2*R*,4*S*-2-(2′-Methyl-3′-hydroxy-5′-hydroxymethylenepyridine-C4′)-5,5-dimethylthiazolidine-4-carboxylic acid, the product of the reaction of D-penicillamine and vitamin B6

R. FAGGIANI, H. E. HOWARD-LOCK,[1] C. J. L. LOCK,[1] AND R. ORGIAS

Laboratories for Inorganic Medicine, Departments of Chemistry and Pathology, McMaster University, ABB-266A, Hamilton, Ont., Canada L8S 4M1

Received November 3, 1989[2]

R. FAGGIANI, H. E. HOWARD-LOCK, C. J. L. LOCK, and R. ORGIAS. Can. J. Chem. **69**, 1 (1991).

We have studied the reaction of both D- and L-penicillamine with pyridoxal hydrochloride and examined the products by single crystal X-ray diffraction. The structure of the title compound, **A**, formed by the reaction of D-penicillamine and pyridoxal was determined. Crystals are orthorhombic, $P2_12_12_1$, with cell dimensions $a = 9.507(5)$, $b = 19.185(5)$, $c = 7.766(2)$ Å and $Z = 4$. The structure was solved by standard methods and refined to $R = 0.088$, $R_w = 0.079$ for 2433 independent reflections. **A** exists as a zwitterion, and bond lengths and angles are normal. In the solid state, **A** and the corresponding product obtained from L-penicillamine, **B**, have identical geometrical structure but are of opposite chirality; that is, D-penicillamine produces the 2*R*,4*S* diastereomer and L-penicillamine produces the 2*S*,4*R* diastereomer (with no *S*,*S* and *R*,*R* components). In solution, however, NMR spectra show the presence of both pairs of diastereomers (2*R*,4*S* and 2*S*,4*S*; 2*S*,4*R* and 2*R*,4*R*). In neutral or alkaline solution there appears to be a rapid epimerization at the thiazolidine carbon atom attached to the pyridoxal moiety. Features of the mass, ^{1}H NMR, vibrational, and electronic spectra are also discussed.

Key words: D-penicillamine, vitamin B6, pyridoxal hydrochloride, therapeutic uses, bischemical reactions, structures.

R. FAGGIANI, H. E. HOWARD-LOCK, C. J. L. LOCK et R. ORGIAS. Can. J. Chem. **69**, 1 (1991).

On a étudié la réaction des D- et L-pénicillamines avec le chlorhydrate du pyridoxal et on a examiné la nature des produits obtenus par diffraction des rayons-X par un cristal unique. On a déterminé la structure du composé **A** mentionné dans le titre et formé par la réaction de la D-pénicillamine avec le pyridoxal. Les cristaux sont orthorhombiques, $P2_12_12_1$, avec $a = 9{,}507(5)$, $b = 19{,}185(5)$ et $c = 7{,}766(2)$ Å et $Z = 4$. On a résolu la structure par les méthodes standards et on l'a affinée jusqu'à des valeurs de $R = 0{,}088$ et $R_w = 0{,}079$ pour 2433 réflexions indépendantes. Le composé **A** existe sous le forme d'un zwitterion; ses angles et les longueurs de ses liaisons sont normaux. À l'état solide, les composés **A** et **B** possèdent des structures géométriques identiques, mais de chiralités opposées; c'est-à-dire que la D-pénicillamine conduit au diastéréoisomère 2*R*,4*S* alors que la L-pénicillamine conduit au diastéréoisomère 2*S*,4*R* (sans contamination par les composantes *S*,*S* ou *R*,*R*). Toutefois, en solution, les spectres RMN montrent qu'il existe deux paires de diastéréoisomères (2*R*,4*S* et 2*S*,4*S*; 2*S*,4*R* et 2*R*,4*R*). Il semble que, en solutions neutres ou alcalines, il se produit une épimérisation rapide de l'atome de carbone de la thiazolidine qui est attaché à la portion pyridoxal. On discute aussi des caractéristiques spectrales (masse, RMN du ^{1}H, vibrationnels et électroniques) de ces produits.

Mots clés : D-pénicillamine, vitamine B6, chlorhydrate du pyridoxal, usage thérapeutique, réactions bischimiques, structures.

[Traduit par la revue]

Introduction

D-(−)-Penicillamine is a synthetic amino acid, which has been used in the treatment of rheumatoid arthritis since 1973 when its efficacy as an anti-arthritic drug was firmly established. In addition, D-(−)-penicillamine has an older, well-established use in the treatment of patients suffering from Wilson's disease, as well as uses in the treatment of heavy metal poisoning, cystinuria, multiple sclerosis, and chronic aggressive hepatitis (1).

Only the stereochemically pure D-isomer of penicillamine is employed as a therapeutic agent because it has been shown that the administration of the racemate or the L-isomer causes greater toxicity. Penicillamine causes inhibition of the kynurenine pathway and pyridoxine metabolism (2), the reduction of the activities of liver transaminases and liver cysteine desulfhydrase (3, 4), the inhibition of collagen fibre crosslinking (5), and the inhibition in bone marrow of DNA, RNA, and protein synthesis (6). In all but the last of the toxic effects cited above, penicillamine is acting on an ubiquitous coenzyme called pyridoxal-5-phosphate. This fact is borne out by studies that have shown that the administration of penicillamine creates a need for supplements of vitamin B_6, a pyridoxal-5-phosphate precursor (2, 7).

The principal derivatives of vitamin B_6 are pyridoxal, pyridoxal-5-phosphate, pyridoxamine, and pyridoxine, all of which are interconvertible in vivo (2). The postulated targets of penicillamine are the aldehydes, pyridoxal and pyridoxal-5-phosphate. The aldehydic function present in these structures has been shown to be the site through which the coenzyme binds to different apoenzymes to form active holoenzymes. This binding takes the form of a Schiff's base linkage (8).

Penicillamine, being an aminothiol, reacts with aldehydes to form five-membered ring thiazolidine-4-carboxylic acids, which are stable under physiological conditions (9). More significantly, competition experiments have shown that aminothiols can react with Schiff's bases to form thiazolidines (10). This result implies that penicillamine can interact directly with enzyme bound pyridoxal, and such a reaction is believed to occur when penicillamine is administered as a drug.

Previous work has provided substantial evidence that the thiazolidine products of the reactions are formed in solution (9), but the preparation of the reaction products in the solid state has been dealt with only fleetingly. Heyl *et al.* (11) reported the preparation of a thiazolidine product from pyridoxal and penicillamine but their characterization of the product was minimal, and was confined to an elemental analysis and a melting point.

We became interested in the factors that control the absolute

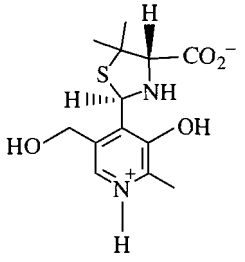
[1]Authors to whom correspondence may be addressed.

[2]Revision received June 26, 1990.

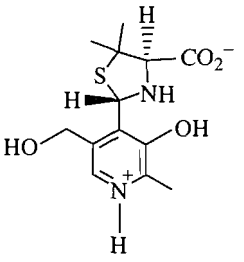
Can. J. Chem. Downloaded from www.nrcresearchpress.com by 195.138.81.100 on 09/07/12
For personal use only.

Can. J. Chem. Downloaded from www.nrcresearchpress.com by 195.138.81.100 on 09/07/12
For personal use only.

stereochemistry at the C2 position of the thiazolidine ring. In this study, we have attempted to add to the present understanding of the chiral nature of the penicillamine – vitamine B_6 interaction by preparing and characterizing the thiazolidine products (**A** and **B**) arising from the separate reactions of D-(−)- and L-(+)-penicillamine, respectively, with pyridoxal.



A



B

The reaction products 2-(2′-methyl-3′-hydroxy-5′-hydroxymethylenepyridine-C4′)-5,5-dimethyl-4-thiazolidine carboxylic acid (**A** = 2*R*,4*S*; **B** = 2*S*,4*R*) were prepared in a crystalline form to allow study of their configurations by single crystal X-ray diffraction. Although the crystal structures of both **A** and **B** were determined, they are enantiomers with no significant differences in their structures; hence only data for **A** are reported here. Spectroscopic characterization (NMR, vibrational, electronic, mass) of the reaction products was also undertaken.

Experiments

Pyridoxal hydrochloride, L-(+)-penicillamine (free base), and D-(−)-penicillamine (free base) were of reagent grade as supplied by Sigma Chemical Co., St. Louis, MO. All other reagents were of standard laboratory grade.

*2-(2′-Methyl-3′-hydroxy-5′-hydroxymethylenepyridine-C4′)-5,5-dimethyl-4-carboxylic acid (**A** and **B**)*

Pyridoxal hydrochloride (0.5000 g, 2.5 mmol) was dissolved in 50 mL of water and the pH adjusted to 8.0 by the dropwise addition of dilute NH_4OH. The pH was monitored with a pH meter (Corning model 120). To this solution was added 0.3665 g (2.5 mmol) of D- or L-penicillamine (to give the products **A** and **B**, respectively). The mixture was stirred at room temperature with a magnetic stirrer until the gradual disappearance of the characteristic yellow colour of pyridoxal signalled that the reaction was complete (about1 h). The solution was filtered by suction to remove any unreacted solids, and was stored undisturbed at room temperature in the dark. Some crystallization was evident after 24 h but the solution was allowed to sit for 4 days before being filtered. The pale yellow crystals were collected by suction on a fritted glass filter and washed successively with water, ethanol, and ether. Yield: 0.5661 g (77.4%) (**A**), 0.5968 g (81.5%) (**B**).

Analysis (by Guelph Chemical Laboratories Ltd., Guelph, Ontario) for **B**: calcd. for $C_{13}H_{18}N_2O_4S$: C 52.5, H 6.0, N 9.4, S 10.7; found: C 52.5, H 6.2, N 9.4, S 9.9. For **A**, $[\alpha]_D^{27}$ +19.4° (*c* 1, 0.1 N HCl); for **B**, $[\alpha]_D^{27}$ −19.7° (*c* 1, 0.1 N HCl). **A** and **B** were insoluble in saturated hydrocarbon solvents, chlorinated methanes, and ether. They were slightly soluble in methanol and ethanol and were soluble in dimethyl sulfoxide on warming. Solubility in water depended on pH; they were insoluble in neutral water but soluble in acidic or basic solutions.

*2-Phenyl-5,5-dimethylthiazolidine-4-carboxylic acid (**C** and **D**)*

Benzaldehyde (0.05 mL, 0.5 mmol) was mixed with 0.0733 g (0.5 mmol) of either D- or L-penicillamine (to give the products **C** and **D**, respectively) in 10 mL of water at pH 8.0 (pH adjusted with dilute NH_4OH). The solution yielded a white precipitate after 2 h of stirring. The precipitate was collected by suction and washed with ethanol and ether. Yield: 0.0490 g (41%) (**C**), 0.0341 g (29%) (**D**).

Spectral measurements

Infrared specrtra were recorded over the range 4000–200 cm^{-1} on a Perkin Elmer model 283 spectrophotometer with samples in the form of KBr pellets (at a concentration of ~1–10% by weight). The spectra were calibrated with polystyrene. Infrared spectra were also recorded in the range 500–100 cm^{-1} on a Nicolet 7199 FT-IR spectrometer with samples prepared as Nujol mulls between polyethylene plates. These spectra were automatically corrected for background noise. Raman spectra were obtained by excitation of solid samples with λ 5145 Å radiation from an Innova 90 series argon ion laser operating at an output power of 0–2 W. The spectra were recorded on a Spex 14018 double monochromator. The spectrometer was calibrated against neon and indene, and the wavenumber readout was accurate to ±2 cm^{-1}. Ultraviolet–visible spectra were recorded on a Hewlett Packard 8451 Å diode array spectrophotometer. The samples were contained in quartz cuvettes with path lengths of 1 cm; sample concentrations were 10^{-5}–10^{-4} molar. All spectra were of water solutions and run against an overlaid water reference. Sample solutions of varied pH were prepared by the addition of 0.1 N HCl or 0.1 N KOH to standard solutions. The optical activities of aqueous solutions were measured with use of the sodium D line (589 nm) and a Perkin Elmer 241 MC polarimeter, the sample chamber temperature being kept at 27°C. Samples were prepared in 0.1 N HCl solution at concentrations of 10 g L^{-1} and were measured against an overlaid reference solution. Mass spectral data were obtained with a VG micromass 7070F spectrometer equipped with a Digital PDP-8 computer. The electron impact method of ionization was used, with an electron potential of 70 eV, direct probe introduction, an ion source temperature of 220°C, and an emission current of 100 μA. The ^1H NMR spectra were recorded at 90 MHz on a Varian EM 390 spectrometer. Samples were prepared in DMSO-d_6 and D_2O solutions at concentrations of approximately 20 g L^{-1} of solvent. Tetramethylsilane and trimethylsilylpropionic acid were used as internal standards.

Collection of the X-ray diffraction data

The X-ray studies were carried out on single crystals sealed in Lindeman capillary tubes, in order to protect against decomposition. Precession photographs of the crystals indicated that they were orthorhombic. The unit cell parameters were obtained from least-squares fit of χ, φ, and 2θ for 15 reflections in the range $19.1° < 2\theta < 31.8°$, measured on a Syntex $P2_1$ diffractometer having graphite monochromated MoKα radiation (λ = 0.71069 Å). Crystal data and other parameters related to data collection are summarized in Table 1. The density of the crystals was measured by suspension in a dichloromethane–bromoform mixture. Intensities were also measured with use of the Syntex $P2_1$ diffractometer and a coupled θ(crystal)–2θ(counter) scan. The methods of selection of scan rates and initial data treatment have been described (12, 13). Corrections have been made for Lorentz and polarization effects but not for absorption. This will make a maximum error in F_o of 1.0%.

Solution of the structure

Phases were determined by direct methods with use of 230 reflections with $|E| > 1.789$ and 12 sets of starting phases. All non-hydrogen atoms were found in the resulting *E* map. Subsequent refinement and electron density difference syntheses revealed all the hydrogen atoms except one. Attempts to refine hydrogen atoms led to divergent functions, so the hydrogen atoms were placed at the positions given in the difference synthesis with temperature factors of about twice those of the atoms to which they were attached, and were not refined in further cycles. Temperature factors for sulfur and oxygen atoms and adjacent carbon atoms were made anisotropic. The significance of the additional parameters was tested at each stage (14). Full-matrix least-squares refinement, which minimized $\Sigma w(|F_o|-|F_c|)^2$, was continued until the maximum shift/error was <0.1. No corrections were needed for secondary extinction.

TABLE 1. Crystal data

Formula	$C_{13}H_{18}N_2O_4S$
Formula weight	298.36
Crystal shape, size (mm)	Acicular, 0.10 × 0.11 × 0.35
Systematic absences	$h00$, $h = 2n + 1$, $0k0$, $k = 2n + 1$, $00l$, $l = 2n + 1$
Space group	$P2_12_12_1$ (No. 19)
Unit cell (Å)	a = 9.507(5), b = 19.185(5), c = 7.766(2)
Volume (Å^3)	1416.5(9)
Z	4
ρ_{calc}, ρ_{obs} (g cm^{-3})	1.399, 1.40(1)
Temperature (°C)	22
Linear absorption coeff (cm^{-1})	2.44
Reflections collected, max 2θ	h, k, $\pm l$, 55°
Standard reflections (esd)	3 0 2 (0.016), 2 2 −1 (0.015)
No. of reflections collected	5354
R_{merg}	0.0284
No. of unique reflections	2510
No. with $I > 0$, used	2433
Final R,[a] R_w[a]	0.0876, 0.0787
Final shift/error, max, ave.	0.013, 0.002
Final difference map, max, min (e Å^{-3})	1.10, −0.73
Weighting scheme	$w = (\sigma_F^2 + 0.00090F_o^2)^{-1}$
Error in an observation of unit wt., S[b]	1.422

[a] $R = \Sigma||F_o| - |F_c||/\Sigma|F_o|$; $R_w = \{\Sigma w(|F_o| - |F_c|)^2/\Sigma wF_o^2\}^{1/2}$.
[b] $S = [\Sigma w(|F_o| - |F_c|)^2/(m-n)]^{1/2}$.

Scattering curves were taken from Cromer and Waber (15) and anomalous dispersion corrections were taken from Cromer (16) and applied to the curves for S, N, O, and C. The atom parameters are listed in Table 2.[3,4]

Discussion

The structure of **A** is shown in Fig. 1 and bond distances and angles are given in Table 3. As can be seen, the configuration at the chiral C2 carbon atom is *R* while that at C4 is *S*. The conformation is such that the hydrogen atoms at C2 and C4 are *trans*. The thiazolidine ring resembles an open envelope with C5 lying 0.682(5) Å out of the rough plane of the other four atoms. This is different from both (*S*)-2,2,5,5-tetramethylthiazolidine-4-carboxylic acid (21) and (*R*)-thiazolidine-4-carboxylic acid (22). The small N3,C4,C1,O1 torsion angle (11.9(4)°) is in agreement with those in related structures we and others have examined (21–25) and again appears to be caused by non-bonding steric interactions rather than intramolecular hydrogen bonding. Although the N3...O1 distance is short, the N3—H3...O2 angle (118°) lies well outside the N...O/N—H...O relationship established by Brown (26). The pyridine ring (max. dev. C2′, 0.007(6) Å) and the exocyclic atoms (largest dev. C51′, 0.035(9); O5′, 0.066(9); C2, 0.053(8) Å) are very close to planar. The dihedral angle of 60.7(2)° between the pyridine ring and the thiazolidine ring is determined by the strong internal hydrogen bond between O3′—H3′ and N3. Since N3 is roughly coplanar with the pyridine ring, the thiazolidine ring may be regarded as bent out of the pyridine ring plane about a C2—N3 hinge.

TABLE 2. Atomic positional parameters (×10^4) and temperature factors (Å^2 × 10^3).

Atom	x	y	z	U_{eq}[a]
S1	281(2)	1024(1)	2522(2)	40
C2	1004(5)	1009(2)	4722(6)	26
N3	603(5)	1681(2)	5524(5)	28
C4	−298(5)	2115(2)	4408(6)	28
C5	104(5)	1975(2)	2509(7)	30
C1	−124(5)	2890(2)	4917(6)	31
O1	858(4)	3043(2)	5901(5)	40
O2	−1023(5)	3303(2)	4304(5)	51
C51	1489(7)	2320(3)	1991(8)	49
C52	−1102(8)	2157(3)	1266(8)	55
N1′	−369(4)	−779(2)	7499(6)	32
C2′	−838(5)	−160(2)	8020(6)	28
C3′	−433(5)	436(2)	7113(5)	22
C4′	476(5)	372(2)	5706(6)	23
C5′	948(5)	−298(2)	5230(6)	27
C6′	505(6)	−856(2)	6166(6)	32
C21′	−1805(6)	−135(3)	9532(7)	43
O3′	−940(4)	1041(2)	7667(5)	42
C51′	1964(7)	−405(3)	3736(8)	47
O5′	2304(5)	−1101(2)	3460(6)	51

[a] $U_{eq} = 1/3\ (U_{11} + U_{22} + U_{33})$.

[3]Tables of anisotropic temperature factors, hydrogen atom positions, bond lengths and angles involving hydrogen atoms, best planes, dihedral and torsional angles, moduli of F_o and F_c for **A**, and all vibrational bands in the region 4000–100 cm^{-1} for D-penicillamine, **A** (or **B**), and **C** (or **D**) may be purchased from the Depository of Unpublished Data, CISTI, National Research Council of Canada, Ottawa, Ont., Canada K1A 0S2.

Tables of hydrogen atom positions and bond lengths and angles involving hydrogen atoms have also been deposited with the Cambridge Crystallographic Data Centre and can be obtained on request from The Director, Cambridge Crystallographic Data Centre, University Chemical Laboratory, Lensfield Road, Cambridge CB2 1EW, U.K.

[4]All calculations were carried out on a CYBER 170/815 computer. Initial data treatment was performed with programs from the XRAY76 package (17). The structure was solved by means of SHELX (18). The least-squares planes calculations used NRC-22 (19) and diagrams were prepared with the use of SNOOPI (20).

Can. J. Chem. Downloaded from www.nrcresearchpress.com by 195.138.81.100 on 09/07/12
For personal use only.

TABLE 3. Interatomic distances (Å) and angles (°)

S1—C2	1.842(5)	C2–N3	1.481(6)	N3—C4	1.476(6)
C4—C5	1.547(7)	C5—S1	1.833(4)	C2—C4′	1.526(6)
C4—C1	1.548(7)	C1—O1	1.241(6)	C1—O2	1.260(6)
C5—C51	1.528(8)	C5—C52	1.539(8)	N1′—C2′	1.332(6)
C2′—C3′	1.396(6)	C3′—C4′	1.399(6)	C4′—C5′	1.411(6)
C5′—C6′	1.360(7)	C6′—N1′	1.336(7)	C2′—C21′	1.492(7)
C3′—O3′	1.330(6)	C5′—O51′	1.524(8)	C51′—O5′	1.390(6)
C5—S1—C2	93.1(2)	S1—C2—N3	106.3(3)	C2—N3—C4	113.2(4)
N3—C4—C5	108.6(4)	C4—C5—S1	101.0(3)	S1—C2—C4′	110.7(3)
C4′—C2—N3	113.7(4)	N3—C4—C1	109.3(4)	C1—C4—C5	112.5(4)
C4—C1—O1	117.7(4)	C4—C1—O2	115.9(4)	O1—C1—O2	126.4(5)
C4—C5—C51	112.9(4)	C4—C5—C52	112.0(4)	S1—C5—C51	110.7(4)
S1—C5—C52	107.3(3)	C6′—N1′—C2′	122.9(4)	N1′—C2′—C3′	118.9(4)
C2′—C3′—C4′	119.6(4)	C3′—C4′—C5′	118.7(4)	C4′—C5′—C6′	118.6(4)
C5′—C6′—N1′	121.3(4)	N1′—C3′—C31′	118.3(4)	C3′—C2′—C21′	122.8(4)
C2′—C3′—O3′	116.8(4)	C4′—C3′—O3′	123.6(4)	C3′—C4′—C2	121.7(4)
C3′—C4′—C2	119.6(4)	C4′—C5′—C51′	121.6(4)	C6′—C5′—C51′	119.8(4)
C5′—C51′—O5′	113.2(4)	C51—C5—C52	112.1(5)		

Possible hydrogen bonds

O3′...N3	2.535(5)	O3′—H3′	0.69[c]	H3′...N3	1.89	O3′—H3′...N3	156
N1′...O1[a]	2.620(5)	N1′—H1′	0.96	H1′...O1	1.67	N1′—H1′...O1	169
O5′...O2[b]	2.719(6)						

[a,b]Atoms are related to those in Table 2 by the relationships *a*; -*x*, *y*-1/2, 3/2-*z*; *b*; -*x*, y-1/2, 1/2-*z*.
[c]No errors are given since the hydrogen atom parameters were not refined.

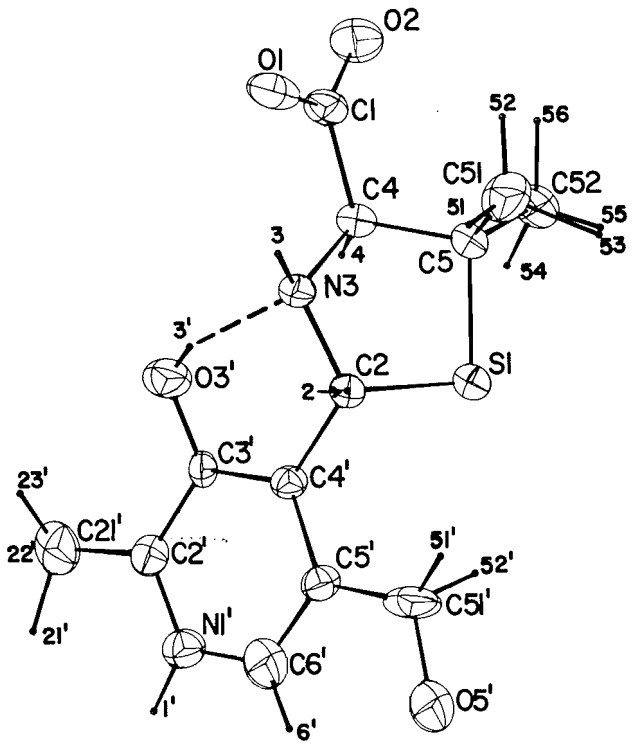


FIG. 1. The molecule of **A** showing the atom numbering. The view is down the H2—C2 bond. Hydrogen atoms are indicated by affixes only in smaller print.

The bond lengths and angles within the thiazolidine ring are consistent with values found for (*S*)-2,2,5,5-tetramethylthiazolidine-4-carboxylic acid, except for the C2—N3—C4 angle, which is significantly larger (113.2(4)° vs. 108.6(4)°, 107.9(4)°) (21) and closer to the value found for protonated amines as in bis((*S*)-5,5-dimethylthiazolidine-4-carboxylic acid)hydrogen chloride hydrate (112.2°, 109.7°) (27). The structural results show no protonation of the nitrogen atom, although there is a very strong internal hydrogen bond to it (N3...O3′, 2.535(5) Å). In the difference map, however, a small peak appeared on the same N3...O3′ axis, about 1 Å from the nitrogen atom, but this disappeared when attempts were made to refine it with partial occupancy. It may be that, in the crystal, there is a small amount of the $O^-...NH_2^+$ tautomer, as well as the major OH...NH tautomer, which could not be detected by the X-ray refinement procedure. The distances and angles within the carboxylate ion differ from those found in both the above structures and are close to those found in (*R*)-thiazolidine-4-carboxylic acid, which exists as the zwitterion tautomer (22). The bond lengths and angles in the pyridoxal ring agree well with average values for a number of N-protonated pyridoxyl rings (28–34). In particular the C6′—N1′—C2′ angle is significantly larger (122.9(4)° vs. 111.3°) than a comparable angle in a non-protonated pyridoxyl ring (35), an effect first noted by Singh (36).

The packing is shown in Fig. 2 and is dominated by the strong hydrogen bonds between adjacent molecules related by the 2_1 axes along the *b* direction. N1′...O1 (2.620(5) Å) is between molecules related by the axis at $x = 0$, $z = 3/4$, whereas O5′...O2 (2.70(5) Å) is between molecules related by the $x = 0$, $z = 1/4$ axis. The resultant bonding of one molecule to four others provides a hydrogen bonding net in the *c* direction as well. Interactions in the *a* direction are van der Waals.

The ^{1}H NMR chemical shifts and assignments for **A** and **B** are presented in Table 4 together with those of **C** and **D** so that analogies can be drawn between the spectra. Both sets of spectra can be readily interpreted if it is assumed that pairs of diastereomers are present in solution for each compound (**A** has *S*,*S* and 2*R*,4*S* and **B** has *R*,*R* and 2*S*,4*R*). This is shown by the splitting of all peaks except that for H6′. We assume that the lack of visible splitting of the H6′ proton peak is caused by limita-

Can. J. Chem. Downloaded from www.nrcresearchpress.com by 195.138.81.100 on 09/07/12
For personal use only.

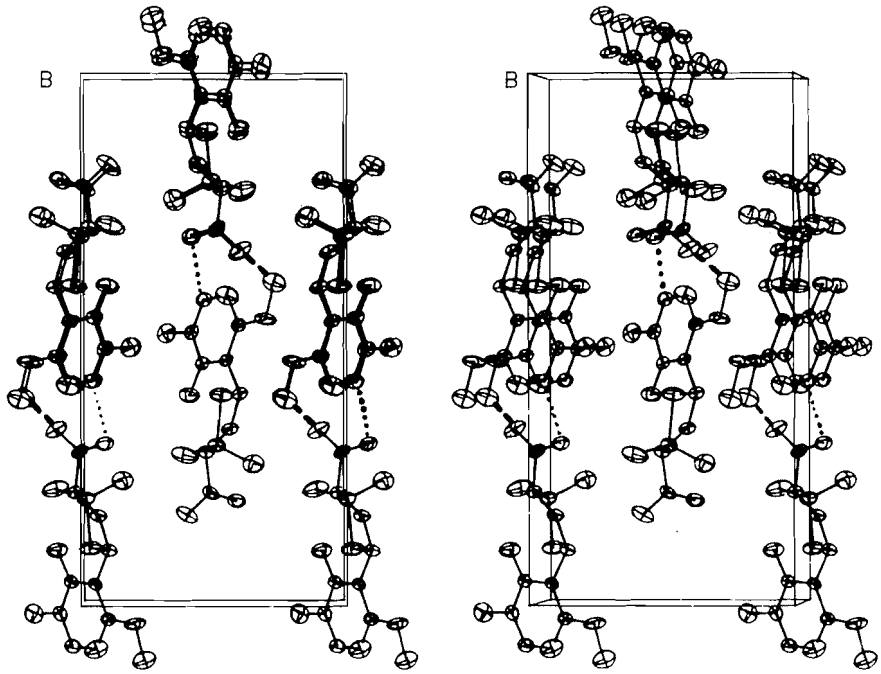


FIG. 2. The packing **A** within the unit cell. *a* and *b* are parallel to the bottom and side of the page and the view is down *c*. Hydrogen bonds are given by dashed (O5′---O2) or dotted (N1′...O1) lines.

TABLE 4. ^{1}H NMR chemical shifts of various thiazolidine-4-carboxylic acids

Compound[a]	%	Diastereomer	α-CH_3 H-7	β-CH_3 H-8	H2i′ *i* = 1–3	H2	H5i′ *i* = 1,2	H4	H6′	Aromatic
A	22	*S,S*	1.38	1.58	2.30	3.88	4.45	6.33	7.82	—
	78	2*R*,4*S*	1.43	1.63	2.35	3.75	4.45	5.93	7.82	—
B	20	*R,R*	1.38	1.59	2.30	3.90	4.45	6.33	7.84	—
	80	2*S*,4*R*	1.44	1.63	2.35	3.76	4.45	5.95	7.84	—
C	30	*S,S*	1.33	1.58	—	3.63	—	5.90	—	7.4 m
	70	2*R*,4*S*	1.40	1.70	—	3.72	—	5.67	—	7.4 m
D	33	*R,R*	1.33	1.56	—	3.60	—	5.88	—	7.4 m
	67	2*S*,4*R*	1.38	1.68	—	3.67	—	5.65	—	7.4 m

m = multiplet

[a]**A** and **B** are solutions of 2*R*,4*S* and 2*S*,4*R* 2-(2′methyl-3′-hydroxy-5′-hydroxymethylenepyridine-C4′)-5,5-dimethylthiazolidine-4-carboxylic acid. **C** and **D** are solutions of the 2-phenyl-5,5-dimethylthiazolidine-4-carboxylic acids derived from *S*-penicillamine and *R*-penicillamine respectively.

tions in resolution of the NMR instrument or chance coincidence. Comparison of the spectra of **C** and **D** with those of **A** and **B**, together with consideration of the intensities, shows that the peak at $\delta \approx 2.3$ is caused by the methyl group of the substituted pyridine ring. The resonance at $\delta \approx 7.82$ is assigned to the hydrogen atom at the C6′ position of the substituted pyridine ring and the resonance at $\delta \approx 4.45$ to the CH_2 protons at the 5′ position. The proton of the C4 position of the thiazolidine ring can be assigned the resonances at ≈5.92 and ≈6.3. The assignment is consistent with assignments of similar compounds examined by other workers (37). The C51 and C52 methyl group protons are assigned by analogy to penicillin (38).

The assignment of the resonances to *S,R* and *S,S* (or *R,S* and *R,R*) is based on the work of McMillan and Stoodley (37). Talking about the protons at C2 and C4 in similar compounds, they state: "In particular, if both stereoisomers at C2 are available, the isomer in which the C4 proton appears at lower field possesses the *trans* configuration." Thus the "*trans*" diastereomer, which is the one of which the structure was determined, is the major component in solution and this is more stable. The apparent contradiction, that only one diastereomer was found in the solid state, whereas the ^{1}H NMR spectra showed that in solution both diastereomers were present (that is, a solution of **A** contained both 2*R*,4*S* and *S,S* diastereomers with the corresponding pair for **B**), can be explained in two ways:

(a) The products **A** and **B** were obtained from a mixture of diastereomeric crystals but the crystals chosen for study just happened to be 2*R*,4*S* and 2*S*,4*R*.

(b) The products **A** and **B** in the solid state are single diastereomers that undergo epimerization in solution to give a mixture of diastereomers.

Possibility (a) was tested by performing a powder diffraction study on the product **B**. The measured diffraction pattern agreed with that calculated from the single crystal parameters. It was concluded therefore that possibility (b) holds: rapid epimerization of the thiazolidine products **A** and **B** occurs in solution probably by means of a Schiff's base intermediate (39). The

Can. J. Chem. Downloaded from www.nrcresearchpress.com by 195.138.81.100 on 09/07/12
For personal use only.

TABLE 5. Selected vibrational bands[a]

D-Penicillamine[b]	Pyridoxal·HCl[b]	A[b]	Assignment[c]
		2480, IR	O—H...N bonding
2008, IR		2080, IR	
	1638, IR	1650, IR	ν C=N
	1630, R		
1616, IR		1610, IR	ν_a CO_2^-
1597, IR			
1558, IR			δ_a NH_3^+
	1552, IR	1540, IR	δ NH, δ NH^+
1524, IR			δ_s NH_3^+
1518, R			
1400, R		1400, IR	ν_s CO_2^-
1397, IR		1395, R	

[a]Infrared bands (IR) and Raman shifts (R), in cm^{-1}.
[b]Compounds as defined in the Experiments. D-Penicillamine in single enantiomer, zwitterionic, non single crystalline form; **A** in crystalline form.
[c]Notations: ν = stretching frequency, a = antisymmetric, s = symmetric, δ = deformation.

TABLE 6. Electronic spectra of **A** and pyridoxal as a function of pH

A			Pyridoxal		
pH	λ_{max}[a]	Absorbance (M^{-1} cm^{-1})	pH	λ_{max}	Absorbance (M^{-1} cm^{-1})
3.0	245sh[b]	~2500	1.1		
	295sh	~2500		286	8524
	326	5330			
7.0	245sh	~2500	6.2	250	5574
	295sh	~2500			
	326	4887		314	8463
10.0	245sh	~4000	12.5	236	8437
	318	5249		298	5654
				392	1870

[a]λ_{max}, wavelength in nanometers of band maximum.
[b]sh = shoulder.

diastereomer found in the solid state is that which is least soluble and will be determined not only by molecular stability but also by intermolecular interactions.

The infrared and Raman spectra of **A** and **B** were identical (as were those of **C** and **D**). The frequencies and assignments of the major vibrational bands of the starting materials D-penicillamine and pyridoxal hydrochloride, and of **A**, are listed comparatively in Table 5.[3] The two strong bands between 2500 and 1900 cm^{-1} are typical of medium strong O—H...N bonding in the solid state. That the compounds **A** and **B** exist as zwitterions in the solid state is shown by the presence of strong bands at ca. 1620 and 1400 cm^{-1}, typical of ν_a and ν_s of the CO_2^- group, and the absence of a strong νC=O absorption at 1720 cm^{-1}. Assignments are based on previous work by ourselves (23) and others (40, 41).

The electronic spectra were of interest because the reaction between penicillamine and pyridoxal was monitored by the appearance of a peak at 326 nm, which is characteristic of thiazolidines of pyridoxal (42). The ultraviolet–visible spectra of **A** were examined at three pH values: 3.2, 7, and 10.2. The spectral results are given in Table 6. The spectra of the starting material, pyridoxal hydrochloride, were also obtained at several pH values. For pyridoxal at pH 1.5, where the pyridine nitrogen

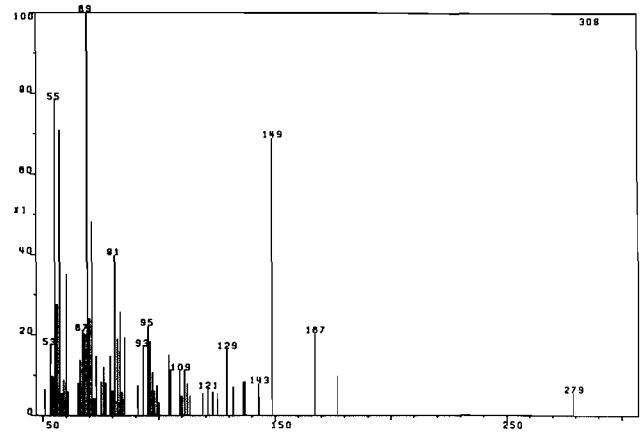


FIG. 3. The mass spectrum of **A**.

atom is protonated, only one absorption maximum at 286 nm is evident, while at pH 12.5, where the phenolic group is deprotonated, three maxima are present. Pyridoxal forms bright yellow solutions at pH values greater than 7.5 because of the presence of the phenoxide-like chromophore.

Compound **A** also has a pH dependent UV spectrum. Formation of the thiazolidine reduces the extent of the delocalization of the phenoxide-like chromophore, and hence the absorption maxima occur at lower wavelengths and the characteristic yellow colour observed for pyridoxal solutions is not present.

A titration of **B** against 0.01 N HCl shows the presence of three titratable protons at pK values of 4.5, 7.5, and 10.1. By comparison with ^{13}C NMR studies done by other workers (43), we have made the following assignments: pK_a 4.5, proton of pyridinium nitrogen; pK_a 7.5, proton of N3 of thiazolidine ring; pK_a 10.1, phenolic hydrogen. These assignments can also be seen to support the pH dependent ultraviolet data.

The mass spectrum is shown in Fig. 3. No parent peak, P^+, is seen; the highest peak at m/e = 279 corresponds to $(P-OH_3)^+$, but the fragment cannot be identified. The principal features below m/e = 200 are very similar to the corresponding spectra for pyridoxal phosphate and pyridoxal, for which the fragmentation patterns have been fully discussed (44, 45). There is little evidence of fragments from the thiazolidine ring through the normal 1,4 cleavage. Peaks at m/e = 69 and 55 have been observed previously for decompositions of thiazolidines derived from D-penicillamine (21). In that case the m/e = 69 peak was derived from a 1,4 fragmentation, whereas in this case it can only be derived from a 2,5 fragmentation. The m/e = 55 peak can also arise from the 2,5 fragmentation, even though the first fragment (m/e = 114) is not observed.

Acknowledgements

We acknowledge, with thanks, financial support from the Natural Sciences and Engineering Research Council of Canada, and McMaster University Science and Engineering Research Board.

1. H. E. HOWARD-LOCK, C. J. L. LOCK, A. MEWA, and W. F. KEAN. Semin. Arthritis Rheum. **15**, 261 (1986), and references therein.
2. I. A. JAFFE, K. ALTMAN, and P. MERRYMAN. J. Clin. Invest. **43**, 1869 (1964).
3. V. DU VIGNEAUD, E. J. KUCHINSKAS, and A. HORVATH. Arch. Biochem. Biophys. **69**, 130 (1957).
4. H. V. APHOSIAN and L. S. BRADHAM. Biochem. Pharmacol. **3**, 38, (1959).

Can. J. Chem. Downloaded from www.nrcresearchpress.com by 195.138.81.100 on 09/07/12
For personal use only.

5. M. E. NIMNI and L. A. BUETHA. Science, **150**, 905 (1965).
6. G. TISMAN, V. HERBERT, L. T. GO, and L. BRENNER. Proc. Soc. Exp. Biol. Med. **139**, 355 (1972).
7. C. A. MCAULIFFE and S. G. MURRAY. Inorg. Chim. Acta, **6**, 103 (1972).
8. E. H. FISCHER, A. B. KENT, E. R. SNYDER, and E. G. KREBS. J. Am. Chem. Soc. **70**, 3429 (1948).
9. E. J. KUCHINSKAS and V. DU VIGNEAUD. Arch. Biochem. **66**, 1 (1957).
10. N. D. SCHONBECK. J. Biol. Chem. **250**, 5343 (1975).
11. D. HEYL, S. A. HARRIS, and K. FOLKERS. J. Am. Chem. Soc. **70**, 3429 (1948).
12. R. P. HUGHES, N. KRISHNAMACHARI, C. J. L. LOCK, J. POWELL, and G. TURNER. Inorg. Chem. **16**, 314 (1977).
13. B. LIPPERT, C. J. L. LOCK, B. ROSENBERG, and M. ZVAGULIS. Inorg. Chem. **16**, 1525 (1977).
14. W. C. HAMILTON. Acta Crystallogr. **18**, 504 (1965).
15. D. T. CROMER and J. T. WABER. *In* International tables for X-ray crystallography. Vol. IV. *Edited by* J. A. Ibers and W. C. Hamilton. Kynoch Press, Birmingham, England. 1974. Table 2.2B, pp. 99–101.
16. D. T. CROMER. *In* International tables for X-ray crystallography. Vol. IV. *Edited by* J. A. Ibers and W. C. Hamilton. Kynoch Press, Birmingham, England. 1974. Table 2.3.1, pp. 149, 150.
17. J. M. STEWART. The XRAY76 system. Tech. Rept. TR-446, Computer Science Center, University of Maryland, College Park, MD. 1976.
18. G. M. SHELDRICK. SHELX. Program for crystal structure determination. University of Cambridge, England. 1976.
19. F. A. AHMED and M. E. PIPPY. NRC-22, Mean plane and torsional angles. National Research Council of Canada, Ottawa, Canada. 1976.
20. K. DAVIES. CHEMGRAF Suite, Program SNOOPI, Chemical Design Ltd., Oxford, England. 1983.
21. H. E. HOWARD-LOCK, C. J. L. LOCK, and P. S. SMALLEY. Can. J. Chem. **63**, 2411 (1985).
22. J. LOSCALZO, R. G. KALLEN, and D. VOET. Arch. Biochem. Biophys. **157**, 426 (1973).
23. H. E. HOWARD-LOCK, C. J. L. LOCK, and P. S. SMALLEY. J. Crystallogr. Spectrosc. Res. **13**, 333 (1983).
24. A. CALVO, R. FAGGIANI, D. A. HARVEY, H. E. HOWARD-LOCK, W. F. KEAN, and C. J. L. LOCK. J. Crystallogr. Spectros. Res. **14**, 59 (1984).
25. R. FAGGIANI, H. E. HOWARD-LOCK, C. J. L. LOCK, M. L. MARTINS, and P. S. SMALLEY. Can. J. Chem. **62**, 1127 (1984).
26. I. D. BROWN. Acta Crystallogr. Sect. A: Cryst. Phys. Diffr. Theor. Gen. Crystallogr. **A32**, 24 (1976).
27. H. E. HOWARD-LOCK, C. J. L. LOCK, M. L. MARTINS, R. FAGGIANI, and M. DUARTE. Can. J. Chem. **65**, 878 (1987).
28. S. P. S. RAO, M. D. POOJARY, and H. MANOHAR. Curr. Sci. **51**, 410 (1982).
29. A. MOSSET, F. NEPEV.-JURAS, R. HARAN, and J.-J. BONNET. J. Inorg. Nucl. Chem. **40**, 1259 (1978).
30. F. HANIC. Acta Crystallogr. **21**, 332 (1966).
31. F. GIORDANO and L. MAZZARELLA. Acta Crystallogr. Sect. B: Struct. Crystallogr. Cryst. Chem. **B27**, 128 (1971).
32. J. LONGO and M. F. RICHARDSON. Acta Crystallogr. Sect. B: Struct. Crystallogr. Cryst. Chem. **B36**, 2456 (1980).
33. G. E. BACON and J. S. PLANT Acta Crystallogr. Sect. B: Struct. Crystallogr. Cryst. Chem. **B36**, 1130 (1980).
34. T. FUJIWARA. Bull. Chem. Soc. Jpn. **46**, 863 (1973).
35. J. LONGO, K. J. FRANKLIN, and M. F. RICHARDSON. Acta Crystallogr. Sect. B: Struct. Crystallogr. Cryst. Chem. **B38**, 2721 (1982).
36. C. SINGH. Acta Crystallogr. **19**, 861 (1965).
37. I. MCMILLAN and R. J. STOODLEY. Chem. Commun. 11 (1968).
38. R. A. ARCHER, R. D. G. COOPER, P. V. DEMARCO, and L. F. JOHNSON. Chem. Commun. 1291 (1970).
39. L. SZILAGYI and Z. GYORGYDEAK. J. Am. Chem. Soc. **101**, 427 (1979).
40. D. HEINERT and A. E. MARTELL. J. Am. Chem. Soc. **84**, 3257 (1962).
41. D. HEINERT and A. E. MARTELL. J. Am. Chem. Soc. **81**, 3933 (1959).
42. M. V. BUELL and R. E. HANSEN. J. Am. Chem. Soc. **82**, 6042 (1960).
43. R. C. HARRUFF and W. JENKINS. Org. Magn. Reson. **8**, 548 (1976).
44. G. P. TRYFIATES and R. R. SMITH. *In* Coenzymes and cofactors. Vol. I. Vitamin B6, pyridoxal phosphate. Part A. *Edited by* D. Dolphin, R. Poulson, and O. Avramovic. John Wiley and Sons, New York. 1986.
45. D. C. DEJONGH, S. C. PERRICONE, M. L. GRAY, and W. KORYTNYK. Org. Mass Spectrom. **1**, 155 (1968).

Can. J. Chem. Downloaded from www.nrcresearchpress.com by 195.138.81.100 on 09/07/12
For personal use only.

Corossolone et corossoline, deux nouvelles γ-lactones mono-tétrahydrofuraniques cytotoxiques

DIEGO CORTES[1]

Laboratoire de pharmacognosie, Faculté de médecine et de pharmacie, Université de Rouen, 76800 Saint Etienne du Rouvray, France

ET

SAW HLA MYINT, ALAIN LAURENS, REYNALD HOCQUEMILLER, MICHEL LEBOEUF ET ANDRÉ CAVÉ

Laboratoire de pharmacognosie, Unité de recherche associée n° 496 du Centre national de la recherche scientifique, Faculté de pharmacie, Université Paris-Sud, 92290 Châtenay-Malabry, France

Reçu le 16 mai 1990

DIEGO CORTES, SAW HLA MYINT, ALAIN LAURENS, REYNALD HOCQUEMILLER, MICHEL LEBOEUF et ANDRÉ CAVÉ. Can. J. Chem. **69**, 8 (1991).

Le fractionnement par solvants du contenu des graines d'*Annona muricata* (Annonaceae), guidé par l'activité toxique envers les larves de crevettes et les cellules cancéreuses KB, a permis d'isoler deux nouvelles γ-lactones mono-tétrahydrofuraniques cytotoxiques : la corossolone **1** et la corossoline **2**. La structure de ces deux acétogénines cytotoxiques a été déterminée par analyse des données spectrales, en particulier RMN et SM. La corrélation chimique entre **1** et **2** a été établie par réduction de la corossolone par $NaBH_4$. **1** et **2** constituent les premiers exemples d'acétogénines mono-tétrahydrofuraniques non fonctionnalisées en 4.

Mots clés : Annonaceae, acétogénines, cytotoxicité, corossol, *Annona muricata*.

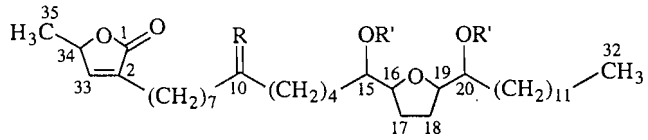
DIEGO CORTES, SAW HLA MYINT, ALAIN LAURENS, REYNALD HOCQUEMILLER, MICHEL LEBOEUF, and ANDRÉ CAVÉ. Can. J. Chem. **69**, 8 (1991).

The fractionation by solvents of the contents of the seeds of *Annona muricata* (Annonaceae), guided by the toxic activity towards the brine shrimp larva and the KB cancer cells, has enabled us to isolate two new cytotoxic mono-tetrahydrofuran γ-lactones: corossolone **1** and corossolin **2**. The structure of these two cytotoxic acetogenins was determined by analysis of the spectral data, NMR and MS in particular. The chemical correlation between **1** and **2** was established by the $NaBH_4$ reduction of corossolone. **1** and **2** constitute the first examples of mono-tetrahydrofuran acetogenins with an unfunctionalized C-4.

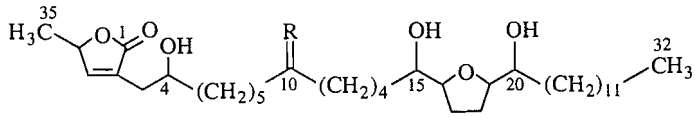
Key words: Annonaceae, acetogenins, cytotoxicity, soursop, *Annona muricata*.

Introduction

Depuis l'isolement de l'uvaricine en 1982 (1), près d'une trentaine de γ-lactones tétrahydrofuraniques ont été isolées, toutes à partir d'espèces de la famille des Annonacées (2, 3). La plupart d'entre elles comportent un enchaînement bis-tétrahydrofuranique (2); seules quelques unes ne possèdent qu'un seul noyau tétrahydrofurane (4–6). Dans ce dernier groupe tous les produits isolés jusqu'ici ont une fonction oxygénée sur le C-4. L'étude des graines d'*Annona muricata* nous a conduits à l'isolement de cinq acétogénines, dont deux produits originaux : la corossolone **1** et la corossoline **2**, premiers représentants d'un nouveau groupe d'acétogénines mono-tétrahydrofuraniques caractérisées par l'absence de fonctionnalisation en position 4, et trois déjà décrites : l'annonacine **3** (4), l'annonacinone **4** (6) et la murisoline **5** (7). Les cinq acétogénines isolées présentent, à des degrés divers, une cytotoxicité sur lignées cellulaires KB et VERO.



1: R = O; R' = H : corossolone
2: R = H,OH; R' = H : corossoline
6: R = O; R' = Ac
7: R = H,OAc; R' = Ac



3: R = H,OH : annonacine
4: R = O : annonacinone
5: R = H,H : murisoline

Résultats et discussion

Le spectre IR de la corossolone **1** contient une bande de carbonyle de γ-lactone insaturée (1745 cm^{-1}), ainsi qu'une bande à 1700 cm^{-1} attribuable à un carbonyle cétonique non conjugué. La formule moléculaire de **1**, $C_{35}H_{62}O_6$, est déduite du spectre de masse à haute résolution de son dérivé diacétylé **6** : MH^+ *m/z* 663,4844 (trouvé); 663,4835 (calculé pour $C_{39}H_{67}O_8$).

Sur le spectre de RMN du ^1H dont l'attribution est réalisée par analyse du spectre 2D ^1H–^1H COSY, on remarque tout d'abord l'aspect typique des signaux dus à une γ-lactone α,β-insaturée substituée en α par une chaîne aliphatique (1) : δ 6,99 (d), 4,99 (dq) et 1,40 (d). La corrélation hétéronucléaire ^1H–^{13}C permet d'attribuer les résonances des carbones C-33, C-34 et C-35 à respectivement δ 148,9, 77,4 et 19,2 (tableau 1). L'existence d'un seul cycle tétrahydrofuranique, comme dans le cas de l'annonacine (4), de la goniothalamicine (5) et de la murisoline (7), est mise en évidence par corrélation entre la RMN du ^1H (δ 3,78, m, H-16 et H-19) et du ^{13}C (δ 82,6 et 82,5). La présence habituelle des deux hydroxyles en α et α′ du cycle tétrahydrofuranique est constatée par corrélation ^1H (δ 3,40, m, H-15 et H-20) et ^{13}C (δ 74,0 et 73,7) : voir tableau 1. En RMN du ^1H, l'absence du système ABX caractéristique des acétogénines hydroxylées en position 4 (8), ainsi que la présence de deux triplets (δ 2,38, 4H, H-9 et H-11 et

1. Auteur à qui adresser toute correspondance.

Printed in Canada / Imprimé au Canada

Can. J. Chem. Downloaded from www.nrcresearchpress.com by 195.138.81.100 on 09/07/12
For personal use only.

TABLEAU 1. Déplacements chimiques de RMN du ^1H ($CDCl_3$, 200 MHz, δ) et de RMN du ^{13}C ($CDCl_3$, 50 MHz, δ) de la corossolone **1**, de la corossoline **2** et de leurs dérivés acétylés **6** et **7**

$^1H/^{13}C$	1*	6	2	7
1	— /173,8	— /173,9	— /174,0	— /173,9
2	— /134,2	— /134,4	— /134,2	— /134,2
3	2,25/ 25,6	2,26/ 25,1	2,25/ 25,1	2,25/ 25,1
4	1,54/ 27,3	1,53/ 27,3	1,52/ 27,3	1,53/ 27,3
5–7	1,25/ 29,6–29,0	1,25/ 29,6–29,0	1,24/ 29,6–29,0	1,26/ 29,6–29,0
8	1,54/ 23,7	1,53/ 23,6	1,24/ 29,6–29,0	1,26/ 29,6–29,0
9	2,38/ 42,8	2,38/ 42,7	1,32/ 37,3	1,53/ 33,9
10	— /211,4	— /211,0	3,57/ 71,6	4,85/ 74,1
11	2,38/ 42,7	2,38/ 42,5	1,32/ 37,2	1,53/ 34,0
12	1,54/ 23,7	1,53/ 23,5	1,24/ 29,6–29,0	1,26/ 29,6–29,0
13	1,25/ 25,1	1,25/ 25,3	1,24/ 25,5	1,26/ 25,2
14	1,38/ 33,4	1,25/ 30,8	1,32/ 33,3	1,53/ 30,7
15	3,40/ 74,0	4,86/ 74,9	3,39/ 73,9	4,85/ 74,9
16	3,78/ 82,6	3,96/ 79,5	3,78/ 82,6	3,97/ 79,5
17–18	1,64, 1,97/ 28,7	1,65, 1,93/ 28,0	1,64, 1,96/ 28,7	1,60, 1,95/ 28,0
19	3,78/ 82,5	3,96/ 79,3	3,78/ 82,6	3,97/ 79,4
20	3,40/ 73,7	4,86/ 74,6	3,39/ 73,9	4,85/ 74,7
21	1,38/ 33,2	1,25/ 30,8	1,32/ 33,2	1,53/ 30,7
22	1,25/ 25,2	1,25/ 25,3	1,24/ 25,5	1,26/ 25,3
23–29	1,25/ 29,6–29,0	1,25/ 29,6–29,0	1,24/ 29,6–29,0	1,26/ 29,6–29,0
30	1,25/ 31,9	1,25/ 31,9	1,24/ 31,8	1,26/ 31,8
31	1,25/ 22,7	1,25/ 22,6	1,24/ 22,6	1,26/ 22,6
32	0,87/ 14,1	0,88/ 14,1	0,87/ 14,0	0,88/ 14,1
33	6,99/148,9	6,99/148,9	6,96/148,9	6,99/148,8
34	4,99/ 77,4	4,99/ 77,4	4,97/ 77,4	5,00/ 77,3
35	1,40/ 19,2	1,40/ 19,2	1,39/ 19,1	1,41/ 19,1
Ac-15,20	— —	2,06/ 21,1, 170,9	— —	2,07/ 21,2–170,9
Ac-10	— —	— —	— —	2,04/ 21,1–170,9

*Attributions réalisées grâce aux spectres de corrélation homonucléaire (^1H–^1H COSY), de corrélation hétéronucléaire (^1H–^{13}C) et de RMN du ^{13}C SPIN ECHO (10). RMN du ^1H, constantes de couplage (J, Hz) : J_{3-4} = 7,2; J_{8-9} = J_{11-12} = 7,5; J_{31-32} = 5,8; J_{33-34} = 1,5; J_{34-35} = 6,7.

δ 2,25, 2H, H-3), indiquent que la corossolone **1** est l'une des rares acétogénines non substituées en 4 (1, 9), mais substituée par une fonction cétonique sur l'une des chaînes aliphatiques (δ 211,4 en RMN du ^{13}C et ν 1700 cm^{-1} en IR). La position en 10 du carbonyle de **1** est déduite de l'étude des fragments observés sur les SM de la corossolone **1** et de la diacétylcorossolone **6** (tableau 2).

Le pic moléculaire en SM de la corossoline **2** (MH^+ 581), ainsi que les pics provenant de la fragmentation entre les carbones C-10 et C-11 (fragment b: voir tableau 2), comportent deux unités de masse de plus que dans le cas de la corossolone **1**, ce qui indique la présence d'un hydroxyle sur le C-10. Les déplacements chimiques observés en RMN du ^1H et du ^{13}C (tableau 1) ont été attribués par le même raisonnement que pour **1**. Enfin, la corrélation chimique entre **1** et **2** a été établie par réduction du carbonyle de la corossolone **1** : l'action de $NaBH_4$ conduit à la formation d'une dihydrocorossolone, identique (co-CCM, IR, RMN et SM) à la corossoline naturelle **2**.

En ce qui concerne la stéréochimie des acétogénines **1** et **2**, nous avons tenté de déduire la configuration relative des centres chiraux du système tétrahydrofuranique α,α′-dihydroxylé (C-15/C-16 et C-19/C-20) de l'étude détaillée des déplacements chimiques en RMN du ^1H de leurs dérivés acétylés **6** et **7**, par rapport aux données des différents stéréoisomères bis-tétrahydrofuraniques diacétylés préparés récemment par synthèse (11, 12). Comme dans le cas de la murisoline **5** (7), les dérivés acétylés de la corossolone **1** et de la corossoline **2**, mais aussi ceux de l'annonacine **3** et de l'annonacinone **4**, présentent des déplacements chimiques très proches pour les paires de carbones C-15/C-20 et C-16/C-19, ce qui permet d'envisager pour ces acétogénines la même configuration relative que celle de la murisoline : *threo, trans, threo* (7).

Les cinq acétogénines isolées des graines d'*A. muricata* présentent donc une certaine homogénéité structurale, puisqu'elles appartiennent toutes au groupe des acétogénines monotétrahydrofuraniques. Disposant de ces cinq acétogénines, il a paru utile de dégager les données spectrales pouvant permettre de différencier les acétogénines de ce type, selon qu'elles sont substituées ou non en 4 et (ou) en 10 par une fonction oxygénée.

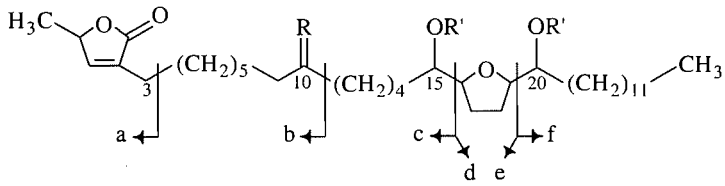
(a) En RMN du ^1H, on constate un blindage des protons en 33 et 34 de la lactone (−0,20 et −0,04 ppm respectivement) des produits non hydroxylés en 4 (corossolone **1**, corossoline **2** et dérivés), par rapport aux produits hydroxylés en 4 (annonacine **3**, annonacinone **4** et murisoline **5**). Cet effet est également observé en RMN du ^{13}C (−3,1 et −0,7 ppm respectivement) (voir figure 1).

(b) Le système ABX, mis en évidence sur le spectre de RMN du ^1H des acétogénines hydroxylées en 4, est absent dans le cas des acétogénines non hydroxylées en 4; ces dernières présentent en revanche un triplet vers δ 2,25 correspondant au CH_2-3 (voir figure 1).

(c) Le spectre de masse, en ionisation chimique, des acétogénines hydroxylées en position 10 (corossoline **2** et annonacine **3**), ne présente pas les coupures caractéristiques en α du cycle tétrahydrofuranique (pics c et e, tableau 2); cependant, les fragments correspondant à la perte d'une

Can. J. Chem. Downloaded from www.nrcresearchpress.com by 195.138.81.100 on 09/07/12
For personal use only.

TABLEAU 2. Fragmentations de **1**, **2**, **6** et **7** en spectrométrie de masse*



	MH^+ (ic)	a	b	c	d	e	f
1	579 (1) 561 (1) 543 (1) 525	111	223 (2) 195	309 (1) 291 (1) (2) 273 263	269 (1) 251	[379] (1) 361 (1) 343	199 (1) 181
2	581 (1) 563 (1) 545 (1) 527	111	225 (1) 207	[311] (1) 293 (1) (2) 275 265	269 (1) 251	[381] (1) 363 (1) 345	199 (1) 181
6	663 (3) 603 (3) 543	111	223 (2) 195	—	311 (4) 269 (1) 251	421 (4) [379] (1) 361 (1) 343	—
7	707 (3) 647 (3) 587 (3) 527	[111]	[267] (4) 225	—	311 (4) [269] (1) 251	465 (3) 405 (3) 345	—

*(1) : perte de H_2O; (2) : perte de CO; (3) : perte de AcOH; (4) : perte de Ac; [ ] : pic très peu abondant.

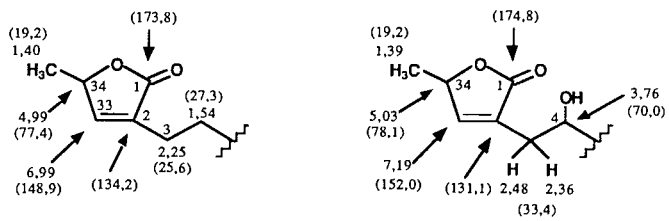


FIG. 1. Différences en RMN du ^1H et du ^{13}C (entre parenthèses), entre la corossolone **1** (acétogénine non hydroxylée en position 4) et la murisoline **5** (7) (acétogénine hydroxylée en 4).

molécule de H_2O à partir de la coupure en α ou α′ du tétrahydrofurane constituent fréquemment les pics de base de ces molécules. Dans le cas des acétogénines portant une cétone en 10 (corossolone **1**, annonacinone **4**), les pics c et e sont présents, mais avec une intensité d'environ 60% par rapport aux fragments c − H_2O ou e − H_2O. En revanche, chez les acétogénines non hydroxylées en 10, telles que la murisoline **5**, on constate la présence de pics de forte intensité correspondant à la coupure entre les carbones C-15 et C-16 (pic c) et entre les carbones C-19 et C-20 (pic e). Ces observations peuvent être aussi appliquées à d'autres acétogenines mono- et bis-tétrahydrofuraniques (1–3).

Enfin, l'étude de l'activité cytotoxique de la corossoline et de la corossolone a été réalisée. La cytotoxicité de la corossoline **2** sur cellules KB ($0,3 \times 10^{-2}$ μg/mL) et sur cellules VERO (10^{-1} μg/mL) est légèrement supérieure à celle de la corossolone **1** (KB : $0,3 \times 10^{-1}$ μg/mL; VERO : 3×10^{-1} μg/mL). D'autre part, ces acétogénines sont plus actives sur la lignée cancéreuse KB que sur les cellules fibroblastiques de rein de singe (VERO).

Partie expérimentale

Pouvoirs rotatoires mesurés sur polarimètre Schmidt–Haensch, type Polartronic I. Spectres enregistrés sur les appareils suivants : UV, Unicam SP 1800; IR, Perkin–Elmer 257; RMN du ^1H et du ^{13}C, Bruker AC-200, respectivement à 200 et à 50 MHz; SM, Nermag–Sidar; SM haute résolution, Kratos MS-80.

Matériel végétal

Les graines d'*A. muricata* ont été récoltées en Guyane française, à Cayenne. Un échantillon d'herbier est conservé au Centre ORSTOM, à Cayenne, sous la référence HJ 2395.

Cytotoxicité

La cytotoxicité a été évaluée par le Laboratoire de virologie–immunologie de la Faculté de pharmacie de Châtenay-Malabry, selon le protocole standard sur cellules épithéliales humaines provenant d'un carcinome de l'épiderme buccal (KB) et sur cellules fibroblastiques de rein de singe (VERO).

Extraction et isolement

Les graines broyées (860 g) sont traitées successivement par l'éther de pétrole, le dichlorométhane et le méthanol. À partir de l'extrait à l'éther de pétrole partiellement évaporé et filtré, on obtient 2,1 g d'un précipité blanc (A). La concentration du filtrat fournit 175 g d'une huile qui est extraite plusieurs fois par le méthanol. Les extraits méthanoliques, après évaporation du solvant sous pression réduite, livrent 8,3 g d'un extrait solide (B). (A) et (B) donnent les réactions des γ-lactones α,β-insaturées (Kedde). Par chromatographie sur colonne de gel de silice 60 H de 1,5 g de (A) et élution par le mélange CH_2Cl_2/AcOEt (4 : 6), les acétogénines suivantes sont successivement obtenues : corossolone **1** (20 mg), corossoline **2** (25 mg), annonacine **3** (230 mg), annonacinone **4** (60 mg) et murisoline **5** (80 mg). Les mêmes acétogénines sont ensuite obtenues par chromatographie de (B).

Corossolone 1

$C_{35}H_{62}O_6$; F 55–57°C (acétate d'éthyle); $[\alpha]_D$ +15° (*c* 0,13;

Can. J. Chem. Downloaded from www.nrcresearchpress.com by 195.138.81.100 on 09/07/12
For personal use only.

MeOH); UV, λ_{max}, EtOH, nm (log ε) : 219 (3,58); IR, ν_{max} (film) : 3415, 2910, 2840, 1745, 1700, 1465, 1410, 1375, 1310, 1065, 1030, 955, 715 cm^{-1}; SM, IC (NH_3) : m/z 596 $(M + NH_4)^+$, voir tableau 2; RMN du ^1H et du ^{13}C : voir tableau 1.

Diacétylcorossolone ***6***

À 5 mg de corossolone **1**, dissous dans 0,1 mL de pyridine, on ajoute 0,2 mL de Ac_2O et on laisse agir 1 nuit à température ambiante. La diacétylcorossolone **6** est obtenue quantitativement. SM haute résolution, IC : m/z 663,4844 (MH^+) trouvé; 663,4835 calculé pour $C_{39}H_{67}O_8$; m/z 603,4633 $(MH - AcOH)^+$ trouvé; 603,4624 calculé pour $C_{37}H_{63}O_6$; m/z 543,4372 $(MH - 2AcOH)^+$ trouvé; 543,4413 calculé pour $C_{35}H_{59}O_4$; m/z 421,2603 (coupure C-19/C-20 : tableau 2) trouvé; 421,2589 calculé pour $C_{24}H_{37}O_6$, tableau 2; RMN du ^1H et du ^{13}C : tableau 1.

Dihydrocorossolone (= corossoline 2)

Le composé **1** (5 mg) en solution dans 1 mL de MeOH est traité par 3 mg de $NaBH_4$ à température ambiante pendant 4 h. Après traitement habituel, la dihydrocorossolone obtenue s'avère identique au produit **2** : corossoline (co-CCM, IR, RMN et SM). SM, IC (CH_4) : m/z 581 (MH^+).

Corossoline 2

$C_{35}H_{64}O_6$; F 45–50°C (acétate d'éthyle); $[\alpha]_D$ +19° (c 0,2; MeOH); UV, λ_{max}, EtOH, nm (log ε) : 212 (4,08); IR, ν_{max} (film) : 3420, 2910, 2840, 1740 cm^{-1}; SM, IC (CH_4): m/z 581 (MH^+), tableau 2; RMN du ^1H et du ^{13}C : tableau 1.

Triacétylcorossoline 7

Obtenue à partir de **2** (Ac_2O/Pyr); SM, IC (CH_4): m/z 707 (MH^+), tableau 2; RMN du ^1H et du ^{13}C : tableau 1.

Remerciements

Le présent travail a été partiellement financé par une subvention DR 8911 du Département de recherche de la Faculté de pharmacie de Châtenay-Malabry, Université de Paris-Sud.

Les auteurs expriment leur gratitude au Dr. J. Cotte-Laffite, du Laboratoire de virologie–immunologie de la Faculté de pharmacie de Châtenay-Malabry, pour l'étude de cytotoxicité réalisée sur les acétogénines d'*A. muricata*.

L'un des auteurs (S.H.M.) remercie le gouvernement français pour l'attribution d'une bourse de coopération France-Birmanie.

1. S. D. Jolad, J. J. Hoffmann, K. H. Schram, J. R. Cole, M. S. Tempesta, G. R. Kriek et R. B. Bates. J. Org. Chem. **47**, 3151 (1982).
2. Y. H. Hui, J. K. Rupprecht, J. E. Anderson, Y. M. Liu, D. L. Smith, C. J. Chang et J. L. McLaughlin. Tetrahedron, **45**, 6941 (1989), et références citées.
3. Y. Fujimoto, C. Murasaki, K. Kakinuma, T. Eguchi, N. Ikekawa, M. Furuya, K. Hirayama, T. Ikekawa, M. Sahai, Y. K. Gupta et A. B. Ray. Tetrahedron Lett. **31**, 535 (1990).
4. T. G. McCloud, D. L. Smith, C. J. Chang et J. M. Cassady. Experientia, **43**, 947 (1987).
5. A. Alkofahi, J. K. Rupprecht, D. L. Smith, C. J. Chang et J. L. McLaughlin. Experientia, **44**, 83 (1988).
6. L. Xu, C. J. Chang, J. G. Yu et J. M. Cassady. J. Org. Chem. **54**, 5418 (1989).
7. S. H. Myint, A. Laurens, R. Hocquemiller, A. Cavé, D. Davoust et D. Cortes. Heterocycles, **31**, 861 (1990).
8. J. K. Rupprecht, C. J. Chang, J. M. Cassady, J. L. McLaughlin, K. L. Mikolajczak et D. Weisleder. Heterocycles, **24**, 1197 (1986).
9. K. Kawazu, J. P. Alcantara et A. Kobayashi. Agric. Biol. Chem. **53**, 2719 (1989).
10. C. Le Cocq et J. Y. Lallemand. J. Chem. Soc. Chem. Commun. 150 (1981).
11. T. R. Hoye et J. C. Suhadolnik. J. Am. Chem. Soc. **109**, 4402 (1987).
12. T. R. Hoye et Z. P. Zhuang. J. Org. Chem. **53**, 5578 (1988).

Can. J. Chem. Downloaded from www.nrcresearchpress.com by 195.138.81.100 on 09/07/12
For personal use only.

Polycarboxylate crown ethers from *meso*-tartaric acid

FRANK R. FRONCZEK AND RICHARD D. GANDOUR
Department of Chemistry, Louisiana State University, Baton Rouge, LA 70803-1804, U.S.A.

AND

THOMAS M. FYLES,[1] PHILIPPA J. HOCKING, SUSAN J. MCDERMID, AND P. DANIEL WOTTON
Department of Chemistry, The University of Victoria, Victoria, B.C., Canada V8W 2Y2

Received, April 17, 1990

FRANK R. FRONCZEK, RICHARD D. GANDOUR, THOMAS M. FYLES, PHILIPPA J. HOCKING, SUSAN J. MCDERMID, and P. DANIEL WOTTON. Can. J. Chem. **69**, 12 (1991).

The synthesis of crown ethers derived from *meso*-tartaric acid was investigated. The sodium salt of the bis(dimethylamide) of *meso*-tartaric acid reacted with diethylene glycol ditosylate to give a mixture of 18-crown-6 tetraamide and 27-crown-9 hexaamide crown ethers. The 2*R*,3*S*,11*S*,12*R* 18-crown-6 isomer crystallized in triclinic space group $P\bar{1}$ (a = 7.557(2), b = 8.866(2), c = 10.4133(13) Å, α = 94.13(2). β = 95.86(2), γ = 99.26(2)°, R = 0.040 for 2090 observed of 3129 unique reflections). The structures of the remaining products were then assigned from the NMR spectra. The solution conformations of the amide crown ethers were examined by NMR, and provide a rationale for the product distribution obtained. One of the 18-crown-6 isomers and a mixture of the two 27-crown-9 isomers were hydrolyzed to the respective crown ether carboxylic acids, and the stability constants for complexation of cations were determined by potentiometric titration. The *meso* tetra- and hexacarboxylates are remarkably nonselective and inefficient cation complexing agents, compared to related crown ethers from *R*,*R*-(+)-tartaric acid, due to the unfavorable conformational control exerted by the tartaro units.

Key words: crown ether synthesis, complexation, crown ether conformation, *meso*-tartaric acid, crystal structure.

FRANK R. FRONCZEK, RICHARD D. GANDOUR, THOMAS M. FYLES, PHILIPPA J. HOCKING, SUSAN J. MCDERMID et P. DANIEL WOTTON. Can. J. Chem. **69**, 12 (1991).

On a réalisé des synthèses d'éthers couronnes dérivés de l'acide *méso*-tartrique. On a fait réagir le sel de sodium du bis-diméthylamide de l'acide *méso*-tartrique avec le ditosylate du diéthylèneglycol et on a obtenu un mélange des éthers 18-couronne-6 tétramide et 27-courone-9 hexamide. L'isomère 2*R*,3*S*,11*S*,12*R* de l'éther 18-couronne-6 cristallise dans le groupe d'espace $P\bar{1}$ (a = 7,557(2), b = 8,866(2) et c = 10,4133(13) Å, α = 94,13(2), β = 95,86(2) et γ = 99,26(2)°; R = 0,040 pour 2090 observées à partir de 3129 réflexions uniques). On a attribué les autres structures sur la base de leurs spectres RMN. En se basant sur la RMN, on a examiné les conformations en solution de l'amide des éthers couronnes et on a ainsi obtenu une explication pour la distribution des produits. On a hydrolysé un des isomères de l'éther 18-couronne-6 ainsi qu'un mélange de deux isomères de l'éther 27-couronne-9 et on a ainsi obtenu les acides correspondants; faisant appel à un titrage potentiométrique, on a déterminé leurs constantes de stabilité pour la complexation de cations. Comparés aux composés correspondants issus de l'acide *R*,*R*-(+)-tartrique, les tétra- et hexa-carboxylates *méso* sont des agents complexants de cations remarquablement inefficaces et non-sélectifs; cet propriété est le résultat d'un contrôle conformationnel non favorable exercé par les unités tartriques.

Mot clés: synthèse d'éthers couronnes, complexation, conformation d'éthers couronnes, acide *méso*-tartrique, structure cristalline.

[Traduit par la Rédaction]

Conformational control of ligand structure is a well-established strategy of ligand design (1, 2), and typically involves the incorporation of a conformationally well-behaved sub-unit into the ligand structure. Nowhere is this more evident than in the numerous macrocycles derived from *R*,*R*-(+)-tartaric acid (3–16). The tartaric acid units exhibit a strong preference for an *anti* disposition, resulting in well-defined conformations in solution (4, 6–8, 13) and in the solid state (17–19). This offers control over lateral interactions from the side arms derived from the carboxylic acid groups (4, 6, 20), results in partial rigidification of flexible ligands (7, 8, 15, 20), and places charged carboxylates in close proximity to bound cations thereby enhancing complex stability (6, 15).

The solution conformation of the parent *R*,*R*-(+)-tartaric acid (21) has *anti* carboxylates. In contrast, the conformation of the *meso* isomer is *gauche* between the carboxylates, observed as an equilibrium mixture of two equivalent *gauche* isomers (21). We expected that a crown ether derived from *meso*-tartaric acid would be capable of a similar conformational equilibrium, and would offer an alternative architecture for manipulation of substituents. We had previously prepared a crown ether diacid derived from *meso*-tartaric acid as a reference compound for comparison with the *R*,*R*-(+)-18-crown-6 diacid (15). The *meso*-diacid crown ether was an ineffective cation-complexing agent; we naively ascribed this to an unfavorable entropy component of the complexation (15).

To more fully explore the complexation chemistry of the *meso* series, we set out to prepare the *meso* 18-crown-6 tetracarboxylic acid incorporating two equivalents of tartaric acid. Unlike the *R*,*R* case, where a single isomer is formed, the *meso* series produces two isomers; a C_{2v} isomer (**3**, Fig. 1), and a C_{2h} isomer (**4**). This report examines the synthesis of the *meso* 18-crown-6 tetraacids, obtained as a mixture with 27-crown-9 hexaacids, and the conformational and complexation properties of all these materials. The study provides further insight into the role of conformational control as a factor in both macrocycle synthesis and complex formation.

Results and discussion

Synthesis

Following the synthetic approach used in the *R*,*R* series (3, 11), the sodium salt of the bis(dimethylamide) of *meso*-tartaric

[1]Author to whom correspondence may be addressed.

Can. J. Chem. Downloaded from www.nrcresearchpress.com by 195.138.81.100 on 09/07/12
For personal use only.

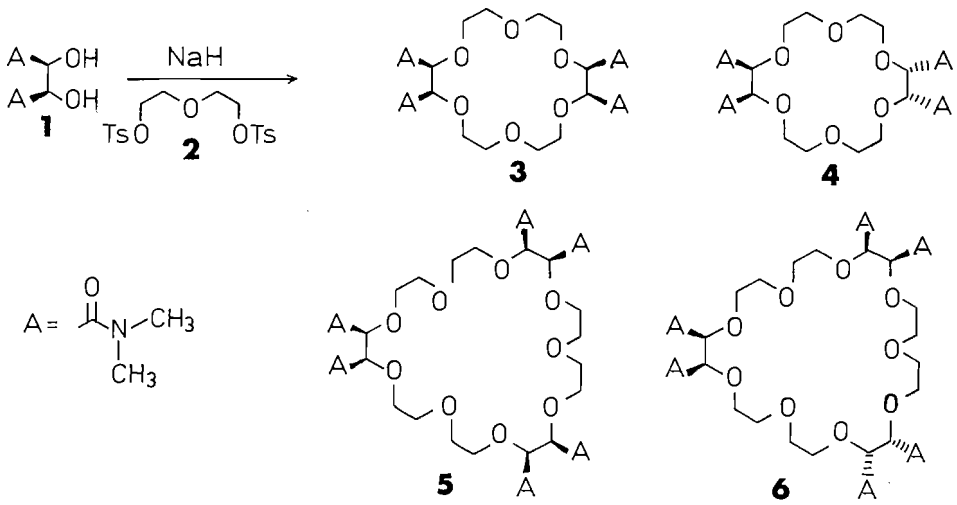


FIG. 1. Synthesis of crown ether amides from *meso* tartaramide.

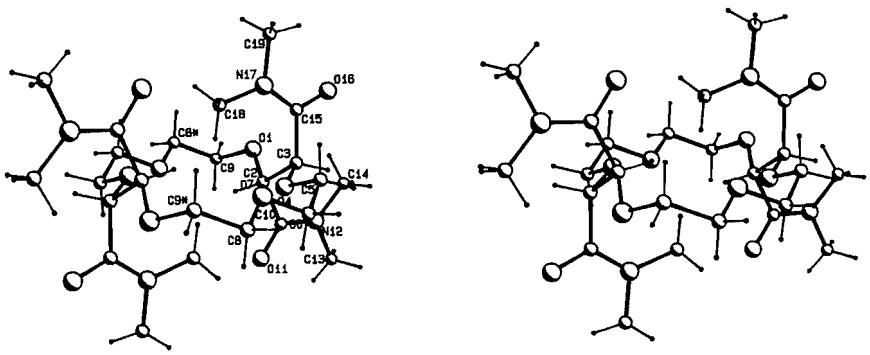


FIG. 2. Stereoscopic view of the solid state structure of **4** showing atom numbering.

acid (**1**) in DMF was treated with an equivalent amount of the ditosylate of diethylene glycol (**2**, Fig. 1). The resulting mixture of oily products was subjected to column chromatography and the fractions were examined by ^{1}H and ^{13}C NMR. Ultimately we were able to recognize four crown ether components. The first could be isolated by acetone trituration of partly purified fractions. Crystals suitable for X-ray structure determination were obtained; Fig. 2 illustrates the structure and identifies the C_{2h} isomer **4**. A second compound mixed with **4** in some fractions was shown to be an isomer by MS and elemental analysis, thus must be the C_{2v} isomer **3**. Other fractions contained a mixture of a compound characterized by a single methine peak in the ^{13}C NMR (78.4 ppm.) and a compound with three methine peaks in the ^{13}C NMR (77.1, 77.5, and 77.8 ppm). Careful gel permeation chromatography of fractions enriched in the "1 methine" product allowed a purified sample to be characterized. It too was an isomer by elemental analysis, but showed a molecular ion in the mass spectrum corresponding to the next higher oligomer, 27-crown-9. From the symmetry implied by the ^{13}C NMR spectrum, this material must be the threefold symmetric isomer **5**. An approximately 1:1 mixture of the "3 methine" material and **5** gave the elemental analysis expected of an isomer and the same mixture gave a mass spectrum identical to **5** alone. On this basis we identified the 3 methine isomer with **6**.

The yields of **3**–**6** are modest. From an initial charge of 40 mmol of **1**, the yields of **3**–**6** are 0.13, 0.45, 0.43, and 0.46 mmol respectively. These correspond to yields of 0.7, 2.2, 3.2, and 3.4% based on the theoretical formation of either 20 mmol of 18-crown-6 or 13.3 mmol of 27-crown-9 derivatives. The total yield of crown ether products is thus 9.5%, compared with yields of 16 (11) and 19% (3) of the single isomer in the *R*,*R* series. Minor amounts of the *R*,*R* series 27-crown-9 derivative can be isolated from the reaction mixture, but these amount to "less than 1% yield" (6). There are thus some key differences between the *R*,*R* and *meso* series: the latter give lower overall yield of crown ethers of any type, but a substantially higher yield of the higher oligomer.

To complete the synthesis, purified **4** and a 1:1 mixture of **5** and **6** were separately hydrolyzed in aqueous acid to give the 2*R*,3*S*,11*S*,12*R*-tetraacid (RSSR18C6A$_4$) and mixed hexaacids m27C9A$_6$ (Fig. 3). Both products gave the expected elemental analysis and equivalent weight by potentiometric titration. Surprisingly, RSSR18C6A$_4$ is relatively insoluble in water: a saturated solution is only 5×10^{-3} M. This is in contrast to the *R*,*R* isomer, which is at least 100-fold more soluble.

Complexation of cations

Complex formation in solution can be described in terms of a cumulative formation constant β_{lmh} defined by the equilibrium between l ligands of charge $-z$, m cations of charge $+y$, and h protons (eq. [1]:

$$[1]\quad lL^{-z} + mM^{+y} + hH^{+} \rightleftharpoons L^{-z}{}_l M^{+y}{}_m H^{+}{}_h$$

$$[2]\quad \beta_{lmh} = \frac{[L^{-z}{}_l M^{+y}{}_m H^{+}{}_h]}{[L^{-z}]^l [M^{+y}]^m [H^{+}]^h}$$

The cumulative formation constants are defined in terms of concentrations. We use corrections for calibration of the pH meter in terms of hydrogen ion concentration (22–26) to give

Can. J. Chem. Downloaded from www.nrcresearchpress.com by 195.138.81.100 on 09/07/12
For personal use only.

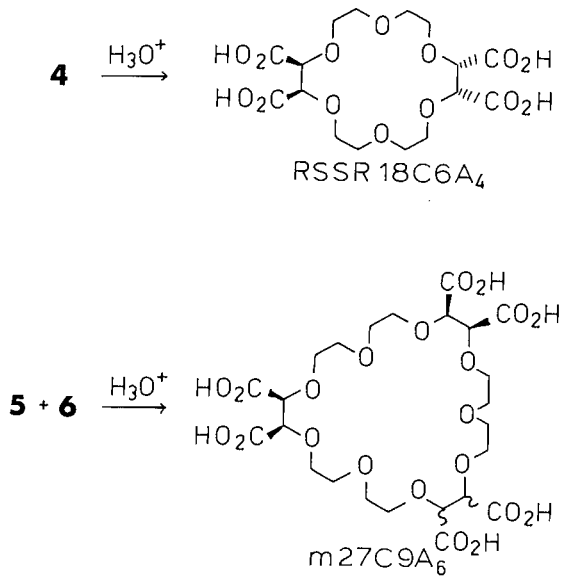


FIG. 3. Synthesis of crown ether polycarboxylic acids.

β_{lmh} values (27) that can be converted to thermodynamic constants through activity coefficient corrections (28, 29).

The acidity and formation constants for complexation of cations by the ligands derived from *meso*-tartaric acid were determined by potentiometric titration (15, 27, 30) (Table 1). These values may be compared with previously determined values for RRRR18C6A$_4$ (15), supplemented by a few new results, also given in Table 1. A cursory inspection of the data shows that the *meso* tetraacid is an inferior cation complexing agent compared to the *R,R* derivative. The differences range from a factor of about 20 for the Na^+ and K^+ to factors of 20–100 000 for the Ca^{2+} and Cd^{2+} complexes. In contrast, the Li^+ and Cs^+ complexes of the *meso* tetraacid are both *more* stable than the corresponding complexes of the *R,R* isomer. The Li^+ complex is 50-fold more stable for the *meso* ligand. The extent of the enhancement is not clear for the Cs^+ complex, because the formation constant could not be determined for the *R,R* derivative.

There are also clear selectivity differences between the two series. Among the univalent cations, the *R,R* derivative favors the larger cations Tl^+ and K^+ and exhibits an 18-crown-6 selectivity modified by a strong electrostatic component (15). The "crown ether" selectivity is absent in the *meso* case. Indeed, K^+ is the most weakly bound of the monovalent ions. As well, the alkaline earth selectivity is reversed between the two series. Even more dramatic is the reversal of the Zn^{2+}/Cd^{2+} selectivity, which involves relatively little difference in the values for zinc, coupled to drastic destabilization of the cadmium complex in the *meso* case.

In contrast, the *meso* 27-crown-9 mixture of isomers offers relatively few surprises. The mixture is relatively unselective apart from a divalent/monovalent selectivity expected from electrostatic considerations. The 27-crown-9 isomer from the *R,R* series binds K^+ with a formation constant of $\log \beta_{110} = 4.0$ (6); thus it appears that the *meso* isomers are less effective cation complexing agents at this ring size as well. A trend favoring larger cations can be discerned, but the selectivities are modest. We rationalize the complexation results in terms of the different macrocycle conformations in the two series; a detailed discussion follows.

Conformational analysis: solid state

An analysis of the conformational differences between the *meso* and *R,R* series explains the complexation and synthetic results. Numerous studies confirm that crown ethers from *R,R*-(+)-tartaric acid adopt a conformation with the carboxylate-derived groups in axial positions on the macrocycle, both in the solid state (17–19) and in solution (4, 6–8, 13). This conformational preference results from preference for an *anti* torsion angle between the carboxylates of the parent tartaric acid (21).

The solid state structure of **4** (Fig. 2) illustrates this conformational bias in the *meso* series. The carboxamide groups are *anticlinal* (C10—C2—C3—C15 torsion angle = 145.8(2)°), as are the tartaro oxygens (O1—C2—C3—O4 torsion angle = 147.1(2)°). The methine hydrogen on C2 points into the cavity, and the oxygen O1 lone pairs out from the macrocycle (Fig. 2). A convergent six-oxygen binding site can only be formed by rotation about both O1—C2 units. The other structural features are typical of crown ethers; the crown C—O bond lengths vary little (1.426 ± 0.005 Å), the C—C bond lengths of the ethylene units are relatively short (1.494 (2) and 1.501 (2) Å), and the average C—O—C bond angle (112.4 ± 1.0°) is somewhat larger than the average C—C—O bond angle (109.5 ± 2.8°) (31).

The observed centrosymmetric conformation is not identical to the "C_i" conformation adopted by uncomplexed 18-crown-6 (32). Polar maps of the torsion angles (Fig. 4)[2] compare the solid-state structures of **4** and 18-crown-6. The major differences are the two torsion angles involving CH_i—O—C—C, where CH_i refers to the carbons with a hydrogen pointing into the cavity. These torsion angles in **4** (C2—O1—C9—C8', 88.8(2)°) and in 18-crown-6 (C9'—O1—C2—C3, −79.7°) differ only in the sign of the torsion angle. Otherwise the remaining 16 torsion angles differ by less than 27.5°. A recently reported structure of a complex of 18-crown-6 with succinic acid (35) has a polar map similar to **4** (Fig. 4). Again the principal differences are a single pair of torsion angles, which in this case involves the rotation about O—CH_i—C—O. The torsion angles are *anticlinal* in **4** (O1—C2—C3—O4, 147.1(2)°) and *gauche* in the succinic acid complex (O8—C9—C12—O11, 73.6(2)° (ref. 35)). From a frequency analysis, Parenteau and Brisse (35) show the torsion angle in the complex (C6—C7—O8—C9, 90.1(2)°) differs "significantly from that normally found" in 18-crown-6-complexes. In **4**, this angle corresponds to the C8'—C9—O1—C2 (88.8(2)°). In addition, the 16 similar torsion angles differ by less than 15.8°.

Conformational analysis: solution

The solid state conformation of **4** prompted us to investigate

[2]Polar maps offer a means to recognize similarity of torsion angles between dissimilar structures (33, 34).[3,4] For an 18-membered ring, the endocyclic torsion angle of each bond is plotted on polar coordinates as the vertices of an octadecagon. A positive torsion angle is plotted from the center of the circular map (0° plus the torsion angle) and a negative torsion angle is plotted from the outer edge (360° minus the torsion angle). In the first instance, the bonds are numbered starting from the O—C bond adjacent to a tartaro unit following the nomenclature convention, thus there are four possible starting points for **4**; the other possible maps of the conformations can be generated by rotation, reflection, and rotation/reflection.[4]

[3]W. D. Celmer. International Symposium on Medicinal Chemistry. Berlin. 1986; personal communication.

[4]P. J. Dutton, F. R. Fronczek, T. M. Fyles, R. D. Gandour, and V. V. Suresh. In preparation.

Can. J. Chem. Downloaded from www.nrcresearchpress.com by 195.138.81.100 on 09/07/12
For personal use only.

TABLE 1. Logarithm of the cumulative and stepwise formation constants of crown ether carboxylic acids[a]

Metal	β_{lmh}	Ligand		
		RSSR18C6$_4$	m27C9A$_6$	RRRR18C6A$_4$[b]
H^+	1 0 1	4.94	5.43	4.88
	1 0 2	8.61 (3.67)	9.66 (4.23)	(4.29)
	1 0 3	11.53 (2.92)	12.02 (2.36)	(2.84)
	1 0 4	14.55 (3.02)	*	(2.13)
L^+	1 1 0	3.8	*	2.1[c]
	1 1 1	8.5 (3.5)	*	—[c]
Na^+	1 1 0	3.3	*	4.5
	1 1 1	7.9 (3.0)	*	(4.1)
K^+	1 1 0	2.9	2.9	4.8
	1 1 1	7.4 (2.5)	8.3 (2.9)	(4.7)
Cs^+	1 1 0	3.3	*	*[c]
	1 1 1	8.1 (3.1)	*	*[c]
Tl^+	1 1 0	3.9	3.4	3.6
	1 1 1	8.3 (3.4)	8.0 (2.5)	4.8
Mg^2	1 1 0	3.3	2.8	*[c]
	1 1 1	8.0 (3.0)	—	*[c]
Ca^{2+}	1 1 0	4.3	5.6	8.6
	1 1 1	8.5 (3.6)	9.6 (4.2)	(7.0)
Sr^{2+}	1 1 0	4.9	5.1	8.0
	1 1 1	9.1 (4.2)	9.5 (4.1)	(6.1)
Ba^{2+}	1 1 0	6.2	6.5	7.2
	1 1 1	10.4 (5.4)	10.7 (5.2)	(6.2)
Cu^{2+}	1 1 0	[d]	5.5	5.3
	1 1 1	[d]	9.5 (4.0)	—
Zn^{2+}	1 1 0	3.8	4.6	4.0
	1 1 1	8.2 (3.3)	8.5 (3.1)	—
Cd^{2+}	1 1 0	2.9	5.5	7.9
	1 1 1	7.4 (2.5)	9.0 (3.6)	(6.0)
Pb^{2+}	1 1 0	7.6	7.7	9.6[c]
	1 1 1	11.6 (6.7)	—	—

[a]Determined at 25°C, I = 0.1 M with tetramethylammonium nitrate. Values in parentheses are for 1:1 association of metal with protonated ligand. The symbol * indicates that no complex was detected. The symbol — indicates that a complex of that stoichiometry was not required to achieve a fit to the titration data. The "proton complexes" are dissociation equilibria and follow the convention of pK_a; uncertainty, +/− 0.1. Uncertainty in log β, +/− 0.2.

[b]Results from ref. 15, I = 0.05 M, tetramethylammonium chloride unless otherwise indicated.[c]

[c]This work.

[d]Precipitation of the ligand precludes titration.

the solution conformations of these crown ethers, by measuring the $^1H-^1H$ coupling constants for the tartaro units. The two hydrogens are equivalent, but the ^{13}C satellites on either side of the resonance arise from an AA'X spin system, from which we can measure $^3J_{HH}$. A similar study of the *R,R* series has been reported (4). The amides **3**, **4**, and **5** give values of $^3J_{HH}$ of 5.0, 5.8, and 7.4 (±0.1) Hz respectively. Using either a single Karplus equation or one extended to correct for the electronegativity of the substituents (8, 36) gives an estimated value of $^3J_{HH}$ of 8.3 Hz for the *anticlinal* conformation in the solid state. The equations predict a value of 2 Hz for the *gauche* conformation. Neither of these limiting cases is the exclusive conformation, and the data compel a significant population of conformations having an *anti* or *anticlinal* relationship between the carboxamides in solution. This conclusion provides a rationalization of the synthetic results and an understanding of the complexation differences between the *meso* and *R,R* series of crown ethers.

Ring closure

From the synthetic perspective, the critical feature is the conformation of the acyclic precursor immediately preceding ring closure to the 18-crown-6 ring size. In the *R,R* isomers, an *anti* disposition of carboxamides places the adjacent oxygens *gauche*, as found in the final product and which facilitates ring

Can. J. Chem. Downloaded from www.nrcresearchpress.com by 195.138.81.100 on 09/07/12
For personal use only.

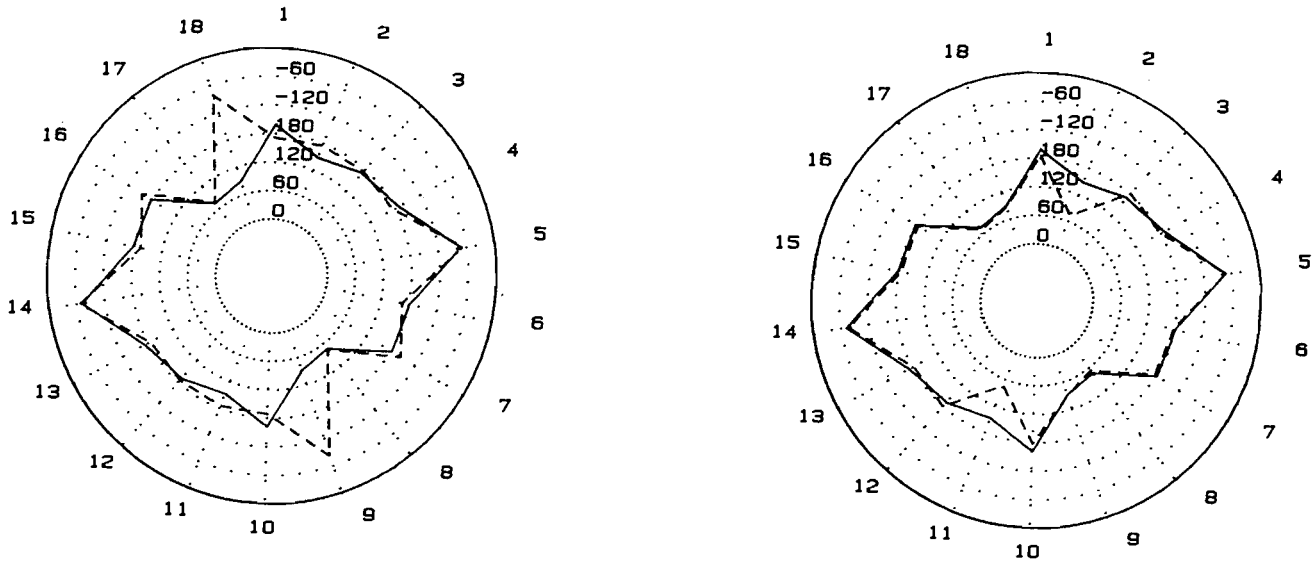


FIG. 4. Polar maps of endocyclic torsion angles. Left: overlap of **4** (—) and 18-crown-6 (32) (---); Right: overlap of **4** (—) and 18-crown-6·succinnic acid complex (35) (---).

closure. If the *meso* acyclic precursor adopts a similar *anticlinal* disposition of carboxamides, the oxygens are also *anti* to one another. This retards ring closure to the 18-crown-6 macrocycle, and prolongs the precursor lifetime in solution. This enhances intermolecular oligomerization and leads to larger ring sizes. It is sufficient to postulate a conformational bias toward an *anti* disposition of oxygens that would be less prone to closure of any ring size. Similar conformational effects on macrocyclization yield are known, notably in the opposite case of enhanced yields of benzo crown ethers relative to unsubstituted crown ethers (37). Precursor lifetime clearly plays a role in determining the ultimate ring size distribution in unsubstituted crown ethers (38); our case is a conformationally biased version of the same process.

Cation complexation

Given a conformational bias in the amides, the carboxylic acids should lie even further towards an *anti* disposition of carboxylates due to electrostatic and dipole effects. A conformation akin to the solid state structure of the precursor amide is thus likely for the tetraacid RSSR-18C6A$_4$ in aqueous solution. Such a conformation offers two scenarios for cation complexation. In cases of favorable cation size or charge, the ligand could act as a simple chelate without reorganization. This might be occurring in the Li^+, Mg^{2+} (high surface charge density), and Cs^+ (large ionic radius) complexes of RSSR-18C6A$_4$, all of which are more stable than their *R,R* counterparts. Conversely, reorganization could accompany cation binding to produce complexes similar to those of the *R,R* series. The energy costs of the reorganization would be exhibited as a smaller stability constant for cation complexation. This scenario is apparently more likely and predicts the general observation of lower stability constant in the *meso* series. The reorganization energy cost and the ultimate stability constant in the 27-crown-9 ring size are both smaller, hence the differences are less pronounced.

The picture that emerges of either *meso* or chiral tartaric acid crown ethers is one of controlled conformations dominated by the influence of the tartaro units. In the *R,R* series, the favored *gauche* conformation of the two oxygens enhances both the synthesis and the cation complexation. In the *meso* series, the favored *anticlinal* conformation diminishes both the synthetic efficiency and the cation complexation.

Experimental

General details

Melting points were taken on a Reichardt hot stage microscope (uncorrected). Proton NMR spectra were recorded with a Perkin–Elmer R32 (90 MHz, CW) or Bruker WM 250 (250 MHZ, FT) spectrometer in $CDCl_3$ or CD_3OD solvent with Me_4Si as internal standard or in D_2O with external Me_4Si in $CDCl_3$ as reference. Carbon NMR spectra were recorded at 62.8 MHz (WM 250) in $CDCl_3$ or CD_2Cl_2 with the central solvent line as standard, or in D_2O with a frequency reference for this solvent previously calibrated against external Me_4Si in $CDCl_3$. Simulation of the second order AA'X spectra for determination of $^3J_{HH}$ was done using a locally constructed package[5] based on UEAITR (39) and NMRPLOT (39). The mass spectra were recorded with a Finnegan 3300 GC–MS instrument with methane chemical ionization. Elemental analyses were performed by Canadian Microanalytical Services, New Westminster, B.C., and are quoted in percentages.

Dimethylformamide was dried over freshly activated 4 Å molecular sieves and dichloromethane was distilled prior to use; other chemicals were used as received. Diethylene glycol ditosylate (**2**) (40) and *meso-N,N,N'N'*-tetramethyltartaramide (**1**) (15) were prepared as previously reported.

2R,3S,11S,12R-N,N,N',N',N'',N'',N''',N'''-Octamethyl-1,4,7,10,13,16-hexaoxacyclooctadecane-2,3,11,12-tetracarboxamide (4)

A 1-L three-necked flask was purged with nitrogen and charged with 3.20 g of NaH (60% in oil, 80 mmol). The solid was washed with four 20-mL portions of pentane, suspended in 100 mL of dry DMF, and a slurry of 8.28 g of **1** (40 mmol) was added in 250 mL of dry DMF. The mixture was allowed to stir at ambient temperature overnight to produce a clear solution, to which 16.64 g of **2** (40 mmol) in 100 mL of dry DMF was added. The mixture was heated to 70°C for 7 h, the DMF was removed under reduced pressure at 40°C, and the resultant off-white solid was evacuated overnight. The solid was slurried in dichloromethane, filtered through Celite, and the filtrate was evaporated to an oil. The oil was dissolved in water (250 mL) and successively extracted with two 250-mL portions each of pentane, ether, dichloromethane, and chloroform. The aqueous layer was further extracted in a

[5]K .R. Dixon and A. Tweedale. Unpublished material, University of Victoria, 1975.

Can. J. Chem. Downloaded from www.nrcresearchpress.com by 195.138.81.100 on 09/07/12
For personal use only.

Can. J. Chem. Downloaded from www.nrcresearchpress.com by 195.138.81.100 on 09/07/12
For personal use only.

continuous liquid/liquid extractor with dichloromethane for 24 h. The combined chlorocarbon extracts were dried over $MgSO_4$, evaporated to an oil, and evacuated for several hours to yield 5.8 g of crude product. Addition of acetone (75 mL) and filtration gave white crystals, which were recrystallized from acetone to give 0.13 g of **4**. The acetone filtrate and mother liquors were combined and evaporated to give 5.5 g of an oil used for the isolation of more **4**, plus **5** and **6** by chromatography as outlined below.

The configuration of **4** was established by X-ray crystallography (below). The total yield of **4** in this preparation, including the material isolated by chromatography (see below), was 0.25 g (2.4%): mp 198°C, ^{1}H NMR (δ, $CDCl_3$): 2.98 and 3.24 (2s, 24H, N $(CH_3)_2$), 3.56 (m, 24H, OCH_2), 4.80 (s, 4H, OCH); ^{13}C NMR (δ, CD_2Cl_2): 36.2 and 37.3 (N $(CH_3)_2$), 69.2 and 71.3 (OCH_2), 80.6 (OCH), 169.2 (CO); MS (*m/z*): 549 (M + 1), 503 (−Me_2NH), 472 (−DMF). Anal. calcd. for $(C_{12}H_{22}N_2O_5)_n$: C 52.56, H 8.08, N 10.21; found: C 52.51, H 8.17, N 10.19.

2R,3S,11R,12S,20R,21S-N,N,N′,N′,N″,N″,N‴,N‴,N⁗,N⁗,N⁗⁗,N⁗⁗-Dodecamethyl-1,4,7,10,13,16,19,22,25-nonaoxacycloheptacosane-2,3,11,12,20,21-hexacarboxamide (5) and 2R,3S,11R,12S,20S,21R-N,N,N′,N′,N″,N″,N‴,N‴,N⁗,N⁗,N⁗⁗,N⁗⁗-dodecamethyl-1,4,7,10,13,16,19,22,25-nonaoxacycloheptacosane-2,3,11,12,20,21-hexacarboxamide (6)

The acetone filtrate from the preparation of **4** (5.5 g) was adsorbed on 28 g of neutral alumina, which was added to a column of neutral alumina (3.5 × 35 cm, 245 g) and eluted with a CH_2Cl_2/MeOH solvent gradient (0, 0.25%, 0.5%, 1.0%, 5.0% MeOH, 1 L each, 500-mL fractions). The fractions eluting with 1% MeOH contained 1.17 g of mixed crown ethers **3**–**6**. Trituration of the oily mixture with acetone yielded solid **4** with **3** as a minor contaminant (see below for isolation of **3**).

The acetone soluble materials were dissolved in a minimum volume of 0.5% MeOH in CH_2Cl_2 and chromatographed on neutral alumina (2.5 × 30 cm, 150 g) using a CH_2Cl_2/MeOH solvent gradient (800 mL 0.5%, 800 mL 0.75%, 1.5 L 1.0% MeOH in CH_2Cl_2). The first 200 mL of the 0.75% MeOH fraction contained **3** mixed with small amounts of **5** and **6** (86 mg). The remaining 600 mL of the 0.75% MeOH fraction and the first 1 L of the 1% MeOH fraction contained **5** and **6** as a mixture (0.68 g). From NMR, the yields of **5** and **6** are 3.2 and 3.4% respectively. The final 500 mL of the 1% MeOH fraction contained **5** and **6** together with additional components not included in the yield calculation.

A small sample of purified **5** was obtained by gel filtration of the 86 mg fraction mixture of **3**, **5**, and **6** on Sephadex LH20 using 4:3 CH_2Cl_2/MeOH as eluent. The first fraction running at the void volume (8.8 mg) was "pure" **5** by NMR analysis; the remaining fractions were mixed, but could be used for the isolation of **3** (below). A further amount of **5** was obtained by gel filtration of the final 1% MeOH fraction. In total, 65 mg of **5** was isolated from various fractions by this tedious gel filtration process, which permitted characterization and $^3J_{HH}$ coupling constants to be determined.

5: clear oil; ^{1}H NMR (δ, $CDCl_3$): 2.95 and 3.11 (2s, 36H, $N(CH_3)_2$), 3.48 (m, 36H, OCH_2), 4.60 (s, 6H, OCH); ^{13}C NMR (δ, CD_2Cl_2): 36.3 and 37.5 ($N(CH_3)_2$), 69.9 and 71.1 (OCH_2), 78.4 (OCH), 169.8 (CO); MS (*m/z*): 823 (M + 1), 777 (−Me_2NH), 749 (−DMF). Anal. calcd. for $(C_{12}H_{22}N_2O_5)_n$: C 52.56, H 8.08, N 10.21; found: C 52.61, H 8.10, N 10.25.

6: obtained only as a mixture with **5**; clear oil; ^{1}H NMR (δ, $CDCl_3$): 2.95 and 3.11 (2s, 36H, $N(CH_3)_2$), 3.48 (m, 36H, OCH_2), 4.62 (br s, 6H, OCH); ^{13}C NMR (δ, CD_2Cl_2): 36–38 (6 lines, $N(CH_3)_2$), 69–71 (m, OCH_2), 77.1, 77.5, and 77.8 (OCH), 170.2 (br, CO); MS (*m/z*) mixture (1:1) with **5**: 823 (M + 1), 777 (−Me_2NH), 749 (−DMF). Mixture (1:1) with **5**, Anal. calcd. for $(C_{12}H_{22}N_2O_5)_n$: C 52.56, H 8.08, N 10.21; found: C 52.56, H 8.27, N 10.22.

2R,3S,11R,12S-N,N,N′,N′,N″,N″,N‴,N‴-Octamethyl-1,4,7,10,13,16-hexaoxacyclooctadecane-2,3,11,12-tetracarboxamide (3)

The mixed fractions from the gel filtration of **3**, **5**, and **6** could be used as a source of pure **3**. Thus an 80 mg fraction, free of **4**, was chromatographed on neutral alumina using 0.75% MeOH in CH_2Cl_2 as eluent (isocratic). A total of 72 mg of **3** was isolated from the early fractions. Yield 0.7%; ^{1}H NMR (δ, $CDCl_3$): 2.97 and 3.22 (2s, 24H, $N(CH_3)_2$), 3.64 (m, 24H, OCH_2), 4.64 (s, 4H, OCH); ^{13}C NMR (δ, CD_2Cl_2): 36.2 and 37.3 ($N(CH_3)_2$), 69.1 and 71.3 (CH_2), 81.0 (OCH), 168.9 (CO); MS (*m/z*): 549 (M + 1), 503 (−Me_2NH), 472 (−DMF). Mixture (1:1) with **4**, Anal. calcd. for $(C_{12}H_{22}N_2O_5)_n$: C 52.56, H 8.08, N 10.21; found: C 52.50, H 8.09, N 10.18.

2R,3S,11R,12S-1,4,7,10,13,16-Hexaoxacyclooctadecane-2,3,11,12-tetracarboxylic acid (RSSR18C6A4)

The tetraamide **4** (0.19 g, 0.35 mmol) was dissolved in 2.5 M HCl (30 mL) and heated at 80°C for 24 h to produce a suspension of a white solid. Removal of the solvent at reduced pressure and evacuation to remove the bulk of the HCl gave a white solid, which was suspended in 20 mL of water and recovered by filtration to yield 120 mg of RSSR18C6A$_4$ (0.25 mmol, 72% yield); ^{1}H NMR (δ, CD_3OD): 3.72 (m, 16H, OCH_2), 4.48 and 4.53 (2s, 4H, OCH); ^{13}C NMR ((δ, CD_3OD): 71.4 and 71.9 (OCH_2), 81.3 (br, OCH), 172.6 (CO). Anal. calcd. for $C_{16}H_{24}O_{14}\cdot 2H_2O$: C 40.34, H 5.93; found: C 40.52, H 5.83. Equivalent weight calcd. for RSSR18C6A$_4\cdot 2H_2O$: 119 g/equiv.; found: 117.9 g/equiv.

Mixture of 2R,3S,11R,12S,20R,21S- and 2R,3S,11R,12S,20S,21R- 1,4,7,10,13,16,19,22,25-nonaoxacyclohepacosane-2,3,11,12,20,21-hexacarboxylic acids (m27C9A6)

A mixture of **5** and **6** (1:1, 0.21 g, 0.25 mmol) was dissolved in 2.5 M HCl (30 mL) and heated at 80°C overnight. The solvent was removed by evaporation at reduced pressure and the bulk of the excess HCl was removed by evacuation to give an oily solid. The solid was dissolved in water (50 mL) and passed down an acidic ion exchange column (Dowex 50W, 250 g). The resin was washed with water and the eluent fractions with pH <3 were combined, evaporated, and evacuated overnight to yield 0.14 g of m27C9A$_6$ (0.20 mmol, 80% yield): ^{1}H NMR (δ, D_2O): 3.5 (m, 28H, CH_2O), 4.4 (m, 6H, OCH); ^{13}C NMR (δ, D_2O): 69.7–70.7 (OCH_2), 79.9 (br, OCH), 172.6 (CO). Anal calcd. for $C_{24}H_{36}O_{21}\cdot 3H_2O$: C 40.34, H 5.93; found: C 40.21, H 5.91. Equivalent weight calcd. for m27C9A$_6\cdot 3H_2O$: 119 g/equiv.; found: 118.1 g/equiv.

Stability constant determinations

Solutions of acid (0.05 M HNO_3) and base (0.05 M tetramethylammonium hydroxide (TMAOH)) were prepared and standardized against primary standards. A constant ionic strength was maintained (0.1 M) by the addition of tetramethylammonium nitrate (TMAN) to both the standard acid and base, as well as by using a 0.1 M TMAN medium for titrations. Standard metal ion solutions (0.05 M) were made from the corresponding nitrates. All reagents were analytical grade or better and were dried before use. The equivalent weight was determined from the average of several titrations and was used to establish ligand homogeneity and purity before the stability constant determinations.

The general procedures and apparatus have been described previously (5, 8, 27). The electrode system was calibrated using commercially available buffers at pH 2.00 and pH 9.18 and linearity was confirmed at pH 6.86 and 4.01. For pK_a determinations, a 4 mL solution of the ligand (approx. 4×10^{-4} M) in 0.1 M TMAN was titrated with standard Me_4NOH containing 0.1 M TMAN to beyond the strong acid – strong base end point (60 μL per ligand equivalent with 0.05 M base) in 2–4 μL aliquots (min. 18 points per ligand equivalent). The data file was processed using SCOGS (30) to yield β_{l0h} for the ligand.

For stability constant determinations, two procedures were used. One followed the procedure for pK_a determination directly, with the addition of an equivalent of metal nitrate solution to the free acid before titration with the base. The other used the solution resulting from the pK_a titration by addition of an equivalent of metal nitrate to the basic solution. This mixture was then back-titrated with standardized 0.05 M HNO_3 (containing 0.1 M TMAN) to the starting acidic pH. The second method, however, is inappropriate for metals that form insoluble

TABLE 2. Crystal data

Crystal size 0.5 × 0.18 × 0.40 mm		$C_{24}H_{44}N_4O_{10}$	FW = 548.63
	Triclinic	Space group $P\bar{1}$	
a = 7.557(2)	b = 8.866(2)	c = 10.4133(13) Å	α = 94.13(2)
β = 95.86(2)	γ = 99.26(2)°	V = 682.2(3) Å^3	d_c = 1.335 g cm^{-3}
μ(MoKα) = 1.0 cm^{-1}	F(000) = 296 e	Z = 1	T = 297 K

TABLE 3. Coordinates for tetraamide **4**

Atom	x	y	z	B_{eq}(Å^2)[a]
O1	−0.1374(2)	−0.3312(1)	0.7319(1)	2.59
O4	0.1023(2)	0.0458(1)	0.8162(1)	2.32
O7	0.1572(2)	0.3309(1)	0.9796(1)	2.58
O11	0.3070(2)	−0.2904(2)	0.8421(1)	3.60
O16	−0.2310(2)	−0.0751(2)	0.5527(1)	3.19
N12	0.2165(2)	−0.3317(2)	0.6279(1)	3.02
N17	−0.2923(2)	0.0006(2)	0.7521(1)	2.67
C2	0.0218(2)	−0.2227(2)	0.7768(2)	2.11
C3	0.0089(2)	−0.0687(2)	0.7188(2)	2.04
C5	0.1347(3)	0.1949(2)	0.7709(2)	2.59
C6	0.2543(3)	0.3016(2)	0.8734(2)	2.65
C8	0.2665(3)	0.4340(2)	0.0785(2)	2.81
C9	0.1623(3)	0.4594(2)	0.1912(2)	2.74
C10	0.1943(2)	−0.2834(2)	0.7501(2)	2.32
C13	0.3831(3)	−0.3862(3)	0.6038(2)	4.80
C14	0.1006(3)	−0.3109(2)	0.5118(2)	3.31
C15	−0.1844(2)	−0.0500(2)	0.6704(2)	2.25
C18	−0.2610(3)	0.0095(3)	0.8927(2)	3.90
C19	−0.4644(3)	0.0388(3)	0.6985(2)	3.99

[a] $B_{eq} = (8\pi^2/3)\Sigma_i\Sigma_j U_{ij} a_i^* a_j^* a_i \cdot a_j$

TABLE 4. Torsion angles in degrees for tetraamide **4**

Atom 1	Atom 2	Atom 3	Atom 4	Angle
C9	O1	C2	C3	−162.5(2)
C9	O1	C2	C10	71.6(2)
C2	O1	C9	C8′	88.8(2)
C5	O4	C3	C2	168.8(2)
C5	O4	C3	C15	−65.1(2)
C3	O4	C5	C6	−172.3(2)
C8	O7	C6	C5	−179.2(2)
C6	O7	C8	C9′	−178.4(2)
C13	N12	C10	O11	−3.2(3)
C13	N12	C10	C2	178.8(2)
C14	N12	C10	O11	−172.3(2)
C14	N12	C10	C2	9.6(3)
C18	N17	C15	O16	169.5(2)
C18	N17	C15	C3	−14.8(3)
C19	N17	C15	O16	−5.0(3)
C19	N17	C15	C3	170.7(2)
O1	C2	C3	O4	147.1(2)
O1	C2	C3	C15	19.9(2)
C10	C2	C3	O4	−87.1(2)
C10	C2	C3	C15	145.8(2)
O1	C2	C10	O11	−121.9(2)
O1	C2	C10	N12	56.2(2)
C3	C2	C10	O11	113.8(2)
C3	C2	C10	N12	−68.1(2)
O4	C3	C15	O16	138.6(2)
O4	C3	C15	N17	−37.4(2)
C2	C3	C15	O16	−100.1(2)
C2	C3	C15	N17	84.0(2)
O4	C5	C6	O7	−70.9(2)
O7	C8	C9′	O1′	73.8(2)

hydroxo complexes. Formation constants of the hydroxo complexes for the relevant metal ions were chosen from the literature (41): log β [species]: 0.7 [$CaOH^+$, $SrOH^+$, $BaOH^+$]; 4.3 [$NiOH^+$]; 5.7 [$CuOH^+$]; 13.1 [$Cu(OH)_2$]; 16.9 [$Cu_2(OH)_2^{2+}$]; 33.7 [$Cu_3(OH)_4^{2+}$]; 4.7 [$ZnOH^+$]; 9.86 [$Zn(OH)_2$]; 5.7 [$Zn(OH)_3^-$]; 3.8 [$CdOH^+$]; 6.9 [$PbOH^+$]; 10.8 [$Pb(OH)_2$]; 13.3 [$Pb(OH)_3^-$]. The reliability of the values, assessed from reproducibility between duplicate solution preparations from salts, is ±0.1 in pK_a and ±0.2 in log β.

Crystal structure determination

Intensity data were collected by ω–2θ scans of variable rate designed to yield measurements with $I = 50\sigma(I)$ for all significant reflections, using an Enraf–Nonius CAD4 diffractometer equipped with Mo Kα radiation (λ = 0.71073 Å) and a graphite monochromator. Unit-cell dimensions and crystal orientation were determined by a least-squares fit to the setting angles of 25 reflections having 20° < 2θ < 24°. A maximum of 120 s was placed on the scan time spent on any reflection; scan rates varied from 0.61 to 4.0 deg min^{-1}. One hemisphere of data ($h \pm k \pm l$) having 2° < 2θ < 55°, $0 \leq h \leq 9$, $-11 \leq k \leq 11$, $-13 \leq l \leq 13$, was collected. Crystal data are given in Table 2. Data reduction included corrections for background, Lorentz, polarization, and a 4.5% linear intensity decay correction. A total of 3129 unique data was collected, of which 2090 had $I > 3\sigma(I)$ and were used in the refinements. $Z = 1$ in space group $P\bar{1}$ requires that the molecule be centrosymmetric. The structure was solved by direct methods and refined by full-matrix least squares minimizing $\Sigma w (|F_o| - |F_c|)^2$ with weights $w = \sigma^{-2}(F_o)$ using the scattering factors of Cromer and Waber (42) and the Enraf–Nonius SPD programs. Non-hydrogen atoms were refined anisotropically, and hydrogen atoms were located on difference maps and refined isotropically. Thermal parameters for three hydrogen atoms tended to refine to slightly negative values and thus were fixed. The refinement converged with maximum of 0.21 σR = 0.40, R_w = 0.044, S = 2.063, and residual densities of 0.25 and −0.17 e Å^{-3}. Definitions are $R = \Sigma||F_o| - |F_c||/\Sigma|F_o|$; $R_w = (\Sigma w(|F_o| - |F_c|)^2/\Sigma w(F_o)^2)^{1/2}$; $S = (\Sigma w(|F_o| - |F_c|)^2/(NO - NV))^{1/2}$, where NO = 2090 observations and NV = 257 variables. Table 3 gives the atomic positional parameters and Table 4 gives the torsion angles of non-hydrogen atoms.[6]

Acknowledgements

This ongoing project was supported by the Natural Sciences and Engineering Research Council through Operating Grants and a Summer Studentship Award to P.D.W.

[6]Tables of atomic positions of hydrogen atoms, bond distances, bond angles, anisotropic thermal parameters, and structure factor amplitudes have been deposited, and may be purchased from the Depository of Unpublished Data, CISTI, National Research Council of Canada, Ottawa, Ont., Canada K1A 0S2.

Tables of bond distances and angles, and of hydrogen atom coordinates, have also been deposited with the Cambridge Crystallographic Data Centre and can be obtained on request from The Director, Cambridge Crystallographic Data Centre, University Chemical Laboratory, Lensfield Road, Cambridge CB2 1EW, U.K.

Can. J. Chem. Downloaded from www.nrcresearchpress.com by 195.138.81.100 on 09/07/12
For personal use only.

1. J. M. LEHN. Struct. Bonding (Berlin), **16**, 1 (1973); Pure Appl. Chem. **50**, 871 (1978); Pure Appl. Chem. **51**, 979 (1979); Science, **227**, 849 (1985); D. J. CRAM and K. N. TRUEBLOOD. Top. Curr. Chem. **98**, 43 (1981); D. J. CRAM. Angew. Chem. Int. Ed. Engl. **25**, 1039 (1986); J. M. LEHN. Angew. Chem. Int. Ed. Engl. **27**, 89 (1988).
2. J. F. STODDART. Chem. Soc. Rev. **8**, 85 (1979).
3. J. P. BEHR, J. M. GIRODEAU, R. C. HAYWARD, J. M. LEHN, and J. P. SAUVAGE. Helv. Chim. Acta, **63**, 2096 (1980).
4. J. P. BEHR and J. M. LEHN. Helv. Chim. Acta, **63**, 2112 (1980).
5. L. A. FREDRICH, T. M. FYLES, N. P. GURPRASAD, and D. M. WHITFIELD. Can. J. Chem. **59**, 1724 (1981).
6. J. P. BEHR, J. M. LEHN, and P. VIERLING. Helv. Chim. Acta, **65**, 1853 (1982).
7. H. DUGAS, P. KEROACK, and M. PTAK. Can. J. Chem. **62**, 489 (1984).
8. T. M. FYLES and D. M. WHITFIELD. Can. J. Chem. **62**, 507 (1984).
9. T. M. FYLES, C. A. MCGAVIN, and D. M. WHITFIELD. J. Org. Chem. **49**, 753 (1984).
10. J. P. BEHR, C. J. BURROWS, R. HENG, and J. M. LEHN. Tetrahedron Lett. **26**, 215 (1985).
11. A. ANANTANARAYAN, V. A. CARMICHEAL, P. J. DUTTON, T. M. FYLES, and M. J. PITRE. Synth. Commun. **16**, 1771 (1986).
12. A. BASAK and H. DUGAS. Tetrahedron Lett. **27**, 3 (1986).
13. J. DESROCHES, H. DUGAS, M. BOUCLAR, T. M. FYLES, and G. D. ROBERTON. Can. J. Chem. **65**, 1513 (1987).
14. J. P. BEHR, J. BERGDOLL, B. CHEVRIER, P. DUMAS, J. M. LEHN, and D. MORAS. Tetrahedron Lett. **28**, 89 (1987).
15. P. J. DUTTON, T. M. FYLES, and S. A. MCDERMID. Can. J. Chem. **66**, 1097 (1988).
16. J. M. LEHN and P. POTVIN. Can. J. Chem. **66**, 195 (1988).
17. J. P. BEHR, J. M. LEHN, A. C. DOCK, and D. MORAS. Nature, **295**, 526 (1982); Acta Crystallogr. Sect. C: Cryst. Struct. Commun. **C39**, 1001 (1983).
18. J. P. BEHR, J. M. LEHN, D. MORAS, and J. C. THEIRRY. J. Am. Chem. Soc. **103**, 701 (1981).
19. J. J. DALY, P. SCHONHOLZER, J. P. BEHR, and J. M. LEHN. Helv. Chim. Acta, **64**, 1444 (1981).
20. D. GEHIN, P. A. KOLLMAN, and G. WIPFF. J. Am. Chem. Soc. **111**, 3011 (1989).
21. J. ASCENSO and V. M. S. GIL. Can. J. Chem. **58**, 1376 (1980).
22. W. A. E. MCBRYDE. Analyst, **94**, 337 (1969).
23. W. A. E. MCBRYDE. Analyst, **96**, 739 (1971).
24. G. R. HEDWIG and H. K. J. POWELL. Anal. Chem. **43**, 1206 (1971).
25. A. AVDEEF and J. J. BUCHER. Anal. Chem. **50**, 2137 (1978).
26. R. F. JAMESON and M. F. WILSON. J. Chem. Soc. 2607 (1972).
27. A. ANANTANARAYAN and T. M. FYLES. Can. J. Chem. **68**, 1338 (1990).
28. W. J. HAMER and Y.-C. WU. J. Phys. Chem. Ref. Data, **1**, 1047 (1972).
29. P. C. MEIER. Anal. Chim. Acta, **236**, 363 (1982).
30. I. G. SAYCE. Talanta, **15**, 197 (1968); **18**, 653 (1971).
31. J. D. DUNITZ, M. DOBLER, P. SEILER, and R. P. PHIZACKERLEY. Acta Crystallogr. Sect. B: Struct. Crystallogr. Cryst. Chem. **B30**, 2733 (1974).
32. J. D. DUNITZ and P. SEILER. Acta Crystallogr. Sect. B: Struct. Crystallogr. Cryst. Chem. **B30**, 2739 (1974).
33. J. P. OUNSWORTH and L. J. WEILER. J. Chem. Educ. **64**, 568 (1987).
34. H. OGURA, K. FURUHATA, Y. HARADA, and Y. IITAKA. J. Am. Chem. Soc. **100**, 6733 (1978).
35. L. PARENTEAU and F. BRISSE. Can. J. Chem. **67**, 1293 (1989).
36. K. G. R. PASCHLER. J. Chem. Soc. Perkin Trans. 2, 1936 (1972).
37. J. S. BRADSHAW and P. E. STOTT. Tetrahedron, **36**, 461 (1980).
38. C. A. VITALI and B. MASCI. Tetrahedron, **45**, 2201 (1989).
39. R. B. JOHANNSEN, J. A. FERRETI, and R. K. HARRIS. J. Magn. Reson. **3**, 84 (1970).
40. J. D. SWALEN. *In* Computer programs for chemistry. Vol. I. *Edited by* D. F. DeTar. W. A. Benjamin, New York. 1968.
41. L. G. SILLEN and A. E. MARTELL (*Editors*). Chem. Soc. Special Publication No. 17. 1964; No. 24. 1971.
42. D. T. CROMER and J. T. WABER. International tables for X-ray crystallography, Vol. IV. Kynoch Press, Birmingham. 1974. Table 2.2B.

Can. J. Chem. Downloaded from www.nrcresearchpress.com by 195.138.81.100 on 09/07/12
For personal use only.

The structure and partial synthesis of imbricatine, a benzyltetrahydroisoquinoline alkaloid from the starfish *Dermasterias imbricata*

DAVID L. BURGOYNE, SHICHANG MIAO, CHARLES PATHIRANA, AND RAYMOND J. ANDERSEN[1]
Departments of Chemistry and Oceanography, University of British Columbia, Vancouver, B.C., Canada V6T 1W5

WILLIAM A. AYER, PETER P. SINGER, AND WILLIAM C. M. C. KOKKE
Department of Chemistry, University of Alberta, Edmonton, Alta., Canada T6G 2E9

AND

DONALD M. ROSS[2]
Department of Zoology, Biological Sciences Centre, University of Alberta, Edmonton, Alta., Canada T6G 2E9

Received February 19, 1990[3]

This paper is dedicated to Professor Ross Stewart on the occasion of his 65th birthday

DAVID L. BURGOYNE, SHICHANG MIAO, CHARLES PATHIRANA, RAYMOND J. ANDERSEN, WILLIAM A. AYER, PETER P. SINGER, WILLIAM C. M. C. KOKKE, and DONALD M. ROSS. Can. J. Chem. **69**, 20 (1991).

The structure of imbricatine (**1**), a cytotoxic metabolite of the starfish *Dermasterias imbricata*, has been determined by spectroscopic analysis and chemical degradation. Synthesis of model compounds **7** and **18** provided evidence for the absolute configuration and constitution of the benzyltetrahydroisoquinoline substructure of imbricatine.

Key words: imbricatine, asteroid, alkaloid.

DAVID L. BURGOYNE, SHICHANG MIAO, CHARLES PATHIRANA, RAYMOND J. ANDERSEN, WILLIAM A. AYER, PETER P. SINGER, WILLIAM C. M. C. KOKKE et DONALD M. ROSS. Can. J. Chem. **69**, 20 (1991).

Faisant appel à des analyses spectroscopiques et à une dégradation chimique, on a déterminé la structure de l'imbricatine (**1**), un métabolite cytotoxique de l'étoile de mer *Dermasterias imbricata*. La synthèse des composés modèles **7** et **18** fournit une preuve de la configuration absolue et de la constitution de la sous-structure benzyltétrahydroisoquinoléine de l'imbricatine.

Mots clés : imbricatine, astéroïde, alcaloïde.

[Traduit par la revue]

Many marine invertebrates exhibit escape responses to chemicals released by their predators. One of the best known examples is the detachment and swimming behavior of the sea anemones *Stomphia coccinea* and *S. didemon* in reaction to contact with certain species of marine asteroids (1, 2). Sea anemones are sessile animals that normally respond to tactile stimulation by contracting and covering their oral disc with a portion of their body column. However, *S. coccinea* and *S. didemon* respond to contact with the starfish *Dermasterias imbricata* in a "striking and extraordinary manner: the anemones release their basal discs from the substratum, and then propel themselves through the water by means of a series of whiplike motions" (2). A number of years ago it was shown that a single metabolite of *D. imbricata* was responsible for eliciting the "swimming response" in *S. coccinea* and *S. didemon* (1–4). Subsequently, we reported the constitution and partial stereochemistry of imbricatine (**1**), the *D. imbricata* metabolite responsible for eliciting the unusual anemone "swimming" behavior (5–7). We now wish to report additional details of the structure elucidation of imbricatine (**1**), including the determination of its absolute configuration and confirmation of the nature of the benzyltetrahydroisoquinoline substructure by synthesis.

Specimens of *Dermasterias imbricata* were collected by hand using SCUBA (−5 to −20 m) in Howe Sound and Barkley Sound, British Columbia. Freshly collected animals were immediately immersed in methanol and allowed to soak at room temperature for 3 days. The methanol was decanted and filtered through Celite to give a crude extract that was capable of eliciting the swimming response in specimens of *S. coccinea* maintained for bioassay purposes in a running seawater aquarium (4, 6, 7). Concentration of the crude methanol extracts *in vacuo* gave an aqueous slurry that was diluted with three equivalent volumes of water and then passed over XAD-4 resin. Elution of the retained substances from the XAD-4 resin with hot methanol gave an active eluate that was further fractionated on a Biogel-P2 column (eluent: H_2O/HOAc 99:1). All of the fractions from the Biogel-P2 chromatography that showed a uv λ_{max} at both 283 and 292 nm and elicited anemone swimming were pooled and further purified by Sephadex LH-20 chromatography (eluent: MeOH/H_2O 8:2) to give pure imbricatine (**1**) (6–7 mg/starfish) as a water soluble white solid. As little as 50 nanograms (50 μL of a 2×10^{-6} M solution) of pure imbricatine (**1**) was capable of eliciting the swimming response in 100% of the bioassay specimens of *S. coccinea* (6). No other swimming elicitors were found in the *D. imbricata* extracts. Imbricatine also displays significant activity in the L1210 (ED_{50} < 1 μg/mL) and P388 (T/C 139 at 0.5 mg/kg) cytotoxicity assays.

The molecular formula of imbricatine, $C_{24}H_{26}N_4O_7S$, was determined from the mass spectra of the parent compound (FABMS (M^+ + H), *m/z*: 515 Da) and the dimethylpentacetyl derivative **2** (FABMS, *m/z*: M^+ + H) 753; HREIMS (M^+ − OAcbenzyl), *m/z*: 603.1756, $C_{27}H_{31}N_4O_{10}S$ (ΔM −0.5 mmu)) prepared from **1** by esterification (MeOH/HCl) and acetylation (Ac_2O/pyridine).

A *N*-methyl-5-thiohistidine fragment could be identified in **1** by comparing ^1H and ^{13}C nmr resonances in the spectrum of

[1]Author to whom correspondence may be addressed.
[2]Deceased.
[3]Revision received September 5, 1990.

Can. J. Chem. Downloaded from www.nrcresearchpress.com by 195.138.81.100 on 09/07/12
For personal use only.

TABLE 1. ^{1}H nuclear magnetic resonance data. Chemical shifts are in ppm from internal TMS

Proton	**1**[a]	**5**[b]	**6a**[a]	**9**[c]	**18**[c]
1	4.67,dd(8.4,4.5)		4.57,dd(8,4)	4.73,dd(8,7)	5.06,dd(8,7)
3	3.76,dd(12.5,5)		3.12,dd(12,4)	4.49,t(10)	4.48,dd(9,11)
4_{ax}	2.71,dd(12.5,16)		2.71,dd(12,16)	3.21,m	3.24,m
4_{eq}	4.03,dd(16,5)		2.90,dd(16,4)	3.21,m	3.24,m
5	—		6.08,d(2)	7.10,s	6.94,d(2)
7	6.42,s		6.22,d(2)		6.88,d(2)
8				6.67,s	
12	3.22,dd(13.9,4.5)		3.20,dd(14,4)	3.28,dd(14,8)	3.32,dd(14,8)
12	2.85,dd(13.9,8.4)		2.80,dd(14,8)	2.88,dd(14,7)	2.88,dd(14,7)
14	7.04,d(8)		7.01,d(8)	7.15,d(8)	7.04,d(8)
15	6.71,d(8)		6.70,d(8)	6.84,d(8)	7.29,d(8)
2′	7.73,s:8.73,s[b]	8.95,s			
6′	3.30,dd(15,9): 3.34,d(8:2H)[b]	3.44,d(7.5:2H)			
6′	3.02,dd(15,5)	—			
7′	3.60,dd(5,9): 4.31,t(8)[b]	4.29,t(7.5)			
NMe	3.66,s:3.87,s[b]	3.94,s			
CO_2Me				3.84,s	3.85,s
OAc				2.28,s	2.29,s
OAc				2.25,s	2.28,s
OAc					2.20,s
NAc				1.87,s	1.80,s

[a]Recorded in Me_2SO-d_6.
[b]Recorded in D_2O.
[c]Recorded in $CDCl_3$.

imbricatine to the values reported for the symmetrical disulfide **3** first isolated from echinoderm eggs (8, 9) (Tables 1 and 2). Reduction of imbricatine (**1**) with Raney nickel (Scheme 1) liberated *N*-methyl histidine, which was shown by tlc analysis to be identical to 3-methylhistidine and different from 1-methylhistidine. This result indicated that the position of *N*-methylation in the histidine residue of imbricatine (3-methyl) was different from that reported for the disulfide from echinoderm eggs (1-methyl). It was subsequently shown by an unambiguous synthesis of disulfide **5** that the structure originally assigned to the disulfide from echinoderm eggs (i.e., **3**) was incorrect and needed to be revised as **5** (9). Treatment of imbricatine with red phosphorus in refluxing HI (Scheme 1) liberated the histidine thiol **4**, which was oxidized by iodine in aqueous HCl to the disulfide **5** (10). The spectral data collected on the disulfide **5** obtained from imbricatine were in complete agreement with the literature values (8, 9) and its specific rotation ($[\alpha]_D$ +67° (lit. (9) $[\alpha]_D$ +77°) indicated that the histidine residues had the L configuration.

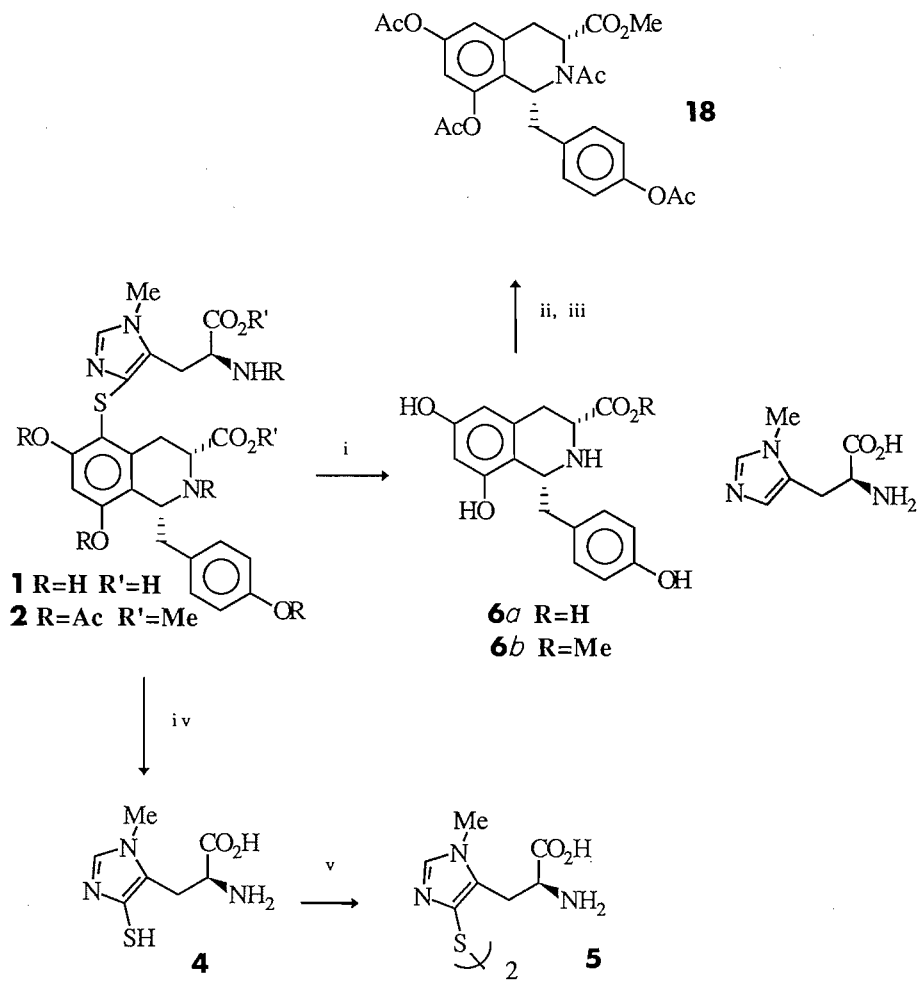
The second product obtained from the Raney nickel reduction of imbricatine was the benzyltetrahydroisoquinoline fragment **6a**. Compound **6a** gave a parent ion ($M^+ + H$) in the CIMS at *m/z* 316 Da and fragment ions at 270 ($M^+ - CO_2H$), 242 ($M^+ - NH{=}CHCO_2H$ via a retro Diels–Alder), 208 ($M^+ -$ HO-benzyl) and 164 ($M^+ -$ (HO-benzyl + CO_2)) Da typical of benzyltetrahydroisoquinolines with a carboxylic acid substituent at C3 (11). The EIHRMS spectrum of **6a** failed to show a parent ion; however, an intense fragment ion at *m/z* 208.1611 Da ($C_{10}H_{10}NO_4$, ΔM +0.1 mmu), which was assigned to a $M^+ -$ (HO-benzyl) fragment ion, was consistent with a molecular formula of $C_{17}H_{17}NO_5$ for the intact molecule. Only 15 resonances were observed in the ^{13}C nmr spectrum of **6a** (Table 2), demonstrating that the molecule contained some element of symmetry. The ^{1}H nmr resonances at δ 6.70 (d, J = 8 Hz, 2H) and 7.01 (d, J = 8 Hz, 2H) (Table 1) and ^{13}C nmr resonances at δ 126.9 (C), 130.2 (2 × CH), 115.0 (2 × CH), and 156.0 (C) (Table 2) were assigned to the phenyl ring in the benzyl residue of **6a**. The ^{1}H and ^{13}C chemical shifts of these resonances were in close agreement with those that we recorded for tyrosine, suggesting that the phenyl ring in **6a** contained only a *para*

TABLE 2. ^{13}C nuclear magnetic resonance assignments

Carbon	**1**[a]	**6**[a]	**5**[b]
1	52.9	53.0	
3	54.9	55.0	
4	27.2	30.0	
5	110.0	106	
6	159.7	157.0	
7	104.0	100.9	
8	155.8	154.7	
9	112.7	110.8	
10	137.7	136.0	
11	169.7	169.2	
12	37.3	37.8	
13	126.5	126.9	
14	130.5	130.2	
15	115.3	115.0	
16	156.4	156.0	
2	137.8		141.1
4′	126.8		130.0
5′	131.1		134.8
6′	25.1		25.5
7′	52.3		54.5
8′	170.5		173.3
9′	32.3		34.0

[a]Recorded in Me_2SO-d_6.
[b]Recorded in D_2O.

Can. J. Chem. Downloaded from www.nrcresearchpress.com by 195.138.81.100 on 09/07/12
For personal use only.



Reagents and reaction conditions: (i) Raney nickel, reflux, 1 h; (ii) HCl, MeOH, reflux, 2.5 h; (iii) Ac_2O, pyridine, r.t., 24 h; (iv) red phosphorus, aqueous HI (57%), N_2, reflux, 48 h; (v) 0.1 N HCl, I_2, r.t., 26 h.

SCHEME 1.

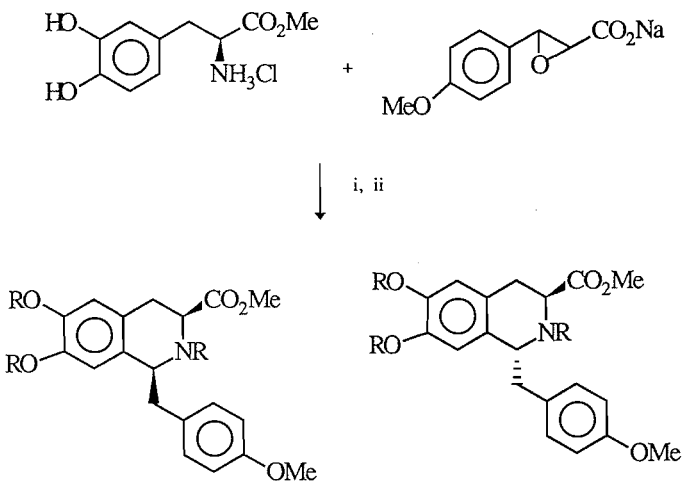
hydroxyl substituent, thereby accounting for the symmetry required by the ^{13}C nmr data. Additional deshielded ^1H resonances at δ 6.08 (d, J = 2 Hz) and 6.22 (d, J = 2 Hz) were assigned to protons on the aromatic ring of the tetrahydroisoquinoline moiety. The magnitude of the scalar coupling between these protons (2 Hz) showed that they were *meta* to each other and their chemical shifts suggested that the other substituents on the ring were a pair of *meta* hydroxyls. The remaining resonances in the ^1H nmr spectrum of **6***a* were assigned to the two CH-CH_2 fragments (δ (4.57, dd, J = 8, 4 Hz, H1), 3.12 (dd, J = 14, 4 Hz, H12), 2.80 (dd, J = 14, 8 Hz, H12′), 3.20 (dd, J = 12, 4 Hz, H3), 2.90 (dd, J = 16, 4 Hz, H4), 2.71 (dd, J = 12, 16 Hz, H4′)) in the reduced ring and the benzyl substituent of the isoquinoline nucleus.

The ^1H nmr spectrum of imbricatine (**1**), in contrast to that of the Raney nickel reduction product **6***a*, contained only a single resonance (δ 6.42, s) that could be assigned to a proton on the aromatic ring of the tetrahydroisoquinoline portion of the molecule (Table 1). Therefore, the other nonphenolic position of the ring had to be occupied by a thioether linkage to the methylhistidine residue. Both the $H4_e$ and $H3_a$ resonances were strongly deshielded in imbricatine (**1**: δ 4.03, $H4_e$: 3.76, $H3_a$) relative to the resonances assigned to the corresponding protons in the Raney nickel reduction product (**6***a*: δ 2.90, $H4_e$: 3.12, $H3_a$). The observed difference in chemical shifts for these two protons in compounds **1** and **6***a* could best be explained if the thioether linkage in imbricatine was attached to C5 of the isoquinoline nucleus, which in turn placed the two phenolic hydroxyls at C6 and C8. A pair of SINEPT experiments optimized for polarization transfer through a J $^{13}C/^1H$ of 7 Hz supported this assignment. Irradiation of H1 (δ 4.67) in imbricatine (**1**) gave polarization transfer into C8 (δ 155.8) and C10 (137.7), while irradiation of H7 (δ 6.42) gave polarization transfer into C5 (δ 110.0), C6 (159.7), C8 (155.8), and C9 (112.7).

Difference nOe experiments involving irradiation of H1 and H3 in imbricatine (**1**) failed to provide definitive proof for the relative stereochemistries at C1 and C3. Therefore, we synthesized the model compounds **9** and **10**, starting from optically pure L-dopa, in order to obtain reference data for the determination of both the relative and absolute configurations at C1 and C3 in the Raney nickel reduction product **6** and ultimately in imbricatine (**1**) itself.

Scheme 2 outlines the synthetic route used to prepare model compounds **9** and **10**. Earlier workers had found that the *cis* isomer was the major product (3.2:1 *cis*/*trans*) formed in the Pictet–Spengler coupling reaction when the phenylglycidate reactant contained methoxy substituents at both C3 and C4 on the phenyl ring (12). We found an identical 3.2:1 ratio of the *cis* to *trans* products with the 4-methoxyphenylglycidate shown. The *cis* configuration of the C1 and C3 substituents in **9** was

Can. J. Chem. Downloaded from www.nrcresearchpress.com by 195.138.81.100 on 09/07/12
For personal use only.



7 R=H
9 R=Ac

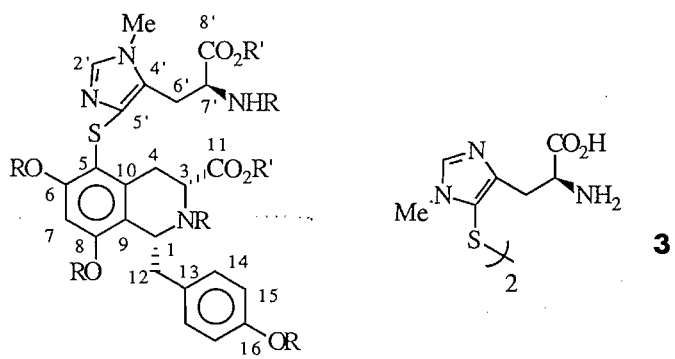
8 R=H
10 R=Ac

Reagents and reaction conditions: (i) H_2O, HOAc, 35°C, 36 h; (ii) Ac_2O, pyridine, r.t., 24 h

SCHEME 2.

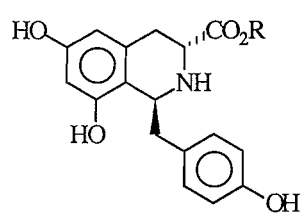
confirmed by a difference nOe experiment involving irradiation of H1 in compound **7** that induced nOe's in H3 and one of the H12 protons. Comparison of the ^1H nmr spectra of the model compounds **9** ($(CDCl_3)$ δ: 1.87 (s, CH_3CON), 2.88 (dd, J = 14, 8 Hz, H12), 3.21 (m, $H4_a$ and $H4_e$), 3.28 (dd, J = 14, 6 Hz, H12′), 4.49 (t, J = 10 Hz, $H3_a$), 4.73 (dd, J = 8, 6 Hz, $H1_a$)) and **10** (see Experimental) to that of derivative **18** ($(CDCl_3)$ δ: 1.80 (s, CH_3CON), 2.88 (dd, J = 14, 8 Hz, H12), 3.24 (m, $H4_a$ and $H4_e$), 3.30 (dd, J = 14, 6 Hz, H12′), 4.48 (t, J = 10 Hz, $H3_a$), 5.04 (dd, J = 8, 6 Hz, $H1_a$)) confirmed the benzyltetrahydroisoquinoline nature of the reduction product **6***a* and demonstrated that the C1 and C3 substituents in **6***a* were *cis* as shown.

A more direct proof of the C1, C3 relative stereochemistry in **6***a* was obtained from a difference nOe experiment carried out on its methyl ester **6***b*. Irradiation of the resonance assigned to H1 (δ 4.45: acetone-d_6 plus four drops of benzene-d_6) in **6***b* induced nOe's in the resonances assigned to H3 (δ 3.42) and H12 (δ 3.48) consistent with the *cis* relative stereochemistry shown. The *trans* reduction product **20***a* was produced as a minor side product in the Raney nickel reduction reaction (Scheme 1) if the catalyst was added in large excess and the reaction was allowed to reflux for at least 3 h. The circular dichroism (CD) spectrum of **20***b* (Fig. 1, see discussion below) indicated that it was epimeric with **6***b* at C1.



1 R=H R′=H
2 R=Ac R′=Me

3



20*a* R=H
20*b* R=Me

The CD spectra of model compounds **7** and **8** prepared from L-dopa, as indicated in Scheme 2, and the CD spectra of the methyl esters **6***b* and **20***b* of the *cis* and *trans* Raney nickel reduction products **6***a* and **20***a* are shown in Fig. 1. The Cotton effects observed for the *cis* (1*S*,3*S*) model compound **7** and the *cis* Raney nickel reduction product methyl ester **6***b* in the long wavelength region (290–298 nm), the middle range wavelength region (234–238 nm), and in the short wavelength region (200–220 nm) are each of opposite signs for the two compounds. Since the model compound **7** has the 1*S*,3*S* absolute configuration, the CD results demonstrate that the *cis* Raney nickel reduction product **6***a* and its methyl ester **6***b* have the 1*R*,3*R* absolute configuration. Similarly, the CD curve of the *trans* Raney nickel reduction product methyl ester **20***b* corresponds to the mirror image of the spectrum for the *trans* model compound **8** (Fig. 1) and, therefore, **20***b* must have the 1*S*,3*R* absolute configuration. Imbricatine has the same absolute configurations at C1 and C3 as the *cis* Raney nickel reduction product **6***a* and its methyl ester **6***b*; therefore, the absolute configuration of imbricatine (**1**) is 1*R*,3*R*,7′*S* as shown.

Imbricatine (**1**) is apparently the first example of a benzylisoquinoline alkaloid to be isolated from a nonplant source and it appears to be the first member of this class of alkaloids to have the C6/C8 hydroxylation pattern and a thiohistidine substituent. The biogenetic origin of the hydroxyl substitutents at C6/C8 is of considerable interest since all the plant alkaloids in this family are derived from L-dopa, which gives rise to C6/C7 hydroxylation (13). Then D amino acid configuration at C3 and the C6/C8 hydroxylation pattern indicate that the isoquinoline fragment of imbricatine (**1**) is probably not derived from L-dopa but rather from some other precursor such as D-3-(3,5-dihydroxyphenyl)-alanine, an amino acid that has not been previously described. We have prepared 3-(3,5-dihydroxyphenyl)alanine methyl ester **13** as the racemate and used it as a starting point in a biogenetic-type synthesis of **18**, a derivative of the benzyltetrahydroisoquinoline alkaloid fragment of imbricatine (**1**). Compound **18** was independently prepared from the Raney nickel reduction product **6***a* (Scheme 1), providing synthetic verification of the constitution of the benzyltetrahydroisoquinoline fragment of imbricatine (**1**). Scheme 3 outlines the synthesis of both **13** and **18**.

The synthesis of **13** started with methyl 3,5-dihydroxybenzoate, a readily available precursor that contains the required arrangement of alkyl and hydroxyl substituents on the benzene ring. Protection of the phenols as the benzyl ether derivatives, followed by LAH reduction of the methyl ester and tosylation of the resulting benzyl alcohol, gave the alkylating agent **11**. Alkylation of diethyl acetamidomalonate with the tosylate **11** following literature procedures gave **12** in excellent yield (14). Hydrolysis and decarboxylation of **12** gave the protected amino acid, which was routinely converted into the amino acid methyl ester **13**. The Pictet–Spengler reaction of methyl

Can. J. Chem. Downloaded from www.nrcresearchpress.com by 195.138.81.100 on 09/07/12
For personal use only.

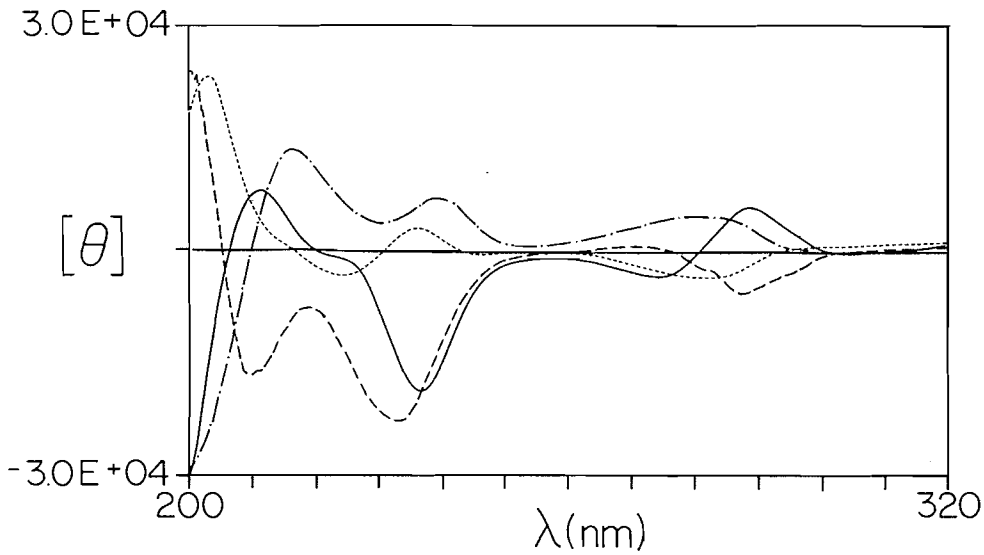
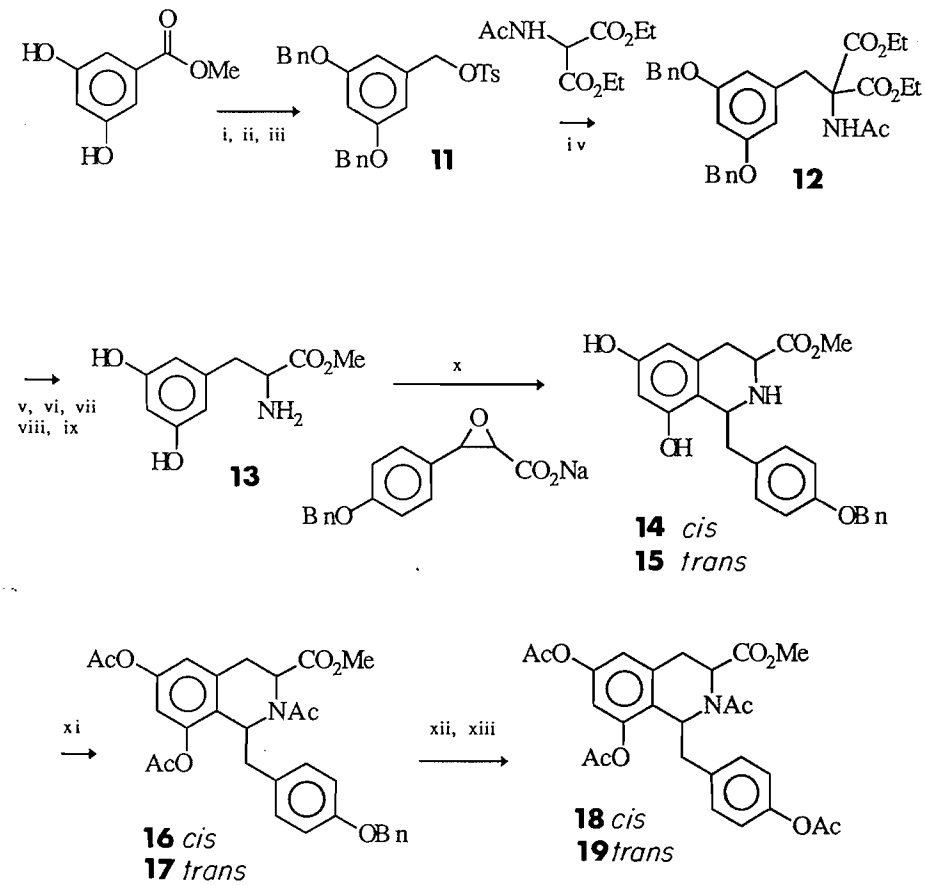


FIG. 1. CD spectra recorded in 0.1 N HCl/MeOH. (———) *cis* model compound **7**(0.1 g/L); (– – – –) *trans* model compound **8**(0.2 g/L); (- - - - -) methyl ester **6*b*** of the *cis* Raney nickel reduction product (0.15 g/L); (— · —) methyl ester **20*b*** of the *trans* Raney nickel reduction product (0.15 g/L).



Reagents and reaction conditions: (i) K_2CO_3, acetone, benzylbromide, reflux 1 h; (ii) LAH, ether, reflux, 2.5 h; (iii) NaH, benzene, tosylchloride, r.t.; (iv) NaH, benzene, DMF, r.t., 6 h; (v) NaOH, dioxane, reflux, 3 h; (vi) HOAc, reflux, 1 h; (vii) hydrazine, 100°C, 24 h; (viii) MeOH, HCl, reflux, 1 h; (ix) H_2, Pt/C, MeOH, r.t., 10 h; (x) MeOH, HOAc, 35°C, 17 h; (xi) Ac_2O, pyridine, r.t., 24 h; (xii) H_2, Pt/C, MeOH, r.t., 3 h; (xiii) Ac_2O, pyridine, r.t., 24 h.

SCHEME 3

Can. J. Chem. Downloaded from www.nrcresearchpress.com by 195.138.81.100 on 09/07/12
For personal use only.

Can. J. Chem. Downloaded from www.nrcresearchpress.com by 195.138.81.100 on 09/07/12
For personal use only.

ester **13** with sodium 3-(4-benzyloxyphenyl)glycidate gave an inseparable mixture of the *cis* and *trans* benzyltetrahydroisoquinoline products **14** and **15** (12). Acetylation of the mixture of **14** and **15** gave the triacetoxy derivatives **16** and **17**, which could be separated by preparative thin-layer chromatography. The relative stereochemistries at C1 and C3 in **16** and **17** were established by comparison of their H1 and H3 coupling constants to those observed for the model compounds **9** and **10** where the relative stereochemistries had been rigorously established. The *trans* isomer was the major product (**17**:*trans*/**16**:*cis* 6.5:1) formed in the Pictet–Spengler reaction of methyl ester **13**, presumably due to an unfavorable steric interaction between the benzyl substituent at C1 and the C8 hydroxyl during the formation of the *cis* isomer. Removal of the benzyl protecting group in **16** by catalytic hydrogenation and acetylation of the resulting phenolic product gave the *cis* benzyltetrahydroisoquinoline derivative **18**, which was identical by tlc, ^{1}H nmr, and mass spectral comparison to compound **18** prepared by methylation (HCl/MeOH) and acetylation (Ac_2O/pyridine) of the Raney nickel reduction product **6***a*. The *trans* isomer **19** prepared from **17** by the same sequence of reactions had tlc and ^{1}H nmr characteristics different from compound **18** prepared from **6***a*.

It is well documented that many marine invertebrates utilize chemical cues to recognize their predators; however, relatively little information is available concerning the chemical structures of the messengers (16). Several studies examining the basis of escape and avoidance of marine invertebrates to seastars have found that saponins are the active substances (16*a*, 16*c*, 17). These results, in combination with the widespread occurrence of saponins in seastars (18), have fostered the common perception that most seastar initiated behavioral responses are elicited by saponins. Our results have shown that the metabolite of the seastar *D. imbricata* responsible for eliciting swimming in *Stomphia* sp. is not a saponin, but rather the very interesting new alkaloid imbricatine (**1**). This discovery suggests that a blanket assumption that other seastar initiated avoidance responses are caused by saponins is probably unjustified. Careful quantitative bioassay guided fractionation of seastar extracts is required to fully characterize the chemical mediator(s) of the responses.

Experimental

Imbricatine (1)

Imbricatine (**1**) was extracted and purified as described in the text. White amorphous solid; ir (KBr disc): 3700–2500 (b), 1630, 1595, 1515, 1447, 1397, 1244, 1175, 1080, 840 cm^{-1}; ^{1}H nmr see Table 1; ^{13}C nmr see Table 2; FABMS, *m/z* (M^+ + H): 515, $C_{24}H_{26}N_4O_7S$ + H.

Methylation and acetylation of imbricatine to give 2

Imbricatine (**1**) (9 mg) was dissolved in methanol saturated with gaseous HCl and the solution was refluxed for 2.5 h. The solvent was evaporated to dryness *in vacuo* and acetic anhydride (2 mL) and pyridine (2 mL) were added to the residue. After stirring 24 h at room temperature the acetylation reagents were removed *in vacuo* and the residue was purified by reverse phase hplc (CH_3CN/H_2O 3:7) to give derivative **2** (9 mg). **2**: ^{1}H nmr (400 MHz, $CDCl_3$) δ: 7.34,(s,1H), 7.29(d, *J* = 8 Hz,2H), 7.02(d, *J* = 8 Hz,2H), 6.89(bs,1H), 6.15(bd, *J* = 8 Hz,1H), 5.06(bt, *J* = 6 Hz,1H), 4.73(bdd, *J* = 6, 12 Hz,1H), 3.87(s), 3.75(s,1H), 3.61(s,3H), 3.36(dd, *J* = 6, 14 Hz,1H), 3.17(m,1H), 3.10(bd, *J* = 16 Hz,1H), 2.89 (dd, *J* = 6, 14 Hz,1H), 2.41(s,3H), 2.28(s,3H), 2.18(s,3H), 1.90(s,3H), 1.74(s,3H) ppm; FABMS, *m/z*: 753 ($C_{36}H_{40}N_4O_{12}S$ + H); EIHRMS, *m/z*: 603.1756 (M^+ − OAcbenzyl), $C_{27}H_{31}N_4O_{10}S$ (Δ*M* −0.5 mmu).

Raney nickel reduction of imbricatine (1)

Imbricatine (**1**) (16 mg) was refluxed with 0.5 mL of Ra-Ni suspension for 1 h under N_2. The reaction mixture was vacuum filtered and the Ra-Ni residue was washed with hot MeOH. The combined filtrate, after removal of MeOH under vacuum, was chromatographed on Sephadex LH20 using 9:1 MeOH/H_2O as the eluent to give crude compound **6***a*, which was further purified on reverse phase HPLC (20:80 MeOH/H_2O) to obtain pure **6***a* (8 mg). **6***a*: ^{1}H nmr, see Table 1; ^{13}C nmr, see Table 2; CIMS, *m/z*: 316 (M^+ + H), 272, 242, 270, 208, 198, 164, 162, 152, 137, 124, 121, 109, 108, 107; EIHRMS, *m/z*: 208.1611 (M^+ − HObenzyl), $C_{10}H_{10}NO_4$ (ΔM +0.1 mmu). When imbricatine was refluxed with a large excess of Ra-Ni suspension for longer than 3 h, the reaction mixture turned a dark red and a mixture of the *cis* reduction product **6***a* and its C1 epimer **20***a* was formed. Methylation of the mixture as described below for **6***a* gave a mixture of **6***b* and **20***b* that was separated by preparative reverse phase tlc (6:4 MeOH/H_2O).

*Methylation of compound 6*a

The Raney nickel reduction product **6***a* was refluxed with HCl/MeOH for 1 h under nitrogen. After removal of the solvent, the reaction mixture was chromatographed on normal phase tlc(4:1 EtOAc/$CHCl_3$) to afford pure **6***b* as a yellow solid; ^{1}H nmr (400 MHz, acetone-d_6) δ: 7.02 (d, *J* = 8.6 Hz, H15, H17), 6.71 (d, *J* = 8.6 Hz, H14, H18), 6.33 (d, *J* = 1.9 Hz, H5), 6.12 (d, *J* = 1.9 Hz, H7), 4.41 (dd, *J* = 7.8, 3.0 Hz, H1), 3.68 (s, 3H, $COOCH_3$), 3.43 (dd, *J* = 13.5, 3.0 Hz, H12a), 3.42 (dd, *J* = 11.0, 3.0 Hz, H3), 2.71 (dd, *J* = 13.4, 7.8 Hz, H12b), 2.69 (dd, *J* = 15.2, 3.0 Hz, $H4_{eq}$), 2.47 (dd, *J* = 15.2, 11.0 Hz, $H4_{ax}$) ppm: EIMS, *m/z* (rel. int.): 236 (50, M^+ − HOphenyl), 222 (49, M^+ − HObenzyl), 191 (8), 176 (30), 162 (53).

*Compound 20*b: obtained as a pale yellow solid; ^{1}H nmr (400 MHz, acetone-d_6) δ: 7.13 (d, *J* = 8.5 Hz), 6.80(d, *J* = 8.5 Hz), 6.31(d, *J* = 1.8 Hz), 6.17(d, *J* = 1.8 Hz), 4.22(dd, *J* = 10.0, 2.5 Hz), 4.01(dd, *J* = 10.5, 4.5 Hz), 3.70(s, 3H), 3.14(dd, *J* = 13.5, 2.5 Hz), 2.88(dd, *J* = 15.3, 4.5 Hz), 2.73(dd, *J* = 15.3, 10.5 Hz), 2.68(dd, *J* = 13.5, 10.0 Hz) ppm; EIMS, *m/z*(rel. int.): 270(5, M^+ − CO_2Me), 222(100, M^+ − HObenzyl); CIMS, *m/z*: 330(100).

Reductive hydrolysis of imbricatine (1)

Red phosphorus (150 mg) was added to a solution of imbricatine (**1**) (100 mg) in 57% aqueous HI and the reaction mixture was refluxed under N_2 for 48 h. At the end of this period, the reaction mixture was filtered to remove the solid phosphorus and the filtrate was evaporated under vacuum. The residue was taken up with 5 mL aqueous HCl (pH 2) and chromatographed on Sephadex LH20 using 1:1 MeOH/H_2O as an eluent to give the histidine thiol **4** (34 mg).

Oxidation of the thiol 4 to the disulfide 5

To a solution of histidine thiol **4** (17 mg) in 2 mL 0.1 N aqueous HCl was added a few crystals of I_2. The reaction mixture was stirred at room temperature for 26 h, diluted with 4 mL water, extracted with $CHCl_3$ to remove I_2, and then chromatographed on Sephadex LH20 using 1:1 MeOH/H_2O as an eluent. Disulfide **5** (15 mg) was obtained. **5**: ^{1}H nmr(300 MHz, D_2O) δ: 8.78(s, 1H), 4.20(t, *J* = 8 Hz, 1H), 3.85(s, 3H), 3.30(dd, *J* = 15, 8 Hz, 1H), 3.35(dd, *J* = 15, 8 Hz, 1H) ppm.

Measurement of the optical rotation of disulfide 5

Disulfide **5** (10 mg) was dissolved in 1.0 mL 0.1 N aqueous HCl and the optical rotation was measured using a 1-dm cell. The specific rotation $[\alpha]_D^{20}$ was found to be +67°.

Synthesis of the model compounds 7 and 8

Methyl-L-dopa (580 mg) in 10 mL MeOH was added to a solution of sodium 3-(4-methoxyphenyl)glycidate in 15 mL of water. The mixture was brought to pH 4 with AcOH and stirred at 35°C for 36 h. At the end of the reaction period, the mixture was concentrated under vacuum to yield an aqueous suspension which was partitioned between EtOAc (15 mL) and 10% HCl (15 mL). The aqueous layer was neutralized with K_2CO_3 and extracted with EtOAc (15 mL × 3). The EtOAc solution was washed with water, dried over Na_2SO_4, and concentrated under

Can. J. Chem. Downloaded from www.nrcresearchpress.com by 195.138.81.100 on 09/07/12
For personal use only.

vacuum to afford a brown residue that was chromatographed on normal phase hplc (3:2 EtOAc/$CHCl_3$) to give **7** (145 mg) and **8** (45 mg).

Compound 7: obtained as a white solid; ^{1}H nmr (270 MHz, DMSO-d_6) δ: 7.17(d, J = 8 Hz, 2H), 6.84(d, J = 8 Hz, 2H), 6.70(s, 1H), 6.43(s, 1H), 4.00(J = 8, 4 Hz, 1H), 3.70(s, 3H), 3.58(s, 3H), 3.48(dd, J = 11, 5 Hz, 1H), 3.21(dd, J = 14, 4Hz, 1H), 2.71(dd, J = 16, 5 Hz, 1H), 2.56(dd, J = 14, 8 Hz, 1H) ppm; CIMS, m/z(rel. int): 344 (M^+ + H, 16), 284(1), 222(100), 162(11), 134(1), 121(13); EIHRMS, m/z: 343.1403 (M^+), $C_{17}H_{21}NO_5$ (ΔM −1.7 mmu).

Compound 8: obtained as a pale yellow oil; ^{1}H nmr (400 MHz, DMSO-d_6) δ: 7.18 (d, J = 8 Hz, 2H), 6.88 (d, J = 8 Hz, 2H), 6.60 (s, 1H), 6.47 (s, 1H), 4.00(dd, J = 10, 4 Hz, 1H), 3.87(dd, J = 9, 5 Hz, 1H), 3.74(s, 3H), 3.63(s, 3H), 2.86(dd, J = 14, 4 Hz, 1H), 2.79(dd, J = 16, 5 Hz, 1H), 2.74(dd, J = 14, 4 Hz, 1H), 2.64(dd, J = 16, 8 Hz, 1H) ppm; EIHRMS, m/z: 343.1412 (M^+), $C_{17}H_{21}NO_5$ (ΔM −0.8 mmu).

Acetylation of model compounds 7 and 8

Compounds **7** (25 mg) and **8** (25 mg) were reacted independently with acetic anhydride (2 mL) and pyridine (2 mL) at room temperature for 24 h to give the triacetyl derivatives **9** and **10** respectively.

Compound 9: white solid; ^{1}H nmr see Table 1; ^{13}C nmr (75 MHz, $CDCl_3$) δ: 172.7(s), 170.6(s), 168.1(s), 168.0(s), 158.5(s), 141.2(s), 140.4(s), 135.5(s), 130.6(d), 129.3(s), 122.7(d), 121.7(d), 114.0(d), 61.2(d), 55.4(d), 55.1(q), 52.3(q), 42.5(t), 29.7(t), 21.2(q), 20.4(q), 20.5(q) ppm; CIMS, m/z: 470(M^+ + H), 428, 348, 306, 264, 222, 162, 121; EIHRMS, m/z: 348.1093 (M^+ − MeObenzyl), $C_{17}H_{18}NO_7$ (ΔM +1.0 mmu).

Compound 10: clear oil; ^{1}H nmr (400 MHz, $CDCl_3$: exists as a 1: 1.4 mixture of conformers) δ: 6.98 (s), 6.89(s), 6.87(d, J = 8 Hz), 6.79(d, J = 8 Hz), 6.70(s), 6.69(s), 6.53(s), 5.36(t, J = 5 Hz), 4.92(t, J = 7 Hz), 4.86(dd, J = 8, 4 Hz), 4.63(dd, J = 6, 3 Hz), 3.78(s), 3.75(s), 3.58(s), 3.51(s), 3.3(m), 3.1–2.85(m), 2.43(dd, J = 16, 6 Hz), 2.26(s), 2.25(s), 2.24(s), 2.23(s), 2.13(s), 2.06(s) ppm; CIMS, m/z: 470 (M^+ + H); EIHRMS, m/z: 348.1090 (M^+ − MeObenzyl), $C_{17}H_{18}NO_7$ (ΔM +0.7 mmu).

Preparation of methyl 3,5-dibenzyloxybenzoate

Methyl 3,5-dihydroxybenzoate (5.0 g, 29 mmol) and K_2CO_3 (20.0 g) were stirred in 100 mL of anhydrous acetone for 30 min. Benzyl bromide (7.5 mL) was added slowly over a period of 5 min and the mixture was refluxed for 1 h. Filtration and evaporation to dryness *in vacuo* yielded a crude product that was purified by flash chromatography (400 mL 9:1 Hex/EtOAc, 400 mL, 8:2 Hex/EtOAc, 400 mL 7:3 Hex/EtOAc) to yield methyl 3,5-dibenzyloxybenzoate (9.4 g, 27 mmol: 92%), mp 66.0–67.5°C; ^{1}H nmr (400 MHz, $CDCl_3$) δ: 7.32(m, 10H), 7.28(d, J = 2.3 Hz, 2H), 6.76(t, J = 2.3 Hz, 1H), 4.97(s, 4H), 3.82(s, 3H) ppm; EIHRMS, m/z: 348.1364 (M^+), $C_{22}H_{20}O_4$ (ΔM +0.2 mmu).

Preparation of 3,5-dibenzyloxybenzyl alcohol

$LiAlH_4$ (0.012 g) was added slowly to methyl 3,5-dibenzyloxybenzoate (0.1 g, 0.29 mmol) in 10 mL of diethyl ether. The mixture was refluxed for 2.5 h and quenched with 10 mL of water. 20% NaOH (10 mL) was added and the mixture was extracted three times with diethyl ether (3 × 15 mL) and the ether layers were dried over magnesium sulfate. Evaporation *in vacuo* gave 3,5-dibenzyloxybenzyl alcohol (0.087 g, 0.27 mmol, 95% yield), mp 78.5–79.0°C; ^{1}H nmr (400 MHz, $CDCl_3$) δ: 7.31(m, 10H), 6.56(bs, 2H), 6.50(bs, 1H), 4.94(s, 4H), 4.50(s, 2H), 2.29(bs, 1H) ppm.

Preparation of 3,5-dibenzyloxybenzyl tosylate (11)

Sodium hydride (0.019 g 80% dispersion in oil) was added to a stirred solution of 3,5-dibenzyloxybenzyl alcohol (0.20 g, 0.63 mmol) in 10 mL of benzene. Tosyl chloride (0.12 g) was added slowly over a period of 10 min and the mixture was stirred for 9 h at room temperature. The resulting solution was centrifuged and the supernatant withdrawn. Evaporation of the benzene *in vacuo* yielded a mixture of the product 3,5-dibenzyloxybenzyl tosylate and starting material. Purification using flash chromatography (7:3 Hex/EtOAc) yielded the desired tosylate **11** (0.11 g, 0.23 mmol); ^{1}H nmr (400 MHz, $CDCl_3$) δ: 7.76(d, J = 8.2 Hz, 2H), 7.34(m, 10H), 7.28(d, J = 8.2 Hz, 2H), 6.54(t, J = 2.2 Hz, 1H), 6.46(d, J = 2.2 Hz, 2H), 4.96(s, 2H), 4.94(s, 4H), 2.39(s, 3H) ppm.

Preparation of benzylacetamidomalonate 12

Diethyl acetamidomalonate (0.13 g, 0.61 mmol) and sodium hydride (0.018 g 80% dispersion in oil) were stirred in benzene (5 mL) and DMF (5 mL) for 15 min. 3,5-Dibenzyloxybenzyl tosylate **11** (0.068 g, 0.14 mmol) was added slowly and the mixture was stirred at room temperature for 6 h. Evaporation *in vacuo* followed by flash chromatography (3:2 EtOAc/Hex) gave compound **12** (0.069 g, 0.13 mmol, 92% yield), mp 138.5–140.0°C; ^{1}H nmr (400 MHz, $CDCl_3$) δ: 7.34(m, 10H), 6.56(s, 1H), 6.51(t, J = 2.2 Hz, 1H), 6.26(d, J = 2.2 Hz, 2H), 4.98(s, 4H), 4.23(m, 4H), 3.58(s, 2H), 1.95(s, 3H), 1.27(t, J = 7.1 Hz, 6H) ppm; EIHRMS, m/z: 519.2254 (M^+), $C_{30}H_{33}NO_7$ (ΔM −0.3 mmu).

Hydrolysis and decarboxylation of 12

Compound **12** (0.055 g, 0.11 mmol) was dissolved in 10 mL of dioxane and 20% NaOH (2 mL) was added. The mixture was stirred under reflux for 3 h. After cooling, glacial acetic acid (2 mL) was added and the reaction was refluxed for an additional hour. After cooling, the mixture was extracted three times with 10-mL portions of EtOAc. Evaporation of the EtOAc *in vacuo* gave the crude 3,5-dibenzyloxy-*N*-acetamidophenylalanine (0.041 g, 0.099 mmol, 93% yield), which was used directly in the next step; ^{1}H nmr (400 MHz, CD_3OD) δ: 7.35(m, 10H), 6.53(bs, 2H), 6.45(bs, 1H), 4.80(s, 4H), 4.51(bs, 1H), 3.15(dd, J = 4.1, 13.6 Hz, 1H), 2.90(dd, J = 7.5, 13.6 Hz, 1H), 1.88 (s, 3H) ppm.

Preparation of methyl-3-(3,5-dihydroxyphenyl)alanine (13)

N-Acetamido-3-(3,5-dibenzyloxyphenyl)alanine was stirred in hydrazine (2 mL) at 100°C for 24 h. The mixture was evaporated to dryness *in vacuo*, taken up in methanol saturated with HCl, and refluxed for 1 h. The mixture was then evaporated to dryness *in vacuo* and taken up in methanol. Stirring under H_2 in the presence of Pt/C at room temperature for 10 h gave, after reverse phase flash chromatography (100% H_2O, 80% H_2O/acetone, 60% H_2O/acetone), the amino acid methyl ester **13**: ^{1}H nmr (400 MHz, CD_3OD) δ: 6.25(t, J = 1.8 Hz, 1H), 6.22(d, J = 1.8 Hz, 2H), 4.26(t, J = 6.6 Hz, 1H), 3.83(s, 3H, 3.36(s, 1H), 3.10(dd, J = 6.6, 13.8 Hz, 1H), 3.05(dd, J = 6.6, 13.8 Hz, 1H), 2.62 (s, 1H) ppm; EIHRMS, m/z: 211.0851 (M^+), $C_{10}H_{13}NO_4$ (ΔM +0.7 mmu).

Preparation of the benzyltetrahydroisoquinolines 14 and 15

Sodium 3-(4-benzyloxyphenyl)glycidate (15) (0.15 g, 0.53 mmol) in 10 mL of water was added to a solution of compound **13** (0.11 g, 0.53 mmol) in 15 mL of methanol. Acetic acid (2 mL) was added and the mixture was stirred at 35°C for 17 h under N_2. The solvent was evaporated *in vacuo* and the crude material was taken up in EtOAc. The organic layer was washed twice with 1 N HCl and once with H_2O and dried over sodium sulfate. Evaporation of the EtOAc to dryness gave 0.20 g of the crude mixture. Purification was accomplished using silica gel (1:1 Hex/EtOAc) to yield an inseparable mixture (0.079 g, 0.19 mmol, 36% yield) of the tetrahydroisoquinolines **14** and **15**. Data for the mixture of **14** and **15**: EIHRMS, m/z: 419.1728 (M^+), $C_{25}H_{25}NO_5$ (ΔM −0.4 mmu); Compound **15**: ^{1}H nmr (400 MHz, CD_3OD) δ: 7.37(m, 5H), 7.17(d, J = 8.1 Hz, 2H), 6.97(d, J = 8.1 Hz, 2H), 6.22(s, 1H), 6.13(s, 1H), 5.06(s, 2H), 4.31(d, J = 10.0 Hz, 1H), 4.01(d, J = 11.3 Hz, 1H), 3.74(s, 3H), 3.29(m, 2H), 2.85(m, 2H) ppm; Compound **14**: ^{1}H nmr (400 MHz, CD_3OD) δ: 7.37(m, 5H), 7.06(d, J = 8.1 Hz, 2H), 6.88(d, J = 8.1 Hz, 2H), 6.26(s, 1H), 6.06(s, 1H), 5.03(s, 2H), 4.46(bs, 1H), 3.44(m, 1H), 2.78(m, 3H) ppm.

Acetylation of the mixture of 14 and 15:

The tetrahydroisoquinoline mixture (**14** and **15**) (0.030 g, 0.072 mmol) was stirred in pyridine (2 mL) and acetic anhydride (2 mL) for 19 h. Evaporation of the reagents *in vacuo* yielded 0.048 g of the crude mixture. Purification was accomplished on preparative tlc (1:1

Can. J. Chem. Downloaded from www.nrcresearchpress.com by 195.138.81.100 on 09/07/12
For personal use only.

Hex/EtOAc) to yield **16** (0.0035 g, 0.0064 mmol) and **17** (0.023 g, 0.042 mmol). Compound **16**: ir (NaCl window): 3031, 2925, 2853, 1769, 1652, 1615, 1510 cm^{-1}; ^1H nmr(400 MHz, $CDCl_3$) δ: 7.40(m, 5H), 7.22(d, J = 8.7 Hz, 2H), 6.92(d, J = 8.7 Hz, 2H), 6.93(d, J = 2.1 Hz, 1H), 6.88(d, J = 2.1 Hz, 1H), 5.06(s, 2H), 5.03(dd, J = 5.3, 8.0 Hz, 1H), 4.46(t, J = 9.6 Hz, 1H), 3.85(s, 3H), 3.25(m, 3H), 2.81(dd, J = 5.3, 13.7 Hz, 1H), 2.29(s, 3H), 2.20(s, 3H), 1.71(s, 3H) ppm; EIHRMS, m/z: 545.2043 (M^+), $C_{31}H_{31}NO_8$ (ΔM −0.7 mmu). Compound **17** existed as a mixture of conformers. *Major conformer*: ^1H nmr (400 MHz, $CDCl_3$) δ: 7.33(m, 5H), 6.89(d, J = 2.2 Hz, 1H), 6.75(d, J = 8.6 Hz, 2H), 6.67(d, J = 2.2 Hz, 1H), 6.66(d, J = 8.6 Hz, 2H), 5.64(dd, J = 2.8, 6.7 Hz, 1H), 5.01(s, 2H), 4.54(dd, J = 2.4, 5.4 Hz, 1H), 3.49(s, 3H), 3.24(dd, J = 6.7, 13.2 Hz, 1H), 2.86(m, 2H), 2.25(s, 3H), 2.16(s, 3H), 2.12(s, 3H), 2.10(m, 1H) ppm. *Minor conformer*: ^1H nmr (400 MHz, $CDCl_3$) δ: 7.33(m, 5H), 6.93(d, J = 2.2 Hz, 1H), 6.86(s, 4H), 6.79(d, J = 2.2 Hz, 1H), 5.18(t, J = 6.3 Hz, 1H), 5.04(s, 2H), 4.83(dd, J = 3.5, 6.4 Hz, 1H), 3.57(s, 3H), 3.02(dd, J = 3.5, 16.3 Hz, 1H), 2.95 (second order d, J = 6.3 Hz, 1H), 2.93(second order d, J = 6.3 Hz, 1H), 2.86(m, 3H), 2.26(s, 3H), 2.22(s, 3H), 1.99(s, 3H) ppm; EIHRMS, m/z: 545.2043 (M^+), $C_{31}H_{31}NO_8$ (ΔM −0.7 mmu).

Preparation of compound 18

The *cis* benzyltetrahydroisoquinoline **16** (0.0039 g, 0.0071 mmol) was stirred in methanol (2 mL) under H_2 in the presence of Pt/C catalyst for 3 h. The mixture was filtered and evaporated to dryness *in vacuo*. Purification was accomplished using preparative tlc (9:1 EtOAc/Hex) to yield the phenol, which was stirred in pyridine (1 mL) and acetic anhydride (1 mL) at room temperature for 15 h. Evaporation of the reagents *in vacuo* followed by purification using preparative tlc (9:1 EtOAc/Hex) yielded compound **18**: ^1H nmr (400 MHz, $CDCl_3$) see Table 1; EIHRMS, m/z: 497.1691 (M^+), $C_{26}H_{27}NO_9$ (ΔM +0.5 mmu).

Preparation of compound 19

An identical procedure was employed to prepare the *trans* isomer **19** starting from **17**. The *trans* isomer **19** existed as a mixture of conformers. EIHRMS, m/z: 438.1556 ($M^+ - C_2O_2H_3$), $C_{24}H_{24}NO_7$ (ΔM +0.3 mmu). *Major conformer*: ^1H nmr(400 MHz, $CDCl_3$) δ: 6.88(d, J = 2.1 Hz, 1H), 6.86(d, J = 8.6 Hz, 2H), 6.79(d, J = 8.6 Hz, 2H), 6.71(d, J = 2.1 Hz,1H), 5.65(dd, J = 2.8, 7.2 Hz, 1H), 4.59(dd, J = 2.5, 5.3 Hz, 1H), 3.49(s, 3H), 3.21(dd, J = 7.2, 13.0 Hz, 1H), 2.97(m, 3H), 2.26(s, 3H), 2.25(s, 3H), 2.15(s, 3H), 2.13(s, 3H) ppm. *Minor conformer*: ^1H nmr (400 MHz, $CDCl_3$) δ: 6.99(m, 4H), 6.94(d, J = 2.6 Hz, 1H), 6.82(d, J = 2.6 Hz, 1H), 5.21(t, J = 6.2 Hz, 1H), 4.86(dd, J = 3.5, 6.3 Hz, 1H), 3.57(s, 3H), 3.08(dd, J = 3.5, 16.3 Hz, 1H), 2.95(m, 3H), 2.28(s, 3H), 2.27(s, 3H), 2.22(s, 3H), 2.06(s, 3H) ppm.

Acknowledgments

The authors wish to thank M. LeBlanc and the staff of the Bamfield Marine Station for assisting the collection of *D. imbricata* and *S. coccinea*. Financial support was provided by grants from NSERC (R.J.A., W.A.A., D.M.R.) and the National Cancer Institute of Canada (R.J.A.).

1. D. M. Ross and L. Sutton. J. Exp Biol. **48**, 751 (1964).
2. J. A. Ward. J. Exp. Zool. **158**, 357 (1965).
3. W. A. Ayer, D. M. Ross, and P. P. Singer. Am. Zool. **13**, Abstr. 233 (1973).
4. P. P. Singer. An investigation of the swimming response of the sea anemone *Stomphia coccinea* to certain starfish. Ph.D. Dissertation, University of Alberta, Edmonton, Alta. 1975.
5. C. Pathirana and R. J. Andersen. J. Am. Chem. Soc. **108**, 8288 (1986).
6. J. K. Elliott, D. M. Ross, C. Pathirana, S. Miao, R. J. Andersen, P. P. Singer, W. C. M. C. Kokke, and W. A. Ayer. Biol. Bull. (Woods Hole, Mass.), **176**, 73 (1989).
7. C. Pathirana. Secondary metabolites from selected marine organisms. Ph.D. Dissertation, University of British Columbia, Vancouver, B.C. 1986.
8. A. Palumbo, G. Misuraca, M. D'Ischia, F. Donaudy, and G. Prota. Comp. Biochem. Physiol. **78B**, 81 (1984).
9. T. P. Holler, F. Ruan, A. Spaltenstein, and P. B. Hopkins. J. Org. Chem. **54**, 4570 (1989).
10. S. Ito, G. Nardi, A. Palumbo, and G. Prota. J. Chem. Soc. Perkin Trans. 1, 2617 (1979).
11. S. F. Dyke and R. G. Kinsman. *In* Heterocyclic compounds, isoquinolines. Vol. 38. *Edited by* G. Grethe. Wiley, New York. 1981. Part 1. pp. 25–62.
12. M. Konda, T. Shiori, and S. Yamada. Chem. Pharm. Bull. **23**, 1025 (1975).
13. E. McDonald. *In* Heterocyclic compounds, isoquinolines. Vol. 38. *Edited by* G. Grethe. Wiley, New York. 1981. Part 1. Chap. III.
14. K. I. H. Williams, S. E. Cremer, F. W. Kent, E. J. Sehm, and D. S. Tarbell. J. Am. Chem. Soc. **82**, 3982 (1960).
15. Y. Ban and T. Oishi. Chem. Pharm. Bull. (Tokyo), **6**, 574 (1958).
16. (*a*) C. Harvey, F. X. Garneau, and J. H. Himmelman. Mar. Ecol. Prog. Ser. **40**, 79 (1987); (*b*) N. A. Sloan. Oceanogr. Mar. Biol. Annu. **Rev.** 18, 57 (1980); (*c*) A. M. Mackie and P. T. Grant. *In* Chemoreception in marine organisms. *Edited by* P. T. Grant and A. M. Mackie. Academic Press, New York. 1974. pp. 105–141.
17. A. M. Mackie. J. Exp. Mar. Biol. Ecol. **5**, 63 (1970).
18. D. J. Burnell and J. W. ApSimon. *In* Marine natural products. Vol V. *Edited by* P. J. Scheuer. Academic Press, New York. 1983. pp. 287–389.

Hydrolysis of aluminum(III) ion in sodium nitrate medium

NIKOLA B. MILIĆ,[1] ŽIVADIN D. BUGARČIĆ, AND PREDRAG T. DJURDJEVIĆ
Faculty of Science, Svetozar Marković University, R. Domanovića 12, 34000 Kragujevac, Yugoslavia

Received August 4, 1989[2]

NIKOLA B. MILIĆ, ŽIVADIN D. BUGARČIĆ, and PREDRAG T. DJURDJEVIĆ. Can. J. Chem. **69**, 28 (1991).

Hydrolysis of aluminum(III) ion in 3.0 *M* $(Na)NO_3$ medium was studied by emf method at 25°C. Data cover the range 1–78 *mM* Al(III) within the pH range of 2.0–4.5. At a definite pH, the extent of hydrolysis increases with increasing aluminium concentration, thereby indicating the presence of polynuclear hydrolysis products. The least squares treatment of the data indicates the formation of polynuclear hydrolytic complexes $Al_2(OH)_2^{4+}$, $Al_2(OH)_4^{2+}$, and $Al_3(OH)_4^{5+}$. With the reactions written in the form

$$p\ Al^{3+} + qH_2O \rightleftarrows Al_p(OH)_q^{(3p-q)} + qH^+$$

the stability constants obtained were $\log \beta_{2,2} = -7.55 \pm 0.21$, $\log \beta_{2,4} = -16.41 \pm 0.13$, and $\log \beta_{3,4} = -13.24 \pm 0.08$. Distribution curves indicate that the complex $Al_3(OH)_4^{5+}$ is predominant.

Key words: hydrolysis, aluminum(III) ion, hydrolytic complexes, aluminum(III) ion hydrolysis.

NIKOLA B. MILIĆ, ŽIVADIN D. BUGARČIĆ et PREDRAG T. DJURDJEVIĆ. Can. J. Chem. **69**, 28 (1991).

Opérant à 25°C, dans un milieu contenant 3,0 M de $NaNO_3$ et faisant appel à la méthode de la f.e.m., on a étudié l'hydrolyse de l'ion aluminium(III). Les données couvrent les concentrations allant de 1 à 78 mM de Al(III) et les pH allant de 2,0 à 4,5. A un pH donné, le taux d'hydrolyse augmente avec une augmentation de la concentration en aluminium; ce résultat indique qu'il y a des produits d'hydrolyse de nature polynucléaire. L'examen des données par la méthode des moindres carrés indique qu'il y a formation des complexes d'hydrolyse polynucléaires $Al_2(OH)_2^{4+}$, $Al_2(OH)_4^{2+}$ et $Al_3(OH)_4^{5+}$. Avec les réactions écrites sous la forme

$$p\ Al^{3} + qH_2O \rightleftarrows Al_p(OH)_q^{(3p-q)} + qH^+$$

on à obtenu les constantes de stabilité suivantes: $\log \beta_{2,2} = -7{,}55 \pm 0{,}21$, $\log \beta_{2,4} = -16{,}41 \pm 0{,}13$, et $\log \beta_{3,4} = -13{,}24 \pm 0{,}08$. Les courbes de distribution indiquent que le complexe $Al_3(OH)_4^{5+}$ est prédominant.

Mots clés : hydrolyse, ion aluminium(III), hydrolyse de complexes, hydrolyse de l'ion aluminium(III).

[Traduit par la revue]

Introduction

Although aqueous hydrolysis of aluminum(III) ion has been studied extensively (1–20) the composition and stability of its predominating hydrolytic complexes remains unclear. Kubota's data (5) indicate that monomer $Al(OH)^{2+}$ is formed in a wide range of concentration of sodium perchlorate media (0.01–1.0 *M*).[3] Brosset's data (6, 7) in 2 *M* $NaClO_4$ medium at 40°C indicate the formation of only polynuclear species. Aveston (8) found dimer $Al_2(OH)_2^{4+}$ and tridecamer $Al_{13}(OH)_{32}^{7+}$ in 1 *M* $NaClO_4$ medium. Mesmer and Baes (9) found $Al_2(OH)_2^{4+}$, $Al_3(OH)_4^{5+}$, and $Al_{13}(OH)_{32}^{7+}$ at elevated temperatures (62.5–149.8°C). Brown *et al.* (10), in 0.1 *M* KNO_3 medium, found $Al(OH)^{2+}$, $Al(OH)_2^{+}$, $Al(OH)_4^{5+}$ and a species of high nuclearity for which they presented a stoichiometry-dependent equilibrium constant. Formation of tridecamer was observed by Bottero *et al.* (11–13). Akitt's previous ^{27}Al-NMR measurements (14, 15) indicate the formation of dimer $[(H_2O)_4Al(\mu\text{-}OH)_2Al(H_2O)_4]^{4+}$ and tridecamer $[AlO_4Al_{12}(OH)_{24}(OH_2)_{12}]^{7+}$, while recent data (16–18) obtained at very high magnetic fields indicate the presence of tridecamer and trimer $Al_3O_2(OH)_4^{+}$, as well as oligomeric mixture with stoichiometry close to $[Al_n(OH)_{2.5n}(H_2O)_{5n}]^{0.5n+}$. In the presence of acetate (19, 20) only dimer was found.

In our studies (21–23) of the metal ion hydrolysis, an effect of ionic medium on the extent of hydrolysis and on the composition of hydrolytic complexes and their stability, was observed. Thus discordance in explanation of the hydrolytic behaviour of aluminum might be a result of varying experimental conditions under which the hydrolysis was studied. Thus more reliable information on hydrolytic complexes of aluminum can be obtained by investigating its hydrolysis in various types of ionic media under the same experimental conditions. As part of a wider work this study is on the hydrolysis of aluminum(III) ion in 3.0 *M* $(Na)NO_3$. We used an emf method at 25°C over a wide range of aluminum concentration and pH value.

Experimental

Chemical and analysis

Aluminum nitrate stock solution was prepared from recrystallized $Al(NO_3)_3 \cdot 9H_2O$, Merck, p.a. To prevent hydrolysis of aluminum(III) ion in the stock solution, an appropriate amount of nitric acid was added. Its free concentration was determined potentiometrically using a Gran plot method (24). The aluminum content was determined by precipitation with ammonium hydroxide. The precipitates were ignited at 1100°C, and weighed as Al_2O_3. Reproducibility was within ±0.2%.

Sodium nitrate stock solution was prepared from recrystallized $NaNO_3$, Merck, p.a. The content was determined by evaporating a known volume of solution to dryness at 150°C.

Sodium hydroxide stock solution was prepared in polyethylene bottle as a 50% solution from solid NaOH, Merck, p.a. After a few days, Na_2CO_3 was removed by filtering through a G-4 Jena glass filter. The solution was diluted with 3.0 *M* $NaNO_3$ and standardized against potassium hydrogenphthalate, Merck, p.a.

Nitric acid was made by dilution of HNO_3, Merck, Suprapure, and standardized against NaOH. All solutions were prepared using boiled distilled water.

Nitrogen gas, used for stirring and providing an inert atmosphere for titration, was purified by passing through 10% NaOH and 10% H_2SO_4. Before reaching the titrant, the gas was saturated with H_2O vapor by bubbling it through water and 3.0 *M* sodium nitrate.

[1]Author to whom correspondence should be addressed at Faculty of Science, Radoja Domanovića 12, P.O. Box 60, 34000 Kragujevac, Yugoslavia.

[2]Revision received July 16, 1990.

[3]For shortness *M* and *mM* denote mol dm^{-3} and mmol dm^{-3}.

Can. J. Chem. Downloaded from www.nrcresearchpress.com by 195.138.81.100 on 09/07/12
For personal use only.

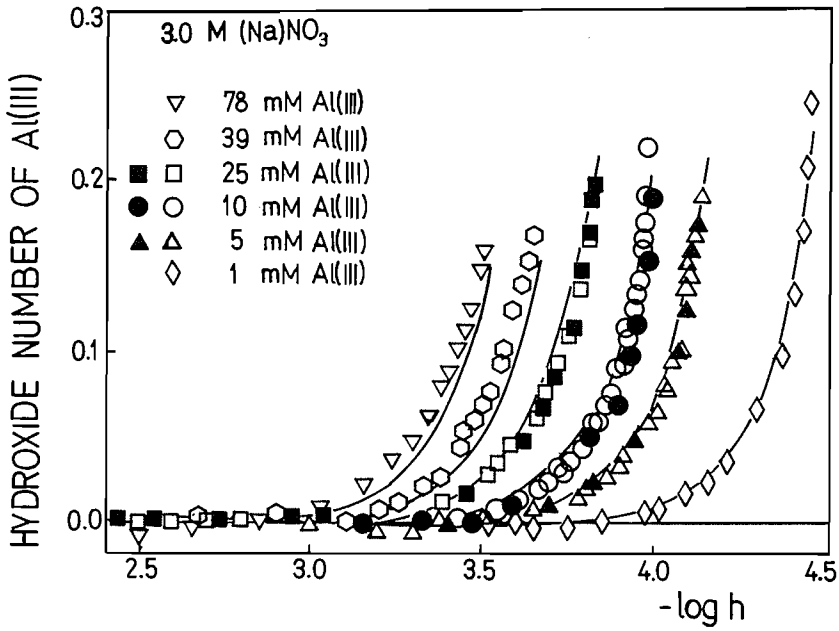


FIG. 1. Hydrolysis of the aluminum(III) ion in sodium nitrate medium (full symbols denote back titrations).

Apparatus and procedure

All emf measurements were carried out as potentiometric titration by using a Wilhelm bridge and constant ionic medium, 3.0 *M* (Na)NO_3[4]. Thus the composition of aluminum(III) solutions was *B* mol dm^{-3} Al^{3+}, *H* mol dm^{-3} H^+, (3.0 − 3*B* − *H*) mol dm^{-3} Na^+, 3.0 mol dm^{-3} NO_3^-, where *B* and *H* denote the total concentration of aluminum(III) and hydrogen ions, respectively.

During measurements the titration vessel and the Wilhelm bridge were inserted in a paraffin oil thermostat at 25.0 ± 0.1°C, which was placed in a room thermostated at 25.0 ± 0.5°C. The cell was

(−) glass electrode | aluminum(III) solution, HNO_3, 3.0 *M* (Na)NO_3 | RE (+)

As reference electrode (RE) the following half cell was used

Ag,AgCl | 3.0 *M* $NaNO_3$, 0.01 *M* $AgNO_3$

The glass electrode was commercial (Beckman, pH 0–11), while the Ag,AgCl electrode was prepared according to Brown (25). Titrations of aluminum(III) solutions were carried out by adding sodium hydroxide from one burette and aluminum(III) solution in the same portion from a second burette. The aluminum solution in second burette was twice the concentration of the aluminum solution in the titration vessel. In this way the total concentration of the aluminum(III) ion was kept constant throughout each titration. Since all solutions were prepared in the corresponding concentration of sodium nitrate, the total concentration of nitrate ions was kept constant, at 3.0 *M* . The concentration of free H^+ (denoted as *h*) at each point was calculated by the Nernst formula

$$E = E_o + E_j + 59.16 \log h$$

where *E* is the measured potential, E_o a constant which includes the standard potential of the glass electrode, and E_j the liguid junction potential. E_o and E_j were both determined in each titration in the area in which the extent of hydrolysis was negligible. The potential was repeatedly measured after each addition of the solutions from the burettes, until a remaining drift of ≤ 0.2 mV/h was reached. In the beginning of the titration a constant value of emf was obtained within 10 min. In the pH range where hydrolysis of the aluminum(III) ion becomes significant, attainment of the equilibrium was rather slow, particularly at higher values of hydroxide number, $Z_{Al} > 0.3$. The emf was measured with a Beckman digital pH meter, Model 4500, with a resolution of ± 0.2 mV.

Results and discussions

The emf data of the hydrolysis of 1.0, 5.0, 10.0, 25, 39, and 78.0 *mM* Al^{3+} ion in 3.0 *M* (Na)NO_3 medium are presented in Fig. 1. This figure gives the average number of hydroxide ions reacted per aluminum(III) ion, Z_{Al}, as function of the free hydrogen ion concentration, −log *h*. Z_{Al} was calculated from the analytical excess of hydrogen ions, *H*, the measured concentration of the free hydrogen ion, *h*, and the total concentration of the aluminum(III) ion, *B*, according to the expression

$$[1] \quad Z_{Al} = (h - H)/B$$

The data obtained show that the aluminum(III) ion in 3.0 M (Na)NO_3 medium starts to hydrolyse between pH 2.0 and 4.5, depending upon its concentration. Thus as the aluminum concentration increases hydrolysis starts at lower pH values (Fig. 2). "Start of hydrolysis" corresponds to the formation of the first hydrolytic complex. From an experimental point of view, the start of hydrolysis corresponds to the first positive hydroxide number, Z_{Al}, beyond the average random error. Thus in Fig. 2, this point occurs when Z_{Al} is 0.01.

The separate curve (Fig. 1) for each concentration of aluminum(III) indicates the formation of polynuclear hydrolytic complexes. The composition of complexes and their stability constants were determined assuming aluminum(III) ion interacts with the water molecules to form one or more hydrolytic complex of the general formula $Al_p(OH)_q^{(3p-q)}$, according to reaction

$$[2] \quad pAl^{3+} + qH_2O \rightleftarrows Al_p(OH)_q^{(3p-q)} + qH^+$$

where the amount of H^+ ions set free is equivalent to the amount of OH^- ions bound to aluminum(III) ion. The general formula $Al_p(OH)_q^{(3p-q)}$ is understood to also include an unknown amount of H_2O as a solvent and possibly also include medium ions. In reaction [2] the hydration of individual ions and complex formation of aluminum(III) ion with nitrate ions are

[4]The notation of the ionic medium is in accordance with refs. 1–3.

Can. J. Chem. Downloaded from www.nrcresearchpress.com by 195.138.81.100 on 09/07/12
For personal use only.

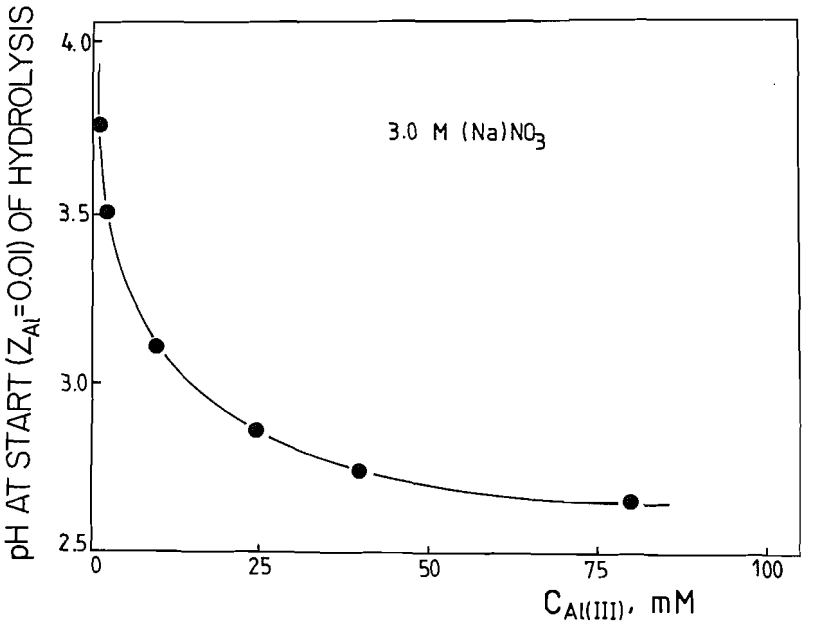


FIG. 2. The correlation between the start of hydrolysis (pH at $Z_{Al} = 0.01$) and the total aluminum(III) ion concentration.

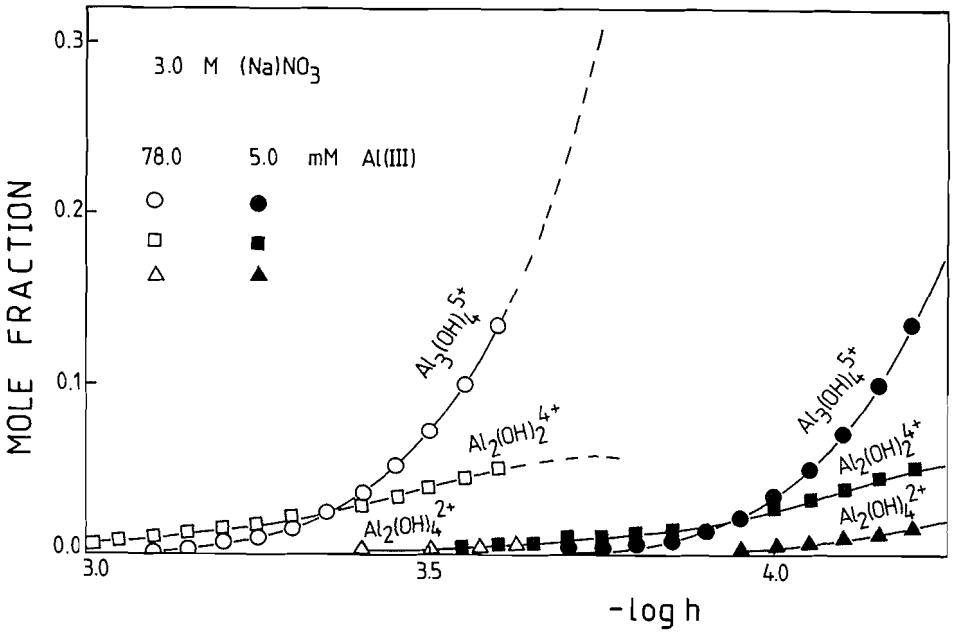


FIG. 3. Distribution of the hydrolytic complexes at 5.0 and 78.0 *mM* Al^{3+}. The distribution curves of the free Al^{3+} ion are omitted due to extension mole fraction scale.

omitted. The concentration of both nitrate ions and water molecules is much higher than the concentration of aluminum(III) ion, therefore it is not possible to determine the changes in concentration of nitrate ions and water molecules. To avoid variable effects of complex formation of aluminum(III) ion with nitrate ion, its concentration was kept high and constant, 3.0 *M* NO_3^-. Under such conditions, an eventual complex formation should appear as a constant effect and should not affect the number of OH^- ions in the hydrolytic complexes.

The composition of the hydrolytic complexes and their stability constants were determined by minimizing the error square sum

$$[3] \quad U = \Sigma(Z_{calc} - Z_{exp})^2$$

where Z_{exp} denotes the experimental value of Z_{Al} (eq. [1]) and Z_{calc} the calculated value using the tested (p,q) values and stability constants

$$[4] \quad Z_{calc} = (\Sigma q\beta_{pq}\, h^{-q}b^p)/(b + \Sigma p\beta_{pq}h^{-q}b^p)$$

In eq. [4] β_{pq} denotes the stability constant of the hydrolytic complex according to eq. [5]

$$[5] \quad \beta_{pq} = c_{pq}h^q b^{-p}$$

c_{pq} denotes the concentration of the hydrolytic complex, and b and h the free concentrations of the metal ion and hydrogen

Can. J. Chem. Downloaded from www.nrcresearchpress.com by 195.138.81.100 on 09/07/12
For personal use only.

Can. J. Chem. Downloaded from www.nrcresearchpress.com by 195.138.81.100 on 09/07/12
For personal use only.

TABLE 1. Tested models for the aluminum(III) ion hydrolysis

(p, q)	$-\log(\beta_{pq} \mp 3\delta)$	$10^{-5}\ U_{min}$
(2, 2)	−6.93 ∓ 0.03	
(1, 1)	—	0.98
(2, 2)	−6.93 ∓ 0.03	
(1, 2)	—	0.98
(2, 2)	−6.93 ∓ 0.03	
(13,32)	—	0.98
(2, 2)	−6.96 ∓ 0.03	
(13, 24)	−73.83 max − 73.56	0.89
(2, 2)	−6.93 ∓ 0.03	
(3, 6)	—	0.98
(2, 2)	−6.95 ∓ 0.30	
(1, 3)	−14.94 ∓ 0.20	0.85
(2, 2)	−7.03 ∓ 0.06	
(2, 3)	−11.78 ∓ 0.19	0.83
(2, 2)	−7.14 ∓ 0.08	
(4, 6)	−19.46 ∓ 0.11	0.65
(2, 2)	−7.52 ∓ 0.25	
(3, 4)	−13.18 ∓ 0.08	0.50
(3, 4)	−13.03 ∓ 0.11	
(1, 1)	—	0.59
(2, 2)	−7.52 ∓ 0.25	
(3, 4)	−13.18 ∓ 0.08	
(13, 24)	—	0.50
(2, 2)	−7.52 ∓ 0.25	
(2, 3)	−11.78 ∓ 0.19	
(13, 14)	—	0.83
(2, 2)	−7.55 ∓ 0.25	
(3, 4)	−13.26 ∓ 0.11	
(2, 3)	−11.98 max − 11.76	0.45
(2, 2)	−7.52 ∓ 0.25	
(3, 4)	−13.18 ∓ 0.08	
(4, 6)	—	0.50
(2, 2)	−7.52 ∓ 0.25	
(3, 4)	−13.18 ∓ 0.08	
(3, 5)	—	0.50
(2, 2)	−7.52 ∓ 0.25	
(1, 2)	—	
(3, 4)	−13.18 ∓ 0.08	0.50
(2, 2)	−7.52 ∓ 0.25	
(3, 4)	−13.18 ∓ 0.08	
(1, 3)	—	0.50
(2, 2)	−7.55 ∓ 0.21	
(1, 2)	—	
(2, 4)	−16.41 ∓ 0.13	
(3, 4)	−13.24 ∓ 0.08	0.30
(2, 2)	−7.55 ∓ 0.21	
(1, 1)	—	
(2, 4)	−16.41 ∓ 0.13	
(3, 4)	−13.24 ∓ 0.08	0.30

ion, respectively. The minimization given by eqs. [3] and [4] has been performed using the generalized least-squares program LETRAGROP (26). The data obtained indicate the formation of two dimeric complexes, $Al_2(OH)_2^{4+}$ and $Al_2(OH)_4^{2+}$, and the trimer, $Al_3(OH)_4^{5+}$, with the following stability constants: log

TABLE 2. Hydrolytic complexes of the aluminum(III) ion in 3.0 *M* $(Na)NO_3$ medium at various levels of the hydroxide number

	Stability constants, $\log(\beta_{pq} \mp 3\delta)$		
Z_{Al}	$Al_2(OH)_2^{4+}$	$Al_2(OH)_4^{2+}$	$Al_3(OH)_4^{5+}$
<0.05	−7.43 ∓ 0.22	—	−13.38 max −13.14
<0.15	−7.41 ∓ 0.17	—	−13.28 ∓ 0.11
<0.30	−7.55 ∓ 0.21	−16.41 ∓ 0.13	−13.24 ∓ 0.08

$\beta_{2,2} = -7.55 \pm 0.21$, $\log \beta_{2,4} = -16.41 \pm 0.13$ and $\log \beta_{3,4} = -13.24 \pm 0.08$, respectively. Many other models were also tested (Table 1) but in all these cases calculation gave either negative values of β_{pq} or larger values of U_{min}.

Since some recent works (10, 16) denied or questioned the presence of $Al_2(OH)_2^{4+}$ we tested for this complex in a number of models (Table 1). The dimer was accepted in all models tested, but with rather high error. A similar controversial situation is true of the tridecamer. Therefore we tested its presence in combinations with other species using all six data for total aluminum concentrations but tridecamer was rejected in every case. We also tested for tridecamer by calculating the concentration of aluminum(III) ion separately. Tridecamer was accepted only at 5 *mM* Al(III) and rejected at all other aluminum concentrations. The presence or absence of dimer and tridecamer complexes may be a result of different experimental conditions, therefore it will be of interest to investigate the aluminum(III) ion hydrolysis by both NMR and emf measurements under the same experimental conditions. In a study of the hydrolysis of thorium(IV) ions (22), we obtained an excellent agreement betweem emf and calorimetric data under the same experimental conditions.

Since some data (5, 10) in very dilute solutions (0.1–1 *mM* Al^{3+}) and at low hydroxide numbers indicated the formation of mononuclear species we have also treated the data of 1 and 5 *mM* Al^{3+} with $Z_{Al} < 0.05$, separately. However, the two monomers $AlOH^{2+}$ and $Al(OH)_2^+$ were rejected in combination with the dimers and trimer. Since polymerization process of monomers to polynuclear species is extensive, the existence of monomers depends very much on the ageing time of hydrolyzed solutions. If potential is measured immediately after the addition of base, the data might indicate the presence of monomers. More reliable information on the composition of the hydrolytic species can be obtained from data at equilibrium state. However, equilibrium, may take a long time to get established, depending on the nature of the metal ion, the degree of hydrolysis, and medium effect. In our work, the time necessary for achieving constant potential readings was between 15 min and 3 h, depending on Z_{Al} values. To check for equilibrium, we measured the potential for more than 10 h (overnight) without adding the base. The results indicate that a "constant potential" reflects the equilibrium state, or, at least a state which is very close to equilibrium. This might be why our data did not indicate the presence of monomeric hydrolytic complexes. A high concentration of ionic medium may be another explanation for our results. In our work the medium was 3.0 *M*. Consequently, the concentration of free water molecules was lowered because of the stoichiometry and hydration of medium ions. Under such conditions one may expect that the formation of polynuclear hydrolytic complexes will be more pronounced.

Using the Haltafall program (27) the distribution of $Al_2(OH)_2^{4+}$, $Al_2(OH)_4^{2+}$, and $Al_3(OH)_4^{5+}$ as a function of pH was calculated (Fig. 3). These plots show that $Al_3(OH)_4^{5+}$ is the predominant complex. Its concentration increases with increasing total aluminum(III) ion concentration.

Assuming that formation of polynuclear hydrolytic complexes is a result of polymerization, it is obvious that polynuclearity should increase with increasing Z_{Al}. To check that, all data were divided into three groups ($Z_{Al} < 0.05$, $Z_{Al} < 0.15$, $Z_{Al} < 0.30$) and each of them was treated separately. The results obtained (Table 2) indicate that at low Z_{Al} values only the formation of dimer $Al_2(OH)_2^{4+}$ is significant. At higher Z_{Al} values, the trimer also appeared. However, two dimers, $Al_2(OH)_2^{4+}$, $Al_2(OH)_4^{2+}$, and one trimer $Al_3(OH)_4^{2+}$ are found over the entire Z_{Al} range, with stability constants differ only slightly from one range of Z_{Al} values to another.

1. L. G. SILLÉN and A. E. MARTELL (*Editors*). Stability constants of metal ion complexes. Special Publication, No. 17. The Chemical Society, London. 1964.
2. L. G. SILLÉN and A. A. MARTELL (*Editors*). Stability constants of metal ion complexes. Special Publication No. 25. The Chemical Society, London. 1971.
3. E. HÖGFELDT (*Editor*). Stability constants of metal ion complexes. IUPAC Chem. Data Series, No. 22, Pergamon Press, Oxford. 1982.
4. C. F. BAES and R. E. MESMER. The hydrolysis of cations. J. Wiley and Sons, New York. 1976.
5. H. KUBOTA. Diss. Abstr. **16**, 864 (1956).
6. C. BROSSET. Acta Chem. Scand. **6**, 910 (1952).
7. C. BROSSET, G. BIEDERMANN, and L. G. SILLÉN. Acta Chem. Scand. **8**, 1917 (1954).
8. J. AVESTON. J. Chem. Soc. 4438 (1965).
9. R. E. MESMER and C. F. BAES. Inorg. Chem. **10**, 2290 (1971).
10. P. L. BROWN, R. N. SYLVA, G. E. BATLEY, and J. ELLIS. J. Chem. Soc. Dalton Trans. 1967 (1985).
11. J. Y. BOTTERO. J. P. MARCHALL, J. E. POIRIER, J. CASSES, and F. FIESSINGER. Bull. Soc. Chim. Fr. 439 (1982).
12. J. Y. BOTTERO, J. E. POIRIER, and F. FIESSINGER. Prog. Water Techn. **12**, 601 (1980).
13. J. Y. BOTTERO, J. M. CASES, F. FIESSINGER, and J. E. POIRIER. J. Phys. Chem. **84**, 2933 (1980).
14. J. W. AKITT and A. FARTHING. J. Chem. Soc. Dalton Trans. 1617 (1981).
15. J. W. AKITT and J. M. ELDERS. Bull. Soc. Chim. Fr. 10 (1986).
16. J. W. AKITT and J. M. ELDERS. J. Chem. Soc. Dalton Trans. 1347 (1988).
17. J. W. AKITT. Prog. Nucl. Magn. Reson. Spectrosc. **21**, 1 (1988).
18. J. W. AKITT, J. M. ELDERS, X. L. R. FONTAINE, and A. K. KUNDU. J. Chem. Soc. Dalton Trans. 1889 (1989).
19. J. W. AKITT and N. B. MILIĆ. J. Chem. Soc. Dalton Trans. 981 (1984).
20. J. W. AKITT, J. M. ELDERS, X. L. R. FONTAINE, and A. K. KUNDU. J. Chem. Soc. Dalton Trans. 1897 (1989).
21. N. B. MILIĆ. Acta Chem. Scand. **25**, 2487 (1971).
22. N. B. MILIĆ. J. Chem. Soc. Dalton Trans. 1445 (1981).
23. T. M. ŠURANJI and N. B. MILIĆ, Croat. Chim. Acta **55**, 295 (1982).
24. G. GRAN, Analyst, **77**, 661 (1952).
25. A. S. BROWN. J. Am. Chem. Soc. **56**, 646 (1934).
26. P. BRAUNER, L. G. SILLÉN, and R. WHITEKER. Ark. Kemi, **31**, 365 (1968).
27. N. INGRI, W. KAKOLOWICZ, L. G. SILLÉN, and B. WARNQUIST. Talanta, **31**, 365 (1967).

Can. J. Chem. Downloaded from www.nrcresearchpress.com by 195.138.81.100 on 09/07/12
For personal use only.

Spinel ferrites as catalysts: A study on catalytic effect of coprecipitated ferrites on hydrogen peroxide decomposition

PREETI LAHIRI AND SUSANTA K. SENGUPTA

Department of Chemistry, Faculty of Science, Banaras Hindu University, Varanasi-221005, India

Received December 5, 1989[1]

PREETI LAHIRI and SUSANTA K. SENGUPTA. Can. J. Chem. **69**, 33 (1991).

Some ferrospinels act as catalysts for the decomposition of H_2O_2, their effectiveness is dependent on the composition of the catalyst. This study is to find the most effective catalyst of stoichiometry $M^{II}Fe_2^{III}O_4$. A set of ferrites of different composition $M^{II}Fe_2^{III}O_4$ (M^{II} = Mn, Co, Ni, Cu, Zn, Cd) was synthesized by co-precipitation and characterized by chemical analysis, X-ray diffractometry, and B.E.T. technique. A comparative assessment of the catalytic power of these ferrites from investigations of their influence on the kinetics of H_2O_2 decomposition in a neutral medium was made. An analysis of the data on specific rate, and the Eyrings activation parameters for the reaction sharply reveal the following: (*a*) The catalytic power follows the order $MnFe_2O_4 > CoFe_2O_4 > CuFe_2O_4 > NiFe_2O_4 > CdFe_2O_4 > ZnFe_2O_4$, $MnFe_2O_4$ is much more highly effective than the others (50–100 fold). (*b*) A compensation effect has been noted from the observed linearity with slightly less than unity slope between $T\Delta^*S^0$ and Δ^*H^0 over the entire series.

Key words: Ferrospinels, catalysis, hydrogen peroxide decomposition kinetics.

PREETI LAHIRI et SUSANTA K. SENGUPTA. Can. J. Chem. **69**, 33 (1991).

Quelques ferrospinelles catalysent la décomposition du H_2O_2; le degré de la catalyse dépend de la composition du catalyseur. On a entrepris la présente étude dans le but de trouver le catalyseur de stoechiométrie $M^{II}Fe_2^{III}O_4$ le plus efficace. Faisant appel à une méthode de coprécipitation, on a synthétisé un ensemble de ferrites de composition $M^{II}Fe_2^{III}O_4$ (M^{II} = Mn, Co, Ni, Cu, Zn, Cd) que l'on a caractérisées par des analyses chimiques, par la diffraction des rayons-x et par la technique BET. On a évalué les pouvoirs catalytiques relatifs de ces ferrites en examinant leur influence sur la cinétique de la décomposition du H_2O_2 en milieu neutre. Une analyse de données spécifiques et des paramètres d'acivation de Eyring conduit aux conclusions suivantes: (*a*) Le pouvoir catalytique décroit dans l'ordre suivant: $MnFe_2O_4 > CoFe_2O_4 > CuFe_2O_4 > NiFe_2O_4 > CdFe_2O_4 > ZnFe_2O_4$; le $MnFe_2O_4$ est toutefois beaucoup plus actif que les autres (de 50 à 100 fois plus). (*b*) On a noté un effet de compensation de la linéarité; sur toute la série, la pente entre le $T\Delta^*S^0$ et la Δ^*H^0 es légèrement inférieure à l'unité.

Mots clés : ferrospinelles, catalyse, peroxyde d'hydrogène, cinétique de décomposition.

[Traduit par la revue]

Introduction

Ferrospinels which form a series of isostructural compounds ($M^{II}Fe_2O_4$, M^{II} a bivalent metal ion) structurally belong to two major types: normal $(M^{II})_{tet}[Fe^{III}Fe^{III}]_{oct}O_4$ and inverse $(Fe^{III})_{tet}[M^{II}Fe^{III}]_{oct}O_4$. These mixed oxides, well known for their use as high frequency transformer cores, magnetic memories and switches, also have attractive catalytic properties. Among the applications mention must be made of highly selective oxidation of butene to butadiene (1), synthesis of ammonia (2), and decomposition of hydrogen peroxide (3). H_2O_2 decomposoiton is catalyzed by a number of ferrites and the effectiveness of the catalysts is dependent on the ferrite composition. Cobalt ferrite, CoF_2O_4, an inverse spinel catalyzes the decomposition of H_2O_2 to such an extent that it is matched only by the highly powerful, expensive catalysts like platinum, palladium, or silver oxide (4). This has, in fact, led to a number of important investigations on the use of cobalt ferrites $Co_xFe_{3-x}O_4$ ($0 \leq x \leq 3$) as electrocatalysts for oxygen reduction electrode process (5). Several catalysts were tried to search for a ferrospinel with optimum catalytic activity for the decomposition of H_2O_2. Examples include $Co_xFe_{3-x}O_4$, $Cu_xFe_{3-x}O_4$, and $Ni_xFe_{3-x}O_4$ ($0 \leq x \leq 3$) (6–8). The intrinsic catalytic power was found to be Co > Cu > Ni. Among the cobalt ferrites, $Co_{1.5}Fe_{1.5}O_4$ is the most active (6). Chemical composition, crystal structure, electronic, electrochemical, topochemical, and microstructural factors have been found to contribute to the overall activity of the catalysts (3). Peroxide decompositions are generally studied in the alkaline media, the media in which H_2O_2 is intrinsically unstable because of base catalysis by OH^- (9). In view of this complication, the present comparative assessment of the intrinsic activity of transition metal ferrites ($M^{II}Fe_2O_4$ where M = Mn, Co, Ni, Cu, Zn, Cd) towards peroxide decomposition was done in a neutral medium (pH 6.6).

Experimental

Preparation and characterisation of ferrospinels

Among the various synthetic routes considered by Goldstein and Tseung, hydroxide coprecipitation is the best for achieving high surface area for the spinel catalyst (3). A series of ferrospinels, MFe_2O_4 (M = Mn, Co, Cu, Ni, Cd, Zn) was synthesized by mixing appropriate amount of metal sulfate solution (Analar Grade) and ferrous ammonium sulfate (Analar Grade) with the appropriate volume of freshly prepared 5 M NaOH at 73 ± 1°C. More base was added until the precipitate formed attained a pH value of 10–10.5. The resultant precipitate was heated for 4 h. The brown deposit was filtered, the residue was washed until alkali-free, dried in an oven at 110°C, and sieved to 200 B.S.S. mesh size.

Chemical analysis was done complexometrically to determine the stoichiometry of the metal ions present in the sample. The powder samples were subjected to X-ray diffraction analysis, carried out on a Philips automatic X-ray diffractometer with a PW 1729 X-ray generator using Cu-K_α (1.5418 Å) radiation. The values obtained for the *d*-plane spacings and their relative intensities of reflection of MFe_2O_4 (M = Zn, Cd, Co, Ni, Cu, Mn) were compared with those in International tables for X-ray crystallography to determine the phases present. The Brunauer, Emmett, and Teller (B.E.T.) specific surface areas of the samples were measured by nitrogen adsorption at 77 K after degassing the catalyst at 301 K for 6 h.

Measurement of catalytic activity of the peroxide decomposition reaction kinetics

The catalytic activity of the ferrospinels for hydrogen peroxide decomposition was evaluated by rate of evolution of oxygen from the

[1]Revision received July 31, 1990.

Can. J. Chem. Downloaded from www.nrcresearchpress.com by 195.138.81.100 on 09/07/12
For personal use only.

TABLE 1. Properties of ferrite series: MFe_2O_4 (M = Zn, Cd, Cu, Ni, Co, Mn)

Catalyst	Cation valency distribution on the spinel structure	g-atom ratio Fe/M	B.E.T. specific surface area ($m^2\ g^{-1}$) (±5%)
$ZnFe_2O_4$	$(Zn^{2+})_{tet}[Fe^{3+}Fe^{3+}]_{oct}\ O_4^{2-}$	2.00	29
$CdFe_2O_4$	$(Cd^{2+})_{tet}[Fe^{3+}Fe^{3+}]_{oct}\ O_4^{2-}$	1.92	37.2
$CuFe_2O_4$	$(Fe^{2+})_{tet}[Cu^{+}Fe^{3+}]_{oct}\ O_4^{2-}$	2.10	73.7
$NiFe_2O_4$	$(Fe^{3+})_{tet}[Ni^{2+}Fe^{3+}]_{oct}\ O_4^{2+}$	2.02	61
$CoFe_2O_4$	$(Fe^{3+})_{tet}[Co^{2+}Fe^{3+}]_{oct}\ O_4^{2-}$	2.15	68.7
$MnFe_2O_4$	$(Mn_{0.5}^{2+}Fe_{0.5}^{3+})_{tet}[Fe_{0.5}^{2+}Fe^{3+}Mn_{0.5}^{3+}]_{oct}\ O_4^{2-}$	2.04	45

TABLE 2. X-ray diffraction results

Catalysts	d(cal) Å have been noted at sharp peak I/I_0 (%) positions	Phases present
$ZnFe_2O_4$	2.96; 2.53; 2.10; 1.61; 1.48 35.7; 100; 13.4; 25.1; 29.0	$ZnFe_2O_4$
$CdFe_2O_4$	3.04; 2.61; 2.53; 1.67; 1.50; 1.49 55.4; 100; 19.2; 40.0; 12.3; 30.2	$CdFe_2O_4$
$CuFe_2O_4$	2.97; 2.52; 2.32; 1.87; 1.61; 1.47 44.5; 100; 22.4; 7.3; 19.2; 49.8	$CuFe_2O_4$, CuO
$NiFe_2O_4$	2.96; 2.52; 2.42; 2.09; 1.61; 1.48 19.2; 100; 9.1; 25.7; 24.8; 37.9	$NiFe_2O_4$
$CoFe_2O_4$	2.52; 2.08; 1.61; 1.47; 1.27; 1.12 100; 17.9; 22.1; 42.7; 12.1; 5.78	$CoFe_2O_4$
$MnFe_2O_4$	2.97; 2.53; 1.71; 1.61; 1.48; 1.17; 1.28 29.2; 100; 8.10; 21.8; 33.2; 5.47; 5.80	$MnFe_2O_4$

liquid phase. A measured amount of catalyst (5–200 mg), depending upon the nature of catalysts, was injected into a thermosttated reaction vessel containing 2 cm^3 of 0.8 M H_2O_2 in 8 cm^3 of distilled water (pH 6.64 ± 0.01) for each specimen, H_2O_2 was standardized immediately before use by standard $KMnO_4$ solution. The peroxide decomposition is represented by

[1] $2H_2O_2 = 2H_2O + O_2$

The rate of evolution of gaseous O_2 was monitored with a gasometric assembly. The time-dependent volume, V_t of the evolved oxygen was monitored at 2 min intervals in all cases. The infinity reading, V_∞ was recorded by completing the reaction at 100°C. pH variation during the reaction was only ±0.04. Eyrings activation parameters were investigated over the temperature range 303–318 K.

Results and discussion

Results of chemical (complexometric) and XRD analyses revealed the presence of only spinel phases of stoichiometry $M^{II}Fe_2O_4$ (Table 2). However, we found contamination of the copper ferrite sample with CuO (Table 2). Moreover, no broad halos characteristic of amorphous phases could be detected on the diffraction pattern. The cation valency distribution between tetrahedral and octahedral sublattices characteristic of the spinel phases detected are included in Table 1. Thus whereas zinc and cadmium ferrites are normal spinels, copper, nickel, and cobalt ferrites are inverse ones, all having the stoichiometry $M^{II}Fe_2O_4$. In manganese ferrite, manganese distribution between tetrahedral and octahedral sublattices is 1:1. It is worth noting that the distribution depends upon the technique of preparation. It is 4:1 in the samples prepared by ceramic method as against 1:1 in the coprecipitated method, a result substantiated by ^{55}Mn NMR spectra (10). The catalytic activity of Fe_3O_4, known to be too low, was excluded in this study (3). It is noteworthy that catalytic activity of simple oxides of M^{II}, Fe^{III}, and their simple mixtures for decomposition of H_2O_2 in neutral media was found to be negligible. Thus for copper ferrite, which is contaminated with CuO, the observed catalysis is completely due to the spinel phase, as is the case of other ferrites. Results of specific surface area (Table 1) as determined by the B.E.T. technique show that this microstructural feature varies to some extent over a range (30–73 m^2/g) among the samples prepared.

TABLE 3. Specific rate constants at different temperatures for ferrite catalysts

Catalyst	Specific rate constants (k) $g^{-1}\ min^{-1}\ 10^2$ (±5%) 303 K	308 K	313 K	318 K
$ZnFe_2O_4$	2.46	4.16	5.60	8.20
$CdFe_2O_4$	11.51	17.22	23.49	35.12
$NiFe_2O_4$	14.96	22.45	33.85	41.45
$CuFe_2O_4$	25.56	39.49	78.87	123.21
$CoFe_2O_4$	221.00	287.80	396.10	495.10
$MnFe_2O_4$	1007.50	1727.00	2256.50	3132.00

Results from the kinetic study showed that H_2O_2 decomposition in neutral media follows first order kinetics for each of the ferrite catalysts. The specific reaction rates were found to be

Can. J. Chem. Downloaded from www.nrcresearchpress.com by 195.138.81.100 on 09/07/12
For personal use only.

TABLE 4. Specific rate constant normalized to unit B.E.T. specific surface area, and activation enthalpy and entropy of ferrite catalysts

Catalyst	Specific rate constant normalized to unit B.E.T. specific surface area (k_n) min^{-1} m^{-2} 10^3 (±5%) 303 K	308 K	313 K	318 K	Δ^*H^0 (kJ mol^{-1}) (±2%)	Δ^*S^0 (J K^{-1} mol^{-1}) (±2%)
$ZnFe_2O_4$	0.84	1.43	1.93	2.82	56.06	−125.96
$CdFe_2O_4$	3.09	4.62	6.31	9.44	61.27	−95.67
$NiFe_2O_4$	2.45	3.68	5.55	6.79	61.27	−93.28
$CuFe_2O_4$	3.47	5.35	10.70	16.72	83.48	−15.16
$CoFe_2O_4$	32.16	41.89	57.65	72.06	38.29	−145.93
$MnFe_2O_4$	223.80	383.30	501.10	696.00	54.70	−79.00

proportional to the mass of the catalyst at least in our experiment (2–200 mg). The data on the rate constant per unit mass (k) of catalyst presented in Table 3 revealed that the catalytic activity of the prepared samples follow the order Mn > Co > Cu > Ni > Cd > Zn in MFe_2O_4. This order holds consistently at four different temperatures (Table 3).

The key objective of our investigation was to establish an order of intrinsic catalytic activities for MFe_2O_4 in the decomposition of H_2O_2 a property far more dependent on composition of the catalyst than on their microstructural differences. One possible way to ascertain an intrinsic catalytic activity is to utilize a kinetic parameter which is normalized for catalyst microstructure. Since B.E.T. specific surface area is a key microstructural factor, we chose the specific decomposition rate per unit B.E.T. surface area (k_n) as the microstructure-normalized parameter. The intrinsic activity in terms of k_n (Table 4) was found to follow the order Mn > Co > Cu > Cd > Ni > Zn ferrite, virtually the same order as k. It is further revealing that whereas Mn, Co or Zn ferrite has significantly different catalytic effectiveness than any other member, Cu, Cd, and Ni ferrites do not exhibit that much difference amongst themselves. Moreover, the order in k_n was found to be the same at the four different temperatures. It may be noted that k_n of copper ferrite, when corrected for activity due to the CuO (an inactive phase) present, would not change the activity order among the ferrites.

The results were analyzed using Eyring's equation

$$\log\left(\frac{k}{T}\right) = \log\left(\frac{K}{h}\right) + \frac{\Delta^*S^0}{2.303R} - \frac{\Delta^*H^0}{2.303R}\left(\frac{1}{T}\right)$$

K = Boltzmann constant. Activation entholpies (Δ^*H^0) and entropies (Δ^*S^0) were calculated using the log (k/T) vs. $1/T$ plot. It is seen that the activation enthalpies show a significant variation (38–83 kJ mol^{-1}) for the series (Table 4). This is not unexpected in view of the differences in composition and structure amongst the catalysts. This wide variation in Δ^*H^0 with composition also minimizes the possibility of diffusion of H_2O_2 to the surface of the catalyst as a major factor controlling the decomposition kinetics (3). It is interesting to note that the order observed in k_n, Δ^*H^0, and Δ^*S^0 among the ferrites differ significantly from one another. The order found is Cu > Ni ≈ Cd > Zn > Mn > Co ferrite in Δ^*H^0 and Cu > Mn > Ni ≈ Cd > Zn > Co ferrite in Δ^*S^0 as against Mn > Co > Cu ≈ Cd ≈ Ni > Zn ferrite in k_n (Table 4). However, $T\Delta^*S^0$ vs. Δ^*H^0 plot yields a straight line of slope slightly less than unity (0.88) (Fig. 1) showing the constancy of peroxide decomposition mechanism over the entire ferrite series and a high degree of compensation between Δ^*H^0 and Δ^*S^0 (11). Evidently, activation entropies which can be related to the entropy of adsorption of the reactant (7) play a key role in determining the order of intrinsic activity among the ferrites. Mn and Zn ferrites have similar Δ^*H^0 values but very different Δ^*S^0 values. Their k_n values are also very different.

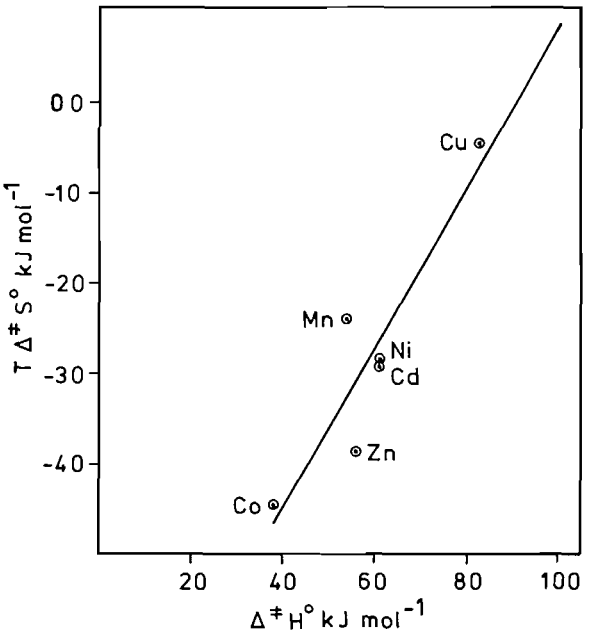


FIG. 1. Compensation effect. Plot of $T\Delta^*S^0$ vs Δ^*H^0 for the decomposition of H_2O_2 on ferrospinels MFe_2O_4 surfaces.

It has been seen from a number of kinetic studies on ferrite-catalyzed decomposition of H_2O_2 (3) that several factors, such as chemical composition, electronic structure, redox characteristics, topochemical effects, and pH, govern the intrinsic activity of ferrospinel catalysts. For the series chosen topochemical factors are insignificant to explain the observed order. pH effects were kept at a minimum level because of the choice of a neutral medium (pH 6.64 ± 0.04).

It is generally agreed that the electronic structure and the ease of M^{II} (or Fe^{II})/Fe^{III} (or M^{III}) redox conversions initiated by M^{II} (or Fe^{II}) centres on the spinel lattice are among the principal factors governing the intrinsic catalytic activity for the decomposition of H_2O_2. Taking these factors into account, the observed order for intrinsic catalytic activity among MFe_2O_4 for H_2O_2 decomposition may be re-expressed as

$$[Mn_{0.5}^{II}—Fe_{0.5}^{III}]_{tet} + [Fe_{0.5}^{II}—Mn_{0.5}^{III}]_{oct} > [Co^{II}—Fe^{III}]_{oct} > [Cu^{I}—Fe^{III}]_{oct} \approx [Cd^{II}]_{tet} \approx [Ni^{II}—Fe^{III}]_{oct} > [Zn^{II}]_{tet}$$

Can. J. Chem. Downloaded from www.nrcresearchpress.com by 195.138.81.100 on 09/07/12
For personal use only.

$[Fe^{II}—Fe^{III}]_{oct}$ is not mentioned because of the known low activity of Fe_3O_4 (3).

The conclusion that emerges is that the operation of the redox couples $(Mn^{II}/Fe^{III})_{tet}$, $(Fe^{II}/Mn^{III})_{oct}$, along with $(Mn_{tet}^{II}/Mn_{oct}^{III})$, must be sufficiently unhindered to make manganese ferrite the most active, and significantly more effective than the well-known cobalt ferrite. The low activity of zinc ferrite is not unexpected in the light of the foregoing discussion. However, $(Cu^{I}/Fe^{III})_{oct}$ as well as $(Ni^{II}/Fe^{III})_{oct}$ redox couples must be sufficiently restricted, more so the latter to make their intrinsic activity comparable to that of cadmium ferrite. The activity of cadmium ferrite compared to that of zinc ferrite appears unexpected in view of the above factors. It needs more examination to find some explanation for its activity. However, the present investigation has led to the finding that manganese ferrite is potentially a very powerful catalyst significantly more so than cobalt ferrite for the decomposition of hydrogen peroxide.

Acknowledgements

One of the authors (P.L.) expresses her heartfelt gratitude to the C.S.I.R., New Delhi, for providing financial support. Both authors thank the Head, Department of Chemistry, B.H.U., Varanasi, for providing laboratory facilities. Our appreciation goes to the Director, R.S.I.C., Nagpur University, Nagpur, for facilitating XRD analysis. Finally, we like to extend our thanks and appreciation to Mr. A. S. K. Sinha, Chemical Engineering Department, I.T., B.H.U., Varanasi, for providing BET surface area measurement facility and Dr. R. S. Tiwari, Department of Physics, B.H.U., for critical suggestions on the XRD analysis.

1. H. K. HAROLD and C. K. MAYFAIR. Adv. Catal. **33**, 159 (1985).
2. R. R. RAJARAM and . A. SERMON. J. Chem. Soc. Faraday Trans. I, **81**, 2577 (1985).
3. J. R. GOLDSTEIN and A. C. C. TSEUNG. J. Catal. **32**, 452 (1974).
4. H. M. COTA, J. KATAN, M. CHIN, and F. J. SCHOENWEIS. Nature, **203**, 1281 (1964).
5. A. C. C. TSEUNG and J. R. GOLDSTEIN. J. Phys. Chem. **76**, 3646 (1972).
6. A. I. ONUCHUKWU and A. B. ZURU. Mater. Chem. Phys. **15**, 131 (1986).
7. A. I. ONUCHUKWU. J. Chem. Soc. Faraday Trans. I, **80**, 1447 (1984).
8. S. V. S. PRASAD and S. RAO. Proceedings of the 7th National Symposium on Advances in Catalysis-Science and Technology, Baroda (India). January 1985, *edited by* T. S. R. Prasada Rao, Wiley Eastern Limited, New Delhi, 1985, p. 41.
9. F. R. DUKE and T. W. HAAS. J. Phys. Chem. **65**, 304 (1961).
10. T. TAKADA, Y. BANDO, M. KIYAMA and T. SHINJO. Proceedings of the International Conference on Ferrites, Japan. July 1970, *Edited by* Y. Hoshino, S. Iida, and M. Sugimoo. University of Tokyo Press, Japan, 1971, p. 29.
11. K. J. LAIDLER. Chemical kinetics, Harper and Row, New York. 1987. p. 211.

Can. J. Chem. Downloaded from www.nrcresearchpress.com by 195.138.81.100 on 09/07/12
For personal use only.

The homogeneous conversion of methane to higher hydrocarbons in the presence of ethylene in the temperature range 925–1023 K

ALAIN R. BOSSARD AND MARGARET H. BACK
Department of Chemistry, University of Ottawa, Ottawa, Ont., Canada K1N 6N5

Received June 26, 1990

ALAIN R. BOSSARD and MARGARET H. BACK. Can. J. Chem. **69**, 37 (1991).

Mixtures of ethylene and methane have been pyrolyzed in the temperature range 925–1023 K for the purpose of converting methane to higher hydrocarbons. Addition of methane to thermally-reacting ethylene increases the rate of formation of propylene but decreases the rates of formation of the other major products, ethane, acetylene, and butadiene. Hydrogen abstraction from methane is a major propagation reaction and causes a shift in the radical distribution from ethyl and vinyl radicals, the main radicals in the pyrolysis reactions of ethylene alone, to methyl radicals, which lead to the formation of propylene. At 1023 K with a pressure of ethylene of 6.5 Torr and of methane of 356 Torr, 1.5 mol of methane is converted to higher molecular weight products for every mole of ethylene reacted. The rate of conversion of methane in the homogeneous system is lower than in catalytic reactions but the product is entirely hydrocarbon and no methane is lost to carbon monoxide or carbon dioxide.

Key words: methane, ethylene, kinetics, pyrolysis, fuels.

ALAIN R. BOSSARD et MARGARET H. BACK. Can. J. Chem. **69**, 37 (1991).

Dans le but de transformer du méthane en hydrocarbures de poids moléculaires plus élevés, on a pyrolysé des mélanges d'éthylène et de méthane à des températures allant de 925 à 1023 K. L'addition de méthane à de l'éthylène qui réagit d'une façon thermique provoque une augmentation de la vitesse de formation du propylène; elle provoque aussi une diminution des vitesses de formation des autres produits majeurs : éthane, acétylène et butadiène. L'abstraction d'un atome d'hydrogène du méthane est une des principales réactions de propagation et elle provoque un déplacement important dans la distribution radicalaire qui passe d'une prépondérance des radicaux éthyles et vinyles, les radicaux principaux dans les réactions de pyrolyse de l'éthylène seul, vers les radicaux méthyles qui conduisent à la formation du propylène. A 1023 K, à des pressions d'éthylène de 6,5 Torr et de méthane de 356 Torr, 1,5 mole de méthane se transforme en hydrocarbures de poids moléculaires plus élevés pour chaque molécule d'éthylène qui réagit. La vitesse de conversion du méthane dans le système homogène est plus faible que dans les réactions catalytiques; toutefois, les produits ne sont que des hydrocarbures et il n'y a pas de perte de méthane en monoxyde et en dioxyde de carbone.

Mots clés : méthane, éthylène, cinétique, pyrolyse, combustibles.

[Traduit par la revue]

Introduction

Most of the efforts directed to the conversion of natural gas into higher molecular weight fuels have focussed on the use of catalysts as a means of overcoming the thermodynamic disadvantage of the overall process. For example, several metal oxides have been found effective in the oxidative coupling reaction of methane and their development and improvement has received considerable attention in recent years (1–4). Catalysts, however, while effective in many regards, have a number of limitations. In the methane conversion the presence of the oxide leads to the formation of carbon monoxide and carbon dioxide and represents a loss of carbon as fuel. Homogeneous conversion of methane would not involve this loss process and such systems therefore warrant investigation along with catalytic processes. Direct thermal decomposition of methane is not practical because of its high stability; at the high temperatures necessary for reaction rapid conversion to carbon occurs (5, 6). To overcome this problem a sensitizer may be used to induce decomposition at lower temperatures, favouring the production of the less stable hydrocarbon products. One such system involves the pyrolysis of mixtures of methane and ethylene. A description of this system and some results from the pyrolysis of these mixtures have been reported (7) and only a brief summary of the reactions will be given here.

The thermal reactions of ethylene at temperatures in the neighbourhood of 800 K involves both decomposition and polymerisation and occurs by a chain reaction mechanism (8). Initiation by the bimolecular reaction of ethylene,

[1] $2C_2H_4 \rightarrow C_2H_3 + C_2H_5$

is followed by addition, abstraction, decomposition, and isomerisation of the ethyl, vinyl, and other radicals. In pure ethylene methane and ethane are the only saturated products and are formed by hydrogen-abstraction by the corresponding radical.

[2] $CH_3 + C_2H_4 \rightarrow CH_4 + C_2H_3$

[3] $C_2H_5 + C_2H_4 \rightarrow C_2H_6 + C_2H_3$

Addition of methane will not add new initiation processes, since methane is stable at these temperatures, but will add a new propagation reaction.

[4] $C_2H_5 + CH_4 \rightarrow C_2H_6 + CH_3$

Thus in the ethylene system, where the ethyl radical is one of the major chain-carrying radicals, methane is converted to ethane.

When the relative amount of methane is small, the actual and relative concentrations of the various radicals in the system will not be altered; only the rate of formation of ethane will be increased. With larger amounts of methane, however, reaction [4] will shift the balance of radicals in favour of the methyl radical and the products of the chain reaction will be altered. As expected under these conditions, propylene becomes the product most affected by the presence of methane. The ratio CH_4/C_2H_4 is therefore an important parameter in the selectivity of the products. Equally important is the concentration of ethylene which controls the overall rate of the reaction. Thus optimum performance of the system with respect to conversion of methane requires a balance between these two factors.

Can. J. Chem. Downloaded from www.nrcresearchpress.com by 195.138.81.100 on 09/07/12
For personal use only.

Can. J. Chem. Downloaded from www.nrcresearchpress.com by 195.138.81.100 on 09/07/12
For personal use only.

In the earlier study covering the temperature range 774–853 K (7) the conversion of methane and the selectivity of the products was measured as a function of the relative and absolute concentrations of methane and ethylene. Although the selectivity for formation of ethane and propylene was high, the rate of the reaction was too slow to be practical; the limitation was the rate of the initiation of the chain reaction by ethylene. These studies have now been extended to higher temperatures, 925–1123 K, for the purpose of increasing the overall rate of the conversion of methane. Significant changes in the mechanism of the reaction which caused considerable shift in the product distribution were observed in the higher temperature region and this paper describes the results of these studies.

Experimental

The experiments were performed in a static pyrolysis system. A quartz reaction vessel of 0.21 L was placed in the center of a three-zone Lindberg Furnace, Model 54457. Mixtures of reactants were admitted to the reactor by expansion from calibrated volumes. Samples were removed for analysis after the required time of reaction. Details of the procedures for preparation of the mixtures were given previously (7, 9).

Products were analyzed using a Hewlett-Packard Gas Chromatograph Model 5710A with flame detector. Two columns were used to obtain analysis for a wide range of products. A silica gel column (40/60 mesh, 1.5 m × 6.5 mm o.d. copper tubing) at 30°C separated small quantities of the product ethane from the large quantities of the reactants. After elution of the ethylene the column was programmed at 16°C min^{-1} to 250°C and analysis was obtained for benzene and toluene. Other C_6 or C_7 compounds of similar structure, such as cyclohexene or cyclohexadiene, may have been included in these peaks but no attempt at further separation was made. A Durapak column (phenylisocyanate/Porasil C, 80/100 mesh, 6 m × 6.5 mm o.d. copper tubing) maintained at 25°C gave good separation of acetylene, allene, propylene, and butenes. A single peak corresponding to a C_5 compound was also detected and analyzed in certain experiments.

Research Grade methane (99.99%) and Research Grade ethylene (99.99%) were obtained from Matheson Gas Products, Whitby, Ont., and, except for rigorous degassing, were used without further purification. Impurities in the reactants, mainly ethane and acetylene, were too small to affect the kinetics of the reaction but correction to the yields of these products were made where necessary.

Results and discussion

Twenty series of experiments, in which yields of products were measured as a function of the reaction time, were done at the following temperatures: 925, 974, and 1023 K. The conditions of initial pressures of ethylene and methane are summarized in Table 1. The pyrolysis of ethylene alone was also studied at each temperature.

A. Initial stages of the reaction

The main products from the pyrolysis of ethylene alone at 925 K are, in order of importance, butadiene, propylene, ethane, methane, acetylene, and butene-1. This distribution remained much the same at the two higher temperatures except that by 1023 K acetylene replaced propylene as the second most abundant product, next to butadiene. At this temperature butadiene accounted for 80% of the products and acetylene 10%. Examples of the yields of the major products as a function of time at 1023 K in the presence and absence of methane are shown in Figs. 1–4. The reaction was too fast in this temperature range to allow accurate measurement of initial rates under all conditions. Relative initial rates were, however, reliably measured by extrapolation of the ratios of the yields of products to zero time. These ratios are summarized in Table 2.

TABLE 1. Initial pressure of ethylene and ratios of methane/ethylene for each temperature

Temperature (K)	Pressure of ethylene (Torr)	$\frac{CH_4}{C_2H_4}$
925	25	4, 16
	12.5	4, 16
974 and 1023	12.5	4, 16
	6.25	4, 16
	6.5	55

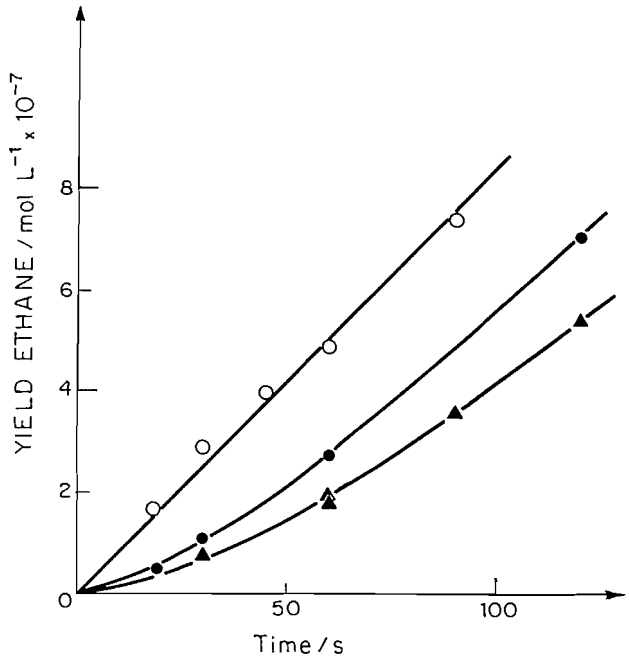


FIG. 1. Yield of ethane as a function of time. Initial pressure of ethylene 12.5 Torr. T = 974 K. Pressure of methane, ○: 0 Torr; ●: 50 Torr; △: 200 Torr.

The mechanism of the thermal reactions of ethylene in the temperature region of 800 K was discussed in an earlier report (7). Following initiation by reaction [1], addition and abstraction reactions of the ethyl and vinyl radicals and addition, isomerization, and decomposition reactions of higher radicals led to the formation of the major products, methane, ethane, propylene, and butene-1. Carbon–carbon bond rupture was the only decomposition process of the radicals which was sufficiently fast to compete with addition to ethylene. In the present experiments the appearance of butadiene and acetylene as major products indicates that at higher temperatures dissociation of radicals by carbon–hydrogen bond splitting is an important loss process. As these dissociation reactions begin to compete effectively with additions to ethylene the product distribution shifts from monoolefins to more unsaturated products, of which butadiene, acetylene, and benzene were the main examples identified in the present experiments. The trend to unsaturation leads also to the formation of polyaromatic

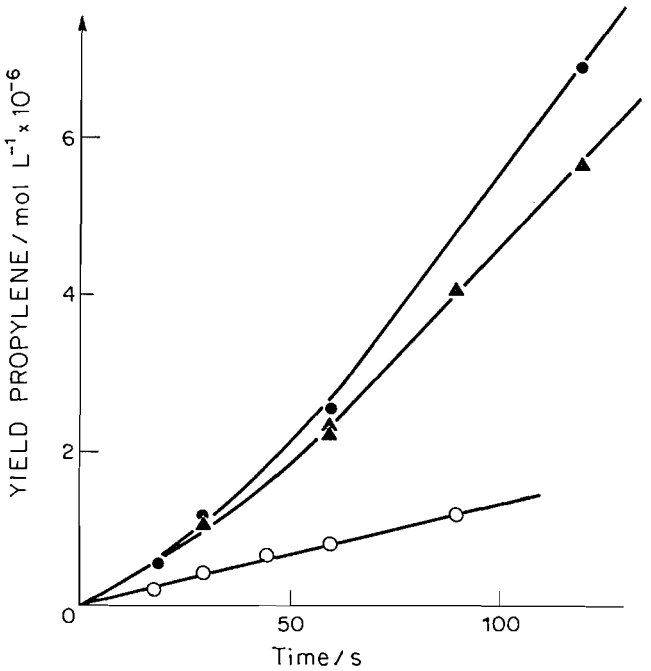


FIG. 2. Yield of propylene as a function of time. Initial pressure of ethylene 12.5 Torr. T = 974 K. Pressure of methane, ○: 0 Torr; ●: 50 Torr; △: 200 Torr.

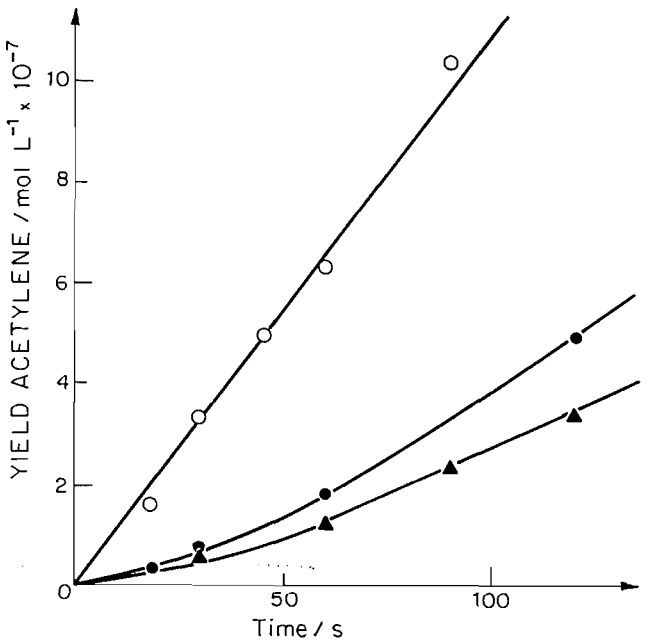


FIG. 3. Yield of acetylene as a function of time. Initial pressure of ethylene 12.5 Torr. T = 974 K. Pressure of methane, ○: 0 Torr; ●: 50 Torr; △: 200 Torr.

hydrocarbons and eventually to carbon. Thus the yields of the light products approached constant or maximum values with time even at conversions less than 1%. This contrasts with the auto-acceleration of the rates of formation of these products observed in the lower temperature region.

The following simplified mechanism shows these modifications to the mechanism outlined for the low temperature region and accounts for the main features of the reaction in the initial stages.

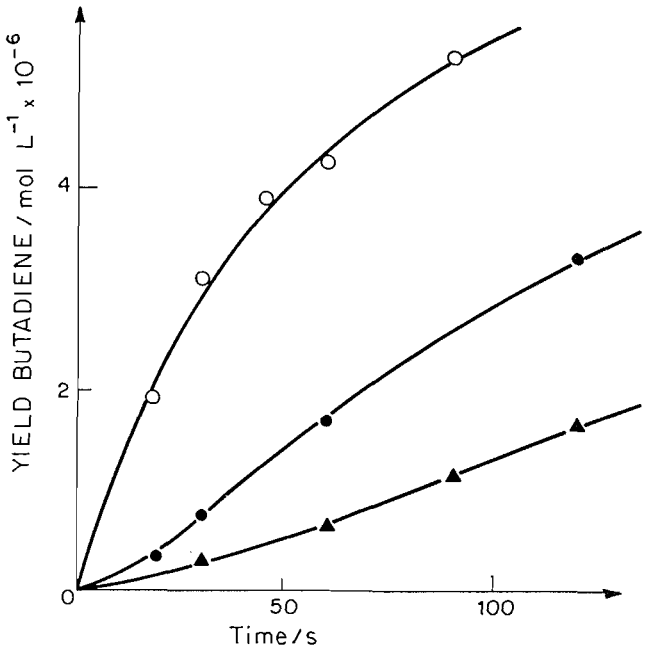


FIG. 4. Yield of butadiene as a function of time. Initial pressure of ethylene 12.5 Torr. T = 974 K. Pressure of methane, ○: 0 Torr; ●: 50 Torr; △: 200 Torr.

[1] $2C_2H_4 \rightarrow C_2H_5 + C_2H_3$

[2] $C_2H_5 + C_2H_4 \rightarrow C_2H_6 + C_2H_3$

[3] $C_2H_5 + C_2H_4 \leftrightarrows n\text{-}C_4H_9$

[4] $C_2H_5 \leftrightarrows C_2H_4 + H$

[5] $n\text{-}C_4H_9 \rightarrow s\text{-}C_4H_9$

[6] $s\text{-}C_4H_9 \rightarrow C_3H_6 + CH_3$

[7] $CH_3 + C_2H_4 \rightarrow CH_4 + C_2H_3$

[8] $CH_3 + C_2H_4 \leftrightarrows C_3H_7$

[9] $C_3H_7 \rightarrow C_3H_6 + H$

[10] $C_2H_3 + C_2H_4 \leftrightarrows C_4H_7$

[11] $C_4H_7 \rightarrow C_4H_6 + H$

[12] $H + C_2H_4 \rightarrow H_2 + C_2H_3$

[13] $C_2H_3 \rightarrow C_2H_2 + H$

[14] $C_2H_5 + CH_4 \rightarrow C_2H_6 + CH_3$

[15] $C_2H_3 + CH_4 \rightarrow C_2H_4 + CH_3$

[16] $H + CH_4 \rightarrow H_2 + CH_3$

No decomposition of methane itself was observed under the conditions of the present experiments; its effect is solely as a source of methyl radicals in the propagation reactions, as indicated by reactions [14]–[16]. The occurrence of these reactions completely changed the product distribution. At the highest temperature in the absence of methane, butadiene accounted for ~80% of the products, whereas with the highest pressure of methane the products contained ~85% propylene. Addition of methane increased the rate of formation of propylene, but decreased the rate of formation of all other products. This trend towards increasing importance of propylene in the presence of methane was observed in the previous experiments and was more noticeable at the higher temperatures. At the

Can. J. Chem. Downloaded from www.nrcresearchpress.com by 195.138.81.100 on 09/07/12
For personal use only.

Can. J. Chem. Downloaded from www.nrcresearchpress.com by 195.138.81.100 on 09/07/12
For personal use only.

TABLE 2. Ratios of rates of formation of products

T (K)	C_2H_4 (Torr)	CH_4 (Torr)	$\frac{C_2H_6}{C_3H_6}$	$\frac{C_2H_2}{C_3H_6}$	$\frac{C_4H_6}{C_3H_6}$	$\frac{C_2H_2}{C_4H_6}$
925	25	0	2.0	0.22	6.4	0.034
		100	0.30	0.026	0.64	0.041
		400	0.20	0.020	0.29	0.069
	12.5	0	1.45	0.30	10.0	0.033
		50	0.18	0.02	0.58	0.04
		200	0.14	0.02	0.32	0.05
974	12.5	0	0.90	0.75	11.4	0.066
		50	0.072	0.050	0.65	0.077
		200	0.063	0.050	0.28	0.18
	6.25	0	0.65	1.2	16	0.075
		25	0.036	0.038	0.42	0.090
		100	0.038	0.054	0.29	0.19
1023	12.5	0	0.43	1.4	8.6	0.16
		50	0.050	0.10	0.60	0.17
		200	0.044	0.08	0.27	0.30
	6.25	0	0.32	1.9	16	0.11
		25	0.035	0.10	0.59	0.17
		100	0.030	0.10	0.25	0.40

lowest temperature, 774 K, methane did not significantly affect the rate of formation of propylene but at 853 K the rate of formation of propylene was increased more than that of ethane.

The rise in importance of propylene is a direct consequence of the participation of methane in the chain propagation reactions. Radical abstraction from methane shifts the radical distribution in favour of methyl radicals at the expense of the ethyl and vinyl radicals and methyl radicals lead directly to propylene. Propylene will therefore become a major product as, with increasing temperature, abstraction is increasingly favoured over addition.

The more surprising observation was that the rates of formation of the other main products, ethane, acetylene, and butadiene, all decreased in the presence of methane. This suggests that abstraction from methane by the radicals depicted in reactions [14] and [15] is not fast enough to compete with their decomposition. Methane therefore reacts mainly with the hydrogen atoms produced in the decomposition rather than with the parent radical. In the absence of methane the hydrogen atoms are converted back to ethyl and vinyl radicals by addition and abstraction from ethylene; in the presence of methane they are converted to methyl radicals. Thus propylene will be formed through reactions [7]–[9] at the expense of the products formed by reactions of the ethyl and vinyl radicals.

On the basis of the simplified mechanism the rates of formation of the main products in the presence of methane are given as follows:

$$[17]\quad R_{C_2H_6} = k_2[C_2H_5][C_2H_4] + k_{14}[C_2H_5][CH_4]$$

$$[18]\quad R_{C_3H_6} = bk_3[C_2H_5][C_2H_4] + ak_8[CH_3][C_2H_4]$$

$$= bk_3[C_2H_5][C_2H_4] + a(1-c)[C_2H_5]\left[bk_3[C_2H_4] + k_{14}[CH_4] + k_{16}K_4\frac{[CH_4]}{[C_2H_4]}\right] + k_{15}[C_2H_3][CH_3]$$

where

$$a = \frac{k_9}{k_{-8}+k_9},\quad b = \frac{k_5}{k_{-3}+k_5},\quad c = \frac{k_7}{k_7+k_8}$$

$$[19]\quad R_{C_2H_2} = k_{13}[C_2H_3]$$

$$[20]\quad R_{C_4H_6} = dk_{10}[C_2H_3][C_2H_4]$$

where

$$d = \frac{k_{11}}{k_{-10}+k_{11}}$$

and

$$[21]\quad [C_2H_3] = [C_2H_5]\left\{\frac{k_2[C_2H_4] + k_{12}K_4 + cbk_3[C_2H_4] + ck_{14}[CH_4] + ck_{16}K_4\frac{[CH_4]}{[C_2H_4]}}{k_{10}[C_2H_4] + (1-c)k_{15}[CH_4] + k_{13}}\right\}$$

and the concentration of hydrogen atoms is controlled through equilibrium of reaction [4].

Table 2 shows that the ratios of the rates of formation of all products to the rate of formation of propylene decrease sharply as methane is added to the system until the ratio of methane/ethylene reaches about four. Further additions of methane have much less effect on the ratios and in some cases a limiting value is obtained. This initial decrease shows that the second term in the expression for the rate of formation of propylene becomes the major contribution to its rate at relatively low ratios of methane/ethylene, before the rates of formation of the other products are affected. With sufficiently large amounts of methane, however, the rates of formation of the other products become dominated by the terms involving methane and the ratios therefore eventually become independent of methane.

This behaviour is illustrated by the ratio $R_{C_2H_6}/R_{C_3H_6}$ shown in Fig. 5 for the three lower temperatures of the previous study and for 925 K. The initial sharp decrease in the ratio observed at 925, 974, and 1023 K was progressively less pronounced with decreasing temperature and in fact at the lowest temperature the ratio increased with additions of methane, but still approached a constant value. These ratios would not be expected to change much with further reaction and the system thus has the advantage of allowing a fixed product distribution by adjustment of the reactant ratio and the temperature.

The limitations of the simplified mechanism are shown by the

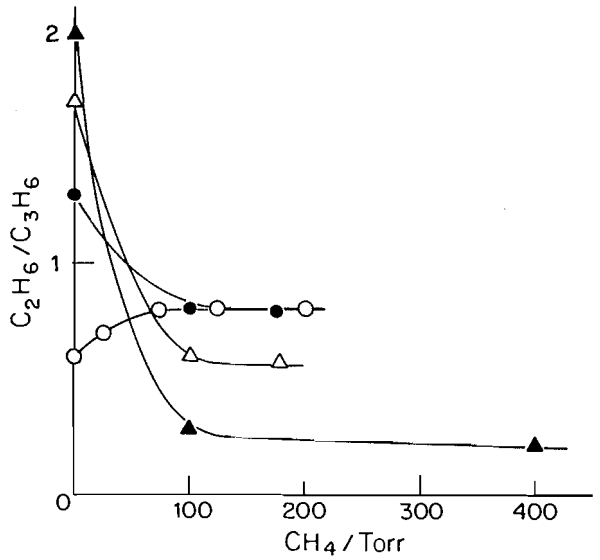


FIG. 5. Ratio of the initial rate of formation of ethane to the initial rate of formation of propylene. Initial pressure of ethylene 25 Torr. Temperature ○: 774 K; ●: 824 K; △: 853 K; ▲: 925 K.

ratios of acetylene/butadiene. These are practically independent of methane concentration, as predicted, except for some increase at the highest ratio of methane to ethylene. They should, however, be inversely proportional to the concentration of ethylene whereas little change in the ratio was observed with a change in the initial concentration of ethylene. A possible loss process for butadiene is the Diels–Alder addition to ethylene. This reaction has been shown to be a major source of cyclic olefins in thermal reactions of ethylene and other light olefins (10) and its occurrence in the present system would act to increase the ratio C_2H_2/C_4H_6 at high pressures of ethylene. An additional source of acetylene could be the alternative decomposition of butenyl radicals,

[22] $C_4H_7 \rightarrow C_2H_2 + C_2H_5$

and the order of the rate of this reaction with respect to ethylene is the same as that for butadiene. Such additional reactions nevertheless represent relatively minor adjustments to the mechanism and it may be concluded that the simple scheme provides a reasonable description of the system.

B. Later stages of the reaction

An important question for this system is the efficiency of the conversion of methane into higher molecular weight products. What fraction of the products arise through reaction with methane and what fraction through reaction with ethylene? A series of experiments was performed at each of the temperatures 974 and 1023 K, using a low pressure of ethylene, 6.5 Torr, and a high pressure of methane, 356 Torr, and allowing the reaction to proceed until the conversion was sufficient to allow quantitative measurement of the amount of ethylene reacted (up to about 15% conversion). At the same time the yields of all products up to C_7 were measured. The relation between the yields of products and the conversion of the reactants is given as follows:

[23] $\Sigma C_{\text{Products}} = \Delta CH_4 + 2\Delta C_2H_4$

At both temperatures propylene was the major product in the initial stages but with increasing conversion passed through a maximum yield and at 1023 K was surpassed by the secondary product, benzene. The results are shown in Figs. 6 and 7.

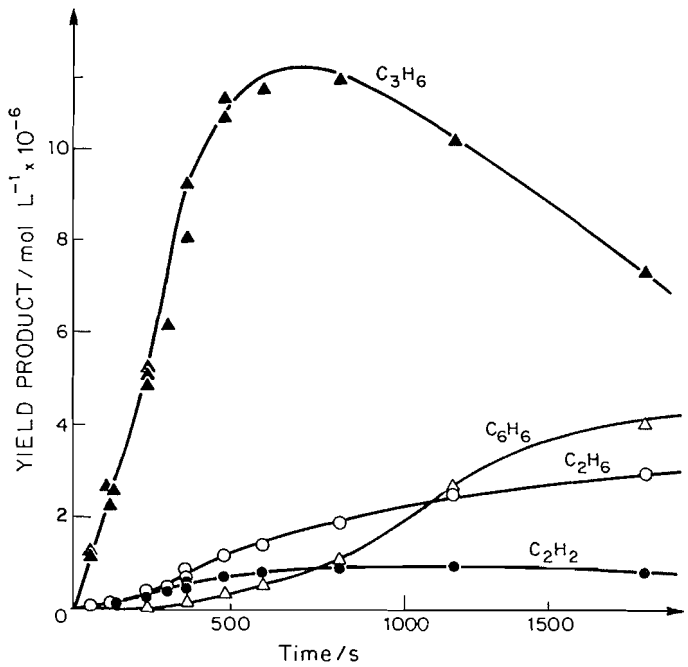


FIG. 6. Yield of products as a function of time at 974 K. Initial pressure of ethylene, 6.5 Torr; initial pressure of methane 356 Torr. ○: C_2H_6; ●: C_2H_2; △: C_6H_6; ▲: C_3H_6.

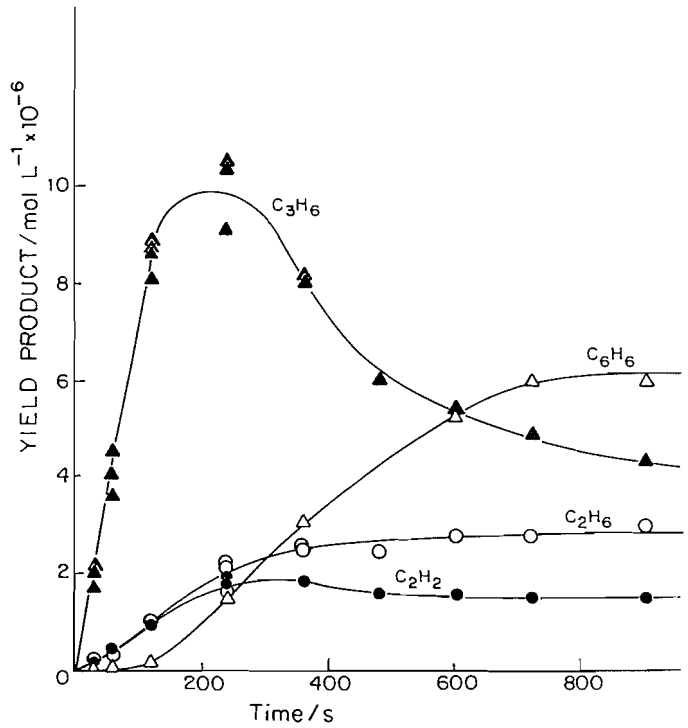


FIG. 7. Yield of products as a function of time at 1023 K. Initial pressure of ethylene 6.5 Torr; initial pressure of methane 356 Torr. ○: C_2H_6; ●: C_2H_2; △: C_6H_6; ▲: C_3H_6.

Butadiene is not shown on these figures because at 1023 K its yield closely matches that of acetylene; at 974 K its yield is slightly less than twice the yield of acetylene. At 1023 K the total quantity of product, expressed as $\Sigma C/2$, is compared to the loss of ethylene over the course of the reaction in Fig. 8. At low conversions the yield of products exceeds the ethylene reacted and the difference represents the product derived from methane

Can. J. Chem. Downloaded from www.nrcresearchpress.com by 195.138.81.100 on 09/07/12
For personal use only.

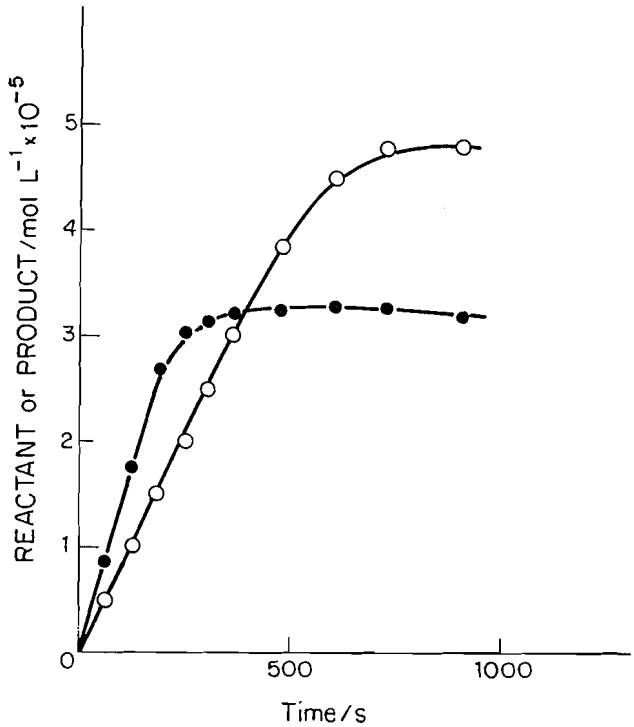


FIG. 8. Relation between ethylene consumed ΔC_2H_4, and total product, $\Sigma C/2$, at 1023 K. Initial pressure of ethylene 6.5 Torr; initial pressure of methane 356 Torr. ○: ΔC_2H_4; ●: $\Sigma C/2$.

according to eq. [23]. At higher conversions the yield of products analyzed (up to C_7) falls below the ethylene consumed and higher molecular weight products, not analyzed, including carbon, are important in this region.

From Fig. 8 the maximum conversion of methane into products occurs at 180 s. At 974 K the maximum occurred at 480 s. Table 3 summarizes the relation between the ethylene reacted and the methane converted for both temperatures. At the maximum, at 974 K, 0.8 mol of methane react for every mole of ethylene, while at 1023 K the ratio is 1.5. This appears to indicate an efficient use of methane, but in the experiments the ratio of methane/ethylene is high, making the percentage conversion of methane low.

An important characteristic of the reaction is the rate of conversion of methane. Because of the small percentage conversion of methane in all the experiments a direct measurement of the rate of conversion was not possible. In the experiments in the lower temperature region the rate of conversion was estimated from the increase in the rate of formation of ethane in the presence of methane. In the higher temperature region the main product increased by the presence of methane is propylene. The rate of loss of methane in these experiments may therefore be estimated from the rate of formation of propylene in the presence, R_a^0, and in the absence, R^0, of methane, as follows:

$$-R_{CH_4} = R_a^0 - R^0$$

The maximum rate of conversion of methane at each temperature, usually obtained at the highest pressure of ethylene, is summarized in Table 4.

Although these rates are below those achieved in catalytic reactions (typically in the neighbourhood of 5% s^{-1}), an important feature of the reaction is that the products are entirely hydrocarbon and no methane is lost to the formation of carbon monoxide or carbon dioxide. The percentage conversion of

TABLE 3. Relation between methane converted and ethylene reacted, $P^0_{C_2H_4} = 6.5$ Torr; $P^0_{CH_4} = 356$ Torr

T (K)	Time of reaction (s)	ΔC_2H_4 (mol L^{-1})	ΣC (mol L^{-1})	ΔCH_4 (mol L^{-1})	$\frac{\Delta CH_4}{\Delta C_2H_4}$
974	480	1.66×10^{-5}	4.61×10^{-5}	1.29×10^{-5}	0.8
1023	180	1.50×10^{-5}	5.33×10^{-5}	2.33×10^{-5}	1.5

TABLE 4. Maximum rate of conversion of methane at each temperature

T (K)	Pressure of ethylene (Torr)	Pressure of methane (Torr)	Rate of conversion (% s^{-1})
774	200	200	1.2×10^{-5}
824	50	350	1.5×10^{-5}
853	50	200	2.0×10^{-5}
925	25	100	1.0×10^{-5}
974	12.5	50	5.0×10^{-3}
1023	12.5	50	1.4×10^{-2}

methane in this system is of necessity low because high concentrations of methane are required to prevent formation of polyaromatic hydrocarbons and carbon. For recovery of the light hydrocarbon products a recycling system would be essential.

Conclusions

As a sensitizer for the conversion of methane, ethylene has certain advantages. The selectivity of the products for ethane or propylene may be controlled through the temperature and the ratio of methane to ethylene. If the conversion is kept low the formation of polyaromatic compounds and carbon can be avoided even at temperatures of 1000 K. The rate of conversion may be increased and controlled through use of additional sensitizers.

Acknowledgments

The authors thank the Department of Energy, Mines and Resources, Canada, for the award of a contract in support of this project. They also thank Dr. J. Z. Galuszka, ERL, CANMET, for his continued interest in the project.

1. S. AHMED and J. B. MOFFAT. J. Catal. **121**, 408 (1990).
2. J. G. MCCARTY, M. A. QUINLAN, and H. WISE. Proc. 9th Int. Congres. Catal. **4**, 1818 (1988).
3. J. S. LEE and S. T. OYAMA. Catal. Rev. Sci. Eng. **30**, 249 (1988).
4. C.-H. LIU, J.-X. WANG, and J. H. LUNSFORD. J. Catal. **111**, 302 (1988).
5. C.-J. CHEN, M. H. BACK, and R. A. BACK. Can. J. Chem. **54**, 3175 (1976).
6. M. H. BACK and R. A. BACK. Pyrolysis: theory and industrial practice. *Edited by* L. F. Albright, B. L. Crynes, and W. H. Corcoran. Academic Press. 1983. p. 1.
7. A. R. BOSSARD and M. H. BACK. Can. J. Chem. **68**, 1401 (1990).
8. M. H. BACK and R. MARTIN. Int. J. Chem. Kinet. **11**, 757 (1979).
9. G. AYRANCI and M. H. BACK. Int. J. Chem. Kinet. **13**, 897 (1981).
10. T. SAKAI. Pyrolysis: theory and industrial practice. *Edited by* L. F. Albright, B. L. Crynes, and W. H. Corcoran. Academic Press. 1983. p. 89.

Can. J. Chem. Downloaded from www.nrcresearchpress.com by 195.138.81.100 on 09/07/12
For personal use only.

Étude chimique et cinétique de l'oxydation homogène en phase gazeuse d'alcanes légers. II. Propane et mécanisme généralisé

B. VOGIN,[1] F. BARONNET[2] ET G. SCACCHI

Département de chimie physique des réactions, Unité de recherche associée n° 328 du Centre national de la recherche scientifique, Institute-national polytechnique de Lorraine – École nationale supérieure des industries chimiques, 1, rue Grandville, BP 451, 54001 Nancy CEDEX, France

Reçu le 31 mai 1990

B. VOGIN, F. BARONNET et G. SCACCHI. Can. J. Chem. **69**, 43 (1991).

Une étude expérimentale détaillée de l'oxydation du propane en phase gazeuse homogène à 350°C et à pression subatmosphérique a été entreprise dans le but d'identifier et de doser les produits primaires principaux de la réaction. Les résultats expérimentaux ont été interprétés par un mécanisme radicalaire en chaînes s'appuyant sur ces résultats et sur l'évaluation des constantes de vitesse des processus élémentaires proposés par les méthodes de la Cinétique Thermochimique. Les processus élémentaires proposés sont discutés et comparés aux observations expérimentales. Les résultats obtenus et leur interprétation font l'objet d'une comparaison avec une étude détaillée de même nature faite sur l'exemple de l'isobutane. Comme dans ce dernier cas, il apparaît deux chemins réactionnels parallèles, l'un prédominant conduisant à l'oléfine conjuguée (ici propylène) et l'autre à la formation de l'époxyde de cette oléfine (ici oxyde de propylène). De substantielles similitudes entre l'oxydation de l'isobutane et celle du propane ont pu être mises en évidence, ce qui renforce la cohérence des résultats obtenus.

Mots clés : oxydation, cinétique, mécanisme réactionnel, propane, cinétique thermochimique.

B. VOGIN, F. BARONNET, and G. SCACCHI. Can. J. Chem. **69**, 43 (1991).

An experimental study of the homogeneous gas phase oxidation of propane at 350°C and subatmospheric pressure has been performed in order to identify and to measure the major primary products of the reaction. The experimental results have been interpreted by a chain radical mechanism, deduced from these results and from estimates of the rate constants for the elementary steps obtained by the methods of Thermochemical Kinetics. The proposed elementary steps are discussed and compared with the experimental observations. The results that we have obtained and their interpretation are compared with a similar detailed investigation performed on the oxidation of isobutane. As in the case of isobutane, two parallel reaction pathways appear, a dominant one leading to the conjugated alkene (propylene) and another one leading to the epoxide of this olefin (here propylene oxide). The oxidation of isobutane and that of propane appear to be quite similar, which corroborates the results that we have obtained.

Key words: oxidation, kinetics, reaction mechanism, propane, thermochemical kinetics.

I. Introduction

I.1. Généralités et rappels

Ce second mémoire fait suite à un premier travail publié sur l'oxydation de l'isobutane (1). Dans ce premier article, nous avions fait une mise au point bibliographique assez complète sur les publications traitant de l'oxydation des alcanes légers. Rappelons seulement que notre objectif est essentiellement de proposer un mécanisme réactionnel suffisamment complet permettant de rendre compte des observations expérimentales effectuées lors de l'oxydation d'alcanes légers vers 300–350°C à relativement faible avancement.

L'étude bibliographique précitée (1) nous avait conduits à conclure que les données publiées dans la littérature ne permettaient pas de construire un mécanisme suffisamment sûr et détaillé. Cette situation nous avait incités à reprendre une étude expérimentale spécifiquement orientée vers les réactions d'oxydation d'alcanes légers à faible avancement.

Nous nous étions d'abord intéressés au cas de l'isobutane (1). Dans le présent travail, nous allons examiner l'exemple du propane et généraliser les conclusions auxquelles nous avons abouti.

I.2. Données bibliographiques de l'oxydation du propane

Il existe un certain nombre d'articles généraux sur les réactions d'oxydation d'alcanes mentionnés dans le mémoire précédent, tels ceux de Pollard (2) et de Benson (3, 4). D'autres travaux de Benson (5, 6) abordent ces questions mais sont plus orientés vers les problèmes liés aux flammes froides ou aux inflammations; une recherche bibliographique a souligné le faible nombre de publications susceptibles d'apporter des réponses aux questions que nous nous posons sur les réactions du propane; c'est ainsi que, dans la mise au point de Pollard (2), aucun article sur la chimie de l'oxydation de cet alcane n'est répertorié.

La majeure partie des articles publiés sur l'oxydation du propane concerne les réactions catalytiques qui ont des applications industrielles plus directes que la réaction non catalytique. Comme dans le cas de l'isobutane, nous avons éliminé les articles correspondant à des études effectuées à trop grand avancement, l'analyse du mécanisme devenant alors quasi impossible, ainsi que les articles décrivant la réaction non-isotherme (flammes froides et inflammations de 2ème stade).

Dans le cas de l'oxydation homogène du propane, il apparaît que les quelques auteurs qui ont étudié la réaction se sont penchés surtout sur les effets de parois. En effet, la grande quantité de CO_2 formée dans les premiers instants de la réaction observée par Shtern et co-auteurs (7–9), ainsi que la formation de propène, ont conduit ces auteurs à associer ces observations à une hétérogénéité de la réaction. Cependant l'addition de gaz inerte ou l'augmentation du rapport surface sur volume du réacteur ne modifiant pas la répartition des produits, ces mêmes auteurs ont conclu, dans une étude postérieure, à l'homogénéité de la réaction, ce qui paraît d'ailleurs plus en accord avec les observations faites sur d'autres alcanes légers, *n*-butane par exemple (10, 11).

Étant donné que notre étude précédente sur l'isobutane suggérait qu'il était illusoire d'appliquer directement les théories de

1. Nouvelle adresse : Rhône-Poulenc, Usine de Chalampé, 68490 Ottmarsheim, France.

2. Auteur à qui adresser toute correspondance.

Printed in Canada / Imprimé au Canada

Can. J. Chem. Downloaded from www.nrcresearchpress.com by 195.138.81.100 on 09/07/12
For personal use only.

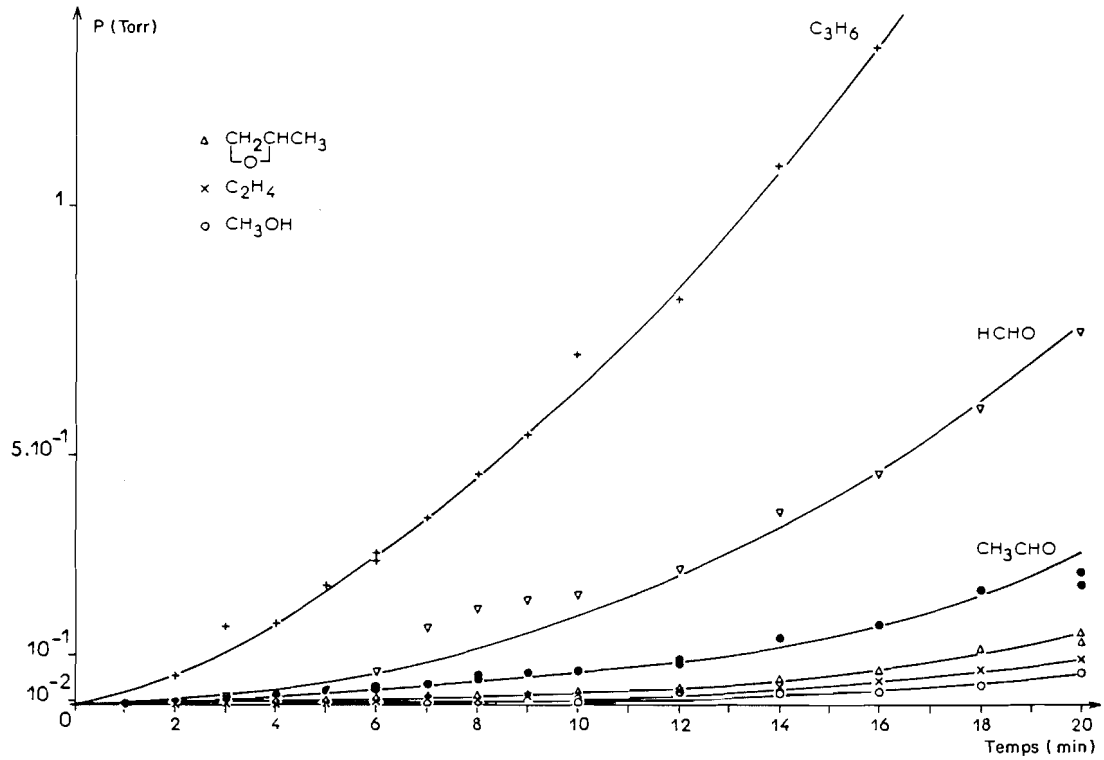


FIG. 1. Oxydation du propane à avancement modéré : courbes de formation des produits principaux en fonction du temps. Pression initiale du mélange équimoléculaire propane–oxygène : 125 Torr. Température de réaction 350°C (623 K).

Fish (12) ou de Knox (13) pour tenter de décrire en détail la chimie du système, une approche rationnelle de l'étude de la réaction d'oxydation du propane à faible avancement nécessitait une investigation expérimentale suffisamment détaillée.

Le choix du propane paraissait justifié également d'un point de vue pratique car il présente l'avantage de posséder un atome de carbone en moins que les butanes, ce qui devrait restreindre la gamme des produits formés et faciliter l'étude expérimentale, en particulier au niveau des analyses.

II. Étude expérimentale de l'oxydation du propane

II.1. Appareillage et analyses

L'appareillage utilisé (réacteur statique à volume constant), le mode opératoire et les méthodes analytiques (chromatographie en phase gazeuse essentiellement) ont été décrits dans notre mémoire précédent (1). Rappelons que le formaldéhyde est dosé par colorimétrie, méthode nettement moins sensible que la chromatographie en phase gazeuse utilisée pour les hydrocarbures, d'où une certaine dispersion des points, car à la moindre sensibilité de la méthode s'ajoutent les erreurs liées au piégeage et à la mise en solution du formaldéhyde formé.

II.2. Conditions expérimentales

La plupart des expériences ont été effectuées à 350°C, à une pression de mélange équimoléculaire C_3H_8/O_2 de 125 Torr (1 Torr = 133,3 Pa), dans un réacteur de Pyrex de 250 cm^3, pour des temps de réaction généralement compris entre 1 et 20 min; l'avancement de la réaction est voisin de 1% pour un temps de réaction de 5 min.

Contrairement au cas de l'isobutane, nous n'avons pas jugé nécessaire de redéterminer un diagramme pression–température, de tels diagrammes ayant été établis à plusieurs reprises par différents auteurs (14–16). Celui de Newitt et Thornes (14) est d'ailleurs un «classique» figurant dans de nombreux ouvrages. À partir de ces diagrammes, corroborés par des modélisations (17), nous avons pu vérifier que les conditions choisies correspondent à une zone de réaction lente.

Les problèmes liés à la reproductibilité des expériences avaient fait l'objet d'investigations détaillées dans le cas de l'isobutane; l'oxydation du propane n'appelle pas de commentaires particuliers de ce point de vue, compte-tenu de l'expérience acquise avec l'isobutane. Comme le montrent les points représentatifs de la formation des produits en fonction du temps, la reproductibilité des expériences apparaît suffisante pour l'étude entreprise.

Par ailleurs nous avons décidé d'étudier directement la réaction à faible avancement, compte-tenu des études faites avec l'isobutane; en effet, nos méthodes d'analyse permettent de mettre en évidence avec une sûreté suffisante les produits primaires principaux de la réaction. Il ne paraissait donc pas nécessaire de faire des bilans à plus fort avancement (de façon à ce qu'ils soient significatifs) entre propane consommé et produits formés. Ceci justifie les conditions expérimentales indiquées précédemment.

II.3. Résultats expérimentaux pour les mélanges propane–oxygène

Les produits dosés se composent d'hydrocarbures : propène, éthylène et méthane, et de produits oxygénés : formaldéhyde, acétaldéhyde, propionaldéhyde, acétone, méthyloxiranne, oxétanne, monoxyde et dioxyde de carbone et eau oxygénée. Le dosage de l'eau présentant des difficultés, les quantités d'eau formée n'ont pas été déterminées, mais sa production est relativement importante.

Les courbes de formation au cours du temps des produits sont rassemblées sur les figures 1–3 comportant des échelles différentes.

Afin de déterminer la nature primaire ou secondaire des produits dosés, nous avons établi figure 4 un «diagramme horizontal» où nous avons représenté en fonction du temps le pourcentage molaire de chaque produit dosé (pression du produit considéré divisée par la somme des pressions des produits dosés) à l'exclusion des réactifs et de l'eau; ceci ne donne que des valeurs relatives puisque l'eau n'est pas comptabilisée et, en particulier, il n'est pas possible de remonter à partir de ce diagramme à des équations stoechiométriques.

Les produits qui s'extrapolent à une valeur non nulle pour $t = 0$ peuvent être considérés comme les produits primaires de la réaction.

La gamme de produits primaires comprend donc le propène, le formaldéhyde, l'acétaldéhyde, l'eau oxygénée, le méthyloxiranne et peut-être l'éthylène.

Can. J. Chem. Downloaded from www.nrcresearchpress.com by 195.138.81.100 on 09/07/12
For personal use only.

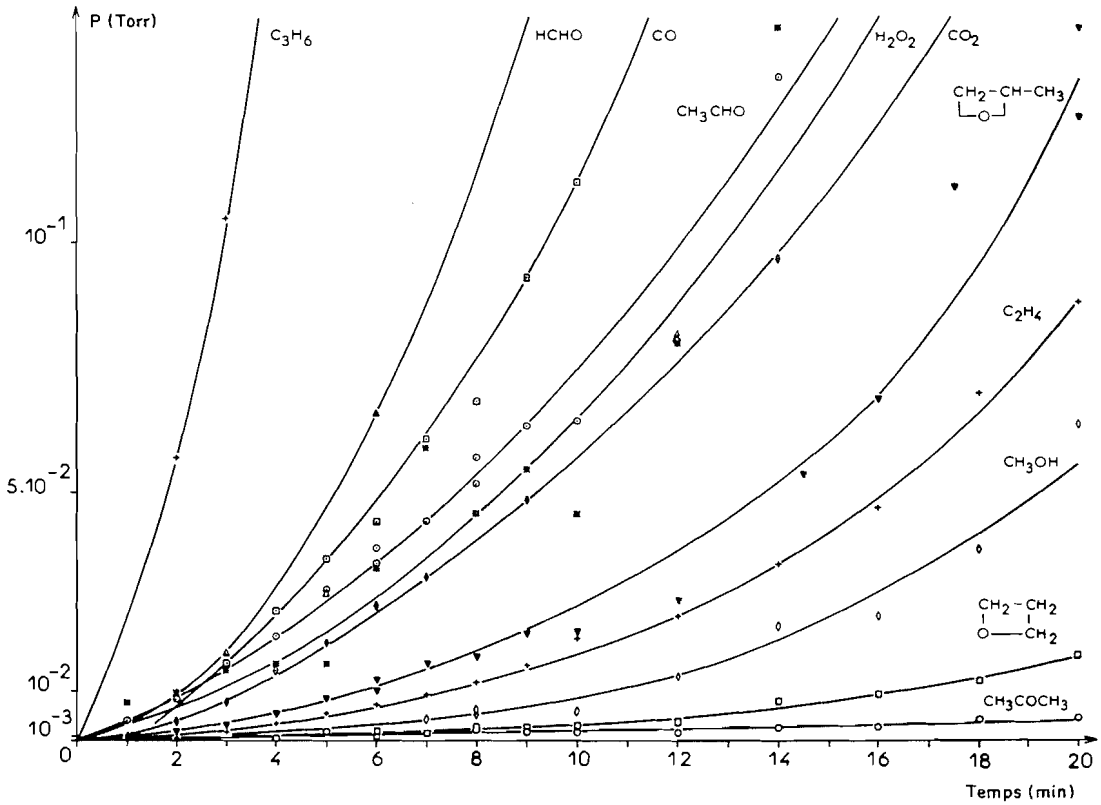


FIG. 2. Oxydation du propane à avancement modéré : courbes de formation des produits en fonction du temps. Mêmes conditions expérimentales que fig. 1.

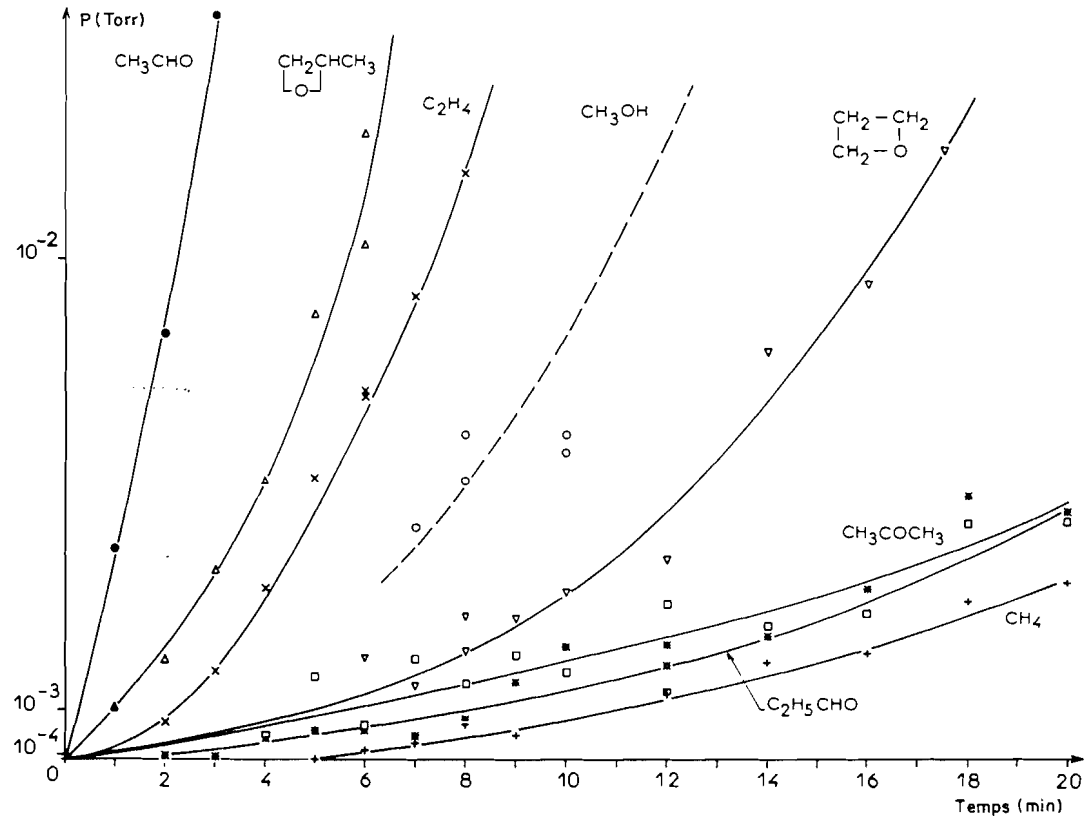


FIG. 3. Oxydation du propane à avancement modéré : courbes de formation des produits en fonction du temps, faisant apparaître les produits mineurs. Mêmes conditions expérimentales que fig. 1.

Can. J. Chem. Downloaded from www.nrcresearchpress.com by 195.138.81.100 on 09/07/12
For personal use only.

Can. J. Chem. Downloaded from www.nrcresearchpress.com by 195.138.81.100 on 09/07/12
For personal use only.

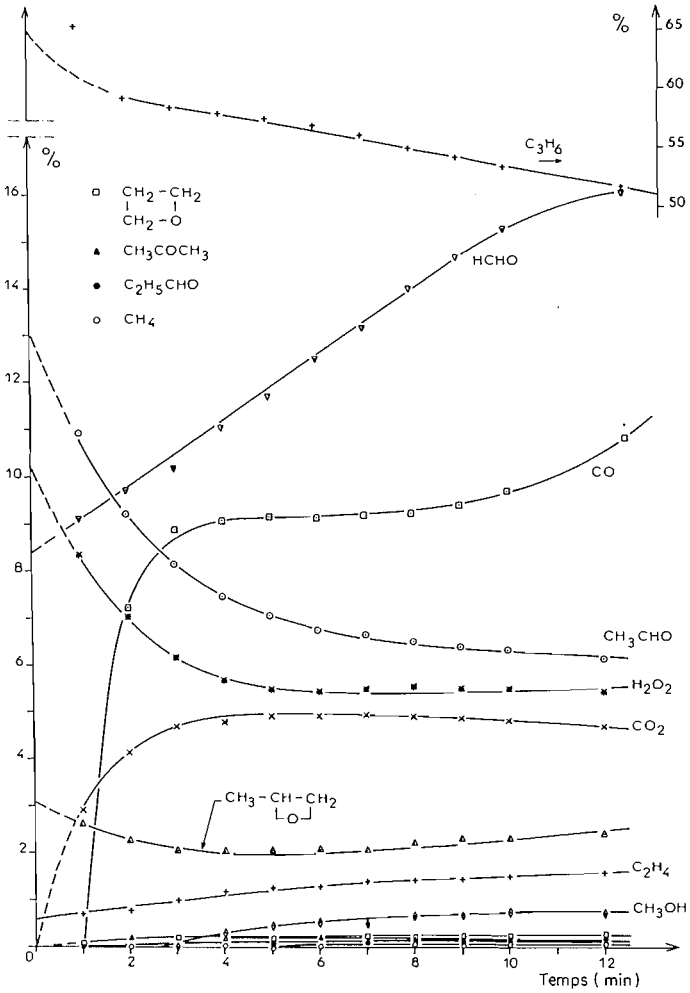


FIG. 4. Représentation du pourcentage molaire des différents produits : pression du produit i/Σ(pressions des produits mesurés) en fonction du temps. Mêmes conditions expérimentales que fig. 1 (l'eau est exclue de cette représentation).

Par ailleurs, les produits secondaires sont composés de monoxyde et dioxyde de carbone, méthanol, oxétanne, acétone, propionaldéhyde et méthane. Le tableau 1 regroupe les estimations du pourcentage initial de ces produits, ainsi qu'à 5 min de réaction (colonnes propane seul).

II.4. Résultats expérimentaux pour les mélanges propane–propène–oxygène

Compte-tenu de la réactivité des alcènes, il paraît logique de supposer que l'alcène conjugué formé lors de l'oxydation d'un alcane s'oxyde à son tour, et vient superposer son mécanisme à celui de l'alcane. Il peut ainsi devenir difficile de déterminer l'origine exacte des produits lorsqu'il y a ambiguïté possible, comme c'est souvent le cas. Nous avons tenté de lever en partie la difficulté en étudiant l'oxydation de l'alcane à très faible avancement pour éviter certaines réactions secondaires parasites. Pour essayer de cerner de plus près la nature des produits formés, nous avons décidé d'effectuer l'étude de l'oxydation du mélange alcane – alcène conjugué en ajoutant du propène au propane dans la proportion de 5% de la pression totale des hydrocarbures, le rapport hydrocarbures–oxygène restant fixé à 1 pour modifier le moins possible le comportement du système par rapport à l'oxydation de l'alcane seul. De même, la température de réaction est maintenue à 350°C et la pression initiale à 125 Torr.

Les courbes de formation au cours du temps des produits de l'oxydation commune propane–propène sont rassemblées sur les figures 5–7 comportant des échelles différentes.

TABLEAU 1. Pourcentages molaires des produits formés dans l'oxydation du propane et de mélanges propane–propène (5% de propène) à 5 min de réaction et extrapolés à avancement nul ($t = 0$), d'après les figures 4 et 8

	Pourcentages molaires			
	Mélange propane–propène		Propane seul	
Produit	$t = 0$	$t = 5$ min	$t = 0$	$t = 5$ min
CH_4	0	0,1	0	0
C_2H_4	2,5	3,4	0,6	1,2
C_3H_6	[9,6]	17,0	64,8	57,4
HCHO	[37,5]	23,9	8,4	11,7
CH_3CHO	9,4	9,1	13,0	7,0
C_2H_5CHO	0	0,2	0	0,1
CH_3COCH_3	Traces	0,1	Traces	0,2
CH_3OH	0	0,9	0	0,5
CO	0	15,0	0	9,2
CO_2	0	6,0	0	4,9
H_2O_2	[30,0]	13,7	10,2	5,5
$CH_3-CH-CH_2$ (O)	10,3	9,9	3,0	2,1
CH_2-CH_2 / CH_2-O	0,7	0,7	Traces	0,2
Total	[100,0]	100,0	100,0	100,0

La distinction des produits primaires est à nouveau réalisée par la construction d'un diagramme horizontal représentant le pourcentage du produit considéré (rapporté à la somme des produits dosés) en fonction du temps (fig. 8). Les valeurs utilisées pour ce diagramme sont obtenues après lissage des valeurs expérimentales par le tracé de courbes optimales : celles des figures 5–7.

Nous pouvons à nouveau tenter une détermination des produits primaires : formaldéhyde, eau oxygénée, méthyloxiranne, acétaldéhyde, propène, éthylène et oxétanne, et secondaires : méthane, propionaldéhyde, acétone, méthanol, monoxyde et dioxyde de carbone.

Les pourcentages initiaux et à 5 min de réaction, sont rapportés dans le tableau 1, où figurent aussi les valeurs des mêmes grandeurs dans le cas de l'oxydation du propane seul.

Il faut noter que la valeur du pourcentage donnée pour le propène dans le cas de l'oxydation du mélange propane–propène n'a guère de signification. D'une part, elle résulte de la différence de deux valeurs du même ordre de grandeur (valeur du dosage – valeur de la quantité initiale) ce qui donne un résultat très faible et par conséquent une incertitude d'un niveau très élevé. D'autre part, ce résultat lui-même représente en réalité la différence entre la quantité de propène produite par la réaction d'oxydation du propane et la quantité consommée par oxydation du propène. Il est donc préférable de comparer les pourcentages relatifs des produits en excluant le propène. Les valeurs correspondantes figurent dans le tableau 2. Ce même tableau mentionne les rapports des pourcentages initiaux des produits primaires : pourcentage pour l'oxydation du mélange propane–propène divisé par le pourcentage pour l'oxydation du propane seul, le propène étant toujours exclu des calculs. On observe alors que l'ajout de propène favorise la formation d'éthylène, de formaldéhyde, d'eau oxygénée, de méthyloxiranne et d'oxétanne, tandis que celle de l'acétaldéhyde est fortement diminuée, ce qui est contraire à des hypothèses utilisées dans des modélisations antérieures (17).

Comme pour l'oxydation de l'isobutane, nous allons proposer un mécanisme qui sera confronté aux résultats expérimentaux.

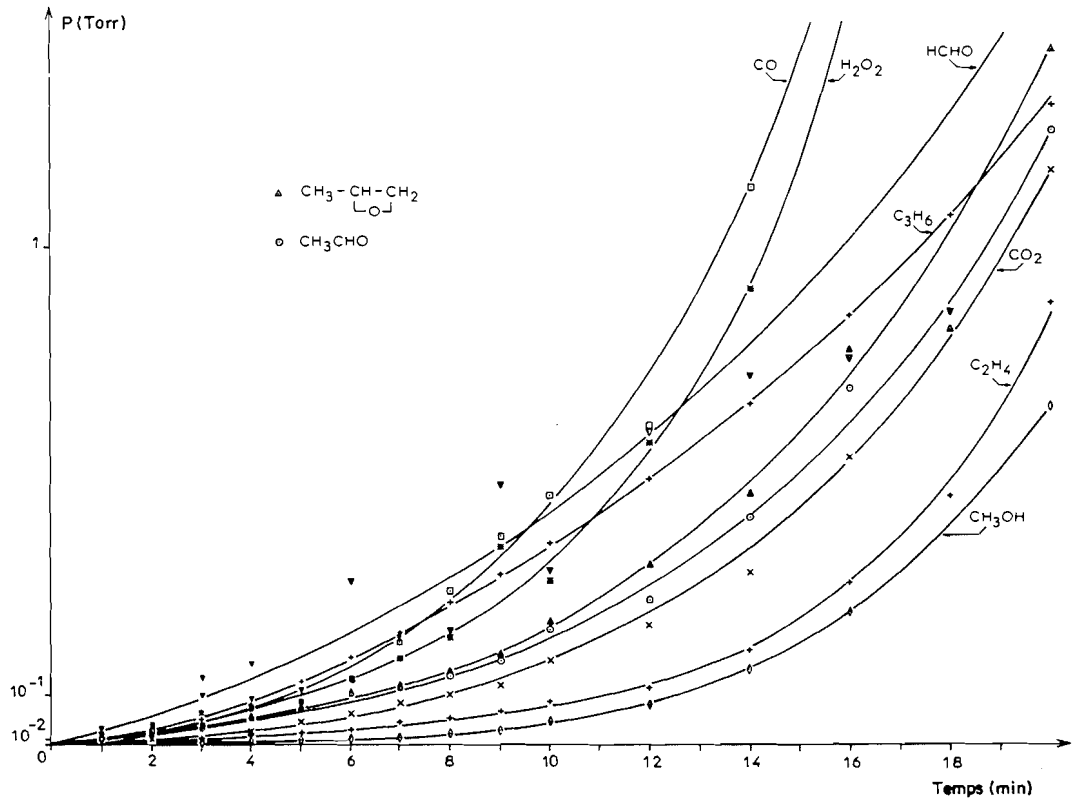


FIG. 5. Oxydation du mélange propane–propène à 5% de propène

$$\frac{\text{propène}}{\text{propène + propane}} = 0{,}05 \qquad \frac{\text{propène + propane}}{\text{propène + propane + oxygène}} = 1$$

Courbes de formation des *produits principaux* en fonction du temps. Pression initiale 125 Torr. Température : 350°C (623 K).

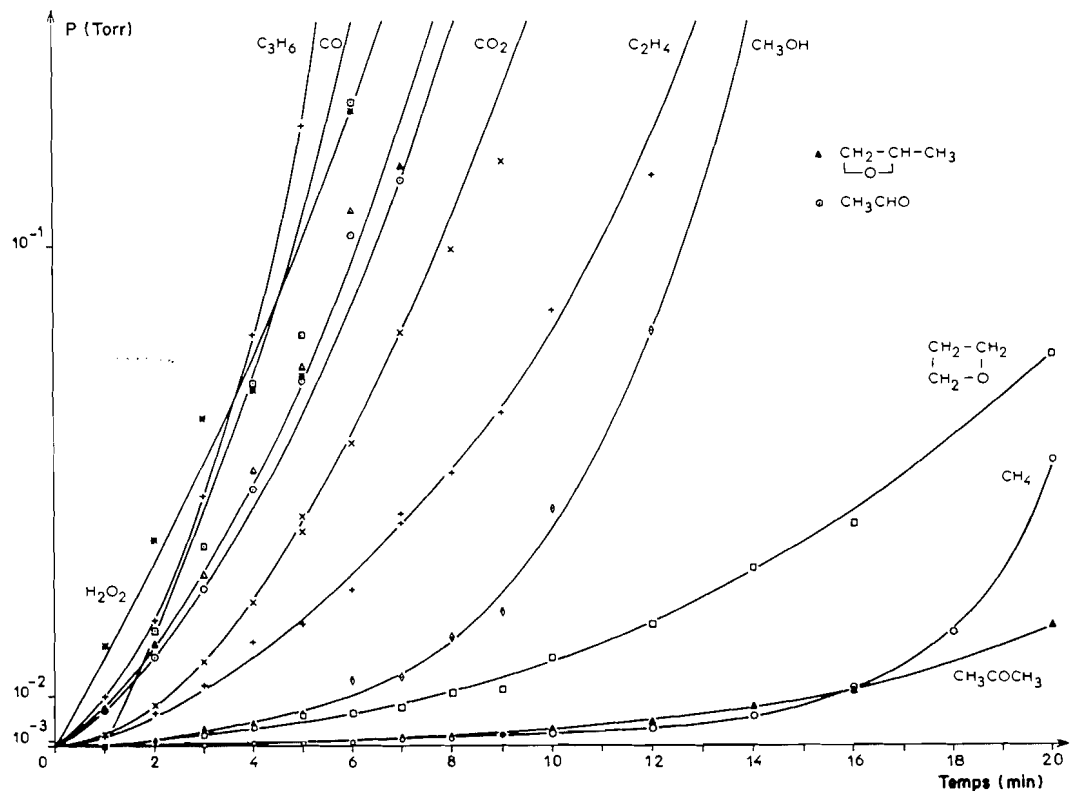


FIG. 6. Oxydation du mélange propane–propène : mêmes conditions que fig. 5. Courbes de formation des produits en fonction du temps.

Can. J. Chem. Downloaded from www.nrcresearchpress.com by 195.138.81.100 on 09/07/12
For personal use only.

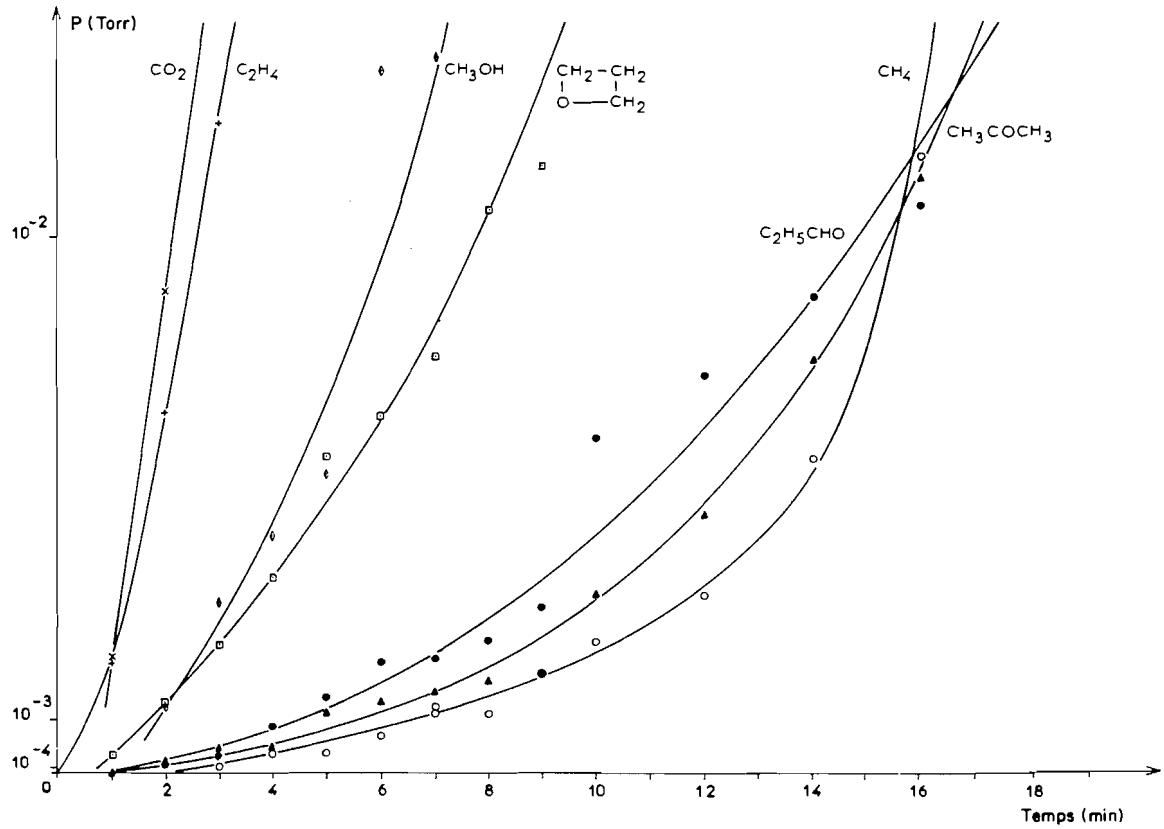


FIG. 7. Oxydation du mélange propane–propène : mêmes conditions que fig. 5. Représentation des produits mineurs.

III. Détermination du mécanisme de la réaction et commentaires

III.1. Détermination du mécanisme[3]

Nous avons suivi la même méthodologie que dans l'étude conduite dans le cas de l'isobutane (1) en nous appuyant d'une part sur les résultats expérimentaux et d'autre part sur les connaissances fondamentales acquises en chimie radicalaire, en utilisant également les techniques d'estimation des constantes de vitesse des processus élémentaires. Ici encore, ce que nous cherchons à écrire, ce ne sont pas des réactions globales mais des processus élémentaires vrais compatibles avec les principes de la cinétique (réversibilité microscopique, moindre changement de structure, etc...) et les données récentes acquises en thermochimie. Comme dans le cas de l'isobutane, les processus retenus tiennent compte aussi des schémas généraux écrits par d'autres auteurs (Fish (12) et Knox (13) en particulier) pour rendre compte des oxydations d'alcanes.

Nous avons cherché à écrire le mécanisme réactionnel de manière rationnelle et systématique, en analysant les diverses catégories de processus élémentaires pouvant intervenir, compte-tenu de la structure des radicaux dérivés de la molécule de propane par arrachement d'hydrogène.

Amorçage

Deux formes isomères du radical propyle $C_3H_7\cdot$ (*iso*- et *n*-) sont susceptibles d'être formées par la réaction :

$$C_3H_8 + O_2 \longrightarrow C_3H_7^{\bullet} + HO_2^{\bullet}$$

généralement retenue comme amorçage primaire dans les réactions d'oxydation en phase gazeuse homogène, bien que sujette à controverse et discutée par certains auteurs (4, 5) en ce qui concerne en particulier les valeurs préconisées pour sa constante de vitesse. En réalité ce point n'est pas fondamental car très rapidement le relais de l'amorçage est pris par les branchements dégénérés.

Les radicaux susceptibles d'être formés sont donc :

(i) par arrachement d'un des deux atomes d'hydrogène secondaires :

$CH_3—{}^{\bullet}CH—CH_3$ radical isopropyle : $(R^{1\bullet})$ ou $i\text{-}C_3H_7^{\bullet}$

$DH^0\ (iC_3H_7 - H) = 95{,}0$ kcal mol^{-1} (18,21)

(ii) par arrachement d'un des six atomes d'hydrogène primaires :

$CH_3—CH_2—{}^{\bullet}CH_3$ radical *n*-propyle : $(R^{2\bullet})$ ou $n\text{-}C_3H_7^{\bullet}$

$DH^0\ (nC_3H_7 - H) = 98{,}0$ kcal mol^{-1} (18,21)

À 350°C, la formation du radical isopropyle est environ 5,5 fois plus rapide que celle du radical *n*-propyle, compte-tenu de la différence des énergies d'activation des deux processus et du nombre d'atomes d'hydrogène arrachables dans les deux cas.

Addition d'une molécule d'oxygène sur les radicaux alcoyle. On considère ensuite l'addition réversible de l'oxygène sur les radicaux isopropyle et *n*-propyle :

$$R^{\bullet} + O_2 \underset{}{\overset{(2)}{\rightleftharpoons}} RO_2^{\bullet}$$

Les deux radicaux peroxyalcoyle obtenus sont :

$CH_3—\underset{\displaystyle OO^{\bullet}}{\underset{|}{CH}}—CH_3$ et $CH_3—CH_2—CH_2OO^{\bullet}$

$(R^1O_2^{\bullet})$ $(R^2O_2^{\bullet})$

3. Dans l'ensemble de ce travail nous utiliserons les unités : L, mol, s, kcal.

Can. J. Chem. Downloaded from www.nrcresearchpress.com by 195.138.81.100 on 09/07/12
For personal use only.

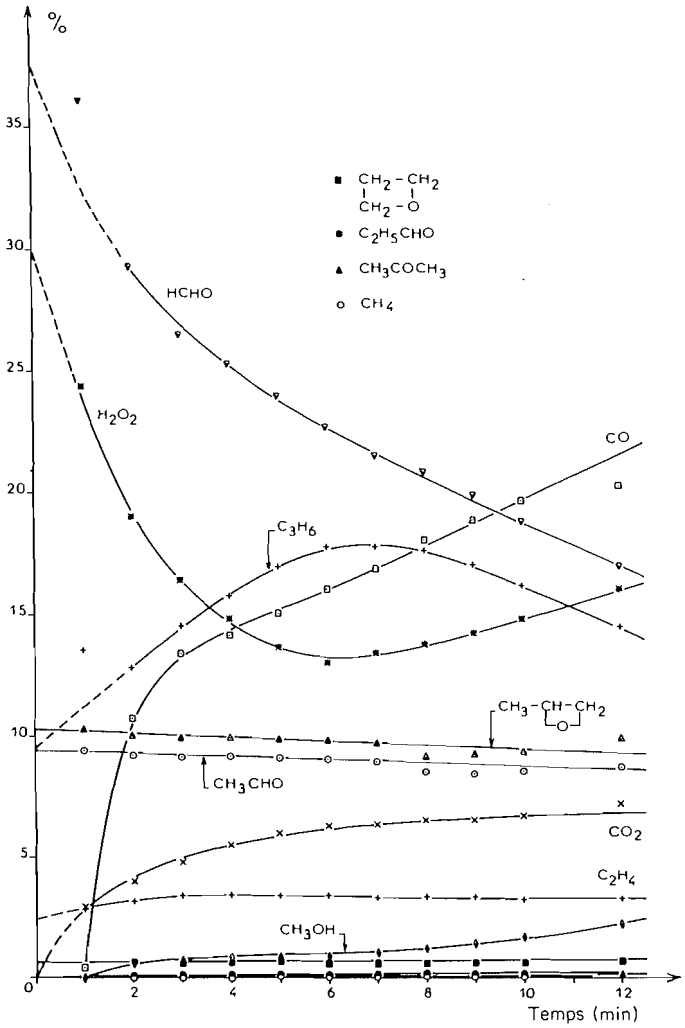


FIG. 8. Représentation du pourcentage molaire en fonction du temps des différents produits formés dans l'oxydation du mélange propane–propène. Mêmes conditions expérimentales que fig. 5.

et ils sont supposés se former avec la même vitesse, comme toute oxydation de radical alcoyle.

Isomérisation des radicaux peroxyalcoyle. En accord avec les schémas retenus par Fish (12), les radicaux peroxyalcoyle sous les deux formes isomères $R^1O_2\cdot$ et $R^2O_2\cdot$, comme dans le cas de l'isobutane, peuvent s'isomériser par transfert interne d'hydrogène en radicaux hydroperoxyalcoyle ·QOOH

$$RO_2\cdot \underset{}{\overset{(3)}{\rightleftharpoons}} \cdot QOOH$$

Ces processus d'isomérisation des deux formes isomères des radicaux peroxyalcoyle conduisent à 5 formes de radicaux hydroperoxyalcoyle $\cdot Q^1OOH$–$\cdot Q^5OOH$ par formation de complexes activés à 6 centres (réaction (3.4)),[4] à 5 centres (réactions (3.1) et (3.3)) et à 4 centres (réactions (3.2) et (3.5)). Ces deux derniers processus sont négligeables devant les autres en raison de l'énergie d'activation élevée nécessaire à la formation du complexe activé à 4 centres.

Les formules semi développées de ces cinq formes seront données ultérieurement dans le tableau 6 qui récapitule les valeurs des grandeurs thermodynamiques nécessaires à l'estimation des constantes de vitesse. Les processus (3.3) et (3.4) issus tous deux du radical $nC_3H_7COO\cdot(R^2O_2\cdot)$ apparaissent plus rapides que le processus (3.1) selon les calculs des constantes de vitesse qui seront donnés plus loin dans le tableau 7. Cette tendance n'est pas compensée par les valeurs des constantes d'équilibre présentées dans le tableau 3, si l'on tient compte du rôle des processus inverses.

Les concentrations des radicaux $\cdot Q^3OOH$ et $\cdot Q^4OOH$ seraient donc a priori plus élevées que celle de $\cdot Q^1OOH$, renversant ainsi l'ordre d'importance estimé à première vue à partir de la facilité de formation des radicaux alcoyle.

Formation des produits de réaction

À partir des différentes formes isomères des radicaux ·QOOH, nous proposons dans le tableau 4 les différents processus élémentaires possibles, y compris dans le souci d'être complet, ceux qui pourraient a priori être considérés comme négligeables; ils portent des numéros supérieurs à 4.7 (cf. tableaux 8 et 9).

Pour interpréter la formation d'aldéhydes, il paraît logique de tenir compte de la décomposition des deux radicaux alcoxy $RO\cdot$ ($R^1O\cdot$ et $R^2O\cdot$) obtenus par dismutation des radicaux peroxyalcoyle $R^1O_2\cdot$ et $R^2O_2\cdot$.

Ces réactions de dismutation sont souvent envisagées et leur constante de vitesse peut être estimée proche de $10^{9,5}$ L mol^{-1} s^{-1}.

Les données relatives aux radicaux alcoxy figurent dans le tableau 5.

Les remarques que nous avons faites dans le cas de l'isobutane (1) demeurent valables dans le cas du propane. Ici encore, l'écriture de *tous* les processus élémentaires possibles conduirait à un mécanisme global particulièrement complexe qui ne serait que d'une efficacité très limitée, voire inexistante, pour interpréter nos résultats expérimentaux. Ce que nous cherchons, c'est à simplifier ce schéma réactionnel pour déterminer les réactions élémentaires *essentielles* permettant de rendre compte des caractéristiques cinétiques et chimiques observées expérimentalement. Il va de soi que les concentrations relatives des diverses espèces radicalaires permettent une première simplification.

Mais, pour mener à bien cette simplification, il faudrait disposer aussi des constantes de vitesse de tous les processus élémentaires pouvant être écrits. Les données disponibles dans la littérature sont généralement incomplètes et peu précises et il peut se poser des problèmes de cohérence entre ces données.

Nous avons donc utilisé à nouveau, comme dans le cas de l'isobutane (1), la méthode semi-empirique d'estimation des constantes de vitesse développée par Benson sous le nom de Cinétique Thermochimique (18). Rappelons que ces méthodes nécessitent d'abord l'estimation des grandeurs thermodynamiques (ΔH^0_f, S^0, C_p^0) par des méthodes d'additivité de groupes pour les molécules ou en tenant compte des paramètres structuraux pour les espèces radicalaires (méthode dite du composé modèle).

Dans cet exemple, nous avons effectué les calculs de ΔH^0_f et S^0 à 300 K; ils sont utilisés à 623 K sans corrections en raison du nombre important de valeurs de C_p^0 non tabulées. Remarquons que les variations en fonction de la température sont généralement relativement faibles et que les erreurs sur ΔH^0 et ΔS^0 se compensent, au moins en partie, lors du calcul de ΔG^0.

Les résultats des calculs des grandeurs thermodynamiques sont donnés dans le tableau 6.

À partir de la relation entre ces grandeurs thermodynamiques

4. La numérotation des réactions correspond à celle des tableaux 8 et 9 présentés plus loin.

Can. J. Chem. Downloaded from www.nrcresearchpress.com by 195.138.81.100 on 09/07/12
For personal use only.

Can. J. Chem. Downloaded from www.nrcresearchpress.com by 195.138.81.100 on 09/07/12
For personal use only.

TABLEAU 2. Pourcentages molaires des produits formés dans l'oxydation du propane et de mélanges propane–propène (5% de propène) calculés en excluant le propène. Valeurs données à 5 min de réaction et à avancement nul ($t = 0$)

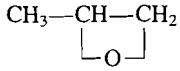
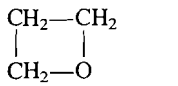
Produit	Pourcentages molaires: Mélange propane–propène $t = 0$	Mélange propane–propène $t = 5$ min	Propane seul $t = 0$	Propane seul $t = 5$ min	Rapport des pourcentages initiaux $\left(\frac{\%\text{ mélange}}{\%\ C_3H_8\text{ seul}}\right)$
CH_4	0	0,1	0	0	—
C_2H_4	2,8	4,1	1,7	2,8	1,65
HCHO	[41,4]	28,8	23,9	27,5	1,73
CH_3CHO	10,4	11,0	36,9	16,4	0,28
C_2H_5CHO	0	0,2	0	0,2	—
CH_3COCH_3	Traces	0,1	Traces	0,5	—
CH_3OH	0	1,1	0	1,2	—
CO	0	18,1	0	21,6	—
CO_2	0	7,3	0	11,5	—
H_2O_2	[33,2]	16,5	29,0	12,9	1,14
	11,4	11,9	8,5	4,9	1,34
	0,8	0,8	Traces	0,5	>>1
Total	100,0	100,0	100,0	100,0	

TABLEAU 3. Constantes d'équilibre à 623 K et tailles des cycles dans l'état de transition lors de l'isomérisation des radicaux peroxyalcoyle ($R^1O_2\cdot$ et $R^2O_2\cdot$) dérivés du propane en radicaux hydroperoxyalcoyle ·QOOH

Réaction	Constante d'équilibre	Taille du cycle dans l'état de transition	Radical formé
3.1	$1{,}25\cdot10^{-2}$	5	$\cdot Q^1OOH$
3.2	13	4	$\cdot Q^2OOH$
3.3	0,11	5	$\cdot Q^3OOH$
3.4	$6{,}0\cdot10^{-3}$	6	$\cdot Q^4OOH$
3.5	1,24	4	$\cdot Q^5OOH$

ΔH^0 et ΔS^0 et la constante d'équilibre K

$$-RT \ln K = \Delta H^0 - T\Delta S^0$$

la connaissance de ΔH^0, ΔS^0 et de la constante de vitesse de la réaction directe k_d ou inverse k_i conduit à l'estimation de la valeur de l'autre, ce qui suppose souvent des approximations raisonnables obtenues par des analogies avec des réactions voisines.

Les résultats de l'évaluation des grandeurs cinétiques sont donnés dans le tableau 7.

Dans ce tableau, nous donnons les valeurs estimées à l'aide des calculs décrits précédemment du facteur préexponentiel A, de l'énergie d'activation E et de la constante k calculée à 623 K (unités : L, mol, s).

Les processus élémentaires, écrits en tenant compte de l'expérience antérieure dans des systèmes voisins (1) et des connaissances acquises en chimie radicalaire, que nous avons retenus, compte-tenu de la discussion précédente et de l'estimation des constantes de vitesse calculées à 623 K, sont donnés dans les tableaux 8 et 9, le premier présentant les processus

TABLEAU 4. Processus élémentaires de décomposition des radicaux hydroperoxyalcoyle ·QOOH intervenant dans l'oxydation du propane

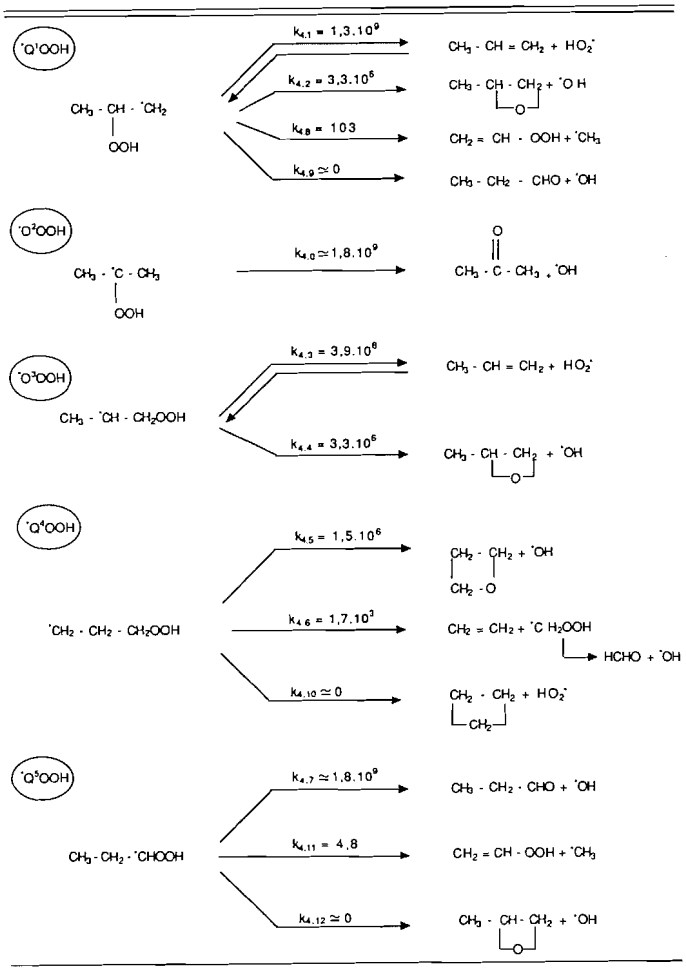
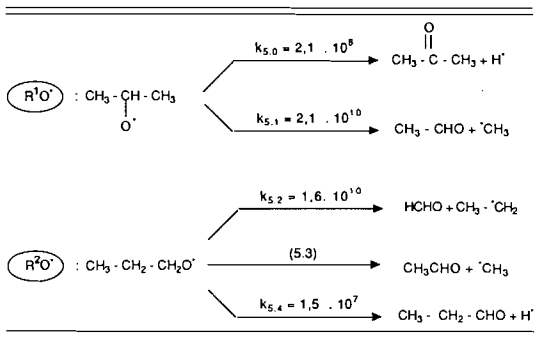


TABLEAU 5. Processus élémentaires de décomposition des radicaux alcoxy à 3 atomes de carbone susceptibles de figurer dans le schéma d'oxydation du propane



élémentaires générés à partir du radical isopropyle, le second à partir du radical *n*-propyle.

III.2. Commentaires sur le mécanisme et discussion

Généralités

Il serait fastidieux de discuter ici chaque chemin réactionnel retenu, d'une part par rapport aux autres chemins réactionnels possibles et d'autre part en le comparant avec les formations de produits observées expérimentalement, d'autant plus que des formations de nature secondaire, au sens cinétique du terme, peuvent compliquer cette analyse. Une telle comparaison détaillée a été faite dans un mémoire de thèse (25); nous n'en donnerons ici que les points les plus importants.

Une première étape dans une telle comparaison est d'estimer les rapports des concentrations des radicaux ·QOOH, en utilisant des calculs effectués à partir de l'approximation de l'état quasi-stationnaire, compte-tenu de l'estimation des constantes de vitesse mentionnée précédemment. Ces calculs font apparaître en particulier des écarts substantiels par rapport aux concentrations évaluées à partir des équilibres isolés. C'est le cas par exemple pour les radicaux $\cdot Q^1OOH$ à la suite du processus (4.1)

(4.1) $CH_3—\underset{\underset{OOH}{|}}{CH}—\cdot CH_2 \longrightarrow CH_3—CH{=}CH_2 + HO_2\cdot$

qui, par sa constante de vitesse élevée ($1{,}3 \times 10^9$), agit comme une sorte de «pompe à radicaux». L'équilibre isolé $(\cdot Q^1OOH)/(R^1OO\cdot)$ peut être estimé à $1{,}25 \times 10^{-2}$ alors que dans notre schéma réactionnel la valeur du rapport des concentrations stationnaires serait de l'ordre de $1{,}9 \times 10^{-5}$ dans nos conditions expérimentales.

Un phénomène analogue est observé avec $\cdot Q^3OOH$ puisque l'on obtient un rapport $(\cdot Q^3OOH)/(R^2OO\cdot)$ voisin de 0,11 à l'équilibre isolé alors que dans notre schéma réactionnel nous obtenons une valeur du rapport des concentrations stationnaires de $(\cdot Q^3OOH)$ et $(R^2OO\cdot)$ voisine de $2{,}4 \times 10^{-4}$, suite à un déplacement analogue dû au processus (4.3):

(4.3) $CH_3—\cdot CH—CH_2—OOH \longrightarrow CH_3—CH{=}CH_2 + HO_2\cdot$

avec $k_{4.3} \cong 3{,}9 \times 10^8$.

On peut obtenir les rapports des concentrations des radicaux hydroperoxyalcoyle en éliminant dans les calculs les concentrations des radicaux peroxyalcoyle. Il apparaît ainsi que pour un radical $\cdot Q^1OOH$, il y a $1{,}2 \times 10^{-5}$ radical $\cdot Q^2OOH$ et que pour un radical $\cdot Q^3OOH$, il y a 20 radicaux $\cdot Q^4OOH$ et $1{,}7 \times 10^{-7}$ radical $\cdot Q^5OOH$, toujours dans les conditions de l'état quasi-stationnaire. Les concentrations des radicaux $\cdot Q^2OOH$ et $\cdot Q^5OOH$ sont donc négligeables. Il est également possible de comparer la concentration des radicaux $\cdot Q^1OOH$ à celles des radicaux $\cdot Q^3OOH$ et $\cdot Q^4OOH$.

Pour un radical $\cdot Q^1OOH$, il y a :

$1{,}2 \times 10^{-5}$ radical $\cdot Q^2OOH$

1,3 radical $\cdot Q^3OOH$

26 radicaux $\cdot Q^4OOH$

$2{,}1 \times 10^{-7}$ radical $\cdot Q^5OOH$

Le radical hydroperoxyalcoyle prépondérant est donc $\cdot Q^4OOH$, $\cdot CH_2$-CH_2-CH_2-OOH, ce qui paraît logique puisqu'il n'est pas consommé par un processus rapide.

TABLEAU 6. Grandeurs thermodynamiques (ΔH^0_f et S^0) pour les espèces intervenant dans le mécanisme proposé d'oxydation du propane (calcul à 300 K)

	Espèce	$\Delta H^0_{f300\,K}$ (kcal mol^{-1})	$S^0_{300\,K}$ (cal mol^{-1} K^{-1})
	C_3H_8	−25,3	64,5
$R^1\cdot$	$i\cdot C_3H_7$	17,1[j]	66,8
$R^2\cdot$	$n\cdot C_3H_7$	20,6[b]	67,8
$R^1OO\cdot$	$iC_3H_7OO\cdot$	−12,9[c]	79,7
$R^2OO\cdot$	$nC_3H_7OO\cdot$	−8,5[c]	81,7
$\cdot Q^1OOH$	$HOOCH(CH_3)\cdot CH_2$	−2,5[b]	87,6
$\cdot Q^2OOH$	$(CH_3)_2\cdot COOH$	−12,5[k]	85,5
$\cdot Q^3OOH$	$CH_3\text{-}\cdot CH\text{-}CH_2OOH$	−1,6[j]	88,4
$\cdot Q^4OOH$	$\cdot CH_2\text{-}CH_2\text{-}CH_2OOH$	1,9[b]	88,2
$\cdot Q^5OOH$	$CH_3\text{-}CH_2\text{-}\cdot CHOOH$	−4,6[d]	88,4
$R^1O\cdot$	$iC_3H_7O\cdot$	−13,6[e]	71,5
$R^2O\cdot$	$nC_3H_7O\cdot$	−9,2[e]	73,5
	$\cdot CH_2OOH$	15,0[f]	69,0
	$HO_2\cdot$	3,0[g]	54,4[g]
	$\cdot OH$	9,4[h]	43,9[h]
	$\cdot CH_3$	34,3[h]	54,4[h]
	$H\cdot$	52,1[h]	27,4[h]
	C_3H_6	4,7	63,8
	C_2H_4	12,5	52,4
	$CH_2—CH_2$ $\quad\quad\llcorner CH_2 \lrcorner$	12,7	56,8
	$CH_3—CH—CH_2$ $\quad\quad\quad\llcorner O \lrcorner$	−21,8	66,2
	$CH_2—CH_2$ $\quad\quad\quad\quad$ $CH_2—CH_2$	−18,6	64,0
	HCHO	−26,0[g]	52,3[g]
	CH_3-CHO	−39,2	63,1
	CH_3-CH_2-CHO	−44,5	72,7
	CH_3COCH_3	−51,6	70,0
	CH_2=CHOOH	−7,9[i]	75,5[i]

[a] Calculé avec DH^0 (tC_4H_9 − H) = 92,0 kcal mol^{-1} (18).
[b] Calculé avec DH^0 (RCH_2 − H) = 98,0 kcal mol^{-1} (18).
[c] Calculé avec DH^0 (ROO − H) = 87,6 kcal mol^{-1} (19).
[d] Calculé avec DH^0 (RCH(OOH) − H) = 91,5 kcal mol^{-1} (21) et d'après la réf. 20.
[e] Calculé avec DH^0 (RO − H) = 104,0 kcal mol^{-1} (18).
[f] Calculé avec DH^0 ($HOOCH_2$ − H) = 98,0 kcal mol^{-1} (21).
[g] Valeur donnée dans la réf. 20.
[h] Valeur donnée dans la réf. 18.
[i] Calculé par la méthode d'additivité de liaisons.
[j] Calculé avec DH^0 ($(CH_3)_2CH$ − H) = 94,5 kcal mol^{-1} (18).
[k] Calculé avec DH^0 (RR'C(OOH) − H) = 88,0 kcal mol^{-1} (21) et d'après la réf. 20.

Can. J. Chem. Downloaded from www.nrcresearchpress.com by 195.138.81.100 on 09/07/12
For personal use only.

Can. J. Chem. Downloaded from www.nrcresearchpress.com by 195.138.81.100 on 09/07/12
For personal use only.

TABLEAU 7. Paramètres cinétiques calculés pour les différents processus élémentaires proposés dans le mécanisme d'oxydation du propane (A, E et constante calculée à 623 K)

Réactions	A		E (kcal mol^{-1})	k (s^{-1}) (à 623 K)
(2.1)	$10^{9,5}$	L mol^{-1} s^{-1}	0	$k(O_2)$ = $5,0\cdot10^6$ (18)
(−2.1)	$10^{15,20}$	s^{-1}	28,7	$1,6\cdot10^5$
(2.2)	$10^{9,5}$	L mol^{-1} s^{-1}	0	$k(O_2)$ = $5,0\cdot10^6$ (18)
(−2.2)	$10^{15,03}$	s^{-1}	27,8	$2,2\cdot10^5$
(3.1)	$10^{13,56}$	s^{-1}	26,3	$2,5\cdot10^4$
(−3.1)	$10^{11,85}$	s^{-1}	15,9	$2,0\cdot10^6$
(3.2)	$10^{13,55}$	s^{-1}	40,0	0,4
(−3.2)	$10^{12,29}$	s^{-1}	39,6	$3,0\cdot10^{-2}$
(3.3)	$10^{13,09}$	s^{-1}	23,3	$9,2\cdot10^4$
(−3.3)	$10^{11,63}$	s^{-1}	16,4	$8,2\cdot10^5$
(3.4)	$10^{12,50}$	s^{-1}	21,0	$1,5\cdot10^5$
(−3.4)	$10^{11,09}$	s^{-1}	10,6	$2,5\cdot10^7$
(3.5)	$10^{13,85}$	s^{-1}	43,0	$7,2\cdot10^{-2}$
(−3.5)	$10^{12,39}$	s^{-1}	39,1	$5,8\cdot10^{-2}$
(4.0)	[10^{11}	s^{-1}]	[5]	[$1,8\cdot10^9$]
(4.1)	$10^{14,33}$	s^{-1}	15,0	$1,3\cdot10^9$
(−4.1)	$10^{9,83}$	s^{-1}	6,0	$5,5\cdot10^7$
(4.2)	$10^{12,78}$	s^{-1}	18,0	$3,3\cdot10^6$
(4.3)	$10^{13,51}$	s^{-1}	14,1	$3,9\cdot10^8$
(−4.3)	$10^{9,18}$	s^{-1}	6,0	$1,2\cdot10^7$
(4.4)	$10^{12,78}$	s^{-1}	18,0	$3,3\cdot10^6$
(4.5)	$10^{12,03}$	s^{-1}	16,8	$15,\cdot10^6$
(4.6)	$10^{14,00}$	s^{-1}	30,9	$1,7\cdot10^3$
(4.7)	[10^{11}	s^{-1}]	[5]	[$1,8\cdot10^9$]
(4.8)	$10^{14,18}$	s^{-1}	34,9	103
(4.9)				≃0
(4.10)				≃0
(4.11)	$10^{13,58}$	s^{-1}	37,0	4,8
(4.12)				≃0
(5.0)	$10^{13,94}$	s^{-1}	16,1	$2,1\cdot10^8$
(5.1)	$10^{14,05}$	s^{-1}	10,7	$2,1\cdot10^{10}$
(5.2)	$10^{13,94}$	s^{-1}	10,7	$1,6\cdot10^{10}$
(5.3)				—
(5.4)	$10^{13,72}$	s^{-1}	18,8	$1,5\cdot10^7$
(6)	$10^{9,5}$	L mol^{-1} s^{-1}	5,0	$k(O_2)$ = $9,2\cdot10^4$ (22)
(10)	$10^{9,5}$	L mol^{-1} s^{-1}	0	$k(O_2)$ = $5,0.10^6$ (18)
(12)	10^9	L mol^{-1} s^{-1}	19,4[a]	k(RH) = 0,28 (23)
			17,1[b]	k(RH) = 1,8
			14,4[c]	k(RH) = 15
(14)	$10^{9,5\pm0,5}$	L mol^{-1} s^{-1}	0	$3,2\cdot10^9$ L mol^{-1} s^{-1}
Parois				≡0,5 (24)

[a]Pour l'arrachement d'un atome H primaire.
[b]Pour l'arrachement d'un atome H secondaire.
[c]Pour l'arrachement d'un atome H tertiaire.

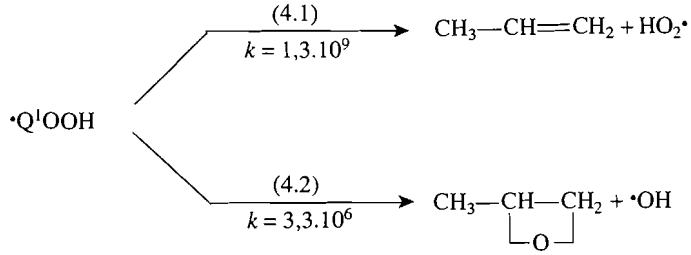
Il est certain que pour vérifier l'adéquation du mécanisme proposé et de l'expérience, l'idéal serait de simuler la formation de l'ensemble des produits formés, pour obtenir en particulier les courbes de pressions partielles des produits en fonction du temps, en effectuant les ajustements requis des valeurs numériques des constantes de vitesse. Une première tentative faite dans ce sens (26) a montré la complexité du problème, tant au niveau des méthodes numériques requises qu'à celui de l'ajustement des constantes puisque les méthodes de Benson ne conduisent qu'à une valeur approximative.

Il nous a donc paru plus réaliste de nous borner dans le cadre de ce mémoire à étudier de manière plus qualitative un certain nombre d'exemples caractéristiques.

Comparaison des formations de propène et de méthyloxiranne

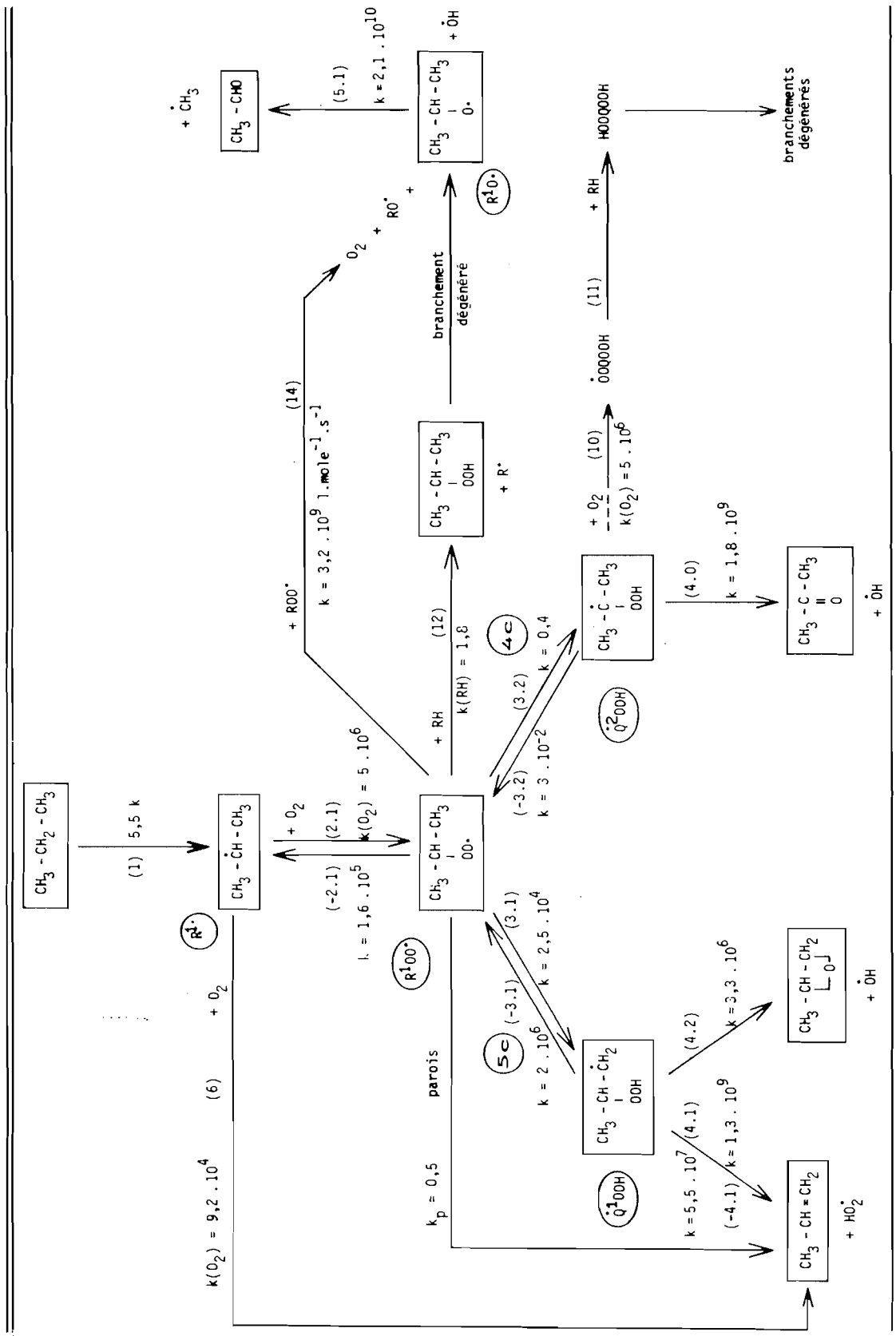
Les chaînes issues des deux radicaux alcoyle produisent conjointement le propène et le méthyloxiranne :

À partir du radical ·Q^{1}OOH :



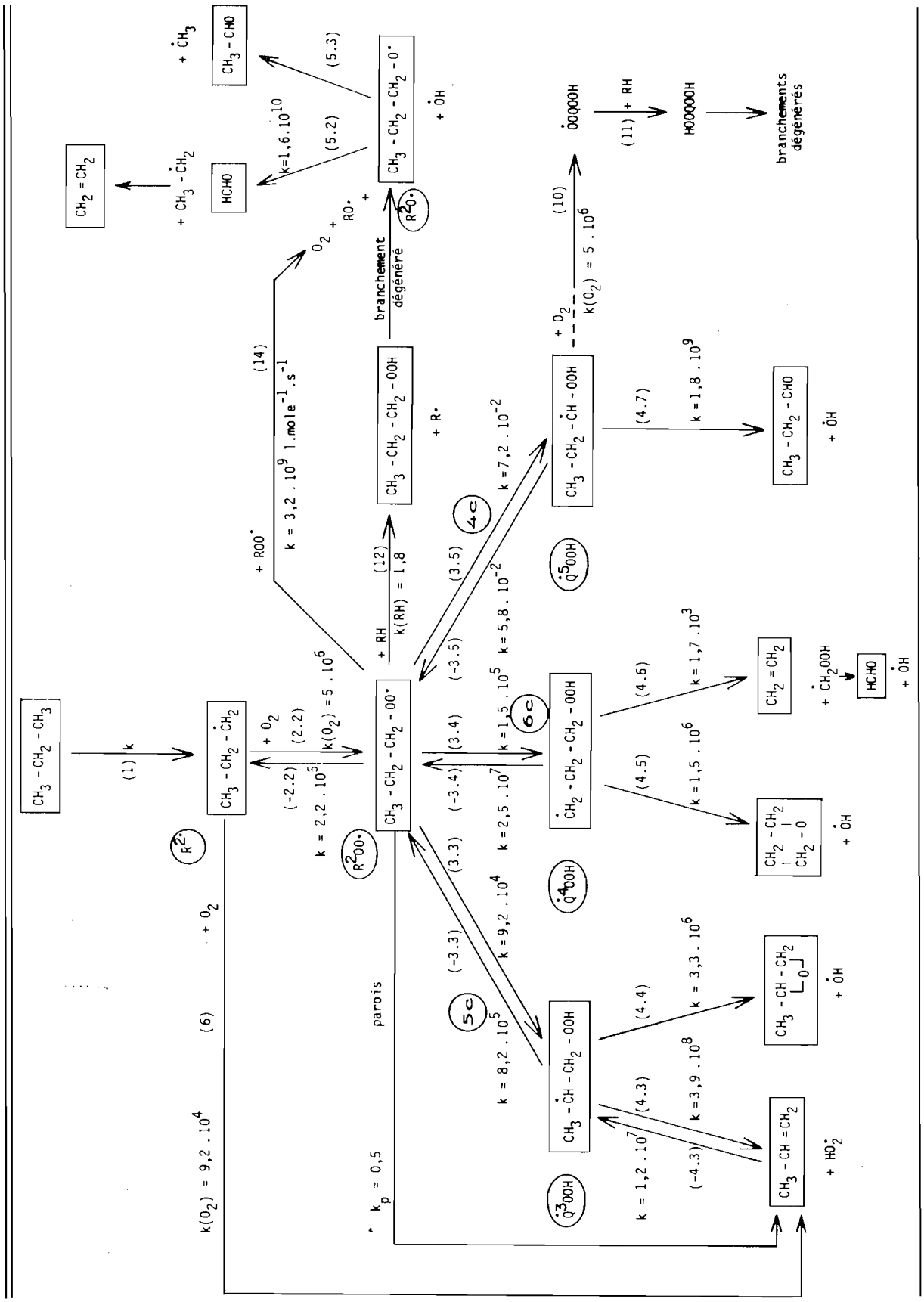
Can. J. Chem. Downloaded from www.nrcresearchpress.com by 195.138.81.100 on 09/07/12
For personal use only.

TABLEAU 8. Mécanisme d'oxydation du propane (processus élémentaires issus du radical isopropyle, CH_3-·CH-CH_3)



Can. J. Chem. Downloaded from www.nrcresearchpress.com by 195.138.81.100 on 09/07/12
For personal use only.

TABLEAU 9. Mécanisme d'oxydation du propane (processus élémentaires issus du radical *n*-propyle, CH_3-CH_2-·CH_2)



Can. J. Chem. Downloaded from www.nrcresearchpress.com by 195.138.81.100 on 09/07/12
For personal use only.

À partir du radical $\cdot Q^3OOH$:

$$\cdot Q^3OOH \xrightarrow[k = 3{,}9.10^8]{(4.3)} CH_3{-}CH{=}CH_2 + HO_2\cdot$$

$$\cdot Q^3OOH \xrightarrow[k = 3{,}3.10^6]{(4.4)} CH_3{-}\underset{\displaystyle O}{\underset{|}{CH}}{-}CH_2 + \cdot OH$$

En négligeant les réactions inverses on obtient le rapport des vitesses de formation :

$$\frac{v_{C_3H_6}}{v_{MeOx}} = \frac{k_{4.1}(\cdot Q^1OOH) + k_{4.3}(\cdot Q^3OOH)}{k_{4.2}(\cdot Q^1OOH) + k_{4.4}(\cdot Q^3OOH)} = \frac{k_{4.1} \times 0{,}78 + k_{4.3}}{k_{4.2} \times 0{,}78 + k_{4.4}}$$

$$\frac{v_{C_3H_6}}{v_{MeOx}} = \frac{1{,}3.10^9 \times 0{,}78 + 3{,}9.10^8}{3{,}3.10^6 \times 0{,}78 + 3{,}3.10^6} \cong \boxed{240}$$

Remarque : le propène est produit en quantités pratiquement équivalentes par les deux processus (4.1) et (4.3).

La valeur expérimentale du rapport des vitesses de formation correspond au rapport des pourcentages initiaux des deux produits :

$$\frac{\%C_3H_6}{\%MeOx} = \frac{64{,}8}{3} \cong \boxed{22}$$

On retrouve les ordres de grandeur obtenus lors de l'étude de l'isobutane et on peut donc admettre également une concordance relativement bonne entre les résultats expérimentaux et les valeurs estimées par la cinétique thermochimique.

Nous n'avons pas tenu compte des parts de propène susceptible d'être formé par la voie oléfinique (6) et aux parois, car elles sont négligeables :

Processus oléfinique :

$$R^{1}\cdot + O_2 \xrightarrow{(6)} C_3H_6 + HO_2\cdot \qquad k_6 \cong 5.10^6\ L\ mol^{-1}\ s^{-1} \quad (23)$$

$$R^{2}\cdot + O_2 \xrightarrow{(6)} C_3H_6 + HO_2\cdot \qquad \Rightarrow k_6(O_2) \cong 8.10^3\ s^{-1}$$

Réactions aux parois :

$$R^1OO\cdot \xrightarrow{\text{parois}} C_3H_6 + HO_2\cdot \qquad k_p \cong 0{,}5\ s^{-1} \quad (24)$$

$$R^2OO\cdot \xrightarrow{\text{parois}} C_3H_6 + HO_2\cdot$$

Importance de la voie oléfinique :

$$\frac{v_{4.1} \times v_{4.3}}{\Sigma v_6} = \frac{k_{4.1}(\cdot Q^1OOH) + k_{4.3}(\cdot Q^3OOH)}{k_6(O_2)(R^1\cdot) + k_6(O_2)(R^2\cdot)} = \frac{(\cdot Q^1OOH)[k_{4.1} + k_{4.3} \times 1{,}3]}{(R^1\cdot) \times k_6(O_2) \times [1 + 0{,}18]} = \boxed{100}$$

La part oléfinique semble très faible : voisine de 1%, ce qui n'est pas en accord avec les théories de Knox. Cependant la valeur du rapport obtenue ne permet pas d'être catégorique, compte-tenu des imprécisions des méthodes d'estimation.

Importance des réactions aux parois :

$$\frac{v_{4.1} \times v_{4.3}}{\Sigma v_p} = \frac{k_{4.1}(\cdot Q^1OOH) + k_{4.3}(\cdot Q^3OOH)}{k_p(R^1OO\cdot) + k_p(R^2OO\cdot)} = \frac{(\cdot Q^1OOH)[k_{4.1} + k_{4.3} \times 1{,}3]}{(R^1OO\cdot) \times k_p \times [1 + 0{,}15]} = \boxed{6.10^4}$$

La formation de propène aux parois serait négligeable d'après nos estimations ce qui n'est pas l'avis d'Atherton *et al.* qui considèrent que l'alcène conjugué est formé de manière prédominante à la surface dans le cas de l'oxydation du propane aux environs de 600 K (24).

Étude de l'éthylène et de l'oxétanne

Le radical $\cdot Q^4OOH$ peut se décomposer principalement selon deux processus :

$$\cdot CH_2{-}CH_2{-}CH_2{-}OOH \xrightarrow[k_{4,5} = 1{,}5.10^6]{(4.5)} \underset{\displaystyle CH_2{-}O}{\underset{|}{CH_2}}{-}CH_2 + \cdot OH$$

$$\cdot CH_2{-}CH_2{-}CH_2{-}OOH \xrightarrow[k_{4,6} = 1{,}7.10^3]{(4.6)} CH_2{=}CH_2 + \cdot CH_2OOH \longrightarrow HCHO + \cdot OH$$

Le rapport théorique des vitesses de formation est alors :

$$\frac{v_{C_2H_4}}{v_{\square_O}} = \frac{k_{4.6}}{k_{4.5}} = \frac{1{,}7.10^3}{1{,}5.10^6} = \boxed{1{,}1.10^{-3}}$$

Comme dans le cas de l'oxydation de l'isobutane, ce résultat fait apparaître une anomalie, car l'expérience montre que l'on obtient au moins 10 fois plus d'éthylène que d'oxétanne. Cependant, lors de l'oxydation du propane, nous avons pu doser cet hétérocycle alors que son homologue (le méthyl-3-oxétanne) n'a pas été mis en évidence dans les produits de l'oxydation de l'isobutane. Nous pouvons examiner le rapport théorique des vitesses de formation du propène et de l'oxétanne pour vérifier la cohérence entre les processus issus de radicaux $\cdot QOOH$ différents.

$$\frac{v_{C_3H_6}}{v_{\square_O}} = \frac{k_{4.1}(\cdot Q^1OOH) + k_{4.3}(\cdot Q^3OOH)}{k_{4.5}(\cdot Q^4OOH)} = \frac{k_{4.1} + k_{4.3} \times 1{,}3}{k_{4.5} \times 26} = \frac{1{,}3.10^9 + 3{,}9.10^8 \times 1{,}3}{1{,}5.10^6 \times 26} \cong \boxed{46}$$

Can. J. Chem. Downloaded from www.nrcresearchpress.com by 195.138.81.100 on 09/07/12
For personal use only.

En utilisant ce rapport et d'après le pourcentage initial expérimental du propène qui est 64,8, celui de l'oxétanne devrait donc être 1,4. Ce résultat est trop élevé car la valeur expérimentale observée est de l'ordre de 0,1; cependant l'écart n'est pas extravagant, compte-tenu des méthodes d'estimation des constantes de vitesse.

Pour en revenir à l'éthylène, il faudrait proposer un autre processus permettant d'expliquer sa formation de façon plus importante. Nous proposons la décomposition du radical alcoxy $R^2O\cdot$:

$$CH_3—CH_2—CH_2—O\cdot \xrightarrow[k = 1{,}6.10^{10}]{(5.2)} HCHO + CH_3—\cdot CH_2$$

$$\downarrow$$

$$CH_2{=}CH_2 + H\cdot$$

Cependant, comme dans le processus (4.6), la formation de propène est accompagnée de celle de formaldéhyde dont le pourcentage initial est 8,4, soit 10 fois plus que l'éthylène. Comme le formaldéhyde n'est pas formé par d'autres processus indépendants, on peut considérer que le radical éthyle s'oxyde plus rapidement qu'il ne donne d'éthylène, ceci pour expliquer le déficit par rapport au formaldéhyde. Les valeurs des constantes confirment cette proposition.

$$C_2H_5\cdot + O_2 \longrightarrow C_2H_5OO\cdot \qquad k = 10^{9,5} \Rightarrow k(O_2) \cong 5.10^6 \quad (18)$$

$$C_2H_5\cdot \longrightarrow C_2H_4 + H\cdot \qquad k \cong 5.10^{-2} \quad (27)$$

Quoi qu'il en soit, une partie non négligeable de radicaux éthyle doivent conduire, directement ou indirectement par «déshydrogénation», à la formation d'éthylène en quantités suffisantes pour expliquer les résultats expérimentaux.

Autres produits dont produits carbonylés

Il paraît intéressant d'examiner également la formation d'autres produits dont les produits carbonylés et les peroxydes.

Acétaldéhyde. Cet aldéhyde est un produit primaire important de l'oxydation du propane. Cependant, sa formation nécessite la perte d'un atome de carbone à partir du squelette du propane et la fermeture d'une double liaison carboxylique. Seul un processus de décomposition du radical alcoxy $R^1O\cdot$ permet d'écrire directement la formation d'acétaldéhyde par coupure relativement facile d'une liaison C—C :

$$CH_3—\underset{\displaystyle O\cdot}{\underset{|}{CH}}—CH_3 \xrightarrow[k = 2{,}1.10^{10}]{(5.1)} CH_3—CHO + \cdot CH_3$$

Pour conserver le caractère primaire du produit, il est indispensable de considérer les radicaux $R^1O\cdot$ provenant de la dismutation des radicaux $R^1OO\cdot$ et non pas ceux provenant de la décomposition d'hydroperoxydes intermédiaires.

Le radical $R^2O\cdot$ peut également donner de l'acétaldéhyde :

$$CH_3—CH_2—CH_2—O\cdot \xrightarrow{(5.3)} CH_3—CHO + \cdot CH_3$$

Cependant ce processus est certainement moins important que le précédent car il nécessite, après la rupture de la liaison C—C, le transfert d'un atome d'hydrogène pour rapprocher le centre radicalaire de l'atome d'oxygène, lui aussi porteur d'un électron célibataire.

La réaction concurrentielle est la fermeture du biradical, supposé formé, en oxiranne. Nous avons déjà mentionné dans l'étude de l'isobutane que Flowers et Parker considèrent que la réaction de transfert est prépondérante devant la formation d'époxyde (28, 29).

Les radicaux méthyle accompagnant la formation d'acétaldéhyde ne donnent pas de méthane puisque les résultats expérimentaux le font apparaître comme nettement secondaire. En effet, l'addition d'une molécule d'oxygène sur un radical méthyle est un processus plus facile que la métathèse.

Formaldéhyde. Nous avons déjà mentionné la formation du formaldéhyde lorsque nous avons exploité les résultats concernant l'éthylène; elle peut avoir lieu par deux processus :

$$\cdot Q^4OOH : \cdot CH_2—CH_2—CH_2—OOH$$

$$\xrightarrow[k = 1{,}7.10^3]{(4.6)} CH_2{=}CH_2 + \cdot CH_2OOH \longrightarrow HCHO + \cdot OH$$

$$R^2O\cdot : CH_3—CH_2—CH_2—O\cdot$$

$$\xrightarrow[k = 1{,}6.10^{10}]{(5.2)} HCHO + CH_3—\cdot CH_2$$

dont le deuxième est très probablement prépondérant. Il faut noter que cet aldéhyde provient exclusivement de la chaîne issue du radical *n*-propyle.

Certains auteurs, comme Quinn (communication privée), envisagent la formation de formaldéhyde à partir de radicaux méthyle, ce qui serait une façon de consommer ces derniers, produits par des processus déjà mentionnés, par exemple :

$$CH_3\cdot + O_2 \longrightarrow CH_3OO\cdot$$

$$CH_3OO\cdot + O_2 \longrightarrow \left[\begin{array}{l} CH_2 \\ H \quad O \\ \cdot \\ O \quad\ O \\ \quad O \end{array}\right] \longrightarrow HCHO + O_2 + \cdot OH$$

On peut se demander si ce processus est réellement élémentaire en raison des multiples ruptures de liaison nécessaires à l'obtention des produits.

On peut comparer les rapports théoriques et expérimentaux des deux aldéhydes en ne considérant que le processus supposé prépondérant : (5.2) pour le formaldéhyde et (5.1) pour l'acétaldéhyde :

$$R^2O\cdot : CH_3—CH_2—CH_2—O\cdot$$

$$\xrightarrow[k = 1{,}6.10^{10}]{(5.2)} HCHO + CH_3—\cdot CH_2$$

$$R^1O\cdot : CH_3—\underset{\displaystyle O\cdot}{\underset{|}{CH}}—CH_3 \xrightarrow[k = 2{,}1.10^{10}]{(5.1)} CH_3CHO + \cdot CH_3$$

$$\frac{v_{CH_3CHO}}{v_{HCHO}} = \frac{k_{5.1}(R^1O\cdot)}{k_{5.2}(R^2O\cdot)}$$

on peut estimer que le rapport des concentrations des radicaux RO· est le même que celui des radicaux ROO· :

$$\frac{(R^1O\cdot)}{(R^2O\cdot)} = \frac{(R^1OO\cdot)}{(R^2OO\cdot)} = \frac{(R^1OO\cdot)}{(R^1\cdot)} \times \frac{(R^1\cdot)}{(R^2\cdot)} \times \frac{(R^2\cdot)}{(R^2OO\cdot)} \cong 10$$

ainsi

$$\frac{v_{CH_3CHO}}{v_{HCHO}} = \frac{2{,}1.10^{10}}{1{,}6.10^{10}} \times 10 = \boxed{13}$$

Can. J. Chem. Downloaded from www.nrcresearchpress.com by 195.138.81.100 on 09/07/12
For personal use only.

Le rapport expérimental étant $\%CH_3CHO/\%HCHO = 13/8,4 \cong \boxed{1,6}$, la cohérence des résultats est correcte.

Propionaldéhyde. Les analyses des produits mettent en évidence la nature secondaire du propionaldéhyde, ce qui est envisageable suite à l'étude des processus de formation :

$$R^2O\cdot : CH_3—CH_2—CH_2—O\cdot \xrightarrow[k = 1,5.10^7]{(5.4)} CH_3—CH_2—CHO + H\cdot$$

$$\cdot Q^5OOH : CH_3—CH_2—\cdot CH—OOH \xrightarrow[k \cong 1,8.10^9]{(4.7)} CH_3—CH_2—CHO + \cdot OH$$

La rupture d'une liaison C—H lors du processus (5.4) rend celui-ci négligeable devant son homologue (5.2) où intervient la rupture d'une liaison C—C :

$$R^2O\cdot : CH_3—CH_2—CH_2—O\cdot \xrightarrow[k = 1,6.10^{10}]{(5.2)} HCHO + CH_3—\cdot CH_2$$

Par contre, le processus (4.7) est rapide, mais le radical $\cdot Q^5OOH$ qui se décompose résulte d'une isomérisation du radical $R^2OO\cdot$ avec passage par un complexe activé à 4 centres, donc difficile et négligeable devant les isomérisations conduisant aux radicaux $\cdot Q^3OOH$ et $\cdot Q^4OOH$. Il est donc logique de n'avoir pas mis en évidence la formation de propionaldéhyde dans les instants initiaux de la réaction d'oxydation du propane.

Acétone. Le cas de l'acétone est exactement identique à celui du propionaldéhyde. Ce dernier était issu exclusivement du radical *n*-propyle de façon à ce que l'atome d'oxygène restant dans la molécule soit situé en bout de chaîne. Dans le cas de l'acétone, l'atome d'oxygène doit être porté par le carbone central impliquant l'oxydation du radical isopropyle. Ainsi le premier processus (5.0) fait intervenir la rupture d'une liaison C—H et le deuxième, (4.0), correspond à la décomposition du radical $\cdot Q^2OOH$ issu d'une isomérisation à 4 centres.

$$R^1O\cdot : CH_3—\underset{\displaystyle O\cdot}{\underset{|}{CH}}—CH_3 \xrightarrow[k = 2,1.10^8]{(5.0)} CH_3—\underset{\displaystyle O\cdot}{\underset{\|}{C}}—CH_3 + H\cdot$$

$$\cdot Q^2OOH : CH_3—\underset{\displaystyle OOH}{\underset{|}{\cdot C}}—CH_3 \xrightarrow[k \cong 1,8.10^9]{(4.0)} CH_3—\underset{\displaystyle O}{\underset{\|}{C}}—CH_3 + \cdot OH$$

L'observation de traces d'acétone à l'instant initial est compatible avec ce qui précède.

Peroxydes. Le dosage des peroxydes a été réalisé en utilisant la méthode que nous avons mise au point au laboratoire et améliorée entre l'étude de l'isobutane (1) et celle du propane (31, 32). Nous avons constaté que l'oxydation du propane donne des quantités notables de peroxydes,[5] ce qui n'était pas le cas de l'oxydation de l'isobutane. En effet, le pourcentage initial obtenu est 10,2, ce qui les place parmi les produits importants, après le propène et l'acétaldéhyde et juste avant le formaldéhyde. Il peut s'agir d'hydroperoxydes provenant de la réaction (12) :

$$ROO\cdot + RH \xrightarrow{(12)} ROOH + R\cdot$$

ou d'eau oxygénée produite selon le même type de processus et selon la réaction entre deux radicaux hydroperoxyle :

$$HO_2\cdot + RH \xrightarrow{(7)} H_2O_2 + R\cdot \qquad k = 1,1.10^3 \text{ L mol}^{-1} \text{ s}^{-1}\ ^6$$

$$HO_2\cdot + HO_2\cdot \xrightarrow{(14a)} H_2O_2 + O_2 \qquad k = 10^{9,3} \text{ L mol}^{-1} \text{ s}^{-1} \quad (34)$$

Nous pouvons estimer un rapport des vitesses de formation des porteurs de chaîne $\cdot OH$ et $HO_2\cdot$ afin de vérifier la cohérence de résultats :

$$\frac{v_{HO_2\cdot}}{v_{\cdot OH}} = \frac{k_{4.1}(\cdot Q^1OOH) + k_{4.3}(\cdot Q^3OOH)}{k_{4.2}(\cdot Q^1OOH) + k_{4.0}(\cdot Q^2OOH) + k_{4.4}(\cdot Q^3OOH) + [k_{4.5} + (\cong k_{4.6})](\cdot Q^4OOH) + k_{4.7}(\cdot Q^5OOH)}$$

$$\frac{v_{HO_2\cdot}}{v_{\cdot OH}} = \frac{k_{4.1} \times 1,3.k_{4.3}}{k_{4.2} + 1,3.k_{4,4} + 26(k_{4.5} + k_{4.6})} \cong \boxed{40}$$

Il y a effectivement prédominance des radicaux $HO_2\cdot$ mais elle n'est pas marquée de façon très nette.

Autres produits. Deux autres produits de réaction ont également retenu notre attention : l'eau et le dioxyde de carbone.

Contrairement au cas de l'isobutane, nous observons une formation secondaire de dioxyde de carbone, ce qui paraît plus logique compte-tenu du schéma mécanistique homogène retenu ainsi que de la nature secondaire de l'oxyde de carbone.

Il est certain que l'eau est formée en quantités importantes mais son analyse présente un certain nombre de difficultés qui nous ont fait renoncer à son dosage : condensation et adsorption dans les tubulures de l'appareillage statique, adsorption dans l'ampoule de chromatographie et difficulté de l'analyse chromatographique elle-même d'où une importante dispersion des résultats. Une estimation à partir d'une comparaison des bilans en carbone et hydrogène laisse prévoir que la formation d'eau est environ 50% plus importante que celle du propène à 5 min de réaction.

III.3. Influence du propène

Il est certain qu'une étude logique de l'influence de cet alcène sur l'oxydation du propane aurait nécessité, à titre de référence, l'étude de l'oxydation homogène du propène, réaction pour laquelle la littérature semble peu abondante. Cependant l'importance de cette tâche et la connaissance limitée atteinte jusqu'à présent des schémas généraux d'oxydation des alcènes nous ont conduits à différer cette étude et à nous contenter d'une étude plus superficielle.

Il avait été montré dans un article publié en 1971 par Sochet *et al.* (35) que les principaux produits d'oxydation du propane et

5. La méthode de dosage ne permettant pas de distinguer les hydroperoxydes de l'eau oxygénée, nous pouvons être amenés à utiliser indifféremment l'un ou l'autre terme pour dénommer l'ensemble des peroxydes dosés. Nous avons déjà mentionné les difficultés d'établir une distinction entre les différents peroxydes (33).

6. Pour l'arrachement d'un atome d'hydrogène secondaire (23).

Can. J. Chem. Downloaded from www.nrcresearchpress.com by 195.138.81.100 on 09/07/12
For personal use only.

du propène sont sensiblement les mêmes ce qui paraît impliquer une certaine similitude dans les mécanismes réactionnels. De même, il apparaît (cf. Lucquin et coll. (36); Shtern (37)) une appréciable similitude dans l'allure des limites de zones réactionnelles (réaction lente, flammes froides, inflammation de 2ème stade) dans le plan pression–température, le propène tendant cependant à s'auto-enflammer pour des pressions moins élevées que le propane, ce qui paraît suggérer une réactivité plus élevée.

L'ajout de propène (5% du total propane + propène) provoque une augmentation de la quantité des produits formés. Une estimation de l'avancement à 5 min de réaction donne 0,47% pour le propane seul et 0,60% pour le mélange propane + propène. Ces résultats sont en accord avec ceux de la littérature (37, 38) qui ont constaté le rôle promoteur du propène lors de l'oxydation du propane. Nous avons mentionné précédemment dans le tableau 2 les rapports des pourcentages de formation des produits primaires, lors de l'oxydation du propane seul et du mélange propane–propène, le propène n'étant pas comptabilisé dans les produits.

Il est connu que la présence de la double liaison dans la molécule de propène modifie les énergies de liaison C—H (18).

propane : $DH^0(nC_3H_7 - H) = 98{,}0$ kcal mol^{-1}
$DH^0(iC_3H_7 - H) = 94{,}5$ kcal mol^{-1}

propène : $DH^0(\text{allyl} - H) = 87$ kcal mol^{-1}
$DH^0((CH_3—CH{=}CH) - H) = 108$ kcal mol^{-1}

$DH^0\left(\left(\begin{matrix}CH_3\\ \diagdown\\ C\\ \diagup\\ CH_2\end{matrix}\right) - H\right) \cong 104$ kcal mol^{-1}

La molécule de propène est ainsi plus réactive que celle du propane en raison de l'affaiblissement des liaisons C—H allyliques.

Ces résultats nous paraissent présenter de plus l'intérêt de conduire à des données sur l'oxydation du radical allyle. En effet, il ne fait aucun doute que le radical, stabilisé par résonance, joue un rôle important dans la réaction. Le radical allyle peut s'oxyder et donner le radical allylperoxy $CH_2{=}CH\text{-}CH_2OO\cdot$. Cependant, cette réaction paraît essentiellement différente de celle de l'oxydation du radical isopropyle; développons un peu cette comparaison en estimant les constantes d'équilibre des réactions (2.1) et (2.1′).

$$CH_3—\cdot CH—CH_3 + O_2 \underset{}{\overset{(2.1)}{\rightleftharpoons}} CH_3—\underset{\displaystyle OO\cdot}{\underset{|}{CH}}—CH_3$$

$$CH_2{=}CH—\cdot CH_2 + O_2 \overset{(2.1')}{\rightleftharpoons} CH_2{=}CH—CH_2—OO\cdot$$

$\Delta_R H^0_{2.1} = -12{,}9 - 0 - 17{,}1 = -30{,}0$ kcal mol^{-1}

$\Delta_R S^0_{2.1} = 79{,}7 - 49{,}2 - 66{,}8 = -36{,}1$ cal mol^{-1} K^{-1}

$\Delta_R H^0_{2,1'} = 22{,}4 - 0 - 39{,}1 = -16{,}7$ kcal mol^{-1}

$\Delta_R S^0_{2.1'} = 78{,}6 - 49{,}0 - 61{,}6 = -32$ cal mol^{-1} K^{-1}

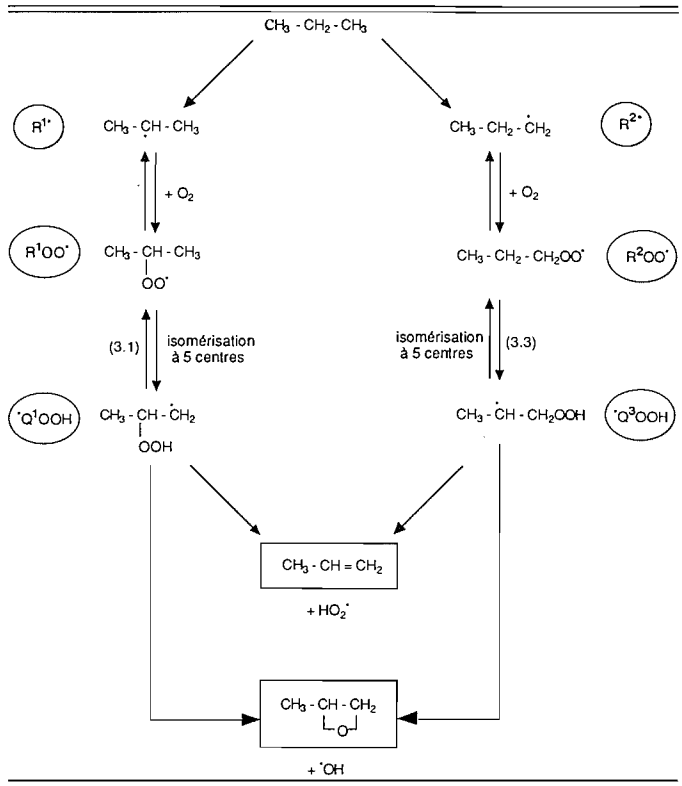
à 623 K :

$$K_{2.1} = \frac{(iC_3H_7OO\cdot)}{(i\cdot C_3H_7)(O_2)} = \frac{k_{2.1}}{k_{-2.1}} = 2{,}2.10^4$$

$$K_{2.1'} = \frac{(ROO\cdot)}{(R\cdot)(O_2)} = \frac{k_{2.1}}{k_{-2.1'}} = 3{,}7$$

Les valeurs des constantes montrent que l'équilibre de la réaction d'oxydation du radical allyle est déplacé, relativement à l'oxydation des autres radicaux alkyle, plutôt dans le sens de la désoxydation. Ceci rejoint donc les conclusions de Benson à propos de l'oxydation des radicaux méthylallyle (3). Ceci confirme aussi des observations récentes de Slagle et Gutman (39).

TABLEAU 10. Mécanisme simplifié d'oxydation du propane



Ces observations nous paraissent également susceptibles de donner une interprétation, au moins qualitative, des caractéristiques spécifiques de l'oxydation du cyclopentane (indice d'octane de recherche de mélange 141) par rapport à d'autres cyclanes, cyclohexane par exemple (indice d'octane recherche 84) (40).

Une étude plus poussée des réactions du radical allylperoxy suggère d'ailleurs que le sort prédominant de ce radical dans la réaction serait le retour au radical allyle par perte d'une molécule d'oxygène et non une isomérisation comme dans le cas de radicaux peroxyalcoyle (25) en accord avec des travaux récents de Slagle et Gutman (39).

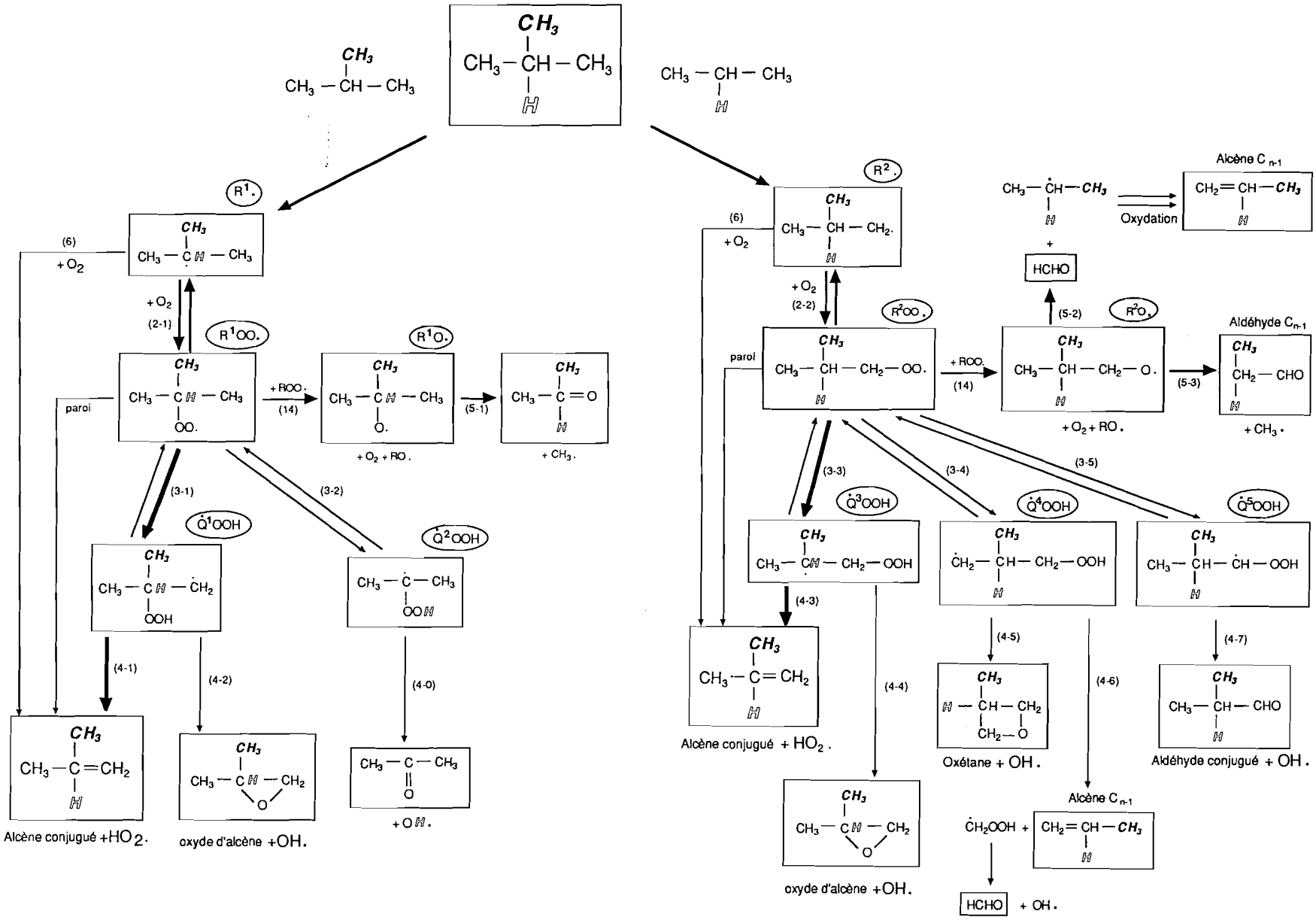
Il paraît ainsi raisonnable de penser que l'oxydation du propène (seul ou en mélange avec C_3H_8) a lieu à la suite de réactions sur la double liaison de la molécule, en particulier de l'addition de radicaux $HO_2\cdot$ et les produits obtenus suggèrent une addition de type anti-Markownikoff (radical $CH_3\text{-}\cdot CH\text{-}CH_2OOH$).

IV. Synthèse des résultats obtenus et comparaison avec l'isobutane

Les résultats expérimentaux que nous avons obtenus et les calculs de Cinétique Thermochimique ont donc conduit à interpréter l'oxydation du propane par le mécanisme présenté dans les tableaux 8 et 9. Comme dans le cas de l'isobutane (1), il apparaît que le propène est formé selon deux processus d'importance voisine après isomérisation des deux radicaux peroxyalcoyle.

Can. J. Chem. Downloaded from www.nrcresearchpress.com by 195.138.81.100 on 09/07/12
For personal use only.

TABLEAU 11. Mécanisme généralisé permettant de rendre compte de l'oxydation de l'isobutane et du propane



Can. J. Chem. Downloaded from www.nrcresearchpress.com by 195.138.81.100 on 09/07/12
For personal use only.

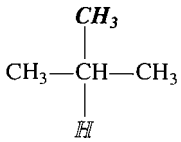
La formation de méthyloxiranne (oxyde de propène) a lieu parallèlement à celle du propène. L'eau oxygénée est produite en quantités notables à partir des radicaux hydroperoxyle $HO_2\cdot$ dont la formation est relativement importante dans les premiers instants de la réaction.

Le schéma réactionnel très simplifié des processus prépondérants est représenté dans le tableau 10. Cette représentation schématique du mécanisme de l'oxydation du propane apparaît très similaire à celle du mécanisme d'oxydation de l'isobutane qui a été présentée dans le mémoire correspondant (1).

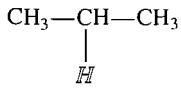
En réalité, si l'on compare de manière plus précise le mécanisme détaillé de l'oxydation de l'isobutane présenté dans notre premier mémoire (1) et le mécanisme détaillé qui figure dans les tableaux 8 et 9 du présent mémoire une nette similitude apparaît. Une comparaison détaillée, par exemple en prenant les processus élémentaires un par un ou même en les regroupant par classes (décomposition, isomérisation, etc...) serait particulièrement fastidieuse.

Nous préférons faire cette comparaison sur une base plus originale en regroupant les mécanismes rendant compte de l'oxydation du propane et de l'isobutane sur un seul tableau, en adoptant une présentation adaptée à cette comparaison.

La molécule de propane et celle d'isobutane sont représentées par la même formule :



Lorsqu'on s'intéresse au propane, la formule correspondante s'écrit



pour passer du propane à l'isobutane, il suffit de remplacer dans la formule générale l'atome d'hydrogène représenté par $\mathcal{H}$ par un groupe méthyle $\boldsymbol{CH_3}$.

En effectuant cette substitution, on s'aperçoit dans le tableau 11 que les deux mécanismes sont remarquablement semblables. Il existe donc une bonne cohérence entre les deux mécanismes d'oxydation présentés : isobutane (1) et propane (présent travail) ce qui conduit ainsi à un schéma général d'oxydation des alcanes légers.

V. Conclusion

En dehors de la généralisation mentionnée ci-dessus, le présent travail, ainsi d'ailleurs que celui effectué sur l'exemple de l'isobutane, souligne l'importance d'allers et retours constants entre l'expérience et le calcul. L'évaluation des constantes de vitesse des processus élémentaires par les méthodes de la Cinétique Thermochimique constitue un guide précieux pour la simplification des schémas réactionnels.

Il aurait pu être intéressant de développer également dans le cadre de ce travail une comparaison plus poussée avec les résultats d'autres auteurs. Cependant cette comparaison est déjà partiellement implicite, en particulier au niveau des estimations des constantes de vitesse et lors de l'utilisation des données de la littérature, le présent mécanisme reprenant fréquemment des réactions élémentaires déjà proposées par d'autres auteurs comme Benson (4, 5), Fish (12) ou Knox (13).

L'aspect original de cette contribution, en dehors de l'utilisation systématique de la Cinétique Thermochimique et de la comparaison interactive avec l'expérience, nous paraît aussi d'avoir toujours insisté sur la nature *primaire* des processus présentés, afin de proposer un mécanisme d'oxydation de l'alcane étudié, et non pas des produits de cette réaction, comme l'alcène conjugué. Un rapide examen d'articles traitant de l'oxydation d'alcanes légers montre que ces préoccupations sont souvent absentes de l'esprit de la plupart des auteurs ayant travaillé dans ce domaine. Les processus écrits ne sont pas toujours des processus élémentaires et la nature, primaire ou secondaire, des produits en résultant est le plus souvent ignorée. Les tentatives de corrélation semi-quantitatives (comparaison entre vitesses de formation des produits et ordre de grandeur des constantes de vitesse) sont généralement inexistantes. C'est également pour cette raison que nous ne nous sommes pas intéressés aux réactions faisant intervenir des flammes froides, où les résultats expérimentaux sont plus spectaculaires, mais où, également, les mécanismes d'oxydation présentent une bien plus grande complexité, ne serait-ce qu'en raison de la non isothermicité de la réaction. Or, pour faire de la cinétique, il est essentiel de maîtriser le paramètre température.

Il nous semble également intéressant de mentionner que, compte-tenu de la complexité des réactions abordées, un certain nombre de points seraient susceptibles de justifier des développements supplémentaires. Il serait certainement intéressant de tenter une simulation de la réaction à partir du schéma que nous proposons. Cependant, les premiers essais que nous avons faits ont montré la complexité d'une telle tâche, complexité pouvant provenir d'une part de l'imprécision des constantes de vitesse et d'autre part de l'insuffisance des méthodes numériques mises en oeuvre dans ces essais.

Des progrès très importants ont certainement été réalisés grâce à des mécanismes complexes comportant un nombre très élevé de processus comme ceux proposés par Dryer et co-auteurs (41) sur l'exemple du *n*-butane. À l'opposé tout en reconnaissant les mérites de tels travaux, P. Gray (30) insiste également sur l'apport très positif de schémas très simples. La présente approche nous paraît un compromis entre ces deux points de vue qui a surtout l'intérêt de mettre en évidence les étapes essentielles permettant de rendre compte de la chimie de la réaction.

Remerciements

Les auteurs remercient la Société ATOCHEM (initialement PCUK) pour l'aide matérielle apportée sous la forme d'une bourse de thèse (B.V.) lors de la réalisation de ce travail.

1. B. Vogin, F. Baronnet et G. Scacchi. Can. J. Chem. **67**, 759 (1989).
2. R. T. Pollard. *Dans* Comprehensive chemical kinetics. Vol. 17. *Éditeurs* : C. H. Bamford et C. F. H. Tipper. Elsevier, Amsterdam. 1977. p. 249.
3. S. W. Benson. *Dans* The mechanisms of pyrolysis, oxidation and burning of organic materials. *Éditeur* : L. A. Wall. NBS Publication, U.S. Government Printing Office, Washington, DC. 1972. p. 121.
4. S. W. Benson et P. S. Nangia. Acc. Chem. Res. **12**, 223 (1979).
5. S. W. Benson. Prog. Energy Combust. Sci. **7**, 125 (1981).
6. S. W. Benson. Oxid. Commun. **2**, 169 (1982).
7. I. A. Ogorodnikov, S. S. Polyak et V. Ya. Shtern. Kinet. Katal. **10**, 1210 (1969).
8. M. M. Aleksishvili, S. S. Polyak et V. Ya. Shtern. Ref. Zh. Khim. Abstr. n° 3, N4 (1972).
9. M. M. Aleksishvili, S. S. Polyak et V. Ya. Shtern. Kinet. Katal. **15**, 290 (1974).

10. C. A. EUKER et J. P. LEINROTH. Combust. Flame, **15**, 275 (1970).
11. R. R. BALDWIN et R. W. WALKER. Combust. Flame, **21**, 55 (1973).
12. A. FISH. Adv. Chem. Ser. **76**, 69 (1968).
13. J. H. KNOX. *Dans* Photochemistry and reaction kinetics. *Éditeurs* : P. G. Ashmore, T. M. Sugden et F. S. Dainton. Cambridge University Press, Cambridge. 1967. p. 250.
14. D. M. NEWITT et L. S. THORNES. J. Chem. Soc. 1656 (1937).
15. J. F. GRIFFITHS, B. F. GRAY et P. GRAY. 13th Symp. (Int.) on Combustion, The Combustion Institute, Pittsburgh, PA. 1971. p. 239.
16. A. ANTONIK et M. LUCQUIN. Combust. Flame, **19**, 311 (1972).
17. F. BARONNET, M. P. HALSTEAD, A. PROTHERO et C. P. QUINN. C.R. Acad. Sci. **275 C**, 17 (1972).
18. S. W. BENSON. Thermochemical kinetics, 2^{e} éd. John Wiley, New York. 1976.
19. M. WEISSMAN, L. G. S. SHUM, S. P. HENEGHEN et S. W. BENSON. J. Phys. Chem. **85**, 2863 (1981).
20. J. C. BROCARD, F. BARONNET et H. E. O'NEAL. Combust. Flame, **52**, 25 (1983).
21. D. F. MACMILLEN et D. M. GOLDEN. Annu. Rev. Phys. Chem. **33**, 493 (1982).
22. M. M. ALEKSISHVILI, S. S. POLYAK et V. YA SHTERN. Kinet. Katal. **17**, 1110 (1976).
23. R. W. WALKER. React. Kinet. **1**, 161 (1975).
24. J. G. ATHERTON, A. J. BROWN, G. A. LUCKETT et R. T. POLLARD. 14th Symp. (Int.) on Combustion, The Combustion Institute, Pittsburgh, PA. 1973. p. 513.
25. B. VOGIN. Thèse de Docteur-Ingénieur, INPL, Nancy (1984).
26. M. H. AMETRANO. Diplôme d'Études Approfondies en Génie des Procédés, Nancy (1987).
27. Y. SIMON, J. F. FOUCAUT et G. SCACCHI. Can. J. Chem. **66**, 2142 (1988).
28. M. C. FLOWERS et R. M. PARKER. J. Chem. Soc. B, 1980 (1971).
29. M. C. FLOWERS et R. M. PARKER. Int. J. Chem. Kinet. **3**, 443 (1971).
30. P. GRAY. Conférence aux Journées de chimie physique, École nationale supérieure de chimie de Paris. 22–24 mai 1989.
31. B. VOGIN, F. BARONNET et J. C. ANDRE. Oxid. Commun. **3**, 51 (1983).
32. B. VOGIN, F. BARONNET et J. C. ANDRE. Anal. Chem. Acta, **142**, 293 (1982).
33. Z. F. SAVAYA. Ph.D. Thèse, Dundee University (1982).
34. S. N. FONER et R. L. HUDSON. Adv. Chem. Ser. **36**, 34 (1962).
35. L. R. SOCHET, N. V. HAI et M. LUCQUIN. Bull. Soc. Chim. Fr. 1571 (1971).
36. N. VAN HAI, S. ANTONIK, L. R. SOCHET et M. LUCQUIN. Bull. Soc. Chim. Fr. 2150 (1970).
37. V. YA. SHTERN. The gas phase oxidation of hydrocarbons. Pergamon Press, Oxford. 1964.
38. C. N. SATTERFIELD et R. C. REID. 5th Symp. (Int.) on Combustion, The Combustion Institute, Pittsburgh, PA. 1955. p. 511.
39. I. R. SLAGLE et D. GUTMAN. 21st Symp. (Int.) on Combustion, The Combustion Institute, Pittsburgh, PA. 1986. p. 875.
40. F. BARONNET. Communication au Congrès Commun des Sections Britannique et Française du Combustion Institute, Rouen, 18–21 avril 1989, Recueil des Actes du Congrès. p. 81.
41. W. J. PITZ, C. K. WESTBROOK, W. M. PROSCIA et F. L. DRYER. 20th Symp. (Int.) on Combustion, The Combustion Institute, Pittsburgh, PA. 1984. p. 831.

Can. J. Chem. Downloaded from www.nrcresearchpress.com by 195.138.81.100 on 09/07/12
For personal use only.

Controlled diastereoselection in 2-lithio-1,3-dithiane additions onto α-substituted γ-lactols. Model studies toward bryostatins from (*R*)-pantolactone

RENÉ ROY[1] AND ALLAN W. REY
Department of Chemistry, University of Ottawa, Ottawa, Ont., Canada K1N 6N5

Received July 30, 1990

RENÉ ROY and ALLAN W. REY. Can. J. Chem. **69**, 62 (1991).

Homochiral α-substituted γ-lactols **3** and **4** derived from (*R*)-pantolactone **1** were used in 2-lithio-1,3-dithiane additions to afford very high controls in diastereoselectivities arising from 1,2-asymmetric inductions. Thus non-chelation controlled nucleophilic addition on **3** gave the *anti* diastereomer **5** as the major product (92% de), while the chelation controlled addition on **4** furnished the *syn* diastereomer **7** (96% de) as the almost exclusive product. The stereochemical outcomes of these reactions were proven unambiguously by locking the conformation of the *syn*- and *anti*-triol adducts **7** and **8** through their respective acetonides and by nuclear Overhauser enhancement measurements. The lack of 1,3-dioxolane formation in the case of the *anti*-triol **8** was taken as a further confirmation of the absolute configuration at the newly created stereocenter.

Key words: byrostatin, pantolactone, α-hydroxylactol, dithiane.

RENÉ ROY et ALLAN W. REY. Can. J. Chem. **69**, 62 (1991).

Les γ-lactols homochirals **3** et **4** α-substitués dérivés de la (*R*)-pantolactone **1** ont été utilisés dans des réactions d'additions avec le carbanion lithié du 1,3-dithiane pour fournir un très haut contrôle diastéréosélectif provenant d'une induction asymétrique-1,2. Le stéréocontrôle de l'addition nucléophilique sur **3** en l'absence de phénomène de chélatation a donné le diastéréomère *anti* **5** comme produit majeur tandis que la chélatation comme moyen de stéréocontrôle de l'addition nucléophilique sur **4** a conduit presque exclusivement au diastéréomère *syn* **7** comme produit final. Les résultats stéréochimiques de ces réactions ont été prouvés de façon non-ambigüe en fixant la conformation des adduits *syn*- et *anti*-triol **7** et **8** par la formation de leurs dérivés acétals respectifs et par des mesures d'effets nOe. L'absence de formation de 1,3-dioxolane dans le cas du triol-*anti* **8** a été considérée comme preuve supplémentaire de la configuration absolue au nouveau centre stéréogénique formé.

Mots clés : byrostatine, pantolactone, α-hydroxylactol, dithiane.

Can. J. Chem. Downloaded from www.nrcresearchpress.com by 195.138.81.100 on 09/07/12
For personal use only.

Introduction

During synthetic endeavors (1–3) toward the construction of the antineoplastic macrolides bryostatins (4), chiral fragments containing quaternary *gem*-dimethyl carbon centers were required. Within the chiral pool, (*R*)-pantolactone **1** was sought as a useful chiral template. As such, **1** has scarcely been utilized for the enantiomeric synthesis of complex natural products (5, 6). On the other hand, **1** and its (*S*)-enantiomer (7) have received increased interest as chiral auxiliaries in asymmetric Diels–Alder cycloadditions (7, 8) and in diastereoselective ketene protonations (9).

Although there have been numerous examples of 1,2-induction in acyclic stereoselections (10), examples of similar or remote inductions in γ- or δ-lactols have received limited attention (11). We wish to describe herein the results obtained with 2-lithio-1,3-dithiane additions onto α-substituted γ-lactols. The effects of 1,2-chelation and non-chelation on the diastereoselectivities will be evaluated. The above findings should provide important clues for the choice of (*R*)-pantolactone derived chiral templates.

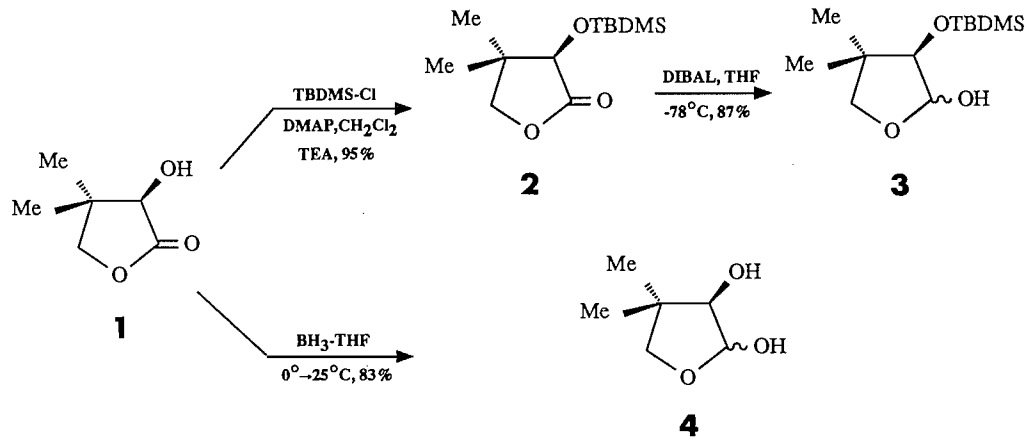
Results and discussion

2-Lithio-1,3-dithiane additions onto 3 and 4

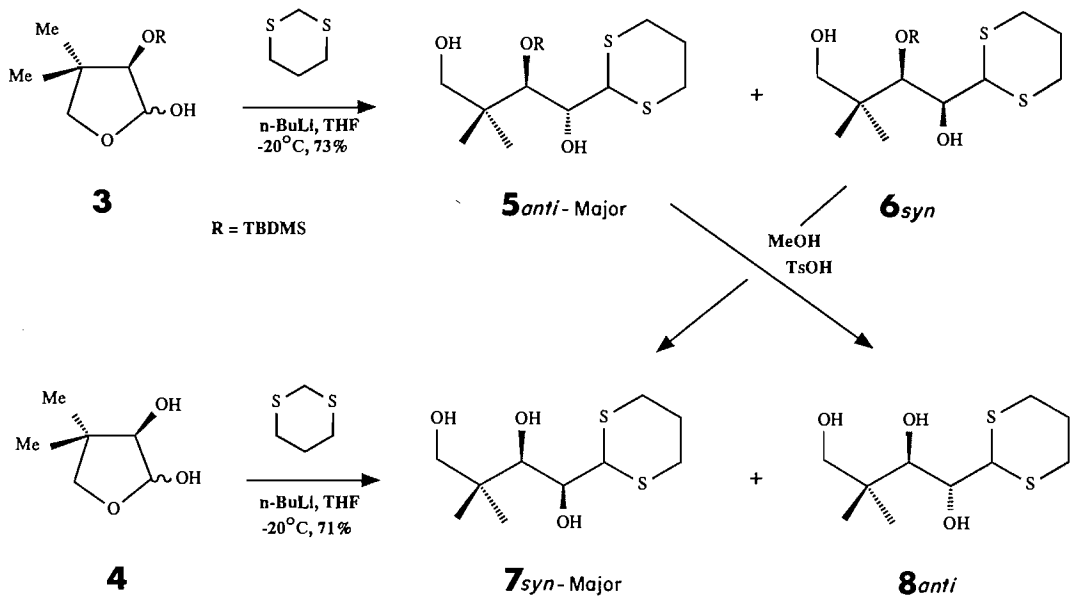
To evaluate the extent of the asymmetric induction onto homochiral α-substituted γ-lactols, we required derivatives **3** and **4**. The silyl ether protecting group was chosen because it has been clearly established as a non-chelating group in nucleophilic addition assisted by Lewis acid (12). Thus, we anticipated good *syn*/*anti* complementary diastereoselection upon addition of 2-lithio-1,3-dithiane on **3** and **4** since the α-hydroxylactol derivative **4**, as opposed to **3**, should allow strong 1,2-chelation. First, protection of the hydroxyl group of (*R*)-pantolactone **1** as its *tert*-butyldimethylsilyl ether in the usual manner (TBDMSiCl, CH_2Cl_2, DMAP) furnished the crystalline lactone **2** in 95% yield. Reduction of the lactone with diisobutylaluminum hydride (DIBAH, THF, −78°C) afforded the lactol **3** (87%) as an anomeric mixture (2.3:1). When the above reduction was attempted in toluene, over-reduction occurred to a large extent. Attempts to reduce the α-hydroxylactone **1** to the γ-lactol **4** under a similar set of conditions (DIBAH/THF or toluene) inevitably gave the triol as the major product. Reduction with slightly acidic (H_2SO_4) sodium borohydride (13) also gave the triol as the major product. Finally, controlled reduction to the lactol **4** was achieved using borane–THF complex (83%) (14) (Scheme 1).

Metalation of 1,3-dithiane according to Seebach and Corey (15) (*n*-BuLi, THF, −20°C, 2 h) and subsequent addition of the resulting 2-lithio-1,3-dithiane onto **3** afforded a mixture of *anti* and *syn* adducts **5** and **6** with very high diastereoselectivity in favour of the predicted *anti* diastereomer **5** (73% yield) (Scheme 2). Due to the complexity of the ^{1}H NMR spectrum of the crude reaction mixture, the ratio of **5** to **6** was assessed from the ^{1}H NMR spectra of the unprotected triols **7** and **8** obtained by acidic methanolysis of the crude mixture (MeOH, TsOH, ~quant.). The relative integration for the dithianyl protons (identified as H1′) at 4.04 ppm ($J_{1',1}$ = 8.8 Hz) for the *syn* diastereomer **7** and at 4.55 ppm ($J_{1',1}$ = 2.7 Hz) for the *anti* and major diastereomer **8** indicated an *anti* to *syn* (**5**,**8**:**6**,**7**) ratio (*vide infra*) of 96:4 (92% de). The same ratio was obtained from the integrations of the chemical shifts of the H2 protons at 3.79 ppm ($J_{1,2}$ ~ 0 Hz) for **7** and at 3.58 ppm ($J_{1,2}$ = 8.4 Hz) for **8**. The small coupling constant (~0 Hz) between H1 and H2 in **7** (*syn*) and the larger one (8.4 Hz) for the same protons in **8** (*anti*) was diagnostic of the absolute stereochemistries of the diastereomers based upon previous empirical rules with aldol adducts (16). For instance, when seen as a Newman projection,

[1]Author to whom correspondence may be addressed.



SCHEME 1



SCHEME 2

the conformer **7**-*A* should be preferred over conformer **7**-*B* because of a dominant unfavourable interaction between the dithiane residues (Di) and the neopentyl group (R), thus bringing the H1 and H2 protons into a *gauche* relationship (<~60°, $J_{1,2} \sim 0$ Hz). Likewise the conformer **8**-*A* should be favoured over **8**-*B* for similar reasons, thus bringing the H1 and H2 protons into an *anti* relationship (<~180°, $J_{1,2} = 8.4$ Hz). A third rotamer for each of the above Newman projections was not accounted for, since they would be equivalent to the unfavourable rotamers **7**-*B* and **8**-*B* with the dithianyl and neopentyl groups in *gauche* relationships (Fig. 1).

When the above 2-lithio-1,3-dithiane addition was effected onto the unprotected α-hydroxylactol **4**, a high stereocontrol for the reversed diastereofacial selectivity was achieved based on α-chelation (1,2-induction) (Scheme 2). Indeed, the *syn* diastereomer **7** was obtained as the major product (71%) after silica gel chromatography, together with a small amount of the *anti* diastereomer **8**. The ratio of *syn*-**7** to *anti*-**8** was also determined from the ^{1}H NMR spectrum of the crude reaction mixture, which indicated a ratio of *syn*/*anti* of 98:2 (96% de) (Table 1).

Determination of the absolute stereochemistries of 7 and 8

The coupling constants between the protons at the two

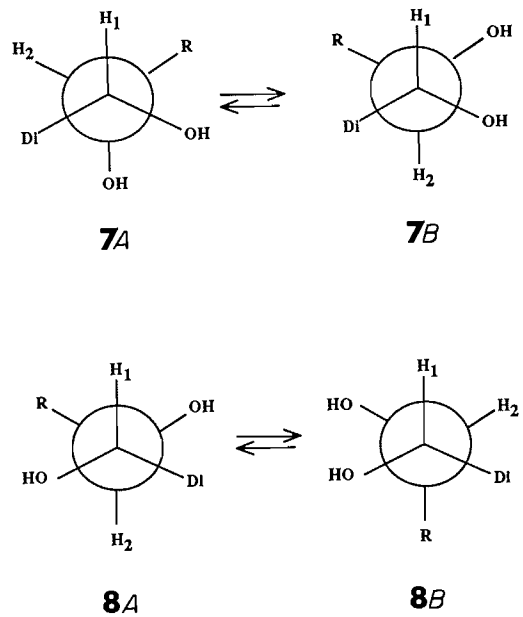
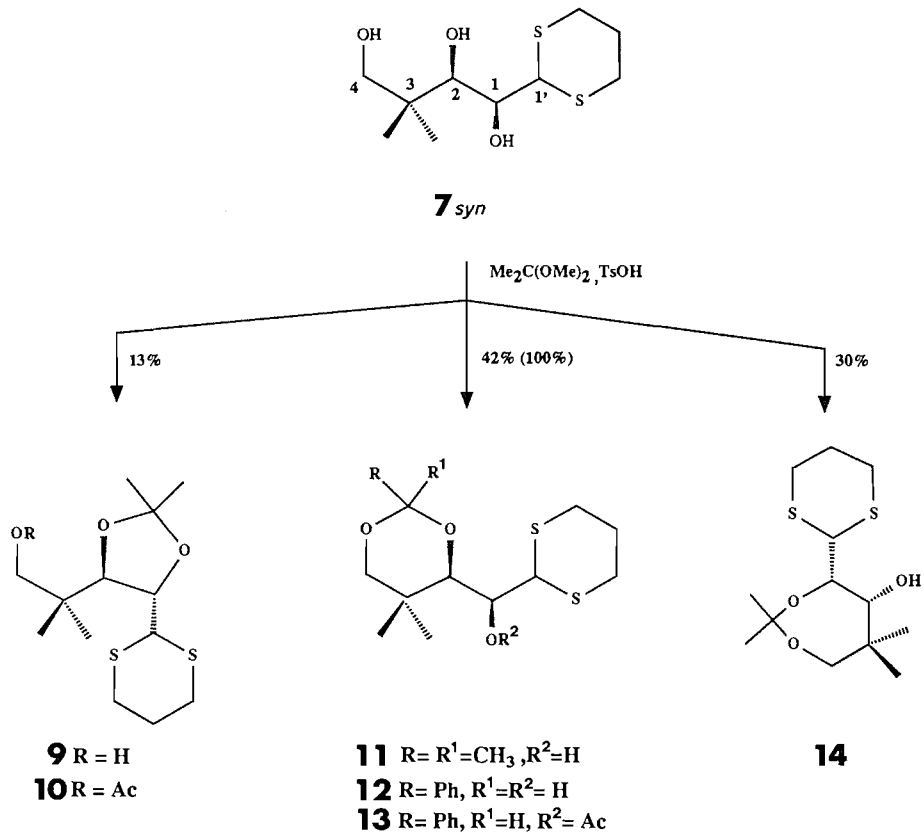


FIG. 1

Can. J. Chem. Downloaded from www.nrcresearchpress.com by 195.138.81.100 on 09/07/12
For personal use only.



SCHEME 3

TABLE 1. Results of the addition of 2-lithio-1,3-dithiane onto **3** and **4**

			δ ppm (Hz)[a]		
γ-Lactol	Yields	*anti*/*syn*	*H1'*	H1 ($J_{1',1}$)	H2 ($J_{1',2}$)
3	**5(8)** (73%)	96 : 4	4.55[b]	3.93 (2.7)	3.58 (8.4)
4	**7** (71%)	2 : 98	4.04	3.93 (8.8)	3.79 (~0)

[a]Taken at 300 MHz in $CDCl_3$.
[b]For free *anti*-triol **8**.

stereocenters did not allow unambiguous determination of the absolute chirality at the newly created stereogenic center. Therefore, to obtain confirmation of the diastereofacial selectivities, a series of transformations was initiated in order to lock the conformation of the acyclic adducts. To achieve this goal, we elected to tether the C-1 and C-2 hydroxyl groups through formation of their respective 1,3-dioxolanes, following Gerlach's strategy (17). It was expected that proton nuclear Overhauser enhancement (nOe) studies would provide definitive establishment of the C-1 chirality.

Thus, the anticipated *syn* adduct **7** was first subjected to standard acetonation conditions (2,2-dimethoxypropane, TsOH, benzene, 25°C, 18 h). An unexpected mixture of acetonides was obtained. Further studies revealed that three regioisomeric acetonides **9**, **11**, and **14**, which could be separated by silica gel chromatography, were produced in 13%, 42%, and 30% yields respectively (Scheme 3). Equilibration to the expected thermodynamic 1,3-dioxolane **9** was apparently slow under the above experimental conditions. However, later experimentation demonstrated that this equilibration was significantly faster when acetone and TsOH alone were used. In this case, exclusive

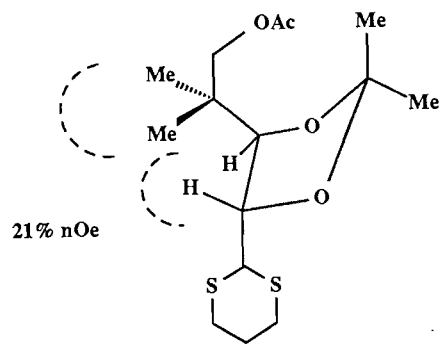


FIG. 2

formation of **9** occurred in only 3 h at room temperature (Scheme 3). The regioselectivity of the 1,3-dioxolane **9** was confirmed by acetylation of the remaining primary hydroxyl group (Ac_2O, pyridine, 92%). This resulted in an expected downfield shift (~0.5 ppm) of the diastereotopic C-4 methylene protons of **10** (3.97 and 3.86 ppm) relative to those of **9** (3.47 and 3.42 ppm). ^1H NMR nOe experiments demonstrated that, for the acetylated 1,3-dioxolane **10**, there was a 21% intensity enhancement between the H-1 proton (dd at 4.14 ppm) and the *gem*-dimethyl protons (2 s at 0.96 and 0.99 ppm). This observed nOe is only consistent with the proposed (1*S*,2*R*)-1,2-*syn* stereochemistry. No nOe should result in the *anti* configuration (Fig. 2).

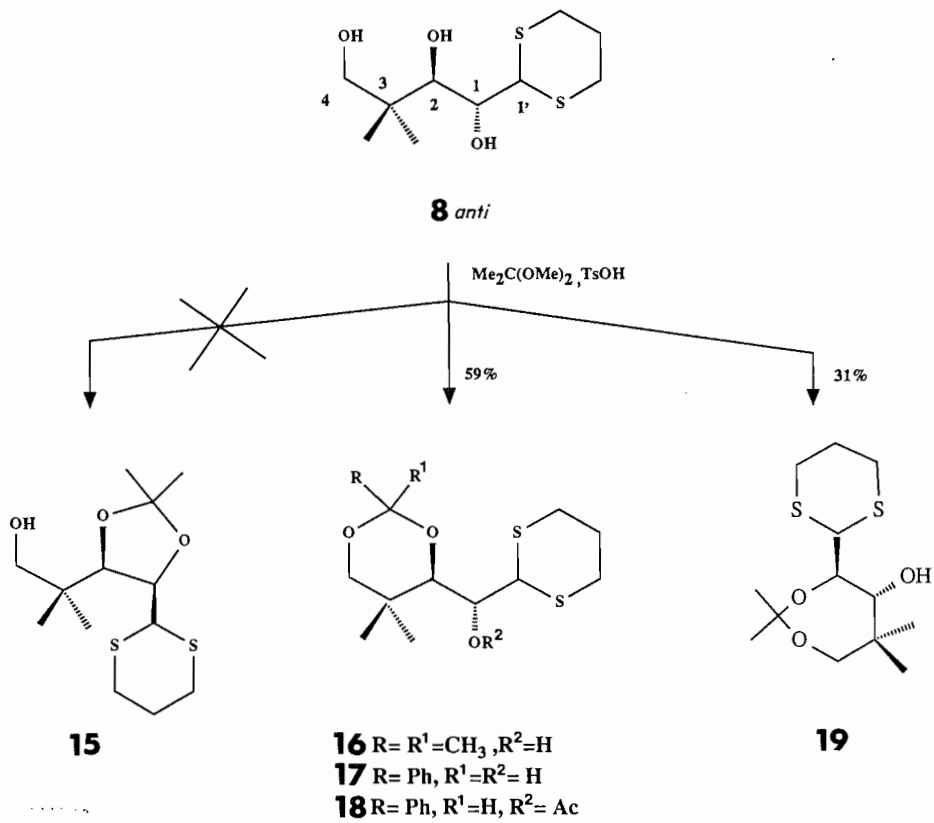
The identity of the 1,3-dioxane acetonide **11** was determined by comparing its ^1H NMR spectral data to those of its related benzylidene acetal **12**. The pertinent ^1H NMR data are given in

Can. J. Chem. Downloaded from www.nrcresearchpress.com by 195.138.81.100 on 09/07/12
For personal use only.

TABLE 2. Selected chemical shifts (ppm) and coupling constants (Hz) for the acetals

Parent triol	Acetal	H1′[a]	H1	H2
syn-**7**	**9**	4.12 ($J_{1',1}$ 4.6)	4.11 (4.6, ~0)	4.12 ($J_{1,2}$ ~0)
	11	4.12 ($J_{1',1}$ 6.6)	3.80 (6.6, ~0)	3.93 ($J_{1,2}$ ~0)
	12	4.23 ($J_{1',1}$ 6.6)	3.90 (6.6, ~0)	3.95 ($J_{1,2}$ ~0)
	14	4.38 ($J_{1',1}$ 10.2)	3.98 (10.2, ~0)	3.55 ($J_{1,2}$ ~0)
anti-**8**	**16**	4.52 ($J_{1',1}$ 1.9)	3.82 (1.9, 8.9)	3.70 ($J_{1,2}$ 8.9)
	17	4.59 ($J_{1',1}$ 1.8)	3.96 (1.8, 9.0)	3.74 ($J_{1,2}$ 9.0)
	19	4.45 ($J_{1',1}$ 2.7)	3.97 (2.7, 9.2)	3.35 ($J_{1,2}$ 9.2)[b]

[a]H1′ refers to the 2-dithianyl proton.
[b]Observed $J_{2,OH}$ = 5.6 Hz.



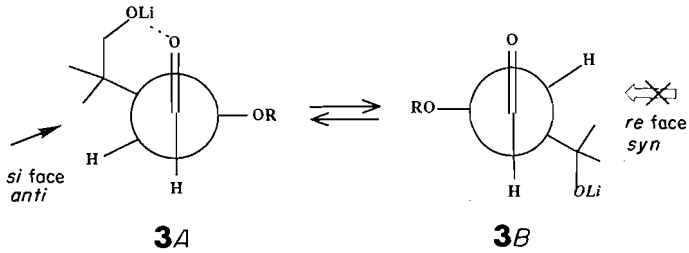
SCHEME 4

Table 2. The six-membered benzylidene acetal **12** formed between the C-2 and C-4 hydroxyl groups of the *syn*-triol **7** was the sole product obtained upon *trans*-acetalization of **7** with benzaldehydedimethylacetal (TsOH, benzene, 1 h, 25°C, 87%). The structure of **12** was further confirmed by acetylation of the remaining secondary C-2 hydroxyl group (Ac_2O, DMAP, pyridine, 86%).

When the expected *anti*-triol **8** was exposed to the same acetonide-forming conditions described above for the *syn*-triol **7** (2,2-dimethoxypropane, TsOH, 18 h, 90%), only two products were obtained in a ratio of 2:1 (Scheme 4). They were assigned structures **16** (59%) and **19** (31%) following similar arguments and derivatization (Ac_2O, pyridine) to those described above. No 1,3-dioxolane product corresponding to **15** was obtained. The only valid explanation for the lack of formation of the five-membered acetonide **15** is that it would require an unfavourable *cis* orientation of both the *gem*-dimethyl and the 1,3-dithiane substituents. Inspection of Dreiding models illustrates that this situation would be extremely sterically demanding, hence this product was not formed. This offers further evidence for the absolute stereochemistry at C-1.

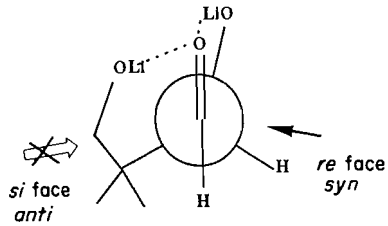
Again, the structure of the 1,3-dioxane acetonide **16** was confirmed by comparison of its coupling patterns and chemical shifts to the analogous six-membered benzylidene acetal **17** ($PhCH(OMe)_2$, TsOH, benzene, 84%). Table 2 gives the relevant ^1H NMR data. Acetylation of the benzylidene acetal **17**

Can. J. Chem. Downloaded from www.nrcresearchpress.com by 195.138.81.100 on 09/07/12
For personal use only.



3A 3B

FIG. 3



4

FIG. 4

(Ac_2O, DMAP, pyridine, 74%), as described above for **12**, demonstrated that the secondary C-1 hydroxyl group was, as expected, free.

Rationale for the observed diastereoselection

Felkin–Anh modification (18) of the Cram model (19) can provide a satisfactory explanation for the observed diastereoselection in the non-chelated situation with **3**. Indeed, as shown by the Newman projections (Fig. 3), conformer **3**-*A* of the protected γ-lactol **3** should be favoured over conformer **3**-*B* for the nucleophilic attack on the *si* face of the carbonyl following the Bürgi–Dunitz (20) trajectory. The *re*-face attack on conformer **3**-*B* is hindered by the neo-pentyl function. If one would consider the bulky neopentyl group as the one perpendicular to the carbonyl group, the reversed diastereoselection would have been obtained. It is also conceivable that the high diastereoselection obtained through conformer **3**-*A* might have been assisted by an added interplay of 1,4-chelation with the neopentylic alkoxide. The above results indicate that the more polar silyloxy protecting group might override the bulkier neopentyl group in its perpendicular arrangement to the carbonyl group in order to maximize electronic effect (σ*-orbital energies).

This situation may be contrasted to the one obtained from the unprotected γ-lactol **4** in which strong 1,2-chelation (and possibly added 1,4-chelation) surely favours *re*-face attack to provide the *syn*-triol adduct **7** as the almost exclusive diastereomer formed (Fig. 4).

In conclusion, good yields and a high degree of diastereoselection have been obtained in 2-lithio-1,3-dithiane additions onto both α-protected and α-unprotected γ-lactols. The absolute stereochemistry of the diastereomers has been unequivocally established using nOe measurements on locked conformers using acetal formations. These model studies are being used for the construction of bryostatin fragments (2). Moreover, it is also of interest to mention that there are only limited examples of diastereoselections in α-substituted γ-lactols. An interplay of 1,2- and possibly 1,4-chelation has been invoked to explain the stereochemical outcome of the nucleophilic additions observed during this study. Further work is in progress to delineate the above factors.

Experimental

Melting points were determined on a Gallenkamp apparatus and are uncorrected. The ^1H and ^{13}C NMR spectra were recorded on a Varian XL-300 or a Varian Gemini 200 spectrometer at 300 and 200 MHz respectively for protons and at 75.4 and 50.3 MHz respectively for carbons. The proton chemical shifts (δ) are given relative to internal Me_4Si (δ = 0) for $CDCl_3$ solutions. The carbon chemical shifts are given relative to deuterochloroform at 77.0 ppm. The analyses were done as a first-order approximation. Optical rotations were measured on a Perkin Elmer 241 polarimeter and were run at room temperature (~25°C). IR spectra were taken in chloroform using a Perkin Elmer 783 spectrophotometer. Mass spectra were recorded on a VG 7070-E spectrometer for CI and EI. Elemental analyses were performed by Guelph Chemical Laboratories Ltd. (Ont.) or M-H-W Laboratories (Phoenix, AZ). Thin-layer chromatography (TLC) was performed using silica gel 60-F254 plates and column chromatography on silica gel 60 (230–400 mesh, E. Merck No. 9385). The developed plates were sprayed or dipped with a solution of ceric sulfate (1%) and ammonium molybdate (2.5%) in 10% aqueous sulfuric acid and heated at ~150°C. Purifications by Chromatotron were performed on a Harrison Research Chromatotron model 7924 using silica gel 60-F254 rotors (1, 2, or 4 mm thickness). (*R*)-(−)-Pantolactone (Aldrich) was dried in a Dean–Stark apparatus using benzene as solvent. All solvents and reagents used were reagent grade and, when required, further purifications were accomplished following published procedures (21). Titrations of the organolithium reagents were done using diphenylacetic acid (22).

(R)-[(tert-Butyldimethylsilyl)oxy]pantolactone 2

To a solution of dry (*R*)-pantolactone (**1**) (2.00 g, 15.4 mmol) in dichloromethane (40 mL) was added triethylamine (2.69 mL, 19.3 mmol), *tert*-butyldimethylsilyl chloride (2.79 g, 18.5 mmol), and DMAP (0.39 g, 3.2 mmol). After stirring for 1 day at room temperature, the mixture was diluted with ether (100 mL) and washed with 0.2 N HCl, saturated aqueous $NaHCO_3$, and brine (50 mL of each). The organic layer was dried over Na_2SO_4 and concentrated *in vacuo*. The white amorphous residue was recrystallized in hexanes, yielding 3.76 g (95%) of the silyl ether **2** as white needles melting at 95.6–96.3°C; $[\alpha]_D$ +33.8° (*c* 1.0 in $CHCl_3$); IR (CH_2Cl_2) ν_{max}: 3050, 2959, 2858, 2302, 1791, 1252, 1132 cm^{-1}; ^1H NMR (300 MHz) δ: 3.97 (d, A of AB, J = 8.9 Hz, 1H, H4), 3.97 (s, 1H, H2), 3.86 (d, B of AB, J = 8.9 Hz, 1H, H4'), 1.12 (s, 3H, *gem* CH_3), 1.03 (s, 3H, *gem* CH_3), 0.91 (s, 9H, $C(CH_3)_3$), 0.18 (s, 3H, $SiCH_3$), 0.11 (s, 3H, $SiCH_3$); ^{13}C NMR (50.4 MHz) δ: 176.9 (C1), 76.5 (C2), 75.5 (C4), 40.7 (C3), 25.4 ($C(CH_3)_3$), 22.7, 18.8 (*gem* CH_3's), 18.0 ($SiC(CH_3)_3$), −4.8, −5.7 ($Si(CH_3)_2$); MS (EI) *m/z*: 187 (M^+−57, 20%), 143 (M^+−101, 35%). HRMS calcd. for $C_8H_{15}O_3Si$ (M^+−$C(CH_3)_3$): 187.0791; found: 187.0796.

(R)-[(tert-Butyldimethylsilyl)oxy]pantolactol 3

The silylated γ-lactone **2** (1.91 g, 7.81 mmol) was dissolved in THF (30 mL) and cooled to −78°C. Diisobutylaluminum hydride (1.0 M in THF, 10.9 mL, 10.9 mmol) was added over a 15 min period via a pressure-equalizing addition funnel. This mixture was stirred for 3 h and then quenched by addition of Glauber's salt ($Na_2SO_4 \cdot 10H_2O$, ~6 g). After warming to ambient temperature, the Glauber's salt was removed by filtration under suction. The filter cake was returned to the flask and refluxed with 50 mL of ethyl acetate (5 min), and filtered. This procedure was repeated with another 50 mL of ethyl acetate. The filtrates were combined and washed with 0.2 N HCl (2 × 50 mL), saturated aqueous $NaHCO_3$ (50 mL), and brine (50 mL), dried over Na_2SO_4, and concentrated *in vacuo* to yield a white amorphous solid. Purification by silica gel flash chromatography (2:8 ether/hexanes) and recrystallization from hexanes afforded 1.67 g (87%) of the silylated γ-lactol **3** as white needles melting at 48.5–51.5°C. When different,

Can. J. Chem. Downloaded from www.nrcresearchpress.com by 195.138.81.100 on 09/07/12
For personal use only.

Can. J. Chem. Downloaded from www.nrcresearchpress.com by 195.138.81.100 on 09/07/12
For personal use only.

data for the minor anomer (2.3:1 anomeric ratio) are given in brackets; $[\alpha]_D$ −13.3° (*c* 2.0 in $CHCl_3$); IR (CH_2Cl_2) ν_{max}: 3591, 3050, 2959, 2931, 2859, 1472, 1256, 1048 cm^{-1}; ^1H NMR (300 MHz) δ: 5.12 (app t, OH coupling, 1H, H1), 5.35 (dd, *J* = 4.2, 9.8 Hz, 1H, H1), (3.82) (d, *J* = 9.8 Hz, 1H, H2), 3.76 (d, A of AB, *J* = 8.2 Hz, 1H, H4), 3.64 (d, <1 Hz, 1H, H2), 3.63 (d, B of AB, *J* = 8.2 Hz, 1H, H4′), (3.60) (s, 2H, H4), 1.03 (s, 3H, *gem* CH_3), 0.97 (s, 3H, *gem* CH_3), 0.88 (0.92) (s, 9H, $C(CH_3)_3$), 0.07, 0.05 (0.10, 0.08) (s, 6H, $Si(CH_3)_2$); ^{13}C NMR (50.4 MHz) δ: 98.0 (104.6) (C1), 79.2 (85.5) (C2), 76.3 (78.4) (C4), 42.0 (42.1) (C3), 25.6 ($C(CH_3)_3$), 25.4, 19.9 (23.6, 19.9) (gem CH_3's), 18.0 (17.9) ($SiC(CH_3)_3$), −5.4 (−4.8) ($Si(CH_3)_2$). MS (CI ether) *m/z*: 247 (M^++1, 1%), 229 ((M^++1)-18, 100%), 189 (M^+−57, 23%). Anal. calcd. for $C_{12}H_{26}O_3Si$: C 58.49, H 10.63, Si 11.40; found: C 58.45, H 10.59, Si 11.33.

(R)-(−)-Pantolactol ***4***

Over a period of 1 h, borane–tetrahydrofuran complex (1.0 M in THF) was added to (*R*)-(−)-pantolactone (**1**) (6.00 g, 46.1 mmol) in THF (100 mL) at 0°C. After stirring for 12 h at room temperature, the reaction was quenched by careful addition of water until the evolution of hydrogen had ceased. The solvent was then removed *in vacuo* to leave a colourless syrup. Several coevaporations with 60 mL of a 2% acetic acid in methanol solution were accomplished, followed by silica gel flash chromatography (7:3 ether/hexanes). This yielded the hydroxy γ-lactol **4** (5.00 g, 82%) as a colourless oil. When different, the data for the minor anomer (1.4:1 anomeric ratio) are given in brackets; $[\alpha]_D$ −2.7° (*c* 2.2 in $CHCl_3$); IR (thin film) ν_{max}: 3395, 2971, 2881, 1471, 1382, 1031 cm^{-1}; ^1H NMR (200 MHz) δ: 5.41–5.47 (5.21–5.26) (m, 1H, H1), (3.82) (d, A of AB, *J* = 8.4 Hz, 1H, H4), 3.73) (d, B of AB, *J* = 8.4 Hz, 1H, H4′), 3.66 (d, A of AB, *J* = 8.1 Hz, 1H, H4), 3.62–3.69 (m, 1H, H2), 3.45 (d, B of AB, *J* = 8.1 Hz, 1H, H4′), 2.85–2.91 (2.51–2.61) (br s, 1H, OH exchangeable), 1.06, 1.04 (1.10, 1.06) (s, 6H, *gem* CH_3's); ^{13}C NMR (50.4 MHz) δ: 97.5 (103.4) (C1), 78.2 (84.1) (C2), 77.2 (78.5) (C4), 41.5 (41.6) (C3), 25.4, 19.5 (23.7, 19.3) (*gem* CH_3's); MS (CI ether) *m/z*: 133 (M^++1, 15%), 131 (M^+−1, 8%), 115 ((M^++1)-18, 96%). Anal. calcd. for $C_6H_{12}O_3$: C 54.53, H 9.15; found: C 54.34, H 8.97.

*(1R,2R)-1,2-*anti*-3,3-Dimethyl-1-(1,3-dithian-2-yl)-2-[(*tert*-butyldimethylsilyl)oxy]-1,4-butanediol* ***5***

To 1,3-dithiane (1.26 g, 10.5 mmol, purified by vacuum sublimation) in THF (30 mL) at 20°C was added *n*BuLi (1.5 M in hexane, 7.00 mL, 10.5 mmol) and the solution was stirred for 2 h, whereupon a solution of the silylated γ-lactol **3** (1.03 g, 4.18 mmol) in THF (5 mL) was added via canula. The mixture was stirred a further 2 h and then placed in the refrigerator (−10°C) for 18 h, whereupon it was quenched by addition of 2 mL of saturated aqueous NH_4Cl and allowed to warm to room temperature. The solution was then diluted with ethyl acetate (80 mL) and extracted with 0.2 N HCl (30 mL), saturated aqueous $NaHCO_3$ (30 mL), and brine (30 mL), dried over Na_2SO_4, and concentrated *in vacuo* to provide a syrup. Further purification by flash chromatography (4:6 ether/hexanes) yielded 1.12 g (73%) of the diol adduct **5** as a colourless syrup; $[\alpha]_D$ −6.2° (*c* 1.8 in $CHCl_3$); ^1H NMR (300 MHz) δ: 4.30 (d, *J* = 5.9 Hz, 1H, H1′), 3.90 (dd, *J* = 5.1, 5.9 Hz, 1H, H1), 3.84 (d, *J* = 5.1 Hz, H2), 3.61 (d, A of AB, *J* = 11.3 Hz, 1H, H4), 3.35 (d, B of AB, *J* = 11.3 Hz, 1H, H4′), 2.66–2.96 (m, 4H, $CH_2(CH_2S)_2$), 2.41–3.00 (br s, 2H, OH exchangeable), 1.88–2.16 (m, 2H, $CH_2(CH_2S)_2$), 1.04, 0.93 (s, 6H, *gem* CH_3's), 0.92 (s, 9H, $C(CH_3)_3$), 0.18, 0.11 (s, 6H, $Si(CH_3)_2$); MS (CI ether) *m/z*: 367 (M^++1, 1%), 329 (M^+−37, 83%).

*(1S,2R)-1,2-*syn*-3,3-Dimethyl-1-(1,3-dithian-2-yl)-1,2,4-butanetriol* ***7***

This material was prepared using a procedure similar to the one described above for the conversion of **3** to **5**. Thus, the 2-hydroxy γ-lactol (**4**) (0.44 g, 3.33 mmol) when treated with 2-lithio-1,3-dithiane (11.7 mmol) yielded, after purification by flash chromatography (6:4 ether/hexanes), 0.60 g (71%) of the *syn*-triol adduct **7** as a white solid melting at 63.0–64.5°C; $[\alpha]_D$ −36.4° (*c* 2.5 in $CHCl_3$); ^1H NMR (300 MHz) δ: 4.04 (d, *J* = 8.8 Hz, 1H, H1′), 3.93 (d, *J* = 8.8 Hz, 1H, H1), 3.79 (s, 1H, H2), 3.63 (d, A of AB, *J* = 11.4 Hz, 1H, H4), 3.34 (d, B of AB, *J* = 11.4 Hz, 1H, H4′), 2.71–3.00 (br s, 3H, OH exchangeable), 2.62–2.93 (m, 4H, $CH_2(CH_2S)_2$), 1.99–2.07 (m, 2H, $CH_2(CH_2S)_2$), 1.00, 0.95 (s, 6H, *gem* CH_3's); MS (CI ether) *m/z*: 253 (M^++1, 92%), 235 ((M^++1)-18, 73%), 149 (M^+−103, 68%), 133 (M^+−119, 64%).

*(1R,2R)-1,2-*anti*-3,3-Dimethyl-1-(1,3-dithian-2-yl)-1,2,4-butanetriol* ***8***

The silyl ether **5** (0.96 g, 2.62 mmol) was dissolved in methanol (30 mL), catalytic TsOH (~10 mg) was added, and the solution was stirred at ambient temperature for 5 h. At this point, TLC (ether) indicated the reaction to be complete and it was subsequently processed by addition of an excess of Dowex 1-X8 resin in the ^-OH form, filtration, and removal of solvent *in vacuo* to yield a resinous material. This was further purified by flash chromatography (7:3 ether/hexanes) to provide a quantitative yield (0.66 g) of the triol adduct **8** as a solid melting at 108.0–109.1°C; $[\alpha]_D$ −33.3° (*c* 2.5 in $CHCl_3$); ^1H NMR (300 MHz) δ: 4.55 (d, *J* = 2.7 Hz, 1H, H1′), 3.93 (dd, *J* = 2.7, 8.4 Hz, 1H, H1), 3.58 (d, *J* = 8.4 Hz, 1H, H2), 3.54 (d, A of AB, *J* = 11.3 Hz, 1H, H4), 3.45 (d, B of AB, *J* = 11.3 Hz, 1H, H4′), 2.86–3.01 (m, 4H, $CH_2(CH_2S)_2$), 2.52–2.79 (br, s, 3H, OH exchangeable), 1.85–2.14 (m, $CH_2(CH_2S)_2$), 1.04, 0.93 (s, 6H, *gem* CH_3's); MS (EI) *m/z*: 149 (M^+−103, 6%); MS (CI ether) *m/z*: 253 (M^++1, 24%), 235 ((M^++1)-18, 11%), 149 (M^+−103, 20%), 133 (M^+−119, 27%).

Acetonide formation on the syn*-triol* ***7***

Triol **7** (0.89 g, 3.53 mmol) was dissolved in 10 mL of a 40% 2,2-dimethoxypropane in benzene solution containing a catalytic amount of TsOH (~15 mg) and the solution was stirred at ambient temperature. After overnight contact, the reaction mixture was neutralized by the addition of triethylamine and the solvent was evaporated under vacuum. The residue was diluted in ethyl acetate (40 mL) and washed with 0.2 N HCl, saturated aqueous $NaHCO_3$, and brine (30 mL portions). Drying over Na_2SO_4 and concentration *in vacuo* afforded a colourless oil. Purification by preparative TLC (1:1 ether/hexanes) yielded three products: 0.13 g (13%) of **9**, 0.43 g (42%) of **11**, and 0.31 g (30%) of **14** (five, six-, and seven-membered ring acetonides, respectively) as colourless oils. The order of polarity in the above solvent was (R_F): **14**(0.33), **9**(0.38), **11**(0.50). Submitting triol **7** (55.6 mg, 0.221 mmol) to the acetonide-forming conditions acetone/catalytic TsOH (25°C) afforded the thermodynamic 1,3-dioxolane acetonide **9** as the exclusive product after 3 h (85%).

*(1S,2R)-1,2-*syn*-1,2-O-Isopropylidene,3,3-dimethyl-1-(1,3-dithian-2-yl)-4-butanol* ***9***: ^1H NMR (300 MHz) δ: 4.12 (d, *J* = 4.6 Hz, 1H, H1′), 4.13 (s, 1H, H2), 4.11 (d, *J* = 4.6 Hz, 2H, H1), 3.47 (d, A of AB, *J* = 11.2 Hz, 1H, H4), 3.42 (d, B of AB, *J* = 11.2 Hz, 1H, H4′), 2.77–3.00 (m, 4H, $CH_2(CH_2S)_2$), 1.95–2.20 (br, s, 1H, OH exchangeable), 1.92–2.17 (m, 2H, $CH_2(CH_2S)_2$), 1.46, 1.40 (s, 6H, $(RO)_2C(CH_3)_3$), 0.98, 0.93 (s, 6H, *gem* CH_3's); MS (CI ether) *m/z*: 293 (M^++1, 53%), 2.75 ((M^++1)-18, 1%), 235 ((M^++1)-58, 58%).

*(1S,2R)-1,2-*syn*-4-Acetoxy-1,2-O-isopropylidene,3,3-dimethyl-1-(1,3-dithian-2-yl)-butane* ***10***

To the acetonide **9** (52.5 mg, 0.180 mmol) in pyridine (5.0 mL) was added acetic anhydride (1.0 mL) and the solution was stirred at room temperature for 4 h. At this point, methanol (1.0 mL) was added and allowed to react for 1 h to destroy the excess acetic anhydride. The solvent was then removed *in vacuo*. The remaining oil was dissolved in 50 mL of ethyl acetate and washed with 30 mL portions of 0.2 N HCl, saturated aqueous $NaHCO_3$, and brine. The organic layer was dried over Na_2SO_4 and concentrated *in vacuo*. Further purification by preparative TLC (2:8 ether/hexanes) afforded the acetate **10** as a colourless oil (55 mg, 92%); ^1H NMR (300 MHz) δ: 4.14 (dd, *J* = 3.2, 7.5 Hz, 1H, H1), 4.06 (d, *J* = 3.2 Hz, 1H, H2), 4.05 (d, *J* = 7.5 Hz, 1H, H1′), 3.97 (d, A of AB, *J* = 11.0 Hz, 1H, H4), 3.86 (d, B of AB, *J* = 11.0 Hz, 1H, H4′), 2.71–3.01 (m, 4H, $CH_2(CH_2S)_2$), 2.08 (s, 3H, OAc), 1.91–2.16 (m, 2H, $CH_2(CH_2S)_2$), 1.45, 1.37 (s, 6H,

Can. J. Chem. Downloaded from www.nrcresearchpress.com by 195.138.81.100 on 09/07/12
For personal use only.

$(RO)_2C(CH_3)_2$), 0.99, 0.96 (s, 6H, *gem* CH_3's); MS (CI ether) *m/z*: 335 ($M^+ + 1$, 45%), 276 (($M^+ + 1$)-59, 100%).

*(1S,2R)-1,2-*syn*-2,4-O-Isopropylidene,3,3-dimethyl-1-(1,3-dithian-2-yl)-1-butanol* ***11****:* ^{1}H NMR (300 MHz) δ: 4.12 (d, *J* = 6.6 Hz, 1H, H1′), 3.93 (s, 1H, H2), 3.80 (d, *J* = 6.6 Hz, 1H, H1), 3.65 (d, A of AB, 1H, *J* = 11.4 Hz, H4), 3.27 (d, B of AB, *J* = 11.4 Hz, 1H, H4′), 2.85–3.00 (br s, 1H, OH exchangeable), 2.71–2.88 (m, 4H, $CH_2(CH_2S)_2$), 1.83–2.16 (m, 2H, $CH_2(CH_2S_2)$, 1.47, 1.42 (s, 6H, $(RO)_2C(CH_3)_2$), 1.12, 0.78 (s, 6H, *gem* CH_3's); MS (CI ether) *m/z*: 293 ($M^+ + 1$, 80%), 275 (($M^+ + 1$)-18, 2%), 235 (($M^+ + 1$)-58, 100%).

*(1S,2R)-1,2-*syn*-1,4-O-Isopropylidene,3,3-dimethyl-1-(1,3-dithian-2-yl)-2-butanol* ***14****:* ^{1}H NMR (300 MHz) δ: 4.38 (d, *J* = 10.2 Hz, 1H, H1′), 3.98 (d, *J* = 10.2 Hz, 1H, H1), 3.55 (s, 1H, H2), 3.66 (d, A of AB, *J* = 12.5 Hz, 1H, H4), 2.96 (d, B of AB, *J* = 12.5 Hz, 1H, H4′), 2.82–2.87 (m, 4H, $CH_2(CH_2S)_2$), 2.41–2.60 (br, s, 1H, OH exchangeable), 1.79–2.10 (m, 2H, $CH_2(CH_2S)_2$), 1.41, 1.38 (s, 6H, $(RO)_2C(CH_3)_2$), 0.99, 0.87 (s, 6H, *gem* CH_3's); MS (CI ether) *m/z*: 293 ($M^+ + 1$, 96%), 275 (($M^+ + 1$)-18, 6%), 235 (($M^+ + 1$)-58, 95%).

*(1S,2R)-1,2-*syn*-1,4-O-Benzylidiene,3,3-dimethyl-1-(1,3-dithian-2-yl)-1-butanol* ***12***

To the triol **7** (98.5 mg, 0.39 mmol) in benzene (10 mL) was added benzaldehyde dimethylacetal (234 μL, 1.56 mmol) and a catalytic amount of TsOH (~10 mg). After stirring for 1 h at ambient temperature, the reaction mixture was neutralized with triethylamine and the solvent removed under vacuum. The residue was diluted in ethyl acetate (40 mL) and washed successively with 0.2 N HCl, saturated aqueous $NaHCO_3$, and brine (30 mL of each), dried over Na_2SO_4, and concentrated under reduced pressure. The oil was further purified by Chromatotron chromatography (2:8 ether/hexanes), providing the benzylidene acetal **12** as a colourless oil (115 mg, 87%); ^{1}H NMR (300 MHz) δ: 7.33–7.53 (m, 5H, aromatic), 5.63 (s, 1H, CHPh), 4.23 (d, *J* = 6.6 Hz, 1H, H1′), 3.95 (s, 1H, H2), 3.90 (d, *J* = 6.6 Hz, 1H, H1), 3.73 (d, A of AB, *J* = 11.1 Hz, 1H, H4), 3.66 (d, B of AB, *J* = 11.1 Hz, 1H, H4′), 2.80–3.02 (br s, 1H, OH exchangeable), 2.74–2.91 (m, 4H, $CH_2(CH_2S)_2$), 1.84–2.15 (m, 2H, $CH_2(CH_2S)_2$), 1.25, 0.85 (s, 6H, *gem* CH_3's); MS (CI ether) *m/z*: 341 ($M^+ + 1$, 79%), 323 (($M^+ + 1$)-18, 4%), 235 (($M^+ + 1$)-106, 59%).

*(1S,2R)-1,2-*syn*-1-Acetoxy-2,4-O-Benzylidene-3,3-dimethyl-1-(1,3-dithian-2-yl)-butane* ***13***

The alcohol **12** (61.2 mg, 0.180 mmol) was stirred at room temperature in pyridine (5.0 mL) containing acetic anhydride (1.0 mL) and DMAP (8.2 mg, 0.067 mmol). After 5 h, the excess acetic anhydride was quenched by addition of methanol (1 mL) for 1 h and the solution was concentrated under reduced pressure. The remaining syrup was taken up in ethyl acetate (30 mL) and washed with 0.2 N HCl, saturated aqueous $NaHCO_3$, and brine (20 mL of each). The organic layer was dried over Na_2SO_4 and concentrated *in vacuo*. Further purification was accomplished by Chromatotron chromatography (1:9 ether/hexanes) to yield 59.3 mg (86%) of the acetate **13** as a colourless oil; ^{1}H NMR (300 MHz) δ: 7.32–7.52 (m, 5H aromatic), 5.60 (dd, *J* = 1.3, 10.1 Hz, 1H, H1), 5.48 (s, 1H, CHPh), 4.35 (d, *J* = 1.3 Hz, 1H, H1′), 3.91 (d, *J* = 10.1 Hz, 1H, H2), 3.70 (d, A of AB, *J* = 10.7 Hz, 1H, H4), 3.63 (d, B of AB, *J* = 10.7 Hz, 1H, H4′), 2.88–3.00 (m, 2H, $CH_2(CH_2S)_2$), 2.48–2.63 (m, 2H, $CH_2(CH_2S)_2$), 2.11 (s, 3H, OAc), 1.96–2.10 (m, 2H, $CH_2(CH_2S)_2$), 1.15, 0.91 (s, 6H, *gem* CH_3's).

Acetonide formation on the anti*-triol* ***8***

The acetonides on triol **8** were prepared in a manner similar to the one described above for the conversion of **7** to **9**, **11**, and **14** (40% 2,2-dimethoxypropane in benzene, 25°C, 18 h). Thus, 155 mg (0.613 mmol) of triol **8** yielded two products. They were identified as the six-membered (**16**) and seven-membered (**19**) ring acetonides (**16** less polar than **19**). The yields for **16** and **19** were 59% and 31%, respectively, and both products were obtained as colourless oils.

*(1R,2R)-1,2-*anti*-2,4-O-Isopropylidene,3,3-dimethyl-1-(1,3-dithian-2-yl)-1-butanol* ***16****:* ^{1}H NMR (300 MHz) δ: 4.52 (d, *J* = 1.9 Hz, 1H, H1′), 3.82 (dd, *J* = 1.9, 8.9 Hz, 1H, H1), 3.70 (d, *J* = 8.9 Hz, 1H, H2), 3.56 (d, A of AB, *J* = 11.6 Hz, 1H, H4), 3.20 (d, B of AB, *J* = 11.6 Hz, 1H, H4′), 2.79–3.02 (m, 4H, $CH_2(CH_2S)_2$), 1.96–2.41 (br s, 1H, OH exchangeable), 1.81–2.16 (m, 2H, $CH_2(CH_2S)_2$), 1.39, 1.36 (s, 6H, $(RO)_2C(CH_3)_2$), 1.07, 0.92 (s, 6H, *gem* CH_3's); MS (CI ether) *m/z*: 293 ($M^+ + 1$, 15%), 275 (($M^+ + 1$)-18, 1%), 235 (($M^+ + 1$)-58, 52%).

*(1R,2R)-1,2-*anti*-1,4-O-Isopropylidene,3,3-dimethyl-1-(1,3-dithian-2-yl)-2-butanol* ***19****:* ^{1}H NMR (300 MHz) δ: 4.45 (d, *J* = 2.7 Hz, 1H, H1′), 3.97 (dd, *J* = 2.7, 9.2 Hz, 1H, H1), 3.56 (d, A of AB, *J* = 12.5 Hz, 1H, H4), 3.35 (dd, *J* = 5.6, 9.2 Hz, 1H, H2), 3.04 (d, B of AB, *J* = 12.5 Hz, 1H, H4′), 2.81–3.01 (m, 4H, $CH_2(CH_2S)_2$), 2.19 (d, *J* = 5.6 Hz, 1H, OH exchangeable), 1.91–2.15 (m, 2H, $CH_2(CH_2S)_2$), 1.39, 1.35 (s, 6H, $(RO)_2C(CH_3)_2$), 0.98 (s, 6H, *gem* CH_3's); MS (CI ether) *m/z*: 293 ($M^+ + 1$, 35%), 275 (($M^+ + 1$)-18, 3%), 235 (($M^+ + 1$)-58, 95%).

*(1R,2R)-1,2-*anti*-2,4-O-Benzylidene,3,3-dimethyl-1-(1,3-dithian-2-yl)-1-butanol* ***17***

This material was prepared and purified in the same manner as described above for the conversion of **7** to **12**. Thus, the triol **8** (81.2 mg, 0.322 mmol) yielded the benzylidene acetal **17** as a colourless oil (92 mg, 84%); ^{1}H NMR (300 MHz) δ: 7.33–7.49 (m, 5H, aromatic), 5.44 (s, 1H, CHPh), 4.59 (d, *J* = 1.8 Hz, 1H, H1′), 3.96 (dd, *J* = 1.8, 9.0 Hz, 1H, H1), 3.74 (d, *J* = 9.0 Hz, 1H, H2), 3.65 (d, A of AB, *J* = 11.3 Hz, 1H, H4), 3.60 (d, B of AB, *J* = 11.3 Hz, 1H, H4′), 2.81–2.99 (m, 4H, $CH_2(CH_2S)_2$), 1.80–2.16 (m, 2H, $CH_2(CH_2S)_2$), 1.51–1.80 (br s, 1H, OH exchangeable), 1.21, 0.97 (s, 6H, *gem* CH_3's); MS (CI ether) *m/z*: 341 ($M^+ + 1$, 37%), 323 ($M^+ + 1$)-18, 3%), 235 ($M^+ + 1$)-106, 23%).

*(1R,2R)-1,2-*anti*-1-Acetoxy-2,4-O-Benzylidene-3,3-dimethyl-1-(1,3-dithian-2-yl)-butanol* ***18***

This material was prepared and purified in the same manner as described above for the conversion of **12** to **13**. Thus, 42.0 mg (0.123 mmol) of the alcohol **17** yielded the acetate **18** as a colourless oil (34.6 mg, 74%); ^{1}H NMR (300 MHz) δ: 7.35–7.50 (m, 5H, aromatic), 5.47 (s, 1H, CHPh), 5.44 (dd, *J* = 2.2, 9.2 Hz, 1H, H1), 4.55 (d, *J* = 2.2 Hz, 1H, H1′), 3.74 (d, *J* = 9.2 Hz, 1H, H2), 3.61 (s, 2H, H4,4′), 2.76–2.98 (m, 4H, $CH_2(CH_2S)_2$), 2.14 (s, 3H, OAc), 1.85–2.12 (m, 2H, $CH_2(CH_2S)_2$), 1.18, 0.78 (s, 6H, *gem* CH_3's).

Acknowledgments

We are grateful to the Natural Sciences and Engineering Research Council of Canada (NSERC) for support of this project. Mr. A. W. Rey wishes to express his gratitude to the Ontario Ministry of Colleges and Universities for an Ontario Graduate Scholarship (OGS). We also thank Mr. R. Capoor and Dr. H. Dettman for running some of the NMR experiments and Dr. C. Kazakoff for the mass spectra.

1. R. Roy and A. W. Rey. Synlett, 448 (1990).
2. R. Roy, A. W. Rey, M. Charron, and R. Molino. J. Chem. Soc. Chem. Commun. 1308 (1989).
3. R. Roy and A. W. Rey. Tetrahedron Lett. **28**: 4935 (1987).
4. G. R. Pettit, J. E. Leet, C. L. Herald, Y. Kamano, F. E. Boettner, L. Baczynskyj, and R. A. Nieman. J. Org. Chem. **52**, 2854 (1987), and references cited therein.
5. R. E. Dolle and K. C. Nicolaou. J. Am. Chem. Soc. **107**, 1691 (1985); **107**, 1695 (1985).
6. P. Lavallé, R. Ruel, L. Grenier, and M. Bissonnette. Tetrahedron Lett. **27**, 679 (1986).
7. E. J. Corey and H.-C. Huang. Tetrahedron Lett. **30**, 5235 (1989).
8. T. Poll, A. Sobczak, H. Hartmann, and G. Helmchen. Tetrahedron Lett. **26**, 3095 (1985).
9. R. D. Larsen, E. G. Corley, P. Davis, P. J. Reider, and E. J. J. Grabowski. J. Am. Chem. Soc. **111**, 7650 (1989).
10. J. D. Morrison and H. S. Mosher. *In* Asymmetric organic reactions. Prentice–Hall, Englewood Cliffs, NJ. 1971. pp. 84–132; E. L. Eliel. *In* Asymmetric synthesis. Vol. 2. *Edited by* J. D. Morrison. Academic Press, New York. 1983. pp. 125–156;

C. H. HEATHCOCK. *In* Asymmetric synthesis. Vol. 3. *Edited by* J. D. Morrison. Academic Press, New York. 1984. Part B; W. C. STILL and J. H. MCDONALD III. Tetrahedron Lett. **21**, 1031 (1980); W. C. STILL and J. A. SCHNEIDER. Tetrahedron Lett. **21**, 1035 (1980); M. NÓGRÁDI. *In* Stereoselective synthesis. VCH, New York. 1987. Chap. 5.

11. K. TATSUTA, H. TAKAHASHI, Y. AMEMIYA, and M. KINOSHITA. J. Am. Chem. Soc. **105**, 4096 (1983); K. TOMOOKA, T. OKINAGA, K. SUZUKI, and G.-i. TSUCHIHASHI. Tetrahedron Lett. **28**, 6335 (1987); K. TOMOOKA, K. MATSUZAWA, K. SUZUKI, and G.-i. TSUCHIHASHI. Tetrahedron Lett. **28**, 6339 (1987); K. TOMOOKA, T. OKINAGA, K. SUZUKI and G.-i. Tsuchihashi. Tetrahedron Lett. **30**, 1563 (1989).
12. G. E. KECK and E. P. BODEN. Tetrahedron Lett. **25**, 265 (1984); G. E. KECK and S. CASTELLINO. Tetrahedron Lett. **28**, 281 (1987).
13. G. STORK, T. TAKAHASHI, I. KAWAMOTO, and T. SUZUKI. J. Am. Chem. Soc. **100**, 8272 (1978).
14. S. S. BHATTACHARJEE, J. A. SCHWARCZ, and A. S. PERLIN. Carbohydr. Res. **42**, 259 (1975).
15. D. SEEBACH and E. J. COREY. J. Org. Chem. **40**, 231 (1975).
16. D. A. EVANS, J. V. NELSON, and T. R. TABER. Top. Stereochem. **13**, 1 (1982).
17. H. GERLACH and H. WETTER. Helv. Chim. Acta, **57**, 2306 (1974).
18. M. CHÉREST, H. FELKIN, and N. PRUDENT. Tetrahedron Lett. 2199 (1968); N. T. ANH and O. EISENSTEIN. Nouv. J. Chim. **1**, 61 (1977).
19. D. J. CRAM and F. A. ELHAFEZ. J. Am. Chem. Soc. **74**, 3210 (1952); D. J. CRAM and K. R. KOPECKY. J. Am. Chem. Soc. **81**, 2748 (1959).
20. H. B. BÜRGI, J. D. DUNITZ, and E. SHEFTER. J. Am. Chem. Soc. **95**, 5065 (1973).
21. D. D. PERRIN, W. L. ARMAREGO, and D. R. PERRIN. *In* Purification of laboratory compounds. 2nd ed. Pergamon Press, London. 1980.
22. W. G. KOFRON and L. M. BACLAWSKI. J. Org. Chem. **41**, 1879 (1976).

Can. J. Chem. Downloaded from www.nrcresearchpress.com by 195.138.81.100 on 09/07/12
For personal use only.

The photochemistry of 1-cyano-2,3-benzobicyclo[4.2.0]octa-2,4,7-triene

CHRISTOPHER OWEN BENDER,[1] DEAN SUTHERLAND CLYNE, AND DOUGLAS DOLMAN
Department of Chemistry, University of Lethbridge, Lethbridge, Alta., Canada T1K 3M4

Received June 13, 1990

CHRISTOPHER OWEN BENDER, DEAN SUTHERLAND CLYNE, and DOUGLAS DOLMAN. Can. J. Chem. **69**, 70 (1991).

The title compound (**10**) was prepared, along with the 4-cyano isomer (**11**), by the direct irradiation of 5-cyanobenzocyclooctatetraene (**9**); the yields were 82% (Φ_{10} = 0.0030) and 12% (Φ_{11} = 0.0004) respectively. Triene **10** was thermally and photochemically reactive. Heating solutions of **10** at 150°C for 1 h gave COT **9** quantitatively. On direct irradiation **10** forms 5-cyanobenzosemibullvalene (**12**; 5%, Φ = 0.019), COT **9** (70%, Φ = 0.56), and 1-cyanonaphthalene (14%, Φ = 0.078). Sensitized irradiation of **10** gave **9** exclusively (92%, Φ = 0.88). COT **9** was also produced by the direct irradiation of semibullvalene **12** (75%, Φ = 0.13). Studies with deuterium labelled **10** suggest that the photoformation of COT **9** involves a simple electrocyclic opening of the cyclobutene ring of the triene. Additionally, the labelling results indicate that the formation of semibullvalene **12** from **10** derives from the operation of two reaction pathways, the major one of which appears to be a Zimmerman di-π-methane rearrangement. The mechanism proposed for the minor pathway to **12** has not been observed in other bicyclo[4.2.0]octatrienes.

Key words: mechanisms, rearrangements, photochemistry, di-π-methane.

CHRISTOPHER OWEN BENDER, DEAN SUTHERLAND CLYNE et DOUGLAS DOLMAN. Can. J. Chem. **69**, 70 (1991).

La photolyse directe du cyano-5 benzocyclooctatetraène (**9**) conduit aux cyano-1 et -4 benzo-2,3 bicyclo[4.2.0]octatriènes-2,4,7 (**10** et **11**) avec des rendements de 82% (Φ_{10} = 0.0030) et 12% (Φ_{11} = 0.0004) respectivement. Le triène **10** est réactif thermiquement et photochimiquement. À 150°C, des solutions de **10** se transforment en **9** en rendements quantitatifs. Par irradiation directe, **10** conduit au cyano-5 benzo semi-bullvalène (**12**; 5%, Φ = 0.019), à **9** (70%, Φ = 0.56) et au cyano-1 naphtalène (14%, Φ = 0.078). Par irradiation sensibilisée, **10** conduit à **9** uniquement (92%, Φ = 0.88). Le composé **9** se forme aussi de la photolyse directe du semi-bullvalène **12** (75%, Φ = 0.13). Des études de marquages au deuterium suggèrent que **9** se produit photochimiquement du triène par un mécanisme qui comporte l'ouverture électrocyclique de l'anneau du cyclobutène de **10**. De plus, des études de marquages démontrent qu'il y a deux mécanismes qui entrent en jeux dans la transformation **10** → **12**. Le mécanisme majeur dérive d'une transposition di-π-méthane de Zimmerman. Un nouveau mécanisme est proposé pour la voie mineure qui fournit **12**.

Mots clés : mécanismes, transpositions, photochimie, di-π-méthane.

Introduction

It has been shown recently that semibullvalenes (i.e., SBs) can be produced from the light-induced isomerization of benzobicyclo[4.2.0]octa-2,4,7-trienes (1–5). Mostly their formation can be rationalized by a Zimmerman di-π-methane rearrangement (6) involving initial bridging between C-5 and C-7 of the two vinyl portions of the trienes (e.g., **1** → **4**; Scheme 1).[2] In one case, however, that of 5-CN derivative **5** (4), the results of deuterium labelling experiments suggested that an alternative mechanism gives SB product through initial bridging of C-4 to C-8 (note **5** → **8**; Scheme 1). We have now examined the photochemistry of 1-cyano-2,3-benzobicyclo[4.2.0]octa-2,4,7-triene (**10**) and herein report on yet a third pathway to SB formation in this intriguing triene system.

Results

Compound **10** was obtained as the major product from the direct irradiation of 5-cyanobenzocyclooctatetraene (i.e., 5-CN-BCOT, **9**), a known compound (10), with light of wavelength ≥318 nm; small amounts (ca. 11–12%) of the alternate 2π + 2π ring closure isomer **11** were also produced (see Scheme 2). Like the cyanolated trienes **1** and **5** (2, 4), **10** was found to be thermally labile, and readily reverted to COT **9** upon modest warming (e.g., $t_{1/2}$ = 4.0 h at 70°C) and at all useful working temperatures on the gc. The isomerization is essentially quantitative on heating at ca. 150°C for 1.0 h.

The structure of **10** was assigned on the basis of spectral evidence. Importantly, the proton nmr spectrum revealed the coupling constant between H-7 and H-8 to be 2.8 Hz, which falls within the characteristic range (2.5–3.7 Hz) of vinylic coupling in cyclobutenes (11). Additionally, all other features of the spectrum are closely analogous to those reported for the related positional isomers **1** (2) and **5** (4), and a comparison of their spectral details is given in Table 1.

Photochemically, triene **10** reacts efficiently under both direct (Pyrex-filtered light transmitting at ≥295 nm) and sensitized (uranium-glass-filtered light transmitting at ≥315 nm; dimethylaminobenzophenone) irradiation conditions to give COT **9** as the major product.[3] Chemical yields (gc analysis) and quantum yields (Φ's) for the reactions are given in Scheme 2. Photoproduct **12**, a new compound, was found to be a stable crystalline solid, unlike 6-, 7-, and 8-cyanobenzosemibullvalene, all of which undergo facile polymerization upon solvent removal (refs. 3, 2, 4, respectively). The structure of 5-cyanobenzotricyclo[3.3.0.$0^{2,8}$]octa-3,6-diene (i.e., SB **12**) was deduced from spectroscopic data alone. Most informative was the proton nmr spectrum, which shows the coupling constants and chemical shifts that are diagnostic for the rigid benzosemibullvalene skeleton. The nmr data of **12** are compared with those of the related benzosemibullvalenes **13** (12) and **4** (10) in Table 2 (note structures in Scheme 3).

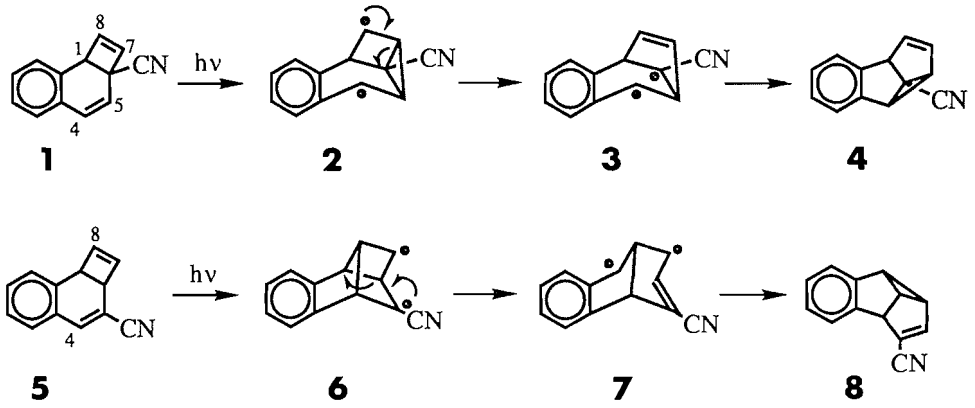
Next, the photochemistry of SB **12** was examined to ascertain

[1]Author to whom correspondence may be addressed.

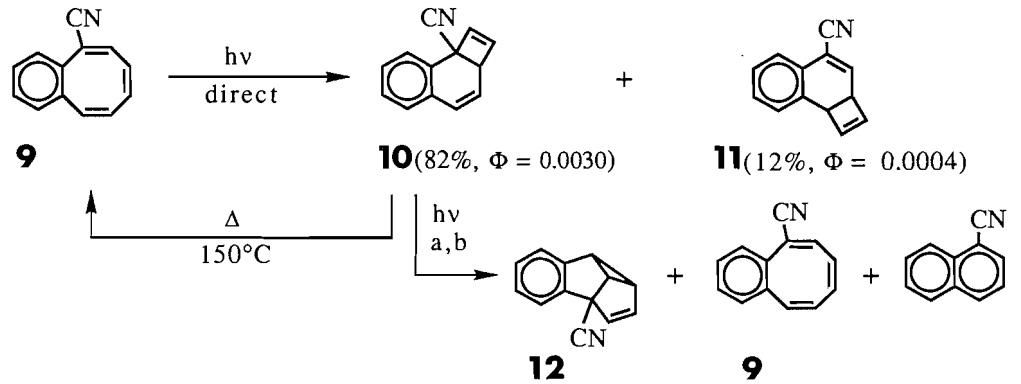
[2]The original version of the Zimmerman di-π-methane rearrangement mechanism (6) is used throughout this article. For leading publications on the issue of "1,3-vinyl, vinyl-bridging" and "1,2-vinyl-migration" versions of the rearrangement see refs. 7–9.

[3]Under the conditions used in this study, detectable amounts of triene **11** and of its major photoproduct 2-cyanobenzotricyclo-[3.3.0.$0^{2,8}$]octa-3,6-diene were not observed during irradiations of **10**; SB **12** is not a photoproduct of **11**. The photochemistry of **11** will be reported in a subsequent paper.

Can. J. Chem. Downloaded from www.nrcresearchpress.com by 195.138.81.100 on 09/07/12
For personal use only.



SCHEME 1



Chemical and quantum (Φ) yields

a, Direct	5%(0.019)	70%(0.56)	14%(0.078)
b, Sensitized		92%(0.88)	

SCHEME 2

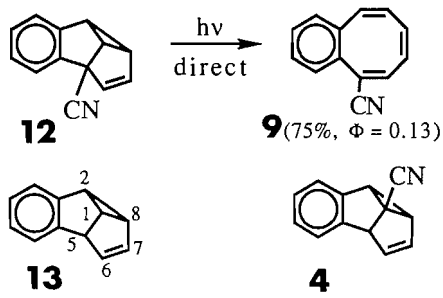
TABLE 1. The ^{1}H nmr of trienes **1**, **5**, and **10**

	Description and signal positions, $\delta^{a,b}$		
Assignment	**10**	**1**	**5**
Aromatics	7.11–7.48 m	7.11–7.28 m	7.15–7.35 m
H-1	—	4.46 br s	4.27 d
H-4	6.39 d	6.46 d	6.99 br s
H-5	5.90 dd	5.85 d	—
H-6	4.00 br d	—	3.82 br d
H-7	6.18 br d	6.19 dd	6.25 br d
H-8	6.10 d	6.07 dd	6.13 dd

[a]Run in $CDCl_3$ solvent.

[b]Coupling constants for **10** are $J_{4,5} = 10$, $J_{5,6} = 4.5$, $J_{6,7} < 1.0$, and $J_{7,8} = 2.8$ Hz; corresponding coupling constants for **1** and **5** are within 0.5 Hz.

its possible involvement in the production of COT **9**. Under the conditions used in the direct (Pyrex-filtered light) and sensitized (*p*-dimethylaminobenzophenone) irradiations of triene **10**, SB **12** was found to be stable. However, upon direct irradiation with light filtered through Corex glass, SB **12** efficiently ($\Phi = 0.13$) and cleanly rearranged to give COT **9** as the exclusive product (Scheme 3). The triplet excited state of SB **12** appears to be unreactive since attempts at sensitization with acetone led only



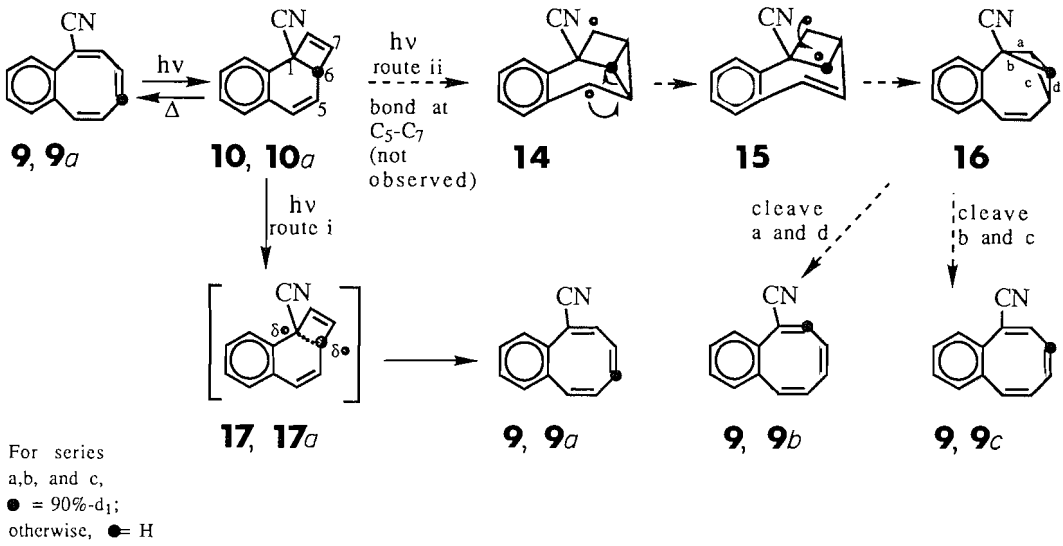
SCHEME 3

to the slow disappearance of starting material without the formation of isomeric products (gc evidence).

Mechanistic considerations

The formation of COT **9** from triene **10** can be rationalized by two literature precedented mechanisms. One is formally equivalent to a simple $2\sigma_s + 2\pi_s$ electrocyclic opening of the cyclobutene ring of triene **10** (route i, Scheme 4), a mechanism that has extensive documentation (13). A second possible pathway to COT **9** is a DPM rearrangement involving initial C-5 to C-7 bridging with subsequent formation of octavalene **16** and thermal reorganization to COT **9** (route ii, Scheme 4); independently generated 1,3-cyclobutanediyls similar to the proposed intermediate **15** have been reported to undergo coupling of the radical centres to give bicyclobutanes (14). A related mechanis-

Can. J. Chem. Downloaded from www.nrcresearchpress.com by 195.138.81.100 on 09/07/12
For personal use only.



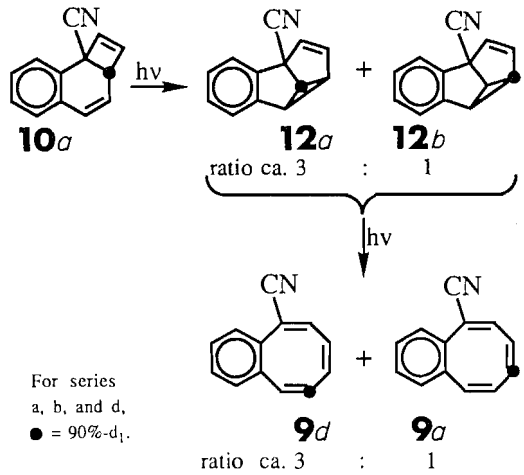
SCHEME 4

TABLE 2. The ^{1}H nmr of semibullvalenes **4**, **12**, and **13**

	Description and signal positions, $\delta^{a,b}$		
Assignment	**12**	**4**	**13**
Aromatics	7.20–7.40 m	7.00–7.44 m	6.80–7.33 m
H-1	3.69 t	—	3.14 q
H-2	3.25 t	3.66 d	2.86 t
H-5	—	4.22 d	3.81 dd
H-6	5.62 d	5.70 dd	5.47 dd
H-7	5.31 dd	5.20 dd	5.08 dd
H-8	2.91 dt	3.33 dd	2.60 dt

[a]Run in $CDCl_3$ (**4** and **12**) or CCl_4 (**13**) solvent.

[b]Coupling constants for **12** are $J_{1,2} = J_{1,8} = 6.0$, $J_{2,8} = 6.5$, $J_{6,7} = 5.0$, and $J_{7,8} = 2.5$ Hz; corresponding coupling constants for **4** and **13** are within 0.5 Hz.



SCHEME 5

tic proposal was invoked by us to account for the formation of 6- and 7-cyano BCOT from 8-cyano-2,3-benzobicyclo[4.2.0]-octa-2,4,7-triene (3). Routes i and ii are skeletally nonequivalent and experiments with the deuterated compound **10***a* were undertaken to distinguish between them. Labelled **10***a* was obtained photochemically from the known (10) deuterated COT **9***a* (ca. 90%-d_1 at C-8). The direct and sensitized irradiation of **10***a* gave COT product with the deuterium attached exclusively to C-8, as determined by proton nmr analysis. Thus the DPM mechanism depicted by route ii (Scheme 4) does not participate in the formation of **9** from triene **10** (the integration results for COT **9***a* and all other labelled compounds are given in the Experimental).

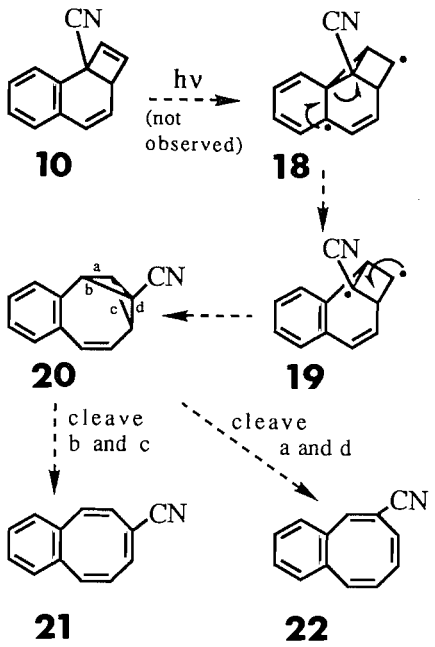
The most surprising result from the labelling experiments was the observation that the semibullvalene material formed in the direct irradiation of **10***a* gave low proton integrations at two positions, 0.30H at C-1 and 0.80H at C-8, and corresponding to the presence of a mixture of two label isomers of structures **12***a* (66%) and **12***b* (24%), and nondeuterated SB **12** (10%). This finding was corroborated by the deuterium nmr spectrum of the sample, which comprised two peaks in the ratio of 3 (C1-D):1 (C8-D). The formation of **12***a* and **12***b* cannot be accounted for in terms of a single DPM rearrangement (*vide infra*).

Lastly, in connection with the labelling studies, the nmr proton integrations of the COT product obtained from the direct irradiation of the mixture of label isomers **12***a* and **12***b* were found to be unexceptional, and corresponded to the formation of COTs **9***a* and **9***b* in the ratio of 3:1, respectively. Mechanistically, this isomerization (**12** → **9**) is interpreted as being analogous to that invoked by Zimmerman, Pagni, and Givens to account for the conversion of parent benzosemibullvalene to benzocyclooctatetraene (12), and involves cleavage of the C1—C5 and C2—C8 bonds of the semibullvalene (Scheme 5).

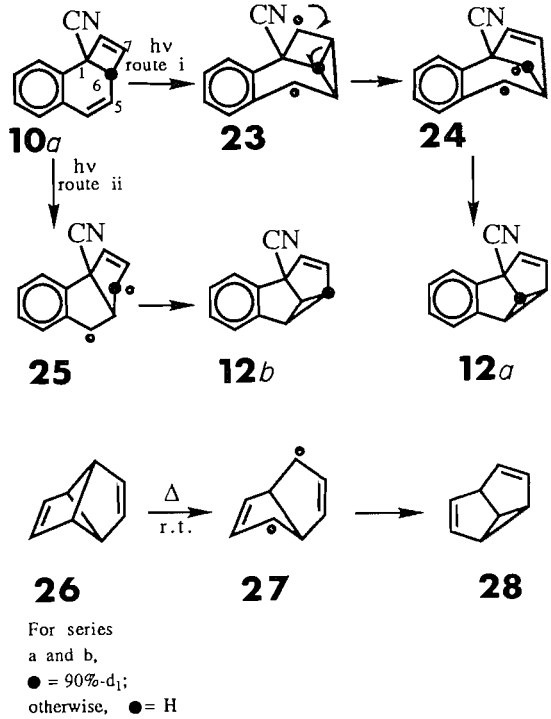
Discussion

Despite the structural similarities of trienes **1** and **10**, which differ only in respect to which one of the two bridgehead carbons the cyano group is attached (C-6 or C-1, respectively), there are major differences in their photochemistry. The most dramatic is that found for the triplet reactivities: **1** (2) gives a semibullvalene (**4**) as the major product (90%), whereas **10** gives exclusively a COT (**9**) in 92% yield. The formation of COT **9** from T_1 of **10** is a striking result, since all previous studies with benzobicyclo[4.2.0]octatrienes have found SBs and (or) naphthalenes to be the triplet products (1–5). The SB **4** formed in the case of **1** was rationalized by the Zimmerman DPM rearrangement depicted in Scheme 1 (2), and the high efficiency of the process

Can. J. Chem. Downloaded from www.nrcresearchpress.com by 195.138.81.100 on 09/07/12
For personal use only.



SCHEME 6



SCHEME 7

($\Phi_{1\rightarrow3}$ = 0.68) was attributed to the presence of the radical delocalizing cyano group on the methane carbon (C-6) of the vinyl–vinyl DPM system.[4]

For triene **10**, the deuterium labelling experiments clearly rule out the involvement of a vinyl–vinyl DPM rearrangement in the formation of COT **9**, since no deuterium was found at C-6 or at C-7 of the product (i.e., route ii, Scheme 4, does not operate). Also, the possible operation of a benzo–vinyl DPM rearrangement, which *a priori* might be promoted by the cyano group on the methane carbon (C-1), seems unlikely since this would give the octavalene **20** and subsequently[5] the COTs **21** and **22** (see Scheme 6), neither of which was observed in photolysates of **10**; both **21** and **22** are known compounds (10) and were used for gc comparisons.

Formation of COT **9** via route i (Scheme 4), the mechanism in accord with the labelling results from both direct and sensitized irradiations, involves cleavage of the C1—C6 bond of triene **10**. The facile nature of this possibly concerted reaction is attributed to the weakened character of the bridging σ-bond, due to a "diradical-like" transition state (note structure **17**) in which the developing electron densities at C-1 and C-6 are afforded extensive delocalization. No similar degree of stabilization appears to be available to radical intermediates from potential vinyl–vinyl or benzo–vinyl DPM rearrangements of **10** (note structures **14** and **15** in Scheme 4, structures **18** and **19** in Scheme 6, and structures **23** and **24** in Scheme 7), or to their transition states, which they presumably resemble, and hence these isomerizations are less favorable.

Turning now to the direct irradiation of triene **10**, the product types formed are the same as those found in the case of triene **1** (2), though the SB formation from **10** is much less predominant than from **1**. Furthermore, the results from the deuterium runs indicate that the limited SB that is formed from **10** is furnished by two routes. The major route is consistent with a DPM rearrangement involving initial C5–C7 bridging (route i, Scheme 7), and is the same mechanism as suggested for the formation of SB **4** from triene **1** (2) (note Scheme 1). For this major pathway, perhaps SB **12** is formed to a lesser extent from triene **10** than is SB **4** from triene **1**, since delocalization of the radical centres of intermediate **24** is not as extensive as that available to radical centres in the corresponding intermediate (**3**) from triene **1**.

The minor pathway of SB **12** can be accounted for by a 1,2-shift mechanism that involves cleavage of the cyclobutene C1—C6 bond and rebonding between C-1 and C-5 to give intermediate **25** (route ii, Scheme 7). A species like **25**, viz. **27**, was invoked by Meinwald *et al.* (17) and by Zimmerman *et al.* (18) to account for the transformation of diene **26** to semibullvalene **28** at room temperature. Route ii is a novel pathway in bicyclo[4.2.0]octatriene photochemistry, and its operation here is seen as a further indication of the weakened character of the ring-junction σ-bond.

Finally, it is noteworthy that the formation of SB **12** from triene **10** is probably exclusively singlet derived, since it is not a product of sensitized irradiations. This is an unusual finding and contrary to the general observation that DPM rearrangements in rigid systems show a preference for triplet initiation (19).

Experimental

The nmr spectra were recorded on Bruker 300- or 400-MHz instruments, with TMS as internal standard. The chemical shifts are in δ units and the coupling constants (*J*) in Hz. The abbreviations br, s, d, t, q, and m refer to broad, singlet, doublet, triplet, quartet, and multiplet, respectively. The ir spectra were recorded on a Bomem MB 102 FT spectrometer. The uv spectra were measured on a Varian DMS 100S spectrometer; maxima are given in nm, with λ_{max} values in parentheses; sh = shoulder. Melting points are uncorrected. Elemental analyses were performed by Galbraith Labs, Inc., Knoxville, TN. Unless stated otherwise, column chromatography was carried out on Silica Gel 60

[4]For a discussion of the influence of substitution at the methane carbon in di-π-methane photochemistry, note the publications of Zimmerman *et al.* (15) and Paquette *et al.* (16).

[5]The possible intermediacy of octavalene **20** and its thermal reorganization to a ca. 1:1 mixture of **21** and **22** was discussed by us in a previous publication (3).

Can. J. Chem. Downloaded from www.nrcresearchpress.com by 195.138.81.100 on 09/07/12
For personal use only.

Can. J. Chem. Downloaded from www.nrcresearchpress.com by 195.138.81.100 on 09/07/12
For personal use only.

(Merck; 230–400 mesh) mixed with Sylvania 2282 phosphor and slurry packed into quartz columns permitting monitoring by a hand uv lamp, or on Lobar columns (Merck; size B, LiChroprep Si 60). The gc analyses were made on a Varian 3700 instrument (FID), coupled to a Varian CDS 111 computing integrator, and fitted with, unless otherwise stated, an SE-30 fused silica capillary column 30 m × 0.32 mm. For preparative gc separations, a Varian AP-90 instrument was used (0.25 in. × 8 ft of 7.5% SE-30 on DMCS 45/50; helium gas; 190°C). Cyclohexane solvent for photolyses was prepared by scrubbing with 20% fuming sulfuric acid, followed by washing with 10% aqueous sodium hydroxide, drying ($MgSO_4$), and finally distilling from calcium hydride. Sensitizers were distilled or recrystallized (after sublimation) prior to use.

General procedures for preparative photolyses

The apparatus consisted of a 450-W Hanovia medium pressure mercury arc surrounded by a water-cooled quartz immersion well. Unless otherwise stated, the light was filtered through either a cylindrical sleeve of Pyrex, or Corex, or uranium glass (Ace) or an aqueous lead nitrate solution (1 g $Pb(NO_3)_2$ and 100 g NaBr in 1 L water; transmittance was 0% below 318 nm) contained in a concentric filter jacket (10 mm path length). Four types of sample cell were used. Cell A (250 mL sample volume) consisted of a cylindrical vessel (Pyrex), which surrounded the immersion well. Cell B (200 mL sample volume) consisted of a cylindrical collar (Pyrex), which surrounded the aqueous filter jacket. Both Cells A and B were fitted with gas inlet and exit ports, and sample solutions were purged with argon prior to, and during, irradiations. Cell C (35 mL sample volume) was a quartz test-tube-like vessel, and Cell D (3.5 mL) was a quartz cuvette; sample solutions contained therein were deoxygenated by flushing with argon and sealed under a positive pressure; the solutions were magnetically stirred throughout the course of the irradiations.

Unless stated otherwise, compositions of photolysates containing the thermally unstable triene **10** were obtained by a combination of nmr spectroscopy and gc analyses. The gc runs were carried out at ≥185°C, at which temperatures the triene rearranged on the column to give COT **9** quantitatively, as determined by calibration against an internal standard (tetradecane).

Direct irradiation of cyclooctatetraene ***9***

A solution of 145.3 mg (0.81 mmol) of COT **9** (10) in 200 mL of cyclohexane was photolyzed at >318 nm for 12.75 h in Cell B. The photolysate analysed (nmr) for a triene photoproduct ratio (**10**:**11**) of ca. 7:1. The photolysate was concentrated and chromatographed on a Lobar column (2.5% ether–cyclohexane) into two bands. The second band contained 60.9 mg (42%) of triene **10**, mp 65–67°C (from hexane); ir (CCl_4): 2234 (C≡N) cm^{-1}; uv (hexane): 257 sh (5210), 265 (6460), 270 sh (5900), 283 sh (3120), 291 sh (1410), 294 sh (910), and 300 (660); ^1H nmr (400 MHz; $CDCl_3$), see Table 1; spin decoupling experiments: irradiation of H-4 collapsed H-5 to a d ($J_{5,6}$ = 4.5); irradiation of H-5 collapsed H-4 and H-6 to singlets; irradiation of H-6 collapsed H-5 to a d ($J_{5,4}$ = 10), and H-7 to a d ($J_{7,8}$ = 2.8); irradiation of H-7 collapsed H-8 to an s; irradiation of H-8 collapsed H-7 to an s; ^{13}C nmr (75.5 MHz; $CDCl_3$): 146.13, 140.29, 137.31, 130.27, 128.70, 128.33, 127.52, 126.49, 124.86, 121.32, 48.90, and 41.75 (one C not observed). Mass spectrum showed molecular ion at m/e = 179.0727 (94%), 178 (base peak); $C_{13}H_9N$ requires 179.0734. Anal. calcd. for $C_{13}H_9N$: C 87.12, H 5.06, N 7.82; found: C 87.09, H 5.15, N 7.81.

The first band was concentrated and the residue crystallized from 3 mL of hexane to give 62.8 mg (43%) of recovered COT **9**. The mother liquors were rechromatographed on a Lobar column (1% ethyl acetate – 20% toluene – 79% hexane) into two bands, the second of which contained 8.0 mg (6%) of COT **9**. The first band gave 8.6 mg (6%) of triene **11**, mp 74–76°C (from hexane); ir (CCl_4): 2224(C≡N) cm^{-1}; uv (hexane): 227 (17 800), 234 (15 800), 281 (5820), and 309 (1510); ^1H nmr (400 MHz; $CDCl_3$): 7.52 (m, 1H, 1 aromatic), 7.27 (m, 2H, 2 aromatics), 7.13 (m, 1H, 1 aromatic), 6.76 (d, 1H, H-5, $J_{5,6}$ = 4.5), 6.11 (br d, 1H, H-8, $J_{8,7}$ = 2.5), 6.07 (br d, 1H, H-7, $J_{7,8}$ = 2.5), 4.17 (d, 1H, H-1, $J_{1,6}$ = 4.5), and 3.79 (t, 1H, H-6, $J_{6,5} = J_{6,1}$ = 4.5); spin decoupling experiments: irradiation of H-6 collapsed H-1 and H-5 to singlets and modified H-7; irradiation of H-1 collapsed H-6 to a d ($J_{6,5}$ = 4.5) and modified H-8; irradiation of H-5 collapsed H-6 to a d ($J_{6,1}$ = 4.5); ^{13}C nmr (75.5 MHz; $CDCl_3$): 142.64, 141.40, 138.04, 134.53, 129.76, 128.11, 127.34, 126.46, 126.09, 117.44, 112.31, 43.69, and 42.87. Mass spectrum showed molecular ion at m/e = 179.0727 (93%), 178 (base peak); $C_{13}H_9N$ requires 179.0734.

Thermolysis of triene ***10***

A solution of 10.7 mg (0.060 mmol) of **10** in 2 mL of *n*-nonane was refluxed (ca. 150°C) for 1 h. The thermolysis product was chromatographed on Silica Gel 60 (0.9 cm × 10 cm; 5% ether–cyclohexane). Crystallization of the main band from hexane gave 10.3 mg (96%) of COT **9**, mp 65–67°C (lit. (10) mp 66–68°C).

Direct irradiation of triene **10**

A solution of 91.8 mg (0.51 mmol) of **10** and 8.6 mg of tetradecane (gc standard) in 250 mL of cyclohexane was irradiated (Pyrex filter) for 3.0 h in Cell A. The photolysate composition analysed (gc and nmr) for 7.7 mg (11%) of 1-cyanonaphthalene, 52.1 mg (57%) of COT **9**, 3.7 mg (4%) of SB **12**, and 17.4 mg (19%) of triene **10**. The photolysate was concentrated and chromatographed on a Lobar column (2.5% ether–cyclohexane). The first band eluted was 5.9 mg (9%) of 1-cyanonaphthalene (identified by gc, tlc, and nmr comparison with an authentic sample). The second band was a mixture of COT **9** and SB **12**. The third band contained 15.3 mg (17%) of recovered triene **10**. Preparative gc of the bulk of the second band on an SE-30 column eluted firstly 2.2 mg (2%) of SB **12**, followed by 39.6 mg (43%) of COT **9**, mp 65–67°C. For SB **12** (gc purity > 99%), mp 81–83°C (from hexane); ir (CCl_4): 2245 (C≡N) cm^{-1}; uv (hexane): 266 (290), 272 (370), and 280 (340); ^1H nmr (400 MHz, $CDCl_3$), see Table 2; spin decoupling experiments: irradiation of H-6 collapsed H-7 to a d ($J_{7,8}$ = 2.5); irradiation of H-7 collapsed H-6 to an s, and H-8 to a t ($J_{8,1} \approx J_{8,2}$ = 6.5); irradiation of H-1 collapsed H-2 to a d ($J_{2,8}$ = 6.5), and H-8 to a dd ($J_{8,7}$ = 2.5, $J_{8,2}$ = 6.5); irradiation of H-2 collapsed H-1 to a d ($J_{1,8}$ = 6.0) and H-8 to a dd ($J_{8,1}$ = 6.0, $J_{8,7}$ = 2.5); irradiation of H-8 collapsed H-1 to a d ($J_{1,2}$ = 6.0), H-2 to a d ($J_{2,1}$ = 6.0), and H-7 to a d ($J_{7,6}$ = 5.0). Mass spectrum showed molecular ion at m/e = 179.0724 (84%), 178 (base peak); $C_{13}H_9N$ requires 179.0734.

Sensitized irradiation of triene ***10***

A solution of 10.3 mg (0.058 mmol) of **10**, 10.5 mg of tetradecane (gc standard), and 6.3 mg (0.028 mmol) of *p*-dimethylaminobenzophenone in 15 mL of cyclohexane was irradiated for 25 min in Cell C with light filtered through a uranium glass sleeve. The photolysate composition analysed (gc and nmr) for 9.5 mg (92%) of COT **9** and 0% of **10** (i.e., complete conversion). The photolysate was concentrated and chromatographed on Silica Gel 60 (0.9 cm × 15 cm; 5% ether–cyclohexane). The first band gave 9.1 mg (88%) of COT **9**, mp 65–67°C (from hexane). The second band gave 5.6 mg (89%) of recovered sensitizer. No 1-cyanonaphthalene was observed in the photolysate (gc monitoring).

Direct irradiation of SB ***12***

A solution of 3.6 (0.020 mmol) of **12** and 2.8 mg of tetradecane (gc standard) in 3.5 mL of cyclohexane contained in Cell D was irradiated for 30 min with Corex-filtered light. The photolysate composition analysed (gc) for 1.2 mg (33%) of COT **9** and 2.0 mg (56%) of SB **12**. The photolysate was concentrated and chromatographed on a short column of Silica Gel 60 (0.9 cm × 5 cm; 3% ether–cyclohexane) to remove the tetradecane. The band containing the COT **9** and SB **12** was separated by preparative gc on an SE 30 column. The first component eluted was 1.2 mg (33%) of SB **12**. The second was 0.7 mg (19%) of COT **9** (identified by nmr).

Attempted sensitized irradiation of SB ***12***

(a) With p*-dimethylaminobenzophenone*

A solution of 2.7 mg (0.015 mmol) of **12**, 3.3 mg (0.015 mmol) of *p*-dimethylaminobenzophenone, and 3.6 mg of tetradecane (gc standard) in 3.5 mL of cyclohexane contained in Cell D was irradiated for 20 min with light filtered through a WG-360 glass (Schott) filter. The

Can. J. Chem. Downloaded from www.nrcresearchpress.com by 195.138.81.100 on 09/07/12
For personal use only.

photolysate composition analysed (gc) for 2.6 mg (96%) of SB **12** and 0.8 mg (24%) of the sensitizer; no other products were detected. The photolysate was concentrated and chromatographed on Silica Gel 60 (0.9 cm × 10 cm; 5% ether–cyclohexane) to give 2.2 mg (81%) of **12** (identified by nmr).

(b) With acetone

A solution of 2.7 mg (0.015 mmol) of SB **12**, and 1.9 mg of tetradecane (gc standard) in 3.5 mL of acetone was irradiated for 3.5 h in Cell D with Pyrex-filtered light. The photolysate analysed for 1.8 mg (67%) of SB **12**; no other products were detected. The SB **12** (1.4 mg; 52%) was recovered from the photolysate and identified as in part (a) above.

Labelled COT **9**a

Deuterated COT **9***a* (ca. 90% d_1 at C-8) was obtained as previously described (10); ^{1}H nmr (400 MHz; $CDCl_3$): 7.23–7.36 (m, 3.79H, 3 aromatics + residual $CHCl_3$), 7.00–7.05 (m, 1.00H, 1 aromatic), 6.90 (dd, 0.95H, H-6, $J_{6,7}$ = 4.5, $J_{6,9}$ = 1.5), 6.65 (d, 1.00H, H-10, $J_{10,9}$ = 11.5), 6.06 (d, 1.05H, H-9 + residual H-8, $J_{9,10}$ = 11.5), and 5.91 (br d, 0.97H, H-7, $J_{7,6}$ = 4.5). Integrations for **9***a* and for all subsequent deuterium labelled compounds were normalized by assigning integer values to one or more aromatic proton signals, unless otherwise stated; integration uncertainties are estimated to be within ca. ±0.05H.

Labelled triene **10**a *from COT* **9**a

A solution of 198.0 (1.10 mmol) of COT **9***a* in 200 mL of cyclohexane was photolyzed at >318 nm for 11.30 h in Cell B. The photolysate was worked up as in the case of the direct irradiation of unlabelled COT **9** to give 128.8 mg (65%) of triene **10***a*; ^{1}H nmr (400 MHz; $CDCl_3$): 7.45–7.48 (m, 1.00H, 1 aromatic), 7.24–7.31 (m, 3.35H, 2 aromatics + residual $CHCl_3$), 7.10–7.14 (m, 1.01H, 1 aromatic), 6.39 (d, 1.01H, H-4, $J_{4,5}$ = 10), 6.18 (d, 0.99H, H-7, $J_{7,8}$ = 2.8), 6.10 (d, 1.01H, H-8, $J_{8,7}$ = 2.8), 5.90 (d, 1.04H, H-5, $J_{5,4}$ = 10), and 4.00 (d, 0.08H, H-6, $J_{6,5}$ = 4.5).

Direct irradiation of triene **10**a

A solution of 128.8 mg (0.72 mmol) of **10***a* in 250 mL of cyclohexane was irradiated (Pyrex filter) for 4.0 h in Cell A. The photolysate was worked up as in the case of the direct irradiation of unlabelled triene **10** to give 46.1 mg (36%) of COT **9***a*, ^{1}H nmr (400 MHz; $CDCl_3$): 7.23–7.36 (m, 4.27H, 3 aromatics + residual $CHCl_3$), 7.00–7.05 (m, 1.00H, 1 aromatic), 6.90 (dd, 0.94H, H-6, $J_{6,7}$ = 4.5, $J_{6,9}$ = 1.5), 6.65 (d, 1.01H, H-10, $J_{10,9}$ = 11.5), 6.06 (d, 1.12H, H-9 + residual H-8, $J_{9,10}$ = 11.5), and 5.91 (br d, 0.98H, H-7, $J_{7,6}$ = 4.5); 1.6 mg (2%) of 1-cyanonaphthalene; 1.4 mg (1%) of SB mixture **12***a* and **12***b*, ^{1}H nmr (400 MHz; $CDCl_3$): 7.20–7.40 (m, 7.35H, 3 aromatics + residual $CHCl_3$), 5.62 (d, 0.98H, H-6, $J_{6,7}$ = 5.0), 5.31 (dd, 1.01H, H-7, $J_{7,6}$ = 5.0, $J_{7,8}$ = 2.5), 3.69 (m, 0.30H, H-1), 3.25 (d, 1.00H, $J_{2,8}$ = 7.0), and 2.91 (dd, 0.80H, H-8, $J_{8,2}$ = 7.0, $J_{8,7}$ = 2.5), normalized on the basis that sum of non-aromatic protons is 4.10H; ^{2}H nmr (400 MHz; $CHCl_3$): 3.70 (br s, D-1) and 2.91 (br s, D-8), integration ratio of (D-1):(D-8) was 3 (**12***a*):1 (**12***b*); and 38.9 mg (30%) of recovered triene **10***a*, ^{1}H nmr (400 MHz; $CDCl_3$): 7.45–7.48 (m, 1.00H, 1 aromatic), 7.24–7.31 (m, 2.95H, 2 aromatics + residual $CHCl_3$), 7.10–7.14 (m, 1.01H, 1 aromatic), 6.39 (d, 1.02H, H-4, $J_{4,5}$ = 10), 6.18 (d, 0.95H, H-7, $J_{7,8}$ = 2.8), 6.10 (d, 0.97H, H-8, $J_{8,7}$ = 2.8), 5.90 (d, 1.00H, H-5, $J_{5,4}$ = 10), and 4.00 (d, 0.08H, H-6, $J_{6,5}$ = 4.5).

Thermolysis of triene **10**a

A solution of 6.3 mg (0.035 mmol) of **10***a* in 2 mL of *n*-nonane was refluxed (ca. 150°C) for 40 min. The thermolysis product was worked up as in the case of the unlabelled triene **10** to give 6.2 mg (98%) of COT **9***a*; ^{1}H nmr (400 MHz; $CDCl_3$): 7.23–7.36 (m, 3.80H, 3 aromatics + residual $CHCl_3$), 7.00–7.05 (m, 1.00H, 1 aromatic), 6.90 (dd, 0.99H, H-6, $J_{6,7}$ = 4.5, $J_{6,9}$ = 1.5), 6.65 (d, 0.99H, H-10, $J_{10,9}$ = 11.5), 6.06 (d, 1.13H, H-9 + residual H-8, $J_{9,10}$ = 11.5), and 5.91 (br d, 1.03H, H-7, $J_{7,6}$ = 4.5).

Sensitized irradiation of triene **10**a

A solution of 6.8 mg (0.038 mmol) of **10***a* and 4.6 mg (0.020 mmol) of *p*-dimethylaminobenzophenone in 10 mL of cyclohexane was irradiated for 23 min in Cell C with light filtered through a uranium glass sleeve. The photolysate was worked up as in the case of the sensitized irradiation of unlabelled triene **10** to give 4.9 mg (72%) of COT **9***a*, ^{1}H nmr (400 MHz; $CDCl_3$): 7.23–7.36 (m, 4.15H, 3 aromatics + residual $CHCl_3$), 7.00–7.05 (m, 1.00H, 1 aromatic), 6.90 (dd, 1.00H, H-6, $J_{6,7}$ = 4.5, $J_{6,9}$ = 1.5), 6.65 (d, 0.99H, H-10, $J_{10,9}$ = 11.5), 6.06 (d, 1.11H, H-9 + residual H-8, $J_{9,10}$ = 11.5), and 5.91 (br d, 1.00H, H-7, $J_{7,6}$ = 4.5); and ca. 0.5 mg (ca. 8%) of recovered triene **10***a*, ^{1}H nmr (400 MHz; $CDCl_3$): 7.45–7.48 (m, 1.00H, 1 aromatic), 7.24–7.10 (m, H integration n/a, 3 aromatics + large residual $CHCl_3$), 6.39 (d, 0.95H, H-4, $J_{4,5}$ = 10), 6.18 (d, 0.99H, H-7, $J_{7,8}$ = 2.8), 6.10 (d, 0.96H, H-8, $J_{8,7}$ = 2.8), 5.90 (d, 0.98H, H-5, $J_{5,4}$ = 10), and 4.00 (d, 0.09H, H-6, $J_{6,5}$ = 4.5).

Direct irradiation of labelled SB mixture **12**a *and* **12**b

A solution of 1.6 mg (0.009 mmol) of SB mixture **12***a* and **12***b* in 3.5 mL of cyclohexane contained in Cell D was irradiated for 30 min with Corex-filtered light. The photolysate was worked up as in the case of the direct irradiation of unlabelled SB **12** to give 0.7 mg (44%) of recovered starting material, ^{1}H nmr (400 MHz; $CDCl_3$): 7.20–7.40 (m, 11.5H, 3 aromatics + residual $CHCl_3$), 5.62 (d, 0.99H, H-6, $J_{6,7}$ = 5.0), 5.31 (dd, 1.01H, H-7, $J_{7,6}$ = 5.0, $J_{7,8}$ = 2.5), 3.69 (m, 0.33H, H-1), 3.25 (d, 1.00H, $J_{2,8}$ = 7.0), and 2.91 (dd, 0.78H, H-8, $J_{8,2}$ = 7.0, $J_{8,7}$ = 2.5); and 0.3 mg (19%) of labelled COT mixture **9***a* and **9***d*, ^{1}H nmr (400 MHz; $CDCl_3$): 7.23–7.36 (m, 9.3H, 3 aromatics + residual $CHCl_3$), 7.00–7.05 (m, 1.00H, 1 aromatic), 6.90 (br d, 0.96H, H-6, $J_{6,7}$ = 4.5), 6.64 and 6.65 (s and d, 1.00H, H-10, $J_{10,9}$ = 11.5; ratio of s (**9***d*):d (**9***a*) ≈ 3:1), 6.03–6.08 (m, 1.04H, H-9 + H-8), and 5.89–5.95 (m, 0.96H, H-7).

Quantum yield determinations

Quantum yields were performed on an apparatus previously described (20), which includes an optical bench arranged for beam splitting into a ferrioxalate actinometer (21). Cyclohexane solutions (3.5 mL) of reactants (ca. (4.5–6.5) × 10^{-3} M) and sensitizer, if any (*p*-dimethylaminobenzophenone, ca. 1.0 × 10^{-3} M), were deoxygenated prior to irradiation by flushing with argon. A positive pressure of argon was maintained over the stirred solutions throughout the course of the irradiations. The quantum yields (Φ's) were obtained from several runs extrapolated to zero conversion. Product analyses were determined by a combination of gc (internal tetradecane standard) and high performance liquid chromatography (hplc; for the determination of relative amounts of COT **9** and triene **10**). The hplc analyses were performed on a normal phase 16 μm silica column (Waters, μ Porasil, 3.9 mm × 300 mm) with a Waters 501 hplc pump with detection by a Waters model 481 LC spectrophotometer. The eluting solvent system was 1% ethyl acetate in hexane. Photometric detection was carried out at 300 nm; chromatograms were integrated using a Waters 740 data module, and relative detector responses were calibrated against known mixtures of COT **9** and triene **10**. For the direct irradiation of triene **10**, light of wavelength 280 nm was used. For sensitized runs with *p*-dimethylaminobenzophenone, the sensitizer absorbed >95% of the incident light (366 nm) employed. For the direct irradiation of SB **12**, light of wavelength 275 nm was used.

Acknowledgements

The authors thank the Spectroscopic Services Laboratory of the University of Alberta and the Agriculture Canada Research Station at Lethbridge for the nmr and mass spectra. Financial support from the Natural Sciences and Engineering Research Council of Canada is gratefully acknowledged.

1. C. O. Bender, I. M. Cassis, D. Dolman, L. D. Heerze, and F. L. Schultz. Can. J. Chem. **62**, 2769 (1984).
2. C. O. Bender, D. L. Bengtson, D. Dolman, and S. F. O'Shea. Can. J. Chem. **64**, 237 (1986).
3. C. O. Bender, D. Dolman, and G. K. Murphy. Can. J. Chem. **66**, 1656 (1988).

4. C. O. BENDER and D. DOLMAN. Can. J. Chem. **67**, 82 (1989).
5. J. R. SCHEFFER and M. YAP. J. Org. Chem. **54**, 2561 (1989).
6. H. E. ZIMMERMAN. *In* Rearrangement in ground and excited states. Vol. 3. *Edited by* P. de Mayo. Academic Press, New York. 1980. pp. 131–166.
7. H. E. ZIMMERMAN and A. P. KAMATH. J. Am. Chem. Soc. **110**, 900 (1988).
8. W. ADAM, M. DÖRR, J. KRON, and R. J. ROSENTHAL. J. Am. Chem. Soc. **109**, 7074 (1987).
9. L. A. PAQUETTE, L. D. BURKE, T. IRIE, and H. TANIDA. J. Org. Chem. **52**, 3246 (1987).
10. C. O. BENDER, D. W. BROOKS, W. CHENG, D. DOLMAN, S. F. O'SHEA, and S. S. SHUGARMAN. Can. J. Chem. **56**, 3027 (1978).
11. O. L. CHAPMAN. J. Am. Chem. Soc. **85**, 2014 (1963).
12. H. E. ZIMMERMAN, R. S. GIVENS, and R. M. PAGNI. J. Am. Chem. Soc. **90**, 6096 (1968).
13. R. B. WOODWARD and R. HOFFMANN. *In* The conservation of orbital symmetry. Verlag Chemie, Weinheim, and Academic Press, New York. 1970. p. 63.
14. (*a*) M. B. SPONSLER, R. JAIN, F. D. COMS, and D. A. DOUGHERTY. J. Am. Chem. Soc. **111**, 2240 (1989); (*b*) M. H. CHANG, R. JAIN, and D. A. DOUGHERTY. J. Am. Chem. Soc. **106**, 4211 (1984); (*c*) G. J. SNYDER and D. A. DOUGHERTY. J. Am. Chem. Soc. **111**, 3942 (1989).
15. (*a*) H. E. ZIMMERMAN and R. L. SWAFFORD. J. Org. Chem. **49**, 3069 (1984); (*b*) H. E. ZIMMERMAN and R. E. FACTOR. Tetrahedron, **37**, 125 (1981); (*c*) H. E. ZIMMERMAN, D. ARMESTO, M. G. AMEZUA, T. P. GANNETT, and R. P. JOHNSON. J. Am. Chem. Soc. **101**, 6367 (1979); (*d*) H. E. ZIMMERMAN, R. J. BOETTCHER, and W. BRAIG. J. Am. Chem. Soc. **95**, 2155 (1973).
16. (*a*) L. A. PAQUETTE and E. BAY. J. Am. Chem. Soc. **106**, 6693 (1984); (*b*) L. A. PAQUETTE, A. VARADARAJAN, and E. BAY. J. Am. Chem. Soc. **106**, 6702 (1984).
17. (*a*) J. MEINWALD and D. SCHMIDT. J. Am. Chem. Soc. **91**, 5877 (1969); (*b*) J. MEINWALD and H. TSURUTA. J. Am. Chem. Soc. **91**, 5878 (1969).
18. H. E. ZIMMERMAN, J. D. ROBBINS, and J. SCHANTL. J. Am. Chem. Soc. **91**, 5878 (1969).
19. S. S. HIXSON, P. S. MARIANO, and H. E. ZIMMERMAN. Chem. Rev. **73**, 531 (1973).
20. C. O. BENDER, D. L. BENGTSON, D. DOLMAN, C. E. L. HERLE, and S. F. O'SHEA. Can. J. Chem. **60**, 1942 (1982).
21. (*a*) C. G. HATCHARD and C. A. PARKER. Proc. R. Soc. London, Ser. A, 235, 518 (1956); (*b*) W. D. BOWMAN and J. N. DEMAS. J. Phys. Chem. **80**, 2434 (1976).

Can. J. Chem. Downloaded from www.nrcresearchpress.com by 195.138.81.100 on 09/07/12
For personal use only.

A stereocontrolled intramolecular cycloaddition – sigmatropic rearrangement approach to a tricyclo[7.4.0^{1,6}.0^{1,10}]tridecane precursor for (±) gascardic acid

GERVAIS BÉRUBÉ AND ALEX G. FALLIS[1]

The Ottawa–Carleton Chemistry Institute, Department of Chemistry, University of Ottawa, Ottawa, Ont., Canada K1N 6N5

Received June 7, 1990

GERVAIS BÉRUBÉ and ALEX G. FALLIS. Can. J. Chem. **69**, 77 (1991).

A general intramolecular Diels–Alder anionic oxy-Cope strategy for the synthesis of tricyclic skeletons and its application to the preparation of the gascardic acid precursor **21** is described. *In situ* generation of the appropriate cyclopentadiene **9** by isomerization (Et_3N) afforded the [4+2] adduct directly or with $EtAlCl_2$ as catalyst. The requisite potassium salt of the 1,5 diene **16** rearranged with concomitant epimerization at 67°C to the fused ring ketone **18**. Selective allylic oxidation and reduction provided **21**.

Key words: Diels–Alder, oxy-Cope, sesterterpene, synthesis, cycloaddition.

GERVAIS BÉRUBÉ et ALEX G. FALLIS. Can. J. Chem. **69**, 77 (1991).

On décrit une stratégie générale, basée sur des réactions de Diels–Alder intramoléculaire et d'oxy-Cope anionique, pour effectuer la synthèse des squelettes tricycliques ainsi que son application à la préparation du précurseur **21** de l'acide gascardique. Utilisant une isomérisation (Et_3N), on a réalisé une génération *in situ* du cyclopentadiène approprié **9** qui a fourni l'adduit [4+2] soit directement ou sous l'influence du $EtAlCl_2$ comme catalyseur. À 67°C, le sel de sodium approprié **16** du 1,5-diène se transpose avec une épimérisation concomitante qui conduit à la cétone cyclique condensée **18**. Son oxydation allylique sélective et une réduction subséquente conduisent au produit **21**.

Mots clés : Diels–Alder, oxy-Cope, sesterterpène, synthèse, cycloaddition.

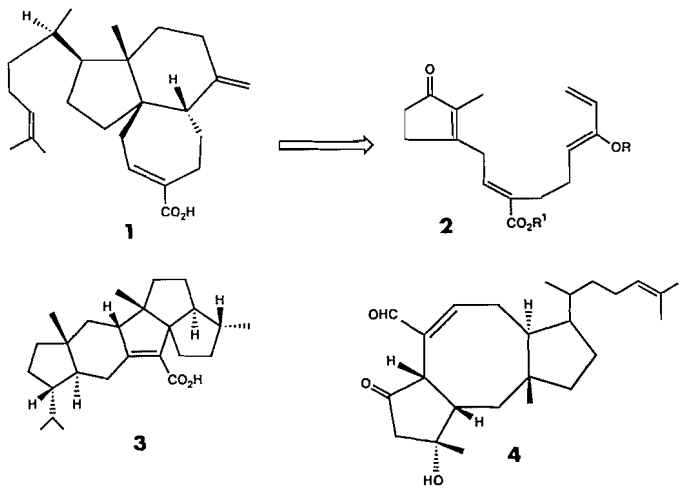
[Traduit par la revue]

Introduction

The sesterterpenes represent a structurally diverse family of C_{25} terpenes. The major polycyclic members include gascardic acid (**1**) (1), retigeranic acid (**3**) (2), and ophiobolin C (**4**) (3). These novel ring systems have attracted considerable synthetic interest and consequently all of them have succumbed to total synthesis (4). Gascardic acid possesses a unique tricyclo-[7.5.0^{1,7}.0^{1,11}]tetradecane skeleton whose structure was established via total synthesis (5) and X-ray diffraction (6). At present, this fused arrangement of five, six, and seven membered rings has not been encountered elsewhere in nature, although this structure shares with other angular triquinane natural products, such as retigeranic acid, a related spiro-fused tricyclic nucleus.

The presence of a spiro center in both gascardic and retigeranic acid that is common to the three fused rings suggested that a common synthetic approach to these skeletons was possible. In a retrosynthetic sense the double disconnection of the cyclohexene ring in gascardic acid would, in principle, allow the construction of the tricyclic framework by an intramolecular Diels–Alder cycloaddition **2** to **1**. However, cyclizations in which the diene and dienophile are linked by five atoms are difficult, particularly in carbocyclic systems (7–9). In addition, for retigeranic acid (**3**), a ring contraction of the cyclohexanone and the expulsion, from an unactivated center, of the extra carbon atom would be required. Closer scrutiny indicated that a more powerful combination would be to employ a different intramolecular cycloaddition followed by a [3,3] sigmatropic rearrangement. Thus in general, a stereocontrolled route to many multicyclic skeletons is available from a combination of these pericyclic transformations via an intramolecular Diels–Alder anionic oxy-Cope rearrangement strategy. As illustrated in Scheme 1, the length of the side chain may be varied and the resulting cyclohexanone contracted or expanded as required.

[1]Author to whom correspondence may be addressed.

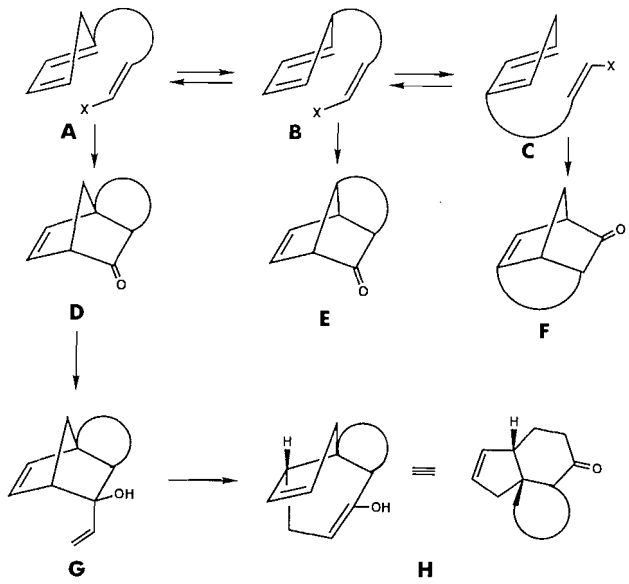


Over several decades the Diels–Alder reaction has remained one of the most useful organic transformations. There is also considerable current interest in the intramolecular Diels–Alder reaction, which has been applied to a number of natural product syntheses with notable success due to the complex systems that can be assembled in a relatively rapid manner (9). Similarly, [3,3] sigmatropic (Cope) rearrangements are a powerful construction tool within the arsenal of the organic chemist. Thus the oxy-Cope variant has recently received increased attention as a versatile method for the synthesis of diverse natural product skeletons (10). We wish to report the details for the successful application of this combined strategy (**A–D–G–H**) to the synthesis of the gascardic acid intermediate **21**, in which the key ring junctions and substituents have the correct relative stereochemistry (11).

Results and discussion

Previous studies established that, in spite of the rapid [1,5] sigmatropic rearrangement that occurs at room temperature in

Can. J. Chem. Downloaded from www.nrcresearchpress.com by 195.138.81.100 on 09/07/12
For personal use only.



SCHEME 1

cyclopentadienes **A**–**C**, the cycloadditions will proceed to give the fused ring product **D** rather than the isomeric bridged ring or Bredt olefin adducts **E** and **F** (7, 8, 12). Our earlier investigations revealed that the cycloheptane ring could not be generated directly and that ultimately a ring expansion would be required (7). In addition, it was established that carrying the dimethylhexenyl substituent caused difficulties, due to competing ene reactions during the cycloaddition step. Furthermore, it is well known that nucleophilic addition to 2-norbornanone type ketones occurs preferentially from the *exo* face. Thus, we developed an epimerization procedure for cyclic vinyl tertiary alcohols via a [2,3] sulfoxide sigmatropic rearrangement, which may be utilized to circumvent this potential difficulty (13, 10*d*).

The detailed synthetic route is outlined in Scheme 2 and commences with the keto-enol ether **5** derived from 2-methyl-1,3-cyclopentanedione upon treatment with *p*-toluenesulfonic acid, molecular sieves, and ethanol in refluxing benzene (90%) (7). Ethyllithium, generated *in situ* in an ultrasonic bath (14) from bromoethane and Li/Na alloy, was condensed with **5** to give the cyclopentenone (98%). The dianion derived from methyl acetoacetate (15), by sequential treatment with sodium hydride and *n*-butyllithium, was added to this cyclopentenone and dehydration of the resulting alcohol was effected with 3 M HCl to afford the dienone-ester **7**. This material was a single regioisomer, formed as a consequence of the nonbonded interactions between the ring vinyl methyl function and carbonyl substitutent that are avoided in the *E* olefin. Alkylation of this keto-ester with methyl 4-bromocrotonate provided the triene-diester **8** (64%) accompanied by a small amount (8.5%) of the dialkylated product.

The requisite Diels–Alder precursor **9** was generated *in situ* from **8**. Treatment of **8** with $EtAlCl_2$ in dichloromethane at room temperature (21°C) catalyzed the cycloaddition with a high level of stereocontrol to give the single isomer **10** in modest yield (30%). This adds to the growing list of examples where alkylaluminum halides are the most satisfactory catalysts for effective control of intramolecular [4+2] cycloadditions (16). As discussed above, several different cyclopentadiene adducts might be envisaged but, as expected, only the tricyclo[6.2.1.$0^{1,6}$]undecene nucleus was formed. On a preparative scale it was more efficient to conduct the cyclization directly in refluxing toluene containing triethylamine (99%). Unfortunately the base created a mixture of stereoisomers that consisted of keto-ester epimers (~1:1) and *endo*/*exo* ester isomers (5:1.5). As a result, this material was used directly in subsequent transformations and the offending epimers transformed as follows. Selective hydrolysis and decarboxylation of the α-ester was effected with lithium chloride in aqueous dimethyl sulfoxide and the resulting cyclohexanone protected as its ethylene ketal to afford the ester **11** in which the adjacent cyclohexane bond was *exo* (43% overall yield from **8**). The identical sequence was employed, commencing with **10** to generate **11**.

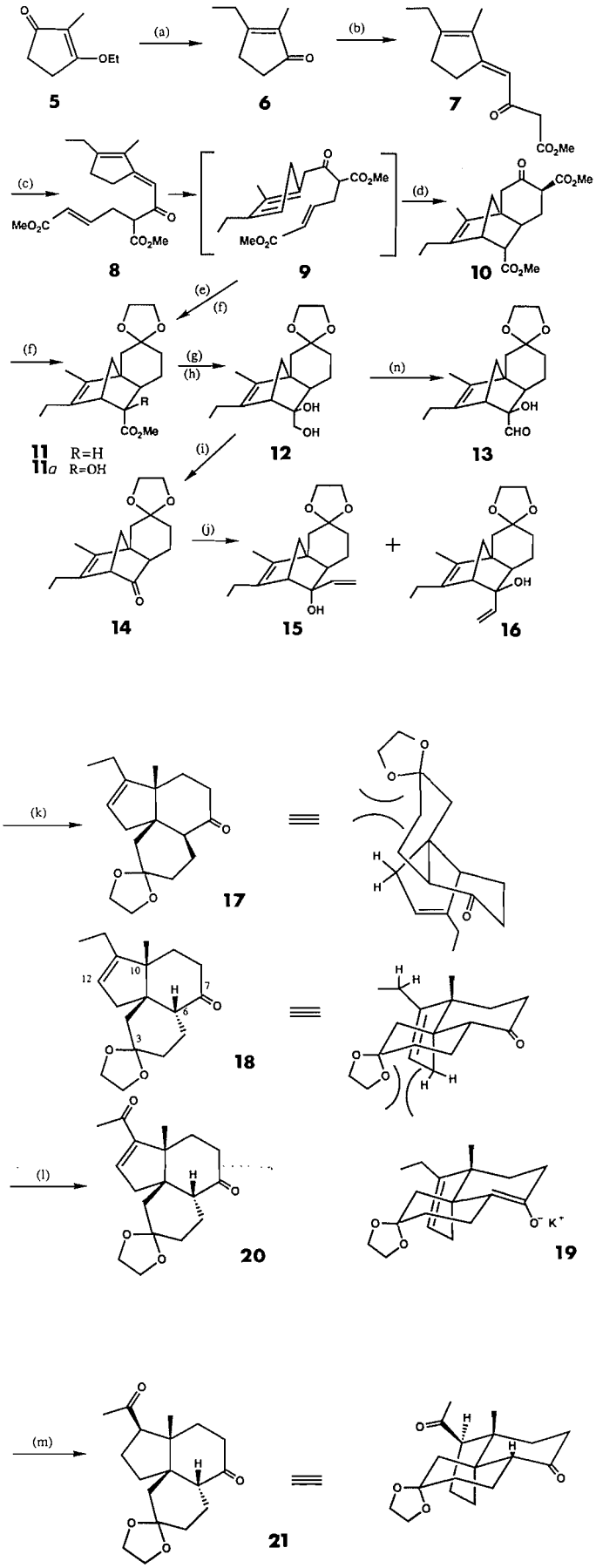
Two different approaches to the tricyclic 1,5-diene **16** were examined. The ester enolate of **11** was generated at −78°C with lithium diisopropylamide (LDA) and quenched with oxygen to afford the hydroxy ester as a single isomer. Reduction of the methyl ester with $LiAlH_4$ gave the diol **12**. It had been anticipated that the alcohol **16** could be prepared directly by oxidation of the primary alcohol followed by Wittig reaction on the resulting aldehyde **13**. The desired oxidation was accomplished under Swern conditions (17), but unfortunately this hydroxy-aldehyde was very unstable and rendered this route impractical since the best yield was 23%. Consequently, the diol **12** was converted to the ketone **14** by periodate oxidation. In spite of the *exo* orientation of the adjacent cyclohexane ring, the carbonyl was attacked preferentially from the top face with vinyl magnesium bromide to give a 3:1 ratio of *endo* and *exo* alcohols **15** and **16**. Conditions to improve this ratio, using a variety of Lewis acids ($CdCl_2$, $ZnCl_2$, $TiCl_4$, $EtAlCl_2$, Et_2AlCl, etc.), were investigated with a view to preferentially complexing the *exo* surface, but the ratio did not change significantly.

Previous studies (18) established that significant acceleration is induced by potassium salts in anionic oxy-Cope rearrangements. Thus, as anticipated, the potassium salt of **16** underwent smooth sigmatropic rearrangement in refluxing THF to the tricyclic ketones **17** and **18** in 67% isolated yield. The initial product was a 1:1 mixture of these *trans* and *cis* cyclohexanones. The *trans* ring junction was strongly favored in the cycloheptane series required for gascardic acid (5) but this is not the case for these cyclohexanes. To generate the natural product stereochemistry, the *exo* cyclohexane bond in **16** must be isomerized via the intermediacy of enolate **19**. However, protonation was not selective as a consequence of the very similar nonbonded interactions that are present in each isomer, particularly between the cyclopentenyl methylene hydrogens and the ketal. This was confirmed by epimerizing **17** with sodium methoxide to give a 1:1 mixture of **17** and **18**. Nevertheless the ketal is important for the subsequent steps.

As illustrated, the cyclopentene ring C13 methylene group in **18** is relatively hindered, compared to the side-chain ethyl group attached to C11, due to the juxtaposition of the oxygen ketal at C3. Thus allylic oxidation with selenium dioxide followed by oxidation of the secondary alcohol with pyridinium chlorochromate (PCC) afforded the conjugated methyl ketone **20** rather than the corresponding cyclopent-11-en-13-one. Treatment of this unsaturated ketone **20** with lithium/ethylene diamine, followed by PCC to correct some reduction of the carbonyl function, provided the tricyclic triketone **21**. In view of the concave nature of the skeleton **20**, dissolving metal reduction should generate the methyl ketone with a *cis* orientation relative to the bridgehead C10 methyl group. This was

Can. J. Chem. Downloaded from www.nrcresearchpress.com by 195.138.81.100 on 09/07/12
For personal use only.

Can. J. Chem. Downloaded from www.nrcresearchpress.com by 195.138.81.100 on 09/07/12
For personal use only.



confirmed by ^{1}H nmr nOe difference spectra, which displayed strong (20–27%) signal enhancements for the methyl ketone (δ 2.19) and tertiary methyl (δ 0.74) signals consistent with the stereochemistry illustrated.

In conclusion, as illustrated by the synthesis of **21**, this intramolecular cycloaddition – [3,3] sigmatropic rearrangement strategy provides a general entry to diverse multicyclic skeletons contained in natural products such as gascardic acid. Several steps are required to complete the total synthesis, including exocyclic methylene introduction via a Wittig reaction, side-chain attachment, diazoester-based ring expansion, reductive elimination, and hydrolysis, but they have ample literature precedent in simpler systems. A related approach, based on these cycloaddition and rearrangement concepts, and which combines different pericyclic reactions, is being developed for the total synthesis of retigeranic acid.

Experimental

Melting points were determined in capillary tubes with a Thomas–Hoover Uni-Melt apparatus or a Fisher–Johns melting point apparatus, and are uncorrected. Infrared (ir) spectra were recorded on a Perkin–Elmer 783 or 983G infrared spectrophotometer. Proton magnetic resonance spectra (^{1}H nmr) were measured at 60 MHz with a Varian model EM 360 spectrometer, at 200 MHz with a Varian Gemini spectrometer, or at 300 MHz with a General Electric GN 300 spectrometer or a Varian XL-300 spectrometer in deuterochloroform. Carbon magnetic resonance spectra (^{13}C nmr) were measured at 75 MHz with a General Electric GN 300 spectrometer or a Varian XL-300 spectrometer. Chemical shifts are reported in ppm downfield from tetramethylsilane (δ scale) as an internal standard; the numbers of protons, multiplicity, and coupling constants are indicated in parentheses. Mass spectra were determined on a V. G. Micromass 7070 HS instrument using an ionization energy of 70 eV, or on a Hewlett Packard 5890A gas chromatograph 5970B mass selective detector equipped with a 12.5-m capillary column (0.2 mm i.d.) coated with cross-linked dimethyl silicone (0.33 μm). Flash column chromatography using E. Merck silica gel 60 (230–400 mesh) was employed for all column chromatography. Analytical thin-layer chromatography (tlc) was carried out on aluminum sheets precoated (0.2 mm layer thickness) with silica gel 60 F_{254} (E. Merck). The purity of all title compounds was judged to be ≥95% as determined by a combination of gc–ms, ^{1}H nmr, and ^{13}C nmr analysis.

Petroleum ether refers to a fraction with boiling range 30–60°C. Anhydrous diethyl ether (ether), tetrahydrofuran (THF), dimethoxyethane (DME), and dioxane were obtained by distillation from $LiAlH_4$ or potassium/benzophenone. Methanol and absolute ethanol were dried by distillation from magnesium. Dry hexamethylphosphoramide (HMPA), dimethylformamide (DMR), dimethyl sulfoxide (DMSO),

Reagents: (a) EtBr, ether, Li/Na)))))) 10°C, 1 h, 98%; (b) $CH_3COCH_2COOCH_3$, NaH, THF, 0–60°C, 20 min; BuLi, 0°C, 10 min; **6**, 0°C, 20 min; 10% aq. HCl, 21°C, 1 h, 64%; (c) KH, THF, 0–21°C, 20 min; $BrCH_2CH{=}CHCOOCH_3$, 21°C, 2 h, 64%; (d) $EtAlCl_2$, 21°C, 16 h, 30%; (e) Et_3N, MeC_6H_5, 110°C, 72 h, 100%; (f) LiCl, H_2O. DMSO, 160°C, 1 h, 75%; $HOCH_2CH_2OH$, $MeC_6H_4SO_3H$, C_6H_6, 80°C, 6 h, 43% from **8**; (g) iPr$_2$NH, nBuli, THF, 0°C, 10 min; **11**, −78°C, 1 h; O_2, −78°C, 2 h, 43%; (h) $LiAlH_4$, ether/CH_2Cl_2 1:1, 0–21°C, 30 min; (i) $HIO_4{\cdot}2H_2O$, ether/CH_2Cl_2 1:1, 0–21°C, 1 h, 30% from **11**; (j) $CH_2{=}CH_2MgBr$, 21°C, 30 min, 84% 1:3 *exo*/*endo* alcohol; (k) KH, I_2, THF, 21°C, 10 min; **10**, 21–67°C, 30 min, 67% 1:1; (l) SeO_2, dioxane, 80°C, 4 h; PCC, NaOAc, 4Å sieves, CH_2Cl_2, 0–21°C, 1 h, 49%; (m) Li, $NH_2CH_2CH_2NH_2$, dioxane, t-BuOH, 30 min; PCC, NaOAc, 4Å sieves, CH_2Cl_2, 0–21°C, 1 h, 24%; (n) DMSO, $(COCl)_2$, CH_2Cl_2, 0°C, 20 min, 23%.

SCHEME 2

Can. J. Chem. Downloaded from www.nrcresearchpress.com by 195.138.81.100 on 09/07/12
For personal use only.

and diisopropylamine were prepared by distillation from calcium hydride. Solutions in organic solvents were dried over anhydrous magnesium sulfate and stripped of solvent with a Büchi rotary evaporator connected to a water aspirator. Unless otherwise indicated, all reactions were conducted under an atmosphere of dry nitrogen.

*2-Methyl-3-ethylcyclopentenone (**6**)*

The Li/Na "alloy" was prepared as follows. Lithium (510 mg) and sodium (25 mg) were washed with petroleum ether and placed in a round bottom flask previously flushed with nitrogen. The metals were heated, with a heat gun, under vacuum until the sodium had melted. This initiated contact between the molten sodium and the solid lithium and the flask was allowed to cool to room temperature. The "activated lithium" prepared in this manner was highly effective for the preparation of alkyl lithiums using ultrasound.

The enone **5** (5.0 g, 35.7 mmol) was added to a suspension of activated lithium (570 mg Li/25 mg Na, 82 mmol) in ether. The mixture was irradiated with ultrasound (cleaning bath) while ethyl bromide was added dropwise. The irradiation was continued for 1 h (i.e., until the activated lithium disappeared); then the reaction mixture was quenched with water. The ethereal phase was washed thoroughly with water, dried, filtered, and concentrated to give **6**, 4.35 g (98%); ir (neat): 1695 (C=O), 1645 (C=C) cm^{-1}; ^1H nmr ($CDCl_3$) δ: 2.4 (6H, m, -CH_2CH_2-, CH_2CH_3), 1.69 (3H, br s, =C-CH_3), 1.1 (3H, t, J = 7.5 Hz, -CH_2CH_3).

*Methyl 3-oxo-4-*E*-(2-methyl-3-ethyl-2-cyclopentyl)butenoate (**7**)*

Methyl acetoacetate (4.1 mL, 4.4 g, 38 mmol) was added dropwise to a suspension of sodium hydride (1.52 g (60% in mineral oil), 38 mmol) in dry tetrahydrofuran (100 mL) maintained at 0°C. The reaction mixture was warmed to 60°C and stirring was continued for a further 20 min. The reaction was recooled to 0°C, butyllithium (14.7 mL of a 2.6 M solution in hexanes, 38 mmol) added, and the mixture stirred for a further 10 min. The enone **6** (4.15 g, 33.4 mmol) was added dropwise and the resulting solution was stirred for a further 20 min. The reaction mixture was diluted with ether (400 mL) and was stirred vigorously with 10% aqueous hydrochloric acid (100 mL) for 2 h. The organic portion was washed with water (5 × 50 mL), dried, filtered, and concentrated. This material was purified by flash chromatography (9:1, petroleum ether/acetone) to give 4.74 g (64%) of β-ketoester **7**; ir (neat): 1735 (C=O, ester), 1675 (C=O, enone), 1580 (C=C), 1145 (C—O) cm^{-1}; ^1H nmr ($CDCl_3$) δ: 6.05 (1H, s, -C=CH-), 3.72 (3H, s, -CO_2CH_3), 3.53 (2H, s, -$CH_2CO_2CH_3$), 3.01 (2H, m, -CH_3CH_2C=CH-), 2.51 (2H, br s, -CH_2CH_2C=CCH), 2.37 (2H, q, J = 7.7 Hz, -CH_2CH_3), 1.73 (3H, s, -C=CCH_3), 1.07 (3H, t, J = 7.7 Hz, -CH_2CH_3); ^{13}C nmr ($CDCl_3$) δ: 190.9, 172.2, 168.3, 164.0, 133.7, 110.9, 51.7, 49.9, 34.1, 31.0, 12.1, 9.6. Exact Mass calcd. for $C_{13}H_{18}O_3$: 222.1256; found: 222.1254.

*Methyl 5-carbomethoxy-6-oxo-7-(*E*)-(2-methyl-3-ethyl-2-cyclopentenyl)-2-(*E*)-heptenoate (**8**)*

A solution of β-ketoester **7** (725 mg, 3.26 mmol) in dry THF (5 mL) was added dropwise (cannula) to a suspension of potassium hydride (145 mg, 3.6 mmol) in dry THF (5 mL) maintained at 0°C. The reaction mixture was allowed to warm to room temperature and stirred for 20 min. Methyl 4-bromocrotonate (0.5 mL (85%), ≅637 mg, ≅3.5 mmol, Aldrich) was added and the resulting solution stirred at room temperature for 2 h. The reaction was diluted with ether (100 mL), washed with water (5 × 25 mL), dried, filtered, and concentrated. The residue was purified by flash chromatography (9:1, petroleum ether/acetone) to give 665 mg (64%) of triene **8** and 116 mg (8.5%) of dialkylated product; ^1H nmr ($CDCl_3$) δ: 6.91 (1H, d of t, J = 15.7 Hz, J = 7.2 Hz, -CH=$CHCO_2CH_3$), 6.07 (1H, s, -C=CH-), 5.89 (1H, d, J = 15.7 Hz, =$CHCO_2CH_3$), 3.73 and 3.71 (6H, 2 s, 2 × OCH_3), 3.69 (1H, t, J = 7.4 Hz, $CHCH_2$), 3.03 (2H, m, -CH_2-CH_2C=CH), 2.79 (2H, t (dd), J = 7.0 Hz, -$CHCH_2CH$=CH-), 2.54 (2H, br s, -CH_2CH_2C=CH-), 2.38 (2H, q, J = 7.6 Hz, -CH_2CH_3), 1.74 (3H, s, -C=CCH_3), 1.08 (3H, t, J = 7.6 Hz, -CH_2CH_3); ^{13}C nmr ($CDCl_3$) δ: 191.9, 174.0, 170.1, 166.6, 165.3, 145.5, 134.1, 122.9, 110.2, 58.0, 52.5, 51.5, 34.4, 31.6, 31.0, 23.3, 12.4, 9.9. Exact Mass calcd. for $C_{18}H_{24}O_5$: 320.1624; found: 320.1623.

Dialkylated product: ^1H nmr ($CDCl_3$) δ: 6.72 (2H, d of t, J = 15.5 Hz, J = 7.7 Hz, 2 × -CH=$CHCO_2CH_3$), 5.95 (1H, s, -C=CH-), 5.87 (2H, d, J = 15.5 Hz, 2× =$CHCO_2CH_3$), 3.74 (3H, s, -CO_2CH_3), 3.71 (6H, s, 2× =$CHCO_2CH_3$), 3.05 (2H, m, -CH_2CH_2C=CH-), 2.81 (4H, d, J = 7.7 Hz, 2× -CH_2CH=CH-), 2.52 (2H, br s, -CH_2CH_2C=CH-), 2.38 (2H, q, J = 7.5 Hz, -CH_2CH_3), 1.70 (3H, s, -C=CCH_3), 1.09 (3H, t, J = 7.5 Hz, -CH_2CH_3).

Diels–Alder cyclization

(a) With $EtAlCl_2$

Ethyl aluminum dichloride (1.8 mL of 1.8 M toluene solution, 0.96 equiv., Aldrich) was added to a solution of triene **8** (108 mg, 0.34 mmol) in dry dichloromethane (3 mL). After stirring for 16 h at 21°C, ether (30 mL) was added and the resulting solution was washed sequentially with 10% aqueous HCl (2 × 5 mL), with 5% aqueous sodium carbonate (2 × 5 mL), and with water (3 × 5 mL). The organic phase was dried, filtered, and concentrated. The residue was purified by flash chromatography (96:4, toluene/acetone) to give 32 mg (30%) of β-ketoester **10**; ir (neat):1720 (br C=O, β-ketoester and ester), 1645 (C=C), 1170 (C—O) cm^{-1}; ^1H nmr ($CDCl_3$) δ: 3.69 and 3.67 (6H, 2 s, 2× -CO_2CH_3), 3.37 and 3.10 (2H, 2 d, part A and B of an AB system, J_{AB} = 16.10 Hz, -CH_2C=O), 3.26 (1H, t, J ≅ 7.5 Hz, O=$CCHCO_2CH_3$), 2.82 (1H, m, -C=CCH-), 2.51 (1H, br s, -$CHCO_2CH_3$), 2.06 (2H, m, -$CHCH_2CH$-), 1.77 (3H, s, -C=CCH_3), 1.68–1.82 (3H, m, =$CCHHCH_3$, CHH bridge, -$CHCHCH_2$-), 1.40–1.50 (2H, m, =$CCHHCH_3$, CHH bridge), 0.90 (3H, t, J = 7.3 Hz, -CH_2CH_3); ^{13}C nmr ($CDCl_3$) δ: 200.0, 175.4, 170.5, 143.5, 132.9, 63.1, 52.1, 51.9, 51.7, 51.5, 48.2, 44.9, 44.4, 43.9, 32.2, 21.3, 10.8, 8.9.

(b) Thermal

The triene **8** (3.0 g, 9.37 mmol) and triethylamine (1.89 g, 2.6 mL, 18.6 mmol) were dissolved in dry toluene (140 mL) and refluxed for 72 h. The solvent was evaporated to give the Diels–Alder adducts **10** (≅3.0 g, 100%). The crude material was used directly in the next step. A sample was purified by flash chromatography (9:1, petroleum ether/acetone); ^1H nmr ($CDCl_3$) (60 MHz) *endo/exo* mixture, characteristic peaks, δ: 3.60–3.76 (6H, s, 2× CO_2CH_3), 1.60 (3H, s, -C=CCH_3), 0.8–1.2 (3H, t, J = 7.5 Hz, -CH_2CH_3). The Diels–Alder adducts **10** (~3.0 g, 9.37 mmol), lithium chloride (0.9 g, 21 mmol), and water (230 mg, 12.7 mmol) were dissolved in dimethyl sulfoxide (23 mL) and heated at 160°C for 1 h. Water (50 mL) was added and the resulting solution extracted with a mixture of ether/petroleum ether (1:4, 4 × 100 mL). The organic phase was washed with water (4 × 50 mL), dried, filtered, and concentrated. The oily residue (1.85 g, 75.5% of crude ketone, unprotected **11**) was used directly in the next step. A sample of this keto-ester was purified by flash chromatography (96:4, toluene/acetone); ^1H nmr ($CDCl_3$) (60 MHz) *endo/exo* mixture, characteristic peaks, δ: 3.65 and 3.58 (3H, s, -CO_2CH_3), 1.58 (3H, s, -C=CCH_3), 0.8–1.2 (3H, t, J = 7.5 Hz, -CH_2CH_3). The crude tricyclic ketone (unprotected **11**) (1.85 g, 7 mmol), ethylene glycol (556 mg, 500 mL, 9 mmol), and pyridinium *p*-toluenesulfonate (170 mg, 0.66 mmol) were dissolved in dry benzene (50 mL) and refluxed (Dean–Stark) for 6 h. The solvent was evaporated and the residue dissolved in ether (100 mL). The ether solution was washed with water (4 × 25 mL), dried, filtered, and concentrated. The residue was purified by flash chromatography to give 1.24 g (43%, for three steps) of dioxolane **11**; ir (neat):1725 (C=O, ester), 1650 (C=C) cm^{-1}; ^1H nmr ($CDCl_3$) δ: 3.93 (4H, s, -OCH_2CH_2O-), 3.67 and 3.60 (3H, 2 s, 2× -OCH_3, *exo/endo* 1.5:5), 3.00 (1H, m, -C=CCH-), 2.53 (1H, t (dd), J = 3.7 Hz, -$CHCO_2CH_3$), 1.63 and 1.53 (3H, 2 s, 2× C=CCH_3), 1.10–2.80 (11H, m, -$CHCH_2CH_2$-C-CH_2-, -CH_2CH_3, -CH_2- bridge), 0.96 and 0.85 (3H, 2 t, J = 7.5 Hz and 7.4 Hz, 2× -CH_2CH_3); ^{13}C nmr ($CDCl_3$) δ: (*endo*) 174.9, 141.1, 138.9, 109.3, 64.5, 63.9, 55.1, 54.5, 51.1, 49.8, 48.3, 39.8, 36.3, 34.0, 29.5, 20.6, 13.0, 9.3; (*exo*) 176.5, 140.0, 137.5, 111.1, 64.3, 63.6, 62.5, 53.4, 51.4, 44.6, 47.8, 46.1, 38.6, 31.6, 26.5, 21.5, 11.0, 8.5.

Can. J. Chem. Downloaded from www.nrcresearchpress.com by 195.138.81.100 on 09/07/12
For personal use only.

7-endo-*Carbomethoxy-9-ethyl-10-methyl-3,3-ethylenedioxytricyclo-[6.2.1.0^{1,6}]-9-undecene (**11**)*

The decarboalkoxylation and the acetalyzation of isomerically pure β-ketoester **10** was conducted as described above, using the following quantities: A. decarboalkoxylation: β-ketoester **10** (28 mg, 8.75 × 10^{-2} mmol), lithium chloride (10 mg, 0.23 mmol), and water (10 mg, 0.55 mmol) in dimethyl sulfoxide (3 mL). B. acetalyzation: ketone intermediate (15 mg, 5.7 × 10^{-2} mmol), ethylene glycol (27.8 mg, 25 mL, 0.45 mmol), and pyridinium *p*-toluenesulfonate (10 mg, 3.88 × 10^{-2} mmol) in benzene (20 mL). The crude material was purified by flash chromatography (96:4, petroleum ether/acetone) to give 4.5 mg (17%, 2 steps) of dioxolane **11**; ^{1}H nmr ($CDCl_3$) δ: 3.94 (4H, s, -OCH_2CH_2O-), 3.60 (3H, s, -CO_2CH_3), 3.00 (1H, m, -C═CCH), 2.53 (1H, t (dd), J = 7.7 Hz, -$CHCO_2CH_3$), 1.53 (3H, s, -C═CCH_3), 1.10–2.40 (11H, m, -$CHCH_2CH_2$-C-CH_2-, -CH_2CH_3, -CH_2- bridge), 0.96 (3H, t, J = 7.53 Hz, -CH_2CH_3).

7-endo-*Carbomethoxy-9-ethyl-10-methyl-3,3-ethylenedioxytricyclo-[6.2.1.0^{1,6}]-9-undecen-7-ol (**11**a)*

A solution of *n*-butyllithium (5.2 mL, 2.5 M in hexane, 13 mmol, Aldrich) was added dropwise to a stirred solution of dry diisopropylamine (1.44 g, 2 mL, 14.2 mmol) in dry tetrahydrofuran (10 mL) maintained at 0°C. After 10 min, the mixture was cooled to −78°C and a solution of ester **11** (800 mg, 2.6 mmol) in tetrahydrofuran (5 mL) was added dropwise. The resulting solution was stirred 1 h and dry oxygen was slowly bubbled through the solution for a period of 2 h (1 h at −78°C and 1 h from −78 to −10°C) after which time dimethyl sulfide (3 mL) was added. The solvent was evaporated and the residue dissolved in ether (200 mL). The ether solution was washed with water (5 × 50 mL), dried, filtered, and the solvent evaporated. The crude product was purified by flash chromatography (9:1, petroleum ether/acetone) to give starting material **11** (82 mg, 10%) and α-hydroxy ester intermediate **11***a* (360 mg, 43%); ir (KBr): 3395 (OH), 1734 (C═O), 1000–1170 (C—O) cm^{-1}; ^{1}H nmr ($CDCl_3$) δ: 3.94 (4H, m, -CH_2CH_2O-), 3.68 (3h, s, -CO_2CH_3), 2.80 (1H, s, -OH), 2.56 (1H, s, -C═CCH-), 2.30 and 1.26 (2H, d apparent, J = 8.8 Hz and d of t apparent, J = 8.8 Hz, J = 1.5 Hz, -CH_2- bridge), 2.14 (1H, sextet (d of q), J = 7.3 Hz, -$CHHCH_3$), 1.51 (3H, s, C═CCH_3), 1.45–2.05 (8H, m, -$CHHCH_3$, -$CHCH_2CH_2$-C-CH_2-), 0.94 (3H, t, J = 7.5, -CH_2CH_3); ^{13}C nmr ($CDCl_3$) δ: 175.8, 140.8, 139.3, 109.0, 83.4, 64.5, 63.8, 57.2, 54.9, 52.3, 48.8, 43.4, 36.4, 33.0, 22.4, 20.4, 13.0, 9.8. Anal. calcd. for $C_{18}H_{26}O_5$: C 67.06, H 8.13; found: C 66.78, H 8.11.

*9-Ethyl-10-methyl-3,3-ethylenedioxytricyclo[6.2.1.0^{1,6}]-9-undecen-7-one (**14**)*

Lithium aluminum hydride (1.48 g, 39 mmol) was added to a stirred solution of the α-hydroxy ester intermediate **11***a* (3.15 g, 9.78 mmol) in a mixture of dry ether and dichloromethane (1:1, 250 mL) maintained at 0°C. After the addition was complete, the ice bath was removed and the reaction mixture was stirred for 30 min after reaching room temperature. The reaction was recooled to 0°C, excess Glauber's salt (10 g) was slowly added, and the mixture was allowed to warm to room temperature and stirred for 1 h. Finally, anhydrous magnesium sulfate (10 g) was added and the slurry filtered and concentrated. The crude diol **12** (2.94 g) was used without further purification in the next step. An analytical sample was obtained by flash chromatography (7:3, petroleum ether/acetone); ir(neat): 3400 (OH), 1090 (C—O) cm^{-1}; ^{1}H nmr ($CDCl_3$) δ: 3.94 (4H, s, -OCH_2CH_2O-), 3.33 and 3.27 (2H, 2 d, part A and B of an AB system, J_{AB} = 10.74 Hz, -CH_2O), 2.68 (2H, br, 2× -OH)), 2.49 (1H, s, -C═CCH-), 1.48 (3H, s, -C═CCH_3), 1.20–2.30 (11H, m, -$CHCH_2CH_2$-C-CH_2-, -CH_2CH_3, -CH_2- bridge), 1.00 (3H, t, J = 7.5 Hz, -CH_2CH_3); ^{13}C nmr ($CDCl_3$) δ: 141.6, 139.3, 109.1, 84.1, 68.9, 64.5, 63.8, 54.4, 52.4, 48.1, 43.7, 36.5, 33.2, 23.2, 20.9, 13.2, 9.8. Exact Mass calcd. for $C_{17}H_{26}O_4$: 294.1831; found: 294.1828.

The diol **12** (2.87 g, 9.76 mmol), dissolved in a mixture of ether and dichloromethane (4:1, 250 mL) maintained at 0°C, was treated with periodic acid (4.4 g, 19 mmol) and sodium acetate (12 g, 146 mmol). The cooling bath was removed and the reaction was stirred for 1 h after reaching room temperature. The solution was filtered through Celite using ether as eluant. The filtrate was washed with water (6 × 50 mL), dried, filtered, and concentrated. The crude product was purified by flash chromatography to give 1.79 g (70% 2 steps) (30%, overall, from ester **11**) of ketone **14** along with 300 mg (14%) of the diketone from acetal cleavage; **14**: ir (neat): 1728 (C═O), 1650 (C═C), 1030–1150 (C—O) cm^{-1}; ^{1}H nmr ($CDCl_3$) δ: 3.94 (4H, s, -OCH_2CH_2O-), 2.85 (1H, s, -C═CCH-), 2.40 (1H, d, J = 14.7 Hz, -$CHCH_2CH_2$-), 1.50 (3H, s, -C═CCH_3), 1.40–2.20 (10H, m, -CH_2CH_2-C-CH_2, -CH_2CH_3, -CH_2- bridge), 0.94 (3H, t, J = 7.5 Hz, -CH_2CH_3); ^{13}C nmr ($CDCl_3$) δ: 216.3, 144.9, 138.5, 108.8, 63.6, 63.9, 59.1, 52.2, 48.7, 44.3, 36.6, 33.4, 23.6, 20.7, 12.8, 10.4. Exact Mass calcd. for $C_{16}H_{22}O_3$: 218.1307; found: 218.1282.

7-endo-*Carboxaldehyde-9-ethyl-10-methyl-3,3-ethylenedioxytricyclo[6.2.1.0^{1,6}]-9-undecen-7-ol (**13**)*

Excess triethylamine (10 drops), dimethyl sulfoxide (5 drops), and oxalyl chloride (3 drops) were added to a dry dichloromethane (2 mL) solution of diol **12** (11 mg, 0.037 mmol) maintained at 0°C. The reaction mixture was stirred for 20 min, then ether (10 mL) was added and the resulting solution washed with water (3 × 3 mL). The ethereal phase was dried, filtered, and concentrated to give an oil, which was purified by flash chromatography (4:1, petroleum ether/acetone) to give **13**, 2.5 mg (23%); ^{1}H nmr ($CDCl_3$) δ: 9.07 (1H, s, HC═O), 3.96 (4H, s, OCH_2CH_2O), 3.51 (1H, s, -OH), 2.53 (1H, s, HC-C═C), 1.58 (3H, s, CH_3-C═C), 1.20–2.40 (11H, m's, CH, CH_2's), 0.98 (3H, t, J = 7.5 Hz, CH_3-CH_2).

7-exo-*Ethenyl-9-ethyl-10-methyl-3,3-ethylenedioxytricyclo-[6.2.1.0^{1,6}]-9-undecen-7-ol (**15**) and 7*-endo-*ethenyl-9-ethyl-10-methyl-3,3-ethylenedioxytricyclo[6.2.1.0^{1,6}]-9-undecen-7-ol (**16**)*

Vinyl magnesium bromide (7 mL of a 1 M solution in tetrahydrofuran, Aldrich) was added dropwise to a stirred solution of ketone **14** (1.64 g, 6.26 mmol) in dry ether (100 mL) at room temperature (21°C). After 30 min, the reaction mixture was quenched with saturated aqueous ammonium chloride. The ethereal phase was washed with water (4 × 50 mL), dried, filtered, and concentrated. The crude products were purified by flash chromatography (95:5, petroleum ether/acetone) to give 370 mg (20.4%) of *exo*-alcohol **16** along with 1.15 g (63.5%) of *endo*-alcohol **15**. **16**: ir (KBr): 3445 (OH), 1622 (C═C), 1050–1130 (C—O) cm^{-1}; ^{1}H nmr ($CDCl_3$) δ: 5.67, 5.18, 4.95 (3H, 3 d of d, parts X, A, and B of an ABX system, J_{AX} = 17.3 Hz, J_{BX} = 10.7 Hz, J_{AB} = 1.5 Hz, -CH_X═CH_AH_B-), 3.95 (4H, m, -OCH_2CH_2O-), 2.36 (1H, s, -C═CCH-), 1.51 (3H, d, J = 0.93 Hz, -C═CCH_3), 1.20–2.35 (12H, m, -O*H*,-$CHCH_2CH_2$-C-CH_2-, -CH_2- bridge, -CH_2CH_3), 0.96 (3H, t, J = 7.5 Hz, -CH_2CH_3); ^{13}C nmr ($CDCl_3$) δ: 145.6, 141.3, 139.4, 110.7, 109.1, 82.8, 64.5, 63.7, 57.2, 51.6, 48.6, 46.7, 36.5, 33.2, 22.2, 21.3, 13.0, 9.7. Anal calcd. for $C_{18}H_{26}O_3$: C 74.44, H 9.02; found: C 74.77, H 8.62. **15**: ir (KBr): 3460 (OH), 16.30 (C═C), 1000–1130 (C—O) cm^{-1}; ^{1}H nmr ($CDCl_3$) δ: 6.05, 5.30, 5.11 (3H, 3 d of d, parts X, A, and B of an ABX system, J_{AX} = 17.26 Hz, J_{BX} = 10.83 Hz, J_{AB} = 1.33 Hz, -CH_X═CH_AH_B-), 3.91 (4H, s, -OCH_2CH2O-), 2.55 (1H, s, -C═CCH-), 2.36 (1H, sextet (d of q), J = 7.2. Hz, -$CHHCH_3$), 1.62 (3H, s, -C═CCH_3), 1.08–2.10 (11H, m, -OH, -$CHCH_2CH_2$-C-CH_2-, -CH_2- bridge, -$CHHCH_3$), 1.01 (3H, t, J = 7.5 Hz, -CH_2CH_3); ^{13}C nmr ($CDCl_3$) δ: 142.3, 141.9, 139.6, 112.0, 108.9, 84.2, 64.4, 63.7, 54.4, 51.3, 49.2, 36.7, 33.7, 25.9, 22.2, 13.1, 9.8. Exact Mass calcd. for $C_{18}H_{26}O_3$: 290.1882; found: 290.1910.

(1R, 6S*, 10R*)-10-Methyl-11-ethyl-3,3-ethylenedioxytricyclo-[7.4.0^{1,6},0^{1,10}]-11-tridecen-7-one (**17**) and (1R*, 6R*, 10R*)-10-methyl-11-ethyl-3,3-ethylenedioxytricyclo[7.4.0^{1,6},0^{1,10}]-11-tridecen-7-one (**18**)*

Potassium hydride (120 mg, 3 mmol), suspended in dry tetrahydrofuran (4 mL), was treated with iodine (72 mg, 0.28 mmol) and stirred at room temperature for 10 min. A solution of alcohol **16** (167 mg, 0.57

Can. J. Chem. Downloaded from www.nrcresearchpress.com by 195.138.81.100 on 09/07/12
For personal use only.

mmol) in dry tetrahydrofuran (3 mL) was added in a single portion, and the resulting mixture was heated at 70°C for 30 min. The reaction was quenched with water and extracted with ether (3 × 40 mL). The organic phase was washed with water (4 × 25 mL), dried, filtered, and concentrated to give an oil. Flash chromatography (9:1, petroleum ether/acetone) afforded 112 mg (67%) of a 1:1 mixture of **17** and **18**. These could be separated by plc (4:1, petroleum ether/acetone). **17**: ir (neat): 3040 (=C-H), 1698 (C=O), 1090 (C—O) cm^{-1}; ^1H nmr ($CDCl_3$) δ: 5.44 (1H, br s, -C=CH-), 3.93 (4H, m, $-OCH_2CH_2O-$), 2.51 (1H, br s, -CHC=O), 1.40–2.60 (14H, m, $-CH_2CH_2-C-CH_2-$, $-CH_2CH_3$, $-C=CHCH_2-$, $-CH_2CH_2C=O$), 1.17 (3H, t, J = 7.3 Hz, $-CH_2CH_3$), 0.80 (3H, s, $-CH_3$); ^{13}C nmr ($CDCl_3$) δ: 213.0, 151.1, 121.8, 109.7, 64.5, 63.8, 55.6, 51.8, 48.1, 42.3, 39.2, 38.2, 32.4, 31.2, 21.3, 19.6, 19.6, 11.7. **18**: ir (neat): 3040 (=C-H), 1704 (C=O), 1090 (C-O) cm^{-1}; ^1H nmr ($CDCl_3$) δ: 5.32 (1H, br s, -C=CH), 3.92 (4H, m, $-OCH_2CH_2O-$), 2.80 (1H, d of d apparent, J = 17.6 Hz, J = 2.3 Hz, -CHC=O), 1.20–2.40 (14H, m, $-CH_2CH_2-C-CH_2-$, $-CH_2CH_3$, $-C=CCHCH_2-$, $-CH_2CH_2C=O$), 1.08 (3H, t, J = 7.3 Hz, $-CH_2CH_3$), 1.04 (3H, s, $-CH_3$); ^{13}C nmr ($CDCl_3$) δ: 213.9, 148.1, 121.1, 109.4, 64.5, 63.4, 54.6, 52.3, 51.1, 41.2, 39.4, 35.8, 33.9, 32.6, 22.0, 20.6, 19.3, 12.2. Exact Mass calcd. for $C_{18}H_{26}O_3$: 290.1880; found: 290.1904. Anal. calcd. for $C_{18}H_{26}O_3$: C 74.44, H 9.02; found: C 74.32, H 8.98.

Equilibration of 17 and 18

An epimeric sample of ketones **17** and **18** (~3:2) (52 mg, 0.178 mmol) dissolved in anhydrous methanol (3 mL) was added to a sodium methoxide solution (1 mL MeOH; Na, 2 mg). The resulting solution was warmed to 60°C over 1.5 h, then cooled to room temperature, concentrated, and ether (20 mL) and water (5 mL) added. The reaction mixture was extracted with ether, washed with brine, dried, filtered, and concentrated. The ^1H nmr analysis of the oil obtained indicated that it was a 1:1 mixture of epimers.

(1R, 6R*, 10R*)-10-Methyl-11-acyl-3,3-ethylenedioxytricyclo-[7.4.0^{1,6},0^{1,10}]-11-tridecen-7-one (20)*

Ketone **18** (33 mg, 0.114 mmol) was dissolved in dioxane (3 mL) containing freshly sublimed selenium dioxide (13.8 mg, 0.125 mmol) and heated at 80°C for 4 h. Water (5 mL) and ether (15 mL) were added to the cooled reaction mixture and the ether extracts were dried, filtered, and concentrated. The resulting oil (34.8 mg, 0.114 mmol) was dissolved in dichloromethane (3 mL) at 0°C and pyridinium chlorochromate (PCC) (40 mg), sodium acetate (20 mg), and 4Å molecular sieves (10 mg) were added. The reaction was stirred for 1 h during which time the temperature was allowed to rise to 21°C. Ether (20 mL) was added, the mixture was filtered through silica gel, concentrated, and chromatographed (hexane/acetone, 9:1) to provide the diketone **20**, 17 mg (49%); ir (neat): 3040 (=C-H), 1705 (C=O), 1658 (C=C-C=O) cm^{-1}; ^1H nmr ($CDCl_3$) δ: 6.84 (1H, br t, J = 1 Hz, HC=C), 3.92 (4H, m, OCH_2CH_2O), 2.93, 2.88 (1H, dt, J = 1, 14 Hz, HC-C=O), 2.69, 2.48 (2H, dd, J = 2, 2.5 Hz, $CH_2C=O$), 2.35 (3H, s, $CH_3-C=O$), 2.2–1.4 (10H, m, CH_2's), 0.96 (3H, s, CH_3-C); ^{13}C nmr ($CDCl_3$) δ: 211.5, 196.5, 149.5, 145.8, 109.4, 64.6, 64.0, 55.6, 52.1, 48.4, 43.2, 39.4, 37.7, 31.7, 31.1, 27.8, 21.4, 19.6. Exact Mass calcd. for $C_{18}H_{24}O_4$: 304.1673; found: 304.1660. Anal. calcd. for $C_{18}H_{24}O_4$: C 71.03, H 7.95; found: C 71.14, H 8.01.

(1R, 6R*, 10S*, 11R*)-10-Methyl-11-acyl-3,3-ethylenedioxytricyclo[7.4.0^{1,6},0^{1,10}]-7-tridecanone- (21)*

Ethylene diamine (~5 mL) was condensed in a round-bottom flask equipped with a Dry Ice condenser, and lithium (2.3 mg, 1.3 mmol) was added, followed by the diketone **20** (14 mg, 0.046 mmol) dissolved in THF (1 mL). The reaction was stirred for 0.5 h, solid NH_4Cl added, the condenser removed, and the reaction warmed to 21°C. Ether (30 mL) was added and the ether solution washed with water (4 × 5 mL), dried, filtered, and concentrated. This material (13.2 mg) was a mixture of keto-alcohols (ir: 3550–3150 (br OH) cm^{-1}) and thus was treated directly with excess pyridinium chlorochromate (PCC) in dichloromethane (2 mL) as above. This afforded, after plc (hexane/acetone 7:3), the saturated diketone **21** in 24% yield; ir (neat):1702 (C=O), 1726 (C=C) cm^{-1}; ^1H nmr ($CDCl_3$) δ: 3.89 (4H, m, OCH_2CH_2O), 3.41 (1H, t, J = 9.1 Hz, HC-$COCH_3$), 2.57 (1H, dd, J = 6.15 Hz, HC-C=O), 2.29, 2.26 (2H, m, CH_2-C=O), 2.19 (3H, s, CH_3-C=O), 1–2 (12H, m, CH_2's), 0.74 (3H, s, CH_3-C); ^{13}C nmr ($CDCl_3$) δ: 210.5, 209.6, 109.4, 64.6, 63.9, 55.1, 54.2, 48.2, 48.1, 38.7, 34.3, 31.9, 30.9, 27.4, 22.8, 21.9, 19.1, 19.1. Exact Mass calcd. for $C_{18}H_{26}O_4$: 306.1829; found: 306.1805.

Acknowledgments

We are grateful to Memorial University of Newfoundland (where this project was initiated), the University of Ottawa, and the Natural Sciences and Engineering Research Council of Canada for financial support of this research, and to Dr. H. Dettman for nmr spectra.

1. (*a*) G. Brochere and J. Polansky. Bull Soc. Chim. Fr. 993 (1960); (*b*) R. Scartazzini. Ph.D., Dissertation, ETH, Zurich, 1966.
2. (*a*) P. S. Rao, K. G. Sarma, and T. R. Seshadri. Curr. Sci. **34**, 9 (1965); (*b*) M. Kaneda, R. Takahashi, Y. Iitaka, and S. Shibata. Tetrahedron Lett. 4609 (1972). (*c*) M. Kaneda, Y. Iitaka, and S. Shibata. Acta Crystallogr. Sect. B: Struct. Crystallogr. Cryst. Chem. **B30**, 358 (1974).
3 (*a*) S. Nozoe, M. Morisaki, K. Tsuda, Y. Iitaka, N. Takahashi, S. Tamura, K. Ishibashi, and M. Shirasaka. J. Am. Chem. Soc. **87**, 4968 (1965); (*b*) S. Nozoe, K. Hirai, and K. Tsuda. Tetrahedron Lett. 2211 (1966).
4. *Retigeranic acid:* (*a*) E. J. Corey, M. C. Desai, and T. A. Engler. J. Am. Chem. Soc. **107**, 4339 (1985); (*b*) L. A. Paquette, J. Wright, G. J. Ortina, and R. A. Roberts. J. Org. Chem. **52**, 2960 (1987); (*c*) J. Wright, G. J. Ortina, R. A. Roberts, and L. A. Paquette. J. Am. Chem. Soc. **110**, 5809 (1988); (*d*) T. Hudlicky, A. Fleming and L. Radesca. J. Am. Chem. Soc. **111**, 6691 (1989); (*e*) P. A. Wender and S. K. Singh. Tetrahedron Lett. **31**, 2517 (1990); *Ophiobolin C*: (*f*) M. Rowley, M. Tsukamoto, and Y. Kishi. J. Am. Chem. Soc. **111**, 2735 (1989); (*g*) R. K. Boeckman, Jr., A. Arvanitis, and M. E. Voss. J. Am. Chem. Soc. **111**, 2737 (1989).
5. R. K. Boeckman, Jr., D. M. Blum, and S. M. Arthur. J. Am. Chem. Soc. **101**, 5060 (1979).
6. R. K. Boeckman, Jr., D. M. Blum, E. V. Arnold, and J. Clardy. Tetrahedron Lett. **48**, 4609 (1979).
7. S. J. Alward and A. G. Fallis. Can. J. Chem. **62**, 121 (1984).
8. B. Lei and A. G. Fallis. J. Am. Chem. Soc. **112**, 4609 (1990).
9. (*a*) A. G. Fallis. Can. J. Chem. **62**, 183 (1984); (*b*) E. Ciganek. Org. React. **32**, 1 (1984); (*c*) D. Craig. Chem. Soc. Rev. **16**, 187 (1987).
10. (*a*) E. Lee, I-J. Shin, and T-S, Kim. J. Am. Chem. Soc. **112**, 260 (1990); (*b*) L. A. Paquette, C. A. Teleha, R. T. Taylor, G. D. Maynard, R. D. Rodgers, J. C. Gallucci, and J. P. Springer. J. Am. Chem. Soc. **112**, 265 (1990); (*c*) L. A. Paquette, N. A. Pegg, G. D. Maynard, and R. D. Rogers. J. Am. Chem. Soc. **112**, 277 (1990); (*d*) R. K. Boeckman, Jr., D. M. Springer, and T. R. Alessi. J. Am. Chem. Soc. **111**, 8284 (1989); (*e*) L. A. Paquette, J. Reagan, S. L. Schreiber, and C. A. Teleha. J. Am. Chem. Soc. **111**, 2331 (1989); (*f*) M. Sworin and K-C. Lin J. Am. Chem. Soc. **111**, 1815 (1989); (*g*) L. A. Paquette and M-A. Poupart. Tetrahedron Lett. **29**, 273 (1988); (*h*) L. A. Paquette, D. T. DeRussy, and R. D. Rogers. Tetrahedron, **44**, 3139 (1988); (*i*) L. A. Paquette, D. T. DeRussy, and C. E. Cattrell. J. Am. Chem. Soc. **110**, 890 (1988); (*j*) J. A. Oplinger and L. A. Paquette. Tetrahedron Lett **28**, 5441 (1987); (*k*) S. L. Schreiber and R. C. Hawley. Tetrahedron Lett. **26**, 5971 (1985); (*l*) M. E. Jung and L. A. Light. J. Am. Chem. Soc. **106**, 7614 (1984); (*m*) S. L. Schreiber and C. J. Santini. J. Am. Chem. Soc. **106**, 4038

(1984); (*n*) P. A. WENDER, J. M. SCHAUS, and A. W. WHITE. J. Am. Chem. Soc. **102**, 6159 (1980).
11. G. BÉRUBÉ and A. G. FALLIS. Tetrahedron lett. **30**, 4045 (1989).
12. (*a*) G. BRIEGER. J. Am. Chem. Soc. **85**, 3783 (1963); (*b*) J. R. STILLE and R. H. GRUBBS. J. Org. Chem. **54**, 434 (1989).
13. W. L. BROWN and A. G. FALLIS. Can. J. Chem. **65**, 1828 (1987).
14. (*a*) J. C. DE SOUSA-BARBOZA, C. PETRIER and J.-L. LUCHE. J. Org. Chem. **53**, 1212 (1988); (*b*) J-L. LUCHE and J. C. DAMIANO. J. Am. Chem. Soc. **102**, 7926 (1980).
15. S. N. HUCKIN and L. WEILER. J. Am. Chem. Soc. **96**, 1082 (1974).
16. (*a*) J. A. MARSHALL, J. E. AUDIA, J. GROTE, and B. G. SHEARER. Tetrahedron, **42**, 2893 (1986); (*b*) J. A. MARSHALL, J. E. AUDIA, and J. J. GROTE. J. Org. Chem. **49**, 5277 (1984); (*c*) K. SAKAN and B. M. CRAVEN. J. Am Chem. Soc. **105**, 3732 (1983); (*d*) K. J. SHEA and J. W. GILMAN. Tetrahedron Lett. **24**, 657 (1983); (*e*) W. R. ROUSH, A. I. KO, and H. R. GILLIS. J. Org. Chem. **45**, 4264 (1980).
17. (*a*) A. B. SMITH III, T. L. LEENAY, H-J. LIU, L. A. K. NELSON, and R. A. BALL. Tetrahedron Lett. **29**, 49 (1988); (*b*) R. E. IRELAND and D. W. NORBECK. J. Org. Chem. **50**, 2198 (1985); (*c*) A. J. MANCUSO and D. SWERN. Synthesis, 165 (1981); (*d*) K. OMURA and D. SWERN. Tetrahedron, **34**, 1651 (1978).
18. (*a*) M. KOREEDA and J. I. LUENGO. J. Am. Chem. Soc. **107**, 5572 (1985); (*b*) H. W. PINNICK. Org. Prep. Proced. Int. **15**, 199 (1983); (*c*) D. A. EVANS and J. V. NELSON. J. Am. Chem. Soc. **102**, 774 (1980); (*d*) D. A. EVANS, D. J. BAILLARGEON, and J. V. NELSON. J. Am. Chem. Soc. **100**, 2242 (1978).

Can. J. Chem. Downloaded from www.nrcresearchpress.com by 195.138.81.100 on 09/07/12
For personal use only.

Vinyl ether hydrolysis. XXIV. 1-Methoxycyclooctene and the question of reversibility of the carbon protonation step[1]

A. J. KRESGE[2] AND Y. YIN

Department of Chemistry, University of Toronto, Toronto, Ont., Canada M5S 1A1

Received July 16, 1990

A. J. KRESGE and Y. YIN. Can. J. Chem. **69**, 84 (1991).

An argument is presented which suggests that hydrolysis of the vinyl ether group of 1-methoxycyclooctene may occur by reversible proton transfer from a catalyzing acid to the β-carbon atom of the substrate, instead of by the conventional reaction mechanism in which this proton transfer is rate determining and not reversible. Hydrolysis of this substrate is then examined by measuring rates of reaction in dilute aqueous solutions of strong mineral acids (perchloric and hydrochloric) as well as in buffer solutions of seven carboxylic acids, biphosphate ion, and 1,1,1,3,3,3-hexafluoro-2-propanol. General acid catalysis is observed and a Brønsted relation with the exponent $\alpha = 0.73$ is constructed. That, plus the isotope effects $k_H/k_D = 2.9$ and 6.0 for catalysis by hydronium ion and acetic acid respectively, as well as the lack of deuterium incorporation into the substrate when the reaction is carried out in D_2O with $D_2PO_4^-/DPO_4^{2-}$ buffer at pD = 8, show that carbon protonation of the substrate is not reversible and that the conventional reaction mechanism is operative.

Key words: 1-methoxycyclooctene, vinyl ether hydrolysis, rate-determining proton transfer, Brønsted relation, solvent isotope effect.

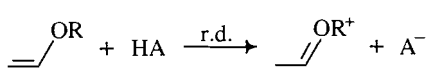
A. J. KRESGE et Y. YIN. Can. J. Chem. **69**, 84 (1991).

On présente un argument qui pourrait suggérer que l'hydrolyse du groupement éther vinylique du 1-méthoxycyclooctène peut se produire par le biais d'un transfert réversible d'un proton d'un catalyseur acide vers l'atome de carbone-β du substrat au lieu du mécanisme conventionnel dans lequel le transfert du proton n'est pas réversible et correspond à l'étape qui détermine la vitesse de la réaction. On a alors étudié l'hydrolyse de ce substrat en mesurant les vitesses de réactions dans des solutions aqueuses diluées d'acides minéraux forts (perchlorique et chlorhydrique) ainsi que dans des solutions tamponnées de sept acides carboxyliques, d'ion biphosphate et de 1,1,1,3,3,3-hexafluoropropan-2-ol. On a observé une catalyse acide générale et on a établi une relation de Brønsted avec un exposant $\alpha = 0{,}73$. Ces données, considérées avec les effets isotopiques $k_H/k_D = 2{,}9$ et 6,0 respectivement pour l'ion hydronium et l'acide acétique ainsi que le fait qu'il n'y a pas d'incorporation de deutérium dans le substrat lorsqu'on réalise la réaction dans le D_2O, avec un tampon de $D_2PO_4^-/DPO_4^{2-}$ et à un pD = 8, montrent que la protonation du carbone du substrat n'est pas réversible et que le mécanisme conventionnel s'applique à cette réaction.

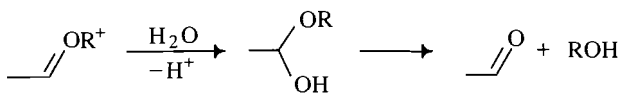
Mots clés : 1-méthoxycyclooctène, hydrolyse d'éther vinylique, transfert du proton qui détermine la vitesse de la réaction, relation de Brønsted, effet isotopique du solvant.

[Traduit par la revue]

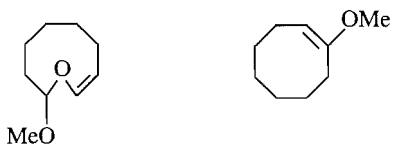
The conventional reaction mechanism for acid-catalyzed hydrolysis of vinyl ethers consists of rate-determining protonation of the substrate on the β-carbon, eq. [1], followed by rapid

[1] 

hydration of the ensuing alkoxycarbocation and decomposition of the hemiacetal intermediate, eq. [2].[3] It was believed at one

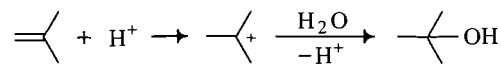
[2] 

time that the hydrolysis of 9-methoxyoxacyclonon-2-ene, **1**, provided the sole exception to this mechanism in that carbon protonation became reversible in its reaction and some subsequent step was consequently rendered rate determining (2). It has been shown recently, however, that this substance does not react through its vinyl ether group but rather by hydrolysis of its acetal function (3), and that the process upon which this mechanistic assignment was based is not a vinyl ether hydrolysis at all. It thus appears that all of the considerable number of vinyl ethers examined so far undergo hydrolysis by non-reversible, rate-determining proton transfer to carbon.



1 **2**

It is likely, however, that the carbon protonation step in at least some of these hydrolyses is not rate determining by a very great margin, i.e., that cation hydration (eq. [2]) is not very much faster than cation deprotonation (reversal of eq. [1]). This is suggested by the fact that in the acid-catalyzed addition of water to simple olefins, eq. [3], cation hydration is only 1–2

[3] 

orders of magnitude faster than deprotonation (4); carbon protonation, moreover, is reversible and not rate determining in the hydrolysis of enamines (5), eq. [4]; vinyl selenides (6), eq. [5]; and ketene thioacetals (7), eq. [6]. It would seem, therefore, that examples of reversible carbon protonation might be found in the hydrolysis of vinyl ethers as well, and that this might be achieved through appropriate structural modification of the vinyl ether functional group.

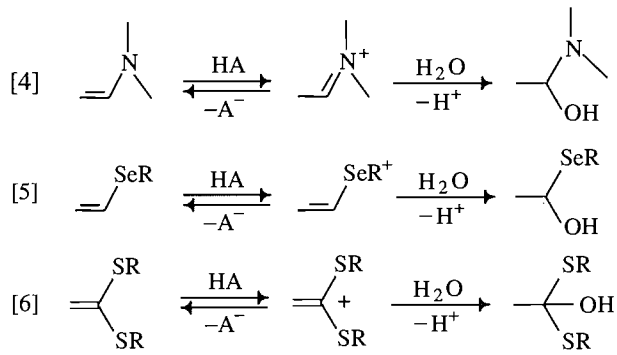
One such structural modification could be incorporation of the vinyl ether group in an eight-membered ring, as in 1-methoxycyclooctene, **2**. This is suggested by the fact that, whereas carbon protonation is fully rate determining in the hydration of isobutene, eq. [3], deprotonation and cation hydration occur at comparable rates in the corresponding

[1]Part XXIII. See ref. 32.

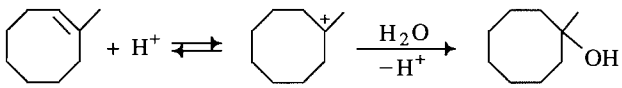
[2]Author to whom correspondence may be addressed.

[3]For a brief review of the evidence and references to earlier literature, see ref. 1.

Can. J. Chem. Downloaded from www.nrcresearchpress.com by 195.138.81.100 on 09/07/12
For personal use only.



reaction of 1-methylcyclooctene (8), eq. [7]. There would thus appear to be some feature of an eight-membered ring, perhaps a conformational effect, that promotes reversibility.



These comparisons of isobutene and 1-methylcyclooctene are for protonation by the hydronium ion in strongly acidic solutions where the only base available to deprotonate the cation is water. The stronger bases present in carboxylic acid and other buffer solutions will be more effective deprotonating agents and should therefore promote reversibility. Unfortunately, olefins such as isobutene and 1-methylcyclooctene are too unreactive to be studied conveniently in buffer solutions, but vinyl ethers are much more labile. We have consequently examined the hydration of 1-methoxycyclooctene in order to determine whether or not its carbon protonation step can be made reversible.

Experimental

Materials

1-Methoxycyclooctene was prepared from the corresponding ketal by *p*-toluenesulfonic acid catalyzed elimination of one equivalent of alcohol, following the procedure we have used before for synthesizing other cyclic vinyl ethers (9); ^{1}H NMR ($CDCl_3$) δ: 4.50 (1H, t, J = 8 Hz), 3.50 (3H, s), 2.5–1.5 (12 H br m); MS calcd. for $C_9H_{16}O$: 140.1201; found: 140.1204. All other materials were best available commercial grades and were used as received.

Kinetics

Rates of hydrolysis of 1-methoxycyclooctene were measured spectroscopically by monitoring the decrease in vinyl ether absorbance at λ = 220 nm. Reactions with half-lives greater than ca. 20 s were examined with a Cary 118 C spectrometer whose cell compartment was thermostatted at 25.0 ± 0.1°C. Runs were initiated by adding 5–10 μL of acetonitrile stock solution of substrate to 3.0 mL of aqueous acid or buffer solution that had come to thermal equilibrium with the spectrometer cell compartment; substrate concentrations in the final reaction solutions were ca. 1×10^{-4} M. Measurements of absorbance were continued for 3–4 half-lives; the data obeyed the first-order rate law accurately and the observed first-order rate constants were obtained by least-squares fitting to an exponential function (10).

Rates of fast reactions with half-lives less than ca. 20 s were determined using a Durrum–Gibson stopped-flow spectrometer operating at 25.0 ± 0.1°C. Measurements were continued for 10–12 half-lives; the data obeyed the first-order rate law accurately and the observed first-order rate constants were evaluated graphically as slopes of plots of $\ln(A - A_\infty)$ vs. time.

Results

Rates of hydrolysis of 1-methoxycyclooctene were measured in aqueous (H_2O) perchloric acid solutions over the concentration range 0.02–0.10 M and in aqueous (H_2O) hydrochloric acid solutions over the concentration range 0.009–0.05 M; ionic strength was maintained at 0.10 M through the addition of NaCl as required.[4] Observed first-order rate constants determined in both media were accurately proportional to acid concentration, and least-squares analysis gave the hydronium ion catalytic coefficients $k_{H^+} = 299 \pm 3\ M^{-1}\ s^{-1}$ for perchloric acid and $k_{H^+} = 291 \pm 7\ M^{-1}\ s^{-1}$ for hydrochloric acid. The mean of these two values, $k_{H^+} = 295\ M^{-1}\ s^{-1}$, is consistent with $k_{H^+} = 299\ M^{-1}\ s^{-1}$ estimated for 1-methoxycyclooctene from $k_{H^+} = 623\ M^{-1}\ s^{-1}$ for 1-ethoxycyclooctene (9*b*) and the rate reduction of 0.48 expected for changing an ethyl vinyl ether to the corresponding methyl vinyl ether (12).

Rates of hydrolysis of 1-methoxycyclooctene were also measured in aqueous D_2O solutions of DCl over the concentration range 0.01–0.05 M at constant ionic strength (μ = 0.10 M, NaCl).[4] Observed first-order rate constants were once again accurately proportional to acid concentration, and least-squares analysis gave the catalytic coefficient $k_{D^+} = 102 \pm 3\ M^{-1}\ s^{-1}$. Combination of this with the corresponding value for H_2O solutions provides the isotope effect $k_{H^+}/k_{D^+} = 2.89 \pm 0.09$.

Rate measurements were also made in buffer solutions of seven carboxylic acids, biphosphate ion, and 1,1,1,3,3,3-hexafluoro-2-propanol. To keep hydronium ion concentrations constant while buffer concentrations were varied, series of solutions of constant buffer ratio and constant ionic strength (μ = 0.10 M in all cases but hexafluoropropanol where μ = 0.40 M) were used.[4] Buffer failure (13) nevertheless occurred with some of the stronger carboxylic acids, causing hydronium ion concentrations to change significantly as the buffer concentration was varied. In such cases observed rate constants were adjusted to a common hydronium ion concentration; hydronium ion concentrations required for this purpose were obtained by calculation using literature pK_a's and activity coefficients recommended by Bates (14).

First-order rate constants were in all cases linear functions of buffer concentration, and catalytic coefficients were evaluated as slopes of buffer dilution plots. For three of the systems examined ($CH_3CO_2H/CH_3CO_2^-$, $C_2H_5CO_2H/C_2H_5CO_2^-$, and $H_2PO_4^-/HPO_4^{2-}$) measurements were made at three different buffer ratios; these results showed that the buffers were acting as general acid catalysts, as expected. The catalytic coefficients so obtained are listed in Table 1.

Measurements were also made in acetic acid buffers in D_2O solution; these data gave the catalytic coefficient $k_{DA} = (6.15 \pm 0.32) \times 10^{-2}\ M^{-1}\ s^{-1}$, which, when combined with the acetic acid catalytic coefficient for H_2O solution, provides the isotope effect $k_{HA}/k_{DA} = 5.95 \pm 0.37$.

Discussion

Acid-catalyzed reactions in which proton transfer from the catalyst to the substrate is reversible and some subsequent step is rate determining generally give inverse hydronium-ion isotope effects, $k_{H^+}/k_{D^+} < 1$; rate-determining proton transfer reactions, on the other hand, usually have hydronium-ion isotope effects in the normal direction, $k_{H^+}/k_{D^+} > 1$ (13). The isotope effect observed here for hydrolysis of 1-methoxycyclooctene, $k_{H^+}/k_{D^+} = 2.9$, thus suggests that proton transfer is in this case not reversible. The present isotope effect is also consistent with $k_{H^+}/k_{D^+} = 3.7$, predicted for a vinyl ether of this reactivity from a correlation of hydronium-ion isotope effects for hydrolysis of a group of vinyl ethers known to react by non-

[4]The data are summarized in ref. 11.

Can. J. Chem. Downloaded from www.nrcresearchpress.com by 195.138.81.100 on 09/07/12
For personal use only.

Can. J. Chem. Downloaded from www.nrcresearchpress.com by 195.138.81.100 on 09/07/12
For personal use only.

TABLE 1. Catalytic coefficients for the hydrolysis of 1-methoxycyclooctene in aqueous solution at 25°C[a]

Acid	pK_a	$k_{HA}/M^{-1}\,s^{-1}$
H_3O^+	−1.74	295
$CNCH_2CO_2H$	2.47[b]	16.2
$ClCH_2CO_2H$	2.87[c]	12.1
$CH_3OCH_2CO_2H$	3.57[d]	4.11
HCO_2H	3.75[e]	1.97
$HOCH_2CO_2H$	3.83[f]	2.02
CH_3CO_2H	4.76[g]	0.366
$C_2H_5CO_2H$	4.88[h]	0.373
$H_2PO_4^-$	7.20[i]	0.0667
$(CF_3)_2CHOH$	9.39[j]	0.000156[k]

[a]Ionic strength = 0.10 M except where designated otherwise.
[b]Reference 24.
[c]Reference 25.
[d]Reference 26.
[e]Reference 27.
[f]Reference 28.
[g]Reference 29.
[h]Reference 30.
[i]Reference 31.
[j]C. H. Arrowsmith, A. J. Kresge, and Y. C. Tang, submitted to J. Am. Chem. Soc.
[k]Ionic strength = 0.40 M.

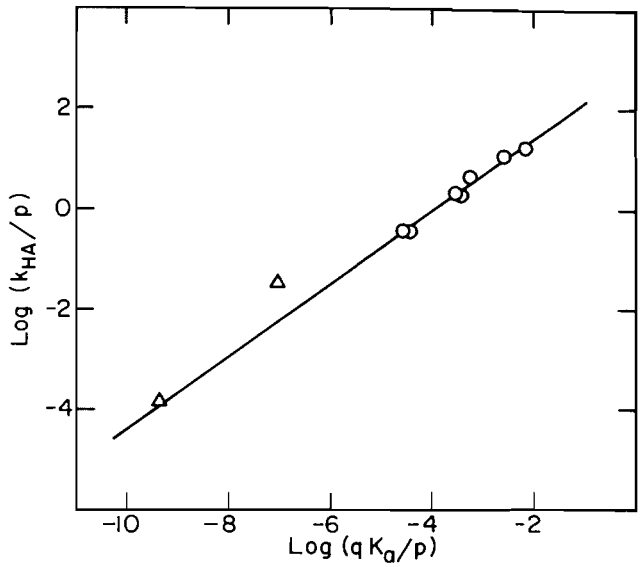


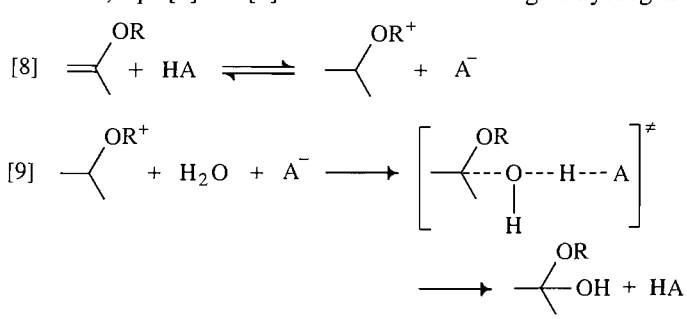
FIG. 1. Brønsted relation for the hydrolysis of 1-methoxycyclooctene in aqueous solution at 25°C catalyzed by carboxylic acids (○); the other points (△) are for, reading from left to right, $(CF_3)_2CHOH$ and $H_2PO_4^-$.

reversible rate-determining proton transfer. This evidence thus indicates that the hydrolysis of 1-methoxycyclooctene catalyzed by the hydronium ion occurs by the conventional mechanism of eqs. [1] and [2].

This conclusion is reinforced by the behavior of the present system in buffer solutions. The reaction shows general acid catalysis, as required for rate-determining proton transfer; reversible proton transfer, on the other hand, would produce specific hydronium ion catalysis.

The presently determined carboxylic acid catalytic coefficients give a Brønsted relation, illustrated in Fig. 1, whose exponent, $\alpha = 0.73 \pm 0.04$, is typical of vinyl ether hydrolysis reactions (9*a*). This Brønsted relation also shows individual deviations similar to those found for other vinyl ether (9*a*) and ketene acetal (15) hydrolyses: the points for chloro- and methoxyacetic acids lie above the correlation line whereas those for cyanoacetic and formic acids lie below. The point for the negatively charged catalyst $H_2PO_4^-$ also lies above the correlation line, as expected on the basis of electrostatic stabilization of the reaction's transition state, and as observed in other vinyl ether hydrolyses (16).

Although general acid catalysis is typical of vinyl ether hydrolysis by the conventional mechanism, it is also consistent with reversible carbon protonation provided that the subsequent rate-determining hydration of the alkoxycarbocation is assisted by base-catalyzed proton removal from the attacking water molecule, eqs. [8] and [9]. Such a scheme would give hydrogen



ion plus general base catalysis, which is operationally equivalent to general acid catalysis. General base catalysis of the reaction of carbocations with water and alcohols has in fact been observed (for some recent examples, see ref. 17). Such catalysis, however, seems to occur only with fairly stable cations in whose hydration the protonated alcohol or ether product that would be formed in the absence of catalysis, eq. [10], is a high-energy intermediate, i.e., lies above the

[10] $R^+ + H_2O \rightarrow ROH_2^+ \rightarrow ROH + H^+$

cation reactant on the free energy scale. With highly reactive cations, such as the methoxycarbenium ion formed in the present study,[5] the protonated alcohol or ether is of lower free energy than the reactant, and this intermediate is consequently no longer a high-energy species. There is therefore no need to avoid this intermediate, and general base catalysis disappears (17, 19).

The mechanism of eqs. [8] and [9] may also be ruled out on the basis of the isotope effect determined here for the hydrolysis of 1-methoxycyclooctene catalyzed by acetic acid. An estimate of the isotope effect expected for the mechanism of eqs. [8] and [9] may be made in the following way. The D:H isotopic fractionation factor for the hydroxyl group of acetic acid, $\phi = 0.96$ (20), is not very different from fractionation factors for carbon–hydrogen bonds of methylene groups, $\phi = 0.93$–1.05 (21), and the isotope effect on the equilibrium of eq. [8] will therefore be close to unity. The isotope effect on the reaction of eq. [9] is also likely to be close to unity. Two isotope effects on such reactions of stable carbocations with water have been reported, and both are small: $k_H/k_D = 1.2$ for the hydration of trianisylmethyl cation (22) and $k_H/k_D = 1.15$ for the hydration of 4,4′-di(*N*,*N*-dimethylamino)triphenylmethyl cation (17*b*). Large isotope effects, moreover, are never found for a reaction such as that of eq. [9], which involves proton transfer between electronegative atoms coupled with heavy atom reorganization (23). An overall isotope effect close to unity is therefore

[5]The rate constant for hydration of a simple analog of the present alkoxycarbocation, $CH_3C(OCH_3)CH_3^+$, has been estimated to be nearly diffusion controlled: $k = 1 \times 10^9\,M^{-1}\,s^{-1}$ (18).

predicted for the mechanism of eqs. [8] and [9]. This is very different from the observed value $k_H/k_D = 6.0$, and that argues strongly against the operation of this mechanism.

A final argument against reversible carbon protonation in the hydrolysis of 1-methoxycyclooctene may be made on the basis of the fact that we could detect no deuterium (by mass spectral analysis) in a sample of substrate recovered from a reaction mixture that had been allowed to go to half-completion in a D_2O–$D_2PO_4^-/DPO_4^{2-}$ buffer solution of pD = 8. Reversible carbon protonation would of course have led to hydrogen exchange and the incorporation of deuterium in the substrate. Evidently the HPO_4^{2-} ion is not sufficiently basic to promote reversibility.

The $(CF_3)_2CHO^-$ ion is also not basic enough to promote reversibility: the fact that the catalytic coefficient for $(CF_3)_2CHOH$ lies on the Brønsted correlation line (see Fig. 1) indicates that reaction in this buffer system occurs by the same mechanism (rate-determining proton transfer) as that established for the carboxylic acid buffers upon which this correlation is based. The property of eight-membered rings that promotes reversibility in olefin hydration thus appears to be insufficiently strong to do the same in vinyl ether hydrolysis.

Acknowledgements

We are grateful to the Natural Sciences and Engineering Research Council of Canada and the Donors of the Petroleum Research Fund, administered by the American Chemical Society, for financial support of this work.

1. A. J. KRESGE. Acc. Chem. Res. **20**, 364 (1987).
2. J. D. COOPER, V. P. VITULLO, and D. L. WHALEN. J. Am. Chem. Soc. **93**, 6294 (1971).
3. R. A. BURT, Y. CHIANG, W. K. CHWANG, A. J. KRESGE, T. OKUYAMA, Y. S. TANG, and Y. YIN. J. Am. Chem. Soc. **109**, 3787 (1987); Y. CHIANG, W. K. CHWANG, A. J. KRESGE, and Y. YIN. J. Am. Chem. Soc. **111**, 7185 (1989).
4. I. DOSTROVSKY and F. S. KLEIN. J. Chem. Soc. 791 (1955); E. GRUNWALD, A. HELLER, and F. S. KLEIN. J. Chem. Soc. 2604 (1957); R. H. BOYD, R. W. TAFT, A. P. WOLF, and D. R. CHRISTMAN. J. Am. Chem. Soc. **82**, 4729 (1960).
5. W. MAAS, M. J. JANSSEN, E. I. STAMHUIS, and H. WYNBERG. J. Org. Chem. **32**, 1111 (1967); J. K. COWARD and T. C. BRUICE. J. Am. Chem. Soc. **91**, 5329 (1969); P. Y. SOLLENBERGER and R. B. MARTIN. J. Am. Chem. Soc. **92**, 4261 (1970).
6. J. L. PIQUARD and L. HEVESI. Tetrahedron Lett. **21**, 1901 (1980); L. HEVESI, J. L. PIQUARD, and H. WAUTIER. J. Am. Chem. Soc. **103**, 870 (1981).
7. T. OKUYAMA. Acc. Chem. Res. **19**, 370 (1986).
8. Y. CHIANG, W. K. CHWANG, A. J. KRESGE, M. F. POWELL, and S. SZILAGYI. J. Org. Chem. **49**, 5218 (1984).
9. (*a*) A. J. KRESGE, H. L. CHEN, Y. CHIANG, E. MURRILL, M. A. PAYNE, and D. S. SAGATYS. J. Am. Chem. Soc. **93**, 413 (1971); (*b*) A. J. KRESGE, D. S. SAGATYS, and H. L. CHEN. J. Am. Chem. Soc. **99**, 7228 (1977).
10. C. G. SWAIN, M. S. SWAIN, and L. F. BERG. J. Chem. Inf. Comput. Sci. **20**, 47 (1980).
11. Y. YA. M.Sc. Thesis, University of Toronto, 1985.
12. Y. CHIANG, W. K. CHWANG, A. J. KRESGE, and S. SZILAGYI. Can. J. Chem. **58**, 124 (1980).
13. J. R. KEEFFE and A. J. KRESGE. *In* Techniques of chemistry. Vol. VI. Investigation of rates of mechanisms of reactions. *Edited by* C. F. Bernasconi. John Wiley, New York. 1986. Part I, Chap. XI.
14. R. G. BATES. Determination of pH. Theory and practise. John Wiley, New York. 1973. p. 49.
15. A. J. KRESGE and T. S. STRAUB. J. Am. Chem. Soc. **105**, 3957 (1983).
16. W. K. CHWANG, R. ELIASON, and A. J. KRESGE. J. Am. Chem. Soc. **99**, 805 (1977).
17. (*a*) R. TA-SHMA and W. P. JENCKS. J. Am. Chem. Soc. **108**, 8040 (1986); (*b*) J. R. GANDLER. J. Am. Chem. Soc. **107**, 8218 (1985).
18. T. L. AMYES and W. P. JENCKS. J. Am. Chem. Soc. **111**, 7888 (1989).
19. J. P. RICHARD and W. JENCKS. J. Am. Chem. Soc. **106**, 1396 (1984).
20. V. GOLD and B. M. LOWE. J. Chem. Soc. A, 1923 (1968).
21. A. J. KRESGE, R. A. MORE O'FERRALL, and M. F. POWELL. *In* Isotopes in organic chemistry. Vol. 7. *Edited by* E. Buncel and C. C. Lee. Elsevier, New York. 1987. Chap. 4.
22. E. A. HILL and W. J. MUELLER. Tetrahedron Lett. **21**, 2565 (1968).
23. C. G. SWAIN, D. A. KUHN, and R. L. SCHOWEN. J. Am. Chem. Soc. **87**, 1553 (1965); A. J. KRESGE. Pure Appl. Chem. **53**, 189 (1981).
24. F. S. FEATES and D. J. G. IVES. J. Chem. Soc. 2798 (1956).
25. D. J. G. IVES and J. H. PRIOR. J. Chem. Soc. 2104 (1955).
26. E. J. KING. J. Am. Chem. Soc. **82**, 3575 (1960).
27. H. S. HARNED and N. D. EMBREE. J. Am. Chem. Soc. **56**, 1042 (1934).
28. L. F. NIMS. J. Am. Chem. Soc. **58**, 987 (1936).
29. H. S. HARNED and R. W. EHLERS. J. Am. Chem. Soc. **55**, 652 (1933).
30. D. H. EVERETT, D. A. LANDSMAN, and B. R. W. PINSENT. Proc. R. Soc. Ser. A, **215**, 403 (1952).
31. A. K. GRZYBOWSKI. J. Phys. Chem. **62**, 555 (1958).
32. A. J. KRESGE and M. LEIBOVITCH. Can. J. Chem. **68**, 2129 (1990).

Can. J. Chem. Downloaded from www.nrcresearchpress.com by 195.138.81.100 on 09/07/12
For personal use only.

Adsorption of tetrahexylammonium – bromothymol blue ion-pairs at the chloroform–water interface

LAWRENCE AMANKWA AND FREDERICK F. CANTWELL[1]
Department of Chemistry, University of Alberta, Edmonton, Alta., Canada T6G 2G2

Received August 15, 1990

LAWRENCE AMANKWA and FREDERICK F. CANTWELL. Can. J. Chem. **69**, 88 (1991).

Porous membrane phase separators are used to study the adsorption of the cation tetrahexylammonium (Q^+), of the anion bromothymol blue (HB^-) and of the ion-pair formed between them (QHB) at the liquid–liquid interface in a rapidly stirred mixture of chloroform and aqueous buffer. Adsorption isotherms in all three cases follow the Langmuir equation. The anion HB^- is much more strongly adsorbed than the ion-pair QHB. The porous membrane technique readily permits measurement of simultaneous adsorption of the two species HB^- and QHB, and thereby allows a study of their competitive adsorption. When QHB is adsorbed in the presence of an excess of HB^- both the saturated (monolayer) interfacial concentration of QHB and the logarithm of the adsorption equilibrium constant for QHB decrease linearly with an increase in interfacial concentration of HB^-. This shows quantitatively that coadsorption of QHB and HB^- involves a direct competition for space at the interface and also that the presence of adsorbed HB^- changes the adsorbent properties of the interface. Analytical implications for solvent extraction are discussed.

Key words: interfacial adsorption, ion-pairs, liquid–liquid interface.

LAWRENCE AMANKWA et FREDERICK F. CANTWELL. Can. J. Chem. **69**, 88 (1991).

On a utilisé des membranes poreuses comme séparateurs de phases pour étudier l'adsorption du cation tétrahexylammonium (Q^+), de l'anion du bleu de bromothymol (HB^-) et de la paire d'ions (QHB) qu'ils forment entre eux, à l'interface liquide–liquide d'un mélange de chloroforme et de tampon aqueux soumis à une agitation rapide. Les isothermes d'adsorption des trois espèces suivent l'équation de Langmuir. L'anion HB^- est plus adsorbé que la paire d'ions QHB. La technique de la membrane poreuse permet de mesurer rapidement l'adsorption simultanée des deux espèces HB^- et QHB, ce qui permet d'étudier leur adsorption compétitive. Lorsque QHB est adsorbé en présence d'un excès de HB^-, la concentration interfaciale saturée (monocouche) de QHB ainsi que le logarithme de la constante d'équilibre d'adsorption de QHB diminuent tous les deux d'une façon linéaire avec une augmentation de la concentration interfaciale de HB^-. Cette observation démontre quantitativement que la coadsorption de QHB et de HB^- implique une compétition directe pour l'espace disponible à l'interface et aussi que la présence de HB^- adsorbé provoque des changements dans les propriétés adsorbantes de l'interface. On discute des implications analytiques pour l'extraction par des solvants.

Mots clés : adsorption interfaciale, paires d'ions, interface liquide–liquide.

[Traduit par la revue]

Can. J. Chem. Downloaded from www.nrcresearchpress.com by 195.138.81.100 on 09/07/12
For personal use only.

Solvent extraction of ion-pairs has been (1) and remains (2, 3) an important technique for the analytical determination of ionic species. The equilibrium aspects of the distribution of ion-pairs between two *bulk* liquid phases have been extensively studied (1, 4) and, more recently, the kinetic aspects of ion-pair extraction between bulk liquid phases have been investigated (5).

Depending on the surface-activity of the sample ion, of the reagent ion and of the ion-pair formed between them, interfacial adsorption may play a major role in determining both the equilibrium and kinetic extraction behavior of ion-pairs. The use of porous membrane phase separators makes possible measurement of the amount of solute adsorbed at the liquid–liquid interface in a vigorously stirred solvent extraction system and therefore permits the measurement of adsorption isotherms of solutes between the interface and the bulk liquid phases (6–9). Adsorption isotherms previously have been measured by this technique for interfacial adsorption of ion-pairs formed between cationic metal–ligand complexes and simple anions (10) and for the ion-pair tetrahexylammonium picrate (QP) (11). Because the technique allows measurement of concentrations in both liquid phases it makes possible the discrimination of two species simultaneously adsorbed at the interface. This is an advantage over conventional techniques for measuring interfacial adsorption such as those based on interfacial tension or pressure. This advantage is utilized in studying the tetrahexylammonium-bromothymol blue system.

[1]To whom correspondence should be addressed.

Bromothymol blue is one of the most often used anionic reagents for ion-pair extraction (1). In the present study bromothymol blue anion, HB^-, which is surface-active, is used to form a surface-active ion pair, QHB, with tetrahexylammonium cation, Q^+, which also is surface-active. Equilibrium adsorption isotherms of the surface-active species at the chloroform–water interface are measured with the aid of a porous membrane phase separator and the competitive adsorption between the strongly adsorbed HB^- and the weakly adsorbed QHB is quantified.

Experimental section

Bromothymol blue is a diprotic acid H_2B with $pK_{a1} \approx 1.5$ (12) and $pK_{a2} \approx 7.1$ (13). The abbreviation BTB will be used when referring to the component, without specifying which conjugate species, H_2B, HB^-, or B^{2-}, are intended.

Reagents

Water was demineralized, distilled, and finally distilled over alkaline permanganate. Aqueous phosphate buffers at pH 5.0 and 6.5 were prepared from sodium hydrogen phosphate and sodium dihydrogen phosphate at an ionic strength of 0.050. Reagent grade chloroform was washed with water shortly before use. A 1×10^{-3} M solution of reagent grade tetrahexylammonium bromide (Eastman Kodak Co., Rochester, NY) was prepared in chloroform. Bromothymol blue (BDH Canada Ltd.) was purified by recrystallization from ethanol and used to prepare a 5×10^{-4} M solution in aqueous phosphate buffer at pH 5.00.

Apparatus

The extraction apparatus includes a thermostatted (20 ± 0.1°C)

Can. J. Chem. Downloaded from www.nrcresearchpress.com by 195.138.81.100 on 09/07/12
For personal use only.

rapid-stir extraction cell with a porous membrane phase separator, a system to pump the separated liquid phase through an 8 μL flow cell in a spectrophotometer, a strip chart recorder and an IBM-XT microcomputer interfaced to the spectrophotometer. The apparatus previously has been described in detail (14). When the *chloroform phase* was being monitored the membrane phase separator consisted of two layers of 7.5 mil thick porous Teflon with 2–5 μm pore size (Zitex, No. E6060223, Chemplast, Wayne, NJ). When the *aqueous phase* was being monitored the membrane phase separator consisted of one layer of Whatman No. 2 filter paper. In all experiments 100.0 mL each of the chloroform and aqueous phases were combined in the rapid-stir cell. Stirring was at a constant speed of 2300 r.p.m. and the pumping rate was 1.0 mL/min. In some experiments the on-line spectrophotometer with flow cell was used to measure the absorbance of the separated phase while in other experiments a portion of the separated phase was collected and analyzed as described below. The latter approach was used for systems which gave a noisy baseline when the separated phase was pumped directly through the on-line spectrophotometer.

A Model 8451A diode array UV-Vis spectrophotometer (Hewlett-Packard) was used to make all absorbance measurements that were not made with the on-line flow-through spectrophotometer. An Accument Model 525 pH meter (Fisher Scientific) with combination electrode (Cat. No. 13-639-90) was used to measure pH.

Interfacial tensions were measured by the drop-volume technique (15) at 22 ± 1°C. Drops of chloroform were formed at a 0.318 cm O.D. Teflon tip using a 2-mL micrometer buret (Roger Gilmont, Great Neck, NY). The chloroform, which had previously been equilibrated with aqueous buffer, was slowly formed as drops in the same kind of chloroform-saturated aqueous buffer solutions as that used in the distribution experiments.

Liquid–liquid distribution

The distributions of tetrahexylammonium and of BTB between chloroform and aqueous bulk-liquid phases were measured by batch equilibration experiments (16). The measurements were repeated at several concentrations in order to generate the liquid-liquid distribution isotherms.

For BTB, chloroform and an aqueous pH 5.0 solution of NaHB were equilibrated. After turning off the stirrer and allowing coalescence of the phases, the concentration of BTB remaining in the aqueous phase was measured from its absorbance at 434 nm. The concentration of BTB in the chloroform phase was calculated from the difference between the initial and equilibrated aqueous phase concentrations.

For tetrahexylammonium at concentrations $\geq 1 \times 10^{-5}$ M, a chloroform solution of tetrahexylammonium bromide (QBr) and an aqueous pH 6.5 buffer were equilibrated. After phase coalescence the concentration of tetrahexylammonium remaining in the chloroform phase was determined by the "picrate method" in which an aliquot of the chloroform was shaken with aqueous sodium picrate and the concentration of tetrahexylammonium picrate in chloroform was measured spectrophotometrically (1, 16). The concentration of tetrahexylammonium in the aqueous phase was calculated by difference. When using initial concentrations of QBr $< 1 \times 10^{-5}$ M calculation by difference became too imprecise. In this case the concentrations of tetrahexylammonium at equilibrium were measured directly in both phases using suitable modifications of the "picrate method" cited above.

Interfacial adsorption

Using the rapid-stir cell, the equilibrium distributions between the chloroform–water interface and the bulk-liquid phases were measured for tetrahexylammonium, for BTB and for the ion-pair formed between them. Repeating the measurements at several concentrations produced the interfacial adsorption isotherms.

In general, the procedure involved combining chloroform and aqueous buffers containing one of the salts QBr, NaHB, or QHB. The two-phase mixture was stirred to achieve distribution equilibrium and, with the aid of the membrane phase separator, the concentration of solute was measured in one of the phases while the stirrer was still on. The stirrer was then shut off and, after the phases completely coalesced, the concentration of solute in the same phase was again measured. The amount of solute adsorbed at the liquid–liquid interface was calculated from the difference in concentrations with the stirrer off and on.

For tetrahexylammonium, the salt QBr was added initially to the chloroform phase, the aqueous buffer was pH 6.5 and the equilibrium concentration of tetrahexylammonium in chloroform was measured by the "picrate method" discussed above. For BTB, the salt NaHB was added initially to the aqueous pH 5.0 phase and the equilibrium concentration of BTB was measured via the absorbance of the aqueous phase at 434 nm. In a related study to demonstrate the effect of the ion-pair QHB on the interfacial adsorption of BTB, the experiment just described for BTB was repeated but with 4.0×10^{-5} M QHB also present, having been added initially to the chloroform phase.

For measuring the interfacial adsorption of the ion-pair QHB, this salt was added initially to the chloroform phase, the aqueous buffer was pH 5.0 and equilibrium concentrations in the chloroform phase were measured via absorbance at 440 nm. In a related study to see the effect of BTB on the adsorption of the ion-pair QHB, the experiment just described was repeated but with NaHB also present, having been added initially to the aqueous phase.

Results and discussion

The goal of the present investigation is a quantitative characterization of the interfacial adsorption of the ion-pair QHB and of the species Q^+ and HB^-. However, to achieve this goal it is necessary also to characterize their liquid–liquid distribution equilibria.

Experiments involving BTB or QHB were performed at pH 5.0, at which the predominant conjugate species of BTB in the aqueous phase is HB^-. Experiments involving QBr were performed at pH 6.5 to allow comparison with another system not reported in this paper. However, the behavior of QBr is expected to be independent of solution pH at all but very high or very low pH values so that its behavior at pH 5.0 can be assumed to be the same as that observed at pH 6.5.

Distribution of QBr

Shown as curve *A* in Fig. 1 is the liquid–liquid distribution isotherm of QBr between chloroform and aqueous buffer. The symbol C represents concentration and the subscripts "a", "o", "s", and "ns" mean "aqueous phase", "organic phase", "with stirring", and "with no stirring", respectively. In the aqueous phase QBr is dissociated into Q^+ and Br^- ions (1). The absence of micelle formation is demonstrated by the lack of a "break" in the Gibbs adsorption isotherm, discussed below.

In the chloroform phase the 1:1 ion-pair QBr is present (1). The anions from the buffer (*e.g.*, $H_2PO_4^-$) cannot be extracted into chloroform as ion-pairs with Q^+ (17, 18). The ion-pair QBr is present at too low concentrations to dimerize in chloroform (1). Dissociation of QBr in chloroform has not been studied but, based on the behavior of similar compounds in solvents of various dielectric constants, its dissociation constant is expected to be about 10^{-7} (19, 20). Thus, in the concentration range studied the undissociated ion-pair will predominate, but at the lower end of the range there could possibly be significant dissociation. If the undissociated ion-pair QBr were the only species present in chloroform curve *A* in Fig. 1 would be expected to show a marked upward concavity, which it does; and a plot of $C_{QBr,o}$ vs. $C^2_{Q^+,a}$ should be linear with slope equal to the ion-pair extraction constant, K_{IP} (1). Such a plot (not shown) is linear with zero intercept and a correlation coefficient $r = 0.985$. Its slope is $(2.1 \pm 0.2) \times 10^6$, which agrees with the literature value of $K_{IP} \approx 1 \times 10^6$ predicted for QBr (21). This suggests that, if present, dissociation is not extensive. However, whether or not ion-pair dissociation occurs in chloroform, the results

Can. J. Chem. Downloaded from www.nrcresearchpress.com by 195.138.81.100 on 09/07/12
For personal use only.

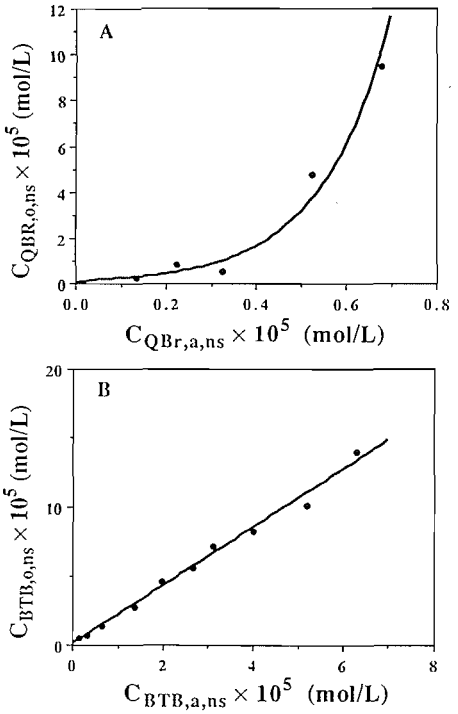


FIG. 1. Liquid–liquid distribution isotherms between chloroform and aqueous buffer of ionic strength 0.050: (*A*) for QBr at pH 6.5, solid line is an arbitrary fit to the data; (*B*) for BTB at pH 5.0, solid line is from linear regression.

obtained in this work can be used in the study of interfacial adsorption, as described below, because the method of measuring the concentration of quaternary ammonium in the chloroform phase is species-independent.

The species of tetrahexylammonium bromide which is adsorbed at the liquid–liquid interface is expected to be the cation Q^+. Electroneutrality near the positively charged interface is provided by an equivalent surface excess of anions in the diffuse part of the electrical double layer in the aqueous phase (22, 23). In the experiment, when the stirrer is turned on Q^+ moves from *both* liquid phases to the newly-created interface (7). The moles of Q^+ adsorbed, $n_{ADS,Q}$ is calculated from the expression:

$$[1] \quad n_{ADS,Q} = C_{QBr,o,ns}\left(V_o + \frac{V_a}{D_{QBr,ns}}\right) - C_{QBr,o,s}\left(V_o + \frac{V_a}{D_{QBr,s}}\right)$$

in which D_{QBr} is the liquid–liquid distribution ratio:

$$[2] \quad D_{QBr} = \frac{C_{QBr,o}}{C_{QBr,a}}$$

When an adsorption isotherm is plotted as $n_{ADS,Q}$ versus $C_{QBr,o,s}$ (not shown) it is found that at $C_{QBr,o,s} \gtrsim 1 \times 10^{-5}$ M the curve flattens out and approaches a limiting value $n_{ADS,Q,SAT}$. In fact, this isotherm follows the Langmuir equation (24):

$$[3] \quad n_{ADS,Q} = \frac{n_{ADS,Q,SAT} K_Q C_{QBr,o,s}}{1 + K_Q \cdot C_{QBr,o,s}}$$

in which $n_{ADS,Q,SAT}$ is the moles of Q^+ adsorbed at monolayer saturation of the interface and K_Q is the equilibrium constant for

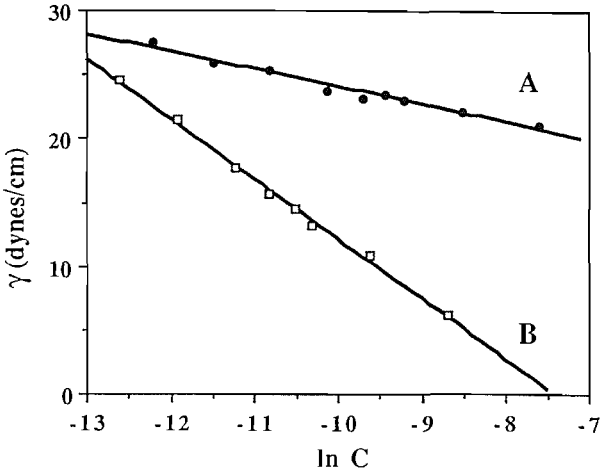


FIG. 2. Gibbs adsorption isotherm plots of interfacial tension versus natural logarithm of equilibrium concentration of: (*A*) QBr in chloroform phase; (*B*) BTB in aqueous phase. Solid lines are from linear regression.

adsorption of Q^+ from chloroform onto the interface. That the data fit the Langmuir equation can be demonstrated by plotting $C_{QBr,o,s}\ (n_{ADS,Q})^{-1}$ versus $C_{Br,o,s}$ (24). A straight line is obtained (not shown) with a slope of $(4.12 \pm 0.02) \times 10^5$ mol^{-1} and an intercept of (0.430 ± 0.035) L^{-1}. The value of K_Q is calculated from the ratio slope/intercept to be $(9.6 \pm 0.8) \times 10^5$ L/mol and the value of $n_{ADS,Q,SAT}$ is calculated from (slope)$^{-1}$ to be $n_{ADS,Q,SAT} = (2.43 \pm 0.01) \times 10^{-6}$ mol.

The quantity $n_{ADS,Q}$ can be converted to interfacial concentration (surface excess, Γ_Q (mol/cm^2), by the expression

$$[4] \quad \Gamma_Q = \frac{n_{ADS,Q}}{A}$$

where A is the total area (cm^2) of the liquid–liquid interface. Knowledge of A would, therefore, make it possible to plot the adsorption isotherm in the more conventional way of Γ_Q versus $C_{QBr,o,s}$. The interfacial area in the stirred liquid mixture can be calculated by comparing $n_{ADS,Q,SAT}$ with the Gibbs isotherm for tetrahexylammonium bromide measured independently in the same concentration range. The Gibbs isotherm is a plot of interfacial tension γ versus ln $C_{QBr,o}$ (6, 9, 24, 25). In the near-saturation region the Gibbs isotherm is expected to be linear with a slope of $-RTn_{ADS,Q,SAT}/A$. If γ is in dyn/cm then R is 8.314×10^7 ergs (mol K)$^{-1}$. As seen in curve *A* of Fig. 2, the experimental plot is linear. From its slope of -1.36 ± 0.09 dyn/cm the value of $n_{ADS,Q,SAT}/A$ is $(5.65 \pm 0.37) \times 10^{-11}$ mol cm^2. Dividing this into the value of 2.43×10^{-6} mol for $n_{ADS,Q,SAT}$ gives $A = 4.3 \times 10^4$ cm^2. This value of A corresponds to an average drop diameter for the dispersed aqueous phase of 0.014 cm which is close to the value predicted from hydrodynamic calculations for stirring at 2300 r.p.m. in this apparatus (14).

The interfacial adsorption isotherm for tetrahexylammonium bromide is shown in Fig. 3 as a plot of Γ_Q versus $C_{QBr,o,s}$. The value of $\Gamma_{Q,SAT}$ is, of course, equal ot $n_{ADS,Q,SAT}/A$, $(5.65 \pm 0.37) \times 10^{-11}$ mol/cm^2, obtained from the slope of the Gibbs isotherm.

Distribution of BTB

At the pH, ionic strength and BTB concentrations used the ion HB^- is the only species of BTB present in significant concentration in the aqueous phase (12, 13). The species of BTB which is

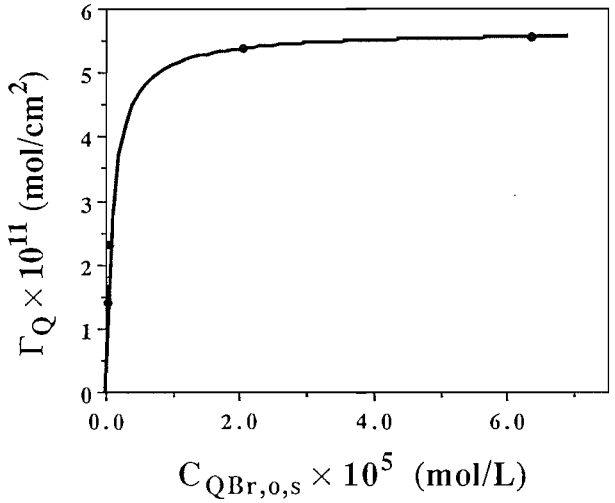


FIG. 3. Adsorption isotherm for QBr at the interface between 100 mL of chloroform and 100 mL of aqueous buffer at pH 6.5 and ionic strength 0.050, while stirring at 2300 r.p.m. Solid line is from linear regression of Langmuir plot (see text).

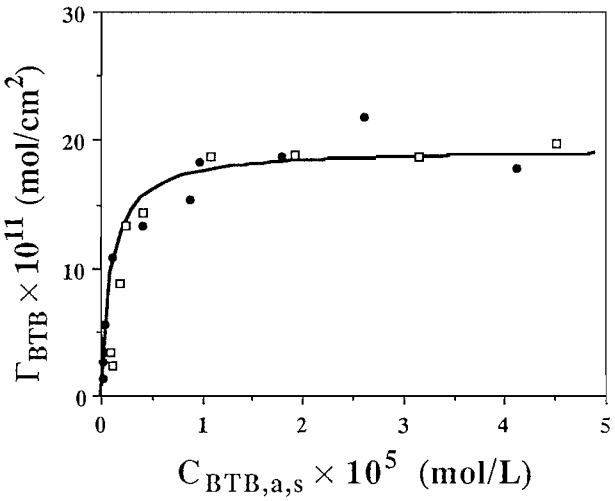


FIG. 4. Adsorption isotherms for NaBTB at the interface between 100 mL of chloroform and 100 mL of aqueous buffer of pH 5.0 and ionic strength 0.050, while stirring at 2300 r.p.m., in the absence (●) of excess QHB and in the presence (□) of 4.0×10^{-5} M added QHB. Solid line is from linear regression of Langmuir plot (see text).

present in the chloroform phase is the free-acid H_2B. The absence of NaHB in the chloroform phase is confirmed by the absence of absorbance at wavelengths greater than 290 nm (13). The liquid–liquid distribution isotherm is shown as a plot of $C_{BTB,o,ns}$ vs. $C_{BTB,a,ns}$ in curve *B* of Fig. 1. It is linear, since $[H_3O^+]_a$ is constant, with a slope of 2.09 ± 0.07 and zero intercept (0.10 ± 0.24).

The species of BTB which is adsorbed at the liquid–liquid interface is HB^-, with electroneutrality provided by an equivalent surface excess of Na^+ in the diffuse part of the electrical double layer. The moles of BTB adsorbed, $n_{ADS,BTB}$, is calculated from the expression:

$$[5] \quad n_{ADS,BTB} = C_{BTB,a,ns}(V_a + V_o D_{BTB,ns}) - C_{BTB,a,s}(V_a + V_o D_{BTB,s})$$

in which D_{BTB} is the liquid–liquid distribution ratio:

$$[6] \quad D_{BTB} = \frac{C_{BTB,o}}{C_{BTB,a}}$$

The analytical concentrations in the organic and aqueous phases, $C_{BTB,o}$ and $C_{BTB,a}$, are obtained from the isotherm in Fig. 1, curve *B*.

The properties of the adsorption isotherm of HB^- are obtained in a manner analogous to that discussed in the previous section: A plot of $C_{BTB,a,s}(n_{ADS,BTB})^{-1}$ versus $C_{BTB,a,s}$ is linear with a slope of $(1.48 \pm 0.06) \times 10^5$ mol^{-1} and an intercept of (0.15 ± 0.11) L^{-1}. The linearity of this plot shows that the isotherm is described by the Langmuir equation (24). The value of the equilibrium constant, K_{BTB}, is $(1.0 \pm 0.7) \times 10^6$ L/mol and that of $n_{ADS,BTB,SAT}$ is $(6.8 \pm 0.1) \times 10^{-6}$ mol. The value of the interfacial area *A* is obtained by dividing $n_{ADS,BTB,SAT}$ by $(1.93 \pm 0.04) \times 10^{-10}$ mol cm^{-2}, which is the value of $n_{ADS,BTB,SAT}(A)^{-1}$ calculated from the slope of the Gibbs isotherm for BTB (curve *B*, Fig. 2; slope is −4.7 ± 0.1). The value of *A* thus obtained is 3.5×10^4 cm^2, which is in reasonable agreement with the value of 4.3×10^4 cm^2 obtained in the previous section from the adsorption of Q^+.

The interfacial adsorption isotherm for BTB, shown as the closed-circle points in Fig. 4, is a plot of Γ_{BTB} versus $C_{BTB,a,s}$. The value of $\Gamma_{BTB,SAT}$ is $(1.93 \pm 0.04) \times 10^{-10}$ mol cm^{-2} from the slope of the Gibbs isotherm.

Distribution of QHB

For the experimental conditions used, the only compound formed between tetrahexylammonium and BTB which is present in significant concentration in chloroform is the 1:1 ion-pair QHB (1). Formation of the 2:1 ion-pair Q_2B (1, 26) and of the dimer $(QHB)_2$ (1, 27) is negligible. As is true for the ion-pair QBr, discussed above, the dissociation constant of the ion-pair QHB in chloroform has not been measured but can be estimated to be about 10^{-7} (1, 19, 20). Therefore, dissociation may or may not be significant at concentrations as high as 10^{-6} M. However, a calibration curve of absorbance at 440 nm versus $C_{QHB,o}$ in chloroform was found to be linear with zero intercept over the range of concentrations of interest. This indicates that either dissociation does not occur or, if dissociation does occur, the molar absorptivity of the species HB^- is the same as that of the species QHB. Either way, the concentration measured in chloroform is species-independent and the difference in absorbance at 440 nm with the stirrer off and on is an accurate measure of interfacial adsorption.

The species adsorbed at the interface is the neutral ion-pair QHB. It is not possible in this experiment to tell whether there is any dissociation of QHB into its constituent ions on the interface (11) because both of these ions are strongly adsorbed, as shown above. The moles of QHB adsorbed, $n_{ADS,QHB}$, is calculated from the expression:

$$[7] \quad n_{ADS,QHB} = (C_{QHB,o,ns} V_o) - (C_{QHB,o,s} V_o)$$

where $C_{QHB,o}$ is the analytical concentration of tetrahexylammonium bromothymol blue in the chloroform phase. Equation [7] is simpler than eqs. [1] and [5] because the ion-pair extraction constant for QHB between chloroform and water is $>10^{10}$ (26) so that D_{QHB} is very large and there is virtually none of this component present in the aqueous phase. The adsorption isotherm of QHB in the absence of an excess of either Q^+ or BTB is shown as a plot of Γ_{QHB} versus $C_{QHB,o,s}$ in curve *A* of Fig. 5. Values of Γ_{QHB} were calculated by dividing the values of $n_{ADS,QHB}$ by an interfacial area of 3.9×10^4 cm^2. This is an

Can. J. Chem. Downloaded from www.nrcresearchpress.com by 195.138.81.100 on 09/07/12
For personal use only.

TABLE 1. Langmuir adsorption behavior of QHB in the presence of excess BTB[a]

Excess NaBTB 10^5 (mol/L)	$C_{BTB,a,s}$[b] 10^6 (mol/L)	$n_{ADS,BTB}$[b] 10^6 (mol)	Langmuir slope[c] 10^{-6} (mol^{-1})	Langmuir intercept[c] (L^{-1})	$n_{ADS,QHB,SAT}$ 10^6 (mol)	$\Gamma_{QHB,SAT}$[d] 10^{11} (mol/cm^2)	K_{QHB} 10^{-5} (L/mol)
0.00	0.00	0.00	0.77 ± 0.05	4.1 ± 1.3	1.30 ± 0.09	3.3 ± 0.2	1.88 ± 0.65
1.00	0.17	0.92	0.87 ± 0.05	7.2 ± 1.8	1.14 ± 0.07	2.9 ± 0.2	1.21 ± 0.29
2.00	0.29	1.92	1.05 ± 0.05	13.8 ± 1.5	0.96 ± 0.05	2.5 ± 0.1	0.76 ± 0.09
4.00	1.17	3.81	1.59 ± 0.26	45.0 ± 8.0	0.63 ± 0.10	1.6 ± 0.3	0.35 ± 0.09
6.00	4.1_3	4.69	2.82 ± 1.00	131.0 ± 31.0	0.35 ± 0.12	0.9 ± 0.3	0.22 ± 0.09

[a]The ± values are standard errors of the mean.
[b]$C_{BTB,a,s}$ and $n_{ADS,BTB}$ are the coordinates of the first five experimental data points measured in the absence of excess QHB in Fig. 4.
[c]Slope and intercept are from plots of $C_{QHB,o,s}\cdot(n_{ADS,QHB})^{-1}$ versus $C_{QHB,o,s}$.
[d]The uncertainty in the interfacial area, A, is ignored in calculating $\Gamma_{QHB,SAT}$ from $n_{ADS,QHB,SAT}$.

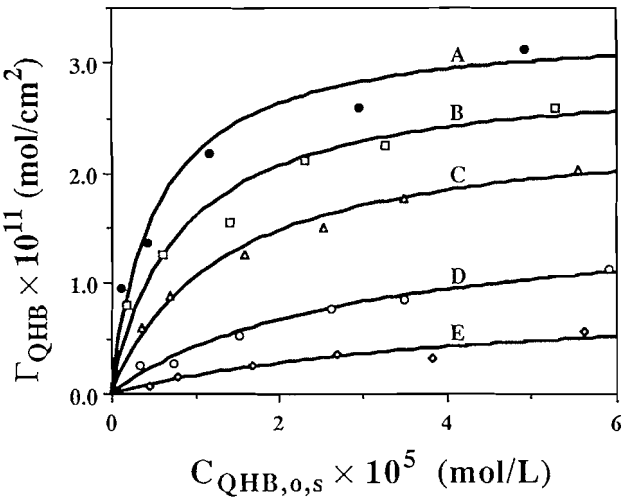


FIG. 5. Adsorption isotherms for QHB ion-pair at the interface between 100 mL of chloroform and 100 mL of aqueous buffer of pH 5.0 and ionic strength 0.050, while stirring at 2300 r.p.m., in the presence of (*A*) (●) 0.0 M; (*B*) (□) 1.0×10^{-5} M; (*C*) (△) 2.0×10^{-5} M; (*D*) (○) 4.0×10^{-5} M; (*E*) (◇) 6.0×10^{-5} M, added NaBTB. Solid lines are from linear regression of Langmuir plots (see text).

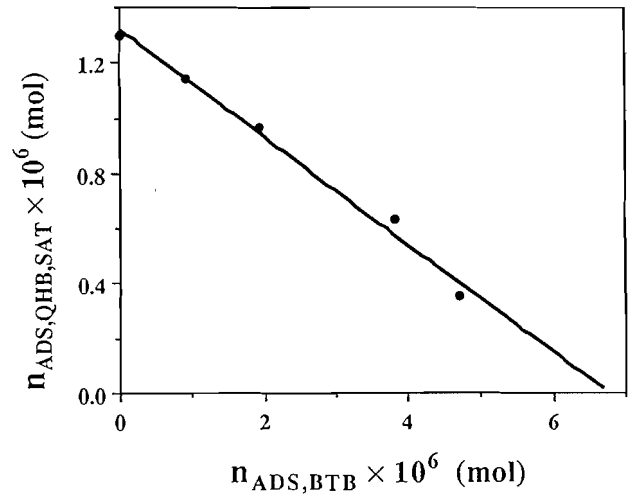


FIG. 6. Plot of moles of QHB adsorbed at interfacial saturation in the presence of excess NaBTB versus moles of BTB adsorbed. Solid line is from linear regression.

average of the values of A measured in the QBr system and in the NaBTB system, discussed above.

Comparing the initial slope of curve A in Fig. 5 with those of the curves in Figs. 3 and 4 shows that QHB is significantly less strongly adsorbed than either Q^+ or HB^-. The fact that the neutral ion-pair exhibits lower surface activity than either of its constituent ions is expected because it has less amphipathic character (24) due to the fact that the charge-centers on the ions tend to be buried in the interior of the ion-pair. The ion HB^- is so much more strongly adsorbed than QHB that the adsorption isotherm of HB^- (Fig. 4) is the same in the presence (closed circles) as in the absence (open squares) of 4.0×10^{-5} M QHB.

In contrast, the adsorption isotherms of QHB is markedly suppressed in the presence of excess NaBTB. This is seen in curves *A–E* in Fig. 5. Curve *A* was measured in the absence of excess NaBTB while curves *B* through *E* were measured in the presence of the indicated fixed concentrations of excess NaBTB. As the concentration of excess NaBTB is raised the adsorption isotherms of QHB show not only a decrease in their initial slope but also a decrease in their saturation plateau. These two effects are due to the coadsorption of HB^- and they can be quantified, in the following way.

When the experimental points for each of the five QHB isotherms in Fig. 5 are re-plotted as $C_{QHB,o,s}\ (n_{ADS,QHB})^{-1}$ versus $C_{QHB,o,s}$ five straight lines are obtained (not shown). Their slopes and intercepts are given in Table 1. The linearity of these plots demonstrates that QHB, both in the presence and absence of excess NaBTB, exhibits Langmuir adsorption behavior (24). The calculated values of K_{QHB} and $n_{ADS,QHB,SAT}$ for the Langmuir equation, as well as the values of Γ_{QHB} are also given in Table 1. In addition, equilibrium values of $C_{BTB,a,s}$ and $n_{ADS,BTB}$ for the experimental points in Fig. 4 are included in Table 1. The quantity $n_{ADS,BTB}$ is the moles of HB^- that are simultaneously adsorbed at the interface with QHB. For a given amount of added excess NaBTB the value of $n_{ADS,BTB}$ is constant, independent of the amount of QHB adsorbed, as discussed above.

When $n_{ADS,QHB,SAT}$ is plotted against $n_{ADS,BTB}$ a straight line results (Fig. 6), with slope of -0.195 ± 0.012 and intercept of $(1.32 \pm 0.03) \times 10^{-6}$ mol QHB. The intercept of this line on the *horizontal* axis is $(6.8 \pm 0.4) \times 10^{-6}$ mol BTB, which is identical to the saturation value of BTB from its isotherm in Fig. 4, $n_{ADS,BTB,SAT} = (6.8 \pm 0.1) \times 10^{-6}$ mol BTB. This indicates that the point at which the interface becomes covered with a monolayer of NaHB is identical to the point at which it will no longer adsorb any QHB. Furthermore, it can be shown that the negative reciprocal of the slope of the line in Fig. 6, *i.e.*, 5.1 ± 0.3, should be equal to the *ratio* of the area occupied per

Can. J. Chem. Downloaded from www.nrcresearchpress.com by 195.138.81.100 on 09/07/12
For personal use only.

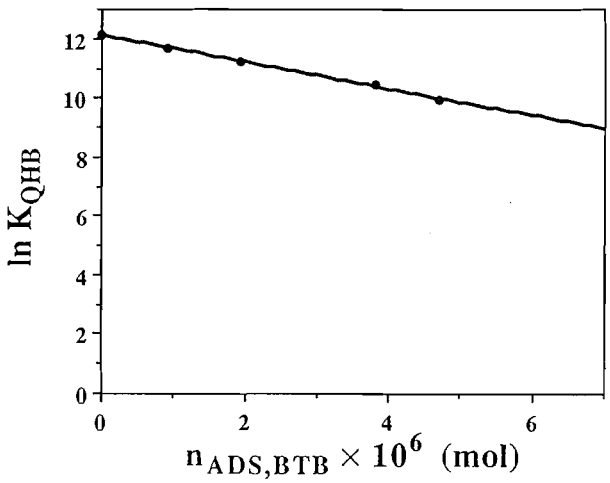


FIG. 7. Plot of natural logarithm of the equilibrium constant for the interfacial adsorption of QHB in the presence of excess NaBTB versus moles of BTB adsorbed. Solid line is from linear regression.

molecule of QHB to the area occupied per molecule of NaHB in their respective monolayers (24). This value of 5.1 ± 0.3 is in good agreement with the ratio $n_{ADS,BTB,SAT}$ $(n_{ADS,QHB,SAT})^{-1}$ = 5.2 ± 0.4 mol HB^- (mol QHB)$^{-1}$ obtained from Figs. 4 and 5*A* and it is also in good agreement with the value of $5._0$ which is estimated from measurements on space-filling molecular models (CPK Models) to be the ratio of the molecular area of QHB to that of HB^-. Thus, the effect of added NaBTB on the saturation plateau of the QHB isotherm is due to a simple competition for space at the interface.

A second effect of added NaBTB is that which leads to a decrease in the initial slope of the QHB isotherm (*i.e.* to a decrease in K_{QHB}). This effect also can be quantified. It is seen in Fig. 7 that a plot of ln K_{QHB} versus $n_{ADS,BTB}$ is also linear with a slope of $(-4.5 \pm 0.1) \times 10^5$ and intercept of 12.10 ± 0.03. The fact that K_{QHB} decreases with increasing coverage of the interface by HB^- implies that the chemical properties of the interface as an adsorbent are altered with the extent of coverage by HB^-. The linearity of the plot in Fig. 7 means that this change in chemical properties of the interface due to adsorbed HB^- occurs in such a way that the molar free energy of adsorption of QHB changes in a linear fashion with an increase in coverage of the interface by adsorbed HB^- (*i.e.*, $\Delta G = -RT \ln K_{QHB}$).

Thus the simultaneous adsorption of the strongly adsorbed ion HB^- with the weakly adsorbed ion-pair QHB involves both a competition of HB^- with QHB for space and a change in the chemical properties of the liquid–liquid interface brought about by adsorbed HB^-. Both effects lead to a decrease in adsorption of QHB with an increase in adsorption of HB^-.

Analytical implication

The interfacial adsorption behavior of the ion-pair QHB, summarized in Fig. 5 and Table 1, reveals that liquid–liquid distribution measurements made in systems where the ratio of interfacial area to bulk phase volume is large are potentially subject to special sources of error. If an analyte ion (*e.g.*, Q^+) is being determined by ion-pair extraction in the presence of a stoichiometric excess of added surface-active reagent ion (*e.g.*, HB^-), the fraction of the surface-active product ion-pair (*e.g.*, QHB) which gets adsorbed at the interface varies with the concentration of excess HB^-. This could lead to a non-linear dependence of optical absorbance in the organic phase on concentration of added analyte Q^+. Systems in which the area-to-volume ratio is large include not only those in which absorbance is measured during stirring (28) but also those, increasingly popular, systems in which automated solvent extraction is performed under segmented flow conditions (solvent extraction/flow injection analysis (2, 29–32)).

Acknowledgments

This work was supported by the Natural Sciences and Engineering Research Council of Canada and by the University of Alberta.

1. G. SCHILL. *In* Ion exchange and solvent extraction. Vol. 6. *Edited by* J. A. Marinsky and Y. Marcus. Marcel Dekker, New York, NY. 1974. Chap. 1.
2. L. FOSSEY and F. F. CANTWELL. Anal. Chem. **54**, 1693 (1982).
3. Y. HIRAI and K. TOMOKUNI. Anal. Chim. Acta. **167**, 409 (1985).
4. F. F. CANTWELL and M. CARMICHAEL. Anal. Chem. **54**, 697 (1982).
5. F. F. CANTWELL and H. FREISER. Anal. Chem. **60**, 226 (1988).
6. E. APRAHAMIAN JR., F. F. CANTWELL, and H. FREISER. Langmuir, **1**, 79 (1985).
7. G. PERSAUD, X-M. TIAN, and F. F. CANTWELL. Anal. Chem. **59**, 2 (1987).
8. H. WATARAI, M. TAKAHASHI, and K. SHIBATA. Bull. Chem. Soc. Jpn. **59**, 3469 (1986).
9. E. APRAHAMIAN JR. and H. FREISER. Sep. Sci. Technol. **22**, 233 (1987).
10. H. WATARAI. Talanta, **32**, 817 (1985).
11. L. AMANKWA and F. F. CANTWELL. Anal. Chem. **62**, 2270 (1990).
12. G. SCHILL. Acta Pharm. Suecica, **1**, 101 (1964).
13. G. SCHILL. Acta Pharm. Suecica, **1**, 169 (1964).
14. L. AMANKWA and F. F. CANTWELL. Anal. Chem. **61**, 1036 (1989).
15. J. L. LANDO and H. T. OAKLEY. J. Coll. Interface Sci. **25**, 526 (1967).
16. L. AMANKWA. Ph.D. Thesis, University of Alberta, Edmonton, Alta. November 1989.
17. K. O. BORG. Acta Pharm. Suecica, **6**, 425 (1969).
18. T. HIGUCHI, A. MICHAELIS, T. TAN, and A. HURWITZ. Anal. Chem. **39**, 974 (1967).
19. C. A. KRAUS. J. Phys. Chem. **60**, 129 (1956).
20. R. M. FUOSS and C. A. KRAUS. J. Am. Chem. Soc. **55**, 1019 (1933).
21. S. MOTOMIZU, S. HAMADA, and K. TOEI. Bunseki Kagaku, **32**, 648 (1983).
22. J. T. DAVIES and E. K. RIDEAL. Interfacial phenomena. Academic Press, New York, NY. 1961. Chap. 2.
23. G. SCIBONA, P. R. DANESI, and C. FABIANI. *In* Ion exchange and solvent extraction. Vol. 8. *Edited by* J. A. Marinski and Y. Marcus. Marcel Dekker, New York, NY. 1981, Chap. 2.
24. P. C. HIEMENZ. Principles of colloid and surface chemistry. Marcel Dekker, New York, NY. 1986. Chap. 7.
25. M. L. DIETZ and H. FREISER. Langmuir, **3**, 467 (1987).
26. G. SCHILL. Acta Pharm. Suecica, **2**, 13 (1965).
27. R. MODIN and G. SCHILL. Acta Pharm. Seucica, **4**, 301 (1967).
28. H. Y. MOHAMMED and F. F. CANTWELL. Anal. Chem. **52**, 553 (1980).
29. M. VALCARCEL and M. D. LUQUE DE CASTRO. J. Chromatogr. **393**, 3 (1987).
30. M. D. LUQUE DE CASTRO. J. Automatic Chem. **8**, 56 (1986).
31. J. F. LAWRENCE. Analyst, **112**, 879 (1987).
32. R. H. ATALLAH, G. D. CHRISTIAN and S. D. HARTENSTEIN. Analyst, **113**, 463 (1988).

Can. J. Chem. Downloaded from www.nrcresearchpress.com by 195.138.81.100 on 09/07/12
For personal use only.

Skeletal scrambling of sulphur diimide radical anions

KETUT BESTARI AND RICHARD T. OAKLEY[1]

Guelph Waterloo Centre for Graduate Work in Chemistry, Guelph Campus, Department of Chemistry and Biochemistry, University of Guelph, Guelph, Ont., Canada N1G 2W1

AND

A. WALLACE CORDES

Department of Chemistry and Biochemistry, University of Arkansas, Fayetteville, AR 72701, U.S.A.

Received May 11, 1990

KETUT BESTARI, RICHARD T. OAKLEY, and A. WALLACE CORDES. Can. J. Chem. **69**, 94 (1991).

In the presence of a catalytic quantity of alkali metal mixtures of sulphur diimides RNSNR and R'NSNR' (R, R' = Ph, 4-C_6H_4Me, 4-C_6H_4OMe, $SiMe_3$, SPh) undergo a rapid scrambling of the R and R' groups. When R and R' are significantly different (*e.g.*, R = Ph, R' = $SiMe_3$ or SPh) the equilibrium is shifted to favour the unsymmetrical sulphur dimmide (R ≠ R'); the procedure thus represents an effective method for preparing such derivatives. A mechanism involving the centrosymmetric association and rearrangement of two sulphur diimide radical anions is suggested for the observed ligand scrambling. The synthesis and X-ray structure determination of the mixed diimide (4-$NO_2C_6H_4$)SNSN(4-C_6H_4OMe) is reported. The crystals are monoclinic, space group $P2_1/n$; the molecules stack as plates along the *a* axis in a head-to-head fashion, producing an interplanar spacing between consecutive S_2N_2 units of 3.421 Å.

Key words: sulphur diimide radical anions, skeletal rearrangements, (4-$C_6H_4NO_2$)SNSN(4-C_6H_4OMe), X-ray structure.

KETUT BESTARI, RICHARD T. OAKLEY et A. WALLACE CORDES. Can. J. Chem. **69**, 94 (1991).

En présence d'une quantité catalytique d'un métal alcalin, des mélanges des diimides du soufre RSNSNR at R'NSNR' (R, R' = Ph, 4-C_6H_4Me, 4-C_6H_4OMe, $SiMe_3$ et SPh) subissent un brouillage rapide des groupements R et R'. Lorsque R et R' sont des groupements assez différents (par exemple, R = Ph et R' = $SiMe_3$ ou SPh), l'équilibre est déplacé vers le diimide de soufre non-symétrique (R ≠ R'); cette procédure représente donc une méthode efficace pour préparer de tels dérivés. Pour expliquer le brouillage observé des ligands, on propose un mécanisme impliquant une association centrosymétrique et une transposition de deux anions radicaux des diimides du soufre. On rapporte la synthèse et la détermination de structure (par diffraction des rayons-X) du dimmide mixte (4-$NO_2C_6H_4$)SNSN(4-C_6H_4OMe). Les cristaux sont monocliniques, groupe d'espace $P2_1/n$; les molécules s'empilent le long de l'axe a sous la forme de plaquettes dans lesquelles elles sont arrangées d'une façon tête-à-tête provoquant un espacement de 3,421 Å entre les plans de deux unité successives de S_2N_2.

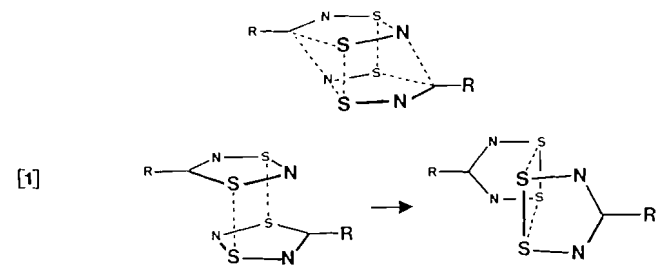
Mots clés : anions radicaux de diimides du soufre; transpositions du squelette; (4-$NO_2C_6H_4$)SNSN(4-C_6H_4OMe), structure par diffractions des rayons-X.

[Traduit par la revue]

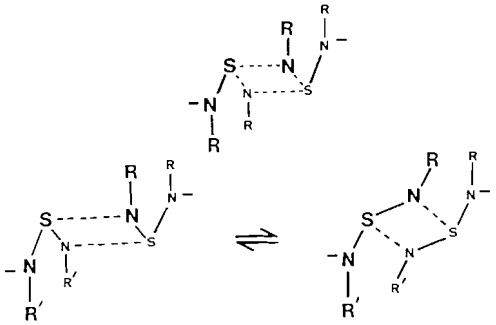
Introduction

The chemistry of molecules built from congugated —S=N— linkages is characterized by a propensity for often baffling rearrangements. Although the mechanistic issues behind these structural changes are clearly complicated, two potentially general pathways for structural change have recently been identified (1). The first is the intramolecular migration of a nitrogen between adjacent sulphur atoms, the so-called "1,3-nitrogen shift" reaction. This process facilitates nitrogen scrambling in RCH_5S_3 molecules (2), and provides a low energy pathway for the *endo*/*exo* isomerization of trithiatetrazocines (3). The second type of skeletal rearrangement involves the association of radical species. In a seminal paper Passmore and co-workers demonstrated that 1,3,2,4-dithiadiazoyl radicals could be photochemically converted to their 1,2,3,5-isomers (reaction [1]) (4). They later proposed a mechanism involving the intermediacy of a radical dimer and, on the basis of CNDO calculations, explained the need for photochemical rather than thermal activation (5) in terms of the orbital symmetries of the reactant and product dimers.

As part of ongoing studies of thiazyl radicals (6) we also have been interested in radical rearrangements, in particular the possibility that simple sulphur diimide radical anions $[RNSNR]^{-\bullet}$ might undergo skeletal scrambling reactions similar to that described by Passmore. Sulphur diimide radical anions, which are isoelectronic with the $SO_2^{-\bullet}$ radical anion, can be generated by either chemical (7) or electrochemical (8) reduction of the corresponding sulphur diimides, but heretofore no study has been performed to test the susceptibility of these systems towards skeletal, and hence ligand, scrambling, as proposed in reaction [2]. In the present paper we provide an account of our work on this topic.



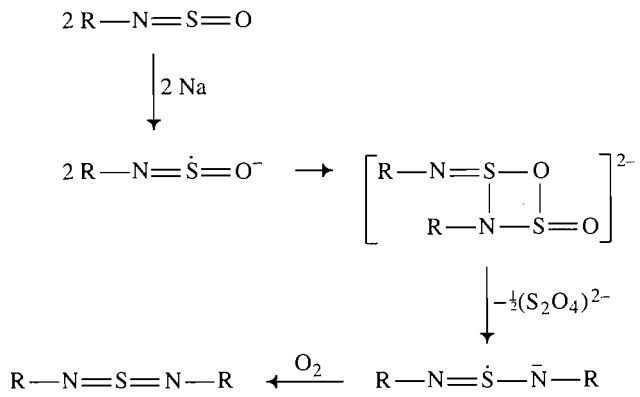
[1]



[2]

[1]To whom correspondence may be addressed.

Can. J. Chem. Downloaded from www.nrcresearchpress.com by 195.138.81.100 on 09/07/12
For personal use only.



SCHEME 1

Results and discussion

Coupling of sulphinylamines

There are several reported routes for the preparation of symmetrically substituted suphur diimides, including (*i*) the condensation of an amide with thionyl chloride (9) and (*ii*) base (10) and (*iii*) alkali metal (11) promoted coupling of sulphinylamines. We have used all these methods (see Experimental section), particularly (*iii*), although this with one important modification; we adjusted the stoichiometry by changing the metal:RNSO ratio from 1:2 to 1:1, and in so doing significantly improved the yields of the products. We view the reaction as being analogous to that proposed (10) for the base-catalysed condensation of sulphinylamines. Accordingly we suggest that the reaction proceeds (Scheme 1) by the generation and association of the radical anions $[RNSO]^{-\bullet}$, followed by elimination of $SO_2^{-\bullet}$ to produce sulphur diimide. The driving force for the reaction can be attributed, in large part, to the lattice energy of the dithionite salt.

Cross coupling of sulphur diimides

The preparation of unsymmetrical sulphur diimides is not always straightforward. The most commonly sought materials are *N*-silylated derivatives (R = Me_3Si), for which the standard synthetic methods (12) are not particularly efficient. We have found that in the presence of catalytic amounts of alkali metals a mixture of two symmetrically substituted sulphur diimides undergo a rapid ligand exchange. We have tested the exchange reaction for a number of aryl- and silyl-substituted systems (R, R′ = Ph, 4-C_6H_4OMe, 4-C_6H_4Me, $SiMe_3$, SPh). In all cases the scrambling was initiated using only a catalytic quantity of reducing agent (typically 5–25 mol% potassium or sodium) to generate the radical anions. Equilibrium was established rapidly, certainly within minutes. The extent of the reaction, *i.e.*, the position of equilibrium of reaction [2], was monitored for most systems by gas chromatography (GC). The results indicate that for similar R and R′ groups the exchange produces a nearly statistical distribution of the three possible products. For less symmetrical combinations, e.g. R = aryl and R′ = Me_3Si or SPh, the equilibrium is displaced sufficiently to the right hand (cross reaction) side that the method can be used as a fast and efficient synthesis of the mixed sulphur diimide.

For the reaction involving —SPh groups GC analysis was not possible as the compounds were too involatile. For these systems, however, we found that ^{14}N NMR spectroscopy provided a useful analytical probe. As Fig. 1 illustrates, the clean formation of PhNSNSPh from the cross coupling of PhNSNPh and PhSNSNSPh was readily confirmed by the appearance of two

TABLE 1. Product distribution (mol %) from reductive scrambling of sulphur diimides, as determined by GC or ^{14}N NMR analysis

R/R′	RNSNR	R′NSNR′	RNSNR′
Ph/4-C_6H_4Me	25	25	50
Ph/4-C_6H_4OMe	25	25	50
Ph/$SiMe_3$	15	15	70[a]
Ph/SPh	—	—	100[b]

[a]Isolated yield 53%.
[b]Isolated yield 55%.

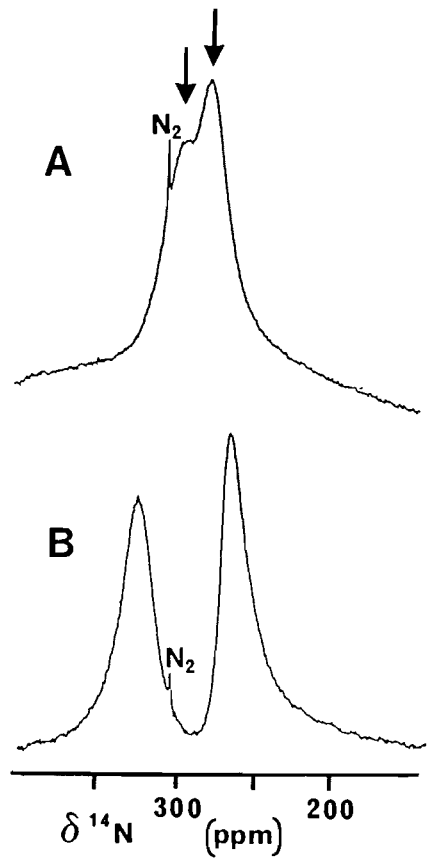


FIG. 1. (*A*) ^{14}NMR spectrum of a mixture PhSNSNSPh (δ 273.3) and PhNSNPh (δ 297.7) in THF. (*B*) Same mixture after reduction with potassium, showing the exclusive production of PhNSNSPh (δ 261.6, 330.4).

signals corresponding to the non-equivalent nitrogens of the product. Neither of the two starting materials was observed in the final reaction mixture.

Preparation and molecular structure of (4-$C_6H_4NO_2$)SNSN(4-C_6H_4OMe)

During the course of this work we became interested in the potential use of highly polar, conjugated sulphur nitrogen compounds as non-linear optical materials (13). To this end we synthesized (4-$C_6H_4NO_2$)SNSN(4-C_6H_4OMe) by condensing the mixed sulphur diimide (4-C_6H_4OMe)NSNSiMe_3 (prepared as described above) with 4-$NO_2C_6H_4SCl$. While the space group of this compound ($P2_1/n$) is not non-centrosymmetric, as would be required for second harmonic generation, it nonetheless reveals some interesting packing features. The molecular structure of this material is shown in Fig. 2*a*, while Fig. 2*b*

Can. J. Chem. Downloaded from www.nrcresearchpress.com by 195.138.81.100 on 09/07/12
For personal use only.

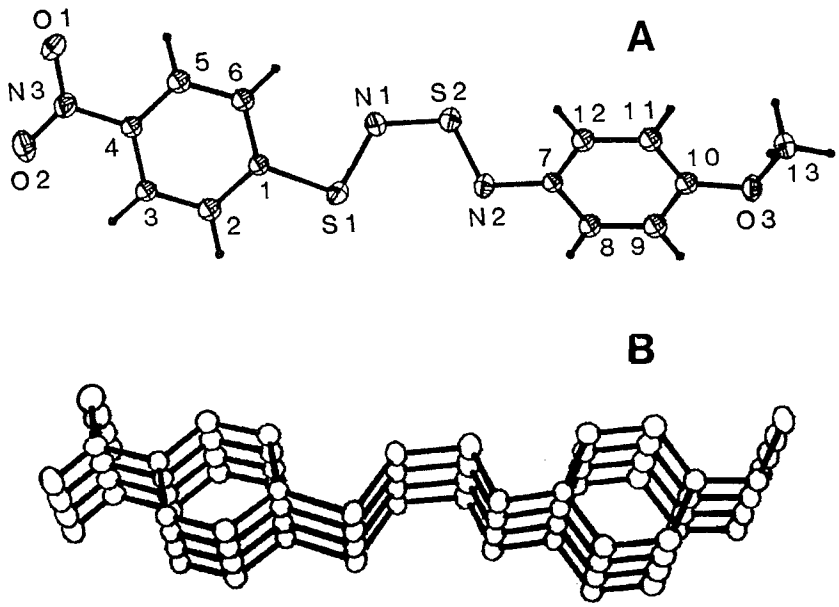


FIG. 2. (*A*) ORTEP drawing of (4-$MeOC_6H_4$)NSNS(4-$C_6H_4NO_2$), showing atom numbering scheme, and (*B*) stacking of (4-$MeOC_6H_4$)-NSNS(4-$C_6H_4NO_2$) molecules along the *a* axis.

TABLE 2. Non-hydrogen atom coordinates in (4-$MeOC_6H_4$)NSNS-(4-$C_6H_4NO_2$)*

Atom	*x*	*y*	*z*	*B*(Å^2)
S(1)	0.7524(5)	0.0893(2)	0.54349(7)	3.42(4)
S(2)	0.8306(5)	0.0889(2)	0.64270(7)	3.68(5)
O(1)	1.350(2)	0.517(5)	0.4243(2)	5.3(2)
O(2)	1.145(2)	0.4041(5)	0.3666(2)	6.1(2)
O(3)	0.251(1)	−0.2130(4)	0.8048(2)	3.5(1)
N(1)	0.894(2)	0.1424(5)	0.5946(2)	3.4(2)
N(2)	0.636(2)	−0.0189(5)	0.6380(2)	3.0(1)
N(3)	1.199(2)	0.4218(5)	0.4085(2)	3.8(1)
C(1)	0.887(2)	0.1903(6)	0.5056(2)	2.4(2)*
C(2)	0.824(2)	0.1747(6)	0.4571(3)	3.1(2)*
C(3)	0.925(2)	0.2500(6)	0.4253(2)	2.7(2)*
C(4)	1.088(2)	0.3411(6)	0.4416(2)	2.7(2)*
C(5)	1.151(2)	0.3588(6)	0.489(3)	3.2(2)*
C(6)	1.048(2)	0.2846(6)	0.5215(2)	2.9(2)*
C(7)	0.543(2)	−0.0625(5)	0.6819(2)	2.4(2)*
C(8)	0.554(2)	−0.1744(6)	0.6876(2)	3.0(2)*
C(9)	0.451(2)	−0.2199(6)	0.7290(3)	3.2(2)*
C(10)	0.346(2)	−0.1588(6)	0.7660(2)	2.9(2)*
C(11)	0.338(2)	−0.0472(6)	0.7613(2)	3.1(2)*
C(12)	0.440(2)	−0.0016(6)	0.7190(3)	3.0(2)*
C(13)	0.130(2)	−0.1498(7)	0.8423(3)	3.8(2)

*Atoms with asterisks were refined isotropically.

†Anisotropically refined atoms are given in the form of the isotropic equivalent thermal parameter defined as: $(4/3)[a^2B(1,1) + b^2B(2,2) + c^2B(3,3) + ab(\cos\gamma)B(1,2) + ac(\cos\beta)B(1,3) + bc(\cos\alpha)B(2,3)]$.

TABLE 3. Selected bond lengths (Å) and angles (deg) in (4-$MeOC_6H_4$)NSNS(4-$C_6H_4NO_2$)

Bond	Length	Bonds	Angle
S1—C1	1.754(7)	N1—S1—C1	98.7(3)
S1—N1	1.663(6)	N1—S2—N2	113.6(3)
S2—N1	1.550(6)	S1—N1—S2	122.2(4)
S2—N2	1.548(6)	S2—N2—C7	113.9(5)
N2—C7	1.424(8)		

shows the stacking arrangement down the *a* axis. Table 2 provides a listing of non-hydrogen atom coordinates, while Table 3 summarizes pertinent bond lengths and angles. Within each molecule the S_2N_2 unit is planar to within ±0.009 Å. The nitrophenyl group makes a 2.5° dihedral angle with the S_2N_2 unit, while the methoxyphenyl ring is markedly twisted (41.2°) with respect to the S_2N_2 plane. Somewhat surprisingly, the molecules do not stack in a head-to-tail pattern (thereby aligning the donor and acceptor centres), but instead pack in a near vertical head-to-head fashion (Fig. 2*b*). The interplanar distance between the S_2N_2 units, 3.421 Å, is similar to the corresponding separations observed in stacked thiazyl heterocycles, *e.g.* benzo-1,3,2,4-dithiadiazine (3.29 Å) (14), naphtho[1,8-*cd*:4,5-*c'd'*]bis[1,2,6]thiadiazine (3.40 Å) (15), and near the graphite value (3.35–3.37 Å) (16). In $Me_3SiNSNSC_6H_4NO_2$, a much wider interplanar spacing (3.75 Å) is observed, and the molecules stack in a far more steeply inclined fashion, one that places the S—N(S) bond of one molecule over the aryl group of the next (17), thereby eliminating repulsive Me_3Si---Me_3Si interactions.

Association and rearrangement of radical anions

The reductive exchange reactions described above provide an important key to the understanding of skeletal rearrangements in sulphur–nitrogen chemistry. A discussion of the various issues requires, as a first step, recognizing the formal isoelectronic analogy between the cyclic internal radical anion **1** (6*a*) and simple acyclic sulphur diimides radical anions of the type $[RNSNR]^{-\bullet}$. The 5-electron 3-orbital π-manifold of these systems is illustrated in Fig. 3.

Association of sulphur diimide radicals can, in principle, occur in a variety of ways.[2] There is no solid state structural evidence on simple acyclic sulphur diimide radical anions, but in the related dithionite ion the dimeric unit is linked by a long S---S contact, with the two $SO_2^{-\bullet}$ anions eclipsed, *i.e.*, **3** (18).

[2]The equilibrium constants that have been measured for association of sulphur nitrogen radicals probably represent the net effect of different binding modes.

Can. J. Chem. Downloaded from www.nrcresearchpress.com by 195.138.81.100 on 09/07/12
For personal use only.

Can. J. Chem. Downloaded from www.nrcresearchpress.com by 195.138.81.100 on 09/07/12
For personal use only.

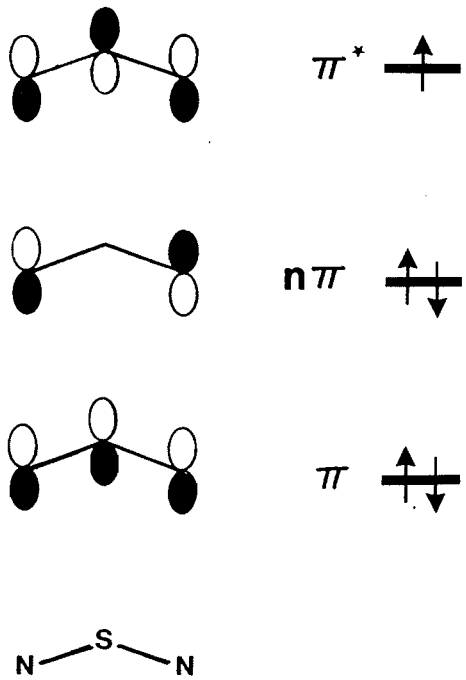
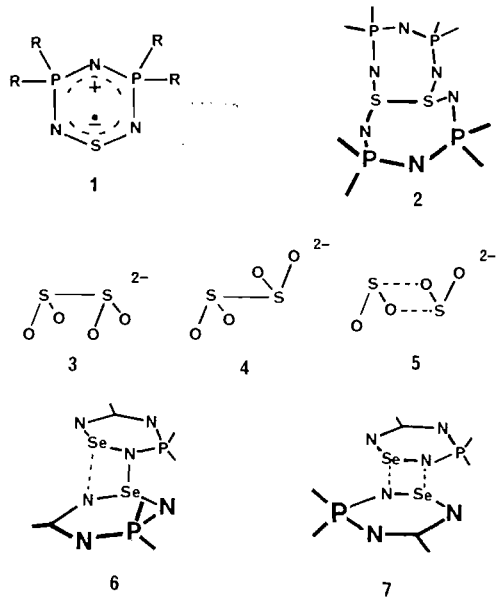


FIG. 3. Qualitative π-MO diagram for $[RNSNR]^{-\bullet}$ radical anions, illustrating nodal patterns.

A similar structure **2** is observed (19) for the dimer of the internal salt **1**, although in the latter case a crossover reaction (*i.e.* reaction [2]) has occurred, generating a twelve-membered ring from two six-membered rings. In orbital terms the weak radical–radical bond originates from the overlap of the two singly occupied molecular orbitals (SOMOs). Thus all the above evidence points to the S---S bridge as the preferred mode of association for $[RNSNR]^{-\bullet}$. Other, presumably higher energy structural possibilities can, however, certainly be imagined. In aqueous solution, for example, where less directional solvation forces replace the specific ion-pairing interactions of the ionic lattice, the dithionite anion is centrosymmetric (20). Structure **4** has been proposed, but we note that the head-to-tail modification **5** also possesses a centre of inversion.

Structure **5** is particularly appealing within the context of structural rearrangements described herein; an analogous head-to-tail fusion of two $[RNSNR]^{-\bullet}$ units provides the proposed pathway for the bond switching reaction of reaction [2]. While there is no direct precedent for this type of structure as a stable ground state, the mode of dimerization recently reported for the selenaphosphatriazinyl radical $[Ph_3PCN_3Se]^{\bullet}$, *i.e.* **6**, can be interpreted as a distortion of the ideal head-to-tail arrangement **7** (6*c*). In terms of chemical reactivity, however, there is no need for the centrosymmetric association to be a potential energy minimum; it needs only to correspond to a relatively accessible point on a reaction profile, one which affords a low energy pathway for rearrangement. Accurate calculations of the energies of such centrosymmetric structures would be useful to further work in this area.



Summary and conclusions

The ease of skeletal scrambling of simple sulfur diimides in the presence of catalytic amounts of reducing agents has many implications in sulphur nitrogen chemistry.[3] Conjugative effects notwithstanding, any open chain or cyclic compound containing the —N=S=N— unit will be susceptible to rearrangement upon reduction. The dimerization of S_2N_2 to S_4N_4 in the presence of reducing agents (21) perhaps represents an example of such a process (1); the necessary intermediate $S_2N_2^{-\bullet}$ anion has certainly been identified in the gas phase (22). Skeletal scrambling reactions can also be used to synthetic advantage, as demonstrated here by the preparation of several unsymmetrical derivatives. As a continuation of this work we are currently pursuing the development of polymeric sulphur diimides, i.e. $(—C_6H_4—NSN—)_x$, by chemical or electrochemical reduction of bifunctional sulphur diimides.

Experimental[4]

Reagents and general procedures

Aniline (Aldrich), 4-methylaniline (Aldrich), 4-methoxyaniline (Aldrich), thionyl chloride (Aldrich), benzene thiol (Aldrich), 4-nitrobenzene thiol chloride (Aldrich), chlorine gas (Matheson) were all commercial products and used as received, except thionyl chloride, which was freshly distilled before use. The sulphinylamines RNSO (R = C_6H_6, 4-MeC_6H_4, and 4-$MeOC_6H_4$) (12*a*), PhSCl (23), the sulphur diimides $Me_3SiNSNSiMe_3$ (9) and PhSNSNSPh (21, 24) were prepared according to standard literature methods. RNSNR (R = C_6H_5, 4-MeC_6H_4, and 4-$MeOC_6H_4$) were prepared by a modification (*vide infra*) of the method of Cramer (6). All solvents were dried (toluene/Na), hexane (CaH_2), diethyl ether (CaH_2), carbon tetrachloride (P_2O_5), methylene chloride (P_2O_5), tetrahydrofuran (K/benzophenone) were distilled immediately before use. All reactions were performed under an atmosphere of nitrogen (99.98% purity). Chemical analyses were performed by MHW Laboratories, Phoenix, AR. Infrared spectra (2000–250 cm^{-1}) were recorded as Nujol mulls (CsI windows) on a Nicolet 20SX/C FTIR spectrometer. Melting points were obtained on an electrothermal melting point apparatus and were uncorrected. Gas chromatograms were recorded on a Varian 3400 gas chromatograph equipped with flame ionization detector (FID). The stainless steel column (6′ × 1/8″ I.D.) was packed with 20% QF-1 (fluorinated hydrocarbon) on chromosorb W-80/100 mesh. The oper-

[3]Sulphur–oxygen chemistry may also be influenced by such reactions. For example, co-reduction of an aqueous mixture of $S^{16}O_2$ and $S^{18}O_2$ should afford $S^{16}O^{18}O$.

[4]Tables of crystallographic data (S1), H-atom coordinates (S2), bond lengths and angles (S3), anisotropic thermal parameters (S4) and observed and calculated structure factors for (4-$MeOC_6H_4$)NSNS(4-$C_6H_4NO_2$) (S5) (18 pages) may be purchased from the Depository of Unpublished Data, CISTI, National Research Council of Canada, Ottawa, Ont., Canada K1A 0S2.

Can. J. Chem. Downloaded from www.nrcresearchpress.com by 195.138.81.100 on 09/07/12
For personal use only.

ating conditions were as follows: hydrogen flow rate 30 mL/min, air flow rate 30 mL/min, carrier gas (N_2) flow rate 30 mL/min, detector temperature 250°C, injector temperature 230°C, column temperature 210°C, chart speed 1 cm min^{-1}, sample volume 1.0 μL. GC–MS analyses were obtained on a VG Mass Lab 12000 equipped with an HP 5790 (GC), and a 30 m DB5 (capillary column). ^{14}N NMR spectra were recorded at 28.906 MHz (in THF ref. $NH_{3(l)}$) on a Bruker WH-400 spectrometer. Pulse widths of 60 μs and pulse delays of 1.0 s were used; good S/N ratios were achieved with 10 000 to 15 000 scans.

Preparation of RNSNR (R = C_6H_5, 4-MeC_6H_4, and 4-$MeOC_6H_4$) (general procedure)

Equimolar amounts of aryl sulfinylamine (RNSO) and freshly cut sodium (or potassium) metal were added to 250 mL of toluene in a round-bottomed flask equipped with a water condenser. The solution was then stirred and heated to reflux under nitrogen. At reflux temperature a vigorous reaction occurred to afford a deep red solution and a heavy precipitate of sodium dithionite. After 2 h, the reaction mixture was cooled to room temperature and finally quenched by bubbling air into the solution for 30 m. The solution was filtered and the resulting filtrate added to a separatory funnel and washed with water three times to remove any remaining water-soluble salts which might have been formed during the reduction. The solution was then dried over Na_2SO_4, and the solvent removed with a rotary evaporator to leave a red oily residue, which was recrystallized from hexane. The purity of the product was checked by GC.

Preparation of PhNSNPh

Starting materials were PhNSO (20.0 g, 0.144 mol) and sodium metal (3.30 g, 0.144 mol); yield (69%) of PhNSNPh (red oil at room temperature) with 96% purity (checked by GC).

Preparation of (4-MeC_6H_4)NSN(4-C_6H_4Me)

Starting materials were (4-MeC_6H_4)NSO (20.0 g, 0.13 mol) and sodium metal (3.0 g, 0.13 mol); yield (61%) of (4-MeC_6H_4)NSN(4-C_6H_4Me) (red crystals), mp 47–48°C. The purity of the product was 99% by GC.

Preparation of (4-$MeOC_6H_4$)NSN(4-C_6H_4OMe)

Starting materials were (4-$MeOC_6H_4$)NSO (15.0 g, 0.089 mol) and sodium metal (2.04 g, 0.089 mol). The residue was recrystallized from a mixture of 100 mL hexane and 5 mL toluene; yield (70%) of (4-$MeOC_6H_4$)NSN(4-C_6H_4OMe) (dark red crystals), mp 46–47°C. The purity of the product was 99% by GC.

General procedure for reductive scrambling of sulphur diimides

Prior to the reduction experiment, all glassware was washed and rinsed with Me_3SiCl and CH_2Cl_2, respectively, then oven dried overnight at 160°C. A solution containing equimolar amounts of the two symmetrical sulphur diimides (RNSNR and R′NSNR′) was prepared in 35 mL of THF. The resulting solution was then degassed by means of three freeze–pump–thaw cycles. A catalytic amount (5–25%) of freshly cut reducing agent (K or Na) was quickly added under nitrogen to the mixture. The deep red reaction mixture was stirred and held under nitrogen for about 2 h (preliminary studies showed that the reaction reached completion within 15 min) to ensure that equilibirum had been reached. The composition of the mixture was determined by removing aliquots via a syringe, quenching them immediately with oxygen, and analysing the resultant solutions by GC and GC–MS.

Scrambling of PhNSNPh and (4-MeC_6H_4)NSN(4-C_6H_4Me)

Materials used were PhNSNPh (0.35 g, 1.65 mmol), (4-MeC_6H_4)NSN(4-C_6H_4Me) (0.40 g, 1.65 mmol) and sodium metal (1.9 mg, 0.082 mmol). GC analysis of the mixture showed an integration of 1:2:1 ratio of PhNSNPh:(4-MeC_6H_4)NSNPh:(4-MeC_6H_4)NSN(4-C_6H_4Me). The unsymmetrical aryl sulphur diimide (4-MeC_6H_4)-NSNPh was identified by GC–MS analysis; mass spectrum (*m/e*) 228 (25), 213 (74), 137 (27), 123 (17), 91 (45), 77 (100).

Scrambling of (4-MeC_6H_4)NSN(4-C_6H_4Me) and (4-$MeOC_6H_4$)NSN(4-C_6H_4OMe)

Materials used were (4-MeC_6H_4)NSN(4-C_6H_4Me) (0.40 g, 1.65 mmol), (4-$MeOC_6H_4$)NSN(4-C_6H_4OMe) (0.45 g, 1.65 mmol) and sodium metal (1.9 mg, 0.082 mmol). GC analysis of the mixture showed an integration of 1:2:1 ratio of (4-MeC_6H_4)NSN(4-C_6H_4Me):(4-MeC_6H_4)NSN(4-C_6H_4OMe):(4-$MeOC_6H_4$)NSN(4-C_6H_4OMe). The unsymmetrical diimide (4-MeC_6H_4)NSN(4-C_6H_4OMe) was identified by GC–MS analysis; mass spectrum (*m/e*) 258 (19), 243 (65), 227 (20), 153 (23), 137 (25), 107 (77), 91 (54).

Scrambling of PhNSNPh and $Me_3SiNSNSiMe_3$

Materials used were PhNSNPh (5.0 g, 0.023 mol), $Me_3SiNSNSiMe_3$ (4.8 g, 0.023 mol), and sodium metal (0.03 g, 1.3 mmol). GC analysis of the equilibrium mixture showed an integration of 1:5:1 ratio of $Me_3SiNSNSiMe_3$:PhNSNSiMe$_3$:PhNSNPh. Evaporation of the solvent and fractional distillation gave PhNSNSiMe$_3$ (5.2 g, 53%) as an orange oil, bp 57–60°C/0.1 Torr (lit. bp 47°C/0.05 Torr (12*a*)). The purity of the distilled product was 96% by GC.

Scrambling of PhNSNPh and PhSNSNSPh

Materials used were PhNSNPh (0.5 g, 2.3 mmol, δN 297.7), PhSNSNSPh (0.65 g, 2.3 mmol, δN 273.4), and sodium metal (2.6 mg, 0.12 mmol). Analysis of the pre- and post-reduction mixture was performed by ^{14}N NMR. After reduction the NMR spectrum showed only two magnetically inequivalent nitrogens of PhNSNSPh at δN 261.7 and 300.6 ppm. Neither starting material was detected. Removal of the solvent (THF) *in vacuo* and subsequent recrystallization of the residual solid from cold hexane afforded PhSNSNPh (0.63 g, 2.7 mmol, 55%). An identical NMR spectrum was obtained from PhSNSNPh prepared by treating PhNSNSiMe$_3$ with PhSCl.

Preparation of (4-$MeOC_6H_4$)NSNS(4-$C_6H_4NO_2$)

A solution of 4-$NO_2C_6H_4SCl$ (0.79 g, 4.2 mmol) in 5 mL CH_2Cl_2 was added dropwise to a solution of (4-$MeOC_6H_4$)NSNSiMe$_3$ (1.0 g, 4.2 mmol) (obtained from a radical rearrangement reaction of (4-$MeOC_6H_4$)NSN(4-C_6H_4OMe) and $Me_3SiNSNSiMe_3$ described above) in CH_2Cl_2 (15 mL). The resulting red solution was allowed to react at room temperature for 1 h. The solvent was then removed *in vacuo*. The resulting solid was redissolved in 25 mL CH_2Cl_2 and placed in a sealed tank containing *n*-pentane. Slow diffusion of *n*-pentane into the CH_2Cl_2 solution led to formation of long red crystals of (4-$MeOC_6H_4$)NSNS(4-$C_6H_4NO_2$) (0.71 g, 53%) mp 167–169°C. *Anal.* calcd for $C_{13}H_{11}N_3O_3S_2$: C 48.59, H 3.45, N 13.08; found: C 48.62, H 3.43, N 13.23. Infrared (2000–250 cm^{-1}): 1575(m), 1496(s), 1458(s), 1377(s), 1317(m), 1289(s), 1247(s), 1211(m), 1184(m), 1085(s), 1026(s), 959(m), 928(w), 829(s), 798(w), 745(s), 722(m), 679(s), 569(w), 518(m), 298(s) cm^{-1}.

X-ray measurements

Red needles of (4-$MeOC_6H_4$)NSNS(4-$C_6H_4NO_2$) suitable for X-ray work were grown from pentane/CH_2Cl_2. The crystals were monoclinic, space group $P2_1/n$, $a = 3.950(1)$, $b = 12.437(2)$, $c = 28.354(5)$ Å, $\beta = 93.07(1)°$, $V = 1390.8(7)$ Å^3, $Z = 4$ at 293 K. The structure was solved by direct methods and refined by full-matrix least-squares analysis. The final R and R_w values of 0.043 and 0.048 were based on 744 unique data with $F > 3\sigma(F)$.

Acknowledgements

We thank NSERC and the NSF (EPSCOR program) for funding.

1. R. T. Oakley. Prog. Inorg. Chem. **36**, 299 (1988).
2. K. Bestari, R. T. Boeré, and R. T. Oakley. J. Am. Chem. Soc. **111**, 1597 (1989).
3. (*a*) R. T. Boeré, A. W. Cordes, and R. T. Oakley. J. Am. Chem. Soc. **109**, 7781 (1987); (*b*) A. W. Cordes, S. W. Liblong, S. G. Phillips, and R. T. Oakley, Inorg. Chem. **28**, 4147 (1989).
4. N. Burford, J. Passmore, and M. J. Schriver. J. Chem. Soc. Chem. Commun. 140 (1986).
5. W. V. F. Brooks, N. Burford, J. Passmore, M. Schriver, and L. H. Sutcliffe. J. Chem. Soc. Chem. Commun. 69 (1987).

6. (*a*) R. T. OAKLEY. J. Chem. Soc. Chem. Commun. 596 (1986); (*b*) K. BESTARI, A. W. CORDES, and R. T. OAKLEY. J. Chem. Soc. Chem. Commun. 1328 (1988); (*c*) K. BESTARI, A. W. CORDES, R. T. OAKLEY, and K. M. YOUNG. J. Am. Chem. Soc. **112**, 2249 (1990).
7. J. A. HUNTER, B. KING, W. E. LINDSELL, and M. A. NEISH. J. Chem. Soc. Dalton Trans. 880 (1980).
8. G. BRANDS and A. GOLLOCH. Z. Naturforsch. **37***b*, 1137 (1982).
9. O. J. SCHERER and R. WEIS. Z. Naturforsch. **25***b*, 1486 (1970).
10. (*a*) V. H. H. HORHÖLD and J. BECK. J. Prackt. Chem. **311**, 621 (1969); (*b*) T. MINAMI, H. MIKI, H. MATSUMOTO, Y. OHSHIRO, and T. AGAWA. Tetrahedron Lett. 3049 (1968).
11. R. CRAMER. J. Org. Chem. **26**, 3476 (1961).
12. (*a*) I. RUPPERT, V. BASTIAN, and R. APPEL. Chem. Ber. **108**, 239 (1975); (*b*) R. APPEL and M. MONTENARH. Z. Naturforsch. **30***b*, 847 (1975); (*c*) O. J. SCHERER, G. WOLMERSHÄUSER, and R. JOTTER. Z. Naturforsch. **37***b*, 432 (1982).
13. (*a*) D. J. WILLIAMS. Ang. Chem. Int. Ed. **23**, 690 (1984); (*b*) D. PUGH and J. N. SHERWOOD. Chem. Brit. 544 (1988); (*c*) J. SIMON, P. BASSOUL, and S. NORVEZ. New J. Chem. **13**, 13 (1989).
14. A. W. CORDES, M. HOJO, H. KOENIG, M. C. NOBLE, R. T. OAKLEY, and W. T. PENNINGTON. Inorg. Chem. **25**, 1137 (1986).
15. A. GIEREN, V. LAMM, R. C. HADDON, and M. L. KAPLAN. J. Am. Chem. Soc. **101**, 7277 (1979).
16. F. LAVES and Y. BASKIN. Z. Kristallogr. Kristallgeom. Kristallphys. Kristallchem. **107**, 337 (1956).
17. R. JONES, D. J. WILLIAMS, P. T. WOOD, and J. D. WOOLLINS. Polyhedron, **8**, 91 (1989).
18. (*a*) J. D. DUNITZ. Acta Crystallogr. **90**, 579 (1956); (*b*) C. TH. KIERS and A. VOS. Acta Crystallogr. **34***b*, 1499 (1978).
19. N. BURFORD, T. CHIVERS, M. N. S. RAO, and J. F. RICHARDSON. Inorg. Chem. **23**, 1946 (1984).
20. H. TAKAHASHI, N. KANEKO, and K. MIWA. Spectrochim. Acta, **38***A*, 1147 (1982).
21. (*a*) M. BECKE-GOEHRING. Inorg. Synth. **6**, 123 (1960). (*b*) M. FEHÉR. Handbook of preparative inorganic chemistry. Vol. 1. *Edited by* G. Brauer. Academic Press, New York. 1963. p. 409.
22. T. B. MACMAHON. Private communication.
23. J. KUYPER and G. B. STREET. J. Am. Chem. Soc. **99**, 7848 (1977).
24. J. WEISS and H. PIECHACZEK. Z. Naturforsch. **18***b*, 1139 (1963).

Can. J. Chem. Downloaded from www.nrcresearchpress.com by 195.138.81.100 on 09/07/12
For personal use only.

Luminescence of excited fragments produced from methyl halides in noble gas flowing afterglow

YUEZHU GU, JINGZHONG GUO, CHUANPU LIU, AND YONGJIA YIN
Department of Chemistry, Shandong University, Jinan, China

AND

DEZHAO CAO AND JIYE CAI
Anhui Institute of Optics and Fine Mechanics, Academia Sinica, Hefei, China

Received January 26, 1990

YUEZHU GU, JINGZHONG GUO, CHUANPU LIU, YONGJIA YIN, DEZHAO CAO, and JIYE CAI. Can. J. Chem. **69**, 100 (1991).

The reaction of metastable He(2^3S) and Ne($^3P_{0,2}$) atoms with methy halides has been investigated by flowing afterglow technique. Emission spectra have been observed and formation rate constants of some fragments have been measured. The rotational and vibrational temperatures of CH($A^2\Delta$) were also estimated.

Key words: flowing afterglow, methyl halides, metastable atoms.

YUEZHU GU, JINGZHONG GUO, CHUANPU LIU, YONGJIA YIN, DEZHAO CAO et JIYE CAI. Can. J. Chem. **69**, 100 (1991).

La réaction des atomes metastables de He(2^3S) et Ne($^3P_{0,2}$) avec halogenures de méthyle a été étudiée par la technique de courant de phosphorescence. Les spectres d'émission ont été observés et les constantes de vitesse de formation de quelques fragments ont été obtenues. Les temperatures rotationelle et vibrationelle de CH($A^2\Delta$) a été aussi determinée.

Mots clés : courant de phosphorescence, halogenures de methyle, atomes métastables.

Introduction

When rare gas atoms He and Ne are subjected to discharge, metastable atoms and ions are generated. The active species can react with the molecules and may produce fragments in electronically excited states. Tsuji *et al.* (1, 2) observed the dissociative charge transfer reaction of He^+ with CCl_4 and CBr_4. Setser and co-workers (3) investigated the reactions of He (2^3S) with diatomic moleclues N_2, CO, O_2, HCl, and HBr. Yencha and Wu (4) have discussed the energy transfer reactions of He(2^3S) and Ne($^3P_{0,2}$) with H_2O, H_2S, and CS_2. The reaction of He(2^3S) with NH_3 has been observed by Someda *et al.* (5). For reactions of He(2^3S) and Ne($^3P_{0,2}$) with five-atom molecules, Jones *et al.* (6) have reported the Penning ionization processes of CCl_4, CH_2Cl_2, $CHCl_3$, CBr_4, and other molecules.

In this work, we investigate the dissociative excitation of polyatomic molecules CCl_4, $CHCl_3$, CH_2Cl_2, CBr_4, CH_2Br_2, $CHBr_3$, CH_3Br, CH_2I_2, and CH_3I in flowing afterglows of helium and neon. The emission spectra of the fragments have been obtained and formation rate constants of CH(A, B, C) in different reactions have been evaluated. The rotational structure of the visible emission spectra from CH(A–X) has been analyzed to obtain information about rotational distribution of CH($A^2\Delta$, $v' = 0$) radical.

Experimental

The experimental assembly is essentially identical to that shown in Fig. 1 of ref. 7. Helium (or neon) gas was passed through a molecular sieve trap cooled by liquid nitrogen and excited to He(2^3S) (or Ne($^3P_{0,2}$)) in a hollow cathode discharge source. A right-angle light trap situated between the discharge source and reaction zone was used to avoid light leakage into the observation region. The system was pumped by a 150 L/s Roots pump. The reagent gases were degassed and purified by vacuum distillation before use and were admitted ca. 15 cm downstream from the discharge section. The total pressure was kept constant at 133 Pa.

Unfocussed emission from flames produced in the reactor was dispersed by a 0.75 m monochromator and detected by a cooled photomultiplier tube (RCA C31034A). Photon counting techniques were used for collecting emssion data. The wavelength response of the detection system had been previously calibrated with standard lamps.

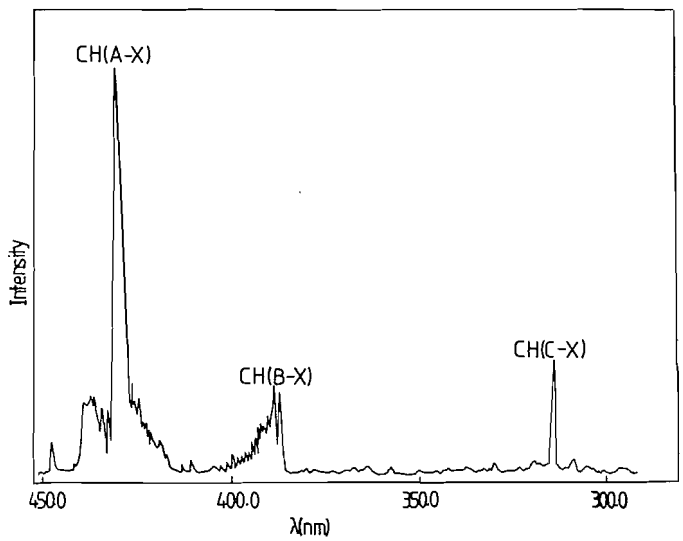


FIG. 1. Emission spectrum from the reaction He(2^3S) + CH_2Br_2.

Results and discussion

Emission spectra of the fragments

Strong conical blue flames were observed from the reactions of He(2^3S) and Ne($^3P_{0,2}$) with various methyl halides. Emission in the 200–500 nm region was recorded and analyzed. Typical emission spectra are shown in Figs. 1 and 2 and fragments with strong emission are listed in Table 1.

When He(2^3S) reacted with H-containing methyl halides strong emission from CH($A^2\Delta$–$X^2\Pi$), CH($B^2\Sigma$–$X^2\Pi$), and CH($C^2\Sigma$–$X^2\Pi$) was observed. Fewer emission bands were observed with Ne($^3P_{0,2}$). For the molecules CH_2Cl_2, $CHCl_3$, CCl_4, $CHBr_3$, CH_2Br_2, and CBr_4, Br_2*, and Cl_2* emission was obtained in the 250–350 nm and 240–260 nm regions, respectively. Tsuji *et al.* (1) reported the reaction between He^+ and CCl_4. Tokue and Ito (8) investigated the dissociation of CBr_4, $CFBr_3$, and $CHBr_3$ using electron-impact induced light emission. Compared with their emission spectra, we conclude that the broad emission in the 250–350 nm region is due to the

Can. J. Chem. Downloaded from www.nrcresearchpress.com by 195.138.81.100 on 09/07/12
For personal use only.

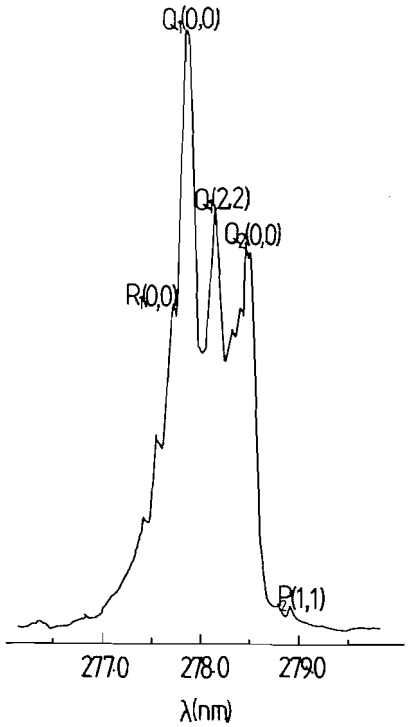


FIG. 2. Emission spectrum from the reaction $Ne(^3P_{0,2}) + CCl_4$.

TABLE 1. Excited fragments produced in the helium flowing afterglow

Reactant	Excited fragments
CCl_4	$CCl(A^2\Delta)$, Cl_2*
CCl_4†	$CCl(A^2\Delta)$
$CHCl_3$	$CH(A^2\Delta)$, $CH(B^2\Sigma)$, $CH(C^2\Sigma)$, $CCl(A^2\Delta)$, Cl_2*, H
CH_2Cl_2	$CH(A^2\Delta)$, $CH(B^2\Sigma)$, $CH(C^2\Sigma)$, $CCl(A^2\Delta)$, Cl_2*, H
CBr_4	Br_2*
$CHBr_3$	$CH(A^2\Delta)$, $CH(B^2\Sigma)$, $CH(C^2\Sigma)$, Br_2*, H
CH_2Br_2	$CH(A^2\Delta)$, $CH(B^2\Sigma)$, $CH(C^2\Sigma)$, Br_2*, H
CH_3Br	$CH(A^2\Delta)$, $CH(B^2\Delta)$, $CH(C^2\Delta)$, H
CH_2I_2	$CH(A^2\Delta)$, $CH(B^2\Sigma)$, $CH(C^2\Sigma)$, H
CH_3I	$CH(A^2\Delta)$, $CH(B^2\Sigma)$, $CH(C^2\Sigma)$, H

†This is the result of the reaction $Ne(^3P_{0,2}) + CCl_4$.

$D0_u^+-X^1\Sigma_g^+$, $D'2_g-A'^3\Pi(2_u)$, $E0_g^+-B^3\Pi(0_u^+)$ and $D'2_g-{}^3\Delta2_u$ transition of Br_2*; the Cl_2* emission is probably from $E^3\Pi_{Og}^+-B^3\Delta_{Ou}^+$ and $D^1\Sigma_u^+-X^1\Sigma_g^+$.

Relative electronically excited fragment populations

The relative populations of excited fragments have been evaluated from emission intensities of the various fragments. In the calculation we have accounted for the wavelength response of the detection system and the predissociation rate of $CH(C^2\Sigma)$ (9). The relation between the fragment yield and emission intensity is given by

$$R_p \propto f(\lambda)\, I_\lambda\, (1 + k\tau)$$

where R_p is the fragment yield, I_λ is the emission intensity, $1/f(\lambda)$ is the wavelength response of the detection system, τ is the level lifetime of the fragment, and k is the predissociation rate of the fragment. The results are listed in Table 2.

TABLE 2. Estimated relative populations of excited fragments produced in the helium flowing afterglow

	Estimated relative population when reagent is					
Fragment	$CHCl_3$	CH_2Cl_2	$CHBr_3$	CH_2Br_2	CH_3Br	CH_3I
$CH(A^2\Delta)$	1.0	1.0	1.0	1.0	1.0	1.0
$CH(B^2\Sigma)$	0.12	0.22	0.19	0.23	0.21	0.20
$CH(C^2\Sigma)$†	0.04	0.04	0.03	0.13	0.18	0.11
$CCl(A^2\Delta)$	0.05	0.02				
Cl_2*	0.30	0.005				
Br_2*			3.38	0.23		

†Assuming a predissociation rate constant $A = 8.6 \times 10^7 s^{-1}$ (9).

TABLE 3. Formation rate constants and branching ratios of some excited fragments in the helium flowing afterglow

	k (10^{-11} cm^3 molecule^{-1} s^{-1})				k/k_Q†	
Fragments	$CHCl_3$	CH_2Cl_2	CH_2Br_2	CH_3I	$CHCl_3$	CH_2Cl_2
$CH(A^2\Delta)$	5.0	8.3	3.1	3.2	0.046	0.083
$CH(B^2\Sigma)$	0.64	1.6	0.63	0.60	0.006	0.016
$CH(C^2\Sigma)$	0.15	0.74	0.42	0.28	0.001	0.007
$CCl(A^2\Delta)$	0.25	0.19			0.002	0.002

†$k_Q(CH_2Cl_2) = 9.9 \times 10^{-10}$ cm^3 molecule s^{-1}; $k_Q(CHCl_3) = 10.7 \times 10^{-10}$ cm^3 molecule s^{-1} (6).

Formation rate constants of excited fragments

Providing there is no quenching, nonradiative decay, or pumping of the excited product state species P* from the observation zone, the steady-state photon emission rate from excited states equals the rate of excited state formation in some energy transfer reaction E^* + AB as expressed in eq. [1]:

$$[1] \quad I_p^* = k_p^*[E^*][AB]$$

If k_p^* is known for some reference molecule AB, the formation rate constant $k_p'^*$ for another reaction E* + BC can be obtained by comparing the relative integrated emission intensities (10):

$$[2] \quad \frac{I_p'^*}{I_p^*} = \frac{k_p'^*[E^*][BC]}{k_p^*[E^*][AB]}$$

$$k_p'^* = k_p^* I_p'^*[AB]/I_p^*[BC]$$

The key to the reference method is, of course, finding a reliable reference reaction. In our experiment, the reference reaction $He(2^3S) + CO(X) \rightarrow CO^+(B) + He$ was used, with a rate constant $k_{CO(B-X)} = 2.1 \times 10^{-11}$ cm^3 molecule s^{-1} (11). The formation rate constants of CH(*A*), CH(*B*), CH(*C*), and CCl(*A*) have been obtained in reactions of $He(2^3S)$ with $CHCl_3$, CH_2Cl_2, CH_2Br_2, and CH_3I. The results are summarized in Table 3.

*Rotational and vibrational distributions of CH(*A*)*

Relative emission intensities were analyzed to estimate the rotational and vibrational populations of $CH(A^2\Delta)$ formed in the reactions of $He(2^3S)$ with various H-containing methyl halides. All the CH(A—X) spectra obtained have complex structure due to overlapping of the different branches from the 0–0, 1–1, and 2–2 bands, but the R-branch lines of the 0–0 band are resolved

Can. J. Chem. Downloaded from www.nrcresearchpress.com by 195.138.81.100 on 09/07/12
For personal use only.

TABLE 4. $CH(A^2\Delta)$ rotational and vibrational temperature obtained in the helium flowing afterglow†

Parameter	Value					
	$CHCl_2$	CH_2Cl_2	$CHBr_3$	CH_2Br_2	CH_3Br	CH_3I
$T_{rot}(v' = 0)$	2900 ± 500	3100 ± 500	2300 ± 500	3100 ± 500	2900 ± 500	3100 ± 500
$T_{vib}(A^2\Delta)$	3000 ± 500	3300 ± 500	2700 ± 500	3200 ± 500	3000 ± 500	2900 ± 500

†P_{He} = 133.32 Pa.

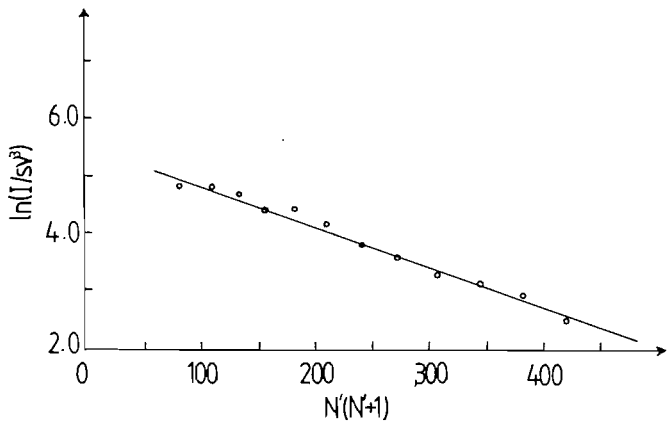


FIG. 3. ln $(I/S_{N'N''}\nu^3)$ plotted against $N'(N' + 1)$ for CH(A—X, 0—0) produced in reaction $He(2^3S) + CHCl_3$.

from those of the 1–1 and 2–2 bands for $N' > 6$. We used the intensities of the R-branch rotational lines from $v' = 0, N' > 6$ to estimated relative rotational populations of $CH(A^2\Delta, v' = 0)$. A semilog plot of $I_{N'N''}/\nu^3 S_{N'N''}$ against $N'(N' + 1)$ is shown in Fig. 3, where $I_{N'N''}$ is the relative emission intensity, ν is the transition and frequency, and $S_{N'N''}$ is the rotational line strength calculated with the Hönl–London formula (12). An approximately linear relationship for $CH(A^2\Delta, v^\circ = 0)$ indicates that the rotational populations can be represented in terms of a Boltzmann distribution. Analogous results were obtained for $CH(A^2\Delta, v' = 0)$ formed from various methyl halides. From the slope $-hcB_{v'}/kT_{rot}$, where $B_{v'}$ is the rotational constant, the effective rotational temperature, T_{rot}, can be evaluated. Table 4 gives the effective rotational temperatures of $CH(A^2\Delta, v' = 0)$ formed from various H-containing methyl halides.

By comparison of the (2, 2) and (0, 0) band Q-branch intensities, the vibrational population ratios (P_2/P_0) were estimated. If Boltzmann distributions are assumed for the vibrational populations, temperatures can be evaluated from these vibrational population ratios (P_2/P_0) with values listed in Table 4.

Taking experimental uncertainties (ca. ±500 K) into account, the rotational and vibrational temperatures of CH(*A*) obtained in this study are very similar to those obtained by electron impact on several methyl halides. In addition, the CH(A—X) emission specta obtained by electron impact on methane, acetylene, and ethylene are similar to those from the methyl halides (13). It is evident that the excess energies with which the excited CH radicals are formed differ in the various molecules excited by different processes, yet their *A* state internal energy distributions are similar. We intend to pursue further experimental and theoretical investigations on this subject.

Formation mechanism of excited fragments

Interactions between metastable atoms and gaseous molecules include several excitation channels, for example Penning ionization, dissociative excitation transfer, rearrangement ionization, ion-pair formation, and associative ionization. It has generally been accepted that for reagents with ionization potentials below the excitation energy of metastable He or Ne, chemiionization is the dominant quenching channel. Thus chemiionization reactions of metastable electronically excited He and Ne atoms have been actively studied in recent years. Jones *et al.* (6) studied the branching ratios for Penning ionization of several compounds, including the diatomic NO, N_2, Cl_2, O_2 and large molecules such as CCl_4, $CHCl_3$, CH_2Cl_2, CH_3Cl, etc., in flowing afterglows of He, Ne, and Ar. The experimental results show that the branching ratio was ~0.7, for the larger molecules in the low reagent concentration region. The data indicate that other channels are available. Much less is known about the dissociative excitation reactions of CH_nX_{4-n} in He and Ne flowing afterglow. Chang *et al.* (11) investigated the reaction of $He(2^3S)$ with CH_4, C_2H_4, and C_2H_2. Dissociative excitation was only 6% of the total quenching for C_2H_2 and even less for CH_4 and C_2H_4.

In the present work, emission spectra from excited neutral species were observed in the reaction of $He(2^3S)$ and $Ne(^3P_{0,2})$ with methyl halides. Branching ratios k/k_Q of $CH(A, B, C)$ and $CCl(A)$ were obtained for CH_2Cl_2 and $CHCl_3$ and listed in Table 3. Here k is the formation rate constant for production of excited fragments and k_Q is the rate constant for all quenching processes. Although the values are smaller than for the ionization channel, dissociative excitation can also be an important exit channel in the reaction of $He(2^3S)$ with CH_nX_{4-n}.

Concerning the formation mechanism of these neutral excited species, it may occur via an electron recombination reaction, analogous to the reaction of $He(2^3S)$ and CS_2 (14). Another possible process is dissociative excitation of the reagent molecule. In order to prove whether the formation of $CH(A, B, C)$ etc. is via ion–electron recombination, a trace amount of SF_6 as an electron scavenger was added to the reaction system. Our result showed the addition of SF_6 has no obvious effect in reducing the fragment emission intensities. This suggests that the fragment formation mechanism is not a process involving ion–electron recombination, but a dissociative excitation transfer process.

Acknowledgement

This work was supported by the National Natural Sciences Foundation of China.

1. M. TSUJI, T. MIZUGUCHI, K. SHINOCHARA, and Y. NISHIMURA. Can. J. Phys. **80**, 838 (1983).
2. M. Tsuji, R. Kuhn, and J. P. MAIER. Chem. Phys. Lett. **119**, 478 (1985).
3. W. C. RICHARDSON and D. W. SETSER. J. Chem. Phys. **58**, 1809 (1973).
4. A. J. YENCHA and K. T. WU. Chem. Phys. **49**, 127 (1980).
5. K. SOMEDA, T. KONDOW, and K. KUCHITSU. J. Phys. Chem. **92**, 368 (1988).

Can. J. Chem. Downloaded from www.nrcresearchpress.com by 195.138.81.100 on 09/07/12
For personal use only.

6. M. T. JONES, T. D. DREILING, D. W. SETSER, and R. N. MCDONALD. J. Phys. Chem. **89**, 4501 (1985).
7. D. C. CAO and D. W. SETSER. J. Phys. Chem. **92**, 1169 (1988).
8. I. TOKUE and Y. ITO. Chem. Phys. **125**, 347 (1988).
9. C. FOTAKIS, M. MARTIN, and R. J. DONOVAN. J. Chem. Soc. Faraday Trans. 2. **78**, 1363 (1982).
10. J. H. KOLTS and D. W. SETSER. Reactive intermediates in the gas phase. Academic Press, New York. 1979. p. 151.
11. R. S. F. CHANG and D. W. SETSER. Chem. Phys. **35**, 201 (1978).
12. R. C. BASS and C. I. M. BEENAKKER. Computer Phys. Commun. **8**, 236 (1974).
13. Y. ITO, A. FUJIMAKI, K. KOBAYASHI, and I. TOKUE. Chem. Phys. **105**, 417 (1986).
14. P. J. MARCOUX, M. V. SWAAY, and D. W. SETSER. J. Phys. Chem. **83**, 3158 (1979).

Can. J. Chem. Downloaded from www.nrcresearchpress.com by 195.138.81.100 on 09/07/12
For personal use only.

Photodegradation of the lignin model α-guaiacoxyacetoveratrone, unusual effects of solvent, oxygen, and singlet state participation[1]

JOHN A. SCHMIDT, ALAIN B. BERINSTAIN, FRANCIS DE REGE, AND CYRIL HEITNER
Pulp and Paper Research Institute of Canada, 570 Boul. St. Jean, Pointe Claire, P.Q., Canada H9R 3J9

AND

LINDA J. JOHNSTON AND J. C. SCAIANO
Division of Chemistry, National Research Council of Canada, Ottawa, Ont., Canada K1A 0R6

Received March 28, 1990

JOHN A. SCHMIDT, ALAIN B. BERINSTAIN, FRANCIS DE REGE, CYRIL HEITNER, LINDA J. JOHNSTON, and J. C. SCAIANO. Can. J. Chem. **69**, 104 (1991).

α-Guaiacoxyacetoveratrone, a lignin model compound, has been studied using a combination of laser flash photolysis and steady state quantum yields. Triplet lifetimes range from 175 to 600 ns while the quantum yields of photodegradation vary from 0.06 to 0.6, depending on the solvent. Singlet processes ($\Phi \sim 0.1$), previously unobserved for aromatic ketones, are implicated in the mechanism, and account for most or all of the degradation in aprotic solvents.

Key words: photodegradation, α-guaiacoxyacetoveratrone.

JOHN A. SCHMIDT, ALAIN B. BERINSTAIN, FRANCIS DE REGE, CYRIL HEITNER, LINDA J. JOHNSTON et J. C. SCAIANO. Can. J. Chem. **69**, 104 (1991).

Utilisant une combinaison de la photolyse éclair au laser et des rendements quantiques dans l'état stationnaire, on a étudié l'α-guaiacoxyacétovératrone, un composé modèle de la lignine. Les temps de vie des triplets vont de 175 à 600 ns alors que les rendements quantiques de la photodégradation varient de 0,06 à 0,6, suivant la nature du solvant. Des processus singulets ($\Phi \sim 0,1$), qui n'ont pas été observés antérieurement avec des cétones aromatiques, sont impliqués dans le mécanisme et ils permettent d'expliquer toutes, ou pratiquement toutes, les dégradations observées dans les solvants aprotiques.

Mots clés : photodégradation, α-guaiacoxyacétovératrone.

[Traduit par la revue]

Mechanical and ultra-high yield pulps are used primarily for the manufacture of low-value grades of short-life papers such as newsprint, advertising, catalog, and directory papers. Their use in higher-value products is severely restricted by the rapid yellowing which occurs upon exposure to indoor illumination or daylight, a phenomenon attributed to photooxidation of lignin (1–6).

Hydrogen abstraction from phenolic groups and β-cleavage of aryloxy ketones are believed to lead to phenoxyl radicals and ultimately to yellowing, probably via quinone formation (6–8). Hydrogen abstraction from phenolic groups cannot be the only source of guaiacoxyl radicals since pulps with fully alkylated phenolic groups still yellow (although to a lower degree than do untreated pulps) (2, 3) and since Gierer and Lin have demonstrated that several nonphenolic phenacyl aryl ethers also undergo efficient degradation and induce yellowing (3). Castellan *et al.* have proposed the use of α-guaiacoxyacetovertatrone (**I**) as a model for the β-cleavage processes in lignin (9). This molecule contains some of the key features of lignin, such as the possibility of β-cleavage to yield phenoxyl radicals and a mechanism for β-phenyl quenching, a common pathway for triplet deactivation in ketones such as β-phenylpropiophenone and α-phenoxyacetophenone (10–12). Further, the lowest lying triplet of **I** is expected to have π,π^* character, a property that is presumably also common to the carbonyls in lignin.

The photochemistry of **I** (Scheme 1) is consistent with the following processes: (*i*) scavenging of phenacyl and phenoxyl radicals by hydrogen donors; (*ii*) *ortho-* and *para*-coupling giving phenacylguaiacols isomeric with **I**; (*iii*) dimerization of phenacyl radicals, and (*iv*) formation of yellow oligomeric material (3, 9). Finally, a non-product forming reaction, the recombination of phenoxyl and phenacyl radicals probably leads to regeneration of **I**. Similar processes are known for several α-aryloxyacetophenones (10–12). Their rate constants for α-C—O cleavage are in the $5 \times 10^6 - 2.7 \times 10^9\ s^{-1}$ range, where the higher values are for ketones with electron-donating substituents (e.g. 4-OCH_3) on the α-phenoxyl ring. Despite these high rate constants, the quantum yield of photocleavage can be low due to competition with efficient intramolecular deactivation via β-phenyl quenching.

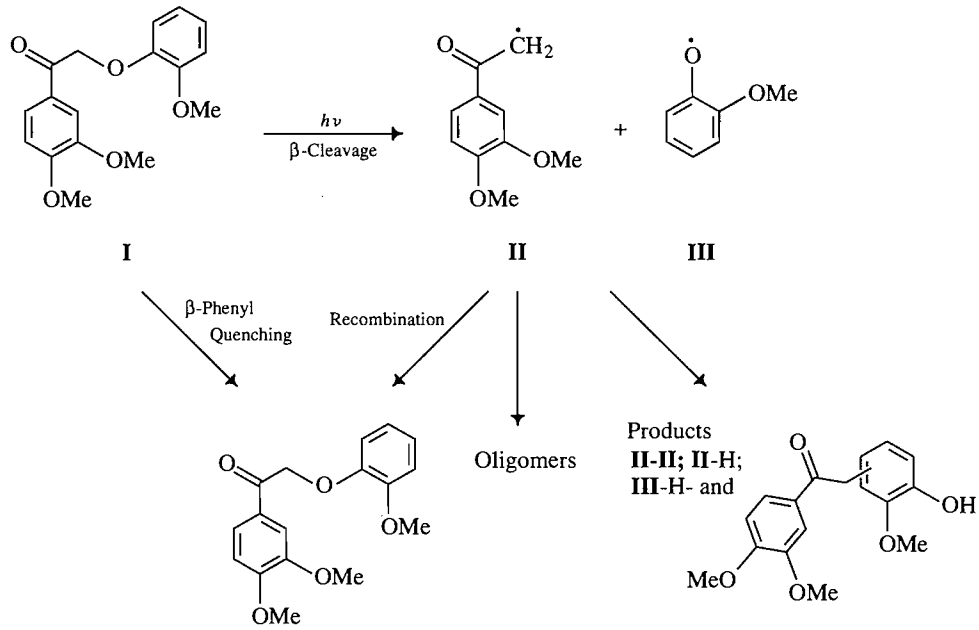
We have carried out additional exploratory work on **I** in an attempt to understand better the mechanism of the light-induced yellowing of lignin. Our results prompt us to communicate them at this time: specifically, we have observed a remarkable solvent dependence of the quantum yields and evidence of important singlet processes in the photodegradation of **I**; in aprotic solvents such as acetonitrile and dioxane degradation may occur exclusively from the singlet manifold.

Laser excitation of the lowest energy absorption band of **I** in deaerated acetonitrile, dioxane, or alcohols generated a transient with $\lambda_{max} = 400$ nm and a weak absorption between 400–500 nm (Fig. 1). This transient is readily identified as triplet **I** on the basis of its similarity to the published spectra for substituted acetophenones (13), and to a previous report on the transient absorption spectrum of **I** in ethanol (9). The triplet decay (at 400 nm, insert in Fig. 1) was monitored in a variety of solvents and the data are listed in Table 1. The lifetimes are independent of the monitoring wavelength and varied from ~200 ns in either dioxane or 1,2-dimethoxyethane to 600 ns in 2-ethoxyethanol. The addition of 40% water to the alcohols leads to shorter lifetimes, while in aqueous aprotic solvents the triplet was substantially longer-lived than in the pure solvent.

To confirm the identity of the triplet state and to determine its reactivity towards the quenchers used in some of our steady-state experiments, we carried out quenching studies with several

[1]NRCC No. 31530.

Can. J. Chem. Downloaded from www.nrcresearchpress.com by 195.138.81.100 on 09/07/12
For personal use only.



SCHEME 1

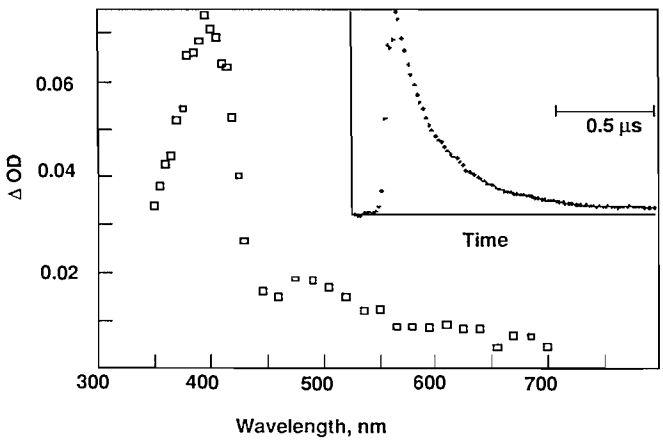


FIG. 1. Transient absorption spectrum measured 50 ns after 337 nm excitation of **I** in acetonitrile. Insert: decay trace at 400 nm for the same sample.

substrates. Plots of the observed rate constant for triplet decay (k_{obs}) as a function of the concentration of quencher were linear and gave, from their slopes, the quenching rate constants (k_q) by various substrates (eq. [1], where k_0 is the rate constant for triplet decay in the absence of quencher). The rate constants obtained are $(3.0 \pm 0.8) \times 10^9\ M^{-1}\ s^{-1}$ for oxygen in ethanol, $(1.9 \pm 0.2) \times 10^9\ M^{-1}\ s^{-1}$ for 1,3-cyclohexadiene in 4:1 2-ethoxyethanol/water and $(2.1 \pm 0.3) \times 10^8\ M^{-1}\ s^{-1}$ for thiophenol in 1,2-dimethoxyethane. These values are typical for triplet quenching and leave no doubt as to the identity of the observed transient.

$$[1] \quad k_{obs} = k_q[\text{Quencher}]$$

Table 1 lists the quantum yields for consumption of **I** in several solvents. The quantum yields in pure alcohols (0.32–0.52) are higher than those observed in aprotic solvents. In the presence of 40% (v/v) water the quantum yields in aprotic solvents increased dramatically, while those in alcohols decreased slightly. The large changes induced by water in

TABLE 1. Triplet lifetimes and disappearance quantum yields for dimer **I** in deaerated solvents, unless otherwise noted

Solvent	Quantum yield	Triplet lifetime (ns)
Dioxane	0.06 ± 0.01	183
w 40% water	0.29 ± 0.02	400
1,2-Dimethoxyethane	0.071 ± 0.002	200
w 40% water	0.49 ± 0.17	390
Ethanol	0.32 ± 0.08	550
w 40% water	0.16 ± 0.04	233
Methanol	0.45 ± 0.02	300
w 40% water	0.28 ± 0.03	175
Isopropanol	0.52 ± 0.12	590
w 40% water	0.30 ± 0.03	310
2-Ethoxyethanol	0.34 ± 0.09	600
w 40% water	0.19 ± 0.03	355
Acetonitrile	0.10 ± 0.01	230
w 40% water	0.47 ± 0.12	288
+ 0.01 M thiophenol*	0.30 ± 0.07	
oxygen (air)*	0.12 ± 0.01	
oxygen + 0.01 M thiophenol*	0.14 ± 0.08	

*In the absence of added water.

solvents such as acetonitrile and dioxane may have four possible origins; (*a*) solvent effects on the amount of radical recombination leading to starting material, (*b*) solvent effects on the competition between β-phenyl quenching and β-C—O bond cleavage of the triplet excited state, (*c*) increased quantum yield of singlet photodegradation pathways in the presence of water, and (*d*) increased involvement of triplet processes in the cleavage of **I**.

For each of the aprotic solvents examined the quantum yields and triplet lifetimes increase upon addition of water, whereas addition of water to protic solvents decreases both quantum yield and triplet lifetime. This may suggest that one of the

Can. J. Chem. Downloaded from www.nrcresearchpress.com by 195.138.81.100 on 09/07/12
For personal use only.

Can. J. Chem. Downloaded from www.nrcresearchpress.com by 195.138.81.100 on 09/07/12
For personal use only.

factors controlling the yields may be the rate of triplet deactivation via β-phenyl quenching, which normally controls the triplet lifetimes in similar ketones, *i.e.* chemical decay is enhanced by a decrease in the rate of competitive processes. While the trends in Table 1 suggest that this is a contributing factor, it is also clear that the magnitudes of the effects on the quantum yields are too large to be solely explained by the changes in the triplet lifetime. In spite of the obvious relationship between lifetimes and quantum yields, further elaboration must await additional results at variable water concentrations, and in the presence of radical scavengers to prevent the back reaction.

It is frequently assumed that the photochemistry of aromatic ketones arises almost exclusively from the lowest triplet state. Quantum yields of intersystem crossing of ca. 1.0 are common in ketones such as benzophenone and acetophenone (15). However, there is clear evidence that this is not the case for **I**. Thus, addition of 0.1 M 1,3-cyclohexadiene has little or no effect on the quantum yield for consumption of **I** in acetonitrile or dioxane and reduces it to 0.1 in ethanol. A simple calculation shows that this diene concentration should quench *ca.* 99% of the triplets. Consumption of **I** under these conditions must reflect processes that occur within the singlet manifold of **I**. The evidence for singlet photoprocesses is not limited to the quantum yield data. Transient studies reveal long-lived transients (presumably singlet-derived) (particularly in polar hydroxylic solvents) that persist after triplet decay and are not quenched by dienes. Although we have not yet positively identified these signals (λ_{max} = 345 nm and 600–700 nm), we are currently examining the possible involvement of phenoxyl radicals and/or radical ions in these reactions, as well as the role of water.

Table 1 also shows the effects of oxygen (as air) and thiophenol on the consumption of **I** in acetonitrile. Oxygen appears to cause a minor increase in consumption yield which is probably due to radical scavenging that prevents the back reaction. That oxygen can scavenge phenacyl radicals is supported by Gierer and Lin's isolation of α-hydroxyacetoveratrone after photolysis of aerated solutions of **I** (3). Addition of thiophenol (0.01 M) increases the quantum yields substantially under conditions where only *ca.* half of the triplets will survive quenching. Radical scavenging may contribute here to the increase in yields (14). However, one must also consider that triplet quenching by thiophenol may involve hydrogen abstraction which would result in the consumption of **I**.[2] In the presence of thiophenol, oxygen decreases the quantum yield. Both observations suggest some triplet photoreduction by thiophenol which is partially prevented by a triplet quencher such as oxygen.

These results have shown that the solvent has a dramatic effect on both the triplet lifetime and the efficiency of photocleavage of **I**. The results point to the rate of triplet deactivation via β-phenyl quenching as one of the factors in controlling the quantum yields, particularly in hydroxylic solvents. Given our observation of previously unobserved singlet processes, it is obvious that other factors related to singlet reactivity must also be involved. Traditional attempts to prevent the photo-yellowing of lignin-rich papers have been largely based on addition of triplet quenchers and elimination of free phenolic groups. However, the results with **I** demonstrate the importance of both β-cleavage and singlet processes, neither of which will be affected by these two methods. It is obviously of interest to explore these processes in more detail, in both the model compound and in lignin, to better understand the processes involved in the yellowing of lignin-rich paper.[3]

Experimental

α-Guaiacoxyacetoveratrone (**I**) was synthesized by condensing α-bromoacetoveratrone and guaiacol in dry acetone in the presence of K_2CO_3 (18).

A description of the laser flash photolysis apparatus has been published (19). A Molectron UV-24 nitrogen laser (337 nm, ~8 nm pulses, <10 mJ/pulse) was used for excitation. Unless otherwise noted samples were deaerated by bubbling nitrogen through the sample and the solutions were flowed through a sample cell constructed from 3 × 7 mm^2 Suprasil tubing. Long-lived residual absorptions resulting from product accumulation were observed if flow samples were not used.

For the quantum yield experiments solutions of **I** (3.0 mL, 0.015 M) were irradiated with monochromatic light at 325 nm in 1 × 1 cm^2 quartz cells. For experiments under oxygen-free conditions the samples were sealed with rubber septa purged with oxygen-free nitrogen for 30 min. The dose absorbed was measured using a commercially available electronically integrating actinometer (QuantaCount, PTI, Deer Park, N.J.) calibrated using azoxybenzene (20). Disappearance of **I** was monitored using gas chromatography (Hewlett-Packard 5890A chromatograph, 25 m capillary column with HP-1 methyl silicone gum). Solutions were irradiated to ~10% conversion. For aqueous solvents the sample was extracted into diethyl ether. After drying and filtering the ether layer, the solvent was evaporated with a stream of nitrogen and the residue was taken up in 3.0 mL of the pure organic solvent employed for the irradiation.

Acknowledgements

The enthusiastic and competent technical assistance of Mr. N. Muradali is much appreciated. F.D. and A.B.B. thank NSERC for Industrial Undergraduate Student Research Awards.

This research was supported by the Canadian Pulp and Paper Industry and a National Centres of Excellence grant provided by the Government of Canada.

1. L. V. Forman. Paper Trade J. **111**, 34 (1940).
2. G. J. Leary. Tappi, **51**, 1257 (1968).
3. J. Gierer and S. Y. Lin. Svensk Paperstidng. **75**, 233 (1972).
4. G. Brunow and B. Eriksson. Acta. Chem. Scand. **25**, 2779 (1971).
5. K. P. Kringstad and S. Y. Lin. Tappi, **53**, 2296 (1970).
6. J. A. Schmidt, C. Heitner, G. P. Kelly, and F. Wilkinson. J. Pulp Paper Sci. **16**, *j*111 (1990).
7. G. Leary. Nature, **217**, 672 (1968).
8. S. E. Lebo, W. F. W. Lonsky, T. J. McDonough, and P. J. Medvecz. J. Pulp Paper Sci. **16**, *j*139 (1990).
9. C. Vanucci, P. Fornier de Violet, H. Bouas-Laurent, and A. Castellan. J. Photochem. Photobiol. A: Chemistry, **41**, 251 (1988).
10. J. C. Scaiano and J. C. Netto-Ferreira. J. Photochem. **32**, 253 (1986).
11. J. C. Netto-Ferreira and J. C. Scaiano. Tetrahedron Lett. **30**, 443 (1989).
12. J. C. Netto-Ferreira, I. G. J. Avellar, and J. C. Scaiano. J. Org. Chem. **55**, 89 (1990).

[2]Note that the ketyl radical generated by hydrogen abstraction might be expected to undergo α-cleavage to produce the enol of acetoveratrone and the 2-methoxyphenoxyl radical (16).

[3]An article published while this report was reviewed (17) suggests that singlet processes may participate in the photochemistry of α(2,6-dimethoxyphenoxy)acetophenone.

13. H. LUTZ, E. BREHERET, and L. LINDQVIST. J. Phys. Chem. **77**, 1758 (1973).
14. P. J. WAGNER and M. J. LINDSTROM. J. Am. Chem. Soc. **109**, 3062 (1987).
15. N. J. TURRO. Modern molecular photochemistry. Benjamin Cummings, Menlo Park, CA. 1978. p. 121.
16. Y. SABURI, T. YOSHIMOTO, and K. MINAMI. Bull. Chem. Soc. Jpn. **90**, 587 (1969).
17. W. U. PALM and H. DRESSKAMP. J. Photochem. Photobiol. A: Chemistry, **52**, 439 (1990).
18. E. ADLER, B. O. LINGREN, and U. SAEDEN. Svensk Paperstidn. **55**, 245 (1952).
19. J. C. SCAIANO. J. Am. Chem. Soc. **102**, 7747 (1980); J. C. SCAIANO, M. TANNER, and D. WEIR. J. Am. Chem. Soc. **107**, 4396 (1985).
20. N. J. BUNCE, J. LAMARRE, and S. P. VAISH. Photochem. Photobiol. **39**, 531 (1984).

Can. J. Chem. Downloaded from www.nrcresearchpress.com by 195.138.81.100 on 09/07/12
For personal use only.

New precursors for organometallic chemical vapor deposition of rhodium

R. KUMAR AND R. J. PUDDEPHATT
Department of Chemistry, University of Western Ontario, London, Ont., Canada N6A 5B7

Received July 4, 1990

R. KUMAR and R. J. PUDDEPHATT. Can. J. Chem. **69**, 108 (1991).

The η-cyclopentadienyl (Cp) and η-allyl (C_3H_5) complexes [RhCp$(CO)_2$], [RhCp(cod)] where cod = 1,5-cyclooctadiene, [Rh(η-C_3H_5)$(CO)_2$], and [Rh(η-C_3H_5)$_3$] have been shown to be useful precursors for the chemical vapour deposition (CVD) of rhodium films. The rhodium films contain carbon impurities but these can be greatly reduced if CVD is carried out in the presence of hydrogen. The films adhere well to a silicon substrate. The pyrolysis of [RhCp$(CO)_2$] gives CO and [$Rh_2Cp_2(CO)_2$(μ-CO)] and [Rh_3Cp_3(μ-CO)$_3$] at intermediate stages. Pyrolysis of [Rh(η-C_3H_5)$_3$] or [Rh(η-C_3H_5)$(CO)_2$] gives 1,5-hexadiene as the only organic product, but similar pyrolysis in the presence of hydrogen gives much propene as well as 1,5-hexadiene.

Key words: rhodium, deposition, allyl, cyclopentadienyl.

R. KUMAR et R. J. PUDDEPHATT. Can. J. Chem. **69**, 108 (1991).

On a démontré que les complexes du η-cyclopentadiényle (Cp) et du η-allyle (C_3H_5) — [RhCp$(CO)_2$], [RhCp(cod)] dans lequel cod = cycloocta-1,5-diène, [Rh(η-C_3H_5)$(CO)_2$] et [Rh(η-C_3H_5)$_3$] — sont des précurseurs utiles pour la déposition chimique de vapeurs (DCV) de films de rhodium. Les films de rhodium contiennent des impuretés; toutefois, on peut les réduire beaucoup si l'on effectue les DCV en présence d'hydrogène. Les films adhèrent bien à un substrat de silicium. La pyrolyse du [RhCp$(CO)_2$] conduit à du CO et à du [$RhCp_2(CO)_2$(μ-CO)] et à du [$RhCp_3$(μ-CO)$_3$] aux étapes intermédiaires. La pyrolyse du [Rh(η-C_3H_5)$_3$] ou du [Rh(η-C_3H_5)$(CO)_2$] ne fournit que de l'hexa-1,5-diène comme produit organique; des pyrolyses semblables réalisées en présence d'hydrogène fournissent aussi du propène, en plus de l'hexa-1,5-diène.

Mots clés : rhodium, déposition, allyle, cyclopentadiényle.

[Traduit par la revue]

Introduction

There has been much recent interest in the formation of thin films of metals using chemical vapour deposition, CVD (1–3). These films have applications in microelectronics, optical devices, wear protection, and catalysis (4). Advantages of CVD include its ease of use, mild conditions of formation, and high performance of the films. Challenges for chemists include the design and synthesis of volatile precursors which decompose to the desired materials in pure form and under mild thermal or photochemical conditions as required for specific applications, and the determination of the mechanisms of CVD to enable the development of a rational approach to precursor design.

Most recent research has been focussed on CVD of gold, palladium, and platinum, noble metals most commonly used in microelectronics (5–9). Rhodium has been much less extensively studied (2, 10). Rhodium films are used in mirror optics, catalysis, and wear protection but, while rhodium has excellent electrical properties and corrosion resistance, its high cost has so far limited its application in microelectronics (11). This paper surveys some volatile organorhodium complexes, and reports on a study of thermal CVD of rhodium films from these compounds. Other researchers have reported CVD of rhodium using the precursors [$Rh_2(CO)_8$], [Rh_2(μ-Cl)$_2(CO)_4$], [Rh($CH_3COCHCOCF_3$)$_3$], [Rh($CH_3COCHCOCH_3$)(C_2H_4)$_2$], [Rh($CH_3COCHCOCF_3$)$(CO)_2$], and, very recently, [Rh(η-C_3H_5)$_3$] (1, 2, 8, 10), and the enhancement of CVD by lasers or by plasma has been demonstrated (1, 10).

Results and discussion

In this work, the new precursors used were the η-cyclopentadienyl derivatives [RhCp(cod)], Cp = μ-C_5H_5, cod = 1,5-cyclooctadiene, and [RhCp$(CO)_2$] and the η-allyl derivatives [Rh(η-C_3H_5)$(CO)_2$] and [Rh(η-C_3H_5)$_3$]. All were prepared by known procedures (12–15). For reference, some CVD experiments were also carried out with the known precursor [Rh_2(μ-Cl)$_2(CO)_4$] (2).

Formation and characterization of rhodium films

In a typical reaction, CVD was carried out in a vertical reactor operating at 10^{-2}–10^{-3} Torr. The substrate was a silicon wafer, which was heated to 130–270°C. Under these conditions, highly reflective rhodium films were formed and the film thickness typically grew at a rate of ~2 μm/h. The films were analyzed by XPS and some typical data are given in Table 1.

The rhodium films are rapidly contaminated by exposure to the atmosphere and, in all cases, the films were cleaned before analysis by argon sputtering for 30 s. Even so, the films consistently contained much carbon and oxygen impurities. These impurities were greatly reduced when the CVD was carried out using hydrogen carrier gas (Table 1). For example, using only 10^{-3} Torr H_2 as carrier gas and [Rh(μ-C_3H_5)$(CO)_2$] as precursor, the rhodium content increased from 48% to 94%, the carbon content decreased from 40% to 6%, and the oxygen content decreased from 12% to undetectably low levels. In other cases, the hydrogen effect was less dramatic (Table 1) but it was always observed.

A similar effect of hydrogen on film purity has been observed for CVD of platinum (8, 9). For CVD of platinum using dimethylplatinum(II) precursors, hydrogen also had a dramatic effect in lowering the temperature required for thermal CVD (9), but this type of effect was not observed for rhodium CVD (Table 1). For CVD using [RhCp(cod)] and [Rh(η-allyl)$_3$], there was a decrease in the temperature required for CVD but no such effect was observed with the precursors [Rh(η-C_3H_5)$(CO)_2$] or [RhCp$(CO)_2$]. Thus the hydrogen effects on film purity and CVD temperature appear to be independent of each other.

The rhodium films adhered strongly to the silicon surface as determined qualitatively by scratch and tape tests. The film resistivity of samples prepared under hydrogen averaged 28 ± 5 μΩ-cm while those prepared without hydrogen averaged 60 ± 20 μΩ-cm. Bulk rhodium has a resistivity at 20°C of 4.51 μΩ-cm. It is clear that residual carbon in the films is partially responsible for the lower conductivity of the rhodium

Can. J. Chem. Downloaded from www.nrcresearchpress.com by 195.138.81.100 on 09/07/12
For personal use only.

Can. J. Chem. Downloaded from www.nrcresearchpress.com by 195.138.81.100 on 09/07/12
For personal use only.

TABLE 1. Minimum CVD temperatures and analytical data for rhodium films[a]

Complex	CVD temperature[b]	Analysis[b]		
$[Rh_2(\mu\text{-}Cl)_2(CO)_4]$	180 (180)	Rh	49	(91)
		C	24	(7)
		O	27	(2)
$[RhCp(CO)_2]$	180 (180)	Rh	75	(89)
		C	20	(7)
		O	5	(4)
[RhCp(cod)]	270 (230)	Rh	81	(97)
		C	19	(3)
		O	0	(0)
$[Rh(C_3H_5)(CO)_2]$	180 (180)	Rh	48	(94)
		C	40	(6)
		O	12	(0)
$[Rh(C_3H_5)_3]$	180 (130)	Rh	86	(96)
		C	14	(4)
		O	0	(0)

[a]Analysis by XPS after sputtering for 30 s.

[b]The minimum temperature or analysis for Rh films formed by CVD in the absence of H_2 are followed, in parentheses, by the corresponding values in the presence of H_2. The analytical data were obtained for CVD at 270°C.

films prepared by CVD. Scanning electron microscopy (SEM) showed the presence of smooth rhodium films composed of crystallites with dimensions of *ca.* 200 Å across.

Studies of the thermolysis reactions

In a crude approximation of the CVD conditions, the precursors (~10 mg) were heated to 140°C in a large (500 mL) vessel sealed under vacuum. The gaseous products of thermolysis were then analyzed by GC, MS, or GC/MS while the residual rhodium complexes present after partial pyrolysis were extracted and examined by MS, IR, and NMR techniques. Pyrolysis of $[Rh_2(\mu\text{-}Cl)_2(CO)_4]$ gave CO as the major product with some $COCl_2$ in the later stages. $RhCl_3$ was also identified at intermediate stages. Thus the loss of CO appears to be the first step in the decomposition stage. Similarly, pyrolysis of $[RhCp(CO)_2]$ gave CO as the only volatile product and, as well as metallic rhodium, the complexes $[Rh_2Cp_2(CO)_2(\mu\text{-}CO)]$ and $[Rh_3Cp_3(\mu\text{-}CO)_3]$ were formed in the early stages of pyrolysis. These complexes were isolated in pure form and were identified by their characteristic NMR and IR spectra (16–20). It is already known that these compounds can be prepared by photolysis of solutions of $[RhCp(CO)_2]$ and that the reaction occurs by initial loss of CO followed by association (16–19). The thermolysis probably occurs in a similar way and it is intriguing to consider whether the cluster complexes may be formed during the CVD of rhodium from $[RhCp(CO)_2]$. The concentration of rhodium complexes in the gas phase during CVD may be too low to allow associative reactions but it is easy to envisage how such processes might occur in surface-bound organometallic complexes. Further studies of this possible mechanism of CVD are planned.

Pyrolysis of [RhCp(cod)] gave a very complex mixture of hydrocarbon products, which were not fully characterized, and the mass spectrum of the residue gave a peak at $m/e = 504$, corresponding to $[Rh_3Cp_3]^+$. However, in this case, attempts to isolate pure complexes from the partly pyrolyzed reaction mixture were unsuccessful. Nevertheless, it does appear that pyrolysis may give rhodium clusters at intermediate stages. The added complexity in this case is probably due to the competition between the loss of Cp or cod groups from rhodium in the initial stage of decomposition (21).

Pyrolysis of $[Rh(\eta\text{-}C_3H_5)_3]$ gave 1,5-hexadiene as the only volatile product, as determined by GC and GC/MS, but no rhodium clusters or dimers could be detected at intermediate stages. In this case, pyrolysis under a partial atmosphere of H_2 had a dramatic effect on the organic product. Thus, propene (32%) and 1,5-hexadiene (67%) were formed under these conditions, along with traces of other unidentified compounds. The product 1,5-hexadiene could be formed by concerted reductive elimination at rhodium or by loss of allyl radicals followed by radical recombination and is the only product in the absence of hydrogen. Hydrogen could react directly with allylrhodium species to give propene, though there are no precedents for reaction of H_2 with rhodium(III) organometallics. Therefore, partial reaction of the precursor to give lower oxidation state rhodium complexes might be necessary before hydrogen could oxidatively add. Formation of propene could then occur by reductive elimination. Alternatively, the reaction might be catalyzed by metallic rhodium, which is known to be a good hydrogenation catalyst. Although the present data do not define a mechanism, the hydrogen effect is shown to influence the temperature of CVD, the rhodium film purity, and the nature of the organic products using $[Rh(\eta\text{-}C_3H_5)_3]$ as precursor. Hence hydrogen is presumed to be involved directly in the mechanism of CVD.

Conclusions

These organometallic precursors for CVD of rhodium have high volatility; they decompose to rhodium at moderate temperatures and, in the presence of hydrogen, they give rhodium films which are of high purity and which adhere well to a silicon substrate. Thus they have considerable advantages over precursors used for CVD of rhodium in the past (1, 2, 10).

Experimental

Organorhodium complexes were prepared by literature methods (12–15) and were purified by sublimation. Their purity was confirmed by ^1H NMR.

The rhodium film thickness was determined by a stylus method using a Sloan Dektak II instrument. Conductivities were determined by a four point probe method (22). The compositions of the metal films were determined by XPS using a SSL SSX-100 instrument with a monochromatized Mg-Kα X-ray source (1253.6 eV). Spectra were computer fitted to 70% Gaussian lineshapes after background subtraction and using no constraint to the final fit. The surfaces were cleaned by sputtering for 30 s with argon ions before analysis. SEM micrographs of rhodium films were taken using a ISL DS-130 scanning electron microscope. Film adherence was tested qualitatively using the scratch and Scotch tape tests. Infrared spectra were obtained by using a Bruker IFS-32 instrument, NMR spectra by using a Varian XL200 spectrometer, and GC/MS by using a Varian 3400 GC coupled to a Finnigan MAT8230 mass spectrometer.

Chemical vapour deposition

The rhodium precursor (50 mg) was placed in a vertical CVD reactor. A silicon wafer substrate (*ca.* 0.5 cm diameter) was heated to the required temperature (130–270°C) and the apparatus was evacuated to 10^{-3} Torr. If necessary the precursor was warmed to give more rapid deposition but in no case was it necessary to heat to more than 50°C. Coatings up to 2 μm in thickness were deposited in 0.5–1 h. In some cases a slow stream of H_2 was passed over the rhodium precursor.

The minimum CVD temperature given in Table 1 is that when most rhodium precursor decomposed to give rhodium metal rather than simply subliming in the equipment. The temperatures 130, 180, 230, and 270°C were checked and the lowest temperature of CVD is given in Table 1. Analytical data were obtained on films prepared at a standard temperature of 270°C.

Thermal decomposition studies

In a typical experiment, $[RhCp(CO)_2]$ (10 mg) in an evacuated vessel (500 mL) was heated slowly to 180°C in an oil bath, until metallic rhodium was visible. The gases evolved were sampled by syringe and analyzed by GC/MS. The residue was extracted with CH_2Cl_2 (2 × 10 mL), then concentrated and separated by preparative thin layer chromatography. This gave red $[Rh_2Cp_2(CO)_3]$ (16) (IR: $\nu(CO)$ = 1986 cm^{-1}; lit. 1989 cm^{-1}, 1841 cm^{-1} in cyclohexane solution; ^1H NMR: δ = 5.50 ppm), and green $[Rh_3Cp_3(\mu\text{-}CO)_3]$ (17) (IR: $\nu(CO)$ = 1850 cm^{-1}, 1791 cm^{-1}; lit. 1849 cm^{-1}, 1793 cm^{-1} in CH_2Cl_2). Similar results were obtained for pyrolysis in the presence of H_2 (0.2 atm).

In similar pyrolyses of $[Rh(\eta\text{-}C_3H_5)(CO)_2]$, the products 1,5-hexadiene and propene were identified by GC/MS by comparison with authentic samples. No new rhodium complexes were identified.

Acknowledgments

We thank the Natural Sciences and Engineering Research Council of Canada and OCMR for financial support and Surface Science Western for surface analytical assistance.

1. K. L. KOMPA. Angew. Chem. Int. Ed. Engl. **27**, 1314 (1988).
2. W. WESTWOOD. Gmelin handbook of inorganic chemistry. Supplement Vol. A1. Technology of platinum-group metals. 8th ed. 1986. pp. 43–50.
3. I. P. HERMAN. Chem. Rev. **89**, 1323 (1989).
4. C. F. POWELL, J. H. OXLEY, and J. M. BLOCHER, JR. Vapor deposition. John Wiley, New York. 1966.
5. T. T. KODAS, T. H. BAUM, and P. B. COMITA. J. Cryst. Growth, **87**, 378 (1988).
6. R. J. PUDDEPHATT and I. TREURNICHT. J. Organomet. Chem. **319**, 129 (1987).
7. J. E. GOZUM, D. M. POLLINA, J. A. JENSEN, and G. S. GIROLAMI. J. Am. Chem. Soc. **110**, 2688 (1988).
8. Z. XUE, J. STROUSE, D. K. SHUH, C. B. KNOBLER, H. D. KAESZ, R. F. HICKS, and R. S. WILLIAMS. J. Am. Chem. Soc. **111**, 8779 (1989); H. D. KAESZ, R. S. WILLIAMS, R. F. HICKS, Y.-J. A. CHEN, Z. XUE, D. XU, D. K. SHUH, and H. THRIDANDAM. Mat. Res. Soc. Symp. Proc. **131**, 395 (1989).
9. R. KUMAR, S. ROY, M. RASHIDI, and R. J. PUDDEPHATT. Polyhedron, **8**, 551 (1989).
10. A. ETSPULER and H. SUHR. Appl. Phys. **48**, 373 (1989).
11. G. HAAS. J. Opt. Soc. Am. **72**, 27 (1982).
12. R. S. DICKSON and G. R. TAILBY. Austral. J. Chem. **23**, 1531 (1970).
13. J. POWELL and B. L. SHAW. J. Chem. Soc. Chem. Commun. 323 (1966).
14. S. O'BRIEN. J. Chem. Soc. Chem. Commun. 757 (1968).
15. J. POWELL and B. L. SHAW. J. Chem. Soc. A, 583 (1968).
16. J. EVANS, B. F. G. JOHNSON, J. LEWIS, T. W. MATHESON, and J. R. NORTON. J. Chem. Soc. Dalton Trans. 626 (1978).
17. R. J. LAWSON and J. R. SHAPLEY. J. Am. Chem. Soc. **98**, 7433 (1976).
18. R. J. LAWSON and J. R. SHAPLEY. Inorg. Chem. **17**, 772 (1978).
19. O. S. MILLS and E. PAULUS. J. Organomet. Chem. **10**, 331 (1967).
20. E. F. PAULUS, E. O. FISCHER, H. P. FRITZ, and H. SCHUSTER-WOLDAN. J. Organomet. Chem. **10**, P3 (1967).
21. R. B. KING. J. Organomet. Chem. **14**, P19 (1968).
22. L. B. VALDES. Proc. I.R.E. **41**, 420 (1953).

Can. J. Chem. Downloaded from www.nrcresearchpress.com by 195.138.81.100 on 09/07/12
For personal use only.

Activity coefficients of NaCl in NaCl–NaOAc–H_2O at 25, 35, and 45°C

S. MANOHAR AND J. ANANTHASWAMY
Department of Chemistry, Osmania University, Hyderabad, India 500 007

Received April 20, 1990

S. MANOHAR and J. ANANTHASWAMY. Can. J. Chem. **69**, 111 (1991).

The activity coefficients of NaCl were estimated by measuring the EMFs of the cell

Na ion-selective electrode | NaCl(m_A), NaOAc(m_B) | Ag/AgCl

at four ionic strengths, *i.e.*, 0.5, 1.0, 2.0, and 3.0 mol/kg and at temperatures 25, 35, and 45°C. The results were analyzed in terms of Harned's rule, the Pitzer and Rush–Johnson–Scatchard treatments. Osmotic coefficients and excess free energies of mixing were calculated at all ionic strengths and temperatures studied.

Key words: activity coefficients, sodium chloride, sodium acetate, Pitzer formalism, Scatchard equation.

S. MANOHAR et J. ANANTHASWAMY. Can. J. Chem. **69**, 111 (1991).

On a évalué les coefficients d'activité du NaCl en mesurant les f.é.m. de la cellule :

électrode ion-sélective au Na | NaCl(m_A), NaOAc(m_B) | Ag/AgCl

à quatre forces ioniques, soit 0,5, 1,0, 2,0 et 3,0 mol/kg et à 25, 35 et 45°C. On a analysé les résultats en fonction de la règle de Harned et des traitements de Pitzer ainsi que de Rush-Johnson-Scatchard. On a calculé les coefficients osmotiques ainsi que les énergies libres en excès de mélange à toutes les forces ioniques et à toutes les températures étudiées.

Mots clés : coefficients d'activité, chlorure de sodium, acétate de sodium, formalisme de Pitzer, équation de Scatchard.
[Traduit par la revue]

Introduction

NaCl–NaOAc–H_2O is an interesting system because the osmotic coefficients of binary solutions of acetates is in reverse order to that of the chlorides (1, 2) *i.e.*, $\phi_{KCl} < \phi_{NaCl}$ but $\phi_{KOAc} > \phi_{NaOAc}$. The activity coefficients of NaCl in aqueous NaCl–NaOAc mixture have been measured by Lanier (3) at ionic strengths 1.0, 3.0, and 5.0 mol/kg with cation-selective glass electrode and a silver – silver chloride electrode at 25°C. Isopiestic vapour pressure measurements were carried out by Jones *et al.* (4) over the concentration range 1.8968–3.1210 mol/kg at 25°C. However, the effect of temperature on the activity coefficients of this sytem is not yet studied. This paper reports measurements of NaCl activity coefficients in aqueous solutions containing sodium acetate. The results were analysed in the light of Pitzer (5) and Scatchard (6, 7) treatments and the corresponding binary and ternary interaction parameters were calculated. The osmotic coefficients and excess free energies were also calculated using the Pitzer parameters ($^s\theta$ and Ψ).

Results

The activity coefficients of NaCl were calculated using the relation:

$$[1] \quad E_{NaCl-NaOAc} = E_0 + k \log (m_{Na} m_{Cl} \gamma^2_{NaCl} + K m_{Na} m_{OAc} \gamma^2_{NaOAc})$$

where $K m_{Na} m_{OAc} \gamma^2_{NaOAc}$ term will take into account the effect of sodium acetate on the cell EMF. $k = 2.303RT/nF$ is the Nernst slope and E_0 is the EMF of the pure NaCl solution at unit activity. The K values were in the range of 1×10^{-5} at all ionic strengths and temperatures studied and hence the $K m_{Na} m_{OAc} \gamma^2_{NaOAc}$ term in eq. [1] could be neglected. Thus eq. [1] could be rearranged as

$$[2] \quad \gamma^2_{\pm} = 1/(m_{Na} m_{Cl})\ 10^{(E_{NaCl-NaOAc} - E_0)/k}$$

Thus the mean activity coefficients ($\gamma_{\pm}$) of NaCl can be obtained by substituting the EMFs of the cell with NaCl–NaOAc aqueous mixtures ($E_{NaCl-NaOAc}$) in eq. [2]. All calculations are done on a computer (PC). The experimental mean activity coefficient data determined at I = 0.5, 1.0, 2.0, and 3.0 mol/kg and at 25, 35, and 45°C are listed in Table 1 as a function of y_B, the ionic strength fraction of NaOAc in the mixture. Thus $y_B = m_B/(m_A + m_B)$. The log γ_{NaCl} vs. y_B plots at 25°C are shown in Fig. 1.

Discussion

The Harned equations (8) given below were fitted to the experimentally determined activity coefficient data at each ionic strength using a least squares procedure.

$$[3] \quad \log \gamma_A = \log \gamma^0_A - \alpha_{AB} y_B$$

$$[4] \quad \log \gamma_A = \log \gamma^0_A - \alpha_{AB} y_B - \beta_{AB} y^2_B$$

The Harned slope (α_{AB}) and intercept (log γ^0_A) were obtained by linear regression. The Harned coefficient at I = 1.0 and at 25°C, viz., −0.0251 is in agreement with −0.0242 reported earlier by Lanier (3). Figure 1 shows that the log γ vs. y_B plots are linear at I = 0.5 and 1.0 mol/kg, whereas these plots are slightly curved at I = 2.0 and 3.0 mol/kg. Therefore, it is evident from the data listed in Table 2 that the linear Harned expression is not so adequate above I = 1.0 mol/kg. There was a good agreement between the experimentally obtained log γ^0_A (from intercept) calculated from the Harned equation involving the β_{AB} term and the literature log γ^0_A values. The same type of trend was also observed at 35 and 45°C. Addition of β_{AB} term indicates the possibility of ternary ionic interactions such as Na–Cl–OAc in these solutions at higher ionic strength.

The activity coefficients and osmotic coefficients of pure sodium chloride (9) and sodium acetate (10, 11) solutions could be calculated using the Pitzer equations given below with the following values of parameters at the experimental temperatures studied.

Printed in Canada / Imprimé au Canada

Can. J. Chem. Downloaded from www.nrcresearchpress.com by 195.138.81.100 on 09/07/12
For personal use only.

Can. J. Chem. Downloaded from www.nrcresearchpress.com by 195.138.81.100 on 09/07/12
For personal use only.

TABLE 1. Activity coefficients of NaCl in the NaCl–NaOAc–H_2O system*

I = 0.5		I = 1.0		I = 2.0		I = 3.0	
y_B	$-\log\gamma$	y_B	$-\log\gamma$	y_B	$-\log\gamma$	y_B	$-\log\gamma$
				T = 25°C			
0.1050	0.1651	0.1005	0.1798	0.1046	0.1709	0.1050	0.1419
0.1900	0.1639	0.1827	0.1777	0.1894	0.1676	0.1900	0.1380
0.2603	0.1628	0.2511	0.1760	0.2595	0.1649	0.2602	0.1348
0.3194	0.1619	0.3090	0.1746	0.3185	0.1626	0.3193	0.1321
0.3697	0.1612	0.3585	0.1733	0.3687	0.1606	0.3696	0.1297
0.4131	0.1606	0.4014	0.1723	0.4121	0.1589	0.4130	0.1277
0.4509	0.1600	0.4390	0.1713	0.4499	0.1574	0.4508	0.1259
0.4841	0.1595	0.4721	0.1705	0.4831	0.1561	0.4840	0.1243
0.5136	0.1591	0.5015	0.1698	0.5125	0.1549	0.5135	0.1229
0.5398	0.1587	0.5278	0.1691	0.5388	0.1539	0.5397	0.1216
0.8967	0.1533	0.8941	0.1598	0.8899	0.1396	0.8774	0.1048
0.8127	0.1546	0.8085	0.1620	0.8017	0.1432	0.7815	0.1096
0.7431	0.1556	0.7379	0.1638	0.7294	0.1462	0.7046	0.1135
0.6845	0.1565	0.6786	0.1653	0.6690	0.1486	0.6414	0.1166
0.6345	0.1572	0.6281	0.1665	0.6179	0.1507	0.5886	0.1192
0.5912	0.1579	0.5847	0.1677	0.5740	0.1524	0.5439	0.1214
0.5535	0.1585	0.5468	0.1686	0.5360	0.1540	0.5055	0.1232
0.5203	0.1590	0.5136	0.1694	0.5027	0.1553	0.4721	0.1248
0.4909	0.1594	0.4841	0.1702	0.4733	0.1565	0.4429	0.1262
				T = 35°C			
0.1002	0.1658	0.1009	0.1789	0.1039	0.1675	0.1033	0.1369
0.1821	0.1647	0.1834	0.1771	0.1882	0.1646	0.1872	0.1336
0.2504	0.1638	0.2520	0.1755	0.2580	0.1622	0.2568	0.1308
0.3081	0.1631	0.3099	0.1743	0.3167	0.1601	0.3154	0.1284
0.3576	0.1624	0.3596	0.1732	0.3669	0.1584	0.3654	0.1264
0.4004	0.1619	0.4025	0.1722	0.4102	0.1569	0.4087	0.1246
0.4380	0.1614	0.4401	0.1714	0.4479	0.1556	0.4464	0.1230
0.4711	0.1610	0.4732	0.1706	0.4811	0.1544	0.4796	0.1216
0.5005	0.1606	0.5026	0.1700	0.5105	0.1533	0.5090	0.1204
0.5268	0.1602	0.5289	0.1694	0.5368	0.1524	0.5353	0.1192
0.8995	0.1553	0.8931	0.1612	0.8888	0.1397	0.8851	0.1038
0.8174	0.1564	0.8068	0.1631	0.7999	0.1429	0.7938	0.1080
0.7490	0.1573	0.7357	0.1647	0.7272	0.1456	0.7197	0.1112
0.6912	0.1581	0.6761	0.1661	0.6666	0.1478	0.6582	0.1139
0.6416	0.1587	0.6255	0.1672	0.6153	0.1496	0.6063	0.1162
0.5987	0.1593	0.5819	0.1682	0.5713	0.1512	0.5621	0.1181
0.5612	0.1598	0.5440	0.1690	0.5332	0.1525	0.5239	0.1197
0.5281	0.1602	0.5107	0.1698	0.4999	0.1537	0.4905	0.1211
0.4987	0.1606	0.4813	0.1704	0.4705	0.1548	0.4611	0.1224
				T = 45°C			
0.0999	0.1675	0.1008	0.1796	0.1126	0.1663	0.1124	0.1347
0.1816	0.1665	0.1832	0.1780	0.2024	0.1634	0.2020	0.1313
0.2497	0.1657	0.2518	0.1766	0.2758	0.1611	0.2752	0.1285
0.3074	0.1650	0.3097	0.1754	0.3367	0.1591	0.3361	0.1262
0.3568	0.1645	0.3593	0.1744	0.3882	0.1575	0.3876	0.1242
0.3997	0.1640	0.4022	0.1736	0.4323	0.1560	0.4317	0.1225
0.4371	0.1635	0.4398	0.1728	0.4705	0.1548	0.4698	0.1210
0.4702	0.1631	0.4729	0.1721	0.5038	0.1537	0.5032	0.1197
0.4996	0.1628	0.5023	0.1716	0.5332	0.1528	0.5326	0.1185
0.5260	0.1625	0.5286	0.1710	0.5593	0.1519	0.5587	0.1175
0.8982	0.1581	0.8930	0.1636	0.8831	0.1412	0.8846	0.1043
0.8152	0.1591	0.8067	0.1654	0.7907	0.1443	0.7931	0.1081
0.7463	0.1599	0.7356	0.1668	0.7158	0.1468	0.7188	0.1111
0.6881	0.1606	0.6760	0.1680	0.6539	0.1488	0.6572	0.1135
0.6383	0.1612	0.6254	0.1691	0.6018	0.1505	0.6053	0.1156
0.5953	0.1617	0.5818	0.1699	0.5574	0.1520	0.5610	0.1174
0.5577	0.1621	0.5439	0.1707	0.5191	0.1532	0.5227	0.1189
0.5245	0.1625	0.5106	0.1714	0.4858	0.1543	0.4894	0.1202
0.4951	0.1629	0.4812	0.1720	0.4564	0.1552	0.4600	0.1213

*E_{25}^0 = 0.1728V, E_{35}^0 = 0.1690V, E_{45}^0 = 0.1678V.

TABLE 2. Harned coefficients for the NaCl–NaOAc–H_2O system

I	α_{AB}	β_{AB}	log $\gamma_A{}^0$ (exp)	log $\gamma_A{}^0$ (cal)	RMSD × 10^5
			T = 25°C		
0.5	−0.0149	—	−0.1667	−0.1667	3.34
1.0	−0.0257	—	−0.1823	−0.1823	3.68
	(−0.0242)*				
2.0	−0.0380	−0.0018	−0.1749	−0.1749	2.12
3.0	−0.0441	−0.0040	−0.1465	−0.1466	2.99
	(−0.0339)*				
			T = 35°C		
0.5	−0.0131	—	−0.1671	−0.1671	2.73
1.0	−0.0224	—	−0.1812	−0.1811	3.41
2.0	−0.0338	−0.0016	−0.1710	−0.1710	2.77
3.0	−0.0383	−0.0041	−0.1409	−0.1409	2.78
			T = 45°C		
0.5	−0.0117	—	−0.1686	−0.1686	2.68
1.0	−0.0202	—	−0.1817	−0.1817	3.23
2.0	−0.0315	−0.0010	−0.1698	−0.1698	2.59
3.0	−0.0370	−0.0023	−0.1389	−0.1389	2.74

*Parenthesized entries are from the work of Lanier (3), RMSD = root mean square deviation.

[5] $$\ln \gamma_{\pm}^{0} = -A_{\phi}[\sqrt{I}/(1 + b\sqrt{I}) + (2/b)\ln(1 + b\sqrt{I})] + m[2\beta^{(0)} + 2\beta^{(1)}/(4I)\{1 - \exp(-2\sqrt{I})(1 + 2\sqrt{I} - 2I)\}] + 1.5m^2C^{\phi}$$

[6] $$\phi^0 = 1 - A_{\phi}[\sqrt{I}/(1 + b\sqrt{I})] + m[\beta^{(0)} + \beta^{(1)}\exp(-2\sqrt{I})] + m^2C^{\phi}$$

			T = 25°C		
$\beta^{(0)}_{NaCl}$	= 0.075373	$\beta^{(1)}_{NaCl}$	= 0.277031	C^{ϕ}_{NaCl}	= 0.001407
$\beta^{(0)}_{NaOAc}$	= 0.13723	$\beta^{(1)}_{NaOAc}$	= 0.34915	C^{ϕ}_{NaOAc}	= −0.00474
			T = 35°C		
$\beta^{(0)}_{NaCl}$	= 0.081915	$\beta^{(1)}_{NaCl}$	= 0.28540	C^{ϕ}_{NaCl}	= 0.000406
$\beta^{(0)}_{NaOAc}$	= 0.13768	$\beta^{(1)}_{NaOAc}$	= 0.33700	C^{ϕ}_{NaOAc}	= −0.005374
			T = 45°C		
$\beta^{(0)}_{NaCl}$	= 0.087048	$\beta^{(1)}_{NaCl}$	= 0.29310	C^{ϕ}_{NaCl}	= −0.000432
$\beta^{(0)}_{NaOAc}$	= 0.13813	$\beta^{(1)}_{NaOAc}$	= 0.33205	C^{ϕ}_{NaOAc}	= −0.006008

According to Guggenheim (12), an electrolyte mixture involves pair-wise interactions of only oppositely charged ions. Moreover, the change in activity coefficient with composition of the mixture can be predicted from the osmotic coefficients (ϕ^0) of the constituent electrolytes. For two univalent electrolytes with a common ion, such as NaCl (m_A) and NaOAc (m_B) the following expression can be written

[7] $$\ln(\gamma_A/\gamma_A^0) = (\phi_B^0 - \phi_A^0)y_B$$

where γ_A^0 is the activity coefficient in a pure solution of component A at the same ionic strength as in the mixture. But Pitzer (5) recognized the possibility of interactions between charges of the same sign as well. Hence, Pitzer included the binary interaction ($^s\theta$) and ternary interaction (Ψ) terms in the mixture equation. The Pitzer equation for the three-ion mixtures such as NaCl–NaOAc–H_2O can be written as

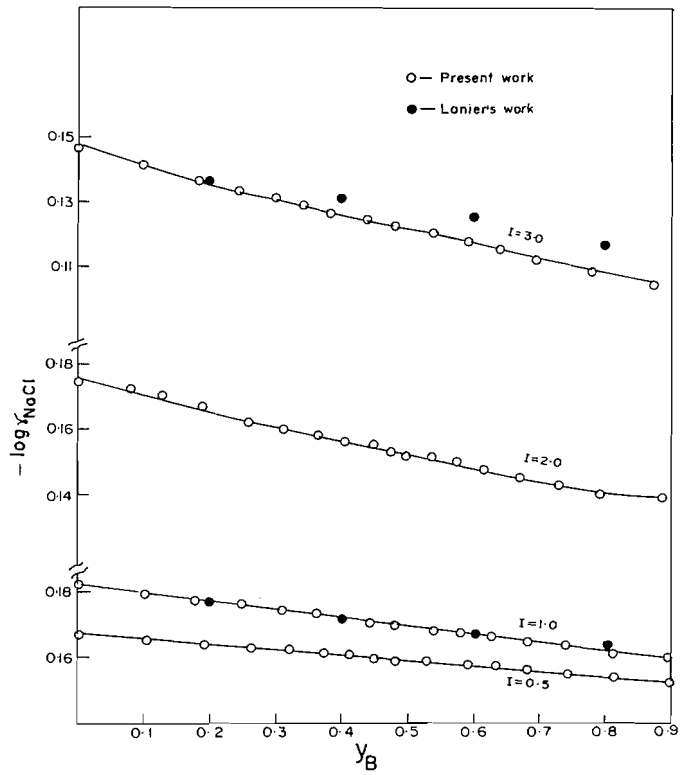


FIG. 1. Activity coefficients of NaCl in the NaCl–NaOAc–H_2O system at 25°C.

[8] $$\ln(\gamma_{NaCl}/\gamma^0_{NaCl}) = y_B(\phi_B^0 - \phi_A^0) + Iy_B{}^s\theta_{Cl-OAc} + 0.5I^2y_B(2 - y_B)\Psi_{Cl-OAc-Na}$$

where ϕ_A^0 and ϕ_B^0 are the osmotic coefficients of pure NaCl and NaOAc solutions at the same ionic strength as the mixture. Equation [8] was fitted to the activity coefficient data at all four ionic strengths at one temperature into a single least-squares program and the common $^s\theta$ and Ψ values were evaluated. The

Can. J. Chem. Downloaded from www.nrcresearchpress.com by 195.138.81.100 on 09/07/12
For personal use only.

TABLE 3. Pitzer and Scatchard parameters for the NaCl–NaOAc–H_2O system

	Pitzer parameters			Scatchard parameters		
T/°C	$^s\theta$	Ψ	RMSD × 10^5	b_{01}	b_{02}	RMSD × 10^5
25	−0.00545	−0.00205	2.90	−0.0109	−0.00405	3.29
35	−0.00451	−0.00202	2.98	−0.00879	−0.00416	3.19
45	−0.00357	−0.00122	2.76	−0.00723	−0.00235	4.67

evaluated $^s\theta$ values are −0.00545, −0.00451, and −0.00357 and Ψ values are −0.00205, −0.00202, and −0.00122 at 25, 35, and 45°C, respectively.

The neutral electrolyte treatment introduced by Scatchard (6) and later extended by Rush and Johnson (7) leads to the expression

$$[9]\quad \ln(\gamma_A/\gamma_A^0) = y_B(\phi_B^0 - \phi_A^0) + 0.5y_B(b_{01}I + b_{02}I^2 + b_{03}I^3 + b_{12}I^2 + b_{13}I^3) - 0.5y_B^2[(1/2)b_{01}I^2 + (2/3)b_{03}I^3 + (3/2)b_{12}I^2 + 2b_{13}I^3] + (1/3)y_B^3 b_{13}I^3$$

where ϕ_A^0 and ϕ_B^0 are the osmotic coefficients of the single components A and B at the same ionic strength as the mixture and can be calculated using the Pitzer equation [6]. The coefficients b_{mn} are mixing parameters accounting for the ion–ion interactions specific to the mixture. It appears that two parameters, namely b_{01}, b_{02}, are required to fit the experimental data accurately. Of these two, b_{01} represents the binary interaction between Cl–OAc and b_{02} represents the binary interaction between Cl–OAc and b_{02} the ternary interaction Na–Cl–OAc. Equation [9] was fitted to the activity coefficient data at all four ionic strengths into a single least-squares program to yield b_{01} and b_{02}. The evaluated values are $b_{01} = -0.0109$, −0.0088, and −0.0072 and $b_{02} = -0.00405$, −0.00416, and −0.00235 at 25, 35, and 45°C, respectively. Jones *et al.* (4) reported $b_{01} = -0.0156$ assuming b_{02} as zero at 25°C. Thus the different treatments of three uni-univalent ion mixtures are equivalent and the mixing parameters of Pitzer (5) and Scatchard (6, 7) models are interrelated because $b_{01} = 2^s\theta_{Cl-OAc}$ and $b_{02} = 2\Psi_{Cl-OAc-Na}$. When only two mixing interaction parameters are considered in each treatment, one gets the comparison as shown in Table 3. By combining eqs. [3], [8], and [9] it is evident that up to $I = 1.0$ mol/kg when the excess free energy of mixing can be accounted for satisfactorily in terms of only $^s\theta_{Cl-OAc}$ or b_{01}, these parameters are related to the Harned slope α_{AB} as

$$[10]\quad \alpha_{AB} = \frac{(\phi_A^0 - \phi_B^0 - I^s\theta_{Cl-OAc})}{2.3026} = \frac{(\phi_A^0 - \phi_B^0 - 0.5Ib_{01})}{2.3026}$$

By substituting $^s\theta_{Cl-OAc}$ or b_{01} values listed in Table 3 in the above equation the α_{AB} value could be calculated as −0.0150 and −0.0256 at $I = 0.5$ and 1.0, respectively. These values are in good agreement with the experimentally determined α_{AB} values of −0.0149 and −0.0257 (cf. Table 2).

Osmotic coefficients of this system were calculated using the Pitzer equation (5)

$$[11]\quad \phi = -A_\phi[\sqrt{I}/(1 + b\sqrt{I})] + \{(1 - y_B)B^\phi_{NaCl} + y_B B^\phi_{NaOAc} + y_B(1 - y_B)^s\theta_{Cl-OAc}\} + I^2\{(1 - y_B)C^\phi_{NaCl} + y_B C^\phi_{NaOAc} + y_B(1 - y_B)\Psi_{Cl-OAc-Na}\} + 1$$

TABLE 4. Osmotic coefficients for the NaCl–NaOAc–H_2O system

	Osmotic coefficient			
y_B	$I = 0.5$	$I = 1.0$	$I = 2.0$	$I = 3.0$
		$T = 25$°C		
0.0	0.9220	0.9363	0.9839	1.045
0.2	0.9289	0.9480	1.002	1.066
0.4	0.9361	0.9603	1.022	1.091
0.6	0.9436	0.9732	1.043	1.118
0.8	0.9513	0.9867	1.066	1.148
1.0	0.9593	1.001	1.091	1.181
		$T = 35$°C		
0.0	0.9233	0.9398	0.9902	1.052
0.2	0.9294	0.9502	1.006	1.071
0.4	0.9357	0.9610	0.1024	1.092
0.6	0.9423	0.9724	1.043	1.117
0.8	0.9490	0.9843	1.063	1.143
1.0	0.9560	0.9968	1.085	1.172
		$T = 45$°C		
0.0	0.9237	0.9416	0.9940	1.056
0.2	0.9291	0.9510	1.009	1.074
0.4	0.9347	0.9608	1.025	1.094
0.6	0.9405	0.9710	1.042	1.115
0.8	0.9464	0.9815	1.060	1.138
1.0	0.9525	0.9924	1.079	1.163

and the resulting data are listed in Table 4 for all temperatures and ionic strengths. Our estimated osmotic coefficients at 25°C are in agreement with the experimental values of Jones *et al.* (4) with an RMSD = 1.690×10^{-3}.

Excess Gibbs free energies of mixing were calculated using the equation (13)

$$[12]\quad \Delta_m G^E = 2y_B(1 - y_B)I^2RT(^s\theta_{Cl-OAc} + I\Psi_{Cl-OAc-Na}/2)$$

and the values are listed in Table 5.

Experimental

Analytical grade sodium chloride (Glaxo India) was purified by precipitation from a saturated solution with hydrogen chloride gas. AR grade sodium acetate (Glaxo India) was used after careful drying at 120°C. The stock solutions of NaCl were standardized by volumetric titrations against standard silver nitrate solution. All solutions were prepared by weight and all titrations and dilutions were done using weight burettes.

The cell consisted of sodium ion-selective electrode and Ag/AgCl electrode:

Na ion-selective electrode	$NaCl(m_A)$ + $NaOAc(m_B)$	Ag/AgCl electrode

Can. J. Chem. Downloaded from www.nrcresearchpress.com by 195.138.81.100 on 09/07/12
For personal use only.

TABLE 5. Excess Gibbs free energies of mixing for the NaCl–NaOAc–H_2O system

	$\Delta_m G^E$/cal kg^{-1}			
y_B	I = 0.5	I = 1.0	I = 2.0	I = 3.0
		T = 25°C		
0.1	−0.177	−0.710	−0.319	−8.17
0.2	−0.296	−1.24	−5.68	−14.5
0.3	−0.355	−1.59	−7.46	−19.0
0.4	−0.414	−1.83	−8.53	−21.8
0.5	−0.414	−1.89 (−2)*	−8.88 (−9)*	−22.7 (−21)*
		T = 35°C		
0.1	−0.122	−0.612	−2.87	−7.47
0.2	−0.244	−1.10	−5.14	−13.2
0.3	−0.306	−1.40	−6.73	−17.4
0.4	−0.367	−1.59	−7.65	−19.9
0.5	−0.367	−1.71	−8.02	−20.7
		T = 45°C		
0.1	−0.126	−0.505	−2.14	−5.50
0.2	−0.189	−0.821	−3.85	−9.86
0.3	−0.252	−1.13	−5.05	−12.9
0.4	−0.316	−1.26	−5.81	−14.7
0.5	−0.316	−1.32	−6.06	−15.3

*Parenthesized entries are from the work of Jones *et al.* (4).

The sodium ion-selective glass electrode was obtained from Elico, India. The Ag/AgCl electrode used was the thermal type (14). These electrodes were immersed in aqueous NaCl(m_A)–NaOAc(m_B) solution placed in a double-walled glass vessel. The temperature was maintained constant within ±0.01 K by circulating thermostatted water. The electrodes were connected to a high impedance ($\approx 10^{12}\ \Omega$) unit gain amplifier. The output of this amplifier was measured by a Keithley 5½ digit electrometer/multimeter (model: DMM 191). The accuracy of EMF measurements was ±0.01 mV. The potentials of the sodium ion-selective electrode vs. Ag/AgCl electrodes were measured at all four ionic strengths studied and the potentials were plotted against log a_{NaCl}. The E_0 values were obtained from the intercept, where the activity of NaCl is unity. These values are given as a footnote to Table 1. Further experimental details are given earlier (15, 16).

Acknowledgements

The authors wish to thank Professor T. Navaneeth Rao, Vice Chancellor, Osmania University, Hyderabad and Professor G. Atkinson, University of Oklahoma, Norman, USA, for constant encouragement and helpful discussions. S.M. is thankful to CSIR, Govt. of India, for the award of a fellowship.

1. G. SCATCHARD and S. S. PRENTISS. J. Am. Chem. Soc. **55**, 4355 (1933).
2. G. SCATCHARD and S. S. PRENTISS. J. Am. Chem. Soc. **56**, 807 (1934).
3. R. D. LANIER. J. Phys. Chem. **69**, 3992 (1965).
4. R. A. JONES and J. E. PRUE. J. Solution Chem. **3**, 585 (1974).
5. K. S. PITZER. J. Phys. Chem. **77**, 268 (1973).
6. G. SCATCHARD. J. Am. Chem. Soc. **83**, 2636 (1961).
7. R. M. RUSH and J. S. JOHNSON. J. Phys. Chem. **72**, 767 (1968).
8. H. S. HARNED and B. B. OWEN. The physical chemistry of electrolyte solutions. 3rd ed. Reinhold, New York. 1958. Chap. 14.
9. K. S. PITZER, J. C. PEIPER, and R. H. BUSEY. J. Phys. Chem. Ref. Data, **13**, 1 (1984).
10. H. T. KIM and W. J. FREDERICK, JR. J. Chem. Eng. Data, **33**, 177 (1988).
11. P. C. RAMESH and K. S. PITZER. J. Solution Chem. **15**, 649 (1986).
12. E. A. GUGGENHEIM. Philos. Mag. **19**, 588 (1935).
13. H. F. HOLMES, C. F. BATES, JR., and R. E. MESMER. J. Chem. Thermodyn. **11**, 1035 (1979).
14. D. J. G. IVES and G. J. JANZ. Reference electrodes. Academic Press, New York. 1961. Chap. IV.
15. S. MANOHAR, S. SARADA, and J. ANANTHASWAMY. J. Chem. Thermodyn. **21**, 969 (1989).
16. J. ANANTHASWAMY and G. ATKINSON. J. Solution Chem. **11**, 509 (1982).

Can. J. Chem. Downloaded from www.nrcresearchpress.com by 195.138.81.100 on 09/07/12
For personal use only.

Studies on the thermal coking of bitumen. I. The use of pyrene-d_{10} as a probe for evaluating the extent of hydrogen shuttling reaction

M. J. KIRK AND T. S. SORENSEN[1]

The Department of Chemistry, University of Calgary, Calgary, Alta., Canada T2N 1N4

Received July 16, 1990

M. J. KIRK and T. S. SORENSEN. Can. J. Chem. **69**, 116 (1991).

The organic reactions that take place during the thermal coking of bitumen are extremely complex and deep-seated, but obviously hydrogen atoms originally attached to carbons that form coke will have moved to a new carbon site (net addition of hydrogen, resulting in upgraded bitumen). Accompanying this process, one expects some general hydrogen shuttling between non-coking molecules. This paper describes an approach to determing the extent of this latter process by the addition of a small amount of perdeuterated pyrene to the bitumen prior to the coking operation. The *in situ* pyrene functions as in indicator, allowing one to establish the extent and other mechanistic details of the "hydrogen donor" reactions that take place during coking. There is no indication that the pyrene substantially modifies the normal course of the reaction, hence the analogy to an indicator.

Key words: bitumen coking, pyrene, hydrogen exchange, donor solvent, free radicals.

M. J. KIRK et T. S. SORENSEN. Can. J. Chem. **69**, 116 (1991).

Les réactions organiques qui se produisent au cours du cokage thermique du bitume sont extrêmement complexes et fondamentales; il est toutefois évident que les atomes d'hydrogène qui sont originalement attachés aux atomes de carbone qui donnent naissance au coke devront se déplacer vers de nouveaux sites carbonés (avec une addition nette d'hydrogène qui donne naissance à un bitume amélioré). On peut s'attendre à ce que ce processus soit accompagné d'un déplacement général des hydrogènes entre les molécules qui ne donnent pas de coke. Dans ce travail, on décrit une approche qui permet de déterminer l'importance de ce dernier processus; elle est basée sur l'addition d'une faible quantité de pyrène perdeutéré au bitume avant l'opération de cokage. Le pyrène fonctionne comme indicateur *in situ* qui permet d'évaluer l'importance ainsi que les autres détails mécanistiques des réactions des «donneurs d'hydrogène» qui se produisent durant le cokage. Il n'existe pas de données permettant de croire que le pyrène affecte d'une façon substantielle le cours de la réaction; d'où l'analogie à un indicateur.

Mots clés : cokage du bitume, pyrène, échange d'hydrogène, solvant donneur, radicaux libres.

[Traduit par la revue]

Introduction

Operational oil-sands (bitumen) plants in Alberta, Canada, use thermal coking as the primary upgrading method for converting bitumen into usable hydrocarbon fractions (coker gas oil). The coke produced (ca. 15% by weight of the raw bitumen) is high in sulphur and the utility of this material depends largely on extraneous factors such as the allowable levels of plant SO_2 emission, etc.

In looking chemically at coking there are two general aspects to consider:

1. what type of organic chemical reactions are responsible for coke formation?

2. what organic reactions or rearrangements have occurred in the production of the coker gas oil?

There have been many studies of the organic reaction mechanisms involved in the related coal upgrading area, particularly those involving donor solvents (for recent reviews, see ref. 1). Like the present study, several of these have involved deuterium labelling approaches (2). In the case of bitumen coking, there are fewer published studies, but the mechanisms involved in "cracking" have been studied extensively, often using model compounds (3).[2]

We have been interested in the possibility of adding substances (additives) to the bitumen prior to coking, in the hope that these additives could modify the subsequent coking process in desirable ways. There are two major improvements that one might ideally hope for: (1) a higher yield of coker gas oil and correspondingly less coke, and (2) in the coker gas oil produced, a reduction of aromatics in the diesel range distillates. When one heats a complex mixture such as bitumen to 475°C, homolytic cleavage of bonds will ensue. The resulting carbon or heteroatom centered radicals can be quenched by natural hydrogen atom donor sources in the bitumen but, when these are in short supply, radical recombination processes can also occur. The latter reactions in some instances probably lead to high molecular weight "mesophases" and eventually to coke. Hydrogen atom donor processes (and the extent of these) are thus expected to occupy a key role in the overall coking reaction. In the absence of added hydrogen gas (hydrocracking) or donor solvents (donor solvent upgrading), there is of course a fixed finite amount of donor hydrogen available in the bitumen itself, but one might speculate that certain additives would increase the hydrogen atom transfer rates during the coking process (hydrogen shuttling reactions) and that such rate increases might have desirable consequences on both coker gas oil yield and on its detailed composition.

In the present work, we describe a methodology for determining the extent of hydrogen atom transfer reactions accompanying the coking of bitumen, in the absence of additives. This study involves the addition of a relatively small amount of perdeuterated pyrene to the raw bitumen, which is subsequently coked in a laboratory-scale coker. The rationale behind this experiment is multifold:

1. Pyrene has a boiling point that is high enough so that it remains dissolved in the bitumen well into the coking temperature range. Pyrene itself is not prone to charring (coking) when distilled by itself, although the actual behaviour in a bitumen mixture could be different.

2. Pyrene has the potential to serve as a hydrogen donor but only if it is first reduced, i.e., it would obviously not initiate

[1]Author to whom correspondence may be addressed.

[2]For a recent study of thermal aromatic hydrocarbon condensations, see refs. 3*b* and *c*.

Can. J. Chem. Downloaded from www.nrcresearchpress.com by 195.138.81.100 on 09/07/12
For personal use only.

Can. J. Chem. Downloaded from www.nrcresearchpress.com by 195.138.81.100 on 09/07/12
For personal use only.

hydrogen donor processes but is capable of serving as a convenient "detector" for such reactions (hydrogen shuttling, see also ref. 4).

3. If indeed deuterium donor reactions do occur, then the recovered pyrene can be analyzed for proton content. Since there are initially three different types of deuterons in pyrene, any preferential exchange involving these different sites should provide specific mechanistic information as to the type and specificity of reactions occurring during the coking.

4. If deuterium donor reactions do occur, the resulting deuterium content in the coker gas oil fractions can be investigated on a "global" basis by ^{2}H NMR spectroscopy or by MS for the individual components.

5. Some of these deuterium atoms transferred to the coker gas oil may be irreversibly incorporated, whilst others may be back exchangeable if one reexposes the gas oil to ordinary pyrene-h_{10} under conditions similar to those used in the original coking reaction. Such exchange reactions would provide information on the kinds of reactive radical intermediates that are produced either reversibly or irreversibly during the coking process.

Experimental

Chemicals

The coker feed bitumen used in these experiments was supplied by Alberta Research Council from Syncrude, Fort McMurray, Alberta, Canada. The pyrene-d_{10} (98+ at.% D) was supplied by MSD Isotopes, the tetralin-d_{12} (98+ % D) and pyrene-h (99+ 1%) were supplied by Aldrich Chemical company, and all were used without further purification.

Instruments

The deuterium NMR spectra were measured on a Varian XL 200 spectrometer operating at 30.7 MHz. The proton NMR spectra were carried out on a Bruker AC 200 instrument at 200 MHz. The direct probe MS analyses were carried out on a VG Micromass 7070F instrument.

Reaction vessels

The lab scale model coker, patterned from a design described by George (5), was built of 316 stainless steel. The coker consists of a pot (the height was 110 mm, the inner diameter was 100 mm) into which the bitumen was placed. The heating was provided by an arrangement of Nichrome wire embedded in a ceramic paste (1 cm thickness), which provided insulation and protected the element. The length of Nichrome was calculated on the basis of amperage required for the desired heating rate. A high output variac (20 amp) was required to provide power to the heating element. A positive pressure of nitrogen (100 mL/min) was continually flushed through the system so that the cracked products could be distilled over before further reaction occurred. The liquid products were collected successively in an ice (0°C) and then a Dry Ice/acetone (−78°C) cooled receptacle.

The tube bomb was constructed of 316 stainless steel. The length of the bomb was 160 mm, the internal diameter was 8 mm, and the approximate volume was 8 cm^3. The loaded tube bomb was placed in a preheated muffle furnance, which allows the tube bomb to reach operating temperatures within a few minutes. After reaction, the hot tube bomb was "quenched" with water, so the cool-down period is also very short.

Bitumen coking procedure

Bitumen (25 g) with pyrene-d_{10} (0.4 g) slurried into it was placed into the lab scale coker and the power was switched on. Heat-up, from room temperature to the final coking temperature of around 480°C, took 2 h to achieve.

Fractional distillation of the coker gas oil (20.3 g) was carried out using a spinning band column (10 × 670 mm), employing a ca. 10:1 reflux ratio. Fractions below 175°C were distilled under water aspirator vacuum and fractions from 175 to 425°C using a vacuum pump. The bp data reported were converted to 760 Torr (1 Torr = 133.3 Pa) pressure. Coking runs were made using both the pyrene additive and with no additives. The yield of coke was also quantified (4.8 g).

Fraction	Corrected boiling pt. (°C)	Weight (g)	Cumulative weight percentage
0	0–145	0.8	4.1
1	145–175	0.6	7.2
2	175–225	1.4	14.4
3	225–275	2.45	26.9
4	275–325	1.4	34.1
5	325–375	5.2	60.7
6	375–425	4.3	82.7
7	>425 (residue)	3.4	100

The coker gas oil fractions were then subjected to ^{2}H NMR analysis to examine deuterium incorporation into the different boiling ranges. The residual pyrene-d was then collected (mainly from fraction 5) and analyzed using direct probe MS, in order to quantify the amount of exchange occurring during the coking reaction. The recovered pyrene-d was finally analyzed using ^{1}H NMR, to study the selectivity of exchange from the pyrene-d_{10}. These experiments were performed in duplicate.

Exchange of pyrene-h_{10} *and tetralin-*d

A weight ratio of 2 parts of the tetralin and 1 part of the pyrene (2.8:1 molar ratio) was heated in the tube bomb for a period of 1 h at the preset temperatures 400, 425, and 450°C. The pyrene was isolated and analysed by mass spectrometry and by ^{1}H NMR spectroscopy. The former measurement gives the deuterium incorporation data shown in Fig. 1, while the NMR data give the positional substitution ratios shown in Fig. 2. The absolute values shown in Fig. 2 were based on the data in Fig. 1. The results shown in Fig. 2 for 450°C are close to the thermodynamic equilibrium result (there is a total of 63 mol% D in the total hydrogen (H + D) system).

Results and discussion

There is in fact extensive deuterium incorporation into the coker gas oil fractions. Table 1 summarizes the ^{2}H NMR data obtained for the different boiling fractions. The fraction containing the majority of the recovered pyrene-d (fraction 5, 325–375°C) is not shown because it was completely dominated by a ^{2}H peak for the recovered pyrene. ^{1}H NMR spectroscopy can be used to assign a number of proton environments but ^{2}H NMR involves a chemical shift dispersion of one seventh that of ^{1}H and also involves somewhat broader lines (quadripolar nucleus) and therefore only three regions are assignable.

We have assigned these three deuterium (proton) NMR regions as follows:

1. aromatic (6–10 ppm)
2. benzylic, allylic etc. (1.9–3.2 ppm)
3. aliphatic (0.5–1.9 ppm)

The latter division is somewhat arbitrarily set and represents only a qualitative measure of the corresponding deuterium/hydrogen types.

For comparison purposes, we have made the corresponding measurements for coker gas oil fractions, produced without pyrene addition, where ^{1}H NMR spectra have been obtained. A comparison of the two sets of data gives some idea of those degraded molecules that have interacted at some point with pyrene (or dihydropyrenes) in contrast to species that may have formed in other ways. By comparing the fractions of deuterium/hydrogen types in Table 1, it is evident that deuter-

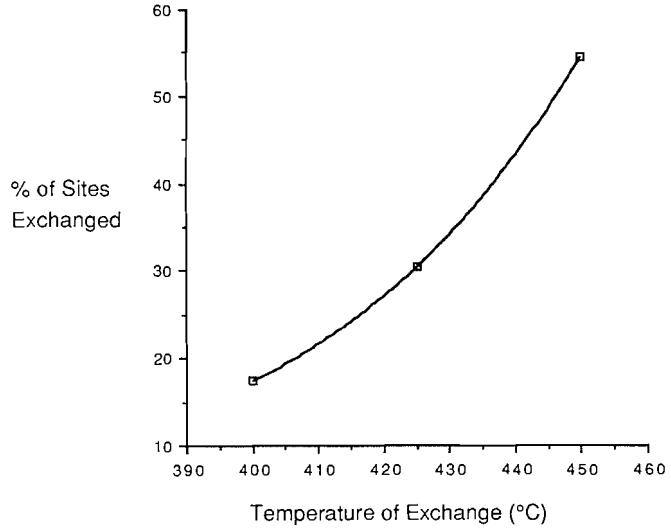


FIG. 1. Direct probe MS analysis of the recovered exchanged (originally h_{10}) pyrene.

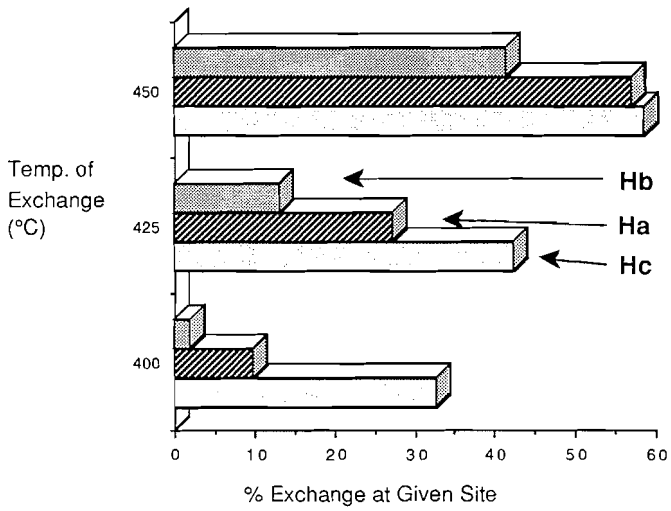


FIG. 2. ^{1}H NMR analysis of recovered (partially deuterated) exchanged pyrene-*h* in the model exchange reactions.

ium has found its way into more benzylic and aromatic sites than expected on a purely statistical basis.

The pyrene can be recovered in near quantitative yield (both by actual recovery and estimates based on quantitative GC measurements). The ^{1}H NMR spectrum of the recovered pyrene is compared in Fig. 3 to that of the ordinary pyrene-*h*. It is immediately obvious that selective H/D substitution has occurred in the pyrene-d_{10} and that the ring positions most exchanged are c and a followed by least substitution in position b. This selectivity can be explained if one considers the energies of the radicals produced on addition of a hydrogen atom to the pyrene-d_{10} molecule. Theoretical calculations carried out by Herndon *et al.* (6) and Stein and Golden (7) suggest that the most stable radical is formed by addition of a hydrogen atom to position c followed by a and lastly b.

The total amount of exchange can be roughly calculated from a direct probe MS of the recovered pyrene. The most intense peak in the molecular-ion envelope is still the d_{10} species and an approximate averaging of the various peaks gives an overall proton incorporation of 7.5 ± 1.5% (this small proton incorporation accounts for the singlets observed in the ^{1}H NMR

TABLE 1. NMR analysis of coker gas oil fractions in both spiked and non-spiked experiments

Boiling point range of fraction (°C)	Aliphatic (0–1.9 ppm)		Benzylic (1.9–3.2 ppm)		Aromatic (6.0–10.0 ppm)	
	^{2}H	^{1}H	^{2}H	^{1}H	^{2}H	^{1}H
145–175	0.57	0.84	0.34	0.14	0.09	0.02
175–225	0.53	0.80	0.38	0.14	0.09	0.06
225–275	0.50	0.78	0.35	0.16	0.15	0.06
>425	0.37	0.77	0.47	0.17	0.16	0.07

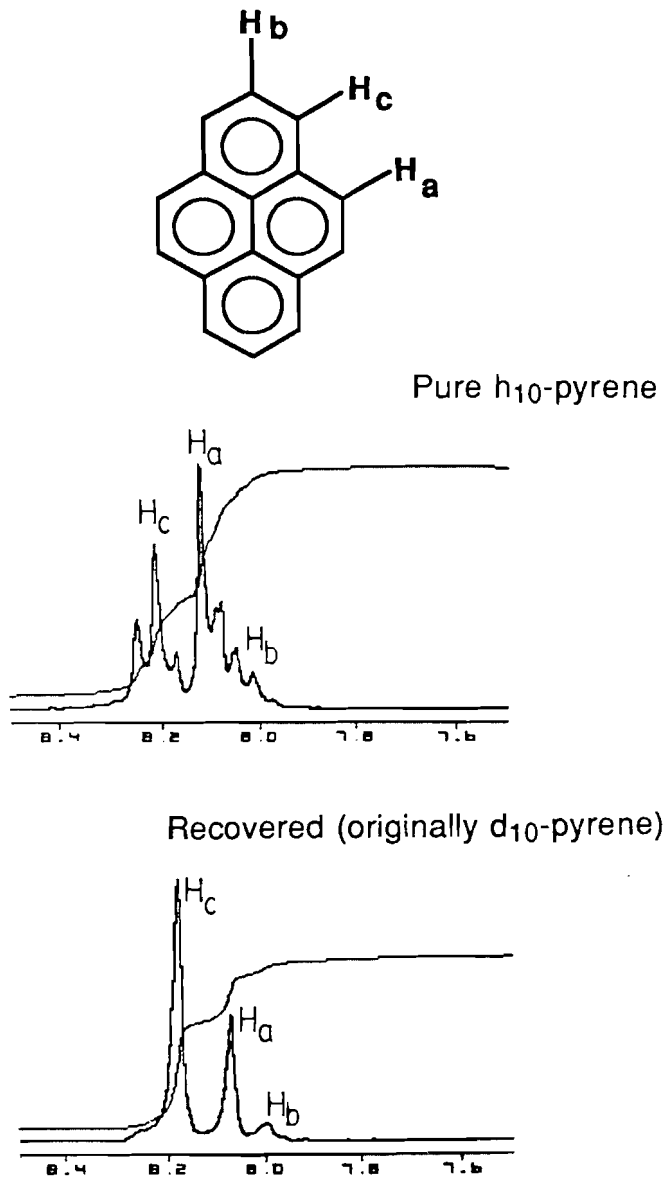


FIG. 3. ^{1}H NMR of recovered pyrene compared to pure pyrene-h_{10}.

spectrum shown in Fig. 3, i.e., the protons H_a, H_b, and H_c will overwhelmingly have deuterium neighbors and hence no ^{1}H–^{1}H couplings are evident). Assuming that this deuterium has all gone into the coker gas oil fractions, the total D/H content of the latter is calculated to be about 0.15%. The presence of the residual pyrene in the middle coker gas oil fractions makes a direct D/H analytical determination difficult.

Can. J. Chem. Downloaded from www.nrcresearchpress.com by 195.138.81.100 on 09/07/12
For personal use only.

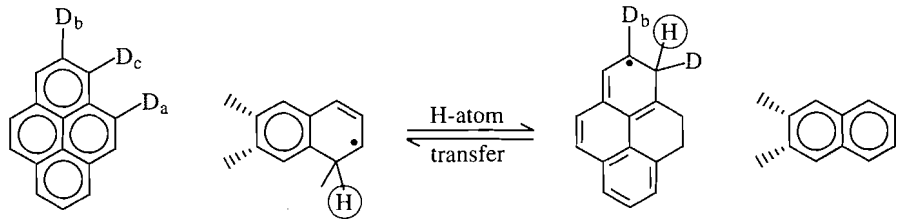


FIG. 4. Reversible H-donor reactions.

The 7.5% proton incorporation into the pyrene-d_{10} should be compared with the potential equilibrium value, and a rough estimate based on the relative weights of the pyrene and bitumen would suggest a number like 98–99% for the equilibrium proton incorporation. Clearly the experimental exchange value is very non-equilibrium and one would have considerable leeway in trying to find "additives" that might increase this proton incorporation. Another indication of the non-equilibrium nature of the exchange is found in the Table 1 data. Thus, the 7.5% deuterium exchanged out of the pyrene is found in many different environments, but benzylic and aromatic positions are favored, as we have noted previously, and as one might expect on established mechanistic grounds.

To assess whether coker gas oil deuterium incorporation is reversible, we carried out a further experiment in which a high boiling coker gas oil fraction (375–410°C) was heated to approximately 450°C for an hour in a tube bomb, in the presence of pyrene-h_{10}. The pyrene was then recovered and monitored for deuterium content using ^{2}H NMR, as was the recovered coker gas oil fraction. The result of this experiment indicated that there is indeed a reversible element of the whole deuterium incorporation. The deuterium type involved is the benzylic/allylic portion, i.e., the ^{2}H NMR spectrum of the recovered coker gas oil fraction is now depleted in benzylic deuterium, which is found to have exchanged into the recovered (initially h_{10}) pyrene, again with the selectivity already described (but in reverse).

To verify that the observed selectivity of exchange into the labelled pyrene is indeed a property of naturally present hydrogen-donor-type molecules in the bitumen, it was decided that a series of model exchange reactions should be carried out between a suitable D donor and pyrene-h_{10} at temperatures similar to those experienced in the coking experiment. We hoped to see the same selectivity in the exchange of deuterium into the pyrene as we saw in the bitumen experiment (in a reversed sense). These model exchange reactions were carried out in tube bombs at the temperatures shown in Fig. 1 for a period of 1 h. Once the pyrolyses were complete, the exchanged pyrene was recovered and analysed by direct probe MS, in order to discover the extent of substitution of deuterium into the pyrene-h. The results of this analysis are shown in Fig. 1.

From the MS data one can see that the extent of exchange varies with the temperature of the exchange reaction, as indeed one would expect. At 400°C the extent of exchange amounts to about 17% of the available sites in the pyrene. At 450°C the extent of exchange has increased substantially to about 55% of the available sites. If one remembers the statistical proportion of the three different available sites, 40% H_c, 40% H_b, and 20% H_a, we know, even before ^{1}H NMR analysis, that the site selectivity at 450°C will be lower because of the high degree of overall exchange.

The next step was the analysis of the recovered pyrene, using

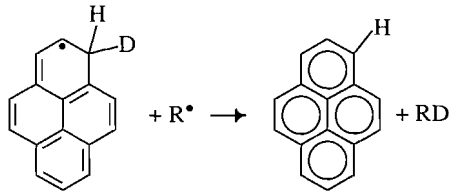


FIG. 5. Irreversible quenching of reactive radicals.

^{1}H NMR spectroscopy, in order to learn the site selectivity of the substituted deuterium atoms. Results of this analysis are illustrated in Fig. 2.

Looking at the results of the ^{1}H NMR spectra, it is evident that at 400°C the site selectivity is high and that the preferred exchange site is H_c followed by H_a and lastly H_b. This matches exactly the order seen in the bitumen/pyrene-d_{10} coking experiment.

Mechanistic considerations

In the coking of bitumen, one is dealing with a very complex mixture of compounds (for a recent discussion, see ref. 8) and mechanistic studies must deal with broad classes of reactions. Based on the results outlined in this work, and in fact on numerous previous studies in the coal area, the following two categories are both envisaged:

1. Reversible H-donor reactions (Fig. 4), where the dihydronaphthalene radical is used only for illustrative purposes to represent possible naturally occurring hydrogen donor molecules present in the bitumen. The formed dihydropyrenyl radical can in principle then reversibly react with a variety of naturally occurring aromatic compounds, transferring a deuterium atom or reversing the hydrogen atom transfer. This deuterium "shuttling" mechanism accounts for the deuterium incorporation into both aromatic and benzylic sites in the coker gas oil produced, and the extent of these reactions can be quantified.

2. Irreversible quenching of reactive radicals (Fig. 5). There are several ways in which the formation of reactive radicals can be envisioned. Side-chain cleavage from an aromatic radical is one well-known route (Fig. 6). Cleavage β to the aromatic ring also explains the high level of exchange into benzylic environments.

Reactive radicals, on quenching, can eventually produce alkane-type deuterium NMR signals. Such deuterium atoms are not expected to back exchange with pyrene-h_{10}, as indeed one observes. Again, this process can be quantified.

The amount of pyrene-d_{10} added to the bitumen is relatively small and we do not notice any particular changes in the overall coking reaction occurring in the presence of the pyrene, i.e., overall yield of the coker gas oil, the amounts of various boiling point cuts, aromaticity of these cuts, etc. (However, in coal upgrading, pyrene addition has been shown to affect the pro-

Can. J. Chem. Downloaded from www.nrcresearchpress.com by 195.138.81.100 on 09/07/12
For personal use only.

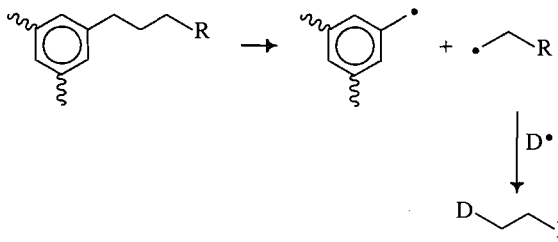


FIG. 6. Dealkylation resulting in formation of reactive radicals.

cesses (4) so some caution is perhaps warranted.) These pyrene-d_{10} exchange reactions therefore function very much like an indicator (i.e., an indicator of broad reaction types). In studying the effect of additives in the coking of bitumen, one now has some quantitative markers for comparison purposes.

Conclusions

The use of a deuterated polynuclear aromatic as a hydrogen shuttling probe is described. From the selectivity of H/D exchange in pyrene we know, not unexpectedly, that the pyrolysis reactions involve free radical processes. From analysis of the exchanged fraction, before and after the back exchange, we know something of the environments in which the mobile, exchanging species find themselves, and that some of these exchange reactions are reversible, i.e., the benzylic and aromatic protons/deuterons, and some (mainly aliphatic protons/deuterons) are not reversible.

The reaction mechanisms discussed in this work are not new, and in this regard we have added no new insights into this rather speculative area. We are primarily interested in developing *quantitative procedures for evaluating changes* in the extent and type of hydrogen shuttling reactions, and in this regard, the pyrene-d_{10} indicator fits most of our criteria.

Acknowledgements

We thank the Natural Sciences and Engineering Research Council of Canada for generous financial support and AOSTRA for a scholarship to M. J. Kirk. We thank Dr. Z. George for his technical advice.

1. (*a*) M. L. POUTSMA. A review of model compounds relevant to processing of coal. U.S. Dept. of Energy Contract No. DE-AC05-840R21400, Nov. 1987; (*b*) M. L. POUTSMA. Energy Fuels, **4**, 113 (1990); (*c*) S. E. STEIN. A.C.S. Symp. Ser. No. 69. 1981. p. 97; (*d*) S. E. STEIN. *In* Chemistry of coal conversion. *Edited by* R. H. Schlosberg. Plenum Press, New York. 1985. Chap. 2. p. 13; (*e*) L. M. STOCK. *In* Chemistry of coal conversion. *Edited by* R. H. Schlosberg. Plenum Press, New York. 1985. Chap. 6. p. 253.
2. (*a*) H-H. KING and L. M. STOCK. Fuel, **61**, 257 (1982); (*b*) R. A. FRIEDEL, B. C. BOCKRATH, and H. L. RETCOFSKY. Anal. Chem. **48**, 1255 (1976); (*c*) R. P. SKOWRONSKI, J. J. RATTO, I. B. GOLDBERG, and L. A. HEREDY. Fuel, **63**, 440 (1984); (*d*) C. W. CURTIS and W. J. CLUNG. A.C.S. Division of Fuel, Preprints, **33** (1), 65 (1988); (*e*) M. A. WILSON, P. J. COLLIN, P. F. BARRON, and A. M. VASSALLO. Fuel Process. Technol. **5**, 281 (1982); (*f*) J. J. RATTO, L. A. HEREDY, and R. P. SKOWRONSKI. A.C.S. Symp. Ser. **139**, 347 (1980); (*g*) D. C. CRONAUER, R. I. MCNEIL, A. C. YANG, and R. C. RUBERTO. Trans. Am. Nucl. Soc. 365 (1980).
3. (*a*) K. BELINKO and J. M. DENIS. A review of some chemical aspects of the formation of coke during thermal hydrocracking of bitumen. CANMET (Dept. of Energy, Mines and Resources, Government of Canada, Ottawa) Report, Sept. 1976; (*b*) V. P. SENTHILNATHAN and S. E. STEIN. J. Org. Chem. **53**, 3000 (1988), and references therein; (*c*) I. C. LEWIS and L. S. SINGER. A.C.S. Symp. Ser. **217**, Chap. 16 (1988).
4. (*a*) F. J. DERBYSHIRE and D. D. WHITEHURST. Fuel, **60**, 655 (1981); (*b*) F. J. DERBYSHIRE, P. VARGHESE, and D. D. WHITEHURST. **61**, 859 (1982).
5. Z. GEORGE. Fuel, **61**, 169 (1982).
6. W. C. HERNDON. J. Org. Chem. **46**, 2119 (1981); (*b*) L. V. SZENTPALY and W. C. HERNDON. A.C.S. Symp. Ser. No. 217. 1981. Chap. 17.
7. S. E. STEIN and D. M. GOLDEN. J. Org. Chem. **42**, 839 (1977).
8. O. P. STRAUSZ. *In* Technical handbook on oilsands, bitumens and heavy oils. *Edited by* L. G. Hepler and C. Hsi. AOSTRA, Edmonton. 1989. Chap. 3. p. 33.

Can. J. Chem. Downloaded from www.nrcresearchpress.com by 195.138.81.100 on 09/07/12
For personal use only.

Solid state and solution structural investigation of homoleptic tin(IV) alkoxide compounds. Part I. $Sn(O—t\text{-}Bu)_4$ and $[Sn(O—i\text{-}Pr)_4 \cdot HO—i\text{-}Pr]_2$

MARK J. HAMPDEN-SMITH[1] AND TERESA A. WARK
Department of Chemistry and Center for Micro-Engineered Ceramics, University of New Mexico, Albuquerque, NM 87131, U.S.A.

ARNOLD RHEINGOLD
Department of Chemistry, University of Delaware, Newark, DE 19716, U.S.A.

AND

JOHN C. HUFFMAN
Indiana University Molecular Structure Center, Indiana University, Bloomington, IN 47405, U.S.A.

Received July 3, 1990

MARK J. HAMPDEN-SMITH, TERESA A. WARK, ARNOLD RHEINGOLD, and JOHN C. HUFFMAN. Can. J. Chem. **69**, 121 (1991).

The crystal and molecular structures of $Sn(O—t\text{-}Bu)_4$ and $[Sn(O—i\text{-}Pr)_4 \cdot HO—i\text{-}Pr]_2$ have been determined by single-crystal X-ray diffraction. $Sn(O—t\text{-}Bu)_4$ crystallizes in the monoclinic crystal system with space group $C2/c$, where $a = 17.382(6)$ Å, $b = 8.742(2)$ Å, $c = 15.518(5)$ Å, $\beta = 116.44(1)°$, $Z = 4$, and $R = 2.5\%$. $Sn(O—t\text{-}Bu)_4$ is monomeric in the solid state, with a distorted tetrahedral tin coordination environment. $[Sn(O—i\text{-}Pr)_4 \cdot HO—i\text{-}Pr]_2$ crystallizes in the monoclinic crystal system with space group $P2_1/n$, where $a = 11.808(3)$ Å, $b = 14.356(3)$ Å, $c = 12.380(2)$ Å, $\beta = 95.27(2)°$, $Z = 2$, and $R = 4.9\%$. $[Sn(O—i\text{-}Pr)_4 \cdot HO—i\text{-}Pr]_2$ exhibits an edge-shared, bi-octahedral structure in the solid state that is distorted due to the presence of asymmetric hydrogen bonding between axially coordinated alcohol ligands and an isopropoxide ligand. ^{13}C NMR and IR spectroscopic data have been recorded for $Sn(O—t\text{-}Bu)_4$ and $Sn(O—t\text{-}Bu\text{-}d_9)_4$ to establish criteria for unambiguous identification of solution structures of tin(IV) alkoxides. It is demonstrated that the two-bond $^2J_{^{13}C—O—^{119}Sn}$ coupling constant is larger for terminal alkoxide ligands than for μ^2-alkoxide bridges, and the $\nu(Sn—O)$ stretching frequency has been assigned. The dynamic solution behaviour of $[Sn(O—i\text{-}Pr)_4 \cdot HO—i\text{-}Pr]_2$ has been studied using variable temperature ^1H and ^{13}C NMR spectroscopy. The data obtained are consistent with a process that involves rapid reversible dissociation of isopropanol at room temperature. Upon cooling, the equilibrium concentration of the species with coordinated alcohol increases, and the molecule undergoes rapid intramolecular proton transfer ($\Delta G^{\ddagger} < 11.9$ kcal mol^{-1}). Upon further cooling, the ^{13}C NMR data are consistent with a solution structure analogous to that found in the solid state.

Key words: tin, alkoxide, NMR, dynamic, structure.

MARK J. HAMPDEN-SMITH, TERESA A. WARK, ARNOLD RHEINGOLD et JOHN C. HUFFMAN. Can. J. Chem. **69**, 121 (1991).

On a déterminé les structures cristallines et moléculaires du $Sn(O—t\text{-}Bu)_4$ et du $[Sn(O—i\text{-}Pr)_4 \cdot HO—i\text{-}Pr]$ par diffraction des rayons-X par des cristaux uniques. Le $[Sn(O—t\text{-}Bu)_4$ cristallise dans le système monoclinique, groupe d'espace $C2/c$, $a = 17,382(6)$, $b = 8,742(2)$ et $c = 15,518(5)$ Å, $\beta = 116,44(1)°$, $Z = 4$ et $R = 2,5\%$. À l'état solide, le $[Sn(O—i\text{-}Pr)_4 \cdot HO—i\text{-}Pr]$ est un monomère dans lequel la coordination de l'étain est un tétraèdre déformé et il cristallise dans le système monoclinique, groupe d'espace $P2_1/n$, $a = 11,808(3)$, $b = 14,356(3)$ et $c = 12,380(2)$ Å, $\beta = 95,27(2)°$, $Z = 2$ et $R = 4,9\%$. À l'état solide, le $[Sn(O—i\text{-}Pr)_4 \cdot HO—i\text{-}Pr]$ se présente sous une structure bi-octaédrique partageant une arète; elle est déformée à cause de la présence de liaisons hydrogènes asymétriques entre des ligands alcooliques coordonnés d'une façon axiale et un ligand isopropylate. On a déterminé les spectes IR et RMN du ^{13}C du $Sn(O—t\text{-}Bu)_4$ et du $Sn(O—t\text{-}Bu\text{-}d_9)_4$ afin d'avoir des critères non-ambigues pour caractériser les structures des alcoolates d'étain(IV) en solution. On a démontré que la constante de couplage à travers deux liaisons $^2J_{^{13}C—O—^{119}Sn}$, est plus grande pour les ligands alcoolates terminaux que pour les ponts alcoolates-μ^2; de plus, on a attribué la fréquence de, vibration $\nu(Sn—O)$. Faisant appel à la rmn du ^1H et du ^{13}C, à température variable, on a étudié le comportement dynamique du $[Sn(O—i\text{-}Pr)\cdot HO—i\text{-}Pr]$ en solution. Les données obtenues sont en accord avec un processus qui implique une dissociation réversible rapide de l'isopropanol, à la température ambiante. Par refroidissement, la concentration de l'espèce avec de l'alcool isopropylique augmente et la molécule subit un transfert intramoléculaire rapide de proton ($\Delta G^{\ddagger} < 11,9$ kcal mol^{-1}). Si on continue le refroidissement, les données de la rmn du ^{13}C obtenues sont en accord avec une structure en solution qui serait analogue à celle qui est trouvée à l'était solide.

Mots clés : étain, alcoolates, RMN, dynamque, structure.

[Traduit par la revue]

Introduction

The conversion of homoleptic metal alkoxides to metal oxides is currently under intense investigation as a route to new and existing ceramic materials (for recent reviews see ref. 1). The sol–gel process is suitable for the hydrolytic conversion of *soluble* metal alkoxides to metal oxides (2); whereas chemical vapour deposition (CVD) has been used for the preparation of thin films of metal oxides from *volatile* metal alkoxide precursors (3). A sound understanding of the mechanistic aspects of the conversion of metal alkoxides to metal oxides is an important aspect of this work since this knowledge may result in lower processing temperatures and better control over the particle size, morphology, and homogeneity of the final ceramic materials.

Studies of the *thermal* decomposition of titanium (4), zirconium (4), tin (5), and most recently, cerium alkoxides have been addressed (6). Many examples of hydrolytic decomposition of metal alkoxides have been published, but mechanistic data are relatively sparse even though the sol–gel hydrolysis of tetraethylorthosilicate has been extensively investigated (see *e.g.* ref. 7). For example, hydrolysis and subsequent thermal treat-

[1]To whom correspondence should be addressed.

Can. J. Chem. Downloaded from www.nrcresearchpress.com by 195.138.81.100 on 09/07/12
For personal use only.

Can. J. Chem. Downloaded from www.nrcresearchpress.com by 195.138.81.100 on 09/07/12
For personal use only.

ment of tin alkoxide compounds yield high purity tin(IV) oxide powder (8), but there is little solid-state or solution structural data available on which to base mechanistic studies for homoleptic tin(IV) alkoxide compounds. Furthermore, there are no satisfactory spectroscopic criteria developed for the unambiguous assignment of solution structures of these species. On the other hand, homoleptic tin(II) alkoxide compounds have received much more attention, and a number of examples have been characterized in the solid state by single crystal X-ray diffraction (9). We have recently structurally characterized a homoleptic thallium(I)–tin(IV) alkoxide compound, which is polymeric in the solid state, but monomeric in benzene solution (10).

The work described here, concerning the characterization of simple homoleptic tin(IV) alkoxide compounds, is the first step in a systematic investigation of their solid-state and solution structures, the mechanistic aspects of condensation and characterization of the kinetic products of thermal and hydrolytic decomposition (11). Here we report the solid-state and solution structures of $Sn(O—t\text{-}Bu)_4$ and $[Sn(O—i\text{-}Pr)_4 \cdot HO—i\text{-}Pr]_2$.

Experimental section

All manipulations were carried out under an atmosphere of dinitrogen that had been dried and deoxygenated by passage through finely divided MnO and molecular sieves (12). All aromatic and hydrocarbon solvents used were distilled from sodium benzophenone ketyl and stored under nitrogen over 4 Å molecular sieves. Alcohols were purchased from Aldrich Chemical Co. and were dried by distillation from magnesium turnings under dinitrogen and stored over 4 Å molecular sieves (13). Infrared spectra were recorded on a Perkin-Elmer Model 1620 spectrometer, and NMR data were recorded on Bruker AC-250 spectrometer. NMR solvents were degassed with dry dinitrogen and stored over 4 Å molecular sieves. ^1H NMR spectra were referenced to the protio impurity in the deuterated solvents, and ^{13}C NMR spectra were referenced to the ^{13}C NMR resonance of the deuterated solvent. ^{119}Sn NMR spectra were referenced to the protio impurity in the deuterated solvents, and ^{13}C NMR spectra were referenced externally to $SnMe_4$ (= 0 ppm, $\Delta\nu_{1/2}$ = 1 Hz) and are quoted using the downfield positive sign convention. Molecular weights were determined cryoscopically by the freezing point depression of benzene.

I. Synthesis of Sn(O—t-Bu)$_4$

$Sn(O—t\text{-}Bu)_4$ was prepared by a modified method of Chandler *et al.* (14) as follows. To a three-necked, round-bottomed, one-litre flask fitted with a dinitrogen inlet, reflux condensor, pressure-equalized addition funnel, and magnetic stir bar was added 250 mL of *n*-pentane and 30.2 g (0.5 mol) of $SnCl_4$. The solution was cooled to 0°C, and 90 mL of Et_2NH dissolved in 40 mL of *n*-pentane was added dropwise over a period of 2 h. An exothermic reaction ensued with the formation of a white precipitate. A further 120 mL of Et_2NH in 100 mL of *n*-pentane was added, after which the solution was stirred at room temperature for 4 h. The mixture was then cooled to 0°C, the addition funnel charged with four 50 mL portions of *t*-BuOH (an excess), and each portion was added over 10 min. When the addition was complete, the ice bath was removed, the addition funnel replaced by a mechanical stirrer, and the mixture stirred for 14 h at room temperature. The stirrer was stopped and the mixture allowed to stand for 2 h and was then filtered. The remaining white solid was transferred to a Sohxlet extractor and extracted with 300 mL of *n*-pentane. All the *n*-pentane washings were combined to give a pale yellow solution from which the volatile components were removed *in vacuo* (10^{-2} Torr) to give a pale yellow solid. The solid was pumped *in vacuo* for two more hours to ensure removal of excess *t*-BuOH at the expense of losing some of the final product. The pale yellow solid was then sublimed at 10^{-2} Torr and 40°C onto a cold finger maintained at −78°C to give 168.9 g (0.41 mol) of large white crystals, a yield of 82.2% based on $SnCl_4$. Melting point 40.2–42.0°C (uncorrected). ^1H NMR data (C_6D_6, 20°C, 250 MHz): 1.57 ppm (s), $OC(CH_3)_3$; $^{13}C\{^1H\}$ NMR data (C_6D_6, 10°C, 62.9 MHz): 74.6 ppm (s), $^2J_{Sn—C}$ = 45 Hz, $OC(CH_3)_3$; 33.7 ppm (s) $^3J_{Sn—C}$ = 27 Hz, $OC(CH_3)_3$: ^{13}C NMR data (^1H coupled): 74.6 ppm (m), $^2J_{C—H}$ = 4 Hz, $OC(CH_3)_3$; 33.7 ppm, septet × quartet, $^1J_{C—H}$ = 125 Hz, $^3J_{C—H}$ = 4 Hz, $OC(CH_3)_3$: ^{119}Sn NMR data (C_6D_6, 20°C, 93.27 MHz): —371.4 ppm (s). Infrared data (KBr disc, cm^{-1}): 2976(m), 2914(m), 1468(m), 1393(s), 1362(s), 1246(s), 1183(s), 1031(m), 937(s, br), 775(s), 605(s), 462(s).

II. Synthesis of Sn(O—t-Bu-d$_9$)$_4$

$Sn(O—t\text{-}Bu\text{-}d_9)_4$ was prepared by a method analogous to that described for $Sn(O—t\text{-}Bu)_4$ above. The quantities of the reagents employed were as follows: $SnCl_4$, 1.75 mL (3.90 g, 0.015 mol); Et_2NH, 10 mL (an excess); DO—*t*-Bu-d_9, 6.44 g; *n*-pentane, 205 mL total. The final mixture obtained was filtered and extracted with three 50 mL portions of *n*-pentane. The *n*-pentane washings were combined and the volatile components removed *in vacuo*. The white solid obtained was sublimed to give 5.363 g of $Sn(O—t\text{-}Bu\text{-}d_9)_4$ (0.012 mol), a yield of 80%. ^{13}C NMR data (C_6D_6, 20°C, 62.9 MHz): 74.13 ppm (s), $^2J_{Sn—C}$ = 45 Hz, $OC(CD_3)_3$; 32.6 ppm, septet, approximately 1:3:6:7:6:3:1, $J_{C—D}$ = 19 Hz, $OC(CD_3)_3$. Infrared data (KBr disc, cm^{-1}): 2227(m), 2128(w), 2053(w), 1222(m), 1135(s), 1076(m), 1052(s), 873(s), 821(w), 737(w), 686(m), 568(s).

III. Single crystal X-ray diffraction study of Sn(O—t-Bu)$_4$

General operating procedures of the Indiana University Molecular Structure Center have previously been reported (15). A summary of the crystal data is given in Table 1.

A suitable crystal was selected and transferred to a goniostat by using standard inert atmosphere techniques and cooled to −155°C. A systematic search of a limited hemisphere of reciprocal space revealed a set of diffraction maxima that could be indexed to the space group $C2/c$. Subsequent solution and refinement confirmed this choice. Data were collected using a continuous θ–2θ scan with fixed backgrounds.

The structure was solved by a combination of direct methods (MULTAN) and Fourier techniques and refined by full-matrix least squares. All hydrogen atoms were clearly visible in a difference Fourier map phased on the non-hydrogen parameters. All hydrogen atoms were refined isotropically and all non-hydrogen atoms anisotropically. No absorption correction was performed. A final difference Fourier map contained four peaks of 0.5–07 e/Å^3 located within 1.1 Å of the Sn atom. All other peaks were less than 0.3 e/Å^3.

Fractional coordinates and isotropic thermal parameters are given in Table 2, atomic coordinates in Table 3, and atomic distances and angles are given in Tables 4 and 5, respectively. Figure 1 shows a view of the molecule that emphasizes the approximate tetrahedral coordination environment of the central tin atom.

IV. Synthesis of [Sn(O—i-Pr)$_4$·HO—i-Pr]

$Sn(O—t\text{-}Bu)_4$ (2.00 g; 4.9 mmol) was dissolved in 30 mL of THF and cooled to 0°. An excess of isopropanol (5.6 mL, 73 mmol) was added and the solution warmed to room temperature. After stirring for 1 h, the volatile components were removed *in vacuo*. The residue was taken up in the minimum amount of diethyl ether and cooled to −30°C for 12 h. During this time, clear colourless crystals formed and were filtered at 0°C. A total of 2.02 g of crude solid was recovered: a yield of 99.2%. In addition 1.25 g of crystalline material that analyzed as $[Sn(O—i\text{-}Pr)_4 \cdot HO—i\text{-}Pr]$ was recovered, a crystalline yield of 62.5%.

^1H NMR data (toluene-d_8; 250.13 MHz): 40°C, 7.25 ppm (br), 1H, O*H*; 4.66 ppm, septet, 5H $J_{n—n}$ = 6 Hz, OC*H*Me$_2$; 1.40 ppm (d), 30H, OCH*Me*$_2$: 25°C, 7.85 ppm (b), 1H, O*H*; 4.67 ppm (m, s), OCHMe$_2$; 1.45 ppm (d), 6 Hz, 30 H, OCH*Me*$_2$; 0°C, 8.54 ppm (b), 1H, O*H*; 4.60 ppm (b, m), 5H OC*H*Me$_2$; 4.68 ppm (b), ~1H, OC*H*Me$_2$; 4.47 ppm (b), ~3H, OC*H*Me$_2$; 1.74 ppm (b), ~6H, OCH*Me*$_2$; 1.43 ppm (b), ~24H, OCH*Me*$_2$: −50°C, 8.75 ppm (b), 1H, O*H*; 5.52 ppm (b), 1H, OC*H*Me$_2$; 4.72 ppm (b), 1H, OC*H*Me$_2$; 4.45 ppm (b), 3H, OC*H*Me$_2$; 1.76 ppm (d), 6 Hz, 6H, OCH*Me*$_2$; 1.49 ppm (d), 6 Hz, OCH*Me*$_2$; 1.42 ppm (b), OCH*Me*$_2$: −60°C, 8.88 ppm (t), 4.5 Hz, 1H, O*H*; 5.55 ppm (b), 1H, OC*H*Me$_2$; 4.72 ppm (b), 1H, OC*H*Me$_2$; 1.78

Can. J. Chem. Downloaded from www.nrcresearchpress.com by 195.138.81.100 on 09/07/12
For personal use only.

TABLE 1. Summary of crystal data for $Sn(O—t\text{-}Bu)_4$, **1**, and $[Sn(O—i\text{-}Pr)_4 \cdot HO—i\text{-}Pr]_2$, **2**

Parameter	Value	
	1	**2**
Empirical formula	$SnC_{16}H_{36}O_4$	$C_{30}H_{72}O_{10}Sn_2$
Colour of crystal	Colourless	Colourless
Crystal dimensions (mm)	0.25 × 0.25 × 0.25	0.30 × 0.31 (conical)
Space group	$C2/c$	$P2_1/n$
Cell dimensions		
Temperature (°C)	−155	25
a (Å)	17.382(6)	11.808(3)
b (Å)	8.742(2)	14.356(3)
c (Å)	15.518(5)	12.380(2)
β (deg)	116.44(1)	95.27(2)
Z (molecules/cell)	4	2
Volume (Å)^3	2111.41	2089.9(7)
Calculated density (g/cm^3)	1.293	1.319
Wavelength (Å)	0.71069	0.71073
Molecular weight	411.15	830.25
Two-θ range (deg)	6–45	4–52
Total number of reflections	1592	4482
Number with $F_o > X\sigma(F_o)$	1332 (X = 2.33)	2672 (X = 3.0)
$R(F)$	0.0247	0.0485
$R_w(F)$	0.0266	0.0556
Goodness-of-fit for last cycle	1.055	1.722
Maximum Δ/σ for last cycle	0.35	0.48

TABLE 2. Fractional coordinates and isotropic thermal parameters for $Sn(O—t\text{-}Bu)_4$[a]

Atom	x	y	z	B_{iso}
SN(1)	10000*	2203.3(4)	7500*	15
O(2)	11005(1)	1008(3)	8324(2)	19
C(3)	11110(2)	208(4)	9186(2)	20
C(4)	10292(3)	−679(5)	8993(3)	27
C(5)	11323(3)	1360(5)	9993(3)	24
C(6)	11854(3)	−876(5)	9408(3)	28
O(7)	10344(1)	3387(3)	6665(2)	20
C(8)	11164(2)	4152(4)	6990(2)	21
C(9)	11394(3)	4956(5)	7938(3)	30
C(10)	11049(3)	5284(5)	6209(3)	30
C(11)	11849(3)	2981(5)	7100(4)	30

[a]Fractional coordinates are ×10^4 for non-hydrogen atoms and ×10^3 for hydrogen atoms. B_{iso} values are ×10. Isotropic values for these atoms refined anisotropically are calculated by using the formula given by Hamilton (24).

TABLE 3. Atomic coordinates (×10^4) and isotropic thermal parameters (Å^2×10^3)

Atom	x	y	z	U*
Sn	979.3(4)	5839.5(3)	5285.8(5)	62.9(2)
O(1)	−720(4)	5601(3)	4731(4)	53(2)
O(2)	1196(5)	5608(4)	3617(4)	72(2)
O(3)	2590(6)	5698(5)	5787(7)	120(4)
O(4)	835(7)	7171(5)	5153(9)	145(5)
O(5)	356(5)	5748(4)	6826(4)	80(2)
C(1)	−1528(9)	6329(8)	4405(9)	102(4)
C(2)	−2327(10)	6547(9)	5221(10)	135(6)
C(3)	−1740(11)	6447(10)	3277(10)	141(6)
C(4)	2002(8)	6075(7)	2982(8)	93(4)
C(5)	1427(15)	6541(16)	2105(13)	243(13)
C(6)	2769(11)	5389(11)	2548(15)	199(10)
C(7)	3433(9)	6200(10)	6209(13)	132(6)
C(8)	4268(15)	6489(17)	5603(18)	275(15)
C(9)	3980(14)	5735(12)	7226(18)	217(12)
C(10)	1079(12)	7966(9)	5213(17)	182(10)
C(11)	252(18)	8612(12)	5621(22)	285(17)
C(12)	1941(16)	8465(13)	4827(18)	245(13)
C(13)	667(8)	6283(7)	7755(7)	85(4)
C(14)	−297(14)	6892(12)	7993(16)	133(12)
C(15)	1018(16)	5679(10)	8673(11)	192(10)

*Equivalent isotropic U defined as one third of the trace of the orthogonalized U_{ij} tensor.

ppm (d), 6 Hz, 6H, OCHMe_2; 1.50 ppm (d), 6 Hz, ~6H, OCHMe_2; 1.42 ppm (d), 5Hz, ~18H, OCHMe_2. No further changes to −100°C.

^{13}C NMR data (toluene-d_8, 62.9 MHz): +40°C, 67.9 ppm (s), OCHMe$_2$; 26.6 ppm (s), OCHMe_2: 25°C, identical; −10°C, ~67 ppm (v. br), OCHMe$_2$: 26.7 ppm (br), OCHMe_2: −20°C, 69.9 ppm, 68.3 ppm, 66.1 ppm (br), OCHMe$_2$; 27.4 ppm, 26.4 ppm, 24.4 ppm (br), OCHMe_2; −30°C, 69.9 ppm (s), 68.5 ppm. (s), 66.1 ppm (br), OCHMe$_2$; 27.4 ppm (br), 26.4 ppm (s), 24.5 ppm (s), OCHMe_2: −40°C, 69.9 ppm (s), 68.5 ppm (s), 66.5 ppm (br), 65.6 ppm (br), OCHMe$_2$; 28.0 ppm (br), 27.3 ppm (br), 26.4 ppm (s), 24.5 ppm (s), OCHMe_2. The low solubility of $[Sn(O—i\text{-}Pr)_4 \cdot HO—i\text{-}Pr]$ in toluene below these temperatures precluded further ^{13}C NMR experiments at lower temperatures.

^{119}Sn NMR data (toluene-d_8, 93.3 MHz): +30°C, −648.9 ppm (br): −40°C, −648.2 ppm (s), $^2J_{^{119}Sn—^{117}Sn}$ = 317 Hz, satellite intensity = ~7%. Infrared data (KBr disc, cm^{-1}): 2964.1 (s), 2930.6 (s), 1466.2 (m), 1384.1 (m), 1374.0 (s), 1359.9 (m), 1164.5 (m), 1123.5 (s), 986.7 (s), 925.9 (m), 839.6 (m), 811.5 (m), 608.8 (m), 593.1 (m), 536.1 (w). *Anal.* calcd. for $C_{15}H_{36}O_5Sn$: C 43.40, H 8.74; found: C 43.22, H 8.85.

The molecular weight was measured at two different concentrations: 0.019 and 0.039 M. The values obtained were 649 ±(45) and 697 ±(27) Daltons, respectively. Calculated value for $[Sn(O—i\text{-}Pr)_4 \cdot HO—i\text{-}Pr]_2$ = 830 Daltons. Each value was determined by two measurements.

Can. J. Chem. Downloaded from www.nrcresearchpress.com by 195.138.81.100 on 09/07/12
For personal use only.

TABLE 4. Bond distances for $Sn(O—t\text{-}Bu)_4$

Atom A	Atom B	Distance (Å)
Sn(1)	O(2)	1.946(2)
Sn(1)	O(7)	1.949(2)
O(2)	C(3)	1.447(4)
O(7)	C(8)	1.447(4)
C(3)	C(4)	1.527(5)
C(3)	C(5)	1.519(5)
C(3)	C(6)	1.514(5)
C(8)	C(9)	1.514(5)
C(8)	C(10)	1.507(5)
C(8)	C(11)	1.521(6)

TABLE 5. Bond angles for $Sn(O—t\text{-}Bu)_4$

Atom A	Atom B	Atom C	Angle (deg)
O(2)	Sn(1)	O(2)′	115.06(15)
O(2)	Sn(1)	O(7)	105.70(10)
O(2)	Sn(1)	O(7)′	107.44(10)
O(2)	Sn(1)	O(7)	105.70(10)
O(7)	Sn(1)	O(7)′	115.83(16)
Sn(1)	O(2)	C(3)	125.03(19)
Sn(1)	O(7)	C(8)	124.09(20)
O(2)	C(3)	C(4)	109.9(3)
O(2)	C(3)	C(5)	109.0(3)
O(2)	C(3)	C(6)	104.9(3)
C(4)	C(3)	C(5)	111.2(3)
C(4)	C(3)	C(6)	110.6(3)
C(5)	C(3)	C(6)	110.9(3)
O(7)	C(8)	C(9)	110.3(3)
O(7)	C(8)	C(10)	105.5(3)
O(7)	C(8)	C(11)	109.2(3)
C(9)	C(8)	C(10)	111.1(4)
C(9)	C(8)	C(11)	110.3(3)
C(10)	C(8)	C(11)	110.4(3)

V. Single crystal X-ray diffraction study of [Sn(O—i-Pr)$_4$·HO—i-Pr]$_2$

Crystallographic data are given in Table 1. Crystals of [Sn(O—*i*-Pr)$_4$·HO—*i*-Pr]$_2$ were grown from diethyl ether solution −30°C, and a conically shaped specimen was mounted in a capillary tube. Photographic and diffraction data revealed $2/m$ Laue symmetry, and systematic absences indicated the space group $P2_1/n$. Unit-cell parameters were obtained from the angular settings of 25 reflections ($20° \leq 2\theta \leq 30°$). The data were empirically corrected for absorption.

A Patterson map was used to locate the unique Sn atom, and the structure was completed by difference Fourier synthesis. The crystallographic asymmetric group consists of one half of the dimer formula; the central Sn_2O_2 rhombus is located on a site of $\bar{1}$ symmetry. All non-hydrogen atoms were refined with anisotropic thermal parameters, and all hydrogen atoms were included as idealized, riding isotropic contributions (d(CH) = 0.96 Å).

All software and sources of scattering factors are contained in the SHELXTL (5.1) library (G. Sheldrick, Nicolet xRD, Madison, WI). Atomic coordinates are provided in Table 3 and selected bond distances and angles in Table 6.

Results and discussion

The title compounds were prepared by modifications of the literature methods (14, 16). Since $Sn(O—t\text{-}Bu)_4$ is a good source of other tin alkoxide compounds, its synthesis is described here in detail. As with alcoholysis of metal amides, precautions must be taken during *trans*-alcoholysis experiments to ensure that the starting-material substituents are completely removed. This generally involves thermal treatment, a dynamic inert atmosphere purge, or the addition of a large excess of alcohol.

TABLE 6. Selected bond distances and angles for [Sn(O—*i*-Pr)$_4$·HO—*i*-Pr]$_2$

(*a*) Bond distances (Å)

Bond	Distance	Bond	Distance
Sn—O(1)	2.080(4)	Sn—O(4)	1.923(7)
Sn—O(1a)	2.091(4)	Sn—O(5)	2.142(6)
Sn—O(2)	2.098(6)	Sn...Sn(a)	3.361(1)
Sn—O(3)	1.964(7)		

(*b*) Bond angles (deg)

Bonds	Angle	Bonds	Angle
O(1)—Sn—O(1a)	72.6(2)	O(3)—Sn—O(4)	101.7(3)
O(1)—Sn—O(2)	82.5(2)	O(3)—Sn—O(5)	95.4(3)
O(1)—Sn—O(3)	164.5(2)	O(4)—Sn—O(5)	95.0(4)
O(1)—Sn—O(4)	93.8(3)	O(2)—Sn—O(1a)	83.1(2)
O(1)—Sn—O(5)	82.7(2)	O(3)—Sn—O(1a)	91.9(2)
O(2)—Sn—O(3)	96.0(3)	O(4)—Sn—O(1a)	166.3(3)
O(2)—Sn—O(4)	96.3(4)	O(5)—Sn—O(1a)	82.6(2)
O(2)—Sn—O(5)	161.9(2)	Sn—O(1)—Sn(a)	107.4(2)

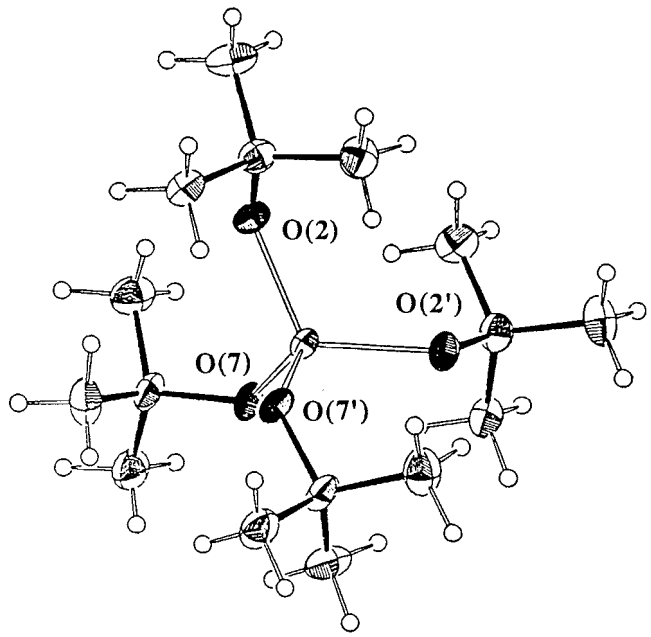


FIG. 1. Molecular structure $Sn(O—t\text{-}Bu)_4$.

(a) Solid-state structure Sn(O—t-Bu)$_4$

$Sn(O—t\text{-}Bu)_4$ is monomeric in the solid state and possesses a distorted tetrahedral coordination environment about the tin atom, as shown in Fig. 1. This probably results from the steric demands of the tertiary butoxide ligands. While the O(2)—Sn—O(2) and O(7)—Sn—O(7′) angles are enlarged, the other O—Sn—O angles are reduced compared to the tetrahedral angle. The Sn—O bond distances are shorter than the sum of their covalent radii and are comparable to the terminal Sn—O—*i*-Pr bond lengths in [Sn(O—*i*-Pr)$_4$·HO—*i*-Pr]. The only other structurally characterized homoleptic tin alkoxide compounds with terminal Sn—OR bonds are the tin(II) dimer $[Sn(O—t\text{-}Bu)_2]_2$

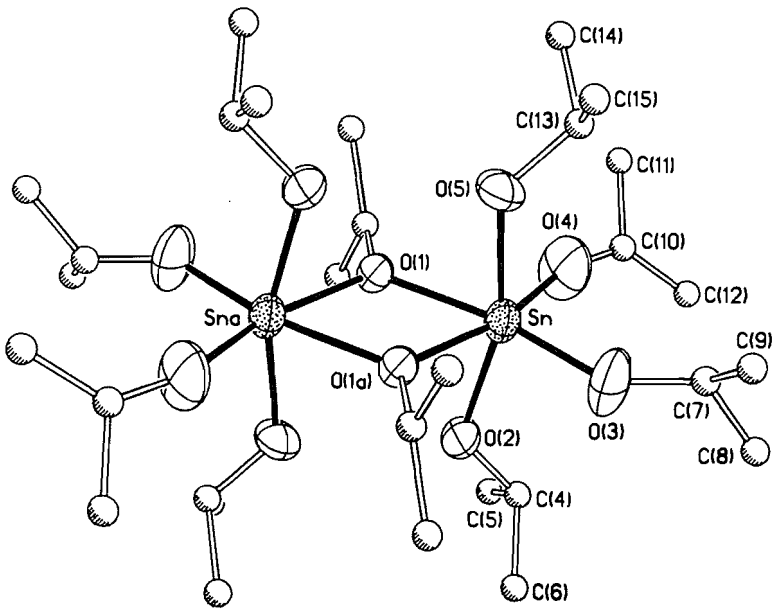


FIG. 2. Molecular structure of [Sn(O—*i*-Pr)$_4$·HO—*i*-Pr]$_2$. High thermal activity in the —*i*-Pr carbon atoms required their depiction with arbitrary-radius spheres.

where Sn—O = 1.97(2) Å (17) and [Sn(O—*i*-Pr)$_3$(acac)]$_2$ where Sn—O = 1.974(3) and 1.957(7) Å (14). The angles at O(2) and O(7) are 125.0(2) and 124.1(2)°, respectively, in the region expected for an alkoxide ligand not involved in π-donation to the metal centre. Other bond lengths and angles within the tertiary butoxide ligands are normal.

*(b) Solution characterization of Sn(O—*t*-Bu)$_4$*

It has previously been demonstrated that Sn(O—*t*-Bu)$_4$ is monomeric in benzene solution (16*a*, 18). This is consistent with its high solubility in hydrocarbon solvents. Since this species contains terminal alkoxide ligands only, the solution spectroscopic data were examined carefully to explore whether or not a spectroscopic criterion could be set for unambiguously identifying terminal tin — tertiary butoxide bonds in solution. For example, using solution NMR spectroscopy, it should be possible to examine coupling constants to the NMR active isotopes of tin (^{119}Sn, 8.58% natural abundance, I = 1/2 and ^{117}Sn, 7.61% natural abundance, I = 1/2) (19) as a means of distinguishing terminal and bridging alkoxide ligands. While no $^4J_{^{119}Sn—O—C—C—^1H}$ is observed in the ^{1}H NMR spectrum of Sn(O—*t*-Bu)$_4$, we have measured $^2J_{^{119}Sn—O—^{13}C}$ = 45 Hz and $^3J_{^{119}Sn—O—C—^{13}C}$ = 27 Hz for the *terminal* tertiary butoxide ligands. This can be compared to the values of $^2J_{^{119}Sn—O—^{13}C}$ = 28 Hz and $^3J_{^{119}Sn—O—C—^{13}C}$ = 29 Hz obtained for $Tl_2Sn(OEt)_6$ where it was demonstrated that the ethoxide ligands were doubly bridging in solution (10). $^2J_{^{119}Sn—O—^{13}C}$ is expected to decrease in the following order: terminal alkoxide > μ^2-alkoxide > μ^3-alkoxide, as a result of the increasing Sn—O bond lengths and therefore decreasing *s*-character in the bonds).

We have also examined the solid state IR spectra of Sn(O—*t*-Bu)$_4$ and its deuterated analogue, Sn(O—*t*-Bu-d_9)$_4$, in some detail in order to unambiguously assign the position of the ν(Sn—O) terminal stretching frequency. In a number of studies, the position of ν(M—O) has been tentatively assigned (20), although there are little data concerning ν(Sn—O) stretches in homoleptic tin alkoxide compounds. Several workers (21) have tentatively assigned a band near 500 cm^{-1} to the ν(Sn—O) stretch in alkyl tin alkoxide compounds. The ν(Sn—C) symmetric and asymmetric stretches, however, occur in a region similar to ν(Sn—O), and there is some evidence for the coupling of these vibrations. Mazdiyasni and co-workers (22) examined the IR spectra of B, Al, Y, Ti, Zr, Hf, and Th isoproxide compounds and Ti, Zr, Hf, and Th tertiary-butoxide compounds, but did not venture to assign ν(M—O). The characteristic IR absorption frequencies of the tertiary butoxy group have been assigned by Ory (23). From a comparison of these data with those published for Ti(O—*t*-Bu)$_4$, it appears that the ν(Sn—O) terminal stretch in Sn(O—*t*-Bu)$_4$ occurs at 605 cm^{-1}. To confirm this value, the perdeuterated analogue, Sn(O—*t*-Bu-d_9)$_4$, was prepared. Using a simplified "diatomic molecule" approach, the ν(Sn—O) stretching frequency in Sn(O—*t*-Bu-d_9)$_4$ was calculated to be ~580 cm^{-1} by treating the labelled and unlabelled tertiary butoxide groups as point masses (82 and 73 mass units, respectively). This assumption has previously yielded satisfactory results in analogous ^{18}O labelling experiments (ref. 18, p. 119). The most notable differences in the IR spectra of the labelled and unlabelled compounds are the positions of ν(C—O) and ν(Sn—O) assigned to the two intense bands at 937 cm^{-1} and 605 cm^{-1} in Sn(O—*t*-Bu)$_4$, respectively. Two new intense bands for Sn(O—*t*-Bu-d_9)$_4$ appear at 873 cm^{-1} and 568 cm^{-1} that we assign to ν(C—O*) and ν(Sn—O*), respectively where O* = O—*t*-Bu-d_9). Both bands are observed at lower energy than predicted, but are in the range expected, based on this crude model. An empirical term can be defined as Δν(Sn—O—*t*-Bu): the difference observed between ν(Sn—O—*t*-Bu) and ν(Sn—O—*t*-Bu-d_9) stretching frequencies. From these data, Δν(Sn—O—*t*-Bu) = 37 cm^{-1}.

*(c) Solid-state structure of [Sn(O—*i*-Pr)$_4$·HO—*i*-Pr]$_2$*

This compound is dimeric in the solid state (see Fig. 2) and possesses a structure similar to that proposed by Bradley *et al.* (25), that has recently been confirmed by Caulton and co-workers for zirconium and cerium analogues (26). The molecular architecture of [Sn(O—*i*-Pr)$_4$·HO—*i*-Pr]$_2$ can be described as distorted edge-shared, bi-octahedral containing two doubly bridging isopropoxide ligands, with four terminal alkoxide ligands (two bonded to each tin) in the same plane and four other

Can. J. Chem. Downloaded from www.nrcresearchpress.com by 195.138.81.100 on 09/07/12
For personal use only.

Can. J. Chem. Downloaded from www.nrcresearchpress.com by 195.138.81.100 on 09/07/12
For personal use only.

ligands perpendicular to this plane (two on each metal) that are involved in hydrogen bonding. The molecule has a crystallographically imposed inversion centre. In the $(RO)_2Sn(\mu\text{-}OR)_2Sn(OR)_2$ plane, the terminal Sn—O distances (1.964(7) and 1.923(7) Å) are comparable to those observed in Sn(O—*t*-Bu)$_4$ (1.956(2) and 1.949(2) Å), while the Sn—(μ-OR) distances (2.080(4) and 2.091(4) Å) are significantly longer, but analogous to those of $[Tl_2Sn(OEt)_6]_\infty$ (2.02(3) and 2.05(4) Å) (10). Interestingly, the angles at the oxygen atoms of the terminal isopropoxide ligands in this plane are enlarged 139(8)° for O(3) and 160(9)° for O(4)), but not to the same extent as in the Zr analogue. In the zirconium analogue, this has been ascribed to O→Zr π-donation, and we note that in tin, the most obtuse Sn—O—C angle is associated with the shortest Sn—O bond. The bridging isopropoxide ligands are approximately planar, the sum of the angles about oxygen being 359.9°.

Perpendicular to the $(RO)_2Sn(\mu\text{—}OR)_2Sn(OR)_2$ plane, there are two isopropoxide ligands and two coordinated isopropanol ligands that are involved in hydrogen bonding. This results in a significant deviation from octahedral coordination about tin. The hydrogen bonding interaction in the solid state is evidenced by (*i*) the relatively long Sn—O(5) bond distances of 2.142(6) Å, (*ii*) the acute Sn—Sn—O(2) and Sn—Sn—O(5) angles of 81.1(2) and 80.9(2)°, respectively, (*iii*) the relative orientation of both organic fragments. These data are consistent with a markedly asymmetric hydrogen bond between O(2) and O(5), although the hydrogen atom was not located in the final difference map. The metrical parameters of the ligands containing O(5) and O(5a) are consistent with a coordinated alcohol; whereas the ligands containing O(2) and O(2a) (Sn—O(2) = 2.098(6) Å) are clearly deprotonated. Analogous features were recently observed in the solid state structures of [Zr(O—*i*-Pr)$_4$·HO—*i*-Pr]$_2$ and [Ce(O—*i*-Pr)$_4$·HO—*i*-Pr]$_2$ (26).

*(d) Solution characterization of [Sn(O—*i*-Pr)$_4$·HO—*i*-Pr]*

At room temperature, benzene-d_6 and toluene-d_8 solutions of [Sn(O—*i*-Pr)$_4$·HO—*i*-Pr] exhibit only one time-averaged type of alkoxide ligand, as determined by ^{1}H and ^{13}C NMR spectroscopy. The presence of one equivalent of alcohol and four alkoxides is established by integration of the hydroxylic proton at 7.85 ppm versus the methine and methyl resonances. The resonances are slightly broadened at room temperature, but are sharp at +40°C. The other noteworthy feature of these spectra is the absence of *any* coupling to ^{119}Sn or ^{117}Sn in either the ^{13}C or the ^{1}H NMR spectra. This is consistent with an exchange process involving cleavage of the Sn—O bonds. Cryoscopic molecular weight determintion indicates the [Sn(O—*i*-Pr)$_4$·HO—*i*-Pr] exhibits a molecular weight slightly less than that of a dimer in benzene solution at approximately 5°C.

Upon cooling toluene-d_8 solutions of [Sn(O—*i*-Pr)$_4$·HO—*i*-Pr], the ^{1}H NMR methine and methyl resonances broaden and coalesce until, at −50°C, three types of alkoxide ligands are observed in a 1:1:3 ratio, as shown in Fig. 3. The hydroxylic proton moves downfield to a chemical shift of 8.8 ppm and is observed as a triplet at −60°C. The coupling constant of 4.5 Hz is consistent with values of $^3J_{HOCH}$ observed in alcohols (27) and is consistent with facile, reversible proton exchange between coordinated alcohol and alkoxide ligands on the ^{1}H NMR timescale at this temperature. The ratio of these resonances seemed inconsistent with the solid-state structure adopted by [Sn(O—*i*-Pr)$_4$·HO—*i*-Pr]$_2$, so 2D ^{1}H NMR chemical shift-correlated experiments were performed at different temperatures.[2] While this *apparently* demonstrated that none of the chemically distinct methine protons were associated with diastereotopic isopropoxide ligands, it was not possible to distinguish accidental degeneracy of methyl groups by using this experiment.

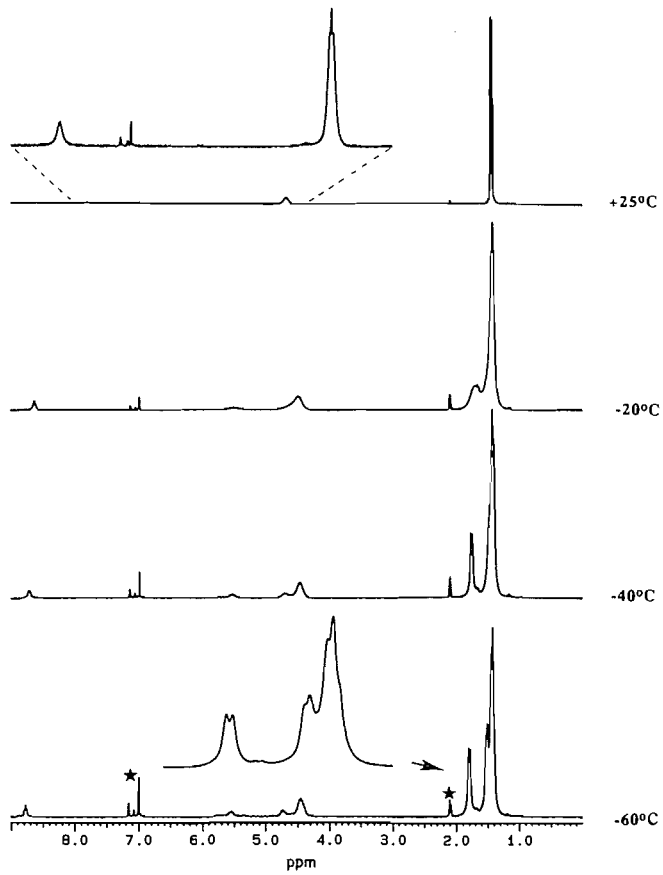


FIG. 3. Variable temperature ^{1}H NMR spectra of [Sn(O—*i*-Pr)$_4$·HO—*i*-Pr]$_2$ in toluene-d_8; * marks the protio impurity of the solvent.

To gain further insight, variable temperature ^{13}C NMR spectra were measured and are shown in Fig. 4. As the solution was cooled to −20°C, three types of O—*i*-Pr resonances were observed in a 1:2:2 ratio. Upon further cooling to −40°C, one of the resonances of relative intensity two broadened and began to coalesce into two different resonances of equal intensity. Unfortunately, the low solubility of this compound in toluene-d_8 below −40°C precluded further ^{13}C measurements. In the ^{119}Sn NMR sectrum at −40°C, a single type of tin environment was observed at −648.2 ppm (upfield of $SnMe_4$) with one set of ^{117}Sn satellites. The intensity and coupling constant (317.2 Hz) was consistent with the values expected for two-bond ^{119}Sn—^{117}Sn coupling constants (28) and established the dimeric nature of this compound at −40°C. Whether or not the ^{13}C NMR resonances of [Sn(O—*i*-Pr)$_4$·HO—*i*-Pr]$_2$ of relative intensity two are chemically equivalent or accidentally isochronous is not clear. The ^{13}C NMR data recorded at −20°C appear consistent with approximate D_{2h} symmetry shown below and can be assigned the following ratios: **A**:**B**:**C** = 1:2:2.

[2]A complete set of material may be purchased from the Depository of Unpublished Data, CISTI, National Research Council of Canada, Ottawa, Ont., Canada K1A 0S2.

Can. J. Chem. Downloaded from www.nrcresearchpress.com by 195.138.81.100 on 09/07/12
For personal use only.

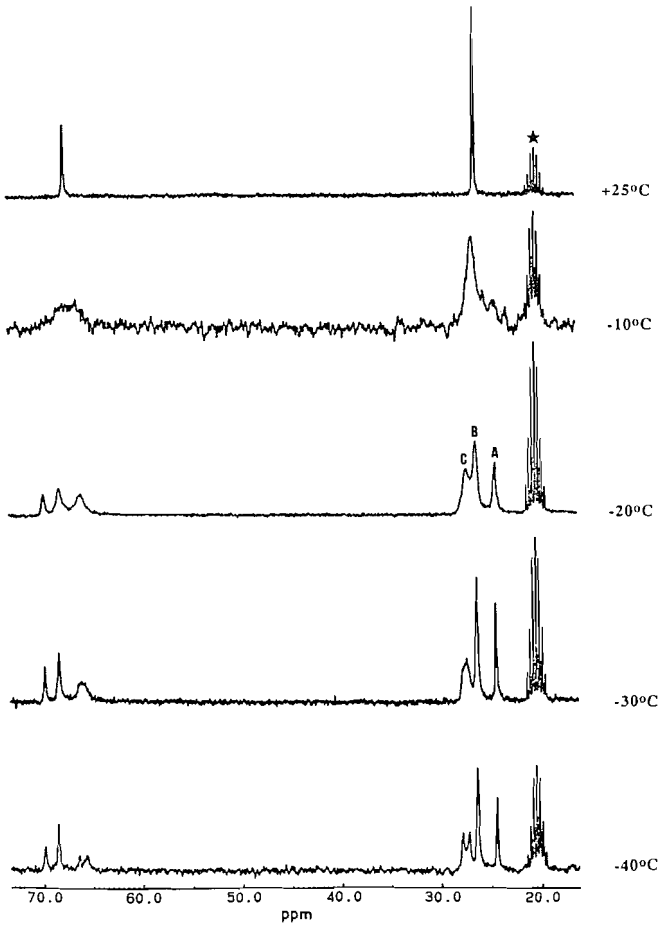
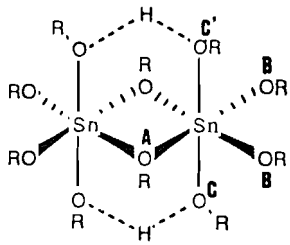
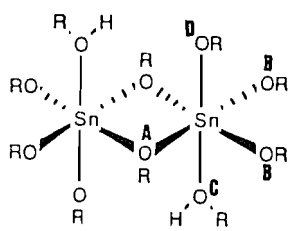


FIG. 4. Variable temperature. ^{13}C NMR spectra of [Sn(O—*i*-Pr)$_4$·HO—*i*-Pr]$_2$ in toluene-d_8; * marks the ^{13}C NMR resonance of the solvent.



All of the isopropoxide ligands should be diastereotopic as a result of fast proton exchange between **C** and **C′**. As the solution is cooled further, the resonance of relative intensity two splits into two resonances. These data are consistent with a solution structure in which the molecule has average C_{2h} symmetry, as shown below.



The resonances previously attributed to rapidly exhanging **C** and **C′** should now be split into two of equal intensity. The methyl groups of isopropoxide ligands **B** should be diastereotopic, but may be isochronous. This interpretation assumes that proton exchange between **C** and **D′** (or **C′** and **D**) is slow compared to the ^{13}C NMR timescale. The activation barrier calculated for this process, based on the coalescence of **C** to **C′** and **D**, is 11.9 ±0.5 kcal mol^{-1}. Since the low-temperature limiting spectrum cannot be recorded, however, the frequency difference ($\delta\nu$) may be larger than that measured at −40°C, so $\Delta G^{\ddagger} < 11.9$ kcal mol^{-1}.[3]

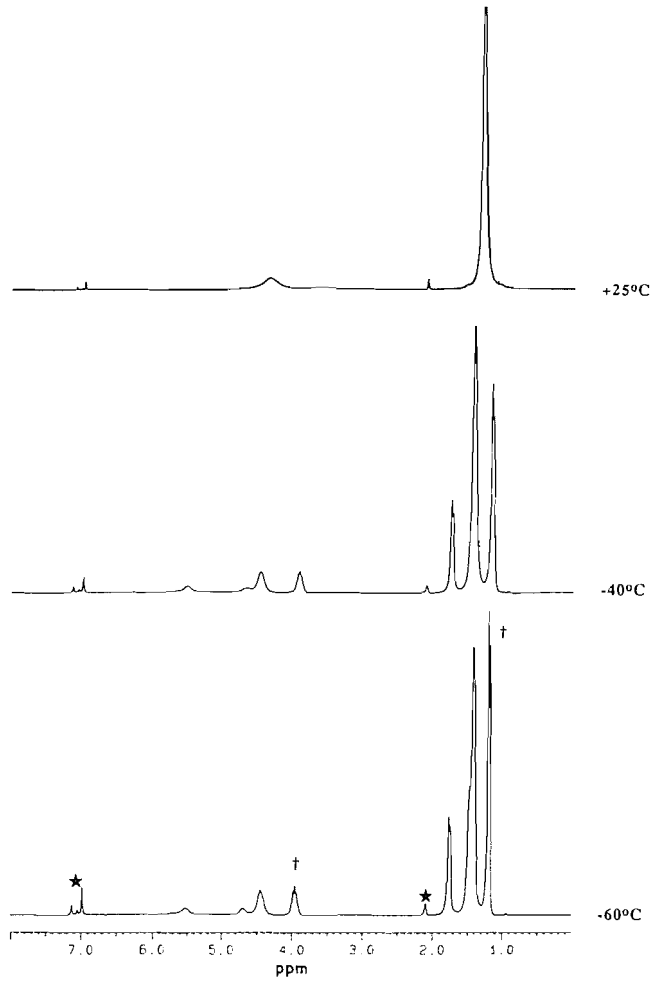
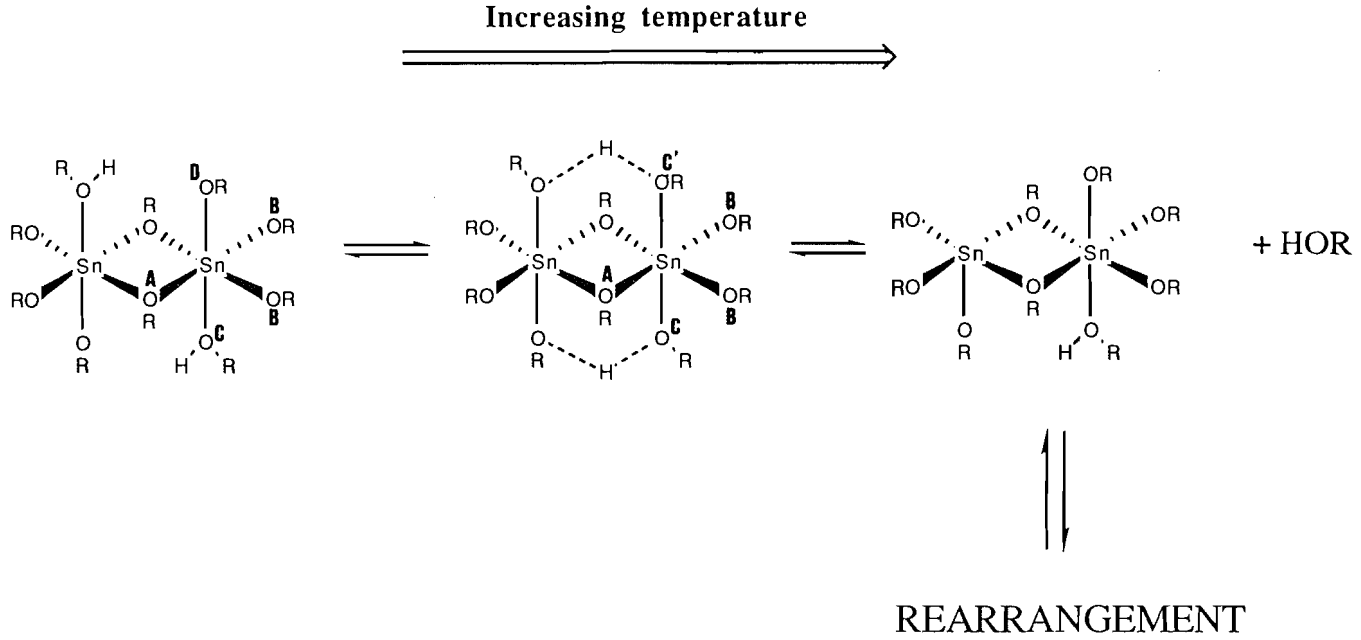


FIG. 5. Variable temperature ^1H NMR spectra of [Sn(O—*i*-Pr)$_4$·HO—*i*-Pr]$_2$ in toluene-d_8 to which three equivalents of HO—*i*-Pr have been added; * marks the protio impurity of the solvent; † marks the resonances due to HO—*i*-Pr.

As noted above, at −60°C, the hydroxylic proton was observed as a triplet in the ^1H NMR spectrum (Fig. 3), presumably due to rapid intramolecular exchange at this temperature on the ^1H NMR timescale. Since the intramolecular proton transfer is a degenerate process, only the $^3J_{H—O—C—H}$ coupling constant should be averaged when the coalescence temperature is reached for this process. The coalescence temperature calculated for the hydroxylic proton in the ^1H NMR spectrum based on $\Delta G^{\ddagger} < 11.9$ kcal mol^{-1} derived from the ^{13}C NMR data is ≤ ~−60°C. The interpretation of the ^{13}C NMR spectra is therefore consistent with the ^1H NMR data. The variable temperature ^1H NMR data can be explained if it is assumed that the methyl

[3]For example of $\delta\nu = 80$ Hz (same coalescence temperature) $\Delta G^{\ddagger} = 11.6$ kcal mol^{-1}.



SCHEME 1. Dynamic solution behaviour of [Sn(O—*i*-Pr)$_4$·HO—*i*-Pr]$_2$

and methine resonances of relative intensity three are due to two superimposed types of isopropoxide ligands of relative intensities two and one. There is some evidence for this, as shown by expansion of the methyl region at −60°C (See Fig. 3).

We therefore propose the following mechanism to account for the observed exchange pheonomena in this system. (*i*) At room temperature, facile intermolecular isopropanol exchange occurs from dimeric [Sn(O—*i*-Pr)$_4$·HO—*i*-Pr]$_2$ to give a coordinatively unsaturated tin centre capable of subsequent rapid intramolecular rearrangement. (*ii*) Upon cooling, the equilibirum of Scheme 1 is displaced to the left until the free alcohol is completely bound to form a dimeric species in which intramolecular proton transfer occurs rapidly between coordinated alcohol and axial alkoxide ligands bonded to adjacent tin centres. (*iii*) Upon further cooling, the proton transfer is slowed and [Sn(O—*i*-Pr)$_4$·HO—*i*-Pr]$_2$ is structurally analogous to the geometry observed in the solid state. These processes are illustrated in Scheme 1.

To test this hypothesis, free isopropanol (3 equiv.) was added to a toluene-d_8 solution of [Sn(O—*i*-Pr)$_4$·HO—*i*-Pr]$_2$, and variable temperature ^{1}H NMR spectra were recorded. At room temperature, only one type of O—*i*-Pr species was observed, but upon cooling to −60°C, resonances arising from [Sn(O—*i*-Pr)$_4$·HO—*i*-Pr]$_2$ were observed together with resonances due to the free added HO—*i*-Pr. These data are shown in Fig. 5 and are consistent with the proposed exchange mechanism involving rapid exchange between free and coordinated alcohol at room temperature, but no exchange at −60°C on the ^{1}H NMR timescale. These data are also consistent with the low value (slightly less than dimeric) of molecular complexity determined by cryoscopic molecular weight determination in benzene at ~+5°C.

Finally, we note that, in the solid state, the isoproxide infrared stretching frequencies of [Sn(O—*i*-Pr)$_4$·HO—*i*-Pr]$_2$ are consistent with data previously reported for metal isopropoxide compounds, and we assign the ν(Sn—O) stretches to bands at 609 and 583 cm^{-1}.

Acknowledgments

We thank the UNM/NSF Center for Micro-Engineered Ceramics for supporting this project, Eva Quesnell for typing this manuscript, and the NSF Chemical Instrumentation Program for the purchase of an NMR spectrometer. We thank Professor Ken Caulton for discussing his work prior to publication.

1. (*a*) D. C. BRADLEY. Chem. Rev. **89**, 1317 (1989); (*b*) L. G. HUBERT-PFALZGRAF. New J. Chem. **11**, 663 (1987); (*c*) R. C. MEHROTRA. *In* Better ceramics through chemistry III. Mat. Res. Soc., Symposium Proceedings, Vol. 81, 1988; (*d*) R. ROY. Science, **238**, 1664 (1987).
2. (*a*) W. G. KLEMPERER, V. V. MAINZ, S. D. RAMANURTHI, and F. S. ROSENBURG. *In* Better ceramics through chemistry III. *Edited by* C. J. Brinker, D. E. Clark, and D. R. Ulrich. North Holland. (1988); (*b*) R. E. RIMAN, D. M. HAALAND, C. J. M. NORTHRUP, H. K. BOWEN, and A. BLEIER. Mat. Res. Soc. Symp. Proc. Vol. **32**, 233 (1984); (*c*) J. FUKUSHIMA, K. KODAIRA, and T. MATUSHITA. Ceramic Bulletin **55**, 1064 (1976); (*d*) F. KIRBIR and H. KOMIYAMA. Chem. Lett. 791 (1988); (*e*) M. SHIOTA. J. Materials Sci. **23**, 1718 (1988); (*f*) D. C. BRADLEY and H. HOLLOWAY. Can. J. Chem. **40**, 1176 (1962); (*g*) A. ROUSSET, F. CHASSAGNEUX, and J. PARIS. J. Mat. Sci. **21**, 3111 (1986); (*h*) L. L. HENCH and D. R. ULRICH (*Editors*). Ultrastructure processing of ceramics, glasses and composites. John Wiley and Sons. 1984; (*i*) S. C. GOEL, K. S. KRAMER, P. C. GIBBONS, and W. E. BUHRO. Inorg. Chem. **28**, 3619 (1989); (*j*) M. A. MATCHETT, M. Y. CHIANG, and W. E. BUHRO. Inorg. Chem. **29**, 358 (1990).
3. P. M. JEFFRIES and G. S. GIROLAMI. Chem. Mat. **1**, 8 (1989).
4. D. C. BRADLEY and M. M. FAKTOR. J. Appl. Chem. **9**, 435 (1959); Trans. Faraday Soc. **55**, 2117 (1959).
5. M. J. HAMPDEN-SMITH, D. E. SMITH, and J. C. HUFFMAN. Spring ACS Meeting, Dallas 1989.
6. H. A. STECHER, A. SEN, and A. L. RHEINGOLD. Inorg. Chem. **28**, 3282 (1989).
7. Better ceramics through chemistry III. Mat. Res. Soc., Symposium Proceedings, Part III, IV, and V. 1988.
8. I. M. THOMAS. U.S. Patent 3,946,056. July 24, 1974.

Can. J. Chem. Downloaded from www.nrcresearchpress.com by 195.138.81.100 on 09/07/12
For personal use only.

9. M. VEITH and R. ROSLER. (*a*) Z. Naturforsch. **41***b*, 1017 (1986); (*b*) Angew. Chem. Int. Ed. Eng. **21**, 858 (1982).
10. M. J. HAMPDEN-SMITH, D. E. SMITH, and E. N. DUESLER. Inorg. Chem. **28**, 3399 (1982).
11. (*a*) T. A. WARK, E. A. GULLIVER, L. C. JONES, M. J. HAMPDEN-SMITH, A. L. RHEINGOLD, and J. C. HUFFMAN. *In* Better ceramics through chemistry IV. MRS Symposium Proceedings. To be published; (*b*) M. J. HAMPDEN-SMITH, D. S. WILLIAMS, and A. L. RHEINGOLD. Inorg. Chem. To be published.
12. D. F. SHRIVER and M. A. DREZDEN. The manipulation of air-sensitive compounds. 2nd ed. Wiley-Interscience. 1986. p. 78.
13. D. R. BURFIELD and R. H. SMITHERS. J. Org. Chem. **48**, 2420 (1983).
14. C. D. CHANDLER, G. D. FALLON, A. J. KOPLICH, and B. O. WEST. Aust. J. Chem. **40**, 1427 (1987).
15. M. H. CHISHOLM, K. FOLTING, J. C. HUFFMAN, and C. C. KIRKPATRICK. Inorg. Chem. **23**, 1021 (1984).
16. (*a*) D. C. BRADLEY, E. A. U. CALDWELL, and W. WARDLAW. J. Chem. Soc. A, 4775 (1957); (*b*) I. M. THOMAS. Can. J. Chem. **39**, 1386 (1961).
17. T. FJELDBERG, P. B. HITCHCOCK, M. F. LAPPERT, S. J. SMITH, and A. J. THRONE. J. Chem. Soc. Chem. Commun. 939 (1985).
18. J.-C. MARIE. Ann. Chim. 969 (1961).
19. R. K. HARRIS. Nuclear magnetic resonance spectroscopy. Pitman. 1983.
20. D. C. BRADLEY, R. C. MEHROTRA, and D. P. GAUR. Metal alkoxides. Academic Press, London. p. 116.
21. (*a*) D. P. GAW, G. SRIVASTAVA, and R. C. MEHROTRA. J. Organomet. Chem. **63**, 221 (1973); (*b*) R. C. POLLER. J. Inorg. Nucl. Chem. **24**, 593 (1962); (*c*) T. TANAKA. Organomet. Rev. **5**, 1 (1970).
22. C. T. LYNCH, K. S. MAZDIYASNI, J. S. SMITH, and W. J. CRAWFORD. Anal. Chem. **36**, 2332 (1964).
23. H. A. ORY. Anal. Chem. **32**, 509 (1960).
24. W. C. HAMILTON. Acta Crystallogr. **12**, 609 (1959).
25. D. C. BRADLEY, R. C. MEHROTRA, J. D. SWANWICH, and W. WARDLAW. J. Chem. Soc. 5020 (1952).
26. K. G. CAULTON. Private communication.
27. R. M. SILVERSTEIN, G. C. BASSLER, and T. C. MORRILL. Spectrometric identification of organic compounds. 4th ed. Wiley and Sons. 1981.
28. (*a*) T. P. LOCKHART. Inorg. Chem. **28**, 4265 (1989); (*b*) T. P. LOCKHARD, H. PUFF, W. SHUH, H. REUTER, and T. N. MITCHELL. J. Organomet. Chem. **366**, 61 (1989).

Can. J. Chem. Downloaded from www.nrcresearchpress.com by 195.138.81.100 on 09/07/12
For personal use only.

Cyclodextrin-based enzyme models. Part 1. Synthesis of a tosylate and an epoxide derived from heptakis(6-*O*-*tert*-butyldimethylsilyl)-β-cyclodextrin and their characterization using 2D NMR techniques. An improved route to cyclodextrins functionalized on the secondary face

MARKO J. PREGEL AND ERWIN BUNCEL
Department of Chemistry, Queen's University, Kingston, Ont., Canada K7L 3N6

Received April 2, 1990

MARKO J. PREGEL and ERWIN BUNCEL. Can. J. Chem. **69**, 130 (1991).

An improved route for the synthesis of cyclodextrin (CD)-based enzyme models having catalytic groups on the secondary face is presented. An epoxide derived from heptakis(6-*O*-*tert*-butyldimethylsilyl)-β-CD was prepared via intermediates that can be purified by conventional flash chromatography on a *preparative* scale. Reaction of β-cyclodextrin with *tert*-butyldimethylsilyl chloride in pyridine gave heptakis(6-*O*-*tert*-butyldimethylsilyl)-β-CD (**1**). Treatment of **1** with *N*-tosylimidazole and NaOMe in chloroform gave mono(2-*O*-tosyl) heptakis(6-*O*-*tert*-butyldimethylsilyl)-β-CD (**2**) in 22% yield. The latter was converted smoothly to mono(2^A, 3^A-anhydro) heptakis(6-*O*-*tert*-butyldimethylsilyl)-β-CD (**3**), in which one glucose subunit has been converted to a manno-epoxide, by treatment with KOEt in refluxing ethanol (87% yield). Compounds **1**, **2**, and **3** were characterized by a variety of one- and two-dimensional NMR techniques. These results open the door to attachment of catalytic groups to the cyclodextrin in a well-defined manner. Nucleophilic attack on the epoxide, followed by removal of the silyl groups, can be used to prepare a wide variety of enzyme model systems.

Key words: functionalized cyclodextrins, silylation, 2D NMR, enzyme models.

MARKO J. PREGEL et ERWIN BUNCEL. Can. J. Chem. **69**, 130 (1991).

On présente une méthode améliorée pour la synthèse de modèles basés sur la cyclodextrine (CD) possédant des groupements catalytiques sur la face secondaire. On a préparé un époxyde, à partir de l'heptakis(6-*O*-*tert*-butyldiméthylsilyl)-β-CD, par le biais d'intermédiaires qui peuvent être purifiés, sur une base *préparative*, par la chromatographie éclair conventionnelle. La réaction de la β-cyclodextrine avec le chlorure de *tert*-butyldiméthylsilyle dans la pyridine fournit l'heptakis(6-*O*-*tert*-butyldiméthylsilyl)-β-CD (**1**). Le traitement du produit **1** par du *N*-tosylimidazole et du NaOMe dans le chloroforme conduit au mono(2-*O*-tosyl)-heptakis(6-*O*-*tert*-butyldiméthylsilyl)-β-CD (**2**), avec un rendement de 22%. Ce produit a été facilement transformé en mono(2^A, 3^A-anhydro)heptakis((6-*O*-*tert*-butyldiméthylsilyl)-β-CD (**3**) duquel une unité de glucose a été transformée en manno-époxyde par un traitement avec du KOEt dans l'éthanol au reflux (rendement de 87%). Les composées **1**, **2** et **3** ont été caractérisés par une variété de techniques RMN en une et en deux dimensions. Ces résultats ouvrent la porte à l'attachement de groupements catalytiques dans des positions bien définies de la cyclodextrine. Une attaque nucléophile sur l'époxyde, suivie de l'enlèvement des groupements silyles, peut être utilisée pour préparer une grande variété de systèmes enzymatiques modèles.

Mots clés : cyclodextrines fonctionnalisées, silylation, RMN 2D, modèles d'enzymes.

[Traduit par la revue]

Introduction

Cyclodextrins (CDs) are of interest as enzyme models because they form inclusion complexes with hydrophobic guests in solutions of polar solvents (1–3). This is directly comparable to the formation of an enzyme–substrate complex and leads to saturation (Michaelis–Menten) kinetics, competitive inhibition, and selective rate accelerations in reactions involving cyclodextrins (2). Since cyclodextrins can be modified to attach catalytic groups, they have the two important attributes of enzymes: molecular recognition and multifunctional catalysis (3).

β-Cyclodextrin is a cyclic oligosaccharide made up of seven α-D-glucose subunits. As shown in Fig. 1, the secondary hydroxyl groups make up one face of the toroidal molecule. The secondary face of the cyclodextrin is of interest in making enzyme models because it is more open and is the preferential site for the binding of large molecules, including aromatic guests (4). However, in contrast to functionalization of the primary face of cyclodextrins, which has been extensively studied, the chemistry available for functionalization of the secondary face is less well developed. Preparative methods for secondary-functionalized cyclodextrins generally involve moderate yields and purification of synthetic intermediates by reverse-phase chromatography, which is scale-limited (5–8).

The synthesis of cyclodextrin-based enzyme model systems may be improved to allow for easier purification of intermediates, and consequently for synthesis on a larger scale, if a partially silylated cyclodextrin derivative is used as the framework for further modifications. Silylation of β-cyclodextrin primary hydroxyls should lead to a number of benefits. The resulting compound is expected to be much less polar than the parent cyclodextrin, making it soluble in organic solvents and allowing purification by chromatography on silica gel. The silyl groups are stable under ordinary conditions, but are easily removed when necessary (9–11). Thus, modification of silylated CDs would provide an improvement over previous approaches because the synthetic intermediates should be more easily purified, allowing work on a large scale.

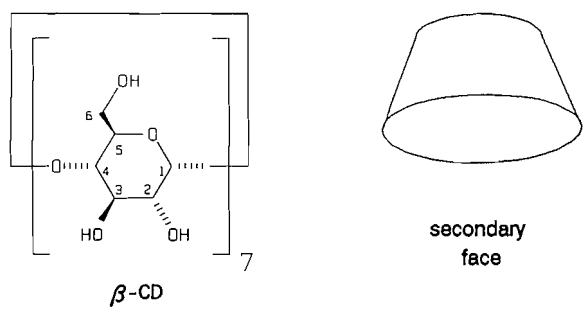


FIG. 1. β-Cyclodextrin and a representation of the shape of the molecule indicating the secondary face.

Can. J. Chem. Downloaded from www.nrcresearchpress.com by 195.138.81.100 on 09/07/12
For personal use only.

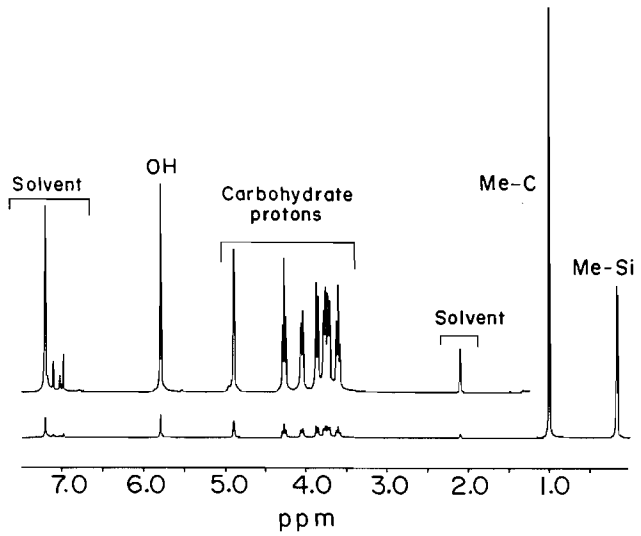


FIG. 2. ^{1}H NMR spectrum of **1** in deuterotoluene (3000–0 Hz). The carbohydrate region is expanded in Fig. 3.

The silylation of β-CD to produce heptakis(6-*O*-*tert*-butyldimethylsilyl)-β-CD (**1**) has been reported previously (12). Szejtli and co-workers originally reported the selective silylation of the primary hydroxyls of β-CD, using pyridine as a catalyst for the reaction of β-CD with *tert*-butyldimethylsilyl chloride; the silylated CD was isolated and characterized as the peracetate (12, 13). Treatment of the peracetate with Bu_4NF removed the silyl groups smoothly (12). Takeo *et al.* have recently prepared **1** in 70% yield by the reaction of β-CD with *t*-$BuMe_2SiCl$ in the presence of imidazole (14) and Fugedi has prepared **1** in 83% yield using pyridine as catalyst and solvent (15).

A number of compounds related to **1** have also been prepared, including heptakis(6-*O*-*tert*-butyldimethylsilyl)-α-CD (11, 16) and heptakis(6-*O*-*tert*-butyldimethylsilyl)-γ-CD (15), as well as 2,6-per(*tert*-butyldimethylsilyl)-α-CD (10, 16) and 2,6-per(*tert*-butyldimethylsilyl)-β-CD derivatives (17, 18).

The present work reports the synthesis and complete characterization of **1**, which is used as a precursor in the synthesis of two new compounds, a tosylate (**2**) and an epoxide (**3**). All three compounds are characterized with the aid of a variety of one- and two-dimensional (2D) NMR techniques. NMR studies of cyclodextrins, including the use of a variety of two-dimensional methods, have recently been reviewed (19). Two-dimensional methods are used because substituted cyclodextrins usually give complex, overlapped spectra. Spreading out overlapped signals into a second dimension often allows individual resonances to be resolved and assigned. This has been shown to be indispensable in the characterization of complex, unsymmetrically modified cyclodextrins (22). For example, Stoddart and co-workers have used COSY, *J*-resolved, and shift correlation experiments to assign the spectra of an unsymmetrical chemically modified CD, 2,6-per-*O*-methyl-3^A-*O*-methyl-β-CD (20).

Results and discussion

As part of our ongoing interest in the construction of cyclodextrin-based enzyme model systems, the use of a cyclodextrin that was soluble in nonpolar solvents as a framework for subsequent transformations appeared to offer a number of advantages. It was expected that such a CD and its derivatives could be easily purified by flash chromatography and this, in turn, would allow syntheses to be carried out on a larger scale than is presently possible. Large amounts of CD derivatives are desirable when multistep syntheses are undertaken and when the modified cyclodextrin is to undergo detailed kinetic studies.

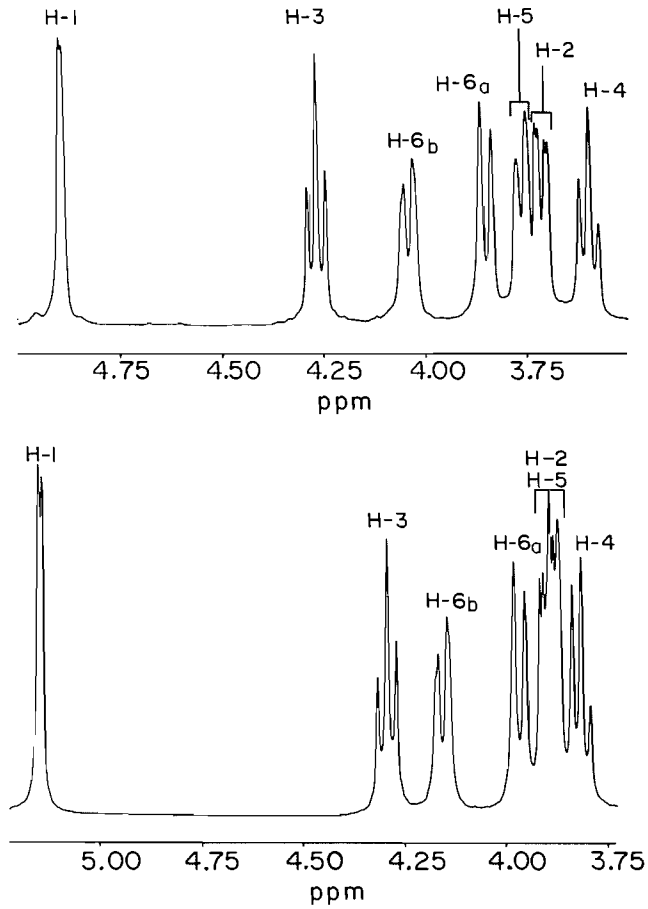


FIG. 3. ^{1}H NMR spectra of **1** in deuterotoluene (upper, 2000–1400 Hz) and deuterochloroform (lower, 2190–1590 Hz), showing resonances due to carbohydrate protons. The H-2 and H-5 resonances overlap in the spectrum recorded in $CDCl_3$.

Accordingly, a cyclodextrin silylated at its primary positions, **1**, was chosen as the starting point and was prepared as follows. Dry β-CD was allowed to react with 7.35 equivalents of *tert*-butyldimethylsilyl chloride in dry pyridine for 18 h at room temperature (eq. [1]). Heptakis(*tert*-butyldimethylsilyl)-β-CD (**1**) was isolated in 73% yield after flash chromatography. The preparative method was analogous to that reported by Fugedi (15). ^{13}C NMR data for **1** in $CDCl_3$ have been previously reported (14, 15), and the ^{13}C NMR data for the product of the present study compare well with the literature data. The ^{1}H, COSY, and ^{13}C–^{1}H shift correlation spectra for **1** have not been previously reported, and are presented below.

The complete ^{1}H NMR spectrum of **1** in deuterotoluene is shown in Fig. 2. The spectrum is remarkably simple because of the sevenfold symmetry of the compound. An expansion of the carbohydrate portion of the spectrum (Fig. 3) reveals distinct resonances for protons on carbons 1, 2, 3, 4, 5, and 6. The two protons on carbon 6, labelled H-6_a nd H-6_b, are nonequivalent (diastereotopic). In $CDCl_3$ solution, resonances assigned to protons on carbons 2 and 5 are overlapped (Fig. 3). Aromatic guests are known to deshield the H-3 and H-5 resonances of cyclodextrins (19), so the difference in spectra in the two

Can. J. Chem. Downloaded from www.nrcresearchpress.com by 195.138.81.100 on 09/07/12
For personal use only.

Can. J. Chem. Downloaded from www.nrcresearchpress.com by 195.138.81.100 on 09/07/12
For personal use only.

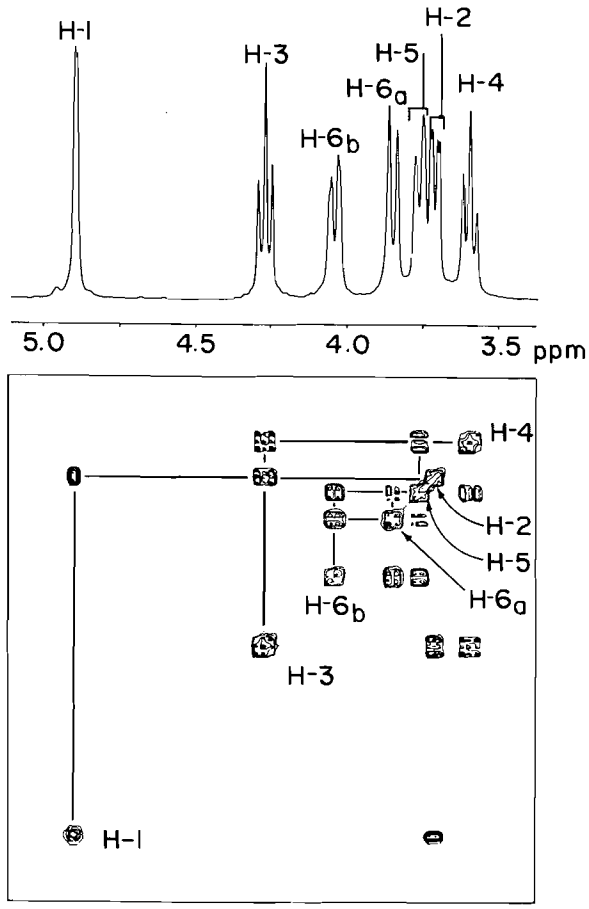


FIG. 4. Contour plot of the carbohydrate region of the COSY spectrum of **1** in deuterotoluene (2044–1349 Hz).

solvents can probably be ascribed to formation of an inclusion complex of deuterotoluene with the silylated CD.

The ^1H spectrum of **1** was assigned unambiguously by means of a COSY experiment, presented in Fig. 4. In this diagram, off-diagonal peaks connect coupled spins. Thus, as shown in Fig. 4, starting from the furthest downfield peak (H-1), all of the remaining resonances can be assigned.

The ^{13}C NMR spectrum of **1** was also recorded (Fig. 5). This is a *J*-modulated spectrum in which the carbon peaks are sorted according to the number of attached protons. Methyl and methine carbons point upwards; methylene and quaternary carbons point downwards. The peaks corresponding to the carbohydrate carbons were assigned by reference to the proton spectrum using a 2D ^{13}C–^1H shift correlation spectrum, presented in Fig. 6. This experiment yields responses that connect carbon peaks in one dimension to proton peaks in the other.

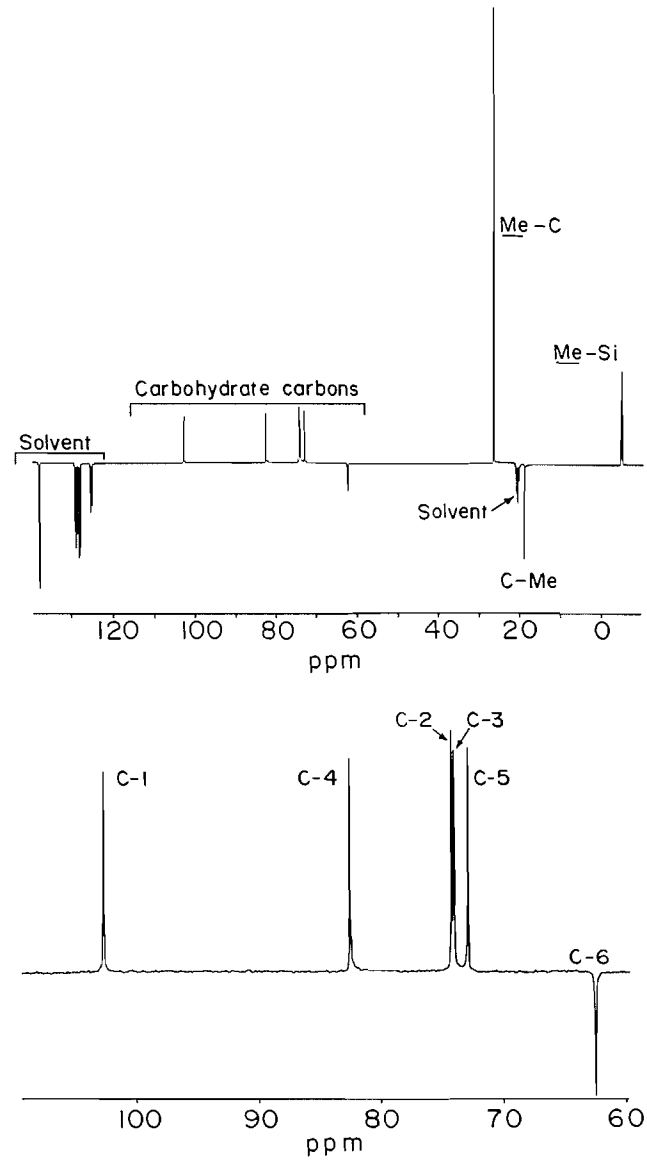
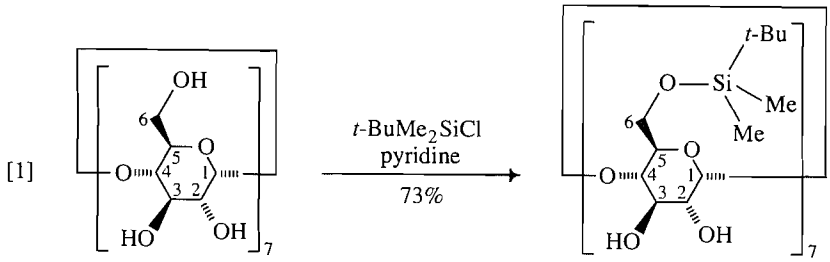


FIG. 5. *J*-Modulated ^{13}C NMR spectra of **1** in deuterotoluene (14 000 to −1000 Hz). The lower spectrum is an expansion showing resonances due to carbohydrate carbons (11 000–6000 Hz).

The title compound has two types of sites that can be modified further, the hydroxyl groups at C-2 and C-3 of each glucose unit. Ideally, tosylation of **1**, to produce **2**, would modify a single glucose subunit and would be specific for one type of hydroxyl on that subunit. In practice, one needs to check whether reaction has occurred at a C-2 hydroxyl, a C-3 hydroxyl, or both.



β-CD **1**

Can. J. Chem. Downloaded from www.nrcresearchpress.com by 195.138.81.100 on 09/07/12
For personal use only.

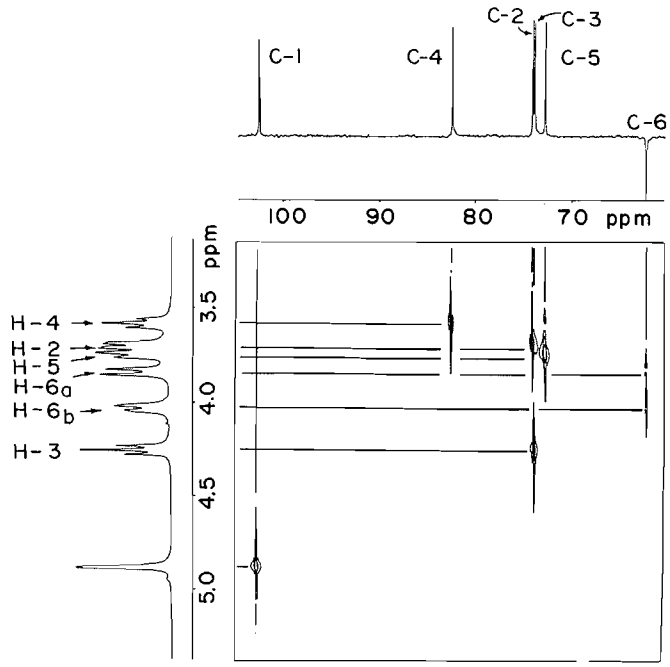


FIG. 6. Contour plot of the carbohydrate region of the $^{13}C-^{1}H$ shift correlation spectrum of **1** in deuterotoluene (^{1}H: 2151–1250 Hz, ^{13}C: 104.6–60.2 ppm).

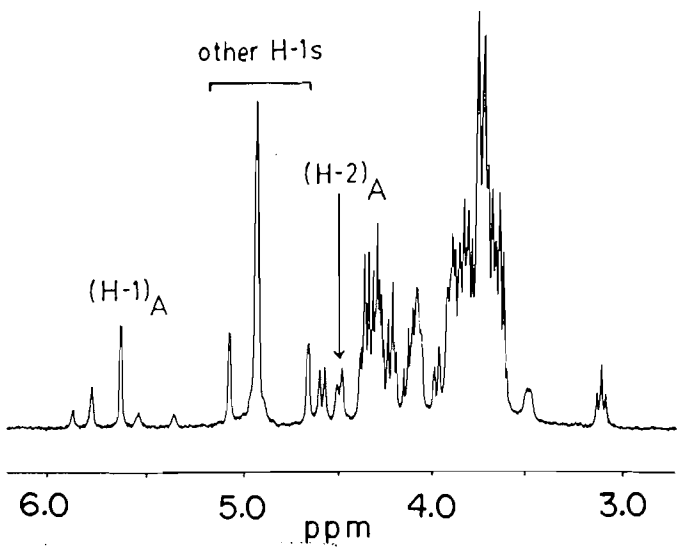


FIG. 7. The carbohydrate region of the ^{1}H NMR spectrum of **2** in deuterotoluene (2483–1092 Hz).

Reaction of **1** with *N*-tosylimidazole and sodium methoxide in chloroform gives **2** in 22% yield after flash chromatography (eq. [2]). This procedure has been shown to yield the C-2 tosylate in the reaction of 4,6-*O*-benzylidene-α-D-glucose (21).

The carbohydrate regions of the ^{1}H and ^{13}C NMR spectra are presented in Figs. 7 and 8, respectively. These spectra are complex and highly overlapped because modification of one of the seven subunits of the cyclodextrin destroys the symmetry of the molecule and all resonances are now nonequivalent.

In practice, resonances for the H-1's of the glucose units are easiest to analyze because they are well separated from other resonances. Three individual H-1 resonances are seen at 5.65, 5.07, and 4.63 ppm, as well as a larger (overlapped) group at

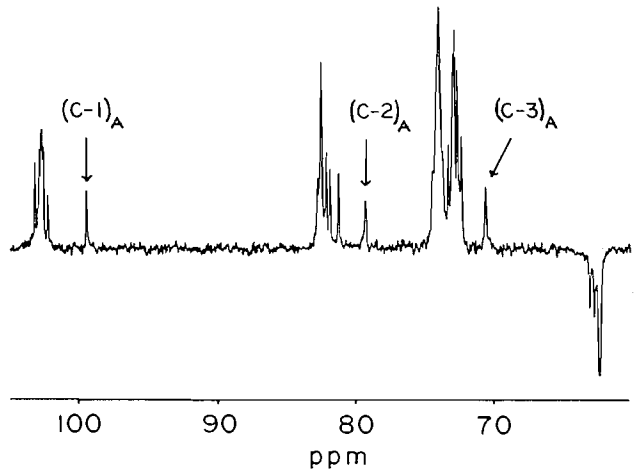


FIG. 8. The ^{13}C NMR spectrum of **2** in deuterotoluene (105.0–60.0 ppm).

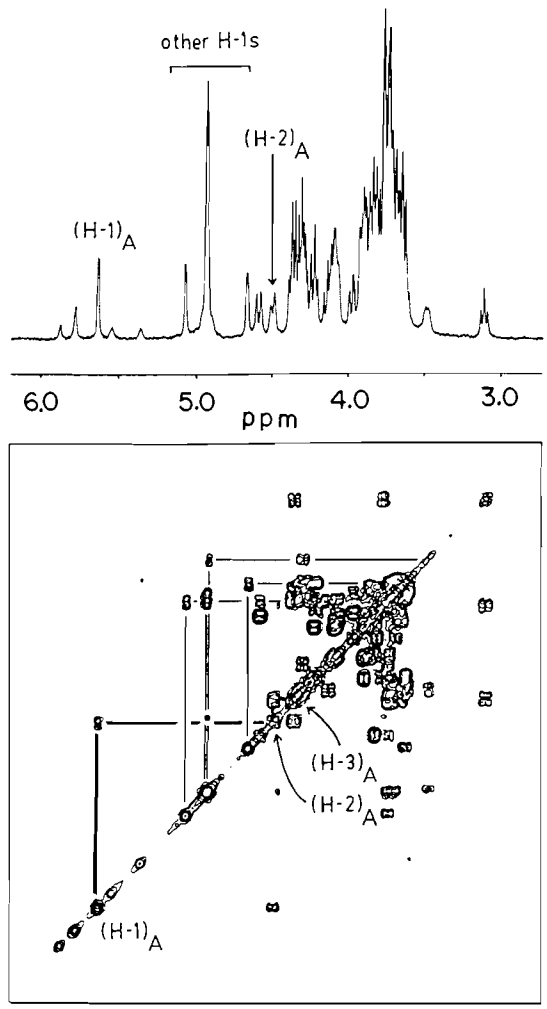


FIG. 9. Contour plot of the carbohydrate region of the COSY spectrum of **2** in deuterotoluene (2483–1092 Hz).

4.91 ppm. The lowest field H-1 signal is assigned to the subunit bearing the tosyl group (this subunit will be called subunit A and $(H\text{-}1)_A$ is labelled in Fig. 7). Examination of the COSY spectrum of **2**, presented in Fig. 9, shows that $(H\text{-}1)_A$ is coupled to an H-2 resonance at 4.50 ppm that is pulled downfield by ca. 0.8 ppm relative to H-2 resonances in parent silylated CD (**1**),

Can. J. Chem. Downloaded from www.nrcresearchpress.com by 195.138.81.100 on 09/07/12
For personal use only.

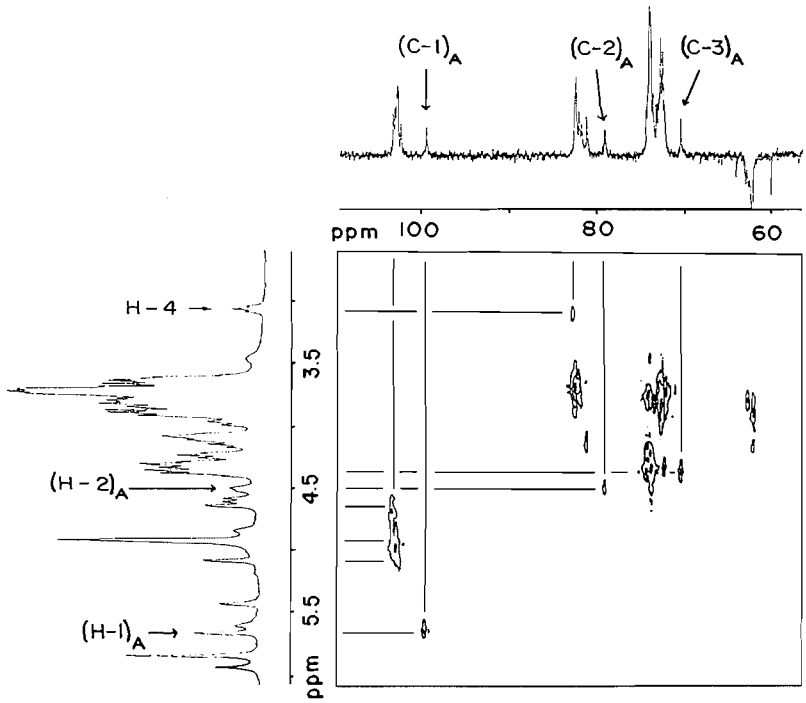


FIG. 10. Contour of the carbohydrate region of the $^{13}C-^{1}H$ shift correlation spectrum of **2** in deuterotoluene (^{1}H: 1047–2418 Hz, ^{13}C: 56.5–110.0 ppm).

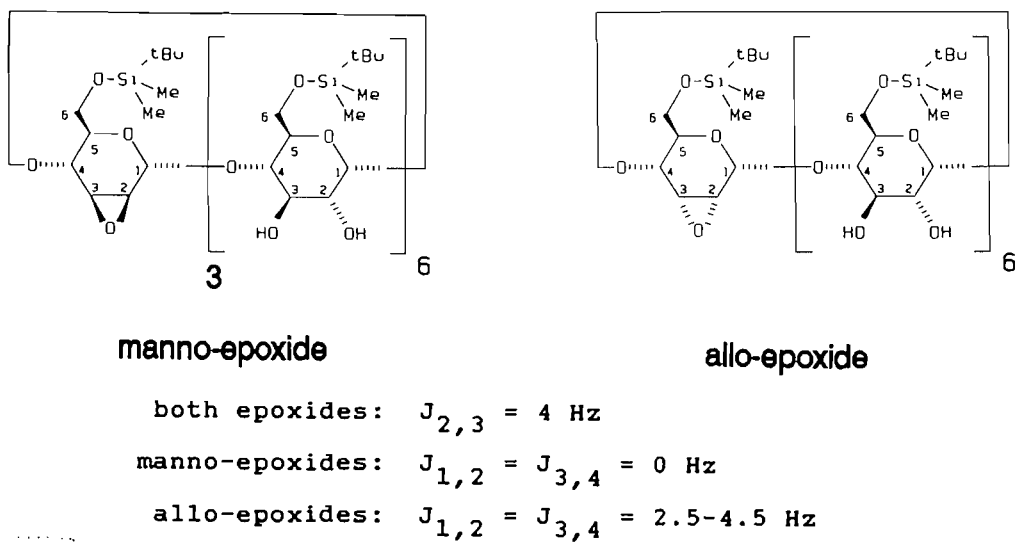
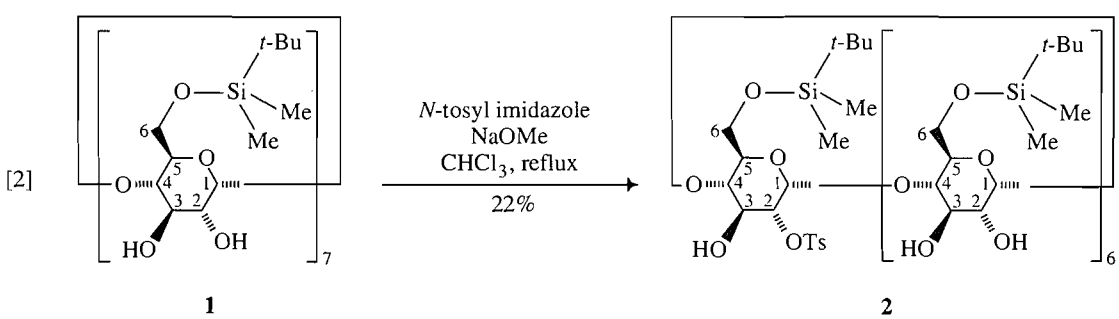


FIG. 11. Structural formulae and ^{1}H coupling constants for the allo- and manno-epoxides derived from **1**.



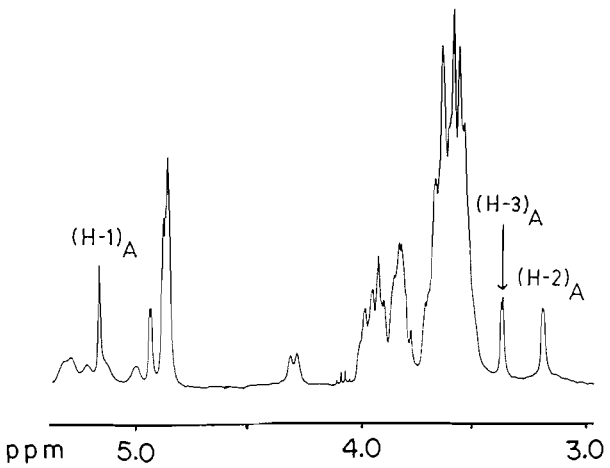


FIG. 12. The carbohydrate region of the ^{1}H NMR spectrum of **3** in deuterochloroform (2151–1185 Hz).

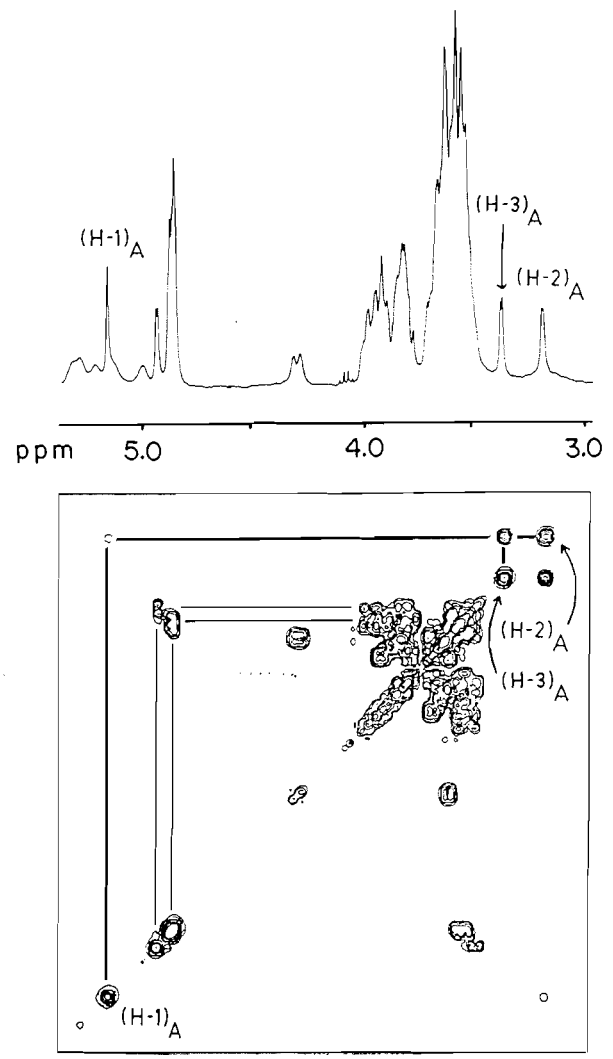


FIG. 13. Contour plot of the carbohydrate region of the COSY spectrum of **3** in deuterochloroform (2149–1192 Hz).

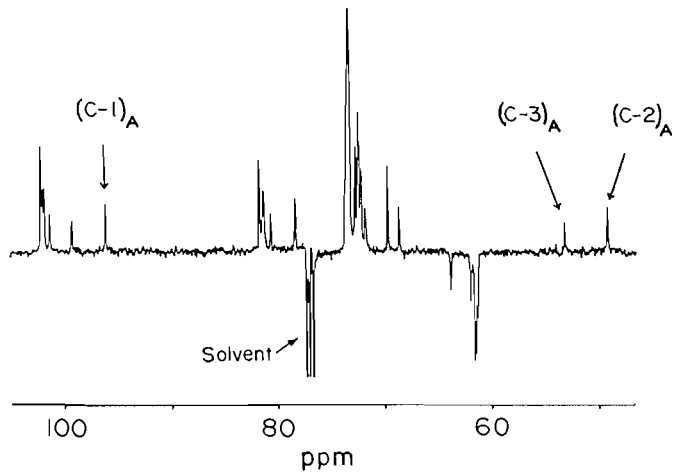


FIG. 14. The carbohydrate region of the *J*-modulated ^{13}C NMR spectrum of **3** in deuterochloroform (105.0–46.5 ppm).

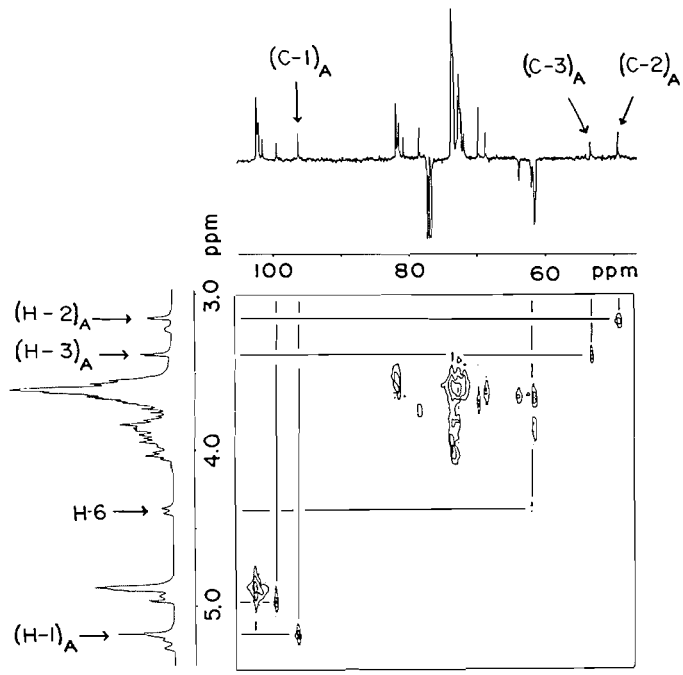
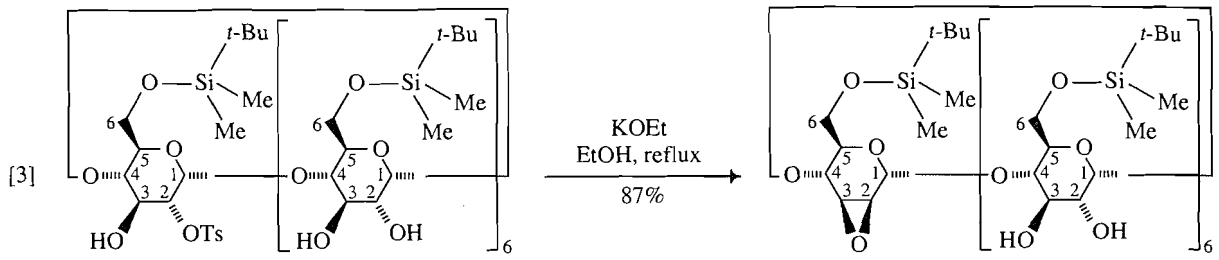


FIG. 15. Contour plot of the carbohydrate region of the ^{13}C–^{1}H shift correlation spectrum of **3** in deuterochloroform (^{1}H: 2151–1183 Hz, ^{13}C: 105.0–46.5 ppm).

which appear at 3.72 ppm. This is consistent with the electron-withdrawing effect of tosylation at C-2 of subunit A. All other H-1 resonances are coupled to H-2 resonances with chemical shifts similar to the H-2 resonances in **1**. The aromatic region shows only one set of ring protons and only one tosyl methyl group is observed. Examination of the ^{13}C spectrum of **2** also shows only one set of aromatic and methyl resonances for the tosyl group. Consequently, it appears that the reaction has produced the C-2 tosylate exclusively.

The ^{13}C–^{1}H shift correlation spectrum of **2** is presented in Fig. 10. It allows the assignment of $(C\text{-}1)_A$, $(C\text{-}2)_A$, and $(C\text{-}3)_A$ resonances from the known $(H\text{-}1)_A$, $(H\text{-}2)_A$, and $(H\text{-}3)_A$ resonances. $(C\text{-}1)_A$ and $(C\text{-}3)_A$ are shifted upfield from the C-1 and C-3 resonances of **1**, respectively, while $(C\text{-}2)_A$ is shifted

Can. J. Chem. Downloaded from www.nrcresearchpress.com by 195.138.81.100 on 09/07/12
For personal use only.



2 3

downfield from the C-2 resonances of **1**. This behavior is expected when a tosylate group is introduced at the C-2 position of **1**, and has been observed in comparisons of the spectra of β-CD and its C-2 tosylate (8).

The silylated CD epoxide **3** is prepared from the tosylate in good yield (87%) by treatment with 1 equivalent of KOEt in refluxing ethanol (eq. [3]).

Confirmation that a C-2 tosylate was produced above is possible from an examination of the spectra of the epoxide. A C-2 tosylate yields a manno-epoxide, while a C-3 tosylate yields an allo-epoxide, and ^{1}H coupling patterns are different in the two epoxides.

In both epoxides, one expects $J_{2,3}$ = 4 Hz. For manno-epoxides, weak coupling between hydrogens that are mutually *trans* results in $J_{1,2} = J_{3,4} = 0$ Hz. In contrast, $J_{1,2} = J_{3,4} =$ 2.5–4.5 Hz for allo-epoxides (22). Consequently, allo- and manno-epoxides are readily distinguished on the basis of the coupling patterns of their epoxide protons, as summarized in Fig. 11.

The H-2 and H-3 resonances of 2,3-anhydroaldopyranoses appear between 3.1 and 3.6 ppm in deuterochloroform solution (22). The carbohydrate region of the ^{1}H spectrum of epoxide **3** (Fig. 12) contains two *doublets* at 3.20 and 3.37 ppm, with coupling constants of 3.4 Hz. There is also one H-1 resonance at 5.19 ppm, which appears as a sharp *singlet*, i.e., coupling to H-2 has been lost. These observations and the absence of any other resonances in the epoxide region with more complex coupling patterns are consistent with a manno-epoxide structure and are parallel to observations for the manno-epoxide derived from unmodified β-CD (5).

The COSY spectrum of the epoxide (Fig. 13) confirms that the resonances assigned to $(H\text{-}2)_A$ and $(H\text{-}3)_A$ are mutually coupled and that $(H\text{-}2)_A$ is weakly coupled to $(H\text{-}1)_A$. Coupling of $(H\text{-}3)_A$ to $(H\text{-}4)_A$ was not detected.

The ^{13}C spectrum of the epoxide (Fig. 14) is also informative. The C-2 and C-3 resonances of 2,3-anhydro-4,6-*O*-benzylidene-α-D-allopyranose appear at 50.4 and 53.0 ppm, respectively, while those of the analogous manno-epoxide appear at 50.6 and 53.9 ppm, respectively (deuterobenzene solution) (23). The ^{13}C spectrum of **3** contains only two peaks in this region, at 49.1 and 53.1 ppm (deuterotoluene solution, spectrum not shown), confirming that the sample contains only one type of epoxide.

The ^{13}C–^{1}H shift correlation spectrum of **3** in $CDCl_3$ is shown in Fig. 15. The sharp downfield singlet at 5.19 ppm ($(H\text{-}1)_A$) correlates with a peak at 96.2 ppm in the ^{13}C spectrum, which is assigned to $(C\text{-}1)_A$. The upfield doublets assigned to $(H\text{-}2)_A$ and $(H\text{-}3)_A$ correlate with peaks at 49.1 and 53.1 ppm (the epoxide carbons, $(C\text{-}2)_A$ and $(C\text{-}3)_A$), as expected. The doublet at 4.30 ppm can now be assigned to an H-6 resonance because it correlates with a peak in the C-6 region of the ^{13}C spectrum.

Conclusions

The manno-epoxide derived from heptakis(6-*O*-*tert*-butyldimethylsilyl)-β-CD was prepared in three steps and 15% overall yield from β-cyclodextrin via intermediates that are easily purified. This allows reactions to be carried out on a larger scale than was previously possible. Synthetic intermediates were characterized by two-dimensional NMR methods and the stereochemistry of the final product was assigned. Attachment of catalytic groups to the cyclodextrin in a well-defined manner is now possible. Nucleophilic attack on the epoxide, followed by removal of the silyl groups, can be used in future work to prepare a wide variety of enzyme model systems.

Experimental

Methods and materials

NMR spectra were recorded on a Bruker AM 400 spectrometer (^{1}H: 400 MHz; ^{13}C: 100 MHz) in deuterotoluene or deuterochloroform solution. Chemical shifts are reported in parts per million downfield from TMS.

Representative parameters used to obtain the two-dimensional spectra were as follows: COSY: spectral width of 2500 Hz, centered at 6150 Hz, 256 experiments, each consiting of 8 scans stored in 1K of data, a recycle delay of 3 s. The transformed spectrum was symmetrized about the diagonal. Heteronuclear shift correlation: ^{1}H: spectral width of 2500 Hz, centered at 6150 Hz, ^{13}C: spectral width of 10 kHz, centered at 52 000 Hz, 256 experiments, each consisting of 48 scans stored in 1K of data, τ_1 = 3.5 ms, τ_2 = 2 ms.

Thin-layer chromatography (TLC) was performed using HP-TLC plates (Merck) coated with silica gel 60 in the following solvent system (A): ethyl acetate – ethanol–water 50:7:4 (v/v). Compounds were visualized by spraying the plates with a solution of 10% sulfuric acid containing 1% cerium sulfate and 1.5% molybdic acid, followed by heating.

Flash chromatography was performed using Kieselgel 60 (Merck, 230–400 mesh), following the procedure of Still *et al.* (24), using the following solvent systems: ethyl acetate – ethanol–water (B) 25:2:1, (C) 16:2:1, (D) 12:2:1, and (E) 50:2:1 (v/v).

Optical rotations were measured with a Perkin–Elmer 241 polarimeter using the sodium D line.

β-CD was dried overnight at 100°C under vacuum (<2 Torr; 1 Torr = 133.3 Pa). Pyridine was distilled from CaH_2 and stored over 3 Å molecular sieves.

Synthesis of 1

In a dry box, dried β-CD (3.72 g, 3.28 mmol) was weighed into a glass bulb fitted with a ground glass joint. The glass bulb was then attached to a three-neck round bottom flask equipped with a stirring bar and the flask was septum-sealed in the dry box. *tert*-Butyldimethylsilyl chloride (3.636 g, 24.1 mmol, 7.35 equiv.) was weighed into a septum-sealed vial.

Dry pyridine (35 mL) was added to the flask by syringe. The weighed CD was added to the stirred pyridine in small portions by inverting the glass bulb. Dry pyridine was also added to the vial containing the silyl chloride and the solution was then added to the CD solution dropwise by syringe. The reaction mixture was stirred overnight (18 h), then

Can. J. Chem. Downloaded from www.nrcresearchpress.com by 195.138.81.100 on 09/07/12
For personal use only.

poured into ice-cold water (350 mL) and stirred vigorously for 10 min.[1] The resulting precipitate was filtered off, washed with ice-cold water, and dissolved in ethyl acetate (70 mL). The solution was washed with 5% aqueous HCl solution (3 × 50 mL), saturated aqueous $NaHCO_3$ solution (50 mL), and saturated brine (50 mL). Finally, the solution was dried (anhydrous Na_2SO_4), filtered, concentrated, and traces of solvent were removed at 100°C under vacuum (<2 Torr) to give 5.69 g (90%) of crude product.

A portion of the crude product (0.423 g) was purified by flash chromatography using a gradient elution with solvents B, C, and D. Pure **1** (0.342 g) was obtained, resulting in an overall yield of 73%, mp 299–300°C (dec., from ethanol) (lit. (14) mp 299–302°C (dec., from ethanol); $[\alpha]_D^{22}$ +111° (*c* 1.04, $CHCl_3$) (lit. (14) $[\alpha]_D^{22}$ +113° (*c* 1.4, $CHCl_3$)); ^1H NMR (toluene-d_8) δ: 0.18 (s, Me-Si), 1.02 (s, Me-C), 3.61 (t, J = 9 Hz, H-4), 3.72 (dd, J = 3.2, 9.5 Hz, H-2), 3.78 (d, J = 9.5 Hz, H-5), 3.86 (d, J = 11 Hz, H-6_a), 4.05 (dd, J = 2.5, 11 Hz, H-6_b), 4.28 (t, J = 9 Hz, H-3), 4.91 (d, J = 3 Hz, H-1); ^{13}C NMR (toluene-d_8) δ: −1.9 (*Me*-Si), 18.4 (Me-*C*), 26.1 (*Me*-C), 62.4 (C-6), 73.0 (C-5), 74.0 (C-3), 74.3 (C-2), 82.6 (C-4), 102.7 (C-1); ($CDCl_3$) δ: −5.2, −5.1 (*Me*-Si), 18.3 (Me-*C*), 25.9 (*Me*-C), 61.6 (C-6), 72.5 (C-5), 73.4 (C-3), 73.6 (C-2), 81.8 (C-4), 102.0 (C-1). Anal. calcd. for $(C_{12}H_{24}O_5Si)_7$: C 52.15, H 8.75; found: C 51.54, H 8.52.

Synthesis of **2**

Compound **1** (0.392 g, 0.203 mmol) and *N*-tosylimidazole (prepared according to ref. 21, 0.067 g, 0.303 mmol) were dissolved in chloroform (2.5 mL), then sodium methoxide (0.162 g, 0.300 mmol) was added and the mixture refluxed for 6 h. Chloroform (6 mL) was added and the reaction mixture was washed with water (10 mL), then dried (anhydrous Na_2SO_4). The crude product was purified by flash chromatography (solvent E), giving pure **2** (0.083 g, 22% yield), mp 199–200°C (dec., from ethanol); $[\alpha]_D^{19}$ +102° (*c* 0.83, $CHCl_3$); ^1H NMR (toluene-d_8) δ: 0.10–0.27 (Me-Si), 0.88–1.12 (Me-C), 2.15 (s, tosyl Me), 3.07 (t, H-4), 3.45 (H-2), 3.61–3.47 (heavily overlapped), 4.50 (d, (H-2)$_A$), 4.59 (d), 4.63 (s, H-1), 4.91 (H-1s), 5.07 (s, H-1), 5.65 (s, (H-1)$_A$), 8.18 (d, tosyl aromatic, other aromatic doublet obscured by solvent); ^{13}C NMR (toluene-d_8) δ: −4.9, −4.6 (Me-Si), 18.3 (*C*-Me), 21.3 (tosyl Me), 26.1 (*Me*-C), 62.3, 62.7, 63.0 (C-6s), 70.5 ((C-3)$_A$), 72.3, 72.6, 72.8, 73.3 (C-2s, C-3s), 74.0 ((C-2)$_A$), 79.2, 81.2, 81.8, 82.1, 82.5, 82.7 (C-4s), 99.5 ((C-1)$_A$), 102.3, 102.6, 102.7, 102.9, 103.2 (C-1s). Anal. calcd. for $C_{91}H_{174}O_{37}Si_7S$: C 52.32, H 8.40; found: C 51.79, H 8.18.

Synthesis of **3**

Following the procedure of Hough *et al.* (25), **2** (0.104 g, 4.96 × 10^{-5} mol) and potassium ethoxide (45 μL of a 1.132 M solution of KOEt in ethanol, 5.09 × 10^{-5} mol, 1.0 equiv.) were added to ethanol (1.2 mL). The solution was refluxed for 70 min, at which point TLC showed a single band. Ice water (10 mL) was added to the reaction mixture and the resultant precipitate was filtered off, washed with cold water, and dried under high vacuum to yield pure **3** (0.083 g, 87% yield), mp 259–260°C (from ethanol); $[\alpha]_D^{19}$ +99.3° (*c* 0.88, $CHCl_3$); ^1H NMR ($CDCl_3$) δ: 0.85 (Me-Si), 1.74 (Me-C), 3.20 (d, (H-2)$_A$), 3.37 (d, (H-3)$_A$), 3.53–4.02 (heavily overlapped), 4.30 (d, H-6), 4.89–4.91 (H-1s), 4.95 (s, H-1), 5.19 (s, (H-1)$_A$); ^{13}C NMR ($CDCl_3$) δ: −5.37 (Me-Si), 18.1 (*C*-Me), 25.8 (*Me*-C), 49.1 ((C-2$_A$), 53.1 ((C-3)$_A$), 61.3, 61.4, 61.6, 61.9, 63.8 (C-6s), 68.6, 69.7, 71.8, 72.2, 72.4, 72.7, 73.3, 78.3, 80.7, 81.3, 81.7 (C-2s, C-3s, C-4s), 96.2 ((C-1$_A$), 99.3, 101.3, 101.8, 102.0, 102.2 (C-1s). Anal. calcd. for $C_{84}H_{166}O_{34}Si_{79}$: C, 52.64; H, 8.73; found: C, 51.89; H, 8.66.

Acknowledgements

This research was supported by the Natural Sciences and Engineering Council of Canada (NSERC). The awards to M.J.P. of a Postgraduate Scholarship by NSERC and a Graduate Award by Queen's University are gratefully acknowledged. The authors wish to thank Dr. C. K. Lee for helpful advice.

[1]The work-up is similar to that of Takeo *et al.* (14).

1. (*a*) R. Bergeron. J. Chem. Educ. **54**, 204 (1977); (*b*) M. L. Bender and M. Komiyama. Cyclodextrin chemistry. Springer-Verlag, New York. 1978; (*c*) J. Szejtli. Cyclodextrins and their inclusion complexes. Akademiai Kiado, Budapest. 1982; (*d*) J. Szejtli. Cyclodextrin technology. Kluwer, Dordrecht. 1988.
2. (*a*) M. Komiyama and M. L. Bender. *In* The chemistry of enzyme action. *Edited by* M. I. Page. Elsevier, Amsterdam. 1984; (*b*) R. L. VanEtten, J. F. Sebastian, G. A. Clowes, and M. L. Bender. J. Am. Chem. Soc. **89**, 3242 (1967); (*c*) O. S. Tee. Carbohydr. Res. **192**, 181 (1989).
3. (*a*) I. Tabushi. Functionalized cyclodextrins as artificial enzymes. *In* Chemical approaches to understanding enzyme catalysis. *Edited by* B. Green, Y. Ashani, and D. Chipman. Elsevier, Amsterdam. 1982; (*b*) E. U. Akkaya and A. W. Czarnik. J. Am. Chem. Soc. **110**, 8553 (1988).
4. R. Breslow and A. Czarnik. J. Am. Chem. Soc. **105**, 1390 (1983).
5. R. Breslow, A. W. Czarnik, M. Lauer, R. Leppkes, J. Winkler, and S. Zimmerman. J. Am. Chem. Soc. **108**, 1969 (1986).
6. K. Fujita, T. Tahara, T. Imoto, and T. Koga. J. Am. Chem. Soc. **108**, 2030 (1986).
7. K. Fujita, S. Nagamura, T. Imoto, T. Tahara, and T. Koga. J. Am. Chem. Soc. **107**, 3233 (1985).
8. (*a*) A. Ueno and R. Breslow. Tetrahedron Lett. **23**, 3451 (1982); (*b*) T. Murakami, K. Harata, and S. Morimoto. Tetrahedron Lett. **28**, 321 (1987).
9. E. J. Corey and A. Venkateswarlu. J. Am. Chem. Soc. **94**, 6190 (1974).
10. T. J. Michalski, A. Kendler, and M. L. Bender. J. Inclusion Phenom. **1**, 125 (1983).
11. K. Takeo, K. Uemura, and H. Mitoh. J. Carbohydr. Chem. **7**, 283 (1988).
12. P. Fugedi and P. Nanasi. Carbohydr. Res. **175**, 173 (1988).
13. A. Liptak, P. Fugedi, Z. Szurmai, J. Imre, P. Nanasi, and J. Szejtli. The chemistry of cyclodextrin derivatives. First Int. Symp. on Cyclodextrins. *Edited by* J. Szejtli. D. Reidel, Dordrecht, Boston, London. 1982. p. 275.
14. K. Takeo, H. Mitoh, and K. Uemura. Carbohydr. Res. **187**, 203 (1989).
15. P. Fugedi. Carohydr. Res. **192**, 366 (1989).
16. J. F. Stoddart and R. Zarzycki. Chemically modified cyclodextrins as second sphere ligands for transition metal complexes. Proc. Fourth Int. Symp. on Cyclodextrins. *Edited by* O. Huber and J. Szejtli. Kluwer, Dordrecht. 1988. p. 197.
17. I. Tabushi, T. Nabeshima, K. Yamamura, and H. Fujita. Bull. Chem. Soc. Jpn. **60**, 3705 (1987).
18. R. L. Wife, D. E. Reed, and H. C. Volger. Cyclodextrin derivatisation: directed reaction of silylated intermediates. First Int. Symp. on Cyclodextrins, *Edited by* J. Szejtli. D. Reidel, Dordrecht, Boston, London. 1982. p. 289.
19. Y. Yamamoto and Y. Inoue. J. Carbohydr. Chem. **8**, 29 (1989).
20. C. M. Spencer, J. F. Stoddart, and R. Zarzycki. J. Chem. Soc. Perkin Trans. 2, 1323 (1987).
21. D. R. Hicks and B. Fraser-Reid. Synthesis, 202 (1974).
22. N. R. Williams. Adv. Carbohydr. Chem. Biochem. **25**, 109 (1970).
23. M. M. Abdel-Malik, Q.-J. Peng, and A. S. Perlin. Carbohydr. Res. **159**, 11 (1987).
24. W. C. Still, M. Kahn, and A. Mitra. J. Org. Chem. **43**, 2923 (1978).
25. L. Hough, P. A. Munroe, and A. C. Richardson. J. Chem. Soc. (C), 1090 (1971).

Can. J. Chem. Downloaded from www.nrcresearchpress.com by 195.138.81.100 on 09/07/12
For personal use only.

Cyclopropylketenes: preparation and nucleophilic additions[1]

ANNETTE D. ALLEN, LYNN M. BAIGRIE, LEYI GONG, AND THOMAS T. TIDWELL[2]
Department of Chemistry, University of Toronto, Toronto, Ont., Canada M5S 1A1

Received July 20, 1990

ANNETTE D. ALLEN, LYNN M. BAIGRIE, LEYI GONG, and THOMAS T. TIDWELL. Can. J. Chem. **69**, 138 (1991).

Phenylcyclopropylketene (**4**), *tert*-butylcyclopropylketene (**5**), and dicyclopropylketene (**6**) were formed by dehydrochlorination of the corresponding acyl chlorides by Et_3N in THF, and are the first cyclopropylketenes to be isolated and purified. Reaction of **4** with *n*-BuLi and capture of the intermediate enolates with Me_3SiCl gave the stereoisomeric silyl enol ethers *c*-PrCPh=C(OSiMe$_3$)-*n*-Bu with a 79:21 preference for formation of the *Z* isomer resulting from nucleophilic attack *syn* to cyclopropyl, whereas the corresponding reaction of *t*-BuLi gave a 9:91 preference for attack *anti* to cyclopropyl. Some isopropyl-, cyclopentyl-, and cyclohexylketenes gave comparable results. Analyses of the relative sizes of the ketene substituents in the ground state by steric parameters, and of the product stabilities by molecular mechanics, both fail to predict the observed similarities in the results with different *secondary* alkyl groups. The hydration reactivities of **4** and **6** show that, in neutral H_2O/CH_3CN, *c*-PrCPh=C=O is more reactive than *i*-PrCPh=C=O, a result ascribed as mainly due to the smaller size of cyclopropyl. *c*-Pr_2C=C=O has the same reactivity in neutral water as Et_2C=C=O, but is 22 times less reactive with acid, a result attributed to the inability of the β-cyclopropyl groups to directly stabilize the cationic transition state for protonation.

Key words: cyclopropylketenes, ketenes, nucleophilic addition, hydration kinetics.

ANNETTE D. ALLEN, LYNN M. BAIGRIE, LEYI GONG et THOMAS T. TIDWELL. Can. J. Chem. **69**, 138 (1991).

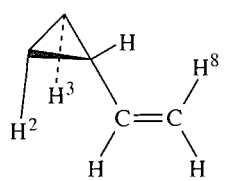
On a obtenu les phénylcyclopropyl- (**4**), *tert*-butylcyclopropyl- (**5**) et dicyclopropyl- (**6**) cétènes par déshydrochloration des chlorures d'acyles correspondants à l'aide du Et_3N dans le THF; il s'agit des premiers cyclopropylcétènes à être isolés et purifiés. La réaction du produit **4** avec le *n*-BuLi, suivie d'une capture des énolates intermédiaires par le Me_3SiCl, fournit les éthers énoliques silylés stéréoisomères *c*-PrCPh=C(OSiMe$_3$)-*n*-Bu qui sont présents dans un rapport de 79:21; l'isomère *Z* qui résulte d'une attaque nucléophile *syn* par rapport au cyclopropyle se forme d'une façon prépondérante. Par ailleurs, lors de la réaction avec le *tert*-BuLi, l'attaque se fait de préférence (9:91) en *anti* par rapport au cyclopropyle. Des analyses, d'une part, des grosseurs relatives des substituants cétènes dans l'état fondamental à l'aide de paramètres stériques et, d'autre part, des stabilités des produits à l'aide de la mécanique moléculaire ne permettent pas de prédire les similarités observées dans les résultats obtenus à l'aide de divers groupements alkyles *secondaires*. Les réactivités des produits **4** et **6** vis-à-vis de l'hydration montrent que, dans un mélange neutre de H_2O/CH_3CN, le *c*-PrCPh=C=O est plus réactif que le *i*-PrCPh=C=O; ce résultat est principalement attribué à une taille plus petite du cyclopropyle. En milieu neutre, le *c*-Pr_2C=C=O et le Et_2C=C=O ont la même réactivité; toutefois, en milieu acide, le dérivé cyclique est 22 fois moins réactif et ce résultat est attribué à l'inhabilité des groupements β-cyclopropyles à stabiliser directement l'état de transition cationique de la protonation.

Mots clés : cyclopropylcétènes, cétènes, addition nucléophile, cinétique d'hydration.

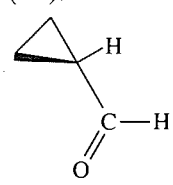
[Traduit par la revue]

Introduction

The conjugative interaction of the cyclopropyl group with adjacent π-systems has long been a source of fascination to chemists (1*a*). Thus both vinylcyclopropane (**1**) (1*b*,*c*) and cyclopropanecarboxaldehyde (**2**) (1*d*) have favored conformations in which the cyclopropane ring is bisected by the plane of the adjacent sp^2 carbon, so that π-conjugation between the cyclopropane ring and the side chain is possible. In **1** the *s-trans* conformation shown is favored with a 2.9 kcal/mol barrier (1*b*) to rotation to a non-bisected *gauche* conformation 1.2 kcal/mol (1*b*) higher in energy. The *s-trans* conformation is favored by π-conjugation whereas the *gauche* conformation is favored by reduced non-bonding interactions involving H^2, H^3, and H^8, and by entropy (1*c*). The π-stabilization is estimated as 1.4 kcal/mol (1*c*). For **2** there is a slight preference for the *syn* conformer shown in the gas phase with a 4.3 kcal/mol barrier for conversion to the *anti* conformer (1*d*).

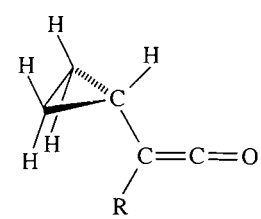


1



2

Cyclopropylketenes (**3**) combine some of the structural features of both **1** and **2**, and a conjugative interaction of the cyclopropyl group might be expected to stabilize ketenes, which are ordinarily prone to dimerization and reaction with various species (2). Surprisingly, however, there are only a few references to cyclopropylketenes in the literature, and these were generated as short-lived intermediates that usually reacted further under their conditions of formation (3) or were detected by their infrared spectra in cold matrices (3*c*) or in dilute solutions at room temperature (3*d*). Cyclopropylketene-derived products were also formed from a chromium carbene complex, but no evidence for the free ketene was obtained (3*f*). Because of our interest both in ketene chemistry (4) and in the conjugative properties of cyclopropane (1*a*) we have examined the preparation and properties of a few representative examples of these species with the goals of elucidating their electronic and chemical properties, providing a general route to their synthesis, and examining their synthetic utility.



3

[1]Reported in part as a preliminary communication, ref. 4*g*.
[2]Author to whom correspondence may be addressed.

Can. J. Chem. Downloaded from www.nrcresearchpress.com by 195.138.81.100 on 09/07/12
For personal use only.

Can. J. Chem. Downloaded from www.nrcresearchpress.com by 195.138.81.100 on 09/07/12
For personal use only.

Results

Phenylcyclopropylketene (**4**), *tert*-butylcyclopropylketene (**5**), and dicyclopropylketene (**6**) were readily prepared from the corresponding cyclopropyl ketones. Conversion of the ketones to the chain-extended carboxylic acids (5, 6) was equally satisfactory by use of the Wittig reagent $CH_3OCHPPh_3$ (*6a*) or a Peterson reaction with $CH_3OCH_2SiMe_3$ and *s*-BuLi (*6b*), following by hydrolysis of the intermediate methyl vinyl ether by HCO_2H/H_2O and oxidation with PDC (eq. [1]), in overall yields of about 40%. The acyl chlorides were obtained from the acids with $SOCl_2$ and converted to the ketenes by Et_3N in THF (eq. [2]). Ketene **5** was formed at reflux but **4** and **6** were

[1] *c*-PrCR=O $\xrightarrow[\text{or (1) } CH_3OCHLiSiMe_3\text{; (2) } H_3O^+]{\text{(1) } CH_3OCHPPh_3\text{; (2) } H_3O^+}$ *c*-PrCHRCH=O

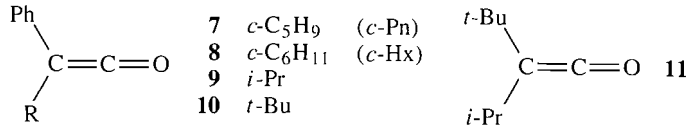
[2] *c*-PrCHRCH=O $\xrightarrow[\text{(3) } Et_3N\text{, THF}]{\text{(1) PDC; (2) } SOCl_2}$ *c*-PrCR=C=O

R = Ph (**4**), *t*-Bu (**5**), *c*-Pr (**6**)

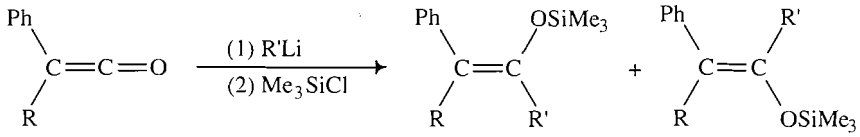
obtained by reaction at room temperature. After removal of the solvent *in vacuo* the ketenes were isolated, by vacuum distillation, as moderately stable yellow liquids in 32–55% yields based on the acyl chlorides.

Ketenes **4–6** were estimated to be greater than 95% pure by their ^1H nmr (200 MHz) spectra, and showed characteristic ir bands for the ketene carbonyl at 2097–2106 cm^{-1}, and uv maxima at 248, 240, and 280 nm ($\varepsilon \cong 10^4$) and 395, 373, and 376 nm ($\varepsilon < 100$) for **4**, **5**, and **6**, respectively. The ^1H and ^{13}C nmr spectra and mass spectra were consistent with the ketene structures, and correct high resolution exact mass parent ions were observed for **4** and **6**.

For comparison to **4–6**, phenylcyclopentylketene (**7**), phenylcyclohexylketene (**8**), phenylisopropylketene (**9**) (*4b*, *7a*), phenyl-*tert*-butylketene (**10**) (*4b*, *7b*), and *tert*-butylisopropylketene (**11**) (*7c*) were also prepared by dehydrochlorination of the acid chlorides by Et_3N (for **7–9** and **11**) or by dehydrohalogenation of the α-bromo acid chloride (for **10**).



Phenylcycloalkylketenes **4**, **7**, and **8** were added to solutions of *n*-BuLi (in hexane–THF) or of *t*-BuLi (in pentane) at −78°C and the resulting enolates were trapped with Me_3SiCl to give *Z*/*E* mixtures of silyl enol ethers **12–17** (eq. [3]). Stereochemical assignments for **12–17** were made based on the ^1H and ^{13}C nmr chemical shifts of the Me_3Si and *t*-Bu groups using the previously established (*4f*, *7d*) relation that the group *syn* to the phenyl group absorbed at higher field, and the *Z*/*E* ratios, estimated to be accurate to ±2%, were derived from the relative ^1H nmr peak areas, as summarized in eq. [3].

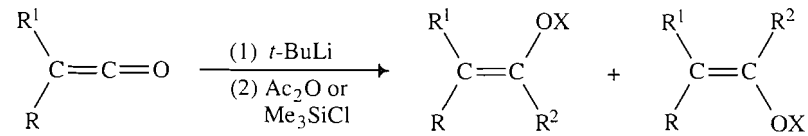
[3] 

R = *c*-Pr (**4**), *c*-Pn (**7**), *c*-Hx (**8**) — **12–17** *Z* — **12–17** *E*

	12	**13**	**14**	**15**	**16**	**17**
R	*c*-Pr	*c*-Pn	*c*-Hx	*c*-Pr	*c*-Pn	*c*-Hx
R'	*n*-Bu	*n*-Bu	*n*-Bu	*t*-Bu	*t*-Bu	*t*-Bu
Z/*E*	79:21	88:12	44:56	9:91	15:85	14:86

It was shown previously (*4f*) that the silylated enolates prepared similarly from phenylmethylketene and phenylethylketene were kinetic products and did not correspond to the product mixtures obtained under equilibrating conditions.

The reactions of **5** and **9–11** with *tert*-butyllithium followed by treatment with acetic anhydride or trimethylsilyl chloride gave the stereoisomeric enol acetates **18–22** or silyl enol ethers **23** and **24** in the *Z*/*E* ratios shown below in eq. [4].

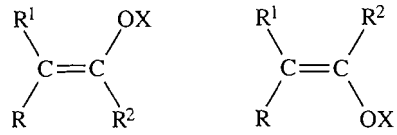
[4] 

Z *E*

R	R^1	R^2	*Z*/*E* (X = Ac)	*Z*/*E* (X = $SiMe_3$)
c-Pr	*t*-Bu (**5**)	*t*-Bu	100:0 (**18**)	—
i-Pr	*t*-Bu (**11**)	*t*-Bu	100:0 (**19**)	—
i-Pr	*t*-Bu (**11**)	H	83:17 (**20**)	—
i-Pr	Ph (**9**)	*t*-Bu	19:81 (**21**) (77%)	14:86 (**23**) (78%)
t-Bu	Ph (**10**)	*t*-Bu	0:100 (**22**) (71%)	0:100 (**24**) (65%)

Can. J. Chem. Downloaded from www.nrcresearchpress.com by 195.138.81.100 on 09/07/12
For personal use only.

TABLE 1. The ^{1}H nmr chemical shifts of enol derivatives



Z *E*

	δ X (X = $SiMe_3$)		δ X (X = OAc)		δ R^2 (R^2 = *t*-Bu)	
	Z	*E*	*Z*	*E*	*Z*	*E*
12	−0.14	0.28				
13	−0.18	0.25				
14	−0.18	0.26				
15	−0.29	0.33			1.34	0.86
16	−0.30	0.31			1.28	0.84
17	−0.30	0.34			1.28	0.83
18			2.12		1.23[a]	
19			2.10		1.20[a]	
20			2.14		1.19[a]	1.07[b]
21			1.38	2.18	1.27	0.81
22				2.13		0.84
23	−0.30	0.32			1.28	0.87
24		0.37				0.79

[a] R^1.
[b] R.

TABLE 2. Rates of hydration in H_2O/CH_3CN of *c*-PrCPh=C=O (**4**) and *c*-Pr_2C=C=O (**6**), 25°C

Neutral hydration				Acid hydration	
[H_2O]		k_{obs} (s^{-1})		[HCl] (M)[a]	
Vol. %	M	**4**	**6**	(20% H_2O)	k_{obs} (s^{-1})
10	5.56	0.0930	0.0102	0.806 (**4**)	0.138
20	11.1	0.297	0.0486	1.21 (**4**)	0.400
30	16.7	0.514	0.112	0.0102 (**6**)	0.0638
40	22.2	0.728	0.200	0.0204 (**6**)	0.0799
50	27.8		0.406	0.0307 (**6**)	0.0978
				0.0409 (**6**)	0.110
				0.0511 (**6**)	0.123

[a] μ = 0.05 (NaCl).

The structures of **18**–**24** follow readily from their spectral properties. The only stereoisomers of **18** and **19** observed were assigned the *Z* configurations on the basis of the downfield ^{1}H nmr chemical shift observed for R^1 = *t*-Bu (δ 1.23 and 1.20, respectively), an effect attributed to the influence of the *syn* acetoxy group. For **20** the chemical shifts of these *t*-Bu groups were δ 1.19 and 1.07 for the structures assigned as *Z* and *E*, respectively, with the lower field signal assigned to the *t*-Bu *syn* to the acetoxy. For **21**–**24** the ^{1}H nmr chemical shifts of the *t*-Bu, CH_3CO, and $(CH_3)_3Si$ groups *syn* to the phenyl group have large upfield shifts relative to the stereoisomeric *anti* groups, as discussed previously (4*f*, 7*d*).

The hydration reactivities of **4** and **6** were measured in H_2O/CH_3CN mixtures, as these ketenes were too reactive for measurement by conventional means at 25°C in solely aqueous solutions. Rates in neutral H_2O/CH_3CN as a function of H_2O concentration, and in 20% H_2O/80% CH_3CN as a function of HCl concentration, were determined by uv as done previously (4*b*,*e*) and are reported in Table 2.

As found previously for other ketenes (4*b*,*e*), reasonable correlations of ketene reactivity with H_2O molarity were found: log k_{obsd} (**4**) = (0.0350 M^{-1} s^{-1}) [H_2O] − 0.901 s^{-1}, r = 0.992; log k_{obs} (**6**) = (0.0543 M^{-1} s^{-1}) [H_2O] − 1.89 s^{-1}, r = 0.998. The plots give extrapolated values of k_{obsd} for 100% (55.5 M) H_2O of 11.1 s^{-1} and 13.4 s^{-1}, respectively. The slope of the plot for **4** is less than that observed for other ketenes (4*b*,*e*) and by direct comparisons the ratio of k_{obs} for **4**/**6** has an average value of 5.8 (Table 2).

The reaction of **6** in 20% H_2O/CH_3CN was catalyzed by HCl with k_{obs} (**6**) = (1.46 M^{-1} s^{-1}) [HCl] + 0.0502 s^{-1}, with the intercept agreeing well with the measured value of k_{H_2O} = 0.0469 s^{-1}. Because of the high reactivity of **4** the value of k_{H^+} was approximated as 0.120 M^{-1} s^{-1} from the relation k_{obs} = k_{H^+}[HCl] + k_{H_2O} using the value of k_{obs} 0.400 s^{-1} at [HCl] = 1.21 M and a separately measured value of 0.255 s^{-1} for k_{H_2O}.

Discussion

The preparation of the cyclopropylketenes **4**–**6** (eqs. [1], [2]) provides a facile route to these interesting species, and other substituted cyclopropylketenes should be accessible by the same methodology. These ketenes show reasonable stability, in accord with the results of preliminary molecular orbital calculations (4*g*) at the 3-21G//3-21G level for the isodesmic reaction in eq. [5], which is calculated to be exothermic as shown by 1.9 kcal/mol. Thus cyclopropyl is predicted to be only modestly less stabilizing as a ketene substituent compared to methyl as opposed to a substituent on ethylene.

[5] *c*-PrCH=C=O + $CH_3CH=CH_2$ → *c*-PrCH=CH_2 + CH_3CH=C=O

The results of the alkyllithium additions to eqs. [3] and [4] show that cyclopropylketenes are also useful synthetic reagents for the preparation of enolate derivatives. These products should be useful for further synthetic transformations or for conversion to the corresponding ketones.

The *Z*/*E* selectivities for *n*-BuLi addition to the phenylcycloalkylketenes **4**, **7**, and **8** (eq. [3]) show that for the cyclopropyl and cyclopentyl substrates most of the product (79 and 88%, respectively) results from nucleophilic attack from the cycloalkyl substituted side, while for the cyclohexyl derivative this percentage drops to 44%. For *t*-BuLi there is a preference for addition to **4**, **7**, **8**, **9**, and **10** *syn* to the phenyl group. For the *secondary* alkyl groups this preference is 86 ± 5% independent of the alkyl group.

For consideration of the *Z*/*E* product ratios of these reactions, some measures of the steric size of some relevant substituents are given in Table 3 (8). These include the E_s parameter of Taft (8*a*), the Winstein–Holness *A* value (8*b*), the υ parameter of Charton (8*c*,*d*), Meyer's *G* and V^a parameters (8*e*), and the Ω parameter (8*f*).

The only steric parameter for cyclopropyl that has been reported is the Charton υ value of 1.06 (8*c*,*d*) but this value, derived from hydrolysis rates of a cyclopropane carboxylate ester, is recognized (8*d*) to contain a polar component and is not a reliable guide to the effective size of this group. By the use of the molecular mechanics program MacroModel (9*a*) we calculate an *A* value of 1.75 for this group, as $\Delta\Delta H_f^0$ between equatorial and axial cyclopropyl substituted cyclohexane or 4-*tert*-butylcyclohexane. Based on this value and those values

TABLE 3. E_s, A, υ, G, V^a, and Ω parameters (ref. 8)

R	Me	Et	*i*-Pr	*c*-Pr	*c*-Bu	*c*-Pn	*c*-Hx	*t*-Bu	Ph
E_s	−1.24	−1.31	−1.71		−1.3	−1.75	−2.03	−2.78	−3.79
A	1.70	1.75	2.15				2.15	5.4	3.0
υ	0.52	0.56	0.76	(1.06)	0.51	0.71	0.87	1.24	0.57–2.15
G	16.42	14.83	14.05		13.10	12.63	12.34	13.45	11.83
$V^{a a}$	2.84	4.31	5.74		5.79	6.16	6.25	7.16	6.10
Ω^b	2.88	3.34	3.77			3.64	3.81	4.21	

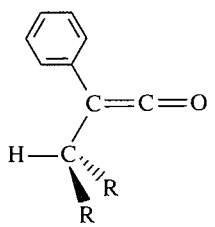
[a] $V^a \times 100$.
[b] $\Omega \times 10$.

in Table 3, the order of effective sizes of secondary alkyl and cycloalkyl groups is *c*-Hx > *c*-Pn ≅ *i*-Pr > *c*-Pr. The effective size of phenyl is variable depending upon the direction of approach to the planar ring.

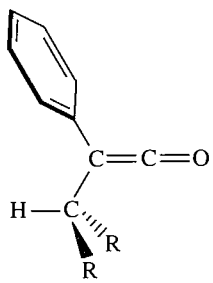
Notably none of the steric parameters in Table 3 predict the observed results for the stereochemistry of attack of the alkyllithiums on the ketenes. Not only are the predicted trends among the *secondary* alkyl groups not observed, but the preferred attack by *t*-BuLi *syn* to phenyl is not anticipated.

The preferred direction of attack of a nucleophilic reagent on a phenylcycloalkylketene is expected to result from the dynamic interplay of a variety of factors, including (a) conjugative stabilization of the ketene by the aryl group favoring coplanarity of the ring and the ketene; (b) steric interactions between the nucleophile and the phenyl group, which will be largest when the phenyl is planar, and smallest when it is perpendicular; (c) steric interactions between the cycloalkyl group and the phenyl group; (d) conjugation of the cyclopropyl group with the ketene; and (e) the effective size of the nucleophile.

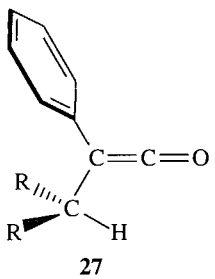
Some limiting conformations of phenylketenes with a *secondary* alkyl substituent are shown. For the ground state of the ketene, **25** is favored, as evidenced by molecular mechanics calculations. Conformations **26** and **27** represent those with



25



26



27

freest access to the carbonyl carbon by a nucleophilic reagent from the phenyl and alkyl sides, respectively, and likely resemble the conformation of the ketene in the actual transition state for nucleophilic addition.

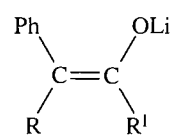
Previous studies have shown a large variation in the stereoselectivity of attack on ketones as a function of the specific organolithium reagent used. Thus reaction of 7-oxabicyclo-[2.2.1]hept-5-en-2-one gave preferences for *exo* attack of 20:1, 11:1, 9:1, and 3.6:1 for CH_3, *n*-Bu, 1-hexynyl, and Ph lithium in Et_2O at 0°C, respectively (10*a*). There are a number of other examples where different organometallic reagents display different stereoselectivities (10*b*). The degree of aggregation of different organolithium reagents is known to vary widely and so it is not simple to evaluate the relative steric bulk of different organolithium reagents (10*b*, 11). There is also evidence that the stereochemistry of nucleophilic additions to ketones is affected by stereoelectronic factors, including the electronegativity of the alkyl portion of the organolithium reagent (10*c*).

TABLE 4. Calculated (MMX) heats of formation for lithium enolates PhCR=C(OLi)-*t*-Bu and *t*-BuC(*i*-Pr)=C(OLi)R

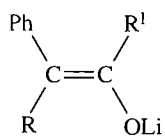
	ΔH_f^0 (kcal/mol)		
	Z	*E*	$\Delta\Delta H^0 (Z - E)$
PhCR=C(OLi)-*t*-Bu			
Et	26.90	31.45	−4.55
i-Pr	25.80	30.68	−4.88
t-Bu	46.19	35.45	10.74
t-BuC(*i*-Pr)=C(OLi)R			
H	37.76	37.55	0.21
t-Bu	−56.62	−45.86	−10.76

Another approach to the study of the stereochemistry of nucleophilic attack on ketones uses a combination of *ab initio* molecular orbital and molecular mechanics methods to predict the relative energies of the stereoisomeric transition states (10*d*,*e*). However, at its present state of development this method does not consider variations in the nucleophile.

The relative importance of steric approach control (or steric strain control) and product stability control have also been examined (10*f*). As a guide to the latter we have used the molecular mechanics program PCMODEL, which uses MMX, an enhanced version of the MMP2 force field (9*b*), to compare the product stability of stereoisomeric lithium enolates **28**, as shown in Table 4.



28*Z*



28*E*

The calculations predict that for PhCR=C(OLi)-*t*-Bu the *Z* isomer with *cis* *i*-Pr and *t*-Bu groups is more stable when R = *i*-Pr, but that for R = *t*-Bu the *E* isomer with the *t*-Bu groups *trans* is predicted to be more stable. In the addition

Can. J. Chem. Downloaded from www.nrcresearchpress.com by 195.138.81.100 on 09/07/12
For personal use only.

Can. J. Chem. Downloaded from www.nrcresearchpress.com by 195.138.81.100 on 09/07/12
For personal use only.

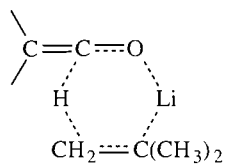
reactions (eq. [4]) the *E* isomer is favored in each case, although to a lesser extent for R = *i*-Pr.

For *t*-BuC(*i*-Pr)=C(OLi)R the calculations predict a slight preference for the *E* isomer with the *t*-Bu *cis* to the added H, whereas experimentally (eq. [4]) there is an 83:17 preference for formation of the *Z* isomer. For R = *t*-Bu the *Z* isomer is predicted to be favored, and this is the only product observed experimentally.

These calculations consider the products and not the transition states, and also ignore the solvent. Particularly in the case of the hydride addition, the reducing agent in the transition state is expected to be much more sterically demanding than the hydrogen in the product. Thus much more sophisticated calculations of the transition states will be needed to reliably predict the stereochemistry of these additions, but the present results do help delineate the complexity of the problem.

The generalization can be made that *t*-BuLi is less likely to add to phenylalkylketenes from the alkyl side compared to *n*-BuLi. However, the quantitative prediction of the stereochemistry of attack in these complex systems is beyond our present capability.

The reduction of *tert*-butylisopropylketene (**11**) by *tert*-butyllithium proceeds with an 83:17 selectivity for hydride delivery *syn* to the isopropyl group, whereas within the limits of detectability addition occurs exclusively from this direction. Hydride attack via a 6-membered transition state (**29**) is expected to have significantly lower steric demands than addition of a *tertiary* carbon nucleophile. There are previous examples of the reduction of ketenes by organometallic reagents and metal hydrides (2*d*, 4*d*).



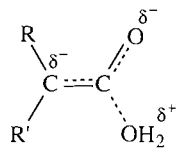
29

A referee has suggested that the stereoelectronic ("Cieplak") (10*c*) effects of the ketene substituents in $RR^1C{=}C{=}O$ may affect the stereochemistry of nucleophilic addition. Experiments to test this intriguing proposal have not been carried out.

Hydration reactivities

The hydration rate constants for *c*-PrCPh=C=O (**4**) (Table 2) with neutral H_2O in 20 and 30% H_2O are an average of 38 times greater than those of *i*-PrCPh=C=O (4*b*). The major cause of this greater reactivity of the cyclopropyl compound is presumably reduced steric crowding in the hydration transition state, which is proposed to resemble **30** (4*b*,*e*,*h*). The same interplay of steric factors involving the nucleophile and the ketene substituents, discussed above for organolithium additions, is expected to occur in the hydration. However, in the hydration the greater reactivity of the cyclopropyl derivative compared to the isopropyl analogue is in accord with the smaller size of the former group calculated by molecular mechanics. There is some evidence (1*a*) that cyclopropyl may stabilize developing negative charge, so an electronic factor may also contribute to the enhanced reactivity of the cyclopropyl derivative.

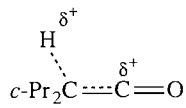
The extrapolated rate constant for *c*-PrCPh=C=O (**4**) in 100% neutral H_2O is 500 times less than that of 4700 s^{-1} for



30

PhCH=C=O (4*h*), indicating that there are significant steric repulsions for cyclopropyl compared to hydrogen. The rate constants of *c*-$Pr_2C{=}C{=}O$ (**6**) in 20, 30, and 50% H_2O/CH_3CN are almost identical to those of $Et_2C{=}C{=}O$ (4*e*), showing that the combined steric and electronic effects of these groups are the same in this process.

Comparison of k_{H^+} for *c*-$Pr_2C{=}C{=}O$ to that of 30.1 M^{-1} s^{-1} for $Et_2C{=}C{=}O$ in 20% H_2O/CH_3CN (4*e*) gives a rate ratio $k(Et_2C{=}C{=}O)/k(c\text{-}Pr_2C{=}C{=}O) = 21$. This result is consistent with results for cyclopropylalkenes (12), in which both *E* and *Z* *c*-PrCH=CH-*c*-Pr are less reactive than $CH_2{=}CH$-*c*-Pr, by an average factor of 30. These results are attributed (12) to ground state stabilization of the alkene by cyclopropyl and inductive destabilization of the cationic transition state resembling **31** by the cyclopropyl group, which cannot stabilize the developing positive charge by π-donation.



31

Summary

Cyclopropylketenes are readily accessible and rather persistent compounds. In reactions of organolithium reagents the stereochemical preferences for attack on ketenes bearing cyclopropyl substituents are comparable to those of other cyclic and acyclic secondary alkyl groups. This behaviour is not predicted by the steric parameters of the substituents or by molecular mechanics calculations of the product stabilities. In neutral hydration, cyclopropylketene **4** is more reactive than the isopropyl analogue, a result consistent with a smaller steric bulk for cyclopropyl. In acid hydration, the cyclopropyl group retards ketene hydration, as expected on the basis of inductive electron withdrawal by this group.

Experimental

Tetrahydrofuran (THF) and diethyl ether were distilled from sodium/benzophenone. Triethylamine and pentane were distilled from CaH_2 after refluxing overnight. Glassware was flame dried and cooled under N_2, and all reactions involving air-sensitive materials were conducted under a N_2 atmosphere. Spectra were measured using Varian T-60, Gemini 200, and (for **20***Z*) XL-400 nmr spectrometers, a Nicolet 5-DX ftir spectrophotometer, a Unicam AR25 Linear "Record" uv spectrophotometer, and VG-70-250S and AEI MS-30 mass spectrometers. Gas chromatographic analyses and separations were carried out using Varian 2700 flame ionization and Varian 90P instruments, respectively, with OV-17 columns unless noted.

2-Cyclopropyl-2-phenylacetic acid

At −78°C, *n*-BuLi (46.8 mL, 75 mmol, 1.6 M in hexane) was added dropwise to a suspension of (methoxymethyl)triphenylphosphonium chloride (25 g, 73 mmol) in 150 mL ether, which was then stirred 1 h at 0°C. Cyclopropyl phenyl ketone (7.16 g, 49 mmol) in 10 mL ether was added to this solution, which was then stirred 12 h at 25°C, poured into H_2O, and extracted with pentane. The organic layer was dried over Na_2SO_4, concentrated, and distilled (80–85°C, 2 Torr; 1 Torr = 133.3 Pa) to give an *E*/*Z* mixture of methyl 2-cyclopropyl-2-phenyl-

Can. J. Chem. Downloaded from www.nrcresearchpress.com by 195.138.81.100 on 09/07/12
For personal use only.

vinyl ethers (6.40 g, 37 mmol, 75%), which was stirred overnight with 10 equivalents HCO_2H at 25°C, poured into H_2O, and extracted with ether. The ether extract was washed with H_2O and $NaHCO_3$, dried over $MgSO_4$, and concentrated to give crude 2-cyclopropyl-2-phenylacetaldehyde (5.92 g): ^{1}H nmr ($CDCl_3$) δ: 0.26 (m, 1), 0.39 (m, 1), 0.64 (m, 1), 0.75 (m, 1), 1.32 (m, 1), 2.80 (dd, J = 9.6 and 4.5 Hz, 1, PhCH), 7.3 (m, 5, Ph), and 9.68 (d, J = 4.5 Hz, 1, CHO).

To the above aldehyde in 50 mL ether was added dropwise a solution of $Na_2Cr_2O_7 \cdot 2H_2O$ (4.40 g), 2.72 mL of 98% H_2SO_4, and 18 mL of H_2O and the solution was stirred overnight, poured into water, and extracted with ether. The ether layer was extracted with NaOH and the aqueous layer was then acidified with HCl and extracted into ether. The ether solution was dried over $MgSO_4$ and evaporated to give the acid (2.00 g, 11.3 mmol, 30%), mp 89–91°C (lit. (*5a*) mp 92–93°C).

Other acids prepared similarly included dicyclopropylacetic acid (*5b*), 2-phenyl-3-methylbutanoic acid (*6a*), 2-phenyl-3,3-dimethylbutanoic acid (*6a*), and *2-cyclopropyl-3,3-dimethylbutanoic acid*, mp 48.5–50°C; ir (CCl_4): 1705 (C=O) cm^{-1}; ^{1}H nmr ($CDCl_3$) δ: 0.23 (m, 2), 0.50 (m, 1), 0.70 (m, 1), 1.05 (m, 1), 1.09 (s, 9, *t*-Bu), and 1.43 (d, J = 10.4 Hz, 1, CHCO); ms m/z: 156 (M^+, 0.3), 100 ($M^+ - C_4H_8$, 88), 57 (*t*-Bu$^+$, 100); hrms m/z calcd. for $C_9H_{16}O_2$ (M^+): 156.1150; found: 156.1159. This latter acid was obtained from the known ketone (*6f*). 2-Cyclopentyl- and 2-cyclohexylphenylacetic acids were obtained from Aldrich, and 2-isopropyl-3,3-dimethylbutanoic acid (*6c,d*) was obtained by the hydroboration/oxidation procedure of Newman *et al.* (*6e*). Some of the acids were also prepared by the use of $CH_3OCHLiSiMe_3$ (eq. [1]), as described previously (*4f*).

2-Cyclopropyl-3,3-dimethylbutanoyl chloride

To a solution of the acid (1.6 g, 10 mmol) in 20 mL CCl_4 was added $SOCl_2$ (50 mmol) dropwise at 25°C. The resulting mixture was stirred overnight, the solvent and excess reagent distilled at atmospheric pressure, and the product distilled (bp 45–46°C, 5 Torr): ir (CCl_4): 1795 (C=O) cm^{-1}; ^{1}H nmr ($CDCl_3$) δ: 0.34 (m, 2), 0.59 (m, 1), 1.08 (m, 1), 1.10 (s, 9, *t*-Bu), 1.96 (d, J = 10.4 Hz, 1, CHCO); ^{13}C nmr ($CDCl_3$) δ: 2.0, 7.1, 9.8, 28.0, 35.2, 73.1, 176.1; hrms m/z calcd. for $C_9H_{15}O$ ($M^+ - Cl$): 139.1119; found: 139.1074. The other acid chlorides were obtained similarly.

Phenylcyclopropylketene (4)

The acid chloride (2.00 g, 10.3 mmol) was dissolved in 30 mL of THF and Et_3N (7.2 mL, 51 mmol) was added at 0°C. The solution was allowed to warm to 25°C and stirred for 1.5 h more. The solvent was evaporated and the product distilled to give **4** (0.74 g, 46%) as a yellow oil: bp 50–52°C, 2 Torr; ir (CCl_4): 2102 (C=O) cm^{-1}; uv (CH_2Cl_2) λ_{max}: 248, 395 nm; ^{1}H nmr ($CDCl_3$) δ: 0.46 (m, 2), 0.96 (m, 2), 1.54 (m, 1), 7.3 (m, 5, Ph); ^{13}C nmr ($CDCl_3$) δ: 4.4, 6.9, 44.7, 124.0, 124.3, 129.0, 133.5, 205.8; hrms m/z calcd. for $C_{11}H_{10}O$ (M^+): 158.0732; found: 158.0724.

tert-*Butylcyclopropylketene (5)* was prepared similarly, in 55% yield after 3.5 days reflux with Et_3N, as a yellow oil distilled at 25°C, 2 Torr; ir (CCl_4): 2097 (C=O) cm^{-1}; uv (CH_2Cl_2) λ_{max}: 240, 373 nm; ^{1}H nmr ($CDCl_3$) δ: 0.28 (m, 2), 0.75 (m, 2), 1.14 (m, 1), 1.15 (s, 9, *t*-Bu); ^{13}C nmr ($CDCl_3$) δ: 3.8, 6.7, 30.1, 30.8, 46.9, 205.0.

Dicyclopropylketene (6) was prepared similarly, in 32% yield after 2 days stirring with Et_3N at 25°C, as a yellow oil distilled at 25°C, 2 Torr; ir (CCl_4): 2106 (C=O) cm^{-1}; uv (CH_2Cl_2) λ_{max}: 280, 376 nm; ^{1}H nmr ($CDCl_3$) δ: 0.26 (m, 4), 0.66 (m, 4), 1.20 (m, 2); ^{13}C nmr ($CDCl_3$) δ: 5.5, 5.8, 46.1, 206.6; hrms m/z calcd. for $C_8H_{10}O$ (M^+): 122.0732; found: 122.0720.

Phenylcyclopentylketene (7) was obtained similarly in 54% yield: bp 82°C, 2 Torr; ir (CCl_4): 2095 (C=O) cm^{-1}; uv (CH_2Cl_2) λ_{max}: 260, 385 nm; ^{1}H nmr ($CDCl_3$) δ: 1.40 (m, 2), 1.72 (m, 4), 2.13 (m, 2), 2.90 (m, 1), 7.3 (m, 5, Ph); ^{13}C nmr ($CDCl_3$) δ: 24.5, 32.3, 34.2, 45.8, 124.3, 124.8, 129.0, 133.4, 205.1; hrms m/z calcd. for $C_{13}H_{14}O$ (M^+): 186.1045; found: 186.1053.

Phenylcyclohexylketene (8) was obtained similarly in 50% yield: bp 110–112°C, 5 Torr; ir (CCl_4): 2091 (C=O) cm^{-1}; uv (CH_2Cl_2) λ_{max}: 264, 388 nm; ^{1}H nmr ($CDCl_3$) δ: 1.1–1.4 (m, 6), 1.8 (m, 2), 2.05 (m, 2), 2.45 (m, 1), 7.3 (m, 5, Ph); ^{13}C nmr ($CDCl_3$) δ: 25.9, 26.2, 32.5, 33.0, 41.0, 124.4, 124.9, 129.0, 132.4, 204.9; hrms m/z calcd. for $C_{14}H_{16}O$ (M^+): 200.1201; found: 200.1207.

Phenylisopropylketene (9) (*7a*) was obtained similarly in 38% yield after 12 h reflux with Et_3N: bp 90–94°C, 1.5 Torr: ir (CCl_4): 2096 (C=O) cm^{-1}; ^{1}H nmr ($CDCl_3$) δ: 1.20 (d, J = 6.5 Hz, 6, CH*Me*$_2$), 2.80 (septet, J = 6.5 Hz, 1, CH), 7.0 (m, 5, Ph).

*Phenyl-*tert*-butylketene (10)* (*7b*)

2-Phenyl-3,3-dimethylbutanoyl chloride (1.0 g, 4.7 mmol) was refluxed with Br_2 (1.5 g, 9.4 mmol) in 10 mL CCl_4. The CCl_4 was distilled and distillation gave the α-bromoacyl chloride (1.3 g, 4.6 mmol, 98%). A portion of this (1.0 g, 3.4 mmol) was added dropwise in 5 mL THF to a suspension of activated Zn dust (0.42 g, 6.4 mmol) in 15 mL of THF and refluxed 10 h. The solution was filtered through glass wool with N_2 pressure and the solvent evaporated. Distillation (73–76°C, 5 Torr) gave **10** (0.35 g, 2.0 mmol, 59%): ir (CCl_4): 2097 (C=O) cm^{-1}; ^{1}H nmr (CCl_4) δ: 1.22 (s, 9, *t*-Bu), 7.14 (s, 5, Ph).

tert-*Butylisopropylketene (11)* (*7c*) was obtained from the acyl chloride (0.15 g, 0.8 mmol) after overnight refluxing with Et_3N in THF. The solution was filtered and evaporated to give crude **11** (0.067 g, 0.48 mmol, 60%), which was purified by vpc (20% OV-17, 100°C): ir (CCl_4): 2090 (C=O) cm^{-1}; ^{1}H nmr ($CDCl_4$) δ: 1.13 (d, J = 7 Hz, 6, CH*Me*$_2$), 1.15 (s, 9, *t*-Bu), 1.74 (septet, J = 7 Hz, 1, CH).

General procedure for reaction of ketenes with n-*BuLi*

To a solution of 30 mL of THF and *n*-BuLi (8.0 mmol, 1.6 M in hexane) at −78°C was added dropwise 2.0 mmol of ketene in 10 mL of THF. The mixture was stirred for 1 h at −78°C, and Me_3SiCl (10 mmol) was added in one portion. The solution was allowed to warm to room temperature, and stirred overnight. The solvent was evaporated, pentane was added, and the solution was removed from the residual white solid by filtration. Evaporation of the solvent left an oil, which was analyzed and purified by vpc. The Z/E isomers of **12–14** were not separated, but spectral assignments were made on the mixtures. For **12***E*, **13***E*, and **14***E* only the Me_3Si peaks in the ^{1}H nmr could be assigned with confidence, at δ 0.28, 0.25, and 0.26, respectively.

*(Z)-1-Cyclopropyl-1-phenyl-2-trimethylsilyloxy-1-hexene (12*Z*)*

Reaction of phenylcyclopropylketene (**4**) (0.25 g, 1.55 mmol) in 30 mL of THF with *n*-BuLi (6.33 mmol) gave 0.38 g of a crude oil by the procedure above. Preparative vpc gve **12***Z* (0.14 g, 0.49 mmol, 31%): ir (CCl_4): 1641 (C=C) cm^{-1}; ^{1}H nmr ($CDCl_3$) δ: −0.14 (s, 9, Me_3Si), 0.16 (m, 2), 0.65 (m, 2), 0.97 (t, J = 7.0 Hz, 3, CH_3), 1.0–2.0 (m, 5), 2.40 (t, J = 7.8 Hz, 2, C=CCH_2), 7.3 (m, 5, Ph); ^{13}C nmr ($CDCl_3$) δ: −0.2, 3.5, 6.2, 12.3, 13.9, 22.5, 29.3, 32.5, 120.9, 125.6, 127.4, 130.4, 140.0, 149.8; hrms m/z calcd. for $C_{18}H_{28}OSi$ (M^+): 288.1909; found: 288.1935.

*(Z)-1-Cyclopentyl-1-phenyl-2-trimethylsilyloxy-1-hexene (13*Z*)* was isolated similarly in 30% yield: ir (CCl_4): 1646 (C=C) cm^{-1}; ^{1}H nmr ($CDCl_3$) δ: −0.18 (s, 9, Me_3Si), 0.95 (t, J = 6.9 Hz, 3, CH_3), 1.2–1.8 (m, 12), 2.24 (t, J = 7.7 Hz, 2, C=CCH_2), 2.81 (m, 1), 7.2 (m, 5, Ph); ^{13}C nmr ($CDCl_3$) δ: −0.05, 13.9, 22.4, 24.5, 29.7, 31.5, 32.0, 41.8, 65.2, 112.4, 125.8, 127.6, 128.6, 128.8, 131.0, 147.0; hrms m/z calcd. for $C_{20}H_{32}OSi$ (M^+): 316.2222; found: 316.2217.

(Z)/(E)-1-Cyclohexyl-1-phenyl-2-trimethylsilyloxy-1-hexene (14) were obtained similarly and were separated by vpc (OV-17, 240°C). **14***Z*: ir (CCl_4): 1644 (C=C) cm^{-1}; ^{1}H nmr ($CDCl_3$) δ: −0.19 (s, 9, Me_3Si), 0.96 (t, 3, J = 7.3 Hz, CH_3), 1.0–1.8 (m, 14), 2.23 (t, 2, J = 7.7 Hz, C=CCH_2), 2.81 (m, 1), 7.2 (m, 5, Ph); ^{13}C nmr ($CDCl_3$) δ: −0.2, 13.8, 22.2, 25.7, 26.6, 29.6, 31.5, 32.5, 40.3, 126.0, 127.5, 130.8, 139.9, 146.5. **14***E*: ir (CCl_4): 1644 (C=C) cm^{-1}; ^{1}H nmr ($CDCl_3$) δ: 0.26 (s, 9, Me_3Si), 0.75 (t, 3, J = 7.2 Hz, CH_3), 1.0–1.8 (m, 14), 2.23 (t, J = 7.7 Hz, 2, C=CCH_2), 2.40 (m, 1), 7.1 (m, 5, Ph); hrms m/z calcd. for $C_{21}H_{34}OSi$ (M^+): 330.2379; found: 330.2373.

Can. J. Chem. Downloaded from www.nrcresearchpress.com by 195.138.81.100 on 09/07/12
For personal use only.

General procedure for reactions of ketenes **4–6** *with* t-*BuLi*

To *t*-BuLi (6.0 mmol) in 30 mL pentane at −78°C was added 1.50 mmol of neat ketene. The mixture was stirred for 2 h at −78°C, the pentane was evaporated, and 15 mL of THF was added. The resulting solution was then quenched with TMSCl or Ac_2O and stirred overnight, the THF was evaporated, and the residue was extracted with pentane and filtered. Evaporation of the pentane gave the crude product, which was then purified by vpc. The minor *Z* isomers of **15–17** were not isolated, but in the ^{1}H nmr the Me_3Si signals at δ −0.29, −0.30, and −0.30 and *t*-Bu signals at 1.34, 1.28, and 1.28 for **15***Z*, **16***Z*, and **17***Z*, respectively, could be assigned with confidence.

*(*E*)-1-Cyclopropyl-3,3-dimethyl-1-phenyl-2-trimethylsilyloxy-1-butene (***15***E)*

The reaction of phenylcyclopropylketene (**4**) (0.30 g, 1.90 mmol) by the procedure above and purification by vpc gave **15***E* (0.14 g, 0.48 mmol, 26%): ^{1}H nmr ($CDCl_3$) δ: 0.1 (m, 2), 0.33 (s, 9, Me_3Si), 0.5 (m, 2), 0.86 (s, 9, *t*-Bu), 1.96 (m, 1), 6.1 (m, 5, Ph); ^{13}C nmr ($CDCl_3$) δ: 0.9, 3.7, 13.8, 30.4, 37.9, 126.5, 127.1, 132.0, 137.6, 154.2; ms *m/z*: 273 ($M^+ - CH_3$).

*(*E*)-1-Cyclopentyl-3,3-dimethyl-1-phenyl-2-trimethylsilyloxy-1-butene (***16***E)*

The reaction of cyclopentylphenylketene (**7**) (0.34 g, 1.83 mmol) by the procedure above and purification by vpc gave **16***E* (0.16 g, 0.51 mmol, 28%): ir (CCl_4): 1616 (C=C) cm^{-1}; ^{1}H nmr ($CDCl_3$) δ: 0.31 (s, 9, Me_3Si), 0.84 (s, 9, *t*-Bu), 1.0–1.7 (m, 8), 3.10 (m, 1), 7.2 (m, 5, Ph); ^{13}C nmr ($CDCl_3$) δ: 1.1, 24.3, 30.3, 30.9, 31.2, 41.9, 126.3, 127.1, 132.4, 139.6, 153.3, hrms *m/z* calcd. for $C_{20}H_{32}OSi$ (M^+): 316.2222; found: 316.2218.

*(*E*)-1-Cyclohexyl-3,3-dimethyl-1-phenyl-2-trimethylsilyloxy-1-butene (***17***E)*

The reaction of cyclohexylphenylketene (**8**) (0.30 g, 1.5 mmol) by the procedure above and purification by vpc gave **17***E* (0.12 g, 0.39 mmol, 26%): ^{1}H nmr ($CDCl_3$) δ: 0.34 (s, 9, Me_3Si), 0.83 (s, 9, *t*-Bu), 0.9–1.2 (m, 10), 2.75 (m, 1), 7.2 (m, 5, Ph); ^{13}C nmr ($CDCl_3$) δ: 1.1, 25.8, 26.6, 30.6, 31.3, 39.4, 126.0, 126.8, 131.7, 136.0, 139.9, 152.0; hrms *m/z* calcd. for $C_{21}H_{34}OSi$ (M^+): 330.2379; found: 330.2392.

*(*Z*)-3-Acetoxy-4-cyclopropyl-2,2,5,5-tetramethyl-3-hexene (***18***Z)*

tert-Butylcyclopropylketene (**5**) (0.25 g, 1.81 mmol) was added dropwise to a solution of *t*-BuLi (9.1 mmol) in 20 mL of pentane at 0°C. The mixture was stirred at 25°C for 0.5 h and was refluxed for 24 h. The pentane was evaporated and 15 mL of THF was added followed by Ac_2O (1.03 mL, 10.9 mmol) in 10 mL of THF and the mixture was stirred overnight at 25°C. Then 10% HCl was added and the mixture was extracted with pentane; the organic layer was washed with $NaHCO_3$, H_2O, and brine, and was dried over $MgSO_4$. The solvent was evaporated and preparative vpc gave **18***Z* (0.08 g, 0.34 mmol, 19%): ir (CCl_4): 1748 (C=O), 1603 (C=C) cm^{-1}; ^{1}H nmr ($CDCl_3$) δ: 0.73 (m, 2), 0.77 (m, 2), 1.22 (s, 9, *t*-Bu), 1.23 (s, 9, *t*-Bu), 1.35 (m, 1), 2.12 (s, 3, CH_3); ^{13}C nmr ($CDCl_3$) δ: 13.7, 21.4, 27.2, 30.0, 30.8, 37.3, 39.0, 136.7, 154.7, 170.1; cims *m/z*: 239 ($M^+ + 1$), 197 ($M^+ - C_3H_5$), 179 ($M^+ - OAc$).

Reaction of tert-*butylisopropylketene (***11***) with* tert-*butyllithium followed by acetic anhydride*

A solution of **11** was generated from the acyl chloride (0.5 g, 2.8 mmol) and Et_3N (0.85 g, 8.4 mmol) in THF as previously described. The filtered ketene solution was transferred to a solution of *t*-BuLi (1.7 M, 8.4 mmol) in 40 mL THF at −78°C. After stirring for 4 h at this temperature, the enolate solution was transferred with a double-tipped needle to a flask containing Ac_2O (0.86 g, 8.4 mmol) at 10 mL of THF at −78°C. The mixture was warmed to 25°C and worked up as before. The crude product (0.38 g, 1.9 mmol, 70%) was separated by vpc (140°C) and gave a 1:5 ratio of **19**/**20**.

The addition was also done in pentane by preparing the ketene in THF, removing the THF under vacuum, and redissolving the ketene in pentane. This solution of ketene in pentane was added at 0°C to a solution of *t*-BuLi (1.7 M, 8.4 mmol) in 20 mL of pentane. The mixture was stirred for 30 min at 0°C and transferred to a flask containing Ac_2O in THF at −78°C. The mixture was warmed to 25°C, poured into saturated aqueous Na_2CO_3, and worked up as before. The **19**/**20** product ratio as determined by vpc (140°C) was 2:1.

*(*Z*)-2,2,5,5-Tetramethyl-3-acetoxy-4-isopropyl-3-hexene (***19***)*: ir (CCl_4): 1746 (C=O) cm^{-1}; ^{1}H nmr ($CDCl_3$) δ: 1.16 (s, 9, *t*-Bu), 1.17 (d, *J* = 7.3 Hz, 3, CH_3), 1.20 (s, 9, *t*-Bu), 1.22 (d, *J* = 7.3 Hz, 3, CH_3), 2.10 (s, 3, OAc), 3.29 (septet, *J* = 7.3 Hz, 1, CH); ^{13}C nmr ($CDCl_3$) δ: 21.6, 21.9, 30.7, 31.9, 37.1, 37.5, 139.7, 151.4, 170.6; hrms *m/z* calcd. for $C_{15}H_{28}O_2$ (M^+): 240.2089; found: 240.2092.

*(*Z*)-1-Acetoxy-2-isopropyl-3,3-dimethyl-1-butene (***20***Z)*: ir (CCl_4): 1755 (C=O) cm^{-1}; ^{1}H nmr ($CDCl_3$) δ: 1.08 (d, *J* = 6.8 Hz, 6, *i*-Pr), 1.19 (s, 9, *t*-Bu), 2.14 (s, 3, OAc), 2.44 (septet, *J* = 6.8 Hz, 1, $CHMe_2$), 6.92 (s, 1, CHO); ^{13}C nmr ($CDCl_3$) δ: 21.1, 21.2, 24.8, 29.8, 35.2, 130.5, 137.7, 167.7; hrms *m/z* calcd. for $C_{11}H_{20}O_2$ (M^+): 184.1463; found: 184.1455. **20***E*: ^{1}H nmr ($CDCl_3$) δ: 1.07 (s, 9, *t*-Bu), 1.14 (d, *J* = 8 Hz, 6, $CHMe_2$), 2.15 (s, 3, OAc), 2.36 (septet of d, *J* = 8, 1 Hz, 1, $CHMe_2$), 6.95 (d, *J* = 1 Hz, 1, C=CH).

*(*E/Z*)-2,2,5-Trimethyl-3-acetoxy-4-phenyl-3-hexene (***21***)*

A solution of **9** (0.5 g, 3.1 mmol) in 5 mL of anhydrous THF was added to a solution of *t*-BuLi (1.7 M in hexane, 6.2 mmol) in 30 mL of THF at −78°C. The solution was stirred at this temperature for 5 h, and then added via a double-tipped needle to a solution of acetic anhydride (1.2 g, 12.0 mmol) in 10 mL of THF at −78°C. The solution was warmed to 25°C, poured into saturated Na_2CO_3, and stirred for 20 min. The product was extracted with ether, dried over $CaSO_4$, and concentrated under vacuum. The crude product was separated by vpc (20% TCEP, 150°C) to give **21** *Z*/*E* (0.62 g, 2.4 mmol, 77%) in a 1:4.3 ratio. **21***Z*: ir (CCl_4): 1749 (C=O) cm^{-1}; ^{1}H nmr (CCl_4) δ: 0.94 (d, *J* = 7.5 Hz, 6, $CHMe_2$), 1.27 (s, 9, *t*-Bu), 1.38 (s, 3, OAc), 3.23 (septet, *J* = 7.5 Hz, 1, $CHMe_2$), 7.1 (m, 5, Ph); ^{13}C nmr ($CDCl_3$) δ: 19.9, 20.8, 21.0, 28.2, 29.9, 35.6, 126.1, 127.2, 129.6, 135.2, 137.4, 150.2, 169.8; hrms *m/z* calcd. for $C_{17}H_{24}O_2$ (M^+): 260.1776; found: 260.1761. **21***E*: ir (CCl_4): 1754 (C=O) cm^{-1}; ^{1}H nmr (CCl_4) δ: 0.81 (d, *J* = 8 Hz, 6, $CHMe_2$), 0.88 (s, 9, *t*-Bu), 2.18 (s, 3, OAc), 2.76 (septet, *J* = 8 Hz, 1, $CHMe_2$, 7.19 (m, 5, Ph); ^{13}C nmr ($CDCl_3$) δ: 20.8, 21.0, 30.0, 30.3, 37.7, 127.2, 127.4, 131.7, 134.0, 136.7, 149.6, 169.9; hrms *m/z* calcd. for $C_{17}H_{24}O_2$ (M^+): 260.1776; found: 260.1773.

The silyl enol ethers **23** *Z*/*E* were prepared similarly by adding Me_3SiCl (12.3 g, 12.2 mmol) to the enolate solution generated from **9** and *t*-BuLi at 0°C. The mixture was warmed to 25°C, stirred for 2 h, filtered to remove LiCl, and the THF was removed under vacuum to give **23** *Z*/*E* in 78% crude yield, in a *Z*/*E* ratio of 1:6, as estimated by ^{1}H nmr. **23***Z*: ^{1}H nmr ($CDCl_3$) δ: −0.30 (s, 9, Me_3Si), 0.95 (d, *J* = 7 Hz, 6, *i*-Pr), 1.28 (s, 9, *t*-Bu), 6.8–7.1 (m, 5, Ph). **23***E*: ^{1}H nmr ($CDCl_3$) δ: 0.32 (s, 9, Me_3Si), 0.80 (d, *J* = 7 Hz, 6, *i*-Pr), 0.87 (s, 9, *t*-Bu), 3.12 (septet, *J* = 7 Hz, 1, CH), 7.08 (m, 5, Ph).

Phenyl-*tert*-butylketene (**10**) was reacted with *t*-BuLi in THF as described for phenyl-*i*-propylketene (**9**). Further reaction with Ac_2O in THF gave *(*E*)-2,2,5,5-tetramethyl-3-acetoxy-4-phenyl-3-hexene* (**22**) in 71% crude yield, which was purified by vpc (200°C): ir (CCl_4): 1754 (C=O) cm^{-1}; ^{1}H nmr (CCl_4) δ: 0.84 (s, 9, *t*-Bu), 0.98 (s, 9, *t*-Bu), 2.13 (s, 3, OAc), 7.2 (m, 5, Ph); ^{13}C nmr ($CDCl_3$) δ: 21.6, 30.7, 31.0, 36.1, 38.3, 126.5, 126.8, 131.5, 136.9, 139.5, 151.9, 170.5; hrms *m/z* calcd. for $C_{18}H_{26}O_2$ (M^+): 274.1933; found: 274.1939.

Crude **24***E* (65%) was prepared similarly by reaction with Me_3SiCl in THF and purified by vpc (150°C): ^{1}H nmr ($CDCl_3$) δ: 0.37 (s, 9, Me_3Si), 0.79 (s, 9, *t*-Bu), 1.02 (s, 9, *t*-Bu), 7.0 (m, 5, Ph).

For reactions of **9** and **10** carried out in pentane/hexane, *t*-BuLi in hexane was added to the ketenes in pentane as above. After warming to 25°C the solvent was evaporated and 10 mL anhydrous THF was added, and the solutions were quenched with Ac_2O or Me_3SiCl. Reaction of **9** gave **21** in a *Z*/*E* ratio of 1:5.4 as determined by vpc, and **23** in a *Z*/*E* ratio of 1:6, as determined by ^{1}H nmr.

Acknowledgement

Financial support by the Natural Sciences and Engineering Research Council of Canada and particularly helpful reports from the referees are gratefully acknowledged.

1. (*a*) T. T. TIDWELL. *In* The chemistry of the cyclopropyl group. Vol. 1. *Edited by* Z. Rappoport. Wiley, New York. 1987. Chap. 10. p. 565; (*b*) B. KLAHN and V. DYCZMONS. J. Mol. Struct. **122**, 75 (1985); (*c*) M. TRAETTEBERG, P. BAKKEN, A. ALMENNINGEN, and W. LÜTTKE. J. Mol. Struct. **189**, 357 (1988); (*d*) J. R. DURIG and T. S. LITTLE. Croat. Chem. Acta, **61**, 529 (1988).
2. (*a*) D. BORRMANN. Methoden der Organischen Chemie. Vol. 7. Part 4. Thieme, Stuttgart. 1968; (*b*) S. PATAI (*Editor*). The chemistry of ketenes, allenes, and related compounds. Parts 1 and 2. Wiley, New York. 1980; (*c*) W. T. BRADY. Tetrahedron, **37**, 2949 (1981); (*d*) H. R. SEIKALY and T. T. TIDWELL. Tetrahedron, **42**, 2587 (1986).
3. (*a*) W. F. BERKOWITZ and A. A. OZORIO. J. Org. Chem. **40**, 527 (1975); (*b*) M. OHKITA, T. TSUJI, M. SUZUKI, M. MURAKAMI, and S. NISHIDA. J. Org. Chem. **55**, 1506 (1990); (*c*) G. MAIER, M. HOPPE, K. LANZ, and H. P. REISENAUER. Tetrahedron Lett. **25**, 5645 (1984); (*d*) W. C. AGOSTA, A. B. SMITH III, A. S. KENDE, R. G. EILERMAN, and J. BENHAM. Tetrahedron Lett. 4517 (1969); (*e*) I. BASNÁK and J. FARKAS. Collect. Czech. Chem. Commun. **41**, 311 (1976); (*f*) B. C. SÖDERBERG, L. S. HEGEDUS, and M. A. SIERRA. J. Am. Chem. Soc. **112**, 4364 (1990).
4. (*a*) T. T. TIDWELL. Acc. Chem. Res. **23**, 273 (1990); (*b*) A. D. ALLEN, A. STEVENSON, and T. T. TIDWELL. J. Org. Chem. **54**, 2843 (1989); (*c*) L. GONG, R. LEUNG-TOUNG, and T. T. TIDWELL. J. Org. Chem. **55**, 3634 (1990); (*d*) L. M. BAIGRIE, D. LENOIR, H. R. SEIKALY, and T. T. TIDWELL. J. Org. Chem. **50**, 2105 (1985); (*e*) A. D. ALLEN and T. T. TIDWELL. J. Am. Chem. Soc. **109**, 2774 (1987); (*f*) L. M. BAIGRIE, H. R. SEIKALY, and T. T. TIDWELL. J. Am. Chem. Soc. **107**, 5391 (1985); (*g*) A. D. ALLEN, L. GONG, and T. T. TIDWELL. J. Am. Chem. Soc. **112**, 6396 (1990); (*h*) A. D. ALLEN, A. J. KRESGE, N. P. SCHEPP, and T. T. TIDWELL. Can. J. Chem. **65**, 1719 (1987).
5. (*a*) A. MAERCKER and J. D. ROBERTS. J. Am. Chem. Soc. **88**, 1742 (1966); (*b*) A. NIERTH, H. M. ENSSLIN, and M. HANACK. Liebigs Ann. Chem. **733**, 187 (1970).
6. (*a*) C. AARON, D. DULL, J. L. SCHMIEGEL, D. JAEGER, Y. OHASHI, and H. S. MOSHER. J. Org. Chem. **32**, 2797 (1967); (*b*) P. MAGNUS and G. ROY. Organometallics, **1**, 553 (1982); (*c*) J. MACPHEE and J. DUBOIS. Tetrahedron, **36**, 775 (1980); (*d*) A. A. SACKS and J. E. ASTON. J. Am. Chem. Soc. **73**, 3902 (1951); (*e*) M. S. NEWMAN, A. ARKELL, and T. FUKUNAGA. J. Am. Chem. Soc. **82**, 2498 (1960); (*f*) R. T. HRUBIEC and M. B. SMITH. J. Org. Chem. **49**, 431 (1984).
7. (*a*) E. V. DEHMLOW, M. SLOPIANKA, and J. PICKARDT. Liebigs Ann. Chem. 572 (1979); (*b*) R. HUISGEN and H. MAYR. Tetrahedron Lett. 2969 (1975); (*c*) E. SCHAUMANN and J. EHLERS. Chem. Ber. **112**, 1000 (1979); (*d*) R. KNORR, M. HINTERMEYER-HILPERT, and P. BÖHRER. Chem. Ber. **123**, 1137 (1990).
8. (*a*) S. H. UNGER and C. HANSCH. Prog. Phys. Org. Chem. **12**, 91 (1976); (*b*) J. A. HIRSCH. Top. Stereochem. **1**, 199 (1967); (*c*) M. CHARTON. Top. Curr. Chem. **114**, 57 (1983); (*d*) M. CHARTON. J. Org. Chem. **41**, 2217 (1976); (*e*) A. Y. MEYER. J. Chem. Soc. Perkin Trans. 2, 1567 (1986); (*f*) T. KOMATSUZAKI, K. SAKAKIBARA, and M. HIROTA. Tetrahedron Lett. **30**, 3309 (1989).
9. (*a*) F. MOHAMADI, N. G. J. RICHARDS, W. C. GUIDA, R. LISKAMP, M. LIPTON, C. CAUFIELD, G. CHANG, T. HENDRICKSON, and W. C. STILL. J. Comput. Chem. **11**, 440 (1990); (*b*) PCMODEL, using the MMX force field from Serena Software, Bloomington, Indiana.
10. (*a*) O. ARJONA, R. F. DE LA PRADILLA, A. MALLO, S. PÉREZ, and J. PLUMET. J. Org. Chem. **54**, 4158 (1989); (*b*) E. C. ASHBY and J. T. LAEMMLE. Chem. Rev. **75**, 521 (1975); (*c*) A. S. CIEPLAK, B. D. TAIT, and C. R. JOHNSON. J. Am. Chem. Soc. **111**, 8447 (1989); (*d*) Y. WU and K. N. HOUK. J. Am. Chem. Soc. **109**, 908 (1987); (*e*) D. MUKHERJEE, Y. WU, F. R. FRONCZEK, and K. N. HOUK. J. Am. Chem. Soc. **110**, 3328 (1988); (*f*) J. FANG, S. SUN, and M. REI. J. Chem. Soc. Perkin Trans. 2, 747 (1989).
11. B. J. WAKEFIELD. Organolithium methods. Academic Press, New York. 1988; The chemistry of organolithium compounds. Pergamon Press. Oxford. 1974.
12. P. KNITTEL and T. T. TIDWELL. J. Am. Chem. Soc. **99**, 3408 (1977).

Can. J. Chem. Downloaded from www.nrcresearchpress.com by 195.138.81.100 on 09/07/12
For personal use only.

The photochemistry of EDA complexes in micellar solutions. II. The stilbene–methylviologen system in the presence of oxygen

M. HAMITY AND R. H. LEMA

Universidad Nacional de Río Cuarto, Departamento de Química y Física, 5800 Río Cuarto, Córdoba, Argentina

Received February 23, 1990

M. HAMITY and R. H. LEMA. Can. J. Chem. **69**, 146 (1991).

The photolyses of electron donor–acceptor (EDA) complexes formed between both *cis*-stilbene (cS) and *trans*-stilbene (tS) as donors and methylviologen (MV^{+2}) as acceptor have been carried out in homogeneous ethanolic and in micellar sodium dodecyl sulfate (SDS) solutions, in the presence of oxygen. The stilbene loss quantum yields (Φ_{-S}) have been determined in both media. Quantum yields were observed to be dependent upon methylviologen concentration and the acidity of media. A reaction scheme is proposed, which accounts for experimental results and can be related to the photochemistry of MV^{+2} and its cation radical $MV^{\bullet+}$.

Key words: EDA complexes, micelles, methyl viologen, stilbene.

M. HAMITY et R. H. LEMA. Can. J. Chem. **69**, 146 (1991).

Opérant en solution éthanolique homogène et en solutions micellaires de dodécylsulfate de sodium (DSS), en présence d'oxygène, on a effectué la photolyse de complexes donneur–accepteur d'électrons (EDA) entre le *cis*-stilbène (cS) ou le *trans*-stilbène (tS) comme donneurs et le viologène de méthyle (MV^{2+}) comme accepteur. On a déterminé les rendements quantiques de perte de stilbène (Φ_{-S}) dans les deux milieux. On a observé que les rendements quantiques varient avec la concentration de viologène de méthyle et l'acidité du milieu. On propose un mécanisme réactionnel qui tient compte des données expérimentales et qui peut être relié à la photochimie du MV^{2+} et de son cation radicalaire $MV^{\bullet+}$.

Mots clés : complexes EDA, micelles, viologène de méthyle, stilbene.

[Traduit par la revue]

Introduction

The photochemistry of stilbenes has been extensively studied (1). The major part of the experimental work in this field has been carried out in homogeneous solution by direct excitation (2, 3) and sensitization (4–6). Some attention has been given to reactions produced by photoexcitation of charge-transfer complexes formed by stilbenes with neutral organic molecules (7, 8).

The *cis*- and *trans*-stilbene cation radicals, ($cS^{\bullet+}$ and $tS^{\bullet+}$) have been proposed as intermediates in the photooxygenation of cS and tS (9) and in the *cis–trans* photoisomerization of cS (10). Both of them, generated via electron transfer reactions, have been detected and characterized (11–14).

Eriksen and Foote (9) obtained photoisomerization and photooxygenation of cS and tS, sensitized by 9,10-dicyanoanthracene in oxygenated acetonitrile, with benzaldehyde (Bzal) as the major oxygenation product. They proposed a mechanism in which the stilbene radical cation $S^{\bullet+}$, formed by electron transfer to excited dicyanoanthracene, reacted with superoxide ion $O_2^{\bullet-}$, produced by the reaction of oxygen with the dicyanoanthracene radical anion, to yield oxygenation products. Lewis *et al.* (10) confirmed for this system that the major photooxygenation product is Bzal and they found that oxygen enhances tS to cS photoisomerization in the polar solvent acetonitrile. They also report that, when the solvent is changed to benzene, oxygen increases 9,10-dicyanoanthracene photosensitized isomerization of both cS and tS, but no oxygenation products are observed. The latter effect is similar to that previously found on tS to cS isomerization via the exciplexes of tS with amines and fumaronitrile, attributed to oxygen-catalyzed intersystem crossing to excited triplet tS (15, 16).

In a previous work we carried out the photolysis, exciting the absorption charge transfer band, of the EDA complexes formed by cS and tS with MV^{+2} in micellar SDS solution and, for the sake of comparison, in homogeneous ethanolic solutions, in the absence of oxygen (17). We report here the results obtained by photolysis of the same systems in the presence of oxygen and the influence exerted on quantum yields by methylviologen concentration and the acidity of the media. We also consider here the possible relationship between the latter effects and the photoreactions of MV^{+2} in the presence of oxygen, studied earlier by several research groups (18, 19).

Experimental

Materials

Commercial methylviologen dichloride (Sigma), *trans*-stilbene (Schuchardt München), and *cis*-stilbene (Koch-Light) were used without further purification. The purity grade of both stilbenes was >99% by GLC.

Sodium dodecyl sulfate (B.D.H.) was washed with diethyl ether and recrystallized from ethanol.

Absolute stilbene loss quantum yields

All the samples, in a 1-cm square quartz cell, were irradiated under similar conditions, at λ >400 nm, with a Philips 1000-W quartz halogen lamp as the light source and a Melles Griot GG 400 filter. The solutions were magnetically stirred, solvent-saturated oxygen was continuously bubbled, and the temperature was maintained at (25 ± 0.1)°C. The concentrations used were as follows. Stilbenes: 1.3×10^{-2} M in 95% ethanol and 6×10^{-4} M in 0.1 M SDS; MV^{+2} was varied between 5×10^{-4} and 5×10^{-3} M in 0.1 M SDS and between 1×10^{-3} M and 2.4×10^{-2} M in ethanol. Ethanolic solutions with HCl concentrations between 0.5×10^{-5} and 1×10^{-5} M were obtained by dilution in 95% ethanol of concentrated commercial hydrochloric acid. In SDS micellar solution, the acidity was varied by adding dilute HCl to obtain a value of pH that was measured with a glass electrode and a Radiometer pHM 64 pH meter. Uranyl oxalate was used as actinometer (20). Oxalate loss was determined by titration with $KMnO_4$.

Stilbene concentrations were monitored by GLC with a Varian 2800 chromatograph using an OV-101 on Chromosorb G H/P 100–120 mesh column. The samples in SDS micellar solutions were treated, after irradiation, with $CaCl_2$ to precipitate SDS and then with *n*-pentane, containing *n*-dodecane as external standard, to extract organic components and separate them from water-soluble MV^{+2} (21). Prior to irradiation, *n*-dodecane was added as internal standard to ethanolic

Can. J. Chem. Downloaded from www.nrcresearchpress.com by 195.138.81.100 on 09/07/12
For personal use only.

Can. J. Chem. Downloaded from www.nrcresearchpress.com by 195.138.81.100 on 09/07/12
For personal use only.

TABLE 1. *trans*-Stilbene loss quantum yields at several methylviologen and hydrochloric acid concentrations in ethanol at constant concentration of tS = 1.3×10^{-2} M

$[MV^{+2}]\ 10^3$ M	$[ClH]\ 10^6$ M	$\Phi_{-tS}\ 10^3$
10.00	10.0	3.8
10.00	8.7	4.0
10.00	7.0	5.1
10.00	5.0	6.6
24.00	—	4.9
10.00	—	10.0
8.68	—	13.0
7.08	—	16.3
5.00	—	27.3
1.00	—	53.1

solutions, which were then photolyzed and chromatographed. The estimated error in quantum yields is 10%.

Results and discussion

Photoreactions of cS complex in ethanol could not be detected under our experimental conditions. In 0.1 M SDS micellar solutions, in turn, the photoisomerization product was obtained, but the quantum yield was appreciably lower than that determined in the absence of oxygen (17) and it was observed to be influenced by acidity of the medium.

Quantum yields for tS loss (Φ_{-tS}) were evaluated in both media. Furthermore, the effect of MV^{+2} concentration and the acidity of the medium was studied.

Photolysis of the EDA complexes in ethanol

In the photolysis of the tS EDA complex, photoisomerization and oxygenation products were detected. During these experiments, an absorption band ($\lambda_{max} \sim 400$ nm) and a fluorescence band ($\lambda_{max} \sim 530$ nm) appeared, whose intensities increased with photolysis time and decreased with acidity of the medium. We believe that these bands are generated from certain products of secondary reactions of methylviologen that have already been observed by several authors (18, 19). Mau *et al.*, in particular, exciting the absorption band of MV^{+2} ($\lambda < 320$ nm) to produce methylviologen cation radical $MV^{\bullet+}$, observed the generation of a green fluorescence, the excitation and emission maxima wavelengths of which are similar to those observed by us and whose intensity decreased with increasing acidity of the solution (19).

In our experiments, tS concentration was kept constant and, to study the effect of secondary reactions, medium acidity (added HCl) or MV^{+2} concentration were varied. Table 1 shows the influence of both acid and methylviologen concentration on quantum yield.

Benzaldehyde (Bzal) was the main product in stilbene photooxygenation reactions (9, 10). In our experiments, the Bzal detected was not enough to get a mass balance. For this reason and to check for the occurrence of secondary reactions, we carried out the photolysis of the tS EDA complex under similar conditions, but with Bzal (0.1 M) added, and we observed an appreciable benzaldehyde consumption. Ethanolic solutions prepared with the same concentrations of Bzal alone and Bzal/tS did not evidence physical or chemical changes. However, a solution containing Bzal and MV^{+2} showed an absorption band ($\lambda_{max} \simeq 430$ nm) and a fluorescence band ($\lambda_{max\ excit} \simeq 440$ nm and $\lambda_{max\ em} \simeq 530$ nm), which disappeared by photolyzing at $\lambda > 400$ nm.[1]

According to the results outlined above, we believe that photolysis of the EDA complex of *trans*-stilbene with MV^{+2}, in the presence of oxygen, yields isomerization and oxygenation products, mainly benzaldehyde, which in turn undergoes secondary photoreactions with MV^{+2}. It is worth note that the fluorescence produced during the photolysis of the EDA complex is not due, at least in part, to the same species as that produced by mixing Bzal and MV^{+2}, because the latter disappears under photolysis, while the former increases with increasing irradiation time.

The following reaction scheme is presented to account for the above detailed experimental results:

$$tS + MV^{+2} \underset{}{\overset{K_{eq}}{\rightleftharpoons}} C \qquad (C = \text{EDA complex})$$

$$C + h\nu \xrightarrow{I_a} C^*$$

$$C^* \xrightarrow{k_0} (tS^{\bullet+} + MV^{\bullet+})$$

[1] $$(tS^{\bullet+} + MV^{\bullet+}) \xrightarrow{k_1} tS + MV^{+2}$$

[2] $$(tS^{\bullet+} + MV^{\bullet+}) \xrightarrow{k_2} tS^{\bullet+} + MV^{\bullet+}$$

[3] $$tS^{\bullet+} + MV^{\bullet+} \xrightarrow{k_3} tS + MV^{+2}$$

[4] $$MV^{\bullet+} + O_2 \underset{k_{-4}}{\overset{k_4}{\rightleftharpoons}} MV^{+2} + O_2^{\bullet-}$$

[5] $$tS^{\bullet+} + O_2^{\bullet-} \xrightarrow{k_5} (tS\ldots O_2) \begin{cases} \rightarrow cS + O_2 \\ \rightarrow tS + O_2 \\ \rightarrow P_{ox.} \end{cases}$$

[6] $$MV^{+2} + O_2^{\bullet-} \xrightarrow{k_6} P_{GF}$$

[7] $$H^+ + O_2^{\bullet-} \xrightarrow{k_7} P$$

The EDA complex C is formed in the first step, for which the equilibrium constant value (K_{eq}) has been already measured (17). The complex is then excited through the absorption of a photon and produces the ionic radical pair in the solvent cage with a rate constant k_0. Solvent cage escape in step [2] competes with deactivation by step [1]. The free radical ions can either recombine (step [3]) or react, $MV^{\bullet+}$ with O_2 to give the superoxide ion $O_2^{\bullet-}$ (step [4]) and $tS^{\bullet+}$, by step [5], to give an intermediate ($tS\ldots O_2$), which in turn renders isomerization and oxygenation products.

The methylviologen ion (step [6]) and the added acid (step [7]) compete with $tS^{\bullet+}$ for the superoxide ion, thus leading to inhibition of reaction step [5] and therefore to a lowering of Φ_{-ts}, as is experimentally observed (Table 1). The quantum yield of stilbene loss is given as

[8] $$\Phi_{-tS} = \eta_c \cdot \eta_r$$

where

[9] $$\eta_c = \frac{k_2}{k_2 + k_1}$$

and

[10] $$\eta_r = \frac{k_5[O_2^{\bullet-}]}{k_5[O_2^{\bullet-}] + k_3[MV^{\bullet+}]}$$

[1] M. Hamity and R. H. Lema. Unpublished results.

Can. J. Chem. Downloaded from www.nrcresearchpress.com by 195.138.81.100 on 09/07/12
For personal use only.

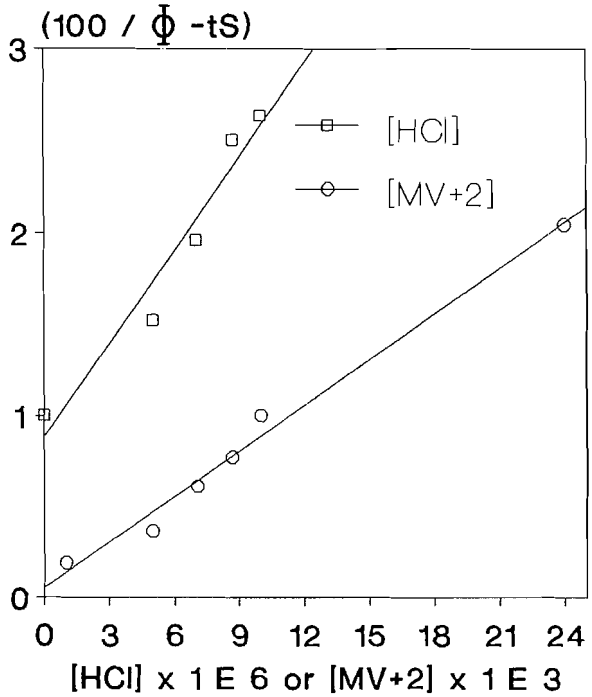


FIG. 1. Inverse of *trans*-stilbene loss quantum yield as a function of hydrochloric acid concentration (correlation coefficient $f_c = 0.974$) and methylviologen concentration ($f_c = 0.994$) in ethanol.

are the efficiencies of generation and of reaction, respectively, of $tS^{\bullet+}$. The rate constant for the reaction between $MV^{\bullet+}$ and O_2 was reported as $k_4 = 7.7 \times 10^8\ M^{-1}$ (23). According to this figure and notwithstanding the value of k_3, we can assume $k_4[O_2] \gg k_3[tS^{\bullet+}]$, because $[O_2] \gg [tS^{\bullet+}]$. Using steady state kinetics and taking $1 \gg \eta_r$, we obtain the following equation for stilbene loss quantum yield Φ_{-tS} and the concentration terms [HCl] and $[MV^{+2}]$:

$$[11] \quad (\Phi_{-tS})^{-1} = a[MV^{+2}] + b[HCl] + (\eta_c)^{-1}$$

where

$$[12] \quad a = \frac{k_3 k_6}{\eta_c k_4 k_5 [O_2]}$$

and

$$[13] \quad b = \frac{k_3 k_7}{\eta_c k_4 k_5 [O_2]}$$

By plotting the inverse of Φ_{-tS} vs. [HCl] at a constant methylviologen concentration and vs. $[MV^{+2}]$ without HCl added, a straight line is obtained in both cases, Fig. 1. The intercept of either line gives the η_c value, which is 0.19 ± 0.02. This is the maximum quantum yield for this system and, according to the proposed mechanism, represents the efficiency of solvent-cage escape for the photogenerated radical ion pair.

From the slopes of both lines, the ratio of rate constants for steps [7] and [6] of the reaction scheme can be obtained as

$$[14] \quad \frac{b}{a} = \frac{k_7}{k_6} = 2.04 \times 10^3$$

These steps correspond to the reactions of $O_2^{\bullet-}$ with H^+ and MV^{+2}, respectively, by which the two latter species are supposed to influence Φ_{-tS} as inhibitors. The value obtained in eq. [14] is in accord with the fact that higher concentrations of MV^{+2} than of HCl must be used to obtain a similar effect on quantum yield.

TABLE 2. *trans*-Stilbene loss quantum yields at several methylviologen concentrations and bulk water-phase proton concentrations in 0.1 M SDS solution at constant analytical concentration of $tS = 6 \times 10^{-4}$ M

$[MV^{+2}]_0\ 10^3$ M	$[MV^{+2}]_m\ 10^2$ M	$[H^+]_w\ 10^6$ M	$\Phi_{-tS}\ 10^3$
1.00	7.22	11.60	1.43
1.00	7.22	7.94	1.61
1.00	7.22	6.31	1.71
0.50	3.61	3.98	3.23
1.00	7.22	3.98	1.90
1.25	8.98	3.98	1.52
1.40	10.10	3.98	1.45

It is noteworthy that steps [4] and [6] in the proposed reaction scheme constitute a simplified mechanism for the photoreaction of MV^{+2} with O_2, yielding fluorescent products via methylviologen radical cation $MV^{\bullet+}$ (18, 19, 24, 25). Leest (24) has proposed that the reaction of $MV^{\bullet+}$ with O_2 regenerates MV^{+2} and takes place in two steps, the first equivalent to step [4] in our reaction scheme and a second slow step, $MV^{\bullet+}$ with $O_2^{\bullet-}$ to yield MV^{+2}. On the other hand, the dependence of Φ_{-tS} on methylviologen concentration suggests that MV^{+2} can react with $O_2^{\bullet-}$ as in step [6], yielding oxidation products from which can arise, at least in part, the green fluorescence observed. Finally, step [7] of the scheme, where HCl is competing with MV^{+2} for $O_2^{\bullet-}$, can account for the dependence of the green fluorescence upon solvent acidity, as observed by Mau *et al.* (19).

Photolysis of EDA complexes in SDS

The photolysis of the tS EDA complex was carried out using constant analytical concentrations of tS and SDS and changing pH (with HCl) or MV^{+2} concentration, as shown in Table 2. The influence of medium acidity and $[MV^{+2}]$ on quantum yield is similar to that observed in ethanol.

When a solution of tS EDA complex containing Bzal (10^{-3} M) is photolyzed, an increase of Bzal concentration is observed, in contrast to the consumption detected in ethanolic solution. A solution of Bzal (10^{-3} M) and MV^{+2} did not show chemical or physical changes similar to those observed in ethanol.

A fluorescence band with λ_{max} at 530 nm, which increased with irradiation periods and decreased with medium acidity, was detected in SDS, but its emission intensity was rather lower than that measured in ethanolic solutions.

The plots of inverse of tS loss quantum yields versus proton or methylviologen concentration are linear, as shown in Fig. 2. This is indicative that the reaction scheme presented to explain the experimental results in ethanol can also be used in SDS solutions. For micelle-bound reactants, as with MV^{+2} and the stilbenes (17), the concentration in the micellar pseudo-phase is given by

$$[MV^{+2}]_m = \frac{[MV^{+2}]_0 - [MV^{+2}]_w}{\bar{V} \cdot [SDS]_m} \simeq \frac{[MV^{+2}]_0}{\bar{V} \cdot [SDS]_m}$$

where the subscripts m, 0, and w indicate micellar, total, and water concentrations, respectively; $\bar{V}$ is the molar volume of micellized detergent; and $[SDS]_m$ is the micellized detergent concentration, i.e., ($[SDS]_0$ − cmc), where cmc is the critical micelle concentration. The values used were $\bar{V} = 0.14$ L/mol and cmc $= 1 \times 10^{-3}$ M (17).

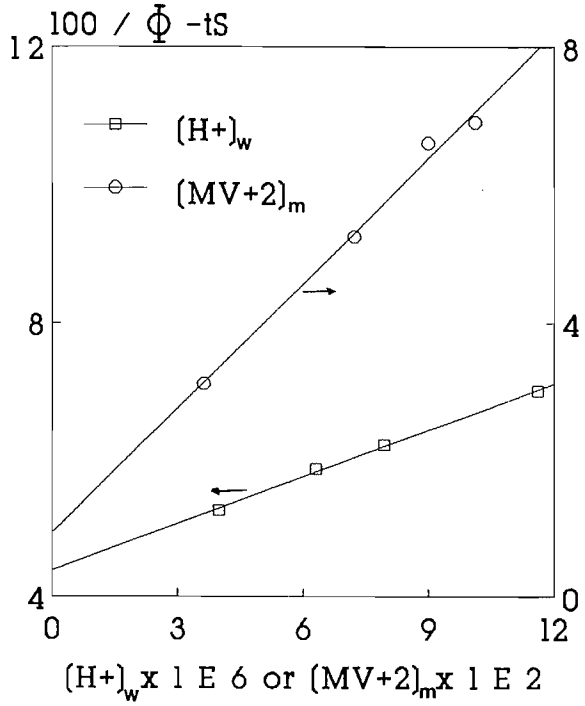


FIG. 2. Inverse of *trans*-stilbene loss quantum yield as a function of bulk water-phase proton concentration (correlation coefficient f_c = 0.999) and micellar-phase methylviologen concentration (f_c = 0.996) in 0.1 M SDS solution.

The medium acidity is given through the bulk water proton activity $a_H{}^w = 10^{-pH} \simeq [H^+]_w$, where pH is measured by a glass electrode. The local interfacial proton activity $a_H{}^m \simeq [H^+]_m$, at the surface of charged micelles, can be expressed by the following equation (26, 27):

$$[15] \quad [H^+]_m = [H^+]_w \cdot \exp -(F\Psi/RT) = [H^+]_w \cdot f$$

where F is Faraday's constant, R is the general gas constant, T is the temperature, and Ψ is the interfacial potential. The value of Ψ depends heavily on the completeness of the binding to the micelles of the probe molecule. When a lipoid dye, closely bound to SDS micelles, is employed, a value of −134 mV is obtained, but using a probe that takes part in an equilibrium at the micelle–water interface, the measured value for SDS micelles is −27 mV (27). Accordingly, eq. [11] can be rewritten as

$$(\Phi_{-tS})_m^{-1} = a_m[MV^{+2}]_m + b_m f[H^+]_w + (\eta_{cm})^{-1}$$

where a_m and b_m are micellar system parameters. From the plot in Fig. 2, the value of the slope a_m is 6.06×10^3 M^{-1}, which is similar to the corresponding ethanol parameter ($a = 7 \times 10^3$ M^{-1}).

According to eq. [12], a is a function of $\eta_c[O_2]$ and therefore, since $a \simeq a_m$, $\eta_c[O_2] \simeq \eta_{cm}[O_2]_m$. In ethanol, $[O_2] = 2.07 \times 10^{-3}$ M and, if $[O_2]_m$ is assumed to be nearly the same as the solubility of oxygen in water (2.65×10^{-4} M) (28), it can be concluded that the efficiency of solvent cage escape in SDS micellar solution (η_{cm}) is higher than that in ethanol (η_c). The mean value obtained from the intercepts of both lines in Fig. 2 is $\eta_{cm} = 0.44$, while from Fig. 1 a value of $\eta_c = 0.19$ was obtained.

If the mechanism in SDS micellar solutions is the same as in ethanol, the ratio of parameters b_m/a_m is approximately the same as that in eq. [14] for b/a in ethanol. From the value of the ratio of the slopes in Fig. 2 ($b_m f/a_m$) and making use of the previous assumption, we obtain $f = 1.8$. This nearly corresponds to the interfacial potential $\Psi = -27$ mV (27). Taking account of the pH value measured for SDS solutions without added acid (Table 2), the local interfacial pH calculated from eq. [15] is 5.1, which is similar to the generally accepted SDS micelle/water interface pH value (≃5).

TABLE 3. Effect of bulk water-phase pH on *cis*-stilbene loss quantum yield in 0.1 M SDS solution at constant analytical concentrations of cS = 6×10^{-4} M and $MV^{+2} = 5 \times 10^{-3}$ M

$(pH)_w$	$[H^+]_w$ 10^6 M	Φ_{-cS} 10^3
5.40	3.98	12.00[a]
5.40	3.98	0.67
4.50	31.63	7.50

[a]In the absence of oxygen.

Experiments with the cS EDA complex were carried out under experimental conditions similar to those for the tS complex. As shown in Table 3, oxygen inhibits the photoreaction of cS (17). An increase of medium acidity decreases this inhibition. A possible explanation is that the radical cation $cS^{\cdot+}$, from the equivalent of step [2] of the reaction scheme, converts irreversibly to $tS^{\cdot+}$:

$$(cS^{\cdot+} + MV^{\cdot+}) \xrightarrow{k_2'} cS^{\cdot+} + MV^{\cdot+}$$

$$cS^{\cdot+} \xrightarrow{k_{isom}} tS^{\cdot+} \longrightarrow tS$$

The radical ion $O_2^{\cdot-}$ can inhibit this reaction path by reacting with $cS^{\cdot+}$ through the equivalent to step [5]:

$$cS^{\cdot+} + O_2^{\cdot-} \xrightarrow{k_5'} (cS\ldots O_2) \longrightarrow cS + O_2$$

Both species, MV^{+2} and H^+, competing with $cS^{\cdot+}$ by $O_2^{\cdot-}$ (steps [6] and [7]), favor the isomerization sequence. This is shown in Table 3 for the case of protons: a decrease in pH supresses the inhibition by oxygen and the quantum yield is raised near to the value obtained in the absence of oxygen.

Conclusions

The results obtained in this work and those reported in a previous paper (17) indicate the occurrence of stilbene radical cation $S^{\cdot+}$ in the photoisomerization and photooxygenation of stilbene by excitation of the stilbene/methylviologen EDA complex.

The *trans*-stilbene radical cation $tS^{\cdot+}$, being much more stable than $cS^{\cdot+}$, is not expected to isomerize. This is confirmed by the lack of photoreaction of the tS complex in the absence of oxygen (17).

Since $cS^{\cdot+}$ is expected to undergo irreversible isomerization (1, 10), the lack of reaction of cS complex in ethanol, with and without oxygen in solution, suggests that the recombination of the radical ion pair in the solvent cage prevents cage escape and subsequent reactions of $cS^{\cdot+}$ · SDS micelles show a catalytic effect on this isomerization process, probably through the stabilization of the radical cation, as has already been observed in micellar systems for radical ions (22). The cS to tS isomerization process is observed in SDS both in the absence and in the presence of oxygen, with lower quantum yield in the latter case. This inhibition by oxygen is probably caused by the trapping of

Can. J. Chem. Downloaded from www.nrcresearchpress.com by 195.138.81.100 on 09/07/12
For personal use only.

$cS^{\bullet+}$ by $O_2^{\bullet-}$ to regenerate starting material. The effect of HCl supports this assumption: the quantum yield is increased, predictably due to step [7], i.e., the reaction of acid with $O_2^{\bullet-}$.

On the other hand, the radical cation $tS^{\bullet+}$, which does not isomerize on its own, gives isomerization as well as oxidation products in the presence of oxygen. According to step [5] of our mechanism, the reaction products could be obtained through an intermediate ($tS...O_2$), which, in contrast to ($cS...O_2$), is reactive enough to give isomerization (probably through internal rearrangement) and oxidation products like Bzal (through a cleavage process). Acid added, in this case, produces a decrease in Φ_{-tS}, and MV^{+2} acts similarly, the probable reason in both cases being reaction with $O_2^{\bullet-}$ (steps [6] and [7]).

Our reaction scheme postulates the superoxide ion radical $O_2^{\bullet-}$ as an intermediate that is common to the reactions of both $S^{\bullet+}$ and MV^{+2}. The latter is proposed to undergo a reaction step (step [6]) as a probable route to fluorescent product generation.

Finally, secondary reactions of the benzaldehyde with MV^{+2} account for the lack of mass balance in stilbene photoreaction. We are currently studying the photochemistry of the benzaldehyde–methylviologen system.

Acknowledgments

Thanks are given to Universidad Nacional de Río Cuarto, CONICOR (Provincia de Córdoba), and CONICET (República Argentina) for financial support.

1. F. D. Lewis. Adv. Photochem. **13**, 165 (1986).
2. G. Fischer, K. A. Muszkat, and E. Fischer. J. Chem. Soc. B, 1156 (1968).
3. J. Saltiel and J. L. Charlton. *In* Rearrangements in ground and excited states. Vol. 3. *Edited by* P. deMayo. Academic Press, New York. 1980. p. 25.
4. L. M. Stephenson and G. S. Hammond. Angew. Chem. Int. Ed. Engl. **8**, 261 (1969).
5. J. D. Simon and K. S. Peters. J. Am. Chem. Soc. **105**, 4875 (1983).
6. K. Gollnick and A. Schnatterer. Photochem. Photobiol. **43**, 365 (1986).
7. B. K. Adams and W. R. Cherry. J. Am. Chem. Soc. **103**, 6904 (1983).
8. J. L. Goodman and K. S. Peters. J. Am. Chem. Soc. **107**, 1441 (1985).
9. J. Eriksen and C. S. Foote. J. Am. Chem. Soc. **102**, 6083 (1980).
10. F. D. Lewis, J. R. Petisce, J. D. Oxman, and M. J. Nepras. J. Am. Chem. Soc. **107**, 203 (1985).
11. T. Shida and W. H. Hamill. J. Chem. Phys. **44**, 2375 (1966).
12. L. T. Spada and C. S. Foote. J. Am. Chem. Soc. **102**, 391 (1980).
13. T. W. Ebbesen. J. Phys. Chem. **92**, 4581 (1988).
14. F. D. Lewis, R. E. Dykstra, I. R. Gould, and S. Farid. J. Phys. Chem. **92**, 7042 (1988).
15. F. D. Lewis and J. T. Simpson. J. Phys. Chem. **83**, 2015 (1979).
16. W. Hub, U. Kluter, S. Schneider, F. Dorr, J. D. Oxman, and F. D. Lewis. J. Phys. Chem. **88**, 2308 (1984).
17. M. Hamity and R. H. Lema. Can. J. Chem. **66**, 1552 (1988).
18. C. L. Bird and A. T. Kuhn. Chem. Soc. Rev. **10**, 49 (1981).
19. A. W-H. Mau, J. M. Overbeek, J. D. Loder, and W. H. F. Sasse. J. Chem. Soc. Faraday Trans. 2, **82**, 869 (1986).
20. J. F. Rabek. Experimental methods in photochemistry and photophysics. Wiley, New York. 1982. Part 2. Chap. 27.
21. D. A. Jaeger and R. E. Robertson. J. Org. Chem. **42**, 3298 (1977).
22. M. A. Fox. Adv. Photochem. **13**, 237 (1986).
23. J. A. Farrington. Biochim. Biophys. Acta, **314**, 372 (1973).
24. R. E. Leest. J. Electroanal. Chem. Interfacial Electrochem. **43**, 251 (1973).
25. R. N. F. Thorneley. Biochim. Biophys. Acta, **333**, 487 (1974).
26. G. S. Hartley and J. W. Roe. Trans. Faraday Soc. **36**, 101 (1940).
27. M. S. Fernández and P. Fromherz. J. Phys. Chem. **81**, 1755 (1977).
28. S. L. Murov. Handbook of photochemistry. Marcel Dekker, New York. 1973. p. 89.

Can. J. Chem. Downloaded from www.nrcresearchpress.com by 195.138.81.100 on 09/07/12
For personal use only.

The influence of dielectric permittivity of the nonaqueous phase on the photooxidation of water at the interface of two immiscible liquids in the presence of a hydrated oligomer of chlorophyll. The role of a proton acceptor

MIKHAIL D. KANDELAKI

Regional Department of the All-Union Research Institute of Applied Molecular Biology and Genetics of VASKhNILL, Tbilisi, USSR

AND

ALEXANDER G. VOLKOV[1]

Centre de Recherche en Photobiophysique, Universite du Quebec a Trois-Rivieres, C.P. 500, Trois-Rivieres, P.Q., Canada G9A 5H7

Received June 4, 1990

MIKHAIL D. KANDELAKI and ALEXANDER G. VOLKOV. Can. J. Chem. **69**, 151 (1991).

We have investigated polarographically the dependence of the dioxygen yield on the concentration of 2,4-dinitrophenol in photooxidation of water in an octane/water system containing hydrated oligomer of chlorophyll, a water-soluble electron acceptor ferricyanide and a buffer. A linear correlation between the rate of dioxygen evolution and the photopotential at the interface between the two liquid phases is observed. Investigation of the dependences of photopotential and rate of dioxygen evolution on the dielectric permittivity of the nonaqueous phase has shown that with increasing dielectric permittivity, one can observe a decrease in both the reaction rate and the potential difference. The lifetime of chlorophyll in the course of water photooxidation reaction has been measured.

Key words: chlorophyll, oxygen, water photooxidation, oil/water interface, artificial photosynthesis.

MIKHAIL D. KANDELAKI et ALEXANDER G. VOLKOV. Can. J. Chem. **69**, 151 (1991).

Faisant appel à la polarographie, on a étudié la relation entre le rendement en dioxygène et la concentration de 2,4-dinitrophénol lors de la réaction de photo-oxydation de l'eau dans un système octane/eau contenant un oligomère hydraté de la chlorophylle, un ferricyanure soluble dans l'eau et accepteur d'électrons et un tampon. On a observé l'existence d'une corrélation linéaire entre la vitesse d'évolution du dioxygène et le photopotentiel à l'interface des deux phases liquides. Une étude sur les relations entre le photopotentiel ou la vitesse d'évolution du dioxygène et la permittivité diélectrique de la phase non-aqueuse montre qu'une augmentation de la permittivité diélectrique conduit à une diminution tant de la vitesse de la réaction que de la différence de potentiel. On a mesuré le temps de vie de la chlorophylle au cours de la réaction de photo-oxydation de l'eau.

Mots clés : chlorophylle, oxygène, photo-oxydation de l'eau, interface huile/eau, photosynthèse artificielle.

[Traduit par la revue]

Introduction

Chemical models of photosynthesis are used for investigation of two types of reactions. In the photosynthesis processes the standard Gibbs free energy of a reaction is positive, and solar energy is used to perform work. In photocatalytic processes the free energy is negative and solar energy is used to overcome the activation barrier.

The interface between two immiscible liquids with immobilized photosynthetic pigments can serve as the simplest model of the biological membrane convenient for investigation of photoprocesses that are accompanied by spatial separation of charges.

It was shown previously by investigating the mass spectra, as well as polarographically on a dropping mercury electrode and on a Clark-type electrode, that illumination of the octane/water interface with visible light in the presence of chlorophyll and proton acceptor pentachlorophenol (PCPh) or 2,4-dinitrophenol (DNPh) in octane and an electron acceptor (NAD^+, $NADP^+$, or $K_3[Fe(CN)_6]$) in water there is evolution of dioxygen from water (1–12). In this case it appeared that with the evolution of one dioxygen molecule four ferricyanide molecules are reduced, and the reaction can be written as

$$[1] \quad 2H_2O + 4[Fe(CN)_6]^{3-} = O_2 + 4[Fe(CN)_6]^{4-} + 4H^+$$

This process is accompanied by the appearance of a photopotential at the octane/water interface and seems to occur on the interface since the photopotential and reaction rate are proportional to the surface concentration of chlorophyll and are independent of the thickness of both the aqueous and octane phases. Investigation of the action spectrum (the rate of dioxygen evolution) has shown that it reproduces the absorption spectrum of hydrated oligomer of chlorophyll (3, 5–8).

The rate of the reaction, accompanied by charge transfer through the interface of two immiscible liquids, as well as the corresponding variation in the interfacial potential difference depend on the dielectric permittivity of the nonaqueous phase (13–18). In this paper we have investigated experimentally the influence of the nature of a nonaqueous solvent on the photopotential and the rate of evolution of molecular dioxygen. It is known that at high concentrations, chlorophyll in nonaqueous solvents is aggregated: tetramers and dimers in dry octane, dimers in benzene and methylbutyl ketone, but appear as monomers or colloid particles in more polar solvents (19). A study of the influence of dielectric permittivity of the nonaqueous phase on the reaction course gives a clue for the interpretation of the mechanism.

Materials and methods

The Volta potential was measured by the vibrating electrode method

[1]Permanent address: A. N. Frumkin Institute of Electrochemistry, Academy of Sciences of the USSR, 31 Leninsky Prospect, 117071 Moscow, USSR.

Can. J. Chem. Downloaded from www.nrcresearchpress.com by 195.138.81.100 on 09/07/12
For personal use only.

in the chain (1–10):

[2]	Au	Air	Oil proton acceptor chlorophyll	Water electron acceptor buffer	Water saturated with KCl	Hg_2Cl_2, Hg

and recorded automatically by a KSP-4 recorder.

The dioxygen, evolved from oil/water system after exposed to light, was determined in a polarographic cell by the usual plotting of polarization curves of oxygen reduction on a dropping mercury electrode dipped in aqueous solution. The duration of dioxygen evolution was also measured using a Clark-type electrode that was designed in the All-Union Institute of Medical Equipment. The diameter of the platinum cathode of the PL-2 grade was 20 μm and the gas-permeable polypropylene membrane (Radiometer, Denmark) was 25 μm thick. The indicator solution is a phosphate buffer. The electrode temperature coefficient is not in excess of 1.5% per °C, which practically rules out the influence of temperature effects on the action spectra. The electrode provided measurement of the oxygen concentration up to 10^{-8} M. The cell with the Clark-type electrode was illuminated by a KGM-300 W iodine incandescent lamp through a water filter and interference light filters ($\lambda_{0.5}$ = 10 nm). For determining the number of incident quanta we used a thermoelement and a ferrooxalate actinometer as described previously (4–8).

Solvents with different dielectric permittivity were chosen as the nonaqueous phase: octane, decane, benzene, methylbutyl ketone, nitrobenzene, and propylene carbonate. The proton acceptor PCPh or DNPh was distributed among the aqueous and organic phases since it was added 24 h before the experiment. Chlorophyll a and a water-soluble acceptor of electrons were introduced just before the start of the experiment. All solutions were prepared with twice-distilled water; and salts were twice-recrystallized. DNPh, PCPh, and potassium ferrocyanide were three times recrystallized by conventional techniques. Chlorophyll a was isolated by the familiar method (20) from nettle and was purified by a sucrose column.

The cell for polarographic measurements was thermostated and before the experiment was blown through to remove oxygen. Experiments were carried out at 20°C.

Results and discussion

During the illumination of the octane/water system containing chlorophyll, DNPh, and ferricyanide, photooxidation of water and evolution of molecular dioxygen occurs. Figure 1 presents the dependence of the concentrations of dioxygen evolved on the concentration of proton acceptor, DNPH, in octane, at different times of light exposure.

If chlorophyll and $K_3[Fe(CN)_6]$ are added to the equilibrated octane/water system containing 2,4-dinitrophenol, illumination at the interface results in a photopotential (Fig. 2) which depends on the wavelength and intensity of the incident light, as well as on the concentration of all reaction components. No photopotential appeared if both solvents, octane and water, were not previously equilibrated and mutually saturated.

Figure 2 presents the results of measurement of the photopotential in the chain (1) and the dependence of the rate of dioxygen evolution on the DNPh concentration. It is evident from Fig. 2 that there is a correlation between the rate of dioxygen evolution and the photopotential value. This signifies that the reaction (1) occurs directly at the interface between water and oil and is accompanied by the spatial separation of charges. Such a correlation between the rate of the charge transfer reaction and the variation in the interfacial potential difference is consistent with the phenomenological theory, developed earlier, of catalytic reactions at the interface between two immiscible liquids (13, 14).

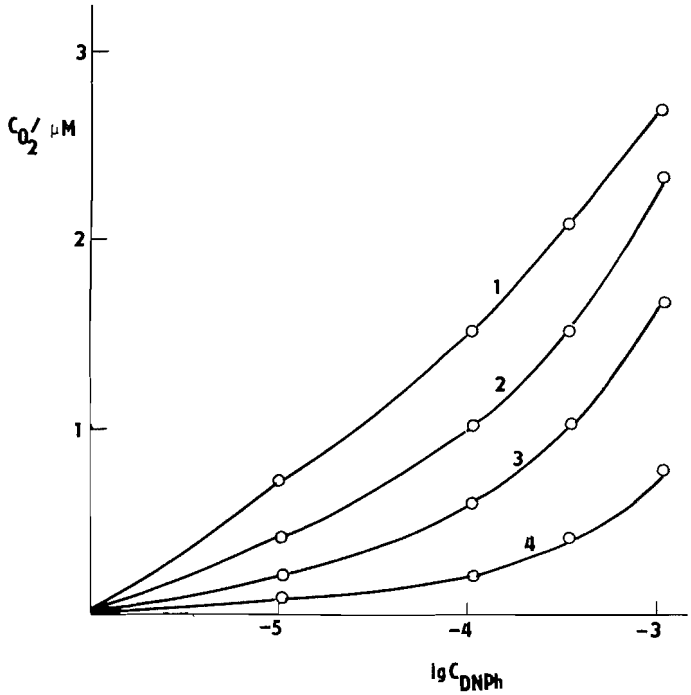


FIG. 1. Dependences of the concentration of dioxygen evolved under illumination on the DNPh concentration. Medium: octane/water, 2×10^{-6} M chlorophyll, 5×10^{-2} M $K_3[Fe(CN)_6]$, 2×10^{-2} M Tris-HCl, pH 7.4. Exposure time: *1*, 60 min; *2*, 45 min; *3*, 30 min; *4*, 15 min. Light intensity is 100 mW/cm^2.

According to the molecular mechanism of photooxydation of water in the octane–water system, as proposed in refs. 9 to 12, DNPh acts as a surface buffer capable of accepting protons, evolved in the course of the reaction (1), and thereby protecting chlorophyll against pheophytinization. DNPh, adsorbed at the interface octane/water, dissociates into $DNPh^-$ and H^+, charging octane negatively relative to water. The change in the Volta potential in the chain (1) as a result of the adsorption of DNPh at the interfaces octane–water or decane/water is −0.2 V. At the start of the photoreaction $DNPh^-$ accepts protons evolved and results in a positive photopotential corresponding to the transfer of protons from water to DNPh anions adsorbed at the interface.

Figures 3 and 4 present the dependences of the photopotential on the time of equilibration between octane and the aqueous phase. The time of contact is the time that has elapsed from the instant of addition of octane to the aqueous phase. Octane, preequilibrated for 24 h with the aqueous phase containing a Tris-HCl buffer at pH 7.4, will be called for brevity "wet". The "dry" octane was not previously in contact with the aqueous phase. It was demonstrated in ref. 3 that the reaction of water oxidation is catalyzed by a hydrated chlorophyll oligomer which is formed in the octane saturated with water. In the case of a brief contact with water for a few minutes, the adsorption spectra show no significant formation of aggregates and the adsorption layer at the interface is formed predominantly from "dry" monomeric chlorophyll. Under these conditions no evolution of dioxygen occurs and, as can be seen from Figs. 3 and 4 (curves 2), no photopotential appears either.

If chlorophyll is dissolved in water-saturated octane, immediately after the preparation of a two-phase system an additional maximum at 742 nm (3, 9, 10) appears; this peak belongs to the hydrated oligomer of chlorophyll. The molecular mechanism of water photooxidation by the hydrated oligomer of chlorophyll

Can. J. Chem. Downloaded from www.nrcresearchpress.com by 195.138.81.100 on 09/07/12
For personal use only.

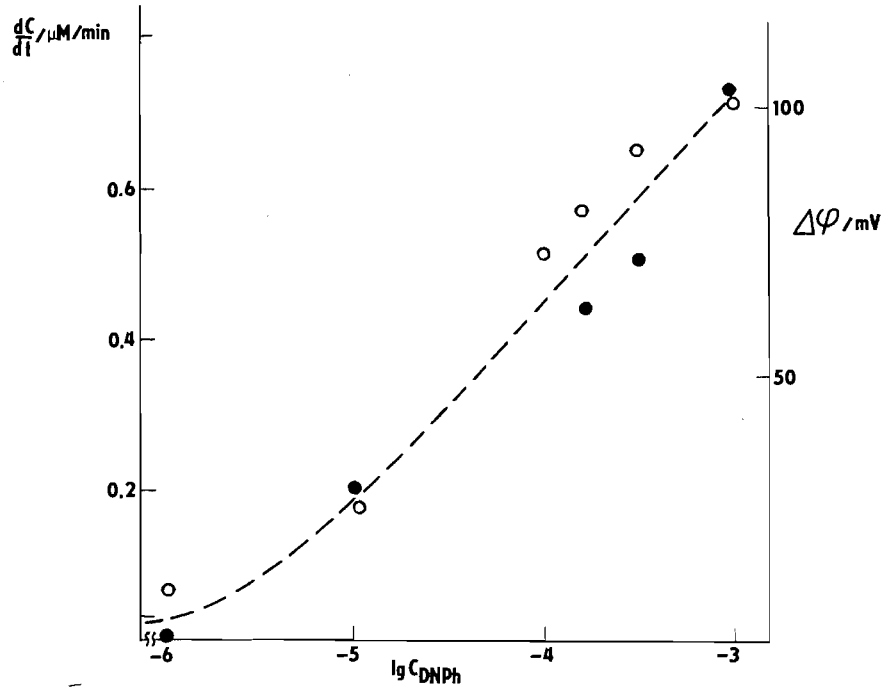


FIG. 2. Dependences of the rate of dioxygen evolution (●) and photopotential generation (○) on the DNPh concentration. The conditions are the same as in Fig. 1.

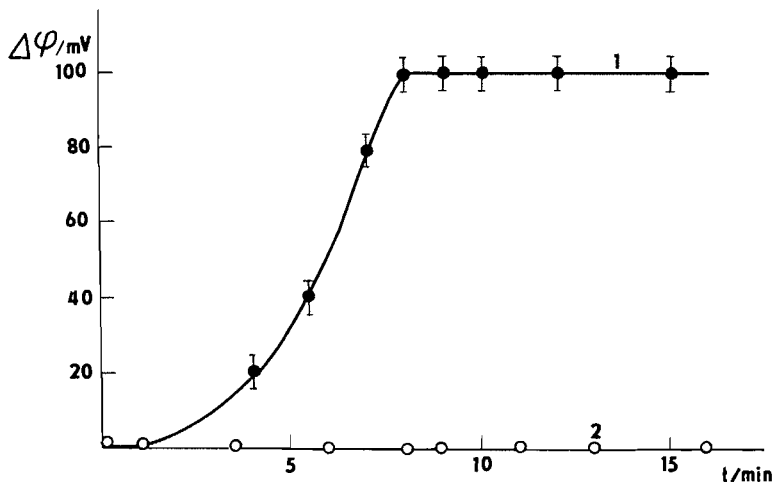


FIG. 3. Dependences of the photopotential, measured in the chain (*2*), on the time of contact of DNPh-free "wet" (*1*) and "dry" (*2*) octane with the aqueous phase. Octane contains 2×10^{-6} chlorophyll a. The aqueous phase contains 10^{-3} M DNPh, 2×10^{-2} M $K_3[Fe(CN)_6]$, 2×10^{-2} M Tris-HCl; pH 7.4.

was proposed in refs. 9 and 10. In all our experiments the photoevolution of molecular dioxygen and the generation of a photopotential were observed only when hydrated oligomers of chlorophyll is present in the system. The hydrated oligomers consist of 4–6 chlorophyll molecules and a few water molecules as shown by circular dichroism spectra (3).

To elucidate the role of DNPh, the results of the experiments are displayed in Figs. 3 and 4 (curve 1). In the first experiment (Fig. 3) DNPh was dissolved beforehand in the aqueous phase but was not added to the "wet" octane. In this case the photopotential appears immediately and increases monotonically for 5 to 10 min, then reaches its limiting value. The characteristic time of increase in the photopotential is limited by the diffusion of DNPh from water to octane. Since the volume of the aqueous phase is 10 times as large as that of octane the DNPh concentration in octane reaches a fairly high value in accordance with the distribution coefficient.

In the second experiment (Fig. 4) DNPh was dissolved beforehand in the "wet" octane but was not added to the aqueous phase. Under illumination a photopotential appeared but after approximately 5 min vanished because of the extraction of DNPh from a small amount of octane (1 mL) into the aqueous phase (10 mL).

Thus the presence of DNPh is indeed necessary in the octane phase for a photopotential to appear. We have detected no photooxidation of water to molecular dioxygen in the absence of a proton acceptor in the nonaqueous phase. As a proton acceptor one can use DNPh, pentachlorophenol, and uncouplers of oxidative phosphorylation.

Special experiments were carried out to determine how the

Can. J. Chem. Downloaded from www.nrcresearchpress.com by 195.138.81.100 on 09/07/12
For personal use only.

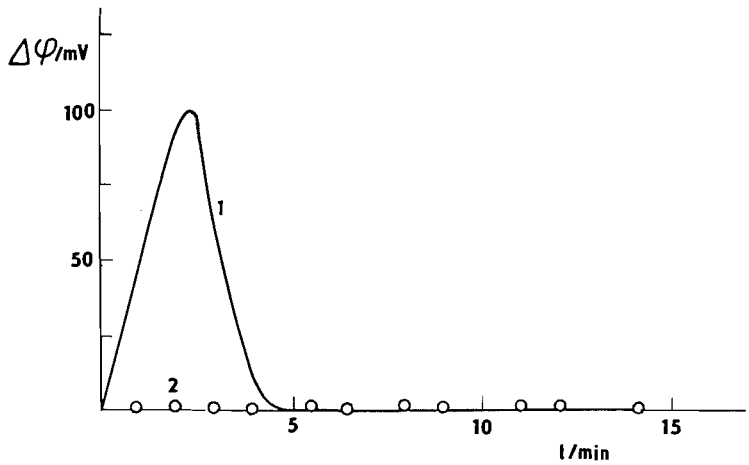


FIG. 4. Dependence of the photopotential, measured in the chain (2), on the time of contact of "wet" (1) and "dry" (2) octane with the aqueous phase. Octane contains 10^{-3} M DNPh and 2×10^{-6} M chlorophyll. The aqueous phase contains 2×10^{-2} M $K_3[Fe(CN)_6]$ and 2×10^{-2} M Tris-HCl and pH 7.4.

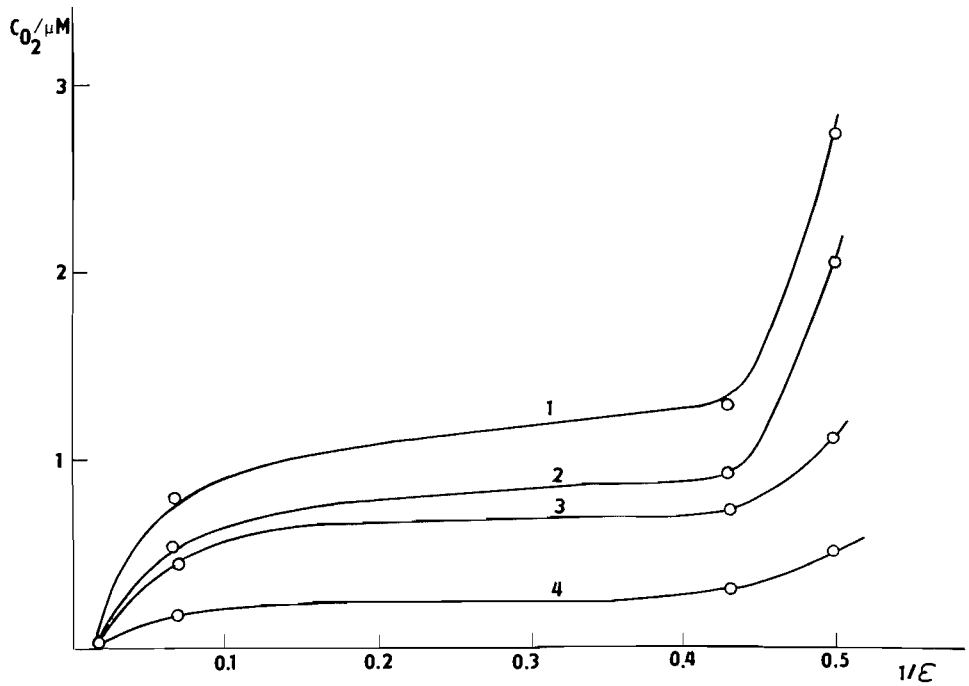


FIG. 5. Dependence of the dioxygen concentration on the dielectric permittivity of the nonaqueous phase ϵ. The medium: oil/water, 10^{-6} M chlorophyll, 10^{-3} M DNPh, 5×10^{-2} M $K_3[Fe(CN)_6]$, 2×10^{-2} M Tris-HCl, pH 7.4. Exposure time: *1*, 60 min, *2*, 45 min; *3*, 30 min; *4*, 15 min.

dielectric permittivity of a nonaqueous phase affects the rate of dioxygen evolution and photopotential. Figure 5 presents the dependence of the concentration of dioxygen evolved on the dielectric permittivity of the nonaqueous solvent, which were obtained at different exposure times. With increasing dielectric permittivity of the organic phase, the dioxygen yield abruptly decreases. Figure 6 is a comparison of the rate of dioxygen evolution and of the photopotential on the dielectric permittivity of a solvent immiscible with water. First of all it should be noted that in the same way as is evident from Fig. 2, there exists a correlation between the photopotential value and the reaction rate. The change in the Volta potential in the chain (2) under illumination, i.e. the photopotential at the octane/water interface, seems to reflect the change in the rate of the photoredox reaction which occurs at the interface.

In accordance with the theory of an elementary act of charge transfer through the interface of two immiscible liquids (13–18, 21, 22), the reaction rate constant in the approximation of Marcus (22, 23) is determined by the following expression

$$[3] \quad k = \frac{\omega}{2\pi} \mathcal{Y} \exp\left[-\frac{U_i}{kT} - \frac{(E_s + \Delta I + U_f - U_i)^2}{4E_s kT} \right]$$

where ω is the effective frequency, $\mathcal{Y}$ is the transmission coefficient, E_s is the energy of reorganization of the solvent, ΔI is the Gibbs energy of the reaction in separating the reagents and the reaction products to infinity, and U_i and U_f are the energies of bringing the reagents together and of separating the reaction products, respectively.

At high substrate concentrations, in accordance with the

Can. J. Chem. Downloaded from www.nrcresearchpress.com by 195.138.81.100 on 09/07/12
For personal use only.

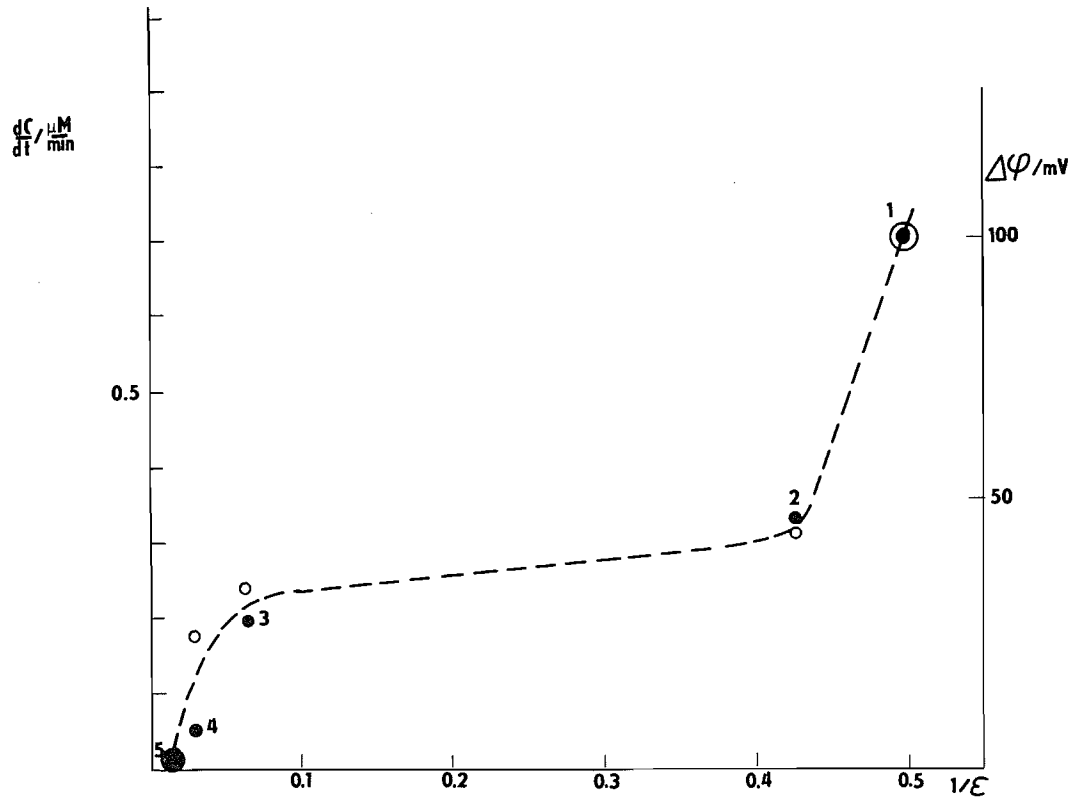


FIG. 6. Dependence of the rate of dioxygen evolution (●) and of the photopotential (○) on the dielectric permittivity of the "wet" nonaqueous phase: *1*, octene, decane; *2*, benzene; *3*, methylbutyl ketone; *4*, nitrobenzene; *5*, propylene carbonate. The conditions are the same as in Fig. 3.

theory developed in refs. 13 and 14, the photopotential is proportional to the reaction rate constant

$$[4] \quad \Delta\varphi = \frac{zFk}{Ck_{dif}}[chl]$$

where C is the capacitance of the electric double layer, [chl] is the concentration of chlorophyll, F is Faraday number, z is the charge of the particle, k_{dif} is rate constant of diffusion.

Substituting eq. [3] into eq. [4] yields

$$[5] \quad \lg \Delta\varphi \approx \frac{1}{\epsilon} \lg \frac{\Delta A}{kT} + \lg \frac{1}{\epsilon}$$

where A includes all the terms independent of the dielectric permittivity of the nonaqueous phase. The first term on the right side of eq. [5] is determined by the influence of the activation energy of the heterogeneous reaction while the second one, by the influence of the capacitance of the electric double layer, C, on the photopotential value. It is evident from Fig. 6 that the reaction rate and photopotential decrease similarly with increasing ϵ, which favours the theoretical calculations of the reaction rate as obtained from refs. 13–18.

The abrupt decrease in the reaction rate and in the photopotential in passing to polar solvents may also be caused by another factor: in nonpolar solvents chlorophyll is aggregated and in polar ones it is a monomer. This effect is distinctly visible on the absorption spectra. For the realization of a four-electron reaction of water photooxidation it seems to be necessary that the chlorophyll should occur as a hydrated oligomer (3). In this case the reaction could occur synchronously as a single act. If the chlorophyll is not aggregated and occurs as a monomer then the course of a synchronous water reaction becomes impossible due to a large value of the reorganization energy of the medium and, consequently, of the activation energy of the reaction. This problem was discussed in detail previously in refs. 9, 10, and 15 to 18. The four-stage one-electron oxidation of water by a chlorophyll monomer is impossible due to a low value of the redox potential ($E^0_{Chl/Chl^+} = 0.76$ V). As a result of these two factors no photooxidation of water by chlorophyll occurs at the water/polar nonaqueous solvent interface.

Thus the change in potential jump at the interface of two immiscible liquids reflects the photoredox reaction rate at the interface in the course of the water photooxidation reaction. The interface of two immiscible liquids can be used as a tool for studying the main processes of photosynthesis involving the spatial separation of charge. The use of solvents with different values of dielectric permittivity will make it possible to verify experimentally the conclusions of the theory of elementary charge transfer.

We have made special experiments on the duration of operation of the octane/water system in the course of the dioxygen photoevolution reaction. O_2 evolved in a stable manner during 3 h of illumination. Between the fourth and fifth hours of exposure the dioxygen evolution decreased and by the end of the fifth hour the evolution of O_2 stopped completely. In this case pH of the aqueous phase containing the Tris-HCl buffer remained neutral but practically all chlorophyll pheophytinized and the octane layer became brown. If any component necessary for the course of the water photooxidation reaction, e.g. DNPh or $K_3[Fe(CN)_6]$, was eliminated from the system then the spectrum of chlorophyll absorption in octane equilibrated with water practically remained unchanged during the 5 h. In the course of the reaction of dioxygen evolution at the interface the buffer capacitance of weak acid (DNPh or PChPh) is insufficient

Can. J. Chem. Downloaded from www.nrcresearchpress.com by 195.138.81.100 on 09/07/12
For personal use only.

to protect the chlorophyll against pheophytinization at long exposure times.

It is very likely that at the earlier stages of the evolution of photosynthesis, chlorophyll was directly involved in photooxidation of water to molecular oxygen. Such a chemical reactor, however, was able to operate only for a few hours. Therefore, the structure and composition of the oxygen-evolving complex could undergo significant changes in the course of evolution of the photosynthesis apparatus to increase its stability and the functioning period.

In natural photosynthesis plastoquinone acts as a transmembrane carrier of electrons and protons between reaction centers of two photosystems in the case of noncyclic electron transfer. In a special experiment we replaced the electron acceptor in water and the proton acceptor in oil by 1,4-naphthoquinone which dissolves both in water and in oil and is able to take on protons as well as electrons. In this case, however, we did not succeed in detecting the dioxygen evolution in the octane/water system.

Elucidation of the mechanism of water photooxidation and of related processes is a major problem in photosynthesis and is of great significance in designing artificial systems for solar energy utilization. The quantum yield of the photocatalytic decomposition of water depends first of all on the efficiency of the photochemical charge separation. The most effective system should be a heterogeneous system in which the oxidant and the reductant are either in different phases or sterically separated. The difference in solubilities of the substrates and reaction products in both phases of such heterogeneous structure as octane/water interface can shift the reaction equilibrium to the other side; the redox potential scale is altered, which makes it possible to carry out the reaction that cannot be performed in homogeneous phase or that proceeds at a slow rate. Extraction of the reaction products and adsorption of the reaction components determine high catalytic properties of the interface between two immiscible liquids, recognized recently as interfacial catalysis (15–18).

Acknowledgments

The authors are grateful to A. Agostiano, P.-F. Blanchet, Yu. A. Chizmadzhev, R. M. Leblanc, V. S. Markin, and G. Munger for helpful discussions and critical remarks.

1. L. I. Boguslavsky, A. G. Volkov, M. D. Kandelaki, and E. A. Nizhnikovsky. Dokl. Akad. Nauk SSSR, **227**, 717 (1976).
2. L. I. Boguslavsky, A. G. Volkov, M. D. Kandelaki, and M. A. Bibikova. Biofizika, **22**, 223 (1977).
3. M. D. Kandelaki, A. G. Volkov, V. V. Shubin, and L. I. Boguslavsky. Electrokhimiya, **24**, 288 (1988).
4. M. D. Kandelaki, A. G. Volkov, A. L. Levin, and L. I. Boguslavsky. Dokl. Akad. Nauk SSSR, **271**, 462 (1988).
5. M. D. Kandelaki, A. G. Volkov, A. L. Levin, and L. I. Boguslavsky. Bioelectrochem. Bioenerg. **11**, 167 (1983).
6. M. D. Kandelaki, A. G. Volkov, A. L. Levin, and L. I. Boguslavsky. *In* Solar energy bioconversion. *Edited by* I. V. Berezin. Acad. Sci. USSR Publ., Pushchino. 1984. pp. 318–321.
7. A. G. Volkov, V. D. Kolev, A. L. Levin, and L. I. Boguslavsky. Electrokhimiya, **22**, 1304 (1986).
8. A. G. Volkov, V. D. Kolev, A. L. Levin, and L. I. Boguslavsky. Photobiochem. Photobiophys. **10**, 105 (1985).
9. A. G. Volkov. Bioelectrochem. Bioenerg. **12**, 15 (1984).
10. A. G. Volkov. Electrokhimiya, **21**, 91 (1985).
11. A. G. Volkov. J. Electroanal. Chem. **205**, 245 (1986).
12. A. G. Volkov. Mol. Biol. **20**, 728 (1986).
13. Yu. I. Kharkats, A. G. Volkov, and L. I. Boguslavsky. Biofizika, **21**, 634 (1976).
14. Yu. I. Kharkats, A. G. Volkov, and L. I. Boguslavsky. J. Theor. Biol. **65**, 379 (1977).
15. Yu. I. Kharkats and A. G. Volkov. J. Electroanal. Chem. **184**, 435 (1985).
16. A. G. Volkov and Yu. I. Kharkats. Kinet. Katal. **26**, 1322 (1985).
17. A. G. Volkov and Yu. I. Kharkats. Khim. Fiz. **5**, 664 (1986).
18. A. G. Volkov and Yu. I. Kharkats. *In* Kinetics of electron transfer in proteins and their models. *Edited by* Yu. Yu. Kulis. Publ. House Acad. Sci. Vil'nius. 1985. pp. 101, 102.
19. J. J. Katz and J. R. Norris. *In* Current topics in bioenergetics. Vol. 4. *Edited by* D. Sanady and L. Packer. Academic Press, New York. 1973. pp. 41–75.
20. Pigments of plastides of green plants and methods of their investigations. Nauka Publ., Moscow. 1964.
21. Yu. I. Kharkats. Electrokhimiya, **12**, 1370 (1976).
22. R. A. Marcus and N. Sutin. Biochim. Biophys. Acta, **811**, 265 (1986).
23. R. A. Marcus. J. Chem. Phys. **24**, 966 (1956).

Can. J. Chem. Downloaded from www.nrcresearchpress.com by 195.138.81.100 on 09/07/12
For personal use only.

Solvent structure effects on solvated electron reactions in mixed solvents: positive ions in 1-propanol/water and 2-propanol/water

SEDIGALLAGE A. PEIRIS[1] AND GORDON R. FREEMAN
Chemistry Department, University of Alberta, Edmonton, Alta., Canada T6G 2G2

Received July 10, 1990

SEDIGALLAGE A. PEIRIS and GORDON R. FREEMAN. Can. J. Chem. **69**, 157 (1991).

In models of the kinetics of chemical reactions in solution the solvent is commonly assumed to be a uniform continuum. An example is the Smoluchowski–Debye–Stokes–Einstein equation for the rate constant k_2 of a bimolecular reaction between charged or polar species:

$$k_2 = \kappa RTfr_r/1.5\ \eta r_d$$

where κ is the probability that a reactant encounter pair will react, R is the gas constant, T is the temperature, f is a factor that reflects the effect of electrostatic interaction between the reactants on their probability of attaining the closeness of approach r_r at which reaction occurs, η is the solvent viscosity, and r_d is the effective radius of the reactant entities for mutual diffusion. The equation is useful in evaluating effects of bulk fluid properties on reaction rates. Residual effects are attributed to more specific solvent behaviour.

Rate constants k_2, activation energies E_2, and pre-exponential factors A_2 of reactions of solvated electrons e_s^- with H_s^+, Ag_s^+, Cu_s^{2+}, and Al_s^{3+} ions vary with the composition of 1-propanol/water and 2-propanol/water mixed solvents. Plots of $k_2\eta/fT$ against solvent composition are nonlinear and change with the solvent pair and with reactant pair. Measured molar conductivities $\Lambda_0(H_s^+, ClO_{4,s}^-)$, $\Lambda_0(Ag_s^+, ClO_{4,s}^-)$, $\Lambda_0(Cu_s^{2+}, 2ClO_{4,s}^-)$, and $\Lambda_0(Al_s^{3+}, 3ClO_{4,s}^-)$ indicate that the values of r_d for the mutual diffusion of the cations and anions have a minimum near 90 mol% water, and that the values in pure propanol-1 or −2 (150–190 pm) are larger than those in pure water solvent (26 pm for H_s^+, 70 pm for the metal ions). The liquid structure influences both the rate of diffusion and the probability of reaction of a reactant encounter pair.

Key words: alcohol/water mixed solvents, positive ions, reaction kinetics, solvated electron, solvent effects.

SEDIGALLAGE A. PEIRIS et GORDON R. FREEMAN. Can. J. Chem. **69**, 157 (1991).

Dans les modèles de la cinétique des réactions chimiques en solution, on fait souvent l'hypothèse que le solvant est un milieu uniforme. Comme exemple, on peut citer l'équation de Smoluchowski–Debye–Stokes–Einstein relative à la constante de vitesse k_2 d'une réaction bimoléculaire entre des espèces polaires ou chargées :

$$k_2 = \kappa RTfr_r/1{,}5\ \eta r_d$$

dans laquelle κ est la probabilité qu'une paire de réactifs qui se rencontrent puissent réagir, R est la constante des gaz, T est la température, f est un facteur qui est le reflet de l'interaction électrostatique entre les réactifs sur la probabilité qu'ils ont de s'approcher jusqu'à une valeur de r_r à laquelle il se produit une réaction, η est la viscosité du solvant et r_d est le rayon effectif des entités qui réagissent pour la diffusion mutuelle. L'équation est utile pour évaluer les effets globaux des propriétés des fluides sur les vitesses de réactions. Les effets résiduels sont attribués à un comportement plus spécifique du solvant.

Les constantes de vitesse k_2, les énergies d'activation E_2 et les facteurs pré-exponentiels A_2 des réactions des ions solvatés e_s^- avec les ions H_s^+, Ag_s^+, Cu_s^{2+} et Al_s^{3+} varient avec la composition des solvants mixtes 1-propanol/eau et 2-propanol/eau. Les courbes de $k_2\eta/fT$ en fonction des compositions de solvants ne sont pas linéaires et elles varient avec la paire de solvant et la paire de réactif. Les conductivités molaires mesurées $\Lambda_0(H_s^+, ClO_{4,s}^-)$, $\Lambda_0(Ag_s^+, ClO_{4,s}^-)$, $\Lambda_0(Cu_s^{2+}, 2ClO_{4,s}^-)$ et $\Lambda_0(Al_s^{3+}, 3ClO_{4,s}^-)$ indiquent que les valeurs de r_d pour la diffusion mutuelle des cations et des anions passent par un minimum près de 90 mol% d'eau et que les valeurs dans le 1- (ou 2-) propanol purs (150 à 190 pm) sont plus grandes que celles dans l'eau pure (26 pm pour H_s^+ et 70 pm pour les ions métalliques). La structure du liquide influence la vitesse de diffusion ainsi que la probabilité qu'une paire des réactifs qui se rencontrent puissent réagir.

Mots clés : solvants mixtes alcool/eau, ions positifs, cinétique de réactions, électrons solvatés, effets de solvants.

[Traduit par la revue]

Introduction

This article continues the study of solvent structure effects on solvated electron reactions in mixed solvents (1–4). The last article (4) reported reactions with negative ions in 1-propanol/water and 2-propanol/water. We here describe solvent effects on rates of solvated electron reactions with several positive ions.

Experimental

Materials

The solvents and the method of their purification were described earlier (4).

Silver perchlorate (Strem, reagent grade), copper(II) perchlorate (Aldrich reagent grade), aluminum(III) perchlorate (98%, Aldrich Chemical Co.), and perchloric acid (70%, Fisher Scientific Co.) were used as received.

Techniques

Methods of sample preparation from solid solutes were as described in ref. 5. Perchloric acid samples were made by measuring 70% perchloric acid solution with a glass pipet to prepare 50 mol/m^3 stock solutions, and then diluting as previously described.

Methods of irradiation, dosimetry and optical measurements were similar to those described in ref. 6.

Electrical conductance measurements were as described in ref. 7. Dissolved CO_2 was removed from the conductance cell by bubbling UHP argon through the solution, then sealing the cell with Parafilm. A small amount of chemical reaction sometimes occurred at the higher temperatures, which was detected by drift of the conductance. In these cases a fresh sample was used for each measurement.

[1]Previously known as Annesley Peiris Sedigallage.

Can. J. Chem. Downloaded from www.nrcresearchpress.com by 195.138.81.100 on 09/07/12
For personal use only.

Can. J. Chem. Downloaded from www.nrcresearchpress.com by 195.138.81.100 on 09/07/12
For personal use only.

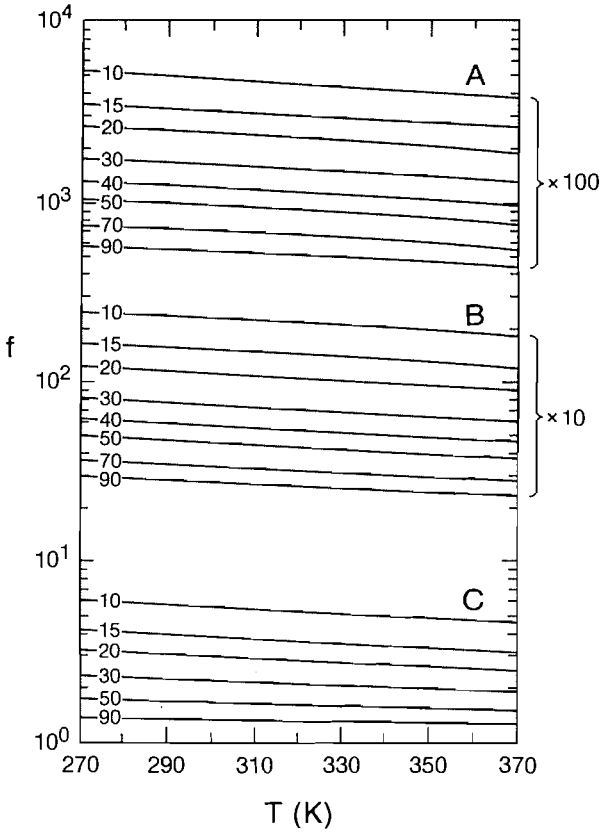


FIG. 1. Temperature dependence of the Debye factor f at different values of dielectric permittivity. A: for $z = +3$ using $r_r = 0.35$ nm. B: for $z = +2$ using $r_r = 0.5$ nm. C: for $z = +1$ using $r_r = 1.0$ nm. Values of ϵ are indicated.

Values of viscosities and relative permittivities of the mixed solvents were obtained from ref. 8.

Results and discussion

The second-order rate constants k_2 were obtained as described in ref. 4.

Diffusion and reaction

The rate constant data were analyzed according to the modified Arrhenius equation (4),

$$[1] \quad k_2/f = A_2 \exp(-E_2/RT)$$

where E_2 is the overall energy of activation of the reaction, and A_2 is the pre-exponential factor. The factor f reflects the effect of electrostatic interaction between the reactants on their probability of attaining the closeness of approach r_r at which reaction occurs:

$$[2] \quad f = \frac{U(r_r)}{k_B T}[\exp(U(r_r)/k_B T) - 1]^{-1}$$

where $U(r_r)$ is the interaction energy of the reactants at distance r_r, k_B is Boltzmann's constant, and T is the temperature.

For the interaction of e_s^- with a solute of charge $z\xi$, $U(r_r)$ is given by

$$[3] \quad U(r_r) = -z\xi^2/4\pi\epsilon_0\epsilon r_r$$

where $-\xi$ is the charge on the electron, ϵ_0 is the permittivity of vacuum, and ϵ is the relative permittivity of the solvent between the electron and the ion.

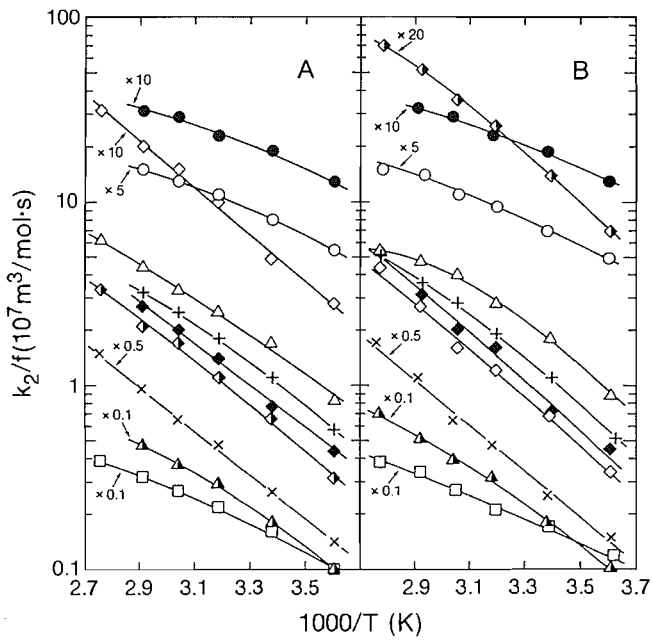


FIG. 2. Arrhenius plots of log $[k_2(e_s^- + H_s^+)/f]$ against T^{-1} in 1-propanol/water (A) and 2-propanol/water (B) mixed solvents. Symbols representing mol% water are given in Table 1, except ▲, (A, 81; B, 80), △, (A, 68; B, 70), +, (A, 51; B, 50), ◆, 35.

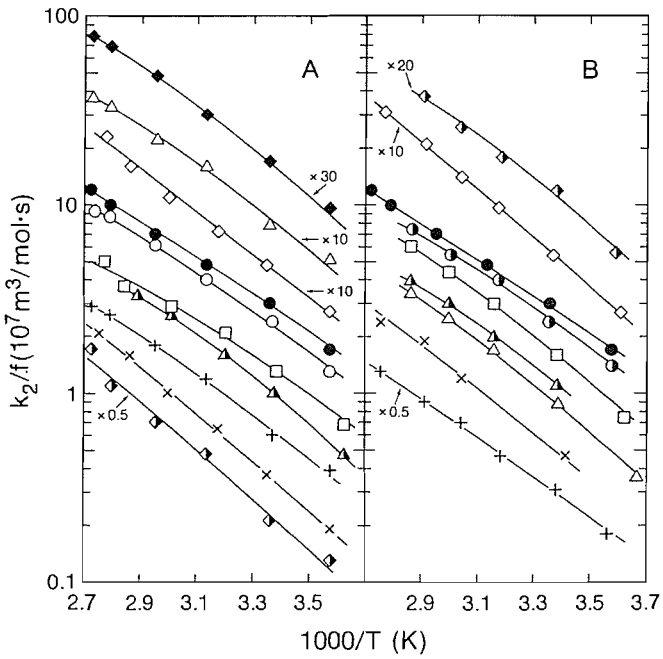


FIG. 3. Arrhenius plots of log $[k_2(e_s^- + Ag_s^+)/f]$ against T^{-1} in 1-propanol/water (A) and 2-propanol/water (B) mixed solvents. Symbols representing mol% water are given in Table 1, except ▲, (A, 80; B, 81); △, (A, 70; B, 71); +, (A, 50; B, 51); ◆, 36.

In Fig. 1 values of f are plotted for ions of different z, using appropriate values of r_r (2), for a range of values of ϵ and T. The value of ϵ of each solvent at each T used in the experiments was obtained by interpolation of data in ref. 8. The value of k_2 was divided by the value of f at the corresponding values of (ϵ, T, r_r).

The second-order rate constant for the counter ion, perchlor-

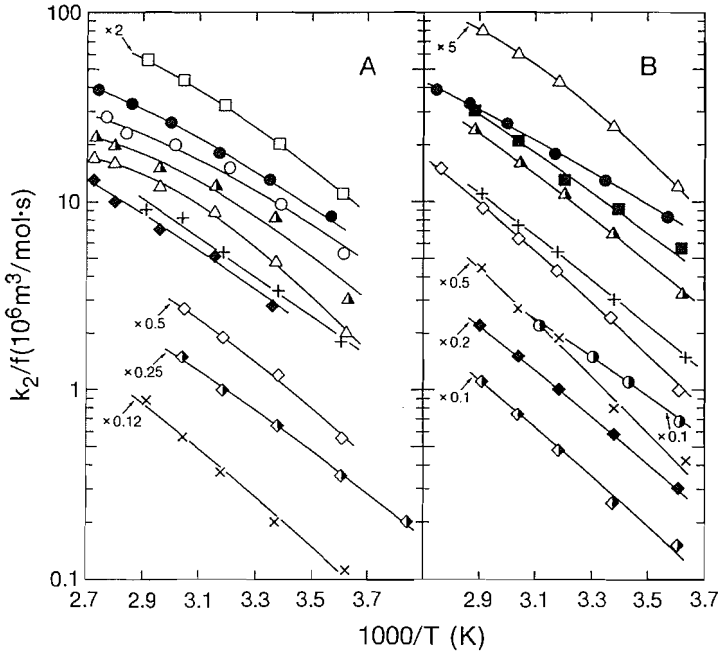


FIG. 4. Arrhenius plots of log $[k_2(e_s^- + Cu_s^{2+})/f]$ in propanol/water (*A*) and 2-propanol/water (*B*) mixed solvents. Symbols representing mol% water are given in Table 1, except: ▲, 81; △, 68; +, (*A*, 51; *B*, 52); ◆, (*A*, 33; *B*, 36).

ate, was less than 10^3 m^3/mol s in water (9). Therefore the observed rate constants are due to H_s^+, Ag_s^+, Cu_s^{2+}, and Al_s^{3+}.

Arrhenius plots of log (k_2/f) against T^{-1} are shown for H_s^+ in Fig. 2, for Ag_s^+ in Fig. 3, for Cu_s^{2+} in Fig. 4, and for Al_s^{3+} in Fig. 5. The mol% water represented by the symbols in these figures are shown in Table 1.

The solvent composition dependences of k_2/f at 298 K are shown in Fig. 6 *A* and *B* for 1-propanol/water and 2-propanol/water, respectively. The variation of k_2/f with the solvent composition is more drastic than that for k_2 itself (Fig. 6 *C* and *D*). In general k_2 increases with increasing charge on the positive ion. However, when the coulombic factor f is taken into account, k_2/f values for Ag_s^+ are greater than those for Cu_s^{2+} and Al_s^{3+}. For H_s^+, k_2/f has the highest values.

Addition of a small amount of water to pure 1-propanol caused k_2/f for Al_s^{3+} to drop, then increase again when more than 2 mol% of water was added (Fig. 6*A*). The initial drop did not occur in 2-propanol (Fig. 6*C*). The value of the optical absorption energy half way up the low energy (red) side of the band, E_r, is an approximate measure of the trap depth of the solvated electrons that react (5). Addition of a small amount of water causes the value of E_r to decrease in 1-propanol and to increase in 2-propanol (10). The decrease in 1-propanol has been explained in terms of the formation of a hydrogen bonded solvent structure which consists of two alcohol tetramers joined together by a water molecule between them, towards 10 mol% of water on the composition scale. This would tend to decrease the availability of OH functional groups to the electron solvation site (10). Thus addition of water to pure 1-propanol would decrease the solvation energy of the electron. The activation energy for $(e_s^- + Al_s^{3+})$ did not change appreciably in this region (Fig. 7*A*), but log A_2 decreased as a small amount of water was added to pure 1-propanol (Fig. 8*A*). Therefore the above-mentioned phenomenon could be linked to a decrease in entropy of activation caused by the structure of the solvent at this composition. This structure apparently does not form in secondary alcohols (10).

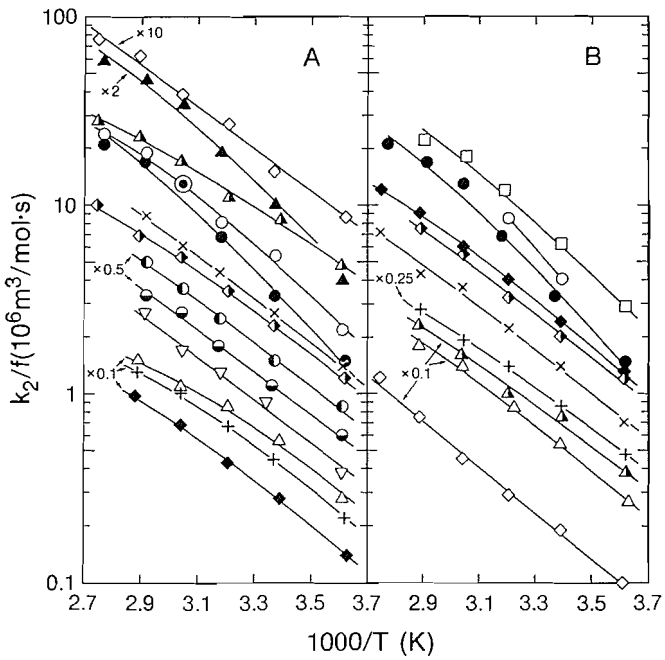


FIG. 5. Arrhenius plots of log $[k_2(e_s^- + Al_s^{3+})/f]$ in 1-propanol/water (*A*) and 2-propanol/water (*B*) mixed solvents. Symbols representing mol% water are given in Table 1, except: ▲, 81; +, (*A*, 51; *B*, 52); ◆, (*A*, 35; *B*, 36).

The plots of E_2 against mol% water in the solvent are *S* curves for Ag_s^+ and Cu_s^{2+} (Fig. 7). The curves for H_s^+ are concave toward the composition axis and those for Al_s^{3+} are convex toward that axis. The differences in curve shapes are due to differences in diffusion behavior of the cations and in the reaction probability of a reactant encounter pair, because the changes in e_s^- properties with solvent composition are the same for each cation.

[4] $e_s^- + C_s^{z+} \rightleftharpoons (e_s^-, C_s^{z+})$

Can. J. Chem. Downloaded from www.nrcresearchpress.com by 195.138.81.100 on 09/07/12
For personal use only.

Can. J. Chem. Downloaded from www.nrcresearchpress.com by 195.138.81.100 on 09/07/12
For personal use only.

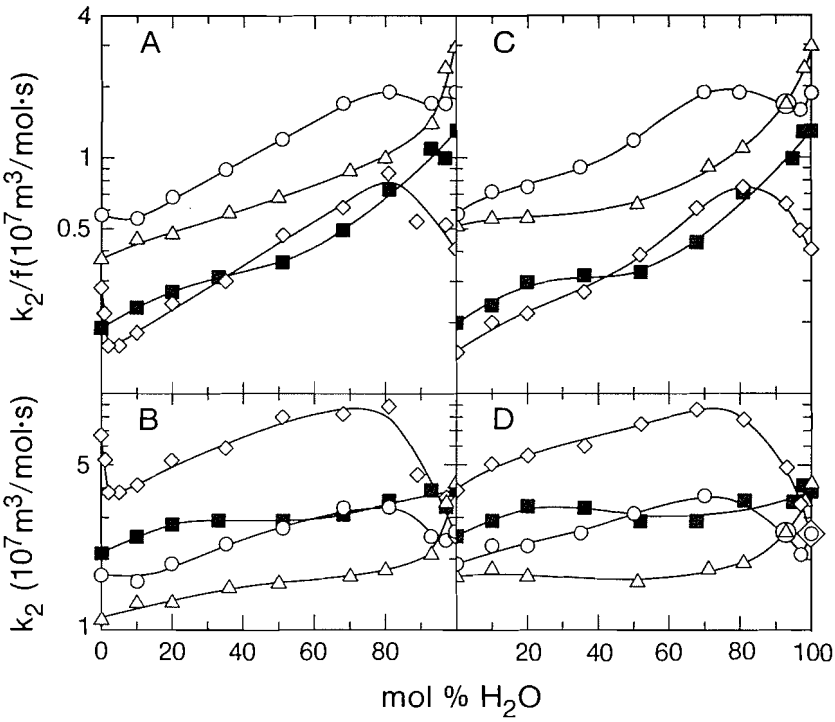


FIG. 6. Solvent composition dependences of k_2/f and k_2 at 298 K. ○, H_s^+; △, Ag_s^+; ■, Cu_s^{2+}; ◇, Al_s^{3+}; in 1-propanol/water mixtures (*A* and *B*), 2-propanol/water mixtures (*C* and *D*).

[5] $(e_s^- + C_s^{z+}) \rightleftharpoons (C^{(z-1)+})$

[6] $(C^{(z-1)+}) \rightarrow C_s^{(z-1)+}$

Reaction [4] represents the reversible formation of the reactant encounter pair, reaction [5] is the reversible electron transfer step, and reaction [6] is the relaxation of the new product and the solvent molecules around it. Reaction [6] in some cases involves further chemical reaction, for example

[6′] $H_3O(H_2O)_n \rightarrow H_s + H_2O_s$

The solvent dependences of log A_2 (Fig. 8) are qualitatively similar to those of E_2 (Fig. 7), with the exception of the $(e_s^- + Al_s^{3+})$ reaction in nearly pure 1-propanol. A correlation between E_2 and log A_2 in a series of reactions of a given type is common (11). It has to do with counterbalancing effects of entropies and enthalpies of activation. A higher $\Delta H^{\ddagger}$ (hence E_2) tends to make a broader reaction path (higher density of states) accessible, which means that $\Delta S^{\ddagger}$ (hence log A_2) is larger.

The activation energy of a reaction that is nearly diffusion-controlled should be similar to that of mutual diffusion of the reacting species. While we cannot measure the diffusion coefficient of e_s^-, the activation energy of conductance $E_{\Lambda 0}$ of the reactant salt gives a rough idea of E_2 values that might be expected for diffusion controlled reactions of the ions. Plots of $E_{\Lambda 0}$ against solvent composition are shown in Fig. 9. The values of $E_{\Lambda 0}$ and E_2 (Fig. 7) are mostly in the vicinity of 20 kJ/mol, but there are many differences in detail between E_2 and $E_{\Lambda 0}$ that cannot yet be interpreted.

Values of the reaction rate parameters are summarized in Tables 2–5.

Effect of solvent viscosity

The Smoluchowski–Debye–Stokes–Einstein equation for the rate constant k_2 of a bimolecular reaction between charged or polar species may be written (4)

[7] $k_2 = \kappa RTfr_r/1.5\,\eta r_d$

where κ = probability that a reactant encounter pair will react, η = solvent viscosity, and r_d = effective radius of the reactant entities for mutual diffusion. Equation [7] can be rearranged to obtain the dimensionless ratio of reaction parameters $\kappa r_r/r_d$:

[8] $\kappa r_r/r_d = k_2\eta/5.5Tf$

The values of this ratio for the present systems at 298 K are approximately in the order $H_s^+ > Ag_s^+ > Cu_s^{2+} > Al_s^{3+}$, and have maxima in the vicinity of 80 mol% water (Fig. 10). The values are similar in the two isomeric propanols at all water contents, with the exception of Al_s^{3+} in the pure propanol solvents. The extra reactivity of Al_s^{3+} in pure 1-propanol has been confirmed by repeated experiments and is not understood.

The effective radius of e_s^- for diffusion is small, presumably due to its deformability: 0.05 nm in water and 0.09 nm in 2-propanol (12). Thus for $\kappa \approx 1$ and $r_r \geq 0.5$ nm one expects $\kappa r_r/r_d > 10$ in water and >6 in 2-propanol. The reaction $(e_s^- + Ag_s^+)$ is approximately diffusion-controlled in the solvents of all compositions. The reaction $(e_s^- + H_s^+)$ is

TABLE 1. Symbols in Figs. 2–5, representing mol% of water in 1-propanol or 2-propanol

Symbol	% H_2O	Symbol	% H_2O	Symbol	% H_2O
×	0	◆	33–36	■	95
◒	1	+	50–52	○	97
▽	2	△	68–71	◑	98
◐	5	◭	80–81	●	100
◇	10	▲	89		
◈	20	□	93		

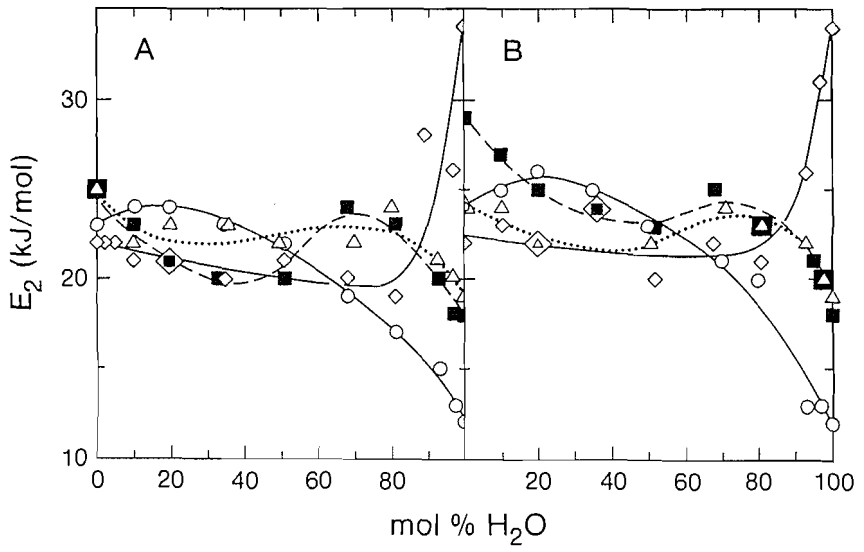


FIG. 7. Solvent composition dependence of the activation energies E_2 in 1-propanol/water (A) and 2-propanol/water (B) mixed solvents near 298 K. Symbols as in Fig. 6.

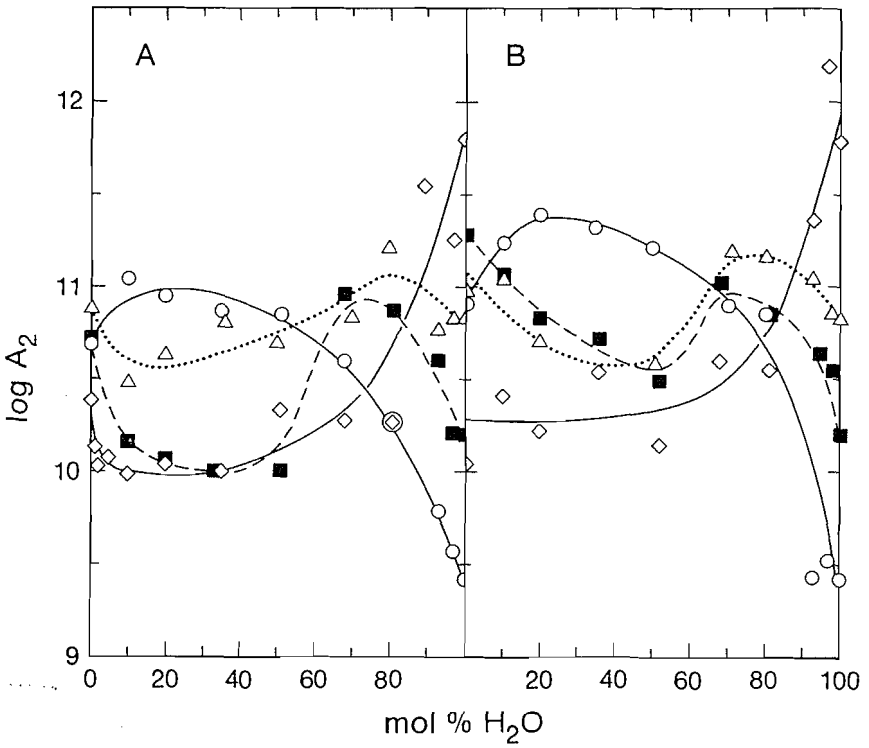


FIG. 8. Solvent composition dependence of log A_2 in 1-propanol/water (A) and 2-propanol/water (B) mixed solvents near 298 K. Symbols as in Fig. 6.

approximately diffusion-controlled in alcohols containing 0–80 mol% water, but in pure water solvent $\kappa \approx 0.5$. The lower efficiency of $(e_s^- + H_s^+)$ in water than in alcohol, with $\kappa = 0.3$ in water and 1.0 in methanol and ethanol, has been attributed to lower efficiencies of reactions [5] and [6] in water (13). The electron is a solvent-structure breaker in water and H^+ is a solvent-structure maker; this difference inhibits the intimate approach of the two species and slows reaction [5]. In alcohols the electron is a weak structure maker (13) and H^+ is a strong structure maker, so their intimate approach is not hindered by the solvent structure. It is also possible that the decomposition of the symmetrical $H_3O(H_2O)_n$, reaction [6′], is slower relative to the solvent viscosity than is that of the unsymmetrical $ROH_2(ROH)_m$:

[6″] $\quad ROH_2(ROH)_m \rightarrow H_s + ROH_s$

The lower values of $\kappa r_r/r_d$ for Cu_s^{2+} and Al_s^{3+} are attributed to difficulty in forming the relatively unstable Cu_s^+ and Al_s^{2+} from e_s^- and Cu_s^{2+} or Al_s^{3+}, respectively. In aqueous solution the Cu_s^+ ion is unstable with respect to Cu_s^{2+} and Cu. The equilibrium

[9] $\quad 2Cu_s^+ \rightleftharpoons Cu_s^{2+} + Cu_s$

Can. J. Chem. Downloaded from www.nrcresearchpress.com by 195.138.81.100 on 09/07/12
For personal use only.

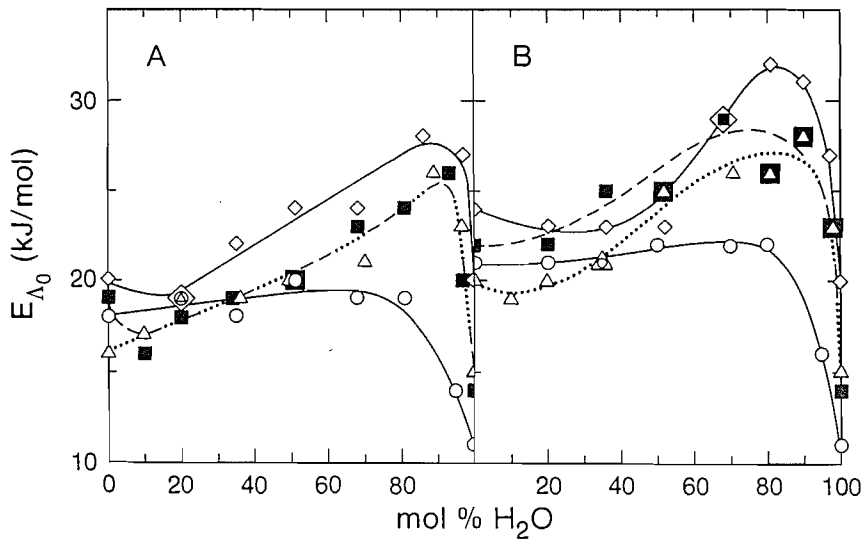


FIG. 9. Arrhenius activation energy of ionic conductances at infinite dilution, $E_{\Lambda 0}$, as functions of water content in 1-propanol (A) and 2-propanol (B). Symbols as in Fig. 6.

TABLE 2. Rate parameters for the reaction of solvated electrons with perchloric acid[a]

X_w[b]	ϵ[c]	η[d] (10^{-3} Pa s)	k_2[e] (10^7 m^3/mol s)	k_2/f[e] (10^7 m^3/mol s)	E_2[f,g] (kJ/mol)	log A_2[g] (A_2 in m^3/mol s)
			1-PrOH/H_2O			
1.00	78.5	0.89	2.6	1.9	12	9.42
0.97	71.7	1.34	2.4	1.7	13	9.57
0.93	65.0	1.86	2.5	1.7	15	9.78
0.81	47.0	2.63	3.3	1.9	17	10.26
0.68	36.0	2.73	3.3	1.7	19	10.60
0.51	28.0	2.56	2.7	1.2	22	10.85
0.35	24.0	2.32	2.3	0.89	23	10.87
0.20	21.7	2.16	1.9	0.68	24	10.95
0.10	20.7	2.06	1.6	0.55	24	11.04
0.00	20.2	1.96	1.7	0.57	23	10.69
			2-PrOH/H_2O			
1.00	78.5	0.89	2.6	1.9	12	9.42
0.97	71.5	1.38	2.1	1.6	13	9.52
0.93	63.2	2.02	2.6	1.7	13	9.43
0.80	45.0	3.03	3.4	1.9	20	10.86
0.70	35.6	3.09	3.7	1.9	21	10.90
0.50	25.0	2.68	3.1	1.2	23	11.21
0.35	21.3	2.38	2.6	0.92	25	11.32
0.20	19.5	2.20	2.3	0.76	26	11.39
0.10	18.6	2.13	2.3	0.72	25	11.24
0.00	18.0	2.08	1.9	0.58	24	10.91

[a]H^+ concentrations 0.01–0.13 mol/m^3.
[b]Mole fraction water.
[c]Static dielectric permittivity at 298 K, ref. 8.
[d]Viscosity at 298 K, ref. 8.
[e]At 298 K.
[f]Near 298 K.
[g]From Arrhenius plots of k_2/f.

lies far to the right, and compounds of Cu(I) are covalent (14). Compounds of Al_s^{2+} are not known. The overall reaction with Al_s^{3+} might be

[10] $Al_s^{3+} + e_s^- \rightarrow [AlOH]_s^{2+} + H_s$

or

[10′] $3Al_s^{3+} + 3e_s^- \rightarrow 3Al_s^{2+} \rightarrow\rightarrow Al_s^0 + 2Al_s^{3+}$

Comparison with ionic conductivities

The diffusion coefficients D_i of the ionic reactants are related to their molar electrical conductivities λ_i, so the solvent dependence of $k_2/f[(\lambda_i/z_i^2) + \lambda_e]T$ indicates the solvent dependence of κr_r (4),

[11] $\kappa r_r = 1.48 \times 10^{-16} k_2/f[(\lambda_i/z_i^2) + \lambda_e]T$

where λ_e is the molar conductivity of e^-.

Can. J. Chem. Downloaded from www.nrcresearchpress.com by 195.138.81.100 on 09/07/12
For personal use only.

TABLE 3. Rate parameters for the reaction of solvated electrons with silver perchlorate[a]

X_w[b]	ϵ[c]	η[d] (10^{-3} Pa s)	k_2[e] (10^7 m^3/mol s)	k_2/f[e] (10^7 m^3/mol s)	$E_2^{f,g}$ (kJ/mol)	log A_2[g] (A_2 in m^3/mol s)
			1-PrOH/H_2O			
1.00	78.5	0.89	4.2	3.0	19	10.83
0.97	71.7	1.34	3.5	2.4	20	10.83
0.93	65.0	1.86	2.1	1.4	21	10.77
0.80	46.2	2.64	1.8	1.0	24	11.21
0.70	37.2	2.74	1.7	0.88	22	10.83
0.50	27.6	2.50	1.6	0.68	22	10.69
0.36	24.2	2.32	1.5	0.58	23	10.80
0.20	21.7	2.16	1.3	0.47	23	10.63
0.10	20.7	2.06	1.3	0.45	22	10.48
0.00	20.2	1.96	1.1	0.37	25	10.88
			2-PrOH/H_2O			
1.00	78.5	0.89	4.2	3.0	19	10.83
0.98	73.0	1.20	3.5	2.4	20	10.85
0.93	63.2	2.02	2.6	1.7	22	11.04
0.81	46.2	3.02	1.9	1.1	23	11.16
0.71	36.3	3.10	1.8	0.92	24	11.19
0.51	25.3	2.72	1.6	0.64	22	10.58
0.20	19.5	2.20	1.7	0.56	22	10.70
0.10	18.6	2.13	1.8	0.56	24	11.04
0.00	18.0	2.08	1.7	0.52	24	10.98

[a] Ag^+ concentrations 3–73 mmol/m^3.
[b–g] As in Table 2.

TABLE 4. Rate parameters for the reaction of solvated electrons with copper(II) perchlorate[a]

X_w[b]	ϵ[c]	η[d] (10^{-3} Pa s)	k_2[e] (10^7 m^3/mol s)	k_2/f[e] (10^7 m^3/mol s)	$E_2^{f,g}$ (kJ/mol)	log A_2[g] (A_2 in m^3/mol s)
			1-PrOH/H_2O			
1.00	78.5	0.89	3.9	1.3	18	10.20
0.97	71.7	1.34	3.4	1.0	18	10.21
0.93	63.0	1.92	3.9	1.1	20	10.60
0.81	47.0	2.63	3.5	0.73	23	11.87
0.68	35.5	2.72	3.1	0.49	24	10.96
0.51	28.0	2.56	2.9	0.36	20	10.00
0.33	23.8	2.30	2.9	0.31	20	10.00
0.20	21.7	2.16	2.8	0.27	21	10.06
0.10	20.7	2.06	2.5	0.23	23	10.16
0.00	20.2	1.96	2.1	0.19	25	10.72
			2-PrOH/H_2O			
1.00	78.5	0.89	3.9	1.3	18	10.20
0.98	73.0	1.20	4.1	1.3	20	10.55
0.95	66.0	1.78	3.5	1.0	21	10.64
0.81	46.2	3.02	3.5	0.71	23	10.85
0.68	34.0	3.07	2.9	0.44	25	11.02
0.52	25.3	2.70	2.9	0.33	23	10.49
0.36	21.6	2.40	3.3	0.32	24	10.72
0.20	19.5	2.20	3.4	0.30	25	10.83
0.10	18.6	2.13	2.9	0.24	27	11.05
0.00	18.0	2.08	2.5	0.20	29	11.29

[a] Cu^{2+} concentrations 2–125 mmol/m^3.
[b–g] As in Table 2.

Can. J. Chem. Downloaded from www.nrcresearchpress.com by 195.138.81.100 on 09/07/12
For personal use only.

Can. J. Chem. Downloaded from www.nrcresearchpress.com by 195.138.81.100 on 09/07/12
For personal use only.

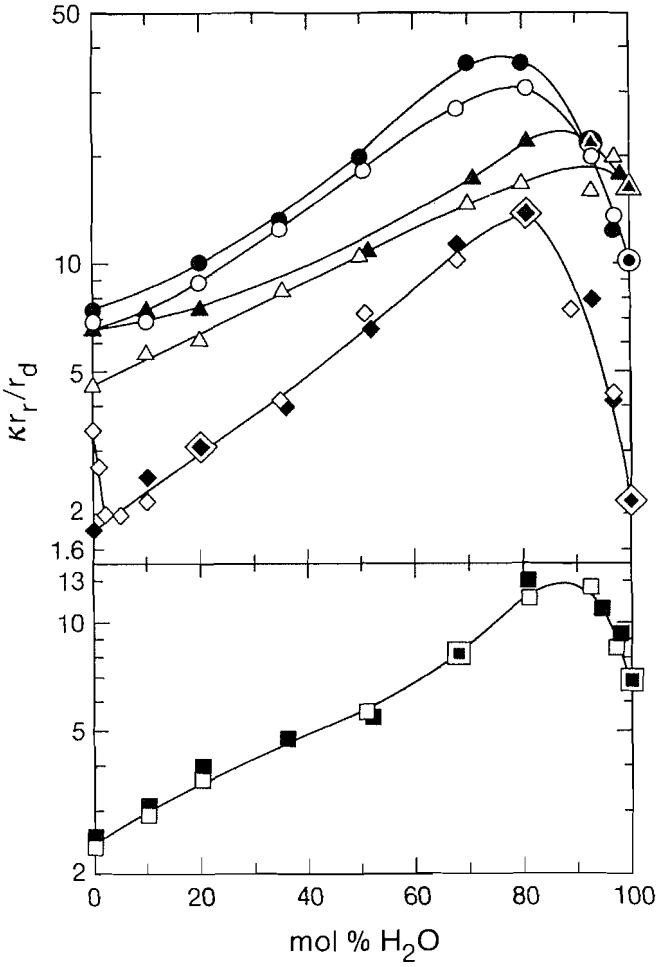


FIG. 10. Solvent composition dependence of reaction-parameter ratio $\kappa r_r/r_d$ at 298 K. Open symbols, 1-propanol/water; solid, 2-propanol/water; otherwise as in Fig. 6.

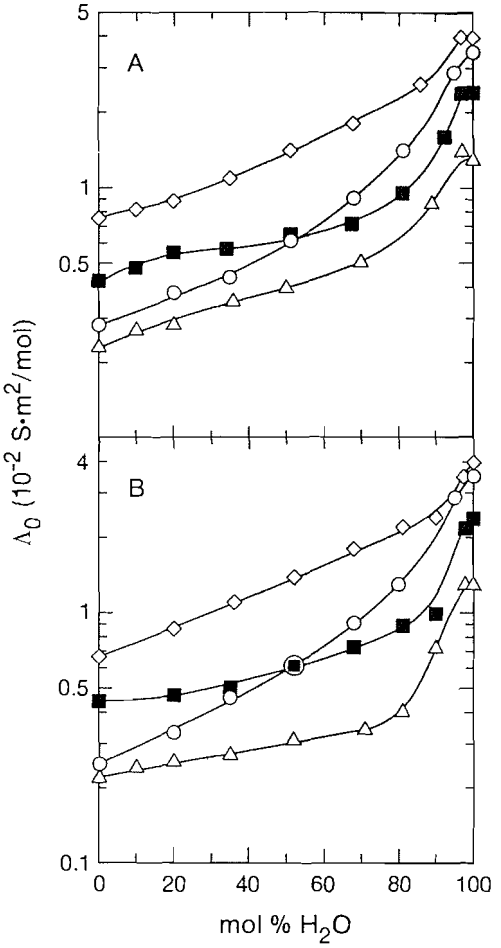


FIG. 11. Solvent composition dependence of molar conductivities at infinite dilution, Λ_0, of $HClO_4$, ○; $AgClO_4$, △; $Cu(ClO_4)_2$, ■; $Al(ClO_4)_3$, ◇; at 298 K in 1-propanol/water (*A*) and 2-propanol/water (*B*) mixed solvents. S = siemens = C/V.s.

The solvent dependences of the molar conductivities of the acid and salts at 298 K are shown in Fig. 11. At the low ion concentrations used to measure k_2 (Tables 2–5), $\Lambda = \Lambda_0$ in the alcohols as well as in water (15). The curves do not contain a minimum at about 70 mol% water where the viscosity is at a maximum (Table 2), as might be expected from Walden's rule (Stokes' law). This interesting behavior of ion diffusion through a composite solvent structure is worthy of separate study. The behavior accounts for the maxima in the curves in Fig. 10 (see eq. [8], which involves Stokes' law).

In pure water at 298 K the ratios of the λ's (16, 17) of e_s^-:H_s^+:Ag_s^+:Cu_s^{2+}:Al_s^{3+} are 4.7:9.1:1.6:3.0:4.9, so the diffusion coefficients ($\propto \lambda_i/z_i^2$) are in the ratios 4.7:9.1:1.6:0.8:0.5. Thus diffusion of e_s^- dominates the relative motion of each reactant pair except that with H_s^+.

The values of the individual ionic conductivities in the mixed solvents are not known, so we made approximations. In water the ratio $[\lambda(e_s^-) + \lambda(H_s^+)]/\Lambda_0(H_s^+, ClO_{4,s}^-) = 1.3$, $[\lambda(e_s^-) + \lambda(Ag_s^+)]/\Lambda_0(Ag_s^+, ClO_{4,s}^-) = 1.9$, $[\lambda(e_s^-) + 0.25\lambda(Cu_s^{2+})]/\frac{1}{2}\Lambda_0(Cu_s^{2+}, 2ClO_{4,s}^-) = 1.6$, and $[\lambda(e_s^-) + 0.11\lambda(Al_s^{3+})]/\frac{1}{3}\Lambda_0(Al_s^{3+}, 3ClO_{4,s}^-) = 1.5$. Thus eq. [11] can be approximated as

$$[12] \quad \kappa r_r \approx 1 \times 10^{-16} z_i k_2/f\Lambda_0 T$$

where z_i is the number of charges on the reactant cation.

The values of κr_r are much less dependent on solvent composition (Fig. 12) than are the apparent values of $\kappa r_r/r_d$ (Fig. 10). Thus the Stokes' value of r_d are solvent dependent.

The Stokes radius r_d for mutual diffusion of ions in an electrolyte solution is given by (4)

$$[13] \quad r_d = \left(\frac{1}{r_{d+}} + \frac{1}{r_{d-}}\right)^{-1} = 8.2 \times 10^{-16} \Big/ \eta\left(\frac{\lambda_+}{z_+^2} + \frac{\lambda_-}{z_-^2}\right)$$

Separate values of λ_+ and λ_- in the mixed solvents are not available, so there is a complication in the calculation of r_d when $z_+ \neq z_-$, as in the present Cu_s^{2+}, $ClO_{4,s}^-$, and Al_s^{3+}, $ClO_{4,s}^-$ solutions. In pure water solvent the values (17) of $[(\lambda_+/z_+^2) + \lambda_-] = 9.6$ and 8.8 (10^{-3} S m^2/mol) for the Cu_s^{2+} and Al_s^{3+} salts, respectively, are a bit nearer to the respective values of $\Lambda_0(\text{salt})/z_+$, 12.4 and 13.0 ($10^{-3}$ S m^2/mol), than to those of $\Lambda_0(\text{salt})/z_+^2$, 6.2 and 4.3 ($10^{-3}$ S m^2/mol), respectively. Furthermore, $\lambda_e = 18 \times 10^{-3}$ S m^2/mol (16) is greater than $\lambda_- = \lambda(ClO_{4,s}^-) = 6.7 \times 10^{-3}$ S m^2/mol in water at 298 K, so the value of $[\lambda_+/z_+^2) + \lambda_e]$ would be much closer to $\Lambda_0(\text{salt})/z_+$ than to $\Lambda_0(\text{salt})/z_+^2$. We therefore chose the approximation

$$[14] \quad r_d \approx 8 \times 10^{-16} z_+/\eta\Lambda_0$$

Values of r_d estimated from eq. [14] display a minimum in the vicinity of 90 mol% water (Fig. 13). The decrease of r_d as small amounts of alcohol are added to water indicates that the microscopic viscosity of the fluid in the vicinity of the ions

TABLE 5. Rate parameters for the reaction of solvated electrons with aluminum perchlorate[a]

X_w[b]	ϵ[c]	η[d] (10^{-3} Pa s)	k_2[e] (10^7 m^3/mol s)	k_2/f[e] (10^7 m^3/mol s)	$E_2^{f,g}$ (kJ/mol)	log A_2[g] (A_2 in m^3/mol s)
			1-PrOH/H_2O			
1.00	78.5	0.89	2.5	0.41	34	11.79
0.97	71.7	1.34	3.5	0.52	26	11.25
0.89	57.2	2.26	4.5	0.54	28	11.54
0.81	47.0	2.63	8.8	0.86	19	10.27
0.68	36.0	2.73	8.2	0.62	20	10.27
0.51	28.0	2.56	8.0	0.47	21	10.33
0.35	24.0	2.32	5.9	0.30	20	10.00
0.20	21.7	2.16	5.2	0.24	21	10.04
0.10	20.7	2.06	4.1	0.18	21	9.98
0.05	20.2	2.01	3.8	0.16	22	10.07
0.02	20.2	1.97	3.8	0.16	22	10.03
0.01	20.2	1.97	5.3	0.22	22	10.13
0.00	20.2	1.96	6.7	0.28	22	10.38
			2-PrOH/H_2O			
1.00	78.5	0.89	2.5	0.41	34	11.79
0.97	71.5	2.02	1.38	0.49	31	12.19
0.93	63.2	2.02	4.9	0.64	26	11.36
0.81	46.2	3.02	7.8	0.75	21	10.55
0.68	34.0	3.07	8.6	0.61	22	10.60
0.52	25.3	2.70	7.5	0.39	20	10.14
0.36	21.6	2.40	6.0	0.27	24	10.54
0.20	19.5	2.20	5.5	0.22	22	10.22
0.10	18.6	2.13	5.1	0.20	23	10.41
0.00	18.0	2.08	3.9	0.5	22	10.04

[a] Al^{3+} concentrations 2–34 mmol/m^3.
[b–g] As in Table 2.

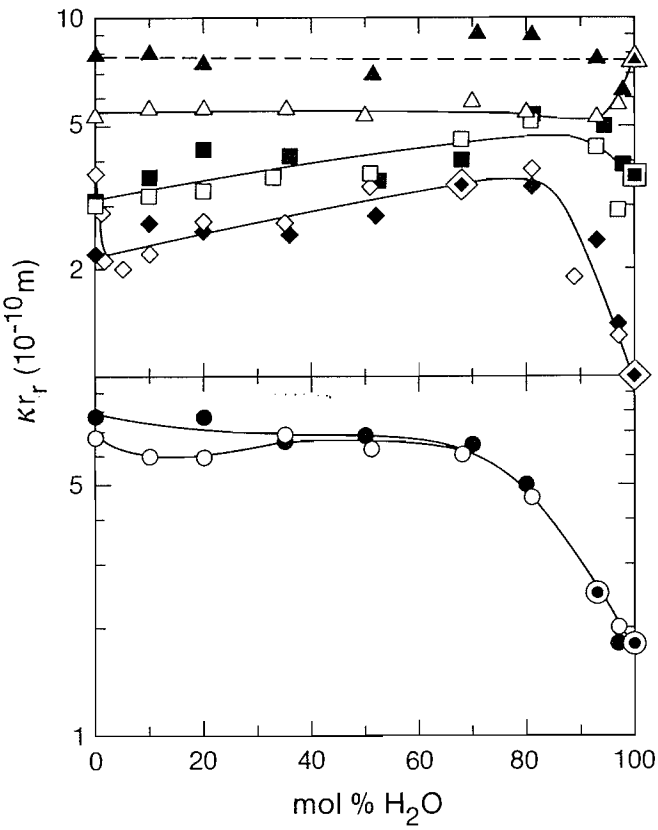


FIG. 12. Solvent composition dependence of κr_r at 298 K. See eq. [12]. Symbols as in Fig. 6. Open symbols, 1-propanol/water; solid, 2-propanol/water.

is lower than the shear viscosity of the bulk fluid. The ions evidently remain in the disordered water and do not associate with the more viscous structures that are nucleated by the alcohol molecules. The increase of r_d at higher alcohol concentrations is attributed to the larger size of the molecules that solvate the ions. The ratio of molar volumes alcohol/water at 298 K are 4.2 for 1-propanol and 4.3 for 2-propanol (18).

The low value of r_d for perchloric acid in water is due to the proton hopping mechanism (19), which is more efficient in water than in alcohol.

Conclusion

The reactivities of solvated electrons with solutes are dependent on the electron affinity of the solute, the electron–solvent and solute–solvent interactions, and the solvent structure. The solvent structure influences both the rate of reactant diffusion and the probability that a reactant encounter pair will react instead of diffusing apart again.

The activation energies E_2 of the reactions e_s^- with H_s^+, Ag_s^+, Cu_s^{2+}, and Al_s^{3+} are similar to the activation energies of conductance $E_{\Lambda 0}$ of the perchlorate electrolyte solutions in all the propanol/water solvents, except for Al_s^{3+} in pure water solvent. The value of E_2 for Al_s^{3+} in pure water solvent is unusually high, probably because the overall reaction is not a single step electron transfer. There are differences in the detailed shapes of the E_2 and $E_{\Lambda 0}$ curves that will provide important information when incorporated into a larger study.

The values of the reaction radius r_r multiplied by the probability of reaction κ of a reactant encounter pair in pure propanol-1 or -2 solvent are in the order $Ag_s^+ \approx H_s^+, > Cu_s^{2+} > Al_s^{3+}$, while in pure water solvent the order has changed to $Ag_s^+ > Cu_s^{2+} > H_s^+, > Al_s^{3+}$. Most of the change occurs in

Can. J. Chem. Downloaded from www.nrcresearchpress.com by 195.138.81.100 on 09/07/12
For personal use only.

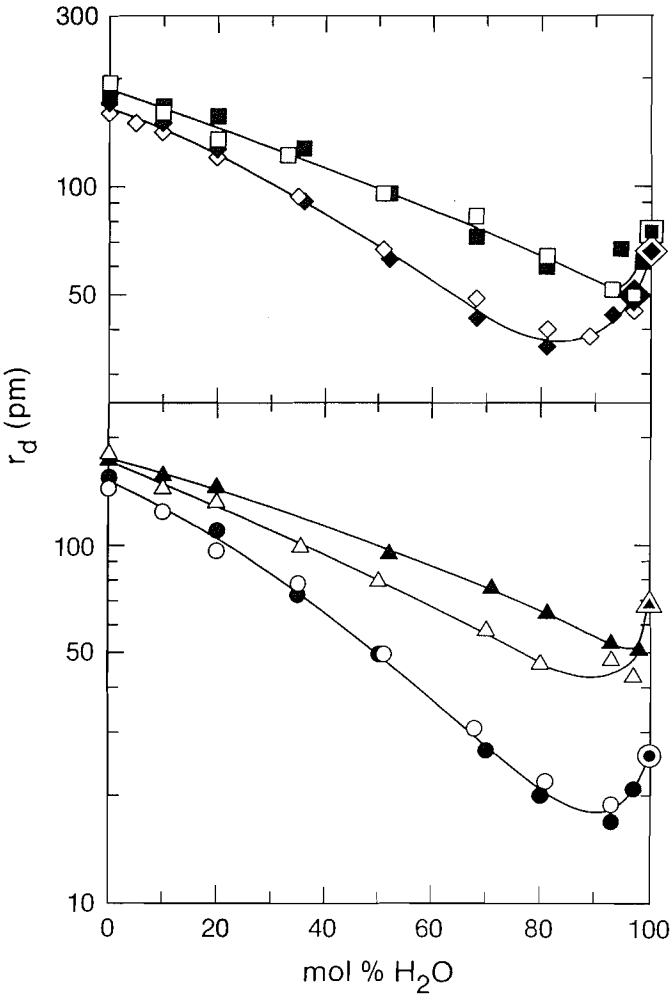


FIG. 13. Solvent composition dependence of r_d (eq. [14]) at 298 K. Open symbols, 1-propanol/water; solid, 2-propanol/water. ○, $H_s^+ + ClO_{4,s}^-$; △, $Ag_s^+ + ClO_{4,s}^-$; □, $Cu_s^{2+} + ClO_{4,s}^-$; ◇, $Al_s^{3+} + ClO_{4,s}^-$.

the solvent composition region 80 to 100 mol% water. The variation of the Stokes radius of ions for mutual diffusion in this composition region indicates that ions remain in the disordered water and do not associate with the more viscous structures that are nucleated by the alcohol molecules.

Acknowledgements

We thank the Natural Sciences and Engineering Research Council of Canada for financial assistance, and the personnel of the Radiation Research Center for maintaining the accelerator and electronic equipment.

1. Y. MAHAM and G. R. FREEMAN. J. Phys. Chem. **92**, 1506 (1988).
2. P. C. SENANAYAKE and G. R. FREEMAN. J. Phys. Chem. **92**, 5142 (1988).
3. C. C. LAI and G. R. FREEMAN. J. Phys. Chem. **94**, 4891 (1990).
4. A. PEIRIS SEDIGALLAGE and G. R. FREEMAN. Can. J. Phys. **68**, 940 (1990).
5. Y. MAHAM and G. R. FREEMAN. J. Phys. Chem. **89**, 4347 (1985).
6. G. L. BOLTON and G. R. FREEMAN. J. Am. Chem. Soc. **98**, 6825 (1976).
7. C. C. LAI. Ph.D. thesis, University of Alberta, Edmonton. 1989.
8. J. TIMMERMANS. Physico-chemical constants of binary mixtures. Vol. 4. Wiley-Interscience, New York. 1960.
9. M. ANBAR, M. BAMBENEK, and A. B. ROSS. Natl. Stand. Ref. Data. Ser. Natl. Bur. Stand. 43 (1973).
10. A. D. LEU, K. N. JHA, and G. R. FREEMAN. Can. J. Chem. **60**, 2342 (1982).
11. A. A. FROST and R. G. PEARSON. Kinetics and mechanism. 2nd ed. Wiley, New York. 1961. pp. 104, 110, 144.
12. P. C. SENANAYAKE and G. R. FREEMAN. J. Phys. Chem. **91**, 2123 (1987).
13. (*a*) K. N. JHA, G. L. BOLTON, and G. R. FREEMAN. Can. J. Chem. **50**, 3073 (1972); (*b*) K. N. GHA and G. R. FREEMAN. J. Chem. Phys. **48**, 5480 (1968).
14. R. S. BOIKESS and E. EDELSON. Chemical principles. 3rd ed. Harper and Row, New York. 1985. p. 796.
15. A. PEIRIS. Ph.D. thesis, University of Alberta, Edmonton. 1990.
16. K. H. SCHMIDT. Int. J. Radiat. Phys. Chem. **4**, 439 (1972).
17. D. DOBOS. Electrochemical data. Elsevier, Amsterdam. 1975. p. 88.
18. R. W. GALLANT. Physical properties of hydrocarbons. Vol. 1. Gulf Publishing Co., Houston, TX. 1968.
19. W. J. MOORE. Basic physical chemistry. Prentice-Hall, Englewood Cliffs, NJ. 1983. p. 364.

Can. J. Chem. Downloaded from www.nrcresearchpress.com by 195.138.81.100 on 09/07/12
For personal use only.

Bimetallic titanium alkoxides: synthesis and structure of $Cp_2Ti(Ph)(\mu\text{-}OCH_2C(CH_3)_2CH_2O)(Ph)TiCp_2$; a precursor to macrocyclic metallocene derivatives

T. TIMOTHY NADASDI AND DOUGLAS W. STEPHAN[1]

Department of Chemistry and Biochemistry, University of Windsor, Windsor, Ont., Canada N9B 3P4

Received June 21, 1990

T. TIMOTHY NADASDI and DOUGLAS W. STEPHAN. Can. J. Chem. **69**, 167 (1991).

The reaction of Cp_2TiPh_2 with 2,2-dimethylpropane-1,3-diol proceeds with the evolution of benzene affording the bimetallic titanocene alkoxide species $Cp_2Ti(Ph)(\mu\text{-}OCH_2C(CH_3)_2CH_2O)(Ph)TiCp_2$, **1**. Complex **1** crystallizes in the monclinic space group *Cc* with $a = 25.448(7)$ Å, $b = 8.483(s)$ Å, $c = 14.512(3)$ Å, $\beta = 101.52(2)°$, $Z = 4$, and $V = 3070(1)$ Å^3. The structure was refined employing 1471 data with $F_o > 3\sigma F_o$ and 138 variables to R values of $R = 0.0588$ and $R_w = 0.0828$. the dimeric nature of **1** is confirmed. The coordination spheres of the two Ti centres are pseudo-tetrahedral. The Ti—C σ bonds were found to be 2.21(1) and 2.25(1) Å. Although the phenyl substituents are directed towards each other, steric effects appear to be overcome by the approximately perpendicular orientation of the phenyl rings (in fact the angle between the planes is 81.9°). The Ti...Ti separation in **1** is 6.725 Å. The implications of the preparation of **1** regarding the mechanism of formation of early metal macrocyclic compounds are discussed. In addition, the ramifications for the synthesis of dissymmetric early metal macrocycles are considered.

Key words: titanium alkoxides, alkoxide bridged, structure.

T. TIMOTHY NADASDI et DOUGLAS W. STEPHAN. Can. J. Chem. **69**, 167 (1991).

Le réaction du Cp_2TiPh_2 avec le 2,2-diméthylpropane-1,3-diol donnent lieu à une évolution de benzène et conduisent à la formation d'alcoolates de titanocène bimétalliques $Cp_2Ti(Ph)(\mu\text{-}OCH_2C(CH_3)_2CH_2O)(Ph)TiCp_2$ (**1**). Le complexe **1** cristallise dans le groupe d'espace *Cc*, avec $a = 25{,}448(7)$, $b = 8{,}483(2)$ et $c = 14{,}512(3)$ Å, $\beta = 101{,}53(2)°$, $Z = 4$ et $V = 3070(1)$ Å^3. On a affiné la structure à l'aide de 1471 données avec $F_o > 3\sigma F_o$ et 138 variables jusqu'à des valeurs de $R = 0{,}0588$ et $R_w = 0{,}0828$. On a confirmé la nature dimère du produit **1**. Les sphères de coordination des deux centres Ti sont pseudo-tétraédriques. On a trouvé que les longueurs de liaisons σ Ti—C sont égales à 2,21(1) et 2,25(1) Å. Même si les groupements phényles sont orientés l'un vers l'autre, il semble que les effets stériques sont éliminés par l'orientation approximativement perpendiculaire des noyaux phényles (l'angle entre les plans est en fait égal à 81.9°). Dans **1**, la séparation Ti...Ti est égale à 6,725 Å. On discute des implications de la préparation du composé **1** sur le mécanisme de formation des premiers termes de composés métalliques macrocycliques. De plus, on considère les ramifications sur la synthèse des premiers termes des macrocycles métalliques dissymétriques.

Mots clés : alcoolates de titane, structure alcoolate pontée.

[Traduit par la revue]

Introduction

Titania or zirconia are often employed as support materials for heterogeneous catalysts (1). These supports may act simply as a dispersent for the late metal centers or may play an active role in the catalytic cycle. In the latter case, such participation gives rise to the phenomenon known as strong metal-support interactions (SMSI) (1). Activation of substrate molecules by a Lewis acidic, early metal and a late metal center may account for the observed effects. We and others have investigated homogeneous systems in which early and late metals are linked in close proximity by bridging ligands (2). Such heterobimetallics are of interest both as models for the heterogeneous catalyst systems and because of their potential as catalysts in their own right. Fewer studies have focused on simple complexes of Ti or Zr that might model the Lewis acidic, early metal centers of titania or zirconia. Several groups (3–5), have reported the syntheses and reaction chemistry of a variety of early metal alkoxide complexes. The similarity of metal-alkoxide species to metal oxides and the propriety of such species as models for metal-oxide surfaces have been considered by others (3). Much of the work to date has focused on systems in which sterically demanding alkoxy or aryloxy ligands inhibit oligomerization and yield mononuclear early metal compounds (4, 5). In our initial investigations in this area, we described the specific formation of bimetallic macrocyclic Zr-alkoxide species via the reaction of dimethylzirconocene with diols (Scheme 1) (6).

In this report we describe the product of the related reaction of Cp_2TiPh_2 with 2,2-dimethylpropanediol, i.e., $Cp_2Ti(Ph)(\mu\text{-}OCH_2C(CH_3)_2CH_2O)(Ph)TiCp_2$ **1**. Compound **1**, which has been crystallographically characterized, may be an analog of the intermediates in the formation of the Zr macrocycles shown in Scheme 1. The ramifications for the mechanism of formation of the macrocyclic species and the implications for macrocycle design are considered and discussed.

Experimental section

General data

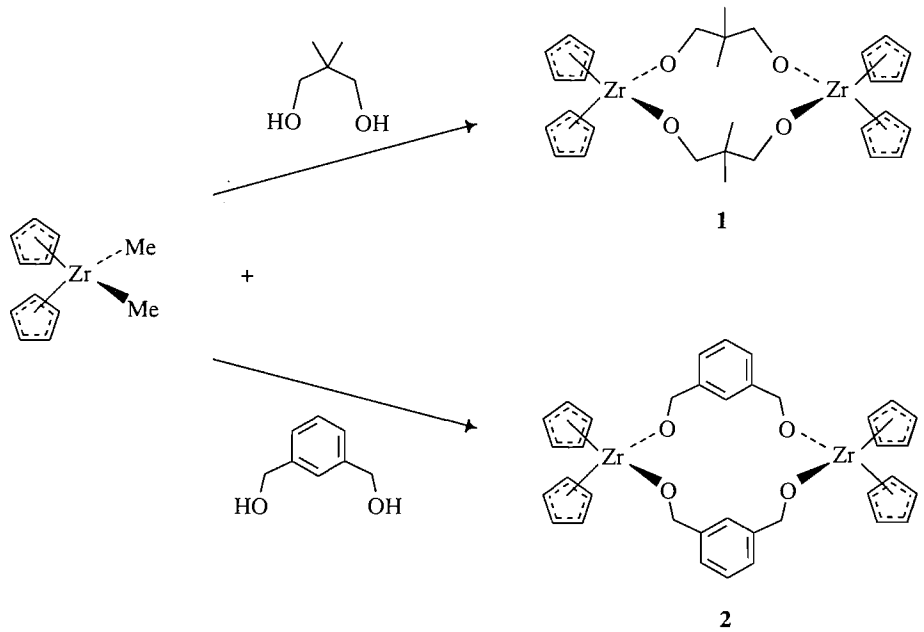
All preparations were done under an atmosphere of dry, O_2-free N_2 employing a Vacuum Atmospheres Inert atmosphere glove box. Solvents were reagent grade, distilled from the appropriate drying agents under N_2, and degassed by the freeze–thaw method at least three times prior to use. ^1H NMR spectra were recorded on a Bruker AC-300 spectrometer operating at 300 MHz. Trace amounts of protonated solvents were used as references and chemical shifts are reported relative to $SiMe_4$. Combustion analyses were performed by Galbraith Laboratories Inc. Knoxville, TN, and Schwarzkoff Laboratories, Woodside, NY. PhLi and Cp_2TiCl_2 were purchased from the Aldrich Chemical Co. Cp_2TiPh_2 was prepared by the literature method (7).

Synthesis of $Cp_2Ti(Ph)(\mu\text{-}OCH_2C(CH_3)_2CH_2O)(Ph)TiCp_2$, 1

To a THF solution (30 mL) of Cp_2TiPh_2 (1.00 g, 3.00 mmol) was added 2,2-dimethylpropane-1,3-diol (0.313 g, 3.00 mmol) and the

[1]A complete set of supplementary material may be purchased from the Depository of Unpublished Data, CISTI, National Research Council of Canada, Ottawa, Ont., Canada K1A 0S2.

Can. J. Chem. Downloaded from www.nrcresearchpress.com by 195.138.81.100 on 09/07/12
For personal use only.



SCHEME 1

solution was stirred for 18 h at 60°C. Yellow blocks crystallized from solution on standing at 25°C in an atmosphere of N_2 for 20 days. (Yield (NMR) 80%.) *Anal.* calcd for $C_{37}H_{40}O_2Ti_2$: C 72.55, H 6.58; found: C 72.99, H 6.58. ^{1}H NMR (d_6-benzene, δ, ppm): 7.15 (m, 10H, Ph), 5.78 (s, 20H, Cp), 3.98 (s, 4H, CH_2), 0.80 (s, 6H, CH_3).

X-ray data collection and reduction

X-ray quality crystals were obained directly from the preparations as described above. The crystals were manipulated and mounted in capillaries in a glove box, thus maintaining a dry, O_2-free environment. Diffraction experiments were performed on a four-circle Syntex $P2_1$ diffractometer with graphite-monochromatized Mo Kα radiation. The initial orientation matrix was obtained from 15 machine-centered reflections selected from a rotation photograph. These data were used to determine the crystal system. Partial rotation photographs around each axis were consistent with a monoclinic crystal system. Ultimately, 49 reflections ($20° < 2\theta < 25°$) were used to obtain the final lattice parameters and the orientation matrix. Machine parameters, crystal data, and data collection parameters are summarized in Table 1. The observed extinctions were consistent with the space groups $C2/c$ and Cc. Successful refinement confirmed the space group as Cc. The data, $h, k, \pm l$, were collected in one shell ($4.5° < 2\theta < 45.0°$) and three standard reflections were recorded every 197 reflections. The intensities of the standards showed no statistically significant change over the duration of the data collection. The data were processed using the TEXSAN program package employing a VAX 3520 workstation. The reflections with $F_o^2 > 3\sigma F_o^2$ were used in the refinement.

Structure solution and refinement

Non-hydrogen atomic scattering factors were taken from the literature tabulations (8). The Ti atom positions were determined using direct methods employing MITHRIL. The remaining non-hydrogen atoms were located from successive difference Fourier map calculations. The refinements were carried out using full-matrix least-squares techniques on F, minimizing the function $w(|F_o| - |F_c|)^2$ where the weight, w, is defined as $4F_o^2/2\sigma(F_o^2)$ and F_o and F_c are the observed and calculated structure factor amplitudes. In the final cycles of refinement the titanium, oxygen, and the methylene and quaternary carbon atoms in the alkoxide bridge were assigned anisotropic temperature factors. The methyl, phenyl, and cyclopentadienyl groups were refined with individual isotropic thermal parameters; however, the geometry of the phenyl and cyclopentadienyl rings were constrained to be that of regular hexagons and pentagons, respectively. Hydrogen atom positions were calculated and recalculated before each successive least-square refinement. C—H bond lengths of 0.95 Å were assumed. Hydrogen atom temperature factors were fixed at 1.10 times the isotropic temperature factor of the carbon atom to which they are bonded. In all cases the hydrogen atom contributions were calculated, but not refined. The final values of R and R_w are given in Table 1. The maximum Δ/σ on any of the parameters in the final cycles of the refinement and the location of the largest peaks in the final difference Fourier map calculation are also given in Table 1. The residual electron densities were of no chemical significance. The following data are tabulated: positional parameters (Table 2) and selected bond distances and angles (Table 3). Thermal parameters (Table S1), hydrogen atom parameters (Table S2), and values of 10 F_o and 10 F_c (Table S3) have been deposited as supplementary material.[1]

Results and discussion

The cleavage of metal–carbon bonds via protolysis with the subsequent formation of a metal–heteroatom bond is well known. Cleavage of an M—C (M = Ti, Zr) bond by reaction with alcohols is known to be a facile route to simple early metal alkoxide species (9, 10). In the same vein, we have shown that reactions of diols with Cp_2ZrMe_2 results in the rapid liberation of methane and the formation of macrocyclic zirconium alkoxides (Scheme 1) (6). While the chemistry of these and related macrocycles is a subject of ongoing study, it is also of interest to develop the means for controlled syntheses of such macrocycles. To that end, the reaction of Cp_2TiPh_2 with a diol was investigated. Reaction of Cp_2TiPh_2 with 2,2-dimethylpropanediol proceeds smoothly at 65°C over an 18 h period. Monitoring of the reaction by ^{1}H NMR showed the gradual growth in the resonance arising from benzene indicative of the protyolysis of the aryl group from Ti. In addition, new resonances attributable to phenyl, cyclopentadienyl, methylene, and methyl protons grew with time. Crystallization of the product was achieved by storage at 25°C for 20 days. The ^{1}H NMR of the isolated product indicated that the compound was the new species originally observed in the NMR scale trials. The ^{1}H NMR and combustion analysis data suggested the formulation $Cp_2Ti(Ph)$-(μ-$OCH_2C(CH_3)_2CH_2O$)(Ph)$TiCp_2$, **1**, and this was later

Can. J. Chem. Downloaded from www.nrcresearchpress.com by 195.138.81.100 on 09/07/12
For personal use only.

Can. J. Chem. Downloaded from www.nrcresearchpress.com by 195.138.81.100 on 09/07/12
For personal use only.

TABLE 1. Crystallographic parameters for molecule 1

Formula	$C_{37}H_{40}O_2Ti_2$
Cryst color, form	Yellow blocks
a (Å)	25.448(7)
b (Å)	8.483(2)
c (Å)	14.512(3)
β (deg)	101.53(2)
Crystal system	Monoclinic
Space group	Cc
Vol (Å^3)	3070(1)
Density (g cm^{-3}) calcd.	
Z	4
Crystal dimension (mm)	0.45 × 0.30 × 0.35
Absorption coefficient, μ (cm^{-1})	5.44
Radiation, λ (Å)	Mo Kα (0.71069)
Temperature (°C)	24
Scan speed (deg/min)	2.0–10.0 (θ/2θ)
Scan range (deg)	1.0 below Kα1 1.0 above Kα2
Background/scan time ratio	0.5
Data collected	2240
2θ range (deg)	4.5–45
Index range	$h, k, \pm l$
Unique data $F_o^2 > 3\sigma(F_o^2)$	1471
Variables	138
R(%)	5.88
R_W(%)	8.28
Maximum shift/error in final cycle	0.01

TABLE 2. Positional parameters for $Cp_2Ti(Ph)$-$(\mu\text{-}OCH_2C(CH_3)_2CH_2O)(Ph)TiCp_2$

Atom	x	y	z
Ti(1)	0.373	0.4927(3)	0.960
Ti(2)	0.11078(8)	0.4921(3)	0.9725(1)
O(1)	0.3112(4)	0.581(1)	0.9755(7)
O(2)	0.1743(4)	0.577(1)	0.9573(8)
C(1)	0.2859(6)	0.680(2)	1.031(1)
C(2)	0.2398(9)	0.780(1)	0.964(2)
C(3)	0.2014(7)	0.683(2)	0.908(1)
C(4)	0.2669(5)	0.876(2)	0.885(1)
C(5)	0.2138(6)	0.900(2)	1.010(1)
C(11)	0.3747(4)	0.311(1)	1.0693(6)
C(12)	0.3260(4)	0.287(1)	1.0975(7)
C(13)	0.3216(4)	0.170(1)	1.1629(8)
C(14)	0.3658(5)	0.077(1)	1.2001(8)
C(15)	0.4145(4)	0.101(1)	1.172(1)
C(16)	0.4189(4)	0.218(1)	1.1064(8)
C(41)	0.1146(4)	0.310(1)	0.8608(7)
C(42)	0.0732(3)	0.209(1)	0.8208(7)
C(43)	0.0817(4)	0.096(1)	0.7555(7)
C(44)	0.1316(4)	0.084(1)	0.7302(7)
C(45)	0.1730(3)	0.185(1)	0.7702(8)
C(46)	0.1645(4)	0.299(1)	0.8355(8)
C(21)	0.3705(5)	0.458(1)	0.792(1)
C(22)	0.3191(4)	0.427(1)	0.808(1)
C(23)	0.3220(4)	0.292(1)	0.8464(9)
C(24)	0.3752(4)	0.240(1)	0.8835(8)
C(25)	0.4052(4)	0.343(1)	0.839(1)
C(31)	0.4689(4)	0.544(1)	1.0076(7)
C(32)	0.4467(4)	0.657(1)	0.9407(5)
C(33)	0.4120(4)	0.751(1)	0.9802(7)
C(34)	0.4127(4)	0.697(1)	1.0715(6)
C(35)	0.4478(4)	0.569(1)	1.0884(5)
C(51)	0.1092(5)	0.460(1)	1.1348(9)
C(52)	0.0818(4)	0.330(1)	1.089(1)
C(53)	0.1186(5)	0.237(1)	1.0534(9)
C(54)	0.1688(4)	0.310(1)	1.077(1)
C(55)	0.1630(4)	0.448(1)	1.1274(9)
C(61)	0.0578(5)	0.647(1)	0.8454(6)
C(62)	0.0770(4)	0.751(1)	0.9196(7)
C(63)	0.0545(4)	0.707(1)	0.9963(6)
C(64)	0.0214(4)	0.576(1)	0.9695(8)
C(65)	0.0235(5)	0.539(1)	0.8762(8)

confirmed by X-ray crystallography (*vide infra*). Attempts to employ this reaction pathway failed to yield Ti macrocycles analogous to those reported for Zr. Neither addition of varying excesses of diol nor prolong refluxing in toluene led to further reaction of **1**. This is perhaps not surprising as it is known that in general, metal–aryl bonds tend to be more resistent to protyolysis than metal–alkyl bonds (11).

Structural study

A crystallographic study showed that **1** crystalizes in the space group *Cc* with four discrete dimeric molecules per unit cell. The closest non-bonded approach between these dimers is 2.400 Å (H42—H32). The Ti atom separation within the dimeric molecule is found to be 6.725 Å; this compares with a Zr...Zr distance of 5.898 Å in the macrocyclic dimer $Cp_2Zr(\mu\text{-}OCH_2C(CH_3)_2CH_2O)_2ZrCp_2$ (6). The coordination spheres of the Ti atoms in **1** are best described as pseudo tetrahedral. Two π-bonded cyclopentadienyl groups, a σ-bonded phenyl ring and an oxygen atom of the dialkoxide complete the coordination spheres of the Ti atoms. An ORTEP drawing of **1** appears in Fig. 1.

The Ti—C distances for the cyclopentadienyl groups averages 2.41(1) Å, typical of Cp_2Ti fragments. The rotational relationship of the cyclopentadienyl rings is between staggered and eclipsed being closer to the latter. The Ti—O bond distances in **1** are 1.80(1) and 1.82(1) Å. These compare with Ti—O distances of 1.855(2) and 1.750(2) Å found in $Cp_2Ti(OEt)Cl$ and $[CpTiCl_2OCMe_2]_2$, respectively (12). The two Ti—O—C angles in **1** were found to be 146.4(9) and 148.0(9)°. These angles are significantly larger than that of 133.2(2)° found in $Cp_2Ti(OEt)Cl$ (12) and significantly smaller than that of 166.2(2)° found in $[CpTiCl_2OCMe_2]_2$ (12). These variations in the Ti—O—C angles are consistent with the expected variations in Ti—O $d\pi$—$p\pi$ multiple bond character based on metal Lewis acidity considerations. Theoretical support for such early-metal–oxygen π-bonding has been previously described (6). The Ti—C distances for the σ-bonded phenyl rings were found to be 2.21(1) and 2.25 Å in **1**. These Ti—C distances are comparable to those found in Cp_2TiPh_2 (2.27(1) Å) (13) and in $(indenyl)_2TiMe_2$ (2.21(2) Å) (14) and yet are considerably longer than those found in $TiBz_4$ (2.14(1) Å) (15). The angle between the planes of the two phenyl rings is 81.9°. Presumably this orientation minimizes the possible intramolecular steric interactions between these groups. The C11 and C41 phenyl rings are oriented 15.2 and 12.4° out of the corresponding C—Ti—O planes, respectively. Again this orientation minimizes steric interactions with the cyclopentadienyl groups on the respective titanium atoms. The C—Ti—O angles in **1** were found to be 95.0(4) and 91.0(5)° at Ti1 and Ti2, respectively. The average of these angles compare with the C—Ti—O angle found in $Cp_2Ti(OEt)Cl$ (12) (93.1(1)°); however, the cause of the 4° variation in the O—Ti—C angles in **1** is not clear. The distances and angles within the bridging dialkoxide moiety are typical and require no further comment.

Can. J. Chem. Downloaded from www.nrcresearchpress.com by 195.138.81.100 on 09/07/12
For personal use only.

TABLE 3. Selected intramolecular distances and angles

(*a*) Selected intramolecular distances

Atom	Atom	Distance (Å)	Atom	Atom	Distance (Å)
Ti(1)	O(1)	1.80(1)	C(1)	C(2)	1.62(2)
Ti(1)	C(11)	2.21(1)	C(2)	C(3)	1.41(2)
Ti(1)	C(21)	2.44(1)	C(2)	C(4)	1.66(3)
Ti(1)	C(22)	2.42(1)	C(2)	C(5)	1.45(3)
Ti(1)	C(23)	2.41(1)	Ti(1)	C(24)	2.42(1)
Ti(1)	C(25)	2.44(1)	Ti(1)	C(31)	2.433(9)
Ti(1)	C(32)	2.39(1)	Ti(1)	C(33)	2.398(9)
Ti(1)	C(34)	2.446(9)	Ti(1)	C(35)	2.468(9)
Ti(2)	O(2)	1.82(1)	Ti(2)	C(41)	2.25(1)
Ti(2)	C(51)	2.38(1)	Ti(2)	C(52)	2.41(1)
Ti(2)	C(53)	2.45(1)	Ti(2)	C(54)	2.45(1)
Ti(2)	C(55)	2.40(1)	Ti(2)	C(61)	2.44(1)
Ti(2)	C(62)	2.424(9)	Ti(2)	C(63)	2.38(1)
Ti(2)	C(64)	2.38(1)	Ti(2)	C(65)	2.41(1)
O(1)	C(1)	1.41(2)	O(2)	C(3)	1.41(2)

(*b*) Selected intramolecular bond angles

Atom	Atom	Atom	Angle (deg)	Atom	Atom	Atom	Angle (deg)
O(1)	Ti(1)	C(11)	95.0(4)	O(2)	Ti(2)	C(41)	91.0(5)
Ti(1)	O(1)	C(1)	146.4(9)	Ti(2)	O(2)	C(3)	148.0(9)
O(1)	C(1)	C(2)	109(2)	C(1)	C(2)	C(3)	112(1)
C(1)	C(2)	C(4)	109(2)	C(1)	C(2)	C(5)	116(2)
C(3)	C(2)	C(4)	103(2)	C(3)	C(2)	C(5)	110(2)
C(4)	C(2)	C(5)	105(1)	O(2)	C(3)	C(2)	116(1)
Ti(1)	C(11)	C(12)	115.2(6)	Ti(1)	C(11)	C(16)	124.8(8)
Ti(2)	C(41)	C(42)	125.7(8)	Ti(2)	C(41)	C(46)	114.2(7)

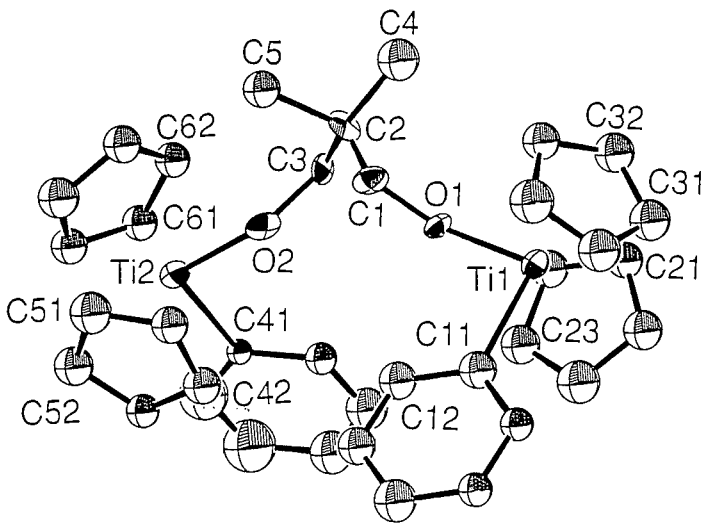
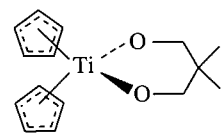


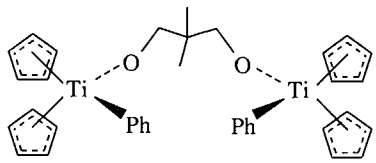
FIG. 1. ORTEP drawing of molecule **1**, 40% thermal ellipsoids are shown. Hydrogen atom are omitted for clarity.



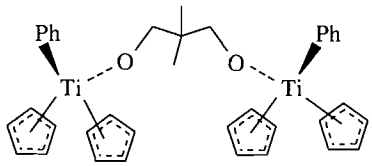
A

The formation of **1** has some implications for the synthesis of early-metal macrocyclic complexes. The driving force behind the quantitative formation of **1** rather than a chelated mononuclear species (**A**) is not understood but may arise as a result of the Ti—O multiple bond character. Such bonding requires a relatively large Ti—O—C angle. Chelation to Ti of a dialkoxide cannot accommodate this structural feature and thus one might conclude that $d\pi$—$p\pi$ bonding inhibits ring closure and favours bridging structures. Implicit in such an argument is, however, the correlation between the Ti—O—C angle and $d\pi$–$p\pi$ bonding. Although this relationship seems intuitively sensible, recent structural studies of Ta and Nb aryloxide complexes imply that the M—O—Ar angle is an extremely flexible parameter (4*x*). It may be that the effects of the extended π system present in such aryloxide species afford the dramatic variation observed. It is noteworthy that both structural and theoretical data support the presence of significant $d\pi$–$p\pi$ bonding between Zr and O in the previously described Zr macrocycles (Scheme 1) (6). A second point that may be relevant to macrocycle formation is the conformation of **1** observed in the solid state. The phenyl rings on the Ti atoms are oriented towards each other. This "inside" conformation (**B**) avoids steric interactions of the cyclopentadienyl rings with the substituents of the bridging dialkoxide moiety that would be present in an "outside" conformation (**C**). If indeed, analogs of **1** are intermediates in the formation of the related Zr macrocycles then the preference for the "inside" conformer may facilitate the formation of the macrocyclic products.

A further implication of the formation of **1** may arise from the kinetic inertness of the second aryl group on Ti. This too, appears to favour bridging dialkoxide groups and thus afford the formation of **1**. It may be possible to employ the differing reactivities of metal-alkyl and metal-aryl groups towards hy-



B



C

drolysis to construct dissymetric early metal macrocycles. This aspect is the subject of ongoing study.

Acknowledgements

Financial support from NSERC of Canada is gratefully acknowledged.

1. (*a*) S. A. Stevenson, J. A. Dumesic, R. T. K. Baker, and E. Ruckenstrin. (*Editors*). Metal–support interactions in catalysis, sintering, and redispersion. Van Nostrand Reinhold Co., New York. 1987; (*b*) R. T. K. Baker, S. J. Tauster, and J. A. Dumesic. (*Editors*). Strong metal-support interactions. American Chemical Society, Washington, D.C. 1986.
2. (*a*) D. W. Stephan. Coord. Chem. Rev. **95**, 41 (1989); (*b*) T. A. Wark and D. W. Stephan. Organometallics, **8**, 2836 (1989); (*c*) T. A. Wark and D. W. Stephan. Inorg. Chem. **29**, 1731 (1990); (*d*) P. Y. Zheng, T. T. Nadasdi, and D. W. Stephan. Organometallics, **8**, 1393 (1989); (*e*) D. G. Dick and D. W. Stephan. Organometallics. In press. (*f*) G. K. Anderson and M. Lin. Organometallics, **7**, 2285 (1988); (*g*) G. S. Ferguson, P. T. Wolczanski, L. Parkanyi, and M. C. Zonnvylle. Organometallics, **7**, 1967 (1988); (*h*) M. Y. Darensbourg, R. Silva, J. Reibenspies, and C. K. Prout. Organometallics, **8**, 1315 (1989).
3. K. C. Malhotra and R. L. Martin. J. Organomet. Chem. **239**, 159 (1982).
4. (*a*) S. M. Beshouri, P. E. Fanwick, I. P. Rothwell, and J. C. Huffman. Organometallics, **6**, 2498 (1987); (*b*) L. D. Durfee, S. L. Latesky, I. P. Rothwell, J. C. Huffman, and K. Folting. Inorg. Chem. **24**, 4569 (1985); (*c*) L. Chamberlain, J. Keddington, and I. P. Rothwell. Organometallics, **1**, 1098 (1982); (*d*) L. D. Durfee, P. E. Fanwick, I. P. Rothwell, K. Folting, and J. C. Huffman. J. Am. Chem. Soc. **109**, 4720 (1987); (*e*) R. W. Chesnut, P. E. Fanwick, and I. P. Rothwell. Inorg. Chem. **27**, 752 (1988); (*f*) L. Chamberlain, I. P. Rothwell, and J. C. Huffman. J. Am. Chem. Soc. **106**, 1502 (1986); (*g*) P. E. Fanwick, A. E. Ogilvy, and I. P. Rothwell. Organometallics, **6**, 73 (1987); (*h*) L. R. Chamberlain and I. P. Rothwell. J. Am. Chem. Soc. **105**, 1665 (1983); (*i*) L. Chamberlain, J. Keddington, I. P. Rothwell, and J. C. Huffman. Organometallics, **1**, 1538 (1982); (*j*) B. D. Steffey, R. W. Chesnut, J. L. Kerschner, P. J. Pellechia, P. E. Fanwick, and I. P. Rothwell. J. Am. Chem. Soc. **111**, 378 (1989); (*k*) L. R. Chamberlain, A. P. Rothwell, and I. P. Rothwell. J. Am. Chem. Soc. **106**, 1847 (1984); (*l*) T. W. Coffindaffer, B. D. Steffy, I. P. Rothwell, K. Folting, J. C. Huffman, and W. E. Streib. J. Am. Chem. Soc. **111**, 4742 (1989); (*m*) B. D. Steffy, L. R. Chamberlain, R. W. Chesnut, D. E. Chebi, P. E. Fanwick, and I. P. Rothwell. Organometallics, **8**, 1419 (1989); (*n*) L. R. Chamberlain, J. L. Kerschner, A. P. Rothwell, I. P. Rothwell, and J. C. Huffman. J. Am. Chem. Soc. **109**, 6471 (1987); (*o*) A. K. McMullen, I. P. Rothwell, and J. C. Huffman. J. Am. Chem. Soc. **107**, 1072 (1985); (*p*) P. E. Fanwick, L. M. Kobriger, A. K. McMullen, and I. P. Rothwell. J. Am. Chem. Soc. **108**, 8095 (1986); (*q*) S. L. Latesky, J. Keddington, A. K. McMullen, I. P. Rothwell, and J. C. Huffman. Inorg. Chem. **24**, 995 (1985); (*r*) S. L. Latesky, A. K. McMullen, G. P. Niccolai, I. P. Rothwell, and J. C. Huffman. Organometallics, **4**, 902 (1985); (*s*) L. R. Chamberlain, L. D. Durfee, P. E. Fanwick, L. M. Kobriger, S. L. Latesky, A. K. McMullen, B. D. Steffy, I. P. Rothwell, K. Folting, and J. C. Huffman. J. Am. Chem. Soc. **109**, 6068 (1987); (*t*) L. D. Durfee, A. M. McMullen, and I. P. Rothwell. J. Am. Chem. Soc. **110**, 1463 (1988); (*u*) S. L. Latesky, A. K. McMullen, G. P. Niccolai, I. P. Rothwell, and J. C. Huffman. Organometallics, **4**, 1896 (1985); (*v*) S. L. Latesky, A. K. McMullen, I. P. Rothwell, and J. C. Huffman. J. Am. Chem. Soc. **107**, 5981 (1985); (*w*) L. R. Chamberlain, L. D. Durfee, P. E. Fanwick, L. M. Kobriger, S. L. Latesky, A. K. McMullen, B. D. Steffy, I. P. Rothwell, K. Folting, J. C. Huffman, W. E. Streib, and R. Wang. J. Am. Chem. Soc. **109**, 390 (1987); (*x*) B. D. Steffey, P. E. Fanwick, and I. P. Rothwell. Polyhedron, **9**, 963 (1990).
5. (*a*) T. V. Lubben, P. T. Wolczanski, and G. D. Van Duyne. Organometallics, **3**, 977 (1984); (*b*) R. E. La Pointe, P. T. Wolczanski, and J. F. Mitchell. J. Am. Chem. Soc. **108**, 6382 (1986); (*c*) R. E. La Pointe, and P. T. Wolczanski. J. Am. Chem. Soc. **108**, 3535 (1986); (*d*) R. Toreki, R. E. La Pointe, and P. T. Wolczanski. J. Am. Chem. Soc. **109**, 7558 (1987); (*e*) R. E. La Pointe, P. T. Wolczanski, and G. D. Van Duyne. Organometallics, **4**, 1810 (1984); (*f*) D. R. Neithamer, R. E. La Pointe, R. A. Wheeler, D. S. Richeson, G. D. Van Duyne, and P. T. Wolczanski. J. Am. Chem. Soc. **111**, 9356 (1989).
6. D. W. Stephan. Organometallics. In press.
7. L. Summers and R. H. Uloth. J. Am. Chem. Soc. **76**, 2278 (1954).
8. (*a*) D. T. Cromer and J. B. Mann. Acta Crystallogr. Sect. A: Cryst. Phys. Diffr. Theor. Gen. Crystallogr. A**24**, 324 (1968); (*b*) D. T. Cromer and J. B. Mann. Acta Crystallogr. Sect. A: Cryst. Phys. Diffr. Theor. Gen. Crystallogr. A**24**, 390 (1968); (*c*) D. T. Cromer and J. T. Waber. *International tables for X-ray crystallography*. Kynoch Press, Birmingham, England. 1974.
9. M. A. Chaudhari and F. G. A. Stone. J. Chem. Soc. 838 (1966).
10. E. A. Babaian, D. C. Hrncir, S. G. Bott, and J. L. Atwood. Inorg. Chem. **25**, 4818 (1986).
11. R. J. Puddephatt and M. A. Stalteri. Organometallics, **2**, 1400 (1983).
12. J. C. Huffman, K. G. Moloy, J. A. Marsella, and K. G. Caulton. J. Am. Chem. Soc. **102**, 3009 (1980).
13. V. Kocman and J. C. Rucklidge. J. Chem. Soc. Chem. Commun. 1340 (1971).
14. J. L. Atwood, W. E. Hunter, D. C. Hrncir, E. Samuel, H. Alt, and M. D. Rausch. Inorg. Chem. **14**, 1757 (1975).
15. I. W. Bassi, G. Allegra, R. Scordamaglia, and G. Chioccola. J. Am. Chem. Soc. **93**, 3787 (1971).

Can. J. Chem. Downloaded from www.nrcresearchpress.com by 195.138.81.100 on 09/07/12
For personal use only.

Towards supported catalyst models: the synthesis, characterization, redox chemistry, and structures of the complexes $Ti(OAr')_4$ ($Ar' = C_6H_4(2\text{-}t\text{-}Bu)$, $C_6H(2,3,5,6\text{-}Me)_4$)

ROBERT T. TOTH AND DOUGLAS W. STEPHAN[1]

Department of Chemistry and Biochemistry, University of Windsor, Windsor, Ont., Canada N9B 3P4

Received, July 9, 1990

ROBERT T. TOTH and DOUGLAS W. STEPHAN. Can. J. Chem. **69**, 172 (1991).

Reaction of substituted phenoxides with $TiCl_4$ affords the species $Ti(OAr')_4$ ($Ar' = C_6H_4(2\text{-}t\text{-}Bu)$, **1**; $Ar' = C_6H(2,3,5,6\text{-}Me)_4$, **2**). The compound $Ti(OC_6H_4(2\text{-}t\text{-}Bu))_4$, **1**, crystallizes in the tetragonal space group $P\bar{4}2_1c$, with a = 15.203(4) Å, c = 8.026(3) Å, Z = 2, and V = 1855(2) Å^3. The compound $Ti(OC_6H(2,3,5,6\text{-}Me)_4)_4$, **2**, crystallizes in the orthorhombic space group *Pbcn*, with a = 16.539(7) Å, b = 16.136(6) Å, c = 27.716(12) Å, Z = 8, and V = 7397(9) Å^3. The geometry of the Ti coordination sphere in these complexes is best described as pseudo-tetrahedral. In the case of **1** strict crystallographic $\bar{4}$ symmetry is imposed. The complex **2** exhibits reversible cyclic voltammetric behaviour consistent with a one electron reduction to the Ti(III) analogue. Chemical reduction of **2** employing sodium amalgam affords the quantitative formation of $(C_6H(2,3,5,6\text{-}Me)_4O)_2Ti(\mu\text{-}OC_6H(2,3,5,6\text{-}Me)_4)_2Na(THF)_2$, **3**. The reaction of **3** with $[(COD)Rh(\mu\text{-}Cl)]_2$ does not afford the Ti(III)/Rh(I) early–late heterobimetallic (ELHB) complex $(C_6H(2,3,5,6\text{-}Me)_4O)_2Ti(\mu\text{-}OC_6H(2,3,5,6\text{-}Me)_4)_2Rh(COD)$. The nature of all products is not known; however, redox chemistry, in which electron transfer from Ti(III) to Rh(I) occurs is evidenced by the generation of **2** and Rh(0). In addition, ligand transfer reactions giving uncharacterized Rh-alkoxides are suggested by the spectral data. The implications and ramifications for the synthesis of alkoxide bridged ELHB models of bimetallic heterogeneous catalyst systems are discussed.

Key words: titanium phenoxides, redox chemistry, structures.

ROBERT T. TOTH et DOUGLAS W. STEPHAN. Can. J. Chem. **69**, 172 (1991).

Les réactions de phénolates substitués avec le $TiCl_4$ fournissent les espèces $Ti(OAr')_4$ [$Ar' = C_6H_4(2\text{-}t\text{-}Bu)$ (**1**) et $Ar' = C_6H(2,3,5,6\text{-}Me)_4$ (**2**)]. Le composé $Ti(OC_6H_4(2\text{-}t\text{-}Bu))_4$ (**1**) cristallise dans le groupe d'espace tétragonal $P\bar{4}2_1c$, avec a = 15,203(4) et c = 8.026(3) Å, Z = 2 et V = 1855(2) Å^3. Le composé $Ti(OC_6H(2,3,5,6\text{-}Me)_4)_4$ (**2**) cristallise dans le groupe d'espace orthorhombique *Pbcn*, avec a = 16.539(7), b = 16.136(6) et c = 27.716(12) Å, Z = 8 et V = 7397(9) Å^3. Dans ces complexes, la meilleure façon de décrire la sphère de coordination du Ti est de la considérer comme pseudo-tétraédrique. Dans le cas du composé **1**, une symétrie cristallographique $\bar{4}$ stricte est imposée. Le complexe **2** présente un comportement voltampérométrique cyclique réversible qui est en accord avec une réduction impliquant un électron et conduisant à l'analogue Ti(III). La réduction chimique du composé **2** à l'aide d'amalgame de sodium conduit à une formation quantitative du $(C_6H(2,3,5,6\text{-}Me)_4O)_2Ti(\mu\text{-}OC_6H(2,3,5,6\text{-}Me)_4)_2Na(THF)_2$ (**3**). La réaction du produit **3** avec du $[(COD)Rh(\mu\text{-}Cl)]_2$ ne fournit pas le complexe hétérobimétallique de la fin des premiers termes (ELHB) du Ti(III)/Rh(I), $(C_6H(2,3,5,6\text{-}Me)_4O)_2Ti(\mu\text{-}OC_6H(2,3,5,6\text{-}Me)_4)_2Rh(COD)$. La nature de tous les produits n'est pas connue; toutefois, la génération du composé **2** ainsi que du Rh(0) fournit des données expérimentales supportant une chimie d'oxydoréduction impliquant un transfert d'électron du Ti(III) au Rh(I). De plus, les données spectrales suggèrent l'existence de réactions de transferts de ligands conduisant à des alcoolates de Rh qui n'ont pas été caractérisés. On discute des implications de ces résultats et de leurs ramifications pour la synthèse d'ELBM pontés par le biais d'alcoolates qui seraient des modèles de systèmes catalytiques bimétalliques hétérogènes.

Mot clés: phénolates de titane, chimie d'oxydoréduction, structures.

[Traduit par la revue]

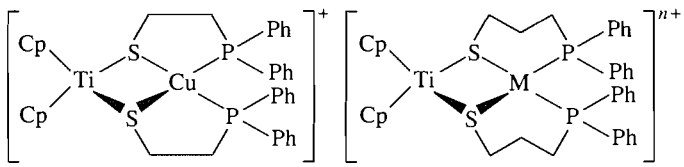
Introduction

In recent years our research has focused on the synthesis, characterization, and reactivity studies of complexes containing both early, oxophilic metals and late, electron-rich metal centres (1–19). Our interest in such species is prompted by the observation of strong metal-support interactions (SMSI) in heterogeneous catalyst systems (20). This phenomenon arises when late metals are dispersed on an early metal support such as titania. The result is a dramatic alteration of the reactivity patterns compared to dispersions of the same metal on other, non-Lewis acidic supports. The cause of the perturbations in reactivity is not clear, but one possibility that has some experimental support, is the direct role of the early metal in substrate activation (20). Alternatively, it has also been suggested that the support may act as an electron sink and thus the effects of the proximity of a Ti(III) centre on the reactivity of a late metal have come into question (20). In our efforts to study such questions, we have prepared several reducible early–late heterobimetallic (ELHB) species. Our initial efforts in this area involved the use of chelating phosphinethiolate ligands giving complexes of the form shown below (2–4). Structural data support the notion of dative interactions between the electron-rich, late metal and the d^0 Ti(IV) centres. Such metal–metal interactions may provide a vehicle for direct electron communication between the early and late metal centres, and thus may be related to the observations of SMSI. The implied role of reduced Ti centres in SMSI led us to study the redox chemistry of these heterobimetallics. These complexes undergo reversible chemical reduction affording the formally Ti(III)/M(I) (M = Cu, Rh) species. In the case of $CP_2Ti(\mu\text{-}SCH_2CH_2CH_2PPh_2)_2Rh$, the observation of coupling of the unpaired electron on Ti to Rh and P further suggests the possibility of a transannular, metal–metal communication (4).

Although these initial systems continue to be of interest, we are actively pursuing synthetic routes to other reducible ELHB compounds that may be more appropriate models for the metal centres in the heterogeneous systems where SMSI are observed. Thus, we have initiated efforts to prepare complexes in which a Ti centre is placed in an oxo environment (17, 18); the reason being that such a Ti environment will more effectively mimic the Ti centres of the support material, TiO_2. In this report, we describe some efforts to that end. The synthesis, characterization, electrochemical and structural studies of two complexes

[1]To whom correspondence may be addressed.

Can. J. Chem. Downloaded from www.nrcresearchpress.com by 195.138.81.100 on 09/07/12
For personal use only.



M = Rh, $n = 1$; M = Ni, $n = 0$

of the general formula $Ti(OAr')_4$ are presented. Chemical reduction of these species with Na affords the Ti(III) species, $Ti(OAr')_4Na(THF)_2$. Attempts to derivatize this reduced material via metal ion exchange employing $[(COD)Rh(\mu\text{-}Cl)]_2$ failed to yield the desired Ti(III)/Rh(I) ELHB species. Rather, electron transfer occurred affording Ti(IV) and Rh(0). The results of these studies are presented and discussed and the utility of Ti(III) aryloxides for reduced ELHB complex synthesis is considered.

Experimental section

All preparations were done under an atmosphere of dry, O_2-free N_2 in a Vacuum Atmospheres' Inert Atmosphere glove box. The quality of the atmosphere was maintained employing a 5 cfm blower with a deoxygenation/drying catalyst column and a molecular sieve prepurifier canister. Solvents were reagent grade, distilled from the appropriate drying agents under N_2, and degassed by the freeze–thaw method at least three times prior to use. ^1H and $^{13}C\{^1H\}$ NMR experiments were performed using a Bruker AC-300 MHz spectrometer employing trace amounts of protonated solvent as the internal reference. Chemical shifts are reported relative to $Si(CH_3)_4$. Cyclic voltammetry was recored on a BAS CV-27 employing THF as the solvent, Bu_4NBF_4 as the supporting electrolyte, and Ag/AgCl as the reference electrode. Combustion analyses were performed by Galbraith Laboratories Inc., Knoxville, TN. Crystalline samples were shipped in ampoules sealed under an atmosphere of N_2.

Preparation of LiOAr'(Ar' = C_6H_4(2-t-Bu), C_6H(2,3,5,6-Me)$_4$)

These salts are prepared in a similar manner and thus a general route is described. HOAr' is stirred in hexane at 0°C while an equivalent of 2.5 M *n*-BuLi is slowly added. The reaction is allowed to stir while warming to 25°C over a 2 h period. The solvent is removed and the residue is washed with hexane. These solids were isolated and manipulated in a dry box and were used without further purification.

*Preparation of Ti(OAr')$_4$(Ar' = C_6H_4(2-t-Bu), **1**; C_6H(2,3,5,6-Me)$_4$, **2**)*

These compounds were prepared in a similar manner and thus only one description is given. To a slurry of $LiOC_6H_4$(2-*t*-Bu) (8.23 g, 52.7 mmol) in hexane (50 mL) was slowly added $TiCl_4$ (2.00 g, 1.16 mL, 10.5 mmol). The reaction was vigorously stirred for 12 h, during which time the mixture became yellow. Filtration of the solution followed by removal of the solvent yields a yellow powder. This material is extracted into benzene, filtered, and the solvent removed.

Recrystallization from pentane affords crystalline compound (yield: 5.85 g, 85%), **1**: ^1H NMR (d_6-benzene): δ (ppm), 7.37 (d of d, H_d), $|J^3_{H-H}| = 7.1$ Hz, $|J^5_{H-H}| = 1.3$ Hz, 7.19 (d of d, H_a), $|J^3_{H-H}| = 7.8$ Hz, $|J^5_{H-H}| = 1.6$ Hz, 6.91 (d of d of d, H_c), $|J^3_{H-H}| = 7.4$ Hz, 6.80 (d of d of d, H_b), 1.49 (s, 9H). $^{13}C\{^1H\}$ NMR (d_6-benzene): 127.09, 123.31, 123.21, 35.03, 30.33 ppm. *Anal.* calcd.: C 74.52; H 8.13; found: C 74.50; H 8.20, **2**: ^1H NMR (d_6-benzene): δ, 6.60 (s, 1H), 2.35 (s, 6H), 2.05 (s, 6H). $^{13}C\{^1H\}$ NMR (d_6-benzene): δ (ppm), 134.15, 128.52, 125.77, 122.82, 19.95, 13.31. *Anal.* calcd.: C 74.52; H 8.13; found: C 74.40; H 8.00.

*Generation of (C_6H(2,3,5,6-Me)$_4O)_2Ti(\mu$-OC_6H(2,3,5,6-Me)$_4)_2$ Na(THF)$_2$, **3***

To a yellow THF solution of **2** (0.070 g, 0.109 mmol) was added sodium amalgam (1.1 equiv. of Na). The mixture was stirred at 25°C for 2 h and the blue THF solution decanted from the amalgam. EPR (THF) g = 1.986.

*Reaction of **3** with $[(COD)Rh(\mu\text{-}Cl)]_2$*

To a THF solution of **3** (0.054 mmol generated as above) was added a THF solution of $[(COD)Rh(\mu\text{-}Cl)]_2$ (0.023 g, 0.054 mmol). With the addition of the Rh species the color of the solution changed from blue to greenish/brown. On standing for 24 h the solution became orange/brown and Rh metal plated on the surface of the flask. Monitoring of the reaction was accomplished by EPR and ^1H NMR. No EPR signal was observed. ^1H NMR data show resonances attributable to **1** and other uncharacterized diamagnetic products.

X-ray data collection and reduction

Diffraction experiments for compound **1** were performed on a four-circle Syntex $P2_1$ diffractometer with graphite-monochromatized Mo Kα radiation (λ = 0.71069 Å) while the diffraction data for **2** was collected on a four-circle Rigaku AFC6 diffractometer also equipped with a graphite monochromator. The initial orientation matrices were obtained from 15 to 20 machine-centred reflections selected from a rotation photograph in the case of **1** and obtained by a zig–zag search routine in the case of **2**. These data were used to determine the crystal systems. Partial rotation photographs around each axis were consistent with a tetragonal crystal system for **1** while intensity measurements of equivalent reflections confirmed the Laue symmetry as *mmm* for the orthorhombic crystal system of **2**. The final lattice parameters and the orientation matrices were determined from 30 and 25 high-angle data ($20° < 2\theta < 25°$) for **1** and ($20° < 2\theta < 24°$) for **2**, respectively. The observed extinctions and ultimate structure refinements confirmed the space groups $P42_1c$ for **1** and *Pbcn* for **2**. *h, k, −l* were collected ($4.5° < 2\theta < 45.0°$) for **1**, while **2** and *h, k, −l* data were collected ($4.5° < 2\theta < 50.0°$). In each case, three standard reflections were recorded regularly during data collection. The intensities of the standards showed no statistically significant change over the duration of the data collection. The data were processed using the TEXSAN program package.

Structure solution and refinement

Non-hydrogen atomic scattering factors were taken from the literature tabulations (21–23). The heavy atom positions were determined using direct methods. The remaining non-hydrogen atoms were located from successive difference Fourier map calculations. The refinement was carried out by using full-matrix least-squares techniques on F, minimizing the function $w(|F_o| - |F_c|)^2$ where the weight, w, is defined as $4F_o^2/2\sigma(F_o^2)$ and F_o and F_c are the observed and calculated structure factor amplitudes. In the final cycles of the refinement of **1**, the titanium, oxygen, and methyl carbon atoms were assigned anisotropic temperature factors, while for **2** only the titanium atom was refined anisotropically. In both cases the phenyl ring carbon atoms were refined as rigid groups with individual isotropic thermal parameters. The hydrogen atom positions were calculated assuming a C—H bond length of 0.95 Å. Hydrogen atom temperature factors were fixed at 1.10 times the isotropic temperature factor of the carbon atom to which they are bonded. The hydrogen atom contributions were calculated, but not refined. The residual electron densities, in each case, were of no chemical significance. Crystal data and data collection parameters are summarized in Table 1. Tables of positional parameters (Table 2) and selected bond distances and angles (Table 3) are reported. Thermal parameters (Table S1), hydrogen atom parameters (Table S2), and calculated and observed structure factors (Table S3) have been deposited.[2]

Results and discussion

The room temperature reaction of $TiCl_4$ with excess of the lithium salt of either 2-*t*-butylphenol or 2,3,5,6-tetramethylphenol led to the isolation, following the standard workup, of yellow microcrystalline solids. The isolated products are soluble in benzene, THF, diethyl ether, and hexane and are stable at room temperature for prolonged periods in the absence

[2]A complete set of data may be purchased from the Depository of Unpublished Data, CISTI, National Research Council of Canada, Ottawa, Ont., Canada K1A 0S2.

Can. J. Chem. Downloaded from www.nrcresearchpress.com by 195.138.81.100 on 09/07/12
For personal use only.

TABLE 1. Crystallographic parameters

Parameter	Value	
	Molecule **1**	Molecule **2**
Formula	$C_{40}H_{52}O_4Ti$	$C_{40}H_{52}O_4Ti$
Crystal color, form	Yellow blocks	Yellow blocks
a (Å)	15.203(4)	16.539(7)
b (Å)		16.136(6)
c (Å)	8.026(3)	27.716(12)
Crystal system	Tetragonal	Orthorhombic
Space group	$P\bar{4}2_1c$ (No. 114)	$Pbcn$ (No. 60)
V (Å^3)	1855(2)	7397(9)
Density (g cm^{-3}) calcd.	1.15	1.16
Z	2	8
Crystal dimensions (mm)	0.40 × 0.30 × 0.35	0.25 × 0.28 × 0.32
Absolute coefficient, μ (cm^{-1})	2.62	2.63
Radiation, λ (Å)	Mo Kα (0.71069)	Mo Kα (0.71069)
T (°C)	24	24
Scan speed (deg/min)	2.0–5.0 (θ/2θ)	16 (θ/2θ)
Scan range (deg)	1.0 below Kα_1 1.0 above Kα_2	0.88 + 0.30 tan θ
Background/scan time ratio	0.5	0.5
Data collected	1447	4189
2θ range (deg)	4.5–40.0	4.5–50.0
Index range	h, k, $-l$	h, k, $-l$
Unique data $F_o^2 > 3\sigma(F_o^2)$	955	852
Variables	60	138
R (%)	5.3	8.7
R_w (%)	6.5	8.2
Largest Δ/σ in final least-squares cycle	0.001	0.000

of moisture and oxygen. The compounds also quickly degrade in protic or halogenated solvents. The ^{1}H NMR spectrum of the 2-*t*-butylphenol derivative showed resonances attributable to the expected aromatic and methyl protons indicative of the incorporation of the phenolate into the product **1**. The aromatic region of the ^{1}H NMR spectrum of **1** shows two doublets of doublets and two overlapping doublets of doublets of doublets (Fig. 1). Homonuclear decoupling experiments were used to confirm the coupling constant assignments. Selective irradiation of the methyl resonances permitted the observation of an NOE enhancement which confirmed the assignment of the resonances as shown in Fig. 1. The data are consistent with conformations of the ring substituents which are symmetric about the Ti atom. Similarly, the 2,3,5,6-tetramethylphenol derivative **2** exhibited the expected singlet resonance arising from the aromatic proton of the phenolate as well as the two singlets from the *ortho* and *meta* methyl groups. These data, in addition to the combustion analysis data, are consistent with the formulation of the products as Ti(OAr′)$_4$ (Ar′ = C$_6$H$_4$(2-*t*-Bu), **1**; Ar′ = C$_6$H(2,3,5,6-Me)$_4$, **2**). These formulations were subsequently confirmed by X-ray crystallographic studies (*vide infra*).

Similar reactions involving 2,6-di-*i*-propylphenolate and 2,6-di-*t*-butylphenolate have been described by Rothwell and co-workers (24, 25). In the former case, the isolated products were the homoleptic species M(OC$_6$H$_3$(2,6-*i*-Pr)$_2$)$_4$ (M = Ti, Zr). In the latter case, the yellow products were identified as M(OC$_6$H$_3$(2,6-*t*-Bu)$_2$)$_3$Cl (M = Ti, Zr). Attempts to effect further substitution were not successful. The authors surmized that the steric demands of the *ortho t*-butyl groups precluded the formation of Ti(OAr′)$_4$. Clearly, in the case of the present

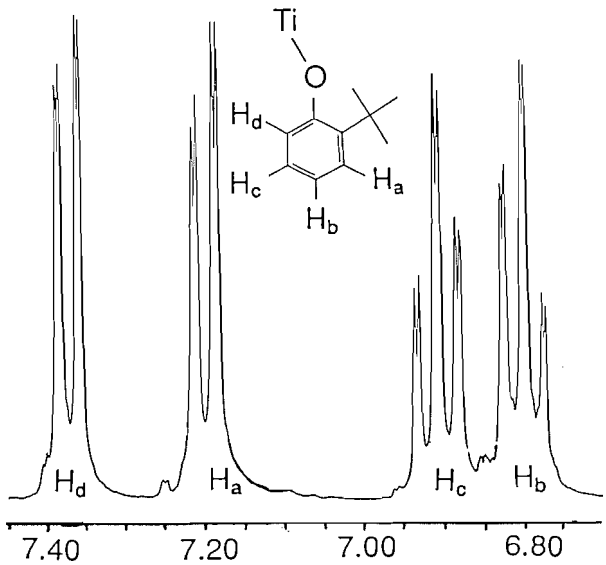


FIG. 1. Aromatic region of the ^{1}H NMR of **1**.

complexes, the lesser steric demands of 2-*t*-butylphenolate and 2,3,5,6-tetramethylphenolate permit ligand and substitutent conformations which allow the formation of tetraphenolate derivatives.

Structural studies

The X-ray crystallographic study of **1** showed that the molecule crystallizes in the space group $P42_1c$ with two independent molecules in the unit cell. The symmetry of the unit cell requires the Ti centre to occupy a site of 4 symmetry. The

Can. J. Chem. Downloaded from www.nrcresearchpress.com by 195.138.81.100 on 09/07/12
For personal use only.

TABLE 2. Positional parameters

(*a*) Molecule **1**

Atom	*x*	*y*	*z*	*B* (eq)
Ti	1/2	1/2	0	3.46(4)
O	0.5037(3)	0.4035(2)	0.1250(4)	4.9(2)
C(1)	0.4679(2)	0.3476(2)	0.2325(4)	3.5(1)
C(2)	0.4189(3)	0.3835(2)	0.3629(5)	5.2(1)
C(3)	0.3813(3)	0.3284(3)	0.4824(4)	6.1(1)
C(4)	0.3927(2)	0.2376(2)	0.4714(4)	6.8(2)
C(5)	0.4417(2)	0.2017(2)	0.3410(5)	5.3(1)
C(6)	0.4793(2)	0.2568(2)	0.2216(4)	3.3(1)
C(8)	0.4932(4)	0.2392(3)	−0.0913(7)	5.4(3)
C(7)	0.5334(4)	0.2169(3)	0.0770(7)	4.1(3)
C(9)	0.6286(4)	0.2498(4)	0.0813(8)	6.8(4)
C(10)	0.5376(4)	0.1158(4)	0.0874(9)	7.1(4)

(*b*) Molecule **2**

Atom	*x*	*y*	*z*	*B* (eq)
Ti(1)	0.8311(3)	0.1314(3)	0.1196(2)	4.0.(2)
O(1)	0.889(1)	0.056(1)	0.0882(6)	5.1(5)
O(2)	0.7791(9)	0.079(1)	0.1659(5)	3.8(4)
O(3)	0.8946(9)	0.209(1)	0.1432(5)	4.2(4)
O(4)	0.763(1)	0.179(1)	0.0776(5)	3.9(4)
C(7)	1.036(1)	0.124(2)	0.0544(9)	5.4(7)
C(8)	1.166(2)	0.002(2)	0.0360(9)	6.7(8)
C(9)	0.982(2)	−0.230(2)	0.081(1)	8(1)
C(10)	0.852(1)	−0.111(2)	0.0963(9)	5.2.(8)
C(17)	0.855(1)	−0.036(2)	0.2257(9)	4.9(7)
C(18)	0.801(2)	−0.050(2)	0.328(1)	9(1)
C(19)	0.605(2)	0.182(2)	0.299(1)	8(1)
C(20)	0.657(2)	0.191(2)	0.196(1)	6.2(8)
C(27)	1.038(2)	0.139(2)	0.185(1)	7.1(8)
C(28)	1.159(2)	0.258(2)	0.221(1)	6.0(8)
C(29)	0.973(2)	0.490(2)	0.181(1)	6.5(8)
C(30)	0.848(1)	0.375(2)	0.1481(8)	5.7(7)
C(1)	0.947(1)	0.004(1)	0.0773(6)	5.3(8)
C(2)	1.023(1)	0.0316(7)	0.0623(6)	4.5(7)
C(3)	1.0851(8)	−0.025(1)	0.0541(5)	2.9(6)
C(4)	1.072(1)	−0.110(1)	0.0609(5)	3.4(6)
C(5)	0.996(1)	−0.1375(7)	0.0759(5)	3.8(6)
C(6)	0.9335(8)	−0.081(1)	0.0840(5)	4.0(6)
C(11)	0.753(1)	0.077(1)	0.2128(4)	3.7(6)
C(12)	0.7886(8)	0.0190(9)	0.2433(6)	3.0(6)
C(13)	0.763(1)	0.0127(8)	0.2911(6)	4.2(7)
C(14)	0.703(1)	0.065(1)	0.3085(4)	5.4(7)
C(15)	0.6672(8)	0.123(1)	0.2780(7)	4.9(6)
C(16)	0.693(1)	0.1296(8)	0.2301(6)	4.5(7)
C(21)	0.949(1)	0.257(1)	0.1649(5)	4.4(7)
C(22)	1.023(1)	0.2303(7)	0.1833(6)	3.2(6)
C(23)	1.0789(8)	0.288(1)	0.2000(5)	3.2(6)
C(24)	1.061(1)	0.372(1)	0.1984(5)	5.8(7)
C(25)	0.987(1)	0.3992(7)	0.1800(6)	5.4(8)
C(26)	0.9309(8)	0.341(1)	0.1632(5)	3.3(6)
C(31)	0.732(1)	0.181(1)	0.0327(4)	3.5(6)
C(32)	0.7641(8)	0.236(1)	−0.0008(7)	3.2(6)
C(33)	0.733(1)	0.240(1)	−0.0475(6)	4.5(7)
C(34)	0.669(1)	0.188(1)	−0.0606(4)	6.4(8)
C(35)	0.6367(9)	0.132(1)	−0.0270(7)	7.0(8)
C(36)	0.668(1)	0.1288(9)	0.0196(6)	3.4(5)
C(37)	0.637(2)	0.070(2)	0.056(1)	7.4(9)
C(38)	0.567(2)	0.078(2)	−0.042(1)	11(1)
C(39)	0.767(2)	0.293(2)	−0.085(1)	9(1)
C(40)	0.830(2)	0.292(2)	0.0133(9)	5.6(7)

Can. J. Chem. Downloaded from www.nrcresearchpress.com by 195.138.81.100 on 09/07/12
For personal use only.

Can. J. Chem. Downloaded from www.nrcresearchpress.com by 195.138.81.100 on 09/07/12
For personal use only.

TABLE 3. Selected bond distances and angles*

(*a*) Molecule **1**

Atom	Atom	Distance	Atom	Atom	Distance
Ti	O	1.779(3)	C(7)	C(6)	1.546(6)
O	C(1)	1.327(5)	C(8)	C(7)	1.521(8)
C(7)	C(9)	1.532(8)	C(7)	C(10)	1.541(8)

Atom	Atom	Atom	Angle	Atom	Atom	Atom	Angle
O	Ti	O	108.6(1)	O	Ti	O	111.3(2)
C(10)	C(7)	C(6)	111.9(4)	O	C(1)	C(2)	117.2(3)
O	C(1)	C(6)	122.8(3)	Ti	O	C(1)	151.9(3)
C(8)	C(7)	C(9)	109.1(5)	C(8)	C(7)	C(10)	106.7(5)
C(7)	C(6)	C(1)	120.1(3)	C(8)	C(7)	C(6)	111.4(4)
C(7)	C(6)	C(5)	119.9(3)	C(9)	C(7)	C(10)	106.6(5)
C(1)	C(6)	C(5)	120.0(3)	C(9)	C(7)	C(6)	111.0(4)

(*b*) Molecule **2**

Atom	Atom	Distance	Atom	Atom	Distance
Ti	O(1)	1.78(2)	Ti	O(2)	1.76(2)
Ti	O(3)	1.76(2)	Ti	O(4)	1.79(2)
O(1)	C(1)	1.31(2)	O(2)	O(11)	1.37(2)
O(3)	C(21)	1.33(2)	O(4)	C(31)	1.35(2)
C(7)	C(2)	1.52(3)	C(8)	C(3)	1.50(3)
C(9)	C(5)	1.51(3)	C(10)	C(6)	1.48(3)
C(17)	C(12)	1.50(3)	C(18)	C(13)	1.56(3)
C(19)	C(15)	1.51(3)	C(20)	C(16)	1.49(3)
C(27)	C(22)	1.50(3)	C(28)	C(23)	1.53(3)
C(29)	C(25)	1.48(3)	C(30)	C(26)	1.54(3)
C(37)	C(36)	1.48(3)	C(38)	C(35)	1.51(4)
C(39)	C(33)	1.47(3)	C(40)	C(32)	1.46(3)

Atom	Atom	Atom	Angle	Atom	Atom	Atom	Angle
O(1)	Ti	O(2)	107.1(8)	O(2)	C(11)	C(12)	117(2)
O(1)	Ti	O(3)	110.2(7)	O(2)	C(11)	C(16)	123(1)
O(1)	Ti	O(4)	108.2(7)	O(2)	Ti	O(3)	111.1(7)
C(17)	C(12)	C(11)	121(2)	O(2)	Ti	O(4)	111.8(7)
C(17)	C(12)	C(13)	119(2)	O(3)	Ti	O(4)	108.4(8)
Ti	O(1)	C(1)	162(1)	C(18)	C(13)	C(12)	123(2)
Ti	O(2)	C(11)	149(1)	C(18)	C(13)	C(14)	117(2)
Ti	O(3)	C(21)	170(1)	Ti	O(4)	C(31)	149(1)
O(1)	C(1)	C(2)	121(2)	C(19)	C(15)	C(14)	118(2)
O(1)	C(1)	C(6)	119(1)	C(19)	C(15)	C(16)	121(2)
C(2)	C(1)	C(6)	120(1)	C(7)	C(2)	C(1)	119(2)
C(20)	C(16)	C(11)	117(2)	C(7)	C(2)	C(3)	121(2)
C(20)	C(16)	C(15)	123(2)	C(8)	C(3)	C(2)	122(2)
O(3)	C(21)	C(22)	125(1)	C(8)	C(3)	C(4)	118(2)
O(3)	C(21)	C(26)	115(1)	C(27)	C(22)	C(21)	118(2)
C(9)	C(5)	C(4)	119(2)	C(27)	C(22)	C(23)	122(2)
C(9)	C(5)	C(6)	121(2)	C(28)	C(23)	C(22)	120(2)
C(10)	C(6)	C(1)	120(2)	C(28)	C(23)	C(24)	120(2)
C(10)	C(6)	C(5)	120(2)	C(29)	C(25)	C(24)	116(2)
C(29)	C(25)	C(26)	124(2)	C(30)	C(26)	C(21)	123(2)
C(30)	C(26)	C(25)	117(2)	O(4)	C(31)	C(32)	119(2)
O(4)	C(31)	C(36)	121(1)	C(40)	C(32)	C(31)	120(2)
C(40)	C(32)	C(33)	120(2)	C(39)	C(33)	C(32)	122(2)
C(39)	C(33)	C(34)	117(2)	C(38)	C(35)	C(34)	119(2)
C(38)	C(35)	C(36)	121(2)	C(37)	C(36)	C(31)	118(2)
C(37)	C(36)	C(35)	122(2)				

*Bond distance in Å, bond angles in degrees. Estimated standard deviations in the least significant figure are given in parentheses.

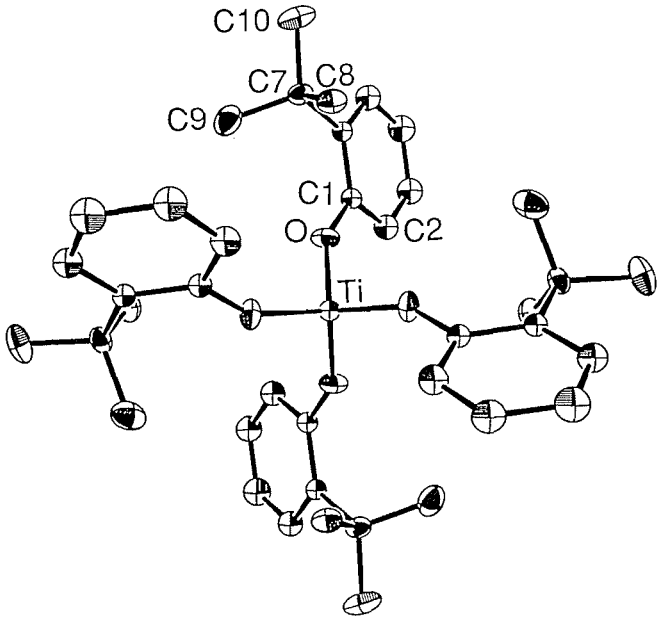


FIG. 2. ORTEP drawing of molecule **1**, 20% thermal ellipsoids are shown. Hydrogen atoms are omitted for clarity.

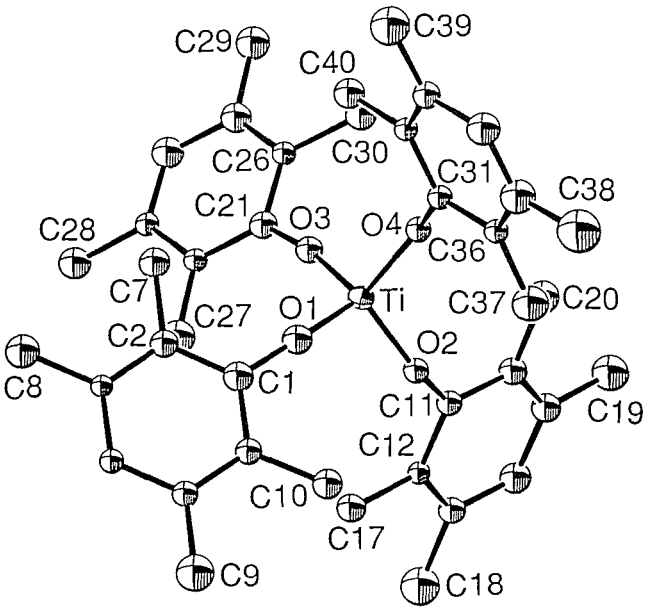


FIG. 3. ORTEP drawing of molecule **2**, 20% thermal ellipsoids are shown. Hydrogen atoms are omitted for clarity.

consequence of this crystallographically imposed symmetry is that the asymmetric unit contains only a single 2-*t*-butylphenolate ligand. Three other symmetry related ligands complete the coordination sphere of the Ti and maintain the strict 4 symmetry. An ORTEP drawing of molecule **1** is shown in Fig. 2. The closest approach between independent molecules is 2.539 Å (H8—H9).

A crystallographic study of **2** shows that the compound crystallizes in the space group *Pbcn* with eight molecules in the unit cell. The closest approach between molecules is found to be 2.205 Å (H47—H47). In this case, no crystallographic symmetry is imposed on the individual molecules and thus, the contents of the asymmetric unit is a single molecule of **2**. An ORTEP drawing of **2** is shown in Fig. 3.

Generally, Lewis acidic complexes readily form aggregates both in solution and in the solid state. For example, the complex $[Ti(OPh)_4 \cdot HOPh]$ has been shown to be a dimer (26). Smaller homoleptic alkoxide complexes of the early metals form higher aggregates, the nuclearity of which can be dependent on solvent, alkyl substituents and the metal (26). The mononuclearity of **1** and **2** is attributed to the bulk of the ligands. Similar complexes have been previously described where bulky substituents stabilize mononuclear complexes despite the Lewis acidity of the metal centre.

The coordination spheres of the Ti atoms of both **1** and **2** are pseudo-tetrahedral in geometry. In the case of **1**, the imposed symmetry results in O—Ti—O′ angles of 108.6(1) and 111.3(2)°. In a similar manner, the O—Ti—O′ angles about the Ti in **2** fall between 107.1(8)–111.8(7)°. The range of the angles about Ti can be attributed to the orientations of the aryl moieties. The conformation or packing arrangement of the aryl rings appears to be an accommodation of the steric demands of the *ortho* substituents. Closer proximity of these substituents to adjacent rings corresponds to the slightly larger O—Ti—O′ angles. The Ti—O distance observed in **1** is 1.779(3) Å while in **2** the Ti—O distances range between 1.76(2) and 1.79(2) Å. These distances are comparable to that of 1.78(1) Å for $Ti(OC_6H_3(2,6\text{-}i\text{-}Pr)_2)_4$ (24) and 1.80(1) Å found for $Ti(OC_6H_3(2,6\text{-}t\text{-}Bu)_2)_3I$ (24). The Ti—O distances found in **1** and **2** are shorter than both the terminal Ti—O bond distances of 1.86(2) Å found in the related Ti(III) species $(2,6\text{-}i\text{-}Pr)_2C_6H_3O)_2Ti(\mu\text{-}OC_6H_3(2,6\text{-}i\text{-}Pr)_2)_4Na(THF)_2$ (25) and the Ti—O distance of 1.807(8) Å found in $Ti(OC_6H_3(2,6\text{-}t\text{-}Bu)_2)(THF)_2Cl_2$ (27). This is consistent with the greater π-acceptor ability of Ti(IV) compared to that of Ti(III). The relatively short Ti—O distances are consistent with the proposition of Ti—O $d\pi$—$p\pi$ bonding. Such π interactions between a Lewis acidic titanium centre and oxygen, nitrogen, and phosphorus donors has been previously suggested (16–19). The Ti—O—C angle found in **1** is 151.9(3)°. For **2** the corresponding angles are 149(1), 149(1), 162(1), and 170(1)°. The corresponding angles in $Ti(OC_6H_3(2,6\text{-}i\text{-}Pr)_2)_4$ were found to be 166.1(3) and 164.5(3)° (24) while in $Ti(OC_6H_3(2,6\text{-}t\text{-}Bu)_2)(THF)_2Cl_2$ the Ti—O—C angle is 174.2(9)° (27). Presumably, the broad range observed for the Ti—O—C angles is a reflection of the structural compromise between the steric demands of the substituted phenoxides and the Lewis acidity of the metal centre. Bond distances and angles within the aryl substituents are as expected and require no further comment.

Redox chemistry

Cyclic voltammetric studies of **2** were performed in THF employing Bu_4NBF_4 as the supporting electrolyte and a Ag/AgCl electrode as the reference. The results are illustrated in Fig. 4. A quasi-reversible wave is observed at −1.19 V relative to Ag/AgCl. The peak separation of 220 mV is substantially greater than that expected for a completely reversible one-electron transfer, nonetheless repetitive scans at scan rates between 20 and 500 mV/s showed no decay in the current. The potential at which the redox chemistry occurs is consistent with a Ti(IV)/Ti(III) redox couple suggesting that the reduced species being generated is $[Ti(OC_6H(2,3,5,6\text{-}Me)_4)_4]^-$. Chemical reduction of **2** is achieved employing sodium. The EPR spectrum of the blue THF solution of **3** shows a single centre band resonance at $g = 1.986$, consistent with the

Can. J. Chem. Downloaded from www.nrcresearchpress.com by 195.138.81.100 on 09/07/12
For personal use only.

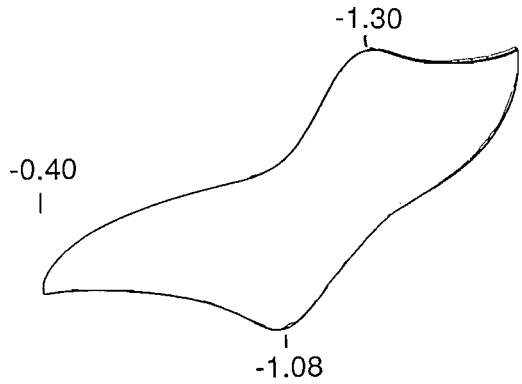
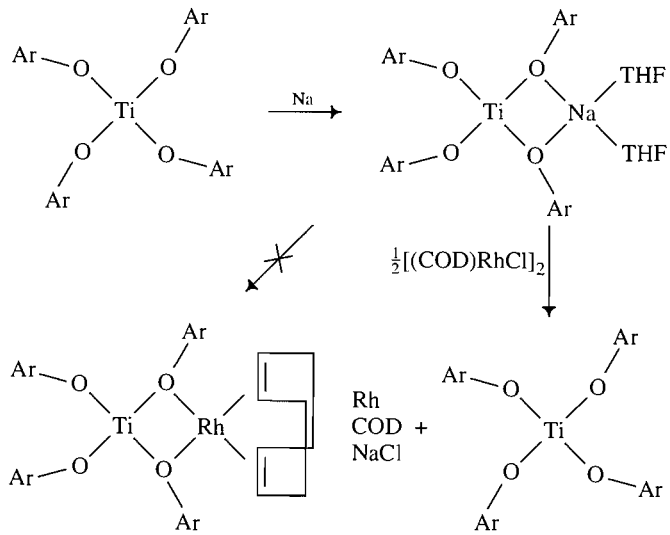


FIG. 4. Cyclic voltamogram of **2** in THF employing NBu_4BF_4 as the supporting electrolyte. The potential shown are referenced to Ag/AgCl electrode. The scan speed employed was 250 mV/s.



SCHEME 1

generation of a metal-based radical. The *extremely* air-sensitive Ti(III) species **3** is formulated as $(C_6H(2,3,5,6\text{-}Me)_4O)_2Ti(\mu\text{-}OC_6H(2,3,5,6\text{-}Me)_4)_2Na(THF)_2$ by analogy to the products of reduction of some related homoleptic early metal aryl-oxides described by Rothwell and co-workers (24).

Attempts to employ this anion as a metalloligand and effect complexation to Rh were undertaken. Reaction of **3** with $[(COD)Rh(\mu\text{-}Cl)]_2$ was performed in THF under strictly anaerobic conditions. Upon addition of the Rh species the solution becomes greenish/brown. Ultimately a grey precipitate appears and the solution becomes orange/brown. Monitoring of the reaction by EPR shows loss of the resonance attributable to **3**. The NMR of the final solution indicates the presence of **2** and other diamagnetic products. In addition Rh metal plates out on the surface of the flask. These data suggest a redox reaction in which the Ti(III) species **3** is oxidized to **2** with concurrent reduction of the Rh(I) to Rh(0). Alternatively, Rh-aryloxide species may be formed in ligand transfer reactions. Similar thiolate ligand transfers from Ti to Rh have been previously described (28). The formation of Rh-aryloxide species may account for the observation of other diamagnetic products; however, no single Rh-containing species could be isolated from the reaction mixtures. It may be that the reaction of **3** with Rh(I) chloride proceeds through the desired ELHB species $[(C_6H(2,3,5,6\text{-}Me)_4O)_2Ti(\mu\text{-}OC_6H(2,3,5,6\text{-}Me)_4)_2Rh(COD)]$; however, no evidence for the existence of this Ti(III)/Rh(I) intermediate has been observed (Scheme 1). This is in contrast to thiolato- and phosphido-bridged systems where Ti(III)/Rh(I) ELHB complexes can be isolated and unequivocally characterized (2–4, 16).

It appears that the oxidation potential of the Ti(III) species **3** is too negative to permit the use of this species as a metalloligand for Rh(I). It may be possible to shift the redox potential in a positive direction by tuning the nature of the substituents on the phenoxides. Presumably more electron-withdrawing substituents will help to stabilize Ti(III) and thus inhibit electron transfer. Alternatively strong electron-donor ligands on Rh would make the Rh centre less electron accepting and thus also serve to inhibit electron transfer from Ti(III). These approaches are being pursued in continuing efforts to mimic the heterogeneous catalyst systems.

Acknowledgement

Financial support from NSERC of Canada is gratefully acknowledged.

1. D. W. STEPHAN. Coord. Chem. Rev. **95**, 41 (1989).
2. G. S. WHITE and D. W. STEPHAN. Inorg. Chem. **24**, 1499 (1985).
3. G. S. WHITE and D. W. STEPHAN. Organometallics, **6**, 2169 (1987).
4. G. S. WHITE and D. W. STEPHAN. Organometallics, **7**, 903 (1988).
5. T. A. WARK and D. W. STEPHAN. Inorg. Chem. **26**, 363 (1987).
6. T. A. WARK and D. W. STEPHAN. Organometallics, **8**, 2836 (1989).
7. T. A. WARK and D. W. STEPHAN. Inorg. Chem. **29**, 1731 (1990).
8. L. GELMINI and D. W. STEPHAN. Inorg. Chim. Acta, **111**, L17 (1986).
9. L. GELMINI and D. W. STEPHAN. Inorg. Chem. **25**, 1222 (1986).
10. L. GELMINI and D. W. STEPHAN. Organometallics, **7**, 849 (1988).
11. L. GELMINI, L. C. MATASSA, and D. W. STEPHAN. Inorg. Chem. **24**, 2585 (1985).
12. L. GELMINI and D. W. STEPHAN. Organometallics. **7**, 1515 (1988).
13. P. Y. ZHENG, T. T. NADASDI, and D. W. STEPHAN. Organometallics, **8**, 1393 (1989).
14. P. Y. ZHENG and D. W. STEPHAN. Can. J. Chem. **67**, 1584 (1989).
15. D. G. DICK and D. W. STEPHAN. Organometallics, **9**, 1910 (1990).
16. D. G. DICK and D. W. STEPHAN. To be published.
17. D. W. STEPHAN. Organometallics, **9**, 2718 (1990).
18. T. T. NADASDI and D. W. STEPHAN. Can. J. Chem. **69**, 167 (1991).
19. D. G. DICK, R. ROUSSEAU, and D. W. STEPHAN. Can. J. Chem. To be published.
20. R. T. BAKER, J. TAUSTER, and J. A. DUMESIC. (*Editors*). *Strong metal-support interactions*. Am. Chem. Soc., Washington, DC, 1986.
21. D. T. CROMER and J. B. MANN. Acta Crystallogr. Sect. A; Cryst. Phys., Diffr. Theor. Gen. Crystallogr. A**24**, 324 (1968).
22. D. T. CROMER and J. B. MANN. Acta Crystallogr. Sect. A; Cryst. Phys., Diffr. Theor. Gen. Crystallogr. A**24**, 390 (1968).
23. D. T. CROMER and J. T. WABER. *International tables for X-ray crystallography*. Kynoch Press, Birmingham, England, 1974.
24. S. L. LATESKY, J. KEDDINGTON, A. E. MCMULLEN, I. P. ROTHWELL, and J. C. HUFFMAN. Inorg. Chem. **24**, 995 (1985).
25. L. D. DURFEE, S. L. LATESKY, I. P. ROTHWELL, J. C. HUFFMAN, and K. FOLTING. Inorg. Chem. **24**, 4569 (1985).
26. K. C. MALHOTRA and R. L. MARTIN. J. Organomet. Chem. **239**, 159 (1982).
27. M. MAZZANTI, C. FLORIANI, A. CHIESI-VILLA, and C. GUASTINI. J. Chem. Soc. Dalton Trans. 1793 (1989).
28. T. A. WARK and D. W. STEPHAN. Can. J. Chem. **68**, 565 (1990).

Can. J. Chem. Downloaded from www.nrcresearchpress.com by 195.138.81.100 on 09/07/12
For personal use only.

π-Facial stereoselectivity in the Diels–Alder reactions of a rigid carbocyclic diene: spiro(bicyclo[2.2.1]heptane-2,1′-[2,4]cyclopentadiene)

D. Jean Burnell[1] and Zdenek Valenta[2]

Department of Chemistry, University of New Brunswick, Bag Service No. 45222, Fredericton, N.B., Canada E3B 6E2

Received August 1, 1990

D. Jean Burnell and Zdenek Valenta. Can. J. Chem. **69**, 179 (1991).

The plane-nonsymmetrical diene spiro(bicyclo[2.2.1]heptane-2,1′-[2,4]cyclopentadiene) (**2**) was synthesized, and the π-facial stereoselectivity of its Diels–Alder cycloadditions with three cyclic dienophiles was examined. Adduct ratios were very similar, and the selectivity is surmised to be mainly the result of steric interactions at the transition state.

Key words: facial stereoselectivity, Diels–Alder, cycloaddition.

D. Jean Burnell et Zdenek Valenta. Can. J. Chem. **69**, 179 (1991).

On a synthétisé le spiro(bicyclo[2.2.1]heptane-2,1′-[2,4]cyclopentadiène), un diène qui n'est pas symétrique par rapport au plan, et on a étudié la stéréosélectivité π-faciale de ses cycloadditions avec trois diénophiles cycliques. Les rapports d'adduits sont très similaires et on fait l'hypothèse que la sélectivité est principalement le résultat d'interactions stériques dans l'état de transition.

Mots clés : stéréosélectivité faciale, Diels–Alder, cycloaddition.

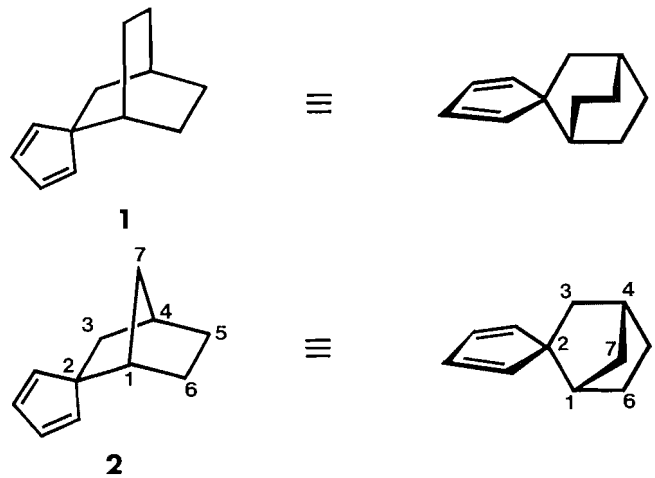
[Traduit par la revue]

Can. J. Chem. Downloaded from www.nrcresearchpress.com by 195.138.81.100 on 09/07/12
For personal use only.

Introduction

The last decade has seen a great deal of interest in π-facial stereoselectivity in Diels–Alder reactions with plane-nonsymmetrical addends. Steric interactions between the diene and an incoming dienophile have been invoked to explain π-facial stereoselectivity in many instances (1–3). Enantioselective Diels–Alder reactions (4) work in this way, too, because the interaction of a plane-symmetrical diene with a chiral auxiliary on a dienophile, or with an achiral dienophile in the presence of a chiral Lewis acid catalyst, leads to steric interactions at the transition state that are different at the two diene faces.

The best known examples of kinetically controlled Diels–Alder reactions leading to sterically disfavored products are the reactions of 5-heteroatom-substituted cyclopentadienes (5, 6). More recently some other cyclic and acyclic heteroatom-substituted dienes have shown a similar proclivity (7).[3] However, some cyclic, purely hydrocarbon, diene molecules give cycloaddition products that arise predominantly by addition to the sterically more hindered face, and this has been rationalized as a result of mixing of framework σ orbitals into the diene π system (11). Previously we synthesized the plane-nonsymmetrical diene **1**, and we used the results of its reactions with various dienophiles to shed light on the transition state geometry of the Diels–Alder reaction (12). Our conclusions were based on an assumption that π-facial stereoselectivity in **1** should be governed by steric interactions between either face of the diene and the incoming dienophile. This assumption and some of our conclusions regarding the transition state geometry were consistent with MM2 models of the reactions of **1** (13). The synthesis of the bicyclo[2.2.1]heptane analog **2** is outlined in this paper. The results of thermally induced and Lewis acid catalysed reactions of **2** are described, and these results are used to help delineate the parameters that control π-facial stereoselectivity.



Results

Synthesis of diene 2

The synthesis of diene **2** was based on our route to diene **1** (12). The enamine **3** alkylated slowly with 2-chloro-3-iodo-1-propene in acetonitrile to give the chloro-aldehyde **4**, which was taken to the alcohols **7** and **8** without purification. Thus, hydrolysis of the vinyl chloride by mercuric acetate in formic acid provided the keto-aldehyde **5**, which cyclized readily in ethanolic KOH to the enone **6**, and reduction with sodium borohydride in the presence of cerium(III) chloride (14) yielded a 7:3 mixture of the epimeric alcohols.[4] Structure **7** was assigned to the major product based on a lanthanide-induced shift nmr study. The mixture of **7** and **8** was treated with *para*-toluenesulfonyl isocyanate, then heated in boiling benzene for 2 days to effect elimination. After chromatography through a short silica column, pure diene **2** was obtained as a colorless liquid. The diene showed absorptions at 205 and 258 nm in the ultraviolet, just like **1** (12). The four olefinic protons of **2** were completely resolved in its 360 MHz ^{1}H nmr spectrum,

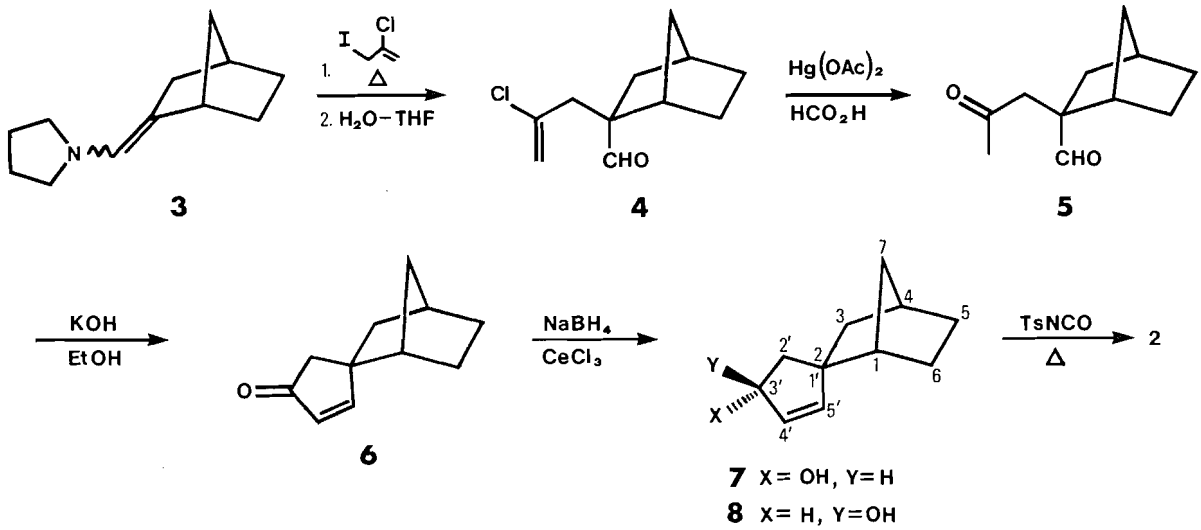
[1]Present address: Department of Chemistry, Memorial University of Newfoundland, St. John's, Nfld., Canada A1B 3X7.

[2]Author to whom correspondence may be addressed.

[3]These results have been explained in terms of a number of through-space and through-bonds orbital interactions (6, 8), torsional considerations (9), and repulsive electrostatic effects (10).

[4]In contrast, reduction of the corresponding cyclopentenone attached to a bicyclo[2.2.2]octane system proceeded without any selectivity (12).

Can. J. Chem. Downloaded from www.nrcresearchpress.com by 195.138.81.100 on 09/07/12
For personal use only.



and the ^{13}C nmr shifts were unremarkable except for the shifts of C-1 (δ 44.1) and C-3 (δ 33.9) that were significantly upfield of their expected positions. The overall, unoptimized, yield of diene **2** from the enamine **3** was 16.5%.

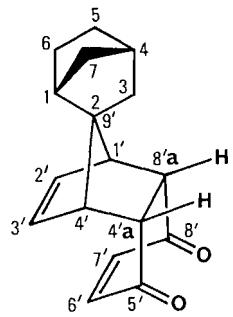
Diels–Alder reactions with 2

The diene **2** reacted readily with *para*-benzoquinone, maleic anhydride, and *N*-phenylmaleimide in boiling dichloromethane with yields of 96%, 98%, and 100%, respectively. Also, Lewis acid catalysed addition of *N*-phenylmaleimide to **2** in the presence of boron trifluoride etherate proceeded at −78°C in a yield of 95%. Each product showed two sets of signals in its 360 MHz ^1H nmr spectrum, attributable to a major and a minor adduct. Ratios of major to minor were obtained by careful integration of the nmr spectra. Thus, for the *para*-benzoquinone adducts the ratio was 69:31 (i.e. $\Delta\Delta G^{\neq} = 0.50$ kcal mol^{-1} at 40°C), for the maleic anhydride adducts it was 72:28 ($\Delta\Delta G^{\neq} = 0.58$ kcal mol^{-1}), and for the thermally produced *N*-phenylmaleimide adducts it was 69:31 ($\Delta\Delta G^{\neq} = 0.50$ kcal mol^{-1}). The rates of the three thermal reactions were similar, but the rate of the Lewis acid catalysed reaction was very much faster. Nevertheless, the ratio of adducts obtained from the catalysed *N*-phenylmaleimide reaction was 73:27 ($\Delta\Delta G^{\neq} = 0.39$ kcal mol^{-1} at −78°C), only slightly different from the corresponding thermal reaction.

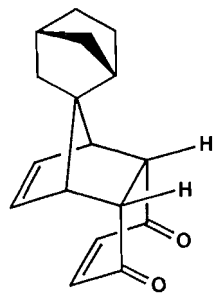
Assignment of the structures of the major and the minor adducts

A detailed ^1H nmr assignment was made using one of the mixtures of *N*-phenylmaleimide adducts. Fortunately, the ^1H nmr spectra of the adduct mixtures derived from the other dienophiles were *very* similar, so this assignment could also be applied to the other mixtures.

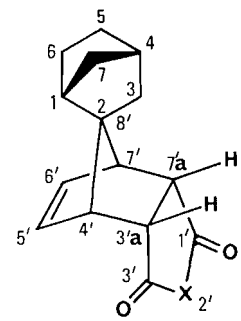
The spectrum, excluding the aromatic signals, of the mixture of *N*-phenylmaleimide adducts is shown in Fig. 1(a). Signals due to the major and the minor adducts are evident. The eight-line pattern (the AB portion of an ABMX system) centred at δ 3.54 was readily assigned by its size, its chemical shift, and from a spin–spin decoupling study to the methines α to the carbonyls (C-3′a and C-7′a) of the major adduct. Irradiation at δ 3.54 with a fairly wide bandwidth resulted in nuclear Overhauser enhancement (nOe) of two geminally coupled (J = 12.5 Hz) signals: a doublet of doublets at δ 1.075 (7% enhancement) and a doublet of apparent triplets at δ 1.434 (8% enhancement). The latter had been buried in a complex part of the spectrum (see Fig. 1(b)). These two signals could only arise from the two protons on the C-3 methylene of the adduct. This result placed this methylene group in the proximity of the methine α to the carbonyls, i.e., the major adduct could only have been **11***a*. (A significant nOe had been observed between the corresponding protons in a major adduct derived from the symmetrical diene **1** (12), and that structure has since been corroborated unequivocally by X-ray crystallography (15).) Given the structure of the major adduct **11***a*, other signals in its nmr spectrum could be assigned with more precision. Since the doublet of doublets at δ 1.075 had less coupling than its geminal partner at δ 1.434, we assigned the former to the *endo* proton at C-3 and the latter was assigned to the *exo* C-3 proton (16). Irradiation of the C-3 *endo* proton's signal (δ 1.075) resulted in nOe of the upfield half of the eight-line pattern centered at δ 3.54, which was therefore attributed to the closer methine proton, i.e., the one on C-7′a. The decoupling experiments



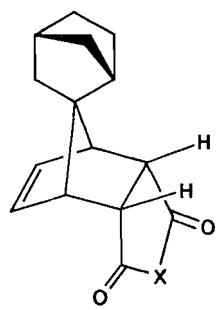
9*a*



9*b*



10*a* X = O
11*a* X = NPh



10*b* X = O
11*b* X = NPh

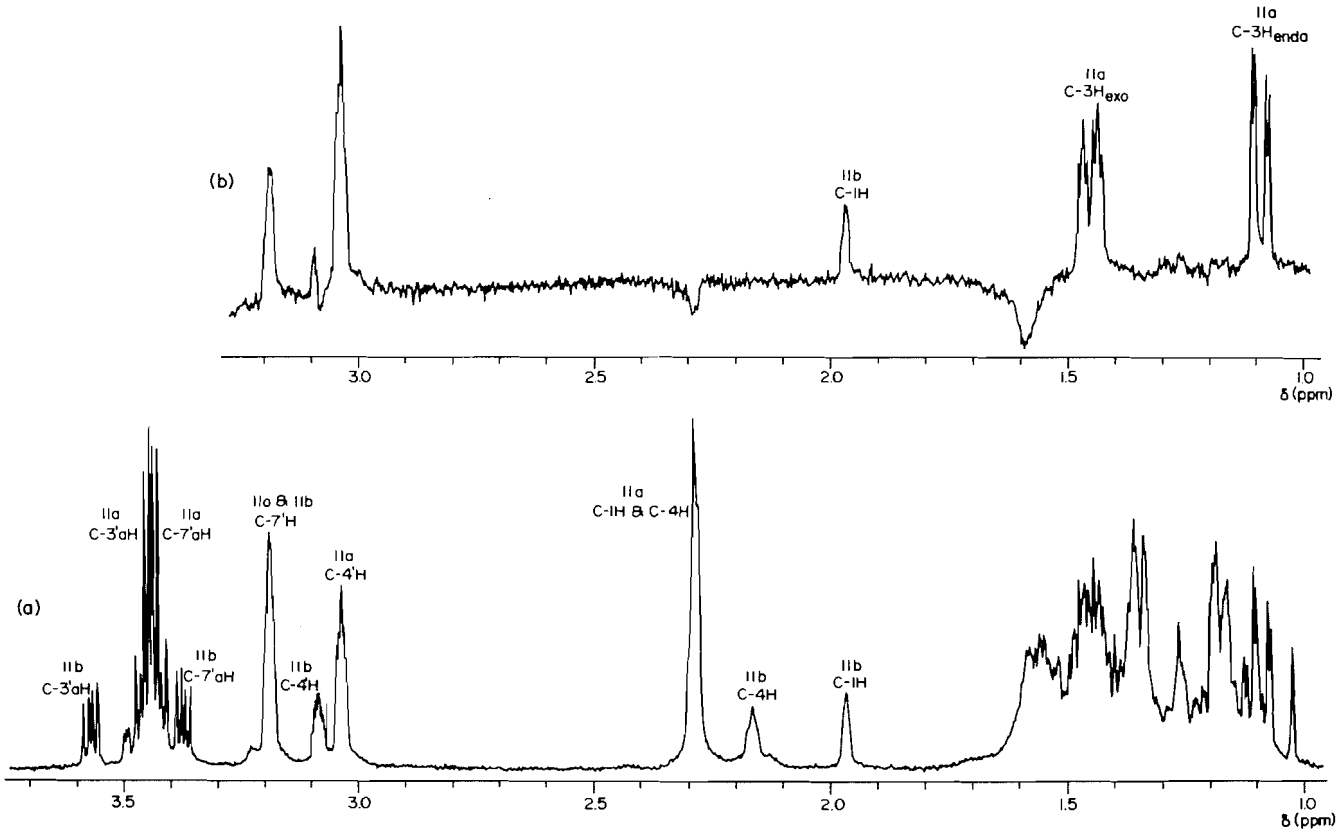


FIG. 1. (a) The upfield portion of the ^{1}H nmr spectrum (400 MHz) of the crude mixture of the adducts **11***a* (major) and **11***b* (minor) in $CDCl_3$. (b) Nuclear Overhauser difference spectrum (×16) of this mixture with irradiation centered at δ 3.54.

were then used to assign the remaining resonances, which are reported in detail in the Experimental.

Smaller doublet-of-doublet systems arising from the methines α to the carbonyls of the minor adduct flanked the corresponding signals from the major isomer (Fig. 1(a)). Irradiation at δ 3.54 affected the signals of the minor adduct, also. However, in this isomer it was a signal at δ 1.953, due to to one of the bridgehead methines of the saturated bicyclo[2.2.1]heptane moiety, that showed the greatest nOe (see Fig. 1(b)), so the minor adduct was assigned structure **11***b*. The relative positions of the signals for the major and the minor adduct were so similar for every adduct pair that it was clear that every major adduct has the same relative stereochemistry, i.e., the result of an *endo* addition *syn* to the C-3 methylene of **2** (**9***a*, **10***a*, and **11***a*), and every minor adduct had the same relative stereochemistry, i.e., the result of an *endo* addition *syn* to the C-1 methine of **2** (**9***b*, **10***b*, and **11***b*). Unfavorable steric interactions were expected to preclude the formation of *exo* addition products. In fact, no *exo* addition products were found.

Discussion

The π-facial stereoselectivity observed in the Diels–Alder reactions of isodicyclopentadiene and many related systems is controlled primarily by an electronic effect stemming from mixing of some σ orbitals from the plane-nonsymmetrical framework into the diene π system (11). Paquette *et al.* (17) have shown that some plane-symmetrical modifications to the isodicyclopentadiene system can reverse its π-facial stereoselectivity, and they correlated π-facial stereoselectivity with differences in nmr chemical shifts. Recently, Ipaktschi *et al.* (18) reported additions to a homo derivative of isodicyclopentadiene that also has π-facial stereoselectivity opposite to the parent compound. Thus, small differences in structure can produce large differences in π-facial stereoselectivity when there is appreciable mixing of framework σ orbitals and the diene π system. However, small differences are unlikely to produce large changes in selectivity when that selectivity is governed by steric interactions.

In our previous work with diene **1** we concluded tentatively that steric interactions were governing the π-facial stereoselectivity (12). However, we did note unusually high field ^{13}C nmr shifts for the C-1 and C-3 carbons of its bicyclo[2.2.2]octane moiety (δ 31.4 and 28.9, respectively). This suggested that some mixing of the framework σ orbitals into the π system might have been present, which in turn might have modulated the π-facial stereoselectivity. Diene **2** was intended to provide a diene similar to **1** from the point of view of the steric interactions that it would present to an incoming dienophile, but the dienes were different with respect to the composition of their plane-nonsymmetrical frameworks. However, just as in the case of diene **1** (12), the shifts of two of the carbons of the bicyclo-[2.2.1]heptane moiety of **2** were significantly upfield of their "expected" positions. (This is evident if one simply compares the shifts of the carbons of **2** with the shifts for the corresponding carbons in its synthetic precursors. Thus, the C-1 methine of **2** resonates at δ 44.1, but in **6**, **7**, and **8** these are at δ 49.4, 50.5, and 48.4, respectively. More dramatically, the C-3 methylene of **2** is at δ 33.9, whereas in **6**, **7**, and **8** these are at δ 45.4, 45.9, and 47.3, respectively. These differences are almost certainly too large to be dismissed as δ-substituent effects.)

We hoped that a comparison of the reactions of **2** with the reactions of **1** (12) might help to determine the relative

Can. J. Chem. Downloaded from www.nrcresearchpress.com by 195.138.81.100 on 09/07/12
For personal use only.

Can. J. Chem. Downloaded from www.nrcresearchpress.com by 195.138.81.100 on 09/07/12
For personal use only.

importance of the various effects that contribute to π-facial stereoselectivity in the Diels–Alder reaction. Diene **2** proved to be only slightly less selective than **1** with the same dienophiles. Furthermore, the ratios of adducts derived from **2** were very similar for the three dienophiles tested. The Lewis acid catalysed reaction with *N*-phenylmaleimide was, in terms of product ratio, only slightly more selective (but with a *smaller* $\Delta\Delta G^{\neq}$) than the thermally induced reaction, in spite of the large differences in rate and the fact that the Lewis acid complexed dienophile must be unsymmetrical. This parallels our earlier findings (2, 12) and recent results from Paquette's group (3). Furthermore, it serves to reinforce our assertion (2, 12) that the geometry of the transition state of the Diels–Alder reaction is much more sensitive to reaction rate in the *endo* region than in the *exo* region, where the plane-nonsymmetry resides in diene **2**.

The similarity of adduct ratios in reactions of **1** and **2** is expected when the π-facial stereoselectivity is controlled by steric interactions. What is more compelling is that a computational study (13) has confirmed that the π-facial stereoselectivity observed in the reactions of **2**, as well as in our previous study with **1**, can be attributed to steric interactions between the incoming dienophile and hydrogens on the bicyclo[2.2.1]heptane, or bicyclo[2.2.2]octane, moiety.

Experimental

Ultraviolet (uv) spectra were obtained with a Beckman model 25 spectrophotometer. Infrared (ir) spectra were recorded on a Perkin–Elmer 727B spectrophotometer in $CHCl_3$ solution. Routine ^1H nuclear magnetic resonance (nmr) spectra were obtained on a Varian T-60 instrument, and routine ^{13}C nmr spectra were run on a Varian CFT-20 instrument. The ^1H nmr spectra at 360 MHz of **2** and its adducts were via Mr. Alan Lee, Department of Medical Genetics, University of Toronto. The nOe and spin–spin decoupling work with a mixture of **11***a* and **11***b* was performed on a Bruker WH-400 instrument by Dr. Thomas T. Nakashima, Department of Chemistry, University of Alberta. Low resolution mass spectra (ms) were obtained on an Hitachi Perkin–Elmer RMU-6D instrument. High resolution mass spectra were determined by Dr. A. M. Hogg, Department of Chemistry, University of Alberta, on an AEI MS-50 spectrometer. Reactions were run under an atmosphere of dry nitrogen. Solvents were distilled, and aqueous solutions are implied by saturated NaCl, dilute $NaHCO_3$, etc.

2-(Pyrrolidinomethylene)-bicyclo[2.2.1]heptane (3)

Crude enamine **3** was obtained from a mixture of *endo* and *exo* bicyclo[2.2.1]heptane-2-carboxaldehyde by the method described in ref. 12. For **3**: ir ν_{max}: 3200 (very broad), 1720, and 1675 cm^{-1}; ^1H nmr δ: 5.89 (1H, apparent t), 3.07 (4H, br t), and 1.0–2.65 (m).

(1RS,2RS,4SR)-2-(2-Chloro-2-propenyl)-bicyclo[2.2.1]heptane-2-carboxaldehyde (4)

2-Chloro-3-iodo-1-propene (9.30 g, 46.0 mmol) and crude **3** (2.6 g, 14.7 mmol assuming pure **3**) in dry acetonitrile (approx. 200 mL) were heated under reflux for 4 days. The solution was evaporated to half its volume and 100 mL of a 1:1 mixture of H_2O and THF was added to the dark red solution. The mixture was stirred at room temperature overnight. Ether (100 mL) and H_2O (200 mL) were added. The organic extract was washed with 5% HCl (100 mL), 10% $Na_2S_2O_3$ (100 mL), saturated $NaHCO_3$ (100 mL), and saturated NaCl (2 × 200 mL). The solution was dried ($MgSO_4$) and concentrated. Column chromatography on silica gel (hexanes – ethyl acetate) provided 1.25 g (43%) of **4** as a pale yellow oil; ir ν_{max}: 2950, 2870, 2820, 2730 (m), 1720, 1635, and 885 cm^{-1}; ^1H nmr δ: 9.68 (1H, s), 5.22 (1H, d, J = 1.5 Hz), 5.07 (1H, br s, $W_{1/2}$ = 3 Hz), 3.03 (1H, br d, J = 16 Hz), 2.53 (1H, d, J = 16 Hz), and 1.1–2.4 (10, m); ^{13}C nmr δ: 205.5 (CHO), 138.5 (=CCl), 115.5 (=CH_2), 57.4 (C-2), 46.2 (CH_2), 45.0 (C-1), 38.1 (2C, C-4 and C-7), 34.7 (C-3), 27.6 (C-5), and 25.1 (C-6); ms m/z (%): 200 and 198 (0.6 and 1.9, M^+), 163 (19), 122 (76), 105 (20), 95 (36), 93 (64), 91 (37), 81 (41), 80 (40), 79 (52), 77 (33), 67 (100), 66 (46), 65 (28), 55 (23), and 53 (25).

(1RS,2RS,4SR)-2-(2-Oxopropyl)-bicyclo[2.2.1]heptane-2-carboxaldehyde (5)

Mercuric acetate (2.01 g, 6.29 mmol) was added to a solution of **4** (1.25 g, 6.29 mmol) in 98% formic acid (32 mL). This mixture was stirred at room temperature for 25 h. The mixture was poured into 300 mL of saturated NaCl and extracted with ether (3 × 100 mL). The combined organic layers were washed with saturated $NaHCO_3$ until gas evolution ceased, then with saturated NaCl (200 mL). The solution was dried ($MgSO_4$) and concentrated to provide crude **5** as a brown oil (0.62 g, 55%). A small portion was purified by preparative tlc to give a low-melting solid; ^1H nmr δ: 9.73 (1H, s), 3.33 (1H, d, J = 18 Hz), 2.53 (1H, d, J = 18 Hz), 2.10 (3H, s), and 1.9–2.5 (10H, m); ^{13}C nmr δ: 207.9 (CHO), 206.3 (C=O), 54.0 (C-2), 52.5 (CH_2), 45.7 (C-1), 40.2 (C-3), 38.8 (C-7), 37.9 (C-4), 29.9 (CH_3), 27.9 (C-5), and 25.0 (C-6).

(1RS,2RS,4SR)-Spiro(bicyclo[2.2.1]heptane-2,1'-[4]cyclopenten-3-one) (6)

A solution of crude **5** (533.6 mg, 2.96 mmol) in 50 mL of freshly prepared 5% (w/v) KOH in degassed absolute ethanol was heated under reflux for 2 h. The mixture was poured into cold H_2O (150 mL), which was extracted with ether (3 × 50 mL). The combined organic extracts were washed with H_2O (150 mL), 5% HCl (150 mL), dilute $NaHCO_3$ (100 mL), and saturated NaCl (100 mL). The solution was dried ($MgSO_4$) and the solvent was evaporated to provide the crude enone **6** as an oil (397.5 mg, 83%). A small portion was purified by preparative tlc: ^1H nmr δ: 7.62 (1H, d, J = 6 Hz), 6.05 (1H, d, J = 6 Hz), 2.4 (1H, br m), 2.39 (1H, d, J = 19 Hz), 2.19 (1H, d, J = 19 Hz), and 1.0–2.3 (9H, m); ^{13}C nmr δ: 209.8 (C=O), 171.0 (β =CH), 132.7 (α =CH), 53.3 (CH_2), 51.6 (C-2), 49.4 (C-1), 45.4 (C-3), 39.3 (C-7), 37.5 (C-4), 29.1 (C-5), and 24.4 (C-6); ms m/z (%): 162 (62, M^+), 134 (39), 95 (100), 94 (30), 91 (27), 79 (29), 77 (30), 68 (44), 67 (69), 66 (61), 65 (24), 55 (23), 53 (28), and 52 (21).

(1RS,2RS,4SR,4'SR)- and (1RS,2RS,4SR,4'RS)-Spiro(bicyclo-[2.2.1]heptane-2,1'-[4]cyclopenten-3-ol] (7 and 8, respectively)

A solution of **6** (138.7 mg, 0.855 mmol) in methanol (5 mL) was cooled in an ice-bath as $CeCl_3 \cdot 7H_2O$ (376.2 mg, 1.00 mmol) was added, followed by $NaBH_4$ (approx. 200 mg, 5.3 mmol) in small portions. The mixture was stirred at room temperature for 1 h. Addition of H_2O (15 mL) and ether (20 mL) produced some sticky material that necessitated filtration through Celite. The aqueous layer of the filtrate was reextracted with ether, and the combined organic extracts were washed with saturated NaCl, dried ($MgSO_4$), and concentrated to provide a mixture of the epimeric alcohols **7** and **8** (7:3, respectively, by ^{13}C nmr gated to suppress the nOe) as an oil (140.2 mg, 99%); ir ν_{max}: 3600, 3440 (br), 2945, and 2860 cm^{-1}; ^1H nmr δ: 5.6–6.0 (m) and 4.6–4.9 (m), 2.6 (br s, disappeared with D_2O), 2.43 (center of AB signal due to **8**), 2.22 (center of AB signal due to **7**), and 0.7–2.3 (m); ^{13}C nmr for **7** (from the mixture) δ: 142.0 (=CH), 133.1 (=CH), 77.2 (CHOH), 54.5 (C-2), 52.6 (CH_2), 48.4 (C-1), 47.3 (C-3), 39.0 (C-7), 37.3 (C-4), 29.0 (C-5), and 25.2 (C-6); ^{13}C nmr for **8** (from the mixture) δ: 143.3 (=CH), 132.0 (=CH), 76.8 (CHOH), 54.1 (C-2), 52.1 (CH_2), 50.5 (C-1), 45.9 (C-3), 39.0 (C-7), 37.2 (C-4), 29.0 (C-5), and 24.6 (C-6); ms m/z (%): 164 (23, M^+), 146 (5), 121 (28), 96 (75), 95 (100), 91 (23), 83 (23), 82 (27), 81 (35), 80 (39), 79 (38), 67 (54), 66 (25), 55 (23), 53 (21), and 41 (42).

Lanthanide-induced shift study of the mixture of 7 and 8

A solution of 140 mg of a mixture of **7** and **8** in $CDCl_3$ was doped with a small amount of tris(2,2,6,6-tetramethyl-3,5-heptanedionato)-europium(III) (Aldrich). After a few hours the solution was filtered through a glass-wool plug, and the proton noise-decoupled ^{13}C nmr spectrum was obtained in the usual manner. The molar ratio of shift reagent to alcohols was determined by comparing the magnitude of the signal due to the methyl groups of the ligand with the signals due to **7** and **8**. More shift reagent was added until spectra were obtained for six molar ratios. Plots of lanthanide-induced shift versus molar ratio of

Can. J. Chem. Downloaded from www.nrcresearchpress.com by 195.138.81.100 on 09/07/12
For personal use only.

lanthanide were linear. The magnitudes of the shifts, extrapolated to a 1:1 substrate-to-lanthanide ratio, were as follows: for the major alcohol (**7**): C-1, 4.0 ppm; C-2, 10.0 ppm; C-3, 6.5 ppm; C-4, 3.5 ppm; C-5, 3.0 ppm; C-6, 3.3 ppm; C-7, 3.4 ppm; C-2′, 11.0 ppm; C-3′, 14.0 ppm; C-4′, 58.7 ppm; and C-5′, 17.3 ppm; for the minor alcohol (**8**): C-1, 9.6 ppm; C-2, 12.2 ppm; C-3, 4.1 ppm; C-4, 4.2 ppm; C-5, 3.0 ppm; C-6, 5.0 ppm; C-7, 4.7 ppm; C-2′, 13.8 ppm; C-3′, 16.2 ppm; C-4′, 64.4 ppm; and C-5′, 17.5 ppm. Shift reagent was removed from the solution by passage through a silica gel column. This proved to be costly as much alcohol was not recovered.

*Spiro(bicyclo[2.2.1]heptane-2,1′-[2,4]cyclopentadiene) (**2**)*

A large excess of *para*-toluenesulfonyl isocyanate (0.5 mL) was added to a solution of **7** and **8** (40.0 mg, 0.244 mmol) in dry benzene. The mixture was stirred at room temperature for 0.5 h, then heated under reflux for 50 h. The benzene was evaporated, and the residue was immediatedly passed through a short silica gel column with hexane as the eluant to provide **2** as a clear colorless liquid (29.9 mg, 84%); ir ν_{max}: 2955, 2865, and 1455 (m) cm^{-1}; uv λ_{max} (hexane): 205 nm (ϵ = 1200) and 258.5 (ϵ = 960); ^1H nmr (360 MHz) δ: 6.379 (1H, ddd, J = 1.3, 2.0, 5.3 Hz), 6.299 (1H, ddd, J = 1.5, 2.0, 5.2 Hz), 6.237 (1H, ddd, J = 1.5, 1.7, 5.3 Hz), 6.121 (1H, ddd, J = 1.3, 1.7, 5.2 Hz), 2.43 (1H, m, $W_{1/2}$ = 9 Hz), 0.8–2.1 (complex m); ^{13}C nmr δ: 145.9 (=CH), 143.2 (=CH), 129.2 (=CH), 126.6 (=CH), 62.8 (C-2), 44.1 (C-1), 39.7 (C-7), 38.0 (C-4), 33.9 (C-3), 29.1 (C-5), and 28.6 (C-6); ms m/z (%, elemental composition): 146.1095 (100, M^+, $C_{11}H_{14}^+$ requires 146.1095), 131.0860 (6, $C_{10}H_{11}^+$), 117.0705 (49, $C_9H_9^+$), 105.0703 (7, $C_8H_9^+$), 91.0550 (10, $C_7H_7^+$), and 67.0555 (12, $C_5H_7^+$).

*Diels–Alder reactions with **2***

The commercially available dienophiles were purified before reaction. In order that the adduct ratios be undisturbed, 360 or 400 MHz ^1H nmr spectra were obtained on the crude reaction mixtures, which in every instance contained a small amount of unreacted dienophile but no unreacted **2**. Adduct ratios were determined by careful integration of the best resolved pairs of signals in these spectra.

Addition of para*-benzoquinone to **2**: (1*RS,2s,*4*SR,*1′*R,*4′*S,*4′a*R,*8′a*S)- and (1*RS,2r,*4*SR,*1′*R,*4′*S,*4′a*R,*8′a*S)-1′,4′,4′a,8′a-tetrahydrospiro(bicyclo[2.2.1]heptane-2,9′-[1,4]methanonaphthalene)-5′,8′-dione (**9**a and **9**b)*

A solution of *para*-benzoquinone (2.21 mg, 0.0205 mmol) in CH_2Cl_2 (1.1 mL) was added to a stirred solution of diene **2** (2.99 mg, 0.0204 mmol) in CH_2Cl_2 (2.5 mL). This mixture was heated under reflux for 15 h. The solvent was evaporated to provide 5.0 mg (96%) of pale yellow needles (which decomposed rapidly in light), composed of **9***a* and **9***b* in a ratio of 69:31, respectively; ir of mixture ν_{max}: 1750, 1730, 1705, and 1675 cm^{-1}; ^1H nmr (360 MHz) resolved signals from **9***a* in the mixture in $CDCl_3$ [C_6D_6] δ: 6.579 [6.072] (2H, s, C-6′H and C-7′H), 6.091 [5.806] (1H, ddd, J = 0.7, 3.1, 5.8 Hz, C-3′H), 6.034 [5.767] (1H, ddd, J = 0.8, 2.7, 5.8 Hz, C-2′H), and [0.565] (1H, dd, J = 2.6, 12.2 Hz, C-3H$_{endo}$); ^1H nmr (360 MHz) resolved signals from **9***b* in the mixture in $CDCl_3$ [C_6D_6] δ: 6.574 [6.072] (2H, s, C-6′H and C-7′H), 6.379 [5.78[5]] (1H, ddd, J = 0.8, 3.0, 5.8 Hz, C-3′H), 6.321 [5.710] (1H, ddd, J = 0.8, 3.1, 5.8 Hz, C-2′H), and [0.771] (1H, dd, J = 2.8, 12.9 Hz, C-3H$_{endo}$); ms of mixture m/z (%, elemental composition): 254.1307 (100, M^+, $C_{17}H_{18}O_2^+$ requires 254.1307), 226.1356 (23, $C_{16}H_{18}O^+$), 161.0966 (12, $C_{11}H_{13}O^+$), 146.1094 (27, $C_{11}H_{14}^+$ by *retro*-Diels–Alder), 117.0703 (31, $C_9H_9^+$), 110.0368 (31, $C_6H_6O_2^+$, some unreacted quinone, also), 91.0548 (27, $C_7H_7^+$), and 67.0555 (19, $C_5H_7^+$).

*Addition of maleic anhydride to **2**: (1*RS,2s,*4*SR,*3′a*R,*4′*S,*7′R,*7′a*S)- and (1*RS,2r,*4*SR,*3′a*R,*4′*S,*7′R,*7′a*S)-3′a,4′,7′,7′a-tetrahydro-1′,3′-dioxospiro(bicyclo[2.2.1]heptane-2,8′-[4,7]methanoisobenzofuran) (**10**a and **10**b)*

A solution of maleic anhydride (2.01 mg, 0.0205 mmol) in CH_2Cl_2 (1.0 mL) was added to a stirred solution of the diene **2** (2.99 mg, 0.0204 mmol) in CH_2Cl_2 (2.5 mL). This mixture was heated under reflux for 15 h. Evaporation of the solvent yielded 4.9 mg (98%) of a clear liquid (which solidified some days later) composed of **10***a* and **10***b* in a ratio of 72:28, respectively; ir of the mixture ν_{max}: 1815 (m), 1755 (s), 1080, and 910 cm^{-1}; ^1H nmr (360 MHz) resolved signals from **10***a* from the mixture in $CDCl_3$ [C_6D_6] δ: 6.361 [5.788[5]] (1H, ddd, J = 0.8, 2.7, 5.9 Hz, C-5′H), 6.309[5] [5.747[5]] (1H, ddd, J = 0.8, 3.1, 5.9 Hz, C-6′H), 3.575 [2.52] (1H, dd, J = 4.4, 8.1 Hz, C-3′aH), 3.545 [2.48[5]] (1H, dd, J = 4.2, 8.1 Hz, C-7′aH), 3.150[5] [2.46[5]] (1H, m, $W_{1/2}$ = 9 Hz, C-7′H), 3.006 [2.269] (1H, m, $W_{1/2}$ = 8 Hz, C-4′H), 2.275[5] [1.874] (1H, apparent br t, $W_{1/2}$ = 10 Hz, C-4H), 2.249[5] [1.796] (1H, apparent br d, $J \approx$ 3.9 Hz, C-1H), 0.994 [0.224] (1H, dd, J = 2.6, 12.6 Hz, C-3H$_{endo}$), and [0.524] (1H, ddd, J = 3.1, 4.4, 12.6 Hz, C-3H$_{exo}$); ^1H nmr (360 MHz) resolved signals from **10***b* from the mixture in $CDCl_3$ [C_6D_6] δ: 6.267[5] [5.78[5]] (1H, ddd, J = 0.9, 3.0, 5.8 Hz, C-5′H), 6.240 [5.703] (1H, ddd, J = 1.0, 3.0, 5.8 Hz, C-6′H), 3.695 [2.570] (1H, dd, J = 4.8, 8.0 Hz, C-3′aH), 3.486 [2.400] (1H, dd, J = 4.6, 8.0 Hz, C-7′aH), 3.17[5] [2.43[5]] (1H, m, C-7′H), 3.054 [2.336] (1H, m, $W_{1/2}$ = 10 Hz, C-4′H), 2.159 [1.768] (1H, apparent br t, $W_{1/2}$ = 10 Hz, C-4H), 1.818 (1H, apparent br d, $J \approx$ 3.9 Hz, C-1H), and 1.074 [0.575] (1H, dd, J = 2.8, 13.0 Hz, C-3$_{endo}$); ms of mixture m/z (%, elemental composition): (M^+ not apparent), 216.1148 (5, $M^+ - CO$, $C_{14}H_{16}O_2^+$ requires 216.1151), 171.1174 (100, $C_{13}H_{15}^+$), 117.0704 (14, $C_9H_9^+$), 104.0630 (19, $C_8H_8^+$), 91.0548 (28, $C_7H_7^+$), and 67.0054 (32, $C_5H_7^+$).

Addition of N*-phenylmaleimide to **2**: (1*RS,2s,*4*SR,*3′a*R,*4′*S,*7′R,*7′a*S)- and (1*RS,2r,*4*SR,*3′a*R,*4′*S,*7′R,*7′a*S)-3′a,4′,7′,7′a-tetrahydro-1′,3′-dioxo-2′-phenylspiro(bicyclo[2.2.1]heptane-2,8′-[4,7]methanoisoindole) (**11**a and **11**b)*

Thermal reaction

A solution of *N*-phenylmaleimide (3.54 mg, 0.0205 mmol) in CH_2Cl_2 (1.0 mL) was added to a stirred solution of the diene **2** (2.99 mg, 0.0204 mmol) in CH_2Cl_2 (2.5 mL). The mixture was heated under reflux for 15 h, then the solvent was evaporated to yield 6.7 mg (100%) of a mixture composed of **11***a* and **11***b* in a ratio of 69:31, respectively; ir ν_{max}: 1710 and 1600 cm^{-1}; ^1H nmr (360 MHz) resolved signals from **11***a* from the mixture in $CDCl_3$ [C_6D_6] δ: 6.273 [5.949] (1H, ddd, J = 0.8, 2.8, 5.9 Hz, C-5′H), 6.232[5] [5.911] (1H, ddd, J = 0.8, 3.0, 5.9 Hz, C-6′H), 3.454 [2.692] (1H, dd, 4.2, 7.5 Hz, C-3′aH), 3.423 [2.674] (1H, dd, 4.2, 7.5 Hz, C-7′aH), 3.183 [2.754] (1H, dddd, J = 0.8, 1.0, 3.0, 4.2 Hz,[6] C-7′H), 3.029 [2.560] (1H, dddd, J = 0.8, 1.0, 2.8, 4.2 Hz,[6] C-4′H), 2.174[5] [2.009] (1H, apparent br d, $J \approx$ 3.6 Hz, C-1H), 2.174[5] [1.976] (1H, apparent br t, $J \approx$ 3.9 Hz, C-4H), 1.434[5,7] (1H, dt, J = 3.9, 12.5 Hz, C-3H$_{exo}$), and 1.075 [0.505] (1H, dd, J = 2.7, 12.5 Hz, C-3H$_{endo}$); ^1H nmr (360 MHz) resolved signals from **11***b* from the mixture in $CDCl_3$ [C_6H_6] δ: 6.205[5] [5.91[5]] (1H, ddd, J = 0.7, 2.9, 5.5 Hz,[6] C-5′H), 6.180[5] [5.860] (1H, ddd, 0.7, 3.0, 5.5 Hz, C-6′H), 3.568 [2.843] (1H, dd, J = 4.7, 7.5 Hz, C-3′aH), 3.368 [2.599] (1H, dd, J = 4.6, 7.5 Hz, C-7′aH), 3.18[5] [2.73[5]] (1H, m, C-7′H), 3.080 [2.63] (1H, m, $W_{1/2}$ = 9 Hz, C-4′H), 2.154 [1.860] (1H, apparent br t, $J \approx$ 3.9 Hz, C-4H), 1.953 [1.399] (1H, apparent br d, $J \approx$ 3.6 Hz, C-1H), and 1.095 [0.778[5]] (1H, dd, J = 2.9, 13.0 Hz, C-3H$_{endo}$). Recrystallization of this product plus some of the product of the catalysed reaction (below) from ethyl acetate gave a colorless material free of unreacted *N*-phenylmaleimide. Anal. calcd. for $C_{21}H_{21}NO_2$: C 78.97, H 6.63, N 4.39; found: C 78.85, H 6.53, N 4.50.[8]

Catalysed reaction

A stirred solution of *N*-phenylmaleimide (3.54 mg, 0.0205 mmol) in CH_2Cl_2 (1.5 mL) as cooled in a Dry Ice – acetone bath, and 25 μL (0.020 mmol) of a 10% solution of BF_3 etherate in CH_2Cl_2 was added by syringe, followed by a solution of the diene **2** (2.99 mg, 0.0204

[5]Partially overlapped signal.

[6]Determined from decoupling experiments.

[7]Identified in a nuclear Overhauser difference spectrum.

[8]We thank Mr. Hector Seguin, National Research Council, Ottawa, for this analysis.

mmol) in CH_2Cl_2 (2.5 mL). After 2.5 h, the mixture was allowed to attain room temperature and H_2O (approx. 2 mL) was added. The H_2O was removed by Pasteur pipet, and the solution was washed in this way with 10% $NaHCO_3$ and H_2O again. The organic solution was passed through a short plug of anhydrous Na_2SO_4, then evaporated to yield 6.2 mg (95%) of a yellow solid composed of **11***a* and **11***b* in a ratio of 73:27, respectively.

Acknowledgements

We thank Dr. Žarko Stojanac of this Department for many fruitful discussions. We are grateful to the Natural Sciences and Engineering Research Council of Canada for financial support.

1. V. A. Mironov, T. M. Fadeeva, and A. A. Akhrem. Dokl. Akad. Nauk SSSR, **174**, 852 (1967); E. J. Corey, N. M. Weinshenker, T. K. Schaaf, and W. Huber. J. Am. Chem. Soc. **91**, 5675 (1969); D. Bellus, G. Helferich, and C. D. Weis. Helv. Chim. Acta, 463 (1971); R. Breslow, J. M. Hoffman, Jr., and C. Perchonock. Tetrahedron Lett. 3723 (1973); J. Das, R. A. Dickinson, M. Kakushima, G. M. Kingston, G. R. Reid, Y. Sato, and Z. Valenta. Can. J. Chem. **62**, 1103 (1984); A. P. Kozikowski, T. R. Nieduzak, T. Konoike, and J. P. Springer. J. Am. Chem. Soc. **109**, 5167 (1986); T. Koizumi, Y. Arai, H. Takayama, K. Kuriyama, and M. Shiro. Tetrahedron Lett. **28**, 3689 (1987); P. Yates, A. Gomes, D. J. Burnell, D. D. Cong, and J. F. Sawyer. Can. J. Chem. **67**, 37 (1989); G. Mehta, S. Padma, V. Pattabhi, A. Pramanik, and J. Chandrasekhar. J. Am. Chem. Soc. **112**, 2942 (1990).
2. D. J. Burnell and Z. Valenta. J. Chem. Soc. Chem. Commun. 1242 (1985).
3. L. A. Paquette, C. Vanucci, and R. D. Rogers. J. Am. Chem. Soc. **111**, 5792 (1989).
4. W. Oppolzer. Angew. Chem. Int. Ed. Engl. **23**, 876 (1984); L. A. Paquette. *In* Asymmetric synthesis. Vol. 3. *Edited by* J. D. Morrison. Academic Press, New York. 1984. Chap. 4; C. J. Northcott and Z. Valenta. Can. J. Chem. **65**, 1917 (1918); D. A. Evans, K. T. Chapman, and J. Bisaha. J. Am. Chem. Soc. **110**, 1238 (1988); K. Narasaka, N. Iwasawa, M. Inoue, T. Yamada, M. Nakashima, and J. Sugimori. J. Am. Chem. Soc. **111**, 5340 (1989); E. J. Corey, R. Imwinkelried, S. Paul, and Y. B. Xiang. J. Am. Chem. Soc. **111**, 5493 (1989).
5. S. Winstein, M. Shatavsky, C. Norton, and R. B. Woodward. J. Am. Chem. Soc. **77**, 4183 (1955); V. A. Mironov, M. E. Dolgaya, V. T. Lukyanov, and S. A. Yankovskii. Zh. Org. Khim. **12**, 1436 (1976); D. W. Jones. J. Chem. Soc. Chem. Commun. 739 (1980).
6. K. L. Williamson, Y.-F.L. Hsu, R. Lacko, and C. H. Youn. J. Am. Chem. Soc. **91**, 6129 (1969); K. L. Williamson, and Y.-F.L. Hsu. J. Am. Chem. Soc. **92**, 7385 (1970); A. S. Cieplak, B. D. Tait, and C. R. Johnson. J. Am. Chem. Soc. **111**, 8447 (1989); J. B. Macaulay and A. G. Fallis. J. Am. Chem. Soc. **112**, 1136 (1990).
7. P. G. McDougal, J. G. Rico, and D. Van Derveer. J. Org. Chem. **51**, 4492 (1986); R. Tripathy, R. W. Franck, and K. D. Onan. J. Am. Chem. Soc. **110**, 3257 (1988); I. Agmon, M. Kaftory, P. Ashkenazi, W. von Philipsborn, and D. Ginsburg. Heterocycles, **28**, 33 (1989); P. Ashkenazi and D. Ginsburg. Israel J. Chem. **29**, 281 (1989); J. R. Gillard and D. J. Burnell. J. Chem. Soc. Chem. Commun. 1439 (1989); A. M. Naperstkow, J. B. Macaulay, M. J. Newlands, and A. G. Fallis. Tetrahedron Lett. **30**, 5077 (1989).
8. N. T. Anh. Tetrahedron, **29**, 3227 (1973); S. Inagaki, H. Fujimoto, and K. Fukui. J. Am. Chem. Soc. **98**, 4054 (1976).
9. F. K. Brown and K. N. Houk. J. Am. Chem. Soc. **107**, 1971 (1985).
10. M. J. Fisher, W. J. Hehre, S. D. Kahn, and L. E. Overman. J. Am. Chem. Soc. **110**, 4625 (1988).
11. R. Gleiter and L. A. Paquette. Acc. Chem. Res. **16**, 328 (1983); L. A. Paquette and M. Gugelchuk. J. Org. Chem. **53**, 1837 (1988), and references therein.
12. D. J. Burnell, H. B. Goodbrand, S. M. Kaiser, and Z. Valenta. Can. J. Chem. **65**, 154 (1987).
13. F. K. Brown, K. N. Houk, D. J. Burnell, and Z. Valenta. J. Org. Chem. **52**, 3050 (1987).
14. J.-L. Luche. J. Am. Chem. Soc. **100**, 2226 (1978); J.-L. Luche, L. Rodriguez-Hahn, and P. Crabbé. J. Chem. Soc. Chem. Commun. 601 (1978).
15. M. J. Newlands, D. J. Burnell, Z. Valenta, and E. J. Gabe. Acta Crystallogr. Sect. C: Cryst. Struct. Commun. Submitted.
16. L. M. Jackman and S. Sternhell. Applications of nuclear magnetic resonance spectroscopy in organic chemistry. 2nd ed. Pergamon Press, Oxford. 1969. pp. 288–289 and 334–335.
17. L. A. Paquette and P. Charumilind. J. Am. Chem. Soc. **104**, 3749 (1982); L. A. Paquette, P. Charumilind, M. C. Böhm, R. Gleiter, L. S. Bass, and J. Clardy. J. Am. Chem. Soc. **105**, 3136 (1983).
18. J. Ipaktschi, J. Herber, H.-O. Kalinowski, and R. Boese. Chem. Ber. **123**, 305 (1990).

Can. J. Chem. Downloaded from www.nrcresearchpress.com by 195.138.81.100 on 09/07/12
For personal use only.

Synthesis and X-ray crystal structure determination of 3,4-diphenyl-6-(diphenylmethyl)-1,5-dioxa-2-thiane-2-oxide

L. Breau,[1] N. K. Sharma,[2] I. R. Butler, and T. Durst[3]

Ottawa–Carleton Chemistry Institute, Department of Chemistry, University of Ottawa, Ottawa, Ont., Canada K1N 6N5

Received July 4, 1990

L. Breau, N. K. Sharma, I. R. Butler, and T. Durst. Can. J. Chem. **69**, 185 (1991).

Erythro and *threo*-1,2-diphenyl-2-*tert*-butylsulfinylethanols **5** and **8** were prepared from the condensation of the α-lithio derivative of benzyl-*tert*-butyl sulfoxide with benzaldehyde. Reaction of **5** with sulfuryl chloride gave the title compound, (2*R**,3*S**,4*R**,6*R**)-3,4-diphenyl-6-(diphenylmethyl)-1,5-dioxa-2-thiane-2-oxide **6**, the first representative of a new heterocyclic ring system. Similar treatment of **8** resulted in the formation of **7**, a stereoisomer of **6**. This same compound was also obtained by photolysis of **6**. In both **6** and **7** the S=O bond is in an axial orientation.

Key words: sulfuryl chloride, reaction with β-hydroxy sulfoxides; 1,2-diphenyl-*tert*-butylsulfinylethanol; β-hydroxysulfoxides; β-sultines; *N*-chlorosuccinimide, reaction with β-hydroxysulfoxides.

L. Breau, N. K. Sharma, I. R. Butler et T. Durst. Can. J. Chem. **69**, 185 (1991).

On a préparé les *érythro*- et *thréo*-1,2-diphényl-2-*tert*-butylsulfinyléthanols (**5** et **8**) par condensation du dérivé α-lithien du sulfoxyde de benzyle et de *tert*-butyle avec le benzaldéhyde. La réaction du produit **5** avec le chlorure de sulfuryle fournit le composé mentionné dans le titre, le (2*R**,3*S**,4*R**,6*R**)-3,4-diphényl-6-(diphénylméthyl)-1,5-dioxa-2-thiane-2-oxyde (**6**), le premier représentant d'un nouveau système d'hétérocycles. Lorsqu'on soumet le produit **8** à un traitement semblable, il y a formation du produit **7**, un stéréoisomère du produit **6**. On a obtenu le même composé par photolyse du produit **6**. Dans les produits **6** et **7**, l'orientation de la liaison S=O est axiale.

Mots clés : chlorure de sulfuryle, réaction avec les sulfoxydes β-hydroxy; 1,2-diphényl-*tert*-butylsulfinyléthanol; sulfoxydes β-hydroxy; β-sultines; *N*-chlorosuccinimide, réaction avec les sulfoxydes β-hydroxy.

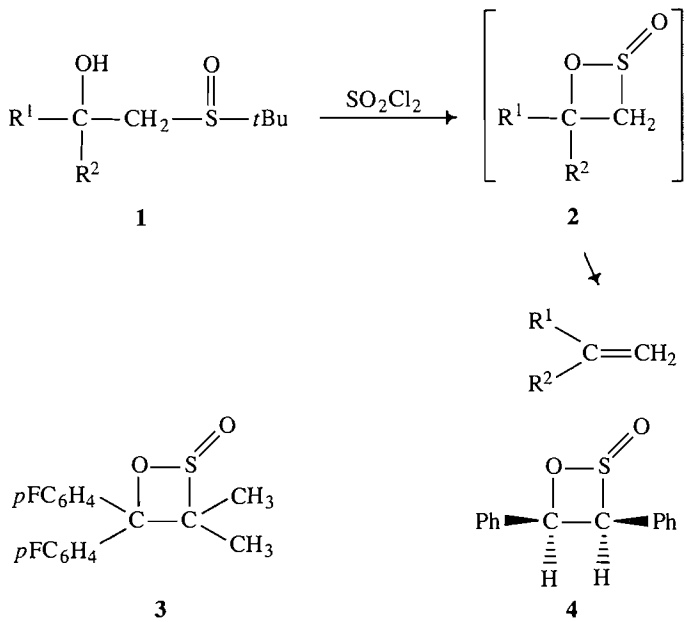
[Traduit par la revue]

Introduction

A number of years ago we reported that β-hydroxy-*tert*-butyl sulfoxides, **1**, reacted with SO_2Cl_2 or *N*-chlorosuccinimide (NCS) to yield alkenes (1). β-Sultines, **2**, were shown to be intermediates in this process. These compounds were generally unstable but we were able to isolate and characterize several tetrasubstituted derivatives (2); an X-ray structure determination was carried out on compound **3** (3). As part of a search for other examples of relatively stable β-sultines we attempted the isolation of *cis*-3,4-diphenyl-1,2-oxathietane-2-oxide, **4**. We had anticipated considerably increased stability for this compound compared to its *trans* isomer. Such a compound was expected to show a significantly puckered four-membered ring to relieve the interaction between the *cis*-phenyl substituents (2, 3), and a relatively slow loss of SO_2 to form *cis*-stilbene.

The expected precursor for **4**, the β-hydroxysulfoxide **5**, was prepared in an unambiguous manner from *trans*-stilbene oxide via the series of reactions shown in Scheme 1. Reactions of **4** with NCS in refluxing benzene gave the expected *cis*-stilbene, presumably via **4**, in 50% isolated yield; no trace of *trans*-stilbene was observed. Surprisingly, when **5** was reacted with SO_2Cl_2 at −78°C in CH_2Cl_2 in an effort to observe **4**, a crystalline product, mp 161–162°C, was obtained in up to 60% yield accompanied by diphenylacetaldehyde (35%).

This material analyzed for $C_{28}H_{24}O_3S$. The proton NMR showed four unique hydrogens, each as a doublet with J = 3.0 Hz, at δ 3.49, 4.53, 6.17, and 6.67 ppm, in addition to 20 aromatic hydrogens. The infrared spectrum revealed a strong band at 1125 cm^{-1} indicative of a sultine (4). Attempted structure determinations during our initial studies by chemical transformation carried out on this new material were frustrated by contradictory and ambiguous results (5). In the end the structure was shown by single crystal X-ray structure determination to be the unusual δ-sultine **6** (Fig. 1).[4] This compound, which can be considered as an acetal derived from diphenylacetaldehyde and a β-hydroxysulfinic acid, represents,



[1]NSERC Scholarship holder 1986–1989.

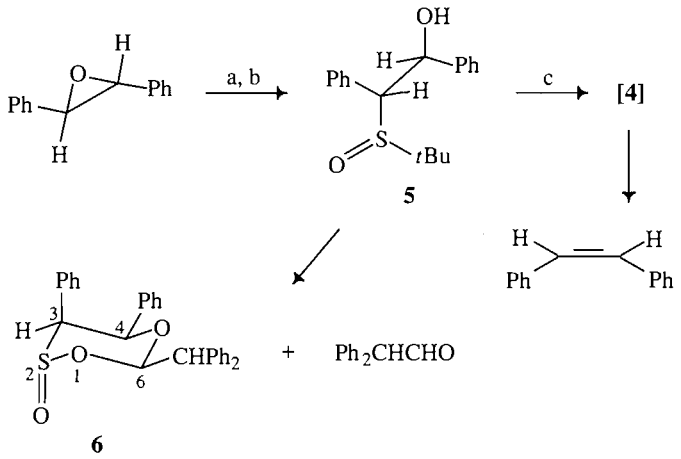
[2]Deceased.

[3]Author to whom correspondence may be addressed.

[4]Tables of observed and calculated structure factors, anisotropic temperature factors, bond distances and angles, and atomic parameters have been deposited and may be purchased from the Depository of Unpublished Data, CISTI, National Research Council of Canada, Ottawa, Ont., Canada K1A 0S2.

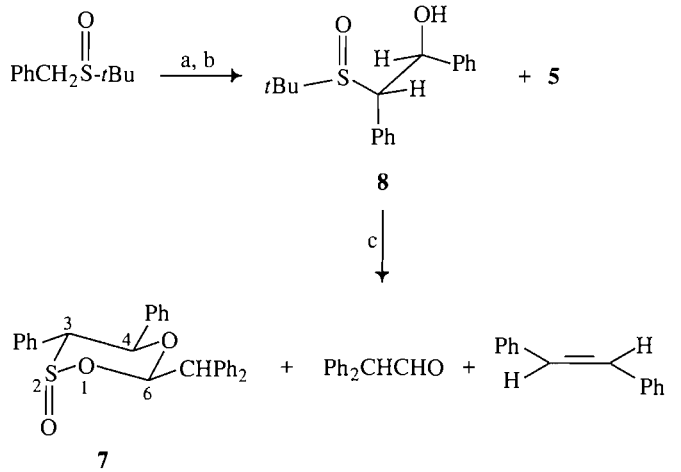
Tables of unit cell parameters and bond distances and angles have also been deposited with the Cambridge Crystallographic Data Centre and can be obtained on request from The Director, Cambridge Crystallographic Data Centre, University Chemical Laboratory, Lensfield Road, Cambridge, CB2 1EW, U.K.

Can. J. Chem. Downloaded from www.nrcresearchpress.com by 195.138.81.100 on 09/07/12
For personal use only.



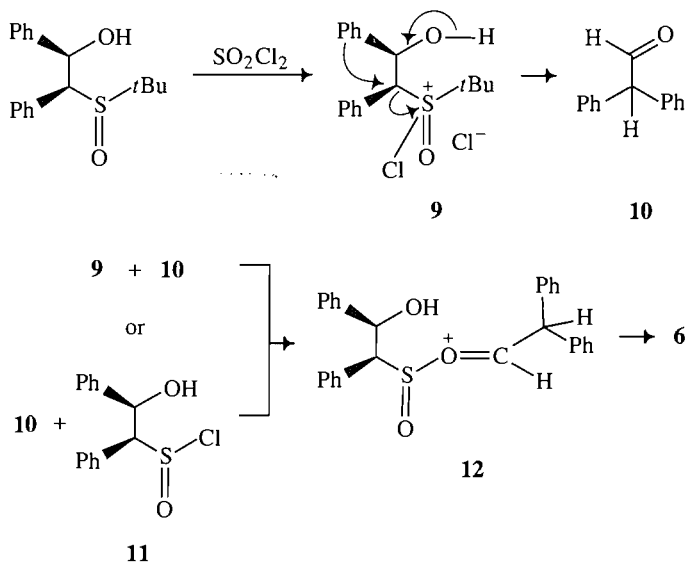
(a) *t*BuSH/KOH; (b) MCPBA;
(c) NCS/benzene/Δ; (d) $SO_2Cl_2/CH_2Cl_2/-78\,°C$

SCHEME 1



(a) LDA/THF−78°C; (b) PhCHO; (c) $SO_2Cl_2/CH_2Cl_2/-78\,°C$

SCHEME 2



Proposed mechanisms for the formation of **6**

SCHEME 3

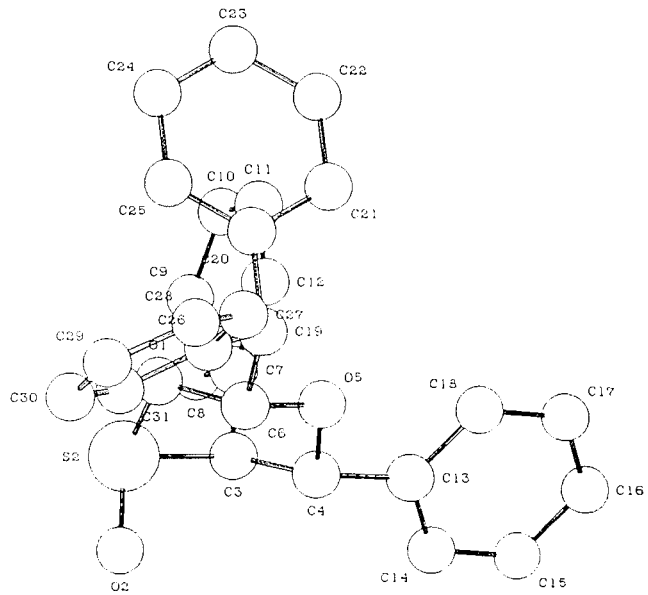


FIG. 1. The molecular structure of (2*R**,3*S**,4*R**,6*R**)-3,4-diphenyl-6-(diphenylmethyl)-1,5-dioxa-2-thiane-2-oxide **6** showing the atomic numbering. Hydrogen atoms have been omitted.

to the best of our knowledge, a new heterocyclic system, namely a 1,5-dioxa-2-thiane-2-oxide.

The X-ray structure of **6** (Fig. 1) shows a *cis* arrangement between the two phenyl groups on the six-membered ring with the C-3 substituent taking up an axial orientation. The 3 Hz coupling constant observed for the remaining hydrogens at C-3 and C-4 shows that a similar conformation exists in solution. The observed axial configuration of the S=O bond is preferred in δ-sultines (4, 6).

Photolysis of **6** in a quartz apparatus with a medium pressure mercury lamp gave an isomeric sultine **7** in quantitative yield. This same compound was obtained by reaction of the *erythro*-β-hydroxysulfoxide, **8**, prepared as shown in Scheme 2. In the latter reaction diphenylacetaldehyde was again a by-product; *trans*-stilbene was also formed.

The NMR spectrum for the isomeric sultine **7** (ir: 1120 cm^{-1}) shows a clear diaxial relationship for the C-3 and C-4 hydrogens (δ 4.02 and 5.86, J = 11 Hz); the remaining non-aromatic hydrogens appear as doublets at δ 4.43 and 6.67 (J = 4 Hz). These data together with the two modes of preparation secure the structure as **7**.

Examples of the photolability of benzylic carbon sulfur bonds in sulfoxides are known (7). Cleavage of this bond in **6** should lead to a diradical, which, after bond rotation, can recombine to give **7**. Complete isomerization of **6** to **7** is reasonable since this places all carbon substituents of the ring in the favorable equatorial position. The S=O bond continues to be axial.

The mechanism for the formation of these unusual heterocycles has not been investigated. A possible route to **6** is shown in Scheme 3.

Reaction of the hydroxysulfoxide **5** with SO_2Cl_2 should give the chlorooxosulfonium species **9** (6*c*). This species can react further in several possible ways: (i) cyclization to the β-sultine **4**, (ii) fragmentation to diphenylacetaldehyde and *t*-BuS(O)Cl, or (iii) loss of *t*-BuCl, or 2-methylpropene and HCl, to give the β-hydroxysulfinyl chloride **11**. Interaction of diphenylacetaldehyde or its enol with either **9** or **11** could lead to the oxonium ion **12**, or the related enol ether, either of which should cyclize to **6**. A similar pathway would hold for the conversion of **8** to **7**.

Can. J. Chem. Downloaded from www.nrcresearchpress.com by 195.138.81.100 on 09/07/12
For personal use only.

Can. J. Chem. Downloaded from www.nrcresearchpress.com by 195.138.81.100 on 09/07/12
For personal use only.

Experimental

Melting points were determined by use of a Gallenkamp digital melting point apparatus and are uncorrected. Infrared spectra were run as films on sodium chloride plates for oils, and in chloroform ($CHCl_3$) for solids using a Perkin Elmer 783 spectrophotometer. Mass spectra was recorded on an AEIMS 9025 instrument. Proton NMR spectra were recorded on either Varian EM-306-A or XL-300 spectrometers using $CDCl_3$ – 1% TMS solvent. ^{13}C spectra were obtained using a Varian XL-300 spectrometer. The chemical shifts for carbon and proton are reported in ppm downfield from TMS.

Column chromatography was accomplished using Baker or Terochem 60–200 mesh silica as the adsorbent. Purifications by radial, centrifugally accelerated thin-layer chromatography were performed on a Harrison Research Chromatotron model 7924 using silica gel coated rotors.

Benzyl tert-*butyl sulfide*

Benzyl chloride (70.0 g, 0.55 mol) was added dropwise, at room temperature, to a stirred methanolic solution ($MeOH/H_2O$ 1:1, 250 mL) of *tert*-butyl mercaptan (50.0 g, 0.55 mol) and potassium hydroxide (34 g, 0.60 mol). The mixture was heated under reflux for 16 h, then cooled. The resulting biphasic mixture was extracted into CH_2Cl_2 (300 mL), then washed twice with 5% NaOH (100 mL) and twice with H_2O (100 mL). The organic extract was dried with anhydrous calcium chloride, and removal of solvent gave the crude sulfide, which was further purified by distillation under reduced pressure, yielding benzyl *tert*-butyl sulfide (83.4 g, 84%); bp 80°C at 0.15 Torr (1 Torr = 133.3 Pa); ir ν_{max} (NaCl): 2800, 1600, 1495, 1450, 1362, 1168, 715, and 697 cm^{-1}; nmr: 1.35 (s, 9H), 3.75 (s, 2H), 7.1–7.4 (m, 5H).

Benzyl tert-*butyl sulfoxide.*

The purified sulfide was dissolved in ethyl acetate (150 mL), and stirred at −60°C while a solution of *m*-chloroperoxybenzoic acid 80% (28 g, 0.11 mol) in ethyl acetate (100 mL) was added dropwise. After the addition was completed, the solution was stirred at −30°C for 30 min and then at room temperature for 1 h. The reaction was washed with 10% sodium bisulfite solution (3 × 100 mL) followed by 5% sodium hydroxide solution (3 × 100 mL). The ethyl acetate layer was dried ($CaCl_2$) and evaporated under reduced pressure. The residual solid was purified by flash chromatography (gradient elution: CH_2Cl_2/hexane 75:25 to CH_2Cl_2/EtOAc 50:50 and finally with EtOAc), to yield the sulfoxide (15.7 g, 72%) as a white solid. The product was further purified by vacuum sublimation at 79°C (0.05 Torr); mp 74–75°C; ir ν_{max} ($CHCl_3$): 1050 cm^{-1}; nmr: 1.45 (s, 9H), 3.55 (d, J = 12 Hz, 1H), 3.84 (d, J = 12 Hz 1H), 7.28 (br s, 5H).

Threo *and* erythro-*1,2-diphenyl-2*-tert-*butylsulfinylethanol (8) and (5) (Scheme 2)*

From benzyl tert-*butyl sulfoxide.*

Benzyl *tert*-butyl sulfoxide (10.0 g, 51 mmol) was dissolved in THF (50 mL) and cooled to −78°C under N_2. This solution was stirred vigorously while a solution of lithium diisopropylamide (prepared from 2.5 N *n*-butyl lithium in hexanes (21 mL, 52 mmol) and diisopropylamine (7.2 mL, 51 mmol) in THF (150 mL) cooled to −70°C), was added by cannula. Stirring was maintained for a further 30 min, and then a solution of benzaldehyde (5.42 g, 51 mmol) in THF (50 mL) was added dropwise. The reaction mixture was then stirred for an additional 30 min at room temperature, quenched with water (100 mL), and the THF removed under reduced pressure. The aqueous phase was extracted with CH_2Cl_2 (3 × 100 mL). The combined organic extracts were dried ($CaCl_2$) and the solvent was evaporated. The crude product was purified by column chromatography (CH_2Cl_2/hexanes/EtOAc 35:35:30) to provide two products. The first to elute was *threo*-1,2-diphenyl-2-*tert*-butylsulfinylethanol (**8**) as a white solid (7.3 g, 47%); mp 167.5–168°C (dec.); ir ν_{max} ($CHCl_3$): 3500–3180, 1050, 1030, 1005, and 1000 cm^{-1}; nmr: 1.20 (s, 9H), 4.00 (d, J = 8 Hz, 1H), 5.27 (dd, J = 8 and 2 Hz, 1H), 6.08 (d, J = 2 Hz, 1H, -OH), 6.95 (br s, 10H); CIMS m/z: 303 (M^++1, 67%), 229(96), 197(91), 181(96), 180(100), 107(62), 105(60). Anal. calcd. for $C_{18}H_{22}O_2S$: C 71.50, H 7.33, S 10.68; found: C 71.27, H 7.36, S 10.47.

The second compound to elute (with gradient elution CH_2Cl_2/EtOAc 1:1 to 0:1) was the *erythro*-1,2-diphenyl-2-*tert*-butylsulfinylethanol (**5**) as a white solid (3.8 g, 25%); mp 165.5–166°C (dec.); ir ν_{max} ($CHCl_3$): 3340, 1058, 1030, 702 cm^{-1}; nmr: 1.15 (s, 9H), 4.01 (d, J = 3 Hz, 1H), 4.65 (d, J = 6 Hz, 1H, -OH), 5.72 (dd, J = 6 and 2 Hz, 1H), 6.8–7.3 (br s, 10H); CIMS m/z: 303 (M^++, 55%), 229(77), 197(100), 181(58), 180(71), 107(47), 105(41). Anal. calcd. for $C_{18}H_{22}O_2S$: C 71.50, H 7.33, S 10.68; found: C 71.27, H 7.03, S 10.24. This isomer was identical with the compound obtained as in Scheme 1.

From erythro-*1,2-diphenyl-2*-tert-*butylthioethanol (Scheme 1)*

trans-Stilbene oxide (1.96 g, 1 mmol), *tert*-butyl mercaptan (0.99 g, 1.1 mmol), and KOH (0.6 g, 1.1 mmol) were heated under reflux in 1-propanol (20 mL) for 8 h. The reaction mixture was cooled, poured into water, and extracted with dichloromethane (3 × 50 mL). The organic exctract was dried and evaporated. The crude product was distilled at 150–160°C (0.05 Torr) to give 2.2 g (75%) of a pale yellow oil, which solidified on standing to a pale yellow solid; mp 59–61°C; ir ν_{max} ($CHCl_3$): 3350 cm^{-1}; nmr: 1.20 (s, 9H), 2.5 (br s, 1H), 4.2 (d, J = 6 Hz, 1H), 5.0 (d, J = 2 Hz, 1H), 7.2 (m, 10H). The purified *erythro*-1,2-diphenyl-2-*tert*-butylsulfinylethanol (5.6 g, 20 mmol) was oxidized with *m*-chloroperoxybenzoic acid (4.4 g, 25.5 mmol) in dichloromethane (200 mL) to give 4.5 g (75%) of *erythro*-1,2-diphenyl-2-*tert*-butylsulfinylethanol (**5**).

cis-*Stilbene*

Hydroxysulfoxide **5** (604 mg, 2 mmol) and *N*-chlorosuccinimide (280 mg, 2.1 mmol) were refluxed in benzene (100 mL) for 1 h. The reaction mixture was cooled and the solvent removed on a rotary evaporator. The crude residue was purified by column chromatography (CH_2CH_2/hexane 1:1) to afford *cis*-stilbene (185 mg, 51%); nmr: 6.55 (s, 2H), 7.2 (s, 10H).

(2R, 3S*, 4R*, 6R*)-3,4-Diphenyl-6-(diphenylmethyl)-1,5-dioxa-2-thiane-2-oxide (6)*

The *erythro*-1,2-diphenyl-2-*tert*-butylsulfinylethanol (**5**) (0.50 g, 1.6 mmol) in dichoromethane (10 mL) was cooled to −78°C under an inert atmosphere. The solution was stirred vigorously while a 1.0 M solution of sulfuryl chloride in CH_2Cl_2 (1.85 mL, 1.85 mmol) was added dropwise by syringe. Stirring was maintained for a further 20 min at −78°C and the reaction mixture was quenched by addition of 10% $NaHSO_3$ solution (100 mL). Separation of the organic layer, extraction of the aqueous layer with dichloromethane (2 × 25 mL), drying ($CaCl_2$), and removal of solvent from the combined organic layers gave a pale yellow oil. The oily residue was purified on Chromatotron (gradient elution; hex/CH_2Cl_2 1:0 to 0:1) to provide diphenylacetaldehyde (85 mg, 26%), eluted first as a pale yellow oil, and then δ-sultine (**6**) (199 mg, 55%), eluted second as a viscous colourless oil that crystallized on standing; mp 160–162°C; ir ν_{max} ($CHCl_3$): 1125 cm^{-1}; nmr: 3.47 (d, J = 3 Hz, 1H), 4.52 (d, J = 3 Hz, 1H), 6.15 (d, J = 3Hz, 1H), 6.64 (d, J = 3 Hz, 1H), 6.72–7.44 (br m, 20H); ^{13}C nmr: 55.3, 66.3, 73.9, 94.3 132–139 (Ar-C). Anal. calcd. for $C_{28}H_{24}O_3S$: C 76.35, H 5.45, S 7.20, found: C 76.72, H 5.66, S 7.15.

(2R,3R*,4R*,6R*)-3,4-Diphenyl-6-(diphenylmethyl)-1,5-dioxa-2-thiane-2-oxide (7)*

Using the procedure described above, a solution of *threo*-1,2-diphenyl-2-*tert*-butylsulfinylethanol (**8**) (1.0 g, 33 mmol) was treated with SO_2Cl_2 (3.3 mL, 3.3 mmol) to yield *trans*-stilbene (410 mg, 69%), diphenylacetaldehyde (100 mg, 15%), and the δ-sultine (**7**) (49 mg, 7%), as a white solid; mp 162–163°C; ir ν_{max} ($CHCl_3$): 1120 cm^{-1}; nmr: 4.03 (d, J = 11 Hz, 1H), 4.42 (d, J = 5 Hz, 1H), 5.85 (d, J = 11 Hz, 1H), 6.68 (d, J = 4 Hz, 1H), 7.05–7.37 (br m, 20H). Anal. calcd. for $C_{28}H_{24}O_3S$: C 76.35, H 5.45, S 7.20; found: C 76.57, H 5.45, S 7.15.

Photoisomerisation of δ-sultine (6) to δ-sultine (7)

A solution containing sultine (**6**) (300 mg) in benzene: acetone (40 mL + 10 mL) was irradiated for 30 min using a 500-W Hanovia lamp and a Corex filter. The solvent was removed *in vacuo* and the residual material was crystallized from methylene chloride – pentane to

yield 295 mg of a fluffy white compound. All the physical data (mp, ir, nmr) were identical to those of **7**, above.

X-ray structure determination of (2R, 3S*, 4R*, 6R*)-3,4-Diphenyl-6-(1,1-diphenylmethyl)-1,5-dioxa-2-thiane-2-oxide (6)*

Crystal data: $C_{28}H_{24}O_3S$ fw = 440.55

Triclinic, $P\bar{1}$, $a = 9.1150(15)$, $b = 10.126(2)$, $c = 13.316(2)$ Å, $\alpha = 108.57(2)$, $\beta = 95.70(2)$, $\chi = 99.91(2)°$, $V = 1132.0(4)$ Å^3, $\rho_c = 1.293$ g cm^{-3}, $\mu = 1.44$ mm^{-1} (24°C, $CuK_{\alpha 1}$, $\lambda = 1.540562$ Å), $z = 2$. $F(100) = 464$.

Suitable crystals of **6** were obtained by slow diffusion of a diethyl ether top solvent layer into a concentrated solution containing **6** in dichloromethane. A crystal measuring approximately 0.15 × 0.25 × 0.35 mm was selected and mounted on a glass fibre. Intensity data were collected using a Picker diffractometer using the $\theta/2\theta$ scan mode. Unit cell dimensions were obtained from 26 reflections with 2θ between 100 and 117°. The calculated density assumes two molecules per unit cell. The data were collected to a maximum Bragg angle of 120°. Out of 5021 reflections measured, 3372 were unique; of these, 2500 were considered observed with $I_{net} > 2.5\sigma(I_{net})$. No absorption correction was made. The structural solution was made by direct methods followed by least-squares refinement using the NRCVAX series of programmes (8, 9). A Fourier difference map gave all non-hydrogen atoms. Hydrogen atoms were placed at calculated positions and refined. The final least-squares cycle was calculated with 56 atoms, 386 parameters using 2500 significant reflections. Weights based on counting statistics were used. The residuals on significant reflections were $R_F = 0.049$, $R_W = 0.055$, and $G_oF(S) = 2.01$. For all reflections $R_F = 0.070$, $R_W = 0.058$, where $R_F = \Sigma|F_o - F_c|/\Sigma(F_o)$, $R_W = [\Sigma(w(F_o - F_c)^2/\Sigma(wF_o^2)]^{1/2}$, and $G_oF(S) = [\Sigma(w(F_o - F_c)^2/((\text{number of reflections}) - (\text{number of parameters}))]^{1/2}$. The maximum shift-to-$\sigma$ ratio was 0.002. In the last D-map the deepest hole was -0.300 e Å^{-3} and the highest peak 0.430 e Å^{-3}, indicating an absence of solvent molecules.

Acknowledgments

Support for this work by NSERC (Canada) is gratefully acknowledged. We are grateful to Drs. Eric Gabe and Florence Lee for access to an NRC diffractometer and many useful discussions.

1. F. JUNG, N. K. SHARMA, and T. DURST. J. Am. Chem. Soc. **95**, 3420 (1973).
2. T. DURST and B. GIMBARZEVSKY. J. Chem. Soc. Chem. Commun. 724 (1975).
3. M. D. GRAY, D. R. RUSSELL, D. J. H. SMITH, T. DURST, and B. GIMBARZEVSKY. J. Chem. Soc. Perkin Trans. 1, 1826 (1981).
4. D. N. HARPP and J. G. GLEASON. Tetrahedron Lett. 1447 (1969).
5. N. K. SHARMA. Ph.D. Thesis, University of Ottawa. 1975.
6. (*a*) K. S. DHAMI. Chem. Ind. (London), 1004 (1968); (*b*) K. HENRICK and B. L. JOHNSON. Aust. J. Chem. **25**, 2263 (1972); (*c*) N. K. SHARMA, F. REINACH-HIRTZBACH, and T. DURST. Can. J. Chem. **54**, 3012 (1976).
7. E. BLOCK. Q. Rep. Sulfur Chem. **4**, 318 (1969).
8. D. F. GRANT and E. J. GABE. J. Appl. Crystallogr. **11**, 114 (1978).
9. E. J. GABE, F. L. LEE, and Y. LEPAGE. *In* Crystallographic computing. Vol. 3. *Edited by* G. Sheldrick, G. Kruger, and R. Goddard. Clarendron Press, Oxford. (1985). p. 167.

Can. J. Chem. Downloaded from www.nrcresearchpress.com by 195.138.81.100 on 09/07/12
For personal use only.

Two 1*H*-naphtho[2,3-*c*]pyran-1-one metabolites from the fungus *Paecilomyces variotii*

WILLIAM A. AYER,[1] PETER A. CRAW, AND KOOHEI NOZAWA
Department of Chemistry, University of Alberta, Edmonton, Alta., Canada T6G 2G2

Received June 28, 1990

WILLIAM A. AYER, PETER A. CRAW, and KOOHEI NOZAWA. Can. J. Chem. **69**, 189 (1991).

The fungus *Paecilomyces variotii* Bainier, isolated from larvae of *Dendroctonus ponderosa* Hopk. (mountain pine beetle), is antagonistic to *Ophiostoma clavigerum*, the fungus believed responsible for tree mortality caused by blue stain fungi. The metabolites produced by *P. variotii* when grown in liquid culture have been studied and two new 1*H*-naphtho[2,3-*c*]pyran-1-ones related to semi-vioxanthin (**4**) have been isolated. The structures of these two metabolites, semi-viriditoxin (**1**) and semi-viriditoxic acid (**2**), have been determined by chemical and spectroscopic methods.

Key words: fungal metabolites, blue stain disease, *Paecilomyces variotii*, semi-viridotoxin, semi-viridotoxic acid.

WILLIAM A. AYER, PETER A. CRAW et KOOHEI NOZAWA. Can. J. Chem. **69**, 189 (1991).

Le champignon *Paecilomyces variotii* Bainier, isolé des larves du *Dendroctonus ponderosa* Hopk. (des pins de montagne), est un antagoniste du *Ophiostoma clavigerum*, le champignon qui serait responsable de la mort des arbres causée par le champignon de coloration bleue. On a étudié les métabolites obtenus lorsqu'on a fait croître le *P. variotii* dans un milieu de culture liquide et on a isolé deux nouvelles 1*H*-naphtho[2,3-*c*]pyran-1-ones qui sont reliées à la semi-vioxanthine (**4**). Les structures de ces deux métabolites, la semi-viriditoxine (**1**) et l'acide semi-viriditoxique (**2**) ont été déterminées par des méthodes chimiques et spectroscopiques.

Mots clés : métabolites de champignon, maladie de coloration bleue, *Paecilomyces variotii*, semi-viridotoxine, acide semi-viridotoxique.

[Traduit par la revue]

Introduction

The blue stain disease of lodgepole pine (*Pinus contorta* Dougl. var *latifolia* Engelm.) is caused by a number of fungi vectored by the mountain pine beetle (*Dendroctonus ponderosae* Hopk.) (1). As part of our continuing investigation of fungi associated with this economically serious disease, we have examined the metabolites produced in liquid cultures of the fungus *Paecilomyces variotii* Bainier, which shows in vitro inhibitory activity towards *Ophiostoma clavigerum* (Robins.-Jeff. & Davids.) Harrington, a fungus strongly associated with tree mortality caused by blue stain fungi (2). We report herein the isolation and structure determination of two new 1*H*-naphtho[2,3-*c*]pyran-1-ones produced by *Paecilomyces variotii*.

Results and discussion

Paecilomyces variotii Bainier was isolated from an egg gallery of mountain pine beetle in lodgepole pine at Invermere, British Columbia, in September 1986. The fungus was grown in still culture on a modified malt extract medium for 3 weeks. Extraction of the dried mycelium with chloroform and chromatography of the residue gave compound **1**. The filtered culture broth was extracted with dichloromethane and the extract crystallized from chloroform to afford crystals of compound **2**. Chromatography of the crystallization mother liquors gave further compound **2**.

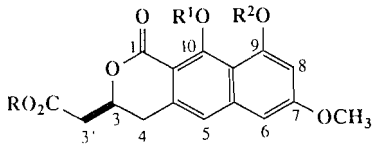
An examination of the spectral data for compounds **1** and **2** suggested a close structural similarity to the 1*H*-naphtho[2,3-*c*]-pyran-1-one fungal metabolites viriditoxin (**3**), semi-vioxanthin (**4**), and vioxanthin (**5**). Semi-vioxanthin (**4**) and vioxanthin (**5**) have been isolated from *Penicillium citro-viride* (3), vioxanthin (**5**) from *Trichophyton violaceum* (4), and viriditoxin (**3**) from *Aspergillus viridi-nutans* (5). By analogy with the naming of these previously reported 1*H*-naphtho[2,3-*c*]pyran-1-ones, we have named compound **1** semi-viriditoxin as it represents the monomeric subunit of the symmetrical dimer viriditoxin (**3**). Compound **2**, semi-viriditoxic acid, is the corresponding carboxylic acid of semi-viriditoxin.

Semi-viriditoxin (**1**) was obtained as microcrystals, mp 168–170°C, and has the molecular formula $C_{17}H_{16}O_7$ as determined by high resolution electron impact mass spectrometry (hreims). The Fourier transform infrared (Ftir) spectrum displays characteristic hydroxyl (3428, 3382 cm^{-1}), aliphatic ester (1736 cm^{-1}), and dihydroisocoumarin carbonyl (1655 cm^{-1}) and C=C (1647, 1582 cm^{-1}) absorptions. The position of the dihydroisocoumarin carbonyl absorption reflects the presence of strong intramolecular hydrogen bonding between the carbonyl group and the C10 phenolic hydrogen. Removal of the effect of this hydrogen bonding as in the methyl ether (**6**) (*vide infra*) shifts the dihydroisocoumarin carbonyl absorption to 1713 cm^{-1}. The ultraviolet spectrum of semi-viriditoxin (**1**) has maxima at 260, 309, and 374 nm, which are very similar in position and intensity to those reported (3) for semi-vioxanthin (**4**).

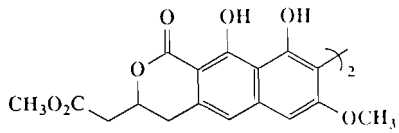
The ^{1}H nmr spectrum of semi-viriditoxin (**1**) was readily assigned by first-order analysis in conjunction with comparisons to the reported spectra of viriditoxin (**3**) (5), and semi-vioxanthin (**4**) and vioxanthin (**5**) (3). The assignments of the aromatic hydrogen signals of semi-viriditoxin (**1**) were confirmed by the observation of large nuclear Overhauser enhancements (nOe) of the *meta*-coupled aromatic hydrogens (J 2.2 Hz) at δ 6.57 (16.6%) and δ 6.61 (13.2%) when the aromatic methoxyl hydrogen signal at δ 3.89 was irradiated. Irradiation of the other aromatic hydrogen signal at δ 6.90 (br s) resulted in a nOe to the doublet at δ 6.61 (H6, 13%) (hence the doublet at δ 6.57 must be due to H8) and a nOe to a doublet of doublets (J 15.8, 3.5 Hz) at δ 3.14 (H4, 3.4%). The signal due to H4β (δ 3.04) displays the expected geminal coupling (J 15.8 Hz) to H4α and vicinal coupling (J 10.0 Hz) to H3, as well as a small benzylic coupling (J 1.0 Hz) to H5. When the signal at δ 6.90 was irradiated, the signal due to H4β simplified to a doublet of doublets (J 15.8, 10.0 Hz). The ^{13}C nmr spectrum of semi-viriditoxin (**1**) was readily assigned by comparison with the reported spectrum (3) of semi-vioxanthin (**4**) (Table 1). The additional signals at

[1]Author to whom correspondence may be addressed.

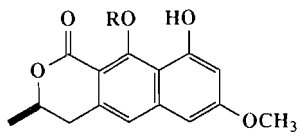
Can. J. Chem. Downloaded from www.nrcresearchpress.com by 195.138.81.100 on 09/07/12
For personal use only.



	R	R^1	R^2
1	CH_3	H	H
2	H	H	H
6	CH_3	CH_3	H
7	CH_3	CH_3	CH_3

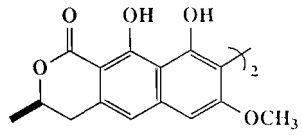


3



4 R = H

8 R = CH_3



5

TABLE 1. ^{13}C chemical shifts of semi-viriditoxin (**1**), semi-viriditoxic acid (**2**), and semi-vioxanthin (**4**) (3)

	Compound		
Carbon	**1**[a]	**2**[b]	**4**[b]
C1	169.8	169.9	170.5
C3	75.8	76.0	76.0
C4	39.4	39.1	33.8
C4a	132.2	133.7	134.0
C5	116.4	115.7	115.4
C5a	140.6	140.7	140.3
C6	101.8	101.0	100.9
C7	163.2	162.1	161.9
C8	99.7	99.2	99.1
C9	162.8	161.9	161.7
C9a	99.1	99.4	99.4
C10	158.6	157.8	157.6
C10a	108.4	108.1	107.9
C3′	32.7	31.6	20.3
CO_2CH_3	170.7	170.9	
CO_2CH_3	52.2		
7-OCH_3	55.5	55.4	55.3

[a]In $CDCl_3$.
[b]In $(CD_3)_2SO$.

δ 170.7 and δ 52.2 in the spectrum of semi-viriditoxin (**1**) are typical of those expected for an aliphatic methyl ester (6).

Semi-viriditoxic acid (**2**) was obtained as pale yellow leaves, mp 172–175°C, and has a molecular formula of $C_{16}H_{14}O_7$ as determined by hreims. The differences between the spectra of **2** and **1** are as expected. Thus, a broad carboxylic absorption is observed from 3200 to 2400 cm^{-1} in the Ftir spectrum of **2**, the ^1H nmr spectrum of **2** contains only one singlet due to methoxyl hydrogens whereas the spectrum of **1** contains two such singlets, and the ^{13}C nmr spectrum correspondingly contains one less carbon resonance than observed in the spectrum of **1** (Table 1).

Brief exposure of semi-viriditoxic acid (**2**) to a solution of diazomethane resulted in methylation to give semi-viriditoxin (**1**) as well as dimethylation to give semi-viriditoxin 10-methyl ether (**6**). Zeeck *et al.* (3) reported that the C10 phenol of semi-vioxanthin (**4**) is also selectively methylated with diazomethane and both the Ftir and ^1H nmr spectra of semi-viriditoxin 10-methyl ether (**6**) compare favourably with those of semi-vioxanthin 10-methyl ether (**8**). In the absence of intramolecular hydrogen bonding the dihydroisocoumarin carbonyl absorption occurs at 1713 cm^{-1} in the Ftir spectrum of **6** (cf 1655 cm^{-1} in semi-viriditoxin). Methylation of the carboxylic acid and only the C10 phenol of **2** is consistent with a significant nOe (15.5%) to the phenol singlet at δ 9.84 when the C10 methoxyl singlet at δ 4.14 is irradiated. Complete methylation of semi-viriditoxic acid (**2**) was achieved using an excess of methyl iodide and potassium carbonate to give the dimethyl ether (**7**) to semi-viriditoxin.

The circular dichroism (cd) spectra of semi-viriditoxin (**1**) and semi-viriditoxic acid (**2**) are very similar to that reported for semi-vioxanthin (**4**), which has been shown to possess the *R* configuration at C3 (3). Accordingly, we have assigned semi-viriditoxin and semi-viriditoxic acid the absolute stereochemistries indicated in **1** and **2** respectively (*S* configuration at C3). Semi-viriditoxin (**1**) and semi-viriditoxic acid (**2**) both showed weak antibacterial activity against a number of bacteria, but neither compound showed antifungal activity against *Ophiostoma clavigerum*.

Experimental

For general experimental details see ref. 7. Low pressure liquid chromatography (lplc) was performed on an E. Merck silica gel 60 prepacked size A column using a Fluid Metering Inc. model RP-SY pump.

Growth of Paecilomyces variotii *and isolation of metabolites*

Slant tubes of *Paecilomyces variotii* Bainier (NOF-1232) were obtained from Dr. Y. Hiratsuka, Northern Forest Research Centre, Edmonton, and a specimen sample of the fungus was deposited with the University of Alberta Microfungus Collection (register number UAMH

Can. J. Chem. Downloaded from www.nrcresearchpress.com by 195.138.81.100 on 09/07/12
For personal use only.

Can. J. Chem. Downloaded from www.nrcresearchpress.com by 195.138.81.100 on 09/07/12
For personal use only.

6353). Slant cultures of the fungus were maintained at 20°C on Weitzman and Silva–Hunter medium (10 g Pablum baby oatmeal, 10 g Hunt's tomato paste, 1.5 g KH_2PO_4, 1.0 g $MgSO_4 \cdot 7H_2O$, 1.0 g $NaNO_3$, 20 g Alphacel, 20 g agar, in 1 L water). Several slant tubes of potato dextrose agar (PDA, Difco) were then inoculated with the mature maintenance stock of the fungus, and grown at room temperature for 3 weeks. Five slant tubes of the PDA culture of the fungus were used to inoculate 10 2.8-L Fernbach flasks each containing 1 L of modified malt extract medium (20 g malt extract (Difco), 20 g D-glucose, 1.0 g bacto-peptone (Difco), 1 L water) and the still cultures were kept at room temperature for 3 weeks.

The mycelium was separated by filtration through cheesecloth, then air dried and ground to a coarse powder (50 g). Soxhlet extraction with chloroform gave a brown oil (3.1 g), which was subjected to flash chromatography. Elution with chloroform gave an oil (62 mg), which was subjected to lplc, eluting with benzene – ethyl acetate (7:1), to give semi-viriditoxin (**1**) (13 mg). Further elution with ethanol gave an oil (0.60 g), which was subjected to lplc using chloroform–ethanol – acetic acid (100:4:0.5) to give semi-viriditoxic acid (**2**) (17 mg).

The filtered culture broth was concentrated at reduced pressure to approximately 2 L and then extracted several times with dichloromethane. The combined dichloromethane extracts were evaporated to give a residue (0.90 g), which deposited crystals of semi-viriditoxic acid (**2**) (18 mg) from chloroform solutions. The mother liquors were flash chromatographed, eluting with chloroform containing increasing amounts of ethanol. Elution with chloroform–ethanol – acetic acid (100:20:0.5) gave an oil (62 mg), which was subjected to lplc, eluting with chloroform–ethanol – acetic acid (100:4:0.5), to give further semi-viriditoxic acid (**2**) (12 mg).

(*S*)-3,4-Dihydro-9,10-dihydroxy-7-methoxy-1*H*-naphtho[2,3*c*]pyran-1-one-3-acetic acid methyl ester (*Semi-viriditoxin*) (**1**) crystallized from benzene – Skellysolve B as off-white microcrystals, mp 168–170°C; $[\alpha]_D^{20}$ −9.0° (*c* 0.21, $CHCl_3$); cd (*C* 0.36 mM, dioxane) 28°C: $[\theta]_{360}$ +2000, $[\theta]_{320}$ +1300, $[\theta]_{270}$ −26 600; uv (CH_3OH) λ_{max} (log ε): 260 (4.62), 309 (3.64), 374 (3.97) nm; Ftir (KBr): 3428, 3382 (OH), 1736 (C=O), 1655 (lactone C=O), 1647, 1582 (C=C), 1160, 1132 (C—O) cm^{-1}; ^1H nmr ($CDCl_3$) δ: 2.78 (1H, dd, *J* = 16.0, 6.7 Hz, H3′), 2.98 (1H, dd, *J* = 16.0, 6.7 Hz, H3′), 3.04 (1H, ddd, *J* = 15.8, 10.0, 1.0 Hz, H4β), 3.14 (1H, dd, *J* = 15.8, 3.5 Hz, H4α), 3.76 (3H, s, CO_2CH_3), 3.89 (3H, s, 7-OCH_3), 5.06 (1H, dddd, *J* = 10.0, 6.7, 6.7, 3.5 Hz, H3), 6.57 (1H, d, *J* = 2.2 Hz, H8), 6.61 (1H, d, *J* = 2.2 Hz, H6), 6.90 (1H, br s, H5), 9.44 (1H, s, 9-OH), 13.58 (1H, s, 10-OH); ^{13}C nmr: see Table 1; hreims, *m/z* calcd. for $C_{17}H_{16}O_7$ (M^+): 332.0896; found: 332.0888 (100), 314 (19), 282 (35), 258 (26).

(*S*)-3,4-Dihydro-9,10-dihydroxy-7-methoxy-1*H*-naphtho[2,3-*c*]pyran-1-one-3-acetic acid (*Semi-viriditoxic acid*) (**2**) crystallized from chloroform as pale yellow leaves, mp 172–175°C; $[\alpha]_D^{20}$ 0° (*c* 0.10, $CHCl_3$); cd (*c* 0.63 mM, dioxane) 28°C: $[\theta]_{360}$ +5300, $[\theta]_{320}$ +2400, $[\theta]_{268}$ −31 800; uv (CH_3OH) λ_{max} (log ε): 219 (4.18), 260 (4.69), 309 (3.61), 323 (3.51), 368 (3.96), 374 (3.96) nm; Ftir (KBr): 3600–3250 (OH), 3200–2400 (br, CO_2H), 1710, 1646, 1583 cm^{-1}; ^1H nmr ($CDCl_3$) δ: 2.73 (1H, dd, *J* = 16.0, 6.5 Hz, H3′), 2.93 (1H, dd, *J* = 16.0, 6.5 Hz, H3′), 3.01 (1H, ddd, *J* = 16.0, 10.5, 1.0 Hz, H4β), 3.15 (1H, dd, *J* = 16.0, 3.5 Hz, H4α), 3.86 (3H, s, 7-OCH_3), 5.06 (1H, dddd, *J* = 10.0, 6.7, 6.7, 3.5 Hz, H3), 6.50 (1H, d, *J* = 2.2 Hz, H8), 6.55 (1H, d, *J* = 2.2 Hz, H6), 6.88 (1H, br s, H5), 9.41 (1H, s, 9-OH), 13.60 (1H, s, 10-OH); ^{13}C nmr: see Table 1; hreims, *m/z* calcd. for $C_{16}H_{14}O_7$ (M^+): 318.0739; found: 318.0743 (100), 300 (14), 274 ($M^+ - CO_2$, 17), 256 (14), 230 (21).

Methylation of semi-viriditoxic acid (2) with diazomethane

An excess of an ethereal solution of diazomethane was added to a solution of **2** (7 mg) in methanol (2 mL) and the solution allowed to stand for 3 min before being evaporated to a yellow oil. Chromatography (lplc), eluting with benzene–acetone (20:1), gave semi-viriditoxin 10-methyl ether (**6**), which crystallized from benzene as colourless needles (3 mg), mp 175–180°C (dec.); Ftir (KBr): 3430, 3325, 1734, 1713, 1636, 1575, 1161 cm^{-1}; ^1H nmr ($CDCl_3$) δ: 2.74 (1H, dd, *J* = 16.0, 7.0 Hz, H3′), 2.97 (1H, dd, *J* = 16.5, 7.0 Hz, H3′), 3.05 (1H, ddd, *J* = 16.0, 10.5, 1.5 Hz, H4β), 3.14 (1H, dd, *J* = 16.5, 3.5 Hz, H4α), 3.75 (3H, s, CO_2CH_3), 3.89 (3H, s, 7-OCH_3), 4.14 (3H, s, 10-OCH_3), 4.95 (1H, dddd, *J* = 10.5, 7.0, 7.0, 3.5 Hz, H3), 6.58 (1H, d, *J* = 2.5 Hz, H6 or H8), 6.61 (1H, d, *J* = 2.5 Hz, H6 or H8), 7.24 (1H, br s, H5), 9.84 (1H, s, OH); hreims, *m/z* calcd. for $C_{18}H_{18}O_7$ (M^+): 346.1053; found: 346.1047 (100), 315 (19), 268 (24), 244 (23), 229 (23).

Further elution with benzene–acetone (20:1) gave semi-viriditoxin (**1**) (1.5 mg) (correct tlc, ^1H nmr).

Methylation of semi-viriditoxic acid (2) with methyl iodide – potassium carbonate

A mixture of semi-viriditoxic acid (20 mg), potassium carbonate (0.10 g), and methyl iodide (0.10 mL) in dimethylformamide (1.0 mL) was stirred at room temperature for 16 h. Work-up in the usual manner provided a yellow oil, which was purified by flash chromatography. Elution with ethyl acetate – Skellysolve B (1:1) gave the dimethyl ether (**7**) (10.2 mg), which crystallized from ethyl acetate – Skellysolve B as flakes, mp 127–128°C; Ftir ($CHCl_3$ cast): 1730 (br), 1621, 1571 cm^{-1}; ^1H nmr ($CDCl_3$) δ: 2.71 (1H, dd, *J* = 16.0, 6.7 Hz, H3′), 2.95 (1H, dd, *J* = 16.5, 6.5 Hz, H3′), 3.03 (1H, ddd, *J* = 15.5, 10.5, 1.0 Hz, H4β), 3.11 (1H, dd, *J* = 15.5, 3.2 Hz, H4α), 3.81 (3H, s, CO_2CH_3), 3.98 (3H, s, $ArOCH_3$), 4.04 (3H, s, $ArOCH_3$), 4.14 (3H, s, $ArOCH_3$), 4.87 (1H, dddd, *J* = 10.0, 6.5, 6.5, 3.0 Hz, H3), 6.50 (1H, d, *J* = 2.5 Hz, H6 or H8), 6.64 (1H, d, *J* = 2.5 Hz, H6 or H8), 7.22 (1H, br s, H5); hreims, *m/z* calcd. for $C_{19}H_{20}O_7$ (M^+): 360.1209; found: 360.1220 (100), 287 (17), 258 (20).

Acknowledgements

We acknowledge with thanks the financial support of the Natural Sciences and Engineering Research Council of Canada. We wish to thank Dr. Y. Yamaoka and Dr. Y. Hiratsuka of the Northern Forest Research Centre, Edmonton, and Mrs. Lynne Sigler of the University of Alberta Microfungus Collection, Devonian Botanic Garden, for the cultures and for valuable advice.

1. L. Sigler, Y. Yamaoka, and Y. Hiratsuka. Can. J. Microbiol. **36**, 77 (1990).
2. Y. Yamaoka, R. H. Swanson, and Y. Hiratsuka. Can. J. For. Res. **20**, 31 (1990).
3. A. Zeeck, P. Rus, H. Laatsch, W. Loeffler, H. Wehrle, H. Zahner, and H. Holst. Chem. Ber. **112**, 957 (1979).
4. A. S. Ng, G. Just, and F. Blank. Can. J. Chem. **47**, 1223 (1969).
5. D. Weisleder and E. B. Lillehoj. Tetradedron Lett. **48**, 4705 (1971).
6. E. Breitmaier and W. Voelter. Carbon-13 NMR spectroscopy. 3rd ed. VCH Publishers, Weinheim, West Germany. 1987.
7. W. A. Ayer, P. A. Craw, T. J. Stout, and J. Clardy. Can. J. Chem. **67**, 773 (1989).

Photoelectrochemical and optical properties of porphyrin thin films prepared by the electrolytic micelle disruption method

KAZUHIKO TAKEDA, YUTAKA HARIMA, AND KAZUO YAMASHITA[1]

Division of Material and Life Sciences, Faculty of Integrated Arts and Sciences, Hiroshima University, Hiroshima 730, Japan

Received March 23, 1990

KAZUHIKO TAKEDA, YUTAKA HARIMA, and KAZUO YAMASHITA. Can. J. Chem. **69**, 192 (1991).

Photoresponses for various porphyrin films prepared by the electrolytic micelle disruption (EMD) method have been investigated in the indium–tin oxide/porphyrin/I_3^-, I^-/Pt cell. The EMD film of an n-type porphyrin, 5,10,15,20-tetra(4-pyridyl)porphyrin (T(4-Py)P), exhibited a clear optical filtering effect (OFE), while not for the EMD films of p-type porphyrins such as (5,10,15,20-tetraphenylporphyrinato)zinc(II) (ZnTPP). For the EMD-ZnTPP film, the photocurrents at 500–700 nm were remarkably enhanced by increasing the film thickness. These photoelectrochemical properties were explained in terms of the electrolyte-permeability of the EMD films, which were confirmed by the electrochemical measurements and electron microscopic observations. The high conversion efficiency of the EMD-ZnTPP film was explained on the same basis. The difference in the thickness dependence of OFE between T(4-Py)P films prepared by the EMD and physical vapor deposition method was elucidated by the differences in diffusion lengths of excitons and in widths of photoactive layers in the films. In addition, a modified version of the EMD method was described in conjunction with a morphology control of the porphyrin solids.

Key words: porphyrin, organic thin film, photoresponse, micelle, electrochemistry.

KAZUHIKO TAKEDA, YUTAKA HARIMA et KAZUO YAMASHITA. Can. J. Chem. **69**, 192 (1991).

Opérant dans une cellule d'indium-oxyde d'étain/porphyrine/I_3^-, I^-/Pt, on a étudié les photoréponses de divers films de porphyrines préparés par le méthode des dislocations micellaires électrolytiques (DME). Le film de DME d'une porphyrine de type-n, la 5,10,15,20-tétra-(4-pyridyl)porphyrine (T(4-Py)P), présente un net effet de filtrage optique (EFO); ce n'est pas le cas avec les films des porphyrines de type-p, comme celui du (5,10,15,20-tétraphénylporphyrinato)zinc(II) (ZnTPP). Pour le film de DME du ZnTPP, les photocourants de la région allant de 500 à 700 nm augmentent d'une façon remarquable avec une augmentation de l'épaisseur du film. On explique ces propriétés photoélectrochimiques en fonction d'une perméabilité aux électrolytes des films de DME; cette explication est confirmée par des mesures électrochimiques et par des observations de microscopie électronique. La grande efficacité de conversion du film de DME du ZnTPP s'explique de la même manière. La différence observée dans les relations entre l'épaisseur et l'EFO des films de T(4-Py)P préparés soit par la DME ou par la méthode du dépôt de vapeurs physiques est attribuée aux différences dans les longueurs de diffusion des excitons et dans les largeurs des couches photoréactives des films. De plus, on décrit une version modifiée de la méthode de DME qui a été associée à un contrôle de la morphologie des porphyrines solides.

Mots clés : porphyrine; film organique mince; photoréponse; micelle; électrochimie.

[Traduit par la revue]

Introduction

Photoelectric and photoelectrochemical properties of organic solid films have been extensively studied, because the organic photoconductors are very promising functional materials applicable to devices such as photocell, TV vidicon tube, laser printer, etc. Usually, thin films of the organic molecules are prepared by using the physical vapor deposition (PVD) method and casting or spin-coating technique (1–5). Recently, however, a new method called an electrolytic micelle disruption (EMD) method has been developed, which is based on the electrolytic disruption of micelles containing dye particles (6–8). Previously, we have shown that the phthalocyanine (Pc) film prepared by the EMD technique is more efficient in photoactivity than the film prepared by the PVD method (9). A similar enhancement in conversion efficiency was observed with porphyrin films (10). Furthermore, we pointed out that the EMD-Pc film was so porous that the electrolyte solution could be penetrable through the EMD film (11).

In this paper, we present the details on spectroscopic and photoelectrochemical properties of porphyrin films prepared by the EMD and its modified methods compared with those for the films prepared by the PVD method, and discuss the conversion efficiencies in relation to the morphologies of the EMD and PVD films.

Experimental

Porphyrins used were 5,10,15,20-tetraphenylporphyrin (H_2TPP), MgTPP, and ZnTPP, which are characterized as p-type organic semiconductors, and 5,10,15,20-tetra(4-pyridyl)porphyrin (T(4-Py)P) which is an n-type organic semiconductor (12–14). These porphyrins were purchased from Strem Chem. Inc. The surfactant (11-ferrocenyl)undecyltridecaethyleneglycol ether (FPEG), was purchased from Wako Pure Chem. Co. MgTPP was purified by HPLC to remove the free base H_2TPP. Other chemicals were used without further purification. An indium–tin oxide (ITO) film, whose sheet resistance was about 20 ohm and transparency over 80%, was from Matsuzaki Shinku Co. The procedures in the production of a porphyrin film on an ITO substrate by the EMD method were as follows: (*1*) aqueous mixtures containing 1 mmol dm^{-3} (mM) FPEG, 5 mM porphyrin, and 0.1 M LiBr, were sonicated for 30 min and then stirred for 10–30 days, (*2*) the resulting solution was centrifuged for 30 min at 500 × *g*, where *g* is 9.8 m s^{-2}, (*3*) the supernatant solution, where a suitable amount of dye particles was involved as micelles with FPEG, was supplied for the potential-controlled electrolysis, which was carried out at 0.50 V vs. SCE in the three-electrode system. Thickness of the dye film could be controlled by the amount of electricity passing through the electrode (7, 10). A modified version of the EMD technique was also used to produce the dye films, which is abbreviated as mod-EMD method hereafter. The procedures were as follows: (*1*) given amounts of ZnTPP and FPEG were dissolved completely in ethanol, and evaporated to dryness, (*2*) the solid residue consisting of ZnTPP and FPEG was redissolved into distilled water and the solution filtrated through a filter whose pore size was 0.20 μm, (*3*) the filtrate was centrifuged for 15

[1]Author to whom correspondence may be addressed.

Printed in Canada / Imprimé au Canada

Can. J. Chem. Downloaded from www.nrcresearchpress.com by 195.138.81.100 on 09/07/12
For personal use only.

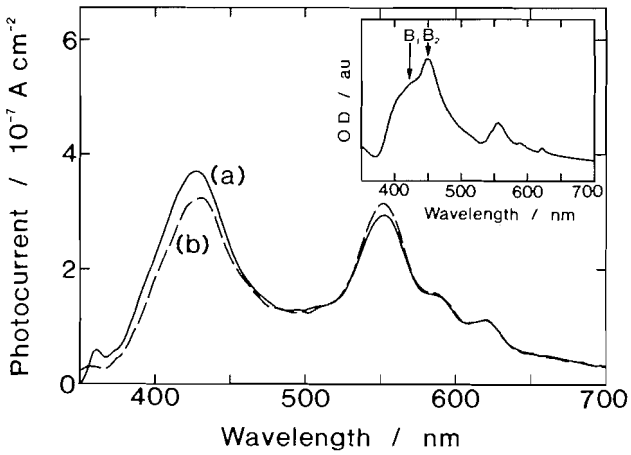


FIG. 1. Photocurrent action spectra for the ITO/EMD-ZnTPP/I_3^-, I^-/Pt cell. Illumination is done through (*a*) the ZnTPP/electrolyte interface and (*b*) the ITO electrode under short circuit conditions. The inset shows the absorption spectrum of the EMD-ZnTPP film.

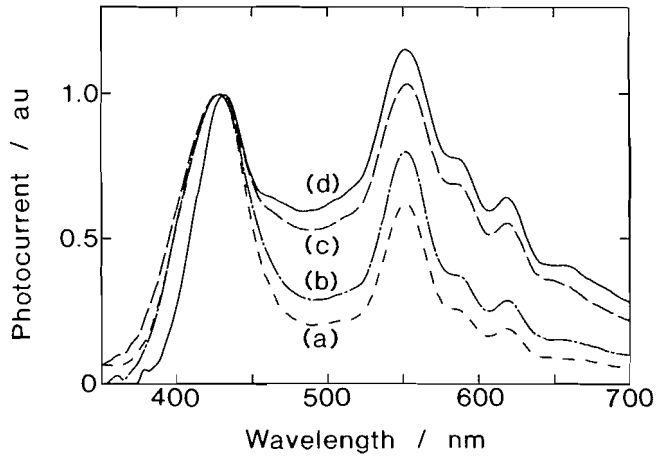


FIG. 2. Thickness dependence of the photocurrent action spectra for ITO/EMD-ZnTPP electrodes. The amount of electricity, which is a measure of a film thickness, was (*a*) 5, (*b*) 10, (*c*) 30, and (*d*) 40 mC cm^{-2}.

min at 16500 × *g* to sediment large particles, and (*4*) the supernatant solution was supplied for the electrolysis which was done in the same manner as described in the EMD method.

The electrolysis and cyclic voltammetry were carried out by a Hokuto-Denko HAB-151 potentiostat. Quantity of electricity (Q) was measured by a home-made coulometer. Thickness of an EMD film was monitored by Q or optical density (OD) of the film. The photocurrent action spectra were measured by a Jasco CT-10S monochromator with a 300W tungsten–halogen lamp and a Takeda Riken TR-8651 electrometer. The redox solution used consisted of 0.5 mM I_2 and 0.1 M KI in an acetate buffer (pH 4.7). The standard redox potential for the I_3^-/I^- couple was 0.29 V vs. SCE. The photocurrents were normalized in such a way that the photon flux of monochromatic light incident on the surface of the porphyrin electrode was constant at 2.5 × 10^{13} photons cm^{-2} s^{-1}. For light source, a 500 W xenon lamp was used with Toshiba ND filters, cut-off filters, or interference filters. The optical absorption spectra were measured by a Shimadzu UV-240 spectrophotometer. The experiments of X-ray diffraction were carried out by a Rigaku Denki RAD-1B diffractometer. All measurements were done at room temperature.

Results and discussion

Figure 1 shows the short-circuit photocurrent action spectra obtained on illumination of the ITO and electrolyte side in the ITO/EMD-ZnTPP/I_3^-, I^-/Pt cell. The inset depicts the optical absorption spectrum of the EMD-ZnTPP film used. The shapes of both action spectra closely resembled each other and all peaks coincided well with those for the ITO/PVD-ZnTPP electrode. No obvious optical filtering effect (OFE) was observed, although the thickness of the EMD porphyrin film was 200 nm, which was usually thick enough for the PVD film to exhibit the OFE (15). The result of the OFE for PVD-ZnTPP films indicated that the PVD-ZnTPP/electrolyte junction was a blocking contact, being stronger than the contact with ITO. It is worthy to note that a new absorption peak B_2 is observed at around 450 nm in addition to the peak B_1 which corresponds to the Soret peak of the PVD-ZnTPP film. The peak B_2 is attributable to the different morphology of ZnTPP crystallines, which may be formed in the course of preparing the micelle solution (10). As shown in Fig. 1, however, the light absorption process responsible for the component B_2 substantially does not contribute to generating a photocurrent, though now the reason is uncertain.

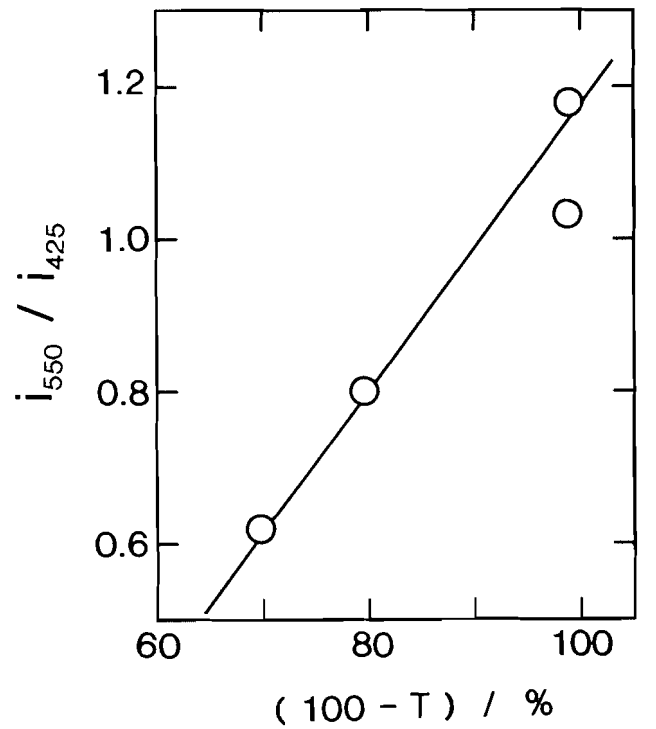


FIG. 3. Plot of the ratio of i_{550} to i_{425} as a function of the transmittance (T) at 550 nm for the EMD-ZnTPP film.

The dependence of film thickness on the photocurrent action spectrum of the EMD-ZnTPP electrode was noticeable as shown in Fig. 2, where illumination was done through the ITO electrode and all photocurrents were normalized with the photocurrent at the Soret band peak (425 nm). The photocurrents at 425 nm were almost independent of the film thickness (or quantity of electricity) in the range from 100 nm (5 mC cm^{-2}) to 800 nm (40 mC cm^{-2}). On the other hand, the photocurrents at wavelengths between 500 and 700 nm increase with the increase of film thickness. Figure 3 is a plot of the ratio (i_{550}/i_{425}) against (100 − T), where i_{550} and i_{425} are photocurrents at Q band and Soret band peaks (550 nm and 425 nm),

Can. J. Chem. Downloaded from www.nrcresearchpress.com by 195.138.81.100 on 09/07/12
For personal use only.

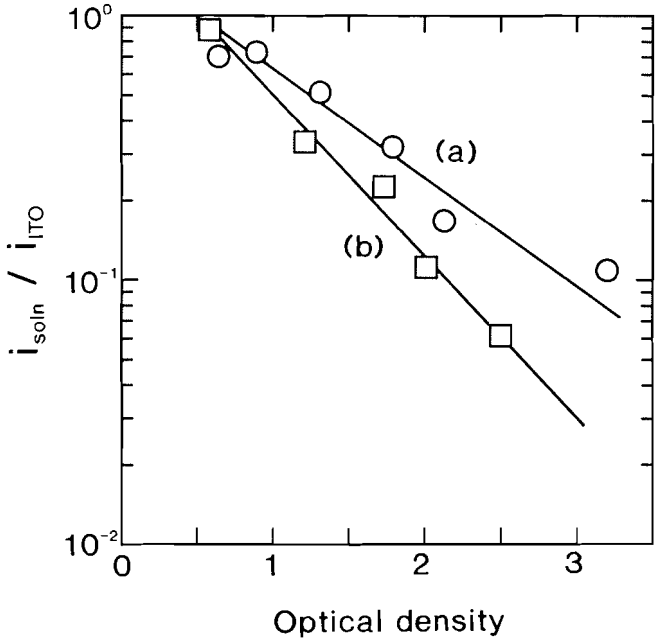


FIG. 4. Plot of i_{soln}/i_{ITO} against the optical density at the Soret band peak (430 nm) for the ITO/T(4-Py)P electrode prepared by (*a*) the EMD and (*b*) PVD methods.

respectively, and T is the transmittance (%) of an EMD-ZnTPP film at 550 nm. The abscissa ($100 - T$) is the percentage of photons absorbed by the ZnTPP films. Figure 3 shows that photocurrents at the Q band peak are proportional to the amount of photons absorbed by the ZnTPP film, since i_{425} is nearly constant. In view of the fact that the absorption coefficient at 425 nm is as high as 2.5×10^5 cm^{-1}, even the thinnest EMD-ZnTPP film (100 nm) can absorb more than 98% of photons incident on the ZnTPP film. Therefore, the photocurrent at the Soret peak must not depend upon the film thickness beyond 100 nm.

The thickness dependence of photocurrents for PVD-ZnTPP films differs from that for EMD-ZnTPP films: the photocurrents for PVD-ZnTPP films decrease with increasing the film thickness up to, at least, 400 nm, and the ratio of photocurrents at the Q band and Soret band peaks is constant at 0.35. The results on the PVD films imply that the photocurrents of PVD films do not correlate with the amount of photons absorbed by the films. In the PVD case, the photocurrents seem to be governed by other factors such as the amount of photons absorbed within the depletion layer formed near the surface of PVD-ZnTPP film, and carrier traps, etc. (15).

Figure 4 shows the OFE observed with T(4-Py)P films. The photocurrents of i_{soln} and i_{ITO} were obtained on illumination of the electrolyte and ITO side at Soret band peak (430 nm), respectively. For both EMD and PVD films, semilogarithmic plots of i_{soln}/i_{ITO} against OD decrease almost linearly with increasing the OD of each film. This is explicable by the OFE due to the T(4-Py)P layer. In other words, a blocking contact is formed at the ITO/T(4-Py)P junction and only photons absorbed near the ITO/T(4-Py)P interface contribute to the carrier generation and thus the photocurrent. On the other hand, the T(4-Py)P/electrolyte contact is ohmic or nearly ohmic. The slope of line (*b*) for the PVD film is slightly steeper than that of line (*a*) for the EMD film. According to the exciton model described previously (15), the gradient of a line becomes steep when the exciton diffusion length (L_{exc}) and/or the apparent

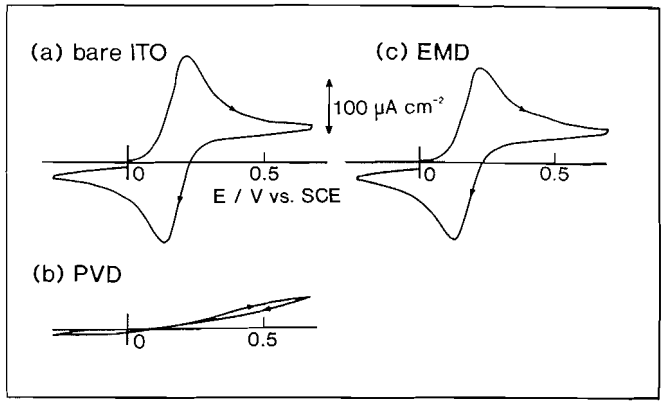


FIG. 5. Cyclic voltammograms of (*a*) bare ITO, (*b*) ITO/PVD-ZnTPP, and (*c*) ITO/EMD-ZnTPP electrodes in 0.1 M KCl solutions containing 1 mM $[Fe(CN)_6]^{4-}$. Potential sweep rate was 100 mV s^{-1}.

barrier width (W_{ap}) are small. It therefore derived from the result shown in Fig. 4 that the L_{exc} or W_{ap} for the EMD porphyrin film is greater than that for the PVD film. The density of the EMD film is likely to be lower than that of the PVD film. This would lead to a result inconsistent with the result in Fig. 4. In regard to L_{exc} and W_{ap}, which relate with the photocurrent and conversion efficiency, Fan and co-workers have demonstrated a very interesting view (16, 17), in that the photoactive region in the photovoltaic CuPc cell is restricted by the grain size of microcrystallines in the sublimed CuPc film, since the exciton diffusion length and the width of photoactive layer (W) being approximately equal to W_{ap} are influenced by the grain size. In our case, the grain size for the EMD-T(4-Py)P film seems to be fairly great compared with that of the PVD film. This inference is drawn from the X-ray diffraction study of the EMD and PVD films. The EMD-ZnTPP film showed a diffraction pattern similar to that of ZnTPP hydrate powders (18), although the diffraction of the former was very weak in comparison with the latter. On the other hand, no X-ray diffraction was observed with the PVD-ZnTPP film. Consequently, it is deduced that the grain size of microcrystallines constituting the EMD film is larger than that for the PVD film on assuming that both EMD and PVD films consist of microcrystallines. Namely, L_{exc} and W (or W_{ap}) for the EMD film are larger than those for the PVD film. This is consistent with the finding that the photocurrent for the EMD-T(4-Py)P film is 2–3 times greater than that of the PVD film, and that the EMD-ZnTPP film is more efficient than the PVD-ZnTPP film as shown before.

Electrochemical studies of the EMD- and PVD-ZnTPP film give important information on the morphologies of EMD and PVD films as shown in Fig. 5, illustrating the cyclic voltammograms of ions $[Fe(CN)_6]^{4-}$ at the bare ITO, ITO/PVD-ZnTPP (80 nm) and ITO/EMD-ZnTPP (300 nm) electrodes in 0.1 M KCl aqueous solutions. Well-defined redox waves were observed at the bare ITO and ITO/EMD-ZnTPP electrodes. This fact shows that the electrolyte solution can penetrate easily through the EMD film and come into contact with the ITO substrate, where $[Fe(CN)_6]^{4-}$ ions are oxidized reversibly. On the other hand, no obvious redox wave was observed at the ITO/PVD-ZnTPP electrode in the potential range studied, suggesting that the PVD-ZnTPP film was so dense that the electrolyte could not permeate in the PVD film and not reach the ITO electrode. Similar results were obtained with EMD films of other porphyrins including T(4-Py)P. The permeable feature of the EMD porphyrin film is also inferred from the scanning electron microscope

Can. J. Chem. Downloaded from www.nrcresearchpress.com by 195.138.81.100 on 09/07/12
For personal use only.

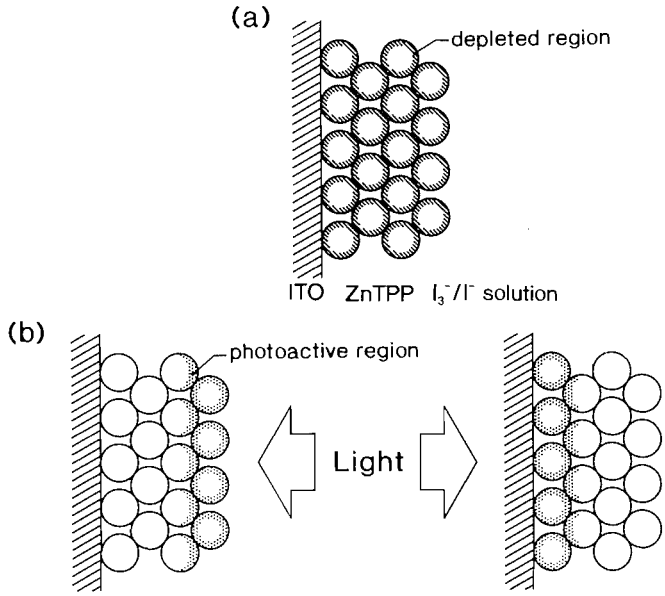


FIG. 6. Schematic illustration for the ITO/EMD-ZnTPP electrode in the I_3^-/I^- redox solution (*a*) in the dark and (*b*) under illumination. The arrows show the illumination direction.

(SEM) pictures in Fig. 9. On the bases of the SEM pictures and results of cyclic voltammograms, the morphological features of the EMD layer on ITO are represented schematically as in Fig. 6. When the ITO/EMD-ZnTPP electrode is dipped into the I_3^-/I^- redox solution, the electrolyte solution permeates the ZnTPP film. Thus a depletion layer can be formed near the surface of every ZnTPP particle contacting the electrolyte solution, because the ZnTPP/electrolyte contact is blocking (Fig. 6 (*a*)). Therefore, there may be no difference in the amount of photons absorbed in the depleted region irrespective of the direction of light illumination (Fig. 6 (*b*)). This explains the experimental finding that the OFE is not observed with the EMD-ZnTPP electrode. The thickness dependence of photocurrent may also be interpreted by the spread of photoactive sites over the entire film. Namely, the photocurrents are proportional to the amount of photons absorbed by the whole film. Similar photoresponses observed with the other p-type porphyrins such as MgTPP and H_2TPP are also understood on the basis of the electrolyte-permeable nature of the EMD films.

Figure 7 illustrates the absorption spectra of micelle solutions centrifuged with various accelerations. The absorption spectrum (*a*) for the non-centrifuged solution having an opaque purple color exhibits two Soret peaks of X_1 and X_2, and an appreciable background resulting from scattering of light due to large ZnTPP particles dispersed in the solution. With the increase in the centrifugal force the peak height of X_2 relative to X_1 decreases, indicating that ZnTPP particles responsible for the absorption X_2 are heavier than for X_1. In addition to this, the increased centrifugal force leads to a narrower half-peak width of X_1; the half-peak width of 20 nm in the spectrum (*e*) for 13000 × *g* is close to 12 nm for that of the Soret peak of ZnTPP molecules in benzene. These results denote that the micelle solution before the centrifugation consist of ZnTPP particles with widely-distributed sizes. In view of the principle of the EMD method, the results suggest a possibility of controlling morphologies of the porphyrin films by changing the size of ZnTPP particles dispersed in the micelle solution. The EMD films of ZnTPP prepared from micelle solutions centrifuged at

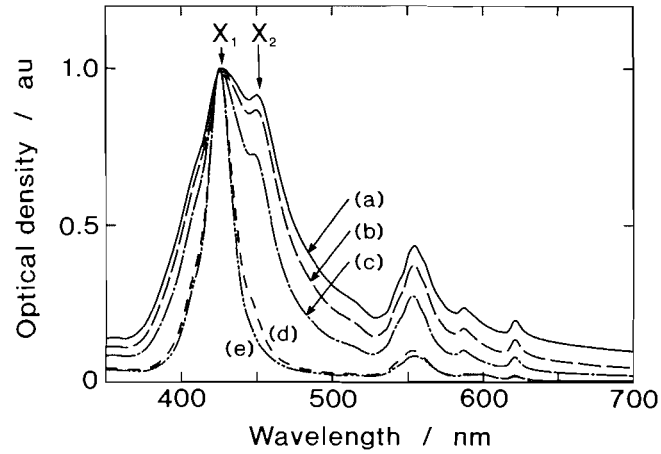


FIG. 7. Optical absorption spectra of the supernatant solutions (*a*) before and after the centrifugal treatments at (*b*) 500 × *g*, (*c*) 2000 × *g*, (*d*) 6800 × *g*, and (*e*) 13000 × *g*. All spectra were normalized at 425 nm.

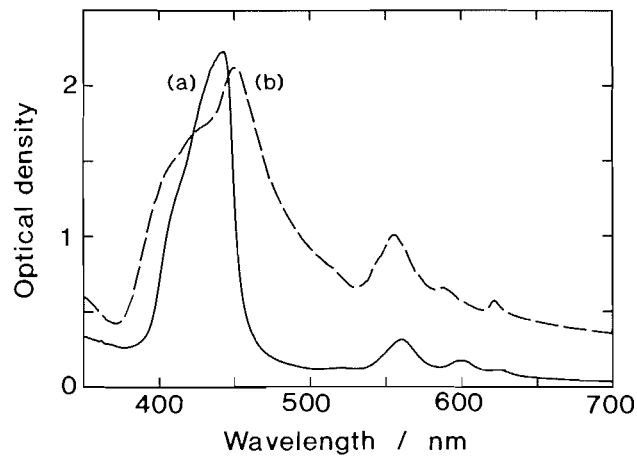


FIG. 8. Absorption spectra of ZnTPP films prepared by (*a*) the mod-EMD and (*b*) EMD methods.

accelerations below about 500 × *g* exhibited the absorption spectra similar with the one for the EMD-ZnTPP film shown in the inset of Fig. 1, where the absorption components of X_1 and X_2 correspond well to B_1 and B_2 for the EMD-ZnTPP film, respectively. On the other hand, an attempt to prepare EMD porphyrin films from the micelle solution treated at 13000 × *g* was unsuccessful, presumably due to the extremely small amount of fine ZnTPP particles in the solution. A successful preparation of EMD films from solutions containing very fine ZnTPP particles was attained only by preparing micelle solutions based on the modified EMD method as described in the Experimental section. Absorption spectrum (*a*) in Fig. 8 was obtained with the mod-EMD-ZnTPP film thus prepared, whose Soret peak was fairly sharp in comparison with that in spectrum (*b*) of the EMD-ZnTPP film. In addition, the absorption background in spectrum (*a*) was small. Comparing SEM pictures (*a*)–(*d*) in Fig. 9, it is clear that the morphology of the mod-EMD film is different from that of the EMD film. The mod-EMD film is studded with ZnTPP particles as large as 1–2 μm, which presumably grew during the electrolysis because the micelle solution supplied for the electrolysis was filtrated with a minipore (0.20 μm) filter before use. Furthermore, it is seen in picture (*b*) that the ITO substrate is covered with a very thin

Can. J. Chem. Downloaded from www.nrcresearchpress.com by 195.138.81.100 on 09/07/12
For personal use only.

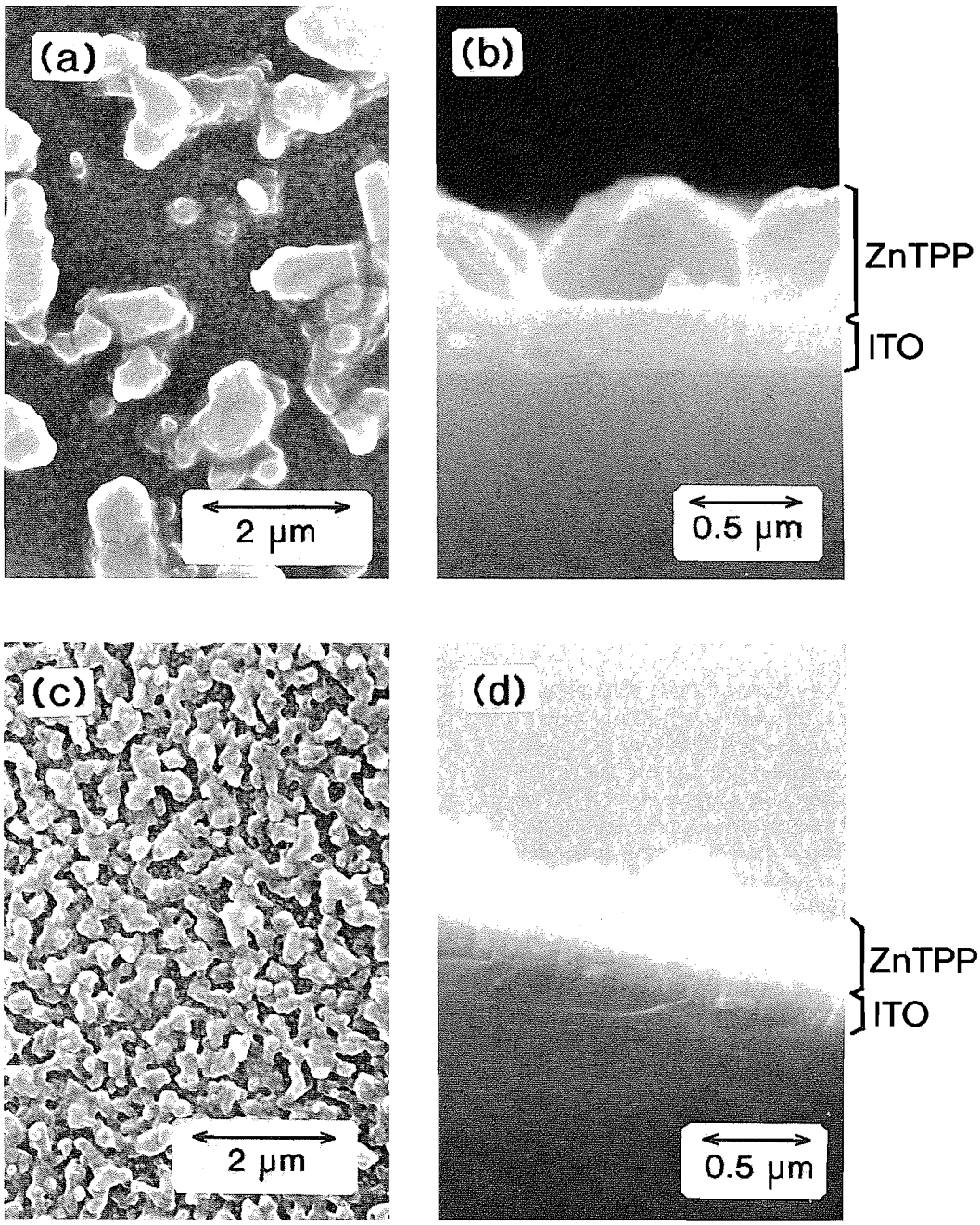


FIG. 9. Scanning electron microscope pictures of the ZnTPP films prepared by (*a*,*b*) the mod-EMD and (*c*,*d*) EMD methods.

ZnTPP layer. This ZnTPP layer seems to be enough not to allow an electrolyte permeation, because any clear redox waves for the $[Fe(CN)_6]^{4-/3-}$ couple were not observed at the ITO electrode coated with the mod-EMD film. It is noted that the transparency of the mod-EMD porphyrin film is superior to the EMD film and comparable to that of the PVD film.

Typical values of photoelectrochemical parameters such as short-circuit photocurrent (i_{sc}) and open-circuit photovoltage (V_{oc}) are summarized in Table 1. V_{oc} and fill factors were independent of the film thickness, irrespective of the film formation techniques. As the thickness increased, i_{sc} increased for the EMD film and was constant for the mod-EMD film, whereas i_{sc} decreased for the PVD film. The power conversion efficiency is about 0.0013% for the mod-EMD-ZnTPP film in the I_3^-/I^- redox system, showing that the mod-EMD-ZnTPP is not efficient compared with the EMD film. Such a small conversion efficiency might be attributed to the surfactants remaining in the mod-EMD film. The presence of FPEG in the mod-EMD film was confirmed indirectly by a determination of Fe atoms, coming from the ferrocenyl moiety of FPEG, by the atomic absorption spectroscopy. The surfactant remaining in the normal EMD films was much smaller than that in the mod-EMD film. The power conversion efficiency of the EMD-T(4-Py)P film was about 0.00018%, which was 3–4 times larger than that of the PVD-T(4-Py)P film.

In conclusion, the EMD porphyrin films were found to be more efficient than the PVD and mod-EMD porphyrin films. The high performance of the ITO/EMD-ZnTPP electrode was

Can. J. Chem. Downloaded from www.nrcresearchpress.com by 195.138.81.100 on 09/07/12
For personal use only.

TABLE 1. Photoelectrochemical parameters[a] of ZnTPP films prepared by EMD, PVD, and Mod-EMD methods

Parameter	Value		
	EMD (260 nm)[b]	PVD (100 nm)[b]	mod-EMD (120 nm)[b]
$i_{sc}/\mu A\ cm^{-2}$	15	1.6	4.0
V_{oc}/mV	155	130	75
f.f.[c]	0.42	0.24	0.42
p.c.e.[d]/%	0.01	0.0005	0.0013

[a]Under a white light of 10 mW cm^{-2}.
[b]Average thickness of the film used.
[c]Fill factor.
[d]Power conversion efficiency for the intensity of light incident on the film.

attributable mainly to the morphological features of the film inferred from the results obtained by the cyclic voltammetry, scanning electron micrography, and X-ray diffractometry. The modified EMD technique provided an organic thin film with a unique morphology, although the photoactivity was comparable with that of a PVD film.

Acknowledgment

The authors wish to thank gratefully Mr. Seiichiro Yokoyama of Idemitsu Kosan Co. for taking the SEM pictures.

1. D. L. MOREL, A. K. GHOSH, T. FENG, E. L. STOGRYN, P. E. PURWIN, R. F. SHAW, and C. FISHMAN. Appl. Phys. Lett. **32**, 495 (1978).
2. F. J. KAMPAS and M. GOUTERMAN. J. Phys. Chem. **81**, 690 (1977).
3. C. D. JAEGER, F.-R. FAN, and A. J. BARD. J. Am. Chem. Soc. **102**, 2592 (1980).
4. R. O. LOUTFY, J. H. SHARP, C. K. HSIAO, and R. Ho. J. Appl. Phys. **52**, 5218 (1981).
5. R. O. LOUTFY and E. R. MENZEL. J. Am. Chem. Soc. **102**, 4967 (1980).
6. K. HOSHINO and T. SAJI. Chem. Lett. 1439 (1987).
7. K. HOSHINO and T. SAJI. J. Am. Chem. Soc. **109**, 5881 (1987).
8. T. SAJI. Chem. Lett. 693 (1988).
9. Y. HARIMA, K. YAMASHITA, and T. SAJI. Appl. Phys. Lett. **52**, 1542 (1988).
10. K. TAKEDA, Y. HARIMA, S. YOKOYAMA, and K. YAMASHITA. Jpn. J. Appl. Phys. **28**, L141 (1989).
11. Y. HARIMA and K. YAMASHITA. J. Phys. Chem. **93**, 4184 (1989).
12. K. YAMASHITA, Y. MATSUMURA, Y. HARIMA, S. MIURA, and H. SUZUKI. Chem. Lett. 489 (1984).
13. Y. HARIMA, K. YAMASHITA, and H. SUZUKI. Appl. Phys. Lett. **45**, 1144 (1984).
14. K. YAMASHITA, Y. HARIMA, and T. MATSUBAYASHI. J. Phys. Chem. **93**, 5311 (1989).
15. K. YAMASHITA, Y. HARIMA, and H. IWASHIMA. J. Phys. Chem. **91**, 3055 (1987).
16. P. LEEMPOEL, F.-R. FAN, and A. J. BARD. J. Phys. Chem. **87**, 2948 (1983).
17. F.-R. FAN and L. R. FAULKNER. J. Chem. Phys. **69**, 3341 (1978).
18. E. B. FLEISCHER, C. K. MILLER, and L. E. WEBB. J. Am. Chem. Soc. **86**, 2342 (1964).

Can. J. Chem. Downloaded from www.nrcresearchpress.com by 195.138.81.100 on 09/07/12
For personal use only.

A new palladium-catalyzed coupling reaction of vinylic and allylic triflates with pyrimidine nucleosides

MOHAMED EZELDIN HASSAN
Chemistry Department, The African University, Aswan, Egypt

Received March 29, 1990

MOHAMED EZELDIN HASSAN. Can. J. Chem. **69**, 198 (1991).

Vinylic trifluoromethane sulfonates (triflates) form palladium intermediates that react with pyrimidine nucleosides to produce C-5 alkyl substituted nucleosides after hydrogenation of the vinylic coupling products with hydrogen and Pd/C in methanol. The reaction, which is run under mild conditions, appears to be a general one since both mono- and disubstituted vinylic triflates, as well as the cyclic ones, gave high yields of the corresponding C-5 alkyl-substituted nucleoside. The reaction with allyl triflate requires the use of the 5-chloromercurinucleoside.

Key words: nucleosides, triflates, palladium catalysis.

MOHAMED EZELDIN HASSAN. Can. J. Chem. **69**, 198 (1991).

Les trifluorométhanesulfonates vinyliques forment des intermédiaires vinyliques que réagissent avec les nucléosides de pyrimidine pour conduire, après hydrogénation des produits de couplage vinyliques à l'aide d'hydrogène et de Pd/C, à des nucléosides substitués en position 5 par des groupements alkyles. Il semble que cette réaction, qui est réalisée dans des conditions douces, est générale puisque des triflates vinyliques mono- ou di-substitués, aliphatiques ou cycliques, donnent des rendements élevés des nucléosides correspondants, substitués en position 5 par des groupements alkyles. La réaction avec le triflate d'allyle nécessite l'utilisation du 5-chloromercurinucléoside.

Mots clés : nucléosides, triflates, catalyse par palladium.

[Traduit par la revue]

Introduction

The direct synthesis of 5-alkyl substituted pyrimidine nucleosides has been reported by two routes (1, 2). A photochemical approach through the generation of an initial reactive species from either a haloalkyl or 5-iodouridine derivative has been reported (1). Alternatively, an approach employing the palladium-catalyzed olefination reaction of 5-chloromercuriuridine derivatives (2) is a useful synthetic procedure, which allows for ready access to these potential antiviral and anticancer agents (3). However, the reaction of C-5 mercurated nucleosides with simple monosubstituted alkenes generally leads to complex product mixtures and in some instances is complicated by the formation of substantial amounts of C-5 methoxyalkyl nucleosides (2). While the palladium-catalyzed reaction of alkenes with vinyl halides has been practically limited to the reactions of vinylic bromides and iodides (4), the ease of preparation of vinylic trifluoromethanesulfonate (triflates) in high regioselective purity persuaded us to investigate the palladium-catalyzed coupling reaction of pyrimidine nucleosides with vinyl triflates.

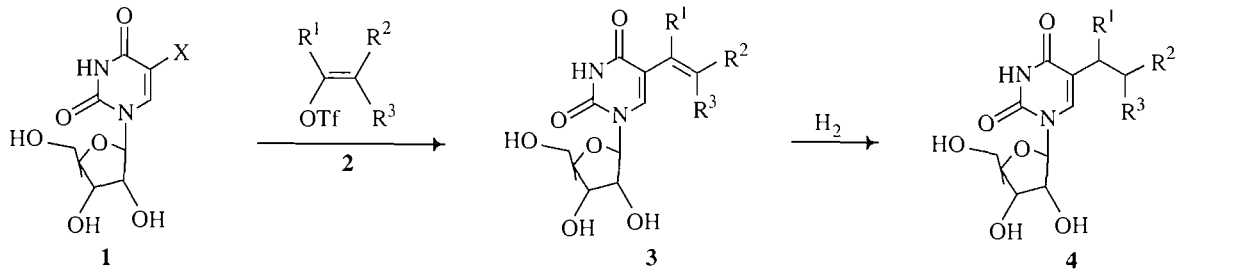
When uridine **1***a* was refluxed for 48 h in tetrahydrofuran under nitrogen with 2-propenyl triflate (5) **2***a* in the presence of tetrakis(triphenylphosphine)palladium(0) and 3 equivalents of lithium chloride, the expected modified nucleoside 5-(2-propenyl)uridine **3***a* was isolated in a moderate yield (54%). The structure of **3***a* was established based on its ^{1}H NMR, mass spectrum, and its catalytic hydrogenation to 5-(2-propyl)uridine **4***a* (2). While alkyl substituted olefins are usually inert in the Heck olefination reaction (6), we observed that both mono- and dialkyl substituted vinyl triflate derivatives react well under these reaction conditions. Therefore, the reaction between uridine **1***a* and 2-methyl-1-propenyl triflate **2***b* (7) afforded 5-(2-methyl-1-propenyl)uridine **3***b* in 43% yield. Catalytic hydrogenation of **3***b* gave 5-(2-methyl-1-propyl)uridine **4***b*. The reaction also was extended to the coupling of uridine **1***a* with cyclic vinylic triflates. 5-(6-Methylcyclohexen-1-yl)uridine **3***c* was obtained from the reaction of **1***a* with 6-methylcyclohexen-1-yl-triflate **2***c* (8).

In an attempt to increase the yield of these reactions, we activated the nucleoside by its conversion to the 5-chloromercuri derivative **1***b*, prior to coupling with **2**. This, however, led to a complicated product mixture. Catalytic hydrogenation of the product mixture obtained from the reaction of **1***b* with **2***a* afforded 5-(2-propyl)uridine **4***a*, with identical melting point and ^{1}H NMR to that obtained from the hydrogenation of **3***a*. In the absence of lithium chloride or when bis(triphenylphosphine)palladium(II) dichloride was used instead of tetrakis palladium(0), a remarkable yield depression was observed. This may indicate that the vinylpalladium(II) triflate, which resulted from the oxidative addition of triflates to palladium, is incapable of entering a catalytic cycle as in the Heck olefination reaction (6). In the presence of lithium chloride, apparently a vinylpalladium(II) chloride complex is generated, which is then capable of undergoing further reaction with the nucleoside **1***a* to afford the coupled product and generate a palladium(0) species (Scheme 2).

It has been reported (9) that the organopalladium(II) complex formed from the transmetalation of the 5-chloromercurinucleoside and palladium chloride undergoes reaction with variously substituted allylic chlorides regioselectively and requires only catalytic amounts of palladium chloride. The difficulty in synthesizing and purifying the allylic chlorides limits this approach. Other allylic derivatives afforded poor yields and (or) additional side products (9). When allyl triflate **2***d* (10) was allowed to react with uridine **1***a* under the above conditions, only starting material was recovered. However, treatment of allyl triflate with 5-chloromercuriuridine **1***b* afforded the expected allylic uridine derivative **3***d* (52% yield). It seems that in this latter case the palladium exchanges initially for the nucleoside mercury to give the transient organopalladium intermediate **5**, which then forms another intermediate **6** with the allylic triflate. This then collapses to 5-allyluridine **3***d*.

Finally, we attempted to extend this reaction to the attachment of a simple unsubstituted alkyl side chain at C-5 of the pyrimidine nucleoside. In all cases these attempts were unsuc-

Can. J. Chem. Downloaded from www.nrcresearchpress.com by 195.138.81.100 on 09/07/12
For personal use only.



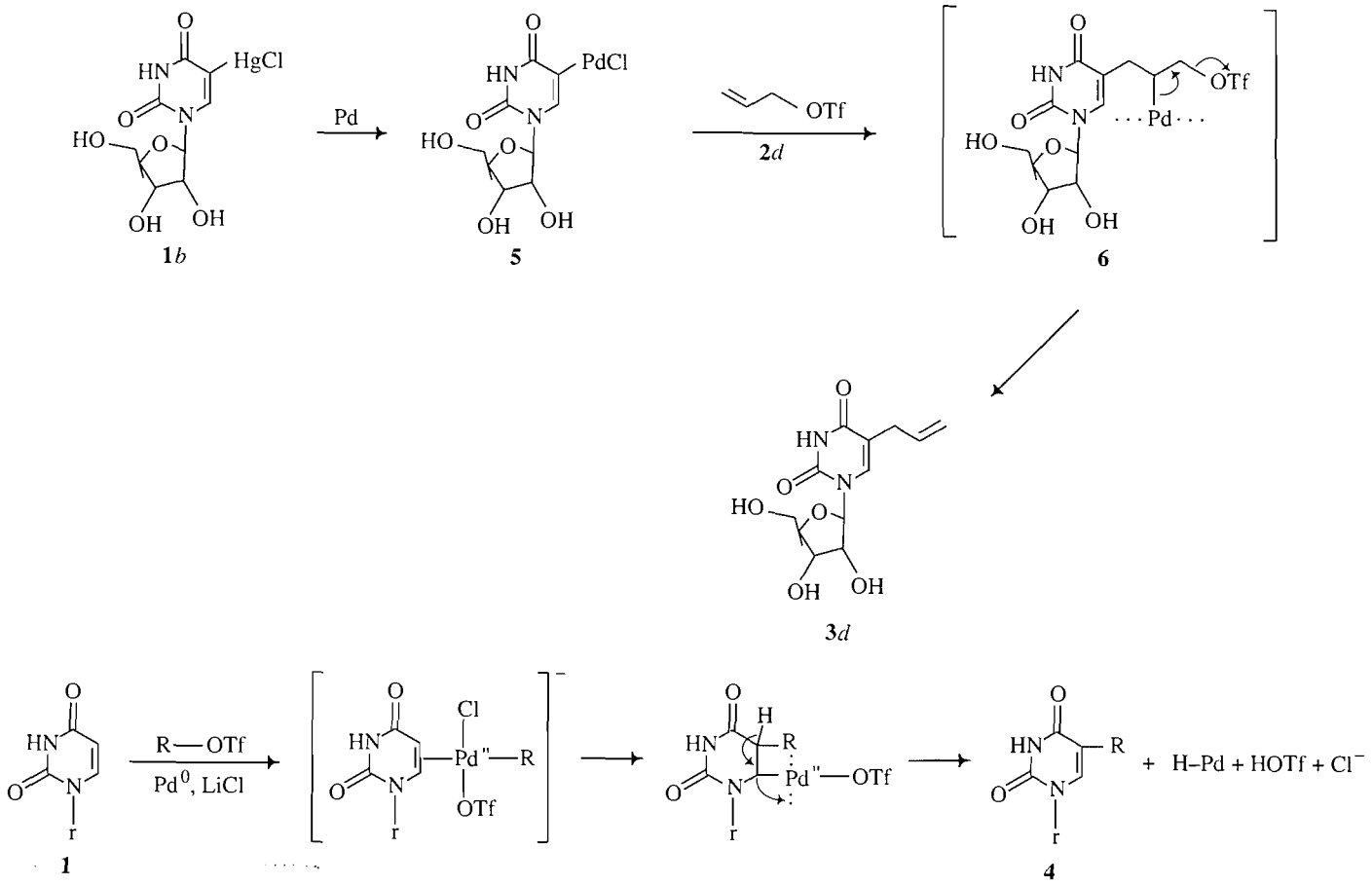
1
a: X = H
b: X = HgCl

2

3

4
a: $R^1 = CH_3$, $R^2 = R^3 = H$
b: $R^1 = H$, $R^2 = R^3 = CH_3$
c: R^1, $R^2 = -(CH_2)_4-$, $R^3 = CH_3$

SCHEME 1



1*b*

5

6

3*d*

1

4

SCHEME 2

cessful. Upon treatment of nucleosides **1***a* or **1***b* with ethyl or propyl triflates (1, 2) under similar conditions, no alkyl substituted nucleoside could be detected. Most probably alkyl palladium triflates containing an sp^3 hydrogen β to the carbon bearing the palladium undergo a facile β-hydride elimination in preference to alkene insertion. It is also quite possible that this type of triflates does not undergo oxidative addition in the first place.

Experimental

Melting points were taken on a Fisher–Johns melting point apparatus and are uncorrected. IR spectra were measured with a Unicam S.P. 2006, and UV spectra with a Perkin–Elmer 554 recording spectrophotometer. ^{1}H NMR spectra were obtained on a Varian 56/69 A and mass spectra on a Varian CH5 mass spectrometer. Unless indicated, C, H, N analyses were ±0.4% of the calculated values, and were performed at the Microanalytical Center, Cairo University. High pressure liquid chromatography was performed using Partisile PXS 10/25 ODS-II, and preparative, Partisile M9-10/50 ODS-2 columns.

5-(2-Propenyl)uridine **3**a *and 5-(2-propyl)uridine* **4**a

Method A

To a stirred suspension of 2-propenyl triflate **2***a* (5) (836 mg, 4.4 mmol), lithium chloride (542 mg, 13 mmol), and $Pd(PPh_3)_4$ (110 mg, 4.4 mol %) in 50 mL of tetrahydrofuran, was added 500 mg of uridine **1***a* (2.05 mmol). The reaction mixture was refluxed under

Can. J. Chem. Downloaded from www.nrcresearchpress.com by 195.138.81.100 on 09/07/12
For personal use only.

nitrogen for 48 h, cooled, and filtered through a Celite pad. It was washed with 10% ammonium hydroxide solution (3 × 25 mL), then with water (2 × 25 mL), dried over magnesium sulfate, and the resulting solution was concentrated under vacuum. The residue was chromatographed (silica gel; 15% methanol in chloroform) to afford 5-(2-propenyl)uridine **3***a* (314 mg, 54% yield) as white crystals after crystallization from CH_3CN, mp 143°C. ^1H NMR (D_2O), δ: 1.91 (3H, s, Me), 3.89 (2H, m), 4.28 (3H, m), 5.30 (1H, d, J = 11 Hz), 5.36 (1H, d, J = 11 Hz), 6.21 (1H, m, anomeric proton), 7.80 (1H, s, C6 proton). Anal. calcd. for $C_{12}H_{16}N_2O_6$: C 50, 70, H 5.63, N 9.86; found: C 50.89, H 5.76, N 9.58.

The nucleoside **3***a* (284 mg, 1 mmol) in 100 mL of methanol was treated with 50 mg of 10% Pd/C and stirred under 24 psi of hydrogen for 10 h (1 psi = 6.9 kPa). The catalyst was removed by filtration and the filtrate evaporated under reduced pressure. The residue was chromatographed over silica gel, using 10% methanol in chloroform as eluent, to give 5-(2-propyl)uridine **4***a* (224 mg, 78.4% yield), mp 192°C (lit. (2) mp 191–193°C). ^1H NMR (D_2O), δ: 1.1 (6H, d, J = 6.2 Hz, 2Me), 2.78 (1H, m, Me-C*H*-Me), 3.9 (2H, s), 4.25 (3H, m), 6.1 (1H, d, J = 3 Hz, anomeric H), 7.8 (1H, s, C6 proton).

Method B

A mixture of 2-propenyl triflate **2***a* (836 mg, 4.4 mmol), lithium chloride (542 mg, 13 mmol), Pd $(PPh_3)_4$ (110 mg, 4.4 mol%), and 5-chloromercuriuridine **1***b* (980 mg, 2.0 mmol) was refluxed in THF under nitrogen for 48 h. Work-up as described above afforded a complicated mixture of vinylic uridines, as proved by ^1H NMR spectroscopy. However, catalytic hydrogenation of this mixture under the same conditions described for hydrogenation of **3***a* gave 5-(2-propyl)uridine **4***a* having a melting point and NMR identical to the product of method A.

5-(2-Methyl-1-propenyl)uridine **3**b

Uridine **1***a* (500 mg, 205 mmol) was added to a stirred mixture of 2-methyl-1-propenyl triflate **2***b* (7) (898 mg, 4.4 mmol), lithium chloride (542 mg, 13 mmol), and Pd $(PPh_3)_4$ (110 mg, 4.4 mmol%) in THF and refluxed under nitrogen for 48 h. Work-up as above afforded **3***b*, crystallizing from CH_3CN as white crystals, mp 168°C (264 g, 43% yield). ^1H NMR (D_2O), δ: 1.83 (6H, s, 2Me), 3.95 (2H, m), 4.20 (2H, m), 4.25 (1H, m), (1H, s, olefinic proton). Anal. calcd. for $C_{13}H_{18}N_2O_6$: C 52.35, H 6.04, N 9.40; found: C 52.29, H 6.26, N 9.63.

5-Isobutyluridine **4**b

Catalytic hydrogenation of 5-(2-methyl-1-propenyl)uridine **3***b*, prepared as in the previous synthesis, gave 5-isobutyluridine **4***b* (74% yield) as white crystals, mp 171°C. ^1H NMR (D_2O), δ: 1.2 (6H, d, 2Me), 1.67 (1H, m, Me-CH-Me), 2.3 (2H, t), 3.91 (2H, m), 4.32 (3H, m), 6.1 (1H, m, anomeric proton), 7.70 (1H, s, C6 proton). Anal. calcd. for $C_{13}H_{20}N_2O_6$: C 5.20, H 6.67, N 9.33; found: C 51.83, H 6.9, N 9.57.

5-(6-Methylcyclohexen-1-yl)uridine **3**c

6-Methylcyclohexen-1-yl triflate (8) (1.70 g, 4.4 mmol) was dissolved in THF (50 mL) and treated successively with lithium chloride (542 mg, 13 mmol), Pd $(PPh_3)_4$ (110 mg, 4.4 mol%), and uridine **1***a* (500 mg, 2.05 mmol) and refluxed under nitrogen for 48 h. Work-up as above afforded **3***c* (316 mg, 45.7% yield), mp 162°C. ^1H NMR (D_2O), δ: 1.89 (d, 3H, Me), 1.61 (4H, m), 2.1 (2H, m), 2.5 (1H, m), 3.9 (2H, m), 4.23 (3H, m), 5.96 (1H, m, anomeric proton), 6.09 (1H, t, J = 4.2 Hz), 7.82 (1H, s, C6 proton). Anal. calcd. for $C_{16}H_{22}N_2O_6$: C 56.80, H 6.50, N 8.28; found: C 56.55, H 6.23, N 8.40.

5-Allyluridine **3**d

5-Chloromercuriuridine, **1***b* (980 mg, 2.0 mmol), was added to a stirred mixture of allyl triflate (**2***d*, 863 mg, 4.4 mmol), Pd $(PPh_3)_4$ (110 mg, 4.4 mol%), and lithium chloride (542 mg, 13 mmol) in tetrahydrofuran and refluxed for 48 h. Work-up as above gave 5-allyluridine **3***d*, as white crystals, mp 176°C (lit. (13) mp 175–176°C) (295 mg, 52% yield). ^1H NMR (D_2O), δ: 3.1 (2H, d, J = 6 Hz), 3.9 (2H, m), 4.25 (3H, m), 5.19 (1H, d, J = 17 Hz), 5.21 (1H, d, J = 11 Hz), 5.95 (2H, m), 7.7 (1H, s).

1. M. E. Hassan. Recl. Trav. Chim. Pays-Bas, **105**, 30 (1986).
2. D. E. Bergstrom and M. K. Ogawa. J. Am. Chem. Soc. **100**, 8106 (1978).
3. E. deClercq, J. Balzarini, J. Descamps, C. F. Gigge, C. T. Chang, P. Kalarities, and M. P. Mertes. Biochem. Pharmacol. **30**, 495 (1981).
4. W. J. Scott, M. R. Peña, K. Swärd, S. J. Stoessel, and J. K. Stille. J. Org. Chem. **50**, 2302 (1985).
5. P. J. Stang and R. H. Summerville. J. Am. Chem. Soc. **91**, 4600 (1969).
6. R. F. Heck. Pure Appl. Chem. **53**, 2323 (1981).
7. P. J. Stang, M. G. Mangum, D. P. Fox, and P. Haak. J. Am. Chem. Soc. **96**, 4562 (1974).
8. J. E. McMurry and W. J. Scott. Tetrahedron Lett. **24**, 979 (1983).
9. D. E. Bergstrom, J. L. Ruth, and P. Warwick. J. Org. Chem. **46**, 1432 (1981).
10. C. D. Beard, K. Baum, and V. Grakauskas. J. Org. Chem. **38**, 3673 (1973).
11. A. Streitwieser, Jr., C. L. Wilkins, and E. Kiehlmann. J. Am. Chem. Soc. **90**, 1598 (1968).
12. G. A. Dafforn and A. Streitwieser, Jr. Tetrahedron Lett. 3159 (1970).
13. H. J. Minnemeyer, H. Tieckelmann, and J. F. Holland. J. Med. Chem. **6**, 602 (1963).

Can. J. Chem. Downloaded from www.nrcresearchpress.com by 195.138.81.100 on 09/07/12
For personal use only.

An *ab initio* study of the structure and intramolecular proton transfer in tropolone

MIGUEL A. RÍOS[1] AND JESÚS RODRÍGUEZ

Departamento de Química Física, Facultad de Química, Universidad de Santiago de Compostela, Santiago de Compostela, Galicia, Spain

Received May 15, 1990

MIGUEL A. RÍOS and JESÚS RODRÍGUEZ. Can. J. Chem. **69**, 201 (1991).

An *ab initio* study of tropolone was carried out at the 3-21G level, with full optimization of the geometry, and the intramolecular proton transfer in the ground state was analysed. The two equivalent C_s structures can be converted to each other via a C_{2v} symmetry transition state with a double minimum potential. The splitting of the ground vibrational state generated by proton tunneling was determined by procedures of variable complexity and found to be in the range $\Delta = 0.1–0.15$ cm^{-1}, i.e., clearly smaller than experimental predictions.

Key words: tropolone, intramolecular hydrogen bond, proton transfer, *ab initio* calculations, molecular structure.

MIGUEL A. RÍOS et JESÚS RODRÍGUEZ. Can. J. Chem. **69**, 201 (1991).

On a réalisé des calculs *ab initio* sur la tropolone, au niveau 3-21G, avec optimisation complète de la géométrie et on a analysé le transfert intramoléculaire de proton dans l'état fondamental. Les deux structures C_s équivalentes peuvent se transformer l'une dans l'autre par le biais d'un état de transition de symétrie C_{2v} comportant un double minimum de potentiel. Le dédoublement de l'état vibrationnel fondamental provoqué par un effet tunnel a été déterminé par des procédures de complexité variable et on a trouvé qu'il est de l'ordre de $\Delta = 0{,}1–0{,}15$ cm^{-1}, soit une valeur beaucoup plus faible que celle prédites sur la base de données expérimentales.

Mots clés : tropolone, liaison hydrogène intramoléculaire, transfert de proton, calculs *ab initio*; structure moléculaire.

[Traduit par la revue]

Introduction

One of the major features of tropolone (2-hydroxy-2,4,6-cycloheptatrien-1-one) is the occurrence in its structure of a strong intramolecular hydrogen bond between the two oxygen atoms present in the molecule. As with other similar instances (e.g., the enol form of malonaldehyde), this situation may result in the occurrence of two equivalent C_s structures (Fig. 1(a)) that can be interconverted by a proton transfer, or in a single symmetrical C_{2v} structure where the H atom is equidistant from the two O atoms (Fig. 1(b)). This in turn implies obtaining either a double or single minimum potential curve, which seems to be determined, among other factors, by the distance between the two electronegative atoms involved in the hydrogen bond. In the case of tropolone, experimental results reported thus far (1–9) appear to confirm the occurrence of a double minimum with a proton transfer, both in the ground and in the excited states.

A double minimum potential curve and proton transfer by tunneling result in the splitting (Δ) of vibrational levels. Redington and Redington (1) reported the results of an IR absorption study of tropolone in neon matrices; however, their spectral data were perturbed by non-homogeneous environmental effects, so that they could not provide a detailed, consistent interpretation. Their average Δ(H) and Δ(D) values (2.2 and 3.0 cm^{-1}) reveal the inversion of the usual isotopic effect. Jackman *et al.* (2) used a straightforward procedure to estimate an upper limit for the rate of exchange of deuterium and postulated that it should be less than 10^{10} s^{-1}, corresponding to $\Delta(D) \leq 0.17$ cm^{-1} via the equation $\tau = h/2\Delta$ (ref. 3). Later, Tomioka *et al.* (4) used a one-dimensional theoretical model, which they fitted with the aid of some IR spectral data, to recalculate the Δ values, which they found to be 6.2 and 0.4 cm^{-1} for the hydrogen atom and deuterium, respectively; as can be seen, these values are quite different from those reported by Redington and Redington and, moreover, the Δ(D) values calculated by both authors exceed the Jackman upper limit.

In contrast to the Δ values, however, consistent results were obtained for the proton transfer barrier, namely 5600 (Redington and Redington) and 5890 cm^{-1} (Tomioka *et al.*).

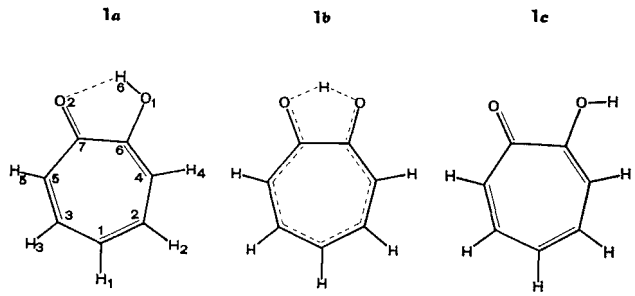


FIG. 1. Structures studied. (a) Stablest conformation: C_s with a hydrogen bond. (b) Structure with a C_{2v} symmetry. (c) C_s conformation with C—O—H angle rotated by 180° and no hydrogen bond.

This paper reports a theoretical *ab initio* study of tropolone with full optimization of its C_s and C_{2v} structures, including calculation of the potential barrier, the frequency of the intramolecular proton transfer by tunneling, and the splitting of the vibrational levels to which it gives rise.

Computation

All computations were made under no constraints by using the program GAUSSIAN 88 (10) and the 3-21G (11) basis set on a CONVEX C-120 computer.

According to our calculations, the intramolecular hydrogen bond in the enol form of malonaldehyde is properly reproduced by the 3-21G basis. Thus the calculated values of O---O = 2.607 Å and barrier height = 7.79 kcal/mol are in better agreement with experimental estimates (12) (2.56 Å and 4–5 kcal/mol) than those obtained with the following basis sets: 4-31G (13) (2.630 Å, 11.6 kcal/mol); C,O(9*s*5*p*/4*s*2*p*) H(4*s*/2*s*) + polarization functions (14) (2.685 Å, 11.4 kcal/mol); 6-31G[2] (2.680 Å, 12.6 kcal/mol); and 6-31G** (15) (2.684 Å, 10.3 kcal/mol). Only a slight improvement is reported for the

[1]Author to whom correspondence may be addressed.

[2]Data obtained by the authors.

Printed in Canada / Imprimé au Canada

Can. J. Chem. Downloaded from www.nrcresearchpress.com by 195.138.81.100 on 09/07/12
For personal use only.

Can. J. Chem. Downloaded from www.nrcresearchpress.com by 195.138.81.100 on 09/07/12
For personal use only.

TABLE 1. Optimized geometric and energetic parameters of the structures studied

	Structures		
	1*a*	**1***b*	**1***c*
Energies (Hartrees):	−415.9177	−415.8954	−415.8998
Lengths (Å):			
C(1)—C(2)	1.343	1.382	1.335
C(1)—C(3)	1.428	1.382	1.436
C(2)—C(4)	1.425	1.380	1.434
C(3)—C(5)	1.341	1.380	1.333
C(4)—C(6)	1.337	1.376	1.335
C(5)—C(7)	1.439	1.376	1.460
C(6)—C(7)	1.476	1.487	1.485
C(6)—O(1)	1.359	1.291	1.366
C(7)—O(2)	1.234	1.291	1.218
C(1)—H(1)	1.073	1.072	1.073
C(2)—H(2)	1.074	1.075	1.074
C(3)—H(3)	1.075	1.075	1.075
C(4)—H(4)	1.072	1.071	1.076
C(5)—H(5)	1.072	1.071	1.072
O(1)—H(6)	0.974	1.234	0.964
O(2)—H(6)	1.930	1.234	3.510
O(1)—O(2)	2.516	2.271	2.546
Angles (deg)			
C(2)—C(1)—C(3)	127.2	127.4	126.7
C(1)—C(2)—C(4)	129.2	130.6	129.0
C(1)—C(3)—C(5)	130.5	130.6	130.0
C(2)—C(4)—C(6)	129.7	128.2	131.3
C(3)—C(5)—C(7)	130.6	128.2	132.5
C(4)—C(6)—C(7)	129.9	127.5	129.3
C(5)—C(7)—C(6)	122.9	127.5	121.2
C(7)—C(6)—O(1)	111.6	107.7	109.4
C(6)—C(7)—O(2)	115.6	107.7	119.3
C(6)—O(1)—H(6)	108.5	95.3	113.4
C(7)—O(2)—H(6)	88.2	95.3	—
O(1)—H(6)—O(2)	116.1	134.0	—
H(1)—C(1)—C(2)	117.4	116.3	117.7
H(2)—C(2)—C(1)	116.6	115.0	117.0
H(3)—C(3)—C(1)	114.2	115.0	114.3
H(4)—C(4)—C(2)	116.0	117.4	113.4
H(5)—C(5)—C(3)	117.7	117.4	117.4

6-31G** basis by including electronic correlation at the MP2 level (15) (2.589 Å, 3.6 kcal/mol). However, this agreement between 3-21G calculations and experimental results is probably due to a cancellation of errors coming from basis set limitations and lack of correlation effect. There is no certainty that an analogous cancellation takes place in the tropolone case, so a confirmation of the results of this work by post-HF calculations with better basis set (e.g., 6-31G**MP2) would be desirable, which is not possible for us at present.

Results and discussion

Structural trends

We studied the structures depicted in Fig. 1 with full optimization; their most representative geometric and energetic parameters are listed in Table 1. The most stable (**1***a*) corresponds to one of the two equivalent C_s structures. The second (**1***b*) corresponds to the saddle point in the transition between the two equivalent C_s structures. As expected, we obtained a double minimum potential with a barrier of 4894.2 cm^{-1}, which is of about the same order as the previously mentioned experimental estimates.

Finally, we also optimized the conformation C_s involving no hydrogen bond (**1***c*); it turned out to be 11.23 kcal/mol less stable than **1***a*. This value is thus indicative of the strength of the hydrogen bond, the energy of which cannot be accurately determined for the intramolecular variety.

The most stable conformation C_s (**1***a*) yielded an O---O distance of 2.516 Å, i.e., significantly smaller than the value obtained for malonaldehyde with the same basis (2.607 Å). However, the energy barrier estimated for tropolone (13.99 kcal/mol) is significantly greater than the value obtained for malonaldehyde (7.79 kcal/mol), which shows the significance of factors other than the O---O bond length on the barrier height.

Our results for the C_s geometry are consistent with the experimental measurements made by Simanouchi and Sasada (5), especially the most interesting parameters related to the hydrogen bond: the experimental and calculated O---O distances were 2.53 and 2.52 Å, and those of the O---H bond were 1.98 and 1.93 Å, respectively. The agreement supports the reliability of the basis used in the reproduction of this kind of hydrogen bond, although no accurate comparisons can be made because the experimental data are referred to the solid phase.

All C—C bonds in the C_{2v} structure except C6—C7, which length is closer to that of a single bond, are virtually of the same length, thereby showing π electrons to be highly delocalized around the ring. The O---O distance (2.27 Å) is considerably shorter than in structure C_s so that the O—H bond can be established at a distance of 1.23 Å.

Finally, we studied the structural effect of the hydrogen bond by comparing structure **1***a* with the conformer **1***c* where no hydrogen bond is present. As expected, the O---O distance and the C—O—H angle decrease upon formation of the hydrogen bond, though only slightly, which appears to be due to the fact that the oxygen atoms are in such a position that the molecule is not compelled to adopt a strained structure for the intramolecular bond to be formed. Thus, the seven-membered ring is scarcely distorted and only the extent of conjugation is modified (increased), which shows in the lengthening of the double and the shortening of the single bonds in the structure **1***a*.

Proton transfer

We studied proton transfer by taking a one-dimensional approach to the process. Other methods (16, 17) involve calculations relying on two-dimensional estimates; however, their increased complexity results in no significantly improved results in treating the transfer process.

The potential energy curve was fitted to the following polynomial function

$$[1] \quad V = ax^4 + bx^2$$

which was used elsewhere by Rossetti and Brus (3) to study proton transfer in tropolone in the excited state. As in earlier work (18), we took the reaction coordinate as the position of the H atom with respect to the overall molecule throughout the transfer process. The pathway followed by the hydrogen atom, referred to the mass centre of the system, was estimated by fitting an arc to the three points defined by the H positions in the two C_s minima (**1***a*) and the C_{2v} transition state (**1***b*). Thus, the x coordinate in eq. [1] corresponds to the H atom position in the arc. The parameters in eq. [1] were obtained from R_0 (the length of the above-mentioned arc, which was found to be 1.0622 Å), V_0 (the energy difference between structures C_s and C_{2v}), and the curvature of the potential function at the singular points, which was estimated from the energy change resulting from the slight variation in the position of the H atom along the

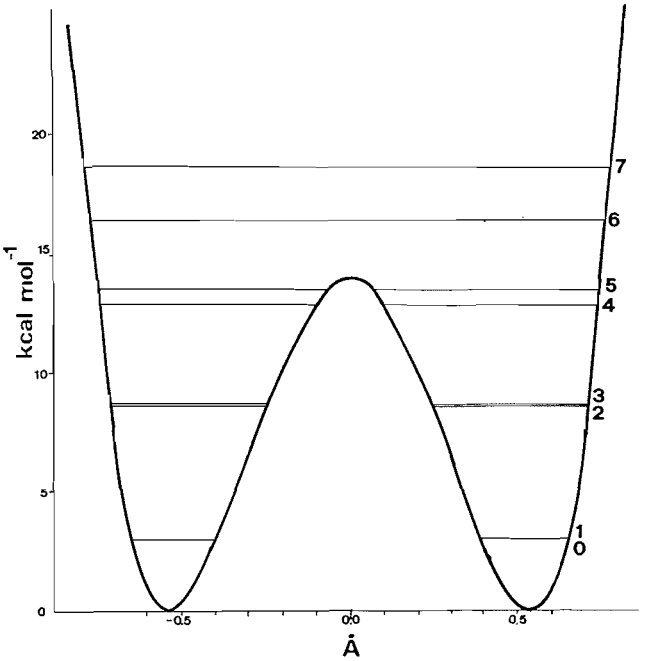


FIG. 2. Potential curve and vibrational levels obtained by fitting the potential curve to eq. [1].

reaction coordinate. Such parameters were found to be $a = 61\,514.4$ cm^{-1} Å^{-4} and $b = -34\,702.4$ cm^{-1} Å^{-2}.

Figure 2 shows the fitted curve and the vibrational levels obtained by the procedure developed by Laane (19), who reported numerical solutions to the Schrödinger vibrational equation obtained from the potential in eq. [1]. The reduced mass of H was taken as its nominal value, as there is evidence that the reduced mass in intramolecular proton transfers with tunneling is similar to that of a free proton (3). The ground vibrational level was found to be subject to a splitting of $\Delta = 0.12$ cm^{-1} (a value of 0.10 cm^{-1} was obtained by fitting the curve to a function defined by a sum of a parabola and a Gaussian (20)). The equation $\tau = h/2\Delta$ yielded a tunneling frequency of 7.2×10^9 s^{-1}.

For contrast, we also calculated Δ by the procedure recently employed successfully by Bicerano *et al.* (14) for the transfer in malonaldehyde, which required the prior calculation of the vibrational frequencies of the initial, final, and transition states. This procedure uses the Wentzel–Kramers–Brillouin (WKB) approximation to calculate the splitting resulting from tunneling at a double minimum potential, which for small splittings is given by (21)

$$[2] \quad \Delta = \frac{\hbar\omega_F}{\pi} e^{-\theta}$$

where ω_F is the classical vibrational frequency at one of the wells and θ is the WKB barrier penetration integral. If the barrier is approximated by the Eckart potential function (see, for example, ref. 22), then θ is given by

$$[3] \quad \theta = \frac{2\pi}{\hbar\omega_i}(V_{eff} - (E_0 V_{eff})^{1/2})$$

where V_{eff} is the effective height of the one-dimensional barrier, E_0 is the energy referred to the bottom of the potential wells, and ω_i is the imaginary frequency at the top of the barrier.

If tunneling is assumed to be an essentially one-dimensional process, the vibrational mode of the "reactant" (structure C_s) to be chosen should be representative of the reaction coordinate; obviously, this can only be the O—H stretching vibration, which will be designated as degree of freedom F, with an ω_F frequency. Thus, we are assuming that the other $(F - 1)$ vibrational modes contribute adiabatically (see, for example, ref. 23) to the determination of the effective one-dimensional barrier. For the ground state,

$$[4] \quad V_{eff} = V_0 + \sum_{k=1}^{F-1} \tfrac{1}{2}(\hbar\omega_k^{\neq} - \hbar\omega_k)$$

$$[5] \quad E_0 = \tfrac{1}{2}\hbar\omega_F$$

where ω_k and $\omega_k^{\neq}$ are the frequencies of the reagent, C_s, and transition state, C_{2v}, respectively, and V_0 is the potential barrier.

TABLE 2. Analytical vibrational frequencies of structures involved in the proton transfer process (C_s and C_{2v})

C_s		C_{2v}	
110.94 a''	1214.32 a''	169.76 a_2	1321.52 b_1
215.10 a''	1281.41 a'	211.28 b_1	1354.67 a_1
388.80 a'	1354.63 a'	395.86 b_2	1373.65 b_2
405.03 a'	1387.27 a'	450.50 b_1	1399.92 b_2
406.72 a''	1434.16 a'	453.64 a_2	1472.61 a_1
460.03 a''	1451.37 a'	457.41 a_1	1527.55 b_2
481.92 a'	1582.23 a'	610.42 b_2	1551.36 a_1
580.57 a'	1596.77 a'	693.22 b_1	1593.22 b_2
663.01 a''	1646.85 a'	736.77 a_1	1653.12 b_2
701.61 a''	1661.60 a'	803.79 b_2	1717.98 a_1
707.02 a'	1776.65 a'	811.75 a_1	1779.82 a_1
814.22 a'	1844.88 a'	858.47 a_2	1798.37 b_2
816.81 a''	1855.50 a'	864.43 b_1	2339.34 a_1
906.93 a''	3326.31 a'	970.21 a_1	3327.98 a_1
967.81 a'	3337.03 a'	1004.42 a_2	3333.84 b_2
1010.01 a''	3360.22 a'	1044.00 a_1	3363.19 a_1
1019.35 a'	3370.71 a'	1073.70 b_1	3380.46 b_2
1090.35 a''	3373.96 a'	1179.56 b_2	3381.89 a_1
1123.96 a'	3769.44 a'	1189.51 a_2	1778.23i b_2
1188.88 a''		1206.12 b_1	

The frequencies, which were calculated analytically, are listed in Table 2; as can be seen, one of them for structure C_{2v} is imaginary, which is consistent with a transition state.

The imaginary frequency obtained was $\omega_i = 1778.13$ cm^{-1}, while the O—H stretching frequency for C_s was 3769.44 cm^{-1}. By using the frequencies listed in Table 2 we found the summation term in eq. [4] to be 970.37 cm^{-1}. This and the V_0 value obtained (4894.2 cm^{-1}) yielded $\Delta = 0.15$ cm^{-1}, i.e., quite similar to that obtained by using the polynomial approximation.

With the described procedure and the same basis (3-21G) we obtained a Δ of 22 cm^{-1} for the splitting in malonaldehyde, a value very close to the experimental one (12) (21 cm^{-1}).

In summary, the procedure based on the calculation of frequencies, at least in this case, does not modify significantly the results obtained by using the other potential functions mentioned, which involve less expensive calculations.

On the other hand, the Δ values obtained in this work (between 0.10 and 0.15 cm^{-1}) are indicative of smaller splitting, and hence a lower frequency for the transfer process, than those reported by Redington and Redington (1) and Tomioka *et al.* (4) from experimental estimates, notwithstanding the fact that the height of the calculated barrier is similar to that obtained by these authors.

It seems logical to assume that the Δ of tropolone must be

Can. J. Chem. Downloaded from www.nrcresearchpress.com by 195.138.81.100 on 09/07/12
For personal use only.

much smaller than that of malonaldehyde, as the experimental barrier of the former is three times as high as that of the latter and only slight differences in their R_0 values are expected according to the experimental O---O distances (2.53 versus $\simeq$2.56 Å). However, further experimental and more precise work and (or) more rigorous calculations will be required to clarify the discrepancy between the results reported here and the experimental estimates available.

Acknowledgement

One of us (J.R.O.) is grateful to the Spanish Ministry of Science and Education for conferral of an FPI grant.

1. R. L. REDINGTON and T. E. REDINGTON. J. Mol. Spectrosc. **78**, 229 (1979).
2. L. M. JACKMAN, J. C. TREWELLA, and R. C. HADDON. J. Am. Chem. Soc. **102**, 2519 (1980).
3. R. ROSSETTI and L. E. BRUS. J. Chem. Phys. **73**, 1546 (1980).
4. Y. TOMIOKA, M. ITO, and N. MIKAMI. J. Phys. Chem. **87**, 4401 (1983).
5. H. SIMANOUCHI and Y. SASADA. Acta Crystallogr. Sect B: Struct. Crystallogr. Cryst. Chem. **B29**, 81 (1973).
6. A. C. P. ALVES, J. M. HOLLAS, H. MUSA, and T. RIDLEY. J. Mol. Spectrosc. **109**, 99 (1985).
7. A. C. P. ALVES and J. M. HOLLAS. Mol. Phys. **23**, 927 (1972).
8. N. M. SZEVERENYI, A. BAX, and G. E. MACIEL. J. Am. Chem. Soc. **105**, 2579 (1983).
9. R. L. REDINGTON, Y. CHEN, G. J. SCHERER, and R. W. FIELD. J. Chem. Phys. **88**, 627 (1988).
10. M. J. FRISCH, M. HEAD-GORDON, H. B. SCHLEGEL, K. RAGHAVACHARI, J. S. BINKLEY, C. GONZÁLEZ, D. J. DEFREES, D. J. FOX, R. A. WHITESIDE, R. SEEGER, C. F. MELIUS, J. BAKER, R. L. MARTIN, L. R. KAHN, J. J. P. STEWART, E. M. FLUDER, S. TOPIOL and J. A. POPLE. Gaussian, Inc., Pittsburgh, PA. 1988.
11. J. S. BINKLEY, J. A. POPLE, and W. J. HEHRE. J. Am. Chem. Soc. **102**, 939 (1980).
12. (*a*) W. F. ROWE JR., R. W. DUERST, and E. B. WILSON. J. Am. Chem. Soc. **98**, 4021 (1976); (*b*) S. L. BAUGHCUM, R. W. DUERST, W. F. ROWE, Z. SMITH, and E. B. WILSON. J. Am. Chem. Soc. **103**, 6296 (1981); (*c*) Z. SMITH, E. B. WILSON, and R. W. DUERST. Spectrochim. Acta, Part A, **39**, 1117 (1983); (*d*) S. L. BAUGHCUM, Z. SMITH, E. B. WILSON, and R. W. DUERST. J. Am. Chem. Soc. **106**, 2260 (1984); (*e*) P. TURNER, S. L. BAUGHCUM, S. L. COY and Z. SMITH. J. Am. Chem. Soc. **106**, 2265 (1984).
13. E. M. FLUDER and J. R. DE LA VEGA. J. Am. Chem. Soc. **100**, 5265 (1978).
14. J. BICERANO, H. F. SCHAEFER III, and W. H. MILLER. J. Am. Chem. Soc. **105**, 2550 (1983), and references therein.
15. M. J. FRISCH, A. C. SCHEINER, H. F. SCHAEFER III, and J. S. BINKLEY. J. Chem. Phys. **82**, 4194 (1985).
16. J. S. HUTCHINSON. J. Phys. Chem. **91**, 4495 (1987).
17. T. CARRINGTON, JR. and W. H. MILLER. J. Chem. Phys. **84**, 4364 (1986).
18. M. A. RÍOS and J. RODRÍGUEZ. J. Mol. Struct. (Theochem), **204**, 137 (1990).
19. J. LAANE. Appl. Spectrosc. **24**, 73 (1970).
20. M. C. FLANIGAN and J. R. DE LA VEGA. J. Chem. Phys. **61**, 1882 (1974).
21. W. H. MILLER. J. Phys. Chem. **83**, 960 (1979), and references therein.
22. H. S. JOHNSTON. Gas phase reaction rate theory. Ronald Press, New York. 1966.
23. D. G. TRUHLAR and A. KUPPERMANN. J. Am. Chem. Soc. **93**, 1840 (1971).

Can. J. Chem. Downloaded from www.nrcresearchpress.com by 195.138.81.100 on 09/07/12
For personal use only.

Phenyltetramethylguanidines: substituent effect on rates and isotope effects in their reaction with bis(4-nitrophenyl)cyanomethane in acetonitrile

PRZEMYSLAW PRUSZYNSKI AND KENNETH T. LEFFEK[1]
Department of Chemistry, Dalhousie University, Halifax, N.S., Canada B3H 4H6
Received May 22, 1990

PRZEMYSLAW PRUSZYNSKI and KENNETH T. LEFFEK. Can. J. Chem. **69**, 205 (1991).

A series of 22 phenyl substituted derivatives of 2-phenyl-1,1′,3,3′-tetramethylguanidine were used as bases in the proton transfer reaction from bis(4-nitrophenyl)cyanomethane in acetonitrile solvent. Brønsted and Hammett type relationships are examined for this family of closely related substrates. The Brønsted relationship constructed from the pK_a values determined in acetonitrile shows $\beta = 0.55 \pm 0.03$. The best fit of the Hammett relationship, with special values for *p*-NO_2 and *p*-CN groups, gives the reaction constant $\rho = -1.39 \pm 0.1$. The kinetic isotope effect, k_H/k_D, increases from 9.6 to 12.4 at 25°C with decreasing base strength, i.e., when the reaction becomes more thermoneutral.

Key words: tetramethylguanidine, proton transfer, deuterium isotope effects.

PRZEMYSLAW PRUSZYNSKI et KENNETH T. LEFFEK. Can. J. Chem. **69**, 205 (1991).

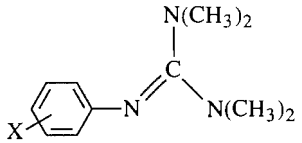
On a utilisé une série de 22 2-phenyl-1,1′,3,3′-tétraméthylguanidines substituées par des groupements phényles comme bases dans des réactions de transfert de proton, à partir du bis(4-nitrophényl)cyanométhane dans l'acétonitrile comme solvant. On a examiné les relations du type de Brønsted et de Hammett pour cette famille de substances intimement apparentées. La relation de Brønsted, établie à partir des valeurs de pK_a déterminées dans l'acétonitrile, présente une valeur $\beta = 0{,}55 \pm 0{,}03$. La meilleure coïncidence de la relation de Hammett, avec des valeurs spéciales pour les groupements *p*-NO_2 et *p*-CN, conduit à une constante de réaction $\rho = -1{,}39 \pm 0{,}1$. Lorsqu'on fait diminuer la force de la base, l'effet isotopique cinétique, k_H/k_D à 25°C, augmente de 9,6 à 12,4; c'est-à-dire que la réaction devient plus thermoneutre.

Mot clés : tétraméthylguanidine, transfert de proton, effets isotopiques du deutérium.

[Traduit par la revue]

Introduction

The synthesis and pK_a measurements of a large series of phenyl substituted derivatives of 2-phenyl-1,1′,3,3′-tetramethylguanidines **1** (1–3) allow the proton transfer reactions



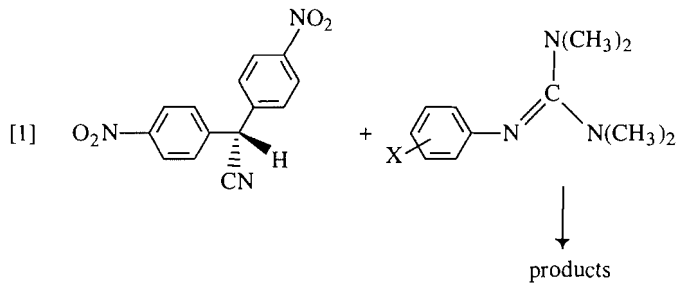
1

from a suitable carbon acid to be studied for a group of strong bases of closely allied structure. Carbon acids that belong to the group of pseudoacids are relatively weak and this creates the need for a series of stronger bases with known pK_a values. The well-known series of bases, such as anilines or pyridines, are much too weak to abstract the proton from most nitro, *p*-nitrophenyl, and cyano activated carbon acids. Previous studies (4, 5) of kinetic isotope effects and activation parameters of proton transfer reactions with respect to the identity of the base have involved bases of somewhat different skeletal structure, which hampered the interpretation of the results.

This paper presents the results of measurements of equilibrium constants and rate constants for the reaction of 24 phenyl substituted derivatives of **1** for the proton transfer reaction from bis(4-nitrophenyl)cyanomethane in acetonitrile solvent, shown in eq. [1]. Six of these reactions have been studied over a range of temperature, the activation parameters evaluated, and the primary deuterium isotope effects have been determined for four of them.

Results and discussion

Many proton transfer reactions from carbon acids to nitrogen bases in acetonitrile have been shown to give an ion-pair product

[1] 

by the application of the Hildebrand–Benesi method (6) of determining the equilibrium constant. However, in a recent publication, Galezowski and Jarczewski (7) have shown that for the reactions of 1-nitro-1-(4-nitrophenyl)alkanes with 1,8-diazabicyclo[5.4.0]undec-7-ene (DBU) in acetonitrile solvent, the ion-pair products are at least 97% dissociated into free ions at the concentrations typically used in kinetic measurements. For proton transfer reactions with large equilibrium constants the Hildebrand–Benesi plots do not easily distinguish between ion-pair products and separated ion products, with both equations showing high correlation coefficients (7).

For a reaction of the type shown in eq. [2],

[2] $$AH + B \rightleftharpoons \underset{\text{ion pair}}{A^-BH^+} \rightleftharpoons \underset{\text{free ions}}{A^- + BH^+}$$

it may be assumed that the interconversion of ions and ion pairs is fast. If the overall equilibrium constant is large, the reverse reaction may be neglected and the overall forward second-order rate constant (k_2) may be determined by measuring the pseudo-first-order rate constants (k_{obs}) at a series of large base concentrations and fitting to eq. [3].

[3] $$k_{obs} = k_2[B]$$

Most of the phenyltetramethylguanidine bases are so strong that the equilibrium constants for the proton transfer reactions are very high. In these cases it is very difficult to determine the

[1]Author to whom correspondence may be addressed.

Can. J. Chem. Downloaded from www.nrcresearchpress.com by 195.138.81.100 on 09/07/12
For personal use only.

TABLE 1. Equilibrium constants for the reaction of bis(4-nitrophenyl)cyanomethane and substituted 2-phenyl-1,1',3,3'-tetramethylguanidines in acetonitrile solvent at 25°C

Substituent in base	ϵ ($dm^3\ mol^{-1}\ cm^{-1}$)	K_{ip} ($dm^3\ mol^{-1}$)	Corr. coeff. (ion pair)	K_i	Corr. coeff. (ions)
4-CN	58 000 ± 200	10 500 ± 100	0.9946	$(9.5 \pm 0.5) \times 10^{-2}$	0.9955
4-NO_2	69 000 ± 1000	4 100 ± 600	0.9724	$(3.7 \pm 0.6) \times 10^{-3}$	0.9727

equilibrium constant quantitatively and this was done only for the two weakest bases, the *p*-nitro and *p*-cyano derivatives. The equilibrium absorptions of the product peak at 645 nm for a series of base concentrations at constant acid concentration were fitted to the Hildebrand–Benesi equations (6) derived for an ion-pair product, eq. [4], and for separated ion products, eq. [5]. *A* is the absorbance at equilibrium, *a* and *b* are the initial

$$[4]\quad a/A = \frac{1}{K_{ip} b \epsilon} + \frac{1}{\epsilon}$$

$$[5]\quad a/A = \frac{A}{K_i b \epsilon^2} + \frac{1}{\epsilon}$$

concentrations of the acid and base respectively, ϵ is the molar extinction coefficient, K_{ip} is the equilibrium constant assuming an ion-pair product, and K_i is the overall equilibrium constant for the reaction yielding separated ions as products. The base was always in large excess over the acid and was varied in the range (1×10^{-3})–(5×10^{-2}) M. Linear plots were obtained for both a/A vs. $1/b$ (eq. [4]) and for a/A vs. A/b (eq. [5]) for both reactions. The results are summarized in Table 1, and the equilibrium constants are sufficiently high that eq. [3] should be obeyed, even if the products are indeed essentially fully ionized.

The pseudo-first-order rate constants, k_{obs}, were determined at a series of base concentrations always in large excess. The second-order rate constants, k_2, were calculated by a least-squares fit to eq. [3] and are collated in Table 2, together with the pK_a values previously determined (3). The plots of the k_{obs} values versus base concentration do pass through the origin, with the possible exception of the *p*-NO_2 derivative, and therefore yield k_2 values that are a very good approximation to the true second-order rate constants for the reaction [1]. The data in Table 2 for the *para* and *meta* substituted bases may be used to construct Brønsted and Hammett correlations, and the *ortho* substituted bases allow the influence of steric factors on the rate of the reaction to be assessed.

The Brønsted relationship between log k_H at 25°C and pK_a of the conjugate acid of the base is shown in Fig. 1 and yields a Brønsted β coefficient of 0.55 ± 0.03 when calculated using only the solid points that represent the various *para* and *meta* substituted bases. This is the same within experimental error as the value of 0.53 reported (5) for the acid 4-nitrophenylphenylcyanomethane reacting with various nitrogen bases in acetonitrile, and also the same as the average value found by Bordwell and Boyle (8) for several arylnitromethanes reacting with bases in water. More O'Ferrall (9) lists values of the Brønsted exponent that vary between 0.38 and 0.79 for the ionization of ketones and nitroalkanes.

The bases containing *ortho* substituents on the phenyl group are shown with open circles in Fig. 1. The points for 2-OMe and 2,4-di-OMe derivatives (points 11 and 12) show a positive deviation from the general relationship for *meta* and *para* substituted bases. This behaviour may be explained by a possible stabilization of the positive charge developed on the base in the transition state by interaction with an oxygen of the *ortho* methoxy group. All the other *ortho* derivatives show a negative deviation, which is most likely caused by simple steric hindrance. This effect is especially pronounced for *ortho* alkyl derivatives (points 19–24).

A Hammett plot, shown in Fig. 2 for nine of the bases, using σ^- values (10) for the *para*-nitro, *para*-cyano, and *para*-trifluoromethyl groups in recognition of the important resonance structures of these bases, gives a ρ value of -1.39 ± 0.10 with a correlation coefficient of 0.987. If σ^0 values (10) are used for all the substituents, the correlation coefficient is almost as good at 0.985 and ρ is -1.94 ± 0.13. These values are consistent with the fact that the positive charge developing on the nitrogen atom directly bonded to the phenyl ring is partially redistributed onto the two other nitrogen atoms and apparently shifted away from the phenyl ring. The Hammet ρ values reported previously for the equilibrium constants of this series of bases (2, 3) were -1.84 ± 0.05 and -2.18 ± 0.16 in water and acetonitrile respectively. These were values determined using σ^- constants where appropriate, and therefore are to be compared with $\rho = -1.39$ for the proton transfer rate constants. This value might be expected to be higher since it is the nitrogen atom directly bonded to the phenyl ring which undergoes protonation. Delocalization of the positive charge, the same effect that is responsible for the unique strength of the guanidine bases, must also lower the sensitivity of this strength to the substituent effect. When the ρ value of -1.39 for $\log_{10} k$ is compared to -2.18 for pK_a, the conclusion may be drawn that the transition state of the reaction comes early on the reaction coordinate. This conclusion is consistent with a Brønsted β value of 0.55 and is also consistent with a Hammett correlation study (11) of cyanocarbon acids reacting with tetramethylguanidine in acetonitrile solvent in which the substituent on a phenyl group in the acid was varied.

The activation parameters for the six reactions studied over a range of temperature are shown in Table 3. The enthalpies of activation are all very low and show no discernable trend. They differ from one another by barely more than the standard deviations, with the slowest reaction of the *p*-NO_2 substituted base yielding the smallest enthalpy of activation. The entropies of activation show a slightly larger variation with the largest negative value found with the *p*-NO_2 substituted base. The stronger electron-withdrawing groups, *p*-NO_2 and *p*-CN, give larger negative entropies of activation but the four weaker groups all yield values between -29 and -30 cal $mol^{-1}\ deg^{-1}$. Negative entropies of activation of this magnitude are typical of proton transfer reactions to carbon acids in acetonitrile solvent. If a major part of the barrier to reaction is the breaking of the initial state solvation shell (12, 13), the small enthalpies of activation are consistent with a transition state that is reached early along the reaction coordinate.

The primary deuterium isotope effects for four of the

Can. J. Chem. Downloaded from www.nrcresearchpress.com by 195.138.81.100 on 09/07/12
For personal use only.

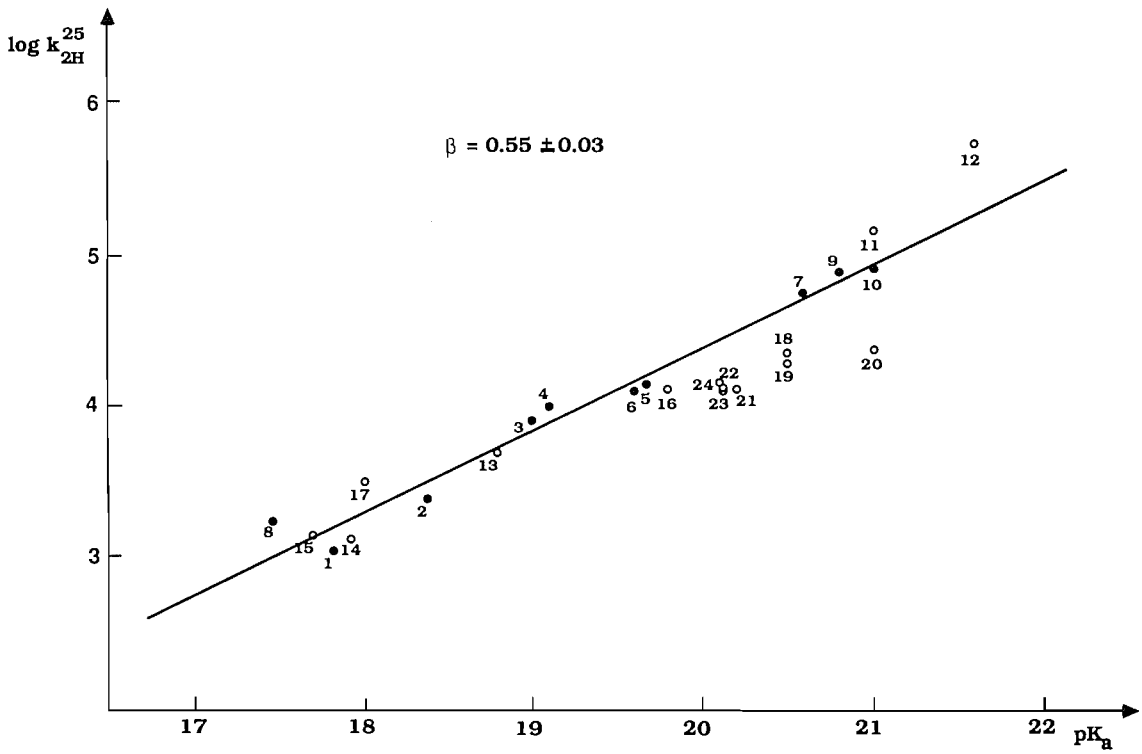


FIG. 1. Brønsted plot for the proton transfer reaction from bis(4-nitrophenyl)cyanomethane to a series of phenyl substituted derivatives of PhTMG in acetonitrile solvent. The numbers refer to the reactions listed in Table 2.

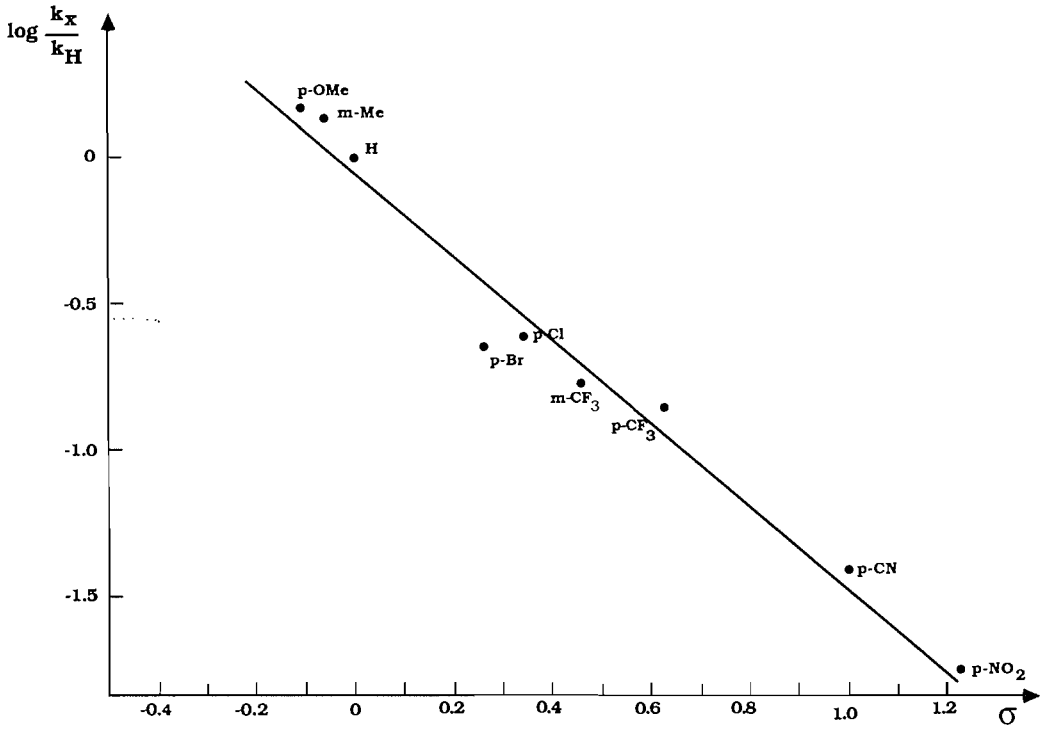


FIG. 2. Hammett plot for the proton transfer reaction from bis(4-nitrophenyl)cyanomethane to a series of phenyl substituted derivatives of PhTMG in acetonitrile solvent.

Can. J. Chem. Downloaded from www.nrcresearchpress.com by 195.138.81.100 on 09/07/12
For personal use only.

TABLE 2. Observed and second-order rate constants for the proton and deuteron transfer reactions from bis(4-nitrophenyl)cyanomethane to a series of phenyl substituted derivatives of PhTMG in acetonitrile solvent

No.	Base	pK_a[a]	L	Temp. (°C)	10^3[B] (M)	k_{obs} (s^{-1})	k_2 ($M^{-1}s^{-1}$)
1.	4-NO_2	17.82 ± 0.07	H	10	2–10	1.87–7.30	770 ± 30
				15		2.10–8.93	850 ± 40
				20		2.29–9.72	940 ± 50
				25		2.49–10.62	1030 ± 30
				30		2.81–12.12	1150 ± 40
			D	10	2.1–10.5	0.12–0.58	54 ± 1
				15		0.14–0.68	63 ± 1
				20		0.16–0.80	75 ± 1
				25		0.19–0.90	83 ± 2
				30		0.21–1.05	100 ± 1
2.	4-CN	18.37 ± 0.08	H	10	1.01–5.06	1.83–8.52	1653 ± 40
				15		2.03–9.53	1860 ± 10
				20		2.30–10.60	2040 ± 20
				25		2.59–11.80	2270 ± 20
				30		3.14–13.60	2580 ± 40
			D	10	1.12–5.61	0.14–0.67	118 ± 1
				15		0.17–0.78	137 ± 1
				20		0.19–0.92	164 ± 5
				25		0.23–1.07	187 ± 2
				30		0.26–1.24	217 ± 3
3.	4-CF_3	19.00 ± 0.09	H	10	1.04–5.21	6.5–30.6	5670 ± 170
				15		6.9–34.3	6350 ± 300
				20		7.5–38.0	7320 ± 100
				25		8.6–42.4	8080 ± 150
				30		9.6–47.4	8920 ± 250
4.	3-CF_3	19.09 ± 0.09	H	10	0.53–2.67	4.5–19.5	7100 ± 400
				15		5.2–21.5	7700 ± 200
				20		6.1–25.2	9100 ± 600
				25		6.3–27.4	9700 ± 300
				30		6.8–30.9	11 600 ± 800
5.	4-Cl	19.7 ± 0.1	H	10	0.52–2.60	5.7–27.1	10 400 ± 100
				15		6.3–30.3	11 600 ± 100
				20		7.0–33.8	12 900 ± 100
				25		7.7–36.6	14 000 ± 200
				30		8.1–40.8	15 700 ± 200
			D	10	0.62–3.10	0.55–2.60	820 ± 10
				15		0.68–3.06	970 ± 20
				20		0.79–3.52	1120 ± 20
				25		0.92–4.09	1280 ± 20
				30		1.10–4.70	1460 ± 20
6.	4-Br	19.6 ± 0.1	H	10	0.75–3.77	8.2–36.2	9400 ± 200
				15		9.2–42.1	11 000 ± 200
				20		10.6–47.0	12 000 ± 300
				25		11.0–50.3	12 900 ± 300
				30		11.9–55.5	14 400 ± 200
			D	10	0.71–3.53	0.67–3.07	850 ± 20
				15		0.79–3.55	1000 ± 30
				20		0.92–4.21	1190 ± 40
				25		1.04–4.80	1350 ± 20
				30		1.22–5.40	1480 ± 10
7.	H	20.6 ± 0.1	H	25	0.46–1.37	19.6–70	57 000 ± 4000
8.	3,5-diCF_3	17.47 ± 0.07	H	25	1.7–6.8	3.1–10.0	1650 ± 80
9.	3-Me	20.8 ± 0.1	H	25	0.21–0.70	25–60	77 000 ± 3000
10.	4-OMe	21.0 ± 0.1	H	25	0.14–0.70	26–68	82 000 ± 2000

Can. J. Chem. Downloaded from www.nrcresearchpress.com by 195.138.81.100 on 09/07/12
For personal use only.

TABLE 2 (*concluded*)

No.	Base	pK_a[a]	L	Temp. (°C)	10^3[B] (M)	k_{obs} (s^{-1})	k_2 ($M^{-1}s^{-1}$)
11.	2-OMe	21.0 ± 0.1	H	25	0.2–0.78	25–112	150 000 ± 10 000
12.	2,4-diOMe	21.6 ± 0.1	H	25	0.088–0.26	46–156	570 000 ± 20 000
13.	2-Cl	18.80 ± 0.09	H	25	0.4–5.65	6–28	4900 ± 200
14.	2,4-diCl	17.93 ± 0.09	H	25	0.25–3.2	0.96–4.64	1270 ± 100
15.	2,5-diCl	17.70 ± 0.07	H	25	0.25–3.3	1.2–5.3	1360 ± 100
16.	2-Ph	19.8 ± 0.1	H	25	0.31–0.93	5.2–11.7	12 900 ± 600
17.	2-OMe-4-NO_2	18.0 ± 0.1	H	25	0.26–1.02	1.5–3.4	3060 ± 200
18.	2-Me	20.5 ± 0.1	H	25	0.13–0.64	3.9–15	22 600 ± 1300
19.	2,6-diMe	20.5 ± 0.1	H	25	0.12–0.31	12.7–74	19 500 ± 1000
20.	2,4-diMe	21.0 ± 0.1	H	25	0.71–3.55	50–116	23 700 ± 1500
21.	2-Et	20.2 ± 0.1	H	25	0.13–0.64	2.5–8.6	12 700 ± 1000
22.	2,6-diEt	20.1 ± 0.1	H	25	0.41–1.65	5.5–23	13 000 ± 1000
23.	2-*i*Pr	20.1 ± 0.1	H	25	0.98–4.88	29–54	12 300 ± 1000
24.	2,6-di-*i*Pr	20.1 ± 0.1	H	25	0.77–2.3	11–37	14 300 ± 1000

[a]pK_a values from ref. 3.

TABLE 3. Activation parameters for the proton and deuteron transfer reactions from bis(4-nitrophenyl)cyanomethane to a series of phenyl substituted derivatives of 2-phenyl-1,1′,3,3′-tetramethylguanidine

Base	$\Delta H_H^{\ddagger}$ kcal mol^1	$\Delta S_H^{\ddagger}$ cal mol^{-1} K^{-1}	$\Delta H_D^{\ddagger}$ kcal mol^{-1}	$\Delta S_D^{\ddagger}$ cal mol^{-1} K^{-1}
p-NO_2	2.8 ± 0.1	−35.4 ± 0.3	4.6 ± 0.2	−34.2 ± 0.7
p-CN	3.1 ± 0.1	−32.6 ± 0.4	4.7 ± 0.1	−32.3 ± 0.5
p-CF_3	3.3 ± 0.1	−29.5 ± 0.4	—	—
m-CF_3	3.5 ± 0.4	−28.5 ± 1.2	—	—
p-Br	2.9 ± 0.2	−30.0 ± 0.9	4.2 ± 0.3	−29.9 ± 1.0
p-Cl	2.9 ± 0.1	−29.8 ± 0.3	4.3 ± 0.1	−29.9 ± 0.2

TABLE 4. Isotope effects for the proton transfer reaction from bis(4-nitrophenyl)cyanomethane to a series of phenyl substituted derivatives of 2-phenyl-1,1′,3,3′-tetramethylguanidine

Parameter	Temp. (°C)	4-NO_2PhTMG	4-CNPhTMG	4-ClPhTMG	4-BrPhTMG
k_{2H}/k_{2D}	10	14.3 ± 0.6	14.1 ± 0.1	12.6 ± 0.3	11.0 ± 0.3
	15	13.5 ± 0.6	13.6 ± 0.2	12.0 ± 0.2	11.0 ± 0.3
	20	12.5 ± 0.7	12.4 ± 0.4	11.5 ± 0.2	10.1 ± 0.4
	25	12.4 ± 0.5	12.1 ± 0.2	10.9 ± 0.2	9.6 ± 0.2
	30	11.5 ± 0.4	11.8 ± 0.2	10.8 ± 0.2	9.7 ± 0.2
$\Delta\Delta H^{\ddagger}$ (kcal mol^{-1})		1.8 ± 0.2	1.6 ± 0.2	1.4 ± 0.3	1.3 ± 0.3
$\Delta\Delta S^{\ddagger}$ (cal mol^{-1} K^{-1})		1.2 ± 0.7	0.2 ± 0.6	0.1 ± 0.3	−0.1 ± 0.3

reactions are given in Table 4. The rate ratios decrease with increasing temperature almost exactly as required for the entire isotope effect to be in the enthalpy of activation, and three of the bases show a $\Delta\Delta H^{\ddagger}$ effect corresponding to the loss of a C–H (or C–D) stretching frequency. The *p*-NO_2 base shows a slightly larger effect, indicating a possible contribution from proton tunnelling. There is a small but clear variation of k_H/k_D with the pK_a of the base. The weakest base, the *p*-nitro derivative, shows the largest isotope effect, in keeping with the theory (14–16) that the maximum isotope effect will occur in the more thermoneutral process.

Experimental

The 2-phenyl-1,1,3,3-tetramethylguanidines were synthesized by the method of Bredereck and Bredereck (17) from 1,1,3,3-tetramethylurea (Aldrich) and the appropriate aniline, in the presence of $POCl_3$. The detailed synthesis including modifications in the work-up procedure was described earlier (2, 3). The purity of these compounds

Can. J. Chem. Downloaded from www.nrcresearchpress.com by 195.138.81.100 on 09/07/12
For personal use only.

was assessed by GC–MS analysis using Hewlett–Packard 5890 A/5970 MSD apparatus.

Bis(4-nitrophenyl)cyanomethane was synthesized by nitration of diphenylcyanomethane according to the procedure described in the paper of Haskelberg and Larie (18). The reaction was performed using fuming nitric acid at −40°C. The crude reaction product was first purified by converting it into the salt by washing with NaOH, extracting the water phase with ether, and reprecipitating the product using acetic acid. The product was further crystallized from benzene and acetic acid until it gave a single spot on a TLC (mp 93–94.5°C exactly as reported earlier by Hojatti and Leffek (11), confirming the validity of this measurement in the light of the earlier reported value of 40–45°C (19)). ^{1}H NMR ($CDCl_3$), δ: 5.4 (1H, s), 7.5 (4H, d, J = 9.0 Hz), 8.2 (4H, d, J = 9.0 Hz).

Bis(4-nitrophenyl)cyanomethane-*d* was prepared by OD^- catalyzed isotopic exchange in a D_2O–dioxan mixture. The neutralization of the anion by DCl/D_2O was followed by evaporation of the solvents. The residue, consisting of the deuterated compound and NaCl, was not separated but dissolved in a new portion of D_2O–dioxan and the procedure was repeated. After five such cycles the residue, after evaporation, was extracted with dry $CHCl_3$ followed by its evaporation. The degree of deuteration was found to be 98% based on ^{1}H NMR and MS spectrometry.

Equilibrium measurements were done using a Cary 219 spectrophotometer at 25°C. The absorbance was measured for the series of solutions with constant acid concentration (in the range of (5×10^{-6})–(2×10^{-5}) M) and varying base concentrations. For stronger bases the change in absorbance due to the increase of their concentration was too small to be reliably measured.

The reaction rate constants were measured using a Durrum –Gibson stopped-flow spectrophotometer, equipped with a computerized data acquisition system, using acid concentrations in the range of (5×10^{-6})–(1×10^{-5}) M with the base concentration high enough to allow for pseudo-first-order kinetics. The rate constants were calculated using the Guggenheim method (20) and the activation parameters obtained by a least-squares fit to the transition state theory equation.

1. J. Oszczapowicz and J. Osek. Pol. J. Chem. **57**, 93 (1983).
2. P. Pruszynski. Can. J. Chem. **65**, 626 (1987).
3. K. T. Leffek, P, Pruszynski, and K. Thanapaalasingham. Can. J. Chem. **67**, 590 (1989).
4. N. Sugimoto and M. Sasaki. J. Chem. Soc. Faraday Trans. **81**, 1441 (1985).
5. M. Dworniczak and K. T. Leffek. Can. J. Chem. **68**, 1657 (1990).
6. H. A. Benesi and J. H. Hildebrand. J. Am. Chem Soc. **71**, 2703 (1949).
7. W. Galezowski and A. Jarczewski. J. Chem Soc. Perkin Trans. 2, 1647 (1989).
8. F. G. Bordwell and W. J. Boyle, Jr. J. Am. Chem Soc. **94**, 3907 (1972).
9. R. More O'Ferrall. *In* Proton transfer reactions. *Edited by* E. F. Caldin and V. Gold. Chapman and Hall, London. 1975. Chap. 8. p. 232.
10. N. S. Isaacs. Physical organic chemistry. Longman Scientific & Technical, Harlow, U.K. 1987. p. 134.
11. M. Hojatti and K. T. Leffek. Can. J. Chem. **62**, 2653 (1984).
12. E. F. Caldin. J. Chem Soc. 3345 (1959).
13. A. Jarczewski and K. T. Leffek. Can. J. Chem. **50**, 24 (1972).
14. L. Melander. Isotope effects on reaction rates. Ronald Press, New York. 1960. Chap. 2.
15. F. H. Westheimer. Chem. Rev. **61**, 265 (1961).
16. R. P. Bell, W. H. Sachs, and R. L. Tranter. Trans. Faraday Soc. **67**, 1995 (1971).
17. H. Bredereck and K. Bredereck. Chem. Ber. **94**, 2278 (1961).
18. L. Haskelberg and D. Larie. J. Am. Chem Soc. **69**, 2267 (1947).
19. M. J. Minch, M. Giaccio, and R. Wolf. J. Am. Chem Soc. **97**, 3766 (1975).
20. E. A. Guggenheim. Philos. Mag. **2**, 538 (1926).

Can. J. Chem. Downloaded from www.nrcresearchpress.com by 195.138.81.100 on 09/07/12
For personal use only.

Sedum alkaloids. XI. Synthesis of sedinone and sedacrine by application of anodic oxidation

FRANK DRIESSENS AND CLAUDE HOOTELÉ[1]

Service de chimie organique, Faculté des sciences, Université Libre de Bruxelles, B-1050 Bruxelles, Belgium

Received April 13, 1990

FRANK DRIESSENS and CLAUDE HOOTELÉ. Can. J. Chem. **69**, 211 (1991).

α-Methoxycarbamate **12**, synthetic precursor of the 2,6-disubstituted alkaloids of *Sedum acre*, was obtained in high yield from 2-phenacylpiperidine **5**; the key step of the synthesis rests on the anodic methoxylation, which allows the functionalization of carbon 6. Nucleophilic substitution of the methoxy group by an acetonyl chain leads, after the required transformations, to sedinone **23**. Bromomethoxylation of the enecarbamate **19** followed by dehydrohalogenation and nucleophilic substitution of the methoxy group leads to sedacrine **33**. In both cases, the nucleophilic substitution of the methoxy group leads to a *cis* 2,6-disubstituted piperidine derivative.

Key words: synthesis, piperidine alkaloids, anodic methoxylation.

FRANK DRIESSENS et CLAUDE HOOTELÉ. Can. J. Chem. **69**, 211 (1991).

L'α-méthoxycarbamate **12**, précurseur synthétique des alcaloïdes 2,6-disubstitués de *Sedum acre* a été obtenu avec un rendement élevé au départ de la 2-phénacylpipéridine **5**; l'étape clé de la synthèse est la méthoxylation anodique qui permet la fonctionnalisation du carbone 6. La substitution nucléophile du groupe méthoxy par une chaîne acétonyle conduit, après aménagement fonctionnel, à la sédinone **23**. La bromométhoxylation du ènecarbamate **19** suivie d'une déhydrohalogénation et de la substitution du groupe méthoxy permet d'accéder à la sédacrine **33**. Dans les deux cas, la substitution du groupe méthoxy conduit à un dérivé pipéridinique *cis* 2,6-disubstitué.

Mots clés : synthèse, alcaloïdes pipéridiniques, méthoxylation anodique.

[Traduit par la revue]

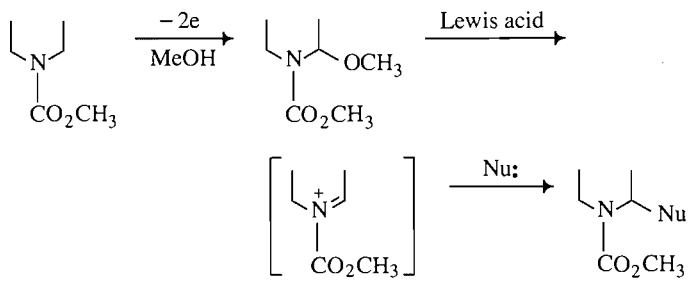
Introduction

Piperidine alkaloids constitute a large family of compounds, many of which exhibit a wide range of physiological activities. Because of this aspect, intense activity has been devoted to the isolation and structure determination of bases of this class and to the development of general routes for their synthesis (1). In this context, during the last few years, several methods were developed for the synthesis of 2,6-disubstituted piperidine alkaloids and especially for the bases isolated from *Solenopsis* species (2). Although electrochemical methoxylation emerged recently as a powerful method for the synthesis of piperidine derivatives (3, 4), no application to the synthesis of 2,6-disubstituted piperidine alkaloids has yet been recorded. Our interest in *Sedum* and related alkaloids prompted us to evaluate the potentiality of anodic methoxylation as a key step for the synthesis of members of this subgroup.

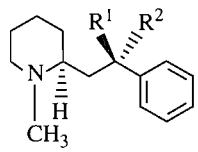
Anodic methoxylation allows the easy preparation of α-methoxyamides and α-methoxycarbamates. These compounds constitute interesting synthetic intermediates because of their facile conversion into the corresponding *N*-acyliminium ions, which have been shown to be versatile electrophiles. The combination of anodic methoxylation and nucleophilic substitution, e.g., with silyl enol ethers, appears to be a choice method for the introduction of a new C—C bond α to the nitrogen atom of cyclic amides and carbamates (Scheme 1).

The electrochemical preparation and the synthetic usefulness of α-methoxycarbamates were investigated by T. Shono in particular, who developed the syntheses of several alkaloids based on the sequence of Scheme 1. In the field of 2-alkylpiperidine alkaloids, application of this sequence leads, *inter alia*, to the synthesis of sedamine **1** and allosedamine **2** (5, 6).

We pointed out, in a preceding communication, that all the 2,6-disubstituted alkaloids isolated from *Sedum acre* contain a (−)-sedamine moiety (7). This feature allows their synthesis to be based on the alkylation at C-6 of a common 2-substituted piperidine derivative. In this respect, the anodic methoxylation process seemed promising because it was observed that the least



SCHEME 1



1 $R^1 = H, R^2 = OH$
2 $R^1 = OH, R^2 = H$

substituted α-carbon atom of *N*-acylpiperidines is oxidized specifically (5); a rationalization of this observation has been offered (8).

Results and discussion

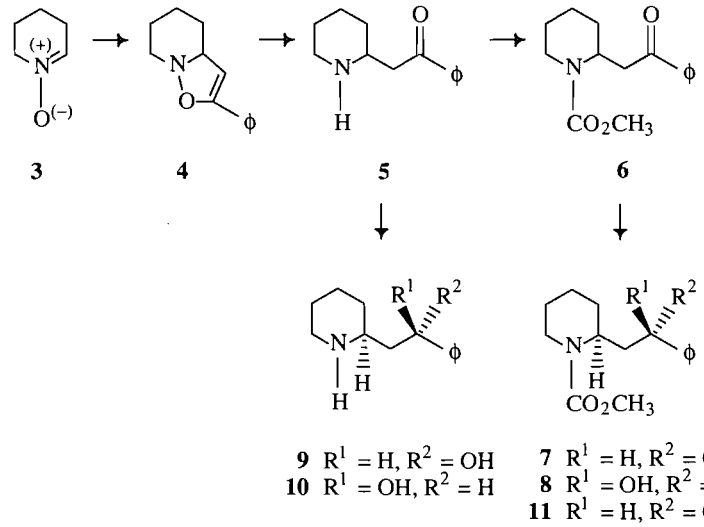
We wish to report here the synthesis of the alkaloids sedinone **23** and sedacrine **33** via the precursor **12** using anodic methoxylation methodology.

Preparation of the precursor 12

2-Phenacylpiperidine **5** was obtained (70% overall yield) by the method we described earlier (9) via hydrogenolysis (H_2, Pd/C) of the isoxazoline **4** resulting from the cycloaddition between the nitrone **3** and phenylacetylene (Scheme 2). Acylation of the nitrogen atom of **5** with methyl chloroformate under

[1]Author to whom correspondence may be addressed.

Can. J. Chem. Downloaded from www.nrcresearchpress.com by 195.138.81.100 on 09/07/12
For personal use only.

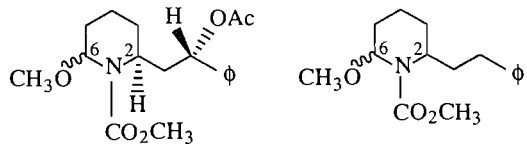


SCHEME 2

Schotten–Baumann conditions yielded quantitatively the carbamate **6**. The same compound had previously been obtained in comparable yield through the sequence anodic methoxylation – nucleophilic substitution (6). Reduction of the keto group of **6** with $NaBH_4$ in MeOH furnished a 70:30 mixture of the diastereoisomeric alcohols **7** and **8**. However, a 98:2 mixture of **7** and **8** was obtained when the reduction was performed with lithium tri-*tert*-butoxyaluminium hydride in THF. Under the same conditions, 2-phenacylpiperidine **5** was transformed into a 35:65 mixture of **9** and **10**. The high selectivity observed for the reduction of the ketone function of the carbamate **6** with $Li(tBuO)_3AlH$ is worthy of note because the sequence described above constitutes a simple and efficient route for the synthesis of sedamine-type derivatives. Thus, norsedamine **9** and sedamine **1** were obtained by basic ethanolysis and by $LiAlH_4$ reduction of **7** respectively. Another efficient stereoselective synthesis of sedamine-type derivatives was described recently (10). On the other hand, it had been established previously that allosedamine-type derivatives are accessible in high yield and with a high stereoselectivity via cycloaddition between nitrone **3**, or derivatives of **3**, and styrene (11).

Acetylation of the alcohol **7** yielded quantitatively **11**, which was submitted to anodic oxidation.

All anodic oxidations performed in this study were carried out at room temperature in methanol containing Et_4NOTs as a supporting electrolyte, in an undivided cell equipped with two vitreous carbon electrodes; a constant potential of 8.00 V was applied. After 8 F/mol of electricity was passed, the oxidation of the acetyl derivative **11** was complete and yielded quantitatively the 6-methoxylated compound **12**. In agreement with structure **12**, the ^{13}C nmr spectrum showed the presence of only 4 methylene groups. In the ^1H nmr spectrum ($CDCl_3$; 250 MHz) of **12**, H-2 and H-6 appeared as broad signals centered at 4.28 and 5.40 ppm respectively; a broadening of signals, due to the "slow" rotation around the N—CO_2CH_3 bond, is observed for all the compounds of this series. The broad signals at 3.28 and 3.72 ppm are attributed to the methoxy group at C-6 and to the N—CO_2CH_3 group, respectively, by comparison with the spectrum of the trideutero derivative obtained after anodic methoxylation of **11** in CD_3OD. When the ^1H nmr spectrum of **12** was recorded at 57°C, sharp signals were observed for the three methyl groups; there was no indication of the presence of another isomer. The configuration at C-6 was, however, not established.



12 **13**

In the same experimental conditions, oxidation of the ketone **6** in methanol furnished regiospecifically the α-methoxycarbamate **13** in 96% yield. On the other hand, anodic methoxylation of the bicyclic derivative **14** (Scheme 3), obtained by transesterification from **7**, gave a mixture of isomers **15**, **16**, and **17** in a 1:1:1 ratio. In this case, the lack of regioselectivity can be ascribed to the strain induced in the less substituted iminium intermediate by the presence of the lactam cycle.

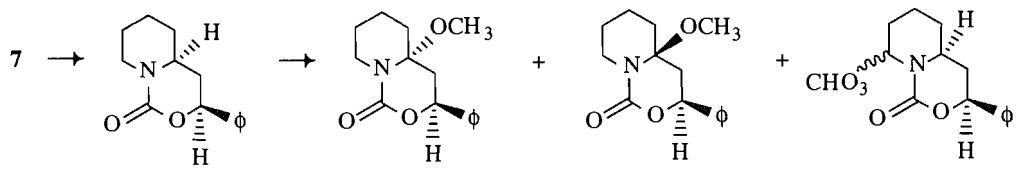
Synthesis of sedinone 23

The replacement of the methoxy group of **12** by an acetonyl side chain was carried out by treatment of **12** with 2-trimethylsilyloxypropene **20** in CH_2Cl_2 in the presence of $TiCl_4$, as a Lewis acid (Scheme 4). After column chromatography only one isomer, the 2,6-disubstituted derivative **18**, was isolated in 70% yield, along with the enecarbamate **19** (10% yield), which results from the elimination of methanol from **12**.

The *cis* configuration of **18** was not established at this stage but rests on the isolation of sedinone **23** as the major isomer after the steps described below (Scheme 5).

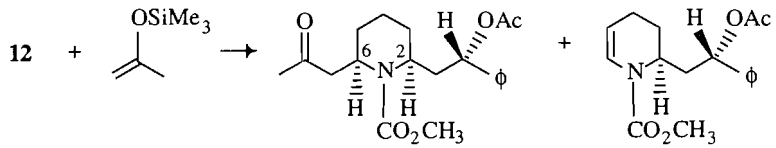
Protection of the keto group of **18** with ethylene glycol yielded quantitatively the dioxolane **21** whose carbomethoxyl and acetyl groups were reduced with $LiAlH_4$ to give the *N*-methyl derivative **22** (82% yield). Deprotection of **22** was carried out in boiling 0.1 N aqueous hydrochloric acid; a 90:10 mixture of sedinone **23** and 6-episedinone **24** was isolated (96% yield). The acetal **21** being a pure compound, the presence of **24** in the hydrolysis mixture must result from a partial epimerization of C-6 during the basic work-up after the deprotection step. While β-aminoketones such as **23** and **24** epimerize readily in basic medium, or simply in methanol, their salts are stereochemically stable. The epimerization therefore involves the nitrogen lone pair and may be accounted for by the path depicted in Scheme 6, as described for pelletierine and related compounds (23). As sedinone **23** is the major compound of the

Can. J. Chem. Downloaded from www.nrcresearchpress.com by 195.138.81.100 on 09/07/12
For personal use only.



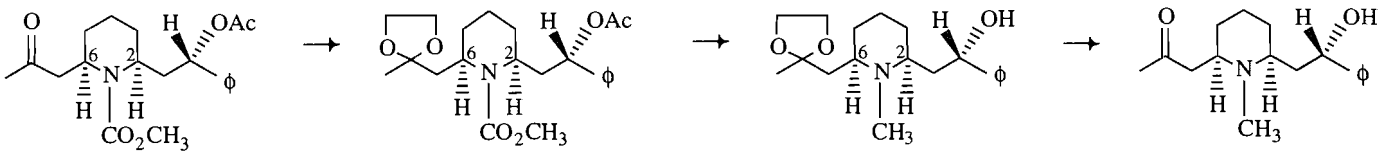
14 **15** **16** **17**

SCHEME 3

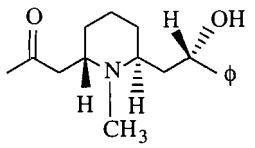


20 **18** **19**

SCHEME 4



18 **21** **22** **23**



24

SCHEME 5

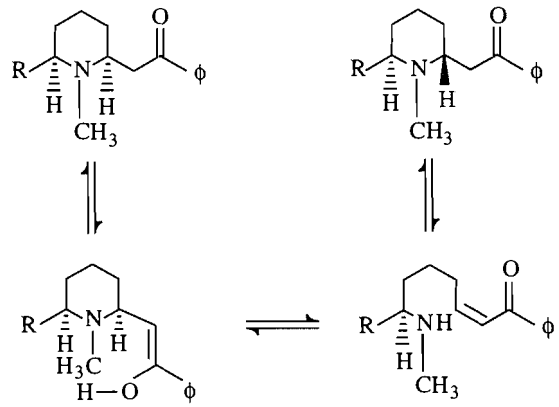
mixture, which is not the equilibrium mixture (8), the relative 2,6 configuration of **18** has to be *cis*.

The same sequence of reactions was applied to (−)-norsedamine **9** (12) as the starting material. After hydrolysis of the optically active acetal **22**, (−)-sedinone hydrochloride was isolated by fractional crystallization from the mixture of the hydrochlorides. The physical properties of the synthetic sample, including the optical rotation, were identical with those of the hydrochloride prepared from a natural sample of (−)-sedinone **23**.

Synthesis of sedacrine 33

The synthesis of sedacrine **33** from the precursor **12** (Scheme 7) requires the introduction of a C=C double bond in position 4. Recently, Shono *et al.* (13) and Torii *et al.* (14) reported that enecarbamates, which are easily obtained from α-methoxycarbamates (15), are suitable precursors of 2-alkyl-6-methoxy-1,2,3,6-tetrahydropyridine derivatives via halomethoxylation followed by dehydrohalogenation. Consequently, the enecarbamate **19** was prepared by treatment of **12** with *p*-toluenesulfonic acid in benzene at room temperature (yield 96%).

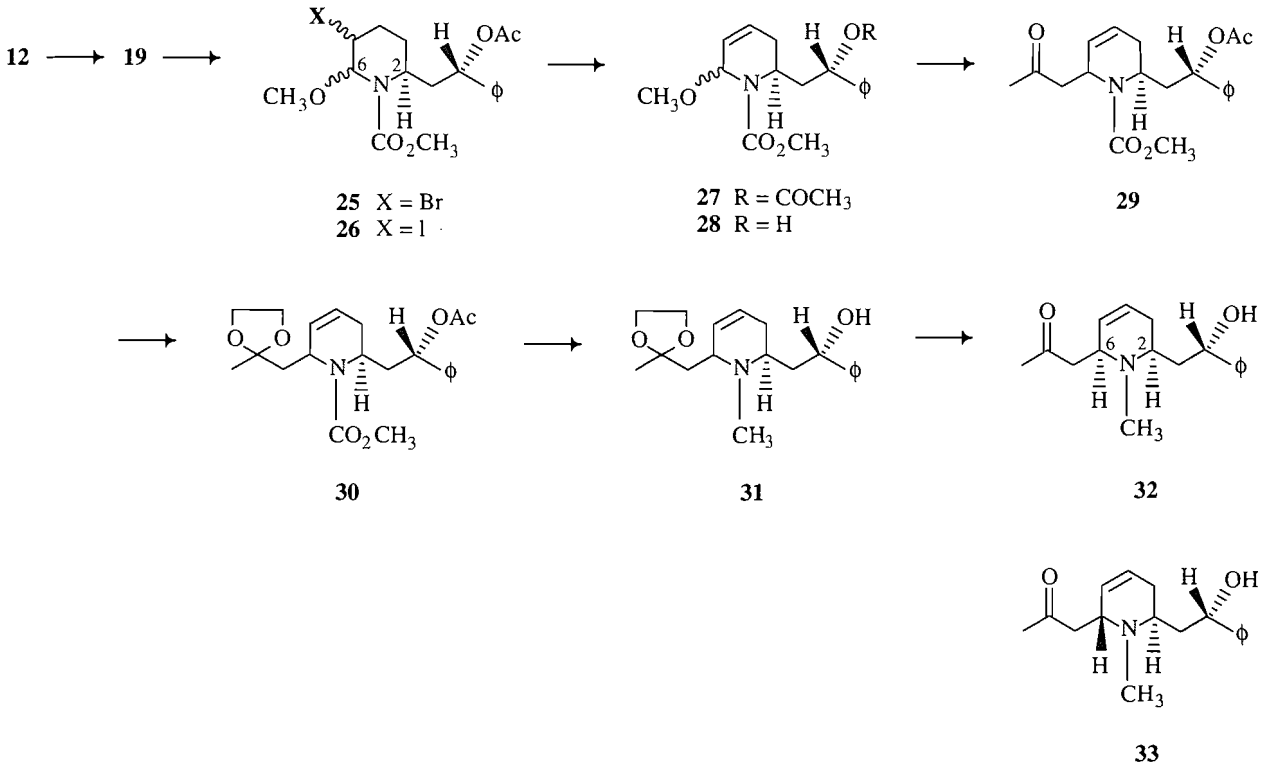
Quantitative bromomethoxylation of **19** was carried out by addition of bromine to a methanolic solution of **19** in the presence of sodium methoxide to give **25**, which is likely to be a mixture of diastereoisomers. The 5-bromo derivative **25** was then subjected to dehydrohalogenation conditions (DBU in



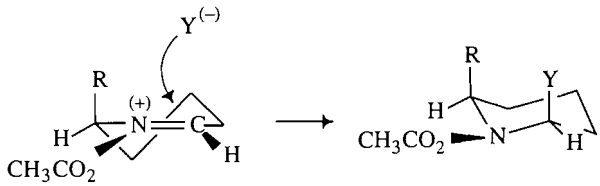
SCHEME 6

toluene at 87°C for 3 h). However, no elimination of HBr occurred. On the other hand, similar treatment of the corresponding 5-iodo derivative **26** (prepared from **19** in 85% yield) furnished a mixture of **27** and the corresponding alcohol **28**; the presence of the alcohol **28** is not surprising since DBU is known as a deprotective agent for acetyl groups (16). Treatment of the crude reaction mixture with acetic anhydride in pyridine led to the isolation of **27** in 93% yield from **26**. The nmr spectra did not allow us to establish whether **27** is a pure compound or a mix-

Can. J. Chem. Downloaded from www.nrcresearchpress.com by 195.138.81.100 on 09/07/12
For personal use only.



SCHEME 7



SCHEME 8

ture of diastereoisomers. The nucleophilic substitution of the methoxy group of **27** by an acetonyl chain was carried out in CH_2Cl_2 at −78°C in the presence of $TiCl_4$; after chromatography, the substitution product was isolated in 64% yield. The stereochemistry at C-6 was not established at this stage but the product must contain at least 90% of the *cis* compound **29**, as can be inferred from the isolation of a 9:1 mixture (by ^1H nmr) of episedacrine **32** and sedacrine **33** (84% overall yield) after a sequence of reactions identical with that described above for the synthesis of sedinone **23**: i.e., protection of the keto group of **29**, $LiAlH_4$ reduction of the acetal **30**, and deacetalization. After equilibration in methanol, a 6:1 mixture (by ^1H nmr) of **33** and **32** was obtained.

When the same sequence was applied to (−)-**12** as the starting material, (−)-sedacrine **33**, identical in all respects with the natural compound, was obtained.

In the two examples discussed above, the nucleophilic substitution of the methoxy group leads with high stereoselectivity to the *cis* 2,6-disubstituted piperidine derivative; this stereochemical control of the C-6 configuration is worthy of note and results from the stereoelectronically preferred axial attack of the nucleophile (8, 17) on the *N*-acyliminium intermediate, whose favoured conformation has an axial alkyl group at C-2 (18, 19) (Scheme 8). Other examples of *cis* stereoselectivity in the substitution of a methoxy group by a nucleophile have already been reported (24, 25).

Experimental

Melting points were determined on a Kofler microscope and are uncorrected. Mass spectral data were obtained on a Micromass 7070 spectrometer. Nuclear magnetic resonance spectra were recorded in $CDCl_3$ with TMS as internal standard on a Bruker WM 250 spectrometer. Optical rotations were measured on a Perkin Elmer 141 polarimeter.

Preparation of the carbamate **6**

K_2CO_3 (5.805 g) and methyl chloroformate (3.9 mL) were successively added to a stirred solution of 2-phenacylpiperidine **5** (3.870 g) in water (100 mL). After 15 h, NH_4OH was added and the basic solution was extracted with $CHCl_3$ (2 × 100 mL). The combined $CHCl_3$ layers were evaporated and the residue was filtered through a short column of alumina to afford quantitatively the carbamate **6** (4.966 g), mp 92°C after crystallization from hexane/ethyl acetate 5:1 (lit. (6) mp 89.2°C); ^1H nmr δ: 7.98 (2H), 7.5 (3H), 4.86 (1H, m, H2), 4.06 (1H, m, H6e), 3.62 (3H, s, CO_2CH_3), 3.29 (1H, dd, J = 9 and 15 Hz, H7), 3.15 (1H, dd, J = 6 and 15 Hz, H7′), 2.93 (1H, dt, H6a), 1.69–1.38 (6H, m); ^{13}C nmr δ: 198.3 (C8), 156.0 (NCO), 137.0, 133.1, 128.7, 128.2, 52.4 (CH_3), 48.3 (C2), 40.0 and 39.3 (C6 and C7), 28.0 and 25.3 (C3 and C5), 18.9 (C4); ms, *m/z*: 261 (11%), 230 (2), 202 (39), 156 (6), 142 (100), 141 (35), 105 (47), 77 (31), 70 (11).

Reduction of **6** *with Li(tBuO)$_3$AlH*

The carbamate **6** (152 mg) was dissolved in THF (15 mL) and Li(*t*BuO)$_3$AlH (1.480 g) was added. The mixture was then refluxed for 4 h. After cooling, some drops of water were added and the mixture was filtered through Celite and evaporated to dryness. The residue was dissolved in water (70 mL), basified with NH_4OH, and extracted with $CHCl_3$ (2 × 70 mL). Evaporation of the solvent gave a mixture (153 mg) of **7** and **8** (98:2 by ^1H nmr). **7** and **8** were separated by chromatography on alumina ($CHCl_3$); **7** (oil): ^1H nmr δ: 7.3 (5H, m), 4.74 (1H, m, H8), 4.43 (1H, m, H2), 3.92 (1H, m, H6e), 3.66 (3H, s), 2.80 (1H, m, H6a), 2.17 (1H, m, H7), 1.89 (1H, m, H7′), 1.61–1.36 (6H, m); ^{13}C nmr δ: 156.5 (NCO), 144.7, 128.3, 127.4, 125.8, 72.4 (C8), 52.5 (CH_3), 48.7 (C2), 39.9 and 39.6 (C6 and C7), 29.0 (C3), 25.4 (C5), 19.1 (C4); ms, *m/z*: 263 (7%), 186 (3), 142 (100). **8** (oil): ^1H nmr δ: 7.3 (5H, m), 4.60 (1H, m), 4.47 (1H, m), 4.05 (1H, m), 3.75 (3H, s),

Can. J. Chem. Downloaded from www.nrcresearchpress.com by 195.138.81.100 on 09/07/12
For personal use only.

Can. J. Chem. Downloaded from www.nrcresearchpress.com by 195.138.81.100 on 09/07/12
For personal use only.

.85 (1H, m, H6a), 2.22 (1H, m, H7), 2–1.3 (7H, m); ms, *m/z*: 263 (7%), 186 (3), 142 (100).

*Reduction of **6** with $NaBH_4$*

The carbamate **6** (131 mg) was dissolved in methanol (5 mL) and $NaBH_4$ (100 mg) was added. After 2 h at room temperature, the solvent was evaporated and water was added to the residue; extraction with $CHCl_3$ afforded, after evaporation of the solvent, 132 mg of a 70:30 mixture (by ^1H nmr) of **7** and **8**.

*Reduction of 2-phenacylpiperidine **5** with $Li(tBuO)_3AlH$*

2-Phenacylpiperidine **5** (143 mg) was treated with $Li(tBuO)_3AlH$ (358 mg) in refluxing THF (10 mL) for 15 h. After addition of some drops of water, the mixture was filtered through Celite and the solvent was evaporated. The residue was dissolved in water (50 mL), basified with NH_4OH, and extracted with $CHCl_3$ (3 × 50 mL). Evaporation of the combined organic layers gave a mixture (140 mg) of norsedamine **9** and norallosedamine **10** (35:65 by ^1H nmr (20)).

*Preparation of norsedamine **9** from **7***

A solution of **7** (144 mg) and KOH (750 mg) in EtOH (7.5 mL) was heated under reflux for 6 h. After evaporation of the solvent, the residue was dissolved in water (15 mL), basified with NH_4OH, and extracted with $CHCl_3$ (2 × 15 mL). Evaporation of the combined organic layers afforded norsedamine **9** (98 mg, 87% yield), whose ^1H nmr and mass spectra were identical with those reported in the literature (20).

*Preparation of sedamine **1** from **7***

To a solution of the carbamate **7** (120 mg) in THF (15 mL) was added $LiAlH_4$ (115 mg) and the mixture was refluxed for 6 h. Some drops of AcOEt and water were added and the mixture was filtered through Celite and evaporated to dryness. The residue was dissolved in 0.2 N aqueous HCl (50 mL) and extracted with $CHCl_3$ (2 × 3 mL). The aqueous phase was then basified with NH_4OH and extracted with $CHCl_3$ (3 × 50 mL). Evaporation of the combined $CHCl_3$ phases and filtration through a short column of alumina afforded homogeneous sedamine **1** (95 mg); the mass and ^1H nmr spectra of the base are identical with those reported in the literature (20).

*Acetylation of the alcohol **7***

The alcohol **7** (1.560 g) was treated at room temperature for 15 h with a mixture of pyridine (7 mL) and Ac_2O (7 mL). After evaporation of the solvent, filtration of the residue through a short column of alumina ($CHCl_3$) yielded **11** quantitatively (1.805 g; oil); ^1H nmr δ: 7.3 (5H), 5.73 (1H, dd, J = 6 and 8 Hz, H8), 4.32 (1H, m, H2), 4.04 (1H, m, H6e), 3.65 (3H, s), 2.93 (1H, m, H6a), 2.37 (1H, m, H7), 2.04 (3H, s), 1.89 (1H, m, H7′), 1.62–1.37 (6H, m); ^{13}C nmr δ: 170.1, 156.0 (NCO), 140.7, 128.5, 128.1, 126.7, 74.3 (C8), 52.4, 48.3 (C2), 39.4 and 36.7 (C6 and C7), 28.6 (C3), 25.5 (C5), 21.1, 19.1 (C4); ms, *m/z*: 305 (1%), 262 (2), 245 (17), 186 (10), 142 (100).

*Preparation of the bicyclic derivative **14***

A solution of the carbamate **7** (169 mg) and KOH (17 mg) in methanol (10 mL) was heated under reflux for 3.5 h. After the solvent was evaporated, the residue was dissolved in water (15 mL), basified with NH_4OH, and extracted with $CHCl_3$ (2 × 15 mL). Evaporation of the $CHCl_3$ and crystallization from hexane afforded **14** (127 mg, 86% yield); mp 97–98°C; ^1H nmr δ: 7.32 (5H), 5.17 (1H, dd, J = 2 and 12 Hz, H8), 4.54 (1H, m, H6e), 3.46 (1H, ddt, J = 2.5 and 11 Hz, H2), 2.73 (1H, dt, J = 3 and 13 Hz, H6a), 2.29 (1H, ddd, J = 2.5 and 14 Hz, H7), 1.97–1.20 (7H, m); ms, *m/z*: 231 (34%), 187 (16), 186 (24), 127 (28), 104 (100).

Anodic methoxylations

All anodic methoxylations were carried out at room temperature in methanol (analytical grade) containing Et_4NOTs as a supporting electrolyte, in an undivided cell equipped with two vitreous carbon electrodes, an exit tube (containing $CaCl_2$) for venting purposes, and a magnetic stirring bar. The carbon electrodes (0.3 cm in diameter, immersed 3.5 cm into the solution) were spaced 1.0 cm apart. The potentiostat was a homemade apparatus. I_0 is the current intensity at the beginning of the anodic oxidation.

*Preparation of **12** by anodic methoxylation*

Into the electrolysis cell were placed **11** (313 mg), Et_4NOTs (80 mg), and 15 mL of methanol. The solution was stirred for 10 min and a constant potential of 8.00 V was applied. After 8 F/mol of electricity was passed (15.5 h, I_0 = 17.1 mA), some drops of NH_4OH were added to the solution and the solvent was evaporated; the residue was dissolved in water (70 mL), basified with NH_4OH, and extracted with $CHCl_3$ (2 × 70 mL). The combined $CHCl_3$ layers were evaporated and the residue was filtered ($CHCl_3$) through a short column of alumina to afford quantitatively the 6-methoxylated derivative **12** (oil, 343 mg); ^1H nmr δ: 7.3 (5H, m), 5.80 (1H, dd, H8), 5.40 (1H, m, H6), 4.28 (1H, m, H2), 3.72 (3H, s, NCO_2CH_3), 3.28 (3H, br, C6-OCH_3), 2.08 (3H, s), 2.4–1.4 (8H, m); ^{13}C nmr δ: 170.3, 156.7, 82.5 (C6), 73.9 (C8), 55.4 (C6-OCH_3), 52.6, 47.9 (C2), 40.0 (C7), 30.5 (C5), 27.5 (C3), 21.2 ($OCOCH_3$), 13.7 (C4); ms, *m/z*: 303 ($M^{+\cdot} - CH_3OH$, 4%), 275 (12), 260 (2), 243 (5), 214 (11), 172 (54), 140 (58), 71 (100).

*Preparation of **13** by anodic methoxylation*

Ketone **6** (82 mg) and Et_4NOTs (45 mg) in 15 mL of methanol were electrolyzed as described above to afford, after 8F/mol of electricity was passed (8.5 h, I_0 = 11.0 mA), the 6-methoxylated derivative **13** (oil, 88 mg, 96% yield), ^1H nmr δ: 8.1–7.3 (5H), 5.44 (1H, m, H6), 4.84 (1H, m, H2), 3.73 (3H, m, NCO_2CH_3), 3.34 (3H, m, C6-OCH_3); ^{13}C nmr δ: 198.7 (C8), 156.8, 137.2, 133.1, 128.6, 82.6 (C6), 55.5 (C6-OCH_3), 52.7, 47.4 (C2), 42.0 (C7), 30.1 and 27.6 (C3 and C5), 13.6 (C4); ms, *m/z*: 259 ($M^{+\cdot} - CH_3OH$, 17%), 172 (21), 154 (60), 140 (43), 105 (52), 77 (28), 75 (16), 71 (100).

*Anodic methoxylation of **14***

The bicyclic compound **14** (296 mg) and Et_4NOTs (150 mg) in 15 mL of methanol were electrolyzed as described above. After 7 F/mol of electricity was passed (9.5 h, I_0 = 28.1 mA) the mixture was treated in the usual way. Fractionation of the residue by chromatography on alumina ($CHCl_3$) afforded four fractions. The first fraction contained the pure 2-methoxylated derivative **15** (or **16**) (oil, 59 mg); ^1H nmr δ: 7.35 (5H, m), 5.11 (1H, dd, J = 2 and 12 Hz, H8), 4.12 (1H, m, H6e), 3.15 (3H, s, OCH_3), 2.93 (1H, dt, J = 3 and 13 Hz, H6a), 2.48 (1H, dd, J = 12 and 14 Hz, H7a), 1.96 (1H, dd, J = 2 and 14 Hz, H7e); ms, *m/z*: 261 (2%), 260 (4), 230 (56), 216 (19), 186 (100), 105 (76), 104 (55), 82 (69), 77 (48), 71 (51), 55 (58). The second fraction (85 mg) was a mixture of the same 2-methoxylated derivative **15** (or **16**) and the 6-methoxylated derivative **17** (1:3 by ^1H nmr); ms *m/z*: 261. **17**: ^1H nmr δ: 7.35 (m), 5.70 (m, H6), 5.18 (dd, J = 2 and 12 Hz, H8), 3.36 (s, OCH_3). The third fraction (34 mg) was a mixture of **17** and the other 2-methoxylated derivative **16** (or **15**) (1:1 by ^1H nmr). The last fraction contained the pure 2-methoxylated derivative **16** (or **15**) (oil, 71 mg): ^1H nmr δ: 7.35 (5H, m), 5.35 (1H, dd, J = 2 and 12 Hz, H8), 4.28 (1H, m, H6e), 3.31 (3H, s, OCH_3), 3.09 (1H, dt, J = 3 and 13 Hz, H6a), 2.45 (1H, dd, J = 2 and 15 Hz, H7e), 1.94 (1H, dd, J = 12 and 15 Hz, H7a); ms, *m/z*: 261 (4%), 260 (2), 230 (73), 186 (100), 105 (30), 104 (75), 82 (63), 77 (29), 55 (48).

*Nucleophilic displacement of the methoxy group of **12***

To a stirred solution of $TiCl_4$ (638 mg) in dichloromethane (10 mL) at −78°C, under an atmosphere of nitrogen, was added dropwise a solution of **12** (1012 mg) in the same solvent (10 mL). After the mixture was stirred for 5 min, a solution of 2-trimethylsilyloxypropene (21) (770 mg), contaminated by ca. 25% of $(CH_3)_3SiOSi(CH_3)_3$) in dichloromethane (10 mL), was added dropwise. The resulting reaction mixture was stirred for 2 h at −78°C and then allowed to reach room temperature (2 h). Cold water (100 mL) was then added and the solution was stirred for 10 min. After basification with NH_4OH, the mixture was extracted with $CHCl_3$ (3 × 100 mL). The combined organic layers were evaporated and the residue was fractionated by chromatography on alumina ($CHCl_3$) to afford **18** (oil, 766 mg, 70% yield) and the enecarbamate **19** (oil, 90 mg, 10% yield). **18**: ^1H nmr δ: 7.3 (5H, m), 5.77 (1H, dd, J = 4 and 10 Hz, H8), 4.67 (1H, m, H6), 4.30 (1H, m, H2), 3.69 (3H, s), 2.65 (2H, m, H9 and H9′), 2.16 and 2.10 (2 × 3H), 2.07–1.5 (8H, m); ^{13}C nmr δ: 206.5, 170.3, 156.2, 140.6, 128.6, 128.1, 126.5, 73.7 (C8), 52.6, 48.4 (C9), 47.5 and 46.4 (C2 and C6), 41.3 (C7), 30.0 (C11), 28.0 and 27.3 (C3 and C5), 21.2,

Can. J. Chem. Downloaded from www.nrcresearchpress.com by 195.138.81.100 on 09/07/12
For personal use only.

13.9 (C4); ms, *m/z*: 361 (<0.5%), 318 (0.5), 301 (15), 242 (10), 212 (4), 198 (19), 154 (10), 140 (100), 85 (11), 83 (18), 75 (6), 43 (16). **19**: ^{1}H nmr δ: 7.29 (5H, m), 6.72 (1H, m, H6), 5.84 (1H, dd, J = 4 and 9 Hz, H8), 4.88 (1H, m, H5), 4.38 (1H, m, H2), 3.75 (3H, s), 2.06 (3H, s), 2.26–1.55 (6H, m); ^{13}C nmr δ: 170.4, 153.8, 140.9, 128.7, 128.2, 126.7, 124.0 (C6), 105.9 (C5), 73.4 (C8), 53.0, 47.7 (C2), 37.7 (C7), 24.2 (C3), 21.3, 17.7 (C4); ms, *m/z*: 303 (8%), 260 (2), 243 (11), 186 (4), 184 (8), 142 (16), 141 (38), 140 (100), 139 (81), 138 (90), 124 (15), 43 (28).

*Preparation of **21** from **18***

A solution of **18** (117 mg), ethylene glycol (128 mg), and $TsOH \cdot H_2O$ (3 mg) in 20 mL of benzene was heated under reflux for 20 h in a Dean–Stark apparatus. After evaporation of the solvent, the residue was dissolved in water (20 mL), basified with NH_4OH, and extracted with chloroform ((2 × 20 mL). The combined organic layers were evaporated and the residue was filtered through a short column of alumina ($CHCl_3$) to yield quantitatively **21** (oil, 131 mg) after evaporation: ^{1}H nmr δ: 7.3 (5H), 5.76 (1H, dd, J = 4 and 10 Hz, H8), 4.4 and 4.3 (2H, m, H6 and H2), 3.92 (4H, m, OCH_2CH_2O), 3.70 (3H, s), 2.09 (3H, s), 1.37 (3H, s), 2.1–1.4 (10H, m); ^{13}C nmr δ: 170.3, 156.1, 140.8, 128.0, 126.5, 109.4 (C10), 73.8 (C8), 64.6 and 64.1 (OCH_2CH_2O), 52.4 (NCO_2CH_3), 47.6 and 47.1 (C2 and C6), 43.1 and 41.3 (C7 and C9), 28.3 and 27.4 (C3 and C5), 23.8 (C11), 21.1 (CH_3COO), 14.0 (C4); ms, *m/z*: 405 (0.5%), 345 (3), 242 (12), 154 (3), 143 (4), 140 (100), 87 (55), 43 (24).

*Preparation of **22** from **21***

To a solution of **21** (125 mg) in THF (15 mL) was added $LiAlH_4$ (117 mg). The mixture was then heated under reflux for 17 h. Some drops of AcOEt and then water were added and the mixture was filtered through Celite and evaporated to dryness. The residue was dissolved in 0.2 N aqueous HCl (30 mL) and extracted with $CHCl_3$ (3 × 7 mL). The organic phases were discarded and the aqueous phase was basified with NH_4OH and extracted with chloroform (2 × 30 mL). Evaporation of the chloroform afforded **22** (oil, 81 mg, 82% yield): ^{1}H nmr δ: 7.25 (5H, m), 4.94 (1H, dd, J = 3 and 11 Hz, H8), 3.92 (4H, m), 3.24–3.04 (2H, m, H2 and H6), 2.26 (3H, s, NCH_3), 1.36 (3H, s), 1.99–1.30 (10H, m); ^{13}C nmr δ: 145.3, 128.2, 126.9, 125.6, 109.5 (C10), 76.1 (C8), 64.9 (C6), 64.6 and 64.3 (OCH_2CH_2O), 59.1 (C2), 43.0 (C9), 40.7 (C7), 26.2 (NCH_3), 24.1 (C11), 25.3, 24.0, and 23.2 (C3, C4, C5); ms, *m/z*: 319 (7%), 276 (8), 218 (47), 198 (100), 98 (17), 96 (34), 87 (50), 43 (21).

*Hydrolysis of the acetal **22***

A solution of the acetal **22** (93 mg) in 0.12 N aqueous HCl (20 mL) was heated under reflux for 30 min. The mixture was then cooled, basified with NH_4OH, and extracted with $CHCl_3$ (2 × 30 mL). Evaporation of the combined organic layers afforded a mixture (77 mg) of sedinone **23** and 6-episedinone **24** (9:1 by ^{1}H nmr).

*Preparation of (−)sedinone **23** from (−)-norsedamine **9***

K_2CO_3 (600 mg) and methylchloroformate (0.4 mL) were successively added to a stirred solution of (−)-norsedamine **9** (401 mg) in water (30 mL). After 4 h, NH_4OH was added and the solution was extracted with $CHCl_3$ (2 × 30 mL). The combined organic layers were evaporated and the residue was filtered through a short column of alumina ($CHCl_3$) to afford quantitatively (−)-**7** (oil, 512 mg) after evaporation of the solvent; acetylation of the alcohol (−)-**7**, as described for racemic **7**, yielded (−)-**11** (oil), $[\alpha]_D$ −98° (*c* 1.7, MeOH), Anodic methoxylation of (−)-**11** afforded (−)-**12** (oil), $[\alpha]_D$ −96° (*c* 1.9, MeOH).

Starting from (−)-**12**, the sequence described for the racemic compound (nucleophilic displacement, acetalization, $LiAlH_4$ reduction, and hydrolysis) afforded a 90:10 mixture (by ^{1}H nmr) of (−)-sedinone **23** (^{1}H nmr, NCH_3 δ: 2.26) and 6-episedinone **24** (^{1}H nmr, NCH_3 δ: 2.33); 184 mg of the above mixture was dissolved in ether (25 mL) and treated with gaseous HCl. Crystallization of the precipitate from 2-butanone afforded (−)-sedinone hydrochloride (138 mg), mp 175–177°C; $[\alpha]_D$ −79° (*c* 2, MeOH) (lit. (22) mp 175°C; $[\alpha]_D$ −79.4° (*c* 1, MeOH)). The mass and ^{1}H nmr spectra of the free base were identical with those reported in the literature (7, 22).

*Preparation of the enecarbamate **19** from **12***

A mixture of **12** (655 mg) and $TsOH \cdot H_2O$ (68 mg) in benzene (50 mL) was stirred for 30 min at room temperature. The solvent was then evaporated and the residue was filtered through a short column of alumina ($CHCl_3$) to afford, after evaporation, the enecarbamate **19** (oil, 570 mg, 96% yield). The spectra of **19** are described above.

*Bromomethoxylation of the enecarbamate **19***

To a mixture of **19** (101 mg) and sodium (8.4 mg) in anhydrous methanol (8 mL) was added dropwise a solution of bromine (68 mg) in anhydrous methanol (7 mL). The mixture was then stirred for 15 min at room temperature. After evaporation of the solvent, the residue was dissolved in dilute NH_4OH (70 mL) and extracted with $CHCl_3$ (2 × 70 mL). The combined organic layers were evaporated and the residue was filtered through a short column of alumina ($CHCl_3$) to yield quantitatively the bromo derivative **25** (oil, 139 mg): ^{1}H nmr δ: 7.3 (5H, m), 5.75 (1H, dd, H8), 5.5 (1H, m, H6), 4.35 (2H, m, H2 and H5), 3.7 (3H, s, $NCOOCH_3$), 3.4 and 3.3 (3H, 2s, C6-OCH_3), 2.1 (3H, s), 2.6–1.4 (6H, m); ms, *m/z*: 383 (18%), 381 (18), 323 (17), 321 (17), 220 (77), 219 (100), 218 (>100), 217 (95), 216 (63), 204 (26), 202 (26), 140 (65), 94 (57), 43 (69).

*Iodomethoxylation of the enecarbamate **19***

To the enecarbamate **19** (288 mg) and sodium (24.2 mg) in anhydrous methanol (10 mL) was added dropwise a solution of iodine (271 mg) in anhydrous methanol (10 mL). After stirring for 1 h, the mixture was treated as described above to afford the 5-iodo derivative **26** (oil, 374 mg, 85% yield): ^{1}H nmr δ: 7.32 (5H, m), 5.79 (1H, dd, J = 5 and 9 Hz, H8), 5.64 and 5.48 (1H, 2m, H6), 4.5–4.2 (2H, m, H2 and H5), 3.76 (3H, s, $NCOOCH_3$), 3.34 (3H, m, C6-OCH_3), 2.09 (3H, s), 2.4–1.6 (6H, m); ms, *m/z*: 430 (2%), 401 (22), 302 (8), 274 (19), 266 (21), 261 (24), 242 (25), 197 (75), 170 (40), 140 (83), 138 (51), 43 (78).

*Dehydroiodation of **26***

(a) A mixture of **26** (154 mg) and DBU (161 mg) in anhydrous toluene (0.5 mL) was heated at 87°C for 4 h. After cooling, pyridine (1 mL) and acetic anhydride (1 mL) were added and the solution was allowed to stand for 16 h at room temperature. Water and NH_4OH were then added and the mixture was extracted with chloroform (2 × 50 mL). The combined $CHCl_3$ layers were evaporated and the residue was filtered through a short column of alumina ($CHCl_3$). Evaporation of the solvent afforded **27** (oil, 103 mg, 93% yield): ^{1}H nmr δ: 7.30 (5H, m), 5.90–5.73 (3H, H4, H5, and H8), 5.47 (1H, m, H6), 4.40 (1H, m, H2), 3.73 (3H, m), 3.40 (3H, m, C6-OCH_3), 2.05 (3H, s), 2.5–1.7 (4H, m); ^{13}C nmr δ: 170.1, 156.5, 140.4, 128.4, 128.0, 126.9, 125.8 and 124.8 (C4 and C5), 80.0 (C6), 73.9 (C8), 56.4 (C6-OCH_3), 52.8, 44.9 (C2), 39.8 (C7), 28.2 (C3), 21.2; ms, *m/z*: 333 (<0.5%), 302 (3), 273 (8), 242 (5), 241 (5), 170 (18), 138 (100), 94 (25), 43 (16).

(b) The iodo derivative **26** (687 mg) in anhydrous toluene (1.5 mL) was treated with DBU (717 mg). After 4 h at 87°C, fractionation of the mixture by chromatography on alumina ($CHCl_3$) afforded the acetyl derivative **27** (oil, 213 mg, 43% yield) and the alcohol **28** (oil, 99 mg, 23% yield): ^{1}H nmr δ: 7.3 (5H), 5.80 (2H, m, H4 and H5), 5.16 (1H, m, H6), 4.77 (1H, dd, J = 3 and 12 Hz, H8), 4.46 (1H, m, H2), 3.82 (3H, m, $NCOOCH_3$), 3.60 (3H, m, C6-OCH_3), 2.5–1.6 (4H, m); ms, *m/z*: 291 (<0.5%), 259 (13), 170 (13), 153 (21), 139 (89), 138 (100), 94 (30).

*Nucleophilic displacement of the methoxy group of **27***

To a stirred solution of $TiCl_4$ (54 mg) in dichloromethane (5 mL) at −78°C, under an atmosphere of nitrogen, was added dropwise a solution of **27** (85 mg) in dichloromethane (5 mL). After the mixture was stirred for 5 min, a solution of 2-trimethylsilyloxypropene (65 mg, contaminated by ca. 25% of $(CH_3)_3SiOSi(CH_3)_3$) in dichloromethane (5 mL), was added dropwise. The solution was stirred for 2 h at −78°C and then allowed to reach room temperature (2 h). Cold water (40 mL) was added and the mixture was stirred for 10 min, basified with NH_4OH, and extracted with $CHCl_3$ (3 × 40 mL). After evaporation of the solvent, chromatography on alumina ($CHCl_3$) of the residue yielded **29** (oil, 59 mg, 64% yield): ^{1}H nmr δ: 7.33 (5H), 5.9–5.7 (3H, m, H4,

H5, and H8), 4.8–4.2 (2H, m, H2 and H6), 3.70 and 3.69 (3H, 2s, $NCOOCH_3$), 2.9–2.6 (2H, m, H9 and H9′), 2.17 and 2.16, 2.11 and 2.09 (2 × 3H, 4s), 2.5–1.8 (4H, m); ms, *m/z*: 302 (7%), 299 (39), 242 (12), 195 (75), 194 (99), 152 (39), 140 (47), 138 (100), 94 (58), 43 (92).

*Preparation of the acetal **30***

A solution of **29** (57 mg), ethylene glycol (62 mg), and $TsOH \cdot H_2O$ (1.5 mg) in benzene was heated under reflux for 16 h in a Dean–Stark apparatus. The solvent was then evaporated and the residue was dissolved in water, basified with NH_4OH, and extracted with $CHCl_3$ (2 × 40 mL) to yield quantitatively the acetal **30** (oil, 64 mg): ^1H nmr δ: 7.3 (5H), 5.98–5.65 (H3, H4, H5, and H8), 4.51 (2H, m, H2 and H6), 3.94 (4H, m), 3.70 (3H, m, $NCOOCH_3$), 2.08 (3H, m, CH_3COO), 1.42 (3H, m), 2.3–1.6 (6H, m); ms, *m/z*: 403 (<0.5%), 344 (3), 343 (2), 302 (7), 242 (7), 194 (9), 140 (39), 138 (100), 87 (91), 43 (43).

*Reduction of **30** with $LiAlH_4$*

To a solution of the acetal **30** (63 mg) in THF (15 mL) was added $LiAlH_4$ (58 mg); the mixture was refluxed for 16 h. Some drops of AcOEt and water were added and the mixture was filtered through Celite and evaporated to dryness. The residue was dissolved in 0.2 N aqueous HCl (50 mL) and extracted with $CHCl_3$ (2 × 3 mL). The aqueous phase was then basified with NH_4OH and extracted with $CHCl_3$ (3 × 50 mL). Evaporation of the combined $CHCl_3$ phases afforded **31** (oil, 43 mg, 86% yield): ^1H nmr δ: 7.3 (5H, m), 5.78–5.56 (2H, m, H4 and H5), 4.95 (1H, dd, J = 2 and 11 Hz, H8), 3.96 (4H, m, OCH_2CH_2O), 3.83 (1H, m, H6), 3.43 (1H, m, H2), 2.21 (3H, s, NCH_3), 1.38 (3H, s), 2.5–1.35 (6H, m); ms, *m/z*: 317 (5%), 216 (72), 196 (28), 98 (71), 96 (81), 94 (100), 87 (93).

*Hydrolysis of the acetal **31***

A solution of the acetal **31** (38 mg) in 0.1 N aqueous HCl (20 mL) was heated under reflux for 30 min. After cooling, NH_4OH was added and the mixture was extracted with $CHCl_3$ (2 × 30 mL) to afford a 9:1 mixture (by ^1H nmr) of 6-episedacrine **32** and sedacrine **33** (32 mg). The mixture was then dissolved in methanol (15 mL) and left at room temperature for 16 h. Evaporation of the solvent yielded a 1:6 mixture (by ^1H nmr) of **32** and **33** (32 mg).

*Synthesis of (−)-sedacrine **33***

Starting from (−)-**12**, the sequence described above afforded a 1:6 mixture of 6-episedacrine **32** and (−)-sedacrine **33**. This mixture was dissolved in 2-butanone and a solution of perchloric acid in acetone was added until neutralization. The solvent was evaporated and fractional crystallizations of the residue from 2-butanone yielded pure (−)-sedacrine perchlorate, mp 168–169°C; $[\alpha]_D$ −114° (*c* 1.7, MeOH) (lit. (7) mp 169°C; $[\alpha]_D$ −115° (*c* 2, MeOH)). The nmr and mass spectra of the free base are identical with those reported in the literature (7, 22).

Acknowledgements

The authors wish to thank Professor J. Nasielski for his stimulating interest. F.D. thanks the Institut pour l'Encouragement de la Recherche Scientifique dans l'Industrie et l'Agriculture (IRSIA) for the award of a fellowship. C.H. is a Research Associate of the National Fund for Scientific Research (FNRS).

1. G. M. STRUNZ and J. A. FINDLAY. *In* The alkaloids. Vol. 26. *Edited by* A. Brossi. Academic Press, New York. 1985.
2. A. NUMATA and T. IBUKA. *In* The alkaloids. Vol. 31. *Edited by* A. Brossi. Academic Press, New York. 1987.
3. T. SHONO. Tetrahedron, **40**, 811 (1984), and references cited therein.
4. L. G. WISTRAND. Janssen Chim. Acta, **4**, 34 (1986), and references cited therein.
5. T. SHONO, H. HAMAGUSHI, and Y. MATSUMURA. J. Am. Chem. Soc. **97**, 4264 (1975).
6. T. SHONO, Y. MATSUMURA, and K. TSUBATA. J. Am. Chem. Soc. **103**, 1172 (1981).
7. B. COLAU and C. HOOTELÉ. Can. J. Chem. **61**, 470 (1983).
8. P. D. PALASZ, J. H. P. UTLEY, and J. D. HARDSTONE. J. Chem. Soc. Perkin Trans. 2, 807 (1984).
9. V. MANCUSO and C. HOOTELÉ. Tetrahedron Lett. **29**, 5917 (1988).
10. P. J. TIREL, M. VAULTIER, and R. CARRIÉ. Tetrahedron Lett. **30**, 1947 (1989).
11. (*a*) J. J. TUFARIELLO and SK. ASROF ALI. Tetrahedron Lett. 4647 (1978); (*b*) C. HOOTELÉ, W. IBEBEKE-BOMANGWA, F. DRIESSENS, and S. SABIL. Bull. Soc. Chim. Belg. **96**, 57 (1987); (*c*) W. IBEBEKE-BOMANGWA and C. HOOTELÉ. Tetrahedron, **43**, 935 (1987); (*d*) A. LIGUORI, R. OTTANÀ, G. ROMEO, G. SINDONA, and N. UCELLA. Chem. Ber. **122**, 2019 (1989).
12. C. SCHÖPF, W. BUNDSCHUH, G. DUMMER, T. KAUFFMANN, and R. KRESS. Annalen, **628**, 101 (1959).
13. T. SHONO, Y. MATSUMURA, O. ONOMURA, and Y. YAMADA. Tetrahedron Lett. **28**, 4073 (1987).
14. (*a*) S. TORII, T. INOKUCHI, F. AKAHOSHI, and M. KUBOTA. Synthesis, 242 (1987); (*b*) S. TORII, T. INOKUCHI, S. TAKAGISHI, F. AKAHOSHI, and K. UNEYAMA. Chem. Lett. 639 (1987).
15. T. SHONO, Y. MATSUMURA, K. TSUBATA, Y. SUGIHARA, S. YAMANE, T. KANAZAWA, and T. AOKI. J. Am. Chem. Soc. **104**, 6697 (1982).
16. L. H. B. BAPTISTELLA, J. F. DOS SANTOS, K. C. BALLABIO, and A. J. MARSAIOLI. Synthesis, 436 (1989).
17. P. DESLONGCHAMPS. *In* Stereoelectronic effects in organic chemistry. Pergamon, New York. 1983. Chap. 6.
18. P. BEAK and W. J. ZAJDEL. J. Am. Chem. Soc. **106**, 1010 (1984), and references cited therein.
19. D. L. COMINS and M. A. FOLEY. Tetrahedron Lett. **29**, 6711 (1988).
20. C HOOTELÉ, F. HALIN, and S. THOMAS. Tetrahedron, **41**, 5563 (1985).
21. H. O. HOUSE, L. J. CZUBA, H. GALL, and H. D. OLMSTEAD. J. Org. Chem. **34**, 2324 (1969).
22. B. FRANCK. Chem. Ber. **91**, 2803 (1958).
23. F. GALINOVSKY, G. BIANCHETTI, and O. VOGEL. Monatsh. Chem. **84**, 1221 (1953).
24. K. IRIE, A. AOE, T. TANAKA, and S. SAITO. J. Chem. Soc. Chem. Commun. 633 (1985).
25. T. SHONO, Y. MATSUMURA, K. TSUBATA, and K. UCHIDA. J. Org. Chem. **51**, 2590 (1986).

Can. J. Chem. Downloaded from www.nrcresearchpress.com by 195.138.81.100 on 09/07/12
For personal use only.

Structure of the O-antigen of *Actinobacillus pleuropneumoniae* serotype 12 lipopolysaccharide[1]

LINDA M. BEYNON, MALCOLM B. PERRY,[2] AND JAMES C. RICHARDS
Division of Biological Sciences, National Research Council of Canada, Ottawa, Ont., Canada K1A 0R6

Received July 18, 1990

LINDA M. BEYNON, MALCOLM B. PERRY, and JAMES C. RICHARDS. Can. J. Chem. **69**, 218 (1991).

The structure of the O-antigen of *Actinobacillus pleuropneumoniae* serotype 12 was determined by 1D and 2D NMR spectroscopic methods, methylation analysis, and partial hydrolytic degradation. The O-polysaccharide was shown to consist of a trisaccharide repeating unit having the structure

$$\begin{array}{l}\rightarrow 5)\text{-}\beta\text{-D-Gal}f\text{-}(1\rightarrow 6)\text{-}\beta\text{-D-Gal}f\text{-}(1\rightarrow \\ \quad\quad\quad\

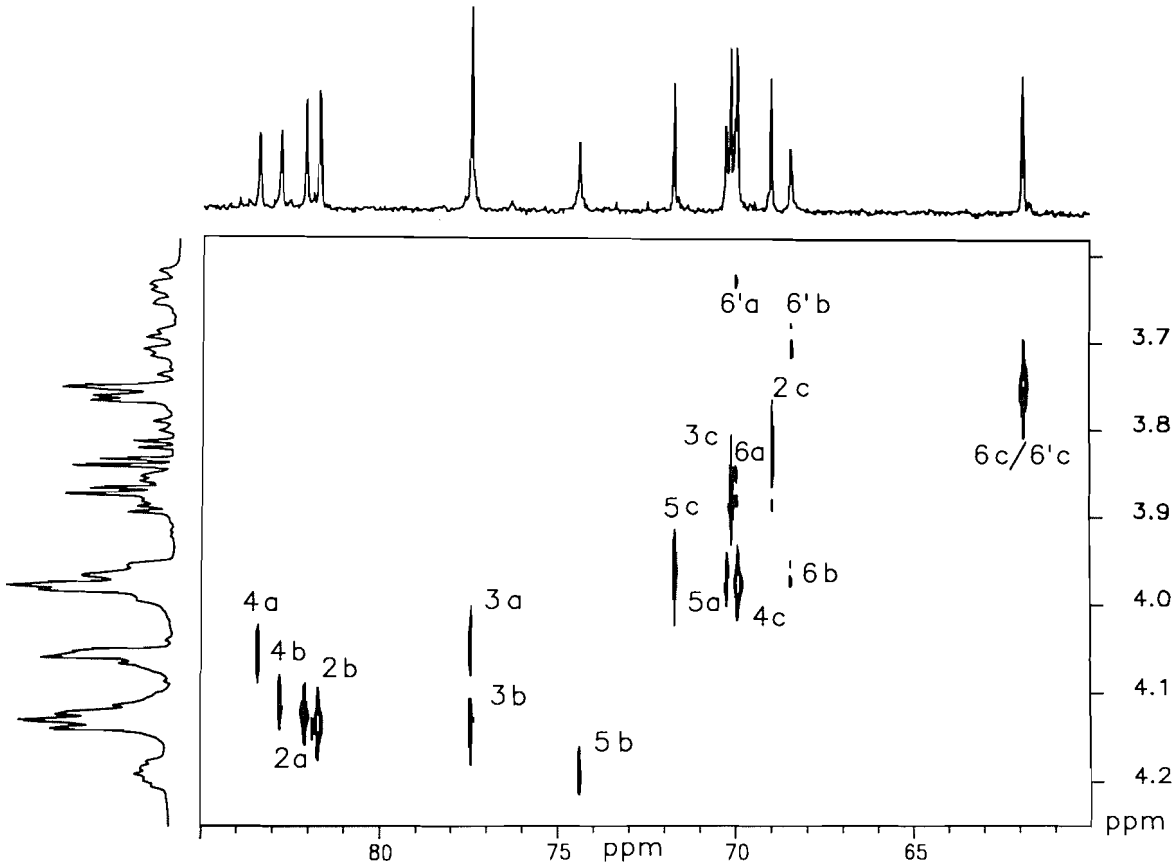


FIG. 1. Heteronuclear $^{13}C-^{1}H$ chemical shift correlation map, for the spectral regions F_2 (85–60 ppm) and F_1 (4.30–3.58 ppm), of the *A. pleuropneumoniae* serotype 12 LPS O-polysaccharide. The respective ^{13}C and ^{1}H 1D projections are displayed along the F_2 and F_1 axes, respectively, and the correlated resonances are labelled.

TABLE 1. Methylation analyses data for *A. pleuropneumoniae* serotype 12 O-antigen and degradation products

Methylated sugar[a] (as alditol acetates)	T_{MG}[d]	Molar ratios[b,c]			
		I	II	III	IV
1,2,3,4,5-Gal	0.7		0.3	0.4	0.5
2,3,5,6-Gal	0.9				0.2
2,3,4,6-Gal	1.0	1.0	1.0	1.0	1.0
2,3,5-Gal	1.4	0.6		0.5	
2,3-Gal	1.7	0.9			

[a]2,3,4,6-Gal represents 1,5-di-*O*-acetyl-2,3,4,6-tetra-*O*-methylgalactitol, etc.

[b]I, O-polysaccharide; II, α-D-Gal$_p$-(1 → 6)-D-Gal-ol; III, α-D-Gal$_p$-(1 → 6)-β-D-Gal$_f$-(1 → 6)-D-Gal-ol; IV, reduced disaccharide fraction.

[c]Uncorrected, fid response.

[d]Retention times relative to that of 1,5-di-*O*-acetyl-2,3,4,6-tetra-*O*-methylgalactitol.

the three sugars in the repeating unit were 6-linked. A third methylene resonance at 61.9 ppm could be attributed to the primary hydroxyl carbon of the galacto*pyranosyl* residue (16).

Methylation and hydrolysis of the O-chain afforded a product that, after reduction ($NaBH_4$) and acetylation, gave GLC–MS results (Table 1) that indicated the polysaccharide to be composed of branched trisaccharide repeating units in which the D-galactopyranosyl residues were present as the non-reducing end groups. Thus, the combined analytical results indicated that the trisaccharide repeating unit consists of a terminal α-D-galactopyranosyl, a 6-*O*-substituted β-D-galactofuranosyl, and a 5,6-di-*O*-substituted β-D-galactofuranosyl residue.

NMR studies of the O-polysaccharide

The structure of the trisaccharide repeating unit was determined by a combination of 1D and 2D NMR methods. A complete assignment of the ^{1}H NMR spectrum was achieved via COSY and relay COSY, followed by subsequent assignment of the ^{13}C resonances from a 2D $^{13}C-^{1}H$ chemical shift correlation experiment (Fig. 1). The three galactosyl residues were labelled **a**, **b**, and **c** according to the order of decreasing anomeric ^{1}H chemical shifts. The resonances corresponding to the terminal α-D-galactopyranosyl residue (residue **c**) were well resolved and the corresponding sub-spectrum was readily identified on the basis of the observed proton coupling constants (Table 2).

Identification of the sub-spectra corresponding to the two β-D-galactofuranosyl residues **a** and **b** was more difficult. The resonances associated with these residues were not well resolved and strong coupling between H-3**a** and H-4**a**, and between H-2**b**, H-3**b**, and H-4**b**, precluded measurement of the related vicinal coupling constants. Fortunately, the H-6 and H-6′ resonances for **a** and **b** could be easily identified, from connectivities to the corresponding methylene carbon (C-6) resonances in the $^{13}C-^{1}H$ chemical shift correlation map (Fig. 1), which permitted additional points of entry into the respective ^{1}H spin-systems. In this way, the resonance associated with H-5**b** (4.19 ppm) was easily assigned from the corresponding cross-peaks to H-6**b** (3.98 ppm) and H-6′**b** (3.70 ppm). In the COSY contour plot, cross-peaks relating the H-4**b**/H-5**b**,

Can. J. Chem. Downloaded from www.nrcresearchpress.com by 195.138.81.100 on 09/07/12
For personal use only.

TABLE 2. ^{1}H Chemical shifts[a] and coupling constants (in parentheses) for the O-antigen of *A. pleuropneumoniae* serotype 12

Proton	Unit **a** → 6)-β-D-Gal$_f$-(1 →	Unit **b** → 5)-β-D-Gal$_f$-(1 → 6 ↑	Unit **c** α-D-Gal$_p$-(1 →
H-1 ($J_{1,2}$)[b]	5.28 (1.8)	5.04 (1.8)	4.99 (3.6)
H-2 ($J_{2,3}$)	4.13 (4.4)	4.14 (—)[c]	3.83 (10.9)
H-3 ($J_{3,4}$)	4.04 (—)	4.13 (—)	3.87 (3.2)
H-4 ($J_{4,5}$)	4.05 (—)	4.11 (4.4)	3.98 (1)
H-5	3.97	4.19	3.97
H-6 ($J_{5,6}$)	3.87 (3.4)	3.98 (5.5)	3.76 (—)
H-6′ ($J_{5,6'}$)	3.63 (7.2)	3.70 (3.6)	3.76 (—)
($J_{6,6'}$)	(10.8)	(10.8)	(—)

[a]Measured at 27°C in ppm from internal acetone (δ 2.225).
[b]First-order coupling constants measured in hertz (Hz).
[c]Unresolved coupling.

H-5**b**/H-6**b**, and H-5**b**/H-6′**b** proton pairs were apparent along a line at the chemical shift value of H-5**b** (4.19 ppm) (Fig. 2). Similarly, it was possible to identify H-4**a** (4.05 ppm), H-5**a** (3.97 ppm), H-6**a** (3.87 ppm), and H-6′**a** (3.63 ppm) from the related cross-peaks in the COSY spectrum. That the resonances of H-2**b** (4.14 ppm) and H-3**b** (4.13 ppm) overlapped was obvious from the relay COSY spectrum, which showed only a single cross-peak relating H-1**b** and both H-2**b** and H-3**b**. The overlapping of the ring proton resonances in β-D-galactofuranosyl residues has been observed previously (17).

The apparent deshielding (17) of resonances corresponding to H-5 and H-6 for residue **b** and H-6 for residue **a** (Table 2) is diagnostic of glycosidation at the respective C-5 and C-6 positions.

The ^{13}C NMR spectrum of the O-polysaccharide contained 17 discrete signals, which were assigned via 2D heteronuclear ^{13}C–^{1}H chemical shift correlation (Fig. 1) and by reference to published data (12, 13, 16) (Table 3). The low-field positions for C-4 and C-2 (81–83 ppm) of residues **a** and **b** are characteristic of galactofuranose residues (12, 13) and, since the chemical shifts of C-1**c** → C-6**c** correlate closely with those published (16) for methyl α-D-galactopyranoside, **c** was identified as a non-reducing terminal sugar.

The arrangement of the three galactose residues within the repeating unit was determined from ^{1}H–^{1}H nOe measurements and selective INEPT experiments.

Saturation of each of the three anomeric protons showed *intra*-residue nOe to the H-2 resonances within the respective ring systems. In addition, significant *inter*-residue effects between H-1**a** and H-5**b**, between H-1**b** and the H-6**a**/H-6′**a** pair, and between H-1**c** and the H-6**b**/H-6′**b** pair indicate the arrangement of the residues within the polysaccharide to be

$$\rightarrow \mathbf{a} \rightarrow \mathbf{b} \rightarrow \mathbf{a} \rightarrow$$
$$\uparrow$$
$$\mathbf{c}$$

Confirmation of this sequence was obtained from selective INEPT experiments. Due to the inherent flexibility of the furanose ring systems (18) within the polymer, it was possible to employ this technique (19) to establish connectivities between the anomeric protons and the aglyconic carbons of adjacent residues. A truncated version of the selective INEPT pulse sequence was employed without broad-band proton decoupling (20), and the ^{13}C NMR spectra obtained from pulsing the

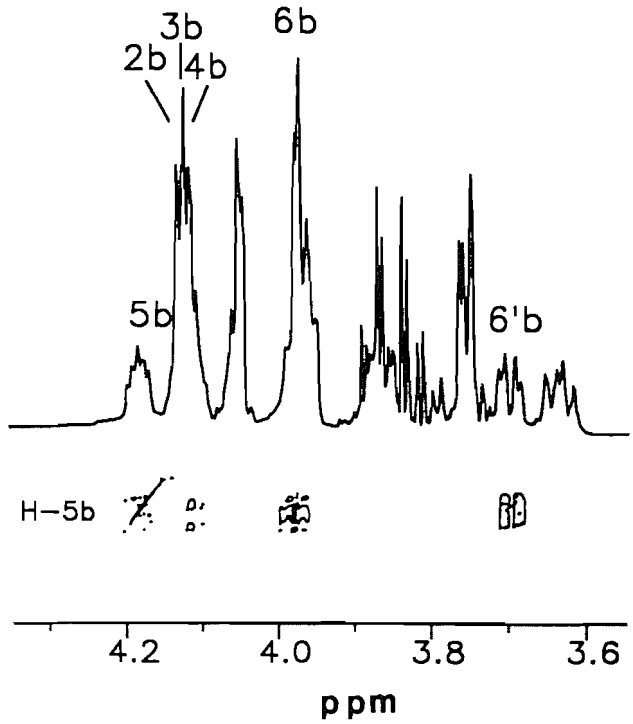


FIG. 2. Cross-peaks relating the H-4, H-5, H-6, and H-6′ resonances belonging to the residue **b** sub-spectrum in the COSY contour plot of the serotype 12 O-polysaccharide at the H5**b** chemical shift value. Resonance assignments associated with residue **b** are indicated in the 1D projection.

anomeric proton resonances of each of the three galactosyl residues are shown in Fig. 3.

The intensity of the ^{13}C signals in the selective INEPT spectra is a function of the efficiency of polarization transfer through a $^3J_{H,C}$ coupling pathway and is conformationally dependent (21). The spectra obtained from pulsing the anomeric protons of the β-D-galactofuranosyl residues (Figs. 3a and 3b) showed intense doublets for C-4 arising from the efficient transfer of polarization within the furanosyl ring systems via H-1 → C-1 → O-4 → C-4, whereas polarization transfer to C-3 via H-1 → C-1 → C-2 → C-3 was absent (Fig. 3a) or very weak (Fig. 3b). Polarization transfer across the respective glycosidic linkages from H-1**a** to C-5**b** (d, 74.4 ppm, Fig. 3a), and from H-1**b** to

Can. J. Chem. Downloaded from www.nrcresearchpress.com by 195.138.81.100 on 09/07/12
For personal use only.

Can. J. Chem. Downloaded from www.nrcresearchpress.com by 195.138.81.100 on 09/07/12
For personal use only.

C-6**a** (t, 70.0 ppm, Fig. 3b) confirmed the sequence of the galactofuranosyl disaccharide backbone unit, → **a** → **b** →. Verification that the terminal α-D-galactopyranosyl residues **c** are 1,6-linked to the galactofuranosyl residues **b** was obtained from pulsing H-1**c** where the selective INEPT experiment (Fig. 3c) showed the connectivity to the methylene carbon triplet from C-6**b** (68.5 ppm) together with proton-coupled signals from C-3**c** (70.2 ppm) and C-5**c** (71.8 ppm) of the α-D-pyranoside.

In the spectrum obtained by pulsing H-1**b** (Fig. 3b), a ^{13}C doublet was observed (70.2 ppm) overlapping the C-6**a** triplet (70.0 ppm). This doublet could only be assigned to C-3**c**, and most likely arises from partial saturation of H-1**c** due to the proximity of the H-1**b** and H-1**c** resonances (ca. 25 Hz separation). Correspondingly, in the spectrum obtained by pulsing H-1**c** (Fig. 3c), the signal from C-4**b** (82.8 ppm) could be attributed to partial saturation of H-1**b**.

Depolymerization of the O-polysaccharide

Depolymerization of the polysaccharide with 48% aqueous hydrogen fluoride for 24 h (4°C), followed by fractionation of the product on Bio-Gel P2, afforded a disaccharide **1** (K_{av} 0.84) which had $[\alpha]_D$ +91.7 (*c* 0.8, water) and showed a single spot on TLC (R_f 0.20). The ^1H NMR spectrum of reduced **1** contained a single doublet ($J_{1,2}$ 3.3 Hz), for the anomeric proton at 4.98 ppm, indicating the presence of an α-linked residue. The ^{13}C NMR spectrum was consistent with the disaccharide alditol possessing a terminal α-D-galactopyranosyl residue (Table 3). GLC–EI–MS of reduced methylated **1** gave a single peak (T_{MS} 1.28) with fragment ions at *inter alia* *m/z* 219, 235, 249, and 133 (Fig. 4). Methylation analysis of reduced **1** gave 2,3,4,6-tetra-*O*-methylgalactitol and 1,2,3,4,5-penta-*O*-methylgalactitol (Table 1). These results permit **1** to be assigned the structure

α-D-Gal$_p$-(1 → 6)-D-Gal
1

In a second experiment depolymerization of the polysaccharide with 48% aqueous hydrogen fluoride for 6 h (0°C), followed by fractionation of the product on Bio-Gel P2, afforded a trisaccharide **2** (K_{av} 0.68) and a disaccharide fraction (K_{av} 0.81). The trisaccharide **2** showed predominantly one spot on TLC analysis (R_f 0.12). The ^1H NMR spectrum of reduced **2** contained two signals, for the anomeric protons, at 5.06 ($J_{1,2}$ 1.7 Hz) and 4.97 ppm ($J_{1,2}$ 2.0 Hz). The presence of two signals at 99.5 and 108.6 ppm (Table 3) in the ^{13}C NMR spectrum indicated that **2** contained both α-D-galactopyranose and β-D-galactofuranose residues. GLC–EI-MS analysis of reduced, methylated **2** gave a major peak (T_{MS} 5.30) with fragment ions at *m/z* 219, 393, 235, and 423 (Fig. 5) as well as a minor peak (7.5%, T_{MS} 1.25) that had a mass spectrum identical to that of reduced methylated **1**. Methylation analysis of the reduced sample gave 1,2,3,4,5-penta-*O*-methylgalactitol, 2,3,4,6-tetra-*O*-methylgalactitol, and 2,3,5-tri-*O*-methylgalactitol (Table 1), which allowed **2** to be assigned the structure

α-D-Gal$_p$-(1 → 6)-β-D-Gal$_f$-(1 → 6)-D-Gal
2

TLC analysis of the disaccharide fraction showed it to be a mixture of two oligosaccharides (R_f 0.17 and 0.29). GLC–EI-MS analysis of the reduced methylated fraction gave two peaks (T_{MS} 1.28 and 1.31, respectively) in the ratios of 1.0:0.28, each having a mass spectrum nearly identical to that of reduced methylated **1** (*m/z* 219, 187, 155, and 235). However, the fragment ion at *m/z* 88 in the mass spectrum of the minor component was of only low intensity (10%), suggesting that this disaccharide contained a non-reducing terminal galacto-

TABLE 3. ^{13}C chemical shifts[a] for the O-antigen of *A. pleuropneumoniae* serotype 12 and its acid hydrolysis products

Compound	Unit **a**						Unit **b**						Unit **c**					
	C-1	C-2	C-3	C-4	C-5	C-6	C-1	C-2	C-3	C-4	C-5	C-6	C-1	C-2	C-3	C-4	C-5	C-6
a →6)-β-D-Gal$_f$-(1→5)-β-D-Gal$_f$-(1→ **b** 6 | 1 α-D-Gal*p* **c**	107.9	82.1	77.5	83.4	70.3	70.0	108.8	81.7	77.5	82.8	74.4	68.5	99.3	69.0	70.2	70.0	71.8	61.9
4																		
c α-D-Gal$_p$-(1→6)-D-Gal-ol[b] **b**							64.0	71.0	70.1	70.1	70.2	69.2	99.3	69.0	70.3	70.2	71.8	62.0
Reduced **1**																		
b β-D-Gal$_f$-(1→6)-D-Gal-ol **a** 6 | 1 α-D-Gal$_p$[b] **c**	64.1	70.9	70.1	70.1	70.3	69.3	108.6	82.0	77.8	84.0	70.8	69.5	99.5	69.5	70.4	70.3	71.8	62.0
Reduced **2**																		

[a]Chemical shifts measured at 27°C in ppm with internal acetone as reference (δ 31.07).
[b]Chemical shifts assigned by comparison with those of the O-polysaccharide and with reference to published data (16).

Can. J. Chem. Downloaded from www.nrcresearchpress.com by 195.138.81.100 on 09/07/12
For personal use only.

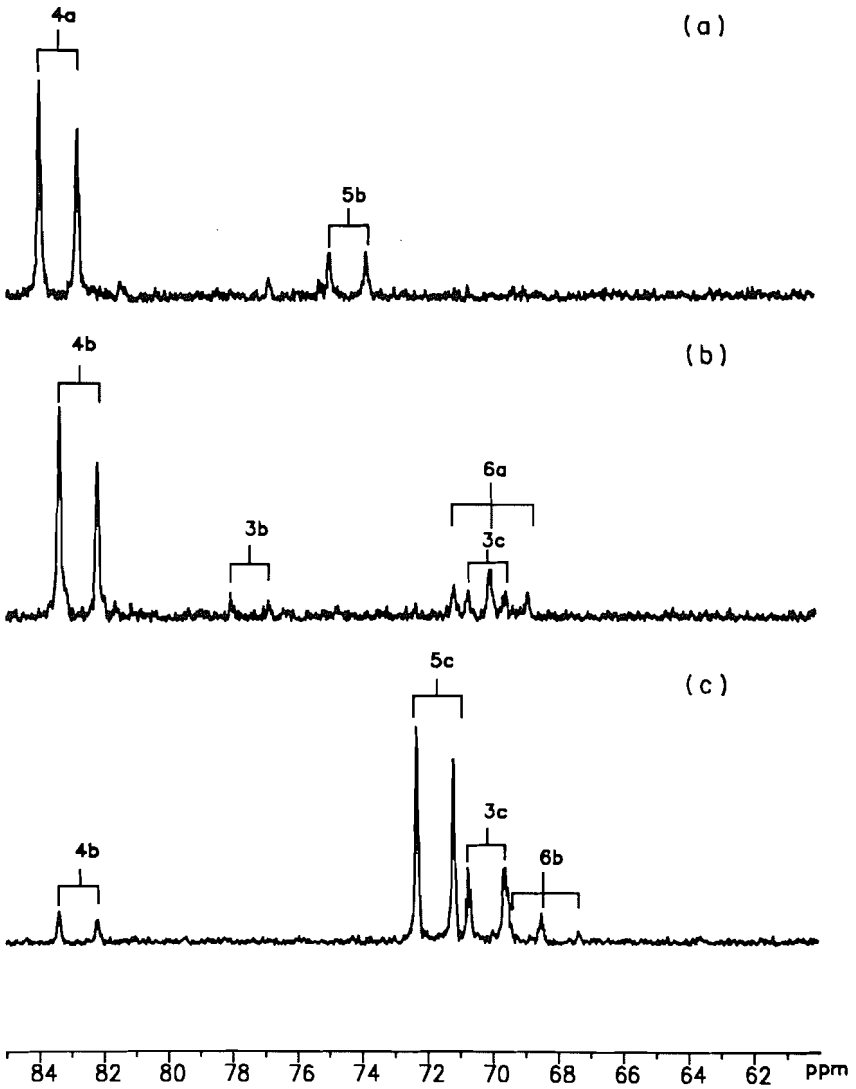


FIG. 3. Proton-coupled selective INEPT ^{13}C NMR spectra obtained from pulsing the H-1 resonances of (a) residue **a**; (b) residue **b**; and (c) residue **c**. Assignments are indicated.

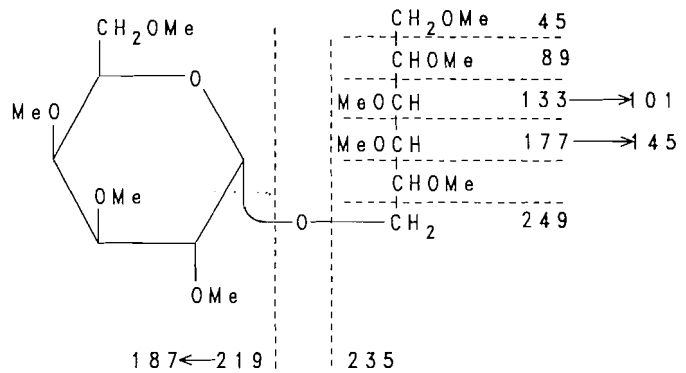


FIG. 4. GLC–EI-MS fragmentation ions from reduced methylated **1**.

furanosyl residue (22). The methylation analysis (Table 1) was in agreement with the major component of the disaccharide fraction having the same structure as **1** and the minor component having a non-reducing terminal galactofuranosyl residue. The lack of a second reducing residue, other than 1,2,3,4,5-penta-*O*-methylgalactitol, suggested that the minor component had the structure

$$\text{Gal}_f\text{-}(1 \rightarrow 6)\text{-Gal}$$

3

and arose from cleavage of the O-polysaccharide at the terminal galactopyranosidic and the 1,5-galactofuranosidic linkages.

Thus, the combined NMR spectroscopic and chemical evidence permits the branched trisaccharide repeating unit of the O-chain polysaccharide of *A. pleuropneumoniae* serotype 12 to be identified as

$$\begin{array}{l}\rightarrow 5)\text{-}\beta\text{-D-Gal}_f\text{-}(1\rightarrow 6)\text{-}\beta\text{-D-Gal}_f\text{-}(1\rightarrow \\ \qquad\qquad\quad 6 \\ \qquad\qquad\quad | \\ \qquad\qquad\quad \alpha\text{-D-Gal}p\end{array}$$

4

A number of other bacteria have been reported (20, 23–28) to possess LPS O-antigen polysaccharides that are composed solely of D-galactose residues. It is noteworthy, in this context, that the galactose content of the LPS from a virulent strain of *A. pleuropneumoniae* serotype 5 is 13 times that of an avirulent strain (28). The serotype 5 LPS O-polysaccharide consists of a homopolymer of 1,6-linked β-D-galactopyranosyl residues (23).

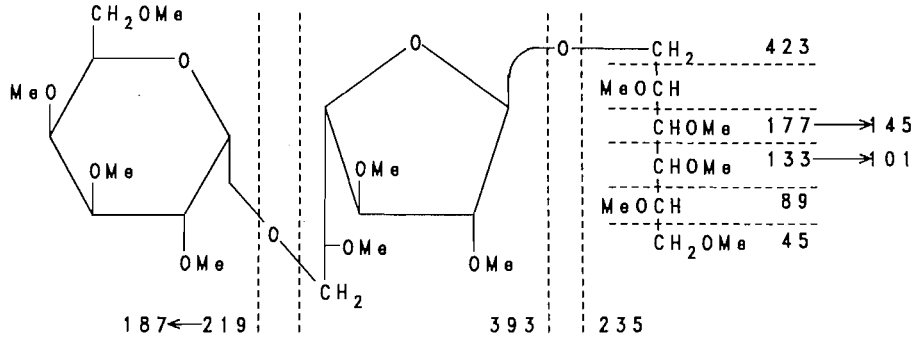


FIG. 5. GLC–EI-MS fragmentation ions from reduced methylated **2**.

Experimental

Production of lipopolysaccharide and O-polysaccharide

Actinobacillus pleuropneumoniae (NRCC 4267) serotype 12 was grown in Bacto PPLO broth (yield 260 g, wet weight) and LPS was isolated by the aqueous-phenol extraction procedure (9). A solution of LPS (0.35 g) in aqueous 1% acetic acid (100 mL) was kept at 100°C for 1.5 h, and the O-polysaccharide recovered by gel filtration on Sephadex G-50 and DEAE–Sephacel as previously described (29).

Analytical methods

Analytical methods were essentially as previously described (30). The following conditions were employed using a Hewlett–Packard 5885B GLC–MS system fitted with a flame ionization detector and an OV-17 fused silica capillary column (Quadrex Corp.): *A* (for alditol acetates), 180°C for 2 min then 4°C/min to 240°C; *B* (for partially methylated alditol acetates), 180°C for 2 min than 2°C/min to 240°C; *C* (for (*R*)-2-butyl acetate derivatives), 180°C for 4 min then 2°C/min to 240°C; *D* (for methylated disaccharide alditols), 220°C for 1 min then 7°C/min to 280°C; *E* (for methylated trisaccharide alditols), 240°C for 1 min then 10°C/min to 280°C. For methylated oligosaccharide alditols, retention times are quoted relative to that of methylated sucrose (T_{MS}).

Methylation of samples (2 mg) was carried out using the methods of either Hakomori (31) or Ciucanu and Kerek (32) and the products were isolated by partition between dichloromethane and water. Methylated oligosaccharide alditols were analysed directly by GLC–MS (programs *D* and *E*), followed by hydrolysis and conversion of the partially methylated glycoses to their alditol acetates, as previously described (33), and analysis by GLC–MS.

TLC was performed on silica gel (Merck) with 6:3:1 (v/v) propanol – conc. NH_3 – water. Sodium dodecyl sulphate (SDS)– PAGE was made under the same conditions as previously recorded (10).

NMR spectroscopy

Measurements were made at 27°C, on solutions in D_2O, using a Bruker AM-500 spectrometer equipped with an Aspect 3000 computer, operating in the pulsed Fourier transform mode with quadrature detection using standard Bruker software.

Proton NMR spectra (500 MHz) were recorded using a spectral width of 1.9 kHz, a 16 K data block, and a 90° pulse width. Chemical shifts are expressed relative to internal acetone (δ, 2.225 ppm). The nOe difference spectra were obtained by using a selective low-power presaturation pulse applied to the proton resonance for 200 ms, in which each line of a multiple resonance was irradiated sequentially for 20 ms, followed by a 90° observation pulse (34).

Broad-band proton-decoupled ^{13}C NMR spectra (125 MHz) were obtained using a spectral width of 31 kHz, a 32 K data block, and a 90° pulse width employing WALTZ decoupling (35). Heteronuclear $^1J_{C,H}$ values were measured using gated decoupling (36) and DEPT spectra (37) were obtained with broad-band proton decoupling, a 135° proton pulse width, and a 3.3 ms delay between pulses.

Homonuclear 2D COSY and relayed coherence transfer experiments were carried out employing conventional pulse sequences (38–40). Spectra were measured using data sets ($t_1 \times t_2$) of 512 × 2048 points for a spectral width of 1319 Hz, with a recycle delay of 1.2 s, and 32 transients were collected for each value of the incrementable delay (t_1). The data were zero-filled to give 1024 × 2048 points and, following resolution enhancement in both dimensions by unshifted sine-bell-window functions, the data were processed to give magnitude spectra with symmetrization.

The 2D ^{13}C–^1H chemical shift correlated spectrum was recorded with proton decoupling in the F_2 domain (41). The initial data matrix ($t_1 \times t_2$) of 128 × 4096 points was zero-filled and Fourier transformed to give a final matrix of 512 × 4096 points. Spectral widths of 7575 and 552 Hz for the respective ^{13}C (F_2) and ^1H (F_1) chemical shift domains and a recycle delay of 1.4 s were employed. Fixed delays τ_1 and τ_2 were set at 3.30 and 1.70 ms, respectively, to select for all multiplicities. Resolution enhancement was applied in both dimensions by means of a Lorentz-to-Gauss transformation and the data were processed to give a power spectrum.

Selective INEPT experiments were carried out without broad-band proton decoupling as described previously (20).

Depolymerization of the O-polysaccharide

O-Polysaccharide (20 mg), dissolved in 48% (w/v) aqueous hydrofluoric acid (1 mL), was kept at 4°C for 24 h. The reaction was quenched by pouring the mixture into a slurry of solid CO_2 – calcium carbonate – dichloromethane (42). The mixture was allowed to warm to room temperature and, after the addition of water, the precipitate and dichloromethane were removed by centrifugation. Disaccharide **1** (yield 6.3 mg), obtained by Bio-Gel P2 gel permeation chromatography, was reduced ($NaBH_4$, 20°C, 3 h). A sample (2 mg) of reduced **1** was methylated (32), analysed by GLC–MS, hydrolysed (4 M TFA, 1 h, 125°C), and the partially methylated glycoses converted to their alditol acetates.

O-Polysaccharide (24 mg) was treated with 48% (w/v) aqueous hydrofluoric acid (1 mL) for 6 h at 0°C and the product worked up as above. The products **2** (yield 2.8 mg) and a disaccharide fraction (yield 3.3 mg) were reduced and methylated (31), analysed by GLC–MS, hydrolysed (4 M TFA, 45 min, 125°C), and the partially methylated glycoses converted to their alditol acetates.

General methods

Concentrations were made under reduced pressure at <40°C. Optical rotations were measured at 20°C in 10-cm microtubes, using a Perkin Elmer 243 polarimeter.

Acknowledgments

We thank Dr. S. Lariviere, University of Montreal, Saint Hyacinthe, for the bacterial culture, Mr. F. P. Cooper for the GLC–MS analyses, and Mr. D. W. Griffith for the large-scale production of bacterial cells.

1. R. A. SCHULTZ, T. F. YOUNG, R. F. ROSS, and J. R. JESKE. Am. J. Vet. Res. **43**, 1848 (1982).
2. T. N. K. SEBUNYA and J. R. SAUNDERS. J. Am. Vet. Med. Assoc. **182**, 1331 (1983).

Can. J. Chem. Downloaded from www.nrcresearchpress.com by 195.138.81.100 on 09/07/12
For personal use only.

3. A. GUNNARSSON, E. L. BIBERSTEIN, and B. HURVELL. J. Am. Vet. Res. **38**, 1111 (1977).
4. S. ROSENDAL and D. A. BOYD. J. Clin. Microbiol. **16**, 840 (1982).
5. R. NIELSEN and P. J. O'CONNOR. Acta Vet. Scand. **25**, 96 (1984).
6. R. NIELSEN. Acta Vet. Scand. **26**, 501 (1985).
7. R. NIELSEN. Acta Vet. Scand. **26**, 581 (1985).
8. R. NIELSEN. Acta Vet. Scand. **27**, 453 (1986).
9. K. G. JOHNSON and M. B. PERRY. Can. J. Microbiol. **22**, 29 (1976).
10. G. M. TSAI and C. E. FRASCH. Anal. Biochem. **119**, 115 (1982).
11. G. J. GERWIG, J. P. KAMERLING, and J. F. G. VLIEGENTHART. Carbohydr. Res. **77**, 1 (1979).
12. P. A. J. GORIN and M. MAZUREK. Can. J. Chem. **53**, 1212 (1975).
13. P. A. J. GORIN and M. MAZUREK. Carbohydr. Res. **48**, 171 (1976).
14. K. BOCK, I. LUNDT, and C. PEDERSEN. Tetrahedron Lett. **13**, 1037 (1973).
15. K. BOCK and C. PEDERSEN. J. Chem. Soc. Perkin Trans. **2**, 293 (1974).
16. K. BOCK and H. THOGERSON. Annu. Rep. NMR Spectrosc. **13**, 1 (1982).
17. S. J. ANGYAL. Carbohydr. Res. **77**, 37 (1979).
18. C. ALTONA and M. SUNDARALINGHAM. J. Am. Chem. Soc. **94**, 8205 (1972).
19. A. BAX, W. EAGAN, and P. KOVAC. J. Carbohydr. Chem. **3**, 593 (1984).
20. J. C. RICHARDS and R. A. LEITCH. Carbohydr. Res. **186**, 275 (1989).
21. A. BAX. J. Magn. Reson. **57**, 314 (1984).
22. N. K. KOCHETKOV and O. S. CHIZHOV. Adv. Carbohydr. Chem. Biochem. **21**, 39 (1966).
23. E. ALTMAN, D. W. GRIFFITH, and M. B. PERRY. Biochem. Cell Biol. **68**, 1268 (1990).
24. M. B. PERRY. Biochem. Cell Biol. **68**, 808 (1990).
25. M. B. PERRY and L. A. BABIUK. Can. J. Biochem. Cell Biol. **62**, 108 (1984).
26. D. OXLEY and S. G. WILKINSON. Carbohydr. Res. **193**, 241 (1989); **195**, 117 (1989).
27. C. WHITFIELD, M. B. PERRY, and B. CLARK. First Congress of the Int. Endotoxin Soc. May 1990.
28. A. E. JENSEN and T. A. BERTRAM. Infect. Immun. **51**, 419 (1986).
29. E. ALTMAN, J.-R. BRISSON, and M. B. PERRY. Carbohydr. Res. **179**, 245 (1988).
30. L. M. BEYNON, M. B. PERRY, and J. C. RICHARDS. Carbohydr. Res. In press.
31. S. I. HAKOMORI. J. Biochem. (Tokyo), **55**, 205 (1964).
32. I. CIUCANU and F. KEREK. Carbohydr. Res. **131**, 209 (1984).
33. L. M. BEYNON, M. MOREAU, J. C. RICHARDS, and M. B. PERRY. Carbohydr. Res. In press.
34. K. KINNS and J. K. M. SANDERS. J. Magn. Reson. **56**, 518 (1984).
35. A. J. SHAKA, J. KEELER, F. FRENKIEL, and R. FREEMAN. J. Magn. Reson. **52**, 335 (1983).
36. O. A. GANSOW and W. SCHMITTENHELM. J. Am. Chem. Soc. **93**, 4294 (1971).
37. D. M. DODDRELL, D. T. PEGG, and M. R. BENDALL. J. Magn. Reson. **48**, 323 (1982).
38. A. BAX, R. FREEMAN, and G. MORRIS. J. Magn. Reson. **42**, 164 (1981).
39. G. WAGNER. J. Magn. Reson. **55**, 151 (1983).
40. A. BAX and G. DROBNY. J. Magn. Reson. **61**, 306 (1985).
41. A. BAX and G. A. MORRIS. J. Magn. Reson. **42**, 501 (1981).
42. A. J. MORT and W. D. BAUER. J. Biol. Chem. **257**, 1870 (1982).

Can. J. Chem. Downloaded from www.nrcresearchpress.com by 195.138.81.100 on 09/07/12
For personal use only.

1,*n*-Radical ions. Photosensitized (electron transfer) carbon–carbon bond cleavage. Formation of 1,6-radical cations[1]

DONALD R. ARNOLD,[2] LAURIE J. LAMONT, AND ALLYSON L. PERROTT
Department of Chemistry, Dalhousie University, Halifax, N.S., Canada B3H 4J3

Received July 13, 1990

DONALD R. ARNOLD, LAURIE J. LAMONT, and ALLYSON L. PERROTT. Can. J. Chem. **69**, 225 (1991).

The reactivity of the radical cations of methyl 2,2-diphenylcyclohexyl ether (**7**), 6,6-diphenyl-1,4-dioxaspiro[4.5]decane (**8**), methyl *cis*- and *trans*-2-phenylcyclohexyl ether (**9***cis* and *trans*), and 6-phenyl-1,4-dioxaspiro[4.5]decane (**10**), generated by photosensitized (electron transfer) irradiation, has been studied. Solutions of the ethers and acetals in acetonitrile–methanol (3:1), with 1,4-dicyanobenzene (**2**) serving as the electron acceptor, were irradiated with a medium-pressure mercury vapour lamp through Pyrex. The diphenyl derivatives **7** and **8** were reactive; **7** gave 6,6-diphenylhexanal dimethyl acetal (**11**) and **8** gave 2-methoxy-2-(5,5-diphenylpentyl)-1,3-dioxolane (**12**). These are the products expected from the intermediate 1,6-radical cation, formed upon carbon–carbon bond cleavage of the cyclic radical cation. The monophenyl derivatives **9***cis* and *trans* and **10** were stable under these irradiation conditions. The mechanism for the carbon–carbon bond cleavage and for the *cis–trans* isomerization is discussed. An explanation, based upon conformation, is offered for the lack of reactivity of **9** and **10**. Molecular mechanics (MM2) calculations were used to determine the preferred conformation of **9***cis* and *trans*, and **10**.

Key words: photosensitization, electron transfer, radical cation, carbon–carbon bond cleavage, conformation.

DONALD R. ARNOLD, LAURIE J. LAMONT et ALLYSON L. PERROTT. Can. J. Chem. **69**, 225 (1991).

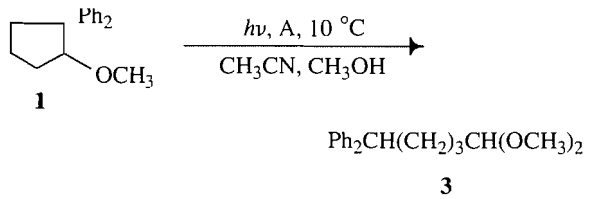
On a étudié la réactivité des cations radicalaires du méthoxy-2,2,-diphénylcyclohexane (**7**), du 6,6-diphényl-1,4-dioxaspiro[4,5]décane (**8**), des *cis*- et *trans*-méthoxy-2-phénylcyclohexane (**9***cis* et *trans*) et du 6-phényl-1,4-dioxaspiro[4,5]décane (**10**) générés par une irradiation photosensibilisée (transfert d'électron). Utilisant une lampe à vapeur de mercure de pression moyenne opérant à travers du Pyrex, on a irradié les éthers et les acétals en solution dans un mélange d'acétonitrile–méthanol (3:1), en présence de 1,4-dicyanobenzène (**2**) servant comme accepteur d'électrons. Les dérivés diphénylés **7** et **8** sont réactifs; **7** conduit à l'acétal diméthylique du 6,6-diphénylhexanal (**11**) alors que **8** fournit le 2-méthoxy-2-(5,5-diphénylpentyl])-1,3-dioxolane (**12**). Ce sont les produits que l'on peut attendre à partir de l'intermédiaire du cation radicalaire-1,6, formé par clivage de la liaison carbone–carbone du cation radicalaire cyclique. Les dérivés monophénylés **9***cis* et *trans* et **10** sont stables dans ces conditions d'irradiation. On discute du mécanisme de clivage de la liaison carbone–carbone ainsi que de l'isomérisation *cis–trans*. On offre une explication, basée sur la conformation, pour le manque de réactivité des dérivés **9** et **10**. On a utilisé des calculs de mécanique moléculaire (MM2) pour déterminer les conformations privilégiées des produits **9***cis* et *trans* et **10**.

Mots clés : photosensibilisation, transfert d'électron, cation radicalaire, clivage d'une liaison carbone–carbone, conformation.
[Traduit par la rédaction]

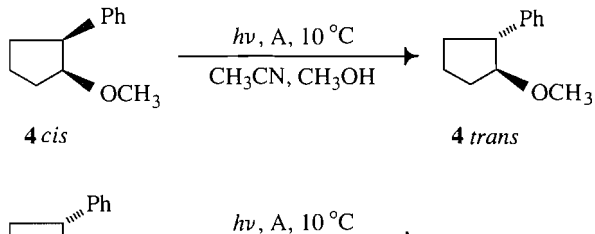
Introduction

Photosensitized (electron transfer) carbon–carbon bond cleavage of five-membered cyclic compounds generates 1,5-radical cations (**2**). When the irradiation is carried out in the presence of a nucleophile, often the solvent, further reaction of these intermediates proceeds by nucleophilic attack on the cationic site, and reduction of the radical site by electron transfer from the radical anion of the photosensitizer, followed by protonation of the resulting anion (**2**). A typical example is shown in reaction [1]: irradiation of an acetonitrile–methanol (3:1) solution of methyl 2,2-diphenylcyclopentyl ether (**1**) and 1,4-dicyanobenzene (**2**) (an electron-accepting photosensitizer) gives the dimethyl acetal of 5,5-diphenylpentanal (**3**) in good yield (>60%) (*2a*).

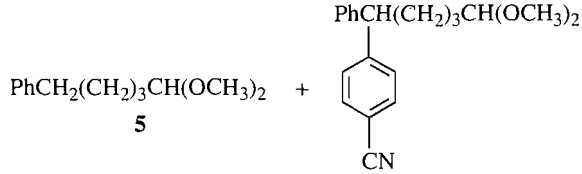
The monophenyl analogue (**4**) behaves similarly (*2b*). In this case, irradiation of the *cis* isomer (**4***cis*) under identical conditions leads to relatively efficient isomerization to a mixture of the *cis* and *trans* isomers. Continued irradiation leads to formation of the expected cleavage product (**5**) and the product (**6**) resulting from attack of the intermediate radical at the *ipso* position of the 1,4-dicyanobenzene radical anion (reaction [2]) (*2b*).[3] It was not clear from this initial report which isomer (*cis*

[1] 

1 **3**

[2] 

4 *cis* **4** *trans* **4** *trans*



5 **6**

[1]This is also part 27 of the series Radical Ions in Photochemistry. Preceding publications in these series are refs. 1 and 2.

[2]Author to whom correspondence may be addressed.

[3]Substitution products such as **6** are expected when the reduction potential of the intermediate radical is greater (more negative) than the reduction potential of the photosensitizer (1,4-dicyanobenene, −1.66 V (sce)) (*2b*, 3). Under these conditions, addition of the radical to the radical anion competes with electron transfer.

Can. J. Chem. Downloaded from www.nrcresearchpress.com by 195.138.81.100 on 09/07/12
For personal use only.

Can. J. Chem. Downloaded from www.nrcresearchpress.com by 195.138.81.100 on 09/07/12
For personal use only.

1. Sensitizer (A) $\xrightarrow{h\nu}$ A*
2. $Ph_2CH{-}R + A^* \longrightarrow Ph_2CH{-}R^{+\cdot} + A^{-\cdot}$
3. $Ph_2CH{-}R^{+\cdot} + A^{-\cdot} \longrightarrow Ph_2CH{-}R + A$
4. $Ph_2CH{-}R^{+\cdot} \longrightarrow Ph_2CH\cdot + R^+$
5. $R^+ + CH_3OH \longrightarrow R{-}OCH_3 + H^+$
6. $Ph_2CH\cdot + A^{-\cdot} \longrightarrow Ph_2CH^- + A$
7. $Ph_2CH^- + CH_3OH \longrightarrow Ph_2CH_2 + CH_3O^-$
8. $Ph_2CH{-}R^{+\cdot} \longrightarrow Ph_2C(\cdot){-}R + H^+$
9. $Ph_2C(\cdot){-}R + A^{-\cdot} \longrightarrow Ph_2C(-){-}R + A$
10. $Ph_2C(-){-}R + H^+(D^+) \longrightarrow Ph_2CH{-}R\ (Ph_2CD{-}R)$

SCHEME 1. The mechanism for the photosensitized (electron transfer) carbon–carbon bond cleavage and deprotonation.

or *trans*) was involved in the carbon–carbon bond cleavage reaction, or whether both isomers were participating in this reaction.

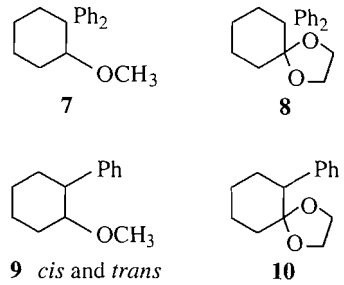
The *cis–trans* isomerization was explained by a mechanism involving deprotonation of the radical cation (**4***cis*$^{+\cdot}$), followed by reduction of the radical by the radical anion of the photosensitizer and reprotonation of the resulting anion. Support for this mechanism came from the observation that deuterium was incorporated at the benzylic position of **4***cis* and *trans* when the irradiation of **4** *cis* was carried out in acetonitrile–methanol-d_4.

The proposed mechanism for the carbon–carbon bond cleavage and for the *cis–trans* isomerization is shown in Scheme 1 (2*b*).

The main objective of this programme is to identify the factors that need to be considered in order to be able to predict whether a particular radical cation will undergo the carbon–carbon bond cleavage reaction. There are few, if any, reports of reactions involving the intermediate formation of 1,6-radical cations.[4] If these intermediates could be formed generally and predictably, reactions involving their formation could have significant synthetic utility. We have extended our investigation to cyclic systems containing six-membered rings in the hope of generating 1,6-radical cations. The compounds chosen for study were similar to those that have been shown to react in the five-membered ring series: methyl 2,2-diphenylcyclohexyl ether (**7**), 6,6-diphenyl-1,4-dioxaspiro[4.5]decane (**8**), methyl *cis*- and *trans*-2-phenylcyclohexyl ether (**9***cis* and *trans*), and 6-phenyl-1,4-dioxaspiro[4.5]decane (**10**) (Chart 1).

The irradiation conditions used in this study were the same as those used previously (2). It is reasonable to expect that the first three steps in the proposed mechanism (Scheme 1, steps 1–3) will proceed as well with these six-membered ring compounds

[4]Griffin and co-workers have reported the formation of a 1,6-radical cation (4). Irradiation of racemic 9,10-dimethoxy-9,10-dimethyl-9,10-dihydrophenanthrene and 1,4-dicyanonaphthalene (an electron-accepting photosensitizer) in acetonitrile solution results in isomerization of the dihydrophenanthrene to a mixture of the diastereomers. The 1,6-radical cation (cleavage of the 9,10 bond of the radical cation of the dihydrophenanthrene) was proposed as an intermediate; however, in this case both the radical and carbocation centres are conjugatively coupled through the π-system. The mechanism may be different.



7 **8**

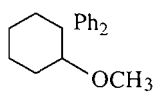
9 *cis* and *trans* **10**

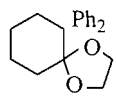
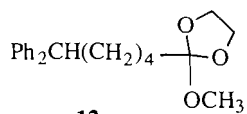
CHART 1

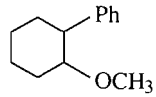
as with those that have a five-membered ring. Two important limitations for step 4 in the proposed mechanism have been identified: (1) Both the nascent fragments, the carbocation and the radical, must be relatively stable, that is, the bond dissociation energy of the radical cation cannot be greater than ca. 55 kJ mol^{-1} or cleavage will not occur (3). (2) A favoured conformation of the radical cation must allow overlap of the singly occupied molecular orbital (SOMO) and the incipient radical or carbocation (2*a*). There was no reason to doubt that all of the compounds chosen for study would satisfy these criteria and carbon–carbon bond cleavage was anticipated. Therefore, it was a surprise to find that **9***cis* and *trans*, and **10**, were stable to irradiation under these conditions. Clearly, additional criteria are required in order to be able to make reliable predictions regarding reactivity in this reaction. As is true for all attempts to define the scope and limitations of any reaction, examples of molecules that do not react are just as informative as examples of those that do.

Results

Solutions of the ether or acetal and photosensitizer, 1,4-dicyanobenzene (**2**), in acetonitrile–methanol (3:1) were degassed and irradiated through a Pyrex filter using a medium-pressure mercury vapour lamp. The results of the irradiations are summarized in Table 1 and in reactions [3]–[6] below. The struc-

[3]  **7** $\xrightarrow[CH_3CN,\ CH_3OH]{h\nu,\ A,\ 10\ °C}$ $Ph_2CH(CH_2)_4CH(OCH_3)_2$ **11**

[4]  **8** $\xrightarrow[CH_3CN,\ CH_3OH]{h\nu,\ A,\ 10\ °C}$  **12**

[5]  **9** *cis* and *trans* $\xrightarrow[CH_3CN,\ CH_3OH]{h\nu,\ A,\ 80\ °C}$ No reaction

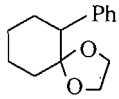
[6]  **10** $\xrightarrow[CH_3CN,\ CH_3OH]{h\nu,\ A,\ 80\ °C}$ No reaction

TABLE 1. Results of the irradiations

Starting material	Products
Methyl *trans*-2-phenylcyclopentyl ether (**4***trans*)	5-Phenylpentanal dimethyl acetal (**5**) 5-(4-Cyanophenyl)-5-phenylpentanal dimethyl acetal (**6**)[a]
Methyl *cis*-2-phenylcyclopentyl ether (**4***cis*)	**4***trans*[b]
Methyl 2,2-diphenylcyclohexyl ether (**7**)	6,6-Diphenylhexanal dimethyl acetal (**11**) (95%)[a]
6,6-Diphenyl-1,4-dioxaspiro[4.5]decane (**8**)	2-Methoxy-2-(5,5-diphenylpentyl)-1,3-dioxolane (**12**) (50%)[a]
Methyl *cis*-2-phenylcyclohexyl ether (**9***cis*)	No reaction[c]
Methyl *trans*-2-phenylcyclohexyl ether (**9***trans*)	No reaction[c]
6-Phenyl-1,4-dioxaspiro[4.5]decane (**10**)	No reaction[c]

[a]Irradiation at 10°C.
[b]No products due to carbon–carbon bond cleavage were observed.
[c]Irradiation at 80°C. No volatile products were detected by gc/ms.

TABLE 2. Summary of the oxidation potential measurements

Compound	E_p(V)[a]	$E_p - E_{p/2}$(mV)
Methyl *trans*-2-phenylcyclopentyl ether (**4***trans*)	2.05	160
Methyl *cis*-2-phenylcyclopentyl ether (**4***cis*)	2.05	120
Methyl 2,2-diphenylcyclohexyl ether (**7**)	2.16	200
6,6-Diphenyl-1,4-dioxaspiro[4.5]decane (**8**)	2.14	210
Methyl *trans*-2-phenylcyclohexyl ether (**9***trans*)	2.25	230
6-Phenyl-1,4-dioxaspiro[4.5]decane (**10**)	2.11	200

[a]The estimated error is ±0.03 V. The oxidation potential ($E_{1/2}^{ox}$) can be taken as 0.03 V less than the anodic peak potential (ref. 19).

tures assigned to the products (**11** and **12**) from reactions [3] and [4] rest firmly on an analysis of the ^1H and ^{13}C nmr spectra.

Deuterium incorporation studies were carried out on the *cis* and *trans* isomers of methyl 2-phenylcyclohexyl ether (**9**), and on 6-phenyl-1,4-dioxaspiro[4.5]decane (**10**). These compounds were irradiated under the usual conditions, except that the solvent was acetonitrile–methanol-d_4 (3:1). Analyses of the photolysate by capillary column gas chromatography with a mass selective detector (gc/ms), using selected ion monitoring, showed that less than 1% of one deuterium had been incorporated in the recovered starting material.

The reactivity of methyl *cis*- and *trans*-2-phenylcyclopentyl ether (**4***cis* and *trans*) was reinvestigated in greater detail. Irradiation of methyl *trans*-2-phenylcyclopentyl ether (**4***trans*) under the usual conditions showed that this isomer undergoes carbon–carbon bond cleavage; the acetal (**5**) and the substitution product (**6**) were detected. There was no evidence for isomerization of **4***trans* to **4***cis*. In marked contrast, no cleavage products were observed during the initial phase of the irradiation of the *cis* isomer; instead, **4***cis* was isomerized to **4***trans*.

The oxidation potentials of the ethers and acetals were measured by cyclic voltammetry (Table 2). All of the anodic waves were typical of irreversible oxidation.

The calculated structures of the *cis* and *trans* isomers of methyl 2-phenylcyclopentyl ether (**4***cis* and *trans*), of methyl 2-phenylcyclohexyl ether (**9***cis* and *trans*), and of 6-phenyl-1,4-dioxaspiro[4.5]decane (**10**) were optimized with the 1987 force field of the MM2 program (5). The dihedral driver option of the program was used to rotate first the methoxy group and then the phenyl group; several energy minima were identified for each compound. The calculated lowest-energy conformers, the global minima, are shown in Figs. 1–5.

Discussion

Based upon the known reactivity of several similar acyclic and five-membered cyclic analogues, it was reasonable a priori to predict that all of the compounds studied (Chart 1) would cleave under these photosensitized (electron transfer) conditions. Therefore, the observed reactivity of **7** and **8** (reactions [3] and [4]) is unexceptional.[5] The cleavage products **11** and **12** were formed in good yield. The proposed mechanism (Scheme 1, steps 1–7), involving the formation of a 1,6-radical cation intermediate in both cases, accounts for these results. The complete lack of reactivity of both **9***cis* and *trans* and **10**, even at the higher temperature (80°C), is surprising and the existing mechanistic criteria do not provide a satisfactory explanation.

There is sufficient evidence to suggest that the first three steps in the proposed mechanism (Scheme 1, steps 1–3) will occur with all of the compounds studied. The free-energy change (ΔG) for the initial electron transfer step (Scheme 1, step 2), calculated using the Weller equation, is exergonic by at least 38 kJ mol^{-1} in every case and the rate should be diffusion controlled (7). Step 3, deactivation by back-electron transfer from the radical anion of the electron acceptor to the radical cation, is the main competing process in every case. There is no reason to expect that this step will be exceptionally rapid in the reactions involving **9** and **10**. The obstacle to reaction must lie within step 4, the crucial carbon–carbon bond cleavage of the radical cation.

The factors that are known to inhibit step 4 of the proposed

[5]There was no evidence for cyclization of the intermediate 1,6-radical cation into the terminal phenyl group in either reaction. This cyclization has been observed only in the case of the 1,4-radical cation where the process 6-*endo*-trig may be relatively favoured (6).

Can. J. Chem. Downloaded from www.nrcresearchpress.com by 195.138.81.100 on 09/07/12
For personal use only.

Can. J. Chem. Downloaded from www.nrcresearchpress.com by 195.138.81.100 on 09/07/12
For personal use only.

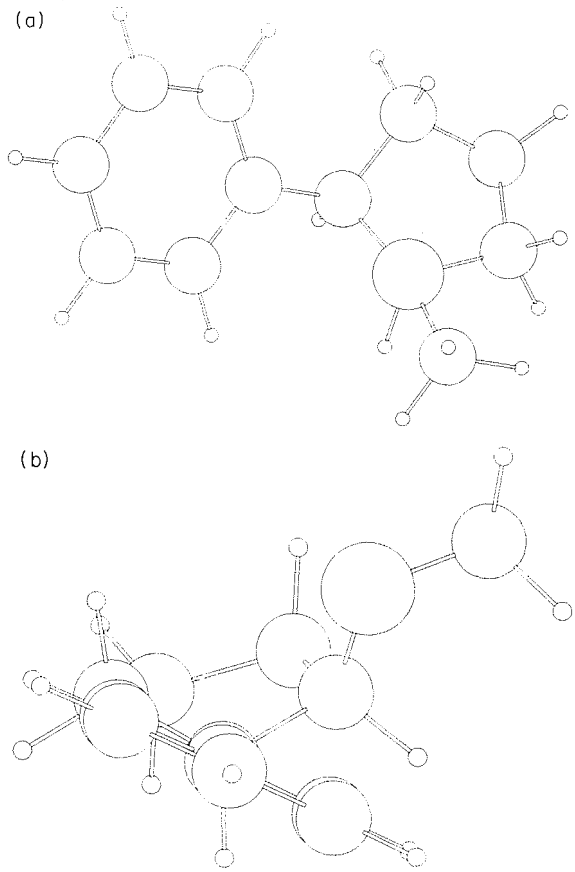


FIG. 1. The global minimum conformer of methyl *cis*-2-phenylcyclopentyl ether (**4***cis*): (a) Looking down the oxygen–carbon bond. The dihedral angle between the benzylic carbon–carbon bond and the oxygen–carbon (methyl) bond is 166°. (b) Viewed along the plane of the phenyl ring. The angle between the plane of the phenyl ring and the benzylic carbon–hydrogen bond is 66°.

mechanism cannot explain the lack of reactivity of $\mathbf{9}^{+\cdot}$ or $\mathbf{10}^{+\cdot}$. The fact that similar 2-phenylalkyl ethers, including **4***trans*, do cleave under these conditions makes it unlikely that the carbon–carbon bond dissociation energy of the radical cation of either **9** or **10** is above the threshold (55 kJ mol^{-1}) for cleavage (2). However, the benzylic carbon–carbon bond dissociation energy for these monophenyl derivatives will be at least 17 kJ mol^{-1} greater than that for the diphenyl derivatives. This is a consequence of the additional delocalization of the bis-benzylic radical relative to the benzylic radical. The bond dissociation energy for the radical cation of the monophenyl derivatives will therefore be closer to the energy threshold and cleavage may demand more stabilization of the incipient carbocation by the methoxy group. The preferred conformation of phenylcyclohexane has the plane of the phenyl ring perpendicular to the cyclohexane (8). This conformation should allow overlap of the SOMO, which is largely associated with the phenyl ring, with the benzylic carbon–carbon bond, sufficient for cleavage to occur. Clearly neither of these considerations can account for the lack of reactivity of **9** or **10**; an additional limitation must be identified.

Perhaps with the monophenyl derivatives, the alkoxy group must provide maximum stabilization of the incipient carbocation fragment for cleavage to occur. One of the nonbonding lone pairs of electrons on the oxygen atom must overlap with the carbon–carbon anti-bonding (σ^*) orbital in order to stabilize the transition state for cleavage. Figure 6b shows the orientation of the alkoxy group, aligned for maximum stabilization, as a Newman projection along the oxygen–carbon bond. Maximum stabilization occurs when the dihedral angle between the nonbonding pair of electrons of the oxygen and the adjacent carbon–carbon anti-bonding (σ^*) orbital is 0°. When this dihedral angle is 90°, stabilization is at a minimum; intermediate dihedral angles provide stabilization as a $\cos^2$ function (9). **Hypothesis**: If a preferred conformation of the ether does not have the alkoxy group oriented in such a way that a lone pair of electrons on the oxygen can overlap with the adjacent carbon–carbon anti-bonding orbital, cleavage may be inhibited.

The fact that neither **9***cis* nor *trans* was isomerized, or incorporated deuterium upon photosensitized (electron transfer) irradiation, must also be explained. For isomerization or deuterium incorporation to occur, the radical cation must deprotonate from the benzylic position (Scheme 1, step 8). It is well established that the acidity of a radical cation is greatly enhanced relative to the neutral molecule (10). However, the conformation of the benzylic carbon–hydrogen bond relative to the SOMO is also important for deprotonation. The SOMO must overlap with the adjacent carbon–hydrogen bond in order for deprotonation to occur (11).

The lowest energy conformer of methyl *cis*-2-phenylcyclohexyl ether (**9***cis*), calculated using the MM2 program, is shown in Fig. 3. The absolute value of the dihedral angle between the methyl group bonded to the oxygen and the carbon–carbon bond to be cleaved was calculated to be 170°. The dihedral angle of the plane of the phenyl group with respect to the benzylic hydrogen was calculated to be 26°. Although the phenyl group is well aligned for carbon–carbon bond cleavage, the orientation of the methyl group on the oxygen prevents interactions of the nonbonding pairs of electrons on oxygen with the carbon–carbon anti-bonding orbital. The search for a conformer with the phenyl and alkoxy groups suitably aligned for cleavage identifies one, but this conformer has a calculated heat of formation that is 24.9 kJ mol^{-1} above that of the global minimum.

The most stable conformation of **9***cis* is also poorly aligned for deprotonation. When the angle between the plane of the phenyl ring and the benzylic carbon–hydrogen bond is 26°, overlap with the SOMO is only 19% effective; deprotonation is inhibited. The conformer next in energy above the global minimum was calculated to have a dihedral angle between the phenyl ring and the benzylic carbon–hydrogen bond of 61°. Deprotonation from this conformer is feasible; however, this structure has a calculated heat of formation that is 7.2 kJ mol^{-1} above that of the global minimum. The equilibrium concentration of this conformer is too small for it to participate in the reactivity of this isomer.

The global minimum structure calculated for methyl *trans*-2-phenylcyclohexyl ether (**9***trans*) (Fig. 4) is similarly consistent with the observed lack of reactivity toward both carbon–carbon bond cleavage and deprotonation. The most stable conformer with both the phenyl and alkoxy groups favourably aligned for carbon–carbon bond cleavage is 8.1 kJ mol^{-1} above the global minimum, and the lowest energy conformer that could conceivably deprotonate is 18.0 kJ mol^{-1} less favourable.

The structure of the lowest energy conformer of methyl *cis*-2-phenylcyclopentyl ether (**4***cis*) is shown in Fig. 1. The orientation of the methoxy group prevents interaction of the nonbonding electrons on oxygen with the carbon–carbon anti-bonding orbital, inhibiting carbon–carbon bond cleavage of the radical cation. However, the preferred orientation of the

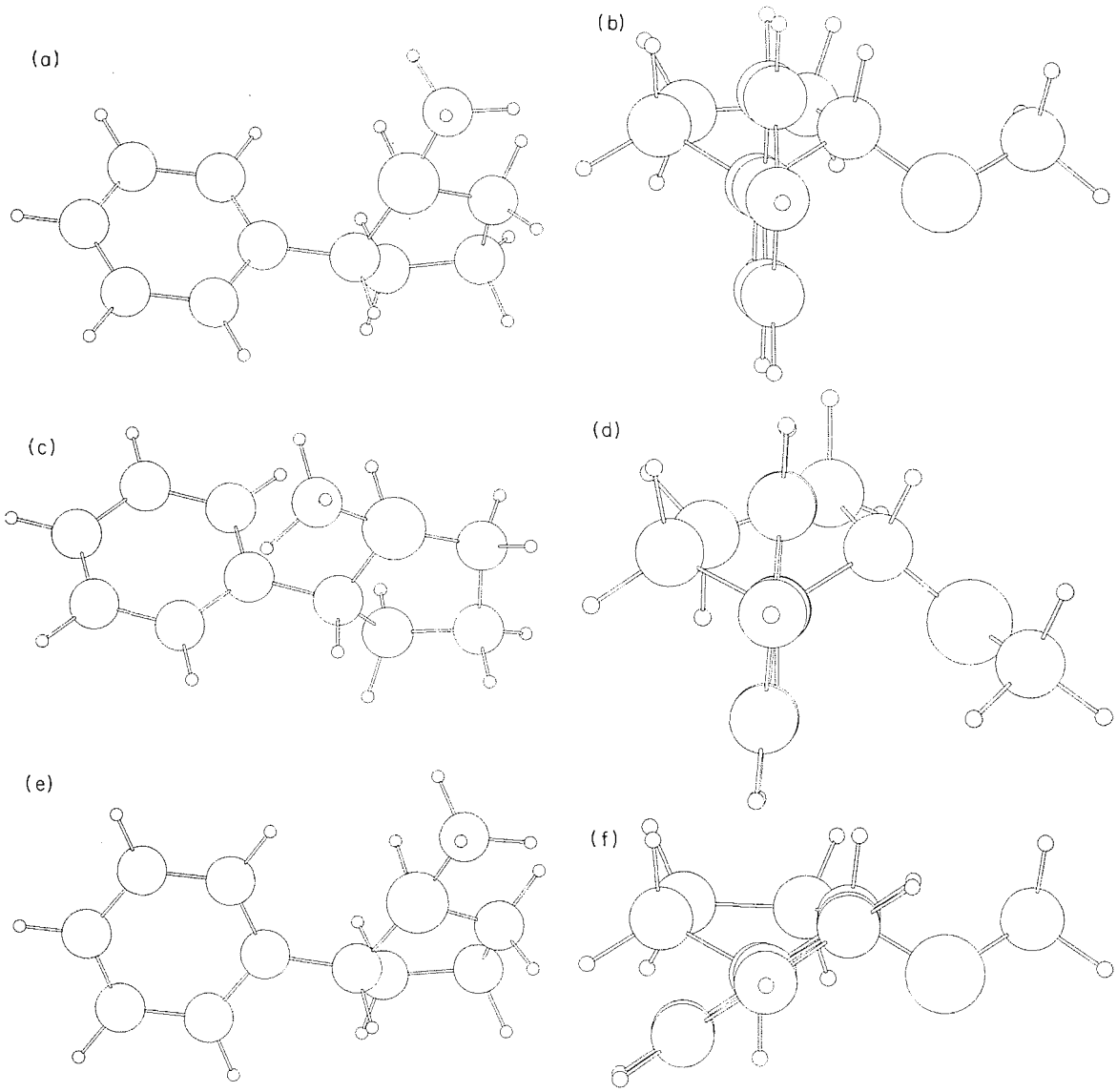


FIG. 2. The low-energy conformers of methyl *trans*-2-phenylcyclopentyl ether (**4***trans*): (a) The global minimum conformer ($\Delta H_f = -93.35$ kJ mol^{-1}). Looking down the oxygen–carbon bond. The dihedral angle between the benzylic carbon–carbon bond and the oxygen–carbon (methyl) bond is 173°. (b) The global minimum conformer. Viewed along the plane of the phenyl ring. The angle between the plane of the phenyl ring and the benzylic carbon–hydrogen bond is 0°. (c) The reactive conformer ($\Delta H_f = -93.14$ kJ mol^{-1}). Looking down the oxygen–carbon bond. The dihedral angle between the benzylic carbon–carbon bond and the oxygen–carbon (methyl) bond is 65° (the optimum angle is 60°). (d) The reactive conformer. Viewed along the plane of the phenyl ring. The angle between the plane of the phenyl ring and the benzylic carbon–hydrogen bond is 5°. (e) An unreactive conformer ($\Delta H_f = -93.14$ kJ mol^{-1}). Looking down the oxygen–carbon bond. The dihedral angle between the benzylic carbon–carbon bond and the oxygen–carbon (methyl) bond is 173°. (f) The same conformer as pictured in (e). Viewed along the plane of the phenyl ring. The angle between the plane of the phenyl ring and the benzylic carbon–hydrogen bond is 56°.

phenyl group should allow sufficient overlap of the SOMO with the benzylic carbon–hydrogen bond to permit deprotonation and, subsequently, isomerization and deuterium incorporation. The angle between the plane of the phenyl ring and the benzylic carbon–hydrogen bond is 66°. An angle of 66° provides 83% effective overlap for the deprotonation reaction. The lowest energy conformer that could participate in the carbon–carbon bond cleavage was calculated to be 5.8 kJ mol^{-1} above the global minimum.

The structural analysis of the *trans* isomer of methyl 2-phenylcyclopentyl ether (**4***trans*) was more complicated. Instead of one clearly recognizable global minimum, structure optimization revealed three conformers with comparable energy minima (Fig. 2). The "global" minimum does not have a conformation favourable for either reaction. However, there are two other conformers within 0.2 kJ mol^{-1} energy, and in one of these conformers the methyl group is not antiperiplanar to the carbon–carbon bond to be cleaved. The dihedral angle between the benzylic carbon–carbon bond and the oxygen–carbon (methyl) bond is 65°, close to the optimum arrangement (Fig. 6b). The nonbonding pair of electrons on oxygen can provide the stabilization of the incipient carbocation required for the cleavage. Experimentally, the radical cation of this isomer does undergo carbon–carbon bond cleavage.

The calculated lowest energy conformer of 6-phenyl-1,4-dioxaspiro[4.5]decane (**10**) is shown in Fig. 5. The orientation of the phenyl group should allow sufficient overlap of the SOMO with the carbon–carbon bond. However, again in this

Can. J. Chem. Downloaded from www.nrcresearchpress.com by 195.138.81.100 on 09/07/12
For personal use only.

Can. J. Chem. Downloaded from www.nrcresearchpress.com by 195.138.81.100 on 09/07/12
For personal use only.

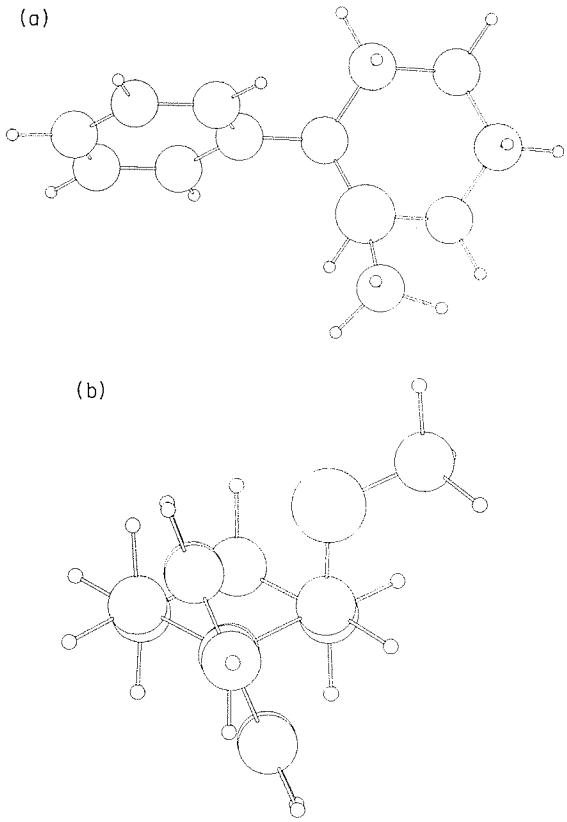


FIG. 3. The global minimum conformer of methyl *cis*-2-phenylcyclohexyl ether (**9***cis*): (a) Looking down the oxygen–carbon bond. The dihedral angle between the benzylic carbon–carbon bond and the oxygen–carbon (methyl) bond is 170°. (b) Viewed along the plane of the phenyl ring. The angle between the plane of the phenyl ring and the benzylic carbon–hydrogen bond is 26°.

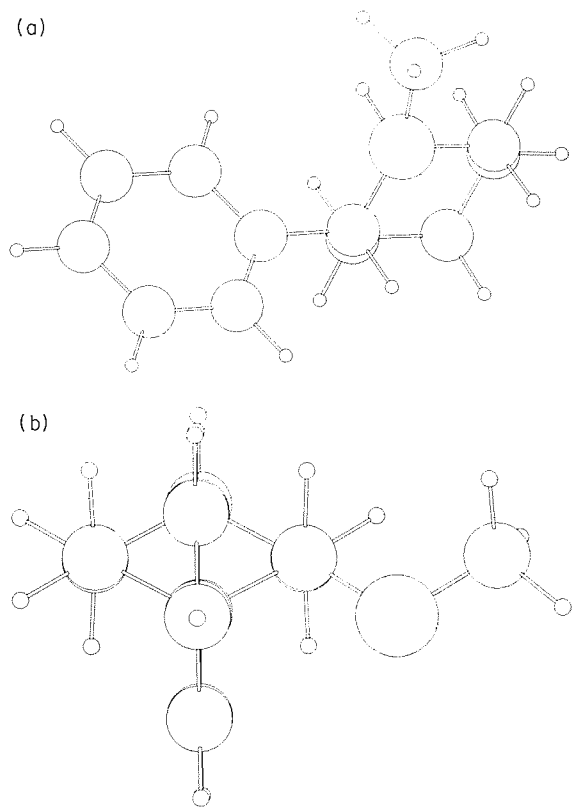


FIG. 4. The global minimum conformer of methyl *trans*-2-phenylcyclohexyl ether (**9***trans*): (a) Looking down the oxygen–carbon bond. The dihedral angle between the benzylic carbon–carbon bond and the oxygen–carbon (methyl) bond is 164°. (b) Viewed along the plane of the phenyl ring. The angle between the plane of the phenyl ring and the benzylic carbon–hydrogen bond is 1°.

case, the dihedral angle between the nonbonding pair of electrons on oxygen and the carbon–carbon σ^* orbital deviates considerably from the optimum and cleavage does not occur.

Conclusions

The reactivity of radical cations, generated by the photosensitized (electron transfer) technique, can be conformationally dependent. Knowledge of the preferred conformation of the neutral molecule, based upon MM2 calculations, has proven to be valuable in explaining the reactivity of radical cations. Not only can the carbon–carbon bond cleavage of the radical cation be predicted, but also the likelihood of deprotonation.

The conformation of the initially formed radical cation must reflect the equilibrium concentration of conformers of the neutral molecules: the electron transfer process (Scheme 1, step 2) is diffusion controlled. The competing deactivation process, back-electron transfer (Scheme 1, step 3), is known to be rapid, 10^7–10^9 s^{-1} (7*b*). The rate of the carbon–carbon bond cleavage and deprotonation (Scheme 1, steps 4 and 8) must be more rapid than back-electron transfer; and the rate of change in conformation, rotation around a carbon–oxygen bond, must be slower than back-electron transfer under these conditions.

In these cyclic ether systems, the carbon–carbon bond dissociation energies of the radical cations are low; the bond cleavage reaction competes with deprotonation. If the alkoxy group were replaced with an alkyl group, the bond dissociation energy would be increased to the point that carbon–carbon bond cleavage will not occur. This leads us to suggest that photosensitization (electron transfer) can be used to isomerize chiral molecules at the saturated centre. This reaction has synthetic utility. It can be used to convert a mixture of diastereomers to a single isomer.

Experimental

General information

The ^1H nmr and ^{13}C nmr spectra were recorded on a Nicolet Magnetics Corporation NB-360 spectrometer. Chemical shifts are reported in parts per million downfield from tetramethylsilane. Infrared spectra were recorded on a Perkin Elmer 180 or a Perkin Elmer 283B spectrometer, as noted. Frequencies are reported in wavenumbers, relative to polystyrene film (1601.8 cm^{-1}). Gas chromatography (gc/ms) was done on a Hewlett Packard 5890A gc equipped with a model 5970 mass selective detector interfaced with a Hewlett Packard 9816 microcomputer. The column used was 25 m × 0.2 mm, 5% phenyl methyl silicone on fused silica with a film thickness of 0.25 μm. Quantitative gas chromatography was done on a Hewlett Packard 5890A equipped with a flame ionization detector (gc/fid). This chromatograph was fitted with a 25 m × 0.25 mm, OV-1701 fused silica column. Melting points were taken on a Thermolyne melting point apparatus and are corrected. Combustion analyses were done by Canadian Microanalytical Service Limited.

Oxidation potentials were obtained by cyclic voltammetry using a three-electrode cell that has been described previously (12). The reference electrode was a saturated calomel electrode (sce). The electrolyte was tetraethylammonium perchlorate (TEAP) (0.1 M) in acetonitrile.

Irradiations were carried out in Pyrex tubes using a Canadian General Electric Co. 1-kW medium-pressure mercury vapour lamp with a

Can. J. Chem. Downloaded from www.nrcresearchpress.com by 195.138.81.100 on 09/07/12
For personal use only.

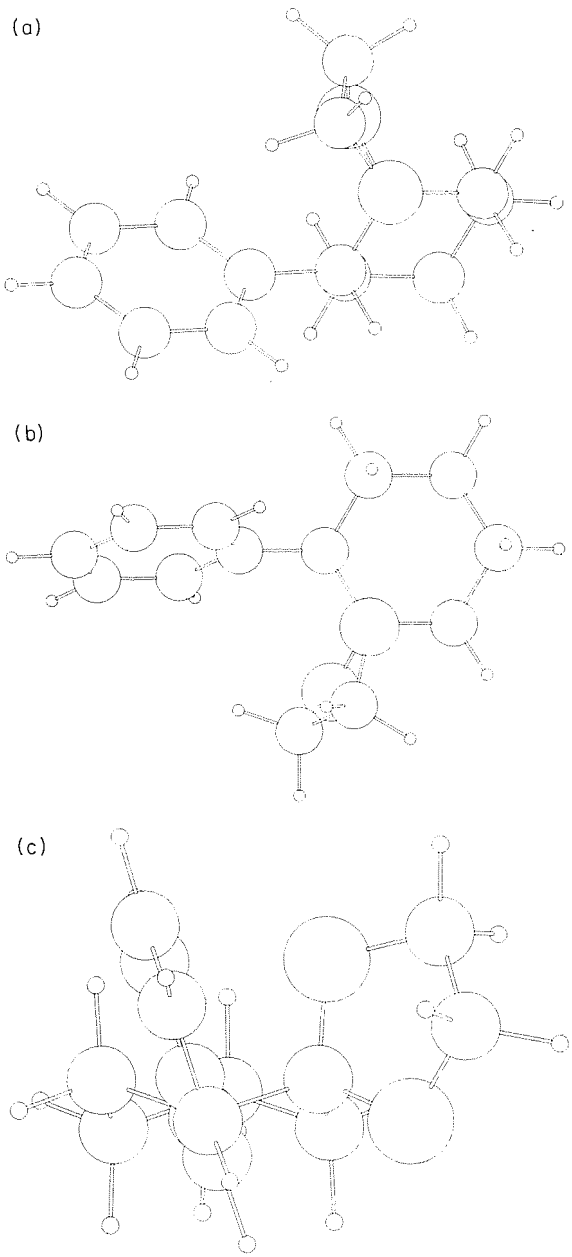


FIG. 5. The global minimum conformer of 6-phenyl-1,4-dioxaspiro[4.5]decane (**10**): (a) Looking down the oxygen (equatorial)–carbon bond. The dihedral angle between the benzylic carbon–carbon bond and the oxygen–carbon (bridge) bond is 112°. (b) Looking down the oxygen (axial)–carbon bond. The dihedral angle between the benzylic carbon–carbon bond and the oxygen–carbon (bridge) bond is 137°. (c) Viewed along the plane of the phenyl ring. The angle between the plane of the phenyl ring and the benzylic carbon–hydrogen bond is 20°.

quartz cooling jacket immersed in a constant temperature bath at either 10°C or 80°C, as noted. Samples were degassed by nitrogen ebullition for 5 min prior to irradiation.

Solvents were distilled prior to use. Acetonitrile and 1,4-dicyanobenzene (**2**) (Aldrich Chem. Co.) were purified as described previously (13). Synthesis and purification of the isomers and methyl 2-phenylcyclopentyl ether (**4**) have been described previously (*2b*). 1-Phenylcyclohexene and 2-phenylcyclohexanone were obtained from Aldrich Chem. Co.

The MM2 calculations were carried out on a VAX 8800 mainframe computer. Structures of the methyl 2-phenylcycloalkyl ethers (**9***cis*

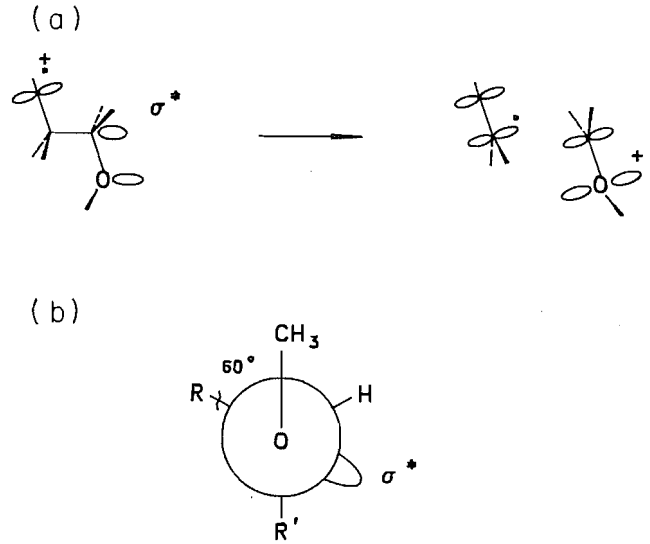


FIG. 6. Carbon–carbon bond cleavage of the radical cation is favoured when the SOMO overlaps with the bonding orbital (σ), and when a non-bonding pair of electrons on the oxygen overlaps with the anti-bonding orbital (σ*). The preferred conformation for carbon–carbon bond cleavage of the radical cation illustrated, (a) with the dashed–wedged line notation, and (b) with the Newman projection.

and *trans* and **4***cis* and *trans*) and **10** were optimized (steric energies were minimized) with the 1987 force field (Quantum Chemistry Program Exchange). For each of the isomers of **4** and **9**, four initial starting conformations were considered. Three conformations of **10** were optimized.

Preparation of compounds

Preparation of methyl 2,2-diphenylcyclohexyl ether (9)

Methyl 2,2-diphenylcyclohexyl ether (**9**) was prepared from 2,2-diphenylcyclohexanone, a known compound (14), by a two-step synthesis. The ketone (3.23 g, 1.29×10^{-2} mol) was reduced, using lithium aluminum hydride (0.35 g, 9.22×10^{-3} mol), to 2,2-diphenylcyclohexanol. The ether was then prepared from this alcohol using NaH (3.0 g, 0.12 mol) and dimethyl sulphate (2.4 mL, 3.2 g, 2.5×10^{-2} mol). The overall yield of **9** for the two steps was 65%; mp 65.6–66.1°C (lit.(15) mp 64–65°C); ^{1}H nmr (360 MHz) in $CDCl_3$: 7.25(m, 10H), 4.04(m, 1H), 3.11(s, 3H), 2.42(m, 2H), 1.91–1.37 (m, 6H).

Preparation of 6,6-diphenyl-1,4-dioxaspiro[4.5]decane (8)

6,6-Diphenyl-1,4-dioxaspiro[4.5]decane (**8**), a new compound, was synthesized from 2,2-diphenylcyclohexanone (1.56 g, 6.25×10^{-3} mol) by a known procedure (16) using chlorotrimethylsilane (5.1 mL) in ethylene glycol (50 mL). The acetal (**8**) was obtained in quantitative yield by flash column chromatography, eluting with 60% methylene chloride and 40% hexanes; mp 113.5–117.1°C; ir (PE 180) KBr: 3020(w), 2960(s), 2920(s), 2880(s), 2860(s), 1590(m), 1490(s), 1440(s), 1340(m), 1270(m), 1260(m), 1210(s), 1180(s), 1150(s), 1130(s), 1080(s), 1070(s), 1020(s), 940(s), 825(m), 740(s), 680(s); ^{1}H nmr (360 MHz) in $CDCl_3$ (−10°C): 7.63(d, 2H), 7.16(m, 8H), 3.82(dd, 1H, J = 6.6 Hz, J = 13.5 Hz), 3.61(dd, 1H, J = 6.6 Hz, J = 12.0 Hz), 3.36(dd, 1H, J = 5.89 Hz, J = 12.0 Hz), 2.74(m, 2H), 2.46(m, 1H, J = 13.5 Hz), 2.29(m, 1H), 1.67(m, 5H); ^{13}C nmr (90 MHz) in $CDCl_3$: 145.2, 130.0, 127 ($W_{1/2}$ = 105 Hz), 125.5, 112.3, 56.7, 65 ($W_{1/2}$ = 260 Hz), 35.1, 34.2, 24.4, 21.4. Anal. calcd. for $C_{20}H_{22}O_2$: C 81.60, H 7.53; found: C 81.74, H 7.71.

Preparation of methyl cis- *and* trans*-2-phenylcyclohexyl ether (9*cis *and* trans*) (17)*

Methyl *cis*- and *trans*-2-phenylcyclohexyl ether (**9**) were prepared by the photosensitized (electron transfer) addition of methanol to 1-phenyl-1-cyclohexene (0.35 g, 2.22×10^{-3} mol) using 1,4-dicyanobenzene (**2**) (0.19 g, 1.48×10^{-3} mol) as an electron-accepting

Can. J. Chem. Downloaded from www.nrcresearchpress.com by 195.138.81.100 on 09/07/12
For personal use only.

photosensitizer and acetonitrile–methanol (3:1) as solvent (18). At 90% conversion (23 h irradiation), a mixture of the *cis* and *trans* ethers (70:30, 75% yield) was obtained by column chromatography on silica gel (Kieselgel 60), using methylene chloride and hexanes as eluent. The *cis* and *trans* isomers were separated by preparative gas chromatography. **9***cis*: ^{1}H nmr (360 MHz) in $CDCl_3$: 7.28(m, 5H), 3.50(m, 1H), 3.09(s, 3H), 2.65(m, 1H, J = 12.9 Hz), 2.11(m, 1H, J = 12.9 Hz), 2.03(m, 1H, J = 3.7 Hz), 1.35–1.86(m, 6H); ^{13}C nmr (90 MHz) in $CDCl_3$: 145.0, 128.0, 127.8, 125.8, 79.8(d), 56.9(q), 48.0(d), 29.1(t), 26.3(t), 19.8(t). **9***trans*: ^{1}H nmr (360 Hz) in $CDCl_3$: 7.29(m, 2H), 7.21(m, 3H), 3.26(ddd, 1H, J = 4.05 Hz, J = 10.23 Hz, J = 10.32 Hz), 3.10(s, 3H), 2.51(m, 1H, J = 10.4 Hz, J = 11.95 Hz), 2.24(m, 1H, J = 12.07 Hz), 1.86(m, 2H), 1.74(m, 1H), 1.24–1.49(m, 4H); ^{13}C nmr (90 MHz) in $CDCl_3$: 144.9, 128.2, 127.5, 126.0, 83.2(d), 56.7(q), 51.1(d), 34.5(t), 31.4(t), 26.1(t), 25.0(t).

*Preparation of 6-phenyl-1,4-dioxaspiro[4.5]decane (**10**)*

6-Phenyl-1,4-dioxaspiro[4.5]decane (**10**), a new compound, was prepared from 2-phenylcyclohexanone according to a known procedure (16). The acetal was purified by column chromatography using silica gel (Kieselgel 60) with methylene chloride and hexanes as the eluent. Pure **10** was obtained in 95% yield; ir (PE 283B) neat: 3040(w), 2940(s), 2880(s), 2860(s), 1600(w), 1500(m), 1450(m), 1340(w), 1260(m), 1220(m), 1155(s), 1140(m), 1095(s), 1045(m), 1030(m), 930(s), 760(m), 700(s); ^{1}H nmr (360 MHz) in $CDCl_3$: 7.32(m, 2H), 7.22(m, 3H), 3.68(m, 2H), 3.43(m, 1H), 2.91(m, 1H), 2.80(dd, 1H, J = 13.2 Hz, J = 3.5 Hz), 2.03(m, 1H), 1.83–1.35(m, 7H); ^{13}C nmr (90 MHz) in $CDCl_3$: 141.4(s), 129.5, 127.7, 126.2, 110.2(s), 65.1(t), 64.7(t), 52.1(d), 36.9(t), 30.5(t), 25.7(t), 24.3(t). Anal. calcd. for $C_{14}H_{18}O_2$: C 77.03, H 8.31; found; C 76.96, H 8.28.

Irradiations

Irradiation of methyl cis- *and* trans-*2-phenylcyclopentyl ether (**4**cis and* trans*)*

A solution of **4***trans* and 1,4-dicyanobenzene (**2**) in acetonitrile–methanol (2 mL, 3:1) was irradiated at 10°C. Progress of the reaction was monitored by gc/fid. After 3 h of irradiation, analysis showed that the product, 5-phenylpentanal dimethyl acetal (**5**), was present; no **4***cis* was detected.

A similar solution of the *cis* isomer was irradiated. After 6 h, analysis of the solution showed two products: **4***trans* and 5-phenylpentanal dimethyl acetal (**5**).

*Irradiation of methyl 2,2,-diphenylcyclohexyl ether (**7**)*

A solution of methyl 2,2-diphenylcyclohexyl ether (**7**) (0.22 g, 8.3×10^{-4} mol) and **2** (0.14 g, 1.1×10^{-3} mol) in acetonitrile–methanol (30 mL, 3:1) was irradiated at 10°C for 5 days. The yield of 6,6-diphenylhexanal dimethyl acetal (**11**) was 94% at 87% conversion, ^{1}H nmr (360 MHz) in $CDCl_3$: 7.23(m, 10H), 4.29(t, 1H, J = 5.66 Hz), 3.87(t, 1H, J = 7.78 Hz), 3.26(s, 6H), 2.04(m, 2H), 1.54(m, 2H), 1.23–1.41(m, 4H); ^{13}C nmr (90 MHz) in $CDCl_3$: 145.1, 128.3, 127.8, 126.0, 104.5, 52.6, 51.2, 35.6, 32.3, 27.8, 24.5.

*Irradiation of 6,6-diphenyl-1,4-dioxaspiro[4.5]decane (**8**)*

A solution of **8** (0.21 g, 7.3×10^{-4} mol) and **2** (0.09 g, 7.3×10^{-4} mol) in acetonitrile–methanol (30 mL, 3:1) was irradiated for 14 h. The *ortho* ester **12** was identified in the reaction mixture by ^{1}H nmr; ^{1}H nmr (360 MHz) in $CDCl_3$: 7.24(m, 10H), 4.08(m, 2H), 3.93(m, 2H), 3.88(t, 1H, J = 7.98 Hz), 3.23(s, 3H), 2.04(m, 2H, J = 7.8 Hz, J = 15.6 Hz), 1.75(m, 2H), 1.47(m, 2H), 1.27(m, 2H). The reaction mixture was added to methanol (5% HCl) and refluxed for 1 h. 2,2-Diphenylcyclohexanone (13%) was recovered and methyl 6,6-diphenylhexanoate was isolated in 50% yield; ^{1}H nmr (360 MHz) in $CDCl_3$: 7.23(m, 10H), 3.88(t, 1H, J = 7.8 Hz), 3.62(s, 3H), 2.26(t, 2H, J = 7.57 Hz), 2.05(m, 2H, J = 7.8 Hz), 1.66(m, 2H), 1.28(m, 2H); ^{13}C nmr (90 MHz) in $CDCl_3$: 174.0, 145.0, 128.4, 127.8, 126.1, 51.4, 51.1, 35.3, 33.9, 27.5, 24.9.

*Irradiation of methyl 2-phenylcyclohexyl ether (**9**)*

A solution of **9***cis* (23 mg, 1.2×10^{-4} mol) and **2** (20 mg, 1.6×10^{-4} mol) in acetonitrile–methanol (2 mL, 3:1) was irradiated at 80°C for 40 h. Neither carbon–carbon bond cleavage nor isomerization products were observed (gc/ms).

A solution of **9***trans* (22 mg, 1.2×10^{-4} mol) and **2** (12 mg, 9.3×10^{-5} mol) in acetonitrile–methanol (2 mL, 3:1) was irradiated at 80°C for 40 h. No products were detected (gc/ms).

A solution of **9***cis* (49 mg, 2.6×10^{-4} mol) and **2** (39 mg, 3.0×10^{-4} mol) in acetonitrile–methanol-d_4 (2 mL, 3:1) was irradiated at 10°C for 4 days. The ratio of the m/m + 1 peaks due to the molecular ion of **9***cis* in the gc/ms was the same before and after irradiation. No deuterium incorporation was observed by selected ion monitoring (SIM).

A solution of **9***trans* (20 mg, 1.1×10^{-4} mol) and **2** (10 mg, 7.8×10^{-5} mol) in acetonitrile–methanol-d_4 (2 mL, 3:1) was irradiated at 10°C for 24 h. No incorporation of deuterium was observed (SIM).

*Irradiation of 6-phenyl-1,4-dioxaspiro[4.5]decane (**10**)*

A solution of **10** (87 mg, $3.7 \times 10^{-}$ mol) and **2** (51 mg, 4.0×10^{-4} mol) in acetonitrile–methanol (3:1) was irradiated at 10°C for 3 days. No product resulting from carbon–carbon bond cleavage was detected (gc/ms).

A solution of **10** (41 mg, 1.9×10^{-4} mol) and **2** (34 mg, 2.7×10^{-4} mol) in acetonitrile–methanol (2 mL, 3:1) was irradiated at 80°C for 25 h. No product resulting from carbon–carbon bond cleavage was observed (gc/ms).

A solution of **10** (48 mg, 2.2×10^{-4} mol) and **2** (32 mg, 2.5×10^{-4} mol) in acetonitrile–methanol-d_4 (2 mL, 3:1) was irradiated at 10°C. Progress of the reaction was followed by gc/ms using SIM. After 35 h of irradiation, less than 1% deuterium incorporation had occurred.

Acknowledgements

This work was supported by a grant from the Natural Sciences and Engineering Research Council of Canada. We thank Dr. D. L. Hooper at the Atlantic Regional Magnetic Resonance Centre at Dalhousie University for running the 360-MHz nmr spectra.

1. (*a*) D. R. Arnold, X. Du, and K. M. Henseleit. Can. J. Chem. In press; (*b*) L. J. Lamont and D. R. Arnold. Can. J. Chem. **68**, 390 (1990).
2. (*a*) D. R. Arnold, B. J. Fahie, L. J. Lamont, J. Wierzchowski, and K. M. Young. Can. J. Chem. **65**, 2734 (1987); (*b*) D. R. Arnold and L. J. Lamont. Can. J. Chem. **67**, 2119 (1989).
3. R. Popielarz and D. R. Arnold. J. Am. Chem. Soc. **112**, 3068 (1990).
4. (*a*) L. W. Reichel, G. W. Griffin, A. J. Muller, P. K. Das, and S. N. Ege. Can. J. Chem. **62**, 424 (1984); (*b*) H. F. Davis, P. K. Das, L. W. Reichel, and G. W. Griffin. J. Am. Chem. Soc. **106**, 6968 (1984).
5. (*a*) U. Burkert and N.L. Allinger. Molecular mechanics. American Chemical Society, Washington, DC. 1982; (*b*) N. L. Allinger. J. Am. Chem. Soc. **99**, 8127 (1977).
6. (*a*) R. A. Neunteufel and D. R. Arnold. J. Am. Chem. Soc. **95**, 4080 (1973); (*b*) S. L. Mattes and S. Farid. J. Am. Chem. Soc. **108**, 7356 (1986).
7. (*a*) D. Rehm and A. Weller. Isr. J. Chem. **8**, 259 (1970); (*b*) I. R. Gould, D. Ege, J. E. Moser, and S. Farid. J. Am. Chem. Soc. **112**, 4290 (1990).
8. N. L. Allinger and M. T. Tribble. Tetrahedron Lett. **35**, 3259 (1971).
9. (*a*) M. Karplus. J. Chem. Phys. **30**, 11 (1959); (*b*) J. Am. Chem. Soc. **85**, 2870 (1963).
10. (*a*) A. M. de P. Nicholas and D. R. Arnold. Can. J. Chem. **60**, 2165 (1982); (*b*) F. G. Bordwell, J.-P. Cheng, and M. J. Bausch. J. Am. Chem. Soc. **110**, 2867 (1988); (*c*) M. M. Green, S. L. Mielke, and T. Mukhopadhyay. J. Org. Chem. **49**, 1276 (1984).
11. (*a*) L. M. Tolbert, R. K. Khanna, A. E. Popp, L. Gelbaum, and L. A. Bottomley. J. Am. Chem. Soc. **112**, 2373 (1990); (*b*) L. M. Tolbert and R. K. Khanna. J. Am. Chem. Soc. **109**, 3477 (1987); (*c*) F. D. Lewis. Acc. Chem. Res. **19**, 401 (1986);

(*d*) P. J. WAGNER, R. J. TRUMAN, A. E. PUCHALSKI, and R. WAKE. J. Am. Chem. Soc. **108**, 7727 (1986).
12. D. D. M. WAYNER and D. R. ARNOLD. Can. J. Chem. **63**, 871 (1985).
13. A. OKAMOTO, M. S. SNOW, and D. R. ARNOLD. Tetrahedron, **42**, 6175 (1986).
14. (*a*) R. L. FRANK, R. E. BERRY, and O. L. SHOTWELL. J. Am. Chem. Soc. **71**, 3889 (1949); (*b*) W. D. EMMONS and J. P. FREEMAN. J. Am. Chem. Soc. **77**, 4387 (1955); (*c*) H. MEERWEIN and W. UNKEL. Ann. Chem. **376**, 152 (1910).
15. I. G. MURSAKULOV, E. A. RAMAZANOV, M. M. GUSEINOV, N. S. ZEFIROV, V. V. SAMOSHIN, and E. L. ELIEL. Tetrahedron, **36**, 1885 (1980).
16. T. H. CHAN, M. A. BROOK, and T. CHALY. Synthesis, 203 (1983).
17. F. GASPARRINI, L. CAGLIOTI, D. MISITI, G. PALMIERI, and R. BALLINI. Tetrahedron, **38**, 3609 (1982).
18. (*a*) A. J. MAROULIS, Y. SHIGEMITSU, and D. R. ARNOLD. J. Am. Chem. Soc. **100**, 535 (1978); (*b*) Y. SHIGEMITSU and D. R. ARNOLD. J. Chem. Soc. Chem. Commun. 407 (1975).
19. R. S. NICHOLSON and I. SHAIN. Anal. Chem. **36**, 706 (1964); **37**, 178 (1965).

Can. J. Chem. Downloaded from www.nrcresearchpress.com by 195.138.81.100 on 09/07/12
For personal use only.

Structural studies of organoboron compounds. XLII.[1] 4,6-Bis(1-cyano-1-methylethyl)-2-mesityl-1,3-dioxa-4,6-diaza-2-boracyclohexane

WOLFGANG KLIEGEL and GOTTFRIED LUBKOWITZ
Institut für Pharmazeutische Chemie der Technischen Universität Braunschweig, Beethovenstrasse 55, 3300 Braunschweig, Bundesrepublik Deutschland
AND
STEVEN J. RETTIG and JAMES TROTTER
Department of Chemistry, University of British Columbia, 2036 Main Mall, Vancouver, B.C., Canada V6T 1Y6
Received April 4, 1990

WOLFGANG KLIEGEL, GOTTFRIED LUBKOWITZ, STEVEN J. RETTIG, and JAMES TROTTER. Can. J. Chem. **69**, 234 (1991).

The condensation of *N,N'*-bis(1-cyano-1-methylethyl)-*N,N'*-dihydroxymethanediamine and mesitylboronic acid gives 4,6-bis(1-cyano-1-methylethyl)-2-mesityl-1,3-dioxa-4,6-diaza-2-boracyclohexane in good yield. Crystals of the latter compound are orthorhombic, a = 15.825(1), b = 17.958(1), c = 14.014(1) Å, Z = 8, space group *Pbca*. The structure was solved by direct methods and was refined by full-matrix least-squares procedures to R = 0.037 and R_w = 0.051 for 2844 reflections with $I \geq 3\sigma(I)$. The molecule has a six-membered cycloboronate structure featuring the first structurally characterized BONCNO ring. The ring was found to have a *C*-envelope conformation in the solid state. Bond lengths include: O—B(sp^2) = 1.356(2) and 1.370(2), and C(aryl)—B = 1.560(2) Å.

Key words: organoboron compound, boron compound, crystal structure.

WOLFGANG KLIEGEL, GOTTFRIED LUBKOWITZ, STEVEN J. RETTIG et JAMES TROTTER. Can. J. Chem. **69**, 234 (1991).

La condensation de la *N,N'*-bis(1-cyano-1-méthyléthyl)-*N,N'*-dihydroxyméthanediamine et de l'acide mésitylboronique fournit le 4,6-bis(1-cyano-1-méthyléthyl)-2-mésityl-1,3-dioxa-4,6-diaza-2-boracyclohexane avec un bon rendement. Les cristaux de ce dernier composé sont orthorhombiques, groupe d'espace *Pbca*, avec a = 15,825(1), b = 17,958(1) et c = 14,014(1) Å et Z = 8. On a résolu la structure par des méthodes directes et on l'a affinée par là méthode des moindres carrés (matrice entière) jusqu'à des valeurs de R = 0,037 et R_w = 0,051 pour 2844 réflexions avec $I \geq 3\sigma(I)$. La molécule possède un cycloboronate à six chaînons comprenant le premier cycle BONCNO à être caractérisé. On a trouvé que, à l'état solide, le cycle existe dans une conformation *C*-enveloppe. Les longueurs des liaisons observées comprennent : O—B(sp^2) = 1,356(2) et 1,370(2) et C(aryl)—B = 1,560(2) Å.

Mot clés : composés organoboriques, composés boriques, structure cristalline.

[Traduit par la revue]

Introduction

N,N'-Dihydroxy-*N,N'*-dialkylaminals **1** react with arylboronic acids to give bicyclic pyroboronates **3** with transannular N—B coordination (1, 2). The bicyclo[3.3.0]octane skeletal structure of these compounds has been established by an X-ray crystallographic analysis of the *N*-methyl/*B*-phenyl-substituted derivative **3***a* (3).

Reaction of **1** and arylboronic acid in various molar ratios (including 1:1) leads to type **3** products, rather than the six-membered "diol boronate" **4**. Cyclic esters derived from 1,3-alkanediols similar to **4** are well-known in the literature (4). The structures of several arylboronates of 1,3-diols have been elucidated by X-ray crystallographic analyses (5–8). To achieve the formation of a type **4** boronate with the "diol" compound **1** we reduced the basicity of the aminal nitrogen atom by incorporation of an α-cyano group into the *N*-alkyl substituent. The decrease in basicity should weaken the dative N—B interaction which is possible in the hypothetical intermediate **2** leading to the bicyclic 2:1 condensate **3**. In addition, steric hindrance of the boronic acid by *ortho* substitution in the aryl residue could impede an extension of the coordination at boron from trigonal planar sp^2 to tetrahedral sp^3. Indeed, the condensation of a *N*-(α-cyanoalkyl)aminal **1** (R = $C(CH_3)_2CN$) and mesitylboronic acid (Ar = 2,4,6-$(CH_3)_3C_6H_2$) gave a crystalline 1:1 condensation product, according to elemental analyses and spectroscopic data. Although mass spectral data were consistent with a monomeric condensate, it was not possible to decide unambiguously between the expected six-membered cycloboronate structure **4** and the less probable *N*-oxide form **5** or its rearrangement product **6**, its dimer **7**, and possible oligomers like **8** (n = 2, 3, or higher). Thus an X-ray crystallographic analysis has been undertaken to determine the molecular structure of the condensate and to provide data on the conformation of the new heterocyclane ring, at least in the solid state.

[1]Previous paper in this series: ref. 25.

Experimental

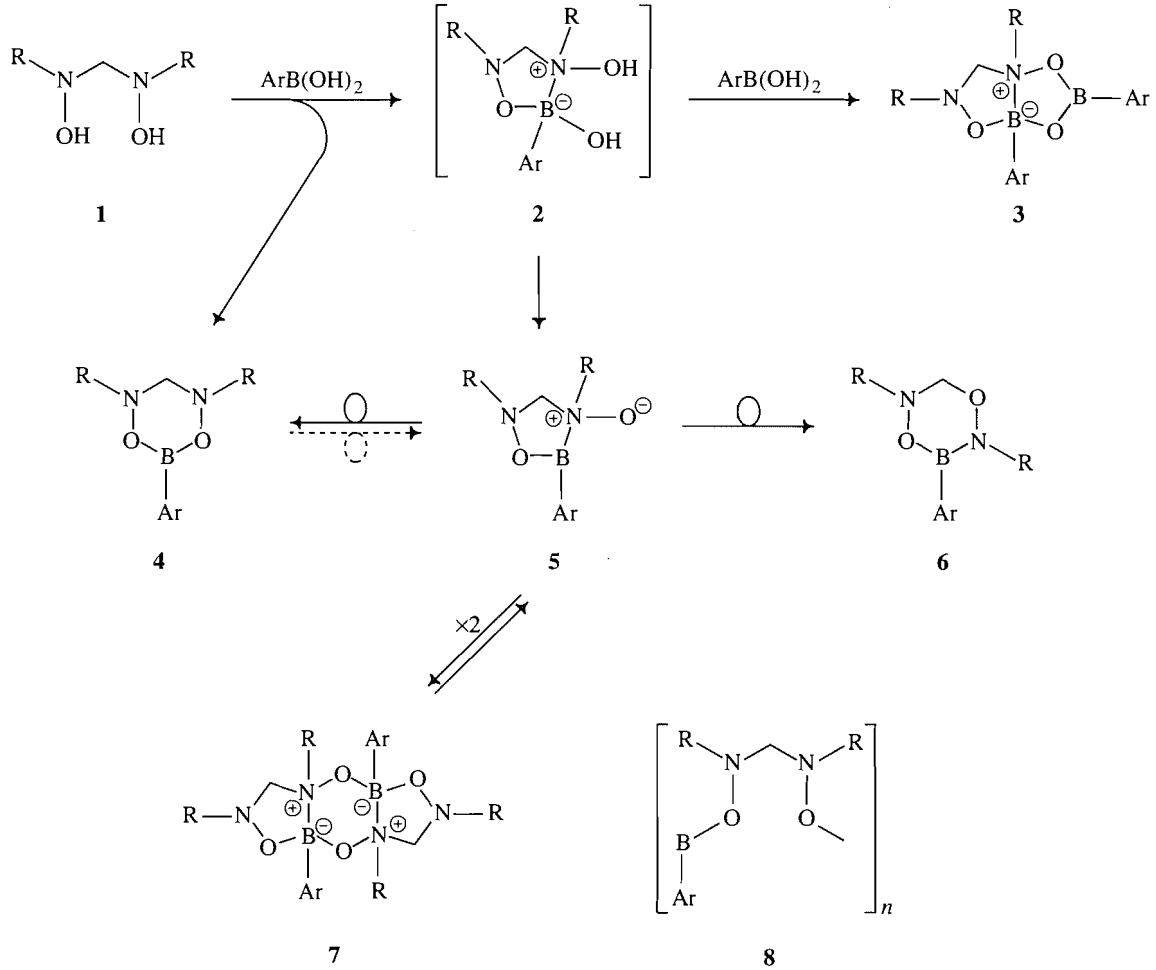
*4,6-Bis(1-cyano-1-methylethyl)-2-mesityl-1,3-dioxa-4,6-diaza-2-boracyclohexane, **4**a (R = $C(CH_3)_2CN$, Ar = 2,4,6-$(CH_3)_3C_6H_2$)*

N,N'-Bis(1-cyano-2-methylethyl)-*N,N'*-dihydroxymethanediamine **1** (R = $C(CH_3)_2CN$) (9) (0.64 g, 3 mmol) and mesitylboronic acid (0.49 g, 3 mmol) are dissolved in 20 mL of benzene and refluxed for 1 h with continuous removal of water. After partial evaporation *in vacuo* colorless crystals formed upon cooling. Yield: 0.83 g (81%). Melting point (decomp.) 158–160°C (from benzene). *Anal.* calcd. for $C_{18}H_{25}BN_4O_2$: C 63.54, H 7.41, B 3.18, N 16.47; found: C 63.55, H 7.59, B 3.20, N 16.47. Infrared (KBr): 2230 (C≡N), 1610 cm^{-1} (aryl-C=C). ^1H nmr (90 MHz, $CDCl_3$/TMS): δ(ppm) = 1.67 (s, 2 $C(CH_3)_2$), 2.27 (s, *p*-CH_3), 2.43 (s, 2 *o*-CH_3), 4.35 (s, N—CH_2—N), 6.78 (s, 2 aromatic H). Mass spectrum (70 eV, 60°C): m/z = 340 (56%, M^+), 298 (14%), 272 (8%, M − $C(CH_3)_2CN$), 241 (14%), 227 (36%, M − H_2C=N(OH)$C(CH_3)_2CN$), 161 (15%), 147 (41%, $(CH_3)_3C_6H_2$), 133 (26%), 113 (76%, H_2C=N(OH)$C(CH_3)_2CN$), 97 (10%), 85 (26%), 68 (100%, $C(CH_3)_2CN$), 56 (8%), 45 (64%, CH_2NOH). Crystals suitable for X-ray analysis were obtained by recrystallization from dry benzene.

*X-ray crystallographic analysis of **4**a*

A crystal *ca.* 0.25 × 0.25 × 0.35 mm in size was mounted on a glass

Can. J. Chem. Downloaded from www.nrcresearchpress.com by 195.138.81.100 on 09/07/12
For personal use only.



fiber. Unit-cell parameters were refined by least squares on setting angles for 25 reflections ($2\theta = 92.4$–$118.1°$) measured on a diffractometer with Cu-K_α radiation ($\lambda = 1.54178$ Å). Crystal data at 21°C are as follows

$C_{18}H_{25}BN_4O_2$ f.w. = 340.23

Orthorhombic, $a = 15.825(1)$, $b = 17.958(1)$, $c = 14.014(1)$ Å, $V = 3982.6(5)$ Å^3, $Z = 8$, $\rho_c = 1.135$ Mg m^{-3}, $F(000) = 1456$, μ(Cu-K_α) = 5.66 cm^{-1}. Absent reflections: $0kl$, k odd, $h0l$, l odd, and $hk0$, h odd, uniquely indicate the space group *Pbca* (No. 61).

Intensities were measured with graphite-monochromated Cu-K_α radiation on a Rigaku AFC6S diffractometer. An ω–2θ scan at 32° min^{-1} over a range of $(1.10 + 0.30 \tan\theta)°$ in ω (with up to eight rescans, background/scan time ratio = 0.5) was employed. Data were measured to $2\theta = 155°$. The intensities of three check reflections, measured every 150 reflections throughout the data collection, showed only small random variations. After data reduction,[2] an empirical absorption correction, based on azimuthal scans for three reflections, was applied. Transmission factors range from 0.909 to 1.00. Of the 4294 independent reflections measured, 2844(66.2%) had intensities greater than or equal to $3\sigma(F^2)$ above background where $\sigma^2(F^2) = [S^2(C + 4B) + (0.035F^2)^2]/\mathrm{Lp}^2$ with S = scan speed, C = scan count, B = total background count, and Lp = Lorentz-polarization factor.

The structure was solved by direct methods, the coordinates of all non-hydrogen atoms being determined from an E-map. The non-hydrogen atoms were refined with anisotropic thermal parameters and the hydrogen atoms were refined with isotropic thermal parameters. A correction for secondary extinction was applied, the final value of the extinction coefficient being 8.35×10^{-6}. Scattering factors for all atoms and anomalous dispersion corrections for the non-hydrogen atoms were taken from ref. 10. The weighting scheme $w = 4F_o^2/\sigma^2(F_o^2)$ gave uniform average values of $w(|F_o| - |F_c|)^2$ over ranges of both $|F_o|$ and $\sin\theta/\lambda$ and was employed in the final stages of full-matrix least-squares refinement of 327 variables. Reflections with $I < 3\sigma(I)$ were not included in the refinement. Convergence was reached at $R = 0.037$ and $R_w = 0.051$ for 2844 reflections with $I \geq 3\sigma(I)$. The function minimized was $\Sigma w(|F_o| - |F_c|)^2$, $R = \Sigma||F_o| - |F_c||/\Sigma|F_o|$, $R_w = (\Sigma w(|F_o| - |F_c|)^2/\Sigma w|F_o|^2)^{1/2}$.

On the final cycle of refinement the maximum parameter shift corresponded to 0.15σ. The mean error in an observation of unit weight was 2.09. The final difference map showed maximum fluctuations of ±0.15 e Å^{-3}. The final positional and (equivalent) isotropic thermal parameters for the non-hydrogen atoms appear in Table 1. Bond lengths and angles are given in Tables 2 and 3 and intra-annular torsion angles in Table 4. Hydrogen atom parameters, anisotropic thermal parameters, torsion angles, intermolecular contacts, least-squares planes, bond lengths and angles involving hydrogen, and structure factors have been deposited.[3]

Results and discussion

The X-ray analysis shows that compound **4***a* has the expected six-membered cycloboronate structure of the type **4** (Fig. 1), and represents (to the best of our knowledge) the first heterocyc-

[2]TEXSAN/TEXRAY structure analysis package which includes versions of the following: MITHRIL, integrated direct methods, by C.J. Gilmore; DIRDIF, direct methods for difference structures, by P.T. Beurskens; ORFLS, full-matrix least-squares, and ORFFE, function and errors, by W.R. Busing, K.O. Martin, and H.A. Levy; ORTEP II, illustrations, by C.K. Johnson.

[3]Supplementary material mentioned in the text may be purchased from the Depository of Unpublished Data, CISTI, National Research Council of Canada, Ottawa, Ont., Canada K1A 0S2.

Can. J. Chem. Downloaded from www.nrcresearchpress.com by 195.138.81.100 on 09/07/12
For personal use only.

Can. J. Chem. Downloaded from www.nrcresearchpress.com by 195.138.81.100 on 09/07/12
For personal use only.

TABLE 1. Final atomic coordinates (fractional) and B (eq)

Atom	x	y	z	B (eq)
O(1)	0.27031(7)	0.54983(5)	0.56908(7)	3.71(4)
O(2)	0.21797(6)	0.44590(5)	0.47966(8)	3.85(5)
N(1)	0.32810(8)	0.50019(7)	0.6197(1)	3.45(5)
N(2)	0.27315(8)	0.39828(6)	0.5366(1)	3.46(5)
N(3)	0.4556(1)	0.6237(1)	0.5003(1)	5.59(8)
N(4)	0.3550(1)	0.3639(1)	0.3138(1)	6.2(1)
C(1)	0.3503(1)	0.44081(8)	0.5531(1)	3.51(6)
C(2)	0.3985(1)	0.54942(8)	0.6483(1)	3.66(6)
C(3)	0.2847(1)	0.33028(8)	0.4779(1)	3.68(6)
C(4)	0.4304(1)	0.5917(1)	0.5644(1)	3.99(7)
C(5)	0.4708(1)	0.5037(1)	0.6906(2)	4.83(9)
C(6)	0.3643(1)	0.6039(1)	0.7222(1)	5.0(1)
C(7)	0.3241(1)	0.3489(1)	0.3849(1)	4.27(7)
C(8)	0.3418(1)	0.2764(1)	0.5324(2)	4.75(9)
C(9)	0.1985(1)	0.2946(1)	0.4605(2)	4.93(9)
C(10)	0.1613(1)	0.57343(7)	0.4423(1)	3.39(6)
C(11)	0.0811(1)	0.59247(8)	0.4759(1)	3.81(6)
C(12)	0.0293(1)	0.6377(1)	0.4201(2)	4.68(8)
C(13)	0.0558(1)	0.66651(9)	0.3341(1)	4.76(8)
C(14)	0.1370(1)	0.6500(1)	0.3039(1)	4.46(8)
C(15)	0.1900(1)	0.60324(8)	0.3553(1)	3.78(6)
C(16)	0.0519(1)	0.5669(1)	0.5725(2)	5.5(1)
C(17)	−0.0012(2)	0.7144(2)	0.2735(3)	7.5(2)
C(18)	0.2768(1)	0.5853(2)	0.3178(2)	5.2(1)
B	0.2195(1)	0.52032(9)	0.5010(1)	3.34(7)

TABLE 2. Bond distances (Å) with estimated standard deviations in parentheses

Atom	Atom	Distance	Atom	Atom	Distance
O(1)	B	1.356(2)	C(3)	C(7)	1.484(2)
O(1)	N(1)	1.461(2)	C(3)	C(9)	1.527(2)
O(2)	B	1.370(2)	C(3)	C(8)	1.529(2)
O(2)	N(2)	1.460(2)	C(10)	C(11)	1.396(2)
N(1)	C(1)	1.460(2)	C(10)	C(15)	1.406(2)
N(1)	C(2)	1.478(2)	C(10)	B	1.560(2)
N(2)	C(1)	1.458(2)	C(11)	C(12)	1.394(2)
N(2)	C(3)	1.484(2)	C(11)	C(16)	1.502(3)
N(3)	C(4)	1.138(2)	C(12)	C(13)	1.378(3)
N(4)	C(7)	1.142(2)	C(13)	C(14)	1.385(3)
C(2)	C(4)	1.488(2)	C(13)	C(17)	1.507(3)
C(2)	C(6)	1.525(2)	C(14)	C(15)	1.388(2)
C(2)	C(5)	1.527(3)	C(15)	C(18)	1.506(3)

lane with a BONCNO ring skeleton to be structurally characterized. The structure is comparable to that of a simple 1,3-diol boronate and possesses a "semi-planar" (C(1)—sofa) conformation for the six-membered heterocyclic ring, similar to those postulated for and established by X-ray analyses of several crystalline phenylboronates of 1,3-diols **9** (5–7) and **10** (8) as well as related ethylboronates (11, 12) and a simple boric acid ester of a 1,3-diol (13).

The essential planarity (to within 0.026 Å) of the N—O—B—O—N moiety in the boronate portion of **4***a* results, as does that of corresponding ring fragments in compounds **9**, **10**, and other known six-membered cyclic esters of ethylboronic or boric aid, from the partial double bond character of the O—B bonds caused by O—B $pp(\pi)$ back donation. This is supported by the relatively short O—B distances in **4***a* (1.356(2) and 1.370(2) Å). Corresponding O—B distances in the related compounds mentioned above range from 1.354 to 1.398 (average 1.373 Å) (5–8,11–13). Correlation of these O—B bond lengths with O—B π-bond order (14) yields a value of around 50%. Thus, a mean bond order of 1.5 is characteristic of the O—B bonds in the cycloboronate **4***a*.

In contrast to phenylboronates like **9** and **10**, in which the phenyl rings lie approximately coplanar with the C—O—B—O—C moieties of the boronate rings (suggesting at least some π-interaction between the aromatic system and the unoccupied boron p_z-orbital), the mesityl group of **4***a* is oriented perpendicular (dihedral angle between normals to the aromatic ring and boron coordination mean planes = 87.2°) to the boronate ring. This is apparently due to the steric hindrance of the ortho methyl substituents. The B—C(aryl) distance in **4***a* (1.560(2) Å) is nearly equal to those in **9***b* (6) (1.564 Å) and **9***c* (7) (1.561 Å), marginally longer than that in **10** (8) (1.554 Å), and distinctly longer than the reported (5) value for **9***a* (1.506 Å). The similarity of the above-mentioned distances suggests that for the B(sp^2)-C(aryl) bonds, in contrast to the O—B(sp^2) bonds, $p\pi-p\pi$ interactions appear to play a relatively minor role.

Compared to the bicyclic pyroboronate **3***a*, the monocyclic boronate **4***a* requires a different configuration at one of the aminal nitrogen atoms. Whereas **3***a* has the same configuration at both amine centres (*R,R* or *S,S*),[4] compound **4***a* has opposite configurations (*R,S*) at the two amine centres. Both of the bulky *N*-cyanoalkyl substituents are found in equatorial positions, resembling the similar influence of *tert*-butyl substituents on the geometry of cyclohexane ring systems (15). Considering the bond lengths and the conformational arrangement of both cyanoalkylamine groups in **4***a*, an anomeric effect (16) seems to contribute to the stabilization of the molecular geometry: the antiperiplanar orientation of both non-bonding electron pairs with respect to the adjoining geminal cyano groups allows the overlap of the nitrogen *n*-orbital with the antibonding σ* orbital of the C—C(cyano) bond. This is supported by relatively short C—N(amine) and long C—C(cyano) bonds within the cyanoalkylamine moiety of **4***a*. The mean C—N distance of 1.481 Å is somewhat shorter than comparable C—N bonds in *N-t*-butyl hydroxylamine derivatives: 1.497 Å (17), 1.496 Å (18). Correspondingly, the mean C—C(cyano) distance of 1.486 Å in **4***a* is longer than the comparable C—C(cyano) distance of 1.460 Å in Me_3C—CN (19) and the average value of 1.469 Å reported for C(sp^3)—C(cyano) bonds (20). An even longer C—C(cyano) bond (1.51 Å) has been reported for the *N*-cyanoalkylpiperidine **11** (21) which has the same *N*-substituent as **4***a* and an analogous conformation of the cyanoalkylamine moiety. Stereoelectronic effects on the geometry of the α-cyanoalkylamine group, similar to those deduced from bond lengths and conformations of both the hydroxylamine derivative **4***a* and the amine derivative **11** (21), have been postulated for α-cyanohydroxylamine derivatives of the general formula **12** (with a preferred axial orientation of the cyano group) on the basis of ^{1}H nmr data (22, 23).

The mean C≡N bond length of 1.140 Å in **4***a* is in good agreement with the average value 1.137 Å reported for cyano groups (20), and is slightly shorter than the values of 1.15 Å in **11** (21) and 1.158 Å in Me_3C—CN (19). The mean C—N and N—O distances in the aminal group (O—N—CH_2—N—O) of 1.460 and 1.461 Å, respectively, are equal within experimental error to the corresponding values of 1.461 and 1.458 Å reported

[4]Equal numbers of enantiomers are found in the crystal (3); formula **3***a* depicts the (1*R*,5*S*,7*R*)-enantiomer.

TABLE 3. Bond angles (deg) with estimated standard devitions in parentheses

Atom	Atom	Atom	Angle	Atom	Atom	Atom	Angle
B	O(1)	N(1)	118.3(1)	C(9)	C(3)	C(8)	110.1(2)
B	O(2)	N(2)	116.2(1)	N(3)	C(4)	C(2)	179.3(2)
C(1)	N(1)	O(1)	106.6(1)	N(4)	C(7)	C(3)	179.1(2)
C(1)	N(1)	C(2)	115.4(1)	C(11)	C(10)	C(15)	119.5(1)
O(1)	N(1)	C(2)	103.8(1)	C(11)	C(10)	B	120.5(1)
C(1)	N(2)	O(2)	106.3(1)	C(15)	C(10)	B	120.0(1)
C(1)	N(2)	C(3)	114.6(1)	C(12)	C(11)	C(10)	119.2(2)
O(2)	N(2)	C(3)	104.6(1)	C(12)	C(11)	C(16)	120.2(2)
N(2)	C(1)	N(1)	106.4(1)	C(10)	C(11)	C(16)	120.6(2)
N(1)	C(2)	C(4)	110.3(1)	C(13)	C(12)	C(11)	122.1(2)
N(1)	C(2)	C(6)	107.5(1)	C(12)	C(13)	C(14)	118.0(2)
N(1)	C(2)	C(5)	110.4(1)	C(12)	C(13)	C(17)	121.7(2)
C(4)	C(2)	C(6)	109.3(1)	C(14)	C(13)	C(17)	120.4(2)
C(4)	C(2)	C(5)	109.1(1)	C(13)	C(14)	C(15)	122.1(2)
C(6)	C(2)	C(5)	110.3(2)	C(14)	C(15)	C(10)	119.1(2)
N(2)	C(3)	C(7)	110.7(1)	C(14)	C(15)	C(18)	119.9(2)
N(2)	C(3)	C(9)	108.9(1)	C(10)	C(15)	C(18)	121.0(2)
N(2)	C(3)	C(8)	108.5(1)	O(1)	B	O(2)	123.1(1)
C(7)	C(3)	C(9)	109.2(2)	O(1)	B	C(10)	118.8(1)
C(7)	C(3)	C(8)	109.4(1)	O(2)	B	C(10)	118.1(1)

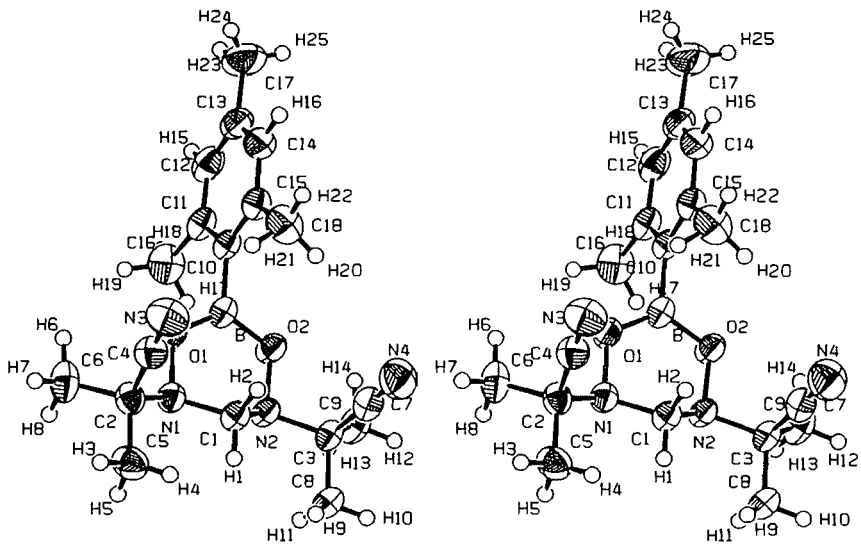
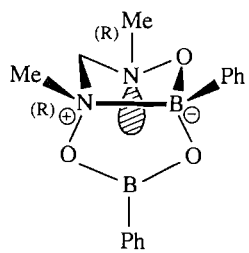
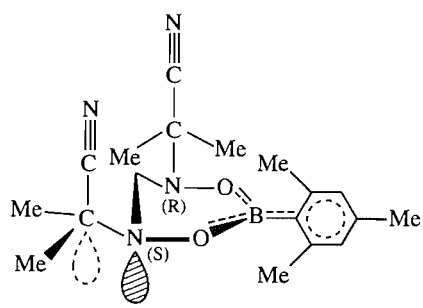


FIG. 1. Stereoview of the 4,6-bis(1-cyano-1-methylethyl)-2-mesityl-1,3-dioxa-4,6-diaza-2-boracyclohexane molecule; 50% probability thermal ellipsoids are shown for the non-hydrogen atoms.

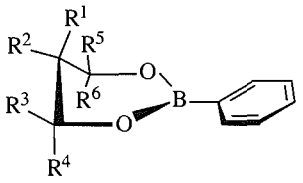


3a

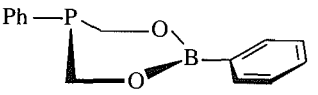


4a

Can. J. Chem. Downloaded from www.nrcresearchpress.com by 195.138.81.100 on 09/07/12
For personal use only.

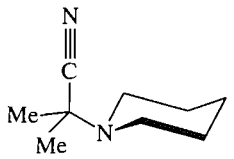


9

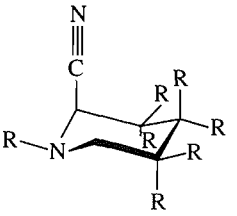


10

9*a*: R^1 = OH, $R^2 = R^3 = R^5$ = H, $R^4/R^6 = CH_2OCH(NHC_6H_4$—4-Br)
9*b*: R^1 = 4-O_2N—C_6H_4CH=N(O)—, R^2 = Me, R^{3-6} = H
9*c*: $R^1 = NO_2$, R^2 = Me, R^{3-6} = H



11



12

TABLE 4. Intra-annular torsion angles

Atoms	Torsion angle
B —O(1)—N(1)—C(1)	30.3(2)
O(1)—N(1)—C(1)—N(2)	−66.8(1)
N(1)—C(1)—N(2)—O(2)	70.9(1)
C(1)—N(2)—O(2)—B	−37.4(2)
N(2)—O(2)—B —O(1)	1.7(2)
O(2)—B —O(1)—N(1)	2.1(2)

for the simple aminal **1** (R = CH_3) (24). The crystal structure of **4***a* consists of molecules separated by normal van deer Waals distances, the shortest intermolecular distance between non-hydrogen atoms being N(3)···C(1) = 3.367(2) Å.

Acknowledgements

We thank the Natural Sciences and Engineering Research Council of Canada and the Fonds der Chemischen Industrie, Frankfurt am Main, for financial support.

1. W. KLIEGEL. J. Organometal. Chem. **253**, 9 (1983).
2. W. KLIEGEL and G. LUBKOWITZ. Unpublished results.
3. W. KLIEGEL, S. J. RETTIG, and J. TROTTER. Can. J. Chem. **62**, 515 (1984).
4. C. F. POOLE and A. ZLATKIS. J. Chromatogr. **184**, 99 (1980).
5. H. SHIMANOUCHI, N. SAITO, and Y. SASADA. Bull. Chem. Soc. Jpn **42**, 1239 (1969).
6. W. KLIEGEL, L. PREU, S. J. RETTIG, and J. TROTTER. Can. J. Chem. **63**, 509 (1985).
7. W. KLIEGEL, L. PREU, S. J. RETTIG, and J. TROTTER. Can. J. Chem. **64**, 1855 (1986).
8. I. A. LITVINOV, O. N. KATAEVA, G. N. NIKONOV, O. A. ERASTOV, V. A. NAUMOV, and B. A. ARBUZOV. Bull. Acad. Sci. USSR, Div. Chem. Sci. 2489 (1986); Izv. Akad. Nauk SSSR, Ser. Khim. 2715 (1986).
9. M. MASUI and C. YIJIMA. Yakugaku Zasshi **89**, 135 (1969).
10. International tables for X-ray crystallography. Kynoch Press: Birmingham, U.K. (present distributor Kluwer Academic Publishers: Dordrecht, The Netherlands), 1974. Vol. IV. pp. 99–102, 149.
11. W. FENZL, C. KRÜGER, and R. KÖSTER. Unpublished results; cit.: Houben-Weyl. Methoden der organischen chemie, Bd. XIII/3c (Organobor-Verbindungen III). Georg Thieme Verlag. Stuttgart. 1984. p. 457.
12. R. KÖSTER and W. V. DAHLHOFF. Liebigs Ann. Chem. 1925 (1976).
13. S. KURIBAYASHI. Bull. Chem. Soc. Jpn. **46**, 1045 (1973).
14. C. A. COULSON and T. W. DINGLE. Acta Crystallogr. Sect. B, **24**, 153 (1968).
15. M. HANACK. Conformation theory. Academic Press, New York. 1965.
16. P. DESLONGCHAMPS. Stereoelectronic effects in organic chemistry. Oxford. 1983; A. J. KIRBY. The anomeric effect and related stereoelectronic effects at oxygen. Berlin. 1983.
17. H. G. AURICH, G. BAUM, W. MASSA, and K.-D. MOGENDORF. Acta Crystallogr. Sect. C, **45**, 760 (1989).
18. H. G. AURICH, H. GRIGAT, W. MASSA, K.-D. MOGENDORF, and G. ZINNER. Chem. Ber. **119**, 1441 (1986).
19. T. SPARSTADT and E. AMBULE. J. Chem. Phys. **27**, 317 (1957).
20. F. H. ALLEN, O. KENNARD, D. G. WATSON, L. BRAMMER, A. G. ORPEN, and R. TAYLOR. J. Chem. Soc. Perkin Trans. II, S1 (1987).
21. L. G. VORONTSOVA, V. I. ANDRIANOV, and B. L. TARNOPOL'SKII. J. Struct. Chem. **10**, 756 (1969); Zh. Strukt. Khim. **10**, 872 (1969).
22. M. PETRZILKA, D. FELIX, and A. ESCHENMOSER. Helv. Chim. Acta, **56**, 2950 (1973).
23. M. RIEDIKER and W. GRAF. Helv. Chim. Acta, **62**, 2053 (1979).
24. W. KLIEGEL, S. J. RETTIG, and J. TROTTER. Can. J. Chem. **67**, 1959 (1989).
25. C. ORVIG, S. J. RETTIG, J. TROTTER, and Z. ZHANG. Can. J. Chem. **68**, 1803 (1990).

Can. J. Chem. Downloaded from www.nrcresearchpress.com by 195.138.81.100 on 09/07/12
For personal use only.

Study of the protonation of simple Schiff bases in solvents of various polarity by means of Raman spectroscopy

S. ALEX, P. TURCOTTE, R. FOURNIER, AND D. VOCELLE[1]

Département de chimie, Université du Québec à Montréal, PO Box 8888, Station A, Montréal (Québec), Canada H3C 3P8

Received August 15, 1989[2]

S. ALEX, P. TURCOTTE, R. FOURNIER, and D. VOCELLE. Can. J. Chem. **69**, 239 (1991).

In this study, the protonation of simple Schiff bases by organic acids in various solvents is investigated by Raman spectroscopy and the spectral response of the C=N$^+$ stretching mode is correlated with the macroscopic properties of the medium surrounding the imine. Upon protonation, the unperturbed C=N stretch increases in frequency due to the combination of the coupling with the C=N$^+$H bend and a partial rehybridization of the C=N bond. Depending on the proton location relative to that of its counterion, one mechanism may prevail over the other. Intensity measurements show that protonation is mostly controlled by the hydrogen bonding properties of the solvent and by the polarity of the medium. However, whatever the solvent, full proton transfer cannot be achieved with organic acids with pK_a similar to the COOH of amino acids found in visual or bacterial pigments, meaning that the protonation mechanism may depend upon particular properties of the protein.

Key words: imines, protonation, Raman spectroscopy, rhodopsin, Schiff base.

S. ALEX, P. TURCOTTE, R. FOURNIER et D. VOCELLE. Can. J. Chem. **69**, 239 (1991).

Cet article porte sur l'étude de la protonation des bases de Schiff simples avec des acides carboxyliques dans divers solvants par spectroscopie Raman. Nous avons établi qu'il est possible d'identifier la nature du milieu entourant l'imine, à partir des réponses spectrales obtenues sur le lien C=N$^+$. Une fois protonée, la vibration d'élongation C=N augmente en fréquence suite à la combinaison d'un couplage avec le mode de déformation C=N$^+$H et d'une rehybridation partielle du lien C=N. Dépendant de la position du proton vis-à-vis de son contre-ion, un des deux mécanismes peut être favorisé au dépend de l'autre. Quant aux mesures des intensités, elles montrent que la protonation de la base de Schiff est principalement contrôlée par la capacité de solvolyse du solvant et par la polarité du milieu. Cependant, quel que soit le milieu choisi, il a été impossible d'obtenir une protonation totale du groupe C=N avec des acides organiques dont l'acidité est comparable à celle rencontrée chez les fonctions COOH des acides aminés présents dans les pigments. Aussi, le mécanisme de transfert du proton semble nécessiter des propriétés particulières de la protéine.

Mots clés : imines, protonation, spectroscopie Raman, rhodopsine, base de Schiff.

Introduction

Bacteriorhodopsin and rhodopsin are proteins able to absorb light in the visible range between 500 and 600 nm. When they are exposed to light, they undergo their respective photocycles, which have been fully investigated and described in the literature (for example, see ref. 1–4 and refs. cited therein for reviews and recent developments). Even if their roles are not essentially the same, they both contain a chromophoric molecule of retinal covalently bound to a lysine residue via a protonated Schiff base linkage. Recently, a large number of articles aimed at finding the proton source and characterizing the local environment of the chromophore have been published (see reviews already quoted).

The work reported here is related to this field of research, and its main objective is to discuss the protonation of the simple Schiff bases and its effect on the C=N and C=N$^+$ stretching vibrations. So far, Raman spectroscopy has been widely used for such systems as pigments and model chromophores and has given valuable information (5–14). We also propose to investigate the influence of protonation and of the environment with the same technique. We decided to use a saturated imine to address this question even if the model is far removed from the visual or bacterial chromophores, since with retinal derivatives the presence of double bonds strongly weakens, or overlaps with, the Raman signal derived from either the C=N or the C=N$^+$ stretching vibration. The results reported are comparable to the early work done by Lussier *et al.* (15) on the state of protonation on similar systems in apolar solvents, using FT-IR. Lussier's data have been used as a basis of comparison and to calibrate the Raman results, Raman spectroscopy being more convenient for this type of study. This work was then extended to other solvents. Finally, the spectral behavior of these models is related to the more general case of the visual and bacterial rhodopsins.

The selected model system is built around mineral or organic acids used as proton sources, and an imine. The acids are chosen either to bracket the pK_a of amino acid residues met in the pigments and (or) to obtain the full protonation of the imine. The following acids have been used: hydrochloric acid (HCl, pK_a = −6.9 in water), trichloroacetic acid (TCA, pK_a = 0.66 in water), dichloroacetic acid (DCA, pK_a = 1.26 in water), monochloroacetic (MCA, pK_a = 2.85 in water), and propionic acid (PRO, pK_a = 4.87 in water).

Experimental section

Preparation of the samples

All the imines were prepared according to the method reported in ref. 15. The preparation and the purity control of these compounds were also described in this article. The following imines were investigated, fully or in part, according to our needs: $(CH_3)_2CHCH{=}NC(CH_3)_3$ (I_1), $(CH_3)_2CHCH{=}NCH(CH_3)_2$ (I_2), $(CH_3)_3CCH{=}NC(CH_3)_3$ (I_3), and $(CH_3)_3CCH{=}NCH(CH_3)_2$ (I_4). Their pK_a's have been evaluated by Favrot *et al.* (16, 17) and fall in the range 6–8 in $CHCl_3$ solution. Most of the investigations were carried out on I_2. These molecules promptly undergo hydrolysis, especially in acidic medium, so great care has been taken to avoid the presence of moisture. All the solvents were Spectrograde and were purchased from the Aldrich Chemical Company, Milwaukee, WI, U.S.A. Most were used without further purification, except chloroform, which was passed at least three times over an activated basic alumina column in order to remove traces of acids, ethanol, and water. The acids used were purchased from the same company and dried over P_2O_5 in a desiccator under vacuum. All liquid acids and solvents were stored over molecular sieves (3Å). The

[1]Author to whom correspondence may be addressed.

[2]Revision received October 17, 1990.

Can. J. Chem. Downloaded from www.nrcresearchpress.com by 195.138.81.100 on 09/07/12
For personal use only.

Can. J. Chem. Downloaded from www.nrcresearchpress.com by 195.138.81.100 on 09/07/12
For personal use only.

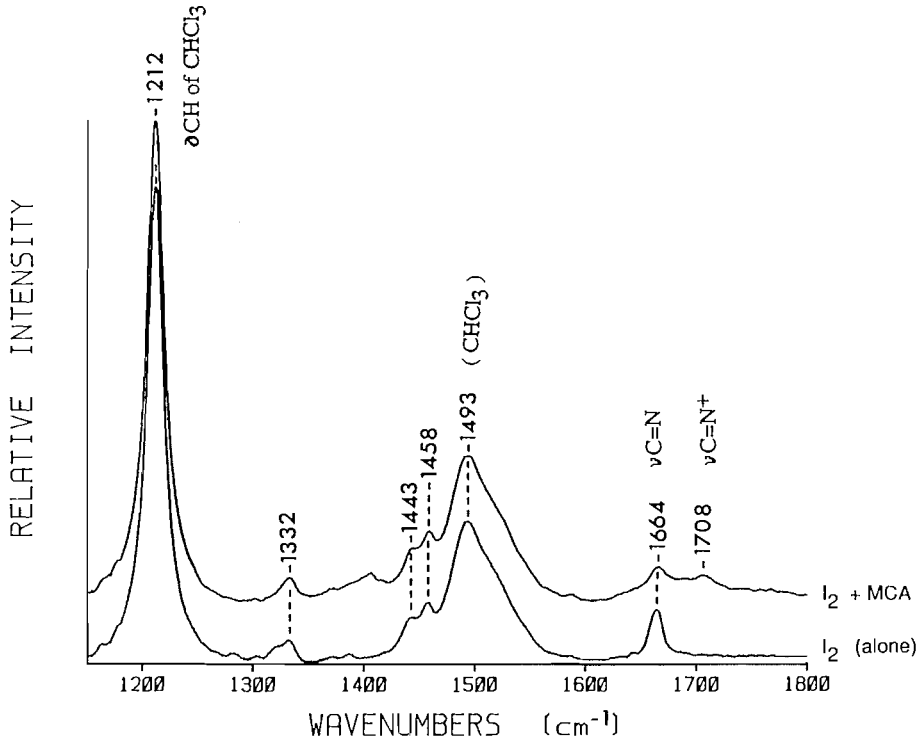


FIG. 1. Raman spectra of a 0.2 M solution of isobutylidene isopropylamine (I_2) in $CHCl_3$ (A) and of an equimolar solution of I_2 – 0.2 M MCA (B). The solvent bands are not substracted (excitation wavelength 488.0 nm).

complexes were synthesized by mixing an equimolar (unless otherwise stated) quantity of the acid with the proper imine in the appropriate solvent. The experiments were run in two types of solvents, the first being apolar, namely chloroform (refractive index or $n_D = 1.443$, dielectric constant or $D = 4.81$), and the second including both protic (methanol, $n_D = 1.3288$, $D = 32.80$) and aprotic (dimethyl sulfoxide or DMSO, $n_D = 1.478$, $D = 46.70$) polar solvents. Tentative experiments were carried out in a low dielectric constant medium, but in this situation the complexes are insoluble and are readily precipitated from solution. Raman spectra of these latter compounds were of little help, as they exhibit strong fluorescence background under laser exposure either in the solid state or from the centrifuged residue (not isolated from the solution).

For the deuteration of acids, the product of interest was dissolved in D_2O (Aldrich Chemical Company) and crystallized under inert atmosphere. This step was repeated as often as necessary, and the purity of the acids as well as the degree of hydrogen exchange were checked by NMR and IR spectroscopy. Then the imine–acid complexes were synthesized and dissolved in the proper solvents.

The Raman spectra were recorded on a Spex Triplemate spectrograph coupled with an EG & G Princeton Applied Research detector, model 1422, and were excited with ca. 100–200 mW of the 488 nm laser line (Spectra Physics CW Ar^+ laser, model 2016) in order to minimize the fluorescence of the sample. The sealed capillary was mounted on a thermally regulated sample holder and maintained at a temperature of 5°C. The spectra were recorded with a 3 cm^{-1} resolution at ca. 1600 cm^{-1} during 15 min. The fluorescence background was routinely subtracted with an appropriate nth order polynomial when necessary. All the Raman intensities reported in this work are normalized to the CH deformation mode of $CHCl_3$ at ca. 1212 cm^{-1}, whatever the solvent used. This is performed by first normalizing the imine bands to a particular peak P of the solvent present, and then, this latter band (P) is converted, by using a suitable factor, to a value related to the deformation mode of $CHCl_3$. In the text this procedure is called renormalization of the intensities. The scaling factors are deduced from Raman spectra of solutions of both solvents mixed in various proportions. Raman bands generated by organic solvents are usually very intense; the linearity of the detector response was also checked for the given laser power and no saturation effect was detected.

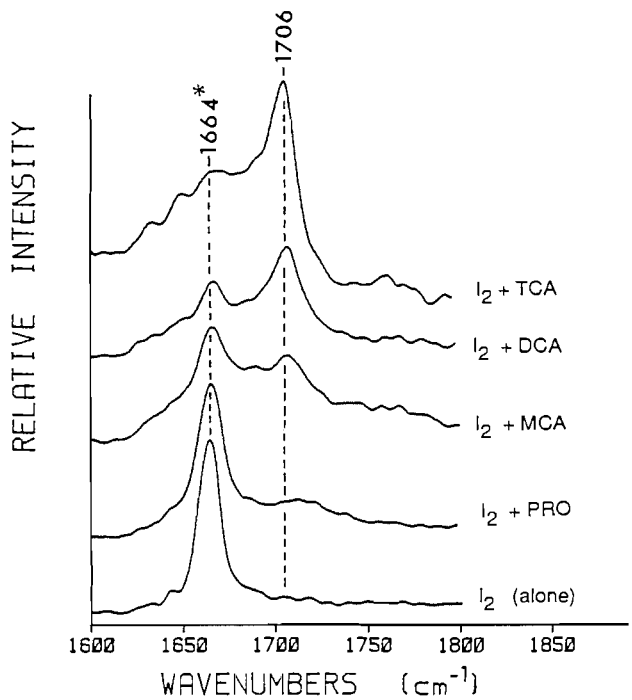


FIG. 2. Raman spectra of a 0.2 M solution of I_2 and its complexes in $CHCl_3$ solution in the region 1500–1800 cm^{-1}. The spectrum are solvent subtracted (excitation wavelength 488.0 nm).

The FTIR spectra were monitored on a Digilab FTS 50 spectrometer using a 2 cm^{-1} resolution and a recording time of about 5 min. The sample was held between two CaF_2 windows of a 0.1 mm optical path.

Results and discussion

The evaluation of the degree of protonation of the Schiff base by an organic or mineral acid is easily achieved by Raman spectroscopy because the signal derives mostly from the imines,

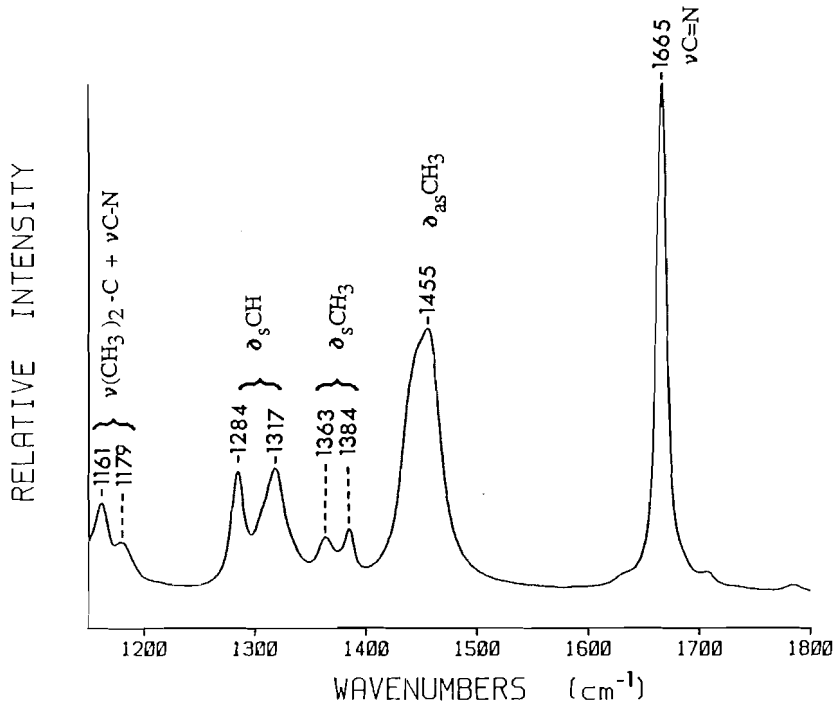


FIG. 3. Raman spectrum of neat isobutylidene isopropylamine (I_2) in the region 1200–1800 cm^{-1}.

since no additional contribution is seen from the unavoidable presence of acids. The complex under investigation can be represented as follows, using symbolic notation:

$$C{=}N + HOOC\text{-}R \rightleftharpoons C{=}N^{+}H\cdots\cdots{}^{-}OOC\text{-}R$$

Raman spectra of these imines mixed with organic acids are shown in Figs. 1 and 2. Only the data collected in chloroform are plotted, the results with other solvents being essentially similar. The discussion is focussed on the 1500–1800 cm^{-1} region where only the $\nu_{C=N}$ or $\nu_{C=N^+}$ stretching vibrations are observed, depending on the protonation state of the molecule. This is always true except in the case of TCA, where a broad emission deriving from the $\nu_{as\ COO^-}$ mode at ca. 1669 cm^{-1} overlaps with these modes; this is indicated by the asterisk in Fig. 2. No particular attention will be given to the rest of the spectra since only the two vibrations $\nu_{C=N}$ and $\nu_{C=N^+}$ are good probes to monitor the local environment and the state of hydrogen bonding (18–22). However, an example of a spectrum of the neat imine I_2 (pK_a = 7.15 in $CHCl_3$) is given in Fig. 3 and the main features pointed out (*vide infra*).

The text is organized as follows: in Sect. I, a frequency analysis of the $\nu_{C=N}$ and $\nu_{C=N^+}$ stretching is reported. In Sect. II, intensity measurements of these modes as a function of the protonation state are discussed. Finally, in Sect. III, some implications for bacterial and visual pigments are mentioned.

I. Frequency analysis of the $\nu_{C=N}$ and $\nu_{C=N^+}$ stretching vibrations in solvents of various polarity

Inspection of Tables 1–3 shows that when a simple imine is dissolved in various solvents both the frequency position and intensity of the $\nu_{C=N}$ mode are modified, compared to its unsolvated state. This is particularly true when the solvent is able to form hydrogen bonds with the imine. This is illustrated with methanol where the $\nu_{C=N}$ peak position is shifted by ca. 4 cm^{-1}. Since methanol or other alcohols are known to form strong hydrogen bonds with C=N (20, 23, 24), the results might be explained accordingly: that is, hydrogen bonding could better localize the π electrons on the C=N group and contributes to increase its vibrational frequency. This might also explain the increase in intensity of the band although this enhancement is probably only related to the variation of the dielectric constant. However, this explanation runs contrary to the usual effect of hydrogen bonding, which shifts stretching vibrations to lower frequencies as is effectively noted in chloroform, where a downward frequency shift of ca. 2 cm^{-1} is monitored upon solvation of imines like I_1 or I_4. This first observation demonstrates that, depending on the solvent, H bonding is differently expressed. For a solvent like dimethyl sulfoxide (DMSO), the $\nu_{C=N}$ position is not affected, meaning that interactions are limited. With imines substituted with *tert*-butyl instead of isopropyl groups, the result is almost similar except that the intensity of the $\nu_{C=N}$ band is split by a factor of 2 due to intensity borrowing through Fermi resonance from a side band at ca. 1653 cm^{-1} (15).

Upon protonation, the $\nu_{C=N}$ mode at ca. 1664 cm^{-1} disappears at the expense of a $\nu_{C=N^+}$ mode detected between 1698 and 1712 cm^{-1} in $CHCl_3$ depending on which kind of acid is used (see Table 1). For this new vibration, the frequency range is not so widely distributed in MeOH (see Table 2) and the average position of this vibration is located at almost the same position (1700–1703 cm^{-1}). In DMSO (see Table 3), lack of significant protonation severely limits the discussion, $\nu_{C=N^+}$ being very weak or absent.

The upward frequency shift observed on the $\nu_{C=N^+}$ (compared to the $\nu_{C=N}$) is not consistent with normal expectations. Protonation of the C=N group should rather shift its stretching mode to lower wavenumbers. This anomaly is, however, well documented in the literature (18–22, 24, 25) and the behavior can be explained by invoking a mixing of the $\nu_{C=N}$ mode and the $C{=}N^{+}H$ bend (19–22), thus propelling the $\nu_{C=N^+}$ Raman vibration to higher frequency. This explanation was based in part on the experimental fact that downward isotopic shifts of ca. 25 cm^{-1} have been noted on substituting hydrogenated acids (HX) by deuterated ones (DX). Using a diatomic oscillator model, Deng and Callender (26) showed that indeed the upward shift on Schiff bases, upon protonation, originated from such a

Can. J. Chem. Downloaded from www.nrcresearchpress.com by 195.138.81.100 on 09/07/12
For personal use only.

Can. J. Chem. Downloaded from www.nrcresearchpress.com by 195.138.81.100 on 09/07/12
For personal use only.

TABLE 1. Frequency positions and intensities of the $\nu_{C=N}$ and $\nu_{C=NH^+}$ stretching vibrations of isobutylidene isopropylamine (I_2) complexes with various acids in chloroform

Complexes	pK_a	Raman shift (cm^{-1})		Intensities[b]		% of protonation
		$\nu_{C=N}$	$\nu_{C=NH^+}$	$\nu_{C=N}$	$\nu_{C=NH^+}$	
I_2	—	1664	—	0.15	—	0.0
PRO	4.87	1664	1712	0.142	0.026[b]	5.3
MCA	2.85	1664	1708	0.081	0.067	46.0
DCA	1.26	1664	1708	0.046	0.100	69.3
TCA	0.66	1664	1706	0.011	0.133[a]	92.4
HCl	−6.90	—	1698	—	0.262	100

[a]The intensities have been corrected for the contribution of the $\nu_{as\ COO^-}$ mode of TCA at ca. 1669 cm^{-1} by spectral stripping.
[b]The values reported are normalized to the δ_{CH} mode of $CHCl_3$ at ca. 1212 cm^{-1}.

TABLE 2. Frequency positions and intensities of the $\nu_{C=N}$ and $\nu_{C=NH^+}$ stretching vibrations of isobutylidene isopropylamine (I_2) complexes with various acids in methanol

Complexes	pK_a	Raman shift (cm^{-1})		Intensities[b]		% of protonation
		$\nu_{C=N}$	$\nu_{C=NH^+}$	$\nu_{C=N}$	$\nu_{C=NH^+}$	
I_2	—	1668	—	0.400		0.0
PRO	4.87	1667	1703	0.334	0.036	17.0
MCA	2.85	1666	1703	0.137	0.146	66.0
DCA	1.26	—	1703	0.000	0.234[b]	100.0
TCA	0.66	—	1704	0.000	0.217[b]	100.0
HCl	−6.90	—	1700	0.000	0.372	100.0

[a]The values reported are renormalized to the δ_{CH} of $CHCl_3$ at ca. 1212 cm^{-1} (see text in experimental section).
[b]The intensities have been uncorrected for the contribution from the $\nu_{as\ COO^-}$ of DCA (1640 cm^{-1}) and TCA (1669 cm^{-1}), as the percentage of protonation is obviously 100%.

TABLE 3. Frequency positions and intensities of the $\nu_{C=N}$ and $\nu_{C=NH^+}$ stretching vibrations of isobutylidene isopropylamine (I_2) complexes with various acids in dimethyl sulfoxide

Complexes	pK_a	Raman shift (cm^{-1})		Intensities[b]		% of protonation[c]
		$\nu_{C=N}$	$\nu_{C=NH^+}$	$\nu_{C=N}$[b]	$\nu_{C=NH^+}$	
I_2	—	1664	—	0.478	—	—
PRO	4.87	1664	(1715)[a]	0.459	—	—
MCA	2.85	1664	(1718)[a]	0.459	—	—
DCA	1.26	1663	1705	0.387	Weak	18.2
TCA	0.66	1666	1700	0.287	Weak	39.1
HCl	−6.90	—	1701	—	0.718	100

[a]Assigned to the $\nu_{C=O}$ mode of the -COOH function of the acid.
[b]The values reported are renormalized to the δ_{CH} mode of $CHCl_3$ at ca. 1212 cm^{-1} (see text in experimental section).
[c]These values are estimated from the loss of intensity monitored on the $\nu_{C=N}$ mode.

coupling since deuteration reduced it greatly. However, even if there has been general agreement about this coupling, Lòpez-Garriga *et al.* (18, 25) have recently cautioned that this should not be taken for granted. They stressed that a redistribution of the electronic density in such a system is conceivable and consequently will give the same spectral response without requiring any coupling. In support of this theory these authors invoked a rehybridization of the C=N bond upon protonation, leading to a shortening of its length by 0.007 Å and a stiffening of its force constant. This raises the question as to which of the two theories is the more valid for our study.

From Tables 1 and 2, it is seen that the frequency differences (between the neat imine and its complexes) appear *a priori* inversely proportional to the acid strength. With weak acids (PRO, MCA, and DCA), the difference is of the order of 48–44 cm^{-1} while from much stronger acids (TCA and HCl), it is around 42–34 cm^{-1}. This means either that the C=N/C=N^+H stretch–bend interaction is reduced with strong acids or that upon protonation the C=N bond is weakened, this compensating for the action of coupling. This latter hypothesis has been ruled out because acids are expected to form fairly strong H-bonds with the imines, at least similar to the ones created with

Can. J. Chem. Downloaded from www.nrcresearchpress.com by 195.138.81.100 on 09/07/12
For personal use only.

the use of methanol, with the same effect on the C=N link. Hence, the frequency distribution of $\nu_{C=N^+}$ seems rather a function of the nature of the counterion. This is consistent with the limited effect of the anion on the $\nu_{C=N^+}$ vibration position in MeOH, where the hydrogen bond network around the chromophore is known to play a buffer electrostatic role (or a levelling effect) (23). The negative charge probably defines the proton position and, in this kind of complex, the proton can be found close to the nitrogen atom (i.e., forming a front H-bond), or close to its counterion (involving a back H-bond), or again hesitating between both moieties (3, 15). Keeping this picture in mind, it is interesting to look at its effect on the $C{=}N^+$ oscillator.

First, the importance of the coupling can be revealed by using deuterated acids, considering that the C=N stretching mode will receive much smaller contributions from the $C{=}N^+D$ bend than from the $C{=}N^+H$ bend. Therefore, as stated before, the isotopic shift between the deuterated and the protonated imines will emphasize the importance of the coupling. This being so, we tested the proposal by using deuterated acids. Results given in Table 4 show that the deuterated Schiff bases have $\nu_{C=N^+}$ at higher frequencies than the unprotonated Schiff bases. If it is assumed that, with deuterium, the coupling between the stretch and the bend is slight, then the upward shift can only be attributed to a rehybridization of the C=N function as in the Lopez–Garriga theory since there exists no other proposal but the two already described. In Table 4, it is also possible to note that the isotopic shifts found in our work are almost the same as those found by Deng and Callender (25 cm^{-1}) in their study (26). So we are dealing with two facts: deuteration indicates that rehybridization is present in our Schiff bases upon protonation, while the isotopic shifts of ca. 25 cm^{-1} indicate that stretch–bend interactions are also important. One way of solving this question is simply to invoke the presence of *both* effects and, from this, try to analyze how both theories could explain our results obtained by using different acids in different solvents.

Let us start with HCl (and DCl). The isotopic shift found is 22 cm^{-1}, a lower value that the one found for the upward frequency shift of the C=N stretching band upon protonation and which is probably due to rehybridization and stretch–bend interaction, the latter being somewhat reduced. However, in methanol, the isotopic shift returns at 26 cm^{-1}. This reduced contribution in $CHCl_3$ could possibly be explained by invoking the high electronegativity of the Cl^- ion and its small ionic radius, both favoring the back H-bond (viz. $N\cdots H^+\cdots Cl^-$) (15, 20). As a consequence, the contribution of δ_{N^+H} to $\nu_{C=N^+}$ should be lower in this context, the -NH link becoming longer and more directional and harder to bend (27).[3] This point of view is consistent with the fact that back H-bridges appear weaker in complexes containing halides such as bromides and iodides as counterions, as described by Lussier *et al.* (15).

For organic acids like TCA, there is no change in the isotopic shift whatever the solvent used. In this case, one can imagine that the front H-bond is favored (viz. $N^+\cdots H\cdots {}^-OOC$), this being justified by the different electronegativity and larger size of the carboxylate anion. In this context, the isotopic shift should be important since the proton, being closer to the nitrogen atom, should allow a strong stretch–bend interaction. This is actually the case since an isotopic value of 26 cm^{-1} is registered.

There is no way here to measure the relative importance of rehybridization and stretch–bend coupling. One can only

[3] δ: deformation mode.

TABLE 4. Effect of isotopic substitution on the frequency positions of the $\nu_{C=NH^+}$ stretching vibrations of I_2 complexes with mineral and organic acids in chloroform and in methanol

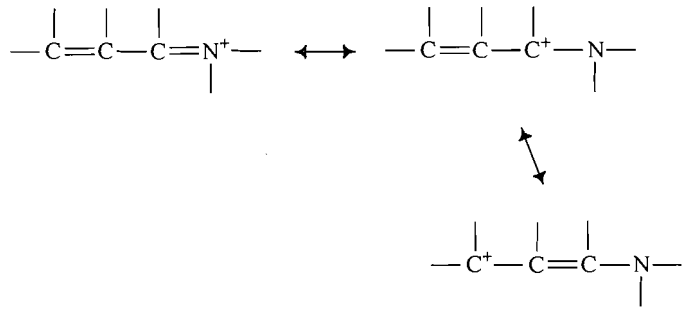
	$CHCl_3$		MeOH or MeOD	
Complexes	$\nu_{C=NH^+}$ (cm^{-1})	Δd^a (cm^{-1})	$\nu_{C=NH^+}$ (cm^{-1})	Δd^a (cm^{-1})
I_2–HCl	1698	—	1700	—
I_2–DCl	1676	(22)	1676	(24)
I_2–TCA	1706	—	1704	—
I_2–TCA-*d*	1679–1680	(27–26)	1678	(26)

[a] Δd represents the isotopic shift between $\nu_{C=N^+H}$ and $\nu_{C=N^+D}$.

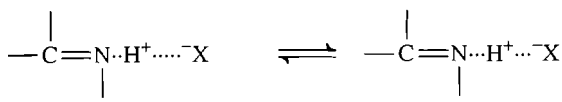
predict that rehybridization will be quite important when the positive charge sits mainly on the nitrogen atom, as shown below:



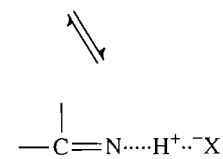
This is the case for the unconjugated Schiff bases (the present work) while for conjugated Schiff bases a somewhat different picture arises:



But acids can protonate the azomethine function in different ways, i.e., the proton could be more or less close to the nitrogen atom as shown below:



(A) (B)



(C)

Thus, the proton could be nearer to the nitrogen atom (A), closer to the counterion (C), or more or less in the middle (B). We have seen that in the stretch–bend theory, structures A and B should give maximal stretch–bend interaction, provided that the coincidence of the energy levels of the two modes is not broken as has been observed on similar complexes (20, 21, 24, 26). It should also give maximal rehybridization, so that both theories are affected the same way. The question of protonation will be discussed in Sect. II.

Can. J. Chem. Downloaded from www.nrcresearchpress.com by 195.138.81.100 on 09/07/12
For personal use only.

II. Analysis of the state of protonation of the imine complexes

Besides the frequency modulation, the intensity changes of both vibrations (viz. $\nu_{C=N}$ and $\nu_{C=N^+}$) are also of interest because they can be used to monitor the extent of proton transfer. The intensities needed for the calculations are normalized to a selected band of solvent present and are reported in Tables 1–3. For convenience, they have been renormalized to the $\delta_{C=H}$ mode of $CHCl_3$ (see experimental section for detail). The degree of protonation is estimated either from the intensity of the $\nu_{C=N}$ or of the $\nu_{C=N^+}$, depending upon which mode is the more intense. Their Raman signals being linear with respect to concentration, the percentage of protonation is easily calculated using basic algebra.

The extent of protonation obtained is summarized in Tables 1–3 for $CHCl_3$, MeOH, and DMSO, respectively. The given percentages are comparable to the data of Lussier *et al.* (15) acquired for chloroform. Clearly, none of the carboxylic acids used are able to completely protonate the Schiff base, and a significant proton transfer appears only with acids having pK_a's lower than ca. 2 units in water (that is, for very strong acids). This situation deteriorates when the imine is less basic. For instance, a drop of 1 unit in the pK_a of the imine group leads to a loss of 10% in proton transfer. Protonation is improved by a factor of approximately 20 percent when the dielectric constant of the solvent is increased from ca. 5 to ca. 33 units (see Tables 1 and 2). These comments only apply when the medium strongly interacts with the analyte, because with a non-interacting but polar solvent like DMSO, protonation is simply absent (see Table 3). This can be understood by looking at the factors affecting imine – carboxylic acid complexes. They generally obey the following equations (written using symbolic notation) (28–30):

[1] $C{=}N + HOOC{-}R \rightleftharpoons C{=}N\cdots\cdots HOOC{-}R$

I II

$C{=}N^+H\cdots\cdots{}^-OOCR$

III

From an experimental point of view, the protonated species quoted in this work correspond to complex III. The protonation is driven by the force associated with the energy gradient corresponding to the pK_a difference between the imine and the acid functions. From one solvent to another, pK_a's are modified by both the electrostatic properties of the medium and its solvation capacity.

This makes it difficult to predict the extent of protonation based solely on this physical factor alone (viz. grad(pK_a) in water). A better analysis can be carried out by separating the electrostatic forces and by using a grad(pK_a) related to a particular solvent (i.e., water, this being more convenient as pK_a's do not have a clear meaning in nonaqueous solvents). Qualitatively, proton transfer occurs when it abides by the following inequality:

[2] $\text{Grad}(pK_a) - (F_c + F_s) > 0$

The position of the balance between the terms in expression [2] will locate the proton. This equation shows that protonation is significant when the driving term grad(pK_a) is not overcome by the attractive electrostatic (or coulombic) force F_c, which tends to retain the proton near its anion in a low dielectric medium. Besides, the solvation capacity of the medium F_s severely reduces the proton motion towards nitrogen. This term (F_s) represents the solvent ability to create a tight ion pair or to solvate charge, this being equivalent to the reaction $RCOOH \rightleftharpoons RCOO^-\cdots H^+$. In other words, only a solvent with a good hydrogen bonding capacity is able to polarize the acid, that is, to make it an ion pair (viz. A^-H^+), this being followed by a total ionization of $RCOO^-\cdots H^+$ (viz. $RCOO^-\cdots H^+ \rightleftharpoons RCOO^- + H^+$) if the medium happens to be sufficiently polar. Using this definition, F_s will be small when the solvent is able to create ion pairs such as $RCOO^-\cdots H^+$ and will tend to infinity otherwise. This image fits the protonation pattern obtained in chloroform and methanol (where F_s and F_c are moderate), as well as in DMSO where F_s is infinite and F_c ineffective. Now, it is clear that for a given grad(pK_a) and polarity of the medium, proton transfer will occur only when ion pairs are present, this being the limiting factor.

III. Implications for bacterial and visual pigments

As reported in Sect. I, the imine–HCl system in $CHCl_3$ is characterized by a reduced isotopic shift resulting from a H^+ located near the counterion (viz. $N^+\cdots\cdots H\cdot\cdot X^-$), thus forming a less ionic complex (15, 20, 31). However, the literature (20, 21, 24, 32) shows that a reduced isotope effect could also be explained in term of a weaker interaction between the protonated Schiff base and its counterion (viz. $N^+\cdot\cdot H\cdots\cdots X^-$), which leads to a less effective C=N/N—H coupling owing to the modification of their vibrational level energy proximities (20, 21, 27). This last statement implies that the counterion is separated by a large gap from the protonated imine and, consequently, the positive charge rests mainly on the nitrogen atom, while in our case the positive charge is located on the proton, which is supposed to be distant from the imine. These facts illustrate that reduced deuterium effect may indicate that the proton is located at either end of the $N^+\cdots H\cdots X^-$ axis, and the $\nu_{C=N^+H}$ frequency position is best explained by the rehybridization model because it assumes a minimal role for the C=N/N—H coupling. As a consequence, for cases where H^+ is located more or less at midpoint along the $N^+\cdots H\cdots X^-$ bridge, the $\nu_{C=N^+}$ frequency position could be explained by both coupling and rehybridization as already demonstrated by Baasov *et al.* (20), and this situation is the most commonly encountered in models.

Intensity measurements may help to solve the protonation problem in rhodopsins. At present protonation of the Schiff base in pigments is believed to involve complex paths. For instance, evidence that aspartic acids 85, 96, 115, and 212 in bacteriorhodopsin are affected in this protonation process has been reported (33). From data for our carboxyl–imine complexes, it is clear that the medium around the chromophore should exhibit strong interactions with the proton source in order to insure full protonation. This statement derives from eq. [2], where the role of these interactions is to minimize the forces F_c and F_s, both factors reducing the effectiveness of grad(pK_a). In other words, the chromophore pocket should be at least chloroform-like or, even better, methanol-like. This idea is not new and has already been widely suggested (see refs. 3 and 4 and refs. therein) and, as an example, the presence of water has been often invoked to suit this requirement (34).

This hypothesis can be tested by mixing an imine with an acid having a protonating capacity similar to aspartic or glutamic acid, and then by adding a water-like molecule in various proportions. This was done in our laboratory by solubilizing an

imine–PRO system in a $CHCl_3$ matrix and adding quantities of methanol ranging from 1 to 20% (v/v). Upon addition of 1, 5, 10, 20% of MeOH by volume to this apolar matrix, an increase in protonation can be observed. Duplicating the same experiments with twice the amount of acid compared to the imine again improves the proton transfer. Even so, this excess of acid is not enough to fully protonate the imine. Therefore the presence of a water-like medium could only partially explain the whole protonation mechanism.

Nevertheless, these model systems should be accepted with reservations for two reasons: first, the model cannot integrate all the factors met in the proteins and, second, the literature (35, 36) reports a pK_a value of 13.3 for the chromophore in bacteriorhodopsin. Similarly, a value of about 2.5 units (33) has been suggested for some aspartic acid residues in the pigments instead of the usual 3.8 units, this giving a grad(pK_a) that cannot be reproduced by our models. In spite of these two weaknesses, our examples prove that the protein has to provide to the chromophore a medium able to "solvate" COO^- and H^+ groups, this condition being fundamental.

Conclusion

Frequency changes experienced by a Schiff base and isotopic substitution on protonated imines may be correlated to the Schiff base – counterion interaction. With regard to protonation, it is clear that this will be eased only if the chromophore cavity is protic and fairly polar. These conditions can be fulfilled in the pigments by invoking the presence of water. This raises the question of how Schiff bases, sensitive to hydrolysis, will be able to survive in pigments? Some explanations suggest that either H_2O molecules have different physical or chemical properties in the proteins, or hydrolysis may be triggered only when a sufficiently large concentration of water is present inside the chromophore pocket. So far no work has been done in this sense and the question remains open.

Acknowledgments

This work was supported by the Natural Sciences and Engineering Research Council of Canada and by the Université du Québec à Montréal.

1. W. Stoeckenius and R. A. Bogomolni. Annu. Rev. Biochem. Biophys. Acta, **505**, 215 (1982).
2. R. Diller and M. Stockburger. Biochemistry, **27**, 7641 (1988).
3. C. Sandorfy and D. Vocelle. Can. J. Chem. **64**, 2251 (1986).
4. C. Sandorfy and D. Vocelle. *In* Molecules in physics, chemistry, and biology. Vol. IV. *Edited by* Jean Maruani. Kluwer Academic Publishers, Norwell, Mass. 1989. pp. 195–211.
5. B. Honig, A. D. Greenberg, U. Dinur, and T. G. Ebrey. Biochemistry, **15**, 4593 (1976).
6. B. Aton, A. G. Doukas, R. H. Callender, B. Becher, and T. G. Ebrey. Biochemistry, **16**, 2995 (1977).
7. R. E. Cookingham, A. Lewis, and A. T. Lemley. Biochemistry, **17**, 4699 (1978).
8. H. Kakitani, T. Kakitani, H. Rodman, B. Honig, and R. Callender. J. Phys. Chem. **87**, 3620 (1983).
9. M. A. Marcus, A. T. Lemley, and A. Lewis. J. Raman Spectrosc. **8**, 22 (1979).
10. M. Braiman and R. Mathies. Biochemistry, **19**, 5421 (1980).
11. I. Palings, J. A. Pardoen, E. van den Berg, C. Winkel, J. Lugtenburg, and R. A. Mathies. Biochemistry, **26**, 2544 (1987).
12. G. R. Loppnow and R. A. Mathies. Biophys. J. **54**, 35 (1988).
13. B. Barry and R. A. Mathies. Biochemistry, **26**, 59 (1987).
14. S. O. Smith, J. A. Pardoen, J. Lugtenburg, and R. A. Mathies. J. Phys. Chem. **91**, 804 (1987).
15. L. S. Lussier, A. Dion, C. Sandorfy, H. Le-Thanh, and D. Vocelle. Photochem. Photobiol. **44**, 629 (1986).
16. J. Favrot, C. Sandorfy, and D. Vocelle. Photochem. Photobiol. **28**, 271 (1978).
17. J. Favrot, D. Vocelle, and C. Sandorfy. Photochem. Photobiol. **30**, 417 (1979).
18. J. J. Lòpez-Garriga, G. T. Babcock, and J. F. Harrison. J. Am. Chem. Soc. **108**, 7241 (1986).
19. T. Baasov and M. Sheves. J. Am. Chem. Soc. **107**, 7524 (1985).
20. T. Baasov, N. Friedman, and M. Sheves. Biochemistry, **26**, 3210 (1987).
21. H. S. Rodman Gilson, B. H. Honig, A. Croteau, G. Zarrilli, and K. Nakanishi. Biophys. J. **53**, 261 (1988).
22. S. O. Smith, A. B. Myers, R. A. Mathies, J. A. Pardoen, C. Winkel, E. M. M. van den Berg, and J. Lugtenburg. Biophys. J. **47**, 653 (1985).
23. P. E. Blatz and J. H. Mohler. Biochemistry, **14**, 2304 (1975).
24. T. Sugihara and T. kitagawa. Bull. Chem. Soc. Jpn. **59**, 2929 (1986).
25. J. J. Lòpez-Garriga, S. Hanton, G. T. Babcock, and J. F. Harrison. J. Am. Chem. Soc. **108**, 7251 (1986).
26. H. Deng and R. H. Callender. Biochemistry, **26**, 7418 (1987).
27. L. J. Bellamy. *In* Advances in infrared group frequencies. Methuen, London. 1968.
28. D. C. Jain, A. M. Sapse, and D. Cowburn. J. Phys. Chem. **92**, 6847 (1988).
29. G. Zundel. J. Mol. Struct. **177**, 43 (1988).
30. H. Merz and G. Zundel. Biochem. Biophys. Res. Commun. **138**, 819 (1986).
31. C. Brissette and C. Sandorfy. Can. J. Chem. **38**, 34 (1960).
32. C. Pande, R. Callender, J. Baribeau, F. Boucher, and A. Pande. Biochem. Biophys. Acta, **973**, 257 (1989).
33. M. S. Braiman, T. Mogi, T. Marti, L. J. Stern, H. G. Khorona, and K. J. Rothschild. Biochemistry, **27**, 8516 (1988).
34. P. Hildebrandt and M. Stockburger. Biochemistry, **23**, 5539 (1984).
35. M. Sheves, A. Albeck, N. Friedman, and M. Ottolenghi. Proc. Natl. Acad. Sci. U.S.A. **83**, 3262 (1986).
36. S. Druckman, M. Ottolenghi, A. Pande, J. Pande, and R. H. Callender. Biochemistry, **21**, 4952 (1982).

Can. J. Chem. Downloaded from www.nrcresearchpress.com by 195.138.81.100 on 09/07/12
For personal use only.

An *ab initio* study of symmetry breaking in calculations on the first excited singlet state of N_2H_2

JANET E. DEL BENE[1]
Department of Chemistry, Youngstown State University, Youngstown, OH 44555, U.S.A.
KYUNGSUN KIM AND ISAIAH SHAVITT
Department of Chemistry, The Ohio State University, Columbus, OH 43210, U.S.A.

Received September 6, 1990

JANET E. DEL BENE, KYUNGSUN KIM, and ISAIAH SHAVITT. Can. J. Chem. **69**, 246 (1991).

Calculation of the vertically excited singlet $n \rightarrow \pi^*$ state of *trans*-N_2H_2 carried out in C_s symmetry at the RHF and RHF-CISD levels results in a broken symmetry solution in which the wave function does not reflect the C_{2h} symmetry of the molecular framework. The excited state RHF energy computed in C_s symmetry is lower than the corresponding energy computed in C_{2h} symmetry, but the single-reference CISD energy based on the C_s RHF configuration is higher than the corresponding C_{2h} result. The symmetry breaking leads to difficulties in the description of the excited state potential energy surface, including the location of stationary points and the calculation of vibrational frequencies, and in the treatment of complexes of excited N_2H_2 with other molecules. The molecular symmetry of the vertically excited state can be restored in C_s calculation by the use of a four-configuration MCSCF wave function. The MCSCF procedure provides consistent data and leads to the prediction that the relaxed excited state has C_2 molecular symmetry. Unlike the RHF case, the UHF wave function does not display symmetry breaking at the C_{2h} geometry, and agrees with the MCSCF model in predicting an equilibrium structure of C_2 symmetry. A low-energy structure of C_2 symmetry has also been found with the UMP2 model, although it could not be positively confirmed that it corresponds to an equilibrium structure. The symmetry-breaking dilemma is not unique to the excited $n \rightarrow \pi^*$ state of N_2H_2, but arises in other molecules in which the two chromophores are similarly symmetry related.

Key words: symmetry breaking, excited state, MCSCF, N_2H_2.

JANET E. DEL BENE, KYUNGSUN KIM et ISAIAH SHAVITT. Can. J. Chem. **69**, 246 (1991).

Des calculs effectués aux niveaux RHF et RHF-CISD, sur l'état singulet excité verticalement $n \rightarrow \pi^*$ de la *trans*-N_2H_2 calculée dans la symétrie C_s, conduisent à une solution avec discontinuité dans la symétrie dans laquelle la fonction d'onde n'est pas un reflet de la symétrie C_{2h} du cadre moléculaire. L'énergie RHF de l'état excité, calculée dans la symérie C_s, est inférieure à l'énergie correspondante calculée dans la symétrie C_s est inférieure à l'énergie corrrespondante calculée dans la symètrie C_{2h}; toutefois l'énergie CISD à référence simple, calculée sur la base de la configuration RHF C_s, est supérieure à la valeur C_{2h} correspondante. La discontinuité dans la symétrie conduit à des difficultés dans la description de la surface d'énergie potentielle de l'état excité, y compris dans la localisation des points stationnaires, dans les calculs des fréquences de vibration ainsi que dans le traitement de complexes du N_2H_2 excité avec d'autre molécules. La symétrie moléculaire de l'état excité verticalement peut être restaurée dans les calculs C_s par l'utilisation d'une fonction d'onde MCSCF à quatre configurations. La méthode MCSCF fournit des données cohérentes et conduit à faire la prédiction que l'état excité relaxé possède une symétrie moléculaire C_2. Par opposition avec le cas RHF, la fonction d'onde UHF ne présente pas de discontinuité dans la symétrie de la géométrie C_{2h} et elle est en accord avec le modele MCSCF pour prédire une structure d'équilibre pour la symérie C_2. Avec le modèle UMP2, on a aussi trouvé une structure de basse énergie de symétrie C_2, même si on n'a pas pu confirmer positivement qu'elle correspond à une structure en équilibre. Le dilemme de la discontinuité dans la symétrie n'est pas unique à l'état excité $n \rightarrow \pi^*$ de la N_2H_2; c'est une situation que l'on retrouve dans d'autres molécules dans lesquelles les deux chromophores sont aussi reliés par la symétrie.

Mots clès : discontinuité dans la symmétrie, état excité, MCSCF, N_2H_2.

[Traduit par la rédaction]

Introduction

In a study of $n \rightarrow \pi^*$ transitions in molecules containing lone pairs of electrons, we have encountered a symmetry-breaking problem in the single-determinant description of the lowest singlet excited state of N_2H_2. In this case, the wave function produced from a restricted Hartree–Fock (RHF) calculation carried out in C_s symmetry fails to reflect the full C_{2h} symmetry of the molecular framework. This symmetry-breaking problem gives rise to discontinuities on the potential energy surface, preventing the correct location of stationary points and the calculation of reliable vibrational frequencies and other properties of excited N_2H_2. In particular, it causes difficulties in the calculation of binding energies of complexes of excited N_2H_2, because these complexes generally possess lower symmetry than N_2H_2 itself. This type of problem, first referred to by Löwdin (1) as the "symmetry dilemma", has been investigated extensively (see, e.g., Čížek and Paldus (2), McKelvey and co-workers (3), Jackels and Davidson (4), Seeger and Pople (5), Paldus and co-workers (6), Englebrecht and Liu (7), Davidson and co-workers (8), McLean *et al.* (9), and Szalay *et al.* (10), and references therein), primarily for the ground doublet state of allyl and other radicals. Interestingly (and similar to the case of the allyl radical (8)), the unrestricted Hartree–Fock (UHF) wave function of singlet-excited N_2H_2 does not break symmetry at the C_{2h} geometry (though the lowest-energy C_{2h} geometry is unstable with respect to asymmetric a_u and b_u distortions of the molecule on the UHF potential energy surface). In an effort to investigate the symmetry-breaking problem for excited N_2H_2, we have used several *ab initio* models and different symmetry contraints to compute the energy of the vertically excited molecule and to search the excited-state potential energy surface for stationary points.

Methods

All the calculations were carried out with the 6-13+G(*d*,*p*) basis set (11, 12). The ground state structure of *trans*-N_2H_2 was

[1]To whom correspondence should be addressed.

Printed in Canada / Imprimé au Canada

Can. J. Chem. Downloaded from www.nrcresearchpress.com by 195.138.81.100 on 09/07/12
For personal use only.

TABLE 1. Total RHF and CISD energies (hartrees) and Mulliken gross atomic populations in the ground and first excited singlet states of N_2H_2, calculated at the ground-state MP2-optimized geometry[a] using different symmetry constraints

	RHF					CISD				
		Populations[b]					Populations[b]			
Symmetry	Energy	N_1	N_2	H_1	H_2	Energy	N_1	N_2	H_1	H_2
					Ground state					
1-ref C_{2h}	−110.002622	7.285	7.285	0.715	0.715	−110.330350	7.274	7.274	0.726	0.726
					First excited singlet state					
1-ref C_{2h}	−109.872701	7.337	7.337	0.663	0.663	−110.201982	7.321	7.321	0.679	0.679
1-ref C_s	−109.878081	7.275	7.381	0.707	0.637	−110.194288	7.277	7.335	0.708	0.659
4-ref C_s	−109.912177	7.324	7.324	0.676	0.676	−110.215141	7.313	7.313	0.687	0.687

[a] R_{NN} = 1.264 Å, R_{NH} = 1.029 Å, ∠NNH = 105.7°.
[b] H_i is bonded to N_1, and H_2 to N_2.

fully optimized with correlation at second-order Møller–Plesset perturbation theory (13–16) (MP2) with this basis. This molecule has C_{2h} symmetry, with a closed-shell ^1A_g ground state. Single-configuration restricted open-shell Hartree–Fock calculations followed by configuration interaction with all single and double excitations (17) (CISD) were carried out to obtain the energy of the vertically excited $n \rightarrow \pi^*$ state. These calculations were done in both C_{2h} symmetry, where the excited state is ^1B_g, and in C_s symmetry, where the excited state is $^1A''$, always maintaining the C_{2h} molecular framework. Similar calculations were done for the UHF and unrestricted second-order Møller–Plesset (UMP2) models. Multiconfigurational SCF (MCSCF) and multireference CISD calculations of the vertically excited state were carried out using C_s symmetry.

Geometry optimizations to determine the structure of the relaxed excited state were carried out using the RHF, UHF, UMP2, and MCSCF models in C_{2h}, C_s, and C_2 symmetries. The UHF and UMP2 optimized structures and vibrational frequencies were calculated using the GAUSSIAN 88 system of computer programs (18). The RHF, MCSCF, and CI calculations were done with the COLUMBUS system of programs (19, 20). The location of stationary points on the RHF and MCSCF potential energy surfaces from computed values of the energy and the energy gradient was accomplished with the MINPT program (21).

The occurrence of symmetry-broken solutions greatly complicates the characterization of symmetrically constrained stationary points and the determination of the corresponding vibrational frequencies, at least when analytically computed second derivatives are not available. On the one hand, if the wave function calculations are carried out without symmetry constraints, the symmetric points usually represent cusps on the complete potential energy surface in symmetry breaking cases. On the other hand, if the calculations at the symmetric points are symmetry constrained, it is not unusually possible to carry out equivalent calculations at asymmetrically distorted geometries. However, it has been found (3, 6, 7) that the symmetrically constrained Hartree–Fock wave function can often be obtained as an unstable solution, presumably a saddle point on the orbital optimization surface (not to be confused with the potential energy surface), of the unconstrained Hartree–Fock equations for the symmetric point, and that corresponding unstable solutions which connect smoothly with it can even be found at slightly distorted geometries (6, 7).

In the RHF calculations described here, it was found possible to find such solutions and to obtain a complete set of frequencies corresponding to symmetrically constrained stationary points using just energies and gradients. First, the orbitals obtained in the symmetrically constrained calculation at the symmetric stationary point were reexpressed in a format appropriate for lower symmetry calculations and were used as starting orbitals in symmetry unconstrained calculations at the same point. These orbitals were found to satisfy the symmetry-unconstrained RHF equations, and produced the same energy as in the constrained calculation. Then, the same starting orbitals were used in calculations on slightly asymmetrically distorted geometries, and were found to produce solutions which connected quite smoothly with the solution at the symmetric point. This procedure can be regarded as an analytical continuation of the symmetry-constrained solution into the asymmetric region of the potential energy surface.

The UHF frequencies were computed with the GAUSSIAN 88 programs using analytical second derivatives, and were not subject to instability problems. However, the UMP2 frequency determinations use energies and gradients only, and require calculations at asymmetrically distorted geometries around the stationary point. Some of these distorted geometries have no symmetry at all, and the UHF solutions at these points collapsed to the ground state (since the excited and ground-state UHF determinants could not be distinguished in this case by differences in the occupancy of spin orbitals of different symmetry or spin), preventing the reliable determination of the UMP2 frequencies and the characterization of the stationary points.

All calculations reported in this work were carried out on the AMDAHL 5868 computer at Youngstown State University and the CRAY Y-MP8/864 at the Ohio Supercomputer Center.

Results and discussion

Vertical excitation energies

The RHF and CISD energies of N_2H_2 in the ground and the first vertically excited $n \rightarrow \pi^*$ state are reported in Table 1, along with the Mulliken gross atomic populations. In C_{2h} symmetry the RHF excited state has ^1B_g symmetry and lies 3.54 eV above the ground state. However, if the RHF calculation is done in C_s symmetry (while maintaining the molecular framework in C_{2h}), a lower energy for the $^1A''$ $n \rightarrow \pi^*$ state is found and the excitation energy decreases to 3.39 eV. This lowering of energy is accompanied by a symmetry breaking of the wave function

Can. J. Chem. Downloaded from www.nrcresearchpress.com by 195.138.81.100 on 09/07/12
For personal use only.

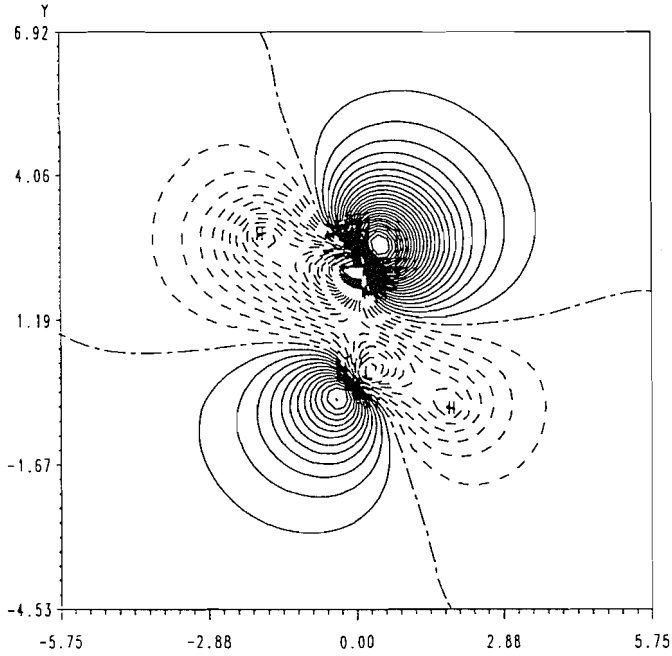


FIG. 1. Cross-section, in the molecular plane, of the singly-occupied $7a'$ RHF orbital for vertically-excited N_2H_2, computed in C_s symmetry. Countour lines range from -0.5 to $+0.5$ in steps of 0.02. Solid lines indicate positive values, dashed lines negative values, and nodes are designated by short–long dashed lines. The nitrogen atoms are located at the origin and on the positive Y axis. The coordinate scales are in units of Bohr radii (a_0).

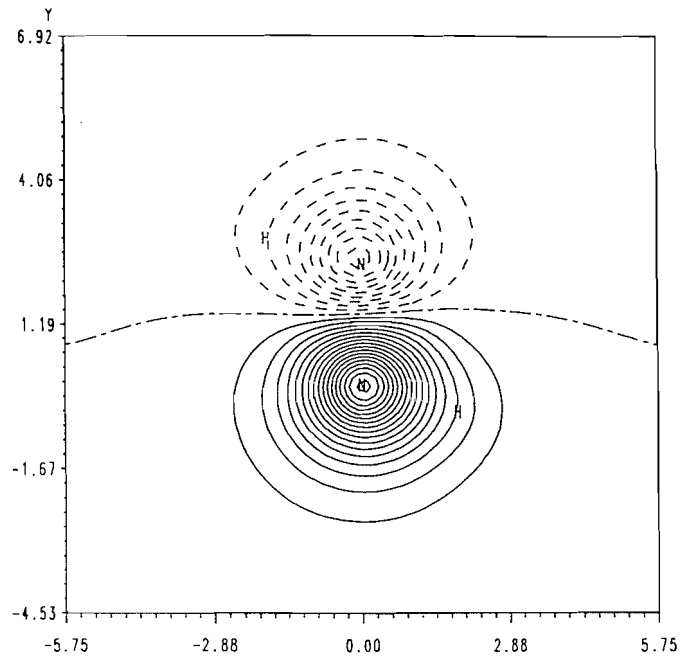


FIG. 2. Cross-section, in a plane 1 a_0 above the molecular plane, of the singly-occupied $2a''$ RHF orbital computed in C_s symmetry. Line values and other details are the same as in Fig. 1.

which makes the two N—H groups nonequivalent, as indicated by the Mulliken population data. Configuration interaction does not restore the equivalency of the two N—H groups in C_s symmetry. Furthermore, the CISD energy based on the C_s single-configuration reference function is now higher than the CISD energy based on the C_{2h} single-configuration reference function. Thus, neither the single-configuration RHF wave function nor the CISD wave function based on it provide an appropriate description of the $n \rightarrow \pi^*$ excited state of N_2H_2.

The restricted open-shell Hartree–Fock calculation in C_s symmetry gives rise to the configuration

$$(1a')^2(2a')^2(3a')^2(4a')^2(5a')^2(6a')^2(1a'')^2(7a')^1(2a'')^1$$

Both the doubly-occupied $6a'$ and singly-occupied $7a'$ orbitals (the two lone-pair orbitals in the ground state) have different contributions from the two N—H groups. Likewise, the two nitrogen atoms make different contributions to the doubly-occupied $1a''$ (π) and the singly-occupied $2a''$ (π^*) orbitals. The singly-occupied $7a'$ orbital is polarized toward one N—H group, while the singly-occupied $2a''$ orbital is polarized toward the other. This is shown in Fig. 1 and 2, respectively, which present contour diagrams of the $7a'$ orbital in the molecular plane and of the $2a''$ orbital in a plane 1 a_0 above the molecular plane.

The symmetry dilemma is resolved when a suitable multiconfiguration wave function is used for the calculation of the excited-state energy. (Obviously, an equivalent multiconfiguration function for the ground state is required for the determination of the excitation energy in this case.) The active space required to make the two NH groups equivalent in C_s-symmetry calculations for the excited state consists of the two highest-energy σ orbital, $6a'$ and $7a'$, and the two lowest-energy π orbitals, $1a''$ and $2a''$. This active space requires that three electrons be distributed in $6a'$ and $7a'$ and three electrons in $1a''$ and $2a''$, and generates four configurations. It is evident from the Mulliken populations shown in Table 1 that the resulting four-configuration MCSCF wave function restores the equivalence of the two N—H groups in C_s symmetry. The MSCSF energy, is of course, lower than any single-configuration energy. The four-reference CISD energy is also lower than any single-reference CISD energy for the excited state. The CI coefficients of the four reference configurations in the multireference CISD wave function are

$\ldots(6a')^2(1a'')^2(7a')^1(2a'')^1$	0.935
$\ldots(6a')^2(1a'')^1(7a')^1(2a'')^2$	0.000
$\ldots(6a')^1(1a'')^2(7a')^2(2a'')^1$	0.000
$\ldots(6a')^1(1a'')^1(7a')^2(2a'')^2$	0.192

The UHF and UMP2 energies and UHF gross atomic populations for the ground and excited state of N_2H_2 are displayed in Table 2. The ground state solutions are identical to the corresponding RHF and MP2 solutions. The excited state calculations produce identical results in C_{2h} and C_s symmetries, displaying no spatial symmetry breaking (though they do not represent a pure singlet spin state).

Excited state geometries

The discrepancy between the RHF and CISD energies computed for excited N_2H_2 in C_{2h} and C_s symmetries suggests that there are discontinuities on the excited state potential energy surface associated with symmetry breaking. To further investigate this surface, we have attempted to optimize the geometry of relaxed N_2H_2 in the first excited singlet state using various theoretical methods and imposing different symmetry constraints. The resulting structures and energies are reported in Table 3.

Using the RHF model, geometry optimizations were done in C_{2h}, C_s, and C_2 symmetries. The C_s structure has two inequivalent N—H groups and a significantly longer N—N bond than in the C_{2h} and C_2 structures. The C_{2h} structure has

Can. J. Chem. Downloaded from www.nrcresearchpress.com by 195.138.81.100 on 09/07/12
For personal use only.

TABLE 2. Total UHF and UMP2 energies (hartrees) and Mulliken gross atomic populations in the ground and first excited singlet states of N_2H_2, calculated at the ground-state MP2-optimized geometry[a] using different symmetry constraints

	UHF					UMP2
		Populations				
Symmetry	Energy	N_1	N_2	H_1	H_2	Energy
		Ground state				
C_{2h}, C_s	−110.002621	7.285	7.285	0.715	0.715	−110.343516
		First excited singlet state				
C_{2h}, C_s	−109.910437	7.325	7.325	0.675	0.675	−110.230839

[a]See Table 1.

TABLE 3. Calculated structures and energies[a] of N_2H_2 in the first excited singlet state

Symmetry	N—N	N_1—H_1	N_2—H_2	∠H_1—N_1—N_2	∠H_2—N_2—N_1	∠H_1—N_1—N_2—H_2	Energy	N_{imag}[b]
				RHF				
C_{2h}	1.241	1.002	1.002	123.1	123.1	180.0	−109.891162	1
C_s	1.297	0.995	1.009	133.6	108.1	180.0	−109.902418	0
C_2	1.227	1.008	1.008	122.5	122.5	111.9	−109.897197	0
				UHF				
C_{2h}	1.253	1.003	1.003	121.3	121.3	180.0	−109.926263	2
C_s	1.271	0.998	1.008	129.2	112.3	180.0	−109.927464	1
C_2	1.236	1.008	1.008	121.4	121.4	112.3	−109.930971	0
				UMP2				
C_{2h}	1.270	1.015	1.015	120.5	120.5	180.0	−110.251138	—[c]
C_2	1.267	1.025	1.025	119.3	119.3	104.7	−110.259732	—[c]
				MCSCF				
C_{2h}	1.274	1.000	1.000	120.9	120.9	180.0	−109.929113	1
C_2	1.260	1.004	1.004	121.4	121.4	121.2	−109.931616	0

[a]Bond lengths in ångströms and angles in degrees; energies in hartrees.
[b]Number of imaginary frequencies.
[c]The frequencies could not be determined reliably in this case (see text).

one imaginary frequency which corresponds to out-of-plane distortion toward a C_2 structure. Both the C_s and C_2 optimized structures are predicted to be true minima, with no imaginary frequencies, but the C_s structure has the lower energy. As seen below, no other model predicts a stable minimum of C_s symmetry.

Though the UHF solution for the excited state at the ground-state geometry does not display symmetry breaking, there is a UHF stationary point of C_s symmetry lower in energy than the UHF C_{2h} stationary point. However, neither of these two points is a true minimum on the UHF potential energy surface, having one and two imaginary frequencies, respectively, and there is a true minimum of lower energy having C_2 symmetry. Although it is not expected that there would be a global minimum of C_1 symmetry, this possibility could not be pursued because of our inability to prevent the collapse of the UHF calculation to the ground state in this case.

Geometry optimization of excited N_2H_2 at the UMP2 level of theory produced just two stationary points. Optimization in C_s symmetry encountered difficulties, but appeared to be converging toward a C_{2h} structure, with equivalent N—H groups. The optimized nonplanar C_2 structure has a lower energy than the optimized C_{2h} structure. It was not possible to obtain consistent frequencies for either of these structures for reasons discussed in the previous section.

The fourth method used to locate the global minimum on the N_2H_2 potential surface was the multiconfigurational MCSCF procedure. At this level of theory only two stationary points were found. The C_{2h} structure has one imaginary frequency corresponding to an out-of-plane twist. The optimized C_2 structure has a lower energy, and with no imaginary frequencies appears to be the global minimum and equilibrium structure for singlet excited N_2H_2.

In summary, while RHF, UHF, UMP2, and MCSCF all exhibited stationary points of C_2 symmetry lower in energy than C_{2h}, the RHF point was not the global minimum, and the UMP2 point could not be reliably confirmed to be a minimum rather than a saddle point. The symmetry-breaking problem has been investigated in detail in this work only for the excited $n \rightarrow \pi^*$ state of N_2H_2, but similar problems are anticipated in other

Can. J. Chem. Downloaded from www.nrcresearchpress.com by 195.138.81.100 on 09/07/12
For personal use only.

molecules, such as glyoxal and the diazines, in which the two chromophores are similarly symmetry related.

Acknowledgements

We wish to thank the Youngstown State University Computer Center and the Ohio Supercomputer Center for support of this work. Helpful discusison with Dr. Ron Shepard are gratefully acknowledged.

1. P.-O. Löwdin. Rev. Mod. Phys. **35**, 496 (1963); Adv. Chem. Phys. **14**, 283 (1969).
2. J. Čížek and J. Paldus. J. Chem. Phys. **47**, 3976 (1967); Phys. Rev. A, **3**, 525 (1971).
3. J. McKelvey and W. J. Hehre. Mol. Phys. **25**, 983 (1973); J. M. McKelvey and G. Berthier. Chem. Phys. Lett. **41**, 476 (1976).
4. C. F. Jackels and E. R. Davidson. J. Chem. Phys. **64**, 2908 (1976).
5. R. Seeger and J. A. Pople. J. Chem. Phys. **66**, 3045 (1977).
6. J. Paldus and A. Veillard. Mol. Phys. **35**, 445 (1978); M. Bénard and J. Paldus. J. Chem. Phys. **72**, 6546 (1980); J. Paldus and E. Chin. Int. J. Quantum Chem. **24**, 373 (1983).
7. L. Engelbrecht and B. Liu. J. Chem. Phys. **78**, 3097 (1983).
8. E. R. Davidson and W. T. Borden. J. Phys. Chem. **87**, 4783 (1983); D. Feller, E. R. Davidson, and W. T. Borden. J. Am. Chem. Soc. **106**, 2513 (1984).
9. A. D. McLean, B. H. Lengsfield III, J. Pacansky, and Y. Ellinger. J. Chem. Phys. **83**, 3567 (1985).
10. P. G. Szalay, A. G. Császár, G. Foragasi, A. Karpfen, and H. Lischka. J. Chem. Phys. **93**, 1246 (1990).
11. P. C. Hariharan and J. A. Pople. Theoret. Chim. Acta, **28**, 213 (1973); J. D. Dill and J. A. Pople. J. Chem. Phys. **62**, 2921 (1975).
12. T. Clark, J. Chandrasekhar, G. W. Spitznagel, and P. v. R. Schleyer. J. Comput. Chem. **4**, 294 (1983); G. W. Spitznagel, T. Clark, J. Chandrasekhar, and P. v. R. Schleyer. J. Comput. Chem. **3**, 363 (1982).
13. R. J. Bartlett and D. M. Silver. J. Chem. Phys. **62**, 3258 (1975).
14. R. J. Bartlett and G. D. Purvis. Int. J. Quantum Chem. **14**, 561 (1978).
15. J. A. Pople, J. S. Binkley, and R. Seeger. Int. J. Quantum Chem. Quantum Chem. Symp. **10**, 1 (1976).
16. R. Krishnan and J. A. Pople. Int. J. Quantum Chem. **14**, 91 (1978).
17. I. Shavitt. The method of configuration interaction. *In* Methods of electronic structure theory. *Edited by* H. F. Schaefer III. Plenum Press, New York. 1977.
18. M. J. Frisch, M. Head-Gordon, H. B. Schlegel, K. Raghavachari, J. S. Binkley, C. Gonzalez, D. J. DeFrees, D. J. Fox, R. A. Whiteside, R. Seeger, C. F. Melius, J. Baker, R. Martin, L. R. Kahn, J. J. P. Stewart, E. M. Fluder, S. Topiol, and J. A. Pople. GAUSSIAN 88. Gaussian, Inc., Pittsburg. 1988.
19. H. Lischka, R. Shepard, F. B. Brown, and I. Shavitt. Int. J. Quantum Chem. Quantum Chem. Symp. **15**, 91 (1981).
20. R. Shepard, I. Shavitt, R. M. Pitzer, D. C. Comeau, M. Pepper, H. Lischka, P. G. Szalay, R. Ahlrichs, F. B. Brown, and J.-G. Zhao. Int. J. Quantum Chem. Quantum Chem. Symp. **22**, 149 (1988).
21. D. C. Comeau, R. J. Zellmer, and I. Shavitt. The location and characterization of stationary points on molecular potential energy surfaces. *In* Geometrical Derivatives of Energy Surfaces and Molecular Properties. *Edited by* P. Jørgensen and J. Simons. D. Reidel Publishing Company, Dordrecht, Holland. 1986.

Can. J. Chem. Downloaded from www.nrcresearchpress.com by 195.138.81.100 on 09/07/12
For personal use only.

The direct electrochemical synthesis of the novel copper(I) complex $Cu_2[OC_6Cl_4(OH)]_2[(C_6H_5)_2PCH_2P(C_6H_5)_2]_2$

THEODORE A. ANNAN, JAMES E. KICKHAM, AND DENNIS G. TUCK[1]

Department of Chemistry and Biochemistry, University of Windsor, Windsor, Ont., Canada N9B 3P4

Received February 8, 1990[2]

THEODORE A. ANNAN, JAMES E. KICKHAM, and DENNIS G. TUCK. Can. J. Chem. **69**, 251 (1991).

The electrochemical oxidation of copper in an acetonitrile solution of an aromatic diol ($R(OH)_2$ = catechol, tetrachloro-1,2-dihydroxybenzene, 2,2′-dihydroxybiphenyl) gives soluble copper(I) products which are reduced to copper at a platinum cathode. In the presence of $R(OH)_2$ + L (L = 2,2′-bipyridine, triphenylphosphine, bis(diphenylphosphino)methane (= dppm)), the products are adducts of copper(I) species in which the anionic ligand is $[R(O)OH]^-$. The crystal structure of $Cu_2[OC_6Cl_4(OH)]_2(dppm)_2$ is triclinic, with a = 22.418(5) Å, b = 11.784(4) Å, c = 13.492(4) Å, α = 61.63(2)°, β = 86.66(2)°, γ = 80.61(2), V = 3093(2) Å^3, Z = 2, and space group $P\bar{1}$. The molecule consists of a Cu—P—C—P—Cu—P—C—P ring, with copper ligated by $[R(O)OH]^-$ groups external to this. Intramolecular O—H---O hydrogen-bonding contributes to the stabilization of this novel complex.

Key words: Copper, electrochemical synthesis, hydrogen bonding, aromatic diols, crystal structure.

THEODORE A. ANNAN, JAMES E. KICKHAM et DENNIS G. TUCK. Can. J. Chem. **69**, 251 (1991).

L'oxydation électrochimique du cuivre en solution avec un diol aromatique ($R(OH)_2$ = catéchol, tétrachloro-1,2-dihydroxybenzène, 2,2′-dihydroxybiphényle) dans de l'acétonitrile conduit à des produits solubles du cuivre(I) qui sont réduits en cuivre à une cathode de platine. En présence de $R(OH)_2$ + L (L = 2,2′-bipyridine, triphénylphosphine, bis(diphénylphosphino)-méthane (= dppm), les produits sont des adduits d'espèces du cuivre(I) dans lesquels le ligand anionique est le $[R(O)OH]^-$. La structure cristalline du $Cu_2[OC_6Cl_4(OH)]_2(dppm)_2$ est triclinique avec a = 22,418(5), b = 11,784(4) et c = 13,492(4) Å, α = 61,63(2), β = 86,66(2) et γ = 80,61(2)°, V = 3093(2) Å^3, Z = 2 et groupe d'espace $P\bar{1}$. La molécule comprend un cycle Cu—P—C—P—Cu—P—C—P dans lequel le cuivre est lié au groupe externe par des groupements $[R(O)OH]^-$. La liaison hydrogène intramoléculaire O—H---O contribue à la stabilisation de ce nouveau complexe.

Mots clés : cuivre, synthèse électrochimique, liaison hydrogène, diols aromatiques, structure cristalline.

[Traduit par la rédaction]

Introduction

One of the advantages of direct electrochemical synthesis is that in producing compounds by oxidising a metallic element in non-aqueous solution, the formation of lower oxidation state species is often favoured. Some examples include the synthesis of $Sn(SPh)_2$ (1), $Pb(SPh)_2$ (1), salts of $Ga_2X_6^{2-}$ (X = Cl, Br, I) (2), $Sn(O_2R)$ (R = catecholate, etc.) (3), InSPh (4), and the unusual indium(I) species In[OR(OH)] ($R(OH)_2$ = 1,2-$C_6H_4(OH)_2$, 2,3-dihydroxynaphthalene, 2,2′-dihydroxybiphenyl, 1,2-dihydroxytetrabromobenzene) (5), and In[SR(SH)] (R = 1,2-C_2H_4, 1,2-C_3H_6, 1,3-C_3H_6, 1,4-C_4H_8, 2,3-C_4H_8, 1,5-C_5H_{10}, 1,6-C_6H_{12}) (6). Similarly investigation of various copper–thiol systems in non-aqueous electrochemical synthesis gave rise to a number of CuSR compounds and their adducts, and some interesting cage structures were identified by X-ray crystallography (7–11). These latter form part of a large group of copper(I)-thiolato and -dithiolato species which illustrate the wide range of stereochemical possibilities in such molecules (12–14).

We now report an unusual copper(I) compound obtained in the extension of earlier work on the electrochemical synthesis of derivatives of aromatic 1,2-diols (3, 5, 15), where the product is the dppm adduct (dppm = bis(diphenylphosphino)methane) of the copper(I) derivative of 2-hydroxy-3,4,5,6-tetrachlorophenolate. The structure of this dimeric species has been established.

Experimental section

General

Copper anodes, in the form of sheets approximately 1 cm × 2 cm × 0.5 mm, were washed successively with dilate nitric acid, water, and acetone before use. Acetonitrile was distilled from calcium hydride immediately before use. All other materials were used as supplied.

Copper analysis was performed by atomic absorption spectrophotometry, using an IL-251 instrument. Microanalysis was by Guelph Chemical Laboratories Ltd. Infrared spectra were run as KBr discs on a Nicolet 5DX instrument; ^1H and ^{13}C nmr spectra were recorded on a Bruker 300 L spectrometer.

Electrochemical synthesis

The experimental techniques were essentially those used in earlier work, with cells of the type

$$Pt_{(-)}/CH_3CN + R(OH)_2 + L/Cu_{(+)}$$

and the diols investigated were catechol (1,2-dihydroxybenzene), tetrachloro-1,2-dihydroxybenzene, 4-*t*-butyl-1,2-dihydroxybenzene, and 2,2′-dihydroxybiphenyl. The neutral ligands used were 2,2′-bipyridine (bpy), triphenylphosphine, and dppm. Not all of these systems gave rise to identifiable products (see below). The composition of the solutions used are given in Table 1. Each experiment was run for 3 h at room temperature in an atmosphere of dry nitrogen, and the solution phase was stirred mechanically at regular intervals. Observations on specific systems are given below.

(*i*) Catechol, etc. When cells containing *ca.* 2.2 mmol of diol and no neutral ligand were used as the electrolyte, copper was dissolved from the anode, but deposition of metal on the cathode became increasingly apparent as the experiment proceeded. The electrochemical efficiency (E_F) for the anodic dissolution of copper, defined as moles Cu dissolved per Faraday of charge, was 1.10 mol F^{-1} for both catechol and tetrachlorocatechol. These experiments were not pursued further.

(*ii*) $Cl_4C_6(OH)_2$ + dppm. As electrolysis proceeded, the colour of the solution turned from pale brown through pink to orange, and after about 90 min, colourless crystals began to deposit and continued to form as current flowed. At the end of the experiment, these crystals were collected by filtration *in vacuo*, washed with acetone (10 mL), dried *in vacuo*, and identified as $Cu[OC_6Cl_4(OH)]$dppm (*Anal.* calcd. C 53.7, H 3.31, Cu 9.14; found C 53.3, H 3.40, Cu 9.25). The material

[1]To whom correspondence should be addressed.

[2]Revision received September 5, 1990.

Can. J. Chem. Downloaded from www.nrcresearchpress.com by 195.138.81.100 on 09/07/12
For personal use only.

TABLE 1. Experimental conditions for the attempted electrochemical synthesis of copper (I) diolato complexes

Diol[a]	Mass (g)	Ligand[b]	Mass (g)	Applied voltage[c] (V)	Metal consumed (mg)	Electrochemical efficiency (mol F^{-1})
$Cl_4C_6(OH)_2$-1,2	0.55	dppm	0.86	24	182	1.14
4-C_4H_9-$C_6H_3(OH)_2$-1,2	0.37	bpy	0.35	40	154	1.09
$(C_6H_4)_2(OH)_2$-2,2′	0.42	bpy	0.35	26	166	1.12
$(C_6H_4)_2(OH)_2$-2,2′	0.42	dppm	0.86	25	160	1.12
$C_6H_4(OH)_2$	0.37	Ph_3P	1.77	8	228	1.07

[a]Dissolved in 50 mL CH_3CN containing ca. 30 mg Et_4NClO_4.
[b]bpy = 2,2′-bipyridine; dppm = bis(diphenylphosphino)methane.
[c]Voltage to give an initial current of 20 mA.

used in the X-ray studies was obtained by recrystallizing the initial product from *N*,*N*-dimethylformamide. The ^1H nmr spectrum consists of a multiplet in the aromatic region, a singlet at 2.08 (d_6-dmso) or 1.64 ($CDCl_3$), which is assigned to CH_2 of dppm, and weak broad resonances at 3.75 (d_6-dmso) or 3.99 ($CDCl_3$) indicative of hydrogen bonding between solvent and the OH of the $[C_6Cl_4O(OH)]^-$ ligand. The ^{13}C spectrum (in dmso; Me_4Si = 0) shows two groups of resonances in the aromatic region; those at 132.4, 129.8, and 128.1 ppm are assigned to the phenyl carbons of dppm, shifted from 138.6, 132.6, and 128.5 ppm in the free ligand, while the remaining features at 150.0, 117.9, and 116.9 arise from Cl + C2, C3 + C6, and C4 + C5 of tetrachlorocatecholate, and are close to the values reported for indium(III) (16) and tin(IV) (17) complexes of this ligand. In addition, a triplet at 25.75, 25.47, 25.18 ppm arises from the CH_2 of dppm. The ^{31}P spectrum of the complex in dmso shows a singlet at −6.26 ppm (relative to external 85% H_3PO_4), shifted from −18.61 ppm for dppm itself in the same solvent.

(*iii*) 2,2′-Dihydroxybiphenyl + dppm. During electrolysis, the solution became deep yellow, but no precipitation occurred. The solvent was subsequently removed by evaporation *in vacuo* to give a pale brown oil (*ca.* 15–20 mL) which was triturated overnight with diethyl ether, in which the oil is insoluble. The ether was decanted away, and the residual oil redissolved in CH_3CN (20 mL); addition of Et_2O (70 mL) precipitated a brown solid, which was washed with Et_2O (5 mL) and dried; yield 0.28 g, 21% on the basis of metal dissolved. Analysis agreed with the formula $Cu[O(C_6H_4)_2OH].0.5dppm.2CH_3CN$ (*Anal.* calcd. C 65.4, H 5.01; found C 65.3, H 4.75). Melting point 185–190°C. The infrared spectrum has a medium intensity band at 2225 cm^{-1}, corresponding to $\nu(C{\equiv}N)$ of CH_3CN. The ^1H spectrum ($CDCl_3$) shows resonances at 7.3–6.5 (phenyl), 2.83 (br) (H-bonding), 2.33 (s) (CH_2 of dppm), and 1.24(s) (CH_3CN): the presence of trace quantities of $CHCl_3$, and the low solubility, did not allow for meaningful integration.

(*iv*) 2,2′-Dihydroxybiphenyl + 2,2′-bipyridine. The solution obtained by dissolving equimolar quantities of these compounds in acetonitrile was deep orange in colour. During electrolysis, this changed to deep red, and a steady increase in the current at constant voltage was observed, implying the formation of charged species; the voltage was decreased at intervals to keep the current at 20 mA. At the end of the electrolysis, small quantities (60 mg) of a brown–red solid were removed by filtration, and the red filtrate was slowly evaporated to dryness over 3 days. The resultant solid was dissolved in CH_3CN (15 mL), and diethyl ether (100 mL) added to precipitate a brown solid which was collected and dried *in vacue*; yield 0.41 g, 41% on the basis of metal dissolved. Analysis agreed with the formula $Cu[O(C_6H_4)_2OH].bpy$ (*Anal.* calcd.: C 65.3, H 4.23, N 6.92, Cu 15.7; found: C 64.7, H 4.25, N 6.54, Cu 15.4). Melting point > 300°C. The infrared spectrum confirmed the presence of 2,2′-bipyridine (18). Attempts to run the nmr spectrum of this compound failed because of the presence of paramagnetic species.

(*v*) Other systems which gave rise to solid products included 4-*t*-butylcatechol + dppm, and catechol + Ph_3P. In the former system, the product of the electrolysis was isolated as a heavy orange oil, but this became deep purple after being kept at 0°C for 3 days, and a purple–blue solid was obtained when this material was taken to dryness *in vacuo*. (Found: C 65.5, H 5.42, Cu 10.8.) Similarly, for catechol + PPh_3, the product of the electrolysis was a dark green solid, which on recrystallization (CH_3CN + Et_2O) gave an unstable green solid; Found: C 67.4, H 4.97, Cu 12.6. In neither case could a satisfactory stoichiometry be established, and no further studies were carried out on these compounds.

TABLE 2. Summary of crystal data, intensity collection, and structural refinement for $Cu_2[OC_6Cl_4(OH)]_2(dppm)_2$, $C_{62}H_{46}Cl_8Cu_2O_4P_4$

a (Å)	22.418(5)
b (Å)	11.784(4)
c (Å)	13.492(4)
α (deg)	61.63(2)
β (deg)	86.66(2)
γ (deg)	80.61(2)
V (Å^3)	3093(2)
Crystal system	Triclinic
Space group	$P\bar{1}$
Mol. wt.	1389.6
Z	2
ρ_c (g cm^{-3})	1.34
ρ_o (g cm^{-3})	1.35
Crystal dimensions (mm)	0.23 × 0.19 × 0.36
Radiation	Mo-K_α, 0.71069 Å
Monochromator	Highly oriented graphite
T (°C)	21°C
Absorption coefficient, μ(cm^{-1})	11.11
2 Φ angle (deg)	4.5–40.0°
Scan type	coupled Φ (crystal)/2 Φ (counter)
Scan width	$K\alpha_1$ − 1° to $K\alpha_2$ + 1°
Scan speed (deg min^{-1})	variable, 2.02–4.88
Background time/scan time	0.5
Total reflections measured	5780
Unique data used	4730
No. of parameters (NP)	386 (271, 115) ($I > 3\ \sigma(I)$)
R	0.0719
R_{WF}	0.0844
Largest residual electron density in diff. Fourier (e Å^{-3})	1.1
Largest shift/esd in final cycle	0.03

Crystallographic analysis

A colourless crystal of $Cu_2[OC_6Cl_4(OH)]_2(dppm)_2$ (**1**) was mounted along its longest dimension on a Syntex $P2_1$ diffractometer, and data collected at room temperature (*ca.* 25°C) by procedures described previously (19). The intensities of three check reflections were monitored regularly, but no significant decay was observed during the

Can. J. Chem. Downloaded from www.nrcresearchpress.com by 195.138.81.100 on 09/07/12
For personal use only.

TABLE 3. Final fractional coordinates and isotropic thermal parameters for non-hydrogen atoms of $Cu_2[OC_6Cl_4(OH)]_2(dppm)_2$, with standard deviations in parentheses

Atom	x	y	z	U_{eq} (Å^2 × 10^3)[a]
Cu(1)	0.2078(1)	0.4640(1)	0.4437(1)	28(1)
Cu(2)	0.2935(1)	0.4595(1)	0.2713(1)	28(1)
Cl(1A)	0.1319(1)	0.6307(3)	0.5177(2)	54(2)
Cl(2A)	0.0536(1)	0.8977(3)	0.4678(3)	85(2)
Cl(3A)	0.0541(1)	0.1368(3)	0.2273(4)	98(2)
Cl(4A)	0.1332(2)	0.1005(3)	0.0405(3)	73(2)
Cl(1B)	0.3739(1)	0.6559(3)	0.9712(2)	61(2)
Cl(2B)	0.4920(1)	0.7748(3)	−0.0494(3)	72(2)
Cl(3B)	0.5247(1)	0.8425(3)	0.1368(3)	74(2)
Cl(4B)	0.4344(2)	0.8058(4)	0.3312(3)	79(2)
P(1)	0.2814(1)	0.3907(2)	0.5763(2)	30(1)
P(2)	0.3674(1)	0.3598(2)	0.4035(2)	28(1)
P(3)	0.1441(1)	0.3600(2)	0.4076(2)	28(1)
P(4)	0.2280(1)	0.3741(2)	0.2173(2)	26(1)
O(1)	0.2125(3)	0.6470(6)	0.3308(5)	36(3)
O(2)	0.2064(3)	0.8477(6)	0.1196(5)	47(3)
O(3)	0.2980(3)	0.6437(5)	0.1603(5)	35(3)
O(4)	0.3251(3)	0.7085(6)	0.3185(5)	44(3)
C(01)	0.3569(4)	0.4055(8)	0.5167(7)	29(4)
C(02)	0.1811(4)	0.2750(8)	0.3311(7)	26(5)
C(1A)	0.1731(3)	0.7529(5)	0.3094(5)	34(5)
C(2A)	0.1354(3)	0.7653(5)	0.3909(5)	42(6)
C(3A)	0.0973(3)	0.8826(5)	0.3640(5)	48(7)
C(4A)	0.0969(3)	0.9875(5)	0.2557(5)	59(7)
C(5A)	0.1345(4)	0.9751(5)	0.1742(5)	45(6)
C(6A)	0.1726(3)	0.8578(5)	0.2010(5)	42(7)
C(1B)	0.3498(4)	0.6910(5)	0.1515(5)	30(6)
C(2B)	0.3899(4)	0.7061(5)	0.0646(5)	24(5)
C(3B)	0.4435(2)	0.7543(5)	0.0593(5)	36(5)
C(4B)	0.4570(2)	0.7875(5)	0.1410(5)	41(6)
C(5B)	0.4169(2)	0.7724(5)	0.2279(5)	40(6)
C(6B)	0.3633(2)	0.7242(5)	0.2332(5)	34(5)
C(11)	0.2856(4)	0.2272(7)	0.6885(6)	49(2)
C(12)	0.3378(3)	0.1566(7)	0.7540(6)	91(4)
C(13)	0.3364(3)	0.0328(7)	0.8450(6)	93(4)
C(14)	0.2828(3)	−0.0205(7)	0.8706(6)	112(4)
C(15)	0.2307(3)	0.0501(7)	0.8050(6)	166(7)
C(16)	0.2333(8)	0.1739(7)	0.7140(6)	147(6)
C(21)	0.2757(4)	0.4880(6)	0.6486(5)	47(2)
C(22)	0.2853(4)	0.6176(6)	0.5880(5)	77(3)
C(23)	0.2774(4)	0.6973(6)	0.6394(5)	103(4)
C(24)	0.2599(4)	0.6475(6)	0.7514(5)	105(4)
C(25)	0.2503(4)	0.5180(6)	0.8121(5)	110(4)
C(26)	0.2582(4)	0.4382(6)	0.7607(5)	132(6)
C(31)	0.4407(2)	0.4016(7)	0.3464(5)	37(2)
C(32)	0.4544(2)	0.4005(6)	0.2446(5)	57(3)
C(33)	0.5102(2)	0.4293(6)	0.1956(5)	73(3)
C(34)	0.5523(2)	0.4593(6)	0.2483(5)	65(3)
C(35)	0.5385(2)	0.4604(6)	0.3501(5)	81(3)
C(36)	0.4827(2)	0.4315(6)	0.3991(5)	67(3)
C(41)	0.3840(3)	0.1823(7)	0.4735(6)	44(2)
C(42)	0.4272(3)	0.1151(7)	0.5608(6)	88(4)
C(43)	0.4405(3)	−0.0207(7)	0.6112(6)	114(5)
C(44)	0.4107(3)	−0.0893(7)	0.5743(6)	102(4)
C(45)	0.3675(3)	−0.0221(7)	0.4870(6)	111(5)
C(46)	0.3542(3)	0.1137(7)	0.4366(6)	84(4)
C(51)	0.0766(3)	0.4546(5)	0.3218(5)	44(2)
C(52)	0.0246(3)	0.4018(5)	0.3274(5)	65(3)
C(53)	−0.0246(3)	0.4786(5)	0.2545(5)	74(3)
C(54)	−0.0213(3)	0.6081(5)	0.1761(5)	90(4)
C(55)	0.0309(3)	0.6608(5)	0.1706(5)	74(3)
C(56)	0.0799(3)	0.5841(5)	0.2434(5)	57(3)
C(61)	0.1146(3)	0.2302(6)	0.5324(5)	43(2)
C(62)	0.1288(3)	0.0988(6)	0.5597(5)	66(3)
C(63)	0.1076(3)	0.0037(6)	0.6588(5)	80(3)
C(64)	0.0721(3)	0.0400(6)	0.7033(5)	85(3)
C(65)	0.0579(3)	0.1715(6)	0.7033(5)	100(4)
C(66)	0.0792(3)	0.2666(6)	0.6042(5)	85(4)
C(71)	0.1765(3)	0.4827(7)	0.1005(5)	36(2)
C(72)	0.1284(4)	0.4412(4)	0.0721(5)	47(2)
C(73)	0.0899(3)	0.5290(4)	−0.0189(5)	67(3)
C(74)	0.0996(3)	0.6584(4)	−0.0815(5)	76(3)
C(75)	0.1476(3)	0.6999(4)	−0.0531(5)	62(3)
C(76)	0.1861(3)	0.6120(4)	0.0379(5)	52(2)
C(81)	0.2677(3)	0.2641(6)	0.1688(5)	43(2)
C(82)	0.2558(3)	0.1380(6)	0.2043(5)	83(4)
C(83)	0.2901(3)	0.0591(6)	0.1642(5)	98(4)
C(84)	0.3363(3)	0.1062(6)	0.0886(5)	92(4)
C(85)	0.3481(3)	0.2323(6)	0.0531(5)	95(4)
C(86)	0.3138(3)	0.3113(6)	0.0932(5)	72(3)

[a] $U_{eq} = \frac{1}{3}[\Sigma_i\Sigma_j U_{ij} a_i^* a_j^* \mathbf{a}_i \cdot \mathbf{a}_j]$

time required for data collection. The cell parameters were measured and refined from 30 strong high angle ($15° < 2\theta < 25°$) reflections. Data used in the structure determination were corrected for Lorentz and polarization effects, and analytically for absorption. Density was measured by the flotation method in carbon tetrachloride – benzene mixtures. No symmetry or extinctions were observed, and the crystal was assigned to the space group $P\bar{1}$.

The structure was solved by first locating the Cu atoms by direct methods using the program SHELX (20), and then proceeding with the usual heavy atom Fourier technique. The structure was refined by block-matrix least-squares methods, using 271 parameters in one block and 115 in the other. The two copper atoms Cu(1) and Cu(2) were common to each block, one of which also contained Cl(1)—Cl(4), P(1)—P(4), O(1)—O(4), C(01), C(02), and C(1)—C(6), while the other contained the remaining carbon atoms (C(11)–C(86). Convergence was achieved at $R = 0.1169$. The anistropic treatment of the atomic thermal vibrations showed several non-positive definite parameters for the carbon atoms of the phenyl rings of dppm, and this treatment was therefore restricted to Cu, Cl, P, O, C(01), C(02), and C(1)—C(6) (see Figs. 1 and 2 for numbering). Geometrical constraints were applied to all the aromatic rings, imposing identical C—C bond lengths of 1.395 Å and bond angles of 120°. The rings bonded through C(11) and C(21) showed unacceptably high thermal vibrations at some of the carbon atoms, indicating disorder in these phenyl groups. Several attempts were made to correct this disorder problem but none of them led to convergence in our refinement, and this uncorrected disorder problem therefore accounts for the residual electron density of 1.1 e/Å^3 located around the phenyl rings in question.

Hydrogen atoms were included on all carbon atoms in idealized position (r(C—H) = 0.95 Å and ∠ CCH = 109.5°), with isotropic thermal parameters assigned values 0.01U (Å^2) greater than those for the appropriate carbon atoms. The hydrogen atoms bonded to O(2) and O(4) were constrained, with bond distances of 1.10 Å. After several cycles of refinement, convergence was achieved, with the final $R = 0.0719$ and $R_w = 0.0844$ for 4730 unique "observed ($I > 3\ \sigma(I)$)" reflections. The function minimized during least-squares calculation was $\Sigma_w(|F_o| - |F_c|)^2$ with $w = (\sigma_2(F) + \rho F^2)$ and final $\rho = 0.00001$.

Details of the crystal size, intensity data collection, and structure refinement are summarized in Table 2. Table 3 gives the atomic coordinates for the non-hydrogen atoms, and Table 4 presents the interatomic distances and angles. Atomic positions of hydrogen atoms, equivalent isotropic temperature factors, the unit cell diagram, and observed and calculated structure factor amplitudes are available as

Can. J. Chem. Downloaded from www.nrcresearchpress.com by 195.138.81.100 on 09/07/12
For personal use only.

TABLE 4. Bond distance (Å) and angles (deg) in $Cu_2[OC_6Cl_4(OH)]_2(dppm_2)$

(*a*) Bond distances

Bond	Distance	Bond	Distance
Cu(1)—P(1)	2.254(2)	C(11)—P(1)	1.788(7)
Cu(1)—P(3)	2.237(3)	C(21)—P(1)	1.813(9)
Cu(1)—O(1)	1.979(5)	C(31)—P(2)	1.813(6)
Cu(2)—P(2)	2.242(2)	C(41)—P(2)	1.821(7)
Cu(2)—P(4)	2.236(3)	C(51)—P(3)	1.816(6)
Cu(2)—O(3)	1.982(5)	C(61)—P(3)	1.839(6)
P(1)—C(01)	1.830(8)	C(71)—P(4)	1.808(5)
P(2)—C(01)	1.838(11)	C(81)—P(4)	1.806(8)
P(3)—C(02)	1.835(11)	C(2A)—Cl(1A)	1.702(6)
P(4)—C(02)	1.827(8)	C(3A)—Cl(2A)	1.724(8)
C(1A)—O(1)	1.323(8)	C(4A)—Cl(3A)	1.736(6)
C(6A)—O(2)	1.3406(11)	C(5A)—Cl(4A)	1.702(6)
C(1B)—O(3)	1.344(9)	C(2B)—Cl(1B)	1.701(9)
C(6B)—O(4)	1.351(9)	C(3B)—Cl(2B)	1.719(7)
C(5B)—Cl(4B)	1.698(9)	C(4B)—Cl(3B)	1.733(7)

(*b*) Non-bonding distances

Atoms	Distance
Cu(1) ..... Cu(2)	2.946(1)
Cu(1) ..... Cl(1A)	2.885(3)
O(1) ..... O(2)	2.696(4)
O(1) ..... O(4)	2.713(3)
O(2) ..... O(3)	2.750(3)
O(3) ..... O(4)	2.713(4)

(*c*) Bond angles

Bonds	Angle	Bonds	Angle
P(1)—Cu(1)—P(3)	131.4(1)	C(71)—P(4)—C(02)	105.7(3)
P(1)—Cu(1)—O(1)	110.2(2)	C(81)—P(4)—C(2)	110.6(3)
P(3)—Cu(1)—O(1)	117.8(2)	C(81)—P(4)—C(02)	104.7(4)
P(2)—Cu(2)—P(4)	129.8(1)	C(81)—P(4)—C(71)	102.2(3)
P(2)—Cu(2)—O(3)	116.0(2)	C(1A)—O(1)—Cu(1)	128.4(5)
P(4)—Cu(2)—O(3)	112.4(2)	C(1B)—O(3)—Cu(2)	119.3(4)
C(01)—P(1)—Cu(1)	112.7(3)	P(2)—C(01)—P(1)	112.9(6)
C(11)—P(1)—Cu(1)	116.9(3)	P(4)—C(02)—P(3)	112.7(5)
C(11)—P(1)—C(01)	106.3(3)	C(2A)—C(1A)—O(1)	123.1(5)
C(21)—P(1)—Cu(1)	111.9(2)	C(6A)—C(1A)—O(1)	116.9(6)
C(21)—P(1)—C(01)	102.9(4)	C(1A)—C(2A)—Cl(1A)	118.5(4)
C(21)—P(1)—C(11)	103.6(4)	C(3A)—C(2A)—Cl(1A)	121.2(5)
C(01)—P(2)—Cu(2)	113.1(3)	C(2A)—C(3A)—Cl(2A)	120.8(5)
C(31)—P(2)—Cu(2)	112.1(2)	C(4A)—C(3A)—Cl(2A)	119.1(4)
C(31)—P(2)—C(01)	104.7(4)	C(3A)—C(4A)—Cl(3A)	119.2(6)
C(41)—P(2)—Cu(2)	118.6(3)	C(5A)—C(4A)—Cl(3A)	120.5(4)
C(41)—P(2)—C(01)	105.8(3)	C(4A)—C(5A)—Cl(4A)	120.8(4)
C(41)—P(2)—C(31)	100.8(3)	C(6A)—C(5A)—Cl(4A)	119.2(5)
C(02)—P(3)—Cu(1)	111.5(3)	C(1A)—C(6A)—O(2)	121.5(5)
C(51)—P(3)—Cu(1)	118.8(3)	C(5A)—C(6A)—O(2)	118.4(5)
C(51)—P(3)—C(02)	102.8(4)	C(2B)—C(1B)—O(3)	121.9(7)
C(61)—P(3)—Cu(1)	115.1(3)	C(6B)—C(1B)—O(3)	118.1(6)
C(61)—P(3)—C(02)	103.5(4)	C(1B)—C(2B)—Cl(1B)	117.4(8)
C(61)—P(3)—C(51)	103.4(3)	C(3B)—C(2B)—Cl(1B)	121.3(5)
C(02)—P(4)—Cu(2)	113.6(4)	C(2B)—C(3B)—Cl(2B)	119.6(6)
C(71)—P(4)—Cu(2)	118.6(2)	C(4B)—C(3B)—Cl(2B)	120.4(5)
C(3B)—C(4B)—Cl(3B)	119.9(5)	C(5B)—C(4B)—Cl(3B)	120.4(5)
C(4B)—C(5B)—Cl(4B)	120.4(5)	C(6B)—C(5B)—Cl(4B)	119.5(5)
C(1B)—C(6B)—O(4)	119.5(6)	C(5B)—C(6B)—O(4)	119.5(4)
P(1)—C(11)—C(12)	123.3(6)	P(2)—C(31)—C(32)	116.2(5)
P(1)—C(11)—C(16)	116.5(5)	P(2)—C(31)—C(36)	123.8(5)

Can. J. Chem. Downloaded from www.nrcresearchpress.com by 195.138.81.100 on 09/07/12
For personal use only.

TABLE 4 (*concluded*)

Bond	Distance	Bond	Distance
P(1)—C(21)—C(22)	118.7(5)	P(2)—C(41)—C(42)	120.9(7)
P(1)—C(21)—C(26)	121.2(6)	P(2)—C(41)—C(46)	119.1(5)
P(3)—C(51)—C(52)	123.2(3)	P(4)—C(71)—C(72)	122.3(3)
P(3)—C(51)—C(56)	116.7(4)	P(4)—C(71)—C(76)	117.7(5)
P(3)—C(61)—C(62)	122.5(5)	P(4)—C(81)—C(82)	115.7(6)
P(3)—C(61)—C(66)	117.4(5)	P(4)—C(81)—C(86)	124.3(5)

supplementary data.[3] The molecular structure is shown in Fig. 1; Fig. 2 isolates the core of the molecule.

Stability of $Cu_2[OC_6Cl_4(OH)]_2(dppm)_2$(1)

This compound darkens on heating, turning brown at *ca.* 200°C; the melting point is not sharp (211–214°C), and a brown liquid is formed above this range.

In an attempt to remove the proton of the $[OC_6Cl_4(OH)]^-$ ligand, a sample of **1** (0.77 g, 0.55 mmol) in acetonitrile (50 mL) was treated with Et_3N (0.1 mL, 0.073 g, 0.71 mmol). The solution, which became pale green, was refluxed for 1.5 h, after which minor solid impurities were removed by filtration and the filtrate taken to dryness to give a colourless powder which was identified as the starting material **1**.

Results and discussion

The structure of $Cu_2[OC_6Cl_4(OH)]_2(dppm)_2$

There are a number of interesting features to this molecule, which can be simply described as two copper(I) units, $Cu[OC_6Cl_4(OH)]$, held together by bridging dppm units (see Fig. 1). One immediate conclusion is that the Cu—Cu distance, 2.946(1) Å, appears to preclude any metal–metal bonding interaction (see refs. 20 and 21 for a discussion of this subject). The absence of any Cu–Cu interaction is also in keeping with the bond angles in the Cu—P—CH_2—P—Cu bridge, in which the phosphorus atom is essentially tetrahedral (sum of all angles 654.3°), and in which the P—C—P angles of 112.9(6)° and 112.7(5)° imply the absence of any strain in this ligand. The sums of the bond angles at copper are 359.4° (Cu(1)) and 358.2° (Cu(2)), establishing a quasi-trigonal planar stereochemistry at these atoms. The core of the molecule is an eight-membered ring, folded along the Cu—Cu axis, as shown in Fig. 2.

The most striking difference between this structure and those of copper(I)—thiolate cages, is that in the latter the thiolate ligand bridges copper atoms to give a range of Cu_2S_2, Cu_4S_4, etc., rings. Neutral monodentate or bidentate ligands then bond to the copper, and may also serve as additional bridges which cap the Cu_nS_n ring. In the present structure, the oxy ligand is monodentate, and external to the central eight-membered Cu—P—C—P—Cu—P—C—P feature. It would be interesting to see if one aspect of this argument, namely, that the softer (S,P) atom bridges while the harder atom (O,N) is external to the ring system, applies in other structures involving low oxidation state d^{10} metal ions.

The Cu—P bond distances (ave. 2.246 Å) are close to those in other copper(I)–dppm complexes with bridging dppm ligands (*e.g.* ave. Cu—P value 2.295 Å in $[Cu_2S_2C_3H_6(dppm)_2]_2$ (11); 2.290 Å in $Cu_4(PPh_2)_4(dppm)_2$ (22)), and the P—C distances and angles equally are very close in all these compounds. An interesting comparison for the Cu—O bond

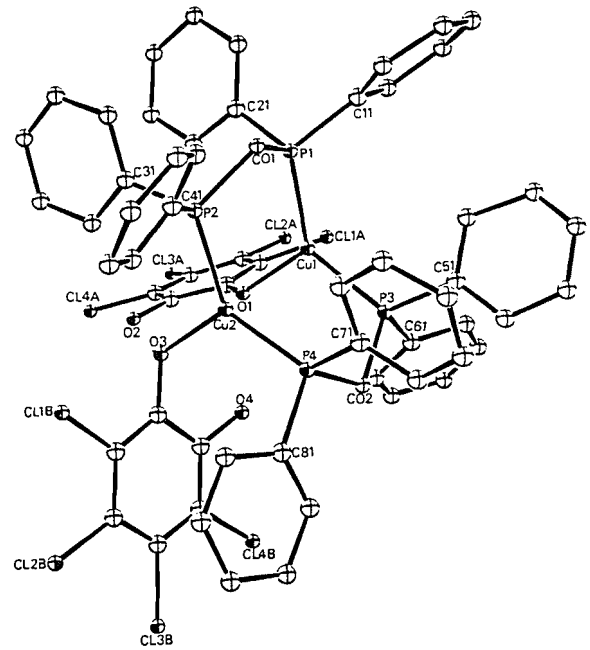


FIG. 1. ORTEP diagram of $Cu_2[OC_6Cl_4(OH)]_2(dppm)_2$; all atoms are shown isotropically, with 30% probability. Hydrogen atoms have been omitted for clarity.

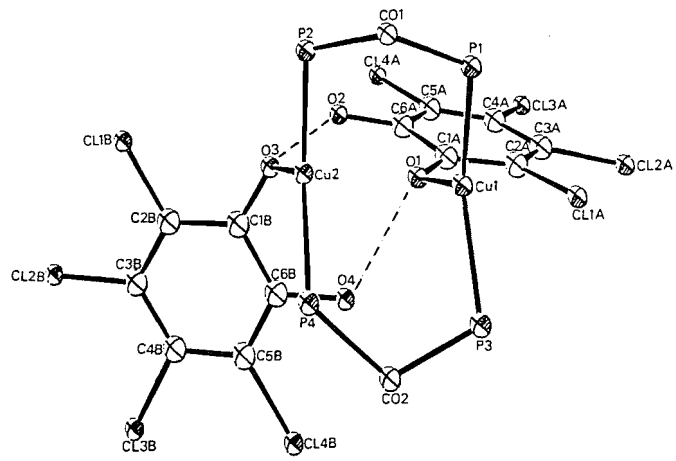


FIG. 2. The core of the structure of $Cu_2[OC_6Cl_4(OH)]_2(dppm)_2$, identifying the intramolecular hydrogen-bonding.

distance (1.986(5) Å) is with the unusual $L_3Cu_4OCl_6(OH)_2.L$ (L = *N*-methylpyrrolidin-2-one) (23), in which Cu—O within the Cu_4OCl_6 core is 1.896 Å (ave), that to the oxygen atom of the external L is 1.918 Å (ave), and that to the aquo ligand is 1.936(6) Å. The Cu—O bond is shorter than that in the compound formed in the oxidation of a phenoxo-bridged binuclear copper(I) species with $Cl_4C_6O_2$-*o* (24); in this product,

[3]Complete set of data may be purchased from The Depository of Unpublished Data, Document Delivery, CISTI, National Research Council Canada, Ottawa, Canada K1A 0S2.

Can. J. Chem. Downloaded from www.nrcresearchpress.com by 195.138.81.100 on 09/07/12
For personal use only.

Can. J. Chem. Downloaded from www.nrcresearchpress.com by 195.138.81.100 on 09/07/12
For personal use only.

two copper(II) atoms are bridged by $Cl_4C_6O_2^{2-}$, with Cu—O distances of 1.995(9) Å.

The final point to be addressed is the nature of the 2-hydroxy-3,4,5,6-tetrachlorophenolate ligand. The loss of only one of two acidic protons from the parent substituted catechol is surprising, since the pK values for the two dissociations do not differ in any unusual degree; the values for $Cl_4C_6(OH)_2$ do not appear to be available, but for catechol itself, pK_1 = 9.45 and, pK_2 = 12.8 (25). It therefore seems unlikely that the presence of one residual acidic hydrogen in the ligand is the result of differences in the pK values, or the energy changes which they represent. Rather one should look for some stabilizing factors in the final complex, and in the case of the present structure this is to be found in the intramolecular hydrogen-bonding which is identified from the crystallographic results. In the crystallographic refinement, the hydrogen atoms were reasonably assumed to be bonded to O(2) and O(4), since O(1) and O(3) are coordinated to copper atoms. The final results show that the distances O(1)—O(4) (2.713(3) Å) and O(2)—O(3) (2.750(3) Å) are well within the range identified for O—H---O distances in hydrogen-bonded solid state structures (26, 27). The stability of this compound in the solid state therefore owes more to these hydrogen bonds than to the energy implicit in the retention of one proton in $[C_6H_4O(OH)]^-$. The failure to deprotonate **1** by reaction with Et_3N, in contrast to the behaviour of In[OR(OH)] (5) and In[SR(SH)] (6), is clearly also due to this intermolecular hydrogen-bonding.

Electrochemical synthesis

For each of the systems studied, the value of the electrochemical efficiency, defined as the number of moles of copper dissolved per Faraday of charge, is in the range 1.11 ± 0.04 mol F^{-1}. This is higher than the value of 1.00 mol F^{-1} which would be required by the sequence

[1] cathode: $R(OH)_2 + e \rightarrow R(O)OH^- + H_2(g)$

[2] anode: $R(O)OH^- + Cu \rightarrow Cu[OR(OH)] + e$

and this deviation is probably related to the problem of maintaining a constant current during E_F measurements because of the deposition of small amounts of copper on the anode in these experiments. An alternative scheme to reactions [1] and [2], involving the formation of RO_2^{2-} anions which subsequently interact with $R(OH)_2$ to give $2R(O)OH^-$ anions, does not affect the conclusion that these copper(I) species are formed in the initial anodic oxidation process [2], and are not the product of the disproportionation of an initially-formed copper(II) product. The systems in Table 1 are clearly further examples of the usefulness of direct electrochemical oxidation of metals in producing low oxidation state complexes as noted in the Introduction.

General conclusions

Given the varied stability and crystallinity of the products described in the Experimental section, it is clear that the synthesis of $Cu_2[OC_6Cl_4(OH)]_2(dppm)_2$ was indeed fortuitous. Equally, given the significance of hydrogen bonding in this structure, it is not surprising that changes in either substituted catechol or in neutral ligand produce structural changes that allow oxidation to copper(II) to occur. It would clearly be imprudent to speculate on the number of structures similar to that shown in Fig. 1 which might be stabilized by suitable variation in the ligands used.

Acknowledgements

This work was supported in part by Operating Grants (to D.G.T.) from the Natural Sciences and Engineering Research Council of Canada. Dr. D. W. Stephan is thanked for helpful discussions of the crystallographic results.

1. J. L. Hencher, M. A. Khan, F. F. Said, R. Sieler, and D. G. Tuck. Inorg. Chem. **21**, 2787 (1982).
2. M. A. Khan, M. J. Taylor, D. G. Tuck, and D. A. Rogers. J. Cryst. Spectr. Res. **16**, 895 (1986).
3. H. E. Mabrouk and D. G. Tuck. J. Chem. Soc. Dalton Trans. 2539 (1988).
4. J. H. Green, R. Kumar, N. Seudeal, and D. G. Tuck. Inorg. Chem. **28**, 123 (1989).
5. H. E. Mabrouk and D. G. Tuck. Can. J. Chem. **67**, 746 (1989).
6. C. Geloso, H. E. Mabrouk, and D. G. Tuck. J. Chem. Soc. Dalton Trans. 1759 (1989).
7. R. K. Chadha, R. Kumar, and D. G. Tuck. Can. J. Chem. **65**, 1336 (1987).
8. M. A. Khan, R. Kumar, and D. G. Tuck. Polyhedron, **7**, 49 (1988).
9. R. K. Chadha, R. Kumar, and D. G. Tuck. Polyhedron, **7**, 1121 (1988).
10. R. Kumar and D. G. Tuck. Inorg. Chem. **29**, 1444 (1990).
11. T. A. Annan, R. Kumar, and D. G. Tuck. Inorg. Chem. **29**, 2475 (1990).
12. I. G. Dance. Polyhedron, **5**, 1937 (1986).
13. P. J. Blower and J. R. Dilworth. Coord. Chem. Rev. **76**, 121 (1987).
14. Ch. P. Rao, J. R. Dorfman, and R. H. Holm. Inorg. Chem. **25**, 428 (1986).
15. H. E. Mabrouk, D. G. Tuck, and M. A. Khan. Inorg. Chim. Acta, **129**, 75 (1987).
16. T. A. Annan and D. G. Tuck. Can. J. Chem. **66**, 2935 (1988).
17. T. A. Annan, R. K. Chadha, D. G. Tuck, and K. D. Watson. Can. J. Chem. **65**, 2670 (1987).
18. A. A. Schilt and R. C. Taylor. J. Inorg. Nucl. Chem. **9**, 211 (1959).
19. M. A. Khan, R. C. Steevensz, D. G. Tuck, J. G. Noltes, and P. W. R. Corfield. Inorg. Chem. **19**, 3407 (1980).
20. D. Coucouvanis, C. N. Murphy, and S. K. Kanodia. Inorg. Chem. **19**, 2993 (1980).
21. P. K. Mehrotra and R. Hoffman. Inorg. Chem. **17**, 2187 (1978).
22. T. A. Annan, R. Kumar, and D. G. Tuck. J. Chem. Soc. Chem. Commun. 446 (1988).
23. G. Davies, M. F. El-Shazly, M. W. Rupich, M. R. Churchill, and F. J. Rotella. J. Chem. Soc. Chem. Commun. 1045 (1978).
24. K. D. Karlin, Y. Gultneh, T. Nicholson, and J. Zubieta. Inorg. Chem. **24**, 3121 (1985).
25. R. P. Agarwal and R. C. Mehrotra. J. Inorg. Nucl. Chem. **24**, 821 (1962).
26. G. C. Pimental and A. L. McClellan. The hydrogen bond. W. H. Freeman and Co., San Francisco. 1960. p. 260.
27. W. C. Hamilton and J. A. Ibers. Hydrogen bonding in solids. W. A. Benjamin, New York. 1968. p. 260 *et seq.*

Liquid assisted secondary ion mass spectrometry of $[(\eta^5\text{-}C_5Me_4R')Rh(SCN)_2(CNR)]$ (R′ = Me, Et) complexes of isocyanides[1]

R. K. BOYD,[2] D. J. EMBREE, A. J. MCALEES,[3] AND A. TAYLOR

Institute for Marine Biosciences, National Research Council of Canada, Halifax, N.S., Canada B3H 3Z1

Received August 14, 1990

R. K. BOYD, D. J. EMBREE, A. J. MCALEES, and A. TAYLOR. Can. J. Chem. **69**, 257 (1991).

It is shown that the primary ionization, under conditions of liquid-assisted secondary ionization mass spectrometry (LSIMS), of neutral complexes of the type $[(\eta^5\text{-}C_5Me_4R')Rh(SCN)_2(CNR)]$, involves the loss of a thiocyanate ligand. The processes leading to the observed spectra have been elucidated using techniques of accurate mass measurement and tandem mass spectrometry, so that the molecular weight and elemental composition of the isocyanide ligand RNC can be deduced with confidence. The greatest sensitivity was found when 3-nitrobenzyl alcohol was used as the matrix. Bimolecular reactions are shown to occur under LSIMS conditions, yielding ions containing two rhodium atoms but not the isocyanide. The implications of these results for the characterization and analysis of isocyanide metabolites of *Trichoderma hamatum* are discussed and illustrated.

Key words: isocyanides, mass spectrometry, rhodium complexes, *Trichoderma hamatum*.

R. K. BOYD, D. J. EMBREE, A. J. MCALEES et A. TAYLOR. Can. J. Chem. **69**, 257 (1991).

On démontre que l'ionisation primaire de complexes neutres du type $[(\eta^5\text{-}C_5Me_4R')Rh(SCN)_2(CNR)]$, dans des conditions de spectrométrie de masse avec ionisation secondaire assistée par un liquide SMISAL), implique la perte d'un ligand thiocyanate. Les processus conduisant aux spectres observés ont été élucidés à l'aide des techniques de mesure des masses exactes et de la spectrométrie de masse en tandem; on a donc pu déduire la masse moléculaire et la composition élémentaire du ligand isocyanure, RNC, avec confiance. On a trouvé que la meilleure sensibilité est obtenue lorsque l'alcool 3-nitrobenzylique est utilisé comme matrice. On a démontré que, dans les conditions de SMISAL, il se produit des réactions bimoléculaires conduisant à des ions qui contiennent deux atomes de rhodium, mais pas d'isocyanure. On discute et on illustre les implications de ces résultats pour la caractérisation et l'analyse des métabolites du *Trichoderma hamatum* qui contiennent de l'isocyanure.

Mots clés : isocyanures, spectrométrie de masse, complexes du rhodium, *Trichoderma hamatum*.

[Traduit par la rédaction]

Interest in the isocyanide metabolites (*e.g.* **1***a*) of *Trichoderma hamatum* lies in their unusual inhibition of growth of functionally important rumen bacteria, *e.g.*, *Fibrobacter succinogenes*, and thus being implicated in poor performance of ruminant animals on pasture (1, 2). Isolation and structural characterization of these isocyanide metabolites has been hampered by their sensitivity to light and their marked tendency to polymerise. The most unstable isocyanides (*e.g.* **1***a*) can be converted to their relatively stable esters **1***b* (3), thus permitting structural studies by X-ray crystallography, nmr spectroscopy, and mass spectrometry (4). We have shown (3, 5) that isocyanides RNC are readily converted into stable crystalline rhodium complexes of the type $[\eta^5\text{-}(C_5Me_4R')Rh(SCN)_2(CNR)]$ **2**, by reaction with the dirhodium complex reagent $[\eta^5\text{-}(C_5Me_4R')\text{-}Rh(SCN)_2]_2$ (R′ = Me, **2***a*; R′ = Et, **2***b*); such complexes prepared from naturally occurring mixtures of isocyanides can be separated (6) by two-dimensional thin layer chromatography (tlc).

Liquid-assisted secondary ion mass spectrometry (LSIMS) of η^5-cyclopentadienylrhodium(III) complexes is well-known (7, 8), and LSIMS analysis of spots on tlc plates has been reported (9). It therefore seemed possible to utilize the inherent sensitivity of the mass spectrometer to explore and characterize the isocyanide metabolites of *T. hamatum*, usually present in low concentration. As a first step towards this goal we have prepared a number of complexes **2** of well-characterised isocyanides RNC, *viz.* cyclohexyl isocyanide (10), phenyl isocyanide, benzyl isocyanide, methyl 2-isocyano-2-methylpropionate (NC—CMe_2—CO_2Me), phenyl 2-isocyano-2-methylpropionate (NC—CMe_2—CO_2Ph), and **1***b*, and studied their LSIMS spectra.

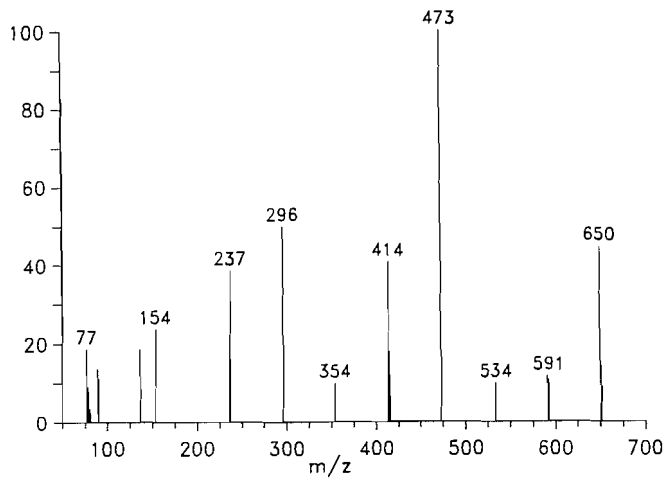


FIG. 1. Positive ion LSIMS spectrum of $[(\eta^5\text{-}C_5Me_5)Rh(SCN)_2\text{-}(RNC)]$ with RNC = **1** (R″ = Me). Peaks below *m/z* 200 may be attributed to the matrix (3-nitrobenzyl alcohol). The primary beam was Cs^+ at 25 keV (17 keV at the sample, maintained at 8 kV); static resolving power (10% valley definition) 1500, scan speed 5s/decade.

Results and discussion

The positive ion LSIMS spectrum of the neutral complex **2***a* with RNC = **1***b* is shown in Fig. 1. In Table 1 a summary of the sample-derived ions in this spectrum, and in analogous spectra of other complexes **2***a* of known structures, is given. In Table 1 only those ions with *m/z* values less than the molecular weight of the neutral complex **2***a* are reported. Ions at *m/z* 650, 592, 591, and 534 (Fig. 1) were observed in the spectra of all

[1]NRCC No. 31942.

[2]Author to whom correspondence should be addressed.

[3]Present address: Department of Chemistry and Biochemistry, University of Guelph, Guelph, Ont., Canada N1G 2W1.

Can. J. Chem. Downloaded from www.nrcresearchpress.com by 195.138.81.100 on 09/07/12
For personal use only.

TABLE 1. Major ions in the positive ion LSIMS spectra of neutral rhodium complexes **2***a*, $[(\eta^5\text{-}C_5Me_5)Rh(SCN)_2(RNC)]$, of known isocyanides RNC[a]

Isocyanide	*M*(RNC), u	*M*(**2**), u	*m/z*, observed
C_6H_5—NC	103	457	399, 341, 340, 296, 238, 237
$C_6H_5CH_2$—NC	117	471	413, 355, 354, 296, 238, 237
cyclo-C_6H_{11}—NC	109	463	405, 347, 346, 296, 238, 237
MeO_2C—$C(Me_2)$—NC	127	481	423, 365, 364, 296, 238, 237
$C_6H_5O_2C$—$C(Me_2)$—NC	189	543	485, 427, 426, 296, 238, 237
1, R″ = Me	177	531	473, 415, 414, 296, 238, 237

[a]Ions observed at *m/z* values greater than *M*(**2**) have been omitted (see text).

TABLE 2. Accurate mass measurements (from manual peak matching at 8 000 resolving power, 10% valley definition); precision of measurements 3–5 ppm

Assigned atomic composition	Mass		Deviation (ppm)
	Calculated	Measured	
$Rh(CH_2.C_5Me_4)$	237.0151	237.0144	3
$Rh(C_5Me_5)(SCN)$	295.9980	295.9965	5
$Rh_2(C_5Me_5)_2(SCN)$	534.0209	534.0199	2
$Rh_2(C_5Me_5)_2(SCN)_3$	649.9711	649.9736	4
$Rh(C_5Me_5)(SCN)(C_6H_5CH_2NC)$[a]	413.0559	413.0552	2
$Rh(C_5Me_5)(SCN)$ (**1**, R″ = Me)[b]	473.0770	473.0782	3

[a,b]$(M - CNS)^+$ ions from complexes **2** of known constitution, for RNC = benzyl isocyanide and **1** (with R″ = Me), respectively.

complexes **2***a* (R′ = Me) investigated in the present work, and thus do not contain the isocyanide moiety. The identities of these ions, as well as of the common low-mass ions at *m/z* 237, 238, and 296 (Table 1), are discussed below.

The same peaks were observed no matter which LSIMS matrix was used, although matrices incorporating thiol groups gave additional peaks corresponding to displacement of ligands by matrix-derived species; these extra peaks were intense in some cases, so such matrices were not suitable. However, use of glycerol, perdeuteroglycerol, and 3-nitrobenzyl alcohol gave simple spectra which were identical to one another, apart from mass peaks readily identifiable as derived directly from the matrix. Use of 3-nitrobenzyl alcohol yielded an ionization efficiency which was at least an order of magnitude greater than that achievable using glycerol, and most of the spectra reported here were obtained using the former matrix. The corresponding negative ion LSIMS spectra were dominated by thiocyanate anion, and did not provide information on the nature of the isocyanide ligand.

The monoisotopic molecular weight of the compound **2***a* with RNC = **1***b* is 531.0521, but the ion at *m/z* 534 (Fig. 1) is not a protonated molecular ion with an additional ligand H_2 (11) since the measured accurate mass (Table 2) is much too low. In addition, as noted above, this ion was observed in the spectra of *all* the complexes **2***a* studied in the present work, and therefore does not contain the RNC ligand. However, the accurate mass of the ion at *m/z* 473 (Table 2) of 473.0782 ($C_{21}H_{26}N_2O_2RhS$ requires 473.0770), corresponds to **3** with RNC = **1***b*, generated by the loss of the thiocyanate ion from the corresponding neutral complex **2***a*. This reaction was observed in the LSIMS spectra of all the model compounds studied (Table 1). The peak at *m/z* 354 in Fig. 1 corresponds to ionization of the neutral complex by expulsion of a $(RNC)^-$ anion (loss of 177 u in this case); this was the only example for which this process was observed to compete with the loss of thiocyanate (as the leaving group), and the process was not investigated further.

Further fragmentations of the $(M - SCN)^+$ ions were complex. Accurate mass measurements on the common fragment ions at *m/z* 296, 238, and 237 (Table 2) were not sufficient, in the absence of any other information, to uniquely specify the atomic compositions. However, if it is specified that these ions contain sub-structures comprised of Rh atoms, SCN^- groups, and (C_5Me_5) ligands, the results summarised in Table 2 do establish the atomic constitutions unambiguously. This question of the sub-structures in these ions, and related questions, were approached by exploiting techniques of tandem mass spectrometry and collision-induced dissociation (CID). Mass-selected ions were transmitted to the RF-only quadrupole *q* of the BEqQ tandem hybrid instrument; the experimental conditions thus involved low-energy collisional activation with a laboratory frame collision energy in the range 30–50 eV. For argon collision gas and the precursor ions studied, this translates into maximum ("elastic-limit") center-of-mass energies 2–7 eV. Multiple collision conditions were used to promote formation of lower mass fragments.

Figure 2 is the CID spectrum of the ion at *m/z* 473 (Fig. 1), the $(M - SCN)^+$ ion **3** (RNC = **1***b*). The most intense fragmentation provided the common (Table 1) fragment ion at *m/z* 296; the accurate mass of such ions formed in the ionization source (Table 2) agreed with an assigned structure $[(C_5Me_5)Rh(SCN)]^+$, and this was consistent with the CID spectrum of these ions (not shown) which comprised an intense peak at *m/z* 237 and a weaker one at *m/z* 238. Hence the fragmentation of the $(M - SCN)^+$ ions to form fragments at *m/z* 296 involves the loss of the neutral organic isocyanide ligand. This ion at *m/z* 296 and its homologue (at *m/z* 310) derived from complexes **2***b* with R′ = Et are of diagnostic importance because the molecular weights and elemental

Can. J. Chem. Downloaded from www.nrcresearchpress.com by 195.138.81.100 on 09/07/12
For personal use only.

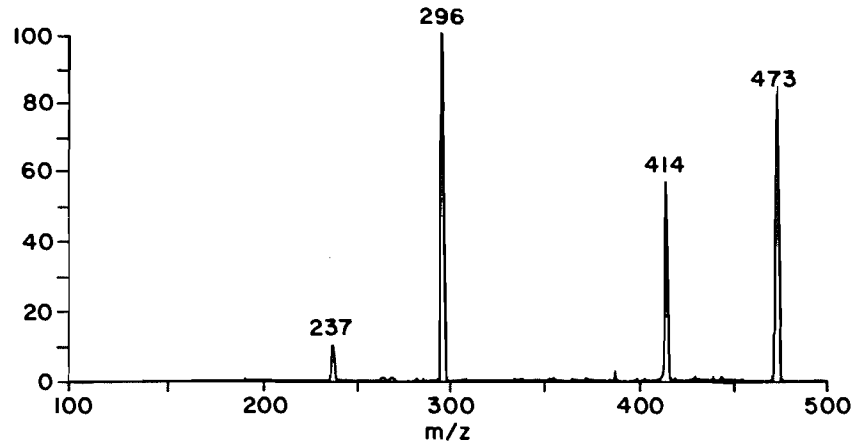
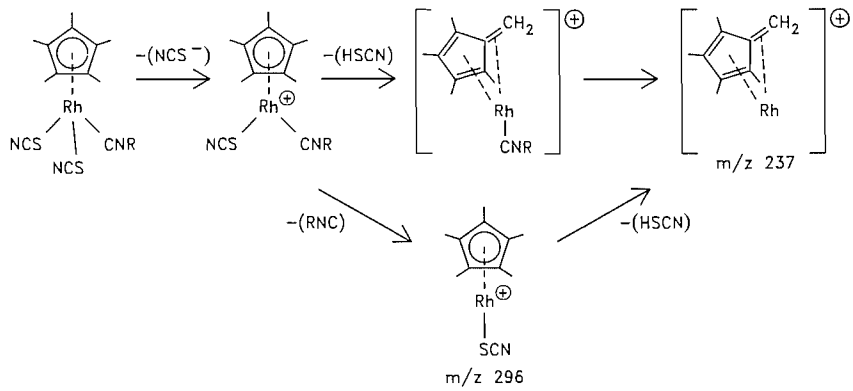


FIG. 2. Low-energy CID spectrum of the ion at m/z 473 in Fig. 1, formed as the $[M - (SCN)]^+$ ion by LSIMS of the rhodium complex **2** with RNC = **1** (R″ = Me). Laboratory-frame collision energy 30 eV, argon collision gas, 60% attenuation of intensity of precursor ion.



SCHEME 1

compositions of the isocyanide ligands can be deduced from the differences between the m/z values of these ubiquitous fragments and those of their $(M - SCN)^+$ precursors.

A competing fragmentation reaction of the $(M - SCN)^+$ ions, shown in Fig. 2, involves the loss of the elements HSCN (59 u). Similar reactions have been reported in the fast atom bombardment (FAB) mass spectra of compounds such as **4**, in which fragment ions observed to correspond to loss of a protonated ligand were formulated (8) as the *ortho*-metallated triphenylphosphine, **5**. In the reactions studied in this work the proton lost can originate only from the isocyanide or the cyclopentadienyl ligands. The former is less likely on the basis of the geometry of the Rh—C≡N—R system in the neutral complex **2***a* in the crystalline state (5), but evidence shown below (Fig. 4) suggests that the proton lost from the $(M - SCN)^+$ ions can originate from either the RNC or (C_5Me_5) ligand. The sequence shown in Scheme 1 is dominant at lower energies (Fig. 2), and is consistent with the accurate mass measurements (Table 2). The structure proposed for the fragment ion at m/z 237 (Scheme 1), incorporating a tetramethylfulvene ligand, suggests a related structure **6** for the fragment ion originally (8) assigned the formula **5**.

Some information on the question of the origin of the hydrogen atom, in the HSCN expelled from the $(M - SCN)^+$ ions, can be obtained from Figs. 3 and 4 which compare the CID spectra of the $[M - 2(SCN)]^+$ and $[M - (SCN) - (HSCN)]^+$ ions at m/z 415 and 414 (Fig. 1), respectively. According to the proposed interpretation these ions correspond to $[(C_5Me_5)Rh(RNC)]^+$ and $\{[(C_5Me_5)Rh(RNC)] - H\}^+$. The CID spectrum of $[(C_5Me_5)Rh(RNC)]^+$ (m/z 415) is shown in Fig. 3. As anticipated the dominant reaction corresponds to expulsion of the intact RNC ligand (177 u in this case) to form a fragment ion at m/z 238, presumably $[(C_5Me_5)Rh]^+$; only a trace of the ion at m/z 237 was observed. However, the situation is not entirely simple, since a fragment ion corresponding to loss of $CH_3\cdot$ is also observed (Fig. 3).

The CID spectrum of $\{[(C_5Me_5)Rh(RNC)] - H\}^+$ (m/z 414) is shown for comparison in Fig. 4. Now the product ion corresponding to the loss of intact RNC (at m/z 237 in this case) is of intensity comparable to that at m/z 238, arising from expulsion of (RNC − H). One possible rationalisation of this observation suggests that, in formation of m/z 414 by expulsion of HSCN from $[(C_5Me_5)Rh(SCN)(RNC)]^+$ ions (m/z 473), some of the expelled hydrogen atoms originated from the RNC moiety, and some from the C_5Me_5 ligand. Expulsion of (RNC − H), *i.e.* 176 u, from the former type of ions at m/z 414 would give the m/z 238 fragments, while expulsion of the intact RNC from the latter type would give the ions at m/z 237 (Fig. 4). Thus the fragment ion at m/z 238 is assigned as $[(C_5Me_5)Rh]^+$, consistent with mass shifts in the corresponding spectra (not shown) of ions derived from a homologous neutral complex **2** with RNC = **1** (R″ = Et); however, the fragmentation route shown in Scheme 1 was the dominant one in all examples studied here. The mass spectra of all the other model compounds (Table 1) can be rationalized by similar analyses.

All LSIMS spectra of the model compounds contained ions of

Can. J. Chem. Downloaded from www.nrcresearchpress.com by 195.138.81.100 on 09/07/12
For personal use only.

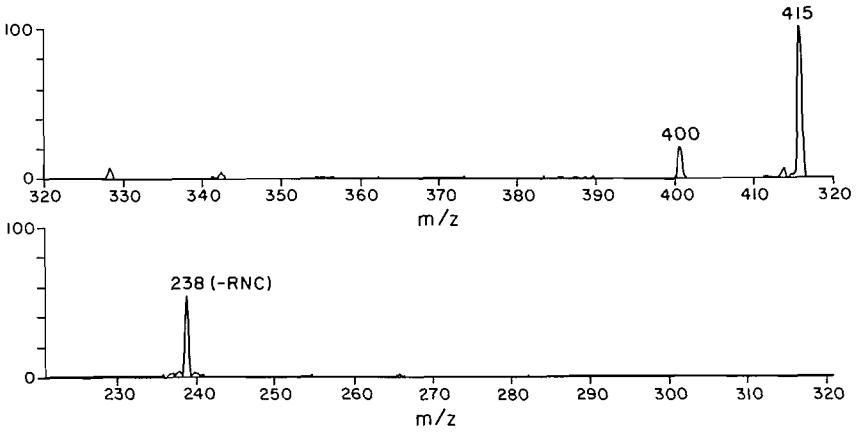


FIG. 3. Low-energy CID spectrum of the ion at m/z 415 in Fig. 1, formed as the $[M - (SCN)_2]^+$ ion by LSIMS of the rhodium complex **2** with RNC = **1** (R″ = Me). Laboratory-frame collision energy 30 eV, argon collision gas, 60% attenuation of intensity of precursor ion.

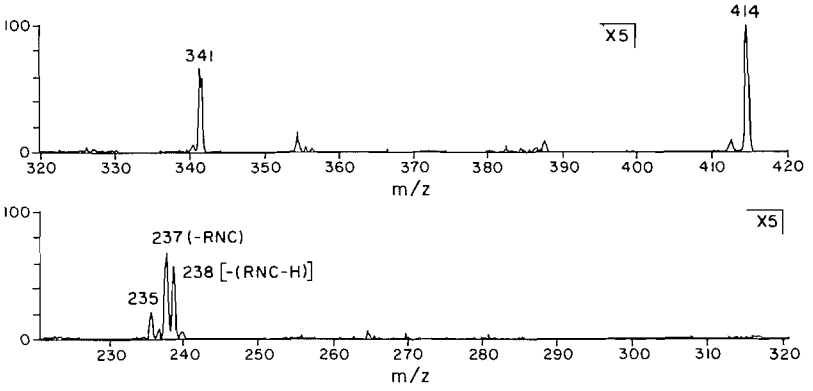
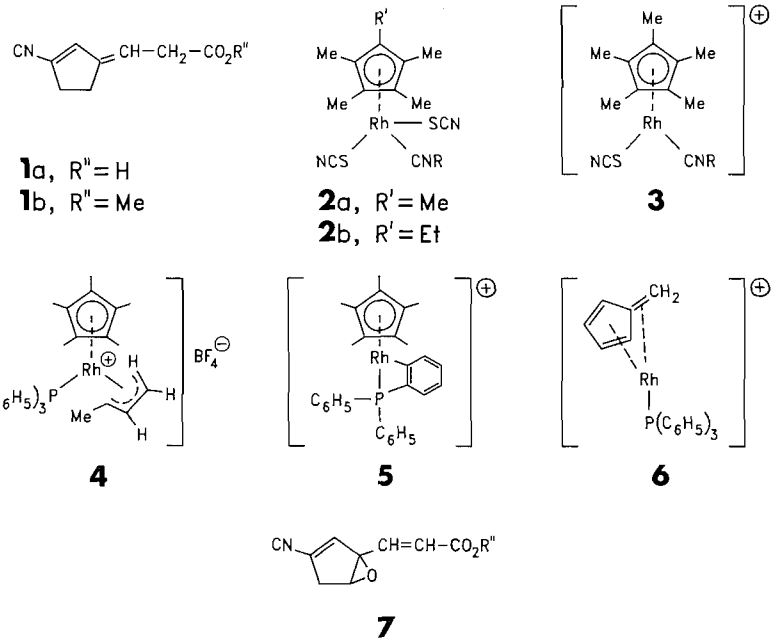


FIG. 4. Low-energy CID spectrum of the ion at m/z 414 in Fig. 1, formed as the $[M - (SCN) - (HSCN)]^+$ ion by LSIMS of the rhodium complex **2** with RNC = **1** (R″ = Me). Laboratory-frame collision energy 30 eV, argon collision gas, 60% attenuation of intensity of precursor ion.



Can. J. Chem. Downloaded from www.nrcresearchpress.com by 195.138.81.100 on 09/07/12
For personal use only.

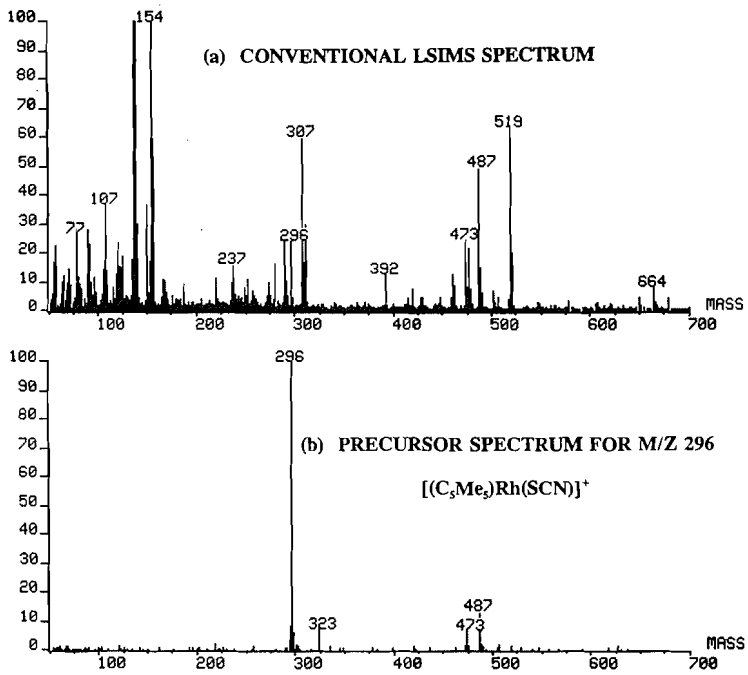


FIG. 5. Positive ion LSIMS spectra of the crude esterified ethyl acetate extract of a fermentation of *T. hamatum*, treated with excess $[(\eta^5\text{-}C_5Me_5)Rh(SCN)_2]_2$. (*a*) Conventional mass spectrum (magnet scan), with detection immediately following double-focus (BE) stage. (*b*) As (*a*), but quadrupole mass filter set to transmit *m/z* 296 and detection after the entire BEqQ train, *i.e.* a precursor scan for *m/z* 296. Conditions in the RF-only quadrupole collision cell *q* were laboratory-frame collision energy 30 eV, argon collision gas, 60% attenuation of intensity of precursor ion.

high abundance at *m/z* values greater than the molecular weight of the complex under study. Similar species have been reported (8) in the cases of other Rh and Ir coordination complexes, where they have been attributed to reactions of the complexes with components of the matrix. In the work reported here such an explanation is untenable because ions of the same mass were observed in spectra when four different matrices were used. The species *m/z* 650, 591, and 534 (Fig. 1) were present in the LSIMS spectra of all the compounds listed in Table 1 and hence did not contain an isocyanide ligand. In the LSIMS spectra of complexes **2***b*, with R′ = Et, a similar triad was observed at *m/z* 678, 619, and 562, *i.e.*, 28 u greater, implying the presence of two cyclopentadienyl groups. The accurate mass measurements (Table 2) of the ions at *m/z* 534 and 650 are consistent with the formulations $[(C_5Me_5)_2Rh_2(SCN)]^+$ and $[(C_5Me_5)_2Rh_2(SCN)_3]^+$, respectively. The same groups of ions were observed in the LSIMS spectra of the reagents $[(\eta^5\text{-}C_5Me_5)Rh(SCN)_2]_2$ and $[(\eta^5\text{-}C_5Me_4Et)Rh(SCN)_2]_2$, and thus the ions at *m/z* 650 and *m/z* 678 may be assigned to $[M - (SCN)]^+$ ions of these dirhodium reagents. Their appearance in the LSIMS spectra of the monorhodium complexes **2***a* implies that bimolecular reactions were proceeding in the ionization source under LSIMS conditions; this conclusion agrees with the observation that the intensities of these dirhodium ions, relative to that of the $(M - SCN)^+$ ions of **2***a*, increased markedly with increasing concentration of sample in the matrix. This hypothesis was also confirmed by examining the LSIMS spectrum of a mixture of the two homologous complexes **2***a* and **2***b* of the same isocyanide. In this case ions at *m/z* 534, 591, 650 and 562, 619, 678 were observed, exhibiting the expected 28 u shifts. In addition, however, a third group of ions at 548, 605, and 664 (*i.e.* 14 u shifts) were present, clearly indicating the occurrence of cross-reactions producing species containing one (C_5Me_5) and one (C_5Me_4Et) ligand.

The question of whether these cross-reactions occurred in the liquid matrix, or in the gas phase immediately above the matrix, was explored using a dual-target sample probe (VG Analytical). Complex **2***a* was loaded on one target, and **2***b* on the other, both in 3-nitrobenzyl alcohol as matrix. The primary beam of Cs^+ ions was adjusted (defocussed) so that both of the targets were activated simultaneously. No cross-reaction products were observed in the secondary ion mass spectrum under these conditions. Thus it is unlikely that the dimerization occurs in the gas phase, though it is possible that the reaction proceeds in the "selvedge" region immediately above the irradiated surface.

The complexes **2** of the model isocyanide compounds were easily separated on analytical tlc plates, where quantities of about 0.5 μg could be detected by sight and 0.05 μg detected by reflected ultraviolet light at 254 nm. Such spots could be eluted by treatment with 3-nitrobenzyl alcohol as described in the Experimental section and excellent mass spectra obtained (*e.g.* Fig. 1) by transferring 1–2 μL of the solution to the probe. An alternative procedure for analysis of isocyanide mixtures, eliminating a chromatographic step, was also investigated. In a mixture of isocyanide complexes **2***a* all provide the daughter ion at *m/z* 296. Thus a scan of the ion reactions leading to *m/z* 296 should reveal parent ions whose masses correspond to the $[(\eta^5\text{-}C_5Me_5)Rh(SCN)(NCR)]^+$ ions for various isocyanide ligands. Figure 5(*a*) is an LSIMS spectrum of the crude esterified ethyl acetate extract of a fermentation of *T. hamatum*, treated with excess $[(\eta^5\text{-}C_5Me_5)Rh(SCN)_2]_2$, while Fig. 5(*b*) is a precursor scan for *m/z* 296 conducted on the same extract. Useful information is difficult to detect in Fig. 5(*a*) but Fig. 5(*b*) shows signals at *m/z* 473 and 487, corresponding to the

Can. J. Chem. Downloaded from www.nrcresearchpress.com by 195.138.81.100 on 09/07/12
For personal use only.

Can. J. Chem. Downloaded from www.nrcresearchpress.com by 195.138.81.100 on 09/07/12
For personal use only.

metabolite methyl esters **1***b* and **7** (R″ = Me). Further work on this rapid screening analytical method is envisaged.

The present work has shown that positive ion LSIMS spectra of complexes **2**, exemplified by Fig. 1, are interpretable in a self-consistent manner to yield the nominal mass of the isocyanide ligand RNC. Indeed mass measurements on the $(M - SCN)^+$ ions give, after subtracting the mass (295.9980) of the $[(\eta^5\text{-}C_5Me_5)Rh(SCN)]$ moiety, the accurate mass and thus information concerning the atomic constitution of RNC; experimental uncertainties in such mass differences will be of the order of 10 ppm. Identification of the $(M - SCN)^+$ ions can be made via the spectral clues discussed in relation to Table 1, and if necessary confirmed by simple tandem mass spectrometry experiments (Fig. 2). The present work also confirms the remarkable properties of 3-nitrobenzyl alcohol as a matrix for LSIMS of transition metal complexes (12).

Experimental

Melting points are not corrected. Infrared spectra were measured on a Perkin-Elmer 283 instrument, and ^1H and ^{13}C nmr spectra in 5 mm tubes on a Bruker MSL-300 instrument at 300 and 75 MHz, respectively. Chemical shifts are given in ppm downfield from the signal of tetramethylsilane. Mass spectra were obtained using a hybrid tandem instrument of BEqQ configuration (ZAB-EQ, VG Analytical, Manchester, U.K.) with a VG 250J data system. A VG Analytical cesium ion gun, operated at a beam energy of 25 keV (and thus an effective energy of 17 keV at the sample probe maintained at 8 kV) was used to provide the primary ion beam for LSIMS. Four liquid matrices were used: dithioerythritol–dithiothreitol (5:1), glycerol, glycerol[$^2H_8$], and 3-nitrobenzyl alcohol. The first three were used as received, the last was distilled under reduced pressure and the middle-third fraction used. Accurate mass measurement (8×10^3 resolving power, 10% valley definition, precision 3–5 ppm) were made by the peak matching method, using either matrix-derived ions or ions derived from alkali iodides added to the matrix as standards. Tandem mass spectrometry involved the selection of precursor ions by the double-focussing (BE) analyser followed by collision-induced dissociation of mass-selected ions in the RF-only quadrupole (q), using a laboratory frame collision energy in the range 30–50 eV and argon collision gas at a pressure sufficient to attenuate the intensity of the precursor ion beam to 50–60% of its initial value.

Mass spectrometry of isocyanide complexes from analytical tlc plates was achieved as follows. The yellow (or orange) spot on the chromatogram was scraped from the plate into a vial and the mixture treated with 3-nitrobenzyl alcohol (50 μL). The mixture was agitated for 2 min, the silica allowed to settle under gravity, and 2 μL of the supernatant liquid transferred to the tip of the direct introduction probe using a syringe; the probe was inserted into the source immediately. In general there was sufficient material for a LSIMS spectrum and for a mass measurement of the $M - 58^+$ ion in a spot containing *ca.* 0.5 μg of the complex. Tetrahydrofuran (THF) was distilled from lithium aluminum hydride immediately before use.

Reaction of phenyl isocyanide with $[(\eta^5\text{-}C_5Me_5)Rh(SCN)_2]_2$

A solution (20 mL) of the rhodium complex (72 mg) in dichloromethane was treated with phenyl isocyanide (ref. 13, 20 mg). After 1 h the solution was concentrated and the concentrate (0.5 mL) applied to two preparative layer chromatography (plc) plates (20 × 20 × 0.1 cm). The plates were developed with methyl alcohol – dichloromethane (1:39) and the main orange band eluted from the silica with THF. The eluate was evaporated and the *complex* ($\eta^5\text{-}C_5Me_5Rh(SCN)_2.CNC_6H_5$) separated from ethyl acetate as stout rods, mp 160–162°C. *Anal.* calcd. for $C_{19}H_{20}N_3RhS_2$: C 49.9, H 4.4, N 9.2, Rh 22.5, S 14.0; found: C 49.6, H 4.4, N 9.4, Rh 22.4, S 13.8. δ_C 130.7, 129.7, 127.3, 121.75 (2CNS), 103.4 (5C $J_{^{13}C,Rh}$ 5 Hz), 9.3 (5C).

Preparation of $[(\eta^5\text{-}C_5Me_5)Rh(SCN)_2(CNCH_2C_6H_5)]$

A solution of the dirhodium complex reagent (ref. 5, 210 mg) in dichloromethane (15 mL) was treated dropwise with a solution (2 mL) of benzyl isocyanide (Aldrich, 30 mg) in dichloromethane. After 2 h at room temperature the reaction solution was concentrated to 2 mL and the concentrate applied to a Florisil (25 g) column (20 × 2 cm). The column was eluted successively with dichloromethane (100 mL), and dichloromethane – methyl alcohol mixtures as follows: 99:1 (100 mL), 49:1 (200 mL), 19:1 (1200 mL), 9:1 (100 mL), and 4:1 (100 mL, containing 1% NaSCN). The product was eluted in the dichloromethane – methyl alcohol (49:1) fraction, and excess reagent appeared in the final fraction. The eluate (49:1) was concentrated to 5 mL, diethyl ether (15 mL) added, and the orange–yellow precipitate (93 mg) collected. The complex separated from ethyl acetate as orange needles, mp 135–136°C. *Anal.* calcd. for $C_{20}H_{22}N_3RhS_2$: C 50.96, H 4.7, N 8.9, Rh 21.8, S 13.6; found: C 51.0, H 4.7, N 9.0, Rh 21.4, S 13.3. Infrared ν_{max} (CH_2Cl_2) 2210, 2102 cm^{-1}; δ_H (C^2HCl_3) 7.5–7.3 (m, 5H), 5.1 (s, 2H), 1.81 (s, 15H).

Preparation of the cyclohexylisocyanide complex of $[(\eta^5\text{-}C_5Me_5)Rh(SCN)_2]$

This complex was prepared from cyclohexylisocyanide (10) on the same scale and in the same way as the benzyl isocyanide complex. The crude product was purified by plc. The major orange band that separated on developing the plate with methyl alcohol – dichloromethane (1:49) was eluted with THF, the eluate evaporated, and the residue recrystallized from ethyl acetate giving the complex as glistening orange leaflets, mp 132–134°C. Anal. calcd. for $C_{19}H_{26}N_3RhS_2$: C 49.2, H 5.7, N 9.1, Rh 22.2, S 13.8; found: C 49.2, H 5.7, N 9.0, Rh 21.8, S 13.5. Infrared ν_{max} (CH_2Cl_2) 2205, 2105 cm^{-1}; δ_C 121.75 (*C*NS), 102.44 (d, $J_{^{13}C,Rh}$ 6 Hz), cyclopentadienyl ring carbons), 55.7 (cyclohexyl methine carbon atom), 32.2, 24.67, 22.82 (cyclohexyl methylene carbons), 9.13 (5 *C*H_3). The isocyanide carbon atom bonded to rhodium was not detected in the proton decoupling experiments (*cf.* ref. 14).

Phenyl 2-N-benzyloxycarbonylamino-2-methylpropionate

2-*N*-Benzyloxycarbonylamino-2-methylpropionic acid (ref. 15, 11.8 g) was suspended in dichloromethane (75 mL) and phenol (5 g) added. When all the solids had dissolved, dicyclohexylcarbodiimide (10.5 g) was added. The mixture was stirred at room temperature for 18 h, when the precipitated urea was removed by filtration, the filtrate evaporated, and the oily residue taken up in toluene (30 mL). The toluene solution was filtered, the filtrate washed with sodium bicarbonate solution (1%, 3 × 100 mL), dilute HCl (*N*, 50 mL) and finally with water. The solution was dried over Na_2SO_4, filtered, and evaporated to give an oil (16 g) which crystallised on standing. The majority of this product was dissolved in boiling petroleum ether (bp 60–80°C, 600 mL). The filtered solution was cooled very slowly, seeded at the first sign of opalescence, and maintained at 4°C for 24 h. The *phenyl ester* separated as colorless rods, mp 61–62°C. *Anal.* calcd. for $C_{18}H_{19}NO_4$: C 69.0, H 6.1, N 4.5, O 20.4; found: C 69.0, H 6.2, N 4.6, O 20.2. Infrared ν_{max} (CCl_4) 3450, 3430, 1760, 1730, 1460, 1280, 1125 cm^{-1}.

Preparation of the phenyl 2-isocyano-2-methylpropionate complex of $[(\eta^5\text{-}C_5Me_5)Rh(SCN)_2]$

The phenyl ester (3.6 g, see preceding paragraph) was dissolved in ethyl formate (75 mL) and formic acid (0.1 mL) added. The solution was treated with palladium on carbon (10%, 0.12 g) and the mixture shaken with hydrogen at 3 atm pressure for 18 h. The shaking should start as soon as possible to prevent crystallisation of the formate on the carbon, thus rendering the catalyst ineffective. Methanol (100 mL) was then added to the reaction mixture, which was filtered through a bed of Celite 545 (1 cm thick), and the filtrate evaporated. The crystalline residue was taken up in hot ethyl acetate (90 mL) and the filtrate kept at 4°C for 24 h. *Phenyl 2-N-formylamino-2-methylpropionate* separated as colorless needles, mp 133–135°C (some sublimation above 110°). *Anal.* calcd. for $C_{11}H_{13}NO_3$: N 6.7, found: N 6.4. This ester (0.25 g) was treated with a solution (3 mL) of triethylamine (6.05 mL) in dichloromethane (25 mL). The solution was introduced into a flame-dried, nitrogen-filled vessel and was stirred and cooled to −5°C. A solution (0.5 mL) of phosphorus oxychloride (2.17 g) in dichloro-

methane (5 mL) was added to the reaction solution with a syringe over a period of 40 min, while maintaining the temperature at −5°C. After a further 1 h at −5°C the reaction mixture was allowed to warm to room temperature and was stirred under nitrogen for 18 h. The mixture was treated with a solution (5 mL) of sodium bicarbonate (0.52 g) and was then diluted with 5 mL of dichloromethane. The phases were separated and the aqueous phase extracted with dichloromethane (2 × 5 mL). The extracts were combined and freeze–dried at −15°C for 18 h. The ice was filtered off, the filtrate treated with $[(\eta^5\text{-}C_5Me_5)Rh(SCN)_2]_2$ (100 mg), and the reaction mixture kept at ambient temperature for 3 h. The resulting solution was concentrated to 3 mL and the concentrate applied to two plc plates, which were developed with dichloromethane–methyl alcohol (19:1). The orange band of greatest R_F was eluted with THF and the eluate evaporated. The residue (70 mg) was chromatographed as before, and the crystalline residue remaining after evaporation of the THF collected (30 mg, mp 149–152°C). The *complex* separated from butyl acetate – isopropyl ether (1:3) as orange needles (mp 150–152°C). *Anal.* calcd. for $C_{23}H_{26}N_3O_2RhS_2$: C 50.8, H 4.8, N 7.7, Rh 18.9, S 11.8; found: C 50.5, H 4.8, N 7.8, Rh 18.4, S 11.8. Infrared ν_{max} ($CHCl_3$) 2205, 2114, 1769, 1725 cm^{-1}; δ_H (C^2HCl_3), 7.1–7.5 (m, 5H), 2.04 (s, 6H), 1.88 (s, 15H); *m/z* 485.0767 ($(M - SCN)^+$, $C_{22}H_{26}N_2O_2RhS$ requires 485.0770).

Preparation of the methyl 2-isocyano-2-methylpropionate complexes of $[(\eta^5\text{-}C_5Me_5)Rh(SCN)_2]$ and $[(\eta^5\text{-}C_5EtMe_4)Rh(SCN)_2]$

Methyl 2-isocyano-2-methylpropionate (ref. 16, 63 mg) was dissolved in dichloromethane (5 mL) and treated with a solution (10 mL) of $[(\eta^5\text{-}C_5Me_5)Rh(SCN)_2]_2$ (170 mg) in dichloromethane. The resulting orange solution was kept at room temperature overnight, then concentrated to 1 mL and the concentrate applied to two plc plates which were developed with dichloromethane – methyl alcohol (93:7). The main orange band was eluted with THF. The complex separated from butyl acetate as yellow needles, mp 138–139°C. *Anal.* calcd. for $C_{18}H_{24}N_3O_2RhS_2$: C 44.9, H 5.0, N 8.7; found: C 44.7, H 5.0, N 8.9. δ_H 3.86 (3H), 1.86 (15H), 1.83 (6H). The homologous complex (R′ = Et) was prepared in exactly the same way using $[(\eta^5\text{-}C_5EtMe_4)Rh(SCN)_2]_2$ (200 mg) and methyl 2-isocyano-2-methylpropionate (60 mg). The complex separated from butyl acetate – isopropyl ether (1:3) as orange needles, mp 74°C. *Anal.* calcd. for $C_{19}H_{26}N_3O_2RhS_2$: C 46.1, H 5.3, N 8.5; found: C 45.9, H 5.3, N 8.3. δ_H 3.85 (s, 3H; ester methyl protons), 2.36 (q, *J* 7.7 Hz, 2H; methylene protons on cyclopentadienyl ring), 1.88 (s, 12H; protons on methyl groups directly bonded to cyclopentadienyl ring), 1.86 (s, 6H; methyl protons on isopropyl moiety), 1.14 (t, *J* 7.7 Hz, 3H; methyl protons on ethyl substituent on cyclopentadienyl ring).

Acknowledgements

The authors are indebted to Dr. J. A. Walter and D. M. Leek for the nmr spectra, to Dr. J. M. Miller for a copy of ref. 12 prior to publication, and to an anonymous referee for suggesting the experiment with the dual-target probe tip.

1. S. N. Liss, D. Brewer, A. Taylor, and G. A. Jones. Can. J. Microbiol. **31**, 767 (1985).
2. D. Brewer, V. O. Parkinson, and A. Taylor. J. Appl. Bacteriol. **69**, 701 (1990).
3. A. J. McAlees, K. Schwartzentruber, and A. Taylor. J. Chem. Soc. Perkin Trans. I, 2115 (1990).
4. D. Brewer, E. J. Gabe, A. W. Hanson, A. Taylor, J. W. Keeping, V. Thaller, and B. C. Das. J. Chem. Soc. Chem. Commun. 1061 (1979).
5. A. W. Hanson, A. J. McAlees, and A. Taylor. J. Chem. Soc. Perkin Trans. I, 441 (1985).
6. R. K. Boyd, A. J. McAlees, A. Taylor, and J. A. Walter. J. Chem. Soc. Perkin Trans. I. In press.
7. M. Barber, R. S. Bordoli, R. D. Sedgwick, and A. N. Tyler. Nature (London), **293**, 270 (1981).
8. R. Bertani, P. Diversi, G. Ingrosso, A. Lucherini, F. Marchatti, V. Adovasio, M. Nardelli, and S. Pucci. J. Chem. Soc. Dalton Trans. 2983 (1988).
9. K. J. Bari and H. Read. Analyst, **112**, 433 (1987).
10. F. Faraone, V. Marsala, and G. Tresoldi. J. Organomet. Chem. **152**, 337 (1978).
11. R. H. Crabtree. Acc. Chem. Res. **23**, 95 (1990).
12. J. M. Miller. Mass Spectrom. Rev. **9**, 319 (1990).
13. W. P. Weber, G. W. Gokel, and I. K. Ugi. Angew. Chem. Intl. Eng. Ed. **11**, 530 (1972).
14. W. D. Jones, R. P. Duttweiler Jr., and F. J. Feher. Inorg. Chem. **29**, 1505 (1990).
15. M. Bergmann, L. Zervas, J. S. Fruton, F. Schneider, and H. Schleich. J. Biol. Chem. **109**, 325 (1935).
16. R. Schroeder and K. Luerssen. Ger. Offen. 2751783 (1979).

Can. J. Chem. Downloaded from www.nrcresearchpress.com by 195.138.81.100 on 09/07/12
For personal use only.

Reactions of silanes with bis(cyclopentadienyl)dialkylzirconium complexes

YING MU, CLARE AITKEN, BRUNO COTE, AND JOHN F. HARROD[1]
Chemistry Department, McGill University, Montreal, P.Q., Canada H3A 2K6

AND

EDMOND SAMUEL
Laboratoire de Chimie Organométallique de l'ENSCP, 75005 Paris, France

Received June 28, 1990

YING MU, CLARE AITKEN, BRUNO COTE, JOHN F. HARROD, and EDMOND SAMUEL. Can. J. Chem. **69**, 264 (1991).

A systematic comparison between the dimethylzirconocene (DMZ) and dimethyltitanocene (DMT) catalyzed dehydrocoupling of organosilanes is reported. The polymerization rates of primary silanes are about ten times faster for DMZ than for DMT, but the characteristics of the polymers produced are essentially identical. Variations of molecular weight and molecular weight distribution with varying monomer and reaction time, and the relative amounts of linear and cyclic polymer are also essentially the same for the two catalysts.

Oligomerizations of phenylmethylsilane, diphenylsilane, and 1,2-diphenyldisilane are described. The compound Cp_2Zr-(SiPhMeH)(μ-H)$_2$(SiPhMe$_2$)ZrCp_2 (**1***b*) is isolated from the reaction of phenylmethylsilane with DMZ and its structure confirmed by crystallography and ^{1}H-NMR spectroscopy. The compound $Cp_2Zr(Me)(\mu\text{-}H)_2(SiPh_2H)ZrCp_2$ (**1***d*) is isolated from the reaction of diphenylsilane with DMZ and its structure assigned by NMR spectroscopy. A number of other hydride bridged species are observed by ^{1}H-NMR in the reactions of DMZ with phenylmethyl-, diphenyl-, and *n*-butylmethylsilanes and their structures are tentatively assigned. The implications of these observations on the mechanism of transformation of DMZ into active catalyst and our current views of the polymerisation mechanism are also discussed.

Key words: silanes, dehydrocoupling, titanocene, zirconocene, polysilanes.

YING MU, CLARE AITKEN, BRUNO COTE, JOHN F. HARROD et EDMOND SAMUEL. Can. J. Chem. **69**, 264 (1991).

On a effecté une comparaison systématique du déshydrocouplage des organosilanes, catalysé par le diméthylzirconocène (DMZ) et par le diméthyltitanocène (DMT). Les vitesses de polymérisation des silanes primaires sont environ dix fois plus rapides avec le DMZ qu'avec le DMT; toutefois, les caractéristiques des polymères obtenus sont essentiellement identiques. Les variations des masses moléculaires et des distributions des masses moléculaires en fonction du monomère et du temps de réaction ainsi que les quantités relatives des polymères linéaires et cycliques sont aussi essentiellement les mêmes pour les deux catalyseurs.

On décrit les oligopolymérisations du phénylméthylsilane, du diphénylsilane et du 1,2-diphényldisilane. On a isolé le composé Cp_2Zr(SiPhMeH)(μ-H)$_2$(SiPhMe$_2$)ZrCp_2 (**1***b*) de la réaction du phénylméthylsilane avec le DMZ et on a confirmé sa structure par cristallographie et par RMN du ^{1}H. On a isolé le composé $Cp_2Zr(Me)(\mu\text{-}H)_2(SiPh_2H)ZrCp_2$ (**1***d*) du mélange réactionnel du diphénylsilane avec le DMZ et on a attribué sa structure à l'aide de la spectroscopie RMN. En se basant sur la rmn du ^{1}H, on a observé un certain nombre d'autres espèces pontées par de l'hydrure dans les mélanges réactionnels du DMZ avec les phénylméthyl-, diphényl- et *n*-butylméthylsilanes et on leur a attribué des structures provisoires. On discute aussi des implications de ces observations sur le mécanisme de transformation du DMZ en catalyseur actif et sur nos vues actuelles concernant le mécanisme de polymérisation.

Mots clés : silanes, déshydrocouplage, titanocène, zirconocène, polysilanes.

[Traduit par la rédaction]

Introduction

In earlier papers we have described the exceptional activity of bis(cyclopentadienyl)dialkylzirconium complexes for the catalytic dehydrocoupling of silanes (1–4). Since our original report, a number of other groups have made important observations on this reaction. Tilley and co-workers have developed general methods for synthesis of silylzirconium complexes and shown how these complexes can generate Si—Si bonds through σ-bond metatheses with other Si—H compounds (5–9). Corey *et al.* have demonstrated catalytic oligomerizations of secondary silanes at higher temperatures with catalysts generated in situ by reaction of zirconocene(IV) chloride with butyl lithium (10–12). Campbell *et al.* have provided unequivocal evidence for the predominant production of cyclic oligosilanes by polymerization of *n*-butylsilane with dimethylzirconocene (13).

In this paper we present the results of a detailed comparison between dimethylzirconocene (DMZ) and dimethyltitanocene (DMT) (14–16) as catalysts for the polymerization of some primary and secondary silanes. The structures and NMR spectra of some important intermediates in these catalytic reactions are also discussed.

[1]To whom correspondence should be addressed.

Results and discussion

Polymerization of primary organosilanes

DMZ exhibits almost identical behavior to DMT in catalyzing the polymerization of primary organosilanes. The only dramatic differences between the two systems are the pronounced induction period for the titanium catalyzed reaction and the essentially complete reduction of the titanium to Ti(III) at the onset of polymerization. The zirconium catalyzed reaction exhibits a slight autoacceleration in the course of the reaction at low catalyst, or monomer, concentrations, but no obvious induction period. In addition, although paramagnetic Zr(III) species are observable in reaction mixtures by EPR spectroscopy, most of the zirconium remains in the form of NMR-observable Zr(IV) species throughout the reaction. A typical reaction profile for a DMZ-catalyzed polymerization of phenylsilane is shown in Fig. 1*b*.

The evolution of the reaction products may be followed by ^{1}H-NMR spectroscopy. Although 1,2-diphenyldisilane is

Can. J. Chem. Downloaded from www.nrcresearchpress.com by 195.138.81.100 on 09/07/12
For personal use only.

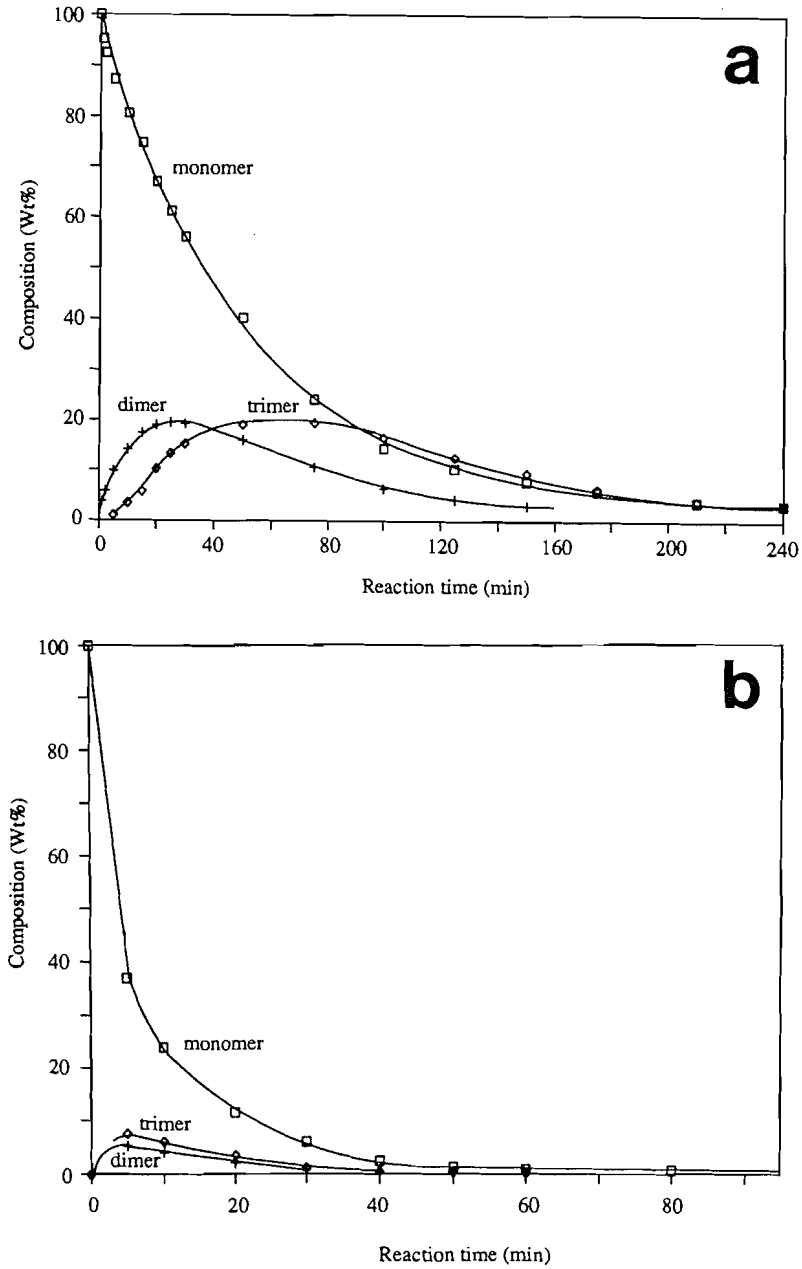


FIG. 1. Reaction rate profile for the polymerisation of phenylsilane catalysed by (*a*) DMT. $[DMT]_i$ = 0.08 M, neat $PhSiH_3$; (*b*) DMZ: $[DMZ]_i$ = 0.04 M, $[PhSiH_3]_i$ = 3.0 M. T = 20°C in both cases.

observable as a product of the reaction, its concentration never rises to more than about 5% of the initial monomer concentration with the DMZ catalyst. We had earlier claimed that no dimer is produced in the DMT-catalyzed reaction (14). This incorrect claim was based on our failure to observe dimer (or any other identifiable oligomer) during the polymerization reaction. More recently we have found that the NMR signals for the dimer are greatly broadened in the presence of the active titanium catalyst, probably as a result of a rapid equilibrium between disilane and the catalyst, and the catalyst must either be destroyed by oxidation, or removed, in order to observe the dimer and trimer at room temperature. Even in the presence of catalyst, these species can be observed at lower temperature (ca. −20°C). Using such procedures it was established that the DMT-catalyzed polymerization leads to a maximum accumulation of about twenty per cent of dimer in the initial stages of the reaction, as illustrated in Fig. 1*a*.

The complex, and different, reaction rate profiles make absolute comparison of the reactivities of the two catalysts difficult. The use of either maximum rates, or times to achieve 80% conversion, lead to the same conclusion: that the DMZ-catalyzed polymerization of phenylsilane is about an order of magnitude faster than the DMT reaction under ambient conditions. The results of a comparison of relative rates for three different primary silanes, shown in Table 1, reveal little difference between the two catalyst systems. No significance can be attached to the small numerical differences since the titanium data were based, in this particular case, on initial rates of reactions where the hydrogen product was completely scavenged by co-hydrogenation of cyclohexene (17), while

Can. J. Chem. Downloaded from www.nrcresearchpress.com by 195.138.81.100 on 09/07/12
For personal use only.

TABLE 1. Relative rates of polymerization of some primary organosilanes with DMT[a] and DMZ[b]

Monomer	Relative rates		
	$PhSiH_3$	$BzSiH_3$	$HxSiH_3$
DMT	13	1	1
DMZ	100	15	5

[a]Data from ref. 16.
[b][DMZ] = 0.020 M; $[silane]_i$ = 1.20 M; in C_6D_6 at 20°C.

the zirconium data are maximum rates. The co-hydrogenation technique could not be applied to the DMZ system since the zirconium is much less active as a hydrogenation catalyst and hydrogen scavenging is only about 50% efficient.

On the basis of their broad, poorly resolved NMR spectra all of the polymers produced with these catalysts may be assumed to be atactic and, within the limits of accuracy of NMR integration, to have the average composition (RSiH). The extreme broadness and lack of resolution of the NMR peaks is attributed to the atacticity of the polymers. The ^{29}Si(DEPT) spectra, with suitable pulse angles for the detection of SiH and SiH_2, reveal the presence of SiH_2 units in the polyphenyl- and polyhexylsilane samples synthesised with DMZ, but no SiH_2 was detected in the polybenzylsilanes. It may therefore be concluded that the phenyl and *n*-hexyl polymers contain at least some linear species, while the benzyl polymer consists uniquely of cyclics. Essentially the same behaviour was reported previously for the DMT catalysed reactions (16).

The molecular weights and molecular weight distributions of the polymers produced by the two catalysts are also remarkably similar. Unfortunately, for both systems, the average degrees of polymerization fall in an awkward range (ca. 10 to 20), where the molecules are a bit too small to be adequately described in purely statistical terms, yet a bit too large to achieve separations of stereoisomers and define exact structures. Nevertheless, the application of a number of different physico-chemical techniques allows some reasonably firm conclusions regarding the structures and compositions of the products.

The phenyl and hexyl polymers give bimodal GP chromatograms with a very narrow distribution low molecular weight fraction and a somewhat broader distribution higher molecular weight fraction. A number of representative chromatograms are illustrated in Fig. 2. Two features of these chromatograms should be noted. In the first place, the formation of the higher molecular weight fraction is favoured by high monomer concentrations. Secondly, very long contact times with the catalyst lead to a reversion of the higher molecular weight fraction to lower molecular weight species. Both of these patterns of behaviour are what would be expected if the lower molecular weight fraction consists of cyclics. In the first case, the formation of cyclics is favoured by low monomer concentration since intramolecular ring closure will be favoured relative to a linear propagation effected via an intermolecular reaction of monomer with the propagating species. In the second case the cyclics result from a classical back-biting depolymerization reaction whose rate becomes more and more significant relative to propagation as the concentration of SiH decreases. These observations also conform with the observation that the polybenzylsilane, which ^{29}Si-NMR indicated to contain no linear species, gives a monomodal chromatogram of narrow dispersity. The polydispersities of the samples in Fig. 2 range from 1.3 to 1.7.

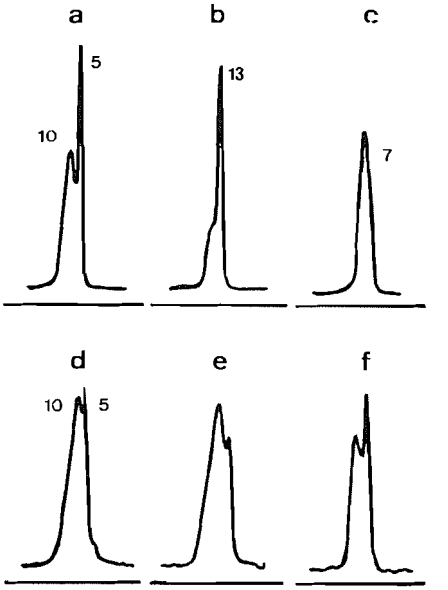


FIG. 2. Some representative chromatograms for polysilanes produced with DMZ catalyst, $[DMZ]_i$ = 0.075 M; toluene solvent; 20°C. (*a*) Poly(phenylsilane), $[PhSiH_3]_i$ = 4.0 M, 20 days; (*b*) poly(*n*-hexylsilane), $[HxSiH_3]_i$ = 3.1 M, 20 days; (*c*) poly(benzylsilane), $[BzSiH_3]_i$ = 3.7 M, 20 days; (*d*) poly(phenylsilane), $[PhSiH_3]_i$ = 4.0 M, 1 day; (*e*) poly(phenylsilane), $[PhSiH_3]_i$ = 4.0 M, 3 days; (*f*) poly(phenylsilane), $[PhSiH_3]_i$ = 2.0 M, 1 day. The figures next to the peaks are the calculated peak maximum degrees of polymerization.

Oligomerization of secondary silanes

We have recently described the stoichiometric reactions of secondary silanes with DMT in some detail (18). Secondary silanes react readily with DMT, in the presence of coordinating ligands, to give titanocene(III)silyl complexes, analogous to those obtained with primary silanes (18). They do not, however, give the binuclear titanocene(III)silyl complexes, readily obtained with primary silanes (15, 18), in the absence of coordinating ligands. In addition, the secondary silanes show very low reactivity under conditions where primary silanes are rapidly dehydrocoupled by catalytic amounts of dialkyltitanocenes. Structural evidence suggests that steric hindrance may prevent formation of both the titanocene(III)silyl dimer and the necessary transition state for dehydrocoupling in the case of secondary silanes (18).

DMT does not couple secondary silanes at an appreciable rate at room temperature. At temperatures in the range of 60–80°C, with the use of relatively high catalyst concentrations, and in the absence of solvent, diphenyl- and phenylmethylsilanes can be coupled. In the case of diphenylsilane, only the dimer is produced, but with sufficiently long reaction times the reaction goes eventually to completion. In the case of phenylmethylsilane the rate of dehydrocoupling is slightly faster than that for diphenylsilane and both the dimer and trimer are produced. At very long reaction times, conversions of up to 70% of trimer have been obtained, but no tetramer has been detected. A typical reaction profile for DMT catalysed phenylmethylsilane oligomerisation is shown in Fig. 3*a*.

We have previously reported the dimerization of secondary silanes with DMZ (1). More recently Corey *et al.* have shown that catalysts generated *in situ* by reaction of dichlorozircono-

Can. J. Chem. Downloaded from www.nrcresearchpress.com by 195.138.81.100 on 09/07/12
For personal use only.

Can. J. Chem. Downloaded from www.nrcresearchpress.com by 195.138.81.100 on 09/07/12
For personal use only.

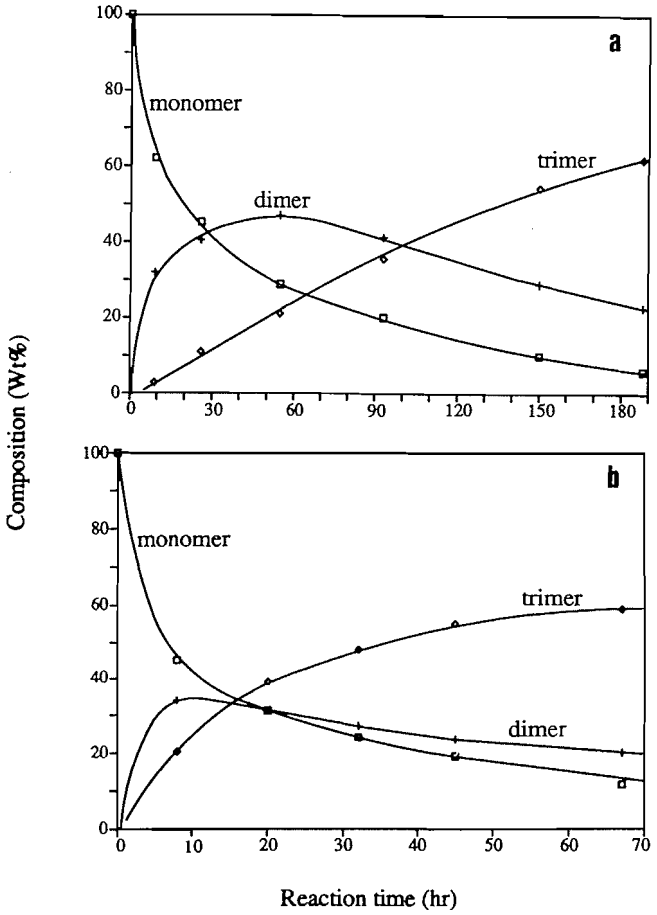


FIG. 3. Evolution of reaction products for oligomerizations of phenylmethylsilane catalyzed by (*a*) DMT, $[DMT]_i = 0.22$ M; (*b*) DMZ, $[DMZ]_i = 0.20$ M. $T = 80°C$ and reactions in neat $PhMeSiH_2$ in both cases.

cene with butyl lithium can oligomerise secondary silanes to products containing several silicon atoms (12). Except for a slightly higher catalytic activity (ca. ×5), DMZ gives essentially the same results with diphenyl and phenylmethylsilanes (see Fig. 3*b*) as obtained with DMT. In particular, we note the failure of the DMZ catalyst to give any oligomers higher than the dimer for diphenylsilane and the trimer for phenylmethyl silane. It is possible that the difference between the results of Corey *et al.* and ours, with regard to the observation of higher oligomers, is due to the effect of excess alkyl lithium in the *in situ* generated catalyst system. In work to be described elsewhere, we have found that excess methyl lithium can have a large effect on the molecular weight of polyphenylsilanes produced with *in situ* generated dimethyltitanocenes.

Neither DMT nor DMZ catalysed the coupling of butylmethylsilane under any condition of concentration, or temperature that were tried.

A dramatic exception to the general behavior described above is the oligomerisation of 1,2-diorganodisilanes. Although formally secondary silanes, these compounds polymerise even more rapidly than their analogous monomers, with both titanium and zirconium based catalysts. It is this behavior which prevents the build up of dimer in the system when starting from monomer and which seems to put the group 4-metallocenes in a category apart from catalysts derived from other transition groups. In all cases of the latter, there is a clear stepwise polymerisation passing from monomer to dimer to trimer etc. (2, 19).

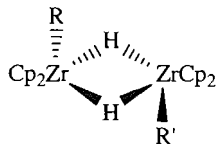
A reaction profile for the polymerization of 1,2-diphenyldisilane is shown in Fig. 4. No trimer was detected in this reaction. Since the NMR resonances of the tetramer and of higher oligomers overlap, it is not possible to estimate the concentration of these species accurately. However, it is clear, from both GPC and ^{29}Si-NMR measurements, that the main initial product is the tetramer and that the reaction is proceeding by dehydrocoupling. The small amount of monomer produced is perhaps due to a catalytic disproportionation reaction, such as shown in reaction [1]. The small amount of trimer, which should also result from such a disproportionation, could have escaped detection because of the greater linewidth of the Si—H resonance relative to that of the dimer and monomer.

[1] $$n H_2PhSiSiPhH_2 \rightarrow (n-1)PhSiH_3 + H_2PhSi(SiPhH)_nH$$

The greater reactivity of the disilane can be attributed, at least in part, to the lower bond energy of a silicon substituted SiH species, relative to one that has no Si—Si bond (20). The bond energy argument is not sufficient to explain the peculiar activity of the group 4 catalysts, since the same effect would be expected to apply to other catalysts, such as vanadocene, which in fact are less active towards the dimer than to the monomer and which produce trimer, rather than tetramer, as the secondary product (2).

Products of reactions of silanes with DMZ

In a preliminary communication we reported the isolation and characterization of the unusual bimetallic silylzirconocene-hydride complex **1***a* from the reaction of DMZ with phenylsilane (1). NMR studies of both stoichiometric and catalytic reactions of phenylsilane and DMZ showed **1***a* to be produced almost quantitatively (ca. 90%) in the early stages of the reaction, and with the passage of time appreciable quantities of other species, both diamagnetic and paramagnetic, were produced. The structural assignment of **1***a* was based on ^{1}H- and ^{29}Si-NMR data and on a single crystal X-ray structure. The quality of the X-ray structure was poor due to a severe disorder problem, resulting from the ordered superposition of the two enantiomers of **1***a* in the crystal, but was sufficiently good to confirm the structure assignment. We have now isolated compound **1***b* from the reaction of methylphenylsilane with DMZ. The compound appeared to give excellent single crystals, but attempts to resolve the X-ray structure were again frustrated by the same type of disorder as encountered in **1***a*. The manner



1

a: R = $PhSiH_2$, R' = PhMeSiH
b: R = PhMeSiH, R' = $PhMe_2Si$
c: R = Ph_2SiH, R' = Ph_2MeSi
d: R = Me, R' = Ph_2SiH
e: R = Me, R' = Ph_2MeSi
f: R = R' = BuMeSiH

in which the two superposed enantiomers lead to a symmetric electron density map is illustrated in Scheme 1. Crystal data, collection and refinement parameters are listed in Table 2. A listing of atomic coordinates and isotropic thermal parameters is given in Table 3. Although the residuals are at the margin of acceptability, the X-ray data confirm the structure assignment based on NMR data. The ^{1}H-NMR spectrum is shown in Fig. 5.

Can. J. Chem. Downloaded from www.nrcresearchpress.com by 195.138.81.100 on 09/07/12
For personal use only.

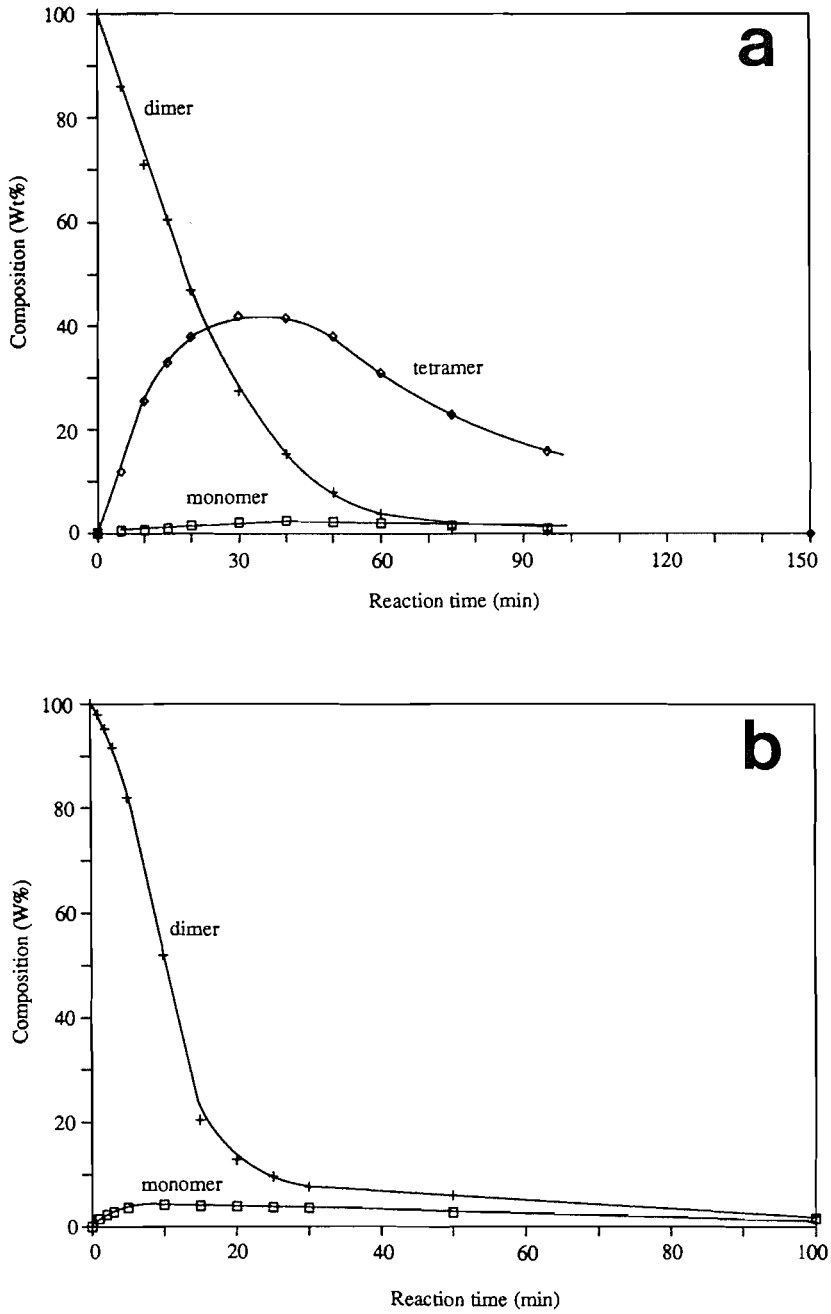
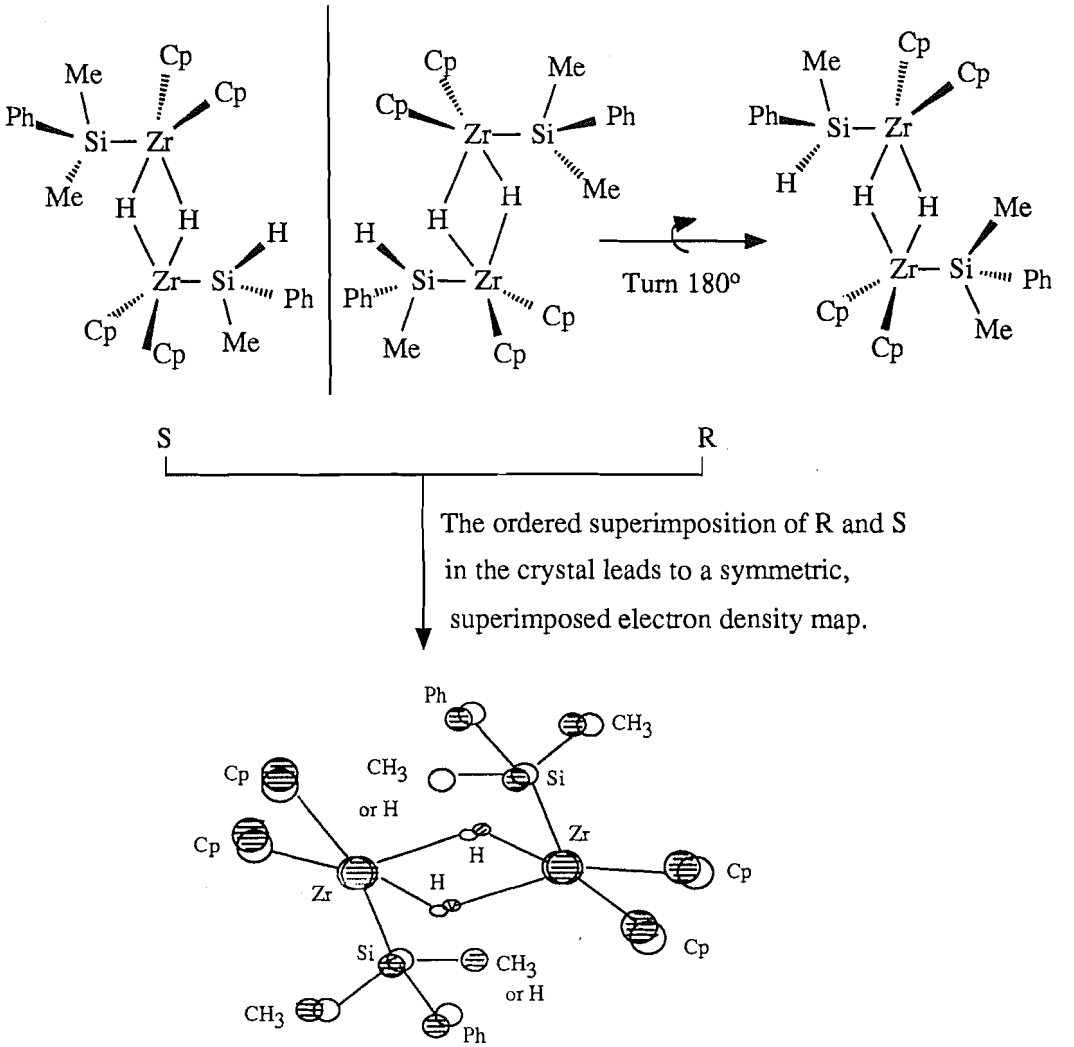


FIG. 4. Catalytic oligomerization of 1,2-diphenyldisilane by (*a*) DMT, $[DMT]_i = 0.02$ M in neat disilane (concentrations estimated by GPC); (*b*) DMZ, $[DMZ]_i = 0.025$ M; $[Ph_2Si_2H_4]_i = 2.5$ M in C_6D_6 solvent (concentrations estimated by ^{1}H-NMR). Both reactions at 20°C.

Homonuclear decoupling confirms that the Si—H resonance (4.88 ppm) is coupled to the weaker methyl resonance at 0.596 ppm. A ball and stick structure showing the atomic numbering scheme is shown in Fig. 6 and an ORTEP diagram of the $[SiZrH]_2$ fragment of **1***b*, showing thermal ellipsoids and relevant molecular parameters, is presented in Fig. 7.[2]

Because of the relatively poor precision of the molecular parameters, detailed comparison with other related structures is of questionable utility. Suffice it to say that the structural parameters are certainly in line with those reported for other bridged Zr(IV) hydrides (22) and Zr(IV) silyl complexes (7, 23). The compounds **1***a* and **1***b* are more remarkable for their overall structure than for the details of their molecular parameters. The presence of two different silyl groups, one derived directly from the starting silane and another derived from methyl transfer to the starting silane, raises two important questions. Firstly, why is the unsymmetrical, rather than the symmetrical, compound preferentially formed? Secondly, is the formation of this particular structure a direct consequence of the mechanism whereby the silanes transform DMZ to active catalyst?

[2]Complete tables of molecular parameters, heavy atom anisotropic thermal parameters, H atom coordinates and isotropic thermal parameters, and observed and calculated structure factors have been deposited. These may be purchased from the Depository for Unpublished Data, CISTI, National Research Council of Canada, Ottawa, Ont., Canada K1A 0S2.



SCHEME 1. The nature of the disorder in compound **1***b*.

TABLE 2. Summary of crystal data and collection and refinement parameters

Formula	$Zr_2Si_2C_{35}H_{42}$
fw	701.39
Crystal system	Monoclinic
Space group	$P2_1/c$
a, Å	9.581(6)
b, Å	16.423(5)
c, Å	10.463(5)
β, deg	92.27(5)
V, Å^3	1.645(1)
Z	2
Crystal size, mm	0.1 × 0.2 × 0.4
μ (Mo Kα)	7.2
ρ_{calcd}, g/cm^3	1.42
T, °C	20
Radiation (graphite monochrometer)	Mo Kα (λ = 0.71069)
2θ limits, deg	3/50
Scan speed	Depending on reflection
No. of reflections collected	3157
No. of reflections used	1379
R	0.082
R_w	0.083

Before attempting to answer these questions, it is helpful to consider the results of an ^{1}H-NMR study of the reactions of several different silanes with DMZ.

The reactions of $PhSiH_3$, $PhMeSiH_2$, Ph_2SiH_2, and $BuMeSiH_2$ with DMZ

In Fig. 8, the ZrH resonances of the reaction products of several silanes with DMZ are shown. It is evident from these spectra that different silanes exhibit dramatically different reactivity towards DMZ. As noted previously, $PhSiH_3$ reacts rapidly and completely at room temperature to give **1***a* and a few other trace products containing bridging Zr—H bonds. The stoichiometry of this reaction is as shown in reaction [2]. Methane was detected by ^{1}H-NMR as CH_4 when the silane was $PhSiH_3$ and CH_3D when $PhSiD_3$ was used. In contrast to the reaction of DMT, only a trace amount of $PhMeSiH_2$ was produced in this reaction. Also, at the time of complete conversion of the DMZ to **1***a*,

[2] $2Cp_2ZrMe_2 + 2PhSiH_3 \rightarrow Cp_2Zr(SiH_2Ph)(\mu\text{-}H)_2(PhMeSiH)ZrCp_2 + CH_4$

2*a*

Can. J. Chem. Downloaded from www.nrcresearchpress.com by 195.138.81.100 on 09/07/12
For personal use only.

Can. J. Chem. Downloaded from www.nrcresearchpress.com by 195.138.81.100 on 09/07/12
For personal use only.

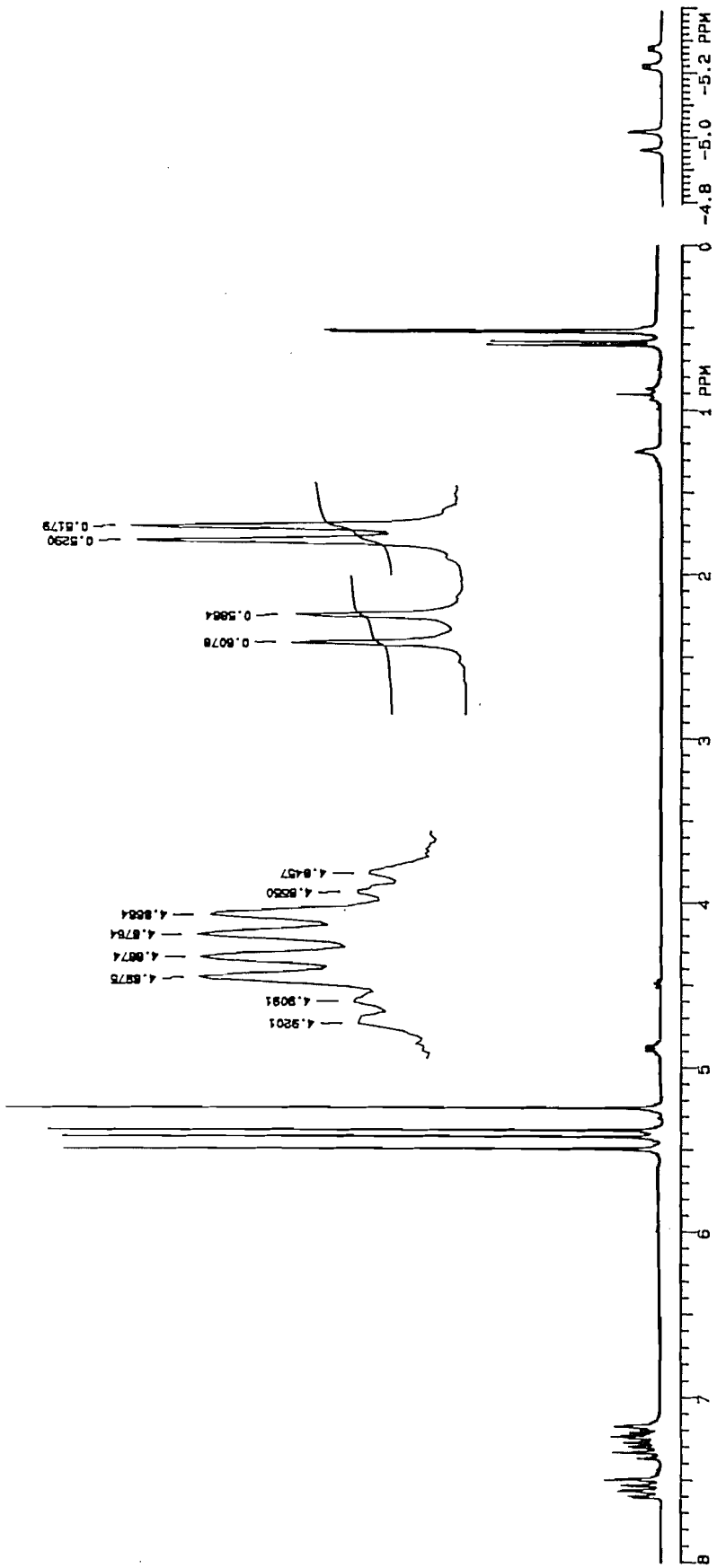


FIG. 5. ^{1}H-NMR spectrum of **1***b* in C_6D_6.

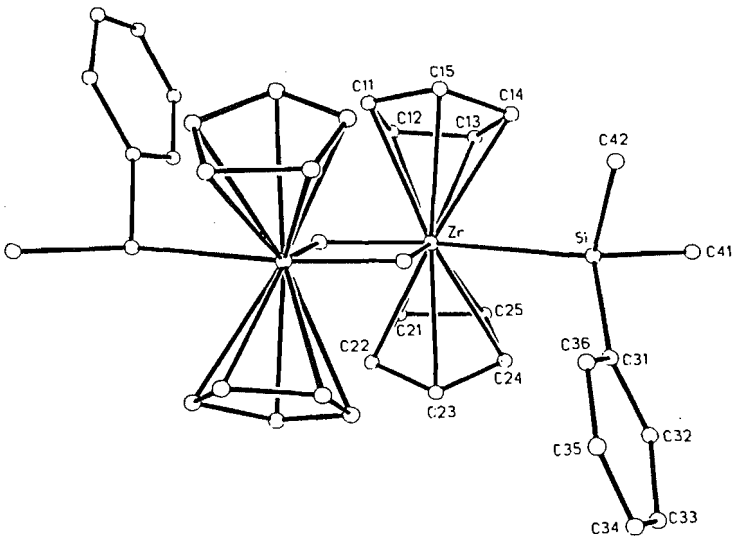


FIG. 6. Ball and stick drawing of the structure of **1***b*, showing atom numbering scheme.

TABLE 3. Atomic coordinates ($\times 10^4$) and isotropic thermal parameters ($\times 2000$) for compound **1***b*

Atom	*x*	*y*	*z*	U^a
Zr	4735(1)	9224(1)	1105(1)	46(1)
Si	7538(4)	9116(2)	1973(4)	59(1)
C11	4045(18)	8393(7)	−838(13)	68(6)
C12	3305(18)	8072(8)	174(14)	73(6)
C13	4217(19)	7715(9)	1040(15)	91(7)
C14	5556(17)	7818(7)	602(12)	77(5)
C15	5425(20)	8232(7)	−621(14)	69(5)
C21	2697(17)	9308(14)	2542(15)	97(8)
C22	3095(19)	10097(10)	2326(15)	83(7)
C23	4344(18)	10237(8)	2890(13)	73(6)
C24	4759(20)	9537(14)	3452(14)	91(8)
C25	3810(17)	8943(11)	3274(13)	72(6)
C31	8349(15)	10113(9)	2574(15)	72(5)
C32	8370(17)	10369(11)	3847(17)	89(7)
C33	8957(24)	11115(14)	4207(19)	122(9)
C34	9578(18)	11594(11)	3359(24)	102(9)
C35	9593(18)	11358(11)	2131(22)	98(8)
C36	9054(14)	10650(8)	1712(15)	66(5)
C41	7961(19)	8337(11)	3253(16)	96(7)
C42	8667(23)	8768(17)	716(22)	55(9)
Ha	5880(107)	9978(65)	157(105)	74(38)

[a]Equivalent isotropic *U* defined as one third of the trace of the orthogonalised U_{ij} tensor.

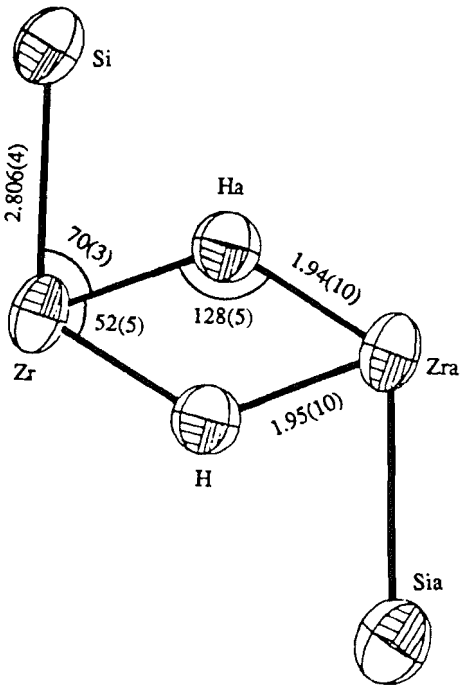


FIG. 7. ORTEP diagram of the $[SiZrH]_2$ fragment of **1***b*.

in contrast to the secondary silanes described below, no hydride signal was evident at −12 ppm.

The reactions of $PhMeSiH_2$ and Ph_2SiH_2 are much slower than that of $PhSiH_3$, requiring 1 to 2 days to go to completion under the same conditions that lead to complete reaction of $PhSiH_3$ in ca. 1–2 h. In the case of $PhMeSiH_2$, the major product is still the unsymmetrical silyl, **1***b*, but this product now only accounts for about 55% of the total observable Zr—H species. The NMR spectrum of the $PhMeSiH_2$ reaction products is more complicated than that of the $PhSiH_3$ products and that of the Ph_2SiH_2 is more complicated still. In the last case, the unsymmetrical silyl complex, **1***c*, only accounts for ca. 10% of the total observable Zr—H species and the major products are the mixed methyl/silyl dimers **1***d* and **1***e*, which are produced in comparable amounts. **1***d* was isolated as a pure product from the reaction of diphenylsilane with DMZ and its structure is assigned on the basis of its NMR spectrum, shown in Fig. 9.

A further feature of the spectra of the secondary silane products is the appearance of a hydride resonance in the region of −12 ppm. This resonance is at unusually high field for a Zr—H resonance and is almost certainly due to a diamagnetic zirconocene(III) species; most likely a zirconium analogue of the previously reported titanocene(III)silyl dimer (15). Unfortunately, these products have thus far resisted our attempts at isolation and characterization in the pure state.

n-Butylmethylsilane is much less reactive than phenylmethyl- or diphenylsilane and it requires heating to achieve reasonable reaction rates. However, the reaction products are very simple. The unresolved multiplet at −5.70 ppm is due to a

Can. J. Chem. Downloaded from www.nrcresearchpress.com by 195.138.81.100 on 09/07/12
For personal use only.

Can. J. Chem. Downloaded from www.nrcresearchpress.com by 195.138.81.100 on 09/07/12
For personal use only.

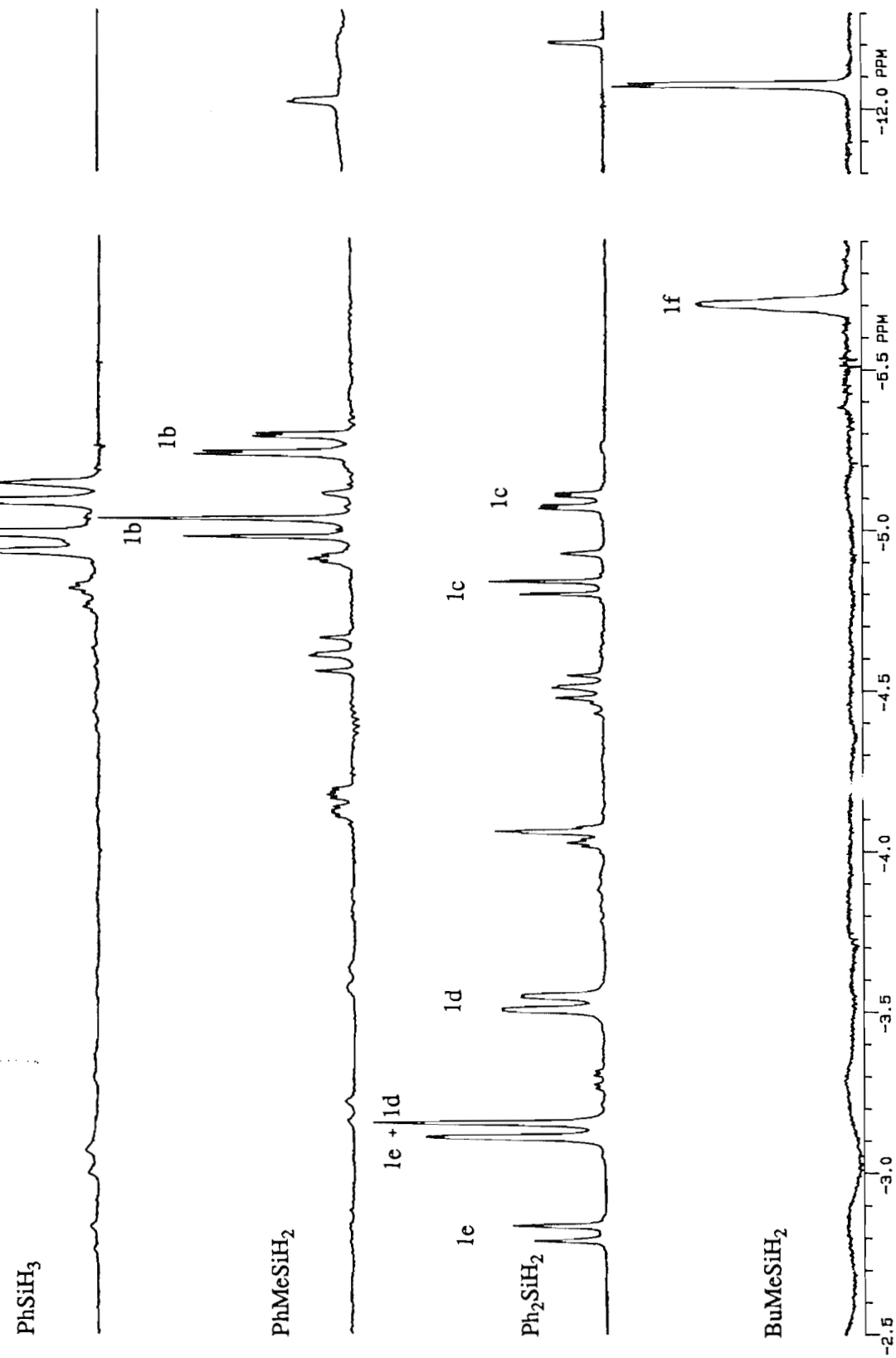


FIG. 8. ZrH region NMR spectra of the reaction products of $PhSiH_3$, $PhMeSiH_2$, Ph_2SiH_2, and $BuMeSiH_2$.

Can. J. Chem. Downloaded from www.nrcresearchpress.com by 195.138.81.100 on 09/07/12
For personal use only.

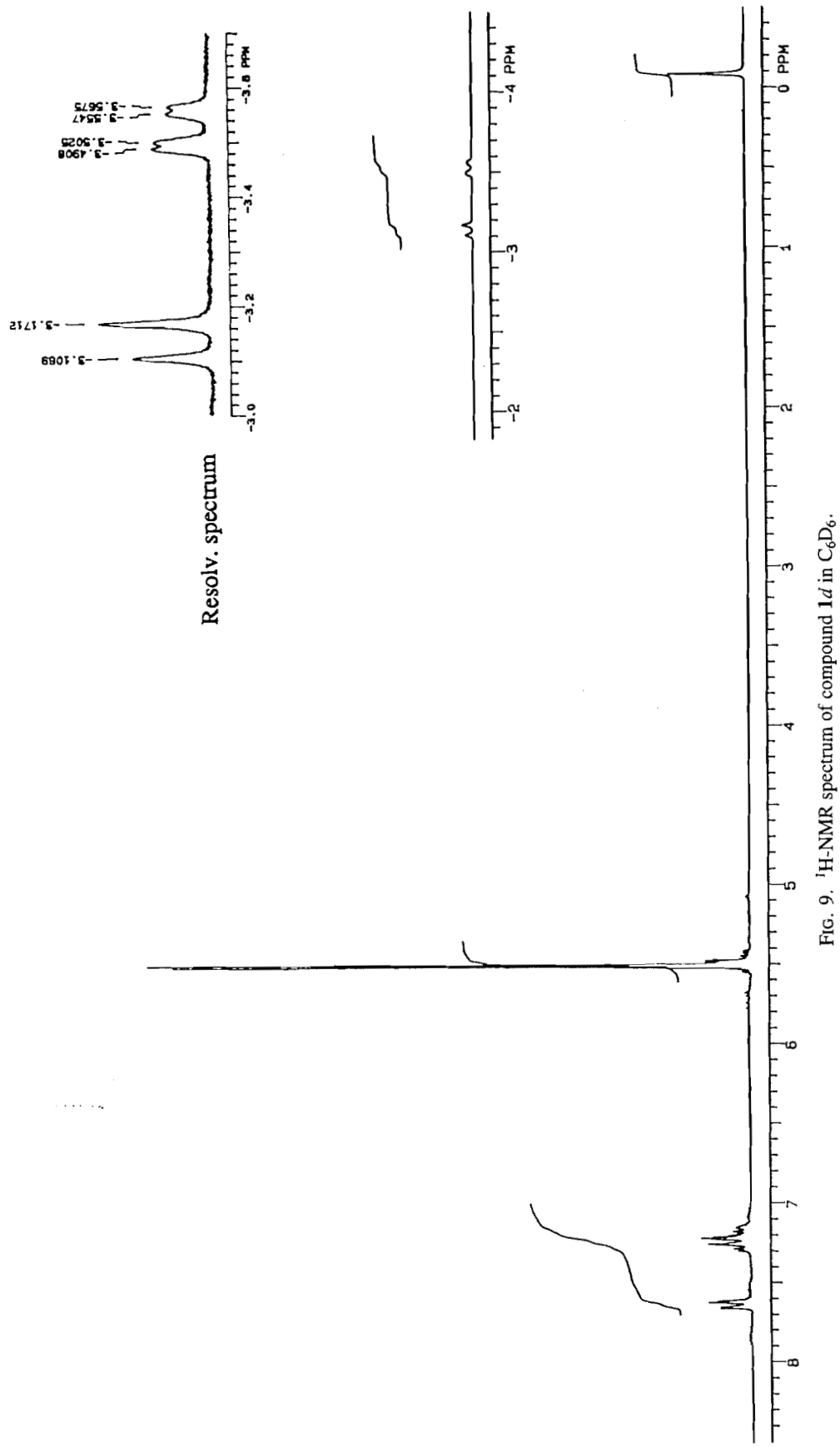


FIG. 9. ^{1}H-NMR spectrum of compound **1***d* in C_6D_6.

Can. J. Chem. Downloaded from www.nrcresearchpress.com by 195.138.81.100 on 09/07/12
For personal use only.

symmetrical hydride-bridged dimer, the most likely candidate being **1***f*. The second resonance, at −12 ppm, is assigned tentatively to the symmetrical zirconocene(III)silyl dimer.

The above results, insofar as they concern phenyl-, phenylmethyl-, and diphenylsilane, show a consistent pattern which suggests that in these cases there is an initial production of $Cp_2Zr(SiRR'H)Me$ (**2***a*) by reaction [3]. There is precedent for

[3] $Cp_2ZrMe_2 + RR'SiH_2 \rightarrow Cp_2Zr(SiRR'H)Me + CH_4$

2*a*

this type of complex, produced by an alternative synthetic route (9). Production of the various hydride species must then be accounted for by reactions which do not produce free RR'MeSiH. The latter constraint precludes formation of $Cp_2Zr(H)Me$, **2***b*, by a metathesis in the reverse sense to [3]. A more likely route to **2***b* is a metathesis between **2***a* and silane as shown in [4], since it is known that compounds of this type react with hydrogen more rapidly via the Zr—Si bond than the Zr—C bond (9).

[4] $Cp_2Zr(SiRR'H)Me + RR'SiH_2 \rightarrow Cp_2Zr(H)Me + HSiRR'SiRR'H$

2*b*

A similar constraint applies to the formation of methylated silyl ligands. The low reactivity of secondary relative to primary, and tertiary relative to secondary silanes, excludes any process which involves formation and subsequent rapid reaction of the free methylated silane. The most likely candidate for the methylation step is a σ-bond metathesis between a ZrMe and a ZrSiRR'H species (reaction [5]). Such reactions can account

[5] $ZrMe + ZrSiRR'H \rightarrow ZrH + ZrSiRR'Me$

for the formation of all the observed hydride and methylsilyl species in the dimers **1** in simple one-step reactions. In the context of [5], one of the main roles of the metal is the activation of the α-Si—H bond of the silyl ligand towards σ-bond metathesis. For such a reaction to be thermodynamically possible, the greater strength of the Zr—H bond, relative to Zr—C bond, must outweigh the loss of stability of the Zr—Si bond resulting from increased steric encumbrance about the silicon (5, 7). This condition is surely satisfied given the generally greater stability of M—H as opposed to M—C bonds.

From the above arguments we conclude that the formation of the unsymmetrical dimers **1***a* and **1***b* is due to the prevalence of reactions [4] and [5] in the early stages of the reaction, during which DMZ is abundant. After the DMZ is exhausted, conversions of **2***a* and **2***b* to the silyl hydride species can occur by analogues of [3] and [5]. In the case of diphenylsilane, conversion of **2***b* to silyl hydride is apparently too slow and dimerization of **2***b* with silylhydrides predominates to give species **1***d* and **1***e*.

Extension of [5] to the propagation reactions suggests [6] and [7] as likely processes. In particular, [7] provides a rationalisation

[6] $ZrSiRR'H + ZrSiRR'H \rightarrow ZrH + ZrSiRR'SiRR'H$

[7] $ZrSiRHSiRH_2 + ZrSiRHSiRH_2 \rightarrow ZrSiRH_2 + ZrSiRHSiRHSiRH_2$

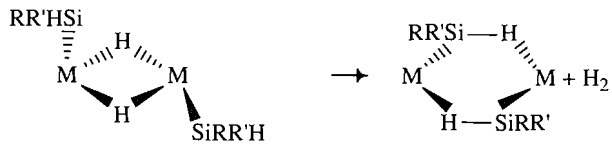
for the redistribution of 1,2-disubstituted disilanes. A precedent for [6] has been reported by Woo and Tilley (6).

The hydrogen evolving step, required to close the dehydrocoupling cycle, presents some problems in terms of simple σ-bond metathesis. It is not clear whether or not the reaction shown in [8] is thermodynamically allowed. We have recently

[8] $M—H + Si—H \rightarrow M—Si + H_2$

calculated the Ti—H and Ti—Si bond energies for the compound $Cp_2Ti(H)(SiH_3)$, **3**, to be ca. 60 and 30 kcal/mol, respectively (25). Assuming a typical Si—H bond energy to be ca. 90 kcal/mol (21, 24) and the bond energy for H_2 to be 104 kcal/mol, the reaction of **3** with a silane in the sense of [8] would be endothermic by ca. 15 kcal/mol. This appears to be far too high to account for the observed reactivities. In addition, the extremely facile reaction of the Zr—Si bond with H_2 in the reverse sense of [8] (9) supports the contra-thermodynamic character of [8]. On the other hand, Woo and Tilley have observed the direct reactions of zirconocene hydrides with silanes, with evolution of hydrogen, in what appears to be a simple bimolecular reaction (6). It is very possible that these seeming contradictions arise from fairly large differences in the thermodynamics, depending on the degree of substitution of the silyl group. It is well established that both silyl metathesis (5) and catalytic dehydrocoupling (3, 4) have rates that vary greatly with the substitution at silicon.

An interesting speculation is that the hydrogen evolution reaction may occur via dimeric species, such as **1**. In a pathway of this type, shown in [9], the energy sacrificed in the cleavage

[9] 

4

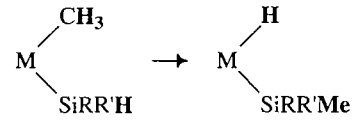
of the M—H bond can be compensated by the formation of a M—H—Si bridge and by the additional strength of a M—Si bond which involves d_π—p_π bonding to the d^1 metal centre. Species such as **4** are well established in titanium chemistry (15) and there is a strong possibility that the high field resonances in the spectra shown in Fig. 8 are due to species of the type **4**.

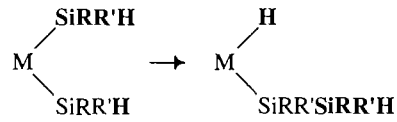
We are continuing our studies of the chemistry of the compounds **1** in an effort to obtain evidence in support of this speculation.

Conclusions

The sum of the observations reported above lead us to two primary conclusions. Firstly, the mechanisms of Si—H activation by the DMT and DMZ catalyst systems are very closely related, since both catalysts give essentially the same kinds of polymer and the molecular weights and molecular weight distributions of the polymers vary in the same way with varying reaction conditions. Secondly, all of the experimental observations can be accommodated within the context of the σ-bond metathesis mechanism proposed by Woo and Tilley (5, 6). These conclusions require the assumption that the obligatory titanium(IV) species be readily available by some kind of rapid equilibrium process such as that previously suggested to explain kinetic results (17), since no titanium(IV) intermediates have been detected in titanocene based reactions, subsequent to the initial reduction of the DMT.

Despite our present preference for the M(IV) σ-bond metathesis mechanism, we still believe that these systems are too poorly understood to prematurely discard several other plausible mechanisms. Among these are the intermediacy of silylene complexes (4, 19), σ-bond metathesis involving M(III) as opposed to M(IV) complexes, intramolecular σ-bond metathesis, as exemplified in reactions [10] and [11], and ligand transfer processes between M(III) and M(IV) species.

[10] 

[11] 

Experimental

The general experimental techniques for purifying solvents, synthesis of reactants and catalysts, and carrying out reactions are the same as described in earlier publications (2, 15, 16). 1,2-Diphenyldisilane was synthesised using the vanadocene catalyzed dimerization of phenylsilane (2).

Polymer characterization

Details of the various experimental methods of polymer characterization have been published elsewhere (16).

Reaction of primary and secondary silanes with DMZ

All these reactions were followed by ^{1}H-NMR. The standard conditions for stoichiometric reactions of DMZ with different silanes were DMZ (5 mg) dissolved in a mixture of degassed benzene-d_6 (0.5 mL) and the appropriate silane (0.06 mmol). Reaction mixtures were sealed in NMR tubes, placed in the temperature controlled cavity of a 200 or 300 MHz FT-NMR spectrometer, and the concentrations of the various species with the passage of time were estimated by integration of ^{1}H spectra. The concentrations of monomer, dimer, and trimer in catalytic oligomerization reactions of phenyl- and diphenylsilanes can usually be followed easily due to the simplicity and sharpness of the spectra and the good separation of the resonances (2). In the case of methylphenylsilane, the dimer and the trimer have more complicated spectra due to the presence of geometric isomers and due to the coupling between the Si—H and C—H protons. The ^{1}H-NMR spectra of these species are as follows: dimer: ∂_{Si-H} = 4.625 (q) and 4.638 (q); ∂_{C-H} = 0.337 (d) and 0.347 (d). Trimer: ∂_{Si-H} = 4.711 (q), 4.718 (q), 4.726 (q), and 4.734 (q); ∂_{C-H} (ter) = 0.343 (d), 0.347 (d), 0.378 (d) and 0.381 (d); ∂_{C-H} (mid) = 0.417 (s), 0.427 (s) and 0.446 (s). From these data it is evident that the dimer and trimer can be monitored by integration of their Si—H resonances.

The oligomerization/redistribution of diphenyldisilane was carried out in a Schlenk tube. DMZ (20 mg, 0.155 mmol)) was rapidly dissolved in a mixture of benzene-d_6 (2 mL), diphenyldisilane (1.0 mL), and cyclohexane (0.10 mL for calibration). Gas evolution commenced immediately and the colour of the solution slowly turned to orange. The reaction mixture was periodically sampled and analyzed by ^{1}H-NMR.

The oligomerization of phenylmethylsilane was studied using neat phenylmethylsilane. The reaction mixture was prepared in a Schlenk tube and placed in a constant temperature oil bath. The progress of the reaction was monitored by periodic sampling and analysis by ^{1}H-NMR.

Synthesis of compounds **1**a, **1**b, *and* **1**d

These three compounds were prepared by the same method. DMZ (200 mg, 0.80 mmol) was dissolved in degassed benzene (**1***a*) or *n*-hexane (**1***b*,*d*) (4.0 mL) containing the silane (2.4 mmol). The solution slowly changed from colourless to orange with a slow gas evolution and the formation of orange crystals over a period of several hours. The crystals were filtered, washed several times with *n*-hexane and dried under vacuum. Yields: **1***a*, 155 mg, 58%; **1***b*, 119 mg, 44%; **1***d*, 54 mg, 21%. **1***a* and **1***b* were obtained as well-formed crystals, **1***d* as a microcrystalline powder.

The crystal structure of compound **1**b

A crystal of dimensions 0.1 × 0.2 × 0.4 mm was sealed in a thin-walled capillary. Diffraction measurements were carried out on a Nicolet R3M/E diffractometer.[3] Computations were performed using the SHELXTL system[4] adapted to an Eclipse S/140 computer. Crystal data and collection parameters are listed in Table 2. The space group $P2_1/c$ was established by systematic absences in the complete data set ($0k0$, $k = 2n + 1$ and $h0l$, $l = 2n + 1$). The intensity data were corrected for absorption and Lorentz-polarization effects. The positions of the independent zirconium and silicon atoms were deduced from the *E*-map. The positions of all other independent non-hydrogen atoms were determined from difference Fourier synthesis and the dimeric structure of the compound was confirmed at this point. After a refinement of the positional and thermal parameters of the non-hydrogen atoms by least squares, all of the hydrogen atoms were calculated from difference Fourier synthesis and refined with isotropic thermal parameters. The largest peak corresponded to the bridging hydrides. Finally, all non-hydrogen atoms were refined by full-matrix least-squares with anisotropic thermal parameters. All atoms other than silicon and zirconium were severely distorted and the electron density for C_{42} showed 1/2 occupancy at the two sites of the dimer, indicating that the crystal contains a pair of enantiomers of **1***b* and the disorder problem results from the ordered superposition of the two enantiomers. The final atomic coordinates are listed in the supplementary material. The final least squares refinement converged with the residuals shown in Table 2.

Acknowledgements

Financial support of this work by the Natural Sciences and Engineering Research Council of Canada and the Fonds FCAR de Québec is gratefully acknowledged.

1. C. A. AITKEN, E. SAMUEL, and J. F. HARROD. Can. J. Chem. **64**, 1677 (1986).
2. C. A. AITKEN, J.-P. BARRY, F. GAUVIN, J. F. HARROD, A. MALEK, and D. ROUSSEAU. Organometallics, **8**, 1732 (1989).
3. J. F. HARROD. Inorganic and organometallic polymers. *Edited by* M. Zeldin, K. Wynne, and H. R. Allcock. Am. Chem. Soc. Symp. Ser. 360; Am. Chem. Soc. Washington, DC. 1988. Chap. 7.
4. J. F. HARROD. Transformation of organometallics into common and exotic materials: design and activation. *Edited by* R. M. Laine. NATO ASI Ser. E; Appl. Sci. No. 141; Martinus Nijhoff, Amsterdam. 1988. p. 103.
5. T. D. TILLEY. Comments Inorg. Chem. **10**, 37 (1990).
6. H.-S. WOO and T. D. TILLEY. J. Am. Chem. Soc. **111**, 8043 (1989).
7. H.-G. WOO and T. D. TILLEY. J. Am. Chem. Soc. **111**, 3757 (1989).
8. T. D. TILLEY. Organometallics, **4**, 1452 (1985).
9. D. M. RODDICK, R. H. HEYN, and T. D. TILLEY. Organometallics, **8**, 324 (1989).
10. J. Y. COREY, L. S. CHANG, and E. R. COREY. Organometallics, **6**, 1596 (1987).
11. L. S. CHANG and J. Y. COREY. Organometallics, **8**, 1885 (1989).
12. J. Y. COREY, X.-H. ZHU, and T. C. BEDARD. XXIII Organosilicon Symposium, Midland, MI. April 20–21, 1990. Abstr. D1.
13. W. H. CAMPBELL, T. K. HILTY, and L. YURGA. Organometallics, **8**, 2615 (1989).
14. C. A. AITKEN, J. F. HARROD, and E. SAMUEL. J. Organomet. Chem. **279**, C11 (1985).
15. C. A. AITKEN, J. F. HARROD, and E. SAMUEL. J. Am. Chem. Soc. **108**, 4059 (1986).
16. C. A. AITKEN, J. F. HARROD, and U. S. GILL. Can. J. Chem. **65**, 1804 (1987).
17. J. F. HARROD and S. S. YUN. Organometallics, **6**, 1381 (1987).

[3]The crystal structure was purchased from Dr. Zhongsheng Jin of Laboratory 26, Changchun Institute of Applied Chemistry, Academia Sinica, Changchun, PRC.

[4]Sheldrick, G. M. SHELXTL, an integrated system for solving, refining and displaying crystal structures from diffraction data, Revision 5; University of Gottingen, Federal Republic of Germany.

Can. J. Chem. Downloaded from www.nrcresearchpress.com by 195.138.81.100 on 09/07/12
For personal use only.

18. E. SAMUEL, Y. MU, J. F. HARROD, Y. DROMZEE, and Y. JEANNIN. J. Am. Chem. Soc. **112**, 3435 (1990).
19. K. BROWN-WENSLEY. Organometallics, **6**, 1590 (1987).
20. I. OJIMA, S. INABA, T. KOGURA, and Y. NAGAI. J. Organomet. Chem. **55**, C7 (1973).
21. J. M. KANABUS-KAMINSKA, J. A. HAWARI, D. GRILLER, and C. CHATGILIALOGLU. J. Am. Chem. Soc. **109**, 5267 (1987).
22. S. B. JONES and J. PETERSEN. Inorg. Chem. **20**, 2889 (1981).
23. K. W. MUIR. J. Chem. Soc. A, 2663 (1971).
24. R. WALSH. Accts. Chem. Res. **14**, 246 (1981).
25. J. F. HARROD, T. ZIEGLER, and V. TSCHINKE. Organometallics, **9**, 897 (1990).

Can. J. Chem. Downloaded from www.nrcresearchpress.com by 195.138.81.100 on 09/07/12
For personal use only.

Synthesis, structure, and magnetic properties of diphenylphosphinates of cobalt(II) and manganese(II). The crystal and molecular structures of the γ forms of poly-bis(μ-diphenylphosphinato)cobalt(II) and manganese(II)

JING-LONG DU, STEVEN J. RETTIG, ROBERT C. THOMPSON,[1] AND JAMES TROTTER
Department of Chemistry, University of British Columbia, 2036 Main Mall, Vancouver, B.C., Canada V6T 1Y6

Received August 8, 1990

JING-LONG DU, STEVEN J. RETTIG, ROBERT C. THOMPSON, and JAMES TROTTER. Can. J. Chem. **69**, 277 (1991).

The synthesis of the β and γ forms of $M(Ph_2PO_2)_2$ where M = Co and Mn are described and the compounds are characterized by infrared spectroscopy, differential scanning calorimetry, X-ray powder diffraction, and low-temperature (2–80 K) magnetic susceptibility studies. Single crystal X-ray diffraction studies are reported on the γ forms. Crystals of the γ forms of poly-bis(μ-diphenylphosphinato)cobalt(II) and poly-bis(μ-diphenylphosphinato)manganese(II) are isomorphous, crystallizing with 4 formula units per unit-cell in the monoclinic space group $P2_1/c$. Lattice constants are a = 8.080(2), 8.161(1), b = 23.550(6), 23.751(1), c = 11.726(3), 11.6946(6) Å, and β = 92.88(2), 93.026(8)° for the Co and Mn derivatives respectively. The structures were solved by heavy atom methods and were refined by full-matrix least-squares procedures to R = 0.039 and 0.045 for 4041 and 2878 reflections with $I \geq 3\sigma(I)$, respectively. Both crystal structures consist of double phosphinate-bridged chain polymers containing tetrahedrally coordinated metal atoms: Co—O = 1.950(2)–1.963(2) Å, O—Co—O = 104.81(8)–117.77(9)°, Mn—O = 2.016(3)–2.033(3) Å, O—Mn—O = 103.2(1)–114.7(1)°. All four compounds exhibit antiferromagnetic coupling and magnetic susceptibilities have been analyzed according to two Heisenberg models for linear chains of metal ions with S = 3/2 for cobalt and S = 5/2 for manganese. The Weng model (with values for the Wagner and Friedberg model in parentheses) gives $-J$ = 0.25 (0.26) cm^{-1} and 0.55 (0.60) cm^{-1} for the β and γ forms, respectively, of $Co(Ph_2PO_2)_2$, and 0.34 (0.36) cm^{-1} and 0.17 (0.17) cm^{-1} for the β and γ forms, respectively, of $Mn(Ph_2PO_2)_2$.

Key words: crystal structure, diphenylphosphinates of cobalt(II) and manganese(II), magnetic properties.

JING-LONG DU, STEVEN J. RETTIG, ROBERT C. THOMPSON et JAMES TROTTER. Can. J. Chem. **69**, 277 (1991).

On décrit la synthèse des formes β et γ des $M(Ph_2PO_2)_2$ dans lesquels M = Co et Mn et on a caractérisé les composés par spectroscopie infrarouge, par calorimétrie à balayage différentiel, par diffraction des rayons-x par des poudres et par des études de susceptibilité magnétique à basse température (2–80 K). On rapporte des études de diffraction des rayons-X effectuées sur des cristaux uniques des formes γ. Les cristaux des formes γ du poly-bis(μ-diphénylphosphinato)cobalt(II) et du poly-bis(μ-diphénylphosphinato)manganèse(II) sont isomorphes et ils cristallisent, avec 4 unités de formule par maille, dans le groupe d'espace monoclinique $P2_1/c$, avec a = 8,080(2) et 8,161(1), b = 23,550(6) et 23,751(1) et c = 11,726(3) et 11,6946(6) Å et β = 92,88(2) et 93,026(8)° respectivement pour les dérivés du Co et du Mn. On a résolu les structures par les méthodes aux atomes lourds et on les a affinées par la méthode des moindres carrés jusqu'à des valeurs respectives de R = 0,039 et 0,045 pour 4041 et 2827 réflexions avec $I \geq 3\sigma(I)$. Les deux structures comportent des doubles chaînes de polymères, liées par des groupements phosphinates, qui contiennent des atomes métalliques coordonnés d'une façon tétraédrique: Co—O = 1,950(2)–1,963(2) Å; O—Co—O = 104,81(8)–117,77(9)°; Mn—O = 2,016(3)–2,033(3) Å; O—Mn—O = 103,2(1)–114,7(1)°. Les quatre composés présentent un couplage antiferromagnétique et on a analysé les susceptibilités magnétiques suivant deux modèles de Heisenberg pour des chaînes linéaires d'ions métalliques avec S = 3/2 pour le cobalt et S = 5/2 pour le manganèse. Le modèle de Weng (avec les valeurs pour le modèle de Wagner et de Friedberg entre parenthèses) conduit à des valeurs respectives de $-J$ = 0,25 (0,26) cm^{-1} et 0,55 (0,60) cm^{-1} pour les formes β et γ du $CO(Ph_2PO_2)_2$, respectivement, et 0.34 (0.36) cm^{-1} et 0.17 (0.17) cm^{-1} pour les formes β et γ, respectivement du $Mn(Ph_2PO_2)_2$.

Mots clés : structure cristalline, diphénylphosphinates du cobalt(II) et du manganèse(II), propriétés magnétiques.

[Traduit par la rédaction]

Introduction

Coates and Golightly first described the preparation of cobalt(II) diphenylphosphinate, $Co(Ph_2PO_2)_2$, and on the basis of its solubility properties and color they suggested a polymeric structure with tetrahedrally coordinated cobalt(II) ions linked in chains by double phosphinate bridges (1). Rose and Block later reported studies on the compound prepared by a different route. This work, which included X-ray powder diffraction and thermogravimetric analysis supported the original proposed structure and, moreover, showed the compound to be isomorphous with the β crystalline modification of zinc(II) diphenylphosphinate (2). Although a second, γ, modification of the zinc compound has been reported (3), no evidence for the γ modification of $Co(Ph_2PO_2)_2$ was found in this earlier work. We report here the synthesis of two forms of both $Co(Ph_2PO_2)_2$ and $Mn(Ph_2PO_2)_2$ which on the basis of X-ray powder diffraction studies appear to be isomorphous with the β and γ forms of $Zn(Ph_2PO_2)_2$. Sufficiently large crystals of the γ forms of both compounds were obtained to permit single crystal X-ray diffraction studies. These reveal tetrahedral metal centres linked by double phosphinate bridges as proposed in the early studies (1). The β forms were obtained only as microcrystalline powders and hence their detailed structures remain uncertain.

Our interest in binary metal phosphinates stems from the fact that such compounds often provide interesting examples of low-dimensional magnetic exchange. For example, copper(II) diphenylphosphinate, a polymeric chain compound in which square planar metal ions are linked by double phosphinate bridges (4) exhibits weak ferromagnetism (5). In the present work, low temperature magnetic susceptibility studies reveal weak antiferromagnetism in all of the materials studied.

Experimental

Preparations

Poly-bis(μ-diphenylphosphinato)cobalt(II), $Co[(C_6H_5)_2PO_2]_2$ (γ form)
Cobalt(II) chloride hexahydrate (1.19 g, 5.00 mmol) was dissolved

[1]To whom correspondence should be addressed.

Can. J. Chem. Downloaded from www.nrcresearchpress.com by 195.138.81.100 on 09/07/12
For personal use only.

Can. J. Chem. Downloaded from www.nrcresearchpress.com by 195.138.81.100 on 09/07/12
For personal use only.

in 30 mL of dimethylformamide and this solution was mixed with a solution containing 2.18 g (10 mmol) of diphenylphosphinic acid and ~1.2 mL of triethylamine dissolved in 50 mL of dimethylformamide. A clear solution was obtained; on standing over 3 months, blue needle-like crystals formed. The crystals were collected by filtration, washed with acetone, and air-dried. *Anal.* calcd. for $CoC_{24}H_{20}P_2O_4$: C 58.44, H 4.09; found: C 58.26, H 4.05.

$Co[(C_6H_5)_2PO_2]_2$ (β form)

Cobalt diphenylphosphinate was prepared according to the method of Coates and Golightly (1). Cobalt(II) chloride hexahydrate (2.67 g, 11.2 mmol) was dissolved in 50 mL of water, then added dropwise to a stirring solution of sodium diphenylphosphinate which was prepared by neutralizing diphenylphosphinic acid (5.27 g, 24.2 mmol) in 100 mL water with sodium hydroxide. Initially a red solution formed and as more of the metal salt solution was added a blue precipitate formed. After addition was complete the mixture was heated gently on a hot plate then filtered. The pink filtrate was heated at 60°C for 2 days during which time product in the form of a blue precipitate formed. This was collected by filtration, washed with warm water then air dried. *Anal.* found: C 58.45, H 4.07. The first precipitate obtained in this synthesis was redissolved in cold water and heating this solution for two days at 60°C yielded more analytically pure product.

Poly-bis(μ-diphenylphosphinato)manganese(II), $Mn[(C_6H_5)_2PO_2]_2$ (γ form)

Diphenylphosphinic acid (2.18 g, 10.0 mmol) was dissolved in 40 mL aqueous methanol (1:3 methanol:water, v/v) and neutralized with potassium carbonate. To this stirring solution was added dropwise, over about 30 min, manganese sulfate monohydrate (0.845 g, 5.00 mmol) in 35 mL of water. A precipitate in the form of a fine white microcrystalline powder formed and the mixture was stirred for an additional 45 min. The powder was then removed by filtration, washed with a 50:50 methanol:water mixture and then air-dried overnight. *Anal.* calcd. for $MnC_{24}H_{20}P_2O_4$: C 58.91, H 4.12; found: C 59.07, H 4.34.

Attempts to prepare a formamide adduct of $Mn[(C_6H_5)_2PO_2]_2$ led instead to the synthesis of the γ form of the binary phosphinate in a crystalline form suitable for single crystal X-ray diffraction studies. The neutralized acid and manganese(II) sulfate solutions were prepared as above. These were then mixed and 60 mL of formamide was added immediately before any precipitate formed. Over a period of 3 months pale-green crystals were collected, washed with water, and dried under vacuum at 60°C for 6 h. That these crystals are the same material as the microcrystalline powder sample described above was confirmed by a detailed comparison of the spectroscopic and other physical properties of the two samples as described later. All of the data (other than the single crystal X-ray data) reported in this experimental section for γ-$Mn[(C_6H_5)_2PO_2]_2$ were obtained on the microcrystalline powder sample.

$Mn[(C_6H_5)_2PO_2]_2$ (β form)

Diphenylphosphinic acid (2.19 g, 10.0 mmol) was dissolved in 70 mL of dimethylformamide and neutralized by the addition of 1.7 mL of triethylamine. To this stirring solution was added dropwise, over about 30 min, a solution of manganese(II) chloride tetrahydrate (1.00 g, 5.06 mmol) in 50 mL of dimethylformamide. A white precipitate formed and the mixture was left stirring overnight. The product was collected by filtration, washed well with acetone, and air-dried. *Anal.* found: C 58.8, H 4.25.

Infrared spectroscopy

Infrared spectra (4000 to 250 cm^{-1}) were recorded using a Perkin-Elmer Model 598 spectrophotometer. Samples were mulled in Nujol and pressed between KRS-5 plates (Harshaw Chemical Co.). Frequencies are considered accurate to within ± 3 cm^{-1}. Bands observed in the range of 1600 to 250 cm^{-1} are given (w = weak, m = medium, s = strong, sh = shoulder, v = very, numbers in parentheses refer to split bands):

γ-$Co(Ph_2PO_2)_2$: 1593 w, 1439 m, 1212 m, 1180 wsh, 1135 vs, 1069 wsh, 1049 vs, 1026 s, 1001 m, 760 wsh, 755 w, 723 s, 700 s, 696 wsh, 576 s, 546 s, 440 w, 420 w, 335 wsh, 324 w, 308 w.

β-$Co(Ph_2PO_2)_2$: 1593 w, 1438 m, 1210 w, 1138 vs, 1070 wsh, 1056 vs, 1025 s, 1001 m, 757 m, 731 s, 696 s, 575 s, 545 s, 470 w, 439 w, 408 w, 400 w.

γ-$Mn(Ph_2PO_2)_2$: 1595 w, 1443 m, 1211 m, 1183 w, (1143, 1150) vs, 1072 w, 1053 vs, 1026 s, 1002 m, (757, 761) w, 727 s, 701 s, 698 wsh, 578 wsh, 572 s, 549 s, 438 w, 415 w, 318 w, 310 w.

β-$Mn(Ph_2PO_2)_2$: 1593 w, 1440 m, 1310 w, 1210 w, 1185 wsh, (1152, 1140) vs, 1073 wsh, 1060 vs, 1028 s, 1002 m, 758 m, 733 s, 696 s, 570 s, 544 s, 466 w, 426 w, 403 w, 390 w.

Differential scanning calorimetry

Differential scanning calorimetry, DSC, measurements were made with a Mettler DSC 20 cell and a Mettler TC10 TA processor operating over the temperature range 35 to 400°C. The β and γ forms of $Co(Ph_2PO_2)_2$ exhibit single endothermic peaks at 366°C (ΔH = 23 J g^{-1}) and 368°C (ΔH = 18 J g^{-1}), respectively. The β form of $Mn(Ph_2PO_2)_2$ shows a single endotherm at 357°C (ΔH = 24 J g^{-1}) while the γ form of this compound exhibits three endothermic peaks at 213°C (ΔH = 29 J g^{-1}), 238°C (ΔH = 4 J g^{-1}), and 356°C (ΔH = 26 J g^{-1}).

X-ray powder diffractometry

X-ray powder diffraction patterns were recorded in the range 2θ = 5–60° using a Rigaku Rotaflex rotating anode X-ray powder diffractometer (Ni filtered Cu-K_α radiation). The powder patterns are depicted for the four compounds in Fig. 1.

Electronic spectroscopy

Electronic spectra of samples of the β and γ forms of $Co(Ph_2PO_2)_2$ mulled in Nujol and smeared on filter paper were obtained on a Shimadzu UV-2100 spectrometer and the spectra are shown in Fig. 2.

Magnetic susceptibility measurements

Magnetic susceptibilities were measured from 2 to 80 K using a PAR model 155 vibrating sample magnetometer, VSM, as described previously (6). Measurements were made at a field of 7501 G. The diamagnetic corrections used were -14, -12, and -127×10^{-6} cm^3 mol^{-1} for Mn^{2+}, Co^{2+}, and $(C_6H_5)_2PO_2^-$, respectively. The magnetic susceptibility values for the cobalt compounds were corrected for temperature independent paramagnetism using a value for TIP of 560×10^{-6} cm^3 mol^{-1} calculated as described below. Values of magnetic susceptibilities and magnetic moments are included as supplementary material.[2]

X-Ray crystallographic analyses of γ-$Co(Ph_2PO_2)_2$ and γ-$Mn(Ph_2PO_2)_2$

Crystallographic data for both compounds appear in Table 1. The final unit-cell parameters were obtained by least-squares on the setting angles for 25 reflections with 2θ = 20.1–30.4° for the cobalt and 66.8–84.8° for the manganese derivative. The intensities of three standard reflections, measured every 200 reflections throught the data collections, were essentially constant for both compounds. The data were processed[3] and corrected for Lorentz and polarization effects, and absorption (empirical, based on azimuthal scans for three reflections).

The structure of the Co complex was solved by heavy atom methods, the Co and P atoms being positioned from the Patterson function and the remaining non-hydrogen atoms from a subsequent difference Fourier synthesis. The refinement of the isomorphous Mn complex was initiated using the non-hydrogen atom positions from the γ-$Co(Ph_2PO_2)_2$ stucture (with the origin shifted by -0.5 along z). The non-hydrogen atoms were refined with anisotropic thermal parameters and hydrogen atoms were refined with isotropic thermal parameters for the Co

[2]Supplementary material mentioned in the text may be purchased from the Depository of Unpublished Data, Document Delivery, CISTI, National Research Council of Canada, Ottawa, Ont., Canada K1A 0S2.

[3]TEXSAN/TEXRAY structure analysis package, containing versions of the following: DIRDIF, direct methods for difference structures, by P. T. Beurskens; ORFLS, full-matrix least-squares, and ORFFE, function and errors, by W. R. Busing, K. O. Martin, and H. A. Levy; ORTEP II, illustrations, by C. K. Johnson.

Can. J. Chem. Downloaded from www.nrcresearchpress.com by 195.138.81.100 on 09/07/12
For personal use only.

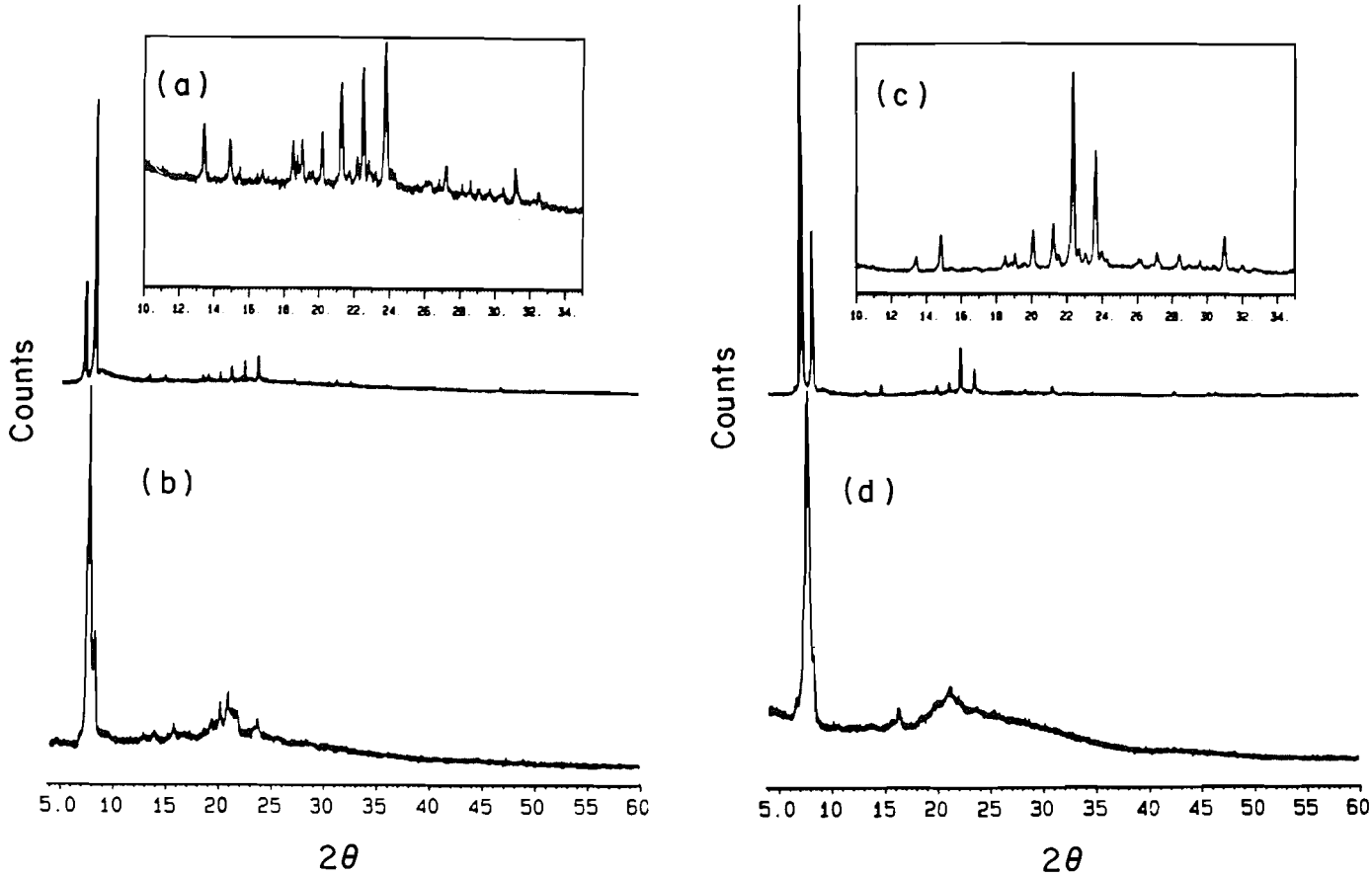


FIG. 1. X-Ray powder diffraction patterns for $M(Ph_2PO_2)_2$: (*a*) γ-Co, (*b*) β-Co, (*c*) γ-Mn, (*d*) β-Mn.

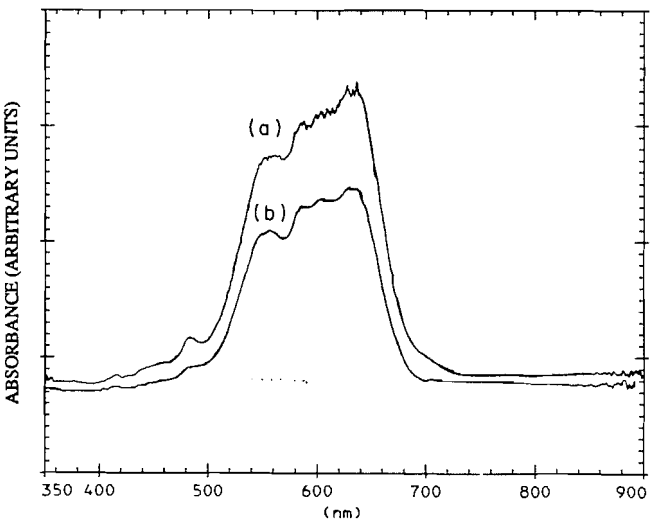


FIG. 2. Electronic spectra for $Co(Ph_2PO_2)_2$: (*a*) γ form, (*b*) β form.

complex and were fixed in idealized positions (C—H = 0.98 Å, $B_H = 1.2B_{\text{bonded atom}}$) for the Mn complex. Secondary extinction corrections were applied, the final values of the extinction coefficient being 1.08×10^{-7} for γ-$Co(Ph_2PO_2)_2$ and 3.63×10^{-6} for γ-$Mn(Ph_2PO_2)_2$. Neutral atom scattering factors and anomalous dispersion corrections for the non-hydrogen atoms were taken from the *International tables for X-ray crystallography* (7). Final atomic coordinates and equivalent isotropic thermal parameters are given in Table 2 and bond lengths and angles appear in Tables 3 and 4, respectively. Hydrogen atom parameters, anisotropic thermal parameters, bond lengths and angles involving hydrogen, general torsion angles, intermolecular distances, least-squares planes, and measured and calculated structure factor amplitudes for both structures are included as supplementary material.[2]

Results and discussion

Cobalt(II) diphenylphosphinate

Two crystalline modifications of $Co(Ph_2PO_2)_2$ were obtained which, based on their X-ray powder diffraction patterns (Fig. 1), appear to be isomorphous with the β and γ modifications of $Zn(Ph_2PO_2)_2$ (3, 8). The β form of the cobalt compound was reported previously by Rose and Block (2) who used a different synthetic route from that employed here, the latter being similar to that described by Coates and Golightly (1). The powder patterns we observed for our β samples showed broad line features at the higher θ values suggesting a lower degree of crystallinity than in the γ samples. The γ form of $Co(Ph_2PO_2)_2$ has not been reported previously; we obtained this in crystalline form suitable for a single crystal X-ray diffraction study.

The crystal structure of γ-$Co(Ph_2PO_2)_2$ consists of fused eight-membered rings, each ring consisting of two cobalt ions bridged by two phosphinate groups (Fig. 3). The coordination about each cobalt is approximately tetrahedral with O—Co—O bond angles ranging from 104.81(8) to 117.77(9)° (Fig. 4). This contrasts with the situation for the dialkylphosphinates of copper(II) where the CuO_4 chromophore is a compressed tetrahedron (O—Cu—O bond angles range from 92.74(5) to 149.85(6)° in the diethylphosphinate, for example) (6, 9) and for copper(II) diphenylphosphinate where the coordination

Can. J. Chem. Downloaded from www.nrcresearchpress.com by 195.138.81.100 on 09/07/12
For personal use only.

TABLE 1. Crystallographic data[a]

Compound	γ-$Co(Ph_2PO_2)_2$	γ-$Mn(Ph_2PO_2)_2$
Formula	$C_{24}H_{20}CoO_4P_2$	$C_{24}H_{20}MnO_4P_2$
fw	493.30	489.31
Color, habit	Blue, prism	Pale green, prism
Crystal system	Monoclinic	Monoclinic
Space group	$P2_1/c$	$P2_1/c$
a, Å	8.080(2)	8.161(1)
b, Å	23.550(6)	23.751(1)
c, Å	11.726(3)	11.6946(6)
β, deg	92.88(2)	93.026(8)
V, Å^3	2229(1)	2263.6(4)
Z	4	4
ρ_{calc}, g/cm^3	1.470	1.436
$F(000)$	1012	1004
Radiation	Mo	Cu
μ, cm^{-1}	9.36	63.63
Crystal size, mm	0.15 × 0.25 × 0.50	0.05 × 0.15 × 0.35
Transmission factors	0.83–1.00	0.59–1.00
Scan type	ω–2θ	ω–2θ
Scan range, deg in ω	1.21 + 0.35 tan θ	1.00 + 0.20 tan θ
Scan speed, deg/min	32.0	16.0
Data collected	$+h, +k, \pm l$	$+h, +k, \pm l$
$2\theta_{max}$, deg	65	155
Crystal decay	Negligible	Negligible
Total reflections	8745	5296
Total unique reflections	8260	4954
R_{merge}	0.051	0.068
No. of reflections with $I \geq 3\sigma(I)$	4041	2878
No. of variables	361	281
R	0.039	0.045
R_w	0.042	0.056
gof	1.42	1.45
Max Δ/σ (final cycle)	0.0007	0.007
Residual density e/Å^3	−0.30 to +0.39	−0.46 to +0.57

[a]Temperature 294 K, Rigaku AFC6S diffractometer, Mo-K_α radiation (λ = 0.71069 Å) or Cu-K_α (λ = 1.54178 Å), graphite monochromator, takeoff angle 6.0°, aperture 6.0 × 6.0 mm at a distance of 285 mm from the crystal, stationary background counts at each end of the scan (scan/background time ratio 2:1, up to eight rescans), $\sigma^2(F^2) = [S^2(C + 4B) + (pF^2)^2]/Lp^2$ (S = scan rate, C = scan count, B = normalized background count, $p = 0.03$ for the Co complex and 0.045 for the Mn complex). Function minimized: $\Sigma w(|F_o| - |F_c|)^2$ where $w = 4F_o^2/\sigma^2(F_o^2)$, $R = \Sigma||F_o| - |F_c||/\Sigma|F_o|$, $R_w = (\Sigma w(|F_o| - |F_c|)^2/\Sigma w|F_o|^2)^{1/2}$, and gof = $[\Sigma(|F_o| - |F_c|)^2/(m - n)]^{1/2}$. Values given for R, R_w, and gof are based on those reflections with $I \geq 3\sigma(I)$.

about the metal is square-planar (4). There is nothing remarkable about the internal phosphinate geometry in the cobalt compound with bond angles and distances being typical for metal phosphinate compounds. A unique feature of the present structure, however, involves the conformation of the Co—O—P—O—Co unit. Here, the two bridged metals are on opposite sides of the plane formed by the O—P—O atoms and, as a consequence, the eight-membered rings are linked in a folded or stepped fashion along the direction of the chain. The two crystallographically unique, centrosymmetric, eight-membered $(Co—O—P—O)_2$ rings have very similar conformations with cross ring Co···Co contacts of 4.329(1) and 4.363(1) Å. In the copper(II) diphenylphosphinate and dialkylphosphinate structures the bridged copper atoms are on the same side of the plane formed by the bridging O—P—O atoms and a more extended linear chain structure results. In copper(II) dihexylphosphinate, for example, the cross ring (Cu···Cu contacts are 4.9277(8) and 4.9310(8) Å (6). It is possible that β-$Co(Ph_2PO_2)_2$, for which we have no detailed structural information, has a chain structure more like that of the copper polmers.

TABLE 2. Final atomic coordinates (fractional) and B_{eq} (Å^2)[a]

Atom	x	y	z	B_{eq}
		[$Co(Ph_2PO_2)_2$]		
Co(1)	0.24621(4)	0.50596(1)	0.43267(3)	1.98(1)
P(1)	0.45808(8)	0.56285(3)	0.65155(6)	2.21(3)
P(2)	0.06473(8)	0.41352(3)	0.60026(6)	2.20(3)
O(1)	0.3750(2)	0.55690(8)	0.5339(2)	2.99(9)
O(2)	0.6041(2)	0.52429(8)	0.6793(1)	2.54(8)
O(3)	0.1477(2)	0.43902(8)	0.5001(2)	2.91(8)
O(4)	−0.0802(2)	0.44552(8)	0.6447(2)	2.87(8)
C(1)	0.5233(3)	0.6353(1)	0.6707(2)	2.5(1)
C(2)	0.4722(5)	0.6779(1)	0.5974(3)	4.6(2)
C(3)	0.5180(6)	0.7337(2)	0.6207(4)	6.1(2)
C(4)	0.6135(5)	0.7466(2)	0.7168(4)	5.1(2)
C(5)	0.6647(5)	0.7044(2)	0.7908(3)	4.4(2)
C(6)	0.6207(4)	0.6493(1)	0.7676(3)	3.5(1)
C(7)	0.3085(3)	0.5543(1)	0.7575(2)	2.5(1)
C(8)	0.1471(4)	0.5710(2)	0.7322(3)	5.0(2)
C(9)	0.0326(5)	0.5700(2)	0.8152(4)	6.8(3)
C(10)	0.0786(5)	0.5540(2)	0.9236(4)	5.4(2)
C(11)	0.2371(5)	0.5365(2)	0.9501(3)	4.3(2)
C(12)	0.3520(4)	0.5364(1)	0.8674(3)	3.2(1)
C(13)	−0.0019(3)	0.3425(1)	0.5625(2)	2.6(1)
C(14)	0.0573(4)	0.3147(1)	0.4693(3)	3.9(2)
C(15)	0.0089(6)	0.2589(2)	0.4456(4)	5.5(2)
C(16)	−0.0938(6)	0.2315(2)	0.5150(5)	5.6(2)
C(17)	−0.1534(5)	0.2582(2)	0.6080(4)	5.2(2)
C(18)	−0.1082(5)	0.3136(2)	0.6304(3)	4.0(2)
C(19)	0.2154(3)	0.4038(1)	0.7167(2)	2.4(1)
C(20)	0.3838(4)	0.4052(1)	0.6993(3)	3.1(1)
C(21)	0.4963(4)	0.3959(1)	0.7910(4)	4.0(2)
C(22)	0.4434(5)	0.3844(1)	0.8973(3)	4.2(2)
C(23)	0.2769(5)	0.3825(2)	0.9151(3)	4.1(2)
C(24)	0.1624(4)	0.3928(1)	0.8262(3)	3.2(1)
		[$Mn(Ph_2PO_2)_2$]		
Mn(1)	0.24352(8)	0.50589(2)	−0.07301(5)	2.51(2)
P(1)	0.4548(1)	0.56443(4)	0.15479(9)	2.75(4)
P(2)	0.0671(1)	0.41106(4)	0.10261(9)	2.73(4)
O(1)	0.3751(4)	0.5571(1)	0.0365(3)	3.6(1)
O(2)	0.6003(3)	0.5270(1)	0.1852(2)	3.1(1)
O(3)	0.1429(4)	0.4379(1)	0.0015(3)	3.7(1)
O(4)	−0.0778(4)	0.4415(1)	0.1495(3)	3.5(1)
C(1)	0.5174(5)	0.6364(2)	0.1729(4)	3.1(2)
C(2)	0.4623(7)	0.6786(2)	0.0989(5)	5.4(3)
C(3)	0.507(1)	0.7338(2)	0.1222(6)	7.1(4)
C(4)	0.6047(8)	0.7473(2)	0.2161(6)	5.7(3)
C(5)	0.6585(7)	0.7061(2)	0.2896(5)	5.1(3)
C(6)	0.6157(7)	0.6502(2)	0.2683(4)	4.1(2)
C(7)	0.3053(5)	0.5562(2)	0.2601(4)	3.1(2)
C(8)	0.3461(6)	0.5364(2)	0.3691(4)	3.9(2)
C(9)	0.2320(8)	0.5361(3)	0.4503(5)	5.4(3)
C(10)	0.0748(9)	0.5550(3)	0.4232(6)	6.5(4)
C(11)	0.0310(8)	0.5733(4)	0.3155(7)	7.5(4)
C(12)	0.1467(7)	0.5741(3)	0.2344(5)	5.6(3)
C(13)	0.0041(5)	0.3408(2)	0.0645(4)	3.1(2)
C(14)	0.0632(7)	0.3132(2)	−0.0289(4)	4.5(2)
C(15)	0.0163(8)	0.2577(2)	−0.0530(6)	5.9(3)
C(16)	−0.0858(8)	0.2299(2)	0.0142(7)	6.2(3)
C(17)	−0.1450(8)	0.2562(3)	0.1067(6)	5.8(3)
C(18)	−0.1018(7)	0.3118(2)	0.1328(4)	4.5(2)
C(19)	0.2201(5)	0.4023(2)	0.2167(4)	2.9(2)
C(20)	0.1711(6)	0.3919(2)	0.3281(4)	3.9(2)
C(21)	0.2883(8)	0.3825(2)	0.4155(4)	4.9(3)
C(22)	0.4517(8)	0.3848(2)	0.3957(5)	5.2(3)
C(23)	0.5023(6)	0.3961(2)	0.2878(5)	4.6(2)
C(24)	0.3853(6)	0.4046(2)	0.1983(4)	3.8(2)

[a]$B_{eq} = (8/3)\pi^2\Sigma\Sigma U_{ij}a_i^*a_j^*(\mathbf{a}_i \cdot \mathbf{a}_j)$.

TABLE 3. Bond lengths (Å) with estimated standard deviations[a]

Atom	Atom	Distance	Atom	Atom	Distance
		[$Co(Ph_2PO_2)_2$]			
Co(1)	O(1)	1.952(2)	C(7)	C(8)	1.380(4)
Co(1)	O(2)′	1.963(2)	C(7)	C(12)	1.383(4)
Co(1)	O(3)	1.951(2)	C(8)	C(9)	1.376(5)
Co(1)	O(4)′′	1.950(2)	C(9)	C(10)	1.360(6)
P(1)	O(1)	1.510(2)	C(10)	C(11)	1.367(6)
P(1)	O(2)	1.511(2)	C(11)	C(12)	1.377(4)
P(1)	C(1)	1.796(3)	C(13)	C(14)	1.379(4)
P(1)	C(7)	1.788(3)	C(13)	C(18)	1.380(4)
P(2)	O(3)	1.506(2)	C(14)	C(15)	1.396(5)
P(2)	O(4)	1.508(2)	C(15)	C(16)	1.355(7)
P(2)	C(13)	1.806(3)	C(16)	C(17)	1.369(6)
P(2)	C(19)	1.798(3)	C(17)	C(18)	1.377(5)
C(1)	C(2)	1.372(4)	C(19)	C(20)	1.386(4)
C(1)	C(6)	1.389(4)	C(19)	C(24)	1.399(4)
C(2)	C(3)	1.388(5)	C(20)	C(21)	1.390(4)
C(3)	C(4)	1.367(6)	C(21)	C(22)	1.366(5)
C(4)	C(5)	1.370(5)	C(22)	C(23)	1.373(5)
C(5)	C(6)	1.369(5)	C(23)	C(24)	1.380(4)
		[$Mn(Ph_2PO_2)_2$]			
Mn(1)	O(4)′	2.016(3)	C(7)	C(12)	1.380(7)
Mn(1)	O(3)	2.028(3)	C(7)	C(8)	1.383(6)
Mn(1)	O(1)	2.032(3)	C(8)	C(9)	1.364(7)
Mn(1)	O(2)′′	2.033(3)	C(9)	C(10)	1.380(9)
P(1)	O(1)	1.508(3)	C(10)	C(11)	1.36(1)
P(1)	O(2)	1.511(3)	C(11)	C(12)	1.373(8)
P(1)	C(7)	1.789(4)	C(13)	C(14)	1.382(6)
P(1)	C(1)	1.793(4)	C(13)	C(18)	1.389(6)
P(2)	O(3)	1.505(3)	C(14)	C(15)	1.398(7)
P(2)	O(4)	1.513(3)	C(15)	C(16)	1.348(9)
P(2)	C(19)	1.791(4)	C(16)	C(17)	1.36(1)
P(2)	C(13)	1.795(4)	C(17)	C(18)	1.397(8)
C(1)	C(6)	1.380(6)	C(19)	C(24)	1.378(6)
C(1)	C(2)	1.384(6)	C(19)	C(20)	1.405(6)
C(2)	C(3)	1.386(8)	C(20)	C(21)	1.381(6)
C(3)	C(4)	1.359(8)	C(21)	C(22)	1.367(8)
C(4)	C(5)	1.361(8)	C(22)	C(23)	1.374(8)
C(5)	C(6)	1.390(7)	C(23)	C(24)	1.394(7)

[a]Here and elsewhere in the report the symbols ′ and ′′ refer to symmetry operations: $1-x, 1-y, 1-z$ and $-x, 1-y, 1-z$ for the Co complex and $1-x, 1-y, -z$ and $-x, 1-y, -z$ for the Mn complex.

Spectroscopically there is relatively little difference between the β and γ forms of $Co(Ph_2PO_2)_2$. The visible spectra are virtually identical (Fig. 2), indicating little difference in the CoO_4 chromophores. The infrared spectra of the two forms are also very similar (see experimental section). Both forms show two strong bands which may be assigned to the antisymmetric and symmetric PO_2 stretching frequencies, the former occurring at 1138 cm^{-1} in both forms and the latter at 1049 and 1056 cm^{-1} in the β and γ forms, respectively. These band frequencies and separations are similar to those observed for the phosphinates of copper(II) (5, 6, 9) and are consistent with relatively symmetrical phosphinate bridging as shown by the X-ray structure determination of the γ form. The most distinctive feature in the infrared spectra which distinguishes the β and γ forms is a band at about 1210 cm^{-1} which is moderately strong in the γ form and appears only very weakly in the β form. There are also some differences in the weak bands which occur below 500 cm^{-1} and which may be ascribed to Co—O or lattice vibrations. The DSC thermograms are very similar for both forms (experimental section). The single endothermic bands observed correspond closely to the β → ϵ (paracrystalline phase) transition reported for $Zn(Ph_2PO_2)_2$ (345°C, ΔH = 21 J g^{-1}, ref. 8) and may be assigned to a similar event.

We have examined the magnetic properties of both forms of $Co(Ph_2PO_2)_2$ at low temperatures (2–82 K) and the data have been deposited.[2] The susceptibilities have been corrected for temperature independent paramagnetism, TIP, calculated from the expression TIP = $8N\beta^2/10Dq$. The value of 10 Dq was estimated from the spectrum of $Co((C_8H_{17})_2PO_2)_2$ (form I), a phosphinate compound previously reported to contain tetrahedral cobalt(II) (10). This compound exhibits broad structured absorptions centred near 6 500 and 16 500 cm^{-1} assigned to $^4A_2(F) \rightarrow 4T_1(F)$ and $^4A_2(F) \rightarrow {}^4T_1(P)$ transitions, respectively (10). From this it is possible to calculate 10 Dq as 3740 cm^{-1} and hence TIP as 560×10^{-6} cm^3 mol^{-1}.

The magnetic moment of cobalt(II) ($^4A_2$ ground state in T_d) in a regular or slightly distorted tetrahedral environment is expected to be temperature independent except possibly at very low temperatures where zero-field splitting (ZFS) effects may impart some temperature dependence (11). The magnetic moments for both the β and γ forms of $Co(Ph_2PO_2)_2$ decrease significantly with decreasing temperature (deposited material). Attempts to fit the experimental magnetic susceptibilities calculated assuming zero-field splitting (11) show that ZFS alone cannot account for the magnetic properties of these materials. The susceptibility data for the γ form pass through a maximum at 3.6 K indicative of antiferromagnetic behavior. The magnetic data for this compound have been analyzed according to two Heisenberg models for linear chains, the scaling model of Wagner and Friedberg with $S = 3/2$ (12) and the Weng model (13) with coefficients generated by Hiller *et al.* (14) for $S = 3/2$. The magnetic parameters generated for the best fits between experiment and theory are given in Table 5. The Weng model reproduced the position of the maximum in the susceptibility better and gave an overall better fit than the other model. The best fit curve using the Weng model is shown in Fig. 5*a*. There is no maximum in the susceptibility data of the β form of $Co(Ph_2PO_2)_2$; nonetheless, the data may be analyzed assuming antiferromagnetic coupling which is somewhat weaker than that in the γ form. In this case there is little difference in the quality of the fit between the two models; the best fit parameters are given in Table 5 and the best fit curve employing the Weng model is shown in Fig. 5*b*.

Manganese(II) diphenylphosphinate

In our investigations on manganese(II) diphenylphosphinate complexes we established synthetic routes to two forms of $Mn(Ph_2PO_2)_2$ which, on the basis of their X-ray powder diffraction patterns, infrared spectra and, in one case, a single crystal X-ray diffraction study, are isomorphous with the β and γ forms of $Co(Ph_2PO_2)_2$ just described. The preparation of the bis(dimethylformamide) complex of manganese(II) diphenylphosphinate is described in the literature (16). We found the complex formed in this preparation to be very susceptible to the loss of dimethylformamide such that, on washing well with acetone followed by drying in air, all of the amide ligand is lost and anhydrous $Mn(Ph_2PO_2)_2$ is obtained. The infrared spectrum (experimental section) and X-ray powder diffraction pattern (Fig. 1) for this material indicate isomorphism with β-$Co(Ph_2PO_2)_2$. The DSC thermogram, like that of the cobalt analog, also shows just one endothermic peak which for the manganese compound is at 357° (ΔH = 24 J g^{-1}).

The preparation of $Mn(Ph_2PO_2)_2$ from aqueous methanol solution gives a microcrystalline powder which, on the basis of

Can. J. Chem. Downloaded from www.nrcresearchpress.com by 195.138.81.100 on 09/07/12
For personal use only.

TABLE 4. Bond angles (deg) with estimated standard deviations

Atom	Atom	Atom	Angle	Atom	Atom	Atom	Angle
			$[Co(Ph_2PO_2)_2]$				
O(1)	Co(1)	O(2)′	107.60(8)	C(2)	C(3)	C(4)	120.4(4)
O(1)	Co(1)	O(3)	117.77(9)	C(3)	C(4)	C(5)	120.1(4)
O(1)	Co(1)	O(4)″	104.83(9)	C(4)	C(5)	C(6)	119.6(3)
O(2)′	Co(1)	O(3)	104.81(8)	C(1)	C(6)	C(5)	121.2(3)
O(2)′	Co(1)	O(4)″	109.51(8)	P(1)	C(7)	C(8)	118.9(2)
O(3)	Co(1)	O(4)″	112.13(9)	P(1)	C(7)	C(12)	122.2(2)
O(1)	P(1)	O(2)	116.6(1)	C(8)	C(7)	C(12)	118.7(3)
O(1)	P(1)	C(1)	108.4(1)	C(7)	C(8)	C(9)	120.3(4)
O(1)	P(1)	C(7)	109.8(1)	C(8)	C(9)	C(10)	120.3(4)
O(2)	P(1)	C(1)	108.8(1)	C(9)	C(10)	C(11)	120.3(4)
O(2)	P(1)	C(7)	109.3(1)	C(10)	C(11)	C(12)	119.9(4)
C(1)	P(1)	C(7)	102.9(1)	C(7)	C(12)	C(11)	120.5(3)
O(3)	P(2)	O(4)	117.0(1)	P(2)	C(13)	C(14)	121.5(2)
O(3)	P(2)	C(13)	108.5(1)	P(2)	C(13)	C(18)	120.1(2)
O(3)	P(2)	C(19)	109.4(1)	C(14)	C(13)	C(18)	118.4(3)
O(4)	P(2)	C(13)	108.7(1)	C(13)	C(14)	C(15)	119.9(4)
O(4)	P(2)	C(19)	108.0(1)	C(14)	C(15)	C(16)	120.2(4)
C(13)	P(2)	C(19)	104.5(1)	C(15)	C(16)	C(17)	120.7(4)
Co(1)	O(1)	P(1)	144.3(1)	C(16)	C(17)	C(18)	119.2(4)
Co(1)′	O(2)	P(1)	125.1(1)	C(13)	C(18)	C(17)	121.5(4)
Co(1)	O(3)	P(2)	147.7(1)	P(2)	C(19)	C(20)	121.2(2)
Co(1)″	O(4)	P(2)	131.3(1)	P(2)	C(19)	C(24)	119.6(2)
P(1)	C(1)	C(2)	122.7(2)	C(20)	C(19)	C(24)	119.2(3)
P(1)	C(1)	C(6)	118.6(2)	C(19)	C(20)	C(21)	119.4(3)
C(2)	C(1)	C(6)	118.6(3)	C(20)	C(21)	C(22)	121.0(3)
C(1)	C(2)	C(3)	120.1(3)	C(21)	C(22)	C(23)	120.0(3)
C(22)	C(23)	C(24)	120.3(3)	C(19)	C(24)	C(23)	120.1(3)
			$[Mn(Ph_2PO_2)_2]$				
O(4)′	Mn(1)	O(3)	114.0(1)	C(4)	C(3)	C(2)	121.3(5)
O(4)′	Mn(1)	O(1)	103.2(1)	C(3)	C(4)	C(5)	119.8(5)
O(4)′	Mn(1)	O(2)″	112.4(1)	C(4)	C(5)	C(6)	120.2(5)
O(3)	Mn(1)	O(1)	114.7(1)	C(1)	C(6)	C(5)	120.2(5)
O(3)	Mn(1)	O(2)″	104.7(1)	C(12)	C(7)	C(8)	118.8(5)
O(1)	Mn(1)	O(2)″	108.0(1)	C(12)	C(7)	P(1)	118.8(4)
O(1)	P(1)	O(2)	116.4(2)	C(8)	C(7)	P(1)	122.1(3)
O(1)	P(1)	C(7)	110.0(2)	C(9)	C(8)	C(7)	120.2(5)
O(1)	P(1)	C(1)	108.9(2)	C(8)	C(9)	C(10)	119.9(6)
O(2)	P(1)	C(7)	109.3(2)	C(11)	C(10)	C(9)	120.8(6)
O(2)	P(1)	C(1)	108.5(2)	C(10)	C(11)	C(12)	119.1(6)
C(7)	P(1)	C(1)	102.9(2)	C(11)	C(12)	C(7)	121.1(6)
O(3)	P(2)	O(4)	116.3(2)	C(14)	C(13)	C(18)	118.2(4)
O(3)	P(2)	C(19)	109.6(2)	C(14)	C(13)	P(2)	122.0(4)
O(3)	P(2)	C(13)	108.9(2)	C(18)	C(13)	P(2)	119.8(4)
O(4)	P(2)	C(19)	108.3(2)	C(13)	C(14)	C(15)	120.2(5)
O(4)	P(2)	C(13)	108.3(2)	C(16)	C(15)	C(14)	121.0(6)
C(19)	P(2)	C(13)	104.9(2)	C(15)	C(16)	C(17)	119.7(5)
P(1)	O(1)	Mn(1)	146.6(2)	C(16)	C(17)	C(18)	120.8(6)
P(1)	O(2)	Mn(1)″	125.9(2)	C(13)	C(18)	C(17)	120.1(5)
P(2)	O(3)	Mn(1)	150.2(2)	C(24)	C(19)	C(20)	118.8(4)
P(2)	O(4)	Mn(1)′	130.9(2)	C(24)	C(19)	P(2)	121.9(3)
C(6)	C(1)	C(2)	119.2(4)	C(20)	C(19)	P(2)	119.3(3)
C(6)	C(1)	P(1)	118.3(3)	C(21)	C(20)	C(19)	119.7(5)
C(2)	C(1)	P(1)	122.4(4)	C(22)	C(21)	C(20)	120.8(5)
C(1)	C(2)	C(3)	119.3(5)	C(21)	C(22)	C(23)	120.4(5)
C(22)	C(23)	C(24)	119.4(5)	C(19)	C(24)	C(23)	120.9(5)

its infrared spectrum (experimental section) and X-ray powder diffraction pattern (Fig. 1), is isomorphous with γ-$Co(Ph_2PO_2)_2$. The DSC thermogram for the manganese compound, however, is more complex than that of the cobalt analog (experimental section). γ-$Mn(Ph_2PO_2)_2$ exhibits a peak at 356°C which may be ascribed, as in the case of the other compounds studied here, to a transition to a paracrystalline phase. However, in addition it shows another major endotherm at 213°C and a minor event at 238°C. On cooling the sample from the paracrystalline phase to 35°C and reheating, the event at 213°C disappears while the weak peak at 235°C and the 356°C event are retained. A possible explanation for these observations is that the γ form converts

Can. J. Chem. Downloaded from www.nrcresearchpress.com by 195.138.81.100 on 09/07/12
For personal use only.

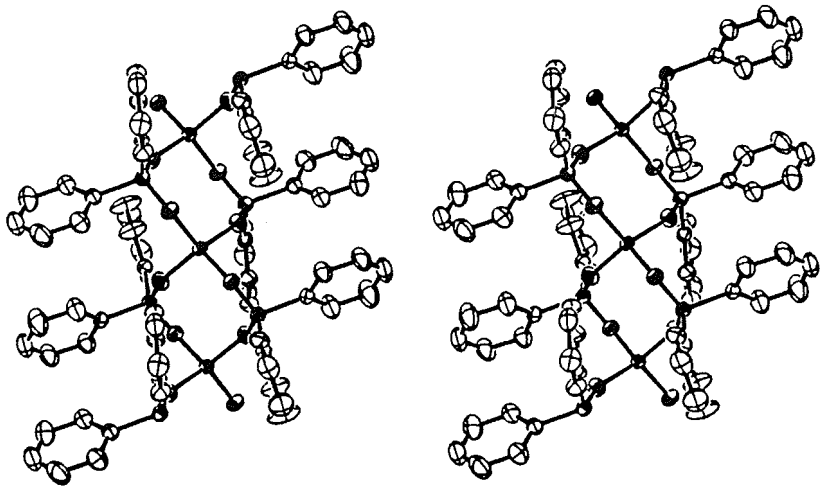


FIG. 3. Stereoview of the γ-$Co(Ph_2PO_2)_2$ structure showing a section of the linear double phosphinate bridged chain structure. γ-$Mn(Ph_2PO_2)_2$ is isomorphous and isostructural.

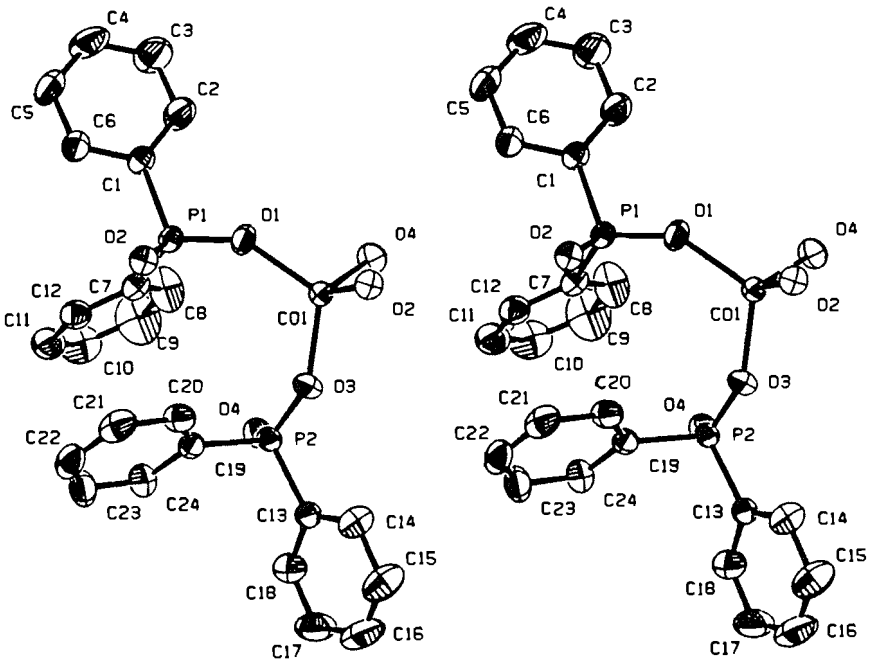


FIG. 4. Stereoview of the asymmetric unit of the γ-$Co(Ph_2PO_2)_2$ structure showing atom labelling and the coordination about the metal atom. 50% probability thermal ellipsoids are shown for the non-hydrogen atoms. γ-$Mn(Ph_2PO_2)_2$ is isomorphous and isostructural.

irreversibly to a third form at 213°C which in turn converts to the β form at 238°C. The transition from β to the paracrystalline phase then occurs at 356°C as observed for an independently prepared sample of β-$Mn(Ph_2PO_2)_2$. Complex thermal behaviour of this type is not uncommon for metal phosphinate polymers (see, for example, ref. 8); it is interesting though that it is seen in γ-$Mn(Ph_2PO_2)_2$ but not in any of the other compounds studied here.

Attempts to prepare a formamide adduct of $Mn(Ph_2PO_2)_2$ by adding formamide to the methanol solution prior to the formation of a precipitate led instead to the slow crystallization of the γ form. Confirmation that these crystals were of the γ form came from a variety of studies. The infrared spectrum and the magnetic susceptibilities of ground samples of these crystals are the same to within experimental error as observed for the microcrystalline powder samples as reported here. The X-ray powder diffraction pattern of powdered samples of these crystals is identical to that shown in Fig. 1 with the exception that some of the relative peak intensities differ. This likely arises from differences in preferred orientation in the powdered samples. Powdered samples of the crystals show only small differences in the DSC thermogram from that of the microcrystalline powder. Three events occur at 210°C (ΔH = 25 J g^{-1}), 240° (ΔH = 7 J g^{-1}), and 358°C (ΔH = 27 J g^{-1}). The irreversibility of the event at 210°C was confirmed in this sample also. Crystals obtained from this preparation were large enough for a single crystal X-ray structure determination.

The crystal structure of γ-$Mn(Ph_2PO_2)_2$ shows the compound to be isomorphous and isostructural with the γ form of cobalt(II) diphenylphosphinate. The Mn—O distances are longer than those in the cobalt complex, ranging from 2.016(3) to 2.033(3) Å (average 2.027 Å), and the angles about the Mn

Can. J. Chem. Downloaded from www.nrcresearchpress.com by 195.138.81.100 on 09/07/12
For personal use only.

Can. J. Chem. Downloaded from www.nrcresearchpress.com by 195.138.81.100 on 09/07/12
For personal use only.

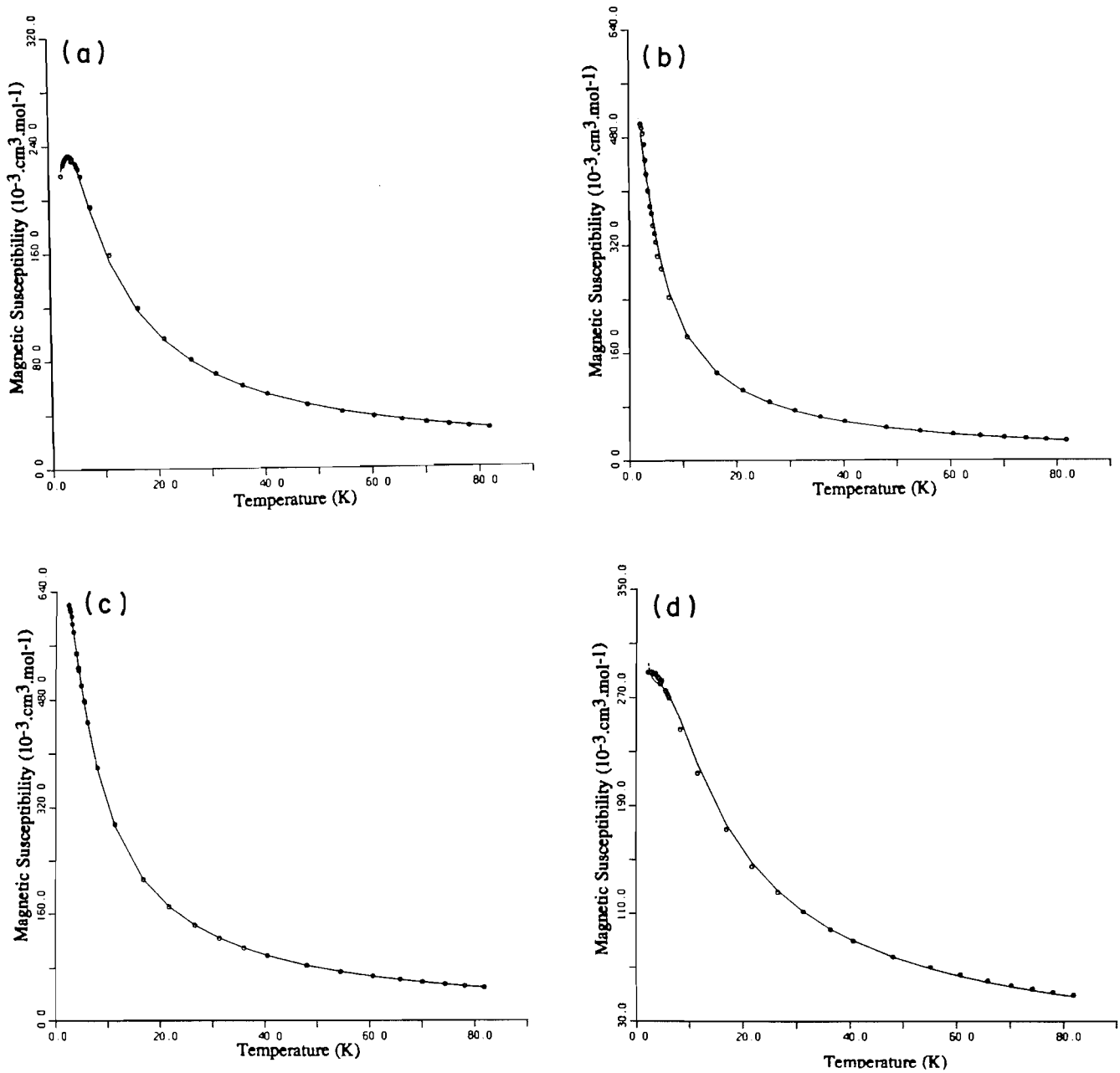


FIG. 5. Magnetic susceptibility versus temperature plots for $M(Ph_2PO_2)_2$: (*a*) γ-Co, (*b*) β-Co, (*c*) γ-Mn, (*d*) β-Mn. Circles are experimental data and solid lines are calculated as described in the text.

atom range from 103.2(1) to 114.7(1)°. The Mn...Mn distances along the chain are 4.417(1) and 4.446(1) Å. All other features of the structure are as described above for γ-$Co(Ph_2PO_2)_2$.

Tetrahedral manganese(II) complexes by virtue of their $^6A_1$ ground state should, in the absence of magnetic exchange, exhibit a temperature independent spin-only magnetic moment of 5.92 μ_B, with possibly small deviations at the lowest temperatures due to weak zero-field splitting effects. Both forms of $Mn(Ph_2PO_2)_2$ exhibit lower than spin-only moments over the entire range studied and, moreover, the moments decrease significantly with temperature (deposited data)[2] thus indicating the presence of antiferromagnetic coupling. The coupling appears to be greater in the case of the β form where the magnetic moment values are lower at all temperatures than those obtained for the γ form and the onset of a maximum in the susceptibility is observed at the lowest temperatures studied. Fits to the Wagner–Friedberg and Weng models for $S = 5/2$ were obtained and the best fit parameters are given in Table 5. For these manganese compounds a better fit between experiment and theory is obtained if allowance is made for a paramagnetic component as was described in an earlier study on manganese(II) monophenylphosphinate (17). The improvement in fit is particularly noticed near the susceptibility maximum in β-$Mn(Ph_2PO_2)_2$. The best-fit parameters, including allowance for the paramagnetic component, are also given in Table 5 and the theoretical curves obtained from the Weng model and employing these parameters are compared with experiment in Fig. 5*c* for the γ form and Fig. 5*d* for the β form.

In summary, β and γ forms of both $Co(Ph_2PO_2)_2$ and $Mn(Ph_2PO_2)_2$ have been synthesized and characterized. All

TABLE 5. Magnetic parameters for $M(Ph_2PO_2)_2$

M	Form	Model[a]	S	g[b]	$-J$ (cm^{-1})	$\%p$[c]	F[d]
Co	γ	W	3/2	2.32	0.55	—	0.0112
		W–F	3/2	2.31	0.60	—	0.0229
	β	W	3/2	2.29	0.25	—	0.0250
		W–F	3/2	2.28	0.26	—	0.0263
Mn	γ	W	5/2	2.00	0.17	—	0.0125
		W	5/2	2.00	0.19	8.1	0.0047
		W–F	5/2	2.00	0.17	—	0.0169
		W–F	5/2	2.00	0.19	6.5	0.0127
	β	W	5/2	2.00	0.34	—	0.0442
		W	5/2	2.00	0.45	4.0	0.0154
		W–F	5/2	2.00	0.36	—	0.0335
		W–F	5/2	2.00	0.41	3.1	0.0132

[a]W = Weng (13, 14); W–F = Wagner-Friedberg (12).
[b]g value set at 2.00 for $S = 5/2$ and allowed to vary for $S = 3/2$.
[c]$\%p$ = % paramagnetic component set at zero where no value indicated.
[d]F = fitting function defined in ref. 15.

four materials show antiferromagnetic behavior which can be analyzed according to Heisenberg models for linear chains. Single crystal X-ray diffraction studies on the γ forms confirm the presence of extended chains in which tetrahedrally coordinated metal atoms are linked by double phosphinate bridges. The magnetic exchange which likely proceeds by a superexchange mechanism via the bridging O—P—O groups is of the same order of magnitude in the γ forms of the cobalt and manganese compounds, which is perhaps not too surprising considering the similarities in structural parameters in the two compounds. On the other hand, it is interesting to note that, whereas the exchange coupling is greater for the γ form of $Co(Ph_2PO_2)_2$ compared to its β form, the opposite is true for the $Mn(Ph_2PO_2)_2$ pair. Whether such a finding is a result of differences in the detailed structures of the two β forms or a consequence of the different metal ion electron configurations and therefore magnetic orbitals involved is something which is difficult to answer without a detailed knowledge of the structures of the β forms.

Finally, it should be noted that earlier studies by Ripamonte and co-workers (18, 19) on zinc(II) and beryllium(II) phosphinate polymers led these authors to suggest that coordination polymers involving bridging phosphinate groups and tetrahedral metal atoms have alternate single and triple phosphinate bridges, rather than the double phosphinate bridge, regardless of the organic side group. That this is not the case is shown by the work presented here as well as the recently reported X-ray structure determination of zinc(II) monophenylphosphinate which also reveals tetrahedral metal centres combined with the double phosphinate bridge system (20).

Acknowledgements

The authors thank the Natural Sciences and Engineering Research Council of Canada for financial support, P. Borda of this department for C and H microanalyses, and E. Mar for the preparation of β-$Co(Ph_2PO_2)_2$.

1. G. E. COATES and D. S. GOLIGHTLY. J. Chem. Soc. 2523 (1962).
2. S. H. ROSE and B. P. BLOCK. J. Polymer Sci. A-1, **4**, 583 (1966).
3. S. H. ROSE and B. P. BLOCK. J. Polymer Sci. A-1, **4**, 573 (1966).
4. A. BINO and L. SISSMAN. Inorg. Chim. Acta, **128**, L21 (1987).
5. J.-L. DU, K. W. OLIVER, and R. C. THOMPSON. Inorg. Chim. Acta, **141**, 19 (1988).
6. J. S. HAYNES, K. W. OLIVER, S. J. RETTIG, R. C. THOMPSON, and J. TROTTER. Can. J. Chem. **62**, 891 (1984).
7. International tables for X-ray crystallography. Vol. IV. Kynock Press: Birmingham, U.K. (present distributor Kluwer Academic Publishers: Dordrecht, The Netherlands), 1974. pp. 99–102, 149.
8. V. GIANCOTTI and A. RIPAMONTE. J. Chem. Soc. (A), 706 (1969).
9. K. W. OLIVER, S. J. RETTIG, R. C. THOMPSON, and J. TROTTER. Can. J. Chem. **60**, 2017 (1982).
10. H. D. GILLMAN. Inorg. Chem. **11**, 3124 (1972).
11. C. J. O'CONNOR. *In* Progress in inorganic chemistry. Vol. 29. *Edited by* S. J. Lippard. John Wiley and Sons, New York. 1982. p. 203.
12. G. R. WAGNER and S. A. FRIEDBERG. Phys. Lett. **9**, 11 (1964).
13. C. H. WENG. Ph.D. Dissertation, Carnegie-Mellon University, Pittsburg, PA. 1968.
14. W. HILLER, J. STRÄHLE, A. DATZ, M. HANACK, W. E. HATFIELD, L. W. TERHAAR, and P. GÜTLICH. J. Am. Chem. Soc. **106**, 329 (1984).
15. W. V. CICHA, J. S. HAYNES, K. W. OLIVER, S. J. RETTIG, R. C. THOMPSON, and J. TROTTER. Can. J. Chem. **63**, 1055 (1985).
16. D. J. COOKSON, R. F. WAKEFIELD, T. D. SMITH, J. F. BOAS, J. R. PILBROW, P. R. HICKS, and D. H. LAMBLE. J. Chem. Soc. Faraday Trans. II, **75**(3), 500 (1979).
17. J.-L. DU and R. C. THOMPSON. Can. J. Chem. **67**, 1239 (1989).
18. V. GIANCOTTI, F. GIORDANO, L. RANDACCIO, and A. RIPAMONTE. J. Chem. Soc. (A), 757 (1968).
19. F. GEMITI, V. GIANCOTTI, and A. RIPAMONTE. J. Chem. Soc. (A), 763 (1968).
20. M. SHIEH, K. J. MARTIN, P. J. SQUATTRITO, and A. CLEARFIELD. Inorg. Chem. **29**, 958 (1990).

Can. J. Chem. Downloaded from www.nrcresearchpress.com by 195.138.81.100 on 09/07/12
For personal use only.

A microstratigraphic investigation of iron ion migration in some ancient Egyptian wall paintings using PIXE Analysis

GEORGE BURNS AND K.M. WILSON-YANG[1]

Lash Miller Chemical Laboratories, University of Toronto, 80 St. George Street, Toronto, Ont., Canada M5S 1A1

Received May 28. 1990

GEORGE BURNS and K. M. WILSON-YANG. Can. J. Chem. **69**. 286 (1991).

The painted murals in the tombs at Beni Hasan (*circa* 2100 B.C.) are obscured by a rock-like grey surface layer. Its formation involves subsurface removal of slightly soluble calcite ($CaCO_3$) under the action of surface-condensed water. To study the mechanism of surface layer formation and the effect of mural cleaning during recent restorations, the PIXE microprobe was used. Iron depth profiles in red-painted samples taken from the murals, both uncleaned and cleaned, have been obtained over depths of 80 μm (the cleaned sample) and 100 μm (the uncleaned sample). It has been found that the uncleaned sample has more Fe at all depths than does the cleaned sample and that portions of the uncleaned pigment appear to be pure Fe_2O_3. The shapes of depth profiles of Fe in the cleaned and uncleaned samples are similar to the shapes of diffusion curves; this finding is in agreement with the mechanism of surface layer formation proposed in our earlier papers. Apparent diffusion coefficients for the ion migration of Fe, D_{Fe}, in the limestone painting substrate have been determined, assuming constant temperature diffusion over 4 000 years: $D_{Fe(u)} = (1.4 \pm 0.5) \times 10^{-16}$ cm^2/s for the uncleaned sample and $D_{Fe(c)} = (0.7 \pm 0.4) \times 10^{-16}$ cm^2/s for the cleaned sample, where errors are given as the 95% C.I. based on standard deviations of the slope of the fitted curve. These coefficients are consistent with the mechanism of slow migration of Fe in the painting substrate in an arid environment. The difference between D_{Fe} values secured for the cleaned and uncleaned samples is attributed to a partial removal of the paint layer in the cleaned sample during the restoration efforts. Thus, if it is assumed that either 20 or 40 μm of paint layer was removed during HCl-cleaning of murals, $D_{Fe(c)} = (1.0 \pm 0.4) \times 10^{-16}$ and $D_{Fe(c)} = (1.4 \pm 0.6) \times 10^{-16}$ cm^2/s, respectively, are obtained. Removal of the top 40 μm of the mural corresponds to elimination, during the restoration, of the order of 60% of the uncleaned paint layer.

Key words: Egypt, PIXE, ancient murals deterioration.

GEORGE BURNS et K. M. WILSON-YANG. Can. J. Chem. **69**, 286 (1991).

Les murales des tombes trouvées à Beni Hasan (environ 2100 BC) sont obscurcies par des couches superficielles grises qui ressemblent à du roc. Leur formation implique l'enlèvement, sous la surface, de calcite ($CaCO_3$) partiellement soluble sous l'action d'eau qui se condense à la surface. Afin d'étudier le mécanisme de formation de la couche superficielle ainsi que l'effet du nettoyage de ces peintures effectué dans le cadre de restaurations récentes, on a fait appel à des microprobes PIXE. On a déterminé les profils de concentration du fer en fonction de la pofondeur (jusqu'à 80 μm pour des échantillon nettoyé et jusqu'à 100 μm pour l'échantillon non-nettoyé) pour des échantillons peints en rouge prélevés sur les murales. On a trouvé que, à toutes les profondeurs, l'échantillon qui n'a pas été nettoyé contient plus de fer que celui qui a été nettoyé et que des portions du pigment non-nettoyé semblent être du Fe_2O_3 pur. Les formes des profils des concentrations du Fe en fonction de la profondeur dans les échantillons nettoyé et non-nettoyé ressemblent aux formes des courbes de diffusion; ce résultat est en accord avec le mécanisme de formation de la couche superficielle qui a été proposé dans nos communications antérieures. Faisant l'hypothèse que la température de diffusion a été constante au cours des derniers 4 000 ans, on a déterminé les coefficients de diffusion apparents pour la migration de l'ion Fe dans le substrat qu'est le calcaire peint; $D_{Fe(u)} = (1,4 \pm 0,5) \times 10^{-16}$ cm^2/s pour l'échantillon qui n'a pas été nettoyé et $D_{Fe(c)} = (0,7 \pm 0,4) \times 10^{-16}$ cm^2/s pour l'échantillon qui a été nettoyé alors que les erreurs sont égales à 95% de l'I.C. basé sur les déviations standard de la pente de la courbe. Ces coefficients sont en accord avec le mécanisme d'une migration lente du Fe dans le substrat peint, dans un environnement aride. Les différences observées pour les valeurs de D_{Fe} obtenues pour les échantillons nettoyés et non-nettovés sont attribuées à un enlèvement partiel de la couche de neinture dans l'échantillon nettoyé qui se serait produit au cours des efforts de restauration. Donc, si on fait l'hypothèse que 20 ou 40 μm de la couche de peinture a été enlevé au cours du nettoyage des muales avec du HCl, on obtient des valeurs respectives de $D_{Fe(c)} = (1,0 \pm 0,4) \times 10^{-16}$ et $D_{Fe(c)} = (1,4 \pm 0,6) \times 10^{-16}$ cm^2/s. L'enlèvement de 40 μm de la surface de la murale correspond à l'élimination, durant la restauration, d'environ 60% de la couche de peinture qui n'a pas été nettoyée.

Mots clés : Égypte, PIXE, détérioration de murales anciennes.

[Traduit par la rédaction]

Introduction

Eco-archaeological chemistry

Extensive degradations of ancient monuments throughout the world, and specifically in Egypt (see, for example, ref. 1), cause considerable concern not only in the scientific community but also to the public at large (1). Study of such processes by chemical means provides an unusual opportunity for elucidation of fundamental physicochemical processes which occur over a very long period of time, of the order of millennia, which is of the order of 10^{11} s. While modern chemical methods now make possible studies of processes down to the order of 10^{-13} s, studies of very slow processes have been difficult to conduct because there are but few systems of well-defined age if this age is of the order of a few millennia. Even if the age can be determined, it is rare to find a system which existed under sufficiently uniform conditions over such a long period of time. However, some archaeological systems satisfy both of these requirements. In addition, such studies are important because prevention of degradation of ancient monuments and development of reliable conservation and restoration methods require, as a first step, an adequate understanding, at a rather fundamental level, of the physicochemical processes responsible for these deteriorations (2).

[1]Senior Chemist, Eco Logic. Present address: 143 Dennis St., Rockwood, Ont., Canada N0B 2K0.

Can. J. Chem. Downloaded from www.nrcresearchpress.com by 195.138.81.100 on 09/07/12
For personal use only.

Can. J. Chem. Downloaded from www.nrcresearchpress.com by 195.138.81.100 on 09/07/12
For personal use only.

Without such understanding, even the most conscientious conservation or restoration effort may not only simply fail, but may even augment the existing damage. These questions are the domain of eco-archaeological chemistry, sometimes considered to be a part of a more general field of eco-archaeometry (2), which combines methods of analytical and physical chemistry and associated (2) fields. In this paper, an attempt is made to study, using some tools of eco-archaeological chemistry, the deteriorating murals of the ancient tombs of Beni Hasan.

Degradation at the Beni Hasan Tombs

The tombs at Beni Hasan, Egypt, contain artistically significant painted murals which constitute important records of First Intermediate Period and Middle Kingdom (*circa* 2100 B.C. to 1800 B.C.) life. These paintings were executed on the tomb walls using the tempera technique (3) on the polished limestone which constitutes the painting substrate. A thin layer (3, 4) of whitewash (5) may have been employed to prepare the rock surfaces for painting; however, in our work, no conclusive evidence has been found to verify this point.

The Beni Hasan wall paintings are now obscured by a rock-like grey deposit (3, 6, 7) and evidence accumulated from historic sources suggests (7) that the development of this surface degradation product has accelerated over the past 150 years.

Investigations of the grey degradation layer and its formation have been conducted (5, 8) on a small collection of fragments, coloured with the yellow and the red iron-based pigments assembled by the authors on site from the Beni Hasan tomb paintings. The first few nanometres of the surface deposit have been analyzed earlier by the X-ray photoelectron spectroscopy (8). The results of this analysis made it possible to propose a mechanism (8) for the formation of the degradation layer which required that, in addition to dust deposition, surface layer formation involves ion migration within and throughout the paint layers and subsurface regions. According to the proposed mechanism (8), it is this ion migration that led to formation of the $CaCO_3$ surface layer in which sand and dust particles are now imbedded. It is this ion migration that also led to eventual subsurface removal of slightly soluble material, mainly $CaCO_3$, from the substrate upon which the murals were painted and the subsequent deposition of this material on the surface. The migration of this material appeared to be possible under the action of surface-condensed water (5).

Although all these predictions could not have been verified from the XPS observations (8), some of them were subsequently confirmed using light microscopy and electron microprobe analyses (5): painted fragments, examined in cross-section, showed some subsurface depletion and associated formation of dendritic structures within the substrate, below the painted layers (5). Such confirmation provides qualitative support for the proposed (8) mechanism; however, this work (8) provided no direct evidence for ion migration within the murals.

The degradation process which results in the subsurface depletion below the paint layer has been suspected also to act directly on the paint layers (5): in the depleted yellow-painted samples, degradation was so extensive that a clear demarcation of the paint layer could not be seen. However, the subsurface degradation associated with the surface layer formation was seen in only one red-pigmented sample (5), although not at the same depth as in the yellow samples. Furthermore, the red paint layer-substrate separation line can be seen both under the microscope and by the electron microprobe (5).

During continuing cleaning endeavour by chemists and conservators of the Egyptian Antiquities Organization, the obscuring grey layer which covers the painted surface at Beni Hasan is being removed from some murals (3). This restoration effort involves use of fairly concentrated HCl on the encrusted painted surface, normally applied with a papier maché poultice, and then rinsing the surfaces with water applied in the same manner. However, Egyptian scientists expressed a continuous concern (the late Professor Z. Iskander, private communication) that during this cleaning, disruption of the both the iron-based paint layer and the limestone substrate may accompany removal of the disfiguring surface layer with HCl.

To further investigate the mechanism of the physicochemical processes responsible for the formation of grey deposits at Beni Hasan and to study the effects of strong acid on wall paintings, a proton-induced X-ray emission (PIXE) microprobe has been used. This technique yields iron concentration and its depth distribution in the red painted samples. In earlier electron microprobe studies (5), the equipment proved to be not sufficiently sensitive for quantitative analysis of iron.

Experimental section

A red-painted, uncleaned sample from Beni Hasan Tomb 15 (the First Intermediate Period), and a red-painted, HCl-cleaned fragment from Beni Hasan Tomb 2 (the Middle Kingdom), were investigated using the PIXE analyses. Representative photographs of pigmented samples assembled in Beni Hasan tombs were reproduced elsewhere (5, 8).

PIXE sample preparation

The samples were grain-mounted in an epoxy resin of low curing temperature (Metaserv Metset SW). Cross-sections were exposed by cutting the sample perpendicular to the surface with a diamond saw (Buehler Isomet) using ethanol as coolant. The exposed surfaces were ground by hand with 600 and 1000 mesh carborundum on plate glass with spectroscopic grade methanol (Fisher ACS) as a lubricant. The surfaces were then polished using, in succession, 9, 3, 1, and 1/4 μm particle-size diamond pastes. Samples were observed at 100× magnification after 1000 mesh grinding, and reexamined after final polishing. When the paint and surface crust strata were clearly visible and no surface irregularities were seen under the microscope, the polishing was judged complete. The final exposed cross-sectional areas were approximately 1 mm^2. The specimens were mounted in 28 mm × 9.5 mm × 1.6 mm aluminum sample holders.

To quantify PIXE results,[2] a pellet whose composition imitates the paint layer composition was prepared. The red paint layer in the wall paintings at Beni Hasan has been found, from microprobe analyses (5), to be a mixture of iron oxide, silica, and calcium sulphate as well as phosphates and calcium carbonate.[3] The standard pellet was prepared from three components: (*1*) 0.3561 g Fe ore, National Bureau of Standards Standard Reference Material, NBS SRM 27e, (*2*)

[2]Quantification in PIXE and related techniques is difficult for thick samples of heterogeneous materials, a category in which most archaeological material falls. In provenance studies of obsidian, peak intensity ratios have been used without correction, see ref. 9*a*. Fundamental parameter methods, similar to those used routinely in electron microprobe analyses (9*b*) have been employed on ceramics (9*c*) and special consideration has been given to the development of computer-based quantification procedures for thick samples (9*d*).

[3]In ancient Egypt, anhydrous iron oxide, Fe_2O_3, has been found mixed with $CaSO_4.2H_2O$ (10*a*). The presence of calcite, quartz, gypsum, and haematite was reported in red pigments from the Tomb of Horemheb (*circa* 1350 B.C.) (10*b*).

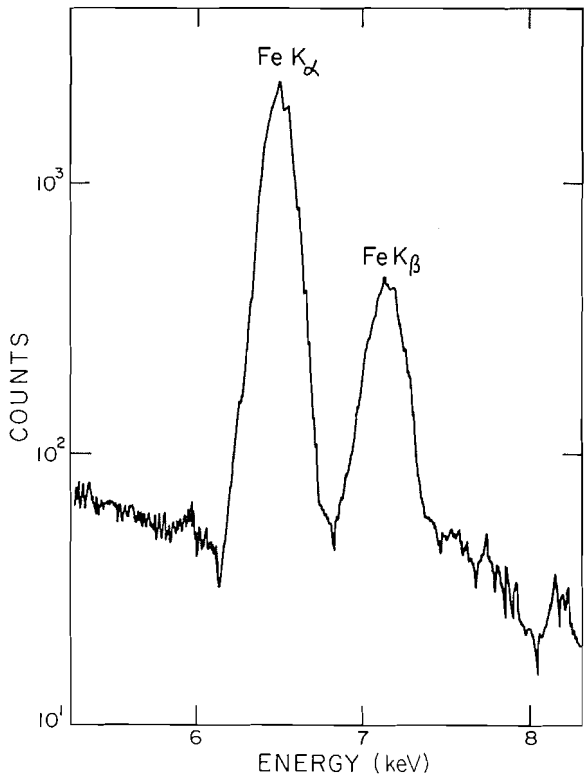


FIG. 1. An example of PIXE spectrum of Fe obtained in the present work.

0.2851 g Opal glass NBS SRM 91, and (*3*) 0.2735 g reagent grade $CaSO_4.2H_20$ (Fisher ACS). This standard contained 26.72% Fe. The three components were mixed by grinding in a mortar and pestle. The mixture was shaken twice in a WIG-L-BUG^R automatic mixer for 15 s a time. A pellet was formed by applying a pressure of 104 kg/cm^2 for 3 min using a Barnes Engineering pellet press. Upon removal, the 9 mm diameter pellet was also mounted on an aluminum sample holder. Both samples and standard were coated with an approximately 10 μm thick layer of carbon, deposited by sublimation in vacuum, to reduce charging and heating effects (11).

PIXE analyses

PIXE spectra were collected at the van de Graaff accelerator, Los Alamos National Laboratories. The superconducting solenoid magnet used as a final lens on this PIXE microprobe provides a finely-focused beam. The instrumentation has been described elsewhere (12). A 3 MeV, 4 namp, proton beam with an approximate diameter of 5 μm was employed to generate the spectra. An aluminum filter was placed in front of the Si:Li detector to reduce the intensity of the spectral background. A piece of Cu foil was placed on each sample to act as a positional reference and a conductive pathway. For the uncleaned sample, a depth profile was assembled from six spectra which were collected in 20 μm steps starting at an Fe maximum. In the cleaned sample, the depth profiles were assembled from five spectra which were collected starting from a point within the limestone substrate and extending into the paint layer as far as it was possible. An example of Fe PIXE spectrum is shown in Fig. 1.

PIXE data reduction

Data reduction was performed in Toronto: Fe concentrations have been calculated from the Los Alamos raw spectral data. The mixed-oxide pellet standard was used to reduce the background-subtracted peak areas to elemental concentrations. Backgrounds were calculated by linear extrapolation under individual peaks. It was assumed that a peak existed when the net count under the peak was greater that 2.3 times the standard deviation of the background.[4]

[4]This is the critical level for detection, $L_c = 1.64$ (2σ background) at 95% significance level (13).

TABLE 1. Concentration of Fe (%wt.) versus distance (μm)

Distance (μm)	[Fe]*	
	Cleaned sample	Uncleaned sample
0	37.9±0.4 (1.1%)	79.9±0.3 (0.4%)
20	27.5±0.3 (1.1%)	79.1±0.3 (0.4%)
40	13.6±0.2 (1.5%)	58.8±0.2 (0.3%)
60	11.9±0.2 (1.7%)	35.4±0.2 (0.5%)
80	5.6±0.1 (1.8%)	28.5±0.1 (0.4%)
100	—	20.1±0.1 (0.5%)

*The errors are the standard deviation compounded from the counting error on the background subtracted counts for each element and the error associated with the calibration standard. Relative standard deviations in percent.

Partially resolved K_a and K_b peaks from Ca were seen also, as well as three well-defined peaks due to elements lighter than calcium. None of these lighter elements was investigated in the present studies: they were expected to be due to elements which have a smaller atomic number than Ca, such as oxygen and silicon; the latter two elements can normally be investigated using the electron microprobe technique since their concentrations are relatively large.

Results

Depth and distributions

Iron concentrations from cleaned and uncleaned samples are summarized in Table 1 and plotted against depth in Fig. 2. The starting point of the scans, 0 μm, is defined as a point closer to the surface than all other points, but inside the paint layer of a sample; at this point a maximum Fe concentration was observed.

Error assessment

In a similar stratigraphic investigation of thick samples of heterogeneous materials (14) where the standards closely mimicked the samples, the error in concentration, due to the method of analysis as a whole, was estimated to be ±5%. This error can be considered, therefore, the lower limit in the present work. In investigations described below, a single standard was used; however, a single standard cannot anticipate all matrix effects in the wide range of compositions which can be encountered in a stratigraphic analysis. The proton stopping-power, the degree of enhancement by secondary X-rays and the sample absorption coefficients all change with composition.

The maximum percentage of Fe in pure Fe_2O_3 is 69.9%. The concentrations of Fe at the first two distances in the uncleaned sample (Table 1) are higher than that possible for pure Fe_2O_3 by 10% by weight or 14% relative error. Therefore, for the present analyses, 14% is assumed to be the relative method error for results whose relative standard deviation (Table 1) is less than 14%. For all other results, the relative method error is estimated by the reported relative standard deviation (Table 1). The difference between two individual results was taken to be significant if it was equal to or larger than 1σ, where σ is estimated by the relative method error as defined above; in our case $\sigma \geq 14\%$, and corresponds to a 68% level of confidence.

Discussion

The most evident findings of this work are that (*i*) the uncleaned paint layer contains appreciably more iron than the cleaned sample and that (*ii*) at least some of the analyzed

Can. J. Chem. Downloaded from www.nrcresearchpress.com by 195.138.81.100 on 09/07/12
For personal use only.

Can. J. Chem. Downloaded from www.nrcresearchpress.com by 195.138.81.100 on 09/07/12
For personal use only.

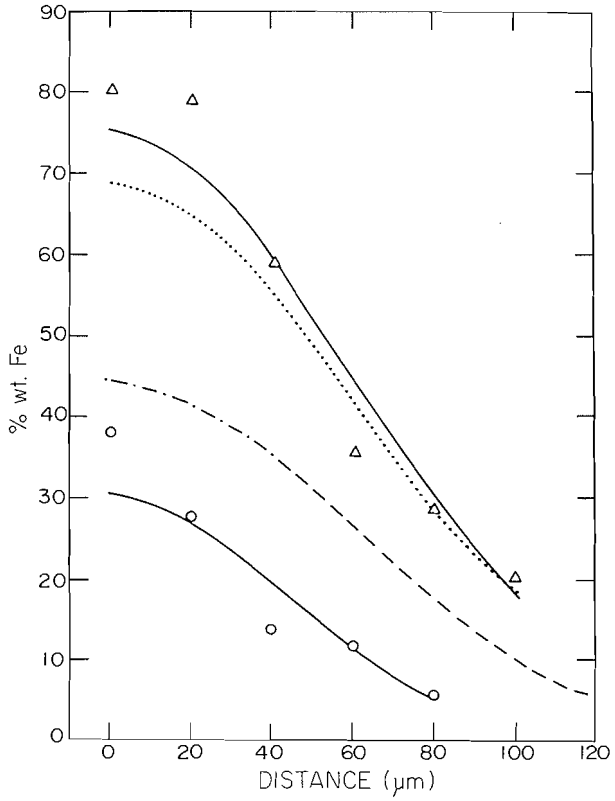


FIG. 2. Iron percentage versus distance in μm. Errors in abundance are given in Table 1; error in distance is 2.5 μm. △, uncleaned sample; upper solid curve, uncleaned sample diffusion curve, $D^{4000y}_{(Fe(u)} = (1.4 \pm 0.5) \times 10^{-16}$ cm²/s. ○, cleaned sample; lower solid curve, cleaned sample diffusion-like curve, $D^{4000y}_{Fe(c)} = (0.7 \pm 0.3) \times 10^{-16}$ cm²/s. These curves were calculated by least-squares fits to experimental data. The dashed-dotted curve was calculated from cleaned sample data plotted, using the assumption that 40 μm of the surface of the cleaned mural were removed during recent restorations; dotted line, see text. The dashed curve is identical to the lower solid curve, but displaced by 40 μm to the right; it extrapolates directly into the dashed- dotted curve.

portion of the uncleaned paint layer is almost pure Fe_2O_3. At 0 μm the Fe content of the cleaned sample is less than that of the uncleaned sample by 42% by weight; this difference is 53% of the Fe content of the uncleaned sample. Indeed, the uncleaned sample has more Fe than the cleaned sample at all distances (Table 1).

Apart from the data in Table 1, and the approximate composition of the pigment layer found in electron microprobe analyses (5), only a few analyses of ancient Egyptian red iron oxide pigments appear in the literature (10). It is suspected that, generally, the range of compositions is broad: in medieval usage, the raw materials from iron oxide red pigments ranged from as little as 20% Fe_2O_3 (14% Fe) to as much as 95% Fe_2O_3 (66% Fe) with clay and quartz making up the balance (14*a*) Two main types of red pigments are known to be used in ancient Egypt: anhydrous oxide of iron, and hydrated oxides of iron, usually referred to as red ochre (14*b*) The present work yields evidence that ancient Egyptians, as early as *circa* 2100 B.C., indeed used pigments which were, at least in part, fairly pure Fe_2O_3. Even if we were to assume that the relative error is 14% (as was done above), the pigment samples analyzed would be 100% pure. However, if the error is larger than 14% purity, purity of sample below 100% would be possible. Red pigments analyzed previously (14*c*) yielded 79.11 and 81.34 pure Fe_2O_3. We are not aware of any analyses which yield purity higher than 81.34. Red ochre, being hydrated ferric oxides, contain smaller concentrations of Fe and hence less Fe_2O_3 than pure Fe_2O_3.

Migration of Fe in uncleaned and cleaned samples

The PIXE depth profiles for Fe extend beyond 30 ± 10 μm, which is the red paint film thickness measured by optical microscopy and seen in electron microprobe depth scans (5). The subsurface depletion and dendrite formation, visible under the light microscope in yellow-painted fragments also extends beyond 30 μm; the dendrites have been found to extend 55 to 230 μm below the surface layer (5). However, these subsurface effects are not as extensive in red-painted samples (5). The depth profiles of iron concentration (Fig. 2) obtained from the PIXE analyses of the red-painted samples are similar to distributions which would arise if changes in Fe concentrations in depth were due to diffusion. Therefore, the Fe depth profiles (Fig. 2) suggest that the red-painted samples are also affected by the subsurface presence of solvent; specifically, they imply that transport of iron away from the paint layer has occurred. This finding had not been detected previously (5) in earlier electron microprobe work.

To calculate apparent diffusion coefficients for Fe ion migration, one can assume that the depth profiles of Fe in both samples are the result of a constant diffusion-like ion migration which has occurred either over 4 000 years, *i.e.*, the approximate age of these paintings, or over 150 years (7), the approximate time of the acceleration of the growth of the surface degradation layer. Then, apparent diffusion coefficients for Fe ion migration in the painting substrate can be calculated from the experimental data (Table 1, Fig. 2) for these two time periods. If it is assumed that diffusion-like migration has occurred from a film of uniform composition into the limestone-based substrate, then the concentration distribution can be described by (15)

$$[1] \qquad C(x) = K \exp(-x^2/4Dt)$$

where D is the apparent diffusion coefficient and concentration at distance x is represented by $C(x)$.[5] The pre-exponential factor, K, is equal to $M/(\pi Dt)^{1/2}$, where M is the initial mass of diffusing substance per unit area in the thin film. Apparent diffusion coefficients can be calculated from the least-squares fitted curve of ln $C(x)$ versus x^2. Error in the diffusion coefficient is reported throughout as the 95% C.I. based on the standard deviation of the slope of the fitted curve.

The apparent diffusion coefficient for Fe in the uncleaned sample, $D^{4000y}_{Fe(u)}$, is $(1.4 \pm 0.5) \times 10^{-16}$ cm²/s assuming constant temperature diffusion over approximately 4 000 years. The dotted line (Fig. 2) was plotted using the assumption that at 0 μm, the Fe weight percent is equal to 69.9%; its diffusion coefficient over 4 000 years, being $(1.5 \pm 0.4) \times 10^{-16}$ cm²/s, did not differ significantly from $D_{Fe(u)}$ reported above. Using

[5]The use of this equation assumes that migration occurs from the thin film in the positive direction x, in our case into the limestone. In a semi-infinite boundary condition, it is implicit that C(0) does not change when $x = 0$; this condition may also be accommodated by the immobilization of pigment in the paint layer. However, it is necessary that the source of the diffusing material exceed some minimum thickness. A minimum layer thickness for the assumption of the semi-infinite boundary condition can be calculated from the expression: $l_{(min)} = 4.3(Dt)^{1/2}$; ref. 15(*a*). Using the estimates of the diffusion coefficient found here, $l_{(min)}$ is approximately 130 μm: the thickness of the paint film is about one quarter of this value.

Can. J. Chem. Downloaded from www.nrcresearchpress.com by 195.138.81.100 on 09/07/12
For personal use only.

the same method of calculation for the diffusion coefficient of Fe in the limestone painting substrate in the cleaned sample, $D^{4000y}_{Fe(c)} = (0.7 \pm 0.3) \times 10^{-16}$ cm^2/s. For diffusion over 150 years, $D^{150y}_{Fe(u)} = (4 \pm 1) \times 10^{-15}$ cm^2/s and $D^{150y}_{Fe(c)} = (2 \pm 1) \times 10^{-15}$ cm^2/s. Note that these apparent diffusion coefficients in the cleaned sample are approximately half of those found for the uncleaned sample. At first sight, these calculations may suggest that Fe in the cleaned sample moved a shorter distance over the equivalent time period as did Fe in the uncleaned sample only because the sample was recently cleaned with HCl. However, this explanation cannot be accepted: it would be unreasonable to suggest a mechanism which would require that apparent diffusion coefficients, obtained from calculations based on diffusion over millennia, are affected by recent HCl cleaning. Furthermore, such a mechanism should account for the fact that the concentration of Fe in the cleaned sample is lower than that of the uncleaned sample at each distance (Table 1). One would expect that the apparent diffusion coefficients in the cleaned and uncleaned samples be the same, if the pigment does not interact chemically with HCl during cleaning. If, on the other hand, one is to assume that red pigment is somewhat soluble in HCl, cleaning should promote migration of iron into the substrate; then the inequality $D_{Fe(c)} > D_{Fe(u)}$ would be predicted. Dissolution of pigment in HCl is indeed possible: it has been reported that 50% HCl has been used to dissolve iron oxides in limestone fractionation experiments (16). However, the inequality $D_{Fe(c)} < D_{Fe(u)}$ is observed.

To explain the differences in Fe ion apparent diffusion coefficients in the cleaned and uncleaned samples, it is first assumed that 20 to 40 μm of paint layer has been removed during restorations. Then, apparent diffusion coefficients were recalculated by translating the cleaned Fe depth profile by 20 μm and by 40 μm (Fig. 2). This yields $D^{4000y}_{Fe(c)}(20\ \mu m) = (1.0 \pm 0.4) \times 10^{-16}$ cm^2/s and $D^{4000y}_{Fe(c)}(40\ \mu m) = (1.4 \pm 0.6) \times 10^{-16}$ cm^2/s. The $D^{4000y}_{Fe(c)}$ calculated in this manner, and especially $D^{4000y}_{Fe(c)}(40\ \mu m)$, are comparable to the apparent diffusion coefficient calculated for the uncleaned sample. Thus, the lower value of the $D^{4000y}_{Fe(c)}$, *i.e.* $D^{4000y}_{Fe(c)} = (0.7 \pm 0.4) \times 10^{-16}$ cm^2/s, from the cleaned sample data, may be attributed to the removal of the paint layer during recent *in situ* cleaning. The removal of 40 μm of paint layer is equivalent to the removal of 60% of the Fe pigment; the latter estimate is deduced by comparing the areas under the two solid % Fe *versus* distance curves for the cleaned sample (Fig. 2). This conclusion should be considered with a measure of caution: apparent diffusion coefficients just overlap at 95% confidence interval. Furthermore, there is no reason to believe that the original thickness of the pigment layers was the same for both samples investigated. Therefore, the 60% number has more qualitative than quantitative significance: the percent of pigment removed by cleaning may have been smaller or larger than 60% depending upon the original thickness of the pigment of the cleaned sample. Nonetheless, present findings suggest that a removal of some 60% of the pigment is possible. Such a removal would constitute major damage to the painted surfaces and should not be considered acceptable. If one were to accept a loss of pigments in order to restore the beauty of the original mural, one would have to face an even graver consequence of current restoration practices: one may expect that a cleaned surface will develop again, relatively quickly, its own new grey crust of dust imbedded in $CaCO_3$. This time it will not be possible to remove the crust with HCl, without removing practically all the remaining pigment.

It is difficult for a technician who is responsible for the cleaning of murals to estimate the amount of pigment removal which occurs during the restoration. His primary responsibility is to produce a good product, *i.e.*, a well-cleaned, fresh-looking mural surface; and indeed visual inspection of restored murals by an interested visitor entice admiration of a beautiful restoration effort. Murals do look lighter in colour, as indeed they should because fresh layers of pigments are exposed and because they contain now an appreciable amount of white calcium carbonate. However, low percent concentrations of Fe_2O_3 in red pigments have often been used in Egypt and elsewhere (10, 14*a*); therefore, the quality of colour may not be questioned. On the other hand, HCl washing using papier-maché sponges yields loose $CaCO_3$ deposits which contain appreciable quantities of sand, an efficient abrasive of an already damaged pigment. Therefore, removal of large quantities of pigments may not be totally unexpected.

A mechanism for Fe migration

Using kinetic parameters found in high temperature diffusion studies for Fe in single Fe_2O_3 crystals[6] (17), a diffusion coefficient of 4×10^{-40} cm^2/s at 25°C has been calculated for Fe, assuming a temperature-independent pre-exponential factor. This number is 10^{25} times smaller than the observed apparent diffusion coefficients. This mechanism for explanation of diffusion-like data (Fig. 2) can therefore, be neglected. The mechanism for solid state diffusion in single crystals involves substitutional and interstitial migration of ions through the crystal lattice, which is indeed a relatively slow process.

For solid state diffusion in a less-ordered system, for example, ground calcite, the diffusion coefficient is considerably higher. Using kinetic parameters obtained elsewhere[7] (18), the diffusion coefficient for the self-diffusion of ^{14}C in ground calcite has been calculated as 2×10^{-28} cm^2/s at 25°C. This represents an increase of 10^{12} over the diffusion coefficient of Fe in single crystals; a change of this magnitude is apparently due to increased migration along calcite microcrystal boundaries. (The factor of 10^{12}, *i.e.* 10^{-40} *vs.* 10^{-28} is probably still too small because the diffusion of ^{14}C may be expected to occur in conjunction with movement of CO_3^{2-}; its diffusion coefficient in single crystals is expected to be considerably smaller than that of iron. Since the diffusion coefficient for ^{14}C in ground calcite is still smaller by a factor 10^{12} than that found for Fe in the painting substrate at Beni Hasan, it can be concluded that this type of self-diffusion process is also too slow to account for apparent diffusion coefficients observed in this work.

On the other hand, diffusion coefficients for ions in free solution are of the order of 10^{-5} cm^2/s. This diffusion process is some 10^{11} times faster than the diffusion in Beni Hasan samples. Therefore, the observed apparent diffusion coefficients cannot be attributed to free diffusion in solution.

Ion migration within solvent-saturated pores, *i.e.*, within rock (19), decreases diffusion coefficients by one to three orders of magnitude from the solution value depending, in part, on the degree of porosity and tortuosity. Room temperature diffusion coefficients for the movement of $Na^+$and Cl^- in unconsolidated sediments are of the order of 10^{-5} cm^2/s in sediments with 80% porosity to 10^{-6} cm^2/s in sediments with

[6] $D_{Fe} = A \times 10^{-9} \exp(-B/k_bt)$ for $T < 1173$ K, $A = 2.8$ eV, $B = 1.8$ eV (17).

[7] $D = D_0 \exp(-E_a/k_bt)$ for 250 – 550°C, $D_0 = 4.6 \times 10^{-16}$ cm^2/s, $E_a = 71$ kJ mol^{-1} (18).

Can. J. Chem. Downloaded from www.nrcresearchpress.com by 195.138.81.100 on 09/07/12
For personal use only.

20% porosity. Room temperature diffusion coefficients of the order of 10^{-7} to 10^{-8} cm^2/s have been reported for 2-propanol in wet portland cement with 21% porosity to 1.2% porosity, respectively (20).[8] Thus, the observed apparent diffusion coefficients cannot be attributed to ion migration in solvent-saturated pores.

Diffusion coefficients measured in some porous materials may be smaller by a factor of 10^6 than those found for the free movement of ions in porous media because the interaction on, or ion exchange with, pore-wall material is slow. For example, in sodium ion/water leaching experiments on powdered silicate-based glasses, apparent ion diffusion coefficients range from 10^{-14} to 10^{-17} cm^2/s at 40°C. The 10^3 spread in the apparent diffusion coefficients is due predominantly to variation in composition of the mixed oxides which were incorporated in the silica lattice of the glasses tested (21). These numbers compare reasonably well with the apparent diffusion coefficients for iron found in this work, which are of the order of 10^{-15} to 10^{-16} cm^2/s.

The magnitude of the Fe ion apparent diffusion coefficients, over the period of 4 000 years, are of the same order of magnitude as those obtained (22) for Ca ion migration across accurately dated clay—cement interfaces. Thus, the apparent diffusion coefficient for Ca ion was found to be 1.34×10^{-16} cm^2/s to 9.77×10^{-17} cm^2/s in masonry samples ranging in age from 68 years to approximately 4 000 years (22). The 150 year Fe-ion apparent diffusion coefficients are only one order of magnitude larger than the Ca-ion apparent diffusion coefficients. It thus appears that the Beni Hasan system is fairly well mimicked by diffusion in clay cement systems.

It thus can be concluded that in the heterogeneous matrix of the limestone painting substrate at Beni Hasan, movement of Fe ions in the limestone can be most appropriately considered in terms of ionic diffusion, with active sites for the migrating ions located on the walls of the rock pores. This movement involves the presence of a solvent (water) which intimately interacts with the active sites. Substrate porosity, and intermittent water (solvent) availability in these arid tombs, appear to be the major factors responsible for the magnitude of the apparent diffusion coefficients found in the Beni Hasan samples.

Since the magnitudes of the 4 000 year and the 150 year Fe-ion apparent diffusion coefficients are both consistent with ionic diffusion within rock pores, it is not possible, on the basis of available data, to establish which of these diffusion times is more appropriate in the description of ion-migration in the painting substrate at Beni Hasan.

Ionic diffusion processes for dating purposes

Diffusion-related phenomena have been studied in ancient materials such as metals (23), obsidians (24), masonry (17) and papers (25). Dating of archaeological and historical materials has been attempted using diffusion-like phenomena and it was shown that it may be appropriate in narrowlydefined situations.[9] Present results indicate, however, that although it may be possible to obtain apparent diffusion coefficients, it is much more ambiguous to establish the reliable age of ancient materials from these diffusion coefficients alone. This latter point is relatively easy to demonstrate using such well-dated ancient materials such as the Beni Hasan murals. For example, it could not be established from the Fe-ion apparent diffusion coefficients found here whether the Fe migration took place predominantly over 4 000 years or over 150 years. The mechanism of ion migration in murals would have to be defined in much greater detail before a reasonably accurate dating would become feasible. Nonetheless, metal ion depth profiles such as found here may prove to be a means of diagnosing and monitoring the effects of industrially generated acid condensation on exposed rock and building materials.

Validity of the approach used

Results and their interpretations discussed above suggest that it is appropriate to conduct scientific studies such as these, to a large extent because they form a technical background for further restoration and conservation initiatives. Nonetheless, it should be stressed that one of the difficulties of the approach is that the samples studied, being taken from irreplaceable ancient historic records some 4 000 years old, have to be small in size and in number. Consequently, only two samples were studied here. Yet, it can also be noted that it is encouraging that much information can be obtained using such a small number of small samples. Efforts, now in progress, are directed toward expanding this work, using a larger number of samples. Generally, it is clear that more work should be done, and although the approach is clearly useful, extrapolation to other colours, murals and tombs is at best risky, if not impossible, at least for the present.

[8]2-Propanol was used to displace water in wet portland cement.

[9]In the dating of obsidian by hydration rind thickness, it has been recognized that composition, chemical reaction, and concurrent diffusion all play roles in the kinetics of hydration (24). The migration of ink in historical papers has been correlated with age, but the mechanism for the movement of Fe-based inks down paper fibrils was not determined (25).

Acknowledgements

The authors wish to thank the Egyptian Antiquities Organization for permission to take samples from the tombs at Beni Hasan. Special thanks are extended to Dr. Ali el Khouli and Mr. Mottawi Balboosh. Mr. George Taylor, Geology Department, University of Toronto, gave useful advice on sample preparation and provided the polishing and grinding compounds. Dr. C.J. Maggiore of the van de Graaff accelerator Laboratory at Los Alamos ran the PIXE spectra. This work was supported in part by the Natural Sciences and Engineering Research Council of Canada and in part by the University of Toronto.

1. (*a*) A. LOWELL. New York Times, Science Section. January 20, 1990; (*b*) a collection of papers in Science, Technology and European Cultural Heritage, Int. Symposium, Bologna, 1989, pre-print; also the Extended Abstracts of the Symposium, in press (1990).
2. G. BURNS, K. M. MATSUI, J. E. SMEATON, and K. M. WILSON-YANG. Ref. 1(*b*), paper No. 11.
3. H. J. PLENDERLITH, P. MORA, G. TORRACA, and G. DE GUICHEN. Conservation problems in Egypt; UNESCO Consultant Report No. 33.591. 1970.
4. N. M. DAVIES. Ancient Egyptian Paintings. Oriental Institute, University of Chicago and Oxford University Press, Oxford, England. 1936. p. xxiii.
5. K. M. WILSON-YANG and G. BURNS. Can. J. Chem. **66,** 2348 (1988).
6. (*a*) A. STOPPELÄERE. Ann. Serv. Antiquit. Egypt. **40**, 941 (1940); (*b*) G. TORRACA. *In* Application of science in the examination of works of art. *Edited by* Wm. Young. Museum of Fine Arts, Boston. 1970. p. 170.
7. K. M. WILSON-YANG and G. BURNS. J. Am. Res. Cent. Egypt, **19**, 119 (1982).

8. K. M. WILSON-YANG and G. BURNS. Can. J. Chem. **65**, 1058 (1987).
9. *(a)* W. R. AMBROSE, T. HACKENS, and A. BOLLAR. Nucl. Inst. Meth. Phys. Res. **191**, 397 (1981); *(b)* K. F. J. HEINRICH. Electron beam X-ray analysis. Van Nostrand-Reinhold, Toronto. 1981. Chapt. 12; *(c)* G. LAGARDE, I. BRISSAUD, J. CAILLERT, P. FONTES, and C. HEITZ. Nucl. Inst. Math. Phys. Res. **B1**, 45 (1984); *(d)* R. D. WILLIS, R. L. WALTER, R. W. SHAW, and W. F. GUTKNECHT. Nucl. Inst. Meth. **142**, 67 (1977); C. J. DUFFY, P. S. Z. ROGERS, and T. M. BENJAMIN. Nucl. Inst. Meth. Phys. Res. **B22**, 91 (1987); J. L. CAMPBELL, A. PERUJO, and W. J. TEESDALE. Nucl. Inst. Meth. Phys. Res. **B30**, 317 (1988).
10. *(a)* A. LUCAS and E. HARRIS. Ancient Egyptian materials and techniques. Arnold, London. 1962. p. 342; *(b)* W. Noll. Neues Jahrb. Mineral. **9**, 416 (1981).
11. J. A. COOKSON. *(a)* J. Radioanal. Chem. **48**, 377 (1979); *(b)* Nucl. Inst. Meth. Phys. Res. **B30**, 324 (1988).
12. *(a)* C. J. MAGGIORE. IEEE Trans. Nucl. Sci. **NS-28**, 1417 (1981); Nucl. Inst. Meth. Phys. Res. **199**, 191 (1981); *(b)* C. J. MAGGIORE, T. M. BENJAMIN, P. J. HYDE, P. S. Z. ROGERS, J. SRINIVASAN, J. TOOMER, and D. S. WOOLUM. IEEE Trans. Nucl. Sci. **NS-30**, 1224 (1983).
13. L. A. CURRIE. Anal. Chem. **40**, 586 (1968).
14. *(a)* K. WEHLTE. The materials and techniques of painting, Dix, U., Trans. Van Nostrand, New York. 1975. p. 98; *(b)* A. LUCAS and E. ARNOLD. Ancient materials and techniques. Arnold, London. 1962. p. 346; *(c)* W. HUGGINS and W. J. RUSSEL. Proc. R. Inst. **14**, 67 (1893—1895).
15. *(a)* B. TUCK. Introduction to diffusion in semiconductors. IEEE Ser. 16. Peter Peregrinus, Stevenage, Herts. 1974; pp. 199—203, p. 225; *(b)* J. CRANK. The mathematics of diffusion. 2nd ed. Clarendon, Oxford. 1983. p. 231.
16. S. P. VARNAVAS and A. G. PANAGOS. Chem. Erde, **40**, 253 (1981).
17. A. ATKINSON and R. I. TAYLOR. At. Ener. Res. Est. UKAEA, Harwell. U.K. Report. 1984 (Chem. Abstr. **102**, 209748*u* (1984)).
18. T. F. ANDERSON. J. Geophys. Res. **74**, 3918 (1969).
19. F. T. MANHEIM. Earth Planet. Sci. Lett. **9**, 307 (1970).
20. R. F. FELDMAN. Cem. Concr. Res. **17**, 602 (1987).
21. G. H. FRISCHAT. Ionic diffusion in oxide glasses. Trans. Tech. Publications, Bay Village, OH. 1975.
22. C. WADDELL and J. C. FOUNTAIN. Geology, **12**, 24 (1984).
23. M. R. NOTIS, C. E. LYMEN, H. MAYER, and C. COWEN. Mat. Res. Symp. Proc. **123**, 183 (1988).
24. *(a)* A. P. W. HODDER. J. Colloid Interfac. Sci. **103**, 45 (1985); *(b)* J. E. ERICSON. Mat. Res. Symp. Proc. **123**, 215 (1988); *(c)* W. B. WHITE. Mat. Res. Symp. Proc. **123**, 225 (1988); *(d)* J. K. BATES, T. A. ABRAJANO, W. L. EBERT, J. J. MAZER, and T. J. GERDING. Mat. Res. Symp. Proc. **123**, 237 (1988).
25. R. J. MCNEIL. *In* Archaeological chemistry. Vol. III. *Edited by* J. B. Lambert. Am. Chem. Soc. Washington D.C. 1984. p. 255.

Can. J. Chem. Downloaded from www.nrcresearchpress.com by 195.138.81.100 on 09/07/12
For personal use only.

Colloidal molybdoantimonic acids as ion exchangers

M. KONÉ, P. COURTIN, AND J. LEMERLE

Laboratoire de chimie des polymères inorganiques, Université P. et M. Curie, 4 place Jussieu, 75252 Paris, Cedex 05, France

Received November 28, 1989[1]

M. KONÉ, P. COURTIN, and J. LEMERLE. Can. J. Chem. **69**, 293 (1991).

Colloidal particles with a c.c.p. structure were obtained from mixtures of antimonic and molybdic acids through a polymerization process. These particles were octahedral and their sizes fits the log-normal distributions. The mean size decreases and the polydispersity increases with increasing Mo content in the particles. The stability of the aqueous dispersions was due to the surface charge density of the particles which was enhanced when increasing the Mo content. Ion exchange reactions can occur with the dispersions. Two different routes lead to Ag^+ fixation: substitution of core H^+ without flocculation of the dispersion or cancellation of external charges with flocculation.

Key words: inorganic exchangers, colloids, antimonic acid, molybdic acid.

M. KONÉ, P. COURTIN et J. LEMERLE. Can. J. Chem. **69**, 293 (1991).

Des particules colloïdales ayant la structure c.f.c. de l'acide antimonique sont préparées par polymérisation de mélanges d'acides antimonique et molybdique. Les liaisons en taille de ces particules octaédriques satisfont une loi log-normale. La taille moyenne diminue et la polydispersité augmente quand la teneur en Mo augmente. La stabilité des dispersions est due aux charges de surface dont la densité est augmentée par la teneur en Mo. Les dispersions de ces particules peuvent être le siège de réactions d'échange d'ions. Ag^+ peut être fixé selon deux processus : substitution des protons de la structure sans floculation de la dispersion ou annulation des charges externes causant la floculation.

Mots clés : échangeurs inorganiques, colloïdes, acide antimonique, acide molybdique.

Introduction

Inorganic ion exchangers are used in large quantities for separation processes, substitution of polyphosphates in detergents, and as inert matrices for catalyst application. Their cavities are responsible for their activities. Inorganic ion exchangers like zeolites are usually manufactured through a sol–gel process involving the mixing of aluminate and silicate solutions. Particles of inorganic oxides of colloidal size can be prepared by spontaneous polymerization of inorganic acids in aqueous solution. This route leads to particles whose composition and size can be controlled.

In previous work (1), inorganic polymers including both molybdic and antimonic acids have been prepared. In this paper we describe the nature and physicochemical properties of the particles.

Experimental

The particles were isolated by preparative ultracentrifugation from aged mixtures of antimonic and molybdic acids (1). The starting mixtures had a constant antimony concentration (6×10^{-2} mol L^{-1}) and variable molybdenum concentration ($0 < Mo/Sb < 1.88$). The preparative centrifugation was performed after 10 months. The particles were packed down to the bottom of the centrifugation tube and obtained after discarding the supernatant liquid. The particles were dried for solid state study or redispersed in water for sol study.

Preparative ultracentrifugations were carried out with a Beckman Microfuge at 10000 rpm for 1 h. In this centrifuge the tube axis is colinear with the centrifugal field.

The Mo and Sb contents of the particles were measured by atomic absorption with an air–acetylene flame for antimony and a nitrous acetylene flame for molybdenum (1). In this paper, r stands for the Mo/Sb ratio in the particles.

The solid particles were studied by electron microscopy with a Jeol 100 CX II microscope. Samples were prepared by deposition of the dilute sol containing the particles on a grid. Analytical electronic microscopy was carried out with Link equipment. X-ray powder patterns were obtained from diffractometry with a CGR Theta 60 diffractometer using CuK_α radiation. Analytical grade NaCl was added to the powders as an internal standard to yield accurate mean crystal size (2).

Analytical ultracentrifuge experiments were carried out with a Beckman model E ultracentrifuge equipped with schlieren and absorption optics. Double sector cells manufactured in Kel F were used. The rotation speed was 8000 rpm. To avoid the effects of electric charges, an electrolyte (LiCl 5×10^{-2} mol L^{-1}) was added to the samples just before the runs. Specific volumes were measured by density measurements carried out with a PAAR automatic densimeter.

Photon correlation spectroscopy (PCS) was made with a Brookhaven BI90 correlator. The samples were clarified through Millipore filters prior to the measurements.

Ion exchange (Ag^+/H^+) experiments were performed using a Methrom pH stat to keep the pH at a constant value of 6.5. $AgNO_3$ was added to the dispersion of particles. The amount of base added to keep the pH constant is recorded simultaneously with the silver electrode potential in the medium. Ion exchange experiments were also performed without addition of base. The silver electrode potential in the dispersion was measured under these conditions.

Viscosity measurements were carried out with an Ubelhode capillary viscosimeter.

Results

The composition of the particles was homogeneous as shown by analytical electron microscopy (standard deviation = 0.007 for Mo/Sb = 0.085). Electronic micrographs (TEM) of the particles showed different shapes: hexagonal, square, or diamond (Fig. 1). These shapes can be considered projections of an octahedron onto a plane. This assumption was confirmed by STEM micrographs. The particles had a tendency to associate, even if the sol is ultrasonically dispersed prior to the grid making. Association of the particles increased with increasing Mo content. Accurate size measurements could not be made for $r > 0.32$. For low Mo content ($r = 0.085$), the particles were ordered. High resolution micrographs showed ordered lattice planes with d spacings = 5.98 Å (Fig. 2). The octahedron edges (e) were measured on the micrographs to give the particle size distributions for each sample (Fig. 3). For each sample about 500 particles were measured. The experimental values fit into the log-normal distributions as are particles obtained by

[1]Revision received July 26, 1990.

Printed in Canada / Imprimé au Canada

Can. J. Chem. Downloaded from www.nrcresearchpress.com by 195.138.81.100 on 09/07/12
For personal use only.

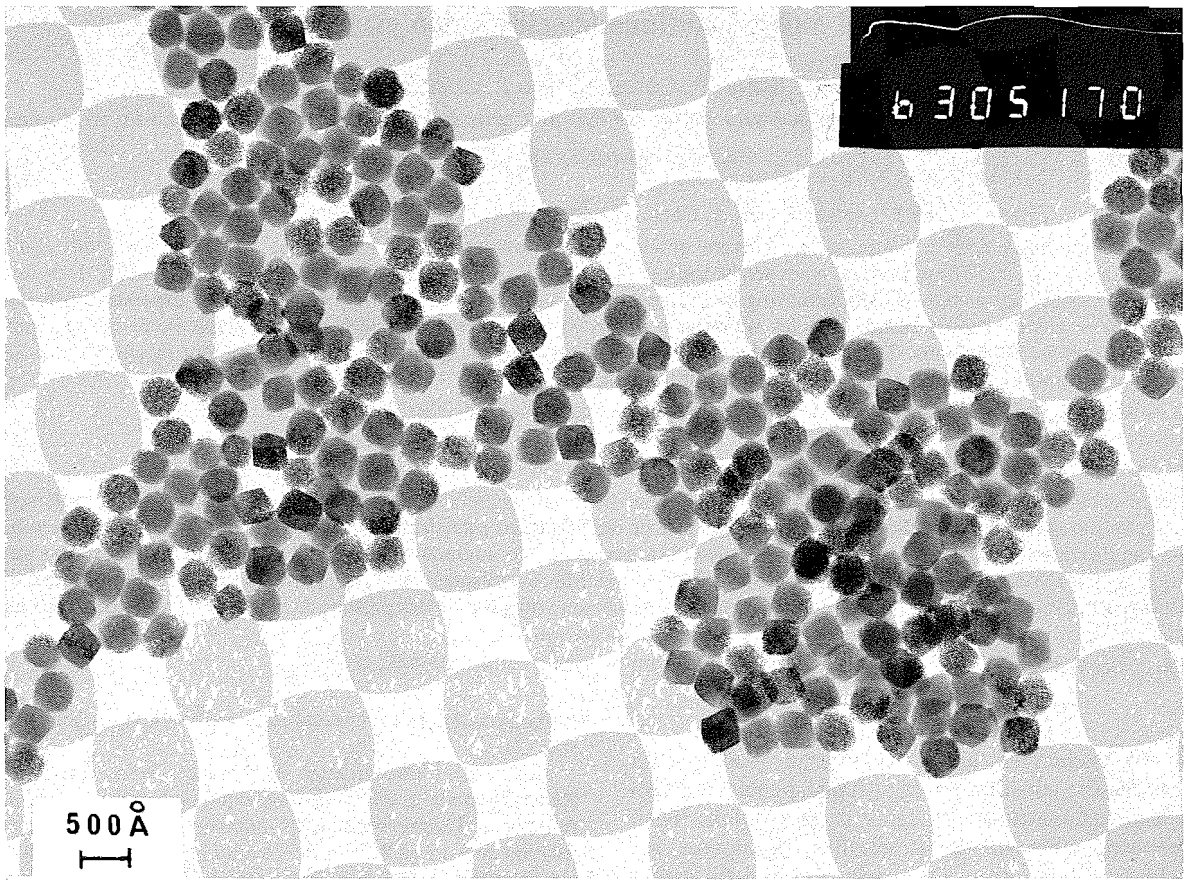


FIG. 1. Electron micrograph (TEM): composition of the particles. r = Mo/Sb = 0.085.

crystallization and/or sol gel process (3, 4). The samples were characterized by the following parameters (Table 1).

Geometric mean size $\bar{e}$:

$$\bar{e} = \sqrt[n]{e_1 e_2 \ldots e_n}$$

Standard deviation σ

$$\ln \sigma = \sqrt{\frac{\Sigma n_i (\ln e_i - \ln \bar{e})^2}{\Sigma n_i}}$$

and e_m corresponds to the maximum value on the distribution curve.

For a given ageing time of the starting mixtures before the preparative centrifugation, the size of the particles decreased when r increased. Moreover, for a given r, the particle size increased when the starting mixture aged.

Powder diffraction patterns agree with a cubic close packing (c.c.p.) structure (pyrochlore type), as in β antimonic acid (5). The unit cell decreased slightly from 10.38 to 10.33 Å when r increases from 0 to 0.32 (Table 2). Such changes have been seen in mixed oxides with a pyrochlore structure (6, 7). The d spacings corresponding to 111 planes are the same as those measured on high resolution micrographs, thus the octahedral faces correspond to 110 planes.

The peak width gave the mean crystal sizes (2) (Table 3). These mean crystal sizes are greater than the mean particle sizes measured by microscopy. Such differences are generally observed. These two measurements may be correlated using the Tronc and Bonnin (8) relationship:

$$e_{RX} = e_{\mu E} \exp [2.5(\ln \sigma)^2]$$

where e_{RX} and $e_{\mu E}$ are the sizes measured by diffractometry and electronic microscopy, respectively.

Aqueous dispersions of the particles were studied by ultracentrifugation and PCS. For a given particle concentration, the measured sedimentation coefficient was dependent on the optics used. Using absorption optics the sedimentation coefficient was about twice that using schlieren optics. With absorption optics, the light scattered is measured by the detector. Thus the heavier particles which scatter the light much more than the others were more heavily weighted in sedimentation coefficients. This artefact does not exist with schlieren optics. Nevertheless, S was independent of the concentration with UV optics ($2 \times 10^{-4} \leq C \leq 2.7 \times 10^{-3}$) and schlieren optics ($2 \times 10^{-3} \leq C \leq 10^{-1}$). As these concentration ranges overlap, S is independent of the concentration in the whole range ($2 \times 10^{-4} \leq C \leq 10^{-1}$). The distribution curves of sedimentation coefficient were calculated from ultracentrifugation patterns (9) (Fig. 4).

The sols had a reduced viscosity which was slightly dependent on the concentration.

The PCS measurements gave apparent diameters of equivalent spheres which are close to the other values (Table 4, Fig. 5).

Molybdoantimonic acids were dispersed in aqueous solutions of tetramethylammonium chloride of various concentrations (tetramethylammonium is not specifically adsorbed (10)). HCl or $N(CH_3)_4OH$ were added to these sols and after equilibrium the pH was measured. Blank solutions were made by adding HCl or $N(CH_3)_4OH$ to solutions of the same electrolyte at the same concentration and the pH measured. In the sols the negative charges (surface charges SO^-, Cl^-, and OH^-) must

Can. J. Chem. Downloaded from www.nrcresearchpress.com by 195.138.81.100 on 09/07/12
For personal use only.

Can. J. Chem. Downloaded from www.nrcresearchpress.com by 195.138.81.100 on 09/07/12
For personal use only.

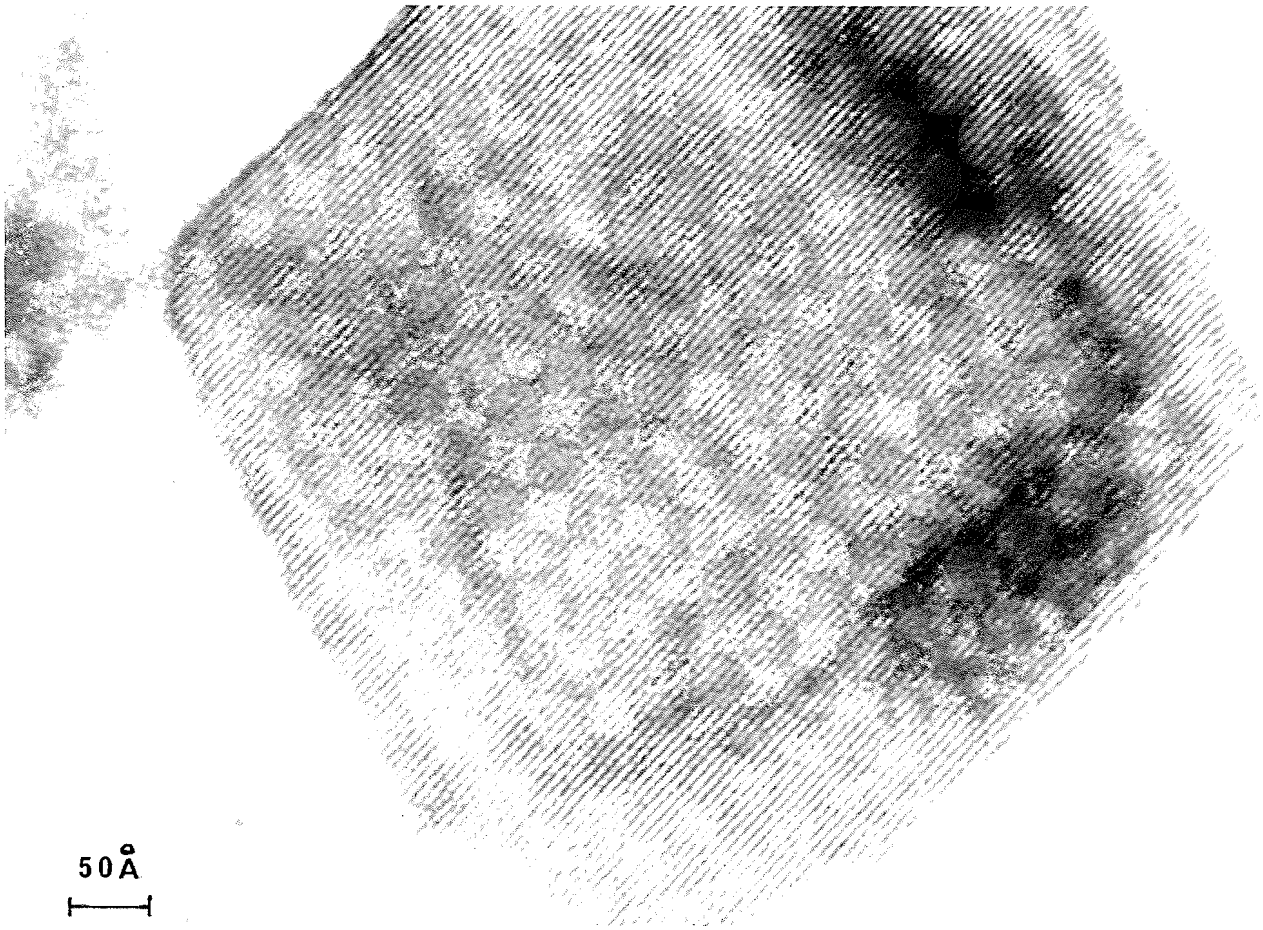


FIG. 2. High resolution electron micrograph (TEM): composition of the particle. r = Mo/Sb = 0.085.

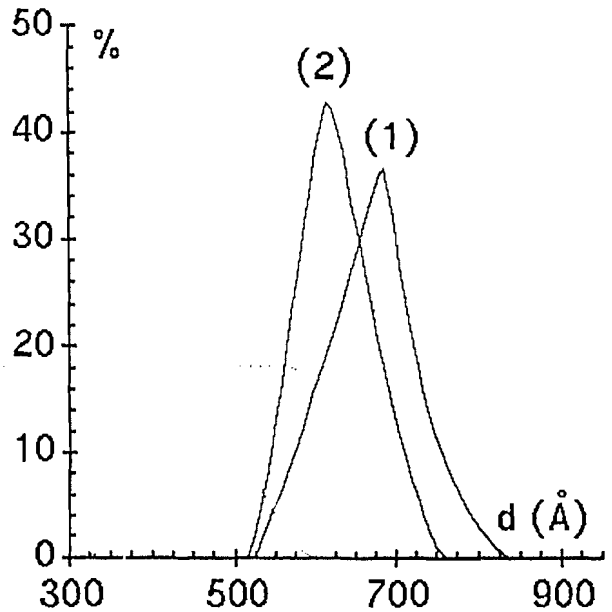


FIG. 3. Distribution curves of particles size measured by electron microscopy, (*1*) Mo/Sb = 0.085, (*2*) Mo/Sb = 0.165.

be balanced by positive charges:

$$[SO^-] + [OH^-] + [Cl^-] = [H^+] + [N(CH_3)_4{}^+]$$

Here $[Cl^-]$ and $[N(CH_3)_4{}^+]$ are known quantities, and $[H^+]$ and $[OH^-]$ were obtained from pH measurements on the sols and the corresponding blank solutions. Thus $[SO^-]$ can be obtained.

TABLE 1. Mean particle size measured by electronic microscopy

$r = \frac{Mo}{Sb}$	$\bar{e}$ (Å)	σ	e_m (Å)
0.085	686	1.065	686
0.165	635	1.074	618
0.32	538	1.112	484

These values are plotted in Fig. 6. The values obtained with different electrolyte concentrations are very close. The intersection point of these curves corresponds to $[SO^-] = 0$ for pH ~ 0.88, corresponding to the PZC of the molybdoantimonic acid (19). In a colloidal dispersion in pure water, H^+ is the cation in the diffuse layer.

The dispersions were titrated by rapid addition of tetramethylammonium hydroxide (maximum addition time 10 s). These protometric titrations were made at constant ionic strength using tetramethylammonium chloride (0.1 mol L^{-1}). The number of H^+ titrated is almost independent of the ionic strength. Under these conditions (fast protometric titrations) the surface of the particles is not modified. The concentration of H^+ in the diffuse layer corresponds to the $[H^+]$ measured and is the same as that from pH measurements, after standardization of the glass electrode for the same ionic strength. The results are reported in Table 5.

The sizes and structure of the particles were not modified (no changes in ultracentrifugation measurements and powder

TABLE 2. d spacing in particles

(a) Molybdo antimonic acids

$r = 0$, $a = 10.38$ Å				$r = 0.085$, $a = 10.36$ Å			$r = 0.32$, $a = 10.33$ Å		
d_{exp}	hkl	d_{calc}	I/I_1	d_{exp}	d_{calc}	I/I_1	d_{exp}	d_{calc}	I/I_1
5.993	111	5.993	100	5.985	5.981	100	5.960	5.964	100
3.129	311	3.129	68	3.127	3.124	68	3.118	3.115	70
2.996	222	2.996	74	2.992	2.991	80	2.984	2.982	83
2.595	400	2.595	16	2.592	2.590	15	2.582	2.582	16
2.381	331	2.381	13	2.379	2.377	11	2.371	2.370	11
1.998	333 511	1.998	18	1.994	1.994	19	1.992	1.988	19
1.835	440	1.835	34	1.832	1.832	33	1.825	1.826	37
1.754	531	1.754	24	1.752	1.751	22	1.743	1.746	20
1.583	533	1.583	9	1.580	1.580	10	1.575	1.575	8
1.565	622	1.565	25	1.563	1.562	24	1.557	1.557	27
1.498	444	1.498	6	1.495	1.495	6	1.490	1.491	6
1.453	711 551	1.453	11	1.451	1.451	11	1.446	1.446	11
1.351	553 731	1.351	11	1.349	1.349	9	1.345	1.345	9

(b) Exchanged materials

$r = 0$, $a = 10.27$ Å				$r = 0.085$, $a = 10.27$ Å			$r = 0.32$, $a = 10.29$ Å		
d_{exp}	hkl	d_{calc}	I/I_1	d_{exp}	d_{calc}	I/I_1	d_{exp}	d_{calc}	I/I_1
2.967	222	2.965	100	2.967	2.965	100	2.976	2.970	100
2.569	400	2.568	33	2.569	2.568	31	2.571	2.572	28
1.815	440	1.815	38	1.815	1.815	38	1.819	1.819	47
1.548	622	1.548	31	1.549	1.548	29	1.552	1.551	29
1.483	444	1.482	9	1.483	1.482	7	1.485	1.485	7
1.284	800	1.284	3	1.284	1.284	3	1.286	1.286	2

TABLE 3. Mean crystal size measured by diffractometry

$r = \frac{Mo}{Sb}$	a (Å)
0.085	814
0.165	644
0.32	559

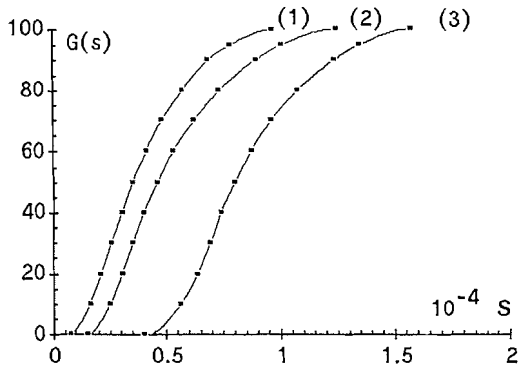


FIG. 4. Cumulative distribution curves of sedimentation coefficient (*1*) Mo/Sb = 0.60, (*2*) Mo/Sb = 0.32, (*3*) Mo/Sb = 0.085.

diffraction patterns) when the addition of base was stopped at pH reaches 7.

The particles had the same structure as β antimonic acid which is an ion exchanger (H^+ in the core particles can be removed by other cations) (5, 11), and they can also have ion exchange properties. In the first experiment, small amounts of Ag^+ were added to a dispersion of particles at constant ionic strength (tetramethylammonium nitrate 0.1 mol L^{-1}). The curve which represents the variation of the silver electrode potential exhibited two steps (Fig. 7). Before the first step the sol is homogeneous. The potential at the Ag-sensitive electrode indicates a low Ag^+ concentration in the solution: Ag is in or on the particles. As the sol is not flocculated during this step, Ag is not quantitatively fixed onto the SO^- sites located at the surface. At higher Ag^+ ratios, addition of Ag to molybdoantimonic acid induces flocculation of the sol. The peptization can only be obtained if the pH is risen to the higher values near 7.5. In the second experiment, the addition of silver nitrate was done at pH = 6.5. After each addition of Ag^+, the pH was kept constant to 6.5 by adding a strong base ($N(CH_3)_4OH$). The concentration of free Ag^+ in solution was measured potentiometrically with a silver electrode. Figure 8 shows the variation of the amount of base added to keep the pH constant versus the amount of Ag^+ added. This curve exhibits three segments of different slopes. Along the segment AB, one H^+ is titrated when one Ag^+ is added. The dispersion remains homogeneous. Along the segment BC, the dispersion flocculates. During this section

Can. J. Chem. Downloaded from www.nrcresearchpress.com by 195.138.81.100 on 09/07/12
For personal use only.

TABLE 4. Sedimentation coefficient (S), density (ρ), and diameters ($\bar{D}$, D_m) of the particles considered as spheres:

$r = \frac{Mo}{Sb}$	S (Svedberg)	ρ (g cm^{-3})	Ultracentrifugation measurements			PCS measurements	
			$\bar{D}$ (Å)	σ	D_m (Å)	D (Å)	σ
0.085	7353	4.42	687	1.144	630	670	1.4
0.11	6476	4.38	665	1.160	610	610	1.4
0.165	6024	4.35	616	1.182	569	540	1.4
0.32	3510	4.24	545	1.237	480		
0.47	3180	4.15	514	1.250	426		
0.60	3055	4.12	495	1.252	425		

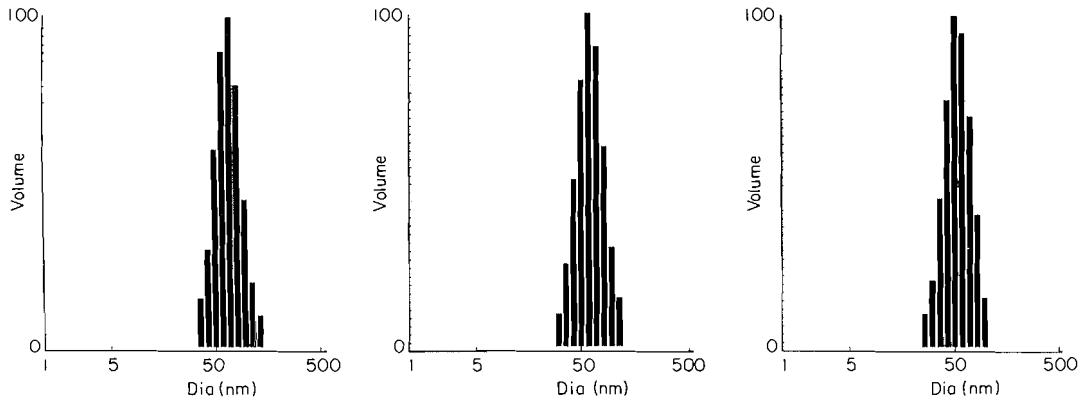


FIG. 5. Log-normal distribution curves measured by PCS. (*1*) Mo/Sb = 0.085, (*2*) Mo/Sb = 0.11, (*3*) Mo/Sb = 0.165.

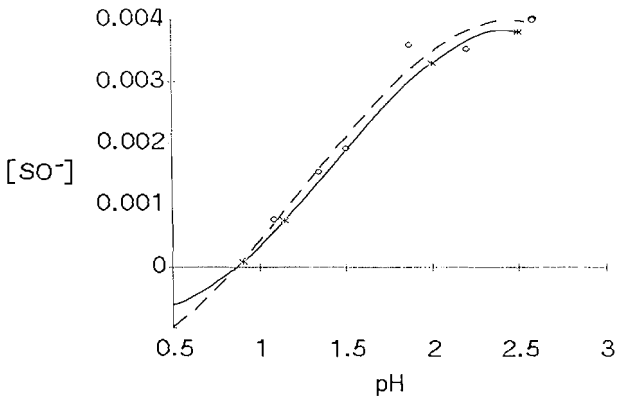


FIG. 6. Concentration of SO^- sites (in mol L^{-1}) as a function of pH of the sol (Mo/Sb = 0.085). ○, $[N(CH_3)_4Cl]$ = 1 mol L^{-1}; +, $[N(CH_3)_4Cl]$ = 0.1 mol L^{-1}.

the number of titrated protons is lower than the number of added Ag^+. Between A and C, Ag^+ obtained from electrode measurements is negligible. After C, Ag^+ does not react. The ratios corresponding to C are reported in Table 6.

These Ag^+/Sb ratios and that corresponding to the composition of the flocculated materials are the same. The amount of Ag fixed in the particles is higher at pH 6.5. than that in acidic medium. The structure of the flocculated materials was that of silver antimonate (c.c.p. pyrochlore type) corresponding to r = 0 (Table 2) (11). The unit cell dimension of the antimonates with a pyrochlore structure is generally decreased when H is substituted by Ag (6, 11, 12).

TABLE 5. Protometric titration of the sols, surface charge density (σ_S) determination

r	C_1[a] (mol L^{-1})	pH	(H^+) titrated (mol L^{-1})	σ_S[b] (μC cm^{-2})	
				(*1*)	(*2*)
0	0.06	2.7	0.003	70	84
0.085	0.065	2.34	0.0097	327	409
0.165	0.070	2.17	0.0126	365	399
0.32	0.079	2.05	0.0190	421	475

[a] C_1 = [Mo] + [Sb] = [Sb] × (1 + r).
[b] (*1*) σ_S at the pH of the dispersion for the given concentration of molybdoantimonic acid, (*2*) σ_S at pH = 6.5.

Discussion

The octahedral particles can be assumed to have approximately the same hydrodynamic behaviour as spheres. Under this condition, their frictional coefficient in the aqueous phase can be estimated from Stokes' law. Assuming the particles are not solvated, the diameter of the rigid sphere (D) can be obtained from the sedimentation velocity S (Table 4) from the following relationship.

$$D = 2\sqrt{\frac{9S\eta}{2(\rho - \rho_0)}}$$

where η is the solvent viscosity, ρ the particle density (Table 4), and ρ_0 the solvent density. The diameter D_m, corresponding

Can. J. Chem. Downloaded from www.nrcresearchpress.com by 195.138.81.100 on 09/07/12
For personal use only.

Can. J. Chem. Downloaded from www.nrcresearchpress.com by 195.138.81.100 on 09/07/12
For personal use only.

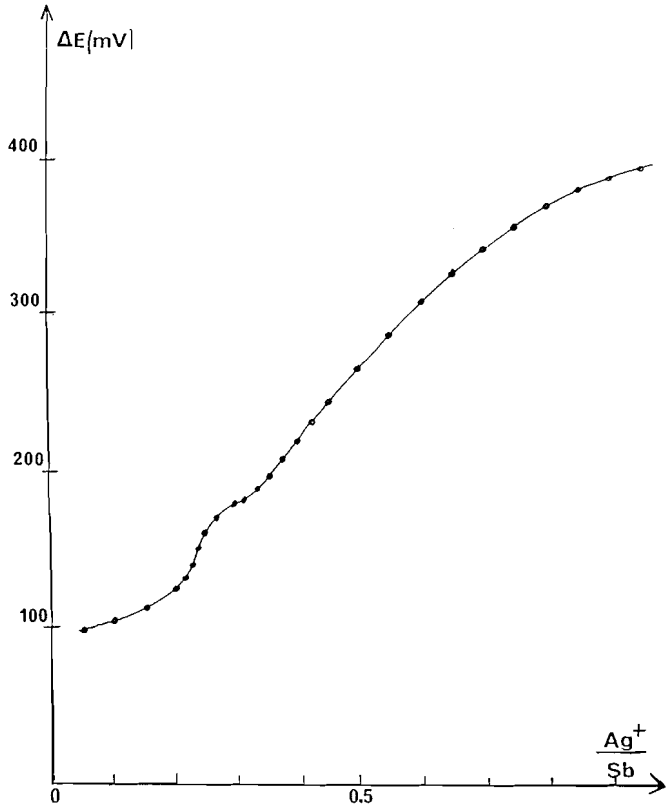


FIG. 7. Ion exchange experiment in acidic medium, $r = 0.085$.

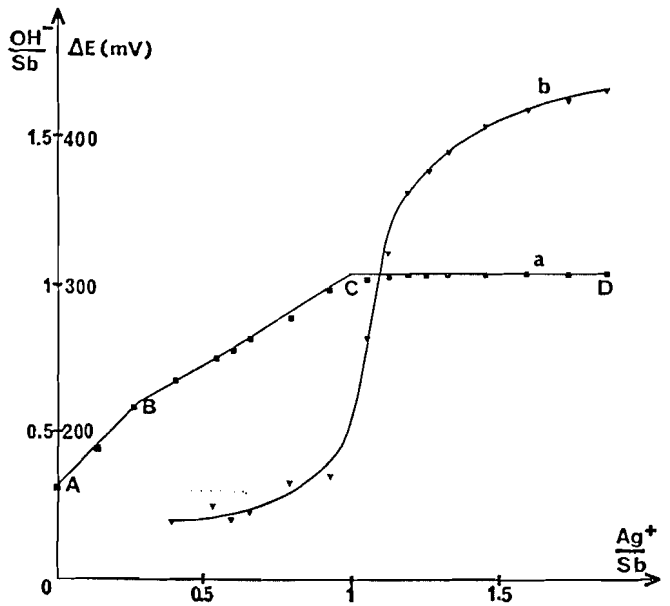


FIG. 8. Ion exchange experiment at pH 6.5; $r = 0.32$; curve a $(OH^-/Sb) = f(Ag^+/Sb)$, curve b, $\Delta E_{Ag} = f(Ag^+/Sb)$.

to the maximum on the distribution curve of sedimentation coefficient, and the geometric mean size are reported in Table 4. The particle sizes measured by different methods are in good agreement. The dispersed phase had the same sedimentation coefficient as the high polymers in the starting mixture before preparative centrifugation (1). Ultracentrifuge and PCS measurements give the hydrodynamic diameter while diffractometry and electronic microscopy give the diameter in the solid state. As these values are close, the solid crystalline particles pre-exist in the dispersed phase.

TABLE 6. Ion exchange properties of the particles

$r = \frac{Mo}{Sb}$	$\frac{Ag^+}{Sb}$	$\frac{H^+}{Sb}$
0	1	1
0.069	1	0.99
0.32	1.04	1.04
0.47	0.795	0.80
0.60	0.66	0.66

The reduced viscosity also leads to the hydrodynamic diameter of the spheres. With our experimental results ($[\eta] = 1.1$ cm^3 g^{-1} for $r = 0.085$), the Stokes–Einstein law or the Hiltner and Krieger formula (13) (suspensions of charged spherical particles) give results which are close. This hydrodynamic diameter is higher than the core diameter measured from electronic micrographs and leads too high a value for the thickness of a water shell. This abnormally high hydrodynamic diameter can be attributed to the electroviscous effects which have not been taken into account in the calculation. Such deviations have already been seen for charged spheres at low ionic strength and low shear rates (14, 15).

The stability of the particle dispersions arises from electric charges located at the surface of the particles (16, 17). The pH at which the surface charge is zero (PZC) is about 0.88. The pH of the dispersions is near 2. The reaction at the surface can be summarized as following.

$$[1]\quad \overline{SOH} \Leftrightarrow \overline{SO}^- + H^+, \qquad k_1 = \frac{\bar{a}_{SO^-}\, a_{H^+}}{\bar{a}_{SOH}}$$

where a_i is activity of species i, and bars refer to values in the dispersed phase. $[H^+]$ can be measured from fast protometric titrations or from pH measurements. This value depends on the pH of the sol.

The number of negative charges (z) per particle is $z = [\overline{SO}^-]/C_0$ where $[SO^-] = [H^+]$, C_0 is number of particles per unit volume, $C_0 = C_1/m$, $C_1 = [Sb + Mo]$, and m = number of atoms in a particle. In a pyrochlore structure the unit cell contains 16 atoms. The number of atoms in a particle is:

$$m = \frac{16V}{v_0}$$

where V, v_0 represents the volume of a particle and a unit cell, respectively. The number of electric charges per unit of surface area σ_S, can be calculated from:

$$\sigma_S = \frac{1.6 \times 10^{-19} z}{S}$$

where S is area of the particle surface, and

$$\sigma_S = \frac{1.6 \times 10^{-19} \times 16[H^+]}{v_0 C_1}\frac{V}{S} = \frac{2.56 \times 10^{-18}[H^+]}{v_0 C_1}\frac{V}{S}$$

For an octahedron

$$V = e^3\frac{\sqrt{2}}{3}$$

$$S = 2e^2\sqrt{3}$$

where e is the octahedron edge.

Can. J. Chem. Downloaded from www.nrcresearchpress.com by 195.138.81.100 on 09/07/12
For personal use only.

Taking into account the log normal distribution of the particle size, these expressions become

$$V = \int_0^\infty \frac{\sqrt{2}}{3} e^3 f(e)\mathrm{d}e$$

$$S = \int_0^\infty 2\sqrt{3} e^2 f(e)\mathrm{d}e$$

with

$$f(e) = \frac{1}{\sqrt{2\pi}\ln\sigma} \exp\left[-\left(\frac{\ln(e/\bar{e})}{\sqrt{2}\ln\sigma}\right)^2\right]$$

We obtain

$$\frac{V}{S} = \frac{\bar{e}\sqrt{2}}{6\sqrt{3}} \exp\left[\frac{7}{2}(\ln\sigma)^2\right]$$

If the particles are spheres

$$\frac{V}{S} = \frac{\bar{e}}{6} \exp\left[\frac{7}{2}(\ln\sigma)^2\right]$$

Antimonic acid particles are spheres and molybdoantimonic acid particles are octahedral. Accurate values for V/S are used according to the shape of the particles. The surface charge of the particles depends on the pH of the sol. The influence of Mo content on σ_S can be shown in two ways: (*i*) σ_S is calculated at the same pH for all samples. Under these conditions $[H^+]$ is measured from the number of protons released from the surface when pH increased from PZC to the fixed value. (*ii*) σ_S is calculated at the pH of the dispersion of molybdoantimonic acids. In this case the concentration in antimony and pH of the sol must be given.

The results are reported in Table 5. When Mo is included in antimonic acid, σ_S is roughly increased. When the Mo content increases, the size of the particles decreases, leading to small changes in σ_S values but an increase in $[SO^-]$.

Ag fixation in the particles can be made through two routes: (*i*) ion exchange in the whole particles (core and surface) as for zeolites (18) antimonates (11, 12).

[2] $\overline{H^+} + Ag^+ \Leftrightarrow H^+ + \overline{Ag^+}$

$$k_2 = \frac{a_H \bar{a}_{Ag}}{\bar{a}_H a_{Ag}}$$

(*ii*) fixation of Ag on the SO^- sites located at the surface

[3] $\overline{SO^-} + Ag^+ \Leftrightarrow \overline{SOAg}$

$$k_3 = \frac{\bar{a}_{SOAg}}{\bar{a}_{SO^-} a_{Ag^+}}$$

The general formulae of these compounds correspond to $Sb_{1-x}Mo_xO_3H_{1-x}$. The protons and antimony atoms are present in the same quantity in the particles. The protons displaced by Ag at pH 6.5 are almost all of the protons present in the particles. Thus both routes have to be taken into account.

If $k_2 > k_3$, ion exchange in the core of particles can occur prior to fixation onto the SO^- sites located at the surface. Under these conditions, if Ag is added in small quantities, no flocculation occurs. Ag can be fixed at the surface if it is added in great quantities. As the concentration of H^+ in solution increases, Ag cannot be exchanged quantitatively according to equilibrium [2]. The concentration of Ag in solution increases, leading to a kick on the curve representative of Ag potential.

In the experiments performed at pH = 6.5, equilibrium [2] is displaced towards the right. The amount of Ag exchanged is increased. During the first step (AB) (Fig. 7), only ion exchange (equilibrium [2]) takes place. During the second step (BC) two equilibria take place. As exchange is favored by increasing pH, the concentration of Ag in solution is kept very low and the representative curve of the Ag potential does not exhibit a step before all the H^+ are removed and all the Ag^+ fixed onto the whole SO^- sites.

The particles are formed through a polymerization process (1) involving water elimination between two adjacent monomers. In acidic medium Mo and Sb are six-coordinated and approximately the same size. MoO_6 octahedra can easily substitute SbO_6 octahedra when building the c.c.p. structure. Mo atoms limit the extension of the polymerization. For $r > 0.32$ the particles are associated and the crystallinity is decreased; therefore the particle size could not be accurately measured. For Mo-rich particles ($r > 0.32$) there is not enough Sb to build defect-free pyrochlore structure. The ion exchange properties of the pyrochlore structure are modified and the amount of H^+ removed from the particle core must decrease.

Conclusion

Colloidal particles with a narrow size distribution were formed through a polymerization process and no noticeable aggregation occurs in the solid state. These particles are ion exchangers. The fixation of cations is done through two different reactions: substitution of protons in the structure or cancellation of the external charges. The relative occurrence of these two processes is monitored by the Mo content of the particles which controls their charge surface density.

1. M. Koné, P. Courtin, and J. Lemerle. Can. J. Chem. **68**, 36 (1990).
2. R. Guinier. Théorie et technique de la radiocristallographie. Dunod, Paris. 1964. p. 464.
3. R. R. Irani and C. F. Callis. Particle size measurement, interpretation and application. J. Wiley, New York. 1963. pp. 39–41.
4. F. Tourinho, R. Frank, and R. Massart. J. Mat. Sci. In press.
5. J. Lemerle. Rev. Chim. Min. **9**, 863 (1972).
6. D. Groult, C. Michel, and B. Raveau. J. Inorg. Nucl. Chem. **35**, 3095 (1973).
7. J. Lemerle and J. Lefebvre. Bull. Soc. Chim. **34**, 409 (1976).
8. E. Tronc and D. Bonnin. J. Phys. Lett. **46**, 437 (1985).
9. V. N. Schumaker and H. K. Schachman. Biochim. Biophys. Acta, **23**, 628 (1957).
10. J. Lemerle and J. Lefebvre. J. Chim. Phys. **1**, 97 (1974).
11. J. P. Jolivet and J. Lefebvre. Rev. Chim. Min. **9**, 845 (1972).
12. M. Abe and T. Itoh. J. Inorg. Chem. **42**, 1641 (1980).
13. P. A. Hiltner and I. M. Krieger. J. Phys. Chem. **73**, 2386 (1969).
14. J. Stone-Masui and A. Watillon. J. Colloid Interface Sci. **28**, 187 (1968).
15. J. Stone-Masui and A. Watillon. J. Colloid Interface Sci. **34**, 327 (1970).
16. G. A. Parks and P. L. De Bruyn. J. Phys. Chim. **66**, 967 (1962).
17. G. A. Parks. Chem. Rev. **65**, 177 (1965).
18. R. M. Barrer and D. C. Sammon. J. Chem. Soc. 2838 (1955).
19. J. Lyklema. *In* Solid liquid dispersions. *Edited by* Th. F. Tadros, Academic Press. 1987. pp. 63–89.

Étude conformationnelle et structurale de 1,5-diacétoxy-3,4-bis(bicyclophosphoranylato)quinate de méthyle

MICHEL BALTAS, LATIFA CHAHOUA, LILIANE GORRICHON[1] ET PIERRE TISNÈS

Synthèse et physicochimie organique, Unité de recherche associée au Centre national de la recherche scientifique, n° 471, Université Paul Sabatier, 118 route de Narbonne, 31062, Toulouse CEDEX, France

DOURAID HOUALLA ET ROBERT WOLF

Synthèse, structure et réactivité des molécules phosphorées, Unité de recherche associée au Centre national de la recherche scientifique, n° 454, Université Paul Sabatier, 118 route de Narbonne, 31062, Toulouse CEDEX, France

ET

JOËL JAUD

Centre d'élaboration des matériaux et d'études structurales du Centre national de la recherche scientifique, 29 rue Jeanne Marvig, 31400 Toulouse, France

Reçu le 3 juin 1990

MICHEL BALTAS, LATIFA CHAHOUA, LILIANE GORRICHON, PIERRE TISNÈS, DOURAID HOUALLA, ROBERT WOLF et JOËL JAUD. Can. J. Chem. **69**, 300 (1991).

Au cours d'un travail de synthèse de dérivés de l'acide quinique, régulateurs potentiels de la biosynthèse des acides aminés aromatiques, nous avons préparé un intermédiaire 1,5-diacétoxy-3,4-bis(bicyclophosphoranylato)quinate de méthyle **7**. Ce dernier a été caractérisé par RMN ^1H, ^{31}P, infrarouge, analyse élémentaire et spectrométrie de masse. Sa structure moléculaire a été déterminée par diffraction des rayons X et une étude conformationnelle complète a été effectuée. Le cycle quinique adopte une forme chaise presque parfaite. Les deux groupements bicyclophosphoranes présentent une géométrie bipyramidale trigonale avec une annelation axiale–équatoriale–axiale. Les cycles pentagonaux adoptent une forme enveloppe avec l'atome de carbone tétrasubstitué à la pointe du rabat.

Mots clés : voie de l'acide shikimique, 1,5-diacétoxy-3,4-bis(bicyclophosphoranylato)quinate de méthyle, analyse conformationnelle, RMN ^1H et ^{31}P, structure cristalline.

MICHEL BALTAS, LATIFA CHAHOUA, LILIANE GORRICHON, PIERRE TISNÈS, DOURAID HOUALLA, ROBERT WOLF, and JOËL JAUD. Can. J. Chem. **69**, 300 (1991).

In connection with our work on quinic acid derivatives, which are supposed to regulate the biosynthesis of aromatic amino acids, we have prepared the methyl 1,5-di-*O*-acetyl-3,4-bis-*O*-(bicyclophosphoranylato)quinate **7**. The compound obtained has been characterized by NMR (^1H and ^{31}P), IR, elemental analysis, and mass spectrometry. Its molecular structure has been determined by X-ray diffraction and an exhaustive conformational study has been accomplished. The quinic ring adopts an almost perfect chair form. Both bicyclophosphoranyl groups present a trigonal bipyramidal geometry with an axial–equatorial–axial type annelation. The pentagonal rings adopt an envelope form in which the tetrasubstituted carbon atom is at the top of the fold.

Key words: shikimic acid pathway, methyl 1,5-di-*O*-acetyl-3,4-bis-*O*-(bicyclophosphoranylato)quinate, conformational analysis, ^1H and ^{31}P NMR, crystal structure.

Récemment, nous nous sommes intéressés à la formation d'acétals et de borates dérivés des acides shikimique et quinique (1–3). Ces acides interviennent dans la biosynthèse des acides aminés aromatiques, un processus fondamental et spécifique des végétaux et des microorganismes (4–6) (schéma 1).

Nous abordons maintenant l'étude de la phosphorylation de l'acide quinique. En effet, si l'importance de l'acide shikimique et des dérivés ou analogues phosphorés est bien établie et largement étudiée (7, 8), le rôle de l'acide quinique reste mal connu.

L'acide quinique n'apparaît que chez les végétaux mais il peut constituer une source de carbone chez les microorganismes (9); sa présence permet d'observer, ou d'induire, une régulation de la voie de l'acide shikimique (10). Cependant, la formation de l'acide quinique en quantités importantes, dans certains cas plus de 5% du poids du végétal sec, suggère d'autres activités métaboliques encore indéterminées et (ou) d'autres interférences avec la voie de l'acide shikimique, par exemple par le biais des dérivés phosphorylés de l'acide quinique.

La synthèse des dérivés phosphorylés de l'acide quinique fait intervenir deux étapes principales :

(i) La protection sélective des fonctions hydroxylées qui ne doivent pas être touchées lors de la phosphorylation.

(ii) Le choix de la réaction de phosphorylation et des réactifs pouvant permettre selon le cas l'accès à des dérivés mono-, di- ou poly-phosphorylés sur le squelette quinique.

La synthèse des dérivés phosphorylés de l'acide quinique relève du procédé général de phosphorylation des alcools. Jusqu'à une date récente celle-ci était réalisée soit par action d'un dérivé du phosphore tétracoordonné possédant un groupement phosphoryle et un groupement partant X (méthode de Khorana et coll. (11))

$$ROH + \underset{\underset{O}{\|}}{>P—X} \rightarrow HX + RO—\underset{\underset{O}{\|}}{P<}, \quad X = Cl, NR_2..$$

soit par action d'un dérivé du phosphore tricoordonné (phosphitation) suivie d'une oxydation (méthode de Letsinger *et al.* (12*a*), Caruthers (12*b*))

$$ROH + X—P< \rightarrow HX + RO—P< \xrightarrow[\frac{1}{2}O_2]{} RO—\underset{\underset{O}{\|}}{P<}$$

1. Auteur à qui adresser toute correspondance.

Can. J. Chem. Downloaded from www.nrcresearchpress.com by 195.138.81.100 on 09/07/12
For personal use only.

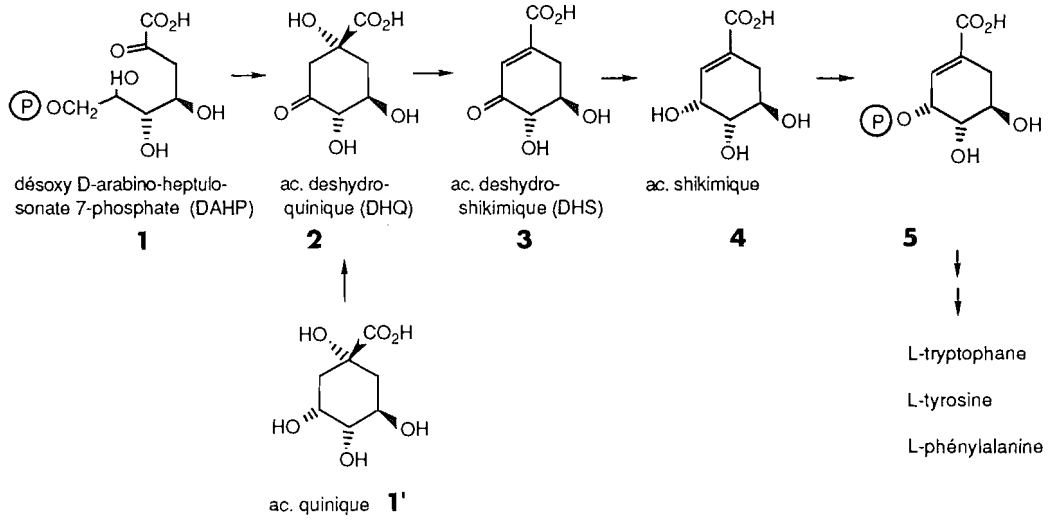


SCHÉMA 1

En 1988, Duthu *et al.* (13) ont décrit un autre procédé de phosphorylation qui exploite l'aptitude des bicyclophosphanes (**I**) à subir l'addition oxydante des alcools pour conduire à un bicyclophosphorane à liaison P—H (**II**). L'oxydation de ce dernier fournit les dérivés du phosphore tétracoordonné (**III**) et (**IV**) dont l'hydrolyse aboutit au monoester phosphorique recherché (**V**) (schéma 2):

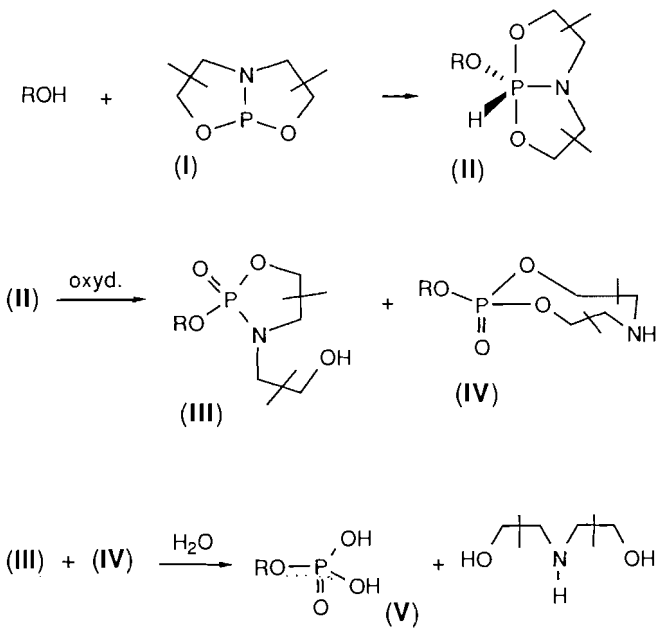
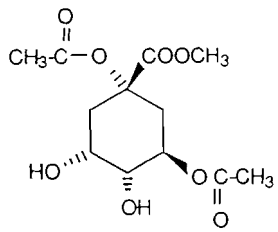


SCHÉMA 2

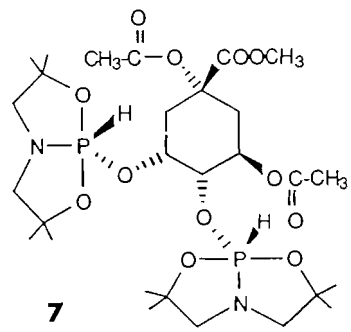
Dans les deux premiers procédés, la présence des fonctions alcools sur deux atomes de carbone vicinaux conduit en cas de non protection à un fort taux de cyclisation. Par contre dans le cas de la phosphoranylation une telle cyclisation n'a jamais été observée. Nous avons donc choisi cette dernière méthode de phosphorylation.

L'approche expérimentale de ce problème nous a amené à choisir dans un premier temps le composé **6** comme produit de départ.

Dans ce premier article nous rapportons la synthèse du bicyclophosphorane **7**, son analyse conformationnelle par RMN ainsi que sa structure moléculaire par diffraction des rayons X.



6



7

Résultats et discussion

Le diol **6** a été obtenu suivant le schéma 3. L'action de l'acide D(−)quinique **1'** avec le benzaldéhyde conduit à l'acétal lactonique **8**. Il est connu (14) que cette méthode ne conduit pas à des produits de racémisation de l'acide D(−)quinique. La méthanolyse de **8** en présence de méthylate de sodium, puis l'acylation des fonctions hydroxy en C4 et C6 en présence de 4-*N*,*N*-diméthylaminopyridine (DMAP) et d'anhydride acétique conduit à l'ester complètement protégé **10**. Le diol **6** est alors obtenu par déprotection acide de la fonction acétal avec un rendement global de 65%. Il a été identifié par RMN ^{1}H et ^{13}C, IR, analyse élémentaire et spectrométrie de masse.

La synthèse du bicyclophosphane **11** a été effectuée suivant la méthode décrite dans la littérature (13).

Enfin le dérivé **7** a été obtenu par action de deux équivalents du bicyclophosphane **11** sur le diol **6**. Après recristallisation dans le toluène il est obtenu sous forme de cristaux blancs avec un rendement de 62% par rapport à **6**.

Le composé **7** a été caractérisé par spectrométrie de masse, analyse élémentaire et spectroscopies IR, RMN ^{1}H et ^{31}P (cf. partie expérimentale). Sa structure moléculaire a été établie par diffraction des rayons X.

Étude de RMN

Attribution des signaux

Le spectre RMN ^{31}P{^{1}H} (fig. 1a) du composé **7** contient deux pics à $\delta = -40{,}4(5)$ ppm et $\delta = -41{,}9(1)$ ppm alors que sans découplage de proton (fig. 1b) chacun de ces pics se présente comme un doublet avec un écart entre les branches égal à $^1J_{P-H} = 815$ Hz et $^1J_{P-H} = 809$ Hz. Chacun des membres des doublets présente une structure fine ou un élargissement lié

Can. J. Chem. Downloaded from www.nrcresearchpress.com by 195.138.81.100 on 09/07/12
For personal use only.

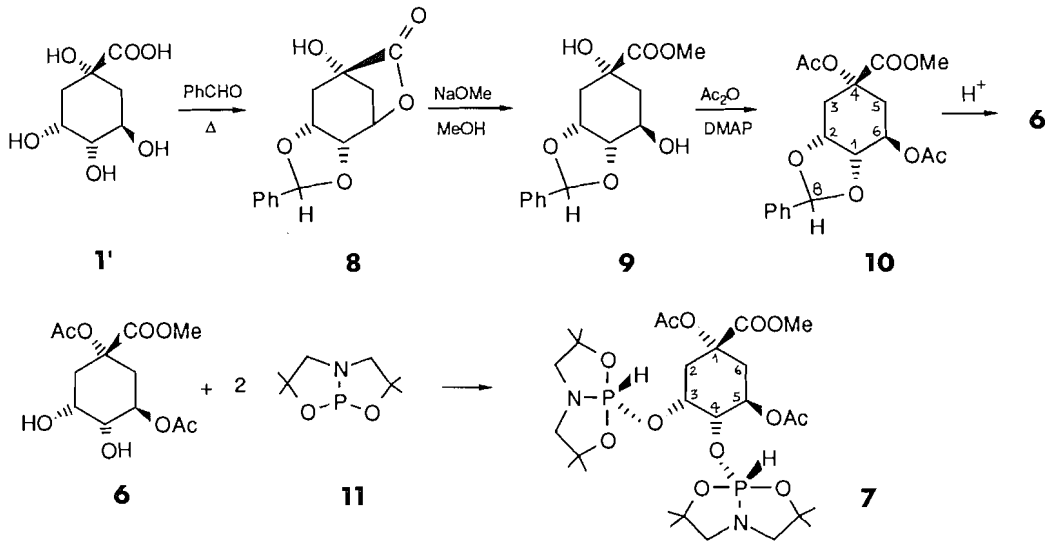


SCHÉMA 3

à des couplages ^3J avec d'autres protons. Les déplacements chimiques des noyaux de ^{31}P ainsi que les grandes constantes de couplage montrent qu'on est en présence d'un composé à deux atomes de phosphore pentacoordonné ayant chacun un atome d'hydrogène directement lié au phosphore (bis-phosphorane à liaison P—H).

Le spectre RMN ^1H du composé **7** enregistré à une radiofréquence de 250 MHz (dans C_6D_6) (fig. 2) confirme la présence de deux protons liés chacun à un phosphore. Ces protons résonnent à $\delta = 7{,}35$ ppm et $\delta = 7{,}30$ ppm et se présentent sous la forme de deux doublets avec des écarts entre les branches de 815 Hz et 809 Hz respectivement.

L'analyse spectrale du cycle quinique a été effectuée après irradiation des deux noyaux de ^{31}P.

Les troix protons méthine H3, H4 et H5 donnent naissance à trois massifs bien séparés entre 4,7 et 5,8 ppm. Lorsque les noyaux ^{31}P sont irradiés les deux massifs les plus blindés, centrés respectivement à 4,81 et 5,30 ppm, sont perturbés (fig. 3). On peut donc les attribuer aux protons H3 ou H4 et par conséquent le massif le plus déblindé ($\delta = 5{,}70$ ppm) au proton H5.

Le proton H4 doit présenter un doublet dédoublé par couplage avec H3 et H5 et il correspond au massif le plus blindé (4,81 ppm). Cette attribution est confirmée par l'irradiation du massif du proton H5 à 5,70 ppm qui le simplifie en un doublet.

Outre les signaux correspondants au groupe méthoxy à $\delta = 3{,}37$ ppm et aux deux CH_3 des fonctions acétyles à $\delta = 1{,}89$ et $\delta = 1{,}72$ ppm on distingue à $\delta = 2{,}90$ et $\delta = 2{,}10$ ppm deux massifs représentant chacun un proton. Ils sont attribuables aux protons méthyléniques portés par les carbones C2 ou C6. L'irradiation du proton H5 entraîne seulement la modification du massif à $\delta = 2{,}10$ ppm alors que l'irradiation du proton H3 entraîne celle du massif à $\delta = 2{,}90$ ppm. Ceci permet d'attribuer le premier à un des protons H6 et le massif à $\delta = 2{,}90$ ppm à un des protons H2. Les deux autres protons donnent naissance à des signaux qui se trouvent confondus avec ceux des protons NCH_2 des cycles pentagonaux phosphoraniques ($\delta = 2{,}76$–$2{,}40$ ppm; 10 protons). Pour terminer nous trouvons un ensemble de pics entre 1,5 et 1,1 ppm attribuables aux groupements méthyles des groupes bicyclophosphoraniques (24 protons).

Conformation du cycle quinique

La conformation du cycle quinique a été établie à partir de l'analyse des constantes de couplage entre les différents protons du cycle. L'accès à ces paramètres a été facilité par l'irradiation des deux noyaux de phosphore et dans certains cas par des découplages homonucléaires proton–proton. Les spectres obtenus ont été analysés dans les conditions du premier ordre. Les déplacements chimiques des protons du cycle quinique ainsi que les constantes de couplages sont rassemblés dans le tableau 1.

Les valeurs des constantes de couplage mesurées sur les différents massifs sont en accord avec la stéréochimie relative des différents carbones asymétriques C3, C4, C5 en série quinique. En les comparant avec celles déterminées par Corse *et al.* (15) d'une part et Haslam et Turner (16) d'autre part dans cette même série quinique, elles permettent d'établir une conformation chaise pour le composé **7** où le substituant carboxylate de méthyle du carbone C1 est en position équatoriale. En effet le proton H4 possède une constante de couplage de 7,8 Hz avec le proton H5 typique dans cette série d'un couplage axial–axial; l'autre valeur de couplage de 3,4 Hz conduit à attribuer au proton H3e l'orientation équatoriale. Les valeurs trouvées sur les massifs des protons H3 et H5 vérifient cette stéréochimie et permettent de plus d'attribuer les massifs à 2,90 et 2,10 ppm respectivement aux protons H2a et H6a. La valeur de 14,8 Hz du couplage $^2J_{2a-2e}$ est plus grande que celle observée habituellement dans cette série. Elle pourrait être interprétée par un aplatissement de la forme chaise au niveau de l'enchaînement C1–C2–C3 qui a été reconnu comme responsable de l'augmentation d'une telle constante (17). Cette déformation serait également responsable du fait que le proton H2a résonne à champ plus faible que H2e, ce qui constitue une inversion de la règle de Lemieux (18). Le massif à 2,10 ppm du proton H6a présente des constantes de couplage de 13,5 et 7,8 Hz proches de celles habituellement rencontrées. Cette observation ainsi que le fait que δH6a < δH6e en accord avec la règle de Lemieux montrerait qu'il n'y a pas de déformation dans le fragment C5–C6–C1 du cycle quinique.

Stéréochimie des groupes bicyclophosphoraniques

La stéréochimie sera déduite de l'analyse des paramètres de RMN des substituants CH_3 et des protons NCH_2.

Les déterminations structurales par diffraction des rayons X effectuées sur des bicyclophosphoranes comparables ont montré que ces composés adoptent généralement une géométrie bipyra-

Can. J. Chem. Downloaded from www.nrcresearchpress.com by 195.138.81.100 on 09/07/12
For personal use only.

Can. J. Chem. Downloaded from www.nrcresearchpress.com by 195.138.81.100 on 09/07/12
For personal use only.

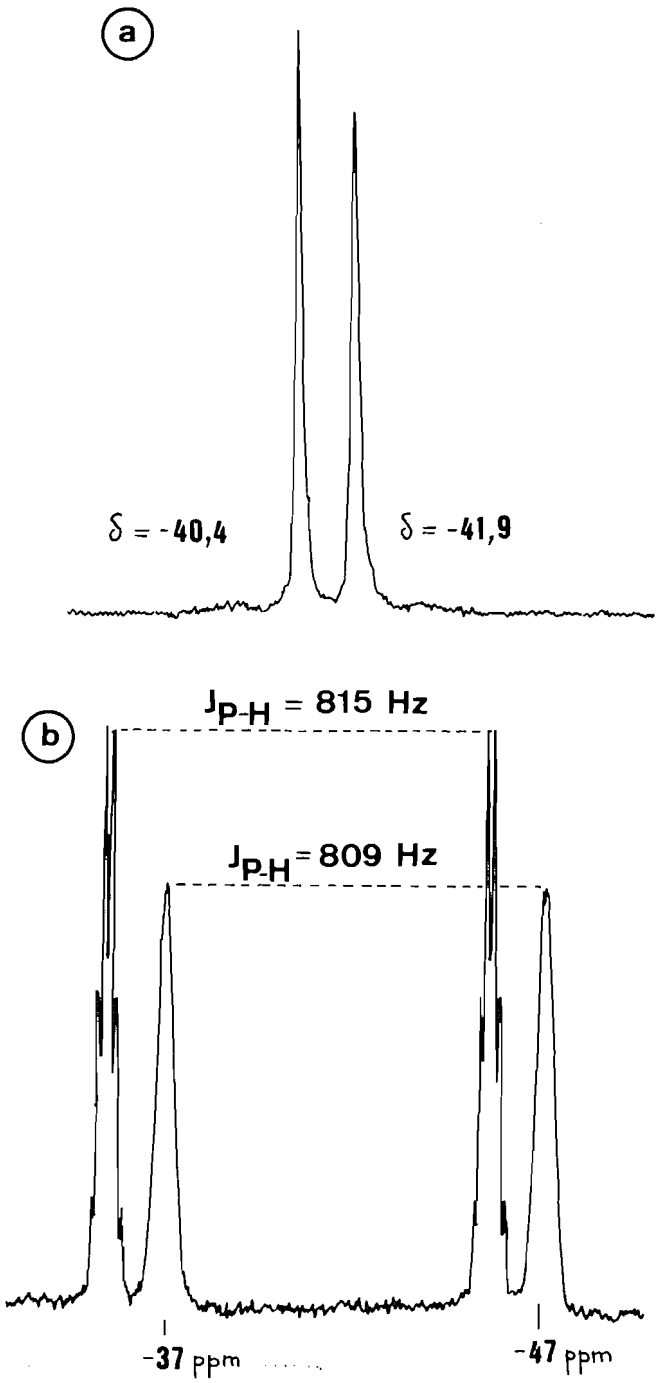
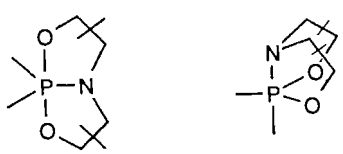


FIG. 1. Spectre RMN ^{31}P (81,01 MHz) du composé **7** dans C_6D_6 (a) spectre découplé du proton; (b) spectre couplé du proton.

midale trigonale avec soit une annelation axiale–équatoriale–axiale (a-e-a) soit une annelation équatoriale–axiale–équatoriale (e-a-e) (19). Dans l'une comme dans l'autre il existe un élément de symétrie qui permute les deux cycles pentagonaux symétriquement substitués. La présence sur l'atome de phosphore de deux substituants différents rend diastéréotopes les groupes CH_3 portés par le même atome de carbone ainsi que les protons NCH_2. Quelle que soit la géométrie effectivement adoptée par les groupes bicyclophosphoraniques on peut s'attendre à ce que dans chaque bicyclophosphorane les quatre substituants CH_3 ainsi que les quatre protons NCH_2 soient deux à deux équivalents. On devrait donc observer quatre signaux correspondant aux substituants CH_3 et deux systèmes ABX pour les protons NCH_2.



Pour le composé **7** ceci n'est pas le cas. En effet, l'examen du domaine spectral à $\delta = 1,5$ et $\delta = 1,1$ ppm où l'on attend les signaux correspondants aux substituants CH_3 montre la présence de cinq pics (fig. 2) dont les intensités sont comme 3 : 3 : 6 : 9 : 3. Il en résulte que les groupements méthyles de deux bicyclophosphoranes ne sont plus permutés par l'élément de symétrie locale propre à chaque bicycle : ils sont tous distincts. Ce fait traduit l'existence d'un centre chiral C3 et C4 en β de chaque atome de phosphore qui différencie l'environnement spatial des cycles pentagonaux. Le même effet est observé sur les protons NCH_2 (fig. 4). En effet le massif correspondant à ces protons ($\delta = 2,76$–$2,40$ ppm) ne comporte pas les 16 pics attendus pour les deux parties AB des deux systèmes ABX (X = P) mais présente une multiplicité bien plus grande confirmant ainsi la différenciation des quatre groupes de protons NCH_2 (fig. 5).

L'analyse du spectre enregistré à 250 MHz comme à 300 MHz ne nous a pas permis la détermination complète des constantes de couplage et en particulier celles attribuables à $^3J_{H-C-N-P}$. Nous avons pu établir toutefois, par irradiation des deux atomes de phosphore, que le massif résiduel s'analyse comme un ensemble de trois systèmes AB et d'un système AM (tableau 2). Ainsi nous obtenons quatre groupes de protons NCH_2 distincts dont un se trouve beaucoup plus différencié que les trois autres. À notre sens celà doit traduire l'existence d'un effet d'anisotropie dû au reste de la molécule qui s'exerce préférentiellement sur un seul des quatre cycles pentagonaux. L'étude de la structure moléculaire par diffraction des rayons X nous permettra de confirmer cette proposition.

Étude cristallographique

Les paramètres atomiques finaux issus de l'analyse structurale par diffraction des rayons X sont rassemblés dans le tableau 3,[2] et certaines données utiles de géométrie moléculaire dans les tableaux 4–6. La figure 5 représente une vue perspective de la molécule où sont indiqués les numéros des différents atomes. Dans un souci de clarté, les atomes d'hydrogène n'ont pas été représentés. Nous commenterons d'abord les données relatives au cycle quinique puis celles concernant les deux groupes bicyclophosphoraniques.

La conformation du cycle quinique est celle d'une chaise presque parfaite. Les atomes de carbone C3, C4, C6, C1 sont dans un plan alors que les atomes de carbone C2 et C5 se trouvent de part et d'autre de ce plan à des distances de 0,602 Å et −0,670 Å respectivement (tableau 6). L'écart entre les

2. Une documentation supplémentaire concernant les amplitudes des facteurs de structure, les paramètres d'agitation thermique anisotrope, les valeurs en Å des amplitudes d'agitation thermique, les tableaux des paramètres positionnels, des angles et distances de liaison et des principaux plans des moindres carrés peut être acheté du Service de fourniture de documents, ICIST, Conseil national de recherches du Canada, Ottawa (Ontario), Canada K1A 0S2.

On peut egalement les tableaux des paramètres positionnels et des angles et distances de liaison obtenir en s'adressant au directeur, Cambridge Crystallographic Data Centre, University Chemical Laboratory, Lensfield Road, Cambridge CB2 1EW, Royaume-Uni.

Can. J. Chem. Downloaded from www.nrcresearchpress.com by 195.138.81.100 on 09/07/12
For personal use only.

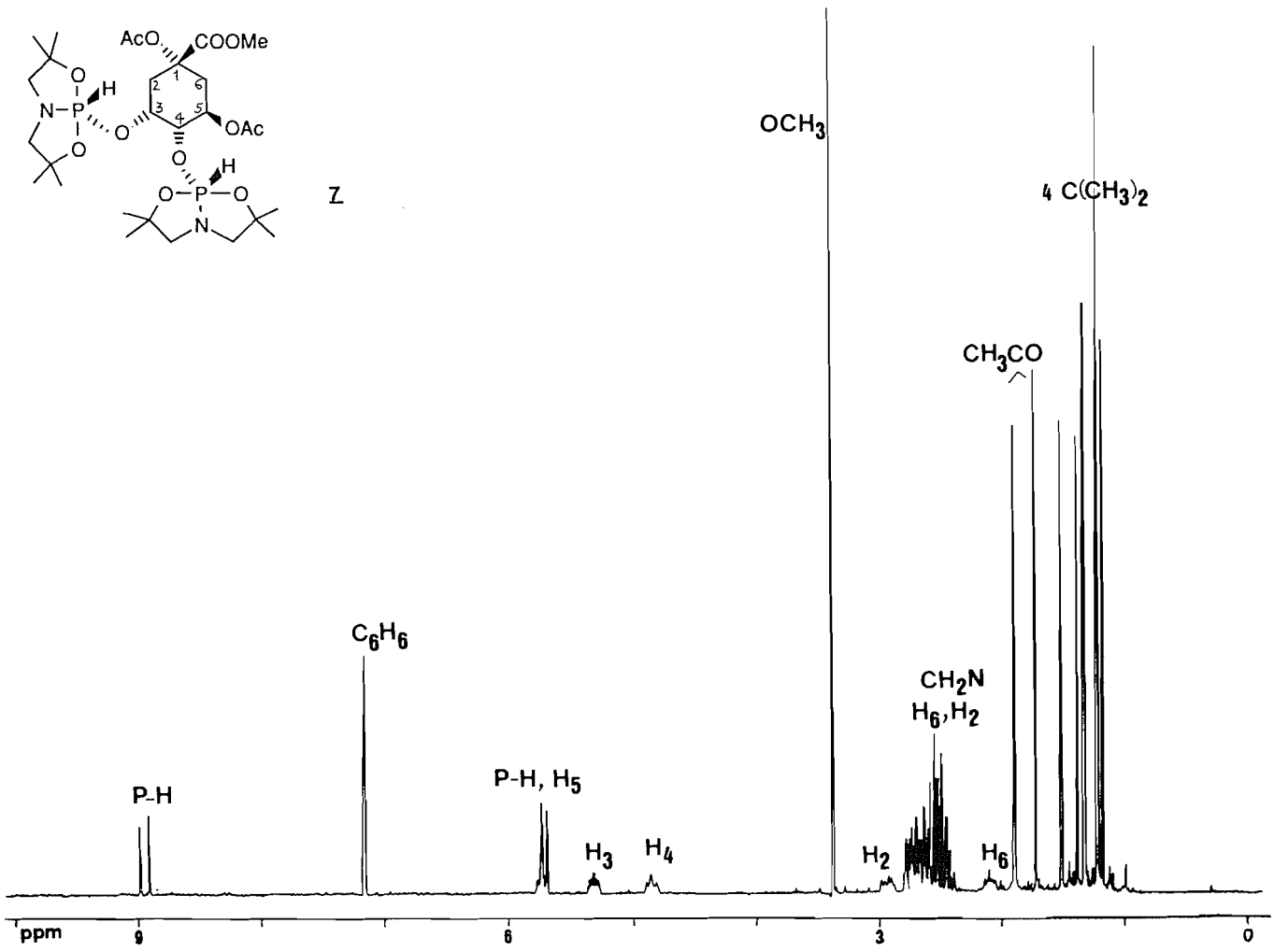


FIG. 2. Spectre RMN ^1H (250 MHz) du composé **7** dans C_6D_6.

TABLEAU 1. Données spectrales en RMN ^1H du composé **7** (250 MHz, $CDCl_3$)

Proton	δ (ppm)	*J* (Hz)	Proton	δ (ppm)	*J* (Hz)
P-H	7,35 (d) 7,30 (d)	815 809	H2a	2,90 (m)	J_{2a-3e} = 6,7 J_{2a-2e} = 14,8
H5	5,70 (m)	J_{5-6a} = 7,8 J_{5-6e} = 4,0 J_{5-4a} = 4,8	NCH_2, H2e,[a] H6e	2,76–2,40	
H3	5,29 (m)	J_{3e-4a} = 3,4 J_{3e-2a} = 6,7 J_{3e-2e} = 3,4	H6a	2,12 (m)	J_{5-6a} = 7,8 J_{6a-6e} = 13,5
H4	4,81 (m)	J_{4a-3e} = 3,4 J_{4a-5a} = 7,8	O=C—CH_3	1,89 (s) 1,72 (s)	
OCH_3	3,41 (s)		$(CH_3)_2C$<	1,50 1,32 (6H) 1,18	1,38 1,21 (9H)

[a]L'analyse de ce massif est donnée dans le tableau 2.

distances des atomes C2 et C5 par rapport à ce plan pourrait être dû à un léger applatissement de la chaise du côté de C2 qui le rapprocherait du plan indiqué ci-dessus. La valeur moyenne absolue des angles de torsion intraannulaire est égale à 54,07° (tableau 5). Cette valeur est comparable à celle correspondante à l'acide D(−)quinique (54,9°) (20) ainsi qu'à celle obtenue pour un cyclohexane libre par un calcul théorique après minimisation de l'énergie (55,5°) (21). Une analyse plus fine montre que les angles de torsion d'un côté du cycle (C4–C5–C6) sont plus grands que ceux de l'autre côté (C1–C2–C3) rejoignant ainsi la différence observée quant à la position des carbones C2 et C5 par rapport au plan moyen du cycle. Cette distorsion pourrait

Can. J. Chem. Downloaded from www.nrcresearchpress.com by 195.138.81.100 on 09/07/12
For personal use only.

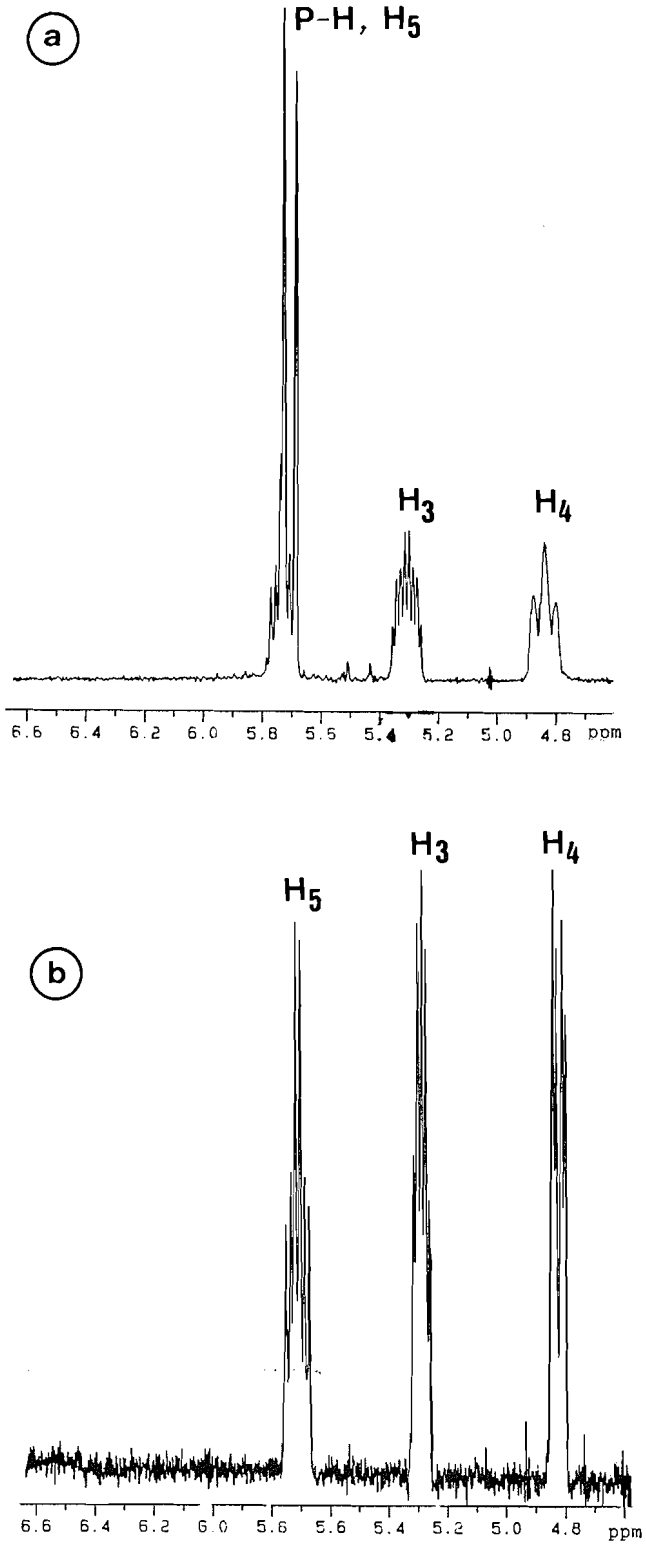


FIG. 3. Partie du spectre RMN ^1H (250 MHz) du composé **7** dans C_6D_6 correspondant aux protons H3, H4 et H5 avant (a) et après (b) irradiation des deux atomes de ^{31}P.

TABLEAU 2. Analyse spectrale des protons méthyléniques des quatre cycles pentagonaux phosphoraniques du composé **7**

Système	CH_2(AB)	CH_2(AB)	CH_2(AB)	CH_2(AM)
δ (ppm)	2,55	2,64	2,75	2,71
	2,49	2,52	2,62	2,52
J (Hz)	7,7	7,85	8,05	7,7

TABLEAU 3. Coordonnées atomiques et déviations standards de **7**

Atome	*x*	*y*	*z*	B(A^2)[a]
P1	0,1370(1)	0,39307(7)	0,76243(6)	3,82(2)
P2	0,3369(1)	0,19699(7)	0,61749(6)	3,84(2)
O1	0,2278(3)	0,3201(2)	0,7733(2)	3,60(6)
O2	0,3165(3)	0,1934(2)	0,6995(1)	4,14(6)
O3	0,4140(3)	0,1061(2)	0,8060(2)	4,16(6)
O4	0,2993(3)	0,3092(2)	0,9163(1)	3,43(6)
O5	0,6074(3)	0,3756(3)	0,9199(2)	7,1(1)
O6	0,4925(3)	0,3189(2)	1,0020(2)	5,28(8)
O7	0,3187(3)	0,4369(2)	0,9446(2)	4,80(7)
O8	0,2584(5)	0,0533(2)	0,8606(3)	12,2(1)
O9	0,0260(3)	0,3446(2)	0,8049(2)	4,72(7)
O10	0,2395(3)	0,4484(2)	0,7188(2)	5,33(7)
O11	0,4871(3)	0,2213(2)	0,6204(2)	4,52(7)
O12	0,1890(3)	0,1765(2)	0,6031(2)	5,05(7)
N1	0,0426(5)	0,4018(3)	0,6959(2)	5,7(1)
N2	0,3724(4)	0,1158(3)	0,5758(2)	5,51(8)
C1	0,4216(4)	0,3090(2)	0,8867(2)	3,31(8)
C2	0,4307(4)	0,3530(2)	0,8192(2)	3,41(8)
C3	0,3573(4)	0,3161(2)	0,7595(2)	3,33(8)
C4	0,3900(4)	0,2295(2)	0,7509(2)	3,30(8)
C5	0,3710(4)	0,1854(2)	0,8177(2)	3,26(8)
C6	0,4486(4)	0,2206(2)	0,8758(2)	3,73(9)
C7	0,5182(4)	0,3401(3)	0,9377(3)	4,5(1)
C8	0,5821(6)	0,3454(4)	1,0527(3)	7,5(2)
C9	0,2576(4)	0,3781(2)	0,9431(2)	3,68(9)
C10	0,1293(5)	0,3687(3)	0,9694(3)	5,4(1)
C11	0,3490(5)	0,0462(3)	0,8291(3)	5,4(1)
C12	0,4028(6)	−0,0306(3)	0,8050(4)	6,9(2)
C13	−0,0651(4)	0,3092(3)	0,7628(3)	5,4(1)
C14	−0,0794(6)	0,3664(4)	0,7020(4)	8,3(2)
C15	0,2022(5)	0,4814(3)	0,6542(3)	5,0(1)
C16	0,0765(8)	0,4495(6)	0,6397(4)	16,5(2)
C17	0,5735(5)	0,1610(3)	0,5999(3)	5,3(1)
C18	0,4980(6)	0,1059(4)	0,5536(3)	8,5(2)
C19	0,1602(6)	0,0972(3)	0,5841(3)	6,4(1)
C20	0,2747(6)	0,0710(4)	0,5450(3)	7,5(2)
C21	−0,0215(6)	0,2287(4)	0,7377(4)	7,6(2)
C22	−0,1845(5)	0,3031(4)	0,8040(4)	8,4(2)
C23	0,2062(9)	0,5667(4)	0,6582(4)	10,8(2)
C24	0,2830(9)	0,4520(5)	0,5989(3)	11,4(2)
C25	0,6205(6)	0,1175(4)	0,6633(3)	7,3(2)
C26	0,6786(6)	0,2009(5)	0,5618(4)	9,3(2)
C27	0,0473(7)	0,0982(5)	0,5387(4)	9,9(2)
C28	0,1384(8)	0,0482(4)	0,6484(4)	9,0(2)

[a]Les atomes affinés anisotropiquement sont donnés sous la forme d'équivalents isotropiques définis ainsi au moyen des paramètres de la maille : $B_{eq} = 4/3[a^2B(1,1) + b^2B(2,2) + c^2B(3,3) + ab(\cos\gamma)B(1,2) + ac(\cos\beta)B(1,3) + bc(\cos\alpha)B(2,3)]$.

être le résultat des interactions diaxiales entre le groupement acetoxy en C1 et le groupement phosphoranique en C3. En outre les angles C2—C1—O4 et C6—C1—O4 ont des valeurs sensiblement différentes de celles observées dans l'acide quinique (20) (C2—C1—O4 = 113,6° et C6—C1—O4 103,4° contre 107,9° et 111° respectivement). Cette variation pourrait très bien s'expliquer par l'interaction diaxiale signalée ci-dessus.

L'atome d'oxygène O7 (C=O) de la fonction acetoxy en C1 se trouve dans le même plan que l'atome de carbone C1 (C1–O4–C9–O7 = −2°), le plaçant ainsi dans une position

Can. J. Chem. Downloaded from www.nrcresearchpress.com by 195.138.81.100 on 09/07/12
For personal use only.

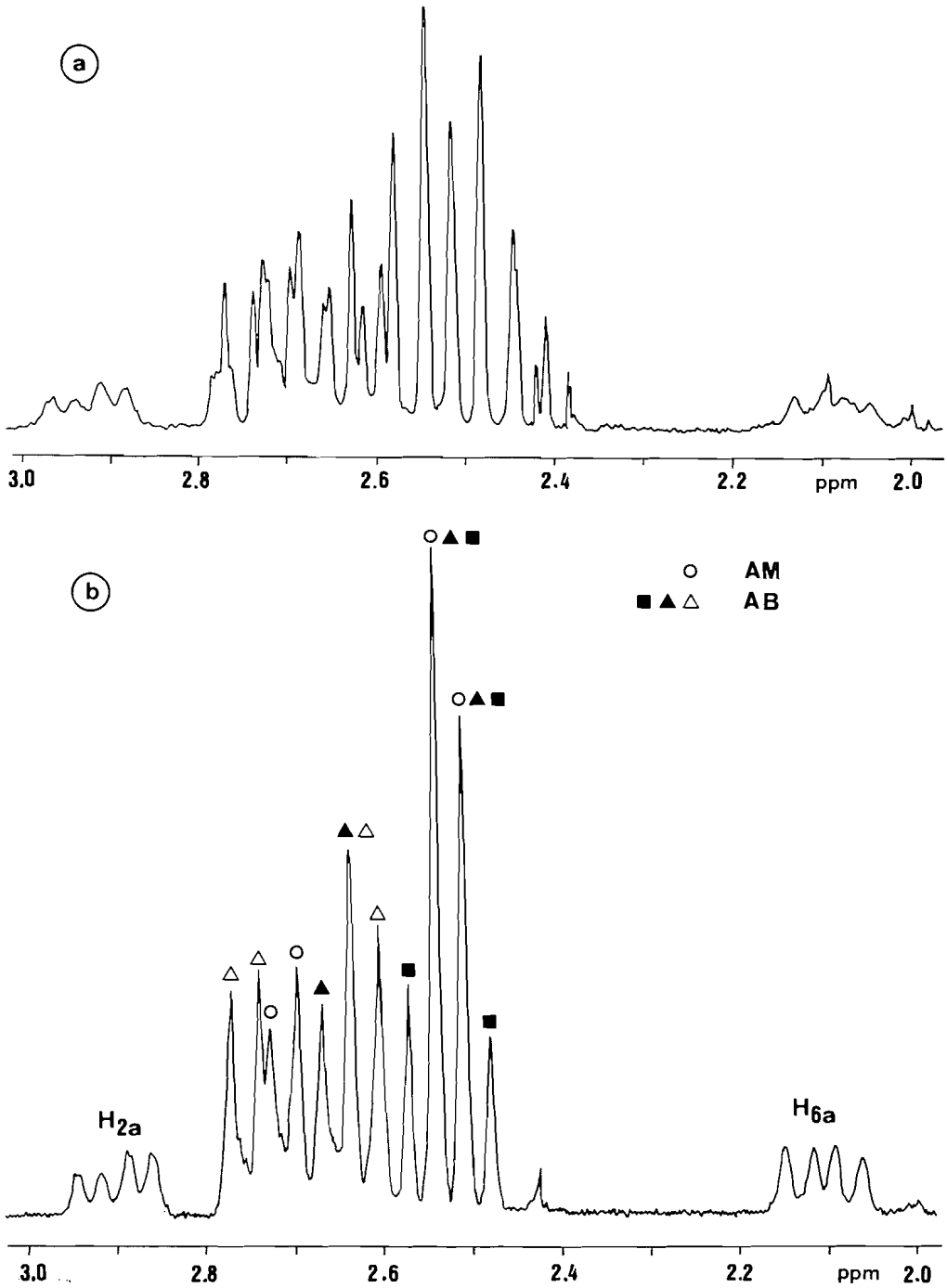


FIG. 4. Région de δ = 2–3 ppm du spectre RMN ^1H (250 MHz) du composé dans C_6D_6 (a) avant découplage des deux atomes de phosphore et (b) après irradiation.

eclipsée. L'atome d'oxygène O5 de la fonction acétate en C1 est orienté du côté C5–C6 du cycle quinique. Enfin, le carbonyle du groupement acetoxy en C5 est orienté vers l'intérieur du cycle quinique avec l'atome d'oxygène O8 (C=O) dans le même plan que C5 (C5–O3–C11–O8 = 1,91°) (tableau 5).

Les deux bicyclophosphoranes adoptent une géometrie bipyramidale trigonale avec une annelation axiale–équatoriale–axiale. Les atomes d'oxygène des cycles pentagonaux sont bien en position axiale : O9–P1–O10 = 174,9° et O11–P2–O12 = 172° alors que les atomes d'oxygène O1, O2 liés au cycle quinique ainsi que les atomes d'azote N1, N2 sont dans le plan équatorial (tableau 4). Dans chaque cycle oxazaphospholane les atomes de phosphore, d'oxygène, d'azote et de carbone NCH_2 sont dans un plan, l'atome de carbone tétrasubstitué étant en dehors de ce plan. Il en résulte que ces cycles adoptent la conformation d'une enveloppe, l'atome de carbone lié à l'oxygène étant à la pointe du rabat. Ce résultat confirme les conclusions précédemment obtenues à partir de l'étude RMN de bicyclophosphoranes comparables (22). Les orientations des deux bicyclophosphoranes par rapport au cycle quinique sont différentes. Le plan moyen du bicyclophosphorane lié à C3 (P1–O10–C16–N1–C14–O9) est quasiment perpendiculaire au plan moyen du cycle quinique (O9–P1–O1–C3 = −170,41° et O10–P1–O1–C3 = 9,65°) alors que celui du bicyclophos-

TABLEAU 4. Angles de liaison (en degrés) du composé **7**

Atome 1	Atome 2	Atome 3	Angle	Atome 1	Atome 2	Atome 3	Angle
O1	P1	O9	89,9(2)	C14	N1	C16	122,6(5)
O1	P1	O10	95,2(2)	P2	N2	C18	117,9(4)
O1	P1	N1	123,8(2)	P2	N2	C20	118,4(4)
O9	P1	O10	174,9(2)	C18	N2	C20	120,9(5)
O9	P1	N1	88,9(2)	O4	C1	C2	113,6(3)
O10	P1	N1	88,3(2)	O4	C1	C6	103,4(3)
O2	P2	O11	96,3(2)	O4	C1	C7	111,9(3)
O2	P2	O12	91,4(2)	C2	C1	C6	110,6(3)
O2	P2	N2	119,1(2)	C2	C1	C7	110,0(3)
O11	P2	O12	172,0(2)	C6	C1	C7	107,1(3)
O11	P2	N2	89,7(2)	C1	C2	C3	114,5(3)
O12	P2	N2	88,2(2)	O1	C3	C2	110,5(3)
P1	O1	C3	128,2(2)	O1	C3	C4	107,2(4)
P2	O2	C4	127,0(3)	C2	C3	C4	110,9(3)
C5	O3	C11	119,6(3)	O2	C4	C3	111,4(3)
C1	O4	C9	117,4(4)	O2	C4	C5	108,1(3)
C7	O6	C8	114,2(5)	C3	C4	C5	110,7(3)
P1	O9	C13	115,4(3)	O3	C5	C4	106,5(3)
P1	O10	C15	118,1(4)	O3	C5	C6	107,6(3)
P2	O11	C17	116,5(3)	C4	C5	C6	111,2(3)
P2	O12	C19	116,7(3)	C1	C6	C5	112,1(3)
P1	N1	C14	117,6(5)	O5	C7	O6	125,4(5)
P1	N1	C16	119,4(4)	O5	C7	C1	123,1(4)
O6	C7	C1	111,5(4)	C16	C15	C24	106,6(5)
O4	C9	O7	122,9(5)	C23	C15	C24	111,1(6)
O4	C9	C10	110,4(4)	N1	C16	C15	107,7(6)
O7	C9	C10	126,7(4)	O11	C17	C18	104,3(4)
O3	C11	O8	123,5(4)	O11	C17	C25	110,0(4)
O3	C11	C12	110,9(5)	O11	C17	C26	107,8(5)
O8	C11	C12	125,5(5)	C18	C17	C25	110,8(5)
O9	C13	C14	104,1(4)	C18	C17	C26	113,0(5)
O9	C13	C21	110,3(4)	C25	C17	C26	110,8(5)
O9	C13	C22	108,7(5)	N2	C18	C17	105,1(5)
C14	C13	C21	110,9(5)	O12	C19	C20	102,9(4)
C14	C13	C22	111,0(5)	O12	C19	C27	108,4(5)
C21	C13	C22	111,6(5)	O12	C19	C28	109,9(5)
N1	C14	C13	103,5(5)	C20	C19	C27	112,2(5)
O10	C15	C16	106,3(5)	C20	C19	C28	112,1(5)
O10	C15	C23	109,8(5)	C27	C19	C28	110,9(6)
C10	C15	C24	109,4(5)	N2	C20	C19	104,1(5)
C16	C15	C23	113,5(6)				

phorane en C4 (P2–O11–C18–N2–C20–O12) est légèrement incliné par rapport au même plan (O11–P2–O2–C4 = 20,77 et O12–P2–O2–C4 = −157,28°).

L'examen d'un modèle moléculaire reproduisant ces données structurales et tenant compte du fait que le groupement carbonyle du substituant acetoxy porté par l'atome de carbone C5 (C11O8) pointe vers l'intérieur du cycle quinique complète les observations faites en RMN ^{1}H concernant les protons méthyléniques NCH_2. En effet les protons CH_2 portés par le carbone C18 du bicyclophosphorane lié en C4 du cycle quinique peuvent se trouver dans le cône d'anisotropie du carbonyle C11O8 (le cône est défini par un angle de 43° entre la verticale menée de l'atome d'oxygène au plan du carbonyle C=O et l'axe de ce dernier (23)). Les autres protons CH_2 des bicyclophosphoranes portés en C3 ou en C4 du cycle quinique sont tout à fait en dehors du cône d'anisotropie des groupements carbonyles en C5 ou en C1 (C7O5, C9O7). Cet effet d'anisotropie peut se traduire par une augmentation de l'écart entre les déplacements chimiques des protons CH_2 en C18. Ainsi de ce fait ces protons se présentent en RMN comme un système AM, alors que les autres protons NCH_2 sont des systèmes AB.

Enfin la structure cristalline est stabilisée par un ensemble des liaisons hydrogènes intermoléculaires faisant intervenir l'atome d'oxygène des groupements carboxylate en C1 (O5) avec un des protons portés par C20 (C20H220...O5 d = 2,61 Å; C2—H220—O5 : 162°) et l'atome d'oxygène O7 de l'acetoxy en C1 avec les protons portés par les atomes de carbone C18 et C24 :

C18H118..O7 = 2,58 Å et C18—H118—O7 153°

C24H124..O7 = 2,76 Å et C24—H124—O7 151°

Partie expérimentale

Méthodes spectroscopiques

Les spectres de RMN ^{1}H, ^{13}C et ^{31}P ont été enregistrés avec différents appareils Bruker : WP-60, AC-80, WH-90, WM-250 et AM-300 WB.

Les déplacements chimiques, exprimés en parties par million du

Can. J. Chem. Downloaded from www.nrcresearchpress.com by 195.138.81.100 on 09/07/12
For personal use only.

Can. J. Chem. Downloaded from www.nrcresearchpress.com by 195.138.81.100 on 09/07/12
For personal use only.

TABLEAU 5. Distances de liaison en Å et déviations standards estimées (entre parenthèses) pour le composé **7**

Atome 1	Atome 2	Distance	Atome 1	Atome 2	Distance
P1	O1	1,597(3)	N1	C14	1,458(8)
P1	O9	1,674(3)	N1	C16	1,405(9)
P1	O10	1,682(3)	N2	C18	1,439(9)
P1	N1	1,652(4)	N2	C20	1,435(8)
P2	O2	1,600(3)	C1	C2	1,508(6)
P2	O11	1,683(3)	C1	C6	1,542(6)
P2	O12	1,666(3)	C1	C7	1,532(6)
P2	N2	1,641(4)	C2	C3	1,535(6)
O1	C3	1,432(5)	C3	C4	1,521(5)
O2	C4	1,413(5)	C4	C5	1,507(6)
O3	C5	1,442(5)	C5	C6	1,525(6)
O3	C11	1,315(6)	C9	C10	1,492(8)
O4	C1	1,446(5)	C11	C12	1,503(7)
O4	C9	1,357(5)	C13	C14	1,530(9)
O5	C7	1,191(7)	C13	C21	1,524(8)
O6	C7	1,323(6)	C13	C22	1,526(9)
O6	C8	1,451(7)	C15	C16	1,49(1)
O7	C9	1,198(5)	C15	C23	1,450(8)
O8	C11	1,163(8)	C15	C24	1,470(9)
O9	C13	1,415(6)	C17	C18	1,532(9)
O10	C15	1,429(6)	C17	C25	1,519(8)
O11	C17	1,443(6)	C17	C26	1,518(9)
O12	C19	1,430(6)	C19	C20	1,521(9)
C19	C27	1,508(9)	C19	C28	1,512(9)

C1—C1—C2—C3	50,07(0,45)	C5—O3—C11—O8	−1,91(0,79)
C2—C1—C6—C5	−51,53(0,45)	C1—O4—C9—O7	−2,00(0,57)
C1—C2—C3—C4	−52,61(0,45)	O9—P1—O1—C3	−170,41(0,32)
C2—C3—C4—C5	55,36(0,43)	O10—P1—O1—C3	9,65(0,33)
C3—C4—C5—C6	58,27(0,43)	O11—P2—O2—C4	20,77(0,35)
C4—C5—C6—C1	56,59(0,45)	O12—P2—O2—C4	−157,28(0,33)

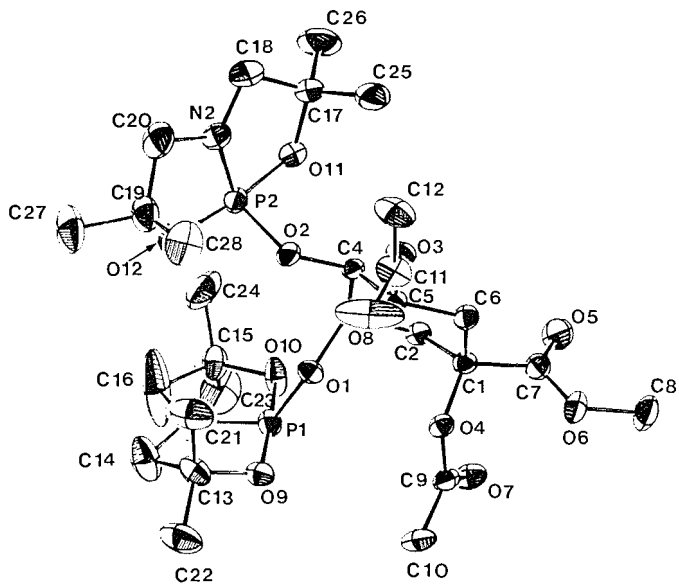


FIG. 5. Vue perspective de la structure de **7** montrant la numérotation des atomes.

champ inducteur (ppm) sont mesurés avec une précision de ± 0,005 ppm pour ^{1}H, ± 0,03 ppm pour ^{31}P et ^{13}C (références : TMS pour ^{1}H et ^{13}C, H_3PO_4 à 85% pour ^{31}P). Les constantes de couplage, exprimées en Hz, sont mesurées avec une précision de ± 0,2 Hz.

Les spectres infrarouge ont été effectués sur un appareil Perkin–Elmer 783, les spectres de masse sur Nermag R10-10. La chromatographie haute performance est réalisée sur un appareil Jobin–Yvon avec de la silice 6–35 μm Amicon.

*(1S,2R,4R,6R,8S)-4(Méthoxycarbonyl)-8 phenyl-7,9 dioxabicyclo-[4.3.0]nonane-2,4-diol (**9**)*

Ce composé a été préparé comme indiqué par Lesuisse et Berchtold (14).

*(1S,2R,4R,6R,8S)-2,4-Diacétoxy 4-(méthoxycarbonyl)-8 phenyl-7,9 dioxabicyclo[4.3.0]nonane (**10**)*

À une solution de **9** (1,6 g; 5,71 mmol) dans le chlorure de méthylène (40 mL) on ajoute successivement 12 mmol (1,4 g) de 4-*N,N*-dimethylaminopyridine (DMAP) et 12 mmol (1,08 mL) d'anhydride acétique. Après 2 h d'agitation à la température ambiante, on lave à l'eau, on extrait la phase organique, on sèche sur $MgSO_4$ et on évapore le solvant. Le produit désiré **10** est obtenu sous la forme de cristaux blancs (1,79 g, rendement = 83%); F = 132–133°C; ν_{max} ($CHCl_3$, cm^{-1}) : 1740 (C=O). RMN ^{1}H ($CDCl_3$) δ : 7,50 (m, 2H, Ar), 7,37 (m, 3H, Ar), 5,83 (s, 1H, C8-H), 5,33 (m, 1H, C6-H, J_{6-5} = 11,10, $J_{6-5'}$ = 4,50, J_{6-1} = 6,75), 4,50 (m, 1H, C2-H, J_{2-1} = 6,50, J_{2-3} = 3,15, $J_{2-3'}$ = 5,00 Hz), 4,24 (dd, 1H, C1-H, J_{1-6} = 6,75, J_{1-2} = 6,50), 3,71 (s, 3H, OCH_3), 2,87 (m, 1H, C3-H, $J_{3-3'}$ = 16,0, J_{3-2} = 3,15, J_{3-5} = 2,30), 2,46 (m, 1H, C3-H', $J_{3-3'}$ = 16,0, $J_{3'-2}$ = 5,0), 2,43 (m, 1H, C5-H, $J_{5-5'}$ = 13,50, J_{5-6} = 4,50, J_{5-3} = 2,30 Hz), 2,06 (s, 3H, CH_3CO), 2,05 (s, 3H, CH_3CO), 1,88 (m, 1H, C5-H', $J_{5'-5}$ = 13,50, $J_{5'-6}$ = 11,10). RMN ^{13}C ($CDCl_3$) δ : 171,44 (C=O), 170,07 (C=O), 136,99, 129,59, 128,42, 126,86 (C_6H_5), 104,43 (C8), 78,11 (C4), 75,97 (C6), 74,99 (C1), 70,96 (C2), 52,77 (OCH_3), 34,50 (C5), 30,74 (C3), 21,05 (CH_3CO), 20,86 (CH_3CO). SM *m/e* (intensité relative) : 378 M^+ (17), 136 (12), 105 (53), 43 (100). Anal. calc. pour $C_{19}H_{22}O_8$: C 60,31, H 5,86; trouvée : C 60,33, H 5,82.

TABLEAU 6. Plans moyens caractéristiques du composé **7**[a]

	A	*B*	*C*	*D*
Plan n° 1	0,9408	0,2346	−0,2445	8,1331

Atomes dans le plan :

Atome	*x*	*y*	*z*	Distance	esd
C3	6,9715	11,6074	4,6492	0,012	0,006
C4	6,6203	13,0800	4,8119	−0,012	0,006
C6	5,9796	13,2385	2,3974	0,012	0,006
C1	6,2748	11,7321	2,1871	−0,012	0,006

Autres atomes :

Atome	*x*	*y*	*z*	Distance	esd
C5	6,8241	13,8243	3,5193	0,670	0,006
C2	6,1761	10,9782	3,4988	−0,602	0,006
P1	9,3661	10,2994	4,5919	1,972	0,002
P2	7,1965	13,6268	7,3922	0,027	0,002
O3	6,3596	15,1653	3,7463	0,492	0,004
O4	7,6053	11,7249	1,6153	1,378	0,004
C6	5,2249	11,1998	1,1964	−0,882	0,007
O1	8,3810	11,5389	4,3829	1,387	0,004
O2	7,4161	13,6856	5,8045	0,636	0,004

Plan n° 2	0,3530	−0,8631	−0,3661	−7,2343

Atomes dans le plan :

Atome	*x*	*y*	*z*	Distance	esd
P1	9,3661	10,2994	4,4519	−0,007	0,002
N1	10,3956	10,1620	5,8847	0,008	0,006
O9	10,5759	11,1233	3,7733	0,005	0,005
C14	11,7192	10,7637	5,7800	−0,006	0,010

Autres atomes :

Atome	*x*	*y*	*z*	Distance	esd
C13	11,5618	11,7296	4,5949	−0,467	0,008
C15	8,8685	8,8045	6,6864	0,277	0,007

Plan n° 3	0,3939	−0,8230	−0,4092	−6,6706

Atomes dans le plan :

Atome	*x*	*y*	*z*	Distance	esd
P1	9,3661	10,2994	4,5919	0,005	0,002
N1	10,3956	10,1620	5,8847	−0,006	0,006
O10	8,2502	9,3576	5,4305	−0,003	0,004
C16	9,9966	9,3995	7,0098	0,004	0,010

Autres atomes :

Atome	*x*	*y*	*z*	Distance	esd
C13	11,5618	11,7296	4,5949	−0,309	0,008
C15	8,6585	8,8045	6,6864	0,099	0,007

Plan n° 4	−0,1434	0,5141	−0,8457	−0,2389

Atomes dans le plan :

Atome	*x*	*y*	*z*	Distance	esd
P2	7,1965	13,6268	7,3922	−0,039	0,002
N2	6,8178	15,0156	8,1993	0,047	0,006
O11	5,5637	13,2067	7,3382	0,025	0,004
C18	5,4538	15,1891	8,6308	−0,033	0,009

Autres atomes :

Atome	*x*	*y*	*z*	Distance	esd
C17	4,6225	14,2345	7,7317	0,356	0,007
C19	9,1165	15,3437	8,0319	0,028	0,008

Plan n° 5	0,9408	0,2346	−0,2445	8,1331

Atomes dans le plan :

Atome	*x*	*y*	*z*	Distance	esd
P2	7,1965	13,6268	7,3922	−0,017	0,002
N2	6,8178	15,0156	8,1993	0,021	0,006
O12	8,8047	13,9734	9,6737	0,011	0,005
C20	7,8765	15,7862	8,7901	−0,015	0,009

Autres atomes :

Atome	*x*	*y*	*z*	Distance	esd
C17	4,6225	14,2345	7,7317	−0,111	0,007
C19	9,1165	15,3437	8,0319	0,453	0,008

[a]L'équation du plan est de la forme $Ax + By + Cz - D = 0$ où A, B, C, D sont des constantes et x, y, z sont les coordonnées orthogonalisées.

(1R,3R,4S,5R)-1,5-Diacétoxy 3,4-dihydroxycyclohexane carboxylate de méthyle (6)

À une solution d'acide acétique à 80% (50 mL) on ajoute 1,79 g (4,73 mmol) de **10** et on laisse sous agitation pendant 12 h à la température ambiante. Après évaporation du solvant et purification par chromatographie sur gel de silice (éluant acétate d'éthyle) on récupère 1,27 g de produit désiré **6** (rendement = 92%) sous la forme d'un solide blanc; F = 114–115°C; ν_{max} (KBr, cm^{-1}) : 3480, 3400 (OH), 1750 (C=O), 1740 (C=O). RMN ^1H ($CDCl_3$) δ : 5,22 (m, 1H, C5-H, J_{5-4} = 9,0, J_{5-5a} = 10,5, J_{5-6e} = 4,50 Hz), 4,19 (m, 1H, C3-H, J_{3-4} = 3,0, J_{3-2a} = 3,80, J_{3-2e} = 3,50 Hz), 3,68 (s, 3H), 3,60 (m, 1H, C4-H, J_{4-5} = 9,0, J_{4-3} = 3,0 Hz), 2,57 (m, 1H, C2-He, J_{2e-2a} = 15,50, J_{2e-3} = 3,50, J_{2e-6e} = 2,50 Hz), 2,43 (m, 1H, C6-He, J_{6e-6a} = 13,50, J_{6e-5} = 4,50, J_{6e-2e} = 2,50 Hz), 2,14 (m, 1H, C2-Ha, J_{2a-2e} = 15,50, J_{2a-3} = 3,80), 2,06 (s, 3H), 2,05 (s, 3H), 1,82 (m, 1H, C6-Ha, J_{6a-6e} = 13,50, J_{6a-5} = 10,50 Hz). RMN ^{13}C ($CDCl_3$) δ : 171,5 (C=O), 171,18 (C=O), 170,33 (C=O), 79,41 (C1), 72,65 (C4), 69,92 (C5), 68,49 (C3), 52,70 (OCH_3),

Can. J. Chem. Downloaded from www.nrcresearchpress.com by 195.138.81.100 on 09/07/12
For personal use only.

Can. J. Chem. Downloaded from www.nrcresearchpress.com by 195.138.81.100 on 09/07/12
For personal use only.

TABLEAU 7. Données cristallographiques

Formule brute : $C_{28}H_{50}N_2O_{12}P_2$
Densités calculées : $\rho_c = 1{,}25$ g cm^{-3}
Masse moléculaire relative : 668,6
Système : orthorombique
Groupe : $P2_12_12_1$
Maille en Å $a = 10{,}853(9)$
$b = 16{,}971(6)$
$c = 19{,}326(5)$
Volume de la maille Å^3 $V = 3560$
Nombre de molécules par maille $Z = 4$
$\mu(\text{MoK}\alpha) = 1{,}73$ cm^{-1}
$F[000] = 1428$
Temperature : 20°C
Radiation : MoKα $\lambda = 0{,}71069$ Å; monochromateur : graphite
Distance cristal–détecteur : 207 mm
Fenêtre détecteur : hauteur : 4 mm; largeur : 4 mm
Angle de «take-off» : 3,2°
Mode de balayage : $\theta/2\theta$
Angle de Bragg maximum : 28°
Largeur de balayage : $(0{,}8 + 0{,}35 \text{ tg } \theta)°$ en ω
Paramètres pour la détermination de la vitesse de balayage :
SIGPRE : 0,75; SIGMA : 0,018; VPRE : 10° min^{-1}; T_{max} : 120
périodicité : 3600 s 100 réflexions
Nombre de réflexions pour affinement des paramètres cristallins : 25
Nombre de réflexions indépendantes : 4801
Nombre de réflexions observées ($I > 3\sigma'(I)$) : 3324
Nombre de paramètres affinés : 398
Facteurs de convergence finaux : $R = 0{,}046$ $R_w = 0{,}045$
$R = \Sigma||F_o| - k|F_c||/\Sigma|F_o|$
$R_w = [\Sigma_w(|F_o| - k|F_c|)^2/\Sigma_w|F_o|^2]^{1/2}$
$w = 4F_o^2/(\sigma F_o^2)^2$ $S = 1{,}135$

36,13 (C6), 33,79 (C2), 21,12 (CH_3CO). SM *m/e* (intensité relative) : 291 MH^+ (3), 273 (19), 89 (27), 61 (16), 43 (100). Anal. calc. pour $C_{12}H_{18}O_8$: C 49,65, H 6,25; trouvée : C 49,82, H 6,24.

(1R,3R,4S,5R)-1,5-Diacétoxy 3,4-di[3,3,7,7-tétraméthyl 2,8-dioxa 5-aza 1-phospha^V bicyclo[3.3.0]octyl-1-oxy]cyclohexane carboxylate de méthyle (7)

À une solution de 1 g (3,45 mmol) de **6** dans le toluène (5 mL) anhydre et sous atmosphère d'argon on ajoute 1,33 g (7 mmol) de **11**. Après 1 nuit d'agitation à température ambiante le solvant est évaporé. Le solide blanc obtenu est recristallisé dans l'éther anhydre pour donner le composé **7** (1,42 g; $R = 62\%$); $F = 143$–144°C; ν_{max} (KBr, cm^{-1}) : 2380 (PH), 1745 (C=O), 1130 (P—O). SM *m/e* (intensité relative) : 667 $(M - 1)^+$ (0,3), 401 (1,5), 335 (20), 285 (12), 169 (100), 150 (34), 119 (14), 69 (75). Anal. calc. pour $C_{28}H_{50}N_2O_{12}P_2$: C 50,29, H 7,48, N 4,19; trouvée : C 49,69, H 7,53, N 4,21.

Étude cristallographique et collection des données

Le monocristal du composé **7** a été obtenu par évaporation lente sous atmosphère inerte et à température ambiante d'une solution de bicyclophosphorane **7** dans le toluène. Le cristal transparent choisi pour l'étude se présente sous la forme approximative d'un cube de 0,3 mm de côté.

Les mesures ont été effectuées à l'aide d'un diffractomètre automatique Enraf–Nonius de type CAD4. Le composé cristallise dans le système orthorombique, le groupe spatial étant $P2_12_12_1$. L'affinement de 25 réflexions *hkl* réparties aléatoirement dans l'espace réciproque conduit aux paramètres de la maille cristalline suivants : *a* : 10,853 (9) Å; *b* : 16,971 (6) Å; *c* : 19,326 (5) Å; *V* 3560 Å^3.

L'ensemble des calculs a été effectué sur un ordinateur Digital Vax 730; la chaîne SDP a été utilisée. L'intensité des réflexions *hkl* a été corrigée des facteurs de Lorentz et de la polarisation. Aucune décroissance des tâches de contrôle d'intensité n'étant observée, cette correction n'a pas été nécessaire. Une correction d'absorption expérimentale a également été effectuée malgré une valeur faible (1,73 cm^{-1}) du coefficient d'absorption. Ceci a conduit à des coefficients de transmission variant de 0,93 à 1,0.

La détermination de la structure cristalline a été effectuée par l'utilisation des méthodes directes (programme MULTAN). L'affinement des positions atomiques et de l'agitation thermique de tous les atomes exceptés les hydrogènes nous a conduit à un facteur de reliabilité $R = 0{,}15$ puis $R = 0{,}07$ après introduction de l'agitation thermique anisotrope. À ce stade d'affinement une série de Fourier-différence nous a permis de localiser les atomes d'hydrogène à l'exception des deux hydrogènes liés aux atomes de phosphore. Un calcul théorique nous a permis de confirmer nos observations et de fixer les longueurs entre atomes de carbone et hydrogène à 0,97 Å. La contribution des atomes d'hydrogène a été introduite dans le dernier affinement mais ni leurs positions ni leurs agitations thermiques n'ont été affinées.

L'affinement final incluant également l'extinction secondaire ($3{,}17 \times 10^{-7}$) conduit à un facteur de reliabilité final $R = 0{,}046$. Le tableau 3 donne les coordonnées atomiques. Les paramètres angulaires et de liaison ainsi que les valeurs de torsion les plus significatives sont données dans les tableaux 4 et 5. Les tableaux des plans moyens caractéristiques de la molécule sont regroupés dans le tableau 6. Enfin, les données cristallines du composé sont consignées dans le tableau 7.

1. E. DELFOURNE, L. GORRICHON et C. ZEDDE. Tetrahedron Lett. **29**, 4555 (1988).
2. E. DELFOURNE, J. VERONIQUE, L. GORRICHON, A. MUNOZ et L. LAMANDE. Tetrahedron, **45**, 2605 (1989).
3. J. VERONIQUE. Thèse de l'Université Paul Sabatier, Toulouse, France. 1988.
4. B. GANEM. Tetrahedron, **34**, 3353 (1978).
5. P. A. BARTLETT. Recent Adv. Phytochem. **20**, 119 (1986).
6. S. CHAUDHURI, J. M. LAMBERT, L. A. MCCOLL et J. R. COGGINS. Biochem. J. **239**, 699 (1986).
7. (*a*) D. A. MCGOWAN et G. A. BERCHTOLD. J. Am. Chem. Soc. **104**, 7036 (1982); (*b*) P. M. CHOUINARD et P. A. BARTLETT. J. Org. Chem. **51**, 75 (1986).
8. (*a*) P. A. BARTLETT et L. A. MCQUAID. J. Am. Chem. Soc. **106**, 7854 (1984); (*b*) CHIA-YU P. TENG, Y. YUKIMOTO et B. GANEM. Tetrahedron Lett. **24**, 21 (1985).
9. R. S. CHARLEFF. J. Gen. Microbiol. **81**, 337 (1974).
10. A. GRAZIANA et A. M. BOUDET. Plant Cell Physiol. **21**, 793 (1980).
11. K. L. AGARWAL, A. YAMAZAKI, P. T. CASHION et M. G. KHORANA. Angew. Chem. Int. Ed. Engl. **11**, 457 (1972).
12. (*a*) R. L. LETSINGER et W. B. LUNSFORD. J. Am. Chem. Soc. **98**, 3655 (1976); (*b*) M. H. CARUTHERS. Science, **230**, 281 (1985).
13. (*a*) D. HOUALLA, F. H. OSMAN, M. SANCHEZ et R. WOLF. Tetrahedron Lett. **35**, 3041 (1977); (*b*) B. DUTHU, D. HOUALLA et R. WOLF. Can. J. Chem. **66**, 2965 (1988).
14. D. LESUISSE et G. A. BERCHTOLD. J. Org. Chem. **50**, 888 (1985).
15. J. CORSE, R. E. LUNDIN, E. SONDHEIMER et A. C. WAISS. Phytochemistry, **5**, 767 (1966).
16. E. HASLAM et M. J. TURNER. J. Chem. Soc. (C), 1496 (1971).
17. R. C. COOKSON, J. J. FRANKEL, L. HUDEC et T. A. CRABB. Tetrahedron (Suppl.), **7**, 335 (1966).
18. R. U. LEMIEUX et J. D. STEVENS. Can. J. Chem. **43**, 2059 (1965).
19. (*a*) W. S. SHELDRICK, A. SCHMIDPETER et J. H. WEINMAIER. Angew. Chem. Int. Ed. Engl. **14**, 490 (1975); (*b*) R. CONTRERAS, A. MURILLO et P. JOSEPH-NATHAN. Phosphorus Sulfur Silicon Relat. Elem. **47**, 215 (1990).
20. C. ABELL, F. H. ALLEN, T. D. H. BUGG, M. J. DOYLE et P. R. RAITHBY. Acta Crystallogr. Sect. C: Cryst. Struct. Commun. **C44**, 1287 (1988).
21. R. BUCOURT et D. HAINAUT. Bull. Soc. Chim. Fr. 1366 (1965).
22. J. DEVILLERS, D. HOUALLA, J. MOUHEICH et R. WOLF. Org. Magn. Reson. **8**, 558 (1976).
23. M. L. MARTIN et G. J. MARTIN. *Dans* Manuel de résonance magnétique nucléaire. Azoulay, Paris. 1971. p. 43.

Isobaric vapor–liquid equilibria of 1-bromobutane + chloroethane systems[1]

K. RAMBABU, P. VENKATESWARLU,[2] AND G. K. RAMAN
Thermo Chemical Laboratories, Department of Chemistry, College of Engineering, Sri Venkateswara University, Tirupati-517 502, (A.P.), India

AND

Y. V. L. RAVI KUMAR
Chemical Engineering Division, Indian Institute of Chemical Technology, Hyderabad-7, India

Received December 21, 1989

K. RAMBABU, P. VENKATESWARLU, G. K. RAMAN, and Y. V. L. RAVI KUMAR. Can. J. Chem. **69**, 311 (1991).

The boiling point data for the binary liquid mixtures of 1-bromobutane with 1,2-dichloroethane, 1,1,1-trichloroethane, and 1,1,2,2-tetrachloroethane were obtained over the entire composition range by using a standard Swietoslawski type ebulliometer at 715 Torr. The experimental t–x data were used to estimate Wilson parameters and also to calculate the equilibrium vapor compositions for these systems. These Wilson parameters were used to calculate activity coefficients and these in turn were used to compute excess Gibbs free energy.

Key words: Wilson parameters, 1-bromobutane + chloroethane systems.

K. RAMBABU, P. VENKATESWARLU, G. K. RAMAN et Y. V. L. RAVI KUMAR. Can. J. Chem. **69**, 311 (1991).

Opérant à une pression de 715 Torr et utilisant un ébulliomètre standard de type Swietoslawski, on a déterminé les données relatives aux points d'ébullition de mélanges liquides binaires du 1-bromobutane avec le 1,2-dichloroéthane, le 1,1,1-trichloroéthane et le 1,1,2,2-tétrachloroéthane couvrant l'ensemble des compositions. On a utilisé les données expérimentales t–x pour évaluer les paramètres de Wilson ainsi que pour calculer les compositions des vapeurs à l'équilibre de ces systèmes. On a utilisé ces paramètres de Wilson pour calculer les coefficients d'activité et on a utilisé ces derniers pour calculer l'énergie libre de Gibbs en excès.

Mots clés : paramètres de Wilson, systèmes de 1-bromobutane + chloroéthane.

[Traduit par la rédaction]

Introduction

Distillation has been used as an effective means of separation in chemical processing. Evidently an accurate and complete knowledge of vapor–liquid equilibrium data for the mixture under consideration is necessary for the design of separation equipment. Generally, vapor–liquid equilibrium data are obtained under two fixed conditions, namely, isothermal and isobaric. Most distillation processes are carried out at constant pressure rather than at constant temperature, so that the temperature–composition curves are more practical in making such calculations as the number of plates, although for theoretical consideration the pressure–composition curves are preferable. Hence, an attempt is made to determine the isobaric boiling points and to calculate vapor compositions, activity coefficients, and excess Gibbs free energies for the systems of 1-bromobutane with chloroethanes at 715 Torr (1 Torr = 133.3 Pa).

Experimental

A Swietoslawski ebulliometer (Hala *et al.*, ref. 1) was used to measure the boiling points of the mixtures. The ebulliometer was connected to a vacuum system. Pressure was measured with a mercury manometer with an accuracy of ±1 Torr. The temperatures were measured with a PT 100 thermometer, which gave an accuracy of ±0.1°C. The detailed procedure was described previously (1).

Isobaric binary systems

The isobaric boiling points of the systems 1-bromobutane with 1,2-dichloroethane, with 1,1,1-trichloroethane, and with 1,1,2,2-tetrachloroethane were determined over the entire range of compositions. Mixtures of different compositions were made by taking suitable quantities (by weight) of the pure materials. The equilibrium compositions were not determined gravimetrically. The liquid compositions were assumed from the gravimetric compositions of the mixture. Vapour compositions were estimated by using the Wilson model. The boiling points for the known binary compositions were measured at 715 Torr.

Purification of materials

All materials were purified by the methods described by Riddick and Bunger (2). 1-Bromobutane, Fluka (AG 99%, GC pure), was used without further purification. 1,2-Dichloroethane (BDH) was purified as described by Choudary and Naidu (3). 1,1,1-Trichloroethane (Koch–Light) was washed with concentrated hydrochloric acid, followed by 10% potassium carbonate solution, and then with 10% sodium chloride solutions. It was dried over calcium chloride, distilled twice, and the middle fraction collected. During the distillation about 0.5 g of phenol was added as a stabilizer. 1,1,2,2-Tetrachloroethane (Riedel) was shaken with concentrated sulphuric acid for 10 min. The operation was repeated until the acid developed no more colour. The chloroalkane was then washed with water, steam distilled, dried with potassium carbonate, and finally fractionated.

The purity of the samples was checked by comparing the measured densities and boiling points of the compounds with those reported in the literature (4, 5). Densities were determined using a bicapillary type pycnometer that offered an accuracy of 2 parts in 10^5.

Results

Isobaric t–x measurements are used for the data reduction. The model for expressing the composition and temperature dependence is chosen to be the Wilson equation (6):

$$[1]\quad \ln \gamma_1 = -\ln [X_1 + \Lambda_{12}X_2] + X_2\left[\frac{\Lambda_{12}}{X_1 + \Lambda_{12}X_2} - \frac{\Lambda_{21}}{X_2 + \Lambda_{21}X_1}\right]$$

$$[2]\quad \ln \gamma_2 = -\ln [X_2 + \Lambda_{21}X_1] + X_1\left[\frac{\Lambda_{21}}{X_2 + \Lambda_{21}X_1} - \frac{\Lambda_{12}}{X_2 + \Lambda_{12}X_1}\right]$$

[1]This paper is being published without the author having checked the proofs.

[2]Author to whom correspondence may be addressed.

Can. J. Chem. Downloaded from www.nrcresearchpress.com by 195.138.81.100 on 09/07/12
For personal use only.

Can. J. Chem. Downloaded from www.nrcresearchpress.com by 195.138.81.100 on 09/07/12
For personal use only.

TABLE 1. Wilson constants $(\lambda_{12} - \lambda_{11})/R$ and $(\lambda_{12} - \lambda_{22})/R$ along with the standard deviation, $\sigma(t)$

System	$(\lambda_{12} - \lambda_{11})/R$	$(\lambda_{12} - \lambda_{22})/R$	$\sigma(t)$
1-Bromobutane + 1,2-dichloroethane	−206.14	440.89	0.5
1-Bromobutane + 1,1,1-trichloroethane	−267.58	682.95	0.5
1-Bromobutane + 1,1,2,2-tetrachloroethane	−265.14	41.81	0.4

TABLE 2. Antoine constants of pure components

Component	Antoine constants		
	A	*B*	*C*
1-Bromobutane	6.92254	1298.61	219.720
1,2-Dichloroethane	6.66301	1073.99	200.406
1,1,1-Trichloroethane	6.51385	988.54	197.936
1,1,2,2-Tetrachloroethane	6.81569	1361.62	199.858

TABLE 3. T, X_1, Y_1, γ_1, γ_2 data for 1-bromobutane with chloroethanes at 715 Torr

T, °C	X_1	Y_1	γ_1	γ_2
1-Bromobutane + 1,2-dichloroethane				
83.0	0.1026	0.0688	1.1262	1.0002
84.1	0.1997	0.1385	1.1206	1.0012
85.1	0.2991	0.2143	1.1122	1.0040
85.6	0.4024	0.2978	1.1003	1.0101
88.3	0.5087	0.3890	1.0846	1.0228
91.6	0.6949	0.5640	1.0498	1.0777
92.9	0.7954	0.6715	1.0288	1.1446
95.3	0.8943	0.7984	1.0101	1.2682
1-Bromobutane + 1,1,1-trichloroethane				
74.9	0.0998	0.0406	0.9072	0.9985
76.8	0.2044	0.0931	0.9366	0.9933
79.3	0.3039	0.1545	0.9636	0.9847
81.2	0.4077	0.2324	0.9894	0.9715
84.6	0.5038	0.3184	0.0100	0.9573
85.7	0.5944	0.4122	1.0248	0.9428
89.3	0.6904	0.5237	1.0335	0.9316
92.0	0.8052	0.6698	1.0310	0.9444
94.7	0.8913	0.7878	1.0184	1.0201
1-Bromobutane + 1,1,2,2-tetrachloroethane				
136.7	0.0955	0.2407	0.9320	0.9994
130.8	0.2107	0.4563	0.9442	0.9969
125.8	0.2947	0.5755	0.9529	0.9936
120.5	0.4077	0.7000	0.9642	0.9870
116.5	0.4971	0.7763	0.9726	0.9797
111.7	0.6023	0.8472	0.9816	0.9683
108.9	0.7046	0.9010	0.9891	0.9541
106.6	0.7751	0.9312	0.9934	0.9422
101.8	0.8946	0.9723	0.9984	0.9176

The Wilson parameters Λ_{12} and Λ_{21} are given by

$$[3] \quad \lambda_{12} = \frac{V_2^L}{V_1^L} \exp\left[-\frac{\lambda_{12} - \lambda_{11}}{RT}\right]$$

$$[4] \quad \lambda_{21} = \frac{V_1^L}{V_2^L} \exp\left[-\frac{\lambda_{12} - \lambda_{22}}{RT}\right]$$

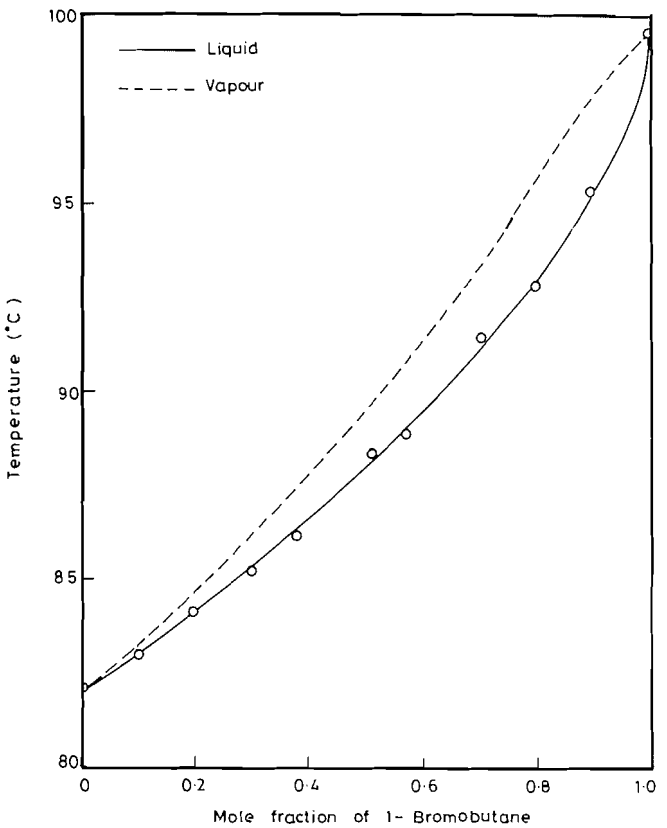


FIG. 1. 1-Bromobutane + 1,2-dichloroethane (○) at 715 Torr.

where V_1^L and V_2^L are liquid molar volumes, and $(\lambda_{12} - \lambda_{11})$ and $(\lambda_{12} - \lambda_{22})$ are temperature independent (to some extent) Wilson parameters. λ's are the energies of interaction between the molecules designated in the subscripts.[3]

Discussion

The optimum Wilson parameters λ_{12} and λ_{21} are obtained by minimizing the objective function ϕ, using Nelder–Mead optimization techniques (7), and the values are presented in Table 1 along with the standard deviation of the fit.

$$[5] \quad \phi = \Sigma(P_{calc}/P_{exp} - 1.0)^2$$

Since the prediction of vapor–liquid equilibrium data involves the vapor pressure data of the pure compounds, these same data have been determined for 1-bromobutane, 1,2-dichloroethane, 1,1,1-trichloroethane, and 1,1,2,2-tetrachloroethane.

[3] *Glossary*: *A*,*B*,*C*: Antoine constants; *P*: pressure, Torr; *t*: temperature, °C; X_1: mole fraction in liquid phase; *Y*: vapor composition; γ activity coefficients; Λ Wilson parameter. Subscript 1 refers to 1-bromobutane, and subscript 2 to the chloroethanes.

TABLE 4. Excess Gibbs energy data at 25°C for the mixtures 1-bromobutane with chloroethanes

	G^E, J/mol		
X_1	1-Bromobutane + 1,2-dichloroethane	1-Bromobutane + 1,1,1-trichloroethane	1-Bromobutane + 1,1,2,2-tetrachloroethane
0.0500	9.07	−24.27	−3.05
0.1000	18.46	−46.24	−5.80
0.1500	28.12	−65.77	−8.24
0.2000	37.99	−82.72	−10.37
0.2500	47.99	−96.94	−12.18
0.3000	58.04	−108.28	−13.68
0.3500	68.01	−116.57	−14.85
0.4000	77.75	−121.63	−15.69
0.4500	87.08	−123.30	−16.21
0.5000	95.77	−121.41	−16.39
0.5500	103.51	−115.81	−16.24
0.6000	109.92	−106.39	−15.76
0.6500	114.51	−93.12	−14.94
0.7000	116.64	−76.10	−13.79
0.7500	115.45	−55.70	−12.31
0.8000	109.81	−32.76	−10.49
0.8500	98.16	−9.04	−8.34
0.9000	78.32	11.80	−5.88
0.9500	47.17	21.65	−3.09

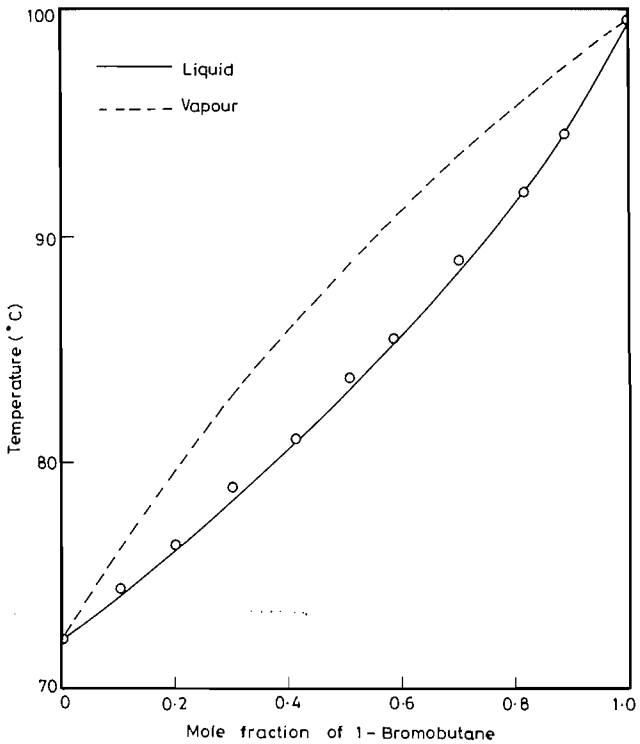


FIG. 2. 1-Bromobutane + 1,1,1-trichloroethane (○) at 715 Torr.

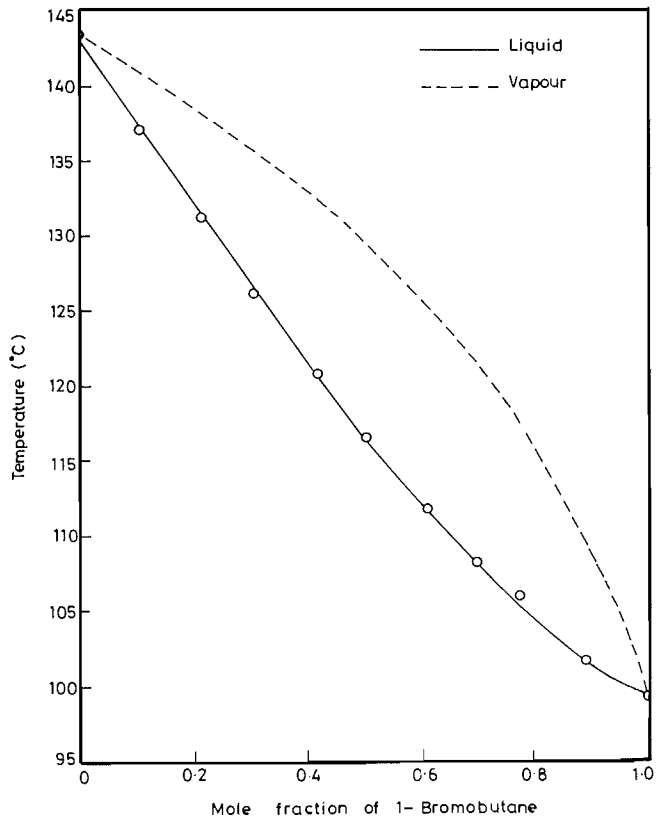


FIG. 3. 1-Bromobutane + 1,1,2,2-tetrachloroethane (○) at 715 Torr.

The Antoine constants for the pure compounds were obtained by non-linear regression analysis of the experimental data (8). The observed Antoine constants are presented in Table 2. The liquid composition, measured boiling points, vapour compositions, and activity coefficients using the Wilson equation are presented in Table 3 and shown in Figs. 1–3. If vapor-phase non-idealities are neglected, which is justified at these low pressures, the vapor compositions can be calculated by using the following equation.

$$[6] \quad Y_1 = \frac{X_1 P_1^S \gamma_1^S}{P_{calcd}}$$

The excess Gibbs free energies at 25°C for the three systems were also calculated with these model parameters by using

Can. J. Chem. Downloaded from www.nrcresearchpress.com by 195.138.81.100 on 09/07/12
For personal use only.

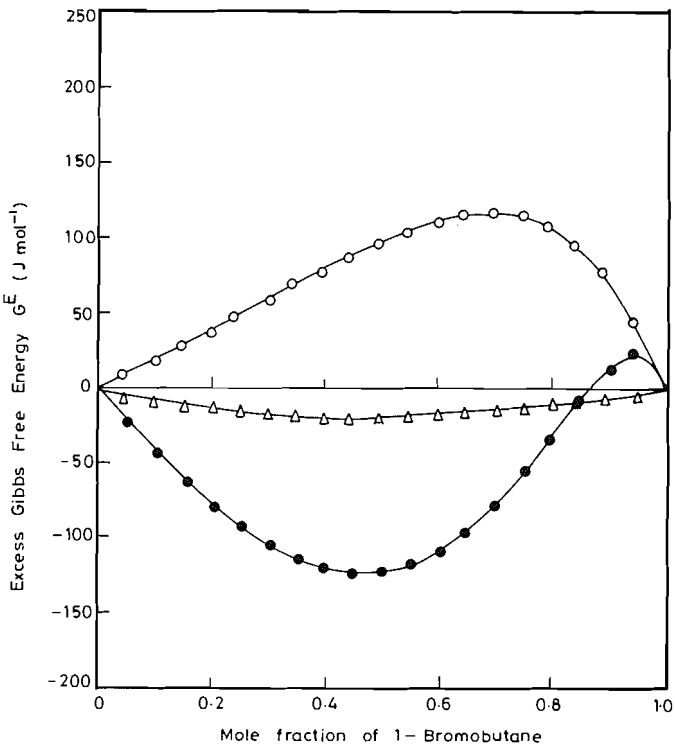


FIG. 4. 1-Bromobutane + 1,2-dichloroethane (○), + 1,1,1-trichloroethane (●), and + 1,1,2,2-tetrachloroethane (△) at 298.15 K.

eq. [7]:

[7] $G^E/RT = X_1 \ln \gamma_1 + X_2 \ln \gamma_2$

and are presented in Table 4 and shown in Fig. 4.

1. E. HALA, J. PICK, V. FRIED, and O. VILIM. Vapor–liquid equilibrium. Pergamon Press, Oxford.
2. J. A. RIDDICK and W. B. BUNGER. Techniques of chemistry. 3rd ed. Vol. II. Wiley–Interscience, New York. 1970.
3. N. V. CHOUDARY and P. R. NAIDU. Can. J. Chem. **59**, 2210 (1981).
4. J. TIMMERMANS. Physico-chemical constants of pure organic compounds. Elsevier, Amsterdam. 1950.
5. J. A. DEAN. Langes handbook of chemistry. McGraw–Hill, New York. 1973.
6. G. M. WILSON. J. Am. Chem. Soc. **86**, 127 (1964).
7. R. T. KUESTER and J. H. MIZE. Optimization techniques with Fortran. McGraw–Hill, New York. 1973.
8. C. R. REID, J. M. PRAUSNITZ, and K. T. SHERWOOD. The properties of liquids and gases. 3rd ed. Properties Data Bank A, New York. 1977.

Can. J. Chem. Downloaded from www.nrcresearchpress.com by 195.138.81.100 on 09/07/12
For personal use only.

Synthesis, electrochemical and spectroscopic investigations of 2,2′:4,4″-terpyridine and 2,2′:4,4″:6,2″-quaterpyridine ligands for metal complex photoelectrochemistry

L. PERSAUD[1] AND G. BARBIERO

Department of Chemistry, University of Sherbrooke, Sherbrooke (Québec), Canada J1K 2R1

Received August 13, 1990

L. PERSAUD and G. BARBIERO. Can. J. Chem. **69**, 315 (1991).

The synthesis of 2,2′:4,4″:6,2‴-quaterpyridine and 2,2′:4,4″-terpyridine was accomplished by a reverse aldol condensation reaction of the appropriate aldehyde with alkyl and pyridyl acetyls. A selective quaternization method in toluene is described. In this method the 1,1′ nitrogens survive alkylation and are free to coordinate with metals to form metal complexes. The electrochemical behaviour of the neutral ligands as well as the monoquaternized cations was established by linear sweep cyclic voltammetry. Spectroelectrochemical techniques were used to establish the electronic spectral behaviour and stability of the radicals obtained upon reduction.

Key words: 2,2′:4,4″-terpyridine, quaterpyridine, selective quaternization.

L. PERSAUD et G. BARBIERO. Can. J. Chem. **69**, 315 (1991).

Les aldéhydes appropriés soumis à des réactions de retroaldolisation avec les acétyles d'alkyle de pyridine fournissent la 2,2′:4,4″:6,2‴-quaterpyridine et la 2,2′:4,4″-terpyridine. La formation sélective des sels quaternaires est favorisée dans le toluène où les azotes 1,1′ sont libres pour donner des complexes avec des ions métalliques. Par voltampérométrie à balayage cyclique, les caractéristiques électrochimiques des espèces neutres ainsi que celles des cations monoquaternaires ont été établies. Les caractéristiques spectrales UV et la stabilité des radicaux anions ont été déterminées par spectroélectrochimie.

Mots clés : 2,2′:4,4″-terpyridine, quaterpyridine, quaternisation sélective.

Introduction

The diimine ligand, 2,2′-bipyridine, continues to find extensive usage in the preparation of metal complexes for photochemical and photophysical studies. It has been modified by a number of substituents in an effort to tune and control excited states behaviour. Reviews by Kalyanasundaram (1), Juris *et al.* (2), and more recently by Krause (3) have summarized a number of substituted 2,2′-bipyridines and their metal complexes along with some of their excited states behaviour. Most of the modifications were accomplished by adding the same group to both rings to obtain disubstituted derivatives. Small and simple groups such as chloride as well as the larger and strongly interacting aromatic phenyl rings were used. Among these groups the latter appear to be particularly interesting.

Metal complexes of 4,4′-diphenyl-2,2′-bipyridine were shown to exhibit an enhanced absorbance in the MLCT band (4). In addition, their excited states lifetimes are longer than others in which the substituent is nonaromatic. This behaviour was also observed for other molecules derived from the closely related 1,10-phenanthroline ligand with phenyl substituents in the 4 and 7 positions (5). The phenyl ring appears to be the factor that is responsible for this behaviour. The aromatic nature and its ability to undergo resonance isomerism have been suggested as the explanation (6). These groups are in conjugation with the π system of the parent ligand and extend it away from the metal center. This affects the dipole transition, which in turn influences the absorptivity.

Pyridine groups are similar to the phenyl rings. They are aromatic and can undergo conjugation. 2,2′-Bipyridine with a pyridine substituent in the 4 position is therefore an interesting ligand since it can exhibit behaviour similar to the phenyl derivatives. In addition, a quaternized pyridine substituent can undergo redox reaction and thereby provide a site away from the metal center, but in conjugation with it, for the acceptance or donation of an electron. The combined features of a redox site and electronic conjugation effects in this molecule make it a new and different ligand system for excited states electron transfer studies. In spite of this, such a system was only recently prepared when Morgan and Baker (7) catalytically coupled two molecules of 4,4′-bipyridine to produce a 2,2′:4,4″:4′,4″-quaterpyridine.

As part of the general effort to develop new ligands and new modifications of known ligands for the preparation of molecular complexes to investigate photoelectrocatalysis and photoinduced electron transfer we have successfully synthesized 2,2′:4,4″-terpyridine (**1**) and 2,2′:4,4″:6,2‴-quaterpyridine (**2**). These molecules were selectively quaternized at the N″ nitrogen to give the corresponding *N*″-methylterpyridinium (**3**) and *N*″-methylquaterpyrindium (**4**) cations. Their preparation and electrochemical and spectroscopic behaviour are described.

Experimental

Reagents

4-Pyridinecarboxaldehyde, 2-acetylpyridine, pyruvic acid, tetrabutylammonium hexafluorophosphate, and ammonium hexafluorophosphate were purchased from Aldrich. *N*,*N*-Dimethylformamide was either spectrophotometric or anhydrous sure/seal grade, also from Aldrich. Other solvents and chemicals were reagent grade obtainable from commercial sources.

Apparatus

Cyclic voltammetry and other electrochemical measurements were done on a PAR 273 potentiostat/galvanostat in conjugation with an EG&G model RE0089 X–Y recorder. The working electrode was a platinum disk, the counter electrode was a platinum wire, and the reference electrode was a Ag/Ag^+ (0.1 M $AgNO_3/CH_3CN$) the potential of which was measured as −0.31 vs. the standard calomel electrode. For cyclic voltammetric measurements millimolar quantities of samples were used in anhydrous sure/seal grade DMF with 0.1 M tetra-*n*-butylammonium hexafluorophosphate as supporting electrolyte. The latter was recrystallized from ethanol and dried under vacuum at 80°C. Spectroelectrochemical measurements were obtained by electrolyzing the solution in a locally made cell with a 1-cm spectrophotometric cuvette that fitted directly in the path of the light beam. The counter electrode was separated from the bulk solution by a fritted glass disk.

[1]Author to whom correspondence may be addressed.

Can. J. Chem. Downloaded from www.nrcresearchpress.com by 195.138.81.100 on 09/07/12
For personal use only.

TABLE 1. ^{13}C NMR resonances for Qpy,[a] $[QpyMe]^+(I^-)$,[b] Terpy,[a] and $[TerpyMe]^+(I^-)$[b]

C	Qpy **2**	$[QpyMe]^+(I^-)$ **4**	Terpy **1**	$[TerpyMe]^+(I^-)$ **3**
1	—	—	—	—
2	156.29	156.37	157.07	157.80
3	118.52	118.60	118.70	118.77
4	145.83	143.76	145.62	143.56
5	118.52	118.60	123.99	124.09
6	156.29	156.37	149.15	146.16
1′	—	—	—	—
2′	155.64	154.19	155.53	153.91
3′	121.24	121.14	121.17	121.07
4′	136.83	137.62	136.93	137.72
5′	123.99	124.62	124.40	125.01
6′	149.10	146.11	149.93	146.93
1″	—	47.50	—	47.30
2″	150.48	149.36	150.54	149.44
3″	121.56	125.44	121.80	125.68
4″	147.33	152.21	146.37	151.22
5″	121.56	125.44	121.80	125.68
6″	150.48	149.36	150.54	149.44
1‴	—	—	—	—
2‴	155.64	154.19	—	—
3‴	121.24	121.14	—	—
4‴	136.83	137.62	—	—
5‴	123.99	124.62	—	—
6‴	149.10	146.11	—	—

[a]Saturated solution in $CDCl_3$.
[b]Saturated solution in DMSO-d_6.

TABLE 2. Proton NMR chemical shifts for Qpy,[a] $[QpyMe]^+(I^-)$,[b] Terpy,[a] and $[TerpyMe]^+(I^-)$[b]

H	Qpy **2**	$[QpyMe]^+(I^-)$ **4**	Terpy **1**	$[TerpyMe]^+(I^-)$ **3**
H1	—	—	—	—
H2	—	—	—	—
H3	8.72 (m)	8.91 (s)	8.80 (d)	8.76 (s)
H4	—	—	—	—
H5	8.72 (m)	8.91 (s)	7.56 (dd)	8.06 (m)
H6	—	—	8.72 (m)	8.95 (d)
H1′	—	—	—	—
H2′	—	—	—	—
H3′	8.65 (d)	8.77 (m)	8.48 (d)	8.47 (d)
H4′	7.85 (t)	8.11 (t)	7.88 (dt)	8.06 (m)
H5′	7.36 (m)	7.60 (t)	7.35 (q)	7.56 (m)
H6′	8.70 (m)	8.79 (m)	8.71 (m)	8.74 (m)
H1″	—	4.42 (s)	—	4.34 (s)
H2″	8.75 (m)	9.16 (d)	8.76 (dd)	9.14 (d)
H3″	7.75 (dd)	8.72 (d)	7.67 (dd)	8.69 (d)
H4″	—	—	—	—
H5″	7.75 (dd)	8.72 (d)	7.67 (dd)	8.69 (d)
H6″	8.75 (m)	9.16 (d)	8.76 (dd)	9.14 (d)
H1‴	—	—	—	—
H2‴	—	—	—	—
H3‴	8.65 (d)	8.77 (m)	—	—
H4‴	7.85 (t)	8.11 (t)	—	—
H5‴	7.36 (t)	7.60 (t)	—	—
H6‴	8.70 (m)	8.79 (m)	—	—

[a]Solution in $CDCl_3$.
[b]Solution in DMSO-d_6.

Spectrophotometric measurements were recorded on an HP 8452A diode array spectrophotometer. NMR data were collected on a Bruker 250 MHz spectrometer with an Aspect 2000 computer. The ionic compounds or salts were taken in deuterated DMSO while the neutral materials were measured in deuterated chloroform. Molecular mass information was obtained on a 70 eV V.G. Micromass ZAB-1F spectrometer.

*Preparation of 2,2′:4,4″ terpyridyl (**1**) [Terpy]*

To a stirring solution of 4-pyridinecarboxaldehyde (0.1047 mol) in 40 mL of methanol cooled at −25°C, pyruvic acid (28 mL) neutralized at 0°C with 84 mL of 20% aqueous NaOH and 20 mL of 20% aqueous NaOH were simultaneously added dropwise over a 30 min period. A solution of 2-acetylpyridine (0.0891 mol) in 25 mL of methanol was cooled to −25°C and added dropwise to the reaction mixture over a 40 min period, followed by the dropwise addition of 40 mL of 20% aqueous NaOH over a 90 min period while always maintaining the reaction temperature between −15 and −20°C. The reaction mixture was stirred for an additional 4 h, warmed to room temperature, filtered, and washed with water. The precipitate was dissolved in methanol and treated at reflux with ammonium acetate to yield 7.25 g (54%) of the quaterpyridine. The original filtrate solution was heated with stirring to 80°C with ammonia gas bubbling through. After 1 h the mixture was filtered hot and washed with hot water. The filtrate was cooled to room temperature and treated with concentrated HCl to induce precipitation. The crude precipitate was reprecipitated twice from a saturated aqueous NaOH/concentrated HCl solution system, to give 4.7 g (23%) of 6-carboxyl-2,2′:4,4″ terpyridine acid as a white precipitate; MS, *m/e* 277.

*Preparation of 2,2′:4,4″:6,2‴-quaterpyridine (**2**) [Qpy]*

To a stirring solution of 4-pyridinecarboxyaldehyde (0.1047 mol) in 40 mL of methanol cooled to −15°C, 2-acetylpyridine in 20 mL of methanol and 40 mL of 20% aqueous NaOH were simultaneously added dropwise over a 20 min period. The reaction mixture was stirred for 3 h maintaining a temperature of −10 to −15°C, warmed to room temperature, and filtered. The filtrate solution was refluxed with 40 g of ammonium acetate for 4 h, filtered, and washed several times with hot water and hot ethanol, yielding 10.31 g of crude product, which was recrystallized from a minimum quantity of 15% DMF in methanol to give 9.46 g (69%) of **2** as white crystals, mp 216°C. The ^{13}C and ^1H nuclear magnetic resonance values are summarized in Tables 1 and 2 respectively. Anal. calcd. for $C_{20}H_{14}N_4$: C 77.40, H 4.55, N 18.05; found: C 77.42, H 4.58, N 18.04.

The carboxylic acid mentioned above (1.2 g) was heated to 280°C for 10 min to give a brown oil, which solidified upon cooling. The precipitate was purified twice, once in hot toluene and secondly by suspending the product in 10% aqueous NaOH and extracting with toluene. The organic extract was treated with charcoal, filtered, evaporated to dryness, and kept under reduced pressure overnight, to give 2,2′:4,4″-terpyridine (0.71 g, 59%) as white microcrystals, mp 84–85°C. The ^{13}C and H NMR are summarized in Tables 1 and 2 respectively. Anal. calcd. for $C_{15}H_{11}N_3$: C 77.23, H 4.75, N 18.01; found: C 77.28, H 4.65, N 18.03.

*Preparation of N″-methyl-2,2′:4,4″-terpyridinium iodide (**3**) [TerpyMe]$^+(I^-)$ and hexafluorophosphate (salts of **1**)*

To a solution of 2,2′:4,4″-terpyridine (300 mg) in 300 mL of toluene maintained at 50°C with stirring, methyl iodide (1 mL) in 10 mL of toluene was added dropwise and left to react for 24 h. The mixture was filtered hot, washed with hot toluene, and dried under vacuum. The crude iodide salt was recrystallized from ethanol to give *N″*-methyl-2,2″:4,4″-terpyridinium iodide salt (433 mg, 90%). The ^{13}C and ^1H chemical shifts are summarized in Tables 1 and 2 respectively. Anal. calcd. for $C_{16}H_{14}N_3$: C 51.22, H 3.76, N 11.20; found: C 51.24, H 3.76, N 11.27.

The hexafluorophosphate salt was prepared by dissolving 200 mg of the iodide salt **2** in 22 mL of water, followed by excess addition of a saturated aqueous ammonium hexafluorophosphate solution. The white slurry solution was filtered, washed with water, and recrystallized from methanol to give 189 mg of the hexafluorophosphate salt.

Can. J. Chem. Downloaded from www.nrcresearchpress.com by 195.138.81.100 on 09/07/12
For personal use only.

Can. J. Chem. Downloaded from www.nrcresearchpress.com by 195.138.81.100 on 09/07/12
For personal use only.

Preparation of N″*-methyl-2,2′:4,4″:6,2‴-quaterpyridinum iodide (4) [QpyMe]$^+$(I$^-$) and hexafluorophosphate (salts of 2)*

The selective monoquaternization of the N″ of quaterpyridine (**2**) was synthesized in the same manner as the terpyridine compound to give *N*″-methyl-2,2′:4,4″:6,2‴-quaterpyridinium iodide salt (90%). The ^{13}C and ^1H resonance values are summarized in Tables 1 and 2 respectively. Anal. calcd. for $C_{21}H_{17}N_4$: C 55.77, H 3.79, N 12.39; found: C 55.72, H 3.74, N 12.37. The exchange of the iodide ion for hexafluorophosphate was achieved in the same manner as mentioned above.

Results and discussion

Synthesis

The coupling methods (8, 9) known for preparing bi-, ter-, and other pyridines were not chosen because of the anticipated difficulty that may incur in product separation.

We initially contemplated using the route described by Krohnke (10) to obtain compounds **1** and **2** by first preparing the 4-pyridyl-2′-acetylpyridine from 4-pyridinecarboxaldehyde and 2-acetylpyridine and then using this unsaturated pyridyl ketone in the reaction with Ortoleva–King reagent (11). Despite repeated attempts, the desired unsaturated ketone was not successfully isolated. It appears that the pyridine aldehyde undergoes a condensation reaction with two molecules of the acetylpyridine to give a diketone. Reactions of this type in which two molecules of methyl ketone react with one molecule of an aldehyde have been reported (12). A similar reaction is inferred here since the product of the reaction between the 4-pyridinecarboxaldehyde and 2-acetylpyridine always produces the quaterpyridine **2** when refluxed with ammonium acetate or ammonia gas. The isolation of 6-carboxy-2,2′:4,4″-terpyridine when pyruvic acid is present in the reaction mixture also supports the 1:2 ratio aldehyde/acetyl reaction.

NMR measurements and assignments

^{13}C NMR assignments were based on spectral models of pyridine, bipyridine, and their substituted derivatives (13–17), while the proton chemical shifts were analyzed with the aid of 2D carbon–proton correlation data and by comparison with literature values (18–23).

Reaction with ferrous sulfate

In addition to the NMR data, the reaction with ferrous sulfate is a simple chemical indicator test to show the α-diimine nitrogens do not undergo alkylation in the quaternization reaction. Ligands **1**–**4** readily form a red to purple coloration with this metal ion. For ligands **1** and **3** the absorbance maxima in the visible are 532 and 562 nm respectively while a shift to lower wavelength was observed for **2** and **4**.

Electrochemical measurements

Molecules **1**–**4** are designed for the preparation of metal complexes that are to be used as catalytic materials in photoelectrochemical studies. It is therefore important that the energetics of the free ligands be established in order to aid in the redox characterization of the more complicated metal complex systems. The half-wave potentials were obtained by linear sweep cyclic voltammetry. All the potentials referred to herein are experimental room temperature values referenced to the Ag/Ag^+ electrode referred to above. Scan speeds were 100 mV/s unless otherwise mentioned.

The redox behaviour of 2,2′:4,4″-terpyridine (**1**) is depicted in the voltammogram of Fig. 1A. There are three redox couples within the potential range of −0.5 to −3.5 V. For convenience the waves of each couple are numbered. Within the scan range

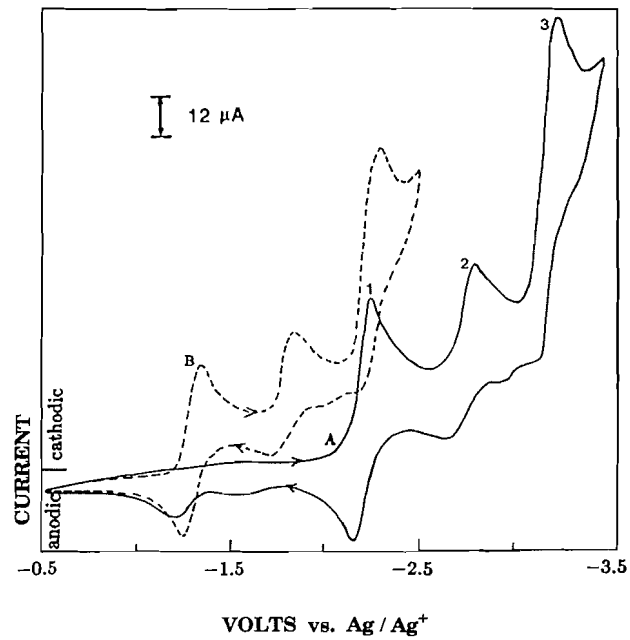


FIG. 1. Cyclic voltammograms of 2,2′:4,4″-terpyridine in 0.1 M $TBAPF_6$/DMF solution at 100 mV/s. (A) Fresh solution −0.5 to −3.2 V; (B) after electrolysis at −2.3 V vs. Ag/Ag^+.

of −0.5 to −2.3 V one reversible couple with a half-wave potential of −2.047 V was found. The profile, ratio of cathodic to anodic peak current, and peak to peak separation would suggest that this is one-electron transfer process. Beyond −2.3 V a quasi reversible wave at $E_{1/2}$ −2.507 V and an irreversible cathodic wave at −2.99 V were found. Successive scans in the potential range of −0.5 to −2.3 V revealed a small anodic wave at −1.503 V as well as a pre-wave at the foot of the ascending portion of the cathodic wave. There was no other change in the voltammogram and it remained this way after a number of repeated scans. Scans covering the first and second redox couples within the potential range of −0.5 to −2.8 V revealed another small anodic wave at −1.155 V. This wave increased as the scan encompassed the third cathodic wave at −2.970 V. Multiple scans did not indicate any increase in these peaks. The voltammogram remained unchanged. At 30 mV/s these small anodic waves were not seen but when the electrode was polarized beyond the second redox couple they showed up with an increase in current. To determine the origin of these transient waves the solution was electrolyzed at −2.3 V. A green coloration resulted, and the voltammogram of this solution is shown in Fig. 1B. A new reversible couple with $E_{1/2}$ at −1.201 V and a quasi reversible one at $E_{1/2}$ −1.621 V were observed. They are in the potential range where the anodic transients were found. These findings are indications that a slow chemical reaction follows the reduction process. At fast scan speeds the reaction product cannot completely diffuse away from the electrode interface and reacts with the electrode at the appropriate potential. At slow scan speeds there is adequate time for it to diffuse far enough from the electrode for any reaction to occur.

The voltammogram for 2,2′:4,4″:6,2‴-quaterpyridine (**2**) is given in Fig. 2. There are four major redox waves in the potential range −1.0 to −3.5 V. Scans taken within the potential range −1.8 to −2.5 V showed the first couple to be electrochemically reversible with characteristic one-electron transfer behaviour. The $E_{1/2}$ value was determined as −2.181 V and

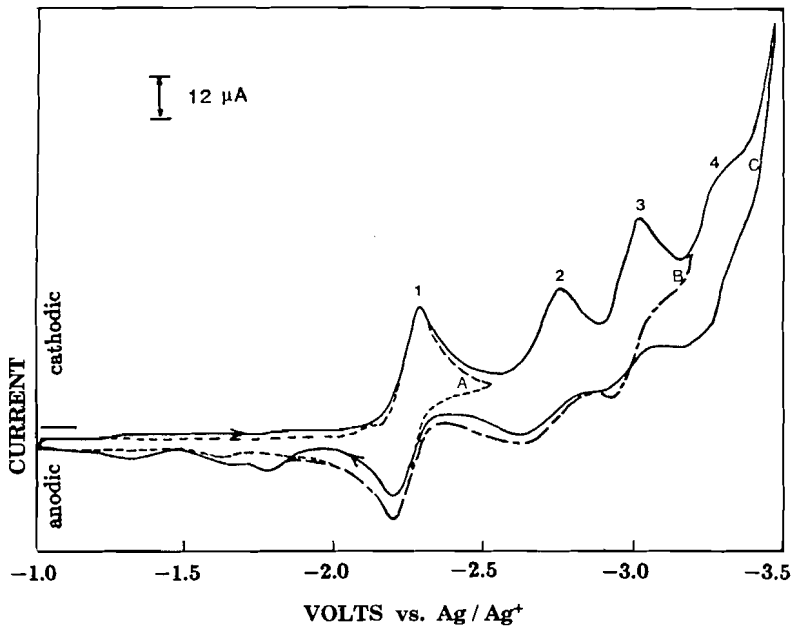


FIG. 2. Cyclic voltammograms of 2,2′:4,4″:6,2‴-quaterpyridine in 0.1 M $TBAPF_6$/DMF solution at 100 mV/s. (A) −1.0 to −2.5 V; (B) −1.0 to −3.2 V; (C) −1.0 to −3.5 V.

TABLE 3. Half-wave or peak potential of bipyridines and substituted bipyridines[a]

Compound	First redox wave		Second redox wave		Third redox wave	
	$E_{1/2}$ (V)	ΔE (mV)	$E_{1/2}$ (V)	ΔE (mV)	$E_{1/2}$ (V)	ΔE (mV)
4,4′ Bipyridine	−2.015	180	—	—	—	—
2,2′ Bipyridine	−2.549	201	−3.396	—	—	—
2,2′:6′,2″-Terpyridine	−2.362	151	−2.952	221	—	—
2,2′:4,4′-Terpyridine	−2.047	65	−2.507	121	−2.993[a]	193
2,2′:4,4″:6,2‴-Quaterpyridine	−2.181	69	−2.654	119	−2.946[b]	—
N″-Methyl-4,4′-bipyridine	−1.359	65	−2.014	84	—	—
N″-Methyl-2,2′:4,4″:6,2‴-quaterpyridinium salt	−1.375	68	−2.039	73	—	—
N″-Methyl-2,2′:4,4″-terpyridinium salt	−1.419	71	−2.041	120	—	—

[a]Volts vs. Ag/Ag^+ (0.1 M/CH_3CN) in 0.1 M $TBAPF_6$/DMF solution.
[b]Refers to cathodic peak potentials for irreversible process.

the ratio of peak currents as 0.98. Successive scans at 100 mV/s showed only a very slight decrease in the peak currents. When the scan range was extended from −1.0 to −2.5 V a small anodic wave at −1.545 V and a pre-wave at the foot of the cathodic wave was observed. After the first few successive scans these transient waves did not increase and the voltammogram showed no further change. Between −1.0 and −2.85 V a second redox couple with $E_{1/2}$ of −2.654 V was observed. This is a quasi reversible couple with ΔE of 119 mV and an obvious larger cathodic wave. Further in the cathodic region quasi reversible and irreversible couples are seen at potentials of −2.993 V, and a broad wave between −3.2 and −3.4 V. When the scan is taken over the potential range of −1.0 to −3.5 V two additional small anodic waves in the reverse direction were observed at −1.178 and −1.670 V. These appear to be associated with the third and fourth redox processes. Multiple scans over this range do not indicate any changes in the voltammogram. Polarizing the electrode beyond the third redox couple resulted in an increase in the peaks in the region −1.178 to −1.670 V. At a scan rate of 30 mV/s these waves were absent. This behaviour is identical to that described for 2,2′:4,4″-terpyridine and the same explanation is applicable. From Table 3 it can be seen that the $E_{1/2}$ values of the first redox couple of 4,4-bipyridine, 2,2′:4,4″-terpyridine, and 2,2′:4,4″:6,2‴-quaterpyridine are very close within the potential range of −2.015 to −2.181 V. The latter are ca. 368 and 181 mV more positive than the half-wave potentials of 2,2′-bipyridine and 2,2′:4,4″:6,2‴-terpyridine, respectively. Unsubstituted pyridine and 2,2′-bipyridine are known to be more difficult to reduce (24, 25). The added electron is localized in the 4 position of the pyridine ring and an electron-withdrawing substituent in this position makes the reduction process easier. This may explain the more positive redox potential of the 4-substituted derivatives.

The electrochemical behaviour of the *N*″-methyl-monoquaternary cations **3** and **4** is different from that of their corresponding neutral compounds. No redox couple is detected at the extreme negative potentials. Figure 3 shows the voltammograms of both cations. Voltammogram A is that of the quaternized terpyridinium ion while B depicts the behaviour of the *N*″-quarternized quaterpyridinium moiety. The $E_{1/2}$ values are set out in Table 3. The current ratios of the cathodic to anodic waves are very close to unity. The peak to peak separations are slightly larger than the 60 mV value for an electrochemically

Can. J. Chem. Downloaded from www.nrcresearchpress.com by 195.138.81.100 on 09/07/12
For personal use only.

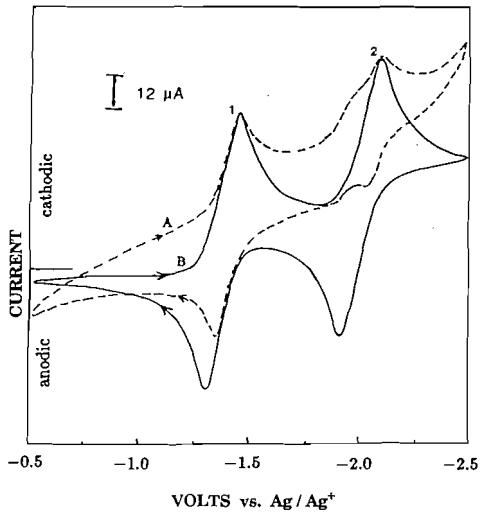


FIG. 3. Cyclic voltammogram in 0.1 M $TBAPF_6$/DMF solution of (A) *N*″-methyl-2,2′:4,4″-terpyridinium hexafluorophosphate; (B) *N*″-methyl-2,2:4,4″:6,2‴-quaterpyridinium hexafluorophosphate at 100 mV/S.

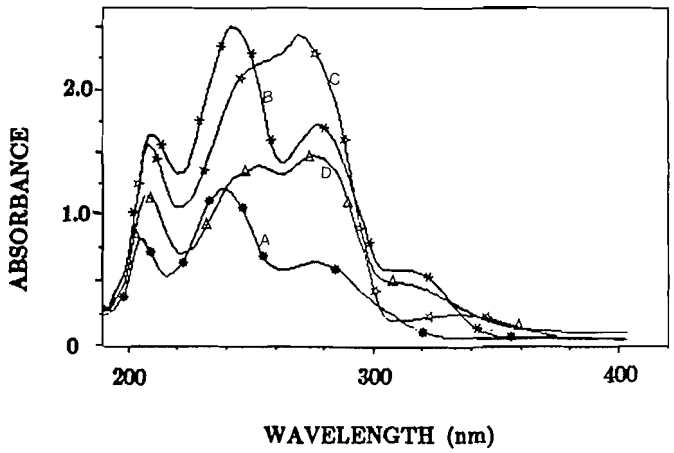


FIG. 4. Ultraviolet spectrum in methanol of (A) 2,2′:4,4″-terpyridine; (B) 2,2′:4,4″:6,2‴-quaterpyridine; (C) *N*″-methyl-2,2′:4,4″-terpyridinium perchlorate; (D) *N*″-methyl-2,2′:4,4″-quaterpyridinium perchlorate.

TABLE 4. Peak wavelengths and molar extinction coefficients

Compound	Wavelength (nm)	Extinction coefficient × 10^4 (M^{-1} cm^{-1})
2,2′:4,4″-Terpyridine	208	1.42
	240	2.82
	276	1.76
2,2′:4,4″:6,2‴-Quaterpyridine	206	5.58
	242	6.68
	278	4.53
	312	1.36
N″-Methyl-2,2′:4,4″:6,2‴-terpyridinium salt	206	1.71
	252	1.97
	272	2.24
	318	0.351
N″-Methyl-2,2′:4,4″:6,2‴-quaterpyridinium salt	206	3.15
	254	3.53
	274	3.76
	336	0.551

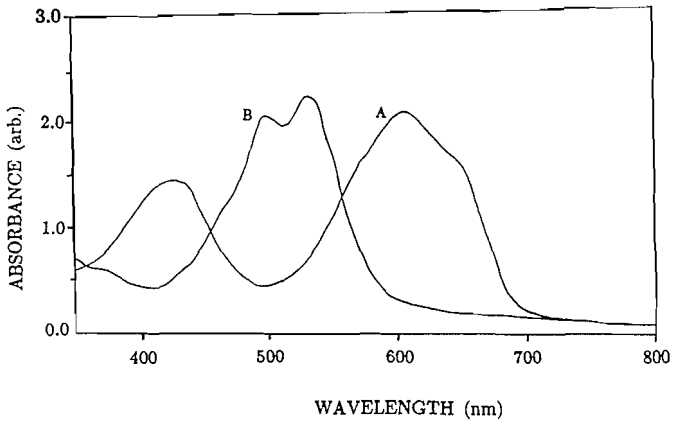


FIG. 5. Visible spectra of radical ions of (A) 2,2′:4,4″-terpyridine; (B) 2,2′:4,4″:6,2‴-quaterpyridine, obtained upon reduction at −2.2 and −2.45 V vs. Ag/Ag^+ respectively.

reversible process but this is normal for organic solvents. Successive scans do not introduce any changes in the voltammograms, indicating that on this time scale the reduced species are stable and can be reversibly generated at the electrode.

The electrochemical behaviour of these monoquaternary cations is similar to that of *N*-alkylpyridinium species bearing an electron-withdrawing substituent in the 4 position (24, 26). Voltammetric reduction of *N*′-methyl-4,4′-bipyridine was recorded and supports this suggestion. Half-wave values are given in Table 3 and are in close agreement with those obtained for the monoquaternary compounds **3** and **4**. The primary reduction process results in the formation of a neutral electron septet (24). For the *N*′-methyl-4,4-bipyridinium and monoquaternized compounds **3** and **4**, this septet is stable and undergoes further reduction at $E_{1/2}$ −2.014, −2.041, and −2.039 V respectively. These values are very nearly identical to that of the first redox couple of the 4,4′-bipyridine, which is 534, and 347 mV more positive than the corresponding couple of 2,2′-bipyridine and 2,2′:6,2″-terpyridine. The difference of 500 mV is large enough to suggest that the septet of 2,2′:4,4″-terpyridine is behaving more as a 4,4′-bipyridine than a 2,2′-bipyridine.

Electronic spectra

The electronic absorption spectra for compounds **1**, **2**, **3**, and **4** were determined in methanol. For these measurements the positive charge on the quaternized molecules was balanced by a perchlorate anion. The spectrum of 2,2′:4,4″-terpyridine is shown in Fig. 4A and it consists of three major band systems at 208, 240, and 276 nm. The profile of the long wavelength band may suggest more than one transition. The 2,2′:4,4″:6,2″-quaterpyridine shows spectral features similar to those of the terpyridine with an additional band clearly resolved at the long wavelength region. The spectrum is shown in Fig. 4B. It consists of four bands, positions of which are given in Table 4.

The spectral profiles of the perchlorate salts of the quaternized molecules are different from their corresponding neutral counterparts. The spectrum of the *N*″-methyl-2,2′:4,4″-terpyridinium cation, Fig. 4C, shows three major bands at 206, 252, and 318 nm with a clearly discernable shoulder on the higher energy portion of the 252 nm band. This shoulder is assigned at 272 nm. It appears that the long wavelength transition referred to in the neutral compound has now been resolved by shifting to lower energy. The *N*″-methyl-quaterpyridinium cation shows similar shifts in the spectrum when compared to the neutral molecule. The long wavelength band is shifted by 24

Can. J. Chem. Downloaded from www.nrcresearchpress.com by 195.138.81.100 on 09/07/12
For personal use only.

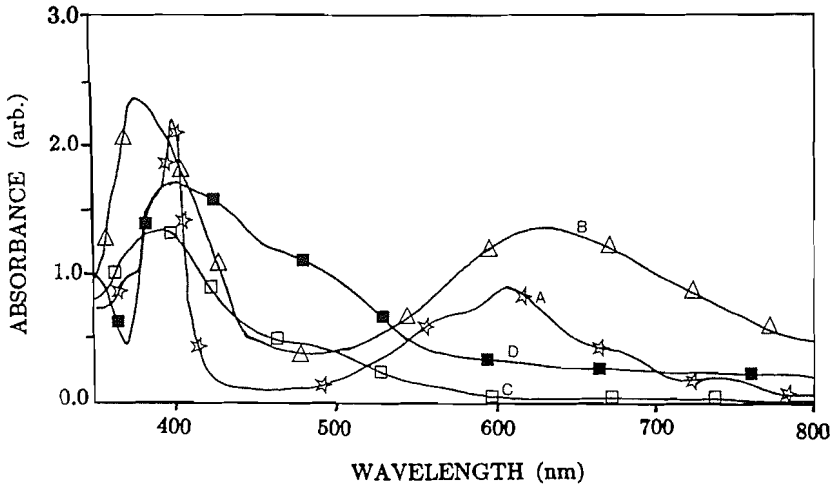


FIG. 6. Visible spectra of radicals of (A) *N*″-methylterpyridinium (**3**), and (B) *N*″-methylquaterpyridinium (**4**), obtained upon reduction at −1.6 V vs. Ag/Ag^+; (C) and (D) are the respective decomposition products.

nm to the red while the 242 nm band is displaced to 254 nm. The spectral profile is given in Fig. 4D.

Assignments of each absorption band cannot be made with certainty but, as in the case of the bipyridines (23), the lowest energy transition is long-axis polarized. The positions and apparent extinction coefficients are summarized in Table 4 while the spectra are shown in Fig. 4.

The electronic spectra of the first reduced species were obtained by spectroelectrochemical means. Each spectrum was generated by reduction beyond the cathodic wave of the redox couple. Figure 5A shows the visible spectrum of 2,2′:4,4″-terpyridine obtained upon controlled potential reduction at −2.2 V in DMF. As the reduction proceeds, the colorless solution becomes blue green with absorption bands at 425 and 606 nm. The latter bears a shoulder at 650 nm. The spectrum is different from the radical anion of 2,2′-bipyridine (25, 27–29) but appears to be similar to the radical anion of 4,4′-bipyridine. The latter was reduced at −2.2 V and spectral changes were compared in the 400 and 600 nm regions. This radical anion was found to be unstable over long periods. The solution turned yellow with an absorbance maximum at 406 nm. Reduction of similar molecules is known to form dimers (24, 26, 30–32). This is also likely to occur here. The close similarity in the spectral changes accompanying reduction of the terpyridine suggests that this molecule is behaving as a 4,4′-bipyridine rather than a 2,2′-bipyridine. This is in agreement with the suggestion deduced from the electrochemical results.

Figure 5B shows the spectrum of 2,2′:4,4″:6,2‴-quaterpyridine obtained upon electrolysis at −2.45 V. Two major bands, not far apart, are seen at 496 and 532 nm. A shoulder is discernable on the higher energy slope of the 496 nm band at approximately 460 nm. This spectrum is closely identical to that of the 2,2′-bipyridine radical anion (25, 27, 28) and not that of 4,4′-bipyridine. This indicates that the quaterpyridine is more likely to behave as a 2,2′-bipyridine than a 4,4′-bipyridine. The electronic influence of pyridine groups in both the 2 and 6 positions appears to outweigh the effects of the one in the 4 position.

The spectra of the reduced monoquaternized compounds **3** and **4** are different from those of the neutral species. The spectrum of the *N*″-methyl-terpyridinium cation obtained upon reduction at −1.6 V is presented in Fig. 6A. Major bands are found at 374, 570, 670, and 744 nm. The spectral changes are in agreement with those obtained upon reduction of *N*-alkylpyridinium salts (26). The spectrum of the radical of monoquaternary 4,4′-bipyridinium was generated by reduction at −1.5 V in order to verify this. Two characteristic absorption bands are found at 602 and 394 nm. The other features are identical to the radical species of *n*-alkylpyridinium and diquaternary 4,4′-bipyridinium cations (32, 33). The radical of 2,2′:4,4″-terpyridinium is not stable over long periods. It gave a yellow coloration, spectrum C, Fig. 6, upon standing.

Quaternization of the *N*″ nitrogen of the quaterpyridine also produces a radical with a different spectrum than that derived from the neutral compound. This is shown in Fig. 6B and was obtained after controlled potential reduction of the quaternized cation at −1.6 V. Two broad bands with maxima at 376 and 630 nm are obvious. The former has a shoulder at 422 nm. The absorption in the 600 nm region is similar to that of the reduction products of *N*″-methyl-4,4″-bipyridinium and *N*″-methyl-2,2′:4,4″-terpyridinium cations except for a shift in the peak maximum by 30 nm and some loss of fine structure. As in the case of the others, this radical is not stable over long periods. The blue color initially seen upon reduction is replaced by yellow. The spectrum of this yellow solution is given in Fig. 6D and is assigned to a dimeric species.

All the radicals obtained by electrochemical reduction were stable enough to obtain reliable spectral profiles. They undergo a slow chemical reaction. This is in agreement with the electrochemical observations. The question of the actual solution composition is an important one and, since the possibility exists that not only the desired species is in solution but that others may be present in small quantities, no extinction coefficients are included at this time.

Conclusion

Two new structural modifications of 2,2′-bipyridine were successfully prepared by condensation and cyclization procedures. The synthetic route is straightforward and does not require expensive catalytic materials as in the coupling reactions. A selective quaternization method was established in which the 1,1′ nitrogens survive the process and remain free to coordinate to metal ions for the preparation of metal complexes. The electrochemistry and spectroelectrochemistry are influenced by the position and degree of substitution. These results have indicated that the behaviour of the parent 2,2′-bipyridine ligand

Can. J. Chem. Downloaded from www.nrcresearchpress.com by 195.138.81.100 on 09/07/12
For personal use only.

is altered by the structural modifications. These changes are expected to be reflected in the chemistry of ground and excited states of metal complexes, to be investigated shortly.

Acknowledgements

Financial support by the Natural Sciences and Engineering Research Council of Canada and the University of Sherbrooke is gratefully acknowledged. L. P. would also like to thank Prof. Jean Lessard for helpful discussion and advice, Mr. Serge Bérubé and Mr. Gaston Boulay for acquiring NMR and mass spectral data, respectively, and Mrs. Solange Thériault for typing the manuscript.

1. K. KALYANASUNDARAM. Coord. Chem. Rev. **46**, 159 (1982).
2. A. JURIS, V. BALZANI, F. BORIGELLETTI, S. CAMPAGNA, A. BELSER, and A. VON ZELEWSKY. Coord. Chem. Rev. **84**, 85 (1988).
3. R. A. KRAUSE. Struct. Bonding (Berlin), **67**, 3 (1987).
4. (*a*) C. T. LIN, W. BOETTCHER, M. CHOU, C. CREUTZ, and N. SUTIN. J. Am. Chem. Soc. **98**, 6536 (1976); (*b*) M. J. COOK, A. P. LEWIS, G. S. G. MCAULIFFE, V. SKARDA, A. J. THOMPSON, J. L. GLASPER, and D. J. ROBBINS. J. Chem. Soc. Perkin Trans. **2**, 1293 (1984).
5. (*a*) P. C. ALFORD, M. J. COOK, A. P. LEWIS, G. S. G. MCAULIFFE, V. SKARDA, A. J. THOMSON, J. L. GLASPER, and D. J. ROBINS. J. Chem. Soc. Perkin Trans. 2, 705 (1985; (*b*) M. J. COOK and A. J. THOMPSON. Chem. Ber. 914 (1984).
6. C. C. PHIFER and D. R. MCMILLIN. Inorg. Chem. **25**, 1329 (1986).
7. R. J. MORGAN and A. D. BAKER. J. Org. Chem. **55**, 1986 (1990).
8. L. A. SUMMERS. *In* Adv. Heterocycl. Chem. **25**, 281 (1984).
9. M. TIECCO, L. TESTAFERRI, M. TINGOLI, D. CHIANELLI, and M. MONTANUCCI. Synthesis, 736 (1984).
10. F. KROHNKE. Synthesis, 1 (1976).
11. (*a*) F. KROHNKE. Angew. Chem. **75**, 189 (1963); (*b*) L. C. KING. J. Am. Chem. Soc. **66**, 894 (1944); (*c*) L. C. KING and M. MCWHISTER. J. Am. Chem. Soc. **68**, 717 (1946).
12. R. L. FRANK and R. P. SEVEN. J. Am. Chem. Soc. **71**, 2629 (1949).
13. L. A. SUMMERS. The bipyridinum herbicides. Academic, New York, NY. 1980. pp. 30–43.
14. (*a*) O. JOHNSON. Aust. J. Chem. **34**, 981 (1981); (*b*) R. P. THUMMEL, F. LEFOULON, S. CHERAYIL, and V. GOULLI. J. Org. Chem. **53**, 4757 (1988).
15. H. L. RETCOFSKY and R. A. FRIEDEL. J. Phys. Chem. **72**, 290 (1968); **72**, (1968).
16. A. MARKER, A. J. CANTY, and R. T. C. BROWNLEE. Aust. J. Chem. **31**, 1255 (1978).
17. A. J. DEKONING, P. H. M. BUDZELAAR, J. BOERSMA, and G. J. M. VAN DER KERK. J. Organomet. Chem. **199**, 153 (1980).
18. T. MCL. SPOTSWOOD and C. I. TANZER. Aust. J. Chem. **20**, 1227 (1967).
19. S. CASTELLANO, H. GUNTHER, and S. EBERSOLE. J. Phys. Chem. **65**, 4166 (1965).
20. H. ELSBERND and J. K. BEATTIE. J. Inorg. Nucl. Chem. **34**, 771 (1972).
21. S. CASTELLANO and R. KOSTELNIK. J. Am. Chem. Soc. **90**, 141 (1968).
22. I. C. SMITH and W. G. SCHNEIDER. Can. J. Chem. **39**, 1158 (1961).
23. I. C. CALDER, T. MCL. SPOTSWOOD, and C. I. TANZER. Aust. J. Chem. **20**, 1195 (1967).
24. J. VOLKE and V. VOLKOVA. Collect. Czech. Chem. Commun. **37**, 3686 (1972) and references therein.
25. M. NAAROVA and J. VOLKE. Collect. Czech. Chem. Commun. **38**, 2671 (1973).
27. B. GAS, J. KLIMA, S. ZALIS, and A. A. VLECK. J. Electroanal. Chem. **222**, 161 (1987).
28. E. KONIG and S. KREMER. Chem. Phys. Lett. **5**, 87 (1970).
29. G. A. HEATH and L. J. YELLOWLEES. J. Chem. Soc. Chem. Commun. 287 (1981).
30. C. L. BIRD and A. T. KUHN. Chem. Soc. Rev. **10**, (1981).
31. E. STECKHAM and T. KUWANA. Rev. Bunsen-ges Phys. Chem. **78**, 253 (1974).
32. E. M. KOSOWER and J. L. COTTER. J. Am. Chem. Soc. **86**, 5524 (1964).
33. T. WATANABE and K. HONDA. J. Phys. Chem. **86**, 2617 (1982).

Can. J. Chem. Downloaded from www.nrcresearchpress.com by 195.138.81.100 on 09/07/12
For personal use only.

Chemical state detection of dibutyl phosphate using ^{31}P NMR chemical shift change

NAOHITO UETAKE
Energy Research Laboratory, Hitachi, Ltd., Hitachi-shi, Ibaraki-ken 316, Japan

Received January 29, 1990

NAOHITO UETAKE. Can. J. Chem. **69**, 322 (1991).

Chemical shift changes of ^{31}P NMR were investigated for dibutyl phosphate (DBP) in several polar solvents and compared with tributyl phosphate (TBP). The chemical shift differences between DBP and TBP in the same solvents were found to reflect only the intermolecular interaction on P—OH in DBP, a moiety that is not present in TBP. Acid dissociation constants, K_a, in several polar solvents were determined using such chemical shift differences of DBP. The K_a determined in pure water is in good agreement with the literature value. The intermolecular interaction between alkaline ions and DBP was also investigated using a similar method. No interactions with Na^+ ion and K^+ ion were detected from chemical shift change. However, ion association between the tetramethylammonium ion and the DBP^- ion was detected and the complex formation constant was determined as $K_c = 0.49 \pm 0.02\ M^{-1}$.

Key words: Fourier transform nuclear magnetic resonance spectrometry, dibutyl phosphate, chemical shift, acid dissociation, intermolecular interaction.

NAOHITO UETAKE. Can. J. Chem. **69**, 322 (1991).

On a étudié les changements de déplacements chimiques dans les spectres RMN du ^{31}P du phosphate de dibutyle (PDB) en solution dans plusieurs solvants polaires et on les a comparés avec ceux obtenus avec le phosphate de tributyle (PTB). On a trouvé que les différences dans les déplacements chimiques entre PDB et PTB, dans les mêmes solvants, ne sont que le reflet de l'interaction intramoléculaire avec le P—OH présent dans de PDB, une portion qui n'est pas présente dans le PTB. Utilisant ces différences dans les déplacements chimiques du PDB, on a déterminé les constantes de dissociation acide, K_a, dans plusieurs solvants polaires. Utilisant une méthode semblable, on a aussi étudié l'interaction intermoléculaire entre les ions alcalins et le PDB. Sur la base des changements dans les déplacements chimiques, on n'a pas détecté d'interactions ioniques avec le Na^+ et le K^+. Toutefois, on a détecté une association ionique entre l'ion tétraméthylammonium et l'ion PDB^- et on a déterminé que la constante de formation du complexe, K_c, est égale à $0{,}49 \pm 0{,}02\ M^{-1}$.

Mots clés: spectrométrie de résonance magnétique nucléaire par transformation de Fourier, phosphate de dibutyle, déplacement chimique, dissociation acide, interaction intermoléculaire.

[Traduit par la rédaction]

Introduction

The chemical shifts of NMR spectra reflect the chemical state of the measured nuclei. The formation of chemical bonds changes the electron densities on the nuclei and gives different chemical shift values. Intermolecular interactions also contribute to the chemical shift change, but the degree of change is much smaller than for a true chemical bond. Neighboring molecules that have an intermolecular interaction in solution commonly exchange rapidly with each other. When the exchange frequency between two states is rapid, the NMR spectrum is observed in the averaged chemical shift, which depends on the relative population of the different states (1). If chemical states A and A·B are assumed to exchange very rapidly ($> 50|\nu_A - \nu_{A\cdot B}|$),

[1] $$A + B \leftrightarrows A\cdot B$$

the chemical equilibrium describes the relation between two states. The observed chemical shift is expressed in the equation

[2] $$\nu_{ob} = P_A\nu_A + P_{A\cdot B}\nu_{A\cdot B}$$

where ν_{ob} is the observed chemical shift, ν_A and $\nu_{A\cdot B}$ are chemical shifts of measured nuclei in A and A·B, respectively, and P_A and $P_{A\cdot B}$ are relative populations of A and A·B. Then, the equilibrium constant, K, for eq. [1] is defined by

[3] $$K = \frac{[A\cdot B]}{[A][B]}$$

The equilibrium constant K expresses the strength of the interaction between A and B. It is often difficult to determine the concentrations of A and A·B individually when they exchange rapidly with each other. Chemical shift measurements should offer a powerful method to detect and measure the K values. There must be suitable magnetic nuclei in the molecule in order to use NMR for such a purpose. Phosphorus is one such common element and it has a magnetic nucleus, ^{31}P ($I = 1/2$), that has a 100% natural abundance, relatively high sensitivity, and a wide chemical shift range (2). Since these properties of phosphorus are convenient for NMR study of weak intermolecular interactions, dibutyl phosphate (DBP), which is an organic acid containing phosphorus, was used and its intermolecular interactions in aqueous solutions and other polar solvents were investigated. DBP is one of the main degradation products of tributyl phosphate (TBP), which is used as an extraction solvent in nuclear fuel reprocessing. Therefore, the molecular structure of DBP resembles that of its precursor TBP. The main differences are the number of butyl groups and the existence of OH in DBP, which can undergo acid dissociation. In actual solvents, there are various contributions to the chemical shift and these cannot readily be separated. Thus an alternative is to consider chemical shift differences between two similar molecules, such as DBP and TBP. Therefore, DBP chemical shifts were measured and compared with those of TBP to evaluate the chemical state of DBP.

Experimental

Samples

Dibutyl phosphate (DBP) was obtained from Tokyo Chemical Industries. The ^{31}P NMR spectrum of the reagent DBP showed no other peaks from phosphorus compounds. Therefore, the purity of the reagent DBP was determined as 99.0% based on chemical analysis of the total phosphorus content. The TBP and solvents were of analytical reagent grade and obtained from Wako Chemical Industries. Tetramethylammonium hydroxide (TMAH) solution was also obtained from Wako Chemical Industries. Saturated tetramethylammonium hydroxide

Printed in Canada / Imprimé au Canada

Can. J. Chem. Downloaded from www.nrcresearchpress.com by 195.138.81.100 on 09/07/12
For personal use only.

solution was prepared by dissolving tetramethylammonium hydroxide pentahydrate (Kodak Organic Chemicals) in pure water.

The DBP was added to several polar solvents and alkaline solutions to give a concentration of 30 g/L. The TBP was also added to the polar solvents to give a concentration of 30 g/L and to one alkaline solution to give a saturated solution. Both DBP and TBP dissolve in pure water only below 30 g/L and so their saturated solutions were prepared for the experiments.

Procedures

All spectra were obtained on a Hitachi R-90H FT-NMR spectrometer with ^2D external lock operating at 36.4 MHz for ^{31}P and 22.6 MHz for ^{13}C in a field of 2.114 T. All spectra were measured at 32°C in a sample tube of 8 mm diameter. The ^1H decoupling procedure was adopted for ^{13}C. ^{31}P chemical shifts were measured relative to external P_4O_6 and ^{13}C shifts were relative to internal TMAH.

Since FT-NMR produces a high magnetic field by using a permanent magnet in a thermostat controlled at 35°C, the magnetic field applied to the sample is very stable. Moreover, room temperature was controlled at 22 ± 0.5°C in order to get even better magnetic field stability.

The P_4O_6 external standard was sealed in a capillary tube and placed in the sample tube. Free induction decays (FIDs) for a spectral width of 200 ppm were collected with 90° pulse angle for 16K data points. Fourier transformation was performed on the FID accumulated 100 times, giving a digital resolution of 0.02 ppm per data point. Sensitivity enhancement filters were not used.

The chemical shifts measured were corrected for the values for the pure water magnetic susceptibility condition using the equation

$$[4] \quad \delta_{corr} = \delta_{obs} - \frac{2}{3}\pi \times 10^6 (K_R - K_S)$$

where δ_{corr} and δ_{obs} are corrected and observed chemical shifts respectively, and K_R and K_S are magnetic susceptibilities of pure water and sample, respectively. The magnetic susceptibilities of pure solvents were obtained from the literature (3). The magnetic susceptibilities of TMAH solutions were determined from the ^{13}C NMR chemical shift of TMAH.

Results and discussion

Dissociation of DBP in polar solvents

The DBP is partially dissociated in polar solvents such as water and the following equilibrium is established:

$$[5] \quad HDBP \leftrightarrows H^+ + DBP^-$$

where HDBP is undissociated DBP and DBP^- is the dissociated DBP ion. The equilibrum of eq. [5] is described by the acid dissociation constant, K_a, which is defined in the following equation.

$$[6] \quad K_a = \frac{[H^+][DBP^-]}{[HDBP]}$$

HDBP and DBP^- interact with solvent molecules or solute molecules other than those of eq. [5] in the actual polar solvents. DBP can be categorized as having three parts when such interactions are considered. One of them is P—OBu, in which the butyl group contacts the other molecules. However, as the alkyl group is hydrophobic, it is expected to have few interactions with polar molecules such as water. Another is the P=O moiety, which acts as a base. The third is P—OH, which can dissociate and release a H^+ ion. Intermolecular interactions must be considered for each individual part. The effects of each part affect the ^{31}P nuclei in DBP.

TBP also has P=O and P—OBu in common with DBP, but does not have the P—OH group. Therefore, ^{31}P NMR chemical shifts of DBP and TBP in several polar solvents were measured

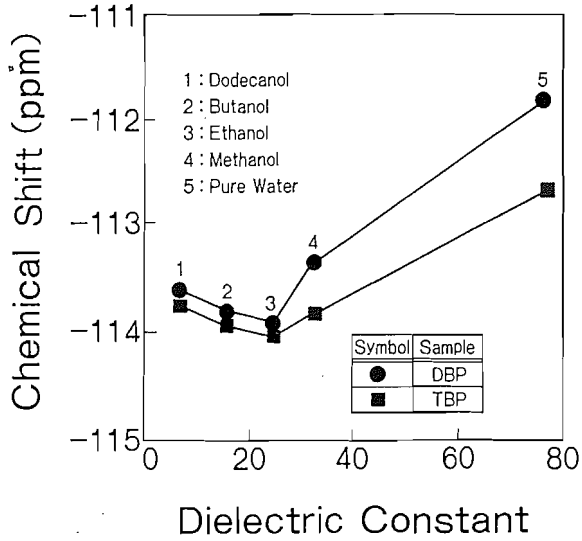


FIG. 1. ^{31}P chemical shifts of DBP and TBP in pure water and alcohols.

in order to evaluate the contributions from each part. The results in a group of normal alcohol solvents are shown in Fig. 1. The chemical shifts of DBP and TBP indicate the similar dependency on the solvent dielectric constant. The chemical shift difference between DBP and TBP is constant, 0.14 ppm from dodecanol to ethanol. This result indicates that the chemical shift of DBP depends on the intermolecular interaction of P=O or P—OBu in these solvents.

On the other hand, the chemical shift difference becomes larger as the dielectric constant becomes higher than that of ethanol. When the dielectric constant of solvent becomes higher and close to that of water, HDBP also begins to dissociate as shown in eq. [5]. If the intermolecular interactions on the P=O and P—OBu parts are the same as in DBP and TBP, the increase in chemical shift above ethanol in Fig. 1 is considered to be caused by dissociation of DBP. The fact that the chemical shift difference between DBP and TBP is constant in lower dielectric constant solvents supports the above assumption, in which the effects of intermolecular interactions on P=O and P—OBu are the same for both DBP and TBP. As TBP has one more butyl group than DBP and the resultant effect from the interaction on P—OBu is considered to be different for DBP and TBP, the main contribution to chemical shift change of HDBP or TBP is considered to be due to solvent–solute interaction on the part of P=O, of which there is only one moiety in each molecule. Hydrogen bonding between P=O and OH in alcohols seems to be the main interaction.

Therefore, adopting the chemical shift difference $\delta_{DBP} - \delta_{TBP}$, one can eliminate the contribution from the P=O part and determine the degree of dissociation of DBP. The chemical shift differences $\delta_{HDBP} - \delta_{TBP}$ and $\delta_{DBP^-} - \delta_{TBP}$ are required for such a calculation. Then, $\delta_{HDBP} - \delta_{TBP}$ can be determined from the value in the lower dielectric constant alcohol:

$$[7] \quad \delta_{HDBP} - \delta_{TBP} = 0.14 \pm 0.04 \text{ ppm}$$

The value of $\delta_{DBP^-} - \delta_{TBP}$ can be determined in 1 M NaOH solution, in which DBP dissociates completely as described in the next section.

$$[8] \quad \delta_{DBP^-} - \delta_{TBP} = 1.18 \pm 0.04 \text{ ppm}$$

As the total DBP concentration is already known, the concentra-

Can. J. Chem. Downloaded from www.nrcresearchpress.com by 195.138.81.100 on 09/07/12
For personal use only.

TABLE 1. Chemical shift differences and calculated dissociation constants

Solvent	Dielectric constant	Chemical shift difference $\delta_{DBP} - \delta_{TBP}$ (ppm)	Calculated dissociation constant pK_a (log M^{-1})
Pure water	76.6	0.85	0.92
Methanol	32.6	0.48	1.64
Ethanol	24.6	0.14	—
Butanol	17.8	0.14	—
Dodecanol	6.5	0.14	—
1 M Sodium hydroxide	—	1.18	(Complete dissociation)
Pyridine	12.3	1.07	−0.03
Ethylene glycol	37.7	0.36	2.09
Formamide	111.0	0.76	0.90

tions of HDBP and DBP^-, respectively, can be determined using eq. [2]. The concentration of H^+ is equal to that of DBP^- in pure solvent. The equilibrium constant, K_a, can be calculated using eq. [6]. Measured $\delta_{DBP} - \delta_{TBP}$ and calculated pK_a's in several solvents are listed in Table 1. Dyrssen (4) reported a value $pK_a = 1.00 \pm 0.01$ from the distribution of DBP between hexene and a $HClO_4$–$NaClO_4$ solution. This value is in good agreement with the value in pure water in Table 1, which indicates that the above mentioned method can lead to proper pK_a values.

There are no reported values except for aqueous solution, so the values in Table 1 cannot be compared with those from other methods. If $\delta_{DBP} - \delta_{TBP}$ expresses only acid dissociation of DBP as for normal alcohols, the values in Table 1 become reliable. Since the main solvent–solute interactions are considered to be hydrogen bonding on P=O in these solvents, it seems to be a reasonable assumption.

Acid dissociation in solvents can be divided into two steps. The first step is ionization, as described by

[9] $$HDBP + S + \leftrightarrows HS^+ \cdot DBP^-$$

where S is solvent.

The second step is dissociation of the ion pair, as described by the following equation:

[10] $$HS^- \cdot DBP^- \leftrightarrows HS^- + DBP^-$$

Since eq. [9] depends on basicity or acidity of the solvent and eq. [10] depends on the dielectric constant (5), K_a depends on both basicity or acidity and dielectric constant of the solvent. The obtained dissociation constants, in Table 1, reflect such a relationship. It is important for the evaluation of specific intermolecular interactions to remove the contribution from the other interactions using adequate reference. Gutowsky and Saika (6) used ^1H NMR chemical shifts for determination of dissociation constants. However, their method is useful only for high concentration solutions because hydrogen exchanges between solute and solvent. Moreover, the atom located on the outer surface of molecules, like hydrogen, is directly affected by contact solvent molecules, and such interactions are complex. Their method can be applied for aqueous solution, because solute molecules are always solvated by water molecules and protected for other intermolecular interactions in aqueous solutions. However, application for other solvents is doubtful.

Intermolecular interaction in alkaline solutions

Since TBP is a base and mainly coordinated by water molecules in alkaline solutions, its chemical shift in alkaline solution is estimated to be constant and does not depend on concentration and alkaline species. The P=O moiety in DBP also has a base functionality and is mainly coordinated by water molecules in alkaline solutions. On the other hand, the P—OH functionality is acid in character and may interact with cations in alkaline solutions. Therefore, the chemical shift of DBP was measured in several alkaline solutions in order to detect solute–solute interactions. The chemical shift of TBP in 1 N NaOH, Na_2CO_3, and TMAH solutions is evaluated as −112.65 ppm, the same as in pure water. Therefore, the evaluation of intermolecular interactions of DBP can be discussed using the absolute chemical shift value instead of the difference between TBP and DBP. This reduces errors caused by taking the difference between two values obtained by individual measurements.

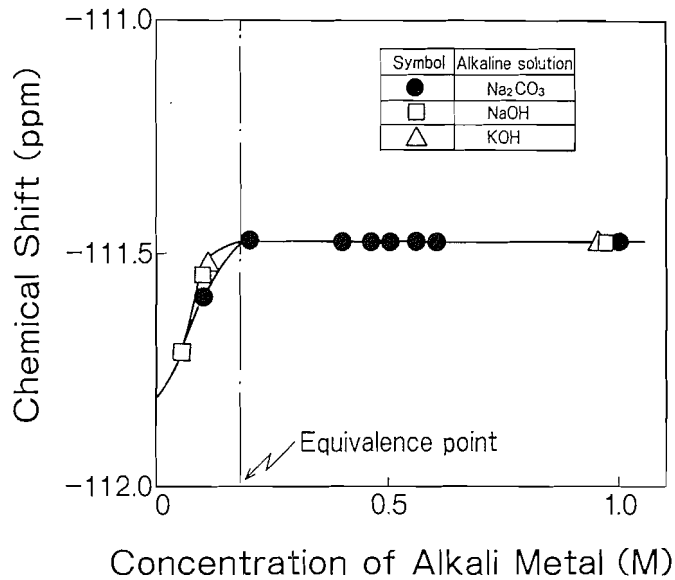


FIG. 2. ^{31}P chemical shifts of DBP in alkaline solutions.

The chemical shift measurement results of DBP in NaOH, Na_2CO_3, and KOH solutions are shown in Fig. 2. Chemical shifts of DBP become higher as alkaline concentration increases from pure water to the equivalent concentration for DBP. Above the equivalence point for DBP, chemical shifts of DBP become constant ($\delta_{DBP} = -111.47$ ppm). This chemical shift value does not depend on the kind of alkaline solution. Since HDBP is dissociated in alkaline medium and only DBP^- can exist above the equivalence point, the chemical shift value, −111.47 ppm,

Can. J. Chem. Downloaded from www.nrcresearchpress.com by 195.138.81.100 on 09/07/12
For personal use only.

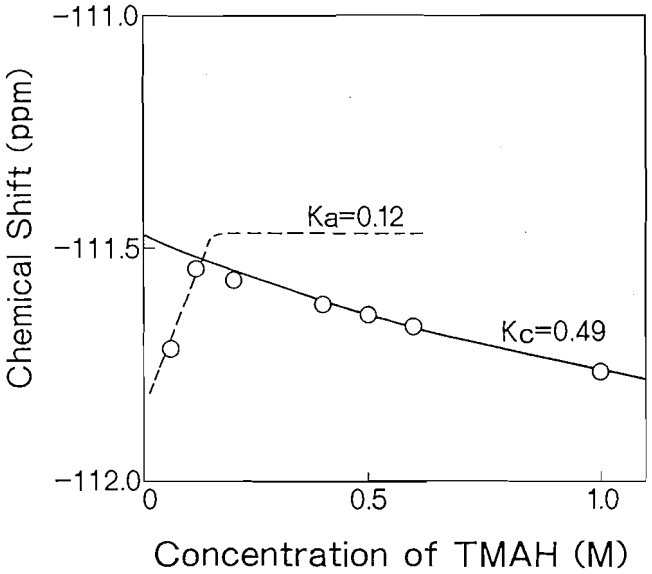


FIG. 3. ^{31}P chemical shifts of DBP in TMAH solutions.

is estimated to be that of DBP^-. The ^{31}P NMR spectra of DBP indicate no differences between NaOH and KOH solution and so it is concluded that any interaction of DBP with Na^+ ion and K^+ ion is too small to be detected by ^{31}P NMR.

Regarding alkaline concentration below the equivalence point for DBP, the chemical shift of DBP in Na_2CO_3 solution is slightly lower than that in NaOH and KOH. Carbonate ion in Na_2CO_3 solution reduces the hydroxide ion concentration and prevents the dissociation of DBP, resulting in a relatively lower chemical shift. However, the chemical shift agrees with that in NaOH and KOH above the equivalent Na_2CO_3 concentration for DBP. This indicates that there are no intermolecular interactions between carbonate ion and DBP.

Although TMAH is strongly alkaline, like NaOH and KOH, the chemical shift change of DBP in TMAH solution is different from that in other alkaline solutions, as shown in Fig. 3. Regarding the equivalence point for DBP, chemical shifts of DBP in TMAH solution are quite similar to those in NaOH and KOH solution. However, the chemical shift of DBP in TMAH solution decreases as TMAH concentration increases. This result indicates that DBP has some intermolecular interactions with TMAH. Since such an intermolecular interaction confirms the above equivalent TMAH concentration for DBP, it is not HDBP but also DBP^- that interacts with TMAH in solution. The following chemical equilibrium must be established:

[11] $DBP^- + TMA^+ \leftrightarrows DBP \cdot TMA$

Such a reaction can be considered as a kind of complex formation and its complex formation constant, K_c, is expressed by the following equation:

$$[12] \quad K_c = \frac{[DBP \cdot TMA]}{[DBP^-][TMA^+]}$$

Here, K_c expresses the strength of the intermolecular interaction (1).

To determine K_c using eq. [2], chemical shift values of DBP^- and DBP·TMA are needed. The former has already been determined and the latter can be determined by measuring the chemical shift of DBP in a TMAH saturated solution. The results are

$$\delta_{DBP \cdot TMA} = -112.39 \pm 0.02 \text{ ppm}$$
$$\delta_{DBP^-} = -111.47 \pm 0.02 \text{ ppm}$$

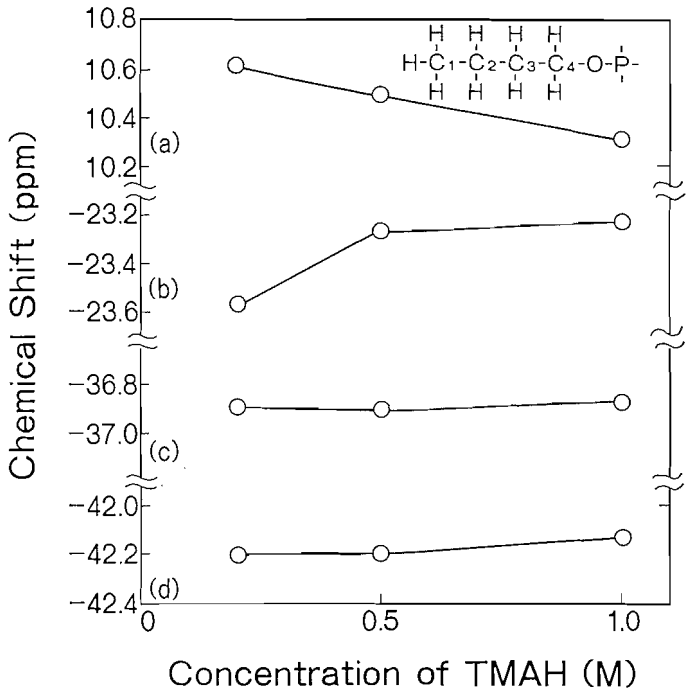


FIG. 4. ^{13}C chemical shifts of DBP in TMAH solution: (a) C_4, (b) C_3, (c) C_2, (d) C_1.

The K_c was determined using chemical shift values in TMAH concentrations between 0.1 and 0.4 M, and the following averaged value was obtained:

$$K_c = 0.49 \pm 0.02 \text{ M}^{-1}$$

To date, the intermolecular interaction between TMA^+ ion and DBP^- ion has not been reported. Larsen and Wahl (7) reported that there is an ion association between TMA^+ and hexacyanoferrate ion and that the complex formation constant (K_c) is 21 M^{-1}. On the other hand Lindman *et al.* (8) found an intermolecular interaction between tetraalkylammonium and bromine ions. They did not determine the K_c values, but did suggest such a intermolecular interaction was caused by an "iceberg structure" around the alkyl groups of the tetraalkylammonium ion. These reports indicate that alkylammonium ions have relatively stronger interactions with inorganic anions than alkali metal ions.

However, the K_c value for DBP·TMA is considerably lower than that for ion association between TMA^+ ion and the hexacyanoferrate ion. The origin of the intermolecular interaction may not always be similar for different species. Therefore, ^{13}C NMR chemical shift measurements were performed in order to investigate the interaction mechanism. The results were compared with those of ^{31}P NMR in order to clarify the effects of the location of measured nuclei.

The ^{13}C NMR chemical shift change is shown in Fig. 4 for each carbon in the butyl group of DBP in TMAH solution. The carbons C_1 and C_2, located on the outer surface of the DBP molecule, show little change. On the other hand, C_3 and C_4, located near the phosphorus atom of DBP, show a relatively larger chemical shift change. However, the chemical shift of C_3 changes in the opposite direction from that of C_4. Alkyl chains are easily distorted by intermolecular interactions and the relative location of each carbon changes in comparison with the non-interacting state. Therefore, secondary intermolecular interaction effects for the chemical shift will appear on alkyl carbons, adding to the effect expressed by eq. [2]. As C_4 is fixed

Can. J. Chem. Downloaded from www.nrcresearchpress.com by 195.138.81.100 on 09/07/12
For personal use only.

by the C—O bond and cannot change its location, the chemical shift change of C_4 corresponds to that of ^{31}P. A large secondary effect caused by the alkyl chain distortion is observed on C_3. These results suggest that P—O^- or P=O of the DBP^- ion is the main contributor to the intermolecular interaction. Large chemical shift changes of C_3 and C_4 are considered to be caused by the change in electron state of the oxygen that is bonded to phosphorus. As the ^{31}P chemical shift value of HDBP in alkaline solution estimated from eq. [7] is -112.51 ± 0.06 ppm and resembles that of DBP·TMA, the electronic states of phosphorus in these two species are considered to be similar. The kind of intermolecular interaction seems to be ion association through the P—O^-. As the K_c value is small and the intermolecular interaction is very weak, it is considered difficult to detect such an interaction using methods other than NMR. Although such a detection is possible by ^{13}C NMR as well as ^{31}P NMR, the secondary effect caused by the alkyl chain distortion makes quantitative evaluation using the ^{13}C NMR chemical shift difficult. It is important to select nuclei that cannot have such a molecular structure distortion when quantitative evaluation of intermolecular interaction using eq. [2] is required.

Conclusion

Intermolecular interactions of DBP were investigated for DBP in polar solvents using the ^{31}P NMR chemical shift. The adoption of chemical shift differences, $\delta_{DBP} - \delta_{TBP}$, could eliminate the effects on P=O, and allowed detection of the intermolecular interaction on P—OH separately. Acid dissociation constants in several polar solvents were determined using $\delta_{DBP} - \delta_{TBP}$. The K_a determined in pure water is in good agreement with that obtained by a conventional method. The intermolecular interaction of DBP in alkaline solution was also investigated. No intermolecular interactions with Na^+ and K^+ ions were detected by ^{31}P NMR chemical shift data. However, intermolecular interaction, possibly as an ion association between TMA^+ ion and DBP^- ion, was detected and the complex formation constant was determined as $K_c = 0.49 \pm 0.02\ M^{-1}$. The NMR chemical shift should be a powerful method of evaluating intermolecular interactions if careful attention is paid to the origin of the chemical shift.

Acknowledgment

The author thanks Dr. M. Yoshida of Naka Works, Hitachi, Ltd. for his help with the NMR measurements.

1. J. HOMER. Appl. Spectrosc. Rev. **9**, 103 (1975).
2. C. BREVARD and P. GRANGER. Handbook of high resolution multinuclear NMR. John Wiley & Sons, New York. 1981. p. 102.
3. R. TAMAMUSHI. *et al.* Kagakubinran. 2nd ed. Maruzen, Tokyo. 1975. p. 1236.
4. D. DYRSSEN. Acta Chem. Scand. **11**, 1771 (1957).
5. W. R. GILKERSON. J. Chem. Phys. **25**, 1199 (1956).
6. H. S. GUTOWSKY and A. SAIKA. J. Chem. Phys. **21**, 1688 (1953).
7. D. W. LARSEN and A. C. WALL. Inorg. Chem. **4**, 1281 (1965).
8. B. LINDMAN, S. FORSEN, and E. FORSLIND. J. Phys. Chem. **72**, 2805 (1968).

Can. J. Chem. Downloaded from www.nrcresearchpress.com by 195.138.81.100 on 09/07/12
For personal use only.

Polar trifluoromethylation reactions: the formation of bis(trifluoromethyl)iodine(III) compounds and trifluoromethyl iodine(III) cations and anions[1]

WIELAND TYRRA AND DIETER NAUMANN[2]

Institut für Anorganische Chemie, Universität zu Köln, Greinstr. 6, D-5000 Köln 41, Federal Republic of Germany

Received May 23, 1990

WIELAND TYRRA and DIETER NAUMANN. Can. J. Chem. **69**, 327 (1991).

IX_3 (X = Cl, $OCOCF_3$, ONO_2) reacts with $Cd(CF_3)_2$ complexes or $Bi(CF_3)_3$ to yield the corresponding CF_3IX_2 derivatives. ^{19}F nuclear magnetic resonance spectroscopic evidence is found for $[I(CF_3)_2]^+$ and $I(CF_3)_2X$ (X = Cl, $OCOCF_3$) in the reactions of CF_3IX_2 with $Cd(CF_3)_2$ complexes. During the reaction of CF_3IF_2 and $Hg(CF_3)_2$ the new species $I(CF_3)_2F$ and *cis*-$[I(CF_3)_2F_2]^-$ are identified by nuclear magnetic resonance spectroscopy. The reactions proceed under polar conditions and can be accelerated by the addition of a Lewis acid such as BF_3, $B(OCOCF_3)_3$, or Sb(V) compounds. Difluoromethyl compounds are formed as by-products.

Key words: polar trifluoromethylations, trifluoromethyl iodine(III) compounds, difluoromethyl group formation.

WIELAND TYRRA et DIETER NAUMANN. Can. J. Chem. **69**, 327 (1991).

Le IX_3 (X = Cl, $OCOCF_3$, ONO_2) réagit avec les complexes du $Cd(CF_3)_2$ ou avec le $Bi(CF_3)_3$ pour conduire aux dérivés CF_3IX_2 correspondants. Utilisant la résonance magnétique nucléaire du ^{19}F, on a mis en évidence la présence de $[I(CF_3)_2]^+$ et de $I(CF_3)_2X$ (X = Cl, $OCOCF_3$) lors des réactions du CF_3IX_2 avec les complexes du $Cd(CF_3)_2$. Dans les réactions du CF_3IF_2 et du $Hg(CF_3)_2$, on a identifié les nouvelles espèces $I(CF_3)_2F$ et *cis*-$[I(CF_3)_2F_2]^-$ par spectroscopie de résonance magnétique nucléaire. Les réactions se produisent dans des conditions polaires et on peut les accélérer par l'addition d'un acide de Lewis, comme les composés BF_3, $B(OCOCF_3)$ ou Sb(V). Les composés difluorométhylés se forment comme produits secondaires.

Mots clés : trifluorométhylations polaires, composés du trifluorométhyl-iode(III), formation du groupement difluorométhyle.

[Traduit par la rédaction]

Introduction

While organoiodine(III) and non-fluorinated diorganoiodonium compounds are well-characterized versatile synthetic reagents, especially in organic reactions, only a few examples of fluorinated diorganoiodine(III) compounds with perfluoroalkyl groups are known in the literature. The mixed arylperfluoroalkyliodonium salts $[C_6H_5IR_f]^+[BF_4]^-$ (2) and $[C_6H_4(CH_3)IR_f]^+Cl^-$ (3) (R_f = C_3F_7, C_6F_{13}) have been described by Yagupolskii and co-workers and $[C_6H_5I(CF_2)_nF]^+X^-$ (n = 2, 3, 6, 7, 8, 10; X = $OCOCF_3$, OSO_2CF_3) by Umemoto *et al.* (4). Frohn *et al.* (5) have reported on the existence of the $[I(C_6F_5)_2]^+$ cation.[3] We have also prepared this cation from the reactions of C_6F_5I with $[XeC_6F_5]^+$ and of $C_6F_5IF_2$ with $B(C_6F_5)_3$, respectively (6). Christe and co-workers (7, 8) characterized the compounds i-$C_3F_7I(OSO_2F)_2$ and $R_fI(OClO_3)_2$ (R_f = i-C_3F_7, C_7F_{15}). Based on Raman spectra, they postulated the ionic structures $[I(R_f)_2]^+[IX_4]^-$ and were first to point out the existence of bis(perfluoroalkyl)iodonium salts. These authors also postulated for $CF_3I(ONO_2)_2$ the ionic structure $[I(CF_3)_2]^+$-$[I(ONO_2)_4]^-$, based on the observed decomposition reaction (9).

During our investigations of polar trifluoromethyl transfer reactions, the preparation of bis- and tris(trifluoromethyl)iodine(III) compounds was studied. In this paper we wish to report spectroscopic evidence for the successful preparation of these compounds.

Experimental

Materials

All commercially available compounds were purified by common methods. The following compounds were prepared according to literature procedures: $Cd(CF_3)_2 \cdot 2D$ (D = CH_3CN or diglyme) (10); $I(OCOCF_3)_3$ (11); $I(ONO_2)_3$ (12); $Bi(CF_3)_3$ (13); CF_3IF_2 (14); $CF_3I(OCOCF_3)_2$ (15); CF_3ICl_2 (16); $Zn(CF_3)Br$ (17); $Hg(CF_3)_2$ (18).

Nuclear magnetic resonance spectra were recorded with the Bruker FT NMR spectrometer AM 300; ^{19}F nmr 282.4 MHz (CCl_3F, ext.); ^{113}Cd 66.5 MHz (50 vol% $(CH_3)_2Cd$ in $CDCl_3$, ext.); negative values indicate high field shifts. The ^{19}F nmr chemical shifts and coupling constants for some of the new iodine derivatives are summarized in Table 1.

General procedure

All reactions were carried out in a dry nitrogen atmosphere. Carefully dried 25 mL glass Schlenk tubes were used as reaction vessels. Yields were determined by ^{19}F nmr spectroscopy.

Method A

The iodine component was dissolved or suspended in the appropriate solvent. The non-dissolved trifluoromethyl metal compound was added.

Method B

The solid iodine compound was added to a solution of the trifluoromethyl metal derivative in the appropriate solvent.

Method C

The iodine derivative and the trifluoromethyl metal compound were dissolved or suspended in the appropriate solvent. The solutions were combined.

Method D

The iodine derivative was dissolved or suspended in the appropriate solvent. The Lewis acid was added. Colour effects were observed after adding BF_3 or SbF_5. Solid bis(trifluoromethyl)cadmium complexes were added after approximately 12 h.

The reactions are summarized in Tables 2–4; the products are listed in order of decreasing yields (intensities of the nmr signals). Main products are printed in bold letters.

Results and discussion

Reactions of iodine(III) compounds with trifluoromethyl cadmium compounds and tris(trifluoromethyl)bismuth in pyridine and acetonitrile

Bis(trifluoromethyl)cadmium complexes are excellent reagents for the syntheses of many new or otherwise not readily available trifluoromethyl element compounds (13).

These reactions proceed via an ionic mechanism. A solvent stabilized cation reacts with the cadmium complex to form the

[1]Taken from ref. 1.

[2]Author to whom correspondence may be addressed.

[3]For mass spectrometric evidence for $[I(C_6F_5)_2]^+$, see ref. 5*b*.

Can. J. Chem. Downloaded from www.nrcresearchpress.com by 195.138.81.100 on 09/07/12
For personal use only.

TABLE 1. The ^{19}F nmr data of trifluoromethyliodine derivatives[a]

Compound, T (°C), solvent	Chemical shift $\delta(CF_3)$ (ppm)	Chemical shift $\delta(IF)$ (ppm)	Couplings from ^{13}C satellite spectra $^1J(^{19}F-^{13}C)$ (Hz)	$^1\Delta(^{19}F-^{12/13}C)$ (ppm)	$^3J(^{19}F-^{19}F)$ (Hz)
$I(CF_3)F_2$, −20, CH_3CN	−34.83, t	−176.35, q	354.0	0.1351	6.1
−30, CH_2Cl_2	−29.34, t	−175.49, q			6.1
−30, C_5H_5N	−36.97, t	−170.14, q			6.0
$I(CF_3)(OCOCF_3)_2$,[b] −30, CH_3CN	−26.10, s		360.1	0.1369	
$I(CF_3)Cl_2$, −70, CH_2Cl_2	−26.89, s		364.5	0.1312	
−30, CH_3CN	−28.50, s				
$[I(CF_3)F]^+$, −30, CH_3CN	−32.80, d	−166.60, q			8.4
$[I(CF_3)_2]^+$,[c] −70, SO_2	−21.20, s		361.9	0.1312	
−70, CH_2Cl_2	−23.79, s				
$I(CF_3)_2F$,[d] −33, CH_2Cl_2	−26.21, d	−131.54, sept	357.0	0.1312	6.1
cis-$[I(CF_3)_2F_2]^-$, −33, CH_2Cl_2	−25.48, dd	−150.90, qq	361.0	0.1389	*trans* 9.1
					cis 2.1

[a]s: singlet, d: doublet, dd: doublet of doublets, t: triplet, q: quartet, qq: quartet of quartets, sept: septet.
[b]$\delta(OCOCF_3)$ −73.30 ppm.
[c]$^4J(^{19}F-^{19}F) = 4.4$ Hz.
[d]$^4J(^{19}F-^{19}F) \approx 4$ Hz.

new trifluoromethyl species and a cadmium cation (eq. [1]).

[1*a*] $$EX_n \rightleftharpoons [EX_{n-1} \cdot D]^+ + X^-$$

[1*b*] $$[EX_{n-1} \cdot D]^+ + Cd(CF_3)_2 \cdot D' \longrightarrow CF_3EX_{n-1} \cdot D + [Cd(CF_3) \cdot D']^+$$

E: e.g., Sb, Bi; X: Cl, Br; D: e.g., Et_2O, MeCN;
D': 2 MeCN, glyme, diglyme

The dissociation shown in eq. [1*a*] is established by conductivity measurements. Iodine trichloride shows a molar conductivity of 76 Ω^{-1} cm^2 mol^{-1} (22) in acetonitrile solution, which can be attributed to an equilibrium according to eq. [2].

[2] $$2ICl_3 \rightleftharpoons ICl_2^+ + ICl_4^-$$

This amphoteric behaviour explains the existence of many salts containing ICl_2^+ and ICl_4^- units (23–26). Therefore we reacted ICl_3, $I(OCOCF_3)_3$, and $I(ONO_2)_3$ with bis(trifluoromethyl)cadmium complexes or tris(trifluoromethyl)bismuth at low temperature in various aprotic solvents.

In all cases we obtained the monotrifluoromethyl iodine derivatives; no evidence for a further substitution could be found.

[3] $$IX_3 + Cd(CF_3)_2 \cdot D \longrightarrow CF_3IX_2 + Cd(CF_3)X \cdot D$$
$$IX_3 + Cd(CF_3)X \cdot D \longrightarrow CF_3IX_2 + CdX_2 \cdot D$$
$$IX_3 + Bi(CF_3)_3 \longrightarrow CF_3IX_2 + Bi(CF_3)_2X$$
$$IX_3 + Bi(CF_3)_2X \longrightarrow CF_3IX_2 + Bi(CF_3)X_2$$
$$IX_3 + Bi(CF_3)X_2 \longrightarrow CF_3IX_2 + BiX_3$$
$$X = Cl, OCOCF_3, ONO_2$$

This behaviour is similar to that observed during reactions with tellurium tetrachloride (27). The reactions of $Cd(CF_3)$ complexes with $TeCl_4$ yielded only the bis(trifluoromethyl)tellurium species. No evidence was found for tris- or tetrakis(trifluoromethyl)tellurium compounds. However, $Te(CF_3)_4$ is formed when $Te(CF_3)_2Cl_2$ is reacted with the cadmium complex in a second separate reaction (28).

[4] $$Te(CF_3)_2Cl_2 + Cd(CF_3)_2 \cdot D \rightarrow Te(CF_3)_4 + CdCl_2 \cdot D$$

In analogy to these results, we studied the reactions of CF_3IX_2 (X: F, Cl, $OCOCF_3$) with $Cd(CF_3)_2$ complexes in acetonitrile and pyridine solutions. The results of reactions in the less polar solvents $CHCl_3$ and CH_2Cl_2 are described later.

When CF_3IF_2 is reacted with $Cd(CF_3)_2 \cdot D$ in pyridine or acetonitrile solution, ^{19}F nmr spectroscopic evidence is found for more highly trifluoromethyl-substituted iodine derivatives, but an assignment of the resonances could not be made. A number of by-products were identified: 2-, 3-, and 4-trifluoromethyl pyridine were formed during these reactions in addition to traces of 2,6-bis(trifluoromethyl)pyridine. The pyridine derivatives can be identified by their ^{19}F nmr spectra compared with data published earlier (19). Similar results were obtained when the reaction was carried out under modified conditions in CH_3CN solution. When CF_3ICl_2 in CH_3CN/CH_2Cl_2 mixtures is used as a starting material instead of CF_3IF_2, ^{19}F nmr spectroscopic evidence is found for $[I(CF_3)_2]^+$ and $I(CF_3)_2Cl$ as well as CF_3IF_2; the presence of CF_3IF_2 is indirect evidence for $I(CF_3)_3$. The large number of CF_2 products and the formation of CF_3IF_2, together with the absence of higher trifluoromethylated intermediates such as the sufficiently stable $I(CF_3)_2F$, allow the conclusion that $I(CF_3)_3$ must have been formed as an intermediate.

Thus, tris(trifluoromethyl)iodine can decompose via two possible pathways, either by the elimination of hexafluoroethane to yield CF_3I or by an elimination of two difluorocarbene units to form CF_3IF_2.

$I(CF_3)_2Cl$ can undergo a reductive elimination of CF_3Cl.

[5] $$CF_3ICl_2 + Cd(CF_3)_2 \cdot D \longrightarrow "I(CF_3)_3" + "I(CF_3)_2Cl"$$

[6] $$"I(CF_3)_2Cl" \longrightarrow CF_3I + CClF_3$$

[7] $$"I(CF_3)_3" \longrightarrow CF_3I + CF_3CF_3$$

[8] $$"I(CF_3)_3" \longrightarrow CF_3IF_2 + 2\,CF_2$$

One of the by-products formed during these reactions was

Can. J. Chem. Downloaded from www.nrcresearchpress.com by 195.138.81.100 on 09/07/12
For personal use only.

TABLE 2. Reactions of $Cd(CF_3)_2 \cdot D$ and $Bi(CF_3)_3$ with iodine(III) derivatives

Components		Solvent				
A (mmol)	B (mmol)	(mL)	Method	Temp. (°C)	Reaction time	Detected compounds (ref.)
ICl_3 (0.62)	$Cd(CF_3)_2 \cdot$diglyme (0.88)	Pyridine (5)	A	−50	24 h	**CF_3ICl_2**,[a] CF_3I, $Cd(CF_3)_2 \cdot$2pyridine, $Cd(CF_3)Cl \cdot$2pyridine, CF_3H, CF_3-pyridine derivatives (19)
ICl_3 (1.07)	$Bi(CF_3)_3$ (1.20)	Pyridine (5)	B	−40	3 h	**CF_3ICl_2**, CF_3I, CF_3H, $Bi(CF_3)_2Cl$, $Bi(CF_3)Cl_2$, CF_3-pyridine derivatives (19)
ICl_3 (0.64)	$Cd(CF_3)_2 \cdot 2CH_3CN$ (1.00)	CH_3CN (5)	B	−40	16 h	**CF_3I**,[b] CF_3ICl_2, $Cd(CF_3)_2 \cdot 2CH_3CN$, $Cd(CF_3)Cl \cdot 2CH_3CN$, CF_3H
ICl_3 (0.94)	$Bi(CF_3)_3$ (0.96)	CH_3CN (5)	B	−40	4 h	**CF_3ICl_2**,[c] $Bi(CF_3)_3$, $Bi(CF_3)_2Cl$, $Bi(CF_3)Cl_2$, CF_3I, $CClF_3$, CF_3H
$I(OCOCF_3)_3$ (0.60)	$Cd(CF_3)_2 \cdot$diglyme (1.51)	Pyridine (5)	A	−40	24 h	**CF_3I**, $Cd(CF_3)_2 \cdot$2pyridine, $Cd(CF_3)(OCOCF_3) \cdot$2pyridine, CF_3H, $CF_3I(OCOCF_3)_2$
				−40	18 days	**CF_3I**, CF_3H, $CF_3I(OCOCF_3)_2$, CF_3IF_2, CF_3IF_4, IF_5
$I(OCOCF_3)_3$ (0.90)	$Bi(CF_3)_3$ (1.08)	Pyridine (6)	B	−40	2 days	**$CF_3I(OCOCF_3)_2$**, CF_3I, CF_3H, $Bi(CF_3)_3$, $Bi(CF_3)_2(OCOCF_3)$,[d] $Bi(CF_3)(OCOCF_3)_2$[e]
$I(OCOCF_3)_3$ (0.64)	$Cd(CF_3)_2 \cdot 2CH_3CN$ (0.90)	CH_3CN (4)	A	−35	12 h	**$CF_3I(OCOCF_3)_2$**,[f] $Cd(CF_3)_2 \cdot 2CH_3CN$, CF_3I, $Cd(CF_3)(OCOCF_3) \cdot 2CH_3CN$[g]
$I(OCOCF_3)_3$[h]	$Bi(CF_3)_3$	CH_3CN	A	−35	12 h	**$CF_3I(OCOCF_3)_2$**,[i], $Bi(CF_3)_3$, $Bi(CF_3)_2(OCOCF_3)$, $Bi(CF_3)(OCOCF_3)_2$, CF_3I
$I(ONO_2)_3$ (1.12)	$Cd(CF_3)_2 \cdot 2CH_3CN$ (2.25)	Pyridine (7)	C	−35	2 days	**$CF_3I(ONO_2)_2$**,[j], CF_3I
$I(ONO_2)_3$ (1.15)	$Cd(CF_3)_2 \cdot 2CH_3CN$ (1.98)	CH_3CN (5)	C	−35	2 days	**CF_3I**,[k], $CF_3I(ONO_2)_2$, CF_3H

[a]Ratio CF_3ICl_2:CF_3I = 5:1.
[b]Ratio CF_3I:CF_3ICl_2 = 10:1.
[c]Ratio CF_3ICl_2:CF_3I = 9:1.
[d]$\delta(CF_3)$ −37.36 ppm.
[e]$\delta(CF_3)$ −42.80 ppm.
[f]Ratio $CF_3I(OCOCF_3)_2$:CF_3I:all other compounds = 10:3:1.
[g]A number of signals between δ −74 and δ −78 ppm could not be firmly assigned.
[h]Non-stoichiometric, excess $Bi(CF_3)_3$.
[i]Ratio $CF_3I(OCOCF_3)_2$:CF_3I:all other compounds 10:2:1.5.
[j]Ratio $CF_3I(ONO_2)_2$:CF_3I = 5:1.
[k]Ratio CF_3I:$CF_3I(ONO_2)_2$:CF_3H = 20:1:0.5.

$CHClF_2$. This compound can be explained by an insertion of CF_2 into HCl, which has been formed by solvolysis of the starting material CF_3ICl_2. Insertion reactions into trifluoroacetic acid or trifluoromethylsulfonic acid are known (29) and will be discussed later.

Whether a reaction occurs or not, depends on the basicity of the solvent. The stronger the basicity of the solvent, the more the reactivity decreases. In solvents such as pyridine or DMF, the starting material CF_3ICl_2 forms adducts as also does $Cd(CF_3)_2$, and both reaction partners lose reactivity. The highest reactivity has been found in CH_3CN solution.

Similar results could be obtained using $CF_3I(OCOCF_3)_2$ instead of the dichloride. We also found spectroscopic evidence for $I(CF_3)_2OCOCF_3$ and CF_3IF_2. The by-products from difluorocarbene reactions could also be identified by their nmr spectra.

Although $Cd(CF_3)_2 \cdot D$ is an excellent precursor for CF_2 generation (30, 31) at ambient temperature or above, we never found evidence for CF_2 generated from the Cd complexes under these mild conditions. Identified products are trifluoroacetic acid difluoromethyl ester, $CF_3CO_2CF_2H$, and (difluoro(trifluoroacetato)methyl)trifluoromethyl cadmium, $CF_3CO_2CF_2CdCF_3$. These compounds could easily be identified by ^{19}F nmr and the latter also by ^{113}Cd nmr spectra. A detailed description of these nmr spectra is given later.

These results show that it is very difficult to obtain bis- or tris(trifluoromethyl)iodine(III) derivatives. The complexity of these systems can be confirmed by reactions of CF_3IF_2 with mercury, cadmium, and zinc compounds in less coordinating solvents.

Reactions of trifluoromethyliodine difluoride with trifluoromethyl zinc, cadmium, and mercury compounds in chloroform and dichloromethane

Trifluoromethyliodine difluoride forms 1:1 adducts with acetonitrile, pyridine, and quinoline (32) as well as with CsF.[4] In polar solvents such as DMF, CH_3CN, or pyridine the trifluoromethyliodine derivatives CF_3IX_2 (X = Cl, $OCOCF_3$) also form stable adducts with the solvent. This behaviour proves that a fourfold coordination of iodine is preferred. Because some anions containing the trifluoromethyl group are very stable (33, 34), we decided to carry out reactions to achieve fourfold coordination of the iodine central atom by an additional CF_3 group. Therefore, the reactions of $ZnBr(CF_3) \cdot 2DMF$, $Cd(CF_3)_2 \cdot$diglyme, and $Hg(CF_3)_2$ with CF_3IF_2 in non-coordinating solvents were investigated. In the following section the ^{19}F nmr spectra of the reactions of CF_3IF_2 and $Hg(CF_3)_2$ are

[4]D. Naumann. Unpublished results.

Can. J. Chem. Downloaded from www.nrcresearchpress.com by 195.138.81.100 on 09/07/12
For personal use only.

Can. J. Chem. Downloaded from www.nrcresearchpress.com by 195.138.81.100 on 09/07/12
For personal use only.

TABLE 3. Reactions of trifluoromethyl metal compounds with trifluoromethyl iodine(III) derivatives

A. Reactions in donor solvents

Components						
A (mmol)	B (mmol)	Solvent (mL)	Method	Temp. (°C)	Reaction time	Detected compounds (ref.)
CF_3IF_2 (1.50)	$Cd(CF_3)_2 \cdot 2CH_3CN$ (1.70)	Pyridine (4)	A	−25	4 h	**CF_3I**, CF_3IF_2, $Cd(CF_3)_2 \cdot 2$pyridine, 2-, 3-, and 4-CF_3-C_5H_4N, 2,6-$(CF_3)_2C_5H_3N$ (19)[a]
CF_3IF_2 (1.20)	$Cd(CF_3)_2 \cdot 2CH_3CN$ (1.29)	CH_3CN (4)	A	−33	2 h	**CF_3I**, CF_3IF_2, $Cd(CF_3)_2 \cdot 2CH_3CN$, CF_3IF_4, IF_5, further $Cd(CF_3)$ compounds
CF_3ICl_2 (1.50)	$Cd(CF_3)_2 \cdot 2CH_3CN$ (1.30)	CH_3CN (2.5) $+CH_2Cl_2$ (2.5)	A	−25	4 h	**CF_3ICl_2**, CF_3I, $CClF_3$, CF_3IF_2, $[I(CF_3)_2]^+$, $CClF_2H$, further CF_2H derivatives[b]
CF_3ICl_2 (1.68)	$Bi(CF_3)_3$ (1.25)	CH_3CN (2) $+CH_2Cl_2$ (2)	A	−70	12 h	**CF_3I**, CF_3ICl_2, $CClF_3$, $Bi(CF_3)_3$, $Bi(CF_3)_2Cl$, $Bi(CF_3)Cl_2$, IF_4^+ (?)[c]
$CF_3I(OCOCF_3)_2$ (1.19)	$Cd(CF_3)_2 \cdot 2CH_3CN$ (1.33)	CH_3CN (2) $+CH_2Cl_2$ (2)	A	−30	2 days	**CF_3IF_2**, "$I(CF_3)_3$", $I(CF_3)_2(OCOCF_3)$, CF_3I, $Cd(CF_3)_2 \cdot 2CH_3CN$, $Cd(CF_3)(OCOCF_3) \cdot 2CH_3CN$, $Cd(CF_3)(CF_2OCOCF_3) \cdot 2CH_3CN$, HCF_2OCOCF_3[d]
$CF_3I(OCOCF_3)_2$ (0.36)	$Cd(CF_3)_2 \cdot$diglyme (0.52)	Et_2O (3)	A	−78	6 h	**CF_3I**, $CF_3I(OCOCF_3)_2$, $Cd(CF_3)_2 \cdot$diglyme, CF_3IF_2, CF_3IF_4, $Cd(CF_3)(OCOCF_3) \cdot$diglyme
$CF_3I(OCOCF_3)_2$[e]	$Cd(CF_3)_2 \cdot$glyme	Pyridine (4) $+NMe_3$ (1)	A	−35	3 days	**CF_3I**, CF_3IF_2, CF_3H, CF_3-pyridine derivatives, "$I(CF_3)_3 \cdot$pyridine", "$I(CF_3)_2(OCOCF_3) \cdot$pyridine"[f]

[a]Signals at δ −27.71 ppm and δ −31.80 ppm gave some evidence for higher trifluoromethylated iodine derivatives.
[b]A broad signal at δ −18 ppm might be assigned to "$I(CF_3)_3$". Evidence was also found for $I(CF_3)_2Cl$.
[c]IF_4^+: δ −59.16 ppm (in CH_3CN: δ −58.31 ppm (20)).
[d]Further signals between δ −74 and δ −78 ppm could not unambiguously be assigned.
[e]Non-stoichiometric, excess $Cd(CF_3)_2 \cdot$glyme.
[f]"$I(CF_3)_3 \cdot$pyridine": δ −25 ppm, "$I(CF_3)_2(OCOCF_3)$": δ −30 ppm.

B. Reactions in non-coordinating solvents

Components						
A (mmol)	B (mmol)	Solvent (mL)	Method	Temp. (°C)	Reaction time	Detected compounds (ref.)
CF_3IF_2 (0.43)	$ZnBr(CF_3) \cdot 2$dmf (0.35)	$CDCl_3$ (0.3)	A	−30	3 h	**CF_3IF_2**, $ZnBr(CF_3) \cdot 2$dmf, $Zn(CF_3)_2 \cdot 2$dmf, CF_3I, $CBrF_3$, $[I(CF_3)_2F_2]^-$, $[I(CF_3)F]^+$[a]
CF_3IF_2 (0.56)	$Cd(CF_3)_2 \cdot$diglyme (0.50)	$CDCl_3$ (0.4)	B	−33	3 h + 6 days	**CF_3IF_2**, **$Cd(CF_3)_2 \cdot$diglyme**, IF_5, CF_3I, CF_3IF_4 CF_3IF_2, CF_3I, $Cd(CF_3)_2 \cdot$diglyme, IF_5, $[I(CF_3)_2F_2]^-$, CF_3IF_4
CF_3IF_2 (0.47)	$Hg(CF_3)_2$ (0.58)	$CDCl_3$ (0.4)	A	−30	50 h	**CF_3IF_2**, CF_3I, $[I(CF_3)_2F_2]^-$, $I(CF_3)_2F$, $Hg(CF_3)_2$[b]
CF_3IF_2 (0.99)	$Hg(CF_3)_2$ (1.00)	CH_2Cl_2 (2)	A	−30	24 h	**CF_3IF_2**, CF_3I, $[I(CF_3)_2F_2]^-$, $I(CF_3)_2F$, $Hg(CF_3)_2$

[a]Ratio CF_3IF_2:$[I(CF_3)_2F_2]^-$:$[I(CF_3)F]^+$ = 10:1.5:0.5.
[b]Ratio CF_3IF_2:CF_3I:$[I(CF_3)_2F_2]^-$:$I(CF_3)_2F$ = 31:15:10:2.

Can. J. Chem. Downloaded from www.nrcresearchpress.com by 195.138.81.100 on 09/07/12
For personal use only.

TABLE 4. Reactions of bis(trifluoromethyl)cadmium complexes with CF_3IF_2 and $CF_3I(OCOCF_3)_2$ in the presence of a Lewis acid[a]

Components: A (mmol)	B(mmol)	C (mmol)	Solvent (mL)	Method	Temp. (°C)	Reaction time	Detected compounds
CF_3IF_2 (0.60)	$Cd(CF_3)_2 \cdot$ glyme (excess)	BF_3 (excess)	CH_2Cl_2 (5)	D	−78	4 h	**CF_4**, CF_3I, BF_4^-, $Cd(CF_3)^+$, CF_2HOR
CF_3IF_2 (0.55)	$Cd(CF_3)_2 \cdot 2CH_3CN$ (1.05)	SbF_5 (0.50)	CH_2Cl_2 (5)	D	−78	1 h	**CF_4**, **CF_3I**, **CF_2H_2**, CF_3H, $CClFH_2$, CCl_3F
CF_3IF_2 (0.64)	$Cd(CF_3)_2 \cdot$ diglyme (1.12)	SbF_5 (0.50)	SO_2 (5)	D	−60	2 h	**CF_3I**, **CF_4**, IF_5, SO_2F_2, CF_3SO_2F
$CF_3I(OCOCF_3)_2$ (0.50)	$Cd(CF_3)_2 \cdot 2CH_3CN$ (1.00)	$B(OCOCF_3)_3$ (0.90)	SO_2 (4)	D	−57	12 h	**$[I(CF_3)_2]^+$**, **CF_3I**, **$Cd(CF_3)(CF_2OCOCF_3) \cdot 2CH_3CN$**, **$HCF_2OCOCF_3$**, $[CF_3IOCOCF_3]_2O$,[b] $Cd(CF_3)^+$, $Cd(CF_3)_2 \cdot 2CH_3CN$, $Cd(CF_2OCOCF_3)_2 \cdot 2CH_3CN$, CF_3SO_2F, mixed fluoro-trifluoroacetato borates[c]
$CF_3I(OCOCF_3)_2$ (0.49)	$Cd(CF_3)_2 \cdot 2CH_3CN$ (1.20)	$B(OCOCF_3)_3$ (0.50)	CH_2Cl_2 (4)	D	−70	4 h	**$[I(CF_3)_2]^+$**, **CF_3I**, "$I(CF_3)_3$", $CF_3I(OCOCF_3)_2$, $Cd(CF_3)_2 \cdot 2CH_3CN$, CF_3IF_2, $Cd(CF_3)(CF_2OCOCF_3) \cdot 2CH_3CN$, several CF_2H groups containing compounds, fluorotrifluoroacetato borates[d]
$CF_3I(OCOCF_3)_2$ (0.90)	$Cd(CF_3)_2 \cdot 2CH_3CN$ (2.10)	$B(OCOCF_3)_3$ (1.00)	SO_2ClF (2.5)	D	−78	2 days	**CF_3I**, $CClF_3$, CF_3H, $Cd(CF_3)(CF_2OCOCF_3) \cdot 2CH_3CN$, $Cd(CF_2OCOCF_3)_2 \cdot 2CH_3CN$, several CF_2H groups containing compounds

[a]Reactions in CH_3CN at −25°C (24 h) and of the system $CF_3IF_2/B(OCOCF_3)_3/Cd(CF_3)_2 \cdot 2CH_3CN/CH_2Cl_2$ (−70°C; 30 h) did not proceed successfully. The main product of these reactions was CF_3I, besides a great number of by-products as mentioned above.

[b]δ −31.60 ppm.

[c]δ −140.57 ppm $[BF_3(OCOCF_3)]^-$, δ −142.03 ppm $[BF_2(OCOCF_3)_2]^-$, δ −147.16 ppm $[BF(OCOCF_3)_3]^-$ (21).

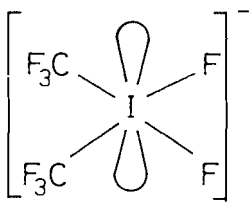
[d]When the nmr tube was warmed to 0°C, only the resonances of CF_3I and $CF_2HOCOCF_3$ could be detected unambiguously beside the collapsing signals of $[I(CF_3)_2]^+$, $CF_3I(OCOCF_3)_2$, and CF_3IF_2.

discussed. When the reaction mixture was studied by ^{19}F nmr spectroscopy, four new signal groups appeared, which could be assigned to bis(trifluoromethyl)iodine fluoride and the *cis*[bis-(trifluoromethyl)difluoro iodate(III)]anion.

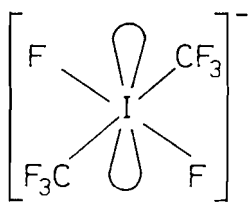
$I(CF_3)_2F$	$\delta(CF_3)$ −26.21 ppm, d $\delta(IF)$ −131.54 ppm, sept Relative intensities: 5.6:1 $^3J(F–F) = 6.1$ Hz $^1J(F–C) = 357.0$ Hz $^1\Delta(^{19}F–^{12/13}C) = 0.1312$ ppm
cis-$[I(CF_3)_2F_2]^-$	$\delta(CF_3)$ −25.48 ppm, dd $\delta(IF_2)$ −150.90 ppm, qq Relative intensities: 2.7:1 *trans*-$^3J(F–F) = 9.1$ Hz *cis*-$^1J(F–F) = 2.1$ Hz $^1J(F–C) = 361.0$ Hz $^1\Delta(^{19}F–^{12/13}C) = 0.1389$ ppm

The splitting of the signals in the ^{19}F nmr spectrum strongly depends on the spatial arrangement of the ligands. The observed multiplicities indicate an A_6X spin system for $I(CF_3)_2F$. Therefore the structure of the molecule may be T-shaped with an axial arrangement of the CF_3 groups or it can be trigonal-planar. An arrangement with one CF_3 group in the axial and one in the equatorial position would cause an $A_3A_3'X$ spin system and can therefore be excluded.

Two conformers are possible for the anionic species $[I(CF_3)_2F_2]^-$. A square-planar arrangement of the four ligands is the most probable structure according to the VSEPR model.



cis conformer



trans conformer

The ^{19}F nmr spectra of this anion favour the *cis* conformer. In the *cis* conformer the F ligands are magnetically nonequivalent due to different couplings to the *cis* and *trans* CF_3 groups. The same arguments apply for the CF_3 groups. Therefore the trifluoromethyl groups split into doublets of doublets resulting from the spin–spin interactions with the *cis* and *trans* fluorine atoms. By analogy, the fluorine signals split into quartets of quartets ($A_3A_3'XX'$ spin system).

Fluorine exchange equilibria in solution could not be observed by ^{19}F nmr spectroscopy because $I(CF_3)_2F$ as well as $[I(CF_3)_2F_2]^-$ decompose in solution at approximately −10°C to give CF_4 and CF_3I.

It should be pointed out that the $CdCF_3$ and $ZnCF_3$ compounds are used as complexes. Therefore, an interaction of the iodine compound with the donor molecules must also be taken into consideration. A decomplexation of the cadmium species, for example, would lead to a naked $Cd(CF_3)_2$. This compound is stable up to 0°C (35). Uncomplexed $Zn(CF_3)_2$ decomposes at approximately −40°C.

[9] $Cd(CF_3)_2 \cdot \text{diglyme} + CF_3IF_2 \rightleftharpoons Cd(CF_3)_2 + CF_3IF_2 \cdot \text{diglyme}$

[10] $Cd(CF_3)_2 \longrightarrow$ dec.

Because Cd and Zn compounds are stronger Lewis-base acceptors than iodine(III) derivatives, the equilibrium [9] should strongly be shifted to the left side.

Polar trifluoromethylation reactions in the presence of a Lewis acid

We have previously shown that trifluoromethyliodine(III) derivatives are extremely stable in a pseudo-octahedral environment (16, 32). It is also known that diorgano iodonium cations (36) and dihalo iodonium cations (23–25) are stable species. Due to the VSEPR model we assume maxima in stability for disubstituted iodine cations with two identical ligands, because neither Yagupol'skii (2, 3) nor Umemoto (4) were able to prepare aryl-trifluoromethyl iodonium salts.

It is known that $Cd(CF_3)_2 \cdot D$ reacts with boron trifluoride or tantalum pentafluoride to form the cation $Cd(CF_3)^+$ (33). Therefore we can suggest that, if BF_3 is used, the anion $[B(CF_3)F_3]^-$ might be formed as an intermediate. This anion could interact with CF_3IF_2 to form $[I(CF_3)_2]^+$ and $[BF_4]^-$ as well as CdF_2.

[11] $Cd(CF_3)_2 \cdot D + BF_3 \longrightarrow [Cd(CF_3)]^+ + [B(CF_3)F_3]^-$

[12] $CF_3IF_2 + [B(CF_3)F_3]^- \longrightarrow [I(CF_3)_2]^+ + [BF_4]^- + F^-$

[13] $[Cd(CF_3) \cdot D]^+ + F^- \rightleftharpoons Cd(CF_3)F \cdot D$

Another reaction is possible as well. The short-lived species $[CF_3IF]^+[BF_4]^-$ may react directly with the cadmium complex to form $[I(CF_3)_2]^+[BF_4]^-$ and $Cd(CF_3)F \cdot D$. Unfortunately, these attempts failed. The Lewis acidity of BF_3 is obviously too high to form either $[CF_3IF]^+$ or $[B(CF_3)F_3]^-$ under the conditions applied. Both intermediates rapidly decompose to give CF_4, CF_3I, $[BF_4]^-$, and CF_2, which can be identified from its subsequent reactions. The low temperature at which we had to work may not have supplied the activation energy necessary for a trifluoromethyl transfer by the cadmium complex. Similar results were obtained using the Lewis acid SbF_5. Therefore, we studied the reactions of CF_3IF_2 and $CF_3I(OCOCF_3)_2$ with $Cd(CF_3)_2 \cdot D$ in the presence of $B(OCOCF_3)_3$, in order to make use of the increased stability of a $[CF_3I(OCOCF_3)]^+$ cation.

[14] $CF_3IF_2 + B(OCOCF_3)_3 \longrightarrow [CF_3I(OCOCF_3)]^+[BF_{4-x}(OCOCF_3)_x]^-$

[15] $[CF_3I(OCOCF_3)]^+ + Cd(CF_3)_2 \cdot D \longrightarrow [I(CF_3)_2]^+ + Cd(CF_3)(OCOCF_3) \cdot D$

We found ^{19}F nmr spectroscopic evidence for the bis(trifluoromethyl)iodine cation in the reaction mixture if sulphur dioxide or dichloromethane were used as solvents. No evidence was found for $[I(CF_3)_2]^+$ in CH_3CN or SO_2ClF. Although we could not isolate $[I(CF_3)_2]^+[BF_4]^-$ from the reaction mixtures, we could easily identify the cation by its ^{19}F nmr resonance. The ^{13}C satellites of $[I(^{12}CF_3)(^{13}CF_3)]^+$ form an $A_3A_3'X$ spin system in the ^{19}F nmr spectrum; they are split into quartets proving that two CF_3 groups are bound to iodine. The nmr data obtained are comparable to those of the isoelectronic bis(trifluoromethyl)tellurium (37).

During these reactions a great number of by-products were formed. Most of them could easily be identified by their nmr spectra.

Description and identification of the by-products formed during the reactions of $CF_3I(OCOCF_3)_2$ with $Cd(CF_3)_2 \cdot 2CH_3CN$

Many by-products were formed during the reactions of

Can. J. Chem. Downloaded from www.nrcresearchpress.com by 195.138.81.100 on 09/07/12
For personal use only.

$CF_3I(OCOCF_3)_2$ and $Cd(CF_3)_2 \cdot 2CH_3CN$ in CH_3CN or SO_2 solution, as mentioned above.

The by-products that could be identified from the reaction in acetonitrile solution were CF_3IF_2, CF_3COOCF_2H, $Cd(CF_3)(CF_2OCOCF_3)$, and $Cd(CF_2OCOCF_3)_2$. Evidence was found for further compounds containing CF_2H groups but a conclusive assignment of the ^{19}F nmr resonances was impossible.

Because "$I(CF_3)_3$" and $Cd(CF_3)_2$ complexes undergo difluorocarbene eliminations under distinct conditions we propose a carbene or carbenoid mechanism.

Trifluoroacetic acid difluoromethyl ester shows two signals in the ^{19}F nmr spectrum: a singlet at δ −75.11 ppm, which can be assigned to the CF_3 group, and a doublet at δ −91.88 ppm, $^2J(^{19}F-^1H) = 68.7$ Hz, $^1J(^{19}F-^{13}C) = 252.3$ Hz, $^1\Delta = 0.1531$ ppm, which can be assigned to the CF_2H group (29).

$Cd(CF_3)(CF_2OCOCF_3)$ can be identified by its ^{19}F nmr and ^{113}Cd nmr spectra. The compound shows three different ^{19}F resonances. The CF_3 group is detected as a singlet at δ −36.58 ppm, $^2J(^{111/113}Cd-^{19}F) = 459.9/480.7$ Hz. The CF_2 group, directly bound to the cadmium atom, gives a resonance at δ −57.42 ppm, $^2J(^{111/113}Cd-^{19}F) = 318.3/332.7$ Hz, and the $OCOCF_3$ group is observed at δ −75.80 ppm. A spin–spin interaction between the CF_3 group and the CF_2 group bound to cadmium could not be observed. The existence of this structural element is proven by its ^{113}Cd nmr resonance. This signal is split into a quartet of triplets caused by the spin–spin interaction of the ^{113}Cd nucleus with three equivalent fluorine atoms of the CF_3 group and two of the CF_2 group. The coupling constants $^2J(^{113}Cd-^{19}F)$ have the absolute values of 483 Hz and 332 Hz, respectively, and are identical to those obtained from the ^{19}F nmr spectra within experimental error.

The chemical shift δ (^{113}Cd) −492 ppm is nearly identical to that of the bis(trifluoromethyl)cadmium complex (33), indicating similar electronic effects for these compounds.

These studies on trifluoromethyl iodine(III) derivatives clearly show the complexity of the system. We have been able to show that it is possible to generate bis(trifluoromethyl)iodine derivatives as neutral, cationic, and anionic species by varying the conditions, and to identify the new derivatives by their ^{19}F nmr spectra.

Further work is being done to isolate these compounds and to obtain more information about the mechanism that leads to by-products containing the CF_2H group.

Acknowledgements

We thank Stephan Menzer for his assistance in the experimental work. Financial support by the Minister für Wissenschaft und Forschung des Landes Nordrhein-Westfalen, the Fonds der Chemischen Industrie, and the Kali-Chemie AG, Hannover, is gratefully acknowledged.

1. W. Tyrra. Dissertation, Universität Dortmund, 1989.
2. L. M. Yagupol'skii, A. A. Mironova, I. I. Maletina, and V. V. Orda. Zh. Org. Khim. **16**, 232 (1980).
3. V. V. Lyalin, V. V. Orda, L. A. Alekseeva, and L. M. Yagupol'skii. Zh. Org. Khim. **7**, 1473 (1971).
4. T. Umemoto, Y. Kuriu, H. Shuyama, O. Miyano, and S.-I. Nakayama. J. Fluorine Chem. **20**, 695 (1982).
5. (*a*) H. J. Frohn, J. Helber, and W. Kaminski. 6th European Symposium on Fluorine Chemistry, Dortmund, 1977, Abstract I8; (*b*) H. J. Frohn, J. Helber, and A. Richter. Chem. Ztg. **107**, 169 (1983).
6. D. Naumann and W. Tyrra. J. Chem. Soc. Chem. Commun. 47 (1989).
7. C. J. Schack and K. O. Christe. J. Fluorine Chem. **16**, 63 (1980).
8. C. J. Schack, D. Pilipovich, and K. O. Christe. Inorg. Chem. **14**, 145 (1975).
9. K. O. Christe, C. J. Schack, and R. D. Wilson. Inorg. Chem. **13**, 2811 (1974).
10. H. Lange and D. Naumann. J. Fluorine Chem. **26**, 1 (1984).
11. M. Schmeisser, K. Dahmen, and P. Sartori. Chem. Ber. **100**, 1633 (1967).
12. G. Brauer (*Editor*). Handbuch der präparativen anorganischen Chemie. Band 1. Enke Verlag, Stuttgart. 1975 acc. to K. Brändle. Dissertation, RWTH Aachen, 1958.
13. D. Naumann and W. Tyrra. J. Organomet. Chem. **334**, 323 (1987).
14. M. Schmeisser and E. Scharf. Angew. Chem. **71**, 524 (1959).
15. D. Naumann and J. Baumanns. J. Fluorine Chem. **8**, 177 (1976).
16. W. Tyrra and D. Naumann. J. Fluorine Chem. **45**, 401 (1989).
17. D. Naumann, W. Tyrra, B. Kock, W. Rudolph, and B. Wilkes. Eur. Pat. App. EP 0291860 A1, 23.11.88. DE App. 3717358, 22.05.87.
18. I. L. Knunyants, Y. F. Kommissarov, B. L. Dyatkin, and L. T. Lantseva. Izv. Akad. Nauk SSSR, Ser. Khim. **4**, 943 (1973).
19. D. Naumann, B. Wilkes, and J. Kischkewitz. J. Fluorine Chem. **30**, 73 (1985).
20. H. J. Frohn and H. Maurer. J. Fluorine Chem. **34**, 129 (1986).
21. S. Brownstein. Can. J. Chem. **56**, 343 (1978).
22. Landolt-Börnstein. Zahlenwerte und Funktionen aus Physik, Chemie, Astronomie, Geophysik und Technik, Eigenschaften der Materie in ihren Aggregatzuständen. 7. Teil: Elektrische Eigenschaften II (Elektrochemische Systeme). Springer-Verlag, Berlin. 1960.
23. P. A. Yeats, W. W. Wilson, and F. Aubke. Inorg. Nucl. Chem. Lett. **9**, 209 (1973).
24. T. Birchall and R. D. Myers. Inorg. Chem. **20**, 2207 (1981).
25. C. G. Vonk and E. H. Wiebenga. Recl. Trav. Chim. Pays-Bas, **78**, 913 (1959).
26. N. N. Greenwood and A. Earnshaw. Chemistry of the elements. 1st ed. Pergamon Press, Oxford. 1984. pp. 978–988, and literature cited therein.
27. F. Leifeld. Dissertation, Universität Dortmund, 1985.
28. B. Wilkes and D. Naumann. J. Fluorine Chem. **27**, 115 (1985).
29. R. A. Mitsch and J. E. Robertson. J. Heterocycl. Chem. **2**, 152 (1965).
30. L. J. Krause and J. A. Morrison. J. Am. Chem. Soc. **103**, 2995 (1981).
31. H. Lange and D. Naumann. J. Fluorine Chem. **27**, 299 (1985).
32. J. Baumanns, L. Deneken, D. Naumann, and M. Schmeisser. J. Fluorine Chem. **3**, 323 (1973/74).
33. D. Naumann and W. Tyrra. J. Organomet. Chem. **368**, 131 (1989).
34. W. Dukat and D. Naumann. Rev. Chim. Min. **23**, 589 (1986).
35. M. A. Guerra, T. R. Bierschenk, and R. J. Lagow. J. Am. Chem. Soc. **108**, 4103 (1986).
36. G. A. Olah. Halonium ions. John Wiley and Sons, New York. 1975.
37. W. Dukat. Dissertation, Universität Dortmund, 1986.

Can. J. Chem. Downloaded from www.nrcresearchpress.com by 195.138.81.100 on 09/07/12
For personal use only.

Nucleic acid related compounds. 63. Synthesis of 5′-deoxy-5′-methyleneadenosine and related Wittig-extended nucleosides[1]

STANISLAW F. WNUK AND MORRIS J. ROBINS[2]

Departments of Chemistry, Brigham Young University, Provo, UT 84602, U.S.A., Academy of Agriculture, 60625 Poznań, Wojska Polskiego 75, Poland, and University of Alberta, Edmonton, Alta., Canada T6G 2G2

Received August 1, 1990

STANISLAW F. WNUK and MORRIS J. ROBINS. Can. J. Chem. **69**, 334 (1991).

Treatment of the purified 5′-aldehyde (**2***a*) (derived from 6-*N*-benzoyl-2′,3′-*O*-isopropylideneadenosine (**1***a*)) with methylenetriphenylphosphorane and successive deprotection with ammonia and acid gave 9-(5,6-dideoxy-β-D-*ribo*-hex-5-enofuranosyl)adenine (5′-deoxy-5′-methyleneadenosine) (**4**). Oxidation of **1***a* or 2′,3′-*O*-isopropylideneadenosine (**1***b*) and treatment of the crude 5′-aldehydes (**2***a* or **2***b*) with (*p*-toluenesulfonylmethylene)triphenylphosphorane gave high yields of the 5′-deoxy-5′-tosylmethylene derivatives (**5***a* or **5***b*). Removal of the tosyl group from **5***b* to give **3***b* was effected with tributylstannyllithium, but sulfone cleavage by the usual reductive methods failed. Reduction and deprotection of **5***a* or **5***b* gave 9-[5,6-dideoxy-6-(*p*-toluenesulfonyl)-β-D-*ribo*-hexofuranosyl]adenine (**6***b*). Isomerization of the vinyl tosyl (**5***b*) to a 4′,5′-unsaturated allylic tosyl derivative (**7**) occurred under cleavage conditions and in solutions of aqueous or organic bases.

Key words: adenosine, 5′-deoxyadenosine, 5′-methylene-5′-deoxyadenosine, nucleosides.

STANISLAW F. WNUK et MORRIS J. ROBINS. Can. J. Chem. **69**, 334 (1991).

La réaction du 5′-aldéhyde purifié (**2***a*) (obtenu à partir de la 6-*N*-benzoyl-2′,3′-*O*-isopropylidèneadénosine (**1***a*)) avec le méthylènetriphénylphosphorane, suivie d'une déprotection à l'aide d'ammoniac et d'acide, conduit à la 9-(5,6-didésoxy-β-D-*ribo*-hex-5-énofuranosyl)adénine (5′-désoxy-5′-méthylèneadénosine) (**4**). L'oxydation de **1***a* ou de la 2′,3′-*O*-isopropylidèneadénosine (**1***b*)), suivie d'une réaction des 5′-aldéhydes bruts (**2***a* ou **2***b*) avec le (*p*-toluènesulfonylméthylène)triphénylphosphorane fournit les dérivés 5′-désoxy-5′-tosylméthylènes (**5***a* ou **5***b*) avec d'excellents rendements. On a effectué l'enlèvement des groupements tosyles du produit **5***b* à l'aide de tributylstannyllithium et on a obtenu le produit **3***b*; toutefois le clivage de la sulfone par les méthodes réductrices habituelles s'est avéré inefficace. La réduction et la déprotection des produits **5***a* ou **5***b* a fourni la 9-[5,6-didésoxy-6-(*p*-toluènesulfonyl)-β-D-*ribo*-hexofuranosyl]adénine (**6***b*). L'isomérisation du dérivé vinyl tosyl (**5***b*) en un dérivé tosylé allylique 4′,5′-insaturé (**7**) se produit dans les conditions de clivage ainsi qu'en solutions aqueuses ou organiques de bases.

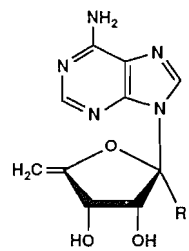
Mots clés : adénosine, 5′-désoxyadénosine, 5′-méthylène-5′-désoxyadénosine, nucléosides.

[Traduit par la rédaction]

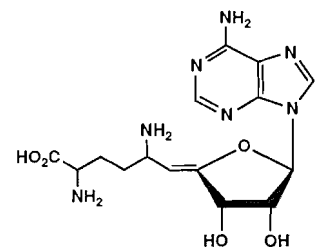
Introduction

Examples of naturally occurring 4′,5′-unsaturated nucleosides include the antibiotics angustmycin A (decoyinine) (**A**) (1–3) and A9145C (**C**), a 4′,5′-didehydrosinefungin derivative (4). Synthetic 5′-deoxy-4′,5′-didehydroadenosine (**B**) (3) was found to be accepted by *S*-adenosylhomocysteine hydrolase as an alternative substrate (5). Sinefungin and antibiotic A9145C (**C**) are inhibitors of methyl transferase enzymes, and this inhibition can be reversed by the addition of *S*-adenosylmethionine (**D**) (4). We are developing inhibitors of enzymes utilized in pathways involving *S*-adenosylmethionine metabolism and wanted to examine nucleoside analogues with unsaturated groups at C5′.

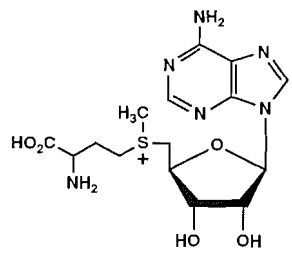
Chain extensions and other carbon–carbon bond-forming reactions at C5′ of nucleosides have generally involved oxidation to 5′-aldehyde derivatives and treatment with Wittig-type reagents, or conversions with 5′-deoxy-5′-halonucleosides (6). Wittig-type reactions of nucleoside 5′-aldehydes with electronegatively substituted ylides have provided several 6′-substituted-5′,6′-unsaturated hexofuranosyl nucleosides (7–11). However, direct introductions of alkylidene groups (particularly the methylene group) at C5′ have met with limited success, presumably owing to the instability of the 5′-aldehyde (or intermediates/products) under the experimental conditions (8, 10). Ueda and co-workers reported successful Wittig reactions of 3′,5′-*O*-(1,1,3,3-tetraisopropyldisiloxan-1,3-diyl)-2′-keto adenosine (12) and uridine (13) derivatives with methylene-



A, R = CH_2OH
B, R = H



C



D

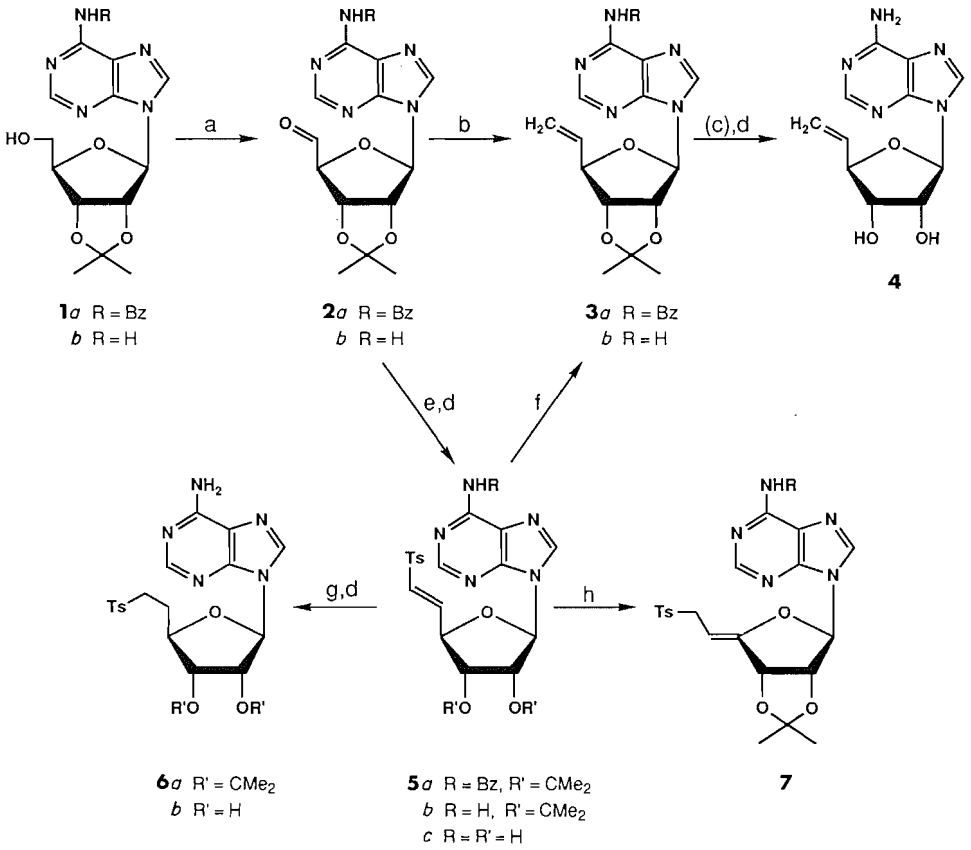
triphenylphosphorane to give 2′-deoxy-2′-methylene nucleosides. We also have developed efficient procedures for syntheses of purine and pyrimidine 2′-deoxy-2′-methylene and 3′-deoxy-3′-methylene nucleoside analogues with direct Wittig reactions (14). Seebach's silyl nitronate (nitro-aldol) methodology has been used in an efficient variation of the Henry reaction for chain extension of aldehydo sugars including a uridine 5′-aldehyde derivative (15). Barton *et al.* have developed a radical-mediated strategy that has been applied to the synthesis

[1]For the previous paper in this series see ref. 14.

[2]Author to whom correspondence may be addressed at Brigham Young University.

Printed in Canada / Imprimé au Canada

Can. J. Chem. Downloaded from www.nrcresearchpress.com by 195.138.81.100 on 09/07/12
For personal use only.



(a) Cl_2CHCO_2H/DCC/DMSO. (b) $Ph_3PCH_3Br/NaOC_5H_{11}/Et_2O/C_6H_6$/THF. (c) NH_3/MeOH. (d) CF_3CO_2H/H_2O. (e) Ph_3P=CHTs. (f) Bu_3SnLi/THF. (g) $NaBH_4$/MeOH/H_2O. (h) DBU/THF or NaOH/H_2O/CH_3CN.

SCHEME 1

of chain-lengthened nucleoside phosphonates and vinyl sulfonates (16).

A multistep synthesis of 5′-deoxy-5′-methyleneadenosine (9-(5,6-dideoxy-β-D-*ribo*-hex-5-enofuranosyl)adenine) (**4**) (Scheme 1) by conversion of D-allose to methyl 2,3-di-*O*-benzoyl-5,6-dideoxy-β-D-*ribo*-hex-5-enofuranoside, activation, coupling with the chloromercury salt of 6-benzamidopurine, and deprotection was reported in 1978 (17). We now describe two Wittig-based syntheses of **4** from adenosine, and transformations of related vinyl sulfone intermediates.

Results and discussion

Adenosine was protected, oxidized, and purified as described (18) to give the 6-*N*-benzoyl-2′,3′-*O*-isopropylidene-5′-aldehyde derivative (**2***a*). Treatment of **2***a* with methylenetriphenylphosphorane (generated (14, 19) from methyltriphenylphosphonium bromide and sodium 2-methyl-2-butoxide in benzene/ether) in tetrahydrofuran at −20°C resulted in formation of 6-*N*-benzoyl-9-(5,6-dideoxy-2,3-*O*-isopropylidene-β-D-*ribo*-hex-5-enofuranosyl)adenine (**3***a*) in 58% yield. The ^{1}H nmr spectrum of **3***a* had characteristic peaks for H6′ and H6″ at δ 5.17 and 5.27 as doublets of triplets with $J_{6'-6''} = J_{6'/6''-4'} =$ 1.3 Hz, $J_{6'-5'} = 10.4$ Hz (*cis*), and $J_{6''-5'} = 17.2$ Hz (*trans*). Removal of the benzoyl group from **3***a* with methanolic ammonia, treatment of the resulting **3***b* with aqueous trifluoroacetic acid, and purification on a column of Dowex 1 × 2 (OH^-) resin gave **4** in 36% overall yield from **2***a*.

Our second approach utilized the Wittig reaction of **2***a* with a stabilized ylid, (*p*-toluenesulfonylmethylene)triphenylphosphorane (20, 21), to give the vinyl sulfone product (**5***a*) in 85% yield. The large vinyl coupling constant ($^3J_{6'-5'} = 15$ Hz) indicated an *E* configuration for **5***a*. Treatment of crude **2***a* (from Moffatt oxidation (7, 22) of 6-*N*-benzoyl-2′,3′-*O*-isopropylideneadenosine (**1***a*)) with (*p*-toluenesulfonylmethylene)triphenylphosphorane gave the same high yield (86%) of **5***a*. Analogous oxidation of 2′,3′-*O*-isopropylideneadenosine (**1***b*) and treatment of crude **2***b* with the stabilized Wittig reagent gave **5***b* in 63% yield. It was hoped that removal of the sulfone group from **5***a* or **5***b* could be readily effected to provide a more efficient route to 5′-deoxy-5′-methyleneadenosine (**4**).

Methods for the reductive cleavage of carbon–sulfur bonds in saturated (23, 24) and α,β-unsaturated (25–27) sulfones have been reported. Unfortunately, our attempted application of these procedures to remove the *p*-toluenesulfonyl group from **5***a* or **5***b* failed to give significant quantities of **3***a* or **3***b*. The Corey sulfone cleavage (23) with sodium (24) or aluminum (25) amalgam, and the sodium dithionite procedure of Julia (26, 27) resulted primarily in rearrangement of the vinyl to allylic sulfones and recovery of starting material. Formation of more complex mixtures was observed under more vigorous conditions. Isomerization of the vinyl sulfone **5***b* to a single allylic sulfone (**7**, tentatively assigned the *Z* configuration with a less-hindered exocyclic 4′–5′ double bond) occurred under basic conditions. Formation of the allyl sulfone **7** was conveniently monitored by ultraviolet absorption spectroscopy. A major bathochromic shift and hypochromic effect were observed as the conjugated vinyl sulfone **5***b* (λ_{max} 236 nm (ε 23 500)) was converted into the allylic sulfone **7** (λ_{max} 258 nm

Can. J. Chem. Downloaded from www.nrcresearchpress.com by 195.138.81.100 on 09/07/12
For personal use only.

Can. J. Chem. Downloaded from www.nrcresearchpress.com by 195.138.81.100 on 09/07/12
For personal use only.

(ε 15 200)) in solutions of aqueous sodium hydroxide or 1,8-diazabicyclo[5.4.0]undec-7-ene (DBU) in acetonitrile or THF.

Desulfonylation of **5***b* was effected (61% yield) via conjugate addition of tributylstannyllithium (28). However, ^{1}H nmr spectra of the crude product showed contamination by the allylic sulfone **7** (5–10%). Treatment of this mixture with aqueous trifluoroacetic acid and purification on a column of Dowex 1 × 2 (OH^-) resin gave pure **4** (39%). The contaminating allylic sulfone **7**, with 4′–5′ unsaturation, suffers acid-catalyzed decomposition as expected (3) from its exocyclic vinyl ether skeleton.

Treatment of **5***b* with sodium borohydride in aqueous methanol resulted in conjugate reduction of the vinyl sulfone to give **6***a* (~75% yield). Deprotection of **6***a* with aqueous trifluoroacetic acid gave 9-[5,6-dideoxy-6-(*p*-toluenesulfonyl)-β-D-*ribo*-hexofuranosyl]adenine (**6***b*, 83%). Parallel treatment of the 6-*N*-benzoyl derivative (**5***a*) gave an equivalent yield of **6***b*. Deprotection of **5***b* proceeded without incident in aqueous trifluoroacetic acid to give 9-[5,6-dideoxy-6-(*p*-toluenesulfonyl)-β-D-*ribo*-hex-5(*E*)-enofuranosyl]adenine (**5***c*, 89%).

Thus, direct Wittig treatment of the protected adenosine 5′-aldehyde (**2***a*) with methylenetriphenylphosphorane provided the most efficient sequence to 5′-deoxy-5′-methyleneadenosine (**4**). This route circumvented complications inherent in the multistep preparation of unsaturated sugar derivatives and coupling with a nucleobase (17). A sulfonyl-stabilized Wittig reagent gave high yields of protected vinyl sulfone intermediates, but removal of the *p*-toluenesulfonyl group proved to be difficult.

Experimental

Uncorrected melting points were determined on a microstage block. The uv spectra were recorded on a Beckman Acta M IV spectrophotometer. The ^{1}H nmr spectra were recorded on Bruker WH-200 or Varian Gemini-200 spectrometers. Mass spectra (ms) were obtained with AEI MS-12 or Jeol JMS-D-100 instruments. Elemental analyses were determined by the microanalytical laboratories of the University of Alberta or Adam Mickiewicz University, Poznań. Reagents and solvents were of commercial reagent quality. Diethyl ether and tetrahydrofuran (THF) were dried by distillation from sodium benzophenone ketyl. Acetonitrile was dried by distillation from P_4O_{10}. (*p*-Toluenesulfonylmethylene)triphenylphosphorane (73% (crystallized from CH_2Cl_2/hexane), mp 182–183°C (lit. (20) mp 186–187°C; (21) mp 182–184°C) was prepared (20) from bromomethyl *p*-tolyl sulfone (21) and triphenylphosphine. Tributylstannyllithium was prepared by treatment of tributyltin chloride with excess lithium in anhydrous THF under N_2 at ambient temperature (29). 6-*N*-Benzoyl-2′,3′-*O*-isopropylideneadenosine 5′-aldehyde (**2***a*, 55%, as the dehydrated aldehyde) was prepared from 6-*N*-benzoyl-2′,3′-*O*-isopropylideneadenosine (**1***a*) with isolation of the crystalline 1,3-diphenylimidazolidine intermediate (18). Sodium 2-methyl-2-butoxide was prepared by refluxing *tert*-amyl alcohol with excess sodium beads in benzene under N_2 for 10 days (30).

*6-*N*-Benzoyl-9-(5,6-dideoxy-2,3-*O*-isopropylidene-β-D-*ribo*-hex-5-enofuranosyl)adenine* **3***a*

To a magnetically stirred suspension of methyltriphenylphosphonium bromide (464 mg, 1.3 mmol) in dry Et_2O (75 mL) in a flame-dried flask under N_2 was added a solution of sodium 2-methyl-2-butoxide (1.115 mL of a 1.13 M solution in benzene, 1.26 mmol). The bright yellow solution was stirred for 1.5 h at ambient temperature and cooled to −40°C. Dehydrated **2***a* (18) (258 mg, 0.63 mmol) in anhydrous THF (50 mL) was added by syringe and stirring continued at −20°C for 2 h and overnight at ~0°C. NH_4Cl/H_2O was added, the layers separated, and the aqueous layer extracted with $CHCl_3$. The two organic fractions were washed separately with $NaHCO_3/H_2O$ and $NaCl/H_2O$, dried (Na_2SO_4), and evaporated. The combined residues were purified by silica column chromatography (EtOAc). Evaporation of appropriately pooled fractions gave 149 mg (58%) of **3***a* as a white solid foam: uv (MeOH): max 278, 229 nm (ε 20 100, 14 100), min 246 nm (ε 12 200); ^{1}H nmr ($CDCl_3$) δ: 1.43 and 1.57 (s,s; 3,3; CH_3's), 4.71–4.78 (m, 1, H4′), 5.04 (dd, $J_{3'-2'}$ = 6.2 Hz, $J_{3'-4'}$ = 3.4 Hz, 1, H3′), 5.17 (dt, $J_{6'-4'}$ = 1.3 Hz, $J_{6'-5'}$ = 10.4 Hz (*cis*), $J_{6'-6''}$ = 1.3 Hz, 1, H6′), 5.27 (dt, $J_{6''-4'}$ = 1.3 Hz, $J_{6''-5'}$ = 17.2 Hz (*trans*), 1, H6″), 5.58 (dd, $J_{2'-1'}$ = 2 Hz, 1, H2′), 5.90 (ddd, $J_{5'-4'}$ = 6.9 Hz, 1, H5′), 6.20 (d, 1, H1′), 7.5–7.7 (m, 3, Bz), 8.05–8.16 (m, 2, Bz), 8.12 (s, 1, H2), 8.82 (s, 1, H8), 9.15 (s, 1, NH); ms *m/z*: 407 (34, M^+), 378 (100), 277 (79). Anal. calcd. for $C_{21}H_{21}N_5O_4$ (407.4): C 61.91, H 5.20, N 17.19; found: C 61.82, H 5.32, N 17.28.

*9-(5,6-Dideoxy-β-D-*ribo*-hex-5-enofuranosyl)adenine (5′-deoxy-5′-methyleneadenosine)* **4**

Removal of the benzoyl group

Saturated NH_3/MeOH (15 mL) was added to a solution of **3***a* (203 mg, 0.5 mmol) in MeOH (15 mL) and stirring was continued at ~4°C overnight. Thin-layer chromatography (tlc) ($MeOH/CHCl_3$, 7:93) showed a new polar compound and the absence of **3***a*. Evaporation of the solution gave 198 mg of crude **3***b*, which can be deprotected directly in the next step. For spectroscopic characterization this material was purified by chromatography on silica ($MeOH/CHCl_3$, 1:49) to give 140 mg (92%) of **3***b* as a white solid foam: ^{1}H nmr ($CDCl_3$) δ: 1.40 and 1.65 (s,s; 3,3; CH_3's), 4.64–4.72 (m, 1, H4′), 5.00 (dd, $J_{3'-2'}$ = 6.2 Hz, $J_{3'-4'}$ = 3.2 Hz, 1, H3′), 5.13 (dt, $J_{6'-4'}$ = 1.3 Hz, $J_{6'-5'}$ = 10.4 Hz (*cis*), $J_{6'-6''}$ = 1.2 Hz, 1, H6′), 5.25 (dt, $J_{6''-4'}$ = 1.3 Hz, $J_{6''-5'}$ = 17.2 Hz (*trans*), 1, H6″), 5.50 (dd, $J_{2'-1'}$ = 1.8 Hz, 1, H2′), 5.75 (br s, 2, NH_2), 5.90 (ddd, $J_{5'-4'}$ = 6.2 Hz, 1, H5′), 6.10 (d, 1, H1′), 7.89 (s, 1, H2), 8.35 (s, 1, H8); ms *m/z*: 303 (12, M^+), 277 (100).

Removal of the isopropylidene group

A solution of crude **3***b* (198 mg) in CF_3CO_2H/H_2O (17:3) was stirred for 20 min at ~0°C and evaporated. The residue was dissolved in EtOH, evaporated, dissolved in MeOH (5 mL), and applied to a column of Dowex 1-X2 (OH^-) resin. Elution was effected with $MeOH/H_2O$ (3:7, 500 mL; followed by 1:1, 500 mL). Evaporation of appropriately pooled fractions gave a colorless product that was recrystallized from Et_2O/EtOH to give 87 mg (62% from **3***a*) of **4**: mp 185–187°C (lit. (17) mp 190–191°C); uv (MeOH): max 259 nm (ε 15 300), min 226 nm (ε 2350); ^{1}H nmr (Me_2SO-d_6) δ: 4.10 (ddd, $J_{3'-2'}$ = 5.0 Hz, $J_{3'-4'}$ = 4.6 Hz, $J_{3'-OH3'}$ = 5.6 Hz, 1, H3′), 4.28–4.34 (m, 1, H4′), 4.65 (ddd, $J_{2'-1'}$ = 5.2 Hz, $J_{2'-OH2'}$ = 5.7 Hz, 1, H2′), 5.17 (dt, $J_{6'-4'}$ = 1.5 Hz, $J_{6'-5'}$ = 10.6 Hz (*cis*), $J_{6'-6''}$ = 1.5 Hz, 1, H6′), 5.28 (dt, $J_{6''-4'}$ = 1.5 Hz, $J_{6''-5'}$ = 17.3 Hz (*trans*), 1, H6″), 5.35 (d, 1, OH3′), 5.52 (d, 1, OH2′), 5.90 (d, 1, H1′), 6.07 (ddd, $J_{5'-4'}$ = 6.8 Hz, 1, H5′), 7.30 (br s, 2, NH_2), 8.15 (s, 1, H2), 8.30 (s, 1, H8); ms *m/z*: 263 (12, M^+), 178 (26), 104 (45), 136 (67), 135 (100), 108 (44). Anal. calcd. for $C_{11}H_{13}N_5O_3$ (263.3): C 50.19, H 4.98, N 26.60; found: C 50.32, H 5.11, N 26.49.

*6-*N*-Benzoyl-9-[5,6-dideoxy-2,3-*O*-isopropylidene-6-(*p*-toluenesulfonyl)-β-D-*ribo*-hex-5(*E*)-enofuranosyl]adenine* **5***a*

Method A

A solution of **1***a* (411 mg, 1 mmol) and dicyclohexylcarbodiimide (DCC, 619 mg, 3 mmol) in anhydrous Me_2SO (2.5 mL) was stirred with cooling (ice bath) while Cl_2CHCO_2H (0.041 mL, 65 mg, 0.5 mmol) was added. Stirring was continued at ambient temperature for 90 min and then (*p*-toluenesulfonylmethylene)triphenylphosphorane (20, 21) (516 mg, 1.2 mmol) was added. After stirring overnight, tlc indicated complete conversion to a product that migrated faster than **1***a*. Oxalic acid dihydrate (252 mg, 2 mmol) in MeOH (5 mL) was added (to hydrolyze excess DCC) and, after 20 min, *N,N′*-dicyclohexylurea was filtered and the filtrate evaporated *in vacuo*. The residue was partitioned ($EtOAc/H_2O$) and the organic layer washed with H_2O (3 × 50 mL, to remove Me_2SO), $NaHCO_3/H_2O$, and $NaCl/H_2O$, dried ($MgSO_4$), and evaporated to give a slightly yellow foam. Silica column chromatography ($MeOH/CHCl_3$, 1.25:98.75) and "diffusion

Can. J. Chem. Downloaded from www.nrcresearchpress.com by 195.138.81.100 on 09/07/12
For personal use only.

crystallization" (31) from EtOH/pentane/hexanes gave 482 nm (86%) of **5***a*: mp 106–108°C; uv (MeOH): max 279, 234 nm (ε 19 500, 29 700), min 256 nm (ε 12 800); ^{1}H nmr (Me_2SO-d_6) δ: 1.34 and 1.56 (s,s; 3,3; CH_3's), 2.38 (s, 3, $PhCH_3$), 4.95 (ddd, $J_{4'-3'}$ = 3.2 Hz, $J_{4'-5'}$ = 5.6 Hz, $J_{4'-6'}$ = 1.5 Hz, 1, H4′), 5.26 (dd, $J_{3'-2'}$ = 6.2 Hz, 1, H3′), 5.58 (dd, $J_{2'-1'}$ = 1.8 Hz, 1, H2′), 6.40 (d, 1, H1′), 6.77 (dd, $J_{6'-5'}$ = 15 Hz, 1, H6′), 6.91 (dd, 1, H5′), 7.40 (d, $J_{H_A-H_B}$ = 8.5 Hz, 2, aromatic H_A), 7.55–7.68 (m, 5, Bz), 8.07 (d, 2, aromatic H_B), 8.60 (s, 1, H2), 8.63 (s, 1, H8), 11.2 (s, 1, NH); ms (CI, NH_3) *m/z*: 562 (22, M + 1). Anal. calcd. for $C_{28}H_{27}N_5O_6S$ (561.6): C 59.88, H 4.85, N 12.47, S 5.71; found: C 60.18, H 4.86, N 12.71, S 5.58.

Method B

(*p*-Toluenesulfonylmethylene)triphenylphosphorane (537 mg, 1.25 mmol) in dry CH_3CN (20 mL) was added dropwise to a stirred solution of dehydrated **2***a* (18) (0.41 g, 1 mmol) in dry CH_3CN (5 mL) under N_2 and stirring was continued at ambient temperature for 10 h. The solution was evaporated to give a white solid that was purified by silica column chromatography and crystallized as in Method A to give 477 mg (85%) of **5***a* with identical physical and spectral data.

*9-[5,6-Dideoxy-2,3-*O*-isopropylidene-6-(*p*-toluenesulfonyl)-β-*D*-*ribo*-hex-5(*E*)-enofuranosyl]adenine* **5**b

Treatment of **1***b* (307 mg, 1 mmol) by Method A (as described above for **5***a*) gave 288 mg (63%) of **5***b* (after diffusion crystallization (31) from EtOAc/hexanes): mp 114–116°C; uv (MeOH): max 257, 236 nm (ε 16 600, 23 500), min 252, 222 nm (ε 16 000, 16 500); ^{1}H nmr (Me_2SO-d_6) δ: 1.32 and 1.53 (s,s; 3,3; CH_3's), 2.40 (s, 3, $PhCH_3$), 4.88 (ddd, $J_{4'-3'}$ = 3.3 Hz, $J_{4'-5'}$ = 6.0 Hz, $J_{4'-6'}$ = 1.25 Hz, 1, H4′), 5.20 (dd, $J_{3'-2'}$ = 6.0 Hz, 1, H3′), 5.49 (dd, $J_{2'-1'}$ = 2.0 Hz, 1, H2′), 6.26 (d, 1, H1′), 6.74 (dd, $J_{6'-5'}$ = 15 Hz, 1, H6′), 6.90 (dd, 1, H5′), 7.34 (s, 2, NH_2), 7.39 (d, $J_{H_A-H_B}$ = 8.5 Hz, 2, aromatic H_A), 7.58 (d, 2, aromatic H_B), 8.01 (s, 1, H2), 8.27 (s, 1, H8); ms *m/z*: 457.1406 (0.4, M^+ (calcd. for $C_{21}H_{23}N_5O_5S$ = 457.1419)), 442.1172 (1.8, M − CH_3), 302.1254 (100, M − Ts). Anal. calcd. for $C_{21}H_{23}N_5O_5S$ (457.5): C 55.13, H 5.07, N 15.13; found: C 55.27, H 5.11, N 15.37.

Desulfonylation of **5**b *to give 9-(5,6-dideoxy-2,3-*O*-isopropylidene-β-*D*-*ribo*-hex-5-enofuranosyl)adenine* **4**

A solution of **5***b* (183 mg, 0.4 mmol) in anhydrous THF (6 mL) was added to a stirred solution of tributylstannyllithium (29) (1.2 mL of a 1 M solution in anhydrous THF, 1.2 mmol) under N_2 at −78°C. After 1 h, $CHCl_3$ (10 mL) and silica gel (0.9 g; Merck 60, 200–400 mesh) were added and the resulting mixture stirred at ambient temperature for 20 h. The silica gel was filtered, washed with $CHCl_3$ (2 × 10 mL), and the combined mother liquors shaken with NH_4Cl/H_2O (15 mL) and $CHCl_3$ (10 mL). The organic layer was washed with $NaHCO_3/H_2O$ and $NaCl/H_2O$, dried ($MgSO_4$), and evaporated to give a yellow foam. Silica column chromatography (MeOH/$CHCl_3$, 1.75:98.25) of this material gave 74 mg (61%) of **3***b* as a white solid foam. The ^{1}H nmr spectrum of this tlc-homogeneous product had peaks identical to those noted above for **3***b*, but also had other peaks (5–10% integrated intensity) corresponding to the allyl-tosyl compound **7**. Deprotection of this material and purification (as described above for pure **3***b*) gave 41 mg (39%) of **4** with identical physical and spectral data.

*9-[5,6-Dideoxy-6-(*p*-toluenesulfonyl)-β-*D*-*ribo*-hex-5(*E*)-enofuranosyl]adenine* **5**c

A solution of **5***b* (137 mg, 0.3 mmol) in CF_3CO_2H/H_2O (17:3, 5 mL) was stirred for 20 min at ~0°C, evaporated, and coevaporated with EtOH. Crystallization and recrystallization of the residue from EtOH/hexanes gave 111 mg (89%) of **5***c*: mp 128–130°C; uv (MeOH): max 259, 239 nm (ε 16 700, 22 800), min 256, 223 nm (ε 16 500, 14 800); ^{1}H nmr (Me_2SO-d_6) δ: 2.38 (s, 3, $PhCH_3$), 4.26 (ddd, $J_{3'-2'}$ = 5.1 Hz, $J_{3'-4'}$ = 4.1 Hz, $J_{3'-OH3'}$ = 5.6 Hz, 1, H3′), 4.57 (dd, $J_{4'-5'}$ = 4.7 Hz, 1, H4′), 4.74 (ddd, $J_{2'-1'}$ = 5.4 Hz, $J_{2'-OH2'}$ = 5.5 Hz, 1, H2′), 5.58 (d, 1, OH3′), 5.60 (d, 1, OH2′), 5.94 (d, 1, H1′), 6.92 (d, $J_{6'-5'}$ = 15.1 Hz, 1, H6′), 7.07 (dd, 1, H5′), 7.43 (d, $J_{H_A-H_B}$ = 8.8 Hz, 2, aromatic H_A), 7.72 (d, 2, aromatic H_B), 7.91 (br s, 2, NH_2), 8.08 (s, 1, H2), 8.43 (s, 1, H8); ms *m/z*: 417 (1, M^+), 358 (3), 278 (10), 156 (14), 139 (32), 135 (100). Anal. calcd. for $C_{18}H_{19}N_5O_5S$ (417.4): C 51.79, H 4.59, N 16.78; found: C 51.66, H 4.39, N 16.61.

*9-[5,6-Dideoxy-2,3-*O*-isopropylidene-6-(*p*-toluenesulfonyl)-β-*D*-*ribo*-hexofuranosyl]adenine* **6**a

To a magnetically stirred solution of **5***b* (274 mg, 0.6 mmol) in $MeOH/H_2O$ (2:1, 30 mL) was added sodium borohydride (45 mg, 1.2 mmol). After stirring for 16 h at ambient temperature, the solution was concentrated to one-half volume and $CHCl_3$ (20 mL) and H_2O (10 mL) were added. The organic layer was separated and the aqueous layer washed with $CHCl_3$ (10 mL). The combined organic phase was washed with $NaCl/H_2O$ and H_2O, dried ($MgSO_4$), and evaporated to give a slightly yellow solid foam that was purified by silica column chromatography (MeOH/$CHCl_3$, 1.5:98.5). Evaporation of appropriately pooled fractions gave 208 mg (76%) of **6***a* as a tlc-homogeneous white solid that could be deprotected directly in the next step; ^{1}H nmr (Me_2SO-d_6) δ: 1.20 and 1.42 (s,s; 3,3; CH_3's), 1.80–1.98 (m, 2, H5′,5″), 2.33 (s, 3, $PhCH_3$), 3.10–3.45 (m, 2, H6′,6″), 4.08–4.16 (m, 1, H4′), 4.83 (dd, $J_{3'-2'}$ = 6.0 Hz, $J_{3'-4'}$ = 3.0 Hz, 1, H3′), 5.36 (dd, $J_{2'-1'}$ = 2.2 Hz, 1, H2′), 5.99 (d, 1, H1′), 7.27 (s, 2, NH_2), 7.31 (d, $J_{H_A-H_B}$ = 8.5 Hz, 2, aromatic H_A), 7.50 (d, 2, aromatic H_B), 7.97 (s, 1, H2), 8.16 (s, 1, H8); ms *m/z*: 459 (4, M^+), 444 (12), 401 (36), 304 (100).

Compound **5***a* was reduced with $NaBH_4$ by the same procedure to give **6***a* in the same yield.

*9-[5,6-Dideoxy-6-(*p*-toluenesulfonyl)-β-*D*-ribo-hexofuranosyl]adenine* **6**b

A solution of **6***a* (161 mg, 0.35 mmol) in CF_3CO_2H/H_2O (17:3, 5 mL) was stirred for 25 min at ~0°C, evaporated, and coevaporated with EtOH to give an amorphous glass. Crystallization and recrystallization from MeOH gave 122 mg (83%) of **6***b* (two crops): mp 158–160°C; uv (MeOH): max 261, 223 nm (ε 15 400, 15 600), min 240 nm (ε 7300); ^{1}H nmr (Me_2SO-d_6) δ: 1.90–2.03 (m, 2, H5′,5″), 2.38 (s, 3, $PhCH_3$), 3.20–3.43 (m, 2, H6′,6″), 3.88–3.98 (m, 1, H4′), 4.09 (dd, $J_{3'-2'}$ = 5.6 Hz, $J_{3'-4'}$ = 4.0 Hz, 1, H3′), 4.59 (dd, $J_{2'-1'}$ = 4.8 Hz, 1, H2′), 5.30 (br s, 2, OH2′, OH3′), 5.84 (d, 1, H1′), 7.41 (d, $J_{H_A-H_B}$ = 8.5 Hz, 2, aromatic H_A), 7.76 (d, 2, aromatic H_B), 8.26 (s, 1, H2), 8.50 (s, 1, H8), 8.52 (s, 2, NH_2); ms *m/z*: 419 (0.5, M^+), 278 (8), 246 (100), 157 (18), 139 (30), 135 (42). Anal. calcd. for $C_{18}H_{21}N_5O_5S$ (419.5): C 51.54, H 5.05, N 16.70; found: C 51.29, H 4.96, N 16.79.

*9-[5,6-Dideoxy-2,3-*O*-isopropylidene-6-(*p*-toluenesulfonyl)-β-*D*-erythro-hex-4(*Z*)-enofuranosyl]adenine* **7**

To a stirred solution of **5***b* (183 mg, 0.4 mmol) in CH_3CN/H_2O (4:1, 10 mL) was added 1 M $NaOH/H_2O$ (1 mL). (Alternatively, THF (10 mL) as solvent and DBU (0.06 mL, 60 mg, 0.4 mmol as base can be used.) After 4 h at ambient temperature, the solution was concentrated to one-half volume and EtOAc (10 mL) and HCl/H_2O (0.05 M, 2 mL) were added. The organic layer was separated and the aqueous layer washed with EtOAc (2 × 10 mL). The combined organic phase was washed with $NaHCO_3/H_2O$, $NaCl/H_2O$, and H_2O, dried ($MgSO_4$), and evaporated to a white foam that was crystallized from EtOH/hexanes to give 163 mg (89%) of **7**: mp 115–116°C; uv (MeOH): max 258, 227 nm (ε 15 200, 13 900), min 240 nm (ε 9700); ^{1}H nmr ($CDCl_3$) δ: 1.39 and 1.48 (s,s; 3,3; CH_3's), 2.35 (s, 3, $PhCH_3$), 3.83 (d, $J_{6'/6''-5'}$ = 8 Hz, 2, H6′,6″), 4.81 (t, 1, H5′), 5.19 (d, $J_{3'-2'}$ = 6 Hz, 1, H3′), 5.62 (d, 1, H2′), 6.02 (s, 2, NH_2), 6.14 (s, 1, H1′), 7.16 (d, $J_{H_A-H_B}$ = 8.5 Hz, 2, aromatic H_A), 7.67 (d, 2, aromatic H_B), 7.74 (s, 1, H2), 8.14 (s, 1, H8); ms *m/z*: 442.1178 (1.7, M − CH_3 [$C_{20}H_{20}N_5O_5S$] = 442.1185), 302.1257 (100, M − Ts). Anal. calcd. for $C_{21}H_{23}N_5O_5S$ (457.5): C 55.13, H 5.07, N 15.31, S 7.01; found: C 55.03, H 5.09, N 15.08, S 7.12.

Acknowledgements

We thank the American Cancer Society (Grant No. CH-405), the Natural Sciences and Engineering Research Council of Canada, Brigham Young University development funds, and

the Academy of Agriculture for generous support. We thank Mrs. Kathryn M. Rollins for assistance with the manuscript.

1. R. J. SUHADOLNIK. Nucleoside antibiotics. Wiley–Interscience, New York. 1970. pp. 115–119.
2. R. J. SUHADOLNIK. Nucleosides as biological probes. Wiley–Interscience, New York. 1979. pp. 279–281.
3. J. R. MCCARTHY, JR., R. K. ROBINS, and M. J. ROBINS. J. Am. Chem. Soc. **90**, 4993 (1968).
4. R. J. SUHADOLNIK. Nucleosides as biological probes. Wiley–Interscience, New York. 1979. pp. 19–23.
5. J. L. PALMER and R. H. ABELES. J. Biol. Chem. **254**, 1217 (1979).
6. J. G. MOFFATT. *In* Nucleoside analogues: chemistry, biology, and medical applications. *Edited by* R. T. Walker, E. De Clercq, and F. Eckstein. Plenum Press, New York. 1979. pp. 71–164.
7. G. H. JONES and J. G. MOFFATT. J. Am. Chem. Soc. **90**, 5337 (1968).
8. P. HOWGATE, A. S. JONES, and J. R. TITTENSOR. Carbohydr. Res. **12**, 403 (1970).
9. J. A. MONTGOMERY, A. G. LASETER, and K. HEWSON. J. Heterocycl. Chem. **11**, 211 (1974).
10. R. A. SHARMA and M. BOBEK. J. Org. Chem. **43**, 367 (1978).
11. J. M. J. TRONCHET and M. J. VALERO. Helv. Chim. Acta, **62**, 2788 (1979).
12. H. USUI and T. UEDA. Chem. Pharm. Bull. **34**, 1518 (1986).
13. K. TAKENUKI, A. MATSUDA, T. UEDA, T. SASAKI, A. FUJII, and K. YAMAGAMI. J. Med. Chem. **31**, 1063 (1988).
14. V. SAMANO and M. J. ROBINS. Synthesis. In press.
15. O. R. MARTIN, F. E. KHAMIS, H. A. EL-SHENAWY, and S. P. RAO. Tetrahedron Lett. **30**, 6139 (1989).
16. (*a*) D. H. R. BARTON, S. D. GÉRO, B. QUICLET-SIRE, and M. SAMADI. J. Chem. Soc. Chem. Commun. 1372 (1988); (*b*) J. Chem. Soc. Chem. Commun. 1000 (1989); (*c*) Tetrahedron Lett. **30**, 4969 (1989).
17. L. M. LERNER. J. Org. Chem. **43**, 2469 (1978).
18. R. S. RANGANATHAN, G. H. JONES, and J. G. MOFFATT. J. Org. Chem. **39**, 290 (1974).
19. J.-M. CONIA and J.-C. LIMASSET. Bull. Soc. Chim. Fr. 1936 (1967).
20. A. J. SPEZIALE and K. W. RATTS. J. Am. Chem. Soc. **87**, 5603 (1965).
21. A. M. VAN LEUSEN, B. A. REITH, A. J. W. IEDEMA, and J. STRATING. Recl. Trav. Chim. Pays-Bas, **91**, 37 (1972).
22. K. E. PFITZNER and J. G. MOFFATT. J. Am. Chem. Soc. **85**, 3027 (1963).
23. E. J. COREY and M. CHAYKOVSKY. J. Am. Chem. Soc. **87**, 1345 (1965).
24. B. M. TROST, H. C. ARNDT, P. E. STREGE, and T. R. VERHOEVEN. Tetrahedron Lett. **17**, 3477 (1976).
25. V. PASCALI and A. UMANI-RONCHI. J. Chem. Soc. Chem. Commun. 351 (1973).
26. J. BREMNER, M. JULIA, M. LAUNAY, and J. P. STACINO. Tetrahedron Lett. **23**, 3256 (1982).
27. M. JULIA, .H. LAURON, J. P. STACINO, J. N. VERPEAUX, Y. JEANNIN, and Y. DROMZEE. Tetrahedron, **42**, 2475 (1986).
28. M. OCHIAI, T. UKITA, and E. FUJITA. J. Chem. Soc. Chem. Commun. 351 (1983).
29. C. TAMBORSKI, F. E. FORD, and E. J. SOLOSKI. J. Org. Chem. **28**, 237 (1963).
30. L. F. FIESER and M. FIESER. Reagents for organic synthesis. Vol. 1. Wiley, New York. 1967. p. 1096.
31. M. J. ROBINS, R. MENGEL, R. A. JONES, and Y. FOURON. J. Am. Chem. Soc. **98**, 8204 (1976).

Can. J. Chem. Downloaded from www.nrcresearchpress.com by 195.138.81.100 on 09/07/12
For personal use only.

The aldol condensation of acetophenone with acetone

J. PETER GUTHRIE[1] AND XIAO-PING WANG
Department of Chemistry, University of Western Ontario, London, Ont., Canada N6A 5B7

Received January 26, 1990[2]

J. PETER GUTHRIE and XIAO-PING WANG. Can. J. Chem. **69**, 339 (1991).

The kinetics and equilibria involved in the aldol condensation of acetophenone, acting as carbon acid, and acetone have been studied in aqueous alkaline solution. The reactions are all first order in hydroxide, with rate and equilibrium constants (defined for enone as initial compound) of: $k_{12} = 3.3 \times 10^{-4}\ M^{-1}\ s^{-1}$, $k_{21} = 3.2 \times 10^{-5}\ M^{-1}\ s^{-1}$, $K_{12} = 10.2$, $k_{23} = 8.0 \times 10^{-2}\ M^{-1}\ s^{-1}$, $k_{32} = 3.3 \times 10^{-4}\ M^{-2}\ s^{-1}$, $K_{32} = 4.1 \times 10^{-3}\ M^{-1}$. The series methylbutenal, mesityl oxide, and 3-methyl-1-phenyl-2-buten-1-one can now be compared with regard to regularities and deviations from regularity. The related series cinnamaldehyde, benzalacetone, and chalcone also provides insights into the behaviour of this system.

Key words: aldol, dehydration, equilibrium, acetophenone, acetone.

J. PETER GUTHRIE et XIAO-PING WANG. Can. J. Chem. **69**, 339 (1991).

Opérant en solution aqueuse alcaline, on a étudié la cinétique et l'équilibre impliqué dans la condensation aldolique de l'acétophénone, agissant comme acide carboné, et de l'acétone. Les réactions sont du premier ordre en ion hydroxyde; les constantes de vitesse et d'équilibre (définies pour l'apparition de l'énone) sont $k_{12} = 3{,}3 \times 10^{-4}\ M^{-1}\ s^{-1}$, $k_{21} = 3{,}2 \times 10^{-5}\ M^{-1}\ s^{-1}$, $K_{12} = 10{,}2$, $k_{23} = 8{,}0 \times 10^{-2}\ M^{-1}\ s^{-1}$, $k_{32} = 3{,}3 \times 10^{-4}\ M^{-2}\ s^{-1}$, $k_{32} = 4{,}1 \times 10^{-3}\ M^{-1}$. On peut maintenant comparer la série méthylbuténal, oxyde de mésityle et 3-méthyl-1-phénylbutèn-3-one-1 et déterminer les régularités ainsi que les déviations de la régularité. La série apparentée du cinnamaldéhyde, de la benzalacétone et de la chalcone éclaire aussi le comportement de ce système.

Mots clés : aldol, déshydratation, équilibre, acétophénone, acétone.

[Traduit par la rédaction]

Can. J. Chem. Downloaded from www.nrcresearchpress.com by 195.138.81.100 on 09/07/12
For personal use only.

Introduction

We have studied various examples of simple aldol condensations (1–7). Although previously studied cases include both conjugated (5–9) and non-conjugated enones (2–4), there has been no detailed study of a cross-conjugated system where a ketone such as acetophenone acts as carbon nucleophile towards an unconjugated aldehyde or ketone in the aldol reaction. Chalcone has been studied (5, 9) but in this case there is through-conjugation by the phenyl derived from benzaldehyde as well as cross-conjugation for the phenyl derived from acetophenone. The present case allows us to assess the effects of cross-conjugation uncomplicated by competing through-conjugation. This system was also of interest to us in connection with enzyme model studies (10, 11), so it seemed appropriate to investigate it carefully. We also wished to compare a series of related enones, which have now been studied, namely 3-methyl-2-butenal, mesityl oxide (4-methyl-3-penten-2-one), and 3-methyl-1-phenyl-2-buten-1-one, the present compound. We have already seen effects of crowding on the rates and equilibria of the steps in the overall condensation in the series propenal, 2-butenal, and 3-methyl-2-butenal. One would expect similar but larger effects in the present series.

Results

The retroaldol cleavage of 3-methyl-1-phenyl-2-buten-1-one is expected to involve two stages, hydration of the enone followed by retroaldol cleavage of the ketol. This mechanism frequently leads to biphasic kinetics. In the present case the observed behavior was deceptively simple.

[1] $\text{Ph-CO-CH=C(CH}_3)_2 \rightleftharpoons \text{Ph-CO-CH}_2\text{-C(OH)(CH}_3)_2 \rightleftharpoons \text{Ph-CO-CH}_3 + \text{CO(CH}_3)_2$

The kinetics of the retroaldol reaction of the enone, 3-methyl-1-phenyl-2-buten-1-one, could be followed conveniently by UV spectroscopy. The reaction exhibited simple first-order behavior, with no sign of the two-phase behavior that might have been expected for a reaction proceeding by an addition, retroaldol cleavage sequence. The rate constants that we measured are found in Table 1(a). The apparent rate constants showed a first-order dependence on hydroxide concentration, leading to a second-order rate constant of $(3.26 \pm 0.30) \times 10^{-4}\ M^{-1}\ s^{-1}$.

The kinetics of the breakdown of the ketol, 3-hydroxy-3-methyl-1-phenyl-1-butanone, were also studied in hopes of being able to detect formation of the enone and so determine the partitioning ratio for the ketol. However, we found that the ketol also showed only simple first-order kinetics behavior, with no detectable formation of the enone. The rate constants that we measured are also found in Table 1(b). Here too the apparent rate constants were first order in hydroxide concentration, leading to a second-order rate constant of $(8.04 \pm 0.71) \times 10^{-2}\ M^{-1}\ s^{-1}$.

Clearly, dehydration of the ketol is slow relative to retroaldol cleavage. Since we see no sign of biphasic kinetics with either enone or ketol as starting material, we cannot evaluate k_{21} directly.

To evaluate k_{21}, we determined the equilibrium constant for hydration of the enone in acid where retroaldol cleavage is slow relative to establishment of hydration equilibrium. This shift in relative rates was expected on the basis of several literature analogies (12–14).

For the kinetic model

$$A_1 \underset{k_{21}}{\overset{k_{12}}{\rightleftharpoons}} A_2 \xrightarrow{k_{23}} A_3$$

where A_1 = enone, A_2 = ketol, A_3 = acetone + acetophenone, we may derive (15) the following rigorously correct equation for the absorbance A as a function of time for reaction starting with

[1]Author to whom correspondence may be addressed.
[2]Revision received October 17, 1990.

TABLE 1. Kinetics of base-catalyzed retroaldol cleavage reactions[a]

(a) Starting with the enone, 3-methyl-1-phenyl-2-buten-1-one:

$[OH^-]$	α	β	$\lambda_3 \times 10^4$ (s^{-1})	$\lambda_3/[OH^-] \times 10^4$ ($M^{-1}\ s^{-1}$)
0.0954[b]	1.861	−0.269	0.294±0.0008	3.08±0.008
0.480[b,c]	1.824	−0.253	1.61±0.020	3.35±0.042
0.285[b,c]	1.818	−0.243	0.883±0.008	3.10±0.030
0.969[b,c]	1.815	−0.276	3.49±0.018	3.60±0.019
0.714[b,c]	1.841	−0.307	2.64±0.157	3.70±0.015
			avg.	3.26±0.30

(b) Starting with the ketol, 3-hydroxy-3-methyl-1-phenyl-1-butanone:

$[OH^-]$	α	β	$\lambda_2 \times 10^3$ (s^{-1})	$\lambda_2/[OH^-] \times 10^2$ ($M^{-1}\ s^{-1}$)
0.102[d]	1.723	−0.0988	8.75±0.07	8.58±0.07
0.102[e]	1.578	0.1046	6.07±0.247	5.95±0.24
0.102[f]	0.653	0.2919	5.49±0.17	5.38±0.17
0.0192[e]	1.503	0.0715	1.35±0.013	7.03±0.07
0.0192[d]	1.611	−0.0974	1.63±0.02	8.49±0.10
0.0192[g]	1.600	−0.0740	0.941±0.084	4.90±0.44
0.0192[h]	1.134	0.1794	1.58±0.013	8.23±0.07
0.005[h]	1.131	0.1843	0.442±0.0038	8.84±0.08
0.005[d]	1.555	−0.1075	0.437±0.0068	8.74±0.14
0.005[f]	0.636	0.2419	0.407±0.0017	8.14±0.03
0.0073[f]	0.639	0.2353	0.621±0.003	8.51±0.04
0.0073[h]	1.122	0.2002	0.559±0.003	7.66±0.04
0.0073[d]	1.652	−0.1065	0.735±0.016	10.00±0.22
0.0073[e]	1.512	0.0248	0.613±0.208	8.40±2.85
0.0073[d]	1.658	−0.1262	0.407±0.008	5.58±0.11
			avg.	8.04±0.71

[a]In aqueous solution at 25°C, ionic strength 0.1 (KCl) unless otherwise noted. Absorbance–time data were fitted to $A = \alpha + \beta \exp(-\lambda_i t)$ by non-linear least squares. We use λ_2 for the faster process, and λ_3 for the slower one to emphasize that the two kinds of experiment measure different phases of the expected double exponential integrated rate law. Standard deviations for the parameters are calculated by the least-squares procedure. Average values are weighted means.
[b]Followed at 247.5 nm.
[c]Ionic strength 1.0 (KCl).
[d]Followed at 243 nm.
[e]Followed at 250 nm.
[f]Followed at 260 nm.
[g]Followed at 245 nm.
[h]Followed at 255 nm.

the enone:

$$[2]\quad A = [A_1]\epsilon_1 + [A_2]\epsilon_2 + [A_3]\epsilon_3$$
$$= \{[A_1]^0 k_{12}/\lambda_2\}\{\epsilon_1(\lambda_2 - k_{23})/(\lambda_2 - \lambda_3) - \epsilon_2 + \epsilon_3 k_{23}/(\lambda_2 - \lambda_3)\}\exp(-\lambda_2 t) + \{[A_1]^0 k_{12}/(\lambda_2 - \lambda_3)\}\{\epsilon_1(k_{23} - \lambda_3)/\lambda_3 + \epsilon_2 - \epsilon_3 k_{23}/\lambda_3\}\exp(-\lambda_3 t) + \epsilon_3[A_1]^0$$

where $\lambda_2 = (p + q)/2$, $\lambda_3 = (p - q)/2$, $p = k_{12} + k_{21} + k_{23}$, $q = (p^2 - 4k_{12}k_{23})^{1/2}$.

There are two interesting special cases. The first pertains to reaction in acid where the hydration–dehydration equilibrium is established rapidly with respect to retroaldol cleavage. Then if k_{23} (and λ_3) are negligible relative to k_{12}, k_{21} and $\lambda_2 \approx k_{12} + k_{21}$, eq. [1] can be simplified to

$$A = \epsilon_1\{[A_1]^0 k_{21}/\lambda_2\} + \epsilon_2\{[A_1]^0 k_{12}/\lambda_2\} + (\epsilon_1 - \epsilon_2)\{[A_1]^0 k_{12}/\lambda_2\}\exp(-\lambda_2 t)$$
$$= \alpha + \beta \exp(-\lambda_2 t)$$

Defining K_{12} as the equilibrium constant for hydration, $K_{12} = k_{12}/k_{21}$, we see that

$$\alpha = [A_1]^0\{\{\epsilon_1 k_{21}/\lambda_2\} + \{\epsilon_2 k_{12}/\lambda_2\}\}$$
$$= [A_1]^0\{\epsilon_1/(1 + K_{12}) + \epsilon_2/(1 + 1/K_{12})\}$$

$$[3]\quad K_{12} = (\epsilon_2[A_1]^0 - \alpha)/(\alpha - \epsilon_2[A_1]^0)$$
$$\beta = [A_1]^0(\epsilon_1 - \epsilon_2)/(1 + /K_{12})$$
$$\alpha + \beta = \epsilon_1[A_1]^0$$
$$[A_1]^0 = (\alpha + \beta)/\epsilon_1$$

$$[4]\quad K_{12} = 1/[(\alpha/\beta)(1 - \epsilon_2/\epsilon_1) - \epsilon_2/\epsilon_1]$$

The second special case pertains to reaction in base where $k_{23} \gg k_{12}$, k_{21}. Under these circumstances, $\lambda_2 \approx k_{23}$, $\lambda_3 \approx k_{12}$, and eq. [1] becomes

$$A = [A_1]^0\epsilon_3 + (\epsilon_1 - \epsilon_3)\exp(-\lambda_3 t)$$
$$= \alpha + \beta \exp(-\lambda_3 t)$$

which is the equation one would derive for a single step reaction starting with A_1. Only the exponential in λ_3 is observable because the pre-exponential term for λ_2, approximately $[A_1]^0 k_{12}(\epsilon_1 - \epsilon_2)/k_{23}$, is very small. Thus the experimental data lead directly to k_{12}.

Similarly we may derive a rigorously correct equation for the absorbance as a function of time starting with the ketol:

$$[5]\quad A = \epsilon_1[A_1] + \epsilon_2[A_2] + \epsilon_3[A_3]$$
$$= \{[A_2]^0/(\lambda_2 - \lambda_3)\}\{-\epsilon_1 k_{21} - \epsilon_2(k_{12} - \lambda_2) + \epsilon_3(\lambda_3 - k_{23})\}\exp(-\lambda_2 t) + \{[A_2]^0/(\lambda_2 - \lambda_3)\}\{\epsilon_1 k_{21} + \epsilon_2(k_{12} - \lambda_3) - \epsilon_3(\lambda_2 - k_{23})\}\exp(-\lambda_3 t) + [A_2]^0\epsilon_3$$

Here also there are two special cases of interest. In the case of acid-catalyzed reactions, where $k_{23} \ll k_{21}$, k_{12}, and $\lambda_2 \approx k_{12} + k_{21}$, eq. [4] can be simplified to

$$A = [A_2]^0(\epsilon_1 k_{21} + \epsilon_2 k_{12})/\lambda_2 + [A_2]^0(\epsilon_2 - \epsilon_1)(k_{21}/\lambda_2)\exp(-\lambda_2 t)$$
$$= \alpha + \beta \exp(-\lambda_2 t)$$

and

$$K_{12} = (\epsilon_2[A_2]^0 - \alpha)/(\alpha - \epsilon_2[A_2]^0)$$
$$[A_2]^0 = (\alpha + \beta)/\epsilon_2$$

K_{12} was calculated from the least-squares parameters, using eq. [4].

In the case of base-catalyzed reactions, where $k_{23} \gg k_{12}$, k_{21}, $\lambda_2 \approx k_{23}$, $\lambda_3 \approx k_{12}$, and eq. [5] becomes

$$A = [A_2]^0\epsilon_3 + [A_2]^0\epsilon_1 k_{21}/k_{23} + [A_2]^0(\epsilon_2 - \epsilon_3 - \epsilon_1 k_{21}/k_{23})\exp(-\lambda_2 t)$$

For this condition the major reaction path for ketol is breakdown to acetone and acetophenone (k_{23}) with dehydration being a very minor side reaction. Thus the second phase controlled by λ_3 is both slow and of very small amplitude; the pre-exponential term for λ_3 is approximately $[A_2]^0\epsilon_1 k_{21}/k_{23}$. Provided that $\epsilon_1 k_{21}/k_{23} \ll \epsilon_1$, ϵ_2 we can further simplify the equation to

$$A = [A_2]^0\epsilon_3 + [A_2]^0(\epsilon_2 - \epsilon_3)\exp(-\lambda_2 t)$$
$$= \alpha + \beta \exp(-\lambda_2 t)$$

Substitution of the values derived from our analysis shows that the approximations employed are valid. For reactions starting with the ketol, the experimental data lead directly to k_{23}.

We measured rates of approach to hydration equilibrium in

Can. J. Chem. Downloaded from www.nrcresearchpress.com by 195.138.81.100 on 09/07/12
For personal use only.

TABLE 2. Kinetics of acid-catalyzed hydration–dehydration reactions[a]

(a) Starting with ketol, 3-hydroxy-3-methyl-1-phenyl-1-butanone:

[Ketol] $\times 10^5$	[HCl]	α	β	λ $\times 10^5$	$\lambda/[H^+]$ $\times 10^5$	K_{12}
1.55	1.011	0.842	−0.140	4.67±0.036	4.62±0.036	12.62
1.55	1.011	0.857	−0.161	4.22±0.040	4.17±0.040	10.74
0.873	0.952	0.440	−0.090	2.90±0.026	3.05±0.027	9.53
0.897	0.952	0.459	−0.091	3.36±0.23	3.53±0.24	10.01
					avg. 3.74±0.81	10.72±1.17

(b) Starting with enone, 3-methyl-1-phenyl-2-buten-1-one:

[Enone] $\times 10^5$	[HCl]	α	β	λ $\times 10^5$	$\lambda/[H^+]$ $\times 10^5$	K_{12}
0.847	1.001	0.545	1.139	3.72±0.0032	3.72±0.0032	12.40
1.485	0.952	1.001	1.847	3.52±0.010	3.70±0.011	7.87
0.895	0.952	0.508	0.959	3.50±0.059	3.68±0.062	8.47
					avg. 3.72±0.007	9.58±2.01

[a]In aqueous solution at 25°C, followed at 266 nm. Absorbance–time data were fitted to $A = \alpha + \beta \exp(-\lambda t)$ by non-linear least squares. Standard deviations for the parameters are calculated by the least-squares procedure. K_{12} = [ketol]/[enone] is the equilibrium constant for hydration of the enone. The average for $\lambda/[H^+]$ is the weighted mean; for K_{12} it is the simple mean.

TABLE 3. Kinetics of base-catalyzed enone formation reactions[a]

[Acetophenone]	[Acetone]	[OH]	α (mm)	β (mm)	λ $\times 10^5$ (s^{-1})	K_{31} $\times 10^4$ (M^{-1})
0.0101[b]	0.213	0.1	30.2	−26.3	1.88±0.39	3.68
0.0103[b]	0.528	0.1	77.6	−68.7	1.77±0.17	3.80
0.0103[b]	0.723	0.1	112.	−100.	1.62±0.21	4.01
0.0102[b,c]	0.972	0.1	156.	−139.	1.59±0.37	4.22
0.0122[b,c,d]	1.054	0.1	12.5	173.	1.68±0.046	4.08
0.010[e]	1.083	0.102	212.	−212.	2.30±0.37	3.93
0.00885[e]	1.083	0.102	145.	−143.	3.01±0.14	5.10
0.0085[e]	1.08	0.100	133.	−133.	3.25±0.25	4.27
0.0085[e]	0.810	0.100	84.	−84.	3.49±0.30	2.85
						avg. 3.99±0.56[f]
						4.04±0.81[g]

[a]In aqueous solution, ionic strength 0.1, followed by HPLC analysis on quenched samples; growth or disappearance of the peak due to 3-methyl-1-phenyl-2-buten-1-one was followed. Data were fitted to: peak height (mm) = $\alpha + \beta \exp(-\lambda t)$.

[b]Reactions carried out at room temperature.

[c]Included in Fig. 1.

[d]Initial enone concentration was 1.3×10^{-4} M.

[e]Reactions carried out at 25.0°C.

[f]All experiments.

[g]Experiments at 25.0°C.

acidic solutions and demonstrated by HPLC analysis that at the end of the initial kinetics process, as followed by UV spectroscopy, there was only a small amount of acetophenone present. Furthermore, the proportions of enone and ketol were the same whether reaction started with the enone or the ketol. The kinetics data are found in Table 2. The hydration reaction went to equilibrium, following first-order behavior, with a rate constant in 1 N HCl of $(3.74 \pm 0.81) \times 10^{-5}$ s^{-1} (starting from ketol), or $(3.72 \pm 0.007) \times 10^{-5}$ s^{-1} (starting from the enone). Combining all the data we obtain $(3.72 \pm 0.12) \times 10^{-5}$ s^{-1}. There was a slower subsequent change in absorbance. The equilibrium constant, K_{12} = [ketol]/[enone] is 10.72 ± 1.17 using data for reactions starting with the ketol, 9.58 ± 2.01 starting with the enone, and 10.24 ± 1.68 using all of the data. Then, since K_{12} must be the same in acid or base, and $K_{12} = k_{12}/k_{21}$, we may calculate the hydroxide-catalyzed rate constant, $k_{21} = (3.18 \pm 0.60) \times 10^{-5}$ M^{-1} s^{-1}.

To complete the description of this aldol reaction, we have measured the kinetics and equilibrium constants for enone formation from acetone and acetophenone. Although the HPLC peak assigned to 3-methyl-1-phenyl-2-buten-1-one in reaction mixtures of acetone plus acetophenone is small, and there are other small peaks, we are confident of our assignment because it corresponds to the major peak found for authentic samples of 3-methyl-1-phenyl-2-buten-1-one and because the rate constant for formation of this peak (starting from acetophenone at

Can. J. Chem. Downloaded from www.nrcresearchpress.com by 195.138.81.100 on 09/07/12
For personal use only.

TABLE 4. Comparison of microscopic rate constants for the two stages of the retroaldol reaction[a]

Enone	k_{12}[b] $\times 10^4$ ($M^{-1}\,s^{-1}$)	k_{21}[c] $\times 10^4$ ($M^{-1}\,s^{-1}$)	k_{23}[d] $\times 10^2$ ($M^{-1}\,s^{-1}$)	k_{32}[e] $\times 10^2$ ($M^{-1}\,s^{-1}$)	K_{12}[f]	K_{32}[g] (M^{-1})
Methylbutenal[h]	34.	2500.	17.1	6.8	0.136	0.4
Mesityl oxide	1.14[i]	0.126[j]	0.78[k]	1.82[l]	9.05	0.039
3-Methyl-1-phenyl-2-buten-1-one[m]	3.3	0.31	8.0	0.033	10.24	0.0041
Cinnamaldehyde[n]	22.	4560.	9.08	63.	0.0048	6.9
Benzalacetone[o]	3.2	75.	1.4	17.	0.042	12.
Chalcone[p]	10.5	260.	19.4	84.	0.04	4.3

[a]All in aqueous solution at 25°C.
[b]Rate constant for hydroxide-catalyzed hydration of the enone.
[c]Rate constant for hydroxide-catalyzed dehydration of the aldol or ketol.
[d]Rate constant for hydroxide-catalyzed retroaldol cleavage of the aldol or ketol.
[e]Rate constant for hydroxide-catalyzed aldol addition to form the aldol or ketol.
[f]Equilibrium constant for hydration of the enone.
[g]Equilibrium constant for the aldol addition step.
[h]From ref. 4; corrected for covalent hydration of the aldehydes.
[i]Calculated from data at higher temperatures in ref. 24.
[j]Calculated from k_{12} and K_{21} (13).
[k]From ref. 25.
[l]Calculated from k_{23} and K_{23} (1, 26, 27).
[m]This work.
[n]From ref. 6; corrected for covalent hydration of the aldehydes.
[o]From ref. 7.
[p]From ref. 5.

Can. J. Chem. Downloaded from www.nrcresearchpress.com by 195.138.81.100 on 09/07/12
For personal use only.

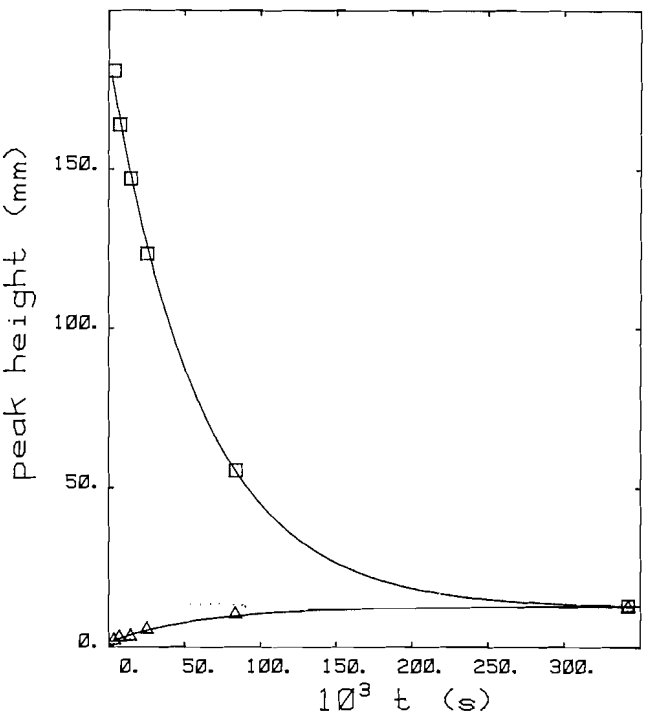


FIG. 1. Kinetics for cleavage and formation of 3-methyl-1-phenyl-2-buten-1-one, followed by HPLC. Initial conditions were as follows: cleavage, [enone] = 0.0013 M, [acetophenone] = 0.0122 M, [acetone] = 1.054 M, [OH^-] = 0.10 M; formation, [acetophenone] = 0.010 M, [acetone] = 0.972 M, [OH^-] = 0.10 M. The points for the formation reaction are corrected by the factor (1.054 × 0.0122)/(0.972 × 0.010) = 1.32, as described in the text.

various concentrations of acetone) and the rate constant for loss of this peak (starting from 3-methyl-1-phenyl-2-buten-1-one) are the same. The kinetics results are found in Table 3.

The rate constant for approach to equilibrium is the sum of the rate constants for the forward and reverse reactions (15). When, as in the present case, formation is much slower than breakdown, the same apparent rate constant, equal to the rate constant for breakdown, is found starting from either direction. Initial experiments to develop the analytical method were carried out at room temperature, 20–25°C, and included reactions followed from both directions; see Fig. 1. Since the equilbrium concentration of enone depends on the product [acetone][acetophenone] and the conditions were not exactly the same for the two reactions, we have corrected the points for the formation run by the ratio $[acetone]_1[acetophenone]_1/[acetone]_2[acetophenone]_2$. As would be expected, the equilibrium constant is relatively insensitive to the small temperature changes involved, but the rates of reaction are quite sensitive, and were faster for reactions thermostatted at 25°C. The rate constant for approach to equilibrium is $(3.06 \pm 0.33) \times 10^{-4}$ $M^{-1}\,s^{-1}$ (weighted mean of rate constants at 25°C, Table 3). Kinetics of breakdown studied by UV led to a rate constant of $(3.1 \pm 0.09) \times 10^{-4}\,M^{-1}\,s^{-1}$. The equilibrium constant for the overall reaction is $K_{31} \times$ [enone]/[acetone][acetophenone] = $(3.99 \pm 0.56) \times 10^{-4}\,M^{-1}$, based on all the experiments, including those at "room temperature", or $(4.04 \pm 0.81) \times 10^{-4}\,M^{-1}$, based on the four reactions carried out at 25°C. Since $K_{31} = K_{32}/K_{12}$, we can now calculate $K_{32} = (4.14 \pm 1.07) \times 10^{-3}\,M^{-1}$. Furthermore, since $K_{32} = k_{32}/k_{23}$, we can calculate $k_{32} = (3.33 \pm 0.91) \times 10^{-4}\,M^{-2}\,s^{-1}$.

Discussion

Examination of the data for two sets of aldol condensations in Table 4 shows both regularities and unexpected deviations from regularity. The reactions included are two sets of reactions of a common carbonyl compound combining with three different carbon acids in the aldol sense: acetone and benzaldehyde with acetaldehyde, acetone, or acetophenone.

For k_{12}, the rate constant for base-catalyzed addition of water to the unsaturated carbonyl compound, we see that the enals are always more reactive then enones. Addition to a cross-conjugated enone derived from acetophenone is faster by

Can. J. Chem. Downloaded from www.nrcresearchpress.com by 195.138.81.100 on 09/07/12
For personal use only.

threefold than addition to the enone derived from acetone. This suggests that there is no extra steric relief upon hydration of an enone with two β-methyls relative to one with a β-phenyl, which can be in the *E* stereochemistry and out of the way. As we have argued previously (4), crowding in the enone (or enal) will not be relieved in the transition state for hydration, but relief of this crowding will affect the overall equilibrium constant for hydration.

For k_{21}, the rate constant for dehydration, the aldehydes are much faster than the ketones. The more dramatic effect is for methylbutenal, where k_{21} is 20 000 times faster than for mesityl oxide, while for cinnamaldehyde, k_{21} is only 60 times faster than for benzalacetone. The change from methyl to phenyl as carbonyl substituent is more regular, with the phenyl compound being 3–4 times faster.

For K_{12}, the equilibrium constant for hydration, the interesting effect is that the aldehydes show a marked preference for dehydration relative to the corresponding ketones. This can be seen to be an effect quite aside from any steric interactions by comparing cinnamaldehyde with benzalacetone or chalcone. Where there is a steric interaction as well, comparing methylbutenal with mesityl oxide or 3-methyl-1-phenyl-2-buten-1-one, the difference between enal and enone is almost 10 times larger. Conjugation clearly favors dehydration, with phenyl as β-substituent favoring dehydration by 30- to 200-fold relative to two β-methyl substituents. There is clearly no major effect of cross-conjugation; K_{12} values for mesityl oxide and 3-methyl-1-phenyl-2-buten-1-one are very similar as are K_{12} values for chalcone and benzalacetone.

For k_{23}, the actual retroaldol step, expulsion of acetone is always slowest, but relative leaving tendencies of acetaldehyde and acetophenone vary. Both are more acidic, hence better leaving groups, than acetone: acetaldehyde, pK_a 16.9 (16), 16.73 (17); acetophenone, 18.4 (18), 18.24 (19); acetone, 19.4 (20), 19.27 (21).

The aldol addition step, k_{32}, is the most surprising; relative rates for attack by the anions of acetaldehyde and acetone are the same for both series, but acetophenone anion is the most reactive nucleophile of the three towards benzaldehyde and the least reactive towards acetone. Part of the reason for this unexpected behavior may be a stabilization of the transition state for the attack of acetophenone on benzaldehyde because of favorable contacts between the aromatic rings. Part of the reason is the less favorable equilibrium constant for the addition step.

Experimental

Materials

3-Hydroxy-3-methyl-1-phenyl-1-butanone, "ketol"

Attempts to prepare this compound by directed aldol condensation of the lithium enolate of acetophenone with acetone led to mixtures containing 4-hydroxy-4-phenyl-2-pentanone, which could not be separated. A less direct synthesis gave pure material. Sodium borohydride (98%, Metal Hydrides Inc.), 0.6 g (15.5 mmol), dissolved in aqueous 0.005 M NaOH, 50 mL, was added to a solution of ethyl benzoylacetate, 2.0 g (10.4 mmol), in 95% ethanol, 100 mL. The reaction was followed by monitoring the UV absorbance at 250 nm in a 1-cm cell, and stopped after 1 h when the absorbance was 0.245. Ice, 50 g, was added to the reaction mixture and 4 M H_3PO_4, 3 mL, was added to adjust the pH to less than 7 (gas evolution). Extraction (chloroform, 1 × 200 mL, 2 × 50 mL), drying (Na_2SO_4), and evaporation gave 1.80 g, 90% crude ethyl 1-hydroxy-1-phenylpropionate. Following the procedure of Wroblewski (22), this crude hydroxy ester was reacted with excess methyl magnesium iodide to give 3-methyl-1-phenyl-1,3-butanediol, which was immediately oxidized to give 3-hydroxy-3-methyl-1-phenyl-1-butanone. The crude product was purified by column chromatography on silica gel, eluting with a linear gradient (0–10%) of ethyl acetate in petroleum ether. Fractions containing only ketol (judged by TLC) were pooled; UV (H_2O): λ_{max} 247.5, ϵ_{max} 12 800, ϵ_{260} 4440, ϵ_{255} 11 100, ϵ_{243} 11 800; ^{1}H NMR (200 MHz, $CDCl_3$) δ (TMS): 1.35 (6H, s) $(CH_3)_2C$, 3.16 (2H, s) CH_2-CO, 4.19 (1H, br s) O*H*, 7.47–7.60 (3H, complex) and 7.93–7.98 (2H, complex) C_6H_5-. Literature (22) ^{1}H NMR (90 MHz, $CDCl_3$) δ (TMS): 1.25 (6H, s), 3.05 (2H, s), 3.75 (1H, s), 7.25–8.1 (5H, m).

3-Methyl-1-phenyl-2-buten-1-one, "enone"

3-Hydroxy-3-methyl-1-phenyl-1-butanone (0.2 g, 1.25 mmol) was added to a crucible containing silica gel (4 g), a few drops of 12 N HCl and a small amount of methanol were added, and the mixture was heated (steam bath) for 1 h. Then the mixture was filtered and washed thoroughly with ethyl acetate. TLC analysis showed approximately 95% enone and 5% ketol. Two column chromatographies on silica gel, the first with a linear gradient (0–20%) of ethyl acetate in petroleum ether, the second with a linear gradient (0–10%) of ethyl acetate in CCl_4, gave pure material; UV (H_2O, 0.1 M KCl): λ_{max} 266 nm, ϵ_{max} 16 500, ϵ_{255} 13 300, $\epsilon_{247.5}$ 9920, ϵ_{243} 7550; ^{1}H NMR (200 MHz, $CDCl_3$) δ (TMS): 2.02 (3H, d, J = 1.4 Hz) CH_3—C=C, 2.22 (3H, d, J = 1.3 Hz) CH_3—C=C, 6.76 (1H, m, J = 1.3 Hz) *H*—C=C, 7.26–7.50 and 7.91–7.96 (5H, complex) C_5H_6-. Literature (23) ^{1}H NMR ($CDCl_3$) δ (TMS): 2.0 (s, 3H), 2.25 (s, 3H), 6.75 (br s, 1H), 7.2–8.0 (m, 6H).

Methods

The procedure for UV kinetics was as previously described (3, 4). Reactions followed by UV were carried out in 10-cm cells, so that low concentrations, ensuring complete solubility, could be used. For reactions followed by HPLC, reactions were carried out in thermostatted flasks, from which samples were removed at suitable intervals and quenched by addition of phosphoric acid. Analysis was carried out using Waters C-18 Radial-Pak columns, with aqueous methanol as eluting solvent. The concentration of materials eluted was monitored at suitable wavelengths: enone, 260 nm; ketol, 248 nm; acetophenone, 245 nm. For equilibrium constant (K_{31}) determinations, calibrations were carried out using suitable stock solutions of pure enone.

NMR spectra were recorded using Varian EM360 or XL200 spectrometers. TLC was carried out using Analtech Silica gel GF uniplates. Column chromatography was carried out using Terochem silica gel 1918.

Acknowledgments

We thank the Natural Sciences and Engineering Research Council of Canada for financial support of this work.

1. J. P. GUTHRIE. Can. J. Chem. **56**, 962 (1978).
2. J. P. GUTHRIE. Can. J. Chem. **52**, 2037 (1974).
3. J. P. GUTHRIE. Can. J. Chem. **59**, 45 (1981).
4. J. P. GUTHRIE and B. A. DAWSON. Can. J. Chem. **61**, 171 (1983).
5. J. P. GUTHRIE, J. COSSAR, P. A. CULLIMORE, N. M. KAMKAR, and K. F. TAYLOR. Can. J. Chem. **61**, 2621 (1983).
6. J. P. GUTHRIE, K. J. COOPER, J. COSSAR, B. A. DAWSON, and K. F. TAYLOR. Can. J. Chem. **62**, 1441 (1984).
7. J. P. GUTHRIE, J. COSSAR, and K. F. TAYLOR. Can. J. Chem. **62**, 1958 (1984).
8. D. S. NOYCE and W. L. REED. Can. J. Am. Chem. Soc. **81**, 624 (1959).
9. A. DE BLIC and P. MARONI. Bull. Soc. Chim. Fr. 512 (1975).
10. J. P. GUTHRIE and S. O'LEARY. Can. J. Chem. **53**, 2150 (1975).
11. J. P. GUTHRIE, J. COSSAR, and B. A. DAWSON. Can. J. Chem. **64**, 2456 (1986).
12. D. S. NOYCE, W. A. PRYOR, and P. A. KING. J. Am. Chem. Soc. **81**, 5423 (1959).
13. J. L. JENSEN and D. J. CARRE. J. Org. Chem. **39**, 2103 (1974).
14. Y. K. KIM and J. D. HATFIELD. J. Chem. Eng. Data, **30**, 149 (1985).

15. J. W. MOORE and R. G. PEARSON. Kinetics and mechanism. 3rd ed. Wiley, New York. 1981. p. 296.
16. J. P. GUTHRIE and J. COSSAR. Can. J. Chem. **64**, 2470 (1986).
17. Y. CHIANG, M. HOJATTI, J. R. KEEFE, A. J. KRESGE, N. P. SCHEPP, and J. WIRZ. J. Am. Chem. Soc. **109**, 4000 (1987).
18. J. P. GUTHRIE, J. COSSAR, and A. KLYM. Can. J. Chem. **65**, 2154 (1987).
19. Y. CHIANG, A. J. KRESGE, and J. WIRZ. J. Am. Chem. Soc. **106**, 6392 (1984).
20. J. P. GUTHRIE, J. COSSAR, and A. KLYM. J. Am. Chem. Soc. **106**, 1351 (1984).
21. Y. CHIANG, A. J. KRESGE, Y. S. TANG, and J. WIRZ. J. Am. Chem. Soc. **106**, 460 (1984).
22. A. E. WROBLEWSKI. Phosphorus Sulfur, **28**, 371 (1986).
23. H. SANO, M. OKAWARA, and Y. UENO. Synthesis, 933 (1984).
24. J. L. JENSEN and H. HASHTROODI. J. Org. Chem. **41**, 3299 (1976).
25. C. C. FRENCH. J. Am. Chem. Soc. **51**, 3215 (1929).
26. K. KOELICHEN. Z. Phys. Chem. **33**, 129 (1900).
27. A. A. FROST and R. G. PEARSON. Kinetics and mechanism. 2nd ed. Wiley, New York. 1963. p. 340.

Can. J. Chem. Downloaded from www.nrcresearchpress.com by 195.138.81.100 on 09/07/12
For personal use only.

The VCD spectrum of 2-methylthietane: measured (800–1500 cm^{-1}) and computed with semi-empirical models

R. A. SHAW, N. IBRAHIM, AND H. WIESER[1]

Department of Chemistry, University of Calgary, Calgary, Alta., Canada T2N 1N4

Received September 12, 1990

R. A. SHAW, N. IBRAHIM, and H. WIESER. Can. J. Chem. **69**, 345 (1991).

The vibrational circular dichroism (VCD) spectrum (800 to 1500 cm^{-1}) is reported for 2-methylthietane (2MT). Fixed partial charge (FPC), atomic polar tensor (APT), and charge flow (CF) methods are used to compute the VCD spectra for both stable conformers (CH_3 in the axial or equatorial orientation) for the complete range of fundamental vibrations, based on 3-21G and 6-31G* harmonic force fields. The experimental and computed absorption and VCD spectra of *R*-(+)-2MT are compared to the previously reported spectra of *R*-(−)-2-methyloxetane. The success of the APT and CF models for reproducing the dominant ring stretching IR and VCD features of that compound is rationalized by a comparison of APT and FPC intensity expressions. Further comparison of the APT and FPC calculated electric dipole moment derivatives are interpreted to suggest values for the diagonal CS and CH stretching charge flow terms for 2MT. These investigations then provide a rationale for previously reported successes of the FPC model, and permit identification of specific vibrational modes of 2MT that are amenable to FPC-VCD modeling. The previously established conformational mixture of ~30% axial and 70% equatorial is shown to be in accord with FPC-VCD predictions for the most appropriate (β-CH_2 wagging) mode.

Key words: vibrational circular dichroism, 2-methylthietane, fixed partial charge, atomic polar tensor, charge flow.

R. A. SHAW, N. IBRAHIM et H. WIESER. Can. J. Chem. **69**, 345 (1991).

On a déterminé le spectre de dichroïsme circulaire vibrationnel (DCV) (de 800 à 1500 cm^{-1}) du 2-méthylthiétane (2MT). On a utilisé les méthodes des charges partielles fixes (CPF), des tenseurs polaires atomiques (TPA) et de l'écoulement des charges (EC) pour calculer le spectre de DCV des deux conformères stables (CH_3 dans les orientations axiale et équatoriale) de l'ensemble complet des vibrations fondamentales, basé sur les champs de force harmonique 3-21G et 6-31G*. On a comparé les absorptions expérimentale et calculée ainsi que le spectre de DCV du *R*-(+)-2MT avec le spectre rapporté antérieurement pour le *R*-(−)-méthyloxétane. Le succès des modèles des TPA et de l'EC à reproduire les caractéristiques principales des élongations en IR et en DCV est rationalisé par comparaison des expressions des intensités des TPA et des CPF. On croit qu'une autre comparaison des dérivées des moments dipolaires électriques, calculées à l'aide des TPA et des CPF, suggère des valeurs pour les termes d'écoulement des charges des élongations diagonales du CS et du CH du 2MT. Ces études ont fourni une base d'interprétation pour les succès rapportés antérieurement par le modèle CPF et elles permettent d'identifier des modes vibrationnels spécifiques du 2MT qui pourraient être examinés par le modèle des CPF-DCV. On montre que, pour le mode le plus approprié de la vibration de balancement du β-CH_2), le mélange conformationnel (d'environ 30% axial et 70 équatorial) qui a été mis en évidence antérieurement est en accord avec les prédictions de la CPF-DCV.

Mots clés : dichroïsme circulaire vibrationnel, 2-méthylthiétane, charges partielles fixes, tenseurs polaires atomiques, l'écoulement des charges.

[Traduit par la rédaction]

Introduction

Vibrational circular dichroism (VCD) spectroscopy measures the differential absorption of left versus right circularly polarized light in the infrared region (for reviews, see for example, ref. 1). The spectrum complements the conventional infrared absorption spectrum, displaying in principle either a positive or negative feature accompanying each vibrational transition. Measurement of VCD is currently feasible to a lower limit of about 600 cm^{-1}, with one of the present challenges being the extraction of structural and conformational details from the observed spectrum. One important theme involves measuring the spectra of small chiral molecules, both to provide a basis for testing theoretical models and to permit identification of spectral features which show a consistent correlation with common structural characteristics. Of particular interest are three- and four-membered rings which, owing to their limited conformational freedom, can serve as effective test cases for model calculations.

We present here the VCD spectrum of 2-methylthietane (2MT, Fig. 1) in the 800–1500 cm^{-1} range, and a series of model calculations based upon the scaled *ab initio* force fields reported earlier (2). This molecule is of particular interest since skeletal flexibility allows inversion between an equatorial and axial orientation of the methyl group, separated by a potential barrier of 341 cm^{-1} (3). The two conformers are suggested to exist in the ratio of approximately 70 to 30%, respectively, at ambient temperatures (2). The influence of ring inversion on the VCD signals may be assessed directly whenever corresponding transitions of the two conformers are resolved in the spectrum.

The 3-21G and 6-31G* force fields reported previously (2) are used here as the basis for calculating the VCD and infrared absorption intensities with the fixed partial charge (FPC), atomic polar tensor (APT), and charge flow (CF) models (4–6). While neither the FPC nor the APT model is universally applicable, even FPC as the simplest reproduces the observed VCD spectrum for certain molecules remarkably well, the most striking examples being *trans*-1,2-dideuteriocyclobutane (DDCB) and *trans*-1,2-dideuteriocyclopropane (DDCP) (7, 8). In the FPC approximation each atom is assigned a net charge which does not vary as the nuclei are displaced from the equilibrium positions. The success of the model for these two saturated hydrocarbons may thus be rationalized by suggesting that vibrational displacements do not induce significant redistribution of electronic charge such as might be anticipated for molecules containing readily polarizable bonds or heteroatoms. FPC calculations for molecules that do contain such groups

[1]Author to whom all correspondence should be addressed.

Can. J. Chem. Downloaded from www.nrcresearchpress.com by 195.138.81.100 on 09/07/12
For personal use only.

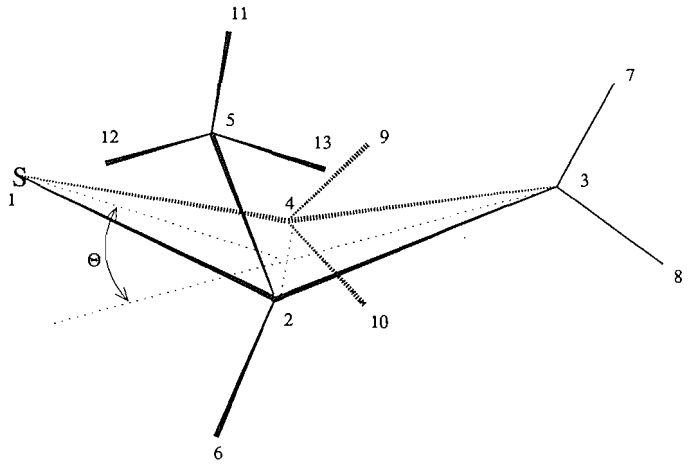


FIG. 1. *R*-(+)-2-methylthietane.

might then be expected to serve as a guide for understanding and modeling, by means of charge flow, such charge rearrangements as do occur.

In a recent report we employed both the FPC and APT models to predict the VCD and infrared absorption intensities of 2-methyloxetane (2MO) (9). From 800 to 1500 cm^{-1} FPC was found to reproduce the signs of nearly all VCD bands; however, the relative intensities were not accurate. The absorption intensities were adequately predicted only for the $CH/CH_2/CH_3$ bending modes in the 1100 to 1500 cm^{-1} range. These observations prompted a detailed comparison of the FPC and APT calculations, with emphasis focussed on attempts to rationalize similarities and differences between the two sets of calculated electric dipole moment derivatives with respect to local symmetry coordinates. This comparison suggested that for FPC the discrepancies in ring stretching absorption intensities might be diminished by including a term reflecting a flow of negative charge along the CO bond from carbon to oxygen as the bond elongates. The resulting improvement toward better agreement between computed and observed absorption and VCD intensities was taken as evidence to indicate that the heteroatom, oxygen in this case, may be viewed as a perturbation upon the otherwise saturated hydrocarbon structure. In this view, charge flow parameters are required to model electronic redistributions that occur solely as a consequence of the heteroatom, and it might be expected readily that the intensities of deformation modes localized at positions remote from the heteroatom can be modeled with FPC just as accurately as for DDCB and DDCP. The β-CH_2 wagging mode in particular was identified as being amenable to FPC modeling, enabling us to establish that the equatorial conformer predominates in solution.

The present study extends this approach, first examining the accuracy of the FPC and APT calculations, and then comparing the two in order to rationalize their strengths and weaknesses in reproducing the observed spectra of 2-methylthietane. We present evidence to suggest that CS stretching leads to charge flow along the CS bonds, allowing us to further assess the influence of a corresponding charge flow parameter on the calculated absorption and VCD intensities. In addition, we examine the effect of charge flow in the CH stretching region by including a diagonal term of the type $\partial\xi_{CH}/\partial R_{CH}$. Finally, we compare in detail the theoretical and experimental VCD spectra of 2MT to those of 2-methyloxetane, stressing in particular the correspondence between both calculated and observed features arising from normal modes that most closely resemble one another.

Theoretical background

The expressions for the dipole and rotatory strengths,

$$[1] \quad \mathcal{D}_i = |\langle 0|\mu|i\rangle|^2$$

$$[2] \quad \mathcal{R}_i = \mathrm{im}\{\langle 0|\mu|i\rangle\cdot\langle i|m|0\rangle\}$$

illustrate the role of the electric and magnetic dipole transition moments governing the calculated infrared absorption and VCD intensities for a transition from the ground state (0) to an excited vibrational state (i). While the former may be evaluated in a straightforward fashion, exact and tractable expressions for the latter have been derived and tested only recently.[2] The FPC, APT, and localized molecular orbital (LMO) (11) models account for the electronic contributions to the magnetic dipole transition moment with progressively less severe approximations in that order, each giving at the same time a clear physical interpretation for the underlying source of the VCD intensities. The CF model extends FPC to include the influence of vibrationally induced charge flow along bonds.

The following discussion rationalizes the success of the charge flow term $\partial\xi_{CO}/\partial R_{CO}$ introduced for 2-methyloxetane (9), while demonstrating simultaneously certain relationships among the FPC, CF, and APT. The expressions for the rotatory strength $\mathcal{R}_i$ are:

$$[3] \quad \mathcal{R}_i^{\mathrm{FPC}} = \frac{e^2\hbar}{4c}\left[\sum_n Z_n\left(\frac{\partial X_n}{\partial Q_i}\right)\right]\cdot\left[\sum_n X_{n,0}\times Z_n\left(\frac{\partial X_n}{\partial Q_i}\right)\right]$$

$$[4] \quad \mathcal{R}_i^{\mathrm{CF}} = \frac{e^2\hbar}{4c}\left[\sum_n Z_n\left(\frac{\partial X_n}{\partial Q_i}\right) + \sum_\alpha Y_\alpha\left(\frac{\partial \xi_\alpha}{\partial Q_i}\right)\right]\cdot \left[\sum_n X_{n,0}\times Z_n\left(\frac{\partial X_n}{\partial Q_i}\right) + \sum_\alpha X_\alpha \times Y_\alpha\left(\frac{\partial \xi_\alpha}{\partial Q_i}\right)\right]$$

$$[5] \quad \mathcal{R}_i^{\mathrm{APT}} = \frac{e^2\hbar}{4c}\left[\sum_n \frac{\partial\mu}{\partial X_n}\left(\frac{\partial X_n}{\partial Q_i}\right)\right]\cdot\left[\sum_n X_{n,0}\times\frac{\partial\mu}{\partial X_n}\left(\frac{\partial X_n}{\partial Q_i}\right)\right]$$

where Z_n and ξ_α denote the net equilibrium atom and bond charges, $X_{n,0}$ and X_α the position vectors for atom n and bond α (note that for the latter the bond position may be specified at any point along the line connecting the two atoms defining the bond), Y_α is a vector running from atoms A to B defining bond α (6), and Q_i the ith normal coordinate.

While several applications of APT and FPC expressions have been reported, the CF model remains largely unexplored. This is due primarily to the difficulty in obtaining reliable values for the charge flow parameters $\partial\xi_\alpha/\partial R_j$, *i.e.* the charge flow along bond α in response to a displacement in the internal (or local symmetry) coordinates R_j. The observed infrared absorption intensities have been successfully reproduced for a number of molecules by least squares adjustments of the formally equivalent electro-optical parameters (EOPs) (for a review, see ref. 12). Simplifying assumptions are inevitably required to reduce the number of variables in such refinements, and hence it is not assured that the corresponding charge flow terms reflect genuine electronic redistributions contributing to the observed

[2]For development of the exact theoretical expressions, see ref. 10*a*,*b*; for calculated results, see ref. 10*c*, *d*, and *e*.

Can. J. Chem. Downloaded from www.nrcresearchpress.com by 195.138.81.100 on 09/07/12
For personal use only.

intensities. A preferable approach may be to evaluate EOPs from first principles, as was suggested by Gribov and co-workers over several years with the MINDO/3 molecular orbital method (13).

In this paper, we examine the influence of diagonal charge flow terms involving the CS and CH bonds only, *i.e.* terms of the type $\partial\xi_{CX}/\partial R_{CX}$, X = S and H. The following discussion demonstrates certain relationships among the CF, FPC, APT, and LMO models, leading to a method for rationalizing these charge flow terms. To illustrate we write the rotatory strength $\mathcal{R}_i$ in the general form:

$$[6] \quad \mathcal{R}_i = \text{constant}[\text{E}]\cdot[\text{M}]$$

where E and M represent, respectively, the electric and magnetic dipole transition moment terms in square brackets in eqs. [3] to [5]. The contribution of *stretching* displacements R_j to the E term can be written for the APT model, and respectively for the CF model assuming only diagonal terms, as follows:

$$[7] \quad \sum_j \frac{\partial\mu}{\partial R_j}\frac{\partial R_j}{\partial Q_i}$$

$$[8] \quad \sum_j \left(Y_\alpha \frac{\partial\xi_\alpha}{\partial R_j} + Z_A^\alpha \frac{\partial X_A}{\partial R_j} + Z_B^\alpha \frac{\partial X_B}{\partial R_j} \right) \frac{\partial R_j}{\partial Q_i}$$

In the second expression, the letters A and B refer to the atoms defining the bond α. The first term denotes the diagonal charge flow upon displacement in R_j, while the last two are the fixed partial charge terms. Provided that the dipole moment derivative $\partial\mu/\partial R_j$ lies along the direction of the bond, as implied by the assumption of only diagonal charge flow contributions, these two expressions may be equated by choosing an appropriate value for $\partial\xi_\alpha/\partial R_j$. Under these conditions,

$$[9] \quad \frac{\partial\mu}{\partial R_j} \approx Y_\alpha \frac{\partial\xi_\alpha}{\partial R_j} + Z_A^\alpha \frac{\partial X_A}{\partial R_j} + Z_B^\alpha \frac{\partial X_B}{\partial R_j}$$

This approximate equality demonstrates that one way of assessing the possible role of charge flow, and of assessing the physical significance of such terms, is to compare the electric dipole moment derivatives as determined by APT given on the left with the fixed partial charge term augmented by charge flow given on the right. Assuming that the atomic polar tensors determined by *ab initio* means give essentially correct values for the dipole moment derivatives, discrepancies in direction and magnitude with the FPC values may be attributed to the neglect of charge flow in the FPC model. Consequently, for bond stretches the diagonal term $\partial\xi_\alpha/\partial R_j$ may be adjusted to best satisfy eq. [9].

The same reasoning for the magnetic dipole moment M lead to the corresponding approximate equality between APT and CF, again limiting R_j to stretching coordinates,

$$[10] \quad X_{A,0} \times \frac{\partial\mu}{\partial R_j} \approx X_{A,0} \times \left(Y_\alpha \frac{\partial\xi_\alpha}{\partial R_j} + Z_A^\alpha \frac{\partial X_A}{\partial R_j} + Z_B^\alpha \frac{\partial X_B}{\partial R_j} \right)$$

where all moment arms X_α, $X_{B,0}$, and $X_{A,0}$ have been moved to a common vector, $X_{A,0}$. These shifts are possible provided that the two contributions $(\partial\mu/\partial X_{A,0})(\partial X_{A,0}/\partial R_j)$ and $(\partial\mu/\partial X_{B,0})(\partial X_{B,0}/\partial R_j)$ to the electric dipole moment derivative for the APT expressions (left side of the equation) both follow the bond direction, and the three contributions to the right side of the equation, arising separately from the diagonal charge flow parameter $\partial\xi_\alpha/\partial R_j$ and the fixed partial charges on the two atoms, lie along the same inter-bond axis.

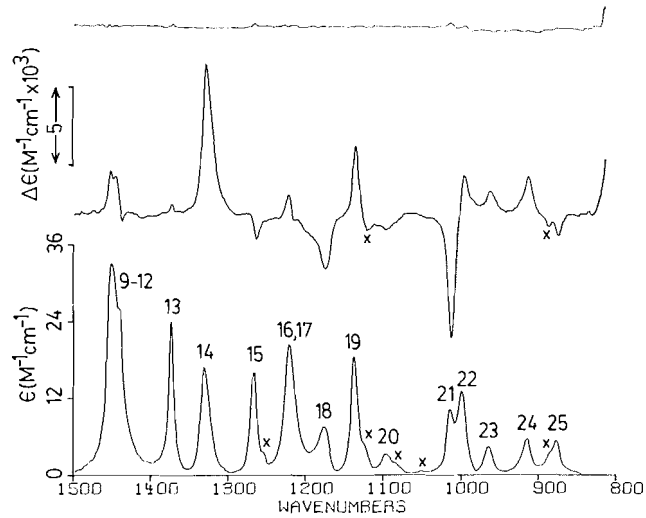


FIG. 2. Experimental infrared absorption (lower trace) and VCD (middle trace) spectra of *R*-(+)-2-methylthietane. The top trace is an estimate of the noise level in the VCD spectrum, i.e. one half of the difference between two separate VCD spectra that are averaged to give the spectrum displayed here. The symbol "×" denotes minor impurities in one of the enantiomers (*R*-(+)) and resulting absorption dependent artifacts in the VCD spectrum.

Analogous arguments may also be applied to the LMO model, assuming all localized molecular orbitals either follow the displaced nuclei exactly if the LMOs are tightly bound to an associated nucleus, or follow the displacement, *e.g.* the direction of bond stretching, if they are bonding molecular orbitals. In that case, expressions identical to APT are obtained.

The above arguments suggest that the APT model, and the CF model incorporating only diagonal charge flow terms, might be anticipated to yield similar intensities, and to reproduce the experimental VCD for those stretching modes involving bonds which are electrically independent, *i.e.* are not linked by charge flow coupling terms. For 2-methyloxetane the FPC value for $\partial\mu/\partial R_{CO}$ matched the APT derived dipole moment derivative in direction, namely parallel to the CO bond, but underestimated the magnitude (9). The discrepancy in absorption intensities for modes containing appreciable CO stretching was largely removed by including the charge flow parameter $\partial\xi_{CO}/\partial R_{CO} = 0.35$ e/Å transferring negative charge from carbon to oxygen as the bond stretches. For the rotatory strength the inclusion of this parameter, while relatively less effective, also leads to closer agreement with observed VCD intensities.

Experimental and computational details

R-(+)- and *S*-(−)-2-methylthietane were made from commercial *R*-(−)- and *S*-(+)-1,3-butanediol (Aldrich, $[\alpha]_D = -24.6°$ and $+25.0°$), respectively, following procedures published for the racemic compounds (14, 15). The methods involved the consecutive syntheses of the *R*-(−)- and *S*-(+)-dimesylates ($[\alpha]_D = -33.0°$ and $+32.6°$ crude, 97% and 96% yield, respectively), and *S*-(+)- and *R*-(−)-dibromides ($[\alpha]_D = +89.9°$ and $-89.0°$ crude, 85% and 90% yield, respectively). After fractional distillation with a Vigreux column from CaH_2 the final products were obtained in about 15% yield in the final step and 98% chemical purity. Chiral complexation chromatography using a Ni-Nop column (CC&CC, FRG) showed an enantiomeric excess of 80% for both enantiomers. The VCD spectrum of *R*-(+)-2-methylthietane is displayed in Fig. 2. It represents one half of the difference of the average of 20 000 scans for each enantiomer, obtained with 4 cm^{-1} resolution on the VCD spectrometer described previously (9).

For each conformer we have computed the VCD and absorption

Can. J. Chem. Downloaded from www.nrcresearchpress.com by 195.138.81.100 on 09/07/12
For personal use only.

TABLE 1. Scaled 6-31G* Mulliken charges for 2-methylthietane

Atom[a]	Charge[b]	Atom[a]	Charge[b]	Atom[a]	Charge[b]
S1	0.0307	H6	0.0649	H10	0.0647
C2	−0.102	H7	0.0588	H11	0.0559
C3	−0.103	H8	0.0611	H12	0.0574
C4	−0.153	H9	0.0641	H13	0.0530
C5	−0.153				

[a]See Fig. 1 for atom numbering.
[b]Units of electronic charge.

intensities with the APT, FPC, and CF models based on the scaled 3-21G and 6-31G* force fields reported earlier (2). The atomic charges (Table 1) were derived by scaling the 6-31G* Mulliken values to give an average charge on hydrogen of +0.06 e, chosen to be in accord with the average of the STO-3G charges on the hydrogen atoms of 2-methyloxetane which reproduce qualitatively the experimental absorption intensities over the CH bending region 1100–1500 cm^{-1} (9). The atomic polar tensors were evaluated analytically for both basis sets as described previously (2).

Table 2 compares the electric dipole moment derivatives calculated with the FPC and APT expressions. The most prominent differences occur for the CH and CS stretching vibrations. For the former the direction of the dipole moment derivative is almost exactly opposite for FPC than for APT. This anomaly has been resolved in the framework of electro-optical parameters by introducing the term $\partial\xi_{CH}/\partial R_{CH} \approx 0.2$ e/Å carrying positive charge from hydrogen to carbon as the CH bond is stretched (12). The present charge flow computation includes this parameter. Although the value of 0.2 e/Å is probably not optimal for 2MT, it demonstrates the general influence of the term as discussed in the following section. For the stretching of the CS bonds FPC underestimates the dipole moment derivative $\partial\mu/\partial R_{CS}$. The charge flow term $\partial\xi_{CS}/\partial R_{CS} = 0.2$ e/Å optimizes the agreement between the CF and APT values of $\partial\mu/\partial R_{CS}$. Clearly the diagonal charge flow term cannot reproduce the difference between the APT values for the two distinct CS bonds, *i.e.* $\partial\mu/\partial R_{C(2)S}$ and $\partial\mu/\partial R_{C(4)S}$, but it does give the average value.

The calculated dipole and rotatory strengths for all calculations are listed in Tables 3 to 6. The experimental rotatory strengths reported in Table 7 were determined from the observed integrated VCD band areas derived from full width at half height measured by means of the band fitting program CAPR supplied by Nicolet. These values, however, are not true rotatory strengths for individual modes since the contributions from the two conformations were not separated. Theoretical spectra, reflecting the 7 to 3 ratio of equatorial to axial conformers deduced previously (2), are compared to the experimental spectra in Figs. 3 to 6.

Results and discussion

Empirical correlations

Two VCD features are of particular interest compared with the spectra of related molecules. Most striking is the strong positive band (for the *R*-(+) enantiomer) observed at 1329 cm^{-1}, arising from the C*—H out-of-plane deformation (peak 14 in Fig. 2). The absolute configuration at the chiral centre and the observed VCD sign for this mode are the same as for propylene sulfide (16), where this band is also the strongest observed feature ($\Delta\epsilon/\epsilon = 4.3 \times 10^{-4}$), and for the oxygen analogues 2-methyloxetane (9) and propylene oxide (17), providing further evidence confirming the C*—H out-of-plane deformation VCD band as a useful probe of the absolute configuration of the X—C*H(CH_3)—CH_2 fragment. It is of further interest to note that the VCD signal of this mode is insensitive to conformational change, *i.e.* ring inversion in this case; the observed and calculated absorption peaks arising from the equatorial and

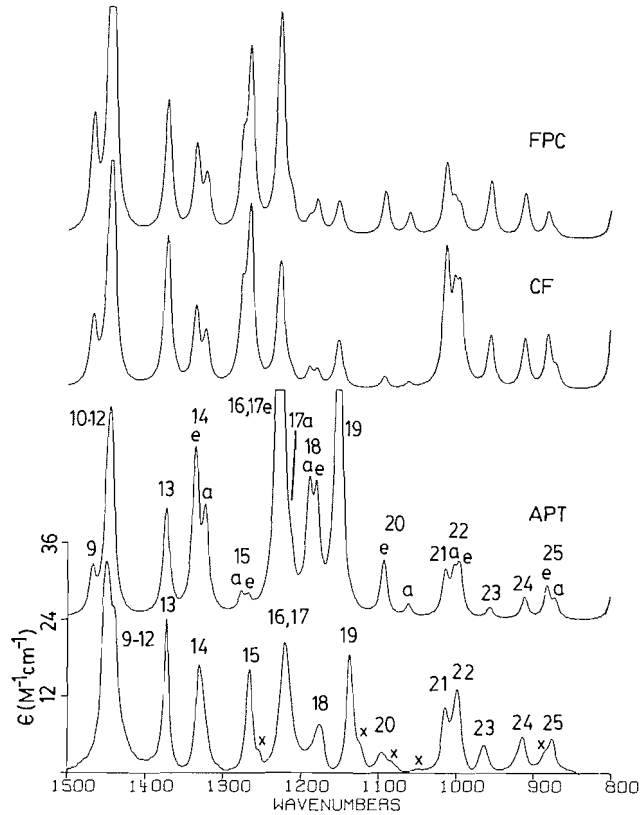


FIG. 3. Experimental (bottom trace) and theoretical absorption spectra (remaining traces) of 2-methylthietane computed with the models as indicated and based on the **6-31G*** force field.

axial conformers are sufficiently separated that a change in sign would be distinctly visible in the VCD spectrum (14.5 cm^{-1} in the vapour phase and 12.8 cm^{-1} by 6-31G*, respectively (2)).

The VCD band corresponding to the methyl symmetric deformation is very weak, as was found also for propylene sulfide (16). In contrast, both 2-methyloxetane (9) and propylene oxide (17) give strong positive VCD bands for the *R* configuration. The different intensities for the sulfur and oxygen analogs cannot be ascribed to changes in the nature of the normal mode which is essentially a pure umbrella motion coupled weakly with the C*—H out-of-plane bend. With the similarity in structure and the normal modes, the difference in the VCD intensities can be attributed, therefore, to electronic influences beyond the FPC model. One possible mechanism involving ring currents has been described qualitatively for 2-methyloxetane (9). It should be noted also that calculations using Stephens' exact formalism (10*b*) do reproduce the observed trend, yielding rotatory strengths of 3.8×10^{-44} (6-31G*) and 11.5×10^{-44} (6-31G**) esu² cm^2 for (*R*)-propylene sulfide (18) and (*R*)-propylene oxide (10*e*), respectively.

Comparison with the VCD spectrum of 2-methyloxetane

For two molecules with common sets of local symmetry coordinates, the normal coordinates of one may be used as the basis for describing the normal modes of the other (2):

$$\mathbf{Q}_2 = \mathbf{L}_2^{-1}\mathbf{L}_1\mathbf{Q}_1$$

where $\mathbf{L}_1$ is the matrix of eigenvectors for molecule **1**, comprised of elements of the type $\partial R_k/\partial Q_{j,1}$. With structural and/or conformational differences between the two molecules,

Can. J. Chem. Downloaded from www.nrcresearchpress.com by 195.138.81.100 on 09/07/12
For personal use only.

TABLE 2. Electric dipole moment derivatives with respect to local symmetry coordinate displacements for fixed partial charge (FPC) and charge flow (CF) models, compared to atomic polar tensor model (APT) at 6-31G*

Coordinate R_i[a]	$\lvert\partial\mu/\partial R_i\rvert \times 10^2$[b]			Θ[c]	
	FPC	CF	APT	FPC/APT	CF/APT
13 α-CH_2 rock	6		5	4.9	
24 CH_3 asymmetric deformation	5		5	7.8	
23 CH_3 asymmetric deformation	5		6	9.5	
18 β-CH_2 wag	8		6	14.7	
11 Ring deformation	4		6	18.3	
3 C(2)—C(3) stretch	4		3	25.4	
19 β-CH_2 twist	0		1	35.7	
30 CH_3 torsion	0		0	38.4	
4 C(3)—C(4) stretch	3		4	39.7	
28 CH_3 bend (out-of-plane)	9		8	46.5	
22 CH_3 rock	5		5	46.7	
29 Ring pucker	1		8	52.5	
20 CH_3 symmetric deformation	7		4	54.5	
21 CH_3 rock	5		4	58.1	
27 CH_3 bend (in plane)	7		6	60.6	
16 β-CH_2 scissor	5		3	63.1	
17 β-CH_2 rock	6		3	68.6	
14 α-CH_2 wag	9		8	89.4	
5 C(2)—C(5) stretch	1		7	112.4	
25 C*—H bend (in plane)	7		7	114.9	
2 C(4)—S stretch	4	34	26	116.6	2.2
1 C(2)—S stretch	4	35	42	122.9	18.3
12 α-CH_2 scissor	6		3	123.6	
15 α-CH_2 twist	0		3	147.0	
26 C*—H bend (out-of-plane)	5		5	152.8	
7 C(4)—H(9) stretch	6	15	18	153.2	26.8
8 C(4)—H(10) stretch	6	15	18	153.9	26.2
6 C(2)—H(6) stretch	6	15	18	162.4	17.7
32 C(5)—H(12) stretch	6	16	18	163.1	16.5
10 C(3)—H(8) stretch	6	16	22	164.6	15.9
31 C(5)—H(11) stretch	6	16	15	164.8	15.0
9 C(3)—H(8) stretch	6	16	16	165.3	14.9
33 C(5)—H(13) stretch	5	16	21	166.5	14.2

[a]Coordinate definition of ref. 2; see Fig. 1 for atom numbering.
[b]Absolute value of molecular dipole moment derivative with respect to displacements in local symmetry coordinates. Units: e (stretches); e Å/rad (bends).
[c]Angle between $\partial\mu/\partial R_i$ calculated by FPC and CF vs. 6-31G* APT.

this relationship is not rigorously correct since the local symmetry coordinates (the **B** matrix) may not be exactly equivalent. The physical interpretation of this relationship is still clear, however. A diagonal product matrix $\mathbf{L}_2^{-1}\mathbf{L}_1$ implies that the displacements in the local symmetry coordinates comprising the normal modes are identical for the two compounds, while off-diagonal elements express the extent of mixing that occurs. The column vectors of this product matrix then give the normal modes of molecule **1** as a linear combination of a set of coordinates describing the normal modes of molecule **2**.

Having previously reported scaled force fields for 2-methyloxetane at the 3-21G and 6-31G* levels (2, 19), we may use this technique to estimate quantitatively the similarities between the normal modes of the oxygen and sulfur analogues. In Table 7 the calculated frequencies (6-31G*) of 2MO and 2MT are paired according to the most closely matched normal modes (*cf.* Table V, ref. 19, and Table 6, ref. 2, respectively), and the mixing is expressed as the normal modes of the former in terms of those of the latter. Given the flexibility of the four-membered rings and the possibility of two stable conformers in each case, there is some ambiguity in this comparison. We have chosen to compare the vibrational displacements of the optimized 6-31G* structure of 2MO, which is equatorial with a dihedral angle of about 7°, to those of the equatorial conformer of 2MT with a dihedral angle of about 21°.

Several points of interest emerge from this comparison. Although there are exceptions it is generally the case that the leading coefficient in each column vector of the matrix $\mathbf{L}_2^{-1}\mathbf{L}_1$ is double or nearly double the next largest term. This suggests that the majority of normal modes retain much the same character in 2MO as in 2MT. The FPC-VCD calculations are in accord with this conclusion, as the corresponding modes of 2MO and 2MT are predicted with the same sign in 26 of 33 instances despite changes in both the charge distribution and the structure. Differences with respect to corresponding APT-VCD intensities may then be assumed in general to arise from changes in the electronic environment (and hence APTs), with changes in the normal coordinates playing a less important role. Perhaps most interesting is the comparison of the *observed* VCD intensities for *matched* normal coordinates. Most features

Can. J. Chem. Downloaded from www.nrcresearchpress.com by 195.138.81.100 on 09/07/12
For personal use only.

Can. J. Chem. Downloaded from www.nrcresearchpress.com by 195.138.81.100 on 09/07/12
For personal use only.

TABLE 3. Dipole strengths calculated for 2-methylthietane using optimized 6-31G* structures and scaled force fields[a]

	Equatorial conformer				Axial conformer			
		D (esu^2 cm^2) × 10^{40}				D (esu^2 cm^2) × 10^{40}		
ν	ν_{calc}[b]	FPC[c]	CF[d]	APT[e]	ν_{calc}[b]	FPC[c]	CF[d]	APT[e]
1	3002	13.8	66.3	41.7	3002	14.5	69.8	42.0
2	2989	9.4	60.2	53.2	2988	10.3	63.9	66.0
3	2968	8.5	57.9	59.3	2970	8.0	49.6	55.9
4	2965	4.1	25.3	31.9	2966	3.5	26.0	24.1
5	2950	3.2	17.1	60.5	2951	4.3	21.4	70.3
6	2938	1.7	7.1	24.1	2955	0.5	4.2	14.5
7	2922	4.3	24.9	62.1	2925	3.8	23.1	57.4
8	2911	1.8	11.6	39.4	2909	1.9	12.5	44.6
9	1468	10.7	6.3	5.1	1470	11.3	6.5	2.0
10	1451	7.2	4.3	7.3	1448	3.8	1.8	4.8
11	1445	14.6	13.4	17.3	1443	14.6	13.1	12.3
12	1444	14.5	10.5	1.3	1449	16.3	11.9	7.1
13	1374	13.6	16.0	12.6	1372	16.3	17.4	8.5
14	1336	12.9	11.3	24.5	1323	18.4	16.8	33.0
15	1267	27.9	27.4	1.9	1277	26.1	28.3	6.6
16	1229	21.0	7.7	39.7	1228	19.8	7.4	21.5
17	1226	9.2	11.4	32.8	1214	9.2	2.7	11.8
18	1180	5.4	2.5	17.2	1190	3.9	6.5	42.7
19	1151	4.2	6.7	46.5	1155	5.9	7.0	38.7
20	1093	8.5	2.2	10.5	1061	10.3	2.6	5.6
21	1014	13.0	24.3	7.4	1013	2.7	3.4	2.3
22	996	4.0	16.1	9.1	1003	11.5	31.5	15.6
23	956	10.9	10.0	2.0	960	4.2	3.9	0.9
24	911	7.1	8.7	4.0	914	8.6	7.3	2.5
25	882	5.7	12.2	7.2	872	2.6	9.8	9.0
26	797	10.4	22.4	8.6	773	15.5	35.0	13.3
27	705	8.0	42.5	26.8	728	8.3	46.1	24.3
28	634	7.5	24.5	40.5	657	7.8	18.5	32.0
29	523	4.4	18.7	16.9	551	1.6	22.4	28.1
30	399	7.7	9.6	5.8	366	8.1	10.4	4.4
31	280	4.6	12.2	17.3	296	5.3	11.5	14.4
32	225	1.1	2.1	3.1	248	0.5	1.1	1.7
33	105	1.4	1.1	32.0	57	1.3	1.0	72.7

[a]See ref. 2 for scaled force field.
[b]Wavenumbers are ordered such that normal coordinates most closely match the corresponding displacements for the scaled 6-31G* force field of the equatorial conformer. See ref. 2.
[c]Using scaled 6-31G* charges. See text.
[d]Including $\partial\xi_{CH}/\partial R_{CH} = \partial\xi_{CS}/\partial R_{CS} = 0.2$ e/Å, with positive charge flowing to carbon with stretching of the CX bond. See text.
[e]APTs calculated using 6-31G*.

TABLE 4. Dipole strengths calculated for 2-methylthietane using optimized 3-21G structures and scaled force fields[a]

	Equatorial conformer				Axial conformer			
		D (esu^2 cm^2) × 10^{40}				D (esu^2 cm^2) × 10^{40}		
ν	ν_{calc}[b]	FPC[c]	CF[d]	APT[e]	ν_{calc}[b]	FPC[c]	CF[d]	APT[e]
1	3012	14.1	67.7	16.1	3013	13.7	64.7	14.9
2	2990	11.3	72.7	35.5	2990	12.3	75.3	41.2
3	2962	6.2	43.5	21.0	2968	5.3	39.5	24.6
4	2973	4.2	25.2	15.2	2975	4.3	25.8	13.6
5	2949	3.7	19.9	40.0	2950	4.2	21.7	39.6
6	2951	1.0	3.1	7.0	2961	0.9	6.2	2.7
7	2926	3.9	22.9	34.4	2926	3.6	22.0	34.8
8	2909	2.0	14.1	30.7	2909	2.0	14.1	32.8
9	1470	12.4	7.8	5.6	1471	13.1	8.2	5.8
10	1453	10.9	10.5	16.1	1453	16.3	13.8	14.2
11	1448	19.7	13.3	16.5	1447	8.2	4.5	16.6
12	1442	7.0	5.2	18.0	1443	11.3	9.3	19.5
13	1375	23.9	22.8	23.0	1376	25.5	24.0	24.0
14	1330	7.5	7.8	13.2	1323	14.8	13.6	8.0
15	1269	21.8	24.8	30.8	1272	18.6	23.9	57.9
16	1220	9.5	7.8	74.5	1225	14.7	8.7	38.4
17	1225	20.9	11.3	42.3	1208	16.6	4.9	25.0
18	1189	7.5	2.0	3.7	1194	3.4	1.9	14.8
19	1144	4.7	5.0	67.1	1148	5.7	5.5	71.6
20	1125	5.0	0.7	4.2	1085	6.4	0.7	3.2
21	1016	12.1	20.7	20.6	1017	0.9	2.1	2.4
22	991	8.5	23.1	19.9	994	14.6	35.2	32.5
23	974	6.3	7.2	6.4	972	6.4	6.6	5.1
24	912	8.2	8.3	8.6	912	6.1	4.8	5.8
25	879	2.4	7.0	10.3	883	3.4	9.0	12.2
26	797	11.3	29.5	10.9	783	13.8	37.7	24.5
27	716	8.2	47.1	43.5	731	8.9	50.0	44.1
28	649	6.9	25.7	50.6	665	6.9	22.1	44.3
29	519	4.5	15.3	26.2	553	2.3	18.5	42.9
30	411	8.2	9.5	5.9	381	8.3	10.1	5.6
31	285	4.4	10.1	23.1	304	4.9	9.0	17.6
32	234	1.2	2.1	4.0	257	0.4	1.0	1.4
33	95	0.9	0.5	41.7	95	0.9	0.6	48.4

[a–d]See Table 3.
[e]APTs calculated using 3-21G.

contain contributions from both the equatorial and axial conformers. The experimental values listed in Table 7 do not represent true rotatory strengths of the two molecules, but serve as measures of the total integrated intensity of possibly overlapped bands. Nevertheless, there is a close correspondence between signs of observed VCD features that correspond to the matched normal modes. For example, mode 20 in 2MO (1136 cm^{-1}) resembles a combination of modes 22 and 24 in 2MT (996 cm^{-1}), and the corresponding VCD features are both positive. We interpret this correspondence as providing experimental evidence supporting both a similarity in the normal modes and a common mechanism dominating the observed VCD intensities.

Calculated spectra 800–1500 cm^{-1}

Considering first the absorption spectra (Figs. 3 and 4, computed at the 6-31G* and 3-21G levels, respectively, and Tables 3 and 4), we note that with few exceptions FPC reproduces qualitatively the observed intensities in the entire range of 800–1500 cm^{-1} at both levels. The most striking discrepancy occurs for ν_{19} at 1137 cm^{-1} (CH_3 rock and α-CH_2 wag (2)) for which both force fields predict a relatively low intensity. This exception aside, the overall picture of stronger bands above and weaker ones below 1150 cm^{-1} is reproduced by all three models.

Since the charge flow calculations include only diagonal parameters for the CH and CS stretches, the CF spectral features might be anticipated to differ from those of FPC only in the CH stretching region, and for the CS stretching absorptions at 630 and 700 cm^{-1}. All of these transitions lie outside the VCD range presently available and therefore cannot be considered here. The corresponding calculated intensities are discussed separately below. The major unexpected changes relative to FPC absorption intensities occur for the bands observed at 999 and 1015 cm^{-1} (ν_{21} and ν_{22}, Figs. 3 and 4), arising largely from combinations of methyl rock (in-plane) and α-CH_2 twist in both conformers (2). The 6-31G* spectra show three features in this

TABLE 5. Rotatory strengths calculated for *R*-(+)-2-methylthietane using optimized 6-31G* structures and force fields[a]

	Equatorial conformer				Axial conformer			
		R (esu^2 cm^2) × 10^{45}				R (esu^2 cm^2) × 10^{45}		
ν	ν_{calc}[b]	FPC[c]	CF[d]	APT[e]	ν_{calc}[b]	FPC[c]	CF[d]	APT[e]
1	3002	−5.7	−35.2	−23.1	3002	11.1	57.9	23.3
2	2989	3.8	37.0	82.9	2988	−2.8	−1.6	51.8
3	2968	−24.6	−172.4	−141.8	2970	−61.2	−413.2	−431.6
4	2965	33.5	213.0	91.1	2966	40.9	302.7	258.4
5	2950	−12.0	−78.0	−106.3	2951	23.8	138.8	191.6
6	2938	6.4	40.5	69.5	2955	−9.9	−72.7	−97.8
7	2922	−2.5	−3.2	43.0	2925	−4.1	−13.7	2.0
8	2911	0.8	−1.3	−19.7	2909	1.4	3.9	2.4
9	1468	−19.5	−11.5	21.7	1470	−7.8	−5.0	−1.2
10	1451	−8.5	−11.2	−57.7	1448	12.3	4.1	−34.6
11	1445	−11.6	−13.1	−17.6	1443	−44.6	−35.6	−26.1
12	1444	32.9	28.7	32.7	1449	25.0	23.5	47.7
13	1374	8.2	14.2	4.7	1372	8.6	11.6	4.7
14	1336	37.7	52.4	25.8	1323	52.6	63.7	35.6
15	1267	−52.7	−51.6	9.0	1277	9.9	8.3	0.1
16	1229	−66.9	−58.2	−36.5	1228	−37.3	−24.4	−18.5
17	1226	5.2	10.4	4.2	1214	−46.3	−32.6	1.4
18	1180	52.2	19.8	−7.3	1190	29.2	−1.3	−19.6
19	1151	−7.9	−6.9	−11.7	1155	−27.8	−30.2	−21.3
20	1093	42.2	12.7	−8.3	1061	24.3	12.3	4.4
21	1014	−36.8	−67.1	8.5	1013	−7.8	−18.3	−13.1
22	996	26.0	63.3	26.3	1003	4.6	8.1	33.1
23	956	13.6	14.7	5.4	960	−5.9	−1.9	−4.0
24	911	7.3	3.3	−7.3	914	33.1	34.9	12.6
25	882	44.1	47.7	11.1	872	2.7	34.7	7.7
26	797	−45.7	−43.7	−6.4	773	−4.6	−48.2	−9.7
27	705	−15.3	−32.5	−10.3	728	11.0	−58.9	−23.2
28	634	−8.2	23.3	15.3	657	−12.4	43.1	21.6
29	523	4.7	11.4	−2.0	551	−5.9	29.5	9.7
30	399	−3.5	−8.0	−0.5	366	−12.2	−18.9	−1.7
31	280	0.5	−1.7	−10.1	296	0.8	−1.1	−7.4
32	225	1.0	2.0	9.7	248	−0.1	1.2	6.5
33	105	1.3	1.1	2.0	57	−0.7	−0.7	−9.3

[a–e] See Table 3.

region, the central band representing ν_{22} of the axial conformer. For 3-21G this axial absorption coincides with the lower wavenumber equatorial peak. For both levels of theory the intensities calculated for ν_{21} and ν_{22} are significantly enhanced by the inclusion of charge flow (see Tables 3 and 4) resulting in an exaggeration of the computed bands. We believe the effect of the C—S charge flow term $\partial\xi_{CS}/\partial R_{CS}$ may require compensation by other parameters of the type $\partial\xi_{CS}/\partial R_i$ involving one or several other modes, in this case in-plane methyl rocking and/or α-CH_2 twisting. The need for additional parameters is demonstrated further by ν_{20} arising primarily from the H_3C—C stretch, for which the intensity is significantly reduced from FPC to CF. Finally, we note that the 3-21G CF calculation provides good overall agreement with the corresponding APT intensities (see Fig. 4 and Table 4), which is not the case for 6-31G* (Fig. 3 and Table 3).

The APT calculated absorption spectra (6-31G* and 3-21G) were reported previously (2). As noted on that occasion, the former surprisingly is not clearly more accurate than the latter. In each case the intensities are reasonably accurate below 1150 cm^{-1}, whereas major discrepancies are apparent above. Transitions which are exaggerated most conspicuously at both levels of theory are ν_{16}, ν_{17}, and ν_{19}, modes involving C*—H in-plane bend, α-CH_2 wag, β-CH_2 twist, and CH_3 out-of-plane rock. In addition, ν_{15} arising primarily from the β-CH_2 wagging motion is conspicuously underestimated by 6-31G* and overestimated by 3-21G. The APT spectra are not clearly more accurate in terms of overall agreement with experiment than those of either FPC and CF. Major differences occur for ν_{15} (6-31G* only), ν_{16}, ν_{17}, and ν_{19} for which the APTs generally predict dipole strengths greater by at least a factor of two (Tables 3 and 4).

In contrast to the qualitative success in reproducing absorption intensities, none of the VCD models considered here agree in general with all the observed VCD features. Nevertheless, several points of interest emerge, particularly where agreement may be interpreted to suggest a genuine strength of a model.

If the success of FPC for DDCB does imply a general strength of the model for predicting the VCD spectra of saturated hydrocarbons, as mentioned in the Introduction, then equally good agreement might be anticipated in heteroatom substituted hydrocarbons for modes structurally removed and vibrationally isolated from the point of substitution. For 2MT this should be true for the methyl asymmetric deformation and the methylene

Can. J. Chem. Downloaded from www.nrcresearchpress.com by 195.138.81.100 on 09/07/12
For personal use only.

TABLE 6. Rotatory strengths calculated for *R*-(+)-2-methylthietane using optimized 3-21G* structures and force fields[a]

	Equatorial conformer				Axial conformer			
		R (esu^2 cm^2) × 10^{45}				R (esu^2 cm^2) × 10^{45}		
ν	ν_{calc}[b]	FPC[c]	CF[d]	APT[e]	ν_{calc}[b]	FPC[c]	CF[d]	APT[e]
1	3012	−6.2	−37.6	−17.3	3013	7.7	40.0	10.1
2	2990	4.4	39.1	56.4	2990	−3.6	−12.1	31.3
3	2962	−2.0	−3.5	−2.6	2968	13.2	119.4	54.2
4	2973	2.7	−1.0	−70.9	2975	−29.1	−186.3	−127.1
5	2949	−6.7	−43.7	24.0	2950	11.7	73.7	54.1
6	2951	7.0	41.0	29.2	2961	1.4	−24.8	−22.1
7	2926	0.2	9.3	42.4	2926	−2.9	−10.0	6.1
8	2909	0.2	−2.9	−15.4	2909	1.0	2.0	−7.4
9	1470	−14.1	−6.3	16.9	1471	−6.5	−2.8	9.7
10	1453	−27.8	−28.6	−129.6	1453	21.6	17.7	48.6
11	1448	28.5	23.2	69.2	1447	7.9	2.4	−19.6
12	1442	9.3	7.1	22.4	1443	−31.5	−23.9	−49.8
13	1375	7.8	6.8	13.0	1376	8.4	6.6	17.1
14	1330	29.1	48.8	36.7	1323	17.9	30.5	58.8
15	1269	−58.7	−59.0	−21.1	1272	35.1	32.0	15.8
16	1220	−30.8	−29.6	−19.1	1225	−24.0	−25.5	−21.5
17	1225	−48.5	−20.4	29.5	1208	−108.5	−64.1	10.4
18	1189	70.4	32.7	−19.7	1194	45.9	25.7	−39.8
19	1144	12.3	3.1	−41.5	1148	12.3	−7.1	−72.7
20	1125	25.4	5.2	−13.9	1085	10.8	3.8	7.0
21	1016	−20.8	−52.1	−11.8	1017	0.2	−18.0	−26.2
22	991	21.9	57.9	47.8	994	11.9	21.3	48.8
23	974	20.8	20.1	25.6	972	−9.6	−4.3	−3.5
24	912	10.6	9.3	−4.6	912	25.8	24.4	26.7
25	879	24.5	36.0	22.3	883	9.7	40.1	27.6
26	797	−36.5	−56.7	−28.4	783	−8.9	−47.7	−35.7
27	716	−16.0	−29.9	−30.2	731	17.1	−81.5	−75.1
28	649	−8.7	30.6	41.6	665	−14.1	55.0	64.3
29	519	3.0	11.2	2.8	553	−8.2	33.6	33.3
30	411	−4.2	−11.5	−8.0	381	−13.0	−19.7	−10.3
31	285	1.0	−1.1	−17.6	304	0.9	−1.1	−12.0
32	234	0.7	1.5	12.3	257	−0.2	0.9	6.6
33	95	1.3	0.7	3.2	95	−0.4	0.0	−12.8

[a–d]See Table 3.
[e]APTs calculated using 3-21G.

scissors, and they would thus be expected to exhibit VCD features as predicted by FPC. It is therefore disconcerting that the VCD signals observed for these modes in the 1430–1470 cm^{-1} region (Figs. 5 and 6 and Tables 5 and 6) are not reproduced in any of the computed spectra. The discrepancies may be due in part to the force field not quite reproducing the correct spacing and/or ordering among the eight transitions (*i.e.* four equatorial and four axial) in this narrow range. Related to this are relatively large changes in the calculated displacements which may result from minor uncertainties in the force field. The agreement or disagreement between the observed and calculated VCD spectra in this region may therefore be unreliable as a guide for assessing the accuracy of the models.

The VCD signs of the bands observed at 1373, 1331, and 1266 cm^{-1}, arising from ν_{13}, ν_{14}, and ν_{15}, respectively (Figs. 5 and 6), and corresponding to CH_3 symmetric deformation, C*—H out-of-plane bend, and β-CH_2 wag (2), are reproduced by all but one of the calculations. The exception occurs for ν_{15} with the 6-31G* APTs. In this instance, the calculated absorption intensity is also in significant error, indicating that inaccuracies in the APTs are likely responsible and fortuitously magnified for this model in particular. All of the other computations yield opposite VCD signs for ν_{15} for the two conformers, negative for equatorial and positive for axial; the negative observed sign is reproduced only by assuming that the equatorial conformer predominates at the measurement temperature. This behaviour is analogous to that of 2-methyloxetane where the same mode was interpreted to also suggest a preference for the equatorial conformation (9). For the CH_3 symmetric deformation and C*—H bending modes the observed and calculated VCD signs for 2MT also match those of the corresponding modes in 2MO, although the VCD signals are relatively insensitive to conformation in these cases. The large difference in intensity for the CH_3 symmetric deformation between 2MO to 2MT is not reproduced by FPC or APT, suggesting that vibrationally induced electronic displacements likely play an important role governing the observed intensity. For the C*—H out-of-plane deformation (ν_{14}) the equatorial and axial transitions are well separated in the vapour phase absorption spectrum

Can. J. Chem. Downloaded from www.nrcresearchpress.com by 195.138.81.100 on 09/07/12
For personal use only.

TABLE 7. Comparison of corresponding normal coordinates (6-31G*) and VCD intensities of equatorial (*R*)-(+)-2-methylthietane (2MT) and (*R*)-(−)-2-methyloxetane (2MO)

Calculated position/cm^{-1}				Normal mode mixing[b]					$R \times 10^{45}$/esu^2 cm^2					
									APT[c]		FPC[c]		Obs.[d]	
ν	2MT	ν	2MO[a]	$Q_{2MO} = c_1$		$Q_{2MT} + c_2$		Q_{2MT}	2MT	2MO	2MT	2MO	2MT	2MO
1	3002	5	2940	**5**	0.9	**1**	−0.4	**4**	−23	−60	−5	−7		
2	2989	2	2986	**2**	0.9	**2**	0.4	**3**	83	−133	4	−24		
3	2968	3	2976	**3**	0.9	**3**	0.3	**4**	−142	6	−28	7		
4	2965	1	2996	**1**	0.8	**4**	0.4	**1**	91	40	36	11		
5	2950	7	2905	**7**	0.9	**5**	−0.3	**7**	−106	−53	−11	−1		
6	2938	8	2892	**8**	0.9	**6**	−0.3	**5**	70	83	6	2		
7	2922	4	2951	**4**	0.9	**7**	0.3	**1**	43	134	−1	11		
8	2911	6	2917	**6**	1.0	**8**	−0.3	**6**	−20	−16	0	1		
9	1468	9	1486	**9**	0.9	**9**	0.3	**10**	22	5	−18	−4		
10	1451	10	1453	**10**	0.9	**10**	−0.3	**9**	−58	−60	−9	−15	27	
11	1445	12	1440	**12**	1.0	**11**	0.2	**9**	−18	−24	−16	−33	35	−48
12	1444	11	1446	**11**	0.9	**12**	0.4	**10**	33	60	36	33	−14	
13	1374	13	1385	**13**	0.9	**13**	0.4	**14**	5	−20	8	0	5	89
14	1336	14	1346	**14**	0.9	**14**	−0.4	**13**	26	12	41	33	265	42
15	1267	17	1223	**17**	0.8	**15**	−0.5	**17**	9	1	−51	−42	−15	−53
16	1229	15	1327	**15**	0.8	**16**	−0.4	**17**	−36	−22	−68	−24	25	0
17	1226	18	1196	**18**	0.7	**17**	−0.4	**18**	4	0	5	19		49
18	1180	19	1175	**19**	0.7	**18**	0.7	**19**	−7	−17	47	−39	−103	−40
19	1151	16	1257	**16**	0.6	**19**	−0.5	**18**	−12	−3	−7	52	80	14
20	1093	21	1096	**21**	0.9	**20**	0.3	**22**	−8	21	39	25	−36	−35
21	1014	22	1065	**22**	0.7	**21**	0.5	**22**	8	30	−33	−24	−188	−145
22	996	20	1136	**20**	0.7	**22**	0.4	**24**	26	−7	26	25	76	38
23	956	24	956	**24**	0.7	**23**	0.4	**27**	5	20	16	8	45	183
24	911	25	916	**25**	0.9	**24**	0.3	**21**	−7	−3	6	8	73	(+)
25	882	26	878	**26**	0.9	**25**	0.3	**23**	11	17	49	21	−37	0
26	797	28	782	**28**	0.9	**26**	−0.4	**27**	−6	7	−51	−12		
27	705	23	984	**23**	0.8	**27**	0.4	**28**	−10	47	−8	−4		106
28	634	27	856	**27**	0.8	**28**	0.8	**29**	15	−82	−17	−24		−130
29	523	29	713	**29**	0.9	**29**	−0.5	**28**	−2	15	2	5		
30	399	30	431	**30**	1.0	**30**	0.5	**31**	0	9	1	−6		
31	280	31	327	**31**	1.0	**31**	−0.3	**30**	−10	−24	3	−5		
32	225	32	230	**32**	1.0	**32**	−0.1	**31**	10	20	−1	0		
33	105	33	81	**33**	1.1	**33**	0.1	**31**	2	−6	0	1		

[a]Calculated with scaled 6-31G* force field at the optimized (~6° equatorial) 6-31G* structure (ref. 2).

[b]Expresses normal coordinates of 2MO in terms of those of 2MT according to $Q_i^{2MO} = c_{i,j}Q_j^{2MT} + c_{i,k}Q_k^{2MT}$, $c_{i,j}$ and $c_{i,k}$ are the dominant elements in the product matrix $\mathbf{L}_{2MO}^{-1}\mathbf{L}_{2MT}$, derived from the eigenvectors in local symmetry coordinates. See text.

[c]Compares 6-31G* APT and FPC VCD intensities. FPC intensities of 2MO were calculated with the charges in ref. 9 and the force field in ref. 2. 6-31G* APTs were calculated in ref. 2.

[d]Compares observed VCD intensities for corresponding modes of 2MT (this work) and 2MO (ref. 9). Experimental values are not true rotatory strengths, since each observed band is a superposition of the equatorial and axial conformers.

(2), and the 6-31G* force field reproduces this splitting (Figs. 3 and 5). The width of the observed bands in solution must therefore arise from the equatorial and axial transitions, the former occurring at higher wavenumber with greater intensity, and both having the same VCD sign. The axial bands emerge as distinct shoulders upon Fourier self-deconvolution.

These examples illustrate the distinction between VCD configurational and conformational marker bands, the signs of the former being relatively insensitive to conformational change, while the latter strongly depend on it. The C*—H out-of-plane bending and β-CH_2 wagging modes, respectively, demonstrate this behaviour, as seen here for 2-methylthietane in the observed as well as all the model spectra, and earlier for 2-methyloxetane (9).

The 1050–1250 cm^{-1} region contains several heavily mixed bending modes. Four features are clearly visible in the VCD spectrum, occurring at 1222 (+), 1175 (−), 1137 (+), and 1097 (−) cm^{-1} (ν_{16}, ν_{18}, ν_{19}, and ν_{20}, respectively). All FPC and CF calculations predict precisely the opposite sign pattern. The 6-31G* APTs predict the correct sign for only two of the four (namely, ν_{18} and ν_{20}), while those of 3-21G provide better overall agreement in this region with but one exception (ν_{19}). The weak couplet labelled ν_{16} and ν_{17} in Fig. 6 appears to be well modeled by 3-21G APTs (the negative lobe of ν_{17} showing faintly in the observed spectrum is clearly evident upon Fourier self-deconvolution). This agreement may be fortuitous, since the computed ordering of the dominant transitions, namely ν_{16} and ν_{17} of the equatorial conformer, is opposite to that predicted by the 6-31G* force field (see Tables 3 and 4). Finally, the negative band observed at 1096 cm^{-1} (ν_{20} in Figs. 5 and 6) corresponds to the negative band predicted by 3-21G APTs for the equatorial conformer at 1125 cm^{-1} (Table 6 and Fig. 6). The

Can. J. Chem. Downloaded from www.nrcresearchpress.com by 195.138.81.100 on 09/07/12
For personal use only.

Can. J. Chem. Downloaded from www.nrcresearchpress.com by 195.138.81.100 on 09/07/12
For personal use only.

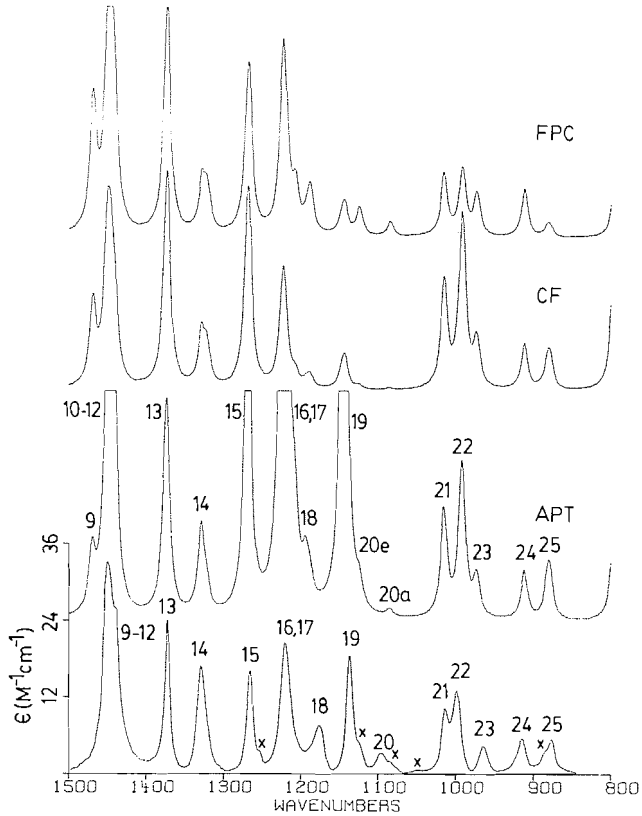


FIG. 4. Experimental (bottom trace) and theoretical absorption spectra (remaining traces) of 2-methylthietane computed with the models as indicated (remaining traces) and based on the **3-21G** force field.

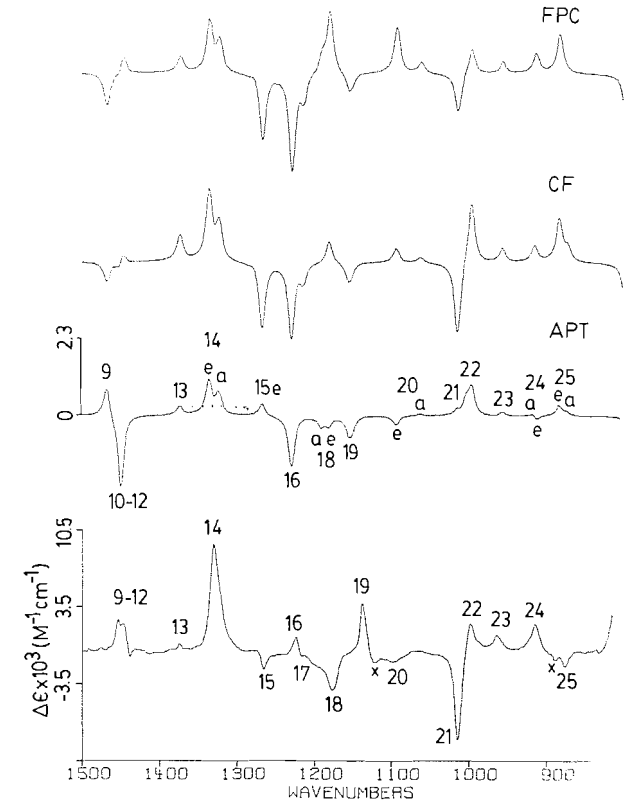


FIG. 5. Experimental (bottom trace) and theoretical VCD spectra (remaining traces) of *R*-(+)-2-methylthietane computed with the models as indicated and based on the **6-31G*** force field.

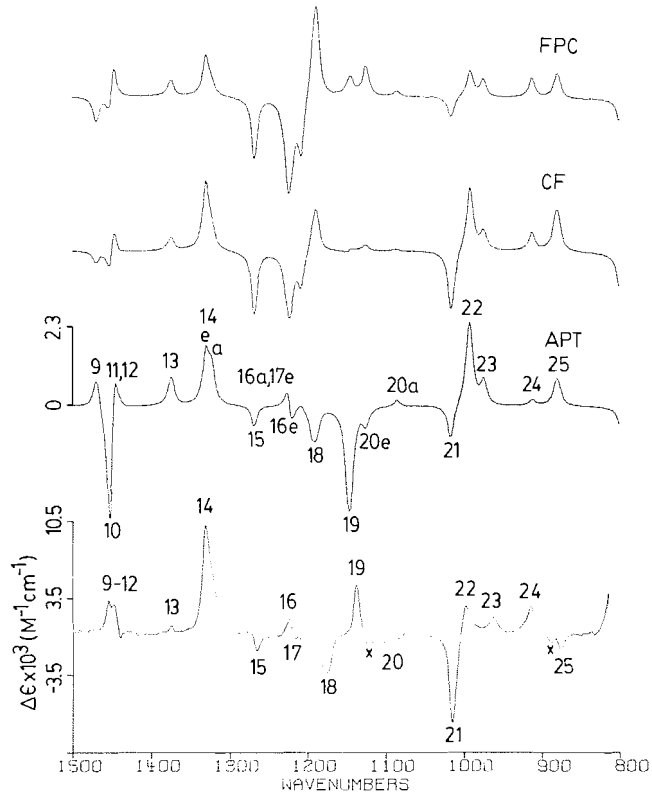


FIG. 6. Experimental (bottom trace) and theoretical VCD spectra (remaining traces) of *R*-(+)-2-methylthietane computed with the models as indicated and based on the **3-21G** force field.

positive VCD feature predicted at 1085 cm^{-1} arises from the same mode of the axial conformer. Both transitions show as clear vapour phase bands at 1101.4 and 1061.5 cm^{-1} (2) and are very well matched by the 6-31G* force field (Tables 3 and 4).

In the 800–1050 cm^{-1} range all of the calculations except 6-31G* APT are remarkably accurate, reproducing four of the five observed VCD signs (ν_{21} to ν_{24} and ν_{25}, respectively). These bands arise from combinations of CH_3 rocking and α-CH_2 twisting (ν_{21} and ν_{22}), H_2C—C stretching (ν_{23}), combination of methyl and methylene rocking (ν_{24}), and CH_3C—C stretching (ν_{25}). The enhancement of the absorption intensities for ν_{21} and ν_{22} upon introducing C—S charge flow with both force fields (3-21G and 6-31G*) was noted earlier in this section. The influence of the C—S stretching charge flow parameter on the intensity of the corresponding VCD couplet is even more striking, improving remarkably the agreement with the observed contour. Although this enhancement does not provide conclusive evidence, it does suggest strongly that the limited charge flow represented by the single parameter improves the physical description of the electronic response to these vibrations.

Calculated spectra in the CH and CS stretching regions

As demonstrated earlier (2), the 6-31G* APTs give a good reproduction of the CH stretching absorptions, whereas FPC underestimates essentially all of these intensities. By including the diagonal charge flow term $\partial\xi_{CH}/\partial R_{CH} = 0.2$ e/Å tranferring positive charge from hydrogen to carbon as the C—H bond is stretched, the discrepancies between FPC and APT are diminished appreciably (Table 3). For FPC the electric dipole moment derivative $\partial\mu/\partial R_{CH}$ is lower by a factor of three or four on average compared to 6-31G* APTs, and the direction is almost exactly *opposite* (see Table 2). The charge flow term

Can. J. Chem. Downloaded from www.nrcresearchpress.com by 195.138.81.100 on 09/07/12
For personal use only.

reverses the direction of $\partial\mu/\partial R_{CH}$ and increases its magnitude to about the 6-31G* APT value.

The computed CF-VCD intensities of the CH stretching modes similarly approach the APT values in most cases (Table 5). Both models reflect similar VCD mechanisms, *i.e.* the disymmetric coupling of separate oscillating moments. The electric moments in each case follow the direction of the bond stretching displacements, as inferred by eqs. [9] and [10]. The FPC model implies a fundamentally different source of VCD intensity for these modes in that the bond dipole moment derivatives lie in the opposite direction to both CF and APT. The fortuitous agreement in sign between FPC and CF is due to the fact that for a given normal coordinate displacement *both* the electric and magnetic dipole moments are reversed in sign for FPC relative to the CF and APT models. The predicted VCD sign is thus unaffected, as the rotatory strength is given by the product of these derivatives. This further explains the reported successes of the FPC model in qualitatively reproducing a number of CH stretching VCD spectra, and the paradox that a set of atomic charges optimized to fit the mid-infrared absorption and VCD features inevitably underestimates the CH stretching VCD intensities. The single charge flow parameter $\partial\xi_{CH}/\partial R_{CH} = 0.2$ e/Å both resolves this paradox and provides a model of electronic behaviour that is in close accord with the requirements dictated by *ab initio* calculations.

The charge flow parameter $\partial\xi_{CS}/\partial R_{CS}$ is most important for the two CS stretches ν_{27} and ν_{28}, as well as ν_{29}, a ring deformation mode that includes some CS stretching. The value of $\partial\mu/\partial R_{CS}$ increases from 0.04 to 0.34 and 0.35 e for the two stretches, compared to the 6-31G* APT values of 0.26 and 0.42 e, respectively, and reduces the orientation of the $\partial\mu/\partial R_{CS}$ vector with respect to APT from 117 and 123° to 2 and 19°, respectively (Table 2). The calculated absorption intensities for all three modes and for both conformers are markedly improved, although the relative intensities for the CS stretches are interchanged relative to APT (Table 3). Most striking are the changes in the VCD intensities for the three modes. Whereas FPC predicts signs opposite from APT in five of the six instances, ν_{27}^{eq} being the exception, CF matches APT in all but one case, namely ν_{29}^{eq} (Table 5). This convergence of CF and APT results suggests that a predominant source of VCD intensity is the coupling of the stretching coordinates, each of which gives rise to a change in dipole moment that is localized along the bond axis. This mechanism is analogous to that discussed above for the CH stretches, and the similarity between the CF and VCD intensities is rationalized by the arguments presented in the Theoretical background section.

In our previous study of the VCD spectrum of 2MO (9) it was demonstrated that by including the analogous charge flow parameter $\partial\xi_{CO}/\partial R_{CO}$ the calculated absorption and VCD intensities, compared with the experimental spectra, are improved relative to FPC for each of the four ring stretching modes. Although the corresponding CS bands lie below the accessible range of our present instrumentation, the computed spectra for 2MT show precisely the same trend as for 2MO. We believe, therefore, that the mechanism discussed in the Theoretical background section plays an important role in generating VCD intensity for the ring stretching modes, and that the CF and APT models represent this mechanism with comparable accuracy.

Summary and conclusions

In this report we present the experimental VCD spectrum of 2-methylthietane (2MT) in the region of 800 to 1500 cm^{-1}, and theoretical VCD spectra in the complete fundamental region. We have tested the approximate models of fixed partial charge (FPC), charge flow (CF) using only two charge flow parameters, one for each of the C—H and C—S bonds, and atomic polar tensors (APT), based on scaled 3-21G and 6-31G* *ab initio* harmonic force fields, against the measured absorption and VCD spectra, and compared the success of each model against one another.

The relatively poor performance of FPC may be traced to significant induced charge displacements that do not follow the direction of nuclear displacements. Morever, FPC generally fails to replicate the APT calculated magnitudes and orientation of the electric dipole transition moments, $\partial\mu/\partial R_i$. This is true even for many of the CH, CH_2, and CH_3 deformations, *i.e.* modes that closely follow FPC behaviour for the saturated hydrocarbons *trans*-1,2-dideuteriocyclobutane and *trans*-1,2-dideuteriocyclopropane. The same analysis for 2-methyloxetane indicated that the β-CH_2 and CH_3 deformations are amenable to FPC modeling based on relatively good agreements among the electric dipole transition moments both in magnitude and direction. The larger discrepancies for 2-methylthietane may be ascribed to polarization induced in the sulfur atom or the CS bond by the motion of fixed partial charges on the hydrogen atoms that are constant throughout the vibrational cycle. Within the charge flow formalism such influences would be reflected in significant terms of the type $\partial\xi_{CS}/\partial R_X$, where ξ_{CS} is the C—S bond charge and X may represent CH, CH_2, or CH_3 deformations.

Despite the generally poor performance of FPC it has been shown that the β-CH_2 wagging mode satisfies the criteria that we have deduced earlier for revealing FPC-like behaviour (9). Namely, (*1*) the FPC model calculation provides a dipole moment derivative $\partial\mu/\partial R_i$ (i = β-CH_2 wag) that closely matches the *ab initio* value, and (*2*), the β-CH_2 moiety is well removed from the sulfur atom and hence deformations such as the wag and localized at this point would be expected to reflect FPC-like behaviour as was found for saturated hydrocarbons. The observation of a negative VCD feature corresponding to the β-CH_2 wag is thus in accord with a preponderance of the equatorial conformer, with both FPC calculations predicting negative and positive features, respectively, for the equatorial and axial conformers. This analysis demonstrates that models such as FPC that are not uniformly accurate may nevertheless prove useful for stereochemical purposes when more elaborate calculations are not practical.

Earlier in the text we described an indirect method with which the dominant diagonal stretching charge flow terms may be determined by constraining the resulting dipole moment derivative to reproduce the *ab initio* value, 6-31G* in the present case (see eq. [9]). This procedure suggested appropriate values for $\partial\xi_{CH}/\partial R_{CH}$ and $\partial\xi_{CS}/\partial R_{CS}$. It also led to the close agreement between the resulting CF and APT intensities, rationalized by showing that for pure stretching modes the two models are formally equivalent with the constraint that each bond stretch contributes to the overall dipole moment change through a term that follows the bond axis exactly. This observation further explains why both the APT and CF methods should reproduce successfully the ring stretching VCD signs for 2-methyloxetane (9) and suggests that similar accuracy might be anticipated for the as yet unmeasured VCD features associated with the CS stretches of 2-methylthietane. The large CH stretching parameter has been recognized previously (12) as being necessary to resolve the fact that charges optimized to best reproduce the mid-infrared absorption intensities provide CH stretching inten-

Can. J. Chem. Downloaded from www.nrcresearchpress.com by 195.138.81.100 on 09/07/12
For personal use only.

sities markedly lower than observed. We have demonstrated here the effectiveness of this term in resolving the corresponding discrepancies in the VCD spectrum, and have further rationalized previous successes of FPC calculations in the CH stretching region by showing that the charge flow and APT models provide essentially the same sign pattern.

A technique, exploited previously as a means of quantitatively estimating the similarities between normal coordinates of isotopically ($10d$) and conformationally (2, $10d$) distinct isomers, has been adopted here to provide a correlation between the normal coordinates of 2-methylthietane and 2-methyloxetane. The computed VCD intensities were then compared for each pair of matched normal coordinates, demonstrating close similarity in the FPC-VCD signs. Most significantly, this analysis permitted correlation between experimental VCD features measured for the two molecules, revealing a nearly unanimous matching of VCD signs observed for common modes and hence implying similar mechanisms underlying the VCD spectra of both compounds. This technique shows promise as a means of separating purely dynamic factors, *i.e.* changes or similarities in normal coordinates, from other influences affecting both computed and experimental spectra of structurally similar molecules ($10d$).

It is clear from this and other studies that the FPC and APT-VCD models are accurate only in favorable circumstances. Close analysis of such calculations has nevertheless proven useful in that they have confirmed the expectation that an extension of the charge flow model incorporating additional terms might lead to systematic improvements in the calculated absorption and VCD spectra. Both this study and that of 2-methyloxetane (9) strongly indicate that the limited set of parameters examined to date, viz. $\partial\xi_{CH}/\partial R_{CH}$, $\partial\xi_{CO}/\partial R_{CO}$, and $\partial\xi_{CS}/\partial R_{CS}$, reflect genuine contributions to the observed vibrational absorption and VCD spectra. Methods are being developed in our laboratory to provide *ab initio* estimates for complete sets of charge flow parameters (20), with preliminary results entirely consistent with this and previous (9) work.

NOTE ADDED IN PROOF. The accuracy of the FPC and APT models for calculating rotatory strengths and hence predicting VCD spectra has been questioned on several occasions, as indeed we emphasize here also for 2-methylthietane. As one of the referees has pointed out in the proof stage, Stephens and co-workers have recently compared in explicit detail the FPC and APT (and also the coupled oscillator) equations to Stephens' rigorous theory of vibrational rotatory strengths for a number of small chiral molecules, with the conclusion that the simple models, APT in particular, omit a magnetic moment contribution, namely the so-called $\mathbf{P}\cdot\mathbf{M}$ term (21). Stephens *et al.* further recommend against the use of the simple semi-empirical models for computing VCD intensities in the future, although they concede, though not believe, that for larger size molecules the $\mathbf{P}\cdot\mathbf{M}$ term may assume less dominance. According to our thinking, which largely coincides with that of Stephens' group, we are attempting to identify systematically those vibrational modes that are amenable to VCD intensity predictions by the simpler models, and extend this experience to larger molecules. In this manner we expect to gain a qualitative appreciation of the VCD mechanism which in the long run may contribute to improving theoretical formalisms. Our recent efforts to interpret the VCD spectrum of 6,8-dioxabicyclo[3.2.1]octane demonstrate this approach (22).

Acknowledgements

This work was supported by an Operating Grant (to H.W.) from the Natural Sciences and Engineering Research Council of Canada (NSERCC) which is hereby gratefully acknowledged. We also wish to thank the Academic Computing Services of the University of Calgary for access to the Honeywell/Multics and Cyber 205 Supercomputer systems, and for their continuing support and good will.

1. T. B. FREEDMAN and L. A. NAFIE. *In* Topics in stereochemistry. Vol. 17. *Edited by* E. L. Eliel and N. L. Allinger. John Wiley and Sons, New York. 1987. pp. 117–206; P. J. STEPHENS and M. A. LOWE. Ann. Rev. Phys. Chem. **36**, 213 (1985).
2. R. A. SHAW, N. IBRAHIM, and H. WIESER. Can. J. Chem. **68**, 90 (1990).
3. J. A. DUCKETT, T. L. SMITHSON, and H. WIESER. J. Mol. Struct. **56**, 157 (1979).
4. J. A. SCHELLMAN. J. Chem. Phys. **58**, 2882 (1973); **60**, 343 (1974).
5. T. B. FREEDMAN and L. A. NAFIE. J. Chem. Phys. **78**, 27 (1983).
6. S. ABBATE, L. LAUX, J. OVEREND, and A. MOSCOWITZ. J. Chem. Phys. **75**, 3161 (1981).
7. A. ANNAMALAI, T. A. KEIDERLING, and J. S. CHICKOS. J. Am. Chem. Soc. **106**, 6254 (1984); **107**, 2285 (1985).
8. M. A. LOWE, G. A. SEGAL, and P. J. STEPHENS. J. Am. Chem. Soc. **108**, 248 (1986); S. J. CIANCIOSI, K. M. SPENCER, T. B. FREEDMAN, L. A. NAFIE, and J. E. BALDWIN. J. Am. Chem. Soc. **111**, 1913 (1989).
9. R. A. SHAW, N. IBRAHIM, and H. WIESER. J. Phys. Chem. **94**, 125 (1990).
10. (*a*) L. A. NAFIE and T. B. FREEDMAN. J. Chem. Phys. **78**, 7108 (1983); (*b*) P. J. STEPHENS. J. Phys. Chem. **89**, 748 (1985); (*c*) A. RAUK and R. DUTLER. J. Am. Chem. Soc. **111**, 6957 (1989); (*d*) R. A. SHAW, H. WIESER, R. DUTLER, and A. RAUK. J. Am. Chem. Soc. **112**, 5401 (1990); (*e*) R. W. KAWIECKI, F. DEVLIN, P. J. STEPHENS, R. D. AMOS, and N. C. HANDY. Chem. Phys. Lett. **145**, 411 (1988).
11. L. A. NAFIE and T. H. WALNUT. Chem. Phys. Lett. **49**, 441 (1977).
12. G. ZERBI, M. GUSSONI, S. ABBATE, and P. JONA. *In* Vibrational intensities in infrared and Raman spectroscopy. *Edited by* W. B. Person and G. Zerbi. Elsevier, Amsterdam. 1982. pp. 301–333.
13. L. A. GRIBOV and S. V. KOTOV. J. Mol. Struct. **198**, 93 (1989).
14. L. A. PAQUETTE and J. P. FREEMAN. J. Org. Chem. **35**, 2249 (1970).
15. Y. ETIENNE, R. SOULAS, and H. LUMBRUSO. *In* Heterocyclic compounds. *Edited by* A. Weissberger. Interscience Publishers, New York – London – Sidney. 1964. p. 725.
16. P. L. POLAVARAPU, B. A. HESS, JR., L. J. SCHAAD, D. O. HENDERSON, L. P. FONTANA, H. E. SMITH, L. A. NAFIE, T. B. FREEDMAN, and W. M. ZUK. J. Chem. Phys. **86**, 1140 (1987).
17. P. L. POLAVARAPU and D. F. MICHALSKA. J. Am. Chem. Soc. **105**, 6190 (1983).
18. H. DOTHE, M. A. LOWE, and J. S. ALPER. J. Phys. Chem. **92**, 6246 (1988).
19. R. A. SHAW, N. IBRAHIM, and H. WIESER. J. Phys. Chem. **93**, 3920 (1989).
20. T. EGGIMANN, F. MAURER, R. A. SHAW, and H. WIESER. Thirteenth Austin Symposium on Molecular Structure, University of Texas, Austin, TX. Paper P45 (1990).
21. P. J. STEPHENS, K. J. JALKANEN, and R. W. KAWIECKI. J. Am. Chem. Soc. **112**, 6518 (1990); A. ANNAMALAI, K. J. JALKANEN, U. NARAYANAN, M.-C. TISSOT, T. A. KEIDERLING, and P. J. STEPHENS. J. Phys. Chem. **94**, 194 (1990).
22. T. EGGIMANN, R. A. SHAW, and H. WIESER. J. Phys. Chem. In press.

Lewis acidic titanium species: the synthesis, structure, bonding and molecular modelling considerations of the complexes $Ti(NR_2)_3Cl$ (R = Me, Et)

DAVID G. DICK, ROGER ROUSSEAU, and DOUGLAS W. STEPHAN[1]

Department of Chemistry and Biochemistry, University of Windsor, Windsor, Ont., Canada N9B 3P4

Received June 29, 1990

DAVID G. DICK, ROGER ROUSSEAU, and DOUGLAS W. STEPHAN. Can. J. Chem. **69**, 357 (1991).

Reaction of simple amides with $TiCl_4$ affords mixed amido-chloride species $Ti(NR_2)_{4-n}Cl_n$. The trisamide-chloride species $Ti(NR_2)_3Cl$ can be prepared directly employing three equivalents of amide or by reaction $Ti(NR_2)_4$ with $TiCl_4$. The compound $Ti(NMe_2)_3Cl$, **1**, crystallizes in the trigonal space group $R\bar{3}c$, with $a = 11.525(5)$, $c = 14.939(3)$ Å, $Z = 6$, and $V = 1718(1)$ Å^3. The compound $Ti(NEt_2)_3Cl$, **2**, crystallizes in the monoclinic space group $P2_1/c$, with $a = 8.385(2)$ Å, $b = 15.958(2)$ Å, $c = 14.230(4)$ Å, $\beta = 107.79(1)°$, $Z = 4$, and $V = 1813(1)$ Å^3. The geometry of the Ti coordination sphere in these complexes is best described as pseudo-tetrahedral. The structural data are consistent with Ti—N multiple bonding. Preliminary results of EHMO calculations are consistent with d_π—p_π Ti—N bonding. Attempts to replace the halides with phosphides ($LiPR_2$, R = Me, Et, Ph) led not to the Ti(IV) phosphido species, but rather to redox chemistry yielding Ti(III) amides and P_2R_4. The barrier to rotation about the Ti—N bonds has been considered. Variable temperature ^1H NMR studies reveal that the barrier is small. Extended Hückel total energy minimization calculations have been performed. In addition, MMX calculations of the barrier to Ti—N rotation are reported. The results of these calculations imply that the rotational barrier is dominated by steric effects.

Key words: titanium amides, structures, Ti—N bonding.

DAVID G. DICK, ROGER ROUSSEAU et DOUGLAS W. STEPHAN. Can. J. Chem. **69**, 357 (1991).

Les réactions d'amides simples avec du $TiCl_4$ fournissent des chlorures d'amides mixtes, $Ti(NR_2)_{4-n}Cl_n$. On peut préparer directement le chlorure de tris(amide), $Ti(NR_2)_3Cl$, en utilisant trois équivalents d'amide ou par réaction du $Ti(NR_2)_4$ avec du $TiCl_4$. Le composé $Ti(NMe_2)_3Cl$, **1**, cristallise dans le groupe d'espace trigonal $R\bar{3}c$, avec $a = 11,525(5)$ et $c = 14,939(3)$ Å, $Z = 6$ et $V = 1718(1)$ Å^3. Le composé $Ti(NEt_2)_3Cl$, **2**, cristallise dans le groupe d'espace monoclinique $P2_1/c$, avec $a = 8,385(2)$, $b = 15,958(2)$, $c = 14,230(4)$ Å, $\beta = 107,79(1)°$, $Z = 4$ et $V = 1813(1)$ Å^3. Un pseudo-tétraèdre est la meilleure façon de décrire la géométrie de la sphère de coordination de ces complexes. Les données structurales sont en accord avec une liaison Ti—N multiple. Les résultats préliminaires de calculs d'OMHE sont en accord avec une liaison Ti—N du type d_π—p_π. Lorsqu'on a voulu remplacer les halogénures par des phosphures ($LiPR_2$, R = Me, Et, Ph) on n'a pas obtenu les espèces Ti(IV)phosphido, mais plutôt une chimie rédox fournissant des amides du Ti(III) et du P_2R_4. On a considéré la barrière à la rotation autour des liaisons Ti—N. Des études de rmn du ^1H à température variable révélent que la barrière est faible. On a effectué des calculs de minimisation de l'énergie totale par le méthode du Hückel étendu. De plus, on a réalisé des calculs MMX de la barrière de rotation Ti—N. Les résultats de ces calculs impliquent que la barrière à la rotation est dominée par des effets stériques.

Mots clés : amides du Ti, structure, liaison Ti—N.

[Traduit par la rédaction]

Introduction

Our interest in Lewis acidic, early metal species stems from our studies of early/late heterobimetallic (ELHB) complexes (1–15). Investigation of such compounds are motivated by the potential for Lewis acid activation of small molecule substrates like CO or CO_2. In initiating efforts to synthesize more reactive ELHB complexes, we are exploring the incorporation of early metal fragments which exclude Cp ligands and offer effective Lewis acidity. To this end, it may be possible to derivatize the species $Ti(NR_2)_3Cl$, and thus incorporate this early metal moiety into an ELHB complex. In this, our initial report on these efforts, we have prepared and structurally characterized two complexes of the form $Ti(NR_2)_3Cl$. Conformational aspects and the nature of the bonding in these Lewis acidic, early metal species are considered. Preliminary attempts to derivatize these species are described and the implications for incorporation in ELHB complexes are discussed.

Experimental section

All preparations were done under an atmosphere of dry, O_2-free N_2 in a Vacuum Atmospheres' Inert Atmosphere glove box. The quality of the atmosphere was maintained employing a 5 cfm blower, a deoxygenation/drying catalyst column and a molecular sieve prepurifier canister. Solvents were reagent grade, distilled from the appropriate drying agents under N_2, and degassed by the freeze–thaw method at least three times prior to use. ^1H and $^{13}C\{^1H\}$ NMR experiments were performed using a Bruker AC-300 MHz spectrometer employing trace amounts of protio solvent as the internal reference. Chemical shifts are reported relative to $Si(CH_3)_4$. $^{31}P\{^1H\}$NMR experiments were performed using a Bruker AC-200 MHz spectrometer. The spectral data were referenced to external 85% H_3PO_4 in D_2O. Combustion analyses were performed by Galbraith Laboratories Inc., Knoxville, TN. Crystalline samples were shipped in ampoules sealed under an atmosphere of N_2. The compounds $Ti(NR_2)_4$ (R = Me, Et) were synthesized employing literature methods (16).

*Preparation of $Ti(NR_2)_3Cl$ (R = Me, **1**; Et, **2**)*

(a) From $Ti(NR_2)_4$

These compounds were prepared in a similar manner and thus only one description is given. To a 50 mL hexane solution $Ti(NEt_2)_4$ (2.00 g, 5.95 mmol) was added $TiCl_4$ (6.0 mL of a 0.33 M solution in benzene, 1.98 mmol) at −65°C. The mixture was allowed to warm to 25°C. The solution was stirred for 2 h. The solvent was removed *in vacuo* and the residue was distilled to give a yellow oil (bp 105°C, 0.1 Torr), yield (0.880 g, 37%).

(b) Direct synthesis

These compounds were prepared in a similar manner and thus only one description is given. To a 50 mL hexane solution $HNEt_2$ (14.80 mL, 0.143 mol) was added *n*-BuLi (57.2 mL, 2.5 M, 0.143 mol) at −65°C. To this solution was added a hexane solution (50 mL) containing $TiCl_4$ (5.25 mL, 0.0477 mol). The addition was performed at −65°C and the mixture was allowed to warm to 25°C. The solvent was removed *in vacuo* and the residue was distilled to give a yellow oil (bp 105°C, 0.1 Torr) yield (11.3 g, 79%). **1**: ^1H NMR (d_8-toluene): δ

[1]To whom correspondence should be addressed.

Can. J. Chem. Downloaded from www.nrcresearchpress.com by 195.138.81.100 on 09/07/12
For personal use only.

TABLE 1. Crystallographic parameters

Parameter	Value	
	Molecule **1**	Molecule **2**
Formula	$C_6H_{18}ClN_3Ti$	$C_{12}H_{30}ClN_3Ti$
Crystal colour, form	Yellow blocks	Yellow blocks
a (Å)	11.525 (5)	8.385 (2)
b (Å)		15.958 (6)
c (Å)	14.939 (3)	14.230 (4)
β (deg)		107.79 (2)
Crystal system	Trigonal	Monoclinic
Space group	$R\bar{3}c$	$P2_1/c$
Vol (Å^3)	1718 (1)	1813 (1)
Density (g cm^{-3}) calcd.	1.25	1.10
Z	6	4
Crystal dimension (mm)	0.40 × 0.30 × 0.35	0.25 × 0.28 × 0.32
Absorption coefficient, μ (cm^{-1})	8.78	5.59
Radiation, λ (Å)	Mo Kα (0.71069)	Mo Kα (0.71069)
T (°C)	24	24
Scan speed (deg/min)	4.50–5.0 (θ/2θ)	2.0–5.0 (θ/2θ)
Scan range (deg)	1.0 below $K\alpha_1$	1.0 below $K\alpha_1$
	1.0 above $K\alpha_2$	1.0 above $K\alpha_2$
Background/scan time ratio	0.5	0.5
Data collected	4963	1880
2θ range (deg)	4.5–45.0	4.5–40.0
Index range	$-h, +k, +l$	$\pm h, +k, +l$
Unique data $F_o^2 > 3\sigma(F_o^2)$	245	1291
Variables	34	156
R (%)	3.23	4.75
R_w (%)	3.33	5.22
Largest Δ/σ in final least squares cycle	0.003	0.002
Maximum residual (e/A^3)	0.67	0.46
Atom associated	Ti	Ti

(ppm), 3.05 (s), $^{13}C\{^1H\}$ NMR (d_8-toluene): 43.40 ppm. **2**: mp (sealed capillary under N_2) 44°C, ^1H NMR (d_8-toluene): δ, 3.52 (q, 2H), 1.05 (t, 3H) $|J_{H-H}| = 7.0$ Hz. $^{13}C\{^1H\}$ NMR (d_8-toluene): δ (ppm), 45.73, 15.02. *Anal.* calcd: C 48.09, H 10.09, N 13.96; found: C 46.98, H 10.65, N 13.96.

Reactions of $Ti(NEt_2)_3Cl$ with $LiPR_2$ (R = Me, Et, Ph)

To a hexane solution of **1** (0.400 mg, 1.350 mmol) was added an equivalent of the Li salt of the phosphide (*i.e.*, $LiPMe_2$, $LiPEt_2$, or $LiPPh_2$). The solution becomes orange brown in colour on stirring. Monitoring the reaction via $^{31}P\{^1H\}$ shows the growth of the resonance attributable to the appropriate P_2R_4 species.

X-ray data collection and reduction

Diffraction experiments were performed on a four-circle Syntex $P2_1$ diffractometer with graphite-monochromatized Mo Kα radiation (λ = 0.71069 Å). The initial orientation matrices were obtained from 15 machine-centred reflections selected from rotation photographs. These data were used to determine the crystal systems. Partial rotation photographs around each axis were consistent with a trigonal crystal system for **1** and a monoclinic crystal system for **2**. The final lattice parameters and the orientation matrices were determined from 30 and 29 high-angle data ($20° < 2\theta < 25°$) for **1** and **2**, respectively. The observed extinctions were consistent with the space groups $R\bar{3}c$ for **1** and $P2_1/c$ for **2**. $-h, +k, +l$ were collected ($4.5° < 2\theta < 45.0°$) for **1**, and $\pm h, +k, +l$ data were collected ($4.5° < 2\theta < 40.0°$) for **2**. In each case, three standard reflections were recorded every 197 reflections. The intensities of the standards showed no statistically significant change over the duration of the data collection. The data were processed using the SHELX-76 program package.

Structure solution and refinement

Non-hydrogen atomic scattering factors were taken from the literature tabulations (17–19). The heavy atom positions were determined using direct methods. The remaining non-hydrogen atoms were located from successive difference Fourier map calculations. The refinement was carried out by using full-matrix least squares techniques on F, minimizing the function $w(|F_o| - |F_c|)^2$ where the weight, w, is defined as $4F_o^2/2\sigma(F_o^2)$ and F_o and F_c are the observed and calculated structure factor amplitudes. In the final cycles of each refinement, the titanium, chlorine, nitrogen, and carbons were assigned anisotropic temperature factors. The hydrogen atom positions were calculated and allowed to ride on the carbon to which they are bonded assuming a C—H bond length of 0.95 Å. Hydrogen atom temperature factors were fixed at 1.10 times the isotropic temperature factor of the carbon atom to which they are bonded. The hydrogen atom contributions were calculated, but not refined. The residual electron densities, in each case, were of no chemical significance. Crystal data and data collection parameters are summarized in Table 1. Tables of positional parameters (Table 2) and selected bond distances and angles (Table 3) are reported. Thermal parameters (Table S1), hydrogen atom parameters (Table S2), and calculated and observed structure factors (Table S3) have been deposited.[2]

Molecular modelling considerations

Energy minimization calculations were performed employing the MMX and MM2 options of the program package PC-MODEL[3] operating on a PC equipped with a 80386 processor and a 80387 numerical coprocessor. Initial molecular coordinates were taken from the X-ray structural studies.

[2]Complete set of tables may be purchased from The Depository of Unpublished Data, Document Delivery, CISTI, National Research Council Canada, Ottawa, Canada K1A 0S2.

[3]Program commercially available from Serena Software, Bloomington, IN.

Can. J. Chem. Downloaded from www.nrcresearchpress.com by 195.138.81.100 on 09/07/12
For personal use only.

TABLE 2. Positional parameters ($\times 10^4$)

Atom	x	y	z	Atom	x	y	z
			Molecule **1**				
Ti	0(0)	0(0)	2743(19)	C1	0(0)	0(0)	1204(19)
N	39(4)	−1466(3)	3238(19)	C1	1108(6)	−1659(6)	2917(18)
C2	−721(6)	−2355Z(5)	3960(19)				
			Molecule **2**				
Ti	971(1)	1385(1)	2196(1)	C1	711(2)	2130(1)	774(1)
Ni	−1031(5)	1405(2)	2509(3)	N2	1509(5)	272(3)	2045(3)
N3	2644(5)	1801(3)	3277(3)	C1	−1411(8)	1623(4)	3427(4)
C2	−1592(9)	866(6)	4031(5)	C3	−2477(7)	1108(4)	1717(4)
C4	−3713(7)	1787(4)	1220(5)	C5	727(7)	−542(4)	2161(4)
C6	1739(13)	−1017(5)	3031(7)	C7	3031(7)	207(4)	1724(4)
C8	2691(9)	−102(5)	667(5)	C9	2453(7)	2708(3)	3424(5)
C10	3751(10)	3242(5)	3160(6)	C11	4047(7)	1395(4)	4028(5)
C12	3617(10)	1187(5)	4963(5)				

TABLE 3. Selected bond distances and angles

(*a*) Molecule **1**

Bond	Distance (Å)	Bond	Distance	Bond	Distance
Ti—C1	2.300 (3)	Ti—N	1.866 (4)	N—C1	1.438 (7)
N—C2	1.444 (6)				

Bonds	Angle (deg)	Bonds	Angle (deg)
N—Ti—C1	113.3 (2)	C1—N—Ti	114.7 (4)
C2—N—Ti	131.1 (3)	C2—N—C1	113.7 (4)
N—Ti—N′	105.4 (2)		

(*b*) Molecule **2**

Bond	Distance (Å)	Bond	Distance (Å)	Bond	Distance (Å)
Ti—C1	2.300 (2)	Ti—N1	1.864 (4)	Ti—N2	1.860 (4)
Ti—N3	1.860 (4)	N1—C1	1.479 (6)	N1—C3	1.460 (6)
N2—C5	1.487 (7)	N2—C7	1.470 (7)	N3—C9	1.479 (7)
N3—C11	1.475 (7)	C1—C2	1.517 (9)	C3—C4	1.517 (8)
C5—C6	1.479 (9)	C7—C8	1.527 (8)	C9—C10	1.516 (9)
C11—C12	1.518 (9)				

Bonds	Angle (deg)	Bonds	Angle (deg)
N1—Ti—C1	110.5 (1)	N2—Ti—C1	110.7 (1)
N3—Ti—C1	112.9 (1)	N1—Ti—N2	108.2 (2)
N1—Ti—N3	107.6 (2)	N2—Ti—N3	106.7 (2)
C1—N1—Ti	132.0 (4)	C3—N1—Ti	114.0 (3)
C5—N2—Ti	133.6 (4)	C7—N2—Ti	111.4 (3)
C9—N3—Ti	112.3 (4)	C11—N3—Ti	132.5 (4)
C1—N1—C3	114.0 (4)	C5—N2—C7	115.0 (4)
C9—N3—C11	115.1 (4)	N1—C1—C2	113.6 (6)
N1—C3—C4	114.6 (5)	N2—C5—C6	112.4 (5)
N2—C7—C8	114.8 (5)	N3—C9—C10	113.5 (5)
N3—C11—C12	112.3 (5)		

Molecular orbital calculations

These calculations and plotting were performed employing the TRIBBL program package (20) operating on a VAX 3520 workstation. Extended Hückel calculations were performed employing the EHT option of TRIBBL. Geometry optimizations were done using the OPT9 routine. Cartesian coordinates of the various models were derived from the perturbations of the crystallographic data presented herein, employing PC-MODEL.

Results and discussion

The complexes $Ti(NR_2)_3Cl$ (R = Me **1**, Et **2**) were initially prepared by the reaction of $Ti(NR_2)_4$ and $TiCl_4$ employing the appropriate ratio to afford the desired product (reaction [1]). In both cases, the orange–yellow distillate crystallizes on standing in an inert atmosphere. Alternatively, these compounds can be prepared by the direct reaction of three equivalents of the

Can. J. Chem. Downloaded from www.nrcresearchpress.com by 195.138.81.100 on 09/07/12
For personal use only.

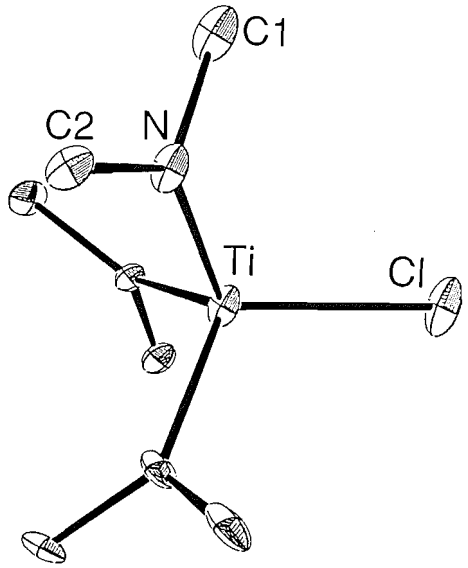


FIG. 1. ORTEP drawing of molecule **1**, 20% thermal ellipsoids are shown. Hydrogen atoms are omitted for clarity.

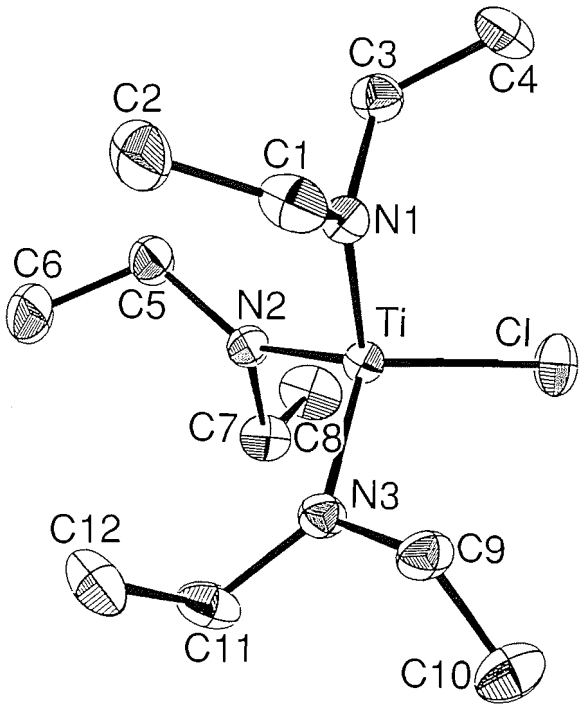


FIG. 2. ORTEP drawing of molecule **2**, 20% thermal ellipsoids are shown. Hydrogen atoms are omitted for clarity.

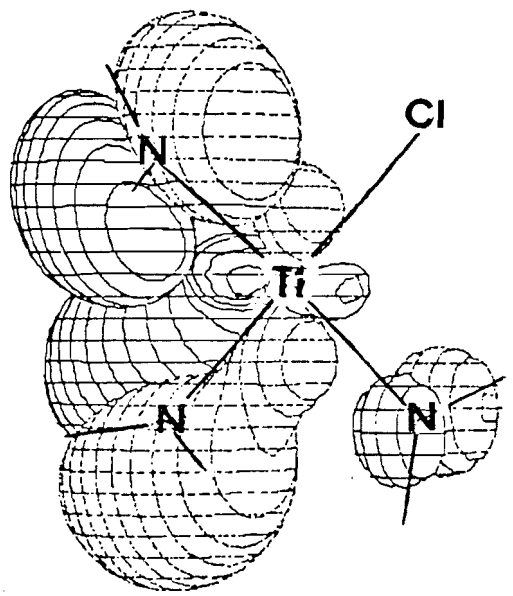


FIG. 3. MOPLOT plot of one of the EHMOs in which d_π—p_π bonding is involved. The contour level is 0.04.

appropriate amide salt with $TiCl_4$ (reaction [2]). The ^1H NMR spectrum of **1** shows the a single resonance attributable to the methyl groups on the amide while the spectrum of **2** confirmed the presence of ethyl groups in the product. The results of combustion analyses were consistent with the formulations of **2** as $Ti(NEt_2)_3Cl$. These formulations were further confirmed by X-ray crystallographic studies (*vide infra*). Similar synthetic routes to these compounds were previously established by Benzing and Kornicker (21) and Chandra and Lappert (22). However, this report is the first to describe the isolation of **2** as a crystalline solid. Small amounts of either other $Ti(NR_2)_{4-n}Cl_n$ species or oxidation or hydrolysis products may account for the oils obtained by previous workers.

[1] $3Ti(NR)_4 + TiCl_4 \rightarrow 4Ti(NR_2)_3Cl$

[2] $3M(NR_2) + TiCl_4 \rightarrow 4Ti(NR_2)_3Cl + 3MCl$

Reactions with phosphides

Attempts to effect substitution reactions in which phosphido groups replace the chloride in **1** or **2** met with failure. Employing lithium disubstitutedphosphides where the substituents were phenyl, methyl, or ethyl groups led not to substitution, but rather to reduction of the Ti, presumably to $Ti(NR_2)_3$. In the case of R = Me this product is known to be dimeric (22). The phosphorus containing oxidation products in these reactions are of the form P_2R_4 where R = Ph, Me, Et. These species were identified by $^{31}P\{^1H\}$ NMR and were the only diamagnetic phosphorus containing products of the reactions. Related results have shown that other Ti(IV) species are reduced by phosphides to Ti(III) compounds. These results do not auger well for the synthesis of Ti(IV) phosphide derivatives and their subsequent use as synthons for ELHB complexes. However, bulkier substituents on the either the amides or the phosphide may inhibit bimolecular redox processes involved in electron transfer and thus stabilize complexes of the form $Ti(NR_2)_3(PR'_2)$. Current efforts are directed at this proposition.

Structural studies

The X-ray crystallographic study of **1** showed that the molecule crystallizes in the space group $R\bar{3}c$ with six independent molecules in the unit cell. An ORTEP drawing of **1** is shown in Fig. 1. The closest approach between molecules is 2.551 Å (H1B—H1B). The symmetry of the space group dictates that the Ti and Cl atoms sit on a crystallographically imposed threefold axis. Thus, the asymmetric unit is comprised of a single dimethylamido group, and one third of the Ti and Cl atoms.

Crystallographic study of **2** shows that the compound crystallizes in the space group $P2_1/c$ with four molecules in the unit cell. An ORTEP drawing of **2** is shown in Fig. 2. The closest approach between molecules is found to be 2.452 Å (H12A—H6C). In this case, no crystallographic symmetry is imposed on the individual molecules and thus, the contents of the asymmet-

Can. J. Chem. Downloaded from www.nrcresearchpress.com by 195.138.81.100 on 09/07/12
For personal use only.

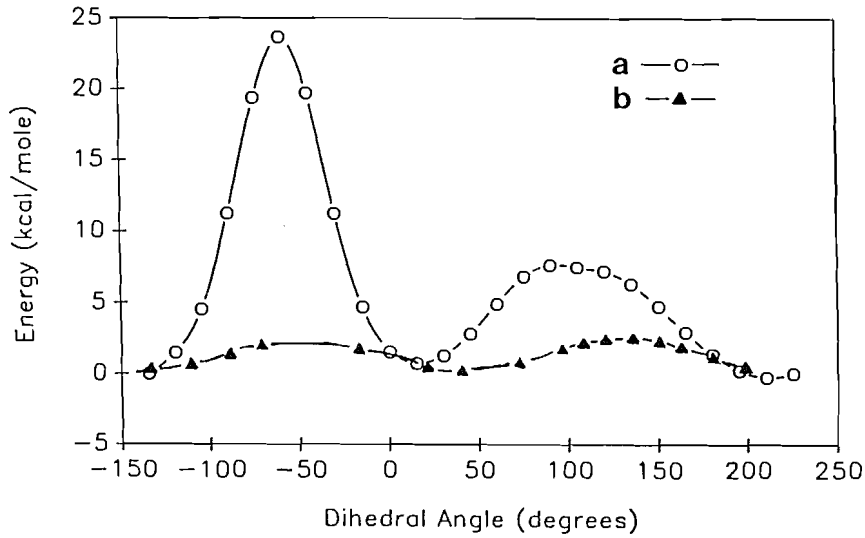


FIG. 4. (*a*) Plot of the energy barrier to Ti—N rotation for $Ti(NH_2)_3Cl$ derived from MMX calcualtions. (*b*) Plot of Extended Hückel total energy minimization curve for Ti—N rotation for $Ti(NH_2)_3Cl$ obtained employing OPT9 of TRIBBLE.

ric unit is a single molecule of **2**. The mononuclearity of the present compounds is in contrast to the tetrameric aggregates formed by $(Me_2N)_2TiF_2$ units (23) and the infinite chain structure formed by $(Et_2N)TiCl_3$ fragments (24).

For both **1** and **2**, the geometry of the Ti atoms of these monomeric species are best described as pseudo-tetrahedral, each being bonded to three nitrogen atoms and a chlorine. The Ti—Cl distances were found to be 2.300(3) Å in both molecules **1** and **2**. This compares to the Ti—Cl distances of 2.360, 2.708, and 2.251 Å found in $[(Et_2N)TiCl_3]_n$ (24). The Ti—Cl distance found in **1** and **2** is slightly shorter than that found in $Cp_2TiCl(C_5H_3N_4)$ (2.338 Å) (25) consistent with the Lewis acidity of the Ti centres in the present compounds. The Ti—N distances are similar being 1.866(4) Å in **1** and averaging 1.861(7) Å in **2**. In comparison, the Ti—N distance found in $[(Et_2N)TiCl_3]_n$ was 1.852(4) Å (25). In $[(Me_2N)_2TiF_2]_4$, the Ti—N distances of 2.14(3) and 2.19(3) Å correspond to the bridging amido groups while the Ti—N distances for terminal amido groups was found to be 1.99(3) Å (23). Similarly, the terminal Ti—N distances in the dimer $[Ti(NMe_2)_2(\mu\text{-N-}t\text{-Bu})]_2$ (1.914(2) Å) (26) were found to be slightly longer than those observed for **1** and **2**. Ti—N distances comparable to those in **1** and **2** were found in $Ti(OC_6H_2(t\text{-Bu})_3)_2(NMe_2)_2$ (1.878(5) Å) (27), $Ti(NMe_2)_2(O_2CNMe_2)_2$ (1.882(5) Å) (28) as well as the metallated Ti species $CpRu(CO)_2Ti(NMe_2)_3$ (1.885 (6) Å) (29). The N—Ti—N′ angle in **1** was found to be 105.4(2)° and ranged from 106.7(2) to 108.2(2)° in **2**. The Cl—Ti—N angle in **1** is 113.3(2)° whereas in **2** it averaged 111.4°. The angles about the nitrogen atoms sum to 360° indicative of the planarity at nitrogen, and suggestive of multiple bond character between the Ti and N. Such bonding is intuitively attributable to the Lewis acidity of the early metal centre. The C—C bond distances and angles within the ethyl moieties of **2** are as expected and precipitate no further comment.

Bonding considerations

The results of preliminary Extended Hückel calculations on the model compound $Ti(NH_2)_3Cl$ were considered. The calculated molecular orbital σ bonding framework of the molecule is as expected. Among the higher energy filled molecule orbitals are those attributable to Ti—N d_π—p_π bonding. One perspective of such bonding is shown in Fig. 3. The HOMO is a nonbonding orbital comprised of *p* orbital contributions from the N atoms. The LUMO is primarily titanium d_{z^2} in character. A more detailed treatment of the bonding in Lewis acidic early metal compounds will be forthcoming.[4]

Conformational considerations

The implication of Ti—N multiple bonding on the basis of structural and theoretical data for **1** and **2** raises the question regarding inhibited rotation about the Ti—N bonds. Variable temperature ^1H NMR studies of **1** and **2** over the temperature range 25 to −95°C were performed. In both cases, no change other than a slight changes in linewidth occurred on cooling to −95°C. This is in contrast to the temperature dependent spectra exhibited by $Zr(N(SiMe_3)_2)_3Cl$, **3** (ref. 30 and footnote 5). In the case of **3**, the spectra are interpreted in terms of the temperature dependence of rotation of the Zr—N bonds. It is intuitively expected on the basis of simple steric considerations, that rotation of the M—N bonds in **1** and **2** would occur more readily than in **3**.

One approach to questions of steric and conformational effects is offered by molecular mechanics calculations. Although this technique is best suited for applications in organic chemistry, it is of interest to examine the utility of these calculations in simple inorganic systems where the metal centre is approximately tetrahedral. Energy minimization calculations were performed on the model compound $Ti(NH_2)_3Cl$. The geometry of the initial model was derived from the crystallographic data. A total energy profile was calculated as a function of rotation of one of the Ti—N bonds. The energy barrier to rotation calculated was to be 25 kcal/mol for $Ti(NH_2)_3Cl$. Geometry optimization based on Extended Hückel energy calculations were also performed. The total energy was calculated as a function of rotation about a single Ti—N bond. The calculated barrier is small, on the order of 2–3 kcal/mol. These calculated energy profiles are shown in Fig. 4. The variable temperature NMR studies indicate that the barrier for **1** and **2** is less than 10 kcal/mol. It is clear from these results that molecular mechanics overestimates the barrier to rotation as this

[4]R. Rousseau and D. W. Stephan. Unpublished results.
[5]D. W. Stephan. Unpublished results.

Can. J. Chem. Downloaded from www.nrcresearchpress.com by 195.138.81.100 on 09/07/12
For personal use only.

approach does not model the cogwheel-like rotation of the three amido-groups. The EHMO calculation suggest that electronically the barrier to rotation is small. This implies that for substituted analogs of the model $Ti(NH_2)_3Cl$ steric factors will dominate the barrier to rotation of Ti—N bonds.

Acknowledgements

Financial support from NSERC of Canada is gratefully acknowledged. D.G.D. is grateful for the award of an NSERC postgraduate scholarship. R.R. is grateful for the award of an NSERC Summer Undergraduate Research Assistantship.

1. D. W. STEPHAN. Coord. Chem. Rev. **95**, 41 (1989).
2. G. S. WHITE and D. W. STEPHAN. Inorg. Chem. **24**, 1499 (1985).
3. G. S. WHITE and D. W. STEPHAN. Organometallics, **6**, 2169 (1987).
4. G. S. WHITE and D. W. STEPHAN. Organometallics, **7**, 903 (1988).
5. T. A. WARK and D. W. STEPHAN. Inorg. Chem., **26**, 363 (1987).
6. T. A. WARK and D. W. STEPHAN. Organometallics, **8**, 2836 (1989).
7. T. A. WARK and D. W. STEPHAN. Inorg. Chem. **29**, 1731 (1990).
8. L. GELMINI and D. W. STEPHAN. Inorg. Chim. Acta, **111**, L17 (1986).
9. L. GELMINI and D. W. STEPHAN. Inorg. Chem. **25**, 1222 (1986).
10. L. GELMINI and D. W. STEPHAN. Organometallics, **7**, 849 (1988).
11. L. GELMINI, L. C. MATASSA, and D. W. STEPHAN. Inorg. Chem. **24**, 2585 (1985).
12. L. GELMINI and D. W. STEPHAN. Organmetallics, **7**, 1515 (1988).
13. P. Y. ZHENG, T. T. NADASDI, and D. W. STEPHAN. Organometallics, **8**, 1393 (1989).
14. P. Y. ZHENG and D. W. STEPHAN. Can. J. Chem. **67**, 1584 (1989).
15. D. G. DICK and D. W. STEPHAN. Organometallics, **9**, 1910 (1990).
16. D. C. BRADLEY and I. M. THOMAS. J. Chem. Soc. 3857 (1960).
17. D. T. CROMER and J. B. MANN. Acta Crystallogr. Sect. A; Cryst. Phys., Diffr. Theor. Gen. Crystallogr. **A24**, 324 (1968).
18. D. T. CROMER and J. B. MANN. Acta Crystallogr. Sect. A; Cryst. Phys., Diffr. Theor. Gen. Crystallogr. **A24**, 390 (1968).
19. D. T. CROMER and J. T. WABER. International tables for X-ray crystallography. Kynoch Press, Birmingham, England. 1974.
20. D. A. PENSAK and J. J. WENDOLOSKI. Quantum Chemistry Program Exchange. No. 529.
21. E. BENZING and W. KORNICKER. Chem. Ber. **94**, 2263 (1961).
22. (*a*) G. CHANDRA and M. F. LAPPERT. Inorg. Nucl. Chem. Lett. **1**, 83 (1965); (*b*) G. CHANDRA and M. F. LAPPERT. J. Chem. Soc. (A), 1940 (1968); (*c*) M. F. LAPPERT and A. R. SANGER. J. Chem. Soc. (A), 1314 (1971).
23. W. S. SHELDRICK. J. Fluorine Chem. **4**, 415 (1974).
24. V. J. FAYOS and D. MOOTZ. Z. Anorg. Allg. Chem. **380**, 190 (1971).
25. A. L. BEAUCHAMP. D. COZAK, and A. MARDHY. Inorg. Chim. Acta, **92**, 191 (1984).
26. D. L. THORN, W. A. NUGENT, and R. L. HARLOW. J. Am. Chem. Soc. **103**, 357 (1981).
27. R. A. JONES, J. G. HEFNER, and T. C. WRIGHT. Polyhedron, **3**, 1121 (1984).
28. M. H. CHISHOLM and M. W. EXTINE. J. Am. Chem. Soc. **99**, 792 (1977).
29. W. J. SARTAIN and J. P. SELEGUE. J. Am. Chem. Soc. **107**, 5818 (1985).
30. R. A. ANDERSEN. Inorg. Chem. **18**, 1724 (1979).

Can. J. Chem. Downloaded from www.nrcresearchpress.com by 195.138.81.100 on 09/07/12
For personal use only.

An ICR mass spectrometry study of ion/molecule reactions between ethyl chloride and alkylamines

GUOYING XU and JAN A. HERMAN
Département de chimie, Université Laval, Québec (Qué.), Canada G1K 7P4

Received July 5, 1990

GUOYING XU and JAN A. HERMAN. Can. J. Chem. **69**, 363 (1991).

Ion/molecule reactions in mixtures of ethyl chloride with C_1–C_4 alkylamines were studied by ICR mass spectrometry. Ethyl cation transfer to C_1–C_4 alkylamines proceeds mainly through diethylchloronium ions with rate constants $\sim 3 \times 10^{-10}$ cm^3 s^{-1}. In the case of *s*-butylamine the corresponding rate constant is 0.5×10^{-10} cm^3 s^{-1}.

Key words: ICR mass spectrometry, ion/molecule reactions, ethylchloride, methylamine, ethylamine, propylamines, butylamines.

GUOYING XU et JAN A. HERMAN. Can. J. Chem. **69**, 363 (1991).

Faisant appel à la spectrométrie de masse ICR, on a étudié les réactions ions/molécules des mélanges du chlorure d'éthyle avec les alkylamines C_1–C_4. Le transfert du cation éthyle vers les alkylamines C_1–C_4 se produit prinicpalement par le biais d'ions diéthylchloroniums avec des constantes de vitesse d'environ 3×10^{-10} cm^3 s^{-1}. Dans le cas de la *s*-butylamine, la constante de vitesse correspondante est $0{,}5 \times 10^{-10}$ cm^3 s^{-1}.

Mots clés : spectrométrie de masse ICR, réactions ion/molécule, chlorure d'éthyle, méthylamine, éthylamine, propylamines, butylamines.

[Traduit par la rédaction]

Can. J. Chem. Downloaded from www.nrcresearchpress.com by 195.138.81.100 on 09/07/12
For personal use only.

Introduction

It is well established that the end-product ions formed in ion/molecule reactions of pure ethylchloride are the diethylchloronium ions, $(C_2H_5)_2Cl^+$, and their solvates, $[(C_2H_5)_2Cl^+\text{-}(C_2H_5Cl)_n]$. Since these products are unreactive toward ethyl chloride neutrals they are found to accumulate in the system with almost 90% yield at a pressure of one Torr in a high pressure mass spectrometer (1, 2).

Dialkylhalonium ions have been used as alkylating agents in both gas and liquid phase reactions (3–7), and it is expected that diethylchloronium ions will react similarly. Such alkylation processes are bimolecular nucleophilic displacement reactions and are usually highly exothermic for bases such as dimethyl ether, ethanol, ammonia, and many aromatic bases (5, 7, 8). The observed relative rates for many of these reactions (5, 7) reveal a negative temperature dependence, which strongly supports evidence for a double well potential model as summarized by Magnera and Kebarle (9).

Our intention was to study the alkylation processes between ethyl chloride and C_1–C_4 monoalkylamines to compare the importance of each of the following two reaction channels for the formation of $(C_2H_5)RNH_2^+$ species: (*a*) ethyl cation transfer from diethylchloronium ion, or (*b*) ethyl radical transfer from ethyl chloride to protonated alkylamine. The first channel being highly exothermic is expected to be the main reaction pathway, but the second channel, even if exothermic by <40 kJ/mol only, might contribute to the formation $(C_2H_5)RNH_2^+$ species especially at low concentration of ethyl chloride in the mixture.

Experimental

The pulsed ICR mass spectrometer used in this work has already been described (10, 11). The usual pulse sequence was started with a 2 ms ionizing pulse of 70 eV electrons followed by a variable delay (5–500 ms) during which ion/molecule processes take place. Then a 2 ms resonant RF frequency excitation pulse of 0.5 V, followed immediately by a 4 ms detection pulse, terminate the measured events. The pulse sequence is ended by a quenching pulse which sweeps out all remaining ions in the ICR cell. The magnetic field was set at 0.8 Tesla allowing to scan ions within a frequency range of 80 to 450 kHz which corresponds to a mass range of 26 to 150 amu. Due to the proximity of one of the trapping plates to the emission filament the temperature of the cell was not uniform. We estimate the average temperature of the cell to be around 50°C.

The pressure at which all experiments were performed was $(1.0 \pm 0.1) \times 10^{-5}$ Torr (1.33×10^{-5} mbar), as measured by an ionization gauge. At that pressure range ions can be kept in the ICR cell for about 2 s, but practical measurements of the intensities of ions limited this time to 0.5 s.

Ethyl chloride and methylamine from Matheson were of the best available purity (~99%). An analysis of methylamine has shown an impurity of 0.4% of dimethylamine. If trimethylamine is present as an impurity in methylamine it should be less than 0.1% which is the sensitivity limit of our analysis. Ethylamine from Matheson and the propyl-, isopropyl-, and butylamines from Aldrich were better than 99% pure and were used without further purification.

The mixtures of ethyl chloride with alkylamines were prepared in a known ratio in a separate high vacuum manifold, which was baked each time between preparation of gaseous samples.

Results and discussion

Since the ionization potential of ethyl chloride (IP = 10.97 eV) is higher than those of alkylamines (RNH_2), an efficient charge transfer from $C_2H_5Cl^+$ to RNH_2 will occur. Consequently, mixtures having a small content (<30%) of ethyl chloride will show peaks, if any, of low intensity of diethylchloronium ions (m/z = 93, 95), and therefore, these mixtures cannot be used to follow in the mass spectrum alkylation processes. For this reason we have measured the time evolution of mass spectra in $EtCl/RNH_2$ mixtures of concentration ratios 1:1 and 1:2. In such mixtures ion/molecule reaction sequences for each of the pure compounds is occurring and any new ion species originating from cross reactions between mixture components are easily observed and their relative rates of formation can be evaluated.

Mixtures of ethyl chloride (EtCl) with methylamine ($MeNH_2$)

Figure 1 shows the time evolution of fractional intensities of major ion species formed in the mixture $EtCl/MeNH_2$ = 1:1. We do not include the disappearance of the fragment ions of methylamine (m/z = 28, 29, and 30) as a function of time,

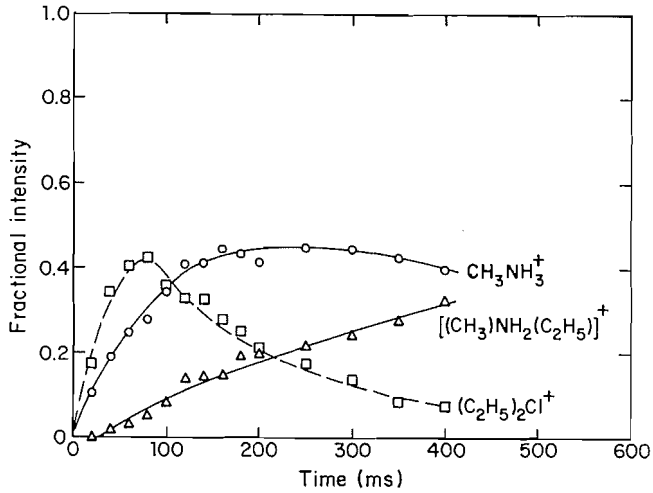


FIG. 1. Time evolution of fractional intensities of some ions of interest in C_2H_5Cl/CH_3NH_2 = 1:1 mixture.

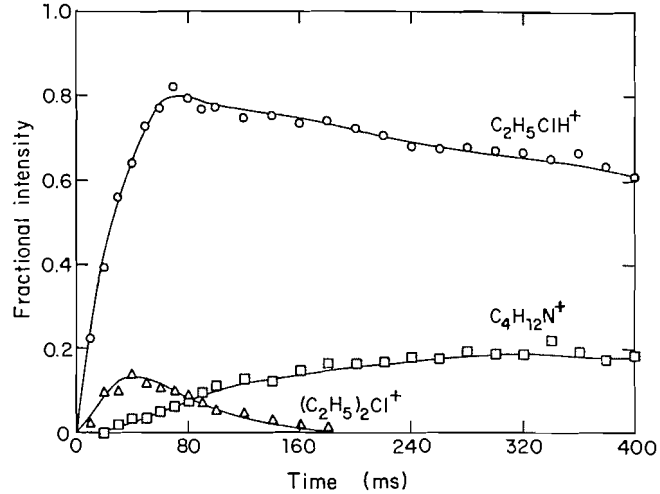


FIG. 2. Time evolution of fractional intensities of some ions of interest in $C_2H_5Cl/C_2H_5NH_2$ = 1:1 mixture.

because all these species vanish very quickly (<40 ms) in the proton transfer processes to form protonated methylamine, $CH_3NH_3^+$ (m/z = 32). Similarly we do not include the disappearance curves of the primary and fragments ions of ethyl chloride, nor the decay of the protonated species, $C_2H_5ClH^+$ (m/z = 65, 67), because within 40 ms the diethylchloronium ions are practically the sole species originating from ethylchloride left in the mass spectrum.

The m/z = 46 ion present in the mass spectrum is assumed to be $(CH_3)_2NH_2^+$ and could be accounted for totally by the presence of the dimethylamine impurity in the mixture, and is therefore omitted from Fig. 1. In the mass spectrum there are also small quantities of ion species of m/z = 56, 57, and 58 (<2% each) wich are usually seen in the high pressure mass spectrum of ethyl chloride. They are assumed to be $C_4H_8^+$, $C_4H_9^+$, and $C_4H_{10}^+$ species (2, 7). These ions do not intervene in any significant ion/molecule reactions with the mixture of neutral components, and therefore, will be systematically ignored in the present figures.

The only possible cross-product ion in the $EtCl/MeNH_2$ system is the m/z = 60 species, which is formed at longer times (>30 ms) and which is assumed to be $[C_2H_5NH_2CH_3]^+$.

[1] $(C_2H_5)_2Cl^+ + CH_3NH_2 \rightarrow [C_2H_5NH_2Cl_3]^+ + C_2H_5Cl$

$\Delta H_4 = -143$ kJ mol^{-1}

In calculating the enthalpy changes the values are taken from ref. 7 for the diethylchloronium ion and from ref. 12 for the other species.

Another possible structure could be $(CH_3)_3NH^+$, originating either from a proton transfer to the trimethylamine impurity, or a methyl group transfer to the protonated dimethylamine:

[2] $CH_3NH_3^+ + (CH_3)_3N \rightarrow (CH_3)_3NH^+ + CH_3NH_2$

$\Delta H_4 = -46.3$ kJ mol^{-1}

[3] $(CH_3)_2NH_2^+ + CH_3NH_2 \rightarrow (CH_3)_3NH^+ + NH_3$

$\Delta H_r = -46.9$ kJ mol^{-1}

As for reaction [2] the low concentration of this impurity (<0.1%) should give at 400 ms a contribution to the fractional intensity of approximately 0.04 (13), which is small compared to the experimental value of 0.33 in Fig. 1. Reaction [3] would contribute to the fractional intensity by around 0.11 if the assumed rate constant for this reaction is 1×10^{-10} cm^3 s^{-1} (14).

An additional argument in favour of an ethyl–methyl–ammonium structure might be inferred from the behaviour of the fractional intensities of the diethylchloronium and the m/z = 60 ions. After an initial rapid growth in intensity of the diethylchloronium ions with a maximum achieved at 40 ms the next systematic decrease in intensity coincides with a corresponding intensity increase of the m/z = 60 species, while the intensity of $CH_3NH_3^+$ ions remains constant, Fig. 1.

Mixtures of ethyl chloride with ethylamine ($EtNH_2$)

The time evolution of fractional intensities of the major species formed in the mixture $EtCl/EtNH_2$ = 1:1 are displayed in Fig. 2. The expected cross-product ion, $(C_2H_5)_2NH_2^+$ (m/z = 74), is clearly seen in the mass spectrum. However, this species can be formed via at least four reaction channels: (*a* and *b*) ethyl group transfer in exothermic processes from either ethylamine or ethylchloride to protonated ethylamine, (*c*) $C_2H_5^+$ transfer from the diethylchloronium species to ethylamine, and (*d*) from the diethylamine impurity. The present experimental data cannot unravel between the four possibilities, and any simulation of the rates would be a hopeless exercise. Therefore, we will not discuss this particular system.

Mixtures of ethyl chloride with n*-propylamine (ProNH2)*

The experimental data for ion-products formed in the mixture $EtCl/ProNH_2$ = 1:1 are shown in Fig. 3. The ion of interest is m/z = 88, which is assumed to be the ethylated propylamine ion: $[(C_3H_7)NH_2(C_2H_5)]^+$, and which is also found with small intensity in pure propylamine (~3% at 400 ms) (14). The intensity of m/z = 88 signal decreases as the concentration of ethyl chloride in the mixtures decreases. In a 4:1 mixture of $C_3H_7NH_2$:C_2H_5Cl, the intensity of this ion is too low to be detected. This suggests that ethyl chloride plays an important role in the formation of m/z = 88 ions:

[4] $(C_2H_5)_2Cl^+ + C_3H_7NH_2 \rightarrow [(C_3H_7)NH_2(C_2H_5)]^+ + C_2H_5Cl$

The heat of formation of $[(n\text{-}C_3H_7)NH_2(C_2H_5)]^+$ is not known, but it should not differ much (a few kJ/mol) from that of the value of 474 kJ mol^{-1} measured for its isomeric species $[(i\text{-}C_3H_7)NH_2(C_2H_5)]^+$ (12). In that case the enthalpy change for reaction [4] would be $\Delta H_r \approx -174$ kJ mol^{-1}.

Can. J. Chem. Downloaded from www.nrcresearchpress.com by 195.138.81.100 on 09/07/12
For personal use only.

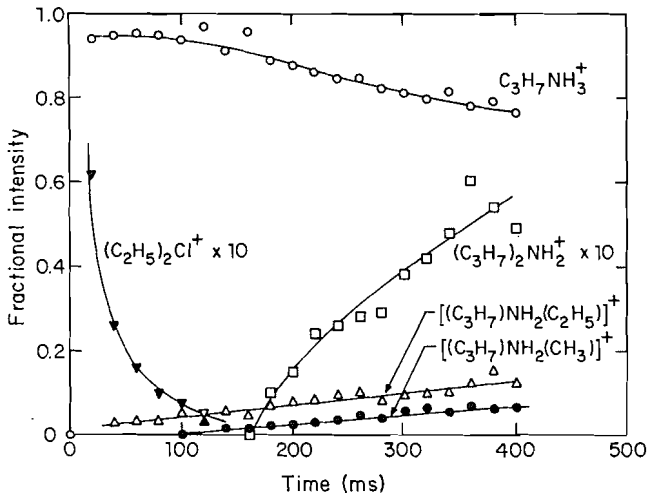


FIG. 3. Time evolution of fractional intensities of some ions of interest in $C_2H_5Cl/n\text{-}C_3H_7NH_2$ = 1:1 mixture.

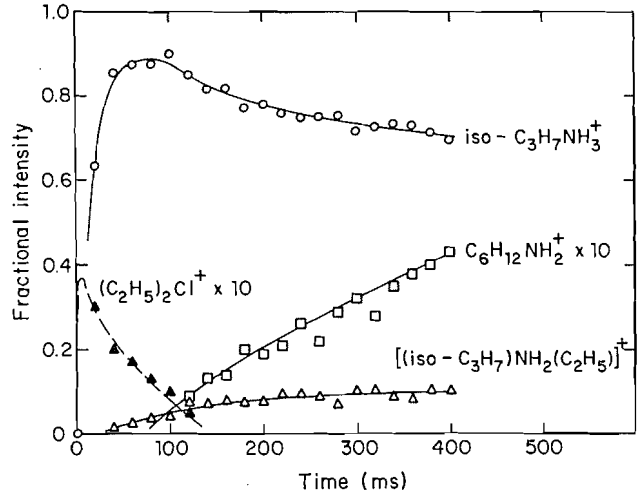


FIG. 4. Time evolution of fractional intensities of some ions of interest in $C_2H_5Cl/iso\text{-}C_3H_7NH_2$ = 1:1 mixture.

On the other hand, the intensity of diethylchloronium ions (m/z = 93, 95) approaches zero within 100 ms, while the intensity of m/z = 88 ions continues to increase long after, Fig. 3. It appears that to some extent the formation of m/z = 88 also corresponds to the consumption of the protonated propylamine (m/z = 60) in the two following reactions:

[5] $C_3H_7NH_3^+ + C_2H_5Cl \rightarrow [(C_3H_7)NH_2(C_2H_5)]^+ + HCl$

[6] $C_3H_7NH_3^+ + C_3H_7NH_2 \rightarrow C_5H_{14}N^+ + CH_3NH_2$

Assuming that $\Delta H_f[(C_3H_7)NH_2(C_2H_5)]^+$ is comparable to that of its isopropyl group containing isomer, the enthalpy of reaction [5] would be around -54 kJ mol^{-1} (12). On the other hand, the enthalpy change of reaction [6] depends on the structure of the $C_5H_{14}N^+$ species, but if it corresponds to $[(C_3H_7)NH_2(C_2H_5)]^+$, which is likely, then the heat of reaction would be slightly exothermic by ≈ -21 kJ mol^{-1}. As mentioned previously, reaction [6] which occurs in pure propylamine with a low rate constant ($<10^{-12}$ cm^3 s^{-1}) (14) might be real, or may reflect the presence of small amounts of impurities. Thus, the contribution from reaction [5] must be quite significant in this system.

The ion with m/z = 74 is assumed to be the methylated propylamonium ion: $[(CH_3)NH_2(C_3H_7)]^+$. It is observed in the mass spectrum of pure propylamine. It probably originates in a decomposition ion/molecule reaction between $C_3H_7NH_3^+$ and $C_3H_7NH_2$, (14) or from some impurity.

Mixtures of ethyl chloride with iso*-propylamine (*iso*-ProNH$_2$)*

In Fig. 4 is shown the time evolution of the fractional intensities of ions of interest formed in a $EtCl/iso\text{-}ProNH_2$ = 1:1 mixture. It is assumed that ions with m/z = 60, 88, and 100 are $[(CH_3)_2CHNH_3]^+$, $[(iso\text{-}C_3H_7)NH_2(C_2H_5)]^+$, and $C_6H_{12}NH_2^+$. The last ion is the main product-ion observed in the high pressure mass spectrum of pure *iso*-propylamine and is formed in a condensation-rearrangement reaction with elimination of ammonia and molecular hydrogen. This ion is not observed in the high-pressure mass spectrum of *n*-propylamine, and conversely the $[(C_3H_7)_2NH_2]^+$ (m/z = 102) ion present in the spectrum of *n*-propylamine is not observed in pure *iso*-propylamine. In pure *iso*-propylamine the ion with m/z = 88 is not observed, but becomes detectable when sufficient amounts of ethylchloride are present in the system. In the $EtCl/iso\text{-}ProNH_2$ = 1:1 mixture the ions with m/z = 88 are more abundant than the ions with m/z = 100 (Fig. 4). In 1:4 mixture these two ions have almost the same fractional intensities, and in 1:8 mixture the m/z = 100 ion species become the major product. This trend indicates that ethyl chloride is an essential compound for the formation of $C_5H_{14}N^+$ (m/z = 88) species, and the main channel for the formation of this ion is reaction [7]:

[7] $(C_2H_5)_2Cl^+ + iso\text{-}C_3H_7NH_2 \rightarrow [(C_3H_7)NH_2(C_2H_5)]^+ + C_2H_5Cl$

$\Delta H_r = -174$ kJ mol^{-1}

Mixtures of ethyl chloride with butylamines (BuNH$_2$)

Mixtures of ethylchloride with *n*-butylamine, *s*-butylamine, and *tert*-butylamine were studied.

In the mass spectrum of $EtCl/n\text{-}BuNH_2$ mixture the ion with m/z = 102, $C_6H_{16}N^+$, which might correspond to the cross-product ion, is also observed in the mass spectrum of pure 1-butylamine and accounts already for ~15% at 400 ms. In this case the probable formation process for this ion is a proton transfer to an unidentified impurity.

In the mass spectrum of $EtCl/n\text{-}BuNH_2$ mixtures the m/z = 102 ion is observed in variable amounts depending on neutral component ratios, but its fractional intensity is smaller than that for the pure *n*-butylamine. The occurrence of reaction [8]

[8] $(C_2H_5)_2Cl^+ + 1\text{-}C_4H_9NH_2 \rightarrow (C_4H_9NH_2C_2H_5)^+ + C_2H_5Cl$

in competition with a possible formation (as mentioned above) of an unidentified impurity with m/z = 102 does not allow us to make an unambiguous assessment of the importance of these two reaction channels. For this reason we did not simulate kinetics for this system as it would be only an arbitrary exercice.

In contradistinction to the previous system the formation of the cross-product ion with m/z = 102 can be unambiguously followed in the $EtCl/s\text{-}BuNH_2$ mixtures. In pure *s*-butylamine the ion with m/z = 102 is not formed, or its amount is within the background (~2%) of the mass spectrum, Fig. 5*a*. In Fig. 5*b* are shown the fractional intensities of the ions of interest in the $EtCl/s\text{-}BuNH_2$ = 1:2 mixture. As mentioned previously we did not draw the time evolution of primary and fragment ions, which disappear very quickly (<50 ms) to form the protonated butylamine and the diethylchloronium ions. In this figure an increase

Can. J. Chem. Downloaded from www.nrcresearchpress.com by 195.138.81.100 on 09/07/12
For personal use only.

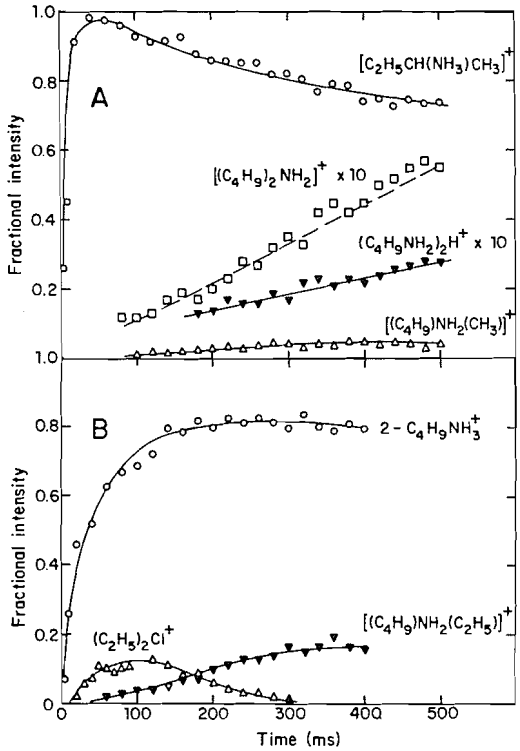


FIG. 5. Time evolution of fractional intensities of some ions of interest: (*A*) in pure *s*-$C_4H_9NH_2$, and (*B*) in C_2H_5Cl/*s*-$C_4H_9NH_2$ = 1:2 mixture.

in the intensity of m/z = 102 species coincides with a decrease of the intensity of the $(C_2H_5)_2Cl^+$ peak. It also seems that the formation of the m/z = 102 species does not correspond to the consumption of the protonated 2-butylamine ions (m/z = 74). Moreover, the relative intensities of the cross-product ion with m/z = 102 decrease to zero in mixtures richer in *s*-butylamine. Therefore the alkylation process is thought to proceed mainly through diethylchloronium ion consumption:

[9] $(C_2H_5)_2Cl^+ + s\text{-}C_4H_9NH_2 \rightarrow [(C_4H_9)NH_2(C_2H_5)]^+ + C_2H_5Cl$

The ΔH_f of butylethylammonium ion is unknown, but the dialkylamine ions of the same formula, $C_6H_{16}N^+$, have heats of formation between 101 and 111 kJ mol^{-1} (12), and it might be assumed that a comparable value characterizes the $[(C_4H_9)NH_2(C_2H_5)]^+$ species. If such is the case, then ΔH_r = -148 ± 10 kJ mol^{-1} for reactions [8] and [9].

Finally in the case of mixtures of *tert*-butylamine and ethyl chloride no cross-product ions with m/z = 102 were observed.

Rates of reaction

The reactivities of alkylamines with $(C_2H_5)_2Cl^+$ ions and chloroethane with RNH_3^+ species (R = CH_3, C_3H_7, and C_4H_9) are shown in Table 1. These values were obtained by numerical simulation by the procedure outlined in ref. 15. In these calculations the available rate constants for diethylchloronium ions formation (5), and those for the protonation of alkylamines in pure amines (14) were used. However, the results of numerical simultion in these complex systems are to be considered cautiously. Usually more than one reaction channel contributes to the formation of the studied species, and in these cases some arbitrariness is expected in assuming the relative importance of each reaction channel, even as in these calculations only exothermic ion/molecule processes were taken into account. Nevertheless, the simulated rate constants in Table 1 compare

TABLE 1. The rate constants of ethyl cation transfer

Reaction	$k \times 10^{10}$ cm^3 s^{-1}
$(CD_3)_2Cl^+ + CH_3NH_2$	145. ± 1.5
$(C_2H_5)_2Cl^+ + CH_3NH_2$	2 ± 1.5
$(C_2H_5)_2Cl^+ + C_2H_5NH_2$	n.d.[a]
$(C_2H_5)_2Cl^+ + n\text{-}C_3H_7NH_2$	3.1 ± 0.6
$(C_2H_5)_2Cl^+ + iso\text{-}C_3H_7NH_2$	3.3 ± 0.6
$(C_2H_5)_2Cl^+ + n\text{-}C_4H_9NH_2$	n.d.
$(C_2H_5)_2Cl^+ + s\text{-}C_4H_9NH_2$	0.5 ± 0.2
$(C_2H_5)_2Cl^+ + tert\text{-}C_4H_9NH_2$	< 0.005

[a]n.d. = not determined.

favourably with those already available for ethylation reactions with ammonia or trimethylamine (5), which are

[10] $[(C_2H_5)Cl(CH_3)]^+ + NH_3 \rightarrow C_2H_5NH_3^+ + CH_3Cl$

$k = 1.6 \times 10^{-10}$ cm^3 s^{-1}

[11] $[(C_2H_5)Cl(CH_3)]^+ + (CH_3)_3N \rightarrow [(CH_3)_3N(C_2H_5)]^+ + CH_3Cl$

$k = 4.0 \times 10^{-10}$ cm^3 s^{-1}

We also present in Table 1 the rate constant for the unambiguous reaction:

[12] $(CD_3)_2Cl^+ + CH_3NH_2 \rightarrow [CH_3NH_2CD_3]^+ + CD_3Cl$

measured on a FT-ICR instrument.[1] The rate constant for reaction [12] (Table 1) is about 20% higher than the rate coefficient for the following similar reaction (7):

[13] $(CH_3)_2Cl^+ + (CH_3)_3N \rightarrow (CH_3)_4N^+ + CH_3Cl$

$k = 11.7 \times 10^{-10}$ cm^3 s^{-1}

which seems reasonable.

The comparison of rate constant values show that the rates of methylation or ethylation of C_1–C_3 alkylamines (reactions [1], [4], [7], and [9]) are comparable, being around 1/5 of the collision rate estimated by trajectory calculation (16). The high uncertainty of the rate constant of reaction [1] results from the occurrence of reactions [2] and [3] the contributions of which are not easy to estimate. In the case of *s*-butylamine (reaction [9]) this rate constant diminishes by a factor of 6, probably due to the size and structure of the amine.

According to Sen Sharma and Kebarle's observation $C_2H_5^+$ transfer from methyl–ethyl–chloronium ion, $CH_3ClC_2H_5^+$, to benzene, toluene, and isopropylbenzene is faster at 305 K than the transfer of CH_3^+ from dimethylchloronium ions, $(CH_3)_2Cl^+$ (5). They suggested that the internal barrier is smaller for the transfer of the more weakly bound $C_2H_5^+$ to a given aromatic. In contrast, Mathews and Stone reported that the $C_2H_5^+$ transfer from diethylchloronium ion, $(C_2H_5)_2Cl^+$, to these aromatics is slower than CH_3^+ transfer from dimethylchloronium species (7). Our results are in agreement with those of Mathews and Stone (7).

The major channels for ethylation of alkylamine by ethyl chloride proceed through reactions [1], [4], [7], and [9] involving diethylchloronium ions. A similar behaviour was found in alkylamine/methyl chloride systems, where methylation occurs mainly in reactions between d_6-dimethylchloronium ions, $(CD_3)_2Cl^+$, and neutral alkylamines.[2]

[1]Department of Chemistry, University of Waterloo, Waterloo.

[2]J. A. Herman, K. Herman, and T. B. McMahon. Unpublished results.

Can. J. Chem. Downloaded from www.nrcresearchpress.com by 195.138.81.100 on 09/07/12
For personal use only.

The other possible methyl group transfer reaction channel:

[14] $RNH_3^+ + CD_3Cl \rightarrow [RNH_2CD_3]^+ + HCl$

where R = CH_3, C_2H_5, C_3H_7, and C_4H_9, is observed, but with very low rate constant values ($\leq 5 \times 10^{-13}$ cm^3 s^{-1}).[3] We expect that processes similar to reaction [14] between protonated alkylamines and ethyl chloride will proceed also at very low rates ($\sim 10^{-13}$ cm^3 s^{-1}), and therefore will not greatly contribute to the formation of ethylated alkylamines, $(C_2H_5)RNH_{2+}$.

Conclusion

In mixtures of alkylamine with ethyl chloride, ethyl cation transfer to methylamine, propylamines, 2-butylamine and most probably also to ethylamine, proceeds mainly through diethylchloronium ion, with rate constants $\sim 3 \times 10^{-10}$ cm^3 s^{-1}. Only *s*-butylamine reacts slower (Table 1). The second competitive pathway of ethylation occurring between protonated alkylamines and neutral ethylchloride, although slightly exothermic or thermoneutral, does not seem to proceed with sufficient rate to contribute evidently.

Acknowledgement

This work was supported by the Natural Sciences and Engineering Research Council (NSERC) of Canada.

[3]J. A. Herman, K. Herman, and T. B. McMahon. Unpublished results.

1. J. L. Beauchamp, D. Holtz, S. D. Woodgate, and S. L. Patt. J. Am. Chem. Soc. **94**, 2798 (1972).
2. Z. Luczynski and H. Wincel. Int. J. Mass Spectrom. Ion Phys. **14**, 29 (1974).
3. G. A. Olah. Halonium ions. Wiley Interscience, New York. 1975.
4. W. J. van der Hart, W. C. M. M. Luijten, and J. van Thuiji. Org. Mass. Spectrom. **15**, 463 (1980).
5. D. K. Sen Sharma and P. Kebarle. J. Am. Chem. Soc. **104**, 19 (1982).
6. J. A. Stone, W. M. Splinter, and D. E. Splinter. Can. J. Chem. **62**, 1373 (1984).
7. P. J. Mathews and J. A. Stone. Can. J. Chem. **66**, 1239 (1988).
8. Z. Łuczynski and J. A. Herman. J. Phys. Chem. **82**, 1679 (1978).
9. T. F. Magnera and P. Kebarle. *In* Ionic processes in the gas-phase. *Edited by* M. A. Almoster Ferreira. D. Reidel Publishing Co. 1982. p. 135.
10. J. A. Herman, R. Neagu-Plesu, and Ł. Wojcik. Can. J. Chem. **67**, 97 (1989).
11. L. Wójcik and J. A. Herman. Nukleonika, **34**, 163 (1989).
12. S. G. Lias, J. E. Bartmess, J. F. Liebman, J. L. Holmes, R. D. Levin, and W. G. Mallard. Gas-phase ion and neutral thermochemistry. J. Phys. Chem. Ref. Data, Vol. 17, Suppl. 1. 1988.
13. J. A. Herman, K. Herman, and T. B. McMahon. J. Am. Soc. Mass Spectrom. In press
14. G. Xu. Ph.D. Thesis. Université Laval, Québec, Qué. 1989.
15. G. Xu, J. A. Herman, and L. Wójcik. Can. J. Chem. **68**, 570 (1990).
16. T. Su and W. J. Chesnavich. J. Chem. Phys. **76**, 5183 (1982).

Can. J. Chem. Downloaded from www.nrcresearchpress.com by 195.138.81.100 on 09/07/12
For personal use only.

Excess properties for binary liquid mixtures of propionic acid with aniline derivatives

BEGOÑA GARCÍA,[1] RAFAEL ALCALDE, AND JOSÉ M. LEAL
Universidad de Valladolid, Departamento de Química Física, Colegio Universitario Integrado, 09001 Burgos, Spain
Received December 21, 1989

BEGOÑA GARCÍA, RAFAEL ALCALDE, and JOSÉ M. LEAL. Can. J. Chem. **69**, 369 (1991).

Excess viscosities, excess volumes, and excess free energies of activation for flow of the binary mixtures containing propionic acid with aniline, *o*-toluidine, *o*-anisidine, and *o*-chloroaniline were determined at five different temperatures from density and viscosity measurements. Based on the Regular Solutions Theory, the empirical parameter θ was calculated; this parameter is related to the viscosity, and also denotes the extent of the non-ideality of the system. The results obtained suggest the existence of acid–base interactions, as well as the formation of 1:2 complexes for the three first mixtures, and 2:1 complexes for *o*-chloroaniline + propionic acid. The extent of the specific interaction decreases with an increase in the strength of the base, and increases with an increase in the dipole moments. The equation $V = V_1^{X_1} \cdot V_2^{X_2}$ is proposed for predicting the mole volume of the mixtures, V, at any composition, X_i, as a function of the mole volumes of the pure components, V_i.

Key words: binary mixture, excess properties, predicting mole volumes, propionic acid.

BEGOÑA GARCÍA, RAFAEL ALCALDE et JOSÉ M. LEAL. Can. J. Chem. **69**, 369 (1991).

En se basant sur des mesures de densité et de viscosité obtenues à cinq températures différentes, on a déterminé les viscosités en excès, les volumes en excès et les énergies libres d'activation en excès pour l'écoulement de mélanges binaires contenant de l'acide propionique et de l'aniline, de l'*o*-toluidine, de l'*o*-anisidine et de l'*o*-chloroaniline. En se basant sur la théorie des solutions idéales, on a calculé le paramètre empirique θ; ce paramètre est relié à la viscosité et il est le reflet de la non-idéalité du système. Les résultats suggèrent qu'il existe des interactions acide–base ainsi qu'il y a formation de complexes 1 : 2 dans les trois premiers mélanges et de complexes 2 : 1 dans le cas de l'*o*-chloroaniline + l'acide propionique. L'importance de ces interactions spécifiques diminue avec une augmentation de la force de la base et elle augmente avec les moments dipolaires. On propose l'équation pour prédire le volume molaire, $V = V_1^{X_1} = V_2^{X_2}$, V, des mélanges à toute composition, X_i, et en fonction des volumes molaires, V_i, des produits purs.

Mot clés : mélange binaire, propriétés en excès, prédiction des volumes molaires, acid propionique.

[Traduit par la rédaction]

Introduction

In previous papers (1–3), the behaviour of binary mixtures containing polar liquids was investigated. Continuing the study of this type of mixtures, we report here excess molar volumes V^E, excess viscosities η^E, and excess free energies of activation for flow ΔG^{*E}, at five different temperatures of binary mixtures containing propionic acid + aniline, + *o*-toluidine, + *o*-anisidine, and + *o*-chloroaniline. From the values of the ionization constants of the *o*-substituted anilinium ions (4–6), an important role of the acid–base interactions may be inferred. The results obtained suggest the existence of proton transfer processes in the three first systems, as well as the probable existence of other interactions responsible for complex formation among the components of the mixtures. A detailed analysis of the relationships existing between η, V, and the empirical parameter θ is made and compared with those reported by other authors. From the proper definition of the magnitude ΔG^{*E}, a simple equation is deduced that permits predicting the molar volume of the mixtures at any composition using the molar volumes of the pure components.

Experimental

The solvents used were commercially available (Merck); aniline and *o*-toluidine were purified by distillation; *o*-anisidine and *o*-chloroaniline were recrystallized according to methods already described (7). The improvement in purity was followed by GC, UV–VIS spectroscopy, and density and viscosity measurements.

Measurements

Densities were measured with a double levelling pycnometer; it was calibrated at the five working temperatures. Viscosities were measured with a Cannon–Fenske viscometer calibrated with distilled water at different temperatures, with the density and viscosity values taken from the literature (8). Temperature was kept constant within ±0.01°C. Densities and viscosities were accurate within ±0.0001 and 0.004 units, respectively.

The purity of the reactants was assessed with a Perkin Elmer 990 gas chromatograph and Perkin Elmer 554 UV–VIS spectrophotometer, since absorptivities of these species had previously been determined (4, 6, 10). Analysis of the data was carried out with an Olivetti M 240 computer.

Results and discussion

In the investigation on binary mixtures of propionic acid with benzene, methylbenzene, ethylbenzene, and propylbenzene, Subha and Rao (11) found that viscosities decreased to a greater extent with the initial addition of hydrocarbons to propionic acid. Although this behaviour was interpreted by Johari (12) as characteristic of systems where at least one of the components exhibits intramolecular hydrogen bonding, Subha and Rao (13) reported maximum values for viscosities around $X = 0.35$ at 25°C for three acid–base mixtures, including aniline – propionic acid, in agreement with our own results. A table containing values of densities and viscosities obtained for the four binary mixtures at different temperatures has been deposited.[2]

In the present paper, the variation of viscosities with mole fraction at different temperatures fitted a polynomial equation for aniline derivatives fairly well. Strong deviations from linearity, characteristic of ideal behaviour, are apparent. According to Fort and Moore (14), such deviations may be attributed to specific interactions arising from the formation of complexes among the mixing molecules.

[1]Author to whom correspondence may be addressed.

[2]This table and others referred to in the text (Tables 2–6) may be purchased from the Depository of Unpublished Data, CISTI, National Research Council of Canada, Ottawa, Ont., Canada K1A 0S2.

Printed in Canada / Imprimé au Canada

Can. J. Chem. Downloaded from www.nrcresearchpress.com by 195.138.81.100 on 09/07/12
For personal use only.

Can. J. Chem. Downloaded from www.nrcresearchpress.com by 195.138.81.100 on 09/07/12
For personal use only.

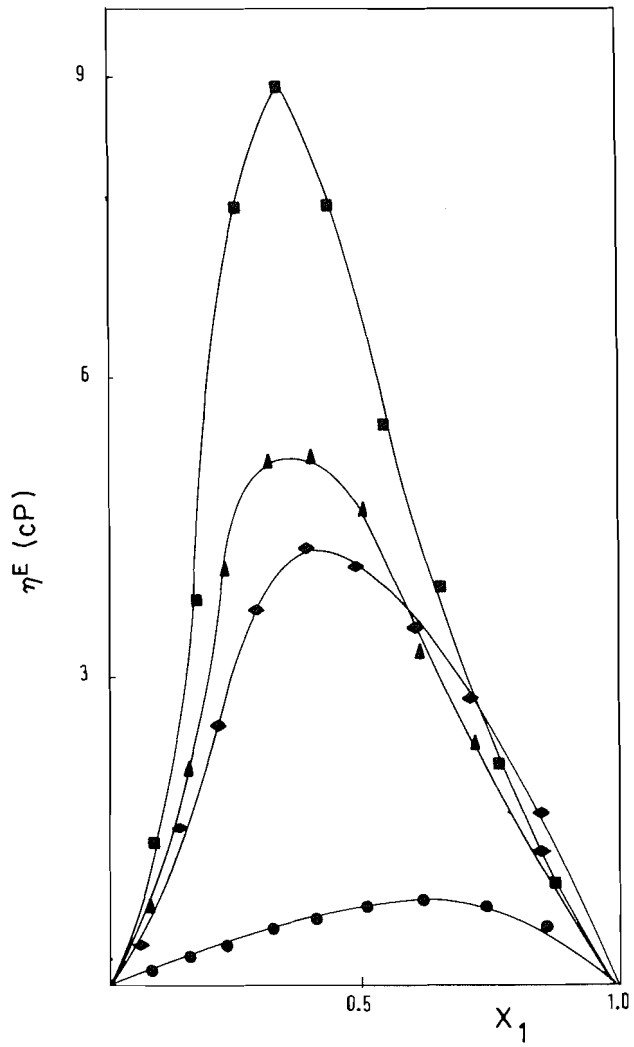


FIG. 1. Variation of the excess viscosity η^E (cP) with aniline derivative mole fraction for mixtures of propionic acid + *o*-chloroaniline (●), + *o*-anisidine (◆), + *o*-toluidine (▲), and + aniline (■); T = 293 K.

The values η^E, V^E, and ΔG^{*E} were fitted, at each temperature for each of the four mixtures studied, to a Redlich–Kister polynomial function. The excess viscosities of the four mixtures exhibited maxima against the mole fraction, these maxima decreasing with an increase in temperature, located at about X = 0.35 for aniline, *o*-toluidine, and *o*-anisidine, and at about X = 0.65 for *o*-chloroaniline (Fig. 1). This behaviour is also observed in liquid mixtures capable of forming complex species by intermolecular hydrogen bonding. The four mixtures showed negative excess volumes with well-defined minima (Fig. 2). Excess free energies of activation for flow behaved similarly to the excess viscosities, with maxima around X = 0.35, except for *o*-chloroaniline (Fig. 3). The solid lines in the figures were generated with the aid of the polynomial coefficients. Tables of the least-squares coefficients of the polynomial regressions for these excess quantities are available from the Depository of Unpublished Data.[2]

The results obtained for the thermodynamic properties of the mixtures indicate that the extent of the interaction increases according to the strength of the base: aniline (pK = 4.60) > *o*-toluidine (pK = 4.40) > *o*-anisidine (pK = 4.38) > *o*-chloroaniline (pK = 2.71), K being the ionization constant of the corresponding anilinium ions according to $RNH_3^+ \rightleftharpoons RNH_2 + H^+$ (4–6). At mole fractions corresponding to η^E maxima, the amount of protons required for the acid–base reactions may be supplied by the acid component of the mixtures (pK = 4.87) (9) in all cases except for *o*-chloroaniline, since its basicity is much lower than the acid strength of propionic acid. Nevertheless, the excess properties of the binary mixtures with *o*-toluidine and *o*-anisidine evidence behaviour less similar than would be expected from the strength of the bases. This fact indicates the existence of interactions, different from hydrogen bonding, responsible for the complex formation; to a first approximation (15), the stoichiometry of these complexes can be determined from the ratio of mole fractions corresponding to the maxima η^E, yielding the values 2:1 for *o*-chloroaniline and 1:2 for the other three mixtures.

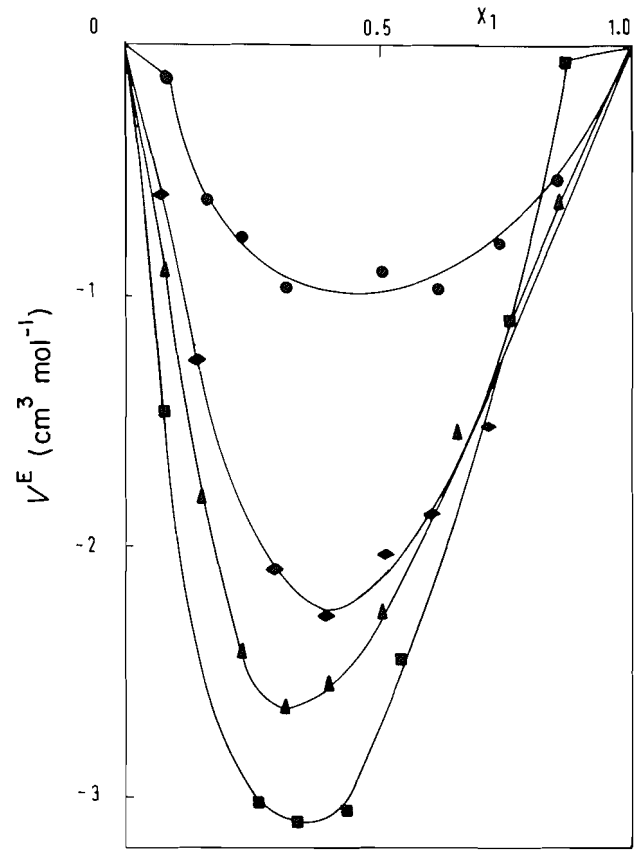


FIG. 2. Variation of the excess volumes V^E (cm^3 mol^{-1}) with aniline derivative mole fraction at 293 K (symbols as in Fig. 1).

Based on the ideas of the Regular Solutions Theory (16, 17), Grunberg and Nissan (18) proposed an empirical expression for viscosities of real liquid mixtures:

$$[1] \quad \ln \eta_{obs} = \ln \eta_{id} + X_1 X_2 \theta$$

where θ denotes the extent of non-ideality of the system, and

$$[2] \quad \ln \eta_{id} = X_1 \ln \eta_1 + X_2 \ln \eta_2$$

The variation of θ with temperature and composition is in the order (a) aniline > *o*-toluidine > *o*-anisidine > *o*-chloroaniline at constant temperature and composition; (b) θ decreases with an increase in temperature for all systems. Values of θ at different temperatures and mole fractions, obtained from eq. [1] have been placed in the Depository of Unpublished Data.[2] These results are in good agreement with those arising from the excess properties.

Prolongo *et al.* (19) reported positive values of θ correspond-

Can. J. Chem. Downloaded from www.nrcresearchpress.com by 195.138.81.100 on 09/07/12
For personal use only.

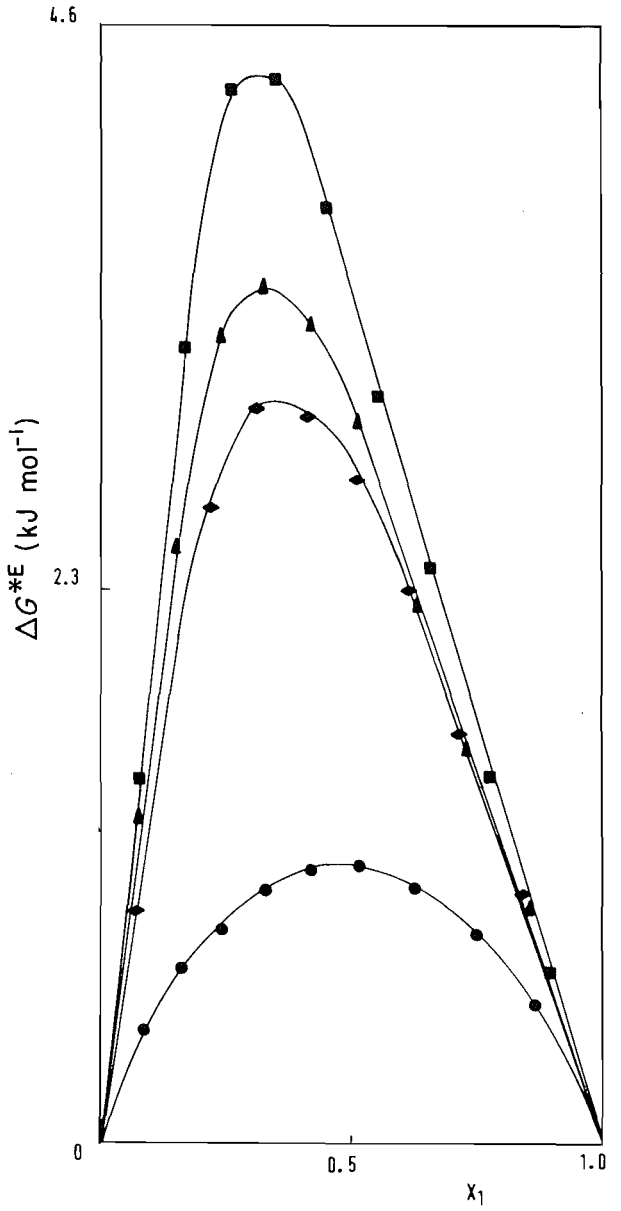


FIG. 3. Variation of the excess free energies of activation for flow ΔG^{*E} (kJ mol^{-1}) with aniline derivative mole fraction at 293 K (symbols as in Fig. 1).

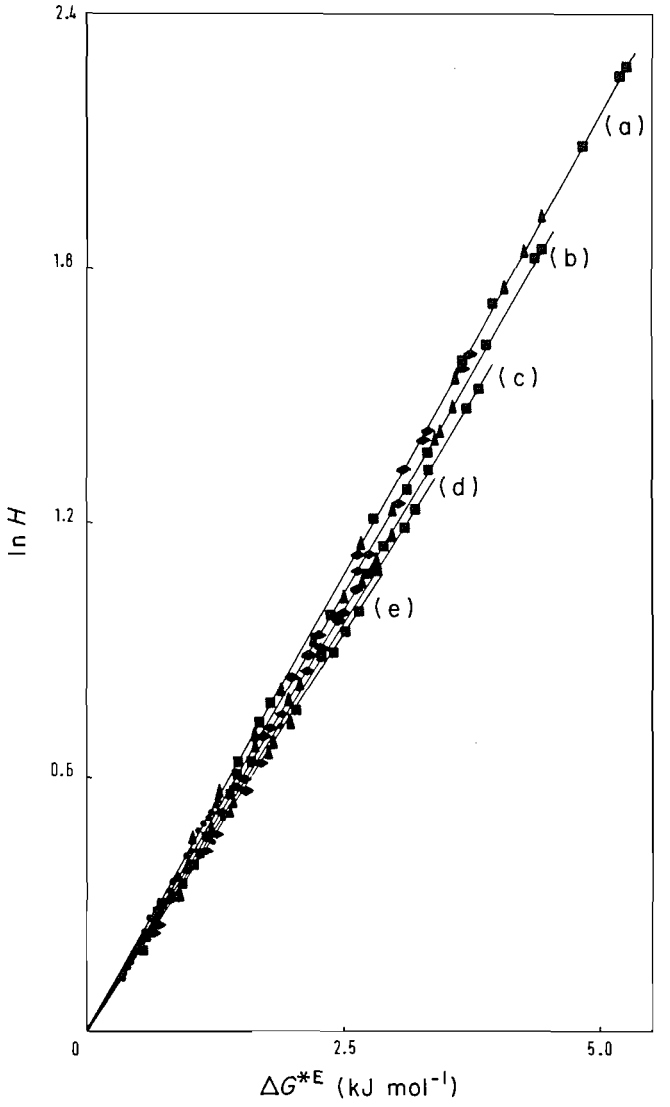


FIG. 4. Plot of ln H against ΔG^{*E} according to eq. [7]; (a) 283 K; (b) 293 K; (c) 303 K; (d) 313 K, and (e) 323 K.

ing to systems with negative excess volumes, which is in agreement with our own results, but the opposite effect was observed by Anantamaran (20).

In view of the different meaning of θ and V^E, it is difficult to establish a general correlation between the two magnitudes. Nevertheless, to pursue the suggested connection between the excess viscosity and the (negative) excess volume, the following correlation was proposed by Stairs (21):

$$[3] \quad H_{max}^{-1} = 0.570 + 1.035\, V_r^E(\max)$$

where

$$[4] \quad \ln H = -(W/RT)\, X_1X_2 = \theta X_1X_2 = \ln \eta_{obs} - \ln \eta_{id}$$

$$[5] \quad V_r^E = 100\,(V^E/V)$$

and where W denotes an interspecific interaction energy.

According to this proposal, the fractional change in the free volume at each composition should be related to our quantity H. Given that the mole fractions of the maxima η^E (plots η^E vs. X_1) and the minima V^E (plots V^E vs. X_1) do not coincide for our mixtures, values of H_{max} experimental and those calculated with eq. [3] also will not coincide. On the other hand, nonlinear plots of H_{max}^{-1} against V_{max}^E were obtained in the present study. This behaviour was also observed by Palepu *et al.* (22) in binary mixtures of *m*-cresol with substituted anilines; they reported a single straight line when ln H was plotted against ΔG^{*E}. This type of result is not unexpected, since the expression for ΔG^{*E} takes into account both viscosity and volume:

$$[6] \quad \Delta G^{*E} = RT\,(\ln \eta V - X_1 \ln \eta_1 V_1 - X_2 \ln \eta_2 V_2)$$

where η, η_1, and η_2 are the viscosities of the mixture and pure components, and V, V_1, and V_2 the molar volumes of the mixture and pure components. Palepu noted that systems with positive η^E and negative V^E led to straight lines, with zero intercept, when ln H was plotted against ΔG^{*E}; this intercept, however, was different from zero for binary mixtures of *m*-cresol with substituted anilines. From eqs. [4] and [6], it is deduced that

$$[7] \quad \ln H = m\, \Delta G^{*E} - \ln D$$

TABLE 1. Experimental and calculated values of the slope m (mol J^{-1}) according to eq. [7]; $S(y)$ = standard deviation; r_{xy} = linear correlation coefficient

T/K	m_{calcd}	m_{expt}	r_{xy}	$S(y)$
283	0.4250	0.4266	0.9999	0.004
293	0.4105	0.4120	0.9999	0.007
303	0.3969	0.3975	0.9999	0.002
313	0.3843	0.3847	0.9999	0.001
323	0.3724	0.3732	0.9999	0.002

where

[8] $$\ln D = \ln V - (X_1 \ln V_1 + X_2 \ln V_2)$$

At constant temperature a straight line should be obtained, with slope $m = 1/RT$ (Fig. 4). Table 1 collects the experimental and theoretical values determined for the slopes m, as well as the linear correlation coefficients, 36 being the number of data points for each of the straight lines; the standard error was estimated to be less than 0.007, and ln D was always less than 0.002. Thus the following equation can be derived from eq. [8]:

[9] $$V = V_1^{X_1} \cdot V_2^{X_2}$$

The percentage of error in V (calculated with eq. [9]) with respect to experimental measurements was always lower than 1%, at any temperature and for any composition of the mixtures.

1. B. GARCÍA and J. C. ORTEGA. J. Chem. Eng. Data, **33**, 200 (1988).
2. B. GARCÍA and J. C. ORTEGA. Thermochim. Acta, **117**, 219 (1987).
3. B. GARCÍA and J. C. ORTEGA. An. Quím. **84**, 267 (1988).
4. F. MATA, J. M. LEAL, and B. GARCÍA. Z. Phys. Chem. Leipzig, **281**, 1059 (1980).
5. B. GARCÍA and J. M. LEAL. Collect. Czech. Chem. Commun. **52**, 299 (1987).
6. L. A. HERRERO. Tesis Licenciatura. Valladolid Univ., Spain. 1986.
7. A. J. RIDDICK and W. B. BUNGER. Techniques of chemistry. 3rd ed. John Wiley & Sons, New York. 1970.
8. R. C. LEAST (*Editor*). Handbook of chemistry and physics. 64th ed. CRC Press, Boca Raton, FL. 1983.
9. Handbook of chemistry. 11th ed. McGraw–Hill, New York. 1973.
10. J. M. LEAL, B. GARCÍA, and F. MATA. An. Quím. **264**, 83 (1987).
11. M. C. S. SUBHA and S. B. RAO. J. Chem. Eng. Data, **33**, 404 (1988).
12. G. P. JOHARI. J. Chem. Eng. Data, **13**, 541 (1968).
13. M. C. S. SUBHA and S. B. RAO. J. Chem. Eng. Data, **33**, 104 (1988).
14. R. J. FORT and W. R. MOORE. Trans. Faraday Soc. **62**, 112 (1966).
15. Y. Y. FIALKOV. Russ. J. Phys. Chem. (Engl. Transl.), **37**, 1051 (1963).
16. E. A. GUGGENHEIM. Mixtures. Clarendon Press, Oxford. 1962.
17. J. H. HILDEBRAND, J. M. PRAUSNITZ, and L. SCOTT. Regular and related solutions. van Nostrand Reinhold, New York. 1970.
18. L. GRUNBERG and L. H. NISSAN. Nature, **164**, 799 (1949).
19. M. G. PROLONGO, R. M. MASEGOSA, I. HERNANDEZ-FUENTES, and A. HORTA. J. Phys. Chem. **89**, 2163 (1984).
20. A. V. ANANTAMARAN. Can. J. Chem. **64**, 46 (1986).
21. R. A. STAIRS. Can. J. Chem. **58**, 296 (1980).
22. R. PALEPU, J. OLIVER, and B. MCKINNON. Can. J. Chem. **63**, 1024 (1985).

Can. J. Chem. Downloaded from www.nrcresearchpress.com by 195.138.81.100 on 09/07/12
For personal use only.

Sense of sequential 1,5-sigmatropic rearrangements of dimethyl-3,3-dialkyl-3*H*-pyrazole-4,5-dicarboxylates. Crystal and molecular structures of two dimethyl-4,5-dialkyl-1*H*-pyrazole-1,3-dicarboxylates

CHRISTOPHER S. FRAMPTON,[1] MICHAEL W. MAJCHRZAK, AND JOHN WARKENTIN[1]
Department of Chemistry, McMaster University, Hamilton, Ont., Canada L8S 4M1

Received April 18, 1990[2]

CHRISTOPHER S. FRAMPTON, MICHAEL W. MAJCHRZAK, and JOHN WARKENTIN. Can. J. Chem. **69**, 373 (1991).

3,3-Dialkyl-3*H*-pyrazole-4,5-dicarboxylic acid dimethyl esters (**4**), obtained by cycloaddition of $R^1R^2C{=}N^+{=}N^-$ ($R^1 = R^2 = CH_3$; $R^1 = CH_3$, $R^2 = CH_2CH_3$) to $CH_3O_2CC{\equiv}CCO_2CH_3$, rearrange thermally by 1,5-sigmatropic alkyl shifts to both N and C. The latter rearrangement is followed by two successive 1,5-sigmatropic shifts of a methoxycarbonyl group. Final products of the threefold rearrangement were shown to be 4,5-dialkyl-1*H*-pyrazole-1,3-dicarboxylic acid dimethyl esters (**6**), rather than the isomeric 3,4-dialkyl-1*H*-pyrazole-1,5-dicarboxylic acid dimethyl esters (**7**), by means of single crystal X-ray diffraction. Those products therefore result from alkyl migration to C-4 of **4**, followed by sequential migration of the methoxycarbonyl group, initially at C-4, to C-3 and then to N-2 of **4**. In the initial alkyl migration step, ethyl migrates in preference to methyl, and in subsequent migration steps the methoxycarbonyl group migrates faster than the ethyl or methyl group. Crystals of 4-ethyl-5-methyl-1*H*-pyrazole-1,3-dicarboxylic acid dimethyl ester (**6***b*) are monoclinic, of space group $P2_1/n$, with $a = 7.907(1)$ Å, $b = 11.087(2)$ Å, $c = 13.199(3)$ Å, $V = 1124.9(4)$ Å^3, $D_c = 1.34$ g cm^{-3}, $D_m = 1.33$ g cm^{-3} for $Z = 4$, and $R_1 = 0.0772$ ($R_2 = 0.0626$) for 1474 reflections ($R_1 = 0.0428$, $R_2 = 0.0422$ for 903 reflections with $I > 3\sigma(I)$. The structure of **6***a* is similar.

Key words: 3,3-dialkyl-3*H*-pyrazoles, 1,5-sigmatropic rearrangements of; 4,5-dialkyl-1*H*-pyrazoles, crystal and molecular structures; 1,5-sigmatropic rearrangements of pyrazoles, sense of.

CHRISTOPHER S. FRAMPTON, MICHAEL W. MAJCHRZAK et JOHN WARKENTIN. Can. J. Chem. **69**, 373 (1991).

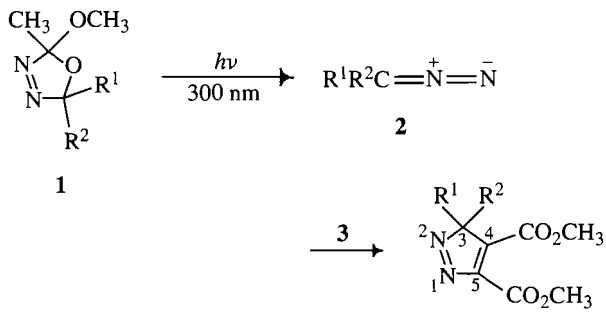
Les esters diméthyliques des acides 3,3-dialkyl-3*H*-pyrazole-4,5-dicarboxyliques (**4**), obtenus par cycloaddition des $R^1R^2C{=}N^+{=}N^-$ ($R^1 = R^2 = CH_3$); $R^1 = CH_3$, $R^2 = CH_2CH_3$) au $CH_3O_2CC{\equiv}CCO_2CH_3$, se réarrangement thermiquement par des transpositions 1,5-sigmatropiques d'alkyles vers le N ainsi que le C. Cette dernière transposition est suivie par deux transpositions 1,5-sigmatropiques successives d'un groupement méthoxycarbonyle. Faisant appel à la diffraction des rayons-X par un cristal unique, on a montré que les produits finaux de ces transpositions ternaires sont les esters diméthyliques des acides 4,5-dialkyl-1*H*-pyrazole-1,3-dicarboxyliques (**6**) plutôt que les esters diméthyliques isomères des acides 3,4-dialkyl-1*H*-pyrazole-1,5-dicarboxyliques. Ces produits sont donc formés par une migration d'un groupement alkyle vers la position C-4 du produit **4**, suivie par la migration séquentielle du groupement méthoxycarbonyle, initialement vers la position C-4, puis C-3 et finalement N-2 du produit **4**. Dans l'étape initiale de migration des groupements alkyles, l'éthyle migre de préférence au méthyle et, dans les étapes subséquentes de migration, le groupement méthoxycarbonyle migre plus rapidement que les groupements éthyle ou méthyle. Les cristaux de l'ester diméthylique de l'acide 4-éthyl-5-méthyl-1*H*-pyrazole-1,3-dicarboxylique (**6***b*) sont monocliniques, groupe d'espace $P2_1/n$, avec $a = 7{,}907(1)$, $b = 11{,}078(2)$ et $c = 13{,}199(3)$ Å, $V = 1124{,}9(4)$ Å^3, $D_c = 1{,}34$ g cm^{-3}, $D_m = 1{,}33$ g cm^{-3}, $Z = 4$ et $R_1 = 0{,}0772$ ($R_2 = 0{,}0626$) pour 1474 réflexions ($R_1 = 0{,}0428$, $R_2 = 0{,}0422$ pour 903 réflexions avec $I \geq 3\sigma(I)$). La structure du composé **6***a* est semblable.

Mots clés : 3,3-dialkyl-3*H*-pyrazoles, transpositions 1,5-sigmatropiques; 4,5-dialkyl-1*H*-pyrazoles, structures cristallines et moléculaires; signification des transpositions 1,5-sigmatropiques des pyrazoles.

[Traduit par la rédaction]

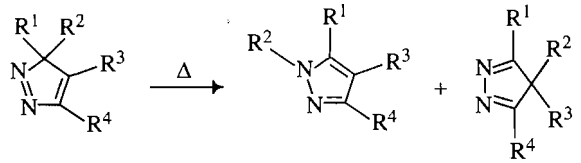
Introduction

Diazoalkanes (**2**), generated conveniently by photolysis of 5,5-dialkyl-2-methoxy-2-methyl-Δ^3-1,3,4-oxadiazolines (**1**) (1), are trapped efficiently, *in situ*, by dimethyl acetylenedicarboxylate (**3**) to afford 3,3-dialkyl-3*H*-pyrazole-4,5-dicarboxylic acid dimethyl esters (**4**), eq. [1].

[1] 

a: $R^1 = R^2 = CH_3$; *b*: $R^1 = CH_3$, $R^2 = CH_2CH_3$

Compounds **4** are of the 1,3-cyclopentadiene type and, as such, are prone to 1,5-sigmatropic rearrangement (2, 3). Examples of thermal rearrangement in the 3,3-dialkyl-3*H*-pyrazole skeleton are known (4–8) and include the reactions illustrated with eq. [2] (8).

[2] 

We found that **4***a* and **4***b* rearranged at 160°C in benzene solution by a mechanism more complicated than the simple competition between the two migration pathways depicted with eq. [2]. The 1*H*-pyrazole products of migration to nitrogen were obtained in each case but the second product was also a 1*H*-pyrazole, not a 4*H*-pyrazole. Although the possible structures of the unexpected products could readily be narrowed down to **6** or **7**, eq. [3], the choice between those two could not be made unambiguously by means of spectroscopy, in the absence of authentic samples.

[1]Authors to whom correspondence may be addressed.
[2]Revision received October 26, 1990.

Can. J. Chem. Downloaded from www.nrcresearchpress.com by 195.138.81.100 on 09/07/12
For personal use only.

TABLE 1. Crystal data for **6***a* and **6***b*

	6*a*	**6***b*
Formula	$C_9H_{12}O_4N_2$	$C_{10}H_{14}O_4N_2$
FW	212.20	226.23
System	Monoclinic	Monoclinic
Syst. Abs.	$h0l$, $l \neq 2n$, $0k0$, $k \neq 2n$	$h0l$, $h + l \neq 2n$, $h00$, $h \neq 2n$ $0k0$, $k \neq 2n$, $00l$, $l \neq 2n$
Space group	$P2_1/c$ No. 14	$P2_1/n$ No. 14[a]
a, Å	7.928(5)	7.907(1)
b, Å	10.570(5)	11.078(2)
c, Å	13.625(7)	13.199(3)
β,°	111.29(4)	103.36(2)
V, Å^3	1064(1)	1124.9(4)
Z	4	4
D_c, g cm^{-3}	1.32	1.34
D_m, g cm^{-3}	1.31	1.33
$F(000)$	448	480
μ(MoKα), cm^{-1}	0.67	0.66
Final, R_1, R_2[b]	0.1770, 0.1386[d]	0.0772, 0.0620[e]
Weighting scheme	$w = (\sigma^2F + 0.0005F^2)^{-1}$	$w = (\sigma^2F + 0.0002F^2)^{-1}$
S[c]	1.5976	1.6362
Highest peak, e Å^{-3}	0.58	0.24
Lowest peak, e Å^{-3}	−0.57	−0.25

[a]This cell may be transformed to an equivalent $P2_1/c$ cell with cell dimensions a = 7.909(2) Å, b = 11.077(2) Å, c = 13.729(4) Å, and β = 110.75(2)° with use of the matrix ((−1, 0, 0), (0, −1, 0), (1, 0, 1)).

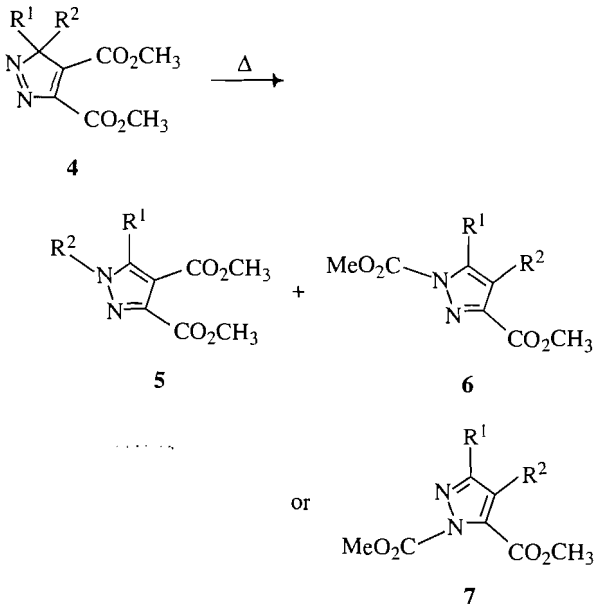
[b]$R_1 = \Sigma||F_o| - |F_c||/\Sigma|F_o|$; $R_2 = (\Sigma w(|F_o| - |F_c|)^2/\Sigma wF_o^2)^{1/2}$,

[c]$S = (\Sigma w(|F_o| - |F_c|)^2/(m - n)^{1/2}$; m = no. of reflections, n = no. of variables.

[d]R_1, R_2 for 504 reflections with $I > 3\sigma(I)$ 0.0664, 0.0608 respectively.

[e]R_1, R_2 for 903 reflections with $I > 3\sigma(I)$ 0.0428, 0.0422 respectively.

[3]



(*a*: $R^1 = R^2 = CH_3$; *b*: $R^1 = CH_3$, $R^2 = CH_2CH_3$)

We now report that the crystal and molecular structures identify the unexpected materials obtained from **4** as **6**, rather than **7**.

Experimental

Syntheses

The pyrazole starting materials (**4***a*, **4***b*) were prepared by photolysis of the appropriate oxadiazoline precursors in the presence of **3**, as described previously (1).

Rearrangements

Thermal rearrangement was carried out by heating a solution (ca. 0.25 M) of the appropriate pyrazole in benzene to 160°C in a sealed nmr tube. Progress of the rearrangement was monitored by ^{1}H nmr spectroscopy. After 8 h at 160°C, rearrangement was complete (>95%).

*4,5-Dimethyl-1H-pyrazole-1,3-dicarboxylic acid dimethyl ester (**6**a)*

Yield 83%; ^{1}H nmr (500 MHz, C_6D_6, residual H at δ 7.15), δ: 2.04 (s, 3H, C-4Me), 2.09 (s, 3H, C-5Me), 3.38 (s, 3H, N-1 ester), 3.51 (s, 3H, C-3 ester); ^{13}C nmr (125.76 MHz, C_6D_6, at 128.0), δ: 8.59, 11.5, 51.3, 53.8, 111.0, 119.7, 141.7, 151.0, 163.2; ms (high resolution), m/z: 212.081; calcd. for $C_9H_{12}N_2O_4$: 212.079.

*4-Ethyl-5-methyl-1H-pyrazole-1,3-dicarboxylic acid dimethyl ester (**6**b)*

Yield 67%; ^{1}H nmr (500 MHz, C_6D_6, residual H at δ 7.15), δ: 1.08 (t, 3H), 2.12 (s, 3H), 2.59 (q, 2H), 3.36 (s, 3H, N-1 ester), 3.50 (s, 3H, C-3 ester).

*1-Ethyl-5-methyl-1H-pyrazole-3,4-dicarboxylic acid dimethyl ester (**5**b)*

Yield 33%; ^{1}H nmr (500 MHz, C_6D_6, TMS), δ: 0.84 (t, 3H), 1.91 (s, 3H), 3.25 (q, 2H), 3.57 (s, 6H); ^{13}C nmr (125.76 MHz, C_6D_6), δ: 9.86, 14.4, 44.1, 51.1, 51.7, 112.0, 142.5, 144.3, 163.6, 163.7.

X-ray crystallography

Crystals of **6***b* were grown from $CHCl_3$/petroleum ether. The density was determined by suspension in an aqueous solution of $ZnCl_2$. Clear parallelepiped crystals were examined under a polarizing microscope for homogeneity. A small well-formed crystal, 0.15 × 0.15 × 0.20 mm, was selected and sealed in a Lindemann capillary. Unit cell parameters were obtained from a least-squares fit of χ, φ, and 2θ for 15 reflections in the range 12.0° < 2θ < 24.2° recorded on a Nicolet P3 diffractometer with use of graphite monochromated MoKα radiation (λ = 0.71069 Å at 22°C). Intensity data were also recorded on a Nicolet P3 diffractometer with a coupled θ(crystal)–2θ(counter)

Can. J. Chem. Downloaded from www.nrcresearchpress.com by 195.138.81.100 on 09/07/12
For personal use only.

Can. J. Chem. Downloaded from www.nrcresearchpress.com by 195.138.81.100 on 09/07/12
For personal use only.

TABLE 2. Positional parameters ($\times 10^4$) and U_{eq} (Å^2) ($\times 10^4$) for $(C_3N_2(CH_3CO_2)_2(CH_3)_2$, **6***a*, with standard errors in parentheses

Atom	*x*	*y*	*z*	U_{eq} (Å^2)[a]
N(1)	4498(9)	1132(5)	6142(5)	484
N(2)	4267(6)	−153(5)	6073(4)	351
C(3)	5929(9)	−593(6)	6495(6)	382
C(4)	7233(9)	363(6)	6842(6)	415
C(5)	6312(10)	1491(6)	6601(6)	442
C(6)	2921(11)	1976(8)	5753(6)	425
C(7)	−261(11)	2060(8)	4960(6)	660
C(8)	6267(13)	−1958(6)	6562(6)	465
C(9)	5033(13)	−3975(6)	6190(6)	679
C(10)	9250(10)	196(6)	7345(6)	653
C(11)	7007(10)	2802(6)	6804(6)	490
O(1)	7738(9)	−2385(5)	6907(6)	864
O(2)	4771(8)	−2604(4)	6170(4)	560
O(3)	3076(6)	3092(5)	5802(5)	665
O(4)	1406(8)	1315(5)	5370(4)	578

[a] $U_{eq} = \frac{1}{3}(U_{11} + U_{22} + U_{33} + 2\cos\beta U_{13})$.

scan, for 1690 reflections in the quadrant h, k, $\pm l$ with $2\theta \leq 45°$. The methods of selection of scan rates and initial data treatment have been described (9, 10). Corrections for Lorentz–polarization effects were applied to all reflections. Two standard reflections (−1, −1, 0; 1.46% and 1, −1, 0; 1.60%) monitored every 48 reflections showed no sign of crystal decomposition or instrument instability. Systematically absent reflections (104) were excluded and 184 symmetry-equivalent data were then averaged (R_{int} = 0.0079) to give 1402 unique reflections. The data collection parameters for **6***a* were similar. A summary of crystal data is given in Table 1.

Solution of the structure

The structure was solved by direct methods on 299 reflections with $|E| > 1.2$ and 50 sets of starting phases with use of the program SHELXS-86 (11). Full-matrix least-squares refinement of the coordinates of all the non-hydrogen atoms followed by a three-dimensional electron density synthesis revealed the positional parameters for most of the hydrogen atoms. The temperaure factors of the non-hydrogen atoms, which were previously isotropic, were made anisotropic and further cycles of refinement and a difference synthesis revealed more hydrogen atoms. These were included, along with calculated positions for the rest of the hydrogen atoms, in subsequent cycles of refinement (U fixed at 0.08 Å^2). Futher refinement using full-matrix least squares minimizing $\Sigma w(|F_o| - |F_c|)^2$ was terminated when the maximum shift/error reached 0.003. Correction for secondary extinction was not necessary. Throughout the refinement, scattering curves were taken from ref. 12. The structure of **6***a* was solved in a similar manner. All calculations were performed on a VAX 8650 computer. Programs used: XTAL (13), data reduction; SHELX-86 (11), structure solution; SHELX-76 (14), structure refinement; MOLGEOM (15) and SNOOPI (16), diagrams. Final atomic positional parameters are given in Tables 2 and 3, selected bond lengths and bond angles are given in Tables 4 and 5. Tables listing full crystal data, least-squares mean planes and dihedral/torsional angles, hydrogen atom positional parameters, bond lengths and bond angles involving hydrogen atoms, and anisotropic temperature factors are available as supplementary material.[3]

[3]This material may be purchased from the Depository of Unpublished Data, Document Delivery, CISTI, National Research Council Canada, Ottawa, Canada K1A 0S2.

Tables of full crystal data, hydrogen atom positional parameters, and bond lengths and angles involving hydrogen atoms have also been deposited with the Cambridge Crystallographic Data Centre and can be obtained on request from the Director, Cambridge Crystallographic Data Centre, University Chemical Laboratory, Lensfield Road, Cambridge CB2 1EW, U.K.

TABLE 3. Positional parameters ($\times 10^4$) and U_{eq} (Å^2) ($\times 10^4$) for $(C_3N_2$-$(CH_3CO_2)_2(CH_2CH_3)(CH_3)$, **6***b*, with standard errors in parentheses

Atom	*x*	*y*	*z*	U_{eq} (Å^2)[a]
N(1)	3430(3)	4080(2)	3881(2)	468
N(2)	3212(3)	5305(2)	3905(2)	459
C(3)	4438(4)	5729(3)	3462(2)	426
C(4)	5452(4)	4808(3)	3153(2)	457
C(5)	4787(4)	3752(3)	3432(2)	469
C(6)	2350(4)	3304(3)	4310(2)	506
C(7)	−41(5)	3211(3)	5070(3)	660
C(8)	4662(4)	7040(3)	3358(2)	527
C(9)	3842(4)	8993(3)	3787(3)	651
C(10)	6909(4)	4931(3)	2600(3)	597
C(11)	6238(4)	5024(3)	1430(3)	679
C(12)	5310(4)	2474(3)	3298(3)	616
O(1)	5695(3)	7486(2)	2928(2)	816
O(2)	3592(3)	7695(2)	3798(2)	578
O(3)	2539(3)	2232(2)	4340(2)	741
O(4)	1150(3)	3924(2)	4629(2)	586

[a] $U_{eq} = \frac{1}{3}(U_{11} + U_{22} + U_{33} + 2\cos\beta U_{13})$.

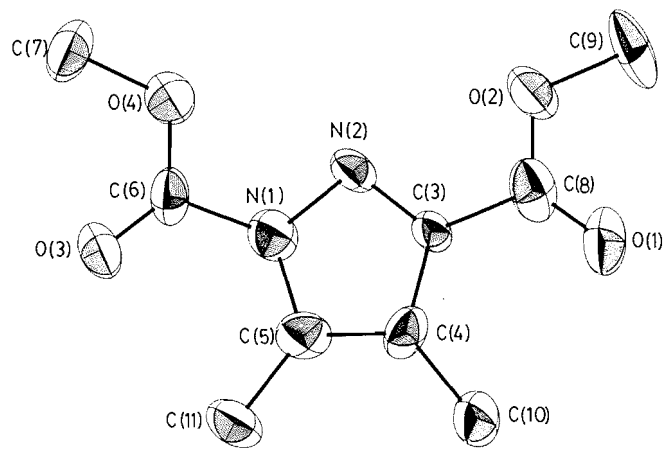


FIG. 1. View of molecule **6***a*.

Results and discussion

Views of molecules **6***a* and **6***b*, with atom numbering schemes, are depicted in Figs. 1 and 2. The molecular structures of **6***a* and **6***b* are similar to those of 1-nitropyrazole (17) and *N*,*N*′-carbonyldipyrazole (18) and do not have any remarkable features. The only reason for determining those structures was to discriminate, unambiguously, between the isomers **6** and **7** (Scheme 1). For that purpose, the best refinement was not necessary and the high *R*-value for **6***a*, which was the result of a large number of reflections with $I < 3\sigma(I)$, is not of great concern. The rearrangement products belong to the family **6**, not **7** (Scheme 1). With the identities of the products firmly established, those rearrangements can now be described in considerable detail.

Thermal isomerizations of conjugated pentadienyl systems are believed to occur, with few exceptions (3), by a concerted process known as a suprafacial 1,5-sigmatropic rearrangement (2). The term denotes an intramolecular shift of a group or atom from one position to another on the same face of a π-system that, at the transition state, has six π-electrons. The migrating entity remains continuously and covalently bonded to the rest of the structure during its migration. Such rearrangements are characterized by low migratory aptitudes for saturated groups

Can. J. Chem. Downloaded from www.nrcresearchpress.com by 195.138.81.100 on 09/07/12
For personal use only.

TABLE 4. Selected bond lengths (Å) and bond angles (°) for $C_3N_2(CH_3CO_2)_2(CH_3)_2$, **6***a*, with estimated standard deviations in parentheses

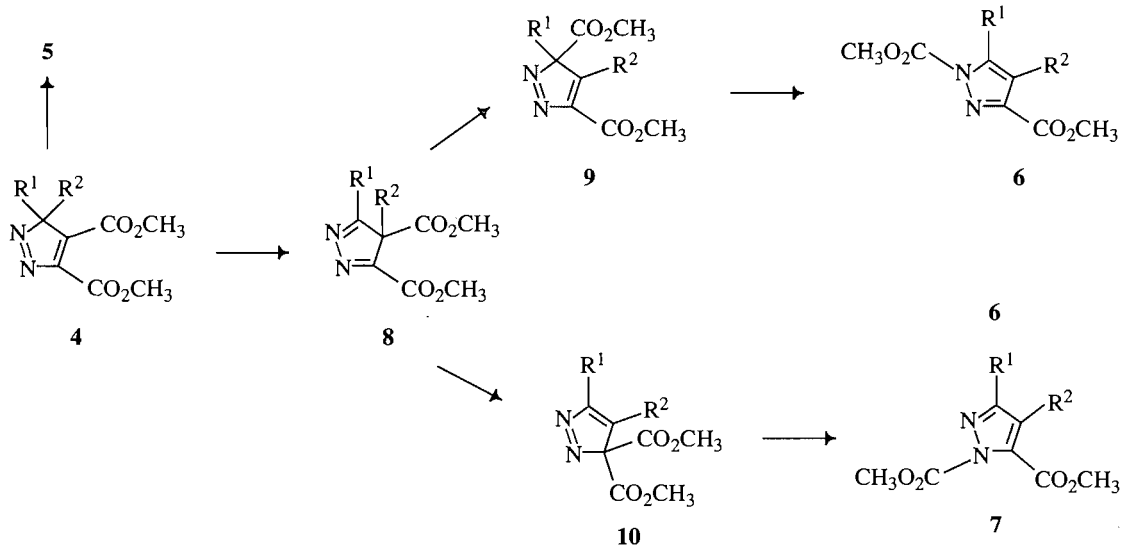
Bond	Length	Bond	Length
N(2)—N(1)	1.369(8)	C(5)—C(4)	1.374(10)
N(2)—C(3)	1.316(8)	C(4)—C(3)	1.399(10)
N(1)—C(5)	1.397(9)	C(5)—C(11)	1.480(10)
C(4)—C(10)	1.504(10)		
C(3)—C(8)	1.466(10)	N(1)—C(6)	1.470(10)
C(8)—O(1)	1.177(11)	C(6)—O(3)	1.186(9)
C(8)—O(2)	1.302(10)	C(6)—O(4)	1.322(9)
O(2)—C(9)	1.463(9)	O(4)—C(7)	1.463(10)
Bonds	**Angle**	**Bonds**	**Angle**
N(1)—N(2)—C(3)	103.4(5)	N(2)—C(3)—C(4)	113.1(6)
N(2)—C(3)—C(8)	120.4(6)	C(4)—C(3)—C(8)	126.5(7)
N(2)—N(1)—C(5)	113.0(6)	N(2)—N(1)—C(6)	120.2(6)
C(5)—N(1)—C(6)	126.8(6)	N(1)—C(5)—C(4)	104.0(6)
N(1)—C(5)—C(11)	126.2(6)	C(11)—C(5)—C(4)	129.7(6)
C(3)—C(4)—C(5)	106.4(6)	C(3)—C(4)—C(10)	127.1(7)
C(10)—C(4)—C(5)	126.5(7)	C(3)—C(8)—O(1)	122.2(8)
C(3)—C(8)—O(2)	111.8(7)	O(1)—C(8)—O(2)	126.0(7)
C(8)—O(2)—C(9)	114.1(6)	N(1)—C(6)—O(3)	121.8(7)
N(1)—C(6)—O(4)	110.7(6)	O(3)—C(6)—O(4)	127.5(7)
C(6)—O(4)—C(7)	115.6(6)		

TABLE 5. Selected bond lengths (Å) and bond angles (°) for $C_3N_2(CH_3CO_2)_2(CH_2CH_3)(CH_3)$, **6***b*, with estimated standard deviations in parentheses

Bond	Length	Bond	Length
N(1)—N(2)	1.370(3)	C(4)—C(5)	1.367(4)
N(2)—C(3)	1.328(3)	C(3)—C(4)	1.415(4)
N(1)—C(5)	1.389(3)	C(5)—C(12)	1.497(4)
C(4)—C(10)	1.505(4)	C(10)—C(11)	1.514(4)
C(3)—C(8)	1.473(4)	N(1)—C(6)	1.419(4)
C(8)—O(1)	1.204(4)	C(6)—O(3)	1.196(3)
C(8)—O(2)	1.344(4)	C(6)—O(4)	1.317(3)
O(2)—C(9)	1.450(4)	O(4)—C(7)	1.451(3)
Bonds	**Angle**	**Bonds**	**Angle**
N(1)—N(2)—C(3)	103.4(2)	N(2)—C(3)—C(4)	113.1(3)
N(2)—C(3)—C(8)	120.3(3)	C(4)—C(3)—C(8)	126.6(3)
N(2)—N(1)—C(5)	112.5(2)	N(2)—N(1)—C(6)	120.1(2)
C(5)—N(1)—C(6)	127.5(3)	N(1)—C(5)—C(4)	106.0(3)
N(1)—C(5)—C(12)	124.0(3)	C(4)—C(5)—C(12)	130.0(3)
C(3)—C(4)—C(5)	105.1(2)	C(3)—C(4)—C(10)	128.5(3)
C(5)—C(4)—C(10)	126.4(3)	C(3)—C(8)—O(1)	123.9(3)
C(3)—C(8)—O(2)	113.1(3)	O(1)—C(8)—O(2)	123.0(3)
C(8)—O(2)—C(9)	115.6(3)	N(1)—C(6)—O(3)	122.2(3)
N(1)—C(6)—O(4)	110.8(3)	O(3)—C(6)—O(4)	127.0(3)
C(6)—O(4)—C(7)	115.2(2)	C(4)—C(10)—C(11)	111.9(2)

(e.g., alkyl) and high migratory aptitudes for unsaturated groups such as phenyl or ester (8*b*).

Although thermal 1,5-sigmatropic rearrangements of 3*H*-pyrazoles had been reported (8), the systems studied did not include any with alkyl groups at C-3 and with ester groups at both C-4 and C-5. The major questions at the outset were the following. First, would alkyl migration occur under thermodynamic control to form **5** (Scheme 1) following the sense of migration of ester, acyl, and cyano groups (5*b*) from C-3 to N-2? Second, if 4*H*-pyrazoles were formed preferentially, would they be isolable (8*a*) or would subsequent rearrangement be too fast? Third, in what sense would **8** rearrange under conditions where **8** are unstable? Although it was predictable that the ester groups of **8** would migrate to the exclusion of R^2 ($R^2 = CH_3$ or C_2H_5) it was not clear whether that group would migrate to form **9** or **10**, or both.



SCHEME 1

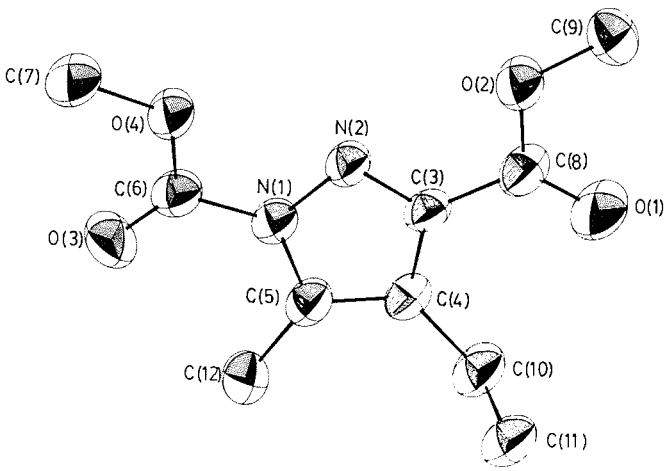


FIG. 2. View of molecule **6***b*.

The results of this study provide clear answers to those three questions. Methyl and ethyl group migrations are largely under kinetic control, **4***a* yielding only 9% of the aromatic product **5***a* and **4***b* leading to only 33% of **5***b*. In each case the major product comes from alkyl group migration to carbon. In this respect compounds **4** are similar to 4,5-diaryl-3,3-dimethyl-3*H*-pyrazoles (8*a*) and 5-methyl-3,3-dialkyl-3*H*-pyrazoles (8*b*); the ester groups of **4** do not have a pronounced effect (relative to H or aryl groups) on the preference for migration under kinetic control. The identity of the migrating group does appear to have a large effect on the site selectivity, on the other hand. Phenyl migrates about seven times faster to N-2 than to C-4 of ethyl and methyl-3,3,5-triphenyl-3*H*-pyrazole-4-carboxylates at 140°C (6), while ester, acyl, and cyano groups migrate exclusively to N-2 of 3-methyl-3-R-3*H*-pyrazole-4,5-dicarboxylic acid dimethyl esters (R = CO_2CH_3, $COCH_3$, CN) (5*b*).

Although the formation of 4*H*-pyrazoles (**8**) is required to account for the major products of rearrangement of **5**, accumulation of **8** to detectable levels did not occur under the reaction conditions. That result was not predictable, despite the fact that the CO_2CH_3 group migrates 19 000 and 826 times faster, respectively, than methyl and ethyl from C-3 of 3*H*-pyrazoles (8*b*). The reason why a prediction could not be made is that some 4*H*-pyrazoles are more stable than 3*H*-pyrazoles.[4] In fact, in many instances (6, 8*a*, 8*b*), 4*H*-pyrazoles have been isolated readily from the thermal rearrangement of their 3*H*-pyrazole isomers. In the present cases, **8** appears to rearrange faster than **4** in spite of the greater stability expected of the ring system **8**, with two CN double bonds.

Finally, the question of the sense of rearrangement of **8** is answered. The ester group migrates to the alkyl-bearing sp^2-carbon only, to form **9**, and as a result the net effect of two sigmatropic shifts is to interchange an alkyl group at C-3 of **4** with the ester group at C-4. Presumably this happens with overall inversion at C-3 because those sigmatropic shifts must be suprafacial. In the new 3*H*-pyrazole (**9**), the migration competition is again between CO_2Me and primary alkyl, and only ester migration, to form **6**, occurs. Presumably **9** also reverts to **8** but that rearrangement would have been invisible in the present study.

With the sense of the second of three sequential sigmatropic rearrangements firmly established by means of X-ray crystallography, it should be easier, in the future, to distinguish between rearrangement products of types **6** and **7** by means of ^1H and ^{13}C nmr spectroscopy.

1. M. W. MAJCHRZAK, M. BÉKHAZI, I. TSE-SHEEPY, and J. WARKENTIN. J. Org. Chem. **54**, 1842 (1989).
2. (*a*) C. W. SPANGLER. Chem. Rev. **76**, 187 (1976); (*b*) J. J. GAJEWSKI. Hydrocarbon thermal isomerizations. Academic Press, New York. 1981; (*c*) I. FLEMING. Frontier orbitals and organic chemical reactions. Wiley, London. 1976; (*d*) R. B. WOODWARD and R. HOFFMANN. The conservation of orbital symmetry. Verlag Chemie GmbH/Academic Press, Weinheim. 1970.
3. M. W. MAJCHRZAK, E. JEFFERSON, and J. WARKENTIN. J. Am. Chem. Soc. **112**, 2449 (1990).
4. (*a*) J. VAN ALPHEN. Recl. Trav. Chim. Pays-Bas, **62**, 485 (1943); (*b*) R. BAUMES, J. ELGUERO, R. JACQUIER, and G. FARRAGO. Tetrahedron Lett. 3781 (1973); (*c*) H. DÜRR and W. SCHMIDT. Justus Liebigs Ann. Chem. 1140 (1974); (*d*) R. HÜTTEL,

[4]Calculation (19) using optimized geometries from INDO and STO-3G energies suggests that the unsubstituted isomers are similar in energy.

Can. J. Chem. Downloaded from www.nrcresearchpress.com by 195.138.81.100 on 09/07/12
For personal use only.

K. FRANKE, H. MARTIN, and J. RIEDL. Chem. Ber. **93**, 1433 (1960); (*e*) G. WITTIG and J. J. HUTCHISON. Justus Liebigs Ann. Chem. **741**, 89 (1970).
5. (*a*) D. SEYFERTH and T. C. FLOOD. J. Organomet. Chem. **29**, C25 (1971); (*b*) M. FRANCK-NEUMANN and C. BUCHECKER. Tetrahedron Lett. 937 (1972); (*c*) M. FRANCK-NEUMANN and C. BUCHECKER. Angew. Chem. Int. Ed. Engl. **12**, 240 (1973); (*d*) M. MARTIN and M. REGITZ. Justus Liebigs Ann. Chem. 1702 (1974); (*e*) L. L. RODINA, V. V. BULUSHEVA, T. G. EKIMOVA, and I. K. KOROBITSYNA. J. Gen. Chem. USSR, **10**, 53 (1974).
6. M. I. KOMENDANTOV and R. R. BEKMUKHAMETOV. Chem. Heterocycl. Compd. 68 (1975).
7. M. FRANCK-NEUMANN and C. DIETRICH-BUCHECKER. Tetrahedron Lett. 2069 (1976).
8. (*a*) W. J. LEIGH and D. R. ARNOLD. Can. J. Chem. **57**, 1186 (1979); (*b*) P. SCHIESS and H. STALDER. Tetrahedron Lett. 1417 (1980).
9. B. LIPPERT, C. J. L. LOCK, B. ROSENBERG, and M. ZAVAGULIS. Inorg. Chem. **16**, 1525 (1977).
10. R. P. HUGHES, N. KRISHNAMACHARI, C. J. L. LOCK, J. POWELL, and C. T. TURNER. Inorg. Chem. **16**, 314 (1977).
11. G. M. SHELDRICK. SHELXS-86, program for crystal structure solution. University of Göttingen, Federal Republic of Germany. 1986.
12. D. T. CROMER and J. B. MANN. Acta Crystallogr. Sect. A: Cryst. Phys. Diffr. Theor. Gen. Crystallogr. **A24**, 321 (1968).
13. J. M. STEWART and S. R. HALL. The XTAL system of crystallographic programs. Tech. Rept. TR-1364, University of Maryland, College Park, MD, U.S.A. 1983.
14. G. M. SHELDRICK. SHELX-76, program for crystal structure determination. University of Cambridge, England. 1976.
15. J. STEPHENS. MOLGEOM adapted from CUDLS, McMaster University, Hamilton, Ont., Canada. 1973.
16. K. DAVIES. CHEMGRAF suite: SNOOPI. Chemical Design Ltd., Oxford, England. 1983.
17. C. TARIMIC and E. SCHEMPP. Acta Crystallogr. Sect. B: Struct. Crystallogr. Cryst. Chem. **B33**, 240 (1977).
18. M. BELLUCE, F. EINSTEIN, L. PETERSON, and P. L. VOGEL. Acta Crystallogr. Sect B: Struct. Crystallogr. Cryst. Chem. **B33**, 266 (1977).
19. J. CATALAN, J. L. G. DE PAZ, M. SANCHEZ-CABEZUDO, and J. ELGUERO. Bull. Soc. Chim. Fr. 429 (1986).

Can. J. Chem. Downloaded from www.nrcresearchpress.com by 195.138.81.100 on 09/07/12
For personal use only.

Transformation of resin abietic acid into a pregnane-type steroid

ANTONIO ABAD,[1] CONSUELO AGULLO, MANUEL ARNO,[1] LUIS R. DOMINGO, JOSÉ ROZALEN, AND RAMON J. ZARAGOZA

Departamento de Química Orgánica, Universidad de Valencia, Dr. Moliner 50, 46100 Burjasot, Valencia, Spain

Received July 13, 1990

ANTONIO ABAD, CONSUELO AGULLO, MANUEL ARNO, LUIS R. DOMINGO, JOSÉ ROZALEN, and RAMON J. ZARAGOZA. Can. J. Chem. **69**, 379 (1991).

Abietic acid (**1***a*) has been converted into the pregnane analogue steroid **10** via a sequence of transformations involving as key step the acetylene-cation cyclization of **9**.

Key words: abietic acid, pregnane steroids, acetylene-cation cyclization.

ANTONIO ABAD, CONSUELO AGULLO, MANUEL ARNO, LUIS R. DOMINGO, JOSÉ ROZALEN et RAMON J. ZARAGOZA. Can. J. Chem. **69**, 379 (1991).

L'acide abiétique (**1***a*) a été converti en un stéroïde analogue du pregnane (**10**) via une séquence de transformation englobant comme étape clé la cyclisation du cation acétylénique **9**.

Mots clés : acide abiétique, steroïdes analogues du pregnane, cyclisation par cation acétylénique.

Introduction

The synthesis of the steroid skeleton from resin acids has attracted the attention of many research groups over the years. In recent years, the conversion of tricyclic diterpenes with pimarane (1), isopimarane (2), podocarpane (3), and abietane (4) skeleton into steroid compounds has been reported, but hitherto none of these syntheses has resulted in the preparation of a pregnane-type steroid structure.

We have recently reported the conversion of dehydroabietic acid into a C-aryl-18-norpregnane steroid (5) and we wish to report in this paper the conversion of the most abundant resin acid, abietic acid (**1***a*), into a pregnane analogue steroid (**10**).

Results and discussion

Since synthesis of the steroidal D-ring possessing the 13-methyl group by the use of the carbon units of the isopropyl group of abietane-type diterpenes had proved to be difficult (4, 6), our strategy for the above-mentioned conversion (**1** to **10**) was founded on the initial deisopropylation of abietic acid, then to build an acetylene alcohol (**9**), which might undergo a stereocontrolled acid-promoted cyclization, through the well-known acetylene-cation cyclization (7), to afford the 20-keto-steroid **10**.

On the basis of the above considerations, methyl abietate (**1***b*) was transformed into enone **3** by a previously described procedure, which involves conversion of **1***b* to diene **2** and subsequent cleavage of the C13—C15[2] double bond (8).

The required side chain at C-14 was introduced by alkylation of the dienolate anion of **3**. Thus, reaction of **3** with 1 equivalent of lithium diisopropylamide (LDA) at −78°C afforded the corresponding lithium dienolate, which was coupled to 1-iodo-3-pentyne[3] at −78°C in the presence of added hexamethylphosphoric triamide (HMPA) for 2 h (−78°C to room temperature) to give the monoalkylated product **4** in 42% yield (82% based on recovered starting material, which could be recycled) along with a small amount of dialkylated product **5** (5%). The monoalkylated product **4** was isolated as a mixture of epimers at C-14, according to the evidence obtained from the gc–ms data and ^{1}H and ^{13}C nmr spectra (see experimental section). Despite numerous attempts, we were unsuccessful in finding conditions to increase the low percent conversion of this reaction. Attempts to improve its efficiency by prolonging the reaction time, or by using a larger excess of the iodide or a different base–solvent system (e.g., $(CH_3)_3$ COK/$(CH_3)_3$COH, CH_3SOCH_2Na/CH_3SOCH_3) resulted in a lower yield of **4**. Presumably, the low percent conversion obtained in this reaction under all attempted conditions reflected the facile elimination of IH from the homopropargylic iodide.

On treatment with hydrochloric acid in methanol, the mixture of C-14 epimeric ketones (**4**) was converted into the α,β-unsaturated ketone **6** in 92% yield. Chemoselective double bond reduction of **6** with lithium in liquid ammonia by inverse addition at −78°C afforded the acetylenic ketone **7** in 74% yield. Although partial reduction of the 4α-methoxycarbonyl function occurred under these conditions (a 5–10% yield of **8** was obtained), the lithium–ammonia reduction of the conjugated double bond took place with no observable reduction of the acetylene group.

The synthesis of the desired acetylenic alcohol **9** was completed by reacting the acetylenic ketone **7** with methyllithium to give, in a 9:1 ratio, the isomeric alcohols **9***a* and **9***b*, which were easily separated by column chromatography. Probably due to steric hindrance towards carbonyl addition, α deprotonation was a serious competition reaction and only 60% conversion took place. By repeated addition of methyllithium to the hydrolysed product, 93% conversion could be achieved. The assigned stereochemistry at C-13 of **9***a* and **9***b* followed from a comparison of their ^{1}H and ^{13}C nmr spectra. Of particular significance was the chemical shift of the methyl group at C-13; this carbon resonates 8.4 ppm upfield in the 13α-alcohol (**9***b*) compared with the epimeric β-alcohol (**9***a*) (20.75 and 29.13 ppm, respectively) due to the cooperative γ-interactions with the two axial hydrogens on C-8 and C-11.

The final step in the synthesis of the pregnane analogue steroid **10** involved the acetylene-cation cyclization of **9**. Both epimeric acetylenic-carbinols (**9***a* and **9***b*) were cyclized as described for related cases (10) by treatment with a mixture of trifluoroacetic acid and trifluoroacetic anhydride at −23°C followed by hydrolysis of the initially formed enol trifluoroacetates with 10% ethanolic potassium hydroxide.[4] Chromatog-

[1]Authors to whom correspondence may be addressed.

[2]Usual diterpene and steroid nomenclature and numbering are used for all tricyclic and tetracyclic compounds respectively.

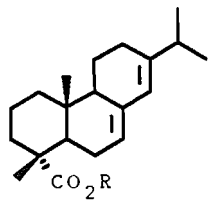
[3]Prepared from 3-pentyn-1-ol as in ref. 9.

[4]The use of higher temperatures had only a small effect on the product distribution. Specifically, the ratio **10**/**11** was 4:1 when the cyclization reaction was conducted at room temperature.

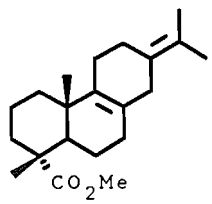
Printed in Canada / Imprimé au Canada

Can. J. Chem. Downloaded from www.nrcresearchpress.com by 195.138.81.100 on 09/07/12
For personal use only.

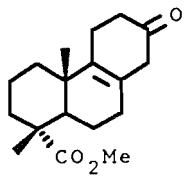
Can. J. Chem. Downloaded from www.nrcresearchpress.com by 195.138.81.100 on 09/07/12
For personal use only.



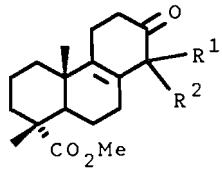
1*a* R=H
b R=Me



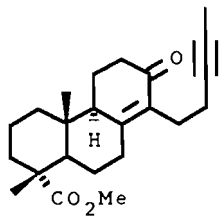
2



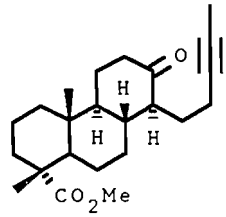
3



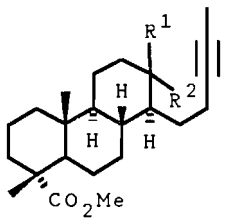
4 R^1, R^2=H, $-CH_2CH_2C{\equiv}CMe$
5 $R^1=R^2=-CH_2CH_2C{\equiv}CMe$



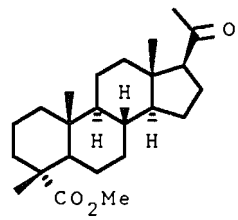
6



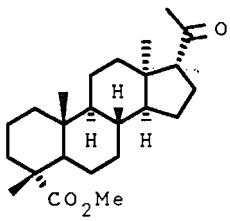
7 R=CO_2Me
8 R=CH_2OH



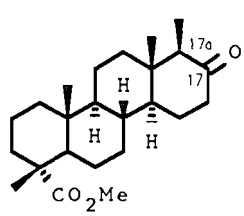
9*a* R^1=β-OH, R^2=α-Me
b R^1=α-OH, R^2=β-Me



10



11



12

raphy of the cyclization product afforded a 4.5:1 mixture (80% yield from alcohol **9***a*)[5] of desired 4α-methoxycarbonyl-4β-methyl-5α-pregnan-20-one (**10**, the major product) and its 13α (C/D *cis*) isomer (**11**), together with a small amount (less than 6%) of the six-membered annulated product (**12**). The mixture of 13-epimeric ketones **10** and **11** was separated by preparative high-pressure liquid chromatography (hplc). The stereochemistry assignments of both compounds were based on a comparison of the C-13 methyl group nmr signals at 0.56 ppm and 0.76 ppm for **10** and **11**, respectively, with the C-13 methyl frequencies of analogous structures.[6] The nmr signal of the methine proton of C-17, which appears at 2.49 ppm in **10** and at 2.96 ppm in the C-13 diastereoisomeric compound **11**, also substantiates the assigned stereochemistries. None of the 17α and 17β epimers of **10** and **11**, respectively, was detected in the ^1H nmr spectrum of the crude cyclization mixture.[6] It is worthwhile mentioning that the results obtained in the above cyclization of **9** seem to be at variance with those previously reported for the cyclization reaction of related acetylene-carbinols (10) for which the formation of C/D-*cis* fused compounds has not been detected. The formation of **12** was also surprising in that no detectable formation of six-membered annulated products took place during the cyclization of bicyclic carbinols (7).

Experimental

Melting points were determined on a Kofler apparatus and are uncorrected. The ir spectra were recorded on a Perkin–Elmer model 281 spectrometer. The ^1H and ^{13}C nmr spectra were measured in deuteriochloroform at 200.13 and 50.32 MHz, respectively, on a Bruker AC-200 spectrometer. Signals multiplicities in the ^{13}C nmr data were determined by DEPT experiments. Mass spectra were run by electron impact (70 eV) on a Varian MAT-311A spectrometer. Elemental analyses were performed by Servicio de semimicroanálisis del CSIC (Barcelona); final purification of all products for microanalysis was done by preparative hplc on a μ-Porasil column. Optical rotations were measured with a BS model A-PI polarimeter. Thin-layer chromatography was carried out on Merck 0.25 mm silica gel 60 HF_{254} analytical aluminium plates. Column chromatography refers to flash chromatography and was performed on Merck silica gel 60, 230–240 mesh. All reactions involving moisture- or air-sensitive materials were executed under an atmosphere of dry argon using oven-dried glassware and freshly distilled and dried solvents.

Methyl 13-oxo-podocarp-8-en-18-oate (3)

Enone **3** was obtained from abietic acid or commercial colophony as described in ref. 8; ^{13}C nmr, δ: 15.71 (C-19), 17.41 (C-2), 18.85 (C-20), 20.58 (C-6), 23.11 (C-11), 30.55 (C-7), 34.54 (C-12), 36.64 (C-10), 38.57 (C-1), 38.87 (C-3), 43.77 (C-14), 45.48 (C-5), 46.78 (C-4), 51.12 (OCH_3), 124.16 (C-8), 138.20 (C-9), 177.97 (C-18), 209.98 (C-13) ppm.

Methyl 13-oxo-14-(3-pentynyl)-podocarp-8-en-18-oate (4)

A stirred solution of the enone **3** (661 mg, 2.28 mmol) in anhydrous tetrahydrofuran (4 mL) containing a few crystals of anhydrous phenanthroline was treated dropwise with a stock solution of lithium diisopropylamide in tetrahydrofuran at −78°C until persistence of the characteristic rust colour of LDA-phenanthroline (approximately 3.9 mL, 0.6 M, 2.34 mmol). The stirring was continued at the same temperature for an additional 5 min. Hexamethylphosphoric triamide (1.2 mL, 6.9 mmol), followed by 1-iodo-3-pentyne (1.33 g, 6.85 mmol), was added and the resulting solution was allowed to warm to room temperature during 2 h. Water was added and the mixture was extracted with ether. The combined extracts were washed with brine until neutral, dried, and filtered. Evaporation of the solvent gave an oily residue, which was purified by flash chromatography (hexane–ether 9:1 as eluent) to give, in order of elution:

Dialkylated ketone 5 (50 mg, 5.2%) as an oil; $[\alpha]_D$ +98.8° (*c* 0.8, $CHCl_3$); ir (film) ν_{max}: 2940, 2860, 1730, 1715, 1465, 1445, 1260,

[5]A similar yield was obtained from the epimeric alcohol **9***b*, but in this case the ratio of **10** to **11** was ca. 9:1.

[6]Reported chemical shifts observed for the 13-Me group of related structures are δ 0.60 ppm in the case of 17β-acyl C/D *trans*-fused compounds (0.90 ppm for 17α epimers) and δ 0.80 ppm in the case of 17α-acyl C/D *cis*-fused isomers (1.20 ppm for 17β epimers). See, for example, refs. 7 and 10.

Can. J. Chem. Downloaded from www.nrcresearchpress.com by 195.138.81.100 on 09/07/12
For personal use only.

1200, 1120 cm^{-1}; ^1H nmr ($CDCl_3$), δ: 1.04 (s, 3H, CH_3-10β), 1.19 (s, 3H, CH_3-4β), 1.71 (t, *J* 2.55 Hz, 6H, 2 × ≡C—CH_3), 1.95 (dd, *J* 12.2 and 2 Hz, 1H, H-5α), 3.65 (s, 3H, CO_2CH_3); ^{13}C nmr, δ: 3.19 (C-5′ and C-5″), 14.45 (C-2′), 14.55 (C-2″), 16.35 (C-19), 17.99 (C-2), 19.68 (C-20), 21.10 (C-6), 22.43 (C-11), 25.08 (C-7), 35.47 (C-12), 35.89 (C-1′), 36.22 (C-3), 38.07 (C-1), 38.19 (C-10), 39.64 (C-1″), 45.95 (C-5), 47.31 (C-4), 51.67 (OCH_3), 54.25 (C-14), 75.74 (C-4′ and C-4″), 78.20 (C-3′), 78.66 (C-3″), 127.59 (C-9), 143.45 (C-8), 178.62 (C-18), 213.64 (C-13); mass spectrum, *m/e* (relative intensity, %): 422 (3), 407 (2.5), 379 (1), 363 (4), 357 (24), 356 (100), 347 (5), 342 (18), 341 (80), 281 (15.5). Anal. calcd. for $C_{28}H_{38}O_3$: C 79.57, H 9.06; found: C 79.31, H 9.22.

*Compound (**4**)* (341 mg, 42%), an oil, which gc–ms analysis (using a 12.5-m fused silica capillary column with dimethylsilicone as the stationary phase) revealed to be a mixture of two compounds with identical mass spectrum (a mixture of C-14 epimers); ir (film), ν_{max}: 2920, 1730, 1715, 1470, 1260 cm^{-1}; ^1H nmr, δ: 1.01 (s, 3H, CH_3-10β), 1.19 (s, 3H, CH_3-4β), 1.74 (t, *J* 2.6 Hz, 3H, ≡C—CH_3), 2.49 and 2.58 (each m, 1H, H-14 of epimers at C-14), 3.64 and 3.65 (each s, 3H, CO_2CH_3 of epimers at C-14); ^{13}C nmr (only signals of the main epimer are given), δ: 3.41 (C-5′), 15.87 (C-2′), 16.44 (C-19), 18.00 (C-2), 19.27 (C-20), 21.22 (C-6), 22.51 (C-11), 28.98 (C-7), 30.25 (C-1′), 35.16 (C-12), 36.45 (C-3), 37.63 (C-10), 38.35 (C-1), 46.50 (C-5), 47.48 (C-4), 51.86 (OCH_3), 52.39 (C-14), 76.14 (C-4′), 78.72 (C-3′), 127.77 (C-9), 140.93 (C-8), 178.95 (C-18), 213.02 (C-13); mass spectrum (from the gc–ms data), *m/e* (relative intensity, %): 357 (M^+ +1, 5), 356 (M^+, 19), 341 (73), 302 (26), 297 (35), 290 (98), 281 (66), 275 (100), 227 (43), 173 (39), 131 (45), 91 (77), 79 (41). Anal. calcd. for $C_{23}H_{32}O_3$: C 77.48, H 9.05; found: C 77.71, H 8.90.

*Unreacted starting material **3*** (320 mg, 48.2%).

*Methyl 13-oxo-14-(3-pentynyl)-podocarp-8(14)-en-18-oate (**6**)*

To a solution of the ketone **4** (256 mg, 0.72 mmol) in methanol (10 mL) was slowly added concentrated hydrochloric acid (1.5 mL) and the mixture was stirred at room temperature for 1 h. Brine was then added and the mixture was extracted with ether. The combined organic layers were washed with aqueous $NaHCO_3$ and brine, dried, and evaporated to yield a yellowish oil. Chromatography with hexane–ether (8:2) as eluent gave the enone **6** (236 mg, 92%) as a solid: mp 62–62.5°C (from hexane); $[\alpha]_D$ +12° (*c* 0.8, $CHCl_3$); ir (film), ν_{max}: 2940, 2880, 1730, 1670, 1620, 1460, 1440, 1265, 1160 cm^{-1}; ^1H nmr ($CDCl_3$), δ: 0.91 (s, 3H, CH_3-10β), 1.19 (s, 3H, CH_3-4β), 1.71 (t, *J* 2.6 Hz, 3H, ≡C—CH_3), 2.02 (dd, *J* 12.2 and 3.2 Hz, 1H, H-5α), 1.87–2.20 (m, 1H, H-7α), 2.21 (dd, *J* 12 and 5.5 Hz, 1H, H-9α), 2.4 (dt, *J* 15.3 and 4.5 Hz, 1H, H-12β), 3.01 (ddd, *J* 15.5, 4.5, and 2.2 Hz, 1H, H-7β), 3.65 (s, 3H, CO_2CH_3); ^{13}C nmr, δ: 3.41 (C-5′), 15.04 (C-20), 16.76 (C-19), 17.85 (C-2), 18.50 (C-2′), 19.66 (C-11), 24.25 (C-6), 24.77 (C-1′), 31.02 (C-7), 36.63 (C-12 and C-3′), 38.87 (C-10), 37.79 (C-1), 47.08 (C-4), 48.20 (C-5), 51.83 (OCH_3), 52.25 (C-9), 75.38 (C-4′), 78.85 (C-3′), 133.75 (C-14), 158.21 (C-8), 198.74 (C-13); mass spectrum, *m/e* (relative intensity, %): 357 (M^+ +1, 23), 356 (M^+, 100), 341 (10), 297 (12), 296 (7), 281 (10), 227 (17), 176 (74), 175 (58), 161 (23), 121 (97). Anal. calcd. for $C_{23}H_{32}O_3$: C 77.48, H 9.05; found: C 77.32, H 9.37.

*Methyl 13-oxo-14β-(3-pentynyl)-podocarpan-18-oate (**7**)*

A solution of lithium (10 mg, 1.4 mmol) in liquid ammonia (5 mL) contained in a cooled (−78°C) addition funnel was slowly added to a well-stirred solution of enone **6** (236 mg, 0.66 mmol) in a mixture of ether (6 mL) and ammonia (10 mL), also at −78°C. After addition of solid ammonium chloride, followed by evaporation of the ammonia, water was added and the resulting mixture was extracted with ether. The organic layer was washed with brine and dried. After removal of the solvent, the residue was chromatographed on silica gel with hexane–ether (8:2) as eluent to give **7** (175 mg, 74%) as a solid: mp 102–102.5°C (from hexane); $[\alpha]_D$ −14.5° (*c* 1.6, $CHCl_3$); ir (KBr disc), ν_{max}: 2960, 2860, 1730, 1715, 1460, 1398, 1265, 1185 cm^{-1}; ^1H nmr, δ: 0.82 (s, 3H, CH_3-10β), 1.16 (s, 3H, CH_3-4β), 1.73 (t, *J* 2.55 Hz, 3H, ≡C—CH_3), 3.64 (s, 3H, CO_2CH_3); ^{13}C nmr, δ: 3.34 (C-5′), 14.27 (C-20), 16.56 (C-19), 16.71 (C-2′), 17.94 (C-2), 24.05 (C-6), 24.80 (C-11), 26.04 (C-1′), 32.75 (C-7), 36.64 (C-10), 36.85 (C-3), 38.26 (C-1), 41.63 (C-12), 42.48 (C-8), 47.30 (C-4), 49.18 (C-5), 51.75 (OCH_3), 54.49 (C-9), 54.68 (C-14), 75.48 (C-4′), 79.06 (C-3′), 179.03 (C-18), 211.90 (C-13); mass spectrum, *m/e* (relative intensity, %): 359 (M^+ +1, 2), 358 (M^+, 8), 343 (1), 299 (2), 293 (19), 292 (100), 274 (10). Anal. calcd. for $C_{23}H_{34}O_3$: C 77.05, H 9.56; found: C 77.19, H 9.30.

Further elution with hexane–ether 6:4 afforded *13-oxo-14β-(3-pentynyl)-podocarpan-18-ol (**8**)* (17.4 mg, 8%) as a foam; $[\alpha]_D$ −4.05° (*c* 1.0, $CHCl_3$); ir (KBr disk), ν_{max}: 3460, 2940, 2880, 1720, 1460 cm^{-1}; ^1H nmr, δ: 0.75 (s, 3H, CH_3-10β), 0.82 (s, 3H, CH_3-4β), 1.73 (t, 3H, *J* 2.5 Hz, ≡C—CH_3, 3.07 and 3.40 (each d, *J* 10.9 Hz, 1H each, 2 × H-18); ^{13}C nmr, δ: 3.43 (C-5′), 14.57 (C-20), 16.75 (C-2′), 17.54 (C-19), 18.10 (C-2), 21.29 (C-6), 24.80 (C-11), 26.40 (C-1′), 32.92 (C-7), 35.19 (C-3), 37.00 (C-10), 38.79 (C-1), 41.81 (C-12), 42.47 (C-8), 37.48 (C-4), 47.61 (C-5), 54.63 (C-9 and C-14), 71.77 (C-18), 75.53 (C-4′), 79.17 (C-3′), 212.57 (C-13); mass spectrum, *m/e* (relative intensity, %): 331 (M^+ +1, 3), 330 (M^+, 11), 315 (1), 299 (1), 266 (2), 265 (18), 264 (100), 246 (7), 234 (11), 233 (61), 216 (21), 215 (42).

*Methyl 13β-hydroxy-13α-methyl-14β-(3-pentynyl)-podocarpan-18-oate (**9**a) and C-13 epimer (**9**b)*

A crystal of 1,10-phenanthroline was added to a solution of acetylenic ketone **7** (110 mg, 0.31 mmol) in dry tetrahydrofuran (2 mL); the mixture was cooled to −78°C and then ca. 0.22 mL of a 1.6 M solution of methyllithium in ether was slowly added until a yellow-brown color persisted. The mixture was stirred for 5 min and then excess methyllithium was destroyed by careful addition of water. The resulting mixture was diluted with water and extracted with ether. The combined organic layers were washed with brine and dried. The ether was distilled off and the residue was dissolved in anhydrous tetrahydrofuran (2 mL). This solution was treated again with methyllithium and worked up as described above. After repeating this procedure once more, ^1H nmr analysis showed the presence of a small amount of **7** (about 5%). The crude product was chromatographed on silica gel, using hexane – ethyl acetate (9:1) as eluent, to afford, in order of elution:

*Starting compound **7*** (6.8 mg, 6.2%)

*Compound **9**a* (89.3 mg, 77.9%)) as a solid, mp 113–115°C (from hexane); $[\alpha]_D$ −34.6° (*c* 1.15, $CHCl_3$); ir (KBr disk), ν_{max}: 3520, 2930, 2860, 1720, 1440, 1395, 1260, 1180 cm^{-1}; ^1H nmr, δ: 0.85 (s, 3H, CH_3-10β), 1.14 (s, 3H, CH_3-4β), 1.18 (s, 3H, CH_3-13α), 1.73 (t, *J* 2.55 Hz, 3H, ≡C—CH_3), 1.93 (dd, *J* 12.6 and 3.4 Hz, 1H, H-5α), 3.62 (s, 3H, CO_2CH_3); ^{13}C nmr, δ: 3.39 (C-5′), 14.58 (C-20), 16.64 (C-19), 18.03 (C-2), 19.02 (C-2′), 19.41 (C-11), 24.36 (C-6), 27.86 (C-1′), 32.09 (C-7), 36.87 (C-3), 37.14 (C-8), 38.08 (C-1 and C-10), 40.50 (C-12), 47.47 (C-4), 49.49 (C-5), 51.05 (C-14), 51.72 (OCH_3), 55.49 (C-9), 71.37 (C-13), 75.55 (C-4′), 79.69 (C-3′), 179.35 (C-18); mass spectrum, *m/e* (relative intensity, %): 374 (M^+, 4), 359 (32), 356 (11), 341 (3), 316 (3), 290 (56), 121 (92), 81 (63), 43 (100). Anal. calcd. for $C_{24}H_{38}O_3$: C 76.96, H 10.22; found: C 77.18, H 10.10.

*Compound **9**b* (10.3 mg, 8.9%) as a clear foam that could not be induced to crystallize; ir (film), ν_{max}: 3500, 2925, 2860, 1720, 1245 cm^{-1}; ^1H nmr, δ: 0.81 (s, 3H, CH_3-10β), 1.02 (s, 3H, CH_3-13β), 1.14 (s, 3H, CH_3-4β), 1.73 (t, *J* 2.55 Hz, 3H, ≡C—CH_3), 3.62 (s, 3H, CO_2CH_3); ^{13}C nmr, δ: 3.42 (C-5′), 14.49 (C-20), 16.64 (C-19), 18.06 (C-2), 20.43 (C-2′), 21.97 (C-11), 24.32 (C-6), 27.85 (C-1′), 32.30 (C-7), 36.27 (C-10), 36.83 (C-3), 38.11 (C-1), 40.22 (C-8), 42.25 (C-12), 47.45 (C-4), 49.49 (C-5), 51.86 (OCH_3), 53.20 (C-14), 55.52 (C-9), 72.89 (C-13), 76.02 (C-4′), 79.95 (C-3′), 179.37 (C-18); mass spectrum, *m/e* (relative intensity, %): 374 (M^+, 1), 359 (17), 356 (4), 290 (22), 281 (4), 243 (5), 231 (10), 180 (19), 121 (62), 81 (49), 43 (100).

*Cyclization of **9**. 4α-Methoxycarbonyl-4β-methyl-5α-pregnan-20-one (**10**) and 13α-(C/D* cis*) isomer (**11**)*

To a mixture of trifluoroacetic acid (1.5 mL) and trifluoroacetic anhydride (0.75 mL) at −23°C was added the alcohol **9***a* (41 mg,

Can. J. Chem. Downloaded from www.nrcresearchpress.com by 195.138.81.100 on 09/07/12
For personal use only.

0.12 mmol) and the resulting mixture was allowed to stand overnight at the same temperature. After evaporation of the solvent under reduced pressure, the residual oil was dissolved in ethanol (3 mL) and was treated with 10% ethanolic potassium hydroxide (1 mL). After stirring at room temperature for 1 h, the mixture was diluted with water and extracted with ether. The combined organic layers were washed with brine, dried, filtered, and evaporated to afford the crude material, which was chromatographed, using hexane – ethyl acetate (95:5) as eluent, to give an epimeric mixture of **10** and **11** (32.7 mg, 79.8%). Further elution gave *4α-methoxycarbonyl-4β,17aβ-dimethyl-D-homo-5α-androstan-17-one (12)* (2.3 mg, 5.6%) as a solid; mp 155–157°C (from hexane – ethyl acetate); ir (KBr disk), ν_{max}: 2930, 2850, 1730, 1715, 1460, 1390, 1250 cm^{-1}; ^1H nmr, δ: 0.60 (s, 3H, CH_3-18β), 0.85 (s, 3H, CH_3-10β), 0.89 (d, *J* 6.7 Hz, 3H, CH_3-17aβ), 1.15 (s, 3H, CH_3-4β), 3.63 (s, 3H, CO_2CH_3); ^{13}C nmr, δ: 7.10 (CH_3-17a), 13.18 (C-18), 14.51 (C-19), 16.64 (CH_3-4β), 18.07 (C-2), 19.88 (C-11), 24.24 (C-6), 26.04 (C-15), 29.68 (C-13), 31.70 (C-7), 35.63 (C-8), 36.28 (C-10), 36.85 (C-3), 38.01 (C-12), 38.45 (C-1), 41.36 (C-16), 47.50 (C-4), 49.42 (C-5), 51.16 (C-14), 51.85 (OCH_3), 55.79 (C-17a), 58.08 (C-9), 179.44 (CO_2), 213.58 (C-17); mass spectrum, *m/e* (relative intensity, %): 375 (M^+ +1, 3), 374 (M^+, 11), 346 (2), 315 (4), 302 (12), 290 (5), 287 (10), 242 (6), 229 (4), 147 (12), 55 (100).

Isomers **10** and **11** were separated from the above mixture by preparative hplc on a μ-Porasil column, with hexane – ethyl acetate (9:1) as eluent, to give pure **10** (26.3 mg, 64.1% from **9***a*) and its 13α(C/D-*cis*)-17β*H*-isomer **11** (5.8 mg, 14.1% from **9***a*).

Compound **10** was a solid; mp 116–116.5°C (from methanol); $[\alpha]_D$ +59.6° (*c* 1.14, $CHCl_3$); ir (KBr disk), ν_{max}: 2930, 2850, 1730, 1715, 1460, 1270 cm^{-1}; ^1H nmr, δ: 0.56 (s, 3H, CH_3-13β) 0.86 (s, 3H, CH_3-10β), 1.14 (s, 3H, CH_3-4β), 2.08 (s, 3H, $COCH_3$), 2.49 (t, *J* 9 Hz, 1H, H-17α), 3.62 (s, 3H, CO_2CH_3); ^{13}C nmr, δ: 13.37 (C-18), 14.60 (C-19), 16.63 (CH_3-4β), 18.08 (C-2), 20.38 (C-11), 22.73 (C-16), 24.18 (C-15), 24.36 (C-6), 31.55 (C-21), 32.34 (C-7), 35.29 (C-8), 36.23 (C-10), 36.92 (C-3), 38.17 (C-12), 38.88 (C-1), 44.08 (C-13), 47.63 (C-4), 50.02 (C-5), 51.83 (OCH_3), 56.28 (C-9), 56.75 (C-14), 63.73 (C-17), 179.47 (CO_2), 209.74 (C-20); mass spectrum, *m/e* (relative intensity, %): 375 (M^+ +1, 7), 374 (M^+, 29), 315 (30), 314 (57), 291 (92), 229 (32), 175 (40), 84 (100). Anal. calcd. for $C_{24}H_{38}O_3$: C 76.96, H 10.22; found: C 76.89, H 10.12.

Compound **11** was a solid; mp 202–202.5°C (from methanol); $[\alpha]_D$ −78.2° (*c* 0.55, $CHCl_3$); ir (KBr disk), ν_{max}: 2935, 2855, 1720, 1700, 1245, 1170 cm^{-1}; ^1H nmr, δ: 0.76 (s, 3H, CH_3-13α), 0.84 (s, 3H, CH_3-10β), 1.14 (s, 3H, CH_3-4β), 2.08 (s, 3H, $COCH_3$), 2.96 (t, *J* 9 Hz, 1H, H-17β), 3.62 (s, 3H, CO_2CH_3); ^{13}C nmr, δ: 14.60 (C-19), 16.70 (CH_3-4β), 18.05 (C-2), 19.42 (C-11), 24.04 (C-16), 24.36 (C-6), 25.46 (C-18), 25.92 (C-15), 31.72 (C-21), 33.13 (C-7), 34.55 (C-12), 36.38 (C-10), 36.87 (C-3), 37.29 (C-8), 38.02 (C-1), 45.33 (C-13), 47.56 (C-4), 49.61 (C-5), 51.83 (OCH_3), 54.25 (C-17), 55.01 (C-9), 55.95 (C-14), 179.44 (CO_2), 210.88 (C-20); mass spectrum, *m/e* (relative intensity, %): 375 (M^+ +1, 1), 374 (M^+, 4), 359 (1), 356 (3), 315 (3), 314 (6), 291 (9), 229 (4), 84 (24), 43 (100).

Acknowledgments

Financial support from CAICYT (Grant No. Pb86-0578) is gratefully acknowledged. We also thank Dr. Donald Craig for manuscript revision.

1. B. Delmond, S. M. Arreguy, and B. Maillard. Tetrahedron Lett. **28**, 2127 (1987), and references cited therein.
2. (*a*) E. Wenkert, M. Curini, R. Coccia, P. Ceccherelli, T. D. J. Halls, and B. Porter. J. Org. Chem. **49**, 2054 (1984); (*b*) F. Bermejo, M. Bordell, and A. Fernandez. Can. J. Chem. **66**, 2200 (1988), and references cited therein.
3. (*a*) R. C. Cambie, W. A. Denny, T. J. Fullerton, and R. C. Hayward. Aust. J. Chem. **27**, 1317 (1974); (*b*) D. M. S. Wheeler and P. R. Witt. J. Org. Chem. **37**, 4211 (1972), and references cited therein.
4. (*a*) A Tahara, Y. Harigaya, and M. Onda. Chem. Pharm. Bull. **24**, 1497 (1976); (*b*) H. Steindl and E. Haslinger. J. Org. Chem. **50**, 3749 (1985); T. Matsumoto, S. Imai, Y. Sunaoka, and T. Yoshinari. Bull. Chem. Soc. Jpn. **61**, 723 (1988), and references cited therein.
5. A. Abad, C. Agullo, M. Arno, L. R. Domingo, and R. J. Zaragoza. J. Org. Chem. **53**, 3761 (1988).
6. M. Shimagaki, A. Anazawa, T. Oishi, and A. Tahara. Heterocyles, **8**, 237 (1977).
7. P. T. Lansbury, T. R. Demmin, G. E. Dubois, and V. R. Haddon. J. Am. Chem. Soc. **97**, 394 (1975).
8. A. Abad, M. Arno, L. R. Domingo, and R. J. Zaragoza. Tetrahedron, **41**, 4937 (1985).
9. M. F. Ansell, J. C. Emmett, and R. V. Coombs. J. Chem. Soc. (C), 217 (1968).
10. (*a*) T. Kametani, K. Suzuki, and H. Nemoto. J. Chem. Soc. Perkin Trans. 1, 2805 (1980); (*b*) Tetrahedron Lett. **21**, 4855 (1980) (*c*) J. Org. Chem. **47**, 2331 (1982).

2-*S*-Methyl-5,5-dimethylimidazolin-4-one: chemical behaviour and crystal structure of its Δ^1 tautomer

FRANCO CRISTIANI, FRANCESCO A. DEVILLANOVA,[1] ANGELO DIAZ, FRANCESCO ISAIA, AND GAETANO VERANI
Dipartimento di Chimica e Tecnologie Inorganiche e Metallorganiche, Via Ospedale 72, 09124 Cagliari, Italy

FRANCESCO DEMARTIN
Istituto di Chimica Strutturistica Inorganica, Via G. Venezian 21, 20133 Milano, Italy

AND

GIUSEPPE SABA
Dipartimento di Scienze Chimiche, Via Ospedale 72, 09124 Cagliari, Italy

Received March 15, 1990[2]

FRANCO CRISTIANI, FRANCESCO A. DEVILLANOVA, ANGELO DIAZ, FRANCESCO ISAIA, GAETANO VERANI, FRANCESCO DEMARTIN, and GIUSEPPE SABA. Can. J. Chem. **69**, 383 (1991).

2-*S*-Methyl-5,5-dimethylimidazolin-4-one can be crystallized as Δ^1 or Δ^2 tautomers, depending on the solvent polarity. The structure, solved on crystals obtained from benzene, showed it to be the Δ^1 tautomer in the *anti* configuration. Δ^1-2-*S*-Methyl-5,5-dimethylimidazolin-4-one is monoclinic, space group $P2_1/c$, *with* a = 8.347(1), b = 10.121(1), c = 9.996(3) Å, β = 107.20(2)°, R = 0.037 for 1395 independent reflections with $I > 1\sigma(I)$. The quantum mechanical (MNDO, PM3, and AM1) calculations indicate that among the four conformers the *anti*-Δ^1 tautomer has both the lowest dipole moment and the lowest enthalpy of formation. The ultraviolet spectrum of the title compound has been recorded in solvents with different dielectric constants. The infrared spectra of the Δ^1 and Δ^2 solid samples are discussed relative to the ν(NH) and ν(CO) absorptions and in comparison with those recorded in carbon tetrachloride and in chloroform solution. Its acid–base behaviour has been studied by determining the pK_a in aqueous solutions and the results are compared with those obtained for some related hydantoins.

Key words: 2-*S*-methyl-5,5-dimethylimidazolin-4-one, tautomerism, hydantoin derivatives, crystal structure.

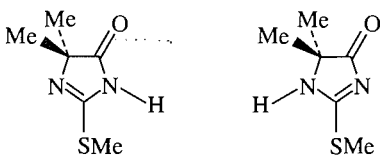
FRANCO CRISTIANI, FRANCESCO A. DEVILLANOVA, ANGELO DIAZ, FRANCESCO ISAIA, GAETANO VERANI, FRANCESCO DEMARTIN et GIUSEPPE SABA. Can. J. Chem. **69**, 383 (1991).

Le 2-*S*-méthyl-5,5-diméthylimidazoline-4-one peut être cristallisé comme tautomères Δ^1 ou Δ^2, selon la polarité du solvant. La structure, qui a été résolue sur des cristaux obtenus d'une solution benzénique, a mis en évidence que la tautomère Δ^1 possède une configuration *anti*. Δ^1-2-*S*-Méthyl-5,5-diméthylimidazoline-4-one est monoclinique, groupe spatial $P2_1/c$, avec a = 8,347(1), b = 10,121(1), c = 9,996(3) Å, β = 107,20(2)°, R = 0,037 pour 1395 réflections indépendantes avec $I > 1\sigma(I)$. Les résultats des calculs de mécanique quantique indiquent que le tautomère *anti*-Δ^1 a le moment dipolaire et l'enthalpie de formation les plus bas parmi les quatre conformères. Les spectres ultraviolets du composé dissous dans des solvants ayant des constantes diélectriques différentes ont été enregistrés. Les spectres infrarouges des tautomères sont discutés par rapport aux absorptions ν(NH) et ν(CO) et en comparaison avec ceux enregistrés dans le tétrachlorure de carbone et le chloroforme. Le comportement acide–base du composé a été étudié par la détermination du pK_a en solution aqueuse et les résultats ont été comparés à ceux obtenus pour certaines hidantoïnes apparentées.

Mots clés : 2-*S*-méthyl-5,5-diméthylimidazoline-4-one, tautomérie, dérivés hydantoïnes, structure cristalline.

Introduction

S-Methylation of 5,5-dimethyl-2-thioxoimidazolidin-4-one (L = ligand) yields Δ^1- or Δ^2-2-*S*-methyl-5,5-dimethylimidazolin-4-one tautomers (**I** or **II**), i.e.,



Δ^1(I) Δ^2(II)

This tautomerism, defined as annular desmotropy, was studied by ir and uv spectroscopies in several hydantoin derivatives (1, 2). Lempert *et al.* (2) determined the X-ray structures of the two desmotropes of 2-*S*-methyl-5,5-diphenylimidazolin-4-one in 1973, and showed that the polarity of the solvent is crucial in obtaining one of the two tautomers. Apolar solvents, such as carbon tetrachloride or benzene, stabilize the Δ^1 tautomer, while solvents such as water stabilize the Δ^2.

Since our main interest is in the coordination chemistry of the **I**/**II** mixture, our main goals will be to ascertain which factors can induce the ligand to coordinate a metal as **I** or **II** and to find out if the nature of the metal is important in determining the coordination by **I** or **II**. For instance, the reaction of 2-*S*-methyl-5,5-dimethylimidazolin-4-one with $CuCl_2$ in Pr^{i}OH at room temperature yielded a complex whose crystal structure was solved as $[CuL_4 \cdot H_2O]^{2+}[CuCl_4]^{2-}$ with the ligand N-coordinated as **II**.[3]

To clarify the chemical behaviour of the ligand, we have carried out a study on 2-*S*-methyl-5,5-dimethylimidazolin-4-one, by several techniques, both in the solid state and in solutions of different solvents.

Experimental section

2-S-Methyl-5,5-dimethylimidazolin-4-one

2-*S*-Methyl-5,5-dimethylimidazolin-4-one was prepared as previously described (3). Its recrystallization from benzene yields **I**, whereas from water **II** is obtained.

[1]Author to whom correspondence may be addressed.

[2]Revision received October 30, 1990.

[3]F. Cristiani, F. Demartin, F. A. Devillanova, A. Diaz, F. Isaia, and G. Verani, unpublished data.

Printed in Canada / Imprimé au Canada

Can. J. Chem. Downloaded from www.nrcresearchpress.com by 195.138.81.100 on 09/07/12
For personal use only.

Can. J. Chem. Downloaded from www.nrcresearchpress.com by 195.138.81.100 on 09/07/12
For personal use only.

Spectroscopic measurements

The ir spectra (3500–3050 cm^{-1} and 1800–1600 cm^{-1}) were recorded in CCl_4 solutions in variable temperature liquid cells Specac P/N 21000 of NaCl with a pathlength of 0.1 cm using a Perkin–Elmer 983 instrument connected with a Perkin–Elmer 7500 data station. The ir spectra (3500–200 cm^{-1}) on the solid samples were recorded as KBr discs.

The uv spectra were recorded in several solvents using a Cary 2300 instrument, connected with a DS15.

X-ray data collection and structure determination of I

The solid obtained from benzene yielded crystals suitable for an X-ray structure determination. Crystal data and other experimental details are summarized in Table 1. The diffraction experiment was carried out on a Enraf–Nonius CAD-4 diffractometer at room temperature using monochromated Mo-K_α radiation (λ = 0.71073 Å). The calculations were performed on a PDP 11/73 computer using the SDP-Plus structure determination package (4). The diffracted intensities were corrected for Lorentz, polarization, and absorption (empirical correction) (5). Scattering factors for all the atomic species and anomalous dispersion corrections for scattering factors of non-hydrogen atoms were taken from ref. 6.

The structure was solved by direct methods (MULTAN), and refined by full-matrix least squares, minimizing the function $\Sigma w(F_o - k|F_c|)^2$. All the hydrogen atoms were located by a difference Fourier synthesis.

Anisotropic thermal factors were refined for all the non-hydrogen atoms, and isotropic temperature factors for the hydrogen atoms. The final difference Fourier synthesis showed maximum residuals of 0.2 e/Å^3. The atomic coordinates of the structure model are listed in Table 2.[4]

Potentiometric measurements

Potentiometric measurements were carried out using a Metrohm E 654 meter equipped with a Metrohm 6.0203 combined glass electrode. The potentiometer was connected with a PC IBM XT controlling the addition of the titrant (KOH) delivered from a Metrohm digital dispenser (model Dosimat E 665); the titrations on 2-*S*-methyl-5,5-dimethylimidazolin-4-one both alone and in presence of an excess of mineral acid (HCl) were performed automatically.

The electrode was standardized on the pH = $-\log C_{H^+}$ scale by titrating HNO_3 (0.01–0.005 mol dm^{-3}) with KOH at 25°C and I = 0.1 mol dm^{-3} (KNO_3). The titrations were carried out over a range of concentrations of 2-*S*-methyl-5,5-dimethylimidazolin-4-one between 0.001 and 0.01 mol dm^{-3}. All titrations were performed in triplicate.

The calculations of the E^0 of the electrode system, the purity of the compound, and the excess of HCl were performed by the least-squares computer program SUPERQUAD (7). The calculations of the ionization constants were performed by SUPERQUAD as well as by PSEQUAD (8). The latter program was modified to obtain a graph of the titration curve.

Conformational calculations

The calculations of the most stable conformations were done using the semiempirical quantum mechanical methods MNDO, AM1, and PM3 (9–12). The first two have been very useful in many chemical applications and AM1, in particular, is gaining major attention because of its ability to correct for the excessive long-range repulsions in the core–core repulsion terms occurring in the original MNDO method. The third, a newly parameterized MNDO method, has been added for comparison; it differs from the parent MNDO in that all two-electron one-center integrals have been optimized and, according to the author, it leads to better estimates of both heats of formation and molecular geometries (12). In the AM1 calculations the parameters of the sulphur atom were taken from the MNDO calculations, as implemented in the MOPAC 5.0 quantum mechanical package (13). The final geometries

TABLE 1. Crystallographic data for Δ^1-2-*S*-methyl-5,5-dimethylimidazolin-4-one

Formula	$C_6H_{10}N_2OS$
FW, (amu)	158.22
Crystal system	Monoclinic
Space group	$P2_1/_c$
a (Å)	8.347(1)
b (Å)	10.121(1)
c (Å)	9.996(3)
β (deg)	107.20(2)
V (Å^3)	806.7(5)
Z	4
D_{calcd} (g cm^{-3})	1.303
μ(Mo–K_α) (cm^{-1})	3.22
Min. transmission factor	0.75
Crystal dimensions (mm)	0.10 × 0.10 × 0.08
Scan mode	ω
ω scan width (deg)	1.1 + 0.35 tan θ
θ range (deg)	3–25
Octants of reciprocal space explored	$+h, +k, \pm l$
Measured reflections	1766
Unique observed reflections $\{I > 1\sigma(I)\}$	1395
Final R and R_w indices[a]	0.037, 0.043
Max. displacement/error	0.08
No. of variables	131
S[b]	1.458

[a] $R = [\Sigma(F_o - k|F_c|)/\Sigma F_o]$; $R_w = [\Sigma w(F_o - k|F_c|)^2/\Sigma w F_o^2]^{1/2}$.
[b] $S = [\Sigma w(F_o - k|F_c|)^2/(N_{observations} - N_{variables})]^{1/2}$; $w = 1/(\sigma(F_o))^2$; $\sigma(F_o) = [\sigma^2(I) + (0.04I)^2]^{1/2}/2F_o$Lp.

TABLE 2. Fractional atomic coordinates with their esd's in parentheses

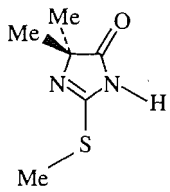
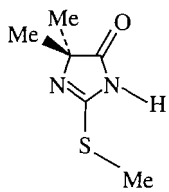
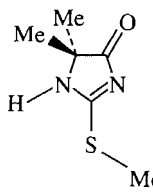
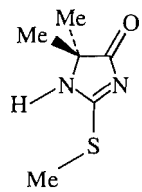
Atom	x	y	z	B (Å^2)
S(6)	0.88177(5)	0.15880(5)	0.63320(5)	3.121(9)
O(7)	1.3754(2)	0.4484(1)	0.8219(1)	3.75(3)
N(1)	1.1220(2)	0.2652(2)	0.5313(1)	2.47(3)
N(3)	1.1430(2)	0.3120(2)	0.7563(1)	2.78(3)
C(2)	1.0592(2)	0.2489(2)	0.6324(2)	2.22(3)
C(4)	1.2755(2)	0.3806(2)	0.7368(2)	2.63(3)
C(5)	1.2719(2)	0.3508(2)	0.5866(2)	2.65(3)
C(8)	1.2542(3)	0.4783(2)	0.5029(2)	4.61(5)
C(9)	1.4315(2)	0.2751(2)	0.5904(2)	4.00(5)
C(61)	0.8003(3)	0.1163(2)	0.4516(2)	3.98(5)
H(3)	1.122(2)	0.305(2)	0.823(2)	3.1(4)*
H(8A)	1.143(3)	0.522(2)	0.494(2)	5.5(6)*
H(8B)	1.346(3)	0.534(2)	0.545(2)	5.0(5)*
H(8C)	1.245(3)	0.461(3)	0.413(3)	6.8(7)*
H(9A)	1.531(2)	0.326(2)	0.634(2)	4.0(5)*
H(9B)	1.439(3)	0.190(2)	0.650(2)	4.7(5)*
H(9C)	1.433(3)	0.254(3)	0.496(3)	6.3(6)*
H(61A)	0.700(3)	0.083(3)	0.444(2)	5.8(6)*
H(61B)	0.780(3)	0.191(3)	0.397(2)	5.6(6)*
H(61C)	0.875(3)	0.055(3)	0.426(3)	7.4(7)*

Starred atoms were refined isotropically. Anisotropically refined atoms are given in the form of the isotropic equivalent thermal parameter defined as: $(4/3)*[a^2*B(1,1) + b^2*B(2,2) + c^2*B(3,3) + ab(\cos\gamma)*B(1,2) + ac(\cos\beta)*B(1,3) + bc(\cos\alpha)*B(2,3)]$.

[4]Tables of observed and calculated structure factor amplitudes, interatomic distances and angles, and temperature factors may be purchased from the Depository of Unpublished Data, Document Delivery, CISTI, National Research Council Canada, Ottawa, Canada, K1A 0S2.

Tables of interatomic distances and angles have also been deposited with the Cambridge Crystallographic Data Centre and can be obtained on request from The Director, Cambridge Crystallographic Data Centre, University Chemical Laboratory, Lensfield Road, Cambridge CB2 1EW, U.K.

TABLE 3. Comparison of the enthalpies of the formation (ΔH_f) and of the dipole moments (μ) of the most stable monomers calculated by AM1, PM3, and MNDO

	anti-Δ^1	*syn*-Δ^1	*anti*-Δ^2	*syn*-Δ^2
				
ΔH_f(kcal/mol)				
AM1[a]	−5.61	[c]	2.00	−0.95
Δ[b]	0	—	7.61	4.66
PM3	−31.06	−27.95	−24.26	−27.73
Δ[b]	0	3.11	6.80	3.33
MNDO	−35.42	[c]	−27.02	−30.76
Δ[b]	0	—	8.40	4.66
μ(D)				
AM1[a]	2.48	[c]	6.26	3.72
PM3	2.37	2.31	6.26	3.33
MNDO	2.39	[c]	5.43	3.67

[a]The parameters used for the sulphur atom have been taken from the MNDO.
[b]Energy difference calculated with respect to the most stable tautomer.
[c]In the AM1 and MNDO approximations the *syn*-Δ^1 tautomer does not correspond to a minimum of energy and the calculation converges to the *anti* tautomer.

of the most stable conformers were refined using the PRECISE keyword, which increases the criteria for terminating electronic and geometric optimization by a factor of 100. Final force constant calculations on the optimized geometries were run with the FORCE keyword to locate ground and (or) transiton states in the potential energy hypersurface.

Results and discussion

For a better understanding of the chemical behaviour of 2-*S*-methyl-5,5-dimethylimidazolin-4-one, we carried out conformational computations both on the Δ^1 and Δ^2 monomers at the MNDO, PM3, and AM1 quantum mechanical level (9–13). Tables 3 and 4 summarize respectively some molecular properties and the optimized geometries of the four most stable conformations of the two monomers obtained with the different calculations. From the values of the enthalpies of formation (ΔH_f), at all levels of quantum mechanical approximations, it is evident that the *anti*-Δ^1 tautomer is the most stable compound, since it has a dipole moment (μ) close to that of the *syn*-Δ^1 and lower than both the Δ^2 conformers and its energy is 3 kcal/mol lower than that of its *syn* analogue and even lower than those of the Δ^2 compounds (see Table 3). It is also evident that the two Δ^2 conformers differ strongly in dipole moment and in spite of the difference in formation energy it is very probable that the solid obtained from water is the *syn*-Δ^2 tautomer. Unfortunately, these crystals are not suitable for an X-ray analysis.

As far as the *syn*-Δ^1 conformer is concerned, we point out that the AM1 and MNDO calculations gave no evidence that it is a stable compound. In fact, on optimization the *syn*-Δ^1 geometry converged to that of *anti*-Δ^1, this being due to the occurrence of a shallow minimum. This was not the case with the PM3 calculation by which a deeper minimum was found. Table 4 also collects the bond lengths and angles of the hydantoin rings found by an X-ray study of crystals obtained from benzene. The

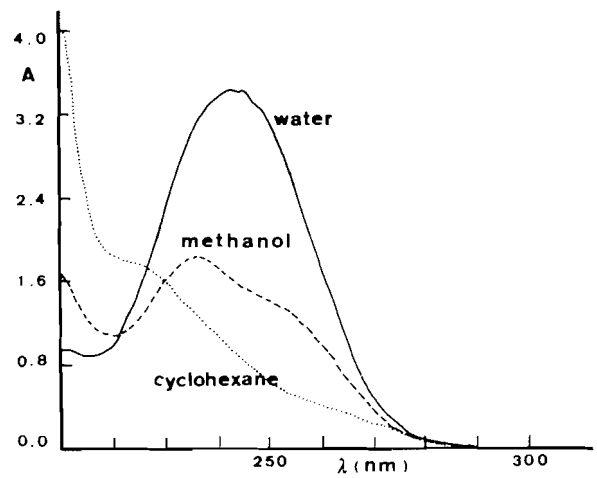


FIG. 1. Ultraviolet spectra of 2-*S*-methyl-5,5-dimethylimidazolin-4-one in solvents at different polarities.

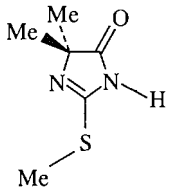
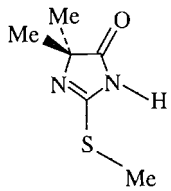
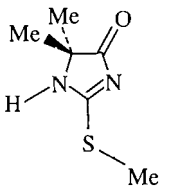
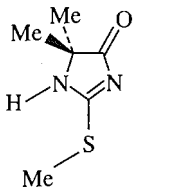
optimized geometry of *anti*-Δ^1 agrees fairly well with the experimental; in particular, this structure is found to be the most planar among the four; the major differences are seen in the C(2)—N(3) and N(3)—C(4) bond lengths. These are almost certainly due to the occurrence in the solid state of hydrogen bonds that were not accounted for in the quantum mechanical calculations. In fact PM3 calculations, carried out not on an isolated molecule but on a doubly hydrogen bonded molecule, have shown a consistent shortening of these two bonds, which become 1.429 and 1.437 Å respectively. However, packing forces in the solid state occur that are not reproduced by the calculations, as suggested by the differences in the dihedral angle N(3)—C(2)—S(6)—C(61).

As regards the comparison of the three quantum mechanical

Can. J. Chem. Downloaded from www.nrcresearchpress.com by 195.138.81.100 on 09/07/12
For personal use only.

Can. J. Chem. Downloaded from www.nrcresearchpress.com by 195.138.81.100 on 09/07/12
For personal use only.

TABLE 4. Some selected bond distances (Å), angles (°), and torsion angles (°) of the hydantoin skeleton, as obtained from X-ray structure and AM1, PM3, and MNDO calculations

Atoms	X-ray structure	*anti*-Δ^1 			*syn*-Δ^1 	*anti*-Δ^2 			*syn*-Δ^2 		
		AM1	PM3	MNDO	PM3[a]	AM1	PM3	MNDO	AM1	PM3	MNDO
N(1)—C(2)	1.280(2)	1.319	1.311	1.312	1.308	1.421	1.433	1.416	1.429	1.447	1.426
C(2)—N(3)	1.385(3)	1.416	1.458	1.407	1.446	1.331	1.318	1.316	1.325	1.314	1.311
N(3)—C(4)	1.368(2)	1.412	1.443	1.422	1.447	1.436	1.458	1.436	1.441	1.461	1.442
C(4)—O(7)	1.212(2)	1.231	1.211	1.218	1.210	1.228	1.205	1.216	1.227	1.204	1.216
C(2)—S(6)	1.741(1)	1.697	1.756	1.677	1.763	1.691	1.753	1.675	1.698	1.759	1.683
S(6)—C(61)	1.792(2)	1.735	1.803	1.731	1.801	1.723	1.804	1.732	1.731	1.801	1.730
N(1)—C(2)—S(6)	128.8(1)	126.1	127.9	127.6	123.1	118.9	120.6	119.2	121.6	125.1	123.7
N(3)—C(2)—S(6)	116.3(1)	118.4	120.7	119.8	125.7	124.7	127.1	126.8	121.3	122.6	122.2
C(2)—N(3)—C(4)	108.8(1)	107.6	107.9	109.3	107.6	106.9	109.8	108.1	106.6	110.1	108.1
N(3)—C(4)—O(7)	127.2(1)	125.3	121.6	122.3	121.4	127.3	123.0	122.6	127.2	123.0	122.4
C(5)—C(4)—O(7)	127.8(1)	129.4	132.0	132.9	132.2	124.6	129.4	132.0	124.6	129.3	128.8
C(2)—S(6)—C(61)	100.9(1)	103.6	104.7	109.7	104.3	105.1	104.7	109.8	104.6	104.5	109.4
H(1)—N(1)—C(2)—S(6)	—	—	—	—	—	−43.0	−40.2	−38.4	−48.2	−45.4	−42.4
H(3)—N(3)—C(2)—S(6)	—	0.0	24.9	0.5	29.7	—	—	—	—	—	—
N(1)—C(2)—S(6)—C(61)	—	—	—	—	—	−173.5	−175.5	−172.8	−5.5	−2.8	−38.8
N(3)—C(2)—S(6)—C(61)	172.2(1)	180.0	177.7	179.9	10.5	—	—	—	—	—	—

[a]The AM1 and MNDO calculations do not indicate *syn*-Δ^1 as a stable compound and the optimization converges to *anti*-Δ^1.

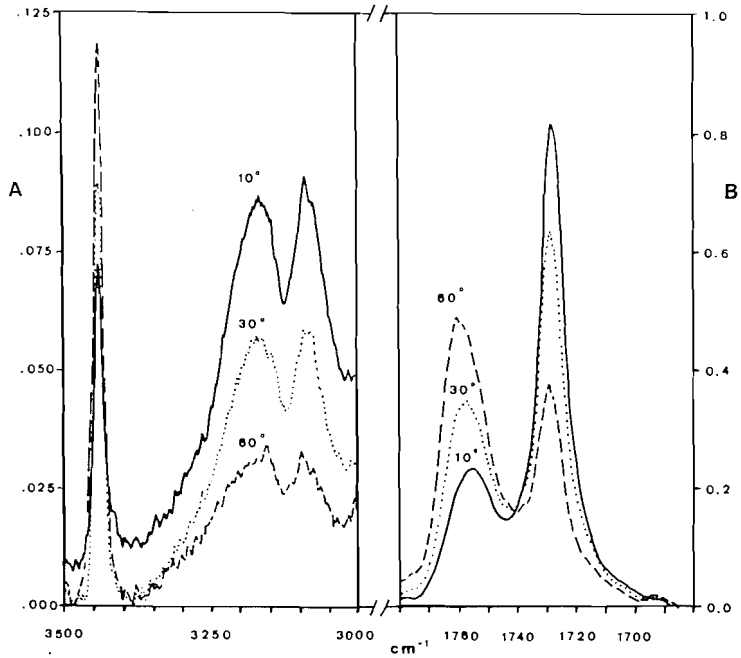


FIG. 2. Infrared spectra of 2-*S*-methyl-5,5-dimethylimidazolin-4-one in CCl_4 solutions at 10, 30, and 60°C; (A) ν(NH) vibrations, (B) ν(CO) vibrations.

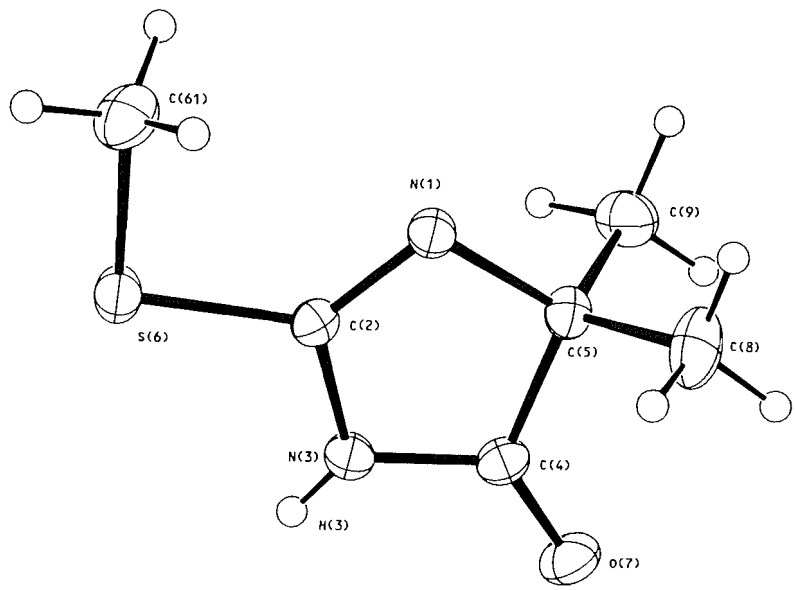


FIG. 3. ORTEP drawing of Δ^1-2-*S*-methyl-5,5-dimethylimidazolin-4-one **I**.

methods, while the data in Tables 3 and 4 indicate a similar ability in giving relative formation enthalpies and molecular electric dipoles, they clearly show a better agreement between the geometries obtained by the AM1 and PM3 methods. In particular, with the PM3 method the calculated C—S bond lengths are very close to the experimental values.

Solution studies

Ultraviolet spectra

The spectra were recorded in solvents with various dielectric constants. They are independent of the starting sample (**I** or **II**) but undergo very large changes on passing from water to MeOH and cyclohexane (see Fig. 1). These changes agree well with those found for similar molecules, and previously assigned on the basis of the spectra of the *N*-methylated derivatives (1). In water, the absorption at higher wavelengths indicates that the conjugated structure **II** is the predominant tautomer (1, 2); vice versa, the unconjugated **I** is predominant in cyclohexane (as a non-polar solvent). The mixture of the two tautomers is clearly evident in a solvent with intermediate polarity such as MeOH.

Infrared spectra

In carbon tetrachloride, as expected, **I** and **II** show the same infrared spectrum. In particular, four ν(NH) stretching vibrations have been identified: one falling at 3442 cm^{-1} due to the free molecule, and three overlapped bands at 3086, 3171, and 3211 cm^{-1} due to the associated hydrogen bonding molecules. Figure 2a reports the spectra recorded between 3500 and 3000

Can. J. Chem. Downloaded from www.nrcresearchpress.com by 195.138.81.100 on 09/07/12
For personal use only.

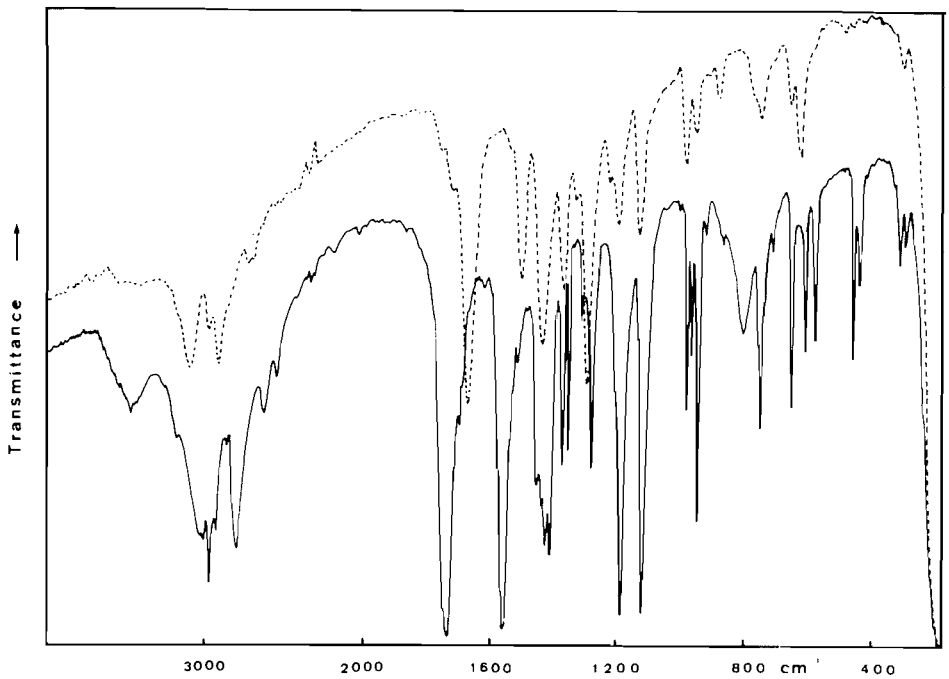


FIG. 4. Infrared spectra of 2-*S*-methyl-5,5-dimethylimidazolin-4-one crystallized from benzene **I** (full line) and from water **II** (dotted line) recorded as KBr discs.

cm^{-1} at three temperatures in the same solution. This solution shows only two peaks at 1760 and 1730 cm^{-1} in the ν(CO) region, attributable to the free and associated hydrogen bonding molecules (Fig. 2b). Both figures show very clearly the influence of temperature on the monomer–dimer equilibrium.

In chloroform, the ν(NH) absorptions show the same pattern as in carbon tetrachloride, except for a broadening of $\nu(NH)_{free}$ (the half-band width, $\Delta\nu_{1/2}$, is 19 cm^{-1} in carbon tetrachloride and 31 cm^{-1} in chloroform). However, this broadening, which could be due to the presence of two overlapped bands attributable to the $\nu(NH)_{free}$ of **I** and **II**, can also be explained on the basis of the different polarities of the two solvents. In the ν(CO) region, the bands due to both the free and associated molecules contribute to one broad absorption at 1738 cm^{-1} ($\Delta\nu_{1/2}$ = 40 cm^{-1}).

Acid–base behaviour

To obtain information on the aqueous solutions, where 2-*S*-methyl-5,5-dimethylimidazolin-4-one is present prevalently as the Δ^2 tautomer, we determined its pK_a both alone and in the presence of hydrochloric acid. The results obtained by the two methods are collected in Table 5, together with those obtained for 5,5-dimethyl-2-thioxo-imidazolidin-4-one (sox), and for its N(1)-methyl (mesox) and N(3)-methyl (soxme) derivatives.

pK_1 and pK_2 arise from the equilibria that involve as acids the LH^+ and L species respectively.

As can be seen, the results obtained from the two different programs practically coincide, as well as the pK_2 values obtained both in the presence and absence of mineral acid. Moreover, it appears very clear that 2-*S*-methyl-5,5-dimethyl-imidazolin-4-one in strong acidic medium is protonated,[5] whereas 5,5-dimethyl-2-thioxoimidazolidin-4-one and the *N*-methylated derivatives are not. The difference of about two pH units between mesox and soxme is due to the fact that mesox loses the hydrogen bonded to N(3), whereas soxme loses the hydrogen that is bonded to N(1). The comparison of pK_2 for sox and mesox clearly shows that the methyl group does not affect the pK values. The calculated value for our compound is exactly intermediate between those for soxme and mesox.

[5]We recently reported the crystal structure of LH^+ with I_3^- as a counterion, obtained by reacting L with I_2 in CH_2Cl_2 solution (14).

TABLE 5. pK_a values measured on 2-*S*-methyl-5,5-dimethylimidazolin-4-one (**I**/**II**), 5,5-dimethyl-2-thioxoimidazolidin-4-one (sox), 1,5,5-trimethyl-2-thioxoimidazolidin-4-one (mesox), and 3,5,5-trimethyl-2-thioxoimidazolidin-4-one (soxme)

	pK_1		pK_2	
	SUPERQUAD	PSEQUAD	SUPERQUAD	PSEQUAD
I/II	3.08(1)	3.16(2)	9.48(2)	9.48(2)
I/II[a]	—	—	9.52(2)	9.54(2)
sox[b,c]	—	—	8.43(4)	8.40(6)
mesox[b]	—	—	8.43(1)	8.43(1)
soxme[b]	—	—	10.49(1)	10.50(1)

[a]Measured without mineral acid.
[b]In the presence of HCl it has been impossible to distinguish between the mineral acid and the protonated compounds.
[c]The loss of the second proton occurs at pH greater than 12.

Solid state studies

Structure of I

The structure of 2-*S*-methyl-5,5-dimethylimidazolin-4-one, solved for a crystal obtained from benzene, shows that it is the Δ^1 tautomer, i.e., **I** in the *anti* configuration (Fig. 3). Bond distances and angles are collected in Table 6. It is interesting to observe that the hydantoin skeleton is substantially unchanged on *S*-methylation; the major changes involve the variation of (i) the N(1)—C(2) bond, which undergoes a strong shortening (1.280(2) in **I** and 1.325(2) in 2-thiohydantoin); (ii) the C(2)—S(6) bond (1.741(1) in **I** and 1.648(2) in 2-thiohydantoin), which still has a significant double-bond character; and (iii) the

Can. J. Chem. Downloaded from www.nrcresearchpress.com by 195.138.81.100 on 09/07/12
For personal use only.

Can. J. Chem. Downloaded from www.nrcresearchpress.com by 195.138.81.100 on 09/07/12
For personal use only.

TABLE 6. Bond distances, angles, hydrogen bonds, and van der Waals contacts of Δ^1-2-*S*-methyl-5,5-dimethylimidazolin-4-one **I**

(a) Selected distances (Å) and angles (deg)

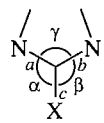
N(1)—C(2)	1.280(2)	C(2)—N(3)	1.385(2)
N(3)—C(4)	1.368(2)	C(4)—C(5)	1.523(2)
C(5)—N(1)	1.488(2)	C(4)—O(7)	1.212(2)
C(5)—C(8)	1.521(3)	C(5)—C(9)	1.528(2)
C(2)—S(6)	1.741(1)	S(6)—C(61)	1.792(2)
N(3)—H(3)	0.74(2)		
H(3)...N(1)^{i}	2.20(2)	N(3)...N(1)^{i}	2.912(2)
S(6)...O(7)^{ii}	3.149(1)	O(7)...C(9)^{iii}	3.434(2)
O(7)...C(61)^{iv}	3.459(2)	O(7)...C(61)^{v}	3.482(2)
N(1)—C(2)—N(3)	115.5(1)	C(2)—N(3)—C(4)	108.8(1)
N(3)—C(4)—C(5)	105.0(1)	C(4)—C(5)—N(1)	104.5(1)
C(5)—N(1)—C(2)	106.1(1)	C(5)—C(4)—O(7)	127.8(1)
N(3)—C(4)—O(7)	127.2(1)	N(1)—C(5)—C(8)	110.8(1)
N(1)—C(5)—C(9)	110.4(1)	C(4)—C(5)—C(8)	110.1(2)
C(4)—C(5)—C(9)	108.2(1)	C(8)—C(5)—C(9)	112.4(2)
N(1)—C(2)—S(6)	128.2(1)	N(3)—C(2)—S(6)	116.3(1)
C(2)—S(6)—C(61)	100.9(1)	N(3)—H(3)...N(1)^{i}	161.7(1)

(b) Torsion angles (deg)

C(61)—S(6)—C(2)—N(1)	−7.3(2)	C(61)—S(6)—C(2)—N(3)	172.2(1)
S(6)—C(2)—N(3)—C(4)	−178.4(1)	S(6)—C(2)—N(1)—C(5)	179.7(1)
C(2)—N(1)—C(5)—C(4)	−1.4(2)	N(1)—C(5)—C(4)—N(3)	2.0(2)
C(5)—C(4)—N(3)—C(2)	−2.0(2)	C(4)—N(3)—C(2)—N(1)	1.2(2)
N(3)—C(2)—N(1)—C(5)	0.2(2)	C(2)—N(1)—C(5)—C(8)	−120.0(2)
C(2)—N(1)—C(5)—C(9)	114.7(2)	C(2)—N(3)—C(4)—O(7)	179.2(2)
N(1)—C(5)—C(4)—O(7)	−179.2(2)	C(9)—C(5)—C(4)—O(7)	63.2(3)
C(8)—C(5)—C(4)—O(7)	−60.1(3)		

Symmetry codes: (i) x, $1/2 - y$, $z - 1/2$; (ii) $2 - x$, $y - 1/2$, $3/2 - z$; (iii) x, $1/2 - y$, $1/2 + z$; (iv) $1 + x$, $1/2 - y$, $1/2 + z$; (v) $2 - x$, $y + 1/2$, $3/2 - z$.

TABLE 7. Bond lengths(Å) and angles(°) around C(2) for some hydantoin derivatives



	I	Triiodide	ss	seox	sse	2-Thiohydantoin
a	1.280(2)	1.34(2)	1.326(2)	1.32(1)	1.308(8)	1.325(2)
b	1.385(2)	1.38(2)	1.339(1)	1.36(1)	1.386(8)	1.378(2)
c	1.741(1)	1.73(2)	1.648(2)	1.805(8)	1.668(7)	1.648(2)
α	128.2(1)	127(1)	130.0(2)	128.2(6)	129.6(5)	128.4(1)
β	116.3(1)	120(1)	124.3(1)	123.7(6)	123.4(5)	124.7(1)
γ	115.5(1)	113(1)	105.7(2)	108.0(7)	107.0(5)	106.8(1)
(α − β)	11.9	7	5.7	4.5	6.2	3.7
Ref.	Present work	14	3	3	3	3

Triiodide = 5,5-dimethyl-2-methylthio-4-oxoimidazolidinium triiodide.
ss = 5,5-dimethylimidazolidine-2,4-dithione.
seox = 5,5-dimethyl-2-selenoxoimidazolidin-4-one.
sse = 5,5-dimethyl-4-selenoxoimidazolidine-2-thione.

N(1)—C(2)—N(3) angle, which undergoes a sensitive increase (115.5(1) in **I** and 106.8(1) in 2-thiohydantoin). To this purpose, it is also interesting to compare the angles around C(2) in the title compound and in some related hydantoin derivatives. Table 7 collects the bond distances and angles of **I**, 5,5-dimethyl-2-methylthio-4-oxoimidazolidinium triiodide (14), 5,5-dimethylimidazolidine-2,4-dithione (3), 5,5-dimethyl-2-selenoxoimidazolidin-4-one (3), 5,5-dimethyl-2-selenoxoimidazoline-2-thione (3), and 2-thiohydantoin (3). The differences in the angles around the C(sp^2) for all these compounds can be easily interpreted in terms of the VSEPR model. As shown in the table, the α values are always greater than the β, as a consequence of the higher conjugation of the lone pair of N(1) with respect to N(3), with a consequent increased repulsion

Can. J. Chem. Downloaded from www.nrcresearchpress.com by 195.138.81.100 on 09/07/12
For personal use only.

between the N(1)—C(2) and C(2)=X bonds. The greater the difference in the repulsion, the higher the difference ($\alpha - \beta$) in the angles.

As expected, the value for this difference of 11.9° found in **I** is the highest among the compounds considered, since only in this compound is N(1)—C(2) practically a double bond. On the other hand, as a consequence of this double bond, the value of the angle γ, internal to the ring, is also the highest. The protonation of **I** on the N(1), observed in the 5,5-dimethyl-2-methylthio-4-oxoimidazolidinium triiodide (14), shifts the angles towards those verified in the hydantoin derivatives.

One of the most interesting features in the structure is that the oxygen atom is not involved in the hydrogen bonding and that the molecules are bound together in the crystal by hydrogen bonds involving only the N(1) and N(3) atoms. Hence, the molecular packing is realized by this hydrogen bond and by some weak van der Waals contacts (see Table 6).

The least-squares planes through the molecule show that the five-membered ring is not rigorously planar, with a deviation of −0.029(2) Å from the "best plane" for C(5).

Infrared spectra

Contrary to what was found in solution, **I** and **II** show two different ir spectra in the solid state, as shown in Fig. 4. It is very interesting to point out the differences in ν(NH) and ν(CO) absorptions. As said above, **I** (full line), obtained from benzene and whose structure has been solved, exhibits a ν(NH) band envelope at about 2800 cm^{-1} and a ν(CO) absorption at 1744 cm^{-1}; while **II** (dotted line) shows the ν(NH) band at 3100 cm^{-1} and ν(CO) at 1670 cm^{-1}.

The low value of ν(NH) found for **I** agrees with the crystallographic results. In fact, by introducing the value of 2.912 Å for the N(1)···N(3) distance R in the equation of Pimentel and Sederholm (15), $\Delta\nu_S = 1.05 \times 10^3 (3.38 - R)$, a shift of about 500 cm^{-1} from $\nu(NH)_{free}$ measured in CCl_4 is calculated, which is not very different from the experimental results.

The infrared spectrum of **II** in the solid state shows a ν(NH) absorption at 3100 cm^{-1}, which indicates a different hydrogen bonding pattern, attributable to an N—H···O interaction. Conversely, the N—H···O hydrogen bonding has been found in both the structures of the Δ^1 and Δ^2 tautomers of 2-*S*-methyl-5,5-diphenylimidazolin-4-one (2). This fact can explain the difference of 74 cm^{-1} between the ν(CO) frequencies of Δ^1 and Δ^2 tautomers of the title compound, a value very high if compared with those of 20 cm^{-1} in the two tautomers of 2-*S*-methyl-5,5-diphenylimidazolin-4-one (2) and 25 cm^{-1} in the two N(1)- and N(3)-methyl isomers of 2-*S*-methyl-5,5-pentamethyleneimidazolin-4-one (1).

Conclusions

The ir spectra of the two tautomers differ mainly in the ν(NH) and ν(CO) frequencies, as seen in Fig. 4. The low value of the ν(NH) frequency (around 2800 cm^{-1}) for **I** in the solid state agrees well with the data obtained from the crystal structure.

As regards the carbon tetrachloride or chloroform solutions, **I** and **II** show the same spectrum, which, on the basis of the position of the ν(CO) absorption, of the uv spectrum, and of the results of the theoretical calculations, must be attributed to the prevailing presence of **I**. Moreover, the calculations indicate that of the two possible tautomers in each of the possible configurations *anti* or *syn* with respect to the N-H hydrogen, the more stable in nonpolar solvent is the *anti*-Δ^1. Contrary to what was found in the solid state, in carbon tetrachloride solutions the more stable hydrogen bonds involve the oxygen atom.

In aqueous solutions, where 2-*S*-methyl-5,5-dimethylimidazolin-4-one is present mainly as the Δ^2 tautomer, the pK_a value clearly shows that proton detachment from N(1) occurs more easily than in the case of the N(3)-alkyl substituted hydantoins. This can be explained on the basis of a high contribution of the oxygen atom to the dispersion of charge of the anion (note the difference in the ν(CO) values between the two desmotrops).

1. J. T. Edward and J. K. Liu. Can. J. Chem. **50**, 2423 (1972).
2. K. Lempert, J. Nytrai, K. Zauer, A. Kalman, Gy. Argay, A. J. M. Duisenbreg, and P. Sohar. Tetrahedron, **29**, 3565 (1973).
3. F. A. Devillanova, A. Diaz, F. Isaia, G. Verani, L. P. Battaglia, and A. Bonamartini Corradi. J. Chem. Res. (S), 192 (1987).
4. B. A. Frenz *et al.* SDP Plus, Version 1.0, Enraf–Nonius, Delft, The Netherlands. 1980.
5. A. C. T. North, D. C. Phillips, and F. S. Mathews. Acta Crystallogr. Sect A: Cryst. Phys. Diffr. Theor. Gen. Crystallogr. **A24**, 351 (1968).
6. International tables for X-ray crystallography. Vol. IV. The Kynoch Press, Birmingham, U.K. 1974.
7. P. Gans, A. Sabatini, and A. Vacca. J. Chem. Soc. Dalton Trans. 1195 (1985).
8. L. Zekany and I. Nagypal. Computational methods for the determination of formation constants. *Edited by* D. J. Legget. Plenum Press, New York. 1985. pp. 291–353.
9. M. J. S. Dewar and W. Thiel. J. Am. Chem. Soc. **99**, 4899 (1977); **99**, 4907 (1977).
10. M. J. S. Dewar. Chem. Br. **11**, 97 (1975).
11. M. J. S. Dewar, E. G. Zoebisch, E. F. Healey, and J. J. P. Stewart. J. Am. Chem. Soc. **107**, 3902 (1985).
12. J. J. P. Stewart. J. Comput. Chem. **10**, 208 (1989); **10**, 221 (1989).
13. MOPAC-QCPE 455, Version 5.0.
14. F. A. Devillanova, A. Diaz, F. Isaia, G. Verani, L. P. Battaglia, and A. Bonamartini Corradi. J. Coord. Chem. **15**, 161 (1986), and refs. therein.
15. G. C. Pimentel and A. L. McClellan. The hydrogen bond. W. H. Freeman and Company, San Francisco. 1960. p. 87.

The crystal and molecular structure of gold tris(fluorosulfate)

H. WILLNER,[1] S. J. RETTIG, J. TROTTER, AND F. AUBKE[2]

Department of Chemistry, The University of British Columbia, Vancouver, B.C., Canada V6T 1Y6

Received September 24, 1990

H. WILLNER, S. J. RETTIG, J. TROTTER, and F. AUBKE. Can. J. Chem. **69**, 391 (1991).

Single crystals of gold(III) tris(fluorosulfate) are obtained by recrystallization from bis(fluorosulfuryl) peroxide, $S_2O_6F_2$, under O_2 pressure. The crystals of $[Au(SO_3F)_3]_2$ are monoclinic, $a = 9.700(4)$, $b = 9.222(2)$, $c = 10.810(4)$ Å, $\beta = 94.43(3)°$, $Z = 2$, space group $P2_1/a$. The structure was solved by heavy atom methods and was refined by full-matrix least-squares procedures, $R(F) = 0.038$ and $R_w(F) = 0.050$ for 1491 reflections with $I \geq 3\sigma(I)$. The structure consists of centrosymmetric $[Au(SO_3F)_3]_2$ dimers containing two bidentate, symmetrically bridging and four monodentate, terminal SO_3F ligands. The Au(III) ions have square-planar coordination geometry with bridging Au—O = 2.020(7) and 2.016(6) Å, and terminal Au—O = 1.959(7) and 1.956(9) Å. The dimeric $[Au(SO_3F)_3]_2$ units are linked in the solid state by weak Au—O interactions (2.757(8) and 2.960(7) Å), resulting in a distorted octahedral coordination geometry about each gold atom.

Key words: gold(III) tris(fluorosulfate), crystal structure.

H. WILLNER, S. J. RETTIG, J. TROTTER et F. AUBKE. Can. J. Chem. **69**, 391 (1991).

On a obtenu des cristaux uniques du tris(fluorosulfate) d'or(III) par recristallization de peroxyde de bis(fluorosulfuryle), $S_2O_6F_2$, sous pression d'O_2. Les cristaux de $[Au(SO_3F)_3]_2$ sont monocliniques, groupe d'espace $P2_1/a$, avec $a = 9{,}700(4)$, $b = 9{,}222(2)$ et $c = 10{,}810(4)$ Å, $\beta = 94{,}43(3)°$ et $Z = 2$. On a résolu la structure par la méthode des atomes lourds et on l'a affinée par la méthode des moindres carrés (matrice complète) jusqu'à des valeurs de $R(F) = 0{,}038$ et $R_w(F) = 0{,}050$ pour 1491 réflexions avec $I \geq 3\sigma(I)$. La structure comprend des dimères centrosymétriques de $[Au(SO_3F)_3]_2$ contenant deux ligands SO_3F bidentates, formant un pont symétrique, et quatre ligands monodentates terminaux. Les ions d'Au(III) possèdent une géométrie de coordination plan-carré dans laquelle les liaisons Au—O (pont) = 2,020(7) et 2,016(6) Å et Au—O (terminales) = 1,959(7) et 1,956(9) Å. À l'état solide, les unités de $[Au(SO_3F)_3]_2$ dimères sont liées par de faibles interactions Au—O (2,757(8) et 2,960(7) Å) qui conduisent à une géometrie de coordination octaédrique déformée autour de l'atome d'or.

Mots clés : tris(fluorosulfate) d'or, structure cristalline.

[Traduit par la rédaction]

Introduction

Gold tris(fluorosulfate), $Au(SO_3F)_3$, first reported by Cady and co-workers (1), is one of the few well-characterized binary gold(III) oxyacid derivatives (2). The compound is conveniently synthesized by the oxidation of gold powder with bis(fluorosulfuryl) peroxide (3), $S_2O_6F_2$, in fluorosulfuric acid, HSO_3F, as reaction medium.

Solid $Au(SO_3F)_3$ redissolved in HSO_3F is one of the strongest monoprotonic superacids (3, 4). The ability of $Au(SO_3F)_3$ to act as a SO_3F^- acceptor is evident from the formation and isolation of a number of tetrakis(fluorosulfato)aurate(III) salts with a variety of cations (3).

Vibrational spectra and the observed diamagnetism of pure $Au(SO_3F)_3$ have suggested an approximately square planar environment of gold, and the presence of both bidentate bridging and monodentate fluorosulfate groups (3). A low degree of intermolecular association is inferred from the appreciable solubility of $Au(SO_3F)_3$ in HSO_3F, and from a recent computer modelling study of electrical conductivity data on the HSO_3F–$Au(SO_3F)_3$–KSO_3F system (5).

We want to report on the molecular structure of gold(III) fluorosulfate, obtained by single crystal X-ray diffraction. Gold(III) fluorosulfate in the solid state consists of weakly associated dimeric $[Au(SO_3F)_3]_2$ units. Its structure reported here is of interest for the following reasons: (*i*) It is the first structure obtained for a binary metal fluorosulfate, other than the ionic fluorosulfates KSO_3F (6*a*) and $LiSO_3F$ (6*b*). (*ii*) Unprecedentedly, solid $[Au(SO_3F)_3]_2$ shows the presence of two distinctly different fluorosulfate groups in the same molecule. (*iii*) A detailed discussion of the dimeric structure will shed some light on the observed high Lewis acidity of gold(III) fluorosulfate, which makes its solution in fluorosulfuric acid one of the strongest, monoprotonic superacid systems (3–5). (*iv*) We have very recently generated defects of the highly unusual (2) cation Au^{2+} in solid $[Au(SO_3F)_3]_2$ (7). Knowledge of the structure of gold(III) fluorosulfate allows a better interpretation of the ESR spectra obtained for Au^{2+} defects (7). (*v*) As recently shown (8), the superacid system HSO_3F–$Au(SO_3F)_3$ has an interesting redox chemistry. Interaction with gaseous CO results in the formation of $[Au(CO)_2]^+$ and $Au(CO)SO_3F$, where an unusual type of CO bonding to gold is encountered.

Experimental

(a) Preparation of single crystals

Gold tris(fluorosulfate) is prepared from gold powder, oxidized by bis(fluorosulfuryl) peroxide, $S_2O_6F_2$ (9) in solution of fluorosulfuric acid, HSO_3F, as reported previously (3*a*). About 100 mg of the polycrystalline powder, obtained after removal of all volatiles, are filled inside an inert atmosphere box into a glass ampul, about 100 mm long with 10 mm o.d. Approximately 1 g $S_2O_6F_2$ are added *in vacuo* and O_2 gas is admitted, to give at room temperature an internal pressure of about 3 atm in the sealed-off ampul. The suspension of $[Au(SO_3F)_3]_2$ in $S_2O_6F_2$ is submersed in a bath of halocarbon wax (Halocarbon Products Corp.) and heated to 80°C for about 2 weeks. During this period orange–red crystals are formed above the $S_2O_6F_2$ level. The ampul is opened *in vacuo*, using an "ampul key", as described previously (10) and all O_2 and $S_2O_6F_2$ are distilled off. Suitable crystals are filled into carefully dried quartz capillaries of 0.5 mm diameter, again inside an inert atmosphere box (Vacuum Atmosphere Corp. Dri Lab. Model HE-493, filled with dry N_2 and equipped with a HE-493 Dri Train).

(b) Crystallographic details

Crystallographic data appear in Table 1. The final unit-cell parameters were obtained by least-squares on the setting angles for 25

[1]Permanent address: Institut Für Anorganische Chemie, Universität Hannover, Callinstr. 9, D-3000 Hannover, F.R.G.

[2]To whom correspondence should be addressed.

Can. J. Chem. Downloaded from www.nrcresearchpress.com by 195.138.81.100 on 09/07/12
For personal use only.

Can. J. Chem. Downloaded from www.nrcresearchpress.com by 195.138.81.100 on 09/07/12
For personal use only.

TABLE 1. Crystallographic data[a]

Compound	$Au_2(SO_3F)_6$
Formula	$Au_2F_6O_{18}S_6$
fw	988.27
Color, habit	Orange prism
Crystal size, mm	0.25 × 0.35 × 0.45
Crystal system	Monoclinic
Space group	$P2_1/a$
a, Å	9.700(4)
b, Å	9.222(2)
c, Å	10.810(4)
β, deg	94.43(3)
V, Å^3	964.1(6)
Z	2
ρ_c, g/cm^3	3.404
$F(000)$	904
Radiation	Mo
Wavelength (Å)	0.71069
μ, cm^{-1}	159.15
Transmission factors	0.25–1.00
Scan type	ω–2θ
Scan range, deg in ω	1.25 + 0.35 tan θ
Scan speed, deg/min	16
Data collected	$+h, +k, \pm l$
$2\theta_{max}$, deg	55
Crystal decay	4.5%
Total no. of reflections	2478
No. of unique reflections	2347
R_{int}	0.081
No. of reflections with $I \geq 3\sigma(I)$	1491
No. of variables	146
R	0.038
R_w	0.050
gof	1.91
Maximum Δ/σ (final cycle)	0.003
Residual density e/Å^3	−3.0 to +3.4 (both near Au)

[a]Temperature 294 K, Rigaku AFC6S diffractometer, graphite monochromator, takeoff angle 6.0°, aperture 6.0 × 6.0 mm at a distance of 285 mm from the crystal, stationary background counts at each end of the scan (scan/background time ratio 2:1), $\sigma^2(F^2) = [S^2(C + 4B) + (0.04F^2)^2]/Lp^2$ (S = scan rate, C = scan count, B = normalized background count), function minimized $\Sigma w(|F_o| - |F_c|)^2$ where $w = 4F_o^2/\sigma^2(F_o^2)$, $R = \Sigma||F_o| - |F_c||/\Sigma|F_o|$, $R_w = (\Sigma w(|F_o| - |F_c|)^2/\Sigma w|F_o|^2)^{1/2}$, and gof = $[\Sigma(|F_o| - |F_c|)^2/(m - n)]^{1/2}$. Values given for R, R_w, and gof are based on those reflections with $I \geq 3\sigma(I)$.

reflections with $2\theta = 41.8$–$45.7°$. The intensities of three standard reflections, measured every 150 reflections throughout the data collection, decayed uniformly by 4.5%. The data were processed[3] and corrected for Lorentz and polarization effects, decay, and absorption (empirical, based on azimuthal scans for four reflections). A total of 2478 reflections was collected on a Rigaku AFC6S diffractometer, of these 2347 were unique ($R_{int} = 0.081$) and those 1491 having $I \geq 3\sigma(I)$ were employed in the solution and refinement of the structure.

The structure was solved by conventional heavy atom methods, the coordinates of the Au and S atoms being determined from the Patterson function and those of the remaining atoms from a subsequent difference Fourier synthesis. All atoms were refined with anisotropic thermal parameters. The thermal parameters of the terminal O and F atoms bonded to S(3) suggest a possible rotational disorder about the S(3)—O(7) bond but no attempt was made to model this disorder, these atoms being refined with full occupancy. Neutral atom scattering factors and anomalous dispersion corrections for all atoms were taken from the International tables for X-ray crystallography (11). A correction for secondary extinction was applied, the final value of the coefficient being 0.645×10^{-6}. Final atomic coordinates and equivalent isotropic thermal parameters, bond lengths, and bond angles appear in Tables 2–4, respectively. Anisotropic thermal parameters, torsion angles, intermolecular contacts, least-squares planes, and measured and calculated structure factor amplitudes are included as supplementary material.[4]

[3]TEXSAN/TEXRAY structure analysis package which includes versions of the following: DIRDIF, direct methods for difference structures, by P. T. Beurskens, ORFLS, full-matrix least-squares, and ORFFE, function and errors, by W. R. Busing, K. O. Martin, and H. A. Levy, ORTEP II, illustrations by C. K. Johnson.

TABLE 2. Final atomic coordinates (fractional) and B_{eq} (Å^2)

Atom	x	y	z	B_{eq}
Au(1)	0.15060(3)	0.50212(4)	0.16969(3)	1.61(2)
S(1)	0.1512(2)	0.6023(3)	−0.1117(2)	1.64(8)
S(2)	0.4497(3)	0.6110(3)	0.1901(3)	3.3(1)
S(3)	0.1936(4)	0.3831(4)	0.4273(3)	4.2(2)
F(1)	0.2016(8)	0.5177(6)	−0.2186(8)	3.6(3)
F(2)	0.483(1)	0.606(2)	0.329(1)	10.3(7)
F(3)	0.063(2)	0.297(2)	0.423(2)	18(1)
O(1)	0.1556(8)	0.4881(6)	−0.0164(7)	1.9(3)
O(2)	0.0082(6)	0.6393(7)	−0.1543(7)	2.3(3)
O(3)	0.2351(7)	0.7225(8)	−0.0904(7)	2.8(3)
O(4)	0.2983(6)	0.6473(7)	0.1854(8)	3.3(4)
O(5)	0.473(1)	0.471(1)	0.148(2)	8.0(8)
O(6)	0.5208(8)	0.732(1)	0.150(1)	5.1(5)
O(7)	0.139(1)	0.5105(9)	0.3494(8)	3.7(4)
O(8)	0.204(2)	0.410(2)	0.546(1)	12(1)
O(9)	0.277(2)	0.300(1)	0.366(1)	12(1)

TABLE 3. Bond lengths (Å) with estimated standard deviations in parentheses[a]

Atom	Atom	Distance	Atom	Atom	Distance
Au(1)	O(1)	2.020(7)	S(1)	O(3)	1.384(7)
Au(1)	O(2)*	2.016(6)	S(2)	F(2)	1.51(1)
Au(1)	O(4)	1.959(7)	S(2)	O(4)	1.504(7)
Au(1)	O(7)	1.956(9)	S(2)	O(5)	1.39(1)
Au(1)	O(6)′	2.757(8)	S(2)	O(6)	1.399(8)
Au(1)	O(3)″	2.960(7)	S(3)	F(3)	1.49(1)
S(1)	F(1)	1.507(7)	S(3)	O(7)	1.52(1)
S(1)	O(1)	1.471(7)	S(3)	O(8)	1.30(1)
S(1)	O(2)	1.467(6)	S(3)	O(9)	1.33(1)

[a]Here and elsewhere in the report; *, ′, and ″ correspond to the symmetry operations: $-x$, $1 - y$, $-z$; $x - \frac{1}{2}$, $\frac{3}{2} - y$, z; and $\frac{1}{2} - x$, $-\frac{1}{2} + y$, $-z$; respectively.

Results and discussion

(a) Single crystal preparation

The method used to obtain suitable single crystals, heating microcrystalline $Au(SO_3F)_3$, suspended in bis(fluorosulfuryl) peroxide, $S_2O_6F_2$, in an O_2-atmosphere for 2 weeks at 80°C was found during an unsuccessful attempt to synthesize a dioxygenyl salt according to

[1] $2O_2 + 2Au(SO_3F)_3 + S_2O_6F_2 \rightarrow 2O_2[Au(SO_3F)_4]$

It is unclear if O_2 is necessary for the preparation of single crystals. Obviously the boiling point of $S_2O_6F_2$, reported to be

[4]Anisotropic thermal parameters, torsion angles, intermolecular contacts, least-squares planes, and measured and calculated structure factor amplitudes may be purchased from the Depository of Unpublished Data, Document Delivery, CISTI, National Research Council of Canada, Ottawa, Ont., Canada K1A 0R6.

TABLE 4. Bond angles (deg) with estimated standard deviations in parentheses

Atom	Atom	Atom	Angle	Atom	Atom	Atom	Angle
O(1)	Au(1)	O(2)*	87.4(3)	O(2)	S(1)	O(3)	113.3(4)
O(1)	Au(1)	O(4)	93.2(3)	F(2)	S(2)	O(4)	99.9(6)
O(1)	Au(1)	O(3)″	67.5(2)	F(2)	S(2)	O(5)	105(1)
O(1)	Au(1)	O(6)′	91.4(3)	F(2)	S(2)	O(6)	105.3(7)
O(1)	Au(1)	O(7)	177.7(3)	O(4)	S(2)	O(5)	112.4(6)
O(2)*	Au(1)	O(4)	177.1(3)	O(4)	S(2)	O(6)	108.4(5)
O(2)*	Au(1)	O(7)	90.4(4)	O(5)	S(2)	O(6)	122.6(7)
O(2)*	Au(1)	O(3)″	73.3(2)	F(3)	S(3)	O(7)	98.2(8)
O(2)*	Au(1)	O(6)′	103.1(2)	F(3)	S(3)	O(8)	98(1)
O(4)	Au(1)	O(7)	89.0(4)	F(3)	S(3)	O(9)	103(1)
O(4)	Au(1)	O(3)″	109.5(2)	O(7)	S(3)	O(8)	113.5(9)
O(4)	Au(1)	O(6)′	74.1(3)	O(7)	S(3)	O(9)	111.6(6)
O(7)	Au(1)	O(3)″	111.9(3)	O(8)	S(3)	O(9)	127(1)
O(7)	Au(1)	O(6)′	89.0(3)	S(1)	O(1)	Au(1)	130.5(4)
O(3)″	Au(1)	O(6)′	158.6(3)	S(1)	O(2)	Au(1)*	124.9(4)
F(1)	S(1)	O(1)	99.9(4)	S(1)″	O(3)″	Au(1)	151.4(5)
F(1)	S(1)	O(2)	103.6(5)	S(2)	O(4)	Au(1)	123.8(4)
F(1)	S(1)	O(3)	108.7(4)	S(2)′	O(6)′	Au(1)	156.6(7)
O(1)	S(1)	O(2)	111.3(4)	S(3)	O(7)	Au(1)	118.6(5)
O(1)	S(1)	O(3)	118.1(5)				

67.1°C at 1 atm (9, 12*a*), is raised beyond the bath temperature of 80°C, and glass attack by $SO_3F\cdot$ radicals in the gas phase (12*b*) is now largely prevented.

The presence of $S_2O_6F_2$, on the other hand, appears to be important. Attempts to sublime solid $[Au(SO_3F)_3]_2$ *in vacuo*, or heating the compound to 125°C *in vacuo* results in the formation of Au^{2+} defects in the solid, presumably with release of $S_2O_6F_2$ (7). The gradual dissociation of $Au(SO_3F)_3$ at 80°C appears to be prevented by the presence of $S_2O_6F_2$. An extension of the method to grow single crystals of other metal fluorosulfates is presently being attempted.

It is interesting to note, that in addition to the plate-like crystals used in this study, one of the synthetic attempts yielded needle-like crystals, which were not investigated further.

(b) Description of the molecular structure of $Au(SO_3F)_3$

An ORTEP view of the molecular structure is shown in Fig. 1 and the packing of molecules in the unit cell is shown in Fig. 2. As can be seen, gold(III) fluorosulfate is dimeric in the solid state, quite in contrast to polymeric AuF_3 (13). On the other hand, there is a structural similarity to the other halides $AuCl_3$ (14) and $AuBr_3$ (15), which are also both dimeric.

The presence of bidentate, symmetrically bridging fluorosulfate groups widens the four-membered metallocycle, found for the two halides $AuCl_3$ and $AuBr_3$ (14, 15), to an eight-membered, centrosymmetric ring, which adopts a chair configuration. The two gold atoms are found in transannular positions with a cross ring distance of 4.510(2) Å, and are linked by two SO_2 moieties from the bridging bidentate fluorosulfate groups.

Both gold(III) centers are found in identical, nearly square coordination environments. The mean deviation from planarity is found to be 0.020 Å, and the maximal displacement is 0.053(7) Å, found for O(4). The close approach to a square planar geometry is evident also from the relevant bond angles (O—Au—O = 87.4(3)–93.2(3), 177.1(3), and 177.7(3)°).

The AuO_4-squares are slightly distorted, because the terminal, monodentate fluorosulfate groups bond more strongly to gold ($Au—O_{av.}$ = 1.957 Å) than do bridging, bidentate groups

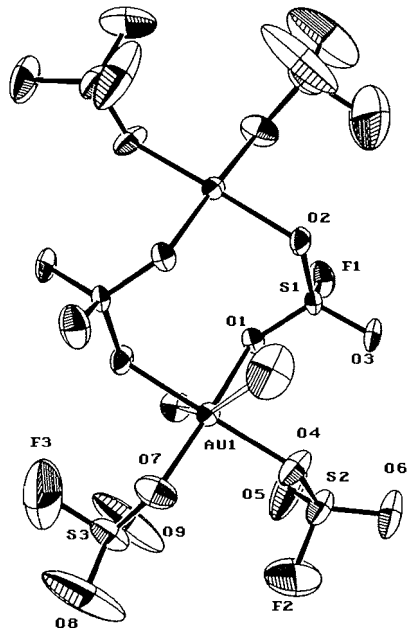


FIG. 1. View of the $[Au(SO_3F)_3]_2$ dimer; 50% probability thermal ellipsoids are shown. Labeled atoms comprise the asymmetric unit.

($Au—O_{av.}$ = 2.018 Å). Similar, slightly larger discrepancies between distances to bridging and terminal halides are reported for the gold–halogen distances in the gold(III) halides, AuF_3 (13), $AuCl_3$ (14), and $AuBr_3$ (15).

In the dimeric molecule, the two AuO_4-planes are positioned parallel to each other transposed by 2.124 Å and connected by bidentate SO_3F groups. The disposition of the four SO_3F groups about the gold(III) ion is interesting. As seen in Fig. 1, the terminal SO_3F groups coordinated to Au(1) are bent below the AuO_4 plane, while the bidentate SO_3F groups are pointing up. For Au(1)* the opposite, pairwise disposition of coordinated fluorosulfate groups is noted, thus generating the chair configuration of the metallocycle. A similar pairwise arrangement of coordinated monodentate nitrate groups is reported for the

Can. J. Chem. Downloaded from www.nrcresearchpress.com by 195.138.81.100 on 09/07/12
For personal use only.

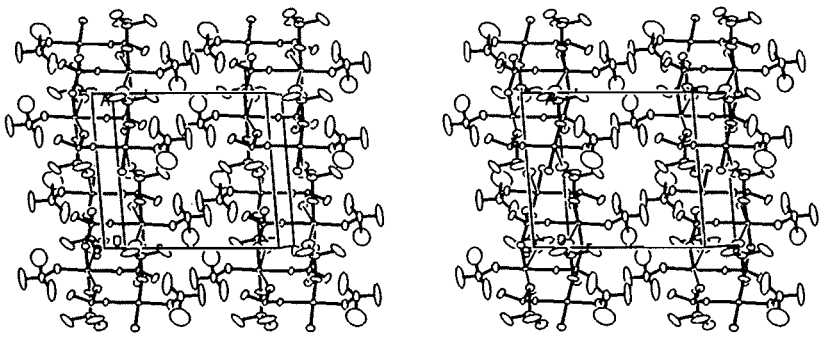


FIG. 2. Stereoview of the packing arrangement of gold(III) tris(fluorosulfate) viewed along the ***b*** axis.

$[Au(NO_3)_4]^-$ anion (16), where for the potassium salt a space group identical to the one found for $[Au(SO_3F)_3]_2$, $P2_1/a$, is reported. Hence the symmetry of the two $Au(SO_3F)_4$ moieties and of the $[Au(NO_3)_4]^-$ anion corresponds approximately to the point group C_{2h}.

Besides the short Au—O bonds, there are two, somewhat longer intermolecular Au···O contacts, Au(1)—O(6)′ at 2.757(8) Å and Au(1)—O(3)″ at 2.960(7) Å, above and below the Au(1)—O_4 plane. They give rise to a very distorted octahedral arrangement about gold(III), with the distortion also reflected in the O(6)′—Au(1)—O(3)″ bond angle, found to be 158.6(3)° rather than the expected 180°. A more regular, tetragonally elongated example for 4:2 coordination is reported for AuF_3 (13*b*), while for $AuCl_3$ (14), $AuBr_3$ (15), and Au_2O_3 (17*a*) several rather long Au···X, X = halogen or oxygen, contacts are found for each gold atom resulting in complex and highly distorted polyhedral geometries. Likewise in the $[Au(NO_3)_4]^-$ anion (16), four relatively short Au···O contacts of ~2.85 Å are observed, but these are intramolecular in nature and involve oxygen atoms of the bonded nitrate groups.

Thus only AuF_3 (13) and $[Au(SO_3F)_3]_2$ may be regarded as examples of 4:2 coordination with the regular arrangement in AuF_3 seemingly a consequence of the compact helical chain structure adopted by this compound. The denser packing in AuF_3 is reflected in the calculated density (13) of 6.78 g cm^{-3} while for $[Au(SO_3F)_3]_2$ a value of 3.404 g cm^{-3} is found, and in the Au···Au distances of 3.461 Å in AuF_3 versus 4.510 Å in $[Au(SO_3F)_3]_2$. The looser packing in $[Au(SO_3F)_3]_2$ and the low degree of intermolecular association contribute in our view to the fairly high solubility in HSO_3F and the acidity of the resulting monoprotonic superacid system.

(c) Discussion of bond parameters

Two aspects remain to be discussed: (*i*) The Au—O bond distances compared to values obtained for other gold(III) oxygen compounds (16–23) and (*ii*) the SO_3F bond parameters, viewed in comparison to relevant precedents. The structural chemistry of gold(III) (18) provides a number of relevant examples, in addition to the binary halides, AuF_3 (13), $AuCl_3$ (14), and $AuBr_3$ (15) already discussed. Nearly square planar AuO_4-groups are found in Au_2O_3 (17*a*), and $[Au(OH)_4]^-$ (17*b*), the selenite-oxide $Au_2(SeO_3)_2O$ (19*a*) and -chloride $Au(SeO_3)Cl$ (19*b*), the tetrakis(nitrato)aurate(III) anion found in $K[Au(NO_3)_4]$ (16), and in aurate(III) anions of various types found in Li_5AuO_4, $KAuO_2$, and $RbAuO_2$, according to X-ray powder data (20), and in $Na_6Au_2O_6$ (21) where a discrete $Au_2O_6^{2-}$ ion is present according to a single crystal diffraction study. A dimeric structure is suggested for $Au(OTeF_5)_3$ (22); however, the structure is disordered. A sulfonate group bonded to Au(III) is found in the organometallic compound $(CH_3)_2Au(H_2O)$-SO_3CF_3 (23). In most instances an approximately square planar coordination environment is found for gold(III).

As can be seen in Table 5, comparable short average Au—O distances of about 2.00 ± 0.02 Å are found for Au_2O_3 (17*a*) and the anion $[Au(OH)_4]^-$ (17*b*) and the oxyacid derivatives $Au_2(SeO_3)_2O$ (19*a*), $Au(SeO_3)Cl$ (19*b*) (considering here distances in the AuO_4 group only), in $[Au(NO_3)_4]^-$ (16) and in $[Au(SO_3F)_3]_2$. The reported crystal structure of dimeric $[Au(OTeF_5)_3]_2$ (22) would normally present a direct analogy and allow a good comparison to the structure of $[Au(SO_3F)_3]_2$. However, the structure is disordered and reported bond parameters, in particular Au—O distances of 1.78(4) and 1.82(3) Å, respectively, are unprecedentedly short and most likely incorrect. Differences within this group are small and probably not overly significant. On the other hand, Au—O distances are longer in the various alkali metal aurates (20, 21) by at least 0.1 Å and also longer in the organogold compound $(CH_3)_2Au(H_2O)OSO_2CF_3$ (23).

The short Au—O bonds are comparable to Au—F distances found in AuF_3 (13) and in $K[AuF_4]$ (24), where average values of 1.975 and 1.95 Å, respectively, are reported with esd's of 0.02 to 0.04 Å. The covalent single bond radius of fluorine is slightly shorter than that of oxygen (25), resulting in shorter Au—F bonds.

Hence it is probable that relativistic effects, which are reportedly at a maximum for gold and its compounds (26), are involved. While no relativistic calculations appear to have been done on AuO_4-containing systems, a recent study (27) on the stability of AuX_4^-, X = F, Cl, Br, or I is available using pseudopotentials, and a calculated Au—F equilibrium distance of 1.93 Å is suggested.

Only a limited number of crystal structures of inorganic fluorosulfates has been reported previously. These examples fall into four groups: (*i*) Ionic fluorosulfates: this group includes examples where the SO_3F-group has approximately C_{3v} symmetry, with S—O distances either the same or only slightly different from one another on account of weak cation–anion contacts. The examples consist of KSO_3F (6*a*), $LiSO_3F$ (6*b*), and NH_4SO_3F (6*c*), $S_4N_4(SO_3F)_2$ (28*a*), $(S_6N_4)(SO_3F)_2$ (28*b*), $Se_{10}(SO_3F)_2$ (28*c*), and 3-methyl-4,5-diphenyl-1,2,3-thiadiazolium fluorosulfate (28*d*); (*ii*) hydrogen bonded fluorosulfates like a 1:1 complex between acetic and fluorosulfuric acid (29) and the mono-solvated anion $[H(SO_3F)_2]^-$ (30), where no bond parameters are reported; (*iii*) non-metal fluorosulfates: $FXeSO_3F$ (31) and $[I(SO_3F)_2]I$ (32), both with monodentate fluorosulfate groups and $[(XeF)_2SO_3F][AsF_6]$ (33) where a

Can. J. Chem. Downloaded from www.nrcresearchpress.com by 195.138.81.100 on 09/07/12
For personal use only.

TABLE 5. Reported gold–oxygen distances and contacts

Compound	Au—O distances (Å)	Au···O contacts (Å)[a]
Au_2O_3 (17*a*)	2.04 (×1), 2.07 (×1), 2.01 (×1), 1.93 (×1) av. 2.0125	2.8 (×1), 2.90 (×1) 3.05 (×1), 3.19 (×1) av. 2.988
$[Au(OH)_4]^-$ in (17*b*) Sr $Au_2(OH)_8$	1.980 (×4)	
$Au_2(SeO_3)_2O$ (19*a*)	2.06 (×2), 1.98 (×1), 2.08 (×1) av. 2.055	
$Au(SeO_3)Cl$[b] (19*b*)	1.975 (×2), 1.998 (×2) av. 1.986	
$K[Au(NO_3)_4]$[c] (16)	2.02 (×2), 1.99 (×2) av. 2.005	2.85 (×2), 2.87 (×2) av. 2.86
$Na_6[Au_2O_6]$[d] (21)	2.12 (×2), 2.17 (×3) av. 2.145	
$(CH_3)_2Au(H_2O)SO_3CF_3$ (23)	2.157 (H_2O), 2.201 (OSO_2CF_3)	
$Au(OTeF_5)_3$[e] (22)	1.78 (×1) 2.23 (×1)	1.82 (×1) 2.29 (×1)
$Au(SO_3F)_3$	1.956 (×1), 1.959 (×1) 2.016 (×1), 2.020 (×1) av. 1.988	2.757 (×1), 2.960 (×1) av. 2.858

[a]Listed only where Au···O contacts are reported.
[b]Besides AuO_4-groups the structure also contains AuO_3Cl- and AuO_2Cl_2-groups which are not considered here.
[c]The Au···O contacts are intramolecular contacts.
[d]Similar long Au—O distances are obtained from powder data for Li_3AuO_3, Li_5AuO_4, $KAuO_2$, and $RbAuO_2$, ref. 20.
[e]For a discussion of the reported bond distances for this molecule see the preceding text.

TABLE 6. Selected SO—F bond distances and angles for $FXeSO_3F$,[a] $[(FXe)_2SO_3F]$,[b] and $Au(SO_3F)_3$

For bidentate, bridging bond type			For monodentate, terminal bond type		
d (Å)[c]	$[(FXe)_2SO_3F]^+$	$Au(SO_3F)_3$	*d* (Å)	$FXeSO_3F$	$Au(SO_3F)_3$
$SO_{(b)}$	1.47 (3)	1.467 (6)	$SO_{(b)}$	1.501 (8)	1.504 (7)
$SO_{(b)}$	1.47 (3)	1.471 (7)	$SO_{(t)}$	1.430 (9)	1.39 (1)
$SO_{(t)}$	1.39 (3)	1.384 (7)	$SO_{(t)}$	1.415 (9)	1.399 (8)
SF	1.53 (3)	1.507 (7)	SF	1.540 (9)	1.51 (1)
$\angle SO_{2(b)}$ (°):	110 (1)	111.3 (4)	$\angle SO_{2(t)}$ (°):	119.6 (6)	122.6 (7) 127 (1)

[a]Reference 32.
[b]Reference 34.
[c]The subscripts used in the table refer to coordinated oxygen, $O_{(b)}$, and terminal oxygen, $O_{(t)}$.

bidentate bridging SO_3F group is found, and (*iv*) organometallic fluorosulfates, with $(CH_3)_2Sn(SO_3F)_2$ (34) with bidentate, symmetrically bridging SO_3F groups as the sole example. In all instances, only a single bonding mode for the fluorosulfate group is observed.

A meaningful comparison to previous work is somewhat more difficult for the bond parameters of the SO_3F group on two accounts: (*i*) due to thermal motion of the non-bonded O and F atoms in the terminal SO_3F groups of $[Au(SO_3F)_3]_2$, only the parameters for bidentate SO_3F-groups are known with a high degree of accuracy and (*ii*) as summarized above most reported structures have ionic SO_3F^- groups with rather small differences in S—O distances for coordinated and non-coordinated oxygen within the fluorosulfate group.

This leaves the two xenon(II) fluorosulfato derivatives $FXeSO_3F$ (31) and the cation $[(FXe)_2SO_3F]^+$ (33) as the most

Can. J. Chem. Downloaded from www.nrcresearchpress.com by 195.138.81.100 on 09/07/12
For personal use only.

reasonable choices for a comparison. The former exhibits a monodentate, and the latter a bidentate bridging fluorosulfate group. The pertinent S—O and S—F distances, as well as some selected SO_2 bond angles for both compounds (31, 33), as summarized in Table 6 and compared to the data for $[Au(SO_3F)_3]_2$. While it may appear that SO_3F bonds are slightly shorter in $[Au(SO_3F)_3]_2$, the differences are either rather small, observed primarily for the monodentate SO_3F-groups, or within the quoted estimated standard deviations. The strong similarity between $Au(SO_3F)_3$ and both xenon-SO_3F derivatives (31, 33) extends also to the pertinent bond angles, and again the largest differences are found for the monodentate fluorosulfate groups in $FXeSO_3F$ (31) and $[Au(SO_3F)_3]_2$.

Summary

The structure of gold(III) fluorosulfate features a dimeric molecule, short Au—O bonds, a distorted example of 4:2 coordination for gold, and two distinctly different fluorosulfate groups. However, neither the Au—O distances nor the SO_3F bond parameters suggest an unprecedented, strong Au—O interaction in $[Au(SO_3F)_3]_2$ as the cause for the observed superacidity of the HSO_3F–$Au(SO_3F)_3$ system (3, 4). The reason for the reported superacidity must be seen in two other structural features: (*a*) the loose packing observed appears to permit sufficient solubility of $[Au(SO_3F)_3]_2$ in fluorosulfuric acid, and (*b*) the dimeric structure suggests, in agreement with computer modelling studies (5), two principle equilibria to be responsible for the high acidium ion concentration (4):

[2] $2HSO_3F + [Au(SO_3F)_3]_{2(solv.)} \rightarrow H_2SO_3F^+ + [Au_2(SO_3F)_7]^-_{(solv.)}$

[3] $2HSO_3F + Au(SO_3F)_{3(solv.)} \rightarrow H_2SO_3F^+ + [Au(SO_3F)_4]^-_{(solv.)}$

In contrast, for the recently reported superacid systems HSO_3F–$Nb(SO_3F)_5$ and HSO_3F–$Ta(SO_3F)_5$ (4) a higher degree of intermolecular association of the Nb- and Ta-species is suggested (5) and lower acidity is observed (4).

Acknowledgements

Financial support by the Deutsche Forschungsgemeinschaft (DFG) and the Natural Sciences and Engineering Research Council of Canada (NSERC) is gratefully acknowledged. The valuable assistance by Mr. F. Mistry is acknowledged.

1. W. M. Johnson, R. Dev, and G. H. Cady. Inorg. Chem. **11**, 2260 (1972).
2. (*a*) R. J. Puddephatt. The chemistry of gold. Elsevier, Amsterdam. 1978; (*b*) R. J. Puddephatt. *In* Comprehensive coordination chemistry. Vol. 7. *Edited by* G. Wilkinson. Pergamon Press, Oxford. 1987. p. 861.
3. (*a*) K. C. Lee and F. Aubke. Inorg. Chem. **18**, 389 (1979); (*b*) K. C. Lee and F. Aubke. Inorg. Chem. **19**, 119 (1980).
4. W. V. Cicha and F. Aubke. J. Am. Chem. Soc. **111**, 4328 (1989).
5. W. V. Cicha, K. C. Lee, and F. Aubke. J. Solution Chem. **19**, 609 (1990).
6. (*a*) K. O'Sullivan-Mailer, R. C. Thompson, and J. Trotter. J. Chem. Soc. (A) 2024 (1967); (*b*) Z. Zak and M. Kosicka. Acta Crystallogr. **B34**, 30 (1976); (*c*) K. O'Sullivan-Mailer, R. C. Thompson, and J. Trotter. J. Chem. Soc. A, 1814 (1970).
7. H. Willner, G. Hwang, F. Mistry, P. Phillips, F. G. Herring, and F. Aubke. To be published.
8. H. Willner and F. Aubke. Inorg. Chem. **29**, 2195 (1990).
9. G. H. Cady and J. M. Shreeve. Inorg. Synth. **7**, 124 (1963).
10. W. Gombler and H. Willner. J. Phys. E. Sci. Instrum. **20**, 1286 (1987).
11. International tables for X-ray crystallography. Vol. IV. Kynoch Press, Birmingham, U.K. (present distributor D. Reidel: Dordrecht, The Netherlands), 1974. pp. 99–102, 149.
12. F. B. Dudley and G. H. Cady. J. Am. Chem. Soc. (*a*) **79**, 513 (1979); (*b*) **85**, 3375 (1963).
13. (*a*) L. B. Asprey, K. H. Jack, H. Kruse, and A. Maitland. Inorg. Chem. **3**, 602 (1964); (*b*) F. W. B. Einstein, P. R. Rao, J. Trotter, and N. Bartlett. J. Chem. Soc. (A), 478 (1967).
14. E. S. Clark, D. H. Templeton, and C. H. MacGillavry. Acta Crystallogr. **11**, 284 (1958).
15. K. P. Lorcher and J. Strähle. Z. Naturforsch. B, **30**, 662 (1975).
16. C. D. Garner and S. C. Wallwork. J. Chem. Soc. (A), 3092 (1970).
17. (*a*) P. G. Jones, H. Rumpel, E. Schwarzmann, and G. M. Sheldrick. Acta Crystallogr. B**35**, 1435 (1979); (*b*) P. G. Jones and G. M. Sheldrick. Acta Crystallogr. C**40**, 1776 (1984).
18. (*a*) P. G. Jones. Gold Bull. **14**, 102 (1981); **14**, 159 (1981); **16**, 114 (1983); **19**, 46 (1986); (*b*) M. Melnik and R. V. Parish. Coord. Chem. Rev. **10**, 157 (1986).
19. (*a*) P. G. Jones, G. M. Sheldrick, E. Schwarzmann, and A. Vielmäder. Z. Naturforsch. **38**B, 10 (1983); (*b*) P. G. Jones, M. Kraushaar, E. Schwarzmann, and G. M. Sheldrick. Z. Naturforsch. **37**B, 941 (1982).
20. H.-D. Wasel-Nielen and R. Hoppe. Z. Anorg. Allg. Chem. **43**, 375 (1970).
21. H. Klassen and R. Hoppe. Naturwissenschaften, **63**, 387 (1976).
22. P. Huppmann, H. Hartl, and K. Seppelt. Z. Anorg. Allg. Chem. **524**, 26 (1985).
23. S. Komiya, J. L. Huffman, and J. K. Kochi. Inorg. Chem. **16**, 2138 (1977).
24. A. J. Edwards and G. R. Jones. J. Chem. Soc. A. 1936 (1969).
25. L. Pauling. The nature of the chemical bond. 2nd ed. Cornell Univ. Press, Ithaca, NY. 1948. p. 164.
26. P. Pyykkö. Chem. Rev. **88**, 563 (1988) and references herein.
27. P. Schwerdtfeger. J. Am. Chem. Soc. **111**, 7261 (1989).
28. (*a*) R. J. Gillespie, J. P. Kent, J. F. Sawyer, R. D. Slim, and J. D. Tyrer. Inorg. Chem. **20**, 3799 (1981); (*b*) R. J. Gillespie, J. P. Kent, and J. F. Sawyer. Inorg. Chem. **20**, 3784 (1981); (*c*) M. J. Collins, R. J. Gillespie, J. F. Sawyer, and G. J. Schrobilgen. Acta Crystallogr. **C42**, 13 (1986); (*d*) P. G. Jones and O. Kennard. Acta Crystallogr. **B34**, 335 (1978).
29. A. Kvick, P.-G. Jonsson, and I. Olovsson. Inorg. Chem. **8**, 2665 (1969).
30. C. Belin, M. Charbonnel, and J. Potier. J. Chem. Soc. Chem. Commun. 1036 (1981).
31. N. Bartlett, M. Wechsberg, G. R. Jones, and R. D. Burbank. Inorg. Chem. **11**, 1124 (1972).
32. M. J. Collins, G. Dénès, and R. J. Gillespie. J. Chem. Soc. Chem. Commun. 1296 (1984).
33. R. J. Gillespie, G. S. Schrobilgen, and D. R. Slim. J. Chem. Soc. Dalton, 1003 (1977).
34. F. H. Allen, J. A. Lerbscher, and J. Trotter. J. Chem. Soc. (A), 2507 (1971).

Can. J. Chem. Downloaded from www.nrcresearchpress.com by 195.138.81.100 on 09/07/12
For personal use only.

Reaction products of ammonium pertechnetate(VII) with triphenylphosphine and crystal structures of *mer*-$Tc(PPh_3)_2Cl_3(DMF)\cdot 2PPh_3$ and $NH_2(CH_3)_2^+DMAH^+[TcCl_6]^{2-}\cdot PPh_3O$

FERNANDE D. ROCHON,[1] ROBERT MELANSON, AND PI-CHANG KONG

Département de chimie, Université du Québec à Montréal, C.P. 8888, Succ. A, Montréal, Canada H3C 3P8

Received August 10, 1990

FERNANDE D. ROCHON, ROBERT MELANSON, and PI-CHANG KONG. Can. J. Chem. **69**, 397 (1991).

The reaction of NH_4TcO_4 with PPh_3 in DMF solution in the presence of HCl produces *mer*-$Tc^{III}(PPh_3)_2Cl_3(DMF)\cdot 2PPh_3$ (**1**). When the reaction is done in acidic DMA, the yellow product isolated was identified as $NH_2(CH_3)_2^+DMAH^+[TcCl_6]^{2-}\cdot PPh_3O$ (**2**). The dimethylammonium cation was produced from the reaction of the solvent (DMA) with aqueous HCl. The reaction of NH_4TcO_4 with PPh_3 in acidic acetone solution produces yellow $(PPh_3H)_2[TcCl_6]$ (≈15% yield) and some orange crystals (≈65% yield) identified by X-ray diffraction as $[Ph_3P\text{-}C(CH_3)_2\text{-}CH_2\text{-}CO\text{-}CH_3]^+[Tc(PPh_3)Cl_5]^-$. The cation was produced from the reaction of acetone used as solvent with HCl and PPh_3. The crystals of **1** are monoclinic with $P2_1/m$ space group, a = 11.393(4), b = 24.993(11), c = 12.398(4) Å, β = 106.98(3)°, Z = 2. The structure was refined to R = 0.072 and wR = 0.058. The Tc—O bond distance is 2.115(12) Å while the Tc—P bond lengths are 2.496(5) and 2.499(5) Å and the Tc—Cl are 2.399(5) and 2.342(3) Å. The C atoms of the DMF ligand are disordered. The crystals of **2** are triclinic, $P\bar{1}$ space group with a = 8.627(5), b = 13.308(7), c = 14.401(9) Å, α = 97.62(5), β = 91.31(5), γ = 106.42(5)°, and Z = 2. The structure was refined to R = 0.060 and wR = 0.076. The proton on $DMAH^+$ is hydrogen bonded to the oxygen of PPh_3O with a distance O···O = 2.48(1) Å.

Key words: technetium, DMF, triphenylphosphine, dimethylacetamide.

FERNANDE D. ROCHON, ROBERT MELANSON et PI-CHANG KONG. Can. J. Chem. **69**, 397 (1991).

La réaction de NH_4TcO_4 avec PPh_3 en solution dans le DMF, produit en présence de HCl, *mer*-$Tc^{III}(PPh_3)_2Cl_3(DMF)\cdot 2PPh_3$ (**1**). Lorsque la réaction est faite dans le DMA, le produit est le sel mixte $NH_2(CH_3)_2^+DMAH^+[TcCl_6]^{2-}\cdot PPh_3O$ (**2**). Le cation diméthylammonium a été produit par la réaction du solvant (DMA) avec HCl aqueux. La même réaction en milieu acétone produit le sel jaune $(PPh_3H)_2[TcCl_6]$ (rendement ≈15%) et des cristaux oranges identifiés par diffraction des rayons-X comme $[Ph_3P\text{-}C(CH_3)_2\text{-}CH_2\text{-}CO\text{-}CH_3]^+[Tc(PPh_3)Cl_5]^-$ (rendement ≈65%). Le cation a été produit par la réaction du solvant (acétone) avec HCl et PPh_3. Les cristaux de **1** sont monocliniques, groupe d'espace $P2_1/m$, a = 11,393(4), b = 24,993(11), c = 12,398(4) Å, β = 106,98(3)° et Z = 2. La structure a été affinée jusqu'à R = 0,072 et wR = 0,058. La distance Tc—O est 2,115(12) Å, tandis que les liens Tc—P = 2,496(5) et 2,499(5) Å et Tc—Cl = 2,399(5) et 2,342(3) Å. Les atomes de C du DMF sont désordonnés. Les cristaux de **2** sont tricliniques, $P\bar{1}$, avec a = 8,627(5), b = 13,308(7), c = 14,401(9) Å, α = 97,62(5), β = 91,31(5), γ = 106,42(5)°, Z = 2, R = 0,060 et wR = 0,076. Le proton sur $DMAH^+$ est lié par pont hydrogène à l'oxygène du PPh_3O avec une distance O···O = 2,48(1) Å.

Mots clés : technécium, DMF, triphénylphosphine, diméthylacétamide.

Introduction

The chemistry of technetium has recently become very important, especially in relation to the use of the isotope 99m in nuclear medicine. This nucleus is a γ-emitter with a half-life of 6.02 h and decays to its isomer technetium-99, which is a β-emitter with a long half-life of 213 000 years. The quantity of ^{99m}Tc needed in radiopharmacy is a few nanograms and for this reason its toxicity is negligible. It is therefore an ideal nucleus for diagnostic studies in nuclear medicine. It has been used for several years for bone scanning and recently it has been used to study the heart, the brain, the kidneys, the liver and other organs, and also tumor tissue. A good review on medical diagnostic imaging with complexes of ^{99m}Tc was published by Clarke and Podbielski in 1987 (1).

We recently started a project on the synthesis of new technetium compounds. The ultimate aim of our research project is to synthesize Tc complexes that could be of some interest for nuclear cardiology. The best heart agent that is being tested at the moment on humans is a Tc(I) hexacoordinated complex with an isonitrile ligand (2, 3). This compound accumulates rapidly in the heart and has a long retention time. But it also accumulates in other organs, which partly limits its use. Therefore, a search for more specific agents is continuing. These studies seem to indicate that such an agent should be charged +1 with a low oxidation state ≤3 for Tc. Other types of ligands producing Tc compounds that accumulate in the heart are phosphines, especially di(alkyl)phosphinoethane (4–6). We have therefore chosen to start a project on the synthesis of mixed-ligand compounds with isonitrile and phosphine derivatives. The synthetic methods must be very simple and adaptable to the use of "kits" (containing $[TcO_4]^-$ as starting material), which are used in nuclear medicine for preparing the ^{99m}Tc compounds. The number of intermediate Tc compounds must also be reduced to a minimum. The use of reducing agents was rejected since they produce secondary products that are difficult to eliminate in the preparation of the radiopharmaceuticals.

The synthesis of $[Tc(isonitrile)_6]^{3+}$ has been reported (7, 8). We first tried to synthesize compounds of the type $[Tc(isonitrile)_xCl_{6-x}]^{y+}$ but without success. We obtained either the hexacoordinated isonitrile compound or decomposition products. Since a few compounds of this type with phosphines $[Tc(phosphine)_xCl_{6-x}]^{y+}$ have been reported in the literature (9, 10), we decided to synthesize this type of compound with monodentate and bidentate phosphines and eventually study the reactions with isonitriles. We started this study with triphenylphosphine. The disubstituted compound $Tc^{IV}(PPh_3)_2Cl_4$ (9) has

[1]Author to whom correspondence may be addressed.

Can. J. Chem. Downloaded from www.nrcresearchpress.com by 195.138.81.100 on 09/07/12
For personal use only.

TABLE 1. Experimental details of the X-ray studies of $Tc(PPh_3)_2Cl_3(DMF)\cdot 2PPh_3$ (**1**) and $NH_2(CH_3)_2^+DMAH^+[TcCl_6]^{2-}\cdot PPh_3O$ (**2**)

	1	**2**
Compound	$C_{75}H_{67}NOP_4Cl_3Tc$	$C_{24}H_{33}N_2O_2PCl_6Tc$
FW	1327.53	724.14
Space group	$P2_1/m$	$P\bar{1}$
a (Å)	11.393(4)	8.627(5)
b (Å)	24.993(11)	13.308(7)
c (Å)	12.398(4)	14.401(9)
α (°)	90	97.62(5)
β (°)	106.98(3)	91.31(5)
γ (°)	90	106.42(5)
Volume (Å^3)	3376(2)	1568.7(16)
Z	2	2
$F(000)$	1372	734
ρ_{calcd} (Mg m^{-3})	1.306	1.528
μ (MoKα) (mm^{-1})	0.459	1.03
2θ max (°)	50	50
Octants	$h, k, \pm l$	$h, \pm k, \pm l$
h, k, l	$0\rightarrow 13, 0\rightarrow 29, -14\rightarrow 14$	$0\rightarrow 10, -15\rightarrow 15, -17\rightarrow 17$
Scan technique	$2\theta/\theta$	$2\theta/\theta$
Std. reflections	2 0 0, 1 5 0, 0 0 −3	3 4 −5, 1 −5 1, 0 1 −10
No. of independent reflections	6138	5557
No. of observed reflections	2232 $I_{net} > 2.5\sigma$	3898 $I_{net} > 3.0\sigma$
$R = \Sigma\|\|F_o\| - \|F_c\|\|/\Sigma\|F_o\|$	0.072	0.060
$wR = [\Sigma w(\|F_o\| - \|F_c\|)^2/\Sigma\|F_o\|^2]^{1/2}$	0.058	0.076
Δ/σ	0.4	0.2
$S = [\Sigma w(\|F_o\| - \|F_c\|)^2/(m-n)]^{1/2}$	1.75	1.11

been reported but no Tc–PPh_3 complex has been prepared yet with a lower oxidation state (≤ 3). The results obtained in our study are discussed below.

Experimental section

Ammonium pertechnetate ($NH_4{}^{99}TcO_4$) was obtained from Oak Ridge National Laboratory. It was recrystallized in nitric acid (**Caution**: ammonium pertechnetate in acid medium will produce some radioactive volatile compound) and dissolved in water. A 0.286 M solution was prepared. All manipulations were made in a laboratory approved for low-level radioactive material (^{99}Tc is a β-emitter with a particle energy of 0.292 MeV and a half-life of 2.13×10^5 years). Triphenylphosphine was bought from Aldrich.

The magnetic susceptibility measurements of the Tc compounds were done by the Faraday method on a Cahn instrument equipped with a millibalance. Corrections were made for diamagnetism. The infrared spectra were measured in the solid state as Nujol mulls on a FT-50 Digilab instrument equipped with a CsI beamsplitter. The microanalyses were performed by Galbraith.

mer-$Tc(PPh_3)_2Cl_3(DMF)\cdot 2PPh_3$

Ammonium pertechnetate (1 mL, 0.286 M) was added to a solution containing 1 mL of concentrated HCl and 0.84 g of triphenylphosphine dissolved in 16 mL of dimethylformamide (DMF). The clear red solution was left overnight and the next day the red crystals were filtered and washed with ethanol and ether. The compound is not soluble in ethanol, ether, or CCl_4, but is slightly soluble in acetone. Yield: ≈70%. IR (cm^{-1}): ν(C=O) 1649, ν(Tc–Cl) 330, 302; main other bands: 1087, 752, 745, 695, 519, 514, and 492. Magnetic moment μ = 3.1 BM.

$NH_2(CH_3)_2{}^+DMAH^+[TcCl_6]^{2-}\cdot PPh_3O$

A solution containing 0.52 g of PPh_3 and 1 mL of NH_4TcO_4 (0.286 M) dissolved in 8 mL of dimethylacetamide (DMA) was added to a second solution containing 1 mL of concentrated HCl dissolved in 6 mL of DMA. A clear red solution was obtained and set aside for crystallization. Ten days later, 6 mL of HCl (6 M) was added to the solution, which became slightly cloudy. About 2 mL of acetone was added to obtain a clear solution, which was covered and left at room temperature. A month later, yellow crystals suitable for X-ray diffraction methods were obtained. Yield: ≈40%. IR (cm^{-1}): ν(N—H) 3125, ν(C=O) 1671, ν(Tc–Cl) 315 (br); main other bands: 1122, 1082, 1070, 995, 722, 695, 544, and 539. Magnetic moment μ = 3.6 BM.

$(PPh_3H)_2[TcCl_6]$ and $(Ph_3P\text{-}C(CH_3)_2\text{-}CH_2\text{-}CO\text{-}CH_3)^+[Tc(PPh_3)Cl_5]^-$

A solution containing 1 mL of NH_4TcO_4 (0.286 M) and 1.5 mL of concentrated HCl dissolved in 30 mL of acetone was added to a second solution containing 0.57 g of PPh_3 dissolved in 20 mL of acetone. The mixture was stirred and refluxed immediately for 15 min. A light yellow precipitate was observed. The precipitate is $(PPh_3H)_2[TcCl_6]$ while $(Ph_3P\text{-}C(CH_3)_2\text{-}CH_2\text{-}CO\text{-}CH_3)[Tc(PPh_3)Cl_5]$ is in solution. The mixture was cooled to room temperature and the precipitate was filtered and washed. Yield of $(PPh_3H)_2[TcCl_6]$: ≈15%. IR (cm^{-1}): ν(P–H) 2440, ν(Tc–Cl) 318 (br); main other bands: 1114, 870, 748, 719, 691, and 498.

The above filtrate was concentrated to 15 mL and placed in a refrigerator to recrystallize. The next day, orange crystals suitable for X-ray diffraction studies were obtained. Yield of $(Ph_3P\text{-}C(CH_3)_2\text{-}CH_2\text{-}CO\text{-}CH_3)[Tc(PPh_3)Cl_5]$: ≈65%. IR (cm^{-1}): ν(C=O) 1718, ν(Tc–Cl) 345, 336, 326, 292; main other bands: 1102, 1087, 996, 748, 722, 692, 524, and 496. Magnetic moment μ = 4.06 BM.

Crystallographic measurements and structure resolution

The two crystals $Tc(PPh_3)_2Cl_3(DMF)\cdot 2PPh_3$ (**1**) and $NH_2(CH_3)_2{}^+\text{-}DMAH^+[TcCl_6]^{2-}\cdot PPh_3O$ (**2**) were selected after examination under a polarizing microscope for homogeneity. The unit cell parameters were obtained by least-squares refinement of the angles 2θ (10–25°), ω, and χ for 15 well-centered reflections on a Syntex $P\bar{1}$ diffractometer using graphite-monochromatized MoKα radiation. Crystal data and other information are summarized in Table 1. Scan rates and data treatment have already been described (12). Corrections were made for Lorentz–polarization effects and, for $Tc(PPh_3)_2Cl_3(DMF)\cdot 2PPh_3$, corrections were made for absorption (11 faces, transmission factors 0.933–0.961).

Can. J. Chem. Downloaded from www.nrcresearchpress.com by 195.138.81.100 on 09/07/12
For personal use only.

Can. J. Chem. Downloaded from www.nrcresearchpress.com by 195.138.81.100 on 09/07/12
For personal use only.

The anomalous dispersion terms of Tc, P, and Cl were included in the calculations (13).

The coordinates of the Tc atom were determined from the three-dimensional Patterson maps and the positions of all the other non-hydrogen atoms were found by the usual Fourier methods. The refinements of the structures were done by block-diagonal least-squares analysis, minimizing $\Sigma w(F_o - F_c)^2$. The atoms of the DMF molecule were found to be disordered. The three C atoms were clearly disordered on the two sides of the mirror plane. The N and O atoms are also probably slightly disordered by different amounts around the mirror. When their y coordinates were varied, the refined value was 0.250. Therefore they were placed on the mirror for the remaining refinements. Most H atoms could be located, but they were fixed at their calculated positions with a $U_{eq} = 0.076$. For the methyl H atoms, at least one H was obtained from a difference Fourier map and the positions of the remaining atoms were calculated. A hydrogen atom was clearly seen at 1.02 Å from the O atom in DMA, confirming the protonation of DMA. The H atoms were not refined. Isotropic secondary extinction corrections (14) were included in the calculations. Individual weights $w = 1/\sigma^2(F)$ were applied. The refinement of the scale factor, coordinates, and anisotropic temperature factors of all the non-hydrogen atoms converged to $R = 0.072$ and $wR = 0.058$ for **1**, to $R = 0.060$ and $wR = 0.076$ for **2**. There were a few residual peaks (<0.33 (for **1**) and <0.7 (for **2**) e Å^{-3}) in the close environment of the Tc atom.

The scattering curves of Cromer and Waber (15) were used except for the hydrogen atoms (16). The calculations were done on a Cyber 830 with programs already described (12).[2]

Results and discussion

We synthesized the Tc(IV) compound $Tc(PPh_3)_2Cl_4$ according to the published method (9). Its reaction with *tert*-butylisonitrile was studied in ethylene glycol following the method described in the literature to synthesize $Tc^{i}(CO)_3(PMe_2Ph)_2Cl$ (17). We obtained only decomposition products. A few trisubstituted compounds of Tc(III) with less crowded ligands have been prepared (9). These compounds were prepared by the reaction of NH_4TcO_4 with PR_3 in ethanol in the presence of HCl. In a 1 to 5 ratio (Tc:PR_3), the disubstituted Tc(IV) compound was prepared, while with a 1 to 15 ratio the trisubstituted Tc(III) complex was obtained. A few complexes of Tc(III) were prepared but not with PPh_3. We assumed that one factor was the solvent, since the disubstituted compound with PPh_3 is very insoluble in the reacting medium (ethanol with HCl). Therefore we decided to study the same reaction but in other solvents. We started the study in DMF with experimental conditions similar to those used to prepare $Tc(PPhMe_2)_3Cl_3$ (9) in an attempt to isolate PPh_3 complexes of Tc(≤III). In these reactions, PPh_3 acts as the reducing agent.

Reaction in DMF

When the reaction was done in acidic DMF, we isolated red crystals. The IR spectrum showed the presence of PPh_3, some ν(Tc–Cl) vibrations at 330 and 302 cm^{-1}, and a ν(C=O) band at 1649 cm^{-1}. The results of the crystal structure analysis showed that it was a Tc(III) compound with a coordinated DMF molecule bonded through its O atom. It is the isomer *mer*-$Tc(PPh_3)_2(DMF)Cl_3 \cdot 2PPh_3$ (**1**) with 2 non-coordinating PPh_3 molecules. This is the first example of a Tc–DMF compound. Molecular models have shown that $Tc(PPh_3)_3Cl_3$ cannot be prepared because the PPh_3 ligand is too bulky. The magnetic susceptibility measurement of *mer*-$Tc(PPh_3)_2(DMF)Cl_3 \cdot 2PPh_3$ showed that it was a low spin d^4 Tc(III) compound with 2 unpaired electrons ($\mu = 3.1$ BM). The preparation of a similar compound with acetonitrile (18) has recently been reported, but the compound is unstable in solution and its crystal structure was not reported. The compound $TcCl_3(PPh_3)_2(CH_3CN)$ was prepared from the reaction of $(n\text{-}Bu_4N)[Tc^{v}OCl_4]$ with PPh_3 in acetonitrile. The DMF compound, which has the advantage of being synthesized directly from $[Tc^{vii}O_4]$, could be an important intermediate for the synthesis of mixed-ligand Tc compounds of low valency.

The refined atomic parameters of the structure are listed in Table 2. A labelled diagram of the molecule is shown in Fig. 1. Several atoms are located on the mirror plane: Tc, Cl(1), P(1), P(2), O(1), N, and four C atoms. The DMF ligand, which is located *trans* to a Cl ligand, is disordered. O(1) and N are on the mirror (probably slightly disordered), while the three C atoms are disordered on the two sides of the mirror plane. The two bonded PPh_3 ligands are located *trans* to each other, as expected, to reduce steric hindrance and the three chlorine atoms are meridional. The structure of **1** is similar to that of $TcCl_3(PPh_3)_2(CO)$ reported recently (18).

The bond distances and angles of crystal **1** are shown in Table 3. The distance Tc—Cl(1) (2.399(5) Å) is significantly longer than the Tc—Cl(2) (2.342(3) Å) distance, which could indicate that DMF has a high *trans* influence. In $TcCl_3(PPh_3)_2(CO)$, the Tc—Cl bond *trans* to CO is also longer (2.397(2) Å) than the other Tc—Cl bonds (2.322(2) Å) (18). The Tc—P are 2.496(5) and 2.499(5) Å, which are very similar to the values (2.46(1) to 2.48(1) Å) obtained for the two Tc—P bonds *trans* to each other in the two independent molecules of *mer*-$Tc(Me_2Ph)_3Cl_3$ (19), but slightly shorter than the value of 2.525(2) Å observed in $TcCl_3(PPh_3)_2(CO)$ (18). The distance Tc—O(1) is 2.115(12) Å. The angles around Tc are close to 90 and 180° except the angle Cl(2)—Tc—Cl(2)′ = 168.5(1)°. This angle is 169.43(8)° in $TcCl_3(PPh_3)_2(CO)$ (18). The P—C distances are normal and vary from 1.81(1) to 1.85(1) Å while the average C—C distance is 1.38(15) Å for the bonded PPh_3 and 1.40(25) Å for the lattice PPh_3. All the non-hydrogen atoms in DMF are coplanar as observed in other DMF compounds (20, 21) and the angles around N are close to 120°.

The crystal consists of layers of Tc complexes located at $b = \frac{1}{4}$ and $\frac{3}{4}$ and parallel to the *ac* plane, separated by the PPh_3 layers located at $b \approx 0$ and $\approx\frac{1}{2}$. The different layers are held together only by van der Waals forces.

Reaction in DMA

A Tc–DMA compound was expected when the reaction was studied in DMA. A larger quantity of acid was used to prevent slow decomposition of the product. We isolated some yellow crystals. The IR spectrum of the compound showed a ν(N–H) stretching band at 3125 cm^{-1}, a carbonyl band at 1671 cm^{-1}, and a broad ν(Tc–Cl) band at 315 cm^{-1}. The product was studied by crystallographic methods. The results have shown that it is a Tc(IV) compound identified as $NH_2(CH_3)_2^+DMAH^+$-

[2]The following tables are available: anisotropic temperature factors (Table S1), hydrogen coordinates (Table S2), bond distances and angles (Table S3), stereoscopic view of the unit cell in the crystal *mer*-$Tc(PPh_3)_2Cl_3(DMF) \cdot 2PPh_3$, stereoscopic view of the packing in the unit cell for the crystal $NH_2(CH_3)_2^+DMAH^+[TcCl_6]^{2-} \cdot PPh_3O$, and observed and calculated structure amplitudes (Table S4). The complete set of tables may be purchased from: The Depository of Unpublished Data, Document Delivery, CISTI, National Research Council Canada, Ottawa, Canada K1A 0S2.

Tables of hydrogen coordinates, bond distances and angles, and stereoscopic views of the unit cells have also been deposited with the Cambridge Crystallographic Data Centre and can be obtained on request from The Director, Cambridge Crystallographic Data Centre, University Chemical Laboratory, Lensfield Road, Cambridge, CB2 1EW, U.K.

Can. J. Chem. Downloaded from www.nrcresearchpress.com by 195.138.81.100 on 09/07/12
For personal use only.

TABLE 2. Refined coordinates and equivalent isotropic temperature factors ($\times 10^4$)[a]

Atom	x	y	z	U_{eq}
$Tc(PPh_3)_2Cl_3(DMF)\cdot 2PPh_3$				
Tc	4754(1)	2500	1687(1)	294
Cl(1)	6849(4)	2500	2844(4)	496
Cl(2)	4552(3)	3432(1)	1567(3)	604
P(1)	5457(4)	2500	−40(4)	384
P(2)	4005(4)	2500	3391(4)	383
P(3)	9545(3)	5633(2)	2207(3)	610
O	2913(10)	2500	653(10)	817
N	959(11)	2500	−397(11)	565
C(1)	4387(9)	3079(5)	4347(8)	359
C(2)	5414(10)	3378(5)	4387(10)	593
C(3)	5682(12)	3822(5)	5124(11)	782
C(4)	5013(12)	3956(5)	5799(10)	674
C(5)	4001(11)	3639(5)	5755(10)	644
C(6)	3705(10)	3219(5)	5059(9)	503
C(7)	2319(15)	2500	2884(12)	438
C(8)	1695(10)	2989(5)	2629(9)	523
C(9)	407(10)	2975(6)	2105(9)	670
C(10)	−233(16)	2500	1857(16)	879
C(11)	4087(14)	2500	−1261(12)	355
C(12)	3532(10)	2020(5)	−1684(10)	545
C(13)	2437(10)	2024(6)	−2518(10)	767
C(14)	1892(14)	2500	−2943(14)	859
C(15)	6368(9)	1928(5)	−274(9)	410
C(16)	7029(10)	1614(5)	626(10)	433
C(17)	7710(11)	1172(5)	430(11)	575
C(18)	7758(11)	1054(5)	−617(11)	667
C(19)	7125(12)	1371(6)	−1495(10)	801
C(20)	6418(10)	1793(5)	−1334(10)	560
C(21)	9914(9)	5999(4)	3542(10)	471
C(22)	10793(10)	6400(5)	3735(11)	619
C(23)	11112(12)	6698(5)	4679(12)	851
C(24)	10574(12)	6624(6)	5517(11)	877
C(25)	9694(13)	6229(6)	5360(11)	854
C(26)	9359(11)	5915(5)	4404(10)	612
C(27)	10747(11)	5111(5)	2488(11)	542
C(28)	10753(14)	4757(5)	1624(12)	847
C(29)	11770(15)	4388(6)	1714(15)	1111
C(30)	12712(15)	4384(5)	2739(16)	1216
C(31)	12638(13)	4723(6)	3666(16)	1183
C(32)	11706(11)	5079(5)	3568(12)	691
C(33)	8150(11)	5280(5)	2191(11)	659
C(34)	7046(12)	5471(6)	1533(13)	982
C(35)	5937(13)	5225(8)	1471(18)	1855
C(36)	5944(17)	4764(8)	2140(17)	1427
C(37)	6993(15)	4547(7)	2787(14)	1044
C(38)	8150(14)	4802(6)	2779(11)	1210
C(39)	2039(19)	2675(7)	184(19)	441
C(40A)	−16(21)	2869(10)	−903(21)	671
C(40B)	696(23)	1873(10)	−574(20)	627
$NH_2(CH_3)_2^+DMAH^+[TcCl_6]^{2-}\cdot PPh_3O$				
Tc	2505.9(6)	1816.3(4)	3684.0(3)	342
Cl(1)	410(2)	1318(1)	2497(1)	454
Cl(2)	3038(2)	3600(1)	3514(1)	564
Cl(3)	1970(2)	13(1)	3857(1)	523
Cl(4)	570(2)	1985(1)	4800(1)	534
Cl(5)	4407(2)	1652(1)	2601(1)	611
Cl(6)	4513(2)	2222(1)	4933(1)	568
P	8894(2)	2866(1)	9880(1)	331
O(1)	7679(7)	4545(4)	2069(3)	593
O(2)	8447(6)	3603(4)	10629(3)	476
N(1)	7539(7)	4823(5)	3590(4)	518
N(2)	2140(7)	382(5)	6193(4)	551
C(1)	8594(10)	3364(6)	2930(6)	617
C(2)	7928(8)	4262(5)	2866(4)	436
C(3)	6850(12)	5703(7)	3469(7)	761
C(4)	7682(13)	4577(9)	4557(5)	849
C(5)	3372(10)	−209(8)	6210(7)	746
C(6)	2281(12)	1248(7)	6993(6)	704
C(11)	11052(7)	3118(4)	9895(4)	346
C(12)	11881(8)	3093(5)	10716(4)	437
C(13)	13554(9)	3335(6)	10794(5)	515
C(14)	14437(8)	3588(6)	10020(5)	525
C(15)	13635(9)	3607(7)	9198(6)	633
C(16)	11955(8)	3370(6)	9118(5)	490
C(21)	8209(7)	3071(5)	8746(4)	354
C(22)	8165(9)	4070(6)	8649(4)	354
C(23)	7705(10)	4303(6)	7789(5)	584
C(24)	7329(11)	3537(7)	7031(5)	627
C(25)	7419(12)	2534(7)	7111(5)	713
C(26)	7817(10)	2285(5)	7974(5)	562
C(31)	8046(7)	1508(4)	10052(4)	356
C(32)	6954(7)	1284(5)	10747(4)	403
C(33)	6371(9)	253(6)	10925(5)	497
C(34)	6824(9)	−535(5)	10413(5)	523
C(35)	7897(9)	−330(5)	9712(5)	516
C(36)	8518(8)	696(5)	9539(4)	435

[a] $U_{eq} = \frac{1}{3}\Sigma_i\Sigma_j U_{ij} a_i^* a_j^* a_i \cdot a_j$.

$[TcCl_6]^{2-}\cdot PPh_3O$. The crystal contained a molecule of triphenylphosphine oxide, a protonated DMA cation, and finally a dimethylammonium cation. The DMA solvent reacted with HCl to produce dimethylamine and some organic carbonyl compound. Triphenylphosphine was oxidized to triphenylphosphine oxide from the reduction of Tc(VII) to Tc(IV) and (or) from the reaction with the carbonyl compound. This kind of oxidation is known in phosphorus chemistry (22). In this experiment, we had to use more acid than in the previous experiment with DMF, since there was decomposition in more dilute solution. The results of the magnetic susceptibility have shown a magnetic moment of 3.6 Bohr magnetons for 3 unpaired electrons, indicating a d^3 configuration for a Tc(IV) compound.

A labelled diagram of the compound $NH_2(CH_3)_2^+DMAH^+$-$[TcCl_6]^{2-}\cdot PPh_3O$ (crystal **2**) is shown in Fig. 2. The bond distances and angles are listed in Table 3. The Tc—Cl bond distances vary from 2.324(2) to 2.379(2) Å with *cis* angles of 88.34(7)–91.68(6)° and *trans* angles of 176.03(7)–179.94(7)°. The P—O(2) bond length is 1.492(5) Å and the average P—C distance is 1.800(6) Å. The angles around the P atom are close to the tetrahedral value (107.2(3)–111.2(3)°). The N(2)—C distances in the dimethylammonium cation are 1.49(1) Å. The bond distances and angles in protonated DMA are normal. All the non-hydrogen atoms are in a plane as expected because of the resonance in the N—C—O segment. The deviations from the best plane are O(1), 0.013(6); N(1), −0.020(6); C(1), −0.002(9); C(2), −0.006(7); C(3), 0.000(10); and C(4), 0.015(11) Å. The angles are also close to 120°. We were able to see the proton on the DMA molecule, which was located at 1.02 Å from O(1) (of DMA) and at 1.48 Å from O(2) of triphenylphosphine oxide. The short distance O(1)···O(2) (2.481(7) Å) clearly indicates hydrogen bonding between the two O atoms. The angles are O(1)—H···O(2) = 168.2 and

Can. J. Chem. Downloaded from www.nrcresearchpress.com by 195.138.81.100 on 09/07/12
For personal use only.

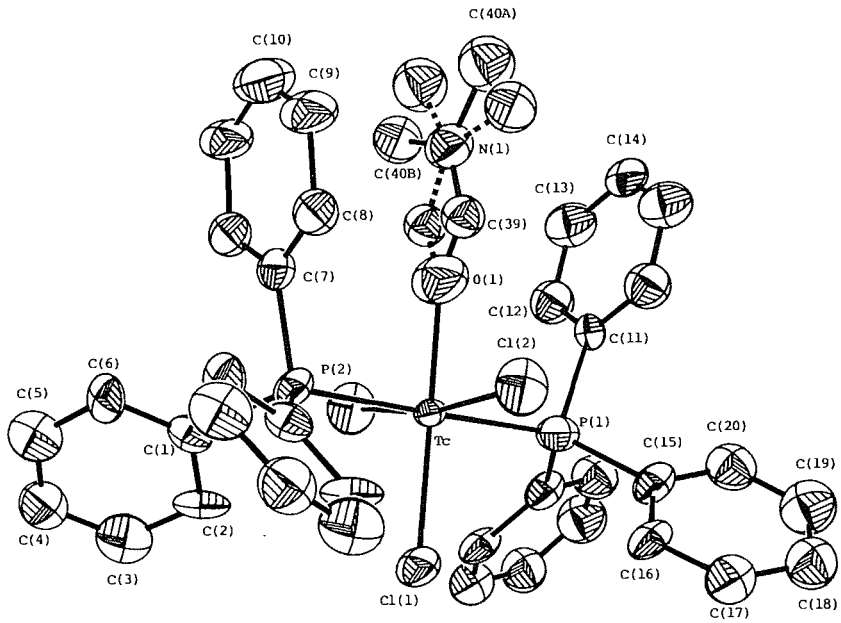


FIG. 1. Labelled diagram of *mer*-$Tc(PPh_3)_2Cl_3(DMF)$.

TABLE 3. Selected bond distances (Å) and angles (°)

$Tc(PPh_3)_2Cl_3(DMF)\cdot 2PPh_3$

Tc—Cl(1)	2.399(5)	Tc—Cl(2)	2.342(3)	Tc—P(1)	2.496(5)
Tc—P(2)	2.499(5)	Tc—O	2.115(12)	P(1)—C(11)	1.83(2)
P(1)—C(15)	1.84(1)	P(2)—C(1)	1.84(1)	P(2)—C(7)	1.84(2)
P(3)—C(21)	1.83(1)	P(3)—C(27)	1.85(1)	P(3)—C(33)	1.81(1)
O—C(39)	1.09(1)	C(39)—N	1.31(1)	N—C(40A)	1.44(3)
N—C(40B)	1.59(2)				
Cl(1)—Tc—Cl(2)	95.7(1)	Cl(2)—Tc—Cl(2)′	168.5(1)	Cl(1)—Tc—P(1)	90.0(1)
Cl(1)—Tc—P(2)	91.2(1)	Cl(1)—Tc—O	179.4(3)	Cl(2)—Tc—P(1)	89.8(1)
Cl(2)—Tc—P(2)	90.1(1)	Cl(2)—Tc—O	84.3(3)	P(1)—Tc—P(2)	178.8(1)
P(1)—Tc—O	89.4(2)	P(2)—Tc—O	89.4(3)	Tc—P(1)—C(11)	107.5(4)
Tc—P(1)—C(15)	118.2(4)	Tc—P(2)—C(1)	118.0(4)	Tc—P(2)—C(7)	107.0(4)
P(1)—C(11)—C(12)	119.8(9)	P(1)—C(15)—C(16)	120.7(8)	P(1)—C(15)—C(20)	121.6(9)
P(2)—C(1)—C(2)	119.3(8)	P(2)—C(1)—C(6)	122.7(8)	P(2)—C(7)—C(8)	119.2(9)
P(3)—C(21)—C(22)	118.7(9)	P(3)—C(21)—C(26)	125.2(9)	P(3)—C(27)—C(28)	118.3(10)
P(3)—C(27)—C(32)	121.7(9)	P(3)—C(33)—C(34)	119.2(10)	P(3)—C(33)—C(38)	122.8(10)
Tc—O—C(39)	156.2(8)	O—C(39)—N	136.7(7)	C(39)—N—C(40A)	121(1)
C(39)—N—C(40B)	121(1)	C(40A)—N—C(40B)	119(2)		

$NH_2(CH_3)_2^+ DMAH^+ [TcCl_6]^{2-}\cdot PPh_3O$

Tc—Cl(1)	2.348(2)	Tc—Cl(2)	2.335(2)	Tc—Cl(3)	2.361(2)
Tc—Cl(4)	2.379(2)	Tc—Cl(5)	2.324(2)	Tc—Cl(6)	2.366(2)
N(2)—C(5)	1.49(1)	N(2)—C(6)	1.49(1)	C(2)—O(1)	1.285(8)
C(1)—C(2)	1.48(1)	C(2)—N(1)	1.307(9)	N(1)—C(3)	1.48(1)
N(1)—C(4)	1.48(1)	P—O(2)	1.492(5)	P—C(11)	1.795(7)
P—C(21)	1.804(6)	P—C(31)	1.801(6)		
Cl(1)—Tc—Cl(2)	91.68(6)	Cl(1)—Tc—Cl(3)	88.38(6)	Cl(1)—Tc—Cl(4)	88.76(6)
Cl(1)—Tc—Cl(5)	91.56(7)	Cl(1)—Tc—Cl(6)	176.03(7)	Cl(2)—Tc—Cl(3)	179.94(7)
Cl(2)—Tc—Cl(4)	90.64(7)	Cl(2)—Tc—Cl(5)	89.45(7)	Cl(2)—Tc—Cl(6)	91.61(7)
Cl(3)—Tc—Cl(4)	89.37(6)	Cl(3)—Tc—Cl(5)	90.55(7)	Cl(3)—Tc—Cl(6)	88.34(7)
Cl(4)—Tc—Cl(5)	179.66(7)	Cl(4)—Tc—Cl(6)	88.97(7)	Cl(5)—Tc—Cl(6)	90.70(7)
C(5)—N(2)—C(6)	116.0(7)	O(1)—C(2)—C(1)	121.2(6)	O(1)—C(2)—N(1)	114.8(6)
C(1)—C(2)—N(1)	124.0(6)	C(2)—N(1)—C(3)	121.0(6)	C(2)—N(1)—C(4)	121.9(7)
C(3)—N(1)—C(4)	117.1(7)	O(2)—P—C(11)	110.6(3)	O(2)—P—C(21)	109.5(3)
O(2)—P—C(31)	111.2(3)	C(11)—P—C(21)	107.8(3)	C(11)—P—C(31)	107.2(3)
C(21)—P—C(31)	110.4(3)	P—C(11)—C(12)	118.8(5)	P—C(11)—C(16)	123.4(5)
P—C(21)—C(22)	117.2(5)	P—C(21)—C(26)	123.2(5)	P—C(31)—C(32)	118.6(5)
P—C(31)—C(36)	121.4(5)				

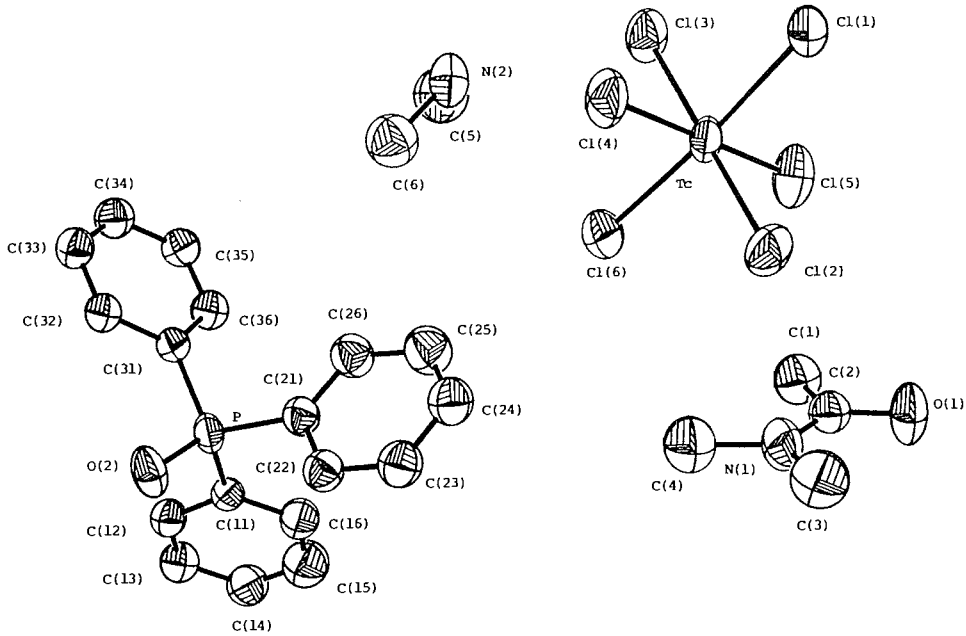


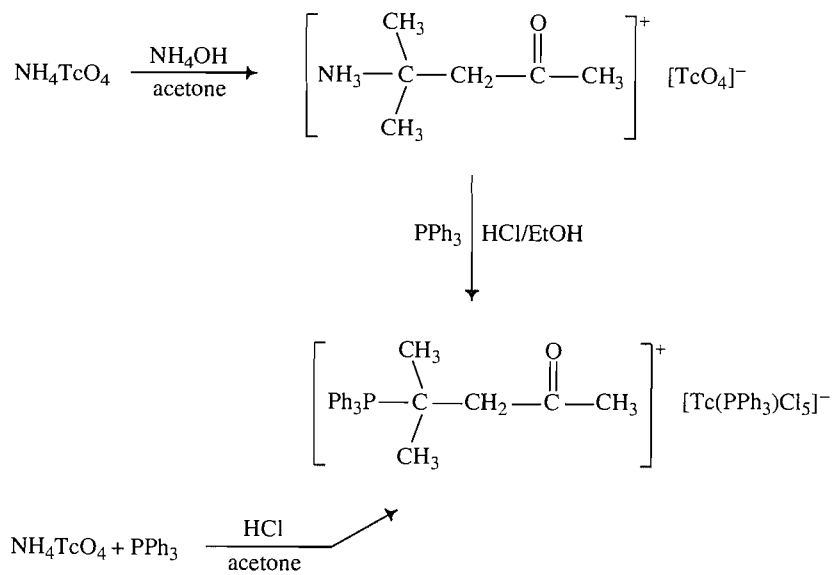
FIG. 2. Labelled diagram of $NH_2(CH_3)_2^+DMAH^+[TcCl_6]^{2-}\cdot PPh_3O$.

C(2)—O(1)···O(2) = 118.8(4)°. The structure is also stabilized by hydrogen bonding between the dimethylammonium cation and the chloride ligands with four distances N(2)···Cl ranging from 3.327(6) to 3.468(7) Å and H···Cl from 2.640 and 2.819 Å, slightly shorter than the sum of the van der Waals radii. The angles N(2)—H···Cl vary from 133.6 to 138.0°.

Reaction in acetone

The reaction of ammonium pertechnetate with triphenylphosphine in acidic acetone produced two compounds, a yellow powder in a low yield (≈15%) and some orange crystals in ≈65% yield. The IR spectra of the two compounds were clearly very different. The yellow compound showed a broad stretching ν(Tc–Cl) vibration at 318 cm^{-1}. The results of the elemental analysis have shown that it was the $(PPh_3H)_2[TcCl_6]$ ionic compound, which has already been reported by Bandoli, Clemente, Mazzi, and Roncari (11). These authors synthesized their compound by refluxing $[AsPh_4][TcO_4]$ with PPh_3 in ethanol and HCl.

The IR spectrum of the orange crystals showed a ν(C=O) band at 1718 cm^{-1}, and two ν(Tc–Cl) bands at 292 and 326 cm^{-1} with shoulders at 336 and 345 cm^{-1}. To identify the compound, the orange crystals were studied by X-ray diffraction methods. The results have shown that it is an ionic compound with $[Tc(PPh_3)Cl_5]^-$ as anion and a surprising cation $[Ph_3P\text{-}C(CH_3)_2\text{-}CH_2\text{-}CO\text{-}CH_3]^+$ produced from the reaction of PPh_3 with acetone in acid medium. The magnetic moment of 4.06 BM confirmed the d^3 configuration of Tc(IV) with three unpaired electrons. The crystal structure of this compound has been published by Bandoli *et al.* (11) who synthesized this compound by the following method:



Can. J. Chem. Downloaded from www.nrcresearchpress.com by 195.138.81.100 on 09/07/12
For personal use only.

The authors isolated and characterized the intermediate compound $[NH_3\text{-}C(CH_3)_2\text{-}CH_2\text{-}CO\text{-}CH_3]^+[TcO_4]^-$, which in the presence of PPh_3 in acetone produced $[PPh_3C(CH_3)_2\text{-}CH_2\text{-}CO\text{-}CH_3]^+[Tc(PPh_3)Cl_5]^-$. We were able to prepare the same final product without the presence of NH_4OH, just by refluxing ammonium pertechnetate with PPh_3 for 15 min in acidic acetone.

Acknowledgement

The authors are grateful to the Medical Research Council of Canada for financial support.

1. M. J. CLARKE and L. PODBIELSKI. Coord. Chem. Rev. **78**, 253 (1987).
2. A. G. JONES, M. J. ABRAMS, A. DAVISON, J. W. BRODACK, A. K. TOOTHAKER, S. J. ADELSTEIN, and A. I. KASSIS. Int. J. Nucl. Med. Biol. **11**, 225 (1984).
3. B. L. HOLMA, A. G. JONES, J. LISTER-JAMES, A. DAVISON, M. J. ABRAMS, J. M. KIRSHENBAUM, S. S. TUMEH, and R. J. ENGLISH. J. Nucl. Med. **25**, 1350 (1984).
4. J. L. VANDERHEYDEN, K. LIBSON, D. L. NOSCO, A. R. KETRING, and E. DEUTSCH. Int. J. Appl. Radiat. Isot. **34**, 1611 (1983).
5. E. DEUTSCH, W. BUSHONG, K. A. GLAVEN, R. C. ELDER, V. J. SODD, K. L. SCHOLZ, S. J. FORTMAN, and S. J. LUKES. Science, **214**, 85 (1981).
6. E. DEUTSCH, K. A. GLAVAN, W. BUSHONG, and V. J. SODD. Appl. Nucl. Radiochem. 139 (1982).
7. M. J. ABRAMS, A. DAVISON, A. G. JONES, C. E. COSTELLO, and H. PANG. Inorg. Chem. **22**, 2798 (1983).
8. B. L. HOLMAN, A. G. JONES, J. LISTERR-JAMES, A. DAVISON, M. J. ABRAMS, J. M. KIRSHENBAUM, S. S. TUMEH, and R. J. ENGLISH. J. Nucl. Med. **25**, 1350 (1984).
9. U. MAZZI, G. DE PAOLI, P. DI BERNADO, and L. MAGON. J. Inorg. Nucl. Chem. **38**, 721 (1976).
10. K. LIBSON, B. L. BARNETT, and E. DEUTSCH. Inorg. Chem. **22**, 1695 (1983).
11. G. BANDOLI, D. A. CLEMENTE, U. MAZZI, and E. RONCARI. J. Chem. Soc. Dalton Trans. 1381 (1982).
12. R. MELANSON and F. D. ROCHON. Can. J. Chem. **53**, 2371 (1975).
13. D. T. CROMER. Acta Crystallogr. **18**, 17 (1965).
14. P. COPPENS and W. HAMILTON. Acta Crystallogr. Sect. A: Cryst. Phys. Diffr. Theor. Gen. Crystallogr. **A26**, 71 (1970).
15. W. T. CROMER and J. T. WABER. Acta Crystallogr. **18**, 104 (1965).
16. R. F. STEWART, E. R. DAVIDSON, and W. T. SIMPSON. J. Chem. Phys. **42**, 3175 (1965).
17. U. MAZZI, A. BISMONDO, N. KOTSEV, and D. A. CLEMENTE. J. Organomet. Chem. **135**, 177 (1977).
18. R. M. PEARLSTEIN, W. M. DAVIS, A. G. JONES, and A. DAVISON. Inorg. Chem. **28**, 3332 (1989).
19. G. BANDOLI, D. A. CLEMENTE, and U. MAZZI. J. Chem. Soc. Dalton Trans. 125 (1976).
20. F. D. ROCHON, P. C. KONG, and R. MELANSON. Can. J. Chem. **61**, 1823 (1983).
21. F. D. ROCHON, P. C. KONG, and R. MELANSON. Can. J. Chem. **58**, 97 (1980).
22. G. M. KOSOLAPOFF and L. MAIER. Organic phosphorus compounds. Vol. 3. Wiley–Interscience, New York. Chap. 6. p. 341.

Can. J. Chem. Downloaded from www.nrcresearchpress.com by 195.138.81.100 on 09/07/12
For personal use only.

Dibenzo-15-crown-5 ether and its sodium thiocyanate complex. X-ray crystallographic and NMR studies in the solid phase and in solution

G. W. BUCHANAN,[1] S. MATHIAS, AND Y. LEAR

Ottawa–Carleton Chemistry Institute, Department of Chemistry, Carleton University, Ottawa, Ont., Canada K1A 5B6

AND

C. BENSIMON

Division of Chemistry, National Research Council of Canada, Ottawa, Ont., Canada K1A 0R9

Received June 22, 1990

G. W. BUCHANAN, S. MATHIAS, Y. LEAR, and C. BENSIMON. Can. J. Chem. **69**, 404 (1991).

For the title systems, single crystal X-ray data indicate the presence of totally asymmetric structures. These features are reflected in the multiplicity of resonances in the solid phase ^{13}C NMR spectra. Some of the ^{13}C chemical shift trends are analyzed in terms of torsional angle influences. In solution, resonance assignments have been made with the aid of 2D methods. Stereochemical inferences are drawn from NOESY spectra and ^{1}H–^{1}H couplings. Low temperature solution experiments indicate that conformational interconversions in both the free ligand and the NaNCS complex are rapid on the NMR timescale down to 163 K.

Key words: crown ethers, NMR, stereochemistry.

G. W. BUCHANAN, S. MATHIAS, Y. LEAR et C. BENSIMON. Can. J. Chem. **69**, 404 (1991).

Pour les systèmes mentionnés dans le titre, les données de la diffraction des rayons-X par un cristal unique indiquent la présence de structures totalement asymétriques. La multiplicité des bandes de résonance dans les spectres RMN du ^{13}C, en phase solide, est le reflet de ces caractéristiques structurales. On a analysé quelques unes des tendances observées dans les déplacements chimiques du ^{13}C en fonction des influences des angles de torsion. En solution, on a fait les attributions des résonances à l'aide de méthodes en 2D. On a tiré des déductions stéréochimiques à partir des spectres COSY et des couplages ^{1}H–^{1}H. Des expériences en solution, à basses températures, indiquent que, jusqu'à 163 K, les interconversions conformationnelles, tant dans le ligand libre que dans le complexe NaNCS, sont rapides à l'échelle de temps de la RMN.

Mots clés : éthers couronne, RMN, stéréochimie.

[Traduit par la rédaction]

Introduction

The 15-crown-5 ether system is of interest because its cavity size (effective radius 1.35 Å) is most suited for complexation of the sodium ion. The original pioneering work of Pedersen (1) described the synthesis of benzo-15-crown-5 and subsequently a series of articles have appeared dealing with the crystal structure (2) and complexation features of this molecule (3–9), as well as 15-crown-5 ether itself (10–14). Also the solid phase ^{13}C NMR features of benzo-15-crown-5 have been reported (15).

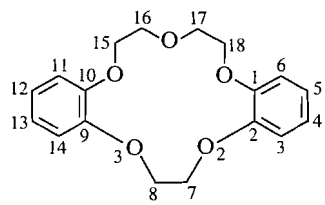
In view of our interest in the dynamic stereochemistry of related systems (16–18), we present herein the preparation of dibenzo-15-crown-5 ether and its NaNCS complex as well as the characterization of their stereochemical features in the solid phase and in solution using X-ray and NMR methods.

Results and discussion

Figure 1 contains the structural formulae and numbering schemes. Bond lengths and angles are listed in Table 1, while torsional angles involving ring skeletal atoms are provided in Table 2. ORTEP diagrams are presented in Fig. 2 while Fig. 3 shows the ^{13}C solid phase NMR spectra. The ^{13}C chemical shifts are collected in Table 3 while the crystallographic data are in Table 4 and the atomic parameters in Table 5.

(i) Dibenzo-15-crown-5 ether (1)

In solution, the ^{13}C NMR of **1** shows nine resonances (down to 163 K) consistent with its symmetry properties and rapid conformational interchange in the central macrocyclic ring on the NMR timescale for this temperature range. The 200 MHz



1

2 ≡ **1**·NaNCS

FIG. 1. Structure and numbering scheme.

^{1}H spectrum shows a complex multiplet centered at δ 6.95 ppm (aromatics), a sharp singlet at δ 4.33 ppm (H-7,8), and multiplets centered at δ 4.16 and 3.89 ppm respectively. A ^{1}H–^{1}H NOESY experiment showed a correlation between the aromatics and the multiplet centered at 4.16 ppm, thereby indicating that these latter protons must be those on the C-15 and C-18 sites. As expected, there was also a NOESY correlation between the aromatics and the singlet at 4.33 ppm due to cross relaxation between protons on C-3 and C-14 with those on C-7 and C-8 respectively.

In the case of C-15, 16, 17, and 18 the geminal protons on each of these carbons are magnetically nonequivalent. Rapid conformational exchange in the 15-membered ring at room temperature results in each member of a geminal pair having the same chemical shift. From a spin coupling viewpoint, however, each member of a geminal pair is unique and hence the occurrence of magnetic nonequivalence (19, 20). As a result a complex multiplet is observed for the four protons on C-15 and C-16 (and by symmetry on C-17 and C-18), which must be analyzed as an AA′XX′ spin system. Such analysis was done using the LAME program (21). Tables 6 and 7 contain ^{1}H data.

[1]Author to whom correspondence may be addressed.

Can. J. Chem. Downloaded from www.nrcresearchpress.com by 198.100.157.202 on 09/07/12
For personal use only.

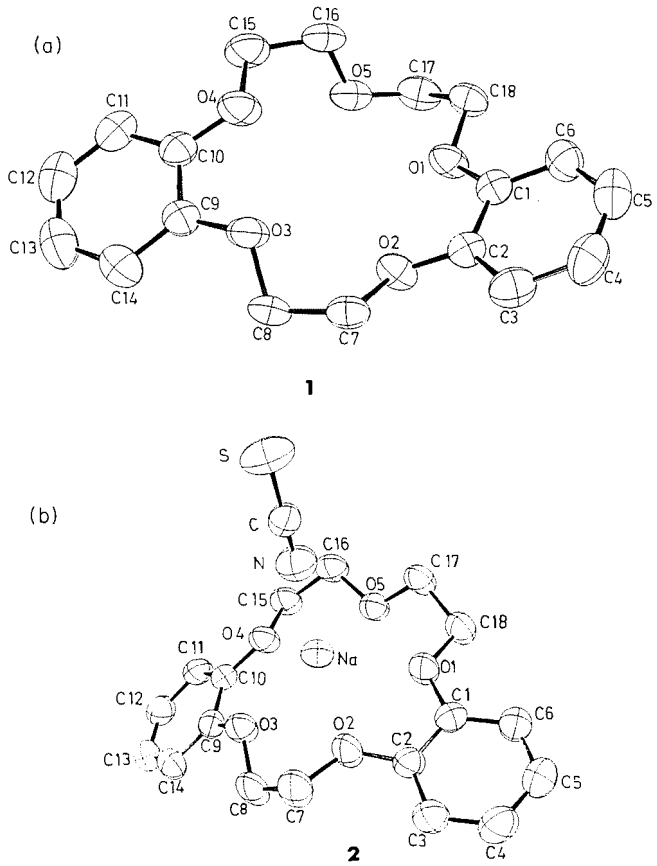


FIG. 2. ORTEP diagrams.

The nine ^{13}C signals observed for **1** at room temperature in solution can be assigned via a combination of methods with limitations as specified. The aromatic region consists of three closely spaced pairs of resonances near 149, 121, and 115 ppm. By analogy with results on related materials (16, 18), the carbons bearing oxygen will be the most deshielded and appear near 149 ppm. The *ortho* sites (C-3, 6, 11, and 14) will be the most shielded and appear near 115 ppm.

For the methylene carbons, unambiguous assignment of the C-7,8 pair to the resonance at 68.38 ppm was made via the one-bond ^{1}H–^{13}C heteronuclear correlation (HETCOR) experiment. Due to their almost identical chemical shifts (69.76 and 69.80 ppm), the C-15,18 vs. C-16,17 pairs could not be distinguished.

Notably, there are *six* clearly resolvable methylene carbon resonances for **1** in the solid state ^{13}C NMR spectrum. This is consistent with the absence of any molecular symmetry elements in the X-ray crystallographic structure. Furthermore, there is a remarkably large range of chemical shifts in the solid for these carbons (8.7 ppm) vs. 1.4 ppm in solution. In view of this, it is instructive to examine the torsional environments of the methylene carbons in the crystal structure as presented in Table 6. Ignoring hydrogens, the C-16 and C-17 sites are involved in four such networks, while the C-7,8 and C-15,18 sites are present in five.

In the attempt to assign resonances in the solid state spectrum to particular carbons, comparison will be made between the torsional environments for pairs of carbons, which are rendered equivalent in solution via conformational averaging. Such averaging is absent in the solid, and hence the steric influences may be more readily apparent in the observed chemical shifts. The basic tenets for the analysis have been presented earlier (16) and involve the known dihedral angle dependence of the γ-steric shift in ^{13}C NMR (22). Generally, carbons situated in a γ-*gauche* relation or bearing such substituents will be shielded by ca. 5 ppm relative to counterparts in γ-*trans* orientations. Also there is a tendency to maximum shielding for *cis* coplanar networks (23) with maximum deshielding for a dihedral angle of 120°.[2]

Comparison of the torsional networks for C-15 vs. C-18 reveals important differences, which would be expected to lead to increased shielding for the C-18 site. For the O—C*—C—O network, the angle for C-18 is 51.5°, whereas that for C-15 has expanded to 70.3°. Most important, however, is the difference in the C—O—C—C* network, where C-15 is involved in an essentially *trans* interaction with C-17 whereas C-18 bears a *gauche* type relation to C-16. Hence one can make a strong case for the attribution of the most shielded resonance at 61.88 ppm to C-18 and that for C-15 to the most deshielded line at 70.59 ppm.

Regarding the C-7 and C-8 sites, data in Table 8 show that their respective torsional environments are quite similar, with offsetting differences present in the dihedral angles in the C—O—C*—C and C—O—C—C* networks. Accordingly we expect these carbons to have nearly identical chemical shifts in the solid, and we assign the resonances at 66.90 and 67.36 ppm to these carbons.

For the remaining C-16 and C-17 methylene carbons, the most significant difference in their torsional environments appears to be the contraction of the O—C—C—O dihedral angle to 51.5° in the case of C-17 in contrast to the value of 70.3° for C-16. Such a contraction should lead to increased shielding at C-17 (23 and footnote 2) and hence we attribute the line at 65.25 ppm to C-17 and that at 68.75 ppm to C-16. Of course all these assignments await unambiguous confirmation, perhaps via ^{13}C–^{13}C INADEQUATE experiments as recently reported for the plastic crystal camphor (24). It may, however, be necessary to synthesize **1** with ^{13}C enrichment to enhance the connectivities in the two-dimensional solid phase experiment. The feasibility of such experiments using ^{29}Si enriched zeolites has been demonstrated recently (25) and the techniques applied to natural abundance samples (26).

In the aromatic region of the solid phase ^{13}C spectrum the effect of nonaveraged conformations is also evident in the increased multiplicity of resonances relative to the solution spectrum. Based on the torsional angle arguments presented above, C-6 is expected to be the most shielded *ortho* aromatic carbon (at 111.11 ppm), since it is nearly coplanar ($\theta = 6.5°$) to C-18.

The spatial disposition of the oxygen lone pairs will also affect the electron density and hence the chemical shift of the nonoxygenated aromatic carbons. The optimal geometry for conjugative electron release will be that in which the lone pairs occupy orbitals that are perpendicular to the plane of the aromatic ring. As a result, the lone pairs on O-1, for example, will influence the electronic environment at the *ortho* carbon (C-6) and the *para* carbon C-4. From the X-ray data, the lone pair orientations can be determined for each oxygen and the values of the angles between these orbitals and the plane of the aromatic ring obtained. Results are as follows, using θ_1 and θ_2 for the two lone pairs on each oxygen respectively. For O-1,

[2]G. W. Buchanan, R. A. Kirby, and J. S. Tse. Unpublished observations.

Can. J. Chem. Downloaded from www.nrcresearchpress.com by 198.100.157.202 on 09/07/12
For personal use only.

Can. J. Chem. Downloaded from www.nrcresearchpress.com by 198.100.157.202 on 09/07/12
For personal use only.

TABLE 1. (*a*) Atomic bond lengths (Å) for compound **1**

O(1)—C(1)	1.372(4)	C(8)—H(8A)	0.99(3)
O(1)—C(18)	1.428(4)	C(8)—H(8B)	1.00(3)
O(2)—C(2)	1.363(4)	C(9)—C(10)	1.404(5)
O(2)—C(7)	1.439(4)	C(9)—C(14)	1.367(5)
O(3)—C(8)	1.425(4)	C(10)—C(11)	1.375(5)
O(3)—C(9)	1.366(4)	C(11)—C(12)	1.380(7)
O(4)—C(10)	1.362(4)	C(11)—H(11)	0.98(4)
O(4)—C(15)	1.441(5)	C(12)—C(13)	1.362(8)
O(5)—C(16)	1.426(5)	C(12)—H(12)	0.98(3)
O(5)—C(17)	1.403(5)	C(13)—C(14)	1.386(6)
C(1)—C(2)	1.402(5)	C(13)—H(13)	0.98(3)
C(1)—C(6)	1.374(5)	C(14)—H(14)	0.93(3)
C(2)—C(3)	1.383(5)	C(15)—C(16)	1.487(6)
C(3)—C(4)	1.378(6)	C(15)—H(15A)	0.96(3)
C(3)—H(3)	0.90(3)	C(15)—H(15B)	1.05(4)
C(4)—C(5)	1.366(7)	C(16)—H(16A)	1.02(3)
C(4)—H(4)	0.97(3)	C(16)—H(16B)	1.02(3)
C(5)—C(6)	1.390(6)	C(17)—C(18)	1.506(6)
C(5)—H(5)	0.97(3)	C(17)—H(17A)	0.97(3)
C(6)—H(6)	0.95(3)	C(17)—H(17B)	1.01(3)
C(7)—C(8)	1.490(5)	C(18)—H(18A)	0.98(4)
C(7)—H(7A)	1.03(3)	C(18)—H(18B)	1.12(3)
C(7)—H(7B)	0.99(3)		

(*b*) Atomic bond lengths (Å) for compound **2**

Na—N	2.3028(23)	C(7)—C(8)	1.462(4)
Na—O(1)	2.3260(16)	C(7)—H(7A)	0.95(3)
Na—O(2)	2.3883(17)	C(7)—H(7B)	1.10(3)
Na—O(3)	2.3520(17)	C(8)—H(8A)	0.93(3)
Na—O(4)	2.3552(17)	C(8)—H(8B)	1.04(3)
Na—O(5)	2.5009(16)	C(9)—C(10)	1.391(3)
S—C(19)	1.617(3)	C(9)—C(14)	1.375(3)
N—C(19)	1.147(3)	C(10)—C(11)	1.370(3)
O(1)—C(1)	1.372(3)	C(11)—C(12)	1.381(4)
O(1)—C(18)	1.438(3)	C(11)—H(11)	0.956(22)
O(2)—C(2)	1.380(3)	C(12)—C(13)	1.360(4)
O(2)—C(7)	1.439(3)	C(12)—H(12)	0.936(25)
O(3)—C(8)	1.418(3)	C(13)—C(14)	1.389(4)
O(3)—C(9)	1.375(3)	C(13)—H(13)	1.04(3)
O(4)—C(10)	1.370(3)	C(14)—H(14)	0.945(25)
O(4)—C(15)	1.433(3)	C(15)—C(16)	1.500(4)
O(5)—C(16)	1.424(3)	C(15)—H(15A)	0.930(23)
O(5)—C(17)	1.424(3)	C(15)—H(15B)	1.033(24)
C(1)—C(2)	1.398(3)	C(16)—H(16A)	0.979(23)
C(1)—C(6)	1.376(3)	C(16)—H(16B)	1.005(22)
C(2)—C(3)	1.377(3)	C(17)—C(18)	1.492(4)
C(3)—C(4)	1.382(4)	C(17)—H(17A)	0.946(24)
C(3)—H(3)	0.915(23)	C(17)—H(17B)	0.964(23)
C(4)—C(5)	1.375(4)	C(18)—H(18A)	1.010(22)
C(4)—H(4)	1.023(23)	C(18)—H(18B)	0.980(22)
C(5)—C(6)	1.391(4)		
C(5)—H(5)	1.021(23)		
C(6)—H(6)	0.980(25)		

(*c*) Bond angles (deg) for compound **1**

C(1)—O(1)—C(18)	118.6(3)	O(4)—C(10)—C(11)	126.0(4)
C(2)—O(2)—C(7)	117.12(24)	C(9)—C(10)—C(11)	119.6(4)
C(8)—O(3)—C(9)	118.7(3)	C(10)—C(11)—C(12)	120.2(4)
C(10)—O(4)—C(15)	119.2(3)	C(10)—C(11)—H(11)	118.8(21)
C(16)—O(5)—C(17)	115.1(3)	C(12)—C(11)—H(11)	121.0(21)
O(1)—C(1)—C(2)	114.4(3)	C(11)—C(12)—C(13)	120.2(4)
O(1)—C(1)—C(6)	125.5(3)	C(11)—C(12)—H(12)	120.6(20)
C(2)—C(1)—C(6)	120.1(3)	C(13)—C(12)—H(12)	119.1(19)

TABLE 1 (*continued*)

O(2)—C(2)—C(1)	116.4(3)	C(12)—C(13)—C(14)	120.2(4)
O(2)—C(2)—C(3)	124.7(3)	C(12)—C(13)—H(13)	120.8(19)
C(1)—C(2)—C(3)	118.9(3)	C(14)—C(13)—H(13)	119.0(19)
C(2)—C(3)—C(4)	120.6(4)	C(9)—C(14)—C(13)	120.3(4)
C(2)—C(3)—H(3)	115.6(19)	C(9)—C(14)—H(14)	121.2(18)
C(4)—C(3)—H(3)	123.8(19)	C(13)—C(14)—H(14)	118.5(18)
C(3)—C(4)—C(5)	120.3(4)	O(4)—C(15)—C(16)	106.6(3)
C(3)—C(4)—H(4)	119.1(19)	O(4)—C(15)—H(15A)	108.7(20)
C(5)—C(4)—H(4)	120.6(19)	O(4)—C(15)—H(15B)	106.1(19)
C(4)—C(5)—C(6)	120.1(4)	C(16)—C(15)—H(15A)	113.3(19)
C(4)—C(5)—H(5)	119.8(18)	C(16)—C(15)—H(15B)	115.4(18)
C(6)—C(5)—H(5)	120.1(18)	H(15A)—C(15)—H(15B)	106(3)
C(1)—C(6)—C(5)	120.0(4)	O(5)—C(16)—C(15)	106.8(4)
C(1)—C(6)—H(6)	120.3(17)	O(5)—C(16)—H(16A)	110.5(16)
C(5)—C(6)—H(6)	119.7(17)	O(5)—C(16)—H(16B)	107.7(17)
O(2)—C(7)—C(8)	107.9(3)	C(15)—C(16)—H(16A)	109.1(15)
O(2)—C(7)—H(7A)	108.3(15)	C(15)—C(16)—H(16B)	112.3(16)
O(2)—C(7)—H(7B)	110.7(15)	H(16A)—C(16)—H(16B)	110.3(23)
C(8)—C(7)—H(7A)	110.9(15)	O(5)—C(17)—C(18)	116.4(3)
C(8)—C(7)—H(7B)	109.2(15)	O(5)—C(17)—H(17A)	110.7(18)
H(7A)—C(7)—H(7B)	109.7(22)	O(5)—C(17)—H(17B)	106.4(17)
O(3)—C(8)—C(7)	107.6(3)	C(18)—C(17)—H(17A)	107.9(19)
O(3)—C(8)—H(8A)	110.3(17)	C(18)—C(17)—H(17B)	104.7(17)
O(3)—C(8)—H(8B)	108.5(17)	H(17A)—C(17)—H(17B)	110(3)
C(7)—C(8)—H(8A)	112.6(16)	O(1)—C(18)—C(17)	107.1(3)
C(7)—C(8)—H(8B)	111.5(16)	O(1)—C(18)—H(18A)	110.3(18)
H(8A)—C(8)—H(8B)	106.3(24)	O(1)—C(18)—H(18B)	109.4(16)
O(3)—C(9)—C(10)	115.2(3)	C(17)—C(18)—H(18A)	111.6(17)
O(3)—C(9)—C(14)	125.4(3)	C(17)—C(18)—H(18B)	111.4(16)
C(10)—C(9)—C(14)	119.5(3)	H(18A)—C(18)—H(18B)	107.1(22)
O(4)—C(10)—C(9)	114.5(3)		

(*d*) Bond angles (deg) for compound **2**

N—Na—O(1)	102.43(7)	H(7A)—C(7)—H(7B)	112.8(21)
N—Na—O(2)	120.95(7)	O(3)—C(8)—C(7)	108.96(23)
N—Na—O(3)	125.47(8)	O(3)—C(8)—H(8A)	107.9(15)
N—Na—O(4)	104.79(7)	O(3)—C(8)—H(8B)	95.9(19)
N—Na—O(5)	96.39(7)	C(7)—C(8)—H(8A)	114.2(15)
O(1)—Na—O(2)	66.93(5)	C(7)—C(8)—H(8B)	111.7(19)
O(1)—Na—O(3)	126.56(6)	H(8A)—C(8)—H(8B)	116.2(23)
O(1)—Na—O(4)	128.38(6)	O(3)—C(9)—C(10)	114.17(19)
O(1)—Na—O(5)	67.63(5)	O(3)—C(9)—C(14)	125.70(21)
O(2)—Na—O(3)	68.62(6)	C(10)—C(9)—C(14)	120.11(22)
O(2)—Na—O(4)	127.83(6)	O(4)—C(10)—C(9)	114.37(19)
O(2)—Na—O(5)	125.75(6)	O(4)—C(10)—C(11)	125.41(21)
O(3)—Na—O(4)	64.79(5)	C(9)—C(10)—C(11)	120.21(21)
O(3)—Na—O(5)	121.56(6)	C(10)—C(11)—C(12)	119.41(25)
O(4)—Na—O(5)	66.43(5)	C(10)—C(11)—H(11)	120.7(13)
Na—Na—C(19)	170.51(19)	C(12)—C(11)—H(11)	119.9(13)
Na—O(1)—C(1)	122.00(12)	C(11)—C(12)—C(13)	120.7(3)
Na—O(1)—C(18)	118.32(13)	C(11)—C(12)—H(12)	117.1(15)
C(1)—O(1)—C(18)	117.74(17)	C(13)—C(12)—H(12)	122.2(15)
Na—O(2)—C(2)	119.10(12)	C(12)—C(13)—C(14)	120.5(3)
Na—O(2)—C(7)	116.15(14)	C(12)—C(13)—H(13)	124.2(13)
C(2)—O(2)—C(7)	116.71(18)	C(14)—C(13)—H(13)	115.3(13)
Na—O(3)—C(8)	112.29(16)	C(9)—C(14)—C(13)	119.1(3)
Na—O(3)—C(9)	121.62(13)	C(9)—C(14)—H(14)	120.2(14)
C(8)—O(3)—C(9)	122.61(18)	C(13)—C(14)—H(14)	120.6(14)
Na—O(4)—C(10)	122.11(13)	O(4)—C(15)—C(16)	105.73(20)
Na—O(4)—C(15)	118.58(13)	O(4)—C(15)—H(15A)	113.4(14)
C(10)—O(4)—C(15)	119.31(17)	O(4)—C(15)—H(15B)	107.5(12)
Na—O(5)—C(16)	97.88(13)	C(16)—C(15)—H(15A)	111.0(14)
Na—O(5)—C(17)	98.24(14)	C(16)—C(15)—H(15B)	114.7(12)
C(16)—O(5)—C(17)	113.48(18)	H(15A)—C(15)—H(15B)	104.7(18)

Can. J. Chem. Downloaded from www.nrcresearchpress.com by 198.100.157.202 on 09/07/12
For personal use only.

TABLE 1 (*concluded*)

O(1)—C(1)—C(2)	115.62(19)	O(5)—C(16)—C(15)	107.98(20)
O(1)—C(1)—C(6)	124.51(20)	O(5)—C(16)—H(16A)	109.7(12)
C(2)—C(1)—C(6)	119.86(21)	O(5)—C(16)—H(16B)	109.9(12)
O(2)—C(2)—C(1)	116.18(19)	C(15)—C(16)—H(16A)	110.7(13)
O(2)—C(2)—C(3)	124.22(20)	C(15)—C(16)—H(16B)	110.0(12)
C(1)—C(2)—C(3)	119.60(21)	H(16A)—C(16)—H(16B)	108.7(17)
C(2)—C(3)—C(4)	120.23(24)	O(5)—C(17)—C(18)	108.37(20)
C(2)—C(3)—H(3)	120.4(14)	O(5)—C(17)—H(17A)	111.3(14)
C(4)—C(3)—H(3)	119.4(14)	O(5)—C(17)—H(17B)	110.0(14)
C(3)—C(4)—C(5)	120.44(24)	C(18)—C(17)—H(17A)	106.6(13)
C(3)—C(4)—H(4)	121.3(12)	C(18)—C(17)—H(17B)	113.1(14)
C(5)—C(4)—H(4)	118.3(12)	H(17A)—C(17)—H(17B)	107.4(19)
C(4)—C(5)—C(6)	119.67(24)	O(1)—C(18)—C(17)	106.57(19)
C(4)—C(5)—H(5)	118.3(13)	O(1)—C(18)—H(18A)	110.4(12)
C(6)—C(5)—H(5)	122.0(13)	O(1)—C(18)—H(18B)	107.8(11)
C(1)—C(6)—C(5)	120.20(23)	C(17)—C(18)—H(18A)	110.2(12)
C(1)—C(6)—H(6)	118.3(13)	C(17)—C(18)—H(18B)	113.5(12)
C(5)—C(6)—H(6)	121.5(13)	H(18A)—C(18)—H(18B)	108.2(16)
O(2)—C(7)—C(8)	110.05(24)	S—C(19)—N	178.82(21)
O(2)—C(7)—H(7A)	108.5(15)		
O(2)—C(7)—H(7B)	105.3(14)		
C(8)—C(7)—H(7A)	113.0(15)		
C(8)—C(7)—H(7B)	106.9(15)		

TABLE 2. (*a*) Torsion angles (deg) for compound **1**

C18—O1—C1—C2	173.7(4)	C18—O1—C1—C6	−6.5(2)
C1—O1—C18—C17	172.3(4)	C7—O2—C2—C1	−151.4(4)
C7—O2—C2—C3	29.2(2)	C2—O2—C7—C8	164.0(4)
C9—O3—C8—C7	179.3(4)	C8—O3—C9—C10	−157.7(4)
C8—O3—C9—C14	22.3(2)	C15—O4—C10—C9	164.8(4)
C15—O4—C10—C11	−15.1(3)	C10—O4—C15—C16	−157.6(5)
C17—O5—C16—C15	−177.3(5)	C16—O5—C17—C18	66.5(3)
O1—C1—C2—O2	−0.9(1)	O1—C1—C2—C3	178.6(4)
C6—C1—C2—O2	179.3(4)	C6—C1—C2—C3	−1.2(2)
O1—C1—C6—C5	−179.4(5)	C2—C1—C6—C5	0.4(2)
O2—C2—C3—C4	−179.9(5)	C1—C2—C3—C4	0.7(2)
C2—C3—C4—C5	0.7(2)	C3—C4—C5—C6	−1.5(2)
C4—C5—C6—C1	1.0(2)	O2—C7—C8—O3	−61.3(3)
O3—C9—C10—O4	1.6(1)	O3—C9—C10—C11	−178.5(5)
C14—C9—C10—O4	−178.5(5)	C14—C9—C10—C11	1.4(3)
O3—C9—C14—C13	178.7(5)	C10—C9—C14—C13	−1.3(2)
O4—C10—C11—C12	178.9(5)	C9—C10—C11—C12	−0.9(2)
C10—C11—C12—C13	0.3(3)	C11—C12—C13—C14	−0.2(3)
C12—C13—C14—C9	0.7(3)	O4—C15—C16—O5	70.3(3)
O5—C17—C18—O1	51.5(2)		

TABLE 2. (*b*) Torsion angles (deg) for compound **2**

O1—Na—N—C19	137.2(2)	O2—Na—N—C19	66.9(2)
O3—Na—N—C19	−17.7(1)	O4—Na—N—C19	−87.1(2)
O5—Na—N—C19	−154.3(2)	N—Na—O1—C1	−121.8(1)
N—Na—O1—C18	74.5(1)	O2—Na—O1—C1	−3.2(1)
O2—Na—O1—C18	−167.0(1)	O3—Na—O1—C1	32.8(1)
O3—Na—O1—C18	−131.0(1)	O4—Na—O1—C1	117.7(1)
O4—Na—O1—C18	−46.1(1)	O5—Na—O1—C1	146.4(1)
O5—Na—O1—C18	−17.4(1)	N—Na—O2—C2	94.6(1)
N—Na—O2—C7	−117.6(2)	O1—Na—O2—C2	3.6(1)
O1—Na—O2—C7	151.4(2)	O3—Na—O2—C2	−146.0(1)
O3—Na—O2—C7	1.8(1)	O4—Na—O2—C2	−118.0(1)
O4—Na—O2—C7	29.8(1)	O5—Na—O2—C2	−31.7(1)
O5—Na—O2—C7	116.1(1)	N—Na—O3—C8	84.3(2)
N—Na—O3—C9	−75.1(1)	O1—Na—O3—C8	−64.7(1)

Can. J. Chem. Downloaded from www.nrcresearchpress.com by 198.100.157.202 on 09/07/12
For personal use only.

TABLE 2 (*concluded*)

O1—Na—O3—C9	135.9(1)	O2—Na—O3—C8	−29.2(1)
O2—Na—O3—C9	171.4(1)	O4—Na—O3—C8	175.0(2)
O4—Na—O3—C9	15.5(1)	O5—Na—O3—C8	−148.9(2)
O5—Na—O3—C9	51.6(1)	N—Na—O4—C10	109.7(1)
N—Na—O4—C15	−70.1(1)	O1—Na—O4—C10	−130.8(1)
O1—Na—O4—C15	49.4(1)	O2—Na—O4—C10	−41.8(1)
O2—Na—O4—C15	138.4(1)	O3—Na—O4—C10	−12.9(1)
O3—Na—O4—C15	167.2(1)	O5—Na—O4—C10	−159.7(1)
O5—Na—O4—C15	20.4(1)	N—Na—O5—C16	57.7(1)
N—Na—O5—C17	−57.5(1)	O1—Na—O5—C16	158.6(1)
O1—Na—O5—C17	43.3(1)	O2—Na—O5—C16	−166.3(1)
O2—Na—O5—C17	78.4(1)	O3—Na—O5—C16	−81.2(1)
O3—Na—O5—C17	163.5(1)	O4—Na—O5—C16	−45.6(1)
O4—Na—O5—C17	−160.9(1)	Na—N—C19—S	39.2(1)
Na—O1—C1—C2	2.5(1)	Na—O1—C1—C6	−176.6(2)
C18—O1—C1—C2	166.4(2)	C18—O1—C1—C6	−12.7(1)
Na—O1—C18—C17	−11.7(1)	C1—O1—C18—C17	−176.2(3)
Na—O2—C2—C1	−3.7(1)	Na—O2—C2—C3	176.2(2)
C7—O2—C2—C1	−151.4(2)	C7—O2—C2—C3	28.6(2)
Na—O2—C7—C8	24.4(1)	C2—O2—C7—C8	173.0(3)
Na—O3—C8—C7	53.2(2)	C9—O3—C8—C7	−147.6(3)
Na—O3—C9—C10	−16.8(1)	Na—O3—C9—C14	164.8(2)
C8—O3—C9—C10	−174.1(3)	C8—O3—C9—C14	7.4(2)
Na—O4—C10—C9	9.5(1)	Na—O4—C10—C11	−169.1(2)
C15—O4—C10—C9	−170.7(2)	C15—O4—C10—C11	10.8(1)
Na—O4—C15—C16	8.7(1)	C10—O4—C15—C16	−171.1(3)
Na—O5—C16—C15	70.9(1)	C17—O5—C16—C15	173.5(3)
Na—O5—C17—C18	−68.6(1)	C16—O5—C17—C18	−171.0(3)
O1—C1—C2—O2	0.9(1)	O1—C1—C2—C3	−179.1(3)
C6—C1—C2—O2	−180.0(3)	C6—C1—C2—C3	0.0(1)
O1—C1—C6—C5	178.4(3)	C2—C1—C6—C5	−0.7(1)
O2—C2—C3—C4	−179.6(3)	C1—C2—C3—C4	0.4(1)
C2—C3—C4—C5	−0.1(1)	C3—C4—C5—C6	−0.5(1)
C4—C5—C6—C1	0.9(1)	O2—C7—C8—O3	−50.1(2)
O3—C9—C10—O4	4.5(1)	O3—C9—C10—C11	−176.8(3)
C14—C9—C10—O4	−177.0(3)	C14—C9—C10—C11	1.7(1)
O3—C9—C14—C13	177.1(3)	C10—C9—C14—C13	−1.2(1)
O4—C10—C11—C12	177.3(3)	C9—C10—C11—C12	−1.2(1)
C10—C11—C12—C13	0.2(1)	C11—C12—C13—C14	0.2(1)
C12—C13—C14—C9	0.3(1)	O4—C15—C16—O5	−56.4(2)
O5—C17—C18—O1	57.3(2)		

$\theta_1 = 66.5°$, $\theta_2 = 53.5°$; for O-2, $\theta_1 = 89.2°$, $\theta_2 = 31.8°$; for O-3, $\theta_1 = 82.3°$, $\theta_2 = 37.7°$; and for O-4, $\theta_1 = 75.1°$ and $\theta_2 = 44.9°$.

If one assumes that the effectiveness of overlap is related to the sine of the angle and that one can treat the two orbitals in an additive fashion, then an order of effectiveness of conjugative lone pair release can be established. Such an order is O-1 > O-4 > O-3 > O-2. In terms of the order of predicted shielding at carbons *ortho* to oxygen, this leads to the prediction that C-6 should be the most shielded, followed by C-11, C-14, and C-3. It is notable that this is the same order of shielding that one predicts based on the simple dihedral angle dependence of the γ-steric shift in butane (23).

Presumably in the case of the observed difference in shielding at the C-4,5,11,12 sites it is the aforementioned stereoelectronic influence of the oxygen lone pairs which dominates. Via the same arguments presented above, the O-1 site is most effective as a conjugative electron donor, and hence it is the carbon *para* to it, i.e., C-4, which is predicted to be the most shielded. Accordingly we attribute the resonance at 118.85 ppm to this carbon. The other three carbons appear as a broad singlet with a shoulder centered at 121.03 ppm.

(ii) Dibenzo-15-crown-5·NaNCS complex (2)

In solution the ^1H and ^{13}C NMR spectra are, with the exception of minor chemical shift differences, quite similar to those of the free ligand **1**. Analysis of the O-CH_2-CH_2-O proton spin coupling pattern as an AA′XX′ system leads to very similar values for all coupling constants, suggesting that there is little change in the average conformation of the 15-membered ring upon complexation *in solution*. The precise K, however, for free and complexed Na^+ is as yet unknown for this system.

Examination of the *solid phase* ^{13}C NMR spectra in Fig. 3, however, reveals substantial differences in chemical shifts between the free and complexed dibenzo-15-crown-5 species. For **1**, all six CH_2-O resonances are resolved with an overall shift difference of 8.71 ppm, whereas in **2**, only four resonances are resolved in this region with an overall shift difference of 4.26 ppm. By contrast, for **2** all eight non-oxygenated aromatic carbons are observed, with a substantially larger range

Can. J. Chem. Downloaded from www.nrcresearchpress.com by 198.100.157.202 on 09/07/12
For personal use only.

Can. J. Chem. Downloaded from www.nrcresearchpress.com by 198.100.157.202 on 09/07/12
For personal use only.

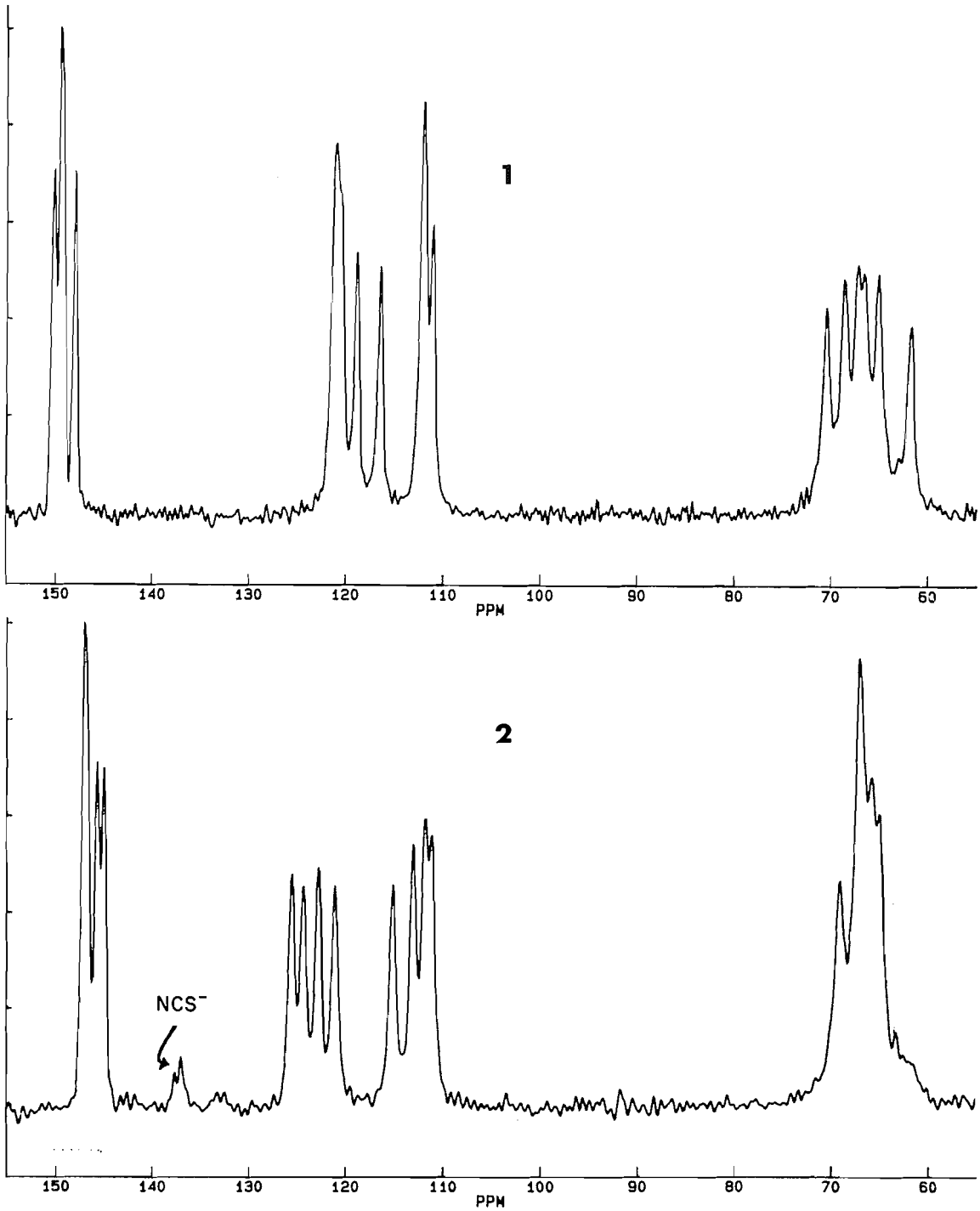


FIG. 3. ^{13}C CPMAS spectra (45.3 MHz).

of shifts than found for **1**. From the total number of ^{13}C lines observed, however, it is clear that neither **1** nor **2** possesses any symmetry elements, in agreement with the X-ray crystallographic structures.

Comparison of the X-ray data for **1** and **2** reveals that the major change in geometry has occurred in the C16—O5—C17—C18 fragment, where a dihedral angle of 66.5° in **1** has changed to 171.0° in **2**. There is also a substantial change in the C9—O3—C8—C7 unit, where the torsional angle of 179.3° in **1** has contracted to 147.6° in **2**. All other dihedral angle changes upon complexation are less than 15°.

Although one cannot rule out steric and electronic effects of the Na^+ and NCS^- species on ^{13}C chemical shifts, it is of interest to attempt an analysis of shielding differences in **2** based on torsional environments of the carbon atoms involved relative to results discussed previously for **1**.

The methylene carbon resonances for solid **2** cover the range 65.00–69.26 ppm. Based on our assignments for **1**, it is mandatory that C-18 (at 61.88 ppm in **1**) must be deshielded by at least 3.12 ppm in **2**. Examination of the torsional environment of C-18 (Table 9) reveals one major reason why this is the case, namely that the C16—O5—C17—C18 torsion angle has

Can. J. Chem. Downloaded from www.nrcresearchpress.com by 198.100.157.202 on 09/07/12
For personal use only.

TABLE 3. ^{13}C NMR chemical shifts (ppm from TMS ∓ 0.01)

Carbon	**1** (soln.)*	**1** (solid)	**2** (soln.)*	**2** (solid)
C-1	(149.54)[a]	(150.17)[e]	(147.52)[i]	(146.94)[o]
C-2	(149.47)[a]	(149.38)[e]	(146.68)[j]	(145.70)[o]
C-3	(115.37)[b]	116.42	(114.37)[k]	115.15
C-4	(121.85)[c]	118.85	(122.64)[m]	124.36
C-5	(121.95)[c]	(121.03)[g]	(123.17)[n]	125.54
C-6	(115.70)[b]	111.11	(113.67)[l]	113.08
C-7	68.38	(66.90)[h]	68.29	(67.14)[q]
C-8	68.38	(67.36)[h]	68.29	(67.14)[q]
C-9	(149.47)[a]	(149.38)[e]	(146.68)[j]	(144.99)[o]
C-10	(149.54)[a]	(147.93)[e]	(147.52)[i]	(146.94)[o]
C-11	(115.70)[b]	(112.10)[f]	(113.67)[l]	(111.87)[p]
C-12	(121.95)[c]	(121.03)[g]	(123.17)[n]	121.10
C-13	(121.85)[c]	(121.03)[g]	(122.67)[m]	122.80
C-14	(115.37)[b]	(112.10)[f]	(114.37)[k]	(111.52)[p]
C-15	(69.80)[d]	70.59	67.13	69.26
C-16	(69.76)[d]	68.75	67.13	(67.14)[q]
C-17	(69.76)[d]	65.25	67.13	(66.01)[q]
C-18	(69.80)[d]	61.88	67.13	(65.00)[q]

*0.1 M solutions in CD_2Cl_2.
[a–q]Parentheses denote possible assignment interchange.

TABLE 4. (*a*) Crystal data for dibenzo-15-crown-5-ether (**1**)

Parameters	Values
Empirical formula	$C_{18}H_{20}O_5$
Formula weight	316.358
Crystal dimension, mm	0.1 × 0.2 × 0.35
Space group	*P bca*, orthorhombic
a, Å	8.4179(8)
b, Å	8.5374(13)
c, Å	45.328(6)
Z (molecules/cell)	8
F (000) electrons	1344
Volume, Å^3	3257.6
D_c, g/cm^3	1.290
Radiation (Cu Kα), Å	1.54056
2θ (max), deg	120
No. reflections measured	4052
No. of unique reflections	2413
No. of reflections with $I_{net} > 2.5\sigma(I_{net})$	1945
Last least-squares cycle calculated with	43 atoms 288 parameters 1945 reflections
R_f (significant reflections)	0.044
R_w (significant reflections)	0.043
Goodness of fit (last cycle)	6.35
R_f (all reflections)	0.054
R_w (all reflections)	0.043
Maximum shift/σ	3.848
Last *D*-map:	
deepest hole, e/Å^3	−0.270
highest peak, e/Å^3	0.120

(*b*) Crystal data for **2**

Parameter	Value
Empirical formula	$C_{19}O_5NSH_{20}Na$
Formula weight	397.42
Crystal dimensions, mm	0.2 × 0.2 × 0.2
Space group	*P* 21/*n*, monoclinic
a, Å	12.1306(13)
b, Å	8.8565(10)
c, Å	18.269(3)
β, deg	99.990(10)
Z (molecules/cell)	4
F (000), electrons	831.87
Vol, Å^3	1932.9(4)
D_c, g/cm^3	1.366
Linear absorption coefficient (μ) mm^{-1}	1.93
Radiation, Å	1.54056
2θ (max), deg	120
No. reflections measured	2965
No. unique reflections	2873
No. unique reflections $I_{net} > 2.5\sigma(I_{net})$	2560
Last least-squares cycle calculated with	47 atoms 325 parameters 2560 reflections
R_f (significant reflections)	0.037
R_w (significant reflections)	0.037
Goodness of fit (last cycle)	6.20
R_f (all reflections)	0.041
R_w (all reflections)	0.037
Maximum shift/σ	0.106
Last *D*-map:	
deepest hole, e/Å^3	−0.30
highest peak, e/Å^3	0.430
Secondary extinction coefficient	4.95886

[a]Throughout this work esd's are in parentheses and refer to the last digit printed.
[b]$R_f = \Sigma||F_o| - |F_c||/\Sigma|F_o|$.
[c]$R_w = [\Sigma w(|F_o| - |F_c|)^2/\Sigma(w|F_o|)^2]^{1/2}$ where $w = 1/\sigma^2 I$.
[d]Goodness of fit = $[\Sigma w(|F_o| - |F_c|)^2/(\text{No. of reflections} - \text{No. of parameters})]^{1/2}$.

increased from 66.5° in **1** to 171.0° in **2**. Resonances for C-16 and C-17 may also be affected, but other angle changes involving these carbons may tend to offset this perturbation.

Conversely, the C-15 resonance of **2** may be expected to be slightly shielded relative to **1**, since there is a contraction of the O4—C15—C16—O5 angle from 70.3° in **1** to 56.4° in **2**. Hence the shift in position of this resonance from 70.59 ppm in **1** to 69.26 ppm in **2** can be explained. Other assignments of methylene carbons of **2** must be regarded as tentative due to peak overlap and the small range of shifts observed.

Regarding assignments for the non-oxygenated aromatic carbons, arguments analogous to those used for **1** lead to a predicted order of shielding of C-14 > C-11 > C-6 > C-3 in **2**. Considering the stereoelectronic influence of the oxygen lone pairs, O-3 in **2** will be the most effective donor of electrons and hence the carbon *para* to it, C-12, will be the most shielded. For the remaining carbons, the predicted order of shielding is C-13 > C-4 > C-5.

Clearly, however, these assignments must be regarded with some caution until methods for unambiguous attribution of solid phase ^{13}C resonances become available or appropriately labelled materials are prepared. The experimental solid phase ^{13}C results for these materials do, however, hold some promise to be of substantial importance in helping to unravel stereochemical contributions to ^{13}C NMR chemical shifts.

(iii) Features of sodium complexation in 2

The geometry of coordination to Na^+ in **2** can best be described as pentagonal pyramidal. From the X-ray data, it is

Can. J. Chem. Downloaded from www.nrcresearchpress.com by 198.100.157.202 on 09/07/12
For personal use only.

TABLE 5. (*a*) Atomic parameters *x*, *y*, *z* and B_{iso} for **1**. ESDs refer to the last digit printed

Atom	*x*	*y*	*z*	B_{iso}[a]
O1	0.0069(3)	0.56531(24)	0.07614(4)	4.03(11)
O2	−0.1658(3)	0.34817(22)	0.09909(4)	3.72(11)
O3	−0.0834(3)	0.3629 (3)	0.15752(5)	4.14(11)
O4	0.1201(3)	0.5823 (3)	0.16255(5)	4.73(12)
O5	0.0863(3)	0.7985 (3)	0.11651(5)	4.56(13)
C1	−0.0040(4)	0.4305 (4)	0.05978(7)	3.34(16)
C2	−0.0991(4)	0.3137 (4)	0.07246(7)	3.30(16)
C3	−0.1205(5)	0.1745 (4)	0.05737(9)	4.39(22)
C4	−0.0478(6)	0.1500 (6)	0.03052(9)	5.36(22)
C5	0.0471(6)	0.2630 (5)	0.01852(8)	5.17(22)
C6	0.0688(5)	0.4046 (5)	0.03310(8)	4.28(19)
C7	−0.1973(5)	0.2190 (4)	0.11864(8)	3.79(18)
C8	−0.2248(5)	0.2840 (4)	0.14873(8)	3.93(19)
C9	−0.0798(4)	0.4346 (4)	0.18445(7)	3.50(16)
C10	0.0338(4)	0.5539 (4)	0.18740(7)	3.71(17)
C11	0.0496(5)	0.6302 (5)	0.21393(9)	4.77(21)
C12	−0.0483(6)	0.5923 (6)	0.23731(10)	5.69(25)
C13	−0.1594(6)	0.4774 (6)	0.23437(9)	5.63(25)
C14	−0.1758(5)	0.3986 (5)	0.20782(9)	4.78(21)
C15	0.2110(6)	0.7250 (5)	0.16047(9)	5.12(22)
C16	0.2364(5)	0.7550 (5)	0.12852(9)	4.63(21)
C17	0.0852(5)	0.8254 (4)	0.08597(10)	4.74(22)
C18	0.1134(5)	0.6850 (4)	0.06657(8)	4.05(19)
H3	−0.180 (4)	0.102 (3)	0.0666 (6)	3.3 (9)
H4	−0.064 (4)	0.051 (4)	0.0204 (7)	6.4 (10)
H5	0.098 (4)	0.245 (3)	−0.0004 (7)	5.3 (8)
H6	0.134 (4)	0.484 (3)	0.0245 (6)	4.2 (9)
H7A	−0.101 (3)	0.146 (3)	0.1184 (6)	4.3 (8)
H7B	−0.293 (4)	0.161 (3)	0.1122 (6)	4.4 (8)
H8A	−0.317 (4)	0.356 (3)	0.1495 (6)	5.2 (9)
H8B	−0.248 (4)	0.199 (3)	0.1634 (5)	5.2 (8)
H11	0.131 (4)	0.712 (4)	0.2159 (8)	5.9 (12)
H12	−0.036 (4)	0.645 (4)	0.2564 (7)	6.3 (10)
H13	−0.227 (4)	0.447 (4)	0.2510 (7)	6.0 (9)
H14	−0.255 (4)	0.322 (4)	0.2062 (6)	4.3 (9)
H15A	0.153 (4)	0.807 (4)	0.1702 (7)	5.7 (11)
H15B	0.315 (5)	0.706 (4)	0.1729 (7)	9.1 (11)
H16A	0.316 (4)	0.844 (3)	0.1261 (6)	5.1 (8)
H16B	0.274 (4)	0.658 (3)	0.1176 (6)	5.1 (9)
H17A	0.163 (4)	0.905 (4)	0.0807 (7)	6.2 (10)
H17B	−0.026 (4)	0.861 (4)	0.0809 (6)	6.1 (9)
H18A	0.224 (4)	0.648 (3)	0.0679 (6)	5.2 (9)
H18B	0.090 (4)	0.713 (4)	0.0427 (7)	6.1 (9)

(*b*) Atomic parameters *x*, *y*, *z* and B_{iso} for **2**. ESDs refer to the last digit printed

Atom	*x*	*y*	*z*	B_{iso}[a]
Na	0.79353(7)	0.84624(9)	0.90598(4)	3.98(4)
S	0.84289(8)	0.46629(9)	1.11510(4)	6.73(4)
N	0.81604(18)	0.65533(24)	0.99287(12)	5.53(11)
O1	0.90976(12)	0.76947(15)	0.82424(8)	3.88(7)
O2	0.94124(13)	1.02079(16)	0.89849(8)	4.16(7)
O3	0.73937(13)	1.09538(17)	0.92682(9)	5.01(8)
O4	0.59932(12)	0.89153(16)	0.88066(8)	4.36(7)
O5	0.69208(12)	0.69176(16)	0.80086(8)	4.07(7)
C1	0.99631(17)	0.85757(23)	0.80945(12)	3.46(10)
C2	1.01272(18)	0.99326(24)	0.84894(12)	3.63(10)
C3	1.09674(20)	1.0898 (3)	0.83684(14)	4.56(12)
C4	1.16402(20)	1.0533 (3)	0.78567(15)	4.85(13)
C5	1.14804(20)	0.9202 (3)	0.74647(15)	4.65(12)
C6	1.06409(20)	0.8215 (3)	0.75890(14)	4.20(12)
C7	0.91843(25)	1.1765 (3)	0.91262(20)	5.65(16)
C8	0.83132(24)	1.1867 (4)	0.95861(19)	5.64(16)
C9	0.63051(18)	1.13112(25)	0.93153(12)	3.72(10)
C10	0.55301(19)	1.02083(24)	0.90325(11)	3.64(10)
C11	0.44102(21)	1.0451 (3)	0.90120(13)	4.33(12)
C12	0.40594(25)	1.1788 (3)	0.92866(15)	5.08(14)
C13	0.48136(24)	1.2862 (3)	0.95735(15)	5.32(14)
C14	0.59517(24)	1.2635 (3)	0.95932(15)	4.79(13)
C15	0.52784(21)	0.7795 (3)	0.84047(16)	4.52(12)
C16	0.60104(21)	0.6448 (3)	0.83523(15)	4.35(12)
C17	0.77460(23)	0.5777 (3)	0.79998(17)	4.52(13)
C18	0.87321(22)	0.6471 (3)	0.77418(15)	4.30(12)
C19	0.82788(19)	0.5760 (3)	1.04327(13)	3.97(11)
H3	1.1073 (19)	1.180 (3)	0.8616 (12)	5.8 (6)
H4	1.2247 (18)	1.1257 (25)	0.7744 (12)	5.5 (6)
H5	1.1971 (19)	0.899 (3)	0.7076 (12)	5.7 (6)
H6	1.0521 (19)	0.725 (3)	0.7328 (12)	6.4 (7)
H7A	0.9864 (21)	1.224 (3)	0.9346 (14)	7.0 (7)
H7B	0.8832 (23)	1.224 (3)	0.8583 (15)	8.7 (9)
H8A	0.8049 (20)	1.283 (3)	0.9636 (14)	6.4 (7)
H8B	0.852 (3)	1.125 (4)	1.0072 (19)	12.0 (12)
H11	0.3871 (18)	0.9706 (24)	0.8811 (12)	5.1 (6)
H12	0.3289 (20)	1.191 (3)	0.9264 (13)	6.2 (7)
H13	0.4601 (20)	1.389 (3)	0.9787 (13)	7.0 (7)
H14	0.6480 (20)	1.335 (3)	0.9825 (13)	6.5 (7)
H15A	0.4671 (19)	0.754 (3)	0.8629 (12)	5.4 (6)
H15B	0.4928 (19)	0.8261 (24)	0.7899 (13)	5.9 (6)
H16A	0.5590 (18)	0.5649 (25)	0.8056 (12)	5.1 (5)
H16B	0.6301 (18)	0.6042 (24)	0.8863 (12)	4.7 (5)
H17A	0.7483 (19)	0.500 (3)	0.7657 (12)	5.2 (6)
H17B	0.7931 (19)	0.532 (3)	0.8483 (13)	5.8 (7)
H18A	0.9349 (18)	0.5701 (24)	0.7754 (11)	4.6 (5)
H18B	0.8559 (17)	0.6887 (22)	0.7238 (12)	4.2 (5)

[a] B_{iso} is the mean of the principal axes of the thermal ellipsoids.

TABLE 6. ^{1}H NMR coupling constants involving methylene protons (Hz ∓ 0.01)

Pathway	**1**	**2**
$^2J_{15,18AA'}$	−12.00	−11.97
$^2J_{16,17XX'}$	−12.12	−11.94
$^3J_{AX}$	6.30	6.05
$^3J_{A'X}$	3.52	3.30
$^3J_{AX'}$	3.52	3.30
$^3J_{A'X'}$	6.30	6.05

TABLE 7. ^{1}H NMR chemical shifts (ppm from TMS ∓ 0.001)[a]

H site	**1**	**2**
3, 6, 11, 14	6.952	7.015
4, 5, 12, 13	6.952	7.015
15, 18	4.155	4.272
16, 17	3.885	4.007
7, 8	4.330	4.443

[a] 0.1 M solutions in CD_2Cl_2.

TABLE 8. Torsional angles (deg) for methylene carbons of **1**

Carbon	C-O-C*-C	O-C-C*-O	C*-O-C-C	C-O-C-C*
C7	164.0	61.3	29.2 (C7-O2-C2-C3) 151.4 (C7-O2-C2-C1)	179.3
C8	179.3	61.3	22.3 (C8-O3-C9-C14) 157.7 (C8-O3-C9-C10)	164.0
C15	157.6	70.3	15.1 (C15-O4-C10-C11) 164.8 (C15-O4-C10-C9)	177.3
C18	172.3	51.5	6.5 (C18-O1-C1-C6) 173.7 (C18-O1-C1-C2)	66.5
C16	177.3	70.3	66.5	157.6
C17	66.5	51.5	177.3	172.3

TABLE 9. Torsional angles (deg) for methylene carbons of **2**

Carbon	C-O-C*-C	O-C-C*-O	C*-O-C-C	C-O-C-C*
C7	170.3	50.1	28.6 (C7-O2-C2-C3) 151.4 (C7-O2-C2-C1)	147.6
C8	147.6	50.1	7.4 (C8-O3-C9-C14) 174.1 (C8-O3-C9-C10)	173.0
C15	171.1	56.4	10.8 (C15-O4-C10-C11) 170.7 (C15-O4-C10-C9)	173.5
C18	176.2	57.3	12.7 (C18-O1-C1-C6) 166.4 (C18-O1-C1-C2)	171.0
C16	173.5	56.4	171.0	171.1
C17	171.0	57.3	173.5	176.2

evident that an approximate pentagonal plane is defined by the five oxygens of the crown ether. For this plane the $(\chi)^2$ value is 6713.492. The distances (in Å) from each oxygen to the mean plane are as follows: O-1, 0.0528 (18); O-2, −0.0031 (20); O-3, −0.0764 (21); O-4, 0.0977 (19); and O-5, −0.0850 (19). Coordination is completed by the N atom of the thiocyanate anion. The plane defined by C-19, N, and S bears an angle of 83.26° to the mean plane defined by the five oxygens. The Na—O distances and the O—Na—O angles are included in Table 1.

Experimental

(a) Spectra

The ^{13}C CPMAS solid phase spectra were recorded at 45.3 MHz on a Bruker CXP-180 spectrometer. Cross polarization (CP) times were typically 3 ms with the radio frequency field amplitude being 60 kHz. Satisfactory signal-to-noise ratios were obtained after a maximum of 400 accumulations. The sweep width was 20 kHz with a recycle time of 4–8 s. Normally 2K data points were collected with zero filling to 8K before Fourier transformation. Magic angle spinning (MAS) rates of ca. 3 kHz were obtained using Kel-F spinners of the Andrew–Beams type. Chemical shifts were measured relative to external solid hexamethylbenzene (HMB) and converted to the TMS scale via the factor of 16.9 ppm, which is the chemical shift for the CH_3 group of HMB.

Solution ^{13}C NMR spectra were recorded at 75.3 MHz on a Varian XL-300 spectrometer under conditions of complete ^1H noise decoupling. The NOESY spectra were obtained on the same instrument with mixing times of 0.3 s. For the ^1H–^{13}C HETCOR experiment, delays were set to correspond to an average $^1J_{CH}$ value of 140 Hz. Standard ^1H spectra were run on a Varian XL-200 system and simulations of spectra were done via the LAME (21) program.

(b) Crystallographic measurements and structure solutions

A summary of the crystal data is given in Table 4. Diffraction intensities were collected on a Picker diffractometer using Cu radiation and the $\theta/2\theta$ scan technique with profile analysis (27). Three standards were measured every 100 reflections. The space group was determined by systematic absences. Unit cell parameters were obtained by least-squares refinement of the setting angles for 24 reflections with a 2θ range between 90 and 110°. Lorentz and polarization factors were applied but no correction for absorption was made.

Structures were solved by direct methods plus Fourier maps and were refined by full matrix least-squares analysis with weights based on counting statistics. H atoms were found from difference maps and their positions were refined isotropically. Non-H atoms were refined anisotropically. All calculations were performed using the NRC VAX Crystal Structure programs (28). A full listing of bond lengths and angles is presented in Table 1, with torsional angles involving non-H atoms in Table 2, and the final atomic positional parameters in Table 5. Anisotropic thermal parameters and final structure factors are available as supplementary data.[3]

(c) Materials

Dibenzo-15-crown-5 (**1**) was prepared by reaction of 1,2-bis(2-chloroethyl)ether with 1,2-bis-(*o*-hydroxyphenoxy) ethane (18) in the presence of 2 molar equivalents of NaOH. A typical procedure follows.

The diol (4.92 g, 0.02 mol), butanol (4 mL), and NaOH (1.72 g, 0.043 mol, dissolved in 3 mL H_2O) were combined and brought to reflux. To this mixture was added dropwise with stirring 2.86 g (0.02 mol) of the 1,2-bis(2-chloroethyl)ether diluted with 4 mL butanol over a period of 20 min. Refluxing was continued for 20 h. The cooled reaction mixture was then acidified with concentrated HCl and the butanol and water were removed by rotary evaporation. The resulting crude product was dissolved in CH_2Cl_2 and washed with water. After the organic layer was dried over $MgSO_4$, the solvent was removed and the material subjected to flash column chromatography on silica gel using CH_2Cl_2 as eluent. Recrystallization from CH_2Cl_2/hexane gave **1**, mp 114–115°C, in 35% overall yield. Mass spectrum (CI), *m/z*: 317 (M + 1).

The NaNCS complex of **1** was prepared according to the following procedure. Equimolar quantities of **1** and NaNCS were dissolved in a minimum volume of dry methanol and allowed to stand for 2–3 h. The solvent was removed by rotoevaporation and the resulting solid recrystallized from 30:70 ethanol/CH_2Cl_2 to give the complex, mp 147–148°C.

1. C. J. PEDERSEN. J. Am. Chem. Soc. **89**, 7017 (1967).
2. I. R. HANSON. Acta Crystallogr. Sect. B: Struct. Crystallogr. Cryst. Chem. **B34**, 1026 (1978).
3. M. A. BUSH and M. R. TRUTER. J. Chem. Soc. Perkin Trans. 2, 341 (1972).
4. J. D. OWEN. J. Chem. Soc. Dalton Trans. 1066 (1980).
5. J. D. OWEN. J. Chem. Soc. Dalton Trans. 1418 (1978).

[3]These data may be purchased from The Depository of Unpublished Data, Document Delivery, CISTI, National Research Council Canada, Ottawa, Canada K1A 0S2.

Can. J. Chem. Downloaded from www.nrcresearchpress.com by 198.100.157.202 on 09/07/12
For personal use only.

6. P. R. MALINSON and M. R. TRUTER. J. Chem. Soc. Perkin Trans. 2, 1818 (1972).
7. N. S. POONIA and M. R. TRUTER. J. Chem. Soc. Dalton Trans. 2062 (1973).
8. N. S. POONIA. J. Am. Chem. Soc. **96**, 1012 (1974).
9. N. S. POONIA, P. BAGDI, and K. S. SIDHU. J. Inclusion Phenom. **4**, 43 (1986).
10. P. GROTH. Acta Chem. Scand. **A35**, 721 (1981).
11. C. CAMBILLAU, G. BRAM, J. CORSET, and C. RICHE. Can. J. Chem. **60**, 2554 (1982).
12. A. I. GARBUNOV, A. P. STOROZHENKO, L. V. IVAKIMA, B. M. BULYCHEV, and A. I. GUSEV. Dokl. Akad. Nauk SSSR, **285**, 129 (1985).
13. N. P. RATH and E. M. HOLT. J. Chem. Soc. Chem. Commun. 665 (1985).
14. M. P. MURCHIE, J. W. BOVENKAMP, A. RODRIGUE, K. A. WATSON, and S. FORTIER. Can. J. Chem. **66**, 2515 (1988).
15. P. S. BELTON, S. F. TANNER, K. M. WRIGHT, M. P. PAYNE, M. R. TRUTER, and J. N. WINGFIELD. J. Chem. Soc. Perkin Trans. 2, 1307 (1985).
16. G. W. BUCHANAN, R. A. KIRBY, and J. P. CHARLAND. J. Am. Chem. Soc. **110**, 2477 (1988).
17. J. P. CHARLAND, G. W. BUCHANAN, and R. A. KIRBY. Acta Crystallogr. Sect. C: Cryst. Struct. Commun. **C45**, 165 (1989).
18. G. W. BUCHANAN, R. A. KIRBY, and J. P. CHARLAND. Can. J. Chem. **68**, 49 (1990).
19. H. BOOTH and J. H. LITTLE. Tetrahedron, **23**, 291 (1967).
20. G. W. BUCHANAN and D. J. LANDRY. Magn. Reson. Chem. In press.
21. C. W. HAIGH. Annu. Rep. NMR Spectrosc. **4**, 311 (1971).
22. N. K. WILSON and J. B. STOTHERS. Top. Stereochem. **8**, 1 (1973).
23. K. SIEDMAN and G. E. MACIEL. J. Am. Chem. Soc. **99**, 659 (1977).
24. R. BENN, H. GRONDEY, C. BREVARD, and A. PAGELOT. J. Chem. Soc. Chem. Commun. 102 (1988).
25. C. A. FYFE, H. GIES, and Y. FENG. J. Am. Chem. Soc. **111**, 7702 (1989).
26. C. A. FYFE, Y. FENG, H. GIES, H. GRONDEY, and G. T. KOKOTAILO. J. Am. Chem. Soc. **112**, 3264 (1990).
27. D. F. GRANT and E. J. GABE. J. Appl. Crystallogr. **11**, 114 (1978).
28. E. J. GABE, F. L. LEE, and Y. LEPAGE. J. Appl. Crystallogr. **22**, 384 (1989).

Can. J. Chem. Downloaded from www.nrcresearchpress.com by 198.100.157.202 on 09/07/12
For personal use only.

Reactions of δ-valerolactone with lithio trithio-orthoformates

PETER YATES,[1] AZZA SEIF-EL-NASR, AND JENNIFER STANTON
Department of Chemistry, University of Toronto, Toronto, Ont., Canada M5S 1A1

JIRI J. KREPINSKY[1]
Department of Molecular and Medical Genetics, University of Toronto, Toronto, Ont., Canada M5S 1A8

Received, July 19, 1990

PETER YATES, AZZA SEIF-EL-NASR, JENNIFER STANTON, and JIRI J. KREPINSKY. Can. J. Chem. **69**, 415 (1991).

δ-Valerolactone (**3**), on treatment with tris(methylthio)methyllithium (**7**) followed by weakly acidic aqueous work-up, gave a tautomeric mixture of 1,1-bis(methylthio)-6-hydroxy-2-hexanone (**8***a*) and tetrahydro-2-bis(methylthio)methyl-2-pyranol (**8***b*). Under analogous conditions **3** reacted with tris(phenylthio)methyllithium (**10**) to form tetrahydro-3-(phenylthiocarbonyl)-2-pyranone (**11**). With 2-(methylthio)-1,3-dithian-2-yllithium (**16**) it gave a tautomeric mixture of 2-(5-hydroxy-1-oxopentyl)-2-(methylthio)-1,3-dithiane (**17***a*) and 2-(tetrahydro-2-hydroxy-2-pyranyl)-2-(methylthio)-1,3-dithiane (**17***b*). Treatment of **17** with methanol in the presence of acidic ion-exchange resin gave a mixture of 2-(5,6-dihydro-3-(methylthio)-2(4*H*)-pyranyl)-1,3-dithiane (**20**), 2-(tetrahydro-2-methoxy-2-pyranyl)-1,3-dithiane (**21**), and 2-(tetrahydro-2-methoxy-4-(methylthio)-2-pyranyl)-1,3-dithiane (**22**). Similar treatment of **20** gave a mixture of **20**, **21**, and **22**. Compound **21** was synthesized independently by similar treatment of 2-(tetrahydro-2-hydroxy-2-pyranyl)-1,3-dithiane (**23**). The origins of the anomalous products are discussed briefly. It is concluded that because of these anomalies the preparation of tetrahydro-2-hydroxypyran-2-carboxylic acid acetals and related glycosides via trithio-orthoformate derivatives can encounter difficulties, although dithioacetals may serve this purpose.

Key words: 1,3-dithianes, α-hydroxy acids, δ-lactones, trithio-orthoformates.

PETER YATES, AZZA SEIF-EL-NASR, JENNIFER STANTON et JIRI J. KREPINSKY. Can. J. Chem. **69**, 415 (1991).

La δ-valérolactone (**3**), par une réaction avec le tris(méthylthio)méthyl-lithium suivie d'une récupération en milieu aqueux, légèrement acide, conduit à un mélange de 1,1-bis(méthylthio)-6-hydroxy-hexan-2-one (**8***a*) et tétrahydro-2-bis(méthylthio) méthyl-pyran-2-ol (**8***b*). Dans des conditions analogues, le composé **3** réagit avec le tris(phénylthio)méthyl-lithium (**10**) pour donner la tétrahydro-3-(phénylthiocarbonyl)-pyran-2-one (**11**). Et avec le 2-(méthylthio)-1,3-dithian-2-yl-lithium (**16**), il donne un mélange tautomère de 2-(5-hydroxy-1-oxopentyl)-2-(méthylthio)-1,3-dithiane (**17***a*) et de 2-(tétrahydro-2-hydroxy-pyran-2-yl)-2-(méthylthio)-1,3-dithiane (**17***b*). Le traitement du composé **17** par du méthanol, en présence d'une résine échangeuse d'ions acide, conduit à un mélange de 2-(5,6-dihydro-3-(méthylthio)-4*H*-pyran-2-yl)-1,3-dithiane (**20**), de 2-(tétrahydro-2-méthoxy-pyran-2-yl)-1,3-dithiane (**21**) et de 2-(tétrahydro-2-méthoxy-4-(méthylthio)-pyran-2-yl)-1,3-dithiane (**22**). Par un traitement similaire, le produit **20** fournit un mélange des composés **20**, **21** and **22**. On a synthétisé le composé **21** par une méthode indépendante en soumettant le 2-(tétrahydro-2-hydroxy-pyran-2-yl)-1,3-dithiane (**23**) à un traitement semblable. On discute brièvement des origines des produits anormaux. Sur la base de ces anomalies, on croit que la préparation des acétals de l'acide tétrahydro-2-hydroxy-pyran-2-carboxylique et des glycosides apparentés, via les dérivés trithio-orthoformiates, peut donner lieu à des difficultés, même si les dithioacétals peuvent être utilisés à leur place.

Mot clés : 1,3-dithianes, acides α-hydroxy, δ-lactones, trithio-orthoformates.

[Traduit par la rédaction]

The reaction of aldehydes or ketones with lithio trithio-orthoformates (**1**) is a well-known method for the preparation of masked α-hydroxy acids (**2**) (1). The corresponding reaction of δ-lactones, including **3** and aldonolactones, to give masked tetrahydro-2-hydroxy-pyran-2-carboxylic acids has also been reported (2) (Scheme 1).[2] The masked α-hydroxy acid derivatives of type **4** are of synthetic interest since acetalization followed by unmasking of the carboxylic acid provides a route to glycosides of type **5**, i.e., of the neuraminic or 3-deoxy-D-manno-2-octulopyranosonic (KDO) acid type, which might circumvent the competing elimination of water that bedevils the glycosylation with the α-hydroxy acids themselves and gives products of type **6** (Scheme 2). We describe here an investigation of the reactions of δ-valerolactone (**3**) with several lithio trithio-orthoformates, which reveals the interesting complications that may arise in the course of the reactions themselves or in subsequent acetalization reactions.[3]

The lithio derivative **7** (**1**, R = Me) was prepared from tris(methylthio)methane by reaction with one equivalent of *n*-butyllithium and was treated with **3** in tetrahydrofuran for 4 h. Under these conditions, attack at the carbonyl group was accompanied by loss of a methylthio group (eq. [1]). In deuteriochloroform the ^1H and ^{13}C nmr spectra of the product showed it to be a 2:1 mixture of the "open" and "closed" tautomers **8***a* and **8***b* (such tautomerism has been reported previously in related cases (3)). In hexadeuteriodimethyl sulfoxide only **8***a* could be detected in the nmr spectra (Tables 1 and 2). Crystallization of the product from ethyl acetate/hexanes gave **8***a* as a crystalline solid, mp 44–46°C, whose elemental composition confirmed the loss of a methylthio group and whose ir spectrum (ν_{max} 3392, 1701 cm^{-1}) confirmed the presence of hydroxyl and carbonyl groups. It is considered that compound **8***a* arises from the first-formed adduct **9** during the work-up under mildly acidic conditions (Scheme 3).

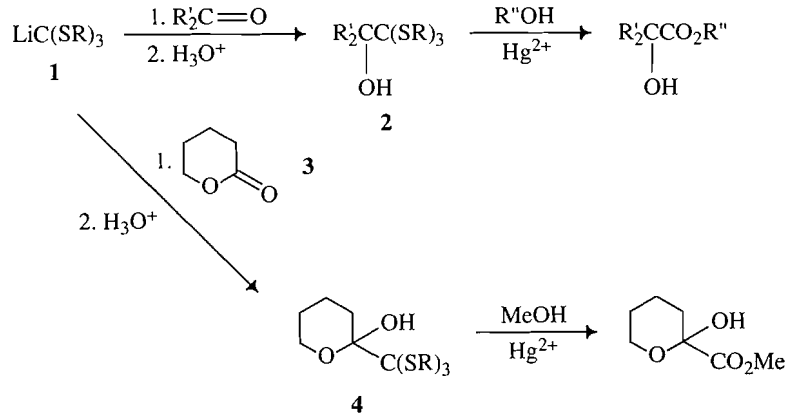
Treatment of δ-valerolactone with the lithio derivative **10** (**1**, R = Ph), prepared from tris(phenylthio)methyllithium and *n*-butyllithium under the same reaction and work-up conditions as those used with **7**, did not lead to the simple adduct. Instead it gave a crystalline product, $C_{12}H_{12}O_3S$, which is assigned structure **11** (eq. [2]). This assignment is based on its ^1H nmr

[1]Authors to whom correspondence may be addressed.

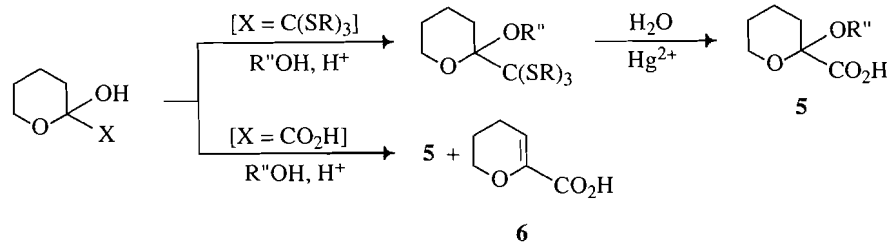
[2]The analogous reaction of δ-lactones with the anion of the dithioacetal 1,3-dithiane was reported earlier (ref. 3 and refs. quoted therein).

[3]For a preliminary account of part of this work, see ref. 4.

Can. J. Chem. Downloaded from www.nrcresearchpress.com by 198.100.157.202 on 09/07/12
For personal use only.



SCHEME 1

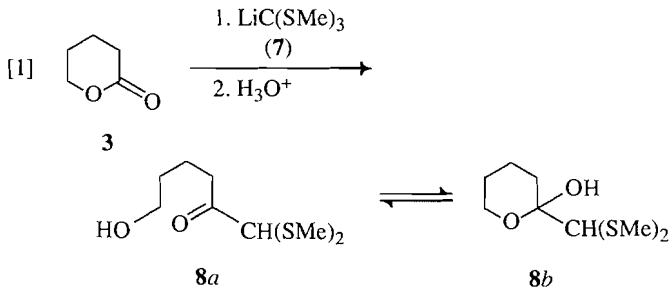


SCHEME 2

TABLE 1. The ^{1}H nmr spectra of compounds **8***a*, **17***a*, **18**, and **19**[a]

	5 4 3 2 1 $ROCH_2CH_2CH_2CH_2COX$			
	2′ $X = CH(SMe)_2$	$X = \begin{matrix} S\text{—}4' \\ 2' \\ CH_3 \quad S\text{—}6' \end{matrix}\!\!>\!\!5'$		
	8*a* R = H	**17***a* R = H	**18** R = $COCH_3$	**19** R = CHO
H-2	2.65 (t)	2.7*	2.7*	2.8*
H-3	1.40	1.8*	1.6*	1.85*
H-4	1.55	1.8*	1.6*	1.85*
H-5	3.37 (t)	3.55 (t)	4.00 (t)	4.15 (t)
H-2′	4.95 (s)	—	—	—
H-4′ }	—	3.15	3.15 (dt)	3.17 (ddd)
H-6′ }	—	2.7*	2.7*	2.8*
H-5′	—	1.8*	1.6*	1.8*
SCH_3	1.99 (s)	1.90 (s)	1.97 (s)	1.92 (s)
CH_3CO	—	—	1.88 (s)	—
CHO	—	—	—	8.02 (s)
OH	4.37 (s)		—	—

[a]δ($CDCl_3$); signals are multiplets unless designated as singlet (s), doublet (d), triplet (t), or a combination of these. Their relative intensities are in accord with the assignments. Signals marked with an asterisk overlap with one or more other signals.



spectrum (δ 1.8–2.5 (m, 4H, H-4 and H-5), 3.95 (t, 1H, H-3), 4.45 (t, 2H, H-6), 7.45 (s, 5H, Ph)), and the presence of two strong bands with ν_{max} 1733 and 1695 cm^{-1} and the absence of a hydroxyl stretching band in its ir spectrum.

We propose that **11** arises as shown in Scheme 4. Tris(phenylthio)methyllithium is known to undergo decomposition in solution to give tetrakis(phenylthio)ethylene (**12**) and lithium thiophenoxide (**13**) (5, 6*a*) (eq. [3]). Reaction of δ-valerolactone (**3**) with the latter could give the anion **14**. Addition of this to **12** and elimination of thiophenoxide would give the intermediate

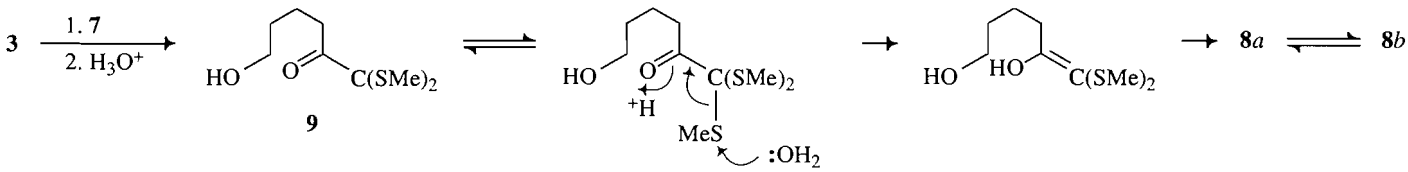
Can. J. Chem. Downloaded from www.nrcresearchpress.com by 198.100.157.202 on 09/07/12
For personal use only.

TABLE 2. The ^{13}C nmr spectra of compounds **8***a*, **17***a*, **18**, and **19**[a]

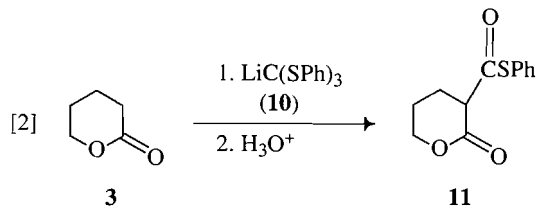
$$ROCH_2CH_2CH_2CH_2COX$$ (5 4 3 2 1)

	X = CH(SMe)$_2$ (2′)	X = 2′-(4′,5′,6′-dithiacyclohexyl)-2′-methyl		
	8*a* R = H	**17***a* R = H	**18** R = $COCH_3$	**19** R = CHO
C-1	202.0	200.6	202.1	200.0
C-2	38.5	35.4	35.2	35.1
C-3	20.3	21.0	21.3[b]	21.2
C-4	31.8	32.4	28.2	28.2
C-5	60.4	62.9	64.5	68.9
C-2′	60.0	68.9	68.9	64.0
C-4′, C-6′	—	27.5	27.8	27.5
C-5′	—	25.0	25.0	25.0
SCH_3	11.9	16.6	16.5	16.6
CH_3CO	—	—	21.3[b]	—
CH_3CO	—	—	171.8	—
CHO	—	—	—	161.8

[a]δ($CDCl_3$); the assignments are in accord with APT spectra.
[b]Superimposed signals; in C_6D_6 separate signals appear at δ 20.9 and 21.6, but are not individually assignable (see Experimental).



SCHEME 3

[2] 

15, which in turn could be converted to the observed product **11** as shown.

The third lithio trithio-orthoformate investigated was 2-lithio-2-(methylthio)-1,3-dithiane (**16**), prepared from *n*-butyllithium and 2-(methylthio)-1,3-dithiane, itself obtained by methylthioylation of 1,3-dithiane (6) and monodemethylthioylation of 2,2-bis(methylthio)-1,3-dithiane, a by-product in the methylthioylation. Reaction of **16** with δ-valerolactone under the usual conditions proceeded without complication and gave a tautomeric mixture of the simple adducts **17***a* and **17***b* (Scheme 5). The complexity of the spectra of this mixture made detailed interpretation difficult and the isolation of a single component was investigated. Acetylation of the mixture with acetic anhydride and pyridine at room temperature gave a single product, the open acetate **18**; the analogous open formate **19** was also obtained by treatment of the mixture with trimethyl orthoformate and cerous chloride heptahydrate (cf. ref. 7).

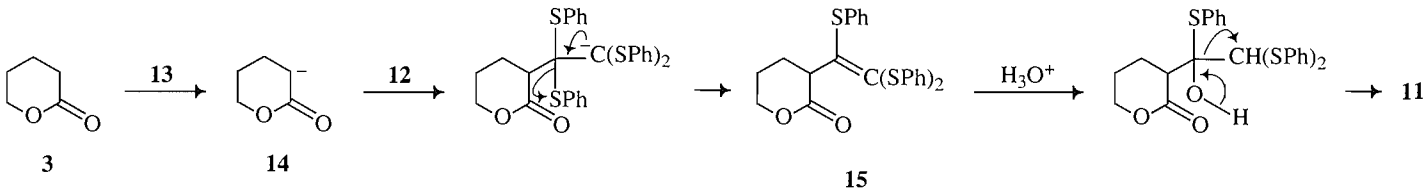
[3] $2(PhS)_3CLi \longrightarrow (PhS)_2C{=}C(SPh)_2 + 2PhSLi$
10 **12** **13**

Hydrolysis of the acetate in weakly basic aqueous methanol gave the single, open adduct **17***a*.[4] It was later found that **17***a* could be obtained by column chromatography of the mixture of **17***a* and **17***b*. The ir spectra of compounds **17***a*, **18**, and **19** show carbonyl stretching bands at ν_{max} 1702–1703 cm^{-1}, establishing the presence of the ketonic group; that of **17***a* also showed a hydroxyl stretching peak at 3389 cm^{-1} and those of **18** and **19** have additional carbonyl stretching peaks at 1735 and 1723 cm^{-1}, respectively, confirming the presence of the acetate and formate groups. The ^1H and ^{13}C nmr spectra of **17***a*, **18**, and **19** are given in Tables 1 and 2, and are in good accord with the structures assigned.

Ironically, although the reaction of δ-valerolactone with **16**, unlike its reactions with the other lithio trithio-orthoformates **7** and **10**, gave the simple adduct without complication, the same was not true of the second reaction of interest, the acetalization of this adduct. This latter problem is not attributable to the fact that **17** was in its open form, since under the reaction conditions used equilibration with closed structures can occur. The acetalization reactions studied all involved reaction with methanol. Initially methanolic hydrogen chloride was used, but it was found that the reactions were complex and capricious. It was later found that the conditions of choice were treatment with methanol in the presence of an acidic ion-exchange resin. Under

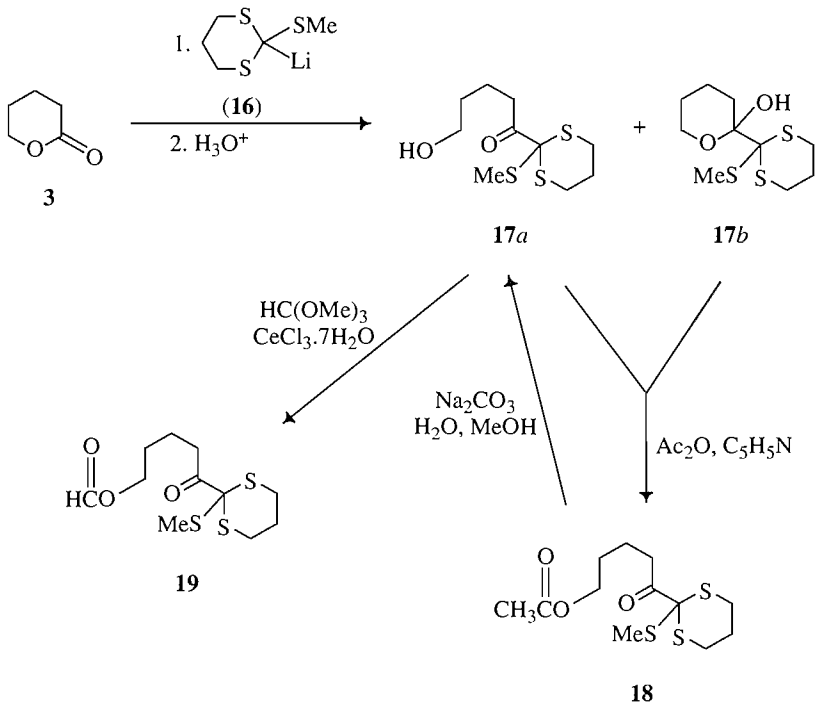
[4]The obtention of **17***a* under some conditions and of a mixture of **17***a* and **17***b* under others must result from failure to reach tautomeric equlibrium.

Can. J. Chem. Downloaded from www.nrcresearchpress.com by 198.100.157.202 on 09/07/12
For personal use only.



3 14 15

SCHEME 4



SCHEME 5

these conditions the reactions were reproducible, although three products were still formed.

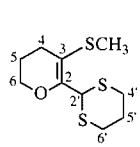
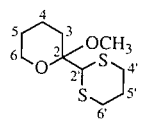
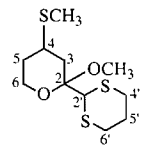
One of these, obtained in 28% yield, was a crystalline compound, $C_{10}H_{16}OS_3$, which is assigned structure **20**. A second product, $C_{10}H_{18}O_2S_2$, isolated in low yield (7%), is considered to have structure **21**, while a third product, $C_{11}H_{20}O_2S_3$, obtained in 23% yield, is assigned structure **22**.

The structures of compounds **20** and **21** readily follow from their origin, composition, and spectra. Neither shows a carbonyl stretching band in its ir spectrum and the signals in their ^1H and ^{13}C nmr spectra can be assigned as in Tables 3 and 4. The structure of compound **21** was confirmed by its preparation as the major product (75%) by acetalization of **23**, the adduct from δ-valerolactone and 1,3-dithiane (3), with methanol and acidic ion-exchange resin (Scheme 6).

The assignment of structure **22** was more challenging. Its composition showed that it is isomeric with the simple acetalization product from **17**. Its ^1H and ^{13}C nmr spectra (Tables 3 and 4) clearly show that it is not the latter; particularly noteworthy are the one-proton signals at $^H\delta$ 3.00 and 4.50, assignable to -C*H*(S-)-S- and -C*H*(S-)-S-, respectively (*vide infra*). These spectra established that the OCH_3 and SCH_3 groups are retained, and the absence of a carbonyl stretching band in its ir spectrum showed that the compound is of the closed type. Its origin, composition, and spectra narrow the choice to one of the diastereomers of **22**, **24** or **25**. Detailed analysis of its ^1H nmr spectra as discussed below permitted the unambiguous choice of structure **22** and the assignment of the relative configuration shown in **26**.

A ^1H–^1H COSY spectrum combined with the chemical shift

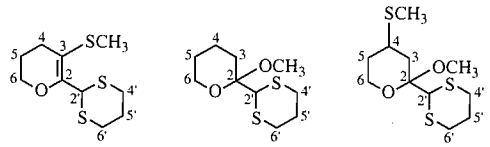
TABLE 3. The ^1H nmr spectra of compounds **20**, **21**, and **22**[a]

	 **20**	 **21**	 **22**
H-3	—	1.5*	1.8*, 2.2*
H-4	2.25 (t)	1.8*, 2.1*	3.00
H-5	1.9*	1.6*	1.8*, 2.2*
H-6	4.04 (t)	3.6–3.75	3.5–3.9
H-2′	5.81 (s)	4.49 (s)	4.50 (s)
H-4′ } H-6′ }	2.94	2.85–2.94	2.85
H-5′	1.9*	1.8*, 2.1*	1.8*, 2.2*
SCH_3	2.17 (s)	—	2.05 (s)
OCH_3	—	3.30 (s)	3.25 (s)

[a]See footnote *a* in Table 1.

Can. J. Chem. Downloaded from www.nrcresearchpress.com by 198.100.157.202 on 09/07/12
For personal use only.

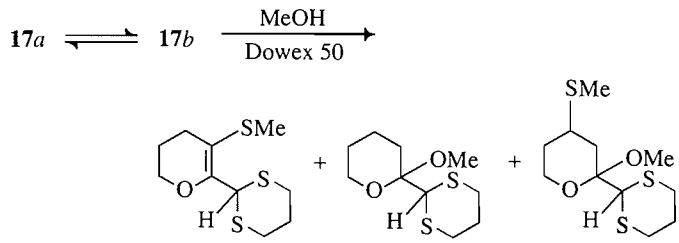
TABLE 4. The ^{13}C nmr spectra of compounds **20**, **21**, and **22**[a]



	20	**21**	**22**
C-2	155.4	99.8	100.7
C-3	104.9	30.9	37.7
C-4	23.5	18.8	37.6
C-5	30.9	25.2[b]	32.1
C-6	67.2	62.1	62.3
C-2′	46.8	54.5	54.0
C-4′ }	26.6	30.5	31.2
C-6′ }		30.5	31.2
C-5′	25.8	26.1[b]	26.4
SCH_3	17.4	—	13.0
OCH_3	—	47.3	48.1

[a]See footnote *a* in Table 2.
[b]Close-lying signals, not individually assignable.

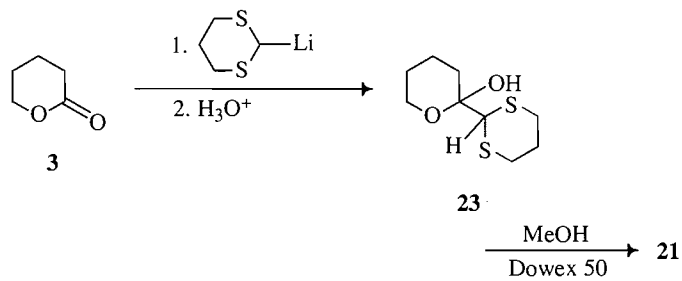
values showed that of the six methylene groups, three form a $-CH_2-CH_2-CH_2-$ sequence with no H–H connectivity with the remainder of the molecule. The proton chemical shift values are in accord with their presence as the C-4′, C-5′, and C-6′ protons of a 1,3-dithiane ring. All but one of the remaining proton signals can be assigned to a $-CH_2CHCH_2CH_2O-$ sequence and the remaining proton signal, which showed no H–H coupling, is assignable on the basis of both its ^1H and ^{13}C nmr chemical shifts to the C-2′ proton of the 1,3-dithiane ring. These results lead to the choice of structure **22** for the product. Confirmatory



20 **21** **22**

evidence was provided by one-bond and multiple bond carbon–proton chemical shift correlation and 1D polarization transfer (INEPT) spectra (see Table 5).[5]

Consideration of the coupling constants shows that the SCH_3

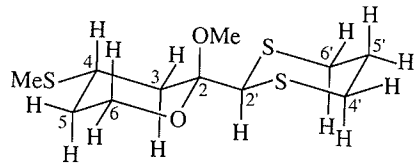


3 **23**

SCHEME 6

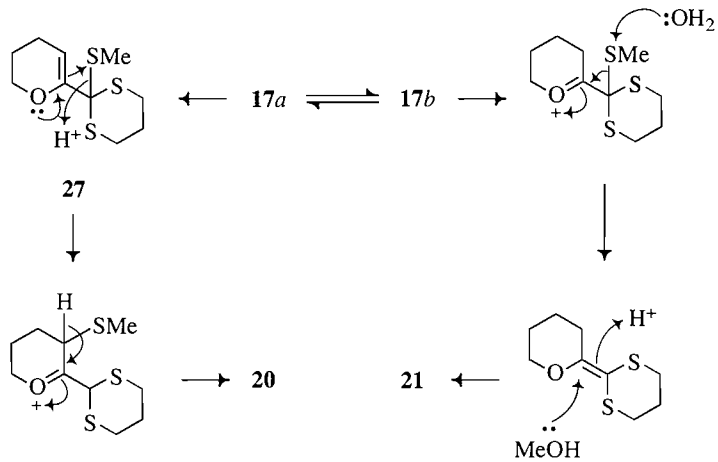
[5]We thank Drs. A. A. Grey and L. R. Radics, Carbohydrate Research Centre, University of Toronto, for obtaining and discussing these and the COSY spectra.

TABLE 5. Correlated nmr spectra of compound **22**[a,b]



	$^C\delta$	$^H\delta$	Long range C–H correlations
2	100.6 (C)	—	C3–H, Cl′–H, OMe
3	38.1 (CH_2)	2.64 (e), 2.20 (a)	C3–H, Cl′–H
4	37.6 (CH)	3.01	SMe
5	32.2 (CH_2)	1.58 (e), 1.45 (a)	C2–H_e, C3–H, OMe
6	61.7 (CH_2)	3.51 (e), 3.38 (a)	C4–H_a, C3–H
2′	53.8 (CH)	4.52	C4′–H, C6′–H
4′	30.43 (CH_2)	2.45 (e), 2.30 (a)	Cl′–H
6′	30.37 (CH_2)	2.45 (e), 2.30 (a)	Cl′–H
5′	26.0 (CH_2)	1.50 (e), 1.36 (a)	C3′–H, C5′–H
OCH_3	47.5 (CH_3)	3.36	C3–H
SCH_3	12.3 (CH_3)	1.73	C4–H

[a]In C_6D_6.
[b]See footnote 5.



SCHEME 7

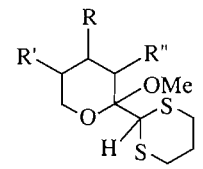
group is located equatorially. Since it would be expected that the 1,3-dithianyl ring would take up the equatorial orientation at C-2, this and the SCH_3 group must be *cis* with respect to the pyran ring, as in **26**. Such a relationship is expected if the introduction of the OCH_3 group is reversible, as is likely.

It is not difficult to postulate types of reaction pathway that would account for the formation of **20** and **21**. As in other cases the reaction sequences may include open or closed intermediates. We illustrate in Scheme 7 two of the latter type, which account for the formation of **20** and **21**.[6] Compound **21** is analogous to compound **8** obtained from **7**; we have previously given in Scheme 3 an open version of this type of reaction.

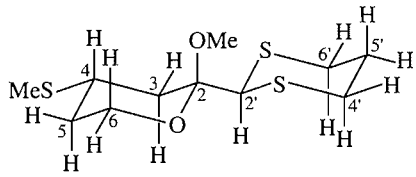
The origin of **22** is more difficult to discern. One possibility is that C-4 develops cationic character in the course of the reaction, for example via intermediates of type **27** and **28** (Scheme 8). The former is also postulated as an intermediate in

[6]The postulated acid-catalyzed nucleophilic attack on sulfur in **27** is closely related to that postulated in Scheme 3 and finds analogy in our observation of the conversion of 2,2-bis(methylthio)-1,3-dithiane to 2-(methylthio)-1,3-dithiane by base-catalyzed nucleophilic attack on sulfur.

Can. J. Chem. Downloaded from www.nrcresearchpress.com by 198.100.157.202 on 09/07/12
For personal use only.



22 R = SMe, R' = R" = H
24 R' = SMe, R = R" = H
25 R" = SMe, R = R' = H

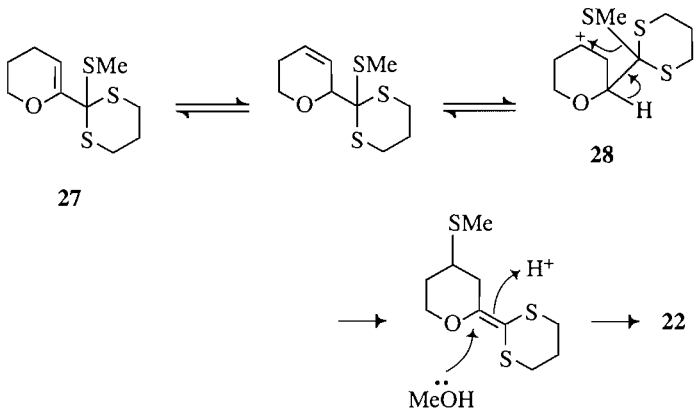


26

the formation of **20** (Scheme 7). Then SCH_3 migration could occur as shown in **28**.[7]

In sum, although we have uncovered several reactions of interest, the reactions of none of the three lithio trithioorthoformates **7**, **10**, and **16** with δ-valerolactone has provided a viable route to acetals of type **5** under the conditions that we have used.[8] Indeed, our results with **16** indicate that under these conditions elimination can still compete with acetalization.

Since we have found that the C-2 acetal **21** can be prepared in acceptable yield from the C-2′ dithioacetal **23**, an alternative avenue worthy of exploration is the unmasking and oxidation of such acetals to give compounds of type **5**.



SCHEME 8

Experimental

Melting points (mp) were determined with a Thomas–Hoover capillary melting point apparatus, and are uncorrected.

Infrared (ir) spectra of the neat compounds were recorded with a Nicolet FTIR 5DX; only strong (s) bands are reported. Proton magnetic resonance (^{1}H nmr) spectra were recorded in deuteriochloroform (unless otherwise specified) with a Varian T-60, Gemini 200, Varian XL-400, or Bruker AM500 spectrometer. Peak positions are reported on the delta (δ) scale in ppm. Signal multiplicities are reported as singlet (s), doublet (d), triplet (t), and multiplet (m). Carbon-13 magnetic resonance (^{13}C nmr) spectra were recorded in deuteriochloroform (unless otherwise specified) with a Varian XL-200 or Varian XL-400 spectrometer, operating in the pulsed Fourier transform mode. Peak positions are reported on the delta (δ) scale in ppm. Mass spectra were recorded with a Bell and Howell CEC 21-490, VG 70-250S, or VG ZAB SE[9] mass spectrometer. Peak positions are reported in mass-to-charge (m/z) units with the relative abundances in parentheses (rel. %). Ionization was effected by electron impact, unless otherwise indicated.

Silica gel (35–70 μm) was used for column chromatography. Analytical thin-layer chromatography was carried out on aluminum-backed plates that had been precoated with 0.20 mm of silica gel.

Reaction of tris(methylthio)methyllithium (7) with δ-valerolactone (3). Formation of 6-hydroxy-1,1-bis(methylthio)-2-hexanone (8a) and tetrahydro-2-bis(methylthio)methyl-2-pyranol (8b)

A solution of tris(methylthio)methane (23.6 g, 153 mmol) in anhydrous THF (130 mL) was cooled at −78°C under argon. One equivalent of *n*-butyllithium in hexane was added, and the mixture was stirred for 30 min. A solution of δ-valerolactone (5.00 g, 49.9 mmol) in anhydrous THF (40 mL) was then added. The mixture was stirred for 4 h, allowed to warm gradually to −20°C, and treated with saturated aqueous ammonium chloride. The mixture was extracted with chloroform and the extract was washed with water, dried over anhydrous magnesium sulfate, and concentrated. The residue was chromatographed on silica gel with hexane/ethyl acetate (7:3 v/v) as the eluent to yield **8***a* and **8***b* (7.05 g, 34.9 mmol; 70%) as a pale yellow oil. Crystals were formed upon storing at −4°C overnight. Recrystallization from hexane/ethyl acetate (9:1 v/v) yielded **8***a* as white crystals, mp 44–46°C; ir ν_{max} (KBr): 1701 (s), 3390 (s) cm^{-1}; ms m/z (rel. %): 208 (2, M^+), 109 (28), 108 (75), 107 (100), 101 (26), 83 (13), 61 (23), 55 (28). Anal. calcd. for $C_8H_{16}O_2S_2$: C 46.20, H 7.74, S 30.78; found: C 46.07, H 7.82, S 30.44.

Reaction of tris(phenylthio)methyllithium (10) with δ-valerolactone (3). Formation of tetrahydro-3-(phenylthiocarbonyl)-2-pyranone (11)

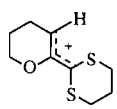
A solution of tris(phenylthio)methane (1.57 g, 4.6 mmol) in anhydrous THF (19.4 mL) was cooled at −78°C under argon. One equivalent of *n*-butyllithium in hexane (2.5 M; 1.84 mL) was added and the mixture was stirred for 15 min. A solution of δ-valerolactone (150 mg, 1.50 mmol) in anhydrous THF (6.75 mL) was added and the reaction mixture was stirred for 4 h. The work-up and purification of the crude product as for **8** yielded **11** (172 mg, 0.73 mmol, 48%) as a pale yellow oil, which crystallized upon being stored in the freezer (−4°C) overnight. Recrystallization from hexane/methanol (9:1 v/v) yielded **11** as white crystals, mp 63–65°C; ir ν_{max}: 1733 (s), 1692 (s) cm^{-1}; ^{1}H nmr (60 MHz) δ: 1.8–2.5 (m, 4H), 3.95 (t, 1H), 4.45 (t, 2H), 7.45 (s, 5H) ppm; ms m/z (rel. %): 236 (12, M^+), 149 (7), 127 (100), 110 (68), 109 (45), 99 (12), 83 (39), 65 (28). Exact Mass calcd. for $C_{12}H_{12}O_3S$: 236.0507; found: 236.0509.

Preparation of 2-(methylthio)-1,3-dithiane

(i) From 1,3-dithiane

Freshly sublimed 1,3-dithiane (2.66 g, 22.1 mmol) was dissolved in anhydrous THF (20 mL) and cooled at −78°C under argon. *n*-Butyllithium in hexane (1.6 M; 16.54 mL, 26.5 mmol) was added over 25 min, and the solution was stirred for 2 h. Dimethyl disulfide (3.61 mL, 40.1 mmol) was added over 10 min, and the reaction mixture was allowed to warm gradually to room temperature and then poured into 0.05 N hydrochloric acid (200 mL). The THF was removed by evaporation, and the aqueous layer was extracted several times with dichloromethane/pentane (1:1 v/v). The extracts were combined and washed with 10% aqueous sodium bicarbonate, water, and saturated aqueous sodium chloride, dried over anhydrous magnesium sulfate,

[7]A referee has suggested that **i** might be an intermediate in the formation of **22** and **20**. We have considered mechanisms such as this where methanethiol is eliminated and re-added. However, we find it difficult to accept that with methanol as solvent the formation of the methoxy analogs of these methylthio compounds is not observed.



i

[8]The differences between certain of our results and those reported earlier (2) may be attributable to differences in reaction conditions, but we have been unable to check this (see ref. 4, footnote §).

[9]We thank Dr. H. Pang, Carbohydrate Research Centre, University of Toronto, for recording and discussing the spectra taken on this spectrometer.

Can. J. Chem. Downloaded from www.nrcresearchpress.com by 198.100.157.202 on 09/07/12
For personal use only.

Can. J. Chem. Downloaded from www.nrcresearchpress.com by 198.100.157.202 on 09/07/12
For personal use only.

and concentrated to give a yellow oil (1.0 g). The crude product was purified by sublimation (50°C, 0.25 Torr; 1 Torr = 133.3 Pa) of the excess 1,3-dithiane present, followed by distillation of the desired 2-(methylthio)-1,3-dithiane (120°C, 0.25 Torr) (lit. (*6b*) bp 50°C, 0.25 Torr), as a colorless oil (886 mg, 24%); ^{1}H nmr (200 MHz) δ: 1.95 (m, 2H), 2.15 (s, 3H), 2.60 (m, 2H), 3.15 (m, 2H), 4.75 (s, 1H) ppm; ^{13}C nmr (200 MHz) δ: 16.8, 25.2, 26.6, 48.1 ppm. The residue was distilled (140°C, 0.25 Torr) to afford 2,2-bis(methylthio)-1,3-dithiane as a colorless oil; ^{1}H nmr (200 MHz) δ: 1.95 (m, 2H), 2.16 (s, 6H), 2.92 (t, 4H) ppm; ^{13}C nmr (200 MHz) δ: 16.0, 24.0, 30.0, 66.4 ppm.

(ii) From 2,2-bis(methylthio)-1,3-dithiane

A solution of 2,2-bis(methylthio)-1,3-dithiane (3.24 g, 15.3 mmol) in anhydrous THF (63.3 mL) was cooled to −78°C under argon. One equivalent of *n*-butyllithium (1.6 M; 9.56 mL) was added, and the mixture was stirred for 1.5 h, allowed to warm to −40°C, added to water, and extracted with carbon tetrachloride. The extract was dried over anhydrous magnesium sulfate, and evaporated to afford a yellow oil. The crude product was identified as a mixture of the starting material and 2-(methylthio)-1,3-dithiane by nmr spectroscopy. Purification was effected by distillation as above to afford the latter compound (69%).

*Reaction of 2-lithio-2-(methylthio)-1,3-dithiane (**16**) with δ-valerolactone (**3**). Formation of 2-(5-hydroxy-1-oxopentyl)-2-(methylthio)-1,3-dithiane (**17**a) and 2-(tetrahydro-2-hydroxy-2-pyranyl)-2-(methylthio)-1,3-dithiane (**17**b)*

A solution of 2-(methylthio)-1,3-dithiane (2.09 g, 12.6 mmol) in anhydrous THF (5 mL) was cooled to −78°C under argon. One equivalent of *n*-butyllithium (1.6 M; 7.78 mL) was added, and the mixture was stirred for 15 min to give **16**. A solution of δ-valerolactone (411 mg, 4.10 mmol) in anhydrous THF (23 mL) was added, and the reaction mixture stirred for 4 h, allowed to warm gradually to −20°C, treated with saturated aqueous ammonium chloride, and extracted with chloroform. The extract was washed with water, dried over anhydrous sodium sulfate, and evaporated to afford a mixture of **17***a* and **17***b* as a yellow oil (2.06 g).

*Acetylation of **17**a and **17**b. Formation of 2-(5-acetyloxy-1-oxopentyl)-2-(methylthio)-1,3-dithiane (**18**)*

The crude product from the above reaction (2.06 g) was dissolved in anhydrous pyridine (4.46 mL), acetic anhydride (71.4 mL) was added, and the mixture was stirred under argon for 4 h. The reaction mixture was poured into ice-water and extracted with chloroform. The extract was washed with water, dried over anhydrous sodium sulfate, and evaporated to afford a yellow oil (1.8 g). Chromatography of the crude product on a silica column with hexane/ethyl acetate (7:3 v/v) as eluent afforded **18** (40% overall yield); ir ν_{max}: 1736 (s), 1700 (s) cm^{-1}; ^{13}C nmr (200 MHz; C_6D_6) δ: 16.5, 20.9, 21.6, 25.2, 27.3, 27.5, 28.6, 35.5, 64.4, 113.2, 199.4 ppm; ms *m/z* (rel. %): 308 (2, M^+), 261 (17), 165 (100), 119 (30). Anal. calcd. for $C_{12}H_{20}O_3S_3$: C 46.72, H 6.54, S 31.18; found: C 46.86, H 6.54, S 30.89.

*Hydrolysis of **18**. Formation of **17**a*

A solution of compound **18** (104 mg, 0.33 mmol) in aqueous basic methanol (70 mg of sodium carbonate/26 mL of 4% aqueous methanol) was stirred for 2.5 h at room temperature. The reaction mixture was treated with water (50 mL), and extracted with chloroform. The extract was washed several times with water, dried over anhydrous sodium sulfate, and evaporated to afford a pale yellow oil (87 mg, 90%); ir ν_{max}: 3389 (s), 2915 (s), 1700 (s) cm^{-1}; ms *m/z* (rel. %): 219 (3.5, $(M - SCH_3)^+$) 165 (35), 119 (100), 91 (32.5).

*Reaction of **17**a with trimethyl orthoformate. Formation of 2-(5-formyloxy-1-oxopentyl)-2-(methylthio)-1,3-dithiane (**19**)*

A solution of compound **17***a* (0.272 g, 1.02 mmol) in trimethyl orthoformate (0.68 mL) with a catalytic amount of cerium(III) chloride heptahydrate (2.5 mg) was stirred at room temperature for 46 h. The excess trimethyl orthoformate was removed under water aspirator pressure to afford a pale yellow oil (199 mg). The crude product was purified by chromatography on a silica column with hexane/ethyl acetate (7:3 v/v) as eluent, giving **19** as the only product eluted (45 mg, 24%); ir ν_{max}: 1723 (s), 1703 (s) cm^{-1}; ms *m/z* (rel. %): 294 (2, M^+), 247 (17), 165 (100), 119 (18), 91 (9).

*Reaction of **17**a with methanol and acidic ion-exchange resin. Formation of 2-(5,6-dihydro-3-(methylthio)-2(4H)-pyranyl)-1,3-dithiane (**20**), 2-(tetrahydro-2-methoxy-2-pyranyl)-1,3-dithiane (**21**), and 2-(tetrahydro-2-methoxy-4-(methylthio)-2-pyranyl)-1,3-dithiane (**22**)*

Dowex 50X8-100 ion-exchange resin (Dowex-50W-hydrogen, strongly acidic cation. 8% cross-linking, 50–100 dry mesh) was treated with 1 N hydrochloric acid, filtered, washed with water, and dried by azeotropic distillation with benzene. It was rinsed several times with anhydrous methanol before use.

Compound **17***a* (208 mg, 0.75 mmol) in anhydrous methanol (45 mL) was added to a tenfold excess of the acidic ion-exchange resin, and the mixture was stirred at room temperature under argon for 44 h. The reaction mixture was filtered through Celite to remove the resin, diluted with water (60 mL), and extracted with chloroform (3 × 25 mL). The combined extracts were washed with water (4 × 20 mL), dried over anhydrous sodium sulfate, and evaporated. Chromatography of the residue on a silica column with hexane/ethyl acetate (6:4 v/v) as eluent gave two major products and one minor product.

Compound **20** (52 mg; 28%) was eluted first as a pale yellow oil that crystallized upon standing in the freezer (−4°C) overnight. Recrystallization from hexane/ethyl acetate (7:3 v/v) afforded white crystals, mp 65.5–66.5°C: ms *m/z* (rel. %): 248 (100, M^+), 201 (24), 159 (83), 119 (21), 73 (10). Anal. calcd. for $C_{10}H_{16}OS_3$: C 48.35, H 6.49, S 38.72; found: C 48.41, H 6.52, S 38.52.

Compound **21** was eluted second as a pale yellow oil (17 mg; 7%). Exact Mass calcd. for $C_{10}H_{18}O_2S_2$: 233.0670 (M − 1); found:[10] 233.0683.

Compound **22** was eluted third as a pale yellow oil (48 mg; 23%); ms *m/z* (rel. %): 279 (9, $(M - 1)^+$), 266 (3), 201 (15), 161 (100), 133 (8), 101 (26), 85 (15), 71 (19). Exact Mass calcd. for $C_{11}H_{20}O_2S_3$: 279.0457 (M − 1); found:[11] 279.0450.

*Reaction of 2-(5-hydroxy-2-oxopentyl)-1,3-dithiane (**23**) with methanol and acidic ion-exchange resin. Formation of **21***

Compound **23** (727 mg, 3.26 mmol) (3) in anhydrous methanol (80 mL) was added to Dowex 50-X8-100 acidic ion-exchange resin prepared as above (7.3 g). The reaction mixture was stirred at room temperature under argon and worked up as before to give a pale yellow oil. Column chromatography on silica with hexanes/ethyl acetate (6:4 v/v) gave **21** as the only major product (580 mg; 75%), as a colorless oil whose spectra were identical with those of **21** obtained from **17***a*.

*Reaction of **20** with methanol and acidic ion-exchange resin. Formation of **21** and **22***

Compound **20** (48.3 mg, 0.195 mmol) in anhydrous methanol was treated with Dowex-50-X8-100 acidic ion-exchange resin as above. Chromatography as before gave compounds **20** (8.7 mg; 18%), **21** (13.8 mg; 30%), and **22** (18.1 mg; 32%), whose spectra were identical with those of the corresponding products obtained from **17***a*.

Acknowledgment

We thank the Petroleum Research Fund of the American Chemical Society for support of this work.

1. A. B. MANAS and R. J. SMITH. J. Chem. Soc. Chem. Commun. 216 (1975); W. D. WOESSNER. Chem. Lett. 43 (1976).

[10]This was obtained in the FAB mode in the mass range 190–250 using the accelerating voltage scan and polyethylene glycol with an average molecular mass of 300 in thioglycerol as an internal standard.

[11]This was obtained as in footnote 10 in the mass range 270–340 and polyethylene glycol with an average molecular mass of 600.

2. J. E. HENGEVELD, V. GRIEF, J. TADANIER, C.-M. LEE, D. RILEY, and P. A. LARTY. Tetrahedron Lett. **25**, 4075 (1984).
3. D. HORTON and W. PRIESE. Carbohydr. Res. **94**, 27 (1981).
4. P. YATES, J. J. KREPINSKY, and A. SEIF-EL-NASR. J. Chem. Soc. Chem. Commun. 177 (1989).
5. D. SEEBACH. Angew. Chem. Int. Ed. Engl. **6**, 443 (1967); G. A. WILDSCHUT, H. J. T. BOS, L. BRANDSMA, and J. F. ARENS. Monatsh. Chem. **98**, 1043 (1967); D. SEEBACH and A. K. BECK. Tetrahedron Lett. 1933 (1970); D. SEEBACH and A. K. BECK. J. Am. Chem. Soc. **91**, 1540 (1969).
6. (*a*) D. SEEBACH. Angew. Chem. Int. Ed. Engl. **6**, 442 (1967); (*b*) E. JUARISTI, J. TAPIA, and R. MENDEZ. Tetrahedron, **42**, 1253 (1986).
7. S. R. SCHOW, J. D. BLOOM, A. S. THOMPSON, K. N. WINZENBERG, and A. B. SMITH III. J. Am. Chem. Soc,. **108**, 2662 (1976).

Can. J. Chem. Downloaded from www.nrcresearchpress.com by 198.100.157.202 on 09/07/12
For personal use only.

The photoaddition of 1,3-diketonatoboron difluorides with benzene derivatives

YUAN L. CHOW AND XINXIN OUYANG
Department of Chemistry, Simon Fraser University, Burnaby, B.C., Canada V5A 1S6

Received July 11, 1990

YUAN L. CHOW and XINXIN OUYANG. Can. J. Chem. **69**, 423 (1991).

The boron difluoride complexes of 2-acetylcyclohexanone, 2-acetylcyclopentanone, and acetylacetone (abbreviated as $ACHBF_2$, $ACPBF_2$, and $AABF_2$) were irradiated in the presence of benzene to give the 1:1 adducts as the primary photoadducts; for certain BF_2 complexes, toluene, chlorobenzene, benzonitrile, and methyl benzoate were also used as substrates. The 1,5-diketone photoadducts were assumed to form by a [2+2] photocycloaddition followed by cyclobutane opening and hydrolysis to give 1,2 adducts. They undergo a variety of secondary thermal reactions, probably acid catalyzed, to give enol ethers, enol acetates, acetophenones, and ketonylacetophenones. The efficiency of these secondary reactions determines the final products. Photoaddition with a monosubstituted benzene preferentially occurs at the 3,4 bond without regioselectivity. Under oxygen, $ACHBF_2$ photolytically reacts with benzene to give a secondary oxidation product of a 10-membered cyclic alkylphenone, which is proven by X-ray crystallographic analysis to have the benzene ring and carbonyl group in orthogonal orientation. It is shown that the singlet excited state $ACHBF_2$ initiates the photoaddition, probably through the formation of the benzene exciplex, which could be detected by its emission. While the Stern–Volmer rates are small, the quantum yield of photoaddition products is as high as 0.12–0.19 under limiting conditions.

Key words: [2+2] photocycloaddition, non-planar alkanophenone, macrocyclic alkanophenone, boron difluoride complexes, photoaddition to benzenes.

YUAN L. CHOW et XINXIN OUYANG. Can. J. Chem. **69**, 423 (1991).

Opérant en présence de benzène, on a irradié les complexes difluorure de bore des 2-acétylcyclohexanone ($ACHBF_2$), 2-acétylcyclopentanone ($ACHBF_2$) et acétylacétone ($AABF_2$) et on a obtenu des photoadduits primaires 1 : 1; pour certains complexes du BF_2 on a aussi utilisé le toluène, le chlorobenzène, le benzonitrile et le benzoate de méthyle comme substrats. On a fait l'hypothèse que les photoadduits 1,5-dicétoniques se forment par une photocycloaddition [2+2] suivie d'une ouverture du cyclobutane et d'une hydrolyse qui conduit aux adduits 1,2. Ils subissent diverses réactions thermiques secondaires, probablement acido-catalysées, qui conduisent à des éthers énoliques, des acétates énoliques, des acétophénones et des cétonylacétophénones. L'efficacité de ces réactions détermine la nature des produits finaux. La photoaddition sur un benzène monosubstitué se produit d'une façon préférentielle, mais sans régiosélectivité, sur la liaison 3,4. En présence d'oxygène, l'$ACHBF_2$ réagit d'une façon photolytique avec le benzène pour donner un produit d'oxydation secondaire comportant une alkylphénone cyclique à dix chaînons dans laquelle on a démontré, par une analyse par diffraction des rayons-X, qu'il existe un cycle benzénique et un groupement carbonyle en position orthogonale. On a démontré que l'état excité singulet du $ACHBF_2$ initie la photoaddition, probablement par le biais de la formation de l'exciplexe du benzène que l'on a pu détecter par son émission. Même si les vitesses de Stern–Volmer sont faibles, le rendement quantique des produits de photoaddition atteint 0,12–0,19, dans des conditions limitantes.

Mots clés : photocycloaddition [2+2], alcanophénone non planaire, alcanophénone macrocyclique, complexes du difluorure de bore, photoaddition à des benzènes.

[Traduit par la rédaction]

We have demonstrated that the singlet excited state of 1,3-diketonatoboron difluorides undergoes photocycloaddition of the diketone moiety to simple olefins, and also sensitizes various electron rich olefins to undergo cation radical reactions (1–3). The primary reaction of the BF_2 complexes has been suggested to involve some degree of electron transfer from excited substrates, as indicated by a correlation of log k_q (where k_q is the quenching rate constant of a BF_2 complex fluorescence) and ionization potentials of substrates (1). Using dibenzoylmethanatoboron difluoride ($DBMBF_2$) as a model, we have described the photocycloaddition with some olefins; such a reaction is shown to be regiospecific and highly stereoselective. Further, its mechanism is shown to be highly unusual in involving the excimer of $DBMBF_2$ (3). While $DBMBF_2$ does not photolytically add to benzene derivatives, we have been surprised to observe that alkyl-type 1,3-diketonatoboron difluorides photolytically add to benzene derivatives. As photoaddition to benzene generally affords unusual products (4–9), we have carried out an investigation, which is the subject of this report.

Results

For this work, acetylacetonatoboron difluoride ($AABF_2$) (10, 11), 2-acetylcyclohexanonatoboron difluoride ($ACHBF_2$) (12), and 2-acetylcyclopentanonatoboron difluoride ($ACPBF_2$) (13) were prepared from the corresponding 1,3-diketones according to the reported procedures. These BF_2 complexes exhibited UV absorption peaks at nearly the same wavelength as the parent 1,3-diketones but with greater optical densities (Fig. 1). For comparison, the UV absorption maxima of the parent 1,3-diketones are as follows: acetylacetone, 271 nm (ϵ 6200); 2-acetylcyclopentanone, 283 nm (ϵ 4000, br); 2-acetylcyclohexanone, 283.5 nm (ϵ 7980).

Photolysis of $ACHBF_2$ in benzene or a mixture of benzene and acetonitrile under nitrogen efficiently consumed the BF_2 complex to yield acetophenone **1** and enol ether **2** in a 1:5 ratio as shown by GC analysis. A similar photolysis under oxygen afforded acetophenone and keto ester **5** in a 1:1 ratio, and a small amount of enol acetate **3**. The enol acetate **3** was known to be a photolabile compound (14, 15); its structure was readily identified from its typical enol acetate IR absorption at 1760, 1229, 1172, 770, and 712 cm^{-1} and the ^{13}C NMR signal for the ester CO at 169.31 ppm without the presence of a ketone CO signal.

While acetophenone was readily determined by coinjection with an authentic sample, the structure of **2** was deduced from its physical data: (i) the ^1H NMR signals of a CH_3 doublet at 1.61

Can. J. Chem. Downloaded from www.nrcresearchpress.com by 198.100.157.202 on 09/07/12
For personal use only.

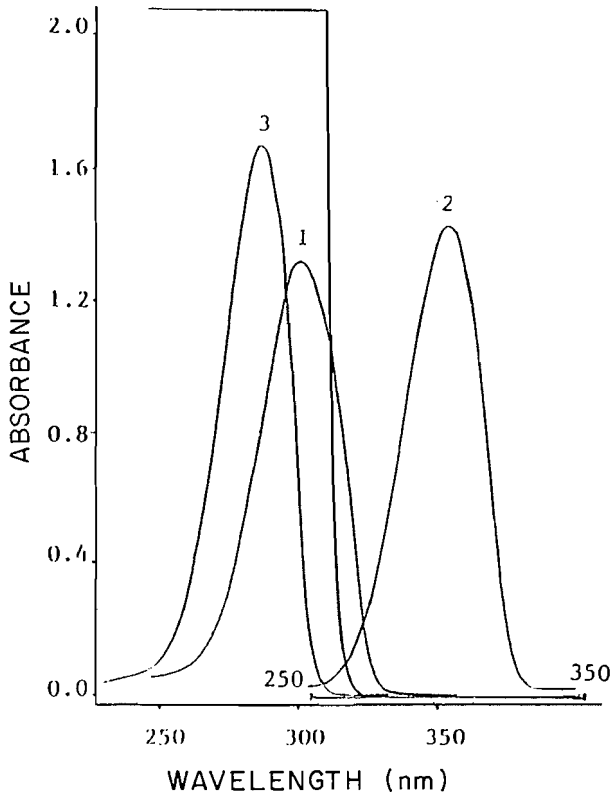


FIG. 1. The absorption spectra of $ACHBF_2$ (**1**, 1.0×10^{-4} M) and $ACPBF_2$ (**2**, 1.0×10^{-4} M) in CH_3CN, and $AABF_2$ (**3**, 1.0×10^{-4} M and 1.0×10^{-3} M) in ether.

ppm and methine quartet at 5.08 ppm (J = 6.4 Hz), and (ii) a tetra-substituted olefinic bond as shown by ^{13}C NMR data as well as the enol ether absorption at 1658 and 1196 cm^{-1}. The keto ester **5** was obtained in high yield by methylene blue sensitized oxygenation of **2** that obviously involved singlet oxygen. The structure of keto ester **5** could be deduced on the basis of an oxidative cleavage of **2** by the cycloaddition of singlet state oxygen to form dioxetane **4**, followed by a ring cleavage (16–18). However, the IR absorption at 1709 cm^{-1} and ^{13}C NMR spectrum for the ketone group at 207.48 ppm are typical for a non-conjugated carbonyl but not common to a conjugated carbonyl group (19), as shown in **5**. In addition, a distinct fluorescence peak at 330 nm is not typical for acetophenone-type compounds. Using X-ray crystallographic analysis, this compound was shown to have the structure shown in **5**. The X-ray computed structure showed that the C=O group was oriented nearly perpendicular to the plane of the benzene ring, therefore would not allow resonance interaction on account of the orthogonal orientation. The ORTEP view of the molecular structure is reproduced in Fig. 2 (20); the torsional angle defined by C(2)—C(1)—C(13)—O(1) is 101.0° and that by C(6)—C(1)—C(13)—O(1) is 80.5°. Inspection of the Dreiding model of structure **5** also showed that the benzyl $CHCH_3$ group strongly interacts with the C=O group at all conceivable conformations and forces the C=O group to orient out of coplanarity. This solved the spectroscopic anomaly shown above.

A similar photoaddition of $ACHBF_2$ to toluene under nitrogen was slower, and yielded product mixtures of positional isomers that defied attempts to separate them. It gave an equal mixture of 3- and 4-methylacetophenone (**6**) and that of enol ethers **7**. A 1:1 mixture of keto ester **8** was obtained either by photooxygenation of the mixture of enol ethers **7** or by a similar

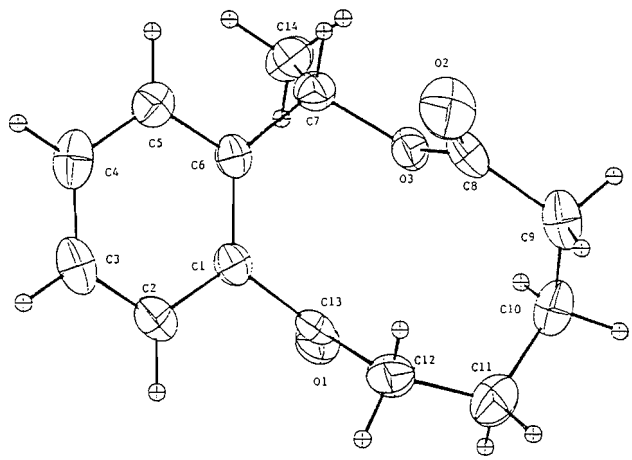


FIG. 2. ORTEP view of the molecular structure of **5**; important torsion angles (°) are: C(2)—C(1)—C(13)—O(1), 101.0 (3); C(6)—C(1)—C(13)—O(1), 80.5 (3); C(1)—C(6)—C(7)—C(14), 93.4 (3).

photoaddition of $ACHBF_2$ in toluene under oxygen. These mixtures gave poorly resolved peaks by GC analysis, could not be easily separated, and hence were analyzed as mixtures. The ^1H NMR spectrum of the mixture of **7** clearly gave two sets of signals similar to those of enol ether **2**. In particular, two sets of broad singlets (6.84 and 6.87 ppm) and double doublets (6.95 and 7.06 ppm, 6.91 and 6.96 ppm) defined two isomers, arising from the 1,2,4- and 1,2,5-substitution patterns on the benzene ring (19). Likewise, the mixture of keto esters **8** also showed two sets of ^1H NMR signals with the two aromatic singlets at 7.01 and 6.84 ppm and double doublets at 6.91 + 6.96 and 7.09 + 7.14 ppm. The ^{13}C NMR spectrum of this mixture showed two carbonyl signals, at 208.0 ppm for the ketone and 172.0 ppm for the ester. Although an X-ray structural analysis was not performed, the ^{13}C NMR signal at 208.0 ppm and the IR absorption at 1720 cm^{-1} for the ketone group unmistakably suggest that the neighboring carbonyl group is not coplanar with the benzene ring.

The photoaddition of $ACHBF_2$ with chlorobenzene, methyl benzoate, and benzonitrile in acetonitrile also occurred; the efficiency of the photoaddition was in the same order as given above. In all cases, mixtures of isomeric acetylated products were obtained as the major products, in addition to small amounts of dehydration products as shown by CI mode mass spectrometry. The minor products were assumed to be the corresponding enol ethers similar to **2** and **7**. For methyl benzoate, the acetylated products were isolated as a mixture and analyzed by ^1H NMR and GC spectra to contain a 3:1 ratio of 3- and 4-acetyl methyl benzoates **9**. However, under similar conditions $ACHBF_2$ failed to photolytically add to anisole, and the BF_2 complex was recovered nearly quantitatively.

The photoaddition of $ACPBF_2$ in benzene–ether (2:3 v/v ratio) gave a mixture of acetophenone, one minor, and one major product in a 5:1:5 ratio. From GC–MS inspection, the major product was shown to be a 1:1 addition product of ACP with benzene, such as 1,5-diketone **10**. The minor product was not isolated and was probably **12**, arising from dehydration in analogy to the formation of **2** and **7**. The yield of acetophenone increased if the photolysate was left untreated at room temperature; washing of the photolysate with water prevented the increase. When the photoaddition was carried out in the presence of either pyridine or tributylamine, the primary adduct **10**, enol ether **12**, and acetophenone were obtained in a 12:1:1 GC

Can. J. Chem. Downloaded from www.nrcresearchpress.com by 198.100.157.202 on 09/07/12
For personal use only.

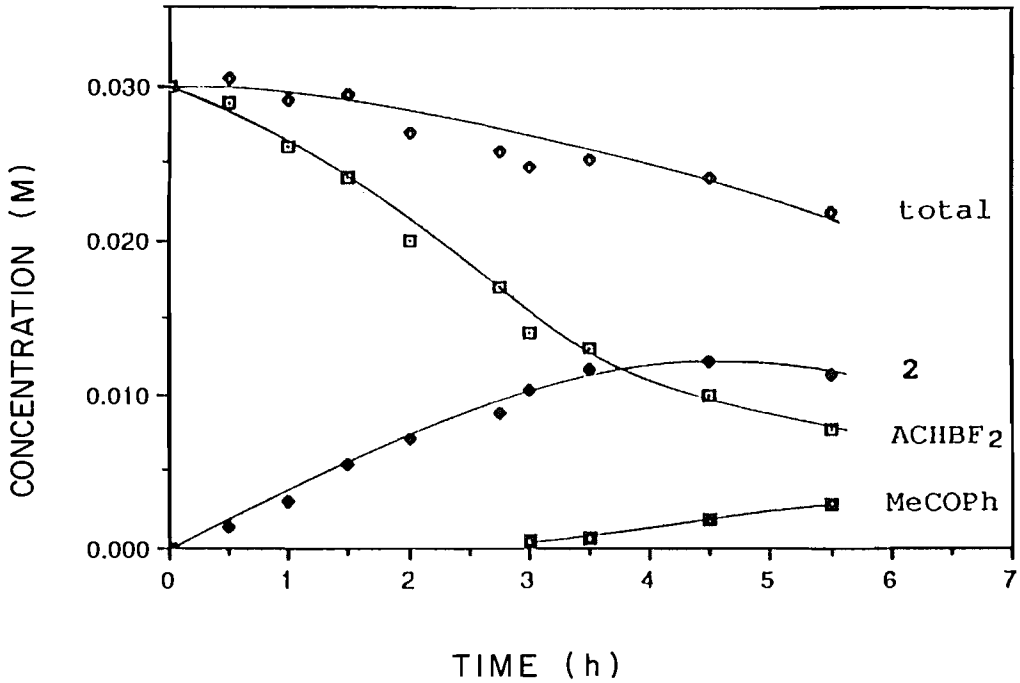


FIG. 3. The profile of the material balance in a photoaddition of $ACHBF_2$ (0.03 M) to benzene (2 M) in dioxane.

ratio. Such a crude product clearly showed allylic protons as a double doublet (3.49 ppm) and a double multiplet (3.05 ppm) with the coupling constant of 8.3 Hz for a *cis* orientation, and four olefinic protons at 5.95 ppm. Column chromatography of the photolysate gave no primary adduct **10** but 2-(2′-acetylphenyl)-cyclopentanone (**11**), which must arise from dehydrogenation of **10** during chromatography.

The photoaddition of $AABF_2$ with benzene was carried out under similar conditions as above and was monitored with GC analysis to show rapid formation of a peak corresponding to the 1:1 adduct **13** (M^+ 178 by CI mode) and a small amount of acetophenone **1**. The peak intensity of **13** started to decrease at about 50% $AABF_2$ conversion and the acetophenone peak started to appear; continuing irradiation of this photolysate afforded a complex mixture. When the photolysate was washed with a base, 1,5-diketone **13** was isolated as a stable compound with a small amount of 2-acetonylacetophenone **14** (21, 22). When the photolysate was not neutralized, **13** underwent facile secondary reactions to give a mixture that was chromatographed to afford a 1:1 mixture of 2-acetonylacetophenone (**14**) and 4-acetonylacetophenone (**15**). The ^1H NMR spectrum of the mixture showed a typical AA′BB′ system at 7.30 and 7.93 ppm (J = 8.3 Hz) for the *para* isomer **15** (21) in addition to other signals for the *ortho* isomer **14** (22). The diketone **15** was shown to be formed by acid-catalyzed thermal, but not by photochemical, reaction. The coupling constant of two allylic protons in **13** was determined to be 7.2 Hz, which confirmed the *cis* orientation of the two ketone side chains.

Mechanistic studies of this photoaddition were carried out using the photoaddition of $ACHBF_2$ to benzene as a model system. In Fig. 3, the profile of $ACHBF_2$ consumption and the formation of acetophenone and enol ether **2** were plotted versus the reaction time. It clearly demonstrated that acetophenone was a secondary photoproduct. $ACHBF_2$ did not show aggregate formation in the ground state, as demonstrated by UV spectroscopy. It showed weak fluorescence in acetonitrile with a peak at 355 nm; the lowest singlet excited state energy level was estimated to be E_s 91 kcal/mol (at 315 nm). The intensity of the fluorescence peak increased on the addition of benzene (0.5 M level), probably owing to emission from an exciplex of $ACHBF_2$ with benzene. The result from our group also showed that the $DBMBF_2$–benzene exciplex emits at about the fluorescence peak of $DBMBF_2$ itself.[1] In ether it showed phosphorescence emission at 77 K with a peak at 469 nm; the lowest triplet state energy is estimated to be 66–67 kcal/mol from the onset of the spectrum at 430 nm. The quantum yield (Φ) of the photocycloaddition was measured at various concentrations of benzene using a quantitative GC determination of enol ether **2**. The plot of the reciprocal of enol ether quantum yield (Φ) against that of benzene concentrations gave a good straight line as shown in Fig. 4. In dioxane, the $K_q\tau_0$ (= 5.4/81) was 0.067 and $\Phi_{limiting}$ (= 1/5.4) was 0.19; in acetonitrile, the $k_q\tau_0$

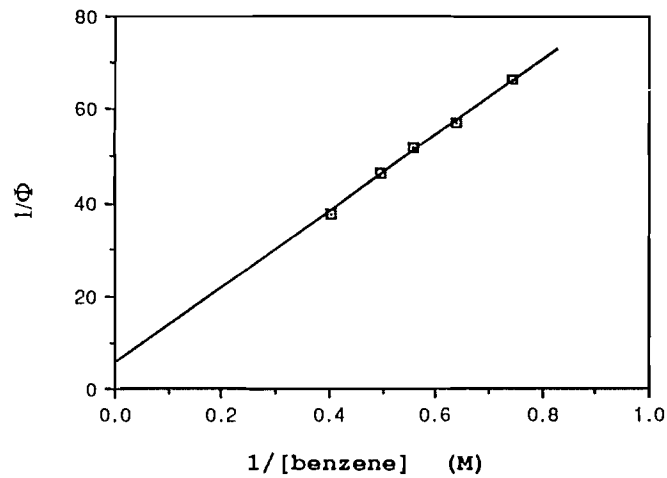
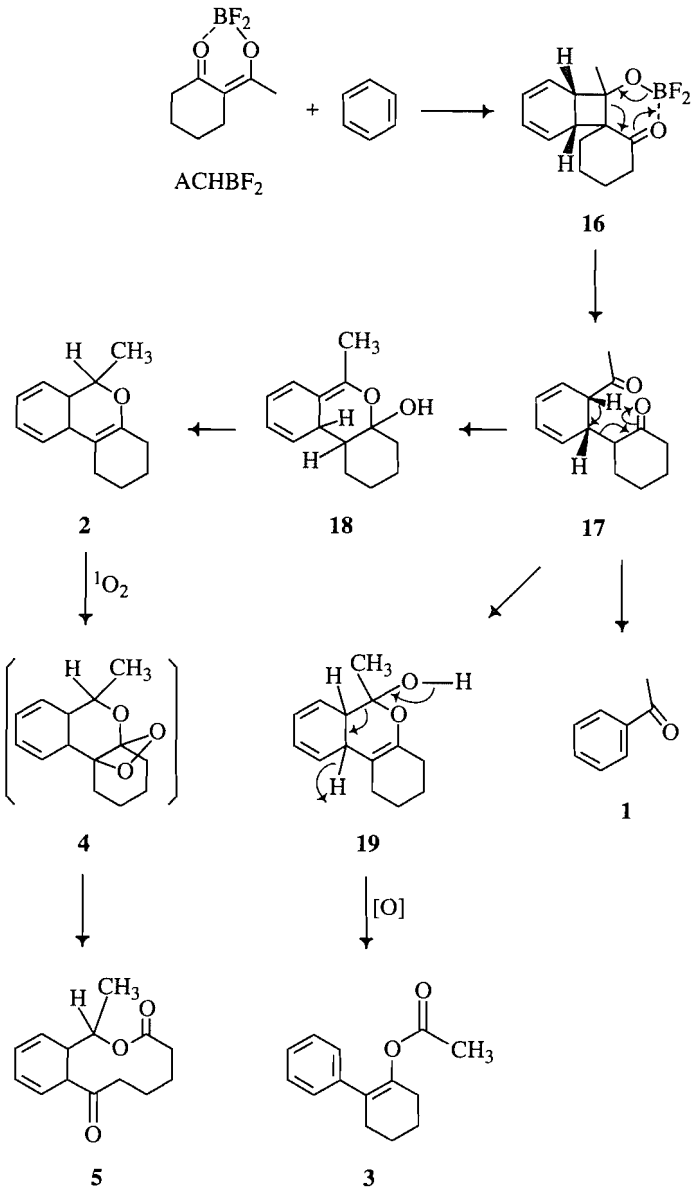


FIG. 4. A plot of the reciprocal of the quantum yields of **2** vs. the reciprocal of benzene concentration in the photoaddition of $ACHBF_2$ in dioxane.

[1]C. I. Johansson. Unpublished results from this group.

Can. J. Chem. Downloaded from www.nrcresearchpress.com by 198.100.157.202 on 09/07/12
For personal use only.



SCHEME 1

(= 8/247) was 0.032 and $\Phi_{limiting}$ (= 1/8) was 0.12. Owing to the long extrapolation, the error margin of intercepts was probably very large, and both $k_q\tau_0$ and $\Phi_{limiting}$ values must be regarded as an approximation. In contrast to the $DBMBF_2$ photoaddition to olefins (3), the quantum yield of **2** in this photoaddition was independent of [$ACHBF_2$] over the range of 0.02–0.04 M. The quantum yield was not affected in the presence of 1,3-pentadiene or 1,3-cyclohexadiene (up to 0.012 M) but was rapidly reduced in the presence of 1,2-dibromoethane in the 0.02–0.06 M range. The effect of this heavy atom containing compound was exponential above a concentration of 0.06 M and could not be analyzed quantitatively. Attempted sensitization of the photoaddition with benzophenone or xanthone as sensitizers failed to give any photoaddition product **2**.

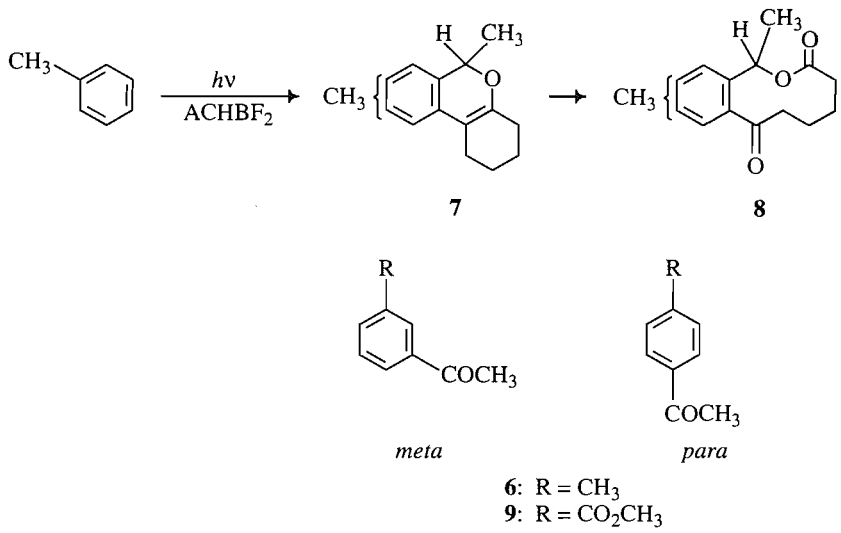
Discussion

As shown in the photoaddition of $ACPBF_2$ and $AABF_2$ to benzene, the primary products are 1:1 adducts of ACP or AA with benzene, i.e., 1,5-diketones such as **10** and **13**. From the structures of subsequent products shown in Scheme 1, the unisolated 1:1 adduct is deduced to be **17**. Indeed **13** is semi-stable and can be isolated and analyzed by ^1H NMR. The primary product is assumed to be formed by a [2+2] photocycloaddition to a BF_2 complex to form a cyclobutane derivative **16** (see Scheme 1); the ring opening and hydrolysis should give 1,5-diketone **17** (or **10** or **13**). This mechanism is proposed in analogy to the photoaddition of dibenzoylmethanatoboron difluoride to olefins (3). The hydrolysis of the BF_2 moiety generates hydrofluoric acid, which promotes acid-catalyzed reactions to be described below. The other photoaddition products arising from the alternative enol isomer (endocyclic double bond) of $ACHBF_2$ and $ACPBF_2$ to benzenes have not formed to a detectable extent as shown by careful searches in GC analysis. Should such photoaddition occur, acetophenone derivatives could not be obtained. It appears that these unsymmetrical BF_2 complexes preferentially react as exocyclic olefin isomers, exclusively, by some unknown reason. It should be pointed out that the proposed mechanism would predict the *cis* orientation of the ketone substituents in 1,5-diketones **10**, **13**, and **17** if the reaction is concerted. While the stereochemistry is eventually lost in aromatization of the ring in the subsequent reactions, the *cis* orientation is proven in the case of **10** and **13**.

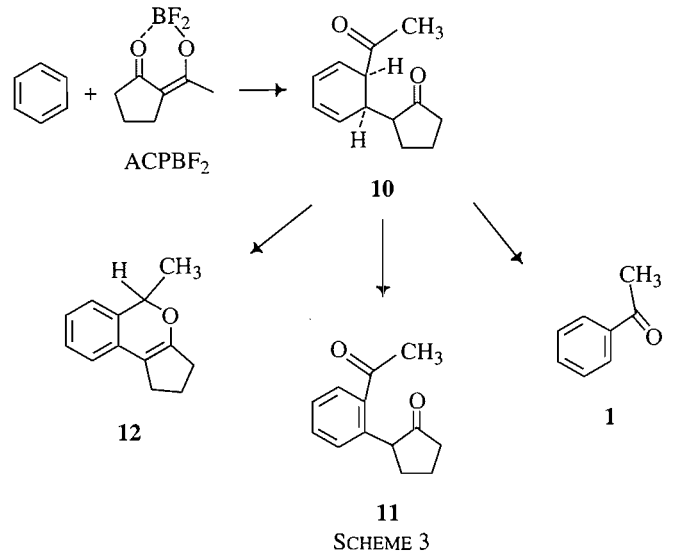
The observed substitution patterns of the photoaddition products in **6**–**9** (Scheme 2) and the lack of *ortho* substituted product could be explained by postulating that $ACHBF_2$ reacts with monosubstituted benzene at the 3,4 position exclusively but without regioselectivity. If photoaddition also occurs at the 2,3 position, the production of *ortho* substituted compound corresponding to **6**–**9** would be expected, since the orientation of $ACHBF_2$ approaching a monosubstituted benzene does not have much regioselective control. The absence of the $ACHBF_2$ attack at the 2,3 position, which may arise from the steric factor of the monosubstituted group, is a significant advantage. However, the complete lack of regioselectivity in the photoaddition of these BF_2 complexes is a major impediment to their synthetic applications.

Having decided the mechanism of primary photoaddition of BF_2 complexes to benzene derivatives, we are in a position to discuss the secondary reactions. The 1,5-diketones **10**, **13**, and **17** and the allied 1:1 adducts in this photoaddition exhibit a wide range of reactivities and patterns. The primary adducts **10** and **13** are obviously more stable than **17** and the allied adducts of $ACHBF_2$ with monosubstituted benzenes under the photolysis conditions. While the adducts of the latter group have undergone thermal reactions during photolysis, **10** and **13** do survive under the experimental conditions. One of the thermal reactions is the elimination of a ketone with aromatization (cyclohexanone in Scheme 1, cyclopentanone in Scheme 3, and acetone in Scheme 4), which is evidently acid catalyzed since pyridine or tributylamine added to neutralize HF formed during the photolysis does reduce the formation of acetophenone. It should be pointed out that acetophenone derivatives could be obtained by photoinitiated Norrish Type II photoreaction (23). A Type II photocleavage appears to contribute insignificantly to the formation of acetophenone since the yield of acetophenone in $ACHBF_2$ is not changed significantly by using a 350 nm irradiation source or a high concentration of $ACHBF_2$ complex. Other BF_2 complex photoadditions should follow the same pattern. This acid-catalyzed elimination drains the primary photoadduct 1,5-diketones to unwanted acetophenone derivatives, which is particularly serious for relatively stable 1,5-diketones such as **10** and **13**. Fortunately, such a process can be controlled with the addition of a tertiary amine.

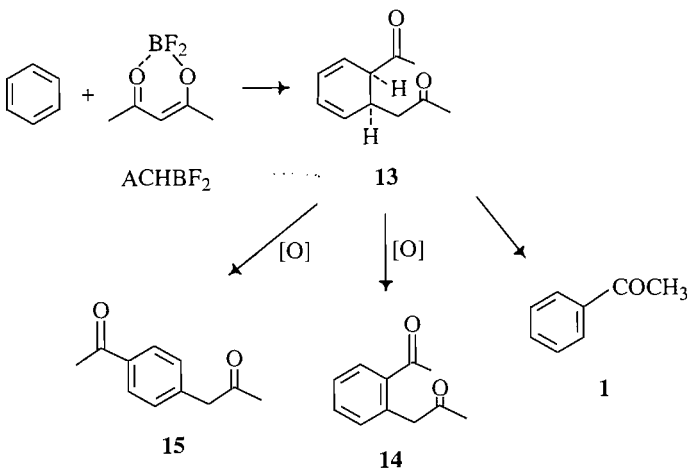
Can. J. Chem. Downloaded from www.nrcresearchpress.com by 198.100.157.202 on 09/07/12
For personal use only.



SCHEME 2



SCHEME 3



SCHEME 4

1,5-Diketone **17** also efficiently undergoes other thermal reactions, most likely acid catalyzed; hence the concentrations of **17** as well as acetophenone are low during the photoaddition as shown by GC examinations. In Scheme 1, the most economical mechanisms are formulated for the formation of **2** and **3**. The enolization of **17** on either site followed by hemiketal formation may proceed readily to give **18** and **19**, probably arising from the particular structural feature (as opposed to **10** and **13**). It is speculated that 1,5-diketone **17** can easily assume conformations convenient for undergoing intramolecular enol ether formations. The process **17** → **18** should be faster than **17** → **19** because of achieving extended conjugation in the dehydration step. However, at this stage the oxidizing species or reduction products involved in the transformation **19** → **3** under nitrogen have not been identified.

The identification of 4-acetonylacetophenone (**15**) in the photoaddition of $AABF_2$ to benzene (Scheme 4) has led us to ascertain that the corresponding dihydro precursor is not formed as a primary photoproduct arising from a [2+4] cycloaddition. The photoaddition of an excited state olefin to benzene or such a photoaddition involving a cyano-substituted substrate generally gives 1,2 adducts (6, 7). The photoaddition involving excited state benzenes with an olefin can give all possible 1,2, 1,3, and 1,4 adducts with retention of stereochemistry, and has been shown to be derived from a common intermediate, which appears to be benzvalene (4, 5, 8). In the present photoaddition, singlet excited state $AABF_2$ is not expected to sensitize benzene from the energetic consideration nor to follow the [2+4] addition pattern. The photolysate has been carefully scrutinized by GC–MS and ^1H NMR analysis to show the absence of other primary photoadducts than **13**. For a heavily functionalized system such as **13**, it may undergo many types of phototransformation by itself. While the acid-catalyzed formation of *para*-isomer **15** from **13** obviously requires a dehydrogenation step, it is premature to suggest a mechanism because pertinent information is scarcely available at this stage.

Having defined the overall reaction pattern, we wish to discuss the primary photoreaction step of the BF_2 complex photoaddition with benzene derivatives. As indicated by the absorption curves of $ACHBF_2$ and other complexes (Fig. 1), undoubtedly the excitation of the BF_2 complexes is the primary step to initiate the photoreaction under the irradiation conditions using a Pyrex filter. $ACHBF_2$ shows only weak fluorescence emission, which overlaps with the exciplex emission with benzene at about 360 nm. This poses a severe limitation to conducting fluorescence quenching experiments. The lack of

Can. J. Chem. Downloaded from www.nrcresearchpress.com by 198.100.157.202 on 09/07/12
For personal use only.

Can. J. Chem. Downloaded from www.nrcresearchpress.com by 198.100.157.202 on 09/07/12
For personal use only.

fluorescence of these BF_2 complexes suggests a fast intersystem crossing, therefore short singlet excited state lifetimes. The photoaddition with benzene most likely occurs from the corresponding exciplex. The quantum yields of the formation of enol ether **2** can be monitored readily by GC analysis. The lack of diene quenching of the quantum yield Φ and the failure to sensitize the photoreaction with a triplet sensitizer suggest that the singlet excited state BF_2 complex undergoes the photoaddition. This is confirmed by a heavy atom effect by 1,2-dibromoethane, which promotes the intersystem crossing of singlet excited state $ACHBF_2$ and reduces the quantum yield of **2**. Therefore, the $k_q\tau_0$ obtained in Fig. 4 must represent the product of the reaction rate constant and lifetime of the singlet excited $ACHBF_2$. The low values of 0.032 M^{-1} in CH_3CN and 0.067 M^{-1} in dioxane must mean that the reactive bimolecular encounter has low probability. This may be caused by the short lifetime of the singlet excited state of $ACHBF_2$ as suggested by weak fluorescence. However, reasonably good limiting quantum yields of 0.12 and 0.19 should suggest that a high proportion of exciplex is partitioned to give product **2**.

Experimental section

Materials and general conditions

Commercially available benzenes were distilled before use. Unless specified otherwise the following conditions prevailed. The boron difluoride complex of β-diketones was prepared from the reactions with BF_2 etherate in methylene chloride according to the published procedures (12). $ACHBF_2$ was recrystallized from CH_2Cl_2/hexanes in 70% yield; mp 79–79.5°C; $ACPBF_2$ was recrystallized from ether/hexanes in 63% yield; mp 65.5–70°C; $AABF_2$ was recrystallized from ether in 45% yield; mp 42.5–43°C (lit. (11) mp 43°C).

Gas chromatographic (GC) analyses were performed on a Hewlett–Packard 5790 chromatograph equipped with an FID and an HP-1 (12 m × 0.20 mm) capillary column, and connected to a Hewlett–Packard 3390A chart integrator. Preparative GC was conducted on a Varian 1700 chromatograph equipped with an OV-1 packed column (4 ft × 0.25 in., 15%, Chromsorb A, 60–80 mesh). Melting points were determined on a Fisher–John apparatus (uncorrected). Infrared (IR) spectra were determined on a Perkin–Elmer 559B (neat film or KBr), and (or) a BOMEM Michelson 120 (FT–IR). Mass spectra (MS) and gas chromatography – mass spectra (GC–MS) were taken with a Hewlett–Packard 5985 GC–MS system in electron impact ionization (EI) and (or) chemical ionization (CI) mode. Nuclear magnetic resonance spectra were obtained on either a Bruker 100SY spectrometer equipped with Aspect 2000 software or a Bruker WH400 spectrometer. Chemical shifts (δ) for ^1H and ^{13}C spectra were reported in ppm with reference to tetramethylsilane. The coupling constants are reported in Hz. Ultraviolet and visible (UV/VIS) spectra were recorded on a Varian Cary 210 spectrophotometer. Emission spectra were obtained on a Perkin–Elmer MPF-44B spectrophotometer (uncorrected).

General procedure of photoaddition

A solution of BF_2 complex was irradiated in a Hanovia-type irradiator with a 200-watt medium pressure mercury lamp (645A 36) under constant purging of nitrogen. Alternatively, a solution of a BF_2 complex was distributed in an appropriate number of Pyrex or quartz tubes (1.2 × 10 cm) and was purged with nitrogen for 15 min. These tubes were irradiated with RPR 3000 Å (16 × 21 watt) or RPR 3500 Å (16 × 24 watt) lamps in a Rayonet photochemical reactor. At intervals, the photolysate was withdrawn for GC analysis. At the end of irradiation, the photolysate was washed twice with water and the solution was evaporated to afford a crude product, which was flash chromatographed. The spectroscopic data of the products are summarized in Tables 1–4.

$ACHBF_2$ to benzene

$ACHBF_2$ (760 mg, 4.0 mmol) in benzene (80 mL) was irradiated with a 200-watt Hanovia lamp for 2.5 h under nitrogen. The photolysate showed GC peaks (170°C) corresponding to acetophenone (R_t 0.91 min), $ACHBF_2$ (R_t 1.99 min), enol ether **2** (R_t 2.38 min), and a minor product in a peak area ratio of 15:1:69:2. The enol ether **2** was isolated as an oil; UV λ_{max} 285 nm (log ε, 4.11) in *n*-heptane; see Tables 1–4 for other data. Anal. calcd. for $C_{14}H_{16}O$: C 83.96, H 8.05; found: C 84.26, H 8.13.

TABLE 1. Infrared spectral data of photoaddition products

Compound	ν_{max} (cm^{-1})
2	3072(w), 3040(w), 2940(s), 2867(m), 2845(m), 1658(s, C═C—O), 1607(m), 1495(s), 1384(m), 1195(s, C—O), 1166(m), 1150(m), 760(s, *o*-C_6H_4RR')
3[a]	3072(m), 3040(m), 2954(vs), 2879(s), 1760(vs, COO-), 1690(m), 1500(s), 1451(s), 1376(vs), 1229(vs), 1172(vs), 1110(vs), 1075(vs), 770(vs), 712(vs, C_6H_5R)
5	3000(m), 2978(s), 2882(w), 1738(vs, COO-), 1709(C═O, vs), 1500(m), 1372(s), 1244(vs), 1226(vs), 1167(s), 1080(vs), 1025(s), 782(s, *o*-C_6H_4RR')
6[a]	2955(s), 1690(vs), 1617(m), 1369(s), 1286(s), 830(s), 800(s), 705(s)
9[a]	3020(w), 2978(m), 1734(vs), 1698(vs), 1613(m), 1443(s), 1368(s), 1314(vs), 1293(vs), 1246(vs), 1120(s), 780(m), 766(s), 710(m), 700(s)
7[a]	3040(m), 2984(s), 2940(vs), 2870(s), 1657(vs), 1503(s), 1450(s), 1373(s), 1200(vs), 1171(vs), 836, 820
8[a]	3012(m), 2960(s), 2902(m), 1750(vs, COO-), 1720(vs, C═O), 1628(m), 1468(s), 1439(s), 1380(s), 1292(s), 1254(s), 1172(s), 1087(s), 875(w), 838(s), 820(m), 768(m)
11	2978(s), 2796(m), 1741(vs), 1690(vs), 1362(s), 1260(vs), 1150(s), 770(s)
13	3020(w), 2970(w), 1730(vs, br), 1580(m), 1430(s), 1365(vs), 1270(s), 1255(s), 1174(s), 776(m), 725(s)
14, **15**[b]	3010(w), 2925(s), 1721(vs, sh), 1713(vs), 1682(vs), 1606(s), 1573(m), 1419(s), 1359(vs), 1267(vs), 1162(s), 959(m), 861(w), 840(w), 763(m), 609

[a]The sample is a mixture of two regioisomers.
[b]The sample contains a 1:1 mixture of 1,2- and 1,4-disubstituted isomers (**14** and **15**).

The photoreaction was repeated in solvent consisting of benzene and acetonitrile (1:2 by volume) under oxygen. The photolysate showed the GC peaks corresponding to acetophenone (37%, R_t 0.91 min), enol acetate **3** (10%, R_t 1.55 min), and keto lactone **5** (37%, R_t 3.43 min). The enol acetate **3**, a known compound (14, 15), was isolated by flash chromatography as an oil. The keto lactone **5** was also obtained in the chromatography operation and was recrystallized from ether/hexane to afford white crystals for X-ray analysis (Fig. 2): mp 116.5–117.5°C; UV absorption, λ_{max} 295 nm (sh) and 258 nm (ε 323) in CH_3OH, 295 nm (ε 73), 286 nm (ε 93), 264 nm (ε 288), and 258 nm (ε 323). Anal. calcd. for $C_{14}H_{16}O_3$: C 72.39, H 6.94; found: C 72.34, H 6.88.

A solution of enol ether **2** (298 mg) in CH_3CN/CH_3OH (3:1 by volume) containing methylene blue (10^{-5} M) was irradiated under oxygen for 75 min with a 200-watt Hanovia lamp through a GWV filter (cutoff at 350 nm). The crude product was filtered through a column of silicic acid to afford keto lactone **5** (238 mg).

$ACHBF_2$ to toluene

A solution of $ACHBF_2$ (932 mg, 5.0 mmol) in toluene (120 mL) was irradiated under nitrogen for 7 h with a 200-watt Hanovia lamp to give a photolysate that showed GC (180°C) peaks for 3- and 4-methylacetophenone (12%, R_t 1.01 min), $ACHBF_2$ (19%, R_t 1.79

TABLE 2. ^{1}H NMR data of photoaddition products ($CDCl_3$)

Compound	δ (ppm)
2	1.61(d, 3H, J = 6.4 Hz), 1.70–1.83(m, 4H), 2.10–2.31(m, 2H), 2.33–2.44(m, 2H), 5.08(q, 1H, J = 6.4 Hz), 7.03(d, 1H, J = 7.6 Hz), 7.06(d, 1H, J = 7.5 Hz), 7.15(dt, 1H, J = 7.6 and 1.3 Hz), 7.25(dt, 1H, J = 7.5 and 1.5 Hz)
3	1.75–1.87(m, 4H), 1.91(s, 3H), 2.25–2.29(m, 2H), 2.39–2.43(m, 2H), 7.20–7.23(m, 3H), 7.28–7.30(m, 2H)
5	1.48–1.55(m, 1H), 1.57(d, 3H, J = 6.6 Hz), 1.66–1.73(m, 1H), 2.13–2.31(m, 3H), 2.56–2.66(m, 2H), 2.71–2.80(m, 1H), 6.05(q, 1H, J = 6.6 Hz), 7.06(dd, 1H, J = 7.5 and 1.5 Hz), 7.21(dd, 1H, J = 7.5 and 0.8 Hz), 7.27(dt, 1H, J = 7.5 and 0.8 Hz), 7.34(dt, 1H, J = 7.5 and 1.5 Hz)
6*a*[a]	2.41(s, 3H), 2.59(s, 3H), 7.36(m, 2H), 7.77(m, 2H)
6*b*[a]	2.41(s, 3H), 2.60(s, 3H), 7.26(dd, 2H, J = 8.3 Hz), 7.86(d, 2H, J = 8.3 Hz)
7*a*[a]	1.560(d, 3H, J = 6.5 Hz), 1.68–1.79(m, 4H), 2.08–2.29(m, 2H), 2.324(s, 3H), 2.34–2.39(m, 2H), 5.06(q, 1H, J = 6.5 Hz), 6.84(s, br, 1H), 6.95(d, 1H, J = 7.4 Hz, became a singlet when decoupled at 7.06 ppm), 7.06(d, 1H, J = 7.4 Hz)
7*b*[a]	1.563(d, 3H, J = 6.5 Hz), 1.68–1.79(m, 4H), 2.08–2.29(m, 2H), 2.331(s, 3H), 2.34–2.39(m, 2H), 5.06(q, 1H, J = 6.5 Hz), 6.87(s, br, 1H), 6.91(d, 1H, J = 7.3 Hz), 6.96(d, 1H, J = 7.3 Hz)
8*a*[a]	1.45–1.55(m, 1H), 1.56(d, 3H, J = 6.7 Hz), 1.67–1.77(m, 2H), 2.13–2.19(m, 1H), 2.22–2.28(m, 3H), 2.35(s, 3H), 2.52–2.64(m, 2H), 2.69–2.77(m, 1H), 5.99(q, 1H, J = 6.7 Hz), 7.01(s, br, 1H), 7.09(d, 1H, J = 8.6 Hz), 7.14(d, 1H, J = 8.6 Hz)
8*b*[a]	1.45–1.55(m, 1H), 1.54(d, 3H, J = 6.7 Hz), 1.63–1.72(m, 2H), 2.13–2.19(m, 1H), 2.22–2.28(m, 3H), 2.32(s, 3H), 2.52–2.64(m, 2H), 2.69–2.77(m, 1H), 6.02(q, 1H, J = 6.7 Hz), 6.84(s, br, 1H), 6.95(d, 1H, J = 8.6 Hz), 7.06(d, 1H, J = 8.6 Hz)
9*a*[a]	2.69(s, 3H), 3.96(s, 3H), 7.56(t, 1H, J = 8.0 Hz), 8.16(dt, 1H, J = 8.0 and 1 Hz), 8.23(dt, 1H, J = 8.0 and 1 Hz), 8.61(s, 1H)
9*b*[a]	2.69(s, 3H), 3.96(s, 3H), 7.78(d, 2H, J = 8.4 Hz), 8.12(d, 2H, J = 8.4 Hz)
11	1.95(m, 1H), 2.20(m, 2H), 2.45(m, 3H), 2.61(s, 3H), 3.92(dd, 1H, J = 8.0 and 1.3 Hz), 7.34(dt, 1H, J = 8.0 and 1.3 Hz), 7.45(dt, 1H, J = 8.0 and 1.3 Hz), 7.75(dd, 1H, J = 8.0 and 1.3 Hz)
13	2.08(s, 3H), 2.19(s, 3H), 2.52(d, 2H, J = 7.0 Hz), 3.19(m, 1H), 3.56(ddt, 1H, J = 7.2, 7.0, and 3.0 Hz), 5.87–5.94(m, 4H), 5.99–6.04(m, 1H)
14[b]	2.29(s, 3H), 2.59(s, 3H), 4.02(s, 2H), 7.19(dd, 1H, J = 7.5 and 1.5 Hz), 7.40(dt, 1H, J = 7.5 and 1.5 Hz), 7.49(dt, 1H, J = 7.5 and 1.5 Hz), 7.86(dd, 1H, J = 7.5 and 1.5 Hz)
15[b]	2.19(s, 3H), 2.58(s, 3H), 3.78(s, 2H), 7.30(d, 2H, J = 8.0 Hz), 7.95(d, 2H, J = 8.0 Hz)

[a]Chemical shifts were read from the ^{1}H NMR spectrum of a mixture of two regioisomers.

[b]^{1}H NMR spectrum was measured for a mixture of 1,2- and 1,4-disubstituted isomers (**14** and **15**).

TABLE 3. ^{13}C NMR data of photoaddition products ($CDCl_3$)

Compound	δ (ppm)
2	150.57, 132.68, 132.43, 127.59, 125.69, 122.86, 119.13, 107.03, 73.01, 27.73, 23.36, 22.84, 22.78, 19.40
3	169.31, 143.42, 139.45, 128.59, 128.17, 127.97, 127.48, 126.66, 125.42, 30.06, 27.44, 22.77, 22.60, 20.69
5	207.48, 171.79, 140.45, 138.16, 128.73, 127.22, 126.46, 124.74, 71.64, 41.53, 34.29, 23.50, 22.54, 20.68
7*a*[a]	150.58, 149.55, 137.09, 135.35, 132.79, 132.40, 129.67, 128.08,
7*b*	126.24, 123.70, 122.79, 119.96, 119.16, 107.40, 73.01, 72.91, 27.76, 27.68, 23.40, 22.85, 22.79, 21.39, 21.20, 19.50
8*a*[a]	208.0, 172.0, 138.5, 138.2, 136.9, 135.2, 130.7, 129.3, 127.8,
8*b*	126.9, 126.3, 125.1, 124.7, 122.2, 71.6, 71.5, 41.57, 41.43, 34.24, 23.45, 23.38, 22.49, 21.05, 20.66
11	217.6, 202.0, 137.7, 137.6, 131.7, 130.6, 129.4, 126.7, 54.5, 38.1, 31.4, 29.1, 20.9
13	208.69, 207.26, 130.28, 125.43, 128.92, 123.69, 51.28, 42.11, 30.44, 30.05, 28.92

[a]^{13}C NMR was measured with a mixture of two regioisomers.

min), and a mixture of enol ethers **7** (63%, R_t 2.63 min). The enol ethers **7** were isolated as a 1:1 mixture of 3- and 4-methyl-substituted isomers as shown by ^{1}H NMR spectra (see Table 2). **6** was isolated as a mixture containing 4-methylacetophenone and 3-methylacetophenone in a 1.1:1 ratio shown by GC analysis at 100°C.

A mixture of the isomers of **7** (248 mg) in CH_3CN/CH_3OH (3:1 by volume) was photooxygenated using methylene blue (10^{-5} M) as the sensitizer under oxygen for 1.5 h. The residue of the photolysate was chromatographed to afford a 1:1 mixture of keto ester **8** (171 mg, 59%).

$ACHBF_2$ with other monosubstituted benzenes

Methyl benzoate (5 mL) and $ACHBF_2$ (205 mg) in acetonitrile (35 mL) were photolyzed under nitrogen as shown above to give two GC peaks. The photolysate was worked up to afford a mixture of methyl 3-acetylbenzoate (72%) and methyl 4-acetylbenzoate (28%). The latter was reported to show ^{1}H NMR signals at 8.15 and 7.97 ppm (24).

Photolysis of $ACHBF_2$ with chlorobenzene or benzonitrile was carried out under conditions similar to the above to give acetylated products as the major products as shown by GC–MS analysis. The photoaddition to the former was faster than that to methyl benzoate, and that to benzonitrile was the slowest.

Photolysis of $ACHBF_2$ in the presence of anisole did not show consumption of $ACHBF_2$.

$ACPBF_2$ with benzene

A solution of $ACPBF_2$ (371 mg, 2.1 mmol) in benzene (16 mL) and anhydrous ether (24 mL) was irradiated with a Hanovia lamp for 45 min under nitrogen to give a photolysate that showed GC (160°C) peaks for acetophenone (R_t 0.92 min), 1,5-diketone **10** (R_t 2.39 min), and what appeared to be enol ether **12** (R_t 2.12 min; GC–MS m/e: 186(M^+, 27), 171(100), 128(13), and 115(11)) in a ratio of 5:5:1. On standing at room temperature for several hours, it showed an additional GC peak for **11** (R_t 2.98 min) at the expense of the peak for **10**. When the photolysis was run in the presence of tributylamine (500 mg) the ratio of these GC peaks was 1:12:1. The photolysate was quickly washed with water and dried–evaporated to give a crude product that showed ^{1}H NMR signals at 3.49 ppm (dd, J = 8.3 and 2.7 Hz, 1H), 3.05 (m, 1H), and 5.95 (m, 4H), and GC–MS (CI) m/e: 205 (M^+ + 1, 78),

Can. J. Chem. Downloaded from www.nrcresearchpress.com by 198.100.157.202 on 09/07/12
For personal use only.

TABLE 4. GC–MS data of photoaddition products

Compound		*m/e* (%)
2	EI	200(M^+, 21), 185($M^+ - CH_3$, 100), 128(12), 115(19)
	CI	201($M^+ + 1$, 100), 185(9)
3	EI	216(M^+, 4), 174($M^+ - 42$, 100), 157(8), 146(18), 115(21), 91(42), 77(17), 43(30)
	CI	217($M^+ + 1$, 100), 199($M^+ + 1 - H_2O$, 4), 175(75)
5	EI	232(M^+, 10), 204(4), 149(100), 131(31), 103(15), 77(25), 55(37)
	CI	233($M^+ + 1$, 100), 149(19)
6*a*	EI	134(M^+, 49), 119($M^+ - CH_3$, 100), 91($M^+ - COCH_3$, 60)
6*b*	EI	134(M^+, 86), 119($M^+ - CH_3$, 100), 91($M^+ - COCH_3$, 44)
7*a*	EI	214(M^+, 15), 199($M^+ - CH_3$, 100), 141(17), 128(32), 115(23), 91(8), 77(17)
	CI	215($M^+ + 1$, 100)
8*a*	EI	246(M^+, 5), 218(6), 163(100), 145(57), 119(47), 91(19), 77(6), 55(17)
	CI	247($M^+ + 1$, 100)
9*a*	EI	178(M^+, 17), 163($M^+ - CH_3$, 100), 147($M^+ - OCH_3$, 20), 135($M^+ - COCH_3$, 25), 119($M^+ - CO_2CH_3$, 7), 91(8), 76(12)
9*b*	EI	178(M^+, 18), 163($M^+ - CH_3$, 100), 147($M^+ - OCH_3$, 20), 135($M^+ - COCH_3$, 21), 119($M^+ - CO_2CH_3$, 6), 103(10), 76(9)
10	EI	204(M^+, 0.2), 186($M^+ - H_2O$, 0.4), 161($M^+ - COCH_3$, 9), 143(15), 126(47), 117(39), 105($M^+ - 91$, 39), 91($M^+ - 105$, 29), 84(100), 77(20)
	CI	205($M^+ + 1$, 78), 187($M^+ + 1 - H_2O$, 44), 121($PhCOCH_3^+ + 1$, 100)
11	EI	202(M^+, 44), 187($M^+ - CH_3$, 56), 160($M^+ - 42$, 30), 145(100), 131(49), 115(20), 103(22), 77(17)
	CI	203($M^+ + 1$, 100), 185($M^+ + 1 - H_2O$, 12)
13	EI	178(M^+, 2), 135($M^+ - COCH_3$, 52), 117(26), 100(33), 91(43), 77(23), 72(17), 62(15), 57(21), 43($COCH_3$, 100)
	CI	179($M^+ + 1$, 100), 121(80)
14	EI	176(M^+, 14), 161($M^+ - CH_3$, 30), 134($M^+ - COCH_2$, 37), 119($M^+ - CH_2COCH_3$, 100), 91(21)
	CI	177($M^+ + 1$, 100), 159(12)
15	EI	176(M^+, 5), 134($M^+ - COCH_2$, 100), 119($M^+ - CH_2COCH_3$, 6), 105(12)
	CI	177($M^+ + 1$, 100)

[a]GC–MS spectrum was taken with a mixture of two regioisomers.

187(44 and 121(100); (EI) *m/e*: 204 (M^+, 0.2), 186(0.4), 161(9), 143(15), 126(47), 117(39), 105(39), 91(29), 84(100), and 77(20).

The crude product was chromatographed to afford acetophenone (75 mg, 29%) and diketone **11** (72 mg, 17%).

$AABF_2$ with benzene

$AABF_2$ (620 mg, 4.2 mmol) in a mixture of benzene (20 mL) and ether (60 mL) was irradiated under nitrogen and the photolysate was monitored by GC analysis (120°C). At the 120 min irradiation, the GC peaks for acetophenone (R_t 1.17 min), $AABF_2$ (R_t 1.46 min), and 1,5-diketone **13** (R_t 2.69 min; GC–MS *m/e*: 178 (M^+, 2), 135(52), 117(26), 77(23) and 43(100)) showed the ratio of 8:46:41; further irradiation resulted in a decrease of **13**. This photolysate was washed with water without the addition of tributylamine. The product was chromatographed to afford acetophenone and a fraction containing a 1:1 mixture of **14** and **15**. Physical data of **13**–**15** are summarized in Tables 1–4.

In a separate experiment, after a 2 h irradiation, tributylamine (0.6 mL) was added to the photolysate, which was worked up in the usual manner to afford a crude product. This was chromatographed to afford a fraction containing 1,5-diketone **13** contaminated with 12% 2-acetonylacetophenone (**14**).

In a separate experiment, a similar photoaddition was run in the presence (1 equivalent) and absence of pyridine; the yield of **13** started to decrease in the latter case but approached a maximum in the former case. Also, the yield of acetophenone built up rapidly in the latter case in contrast to consistently low yields in the former case.

Quantum yield determination

The quantum yields of the enol ether **2** (Φ) were determined in a Rayonet photochemical reactor equipped with a rotating platform and RPR 3000 Å lamps (16 × 21 watt). The solution contained tetradecane as the internal standard and was nitrogen purged. The benzophenone–benzhydrol system in benzene was used for the actinometry with a quantum yield of 0.74 (25). The solution was irradiated for 60–75 min resulting in 6–15% yields of **2**. The yields of enol ether **2** were calculated from the predetermined response plot. The quantum yield calculation details are provided in the M.S. thesis by X. X. Ouyang.[2]

Acknowledgement

The authors wish to acknowledge generous financial support granted by the Natural Sciences and Engineering Research Council of Canada, Ottawa.

1. Y. L. CHOW and X. E. CHENG. J. Chem. Soc. Chem. Commun. 1043 (1990).
2. Y. L. CHOW, X. E. CHENG, and C. I. JOHANSSON. J. Photochem. Photobiol. A, Chem. **51**, 000 (1990).
3. Y. L. CHOW and X. E. CHENG. Can. J. Chem. Submitted.
4. K. E. WILZBACH and L. KAPLAN. J. Am. Chem. Soc. **88**, 2066 (1966).
5. K. E. WILZBACH and L. KAPLAN. J. Am. Chem. Soc. **93**, 2073 (1971).
6. (*a*) D. BRYCE-SMITH, A. GILBERT, and B. H. ORGER. J. Chem. Soc. Chem. Commun. 512 (1966); (*b*) D. BRYCE-SMITH, B. E. FOULGER, A. GILBERT, and P. J. TWITCHET. J. Chem. Soc. Chem. Commun. 794 (1971); (*c*) D. BRYCE-SMITH, B. E. FOULGER, and A. GILBERT. J. Chem. Soc. Chem. Commun. 664 (1972).
7. J. J. MCCULLOUGH. Chem. Rev. **87**, 811 (1987).
8. R. SRINIVASAN. IBM J. Res. Dev. **15**, 34 (1971).
9. (*a*) D. E. REEDICH and R. S. SHERIDAN. J. Am. Chem. Soc. **107**, 3360 (1985); (*b*) H. LEISMANN, J. MATTAY, and H.-D. SHARF. J. Am. Chem. Soc. **106**, 3985 (1984).
10. L. H. TOPERCER, R. E. DESSY, and S. I. E. GREEN. Inorg. Chem. **4**, 1649 (1965).
11. N. M. D. BROWN and P. BLADOM. J. Chem. Soc. (A), 526 (1969).
12. R. A. J. SMITH and T. A. SPENCER. J. Org. Chem. **35**, 3220 (1970).
13. B. P. STARK and M. E. B. JONES. Ger. Patent 1,495, 259 (1973).
14. A. N. KOST and I. P. SUGROBOVA. Vestn. Mosk. Univ. Ser. II, **18**, 75 (1963); Chem. Abstr. **59**, 7460d (1963).
15. S. P. PAPPAS, J. E. ALEXANDER, G. L. LONG, and R. D. ZEHR. J. Org. Chem. **37**, 1258 (1972).
16. S. MAZUR and C. S. FOOTE. J. Am. Chem. Soc. **92**, 3225 (1970).

[2]X. X. Ouyang. M.S. thesis, to be submitted.

Can. J. Chem. Downloaded from www.nrcresearchpress.com by 198.100.157.202 on 09/07/12
For personal use only.

17. P. D. BARTLETT and A. P. SCHAAP. J. Am. Chem. Soc. **92**, 3223 (1970).
18. H. H. WASSERMAN and J. L. IVES. J. Am. Chem. Soc. **98**, 7868 (1976).
19. R. M. SILVERSTEIN, G. C. BASSLER, and T. C. MORRIL. spectrometric identification of organic compounds. John Wiley & Sons, New York. 1981. Chaps. 3–5.
20. F. EINSTEIN and C. REID. Acta Crystallogr. Sect. C: In press.
21. J. F. BUNNET and J. E. SUNDBERG. Chem. Pharm. Bull. **23**, 2620 (1975).
22. J. C. ZHANG and C. S. FOOTE. Tetrahedron Lett. 6153 (1986); P. SCHIESS, M. HUYS-FRANCOTTE, and C. VOGEL. Tetrahedron Lett. 3959 (1985).
23. N. J. TURRO. Modern molecular photochemistry. The Benjamin/Cummings Publishing Co., Menlo Park, CA. 1978. p. 368.
24. H. BEIJAMINS and W. D. CHANDLER. Can. J. Chem. **52**, 597 (1974).
25. W. M. MOORE and M. KETCHUM. J. Am. Chem. Soc. **84**, 1388 (1962).

Can. J. Chem. Downloaded from www.nrcresearchpress.com by 198.100.157.202 on 09/07/12
For personal use only.

Metal pyrazolate polymers. Part 2. Synthesis, structure, and magnetic properties of $[Cu(4\text{-}Xpz)_2]_x$ polymers (where X = Cl, Br, Me, H; pz = pyrazolate)

MARTIN K. EHLERT, STEVEN J. RETTIG, ALAN STORR, ROBERT C. THOMPSON, AND JAMES TROTTER
Department of Chemistry, University of British Columbia, 2036 Main Mall, Vancouver, B.C. Canada V6T 1Y6

Received August 2, 1990

MARTIN K. EHLERT, STEVEN J. RETTIG, ALAN STORR, ROBERT C. THOMPSON, and JAMES TROTTER. Can. J. Chem. **69**, 432 (1991).

Novel and reliable methods for the synthesis of the polymers $[Cu(4\text{-}Xpz)_2]_x$ (where X = H, Cl, Br, and Me; pz = pyrazolate) are presented. The X = Cl compound was obtained as green and brown forms. Single crystals of the polymers with X = Me and X = Cl (green form) suitable for X-ray analysis have been obtained. $[Cu(4\text{-}Mepz)_2]_x$ and $[Cu(4\text{-}Clpz)_2]_x$ are isomorphous, crystallizing with four formula units per unit-cell in the orthorhombic space group *Ibam*, a = 9.7436(6), 9.155(4), b = 12.6106(8), 12.968(6), and c = 7.7482(6), 7.717(5) Å, respectively, for the 4-Me and 4-Cl derivatives. The structures were refined by full-matrix least-squares procedures to R = 0.027 and 0.041 for 430 and 246 reflections with $I \geq 3\sigma(I)$, respectively. Magnetic susceptibility studies over the temperature range 2 to 300 K have revealed that all the polymers exhibit very strong antiferromagnetic exchange between copper(II) centres in the extended linear chains. Discontinuities displayed in the susceptibility versus temperature plots suggest the presence of phase transitions at ~133 and ~108 K in the X = Cl (green form) and X = Br materials, respectively. The four compounds, X = H, Br, Me, and Cl (green form) also exhibit thermochromism over the 77 to 176 K region. The magnetic data have been analyzed employing an isotropic Heisenberg model for antiferromagnetic exchange in extended chain polymers. Values of the exchange coupling constant, J, for the room temperature forms of these materials are determined as −81, −105, −96, −104, and −88 cm^{-1} for 4-X = H, Br, Me, Cl (green form), and Cl (brown form), respectively. The magnitude of the exchange coupling is discussed in relation to structural parameters for the X = H, Me, and Cl (green form) compounds.

Key words: copper(II) 4-substituted pyrazolate polymers, crystal structures, magnetic exchange.

MARTIN K. EHLERT, STEVEN J. RETTIG, ALAN STORR, ROBERT C. THOMPSON et JAMES TROTTER. Can. J. Chem. **69**, 432 (1991).

On présente de nouvelles méthodes fiables de synthèse des polymères $[Cu(4\text{-}Xpz)_2]_x$ (où X = H, Cl, Br et Me; pz = pyrazolate). Le composé avec X = Cl a été obtenu sous des formes verte et brune. On a obtenu des cristaux uniques des polymères avec X = Me et X = Cl (forme verte), appropriés pour des analyses par diffraction des rayons-x. Les composés $[Cu(4\text{-}Mepz)_2]_x$ et $[Cu(4\text{-}Clpz)_2]_x$ sont isomorphes et ils crystallisent avec 4 unités de formules par maille, dans le groupe d'espace orthorhombique *Ibam*, avec a = 9,7436(9), 9,155(5), b = 12,6106(8), 12,968(6) et c = 7,7482(6), 7,717(5) Å, respectivement pour les dérivés 4-Me et 4-Cl. On a affiné les structures par la méthode des moindres carrés jusqu'à des valeurs respectives de R = 0,027 et 0,041 pour 430 et 246 réflexions avec $I \geq 3\sigma(I)$. Des études de susceptibilité magnétique effectuées de 2 à 300 K ont révélé que tous les polymères présentent un échange antiferromagnétique très fort entre les centres cuivre(II) des chaînes linéaires allongées. Les discontinuités observées dans la courbe de susceptibilité en fonction de la température suggèrent la présence de transitions de phase à respectivement ~133 K et ~108 K dans les composés avec X = Cl (forme verte) et X = Br. Les quarte composés, X = H, Br, Me et Cl (forme verte) présentent aussi de la thermochromie entre 77 K et 176 K. On a analysé les données magnétiques à l'aide du modèle isotrope de Heisenberg pour l'échange antiferromagnétique dans les chaînes étendues de polymères. On a déterminé que les valeurs de la constance de couplage, J, pour les formes de ces matériaux existant à la température ambiante, sont respectivement −81, −105, −96, −104 et −88 cm^{-1} pour les produits 4-X = H, Br, Me, Cl (forme verte) et Cl (forme brune). On discute de l'amplitude du couplage d'échange en relation avec les paramètres structuraux des composés X = H, Me et Cl (forme verte).

Mots clés : polymères des pyrazolates de cuivre(II) substitués en position 4, structures cristallines, échange magnétique.

[Traduit par la rédaction]

Introduction

Earlier we reported a novel synthesis of the $[Cu(pz)_2]_x$ polymer and obtained crystals suitable for X-ray analysis (1). Our interests were in metal pyrazolate complexes which would provide examples of extended linear-chain polymers with bridging pyrazolate ligands acting as pathways for strong magnetic exchange between metal centres. These expectations were met in the $[Cu(pz)_2]_x$ polymer which indeed exhibited an infinite chain structure and strong antiferromagnetic coupling. The present account describes the effects of varying the substituent at the 4-position of the pyrazolate bridging ligands on the structural and magnetic properties of these polymeric materials.

Experimental

Pyrazole (Aldrich Chemical Co.) and 4-methylpyrazole (Aldrich Chemical Co.) were used as supplied. $[Cu(pz)_2]_x$ was prepared as described previously (1).

Synthesis

4-Bromopyrazole

Pyrazole (13.6 g, 200 mmol) was dissolved in 50 mL of warm water. Bromine (32.0 g, 200 mmol) was added dropwise, with stirring, to this solution until the yellow color of Br_2 persisted. The resulting solution was refluxed for 30 min and cooled. Concentrated aqueous NaOH was added to the reaction solution until it was slightly basic, resulting in precipitation of an off-white solid. The mixture was suction filtered, the solid washed with cold water and air dried. The solid was then dissolved in a minimum amount of diethyl ether and suction filtered to remove any entrained NaBr. The diethyl ether was removed from the filtrate under vacuum leaving an off-white powder of 4-bromopyrazole. Melting point (recrystallized from petroleum ether) 90.5–92.5°C. *Anal.* calcd. for $C_3H_3BrN_2$: C 24.52, H 2.06, N 19.06; found: C 23.86, H 1.96, N 18.81.

4-Chloropyrazole

4-Chloropyrazole was prepared using a variation of a literature method (2). Pyrazole (13.6 g, 200 mmol) was dissolved in 100 mL of glacial acetic acid. To this solution was added NaOCl (aq) (256 mL of

Can. J. Chem. Downloaded from www.nrcresearchpress.com by 198.100.157.202 on 09/07/12
For personal use only.

Can. J. Chem. Downloaded from www.nrcresearchpress.com by 198.100.157.202 on 09/07/12
For personal use only.

0.780 M, 200 mmol) with stirring. The resulting solution was left for 18 h at room temperature and then neutralized with Na_2CO_3. The neutralized solution was extracted with 3 × 250 mL portions of CH_2Cl_2. The CH_2Cl_2 extracts were combined, condensed under vacuum, and washed with dilute NaOH (aq). The NaOH solution was extracted with 2 × 100 mL portions of CH_2Cl_2. The CH_2Cl_2 extracts were combined and dried *in vacuo* yielding 4-chloropyrazole as a white powder. Yield 85%; mp 72–75°C. *Anal.* calcd. for $C_3H_3ClN_2$: C 35.14, H 2.95, N 27.32; found: C 35.16, H 2.93, N 27.47.

$[Cu(4\text{-}Mepz)_2]_x$

Copper metal shot was cleaned by washing with 12 M HCl, then water, and finally acetone. About 3 g of the cleaned copper shot was combined with 4-methylpyrazole (3 g, 36 mmol) in a 5 mL round bottomed flask fitted with a condenser and gas-tee. The mixture was heated at 115°C (below reflux temperature) with stirring, for 8 h, under a dioxygen atmosphere. The reaction mixture was then allowed to cool, washed with CH_2Cl_2 to both extract the mixture from the flask and to dissolve soluble components. The resulting slurry was then suction filtered and washed with acetone yielding $[Cu(4\text{-}Mepz)_2]_x$ as a fine green powder. The product was dried in air at 110°C for 0.5 h. *Anal.* calcd. for $C_8H_{10}CuN_4$: Cu 28.15, C 42.57, H 4.47, N 24.82; found: Cu 28.20, C 42.57, H 4.42, N 24.82.

Single crystals suitable for X-ray diffraction studies were prepared by a method similar to that used for the preparation of bulk compound. The conditions differed in that the mixture was not stirred, the apparatus was flushed with dinitrogen gas and air was allowed to diffuse into the reaction vessel via a pinhole leak, and the reaction was allowed to proceed for 3 days. The reaction mixture was washed with acetone yielding dark green crystals of $[Cu(4\text{-}Mepz)_2]_x$.

$[Cu(4\text{-}Brpz)_2]_x$

Freshly prepared amorphous $Cu(OH)_2$ (0.487 g, 5.00 mmol) was combined with 4-bromopyrazole (4.41 g, 30.0 mmol) in a 10 mL round-bottomed flask fitted with a condenser and gas-tee. The mixture was heated to 145°C (below reflux temperature) with stirring, for 16 h under a dinitrogen atmosphere. After this time the reaction mixture was cooled and 5 mL of acetone added. The reaction mixture was then refluxed for 3 h causing the sublimed 4-bromopyrazole to be washed back into the flask. At the cessation of the reaction the mixture was allowed to cool and solidify. The solid was then treated with ethanol to remove it from the flask and dissolve soluble components. The slurry thus obtained was suction filtered and washed with water, ethanol, and CH_2Cl_2. The resulting green power was dried *in vacuo* for 2 h at room temperature. Yield 50%. *Anal.* calcd. for $C_6H_4Br_2CuN_4$: Cu 17.81, C 20.27, H 1.13, N 15.76; found: Cu 18.1, C 20.26, H 1.11, N 15.88.

Attempts to grow single crystals of this compound were made by repeating the reaction without stirring. Single crystals did form, however, they were too small for X-ray diffraction studies.

$[Cu(4\text{-}Clpz)_2]_x$

Cu_2O (0.358 g, 5.00 mmol), 4-chloropyrazole (4.39 g, 42.8 mmol), and 1.5 mL of xylene were combined in a 10 mL round-bottomed flask fitted with a condenser and gas-tee. The mixture was heated at 130°C (below reflux temperature) for 8.5 h with vigorous stirring under a dioxygen atmosphere. The mixture was extracted from the flask with CH_2Cl_2, suction filtered, washed with CH_2Cl_2, and finally acetone. The resulting fine green powder was dried in air at 110°C for 0.5 h. Yield 75%. *Anal.* calcd. for $C_6H_4Cl_2CuN_4$: Cu 23.84, C 27.03, H 1.51, N 21.02; found: Cu 23.87, C 27.25, H 1.60, N 21.25.

Single crystals of $[Cu(4\text{-}Clpz)_2]_x$ were grown by combining copper metal shot and 4-chloropyrazole in a test tube, then heating the mixture to 120°C, without stirring, for 3 days. The reaction mixture was washed with acetone, yielding dark green crystals of the desired product in addition to some brown and bluish-grey crystals.[1]

A brown form of $[Cu(4\text{-}Clpz)_2]_x$ was prepared as follows. $Cu(OH)_2$ (0.73 g, 7.5 mmol), 4-chloropyrazole (4.6 g, 45 mmol), and 2 mL of xylene were combined in a 10 mL round-bottomed flask fitted with a condenser and heated at 135°C for 6 days in air, with stirring. The mixture was extracted from the flask with acetone, suction filtered, washed with acetone, and air dried, yielding a fine powder which consisted mostly of a brown material together with a trace of green material. *Anal.* calcd. for $C_6H_4Cl_2CuN_4$: C 27.03, H 1.51, N 21.02; found: C 27.10, H 1.54, N 21.20.

Physical characterization

The $[Cu(4\text{-}Xpz)_2]_x$ materials were found to be insoluble in both polar and non-polar solvents. They are decomposed on dissolution in acid. Differential scanning calorimetry measurements, obtained with a Mettler DSC 20 Standard Cell and TC 10 TA Processor as described previously (3), showed the compounds to decompose, without melting, at the indicated temperatures: $[Cu(4\text{-}Mepz)_2]_x$ (270°C), $[Cu(4\text{-}Brpz)_2]_x$ (290°C), $[Cu(4\text{-}Clpz)_2]_x$ (green) (290°C), $[Cu(4\text{-}Clpz)_2]_x$ (brown) (285°C). All three of the new green copper pyrazolates exhibit thermochromism, as was observed in $[Cu(pz)_2]_x$ but with the new polymers the color at low temperature is more of a blue–green compared to the blue color observed for $[Cu(pz)_2]_x$.

Electronic spectra (350 to 900 nm) were recorded using Nujol mulls suspended on filter paper with a Shimadzu UV-2100 spectrometer.

Infrared spectra (4000–250 cm^{-1}) were obtained using a Perkin-Elmer Model 598 spectrophotometer. Tabulated band frequencies have been deposited.[2] Samples were prepared as mulls in Nujol and hexachlorobutadiene and pressed between KBr and KRS-5 (Harshaw Chemical Co.) plates, respectively.

Magnetic susceptibilities were measured over the temperature range 2–300 K using a Quantum Design (MPMS) SQUID magnetometer (field = 10 000 G). Because the materials studied here have very small magnetic moments, a specially designed sample holder was employed. The sample holder was made from Delron and possessed a constant cross-sectional area, thus minimizing its contribution to the SQUID signal. In addition, all samples were studied over the same temperature range using a combination of vibrating sample magnetometer and Gouy balance equipment as described previously (4). Although there was more scatter in the data points with the latter equipment the agreement with the SQUID data was good. Only the data obtained with the SQUID magnetometer are reported here. Temperature measurement with this instrument was achieved using a combination of Ge and Pt resistance thermometers. Susceptibility calibration was achieved using high purity nickel and bismuth standards. Magnetic susceptibilities were corrected for diamagnetism: copper, −11; $C_3H_3N_2$, −40; $C_4H_5N_2$, −52; $C_3H_2ClN_2$, −57; and $C_3H_2BrN_2$, −67 (values in 10^{-6} cm^3 mol^{-1}). A correction of 60 × 10^{-6} cm^3 mol^{-1} was applied for temperature independent paramagnetism of the copper(II) ion. Tabulated values of temperature, magnetic susceptibility, and magnetic moment have been deposited.[2]

The esr spectra were obtained using an X-band homodyne spectrometer with a Varian 12-inch magnet equipped with a MkII Fieldial control. An Ithaco Dynatrac 391A lock-in amplifier was used to obtain phase-sensitive detection at 100 kHz. Data acquisition was carried out using a Qua-Tech 12-bit data acquisition board (ADM·12-10) together with a Qua-Tech parallel expansion board (PXB-721) incorporated into an IBM XT computer. The relevant data processing software is as described previously (5, 6). The microwave frequency was measured with a HP5246L frequency counter equipped with a HP5255A plug-in. Field calibration was accomplished using a Varian Gaussmeter, the output of which is also collected by the IBM computer. The absolute field is corrected for the placement of the gaussmeter probe by calibrating against peroxylamine sulfate in aqueous solution and is in error by *ca.* 0.01 G. Sample temperature was controlled using a Varian E-257 temperature controller.

X-ray powder diffractograms were collected with a Rigaku Rotaflex rotating anode X-ray powder diffractometer (nickel-filtered Cu-K_α radiation).

[1]The bluish-grey crystals are soluble in polar solvents; however, the material is not stable in solution and was not characterized further.

[2]Supplementary material mentioned in the text may be purchased from the Depository of Unpublished Data, Document Delivery, CISTI, National Research Council Canada, Ottawa, Canada. K1A 0S2.

Can. J. Chem. Downloaded from www.nrcresearchpress.com by 198.100.157.202 on 09/07/12
For personal use only.

TABLE 1. Crystallographic data[a]

Compound	$[Cu(4\text{-}Mepz)_2]_x$	$[Cu(4\text{-}Clpz)_2]_x$
Formula	$C_8H_{10}CuN_4$	$C_6H_4Cl_2CuN_4$
fw	225.74	266.58
Crystal system	Orthorhombic	Orthorhombic
Space group	*Ibam*	*Ibam*
a, Å	9.7436(6)	9.155(4)
b, Å	12.6106(8)	12.968(6)
c, Å	7.7482(6)	7.717(5)
V, Å^3	952.0(2)	916(1)
Z	4	4
ρ_{calc}, g/cm^3	1.575	1.93
$F(000)$	460	524
Radiation	Cu	Mo
μ, cm^{-1}	28.50	29.32
Crystal size, mm	$0.06 \times 0.10 \times 0.12$	$0.08 \times 0.10 \times 0.15$
Transmission factors	0.93–1.00	0.82–1.00
Scan type	ω–2θ	ω–2θ
Scan range, deg in ω	1.05 + 0.20 tan θ	1.10 + 0.35 tan θ
Scan speed, deg/min	16.0	8.0
Data collected	$+h, +k, -l$	$+h, -k, +l$
$2\theta_{max}$, deg	155	65
Crystal decay	Negligible	Negligible
Total unique reflections	570	965
No. of reflcns with $I \geq 3\sigma(I)$	430	246
No. of variables	39	34
R	0.027	0.041
R_w	0.042	0.042
gof	1.96	1.31
Maximum Δ/σ (final cycle)	0.01	0.01
Residual density e/Å^3	0.36	0.62

*Temperature 294 K, Rigaku AFC6S diffractometer, Mo-K_α radiation (λ = 0.71069 Å) or Cu-K_α (λ = 1.54178 Å), graphite monochromator, takeoff angle 6.0°, aperture 6.0 × 6.0 mm at a distance of 285 mm from the crystal, stationary background counts at each end of the scan (scan/background time ratio 2:1, up to eight rescans), $\sigma^2(F^2) = [S^2(C + 4B) + (0.03F^2)^2]/Lp^2$ (S = scan rate, C = scan count, B = normalized background count) function minimized $\Sigma w(|F_o| - |F_c|)^2$ where $w = 4F_o^2/\sigma^2(F_o^2)$, $R = \Sigma||F_o| - |F_c||/\Sigma|F_o|$, $R_w = (\Sigma w(|F_o| - |F_c|)^2/\Sigma w|F_o|^2)^{1/2}$, and gof = $[\Sigma(|F_o| - |F_c|)^2/(m - n)]^{1/2}$. Values given for R, R_w, and gof are based on those reflections with $I \geq 3\sigma(I)$.

C, H, and N microanalyses were performed by P. Borda of this department. Cu analyses were performed using iodometric titrations.

X-ray crystallographic analyses of $[Cu(4\text{-}Mepz)_2]_x$ and $[Cu(4\text{-}Clpz)_2]_x$

Crystallographic data for both compounds appear in Table 1. The final unit-cell parameters were obtained by least-squares on the setting angles for 25 reflections with 2θ = 75.0–117.7° for $[Cu(4\text{-}Mepz)_2]_x$ and 9.4–17.4° for $[Cu(4\text{-}Clpz)_2]_x$. The intensities of three standard reflections, measured every 150 reflections throughout the data collections, were essentially constant for both compounds. The data were processed[3] and corrected for Lorentz and polarization effects and absorption (empirical, based on azimuthal scans for three reflections).

The structures are isomorphous with that of the parent compound $[Cu(pz)_2]_x$ (1). The structure analyses were initiated using the coordinates of the Cu and pyrazolyl ring atoms from the unsubstituted structure, the remaining non-hydrogen atom in both cases being positioned by direct methods for difference structures. The non-hydrogen atoms were refined with anisotropic thermal parameters and hydrogen atoms were fixed in idealized positions (C—H = 0.98 Å,

[3]TEXSAN/TEXRAY structure analysis package, containing versions of the following: DIRDIF, direct methods for difference structures, by P. T. Beurskens; ORFLS, full-matrix least squares, and ORFFE, function and errors, by W. R. Busing, K.O. Martin, and H. A. Levy; ORTEP II, illustrations, by C. K. Johnson.

TABLE 2. Final atomic coordinates (fractional) and B_{eq}*

Atom	x	y	z	B_{eq}
		$[Cu(4\text{-}Mepz)_2]_x$		
Cu(1)	1/2	0	1/4	2.17(3)
N(1)	0.3623(2)	0.0535(2)	0.0871(2)	2.46(7)
C(1)	0.2534(3)	0.1104(2)	0.1388(3)	3.4(1)
C(2)	0.1826(4)	0.1493(4)	0	3.5(2)
C(3)	0.0542(6)	0.2165(6)	0	6.4(3)
H(1)	0.243(4)	0.125(2)	0.250(3)	3.0(6)
H(2)	0.0720	0.2831	0.0614	7.7
H(3)	0.0274	0.2321	−0.1192	7.7
H(4)	−0.0201	0.1780	0.0578	7.7
		$[Cu(4\text{-}Clpz)_2]_x$		
Cu	1/2	0	1/4	1.87(7)
Cl	0.0197(4)	0.2279(3)	0	5.0(2)
N	0.3518(5)	0.0508(4)	0.0876(6)	1.8(3)
C(1)	0.2401(8)	0.1094(6)	0.140(1)	2.5(3)
C(2)	0.168(1)	0.1485(9)	0	2.6(5)
H(1)	0.2138	0.1224	0.2608	2.9

*$B_{eq} = (8/3)\pi^2\Sigma\Sigma U_{ij}a_i^*a_j^*(\mathbf{a}_i \cdot \mathbf{a}_j)$.

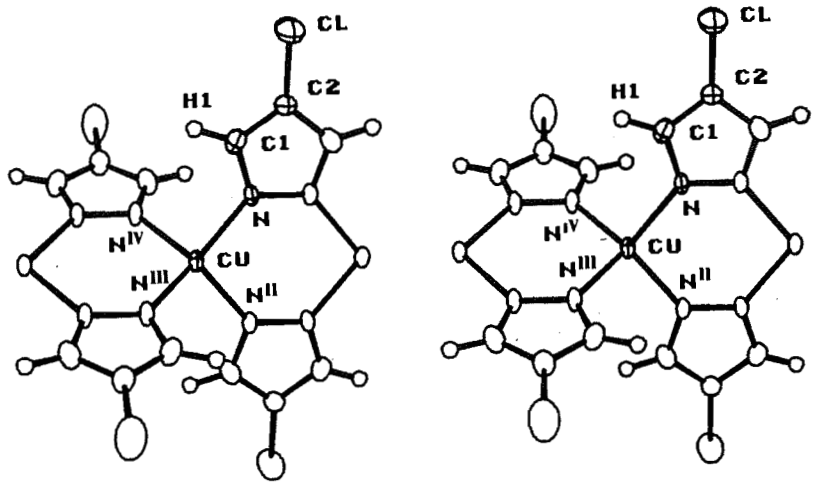


FIG. 1. Stereoview of the coordination about the Cu atom in $[Cu(4\text{-}Clpz)_2]_x$; 50% probability thermal ellipsoids are shown for the non-hydrogen atoms.

TABLE 3. Bond lengths (Å) and angles (deg) for $[Cu(4\text{-}Xpz)_2]_x$ (X = Me, Cl) and selected parameters for the X = H derivative (from ref. 1)*

	Distance		
Atoms	X = H (ref. 1)	X = Me (this work)	X = Cl (this work)
Cu—N	1.957(2)	1.962(2)	1.961(5)
N—N^{I}	1.359(3)	1.351(4)	1.35(1)
N—C(1)	1.345(3)	1.342(3)	1.337(8)
C(1)—C(2)	1.371(3)	1.368(4)	1.361(9)
C(2)—X		1.512(6)	1.70(1)
	Angle		
Atoms	X = H	X = Me	X = Cl
N—Cu—N^{II}	99.4(1)	99.9(1)	100.5(3)
N—Cu—N^{III}	139.5(1)	139.7(1)	140.8(3)
N—Cu—N^{IV}	94.3(1)	93.7(1)	92.4(3)
Cu—N—N^{I}		130.04(5)	129.7(2)
Cu—N—C(1)		122.2(2)	121.9(5)
N^{I}—N—C(1)		107.4(1)	107.5(4)
N—C(1)—C(2)		110.8(2)	110.2(7)
C(1)—C(2)—C(1)^{I}		103.6(3)	104.7(9)
C(1)—C(2)—X		128.2(2)	127.7(4)

*Superscripts refer to symmetry operations: (I) $x, y, -z$; (II) $1-x, -y, z$; (III) $1-x, y, 1/2-z$; and (IV) $x, -y, 1/2-z$.

$B_H = 1.2B_{\text{bonded atom}}$) except for the ring hydrogen atom in $[Cu(4\text{-}Mepz)_2]_x$ which was refined with an isotropic thermal parameter. The methyl hydrogen atoms in $[Cu(4\text{-}Mepz)_2]_x$ were observed to be disordered from a difference map, a (1:1) twofold disordered model was calculated based on the difference Fourier peaks. Neutral atom scattering factors and anomalous dispersion corrections for the non-hydrogen atoms were taken from the International tables for X-ray crystallography (7). Final atomic coordinates and equivalent isotropic thermal parameters are given in Table 2 and bond lengths and angles appear in Table 3. Anisotropic thermal parameters, bond lengths and angles involving hydrogen, general torsion angles, intermolecular distances, least-squares planes, and measured and calculated structure factor amplitudes for the both structures are included as supplementary material.[2]

Results and discussion

Encouraged by our success in preparing the pure polymeric $[Cu(pz)_2]_x$ material by reacting metallic copper with molten pyrazole ligand in the presence of oxygen (1) we have extended our investigations to include substituted pyrazole ligands with the idea of changing the structural parameters of the materials and thus their other physical properties. In the present account we restrict ourselves to 4-substituted pyrazole derivatives and describe the preparation and properties of the $[Cu(4\text{-}Xpz)_2]_x$ polymer species where X = Cl, Br, or Me. In addition to the copper/molten ligand method, syntheses starting with $Cu(OH)_2$ (4-Brpz) and Cu_2O(4-Clpz) are described. Two forms of the 4-Clpz derivative were obtained, one green and one brown. Analytically pure samples of all polymers were obtained and X-ray diffraction quality single crystals were grown for the compounds $[Cu(4\text{-}Mepz)_2]_x$ and $[Cu(4\text{-}Clpz)_2]_x$ (green). The polymers are air-stable, thermally quite robust and, consistent with their extended structures, insoluble in a wide range of solvents.

The crystal structures of the $[Cu(4\text{-}Mepz)_2]_x$ and $[Cu(4\text{-}Clpz)_2]_x$ (green) materials confirm their polymeric nature. The coordination geometry about the Cu atom in $[Cu(4\text{-}Clpz)_2]_x$ is shown in Fig. 1 and the crystal structure of the polymer in Fig. 2. The coordination geometry about the Cu atoms is distorted tetrahedral with Cu—N distances of 1.961(5) and 1.962(2) Å in the 4-Cl and 4-Me structures, respectively, values very similar to the value of 1.957(2) Å previously observed for the $[Cu(pz)_2]_x$ polymer (1). The three unique N—Cu—N angles correspond to N atoms related to one another by three mutually perpendicular twofold axes intersecting at the metal (D_2 symmetry): those within the planar six-membered $Cu(N—N)_2Cu$ rings are 100.5(3) (4-Cl) and 99.9(1)° (4-Me) and the others are 92.4(2) and 140.8(3)° (4-Cl) and 93.7(1) and 139.7(1)° (4-Me). The corresponding values for $[Cu(pz)_2]_x$ are 99.4(1), 94.3(1), and 139.5(1)° respectively.

The X-ray powder diffraction pattern for $[Cu(4\text{-}Brpz)_2]_x$ was indexed to an orthorhombic unit-cell. Fifteen unambiguously indexed diffraction peaks were employed in a least-squares refinement of the unit-cell parameters with the following results: $a = 9.44(1)$, $b = 13.32(2)$, $c = 7.70(1)$ Å. Systematically absent reflections in the diffraction pattern are consistent with the space group *Ibam*. Miller indices, observed d spacings and

Can. J. Chem. Downloaded from www.nrcresearchpress.com by 198.100.157.202 on 09/07/12
For personal use only.

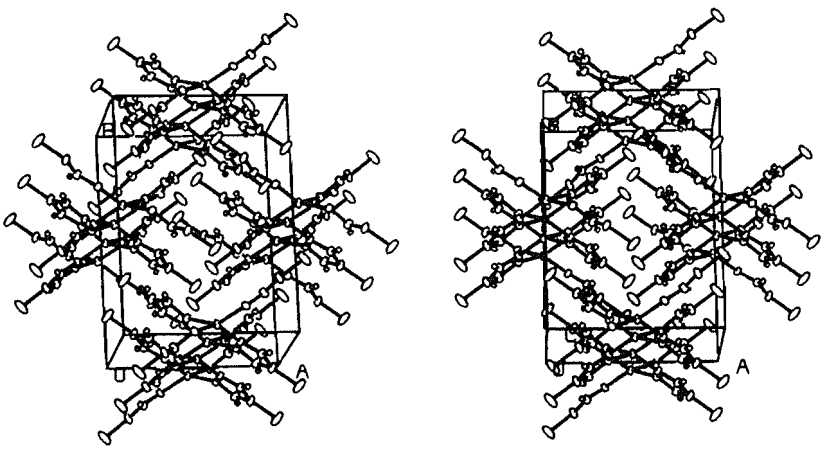


FIG. 2. View down the c axis of the structure of $[Cu(4\text{-}Clpz)_2]_x$.

TABLE 4. X-ray powder diffraction data for $[Cu(4\text{-}Brpz)_2]_x$

h	k	l	d_{obs} (Å)	I_{Rel}	d_{calc} (Å)
1	1	0	7.729	100	7.702
0	2	0	6.692	6	6.664
2	0	0	4.726	72	4.720
1	2	1	4.467	18	4.446
1	3	0	4.026	74	4.012
—	—	—	3.854	52	—
1	1	2	3.469	8	3.445
0	2	2	3.336	16	3.335
—	—	—	2.988	12	—
2	2	2	2.723	53	—
—	—	—	2.567	9	—
3	1	2	2.403	7	2.397
4	0	0	2.358	11	2.360
—	—	—	2.223	7	—
—	—	—	2.142	3	—
—	—	—	2.011	3	—
4	2	2	1.926	7	—
1	7	0	1.867	4	1.866
3	5	2	1.799	3	1.798
1	3	4	1.736	4	1.737
—	—	—	1.723	3	—
3	7	0	1.628	2	1.629
—	—	—	1.571	2	—

their relative intensities and calculated d spacings based on the least-squares refinement of indexed reflections are listed in Table 4. Diffraction peaks not included in the analysis are those which could not be unambiguously indexed because they consist of several overlaping diffraction peaks.

Single crystals of the compound $[Cu(4\text{-}Brpz)_2]_x$ obtained were too small for a single crystal X-ray structure determination; nonetheless, visual observation under a microscope revealed they are of similar color to and possess the same morphology as those of the other 4-substituted pyrazolates. $[Cu(4\text{-}Brpz)_2]_x$ exhibits thermochromism as do the other green copper pyrazolates discussed here. These observations provide substantial evidence that $[Cu(4\text{-}Brpz)_2]_x$ is isomorphous and probably isostructural with $[Cu(pz)_2]_x$, $[Cu(4\text{-}Mepz)_2]_x$, and $[Cu(4\text{-}Clpz)_2]_x$ (green).

As described in the Experimental section, $[Cu(4\text{-}Clpz)_2]_x$ can be prepared in two forms, green and brown polymorphs. It is apparent from X-ray powder diffraction patterns[2] that the two forms are structurally distinct and, furthermore, that a trace of the green form is present in the sample of the brown form. While details of the structure of the brown form of $[Cu(4\text{-}Clpz)_2]_x$ remain unknown, comparison of its solubility and thermal properties with those of the structurally characterized pyrazolate complexes suggest a polymeric structure for this material also. Moreover its magnetic properties are consistent with an extended chain polymeric structure, strongly suggesting a very similar structure to that of the other pyrazolates under discussion here, with differences primarily involving the detailed stereochemistry of the CuN_4 chromophore (see below).

Electronic spectra

Electronic spectra are shown in Fig. 3. The $[Cu(4\text{-}Xpz)_2]_x$ polymers (with the exception of the brown form of $[Cu(4\text{-}Clpz)_2]_x$) all exhibit a single broad asymmetric band in the visible region centered at about 15 600 cm^{-1}. This band compares with the band at 15 400 cm^{-1} which we reported for $[Cu(pz)_2]_x$, and probably involves all four of the d–d transitions, unresolved, expected for a CuN_4 chromophore of distorted tetrahedral geometry (8). The higher energy band at ~25 000 cm^{-1} for the 4-Cl (green) and 4-Me derivatives and at ~27 000 cm^{-1} for the 4Br compound is likely of charge transfer origin as previously suggested (1). The brown form of the 4-Cl derivative shows a very broad absorption over the region studied (Fig. 3) with indications of band maxima at 25 600, 20 000, and 16 700 cm^{-1}. The maximum at 25 600 cm^{-1} is probably charge transfer in origin while the more complex nature of the spectrum in the visible region may indicate a lower symmetry for the CuN_4 chromophore in this material.

Magnetic properties

The strong antiferromagnetic exchange observed previously in $[Cu(pz)_2]_x$ is present also in the $[Cu(4\text{-}Xpz)_2]_x$ polymers. In all four compounds the magnetic moment decreases significantly with temperature; moreover, as in the 4-H compound, susceptibility maxima are seen in the χ_m vs. T plots for the 4-Me, 4-Br, 4-Cl (green), and 4-Cl (brown) compounds occurring at 180, 200, 195, and 160 K, respectively. Plots of susceptibility versus temperature are shown for the 4-Me and 4-Cl (green form) compounds in Fig. 4. All compounds show an increase in susceptibility as temperature decreases at the lowest temperatures studied reflecting the presence of small amounts of paramagnetic impurities in the samples, as discussed previously

Can. J. Chem. Downloaded from www.nrcresearchpress.com by 198.100.157.202 on 09/07/12
For personal use only.

Can. J. Chem. Downloaded from www.nrcresearchpress.com by 198.100.157.202 on 09/07/12
For personal use only.

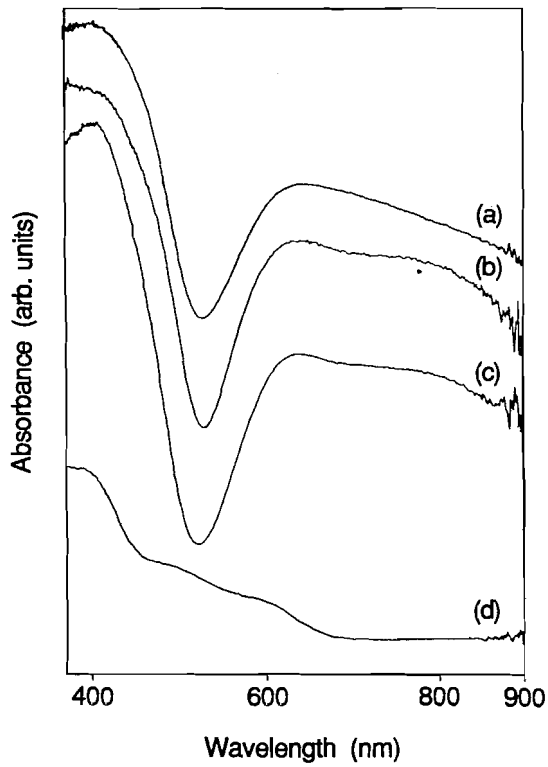


FIG. 3. Electronic spectra for the $[Cu(4\text{-}Xpz)_2]_x$ compounds: (*a*) $[Cu(4\text{-}Mepz)_2]_x$, (*b*) $[Cu(4\text{-}Brpz)_2]_x$, $[Cu(4\text{-}Clpz)_2]_x$ green form, (*d*) $[Cu(4\text{-}Clpz)_2]_x$ brown form.

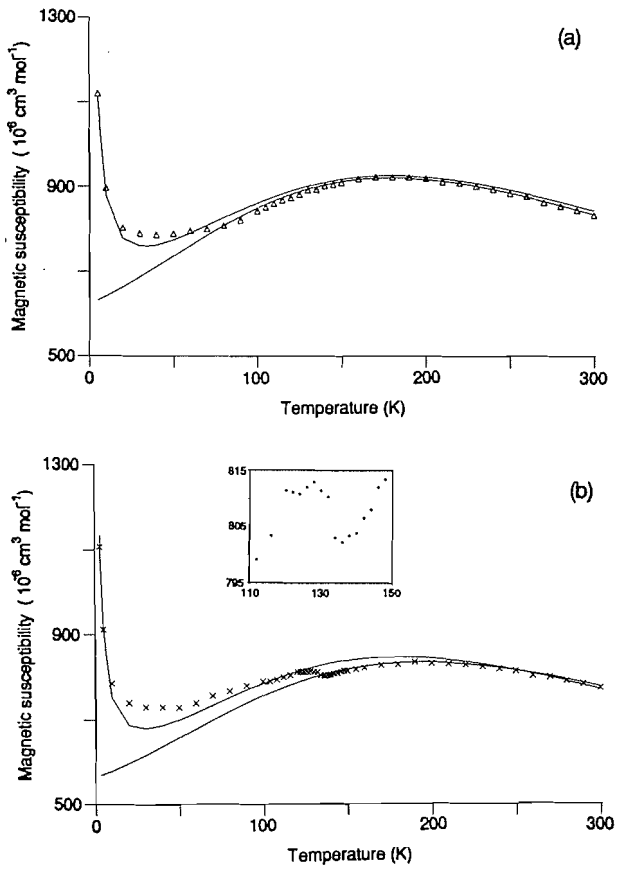


FIG. 4. Plot of magnetic susceptibilty versus temperature for (*a*) $[Cu(4\text{-}Mepz)_2]_x$ (*b*) $[Cu(4\text{-}Clpz)_2]_x$ green form. The lines are calculated from theory. The upper curve represents the best fit to data over the whole temperature range while the lower curve represents the best fit to the high temperature data only as described in the text.

for $[Cu(pz)_2]_x$. An interesting feature of the susceptibility data for the 4-Cl (green) and 4-Br derivatives is a discontinuity occurring at 133 and 108 K, respectively, suggesting the presence of a structural phase change in these materials. Repeated measurements revealed that these discontinuities are reversible and, although small, are reproducible. It is important to note that all four of the green compounds which we have studied show thermochromism in which they reversibly go from a room temperature green to a blue or blue–green color at low temperatures. Qualitative observations using a variety of slush baths indicate this occurs somewhere in the 176 to 77 K range for the 4-Me, 4-Br, and 4-Cl (green) compounds and that for the 4-H compound the color change from green begins at about 176 K and is complete by 133 K. It is possible that the thermochromism and the magnetic discontinuities are linked and that the absence of observable discontinuities in the χ_m vs. T plots for the 4-H and 4-Me compounds is due to the fact that the phase changes in these materials are either too small to affect the magnetic data noticeably or occur over a range of temperatures and hence do not result in a sharp χ_m vs. T discontinuity.

As previously described for $[Cu(pz)_2]_x$ (1), we have analyzed the magnetic data according to the isotropic Heisenberg model for exchange coupled linear chains employing the polynomial developed by Hall and others (9, 10). Computer fits to the model using experimental data over the 2 to 300 K range were made for all five compounds and the best fit values of J, g, and % paramagnetic impurity are given in Table 5. Because of the discontinuity in the data for the 4-Cl (green) and 4-Br derivatives we have also, for these compounds, obtained fits to the data in the high temperature region only and, for comparison, have done the same for the other compounds. In these cases the fits were obtained setting the % paramagnetic impurity arbitrarily to zero. Best fit values of the other parameters are given in Table 5 and these fits are compared graphically for two of the compounds in Fig. 4. For each compound, the parameters J and g differ relatively little whether all the data or only the high temperature data are used in the analysis. Attempts to fit the low temperature data only to the model were, on the other hand, not successful leading to significantly higher $|J|$ values and,

TABLE 5. Derived magnetic parameters for $[Cu(4\text{-}Xpz)_2]_x$ compounds

Compound	Temperature range (K)	$-J^a$ (cm^{-1})	g^a	%P^b	F^c
$[Cu(pz)_2]_x$	135–300	81	2.12	—	0.0014
	2–300	82	2.13	0.31	0.0097
$[Cu(4\text{-}Mepz)_2]_x$	135–300	96	2.15	—	0.0026
	2–300	99	2.18	0.54	0.016
$[Cu(4\text{-}Brpz)_2]_x$	110–300	105	2.20	—	0.0042
	2–300	106	2.21	0.51	0.022
$[Cu(4\text{-}Clpz)_2]_x$ green	140–300	104	2.13	—	0.0020
	2–300	99	2.08	0.42	0.026
$[Cu(4\text{-}Clpz)_2]_x$ brown	135–300	88	2.06	—	0.0012
	2–300	90	2.07	0.72	0.020

[a]The estimated uncertainties in J and g are ± 2 cm^{-1} and ± 0.02, respectively.
[b]%P = percent paramagnetic impurity, arbitrarily set to zero when analysis involved the high temperature data only.
[c]F = fitting function defined in ref. 3.

TABLE 6. Measured g-values for $[Cu(4\text{-}Xpz)_2]_x$ compounds

Compound	Temperature (K)	$g_\parallel$	$g_\perp$	$<g>$
$[Cu(pz)_2]_x$	293	—	—	2.104
	96	2.242	2.078	2.133
$[Cu(4\text{-}Mepz)_2]_x$	293	—	—	2.108
	87	2.223	2.079	2.127
$[Cu(4\text{-}Brpz)_2]_x$	293	—	—	2.108
	86	2.238	2.083	2.135
$[Cu(4\text{-}Clpz)_2]_x$ green	293	—	—	2.107
	86	2.225	2.080	2.128
$[Cu(4\text{-}Clpz)_2]_x$ brown	293	—	—	2.084
	92	—	—	2.084

more importantly, unrealistic g values on the order of 3.0. That such high g values are unrealistic was confirmed by electron spin resonance studies which were made on these compounds at room temperature and at ~90 K. The g values obtained in this study are given in Table 6. At room temperature, all compounds exhibit a single broad esr band at $g_0 \sim 2.11$. At ~90 K the spectrum of the 4-Cl (brown) compound is unchanged while those of the other materials change to typical 2 g-value spectra with $g_\parallel$ values in the range 2.22–2.24 and $g_\perp$ values of ~2.08. An examination of the esr spectrum of $[Cu(pz)_2]_x$ at intermediate temperatures revealed only a gradual change from one type of spectrum to the other. The low temperature isotropic g_0 values calculated from the expression $g_0 = (1/3)(g_\parallel + 2g_\perp)$ agree to within 1% of the values obtained at room temperature (Table 6), indicating no significant change in g_0 with temperature. In addition there is generally good agreement between the esr g values and those obtained from fits to the magnetic data over the whole temperature range or using the high temperature data only. Additional attempts to fit the low temperature data to a Heisenberg two-dimensional model (11) and an Ising linear chain model (12) were also unsuccessful. It would appear then that our inability to fit the low temperature data satisfactorily to the model means either that the low temperature forms of these materials do not model well as Heisenberg chains or sheets, or Ising chains and/or the source of the paramagnetic tail is not being properly modeled here. Finally, it is important to note that the g and J values obtained here for $[Cu(pz)_2]_x$ from the SQUID magnetometer data agree, within experimental error, with those reported earlier from VSM and Gouy balance data (1).

We turn now to a consideration of how the nature of the pyrazolate bridge and structure affect the magnitude of exchange coupling in the compounds under investigation. It seems reasonable to assume that the values of J obtained from the high temperature data analyses properly reflect the magnitude of exchange in the room temperature forms of these compounds and these J values will be used in considerations which follow. Single crystal X-ray diffraction studies show that the 4-H, 4-Me, and 4-Cl (green) derivatives are isomorphous and are very similar structurally. Moreover, the analysis of the X-ray powder pattern of the 4-Br derivative shows it is isomorphous and very probably isostructural with the other three compounds. It is perhaps not too surprising then that these four compounds exhibit very similar magnetic properties: strong antiferromagnetic exchange with $|J|$ values in the range 81 to 105 cm^{-1}. The absolute values of J obtained for the 4-Cl and 4-Br derivatives are the same within experimental error and slightly larger than the value for the 4-Me derivative. The value of $|J|$ for the 4-H

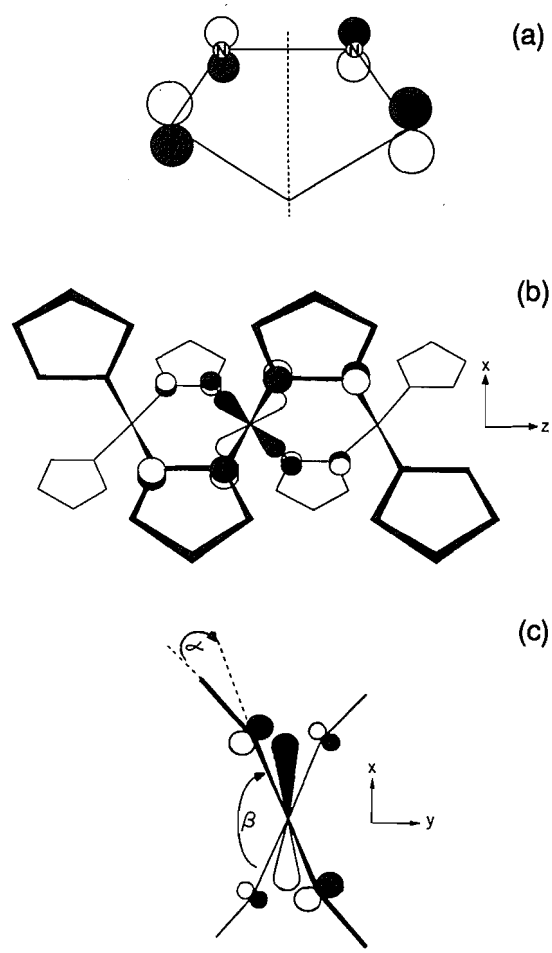


FIG. 5. (a) HOMO for the pyrazolate ion, (b) and (c) two different views of the overlap of the magnetic orbital on copper with the pyrazolate HOMO.

TABLE 7. $[Cu(4\text{-}Xpz)_2]_x$ structural parameters (see Fig. 5(c))

Compound	α	β
$[Cu(pz)_2]_x$	9.1°	126.1°
$[Cu(4\text{-}Mepz)_2]_x$	7.7°	126.6°
$[Cu(4\text{-}Clpz)_2]_x$ green	11.0°	128.2°

derivative is significantly smaller than those obtained for the other three compounds. This variation does not correlate with simple ideas based on relative ligand basicity, since one would expect the halo-substituted pyrazolate ligands to be least basic (as a measure of this: pK_a's for the $H_2$4-Xpz$^+$ cations are 3.09, 2.53, 0.64, and 0.60 for X = Me, H, Br, and Cl, respectively (13–15)), to form the weakest bonds with copper, and therefore to provide the poorest rather than the most efficient pathways for exchange.

We suggested previously (1) that, as for the related neutral pyrazine ligand, it is perhaps the π system of the pyrazolate bridge which provides the pathway for superexchange between the metal ions. A HAM molecular orbital calculation (16) on the pyrazolate ion reveals the highest occupied molecular π orbital shown in Fig. 5a. The orientation of this orbital with respect to the magnetic orbital on copper in $[Cu(pz)_2]_x$ is shown in Figs. 5b and 5c. Defining the angle formed between the plane of the

Can. J. Chem. Downloaded from www.nrcresearchpress.com by 198.100.157.202 on 09/07/12
For personal use only.

pz ring and the Cu—N bond as α and the dihedral angle between adjacent Cu_2N_4 rings as β (Fig. 5*c*) it is clear that increased overlap between the HOMO and the magnetic orbital and therefore increased exchange would be expected as β increases or α decreases. The α and β angles for the three compounds for which the structures are known are given in Table 7. Comparing the 4-Me compound with the 4-H derivative we see that the former has a slightly greater β and a significantly smaller α and hence a higher value of $|J|$ would be expected, as is indeed observed. Unfortunately, there are no other unambiguous comparisons which can be made among these three compounds; for example, on going from the 4-Cl to the 4-H derivative both α and β decrease resulting in opposing effects on orbital overlap and therefore magnitude of exchange. Nonetheless, we feel that our results do indicate that an important factor in determining the magnitude of exchange in metal pyrazolate complexes is the overlap between the pyrazolate π-orbital system and the metal's magnetic orbital. Such a factor, for example, seems likely to account for the difference in $|J|$ between the green and brown forms of $[Cu(4\text{-}Clpz)_2]_x$.

Acknowledgements

Funding for this project has been provided by the Natural Sciences and Engineering Research Council of Canada. We thank F. G. Herring and P. S. Phillips of this department for help in acquiring the esr data and for the use of their esr spectrometer and J. F. Carolan and W. N. Hardy, Department of Physics, U.B.C., for use of the SQUID magnetometer.

1. M. K. Ehlert, S. J. Rettig, A. Storr, R. C. Thompson, and J. Trotter. Can. J. Chem. **67**, 1970 (1989).
2. R. Huttel, O. Schafer, and G. Welzel. Ann. Chem. **598**, 186 (1956).
3. J. S. Haynes, K. W. Oliver, and R. C. Thompson. Can. J. Chem. **63**, 1111 (1985).
4. J. S. Haynes, K. W. Oliver, S. J. Rettig, R. C. Thompson, and J. Trotter. Can. J. Chem. **62**, 891 (1984).
5. F. G. Herring and P. S. Phillips. J. Magn. Reson. **57**, 43 (1984).
6. F. G. Herring and P. S. Phillips. J. Magn. Reson. **62**, 19 (1985).
7. International tables for X-ray crystallography. Vol. IV. Kynoch Press: Birmingham, U.K. (present distributor Kluwer Academic Publishers: Dordrecht, The Netherlands), 1974. pp. 99–102, 149.
8. B. J. Hathaway. J. Chem. Soc. Dalton Trans. 1196 (1972).
9. J. W. Hall. Ph.D. Thesis, University of North Carolina. 1977.
10. W. E. Estes, W. E. Hatfield, J. A. C. van Ooijen, and J. Reedijk. J. Chem. Soc. Dalton Trans. 2121 (1980).
11. M. E. Lines. J. Phys. Chem. Solids, **31**, 101 (1970).
12. M. E. Fisher. J. Math. Phys. **4**, 124 (1963).
13. J. Elguero, E. Gonzales, and R. Jacquier. Bull. Soc. Chim. Fr. 707 (1968).
14. M. W. Austin, J. R. Blackborow, J. H. Ridel, and B. V. Smith. J. Chem. Soc. 1051 (1965).
15. M. Jackman, M. Klenk, B. Fishburn, B. F. Tullar, and S. Archer. J. Am. Chem. Soc. **70**, 2884 (1948).
16. E. Lindholm and L. Åsbrink. Lecture notes in chemistry; Vol. 38: Molecular orbitals and their energies, studied by the semi-empirical HAM method. *Edited by* G. Berthier *et al.* Springer-Verlag, Berlin. 1985.

Can. J. Chem. Downloaded from www.nrcresearchpress.com by 198.100.157.202 on 09/07/12
For personal use only.

A study of the electrolytic solution process using the scaled particle theory. 5. Heat capacity of aqueous ions at elevated temperatures

UTPAL SEN
Central Electrochemical Research Institute, Karaikudi 623 006, Tamilnadu, India

Received February 6, 1990[1]

UTPAL SEN. Can. J. Chem. **69**, 440 (1991).

A theory composite of the scaled particle theory and the Born model of solvent continuum has been used to theoretically calculate the standard heat capacity of hydration as well as the partial molal heat capacity of aqueous ions and electrolytes at elevated temperatures. The uncertainties in the second temperature derivatives of solvent dielectric constant at various temperatures present a barrier to an accurate heat capacity prediction by the theory. Nevertheless, the agreement between the predicted standard heat capacity of electrolytes in solution and the corresponding experimental data, particularly at higher temperatures, is encouraging. Moreover, the composite theory seems to provide the most accurate thermodynamic predictions to date for aqueous electrolytes at higher temperatures without involving any arbitrary adjustable parameter. We therefore use this theory to find the proper ionic scale of the partial molal heat capacities at elevated temperatures.

Key words: scaled particle theory, solvent continuum model of Born, standard heat capacity of aqueous ions, absolute scale for hydration thermodynamic quantities.

UTPAL SEN. Can. J. Chem. **69**, 440 (1991).

On a utilisé une théorie composite, basée sur la théorie des particules scalaires et sur le modèle de Born du continuum de solvant, pour calculer d'une façon théorique la capacité calorifique standard de l'hydratation ainsi que la capacité calorifique molale partielle des ions et des électrolytes aqueux, à températures élevées. On a démontré que les incertitudes liées aux secondes dérivées de la température de la constante diélectrique du solvant à diverses températures empêchent de prédire correctement la capacité calorifique sur une base théorique. Toutefois, on a trouvé encourageante la bonne corrélation qui existe entre les données expérimentales et les capacités calorifiques standard des électrolytes en solution, particulièrement aux températures plus élevées. De plus, il semble que la théorie composite puisse fournir les meilleures prédictions à date pour les électrolytes aqueux, à températures élevées, sans pour cela faire appel à des paramètres arbitraires ajustables. On l'a donc utilisée pour déterminer la bonne échelle ionique des capacités calorifiques molales partielles, à des températures élevées.

Mots clés : théorie des particules scalaires, modèle de Born du continuum du solvant, capacité calorifique standard d'ions aqueux, échelle absolue pour les quantités thermodynamiques d'hydratation.

[Traduit par la rédaction]

1. Introduction

The need for the data related to the thermodynamic behaviour of electrolytes in solution at elevated temperature is obvious, particularly in understanding corrosion problem in electric power industries and the behaviour of minerals in geothermal systems. A few recent experimental efforts to determine high temperature thermodynamic data for aqueous electrolytes suggest that the trend of the thermodynamic behaviour of electrolytes at elevated temperatures is quite unusual and interesting (1–4). However, such data are few and often only partially cover the temperature range between the normal melting point and the critical temperature of water (1–10). There are, of course, a few attempts to theoretically generate high temperature data through empirical equations and through using simplified models (11–29). Horvath (30) compiled some of the advances made in the various attempts for theoretical calculation of entropy and heat capacity of aqueous at various temperatures. Recently, Tanger and Helgeson (31) revised their earlier empirical approach (29) of thermodynamic calculations by introducing additive correction terms to the effective electrostatic radii of aqueous ions to account for the pressure and temperature dependence of the solvent structure and presented the calculated values of various thermodynamic functions of aqueous ions at various temperatures and pressures (30). However, the arbitrariness of the correction terms could not be altogether done away with in spite of generous computer applications.

Very recently, Tanger and Pitzer (32) revised an earlier semi continuum approach (33) which they claim to provide a realistic identification of both inner-shell and outer-shell contributions to the ion-hydration process. Inner shell is assumed to involve six H_2O molecules of hydration whereas the outside of the inner shell region is represented by the Born continuum approach. The prediction has been extended to 1000°C and 5000 bar. An empirical parameter that represents the Born radius has to be used for alkali metal halides and hydroxides. The very complicated calculations are however essentially associated with some experimental data from gas phase mass spectrometric studies for obtaining the equilibrium constant for the successive hydrations for six water molecules per solute ions.

In our earlier communications (14–18), we have developed a simple composite theory which has been remarkably successful in predicting the hydration and partial molal entropies of electrolyte solutions at elevated temperatures. Partial molal heat capacity, however, is probably the most important thermodynamic function for electrolytes over extended temperatures since it can be used to generate enthalpy, free energy, and entropy as functions of temperature. Moreover, it is an extremely scientific probe to the hydration, hydrogen-bonding, and structures of electrolytic solutions.

In this paper we have used the theory and concept to theoretically predict the behaviour of the hydration and the partial molal heat capacities of electrolyte solutions at elevated temperatures. An attempt has also been made to obtain the ionic heat capacity scales at higher temperatures and to find the possible values of the standard partial molal entropy and heat capacity of the aqueous hydrogen ion at different elevated temperatures.

[1]Revision received October 5, 1990.

Can. J. Chem. Downloaded from www.nrcresearchpress.com by 198.100.157.202 on 09/07/12
For personal use only.

Can. J. Chem. Downloaded from www.nrcresearchpress.com by 198.100.157.202 on 09/07/12
For personal use only.

2. Nature of the problem

Standard free energy of solvation (or hydration) has been traditionally accepted as the equivalent of the total work needed for bringing 1 mole of a gaseous solute species at 1 atm pressure from vacuum to a solvent (or water) so that it would form a 1 mole of solution (34).

$$M^+(g, 1\ atm, T) + X^-(g, 1\ atm, T) = M^+(aq, 1\ m, T) + X^-(aq, 1\ m, T)$$

The equilibrium response of the solvent molecules to the incorporated solute species and the nature of the forces that uniquely determine the response are to be defined to gain insight into the solution process. When the solute species is an ion its introduction can bring about several changes in the solvent system. For instance, if sufficient space does not already exist solvent molecules must move apart to accommodate the solute ion. Furthermore, if the solvent is polar as in the case of water, the solvent molecules will align with the ionic field produced by the solute ion. Any theory purporting to accurately describe real ionic solution process must include these as well as other interactions such as hydrogen bonding, etc. The process, no doubt, is complicated. Nevertheless, there is a need to understand the dominant mechanisms that determine the equilibrium properties of solutions, and for this purpose a simplified model is preferred (35).

3. Review of theory

We have, however, found that the overall interaction phenomenon in an ion–solvent system can be conveniently split into two additive parts: (*i*) the interaction due to the presence of an ionic species of finite size in a uniform dielectric solvent system and (*ii*) the so-called specific interactions occurring at various distances apart from the incorporated ion which may result in the formation of the so-called multi layer solvation zones in the solution (16). The free energy involved in the first part of the interaction process as mentioned above may be conveniently estimated with the help of the Born charging equation (36). *A priori* fixation of the value of the interaction free energy for the second part (denoted as ΔG^*), on the other hand, seems difficult and may require various kinds of speculation (37). It has been, however, realized that ΔG^* which apparently has its major contribution from the strong interactions in the vicinity of a dissolved ion, would be relatively insensitive to temperature variations (14–16). An interesting analysis of the Born equation has been put forward by Honig and co-workers (38, 39).

3.1. Methods of calculation

According to the above theory proposed on the basis of the scaled particle approach (which has been extremely successful in thermodynamic predictions for solvation process with neutral gases as solutes (40)) the solvation process of ions can be seen as a simple combination of two steps: (*i*) the formation of a cavity of appropriate size in the solvent system for the accommodation of the solute species and (*ii*) the introduction of the solute ion into the cavity which interacts with the surrounding solvent. Consequently, when this interaction process is again subdivided as stated above into the Born-type electrostatic interaction and the sum of the other kinds of specific interactions occurring in the various regions around the incorporated solute ions, which the Born continuum model cannot recognise, the standard free energy of solvation, ΔG_s^0 for ions can be represented by

[1] $$\Delta G_h^0 = \Delta G_c^0 + \Delta G_i^0 + \Delta G_x$$

[2] $$\Delta G_h^0 = \Delta G_c^0 + (\Delta G_{Born}^0 + \Delta G^*) + \Delta G_x$$

where ΔG_h^0, ΔG_c^0, ΔG_i^0, ΔG_x, ΔG_{Born}^0, and ΔG^* are the free energy of hydration, cavity formation, interactions, standard state alteration, electrostatic free energy calculated from the Born equation (36), and the free energy of specific interactions which the simple Born equation can not recognise. It has been our experience that the term ΔG^* is relatively temperature insensitive. Perhaps the temperature insensitivity may be due to the opposing nature of the temperature variations of the free energy quantities associated with the number of solvent molecule immobilized due to the strong electrostatic field in the near vicinity of the incorporated solute ion on the one hand and the free energy of individual solvent molecules on the other hand. Whatever the solution process, if we consider $(\partial \Delta G^*/\partial T)_P$ $(= -\Delta s^*)$ to be negligible, the calculation of the thermodynamic quantities is simplified and does not as such involve any arbitrary parameters. We may therefore have the following expressions for the entropy and heat capacity of hydration:

[3] $$\Delta s_h^0 = \Delta s_c^0 + \Delta s_{Born}^0 + \Delta s_x$$

[4] $$\Delta c_{P(h)}^0 = \Delta c_{P(c)}^0 + \Delta c_{P(Born)}^0 + \Delta c_{P(x)}$$

Here we are mainly concerned with the calculation of heat capacity and the following are expressions for the various terms associated with the calculation.

[5] $$\Delta c_{P(h)}^0 = c_H \Delta H_c^0 - (c_0 + c_1 d_2 + c_2 d_2^2)$$

[6] $$c_H = (2/T) - \alpha_P + (\partial \ln \alpha_P/\partial T)_P$$

[7] $$\Delta H_c^0 = B_0 + B_1 d_2 + B_2 d_2^2 + B_3 d_2^3$$

[8] $$B_0 = (\alpha_P R T^2 y)/(1 - y)$$

[9] $$B_1 = [(3\alpha_P R T^2 y)/(1 - y)^2]/d_1$$

[10] $$B_2 = (3\alpha_P R T^2 y)[(1 - 2y)/(1 - y)^3]/d_1^2$$

[11] $$B_3 = \pi P N/6$$

[12] $$c_0 = R[(y\alpha_P T)/(1 - y)^2]^2(1 - y)^2$$

[13] $$c_1 = R[(y\alpha_P T)/(1 - y)^2]^2[6(1 - y)]/d_1$$

[14] $$c_2 = R[(y\alpha_P T)/(1 - y)^2]^2[3(4y + 5)]/d_1^2$$

[15] $$\Delta c_{P(Born)}^0 = \left[\frac{N(ze)^2}{d_2}\right]\left[\frac{T}{D^2}\right]\left[\left(\frac{\partial^2 D}{\partial T}\right) - \frac{2}{D}\left(\frac{\partial D}{\partial T}\right)^2\right]$$

[16] $$\Delta c_{P(x)} = 2\alpha_P R T - R + R T^2(\partial \alpha_P/\partial T)_P$$

where $\Delta c_{P(c)}^0$ and ΔH_c^0 are heat capacity and enthalpy respectively of cavity formations calculated using the scaled particle theory (40); y, d_1, d_2, and α_P are the compactness factor (or reduced density), solvent molecular diameter, solute diameter, and volume expansion coefficient at constant pressure, respectively. More details on the equations and the symbols used are available elsewhere (13–15). A comparison of the scale particle theory (SPT) and other hard sphere perturbation approaches in describing the temperature dependence of Δc_P^0 for non-electrolytes has been discussed by Fernandez-Prini and others (41–43). Barta and Hepler (44) recently applied the SPT for calculating thermodynamics of aqueous ions at 25°C with much success and reviewed some earlier applications of the theory for similar purposes.

In the calculation of thermodynamic functions the solute diameter (d_2) was taken to be twice the Pauling's ionic crystal radius (45) which is assumed not to change significantly throughout the temperature range. The solvent diameter (d_1) at

Can. J. Chem. Downloaded from www.nrcresearchpress.com by 198.100.157.202 on 09/07/12
For personal use only.

TABLE 1. Physical parameters at different temperatures used in thermodynamic calculations[a]

T (°C)	P (atm)	V_1 ($cm^3\ mol^{-1}$)	ρ_T ($g\ cm^{-3}$)	α_P ($10^{-5}\ K^{-1}$)	$[\partial\alpha_P/\partial T]_P$ ($10^{-6}\ K^{-2}$)
0	1.000	18.017	0.99986	−6.81	18.33
25	1.000	18.068	0.99708	25.71	9.62
50	1.000	18.233	0.98807	45.78	6.87
75	1.000	18.479	0.97487	61.30	5.70
100	1.000	18.797	0.95838	75.00	5.33
125	2.2907	19.184	0.9391	87.5	5.56
150	4.6978	19.648	0.9169	103.5	6.30
175	8.8087	20.192	0.8922	119.0	6.78
200	15.3484	20.835	0.8647	137.0	8.29
225	25.1724	21.604	0.8339	160.0	11.1
250	39.2589	22.541	0.7992	195.0	17.5
275	58.7137	23.541	0.7594	251.0	26.8
300	84.8001	25.286	0.7125	330.0	48.9

T (°C)	β_T ($10^{-5}\ atm^{-1}$)	y	d_1 (Å)	$D \pm 0.05$	$-[\partial D/\partial T]_P \pm 0.0120$ (K^{-1})
0	5.098	0.3469	2.7060	87.90	0.4015
25	4.524	0.3510	2.7190	78.36	0.3562
50	4.417	0.3454	2.7130	69.88	0.3164
75	4.559	0.3344	2.6960	62.34	0.2821
100	4.890	0.3198	2.6710	55.58	0.2531
125	5.30	0.3047	2.6464	49.35	0.2145
150	6.21	0.2808	2.5959	43.89	0.2055
175	7.20	0.2587	2.5492	39.03	0.1866
200	8.70	0.2322	2.4846	34.59	0.1692
225	11.1	0.1994	2.3904	30.53	0.1569
250	14.7	0.1626	2.2653	26.75	0.1471
275	21.7	0.1121	2.0305	23.15	0.1410
300	33.0	0.0618	1.7047	19.66	0.1390

T (°C)	$[\partial^2 D/\partial T]_P \pm 0.0002$ ($10^{-5}\ K^{-2}$)	B_0 ($J\ mol^{-1}$)	B_1 ($J\ mol^{-1}\ Å^{-1}$)	B_2 ($J\ mol^{-1}\ Å^{-1}$)	B_3 ($J\ mol^{-1}\ Å^{-3}$)
0	188	−20.9	−38.1	−36.5	0.0320
25	164	104.6	174.9	168.4	0.0320
50	145	209.2	354.4	337.2	0.0320
75	128	309.6	518.8	482.5	0.0320
100	113	410.0	674.0	608	0.0320
125	98	506	824	721	0.08
150	84	602	967	809	0.15
175	70	693	1101	884	0.28
200	57	771	1213	930	0.49
225	43	822	1289	942	0.81
250	29	861	1363	952	1.3
275	15	792	1318	895	1.9
300	2	594	1114	782	2.7

T (°C)	C_H ($10^{-3}\ K^{-1}$)	C_0 ($J\ mol^{-1}\ K^{-1}\ Å^{-1}$)	C_1 ($J\ mol^{-1}\ K^{-1}\ Å^{-1}$)	C_2 ($J\ mol^{-1}\ K^{-1}\ Å^{-2}$)	C_x (per ion) ($J\ mol^{-1}\ K^{-1}$)
0	−261.66	−0.00083	−0.0029	−0.0042	2.772
25	43.883	0.0142	0.0485	0.0887	0.084
50	20.737	0.0506	0.1711	0.3075	0.125
75	14.430	0.0954	0.2238	0.5632	0.962
100	11.696	0.1443	0.4770	0.8242	2.510
125	10.503	0.1937	0.6318	1.0711	4.812
150	9.979	0.2431	0.7866	1.2803	8.368
175	8.970	0.2879	0.9079	1.4602	11.883

TABLE 1 (*concluded*)

T (°C)	C_H (10^{-3} K^{-1})	C_0 (J mol^{-1} K^{-1} Å^{-1})	C_1 (J mol^{-1} K^{-1} Å^{-1})	C_2 (J mol^{-1} K^{-1} Å^{-2})	C_x (per ion) (J mol^{-1} K^{-1})
200	8.908	0.3197	1.0042	1.5732	17.908
225	9.352	0.3276	1.0293	1.5564	27.824
250	10.85	0.3335	1.0334	1.5353	48.451
275	11.82	0.2521	0.8368	1.2636	81.504
300	15.01	0.1293	0.4853	0.7950	156.691

[a]Reference 16 and references therein.

different temperatures has been calculated from the respective isothermal compressibility data using Mayer's method (46).

The partial molal heat capacities ($\bar{c}^0_{P_2}$) can be obtained from the standard heat capacities of hydration using the following equation:

$$[17]\quad \Delta c^0_{P(h)} = \bar{c}^0_{P_2} - c^0_{P(GAS)}$$

If c^0_P of monatomic gaseous ions at all temperatures can be taken as 21 J mol^{-1} K^{-1} then eq. [17] can be written as

$$[18]\quad \Delta c^0_{P(h)} = \bar{c}^0_{P_2} - 21n$$

where n is the number of ions in the electrolyte (47).

At temperatures above 100°C, the vapour pressure of the solvent water begins to cause a difference between the standard state functions at 1 atm and those at ambient vapour pressure of the solvent. The effect may be given by

$$[19]\quad [\partial \bar{c}^0_{P_2}/\partial P] = -T[\partial^2 \bar{v}^0_2/\partial T^2]_P$$

If one can assume that $(\partial^2 \bar{v}^0_2/\partial T)$ does not change much over the pressure range involved (which may not be true at very high temperature), one may get

$$[20]\quad \bar{c}^0_{P_2(P)} - \bar{c}^0_{P_2(1)} = -T[\partial^2 \bar{v}^0_2/\partial T^2]_P(P-1)$$

where $\bar{c}^0_{P_2(1)}$ is the partial molal heat capacity at 1 atm, and $(\partial^2 \bar{v}^0_2/\partial T^2)_P$ is the second derivative of the partial molal volume of the electrolyte at infinite dilution. The partial molal volume data for electrolyte at different temperatures have been compiled by Millero (48). Those data for NaCl and $BaCl_2$ from 75 to 200°C (the limit up to which data are available) were fitted to smooth curves and differentiated to give the necessary derivatives. The second derivatives are not very accurately known but the magnitude of correction to the $\bar{c}^0_{P_2}$ data is not large up to 200°C (about 5 units for $BaCl_2$ at 200°C). The same may be higher at higher temperatures, particularly above 250°C or so from where the vapour pressure of water rises quite sharply with increase in temperature. There are other uncertainties in that higher temperature range, for example, uncertainties due to the solvent dielectric constant and its derivatives may be much higher. Therefore the pressure correction on $\bar{c}^0_{P_2}$ has not been included.

4. Results and discussion

Various physical parameters at different temperatures used in the theoretical calculations of the heat capacities are listed in Table 1.

4.1. Standard heat capacities of hydration

Equations [6] and [17] have been used to obtain the standard heat capacity of hydration ($\Delta c^0_{P(h)}$) and the corresponding standard partial molal heat capacity of the electrolytes. Figures

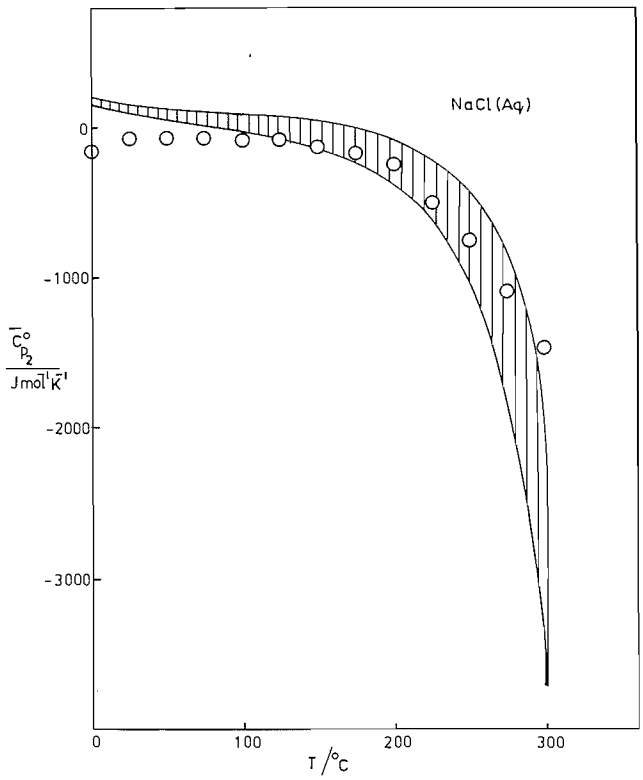


FIG. 1. Predicted (band) and observed (symbol) partial molal heat capacities ($\bar{c}^0_{P_2}$), J mol^{-1} K^{-1} for aqueous NaCl at different temperatures.

1–3, which provide a comparison of the calculated and experimental values of $\bar{c}^0_{P_2}$ for aqueous NaCl, $BaCl_2$, $GdCl_3$ at various temperatures, would give an estimate on the accuracy of the prediction. The agreement is fairly good particularly at the higher temperature ranges. We are, however, concerned about the limit of uncertainty at higher temperatures, which could be large. Yet another way to generate the heat capacity values is to get the derivatives of the corresponding entropy data and use the following equation

$$[21]\quad \Delta c^0_{P(h)} = T(\partial \Delta s^0_h/\partial T)_P$$

To obtain $(\partial \Delta s^0_h/\partial T)_P$ at different temperatures, we have fitted the predicted Δs^0_h values of NaCl and $BaCl_2$ reported in refs. 15, 16 in polynomials of various degrees. Figures 4 and 5 would show the comparison of such $\Delta c^0_{P(h)}$ values with the experimental heat capacity values. Table 2 contains the coefficients of the polynomial fit of third degree which gives the best fit.

As mentioned earlier the specific interaction term Δs^* and its temperature derivative $(\partial \Delta s^*/\partial T)$ and also $T(\partial \Delta s^*/\partial T)$

Can. J. Chem. Downloaded from www.nrcresearchpress.com by 198.100.157.202 on 09/07/12
For personal use only.

Can. J. Chem. Downloaded from www.nrcresearchpress.com by 198.100.157.202 on 09/07/12
For personal use only.

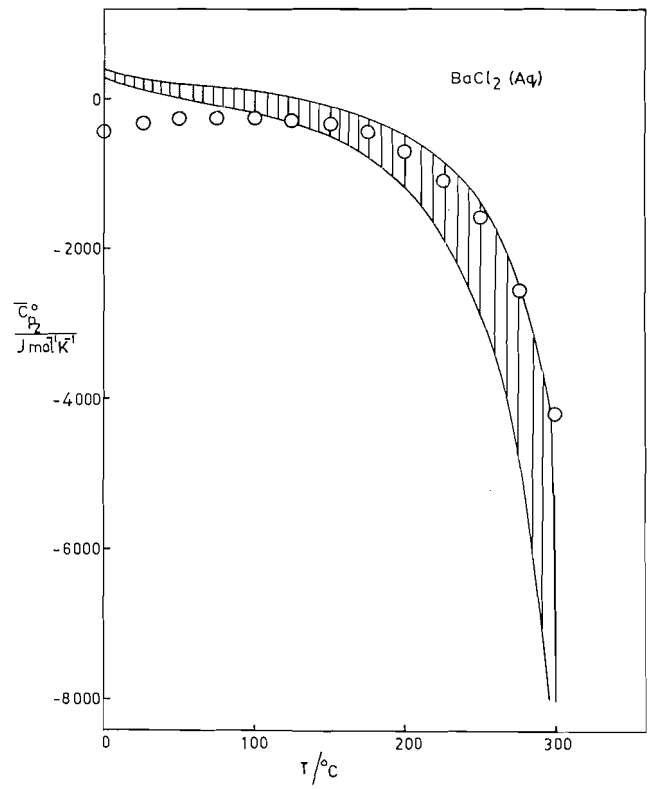


FIG. 2. Predicted (band) and observed (symbol) standard partial molal heat capacities ($\bar{c}^0_{P_2}$), J mol^{-1} K^{-1} for aqueous $BaCl_2$ at different temperatures.

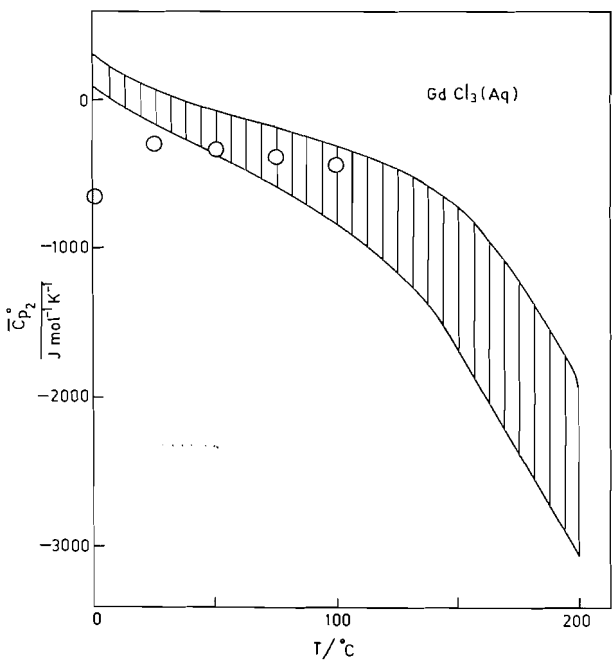


FIG. 3. Predicted (band) and observed (symbol) standard partial molal heat capacities ($\bar{c}^0_{P_2}$), J mol^{-1} K^{-1} for aqueous $GdCl_3$ at different temperatures.

($= \Delta c^*_P$) has been asumed to be negligible in our calculations. Experimental works summarized by Helgeson and co-workers (28, 29, 31) has, however, shown that the contributions of specific interaction to $\Delta c^0_{P(h)}$ which may be close to Δc^*_P in our notation becomes significantly large as the temperature drops to

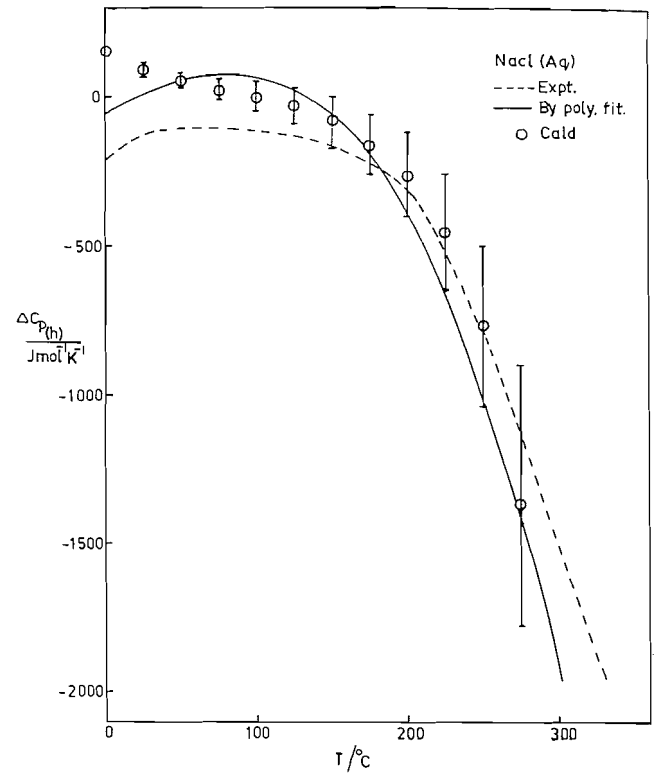


FIG. 4. Calculated and experimental values of standard heat capacity of hydration ($\Delta c^0_{P(h)}$), J mol^{-1} K^{-1} of aqueous NaCl at different temperatures.

room temperature and below. This may be one of the possible reasons of the rather wide disagreements between the predicted and the experimental values of heat capacity of hydration ($\Delta c^0_{P(h)}$) of electrolytes at lower temperatures. Since Helgeson and co-workers did not attempt to avoid arbitrary adjustments for the Born radius of the solute ion, an additional term had to be involved. However, Helgeson and co-workers (31) omitted the standard state correction terms on the plea that it is discontinuous at the critical point of water. The values of such standard state heat capacity terms for hypothetical ions of radii 1 and 2 Å are listed in Table 6.

4.2. Correspondence principle

Criss and Cobble (12) observed that not only the entropy of ions, $\bar{s}^0_T$ at temperature T will be in linear relationship with entropy $\bar{s}^0_{T_R}$ at the reference temperature T_R but there could be a similar linear relationship between the heat capacity $\bar{c}^0_{P(T)}$ at T and the corresponding entropy $\bar{s}^0_{T_R}$ at the reference temperature T_R. However, they use the average heat capacity $\bar{c}^0_{P_2}\Big]_{25}^{T}$ when 25°C is the reference temperature. They give the following relationships

$$[22] \quad \bar{c}^0_{P_2}\Big]_{25}^{T_2} = (\bar{s}^0_{T_2} - \bar{s}^0_{25})/\ln [(T + 273)/298]$$

and

$$[23] \quad \bar{s}^0_{T_2} = a_{T_2} + b_{T_2}\bar{s}^0_{25}$$

They used the average heat capacity data at smaller and smaller intervals to equate them with the actual heat capacity data. However we do not need to go through this exercise and can calculate heat capacities directly. The linear correspondence

Can. J. Chem. Downloaded from www.nrcresearchpress.com by 198.100.157.202 on 09/07/12
For personal use only.

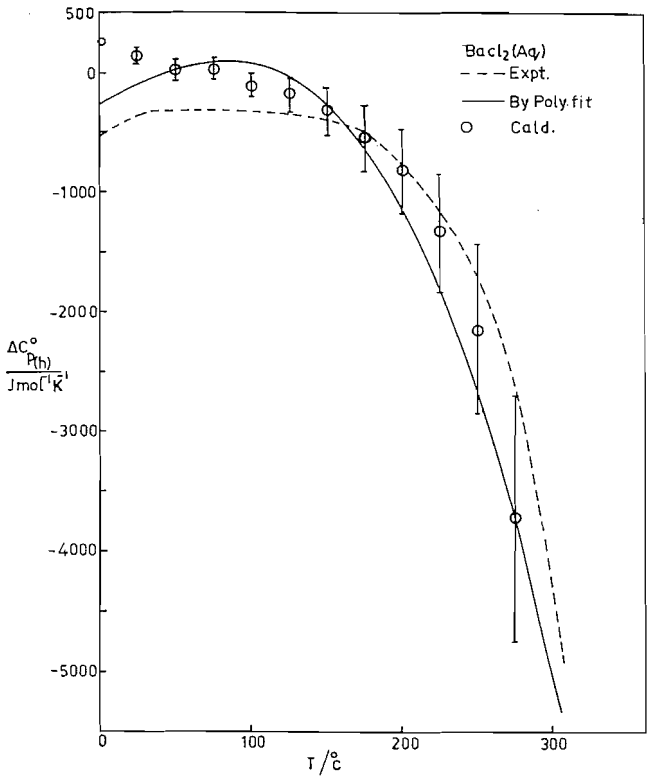


FIG. 5. Calculated and experimental values of standard heat capacity of hydration ($\Delta c^0_{P(h)}$), J mol^{-1} K^{-1} of aqueous $BaCl_2$ at different temperatures.

TABLE 2. Coefficients for the third degree polynomial expressions of the predicted ΔS^0_h values of NaCl(aq) and $BaCl_2$(aq) as the functions of temperature (T K)

$$\Delta S^0_h = A + BT + CT^2 + DT^3$$

Coefficients	Value	
	NaCl	$BaCl_2$
A (J mol^{-1} K^{-1})	731.7	542.0
B (J mol^{-1} K^{-2})	−8.47423	−5.57422
C (J mol^{-1} K^{-3})	2.479493×10^{-4}	1.58454×10^{-2}
D (J mol^{-1} K^{-4})	-2.358253×10^{-7}	-1.50241×10^{-5}

equation involving heat capacities and entropy at a reference temperature is

[24] $\bar{c}^0_{P(T)} = A_T + B_T \bar{s}^0_{100}$

Since our prediction of thermodynamics function is relatively more accurate at higher temperature ranges when the hydrogen bonding in solvent water is considerably weak the reference temperature preferred is 100°C. Table 3 list A_T and B_T in eq. [24] and Fig. 6 shows the typical correspondence plots at these temperatures. We may mention here that the correspondence curves with heat capacity and entropy need not be much different for cations and anions as suggested by Crisis and Cobble (12).

4.3. Single ion heat capacities

There is no direct experimental method which can provide individual ionic heat capacity values at different temperatures. There have been, however, a number of extrathermodynamic non-experimental methods proposed from time to time to generate individual ionic contributions of thermodynamic properties in aqueous systems (49, 50). Most of them were, however, confined to the values at 25°C. The method proposed by Crisis and Cobble (11, 12) is still very much in use to give entropies and heat capacities of aqueous ions, particularly at higher temperatures. However, we have doubts about the validity of the arbitrarily chosen individual ionic values they proposed, particularly those at elevated temperatures (16). Our theory as described above is capable of producing accurate predictions on

TABLE 3. Correspondence constants A_T (in J mol^{-1} K^{-1}) and B_T for the calculated heat capacities of ions at elevated temperatures

$$\bar{c}^0_{P(T)} = A_T + B_T \bar{s}^0_{100}$$

T/(°C)	A_T (J mol^{-1} K^{-1})	B_T
50	−57	1.36
75	−82	1.65
100	−121	1.96
125	−162	2.51
150	−205	3.13
175	−334	4.38
200	−470	5.69
225	−750	8.39
250	−1210	12.70
275	−2050	20.21
300	−3610	38.13

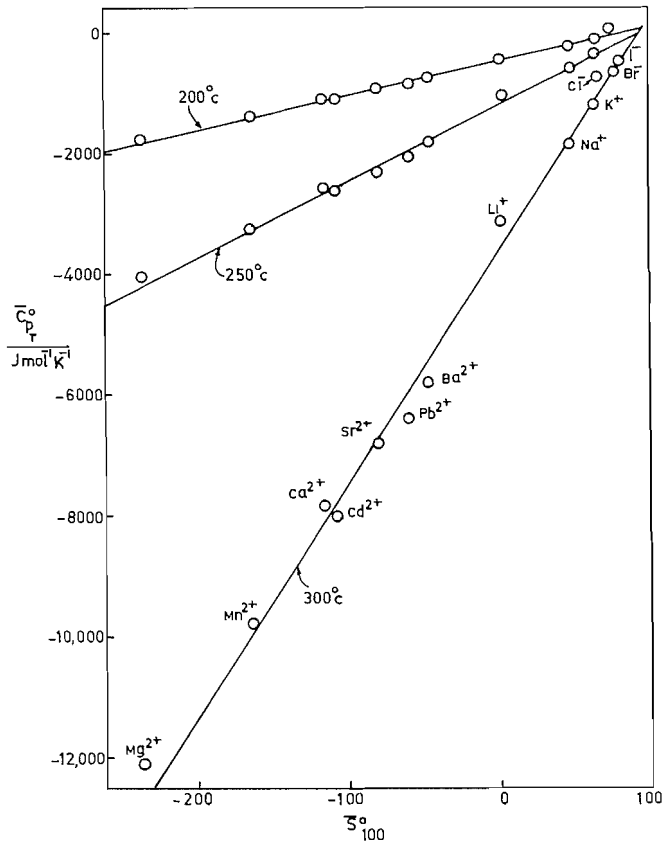


FIG. 6. Correspondence diagram illustrating the linear relationship between the predicted absolute heat capacities of aqueous ion with the absolute entropy of aqueous ions at the reference temperature (100°C).

TABLE 4. Values of the standard heat capacity and entropy of aqueous chloride ion and the respective surface dipole potential corrections at elevated temperatures, recommended for setting the ionic scales (in J mol^{-1} K^{-1})

T/(°C)	$\Delta c^0_{P(h)}$	$\bar{c}^0_{P(Cl^-)}$	$\Delta c^0_{P(corr)}$[a]	Δs^0_h	$\bar{s}^0_{Cl^-}$	Δs^0_{corr}[a]
0	143.0	164.0	223.0	−120.5	31.2	−57.9
25	97.8	118.8	240.3	−111.3	42.2	−38.6
50	80.8	101.7	207.7	−102.9	52.0	−22.2
75	69.0	90.0	105.8	−97.5	58.9	−9.7
100	60.7	81.6	52.8	−92.5	65.7	−3.9
125	54.4	75.3	31.8	−89.1	70.1	−1.5
150	41.0	61.9	18.5	−84.9	75.6	−0.5
175	13.0	33.9	10.0	−85.4	76.3	0
200	16.7	4.2	5.0	−86.2	76.6	0
225	−72.4	−51.5	0	−90.8	73.2	0
250	−150.6	−129.7	0	−98.3	66.9	0
275	−348.1	−327.2	0	−114.2	51.8	0
300	−738.5	−717.6	0	−146.0	20.9	0

[a]For monovalent ions and to be added for cations and to be subtracted for anions.

both entropy and heat capacity values of aqueous electrolytes over a wide range of temperatures. The method does not involve any arbitrary adjustable parameter. It may be seen from Figs. 1–3 that the predictions of heat capacity values are accurate for mono-, di-, and trivalent metal chlorides. We therefore recommend the calculated values of the heat capacity of chloride ion, $\bar{c}^0_{P(Cl^-)}$ for setting up the ionic scale for partial molal heat capacity at different temperatures. Table 4 lists the values of the standard partial molal heat capacity of aqueous chloride ion at different temperatures, recommended for splitting the values of the standard heat capacity of aqueous electrolytes into the corresponding ionic contributions. The predicted standard heat capacity values for a few ions are presented in Table 5. Tanger and Helgeson (31) listed their calculated values of heat capacity of some ions on conventional scale but did not suggest any absolute scale for the ionic values.

4.4. Standard partial molal capacities of the hydrogen ion at different temperatures

One limitation of any prediction of properties of ions by theoretical calculations involving the actual diameter of the ion is that it cannot give a practical value on the property of hydrogen ion (unhydrated) which is generally accepted to have point dimension or zero diameter. In our earlier attempt to generate the value of partial molal entropy of hydrogen ion at different temperatures, we used some experimental emf data involving HCl solution. Recently, results of some calorimetric measurements with HCl solution at some higher temperatures have been reported (10). Those values would be apparently more accurate compared to the values generated using the high temperature emf readings through a number of temperature derivatives. From the experimental values of heat capacity of aqueous HCl at different temperatures obtained from ref. 10 and through some extrapolations our recommended values of standard partial molal heat capacity of aqueous chloride ion at the corresponding temperatures have been subtracted to generate the partial molal heat capacity of the aqueous hydrogen ion at that temperatures. Those values of heat capacity are then used to yield the corresponding partial molal entropy of hydrogen ion in solution. The entropy values were obtained graphically using the following equation

$$[25]\quad \bar{s}^0_T = \bar{s}^0_{T_R} + \int_{T_R}^{T} (\bar{c}^0_P \mathrm{d}T)/T$$

where T_R = 298 K and $\bar{s}^0_{T_R}$ = 22 J mol^{-1} K^{-1}.

It has been already pointed out earlier (16) that if the hydration of an ion is defined as the process where an ion (in the gaseous state) in field-free space is inserted into a large quantity of the solvent, which carries no net electrical charge, then the interaction of the ion in the process of transfer through electrical double layer at the free surface of the solution (51) may have to be considered. This involves the surface dipole potential (χ) (52) and also its temperature derivatives (53) at different temperatures. Such effects on the transfer of cations and anions across the solution surface would obviously be opposite and cancel one another when their neutral combination into the corresponding salt has been considered. It may also be mentioned that the value of the surface dipole potential as well as its temperature derivatives are believed to approach zero with increasing temperature and the potential term vanishes altogether at the critical temperature of the solvent (54). The reported values (53) of the first temperature derivatives of the gas water surface potential ($\partial\chi/\partial T$) at different temperatures have been used for the correction of the calculated values of $\bar{s}^0_{H^+}$ at different temperatures (16). The estimated values of such entropy correction forms at different temperatures have been plotted against temperature and from the slope at each temperature the ionic correction term for heat capacity, $\bar{c}^0_{P(corr)}$ for that temperature can be calculated using $\bar{c}^0_{P(corr)} = T(\partial \bar{s}^0_{corr}/\partial T)$. The estimated correction terms per monovalent ion for the transfer entropy and heat capacity functions have been included in Table 4.

The values of the absolute standard partial molal heat capacity and entropy of aqueous hydrogen ion at different temperatures obtained as described above are listed in Table 6. We believe that the present values of the absolute standard partial molal entropy of hydrogen ion, generated directly using calorimetric data, might be more accurate than those that were generated indirectly through emf data and listed in ref. 16.

Some years ago, Ackermann (55) proposed a model for the arrangement of solvent water molecules in the so-called hydration shell of the hydrogen ion and calculated the heat capacity of the ion at different temperatures. These values were used to yield the partial molar entropy of hydrogen ion using eq. [25]. These values are also included in the table for comparison. Later Criss and Cobble (11, 12) suggested values for partial molal entropy of hydrogen ion at different temperatures up to 200°C with the help of the correspondence principle. When plotted against temperature, these data produce a nearly linear curve at higher temperature ranges. The corresponding values of the heat capacity of aqueous hydrogen ion have been calculated using eq. [21]. All these values are included in Table 5. Figures 7 and 8 would give an idea about the trends of variations of $\bar{s}^0_{H^+}$ and $\bar{c}^0_{P(H^+)}$ with temperature proposed by different authors. It can be seen from these figures that both this work and the work of Ackermann (55) show that $\bar{s}^0_{H^+}$ and $\bar{c}^0_{P(H^+)}$ become more negative with increase in temperature. The values proposed by Criss and Cobble (11, 12) do, however, follow the opposite trend and become increasingly more positive with increase in temperature.

Abraham and Marcus (22) used the TATB assumption (49, 50) viz.,

$$\Delta c^0_{P(h)}{}^{(Ph_4P^+)} = 772 \text{ J mol}^{-1} \text{ K}^{-1} \approx 774 \text{ J mol}^{-1} \text{ K}^{-1} = \Delta c^0_{P(h)}{}^{(Ph_4B^-)}$$

Can. J. Chem. Downloaded from www.nrcresearchpress.com by 198.100.157.202 on 09/07/12
For personal use only.

TABLE 5. Predicted values of standard heat capacities of some common ions in solution ($\bar{c}^0_{P_2}$) (J mol^{-1} K^{-1}, molal scale) at elevated temperature

		$\bar{c}^0_{P_2}$										
Ions	r_c/Å	50°C	75°C	100°C	125°C	150°C	175°C	200°C	225°C	250°C	275°C	300°C
Li^+	0.60	−67	−93	−121	−161	−221	−301	−431	−635	−1017	−1712	−3121
Na^+	0.95	−8	−23	−41	−63	−99	−154	−226	−360	−574	−954	−1854
K^+	1.33	41	29	17	3	−19	−58	−105	−194	−330	−620	−1200
Rb^+	1.48	60	48	37	26	7	−28	−69	−145	−259	−515	−1024
Cs^+	1.69	86	75	66	58	42	12	−21	−84	−173	−390	−818
Ag^+	1.26	34	20	6	−9	−33	−71	−123	−219	−366	−675	−1296
Ti^+	1.40	51	38	26	14	−7	−40	−88	−171	−296	−570	−1115
F^-	1.36	45	33	21	8	−14	−52	−98	−183	−315	−598	−1162
Cl^-	1.81	102	90	82	75	62	34	4	−52	−130	−327	−718
Br^-	1.95	121	110	101	96	93	59	33	−16	−106	−259	−610
I^-	2.16	150	139	131	128	120	96	75	36	−10	−164	−464
Mg^{2+}	0.65	−365	−462	−569	−725	−959	−1300	−1769	−2623	−4040	−6702	−12116
Ca^{2+}	0.99	−204	−268	−339	−439	−590	−812	−1116	−1671	−2585	−4318	−7841
Sr^{2+}	1.13	−161	−216	−280	−365	−498	−689	−955	−1439	−2233	−3747	−6821
Ba^{2+}	1.35	−104	−152	−203	−275	−383	−553	−764	−1164	−1818	−3078	−5788
Cd^{2+}	0.97	−211	−275	−349	−450	−603	−831	−1142	−1709	−2644	−4413	−8011
Mn^{2+}	0.80	−287	−359	−447	−571	−760	−1037	−1415	−2106	−3242	−5403	−9787
Pb^{2+}	1.20	−141	−194	−253	−334	−457	−638	−887	−1342	−2086	−3508	−6397
Al^{3+}	0.50	−1161	−1442	−1766	−2227	−2923	−3924	−5314	−7840	−12040	−19895	−35885
Fe^{3+}	0.64	−893	−1112	−1365	−1724	−2266	−3048	−4131	−6101	−9375	−15504	−27977
Gd^{3+}	1.02	−521	−659	−817	−1040	−1377	−1867	−2542	−3771	−5809	−9638	−17430

TABLE 6. Partial molal entropy ($s^0_{H^+}$) and heat capacity ($\bar{c}^0_{P(H^+)}$) of aqueous hydrogen ion at different temperatures in J mol^{-1} K^{-1}

T/°C	$\bar{s}^0_{HCl}$[a]	$\bar{s}^0_{H^+}$[b]	$\bar{s}^0_{H^+}$[c]	$\bar{s}^0_{H^+}$[d]	$\bar{c}^0_{P(HCl)}$[a]	$\bar{c}^0_{P(H^+)}$[b]	$\bar{c}^0_{P(H^+)}$[c]	$\bar{c}^0_{P(H^+)}$[d]
0	69.7	−19.4	−43.9	−26.4	−177.5	−118.5	24.6	54
25	56.7	−24.1	−20.9	−22.2	−123.3	−1.8	119.6	46
50	47.5	−27.0	−13.0	−18.6	−111.8	−6.1	129.6	29
75	39.2	−29.8	−3.3	−16.1	−110.8	−95.0	139.6	7
100	31.4	−38.2	8.4	−14.7	−119.2	−148.4	149.6	−33
125	22.5	−49.5	16.7	−15.3	−136.0	−179.2	159.6	−84
150	14.3	−62.0	27.2	−18.5	−161.0	−204.5	169.6	−146
175	5.3	−71.3	36.8	−24.6	−200.0[e]	−224.0	179.7	−210
200	−7.0	−80.4	46.4	−34.3	−247[e]	−246.0	189.7	—
225	—	−89.0[e]	56.5	—	—	−265.0[e]	199.7	—
250	—	−97.5[e]	67.4	—	—	−284.0[e]	209.7	—
275	—	−105.0[e]	77.0	—	—	−301.0[e]	219.8	—
300	—	−112.4[e]	86.6	—	—	−317.0[e]	229.8	—

[a]Reference 10, entropy values obtained from the corresponding $\bar{c}^0_{P(HCl)}$ values using $\bar{s}^0_{HCl} = (1/T)[\int_{298}^{T}(c^0_{P(HCl)}/T)dT]$, $\bar{s}^0_{298(HCl)} = 56.73$ J mol^{-1} K^{-1}.
[b]This work.
[c]References 11 and 12. The plot of assigned $s^0_{H^+}$ vs. T is a straight line of slope $(\partial s^0_{H^+}/\partial T) = 0.4010$ J mol^{-1} K^{-2}. Therefore $\bar{c}^0_{P(H^+)} = T(\partial \bar{s}^0_{H^+}/\partial T) = 0.4010T$.
[d]Reference 51.
[e]Extrapolated values.

at 25°C for fixing the absolute scale for heat capacity of hydration of aqueous ion. However, they did not suggest any absolute scale for higher temperatures.

4.5. *Temperature behaviour of cationic and anionic heat capacities*

Ackermann (55) plotted the values of $\bar{c}^0_{P_2}$ of a few cations and anions as a function of temperature. It was observed that for cations, which are comparatively smaller in size, the negative value increases with increase in temperature from the very beginning. However, for anions larger in size, some tendency to decrease the negative value at low temperatures, and then after passing through a rather ill-defined maximum, a trend of increasing the negative value of $\bar{c}^0_{P_2}$ with increase in temperature as in the case of smaller cations were observed. In Fig. 9 we have plotted the predicted values of $\bar{c}^0_{P_2}$ of two hypothetical ions having crystal radii 1 Å, representing the typical monovalent cation and 2 Å representing the typical anion. Our observation is similar to that by Ackermann (55). The sharp increase in the negative value of $\bar{c}^0_{P_2}$ does occur at a comparatively higher temperature if the size of the ion is comparatively large. Thus, as in the case of temperature effects on $\bar{s}^0_2$ (16), the size of the ion plays the most important role to define the temperature effect on the partial molal heat capacity of aqueous ions. Table 7

Can. J. Chem. Downloaded from www.nrcresearchpress.com by 198.100.157.202 on 09/07/12
For personal use only.

Can. J. Chem. Downloaded from www.nrcresearchpress.com by 198.100.157.202 on 09/07/12
For personal use only.

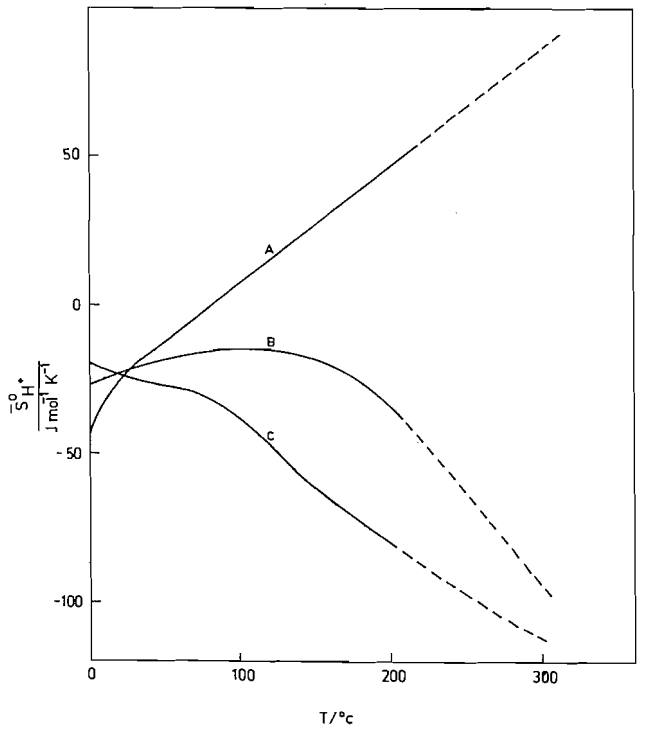


FIG. 7. Comparison of the temperature behaviour of the standard partial molal entropy of aqueous hydrogen ion, assigned by different authors. *A*, Criss and Cobble (11, 12); *B*, Ackermann (55); *C*, this work.

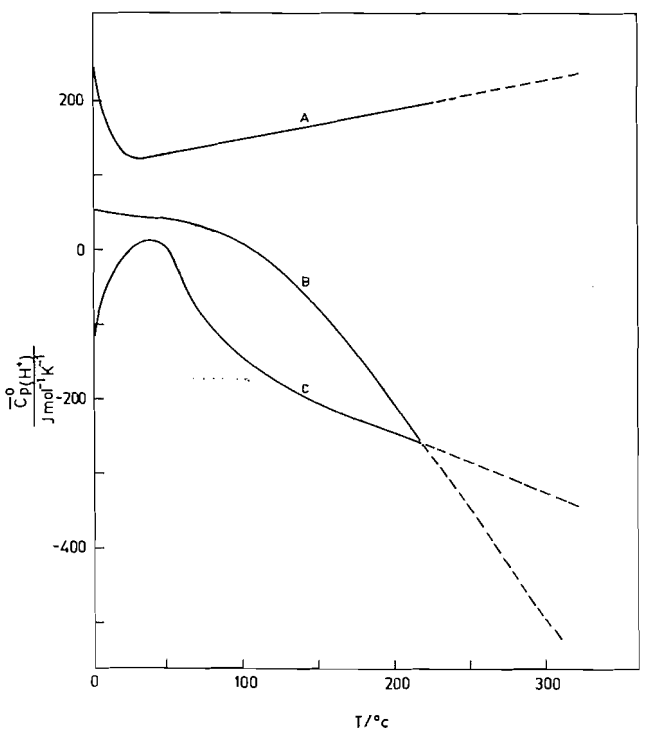


FIG. 8. Comparison of the temperature behaviour of the standard partial molal heat capacity of aqueous hydrogen ion, assigned by different authors. *A*, Criss and Cobble (11, 12); *B*, Ackermann (55); *C*, this work.

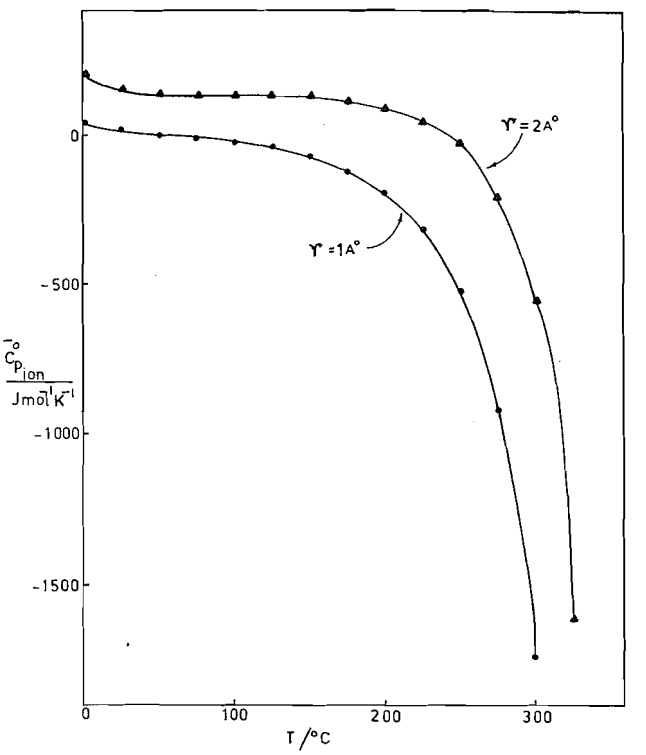


FIG. 9. Variation of the calculated values of $\bar{c}^0_{P_2}$ for monovalent ions of hypothetical radii 1 Å (●, representative of typical monovalent cations) and 2 Å (▲, representative of typical monovalent anions), with temperature.

lists the different contributions to the calculated values of heat capacity for ions of hypothetical radii 1 and 2 Å.

5. Conclusion

The theoretical prediction of partial molal heat capacities of aqueous electrolytes at elevated temperatures using the unified approach consisting of the scaled-particle theory and the Born charging equation (14, 15) may not be as accurate as the prediction of the corresponding entropy data using the same composite theory, but the large uncertainty in the temperature derivatives of the solvent dielectric constant specially at the higher temperatures used in the theoretical calculation seemed to be a major hurdle. Comparatively, contributions to the uncertainty due to some other approximations are of little or no significance to the predicted value. Nevertheless this might be the most accurate and wide ranging theoretical predictions to date without using any arbitrary adjustable parameters, as far as the heat capacity of aqueous electrolytes and ions are concerned. This work thus suggests that the primitive Born continuum dielectric model can be very useful provided some other simple considerations be duly introduced.

Other workers have also been successful in utilizing the Born equation for theoretical thermodynamic predictions for aqueous electrolytes at different temperatures (20, 29, 31, 32). Sometimes, particularly at the temperatures lower than the boiling point of water (100°C), some of these theoretical predictions may seem closer to the experimentally observed values than those in the present work. One example is the recent work of Tanger and Helgeson (31). But the fact that so many complicated assumptions involving several rather arbitrarily chosen adjustable parameters could be altogether avoided with only one simple and experimentally substantiated assumption (14–16)

TABLE 7. Different heat capacity contributions of the calculated values (J mol^{-1} K^{-1})

(*a*) For ions of hypothetical radius 1 Å (representing typical monovalent cations)

T/°C	$\Delta c^0_{P(c)}$	$\Delta c^0_{P(Born)}$	$\Delta c^0_{P(x)}$	$\Delta c^0_{P(h)}$	$\bar{c}^0_{P_2}$
0	63.6	−43.6	2.8	+22.8	43.8
25	50.1	−53.8	0.1	−3.6	17.4
50	48.6	−66.7	0.1	−18.0	3.0
75	50.1	−82.4	1.0	−31.3	−10.3
100	53.4	−100.4	2.5	−44.5	−23.5
125	58.6	−126.3	4.8	−62.9	−41.9
150	64.7	−165.2	8.4	−92.1	−71.1
175	65.6	−221.1	11.9	−143.6	−122.6
200	70.3	−298.7	17.9	−210.5	−189.5
225	75.8	−439.7	27.8	−210.5	−189.5
250	82.2	−674.5	48.5	−543.8	−522.8
275	88.8	−1112.8	81.5	−942.5	−921.5
300	93.9	−2005.5	156.7	−1754.9	−1733.9

(*b*) For ions of hypothetical radius 2 Å (representing typical monovalent anions)

T/°C	$\Delta c_{P(c)}$	$\Delta c^0_{P(Born)}$	$\Delta c_{P(x)}$	$\Delta c^0_{P(h)}$	$\bar{c}^0_{P_2}$
0	198	−21.9	2.8	179	200
25	154	−26.9	0.1	127	148
50	150	−33.4	0.1	117	138
75	152	−41.2	1.0	112	133
100	159	−50.2	2.5	111	132
125	172	−63.2	4.8	114	135
150	184	−82.6	8.4	110	131
175	189	−110.6	11.9	90	111
200	200	−149.9	17.9	68	89
225	214	−219.9	27.8	22	43
250	242	−337.3	48.5	−47	−26
275	247	−556.4	81.5	−228	−207
300	274	−1002.8	156.7	−572	−551

that the free energy involved in the strong ion–solvent interaction in the near vicinity of the solute ion is relatively temperature insensitive, without significantly sacrificing the accuracy of the theoretical prediction, is certainly thought provoking.

The Born charging equation (30) does not distinguish a cation from an anion. It only concerns the size, or in other words, the surface charge density of the solute ionic species. The success of the Born approach, particularly at higher temperatures, perhaps indicates that at temperatures near or above the boiling point of water, hydrogen bonding is weak and therefore the energy involved in solvent orientations around a cation of a particular size may not be much different from that around an anion of the same size. Obviously, an accurate knowledge of the physical parameters of the solvent used, along with an accurate diameter of the solute ion is extremely important in accurate thermodynamic predictions.

Acknowledgement

I thank Professor S. K. Rangarajan, Director, Central Electrochemical Research Institute, Karaikudi 623 006, Tamilnadu, India, for his interest in this work.

1. J. W. COBBLE and R. C. MURRAY. Discuss. Faraday Soc. **64**, 144 (1977).
2. J. W. COBBLE, R. C. MURRAY, and U. SEN. Nature, **291**, 566 (1981).
3. D. S. MAGOWAN and R. H. WOOD. J. Chem. Thermodyn. **13**, 1047 (1981).
4. J. A. GATES, R. H. WOOD, and J. R. QUINT. J. Phys. Chem. **86**, 4948 (1982).
5. W. L. GARDNER, R. E. MITCHELL, and J. W. COBBLE. J. Phys. Chem. **73**, 2025 (1969).
6. H. C. HELGESON. Am. J. Sci. **267**, 729 (1969).
7. C. T. LIU and W. T. LINDAY. J. Soln. Chem. **1**, 45 (1972).
8. P. S. Z. ROGERS and K. S. PITZER. J. Phys. Chem. **85**, 2886 (1981).
9. R. C. PHUTELA and K. S. PITZER. J. Phys. Chem. **90**, 895 (1986).
10. P. R. TREMAINE, K. SWAY, and J. A. BARBERO. J. Soln. Chem. **15**, 1 (1986).
11. C. M. CRISS and J. W. COBBLE. J. Am. Chem. Soc. **86**, 5385 (1964).
12. C. M. CRISS and J. W. COBBLE. J. Am. Chem. Soc. **86**, 5390 (1964).
13. L. F. SILVESTER and K. S. PITZER. J. Phys. Chem. **81**, 1822 (1977).
14. U. SEN. J. Am. Chem. Soc. **101**, 2531 (1979).
15. U. SEN. J. Am. Chem. Soc. **102**, 2181 (1980).
16. U. SEN. J. Chem. Soc. Faraday I, **77**, 2883 (1981).
17. U. SEN. Can. J. Chem. **62**, 2721 (1984).
18. U. SEN. J. Indian Chem. Soc. **63**, 547 (1986).
19. R. H. WOOD and J. R. QUINT. J. Chem. Thermodyn. **14**, 1069 (1982).
20. J. R. QUINT and R. H. WOOD. J. Phys. Chem. **89**, 380 (1985).
21. P. R. TREMAINE and S. GOLDMAN. J. Phys. Chem. **82**, 2317 (1978).
22. M. H. ABRAHAM and Y. MARCUS. J. Chem. Soc. Faraday I, **82**, 3255 (1986).
23. M. H. ABRAHAM and E. MATTEOLI. J. Chem. Soc. Faraday I, **84**, 1985 (1988).
24. M. H. ABRAHAM, E. MATTEOL, and J. LISZI. J. Chem. Soc. Faraday I, **79**, 2781 (1983).
25. P. P. S. SALUJA, K. S. PITZER, and R. C. PHUTELA. Can. J. Chem. **64**, 1328 (1986).
26. R. H. WOOD, D. S. MAGOWAN, K. S. PITZER, and P. S. Z. ROGERS. J. Phys. Chem. **87**, 3297 (1983).
27. H. G. HELGESON. *In* Chemistry and geochemistry of solutions at high temperatures and processes. *Edited by* D. T. Rickard and F. E. Wickman. Pergamon, Oxford. 1982. p. 133.
28. H. C. HELGESON and D. H. KIRKHAM. Am. J. Soc. **274**, 1089 (1974).
29. H. C. HELGESON, D. H. KIRKHAM, and G. C. FLOWERS. Am. J. Soc. **281**, 1249 (1981).
30. A. L. HORVATH. Handbook of aqueous electrolyte solutions. Ellis Horwood, Chicheston, U.K. 1985.
31. J. C. TANGER and H. C. HELGESON. Am. J. Sci. **288**, 19 (1988).
32. J. C. TANGER and K. S. PITZER. J. Phys. Chem. **93**, 4941 (1989).
33. K. S. PITZER. J. Phys. Chem. **87**, 1120 (1983).
34. Y. C. WU and H. L. FRIEDMAN. J. Phys. Chem. **70**, 501 (1966).
35. C. E. WOODWARD and S. NORDHOLM. J. Phys. Chem. **92**, 497 (1988).
36. M. BORN. J. Phys. **1**, 45 (1920).
37. K. W. FRESE, JR. J. Phys. Chem. **93**, 5911 (1989).
38. A. A. RASHIN and B. HONIG. J. Phys. Chem. **89**, 5588 (1985).
39. B. JAYARAM, R. FINE, K. SHARP, and B. HONIG. J. Phys. Chem. **93**, 4320 (1989).
40. R. A. PIEROTTI. Chem. Rev. **76**, 7717 (1976); J. Phys. Chem. **67**, 1840 (1963); **69**, 281 (1965).
41. R. FERNANDEZ-PRINI and M. L. JAPAS. J. Phys. Chem. **90**, 1395 (1986).
42. R. FERNANDEZ-PRINI and M. L. JAPAS. J. Phys. Chem. **93**, 3802 (1989).
43. R. FERNANDEZ-PRINI, R. CROVETTO, M. L. JAPAS, and D. LARIA. Am. Chem. Res. **18**, 207 (1985).

Can. J. Chem. Downloaded from www.nrcresearchpress.com by 198.100.157.202 on 09/07/12
For personal use only.

44. L. BARTA and L. G. HEPLER. J. Phys. Chem. **93**, 5588 (1989).
45. L. PAULING. The nature of the chemical bonds. 3rd ed. Cornell Univ. Press, Ithaca. 1960. p. 514.
46. S. W. MAYER. J. Phys. Chem. **67**, 2160 (1963).
47. G. N. LEWIS and M. RANDALL. Thermodynamics. 2nd ed. *Revised by* K. S. Pitzer and L. Brewer. McGraw-Hill, New York. 1961. p. 502.
48. F. J. MILLERO. *In* Water and aqueous solutions. *Edited by* R. A. Horne. John Wiley, New York. 1972. p. 519.
49. B. E. CONWAY. Ionic hydration in chemistry and biophysics. Elsevier, Amsterdam. 1980; J. Soln. Chem. **7**, 721 (1978).
50. Y. MARCUS. Ion solvation. Wiley, Chichester. 1985.
51. B. CASE and R. PARSONS. Trans. Faraday Soc. **63**, 1224 (1967).
52. J. E. B. RANDLES. Trans. Faraday Soc. **52**, 1573 (1956).
53. J. E. B. RANDLES and D. J. SCHIFFRIN. J. Electroanal. Chem. **10**, 480 (1965).
54. B. E. CONWAY. Physical chemistry. An advanced treatise. Vol. IXA. *Edited by* H. Eyring. Academic Press, New York. 1970. p. 21.
55. T. ACKERMANN. Discuss. Faraday Soc. **24**, 180 (1957).

Can. J. Chem. Downloaded from www.nrcresearchpress.com by 198.100.157.202 on 09/07/12
For personal use only.

Tetrahalogenomercury(II) complexes. A study of their electronic spectra, formation constants, ionic strength, and cation effects

TREVOR R. GRIFFITHS AND RICHARD A. ANDERSON
School of Chemistry, The University, Leeds LS2 9JT, United Kingdom

Received April 5, 1990[1]

TREVOR R. GRIFFITHS and RICHARD A. ANDERSON. Can. J. Chem. **69**, 451 (1991).

The unambiguous electronic absorption spectra of HgX_4^{2-} (X = Cl, Br, or I) in methanol have been determined for the first time. The spectra were resolved into their component Gaussian bands, and assigned using a correlation diagram for T_d symmetry. The effects of second-order spin–orbit coupling account satisfactorily for the observed band intensities and splittings. The formation constants, K_4, as a function of ionic strength were computed over the complete spectral range by multiple linear regression analysis and were, extrapolated to infinite dilution, 0.4 ± 0.1 for HgI_4^{2-} and $HgBr_4^{2-}$, and 5.7 ± 0.2 for $HgCl_4^{2-}$. Significant cation effects were observed upon the spectra of HgX_2 with added X^-, and may partially be explained in terms of the extended Debye–Hückel equation.

Key words: electronic absorption spectra, mercury(II) halide complexes, formation constants, ionic strength, Gaussian band analysis.

TREVOR R. GRIFFITHS et RICHARD A. ANDERSON. Can. J. Chem. **69**, 451 (1991).

On a déterminé pour la première fois le spectre d'absorption électronique non ambiguë du HgX_4^{2-} (X = Cl, Br ou I) dans le méthanol. On a résolu le spectre en ses bandes gaussiennes et on les assignées en se basant sur un diagramme de corrélation pour une symétrie T_d. Les effets de couplage spin-orbite du deuxième ordre expliquent bien les intensités et les couplages des bandes observées. Faisant appel à une analyse de régression linéaire multiple, on a calculé les constantes de formation, K_4, en fonction de la force ionique pour le domaine complet du spectre et on les a extrapolées à dilution infinie : 0,4 ± 0,1 pour le HgI_4^{2-} et le $HgBr_4^{2-}$ et 5,7 ± 0,2 pour le $HgCl_4^{2-}$. On a observé des effets de cation marqués sur les spectres des HgX_2 auxquels on avait ajouté du X^-; on peut les expliquer partiellement en fonction de l'équation de Debye–Hückel étendue.

Mots clés : spectre d'absorption atomique, complexes d'halogénures mercuriques(II), constantes de formation, force ionique, analyse gaussienne des bandes.

[Traduit par la rédaction]

The reaction of HgX_2 (X = Cl, Br, or I) with excess halide, X, to form the tetrahedral anion HgX_4^{2-} is well known in aqueous solution and in dipolar aprotic solvents (1–10). However, only a few studies have been made in protic solvents. Compounds of the type Q_2HgX_4 (where Q = *N*-cetyl-γ-picolium; X = Br, Cl) dissociated in ethanol to give HgX_3^-, HgX_4^{2-} not being detected (11). A similar feature was observed by Deacon and West (12) when investigating the spectra of Q_2HgI_4 (Q = Me_4P or PyH) in ethanol and methanol, but a large excess of added iodide gave the tetraiodo species. Raman studies of $HgCl_2$–LiCl mixtures in methanol indicated (13) the formation of $HgCl_3^-$ and $HgCl_4^{2-}$ but the electronic spectra of $HgBr_4^{2-}$ and $HgCl_4^{2-}$ in methanol have not been reported.

Stability constant measurements for HgX_4^{2-} in water are numerous, but only a few have been reported in dipolar aprotic solvents (5, 6), and none in protic solvents.

This paper describes the electronic spectra of HgX_4^{2-} in methanol, and the assignment of the transitions of their resolved bands, together with the (stepwise) formation constants of HgX_4^{2-} and the effect of cation variation on the equilibrium $HgX_3^- + X^- \rightleftharpoons HgX_4^{2-}$. The analysis of spectra to obtain component bands has previously only been applied for the Gaussian component bands of $HgBr_4^{2-}$ and HgI_4^{2-} in acetonitrile by Day and Seal (10). They obtained the spin–orbit coupling constants and discussed the energy levels and transitions concerned: we use a different theoretical approach, and obtain similar but more complete findings.

Experimental

All chemicals were of analytical or spectrograde quality where available and purified as necessary.

Spectra were recorded using an Applied Physics Cary 14 H spectrophotometer, modified to yield spectra in digital form on paper tape, in addition to the conventional chart output. The details have been published elsewhere (14).

For resolving a spectrum the conventional least-squares method of fitting a set of component bands requires an assumption concerning the type of band distribution involved. The usual distribution functions considered are Gaussian, Cauchy (Lorentzian), or the product or sum functions of both (15). Day and Seal (10) chose the Gaussian function for the resolution of their absorption spectra of HgX_4^{2-}. We tested these functions with our spectra, and found the Gaussian function best fitted our observed spectra. The thermostatted spectra were recorded five times, at 1 nm intervals, and averaged in the Leeds University computer (ICL 1906A) before curve fitting. This improved the convergence rate and the standard deviation.

If the minimised parameters gave a poor fit to the experimental data points it was for one of two reasons (and occasionally both). Reason one, the contribution of the absorption edge at higher energies was not included in the minimisation. This effectively weighted the data points on the high energy side of the band, causing the minimised band position to move to higher energies, the band width to increase, and the band height to increase. The procedure of "band peeling", fitting the low energy data to one band, removing it, fitting the remaining data, and so on was not used because it is less accurate: it demands no contribution to the absorption by the next band at the peak maximum of the first band, and assumes no hidden bands. Our procedure of removing successively the highest energy data point until the calculated band parameters became effectively constant eliminates these difficulties.

Reason two, poor resolutions will be obtained when attempts are made to minimise for too few bands, for example, when an observed single band displaying asymmetry contains hidden bands and a fit is attempted for one or two bands.

Calculation of formation constants

There are several ways of calculating formation constants from spectra, but after testing, the following method was found to be the most reliable and statistically accurate.

[1]Revision received October 24, 1990.

Printed in Canada / Imprimé au Canada

Can. J. Chem. Downloaded from www.nrcresearchpress.com by 195.138.81.100 on 09/07/12
For personal use only.

Can. J. Chem. Downloaded from www.nrcresearchpress.com by 195.138.81.100 on 09/07/12
For personal use only.

At any given wavelength, the absorbance of a solution will be given by $A = \Sigma M_i E_i$, where A is the observed absorbance, M_i and E_i are the molar concentration and molar absorbance at that wavelength of the ith species in solution. This equation holds true for all wavelengths. Thus if A is measured for "n" different wavelengths, then "n" linear equations of "i" unknowns may be derived. For $n \gg i$ these linear equations may be accurately solved for M_i by means of multiple linear regression analysis. A library computer program was amended to perform this analysis for up to six species in solution. In this study only two-species equilibria were used, $HgX_3^- + X^- \rightleftharpoons HgX_4^{2-}$, over the wavelength regions where only the two mercury-containing species absorbed.

The program output consisted of the required concentrations, with their standard error, and parameters indicating the accuracy of the main computation and the precision of the fitted data. These included the residual sum of squares, the regression sum of squares, F ratio, multiple correlation coefficient, degrees of freedom of the F ratio, plus a table of residuals and standardised residuals. Formation constants, with their standard error, were computed from the regression coefficients.

This method has the advantage that conditions of constant ionic strength were not necessary, and hence the variation of formation constant with ionic strength could be studied. Another advantage was the use of complete spectra in a calculation, since the equation is valid for any wavelength range. Thus the formation constants calculated from data covering different wavelength ranges should be the same. If they are significantly different it may be assumed that one of the spectra employed is inaccurate over part of the spectrum. A useful check was that total metal concentration may be computed, and this must tally with the known quantity in solution. In accordance with custom, K_3 and K_4 refer to the formation of HgI_3^- and HgI_4^{2-}, respectively.

Results

The complete conversion of all HgX_2 in solution to HgX_4^{2-} does not occur when the mole ratio of X/Hg (here termed R) is four or slightly greater. This is generally true for dipolar aprotic solvents (7) but is not so for protic solvents (12).

A. Spectra

(1) Spectrum of HgI_4^{2-}

Figure 1 shows that between R values of 100 and 1 000 the two main peaks of HgI_4^{2-} in methanol began to form. Thereafter the spectra rapidly changed as HgI_3^- was converted to HgI_4^{2-} and peaks arose at 268 and 326 nm. Above R = 20 000 little further change was observed but an R value of over 100 000 was required before the molar absorbance values at these peaks were maximised.

No attempt was made in this study to maintain a constant ionic strength for the solutions, particularly since the solubility of the system would be exceeded before complete conversion occurred. However, the effect of dilution at various R values was examined (Fig. 2). For R = 100 the spectra changed only slightly on dilution, but for R = 5 000 the spectral change was from a typical HgI_4^{2-} profile to a HgI_3^- one. This may help explain why somewhat different results and conclusions at times arise from X-ray, Raman, and other techniques employed on HgX_3^- and HgX_4^{2-} studies in solution if solutions of differing concentrations are employed (1–10).

(2) Spectrum of $HgBr_4^{2-}$

The spectral changes accompanying the reaction between $HgBr_2$ and Br^- in methanol at 20°C are shown in Fig. 3. Complete conversion to $HgBr_4^{2-}$, with a peak at 250 nm, occurred when R reached 60 000, after which the spectra did not change.

Potassium bromide was used for R values up to 1 000, but thereafter the more soluble NaBr was employed. The effect of equal mole ratios of KBr and NaBr on the spectra were not identical (Fig. 4), the potassium ion apparently effecting greater conversion to $HgBr_4^{2-}$.

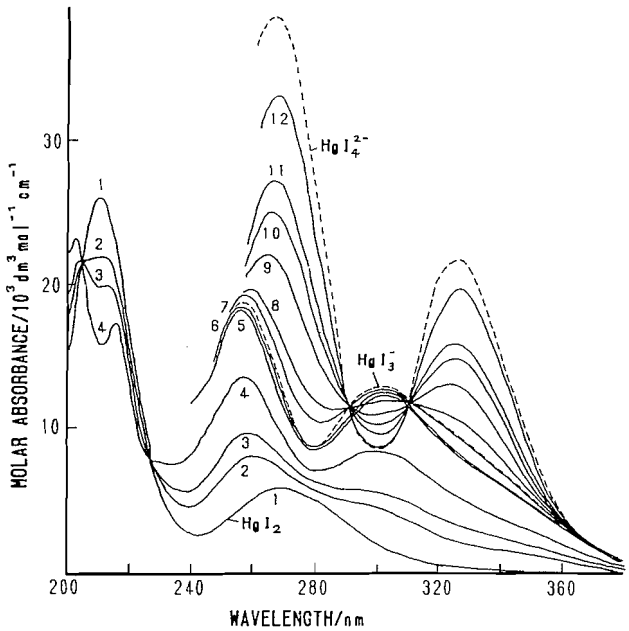


FIG. 1. Ultraviolet absorption spectra changes obtained upon addition of iodide to HgI_2 (6.7×10^{-5} mol dm^{-3}) in methanol at 20°C. Iodide/mercury mole ratios (R) are, progressively: (*1*), 2.0(HgI_2); (*2*), 2.2; (*3*), 2.3; (*4*), 2.4; (*5*), 2.8; (*6*), 8; (*7*), 80; (*8*), 1 000; (*9*), 2 000; (*10*), 3 000; (*11*), 4 000; (*12*), 60 000.

(3) Spectrum of $HgCl_4^{2-}$

The reaction between $HgCl_2$ and added Cl^- in methanol at 20°C is illustrated in Fig. 5. The peak for $HgCl_4^{2-}$ appeared at R = 15 000 but the true peak position at 230 nm could not be identified until higher R values were employed. The minimum R value for complete conversion was 800 000.

Potassium and ammonium chloride were both used, as chloride sources, and Fig. 6 shows their specific cation effect at the same R value. The maximum value with KCl was 1 000, NH_4Cl was usable up to R = 15 000, and further increases in R were made using LiCl.

B. Formation constants

(1) Formation constants for HgI_4^{2-}

Formation constants were computed over a wide range of added iodide concentrations. Data points at 1 nm intervals between 350 and 260 nm were used. At wavelengths below 260 nm the spectra were not considered reliable due to the possibility of uncomplexed iodide absorption contributing to the recorded absorbance.

The formation constants varied with ionic strength over the whole concentration range studied. A plot of log K_4, vs $I^{1/2}$ (I = ionic strength) gave a smooth curve, while that of K_4 vs $I^{1/2}$ yielded a straight line (Fig. 7), which extrapolated to 0.4 at infinite dilution.

(2) Formation constants for $HgBr_4^{2-}$

The formation constants for $HgBr_4^{2-}$ were computed from data points at 1 nm intervals in the range 240–300 nm. The variation of log K_4 and K_4 with $I^{1/2}$ is shown in Fig. 8. For those solutions where NaBr was the added halide, a straight line occurred in both plots. The line involving log K_4 extrapolated to 0.42 ± 0.04 (least-squares fit) at infinite dilution, while that for

Can. J. Chem. Downloaded from www.nrcresearchpress.com by 195.138.81.100 on 09/07/12
For personal use only.

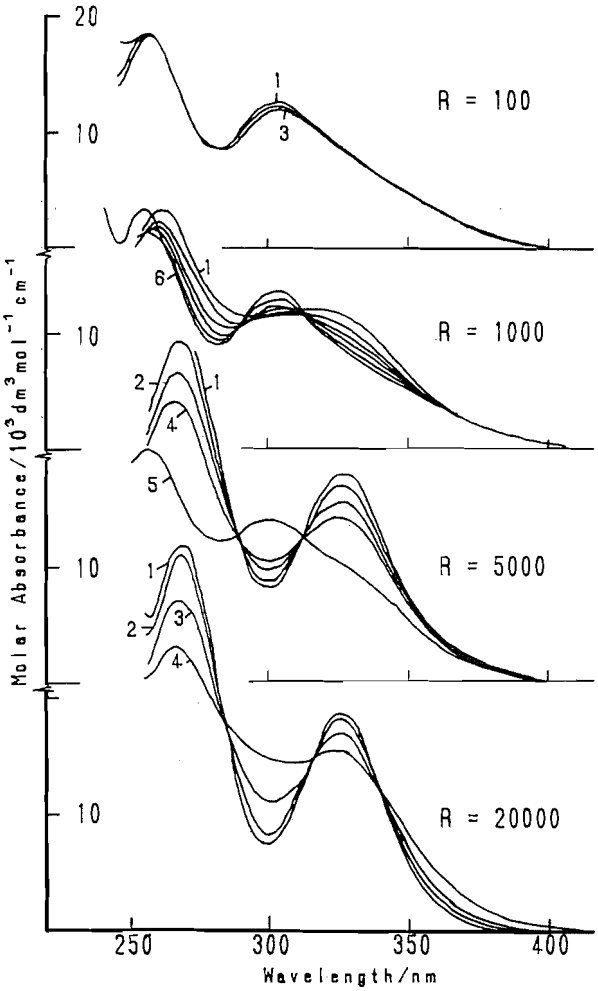


FIG. 2. Effect of ionic strength variation upon the ultraviolet absorption spectra of HgI_2 in methanol at 20°C. At selected iodide/mercury mole ratios (R) the solutions are diluted: note that with increasing dilution the equilibria, $HgI_2 \rightleftharpoons HgI_3^-$ or $HgI_3^- \rightleftharpoons HgI_4^-$, are shifted to the left. At R = 100, ionic strength (I) is (*1*), 0.014; (*2*), 0.005; (*3*), 0.003. At R = 1 000, I is (*1*), 0.072; (*2*), 0.057; (*3*), 0.040; (*4*), 0.028; (*5*), 0.011; (*6*), 0.006. At R = 5 000, I is (*1*), 0.36; (*2*), 0.29; (*3*), 0.20; (*4*), 0.14; (*5*), 0.06. At R = 20 000, I is (*1*), 0.58; (*2*), 0.46; (*3*), 0.23; (*4*) 0.12.

K_4 gave 0.4 ± 0.04 at $I^{1/2} = 0$. The values of K_4 for solutions containing KBr were greater than those for equivalent concentrations of NaBr.

With KBr the K_4 plot gave a straight line with the same intercept as the NaBr plot, but had a different slope. The log K_4 plot employing KBr consisted of two straight lines, that at high ionic strength intercepted at log $K_4 = 0.58 \pm 0.04$. At low ionic strength the slope was greater and the line extrapolated to $I^{1/2} = 0.06 \pm 0.04$.

(3) Formation constants for $HgCl_4^{2-}$

Here formation constants were computed over the range 205–260 nm. The plots of log K_4 and K_4 vs $I^{1/2}$ are shown in Fig. 9. Initially, a linear relationship holds with the line intersecting the abscissa at $I^{1/2} = 0.10$, but above $I^{1/2} = 0.30$, K_4 remained constant at 5.70 ± 0.20 (equivalent log K_4 = 0.75 ± 0.03, which compares well with log K_4 plot intercept of 0.76 ± 0.02). Detailed comparison of cation effects on K_4 values between KCl and NH_4Cl were not possible due to insufficient data points.

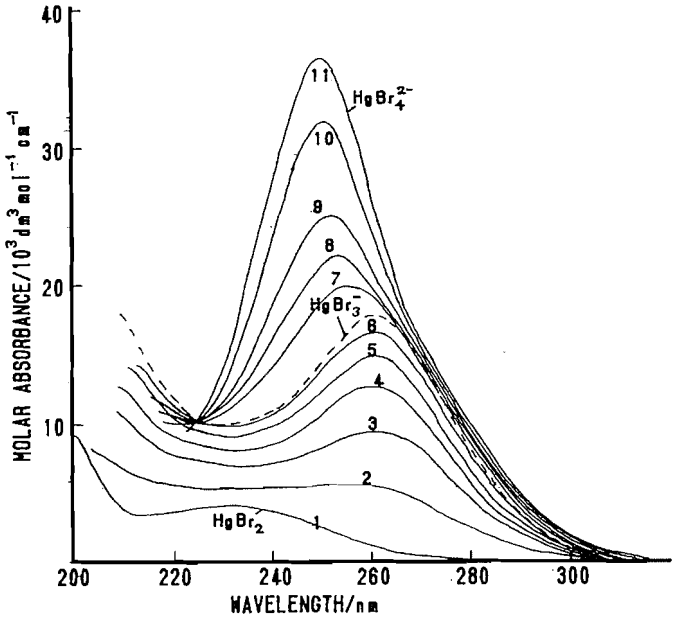


FIG. 3. Ultraviolet absorption spectra changes obtained upon addition of bromide to $HgBr_2$ (1.1×10^{-4} mol dm^{-3}) in methanol at 20°C. Bromide/mercury mole ratios (R) are, progressively: (*1*), 2.0 ($HgBr_2$); (*2*), 4; (*3*), 20; (*4*), 40; (*5*), 90; (*6*), 200; (*7*), 800; (*8*), 1 200; (*9*), 1 600; (*10*), 20 000; (*11*), 60 000 ($HgBr_4^{2-}$). Note that, compared with the iodide system, much greater R values are required initially to produce observable changes, even though essentially the same R values are needed for complete conversion to the tetrahalides. The dotted curve is the calculated spectrum of $HgBr_3^-$ in methanol. A single isosbestic point is seen at 226 nm, for the equilibrium $HgBr_3^- \rightleftharpoons HgBr_4^{2-}$.

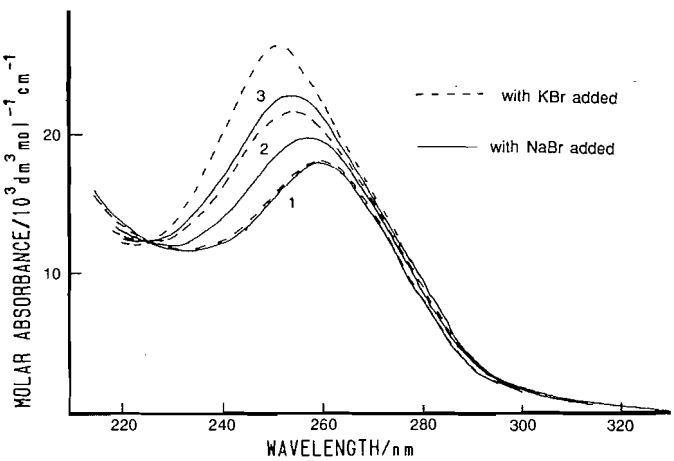


FIG. 4. Effect of cation, and cation size, on the ultraviolet absorption spectra on the reaction between $HgBr_2$ and Br^-. The effect is small below bromide/mercury mole ratios (R) of around 1 000, but more marked when R values refer to the equilibrium $HgBr_3^- \rightleftharpoons HgBr_4^{2-}$, the potassium ion shifting the equilibrium more towards $HgBr_4^{2-}$. Each spectral pair has equal mole ratios of NaBr and KBr. R values are (*1*), 1 000; (*2*), 5 000; (*3*), 10 000, with a fixed concentration of $HgBr_2$ at 8.9×10^{-5} mol dm^{-3}.

C. Gaussian analysis of absorption spectra

The spectra of the tetrahalogenomercurates in methanol were subjected to derivative analysis (16) to determine the number and position of component bands, and then to Gaussian band analysis to determine the band parameters. An example of the ability of derivative analysis to locate the peak position of a band appearing as a shoulder in $HgBr_4^{2-}$ is shown in Fig. 10.

Can. J. Chem. Downloaded from www.nrcresearchpress.com by 195.138.81.100 on 09/07/12
For personal use only.

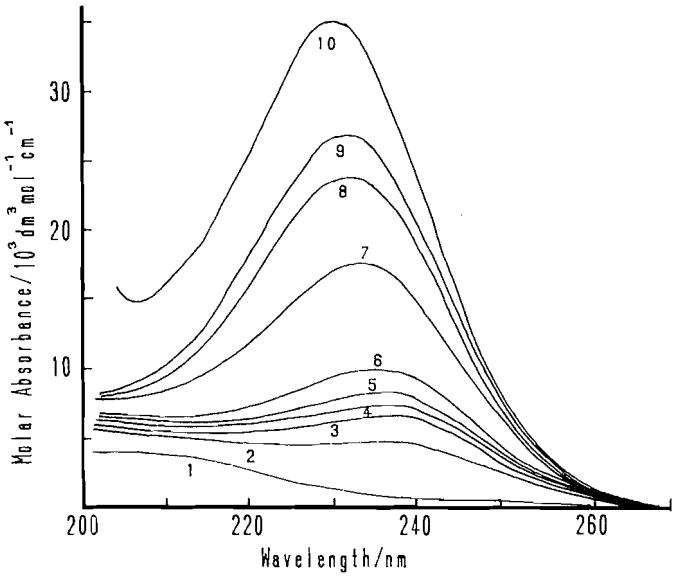


FIG. 5. Ultraviolet absorption spectra changes obtained upon addition of chloride to $HgCl_2$ (3.8×10^{-4} mol dm^{-3}) in methanol at 20°C. Chloride/mercury mole ratios (R) are, progressively: (*1*), 2.0 ($HgCl_2$); (*2*), 50; (*3*), 100; (*4*), 400; (*5*), 3 000; (*6*), 4 000; (*7*), 15 000; (*8*), 800 000 ($HgCl_4^{2-}$). R values are initially required to be higher than those in the iodo or bromo systems to produce observable changes and a much higher R value is necessary for complete conversion to $HgCl_4^{2-}$. No isosbestic points are observed for this system.

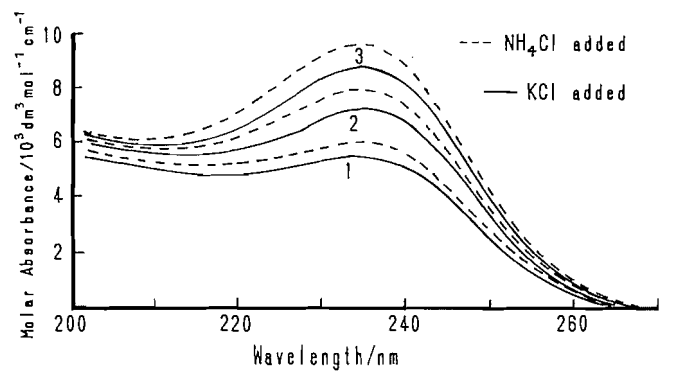


FIG. 6. Effect of cation, and cation size, on the ultraviolet absorption spectra of the reaction between $HgCl_2$ and Cl^-. Compared with the bromide case (Fig. 4), the effect is pronounced at much smaller chloride/mercury mole ratios (R), and the first equilibrium $HgCl_2 \rightleftharpoons HgCl_3^-$, is now affected. Each spectral pair has equal mole ratios of KCl and NH_4Cl. R values are (*1*), 200; (*2*), 300; (*3*), 400. Assuming crystallographic radii apply in methanol for K^+ and NH_4^+, 133 and 143 pm, respectively, the trend is the same as for the bromo system, but more pronounced at lower R values and for smaller differences in cation size.

Day and Seal (10) merely reported the results of their Gaussian analysis: we have found that such analyses are not always straighforward. The spectrum of HgI_4^{2-} was readily resolved into two bands corresponding closely to the observed peaks, but that of $HgBr_4^{2-}$, with its weak shoulder, was more difficult. Using our approach described above, resolution into two bands by Gaussian analysis, using the full spectrum, gave a poor fit to the data, though progressive removal of the high energy data improved the fit. However, over the whole spectral range, resolution into three bands, with one outside the range of

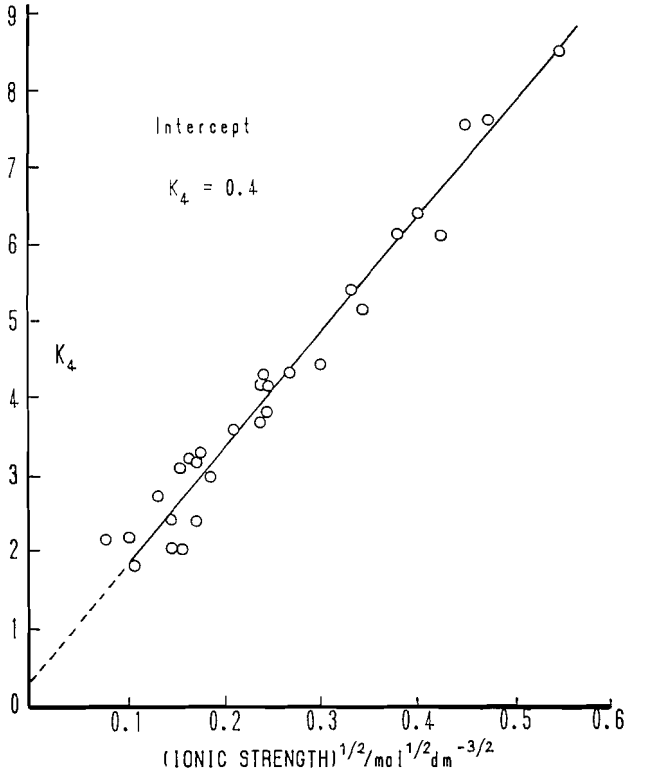


FIG. 7. Variation of K_4 for the formation of HgI_4^{2-} in methanol at 20°C with the square root of the ionic strength (I) of the solutions for which K_4 was determined from spectroscopic data. NaI and KI were both used as added iodide and there is no cationic effect.

the derivative spectra, fitted the data well (Fig. 11). The precision of this fit was confirmed since the band parameters for the two bands in the 'two band improved fit' were identical within experimental error with those of the same bands in the three band fit (Table 1). Day and Seal (10) did not report this third band for $HgBr_4^{2-}$.

The band at around 230 nm for $HgCl_4^{2-}$ could only be resolved into a single Gaussian band upon removal of a considerable proportion of the high energy side of the band profile (Fig. 12*a*). A better fit over the whole spectrum was obtained for three component bands (Fig. 12*b*). Second and fourth derivative spectra, using large convolution arrays, appeared to support the presence of one band, but with small convoluting arrays indicated the possibility of three bands, though the spectra were noisy. It is considered that three bands instead of one (10) should be used to explain the spectrum of $HgCl_4^{2-}$.

Discussion

A. Theory and interpretation

Figure 13 shows a correlation diagram for the molecular orbitals of HgX_4^{2-} species having T_d symmetry with the order of orbital energies as given by Day and Seal (10). Excluding the *d* electrons of the mercury atom there are 32 valency electrons, which fill the available orbitals up to and including the $^1T_1$ orbital. This electron configuration, $(1t_1)^6$, gives a $^1A_1$ ground state term.

Excitation of electrons in the $1t_1$ or $1e$ orbitals to the $3a_1$ orbital is symmetry forbidden, but excitation to it from $3t_2$ is allowed, giving a $(3t_2)^5(3a_1)^1$ configuration and a $^1T_2$ state. The

Can. J. Chem. Downloaded from www.nrcresearchpress.com by 195.138.81.100 on 09/07/12
For personal use only.

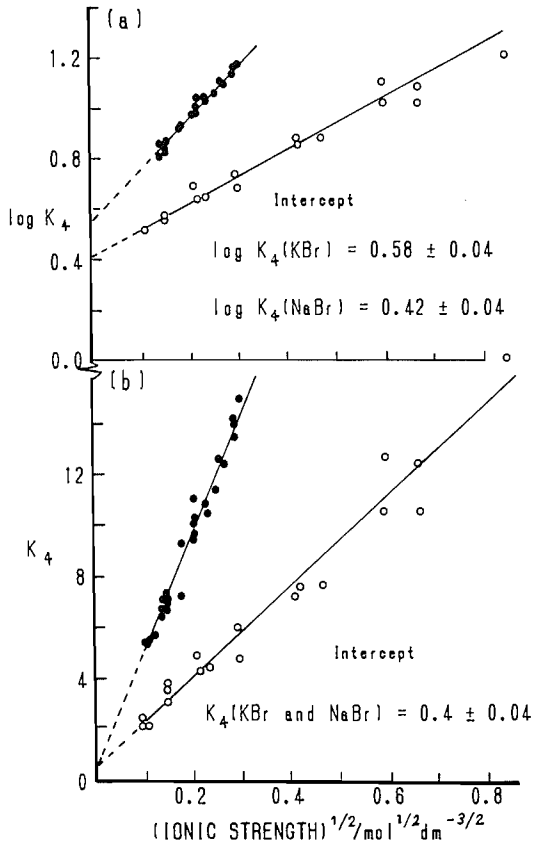


FIG. 8. Variation of log K_4 and K_4 for the formation of $HgBr_4^{2-}$ in methanol at 20°C with the square root of the ionic strength (I) of the solutions for which K_4 was determined from spectroscopic data. Open circles represent data using NaBr as added bromide, full circles, KBr.

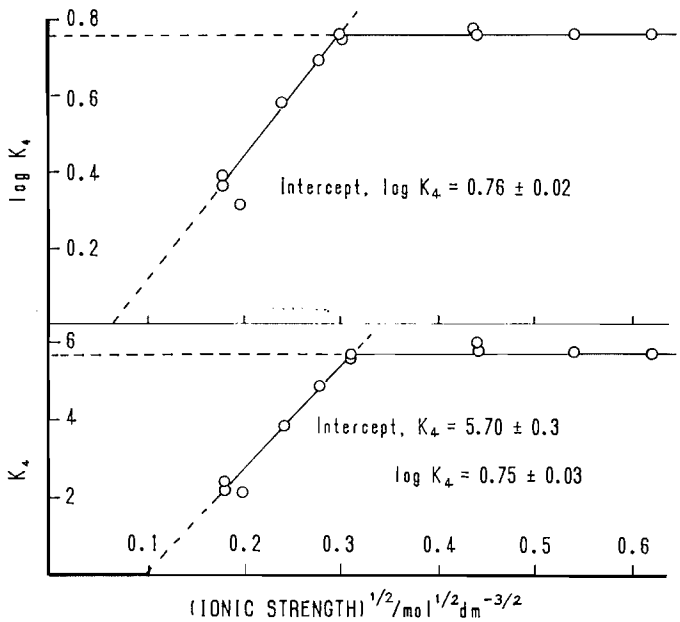


FIG. 9. Variation of log K_4 and K_4 for the formation of $HgCl_4^{2-}$ in methanol at 20°C with the square root of the ionic strength (I) of the solutions for which K_4 was determined from spectroscopic data. KCl and NH_4Cl were both used as added chloride, but the data points were insufficient to determine possible cationic effects.

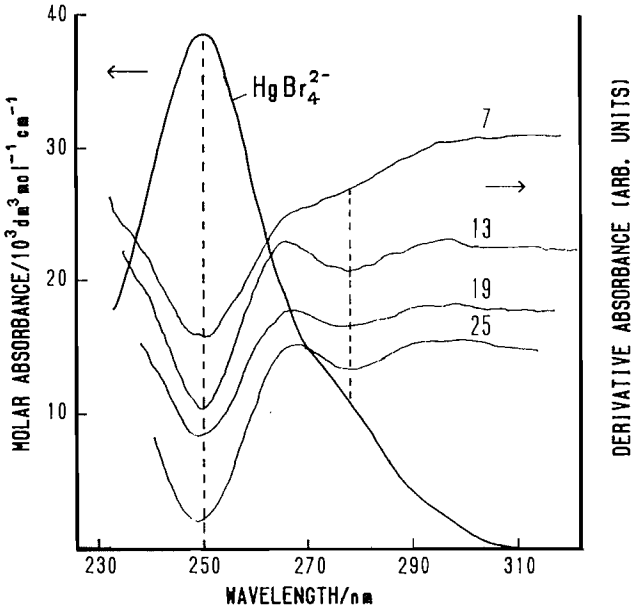


FIG. 10. Second and inverted fourth derivative curves superimposed on the ultraviolet absorption spectrum of $HgBr_4^{2-}$ in methanol at 20°C. The numbers indicate the number of data points used in calculating the derivatives. The curves show that the maxima of the main band and the lower-energy hidden band are clearly resolved only when convolutes > *ca.* 19 are employed.

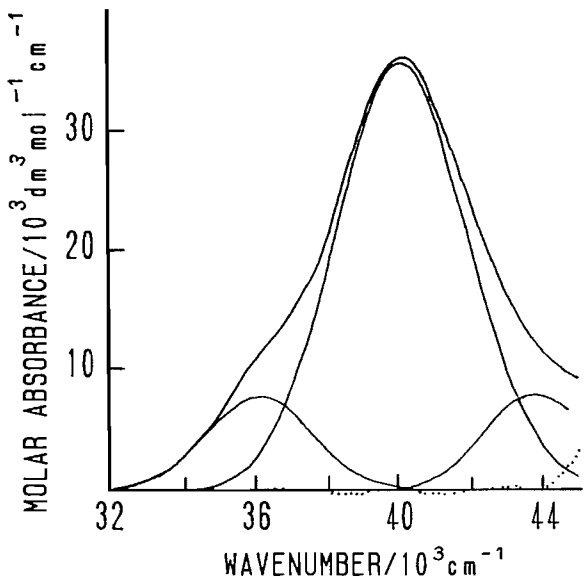


FIG. 11. Gaussian analysis of the ultraviolet absorption spectrum of $HgBr_4^{2-}$ in methanol at 20°C for three bands, fitting all available data points. Dotted line is the difference between the sum of the best fit of the Gaussian curves and the spectrum of $HgBr_4^{2-}$.

$^1A_1 \rightarrow {}^1T_2$ transition should therefore give an intense band in the spectrum of HgX_4^{2-}, which is observed. The allowed transition from the $2t_2$ and $1t_2$ orbitals would occur at much higher energies, outside the range of the recorded spectra.

Spin–orbit coupling may cause forbidden transitions to $^3T_2$, ^3E, and $^3T_1$ states, corresponding to $(3t_2)^5(3a_1)^1$, $(1e)^3(3a_1)^1$ and $(1t_1)^5(3a_1)^1$, respectively, and would be expected at lower energy than the allowed $^1T_2$ transition. The band analysis of the tetrahalide spectra showed a low energy band in HgI_4^{2-} and

Can. J. Chem. Downloaded from www.nrcresearchpress.com by 195.138.81.100 on 09/07/12
For personal use only.

TABLE 1. Band parameters of HgX_4^{2-} from Gaussian analysis of absorption spectra*

		Observed peaks		Resolved bands							
Complex	Solvent	E_{max}	ϵ_m	E_{max}	ϵ_m	w	A	o.s.	Δ	ζx	Reference
HgI_4^{2-}	MeOH	30.77	21.480	30.65	21.050	3.41	15.3	6.61	6.8	5.07	*a*
	MeCN	*b*		30.3	20.600				6.6		10
	MeOH	37.45	38.550	37.45	38.550	4.62	38.0	16.4			*a*
	MeCN			36.9	35.400						10
$HgBr_4^{2-}$	MeOH	40.00	35.880	36.10	7.800	3.32	5.51	2.38	4.0	2.46	*a*
	MeCN			35.5	8.760				4.0		10
	MeOH			40.10	35.500	4.28	32.4	14.0			*a*
	MeCN			39.5	41.400						10
	MeOH			43.80	7.800	3.32	5.51	2.38			*a*
	MeCN			Not found							10
$HgCl_4^{2-}$	MeOH	43.48	35.000	42.20	20.000	3.71	15.8	6.82	2.24	0.59	*a*
	MeCN			42.60	39.200						10
	MeOH			44.40	20.000	3.32	14.1	6.08			*a*
	MeCN			Not found							10
	MeOH			48.50	14.000	2.35	7.02	3.03			*a*
	MeCN			Not found							10

*E_{max} = peak maximum (10^3 cm^{-1}); ϵ_m = molar absorbance (dm^3 mol^{-1} cm^{-1}); w = band width at half-height (10^3 cm^{-1}); A = band area (dm^3 mol^{-1} cm^{-1} × 10); o.s. = oscillator strength; Δ = band separation (10^3 cm^{-1}) of two lowest energy transitions; ζx spin–orbit coupling constants (10^3 cm^{-1}) for halides; *a* = this work; *b* = peak observed but E_{max} not reported by Day and Seal (10).

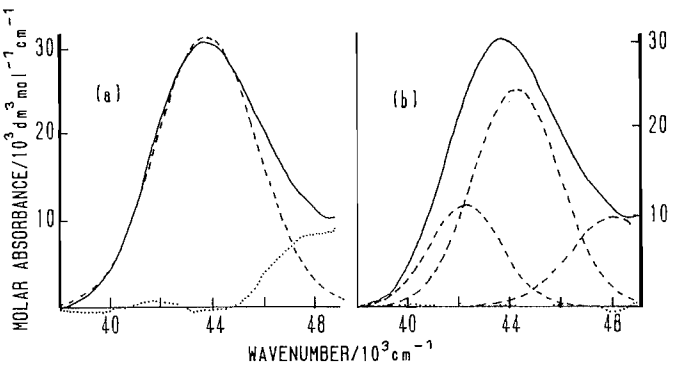


FIG. 12. Comparison of the Gaussian analysis of the ultraviolet absorption spectrum of $HgCl_4^{2-}$ in methanol at 20°C for (*a*) one band, and (*b*) for three bands (see text). Dotted line is the difference between the spectrum of $HgCl_4^{2-}$ and the Gaussian curve, (*a*), or the sum of Gaussian curves, (*b*).

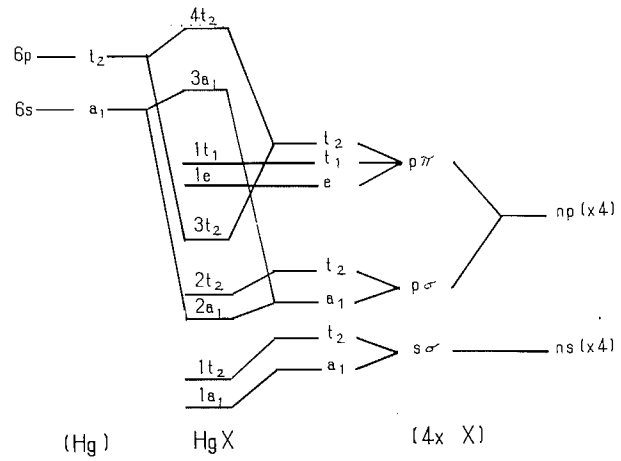


FIG. 13. Correlation diagram for the orbitals of HgX_4^{2-} species with T_d symmetry.

$HgBr_4^{2-}$, and probably one for $HgCl_4^{2-}$. The energy separation between the main band and the forbidden band increases from chloride to iodide, as expected from the spin–orbit coupling constants given by Jorgensen (17). The increased intensity of the second band (from the reliable results of HgI_4^{2-} and $HgBr_4^{2-}$) indicates its origin to be $^1A_1 \rightarrow {}^3T_2$, the $^3T_2$ state mixing with the $^1T_2$ state *via* spin–orbit coupling, thereby becoming partially allowed. Transitions to ^3E and $^3T_1$ states are both spin- and orbital-forbidden on symmetry considerations and are not found for HgX_4^{2-}. The various band parameters for HgX_4^{2-} in methanol are given in Table 1.

Table 1 shows that the band separation is greater than that expected for spin–orbit coupling in the halogen alone, because the transition involves electron transfer between the $3t_2$ and $3a_1$ molecular orbitals, both of which are made up of halogen and mercury atomic orbitals. To a first approximation the $3t_2$ orbital could be considered ligand localised while the $3a_1$ orbital is metal localised.

The trend towards higher energy from HgI_4^{2-} to $HgCl_4^{2-}$ for the main band is simply interpreted in terms of the molecular orbital scheme (Fig. 13): on going from X = I to X = Cl the energy difference between the 6*s* and 6*p* orbitals in mercury and the *np* and *ns* orbitals in the ligand increases. The difference between the bonding and antibonding orbitals, $3t_2$ and $3a_1$, respectively, thus increases from I to Cl.

Essentially the same conclusions are reached by Day and Seal (10), arguing slightly differently, from their analysis of HgX_4^{2-} spectra in acetonitrile, and their results are included in Table 1 for comparison. However, they reported that R values of around 15 were all that were necessary to obtain "essentially complete formation" of $HgBr_4^{2-}$ and $HgCl_4^{2-}$, and around R = 25 for HgI_4^{2-}.

This is much less than our minimum requirements, where the tetrachloro complex required the largest R value. They also reported "satisfactory Beer's law plots under these conditions", which we did not always find in methanol (see Fig. 2). How-

ever, their molar absorbance values were consistently higher than ours, suggesting that molar absorbance values may be solvent dependent, and that further halide addition may possibly lead to still higher values in acetonitrile for HgX_4^{2-}.

B. Formation constants and ionic strength

We have noted earlier (18) how that plots of K_4 (for the formation of HgX_4^{2-}) *vs.* I gave two intersecting straight lines for reactions in water. This was interpreted as a low ionic strength line corresponding to the formation of HgX_4^{2-} in a *three*-species equilibrium with HgX_2 and HgX_3^-. Also, no HgX_4^{2-} could form until HgX_3^- has been formed, and hence the intercept of this line is at $I > 0$, since HgX_3^- will only form in the presence of excess halide (and not by disproportionation of HgX_2 into HgX^+ and HgX_3^-). The intercept gives the minimum ionic strength at which HgX_4^{2-} will occur, and the intersection of the two lines indicates the ionic stength at which the change from a three- to a two-species equilibrium occurs in water. This pattern was followed by only $HgCl_4^{2-}$ in methanol, indicating that $HgCl_4^{2-}$ was not formed in solution until the ionic strength reached around 7×10^{-3} mol dm^{-3}, and that the two species equilibrium obtained above 0.1 mol dm^{-3}.

However, the K_4 plots for the iodo- and bromomercurates in methanol here gave single straight lines which did not cross the abscissa. This shows an absence of a measurable three-species equilibrium for these species in methanol, and almost complete conversion of HgI_2 to HgI_3^- before HgI_4^{2-} forms, which is borne out upon examining the spectra (Fig. 1).

C. Effect of ionic medium and added cation

The difference between the spectra of a solution containing, say KX, and that of one containing an equal molarity of NaX is due to the effect of the cation upon the equilibrium between mercuric halides and X^-, and not to an effect on the spectra of the individual species. We observed that $HgBr_4^{2-}$ has the same profile in KBr and NaBr solutions, although solutions containing $HgBr_3^-$ and $HgBr_4^{2-}$ in equilibrium gave different spectra for equal molarities of these two alkali bromides. Similarly, the effect of dilution or change in ionic strength on solution spectra is also interpreted as a change in equilibrium, and not the individual species changing spectra.

The effect of NaBr and KBr on the formation of $HgBr_4^{2-}$ was significant, and the K_4 values diverged with increasing ionic strength (Fig. 8*b*), but had the same value at infinite dilution.

The effect of cationic size on the activity coefficients of the $HgBr_3^-$ and $HgBr_4^{2-}$ may account for this effect. In the extended Debye–Hückel equation, $-\log \gamma = Az_1z_2I/(1 + aBI^{1/2})$, the mean ionic diameter, a, becomes more important as the ionic strength increases. The thermodynamic formation constant, K_T, is related to the activity coefficients by the equation $\log K_4 = \log K_T - \log \gamma(HgX_4^{2-}) + \log \gamma(HgX_3^-) + \log \gamma(X^-)$. The higher slope of the K_4(KBr) line compared to that of K_4(NaBr) is due to the ionic diameter of K^+ being greater than that of Na^+, and hence having greater effect on the $aBI^{1/2}$ term. Further, the B term also contains the inverse square root of the dielectric constant of the medium, *viz.*, $B = \text{constant}/(DT)^{1/2}$. A change from solvent water to methanol increases B by a factor of around three.

The effect of cationic size on the formation of HgI_4^{2-} using NaI and KI was negligible within experimental error (Fig. 7), whereas the effect of NH_4Cl compared with KCl, on $HgCl_4^{2-}$ formation, was large (Fig. 6).

This simple explanation of the cation effect in terms of the Debye–Hückel $aBI^{1/2}$ term, and dielectric constant change, is probably not complete: the effect of cation upon the entropy and enthalpy changes of the reactions may be significant. Khophar and Naraynankutty (19) have suggested this to explain the effect of different cationic media on the stability of Am(III) and Eu(III) complexes. They found that K values increased with decreasing hydration of medium cations (Li^+, H^+, K^+, and NH_4^+), and concluded that the effect was too large to be related to activity changes alone.

Acknowledgements

We thank the SERC for the provision of the Cary 14 H spectrometer and the UKAEA for the digitising equipment (purchased under EMR 1913). R.A.A. thanks the University of Leeds for a Research Studentship. T.R.G. thanks the Province of Alberta and the University of Leeds for a travel grant and the Chemistry Department, University of Calgary, Calgary, Alta., for hospitality and facilities during the preparation of this paper.

1. T. R. Griffiths and M. C. R. Symons. J. Chem. Soc. Trans. Faraday Soc. **56**, 1752 (1960).
2. F. Gazier and G. Johnansson. Acta Chem. Scand. **22**, 3013 (1968).
3. P. H. Given and M. E. Peover. J. Chem. Soc. 1602 (1959).
4. Y. Matsui and Y. Date. Bull. Chem. Soc. Jpn. **43**, 2052 (1970).
5. R. J. Peterson, P. J. Lingane, and W. L. Reynolds. Inorg. Chem. **9**, 680 (1969).
6. G. Elendt and K. Cruse. Z. Phys. Chem. **201**, 180 (1952).
7. D. N. Waters and Z. Kantarci. J. Raman Spectrosc. **6**, 251 (1977).
8. D. N. Waters, Z. Kantarci, and N. M. Rahman. J. Raman Spectrosc. **7**, 288 (1978).
9. M. Sandström. Actal Chem. Scand. A**31**, 132 (1977).
10. P. Day and R. H. Seal. J. Chem. Soc. (Dalton), 2054 (1972).
11. M. Olteanu and M. Stan. Rev. Roum. Chim. **17**, 1525 (1972).
12. G. B. Deacon and B. O. West. J. Chem. Soc. 3929 (1961).
13. Z. Kecki. Roczniki Chem. **36**, 345 (1962).
14. T. R. Griffiths and P. J. Potts. J. Chem. Soc. (Dalton), 344 (1975).
15. R. N. Jones. Pure Appl. Chem. **18**, 303 (1969).
16. T. R. Griffiths, K. King, H. V. St. A. Hubbard, M-J. Schwing-Weill, and J. Meullemeestre. Anal. Chim. Acta, **143**, 163 (1982).
17. C. K. Jorgensen. Orbitals in atoms and molecules. Academic Press, New York. 1962.
18. T. R. Griffiths and R. A. Anderson. J. Chem. Soc. Faraday Trans. 1, **80**, 2361 (1984).
19. P. K. Khopkar and P. Narayanankutty. J. Inorg. Nucl. Chem. **33**, 495 (1971).

Can. J. Chem. Downloaded from www.nrcresearchpress.com by 195.138.81.100 on 09/07/12
For personal use only.

Thermodynamic investigation of the ternary K–Pb–Sn and Rb–Pb–Sn alloys

PETER J. TUMIDAJSKI

Department of Materials Engineering, The University of Western Ontario, London, Ont., Canada N6A 5B9

Received October 20, 1989[1]

PETER J. TUMIDAJSKI. Can. J. Chem. **69**, 458 (1991).

Activity coefficients for alkali metals in the K–Pb–Sn and Rb–Pb–Sn alloys were measured at 606°C (879 K) for compositions generally less than about 10 at.% alkali metal. An alkali metal concentration cell with a potassium or rubidium substituted β-Al_2O_3 solid electrolyte was used to perform the experiments. A coulometric titration technique was used to electrochemically generate the alkali metal in the Pb–Sn alloys. The results indicated that, for both potassium and rubidium alloys, as solvent composition is varied from pure tin to pure lead the liquid becomes more associated, suggesting the formation of complex species.

Key words: thermodynamics, alkali metals, liquid alloys.

PETER J. TUMIDAJSKI. Can. J. Chem. **69**, 458 (1991).

Opérant à 606°C (879 K) et généralement à des compositions atomiques en métal alcalin inférieures à 10%, on a mesuré les coefficients d'activité des métaux alcalins dans les alliages K–Pb–Sn et Rb–Pb–Sn. On a réalisé les expériences dans une cellule de concentration de métal alcalin dans laquelle on a remplacé l'électrolyte solide β-Al_2O_3 par un potassium ou un rubidium. On a utilisé une technique de titration coulométrique pour générer d'une façon électrochimique le métal alcalin dans les alliages de Pb–Sn. Les résultats indiquent que, pour les alliages de potassium ainsi que de rubidium, le liquide devient plus associé lorsqu'on fait varier la composition du solvant d'étain pur à plomb pur; ce résultat suggère qu'il y a formation d'espèces complexes.

Mots clés : thermodynamique, métaux alcalins, alliages liquides.

[Traduit par la rédaction]

Can. J. Chem. Downloaded from www.nrcresearchpress.com by 195.138.81.100 on 09/07/12
For personal use only.

Introduction

An explanation of the thermodynamic behaviour of liquid alkali metal – lead alloys has proved challenging. Recent experimental results have shown that the thermodynamic properties of K–Pb (1) and Rb–Pb (2) alloys change abruptly at the equiatomic composition, in agreement with electrical resistivity measurements (3, 4). Furthermore, the heat capacities (5, 6), show this abrupt change occurs at equiatomic composition. Neutron diffraction patterns for the structure of equiatomic K–Pb and Rb–Pb display a sharp diffraction peak at low wave vector, indicating intermediate range ordering (7, 8) and a possible existence of the polyvalent anion, Pb_4^{4-}, similar to the Zintl ion which exists in the solid state.

To date, the thermodynamic properties for the binary K–Sn system has been reported only over a limited composition range (9). The thermodynamic properties for the Rb–Sn alloy and the ternary K–Pb–Sn and Rb–Pb–Sn alloys have not been reported. In this paper, we report potassium and rubidium activities in the Pb–Sn alloys. The results can be used to provide an understanding of the thermodynamic behaviour of the ternary systems and how they compare with the constituent binaries. In addition, there is an increased understanding of the influence of multicomponent solvents on the atomic interactions involving the alkali metals.

Experimental

The experimental procedure and technique has been described in detail elsewhere (1, 2, 10). Briefly, the electrochemical cell consisted of two half-cells, a secondary reference half-cell (RE), and a working half-cell (WE), represented schematically as,

$$\underset{\text{(RE)}}{\text{Bi–A}} \;\|\; \beta\text{-}Al_2O_3 \;\|\; \underset{\text{(CE)}}{\text{Bi–A}} \;\|\; \beta\text{-}Al_2O_3 \;\|\; \underset{\text{(WE)}}{\text{Pb–Sn–A}}$$

where A represents the alkali metal potassium or rubidium, respectively. RE contained 5 at.% alkali metal to reduce the alkali metal activity and its vapour pressure. Reference electrodes were calibrated against pure liquid alkali metal using similar concentration cells. The composition of WE was accurately varied by coulometric titration with the counter electrode (CE). Temperatures were measured with a calibrated (Pt–Pt 10 at.% Rh) thermocouple directly immersed in CE.

Results and discussion

The cell reaction for the alkali metal concentration cell is

$$[1] \quad A_{(\text{pure, l})} \rightleftharpoons \underline{A}$$

where $\underline{A}$ represents alkali metal in Pb–Sn alloys. The cell voltage can be expressed as

$$[2] \quad E = -\frac{RT}{F} \ln \gamma_A - \frac{RT}{F} \ln X_A$$

where F, R, and T have their usual meaning and γ_A and X_A are the activity coefficient and atom fraction of alkali metal, respectively. For dilute solutions eq. [2] can be simplified to

$$[3] \quad E = E_A^0 - \frac{RT}{F} \ln X_A$$

where E_A^0 represents the limiting standard potential of alkali metal in molten Pb–Sn alloys. The limiting standard potential defines a hypothetical standard state where the fraction of alkali metal in the Pb–Sn alloy approaches unity, but the alkali metal behaves thermodynamically as if it were infinitely diluted. Nernst plots for $X_A < 0.01$ at 606°C (879 K), as expressed by eq. [3], are given in Figs. 1 and 2 for the potassium and rubidium systems, respectively. Cell voltage is plotted against $\log_{10} X_A$. Also included in Fig. 1 are the results for the K–Sn binary reported earlier by Petric (9). The experimental data are well represented by the indicated least-squares lines. Linear regression analysis for the Nernst plots gave correlation coefficients of almost unity for all cases. Thus the solutions are Henrian. Calculated slopes for the Nernst plots are summarized in Table 1. The results are in excellent agreement with the theoretical values (RT/F) and indicate a one-electron transfer

[1]Revision received August 29, 1990.

Can. J. Chem. Downloaded from www.nrcresearchpress.com by 195.138.81.100 on 09/07/12
For personal use only.

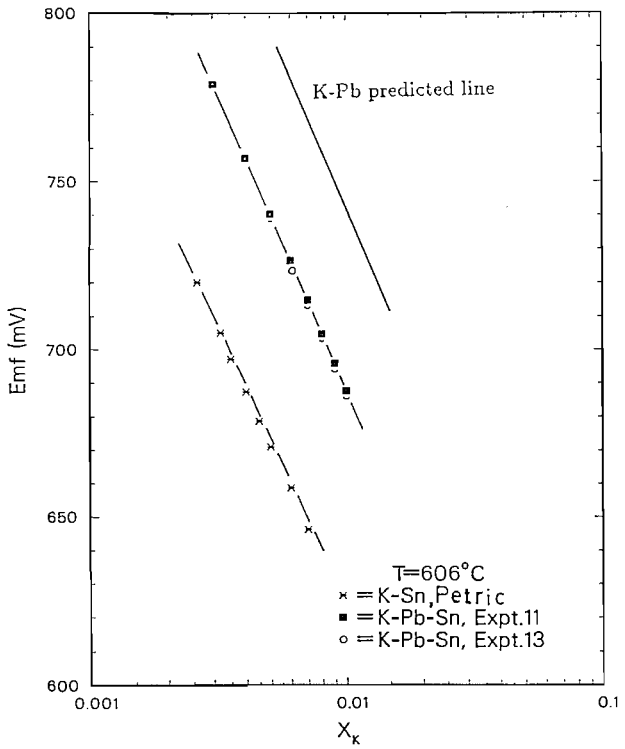


FIG. 1. Nernst plots for K–Pb–Sn systems at 606°C (879 K). Points represent experimental values; the line is the linear least-squares line through the experimental data. The data for the K–Sn binary system were reported previously (9).

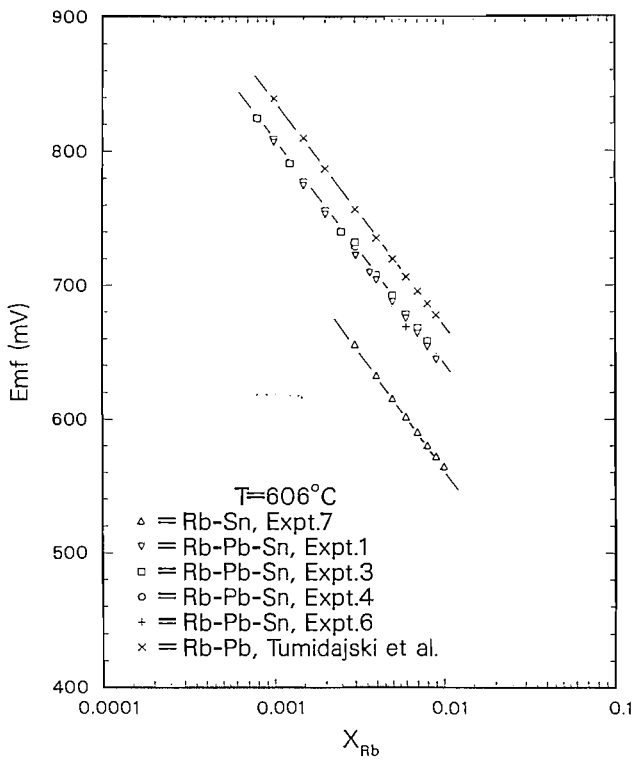


FIG. 2. Nernst plots for Rb–Pb–Sn systems at 606°C (879 K). Points represent experimental values; the line is the linear least-squares line through the experimental data. The data for the Rb–Rb binary system were reported previously (2).

TABLE 1. Values of experimental slopes, limiting potentials, and excess chemical potentials for the A–Pb–Sn systems at 879 K

System	Expt.	Slope	E_A^0 (mV)	$\mu_E^0[A]$ (kJ mol^{-1})
K–Sn	Ref. 9	74.11	278.5	−26.87
K–Pb–Sn	11, 13	76.21	335.9	−32.41
K–Pb	Ref. 1	131.87	394.5	−38.07*
			397.8	−38.38†
Rb–Sn	7	75.56	215.7	−20.81
Rb–Pb–Sn	1, 3, 4, 6	73.44	299.47	−28.89
Rb–Pb	Ref. 2	73.50	330.57	−31.90

*T = 640 K.
†Estimated value for T = 879 K.

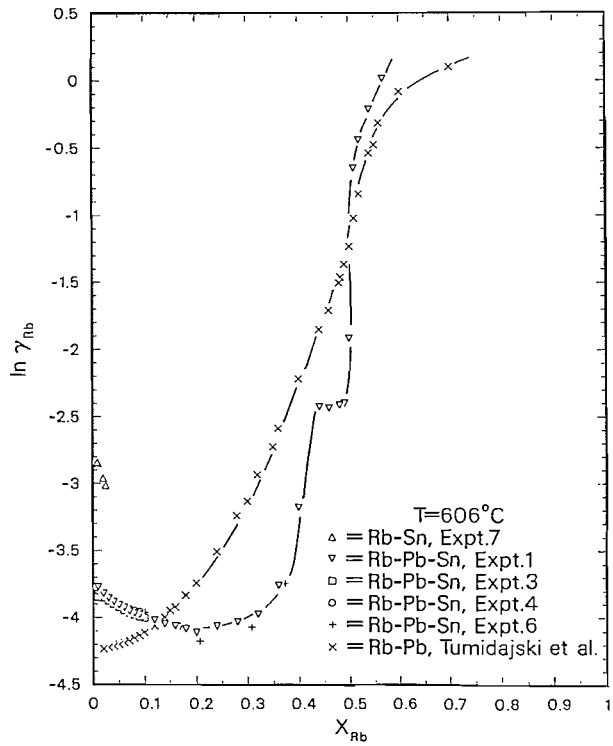


FIG. 3. Variation of ln γ_{Rb} versus composition at 606°C (879 K) for the entire composition range. The data for the Rb–Pb binary system were reported previously (2).

as expected. Values for the limiting standard potential, E_A^0, are included in Table 1, as well as a related thermodynamic property, the limiting excess chemical potential, defined by the expression,

$$[4] \quad \mu_0^E[\underline{A}] = -FE_A^0$$

It can be seen that the magnitudes of the limiting standard potentials and the limiting excess chemical potentials increase in the order Sn → Pb–Sn → Pb for both potassium- and rubidium-based alloys. The result indicates that Pb-based alloys are thermodynamically more stable than Sn-based alloys.

In Table 1 values for the limiting potential and excess chemical potential of the binary K–Pb alloy at 606°C (879 K) have been estimated using a previously proposed relationship (11),

$$[5] \quad E^0_{K-Pb-Sn} = (1 - t)E^0_{K-Pb} + tE^0_{K-Sn}$$

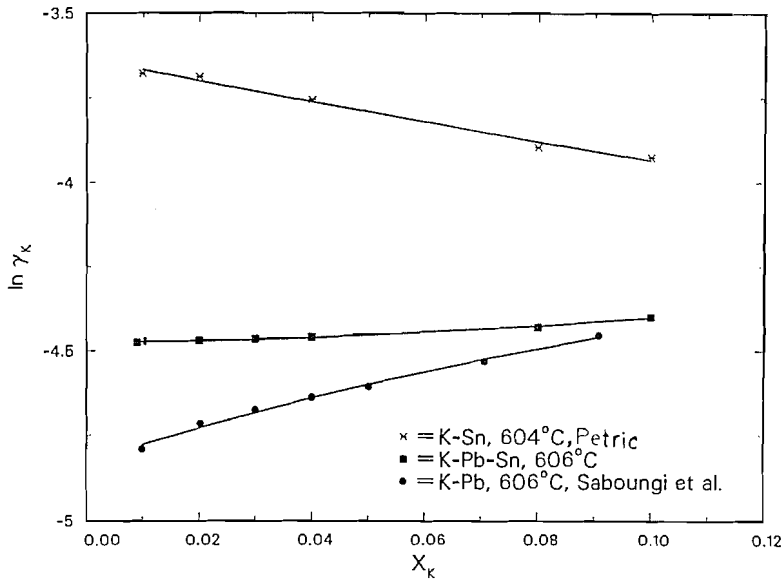


FIG. 4. Variation of ln γ_K versus composition for the limiting slope composition range. The data for the K–Sn binary system were reported previously (9).

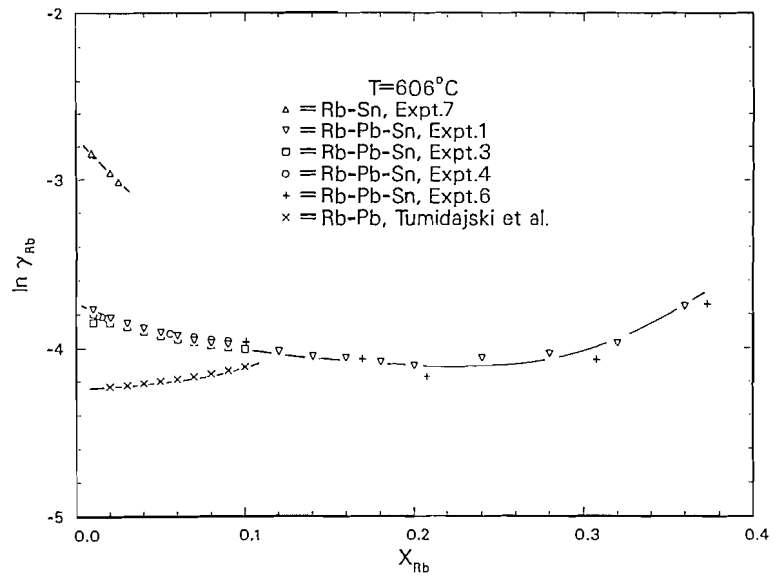


FIG. 5. Variation of ln γ_{Rb} versus composition at 606°C (879 K) for the limiting slope composition range. The data for the Rb–Pb binary system were reported previously (2).

or

[6] $\mu_0^E[K\text{–}Pb\text{–}Sn] = (1 - t)\mu_0^E[K\text{–}Pb] + t\mu_0^E[K\text{–}Sn]$

The t parameter is a solvent composition variable defined as

[7] $$t = \frac{X_{Pb}}{X_{Pb} + X_{Sn}}$$

The estimated values agree very well with previous experimental results (1) at 367°C (640 K). There is a slight increase in magnitude of the limiting potential and limiting excess chemical potential with temperature. The Nernst line for K–Pb in Fig. 1 was constructed using the value for E^0_{K-Pb} calculated with eq. [5] and the ideal Nernst slope.

As the alkali metal content increases beyond the Henrian regime, deviations from the Nernst law become significant. For each alloy composition, γ_A can be calculated from eq. [2] rearranged to,

[8] $$\ln \gamma_A = \frac{FE}{RT} - \ln X_A$$

Figure 3 shows the compositional dependence of ln γ_{Rb} at 606°C (879 K) for the Rb–Pb–Sn alloys. Included in Fig. 3 are results for the Rb–Pb system reported earlier (2). There are several interesting features. The solubility limit of Rb in Rb–Sn alloys was found to be approximately 3 at.% at 606°C (879 K). Beyond 3 at.% there exists a two-phase region as evidenced by a constant cell voltage. For the Rb–Pb–Sn ternary alloy there is a two-phase liquid–solid region in the interval $0.42 < X_{Rb} < 0.49$, and a compound forms at $X_{Rb} = 0.50$.

The limiting slope, ϵ, is defined as

Can. J. Chem. Downloaded from www.nrcresearchpress.com by 195.138.81.100 on 09/07/12
For personal use only.

TABLE 2. Limiting slope values for the A–Pb–Sn systems at 879 K

		$\ln \gamma_A = A + BX_A + CX_A^2$			
System	Expt.	A	B	C	$(\epsilon)_{X_A \to 0}$
K–Sn	Ref. 9	−3.63	−3.51	4.69	−3.5
K–Pb–Sn	11, 13	−4.47	0.82	6.43	0.8
K–Pb	Ref. 1	−4.82	5.20	−12.46	5.2
Rb–Sn	7*	−2.74	−10.79	—	−10.8
Rb–Pb–Sn	1, 3, 4, 6	−3.75	−3.46	9.07	−3.5
Rb–Pb	Ref. 2	−4.26	1.00	2.23	1.0

*T = 877 K over limited composition range.

$$[9] \quad \epsilon = \left(\frac{\partial \ln \gamma_A}{\partial X_A}\right)_{X_A \to 0}$$

The limiting slope is related to the nature and extent of ordering within solutions (12–14). A positive value for ϵ indicates attraction between alkali atoms and solvent atoms and a subsequent high probability of preferred co-ordination (*i.e.* complex formation) in the liquid state. A negative value for ϵ indicates attractive forces between the alkali atoms. A zero value for ϵ represents a random distribution of the neighboring atoms. Limiting slope plots (*i.e.* $\ln \gamma_A$ versus X_A) are presented in Figs. 4 and 5 for potassium and rubidium alloys, respectively. The experimental data points have been fitted to quadratic polynomial equations and are recorded in Table 2. The limiting slopes for K–Sn, Rb–Sn, and Rb–Pb–Sn systems are negative. These results could indicate a pairing between the alkali atoms in dilute solutions. However, the limited number of data points and the presence of phase boundaries precludes a full interpretation and understanding of the limiting slopes for the K–Sn, Rb–Sn, and Rb–Pb–Sn systems. For both the K–Pb and Rb–Pb binary alloys, the limiting slopes suggest an attraction between unlike atoms and a relative repulsion between like atoms. It is surprising that, albeit Pb and Sn are in the same group of the periodic table, they apparently behave differently when alloyed with alkali metal.

Acknowledgements

The author acknowledges helpful discussions with M. L. Saboungi and A. Petric.

1. M. L. SABOUNGI, S. R. LEONARD, and J. ELLEFSON. J. Chem. Phys. **85**, 6072 (1986).
2. P. J. TUMIDAJSKI, A. PETRIC, T. TAKENAKA, M. L. SABOUNGI, and A. D. PELTON. J. Phys. C, **2**, 209 (1990).
3. J. A. MEIJER, W. GEERTSMA, and W. VAN DER LUGT. J. Phys. F: Met. Phys. **15**, 899 (1985).
4. C. VAN DER MAREL, A. B. VAN OOSTEN, W. GEERTSMA, and W. VAN DER LUGT. J. Phys. F: Met. Phys. **12**, 2349 (1982).
5. G. K. JOHNSON and M. L. SABOUNGI. J. Chem. Phys. **86**, 6376 (1987).
6. M. L. SABOUNGI, H. T. J. REIJERS, M. BLANDER, and G. K. JOHNSON. J. Chem. Phys. **89**, 5869 (1988).
7. M. L. SABOUNGI, R. BLOOMQUIST, K. J. VOLIN, and D. L. PRICE. J. Chem. Phys. **87**, 2278 (1987).
8. H. T. J. REIJERS, M. L. SABOUNGI, D. L. PRICE, J. W. RICHARDSON, JR., K. L. VOLIN, and W. VAN DER LUGT. Phys. Rev. B. In press.
9. A. PETRIC. Ph.D. Thesis, Universite de Montreal. November 1987.
10. P. J. TUMIDAJSKI and J. KEUHLER. Can. J. Chem. **68**, 247 (1990).
11. D. R. SADOWAY and S. N. FLENGAS. J. Electrochem. Soc. **122**, 515 (1975).
12. J. G. KIRKWOOD and F. P. BUFF. J. Chem. Phys. **19**, 774 (1958).
13. M. L. SABOUNGI, J. J. MARR, and M. BLANDER. J. Chem. Phys. **68**, 1375 (1978).
14. M. L. SABOUNGI and T. P. CORBIN. J. Phys. F: Met. Phys. **14**, 13 (1984).

Can. J. Chem. Downloaded from www.nrcresearchpress.com by 195.138.81.100 on 09/07/12
For personal use only.

Potential measurements of thorium tetrachloride in alkali halide solutions

P. J. TUMIDAJSKI

Department of Materials Engineering, The University of Western Ontario, London, Ont., Canada N6A 5B9

AND

S. N. FLENGAS

Department of Metallurgy and Materials Science, University of Toronto, Toronto, Ont., Canada M5S 1A4

Received April 12, 1990[1]

P. J. TUMIDAJSKI and S. N. FLENGAS. Can. J. Chem. **69**, 462 (1991).

The thermodynamic behaviour of $ThCl_4$ – alkali chloride solutions was investigated using galvanic and formation cells of the type

$$(-)Th/ThCl_4\text{–}ACl//\text{asbestos diaphragm}//AgCl\text{–}ACl/Ag(+)$$

and

$$(-)Th/ThCl_4\text{–}CsCl/C,Cl_{2(g,\ 1\ atm)}(+)$$

where ACl represents NaCl, KCl, CsCl, or equimolar mixtures of NaCl–KCl, NaCl–CsCl, and KCl–CsCl. In addition, the thermodynamic behaviour of thorium in mixed alkali chloride – alkali fluoride melts was studied using an electrometric titration technique. It was found that these melts are highly nonideal due to the formation of octahedrally coordinated complexes.

Key words: $ThCl_4$ solutions, potentials, thermodynamic properties, titration.

P. J. TUMIDAJSKI et S. N. FLENGAS. Can. J. Chem. **69**, 462 (1991).

On a étudié le comportement thermodynamique de solutions de $ThCl_4$/chlorures alcalins en utilisant des cellules galvanique et de formation du type :

$$(-)Th/ThCl_4\text{–}ACl//\text{diaphragme d'amiante}//AgCl\text{–}ACl/Ag(+)$$

et

$$(-)Th/ThCl_4\text{–}CsCl/C,Cl_{2(g,\ 1\ atm)}(+)$$

où ACl représente NaCl, KCl, CsCl ou les mélanges équimoléculaires de NaCl–KCl, NaCl–CsCl et KCl–CsCl. De plus, utilisant une technique de titration électrométrique, on a étudié le comportement thermodynamique du thorium dans des mélanges de chlorures alcalins/fluorures alcalins fondus. On a trouvé que, à cause de la formation de complexes coordonnés d'une façon octaédrique, ces mélanges fondus sont loin d'être parfaits.

Mots clés : solutions de $ThCl_4$, potentiels, propriétés thermodynamiques, titrage.

[Traduit par la rédaction]

Introduction

Thorium is important for its potential application in the thermonuclear production of electricity. It is used to impart creep resistance in magnesium based alloys, and its low electron work function and high emission current are utilized in electronic devices. $ThCl_4$ – alkali halide solutions are of interest because they can be used for the production or refining of thorium or its alloys by electrolysis.

In a previous publication from this laboratory (1), the standard electrode potentials and the associated thermodynamic properties of dilute solutions of metal chlorides in binary and ternary fused salt solutions were reported. In this work the method is extended to $ThCl_4$ – alkali chloride solutions in the concentration range where $ThCl_4$ conforms to Henrian behaviour.

The electrode potentials in the $ThCl_4$–CsCl system with a higher concentration of $ThCl_4$ were determined using a chloride formation cell. The results are important to confirm the dilute solution behaviour and to provide an insight into the fundamental properties of these mixtures.

Finally, the course of the chemical reaction and the ionic equilibria involved when alkali fluoride is added to the $ThCl_4$–CsCl solutions was determined using an electrometric titration technique. The results indicate that it is possible to control the thermodynamic state of a solute species by using mixed chloride and fluoride ions.

[1]Revision received October 17, 1990.

Experimental

The preparation and purification of the materials used in this investigation have been described previously (1). $ThCl_4$ salts were obtained from Cerac in anhydrous condition in sealed ampoules packed under argon gas. The alkali fluorides were reagent grade; and were dried by vacuum heating at 400°C for several days. Thorium metal electrodes were obtained from Morton Thiokol (Alfa Products Division).

Electrochemical cells

Dilute solutions

The design of the electrochemical cell employed in the present investigation for the dilute solutions has been described in detail elsewhere (1). Briefly, the cell consisted of a thorium metal electrode dipping into a $ThCl_4$ – alkali chloride solution and a Ag–AgCl secondary reference electrode. The half-cell compartments were separated by an asbestos diaphragm.

The spontaneous cell reaction for the Th–Ag galvanic cell is,

$$[1] \quad Th_{(s)} + 4AgCl = ThCl_4 + 4Ag_{(s)}$$

where species in italics denotes species in solution. The corresponding Nernst equation is

Can. J. Chem. Downloaded from www.nrcresearchpress.com by 198.100.157.202 on 09/07/12
For personal use only.

Can. J. Chem. Downloaded from www.nrcresearchpress.com by 198.100.157.202 on 09/07/12
For personal use only.

[2] $$E_{cell} = (E^0_{ThCl_4} - E^0_{AgCl}) - \frac{2.303RT}{4F} \log (X_{ThCl_4}/X^4_{AgCl}) - \frac{2.303RT}{4F} \log (\gamma_{ThCl_4}/\gamma^4_{AgCl})$$

where F is the Faraday's constant of 96 487 J V^{-1} mol^{-1}, and R is the universal gas constant of 8.3144 J K^{-1} mol^{-1}. The standard state in all cases is the pure liquid metal chloride at the temperature of the experiments. $E^0_{ThCl_4}$ and E^0_{AgCl} are the standard cell potentials for the formation of pure liquid $ThCl_4$ and AgCl, respectively. Values for E^0_{AgCl} were obtained from the work of Pelton and Flengas (2). Values for $E^0_{ThCl_4}$ incorporate considerable error. However, the most recent compilation by Pankratz (3) has been used to approximate enthalpies and activity coefficients for the dilute solutions.

Following the development given previously (1) for dilute solutions, where activity coefficients are expected to be constant, eq. [2] can be simplified to,

[3] $$E_{cell} = E^0_{f(ThCl_4)} - E^0_{f(AgCl)} - \frac{2.303RT}{4F} \log \left(\frac{X_{ThCl_4}}{X^4_{AgCl}} \right)$$

$E^0_{f(ThCl_4)}$ and $E^0_{f(AgCl)}$ are the formal formation potentials representing the free energy of formation of unit mole fraction of the salt but behaving as if it were infinitely diluted in a given solvent. For $ThCl_4$ the formal formation potential and its corresponding reaction are given by

[4] $$Th_{(s)} + 2Cl_{2(g,\ 1\ atm)} \rightarrow \mathit{ThCl_4} \qquad \text{at } X = 1, \text{ and at its thermodynamic state of infinite dilution}$$

and

[5] $$E^0_{f(ThCl_4)} = E^0_{ThCl_4} - \frac{2.303RT}{4F} \log (\gamma_{ThCl_4})$$

Because values for $E^0_{f(AgCl)}$ have been determined previously (1), $E^0_{f(ThCl_4)}$ can be calculated from eq. [3].

Concentrated solutions

The cell design was similar to the chloride formation cells described elsewhere (4). The cell consisted of a thorium metal indicator electrode immersed in molten $ThCl_4$–CsCl solution of known composition, and a graphite chlorine electrode, which also dipped into a molten solution of the same composition. The two cell compartments were separated by an asbestos fiber diaphragm fused into silica glass. The spontaneous cell reaction is

[6] $$Th_{(s)} + 2Cl_{2(g,\ 1\ atm)} = \mathit{ThCl_4}$$

The Nernst equation is

[7] $$E_{cell} = E^0_{ThCl_4} - \frac{2.303RT}{4F} \log (\gamma_{ThCl_4} X_{ThCl_4})$$

Chloride-fluoride solutions

The applicability of the electrometric titration technique in fused salt solutions has been demonstrated previously (5–8). The electrochemical cell for the electrometric titration is essentially a chloride formation cell with a port to allow for the addition of alkali fluoride pellets. The cell consisted of a thorium indicator electrode immersed in a $ThCl_4$ – CsCl – alkali fluoride molten solution, and the graphite chlorine gas reference electrode, dipping into a $ThCl_4$–CsCl solution. The half-cell compartments were separated by a diaphragm consisting of an asbestos fiber fused in quartz. The cell can be described schematically as

$$(-)Th/ThCl_4\text{–}CsCl\text{–}AF//\text{asbestos diaphragm}//ThCl_4\text{–}CsCl/C, Cl_{2(g,\ 1\ atm)}(+)$$

where AF represents NaF, KF, or CsF. The concentration of $ThCl_4$ in the reference electrode compartment was fixed at 6.98×10^{-3} mole fraction. At the beginning of an experiment, prior to the addition of alkali fluoride, the composition in both half-cell compartments was equal. Junction potentials caused by compositional differences across the diaphragm due to the addition of alkali fluoride, were minimized by the presence of an excess of CsCl on both sides of the asbestos diaphragm.

Results and discussion

The procedure for a typical experimental run for the dilute and concentrated solutions has been described previously (1). Electrometric titration was performed by adding weighed amounts of NaF, KF, or CsF to the indicator electrode compartment. The emf between the reference and indicator electrode compartments was measured.

Table 1 summarizes the measured cell emf's for dilute $ThCl_4$ solutions. They have been expressed as least-squares lines of the form $E = A + BT$, where E is the cell potential in volts, and T is the temperature in Kelvin. Melt compositions have been expressed in terms of mole fraction of $ThCl_4$. The correlation coefficients in Table 1 indicate that there is a linear relationship between the cell emf and temperature. An estimate for the standard deviations of cell emf for the regression of cell emf on temperature is less than ±2 mV in all cases. Further, the measured emf values were stable and reproducible to within ±1 mV.

As expected for Henrian solutions, there is a linear relationship between the cell emf and the Nernstian concentration term, as expressed by eq. [3]. A linear regression analysis for the concentration term against the cell potential yielded a correlation coefficient of approximately 0.99 for every solvent. Also, the slopes of the lines correspond, within a 99% confidence level, to the theoretical slope for a four-electron electrode reaction. Several $ThCl_4$ – alkali chloride systems have been investigated previously. Yang, Hudson, and Chien (9), Inman, Hills, Young, and Bockris (10), and Martinot (11), investigated the $ThCl_4$–LiCl–KCl melts. Srinivasan and Flengas (12) and Smirnov *et al.* (13–15) performed experiments on the $ThCl_4$–NaCl–KCl system. More recently, Smirnov and Kudyakov (16) re-investigated $ThCl_4$ in alkali chlorides. With the exception of the Soviet work, all investigators found that the single-step reduction

$$Th^{4+} + 4e^- \rightarrow Th$$

is the predominant potential-determining reaction under equilibrium conditions. Smirnov and co-workers (13–15) proposed that the average valency of thorium in alkali chloride melts is less than four, suggesting the existence of thorium subhalides. The experimentally determined potentials in this work did not vary with time, and the absence of thorium metal electrode corrosion suggests that subhalide forming reactions are not significant.

Values for the formal potentials for $ThCl_4$, as calculated with eq. [3], are summarized in Table 2. The formal potentials are expressed in the form

$$E^0_f = A + BT$$

where E^0_f is in volts, and T is the temperature in Kelvin. All potentials represent spontaneous cell reactions and are given with positive signs to conform with the thermodynamic requirement of a decrease in reaction free energy. However, if it is desired to tabulate the emf values in the format of a series against common reference electrode, such as chlorine or silver chloride electrodes, it will be necessary to conform to IUPAC (17) sign convention and assign negative values to the more reactive electrode systems. The uncertainties in the formal potentials listed in Table 2 were obtained as described in a

TABLE 1. E_{cell} versus temperature for the dilute $ThCl_4$ system

Solvent	X_{ThCl_4}	$E = A + BT$ (V) A	$B \times 10^4$	C coeff.	Range (K)
KCl	7.75×10^{-4}	1.750	−2.230	−0.999	1100–1179
	1.53×10^{-3}	1.752	−2.387	−0.999	1071–1174
	2.12×10^{-3}	1.751	−2.455	−0.999	1072–1173
	2.70×10^{-3}	1.752	−2.510	−0.999	1067–1173
CsCl	2.64×10^{-3}	2.207	−5.981	−0.999	981–1087
	4.13×10^{-3}	2.208	−6.082	−0.999	972–1085
	5.52×10^{-3}	2.208	−6.144	−0.999	955–1080
	7.74×10^{-3}	2.206	−6.207	−0.999	960–1079
NaCl–KCl*	6.73×10^{-4}	1.936	−4.007	−0.999	1009–1111
	8.22×10^{-4}	1.937	−4.064	−0.999	982–1092
	2.09×10^{-3}	1.937	−4.260	−0.999	982–1101
	2.88×10^{-3}	1.936	−4.324	−0.999	982–1101
	3.87×10^{-3}	1.937	−4.392	−0.999	981–1100
NaCl–CsCl*	1.71×10^{-3}	1.590	−0.489	−0.999	953–1083
	4.18×10^{-3}	1.588	−0.663	−0.999	948–1079
	6.81×10^{-3}	1.589	−0.777	−0.999	950–1085
	8.85×10^{-3}	1.589	−0.836	−0.999	896–1085
KCl–CsCl*	1.84×10^{-3}	1.903	−3.614	−0.999	961–1095
	3.68×10^{-3}	1.904	−3.769	−0.999	963–1092
	5.65×10^{-3}	1.904	−3.861	−0.998	963–1093
	8.35×10^{-3}	1.903	−3.944	−0.996	948–1093

*Equimolar.

previous publication (1). A comparison of the magnitude of the formal potentials indicates the pronounced effect of CsCl in creating thermodynamically stable solutions. The large magnitudes of the formal potentials for $ThCl_4$ suggest an extremely strong tendency of $ThCl_4$ to form complex species in these melts. The magnitude of the formal potentials decreases with increasing temperature, indicative of complex dissociation at the higher temperatures. The agreement of the present results with those of Srinivasan and Flengas (12) for NaCl–KCl–$ThCl_4$ is good and within experimental error.

The calculation of valid partial molar properties for the $ThCl_4$ – alkali chloride systems is complicated by the lack of reliable data for the free energy of formation of pure molten thorium tetrachloride. The linear approximation for the standard formation potential of $ThCl_4$ (3) is

$$[8] \quad E^0_{ThCl_4} = A^0 + B^0T = 2.8076 - 5.001 \times 10^{-4}T$$

Typical errors expected for standard formation potentials are well over ±200 mV. When the formal formation potential is expressed as

$$[9] \quad E^0_{f(ThCl_4)} = A + BT$$

It follows that

$$[10] \quad \overline{\Delta H}_{ThCl_4} = -4F(A - A^0)$$

and

$$[11] \quad \log \gamma_{ThCl_4} = (E^0_{ThCl_4} - E^0_{f(ThCl_4)}) \frac{4F}{2.303RT}$$

Thermodynamic properties for the $ThCl_4$ systems are summarized in Table 3. The results are informative in a qualitative manner for indicating and confirming general trends. The very small activity coefficients in combination with the exothermic enthalpies of mixing suggest strong interactions usually associated with the formation of complex species. Furthermore, in the presence of larger solvent cations there is an increase in interaction between thorium cation and its surrounding anions.

TABLE 2. Formal potentials in the $ThCl_4$ systems

System	$E_f^0 = A + BT^*$ (V) A	$B \times 10^4$	E_f^0 (V) 1073 K	1173 K	±E
$ThCl_4$–KCl	2.8934	−3.650	2.502	2.465	0.002
$ThCl_4$–CsCl	3.2995	−5.980	2.649	2.603	0.002
$ThCl_4$–NaCl–KCl	3.0244	−5.500	2.434	2.379	0.001
$ThCl_4$–NaCl–CsCl	2.8440	−2.970	2.576	2.534	0.001
$ThCl_4$–KCl–CsCl	3.1873	−5.895	2.555	2.496	0.001

*Temperature range 973–1173 K.

For more concentrated $ThCl_4$–CsCl solutions, it was found that initial saturation of the molten solution with chlorine took about 2 h during which the cell potential rose slowly. Once the melt was saturated with chlorine gas, the cell potential was stable and responded immediately to temperature or chlorine pressure changes. The emf values obtained during heating over a period of 24 h could be retraced on cooling, indicating that the changes are reproducible. The reversibility of the measured emf's was also verified by polarization tests whereby a small current from an external dry cell was passed through the cell. On disconnecting the applied potential, the cell emf returned to its equilibrium value to within ±1 mV. Krasnov and co-workers (18) and Smirnov and co-workers (19, 20) have postulated that for concentrated $ThCl_4$ – alkali chloride solutions, in the presence of thorium the solution process is significant and that the valency of thorium is intermediate between two and four.

Can. J. Chem. Downloaded from www.nrcresearchpress.com by 198.100.157.202 on 09/07/12
For personal use only.

TABLE 3. Thermodynamic properties of dilute $ThCl_4$ solutions in alkali chloride melts*

System	γ_{ThCl_4} at $X_{ThCl_4} \rightarrow 0$		ΔH_{ThCl_4} at $X_{ThCl_4} \rightarrow 0$
	1073 K	1173 K	(kJ mol^{-1})
$ThCl_4$–KCl	4.396×10^{-5}	6.157×10^{-5}	(−33.13)
$ThCl_4$–CsCl	7.607×10^{-8}	2.616×10^{-7}	(−189.87)
$ThCl_4$–NaCl–KCl	8.330×10^{-4}	1.851×10^{-3}	(−83.69)
$ThCl_4$–NaCl–CsCl	1.556×10^{-5}	1.878×10^{-5}	(−14.07)
$ThCl_4$–KCl–CsCl	4.439×10^{-6}	1.805×10^{-5}	(−146.56)

*Parentheses indicate the reported values may have significant uncertainties.

TABLE 4. E_{cell} versus temperature for $ThCl_4$–CsCl systems

	$E = A + BT$ (V)			
X_{ThCl_4}	A	$B \times 10^4$	C coeff.	Range (K)
0.0513	3.583	−8.010	−0.999	940–1097
0.0979	3.527	−7.685	−0.999	916–1092
0.1846	3.487	−7.477	−0.998	963–1083
0.2696	3.435	−7.198	−0.999	886–1034
0.3413	3.370	−6.892	−0.998	908–1025
0.4408	3.307	−6.782	−0.999	898–1029

The stability with time of the measured cell potentials of the thorium electrode, even in the more concentrated solutions, indicates that tetravalent ions are the predominant species in these melts. The results of the emf measurements are summarized in Table 4 expressed as least-squares lines of the form

$$E = A + BT \text{ (V)}$$

An estimate of the standard deviation for the linear regression of Table 4 is 0.5 mV in all cases. Below 0.3413 mole fraction of $ThCl_4$ the volatilities of the salts were low and the loss of $ThCl_4$ did not significantly alter the results. The thermodynamic properties of $ThCl_4$ were not calculated because of the large uncertainty in the free energy of formation of pure liquid $ThCl_4$. However, Fig. 1 is a plot of the Nernst concentration term versus cell potential for the $ThCl_4$–CsCl system at 1073 and 1173 K. The plots include results for the dilute galvanic and concentrated formation cells. It can be seen that the results for the former are consistent with the latter. Figure 1 also includes the standard potential for pure liquid $ThCl_4$ as calculated by Pankratz (3).

For titration experiments, the thorium electrode potential rose slowly for approximately 10 min after each addition of fluoride as dissolution of the pellet continued and mixing occurred; potentials were stable thereafter. For extended reaction times and for the higher alkali fluoride compositions, there was slight corrosion of the silica crucible and some dissolution of the thorium indicator electrode. Therefore, reaction times for these conditions were kept to a minimum. The titration curves obtained for 973 and 1023 K are given in Fig. 2 in which the cell potentials were plotted against the composition variable R, defined as,

[12] R = (total moles of alkali fluoride added/initial moles of $ThCl_4$)

The shapes of the curves indicate that reaction has taken place

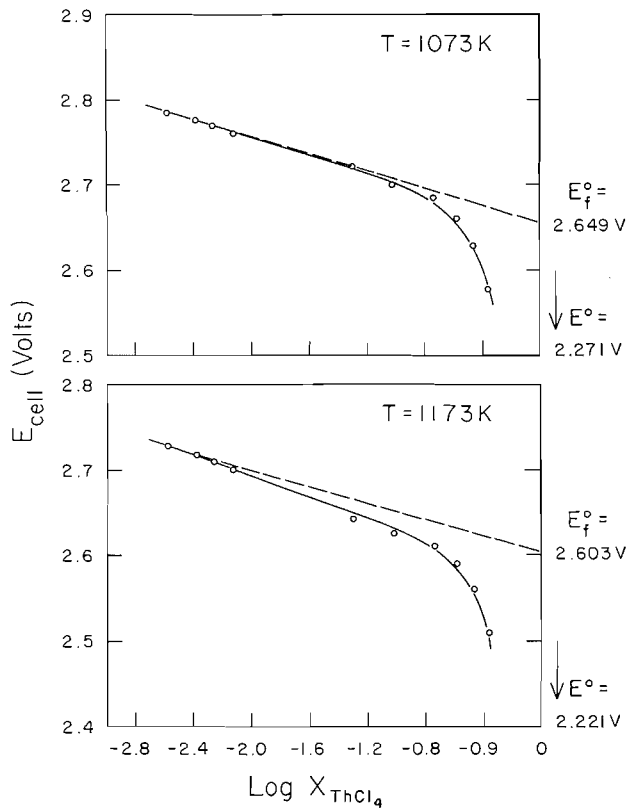


FIG. 1. Nernst plots for the $ThCl_4$–CsCl systems. E^0 represents the standard formation potentials of pure molten $ThCl_4$ at the indicated temperatures. Dotted lines represent a four-electron slope for E_{cell} versus log X_{ThCl_4} for the dilute solutions.

between the initial $ThCl_4$ in the $ThCl_4$–CsCl melt and the added alkali fluoride. A marked change in measured cell potential is expected to occur at the stoichiometric composition corresponding to the predominant species-forming reaction. Figure 2 also includes differential plots of the same titration curves. For both temperatures, and for all titrants, peaks are observed where the parameter R is approximately six. Hence, the addition of fluoride ions sets up an exchange reaction between octahedral complexes according to

[13] $ThCl_6^{2-} + 6F^- = ThF_6^{2-} + 6Cl^-$

For R greater than six, there is a slight but discernible change in cell potential for the addition of different alkali fluorides. The emf's decrease in the order CsF > KF > NaF.

The mass balance for the addition of CsF to a $ThCl_4$–CsCl mixture is given below. Reactions are assumed to occur in two steps. Initially, when $ThCl_4$ is added to CsCl, a chloro complex

Can. J. Chem. Downloaded from www.nrcresearchpress.com by 198.100.157.202 on 09/07/12
For personal use only.

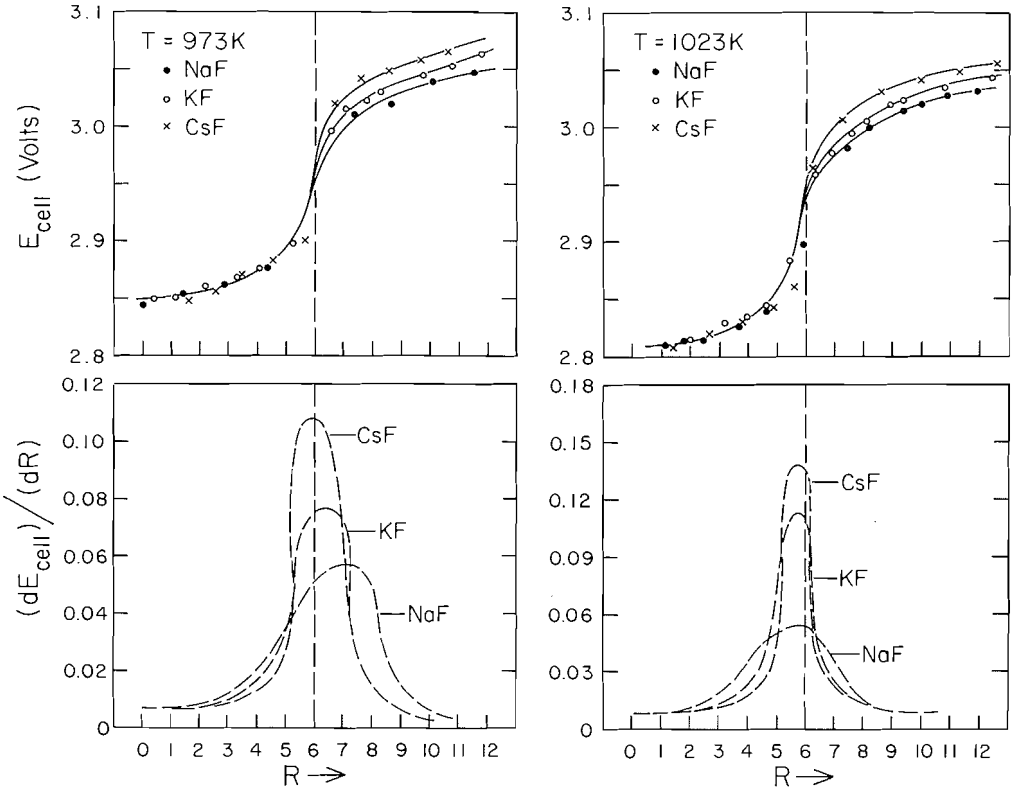


FIG. 2. Potentiometric titration curves during the addition of fluoride ions to $ThCl_4$–CsCl melts. $R = n_{AF}/n_{ThCl_4}$ = (mole ratio). dE/dR is also shown.

is formed, and the reaction is assumed to be complete. Therefore, the initial solution consists of a dilute solution of Cs_2ThCl_6 in CsCl. As CsF is added, the exchange reaction [13] between chloro and fluoro complex develops. The composition of the $ThCl_4$–CsCl–CsF melt is as follows:

	Complex-forming reaction:				
	$ThCl_4$	+	2CsCl	⟶	Cs_2ThCl_6
Initial	y		z		0
Equilibrium	0		$z - 2y$		y

	Exchange reaction:			
	Cs_2ThCl_6 +	6CsF	= Cs_2ThF_6	6CsCl
Initial	y	x	0	$z - 2y$
Equilibrium	$y(1 - \alpha)$	$x - 6\alpha y$	αy	$z - 2y + 6\alpha y$

$\Sigma = x + z - y$
$X_{Cs_2ThCl_6} = y(1 - \alpha)/\Sigma$
$X_{Cs_2ThF_6} = \alpha y/\Sigma$
$X_{CsF} = (x - 6\alpha y)/\Sigma$
$X_{CsCl} = (z - 2y + 6\alpha y)/\Sigma$
Note: α represents the degree of reaction per mole of the complex Cs_2ThCl_6.

The equilibrium constant for reaction [13] is

$$[14] \quad K = \frac{X_{Cs_2ThF_6} X^6_{CsCl}}{X_{Cs_2ThCl_6} X^6_{CsF}} = \frac{\alpha}{1 - \alpha} \frac{z - yz + 6\alpha y}{z - 6\alpha y}$$

The degree of reaction of Cs_2ThCl_6, α, is calculated from the expression for the formal formation potential of the Cs_2ThCl_6–CsCl system as

$$[15] \quad E_{cell} = E^0_{f(Cs_2ThCl_6)} - 2.303RT \log (X_{Cs_2ThCl_6})$$

For dilute solutions of Cs_2ThCl_6 in CsCl, the values for $E^0_{f(Cs_2ThCl_6)}$ are approximated by $E^0_{f(ThCl_4)}$ given in Table 2. At 973 K, with the appropriate substitutions, eq. [15] becomes,

$$[16] \quad E_{cell} = 2.741 - 0.0483 \log (y(1 - \alpha)/\Sigma)$$

For this system, the equilibrium constant is found to be infinitely large. Thus we assumed the exchange reaction to be virtually complete, and only negligible amounts of the chloro complex to be present.

Conclusions

Reversible emf measurements have been used to establish the thermodynamic behaviour of $ThCl_4$ in a number of binary and ternary fused alkali chloride solvents. In dilute solutions, Henrian behaviour is observed, and the calculated formal potentials, activities, and partial molar enthalpies of mixing indicate negative deviations from ideality, which become more negative as the size of the alkali metal cation in the solvent increases from sodium to cesium. Furthermore, thorium is present predominantly as a tetravalent cation.

Results for the more concentrated $ThCl_4$–CsCl solutions are in consonance with the dilute solution behaviour.

The addition of fluoride ions to the $ThCl_4$–CsCl solutions sets up an exchange reaction with the subsequent formation of octahedrally co-ordinated fluoro complexes of the type Cs_2ThF_6. The fluoro complexes represent an activity state for the thorium ions which is much lower than that in the all-chloride melt. Thus, it is possible to control the thermodynamic state of thorium ions by controlling the solvent composition and by using mixed chloride–fluoride melts.

Can. J. Chem. Downloaded from www.nrcresearchpress.com by 198.100.157.202 on 09/07/12
For personal use only.

1. P. J. TUMIDAJSKI and S. N. FLENGAS. J. Electrochem. Soc. **137**, 2717 (1990).
2. A. D. PELTON and S. N. FLENGAS. J. Electrochem. Soc. **117**, 1130 (1970).
3. L. B. PANKRATZ. Bulletin 674 – Thermodynamic properties of halides. U.S. Bureau of Mines. 1984.
4. S. N. FLENGAS. High Temp. High Pres. **5**, 551 (1973).
5. S. N. FLENGAS and E. RIDEAL. Proc. R. Soc. A, **223**, 443 (1956).
6. H. T. TIEN and G. W. HARRINGTON. Inorg. Chem. **2**, 369 (1963).
7. J. JORDAN, J. MEIER, E. J. BILLINGHAM, and J. PENDERGRAST. Anal. Chem. **31**, 1439 (1959).
8. G. BOMBI, M. FIORANI, and G. A. MASSOCCHIN. J. Electroanal. Chem. **9**, 457 (1965).
9. L. YANG, R. G. HUDSON, and C. CHIEN. *In* Physical chemistry of process metallurgy. Part 2. *Edited by* G. R. St. Pierre. Interscience Publishers, New York. 1961. pp. 925–942.
10. D. INMAN, G. J. HILLS, L. YOUNG, and J. O'M. BOCKRIS. Ann. N.Y. Acad. Sci. **79**, 803 (1959).
11. L. MARTINOT. J. Radioanal. Nucl. Chem. Lett. **103**, 357 (1986).
12. R. SRINIVASAN and S. N. FLENGAS. Can. J. Chem. **42**, 1315 (1964).
13. M. V. SMIRNOV and L. D. YUSHINA. Izv. Akad. Nauk, SSSR, Otd. Khim. Nauk, No. 2, 1985 (1956).
14. M. V. SMIRNOV and L. E. IVANOVSKII. Zh. Fiz. Khim. **31**, 641 (1957).
15. M. V. SMIRNOV and L. D. YUSHINA. Izv. Akad. Nauk, SSSR, Otd. Khim. Nauk, No. 2, 251 (1959).
16. M. V. SMIRNOV and V. YA. KUDYAKOV. Electrochim. Acta, **28**, 1339 (1983).
17. T. LICHT and A. DE BETHUNE. J. Chem. Educ. **34**, 443 (1957).
18. K. S. KRASNOV, E. V. MOROZOV, N. V. FILIPPENKO, and N. I. GIRICHEVA. Izv. Vyssh. Ucheb. Zaved. Khim. Khim. Teknol. **16**, 1500 (1973).
19. M. V. SMIRNOV, V. YA. KUDYAKOV, YA. A. LOGINOV, B. G. LOSSOKHIN, YU. V. POSOKHIN, and T. A. PUZANOVA. Fiz. Khim. Elektrokhim. Rasplav. Solei. Shlakov. **1**, 115 (1969).
20. M. V. SMIRNOV, V. YA. KUDYAKOV, and YU. V. POSOKHIN. Tr. In-ta Elektrochimii, Ural'sk. Nauch. Tsentr. AN SSSR, **24**, 18 (1976).

Can. J. Chem. Downloaded from www.nrcresearchpress.com by 198.100.157.202 on 09/07/12
For personal use only.

The proton transfer reaction between bis(2,4-dinitrophenyl)methane and nitrogen bases in dimethyl sulfoxide and toluene solvents

ARNOLD JARCZEWSKI AND GRZEGORZ SCHROEDER
Department of Chemistry, A. Mickiewicz University, Poznań, Poland

AND

KENNETH T. LEFFEK[1]
Department of Chemistry, Dalhousie University, Halifax, N.S., Canada B3H 4H6

Received July 12, 1990

ARNOLD JARCZEWSKI, GRZEGORZ SCHROEDER, and KENNETH T. LEFFEK. Can. J. Chem. **69**, 468 (1991).

Rate constants have been measured for the proton and deuteron transfer reactions of bis(2,4-dinitrophenyl)methane (**1**) with 1,1,3,3-tetramethylguanidine (TMG) and 1,5-diazabicyclo[5.4.0]undec-7-ene (DBU) in dimethyl sulfoxide (DMSO) and toluene solvents. Equilibrium constants, primary deuterium kinetic isotope effects, and activation parameters are reported. The reaction of **1** with DBU is faster than that with TMG by factors of 5 and 50 in toluene and DMSO respectively. The primary deuterium kinetic isotope effects, k_H/k_D = 7–9, which are independent of the polarity of the solvent, indicate an uncoupled mechanism of proton transfer and are in the "classical" region with little or no indication of a tunnelling contribution to the enthalpy of activation for these reactions.

Key words: proton transfer, bis(2,4-dinitrophenyl)methane, deuterium isotope effects.

ARNOLD JARCZEWSKI, GRZEGORZ SCHROEDER et KENNETH T. LEFFEK. Can. J. Chem. **69**, 468 (1991).

On a mesuré les constantes de vitesse des réactions de transfert de proton et de deutéron entre le bis(2,4-dinitrophényl)méthane (**1**) et la 1,1,3,3-tétraméthylguanidine (TMG) ou le 1,5-diazabicyclo[5.4.0]undéc-7-ène (DBU), dans le diméthylsulfoxyde (DMSO) ou le toluène comme solvants. On rapporte les constantes d'équilibre, les effets isotopiques cinétiques primaires du deutérium et les paramètres d'activation. La réaction de **1** avec le DBU est plus rapide que celle avec la TMG par des facteurs de 5 et de 50 respectivement dans le toluène et le DMSO. Les effets isotopiques cinétiques primaires du deutérium, k_H/k_D = 7–9, qui sont indépendants de la polarité du solvant, indiquent que le mécanisme de transfert de proton n'est pas couplé; leur amplitude se trouve dans la région «classique» et ils ne suggèrent que peu ou pas d'existence de contribution d'un effet tunnel à l'enthalpie d'activation de ces réactions.

Mots clés : transfert de proton, bis(2,4-dinitrophényl)méthane, effets isotopiques du deutérium.

[Traduit par la rédaction]

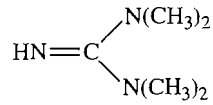
Introduction

The mechanism of proton transfer reactions from carbon acids has been a subject of interest for many years (1–4), and the study of this mechanism has used primary deuterium kinetic isotope effects extensively (5–8), even though the parameters influencing these effects are still not well understood (8–10). From studies of the kinetics of the proton transfer reactions between 4-nitrophenylnitromethane and bases of different structure and strength, Caldin and Mateo (2) deduced that the large difference between the isotope effects in nonpolar and polar solvents could be attributed to the coupling of the proton transfer with the motion of solvent molecules in the polar solvents. This coupling effect was not appreciable in solvents of low polarity, such as toluene. The coupled mechanism causes an increase in the effective mass of the transferred proton, reducing the contribution of tunnelling to the overall process (14), and yielding a small or moderate isotopic rate ratio (4, 11–13). However, this simple picture was first questioned by Rogne and co-workers (15–17) and later by Kresge and Powell (18, 19), who showed that the large isotope effects for the reaction with tetramethylguanidine (TMG) could be artefacts caused by the exchange of hydrogen present on the nitrogen atom of the TMG molecule.

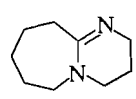
Our results obtained for different proton transfer reactions showed a rather weak dependence of the isotope effect on the polarity of the solvents used (4, 8, 10–12). The isotope effects found for these and other reactions (20, 21) are lower than 8, suggesting that an uncoupled mechanism of proton transfer takes place in polar solvent (4, 8, 10) in which the proton transfer precedes the solvent relaxation (10).

The other important factors governing the isotope effect are the structures of the carbon acid and the base. Steric hindrance was believed to enhance the isotope effect, based on the work of Lewis and Funderburk (22) on the reaction of 2-nitropropane with substituted pyridines in mixed *t*-BuOH/H_2O solvent and this was partly confirmed by our earlier results for other reaction systems (4, 5, 13). Bulky substituents in the reactant molecules could change the height of the potential energy barrier either because of increased repulsive forces or because of crowding of the reaction site, which leads to the exclusion of solvent molecules and so prevents the lowering of the energy barrier by solvent reorganization (23).

The marked dependence of the isotope effect on the presence of substituents close to the reaction site in either the carbon acid or the base was somewhat weakened by several studies (4, 8–10) in which the isotope effect was found to be not very sensitive to the crowding of the reaction site on the carbon acid. For the reaction of 2-methyl-4-nitrophenyl-1-nitropropane with 1,5-diazabicyclo[5.4.0]undec-7-ene (DBU) base, the effect was even reversed, with a larger isotope effect for 4-nitrilophenyl-1-nitroethane, which has much less crowding at the reaction site (10). Therefore, further study of the isotope



(TMG)



(DBU)

[1]Author to whom correspondence may be addressed.

Printed in Canada / Imprimé au Canada

Can. J. Chem. Downloaded from www.nrcresearchpress.com by 198.100.157.202 on 09/07/12
For personal use only.

TABLE 1. Equilibrium constants for the reaction of bis(2,4-dinitrophenyl)methane with TMG and DBU bases in DMSO and toluene solvents

Parameter	Temperature (°C) 25	35	45
Reaction with TMG base in DMSO			
K_i[a]	0.140 ± 0.018	0.130 ± 0.012	0.132 ± 0.012
ε	23900	21800	21700
Corr. coeff.	0.979	0.989	0.989
K_{ip} (apparent) (mol^{-1} dm^3)	3615 ± 300	3420 ± 360	3470 ± 360
Corr. coeff.	0.990	0.984	0.985
Reaction with DBU base in DMSO			
K_i	0.124 ± 0.008	0.124 ± 0.008	0.152 ± 0.002
ε	21600	21300	21100
Corr. coeff.	0.995	0.995	0.999
K_{ip} (apparent) (mol^{-1} dm^3)	2840 ± 110	2860 ± 120	3410 ± 70
Corr. coeff.	0.998	0.997	0.999
Reaction with TMG base in toluene			
K_{ip} (mol^{-1} dm^3)	11.7 ± 4	10.6 ± 5	7.3 ± 4
ε	18500	16500	19000
Corr. coeff.	0.997	0.996	0.997
Reaction with DBU in Toluene			
K_{ip} (mol^{-1} dm^3)	96.2 ± 10	79.1 ± 13	74.1 ± 12
ε	23000	21000	17500
Corr. coeff.	0.995	0.991	0.992

[a] K_i and K_{ip} are the equilibrium constants assuming free-ion or ion-pair products, given by eqs. [2] and [3] respectively.

effect as a function of steric crowding and solvent change is required to resolve these inconsistencies.

In this paper we present a study of the reaction between bis(2,4-dinitrophenyl)methane (**1**) and 1,1,3,3-tetramethylguanidine (TMG) (**2**) and 1,5-diazabicylo[5.4.0]undec-7-ene (DBU) (**3**) in dimethyl sulfoxide (DMSO) and toluene solvents. Both of these bases are very strong, and while TMG has the disadvantage of containing an exchangeable hydrogen and is very hygroscopic, DBU has neither of these problems.

Results and discussion

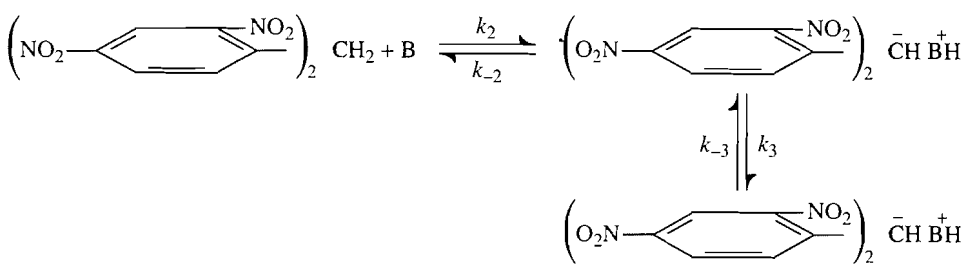
It was recently shown (8, 10) that the products of the proton transfer from 1-nitro-1-(4-nitrophenyl)-alkanes to DBU in acetonitrile exist extensively in the form of free ions rather than ion pairs. It is expected, therefore, that the products of the reaction between **1** and TMG and DBU in dimethyl sulfoxide solvent are probably free ions as shown in eq. [1]. In toluene solvent the product is probably the ion pair in eq. [1].

The reaction shows a strong absorption peak at 715 nm, which is believed to be characteristic of both the ion pair and the free carbanion ion. The absorbances at equilibrium, for a constant acid concentration and varying base concentration, were fitted by the least-squares method to the Hildebrand–Benesi equation for both free ions and ion-paired products, eqs. [2] and [3] respectively, where a and b are the initial concentrations of the carbon acid and base, A is the absorbance at equilibrium, and ε is the molar absorptivity.

$$[2] \quad \frac{a}{A} = \frac{A}{K_i b \varepsilon^2} + \frac{1}{\varepsilon}$$

$$[3] \quad \frac{a}{A} = \frac{1}{K_{ip} b \varepsilon} + \frac{1}{\varepsilon}$$

For the reactions in DMSO the results fitted eqs. [2] and [3] equally well, giving correlation coefficients for a linear least-squares fit of 0.979–0.999 for eq. [2] and 0.984–0.999 for eq.

[1] 

Can. J. Chem. Downloaded from www.nrcresearchpress.com by 198.100.157.202 on 09/07/12
For personal use only.

Can. J. Chem. Downloaded from www.nrcresearchpress.com by 198.100.157.202 on 09/07/12
For personal use only.

TABLE 2. Rate constants for the proton transfer reactions from bis(2,4-dinitrophenyl)methane to TMG and DBU bases in DMSO and toluene solvents

(*a*) Bis(2,4-dinitrophenyl)methane and TMG in DMSO

T (°C)	$10^3[b]$ (M)	$10\,k_{obs}$ (s^{-1})	k_2 ($dm^3\ mol^{-1}\ s^{-1}$)	k_b (s^{-1})	k_H/k_D
Proton transfers					
25	2.0–20.0	13.2–13.92	67.9 ± 4.5	-0.0_3	
30	2.0–20.0	2.41–16.21	78.2 ± 1.9	0.0_5	
40	2.0–20.0	3.68–22.70	108.4 ± 3.3	0.1	
45	2.0–20.0	5.05–27.15	125.2 ± 4.8	0.3	
50	2.0–20.0	6.95–32.50	148.3 ± 6.7	0.3	
Deuteron transfers					
25	2.0–20.0	0.11–1.44	7.3 ± 0.2	-1.8×10^{-3}	9.3 ± 0.3
30	2.0–20.0	0.20–1.76	8.8 ± 0.2	1.9×10^{-3}	8.9 ± 0.3
40	2.0–20.0	0.30–2.44	11.8 ± 0.1	5.2×10^{-3}	9.2 ± 0.3
45	2.0–20.0	0.35–2.97	14.5 ± 0.4	4.8×10^{-3}	8.6 ± 0.4
50	2.0–20.0	0.42–3.60	17.1 ± 1.0	5.9×10^{-3}	8.7 ± 0.7

(*b*) Bis(2,4-dinitrophenyl)methane and DBU in DMSO

T (°C)	$10^3[b]$ (M)	k_{obs} (s^{-1})	$10^{-2}k_2$ ($dm^3\ mol^{-1}\ s^{-1}$)	k_b (s^{-1})	k_H/k_D
Proton transfers					
25	1.0–5.5	2.95–19.80	37.3 ± 1.4	−0.38	
30	1.0–5.5	3.41–25.70	48.4 ± 3.2	−0.19	
40	1.0–5.5	4.09–29.32	56.0 ± 3.8	−0.26	
45	1.0–5.5	6.06–32.92	59.1 ± 2.7	1.02	
50	1.0–5.5	6.85–34.75	63.5–4.4	1.3	
Deuteron transfers					
25	1.0–5.5	0.32–2.48	4.9 ± 0.3	−0.1	7.6 ± 0.6
30	1.0–5.5	0.39_5–2.78	5.4_5 ± 0.4	−0.1	8.9 ± 1.0
40	1.0–5.5	0.41–3.92	7.7 ± 0.5	−0.165	7.3 ± 0.7
45	1.0–5.5	0.54–4.23	8.0 ± 0.7	−0.06	7.4 ± 0.7
50	1.0–5.5	0.97–5.10_5	9.4 ± 0.4	0.08	6.8 ± 0.6

(*c*) Bis(2,4-dinitrophenyl)methane and TMG in toluene

T (°C)	$10^2[b]$ (M)	k_{obs} (s^{-1})	$10^{-1}k_2$ ($dm^3\ mol^{-1}\ s^{-1}$)	k_b (s^{-1})	k_H/k_D
Proton transfers					
5	0.2–4.2	1.42–10.99	24.0 ± 0.3	0.91 ± 0.07	
10	0.2–4.2	2.02–13.31	27.7 ± 0.7	1.6 ± 0.2	
15	0.2–4.2	2.54–16.50	34.9 ± 0.2	1.9 ± 0.1	
25	0.2–4.2	3.41–23.55	49.7 ± 0.8	2.5 ± 0.2	
35	0.2–4.2	4.51–33.08	71.1 ± 0.7	3.0 ± 0.2	
Deuteron transfers					
5	0.2–4.2	0.10–1.14	2.6 ± 0.1	0.05 ± 0.03	9.3 ± 0.7
10	0.2–4.2	0.16–1.60	3.6 ± 0.2	0.15 ± 0.04	7.8 ± 0.5
15	0.2–4.2	0.20–1.97	4.6 ± 0.2	0.04 ± 0.06	7.5 ± 0.3
25	0.2–4.2	0.22–3.07	6.9 ± 0.3	0.18 ± 0.07	7.2 ± 0.3
35	0.2–4.2	0.33–4.30	10.1 ± 0.2	0.08 ± 0.04	7.1 ± 0.2

(*d*) Bis(2,4-dinitrophenyl)methane and DBU in toluene

T (°C)	$10^2[b]$ (M)	k_{obs} (s^{-1})	$10^{-2}k_2$ ($dm^3\ mol^{-1}\ s^{-1}$)	k_b (s^{-1})	k_H/k_D
Proton transfers					
5	0.13–1.60	11.01–33.70	15.6 ± 0.4	8.4 ± 0.3	
10	0.13–1.60	16.1_5–52.10	24.5 ± 0.9	12.0 ± 0.8	
15	0.13–1.60	24.38–68.00	30.0 ± 0.5	19.7 ± 0.4	
25	0.13–1.60	35.15–83.01	33.9 ± 2.0	31.1 ± 2.0	
35	0.13–1.60	46.21–112.02	45.4 ± 2.3	41.8 ± 2.0	

TABLE 2 (*concluded*)

T (°C)	$10^3[b]$ (M)	$10\,k_{obs}$ (s^{-1})	k_2 ($dm^3\ mol^{-1}\ s^{-1}$)	k_b (s^{-1})	k_H/k_D
Deuteron transfer					
5	0.13–1.60	0.24–2.87	$1.80 \pm 0.0_5$	0.04 ± 0.04	8.7 ± 0.3
10	0.13–1.60	0.46–4.59	$2.8 \pm 0.0_5$	0.10 ± 0.02	8.8 ± 0.3
15	0.13–1.60	0.62–6.09	3.8 ± 0.4	0.38 ± 0.33	7.9 ± 0.8
25	0.13–1.60	0.71–7.30	4.6 ± 0.6	0.48 ± 0.52	7.3 ± 1.0
35	0.13–1.60	0.99–9.87	6.3 ± 0.7	0.61 ± 0.63	7.2 ± 0.9

[3]. It seems likely, therefore, that there is a partial, but probably extensive, dissociation of the ion pairs to free ions. Since the two species are indistinguishable by the visible absorption spectrum and it is assumed that the dissociation process, k_3, is much faster than the proton transfer, the kinetic equation [4] for the proton transfer may be applied to the reaction to a good approximation.

For the reactions in toluene a good fit is obtained with eq. [3] but not with eq. [2], confirming that the product is an ion pair. The equilibrium constants, with their standard deviations, for the reactions in DMSO and in toluene are shown in Table 1 for three temperatures, together with the molar absorptivities. The uncertainties in the molar absorptivities are quite large and the values recorded in Table 1 are not considered to be significantly different from each other.

The ion-pair equilibrium constants for the TMG and DBU reactions in toluene reflect the stronger basicity of the DBU base. However, in DMSO solvent, where the ion pairs are probably extensively dissociated into free ions and therefore only the K_i values should be interpreted, these equilibrium constants are almost the same for the two bases. In this case, the overall equilibrium constant, K_i, is the product of the equilibrium constant for the proton transfer to give the ion pair (K_{ip}), multiplied by the ion-pair dissociation constant, k_3/k_{-3}. K_{ip} must be greater for DBU than for TMG since it is the stronger base; therefore the ion-pair dissociation constant for the $TMGH^+$ ion pair has to be greater than that for DBU to yield the experimental result. Given the high degree of resonance delocalization of the positive charge in the $TMGH^+$ ion, this is a possible explanation.

The postulate that each of these strong bases abstracts a proton from DMSO yielding a DMSO anion as the active base would account for the equality of the K_i values, but predicts equal rate constants for the proton transfer reactions, which are not observed.

The pseudo-first-order constants, k_{obs}, were determined from kinetic runs carried out with excess base using a stopped-flow spectrophotometer, and were fitted to eq. [4] where b is the

$$[4] \quad k_{obs} = k_2 b + k_b$$

initial concentration of the base in each run and k_2 is the rate constant for the forward proton transfer reaction. Equation [4] gave a good fit for both proton and deuteron transfers. The results are collated in Table 2 for five different temperatures. In DMSO solvent k_b, the observed intercept of the plot of k_{obs} vs. base concentration, is $k_{-2}k_{-3}[BH^+]/k_3$, assuming that the dissociation of the ion pair and the association of the free ions in DMSO are much faster processes than the proton transfer to and from the carbon acid. Therefore, the figures shown for k_b in Table 2 cannot be readily interpreted for the reactions in DMSO.

Both TMG and DBU are very strong bases; the pK_a values of their conjugate acids in acetonitrile are 23.3 and 23.9 respectively (24). However, the difference in basicity must be larger in DMSO and toluene, since there is a rate factor of about 50 in favour of DBU in DMSO and about 7 in toluene. Such rate differences indicate a Bronsted β value well in excess of unity if the basicity difference is only 0.6 units. DBU is reacting as if it is a much stronger base than TMG in both of these solvents. Such an effect was also observed previously in acetonitrile itself (9), where a rate factor of 66 was observed and is not readily explained. It is possible that these observations could be related to the residual water that is always present in TMG no matter how thoroughly it is dried. However, earlier experiments (25) showed that replacing any ^-OH ion that may be present in the reaction mixture by ^-OD gave no kinetic isotope effect. An isotope effect of 50–80% would be expected if the reacting base was ^-OH (^-OD) rather than TMG.

It is also known that exchange between the deuterated substrate and the TMG hydrogen introduces no error in the determination of k_2 (26, 27). However, it does give spurious values for k_b. The lower values of k_b in Table 2 for the reactions in toluene indicate that some, but not complete, exchange is taking place.

Change of solvent polarity between DMSO and toluene has almost no effect on the second-order rate constant for the reaction with DBU base, whereas the same decrease in solvent polarity increases the rate constant for the TMG reaction by a factor of about 7 at 25°C. This change, which is the reverse of what would be expected for a reaction in which the transition state has more charge separation than the initial state, has been found previously for other proton transfer reactions (17, 28). Since Caldin has concluded that a major part of the energy barrier in proton transfer reactions is the breakdown of the initial state solvation shell (29), the origin of this rate change probably lies in the differences in the specific solvation of the two bases in DMSO and toluene. The observed rate changes require the postulate that the solvation of DBU is roughly the same in DMSO and toluene but the solvation of TMG is significantly greater in DMSO than it is in toluene.

The activation parameters for the reactions are shown in Table 3 and these allow the above free energy differences, measured by the rate constants, to be analyzed in terms of enthalpy and entropy contributions. Table 3 shows that the difference between the two bases for a given solvent lies predominantly in the enthalpy of activation, as would be expected. However, for the TMG base, changing the solvent from DMSO to toluene has a larger effect on the entropy of activation than it does on the enthalpy of activation, i.e., the larger rate constant in toluene is due to an entropy of activation effect, not an enthalpy of activation effect. The same may be true for the DBU reaction but the results are not precise enough to draw this conclusion.

In general, besides electrostatic and specific solvent interactions, the solvent environment in the vicinity of the reaction site

Can. J. Chem. Downloaded from www.nrcresearchpress.com by 198.100.157.202 on 09/07/12
For personal use only.

TABLE 3. Activation parameters for the proton and deuteron transfer reaction from bis(2,4-dinitrophenyl)methane bases in DMSO and toluene solvents

	TMG		DBU	
Parameter	DMSO	Toluene	DMSO	Toluene
ΔH_H^*(kcal mol^{-1})	5.37 ± 0.12	5.66 ± 0.17	3.11 ± 0.6	4.8 ± 1.0
ΔH_D^*(kcal mol^{-1})	5.81 ± 0.22	6.96 ± 0.33	4.42 ± 0.36	6.0 ± 1.0
ΔS_H^*(cal mol^{-1} deg^{-1})	−32.3 ± 0.5	−27 ± 1	−32 ± 2	−26 ± 4
ΔS_D^*(cal mol^{-1} deg^{-1})	−35 ± 1	−27 ± 1	−32 ± 1	−26 ± 4

can affect the proton transfer reactions in two different ways. One is by steric hindrance, which will operate to separate the acid and base, increasing the distance that the proton moves from the carbon acid to the base. The other is to form a solvent cage in which the reaction takes place under much smaller electrostatic effects of the solvent. The first case is common for the coupled mechanism of proton transfer (2, 14) and the second is described as the uncoupled mechanism (8, 10, 14) for which the values of the enthalpy of activation and primary deuterium kinetic isotopic effect are not very sensitive to the polarity of the solvent. The present results generally support the uncoupled mechanism, since the isotopic rate ratios, k_H/k_D at 25°C, lie in the range 9.3–7.2 and are smaller in toluene.

The isotope effects on the enthalpies of activation are substantial, large enough to account for the complete loss of the C–H or C–D stretching vibration, but not large enough to unequivocally indicate a contribution to the rate of the reaction from proton tunnelling.

Overall, these results show that there is no major change in the mechanism of proton transfer between the polar DMSO solvent and the nonpolar toluene solvent, supporting the operation of an uncoupled mechanism under both conditions.

Experimental

Materials

Bis(2,4-dinitrophenyl)methane was prepared using the nitration procedure of Fittig *et al.* (30). Bis(4-nitrophenyl)methane (5 g), prepared as previously described (28), was nitrated with a mixture of 90% HNO_3 (20 mL) and concentrated H_2SO_4 (100 mL) by heating the reaction mixture for 3 h at 120–140°C. The reaction mixture was then cooled and poured onto crushed ice. The solid was separated and recrystallized several times from acetonitrile. Yield 60%, mp 167–168°C; ^{1}H nmr, δ(ppm): 4.77 (s, 2H); 7.44, 7.54 (d, 1H); 8.33, 8.36, 8.43, 8.46 (d, d, 1H); 8.82, 8.80 (d, 1H); MS: 347 (M) (100%), 301 (47.6%), 257 (25.3%), 255 (17.9%), 195 (51.5%), 174 (30.9%), 119 (54.6%), 75 (75.3%).

The deuterated analogue was obtained by exchanging bis(2,4-dinitrophenyl)methane (0.6 g) with a solution of 0.1 M sodium ethoxide in ethanol-*d* (2 mL) in DMSO solvent. After 5 min the reaction mixture was neutralized by addition of 10% DCl in D_2O. This procedure was repeated twice, after which the reaction mixture was poured into excess D_2O. The crystals were filtered and the deuteration was confirmed by the disappearance of the proton nmr signal at δ 4.77 ppm. The mass spectrum indicated 99% deuteration, molecular peak 349.

1,1′,3,3′-Tetramethylguanidine (Aldrich) was dried over KOH pellets and distilled under reduced pressure. Only the middle fraction was collected and used.

1,8-Diazabicyclo[5.4.0]undec-7-ene (Aldrich) was similarly dried with KOH and the middle fraction of a reduced pressure distillation was used. All operations were carried out under nitrogen to exclude atmospheric moisture and CO_2.

Reagent grade DMSO (Reachim) was dried over CaH_2 and distilled over 3 Å molecular sieves at reduced pressure with a small amount of butyl hydrogen phthalate. The middle fraction boiling between 108 and 110°C was collected.

Reagent grade toluene (POCH) was kept for several days over clean sodium wire, then fractionally distilled over sodium. The fraction boiling between 110.5 and 111°C was collected.

Equilibrium measurements

The absorbance at equilibrium for reaction [1] was measured at 715 nm using a Specord M-40 spectrophotometer for a series of reactions with constant carbon acid concentration at either 5×10^{-5} or 2.5×10^{-4} M, and different base concentrations, always in large excess over the acid by a factor of 40–200 in DMSO and 10–400 in toluene.

Kinetic measurements

The kinetic runs were carried out using a stopped-flow spectrophotometer equipped with a thermostating device to keep the cell temperature constant within 0.1°C. An acid concentration of 2.5×10^{-5} M was used with base concentrations shown in Table 2.

Acknowledgement

The authors are grateful for financial support from the CPBP 01.19.04.16 programme.

1. R. P. BELL. The proton in chemistry. 2nd ed. Chapman and Hall, London. 1973.
2. E. F. CALDIN and S. MATEO. J. Chem. Soc. Farday Trans. 1, 112 (1976).
3. L. FUNDERBURK and E. S. LEWIS. J. Am. Chem. Soc. **86**, 2531 (1964).
4. P. PRUSZYNSKI and A. JARCZEWSKI. J. Chem. Soc., Perkin Trans. 2, 1117 (1986).
5. L. MELANDER and W. H. SAUNDERS. Reaction rates of isotopic molecules. Wiley, New York. 1980.
6. E. F. CALDIN and V. GOLD. Proton-transfer reactions. Chapman and Hall, London. 1975. Chaps. 8–10.
7. E. BUNCEL and C. C. LEE. Isotopes in organic chemistry. Vol. 2. Elsevier, Amsterdam. 1976.
8. W. GALEZOWSKI and A. JARCZEWSKI. J. Chem. Soc., Perkin Trans. 2, 1647 (1989).
9. K. T. LEFFEK and P. PRUSZYNSKI. Can. J. Chem. **66**, 1454 (1988).
10. W. GALEZOWSKI and A. JARCZEWSKI. Can. J. Chem. **68**, 2242 (1990).
11. E. F. CALDIN, A. JARCZEWSKI, and K. T. LEFFEK. Trans. Faraday Soc. **67**, 110 (1971).
12. A. JARCZEWSKI and P. PRUSZYNSKI. Pol. J. Chem. **58**, 1175 (1984).
13. A. JARCZEWSKI, P. PRUSZYNSKI, M. KAZI, and K. T. LEFFEK. Can. J. Chem. **62**, 954 (1984).
14. J. L. KURZ and L. C. KURZ. J. Am. Chem. Soc. **94**, 445 (1972).
15. O. ROGNE. Acta Chem. Scand. Ser. A: **32**, 559 (1978).
16. I. HEGGEN, J. LINSTROM, and O. ROGNE. J. Chem. Soc. Faraday Trans. 1, 1263 (1978).
17. J. H. BLANCH and O. ROGNE. J. Chem. Soc. Faraday Trans. 1, 1254 (1978).

Can. J. Chem. Downloaded from www.nrcresearchpress.com by 198.100.157.202 on 09/07/12
For personal use only.

18. A. J. KRESGE and M. F. POWELL. J. Am. Chem. Soc. **103**, 201 (1981).
19. A. J. KRESGE and M. F. POWELL. J. Phys. Org. Chem. **3**, 55 (1990).
20. N. SUGIMOTO, M. SASAKI, and J. OSUGI. Bull. Chem. Soc. Jpn. **57**, 366 (1984).
21. N. SUGIMOTO, M. SASAKI, and J. OSUGI. J. Phys. Chem. **86**, 3419 (1982).
22. E. S. LEWIS and L. H. FUNDERBURK. J. Am. Chem. Soc. **89**, 2322 (1967).
23. E. S. LEWIS. *In* Proton-transfer reactions. *Edited by* E. F. Caldin and V. Gold. Chapman and Hall, London. 1975. Chap. 10, p. 333.
24. K. T. LEFFEK, P. PRUSZYNSKI, and K. THANAPAALASINGHAM. Can. J. Chem. **67**, 590 (1989).
25. A. JARCZEWSKI, P. PRUSZYNSKI, and K. T. LEFFEK. Can. J. Chem. **61**, 2029 (1983).
26. O. ROGNE. Acta Chem. Scand. Ser. A: **32**, 559 (1978).
27. L. MELANDER and W. H. SAUNDERS. Reaction rates of isotopic molecules. Wiley, New York. 1980. Chap. 10.
28. A. JARCZEWSKI and K. T. LEFFEK. Can. J. Chem. **50**, 24 (1972).
29. E. F. CALDIN. J. Chem. Soc. 3345 (1959).
30. R. FITTIG, L. SCHAEFFER, and J. KONIG. Ann. **149**, 324 (1969).

Can. J. Chem. Downloaded from www.nrcresearchpress.com by 198.100.157.202 on 09/07/12
For personal use only.

The conformational behaviour of 2-aryloxytetrahydropyrans and 2-acetoxytetrahydropyran, and barrier to ring inversion[1]

ADAMA OUEDRAOGO AND JEAN LESSARD[2]

Département de chimie, Université de Sherbrooke, Sherbrooke (Québec), Canada J1K 2R1

Received July 27, 1990

ADAMA OUEDRAOGO and JEAN LESSARD. Can. J. Chem. **69**, 474 (1991).

The ^{13}C nuclear magnetic resonance data of a series of 2-(4-substituted-phenoxy)tetrahydropyrans at 156 K and in CF_2Br_2 and $CHFCl_2$ solvents show that the axial preference increases with electron withdrawal in the aryloxy group: from 79% ($\Delta G°_{E\rightarrow A} = -0.4$ kcal mol^{-1}) (4-OCH_3) to 90% ($\Delta G°_{E\rightarrow A} = -0.7$ kcal mol^{-1}) (4-NO_2) in CF_2Br_2. The axial preference (anomeric effect) is smaller in the more polar $CHFCl_2$ solvent, as expected, and the substituent effect is smaller also: change in $\Delta G°_{E\rightarrow A}$ from -0.3 (4-OCH_3) to -0.5 (4-NO_2) kcal mol^{-1}. However, the axial preference of 2-acetoxytetrahydropyran is shown to be smaller than that of 2-phenoxytetrahydropyran in CF_2Br_2 solvent although the acetoxy group is expected to be more electronegative than the phenoxy group. Furthermore, the polarity of the solvent has no effect on the conformational equilibrium of 2-acetoxytetrahydropyran. The results are interpreted in terms of both orbital and electrostatic interactions. The ring-inversion barrier of 2-alkoxy and 2-aryloxytetrahydropyrans, determined by the temperature-coalescence method, is lower than that of tetrahydropyran by about 1.5 kcal mol^{-1}.

Key words: 2-substituted tetrahydropyrans, conformational analysis, anomeric effect, ring inversion.

ADAMA OUEDRAOGO et JEAN LESSARD. Can. J. Chem. **69**, 474 (1991).

Les données de la résonance magnétique nucléaire du ^{13}C à 156 K, dans les solvants CF_2Br_2 et $CHFCl_2$, montrent que la préférence axiale d'une série de tetrahydropyranes portant, en position 2, un groupement phénoxy substitué à la position *para* croît avec le pouvoir électroattracteur du substituant : de 79% ($\Delta G°_{E\rightarrow A} = -0.4$ kcal mol^{-1}) pour un groupement OCH_3 à 90% ($\Delta G°_{E\rightarrow A} = -0.7$ kcal mol^{-1}) pour un groupement nitro dans CF_2Br_2. La préférence axiale (l'effet anomère) est moindre dans $CHFCl_2$, solvant plus polaire, tel qu'attendu, et l'effet de substituant est également plus faible : variation de $\Delta G°_{E\rightarrow A}$ de -0.3 (OCH_3) à -0.5 (NO_2) kcal mol^{-1}. Toutefois, dans CF_2Br_2, la proportion de conformère axial est moins élevée pour le 2-acétoxytétrahydropyrane que pour le 2-phénoxytétrahydropyrane même si le groupement acétoxy est plus électronégatif que le groupement phénoxy. De plus, la polarité du solvant n'a pas d'influence sur l'équilibre conformationnel du 2-acétoxytétrahydropyrane. Les résultats sont interprétés en termes d'intéractions orbitalaires et électrostatiques. La détermination de la barrière d'inversion de cycle d'alcoxy- et d'aryloxytétrahydropyranes par la méthode de coalescence de température montre que la barrière est plus faible que celle du tétrahydropyrane d'environ 1,5 kcal par mole.

Mots clés : tétrahydropyranes substitués en position 2, analyse conformationnelle, effet anomère, inversion de cycle.

Introduction

The preference for the axial orientation of the alkoxy group in 2-alkoxy tetrahydropyrans (*gauche* arrangement about the O(1)—C(2) bond) is known as the anomeric effect (1).[3] The *exo*-anomeric effect refers to the preferred orientation of the O—R bond of the alkoxy group, the R group being *gauche* to the ring oxygen (9–11). The anomeric effect has been explained both by electrostatic interactions destabilizing the antiperiplanar arrangement of a C—O—C—O fragment about the central O—C bond (dipole–dipole repulsions (12, 13) or lone pair – lone pair interactions (14)) and by orbital interactions stabilizing the *gauche* form, mainly the overlap between a nonbonding n orbital on the oxygens and the vacant σ^*_{C-O} orbitals (15–20) (double bond – no bond resonance in the valence bond representation). Evidence for the hyperconjugative stabilizing interactions has been provided by X-ray crystallographic studies (21–23). Theoretical studies support the involvement of n–σ^* stabilizing interactions (17–20, 23–26). Most probably, both electrostatic interactions (mainly dipole–dipole interactions) and orbital interactions (predominantly n–σ^* stabilization) play a role in the preferred conformation of a C—O—C—O—C system (17, 20, 24, 25).

The axial preference of a phenoxy group in 2-substituted tetrahydropyrans has been shown to be larger than that of an alkoxy group, e.g., 81% of conformer A for 2-phenoxytetrahydropyran (R = C_6H_5) as compared to 68% for 2-ethoxytetrahydropyran (R = C_2H_5) at 38°C (neat liquid) (27). This can be readily explained by considering the fact that a phenoxy group is more electron withdrawing than an alkoxy group because of n–π^*_{ring} overlap in the former and because a phenyl ring is more electronegative (sp^2 hybridized carbons) than an alkyl group. Thus a C—O-phenyl bond is a better σ-acceptor (lower energy σ^*_{C-O} orbital) than a C—O-alkyl bond, and the n_{endo} –$\sigma^*_{C(2)-OR}$ stabilization of the conformer with the OR group axial (conformer A) is larger for R = phenyl than for R = alkyl. The n_{exo}–$\sigma^*_{C(2)-O(9)}$ stabilization (*exo*-anomeric effect) for a 2-alkoxy group in a 2-substituted oxane appears to be stronger in the equatorial orientation (conformer E) (11) and so does have some influence on the axial preference. However, because the more electronegative oxygen of a phenoxy group is a poorer n-donor than that of an alkoxy group, the n_{exo}–$\sigma^*_{C(2)-O(1)}$ interaction should be smaller (less stabilizing) in 2-phenoxytetrahydropyran (**1**, R = C_6H_5) and thus have little influence on the axial preference. This might contribute to a small extent to the larger axial preference of the phenoxy group as compared to that of an alkoxy group.

Electrostatic interactions could also be involved in the larger axial preference of the phenoxy group. Since a C—O-phenyl bond might be more polar than a C—O-alkyl bond, dipole–dipole repulsion destabilizing the equatorial form (E) could be stronger in 2-phenoxytetrahydropyran (R = phenyl) than in 2-alkoxytetrahydropyrans (R = alkyl).

In this paper, we report the results of a study of the conforma-

[1]Abstracted from the Ph.D thesis of A. Ouedraogo, Université de Sherbrooke, Sherbrooke (Québec), 1984.

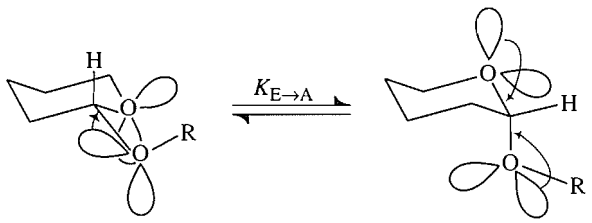
[2]Author to whom correspondence may be addressed.

[3]For reviews on the anomeric effect, see refs. 2–8.

Can. J. Chem. Downloaded from www.nrcresearchpress.com by 198.100.157.202 on 09/07/12
For personal use only.

Can. J. Chem. Downloaded from www.nrcresearchpress.com by 198.100.157.202 on 09/07/12
For personal use only.

tional equilibrium of a series of 2-(4-substituted-phenoxy)tetrahydropyrans **4***a–j*. The purpose of this study was to determine the effect of the substituent on the phenyl ring on the magnitude of the anomeric effect. In such a series, changes in the electron-donating and electron-withdrawing power of the substituent should bring about changes in both electronic and electrostatic interactions but should not have any significant influence on the steric bulk of the aryloxy group. An acetoxy group should be more electron withdrawing than a phenoxy group, and 2-acetoxytetrahydropyran (**3**) was included in the study. We also studied the conformational behaviour of 2-methoxytetrahydropyran (**1**) and 2-isopropoxytetrahydropyran (**2**) in order to evaluate the influence of the size of the R group. Aryloxy and acetoxy groups are bulkier than a methoxy group but probably smaller than an isopropoxy group. Finally, we determined the barrier to inversions of **2**, **4***a*, and **4***c* to see whether or not the anomeric effect has an influence on the inversion barrier of a tetrahydropyran ring.



E A

1 R = CH_3
2 R = *i*-C_3H_7

3 R = $COCH_3$
4 R = 

a X = OCH_3 *f* X = CHO
b X = CH_3 *g* X = $COOCH_3$
c X = H *h* X = CF_3
d X = Br *i* X = CN
e X = $OCOCH_3$ *j* X = NO_2

Results and discussion

The synthesis of the 2-substituted tetrahydropyrans studied is described in the Experimental. All compounds were characterized by infrared, ^{1}H nmr, ^{13}C nmr, and mass spectrometry.

The conformational equilibria were determined from the ^{13}C nmr spectra at 156 K in CF_2Br^2/CD_2Cl_2 (92:8) and in $CHFCl_2/CD_2Cl_2$ (92:8). At 156 K, the conformational equilibrium was frozen and the carbon signals of each conformer were easily distinguished. The proportion of each conformer was determined by integrating the C-3 and C-4 resonances and either one or both of the C-5 and C-6 resonances, then taking the mean value. The spin-lattice relaxation time (T_1) and the nuclear Overhauser effects were assumed to be the same for carbons bearing axial and equatorial substituents. The chemical shifts are given in the Experimental.

2-Aryloxytetrahydropyrans 4

The equilibrium data for the 2-(4-substituted-phenoxy)tetrahydropyrans **4***a–j* are presented in Table 1 (CF_2Br_2) and Table 2 ($CHFCl_2$). In CF_2Br_2 solvent (Table 1), the data show that introducing an electron-donating group such as a methoxy (**4***a*) or a methyl (**4***b*) group at the *para* position of the phenoxy group causes a decrease in the magnitude of the anomeric effect, whereas a strong electron-withdrawing substituent such as a cyano (**4***i*) or a nitro (**4***j*) group leads to a larger anomeric effect. Bromine (**4***d*) and acetoxy (**4***e*), carbomethoxy (**4***j*), formyl (**4***g*), and trifluoromethyl (**4***h*) groups have practically no effect on $K_{E\rightarrow A}$. The overall change in $\Delta G^\circ_{E\rightarrow A}$ is relatively small: from −0.4 (4-OCH_3) to −0.7 (4-NO_2) kcal mol^{-1} ($\Delta\Delta G^\circ_{E\rightarrow A}$ = 0.3 kcal mol^{-1}). In the more polar $CHFCl_2$ solvent (Table 2), the overall change in $\Delta G^\circ_{E\rightarrow A}$ is still smaller: $\Delta\Delta G^\circ_{E\rightarrow A}$ = 0.2 kcal mol^{-1}. Electron-donating substituents have no effect on the magnitude of the anomeric effect (compare **4***a*, **4***b*, and **4***c*), a bromine (**4***d*) has again no effect, but all the remaining substituents that are electron withdrawing according to their substituent σ constants (28–31) bring about some increase of the anomeric effect, the largest influence being observed again with the nitro group (**4***j*), which has the largest σ value. The best Hammett correlation in CF_2Br_2 (r = 0.956; intercept = 0.076) was obtained using σ_p constants, which take into account both resonance and polar effects (28, 29, 31) and gave a ρ value of 0.32. In $CHFCl_2$, σ_p^- constants related to the resonance electron-withdrawing power of the substituent (28, 29) gave the best correlation (r = 0.890, intercept = 0.010) with a ρ value of 0.18.

TABLE 1. Equilibrium data for 2-aryloxytetrahydropyrans **4** in CF_2Br_2[a] at 156 K

Compound	X	% Axial	$K_{E\rightarrow A}$	$-\Delta G^\circ_{156\,K}$[b] (kcal mol^{-1})
4*a*	OCH_3	79	3.8	0.4
4*b*	CH_3	80	4.0	0.4
4*c*	H	86	6.1	0.5_5
4*d*	Br	86	6.1	0.5_5
4*e*	$OCOCH_3$	87	6.7	0.6
4*f*	$COOCH_3$	87	6.7	0.6
4*g*	CHO	87	6.7	0.6
4*h*	CF_3	87	6.7	0.6
4*i*	CN	89	8.1	0.6_5
4*j*	NO_2	90	9.0	0.7

[a] CF_2Br_2/CD_2Cl_2 (92:8).
[b] ±0.1 kcal mol^{-1}.

The larger axial preference with electron withdrawal in the Ar group and the somewhat smaller preference with electron donation could result from changes in n_{endo}–$\sigma^*_{C(1)—OAr}$ orbital interactions in the axial conformer[4] but could result also from changes in dipole–dipole interactions. Both orbital and electrostatic interactions can likewise explain the solvent effects observed, that is, the lower axial preference[5] as well as the smaller influence of the substituent on the phenyl ring on $\Delta G^\circ_{E\rightarrow A}$ in the more polar $CHFCl_2$ solvent, also capable of forming hydrogen bonds. Indeed, the n_{endo}–$\sigma^*_{C(1)—OAr}$ orbital stabilization could be decreased by hydrogen bonding of the ring oxygen to $CHFCl_2$, and dipole–dipole repulsions in the more polar equatorial conformer should be weaker in $CHFCl_2$.

Studies on the influence of a methoxy group and of a nitro group in the *para* position of the phenyl ring on the conformational equilibrium of *trans*-2,3-diaryloxy-1,4-dioxanes (37) were reported before but no significant effect was observed. The

[4] Evidence for an increase in n_{endo}–$\sigma^*_{C(1)—OAr}$ orbital interaction upon increasing the electron withdrawal in the Ar group of 2-aryloxytetrahydropyrans, that is, upon decreasing the energy of the $\sigma^*_{C(1)—OAr}$ orbital, has been provided by bond length changes in a series of axial 2-aryloxytetrahydropyrans (32): the exocyclic C(2)—OAr bond lengthens while the endocyclic C(2)—O(1) bond shortens.

[5] It is well known that the anomeric effect decreases with increasing polarity of the solvent (27, 33–36).

TABLE 2. Equilibrium data for 2-aryloxytetrahydropyrans **4** in $CHFCl_2$[a] at 156 K

Compound	X	% Axial	$K_{E\rightarrow A}$	$-\Delta G^\circ_{156\,K}$[b] (kcal mol^{-1})
4*a*	OCH_3	71	2.5	0.3
4*b*	CH_3	72	2.6	0.3
4*c*	H	72	2.6	0.3
4*d*	Br	70	2.3	0.3
4*e*	$OCOCH_3$	77	3.3	0.3_5
4*f*	$COOCH_3$	76	3.2	0.3_5
4*g*	CHO	79	3.8	0.4
4*h*	CF_3	75	3.0	0.3_5
4*i*	CN	78	3.5	0.4
4*j*	NO_2	83	4.9	0.5

[a]$CHFCl_2/CD_2Cl_2$ (92:8).
[b]± 0.1 kcal mol^{-1}.

conformational equilibria studied by ^{1}H nmr were highly biased (axial preference of 98–99%) and were estimated by an approximate method of analysis so that the small influence of the substituent on the phenyl ring could not be detected.

In their investigation of the conformation equilibria of 2-[(4-substituted-phenyl)selenol]-1,3-dithianes, Pinto *et al.* (38) observed a more pronounced substituent effect than in the case of 2-aryloxytetrahydropyrans. With the 2-arylselenodithianes, the $\Delta G^\circ_{E\rightarrow A}$ (180 K) ranges from −0.61 (4-OCH_3) to −1.10 (4-NO_2) kcal mol^{-1} in CH_2Cl_2 for a $\Delta\Delta G^\circ_{E\rightarrow A}$ value of 0.49 kcal mol^{-1} (180 K) as compared to a $\Delta\Delta G^\circ_{E\rightarrow A}$ value of 0.2 kcal mol^{-1} (156 K) in $CHFCl_2$ for 2-aryloxytetrahydropyrans. The positive ρ values and the variations of ^{13}C and ^{77}Se chemical shifts led the authors to the conclusion that the orbital interaction component predominates over the electrostatic component (38).

It is noteworthy that in the case of 2-(4-substituted-phenoxy)-cyclohexanones studied by Cantacuzene and Tordeux (39), electron-withdrawing substituents have a sizeable effect on the conformational equilibrium, this time leading to a decrease of axial population from 52% (4-H) to 17% (4-NO_2) in CCl_4 solvent at 298 K whereas electron-donating substituents have little effect, the axial population being 54% for a methoxy substituent. The overall substituent effect is thus much larger than in 2-aryloxytetrahydropyrans and 2-(arylseleno)-1,3-dithians, $\Delta G^\circ_{E\rightarrow A}$ (298 K) values ranging from −0.10 (4-OCH_3) to 0.93 (4-NO_2) kcal mol^{-1}. On the other hand, for the analogous 2-(4-substituted-phenoxy)methylenecyclohexanes where the equatorial conformer predominates (75% in $CHFCl_2$ solvent at 220 K), the 4-substituent has no significant effect on the conformational equilibrium (40). The 4-substituent also has no significant effect on the conformational equilibrium of 3-(4-substituted-phenoxy)benzocycloheptenes, where the equatorial orientation (C_e conformation) also predominates over the axial orientation (C_a conformation) in THF-d_8 solvent at 156 K (41).

*2-Acetoxytetrahydropyran (**3**)*

The equilibrium data for the 2-isopropoxy (**2**), 2-methoxy (**1**), 2-phenoxy (**4***c*), and 2-acetoxy (**3**) tetrahydropyrans in CF_2Br_2 and $CHFCl_2$ solvents at 156 K are recorded in Table 3. The lower axial preference of the isopropoxy group (entries 1 and 5) as compared to the methoxy group (entries 2 and 6) has been reported before (^{1}H nmr studies in various solvents (36) and in the neat liquid (27)) and was attributed to the larger steric interactions with the bulkier isopropoxy group in the axial orientation. The larger anomeric effect of the phenoxy group (entries 3 and 7) as compared to the methoxy group has also been observed previously (27) and was discussed in the Introduction. An acetoxy group is also more electronegative than a methoxy group and thus has a larger axial preference than a methoxy group, as shown by a comparison of entries 4 and 8 with entries 2 and 6 respectively and by equilibration of 2-oxy-4-methyltetrahydropyrans and 2-oxy-6-methyltetrahydropyrans (33).

An acetoxy group should be more electronegative than a phenoxy group and the energy of the $\sigma^*_{(C-OR)}$ orbitals should decrease in the following order: $\sigma^*_{C-OCH_3} > \sigma^*_{C-OPh} > \sigma^*_{C-OAc}$ (42). And the $n_{endo}-\sigma^*_{C(1)-OR}$ orbital stabilizing interaction in 2-oxytetrahydropyrans should increase in the order $OCH_3 <$ OPh < OAc. The fact that the axial preference of the acetoxy group is not larger than that of the phenoxy group in the less polar CF_2Br_2 solvent (compare entries 3 and 4 of Table 3) suggests that specific electrostatic interactions might be involved in the case of the acetoxy group, which would more than counteract the larger $n_{endo}-\sigma^*_{C(2)-OAc}$ overlap in the axial conformer. In addition, the acetoxy group is the sole oxygenated substituent among those investigated in this work that does not show a decrease of axial population in going from the less polar (CF_2Br_2) to the more polar ($CHFCl_2$) solvent (compare entries 4 and 8 of Table 3). Again, specific electrostatic interactions associated with the acetoxy group could result in similar polarities for both conformers. In 2-oxymethylenecyclohexanes (43) and benzocycloheptenes (41) bearing an oxygenated substituent (OR, OAr, OCOR) at position 2, the acetoxy group also shows an unexpected conformational behaviour in having a much smaller axial preference than the methoxy group in a nonpolar solvent. Furthermore, the solvent effect is smaller with the acetoxy group than with the methoxy group and is even reversed in the case of 3-acetoxybenzocycloheptene (increase of axial population in the more polar solvent) (41). The peculiar conformational behaviour of the acetoxy group in the latter two series was also tentatively attributed to specific electrostatic interactions by Aubin and St-Jacques (41).

Barrier to ring inversion

The barriers to ring inversion of 2-isopropoxytetrahydropyran (**2**), 2-acetoxytetrahydropyran (**3**), 2-(4-methoxyphenoxy)tetrahydropyran (**4***a*), 2-phenoxytetrahydropyran (**4***c*), and 2-(4-nitrophenoxy)tetrahydropyran (**4***j*) were studied in order to see if the barrier is influenced by the anomeric effect. The activation energies, $\Delta G^{\neq}_{A\rightarrow E}$ and $\Delta G^{\neq}_{E\rightarrow A}$, were calculated from the coalescence temperature (T_c) for the carbon 6 signal using two different methods developed for unequal proportions of conformers (44, 45). Both methods gave practically the same values of activation energies, the largest difference observed being 0.2 kcal mol^{-1}. The mean values are reported in Table 4 for the 2-isopropoxy (**2**), 2-phenoxy (**4***c*), and 2-(4-methoxyphenoxy) (**4***a*) derivatives. In the case of 2-acetoxytetrahydropyran (**3**) and 2-(4-nitro-phenoxy)tetrahydropyran (**4***j*), the coalescence occurred somewhere between 196 and 186 K but it was not possible to determine the coalescence temperature with satisfactory accuracy because of smaller proportions of equatorial conformer and smaller chemical shift differences. However, the temperature range where coalescence was observed indicates that the energies of activation for the ring inversion of **3** and **4***j* must be similar to those reported in Table 4 for **2**, **4***c*, and **4***a*.

The barrier to ring inversion of tetrahydropyran is 10.2 kcal

Can. J. Chem. Downloaded from www.nrcresearchpress.com by 198.100.157.202 on 09/07/12
For personal use only.

TABLE 3. Comparison of equilibrium data for 2-acetoxytetrahydropyran (**3**) with those of 2-isopropoxy (**2**), 2-methoxy (**1**), and 2-phenoxy (**4***c*) tetrahydropyrans in CF_2Br_2[a] and $CHFCl_2$[b] at 156 K

Entry	Solvent	OR (Compound no.)	% Axial	$K_{E\rightarrow A}$	$-\Delta G^\circ_{156\,K}$[c] (kcal mol^{-1})
1	CF_2Br_2	$OCH(CH_3)_2$ (**2**)	62	1.6	0.1_5
2	CF_2Br_2	OCH_3 (**1**)	80	4.0	0.4
3[d]	CF_2Br_2	OC_6H_5 (**4***c*)	86	6.1	0.5_5
4	CF_2Br_2	$OCOCH_3$ (**3**)	83	4.9	0.5
5	$CHFCl_2$	$OCH(CH_3)_2$ (**2**)	32	0.5	−0.2
6	$CHFCl_2$	OCH_3 (**1**)	64	1.8	0.2
7[e]	$CHFCl_2$	OC_6H_5 (**4***c*)	72	2.6	0.3
8	$CHFCl_2$	$OCOCH_3$ (**3**)	84	5.2	0.5

[a] CF_2Br_2/CD_2Cl_2 (92:8).
[b] $CHFCl_2/CD_2Cl_2$ (92:8).
[c] ±0.1 kcal mol^{-1}.
[d] Taken from Table 1.
[e] Taken from Table 2.

TABLE 4. Free energies of activation to ring inversion in 2-oxytetrahydropyrans

Entry	Compound no.	OR	Solvent	$\Delta\delta_{E,A}$[a] for C-6 (ppm)	% Axial	T_c[b] (K)	$\Delta G^{\neq}_{A\rightarrow E}$ (kcal mol^{-1})	$\Delta G^{\neq}_{E\rightarrow A}$ (kcal mol^{-1})
1	**2**	$OCH(CH_3)_2$	CF_2Br_2	6.9	62	200	8.9	8.7
2			$CHFCl_2$	6.8	32	201	8.7	8.9
3	**4***c*	OC_6H_5	CF_2Br_2	5.9	86	190	8.8	8.2
4			$CHFCl_2$	6.0	72	193	8.7	8.3
5	**4***a*	$OC_6H_4OCH_3$	CF_2Br_2	6.1	79	190	8.6	8.2
6			$CHFCl_2$	6.1	71	190	8.5	8.2

[a] Δδ ± 0.2 ppm.
[b] T_c ± 2 K.
[c] $\Delta G^{\neq}$ ± 0.4 kcal mol^{-1}.

mol^{-1} in the nonpolar CS_2 solvent (46) and 10.3 kcal mol^{-1} in the polar $CHFCl_2$–CD_3OD solvent (47). As shown by the $\Delta G^{\neq}_{A\rightarrow E}$ values of Table 4, the polarity of the solvent also has little influence on the barrier of 2-oxytetrahydropyrans. However, the introduction of an oxygenated substituent at position 2 of the tetrahydropyran ring lowers the barrier by 1.4–1.8 kcal mol^{-1}. In contrast, the introduction of an oxygenated group on the cyclohexane ring has virtually no effect on the ring-inversion barrier: $\Delta G^{\neq}_{E\rightarrow A}$ value of 10.4 kcal mol^{-1} for phenoxycyclohexane ($\Delta G^{\neq}_{A\rightarrow E}$ = 9.9 kcal mol^{-1}) (48) compared to a $\Delta G^{\neq}$ value of 10.3 kcal mol^{-1} for cyclohexane (49).[6] Thus, the anomeric effect does lower the barrier to ring inversion of a tetrahydropyran ring. This could be due to the fact that the n_{exo}–$\sigma^*_{C(2)—O(1)}$ orbital overlap (*exo*-anomeric effect) can be maintained throughout the inversion process and thus impart some sp^2 character to carbon 2. Methylenecyclohexane, which has one sp^2-hybridized carbon atom, has a lower inversion barrier ($\Delta G^{\neq}$ = 8.4 kcal mol^{-1} (50)) than cyclohexane. The *endo*-anomeric effect is most probably not the cause of the lower inversion barrier of 2-oxytetrahydropyrans. Indeed, dipole–dipole repulsions as pictured by Edward (12) and by Kabayama and Patterson (13) would be expected to cause an increase of $\Delta G^{\neq}_{A\rightarrow E}$ with respect to the ring-inversion barrier of tetrahydropyran since they would increase during the A→E inversion process. Similarly, the loss of the n_{endo}–$\sigma^*_{C(2)—OR}$ orbital stabilization during the A→E conformational change should also lead to an increase of $\Delta G^{\neq}_{A\rightarrow E}$ with respect to $\Delta G^{\neq}$ for the ring inversion of tetrahydropyran.

Interestingly, 2-methylmethylenecyclohexane (**5***a*) and 2-methoxymethylenecyclohexane (**5***b*) have similar barriers to ring inversion (48): $\Delta G^{\neq}_{E\rightarrow A}$ = 9.9 kcal mol^{-1} and $\Delta G^{\neq}_{A\rightarrow E}$ = 8.9 kcal mol^{-1} for **5***a*, which exists preferentially as the equatorial conformer (95% at 170 K in CF_2Br_2 (51)); $\Delta G^{\neq}_{E\rightarrow A}$ = 9.0 kcal mol^{-1} and $\Delta G^{\neq}_{A\rightarrow E}$ = 9.4 kcal mol^{-1} for **5***b*, in which the axial conformer is more stable (78% at 163 K in CF_2Br_2 (51)). The axial conformer of the latter is stabilized by a π–$\sigma^*_{C—OR}$ orbital interaction (51) (generalized *endo*-anomeric effect (52)) but there should be no significant n_{exo}–$\sigma^*_{C(1)—C(2)}$ overlap, that is, no stabilization akin to the *exo*-anomeric effect, because of the high energy of a $\sigma^*_{C—C}$ orbital.

In 2-oxytetrahydropyrans, the n_{exo}–$\sigma^*_{C(2)—O(1)}$ orbital overlap would be expected to be weaker for a phenoxy group than for an alkoxy group because of the electron-withdrawing effect of the phenyl ring (due to both resonance (n–π^* overlap) and inductive effects). As seen from Table 4 (entries 1–4),

[6] It is noteworthy that tetrahydropyran and cyclohexane have very similar barriers to ring inversion so the replacement of one CH_2 group of cyclohexane by an oxygen atom has virtually no effect on the activation energy for the inversion process.

Can. J. Chem. Downloaded from www.nrcresearchpress.com by 198.100.157.202 on 09/07/12
For personal use only.



E A

5*a* R = CH_3
5*b* R = OCH_3

2-phenoxytetrahydropyran (**4***c*) has a lower $\Delta G^{\neq}_{E\rightarrow A}$ value than 2-isopropoxytetrahydropyran (**2**) but both compounds have similar $\Delta G^{\neq}_{A\rightarrow E}$ values.

Conclusions

In 2-(4-substituted-phenoxy)tetrahydropyrans **4***a–j*, the axial preference, hence the anomeric effect, increases slightly with electron withdrawal in the aromatic ring. The effect is smaller in $CHFCl_2$ than in the less polar CF_2Br_2 solvent. Both orbital and dipole–dipole interactions can account for the substituent and solvent effects.

The axial preference of the acetoxy group is somewhat smaller in CF_2Br_2 than that of the less polar and less electronegative phenoxy group. Electrostatic interactions specific to the acetoxy group might counterbalance the effect of a stronger n_{endo}–$\sigma^*_{C(1)—OAc}$ orbital overlap in the axial orientation. These specific interactions would also be responsible for the absence of a solvent effect on the axial preference of 2-acetoxytetrahydropyran (**3**).

The barrier to ring inversion of 2-alkoxy and 2-aryloxytetrahydropyrans is lower than that of tetrahydropyran by about 1.5 kcal mol^{-1}. This could be due to some sp^2 character of carbon 2, which would be maintained throughout the inversion process through the n_{exo}–$\sigma^*_{C(2)—O(1)}$ overlap (*exo*-anomeric effect).

Experimental[7]

The general information is the same as that given in ref. 43. Variable and low temperature ^{13}C nmr data were obtained with a Bruker WH-400 (±1 K, control unit BVT 1000 calibrated with methanol) Fourier transform spectrometer at the "Laboratoire Régional de RMN de l'Université de Montréal".[8]

Preparation of 2-oxytetrahydropyrans

The 2-oxytetrahydropyrans **1**, **2**, **3**, **4***a*, **4***c*, **4***d*, **4***e*, and **4***h* were prepared from 2,3-dihydropyran and the corresponding alcohol, or acetic acid (freshly distilled over phosphorous pentoxyde),[9] or the corresponding phenol according to the method described by Woods and Kramer (53). For the other 2-oxytetrahydropyrans, the corresponding phenol was not soluble enough in 2,3-dihydropyran and the phenol was dissolved in tetrahydrofuran (preparation of **4***f*), benzene (preparation of **4***g* and **4***j* with the use of *p*-toluene sulfonic acid as catalyst), or dichloromethane (preparation of **4***i*). The physical constants and spectral characteristics of each 2-oxytetrahydropyran are given below. For those already reported in the literature, only the ^{13}Cmr data at room temperature are given (tetramethylsilane as reference).

2-Methoxytetrahydropyran (**1**) (refs. 36, 53): ^{13}Cmr ($CDCl_3$) δ: 19.4 (C-2), 25.5 (C-5), 30.6 (C-3), 55.0 (OCH_3), 61.9 (C-6), 99.9 (C-2) ppm.

2-Isopropoxytetrahydropyran (**2**) (ref. 27): ^{13}Cmr ($CDCl_3$) δ: 20.0 (C-2), 21.6 and 23.6 (2 × CH_3, isopropyl group), 25.7 (C-5), 31.4 (C-3), 62.6 (C-6), 68.3 (O—CH<), 96.8 (C-2) ppm.

2-Acetoxytetrahydropyran (**3**)

The product was isolated as a liquid (83% yield after distillation): bp 55–59°C (3.5 Torr; 1 Torr = 133.3 Pa). It was purified further by distillation: bp 56°C (3.5 Torr); ir ($CHCl_3$) ν_{max}: 1730, 1365, 1220, 1190 cm^{-1}; ^1Hmr ($CDCl_3$) δ: 1.5–1.9 (3 × CH_2), 2.1 (s, CH_3CO), 3.7–4.2 (m, 2H, CH_2O), 6.0 (t, J = 3.2 Hz, H-2) ppm; ^{13}Cmr ($CDCl_3$) δ: 18.7 (C-4), 21.2 (CH_3CO), 25.0 (C-5), 29.2 (C-3), 63.4 (C-6), 92.7 (C-2), 169.8 (C=O) ppm; m/e: 84 ($M^+ - 44$).

2-(4-Methoxyphenoxy)tetrahydropyran (**4**a)

The product was purified by distillation, followed by chromatography on basic alumina (benzene as eluent), and was homogeneous by tlc (74% yield): bp 128°C (4.8 Torr); ir ($CHCl_3$) ν_{max}: 1510, 1210, 1035 cm^{-1}; ^1Hmr ($CDCl_3$) δ: 1.3–2.2 (3 × CH_2), 3.8 (s, CH_3O), 3.4–4.3 (m, CH_2O), 5.4 (t, J = 3 Hz, H-2), 6.8–7.3 (m, 4H) ppm; ^{13}Cmr ($CDCl_3$) δ: 19.0 (C-4), 25.3 (C-5), 30.5 (C-3), 55.6 (CH_3O), 62.1 (C-6), 97.4 (C-2), 114.6 (C-3′), 117.9 (C-2′), 151.2 (C-4′), 154.6 (C-1′) ppm; m/e: 208 (M^+).

2-(4-Methylphenoxy)tetrahydropyran (**4**b)

The product was purified by distillation (80% yield): bp 103°C (2 Torr); ir ($CHCl_3$) ν_{max}: 1610, 1580, 1505, 1220 cm^{-1}; ^1Hmr ($CDCl_3$) δ: 1.3–1.9 (3 × CH_2), 2.1 (s, CH_3), 3.1–3.8 (m, CH_2O), 5.0 (t, J = 3 Hz, H-2), 6.3–6.8 (m, 4H) ppm; ^{13}Cmr ($CDCl_3$) δ: 18.9 (C-4), 20.5 (CH_3), 25.3 (C-5), 30.5 (C-3), 62.0 (C-6), 96.7 (C-2), 116.6 (C-2′), 129.8 (C-3′), 130.9 (C-4′), 155.0 (C-1′) ppm; m/e: 192 (M^+).

2-Phenoxytetrahydropyran (**4**c) (refs. 27, 53): ^{13}Cmr ($CDCl_3$) δ: 18.9 (C-4), 25.3 (C-5), 30.5 (C-3), 62.1 (C-6), 96.5 (C-2), 116.6 (C-2′), 121.6 (C-4′), 129.4 (C-3′), 157.1 (C-1′) ppm.

2-(4-Bromophenoxy)tetrahydropyran (**4**d)

The product was purified by chromatography on basic alumina (benzene as eluent) (72% yield) and was recrystallized from benzene–pentane: mp 55.5–56°C; ir ($CHCl_3$) ν_{max}: 1590, 1580, 1470, 1210 cm^{-1}; ^1Hmr ($CDCl_3$) δ: 1.2–1.9 (3 × CH_2), 3.2–3.8 (m, CH_2O), 5.0 (bs, H-2), 6.3–6.6 (m, 2H), 6.7–7.0 (m, 2H) ppm; ^{13}Cmr ($CDCl_3$) δ; 18.7 (C-4), 25.2 (C-5), 30.3 (C-3), 61.9 (C-6), 96.6 (C-2), 113.8 (C-4′), 118.4 (C-2′), 132.2 (C-3′), 156.3 (C-1′) ppm; m/e: 256, 258 (M^+).

2-(4-Acetoxyphenoxy)tetrahydropyran (**4**e)

The product was purified by chromatography on silica gel (hexane – ethyl acetate 10:90 as eluent) (91% yield) and recrystallized from ether–hexane: mp 55.5–56.5°C; ir ($CHCl_3$) ν_{max}: 1745, 1600, 1500, 1370, 1230, 1180 cm^{-1}; ^1Hmr ($CDCl_3$) δ: 1.6–2.0 (3 × CH_2), 2.3 (s, CH_3CO), 3.3–4.2 (m, CH_2O), 5.4 (br s, H-2), 7.0 (s, 4H) ppm; ^{13}Cmr ($CDCl_3$) δ: 18.8 (C-4), 21.0 (CH_3CO), 25.2 (C-5), 30.4 (C-3), 61.9 (C-6), 96.8 (C-2), 117.2 (C-2′), 122.2 (C-3′), 145.0 (C-4′), 154.9 (C-1′), 169.6 (C=O) ppm; m/e: 236 (M^+). Exact Mass calcd. for $C_{13}H_{16}O_4$: 236.1047; found: 236.1049.

2-(4-Formylphenoxy)tetrahydropyran (**4**f)

The product was isolated as an oil (48% yield) after chromatographic separation on silica gel (ethyl acetate – hexane as eluent): ir ($CHCl_3$) ν_{max}: 2850, 2750, 1700, 1600, 1580, 1505, 1250, 1160 cm^{-1}; ^1Hmr ($CDCl_3$) δ: 1.6–1.9 (3 × CH_2), 3.6–3.9 (m, CH_2O), 5.5 (br s, H-2), 7.1 (m, 2H), 7.8 (m, 2H), 7.9 (s, CHO) ppm; ^{13}Cmr ($CDCl_3$) δ: 18.5 (C-4), 25.1 (C-5), 30.1 (C-3), 62.1 (C-6), 96.2 (C-2), 116.6 (C-2′), 130.5 (C-4′), 131.8 (C-3′), 162.3 (C-1′), 190.9 (CHO) ppm; m/e: 206 (M^+). Exact Mass calcd. for $C_{12}H_{14}O_3$: 206.0942; found: 206.0930.

2-(4-Carbomethoxyphenoxy)tetrahydropyran (**4**g)

The crude product, mp 55–61°C (70% yield), was purified by chromatography on alumina (benzene–ether 1:9) and recrystallization from methylene chloride – petroleum ether 30–60°C: mp 63–64°C; ir ($CHCl_3$) ν_{max}: 1710, 1605, 1580, 1505, 1275, 1240, 1200, 1110 cm^{-1};

[7]The following data may be purchased from the Depository of Unpublished Data, Document Delivery, CISTI, National Research Council Canada, Ottawa, Canada K1A 0R6: ^{13}C chemical shifts at 156 K for each conformer of 2-methoxytetrahydropyran (**1**), 2-isopropoxytetrahydropyran (**2**), 2-acetoxytetrahydropyran (**3**), and 2-(4-substituted-phenoxy)tetrahydropyrans (**4***a–j*); variations of C-2 (or C-4) and C-6 chemical shifts with temperature in CF_2Br_2 and $CHFCl_2$ for **2**, **3**, **4***c*, and **4***j*; data used for the Hammett correlations.

[8]We thank Dr. Minh Tan Phan Viet for his help and availability.

[9]The addition of a catalytic amount of *p*-toluenesulfonic acid did accelerate the reaction.

Can. J. Chem. Downloaded from www.nrcresearchpress.com by 198.100.157.202 on 09/07/12
For personal use only.

^{1}Hmr ($CDCl_3$) δ: 1.2–1.9 (3 × CH_2), 3.3–3.6 (m, CH_2O), 3.7 (s, CH_3O), 5.2 (t, J = 3 Hz, H-2), 6.7 (m, 2H), 7.5 (m, 2H) ppm; ^{13}Cmr ($CDCl_3$) δ: 18.3 (C-4), 24.8 (C-5), 29.8 (C-3), 51.2 (CH_3O), 61.3 (C-6), 94.9 (C-2), 114.5 (C-2′), 121.8 (C-4′), 129.9 (C-3′), 158.9 (C-1′), 169.6 (C=O) ppm; m/e: 236 (M^+). Exact Mass calcd. for $C_{13}H_{16}O_4$: 236.1049; found: 236.1054.

*2-(4-Trifluoromethylphenoxy)tetrahydropyran (***4h***)*

The product was purified by chromatography on silica gel (ethyl acetate – hexane 10:90) (85% yield), then recrystallized from benzene–pentane: mp 38.5–39.5°C; ir ($CHCl_3$) ν_{max}: 1610, 1580, 1510, 1325, 1245, 1200 cm^{-1}; ^{1}Hmr ($CDCl_3$) δ: 1.6–2.1 (3 × CH_2), 3.6–3.9 (m, CH_2O), 5.5 (m, H-2), 7.1–7.2 (m, 2H), 7.5–7.7 (m, 2H) ppm; ^{13}Cmr ($CDCl_3$) δ: 18.6 (C-4), 25.2 (C-5), 30.3 (C-3), 62.1 (C-6), 96.4 (C-2), 116.5 (C-2′), 126.8 (q, J = 3.8 Hz, C-3′), 159.7 (C-1′) ppm (the absorption of C-4′ was not detected); m/e: 246 (M^+). Exact Mass calcd. for $C_{12}H_{13}F_3O_2$: 246.0867; found: 246.0861.

*2-(4-Cyanophenoxy)tetrahydropyran (***4i***)*

The product was purified by recrystallization from ether – petroleum ether 30–60°C (95% yield): mp 69.5–70°C; ir ($CHCl_3$) ν_{max}: 2240, 1605, 1580, 1505, 1245, 1195 cm^{-1}; ^{1}Hmr ($CDCl_3$) δ: 1.3–2.0 (3 × CH_2), 3.3–3.7 (m, CH_2O), 5.2 (m, H-2), 6.7 (m, 2H), 7.1 (m, 2H) ppm; ^{13}Cmr ($CDCl_3$) δ: 18.4 (C-4), 25.0 (C-5), 30.0 (C-3), 62.1 (C-6), 96.3 (C-2), 104.7 (C-4′), 117.0 (C-2′), 119.2 (C-1′), 133.8 (C-3′), 160.5 (C≡N) ppm; m/e: 203 (M^+). Exact Mass calcd. for $C_{12}H_{13}NO_2$: 203.0946; found: 203.0950.

*2-(4-Nitrophenoxy)tetrahydropyran (***4j***)*

The product was purified by recrystallization from ether—hexane (31% yield): mp 59.5–60.5°C; ir ($CHCl_3$) ν_{max}: 1615, 1600, 1515, 1350, 1205 cm^{-1}; ^{1}Hmr ($CDCl_3$) δ: 1.5–2.2 (3 × CH_2), 3.7–4.1 (m, CH_2O), 5.7 (m, H-2), 7.3 (m, 2H), 8.3 (m, 2H) ppm; ^{13}Cmr ($CDCl_3$) δ: 18.3 (C-4), 24.9 (C-5), 29.9 (C-3), 62.1 (C-6), 96.4 (C-2), 116.2 (C-2′), 125.7 (C-3′), 141.9 (C-4′), 162.2 (C-1′) ppm; m/e: 233 (M^+).

Acknowledgements

We are grateful to the Natural Sciences and Engineering Research Council of Canada and to the "Fonds pour la Formation de Chercheurs et l'Aide à la Recherche du Québec" for their financial support. We acknowledge helpful discussions with Professor Deslongchamps, Université de Sherbrooke. We thank Mrs. S. Thériault for typing the manuscript.

1. R. U. Lemieux and N. J. Chü. Abstracts of Papers. Am. Chem. Soc. **133**, 31N (1958).
2. R. U. Lemieux. Pure Appl. Chem. **25**, 527 (1971).
3. N. S. Zefirov and N. M. Shekhtman. Russ. Chem. Rev. **40**, 315 (1971).
4. E. L. Eliel. Agnew. Chem. Int. Ed. Engl. **11**, 739 (1972).
5. S. Wolfe. Acc. Chem. Res. **5**, 102 (1972).
6. W. Szarek and D. Horton. Anomeric effect. Origin and consequences. ACS Symposium Series 87. American Chemical Society, Washington, D.C. 1979.
7. A. J. Kirby. The anomeric effect and related stereoelectronic effects at oxygen. *In* Reactivity and structure concepts in organic chemistry. Vol. 15. Springer Verlag, New York. 1983.
8. P. Deslongchamps. Stereoelectronic effects in organic chemistry. Pergamon Press, New York. 1983. pp. 5–20.
9. R. U. Lemieux, A. A. Pavia, J. C. Martin, and K. A. Watanabe. Can. J. Chem. **47**, 4427 (1969).
10. P. Deslongchamps, D. D. Rowan, N. Pothier, G. Sauvé, and J. K. Saunders. Can. J. Chem. **59**, 1105 (1981); N. Pothier, D. D. Rowan, P. Deslongchamps, and J. K. Saunders. Can. J. Chem. **59**, 1132 (1981).
11. J.-P. Praly and R. U. Lemieux. Can. J. Chem. **65**, 213 (1987), and references therein.
12. J. T. Edward. Chem. Ind. (London), 1102 (1955).
13. M. A. Kabayama and D. Patterson. Can. J. Chem. **36**, 563 (1958).
14. E. L. Eliel. Kem. Tidskr. **81**, NR/6-7, 22 (1969).
15. C. Altona. Ph.D Thesis, University of Leiden. 1964.
16. C. Romers, C. Altona, H. R. Buys, E. Havinga. Top. Stereochem. **4**, 39 (1969).
17. L. Radom, N. J. Hehre, and J. A. Pople. J. Am. Chem. Soc. **94**, 2371 (1972).
18. S. David, O. Eisenstein, N. J. Hehre, L. Salem, and R. Hoffman. J. Am. Chem. Soc. **95**, 3806 (1973).
19. G. Baddeley. Tetrahedron Lett. 1645 (1973).
20. S. Wolfe, M.-H. Wangbo, and D. Mitchell. Carbohydr. Res. **69**, 1 (1979), and references therein.
21. R. U. Lemieux, S. Koto, and D. Voisin. *In* Anomeric effect. Origin and consequences. *Edited by* W. Szarek and D. Horton. ACS Symposium Series 87. American Chemical Society, Washington, D.C. 1979. p. 17.
22. G. A. Jeffrey. *In* Anomeric effect. Origin and consequences. *Edited by* W. Szarek and D. Horton. ACS Symposium Series 87. American Chemical Society, Washington, D.C. 1979. p. 50.
23. P. G. Jones, O. Kennard, S. Chandrasekhar, and A. J. Kirby. Acta Crystallogr. Sect. B: Struct. Crystallogr. Cryst. Chem. **B34**, 2947 (1978); P. G. Jones, O. Kennard, S. Chandrasekhar, and A. J. Kirby. Acta Crystallogr. Sect. B: Struct. Crystallogr. Cryst. Chem. **B35**, 239 (1979); P. G. Jones, O. Kennard, A. J. Kirby, and R. J. Martin. Acta Crystallogr. Sect. B: Struct. Crystallogr. Cryst. Chem. **B35**, 241 (1979).
24. G. A. Jeffrey and J. H. Yates. J. Am. Chem. Soc. **101**, 820 (1979).
25. I. Tvaroska and T. Bleha. Can. J. Chem. **57**, 424 (1979).
26. B. M. Pinto, H. B. Schlegel, and S. Wolfe. Can. J. Chem. **65**, 1658 (1987).
27. G. O. Pierson and O. A. Runquist. J. Org. Chem. **33**, 2572 (1968).
28. J. Hine. Physical organic chemistry. McGraw–Hill, New York. 1962. pp. 87–91.
29. C. G. Swain and E. C. Lupton, Jr. J. Am. Chem. Soc. **90**, 4328 (1968).
30. L. P. Hammett. Physical organic chemistry. 2nd ed. McGraw–Hill, Mexico. 1970. pp. 355–362.
31. C. D. Johnston. The Hammett equation. The University Press, Cambridge. 1973. p. 29.
32. A. J. Kirby. The anomeric effect and related stereoelectronic effects at oxygen. *In* Reaction and structure concepts in organic chemistry. Vol. 15. Springer Verlag, New York. 1983. p. 90.
33. C. B. Anderson and D. T. Sepp. Tetrahedron, **24**, 1707 (1968).
34. E. L. Eliel and C. A. Giza. J. Org. Chem. **33**, 3754 (1968).
35. R. U. Lemieux, A. A. Pavia, J. C. Martic, and K. A. Watanbe. Can. J. Chem. **47**, 4427 (1969).
36. A. J. de Hoog, R. H. Buys, C. Altona, and E. Havinga. Tetrahedron, **25**, 3365 (1969).
37. M. A. Pericàs, A. Riera, and E. Giralt. Tetrahedron, **41**, 3785 (1985).
38. B. M. Pinto, B. D. Johnson, J. Sandoval-Ramirez, and R. D. Sharma. J. Org. Chem. **53**, 3766 (1988).
39. D. Cantacuzene and M. Tordeux. Can. J. Chem. **54**, 2759 (1976).
40. M. T. Phan Viet. Ph.D. Thesis. Université de Sherbrooke. 1979. pp. 70–72.
41. Y. Aubin and M. St-Jacques. Can. J. Chem. **68**, 543 (1990).
42. A. J. Kirby. The anomeric effect and related stereoelectronic effects at oxygen. *In* Reactivity and structure concepts in organic chemistry. Vol. 15. Springer Verlag, New York. 1983. p. 71.
43. A. Ouedraogo, M. T. Phan Viet, J. K. Saunders, and J. Lessard. Can. J. Chem. **65**, 1761 (1987).
44. H. Shanan-Atidi and K. H. Bar-Eli. J. Phys. Chem. **74**, 961 (1970).
45. F. A. Bovey, E. W. Anderson, F. P. Hood, and R. L. Kornegay. J. Chem. Phys. **40**, 3099 (1964).

Can. J. Chem. Downloaded from www.nrcresearchpress.com by 198.100.157.202 on 09/07/12
For personal use only.

46. G. GATTI, A. L. SEGRE, and C. MORANDI. J. Chem. Soc. B, 1203 (1967).
47. J. B. LAMBERT, C. E. MIXAN, and D. H. JOHNSON. J. Am. Chem. Soc. **95**, 4634 (1973).
48. L. DESCHÊNES. M.Sc. Dissertation, Université de Sherbrooke. 1984.
49. F. A. L. ANET, M. AHMAD, and L. D. HALL. Proc. Chem. Soc. 145 (1964), and references therein.
50. J. T. GERIG and R. A. RIMERMAN. J. Am. Chem. Soc. **92**, 1219 (1970).
51. J. LESSARD, P. V. MINH TAN, R. MARTINO, and J. K. SAUNDERS. Can. J. Chem. **55**, 1015 (1977).
52. A. J. KIRBY. The anomeric effect and related stereoelectronic effects. *In* Reactivity and structure concepts in organic chemistry. Vol. 15. Springer Verlag, New York. 1983. pp. 20–22.
53. G. F. WOODS and D. N. KRAMER. J. Am. Chem. Soc. **69**, 2246 (1947).

Can. J. Chem. Downloaded from www.nrcresearchpress.com by 198.100.157.202 on 09/07/12
For personal use only.

Étude thermodynamique des trois isomères du dihydroxybenzène

R. SABBAH[1] ET E. N. L. E. BULUKU

Centre de thermodynamique et de microcalorimétrie du Centre national de la recherche scientifique, 26, rue du 141è RIA, 13003-Marseille, France

Reçu le 2 octobre 1990

R. SABBAH et E. N. L. E. BULUKU. Can. J. Chem. **69**, 481 (1991).

Le présent travail porte sur l'étude thermodynamique des trois isomères du dihydroxybenzène. Cette étude a permis la détermination des enthalpies de combustion, de sublimation, de fusion et de transition des 1,2-, 1,3- et 1,4-dihydroxybenzènes. Les techniques utilisées ont été la calorimétrie de combustion de faibles quantités de substances, la calorimétrie de changement d'état (sublimation), l'analyse thermique différentielle et la mesure des capacités calorifiques. L'ensemble des résultats expérimentaux a permis de : mettre en évidence l'existence d'une liaison hydrogène intramoléculaire dans l'isomère *ortho*; préciser la stabilité relative des trois molécules de dihydrobenzènes; et déterminer : à partir de l'enthalpie de sublimation, une valeur énergétique pour les liaisons intermoléculaires; l'énergie de conjugaison expérimentale et de la comparer à la valeur théorique; l'enthalpie d'atomisation à partir de laquelle a été calculée l'enthalpie de la liaison intramoléculaire C_b—OH.

Mots clés : thermodynamique, calorimétrie, analyse thermique différentielle, 1,2-dihydroxybenzène ou catéchol; 1,3-dihydroxybenzène ou résorcinol; 1,4-dihydroxybenzène ou hydroquinone ou quinol; enthalpies de combustion, de sublimation, de fusion, de transition; énergie de conjugaison; enthalpies d'atomisation, de liaisons inter- et intra-moléculaires; température du point triple et de transition.

R. SABBAH and E. N. L. E. BULUKU. Can. J. Chem. **69**, 481 (1991).

The present work is concerned with a thermodynamic study of the three isomers of dihydroxybenzene. By combustion calorimetry of small amounts of substance, sublimation calorimetry, differential thermal analysis, and heat capacity measurements, it was possible to determine the enthalpies of formation of 1,2-, 1,3-, and 1,4-dihydroxybenzene in the condensed and gaseous phases, their enthalpies of fusion and transition, and the temperature of their triple point and transition. The experimental results are used to discuss the relative stability and determine the conjugation energy of the three compounds. The values are in good agreement with the theoretical values obtained from a quantum chemical calculation. The enthalpies of atomization enabled us to determine an energy value for the intramolecular C_b—OH bond in dihydroxybenzenes and to correlate it with previous results obtained from a study of alkane-diols. The enthalpies of sublimation were discussed. An intramolecular hydrogen bond was displayed in the *ortho* isomer. Intermolecular hydrogen bonds associated with van der Waals interactions exist in dihydroxybenzenes. Their energy contributions were determined.

Key words: thermodynamics, calorimetry, differential thermal analysis, 1,2-benzenediol or 1,2-dihydroxybenzene or catechol; 1,3-benzenediol or 1,3-dihydroxybenzene or resorcinol; 1,4-benzenediol or 1,4-dihydroxybenzene or hydroquinone or quinol; enthalpies of combustion, of sublimation, of fusion, of transition, energy of conjugation, enthalpies of atomization, of inter- and intramolecular bonds; triple point and transition temperatures.

Can. J. Chem. Downloaded from www.nrcresearchpress.com by 195.138.81.100 on 09/07/12
For personal use only.

I. Introduction

Les travaux réalisés jusqu'ici sur l'étude des propriétés thermodynamiques des dihydroxybenzènes (en abrégé DHB) tant en phase condensée que gazeuse sont peu nombreux (1–6). La comparaison précise et rationnelle du comportement des isomères de position, caractérisés par la similitude de leurs propriétés, nécessite une étude globale et homogène.

Soucieux de mettre en évidence et d'interpréter le lien qui existe entre les grandeurs énergétiques et la structure des DHB et de mieux cerner l'importance relative des forces de cohésion cristalline dans ces composés, nous avons été amenés à étudier les trois isomères du DHB. Ces trois diols aromatiques sont présents dans le règne végétal et les produits issus de la pyrolyse du charbon. Compte tenu de leurs propriétés et de leurs applications directes et indirectes (7, 8), la détermination de leurs grandeurs thermodynamiques est souhaitable afin d'élucider certains problèmes liés à leur structure et à leur utilisation courante.

II. Partie expérimentale

II.1. Produits

Les trois molécules de DHB utilisées dans ce mémoire sont des produits Aldrich, de degré de pureté supérieur ou égal à 99%. La pureté du DHB-1,2 (99,92 mol%) et du DHB-1,3 (99,98 mol%), déterminée par ATD, a été jugée satisfaisante. Seul le DHB-1,4, dont l'échantillon commercial a pour degré de pureté 99,79 mol%, a été recristallisé dans l'eau déminéralisée puis sublimé sous une pression résiduelle de 10^{-2} Torr (1 Torr = 133,322 Pa) à 363 K. La pureté du produit ainsi traité est de 99,96 mol%.

La plupart des substances étant sensibles à la lumière, nous avons pris la précaution de les manipuler à l'abri de celle-ci.

II.2. Appareillage, technique et mode opératoire

Pour réaliser l'étude consignée dans ce mémoire, nous avons utilisé comme techniques : la calorimétrie de combustion de faibles quantités de substances, la calorimétrie de sublimation, l'analyse thermique différentielle et la mesure de capacités calorifiques.

II.2.1. Calorimétrie de combustion

Les expériences réalisées par calorimétrie de combustion, l'ont été en utilisant l'appareillage décrit dans la référence 9. Précisons ici que : la microbombe est en acier inoxydable (Superimphy 625, ATGE2); son volume interne est de 42,9 mL à température ambiante; la sensibilité de la pile du calorimètre CRMT est de 62,33 $\mu V\ mW^{-1}$; celle de l'amplificateur est de 30 mV pleine échelle; l'oxygène N45, utilisé dans nos expériences, provient de l'Air Liquide; son degré de pureté est supérieur à 99,995%.

II.2.2. Calorimétrie de sublimation

Pour mesurer directement la quantité de chaleur mise en jeu par la sublimation de nos substances, nous avons utilisé un calorimètre Tian–Calvet associé à une cellule d'effusion de Knudsen. L'appareillage et le mode opératoire ont été décrits dans la référence 10. Toutefois, il y a lieu de préciser ici que le signal issu du calorimètre est amplifié par un nanovoltmètre Keithley modèle 147 (sensibilité utilisée : 30 μV pleine

1. Auteur à qui adresser toute correspondance.

Can. J. Chem. Downloaded from www.nrcresearchpress.com by 195.138.81.100 on 09/07/12
For personal use only.

TABLEAU 1. Degré de pureté, température des points triple et de transition, enthalpies de fusion et de transition des DHB

Paramètre	DHB-1,2	DHB-1,3	DHB-1,4
Pureté (mol%)	99,929±0,002	99,985±0,002	99,965±0,007
$T_{\text{point triple}}$(K)[a]	377,80±0,03	383,54±0,02	445,98±0,03
$\Delta_{\text{fus}}H_{\text{m}}$(kJ mol^{-1})	15,00±0,34	15,25±0,21	21,09±0,40
$T_{\text{trs}}(\alpha \rightarrow \beta)$(K)[a]		366,8±1,4	
$\Delta_{\text{trs}}H_{\text{m}}(\alpha \rightarrow \beta)$(kJ mol^{-1})		0,72±0,06	

[a]Définies par rapport à l'EIPT-68.

TABLEAU 2. Grandeurs physiques à 298,15 K des substances étudiées

Substance	Formule brute	M[a] (g mol^{-1})	ρ (g cm^{-3})	$-(\partial U/\partial P)_T$ (J g^{-1} atm^{-1})[b]
Acide benzoïque	$C_7H_6O_2$	122,1234	1,320 (12)	0,01163 (12)
Coton	$CH_{1.833}O_{0.828}$	27,1061	1,5 (12)	0,029 (12)
DHB-1,2	$C_6H_6O_2$	110,1124	1,149 (13)	(0,013)
DHB-1,3	$C_6H_6O_2$	110,1124	1,272 (13)	(0,013)
DHB-1,4	$C_6H_6O_2$	110,1124	1,328 (13)	(0,013)

[a]Les masses molaires ont été calculées à partir du tableau des masses atomiques de 1987 (14).
[b]1 atm = 101,325 kPa.
Les valeurs placées entre parenthèses ont été estimées.

échelle) puis digitalisé à l'aide d'un voltmètre numérique AOIP modèle MN 5121 ou Keithley modèle 175. L'acquisition et le traitement des données ont été réalisés à l'aide d'un ordinateur Zénith modèle 159 ou Commodore modèle 4032.

Si, pour la molécule de DHB-1,2, nous n'avons eu aucune difficulté à la sublimer à 298,15 K en utilisant un calorimètre dont la sensibilité des piles est de 24,62 μV mW^{-1} et un trou d'effusion de diamètre égal à 1,5 mm, il n'en a pas été de même pour les deux autres molécules.

La faible pression de vapeur saturante du DHB-1,3 et du DHB-1,4 nous a obligés à travailler à 334,6 K. À cette température, la sensibilité des piles du calorimètre est de 17,04 μV mW^{-1} et le diamètre du trou d'effusion utilisé est de 1,5 mm.

II.2.3. Analyse thermique différentielle

Cette technique nous a permis de déterminer le degré de pureté de nos substances, la température de leurs points triple et de transition et de mesurer leur enthalpie de fusion (tableau 1). L'appareillage et le mode opératoire ont été décrits dans la référence 11.

III. Résultats

Nous avons consigné dans le tableau 2 les grandeurs physiques à 298,15 K des substances utilisées qui interviennent dans les calculs menant aux résultats expérimentaux.

III.1. Calorimétrie de combustion

En calorimétrie de combustion, l'équivalent énergétique du calorimètre (U_{cal}) a été obtenu à partir de huit combustions d'acide benzoïque, échantillon 39i du N.B.S., pour lequel $\Delta_c u^0$(s, 298,15 K) = (−26414 ± 3) J g^{-1}. Dans ces expériences, nous avons utilisé environ 5 mg d'acide et 0,2 mg de coton (dont l'énergie de combustion, préalablement déterminée au laboratoire, a pour valeur : $\Delta_c u^0$(s, 298,15 K) = (−16399 ± 23) J g^{-1} (15). Nous trouvons pour U_{cal}(298,15 K) la valeur (16,040 ± 0,006) J V^{-1} s^{-1}.

Les résultats expérimentaux obtenus par calorimétrie de combustion sont consignés dans les tableaux 3–5.

III.2. Calorimétrie de sublimation

En calorimétrie de sublimation, l'étalonnage de notre système calorimétrique a été réalisé par effet Joule avant et après les expériences.

À cause de la faible pression de vapeur saturante des substances étudiées, nous avons admis l'identité $\Delta_{\text{sub}}H_{\text{m}}(T\text{K}) = \Delta_{\text{sub}}H^0_{\text{m}}(T\text{K})$. Par ailleurs, dans le cas du DHB-1,3 et du DHB-1,4, pour calculer $\Delta_{\text{sub}}H^0_{\text{m}}$(298,15 K) à partir de $\Delta_{\text{sub}}H^0_{\text{m}}$(334,6 K), nous avons utilisé la relation suivante :

$$\Delta_{\text{sub}}H^0_{\text{m}}(298{,}15\text{ K}) = \Delta_{\text{sub}}H^0_{\text{m}}(334{,}6\text{ K}) + \int_{334{,}6\text{ K}}^{298{,}15\text{ K}} (C^0_{\text{p,m}}(\text{g}) - C^0_{\text{p,m}}(\text{s}))\,\text{d}T$$

après nous être assurés par ATD que la substance ne présente aucun changement de phase entre 298,15 et 334,6 K. La valeur de $\int_{298{,}15\text{ K}}^{334{,}6\text{ K}} C^0_{\text{p,m}}(\text{s})\text{d}T$ a été obtenue par la méthode de chute en utilisant un calorimètre Tian–Calvet et un four maintenus respectivement à 298,15 et 334,6 K. Quant à l'intégrale $\int_{298{,}15\text{ K}}^{334{,}6\text{ K}} C^0_{\text{p,m}}(\text{g})\text{d}T$, elle a été déterminée à partir d'une méthode incrémentale en utilisant les données des capacités calorifiques à l'état gazeux de la littérature pour les molécules de benzène et d'hydroxybenzène (16).

Nous avons consigné dans le tableau 6 les résultats expérimentaux obtenus par calorimétrie de sublimation.

Signalons qu'aucune valeur aussi bien pour $\Delta_c H^0_{\text{m}}$(s, 298,15 K) que pour $\Delta_{\text{sub}}H^0_{\text{m}}$(298,15 K) pour le DHB-1,2 n'a été trouvée dans la littérature. Nos valeurs expérimentales ne peuvent donc faire l'objet d'aucune comparaison.

En ce qui concerne le DHB-1,3, nous enregistrons un écart respectivement de 0,2% et 9,4% entre nos valeurs de $\Delta_c H^0_{\text{m}}$(s, 298,15 K) et $\Delta_{\text{sub}}H^0_{\text{m}}$(298,15 K) et celles de Desai *et al.* (17). Pour ce qui est de la sublimation, ces auteurs ne précisent pas dans leur publication la technique de mesure utilisée.

En ce qui concerne le DHB-1,4, Pedley *et al.* (1) proposent 99,2 ± 1,7 kJ mol^{-1} comme valeur de $\Delta_{\text{sub}}H^0_{\text{m}}$(298,15 K). Celle-ci a été obtenue par Magnus en 1956 (18) par mesures de pression de vapeur en fonction de la température. Elle diffère de la nôtre de 5,4%. D'autres chercheurs comme de Kruif *et al.* (4) ont déterminé l'enthalpie de sublimation de ce même composé et ont trouvé la valeur de 103,9 ± 1 kJ mol^{-1} toujours à partir de mesures de pression de vapeur en fonction de la

TABLEAU 3. Combustion du DHB-1,2 à 298,15 K

m(subst) (mg)	m(coton) (mg)	S (Vs)	$-\Delta U$ (J)	$-W_1$ (J)	W_2 (J)	$-\Delta_c U_m^0$ (s, 298,15 K) (kJ mol^{-1})
5,6975	0,1419	9,373959	150,360	2,327	0,165	2857,77
5,2314	0,1965	8,675853	139,162	3,223	0,152	2858,10
6,9593	0,2675	11,535756	185,036	4,387	0,204	2855,05
5,2349	0,2563	8,732763	140,075	4,204	0,153	2854,74
6,9775	0,2094	11,492655	184,345	3,434	0,203	2851,74
6,2451	0,2108	10,326705	165,642	3,457	0,182	2856,41
6,2013	0,1573	10,177470	163,249	2,580	0,180	2849,70
6,5952	0,1901	10,874073	174,422	3,118	0,192	2856,87

$\Delta_c U_m^0$ (s, 298,15 K) = $-(2855{,}1 \pm 1{,}1)$ kJ mol^{-1}
$\Delta_c H_m^0$ (s, 298,15 K) = $-(2856{,}3 \pm 1{,}1)$ kJ mol^{-1}
Ces résultats correspondent à la réaction :
$C_6H_6O_2$ (s) + 13/2 O_2 (g) → 6CO_2 (g) + 3H_2O(l)
$\Delta_f H_m^0$ (s, 298,15 K) = $-(362{,}3 \pm 1{,}1)$ kJ mol^{-1}

S = aire des thermogrammes; ΔU = variation de l'énergie interne de la bombe et de son contenu; W_1 = énergie de combustion du coton; W_2 = corrections pour passer à l'état standard.

TABLEAU 4. Combustion du DHB-1,3 à 298,15 K

m(subst) (mg)	m(coton) (mg)	S (Vs)	$-\Delta U$ (J)	$-W_1$ (J)	W_2 (J)	$-\Delta_c U_m^0$ (s, 298,15 K) (kJ mol^{-1})
6,0892	0,2256	10,055757	161,296	3,700	0,178	2846,63
6,3949	0,1810	10,519191	168,730	2,969	0,186	2851,01
6,8682	0,1800	11,257980	180,580	2,952	0,200	2844,57
5,7631	0,2272	9,543072	153,073	3,726	0,169	2850,26
6,8994	0,1841	11,308686	181,394	3,020	0,201	2843,59
6,4726	0,1588	10,595259	169,950	2,605	0,188	2843,70
5,7206	0,2258	9,462438	151,779	3,703	0,167	2847,01

$\Delta_c U_m^0$ (s, 298,15 K) = $-(2846{,}7 \pm 1{,}1)$ kJ mol^{-1}
$\Delta_c H_m^0$ (s, 298,15 K) = $-(2847{,}9 \pm 1{,}1)$ kJ mol^{-1}
Ces résultats correspondent à la réaction :
$C_6H_6O_2$ (s) + 13/2 O_2 (g) → 6CO_2 (g) + 3H_2O(l)
$\Delta_f H_m^0$ (s, 298,15 K) = $-(370{,}7 \pm 1{,}1)$ kJ mol^{-1}

S = aire des thermogrammes; ΔU = variation de l'énergie interne de la bombe et de son contenu; W_1 = énergie de combustion du coton; W_2 = corrections pour passer à l'état standard.

TABLEAU 5. Combustion de DHB-1,4 à 298,15 K

m(subst) (mg)	m(coton) (mg)	S (Vs)	$-\Delta U$ (J)	$-W_1$ (J)	W_2 (J)	$-\Delta_c U_m^0$ (s, 298,15 K) (kJ mol^{-1})
6,5619	0,1518	10,750938	172,447	2,490	0,190	2848,79
6,4255	0,1757	10,537584	169,025	2,882	0,187	2843,96
6,3909	0,1383	10,452186	167,655	2,268	0,185	2846,35
6,9656	0,1678	11,401593	182,884	2,752	0,203	2844,33
6,2185	0,2237	10,263777	164,633	3,669	0,182	2847,01
6,2745	0,2478	10,405191	166,901	4,064	0,184	2854,43
5,2398	0,1966	8,659929	138,907	3,225	0,153	2848,11
6,3303	0,1118	10,305270	165,299	1,834	0,183	2840,21
6,2178	0,1451	10,166751	163,077	2,380	0,180	2842,63
6,5646	0,1740	10,768959	172,736	2,854	0,191	2846,35

$\Delta_c U_m^0$ (s, 298,15 K) = $-(2846{,}2 \pm 1{,}2)$ kJ mol^{-1}
$\Delta_c H_m^0$ (s, 298,15 K) = $-(2847{,}5 \pm 1{,}2)$ kJ mol^{-1}
Ces résultats correspondent à la réaction :
$C_6H_6O_2$ (s) + 13/2 O_2 (g) → 6CO_2 (g) + 3H_2O(l)
$\Delta_f H_m^0$ (s, 298,15 K) = $-(371{,}1 \pm 1{,}3)$ kJ mol^{-1}

S = aire des thermogrammes; ΔU = variation de l'énergie interne de la bombe et de son contenu; W_1 = énergie de combustion du coton; W_2 = corrections pour passer à l'état standard.

Can. J. Chem. Downloaded from www.nrcresearchpress.com by 195.138.81.100 on 09/07/12
For personal use only.

TABLEAU 6. Sublimation des DHB

Substance	T (K)	m (mg)	$\Delta_{sub}H^0_m(T,K)$ (kJ mol^{-1})	$\Delta_{sub}H^0_m(T,K)$ (kJ mol^{-1})	$\Delta_{sub}H^0_m(298,15\ K)$ (kJ mol^{-1})	P (Torr)[a]
DHB-1,2	298,15	15,4191	88,46			
		10,1954	85,69			
		10,6643	87,36			
		10,8020	87,60			
		10,7632	87,74	87,50±0,29	87,50±0,29	$6{,}5\cdot10^{-4}$
		10,6932	87,57			
		10,5882	86,69			
		10,4585	88,48			
		10,6405	87,94			
DHB-1,3	334,6	10,2795	84,73			
		10,7245	84,05			
		10,8125	86,21	85,30±0,52	86,00±0,52	$6{,}5\cdot10^{-3}$
		10,5610	83,77			
		10,7624	86,38			
		10,0871	86,67			
DHB-1,4	334,6	10,4842	95,17			
		10,3790	91,49			
		10,2751	94,45			
		10,6228	94,86	93,71±0,52	94,13±0,53	$6\cdot10^{-4}$
		10,2747	93,09			
		10,5778	94,35			
		10,2813	92,53			

[a]1 Torr = 133,322 Pa.

TABLEAU 7. Grandeurs thermodynamiques à 298,15 K des DHB

Substance	$-\Delta_cH^0_m$ (s, 298,15 K) (kJ mol^{-1})	$-\Delta_fH^0_m$ (s, 298,15 K) (kJ mol^{-1})	$\Delta_{sub}H^0_m$ (298,15 K) (kJ mol^{-1})	$-\Delta_fH^0_m$ (g, 298,15 K) (kJ mol^{-1})
DHB-1,2	2856,3±1,1	362,3±1,1	87,50±0,29	274,8±1,2
DHB-1,3	2847,9±1,1	370,7±1,1	86,00±0,52	284,7±1,2
DHB-1,4	2847,5±1,2	371,1±1,3	94,13±0,53	277,0±1,4

température dans l'intervalle $337 \leq T/K \leq 351$. Les différentes valeurs de l'enthalpie de combustion du DHB-1,4 proposées par Pedley *et al.* (1) sont comprises entre 2825 et 2856 kJ mol^{-1}. À ces valeurs, il faut ajouter celles qui sont consignées par Pilcher et Sutton dans leur mémoire (19) et qui s'échelonnent de 2804–2870 kJ mol^{-1}. Notre valeur (2847,5 ± 1,2 kJ mol^{-1}) est située dans cet intervalle.

Rappelons que les méthodes indirectes de détermination de l'enthalpie de sublimation (ou vaporisation) d'une substance, qui consistent à mesurer des pressions de vapeur en fonction de la température en vue d'appliquer l'équation de Clausius–Clapeyron à l'équilibre solide (ou liquide)–vapeur, sont toujours moins précises que les méthodes calorimétriques directes et ce d'autant plus que la pression de vapeur saturante des composés étudiés est faible.

III.3. Enthalpie de formation des DHB à l'état gazeux

La comparaison des valeurs de $\Delta_fH^0_m$(g, 298,15 K) (tableau 7) permet de constater que la stabilité des trois isomères décroît du *méta*, au *para* et à l'*ortho*. Pareille observation a été faite au laboratoire lors de l'étude des acides aminobenzoïques (20). Le traité de chimie organique (8) nous dit que, du point de vue de la réactivité, l'isomère *méta* serait assez stable car les deux OH s'influencent peu.

III.4. Pression de vapeur saturante des DHB

Comme nous l'avons indiqué dans les références 21 et 22, il nous est possible, à partir de nos essais, d'évaluer la pression de vapeur saturante des substances étudiées en utilisant la relation:

$$P \approx \Delta P = (dm/dt)(1/aF)\,(2\pi RT/M)^{1/2}$$

dans laquelle $\Delta P(T)$ est la différence de pression de vapeur de part et d'autre du trou d'effusion; $P(T)$, la pression mesurée par effusion à la température T; dm/dt, la masse de substance effusée par unité de temps; R, la constance des gaz parfaits; M, la masse molaire de la substance; F, le facteur de Clausing et a, l'aire de l'orifice d'effusion. Les pressions de vapeur saturante à 298,15 K pour le DHB-1,2 et à 334,6 K pour les deux autres isomères sont consignées dans le tableau 6. Le seul résultat qui peut être comparé aux données de la littérature, concerne la pression de vapeur saturante du DHB-1,4. La valeur que nous trouvons à 334,6 K (6×10^{-4} Torr) est compatible avec celle de de Kruif *et al.* (4) ($7{,}5 \times 10^{-4}$ Torr à 330 K).

III.5. Analyse thermique différentielle des DHB

Les principaux résultats obtenus sont consignés dans le tableau 1. Des trois molécules qui nous intéressent, seul le DHB-1,3 présente une transition irréversible entre 298,15 K et la température de fusion. Si l'on se réfère aux tableaux 8 et 9, nous remarquons une parfaite cohérence entre nos valeurs et celles de la littérature pour les températures des points triple et de transition. Il n'en est pas de même en ce qui concerne l'enthalpie de fusion et de transition.

Can. J. Chem. Downloaded from www.nrcresearchpress.com by 195.138.81.100 on 09/07/12
For personal use only.

Can. J. Chem. Downloaded from www.nrcresearchpress.com by 195.138.81.100 on 09/07/12
For personal use only.

TABLEAU 8. Comparaison de nos résultats (T_{pt} et T_{trs}) avec ceux de la littérature

Substance	Nos valeurs	Littérature
	T_{pt}(K)	
DHB-1,2	377,80±0,03	376,85–378,15 (2, 3, 23–26)
DHB-1,3	383,54±0,02	382,55–384,15 (2, 3, 5, 24, 26)
DHB-1,4	445,98±0,03	444,95–447,15 (4, 26)
	T_{trs}(K)	
DHB-1,3	366,8±1,4	366,75–369,15 (3, 5)

TABLEAU 9. Comparaison de nos résultats ($\Delta_{fus}H_m$ et $\Delta_{trs}H_m$) avec ceux de la littérature

Substance	Nos valeurs	Littérature
	$\Delta_{fus}H_m$(kJ mol^{-1})	
DHB-1,2	15,00±0,34	20,50–22,76 (2, 3, 24–27)
DHB-1,3	15,25±0,21	18,90–22,07 (2, 3, 24, 26)
DHB-1,4	21,09±0,40	26,50–27,32 (2, 3, 26)
	$\Delta_{trs}H_m$(kJ mol^{-1})	
DHB-1,3	0,72±0,06	0,92–1,37 (3, 5, 6)

Nous avons essayé d'expliquer la raison pour laquelle nos valeurs de $\Delta_{fus}H_m$ et de $\Delta_{trs}H_m$ sont inférieures à celles de la littérature. Parmi les facteurs éventuellement responsables de la différence observée, nous pouvons citer :

1. La vitesse de chauffage utilisée par nos prédécesseurs; elle est généralement plus élevée que la nôtre (3, 5, 25).
2. La façon d'étalonner l'analyseur thermique. Certains auteurs (3) utilisent l'effet Joule qui n'est pas, à notre avis, le meilleur moyen pour réaliser ce travail. En effet, afin de minimiser les erreurs, il est conseillé de réaliser l'étalonnage de l'appareil dans les mêmes conditions que les mesures en utilisant des substances d'intercomparaison (28).
3. Certains résultats sont fort anciens (26).

III.6. Incertitude expérimentale

L'incertitude qui accompagne les résultats expérimentaux représente l'écart moyen σ_m et tient compte des erreurs sur les termes et facteurs de l'expression conduisant au calcul de la grandeur thermodynamique.

IV. Discussion

L'ensemble des résultats expérimentaux consignés dans le tableau 7 permet la détermination de certaines grandeurs énergétiques liées à la structure des molécules étudiées et à leur réseau cristallin.

IV.1. Energie de conjugaison

Les trois molécules de DHB étudiées dans ce mémoire sont conjuguées. En conséquence, nous avons essayé de déterminer d'abord leur énergie de conjugaison expérimentale puis avons comparé celle-ci à la valeur théorique obtenue en utilisant la méthode de calcul décrite dans la référence 29.

L'énergie de conjugaison est, par définition, égale à la différence entre l'énergie réelle de la molécule et l'énergie qu'elle aurait si les divers systèmes insaturés qu'elle comporte étaient indépendants. Sur le plan pratique, pour la déterminer, nous utilisons les enthalpies standard de combustion à l'état gazeux

TABLEAU 10. Energie de conjugaison des DHB

Substance	$E_{conj,exp}$(kJ mol^{-1})	$E_{conj,théor}$(kJ mol^{-1})
DHB-1,2	177,5	175,0
DHB-1,3	184,4	174,3
DHB-1,4	176,7	174,9

de la molécule réelle et de la molécule fictive, non conjuguée. La première de ces grandeurs s'obtient expérimentalement tandis que la seconde nécessite le recours aux systématiques. En ce qui nous concerne, nous avons utilisé celle de Klages, consignée dans la référence 30. Quant au calcul de l'énergie de conjugaison théorique, nous avons utilisé la méthode décrite dans la référence 29 en utilisant le jeu de paramètres suivant :

$$\alpha_0 = \alpha + 2{,}500\ \beta_0 \qquad \alpha_{c\text{-}(0)} = \alpha$$

$$\beta_{c-0} = 0{,}750\ \beta_0$$

β_0 est l'intégrale de recouvrement dans la molécule de benzène et a, pour valeur absolue, 131,7 kJ mol^{-1}. Les calculs effectués nous ont permis d'obtenir les résultats consignés dans le tableau 10.

Comme nous pouvons le constater, il existe un accord satisfaisant entre les différentes valeurs expérimentales et théoriques de l'énergie de conjugaison. De ce fait, les molécules de DHB seraient planes à l'état gazeux. Signalons, au passage, que les molécules de DHB-1,2 (31), de DHB-1,3 (forme α qui nous intéresse) (32) et de DHB-1,4 (33) sont pratiquement planes à l'état solide. Notons qu'avec le même jeu de paramètres et en utilisant le même procédé de calcul, nous avons obtenu un parfait accord entre les valeurs expérimentale et théorique de l'énergie de conjugaison de l'hydroxybenzène. $E_{conj,exp}$ = 163,1 kJ mol^{-1} et $E_{conj,théor}$ = 162 kJ mol^{-1}. La molécule d'hydroxybenzène serait plane à l'état gazeux; elle l'est pratiquement déjà à l'état condensé (34). Les données numériques nécessaires au calcul de $E_{conj,exp}$ de ce composé ont été empruntées à la référence 1.

IV.2. Enthalpie d'atomisation

Pour déterminer la somme des enthalpies des liaisons intramoléculaires d'une molécule, il est indispensable de connaître son enthalpie d'atomisation. Celle-ci, à l'état standard et à la température T, est liée à la transformation suivante : molécule (considérée comme gaz idéal, état fondamental, T) → atomes (chacun d'eux considéré comme gaz idéal, état fondamental, T).

Sur le plan expérimental, si l'on considère une molécule de formule générale : $C_aH_bO_c$, la réaction d'atomisation s'écrit :

$$C_aH_bO_c(g) \rightarrow aC(g) + bH(g) + cO(g)$$

L'enthalpie liée à cette réaction s'appelle « enthalpie d'atomisation expérimentale » et est égale à :

$$\Delta_{a,exp}H^0_m = a\Delta_fH^0_mC(g) + b\Delta_fH^0_mH(g) + c\Delta_fH^0_mO(g) - \Delta_fH^0_mC_aH_bO_c(g)$$

Aussi, à partir de l'enthalpie de formation d'une molécule à l'état gazeux et de celle des différents constituants C, H et O que l'on emprunte aux tables (35) et qui, à 298,15 K, valent respectivement : 716,67 ± 0,44, 217,997 ± 0,006 et 249,17 ± 0,10 kJ mol^{-1}, est-il possible de calculer son enthalpie d'atomisation expérimentale. Nous trouvons pour nos trois molécules de DHB les valeurs consignées dans le tableau 11.

Pour déterminer l'enthalpie de liaison $H(C_b\text{—}OH)$ dans les molécules de DHB, nous sommes partis de $\Delta_{a,exp}H^0_m$ (298,15 K). En effet, on sait que l'enthalpie d'atomisation est

Can. J. Chem. Downloaded from www.nrcresearchpress.com by 195.138.81.100 on 09/07/12
For personal use only.

TABLEAU 11. Enthalpie d'atomisation expérimentale des DHB

Substance	$\Delta_{a,exp}H^0_m$ (298,15 K)(kJ mol^{-1})
DHB-1,2	6381,1±1,8
DHB-1,3	6391,0±1,8
DHB-1,4	6383,3±1,9

égale à la somme des enthalpies des liaisons intramoléculaires, compte tenu des facteurs de stabilisation et de déstabilisation.

Pour ce qui est des liaisons C_b—C_b, nous avons utilisé le procédé de calcul consigné dans la référence 9. Celui-ci fait intervenir un paramètre lié à la géométrie de la molécule (l'indice de liaison l_{rs} entre deux atomes directement liés r et s) obtenu à partir du calcul théorique de l'énergie de conjugaison (fig. 1). La relation reliant H_{rs} à l_{rs} (9) s'écrit : H_{rs} (kJ mol^{-1}) = 246,0 l_{rs} + 342,6.

Quant à H(C_b—H) nous avons utilisé la valeur 415,88 kJ mol^{-1} (36). Ainsi, dans le cas présent, pour calculer H(C_b—OH), cela revient à retrancher de $\Delta_{a,exp}H^0_m$(298,15 K) la part énergétique des différentes liaisons C_b—C_b et C_b—H. Le calcul effectué nous a permis d'obtenir les valeurs consignées dans le tableau 12. Nous avons adopté la valeur moyenne de 848 kJ mol^{-1} pour H(C_b—OH) dans les DHB. Le même calcul, réalisé avec la molécule d'hydroxybenzène, nous a fourni les résultats suivants : $\Delta_{a,exp}H^0_m$(298,15 K) = 5953,6 ± 1,4 kJ mol^{-1} et H(C_b—OH) = 841 kJ mol^{-1}.

Ces valeurs de H(C_b—OH) nous paraissent cohérentes avec celles qui ont été précédemment trouvées au laboratoire à la suite de l'étude des alcanediols-1,2 et ω-alcanediols (37,38). En effet, dans les alcanediols la distance interatomique C—O est de 1,43 Å et H(C—OH) est comprise entre 819,5 et 827 kJ mol^{-1}. Dans l'hydroxybenzène, cette distance est de 1,39 Å (34); elle est de 1,36 Å dans le DHB-1,3 (32) et de 1,372 Å (31) dans le DHB-1,2. Les distances C_b—O sont ici plus courtes que dans les alcanediols, ce qui explique les valeurs légèrement plus fortes obtenues pour H(C_b—O).

IV.3. Existence de liaisons intermoléculaires dans les DHB

Comme on le sait, l'enthalpie de sublimation d'une substance organique est liée aux interactions intermoléculaires.

Dans le cas des DHB, ces interactions sont du type van der Waals et concernent les forces de dispersion et d'interactions dipolaires. À côté de ces interactions, il existe aussi des liaisons hydrogène intermoléculaires. Il nous a donc paru intéressant de déterminer la part énergétique des forces de van der Waals et des liaisons hydrogène intermoléculaires. Pour ce faire, nous avons appliqué un procédé de calcul qui a déjà été utilisé au laboratoire dans l'étude des acides ω-aminés (39) des alcanediols (37, 38, 40) et des chlorobenzènes (41). Il consiste, dans notre cas, à déterminer la contribution énergétique des forces de dispersion (London) en considérant qu'elle est égale à l'enthalpie de sublimation des diméthylbenzènes, composés isoélectroniques des DHB.

À une température donnée (ici 298,15 K), la différence Δ_1 des enthalpies de sublimation des DHB et des diméthylbenzènes correspondants représente la somme des énergies d'interaction dipolaire et des liaisons hydrogène intermoléculaires, tableau 13. Afin de séparer la contribution énergétique des liaisons hydrogène intermoléculaires, nous avons comparé les enthalpies de sublimation des dichlorobenzènes, qui présentent un moment dipolaire mais ne forment pas de liaisons hydrogène intermoléculaires, à celles des diméthylbenzènes correspondants.

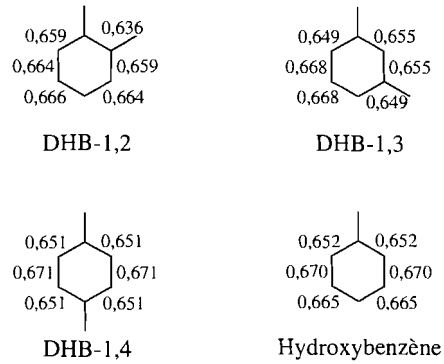


FIG. 1. Indices de liaison dans les trois isomères du DHB et dans l'hydroxybenzène.

TABLEAU 12. Enthalpie de la liaison C_b–OH dans les DHB

Substance	H(C_b–OH)(kJ mol^{-1})
DHB-1,2	845,4
DHB-1,3	850,9
DHB-1,4	846,8

TABLEAU 13. Comparaison des enthalpies de sublimation des DHB, des diméthylbenzènes et des dichlorobenzènes isoélectroniques

	$\Delta_{sub}H^0_m$ (298,15 K) (kJ mol^{-1})		
	−1,2	−1,3	−1,4
di–OH A :	87,50	86,00	94,13
di–Cl B :	64,35	62,78	65,15
di–CH_3 C :	59,82	58,26	60,18
Δ_1 = A − C :	27,68	27,74	33,95
Δ_2 = B − C :	4,53	4,52	4,97
$\Delta_1 - \Delta_2$:	23,15	23,22	28,98

La différence des enthalpies de sublimation des dichlorobenzènes et des diméthylbenzènes Δ_2 représente la contribution énergétique due aux forces d'interaction dipolaire. Comme on peut le constater, celle-ci est faible. La différence $\Delta_1 - \Delta_2$ représente la part énergétique pouvant être attribuée aux liaisons hydrogène intermoléculaires. Comme il ne peut se former que deux ponts hydrogène par molécule de DHB, en prenant la molécule de DHB-1,4, comme référence, il s'en suit que l'enthalpie d'une liaison hydrogène intermoléculaire peut être estimée à 14,5 kJ mol^{-1}.

Les données numériques utiles aux différents calculs précédents ont été empruntées aux références 13,16 et 42–45. Pour calculer $\Delta_{sub}H^0_m$(298,15 K) lorsque celle-ci n'est pas accessible expérimentalement, nous avons utilisé la relation $\Delta_{sub}H^0_m$(298,15 K) = $\Delta_{vap}H^0_m$(298,15 K) + $\Delta_{fus}H_m$(298,15 K). Pour calculer $\Delta_{fus}H_m$(298,15 K) à partir de $\Delta_{fus}H_m$(T_{fus} K), nous avons utilisé la règle de Sidgwick qui consiste à écrire que $\Delta_{fus}H_m(T\text{K}) = \Delta_{fus}H_m$(298,15 K) + $k(T - 298{,}15)$ avec k = 0,055 kJ mol^{-1} K^{-1}.

IV.4. Existence d'une liaison hydrogène intramoléculaire dans l'isomère ortho

Si nous comparons entre elles les valeurs de l'enthalpie de sublimation des isomères *ortho* et *para* de DHB, nous consta-

Can. J. Chem. Downloaded from www.nrcresearchpress.com by 195.138.81.100 on 09/07/12
For personal use only.

tons que celle de l'isomère *para* (ou DHB-1,4) est plus élevée de 6,63 kJ mol^{-1}. Cette différence doit être attribuée au fait que la molécule de DHB-1,2 présente moins de liaisons hydrogène intermoléculaires que les deux autres isomères. En effet, elle est la seule à pouvoir former une liaison hydrogène intramoléculaire. Cependant, cette chélation est moins forte que celle qui existe, par exemple, dans l'acide hydroxy-2 benzoïque. En effet, la différence que l'on note entre les valeurs de l'enthalpie de sublimation des isomères *ortho* et *para* de cet acide est égale à 20,9 kJ mol^{-1} (46). Pour connaître la raison de cette différence, il suffit de comparer entre elles les distances O—H---O dans les molécules de DHB-1,2 et d'acide hydroxy-2 benzoïque. Dans le premier cas, cette distance vaut 2,80 Å (31), dans le second 2,59 Å (47).

D'autres observations faites sur les propriétés physico-chimiques des DHB tendent à prouver l'existence de cette liaison hydrogène intramoléculaire dans la molécule de DHB-1,2.

1. A partir de nos expériences de sublimation, il s'avère que la pression de vapeur saturante du DHB-1,2 est, quelle que soit la température, toujours plus forte que celle du DHB-1,4.

2. L'isomère *para* présente, à l'état liquide, des associations intermoléculaires par liaisons hydrogène plus nombreuses que l'isomère *ortho*. En conséquence, il est insoluble dans un liquide non associé comme le benzène alors que l'isomère *ortho* l'est.

3. La température du point triple (ou de fusion), qui renseigne sur la force des liaisons intermoléculaires, est plus élevée dans le cas du DHB-1,4 que dans celui du DHB-1,2. Il en est de même pour l'enthalpie de fusion (tableau 1).

IV.5. Calcul de l'enthalpie de sublimation du DHB-1,4 par voie incrémentale

Nous avons essayé de retrouver par le calcul à partir des contributions énergétiques apportées par le noyau benzénique et les deux fonctions OH, l'enthalpie de sublimation du DHB-1,4. Dans le réseau cristallin, celui-ci se trouve à l'état moléculaire et ne présente pas de liaison hydrogène intramoléculaire. Afin de tenir au mieux compte des interactions que peuvent avoir le noyau benzénique et les deux fonctions OH au sein du cristal de DHB-1,4, nous avons cherché à calculer ces contributions à partir des grandeurs énergétiques de molécules ayant une nature chimique voisine de celle qui nous intéresse.

Nous avons déterminé la contribution du chaînon OH à partir de deux composés : benzène et hydroxybenzène, en recherchant dans la littérature les principales données qui nous permettaient d'obtenir leur enthalpie de sublimation à 298,15 K. Pour le benzène, il nous fallait calculer cette grandeur à partir de $\Delta_{vap}H^0_m(298{,}15\,K)$ et de $\Delta_{fus}H_m(298{,}15\,K)$. La première de ces deux grandeurs est empruntée à la littérature (45). Quant à la seconde, nous l'avons calculée à partir de $\Delta_{fus}H_m(278{,}68\,K)$ = 9,84 kJ mol^{-1} (16) et en utilisant la règle de Sidgwick signalée ci-dessus. Nous trouvons $\Delta_{sub}H^0_m(298{,}15\,K)$ = 44,83 kJ mol^{-1}. Quant à l'hydroxybenzène, substance solide à 298,15 K, nous avons emprunté à la référence 1 la valeur de $\Delta_{sub}H^0_m(298{,}15\,K)$. Celle-ci est égale à 68,66 kJ mol^{-1}. En conséquence, la part du chaînon OH est égale à 23, 83 kJ mol^{-1}; celle de deux OH à 47,66 kJ mol^{-1}. Il s'en suit que l'enthalpie de sublimation du DHB-1,4, calculée à partir des différentes contributions, est égale à 92,49 kJ mol^{-1}; elle diffère seulement d'environ 1,7% de la valeur expérimentale.

Remerciements

L'un de nous (E.N.L.E.B.) tient à remercier le gouvernement zaïrois pour l'octroi d'une bourse lui ayant permis de réaliser ce travail.

1. J. B. Pedley, R. D. Naylor et S. P. Kirby. Thermochemical data of organic compounds. 2e éd. Chapman and Hall, London. 1986.
2. E. Martin, S. H. Yalkowsky et J. E. Wells. J. Pharm. Sci. **68**, 565 (1979).
3. P. Bret-Dibat et A. Lichanot. Thermochim. Acta, **147**, 261 (1989).
4. C. G. de Kruif, E. J. Smit et H. A. J. Govers. J. Chem. Phys. **74**, 5838 (1981).
5. Y. Ebisuzaki, L. H. Askari, A. M. Bryan et M. F. Nicol. J. Chem. Phys. **87**, 6659 (1987).
6. J. Monteath Robertson et A. R. Ubbelohde. Proc. R. Soc. Ser. A, **167**, 136 (1938).
7. H. G. Franck et J. W. Stadelhofer. Industrial aromatic chemistry. Raw materials, processes, products. Springer-Verlag, Berlin. 1988.
8. V. Grignard, G. Dupont et R. Locquin. Traité de chimie organique. t.VI. Masson, Paris. 1940.
9. R. Sabbah et I. Antipine. Bull. Soc. Chim. Fr. **3**, 392 (1987).
10. R. Sabbah, I. Antipine, M. Coten et L. Davy. Thermochim. Acta, **115**, 153 (1987).
11. (*a*) R. Sabbah et I. Antipine. J. Therm. Anal. **32**, 1929 (1987); (*b*) R. Sabbah et L. El Watik. J. Therm. Anal. Sous presse.
12. W. D. Good et N. K. Smith. J. Chem. Eng. Data, **14**, 102 (1969).
13. R. C. Weast (*Éditeur*). Handbook of chemistry and physics. 58e éd. CRC Press, Cleveland, OH. 1977.
14. Atomic weights of the elements 1987. Pure Appl. Chem. **60**, 841 (1988).
15. R. Sabbah et M. Coten. Thermochim. Acta, **49**, 307 (1981).
16. D. R. Stull, E. F. Westrum, Jr. et G. C. Sinke. The chemical thermodynamics of organic compounds. J. Wiley, New York. 1969.
17. P. D. Desai, R. C. Wilhoit et B. J. Zwolinski. J. Chem. Eng. Data, **13**, 334 (1968).
18. A. Magnus. Z. Phys. Chem. Neue Folge, **9**, 141 (1956).
19. G. Pilcher et L. E. Sutton. J. Chem. Soc. 2695 (1956).
20. M. Nabavian, R. Sabbah, R. Chastel et M. Laffitte. J. Chem. Phys. **74**, 115 (1977).
21. R. Sabbah, R. Chastel et M. Laffitte. Thermochim. Acta, **5**, 117 (1972).
22. R. Sabbah, R. Chastel et M. Laffitte. Can. J. Chem. **52**, 2201 (1974).
23. R. P. Rastogi, N. B. Singh et K. D. Dwivedi. Ber. Bunsen-ges. Phys. Chem. **85**, 85 (1981).
24. R. K. Nigam et M. S. Dhillon. Indian J. Chem. **8**, 614 (1970).
25. N. B. Singh et N. B. Singh. J. Cryst. Growth, **28**, 267 (1975).
26. D. H. Andrews, G. Lynn et J. Johnston. J. Am. Chem. Soc. **48**, 1274 (1926).
27. R. P. Rastogi, N. B. Singh, N. B. Singh et K. D. Dwivedi. Indian J. Chem. **17A**, 431 (1979).
28. A. J. Head et R. Sabbah. IUPAC—Recommended reference materials for the realization of physicochemical properties. *Editeur* : K. N. Marsh. Blackwell, Oxford. 1987. Chap. 9.
29. R. Sabbah, M. Gilbert et A. Julg. Thermochim. Acta, **10**, 345 (1974).
30. G. W. Wheland. Resonance in organic chemistry. J. Wiley, New York. 1955.
31. C. J. Brown. Acta Crystallogr. **21**, 170 (1966).
32. J. Monteath Robertson. Proc. R. Soc. Ser. A, **157**, 79 (1936).
33. A. I. Kitaigorodskii. Struct. Rep. **12**, 408 (1949).
34. Molecular structures and dimensions. Vol. A1. Interatomic distances. 1960–1965. Organic and Organometallic Crystal Laboratory, Cambridge, England. 1972.
35. Report of the Codata Task Group on key values for thermodynamics. 1977. J. Chem. Thermodyn. **10**, 903 (1978).
36. R. Sabbah et M. Laffitte. Thermochim. Acta, **25**, 376 (1978).

37. P. KNAUTH et R. SABBAH. Can. J. Chem. **68**, 731 (1990).
38. P. KNAUTH et R. SABBAH. Thermchim. Acta, **164**, 145 (1990).
39. S. SKOULIKA et R. SABBAH. Thermochim. Acta, **61**, 203 (1983).
40. P. KNAUTH et R. SABBAH. Bull. Soc. Chim. Fr. **5**, 834 (1988).
41. R. SABBAH et X. W. AN. Thermochim. Acta. Sous presse.
42. K. S. PITZER et D. W. SCOTT. J. Am. Chem. Soc. **65**, 803 (1943).
43. X. W. AN et X. ZHENG. Acta Phys. Chim. Sin. **5**, 487 (1989).
44. A. DWORKIN, P. FIGUIÈRE, M. GHELFENSTEIN et H. SZWARC. J. Chem. Thermodyn. **8**, 835 (1976).
45. V. MAJER, V. SVOBODA et H. V. KEHIAIAN. Enthalpies of vaporization of organic compounds: a critical review and data compilation. IUPAC Chemical Series N° 32. Blackwell, Oxford. 1985.
46. M. DAVIES et J. I. JONES. Trans. Faraday Soc. **50**, 1042 (1954).
47. G. C. PIMENTEL et A. L. MCCLELLAN. The hydrogen bond. W. H. Freeman, San Francisco, CA. 1960. p. 272.

Can. J. Chem. Downloaded from www.nrcresearchpress.com by 195.138.81.100 on 09/07/12
For personal use only.

Monohalogénocyclopropanation des esters et des acides α-éthyléniques diversement alkylés. Activation et stéréosélection antithermodynamique

ROGER BARLET,[1] BAHMAN BAHARMAST ET MICHEL VIDAL

Laboratoire d'études dynamiques et structurales de la sélectivité (LEDSS), Université Joseph Fourier, Bâtiment chimie recherche, BP53X, 38041 Grenoble CEDEX, France

Reçu le 28 février 1990

ROGER BARLET, BAHMAN BAHARMAST et MICHEL VIDAL. Can. J. Chem. **69**, 489 (1991).

L'halogénocyclopropanation des acides et des esters α-éthyléniques par le dichlorométhane en présence de MeLi/LiBr est obtenue avec d'excellents rendements. Dans le cas des esters les adduits halogénocyclopropaniques obtenus sont uniquement hydroxylés alors que dans le cas des acides on obtient en sus les adduits carbonylés qui sont majoritaires, même dans le cas d'un excès de MeLi. Dans le cas des acides α-éthyléniques, la cyclopropanation intervient très majoritairement au niveau d'un intermédiaire type hydrate de cétone lithié qui active considérablement le pontage. Le produit primaire de cycloaddition est suffisamment stable pour ne pas être massivement attaqué par le méthyllithium et permettre l'obtention prédominante des cétones halogénocyclopropaniques, obtenues à l'hydrolyse. Dans le cas des esters la réaction est également activée par la formation primaire d'un hémiacétal mais la cycloaddition intervient de façon plus équilibrée, à la fois sur cet intermédiaire et sur l'alcoolate qui en résulte par action ultérieure de MeLi. Dans les deux cas on observe le maintien, comme dans le cas des alcools α-éthyléniques, d'une nette stéréosélection *syn*, malgré les effets stériques et électroniques antagonistes, lorsque le groupement alkyle et le groupement fonctionnel sont en position *cis* par rapport à la double liaison.

Mots clés : halogénocyclopropanation, activation, stéréosélection *syn*.

ROGER BARLET, BAHMAN BAHARMAST, and MICHEL VIDAL. Can. J. Chem. **69**, 489 (1991).

The halogenocyclopropanation of α,β-unsaturated acids and their esters through a reaction with dichloromethane and MeLi/LiBr proceeds with excellent yields. With the esters, the only halogenocyclopropanic adducts obtained are the hydroxylated ones while the acids lead to carbonylated adducts as major products, even when there is an excess of MeLi. With the acids, the cyclopropanation takes place selectively with a lithiated hydrate of ketone type intermediate favouring the formation of the ring. The stability of the primary product of the cycloaddition is such that it does not react massively with the methyllithium and that the halogenocyclopropane ketones can be isolated after hydrolysis. With the esters, the reaction is also activated by the primary formation of an hemiacetal; however, the cycloaddition is more equilibrated between this intermediate and the alkoxide which results from the later action of the MeLi. In both cases, a net *syn* stereoselectivity is observed in the unsaturated alcohols in spite of the opposite steric and stereoelectronic effects operating when the alkyl and functional groups are in a *cis* relation around the double bond.

Key words: halogenocyclopropanation, activation, *syn* stereoselectivity.

[Journal translation]

Can. J. Chem. Downloaded from www.nrcresearchpress.com by 198.100.157.202 on 09/07/12
For personal use only.

Introduction

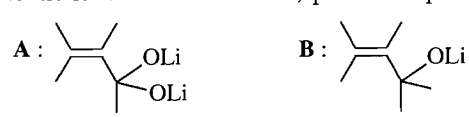
Nous avons pu montrer antérieurement que la réaction de monohalogénocyclopropanation sur les oléfines fonctionnalisées s'avère très générale et fournit d'excellents rendements (1–4). Cette réaction de transfert peut être commodément mise en oeuvre par action du méthyllithium, associé au bromure de lithium, sur divers générateurs de monochlorocarbènes tels que le chlorure de méthylène ou le dichloro-1,1 éthane en présence de substrats variés. Nous avons récemment obtenu des résultats surprenants avec des alcools α-éthyléniques, en mettant en évidence un effet synergique alkyle–alcoolate dans la stéréosélection *syn* majoritaire des alcools α-éthyléniques *cis*-méthylés (5).

Poursuivant ce travail sur les acides et les esters α-éthyléniques nous sommes en mesure, compte tenu de nous derniers résultats, de mettre en évidence un net effet d'activation des fonctions acide et ester par rapport aux fonctions cétone, dioxolanne ou alcool. En même temps on observe, dans le cas où alkyle et groupement fonctionnel sont *cis*, le maintien d'une stéréosélection *syn* (halogène se plaçant du côté du groupement fonctionnel) allant à l'encontre des interactions stériques et électrostatiques attendues. On obtient, en effet, les produits d'addition les plus encombrés (alkyle, halogène et groupement fonctionnel du même côté du cycle) et les plus polaires (halogène et oxygène électronégatifs em position *cis*).

Halogénocyclopropanation des acides α-éthyléniques

Résultats expérimentaux (tableau 1)

Les acides **1**–**5**, diversement méthylés, sont soumis à l'action du générateur de carbénoïde CH_2Cl_2/MeLi/LiBr, à reflux d'éther, selon la méthode que nous avons antérieurement développée (5). Un équivalent de bromure de lithium se trouve en effet associé, sous forme soluble et stable, à une équivalent de méthyllithium formé, de façon commode, à partir du bromure de méthyle et du lithium. La préparation du méthyllithium à partir du chlorure de méthyle entraîne, au contraire, la précipitation du chlorure de lithium et la passivation du lithium par l'halogénure insoluble. De plus, le méthyllithium est alors très réactif et s'enflamme à l'air. En règle générale 4 équivalents de méthyllithium sont utilisés pour 1 équivalent d'acide. Dans ces conditions opératoires deux entités successives, l'hydrate de cétone potentielle **A** et l'alcoolate **B**, peuvent à priori subir la



Structure **A** Structure **B**

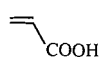
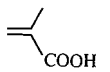
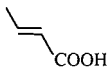
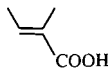
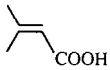
cycloaddition et conduire respectivement, après hydrolyse, aux cétones et aux alcools α-halogénocyclopropaniques comme produits primaires de pontage.

Les acides donnent effectivement, de façon très générale, les adduits carbonylés et les adduits hydroxylés en proportion très variable selon le substrat envisagé et avec d'excellents rende-

1. Auteur à qui adresser toute correspondance.

Printed in Canada / Imprimé au Canada

TABLEAU 1. Cycloaddition sur les acides diversement methylés

		Rdt %	% Adduits hydroxylés	% Adduits carbonylés	% Produits d'add. chlorés		% Produits d'add. bromés		% Dérivés chlorés/ % dérivés bromés
1		90	91		$\mathbf{1}^{c}_{Cl}$ 20	$\mathbf{1}^{t}_{Cl}$ 80	$\mathbf{1}^{c}_{Br}$ 20	$\mathbf{1}^{t}_{Br}$ 80	70 : 30
				9	$\mathbf{1'}^{c}_{Cl}$ 10	$\mathbf{1'}^{t}_{Cl}$ 90	$\mathbf{1'}^{c}_{Br}$ 15	$\mathbf{1'}^{t}_{Br}$ 85	60 : 40
2		70	18		$\mathbf{2}^{c}_{Cl}$ 22	$\mathbf{2}^{t}_{Cl}$ 78	$\mathbf{2}^{c}_{Br}$ 25	$\mathbf{2}^{t}_{Br}$ 75	80 : 20
				82	$\mathbf{2'}^{c}_{Cl}$ 17	$\mathbf{2'}^{t}_{Cl}$ 83	$\mathbf{2'}^{c}_{Br}$ 20	$\mathbf{2'}^{t}_{Br}$ 80	73 : 27
3		70	11		$\mathbf{3}^{c}_{Cl}$ 21	$\mathbf{3}^{t}_{Cl}$ 79	$\mathbf{3}^{c}_{Br}$ 20	$\mathbf{3}^{t}_{Br}$ 80	69 : 31
				89	$\mathbf{3'}^{c}_{Cl}$ 25	$\mathbf{3'}^{t}_{Cl}$ 75	$\mathbf{3'}^{c}_{Br}$ 18	$\mathbf{3'}^{t}_{Br}$ 82	63 : 37
4		90	65			$\mathbf{4}^{t}_{Cl}$ 100		$\mathbf{4}^{t}_{Br}$ 100	73 : 27
				35		$\mathbf{4'}^{t}_{Cl}$ 100		$\mathbf{4'}^{t}_{Br}$ 100	71 : 29
5		95	5		$\mathbf{5}^{c}_{Cl}$ 72	$\mathbf{5}^{t}_{Cl}$ 28	$\mathbf{5}^{c}_{Br}$ 99	$\mathbf{5}^{t}_{Br}$ 1	75 : 25
				95	$\mathbf{5'}^{c}_{Cl}$ 74	$\mathbf{5'}^{t}_{Cl}$ 26	$\mathbf{5'}^{c}_{Br}$ 80	$\mathbf{5'}^{t}_{Br}$ 20	85 : 15

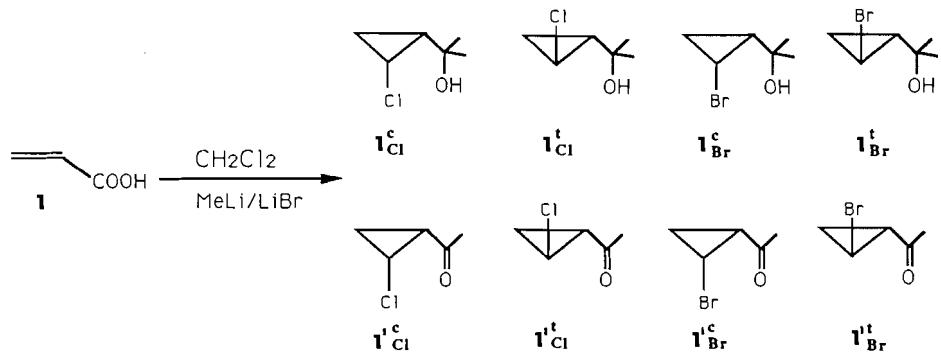


FIG. 1.

ments. Dans chacun des cas on obtient un couple d'adduits chlorés, majoritaire, et un couple d'adduits bromés, obtenu par échange d'halogènes au niveau du carbénoïde ou du complexe carbène–sel. Par contre, on peut limiter ou même inhiber totalement cet échange d'halogène en travaillant à −30°C et ne conserver alors que les adduits chlorés (2). Dans chaque couple les termes *cis* (composé **c** 1′*R**2′*R**) et *trans* (composé **t** 1′*R**2′*S**) précisent la position relative du groupement fonctionnel porté par le carbone 1′ du cycle et de l'halogène porté par le carbone 2′ du cycle. À titre d'exemple figurent ci-dessous les adduits de l'acide acrylique **1** (voir figure 1).

L'obtention d'adduits bromés, à côté des adduits chlorés, malgré l'utilisation du chlorure de méthylène comme générateur de carbène, peut être considérée comme une limitation au plan synthétique qui disparait si on travaille à basse température. L'accés aux adduits bromés, difficile à partir du bromure de méthylène, peut ainsi constituer un avantage dans l'étude de la réactivité comparée des adduits lorsqu'est mis en oeuvre le pouvoir nucléofuge des halogènes. Par exemple, nous menons actuellement des études d'élimination sur de tels composés dont les premiers résultats viennent d'être publiés (12).

Détermination des configurations

De façon générale en CPG les alcools *cis* sont moins retenus que les alcools *trans*, à l'inverse des cétones.

La détermination des diverses configurations prend essentiellement appui sur la spectrographie de RMN.

Les configurations des adduits de cycloaddtion des produits **1** et **2** sont déterminées en RMN ^{1}H par effet LIS après complexation avec les chélates de l'Europium Eu(dpm)$_3$. Cette complexation déplace plus fortement les protons situés en *cis* du groupement fonctionnel que ceux situés en *trans* conformément

Can. J. Chem. Downloaded from www.nrcresearchpress.com by 198.100.157.202 on 09/07/12
For personal use only.

TABLEAU 2. RMN[1] H : déplacements chimiques comparés des protons géminés avec l'halogène dans les couples d'adduits hydroxylés et carbonylés ($CDCl_3$, $\delta \times 10^6$)

Alcools		Cétones	
$\mathbf{1}^c_{Cl}$: 3,20	$\mathbf{1}^t_{Cl}$: 3,04	$\mathbf{1}'^c_{Cl}$: 3,19	$\mathbf{1}'^t_{Cl}$: 3,33
$\mathbf{1}^c_{Br}$: 3,10	$\mathbf{1}^t_{Br}$: 2,90	$\mathbf{1}'^c_{Br}$: 3,10	$\mathbf{1}'^t_{Br}$: 3,29
$\mathbf{2}^c_{Cl}$: 2,93	$\mathbf{2}^t_{Cl}$: 3,36	$\mathbf{2}'^c_{Cl}$: 3,06	$\mathbf{2}'^t_{Cl}$: 3,40
$\mathbf{2}^c_{Br}$: 2,90	$\mathbf{2}^t_{Br}$: 3,33	$\mathbf{2}'^c_{Br}$: 2,94	$\mathbf{2}'^t_{Br}$: 3,38
$\mathbf{3}^c_{Cl}$: 2,85	$\mathbf{3}^t_{Cl}$: 3,10	$\mathbf{3}'^c_{Cl}$: 3,12	$\mathbf{3}'^t_{Cl}$: 3,50
$\mathbf{3}^c_{Br}$: 2,78	$\mathbf{3}^t_{Br}$: 3,00	$\mathbf{3}'^c_{Br}$: 3,10	$\mathbf{3}'^t_{Br}$: 3,45
$\mathbf{5}^c_{Cl}$: 3,01	$\mathbf{5}^t_{Cl}$: 3,10	$\mathbf{5}'^c_{Cl}$: 3,20	$\mathbf{5}'^t_{Cl}$: 3,52
$\mathbf{5}^c_{Br}$: 2,96	$\mathbf{5}^t_{Br}$: 3,05	$\mathbf{5}'^c_{Br}$: 3,19	$\mathbf{5}'^t_{Br}$: 3,50

TABLEAU 3. RMN ^{13}C : déplacements chimiques caracteristiques des couples d'alcools α-chlorocyclopropaniques ($CDCl_3$, $\delta \times 10^6$)

	Carbone porteur de halogène		Carbone cyclopropanique porteur du carbone hydroxylé	
Composés	*cis*	*trans*	*cis*	*trans*
1 *c,t*	33,9	31,2	23,6	28,2
2 *c,t*	41	37,1	27,9	29,8
3 *c,t*	40,1	38,2	35,5	39
5 *c,t*	43,7	39,2	35,7	39,5

à nos résultats antérieurs (2, 6). Les configurations des adduits du produit **3** sont déterminées par l'examen du multiplet présenté par le proton, fortement blindé, lié au carbone porteur du groupement fonctionnel : quadruplet pour les composés *cis* ($^3J_{cis} \simeq 7$–8 Hz, $^3J_{trans} \simeq 4$–5 Hz), triplet grossier pour les composés *trans* (deux $^3J_{trans}$ voisins de 4 Hz). Dans les composés de cycloaddition des acides **4** et **5** le proton lié au carbone porteur de l'halogène présente un couplage $^3J_{trans}$ dans les composés *cis*, inférieur à $^3J_{cis}$ dans les composés *trans*, conformément à ce que nous avons observé antérieurement (5). De façon générale, par effet de dilution, les protons hydroxyliques des composés *cis* sont moins déplacés vers les champs forts que ceux des composés *trans* à cause de la persistance d'une liaison hydrogène intramoléculaire entre ces protons et l'halogène.

Il apparaît cependant, au vu des spectres de RMN ^1H, que l'hydrogène géminé avec l'halogène, systématiquement plus déblindé dans le cas des cétones *trans*, ce qui constituait un critère d'identification stéréochimique (2), ne montre pas ici, dans le cas des alcools nouvellement décrits, un déplacement chimique établissant une corrélation claire avec la nature du stéréoisomère. Le tableau 2 montre en effet que c'est tantôt l'alcool *cis* tantôt l'alcool *trans* qui conduit au blindage le plus élevé pour ce proton. Le carbonyle orienté vers le cycle (conformation *cisoïde* prouvée en particulier par la valeur élevée de ν_{CO} pour les cétones *cis*) déblinde les protons CHX quel que soit l'effet des méthyles substitués sur le cycle. Par contre, l'hydroxyle entraîne un effet d'anisotropie beaucoup moins net et la substitution méthylée joue alors un grand rôle.

Les spectres de RMN ^{13}C montrent que le carbone cyclopropanique porteur de l'halogène est davantage déblindé dans le cas des stéréoisomères *cis* que dans le cas des *trans*. À l'inverse, le carbone cyclopropanique portant le carbone hydroxylé est davantage blindé dans le cas des stéréoisomères *cis* (tableau 3).

La conformation des cétones **1′**–**5′** est de type *cisoïde* comme nous l'avons montré antérieurement lorsque ces adduits étaient issus du pontage des dioxolannes correspondants (2).

Discussion

L'ensemble de nos résultats nous amènent aux conclusions suivantes :

Dans le cas des acides **2**, **3** et **5** la cyclopropanation n'intervient qu'au niveau de l'intermédiaire **A**, même avec un excès de MeLi (figure 2). On obtient en effet sensiblement la même répartition de produits, fortement en faveur des adduits cétoniques, que l'on utilise 3, 4 ou 5 équivalents de MeLi. Dans le cas des acides **1** et surtout **4**, un défaut de MeLi entraîne une augmentation de la proportion de cétones (alcool/cétone = 70 : 30 pour l'acide **1** et 45 : 55 pour l'acide **4** dans le cas de l'utilisation de 3 équivalents de MeLi).

Dans tous les cas de figure nous pensons disposer d'arguments en faveur de la cyclopropanation de l'hydrate de cétone lithié **A** plutôt que de l'alcoolate **B**. Cet hydrate, porteur de 2 atomes d'oxygène, renforcerait l'assistance lithium du carbénoïde-oxygène du substrat, que nous avons invoquée dans le cas des oléfines α-fonctionnalisées faiblement nucléophiles (2, 5), et rendrait compte des rendements de pontage particulièrement élevés dans le cas présent des acides. Cette assistance entraînerait une accélération de la cyclopropanation telle qu'après l'addition de deux équivalents de MeLi on observe déjà, sauf dans le cas de l'acide **1**, la formation de 15–30% de produits de cycloaddition ce qui signifie que la vitesse de l'attaque nucléophile du carboxylate de lithium pour conduire à l'hydrate **A** n'est guère supérieure à la vitesse de cyclopropanation de cet hydrate. Même dans le cas de l'acide **1** le rendement de cyclopropanation, très supérieur à celui de la cétone méthylée correspondante **11** (cf. tableau 4) et conduisant aux mêmes couples d'alcools (90% contre 55%), semble clairement indiquer que l'intermédiaire ponté n'est pas l'alcoolate tertiaire **B** mais bien l'hydrate **A** (voie ② prépondérante par rapport aux voies ① et ②′ dans le schéma réactionnel de la figure 2 mais avec transformation ③ importante).

Ces résultats confirment que, dans les conditions ordinaires de température, lors de l'attaque d'un alkyllithium sur un acide, le complexe intermédiaire **A** a une stabilité suffisante pour ne se transformer majoritairement en cétone qu'à l'hydrolyse (7). On peut ajouter que nos conditions d'hydrolyse, addition lente d'eau au milieu réactionnel ou mélange réactionnel ajouté à un grand excès d'eau, ne modifient pas de façon sensible la répartition entre adduits hydroxylés et adduits carbonylés. L'excès d'eau à l'hydrolyse ne joue donc pas, dans notre cas, de rôle majeur contrairement aux indications de la littérature (7*c*, 8).

Sauf dans le cas de l'acide **1** on peut dire que le méthyllithium en excès s'hydrolyse plus rapidement que l'adduit de l'intermédiaire **A** qui évolue peu en cours de manipulation (transformation ③ faible).

De façon générale, la stéréochimie est indépendante du nombre d'équivalents de MeLi utilisés. La stéréosélection, par cyclopropanation de l'hydrate de cétone, observée ici, s'avère très voisine de celle observée dans le pontage des alcools α-éthyléniques (5), c'est à dire le cas où les substrats primaires de réaction sont des alcoolates. On retrouve l'effet directeur *syn* des substituants alkyles sur la double liaison et l'effet directeur *anti* des groupements hydrate ou alcoolate de lithium lorsque

Can. J. Chem. Downloaded from www.nrcresearchpress.com by 198.100.157.202 on 09/07/12
For personal use only.

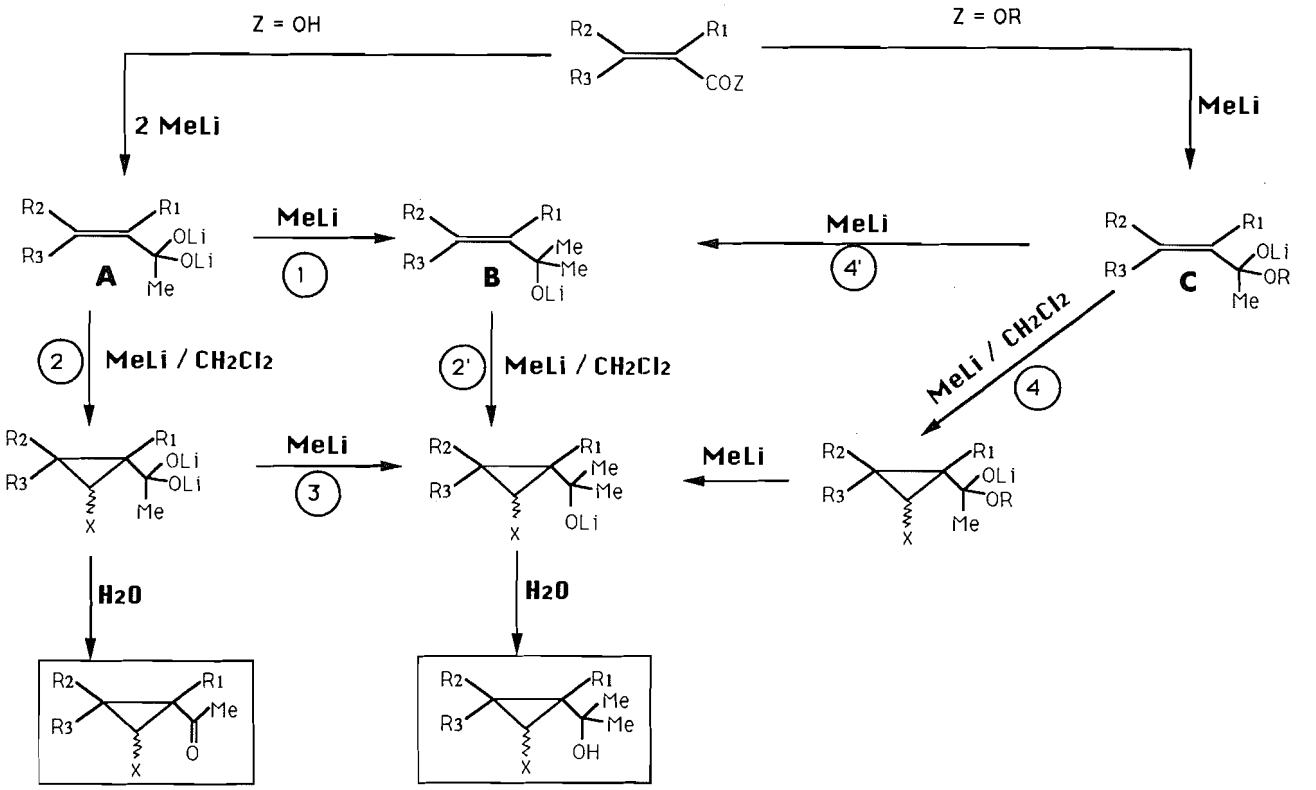


FIG. 2. Halogénocyclopropanation des acides et esters α-éthyléniques. Schéma réactionnel.

ces groupements sont en position *trans*. De même, lorsqu'ils sont *cis* (cas du composé **5**) on retrouve une synergie alkyle – hydrate de lithium encore plus surprenante que la synergie alkyle–alcoolate (5) dans la mesure où l'interaction répulsive stérique et surtout électronique, mise en oeuvre dans l'adduit *cis* majoritaire, devrait être encore accrue par la présence de deux groupements OLi dans l'hydrate de lithium au lieu d'un seul dans l'alcoolate. Cette synergie se manifeste, là encore, par une grande réactivité de l'intermédiaire **A**, traduite par un fort rendement de pontage et une augmentation de la stéréosélection liée à l'accroissement de la pression stérique (cas des adduits bromés).

Nous pensons que cette synergie prend appui sur plusieurs facteurs cumulatifs intervenant tous au niveau de l'état de transition et favorisant un contrôle cinétique en faveur du produit de cycloaddition le plus contraint. Ainsi la diffusion des charges et l'interaction entre l'halogène négatif et la charge partielle positive acquise par le méthyle, en cours de transfert carbénique, explique l'effet directeur *syn* des alkyles (9). Les interactions orbitalaires secondaires, invoquées par Hofmann *et al.* et dues aux hydrogènes de l'alkyle en *cis*, peuvent intervenir dans une telle réaction menée dans des conditions relativement exothermiques où substrat et réactif restent assez éloignés (10). Une assistance, au niveau des intermédiaires **A** et **B**, par les ions Li positif et les halogènes du carbénoïde expliquerait l'effet directeur *syn* du groupement fonctionnel. Nous avons en effet vérifié que cet effet directeur *syn* est sensiblement atténué si le lithium est crypté sélectivement. Cette intervention de Li positif, insuffisante pour orienter de façon *syn*, en l'absence d'alkyle en *cis*, devient au contraire déterminante lorsqu'un alkyle en *cis* permet une synergie des effets. Tout se passe comme si un effet d'accrochage alkyle–halogène rendait alors possible l'assistance Li positif – halogène négatif.

Halogénocyclopropanation des esters α-éthyléniques

Résultats expérimentaux (tableau 4)

Les esters **6–10**, homologues des acides **1–5**, donnent, avec d'excellents rendements, les couples d'adduits hydroxylés, à l'exclusion d'adduits carbonylés. Les alcools obtenus peuvent également résulter de la cyclopropanation des cétones correspondantes **11–15** dont les résultats figurent également dans le tableau 4.

Discussion

Sauf dans le cas du composé **10**, les esters donnent de meilleurs rendements de cycloaddition que les cétones correspondantes. Ceci accrédite à nouveau l'hypothèse d'une cyclopropanation au niveau d'un intermédiaire activé, hémiacétalique **C** tel que mentionné dans le schéma de la figure 2.

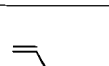
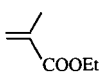
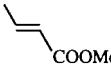
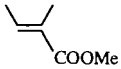
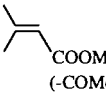
Le fait qu'en général, sauf pour l'ester **10**, le pontage soit déjà de l'ordre de 20–30% après addition de 2 équivalents de MeLi va dans le même sens. Par contre, après addition de 1 équivalent de MeLi, les adduits ne sont formés qu'à l'état de traces. Il semble donc que la vitesse de cyclopropanation et la vitesse de formation de l'alcoolate soient voisines, et que la vitesse de formation de **C** à partir de l'ester soit sensiblement supérieure. La cyclopropanation interviendrait de façon partielle au niveau de l'intermédiaire **C**, apparemment moins activé et moins stable que les intermédiaires de type **A** formés à partir des acides (voie ④ simultanée à la voie ④' dans la figure 2).

Par contre pour l'ester **10**, la cyclopropanation interviendrait surtout au niveau de l'alcoolate comme semblent l'indiquer, tout à la fois, l'absence de tout pontage après l'addition de deux équivalents de MeLi et l'absence d'amélioration, dans ce cas là, du rendement du pontage de l'acide par rapport au pontage de la cétone.

Il est remarquable de constater que le pontage des esters n'a

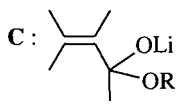
Can. J. Chem. Downloaded from www.nrcresearchpress.com by 198.100.157.202 on 09/07/12
For personal use only.

TABLEAU 4. Cycloaddition sur les esters diversement methylés (comparaison avec cétones correspondantes)

	Rdt %	% Produits d'add. chlorés		% Produits d'add. bromés		Dérivés chlorés/dérivés bromés
6 	80	$\mathbf{1}^{c}_{Cl}$ 24	$\mathbf{1}^{t}_{Cl}$ 76	$\mathbf{1}^{c}_{Br}$ 20	$\mathbf{1}^{t}_{Br}$ 80	72 : 28
(11) (-COMe)	(55)	(19)	(81)	(12)	(88)	(71 : 29)
7 	60	$\mathbf{2}^{c}_{Cl}$ 20	$\mathbf{2}^{t}_{Cl}$ 80	$\mathbf{2}^{c}_{Br}$ 21	$\mathbf{2}^{t}_{Br}$ 79	71 : 29
(12) (-COMe)	(50)	(23)	(77)	(26)	(74)	(76 : 24)
8 	80	$\mathbf{3}^{c}_{Cl}$ 21	$\mathbf{3}^{t}_{Cl}$ 79	$\mathbf{3}^{c}_{Br}$ 20	$\mathbf{3}^{t}_{Br}$ 80	64 : 36
(13) (-COMe)	(65)	(21)	(79)	(20)	(80)	(64 : 36)
9 	80		$\mathbf{4}^{t}_{Cl}$ 100		$\mathbf{4}^{t}_{Br}$ 100	75 : 25
(14) (-COMe)	(70)		(100)		(100)	(74 : 26)
10 	70	$\mathbf{5}^{c}_{Cl}$ 79	$\mathbf{5}^{t}_{Cl}$ 21	$\mathbf{5}^{c}_{Br}$ 99	$\mathbf{5}^{t}_{Br}$ 1	75 : 25
(15) (-COMe)	(90)	(72)	(28)	(97)	(3)	(74 : 26)

*La cycloaddition faite sur l'ester éthylique correspondant donne rigoureusement les mêmes résultats.

jamais, dans nos conditions, conduit aux cétones correspondantes. L'intermédiaire hémiacétalique **C** est suffisamment peu stable pour évoluer vers l'alcoolate soit avant soit, de façon plus limitée, après cyclopropanation. À l'inverse de l'hydrate de cétone **A**, issu des acides, l'hemiacétal **C** serait déstabilisé par cyclopropanation. Aussi bien l'hemiacétal **C** que son produit de cycloaddition évolueraient ainsi plus rapidement vers un alcoolate qu'un ester ordinaire capable de fournir des cétones par action des organolithiens (11).



Structure **A**

Dans le cas de l'ester **10**, où le méthyle et le groupement ester sont *cis*, on observe, à nouveau, une nette stéréosélection en faveur du produit de cycloaddition *cis* malgré les effets stérique et électronique déstabilisants, que ces effets interviennent au niveau de l'alcoolate ou de l'hemiacétal. L'accroissement de cette stéréosélection *syn* dans la cycloaddition de l'ester **10**, comparée à celle de l'ester **15**, semble bien indiquer que l'intermédiaire hémiacétalique **C** subit en partie la cyclopropanation.

Conclusion

La mise en oeuvre d'une telle réaction d'halogénocyclopropanation sur les acides et les esters α-éthyléniques montre que la durée de vie des intermédiaires **A** et **C**, respectivement formés par addition nucléophile initiale sur le carboxylate ou l'ester, est importante. Nous avons pu donner ainsi une nouvelle extension à cette réaction qui autorise l'accès direct à des cétones halogénocyclopropaniques sans passer par la protection du carbonyle sous forme de dioxolanne (2).

La diversité des composés halogénocyclopropaniques fonctionnalisés ainsi accessibles nous permet d'étudier actuellement les réactions d'élimination sur ces substrats, en direction des composés cyclopropéniques ou cyclopropylidéniques correspondants. Nous premiers résultats dans ce domaine laissent présager un cours réactionnel très variable en fonction de la nature des substrats avec accès possible à des composés alléniques ou diéniques (12).

Partie expérimentale

Les spectres de RMN ^{1}H et ^{13}C ont été enregistrés dans la grande majorité des cas, dans $CDCl_3$ sur WP Brücker 80 SY. Les spectres infrarouges ont été réalisés sur un appareil Perkin–Elmer 397 (ou 521 pour les études en solution).

La CPG analytique a été effectuée sur Aérograph 600 D à ionisation de flamme, le plus souvent avec colonnes Carbowax, et la CPG préparative sur Autoprep A 700 et A 705 avec des colonnes Carbowax sauf dans le cas des adduits hydroxyles de l'acide **5** où la séparation a été obtenue sur colonne Ucon Oil. Selon les cas la longueur des colonnes utilisées était de 1 à 3 mètres (3 ou 9 mm de section).

Les analyses élémentaires ont été réalisées par le Service Central de microanalyse du CNRS, échangeur de Solaize, BP 22, 69390 Vernaison, France.

Cyclopropanation des acides et des esters α-éthyléniques

Le méthylithium associé au bromure de lithium est obtenu par barbotage du bromure de méthyle dans un mélange éther diéthylique – lithium martelé en fines lamelles. Avant utilisation l'éther est distillé sur $LiAlH_4$.

La cyclopropanation s'opère selon un mode opératoire conforme à celui décrit antérieurement (2, 3, 5). Le méthyllithium, environ N, est additionné, sous azote, à un mélange de 0,1 mol d'acide ou d'ester et 0.3–0,4 mol de CH_2Cl_2 jouant à la fois le rôle de générateur de carbène et de solvant. L'addition s'opère en 1 h environ, à un rythme tel que le reflux d'éther soit entretenu. Des prélèvements intermédiaires, en cours de réaction (après addition de 2, 3 et 4 équivalents pour les acides, après addition de 1, 2 et 3 équivalents pour les esters), sont immédiatement hydrolysés, par un excès d'eau saturée en chlorure d'ammonium, afin de vérifier l'état d'avancement de la réaction par CPG analytique. Les réactions sont arrêtées après addition de 5 équivalents de MeLi sur les acides et de 3,5 équivalents sur les esters, c'est à dire après addition d'un excès théorique de MeLi de l'ordre de 20–25%, excès tenant compte à la fois de la cyclopropanation et de l'évolution du groupement fonctionnel vers un alcoolate tertiaire. L'hydrolyse, très exothermique, est menée le plus souvent par addition progressive du produit de réaction à un grand excès d'eau glacée. L'addition lente d'eau au milieu réactionnel refroidi est également mise en oeuvre, sur le produit de pontage des acides, afin de vérifier si les conditions d'hydrolyse jouent un rôle dans la répartition entre adduits hydroxylés et carbonylés. Après neutralisation par le chlorure d'ammonium, séparation des phases et extraction de la phase aqueuse à l'éther, on obtient un mélange brut dont les divers constituants ne peuvent pas être séparés par distillation fractionnée mais sont aisément séparables par CPG préparative.

Séparation et détermination des pourcentages d'adduits obtenus

La séparation des mélanges complexes d'adduits obtenus est faite par CPG. Le couple de dérivés chlorés précède normalement le couple de dérivés bromés dans l'ordre de sortie de colonne. Cependant le premier dérivé bromé est parfois moins retenu que le deuxième dérivé chloré.

La détermination des pourcentages est faite, après agrandissement des diagrammes par diminution de l'atténuation, par détermination des surfaces x des pics et étalonnage interne. Une moyenne est effectuée entre plusieurs évaluations qui sont relativement homogènes ($\Delta x/x <$ 0,03).

Identification stéréochimique des adduits

Les adduits hydroxlyés et carbonylés de l'acide 2-méthyl-but-2-

Can. J. Chem. Downloaded from www.nrcresearchpress.com by 198.100.157.202 on 09/07/12
For personal use only.

Can. J. Chem. Downloaded from www.nrcresearchpress.com by 198.100.157.202 on 09/07/12
For personal use only.

ènoïque **4** et de l'acide 3-méthyl-but-2-ènoïque **5** ne sont pas des produits nouveaux. Nous avons décrit antérieurement ces composés (2) de même que les adduits carbonylés issus de l'acide 2-méthyl-prop-2-énoïque **2** (2). Ces derniers adduits carbonylés ont également été, pour certains d'entre eux, décrits par d'autres équipes (13, 14).

Les adduits carbonylés de l'acide acrylique **1** et les adduits hydroxylés de **1**, **2** et **3** n'ont, à notre connaissance, pas été décrits. La caractérisation de ces adduits prend appui sur le faisceau homogène suivant d'observations expérimentales : ordre de sortie en CPG; distinction générale en IR entre les deux stéréoisomères carbonylés *cis* et *trans* (ν_{CO} supérieur d'environ 10 cm^{-1} pour les cétones *cis*, 1705 cm^{-1} contre 1695 cm^{-1} à l'état pur); distinction possible en IR entre les deux stéréoisomères hydroxylés *cis* et *trans* par effet de solvant (l'alcool *cis* en solution à 5×10^{-3} mol L^{-1} donne, le plus souvent, persistance d'une bande ν_{OH} liée vers 3480–3500 cm^{-1} due à une chélation entre l'hydroxyle et l'halogène); distinction en RMN entre les deux stéréoisomères hydroxylés (dans le cas des composés *cis* moindre déplacement du signal dû à OH vers les champs forts par dilution. Ainsi $\mathbf{1}^c_{Cl}$, $\mathbf{2}^c_{Cl}$, $\mathbf{3}^c_{Cl}$, $\mathbf{5}^c_{Cl}$ sont respectivement blindés de 0,45 ppm, 0,40 ppm, 0,48 ppm et 0,38 ppm en passant de $c = 0{,}6$ mol L^{-1} à $c = 0{,}3$ mol L^{-1}. Les isomères chlorés *trans* correspondants sont blindés de 0,70 ppm dans les mêmes conditions), complexation avec les chélates de l'Europium conduisant au fort déblindage d'un seul proton dans le cas de $\mathbf{1}'^c_{Cl}$, $\mathbf{2}^c_{Cl}$, $\mathbf{3}^c_{Cl}$ alors que deux protons sont fortement déblindés dans le cas des homologues $\mathbf{1}'^t_{Cl}$, $\mathbf{2}^t_{Cl}$, $\mathbf{3}^t_{Cl}$ (de même pour $\mathbf{1}'^c_{Br}$, $\mathbf{2}^c_{Br}$, $\mathbf{3}^c_{Br}$ vis-à-vis de $\mathbf{1}'^t_{Br}$, $\mathbf{2}^t_{Br}$, $\mathbf{3}^t_{Br}$).

Caractéristiques des nouveaux produits

Les analyses élémentaires sont satisfaisantes (C, H et O ±0,1%, Cl ±0,15%, Br ±0,25%), à condition qu'elles soient effectuées rapidement après la séparation chromatographique, sinon les écarts sur la composition en halogène deviennent importants bien que les spectres RMN demeurent pratiquement inchangés.

Les spectres IR des alcools sont voisins et montrent à l'état de film pur une vibration $\nu_{C\text{-}H}$ vers 3040–3055 cm^{-1}, une vibration ν_{OH} vers 3400 cm^{-1}, un vibration $\nu_{C\text{-}O}$ vers 1125 cm^{-1} et une vibration persistante à 680 cm^{-1}. Les cétones présentent une bande $\nu_{C\text{-}H}$ vers 3050 cm^{-1}, $\nu_{C=O}$ intense vers 1705 cm^{-1} pour les *cis* et 1695 cm^{-1} pour les *trans*, et des bandes présentes pour tous les stéréoisomères vers 1360 cm^{-1} (COMe), 1325, 1170 et 690 cm^{-1}.

Dans la caractérisation des produits nouveaux ci-après nous rapportons les fréquences en cm^{-1} des maxima d'absorption des spectres IR effectués à l'état de films purs, les données des spectres de RMN ^1H, enregistrés dans $CDCl_3$, selon la nomenclature habituelle ($\delta \times 10^6$, J en Hz, s = singulet, m = multiplet, dd = doublet de doublets, dt = doublet de triplets) et enfin les analyses centésimales :

*1'*R*2'*R** *2'-Chloro-2-cyclopropylpropan-2-ol* ($\mathbf{1}'^c_{Cl}$) : 3610, 3400, 3050, 1120, 910, 800, 750, 680; 1,20 (3H, m), 1,30 (3H, s), 1,44 (3H, s), 3,20 (1H, m, $^3J_c = 7{,}3$, $^3J_t = 4{,}8$). Anal. calc. pour $C_6H_{11}OCl$: C 53,53, H 8,18, O 11,89, Cl 26,38; trouvé : C 53,48, H 8, 27, O 11,79, Cl 26,30.

*1'*R*2'S** *2'-Chloro-2-cyclopropylpropan-2-ol* ($\mathbf{1}'^t_{Cl}$) : 3600, 3390, 3045, 1120, 900, 800, 750, 690; 1,00 (3H, m), 1,22 (3H, s), 1,33 (3H, s), 3,04 (1H, dt, $^3J_t = 7$, $^3J_t = 3{,}5$). Anal. calc. pour $C_6H_{11}OCl$: C 53,53, H 8,18, O 11,90, Cl 26,39; trouvé : C 53,46, H 8,26, O 11,84, Cl 26,27.

*1'*R*2'R** *2'-Bromo-2-cyclopropylpropan-2-ol* ($\mathbf{1}'^c_{Br}$) : 3610, 3400, 3055, 1115, 900, 810, 750, 690; 1,15 (2H, m), 1,32 (3H, s), 1,45 (3H, s), 1,45 (1H, m), 3,10 (1H, m, $^3J_c = 7{,}6$, $^3J_t = 5$). Anal. calc. pour $C_6H_{11}OBr$: C 40,22, H 6,14, O 8,94, Br 44,69; trouvé : C 40,25, H 6,10, O 8,98, Br 44,50.

*1'*R*2'S** *2'-Bromo-2-cyclopropylpropan-2-ol* ($\mathbf{1}'^t_{Br}$) : 3600, 3390, 3050, 1120, 910, 800, 740, 680; 1,04 (2H, m), 1,21 (3H, s), 1,31 (3H, s), 1,50 (1H, m), 2,90 (1H, dt, $^3J_c = 7{,}2$, $^3J_t = 3{,}6$). Anal. calc. pour $C_6H_{11}OBr$: C 40,22, H 6,14, O 8,94, Br 44,69; trouvé : C 40,31, H 6,10, O 8,89, Br 44,63.

*1'*R*2'R** *2'-Chlorocyclopropyl méthyl cetone* ($\mathbf{1}'^c_{Cl}$) : 3050, 2960, 2920, 1705, 1460, 1410, 1355, 1330, 1250, 1170, 1050, 920, 690, 670; 1,10 (1H, m), 1,60 (1H, m), 2,20 (1H, m), 2,30 (3H, s), 3,19 (dt, $^3J_c = 7{,}8$, $^3J_t = 3{,}9$). Anal. calc. pour C_5H_7OCl : C 50,63, H 5,91, O 13,50, Cl 29,96; trouvé : C 50,59, H 5,93, O 13,53, Cl 29,83.

*1'*R*2'S** *2'-Chlorocyclopropyl méthyl cétone* ($\mathbf{1}'^t_{Cl}$) : 3055, 2970, 2920, 1695, 1460, 1400, 1360, 1330, 1250, 1170, 1050, 920, 690; 1,50 (2H, m), 2,10 (1H, m), 2,33 (3H, s), 3,33 (dt, $^3J_c = 7{,}8$, $^3J_t = 3{,}9$). Anal. calc. pour C_5H_7OCl : C 50,63, H 5,91, O 13,50, Cl 29,96; trouvé : C 50,58, H 5,88, O 13,57, Cl 28,79.

*1'*R*2'R** *2'-Bromocyclopropyl méthyl cétone* ($\mathbf{1}'^c_{Br}$) : 3050, 2960, 2900, 1705, 1450, 1390, 1360, 1325, 1250, 1160, 1040, 920, 680; 1,15 (1H, m), 1,70 (1H, m), 2,15 (1H, m), 2,28 (3H, s), 3,10 (dt, $^3J_c = 8$, $^3J_t = 4$). Anal. calc. pour C_5H_7OBr : C 36,81 H 4,29, O 9,82, Br 49,08; trouvé : C 36,90, H 4,36, O 9,79, Br 48,89.

*1'*R*2'S** *2'-Bromocyclopropyl méthyl cétone* ($\mathbf{1}'^t_{Br}$) : 3055, 2970, 2910, 1695, 1460, 1400, 1355, 1320, 1250, 1170, 1050, 920, 680; 1,48 (2H, m), 2,05 (1H, m), 2,30 (3H, s), 3,29 (dt, $^3J_c = 8$, $^3J_t = 4$). Anal. calc. pour C_5H_7OBr : C 36,81, H 4,29, O 9,82, Br 49,08; trouvé : C 36,88, H 4,34, O 9,87, Br 48,83.

*1'*R*2'R** *2'-Chloro-1'-méthyl 2-cyclopropylpropan-2-ol* ($\mathbf{2}^c_{Cl}$) : 3610, 3400, 3055, 1130, 910, 810, 750, 680; 0,81 (1H, dd, $^3J_c = 8{,}5$, $^2J_{gem} = 6$), 1,05 (3H, s), 1,26 (3H, s), 1,43 (3H, s), 1,46 (1H, dd, $^2J_{gem} = 6$, $^3J_t = 5$), 2,93 (1H, dd, $^3J_c = 8{,}5$, $^3J_t = 5$). Anal. calc. pour $C_7H_{13}OCl$: C 56,58, H 8,75, O 10,78, Cl 23,88; trouvé : C 56,52 H 8,71, O 10,83, Cl 23,75.

*1'*R*2'S** *2'-Chloro-1'-méthyl-2-cyclopropylpropan-2-ol* ($\mathbf{2}^t_{Cl}$) : 3600, 3420, 3050, 1120, 900, 810, 740, 680; 0,49 (1H, dd, $^3J_t = 4{,}2$, $^2J_{gem} = 5{,}7$), 1,23 (9H, s), 1,25 (1H, dd, $^2J_{gem} = 5{,}7$, $^3J_c = 8{,}3$), 3,36 (1H, dd, $^3J_c = 8{,}3$, $^3J_t = 4{,}2$). Anal. calc. pour $C_7H_{13}OCl$: C 56,58, H 8,75, O 10,78, Cl 23,88; trouvé : C 56,54, H 8,79, O 10,82, Cl 23,78.

*1'*R*2'R** *2'-Bromo-1'-méthyl-2-cyclopropylpropan-2-ol* ($\mathbf{2}^c_{Br}$) : 3610, 3400, 3040, 1130, 910, 800, 740, 680; 0,92 (1H, dd, $^3J_c = 8$, $^2J_{gem} = 6{,}5$), 1,11 (3H, s), 1,27 (3H, s), 1,43 (3H, s), 1,56 (1H, dd, $^2J_{gem} = 6{,}5$, $^3J_t = 5$), 2,90 (1H, dd, $^3J_c = 8$, $^3J_t = 5$). Anal. calc. pour $C_7H_{13}OBr$: C 43,52, H 6,74, O 8,29, Br 41,45; trouvé : C 43,46. H 6,78, O 8,24, Br 41,31.

*1'*R*2'S** *2'-Bromo-1'-méthyl-2-cyclopropylpropan-2-ol* ($\mathbf{2}^t_{Br}$) : 3620, 3410, 3040, 1125, 900, 810, 750, 690; 0,54 (1H, dd, $^3J_t = 4{,}2$, $^2J_{gem} = 5{,}9$), 1,25 (9H, s), 1,36 (1H, dd, $^2J_{gem} = 5{,}9$, $^3J_c = 7{,}9$), 3,33 (1H, dd, $^3J_c = 7{,}9$, $^3J_t = 4{,}2$). Anal. calc. pour $C_7H_{13}OBr$: C 43,52, H 6,74, O 8,29, Br 41,45; trouvé : C 43,55, H 6,77, O 8,26, Br 41,22.

*1'*R*2'R*3'S** *2'-Chloro-3'-méthyl-2-cyclopropylpropan-2-ol* ($\mathbf{3}^c_{Cl}$) : 3610, 3400, 3055, 1120, 910, 810, 740, 680; 1,10 (3H, d, $J = 5$), 1,15 (1H, m), 1,20 (1H, m), 1,25 (3H, s), 1,40 (3H, s), 2,85 (1H, dd, $^3J_t = 4{,}5$, $^3J_c = 8$). Anal. calc. pour $C_7H_{13}OCl$: C 56,58, H 8,75, O 10,78, Cl 23,88; trouvé : C 56,53, H 8,80, O 10,73, Cl 23,77.

*1'*R*2'S*3'S** *2'-Chloro-3'-méthyl-2-cyclopropylpropan-2-ol* ($\mathbf{3}^t_{Cl}$) : 3600, 3410, 3050, 1125, 910, 800, 740, 690; 1,10 (1H, m), 1,15 (1H, m), 1,20 (3H, d, $J = 6$), 1,25 (6H, s), 3,10 (1H, dd, $^3J_c = 7{,}8$, $^3J_t = 4{,}5$). Anal. calc. pour $C_7H_{13}OCl$: C 56,56, H 8,75, O 10,78, Cl 23,88; trouvé : C 56,54, H 8,78, O 10,76, Cl 23,73.

*1'*R*2'R*3'S** *2'-Bromo-3'-méthyl-2-cyclopropylpropan-2-ol* ($\mathbf{3}^c_{Br}$) : 3610, 3410, 3040, 1115, 900, 800, 750, 680; 1,00 (3H, d, $J = 5{,}5$), 1,05 (1H, m), 1,15 (1H, m), 1,28 (3H, s), 1,40 (3H, s), 2,78 (1H, dd, $^3J_t = 4{,}8$, $^3J_c = 8$). Anal. calc. pour $C_7H_{13}OBr$: C 43,52, H 6,74, O 8,29, Br 41,45; trouvé : C 43,59, H 6,82, O 8,34, Br 41,21.

*1'*R*2'S*3'S** *2'-Bromo-3'-méthyl-2-cyclopropylpropan-2-ol* ($\mathbf{3}^t_{Br}$) : 3600, 3400, 3045, 1120, 910, 800, 745, 690; 0,80 (1H, m), 1,10 (1H, m), 1,20 (3H, s), 1,23 (3H, d, $J = 5{,}5$), 1,28 (3H, s), 3,00 (1H, dd, $^3J_c = 7{,}8$, $^3J_t = 4{,}5$). Anal. calc. pour $C_7H_{13}OBr$: C 43,52, H 6,74, O 8,29, Br 41,45; trouvé : C 43,56, H 6,76, O 8,26, Br 41,32.

1. R. Barlet. Bull. Soc. Chim. Fr. 2767 (1975); Tetrahedron Lett. 4171 (1976).
2. R. Barlet et M. Vincens. Tetrahedron, **33**, 1291 (1977).
3. R. Barlet, R. Le Goaller et C. Gey. Can. J. Chem. **59**, 621 (1981).
4. R. Barlet, R. Le Goaller et C. Gey. Can. J. Chem. **60**, 1933 (1982).

5. R. BARLET, B. BAHARMAST et M. VIDAL. C.R. Acad. Sci. Ser. 2 : **303**, 289 (1986).
6. R. BARLET. J. Org. Chem. **43**, 3500 (1978).
7. (*a*) H. F. BLUM, H. V. DONN, et N. D. ZOOK. J. Am. Chem. Soc. **77**, 4406 (1955); (*b*) H. O. HOUSE et T. M. BARE. J. Org. Chem. **33**, 943(1968); (*c*) T. M. BARE et H. O. HOUSE. Org. Synth. **49**, 81 (1969).
8. M. J. JORGENSEN. Org. React. **18**, 1 (1970).
9. G. L. CLOSS et J. J. COYLE. (*a*) J. Org. Chem. **31**, 2759 (1966); (*b*) J. Am. Chem. Soc. **87**, 4270 (1965).
10. R. HOFFMANN, C. C. LEVIN et R. A. MOSS. J. Am. Chem. Soc. **95**, 629 (1973).
11. B. J. WAKEFIELDS. The chemistry of organolithium compounds. Pergamon Press, Oxford. 1974. p. 138.
12. R. BARLET, B. BAHARMAST et M. VIDAL. Tetrahedron Lett. 3553 (1990).
13. C. A. STEIN et T. H. MORTON. Tetrahedron Lett. 4933 (1973).
14. L. K. SYDNES et L. SKATTEBOL. Acta. Chem. Scand. B, **32**, 547 (1978).

Can. J. Chem. Downloaded from www.nrcresearchpress.com by 198.100.157.202 on 09/07/12
For personal use only.

Theoretical and experimental approaches to the barrier to rotation about the Csp^2—Csp^3 bond in benzyl silane. Hyperconjugative stabilization of the perpendicular conformation

TED SCHAEFER,[1] RUDY SEBASTIAN, AND GLENN H. PENNER[2]
Department of Chemistry, University of Manitoba, Winnipeg, Man., Canada R3T 2N2

Received August 20, 1990

TED SCHAEFER, RUDY SEBASTIAN, and GLENN H. PENNER. Can. J. Chem. **69**, 496 (1991).

The ^{1}H nuclear magnetic resonance spectra of benzyl silane and benzyl trichlorosilane, obtained in CS_2 and benzene-d_6 solutions, are analyzed. The long-range coupling constants between the methylene and *para* ring protons are used to derive apparent twofold barriers about the Csp^2—Csp^3 bonds of 7.4 ± 1.6 and 8.1 ± 1.1 kJ/mol for the silane and the trichlorosilane, respectively. These are higher than that for ethylbenzene and are attributed mainly to the stabilization of the perpendicular conformer, that with the C—Si bond in a plane perpendicular to the phenyl plane, by $\sigma-\pi$ conjugation (hyperconjugation) of the C—Si bond and the π electron system. Molecular orbital computations confirm the predominantly twofold nature of the internal barrier in benzyl silane and also for benzyl germane and stannane. The calculated barriers for the silane derivatives are rather higher than the experimental values. The computed barriers have magnitudes that appear to change with X in much the same order as do the hyperconjugative interactions deduced in other ways for $CH_2X(CH_3)_3$ groups (X = Sn, Ge, Si, C). The angles CCX in benzyl-X (X = CH_3, SiH_3, $SiCl_3$, GeH_3, SnH_3) are all computed to decrease smoothly as $\sin^2\psi$, where ψ is the angle by which the C—X bond twists out of the phenyl plane.

Key words: conformations, benzyl silane and trichlorosilane; NMR, benzyl silane and trichlorosilane; MO calculations, benzyl silane and trichlorosilane.

TED SCHAEFER, RUDY SEBASTIAN et GLENN H. PENNER. Can. J. Chem. **69**, 496 (1991).

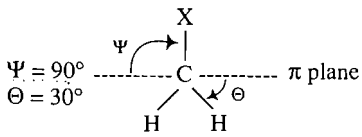
On a analysé les spectres RMN du ^{1}H du benzyl silane et du benzyl trichlorosilane, déterminés en solutions dans le CS_2 ou dans le benzène-d_6. On a utilisé les constantes de couplage à longue distance entre les protons méthyléniques et les protons en *para* du cycle pour évaluer que les barrières binaires apparentes autour des liaisons Csp^2—Csp^3 sont respectivement 7,4 ± 1,6 et 8,1 ± 1,1 kJ/mol pour les dérivés silane et trichlorosilane. Ces valeurs sont plus élevées que celle obtenue avec l'éthylbenzène et on attribue principalement ces différences à la stabilisation de l'isomère perpendiculaire, celui dans lequel la liaison C—Si est maintenue dans un plan perpendiculaire au plan du noyau phényle par une conjugaison $\sigma-\pi$ (hyperconjugaison) de la liaison C—Si et du système électronique π. Des calculs d'orbitales moléculaires confirment la nature principalement binaire de la barrière interne dans le benzyl silane ainsi que dans les benzyl germane et stannane. Les barrières calculés pour les dérivés silanes sont sensiblement plus hautes que les valeurs expérimentales. La variation des amplitudes des barrières calculées pour les dérivés silanes avec X semble suivre l'ordre des interactions d'hyperconjugaison déduites sur d'autres bases pour les groupements $CH_2X(CH_3)_3$ (X = Sn, Ge, Si, C). Les calculs indiquent que les angles CCX, des benzyl-X (X = CH_3, SiH_3, $SiCl_3$, GeH_3 et SnH_3), doivent diminuer doucement comme le $\sin^2\psi$, où ψ est l'angle que fait la liaison C—X avec le plan du noyau phényle.

Mots clés: conformations, benzyl-silane et -trichlorosilane; RMN, benzyl-silane et -trichlorosilane; calculs MO, benzyl-silane et -trichlorosilane.

[Traduit par la rédaction]

Introduction

The stable conformer of ethylbenzene is **1** (X = CH_3) in which the exocyclic C—C bond lies in a plane perpendicular to the benzene plane (1). In solution (2–4), **1** is more stable than



1

the in-plane conformer (ψ = 0°) by 5–6 kJ/mol, with an outlier at 9.6 kJ/mol (5), attributable to $\sigma-\pi$ conjugation (hyperconjugation) of the C—C bond with the π electron system and also, more simply, partially to steric repulsion between the methyl group and the *ortho* C—H bond when ψ = 0° (6). In terms of perturbational molecular orbital theory, the relative stability of **1** arises from a two-orbital four-electron destabilizing interaction when ψ = 0° (7).

When X = $C(CH_3)_3$, the relative stability of **1** rises to more than 20 kJ/mol (8, 9), but drops (10) to about 10 kJ/mol when X is $Si(CH_3)_3$, $Ge(CH_3)_3$, or $Sn(CH_3)_3$, interpretable as a hyperconjugative stabilization (11, 12) of **1** because substitution by chlorine at the *ortho* positions changes the internal barrier by only a small amount. By way of contrast, such substitution in ethylbenzene leads to a very large increase in the stability of **1** (13).

As a further test of the hyperconjugative model we now report ^{1}H nmr data for benzyl silane and benzyl trichlorosilane. The former compound, lacking methyl substituents at silicon, should display even lower residual steric repulsions than in benzyl trimethylsilane for a ψ of 0°. Hence the barrier should be a good estimate of the hyperconjugative stabilization energy of **1** (X = SiH_3). The latter compound may provide a test of the influence of electronegative substituents on the hyperconjugative interaction of the C—Si bond. A derived barrier can then be compared with the type of evidence (12) provided by measurements of ^{13}C chemical shifts, for example. Furthermore, compounds of the type benzyl-XH_3 (S = C, Si, Ge, Sn) lend themselves to reasonably tractable molecular orbital computations. The ensuing conformational predictions can be compared to the available barrier measurements and may provide support for the hyperconjugative model. Such calculations are reported here for X = Si, Ge, Sn and turn out to be useful even though

[1]Author to whom correspondence may be addressed.
[2]Present address: Department of Chemistry of Biochemistry, University of Guelph, Guelph, Ontario.

Can. J. Chem. Downloaded from www.nrcresearchpress.com by 195.138.81.100 on 09/07/12
For personal use only.

TABLE 1. The ^{1}H nmr spectral parameters for benzyl silane and benzyl trichlorosilane at 300 K

Parameter	Benzyl silane		Benzyl trichlorosilane	
	CS_2/C_6D_{12}[a]	C_6D_6[b]	CS_2/C_6D_{12}[a]	C_6D_6[c]
$\nu(SiH_3)$	1104.175(1)[d]	1097.0[e]	—	—
$\nu(CH_2)$	660.754(1)	578.0[e]	842.835(1)	700.000(1)
$\nu_2 = \nu_6$	2097.669(1)	2078.122(3)	2126.667(1)	2066.066(1)
$\nu_3 = \nu_5$	2132.572(1)	2127.545(2)	2159.663(1)	2113.217(1)
ν_4	2095.017(1)	2092.434(3)	2140.290(1)	2093.136(1)
$^3J(CH_2, SiH_3)$	3.966(1)[f]	—	—	—
$^3J_{23}$	7.621(1)	7.686(3)	7.724(1)	7.733(1)
$^3J_{34}$	7.401(1)	7.463(3)	7.488(1)	7.496(1)
$^4J_{24}$	1.125(1)	1.234(3)	1.222(1)	1.225(1)
$^4J_{26}$	1.879(2)	1.951(4)	2.012(1)	2.010(1)
$^4J_{35}$	1.629(1)	1.531(5)	1.469(1)	1.478(1)
$^5J_{25}$	0.616(1)	0.594(2)	0.586(1)	0.592(1)
$^4J(H, CH_2)$	−0.569(1)	−0.551(2)	−0.540(1)	−0.538(1)
$^5J(H, CH_2)$	0.280(1)	0.301(2)	0.286(1)	0.286(1)
$^6J(H, CH_2)$	−0.448(1)	−0.440(4)	−0.401(1)	−0.400(1)
Calcd. transitions	2396[g]	256[h]	332	324
Assigned	1027	158	257	270
Peaks observed	138	—	149	158
Largest difference	0.024	0.046	0.015	0.013
Root-mean-square deviation	0.012	0.017	0.006	0.005

[a] 5 mol% in CS_2 containing also 10 mol% of C_6D_{12} and 0.5 mol% of TMS.
[b] 4 mol% with 0.5 mol% of TMS.
[c] 5 mol% with 0.5 mol% of TMS.
[d] In HZ at 300.135$_2$ MHz to high frequency of internal TMS.
[e] Not included in the analysis.
[f] Numbers in parentheses are standard deviations in the last significant figure.
[g] Including many degeneracies involving the silyl protons. The magnitudes of $^5J(H, SiH_3)$, $^6J(H, SiH_3)$, and $^7J(H, SiH_3)$ are estimated as 0.05(2), 0.02(2), and 0.03(2) Hz, respectively.
[h] Ring protons only.

the benzyl germane and stannane were not available to us for measurements of their ^{1}H nmr parameters.

Experimental

Benzyl trichlorosilane (Fluka) was reduced to the silane with $LiAlH_4$ in the normal way. Solutions of these compounds in CS_2/C_6D_{12}/TMS and C_6D_6/TMS solvent mixtures (Table 1) were filtered into 5 mm o.d. nmr sample tubes. These tubes were degassed by five cycles of the freeze–pump–thaw procedure and were then flame-sealed.

The ^{1}H nmr spectra were accumulated at a probe temperature of 300 K on a Bruker AM300 nmr spectrometer in a manner previously described in detail (14). The spectra of benzyl silane in the CS_2/C_6D_{12}/TMS mixture were rather tightly coupled, the chemical shifts of the ring protons extending over only 37.5 Hz and that between the *ortho* and *para* protons being 2.7 Hz. Small long-range coupling constants between the silyl and ring protons introduced further complications. In the event, the analyses of the spectra were not as precise as could be wished (Table 1). The trichloro derivative gave spectra more amenable to precise analysis.

Ab initio molecular orbital computations utilized an Amdahl 5870 system and the program GAUSSIAN 86 (15). Geometry-optimization procedures allowed all bond angles and lengths to vary, with the constraint, however, that the phenyl moiety remain planar.

Results and discussion

Spectral analyses

The ^{1}H nmr spectra were analyzed with the computer program NUMARIT (16), as extensively modified by R. Sebastian in this laboratory. The spectral parameters obtained in this way appear in Table 1.

The apparent twofold barriers to rotation about the Csp^2—Csp^3 bond

The apparent twofold barriers, V_2, to rotation about the Csp^2—Csp^3 bond are obtainable via the relationship (17, 18) $^6J(H,CH_2) = {}^6J_{90} < \sin^2\theta >$. Here $^6J_{90}$ is the value of the coupling constant for $\theta = 90°$ in **1**, while $<\sin^2\theta>$ is the expectation value determined by the magnitude of V_2, as found from a hindered rotor model or by a classical averaging procedure. In toluene, $^6J_{90}$ is −1.20 Hz (14) and arises from a σ–π coupling mechanism. An α substituent more electronegative than hydrogen reduces σ–π overlap between the α C—H bonds and the π system, causing a reduction in the magnitude of $^6J_{90}$. Thus, in ethylbenzene, $^6J_{90}$ is very likely −1.16 Hz (2) and is −1.02 Hz when X is a methoxy group (19, 20). If the substituent is less electronegative than hydrogen, the magnitude of $^6J_{90}$ is expected to be greater than in toluene and is supported by our INDO MO FPT (21, 22) computations on benzyl silane. These have the maximum magnitude[3] of $^6J_{90}$ as −1.34 Hz, as compared to −1.22 Hz for toluene (17). Another estimate of $^6J_{90}$ for benzyl silane may be had from the general recent agreement that the $Si(CH_3)_3$ and SiH_3 groups are less electronegative than hydrogen (23–25). A lower limit to the magnitude of $^6J_{90}$ is then the −1.20 Hz for toluene. A previous estimate of $^6J_{90}$ for benzyl trimethylsilane is −1.26 Hz (10).

[3] The minimum magnitude lies within 0.01 Hz of that computed for toluene (17); an experimental investigation of the magnitude of ^6J at $\theta = 0$ is available (47).

Can. J. Chem. Downloaded from www.nrcresearchpress.com by 195.138.81.100 on 09/07/12
For personal use only.

TABLE 2. Theoretical components of the internal barriers to rotation about the Csp^2—Csp^3 bonds in benzyl-X (X = CH_3, SiH_3, GeH_3, $SnCH_3$, $SiCl_3$)

Base	X	V_2[a]	V_4[a]	V_6[a]	V_8[a]	$-E$ (min)[d]
STO-3G	CH_3	−6.86(1)	0.97(1)	0.41(1)	−0.15(1)	305.053 256
4-21G	CH_3	−7.85(5)	1.58(5)	0.37(5)	—	308.134 706
6-31G[b]	CH_3	−6.04	1.19	—	—	308.664 033
STO-3G	$SiCH_3$	−12.21(6)	0.66(1)	0.18(1)	−0.18(1)	553.259 814
3-21G	$SiCH_3$	−14.54(1)	0.53(1)	0.42(1)	−0.12(1)	556.790 693
6-31G	$SiCH_3$	−14.04(0)	-0.04_5(0)	0.30(0)	−0.10(0)	559.673 743
STO-3G	$SiCl_3$	−13.36(0)	0.21(0)	−0.34(2)	0.12(0)	1915.426 778
6-31G[c]	$SiCl_3$	−16.62(1)	1.15(6)	—	—	1963.467 574
STO-3G	GeH_3	−11.62(2)	0.48(2)	0.15(2)	−0.17(2)	2319.426 919
STO-3G	SnH_3	−14.23(2)	0.07(2)	0.08(2)	—	6230.959 150

[a]In kJ/mol.
[b]The 6-31 G computations done only for $\psi = 0°$, 45°, and 90°. At $\psi = 0°$, the C—X bond lies in the benzene plane.
[c]For $\psi = 0$, 30, 60, 90°, only.
[d]In au.

$^6J_{90}$ for benzyl silane is probably taken safely as -1.27 ± 0.07 Hz, spanning the value for toluene and the INDO value above. Because $^6J(H,CH_2)$ for the CS_2/C_6D_{12} solution of benzyl silane is −0.448(1) Hz, $<\sin^2\theta>$ follows as 0.353 ± 0.020 and V_2 as $7.4^{+1.7}_{-1.4}$ kJ/mol.

Turning to benzyl trichlorosilane, one recent estimate (26) has the $SiCl_3$ group as 0.1 of a Pauling unit less electronegative than hydrogen, whereas another finds the $SiCl_3$ group as 0.5 units more electronegative than the methyl group (27), for which $^6J_{90}$ appears to be −1.16 Hz (2). It seems safe to take $^6J_{90}$ as -1.16 ± 0.04 Hz for benzyl trichlorosilane, as spanning the range of values indicated by the disparate electronegativity values. Because $^6J(H,CH_2)$ is −0.40 1 (1) Hz (Table 1), $<\sin^2\theta>$ follows as 0.346 ± 0.012 at 300 K. The apparent V_2 is then 8.1 ± 1.1 kJ/mol.

To within experimental error, these apparent twofold barriers are the same as those deduced for benzyl trimethysilane (10). It has been suggested that, for analogous tin compounds, methyl substituents should increase, and chlorine substituents decrease, the extent of hyperconjugation (12). The accuracy of our V_2 estimates is insufficient to confirm such trends for the silicon compounds. Furthermore, small steric contributions to the internal barriers for the methyl and chloro derivatives cannot be excluded (10).

However, the purely hyperconjugative contribution to the barrier should be twofold, the $\sigma-\pi$ conjugation varying as $\sin^2\psi$ (see **1**). Accordingly, molecular orbital computations become of interest and are reported here for benzyl-XH_3 (X = Si, Ge, Sn). These can be compared with the available computations for X = C (2).

Theoretical barriers

The theoretical barriers are reported in Table 2, the relative energies computed at various ψ values being fit to internal potentials as displayed. The striking results are two. First, the twofold barrier is much larger for benzyl silane, germane, and stannane than for ethylbenzene. Second, the fourfold is a much smaller fraction of the twofold component for the former compounds. In ethylbenzene the fourfold component has been attributed to specific steric interactions involving the C—H bonds of the methyl group and those *ortho* to the substituent (2). As the Csp^2—Csp^3 bond is artificially lengthened (2), the fourfold becomes smaller relative to the twofold component. In this interpretation, the decreased importance of the fourfold component of the internal rotational barrier for the silane, germane, and stannane is a consequence of lower short-range repulsive interactions when ψ is 0° in **1**. The large twofold component for these compounds is then evidence for $\sigma-\pi$ conjugation of the C—X bond with the π orbitals of the ring, being a maximum at $\psi = 90°$ and behaving as $\sin^2\psi$, that is, in a twofold manner; this conjugation is also appreciably larger for Si, Ge, Sn than for X = C. The computed twofold components of the internal barrier, using the minimal basis set, decrease in magnitude in the order Sn > Si > Ge > C (Table 2) for benzyl-XH_3, noting also that those for Si and Ge differ by only 0.6 kJ/mol. This order is very similar to that (11) deduced for σ or $\sigma-\pi$ resonance interactions of $CH_2X(CH_3)_3$ groups, which is Sn > Ge ~ Si > C.

The theoretical, mainly twofold, barriers for X = SiH_3 and $SiCl_3$ are rather larger than those deduced from $^6J(H,CH_2)$. Whether this arises from an inadequacy in the size of the employed basis sets, which is possible, or from a solvent effect on the barrier cannot be decided at present. For the similarly nonpolar ethylbenzene the internal barrier is solvent independent in the sense that it is the same in CCl_4, CS_2, acetone-d_6, and in perfluoromethylcyclohexane (2), and very little different from the mean of various magnitudes deduced from experiments on the vapor (28–30). Because benzene, in its influence on the conformational stabilities of solute molecules, behaves as a much more polar solvent than indicated by its dielectric constant (31), the data in Table 1 imply a small or negligible solvent dependence of the internal barriers in benzyl silane and benzyl trichlorosilane. At present, the experimental and theoretical data are qualitatively consistent with a predominantly twofold barrier in benzyl silane arising from a hyperconjugative stabilization of the perpendicular conformer.

Remarks on benzyl trichlorosilane

According to the ^{13}C nmr chemical shifts of the aromatic carbon atoms in benzyl stannane derivatives (12), the extent of $\sigma-\pi$ conjugation decreases as methyl groups are replaced by chlorine atoms at tin. A similar course of events might be expected for benzyl silane and benzyl trichlorosilane. Yet the internal barriers are effectively equal for the two compounds.

Can. J. Chem. Downloaded from www.nrcresearchpress.com by 195.138.81.100 on 09/07/12
For personal use only.

Can. J. Chem. Downloaded from www.nrcresearchpress.com by 195.138.81.100 on 09/07/12
For personal use only.

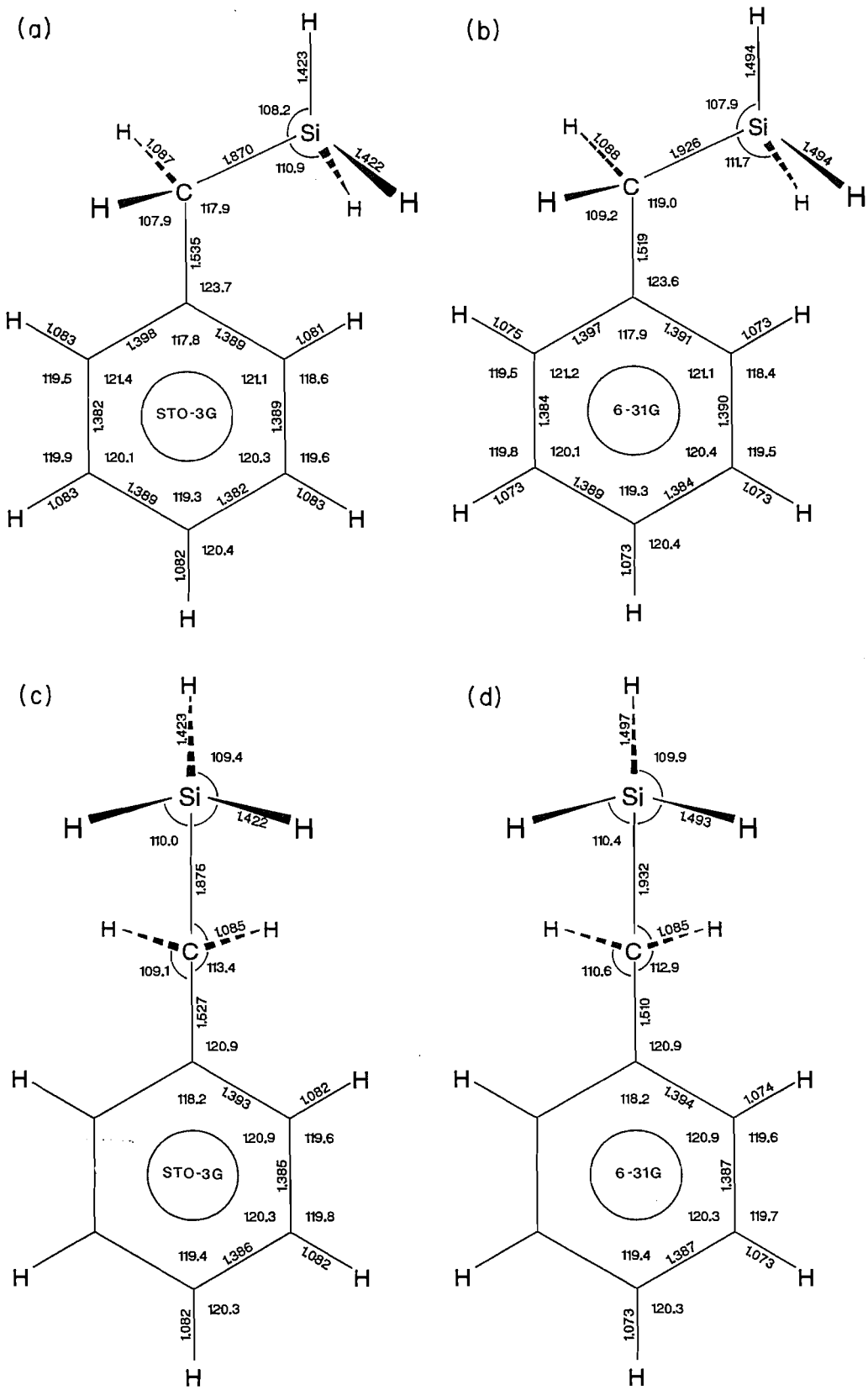


FIG. 1. The structures of the conformations of lowest and highest energies for benzyl silane are shown as computed with the minimal, and with the split-valence, 6-31G basis sets. The computed bond angles within the phenyl group are very close to those predicted (38, 39) from substituent parameters as given for a methyl substituent and determined mainly from X-ray diffraction. The C—Si bond length at the STO-3G level of theory is very close to that of 1.867 Å in methylsilane (40–42), as is the CSiH angle. However, the Si—H bond length in methylsilane is 1.484 Å, so that the STO-3G basis underestimates this length rather badly, whereas it is better reproduced by the split-valence basis set. General comparisons of the performances of the various basis sets can be found in ref. 43, particularly Tables 6.6 and 6.10. The Csp^2—Csp^3 bond length is better found with the larger basis.

Can. J. Chem. Downloaded from www.nrcresearchpress.com by 195.138.81.100 on 09/07/12
For personal use only.

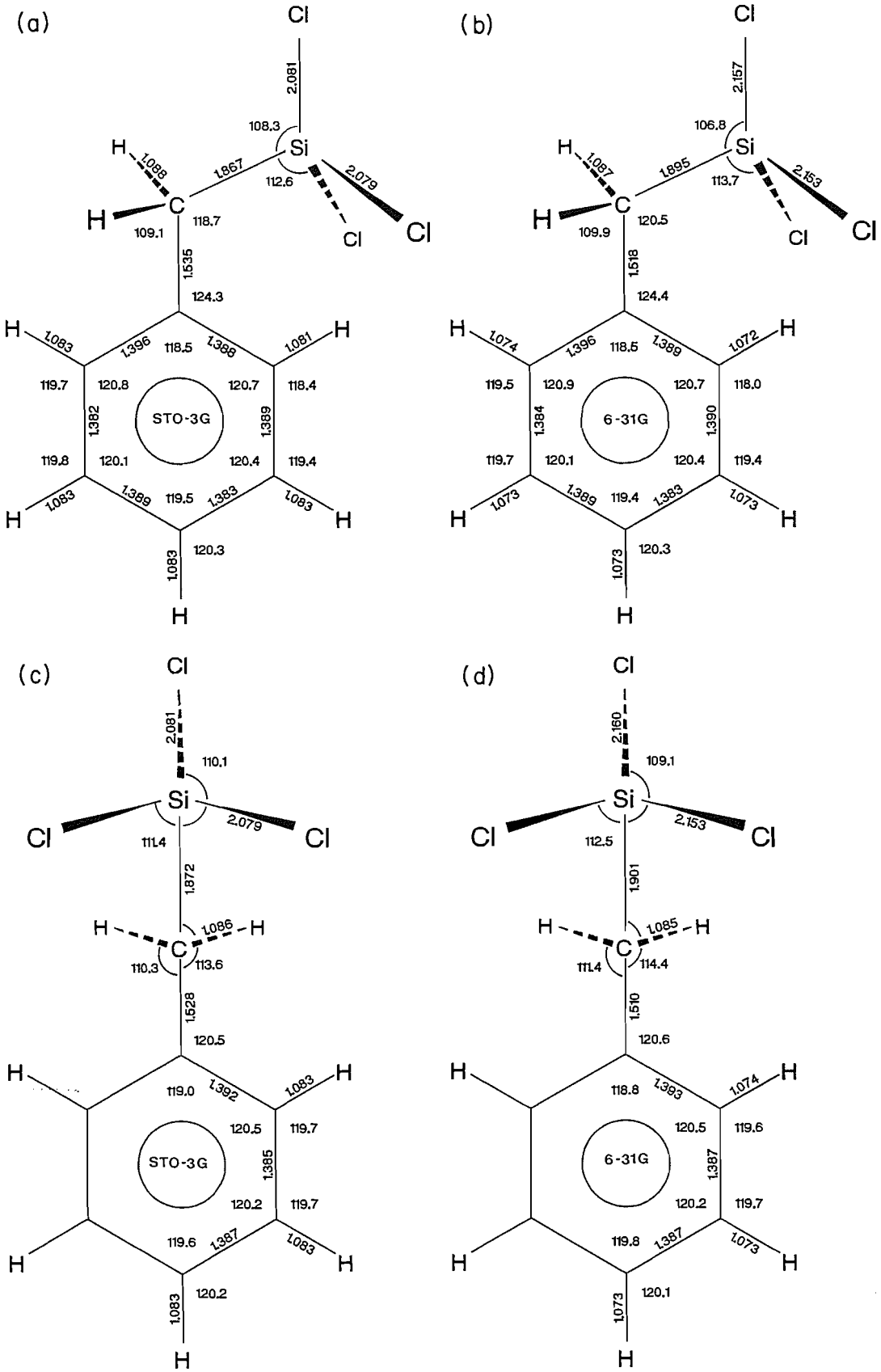


FIG. 2. The structures of the low and high energy conformations of benzyl trichlorosilane are given. Judging by CH_3SiCl_3 (44) and ref. 45, both basis sets overestimate the Si—Cl bond length, the minimal by as much as 0.05 Å. The Si—C bond length in the methyl compound is 1.876(30) Å. From data in ref. 45, the 6-31G basis appears to overestimate this length considerably. These structures can serve as a starting point for computation with larger basis. It does not follow (46) that the larger basis sets will yield more reliable internal barriers.

Can. J. Chem. Downloaded from www.nrcresearchpress.com by 195.138.81.100 on 09/07/12
For personal use only.

Two possibilities present themselves. First, chlorine atoms being larger than hydrogen atoms, a decrease in the hyperconjugative barrier is being compensated by a steric destabilization of the in-plane conformation. However, the internal barriers in benzyl silane and benzyl trimethylsilane (10) are also equal to within experimental error. There are conflicting estimates in the literature concerning the steric sizes of chlorine atoms and methyl groups (32, 33), so that this possibility is moot. Second, it is not at all clear that electron transfer to, or, at least, polarization of, the π electron system of the phenyl group by $\sigma-\pi$ conjugation should be a measure of the size of the internal barrier[4] to rotation about the Csp^2—Csp^3 bond. Thus, for benzyl-X in CS_2 solution, the chemical shift or δ value of the *para* proton is 7.006 (H), 7.019 (CH_3), 6.980 (SiH_3), 7.131 ($SiCl_3$), 7.201 (Cl), and 7.231 (F), while benzene has a δ value of 7.218 (12, 14, 34, 35). These δ values are not simply related to the barriers in these compounds; rather, they more likely are roughly proportional to the electronegativity of X.

The molecular orbital computations (Table 2) with both the minimal and the 6-31G bases imply a larger twofold barrier in the trichlorosilane than in the silane, the former by about 1 kJ/mol, the latter by 2.6 kJ/mol. These *increases* are compatible with the experimental data in solution, perhaps because of the relatively large errors in the latter. At these levels of molecular orbital theory, therefore, the hyperconjugative barriers are not proportional to electron donation to, or rearrangement of the electron densities of, the aromatic ring by the substituents.

Additional considerations

A recent measurement (36) of the free energy of activation for the rotation about the Csp^2—Csp^3 bond in a derivative of $C_6H_5CH(Si(CH_3)_3)_2$ gives a value some 30 kJ/mol lower than that (37) for $C_6H_5CH(C(CH_3)_3)_2$; the lower value is attributed to smaller steric interactions as a consequence of the difference in the C—Si and C—C bond lengths. These results are indirect evidence for the hyperconjugative model of the internal barrier in the title compounds. They are consistent with the measured increase in the barrier to internal rotation in benzyl silane relative to ethyl benzene in the sense that purely steric forces should cause a lower barrier in the silane derivative.

It is interesting, therefore, to compare the theoretical equilibrium structures of the low and high energy conformations of benzyl silane and also of benzyl trichlorosilane. Figure 1 gives the STO-3G and 6-31G structures for benzyl trichlorosilane. The figure captions discuss the reliability of the computed bond lengths involving the silicon atom. Here certain bond angles in the side chain are to be discussed.

The striking bond angles in the conformation of high energy (the silicon atom lies in the benzene plane) are C(2)C(1)C(α) and CCSi, the former being near 124° and the latter as large as 119° in benzyl silane for the larger basis set. In the perpendicular, most stable, conformation the former angle approaches 120°, as expected given the local geometry at C(1), and the latter contracts markedly. These changes are intuitively those expected on the basis of steric repulsions in the planar conformer. In the trichlorosilane, however, the corresponding angles, although somewhat larger, have not increased as much as might be anticipated on the basis of the large chlorine atoms (compare Figs. 1 and 2 for a given basis). Comparison of the CCX angles (X = CH_3, SiH_3, $SiCl_3$, GeH_3, SnH_3), for the seven different ψ values, in the STO-3G computations, reveals that their changes are proportional to $\sin^2\psi$. The CCX angle is given by $A + B\sin^2\psi$, as shown, numbers in parentheses being the standard errors in the fit to seven values of ψ. Note (Table 2) that this dependence on $\sin^2\psi$ holds whatever the relative importance of the various terms in the internal rotational potential. The stabilization of the perpendicular conformer by $\sigma-\pi$ interactions (hyperconjugation) is proportional to $\sin^2\psi$, so that the present relationship is indirect evidence for this phenomenon. Furthermore, for ethylbenzene, the perturbational molecular orbital analysis of Wolfe and co-workers (7), attributing the barrier to a repulsive four-electron, two-orbital interaction for the planar conformer, may be accommodated by the assumption that this interaction decreases as $\sin^2\psi$. The larger deformations in the planar conformers for X = Si, Ge, Sn are not necessarily indicative of larger steric repulsions; their values will depend on the force constants in question, which are not known.

X	A/deg	B/deg
CH_3	116.07(8)	−3.78(12)
$SiCH_3$	118.26(8)	−4.67(12)
$SiCl_3$	118.62(6)	−4.97(10)
$GeCl_3$	118.50(7)	−4.62(12)
SnH_3	119.25(1)	−4.84(2)

In summary, the present experimental and theoretical data, together with the experiments on benzyl trimethyl-X (X = Si, Ge, Sn, Pb) and their 2,6-dichloro derivatives (10), are consistent with a hyperconjugative model for the internal rotational barriers, at least when X = Si, Ge, Sn.

Acknowledgements

We are grateful to the Natural Sciences and Engineering Research Council of Canada for financial assistance. The University of Manitoba is thanked for significant allocations of computing time.

1. P. J. Breen, E. R. Bernstein, and J. I. Seeman. J. Chem. Phys. **87**, 3269 (1987), and references therein.
2. T. Schaefer, G. H. Penner, and R. Sebastian. Can. J. Chem. **65**, 873 (1987).
3. D. Ghesquiere and C. Chachaty. Org. Magn. Reson. **9**, 392 (1977).
4. C. Chachaty, A. Forchioni, and J. C. Ronfard-Haret. Mol. Phys. **31**, 325 (1976).
5. M. Camail, A. Proutiere, and H. Bodot. J. Phys. Chem. **79**, 1966 (1975).
6. W. J. Hehre, L. Radom, and J. A. Pople. J. Am. Chem. Soc. **94**, 1496 (1972).
7. G. H. Penner, T. Schaefer, R. Sebastian, and S. Wolfe. Can. J. Chem. **65**, 1845 (1987).
8. S. Anderson, R. E. Carter, and T. Drakenberg. Acta Chem. Scand. Ser. B, **34B**, 661 (1980).
9. S. Anderson and T. Drakenberg. Org. Magn. Reson. **21**, 730 (1983).
10. T. Schaefer, G. H. Penner, C. S. Takeuchi, and C. Beaulieu. Can. J. Chem. **67**, 1283 (1989).
11. W. Adcock and V. Samkar Tyer. J. Org. Chem. **50**, 1538 (1985), and references therein.
12. J. Holeček, A. Lyčka, K. Handlíř, and M. Nádvorník. Collect. Czech. Chem. Commun. **53**, 571 (1988), and references therein.

[4]It may be possible to rationalize the theoretical barriers in terms of perturbational molecular orbital theory. We have not attempted to do so; the molecular orbitals and their energies for the compounds in Table 2 will be forwarded on request.

13. T. SCHAEFER, L. KRUCZYNSKI, and W. NIEMCZURA. Chem. Phys. Lett. **38**, 498 (1976).
14. T. SCHAEFFER, R. SEBASTIAN, and G. H. PENNER. Can. J. Chem. **63**, 2597 (1985).
15. M. J. FRISCH, J. S. BINKLEY, H. B. SCHLEGEL, K. RAGHAVACHARI, C. F. MELIUS, R. L. MARTIN, J. J. P. STEWARD, F. W. BOBROWICZ, C. F. ROHLFING, L. R. KAHN, D. J. DEFREES, R. SEEGAR, R. A. WHITESIDE, D. J. FOX, E. M. FLUDER, and J. A. POPLE. Carnegie–Mellon Quantum Publishing Unit, Pittsburgh, PA. 1984.
16. J. S. MARTIN, A. R. QUIRT, and K. E. WORVILL. The NMR program library. Daresbury Laboratory, Daresbury, U.K.
17. R. E. WASYLISHEN and T. SCHAEFER. Can. J. Chem. **50**, 1852 (1972).
18. W. J. E. PARR and T. SCHAEFER. Acc. Chem. Res. **13**, 400 (1980).
19. R. LAATIKAINEN. Magn. Reson. Chem. **24**, 588 (1986).
20. R. LAATIKAINEN and K. TUPPURAINEN. J. Chem. Soc. Perkin Trans. 2, 121 (1987).
21. J. A. POPLE, J. W. MCIVER, and N. S. OSTLUND. J. Chem. Phys. **49**, 2965 (1968).
22. P. DEBOSH and N. S. OSTLUND. QCPE, **11**, 281 (1975).
23. J. MULLAY. J. Am. Chem. Soc. **107**, 7271 (1985).
24. R. J. BOYD and K. E. EDGECOMBE. J. Am. Chem. Soc. **110**, 4182 (1988).
25. S. MARRIOTT, W. F. REYNOLDS, R. W. TAFT, and R. D. TOPSOM. J. Org. Chem. **49**, 959 (1984).
26. N. INAMOTO and S. MASUDA. Chem. Lett. 1003 (1982).
27. J. MULLAY. J. Am. Chem. Soc. **106**, 5842 (1984).
28. A. MILLER and D. W. SCOTT. J. Chem. Phys. **68**, 1317 (1978).
29. P. SCHARFENBERG, B. ROZSONDAI, and I. HARGITTAI. Z. Naturforsch. Part A, **35**, 431 (1981).
30. P. SCHARFENBERG. J. Chem. Phys. **77**, 4791 (1982).
31. R. J. ABRAHAM and E. BRETSCHNEIDER. *In* Internal rotation in molecules. *Edited by* W. J. Orville-Thomas. Wiley and Sons, New York. 1974. Chap. 13.
32. H. FÖRSTER and F. VÖGTLE. Angew. Chem. Int. Ed. Engl. **16**, 429 (1977).
33. M. CHARTON and B. CHARTON. J. Am. Chem. Soc. **97**, 6472 (1975).
34. T. SCHAEFER, R. SEBASTIAN, and G. H. PENNER. Can. J. Chem. **64**, 1372 (1986).
35. T. SCHAEFER, J. PEELING, and R. SEBASTIAN. Can. J. Chem. **63**, 3219 (1985).
36. R. OKAZAKI, M. UNNO, N. INAMOTO, and G. YAMAMOTO. Chem. Lett. 493 (1989).
37. A. R. KATRITZKY, V. J. BECKER, and F. M. S. BRITO-PALMA. J. Chem. Soc. Perkin Trans. 2, 143 (1979).
38. A. DOMENICANO and P. MURRAY-RUST. Tetrahedron Lett. 2283 (1979).
39. R. NORRESTAM and L. SCHEPPER. Acta Chem. Scand. Ser. A, **A35**, 91 (1981).
40. R. W. KILB and L. PIERCE. J. Chem. Phys. **27**, 108 (1957).
41. L. PIERCE and D. H. PETERSON. J. Chem. Phys. **33**, 907 (1960).
42. M. WONG, I. OZIER, and W. L. MEERTS. J. Mol. Spectrosc. **145**, 225 (1986).
43. W. J. HEHRE, L. RADOM, P. V. R. SCHLEYER, and J. A. POPLE. *Ab initio* molecular orbital theory. J. Wiley and Sons, New York. 1986.
44. R. MOCKLER, J. H. BAILEY, and W. GORDY. J. Chem. Phys. **27**, 1710 (1953).
45. F. H. ALLEN, O. KENNARD, D. G. WATSON, L. BRAMMER, A. G. ORPEN, and R. TAYLOR. J. Chem. Soc. Perkin Trans. 2, S1 (1987).
46. G. H. PENNER, P. GEORGE, and C. W. BOCK. J. Mol. Struct. (Theochem), **152**, 201 (1987).
47. T. SCHAEFER and C. S. TAKEUCHI. Can. J. Chem. **67**, 1022 (1989)

Can. J. Chem. Downloaded from www.nrcresearchpress.com by 195.138.81.100 on 09/07/12
For personal use only.

2-Phenyladamantane as a model for axial phenylcyclohexane. ^{1}H NMR and molecular orbital studies of motion about the Csp^2—Csp^3 bond

TED SCHAEFER,[1] CHRISTIAN BEAULIEU,[2] AND RUDY SEBASTIAN
Department of Chemistry, University of Manitoba, Winnipeg, Man., Canada R3T 2N2
Received September 4, 1990

TED SCHAEFER, CHRISTIAN BEAULIEU, and RUDY SEBASTIAN. Can. J. Chem. **69**, 503 (1991).

The ^{1}H NMR spectra of the aromatic groups of 2-phenylcyclohexane and 2-phenyladamantane, in CS_2/C_6D_{12} solution at 300 K, are analyzed to yield the long-range coupling constants between the α and ring protons. The coupling over six bonds is related to the internal rotational potential about the Csp^2—Csp^3 bond in these molecules. It is confirmed that the equatorial isomer of phenylcyclohexane has the parallel conformer, that in which the aromatic plane lies in the symmetry plane bisecting the cyclohexane moiety, as the most stable. The apparent twofold barrier to rotation about the exocyclic carbon–carbon bond follows as 7.1 kJ/mol from the six-bond coupling constant. For 2-phenyladamantane, the six-bond coupling constant strongly implies that the perpendicular conformer, perhaps slightly skewed, is that of lowest energy and that the apparent twofold barrier to rotation about the Csp^2—Csp^3 bond is about 7.5 kJ/mol. Insofar as 2-phenyladamantane mimics axial phenylcyclohexane, these results confirm recent conclusions about the conformation of the latter and provide evidence for its internal mobility. Geometry-optimized AM1 and STO-3G MO computations are reported for the internal motion in both isomers of phenylcyclohexane. The former agree best with experiment for the equatorial isomer, but both imply a significant fourfold, of opposite sign to the twofold, component of the internal rotational potential. For the axial isomer, the two sets of computations find a skewed perpendicular conformer as most stable, in rough agreement with force-field results. However, the barrier to rotation about the Csp^2—Csp^3 bond is computed as small and AM1 has the parallel conformer as more stable than the perpendicular.

Key words: 2-phenyladamantane, ^{1}H NMR and internal rotation; phenylcyclohexane, ^{1}H NMR and internal rotation; MO computations, 2-phenyladamantane and phenylcyclohexane.

TED SCHAEFER, CHRISTIAN BEAULIEU et RUDY SEBASTIAN. Can. J. Chem. **69**, 503 (1991).

Afin d'obtenir les constantes de couplage à longue distance entre les protons α et ceux du cycle, on a analysé les spectres RMN du ^{1}H des groupements aromatiques du 2-phénylcyclohexane et du 2-phényladamantane, en solution dans du CS_2/C_6D_{12}, à 300 K. Le couplage à travers six liaisons est lié au potentiel de la rotation interne autour de la liaison Csp^2—Csp^3 de ces molécules. On confirme que l'isomère équatorial le plus stable du phénylcyclohexane est le conformère parallèle, celui dans lequel le plan du noyau aromatique se trouve dans le plan de symétrie bissecteur de la portion cyclohexanique. Sur la base de la constante de couplage à travers six liaisons, il ressort que la barrière binaire apparente à la rotation autour de la liaison carbone–carbone exocyclique est de 7,1 kJ/mol. Pour le 2-phényladamantane, la constante de couplage à travers six liaisons suggère fortement que le conformère perpendiculaire, possiblement un peu décalé, est le plus stable et que la barrière binaire apparente à la rotation autour de la liaison Csp^2—Csp^3 est d'environ 7,3 kJ/mol. En autant que le 2-phényladamantane imite bien le phénylcyclohexane axial, ces résultats confirment les conclusions récentes concernant la conformation de ce dernier et ils fournissent de nouvelles données concernant sa mobilité interne. On rapporte des calculs d'OM AM1 et STO-3G, réalisées sur des molécules dont la géométrie a été optimisée, relatifs au mouvement interne dans les deux isomères du phénylcyclohexane. Les premiers donnent le meilleur accord avec les données expérimentales concernant l'isomère équatorial; toutefois, les deux suggèrent une composante quaternaire importante, de signe opposé à celui de la composante binaire du potentiel de rotation interne. Dans le cas de l'isomère axial, les deux ensembles de calculs suggèrent que le conformère perpendiculaire décalé est le plus stable; ces conclusions se rapprochent des résultats obtenus avec les champs de force. Toutefois, ces calculs indiquent que la barrière à la rotation autour de la liaison Csp^2—Csp^3 est faible; de plus, les calculs AM1 donnent le conformère parallèle comme plus stable que le conformère perpendiculaire.

Mots clés : 2-phényladamantane, RMN du ^{1}H et rotation interne; phénylcyclohexane, RMN du ^{1}H et rotation interne; calculs d'OM, 2-phényladamantane et 2-phénylcyclohexane.

[Traduit par la rédaction]

Introduction

The free energy difference between equatorial, **1** and **2**, and axial, **3** and **4**, phenylcyclohexane is an old and famous problem (1). Recently (1), Squillacote and Neth used a cryogenic trapping technique to show that the equatorial conformer is favored by 11.3 ± 1.1 kJ in free energy in propane-d_8 solution, thereby narrowing considerably the uncertainty in this quantity. Furthermore, the entropy difference between the axial and equatorial forms must be small because the free energy difference changes very little over a range of 800 K.

Squillacote and Neth also use the nuclear Overhauser effect (incoherent transfer of magnetization) in a demonstration that **4**, the perpendicular conformer of axial phenylcyclohexane, is more stable than the parallel conformer, **3**, in solution. In equatorial phenylcyclohexane it is the parallel conformer, with a (bisected) low energy structure analogous to that of isopropylbenzene (2), which is most stable. For 3,5-dichlorophenylcyclohexane the *apparent* twofold barrier to rotation about the Csp^2—Csp^3 bond in benzene-d_6 solution was assessed (3) at 8.4 ± 1.3 kJ/mol on the basis of the conformational dependence of ^6J(H, CH), the σ–π spin–spin coupling constant over six bonds between the α proton in the methine C—H bond and the *para* ring proton. Long-range coupling constants of this kind are generally about 1 Hz in magnitude and would be difficult, perhaps impossible, to extract for axial phenylcyclohexane at −160°C, the temperature at which the trapped molecule is not converting rapidly to the equatorial form, simply because the effective T_2 is too small to allow the requisite narrow ^{1}H NMR peaks. However, it was suggested to us by Craig Takeuchi that

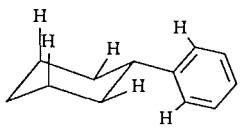
[1]Author to whom correspondence may be addressed.
[2]Undergraduate research participant, 1989–1990.

Can. J. Chem. Downloaded from www.nrcresearchpress.com by 195.138.81.100 on 09/07/12
For personal use only.

Can. J. Chem. Downloaded from www.nrcresearchpress.com by 195.138.81.100 on 09/07/12
For personal use only.

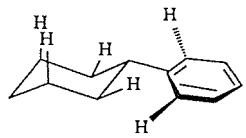
2-phenyladamantane, **5** and **6**, may well serve as a model of axial phenylcyclohexane at ambient temperatures, where high resolution ^{1}H NMR spectra should be reasonably accessible.[3]

Such spectra are reported here for a CS_2 solution. Their analysis yields long-range coupling constants which confirm that the parallel conformation, **5**, is not favored, and which yield an approximate barrier to rotation about the Csp^2—Csp^3 bond. A similar treatment is accorded the ^{1}H NMR spectrum of (equatorial) phenylcyclohexane.



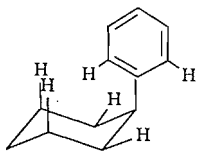
equatorial - parallel

1



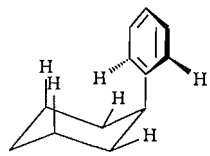
equatorial - perpendicular

2



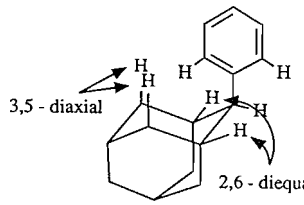
axial - parallel

3



axial - perpendicular

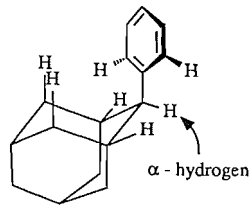
4



3,5 - diaxial

2,6 - diequatorial

5



α - hydrogen

6

In addition, semiempirical AM1 and *ab initio* STO-3G MO computations are reported for the two forms of phenylcyclohexane. The results may be compared with molecular mechanics calculations of conformer stabilities in the literature.

Experimental

The 2-phenyladamantane was prepared by treatment of 2-phenyladamantanone (Aldrich) with C_6H_5MgBr to yield 2-hydroxy-2-phenyladamantane. The latter was reduced to the hydrocarbon with H_2/Pd (charcoal) followed by purification on a silica gel column with hexane as eluent. The yield was poor and this synthesis is not recommended. A later synthesis involved the reduction of the alcohol using the $NaBH_4/CF_3SO_3H$ procedure (4) and gave much better yields.[4] The 2-phenyladamantane gave satisfactory mass, ^{1}H NMR, and ^{13}C NMR (5, 6) spectra.

Solutions of 2-phenyladamantane and phenylcyclohexane (Aldrich), in a CS_2/C_6D_{12}/TMS solvent mixture (see Table 1 for details), were transferred to 5-mm o.d. NMR tubes, were degassed by five freeze–pump–thaw cycles, and the tubes were then flame-sealed under vacuum.

^{1}H NMR spectra were accumulated on a Bruker AM300 spectrometer in a manner described previously (7) and had a digital resolution of 0.12 Hz/point with an acquisition time of 42 s. Those ring protons not coupled appreciably to β-protons give peak widths of about 0.07 Hz. As can be seen in Fig. 1, the *ortho* protons couple by about 0.18 Hz to the β-protons (equatorial 2,6-protons in **5**) in 2-phenyladamantane. The latter resonate at 2.42 ppm (see ref. 1 for their assignment in axial phenylcyclohexane) and were decoupled from the ring protons in the spectrum subjected to spectral analysis. In phenylcyclohexane the corresponding coupling constant is much smaller, rather as in isopropylbenzene (2).

The AM1 (8) and STO-3G (9) molecular orbital computations used the program GAUSSIAN 86 (10). All bond angles and lengths were optimized at each angle of rotation about the Csp^2—Csp^3 bond in axial and equatorial phenylcyclohexane; the nuclei of the phenyl group, however, were constrained to a plane.

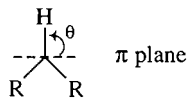
Results and discussion

Spectral analyses

The ^{1}H NMR spectra of the aromatic protons were analyzed with the computer program NUMARIT (11), extensively altered and improved by R. Sebastian. The spectral parameters appear in Table 1. In Fig. 1 the *ortho* region yields broad peaks, some with triplet structure, attributable to coupling constants involving the β-alkyl protons with δ = 2.42. Decoupling procedures caused considerably sharper *ortho* proton peaks, which, however, displayed a greater width than those from *meta* or *para* proton peaks. This residual width, if not due to short spin-lattice relaxation times, may well arise from unresolved coupling constants with the 3,5-axial protons in **5** or **6** because motion about the Csp^2—Csp^3 bond entails occasional short distances between the hydrogen atoms carrying the protons in question. However, the 3,5-proton peaks could not be assigned, leaving the matter uncertain.

Internal motion in equatorial phenylcyclohexane

The coupling constant over six formal bonds, ^6J_p(H, CH) ≡ ^6J, is proportional to $\sin^2\theta$, where the torsion angle, θ, is illustrated in **7** (2, 7, 12); the available evidence (13) is that ^6J



1

effectively vanishes when θ is zero. Furthermore, $^6J_{90}$ is somewhat dependent on the electronegativity of the α-substituents, experimental assessments (14, 15) of this dependence being available. For isopropylbenzene, $^6J_{90}$ is −1.12 Hz (2). Therefore a measurement of ^6J yields an expectations value of $\sin^2\theta$, which can be related to the barrier to rotation about the Csp^2—Csp^3 bond by a hindered rotor model (12) or by a classical averaging procedure; at ambient temperatures for the barrier magnitudes and reduced moments of inertia of many benzene derivatives these two procedures yield essentially the same barrier magnitudes. The measured ^6J is usually an immediate marker of the conformation of lowest energy.

Thus, for phenylcyclohexane (Table 1), ^6J is −0.243 (4) Hz and, with $^6J_{90}$ as −1.12 Hz, $\langle\sin^2\theta\rangle$ follows as 0.217 (4). Were the barrier very high and were the perpendicular form, **2** with θ = 90°, of low energy, $\langle\sin^2\theta\rangle$ would be near unity. Were the barrier high but with the parallel form of low energy, **1** with θ = 0°, $\langle\sin^2\theta\rangle$ would approach zero. For a vanishing barrier, with **1** and **2** then being two of an infinite number of isoenergetic conformations, $\langle\sin^2\theta\rangle$ would be 0.5. Clearly, the value of 0.217 (4) implies a finite barrier with **1** as the conformation of low energy, just as for isopropylbenzene (2). An apparent

[3]In **5**, the numbering of the alkyl protons conforms to that in phenylcyclohexane, facilitating an unambiguous later discussion; of course, the phenyl group is attached at position 2 in adamantane.

[4]We thank George A. Doss (Ashraf Abdel-Sayed) for advice concerning a third method of synthesis, a Friedel–Crafts reaction of 2-bromoadamantane with benzene.

TABLE 1. The ^{1}H NMR spectral parameters of the aromatic protons of phenylcyclohexane, **1**, and 2-phenyladamantane, **6**, in CS_2/C_6D_{12} solution at 300 K

Parameter	**1**[a]	**6**[b,f]	Parameter	**1**[a]	**6**[b,f]
ν_α(CH)	723.73[c]	882.72[c]	$^5J_{om}$	0.579 (0)	0.565 (1)
ν_o	2114.836 (2)[d]	2162.004 (3)	^4J(H,CH)	−0.577 (4)	−1.038 (7)
ν_m	2134.837 (2)	2151.334 (3)	^5J(H,CH)	0.294 (3)	0.367 (5)
ν_p	2102.023 (2)	2106.562 (3)	^6J(H,CH)	−0.243 (4)	−0.889 (5)
$^3J_{om}$	7.742 (4)[e]	7.899 (5)	Calcd. transitions	172	176
$^3J_{mp}$	7.397 (2)	7.353 (3)	Assigned trans.	113	85
$^4J_{oo}$	1.961 (3)	2.109 (5)	Peaks	92	83
$^4J_{op}$	1.259 (2)	1.211 (4)	Largest difference	0.030	0.031
$^4J_{mm}$	1.464 (3)	1.537 (5)	RMS deviation	0.011	0.013

[a]For a 4.0 mol% solution in CS_2, containing also 10 mol% of C_6D_{12} and 0.5 mol of TMS.
[b]For a ca. 1 mol% solution in the CS_2/C_6D_{12}/TMS mixture.
[c]These shifts of the α C—H proton are not optimized, the resonance consisting of a myriad of overlapping peaks.
[d]In Hz at 300.135$_2$ MHz to low frequency of internal TMS.
[e]Numbers in parentheses are the standard deviations of the last significant figure.
[f]The analysis for **6** pertains to a spectrum obtained while decoupling the equatorial 2,6 protons (see **5** in the text); these couple to the *ortho* protons of the phenyl group by ±0.18 Hz (see also the caption to Fig. 1).

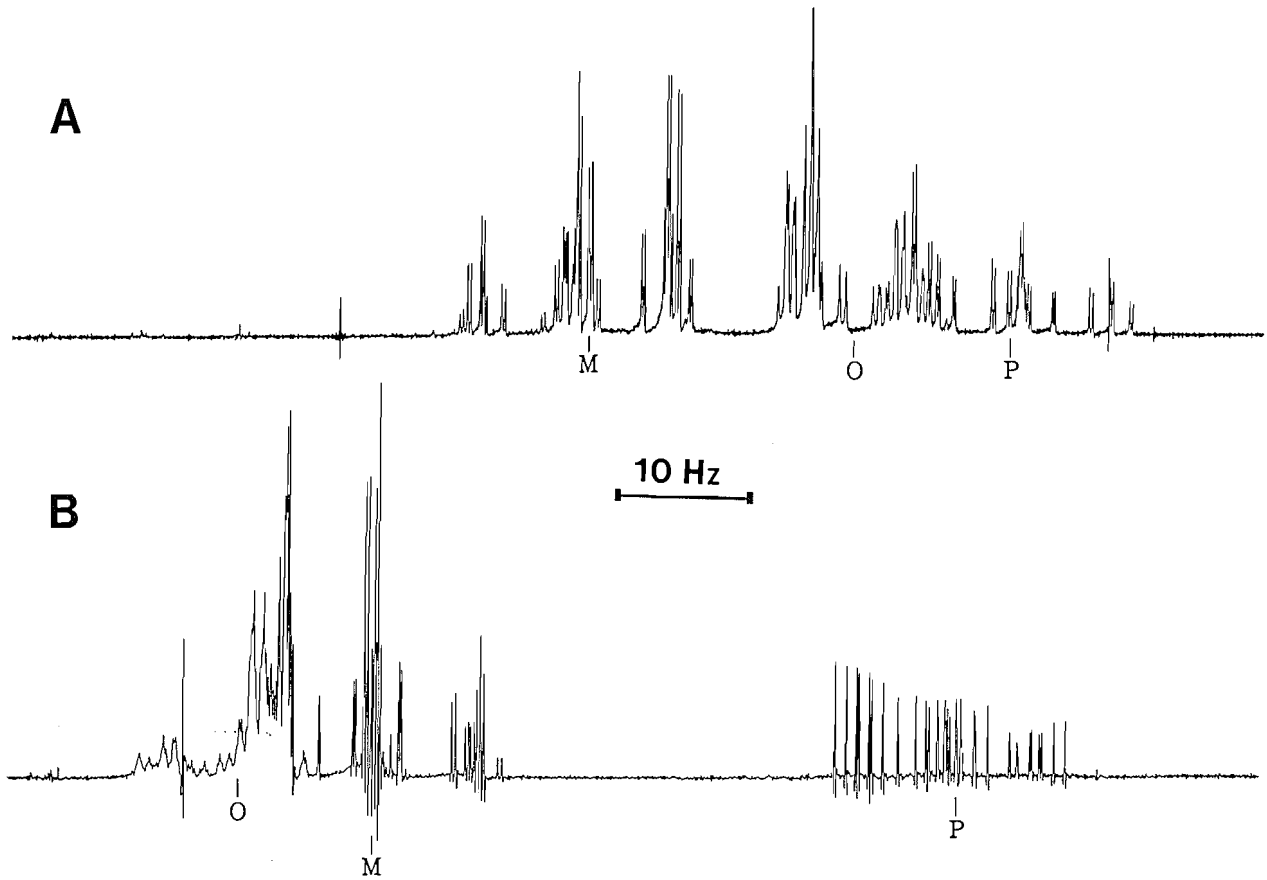


FIG. 1. In A, the ^{1}H NMR spectrum of the phenyl group of a 4 mol% solution of phenylcyclohexane is displayed at 300 Mz and 300 K. The chemical shift positions, obtained from the spectral analysis detailed in Table 1, are indicated. The analogous ^{1}H NMR spectrum for a very dilute solution of 2-phenyladamantane is shown in B. The large relative descreening of the *ortho* protons is similar to that found for axial phenylcyclohexane at 113 K (1). These protons are coupled to the neighbouring β alkyl protons by 0.18 Hz, as deduced from decoupling experiments described in the text. The analysis of the ^{1}H NMR spectrum to yield the parameters in Table 1 used the one in which the β-alkyl protons were decoupled.

twofold barrier, V_2, follows as 7.1 kJ/mol. Were $^6J_{90}$ equal to −1.20 Hz, as in toluene (7), then the apparent V_2 would rise to 7.6 kJ.

The presence of a significant fourfold component will alter the barrier magnitude. This possibility is discussed below in connection with molecular orbital computations of the barrier profile.

Internal motion in 2-phenyladamantane

^6J is −0.889 (5) Hz in 2-phenyladamantane. The discussion

Can. J. Chem. Downloaded from www.nrcresearchpress.com by 195.138.81.100 on 09/07/12
For personal use only.

Can. J. Chem. Downloaded from www.nrcresearchpress.com by 195.138.81.100 on 09/07/12
For personal use only.

in the previous section allows the immediate conclusion that the parallel conformer, **5**, cannot be that of low energy because a rigid **5** would have a vanishing ^6J. If perpendicular **6** has the lowest energy, then the apparent V_2 is 7.5 (1) kJ/mol because $\langle\sin^2\theta\rangle$ is 0.794 (4) at 300 K. This indication, that the internal barriers in equatorial phenylcyclohexane and 2-phenyladamantane are equal, recalls the fact (1) that the entropies of the axial and equatorial forms of phenylcyclohexane are also the same.

An alternative interpretation of ^6J takes a skewed **6** as the conformation of lowest energy. Suppose, as suggested by the computations described below, that a θ near 60° defines the low energy form, the one in which the C(1)—C(2) bond eclipses the C(α)—C(β) bond of the alicyclic group. If this conformer is rigid, then $\langle\sin^2\theta\rangle$ is 0.75 and ^6J follows, in principle, as (−1.12) (0.75) or −0.84 Hz. If motion towards **6** costs less energy than that towards **5**, as would be expected, then $\langle\sin^2\theta\rangle$ would increase somewhat from 0.75, causing a larger magnitude of ^6J, perhaps as large as the measured 0.89 Hz. This interpretation is compatible only with a relatively large barrier to rotation about the Csp^2—Csp^3 bond in 2-phenyladamantane, perhaps in the vicinity of 25 kJ/mol, and, intuitively, appears unlikely but not impossible. To reach **5** does entail a rather close approach of the *ortho* and 3,5-protons.

Of course, 2-phenyladamantane and axial phenylcyclohexane are different molecules. Yet, insofar as the phenyl group in the latter appears (1) to induce geometric distortion of the cyclohexane ring only at the site of attachment, 2-phenyladamantane may provide a reasonable model of the motion of the phenyl group in the cyclohexane derivative. Note also that the order of the chemical shifts (Fig. 1) of the aromatic protons in 2-phenyladamantane is the same as that of axial phenylcyclohexane (1). Furthermore, Squillacote and Neth (1) report that the *ortho* protons in the latter are deshielded by 0.2 ppm relative to their shielding in the equatorial isomer. Table 1 reports a deshielding of 0.160 ppm for the *ortho* protons of the adamantane relative to the cyclohexane derivative. The shift to high frequency is attributed (1) to steric hindrance of the *ortho* by the 2,6 hydrogen atoms, so that **6** and **4** are probably very similar in their internal motional behaviour.[5] Consistent with this statement is the observation that the 2,6-protons of **6** and **4** are both shifted to higher frequencies, in such a way as to isolate their peaks from those of the other alkyl protons, presumably due to steric interactions with *ortho* aromatic hydrogen atoms. In axial cyclohexane at 113 K in propane-d_8, the α-protons are screened less by ca. 0.7 ppm than they are in the equatorial isomer (1). At 184 K, in a 50 vol% solution of $C_6D_{11}H$, the corresponding number is 0.478 (2) ppm (16), whereas at 300 K, for dilute solutions in CS_2/D_6D_{12}, the α-proton of 2-phenyladamantane is deshielded by 0.530 ppm relative to that in equatorial phenylcyclohexane. Given that torsional excursions of the phenyl group about the Csp^2—Csp^3 bond will be of significantly larger amplitude at 300 K than at 113 K, thereby averaging a number of shift values for the α-proton, and that the β-sites are different, this shift is consistent with similar ground state phenyl conformations in the axial adamantane and cyclohexane derivatives.

The existence of a ^5J(H,H) of ±0.18 Hz between the *ortho* and 2,6-protons in 2-phenyladamantane is again evidence for a close approach of the C—H bonds carrying the coupled nuclei in **6**. There is little doubt that this is a proximate (17–21) coupling constant, mediated by overlap of the orbitals on the hydrogen atoms of the β and *ortho* C—H bonds. In a standard model of 2-phenyladamantane, the coupled nuclei are separated by a little less than 2.2 Å in the perpendicular conformer, just as required for a proximate coupling mechanism. The residual extra width of the *ortho* proton peaks in **6** after the decoupling of the 2,6-protons (see experimental) may well be due to a small coupling interaction with the 3,5-protons. In the standard parallel conformation, the internuclear distance would be ca. 1.6 Å, implying a large coupling constant and also, of course, a large repulsion between the hydrogen atoms. The population of this conformer is therefore indicated as small, in line with the nOe studies (1) on axial phenylcyclohexane at 113 K.

The axial isomers are unstable because of steric repulsions even in the perpendicular conformation of the phenyl group. The indication, from ^6J, that the freedom of motion about the exocyclic C—C bond is much the same as in the equatorial isomer implies that the strongly repulsive *ortho*–3,5 interactions in the parallel conformers, **3** and **5**, raise the energy of the axial isomers by roughly the same amount as the repulsive 2,6–*ortho* interactions in the perpendicular, equatorial, **2**, raise its energy relative to **1**. In other words, $E_3 - E_4 \sim E_2 - E_1$, with the caveat, of course, that **6** and **4** are different molecules.

It is of interest whether (practically applicable) molecular orbital calculations on axial and equatorial phenylcyclohexanes bear out the experimental results, previous computations having concentrated on force-field approaches (1).

AM1 and STO-3G MO computations

The computed relative energies of axial and equatorial phenylcyclohexane, as a function of the torsion angle, θ, about the Csp^2—Csp^3 bond are found in Table 2. These energies can be fit to the internal rotational potentials in eqs. [1]–[4]; the angle θ is zero in the parallel conformers, **1** and **3**. The standard

TABLE 2. AM1 and STO-3G geometry-optimized computations of the internal barriers to rotation in axial and equatorial cyclohexane

	Relative energy, kJ mol^{-1}			
	Equatorial		Axial	
θ, deg[a]	AM1[f]	STO-3G[g]	AM1[b]	STO-3G[c]
0	0.000	0.000[d]	0.000	0.000[e]
15	1.039	1.091	0.557	0.090
30	2.479	3.130	0.886	−0.262
45	2.686	4.997	−0.674	−0.966
60	3.941	8.345	−1.189	−2.533
75	7.303	13.633	1.003	−1.380
90	9.271	16.062	2.502	−0.538

[a]For the equatorial isomer, θ = 0° refers to the parallel conformer, **1**, of the text, in which the α C—H bond lies in the aromatic plane. For the axial isomer, θ = 0° again identifies the parallel conformer, **3**, with the α C—H bond in the aromatic plane.

[b]The minimum energy occurs at θ = 55.3°, corresponding to a relative energy of −1.364 kJ mol^{-1}.

[c]The minimum energy is −2.676 kJ mol^{-1}, corresponding to a θ = 57.0°.

[d]The total energy of this conformer is −458.231 326 au.

[e]The total energy of this conformer is −458.223 366 au.

[f]AM1 has the equatorial isomer at θ = 0° as 13.578 kJ mol^{-1} more stable than the axial isomer with θ = 55.3°.

[g]The total energy of the equatorial isomer at θ = 0° is computed as 18.220 kJ mol^{-1} lower in energy than the axial isomer at θ = 57.0° (STO-3G).

[5]The chemical shifts of the *para* protons in **1** and **6** in Table 1 differ by only 0.015 ppm, confirming that redistribution of electron density in the phenyl group is small in going from equatorial to axial conformers.

errors in the fits to the twofold term, in $\sin^2\theta$, and so forth, are given in parentheses.

[1] $V(\theta)/\text{kJ mol}^{-1}$ (equatorial, AM1) = 7.18 (1) $\sin^2\theta$ −1.95 (1) $\sin^2 2\theta$ + 2.11 (1) $\sin^2 3\theta$ + 0.03 (1) $\sin^2 4\theta$

[2] $V(\theta)/\text{kJ mol}^{-1}$ (axial, AM1) = 0.36 (3) $\sin^2\theta$ −1.95 (3) $\sin^2 2\theta$ + 2.21 (3) $\sin^2 3\theta$

[3] $V(\theta)/\text{kJ mol}^{-1}$ (equatorial, STO-3G) = 14.33 (5) $\sin^2\theta$ −3.11 (5) $\sin^2 2\theta$ + 1.87 (5) $\sin^2 3\theta$

[4] $V(\theta)/\text{kJ mol}^{-1}$ (axial, STO-3G) = −1.80 (2) $\sin^2\theta$ −0.98 (2) $\sin^2 2\theta$ + 1.32 (2) $\sin^2 3\theta$ + 0.22 (9) $\sin^2 4\theta$ + 0.26 (2) $\sin^2 6\theta$ − 0.77 (9) $\sin^2 8\theta$

Considering first the AM1 results, and noting that the sixfold term, in $\sin^2 3\theta$, contributes to the barrier height, the latter is 9.3 kJ for the equatorial isomer and corresponds to the perpendicular conformer, **2**, as expected intuitively. The *apparent* V_2 is 7.3–7.6 kJ/mol for a CS_2/C_6D_{12} solution, deduced from ^6J. Note, now, that the potential in eq. [1] corresponds to a $\langle\sin^2\theta\rangle$ of 0.245 at 300 K, somewhat higher than the 0.21 based on ^6J. Were the theoretical fourfold term to vanish, or were it positive, the $\langle\sin^2\theta\rangle$ value would be lower than 0.245. The negative fourfold component in eq. [1] means that out-of-plane motion of the α C—H bond in the low-energy conformer, **1**, is facilitated by its presence. A *pure* V_2 of 9.3 kJ/mol, corresponding to the theoretical barrier *height*, would entail a $\langle\sin^2\theta\rangle$ of 0.167. The experimental value of 0.21 is an upper limit, but cannot distinguish between a pure twofold barrier and a multifold potential. A modest agreement between theory and experiment appears to exist, judging by $\langle\sin^2\theta\rangle$ values; this is not true for the axial isomer, judging by 2-phenyladamantane as a model.

The AM1 data for the axial isomer in Table 2, together with the potential function in eq. [2], imply a very low barrier to rotation about the Csp^2—Csp^3 bond. The $\langle\sin^2\theta\rangle$ value at 300 K is 0.50, quite different from the experimental value of 0.79 for 2-phenyladamantane. It is conceivable that the low theoretical barrier is correct and that the cyclohexane moiety distorts during the rotation so as to lower the torsional barrier, a possibility presumably not available to the rigid adamantyl fragment (but note that any distortion in axial phenylcyclohexane appears (1) to be confined to the attachment site and that the entropy difference (1) between axial and equatorial isomers is apparently zero). An indication that the AM1 results are erroneous comes from its prediction of the perpendicular conformer, **4**, as the least stable, contrary to experiment (1) and to force-field calculations (1, 22, 23). Yet AM1 has the conformation of lowest energy at θ = 55.3°, with a C(1)—C(2) bond of the aromatic ring nearly eclipsing the C(α)—C(β) bond of the alicycle. The MMII computation (1), in the present notation, finds θ as 64° in the minimum-energy, (skewed) perpendicular, conformer. For 2-phenyladamantane, ^6J very clearly indicates that, for the conformer of lowest energy, a θ value nearer 90° than 60° is that of lowest energy. Note that a *rigid* conformer, defined by a θ of 64°, has $\langle\sin^2\theta\rangle$ as 0.81, corresponding to a ^6J of −0.90 Hz, very near the experimental value. Of course, the motion about the Csp^2—Csp^3 bond is not restrained by an infinite potential. Hence the proper interpretation of ^6J likely is that the conformation of lowest energy has a θ *nearer 90° than 60°* and that the potential is such that $\langle\sin^2\theta\rangle$ becomes 0.79 in CS_2/C_6D_{12} at 300 K.

AM1 predicts the axial as 13.6 kJ/mol less stable than the equatorial isomer (footnotes to Table 2). MMII simulations (1) yield 14.3 kJ/mol for this comparison, while the free energy difference at 113 K in propane-d_8 is 11.3 ± 1.1 kJ/mol. Given (1) that the entropies of the two isomers are much the same, small corrections (24) to the computed energies for zero-point energy differences and enthalpy differences between 0 and 113 K are also necessary, as well as for differences in solvation energies at 113 K.

Turning to the STO-3G optimizations, the potential function for internal rotation in eq. [3] for the equatorial isomer has $\langle\sin^2\theta\rangle$ as 0.133. The low value ensues from the large computed barrier height of 16.1 kJ/mol. While qualitatively similar to the AM1 potential in eq. [1], it is likely that it is quantitatively inferior to the latter, as judged by the experimental value of 0.21 for $\langle\sin^2\theta\rangle$ in CS_2/C_6D_{12}. The minimal basis set also overestimates the corresponding internal barrier in isopropylbenzene (2), as measured in solution. It is unlikely that polarity differences between **1** and **2**, causing solvent stabilization of either, are significant. The computed dipole moments at all θ values vary by 0.03 D at most, the largest value being 0.39 D. It may be noted that the corresponding barrier in ethylbenzene does not alter in solvents of widely different polarity (25). The $\langle\sin^2\theta\rangle$ value for isopropylbenzene in CS_2/C_6D_{12} is (2) slightly larger than for phenylcyclohexane, possibly because of easier relaxation of the side chain in the former during the rotational motion. A recent force-field computation (26) has a barrier height of 10.2 kJ/mol for equatorial phenylcyclohexane but the symmetry of the internal potential is not stated. Hence an estimate of $\langle\sin^2\theta\rangle$ cannot be made; if this force field were to predict a predominantly twofold symmetry, then it would be clear that the geometry-optimized AM1 computations agreed best with experimental data in CS_2/C_6D_{12}.

For axial phenylcyclohexane, the STO-3G potential in eq. [4] has $\langle\sin^2\theta\rangle$ as 0.584 at 300 K. In contrast to the AM1 predictions, the perpendicular **4** is correctly found as more stable than **3**, but only by 0.54 kJ/mol. The most stable conformer of this isomer is calculated as that with θ = 57.8, not very different from the θ values of 55.3° from AM1 and 64° from a force field (1). The rather small barrier to rotation about the Csp^2—Csp^3 bond is indicated by the value of 0.584 for $\langle\sin^2\theta\rangle$ (free rotation corresponds to 0.5) and, rather like AM1 above, the STO-3G result contrasts sharply with the experimental value of 0.79 for 2-phenyladamantane (the *rigid* **6**, analogous to *rigid* **4**, has $\langle\sin^2\theta\rangle$ as unity).

In view of the present molecular orbital results for axial phenylcyclohexane and in view of the indications (1) that the slightly skewed perpendicular conformer **4** is rather stable, together with a similar conclusion for 2-phenyladamantane, it would be of great interest to have a molecular mechanics treatment of the internal rotational barrier in **4** and **6**. The barriers are probably predominantly steric in nature, so that the force-field computations may well decide whether the barrier in **4** really is much lower than in **6**, the latter having a rather rigid alicyclic skeleton.

There exists one early CNDO/2 MO computation on axial phenylcyclohexane (30), which, however, does not allow for relaxation of bond lengths and angles during rotation about the Csp^2—Csp^3 bond. The barrier to rotation is calculated as 28.9 kJ/mol; this number appears untenable considering the appearance (1) of the ^{1}H NMR spectrum at 113 K.

The coupling constants, $^4J(H,CH)$ and $^5J(H,CH)$

The coupling constant between the *ortho* and α protons,

Can. J. Chem. Downloaded from www.nrcresearchpress.com by 195.138.81.100 on 09/07/12
For personal use only.

^4J(H,CH)$\equiv^4J$, is dominated by a $\sigma-\pi$ contribution, proportional to $\sin^2\theta$, but also contains a small σ component, going as $\cos^2\theta$ (27, 28). Its actual values for $60° \leq \theta \leq 90°$ for a particular molecule are somewhat uncertain (27). It is -0.994 (6) Hz for fluorene (29) where θ is very near 60° and, for example, has a mean of -0.98 Hz for a molecule (no. 41 in ref. 27) in which the mean $\sin^2\theta$ is 0.72; in another molecule (no. 40 of ref. 27) it has a value of -1.16 Hz for a θ near 90°. For 2-phenyladamantane, ^4J is -1.038 (7) Hz, clearly compatible with a large average θ, characterizing a nonrigid conformer, **6**, with a $\langle\sin^2\theta\rangle$ of 0.79 derived from ^6J. More precisely, the σ component of ^4J has been assessed at -0.32 Hz (27) and, because $\langle\cos^2\theta\rangle$ is 0.21, the $\sigma-\pi$ component of ^4J in **6** becomes -0.97 Hz. Hence this component is implied as $-0.97/0.79$ or about -1.22 Hz at $\theta = 90°$. The latter falls between the limits of the magnitudes implied by the examples cited above. For phenylcyclohexane, ^4J is -0.577 (4), reflecting the small value of $\langle\sin^2\theta\rangle$ for **1** with an appreciable internal barrier; it is also close to the ^4J of -0.559 (1) Hz for isopropylbenzene in the same solvent (2).

^5J(H,CH) consists (7) of a $\sigma-\pi$ term, in $\langle\sin^2\theta\rangle$, and a σ term, in $\langle\sin^2(\theta/2)\rangle$. The latter term is 0.5 for an internal rotational potential containing only evenfold components, as implied by the molecular orbital results in eqs. [1]–[4]. It follows that ^5J should be larger in 2-phenyladamantane than in phenylcyclohexane, as it is, but only by 0.07 (1) Hz instead of the ca 0.17 Hz one might have expected on the basis of about 0.3 Hz for the $\sigma-\pi$ component in toluene. Similar discrepancies are known for ^5J in fluorene (29), for example.

Acknowledgments

We thank the Natural Sciences and Engineering Research Council of Canada for a grant-in-aid of research.

1. M. E. Squillacote and J. M. Neth. J. Am. Chem. Soc. **109**, 198 (1987), and references therein.
2. T. Schaefer, R. Sebastian, and G. H. Penner. Can. J. Chem. **66**, 1495 (1988), and references therein.
3. T. Schaefer, W. Niemczura, and W. Danchura. Can. J. Chem. **57**, 355 (1979).
4. G. A. Olah, A. Wu, and O. Farooq. J. Org. Chem. **53**, 5143 (1988).
5. V. V. Krishnamurthy, P. S. Iyer, and G. Olah. J. Org. Chem. **48**, 3373 (1983).
6. H. Duddeck, F. Hollowood, A. Karim, and M. A. McKervey. J. Chem. Soc. Perkin Trans. **2**, 360 (1979).
7. T. Schaefer, R. Sebastian, and G. H. Penner. Can. J. Chem. **63**, 2597 (1985).
8. M. J. S. Dewar, E. J. Zoebisch, E. F. Healy, and J. J. P. Stewart. J. Am. Chem. Soc. **107**, 3902 (1985).
9. W. J. Hehre, R. Ditchfield, and J. A. Pople. J. Chem. Phys. **56**, 2257 (1972).
10. M. J. Frisch, J. S. Binkley, H. B. Schlegel, K. Raghavachari, C. F. Melius, R. L. Martin, J. J. P. Steward, F. W. Bobrowicz, D. F. Rohlfing, L. R. Kahn, D. J. Defrees, R. Seeger, R. A. Whiteside, D. J. Fox, E. M. Fluder, and J. A. Pople. Carnegie–Mellon Quantum Publishing Unit, Pittsburgh, PA. 1984.
11. J. S. Martin, A. R. Quirt, and K. E. Worvill. The NMR program library. Daresbury Laboratory, Daresbury, U.K.
12. W. J. E. Parr and T. Schaefer. Acc. Chem. Res. **13**, 400 (1980), and references therein.
13. T. Schaefer and C. S. Takeuchi. Can. J. Chem. **67**, 1022 (1989).
14. R. Laatikainen and K. Tuppurainen. J. Chem. Soc. Perkin Trans. **2**, 121 (1987).
15. T. Schaefer, C. Beaulieu, R. Sebastian, and G. H. Penner. Can. J. Chem. **68**, 581 (1990).
16. F. A. Bovey, F. P. Hood, E. W. Anderson, and R. L. Kornegay. J. Chem. Phys. **41**, 2041 (1964).
17. J. Hilton and L. H. Sutcliffe. Prog. NMR Spectrosc. **10**, 27 (1975).
18. I. R. Peat and W. F. Reynolds. Can. J. Chem. **51**, 2968 (1973).
19. T. Schaefer and K. Chum. Can. J. Chem. **54**, 2231 (1976), and references therein.
20. R. H. Contreras, M. A. Natiello, and G. E. Scuseria. Magn. Reson. Rev. **9**, 239 (1985).
21. M. C. Ruiz de Azua, A. C. Diz, C. G. Gribet, R. H. Contreras, and I. D. Rae. Int. J. Quantum Chem. **S20**, 585 (1986).
22. N. L. Allinger and M. T. Tribble. Tetrahedron Lett. **35**, 3259 (1971).
23. E. L. Eliel. J. Mol. Struct. **126**, 385 (1985).
24. K. B. Wiberg and M. A. Murcko. J. Am. Chem. Soc. **110**, 8029 (1988).
25. T. Schaefer, G. H. Penner, and R. Sebastian. Can. J. Chem. **65**, 873 (1987).
26. E. Jaime and E. Osawa. J. Mol. Struct. **126**, 363 (1985).
27. M. Barfield, C. J. Fallick, K. Hata, S. Sternhell, and P. W. Westerman. J. Am. Chem. Soc. **105**, 2178 (1983).
28. M. Barfield, M. J. Collins, J. E. Gready, S. Sternhell, and C. W. Tansey. J. Am. Chem. Soc. **111**, 4285 (1989).
29. T. Schaefer, R. Sebastian, T. A. Wildman, and H. Dettman. Can. J. Chem. **60**, 2274 (1982).
30. C. Leibovici and F. Crasner. J. Mol. Struct. **28**, 219 (1975).

Can. J. Chem. Downloaded from www.nrcresearchpress.com by 195.138.81.100 on 09/07/12
For personal use only.

Dissociation equilibria of picric acid in the binary *N*, *N*-dimethylformamide/2-methoxyethanol solvent system

ANDREA MARCHETTI, CARLO PRETI, MARA TAGLIAZUCCHI, LORENZO TASSI, AND GIUSEPPE TOSI[1]
Department of Chemistry, University of Modena, via G.Campi 183, 41100 Modena, Italy

Received February 9, 1990[2]

ANDREA MARCHETTI, CARLO PRETI, MARA TAGLIAZUCCHI, LORENZO TASSI, and GIUSEPPE TOSI. Can. J. Chem. **69**, 509 (1991).

Three empirical equations are proposed to fit the experimental values of the dissociation constant for picric acid, chosen as guide-solute working in the *N*, *N*-dimethylformamide/2-methoxyethanol solvent system. The work was performed operating at 19 temperatures ranging from −10 to +80°C in the pure solvents and in their nine mixtures, identified by the mole fraction (X) of one component. This empirical treatment, which describes the dependence of the dissociation constant on temperature and composition of the solvent mixture, is represented by functions of the type $K = K(T)$, $K = K(X)$, and $K = K(T, X)$. The $K = K(T, X)$ equation in its complete form is composed of 20 terms, some of which can be eliminated because of small statistical weight; the number and type of these terms vary on passing from one solvent system to another and the best-fitting form is suggested. A comparison among various $K = K(T, X)$ equations proposed in the present and in previous works has been made.

Key words: dissociation equilibria, binary nonaqueous solvent mixtures, picric acid, *N,N*-dimethylformamide, 2-methoxyethanol.

ANDREA MARCHETTI, CARLO PRETI, MARA TAGLIAZUCCHI, LORENZO TASSI et GIUSEPPE TOSI. Can. J. Chem. **69**, 509 (1991).

On propose trois équations pour ajuster les valeurs expérimentales des constantes de dissociation de l'acide picrique comme soluté, guide de travail, dans le système de solvant formé de *N*, *N*-diméthylformamide/2-méthoxyéthanol. On a réalisé le travail en opérant à 19 températures allant de −10 à +80°C, dans les solvants purs et dans neuf de leurs mélanges identifiés par la fraction molaire (X) de l'un des composants. Ce traitement empirique, qui décrit la relation entre la constante de dissociation et la température et la composition des mélanges de solvants, est représenté par des fonctions du type $K = K(T)$, $K = K(X)$ et $K = K(T, X)$. La forme complète de l'équation $K = K(T, X)$ est composée de 20 termes dont quelques-uns peuvent être éliminés parce que leur poids statistique est faible; la quantité et le type de ces termes varie lorsqu'on passe d'un système de solvant à un autre et on suggère la meilleure forme d'ajustement. On présente une comparaison entre les diverses équations $K = K(T, X)$ proposées dans ce travail et antérieurement.

Mots clés: équilibre de dissociation, mélanges de solvants binaires non-aqueux, acide picrique, *N,N*-diméthylformamide, 2-méthoxyéthanol.

[Traduit par la rédaction]

Introduction

The acid–base equilibria of weak electrolytes in solution are, in general, not independent of the solvent; in particular, the role of the medium in ionization and dissociation reactions, in spite of the remarkable work of many authors, has still not been completely elucidated (1). In fact, each solution of any weak solute represents a system quite complex to describe, owing to the multitude of physical-chemical processes that take place therein, sometimes involving species, such as solvated ions or molecules, of unknown stoichiometric composition.

In any case, the ionization and dissociation reactions are related to transport phenomena in solution and are strongly influenced by such thermomechanical properties of the solvent as density, viscosity, and dielectric constant.

The usefulness of employing mixed solvent systems (binary or higher) lies in the possibility of making continuous variations of the properties of the medium. Our interest centres in a more detailed interpretation of the changes observed in the shape of the acid–base conductometric titration curves obtained in nonaqueous solvents (2–4). The trends vary by modifing either the morphological properties (type and molecular size of titrant, titrand, and solvent) of the system, and (or) the structural properties (by temperature variations or by mixing the solvent with a cosolvent); in fact, changes in the nature of the mutual orientation may constrain the medium to assume a significant liquid structure (SLS) (5–7). All these considerations have led to a systematic investigation of the conductometric behavior of a guide-solute in a series of organic solvents, their binary mixtures, and mixtures with water.

For these purposes, the knowledge of the dissociation constants of the weak electrolytes utilized and of the association constants of the adducts formed is necessary and fundamental. In our previous papers, we reported the dissociation constants, evaluated by the conductometric method in the −10 to +80°C temperature range, of picric acid in 1,2-ethanediol (Gliet), 2-methoxyethanol (Gliem) (8), and their binary mixtures (9, 10), in the Gliet/water (11) and Gliem/water (12) solvent systems.

The present work, therefore, represents a further extension of previous studies; it concerns the conductometric determination of the dissociation constants of picric acid in *N,N*-dimethylformamide (DMF) and in a series of binary DMF/Gliem mixtures covering the whole composition range, working at 19 temperatures from −10 to 80°C. Because our purpose was the investigation of the properties of mixed solvent systems, a guide-solute needed to be chosen; picric acid was utilized because it is stable in our experimental conditions, it is a medium-strength electrolyte in water, and it is completely soluble in Gliem, in DMF, in their binary mixtures, and in all the other previously investigated solvent systems.

2-Methoxyethanol (Gliem) is a widely used alcoholic solvent for scientific studies and for industrial applications because of solvating properties associated with its almost-aprotic character (13). In fact, owing to its low autoprotolysis constant ($pK_{autoprot}$ = 20.5) (14) and other physical-chemical properties, it is possible to classify Gliem as a solvent midway between protic

[1]Author to whom correspondence may be addressed.
[2]Revision received November 2, 1990.

Printed in Canada / Imprimé au Canada

Can. J. Chem. Downloaded from www.nrcresearchpress.com by 195.138.81.100 on 09/07/12
For personal use only.

Can. J. Chem. Downloaded from www.nrcresearchpress.com by 195.138.81.100 on 09/07/12
For personal use only.

and dipolar almost-aprotic. DMF, on the contrary, is a quite dipolar aprotic solvent with a high dielectric constant (37.51 at 25°C) and a large dipole moment (μ = 3.82 D at 25°C) (15), which probably enables it to stabilize ions, molecules, and other dissolved species through dipole and induced dipole interactions.

Ionization and dissociation constants in DMF have been determined for a fairly large number of substances (16–19). A few studies, however, have been made on the thermodynamics of ionization of acids in this pure solvent and in binary mixtures with a cosolvent, also operating over a reasonably large temperature range. In view of the importance of DMF as a solvent or cosolvent, it would be desirable to have more data on ionization and dissociation of weak electrolytes in order to achieve a better understanding of these processes in DMF solutions.

In addition, we have chosen this binary system to verify some peculiarities in its behavior and to compare with those results observed in the analogous Gliet/Gliem solvent system (10). In fact, Gliem being the common solvent for these investigations, the most significant differences in the observed behavior of the ionization and dissociation of picric acid are certainly ascribable to the chemical differences between Gliet and DMF.

Experimental section

Materials

2,4,6-Trinitrophenol (picric acid), supplied by BDH (purum ca. 95%), was twice purified by recrystallization from hot ethanol and diethyl ether (mp 122°C (lit. (15) mp 122–123°C)).

The solvents, *N*,*N*-dimethylformamide and 2-methoxyethanol (containing <0.10% and <0.05% water, respectively, by Karl-Fischer titration) were Carlo Erba high purity grade and they were used after purification by passage on a neutral alumina column.

Apparatus

The conductances of the solutions were measured with an Amel model 123 conductivity bridge operating in the 0.1×10^{-6} to 0.3 S (scale-end) range, with a sensitivity of ±1.0%, and using platinized platinum electrodes (cell constant 9.12 cm). Temperature control was provided by a Lauda K2R thermostatic bath maintained to within ±0.02°C. Viscosity measurements were performed using a Schott-Geräte AVS 400 viscosity-measuring system, equipped with a series of Ubbelhode viscometers. The densities at various temperatures were determined with a digital density meter, Anton Paar model DMA 60, equipped with a density measuring cell model DMA 602, with a sensitivity up to 0.000 001 g cm^{-3}. The dielectric constants were measured using a WTW-DM01 dipole meter equipped with two stainless-steel cylindrical cells: MFL2 ($7 < \epsilon < 21$) was calibrated with dichloromethane (ϵ = 9.08 at 20°C), pyridine (ϵ = 12.30 at 25°C), butan-1-ol (ϵ = 17.80 at 20°C), and acetone (ϵ = 20.70 at 25°C) (15); MFL3 ($21 < \epsilon < 90$) was calibrated with ethanol (ϵ = 24.30 at 25°C), methanol (ϵ = 32.63 at 25°C), glycerol (ϵ = 42.50 at 25°C), and water (ϵ = 80.37 at 20°C) (15). A frequency of 2.0 MHz was used. Karl Fischer titrations were performed with an automatic titration system (Crison model KF431) equipped with a digital burette (Crison model 738).

Procedure

The solvent mixtures were prepared by weight. The solutions of picric acid at different concentrations were obtained by successive dilution of stock solutions, freshly prepared by weight; concentrations in volume were then calculated from weight concentrations and densities. Conductance readings were recorded when they became invariant with time; this took about 30 min for each measurement. Solvent conductance corrections were applied to all data at different temperatures.

Results and discussion

To evaluate the experimental dissociation constant of picric acid in this binary solvent system using conductometric measurements performed at 19 temperatures ranging from −10 to +80°C, the equivalent conductances were determined for at least six concentrations for each solution in the two pure solvents and in their nine binary mixtures, which have been identified by the letters A, B, C, ... M; the compositions of the solvent systems appear in Table 2. The conductance data are reported in the Supplementary Tables 1–11 available from the Depository of Unpublished Data[3] and all the conductometric data were corrected for the specific conductances of the relative solvents at each investigated temperature. The corrected values were analyzed and processed by means of the Fuoss–Hsia equation (20), using a computing program kindly supplied by Prof. M. Goffredi and modified by us to take into account the effect of the variation of solution concentrations with density of the solvents at various temperatures.

The equation

$$[1] \qquad \Lambda = \Lambda_0 - S(C\gamma)^{1/2} + EC\gamma \log(C\gamma) + J_1 C\gamma - J_2(C\gamma)^{3/2} - K_A C\gamma f_{\pm}^2 \Lambda$$

was used, where the symbols have their usual meaning (21). The above equation provides the limiting ionic conductivity Λ_0, the association constant K_A (dissociation constant $K = K_A^{-1}$) (21, 22), and the interionic distance parameter $\mathring{a}$.

The calculating procedure starts from an initial value of Λ_0, estimated from a Λ vs. $C^{1/2}$ plot, and a first chosen $\mathring{a}$ value, generally 5 Å; afterwards only a few iterations are necessary to obtain the parameters cited. Table 1 summarizes the dissociation constants K for picric acid in the DMF/Gliem solvent system at each investigated temperature, while the Λ_0 and $\mathring{a}$ values are presented in the Supplementary Tables 12 and 13 respectively, available from the Depository of Unpublished Data.

An immediate comparison between data from the DMF/Gliem solvent system and those from the Gliet/Gliem system appears evident from the analysis of K values of picric acid in the pure Gliet (K_{Gliet}) (10) and those in pure DMF (K_{DMF}) of this work.

In fact, K_{DMF} is always greater than K_{Gliet} (by one or two orders of magnitude) in the temperature range investigated. In addition, this behavior is observed in all the corresponding mixtures from B to L. These differences could probably be explained on the basis of a simple qualitative discussion of the properties of the two pure solvents and their mixtures. DMF is an aprotic solvent having a potentially basic character because of the presence of the amino group in its molecule, while Gliet is a protic, potentially acidic, solvent ($K_{autoprot}$ = 15.8) (23).

It is noteworthy that these characteristics are probably predominant, so that K_{DMF} is always $> K_{Gliet}$, the dielectric constants of the two pure solvents being quite similar (ϵ ranges from 44.08 to 29.12 for DMF and 49.11 to 31.31 for Gliet (8) in the $-10 \leq t(°C) \leq 80$ range, μ_{Gliet} = 2.28 at 25°C) (15). Now, the trend among all the binary mixtures DMF/Gliem and Gliet/Gliem being the same, one may think that preferential or selective solvation of solute takes place and occurs in the DMF/Gliem solvent system through the molecules of DMF, which are more solvating than the Gliem molecules ($20.03 \leq \epsilon_{Gliem} \leq 13.02$ for $-10 \leq t(°C) \leq 80$) (8).

Considering now the values of the experimental dissociation constant relative to the DMF/Gliem solvent system, each set of K data was fitted by an equation of the type

[3]These tables may be purchased from: The Depository of Unpublished Data, Document Delivery, CISTI, National Research Council Canada, Ottawa, Canada K1A 0S2.

Can. J. Chem. Downloaded from www.nrcresearchpress.com by 195.138.81.100 on 09/07/12
For personal use only.

TABLE 1. Experimental dissociation constant values[a] for picric acid in the *N*,*N*-dimethylformamide/2-methoxyethanol solvent system at different temperatures

t (°C)	System A $K \times 10^2$	System B $K \times 10^2$	System C $K \times 10^2$	System D $K \times 10^2$	System E $K \times 10^2$	System F $K \times 10^2$	System G $K \times 10^2$	System H $K \times 10^2$	System I $K \times 10^3$	System L $K \times 10^3$	System M[b] $K \times 10^5$
−10	5.50±0.09	5.12±0.12	4.79±0.10	4.24±0.06	3.97±0.08	3.13±0.04	2.31±0.04	1.25±0.02	8.51±0.12	2.26±0.02	8.48±0.01
−5	5.73±0.11	5.31±0.13	4.91±0.11	3.95±0.05	3.64±0.08	2.72±0.03	2.04±0.03	1.16±0.02	7.49±0.10	1.86±0.02	7.66±0.01
0	5.90±0.11	5.54±0.14	4.99±0.11	3.71±0.04	3.31±0.06	2.49±0.03	1.87±0.03	1.05±0.02	6.68±0.09	1.58±0.02	6.64±0.01
5	6.04±0.12	5.72±0.14	5.14±0.11	3.46±0.04	3.07±0.05	2.33±0.02	1.75±0.03	0.949±0.012	5.98±0.07	1.37±0.02	5.49±0.01
10	6.14±0.12	5.77±0.14	5.24±0.12	3.23±0.03	2.88±0.05	2.12±0.02	1.62±0.02	0.843±0.009	5.30±0.06	1.15±0.01	4.65±0.01
15	6.17±0.12	5.80±0.15	5.29±0.12	3.04±0.03	2.72±0.04	1.91±0.02	1.50±0.02	0.740±0.008	4.70±0.05	0.986±0.007	4.19±0.01
20	6.18±0.13	5.81±0.15	5.19±0.11	2.91±0.03	2.53±0.04	1.79±0.02	1.38±0.02	0.646±0.006	4.20±0.05	0.862±0.006	3.59±0.01
25	6.18±0.13	5.61±0.14	4.95±0.10	2.75±0.03	2.40±0.04	1.62±0.01	1.27±0.02	0.573±0.005	3.56±0.03	0.736±0.005	2.98±0.01
30	6.05±0.12	5.32±0.13	4.66±0.09	2.65±0.03	2.26±0.03	1.47±0.01	1.14±0.01	0.514±0.004	3.11±0.03	0.653±0.005	2.47±0.01
35	5.68±0.11	4.94±0.11	4.34±0.08	2.51±0.03	2.11±0.03	1.35±0.01	1.02±0.01	0.465±0.004	2.75±0.03	0.585±0.004	2.17±0.01
40	5.26±0.09	4.64±0.09	3.94±0.07	2.43±0.03	1.97±0.02	1.27±0.01	0.945±0.008	0.425±0.003	2.53±0.02	0.522±0.004	1.75±0.01
45	5.01±0.09	4.26±0.09	3.67±0.07	2.33±0.03	1.83±0.02	1.23±0.01	0.843±0.006	0.398±0.003	2.30±0.02	0.471±0.004	1.47±0.01
50	4.60±0.08	3.95±0.07	3.43±0.05	2.24±0.02	1.75±0.02	1.21±0.01	0.797±0.006	0.374±0.003	2.08±0.02	0.420±0.003	1.26±0.01
55	4.32±0.07	3.55±0.06	3.18±0.05	2.14±0.02	1.70±0.02	1.17±0.01	0.782±0.006	0.330±0.002	1.99±0.02	0.395±0.003	1.08±0.01
60	3.91±0.06	3.23±0.05	2.88±0.04	2.05±0.02	1.66±0.02	1.14±0.01	0.776±0.005	0.324±0.002	1.94±0.02	0.364±0.003	0.865±0.002
65	3.50±0.05	2.96±0.04	2.61±0.04	2.01±0.02	1.63±0.02	1.11±0.01	0.772±0.005	0.320±0.002	1.88±0.02	0.345±0.003	0.652±0.003
70	3.15±0.04	2.69±0.04	2.39±0.03	1.94±0.02	1.61±0.02	1.08±0.01	0.767±0.005	0.318±0.002	1.82±0.02	0.327±0.003	0.478±0.002
75	2.90±0.04	2.48±0.03	2.21±0.02	1.92±0.02	1.61±0.02	1.04±0.01	0.758±0.005	0.315±0.002	1.78±0.01	0.296±0.002	0.313±0.001
80	2.65±0.03	2.29±0.03	2.03±0.02	1.90±0.01	1.59±0.01	1.02±0.01	0.747±0.005	0.313±0.002	1.75±0.01	0.274±0.002	0.172±0.002

[a]All K values are reported on the molar scale.
[b]From ref. 10.

Can. J. Chem. Downloaded from www.nrcresearchpress.com by 195.138.81.100 on 09/07/12
For personal use only.

[2] $\ln K = a_0 + a_1T + a_2/T + a_3 \ln T$

which certainly represents the most commonly used and the most accurate equation for K vs. T data fit. In fact, eq. [2] reproduces well the experimental K values with an average difference of 1.9% between calculated (Supplementary Table 14 available from the Depository of Unpublished Data) and experimental (Table 1) values. Figure 1 reports the experimental K values and the best-fitting curves, corresponding to the integrated Van't Hoff eq. [2], for our investigated solute in the DMF/Gliem solvent system.

The same trend vs. temperature is observed for the $\mathring{a}$ parameter, as shown by the data of Supplementary Table 13, available from the Depository of Unpublished Data. If we assume, according to Hsia and Fuoss (20), that this adjustment parameter may represent the distance of closest approach of the ions, examination of the $\mathring{a}$ values obtained as a function of the composition X of the mixture may suggest some considerations in terms of solute/solvent properties. Figure 2 shows the plot of $\mathring{a}$ values vs. X and it appears quite interesting; we may observe the presence of maximum values corresponding to X_{DMF} values of ca. 0.2, 0.5, and 0.8 and minimum values for the pure solvents and for ca. 0.33 and 0.70. Relatively high values of $\mathring{a}$ may indicate the presence of "loose" ion pairs, i.e., a greater separation of the ions due to the solvent molecules; on the contrary, when $\mathring{a}$ decreases tight ion pairs are probably formed. In conclusion, in the present case a minimum value of $\mathring{a}$ is observed for the pure Gliem, according also with its low dissociating ability; relatively low $\mathring{a}$ values are evident, corresponding to Gliem/DMF 1:2 and 2:1 ratios, while the highest $\mathring{a}$ values correspond to 1:3, 1:1, and 3:1 Gliem/DMF ratios. This behaviour could suggest that the formation of certain stoichiometrical solvent/cosolvent adducts (1:3, 1:1, and 3:1) may promote dissociation of ion pairs more than the other adduct ratios (1:2 and 2:1).

Turning now to the dissociation constant values, brief examination of Fig. 1 demonstrates the following details: (i) the curves K vs. T change progressively on passing from convex (system A) to concave shape (system M); (ii) the curves A, B, C present a relative maximum in K values in the temperature range investigated, which shifts towards lower temperatures as the X_{DMF} decreases, while all the other curves from D to M show a continuously decreasing trend with temperature. On the basis of these considerations it is possible to evaluate, for the three mixtures cited, values of K_{max} and corresponding T_{max} using the Van't Hoff equation in the following form:

[3] $$\left(\frac{\partial \ln K}{\partial T}\right)_P = 0$$

and employing the proper a_i coefficients for each binary mixture (Table 2). Equation [3] provides the following values of K_{max} and t_{max}(°C): 6.26×10^{-2} and 13.2, 5.92×10^{-2} and 10.1, and 5.30×10^{-2} and 7.9 for systems A, B, and C respectively. For the curve M, the decreasing trend is not very evident by examining the figure because all the curves have been reported in an unique compressed scale that makes the curve M flattened with respect to the others; however, the decreasing trend appears evident if one considers the K values of Table 1. (iii) Taking into account the progressive and regular variation of the shape of the curves in the plane $\pi\{K, T\}$ on passing from A to M and considering that the composition of binary mixtures varies continuously in the range $0 \leq X_{DMF} \leq 1$, one may reasonably think that the property K also varies continuously between the

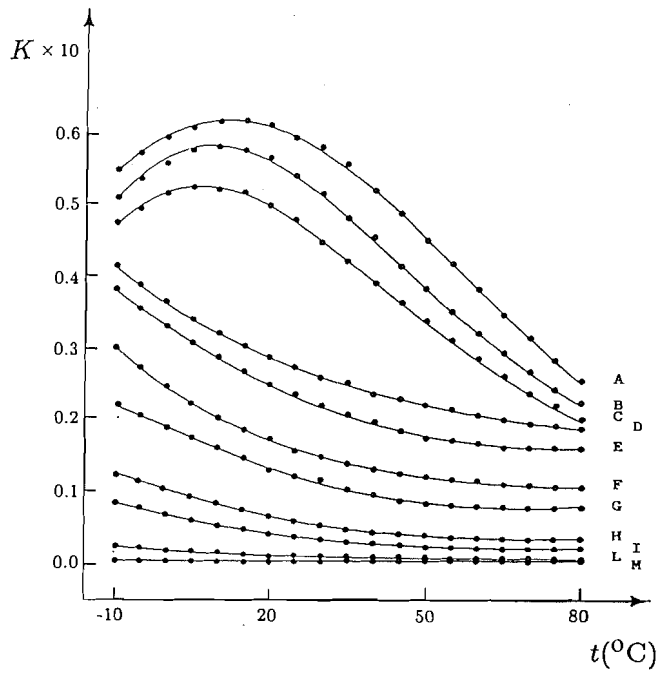


FIG. 1. Experimental dissociation constants of picric acid in the DMF/Gliem solvent system at different temperatures, and best fitting curves calculated by eq. [2].

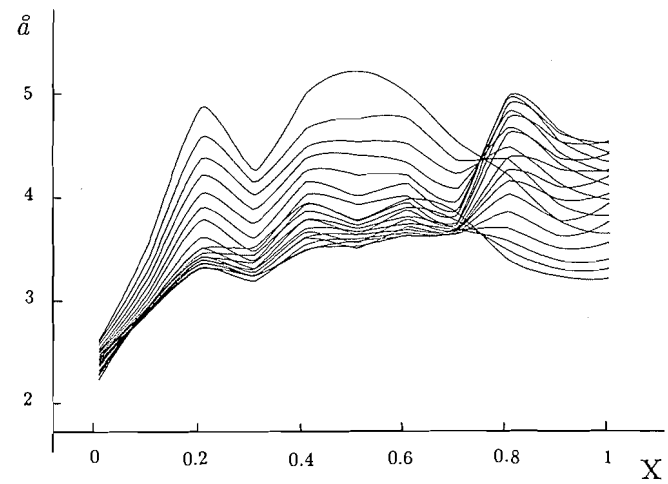


FIG. 2. The graphs of $\mathring{a}$ values plotted vs. X, at different temperatures varying from −10°C (top) to 80°C (bottom).

values obtained in DMF and in Gliem at each temperature investigated.

Now, on the basis of these considerations, we may assume that the dissociation constant of the solute should be described as a function of the two independent variables, temperature and composition, of the binary solvent system. In a general form, we can write:

[4] $K = K(T, X_{DMF})$

where, to simplify the notation, the subscript DMF will hereafter be omitted.

By considering the curves of Fig. 1 and the best-fit eq. [2], we may assume that the dependence of the dissociation constant on the composition of the binary mixture should be implicitly contained in the coefficients of eq. [2] for each solvent system, being defined by the proper X_r ($r = 1, 2, \ldots 11$ for A, B, ... M

TABLE 2. a_i coefficients of eq. [2] for picric acid in the *N*,*N*-dimethylformamide/2-methoxyethanol solvent system

System	X_{DMF}	V_{DMF}(%)	a_0	a_1	a_2	a_3
A	1.00000	100	117.08	−0.04734	−7869.4	−13.932
B	0.90212	90	1385.3	0.31613	−41428	−235.81
C	0.80375	80	1441.4	0.33898	−42440	−246.28
D	0.70529	70	146.41	0.05362	−2567.0	−27.621
E	0.60601	60	1112.5	0.33947	−27514	−197.49
F	0.50632	50	568.17	0.19449	−12216	−103.43
G	0.40624	40	2653.3	0.78671	−67854	−467.69
H	0.30531	30	2836.4	0.84614	−72004	−500.62
I	0.20436	20	2752.5	0.82353	−69567	−486.24
L	0.10252	10	303.84	0.11851	−4497.0	−58.145
M[a]	0.00000	0	−5663.0	−1.7421	145109	997.85

[a]From ref. 12.

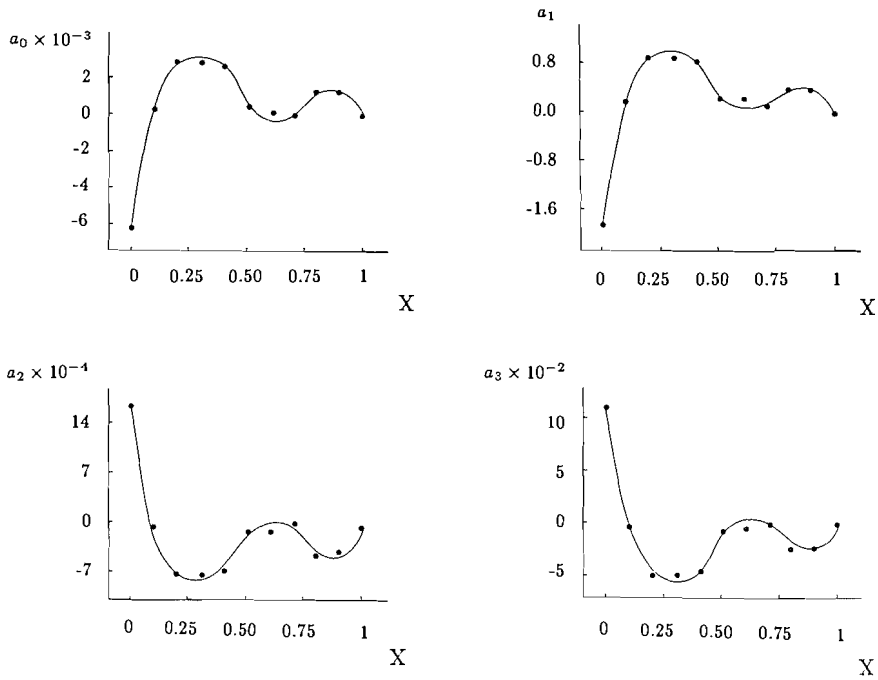


FIG. 3. The graphs of a_i coefficients of eq. [5] vs. X.

respectively). Therefore, we may write:

[5] $a_i = a_i(X)$ for $i = 0, 1, 2, 3$

and consequently, eq. [2] in the form

[2.1] $\ln K = a_0(X) + a_1(X)T + a_2(X)/T + a_3(X) \ln T$

The coefficients a_i, which were determined by analyzing the experimental K values with the multilinear regression package TSP (24), are reported in Table 2, while Fig. 3 reproduces the same table in graphic form. As is clear by examining this last figure, these coefficients show characteristics of "self similarity (25, 26) or *omotetia interna*" (27); in fact, by assuming

$$a_i(X_r) = a_i(X_r) \qquad \text{for } i = 0, 1; \quad r = 1, 2, \ldots 11$$

and

$$a_i(X_r) = -a_i(X_r) \qquad \text{for } i = 2, 3; \quad r = 1, 2, \ldots 11$$

the trend of the four curves is unique and perfectly superimposible. This homotetic (self-similar) behavior was also observed in our previous studies involving similar investigations (9–12).

It is noteworthy that although many studies of other authors (28–31) are present in the literature, no model equation making explicit the function [5] is available. Therefore, to correlate the experimental dissociation constant K with the composition of the binary solvent system, in our previous papers (10–12) we proposed an empirical equation of the type:

$$[6] \qquad \ln K = b_0 + b_1X + b_2\frac{(1 - X)}{(1 + X)} + b_3X^2 + b_4\frac{(1 - X^2)}{(1 + X^2)}$$

Also, the b_j coefficients (Table 3) were determined in the same manner as a_i (24) and they refer to all the $K = K(X)$ isothermal curves, some of which are shown in Fig. 4. By using eq. [6] for each temperature investigated, the calculated K values were obtained (Supplementary Table 15 available from the Depository of Unpublished Data) and they reproduce well the experimental values (average difference of ca. 6.4%).

The same considerations made for a_i may also be applied to b_j, suggesting a homotetic behavior and an implicit dependence on the temperature

Can. J. Chem. Downloaded from www.nrcresearchpress.com by 195.138.81.100 on 09/07/12
For personal use only.

TABLE 3. b_j coefficients of eq. [6] for picric acid in the *N*,*N*-dimethylformamide/2-methoxyethanol solvent system

t (°C)	b_0	b_1	b_2	b_3	b_4
−10	349.97	−481.92	−265.55	129.08	−93.789
−5	328.97	−453.76	−250.78	121.98	−87.673
0	316.35	−436.96	−242.11	117.86	−83.865
5	318.12	−439.62	−243.72	118.79	−84.213
10	311.22	−430.33	−239.01	116.40	−82.190
15	300.03	−415.12	−230.96	112.40	−79.148
20	305.40	−422.35	−234.77	114.26	−80.866
25	301.96	−417.71	−232.48	113.06	−79.906
30	321.31	−443.96	−246.30	119.93	−85.619
35	320.86	−443.31	−245.97	119.65	−85.632
40	338.28	−467.08	−258.71	125.96	−90.520
45	349.05	−481.80	−266.63	129.84	−93.546
50	346.64	−478.37	−265.05	128.73	−92.860
55	334.43	−462.58	−257.54	125.08	−88.327
60	343.63	−475.45	−264.96	128.64	−90.332
65	376.97	−520.90	−289.48	140.64	−99.429
70	404.49	−559.15	−310.49	151.34	−106.25
75	462.55	−637.79	−352.63	171.75	−122.60
80	550.25	−757.42	−416.82	203.60	−146.70

[7] $b_j = b_j(T)$ for $j = 0, 1, 2, 3, 4$

The need to have an available $K = K(T, X)$ function has been resolved, as already done in some previous papers (10–12), by suggesting an empirical approach which leads to:

[8] $f(T, X) = \sqrt{f(T) \cdot f(X)}$

where $f(T)$ and $f(X)$ are eqs. [2] and [6] respectively. The above equation, which in its complete form contains 20 terms, has been simplified by omitting successively the terms having statistical weight ca. <1 (24). The best-fitting equation so obtained is

$$[9] \quad (\ln K)^2 = c_0 + c_1 T + c_4 X + c_5 XT + c_7 X \ln T + c_8 \frac{(1-X)}{(1+X)} + c_9 T \frac{(1-X)}{(1+X)} + c_{12} X^2 + c_{13} X^2 T + c_{15} X^2 \ln T + c_{16} \frac{(1-X^2)}{(1+X^2)} + c_{17} T \frac{(1-X^2)}{(1+X^2)}$$

where $c_0 = 10\,368.2$; $c_1 = -57.7703$; $c_4 = -21\,490.5$; $c_5 = 73.7774$; $c_7 = 1565.21$; $c_8 = -7620.24$; $c_9 = 42.8684$; $c_{12} = 14\,220.9$; $c_{13} = -13.7957$; $c_{15} = -2224.44$; $c_{16} = -2868.50$; $c_{17} = 15.6738$. This equation reproduces the experimental K values with an acceptable approximation, being 9.2% of the average difference between the experimental data of Table 1 and the calculated data of Supplementary Table 16, available from the Depository of Unpublished Data.

Figure 5 is provided by plotting eq. [9] and represents the $K = K(T, X)$ function; obviously the curves of the Figs. 1 and 4 correspond to the intersections of the surface with the $\pi\{K, T\}$ and $\pi\{K, X\}$ planes respectively.

The choice of eq. [9] was made taking into account the criterion of the lowest difference between calculated and experimental values, but at least two other criteria may be considered: (i) the simplicity of the equation and (ii) the possibility of extending the equation to the largest number of

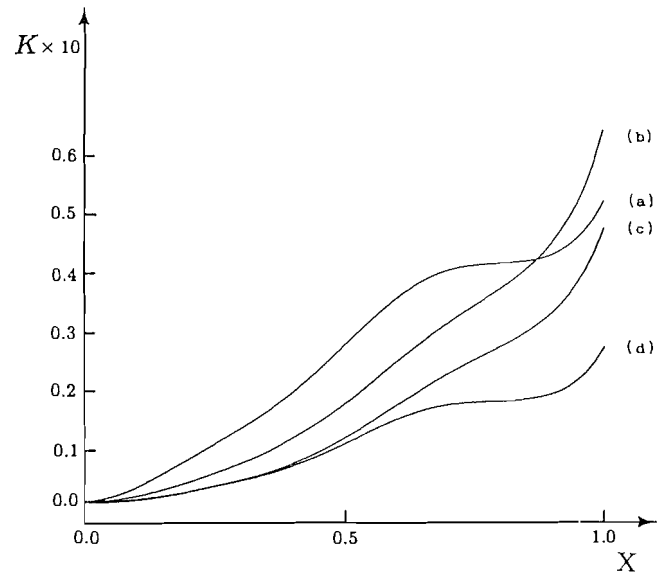


FIG. 4. Dissociation constants of picric acid in the DMF/Gliem solvent system as a function of the composition of the binary solvent system: (a) −10°C, (b) 20°C, (c) 50°C, (d) 80°C.

TABLE 4. c_i coefficients of model equations $K = K(T, X)$ for picric acid in different binary solvent systems

c_i	Variable quantity	Eq. [9]	Eq. [10]	Eq. [11][a]	Eq. [12]
c_0		×	×	×	×
c_1	T	×	×	×	×
c_2	$1/T$			×	×
c_3	$\ln T$				
c_4	X	×	×	×	
c_5	XT	×	×	×	×
c_6	X/T			×	×
c_7	$X \ln T$	×			
c_8	$\frac{(1-X)}{(1+X)}$	×	×	×	×
c_9	$T\frac{(1-X)}{(1+X)}$	×	×	×	×
c_{10}	$\frac{(1-X)}{(1+X)T}$				
c_{11}	$\frac{(1-X)}{(1+X)}\ln T$				
c_{12}	X^2	×	×	×	×
c_{13}	X^2T	×	×	×	×
c_{14}	X^2/T				
c_{15}	$X^2 \ln T$	×			
c_{16}	$\frac{(1-X^2)}{(1+X^2)}$	×	×	×	×
c_{17}	$T\frac{(1-X^2)}{(1+X^2)}$	×	×	×	
c_{18}	$\frac{(1-X^2)}{(1+X^2)T}$			×	×
c_{19}	$\frac{(1-X^2)}{(1+X^2)}\ln T$				
Average difference (%)		9.2	10.6	9.5	10.3

[a]Equation (7) from ref. 10.

Can. J. Chem. Downloaded from www.nrcresearchpress.com by 195.138.81.100 on 09/07/12
For personal use only.

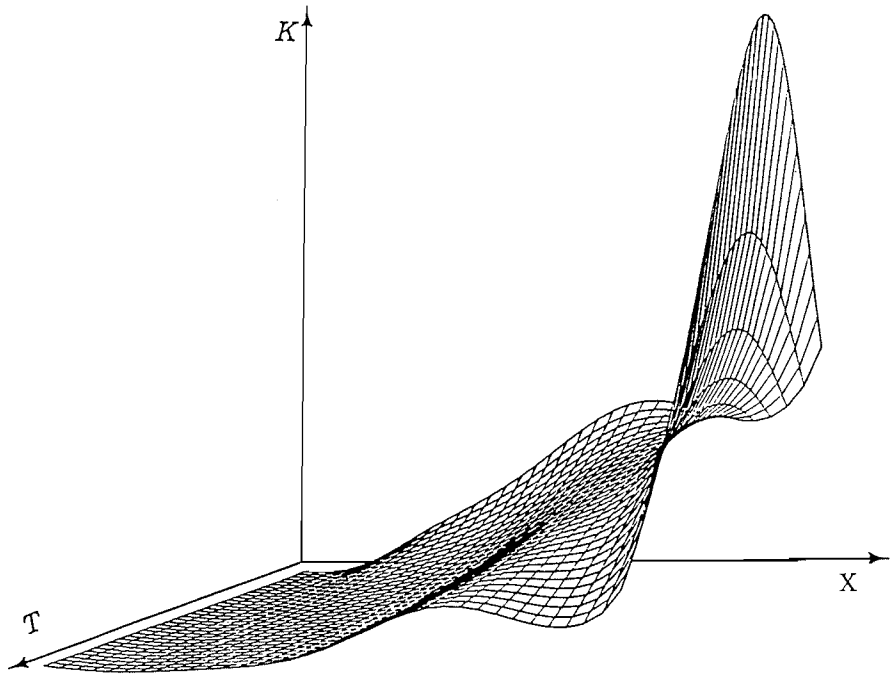


FIG. 5. Plot of $K = K(T, X)$ for picric acid in the DMF/Gliem solvent system.

solvent systems, with the agreement between calculated and experimental values obviously remaining acceptable.

If we apply criterion (i), it is possible to rule out the c_7 and c_{15} terms; in this way a simple and symmetrical equation, without ln T and $1/T$ terms, was obtained:

$$[10]\quad (\ln K)^2 = c_0 + c_1T + c_4X + c_5XT + c_8\frac{(1-X)}{(1+X)} + c_9T\frac{(1-X)}{(1+X)} + c_{12}X^2 + c_{13}X^2T + c_{16}\frac{(1-X^2)}{(1+X^2)} + c_{17}T\frac{(1-X^2)}{(1+X^2)}$$

where $c_0 = 8990.70$; $c_1 = -53.7602$; $c_4 = -12\,197.4$; $c_5 = 73.2864$; $c_8 = -6573.97$; $c_9 = 39.7636$; $c_{12} = 3194.08$; $c_{13} = -19.4608$; $c_{16} = -2523.09$; $c_{17} = 14.7213$; which leads to acceptable calculated K values (average difference of 10.6%).

Criterion (ii) has led us to apply to the present set of 209 K values the best-fit equations suggested in our previous papers (10–12) for three other solvent systems. In general, acceptable differences are observed (about 10%); the best agreement is achieved for the 13-term equation proposed for the Gliet/Gliem solvent system (10) with an average difference of 9.5%:

$$[11]\quad (\ln K)^2 = c_0 + c_1T + c_2\frac{1}{T} + c_4X + c_5XT + c_6\frac{X}{T} + c_8\frac{(1-X)}{(1+X)} + c_9T\frac{(1-X)}{(1+X)} + c_{12}X^2 + c_{13}X^2T + c_{16}\frac{(1-X^2)}{(1+X^2)} + c_{17}T\frac{(1-X^2)}{(1+X^2)} + c_{18}\frac{1}{T}\frac{(1-X^2)}{(1+X^2)}$$

where $c_0 = 4512.90$; $c_1 = -53.9021$; $c_2 = 1\,269\,630$; $c_4 = -9408.45$; $c_5 = 78.7915$; $c_6 = -1\,216\,533$; $c_8 = -9346.79$; $c_9 = 49.6370$; $c_{12} = 4519.54$; $c_{13} = -24.2143$; $c_{16} = 4003.31$; $c_{17} = 6.21057$; $c_{18} = -1\,162\,661$.

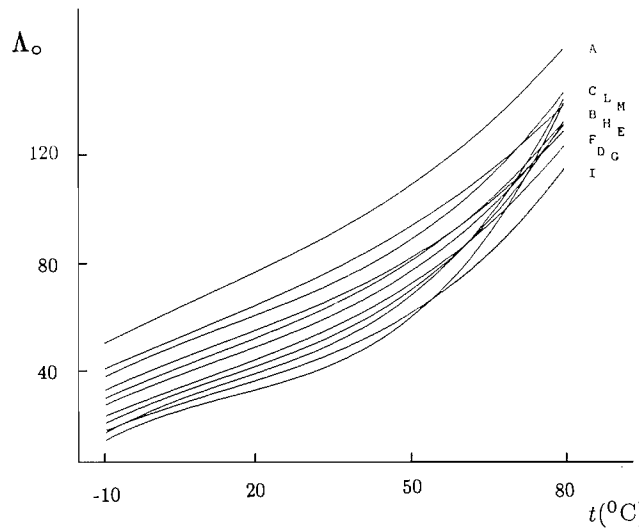


FIG. 6. Λ_0 vs. t (°C) plot for picric acid in the DMF/Gliem solvent system.

Starting from this last equation, if one eliminates the c_4 and c_{17} terms the following equation is obtained:

$$[12]\quad (\ln K)^2 = c_0 + c_1T + c_2\frac{1}{T} + c_5XT + c_6\frac{X}{T} + c_8\frac{(1-X)}{(1+X)} + c_9T\frac{(1-X)}{(1+X)} + c_{12}X^2 + c_{13}X^2T + c_{16}\frac{(1-X^2)}{(1+X^2)} + c_{18}\frac{1}{T}\frac{(1-X^2)}{(1+X^2)}$$

Can. J. Chem. Downloaded from www.nrcresearchpress.com by 195.138.81.100 on 09/07/12
For personal use only.

TABLE 5. λ_i^0 coefficients of eq. [13] for the *N*,*N*-dimethylformamide/2-methoxyethanol solvent system

System	λ_0^0 ($cm^2\,\Omega^{-1}\,mol^{-1}$)	λ_1^0 ($cm^2\,\Omega^{-1}\,mol^{-1}\,t^{-1}$)	$\lambda_2^0 \times 10^{-3}$ ($cm^2\,\Omega^{-1}\,mol^{-1}\,t^{-2}$)	$\lambda_3^0 \times 10^{-5}$ ($cm^2\,\Omega^{-1}\,mol^{-1}\,t^{-3}$)	$\sigma\Lambda_0$ ($cm^2\,\Omega^{-1}\,mol^{-1}$)
A	56.92	0.9154	−3.252	9.404	±0.45
B	46.86	0.7992	−1.829	7.356	±0.57
C	44.33	0.8382	−7.611	15.37	±1.78
D	39.16	0.7913	−5.260	11.45	±1.16
E	36.11	0.7862	−4.822	12.26	±1.21
F	33.62	0.7651	−5.885	14.14	±1.30
G	29.23	0.7242	−3.932	11.71	±1.13
H	27.13	0.7802	−8.906	19.19	±2.17
I	23.72	0.6736	−6.999	15.80	±1.75
L	24.30	0.8662	−13.85	26.20	±2.78
M	21.13	0.7681	−16.27	31.08	±3.25

where $c_0 = -2157.51$; $c_1 = -29.9573$; $c_2 = 1\,071\,488$; $c_5 = 46.1034$; $c_6 = -1\,041\,036$; $c_8 = -3863.85$; $c_9 = 31.6793$; $c_{12} = 1966.16$; $c_{13} = -15.8262$; $c_{16} = 5316.42$; $c_{18} = -982\,071.2$. This last equation (average difference 10.3%) takes into account all the above mentioned criteria and its terms all have high statistical weight. These considerations appear clearly if one examines Table 4, which summarizes all the equations cited.

Some qualitative considerations may be made regarding the trend and the changes of Λ_0 (Supplementary Table 12, available from the Depository of Unpublished Data). These values were fitted vs. temperature by a polynomial equation (32):

$$[13] \qquad \Lambda_0 = \sum_{i=0}^{3} \lambda_i^0 t^i$$

which reproduces well the experimental data (average difference between calculated and experimental values of ±2.2%. Table 5 contains the λ_i coefficients of eq. [13] and the relative standard deviations. Figure 6 shows the Λ_0 vs. temperature (°C) plot derived from eq. [13], which is characterized by a continuous and regular increase with increasing temperature; only in the case of the highest temperatures and for few mixtures are small deviations from the trend observed, probably arising from experimental errors.

Conclusions

The applicability of the empirical equations representing the functions $K = K(T)$ (eq. [2]), $K = K(X)$ (eq. [6]), and $K = K(T, X)$ (eq. [9]) to the dissociation constant of picric acid in the DMF/Gliem solvent system has been verified, giving quite acceptable average differences between experimental and calculated values (1.9% for eq. [2], 6.4% for eq. [6], and 9.2% for eq. [9]).

A comparison among the various $K = K(T, X)$ equations proposed in the present work and in previous studies (10–12) for similar solvent systems has been made by considering the criteria of the smallest difference between calculated and experimental values, of the simplest equation, and of the applicability to the largest number of solvent systems. This comparison has suggested that, in general, quite acceptable agreement between calculated and experimental values is achieved, even if the same equation may be employed with better results for the present system and for the previously studied Gliet/Gliem one.

Some simpler equations may be also utilized because the fitted K values are always in quite good agreement with the experimental results. In conclusion, the availability of $K = K(T, X)$ model equations allows us to calculate K values for any independent variable quantity T and X, if one supposes that the observed differences between experimental and calculated values (ca. 10%) should not be exceeded over all the points of the surface $K = K(T, X)$.

Acknowledgments

The authors wish to thank Prof. M. Goffredi for kindly supplying the computing program, the "Centro Interdipartimentale di Calcolo Automatico ed Informatica Applicata (C.I.C.A.I.A.)" of Modena University for the computing facilities, and the Ministero della Pubblica Istruzione (M.P.I.–40%) of Italy for financial support.

1. J. F. GARST. *In* Solute–solvent interactions. *Edited by* J. F. Coetzee and C. D. Ritchie. Marcel Dekker, New York. 1969.
2. C. PRETI and G. TOSI. Anal. Chem. **53**, 48 (1981).
3. C. PRETI, L. TASSI, and G. TOSI. Anal. Chem. **54**, 796 (1982).
4. E. NEVIANI GILIBERTI, C. PRETI, L. TASSI, and G. TOSI. Ann. Chim. (Rome), **73**, 527 (1983).
5. H. EYRING and M. S. JOHN. *In* Significant liquid structure. J. Wiley & Sons, New York. 1969.
6. G. C. FRANCHINI, C. PRETI, L. TASSI, and G. TOSI. Anal. Chem. **60**, 2358 (1988).
7. G. C. FRANCHINI, A. MARCHETTI, C. PRETI, L. TASSI, and G. TOSI. Anal. Chem. **61**, 117 (1989).
8. G. C. FRANCHINI, E. ORI, C. PRETI, L. TASSI, and G. TOSI. Can. J. Chem. **65**, 722 (1987).
9. G. C. FRANCHINI, L. TASSI, and G. TOSI. J. Chem. Soc. Faraday Trans. 1, **83**, 3129 (1987).
10. G. C. FRANCHINI, A. MARCHETTI, C. PRETI, L. TASSI, and G. TOSI. J. Chem. Soc. Faraday Trans. 1, **85**, 1697 (1989).
11. G. C. FRANCHINI, A. MARCHETTI, L. TASSI, and G. TOSI. J. Chem. Soc. Faraday Trans. 1, **84**, 4427 (1988).
12. A. MARCHETTI, E. PICCHIONI, L. TASSI, and G. TOSI. Anal. Chem. **61**, 1971 (1989).
13. F. FRANKS and D. J. G. IVES. Qt. Rev. **20**, 1 (1966).
14. A. P. KRESHKOV, M. T. SMOLOVA, A. VEVERIS, and B. SPINCE. Zh. Fiz. Khim. **51**, 1827 (1977).
15. R. C. WEAST (*Editor*). Handbook of chemistry and physics. 66th ed. The Chemical Rubber Co., Cleveland, OH. 1985–1986.
16. R. ALEXANDER, E. C. F. KO, Y. C. MAC, and A. J. PARKER. J. Am. Chem. Soc. **89**, 3703 (1967).
17. I. M. KOLTHOFF and M. K. CHANTOONI JR. J. Phys. Chem. **76**, 2024 (1972).

Can. J. Chem. Downloaded from www.nrcresearchpress.com by 195.138.81.100 on 09/07/12
For personal use only.

18. W. R. GILKERSON and M. D. JACKSON. J. Am. Chem. Soc. **101**, 4096 (1979).
19. B. S. KRUMGALZ. J. Chem. Soc. Faraday Trans. 1, **79**, 571 (1983).
20. K. L. HSIA and R. M. FUOSS. J. Am. Chem. Soc. **90**, 3055 (1968).
21. R. M. FUOSS. J. Phys. Chem. **82**, 2427 (1978).
22. J. H. ROBERTS. *In* The chemistry of nonaqueous solvents. *Edited by* J. J. Lagowski. Academic Press, New York. 1976.
23. K. BOSE and K. K. KUNDU. Can. J. Chem. **57**, 2470 (1979).
24. BRONWYN H. HALL. (*Editor*). Time Series Processor (TSP) User's guide. TSP International, Stanford, CA. 1987.
25. B. B. MANDELBROT. Fractal form, chance and dimension. W. H. Freeman and Co., San Francisco, CA. 1977.
26. H. O. PEITGEN and P. H. RICHTER. The beauty of fractals. Springer-Verlag, Berlin. 1986.
27. B. B. MANDELBROT. Gli Oggetti Frattali. Einaudi, Torino, Italy. 1987.
28. T. SHEDLOVSKY and R. KAY. J. Am. Chem. Soc. **60**, 151 (1956).
29. K. NORBERG. Acta Chem. Scand. **20**, 264 (1966).
30. A. D'APRANO and R. M. FUOSS. J. Phys. Chem. **73**, 400 (1969).
31. A. L. DE and A. K. ATTA. Can. J. Chem. **63**, 3129 (1984).
32. M. NAKAHARA. J. Phys. Chem. **88**, 2138 (1984).

Can. J. Chem. Downloaded from www.nrcresearchpress.com by 195.138.81.100 on 09/07/12
For personal use only.

New halogenated sesquiterpenes from the red alga *Laurencia caespitosa*

MANUEL NORTE,[1] RAFAEL GONZÁLEZ, AGUSTÍN PADILLA, JOSÉ J. FERNÁNDEZ, AND JESÚS T. VÁZQUEZ

Centro de Productos Naturales Orgánicos "Antonio González", Instituto Universitario de Bio-Orgánica, Universidad de La Laguna, Carretera de La Esperanza, 2, 38206 La Laguna, Tenerife, Spain

Received August 22, 1990

MANUEL NORTE, RAFAEL GONZÁLEZ, AGUSTÍN PADILLA, JOSÉ J. FERNÁNDEZ, and JESÚS T. VÁZQUEZ. Can. J. Chem. **69**, 518 (1991).

Three new brominated sesquiterpenes have been isolated from the red alga *Laurencia caespitosa*. The structures of these metabolites have been elucidated by spectral analysis and chemical correlations. Their absolute configurations were established by CD methods.

Key words: red alga, Rhodomelaceae, halogenated sesquiterpenes, snyderane.

MANUEL NORTE, RAFAEL GONZÁLEZ, AGUSTÍN PADILLA, JOSÉ J. FERNÁNDEZ et JESÚS T. VÁZQUEZ. Can. J. Chem. **69**, 518 (1991).

On a isolé trois nouveaux sesquiterpènes bromés à partir de l'algue rouge *Laurencia caespitosa*. On a élucidé les structures de ces métabolites en se basant sur des analyses spectrales et sur des corrélations chimiques. On a établi leurs configurations absolues à l'aide de méthodes de DC.

Mots clés : algue rouge, Rhodomelaceae, sesquiterpènes halogénés, snyderane.

[Traduit par la rédaction]

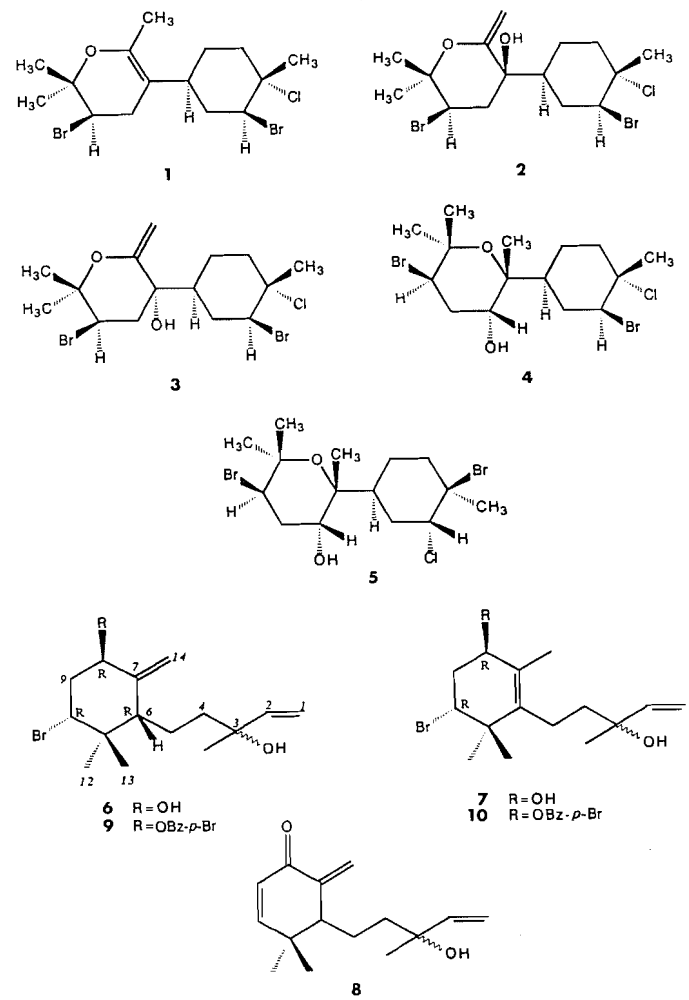
Can. J. Chem. Downloaded from www.nrcresearchpress.com by 195.138.81.100 on 09/07/12
For personal use only.

The red alga *Laurencia caespitosa* collected at La Graciosa (Canary Islands) was found to be a rich source of regular and irregular halogenated sesquiterpenes (1). We recently published the isolation of three new irregular rearranged sesquiterpenoids, the laucapyranoids A, **1**; B, **2**, and C, **3** (2), which are related to caespitol **4** and isocaespitol **5**, metabolites previously isolated from the same alga (3).

We report here the isolation and structure elucidation of the monocyclofarnesane derivatives **6–8**, one of them with an unprecedented γ-snyderol system. In contrast with other kinds of sesquiterpenoid skeletons, the number of halogenated sesquiterpenes with a snyderane skeleton isolated from *Laurencia* is small (4).

These compounds were isolated by chromatography on silica gel followed by gel filtration chromatography on Sephadex LH-20, the final purification being carried out by HPLC.

The major metabolite of this series, compound **6**, was isolated as an oil, $[\alpha]_D$ +8.7 (*c* 0.172, $CHCl_3$). Its molecular formula was established as $C_{15}H_{25}O_2Br$ on the basis of its HRMS. The ^1H NMR spectrum showed the presence of two methines α to heteroatoms (δ 4.28 and 4.50), an exocyclic double bond (δ 4.77 and 5.10), and the characteristic chemical shifts due to the double bond of the last isoprene unit for the monocyclofarnesane derivatives (δ 5.07, 5.21, and 5.91). This was confirmed by the ^{13}C NMR spectrum as well as by the loss of the fragment (C_5H_9O) observed in the mass spectrum. The cyclic proton assignments begin with the direct coupling of H-8 (δ 4.28) to H-9 (δ 2.35 and 2.17) and, further, H-9 to H-10 (δ 4.50), and the direct coupling of protons finishes with the presence of quaternary centers at C-7 and C-11. The relative positions were confirmed by the long range coupling of H-8 to H-14 (δ 5.10). The nature of the heteroatoms at C-8 and C-10 was easily established as oxygen and bromine, respectively, by the correlation of the assigned proton signals to carbons in the ^1H–^{13}C COSY(HETCOR) spectrum: H-8 (δ 74.5) and H-10 (δ 63.5). The relative configurations of the chiral centers at C-6, C-8, and C-10 were established as follows. The coupling constant values observed for H-8 and H-10 (Table 1) showed that the hydroxyl group must be axial and the bromine atom



equatorial, which implies that they possess opposite orientations. On the other hand, the NOEDIFF experiment showed nOe enhancement for the H-10 signal when the H-6 signal at δ 2.3 was irradiated. These spectroscopic data agree with the structure of 8-hydroxy-β-snyderol for compound **6**.

Compound **7**, oil, $[\alpha]_D$ +16.8 (*c* 0.136, $CHCl_3$). Its HRMS

[1]Author to whom correspondence may be addressed.

Printed in Canada / Imprimé au Canada

TABLE 1. NMR spectral data for **6**, **7**, and **8**

	^{13}C			$^{1}H^{c}$		
Carbon	**6**[a]	**7**[b]	**8**[b]	**6**	**7**	**8**
1	112.06	112.34	111.98	5.21 dd, 17.4; 1.2 5.07 dd, 10.7; 1.2	5.23 dd, 17.3; 1.3 5.10 dd, 10.7; 1.3	5.18 dd, 17.3, 1.2 5.04 dd, 10.7; 1.2
2	145.09	144.72	145.20	5.91 dd, 17.4; 10.7	5.92 dd, 17.3; 10.7	5.87 dd, 17.3; 10.7
3	73.56	73.49	73.50	—	—	—
4	41.01	39.96	40.43	1.30 m 1.71 m	1.58 m	1.31 m 1.62 m
5	20.34	24.33	22.03	1.55 m 1.75 m	2.10 m	1.49 m 1.80 m
6	47.26	128.28	53.39	2.30 bd	—	2.32 bd
7	147.72	140.92	145.27	—	—	—
8	74.50	71.14	—	4.28 t, 3.3	3.9 t, 3.4	—
9	42.39	41.49	127.15	2.35 ddd, 13.8; 4.5; 3.3 2.17 ddd, 13.8; 12.4; 3.3	2.38 ddd, 13.8; 4.5; 3.4 2.29 ddd, 13.8; 11.4; 3.4	5.96 d, 10.5
10	63.15	61.52	159.79	4.50 dd, 12.4; 4.5	4.43 dd, 11.4; 4.5	6.65 dd, 10.2, 1.4
11	42.29	41.25	—	—	—	—
12	15.46	17.48	24.48	0.78 s	1.07 s	1.095 s
13	28.20	27.97	29.35	1.18 s	1.19 s	1.185 s
14	111.57	22.56	121.47	4.77 bs 5.10 bs	1.73 s	6.04 d, 2.0 5.22 d, 2.0
15	27.88	26.72	27.94	1.29 s	1.30 s	1.24 s

[a]Assignments made by ^{1}H–^{13}C heteronuclear COSY.
[b]Assignments made by comparison with **6**.
[c]Assignments made by homonuclear COSY.

showed it to be an isomer of **6** and the comparison of their NMR spectra showed that they are structurally related. Thus, the main differences observed, with respect to **6**, in the ^{1}H NMR spectrum of compound **7** were the absence of signals for the protons H-6 and H-14 together with the presence of a vinylic methyl group at δ 1.73. This was confirmed in the ^{13}C NMR spectrum by the presence of a Z tetrasubstituted double bond (δ 128.28, 140.92, and 22.56). On the basis of these data we assigned the structure of **7** as 8-hydroxy-γ-snyderol, which is the first example of a γ-snyderol derivative isolated from marine sources.

Compound **8**, oil, $[\alpha]_D$ +13.6 (*c* 0.77, $CHCl_3$), has a molecular formula of $C_{15}H_{22}O_2$. The presence in the molecule of an α,β-unsaturated carbonyl group was evidenced by the strong absorption at 1660 cm^{-1} in the IR spectrum and by a band in the UV spectrum at 274 nm. It was confirmed by the NMR spectral data, which allowed us to place the carbonyl group at the carbon C-8 and the double bond between the carbons C-9 and C-10.

Moreover, comparison of these data with those observed for **6** and **7** showed that this compound possesses the common side chain and that it belongs to the β-snyderol series. The final confirmation of the structure was obtained through the chemical correlation between **6** and **8**. Treatment of **6** with MnO_2 at room temperature for 2 h gave a compound that showed physical and spectroscopical data identical with those observed for compound **8**.

The circular dichroic exciton chirality method has proved to be an excellent tool for the determination of absolute configurations (5). We have applied the CD allylic benzoate method (6–8) to compounds **6** and **7**, which possess allylic alcohols. Their bromobenzoylation with 4-bromobenzoyl chloride in pyridine with DMAP as catalyst yielded the allylic benzoates **9** and **10** (CH_3CN, 243 nm, ε = 21 300), respectively. Their CD spectra exhibited a negative Cotton effect at 241.5 nm (Δε = −1.5) for **9** and a positive Cotton effect at 241.0 nm (Δε = +13.9) for **10**. Since the sign of the CD Cotton effect represents the chirality of the double bond – benzoate system, the observed negative exciton chirality for **9** and the positive one for **10** led to the absolute configuration shown for these compounds.

Experimental part

NMR spectra were recorded on a Bruker model WP 200 SY spectrometer (200 MHz), chemical shifts are reported relative to Me_4Si (δ, 0), and coupling constants are given in hertz. The 2D-NMR spectra were obtained using Bruker microprograms. Samples for nOe experiments were degassed by bubbling Ar through the solution. IR and UV spectra were recorded on Perkin–Elmer model 257 and Perkin–Elmer model 550D spectrophotometers. CD spectra were recorded on a Jasco J-600 spectropolarimeter. Optical rotations were determined for solution in $CHCl_3$ with a Perkin–Elmer model 241 polarimeter. Low and high resolution mass spectra were obtained from a VG Micromass ZAB-2F spectrometer. HPLC was carried out on a semipreparative silica gel μ-Porasil column attached to a Waters pump model 6000 and monitored with a differential diffractometer detector model R-401. Sephadex LH-20 obtained from Pharmacia was used for gel filtration chromatographies. Silica gel column chromatography, TLC, and PLC were performed on silica gel 60 G. The TLC plates were developed by spraying with 6 N sulphuric acid and heating. All solvents were purified by standard techniques. Anhydrous magnesium sulphate was used for drying solutions.

Collection, extraction, and chromatographic separation

Laurencia caespitosa was collected in shallow water at low tide at the island of La Graciosa in September 1986. The air-dried alga (5 kg) was extracted with acetone and diethyl ether. The solvents were evaporated *in vacuo* to afford 62 g of crude extract. This was chromatographed on a silica gel column eluted with a mixture of *n*-hexane/ethyl acetate of increasing polarity, and 50 fractions of 1 L each were collected. The fractions eluted with *n*-hexane/ethyl acetate 60:40 afforded after solvent evaporation the products **6**, **7**, and **8**.

Can. J. Chem. Downloaded from www.nrcresearchpress.com by 195.138.81.100 on 09/07/12
For personal use only.

Can. J. Chem. Downloaded from www.nrcresearchpress.com by 195.138.81.100 on 09/07/12
For personal use only.

These were chromatographed on Sephadex LH-20 (using as eluent $CHCl_3$/methanol/*n*-hexane 1:1:2) and, after silica gel column chromatography, gave pure **8** (25 mg) and a mixture of **6** and **7** (168 mg). This mixture was chromatographed on HPLC using *n*-hexane/ethyl acetate 70:30, affording the pure products **6** (136 mg) and **7** (30 mg).

Compound 6 (8-hydroxy-β-snyderol)

Oil, $[\alpha]_D$ +8.7 (*c* 0.172, $CHCl_3$). IR ($CHCl_3$) ν_{max}: 3590, 3000, 2970, 1640, and 1370 cm^{-1}. ^1H and ^{13}C NMR (200 MHz, $CDCl_3$), see Table 1. HRMS *m/z*: $C_{14}H_{20}O^{81}Br$ 285.0069 (calcd. 285.0677). MS (EI), *m/z* (relative intensity): 318, 316 (M^+, not obs.), 285, 283 (1, 1); 233, 231 (7, 7); 219 (19); 201 (10); 173 (6); 149 (14); and 133 (29).

Compound 7 (8-hydroxy-γ-snyderol)

Oil, $[\alpha]_D$ +16.2 (*c* 0.136, $CHCl_3$). IR ($CHCl_3$) ν_{max}: 3590, 3000, 2970, 1600, 1410, and 1360 cm^{-1}. ^1H and ^{13}C NMR (200 MHz, $CDCl_3$), see Table 1. HRMS *m/z*: $C_{14}H_{20}O^{81}Br$ 285.0658 (calcd. 285.0677). MS (EI), *m/z* (relative intensity): 318, 316 (M^+, not obs.); 285, 283 (1, 1); 233, 231 (41, 41); 219 (46); 201 (16); 161 (59); and 123 (41).

Compound 8 (8-keto-10-dehydrobrominated-β-snyderol)

Oil, $[\alpha]_D$ +13.6 (*c* 0.77, $CHCl_3$). IR ($CHCl_3$) ν_{max}: 3570, 3010, 3000, 2940, 1660, 1590, and 1420 cm^{-1}. UV (EtOH) λ_{max}: 274 nm (ε 8900). ^1H and ^{13}C NMR (200 MHz, $CDCl_3$), see Table 1. HRMS *m/z*: $C_{15}H_{22}O_2$ 234.1599 (calcd. 234.1620). MS (EI), *m/z* (relative intensity): 234 (M^+, 2), 219 (4), 201 (9), 175 (7), 161 (10), 149 (56), 135 (31), and 121 (40).

Compound 9 (8-(p-bromobenzoyl)-β-snyderol)

To compound **6** (16 mg, 0.05 mmol) dissolved in dry pyridine (2 mL) was added *p*-bromobenzoyl chloride (23 mg, 0.1 mmol) and the mixture was stirred for 5 h at room temperature under Ar. The usual work-up gave an oily residue, which was chromatographed on HPLC to furnish 14 mg of **9**; oil, $[\alpha]_D$ +0.9 (*c* 0.22, $CHCl_3$). ^1H NMR ($CDCl_3$) δ: 7.86 (2H, d, *J* = 8.6 Hz), 7.60 (2H, d, *J* = 8.6 Hz), 5.87 (1H, dd, *J* = 10.6 and 17.1 Hz), 5.53 (1H, t, *J* = 2.8 Hz), 5.34 (1H, s), 5.19 (1H, dd, *J* = 1.2 and 17.1 Hz), 5.04 (1H, dd, *J* = 1.2 and 10.6 Hz), 4.40 (1H, dd, *J* = 4.5 and 12.5 Hz), 2.59 (1H, ddd, *J* = 3.9, 4 and 14.4 Hz), 1.26 (3H, s), 1.23 (3H, s), and 0.85 (3H, s). MS (EI), *m/z* (relative intensity): 416, 414, 412 (8, 16, 8); 334, 332 (2, 2); 267, 265 (5, 6); 254, 252 (8, 7); and 185, 183 (100, 99).

Compound 10 (8-(p-bromobenzoyl)-γ-snyderol)

Compound **7** (16 mg, 0.05 mmol) was converted into **10** under the same conditions employed to transform **6** into **9**. Purification afforded 13 mg of **10**: oil $[\alpha]_D$ +89.5 (*c* 0.19, $CHCl_3$). ^1H NMR ($CDCl_3$) δ: 7.89 (2H, d, *J* = 8.6 Hz), 7.60 (2H, d, *J* = 8.6 Hz), 5.95 (1H, dd, *J* = 10.7 and 17.2 Hz), 5.35 (1H, dd, *J* = 2.5 and 2.8 Hz), 5.26 (1H, dd, *J* = 1.2 and 17.2 Hz), 5.15 (1H, dd, *J* = 1.2 and 10.7 Hz), 4.39 (1H, dd, *J* = 4.4 and 11.9 Hz), 1.65 (3H, s), 1.33 (3H, s), 1.26 (3H, s), and 1.13 (3H, s). MS (EI), *m/z* (relative intensity): 416, 414, 412 (3, 6, 3); 334, 332 (20, 19) and 235, 233 (96, 100); and 219 (10).

Transformation of 6 into 8

To a solution of **6** (16 mg, 0.05 mmol) in CH_2Cl_2 (3 mL) was added MnO_2 (10 mg, 0.12 mmol) and the mixture was stirred for 2 h at room temperature, filtered off, the solvent evaporated, and the residue chromatographed by HPLC. The physical and spectral properties of the ketone obtained were identical with those observed for compound **8**.

Acknowledgments

This research was supported by a grant from the Plan Nacional de Investigación ref. FAR88-0500. R.G. and A.P. thank the Ministry of Education for a F.P.I. fellowship.

1. D. J. Faulkner. Nat. Prod. Rep. **6**, 613 (1988), and references therein.
2. M. Chang, J. T. Vázquez, K. Nakanishi, F. Cataldo, D. M. Estrada, J. J. Fernández, A. Gallardo, J. D. Martín, M. Norte, R. Pérez, and M. L. Rodriguez. Phytochemistry, **28**, 1417 (1989).
3. A. G. González, J. Darias, J. D. Martín, and C. Pérez. Tetrahedron Lett. 1249 (1974).
4. (*a*) B. M. Howard and W. Fenical. Tetrahedron Lett. 41 (1976); (*b*) J. D. Martín and J. Darias. *In* Marine natural products. Vol. I. *Edited by* P. J. Scheuer. Academic Press, New York. 1978. p. 125; (*c*) K. L. Erickson. *In* Marine natural products. Vol. V. *Edited by* P. J. Scheuer. Academic Press, New York. 1983. p. 132.
5. N. Harada and K. Nakanishi. Circular dichroic spectroscopy—Exciton coupling in organic stereochemistry. University Science Books, Mill Valley, CA. 1983.
6. N. Harada, J. Iwabuchi, Y. Yokota, H. Uda, and K. Nakanishi. J. Am. Chem. Soc. **103**, 5590 (1981).
7. N. C. Gonella, K. Nakanishi, V. S. Martín, and K. B. Sharpless. J. Am. Chem. Soc. **104**, 3775 (1982).
8. N. Harada, Y. Yokota, J. Iwabuchi, H. Uda, and M. Ochi. J. Chem. Soc. Chem. Commun. 1220 (1984).

Synthèse, structure et études spectroscopiques RMN ^1H et ^{13}C de dérivés perhydrocyclododéca[*b*]furaniques

MICHEL ALBRAND, RENÉ DOLMAZON[1] ET PATRICK POLLET

Laboratoire de chimie organique, Département de biochimie, Institut national des sciences appliquées, 20 Avenue Albert Einstein, 69621 Villeurbanne CEDEX, France

Reçu le 25 juillet 1990

MICHEL ALBRAND, RENÉ DOLMAZON et PATRICK POLLET. Can. J. Chem. **69**, 521 (1991).

Une voie d'accès à une série de perhydrocyclododéca[*b*]furan-3-ols, perhydrocyclododéca[*b*]furan-3-ones et perhydrocyclododéca[*b*]furanes est décrite. Leurs configurations, en particulier celles de la jonction de cycles, sont précisées. Pour le couple de perhydrocyclododéca[*b*]furan-3-ones ou de perhydrocyclododéca[*b*]furanes, l'isomère *cis* est beaucoup moins stable que son épimère *trans*, en accord avec les résultats de l'analyse conformationnelle conduite par mécanique moléculaire. Leurs caractéristiques spectrales RMN ^1H et ^{13}C sont précisées.

Mots clés : perhydrocyclododéca[*b*]furanes, conformations, mécanique moléculaire, RMN ^1H et ^{13}C.

MICHEL ALBRAND, RENÉ DOLMAZON, and PATRICK POLLET. Can. J. Chem. **69**, 521 (1991).

A synthetic route to perhydrocyclododeca[*b*]furan-3-ols, perhydrocyclododeca[*b*]furan-3-ones, and perhydrocyclododeca[*b*]furan derivatives is described. Their configurations were determined. For the perhydrocyclododeca[*b*]furan-3-one and perhydrocyclododeca[*b*]furan pairs, the *cis* isomer was much less stable than the *trans* isomer. This agrees well with results from a conformational analysis, carried out by molecular mechanics. The ^1H and ^{13}C NMR spectra are reported.

Key words: perhydrocyclododeca[*b*]furans, conformations, force field calculations, ^1H and ^{13}C NMR.

Can. J. Chem. Downloaded from www.nrcresearchpress.com by 198.100.157.202 on 09/07/12
For personal use only.

La configuration *cis* ou *trans* de fusion de cycles à 12 et 5 atomes n'est pas clairement définie. Les tentatives d'assignation de structure effectuées sur les bicyclo[10,3,0]pentadécanones-13 (1–3) ont conduit à des analyses contradictoires, ce qui est dû essentiellement à l'impossibilité de distinguer et d'identifier chaque isomère du couple de jonction *cis* ou *trans*. Dans le cas du couple d'oxa-13 bicyclo[10,3,0]pentadécanes (4–6), les deux isomères ont été observés, mais aucune assignation de structure n'a été effectuée.

En raison de l'intérêt industriel (propriétés olfactives, parfums à odeur musquée) que suscitent ces deux types des composés précités, nous nous sommes intéressés à l'étude d'une série de dérivés oxa-13 bicyclo[10,3,0]pentadécaniques (perhydrocyclododéca[*b*]furanes), l'anisotropie introduite par l'hétéroatome oxygéné devant permettre de différencier spectroscopiquement (RMN ^1H et ^{13}C) le couple d'isomères de jonction. Nous décrivons la synthèse, la structure et les caractéristiques spectrales RMN ^1H (et pour certains ^{13}C) de perhydrocyclododéca[*b*]furanols-3 **4**–**7**, perhydrocyclododéca[*b*]furanones-3 **8**, **9** et perhydrocyclododéca[*b*]furanes **10**, **11**.

Synthèses

Les perhydrocyclododéca[*b*]furanols-3 **4**–**7** ont été obtenus selon deux voies A ou B à partir de l'acétoxyacétyl-2 cyclododécanone (**1**), préparée par acylation du morpholino-1 cyclododécène au moyen du chlorure de l'acide acétoxyacétique (figure 1). Nous avons déjà utilisé ces méthodes lors de la synthèse de perhydrocyclopenta[*b*]furanols-3 (8) et perhydrocyclohepta[*b*]furanols-3 (9).

Voie A : la β-dicétone acétoxylée **1** est préalablement cyclisée, dans l'acide sulfurique concentré, en cétone éthylènique **2**, hydrogénée ensuite, en catalyse hétérogène (Ni de Raney W_4), en alcools **4**, **5** et **6**, séparés et identifiés sous forme d'acétates correspondants **4***a*, **5***a* et **6***a*. La composition du mélange est respectivement la suivante : 53, 35 et 12%.

Voie B : la β-dicétone acétoxylée **1** est réduite par l'hydrogène, en présence de nickel de Raney W_4, en un mélange de dihydroxy acétates **3**, cyclisés ensuite en milieu acide en alcools **5**, **6** et **7**, séparés et identifiés sous forme d'acétates correspondants **5***a*, **6***a* et **7***a*. La composition du mélange est respectivement la suivante : 46, 34 et 20%.

L'oxydation de ces alcools (voies A ou B) dans des conditions décrites comme non épimérisantes (réactif de Jones (10) ou chlorochromate de pyridinium (11)) conduit à des mélanges des perhydrocyclododéca[*b*]furanones-3 **8** et **9** dont la composition varie en fonction de l'origine des alcools (voie A ou B) et aussi des traitements de purification. La cétone **8** a été dosée approximativement (par spectroscopie RMN ^1H) à 80%, dans le meilleur des cas, sur le mélange brut des deux cétones obtenues par oxydation des alcools issus de la voie A au moyen du réactif de Jones. Cette cétone **8** s'est avérée très instable; les tentatives de purification (distillation ou passage sur colonne de silice) n'ont fait que diminuer sa teneur dans les mélanges **8** + **9**. Divers mélanges de ces deux cétones, placés dans des conditions épimérisantes, en présence de triéthylamine (12), ont conduit à un mélange **8** + **9** de composition à l'équilibre 5 : 95.

Les perhydrocyclododéca[*b*]furanes **10** et **11**, composés connus (4–6), ont été obtenus à partir soit du mélange d'alcools saturés **4**–**6** par réduction de leurs tosylates au moyen de $LiAlH_4$ (13, 14), soit du mélange à l'équilibre des cétones saturées **8** + **9** par réduction de Wolff–Kishner dans la modification de Huang–Minlon (15). La stéréochimie de chacune de ces réductions, bien qu'elle soit imprévisible dans le cas d'une réduction de Wolff–Kishner (16), n'a pas fait l'objet d'études de notre part. Dans les deux cas, l'examen en chromatographie préparative en phase vapeur du mélange réactionnel a révélé la présence de deux isomères **10** et **11**, mal séparés, le premier élué (**11**) étant très fortement majoritaire 70–85%. Nos conditions d'analyse chromatographique se sont avérées épimérisantes. Un nouveau passage dans les mêmes conditions d'un échantillon préalablement enrichi en isomère **10** (teneur voisine de 40%, déterminée par RMN ^{13}C) a conduit à un nouveau mélange où la teneur en composé **10** n'était plus que de 15% environ.

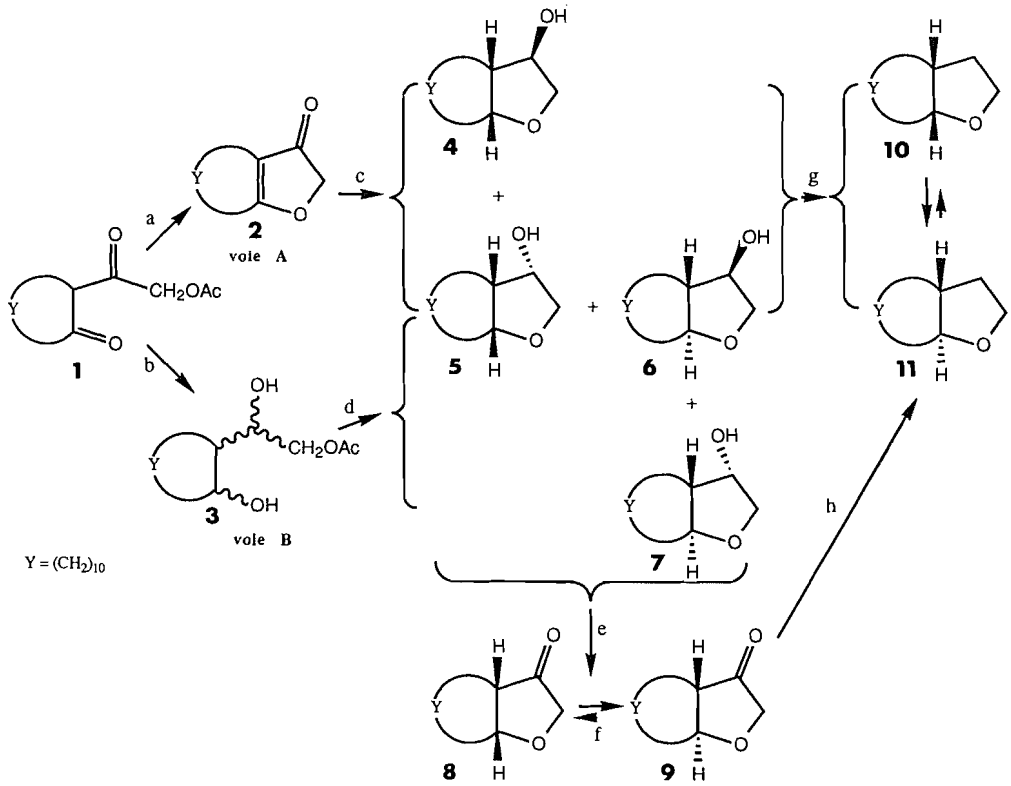
Structures

1. Calculs des structures des bicycles perhydrocyclododéca[b]-furanes 8, 9, 10 et 11

La conformation L = [3333], du cyclododécane possède

1. Auteur à qui adresser toute correspondance.

Printed in Canada / Imprimé au Canada



Les composés de cette publication sont tous des racémiques; le choix pour l'illustration de l'un des énantiomères est arbitraire.

Réactifs : a, H_2SO_4 concentré; b et c, H_2 – nickel de Raney; d, CH_3COCl dans C_2H_5OH; e, réactif de Jones ou chlorochromate de pyridinium; f, Et_3N; g, tosylates puis $LiAlH_4$; h, Wolff–Kishner

FIG. 1

approximativement la symétrie D_4 (figure 2). Cette conformation «carrée», trouvée dans la structure cristalline (17), est en accord avec les données RMN (18, 19) et est celle de plus basse enthalpie calculée (20). En accord avec la littérature (20), nos calculs effectués à l'aide du champ empirique de forces MMX (21) confirment l'existence de quatre conformations compétitives (figure 2) et montrent en particulier que l'enthalpie de la conformation M = [2334] n'est que de 1,02 kcal/mol supérieure à celle de la conformation carrée L. En raison de la moindre symétrie de la conformation M, cette dernière possède une entropie supérieure à celle de L, ce qui entraine une différence d'énergie libre inférieure à la différence d'enthalpie entre les conformères L et M, ce qui montre que les populations de L et M sont du même ordre de grandeur. Pour la suite de notre travail nous avons considéré que seules les conformations L, M et N possèdent une population significative à température ambiante.

Les dérivés tétrahydrofuraniques, comme les dérivés cyclopentaniques (22), sont connus pour leur extrême mobilité conformationnelle (22–25), la conformation évoluant entre deux formes extrêmes d'énergies voisines (1 kcal/mol), demi-chaise C_2 (26) et enveloppe C_s (27).

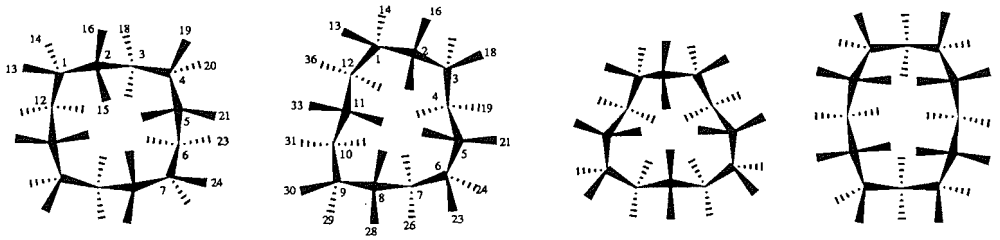
La fusion du cycle tétrahydrofuranique avec le cycle cyclododécane est très restrictive dans la mesure où le cycle à cinq membres ne tolère pas d'angle dièdre endocyclique supérieur à 50° (22) sans introduire rapidement de fortes contraintes stériques.

Les énergies des différentes conformations des bicycles **8**, **9**, **10** et **11** ont été calculées par minimisation des différentes conformations bâties à partir des conformations L, M et N du cyclododécane. Les conformations initiales mettant en jeu une ou deux liaisons de cycle endocyclique par rapport au cyclododécane, ainsi que celles impliquant un angle diédre endocyclique de fusion par rapport au cycle tétrahydrofuranne supérieur à 60° ont été négligées. Une étude systématique, conduite sur les conformations bâties sur L, a confirmé ces restrictions. Trois exemples de conformations optimisées des hétérobicycles sont représentées sur la figure 3. La géométrie et les énergies des cinq conformations privilégiées des composés **8**, **9**, **10** et **11** sont données respectivement dans les tableaux 1 et 2. L'analyse des résultats montre que pour chaque composé les faibles écarts énergétiques calculés entre les différentes conformations n'en privilégient aucune et que l'isomère *trans* est plus stable que l'isomère *cis* (écart énergétique significatif d'environ 2,5 kcal/mol entre les conformations les plus stables).

2. Détermination de structures

La nature de la jonction de cycles des dérivés perhydrocyclododéca[*b*]furaniques est déduite des résultats qui suivent. L'addition, à caractère *syn* stéréospécifique, d'hydrogène par catalyse hétérogène sur la cétone éthylènique **2** devrait conduire à deux alcools de jonction de cycles *cis*. L'obtention de trois alcools **4**, **5** et **6** (voie A) (figure 1) montre que les conditions dures, épimérisantes, nécessaires à la réduction de la double liaison tétrasubstituée, ont entrainé une épimérisation partielle de la cétone intermédiaire énolisable *cis*, comme nous l'avons déjà observé sur des systèmes voisins (28). L'oxydation, non épimérisante, de ce mélange d'alcools conduit à un mélange des cétones **8** et **9** où la cétone **8**, fortement majoritaire (80% au moins), s'avère très instable et s'épimérise très facilement en

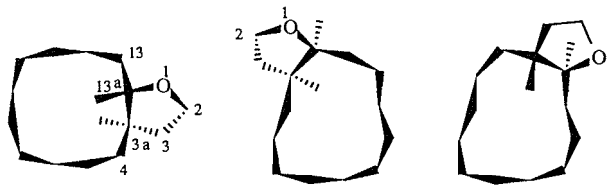
Can. J. Chem. Downloaded from www.nrcresearchpress.com by 198.100.157.202 on 09/07/12
For personal use only.



	L=[3333][a]	M=[2334]	N=[2343]	[2424]
E^b :	12,74	13,76	15,17	17,31
Eo^c :	0	1,02 (1,6)[a]	2,43 (2,9)[a]	4,57 (4,9)[a]

[a]Référence 20.
[b]Energie totale de contrainte calculée en kcal/mol.
[c]Energie relative de contrainte en kcal/mol par rapport à celle de la conformation la plus stable.

FIG. 2. Conformations préférentielles du cyclododécane.



$LO_{21}C_{23}$[a] $MO_{13}C_{36}$ $MO_{18}C_{16}$

[a]L signifie que le conformère est bâti à partir de la conformation L du cyclododécane par substitution des atomes d'hydrogène 21 et 23 par l'atome d'oxygène et un atome de carbone du cycle tétrahydrofurannique.

FIG. 3. Types de conformations préférentielles des composés **8**, **9**, **10** et **11**.

cétone **9** plus stable. L'ensemble de ces données associé aux résultats des calculs précédents conduisent à attribuer une jonction de cycles *cis* à la cétone **8** et *trans* à la cétone **9**, nettement plus stable. Cette plus grande stabilité de l'isomère *trans* par rapport à l'isomère *cis* a été également constatée dans le cas du couple de bicyclo[10,3,0]pentadécène-14-ones-13 *cis* et *trans* (29). La comparaison des compositions des mélanges des alcools **4**, **5** et **6** (53, 35 et 12%) et des cétones *cis* et *trans* **8** et **9** (80 et 20%) obtenus selon la même voie A permet de déduire que les deux alcools fortement majoritaires **4** et **5** possèdent une jonction de cycles *cis*. L'autre couple d'alcools **6** et **7** de jonction de cycles *trans* est obtenu selon la voie B moins stéréosélective. L'assignation de structure au niveau du carbone C-3 pour chaque couple d'alcools de jonction *cis* ou *trans* a été établie à l'examen des données spectroscopiques RMN ^1H de leurs acétates. Pour un couple d'acétates, de jonction donnée, le déplacement chimique du proton carbinolique H-3 est plus important lorsqu'il est en *cis* du proton H-3a que lorsqu'il est en *trans* (8, 9, 30). L'épimérisation du perhydrocyclododéca[*b*]furane (**10**) en son épimère **11**, observé lors de l'analyse chromatographique (colonne DEGS, Chromosorb W NAW), permet d'attribuer la configuration *trans* à l'épimère le plus stable **11**. Cette épimérisation peut s'expliquer par formation d'un ion oxocarbonium (31, 32) (figure 4) obtenu par abstraction d'un ion hydrure (H-13a) (33). Cette dernière est engendrée par le caractère acide du Chromosorb et favorisée par l'assistance des orbitales libres de l'atome d'oxygène voisin.

3. Étude spectroscopique RMN ^1H et ^{13}C des perhydrocyclododéca[b]furanones-3 et perhydrocyclododéca[b]furanes

(a) RMN ^1H (300 MHz)

Les deux cétones isomères *cis* **8** et *trans* **9** sont différenciées par l'examen des signaux des protons en α de l'hétéroatome oxygéné. Le déplacement du proton de jonction H-13a est plus important dans l'isomère *cis* (4,31 ppm) que dans l'isomère *trans* (4,15 ppm), comme pour le couple de bicyclo[10,3,0]-pentadécène-14 ones-13 *cis* et *trans* (29). Un couplage longue distance de 0,7 Hz est observé entre l'un des protons H-2 et le proton H-3a pour la seule cétone *trans* comme dans le cas de la perhydrocyclohepta[*b*]furanone-3 *trans* (9). L'accès aux constantes de couplage vicinal du proton H-3a (8,0; 6,7 et 4,3 Hz) de la cétone *trans* **9**, par irradiation sélective des protons de jonction de cycles, comparées à celles calculées (tableau 2) pour les conformations les plus probables, confirme l'extrême mobilité de cette molécule à température ambiante. Les spectres des deux perhydrocyclododéca[*b*]furanes *cis* (**10**) et *trans* (**11**) ne présentent que de très faibles différences, indiquées dans la partie expérimentale.

(b) RMN ^{13}C

Les spectres des deux diastéréoisomères de chaque couple de cétones **8**, **9** et d'hétérocycles saturés **10**, **11** sont nettement différenciés, principalement au niveau des déplacements chimiques des atomes de carbone de l'hétérocycle oxygéné. Dans les deux cas, en passant de l'isomère *cis* à l'isomère *trans*, les déplacements chimiques des atomes de carbone de jonction sont légèrement plus importants (0,83–2,07 ppm) tandis que ceux des atomes de carbone C-2 sont légèrement plus faibles (1,26–1,35 ppm). Ces faibles variations peuvent être interprétées, dans le cas des deux atomes de jonction, en termes d'effets de substituants aliphatiques (34) introduits par le cycle cyclododécane sur l'hétérocycle. Ces effets seraient dépendants de la conformation du cyclododécane. Les études (19, 20) conduites à basses températures sur le cyclododécane en conformation carrée bloquée, révèlent un blindage de 4,3–4,8 ppm, selon les auteurs, des atomes de carbone «non coin» par rapport à ceux de «coin». Ce blindage est interprété (35, 36) en terme de combinaison d'effets γ-*gauche* pour les atomes de carbones non coin et d'effet «vicinal *gauche*» pour les carbones coin. Cette interprétation permet d'expliquer dans notre cas le faible blindage (0,83–2,07 ppm) des atomes des carbones de jonction, en passant de l'isomère *cis* à l'isomère *trans*. En effet l'examen

Can. J. Chem. Downloaded from www.nrcresearchpress.com by 198.100.157.202 on 09/07/12
For personal use only.

Can. J. Chem. Downloaded from www.nrcresearchpress.com by 198.100.157.202 on 09/07/12
For personal use only.

TABLEAU 1. Angles dièdres endocycliques (en degrés) des cinq conformations optimisées des hétérocycles **8**, **9**, **10** et **11**

Types de conformères[b]	Liaison[a]																
	1–2	2–3	3–3a	3a–13a	13a–1	3a–4	4–5	5–6	6–7	7–8	8–9	9–10	10–11	11–12	12–13	13–13a	13a–3a
								Cétone **8** (*cis*)									
$MO_{13}C_{36}$	31	−8	−15	34	31	−166	163	−50	−56	151	−69	−64	175	−72	−78	74	39
$MO_{30}C_{31}$	−31	9	14	−33	41	156	−175	51	66	−81	−66	173	−64	−71	153	−62	−39
$MO_{36}C_{13}$	24	−1	−20	35	−38	72	−77	−71	174	−64	−69	159	−56	−50	163	−168	40
$MO_{31}C_{30}$	−23	0	20	−35	37	−62	152	−71	64	173	−66	−81	65	51	−174	157	−40
$LO_{21}C_{20}$	22	4	−25	38	−38	68	−158	79	74	−162	61	61	−153	76	81	159	46
								Cétone **9** (*trans*)									
$MO_{18}C_{16}$	29	−9	−13	31	−39	61	56	−167	162	−54	−58	149	−67	−62	174	−63	−86
$LO_{21}C_{23}$	−31	16	4	−22	34	68	68	−175	66	69	−144	68	66	−176	68	67	−141
$MO_{16}C_{18}$	31	−11	−12	30	−39	−62	174	−62	−67	148	−58	−54	162	−167	56	60	−85
$LO_{21}C_{19}$	−29	7	16	−33	40	67	−159	64	65	−157	73	73	−163	62	62	−156	79
$LO_{20}C_{18}$	−28	6	17	−34	39	−158	63	63	−168	74	73	158	65	65	−158	68	79
								Hétérocycle **10** (*cis*)									
$MO_{13}C_{36}$	13	14	−33	42	−35	−165	162	−53	−58	150	−68	−62	176	−69	−80	68	46
$MO_{30}C_{31}$	−12	−15	33	−42	35	160	−171	53	63	−82	−66	174	−63	−69	150	−60	−46
$MO_{36}C_{13}$	7	19	−35	40	−30	69	−80	−63	176	−62	−68	149	−58	−52	164	−164	44
$LO_{20}C_{21}$	15	14	−34	45	−38	−161	78	75	−155	63	62	−163	74	77	−157	68	51
$MO_{31}C_{30}$	−1	−24	36	−39	25	61	151	−70	−64	174	−66	−81	64	52	−173	158	−43
								Hétérocycle **11** (*trans*)									
$LO_{21}C_{23}$	31	−40	33	−16	−9	67	69	−177	65	68	−142	68	65	−177	70	66	−137
$LO_{20}C_{18}$	4	−27	37	−37	22	−168	64	66	−152	70	70	−169	67	67	−145	66	76
$MO_{18}C_{16}$	22	2	−23	37	−37	63	54	−169	161	−52	−56	150	−69	−64	173	−65	−81
$LO_{21}C_{19}$	3	−27	38	−38	22	63	−154	69	69	−162	68	69	−158	68	67	−161	75
$MO_{13}C_{16}$	−11	−17	36	−44	35	−79	−70	173	−65	−70	152	−56	−51	160	−167	47	72

[a]Numérotation UICPA des bicycles.

[b]Formulation utilisée; exemple : $MO_{13}C_{36}$ signifie que le conformère est bâti à partir de la conformation M du cyclododécane (fig. 2) par substitution des atomes d'hydrogène 13 et 36 par respectivement l'atome d'oxygène et d'un atome de carbone du cycle tétrahydrofurannique.

TABLEAU 2. Energie et constantes de couplage vicinal du proton de jonction H-13a, calculées par mécanique moléculaire, pour les conformations les plus stables des composés **8**–**11**

Composés	Conformations[a]	E^b	$E_0{}^c$	$J_{H3a-H13a}{}^d$ (Φ)[e]	$J_{H13-H13a}$ (Φ)
Cétone **8** (*cis*)	$MO_{13}C_{36}$	14,74	0	5,4 (35°)	11,5 (179°); 1,1 (67°)
	$MO_{30}C_{31}$	14,83	0,09	5,6 (34°)	11,2 (173°); 3,9 (59°)
	$MO_{36}C_{13}$	14,99	0,25	5,9 (41°)	11,7 (169°); 0,8 (74°)
	$MO_{31}C_{30}$	15,12	0,38	6,1 (40°)	11,1 (159°); 0,9 (84°)
	$LO_{21}C_{20}$	15,26	0,52	4,9 (38°)	11,5 (179°); 3,2 (65°)
Cétone **9** (*trans*)	$MO_{18}C_{16}$	12,26	0	10,6 (167°)	3,1 (52°); 1,5 (61°)
	$LO_{21}C_{23}$	12,39	0,13	2,9 (109°)	11,5 (179°); 3,3 (63°)
	$MO_{16}C_{18}$	12,40	0,14	10,6 (166°)	10,9 (170°); 4,6 (55°)
	$LO_{21}C_{19}$	12,41	0,15	10,6 (168°)	11,6 (168°); 0,8 (76°)
	$LO_{20}C_{18}$	12,60	0,34	10,6 (168°)	3,9 (46°); 1,1 (67°)
Hétérocycle **10** (*cis*)	$MO_{13}C_{36}$	19,19	0	3,7 (46°)	0,9 (71°); 11,6 (175°)
	$MO_{30}C_{31}$	19,23	0,04	3,6 (47°)	11,4 (176°); 3,6 (61°)
	$MO_{36}C_{13}$	19,27	0,08	7,2 (34°)	0,8 (81°); 11,4 (163°)
	$LO_{20}C_{21}$	19,28	0,09	3 (51°)	7 (68°); 11,6 (176°)
	$MO_{31}C_{30}$	19,38	0,19	7,2 (34°)	1 (87°); 11 (157°)
Hétérocycle **11** (*trans*)	$LO_{21}C_{23}$	16,69	0	1,7 (101°)	11,6 (178°); 1,1 (67°)
	$LO_{20}C_{18}$	17,36	0,67	10,1 (157°)	3,5 (49°); 1,3 (64°)
	$MO_{18}C_{16}$	17,78	1,09	9,3 (151°)	3,2 (51°); 1,5 (62°)
	$LO_{21}C_{19}$	17,85	1,16	10,1 (157°)	11,3 (161°); 0,9 (84°)
	$MO_{13}C_{16}$	17,88	1,19	10,1 (159°)	4,1 (43°); 0,9 (70°)

[a]Types de conformation.
[b]Energie totale de contrainte calculée en kcal/mol.
[c]Energie relative de contrainte par rapport au conformère le plus stable.
[d]Constante de couplage calculée en Hz.
[e]Angle dièdre calculé en degrés.

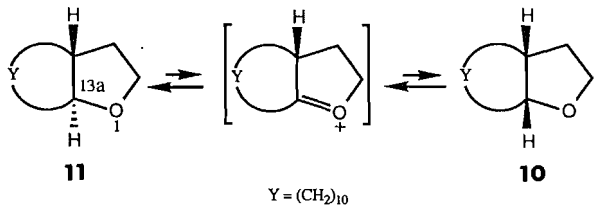


FIG. 4

des conformations calculées révèle que toutes celles de jonction *cis* mettent en jeu un atome de carbone coin du cyclododécane (cette notion de coin à été étendue à la conformation M), tandis que certaines de type $LO_{21}C_{23}$ de jonction *trans* ne mettent en jeu que des atomes de carbones non coin. Ce modeste blindage observé reflète donc simplement une participation des conformations de type $LO_{21}C_{23}$ dans les composés *trans*.

Partie expérimentale

Les points de fusion ont été déterminés au banc chauffant Kofler. Les distillations boule à boule ont été effectuées sur appareil Büchi. Les températures d'ébullition ne sont pas corrigées. Les spectres IR ont été enregistrés sur spectromètre Beckman Acculab 2. Les spectres de RMN ont été réalisés dans le deutériochloroforme sur spectromètres Bruker WP-80 ou AM-300 pour le proton (^{1}H) et Bruker AM-300 à 75,47 MHz pour le carbone 13 (^{13}C). Les déplacements chimiques sont exprimés en ppm par rapport au tétraméthylsilane. Les séparations par chromatographie en phase vapeur ont été réalisées aux températures de 155–190°C, sur un appareil Varian Aerograph 90 P équipé avec la colonne suivante : longeur 6 m; diamètre 1/4 de pouce; phase DEGS (20%) sur Chromosorb W NAW 60/80. Les analyses élémentaires ont été faites au laboratoire de Microanalyses, Centre national de la recherche scientifique, 69390 Vernaison, France.

Synthèse de l'acétoxyacétyl-2 cyclododécanone (1)

Une solution de 0,1 mol de chlorure de l'acide acétoxyacétique dans 50 mL de toluène anhydre est ajoutée lentement à une solution de 0,1 mol de morpholino-1 cyclododécène (2, 37) et 0,1 mol de triéthylamine dans 150 mL de toluène anhydre, placée à température ambiante sous bonne agitation. L'addition terminée, le mélange réactionnel est maintenu sous agitation pendant 48 h puis hydrolysé à température ambiante pendant 5 h avec 70 mL d'acide chlorhydrique environ 2 M. La phase organique est extraite avec du chlorure de méthylène, neutralisée, lavée à l'eau, séchée, concentrée et distillée sous pression réduite, Eb 150–180°C/1 Torr (1 Torr = 133,3 Pa); Rdt 57%; IR (film) : 1750, 1705 et 1625 cm^{-1}. La β-dicétone cristallise lentement. Une recristallisation dans l'éthanol permet d'éliminer la cyclododécanone résiduelle et d'obtenir la β-dicétone pure. Rdt 62%; *F* (éthanol) 72–74°C, RMN ^{1}H (80 MHz) : 1,00–3,00 (m, 20H), 2,14 (s, 3H, OAc), 3,80 (dd, *J* = 10,7 et 3,1 Hz, 1H cétonique), 4,66 (s, 2H, CH_2-O). Anal. calc. pour $C_{16}H_{26}O_4$: C 68,05, H 9,28; tr. : C 68,21, H 9,56. Les formes énoliques de cette β-dicétone ne sont pas détectées dans ces conditions, contrairement à ce que nous avons observé avec des β-dicétones comparables (8, 9). La très faible coloration avec le chlorure ferrique en solution éthanolique confirme le très faible taux d'énolisation de cette β-dicétone.

Synthèse de la décahydro-4,5,6,7,8,9,10,11,12,13(2 H)cyclododéca-[b]furanone-3 (2)

À 40 mL d'acide sulfurique concentré et froid sont ajoutées progressivement, sous bonne agitation, de façon que la température reste inférieure à −5°C, à 20 mmol de β-dicétone **1** recristallisée. Dès que la dissolution est totale, le mélange réactionnel est laissé à température ambiante pendant 0,5 h puis versé sur de la glace et extrait au chloroforme. La phase organique est neutralisée, lavée à l'eau, séchée et concentrée. Le résidu est purifié par passage sur colonne de silice avec l'éther éthylique comme éluant. Rdt 64%; *F* (éthanol) 68–69°C; IR ($CHCl_3$) : 1700, 1620 cm^{-1}, RMN ^{1}H (80 MHz) : 1,00–2,00 (m, 16H), 2,10–2,30 (m, 2H), 2,40–2,60 (m, 2H), 4,35

Can. J. Chem. Downloaded from www.nrcresearchpress.com by 198.100.157.202 on 09/07/12
For personal use only.

Can. J. Chem. Downloaded from www.nrcresearchpress.com by 198.100.157.202 on 09/07/12
For personal use only.

(s, 2H, CH_2-O). Anal. calc. pour $C_{14}H_{22}O_2$: C 75,63, H 9,97; tr. : C 75,82, H 9,90.

Synthèse des (acétoxy-2 hydroxy-1 éthyl)-2 cyclododécanols (3)

Une solution de 30 mmol de dicétone **1** dans 50 mL d'éthanol est hydrogénée en présence de nickel de Raney W_4 sous une pression initiale de 150 atm (1 atm = 101,3 kPa) pendant 24 h à 60°C. Après élimination du catalyseur et du solvant, le résidu est distillé sous pression réduite. L'huile visqueuse obtenue contient les dihydroxy acétates attendus, identifiés par spectroscopie IR. Rdt en composé brut 90%; IR (film) : 3500–3300, 1750–1725 cm^{-1}. Ces composés sont ensuite utilisés sans autre purification.

*Synthèse des perhydrocyclododéca[*b*]furanols-3* **4**–**7** *et de leurs acétates correspondants* **4**a–**7**a

(a) À partir de la cétone éthylènique **2**

Une solution de 50 mmol de cétone **2** dans 60 mL d'éthanol est hydrogénée en présence de nickel de Raney W_4 à 60°C sous une pression initiale de 140 atm pendant 24 h. Après élimination du catalyseur puis du solvant, le résidu est distillé sous pression réduite et conduit à un mélange d'alcools **4**–**6**; Eb 120–130°C/0,1 Torr; Rdt 85%; IR (film) : 3550–3200 cm^{-1}. Le mélange de ces alcools est transformé par l'anhydride acétique dans la pyridine anhydre, en acétates correspondants **4***a*–**6***a*. Ces trois acétates sont difficilement séparés et dosés par chromatographie en phase vapeur sur colonne DEGS à 190°C. L'ordre d'élution est le suivant : **6***a* (12%), **5***a* (35%) et **4***a* (53%). **4***a*–**6***a*, Eb 110–120°C/0,5 Torr; Rdt 80%; IR (film) : 1745 cm^{-1}. Anal. calc. pour $C_{16}H_{28}O_3$: C 71,60, H 10,52; tr. : C 71,35, H 10,39.

(b) À partir des dihydroxy acétates **3**

Une quantité de 10 mmol de dihydroxy acétates **3** est ajoutée à une solution de 2 mL de chlorure d'acétyle dans 60 mL d'éthanol absolu. Le mélange réactionnel est placé à reflux pendant 3 h puis concentré et distillé sous pression réduite pour conduire au mélange d'alcools **5**–**7**; Eb 120–130°C/0,1 Torr; Rdt 50%; IR (film) : 3550–3200 cm^{-1}. Le mélange de ces alcools est transformé en acétates correspondants **5***a*–**7***a* comme précédemment. Les trois acétates sont partiellement séparés par chromatographie en phase vapeur. L'ordre d'élution est le suivant : **6***a* puis **5***a* + **7***a*. Le dosage par chromatographie associé au dosage RMN ^1H (pour **5***a* et **7***a*) permet d'apprécier la composition du mélange : **6***a* (34%); **5***a* (46%) et **7***a* (20%); RMN ^1H (300 MHz) : **4***a*, 1,33–1,50 (m, 19H), 1,70 (m, 1H), 2,08 (s, 3H, OAc), 2,21 (m, ΣJ = 30 Hz, 1H, H-3a), 3,71–3,75 (dd, J = 10,4 et 2,9 Hz, 1H, H-2), 4,06–4,12 (m, 2H, H-2′ et H-13a), 5,24–5,28 (td, J = 5,8 et 2,9 Hz, 1H, H-3); **5***a*, 1,34–1,54 (m, 19H), 1,78 (m, 1H), 2,09 (s, 3H, OAc), 2,13–2,18 (m, 1H, H-3a), 3,73–3,77 (dd, J = 10,5 et 1,6 Hz, 1H, H-2), 3,86–3,91 (ddd, J = 7,7, 5,1 et 1,6 Hz, 1H, H-13a), 4,06–4,11 (dd, J = 10,5 et 4,5 Hz, 1H, H-2), 5,30–5,33 (td, J = 5,2 et 1,6 Hz, 1H, H-3); **6***a*, 1,33–1,50 (m, 19H), 1,75 (m, 1H), 2,06 (s, 3H, OAc), 2,19 (m, ΣJ = 20 Hz, 1H, H-3a), 3,83–3,91 (m, 2H, H-2 et H-13a), 3,92–3,97 (dd, J = 10,7 et 4,7 Hz, 1H, H-2′), 4,89–4,91 (m, ΣJ = 8,6 Hz, 1H, H-3); **7***a*, 1,33–1,50 (m, 19H), 1,76 (m, 1H), 2,07 (s, 3H, OAc), 2,20 (m, 1H, H-3a), 3,65–3,69 (dd, J = 10,8 et 1,6 Hz, 1H, H-2), 3,89–3,95 (m, 1H, H-13a), 4,16–4,21 (dd, J = 10,8 et 5,2 Hz, 1H, H-2′), 4,99–5,01 (m, 1H, H-3).

*Synthèse des perhydrocyclododéca[*b*]furanones-3* cis *(8) et* trans *(9)*

Les cétones **8** et **9** sont obtenues par oxydation non épimérisante des mélanges d'alcools **4**–**6** ou **5**–**7** au moyen du réactif de Jones (10) ou du chlorochromate de pyridinium (11). L'extrême instabilité de la cétone *cis* **8** a nécessité une analyse par RMN ^1H des mélanges bruts de cétones **8** et **9**. Les méthodes de purification utilisées (distillation, séparation sur colonne de silice ou chromatographie en phase vapeur) ont modifié la composition des mélanges (enrichissement en composé *trans*). Le mélange de cétones est obtenu avec un rendement (après distillation) de 85% quel que soit le mode d'oxydation; **8** + **9**, IR (film) : 1755 cm^{-1}. Anal. calc. pour $C_{14}H_{24}O_2$: C 74,95, H 10,78; tr. : C 74,95, H 11,07. La cétone *trans* en équilibre avec environ 5% de cétone *cis* cristallise (F 65–67°C). Les analyses spectrales RMN ^1H et ^{13}C de l'isomère *cis* ont été effectuées sur des mélanges ayant subi une purification rapide et partielle sur colonne de silice avec l'éther éthylique comme éluant; RMN ^1H (300 MHz) : **8**, (seuls les protons en α de l'atome d'oxygène ont été différenciés sans ambiguïté de ceux de l'isomère *trans*) 3,88–3,93 (d, J = 17,2 Hz, 1H, H-2), 3,98–4,04 (d, J = 17,2 Hz, 1H, H-2′), 4,28–4,35 (td, J = 5,8 et 7,5 Hz, 1H, H-13a); **9**, 1,33–1,84 (m, 18H), 2,31–2,38 (m, 1H, H-3a), 3,83–3,88 (d, J = 17,3 Hz, 1H, H-2), 4,06–4,11 (dd, J = 17,3 et 0,7 Hz, 1H, H-2′), 4,11–4,18 (m, J = 8,0, 6,7 et 4,3 Hz, 1H, H-13a); RMN ^{13}C : **8**, 21,46, 23,05, 23,31, 23,76, 24,32, 24,94, 25,00, 25,30, 26,17 (C-4 à C-13), 50,43 (C-3a), 69,48 (C-2), 81,90 (C-13a), 216,91 (C-3); **9**, 20,34, 22,71, 23,32, 23,45, 23,58, 23,92, 24,16, 24,58, 30,18 (C-4 à C-13), 48,36 (C-3a), 70,83 (C-2), 81,07 (C-13a), 218,26 (C-3).

*Synthèse des perhydrocyclododéca[*b*]furanes* cis *(10) et* trans *(11)*

(a) À partir des alcools **4**–**6**

À une solution à 0°C de 2 mmol du mélange d'alcools **4**–**6** provenant de la réduction catalytique de **2**, dans 1,5 mL de pyridine anhydre, sont ajoutées 2,2 mmol de chlorure de l'acide *para*-toluènesulfonique. Le mélange est laissé à 0°C pendant 5 h puis versé sur une solution d'acide chlorhydrique 2 M froid. L'extraction à l'éther conduit après séchage et élimination du solvant à 0,65 g de tosylates partiellement cristallisés. Ce résidu, dilué dans 10 mL de THF anhydre, est additionné à 0°C à une suspension de 0,5 g de $LiAlH_4$ dans 4 mL de THF anhydre. L'addition terminée, le mélange est placé à reflux pendant 2 h puis laissé 1 nuit à température ambiante. Le milieu réactionnel est hydrolysé à l'aide d'une solution aqueuse d'acide chlorhydrique 2 M, puis extrait à l'éther. La phase éthérée lavée à l'eau, séchée et concentrée, conduit à 0,3 g d'une huile contenant les perhydrocyclododéca[*b*]furanes attendus. Le produit brut, examiné en chromatographie en phase vapeur sur colonne DEGS à 155°C, révèle la présence du couple d'isomères *cis* et *trans* mal séparés. Le premier pic (majeur) correspond à l'isomère *trans* qui cristallise (F 30°C).

(b) À partir des cétones 8 et 9

À une solution de 2 mmol d'un mélange à l'équilibre de cétones **8** et **9** dans 2,5 mL de diéthylèneglycol sont ajoutés 0,25 mL d'hydrate d'hydrazine puis 0,3 g de potasse en pastilles. Le mélange est placé à reflux 0,5 h. L'élimination d'eau permet de porter la température du milieu à 200–220°C pendant 0,5 h. Le mélange préalablement refroidi est extrait à l'éther. La phase éthérée est lavée à l'eau, séchée puis concentrée. Le résidu 0,42 g contient le mélange des perhydrocyclododéca[*b*]furanes **10** et **11**, analysé comme précédemment. L'isomère *trans* est très majoritaire. Les deux composés sont identifiés par spectroscopie RMN ^{13}C. Leurs spectres RMN ^1H ne montrent que de très faibles différences. Les spectres de l'isomère *cis* sont tirés des spectres d'un mélange *cis* + *trans*; RMN ^1H (300 MHz) : **10**, 1,00–1,15 (m, 1H), 1,20–1,60 (m, 20H), 1,60–1,75 (m, 1H), 1,93–2,05 (m, 1H), 3,72–3,90 (m, 3H, H-2, H-2′ et H-13a); **11**, 1,20–1,70 (m, 21H), 2,01–2,14 (m, 2H), 3,75–3,88 (m, 3H, H-2, H-2′ et H-13a); RMN ^{13}C : **10**, 23,37, 23,44, 24,18, 24,64, 25,01, 25,72, 25,92, 26,70, 32,36 (C-3 à C-13), 40,62 (C-3a), 65,53 (C-2), 82,39 (C-13a); **11**, 21,75, 22,78, 23,46, 23,47, 23,91, 24,34, 24,83, 30,26, 31,29, 32,52 (C-3 à C-13), 38,83 (C-3a), 66,79 (C-2), 81,33 (C-13a).

1. H. Nozaki, T. Mori, R. Noyori et M. Kawanisi. Can. J. Chem. **45**, 1804 (1967).
2. B. A. McAndrew et S. W. Russell. J. Chem. Soc. Perkin Trans. 1, 1172 (1975).
3. M. Baumann et W. Hoffmann. Ger. Offen. 2 630 428 (1978); Chem. Abstr. **88**, 169677 d (1978).
4. P. Meins et K. Bruns. Ger. Offen. 2 810 107 (1979); Chem. Abstr. **92**, 22377 e (1980).
5. H. Gebauer. Eur. Pat. Appl. EP 75 866 (1983); Chem. Abstr. **99**, 53582 s (1983).
6. M. Kaufhod. Ger. Offen. DE 3 400 690 (1985); Chem. Abstr. **103**, 21514 j (1985).
7. A. S. Bailey, M. L. Gilpin et E. R. H. Jones. J. Chem. Soc. Perkin Trans. 1, 259 (1977).
8. R. Dolmazon. J. Heterocycl. Chem. **25**, 751 (1988).

9. R. DOLMAZON, M. ALBRAND et R. HENRY. Bull. Soc. Chim. Belg. **97**, 357 (1988).
10. K. BOWDEN, I. M. HEILBRON, E. R. H. JONES et B. C. L. WEEDON. J. Chem. Soc. 39 (1946).
11. E. J. COREY et J. W. SUGGS. Tetrahedron Lett. 2647 (1975).
12. H. O. HOUSE et G. H. RASMUSSON. J. Org. Chem. **28**, 31 (1963).
13. P. KARRER, H. ASMIS, K. N. SAREEN et R. SCHWYZER. Helv. Chim. Acta, **34**, 1022 (1951).
14. S. HAGISHITA et K. KURIYAMA. J. Chem. Soc. Perkin Trans. 1, 950 (1980).
15. HUANG-MINLON. J. Am. Chem. Soc. **68**, 2487 (1946); **71**, 3301 (1949).
16. H. O. HOUSE. Modern synthetic reactions. W. A. Benjamin, Menlo Park, CA. 1972. p. 280.
17. J. D. DUNITZ et H. M. M. SHEARER. Helv. Chim. Acta, **43**, 18 (1960).
18. F. A. L. ANET, A. K. CHENG et J. J. WAGNER. J. Am. Chem. Soc. **94**, 9250 (1972).
19. M. MÖLLER, W. GRONSKI, H. J. CANTOW et H. HÖCKER. J. Am. Chem. Soc. **106**, 5093 (1984).
20. F. A. L. ANET et T. N. RAWDAH. J. Am. Chem. Soc. **100**, 7166 (1978).
21. MMX, PCMODEL, Serena Software, Box 3076, Bloomington, IN 47402-3076.
22. B. FUCHS. Top. Stereochem. **10**, 1 (1978).
23. E. L. ELIEL et K. M. PIETRUSIEWICZ. Top. Carbon-13 NMR Spectrosc. **3**, 180 (1979).
24. E. L. ELIEL, V. S. RAO et K. M. PIETRUSIEWICZ. Org. Magn. Reson. **12**, 461 (1979).
25. M. ANTEUNIS et M. VANDEWALLE. Spectrochim. Acta, **27A**, 2119 (1971).
26. P. LUGER et J. BUSCHMANN. Angew. Chem. Int. Ed. Engl. **22**, 410 (1983) ou Angew. Chem. Suppl. 537 (1983).
27. D. CREMER et J. A. POPLE. J. Am. Chem. Soc. **97**, 1358 (1975).
28. R. DOLMAZON et S. GELIN. J. Org. Chem. **49**, 4003 (1984).
29. T. K. JONES et S. E. DENMARK. Helv. Chim. Acta, **66**, 2381 (1983).
30. D. K. DIKSHIT, R. S. KAPIL et N. ANAND. Ind. J. Chem. **13**, 1353 (1975).
31. M. L. SINNOTT. Adv. Phys. Org. Chem. **24**, 197 (1988).
32. F. TURECEK et H. HANUS. Tetrahedron, **39**, 1499 (1983).
33. K. R. BLANCHARD et P. v. R. SCHLEYER. J. Org. Chem. **28**, 247 (1963).
34. D. J. CRAIK. Annu. Rep. NMR Spectrosc. **15**, 72 (1983).
35. H. SAITÔ et I. ANDO. Annu. Rep. NMR Spectrosc. **21**, 232 (1989).
36. T. YAMANOBE, T. SORITA, I. ANDO et H. SATO. Makromol. Chem. **186**, 2071 (1985).
37. C. WAKELSMAN. Bull. Soc. Chim. Fr. **10**, 3763 (1967).

Can. J. Chem. Downloaded from www.nrcresearchpress.com by 198.100.157.202 on 09/07/12
For personal use only.

The photochemistry of the rhodizonate dianion in aqueous solution

B. ZHAO AND M. H. BACK

Department of Chemistry, Ottawa-Carleton Chemistry Institute, University of Ottawa, Ottawa, Ont., Canada KIN 6N5

Received July 10, 1990

B. ZHAO and M. H. BACK. Can. J. Chem. **69**, 528 (1991).

The thermal and photochemical reactions of rhodizonate dianion have been studied in aqueous solution in the presence of various oxidizing agents. Both reactions are initiated by electron transfer to an acceptor which is a sufficiently strong oxidizing agent. With hydrogen peroxide and ferricyanide a square root dependence of the rate on the concentration of additive was observed whereas with tetracyanoethylene the rate was first order with respect to additive. This difference in behaviour is explained on the basis of the rate of separation of ions from the initial charge transfer complex. In most cases the main product was croconic acid. NMR analysis of other products indicated some formation of C—H bonds and possibly incorporation of an oxygen atom into the ring. A maximum quantum yield of 0.04 for disappearance of rhodizonate was observed in the presence of tetracyanoethylene.

Key words: photochemistry, rhodizonic acid, dianion, electron transfer.

B. ZHAO et M. H. BACK. Can. J. Chem. **69**, 528 (1991).

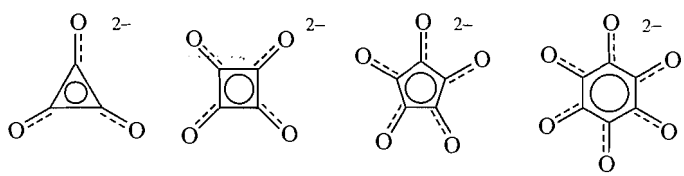
Opérant en solutions aqueuses, en présence de divers agents d'oxydation, on a étudié les réactions thermiques et photochimiques du dianion rhodizonate. Les deux réactions sont initiées par un transfert d'électron vers un accepteur qui est un agent oxydant suffisamment fort. Avec le peroxyde d'hydrogène et le ferricyanure, on a observé que la vitesse dépend du carré de la concentration d'additif; par ailleurs, avec le tétracyanoéthylène, la vitesse est du premier ordre par rapport à l'additif. On explique cette différence de comportement sur la base de la vitesse de séparation des ions à partir du complexe initial de transfert de charge. Dans la plupart des cas, le produit principal est l'acide croconique. Des analyses rmn des autres produits indiquent qu'il y a formation de quelques liaisons C—H et qu'il y a possiblement incorporation d'un atome d'oxygène dans le cycle. On a observé que le rendement quantique maximal est égal à 0,04 pour la disparition du rhodizonate en présence de tétracyanoéthylène.

Mots clés : photochimie, acide rhodizonique, dianion, transfert d'électron.

[Traduit par le rédaction]

Introduction

The dianions of the cyclic oxocarbons, ranging from deltate, $C_3O_3^{2-}$, to rhodizonate, $C_6O_6^{2-}$, were first recognized by West and Niu (1, 2) as members of a new type of aromatic series involving only carbon and oxygen atoms. The high degree of symmetry with the delocalized π bonding around the ring leads to strong absorption in the $\pi-\pi^*$ electronic transition. For the rhodizonic dianion the maximum absorption occurs at 483 nm ($\epsilon = 3.2 \times 10^4$ L mol^{-1} cm^{-1}) and the maximum shifts to lower wavelengths as the ring size decreases. Such strong absorptions usually spark the interest of photochemists for fundamental as well as practical reasons, but it appears that no systematic study of the photochemistry of this series of dianions has been reported.



Rhodizonic acid is a weak diprotic acid whose ionization constants are unusually close ($pK_1 = 4.3$; $pK_2 = 4.7$) (3, 4). The ionization processes are complicated by the strong hydration of both the undissociated acid and the monoanion. The abnormal enthalpy and entropy changes accompanying the second ionization are explained by the concurrent loss of two molecules of water in the formation of the dianion. Aerated, aqueous solutions of rhodizonic acid are unstable and in basic solution (pH > 10) quantitative conversion to croconic acid occurs. Exposure to light accelerates the disappearance of the acid but no mechanism for the photolysis reaction has been proposed.

Rhodizonic acid has been used extensively as an analytical reagent for metal ions, particularly iron, lead, and barium (5–7), and several patents for these procedures have been reported (8). Because of the importance of hydroxyquinones in biological processes (9), and in particular in the degradation of DNA (10), the electrochemical oxidation–reduction cycle of rhodizonic acid – tetrahydroxybenzoquinone – hexahydroxybenzene has been extensively studied (11). Inhibiting action has been observed with some enzymes (12). In another direction, the oxoanions have been fertile ground for theoretical studies of electronic structure (13).

The present study was undertaken to examine the photochemical behaviour of the oxocarbon dianions, starting with rhodizonate. A preliminary report appeared earlier in which it was suggested that electron transfer might occur in the photochemical reaction (14). We have now further explored this possibility using several electron acceptors and investigating the kinetics of the reaction. It will be seen that electron transfer does occur but because of rapid reversal is not efficient.

Experimental

Solutions of rhodizonic dianion were prepared daily from distilled and deionized water and deaerated by thorough flushing with Research Grade nitrogen (99.9995%). Oxygen was also removed by degassing under vacuum, using a cell designed so that the degassed solutions of rhodizonic acid and additive could be mixed directly in the spectrophotometer cell while under vacuum. The two procedures gave results identical within the experimental error. Reactions were studied in the range of pH 6–8, using appropriate buffer solutions, where the acid is fully ionized but the base-catalyzed reaction is negligible.

Solutions were irradiated directly in the spectrophotometer cell (1 cm × 1 cm) using a tungsten filament lamp in conjunction with a Schoeffel monochromator, with a band width of ~20 nm. All photolyses were performed at a wavelength of 483 nm, the maximum

Can. J. Chem. Downloaded from www.nrcresearchpress.com by 198.100.157.202 on 09/07/12
For personal use only.

TABLE 1. Thermal and photochemical oxidation of rhodizonate dianion at 20°C

Additive	pH	Conc. of reactants $M \times 10^{-5}$ [A]	[Rh^{2-}]	Rate/$M\ s^{-1} \times 10^{-9}$ Thermal	Photochem.[a]	Conversion to Cr^{2-}(%)	Φ (10^{-3})
TCNE	7	2.0	2.5	0.52	2.3	<5	6.2
	7	5.0	2.5	1.6	4.9		12
$E^0 = +0.48$ V[b]	7	10.0	2.5	3.8	10.2		23
	7	15.0	2.5	5.3	14.5		33
	7	20.0	1.25	3.2	10.5		35
	7	20.0	2.5	6.6	19.3		45
	7	20.0	5.0	13.5	28.4		44
H_2O_2	7	2.5	2.5	1.5	2.3	33	3.3
	7	5.0	2.5	2.0	3.0		3.9
$E^0 = +1.33$ V	7	10.0	2.5	2.9	4.5		6.3
	7	20.0	2.5	4.1	6.4		8.4
	7	25.0	2.5	4.6	7.0		9.6
	7	50.0	2.5	13.3	16.4		13
$Fe(CN)_6^{3-}$	7	2.5	2.5	1.1	2.3	26	4.4
	7	5.0	2.5	1.6	3.2		5.6
$E^0 = +0.36$ V	7	10.0	2.5	2.1	4.3		7.6
	7	15.0	2.5	2.4	4.9		9.2
	7	20.0	1.25	2.0	4.6		12
	7	20.0	2.5	2.6	5.7		11
	7	20.0	5.0	4.2	7.5		9.7
	7	25.0	2.5	2.9	6.3		12
Cu^{2+}	7	5.0	5.0	0.42	0.42	78	
$E^0 = +0.153$ V	7	25.0	2.5	0.68	0.78		

[a]Total rate (thermal + photochemical).
[b]In CH_3CN solution.

Can. J. Chem. Downloaded from www.nrcresearchpress.com by 198.100.157.202 on 09/07/12
For personal use only.

of the visible absorption of rhodizonic dianion. To keep the absorbance of the solutions below about 0.9 the concentration of the dianion was kept below 2.5×10^{-5} M. The absorption spectra were recorded using a Unicam SP-1800 Spectrophotometer equipped with a thermostattated cell holder. The incident light intensity was measured using the potassium ferrioxalate actinometer, following procedures outlined by Rabek (15). For measurement of the NMR spectra of the products, the solution was concentrated, following photolysis, by removal of water under vacuum. Spectra were recorded on Varian XL-300.

All chemicals were reagent grade. Except for potassium ferricyanide which was recrystallized from warm water–ethanol solution, the chemicals were used without further purification.

Results

Rhodizonic acid is rapidly oxidized in air-saturated solutions in the dark, the rate increasing with increasing pH. Removal of oxygen stabilizes the system, but in the pH range 6–8 of the present experiments a small residual rate of disappearance of rhodizonate dianion remains in all solutions regardless of the procedures used for degassing. The origin is probably a trace of oxidizing impurity, perhaps residual oxygen.

The thermal and photochemical rates of disappearance of rhodizonic dianion were measured at 20°C in deaerated solutions in the presence and absence of several additives. Only the additives cupric ion, $Fe(CN)_6^{3-}$, H_2O_2, and tetracyanoethylene (TCNE) caused a thermal reaction substantially faster than the residual rate and only with the latter three was the rate increased on irradiation. The measurements of the photochemical rates were reproducible within about 5% as were the higher thermal rates. The slow residual dark reaction had more uncertainty, but was generally consistent. The results are summarized in Table 1. In all cases initial rates were measured.

The thermal dark reaction

Rhodizonate dianion is oxidized rapidly by oxygen or hydrogen peroxide in basic solution to give croconic acid. The first step in the reaction is believed to be attack by the hydroxide ion. The present results show that conversion to croconic acid and other products occurs in neutral or slightly acidic solutions and can be initiated by several oxidizing agents as well as oxygen and hydrogen peroxide.

The fact that reagents such as Cu^{2+}, $Fe(CN)_6^{3-}$, and TCNE are effective suggests that the first step is electron transfer and the first stages of the reaction may be written as

[1] $Rh^{2-} + A \rightleftarrows (Rh^{-\bullet} \ldots A^-)$

[2] $(Rh^{-\bullet} \ldots A^-) \rightleftarrows Rh^{-\bullet} + A^-$

[P] $Rh^{-\bullet} \rightarrow$ products

where $(Rh^{-\bullet} \ldots A^-)$ represents the caged complex before separation of the ions.

Two limiting cases may be considered for the kinetics of the reaction. (*a*) Only a small fraction of ions escape the cage before the reverse electron transfer regenerates the reactants but all those that escape react to form products. This corresponds to the condition $k_2 \ll k_{-1}$ and $k_{-2}[Rh^{-\bullet}]^2 \ll k_p[Rh^{-\bullet}]$. The rate of disappearance of rhodizonate is therefore,

$$\frac{-d}{dt}[Rh^{2-}] = k_2 k_1 [Rh^{2-}][A]$$

Can. J. Chem. Downloaded from www.nrcresearchpress.com by 198.100.157.202 on 09/07/12
For personal use only.

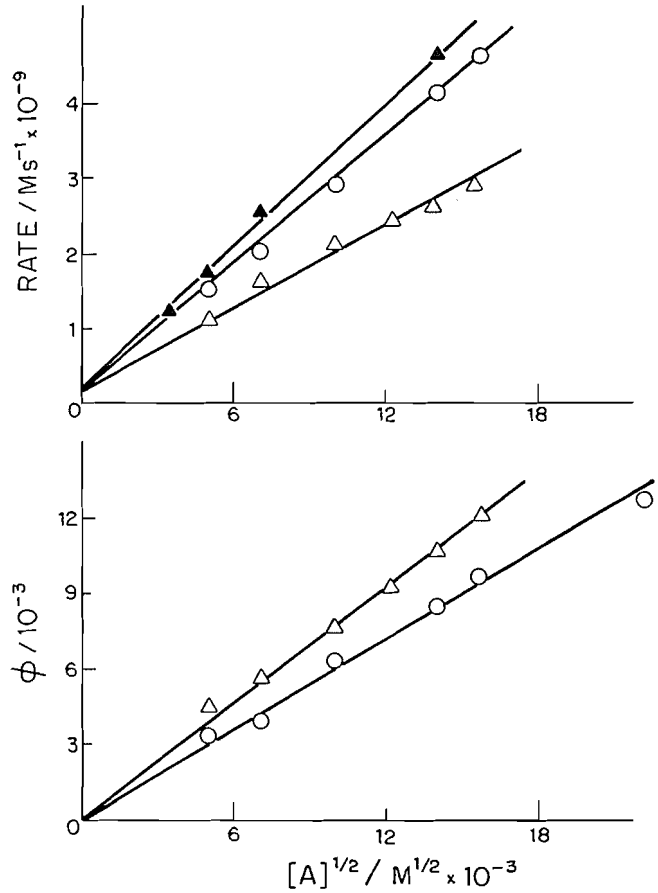


FIG. 1. (*a*) The rate of the thermal dark reaction of rhodizonate dianion with hydrogen peroxide and potassium ferricyanide at pH 7 as a function of the square root of the concentration of oxidizing agent. ○: H_2O_2; △: $Fe(CN)_6^{3-}$, 20°C; ▲: $Fe(CN)_6^{3-}$, 30°C. (*b*) The quantum yield of the photochemical reaction of rhodizonate dianion with hydrogen peroxide and potassium ferricyanide at pH 7 as a function of the square root of the concentration of oxidizing agent. ○: H_2O_2; △: $Fe(CN)_6^{3-}$.

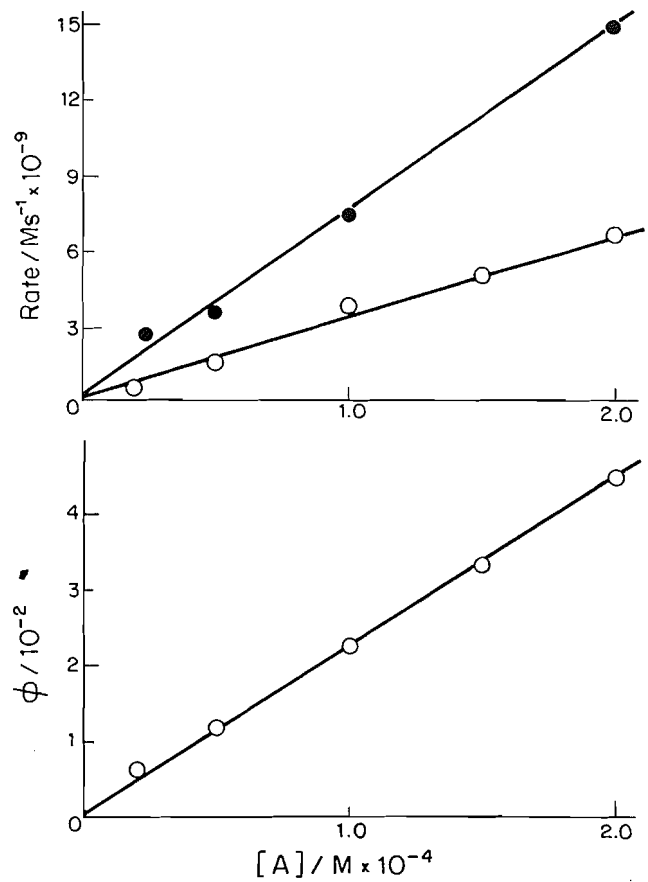


FIG. 2. (*a*) The rate of the thermal dark reaction of rhodizonate dianion with TCNE at pH 7 as a function of the concentration of TCNE. ○: 20°C; ●: 30°C. (*b*) The quantum yield of the photochemical reaction of rhodizonate dianion with TCNE at pH 7 as a function of the concentration of TCNE.

and is first order in concentration of acceptor. (*b*) If the ions escape the cage but still a major fraction undergo the reverse electron transfer and only a small fraction form products, corresponding to the condition $k_p[Rh^{-\bullet}] \ll k_{-2}[Rh^{-\bullet}]^2$, then the concentration of the monoanion radical will be controlled by the equilibrium constants for reactions [1] and [2]. The rate of disappearance of rhodizonate will then be given by

$$\frac{-d}{dt}[Rh^{2-}] = k_p\{K_1K_2[Rh^{2-}][A]\}^{1/2}$$

For this case it is not necessary that the intermediate step [1] attain equilibrium. Only an overall equilibrium involving the electron transfer is indicated and the intermediate step may not be kinetically important.

In the present experiments case (*b*) was observed with the oxidizing agents hydrogen peroxide and potassium ferricyanide. The results are shown in Fig. 1*a* where the rate of the reaction at a fixed concentration of rhodizonate is plotted as a function of $[A]^{1/2}$. Measurements of the rate at 30°C with $Fe(CN)_6^{3-}$ are also included. The rate of the reaction with TCNE, on the other hand, was a linear function of [A] and for this reagent therefore the mechanism corresponds to case (*a*). The results at both 20°C and 30°C are shown in Fig. 2*a*.

Table 1 also includes some experiments with constant concentration of TCNE and $Fe(CN)_6^{3-}$ and variable concentration of Rh^{2-}. Because the rate is measured by the change in absorbance of the rhodizonic acid, its concentration was not varied over a wide range but the results show that with TCNE the rate is proportional to the concentration of rhodizonate and with ferricyanide the rate is proportional to the square root of the concentration of rhodizonate.

At first sight it appears improbable that different limiting cases would be observed for similar reactants, particularly when k_p is the same, and k_{-2} is similar, for each reaction. The difference in rates between $k_{-2}[Rh^{-\bullet}]^2$ and $k_p[Rh^{-\bullet}]$, which governs the order of the rate, arises through the difference in the concentration of the rhodizonate monoanion in the two systems. The change-over in the order occurs when $[Rh^{-\bullet}] = k_p/k_{-2}$. The concentration of the monoanion is largely determined by the rate of separation of the caged complex, which is a function of the structure and properties of the oxidizing agent, including the charge distribution in the complex. It is interesting that similar rates are observed for TCNE and the other two reactants and indicates the compensating effects of k_2, k_{-2}, and k_p. For TCNE the measurements at 30°C, given in Table 2, together with a few measurements at 40°C, suggest an overall activation energy of approximately 40 kJ mol^{-1}.

The equilibrium constant for the over-all one-electron transfer process

[T] $Rh^{2-} + A \rightleftarrows Rh^{-\bullet} + A^-$

Can. J. Chem. Downloaded from www.nrcresearchpress.com by 198.100.157.202 on 09/07/12
For personal use only.

may be expressed as

$$RT \ln K_T = nFE^0$$

where E^0 is the standard cell potential for the cell represented by reaction [T] and

$$E^0 = E^0(A/A^-) - E^0(Rh^{-\bullet}/Rh^{2-})$$

where $E^0(A/A^-)$ and $E^0(Rh^{-\bullet}/Rh^{2-})$ represent the standard reduction potentials for the reactions indicated. Although the experiments were not performed under standard conditions, the concentrations of rhodizonic acid and additive were in the same range, and $[Rh^{-\bullet}] = [A^-]$; hence $E(A/A^-) - E(Rh^{-\bullet}/Rh^{2-})$ will be similar to the cell potential under standard conditions, $E^0(A/A^-) - E^0(Rh^{-\bullet}/Rh^{2-})$. For a particular concentration of rhodizonic acid, K_1 and hence $[Rh^{-\bullet}]$ will therefore be proportional to $E^0(A/A^-)$. From the table it appears that the rate of the thermal reaction correlates roughly with the strength of the oxidizing agents. No oxidation was observed with the following reactants: $S_4O_6^{2-}$ ($E^0 = +0.08$ V); MV^{2+} ($E^0 = -0.42$ V); p-$NO_2C_6H_4CHO$ ($E^0 = -0.86$ V); m-$NO_2C_6H_4CHO$ ($E^0 = -1.02$ v). It may be concluded that oxidizing agents with standard reduction potential below approximately zero volts have not sufficient strength to oxidize rhodizonic acid. This correlation of the rate with potential supports the mechanism of electron transfer.

The photochemical reaction

An increase in rate on irradiation was observed with the reactants hydrogen peroxide, ferricyanide, and tetracyanoethylene. The quantum yields in all cases were low (maximum 4×10^{-2}) as expected when the reverse of reaction [2] is fast. A simple extension of the mechanism for the thermal reaction may be written as follows:

[I_{abs}]	$Rh^{2-} + h\nu$	$\rightarrow Rh^{2-}*$
[D]	$Rh^{2-}*$	$\rightarrow Rh^{2-}$
[1*]	$Rh^{2-}* + A$	$\rightarrow (Rh^{-\bullet} \ldots A^-)$
[−1]	$(Rh^{-\bullet} \ldots A^-)$	$\rightarrow Rh^{2-} + A$
[2]	$(Rh^{-\bullet} \ldots A^-)$	$\rightleftarrows Rh^{-\bullet} + A^-$
[P]	$Rh^{-\bullet}$	$\rightarrow$ products

For the reactants hydrogen peroxide and potassium ferricyanide, corresponding to case (*b*) where $k_p[Rh^{-\bullet}]^2 \ll k_{-2}[Rh^{-\bullet}]^2$, the total rate of disappearance of rhodizonate may be expressed as

$$-\frac{d}{dt}[Rh^{2-}] = k_p\{K_1K_2[Rh^{2-}][A]\}^{1/2} + k_p\left\{\frac{I_{abs}K_2k_1*[A]}{k_{-1}(k_D + k_1*[A])}\right\}^{1/2}$$

Since the rate of disappearance is not independent of [A], $k_D \gg k_1*[A]$, and the quantum yield, obtained by subtraction of the thermal rate from the total rate, may be expressed as

$$\phi = \frac{k_p}{I_{abs}^{1/2}}\left\{\frac{K_2k_1*[A]}{k_{-1}k_D}\right\}^{1/2}$$

The quantum yield for the photochemical reaction with hydrogen peroxide and potassium ferricyanide is shown as a function of $[A]^{1/2}$ for constant concentration of rhodizonate in Fig. 1*b*. The square root dependence on the concentration of additive was observed as predicted for both reactants.

For the reactant TCNE, corresponding to case (*a*), where $k_2 \ll k_{-1}$ and $k_{-2}[Rh^{2-}]^2 \ll k_p[Rh^{-\bullet}]$, the total rate is given as

TABLE 2. Thermal reaction of rhodizonate dianion at 30°C: $[Rh^{2-}] = 2.5 \times 10^{-5}$ M, pH = 7

Additive	Concentration of additive/M	Rate/M s^{-1}
TCNE	2.5×10^{-5}	2.8×10^{-9}
	5.0×10^{-5}	3.6×10^{-9}
	1.0×10^{-4}	7.4×10^{-9}
	2.0×10^{-4}	1.47×10^{-8}
$Fe(CN)_6^{3-}$	1.25×10^{-5}	1.2×10^{-9}
	2.5×10^{-5}	1.7×10^{-9}
	5.0×10^{-5}	2.5×10^{-9}
	2.0×10^{-4}	4.6×10^{-9}

$$-\frac{d}{dt}[Rh^{2-}] = k_2K_1[Rh^{2-}][A] + \frac{k_2I_{abs}k_1*[A]}{k_{-1}(k_D + k_1*[A])}$$

Following the previous reasoning, the quantum yield is given as

$$\phi = \frac{k_2k_1*[A]}{k_{-1}k_D}$$

The linear dependence of the quantum yield for the photochemical reaction with TCNE on the concentration of TCNE is shown in Fig. 2*b*, where the measurements were made with constant concentration of rhodizonic acid.

To test the dependence of the rate on the concentration of rhodizonate dianion, experiments were done with constant concentration of TCNE and ferricyanide with concentrations of rhodizonate of 1.25×10^{-5} M ($I_{abs} = 0.60\ I_0$), 2.5×10^{-5} ($I_{abs} = 0.84\ I_0$) and 5.0×10^{-5} M ($I_{abs} = 0.975 I_0$) and the results are included in Table 1. With TCNE the rate is proportional to I_{abs} while with ferricyanide the rate is proportional to $(I_{abs})^{1/2}$. Thus the mechanism of the oxidation of rhodizonate dianion with the oxidizing agents listed in Table 1 is the same for the thermal and the photochemical reaction. Irradiation of the dianion simply increases the rate of the initial electron transfer.

Products of the reaction

Detection and analysis of products in the dilute solutions used in the present experiments presented some difficulty. In an aqueous solution of ions absorption in the visible or ultraviolet often provides a basis for identification. The only product detected and quantitatively measured by its absorption spectrum was croconic acid. The fraction of rhodizonic acid converted to croconic acid, listed in Table 1, was different with each oxidizing agent. In basic solution rhodizonic acid is quantitatively converted to croconic acid with the oxidizing agents hydrogen peroxide or oxygen. In neutral solution the fraction converted is much less and with oxygen is only about 10%. The most efficient conversion occurred with Cu^{2+}. The fact that each oxidizing agent produced a different rate of conversion to croconic acid indicates that further steps are required for this conversion and these steps, or competing steps, may involve the oxidizing agent. It should be noted that secondary photolysis of croconic acid is not important because the wavelength of maximum absorption of the croconate dianion (363 nm) is far outside the narrow band width of the incident radiation. In basic solution the ring contraction is believed to occur by an α-oxo alcohol rearrangement following attack by hydroxyl ion. The present results show that the ring contraction giving croconic acid may be initiated in neutral solution with several oxidizing agents. No evidence for absorption in the visible and near

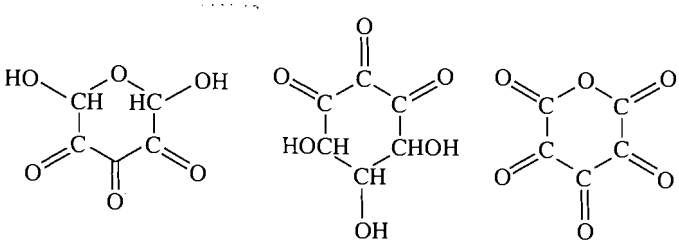
TABLE 3. ^{13}C NMR spectra of the products of the photochemical reaction of rhodizonate dianion

	^{13}C chemical shift for additives =		
Rh^{2-}	$Fe(CN)_6^{3-}$	H_2O_2	O_2
177.0	188.6	188.9	188.8
	176.4	177.2	177.3
	172.6	173.7	176.5
		76.0	170.5
			93.7
			92.6
			90.4
			77.1
			75.1

ultraviolet due to other products was obtained with any of the additives; weak absorbers would, of course, escape detection.

The ^{13}C NMR spectra of the reaction products from the reaction with ferricyanide, hydrogen peroxide and oxygen are summarized in Table 3, which includes the single resonance at 177 ppm observed in the neutral solution of rhodizonic acid before reaction. With all the reactants rhodizonic acid was completely consumed. The resonance at 188 ppm shows the presence of croconic acid dianion, formed in all three reactions. Other carbonyl resonances are present in the products from all reactants. Carbonyl resonances due to oxalic or formic acid are, however, absent. No evidence for products contining C—H bonds was obtained with the additives ferricyanide and hydrogen peroxide and except for the resonance at 76 ppm, the products appear similar from both reactants.

With oxygen the products are more diverse and may include secondary oxidations. The broad band proton decoupled spectra showed that the pairs of resonances with chemical shift 92.6 and 90.4 ppm and 77.1 and 75.1 ppm represent carbon atoms bonded to a single hydrogen atom. The resonance at 93.7 ppm which did not involve a C—H bond may indicate a geminol diol carbon, as suggested by Gelb, Schwargz, and Laufer (4) in their interpretation of the NMR spectra of aqueous solutions of rhodizonic acid. It seems clear that in the oxygen system reduction at a carbon atom has occurred and there is strong indication, particularly from the resonance at 91.5 ppm that an oxygen atom has been incorporated into the ring in an ether linkage. Possible products are ring compounds of the type:



Conclusions

The most important conclusion obtained from the present study is that both the thermal and photochemical conversion of rhodizonic acid to croconic acid and other products in aqueous solution are initiated by electron transfer to an acceptor which is a sufficiently strong oxidizing agent. This conclusion is based on several observations: (*a*) The rate of the thermal reaction in the absence of oxygen is increased in the presence of oxidizing agents with positive standard reduction potentials; (*b*) photolysis of the rhodizonic dianion in the presence of additives increased its rate of disappearance only with those additives which noticeably increased its thermal rate of reaction; (*c*) for any one oxidizing agent, the rates of the thermal and photochemical reactions have the same order with respect to the concentration of additive (either square root or linear).

Details of the subsequent reactions of the monoanion radical following the initial electron transfer step cannot be established at this stage. Because the fraction of the product appearing as croconic acid is not the same with each additive, several competing reactions must occur, which will be dependent on the pH of the solution as well as the reduction potential of the additive. The other products suggest that hydration of the monoanion is important and that oxygen may be incorporated into the ring through a ring-contraction mechanism. This type of mechanism does not invalidate the mechanism involving an α-oxo alcohol rearrangement following attack by hydroxide ion suggested for the conversion of rhodizonic acid to croconic acid in an oxygenated alkaline solution. The present results simply show that this conversion is a more general reaction and can occur in neutral solutions and with other oxidizing agents.

One of the aims of the present study was the exploration of the use of rhodizonic acid as a primary absorber of solar energy with subsequent conversion into a useful chemical system. The low quantum yields of the photochemical reaction observed in the present experiments do not provide much encouragement in the pursuit of this goal. It is nevertheless possible that a more efficient electron acceptor, combined with a suitable reactant for the subsequent conversion of the monoanion radical, might prove useful.

Acknowledgments

The authors thank NSERC for financial support of this work. They also thank Dr. R. A. Back for helpful comments concerning the manuscript.

1. R. WEST and J. NIU. Non-benzenoid aromatics. Vol. 1. *Edited by* J. Snyder. Academic Press New York. 1969. p. 311.
2. R. WEST (*Editor*). Oxocarbons, Academic Press, New York. 1980. Chap. 1.
3. L. M. SCHWARTZ, R. I. GELB, and D. A. LAUFER. Oxocarbons. *Edited by* R. West. Academic Press, New York. 1980. Chap. 3.
4. R. I. GELB, L. M. SCHWARTZ, and D. A. LAUFER. J. Phys. Chem. **82**, 1985 (1978).
5. L. J. SILVESTRI, R. E. HURST, L. SIMPSON, and J. M. SETTINE. Anal. Biochem. **123**, 303 (1982).
6. J. R. PREER and G. B. MURCHISON. Environ. Pollut. Ser. B, **12**, 1 (1986).
7. J. H. GOULD, S. G. CAPAR, R. M. JACOBS, and R. PLUNKETT. Anal. Lett. **21**, 2145 (1988).
8. R. KOSLOW. Chem. Abstr. **111**, 159924*m* (1989); J. H. GOULD. Chem. Abstr. **111**, 193394*y* (1989).
9. M. M. M. SALEEM and M. T. WILSON. Inorg. Chim. Acta, **137**, 139 (1987).
10. R. SCHREBLER, R. ARAYA, A. ARRATIA, D. CIAMPI, M. HOFFMAN, and N. DURAN. Bioelec. Bioenerg. **17**, 523 (1987).
11. G. KOKKINIDIS, D. SAZOU, and I. MOUMTZIS. J. Electroanal. Chem. Interfac. Electrochem. **213**, 135 (1986).
12. S. RAY and M. RAY. J. Biosci. **12**, 405 (1987).
13. T-K. HA and C. PUEBLA. J. Mol. Struct. **137**, 171 (1986); 137, 183 (1986).
14. G. IRACI and M. H. BACK. Can. J. Chem. **66**, 1293 (1988).
15. J. F. RABEK. Experimental methods in photochemistry and photophysics. Wiley–Interscience, New York. 1982.

Can. J. Chem. Downloaded from www.nrcresearchpress.com by 198.100.157.202 on 09/07/12
For personal use only.

Radical reductions of Cu(II)–penicillamine complexes: Evidence for a Cu(II)–disulphide anion intermediate[1]

STEPHEN P. MEZYK
Radiation Laboratory, University of Notre Dame, Notre Dame, IN 46556, U.S.A.

AND

DAVID A. ARMSTRONG[2]
Chemistry Department, University of Calgary, Calgary, Alta., Canada T2N 1N4

Received May 31, 1990[3]

Can. J. Chem. Downloaded from www.nrcresearchpress.com by 198.100.157.202 on 09/07/12
For personal use only.

STEPHEN P. MEZYK and DAVID A. ARMSTRONG. Can. J. Chem. **69**, 533 (1991).

In basic solution Cu(II) ions form planar complexes of stoichiometry Cu(II).L_2 with penicillamine molecules, where both the nitrogen and sulphur atoms of the thiol [$(\ddot{N}H_2)CH(CO_2^-)C(CH_3)_2S^-$] are involved in the coordination. The rates of reduction of this complex by the formate radical and the thiyl radical of penicillamine have been measured by pulse radiolysis.

The rate constant for reaction [14] has been found to be $1.2 \pm 0.2 \times 10^8\ M^{-1}\ s^{-1}$

[14] $\cdot CO_2^- + Cu^{II}(PenS^-)_2 \rightarrow CO_2 + Cu^{I}(PenS^-)_2$

For the thiyl radical, which is not inherently reducing, reduction must involve the PenS.∴SPen$^-$ anion complex.

[2] PenS.∴SPen$^-$ + $Cu^{II}(PenS^-)_2 \rightarrow (PenS)_2 + Cu^{I}(PenS^-)_2$

Under the conditions of this study, ([PenS$^-$] ~ 10^{-2} M, pH = 10.0), this anion exists in free solution equilibrium with PenS·

[1] PenS· + PenS$^- \underset{}{\overset{K_1}{\rightleftharpoons}}$ PenS.∴SPen$^-$ $\quad K_1 = 60.0$

A systematic study of the dependence of the overall reduction rate on [PenS$^-$] showed that the reaction proceeded rapidly even when the PenS.∴SPen$^-$ concentration was negligibly small. This finding can be explained by the formation of an internal PenS.∴SPen$^-$ anion from the reaction of free PenS· with one of the PenS$^-$ ligands of the Cu(II) complex:

[3] PenS· + Cu(II)$(PenS^-)_2 \rightarrow$ (PenS$^-$)Cu(II)(PenS.∴SPen$^-$)

and the subsequent rapid transfer of an electron to Cu(II):

[4] (PenS$^-$)Cu(II)(PenS.∴SPen$^-$) → (PenS$^-$)Cu(I)(PenSSPen)

Analysis of the results gave $k_2 = 2.9 \pm 0.3 \times 10^8\ M^{-1}\ s^{-1}$ and $k_3 = 3.4 \pm 0.4 \times 10^8\ M^{-1}\ s^{-1}$.

Key words: penicillamine, thiyl, reduction, copper(II), radical, disulphide ion.

STEPHEN P. MEZYK et DAVID A. ARMSTRONG. Can. J. Chem. **69**, 533 (1991).

En solution basique, la pénicillamine et les ions Cu(II) forment des complexes plans de stoechiométrie Cu(II).L_2 dans lesquels les atomes d'azote et de soufre du thiol [$(:NH_2)CH(CO_2^-)C(CH_3)_2S^-$] sont impliqués dans la coordination. Utilisant la radiolyse pulsée, on a mesuré les vitesses de réduction de ce complexe par le radical formiate ainsi que par le radical thiyle de la pénicillamine.

On a trouvé que la constante de vitesse pour la réaction [14] est égale à $1{,}2 \pm 0{,}2 \times 10^8\ M^{-1}\ s^{-1}$.

[14] $\cdot CO_2^- + Cu^{II}(PenS^-)_2 \rightarrow CO_2 + Cu^{I}(PenS^-)_2$

Pour le radical thiyle, qui inhéremment n'est pas un réducteur, la réduction doit impliquer le complexe anionique PenS.∴SPen$^-$.

[2] PenS.∴SPen$^-$ + $Cu^{II}(PenS^-)_2 \rightarrow (PenS)_2 + Cu^{I}(PenS^-)_2$

Dans les conditions utilisées au cours de ce travail, ([PenS$^-$] ~ 10^{-2} M, pH = 10,0), cet anion existe en solution, en équilibre libre avec le PenS.

[1] PenS· + PenS$^- \underset{}{\overset{K_1}{\rightleftharpoons}}$ PenS.∴SPen$^-$ $\quad K_1 = 60.0$

Une étude systématique sur la relation entre la vitesse globale de réduction et la [PenS$^-$] montre que la réaction se produit rapidement, même lorsque la concentration de PenS.∴SPen$^-$ est très faible. Cette observation pourrait être expliquée par la formation d'un anion PenS.∴SPen$^-$ interne par la réaction du PenS· libre avec un des ligands PenS$^-$ du complexe du Cu(II):

[3] PenS· + Cu(II)$(PenS^-)_2 \rightarrow$ (PenS$^-$)Cu(II)(PenS.∴SPen$^-$)

---

[1]This research was supported by the Natural Sciences and Engineering Research Council of Canada under Grant A3571 and by the Office of Basic Energy Sciences of the Department of Energy. This is Contribution No: NDRL-3297 from the Notre Dame Radiation Laboratory.

[2]On sabbatical leave as a visiting professor in the Radiation Laboratory at the University of Notre Dame 1989–1990.

[3]Revision received November 1, 1990.

Can. J. Chem. Downloaded from www.nrcresearchpress.com by 198.100.157.202 on 09/07/12
For personal use only.

et le transfert subséquent rapide d'un électron au Cu(II) :

[4] $(PenS^-)Cu(II)(PenS.^{\cdot}.SPen^-) \rightarrow (PenS^-)Cu(I)(PenSSPen)$

Une analyse des résultats conduit à $k_2 = 2{,}9 \pm 0{,}3 \times 10^8\ M^{-1}\ s^{-1}$ et $k_3 = 3{,}4 \pm 0{,}4 \times 10^8\ M\ s^{-1}$.

Mots clés : pénicillamine, thiyle, réduction, cuivre(II), radical, anion disulfure.

[Traduit par la rédaction]

Introduction

The importance of nitrogen- and sulphur-centered ligands in copper-containing enzymes and metallothionenes (1–3) has stimulated fundamental research on the structures of these systems. Because of the catalytic roles of several of the metalloproteins, oxidation–reduction reactions between sulphur species and copper systems are also of interest (4, 5). The bidentate 1,2-aminothiol ligands, cysteine and penicillamine, are among the simplest that can be used for model studies. Recently a report on the kinetics of oxidation of $Cu(I)_nL_{n+1}$ systems ($n = 1$ or 2) by thiyl radicals was made (6) for these two ligands. The thiyl (CysS·, PenS·) radicals are moderately strong one-electron oxidizing agents, with $E^0(RS\cdot/RS^-) = 0.77$ V (7). For typical alkaline conditions with thiol concentrations of 10^{-2} M, however, they are in equilibrium with the $\sigma\sigma^*$ bonded $RS.^{\cdot}.SR^-$ anion radicals (7), for example:

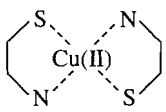
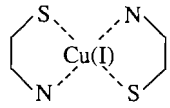
[1]/[−1] $PenS\cdot + PenS^- \rightleftharpoons PenS.^{\cdot}.SPen^-$

These are less strong oxidants ($E^0(RS.^{\cdot}.SR^-/2RS^-) = 0.57$ V (7)), and predictably were found to react less rapidly than the RS· species.

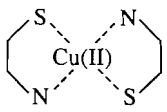
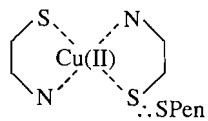
During the course of the study described in ref. 6 it was also confirmed (cf: refs. 8, 9) that the $Cu(II)(PenS^-)_2$ species was stable for several hours at pH values above 10. Earlier work (10) had shown that this species, which was itself the product of the oxidation of $Cu(I)_nL_{n+1}$, could also be reduced by the same sulphur radicals. The purpose of the present investigation was to examine this interesting phenomenon in greater detail.

In principle $R_2CHS\cdot$ radicals with α hydrogens can undergo rearrangement to form the reducing species $R_2C\cdot—S^-$ or $R_2\dot{C}—SH$. However, PenS· has no α hydrogens. Thus the only way for it to be a reducing agent is through the formation of $PenS.^{\cdot}.SPen^-$, which although a mild oxidant is also a strong reductant ($E^0(RSSR/RS.^{\cdot}.SR^-) = -1.6$ V (7)). The rates of reactions [1] and [−1] are sufficiently fast (11) that for typical $PenS^-$ concentrations ($\sim 10^{-2}$ M) the relaxation time $\tau = k_{-1} + k_1[PenS^-]$ is about 0.4 μs. Thus equilibrium [1] would be maintained during the reactions of PenS· and $PenS.^{\cdot}.SPen^-$ with copper species, for which τ is typically 15 μs (data of ref. 6 and below).

Two modes of reduction are possible. The $PenS.^{\cdot}.SPen^-$ present in the bulk solution could directly reduce the Cu(II) species, reaction [2]:

[2] $PensS.^{\cdot}.SPen^- +$  → 

or the free PenS· could react with a $PenS^-$ ligand:

[3] $PensS\cdot +$  → 

I

Due to the strong negative value of $E^0(RSSR/RS.^{\cdot}.SR^-)$, the "internal disulphide anion" would be capable of rapidly transfering an electron to the Cu(II) center, viz.:

[4] $\mathbf{I} \rightarrow Cu(I)(PenS^-)(PenSSPen)$

II

The intermediate **I** should therefore have an extremely short lifetime, and it is reasonable to assume that the reaction rate would be controlled by k_3. The disulphide ligand in **II** should subsequently be replaced by $PenS^-$:

[5] $\mathbf{II} \xrightarrow{(+\ PenS^-)} Cu(I)(PenS^-)_2 + PenSSPen$

The primary object of this investigation was to assess the relative importance of reaction [2] and reactions [3] + [4], and, if possible, to determine their rate constants. At the same time the conditions affecting the photostationary state, reached when the rates of oxidation and reduction were equal (10), were also examined.

The PenS· radicals were produced by the radiolysis of nitrous oxide-saturated aqueous solutions of PenSH, buffered at the desired pHs. The relevant reactions are as follows (12, 13):

[6] $0.43H_2O \rightsquigarrow 0.28e_{aq}^- + 0.28H_3O^+ + 0.29\cdot OH + 0.05H\cdot + 0.05H_2 + 0.07H_2O_2$

(coefficients are in μmoles per J of radiation energy absorbed)

[7] $e_{aq}^- + N_2O + H_2O \rightarrow \cdot OH + N_2 + OH^-$

[8] $\cdot OH\ (\text{or } \cdot H) + PenSH \rightarrow H_2O\ (\text{or } H_2) + PenS\cdot$

[9] $\cdot OH + N_3^- \rightarrow OH^- + \cdot N_3$

[10] $\cdot N_3 + PenS^- \rightarrow N_3^- + PenS\cdot$

Reactions [6] through [8] were used at pH 10 and reactions [6], [7], [9], and [10] at pH 12. Formate radicals ($\cdot CO_2^-$) were formed by reactions [11] and [12]:

[11] $\cdot OH\ (\text{or } \cdot H) + HCO_2^- \rightarrow H_2O\ (\text{or } H_2) + \cdot CO_2^-$

[12*a*] $\cdot OH + OH^- \rightleftharpoons \cdot O^- + H_2O$

[12*b*] $\cdot O^- + HCO_2^- \rightarrow HO^- + \cdot CO_2^-$

Rate constants were determined both from analysis of the photostationary states and by the pulse radiolysis method.

Experimental

Materials

Triply distilled or deionised/chromatographed water was used in the preparation of all solutions. These were buffered with sodium tetraborate (20 mM, Fischer) and carefully deareated by bubbling with N_2O before the weighed amount of PenSH (Aldrich) was added. The desired quantity of CuCl or $CuCl_2$ (Aldrich) was normally added last, and then the final pH adjustment made, care being taken to prevent contact with air. All chemicals were of the highest purity research grade available.

Equipment

Continuous radiolyses were carried out by standard methods (12, 13) in "Gamma Cell" type irradiators, either at the University of Calgary or

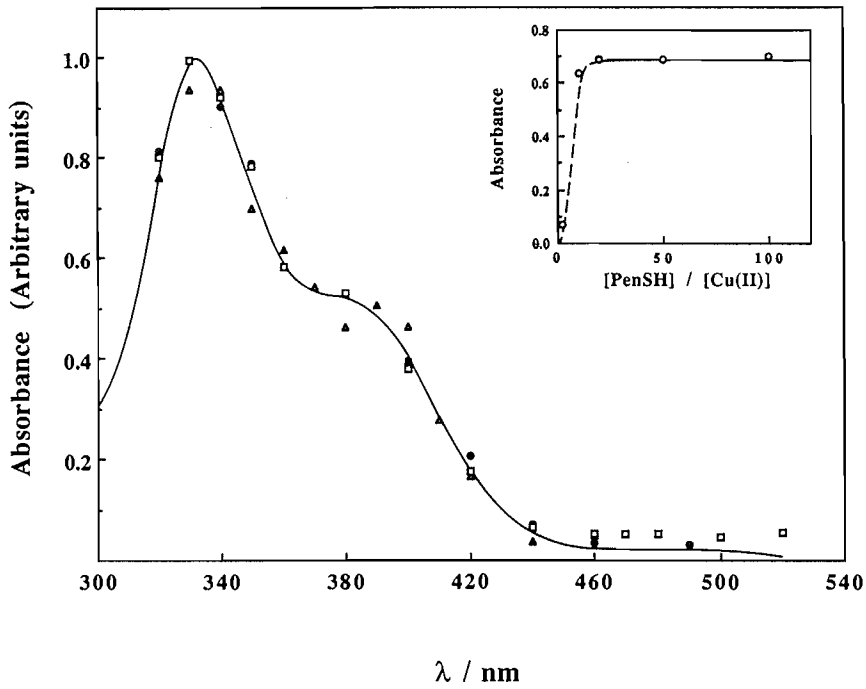


FIG. 1. Spectra and dependence of absorbance on [PenS$^-$]. Main figure: solid line, absorption spectrum of 1×10^{-4} M Cu(II)(PenS$^-$)$_2$ in 10^{-2} M PenSH (total concentration) at pH 10. (▲): Loss of absorbance seen on reaction of $\cdot CO_2^-$ radicals with 10^{-4} M Cu(II)(PenS$^-$)$_2$ complex at pH 10 in pulse radiolysis; (●): as above, but with PenS· radicals; (□): as above, but with PenS· radicals formed in reaction [10] in 0.10 M N_3^- at pH 12. Inset: dependence of peak intensity on ratio of total [PenSH]:[Cu(II)] for 10^{-4} M Cu(II) at pH 10.

the Radiation Laboratory at the University of Notre Dame. Dosimetry was carried out with the Fricke dosimeter solution (12). Pulse Radiolysis experiments were performed using the 1.5 MeV Van de Graaff in the Chemistry Department at the University of Calgary (14) or with the 8 MeV linear accelerator at Notre Dame (15). Experiments were performed at 23 ± 2°C.

Analytical procedures

Concentrations of sulphydryl were determined from the absorbance of PenS$^-$ at 250 nm at pH 10 or above, after quantitative dilution of the concentrations to give intensities in a measurable range. Concentrations of Cu(II)(PenS$^-$)$_2$ were determined from the characteristic absorbance maximum at 335 nm (see Fig. 1). The shape of the spectrum did not change significantly over the concentration range 0.25 to 2.0×10^{-4} M. However, the binding constant of the second PenS$^-$ ligand appears to be only about 1500 M and plots of absorbance versus concentration showed a variation of about 10% in the absorbance coefficient over the range 0.5 to 1×10^{-4} M. Thus, to avoid using an approximate Beer's law relation, concentrations of Cu(II) were read directly from absorbance plots.

For the pulse radiolysis experiments, as in ref. 6, the absorbances at 340 nm were corrected for the contributions of the sulphur radicals. These were calculated from their known absorbance coefficients at 340 nm and from their concentrations, which were determined as a function of time from the absorbances at 470 nm where the Cu(II) and Cu(I) species do not significantly absorb. In some experiments the corrected Cu(II)(PenS$^-$)$_2$ absorbances were plotted as a function of time, and initial rates of Cu(II) loss were found from the slopes. These rates were then divided by the total sulphur radical concentrations produced per pulse to yield k_I, the product of the second order rate constant for reaction with the Cu(II) complex and the concentration of the complex. This procedure has the advantage of eliminating any minor contributions to the rate from second order sulphur radical–radical reactions. It was also used with the $\cdot CO_2^-$ radical studies, but in this case no correction for PenS·/PenS.∴SPen$^-$ absorbance was needed. In other pulse radiolysis experiments the values of k_I were calculated from the decays of the absorbances of the PenS.∴SPen$^-$ radicals at 470 nm.

Results

Spectrum and stability of Cu(II)(PenS$^-$)$_2$

The solid line in Fig. 1 is the spectrum of Cu(II)(PenS$^-$)$_2$ in 10 mM PenSH at pH 10. A similar spectrum was observed at pH 12, and both were in good agreement with the earlier data obtained by Wilson and Martin (8). At pH 10 and above the decay of the absorption spectrum exhibited a first order half life of about 5 h. Experiments with Cu(II)(PenS$^-$)$_2$ were therefore completed within as short a time as possible after the solutions were prepared, in general <45 min. This decay is due to the thermal reaction [13] (8, 9), which occurs much faster with

[13] $$2Cu(II)(PenS^-)_2 + 2PenS^- \rightarrow 2Cu(I)(PenS^-)_2 + PenSSPen$$

amino thiols that do not possess shielding β-methyl groups. The inhibition of this reaction in the case of PenSH is strongest at high pH, where both the amino and sulphydryl groups are deprotonated and available to bind the Cu(II). Thus the intensity and the stability of the 335 nm peak fell off with pH, 10 being the minimum practical pH for the techniques used here. The dependence of intensity on the ratio of PenSH to Cu(II) is shown in the inset of Fig. 1. Experiments were conducted with ratios of 20 to 100 to ensure two ligands were bound to each Cu(II).

^{60}Co γ-radiolysis

The production of PenS· radicals in 0.5 to 2×10^{-4} M Cu(II) solutions caused bleaching of the Cu(II)(PenS$^-$)$_2$ absorption, but eventually a stationary intensity was always reached. At that time the fraction of Cu(II)(PenS$^-$)$_2$ remaining was, within experimental error, independent of total copper concentration over the range studied. At pH 10 the photostationary state was found to be independent of dose rate and of total PenSH concentration over the range 4×10^{-3} to 5×10^{-2} M. Some

Can. J. Chem. Downloaded from www.nrcresearchpress.com by 198.100.157.202 on 09/07/12
For personal use only.

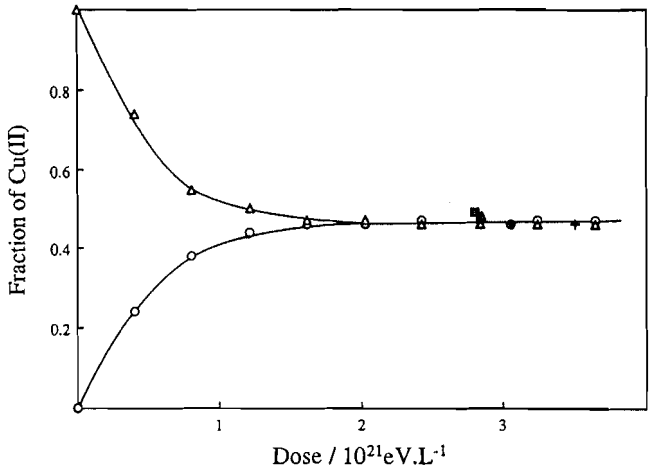


FIG. 2. The approach to stationary state in γ radiolysis at pH 10. Conditions as follows: dose rate = 1.50×10^{21} eV L^{-1} min^{-1} (240 G per min), total [PenSH] = 10^{-2} M, $[Cu(II)]_{initial}$: (●) 5×10^{-5}, (△) 1×10^{-4}, (■) 2×10^{-4} M, respectively; (○) $[Cu(II)]_{initial} = 0.0$, but $[Cu(I)]_{initial} = 1 \times 10^{-4}$ M; [PenSH] = 5×10^{-2} M; $[Cu(II)]_{initial} = 1 \times 10^{-4}$ M, (▲) dose rate = as above, (+) dose rate = 1.13×10^{20} eV L^{-1} min (18.1 G per min).

of these results have been plotted in Fig. 2. This figure also demonstrates that the same fraction of total copper was converted to $Cu(II)(PenS^-)_2$ when the starting reagent was entirely in the form of $Cu(I)_n(PenS^-)_{n+1}$. The initial slopes of the upper and lower curves show that the yields of $Cu(II)(PenS^-)_2$ removal and formation were both 5.7 ± 0.2 molecules per 100 eV or 0.57 ± 0.02 μmoles per J of radiation energy adsorbed. These values agree with the yields of PenS· radicals expected from reactions [6] through [8] (12, 13). This and the identical photostationary fractions of Cu(II) complex obtained from reduction and oxidation lead to the conclusion that the only significant primary products of the reaction of PenS· radicals with $Cu(II)(PenS^-)_2$ are Cu(I)–penicillamine complexes.

In contrast to the above results with PenS· radicals, the production of $\cdot CO_2^-$ radicals via reactions [6], [7], [11], and [12] at pH 12 in 10^{-4} M $Cu(II)(PenS^-)_2$ solutions produced 96+% reduction. That observation is in accord with reaction [14]. This reaction is expected to give a quantitative yield of Cu(I),

$$[14] \qquad \cdot CO_2^- + Cu(II)(PenS^-)_2 \rightarrow CO_2 + Cu(I)(PenS^-)_2$$

since there are no PenS· radicals present and $E^0(CO_2/\cdot CO_2^-)$ is −1.85 to −1.90 V (16, 17). At pH values nearer to the sulphydryl pK (~8.50, where fractions of the various ionic forms were taken from ref. 18), the concentration of PenSH rises and some PenS· are produced via reaction [15] (17).

$$[15] \qquad \cdot CO_2^- + PenSH \rightarrow HCO_2^- + PenS\cdot$$

The level of Cu(II) complex at the photostationary state then rises. However, reaction [15] was negligible at pH 10 with 4×10^{-3} M total PenSH. Pulse radiolysis experiments to determine the rate constant of reaction [14] were therefore done under those conditions — see below.

Because a small amount of H_2O_2 is formed in reaction [6], it was necessary to determine whether this influenced the photostationary concentrations. Hence, reactions of H_2O_2 with PenSH were studied in the presence and absence of Cu(I) and Cu(II) complexes. Millimolar concentrations of H_2O_2 reacted with 10^{-2} M PenSH at pH 10 on the time scale of a minute. This is similar to the observations of Barton *et al.* (19) for other amino thiols. When Cu(I) was present at ~10^{-4} M it was oxidized to about the same extent as seen in the γ radiolysis, suggesting that PenS· radicals were formed as a result of ·OH radical production in a reaction between Cu(I) and H_2O_2. This finding is in accord with observations of Goldstein and Czapski (20). Addition of H_2O_2 to solutions already at the photostationary $Cu(II)(PenS^-)_2$ concentration had no effect on the Cu(I):Cu(II) ratios, but $PenS^-$ was still oxidized, as in the absence of copper.

These observations show that H_2O_2 has no significant effect on the photostationary concentrations of Cu(I) and Cu(II). However, at pH 10 small (~0.003) absorbance increases with a half life of ~70 min occurred after radiolysis to steady state. When the increase in absorbance had ceased, the system reverted to the overall slow ($t_{1/2}$ ~5 h) decay due to reaction [13]. The small post irradiation effect is probably due to rearrangements of liganded copper species, which enhance the $PenS^-$–Cu(II) C.T. transition intensities without causing significant changes in the overall spectrum shape. One rearrangement of this type, involving a Cu(I)–Cu(II) mixed valence species, was observed in ref. 6, but on a shorter time scale.

One important characteristic of the formation of mixed Cu valence species is the presence of absorption bands in the region of 500 nm and above (21, 22). While there was no evidence of significant absorption in that region at the irradiation times required to reach the photostationary state, in radiolyses of very long duration such absorptions were seen. Here it should be stressed that these long term observations were seen on time scales of hours, and do not effect conclusions drawn from the stationary state, measured after 4 min for the higher dose rate and 20 min for the lower, shown in Fig. 2.

Analysis of the photostationary states

The existence of stationary concentrations of Cu(I) and Cu(II) during radiolysis requires that the rate of reduction equal the rate of oxidation. Thus, writing the formulae for the rates of reduction and oxidation on the left and right respectively, one has

$$[16] \qquad \{k_2\theta + k_3\}[Cu(II)(PenS^-)_2][R\cdot]/(1+\theta) = \{(k_{17}\theta + k_{18})[Cu(I)(PenS^-)_2] + k_{19}[Cu(I)_2(PenS^-)_3]\}[R\cdot]/(1+\theta)$$

$$[17] \qquad PenS.\therefore SPen^- + Cu(I)(PenS^-)_2 \rightarrow 2PenS^- + Cu(II)(PenS^-)_2$$

$$[18] \qquad PenS\cdot + Cu(I)(PenS^-)_2 \rightarrow PenS^- + Cu(II)(PenS^-)_2$$

$$[19] \qquad PenS\cdot + Cu(I)_2(PenS^-)_3 \rightarrow Cu(I)(PenS^-)_2 + Cu(II)(PenS^-)_2$$

Here k_{17}, k_{18}, and k_{19} refer to the oxidation reactions [17], [18], and [19], the rate constants of which were reported in ref. 6. The symbol $\theta = K_1(PenS^-)$. The quantity $[R\cdot]$ is the total concentration of sulphur radicals, while $\theta/(1+\theta)$ and $(1+\theta)^{-1}$ are, respectively, the fractions of $PenS.\therefore SPen^-$ and PenS·. Cancelling the $[R\cdot]/(1+\theta)$ terms and rearranging give

$$[20] \qquad \{k_2\theta + k_3\} = \{(k_{17}\theta + k_{18})[Cu(I)(PenS^-)_2]_{ss} + k_{19}[Cu(I)_2(PenS^-)_3]_{ss}\}[Cu(II)(PenS^-)_2]_{ss}^{-1}$$

where the subscripts on the concentration terms signify stationary state concentrations.

Calculation of the quantity on the right hand side of expression [20] requires a knowledge of k_{17}, k_{18}, k_{19}, K_1, and

Can. J. Chem. Downloaded from www.nrcresearchpress.com by 198.100.157.202 on 09/07/12
For personal use only.

Can. J. Chem. Downloaded from www.nrcresearchpress.com by 198.100.157.202 on 09/07/12
For personal use only.

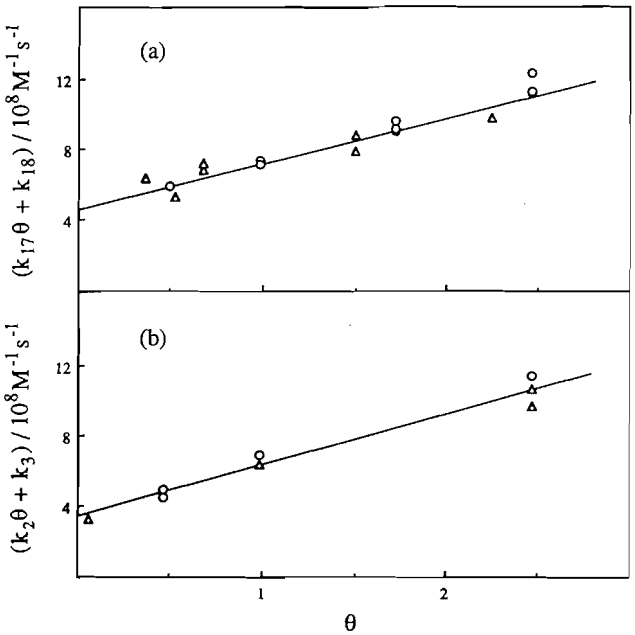


FIG. 3. (*a*) Values of $(k_{17}\theta + k_{18})$ plotted against θ. Circles and triangles are data from this study and ref. 6, respectively. (*b*) Values of $(k_2\theta + k_3)$ plotted against θ. Circles and triangles are data from analyses of the stationary state and pulse radiolysis respectively.

K_{21}, the equilibrium constant for the reaction

[21] $$2Cu(I)(PenS^-)_2 \rightleftharpoons Cu(I)_2(PenS^-)_3 + PenS^-$$

The values of k_{17}, k_{18}, k_{19}, and K_1 as reported in ref. 6 were $<2 \times 10^8$, $(4.5 \pm 0.5) \times 10^8$, and $(5.5 \pm 0.3) \times 10^8$ in $M^{-1}\,s^{-1}$ and 113 ± 14, respectively. The magnitude of K_1 is dependent on pH because of the changes which occur in the charge of the $PenS^-$ species as the amino groups deprotonate. Further work since ref. 6 was published has shown that the value of 16 used for pH 10 was too low.[4] The correct value is 60 ± 3, which is in better agreement with an earlier result of Purdie and co-workers (18). Since K_1 determines the magnitude of θ and the fractions of the two forms of radicals, this finding necessitated a re-evaluation of k_{17} and k_{18}. New pulse radiolysis results on the oxidation at low Cu(I) concentration are presented in the next section, along with the data of ref. 6 recalculated with the correct K_1. These combined data gave $k_{17} = (2.7 \pm 0.3) \times 10^8\ M^{-1}\ s^{-1}$, which is ~40% larger than the upper limit assigned in ref. 6. The magnitude of k_{18} found here was $(4.6 \pm 0.5) \times 10^8\ M^{-1}\,s^{-1}$, essentially unchanged.

The quantity of the right hand side of expression [20] was calculated from the parameters above (with the corrected k_{17} and K_1) for the values of θ and the photostationary state concentrations of the copper species from Fig. 2. These data have been plotted in Fig. 3*b*. Reference to expression [20] shows that the intercept is k_3 and the slope k_2. Further comment is deferred until the pulse radiolysis results have been presented.

Pulse radiolysis experiments

The points in Fig. 1 show the "bleaching spectrum" observed on reacting PenS· and $\cdot CO_2^-$ radicals with $Cu(II)(PenS^-)_2$. The agreement with the spectrum of the starting material demonstrates that no new species absorbing in the 300 to 500 nm region were created. The main process, therefore, is the

[4]S. P. Mezyk. To be published.

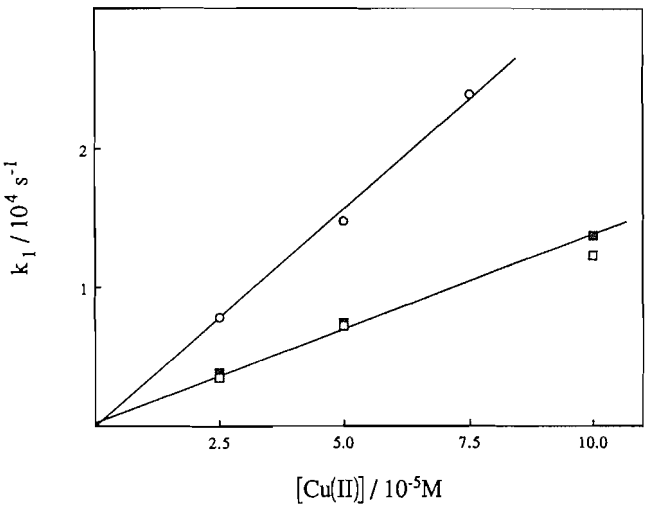


FIG. 4. Dependence of pseudo-first order rate constant obtained in pulse radiolysis experiments on concentration of Cu(II) for reduction by: $\cdot CO_2^-$ radical at pH 10 (■) and 12 (□) respectively, PenS· radical formed via reaction [10] at pH 12 (○).

conversion of $Cu(II)(PenS^-)_2$ to $Cu(I)_nL_{n+1}$ species, which do not have significant absorbance above 300 nm.

The square symbols in Fig. 4 are values of k_1 for the reaction of $\cdot CO_2^-$ radicals with $Cu(II)(PenS^-)_2$ in formate-containing solutions, determined as described in the Experimental section and plotted against the $Cu(II)(PenS^-)_2$ concentration. The results are seen to be independent of pH, and the slope yields $k_{14} = (1.2 \pm 0.2) \times 10^8\ M^{-1}\,s^{-1}$.

Values of k_1 for the reaction between the sulphur radicals of penicillamine and $Cu(II)(PenS^-)_2$ at different concentrations were determined with total PenSH concentrations of 50 and 20 mM at pH 10, and 4 mM at pH 12. The corresponding θ values are 2.47, 0.99, and 0.06, respectively. The conditions for the two solutions at pH 10 were similar to those for the γ radiolyses. Based on the data of ref. 18, the concentration of non-ionized PenSH would have been $>4 \times 10^{-3}$ M and this should be sufficient to convert any C-centered radicals formed by ·OH (23) to PenS· in reactions similar to reaction [15] (24). The pH 12 experiment was done for the purpose of minimizing θ, so that the fraction of PenS· radicals would approach unity. At this pH the non-ionized PenSH concentration is very low and C-centered radicals, would not be converted quantitatively to PenS·. Therefore, 0.1 M N_3^- was incorporated in the solution and PenS· was produced exclusively via reaction [10]. The dependence of k_1 on the Cu(II) concentration has been illustrated for the pH 12 solution in Fig. 4.

Analysis of the data for the PenS· and PenS∴SPen$^-$ reactions requires reference to expression [16]. From the left hand side the rate of the reduction reaction can be written as

$$-d[R\cdot]/dt = (k_2\theta + k_3)[R\cdot](1 + \theta)^{-1}[Cu(II)(PenS^-)_2]$$

The pseudo-first order rate constant determined from pulse radiolysis, k_1, is given by

$$k_1 = -(d[R\cdot]/dt)/[R\cdot]$$

or

[22] $$k_1 = (k_2\theta + k_3)(1 + \theta)^{-1}[Cu(II)(PenS^-)_2]$$

It follows that the slopes of plots of k_1 against $[Cu(II)(PenS^-)_2]$,

TABLE 1. Summary of rate constants for oxidation of Cu(I) and reduction of Cu(II) species liganded by penicillamine (units: $10^8\ M^{-1}\ s^{-1}$)

Radical species	Copper species		
	$Cu(I)(PenS^-)_2$	$Cu(I)_2(PenS^-)_3$	$Cu(II)(PenS^-)_2$
$PenS.\therefore SPen^-$	2.7 ± 0.3 [17][a]	—	2.9 ± 0.3 [2]
$PenS\cdot$	4.6 ± 0.5 [18]	5.5 ± 0.3 [19]	3.4 ± 0.4 [3]
$CO_2\cdot^-$	—	—	1.2 ± 0.2 [14]

[a]Reaction numbers used in the text are given in parentheses.

like the one in Fig. 4, correspond to values of $(k_2\theta + k_3)/(1 + \theta)$. The magnitudes found for this quantity in units of $10^8\ M^{-1}\ s^{-1}$ were 2.8 and 3.1 from two experiments for $\theta = 2.47$, 3.2 for $\theta = 0.99$, and 3.1 for $\theta = 0.06$. These have been multiplied by the values of $(1 + \theta)$ to yield $(k_2\theta + k_3)$, and the latter plotted against θ in Fig. 3*b*. They agree with the data from the photostationary state within the experimental uncertainties of $\pm 10\%$. From a linear least-mean-squares analysis of all the data k_3 was found from the intercept to be $(3.4 \pm 0.4) \times 10^8\ M^{-1}\ s^{-1}$ and the value of k_2 given by the slope was $(2.9 \pm 0.3) \times 10^8\ M^{-1}\ s^{-1}$.

As pointed out above, pulse radiolysis experiments on the θ dependence of the rate of oxidation of Cu(I) were done to correct the value of k_{17}. As in ref. 6, the Cu(I) concentration used (20 μM) was sufficiently low that $Cu(I)(PenS^-)_2$ would have been the only species present. The expression for the pseudo-first order rate constant from the pulse radiolysis experiments is analogous to [22] above, namely:

$$[23] \qquad k_1' = (k_{17}\theta + k_{18})(1 + \theta)^{-1}[Cu(I)(PenS^-)_2]$$

Values of $(k_{17}\theta + k_{18})(1 + \theta)^{-1}$ were obtained from the slopes of plots of k_1' versus $[Cu(I)(PenS^-)_2]$. These have been multiplied by the appropriate values of $(1 + \theta)$ and plotted against θ in Fig. 3*a*. The results from ref. 6, recalculated with $K_1 = 60$, have also been included. A least-mean-squares linear fit to the combined data gave the values of k_{17} and k_{18} reported in the preceding section. A summary of these and other rate constants appears in Table 1.

Discussion

Earlier studies of the reduction of Cu(II) complexes by $\cdot CO_2^-$ have involved a variety of complexing ligands, including the amino compounds glycine and histidine (25). The second order rate constants typically fall into the range $1–7 \times 10^8\ M^{-1}\ s^{-1}$. The rate constant of $1.2 \times 10^8\ M^{-1}\ s^{-1}$ found here for $Cu(II)(PenS^-)_2$ in reaction [14] is, in particular, very similar to $1.0 \times 10^8\ M^{-1}\ s^{-1}$ for oxidized glutathione (26) in which the copper is also bound by S- and N-centered ligands. Thus the present rate for $\cdot CO_2^-$ seems to fall in line with those for other systems with similar types of ligand.

In contrast to the situation with $\cdot CO_2^-$, the rates of reduction of Cu(II) complexes by thiyl radicals and disulphide anions are relatively unknown. The present results confirm the observation in ref. 10 that these reductions are reasonably efficient processes. Actually the rate constants k_2 and k_3 determined here are a factor of ~ 2 smaller than the value of $6.5 \times 10^8\ M^{-1}\ s^{-1}$ estimated in the earlier study (10) for the reduction by $PenS\cdot$ and $PenS.\therefore SPen^-$ combined (the relative contributions were not resolved). However, in that study relatively high concentrations of NH_3 and Cl^- were present due to the NH_4Cl/NH_4OH buffer used, and the copper ion complexes probably contained the smaller NH_3 and Cl^- ligands (6). In the present investigation of the reduction it has been assumed that $Cu(II)(PenS^-)_2$ is the only Cu(II) species of any significance, which is in accord with the results of the ESR study of Davis and co-workers (9).

This work appears to be the first study in which rates of reduction have been resolved in terms of the contributions of the RS and $RS.\therefore SR^-$ species.

It should be stressed that the occurrence of a direct reaction between $RS\cdot$ and $Cu(II)(PenS^-)_2$ was confirmed by the experiments performed at pH 12, where the contribution of the $RS.\therefore SR^-$ species was negligible. The reaction rate was first order in $RS\cdot$ and $Cu(II)(PenS^-)_2$ (see Fig. 4). These findings are consistent with reaction [3] as the rate controlling step and no significant role for [−3]. That conclusion

$$[-3] \qquad \mathbf{I} \rightarrow Cu(II)(PenS^-)_2 + PenS\cdot$$

can be rationalised by the large rate expected for the intra-complex electron transfer reaction [4]. Based on $E^0(Cu(II)L_2/(Cu(I)L_2) \sim 0.2$ V (27) and $E^0(RSSR/RS.\therefore SR^-) = -1.6$ V (7), the driving force of ~ 1.4 V ensures a rate in the region of $10^8\ s^{-1}$ over the short distance involved (28). Reaction [5] would then occur after the oxidation and could not effect the rate. However, it may be noted that ligand substitution reactions with Cu(I) species are normally very rapid (29).

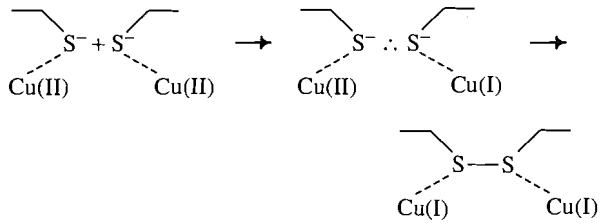
It may be noted that one of the *p* orbital lone pairs of the bound $PenS^-$ ligand would be tied up in coordination with the Cu(II), leaving only one pair available for the $PenS\cdot$ radical attacking in reaction [3]. Since $\sigma\sigma^*$ bonds are readily formed with sulphur species having only one lone pair (30), this should not prevent the formation of the "internal" $PenS.\therefore SPen^-$ complex. However, it may be expected to alter the rate of complexation, and this feature is reflected in the fact that k_3 $(= 3.4 \times 10^8\ M^{-1}\ s^{-1})$ is about 10 times smaller than k_1 $(= 3 \times 10^9\ M^{-1}\ s^{-1})$, the rate of complexation of $PenS\cdot$ radicals by free $PenS^-$ (11).

Quantitative analysis of the photostationary state has provided a second source of rate constant data and a means of ensuring that the rate constants for oxidation and reduction fit into a self-consistent framework. That this is the case is established by the agreement between the values of $(k_2\theta + k_3)$ from pulse radiolysis and analysis of the photostationary concentrations plotted in Fig. 3*b*. The corrected value of k_{17} $(= 2.7 \times 10^8\ M^{-1}\ s^{-1})$ is, as pointed out in the Results section, about 40% larger than the previously estimated upper limit (6). It is now more consistent with the value of the corresponding rate constant for the cysteine species.

The observations reported here provide further information relating to reaction pathways which may occur in the removal of thiyl radicals created in biological systems. They also have relevance to thermal chemical reactions in thiylate species. For example, the rate-controlling step in reaction [13] has been

Can. J. Chem. Downloaded from www.nrcresearchpress.com by 198.100.157.202 on 09/07/12
For personal use only.

shown to be a second order reaction between two $Cu(II)(RS^-)_x$ complex ions (9, 21). It has generally been assumed that they interact to produce two Cu(I) species and a disulphide (RSSR), which is a complex two-electron transfer process. We would suggest that $RS\therefore SR^-$ intermediates also be considered as possible transients in these systems, viz:

[24] 

The shared disulphide ligand would then be replaced by RS^-, as in reaction [5]. Reactions of this kind are also of possible interest in proteins with multiple copper–thiylate ligand sites.

Acknowledgments

One of us (D.A.A.) would like to acknowledge his appreciation to the University of Calgary for a sabbatical leave, and to the University of Notre Dame Radiation Laboratory and the University of Notre Dame for a Visiting Professorship for the period August 1989 through August 1990.

1. P. HEMMERICH and H. LAUTERWEIN. Inorganic biochemistry. Vols. 1 and 2. *Edited by* G. L. Eichhorn. Elsevier, Amsterdam. 1973. Chap. 32.
2. J. A. FEE. Struct. Bonding, **23**, 1 (1975).
3. J. H. R. KAGI, M. NORDBERG, and M. KASAK. Metallothionein, Experientia Suppl. **34**, Bikhauser, Basel (1979).
4. C. G. KUEHN and S. S. ISIED. Prog. Inorg. Chem. **27**, 153 (1980).
5. E. I. SOLOMON, J. W. HAVE, D. M. DOOLEY, J. H. DAWSON, P. J. STEPHENS, and H. B. GRAY. J. Am. Chem. Soc. **102**, 168 (1980).
6. S. P. MEZYK and D. A. ARMSTRONG. Can. J. Chem. **67**, 736 (1989).
7. D. A. ARMSTRONG. *In* Sulphur-centered reactive intermediates in chemistry and biology. NATO-ASI Series, Life Sciences. *Edited by* C. Chatgilialoglu and K.-D. Asmus. Plenum Press, London, New York. 1990.
8. E. W. WILSON and R. B. MARTIN. Arch. Biochem. Biophys. **142**, 445 (1971).
9. F. J. DAVIS, B. C. GILBERT, and R. O. C. NORMAN. J. Chem. Soc. Perkin Trans. **2**, 1763 (1983).
10. A.-D. LEU and D. A. ARMSTRONG. J. Phys. Chem. **90**, 1449 (1986).
11. M. Z. HOFFMAN and E. HAYON. J. Am. Chem. Soc. **94**, 7950 (1972); J. Phys. Chem. **77**, 990 (1973).
12. I. G. DRAGANIĆ and Z. D. DRAGANIĆ. The radiation chemistry of water. Academic Press, New York. 1971.
13. G. V. BUXTON. *In* Radiation chemistry: principles and applications. *Edited by* Farahataziz and M. A. Rodgers. V.C.H., New York. 1987. Chap. 10.
14. A. J. ELLIOT, F. WILKINSON, and D. A. ARMSTRONG. Int. J. Radiat. Biol. **38**, 1 (1980).
15. R. H. SCHULER, A. L. HARTZELL, and B. BEHAR. J. Phys. Chem. **85**, 192 (1981).
16. H. A. SCHWARZ and R. W. DODSON. J. Phys. Chem. **93**, 409 (1989).
17. P. S. SURDHAR, S. P. MEZYK, and D. A. ARMSTRONG. J. Phys. Chem. **93**, 3360 (1989).
18. J. W. PURDIE, H. A. GILLIS, and N. V. KLASSEN. Can. J. Chem. **51**, 3132 (1973).
19. J. P. BARTON, J. E. PACKER, and R. J. SIMS. J. Chem. Soc. Perkin Trans. II, 1547 (1973).
20. S. GOLDSTEIN and G. CZAPSKI. J. Am. Chem. Soc. **105**, 7276 (1983); Inorg. Chem. **24**, 1087 (1985).
21. A. G. LAPPIN and A. J. MCAULEY. J. Chem. Soc. Dalton Trans. 1606 (1978).
22. P. J. M. W. L. BIRKER and H. C. FREEMAN. J. Am. Chem. Soc. **99**, 6890 (1977); H. J. SCHUGAR, C. OU, J. A. THICK, J. A. POTENZA, R. A. LALANCETTE, and W. FINEY. J. Am. Chem. Soc. **98**, 3047 (1976).
23. P. NETA and R. W. FESSENDEN. J. Phys. Chem. **75**, 2277 (1971).
24. G. ADAMS, G. S. MCNAUGHTON, and B. D. MICHAEL. Trans. Faraday Soc. **64**, 902 (1968).
25. P. NETA, R. E. HUIE, and A. B. ROSS. J. Phys. Chem. Ref. Data, **17**, 1027 (1988).
26. M. FARAGGI and J. G. LEOPOLD. Radiat. Res. **65**, 238 (1976).
27. J. ALBERTY. Electrode kinetics. Clarendon, Oxford. 1975. p. 141.
28. R. A. MARCUS and N. SUTIN. Biochim. Biophys. Acta, **811**, 265 (1985).
29. A. G. LAPPIN, M. P. YOUNGBLOOD, and D. W. MARGERUM. Inorg. Chem. **19**, 407 (1980).
30. K.-D. ASMUS. *In* Sulphur-centered reactive intermediates in chemistry and biology. NATO-ASI Series, Life Sciences. *Edited by* C. Chatgilialoglu and K.-D. Asmus. Plenum Press, London, New York. 1990.

Can. J. Chem. Downloaded from www.nrcresearchpress.com by 198.100.157.202 on 09/07/12
For personal use only.

Redox reactions with ferrocene/ferricenium species of radicals derived by H atom abstraction from alcohols and diols

S. R. LOGAN

Department of Applied Physical Sciences, University of Ulster, Coleraine, N. Ireland, BT52 1SA

Received August 30, 1990

S. R. LOGAN. Can. J. Chem. **69**, 540 (1991).

The effect of various alcohols and diols in diminishing the extent of the photo-oxidation of 4-ferrocenylbutanoate ion in the presence of N_2O has been investigated. Where the hydroxyl radical generated in the photo-initiated electron transfer reacts with an alcohol by H atom abstraction at the α-position, the resulting radical is capable of reducing the ferricenium zwitterion to the ferrocenyl anion. Abstraction at other positions produces radicals that are essentially inert in this system and rate constants are derived for the reaction of OH with some such compounds. Non-vicinal diols behave similarly to the corresponding alcohols. With vicinal diols, a dehydration process, which occurs the more slowly the more highly substituted the diol, converts the radical -CR(OH)$\dot{C}$(OH)- into -$\dot{C}$RCO-, which is an oxidizing species. The behaviour of pinacol was found to be anomalous.

Key words: radical reactions, redox behaviour, alcohols.

S. R. LOGAN. Can. J. Chem. **69**, 540 (1991).

On a étudié l'habilité de divers alcools et diols à diminuer le taux de photo-oxydation de l'ion 4-ferrocénylbutanoate en présence de N_2O. Lorsque le radical hydroxyle généré lors du transfert de charge photo-initié réagit avec un alcool par l'enlèvement d'un atome de H en position α, le radical qui en résulte est capable de réduire le zwitterion ferricénium en anion ferrocényle. Des ablations à d'autres positions fournissent des radicaux qui sont essentiellement inertes dans ce système; on a aussi évalué les constantes de vitesse des réactions du OH avec quelques composés de ce type. Les diols qui ne sont pas vicinaux se comportent comme les alcools correspondants. Avec les diols vicinaux, il se produit une déshydratation d'autant plus lente que le diol est plus substitué; elle transforme le radical -CR(OH)$\dot{C}$(OH)- en -$\dot{C}$RCO- qui est une espèce oxydante. On a trouvé que le comportement du pinacol est anormal.

Mots clés : réactions radicalaires, comportement rédox, alcools.

[Traduit par la rédaction]

Introduction

Previously, the use of a photochemical technique was demonstrated (1) for measuring the rate of attack of the hydroxyl radical on an organic solute and the redox behaviour of the resulting radical towards the ferrocene/ferricenium system. The technique is appropriate to any group of water-soluble compounds provided that they are transparent in the relevant range of UV wavelengths.

Since the early work using the Fenton system (2, 3), several studies of the reaction of the hydroxyl radical with alcohols have been carried out. Some (4–6) have used flow systems and ESR spectroscopy to identify the radicals or mixture of radicals formed. Others have been primarily concerned (7–11) with the rate constant for OH attack and these mostly used a pulse radiolysis technique, employing the effect of an added alcohol in reducing the fraction of OH radicals reacting with another solute, where such reaction led to an easily measured intermediate. Since in most cases the observed intermediate is not the original product of the reaction of OH with this solute, but may be formed from the original product in a subsequent reaction, it is desirable that these rate constants be checked by a different method, as it has been shown (12) that such methods are occasionally liable to error.

There have been various other radiation chemical studies focussing on the identity and behaviour of the radicals formed (13–18) by hydroxyl radical attack on alcohols and diols. The present study, using a photochemical technique, is intended to complement these.

The initial photochemical events were established in earlier work (19, 20). The photo-excitation of the ferrocenyl moiety leading to electron transfer to N_2O may be summarized in eq. [1].

[1] $$Fc(CH_2)_3CO_2^- + N_2O \xrightarrow{h\nu} \overset{+}{F}\dot{c}(CH_2)_3CO_2^- + N_2 + O^- (\xrightarrow{H^+} OH)$$

In the presence of a solute RH, the hydroxyl radical formed in reaction [1] may react by either of the following reactions:

[2] $$OH + Fc(CH_2)_3CO_2^- \rightarrow OH^- + \overset{+}{F}\dot{c}(CH_2)_3CO_2^-$$

[3] $$OH + RH \rightarrow H_2O + R$$

Where the solute is an alcohol, the radical formed by OH radical attack at the α-position is usually a reducing species (20), for example:

[4] $$OH + CH_3CH_2OH \rightarrow H_2O + CH_3\dot{C}HOH \text{ (predominantly)}$$

[5] $$CH_3\dot{C}HOH + \overset{+}{F}\dot{c}(CH_2)_3CO_2^- \rightarrow CH_3CHO + H^+ + Fc(CH_2)_3CO_2^-$$

If OH attack on the alcohol were exclusively at the α-position and reaction [5] were fully efficient, then all the ferricenium zwitterions formed in reaction [1] could be reduced back to the ferrocenyl anion at high concentrations of the alcohol.

If, on the other hand, hydroxyl attack on the alcohol were to produce inert radicals (for example, from a tertiary alcohol), then there would be no process corresponding to reaction [5], so the quantum yield of the ferricenium species, denoted by Φ (Fc^+) would be equal to Φ_p, the quantum yield of step [1].

Experimental

4-Ferrocenylbutanoic acid was prepared as previously described (19). The alcohols and diols were BDH Analar or Aldrich 99% or Gold Label grades and were used as supplied. Doubly distilled water was used in the preparation of solutions and in rinsing the apparatus. Solutions were made up in 10^{-2} mol dm^{-3} borax to maintain pH 9.

Printed in Canada / Imprimé au Canada

Can. J. Chem. Downloaded from www.nrcresearchpress.com by 195.138.81.100 on 09/07/12
For personal use only.

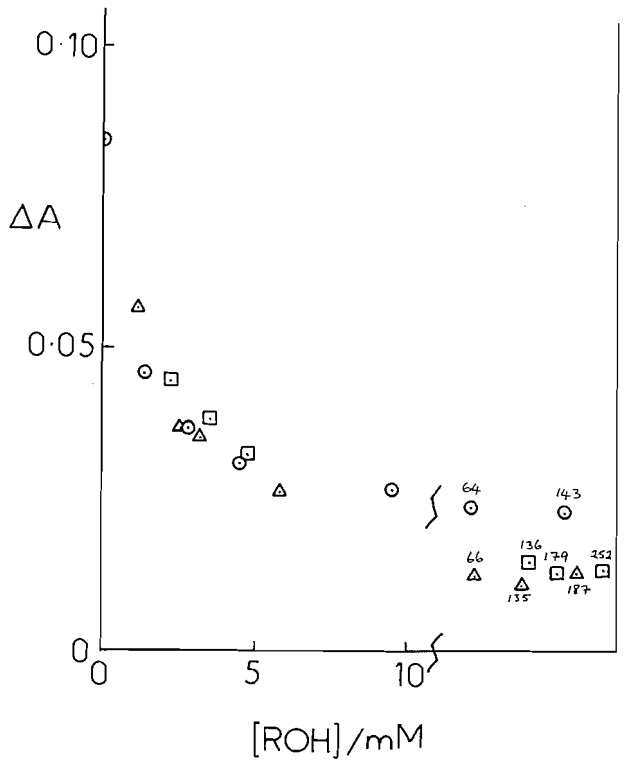


FIG. 1. Absorbance change at 625 nm caused by a flash of 442 J energy as a function of the concentration of added alcohols. The solution contained 2.5×10^{-4} M 4-ferrocenylbutanoate in 0.01 M borax with 0.023 M nitrous oxide: ⊙ 1-propanol; △ 2-propanol; ⊡ 2-propanol-d_1. For the points to the right of the barrier, the number indicates the value of the abscissa.

Since the ferrocenyl anion undergoes slow oxidation from dissolved oxygen, solutions were freshly made up every two days.

After a sample had been degassed by four cycles of freeze–pump–thaw, it was equilibrated with N_2O at a pressure of 85 kPa to give a concentration (21) of 0.023 mol dm^{-3}. The cells and the flash photolysis apparatus have been previously described (22). With the filter compartment filled with distilled water, the cell was mounted in position and the absorbance change at 625 nm (the position of maximum absorbance of the ferricenium zwitterion) caused by the discharge of 442 J through the flash tubes was monitored.

Results and discussion

When 1-propanol was added to the samples of 4-ferrocenylbutanoic acid in borax buffer at pH 9, saturated with N_2O, the absorbance change at 625 nm produced by a 442 J flash was found to decrease, as shown in Fig. 1. However, the plateau achieved at high concentrations corresponds to 0.27 of the original absorbance, in the absence of any added solute that might compete with 4-ferrocenylbutanoate ion for the hydroxyl radical produced (19) concomitantly with photoinduced electron transfer from the anion to N_2O. Thus not all the radicals formed by attack of OH on this alcohol cause reduction of the ferricenium species, Fc^+, that is generated in the photoinduced electron transfer, step [1].

It was initially attempted to treat these results on the basis that the reaction of OH with 1-propanol produces two types of radicals, where the first reduces the ferricenium zwitterion and the second does not. The species concerned are presumably $CH_3CH_2\dot{C}HOH$ and, secondly, a combination of $CH_3\dot{C}HCH_2OH$ and $\dot{C}H_2CH_2CH_2OH$, mainly the former. If one were to assume the formation of these two types to the relative extents of f and $(1 - f)$, then the quantum yield of the ferricenium species can be expressed as follows:

$$[6]\quad \Phi(Fc^+) = \Phi_p\left\{1 + \frac{k_2[Fc]}{k_2[Fc] + k_3[RH]} - \frac{fk_3[RH]}{k_2[Fc] + k_3[RH]}\right\} = \Phi_p\left\{(1 - f) + \frac{(1 + f)k_2[Fc]}{k_2[Fc] + k_3[RH]}\right\}$$

This implies that the addition of RH will cause Φ (Fc^+) to fall as [RH] is increased, levelling out at $(1 - f)\Phi_p$.

However, using the data from the studies of 1-propanol, it would appear as if the fraction f has the value 0.46, whereas earlier work (7, 15, 16) put the yield of the radical $CH_3CH_2\dot{C}HOH$ at around 0.6 of the total. Furthermore, the correspondence between eq. [6] and these 1-propanol data was tested using the relevant reciprocal plot, pertaining to eq. [7].

$$[7]\quad \frac{1}{\Phi(Fc^+) - (1 - f)\Phi_p} = \frac{1}{(1 + f)\Phi_p}\left\{1 + \frac{k_3[RH]}{k_2[Fc]}\right\}$$

The plot did not deviate from linearity but the ratio of slope to intercept gave a value for k_3 well in excess of the literature value of 2.8×10^9 dm^3 mol^{-1} s^{-1} (23).

The resolution of these anomalies was found from the following hypothesis. If only one radical species were produced and it were capable of reducing Fc^+ but with a sufficiently low rate constant for the reaction equivalent to step [5] that other processes such as combination or disproportionation could compete, eq. [6] would still be applicable with f representing the fraction of all radicals that actually do react in this manner. However, it is not to be expected that f would be independent of RH concentration, in that a much greater efficiency of the redox reaction is to be expected at low RH concentrations, where far fewer radicals R· are produced than ferricenium zwitterions, than at high RH concentrations, where the two species are generated in comparable amounts. So if fortuitously the reciprocal plot gives a straight line, deductions from the ratio of slope to intercept using eq. [7] could be quite erroneous since the factor $(1 - f)$ would not be a constant over the range of RH concentrations.

Previous work (1) on this system supports this hypothesis. While the strongly reducing radical $CO_2^{\cdot-}$ reduces Fc^+ with 100% efficiency, even though the rate constant for its dimerization is quite high (24), other reducing radicals such as $CH_3\dot{C}(OH)CO_2^-$ and $\dot{C}H(OH)CO_2^-$ reacted more slowly (1) with Fc^+. Clearly in this system high efficiency in reducing Fc^+ requires that the redox reaction is virtually diffusion controlled. Where the rate constant for this reduction process is substantially less, inter-radical reactions of R· can compete against reaction [5] and the proportion so doing increases with the size of the pool of radicals R·, which increases with RH concentration. Thus with 1-propanol the proposal is that, at high concentrations, of the major radical formed, $CH_3CH_2\dot{C}HOH$, only about three-quarters engage in reducing the ferricenium zwitterion. As the other radicals are inert, the fraction reacting in this way constitute 0.46 of all those formed.

In Fig. 1 there is also shown the effect on ΔA of the addition of 2-propanol. This causes a decrease, eventually to 0.16 of the initial value. Previous studies (4, 5, 13, 14, 16, 18) have

Can. J. Chem. Downloaded from www.nrcresearchpress.com by 195.138.81.100 on 09/07/12
For personal use only.

Can. J. Chem. Downloaded from www.nrcresearchpress.com by 195.138.81.100 on 09/07/12
For personal use only.

TABLE 1. Summary of the plateau values of the absorbance change, ΔA_∞, and of the limiting fractions, f, of the radicals produced by OH attack which actually cause reduction of Fc^+ to Fc, for various alcohols and non-vicinal diols

Alcohol/diol	$\frac{\Delta A_\infty}{\Delta A_0} = \frac{1-f}{2}$	f
1-Propanol	0.27 (±0.02)	0.46 (±0.04)
2-Propanol	0.15	0.70
2-Propanol-d_1	0.16	0.68
2-Butanol	0.26	0.48
2-Methylpropan-1-ol	0.24	0.52
2,2-Dimethylpropan-1-ol	0.28	0.44
2-Methylbutan-3-ol	0.28	0.44
Propane-1,3-diol	0.12	0.76
Hexane-2,5-diol	0.15	0.70
Pentaerythritol	0.02	0.96

shown that hydroxyl radical attack produces mainly the radical $CH_3\dot{C}(OH)CH_3$. Obviously this radical, which is readily oxidized to acetone, does not reduce Fc^+ with a sufficiently high rate constant to avert inter-radical reactions. Studies with the partially deuterated alcohol, $CH_3CD(OH)CH_3$, show that this compound causes a more gradual decrease in ΔA to the same limiting value. These support the earlier conclusions regarding the point of attack and imply that the kinetic isotope effect $k_H/k_D = 1.27 \pm 0.1$. Thus on the basis of the recommended value (23) of 1.9×10^9 dm^3 mol^{-1} s^{-1} for the reaction of OH with 2-propanol, the rate constant for OH + $CH_3CD(OH)CH_3$ is 1.5×10^9 dm^3 mol^{-1} s^{-1}.

The effect of the addition of other alcohols to this system was found to follow the general pattern shown in Fig. 1. However, the position of the final plateau value varied from one compound to another as shown in Table 1, in which in the last column is shown the value of f, the fraction of the radicals (produced by OH attack on the alcohol) that actually cause reduction of Fc^+ to Fc. These values for f pertain to the experimental conditions of the present work.

In the case of 2-butanol, there is evidence (15) that OH attack produces the radicals $CH_3CH_2\dot{C}(OH)CH_3$ and $CH_3\dot{C}HCH(OH)CH_3$, with the former much the more abundant. The f value of 0.52 is consistent with fairly efficient reduction of Fc^+ by this radical. From previous ESR (5) and other (13–15) studies of 2-methylpropan-1-ol, the predominant product radical from OH abstraction is $(CH_3)_2CH\dot{C}HOH$. From the low f value of 0.52, it is apparent that this is a rather inefficient reducing agent. From 2,2-dimethylpropan-1-ol, the expected radical is $(CH_3)_3C\dot{C}HOH$, exclusively. Since f is only 0.44, this also must be an inefficient reducing agent. From 2-methylbutan-3-ol, the product radicals expected are $(CH_3)_2CH\dot{C}(OH)CH_3$ and $(CH_3)_2\dot{C}CH(OH)CH_3$, with the former the more abundant. Since the second radical would be inert in this system, the f value of 0.44 suggests that not all the radicals of the former type are effective in causing reduction.

In Fig. 2 are shown the effects on ΔA of the addition of three tertiary alcohols. With abstraction at the α-position ruled out, it might be anticipated that all will give rise to inert radicals. Addition of *tert*-butanol caused a decrease to 0.54 of the initial ΔA. This slight deviation from one-half may reflect the formation, in addition to the radical $\dot{C}H_2C(CH_3)_2OH$, of a small

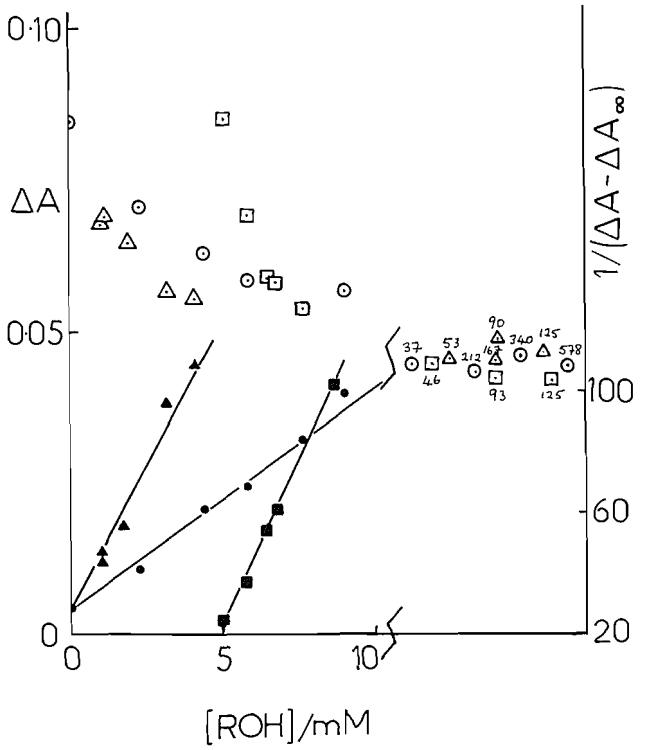


FIG. 2. Absorbance change at 625 nm caused by a flash of 442 J energy as a function of the concentration of added alcohols: ⊙ *tert*-butanol; △ *tert*-amyl alcohol; ⊡ 2,3-dimethylbutan-2-ol. Also (r.h. scale and filled symbols), plots of $(\Delta A - \Delta A_\infty)^{-1}$ against ROH concentration as a test of eq. [7], with $f = 0$.

amount of the radical (16) $(CH_3)_3CO^\bullet$, which is an oxidizing agent. The finding that 2-methylbutan-2-ol lowers ΔA only to 0.54 of its initial value is surprising, since one may anticipate less rather than more abstraction from the hydroxy group, with the radical $CH_3\dot{C}HC(CH_3)_2OH$ predominating.

On addition of 2,3-dimethylbutan-2-ol, it was found that after the flash, the absorbance change decreased over the following ca. 2 ms. The value recorded at the end of the flash was found, at high concentrations, to fall to 0.49 of its original value, consistent with the reaction of the OH radical producing predominantly the radical $(CH_3)_2\dot{C}C(CH_3)_2OH$. The subsequent decrease may then be attributed to a further reaction of some proportion of these radicals.

For these tertiary alcohols, which lead to radicals that do not contain the feature -$\dot{C}$(OH)-, it is possible to apply eqs. [6] and [7] to the value of ΔA found at the end of the flash. On this basis, the relative rate constant k_3/k_2 was determined for each alcohol, and using, as previously (1), the value (12) of 1.09×10^{10} dm^3 mol^{-1} s^{-1} for k_2, the rate constant for the reaction of the hydroxyl radical with the ferrocenyl anion, the rate constants for the reaction of OH with these alcohols were found to be, for *tert*-butanol, 7.6×10^8; 2-methylbutan-2-ol, 1.8×10^9 and 2,3-dimethylbutan-2-ol, 2.4×10^9 dm^3 mol^{-1} s^{-1}. The first two lie within the range of previous determinations (23); for the third, no value is listed in this compilation.

In Fig. 3 are shown the effects on ΔA of the addition of some diols. Ethane-1,2-diol causes a decrease to only 0.82 of the initial value, indicating that the radical resulting from OH attack behaves as an oxidizing agent. This reaction has been intensively studied (4, 15, 16, 18) and it is known that the

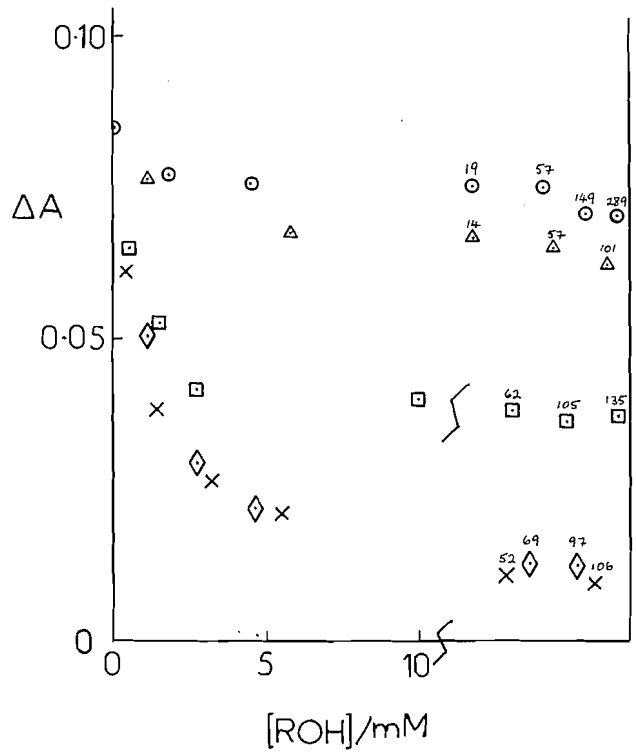


FIG. 3. Absorbance change at 625 nm caused by a flash of 442 J energy as a function of the concentration of added diols: ⊙ ethane-1,2-diol; △ propane-1,2-diol; ⊡ butane-2,3-diol; × propane-1,3-diol; ◇ hexane-2,5-diol.

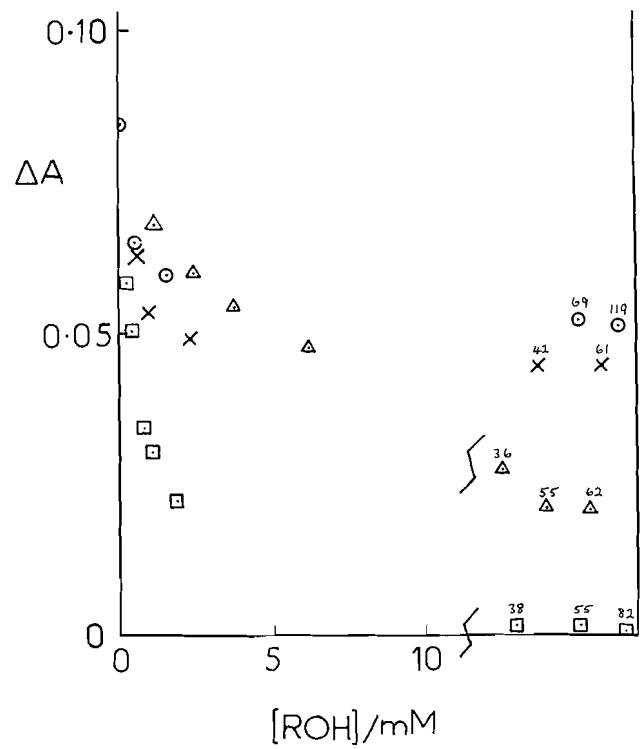


FIG. 4. Absorbance change at 625 nm caused by a flash of 442 J energy as a function of the concentration of added hydroxy compounds: ⊙ glycerol; ⊡ pentaerythritol; × erythritol; △ pinacol.

radical $\dot{C}H(OH)CH_2OH$ initially formed readily dehydrates to $\dot{C}H_2CHO$. In the present system this latter radical oxidizes Fc to Fc^+ at pH 9 with appreciable efficiency.

When propane-1,2-diol, a growth in absorbance was found over a period of ca. 0.5 ms after the flash, with the final figure, at high concentrations, being 0.75 of that found initially. From ESR studies (6), it is known that the hydroxyl radical abstracts chiefly from the middle carbon to give the radical $CH_3\dot{C}(OH)CH_2OH$, with a lesser amount of $\dot{C}H(OH)CH(OH)CH_3$ and a very small yield of $\dot{C}H_2CH(OH)CH_2OH$, which will be inert in this system. Dehydration of the first two radicals yields oxidizing species. The rise in absorbance on the millisecond time scale reflects the slowness of the dehydration of these radicals.

With butane-2,3-diol, a similar increase in absorbance was found over a period of 1–2 ms. At high concentrations, the final absorbance change corresponded to 0.43 of the initial value, which means that the radicals formed are causing net reduction rather than oxidation, but the rise on the ms time scale shows that oxidation is occurring in these later stages. There is ESR evidence (6) that the reaction of OH produces $CH_3\dot{C}(OH)CH(OH)CH_3$ and $CH_3\dot{C}HCOCH_3$, where the latter radical results from the dehydration of the former. But this dehydration process must be sufficiently slow to allow some radicals $CH_3\dot{C}(OH)CH(OH)CH_3$ to engage in reduction of Fc^+. Slow dehydration of the first radical produces the second, which is an oxidizing species whose reaction with Fc is apparent on the millisecond time scale.

On the basis of the reactions of the resulting radicals with tetranitromethane, it has been estimated (16) that OH attack at the methyl group may account for 29% of the total reaction with this diol. The radical $\dot{C}H_2CH(OH)CH(OH)CH_3$, which should be quite inert in the present system, was, however, not detected (6) by ESR, and it might seem surprising that it could be such a significant product. However, the rate constant for OH attack on the six methyl hydrogens of this diol may be estimated from its known rates of reaction (23) with *tert*-butanol and pinacol. On this basis and the quoted overall rate constant (23) of 1.3×10^9 dm^3 mol^{-1} s^{-1}, the figure of 29% would seem quite probable. Moreover, the quoted rate constant (23) for the reaction of OH with this diol is less than that (23) with 2-butanol, which supports the view (1) that H atom abstraction from the grouping $-CH(OH)CH_2-$ is actually impeded by the insertion of another hydroxy group to give $-CH(OH)CH(OH)-$.

Addition of propane-1,3-diol and hexane-2,5-diol causes ΔA to be diminished respectively to 0.12 and 0.15 of the original value. The predominant radicals are expected to be $\dot{C}H(OH)CH_2CH_2OH$ and $CH_3\dot{C}(OH)CH_2CH_2CH(OH)CH_3$, which should behave, respectively, like those from a primary alcohol and from 2-butanol. These non-vicinal diols clearly resemble comparable alcohols.

The effect of other hydroxy compounds on ΔA is shown in Fig. 4. The behaviour of glycerol is similar to that of ethane-1,2-diol, except that less oxidation is caused by the radicals resulting from OH attack. This is consistent with the slower (25) acid-catalysed dehydration of the radicals $CH_2(OH)\dot{C}(OH)CH_2OH$ and $\dot{C}H(OH)CH(OH)CH_2OH$ as compared to $\dot{C}H(OH)CH_2OH$, but not with the reports (26) of faster hydroxide-catalysed dehydration. Erythritol shows similar behaviour.

The addition of pentaerythritol causes ΔA to decrease to 0.02 of its original value. On this molecule, OH attack will produce the radical $(HOCH_2)_3C\dot{C}HOH$, which is apparently

Can. J. Chem. Downloaded from www.nrcresearchpress.com by 195.138.81.100 on 09/07/12
For personal use only.

more efficient in reducing Fc^+ than is $(CH_3)_3C\dot{C}HOH$, the radical formed from neopentyl alcohol. From the manner in which ΔA is decreased, the rate constant for OH reaction is estimated as $4.4 \times 10^9\ dm^3\ mol^{-1}\ s^{-1}$, which is slightly higher than the previous value (23).

Pinacol causes a decrease in ΔA, eventually to 0.23 of the original value. This may seem surprising since the ESR evidence is consistent with the radical formed by OH attack being mostly $\dot{C}H_2C(CH_3)(OH)C(OH)(CH_3)_2$, which should be inert. However, recognizing that the presence of alkyl hydrogens only in methyl groups renders the hydroxyl hydrogen more liable to attack, one product of OH attack should be the radical $(CH_3)_2C(OH)C(CH_3)_2O\cdot$. While alkoxy radicals generally are oxidizing agents, this one is unusual since it readily fragments to give acetone and the reducing radical, $CH_3\dot{C}(OH)CH_3$. However, while such a reaction could account for the decrease in ΔA to less than half its original value, it is difficult to see how it can lead to the final ratio being as small as 0.23. Assuming that the relative rates of reaction of OH with individual methyl and hydroxyl hydrogens are the same in *tert*-butanol and pinacol, and accepting the figure (16) for the former of 4.3% reaction at the hydroxyl, one estimates only a 6.3% yield of this reducing radical from pinacol. This cannot suffice to account for the results obtained.

For all compounds studied, in at least one experiment, after the solution had been flashed as described above, air was allowed into the vessel and the solution was equilibrated with it to give an oxygen concentration of the order of $3 \times 10^{-5}\ mol\ dm^{-3}$. Since this procedure made no difference when no alcohol or diol was present it would seem that any effect in their presence must be due to reactions of O_2 with the radicals formed by OH attack. With all these compounds, except one, the addition of O_2 caused a perceptible growth in absorbance over the few milliseconds after a further flash, consistent with the reaction of the radical with O_2, followed by slow oxidation of the ferrocenyl anion by this peroxy radical. The exception was ethan-1,2-diol, where an oxidizing radical is already formed in the absence of O_2. With propan-1,2-diol a slight rise was observed, of about the same size as was found in the absence of O_2.

Conclusion

These studies show that the radicals formed by H atom abstraction at the α-position from primary or secondary alcohols are not as efficient reducing agents of the ferricenium zwitterion as the corresponding radicals from α-hydroxyacids (1). Thus while the radical $CH_3\dot{C}(OH)CO_2^-$ manages to reduce an equal amount of Fc^+ within 0.5 ms (1), $CH_3\dot{C}(OH)CH_3$ is not correspondingly effective. The behaviour of the tertiary alcohols resembles that of the alkanoates and alkandioates (1) and the data permit the derivation of the rate constant for OH attack.

1. S. R. Logan. J. Chem. Soc. Perkin Trans. 2, 751 (1989).
2. J. H. Merz and W. A. Waters. Discuss. Faraday Soc. **2**, 179 (1947).
3. C. Walling. Acc. Chem. Res. **8**, 125 (1975).
4. R. Livingston and H. Zeldes. J. Am. Chem. Soc. **88**, 4333 (1966).
5. W. T. Dixon and R. O. C. Norman. J. Chem. Soc. 3119 (1963).
6. B. C. Gilbert, J. P. Larkin, and R. O. C. Norman. J. Chem. Soc. Perkin Trans. 2, 794 (1972).
7. K.-D. Asmus, A. Wigger, and A. Henglein. Ber. Bunsen-ges Phys. Chem. **70**, 862 (1966).
8. M. Anbar, D. Meyerstein, and P. Neta. J. Chem. Soc. B: 742 (1966).
9. G. E. Adams, J. W. Boag, and B. D. Michael. Trans. Faraday Soc. **61**, 1417 (1965).
10. C. Walling, G.-M. El-Taliawi, and R. A. Johnston. J. Am. Chem. Soc. **93**, 4275 (1971); **96**, 133 (1974).
11. R. L. Willson, C. L. Greenstock, G. E. Adams, R. Wageman, and L. M. Dorfman. Int. J. Radiat. Phys. Chem. **3**, 211 (1971).
12. S. R. Logan and G. A. Salmon. Radiat. Phys. Chem. **24**, 593 (1984).
13. K.-D. Asmus, A. Henglein, A. Wigger, and G. Beck. Ber. Bunsen-ges. Phys. Chem. **70**, 756 (1966).
14. M. Simic, P. Neta, and E. Hayon. J. Phys. Chem. **73**, 3794 (1969).
15. G. E. Adams and R. L. Willson. Trans. Faraday Soc. **65**, 2981 (1969).
16. K.-D. Asmus, H. Möckel, and A. Henglein. J. Phys. Chem. **77**, 1218 (1973).
17. K. M. Bansal, M. Grätzel, A. Henglein, and E. Janata. J. Phys. Chem. **77**, 16 (1973).
18. M. S. Akhlaq, S. Al-Baghdadi, and C. von Sonntag. Carbohydr. Res. **164**, 71 (1987).
19. E. K. Heaney and S. R. Logan. J. Chem. Soc. Perkin Trans. 2, 1353 (1977).
20. W. P. Armstrong and S. R. Logan. J. Photochem. **22**, 157 (1983).
21. E. Janata and R. H. Schuler. J. Phys. Chem. **86**, 2078 (1982).
22. E. K. Heaney, S. R. Logan, and J. A. Powell. J. Chem. Soc. Faraday Trans. 1, **73**, 669 (1977).
23. G. V. Buxton, C. L. Greenstock, W. P. Helman, and A. B. Ross. J. Phys. Chem. Ref. Data, **17**, 513 (1983).
24. G. V. Buxton and R. M. Sellars. J. Chem. Soc. Faraday Trans. 1, **69**, 555 (1973).
25. S. Steenken, M. J. Davies, and B. C. Gilbert. J. Chem. Soc. Perkin Trans. 2, 1003 (1986).
26. S. Steenken. J. Phys. Chem. **83**, 595 (1979).

Can. J. Chem. Downloaded from www.nrcresearchpress.com by 195.138.81.100 on 09/07/12
For personal use only.

Structural studies of organoboron compounds. XLIII.[1] 4-[(1-Hydroxycyclohexyl)methyl]-2,2,5-triphenyl-1,3-dioxa-4-azonia-2-borata-4-cyclopentene

WOLFGANG KLIEGEL, UTE SCHUMACHER, AND MAHMOOD TAJERBASHI

Institut für Pharmazeutische Chemie der Technischen Universität Brauschweig, Beethovenstrasse 55, 3300 Braunschweig, Bundesrepublik Deutschland

AND

STEVEN J. RETTIG AND JAMES TROTTER

Department of Chemistry, University of British Columbia, 2036 Main Mall, Vancouver, B.C. Canada V6T 1Z1

Received July 10, 1990

WOLFGANG KLIEGEL, UTE SCHUMACHER, MAHMOOD TAJERBASHI, STEVEN J. RETTIG, and JAMES TROTTER. Can. J. Chem. **69**, 545 (1991).

The reaction of *N'*-hydroxy-*N*-[(1-hydroxycyclohexyl)methyl]benzamide and diphenylborinic anhydride gives 4-[(1-hydroxycyclohexyl)methyl]-2,2,5-triphenyl-1,3-dioxa-4-azonia-2-borata-4-cyclopentene in nearly quantitative yield. Crystals of the product are monoclinic, $a = 9.9117(6)$, $b = 13.308(1)$, $c = 17.339(2)$ Å, $\beta = 99.420(7)°$, $Z = 4$, space group $P2_1/c$. The structure was solved by direct methods and was refined by full-matrix least-squares procedures to $R = 0.040$ and $R_w = 0.047$ for 2423 reflections with $I \geq 3\sigma(I)$. The molecule has a normal five-membered hydroxamic acid chelate structure, the BONCO ring having a *B*-envelope conformation. Bond lengths (corrected for libration) (N)O—B = 1.535(3), (C)O—B = 1.569(3), C—B = 1.603(3) and 1.601(3) Å are normal for this type of complex.

Key words: organoboron compound, boron compound, crystal structure.

WOLFGANG KLIEGEL, UTE SCHUMACHER, MAHMOOD TAJERBASHI, STEVEN J. RETTIG et JAMES TROTTER. Can. J. Chem. **69**, 545 (1991).

La réaction du *N'*-hydroxy-*N*-[(1-hydroxycyclohexyl)méthyl]benzamide et de l'anhydride de l'acide diphénylborinique conduit au 4-[(1-hydroxycyclohexyl)méthyl]-2,2,5-triphényl-1,3-dioxa-4-azonia-2-boratacyclopent-4-ène; le rendement est pratiquement quantitatif. Les cristaux de ce produit sont monocliniques, groupe d'espace $P2_1/c$, avec $a = 9,9117(6)$, $b = 13,308(1)$ et $c = 17,339(2)$Å, $\beta = 99,420(7)°$ et $Z = 4$. On a déterminé la structure par des méthodes directes et on l'a affinée par la méthode des moindres carrés (matrice complète) jusqu'à des valeurs respectives de $R = 0,040$ et $R_w = 0,047$; 2423 réflexions avec $I \geq 3\sigma(I)$. La molécule existe dans une structure normale, avec un acide hydroxamique chelate à cinq chainons; le cycle BONCO existe dans la conformation *B*-enveloppe. Les longueurs des liaisons (corrigées pour la libration): (N)O—B = 1,535(3), (C)O—B = 1,569(3), C—B = 1,603(3) et 1,601(3)Å, sont normales pour ce type de complexe.

Mots clés : composé organoborique, composé du bore, structure cristalline.

[Traduit par la rédaction]

Introduction

In a previous attempt to synthesize the five-membered diphenylboron chelate **2** by reaction of the *N*-(2-hydroxyalkyl)salicylohydroxamic acid **1** (R = OH) with the anhydride of diphenylborinic acid we obtained the seven-membered chelate **3**, the structure of which has been determined by X-ray crystallography (1). One of the donor moieties of the bidentate ligand in **3** is a 2-oxazoline *N*-oxide group resulting from an intramolecular condensation reaction that converts the *N*-(2-hydroxyalkyl)hydroxamic acid function into the heterocyclic *N*-oxide. The second donor group in **3** is the phenolate residue.

In order to obtain more information about the reactivity and chelating properties of polyfunctional hydroxamic acids of the type **1**, we synthesized the benzohydroxamic acid **1** (R = H), omitting the phenolic hydroxyl group. The remaining functional groups of **1** (R = H) would still allow cyclocondensation under the influence of the Lewis acid diphenylborinic anhydride leading to the 2-oxazoline *N*-oxide derivative **5**. This parallels the formation of **3**, the difference being that chelate formation involving the phenolic oxygen atom of **3** is not possible with compound **1** (R = H). The reaction of **1** (R = H) with the anhydride $(Ph_2B)_2O$ gave a nearly quantitative yield of a crystalline product with an elemental analysis consistent with the isomers **4**–**7**. Rechelatization of the product with diphenylcarbazone showed an intact diphenylboron moiety in the typical blue color reaction (2). By ^{1}H nmr spectroscopy three phenyl groups could be identified, as well as a single methylene group, a pentamethylene group, and one exchangeable OH proton. Neither the nmr spectrum nor the infrared spectrum (the latter with a distinct C=O/C=N band at 1595 cm^{-1}) allowed a definite assignment of the diphenylboron hydroxamate structure **4**, although the chemical shift of the OH proton signal at δ = 2.68 ppm (in $CDCl_3$) or 4.87 ppm (in d_6-dmso) is suggestive of an alcoholic hydroxyl function. Nevertheless, the isomeric structure **5**, an open-chain complex of diphenylborinic acid with the 2-oxazoline *N*-oxide corresponding to the cyclic derivative **3**, has to be considered. The structure **5** would represent another example of the type of *N*-oxide boron complex recently characterized for the analogous BF_3 adduct (3). Less probable, but not ruled out on the basis of spectroscopic data, are both the six-membered and seven-membered diphenylboron chelates **6** and **7**, respectively. Structure **6** would involve the *N*-hydroxy and the alkanol groups as chelating ligands, and in structure **7** the carbonyl and alkanol oxygen atoms would be available as donors. An X-ray crystallographic analysis has been undertaken in order to make a definitive structural assignment.

Experimental

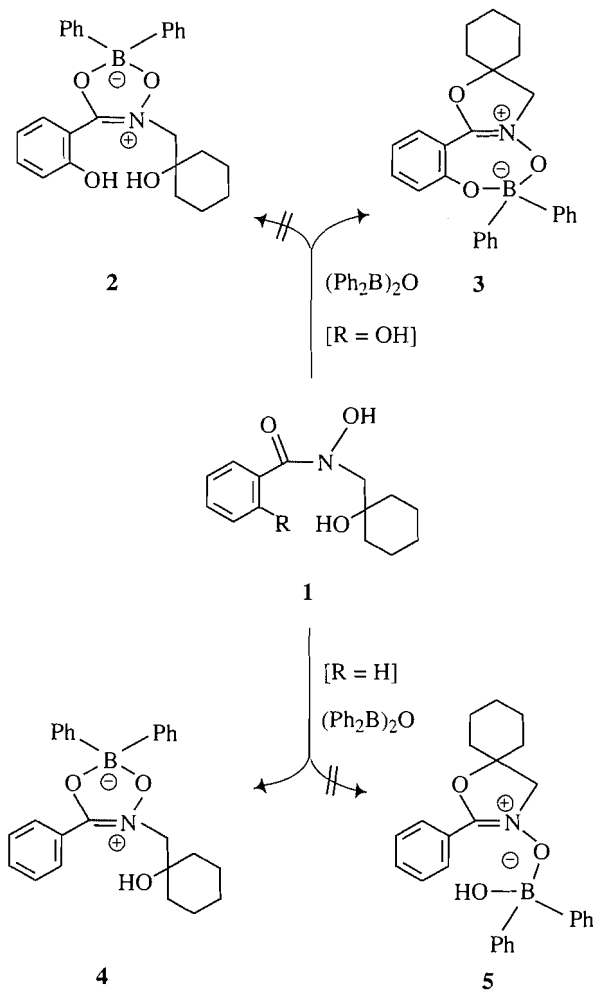
N-Hydroxy-N-[(1-hydroxycyclohexyl)methyl]benzamide, 1 (R = H)

Benzoylchloride (2.81 g, 20 mmol) is diluted in 30 mL dry tetrahy-

[1]Previous paper in this series: ref. 17.

Can. J. Chem. Downloaded from www.nrcresearchpress.com by 195.138.81.100 on 09/07/12
For personal use only.

Can. J. Chem. Downloaded from www.nrcresearchpress.com by 195.138.81.100 on 09/07/12
For personal use only.



drofuran and added dropwise to a solution of 1-(hydroxylamino)cyclohexanol (4) (2.90 g, 20 mmol) and triethylamine (20 mmol in 100 mL dry tetrahydrofuran) at −15°C, with continuous stirring. After stirring for 12 h at room temperature, the solvent is removed *in vacuo*, and the residue is dissolved in 100 mL of 2N NaOH. The alkaline aqueous solution is extracted twice with 100 mL diethylether and is acidified with HCl. The acid solution is extracted with 5 × 100 mL diethylether, and the combined extracts (from the acid solution) are dried over Na_2SO_4. Evaporation of the ether yields 3.51 g (70%) of colorless crystals, mp 124–125°C (from diethylether). *Anal.* calcd for $C_{14}H_{19}NO_3$: C 67.45, H 7.68, N 5.62; found: C 67.35, H 7.69, N 5.56. Infrared (KBr): 3385 and 3140 (broad, O—H), 1630 cm^{-1} (C=O). ^1H nmr (90 MHz): (*a*) ($CDCl_3$/TMS): δ (ppm) = 0.90–1.87 (m, —$(CH_2)_5$—), 3.70 (s, N—CH_2), 7.13–7.67 (m, C_6H_5); (*b*) (d_6-dmso/TMS): δ (ppm) = 0.95–1.85 (m, —$(CH_2)_5$—), 3.67 (s, N—CH_2), 4.27 (s, broad, exchangeable, C—OH), 7.25–7.73 (m, C_6H_5), 9.65 (s, broad, exchangeable, N—OH).

4-[(1-Hydroxycyclohexyl)methyl]-2,2,5-triphenyl-1,3-dioxa-4-azonia-2-borata-4-cyclopentene, 4

1 (R = H; 0.50 g, 2 mmol) and oxybis(diphenylborane) (0.35 g, 1 mmol) are dissolved in a small quantity of ethanol with slight heating. The solution is cooled down until crystallization starts. Yield: 0.63 g (76%), mp 124–126°C (from ethanol). *Anal.* calcd. for $C_{26}H_{28}BNO_3$: C 75.55, H 6.83, B 2.62, N 3.39; found: C 75.35, H 6.88, B 2.61, N 3.39. Infrared (KBr): 3590 (sharp) and 3540 (broad, O—H), 1595 cm^{-1} (C=O/C=N). ^1H nmr (90 MHz): (*a*) ($CDCl_3$/TMS): δ (ppm) = 1.00–1.80 (m, —$(CH_2)_5$—), 2.68 (s, exchangeable, OH), 3.80 (s, N—CH_2), 7.0–7.8 (m, 3 C_6H_5); (*b*) (d_6-dmso/TMS): δ (ppm) = 1.10–1.80 (m, —$(CH_2)_5$—), 3.87 (s, N—CH_2), 4.87 (s, exchangeable, OH), 7.0–8.1 (m, 3 C_6H_5). The substance gives a blue color reaction with diphenylcarbazone in methanolic solution, indicating the presence of a Ph_2B moiety (2). Crystals suitable for X-ray crystallography were obtained by recrystallization from benzene/petroleum ether, mp 128°C.

X-ray crystallographic analysis of 4

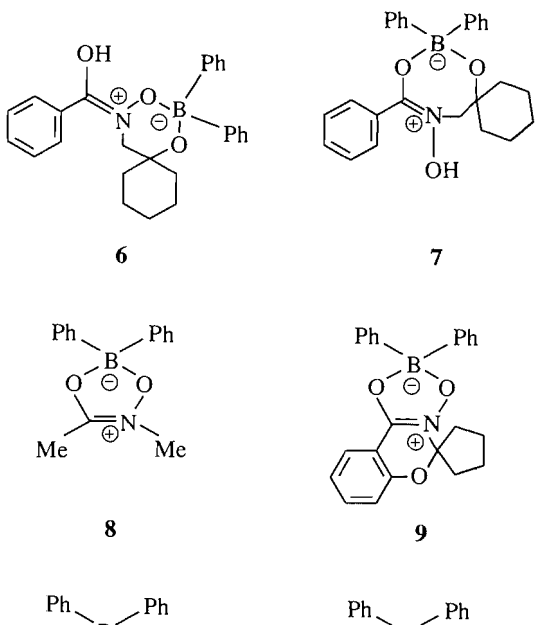
A crystal ca. 0.32 × 0.32 × 0.35 mm in size was mounted on a glass fiber. Unit-cell parameters were refined by least squares on setting angles for 25 reflections (2θ = 30.0–39.4°) measured on a diffractometer with Mo-K_α radiation ($\lambda_{K\alpha 1}$ = 0.70930, $\lambda_{K\alpha 2}$ = 0.71359 Å). Crystal data at 21°C are as follows:

$C_{26}H_{28}BNO_3$ fw = 413.32

Monoclinic, a = 9.9117(6), b = 13.308(1), c = 17.339(2) Å, β = 99.420(7)°, Z = 4, ρ_c = 1.217 Mg m^{-3}, $F(000)$ = 880, μ(Mo-K_α) = 0.73 cm^{-1}. Absent reflections: $0k0$, k odd, and $h0l$, l odd, uniquely indicate the space group $P2_1/c$ (No. 14).

Intensities were measured with graphite-monochromated Mo-K_α radiation on an Enraf-Nonius CAD4-F diffractometer. An ω–2θ scan at 1.1–10.0° min^{-1} over a range of (0.70 + 0.35 tan θ)° in ω (scan extended by 25% on each side for background measurement) was employed. Data were measured to 2θ = 60°. The intensities of three check reflections, measured every hour of X-ray exposure time throughout the data collection, showed only small random variations. The data were processed[2] and corrected for Lorentz and polarization effects. Of the 6551 independent reflections measured, 2423(37.0%) had intensities greater than or equal to 3σ(I) above background where $\sigma^2(I) = [C + 2B + (0.040(C - B))^2]$ with C = scan count, B = normalized total background count.

The structure was solved by direct methods, the coordinates of all



[2]Computer programs used include locally written programs for data processing and locally modified versions of the following: MULTAN80, multisolution program by P. Main, S. J. Fiske, S. E. Hull, L. Lessinger, G. Germain, J. P. Declercq, and M. M. Woolfson; ORFLS, full-matrix least-squares, and ORFFE, function and errors, by W. R. Busing, K. O. Martin, and H. A. Levy; FORDAP, Patterson and Fourier syntheses, by A. Zalkin; ORTEP II, illustrations, by C. K. Johnson.

non-hydrogen atoms being determined from an *E*-map. The non-hydrogen atoms were refined with anisotropic thermal parameters and the hydrogen atoms were fixed in idealized positions (C(sp^2)—H = 0.97, C(sp^3)—H = 0.98 Å, $U_H = 1.2U_{bonded\ atom}$) except for the OH hydrogen atom which was refined with an isotropic thermal parameter. Scattering factors for all atoms and anomalous dispersion corrections for the non-hydrogen atoms were taken from ref. 5. The weighting scheme $w = 1/\sigma^2(F)$ gave uniform average values of $w(|F_o| - |F_c|)^2$ over ranges of both $|F_o|$ and sin θ/λ and was employed in the final stages of full-matrix least-squares refinement of 284 variables. Reflections with $I < 3\sigma(I)$ were not included in the refinement. Convergence was reached at $R = 0.040$ and $R_w = 0.047$ for 2423 reflections with $I \geq 3\sigma(I)$. The function minimized was $\Sigma w(|F_o| - |F_c|)^2$, $R = \Sigma||F_o| - |F_c||/\Sigma|F_o|$, $R_w = (\Sigma w(|F_o| - |F_c|)^2/\Sigma w|F_o|^2)^{1/2}$. On the final cycle of refinement the maximum parameter shift corresponded to 0.17σ. The mean error in an observation of unit weight was 1.45. The final difference map showed maximum fluctuations of ± 0.16 e Å^{-3}.

The thermal motion has been analyzed in terms of the TLS model (6). The rms error in the temperature factors U_{ij} (derived from the least-squares analysis) is 0.0014 Å^2. The five rings in the structure (plus substituent non-hydrogen atoms) were separately analyzed (rms ΔU_{ij} = 0.0018–0.0026 Å^2). The bond lengths have been corrected for libration (6, 7) using shape parameters q^2 of 0.08 for all atoms. The final positional and (equivalent) isotropic thermal parameters for the non-hydrogen atoms appear in Table 1. Bond lengths (corrected and uncorrected) and angles are given in Tables 2 and 3 and intra-annular torsion angles in Table 4. Hydrogen atom parameters, anisotropic thermal parameters, torsion angles, and structure factors have been deposited.[3]

Results and discussion

As already assumed on the basis of the chemical shift value for the OH proton signal in the ^{1}H nmr spectra, the structure is that of the diphenylboron chelate **4** with a free hydroxyalkyl group. In contrast to the intramolecular condensation of the phenolic derivative **1** (R = OH) during the reaction with oxybis-(diphenylborane) leading to **3**, the benzohydroxamic acid without the phenol function, **1** (R = H), does not give a similar cyclocondensate, **5**, stabilization via a seven-membered chelate arrangement like that in **3** no longer being possible. The diphenylboron hydroxamate **4** represents another example of a stable "normal" hydroxamic acid chelate of the diphenylborenium cation (Ph_2B^+), like **8** (8), **9** (9), **10** (10), and others (11).

The short C=N distance[4] of 1.312(2) Å in **4** is similar to the corresponding values of 1.306, 1.300, and 1.309 Å reported for **3** (1), **8** (8), and **9** (9), respectively. From plots of π-bond order vs. bond length for C⋯N bonds (12, 13), these distances have π-bond orders between 0.70 and 0.85. The π-bond order of the C=O bond (1.293(2) Å), estimated to be about 0.5 from a plot of C—O distance vs. MO-π-bond order (13), is considerably less than that expected for a C=O double bond. Comparison of the C=O distance in **4** with those in **8** (8) (1.337 Å) and **9** (9) (1.288 Å) shows the influence of the adjacent (conjugated) aryl substituent on the C=O bond: there is obviously more double bond character in the C—O groups of **4** and **9** than there is in the aliphatic substituted hydroxamate **8**. Nevertheless, the π-interaction between the phenyl group and the hydroxamate system in **4** is somewhat reduced relative to compound **9**. This is manifested not only by the slightly longer C=O bond of **4**, but also by the longer C(1)—C(9, phenyl) bond (1.476(3) Å) in **4**, indicating lesser π contribution than in **9** where the corresponding C(O)—C(aryl) distance is 1.438 Å. Further support for this difference in π interaction is provided by the fact that the approximate coplanarity of the phenyl ring and the hydroxamate chelate ring noted for **9** is not observed for **4**.

The N—O bond in **4** (1.396(2) Å) is the longest yet observed in five-membered boron hydroxamate chelates of the types **8–10**. Only compound **10** ($R^1 = C_6H_{11}$, $R^2 = CH_3$) shows a similar long N—O bond of 1.389 Å. Like compound **4**, **10** possesses a cyclohexyl substituent, separated by one carbon atom from the nitrogen. In both cases the hydroxamate nitrogen atom could gain more basicity by this substitution pattern and thus enhance the single bond character of the N—O bond. In the boron chelates **11** (R = H (14) and R = CH_3 (15)) with a basic hydroxylamine nitrogen each, the N—O bond lengths are 1.409 (uncorr.) and 1.410 Å, respectively.

The two O—B bond lengths in **4** are significantly different (1.535(3) and 1.569(3) Å), which is normal for boron chelates of unsymmetrical ligands like **3**, **9**, or **10**. The mean C—B /mean O—B bond length ratio of 1.031 for **4** is indicative of intermediate overall binding strength of the *O,O*-chelating ligand with respect to the "Ph_2B^+" moiety. These ratios range from 1.017 to 1.066 (mean 1.035) for other "Ph_2BO_2" com-

TABLE 1. Final positional (fractional × 10^5) and isotropic thermal parameters ($U \times 10^3$ Å^2) with estimated standard deviations in parentheses

Atom	*x*	*y*	*z*	U_{eq}
O(1)	31079(13)	29711(10)	41917(9)	52
O(2)	50420(13)	21500(10)	48473(8)	49
O(3)	45999(18)	54459(14)	41526(12)	62
N	43358(15)	33092(12)	39925(10)	44
C(1)	53835(19)	28441(15)	43965(12)	43
C(2)	42282(20)	39876(16)	33296(12)	47
C(3)	37324(20)	50458(15)	34721(12)	46
C(4)	22403(22)	50758(16)	35886(14)	55
C(5)	16550(24)	61278(18)	35782(16)	65
C(6)	18481(26)	66895(19)	28451(16)	74
C(7)	33526(28)	67328(19)	27827(16)	75
C(8)	39460(25)	56819(17)	27712(14)	61
C(9)	68351(19)	30337(16)	43624(12)	45
C(10)	73568(22)	39774(18)	42486(13)	55
C(11)	87475(25)	40842(22)	42436(15)	72
C(12)	96001(24)	32718(27)	43517(17)	81
C(13)	90851(25)	23418(24)	44760(17)	80
C(14)	77074(22)	22125(18)	44858(15)	60
C(15)	27264(20)	18501(16)	53365(13)	49
C(16)	27304(26)	26327(20)	58653(16)	70
C(17)	20444(35)	25585(28)	65021(17)	92
C(18)	13469(32)	17010(34)	66214(19)	94
C(19)	13364(30)	9187(26)	61152(19)	84
C(20)	20210(25)	9863(19)	54861(15)	63
C(21)	32571(21)	10587(16)	39743(12)	47
C(22)	20627(23)	9982(18)	34218(15)	61
C(23)	18141(26)	2002(22)	29081(15)	71
C(24)	27472(31)	−5658(19)	29299(15)	71
C(25)	39298(29)	−5354(19)	34662(17)	70
C(26)	41857(24)	2677(18)	39733(14)	59
B	34734(23)	19586(18)	45916(15)	47

[3]Supplementary material mentioned in the text may be purchased from the Depository of Unpublished Data, Document Delivery, CISTI, National Research Council Canada, Ottawa, Canada K1A 0R6.

[4]Libration-corrected bond distances for compound **4** are employed in the discussion. Bond lengths for other structures determined in this series of papers have been treated in the same way unless otherwise stated. All other bond lengths compared with those in **4** are uncorrected.

Can. J. Chem. Downloaded from www.nrcresearchpress.com by 195.138.81.100 on 09/07/12
For personal use only.

Can. J. Chem. Downloaded from www.nrcresearchpress.com by 195.138.81.100 on 09/07/12
For personal use only.

TABLE 2. Bond lengths (Å) with estimated standard deviations in parentheses

Bond	Length		Bond	Length	
	Uncorr.	Corr.		Uncorr.	Corr
O(1)—N	1.393(2)	1.396	C(11)—C(12)	1.366(4)	1.375
O(1)—B	1.532(3)	1.535	C(12)—C(13)	1.369(4)	1.377
O(2)—C(1)	1.290(2)	1.293	C(13)—C(14)	1.379(3)	1.385
O(2)—B	1.566(3)	1.569	C(15)—C(16)	1.387(3)	1.400
O(3)—C(3)	1.443(3)	1.451	C(15)—C(20)	1.392(3)	1.405
N—C(1)	1.309(2)	1.312	C(15)—B	1.597(3)	1.603
N—C(2)	1.452(3)	1.454	C(16)—C(17)	1.392(4)	1.399
C(1)—C(9)	1.471(3)	1.476	C(17)—C(18)	1.367(5)	1.380
C(2)—C(3)	1.525(3)	1.529	C(18)—C(19)	1.361(4)	1.373
C(3)—C(4)	1.526(3)	1.533	C(19)—C(20)	1.379(4)	1.385
C(3)—C(8)	1.524(3)	1.534	C(21)—C(22)	1.398(3)	1.407
C(4)—C(5)	1.514(3)	1.519	C(21)—C(26)	1.399(3)	1.409
C(5)—C(6)	1.514(4)	1.523	C(21)—B	1.597(3)	1.601
C(6)—C(7)	1.514(4)	1.521	C(22)—C(23)	1.382(3)	1.385
C(7)—C(8)	1.519(3)	1.523	C(23)—C(24)	1.373(4)	1.383
C(9)—C(10)	1.385(3)	1.393	C(24)—C(25)	1.372(4)	1.381
C(9)—C(14)	1.388(3)	1.398	C(25)—C(26)	1.381(3)	1.385
C(10)—C(11)	1.387(3)	1.393			

TABLE 3. Bond angles (deg) with estimated standard deviations in parentheses

Bonds	Angle (deg)	Bonds	Angle (deg)
N—O(1)—B	104.2(1)	C(11)—C(12)—C(13)	119.9(2)
C(1)—O(2)—B	107.0(1)	C(12)—C(13)—C(14)	120.7(2)
O(1)—N—C(1)	111.3(2)	C(9)—C(14)—C(13)	119.5(2)
O(1)—N—C(2)	116.3(1)	C(16)—C(15)—C(20)	116.4(2)
C(1)—N—C(2)	131.8(2)	C(16)—C(15)—B	121.0(2)
O(2)—C(1)—N	113.5(2)	C(20)—C(15)—B	122.6(2)
O(2)—C(1)—C(9)	120.1(2)	C(15)—C(16)—C(17)	121.5(3)
N—C(1)—C(9)	126.3(2)	C(16)—C(17)—C(18)	120.3(3)
N—C(2)—C(3)	115.5(2)	C(17)—C(18)—C(19)	119.4(3)
O(3)—C(3)—C(2)	108.0(2)	C(18)—C(19)—C(20)	120.5(3)
O(3)—C(3)—C(4)	110.0(2)	C(15)—C(20)—C(19)	121.9(3)
O(3)—C(3)—C(8)	107.8(2)	C(22)—C(21)—C(26)	116.1(2)
C(2)—C(3)—C(4)	113.0(2)	C(22)—C(21)—B	120.5(2)
C(2)—C(3)—C(8)	107.1(2)	C(26)—C(21)—B	123.3(2)
C(4)—C(3)—C(8)	110.8(2)	C(21)—C(22)—C(23)	121.8(2)
C(3)—C(4)—C(5)	113.6(2)	C(22)—C(23)—C(24)	120.3(2)
C(4)—C(5)—C(6)	111.4(2)	C(23)—C(24)—C(25)	119.6(2)
C(5)—C(6)—C(7)	109.9(2)	C(24)—C(25)—C(26)	120.1(2)
C(6)—C(7)—C(8)	110.7(2)	C(21)—C(26)—C(25)	122.1(2)
C(3)—C(8)—C(7)	113.4(2)	O(1)—B—O(2)	97.8(1)
C(1)—C(9)—C(10)	123.5(2)	O(1)—B—C(15)	109.8(2)
C(1)—C(9)—C(14)	116.6(2)	O(1)—B—C(21)	111.1(2)
C(10)—C(9)—C(14)	119.9(2)	O(2)—B—C(15)	110.9(2)
C(9)—C(10)—C(11)	119.2(2)	O(2)—B—C(21)	109.3(2)
C(10)—C(11)—C(12)	120.7(2)	C(15)—B—C(21)	116.4(2)

pounds having five-membered chelate rings (refs. 9, 16 and references therein).

The orientation of the two *B*-phenyl rings (angle between normals to the mean planes = 82.9°) is quite different from the symmetrical disposition of the two phenyl rings observed for the symmetrically substituted hydroxamate **8** (8). The hydroxyl group of the cyclohexane ring (which has a chair conformation) is in an axial position and the chelate ring is connected via a methylene link at an equatorial position, a normal orientation for such differently space filling substituents. The five-membered chelate ring has a *B*-envelope conformation with the boron atom displaced 0.415(3) Å from the O(1)O(2)NC(1) mean plane.

The most significant intermolecular contacts correspond to van der Waals interactions across a centre of symmetry between hydroxyl groups (O(3)···H(O3)($1 - x$, $1 - y$, $1 - z$) = 2.55(4) and H(O3)···H(O3) = 1.99(8) Å), the geometry of this interaction being inconsistent with hydrogen bonding. The OH group is, however, involved in a weak intramolecular C—H···O in-

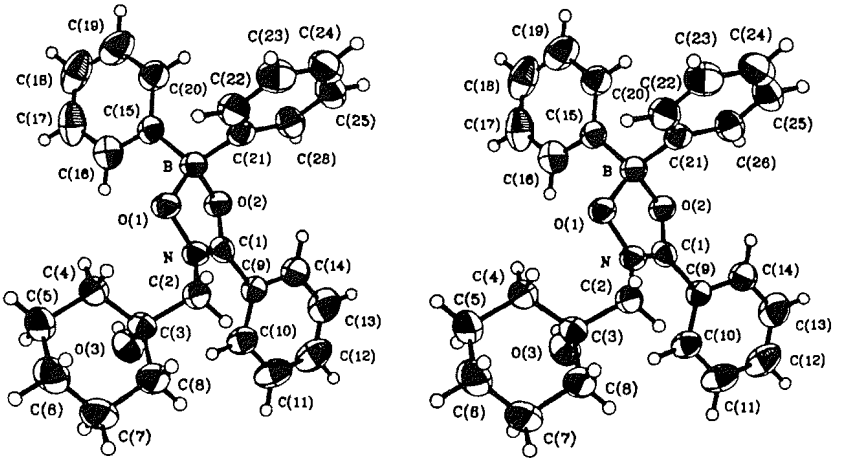


FIG. 1. Stereoview of the 4-[(1-hydroxycyclohexyl)methyl]-2,2,5-triphenyl-1,3-dioxa-4-azonia-2-borata-4-cyclopentene molecule; 50% probability thermal ellipsoids are shown for the non-hydrogen atoms.

TABLE 4. Intra-annular torsion angles (deg) standard deviations in parentheses

Atoms	Value (deg)
B—O(1)—N—C(1)	−18.8(2)
O(1)—N—C(1)—O(2)	3.7(2)
B—O(2)—C(1)—N	13.0(2)
C(1)—O(2)—B—O(1)	−22.2(2)
N—O(1)—B—O(2)	23.3(2)
C(8)—C(3)—C(4)—C(5)	−49.0(3)
C(3)—C(4)—C(5)—C(6)	53.8(3)
C(4)—C(5)—C(6)—C(7)	−57.6(3)
C(5)—C(6)—C(7)—C(8)	58.3(3)
C(6)—C(7)—C(8)—C(3)	−55.6(3)
C(4)—C(3)—C(8)—C(7)	49.9(3)

teraction: C(10)—H(10)···O(3), H···O = 2.44 Å, C···O = 3.341(3) Å, C—H···O = 155°.

Acknowledgements

We thank the Natural Sciences and Engineering Research Council of Canada and the Fonds der Chemischen Industrie, Frankfurt am Main, for financial support.

1. W. KLIEGEL, M. TAJERBASHI, S. J. RETTIG, and J. TROTTER. Can. J. Chem. **66**, 2621 (1988).
2. R. NEU. Z. Anal. Chem. **176**, 334 (1960); B. FRISSE and F. UMLAND. Anal. Chim. Acta **96**, 303 (1978).
3. W. KLIEGEL, U. SCHUMACHER, S. J. RETTIG, and J. TROTTER. Can. J. Chem. To be published.
4. W. KLIEGEL and H. BECKER. Chem. Ber. **110**, 2067 (1977).
5. International tables for X-ray crystallography. Vol. IV. 1974. Kynoch Press, Brimingham, U.K. (present distributor Kluwer Academic Publishers: Dordrecht, The Netherlands), pp. 99–102, 149.
6. V. SCHOMAKER and K. N. TRUEBLOOD. Acta Crystallogr. Sect. B, **24**, 63 (1968).
7. D. W. J. CRUICKSHANK. Acta Crystallogr. **9**, 747 (1956); **9**, 754 (1956); **14**, 896 (1961).
8. S. J. RETTIG, J. TROTTER, W. KLIEGEL, and D. NANNINGA. Can. J. Chem. **56**, 1676 (1978).
9. W. KLIEGEL, M. TAJERBASHI, S. J. RETTIG, and J. TROTTER. Can. J. Chem. **68**, 69 (1990).
10. W. KLIEGEL, D. NANNINGA, S. J. RETTIG, and J. TROTTER. Can. J. Chem. **61**, 2493 (1983).
11. W. KLIEGEL and D. NANNINGA. Chem. Ber. **116**, 2616 (1983).
12. L. M. TREFONAS, R. L. FLURRY, R. MAJESTE, E. A. MEYERS, and R. F. COPELAND. J. Am. Chem. Soc. **88**, 2145 (1966).
13. G. HÄFELINGER. Chem. Ber. **103**, 2902 (1970): **103**, 2922 (1970); **103**, 2941 (1970).
14. S. J. RETTIG, J. TROTTER, and W. KLIEGEL. Can. J. Chem. **52**, 2531 (1974).
15. W. KLIEGEL, H.-W. MOTZKUS, S. J. RETTIG, and J. TROTTER. Can. J. Chem. **62**, 838 (1984).
16. W. O. NELSON, C. ORVIG, S. J. RETTIG, and J. TROTTER. Can. J. Chem. **66**, 132 (1988).
17. W. KLIEGEL, G. LUBKOWITZ, S. J. RETTIG, and J. TROTTER. Can. J. Chem. **69**, 234 (1991).

Can. J. Chem. Downloaded from www.nrcresearchpress.com by 195.138.81.100 on 09/07/12
For personal use only.

On the ground and excited state dipole moments of planar vs. twisted nitroaniline analogues

HEMANT K. SINHA AND KEITH YATES

Department of Chemistry, Lash Miller Chemical Laboratories, University of Toronto, Toronto, Ont., Canada M5S 1A1

Received September 5, 1990

HEMANT K. SINHA and KEITH YATES. Can. J. Chem. **69**, 550 (1991).

Planar and conformationally twisted *p*-nitroaniline (PNA) and *N*,*N*-dimethyl-*p*-nitroaniline (DMPNA) systems have been subjected to electric field study (electrochromism) to understand their charge transfer characteristics in the ground and excited states. The observed values of ground and excited state dipole moments suggest that twisting of either the donor (D) with respect to the acceptor (A) or vice versa can have a large impact on the resultant charge distribution, particularly on the excited state charge distribution. These observations remarkably support the TICT hypothesis and minimum overlap rule, as proposed by Grabowski *et al.* Simple molecular orbital calculations provide adequate explanation for the observed changes in the dipole moment and reasonable agreement has been found in each case studied.

Key words: electrochromism, dipole moments, charge transfer.

HEMANT K. SINHA et KEITH YATES. Can. J. Chem. **69**, 550 (1991).

Afin de mieux comprendre les caractéristiques de transfert de charge dans leurs états fondamentaux et excités, on a étudié des systèmes de *p*-nitroaniline (PNA) et de *N*,*N*-diméthyl-*p*-nitroaniline (DMPNA) plans et conformationnellement déformés en les soumettant à des champs électriques (électrochromisme). Les valeurs observées pour les moments dipolaires des états fondamentaux et excités suggèrent que la déformation soit du donneur (D) par rapport à l'accepteur (A) ou vice versa peut avoir une influence marquée sur la distribution des charges, particulièrement sur la distribution de la charge dans l'état excité. Ces observations apportent un support remarquable à l'hypothèse TICT et à la règle du recouvrement minimal proposée par Grabowski et ses collaborateurs. Des calculs simples d'orbitales moléculaires fournissent une explication raisonnable des changements observés dans le moment dipolaire et l'accord acceptable qui a été trouvé dans chacun des cas étudiés.

Mots clés : électrochromisme, moments dipolaires, transfert de charge.

[Traduit par la rédaction]

Introduction

Numerous examples are available in the literature concerning steric effects on conjugation in the ground state (1). According to the generally accepted maximum overlap rule, the coplanarity of the donor (D) and acceptor (A) orbitals is the first condition for maximum resonance interaction, i.e., maximum charge transfer from the D to A orbitals. Therefore, for conjugated systems significant contribution to the molecular wavefunctions is expected from the intramolecular charge transfer (ICT) structures. The percentage of contribution of ICT structures to molecular wavefunctions is directly reflected in the permanent dipole moment of the molecule. Hence, any deviation from coplanarity between D and A orbitals, which directly hinders their charge transfer interactions, results in a decrease in the molecular dipole moment in the ground state and achieves a minimum value for the perfectly orthogonal conformation, where there will be minimum resonance interactions. Analogously, coplanarity has been found to be equally important for excited state charge transfer processes. Structurally, more pronounced changes in the dipole moment upon electronic excitation have been observed for conjugated planar π-electronic systems of polar organic compounds (2). Experimentally, this has been verified from the direct measurement of the excited state dipole moment, either via solvatochromic shift methods or by more reliable electro-optical methods (2).

However, the maximum overlap rule has been challenged recently for the electronically excited state, on the basis of extensive charge transfer that has been found to occur in systems having completely orthogonal D and A orbitals, for certain kinds of organic molecules (3). The term twisted intramolecular charge transfer (TICT), as coined by Grabowski *et al.*, is characterized by the mutually perpendicular conformation of D and A moieties and a large contribution from ICT structures to molecular wavefunctions (4). Thus it is proposed that, in those molecules that show TICT behaviour, the ICT in the excited state is governed by a *minimum overlap rule*. Several types of experimental and theoretical evidence for the TICT mechanism, and the continuing search for molecules having TICT nature, have given the proposed TICT hypothesis a strong footing. Recent excited state dipole moment determinations by electro-optical fluorescence measurements on the locally excited (LE) state and TICT state (5) provide direct experimental evidence for the more polar character of the TICT state in comparison to that of the LE state, supporting the hypothesis.

It has been observed that excitation of an initially twisted molecule (twisted in the ground state due to steric effects) results in complete population of the TICT state (6). This is manifested by the fact that these molecules show only TICT fluorescence, but no emission from the LE state. Therefore, a study of the excited states of the twisted molecules (twisted across the D–A bond in the ground state) should provide more insight into the TICT phenomena. Until now there has been no effort to probe directly the charge transfer characteristics of twisted molecules in the Franck–Condon excited states. Since the electro-optical absorption method is the most suitable way to determine the dipolar character of a molecule in its vertical excited state, this method has been employed here (2). Furthermore, since we are looking at vertical excited states, solvent-assisted conformational changes during the excited state lifetime will not contribute to our experimental observations and hence will provide a true picture of the excited state charge distribution free of solvent interactions. In our continuing effort to understand the charge transfer characteristics of twisted molecules, we report in this paper a systematic study of ground and excited state dipole moments of some model compounds. Recent study has shown that not only is the nature of the D and A groups important concerning charge transfer in the excited state, but relative localization of HOMO and LUMO is also equally

Can. J. Chem. Downloaded from www.nrcresearchpress.com by 198.100.157.202 on 09/07/12
For personal use only.

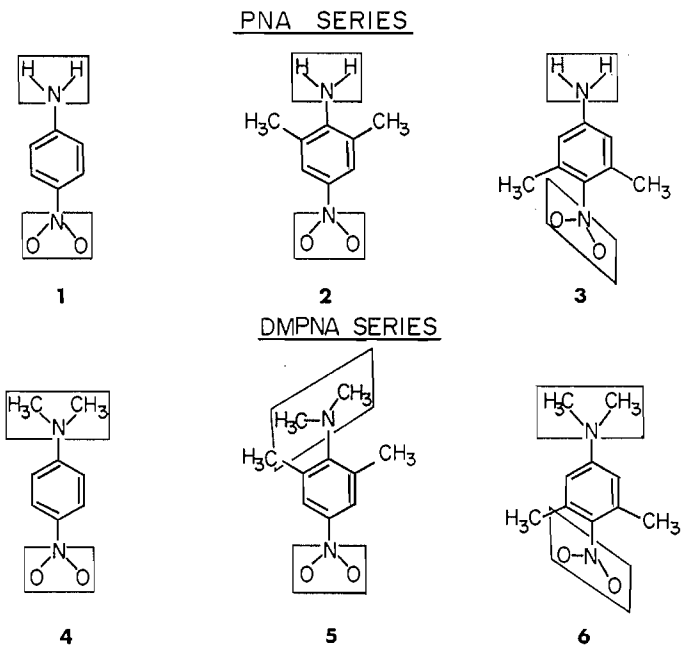


FIG. 1. Planar and conformationally twisted *p*-nitroaniline (PNA) and *N,N*-dimethyl-*p*-nitroaniline (DMPNA) systems.

important (7*a*). In this paper we have carried out an electro-optical absorption study on some carefully selected planar and selectively twisted nitroaniline analogues (see Fig. 1) to look into the factors that determine the charge transfer characteristics in twisted molecular systems. Furthermore, as these molecules are either nonfluorescent or weakly fluorescent, this method is the only suitable way to determine directly the charge distribution in their excited states. Simple molecular orbital calculations have been carried out to emphasize the importance of relative localization of HOMO and LUMO on the ICT in the excited state. These studies will be particularly important in terms of understanding photophysics, photochemistry, and nonlinear optical behaviour of nitroanilines.

Theory of electric field perturbation

The complete experimental and physical description of electro-optical absorption measurements on macroscopic systems has been presented fully in previous papers (7). This will not be repeated, except the basic principles, which are briefly summarized.

The effect of a uniform external electric field, E_{ext}, on the molar absorption coefficient of a molecule in solution phase can be given as

$$[1]\quad \Delta\epsilon = F_{int}^2 \epsilon \left[A_\chi + B_\chi/15h \frac{\partial/\partial\nu(\epsilon/\nu)}{(\epsilon/\nu)} + C_\chi/30h^2 \frac{\partial^2/\partial\nu^2(\epsilon/\nu)}{(\epsilon/\nu)} \right]$$

where F_{int} is the corrected electric field at the location of the molecule in solution, h is Planck's constant, and χ is the angle between the polarization direction of incident light and the direction of the electric field vector. For a molecule possessing a large permanent dipole moment, since the contribution from molecular polarizability terms to field signal can be considered negligible in comparison to that of the dipole moment terms, the A_χ, B_χ, and C_χ terms are related to various dipole moment parameters by the following equations:

$$[2]\quad A_\chi = 1/30(3\cos^2\chi - 1)\beta^2[3(\hat{p}\cdot\mu_g)^2 - \mu_g^2]$$

$$[3]\quad B_\chi = 5\beta(\mu_g\cdot\Delta\mu) + (3\cos^2\chi - 1)\beta[3(\hat{p}\cdot\mu_g)(\hat{p}\cdot\Delta\mu) - (\mu_g\cdot\Delta\mu)]$$

$$[4]\quad C_\chi = 5\Delta\mu^2 + (3\cos^2\chi - 1)[3(\hat{p}\cdot\Delta\mu)^2 - \Delta\mu^2]$$

In these equations, $\hat{p}$ is a unit vector in the direction of the transition moment, μ_g and $\Delta\mu$ are, respectively, the ground state dipole moment and the change in dipole moment on electronic excitation, and $\beta = (\kappa T)^{-1}$, where κ is the Boltzmann constant and T is the temperature.

Methods

The apparatus used for electro-optical absorption measurements is described in detail in ref. 7*a*. For each molecule the electric field signals were collected at three different values of χ and for several wavelengths λ within the absorption band of interest. The derivative terms in eq. [1] were computed numerically from a digitized absorption spectrum. The contribution from the second-derivative term (see eq. [1]) to the electric field signal was found to be very small, as observed in several other polar molecules (7). Therefore, this term has been neglected in the regression analysis. The coefficients A_χ, B_χ, and their standard deviations are obtained by multiple linear regression (see eq. [1]). Finally, the molecular parameters were calculated from the slopes and intercepts of least-squares plots of A_χ and B_χ versus $(3\cos^2\chi - 1)$.

We have used the spherical cavity approximation for correcting the externally applied field to an internal field at the location of the molecule in solution (8). No correction has been made for the effect of dipole reaction field or for the contribution of molecular polarizability to the electric field signal. Since these will be approximately of the same order of magnitude for each molecule studied here, direct comparison of their dipolar character will not be subject to serious error due to lack of the above corrections. Furthermore, recent electric field measurements comparing the gas phase and solution phase results on similar polar molecules, such as *p*-nitroanisole and *p*-cyanoaniline, show that the combined error due to the spherical cavity approximation and lack of a reaction field correction is less than 10% (9).

Materials

p-Nitroaniline (**1**) and *N,N*-dimethyl-*p*-nitroaniline (**4**) were obtained from Aldrich Chemicals. 2,6-Dimethyl-4-nitroaniline (**2**) was obtained by nitration of 1-(*p*-toluenesulphonylamino)-2,6-dimethylbenzene followed by hydrolysis as described in the literature (10). 3,5-Dimethyl-4-nitroaniline (**3**) was synthesized by simple nitration of 3,5-dimethylaniline by nitric acid (11). The above nitration gave both 2-nitro and 4-nitro derivatives, which were separated by thin-layer chromatography. *N,N*,2,6-Tetramethyl-4-nitroaniline (**5**) and *N,N*,3,5-tetramethyl-4-nitroaniline (**6**) were obtained by *N*-methylation of compounds **2** and **3** by freshly distilled dimethyl sulphate (12). All the compounds were recrystallized from appropriate solvents and the purity was checked by various spectroscopic analyses. Spectro-grade dioxane, from Aldrich Chemicals, was used as solvent without further purification. The solution was continuously circulated by a micro pump into the electric field cell from a reservoir to avoid any significant photochemical decomposition.

Theoretical calculations

The basic Hückel molecular orbital method was modified empirically as follows. The Coulomb Integrals H_{ii} for the heteroatoms of the aromatic side chain were scaled to the molecular ionization potentials of the simplest compounds (13), such as nitromethane, methylamine, *N,N*-dimethylamine, etc., using the approximate linear relationship between the E_{HOMO} and I_p reported by Streitwieser for a series of aromatic hydrocarbons (14). This gave heteroatom parameters $h_N(NO_2) = 1.5$, $h_O(NO_2) = 1.66$, $h_N(NMe_2) = 0.95$, and $h_N(NH_2) = 1.3$. The

Can. J. Chem. Downloaded from www.nrcresearchpress.com by 198.100.157.202 on 09/07/12
For personal use only.

Can. J. Chem. Downloaded from www.nrcresearchpress.com by 198.100.157.202 on 09/07/12
For personal use only.

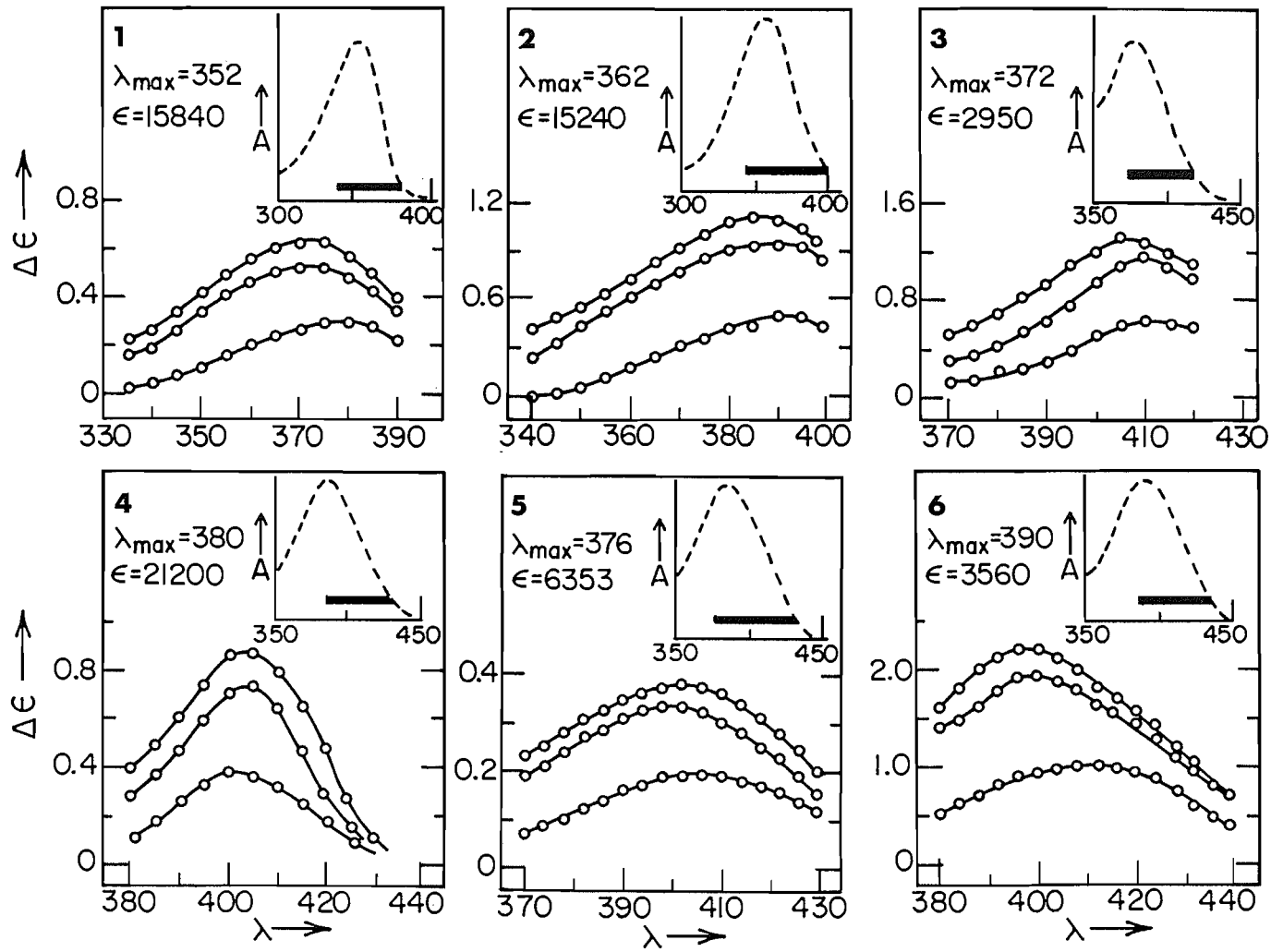


FIG. 2. Electric field spectra of the PNA and DMPNA systems at χ = 0, 25, and 50°. F_{ext} (external field) = 3.77 × 10^4 V/cm (rms). The inserted figures are the absorption spectra and the solid lines indicate the wavelength range on which electric field signals have been collected.

bond integrals H_{ij} for the $C_{aromatic}$—N bond and the N—O bonds were scaled to the curved relationship between k_{XY} and experimental XY bond length (13), also reported by Streitwieser (14). This gave k_{CN} = 0.8 and k_{NO} = 1.65. For the aromatic ring, standard values of H_{ii} and H_{ij} were used unmodified. Overall, the combination of these empirically derived H_{ii} and H_{ij} terms led to calculated values of energy of the HOMOs for compounds **1** and **4**, which gave values of I_p interpolated from the above linear relationship that are close to the reported experimental values. Furthermore, the calculated electron denisty distributions led to values of dipole moments for **1** (6.0 D) and **4** (6.8 D) that were in very good agreement with the experimental values obtained by dielectric methods (6.2 D for **1** and 6.8 D for **4**) (15). The dipole moments for orthogonal forms, i.e., compound **3**, **5**, and **6**, calculated by setting h_{C-N} = 0, were also in good agreement with the experimental values (see Table 1). Excited state dipole moments were calculated by promoting one electron from the HOMO to the LUMO and recalculating the q_i terms. These gave values of μ_e that were consistently higher than the observed values. However, the calculated and observed changes in dipole moments reflect the same trend. μ_e values based on INDO/S calculations on compounds **4**, **5**, and **6**, where σ-electrons are included in the calculation, also result in similar higher μ_e values (16). In addition, the symmetries of the calculated HOMO and LUMO could be be used to predict the directions of the transition moments.

TABLE 1. Ground and excited state dipole moments of the PNA and DMPNA systems obtained from electrochromic measurements in dioxane solution at 298 K

Compound	μ_g	$\Delta\mu\cdot\mu_g$	$\Delta\mu$	μ_e
1	5.5±0.5	45.2±5.0	8.2±0.5	13.7±1.0
2	5.8±0.5	46.3±5.0	8.0±0.5	13.8±1.0
3	3.1±0.4	60.5±6.0	19.5±0.6	22.6±1.0
4	6.0±0.4	37.3±5.0	6.2±0.5	12.2±1.0
5	4.7±0.6	50.1±5.0	10.7±0.5	15.4±1.0
6	5.6±0.6	30.0±5.0	5.4±0.4	11.0±1.0

Experimental results

The electric field signals at three settings of polariztion angle χ are shown in Fig. 2. The continuous lines in these figures were computed from the least-squares values of A_χ and B_χ using eq. [1]. The excellent agreement between the observed and calculated electric field spectrum suggests that eq. [1] adequately describes the field-induced changes in the absorption spectrum.

Can. J. Chem. Downloaded from www.nrcresearchpress.com by 198.100.157.202 on 09/07/12
For personal use only.

The molecular parameters obtained from the experiments are compiled in Table 1.

In the *p*-nitroaniline (PNA) series (compounds **1**, **2**, and **3**), substitution of methyl groups *ortho* to the amino group does not affect the planarity of the molecule, i.e., the D (-NH_2) and A (-NO_2) are still nearly in the same plane. This is evident from the fact that the absorption spectrum of **2** shows a small red shift with respect to that of **1**, as expected, and the extinction coefficients of **1** and **2** are very similar. On the other hand, considerable twisting of the -NO_2 group was observed in the case of **3** due to the steric effect of the *ortho* methyl groups. The twisting of the -NO_2 group was accompanied by a large decrease in the intensity and a small bathochromic shift of the long wavelength charge transfer (CT) transition with respect to that of **1**. Based on the approximate $\cos^2\theta = \epsilon/\epsilon_0$ relationship (ref. 1*a*, p. 414, and ref. 17), the angle between the aniline moiety and the -NO_2 group was calculated to be nearly 60° for compound **3**. The ground state dipole moment calculated from the electric field experiment also leads to a similar conclusion. For example, the μ_g's of **1** (5.5 D) and **2** (5.8 D) are very similar, reflecting the complete conjugation in both and little contribution from the steric factor due to the presence of *ortho* substituents in the latter. On the other hand, a dipole moment of 3.1 D, as observed in case of **3**, is nearly the same as that of nitromethane (3.0 D) (15), which indicates almost complete removal of charge transfer coupling between the -NO_2 group and the aromatic moiety due to deconjugation in the ground state. The μ_e's observed for **1** (13.7 D) and **2** (13.8 D) are also very similar, again suggesting very little difference in the planarity along the whole molecular skeleton. The large change in the dipole moment (μ_e = 22.6 D) observed in the case of **3**, which is nearly twice as large as that of its planar analogues, i.e., molecules **1** and **2**, makes it clear that conjugation between the D and A, in this case, is of little importance in deciding upon the magnitude of charge transfer character in the excited state. Recently, excited state dipole moments of similar magnitude have been reported for twisted nitrobenzene systems (7*b*). In all three cases, the transition moment direction has been found to be approximately in the same direction as μ_g.

The results obtained for the *N,N*-dimethyl-*p*-nitroaniline (DMPNA) series (compounds **4**, **5**, and **6**) are very different when compared with those of the PNA series described above. Similar to compound **3**, the intensity of the first charge transfer transition in the case of **6** was markedly decreased, with a small bathochromic shift in the absorption maximum due to the presence of *ortho* methyl substituents with respect to that of compound **4**. The absorption spectrum of compound **6** resembles as a whole the spectrum of *N,N*-dimethylaniline. When the *ortho* positions of the *N,N*-dimethylamino group in compound **4** are substituted, as in compound **5**, the dimethylamino group will be twisted out of the plane of the aromatic ring. This is accompanied by a marked hypochromic effect and a moderate hypsochromic effect on the first charge transfer band of compound **4**. This results in a spectrum that is closely similar to the spectrum of the correspondingly alkylated nitrobenzene. The smaller μ_g values of compounds **5** and **6** in comparison to that of their planar analogue, i.e., compound **4**, indicate that lack of coplanarity leads to a small degree of overlap between the D (-NMe_2) and A (-NO_2) orbitals, which ultimately leads to a weak charge transfer character in the ground state. The change in the magnitude of μ_g upon twisting either the D or the A group in the DMPNA series is not as pronounced as in the PNA series, indicating that a significant amount of conjugation exists even if the D or A groups are twisted by more than 60° from the plane of the benzene ring. This may be due to the very strong electron-donating ability of the -NMe_2 group in comparison to that of the -NH_2 group, and an equally strong electron-accepting nature of the -NO_2 group. Therefore a small degree of interaction between them could lead to significant charge transfer character in the ground state. The observed μ_e's are substantially different from what was observed in the PNA series. For example, twisting of the nitro group, as in compound **6**, results in a very small change in the dipole moment, whereas twisting of the *N,N*-dimethylamino group, as in compound **5**, brings the largest change in the dipole moment upon electronic excitation in comparison to the change in dipole moment observed in their planar analogue, i.e., compound **4**. The anomalous behaviour observed for these two series of compounds can be given a satisfactory explanation on the basis of simple theoretical calculations (see discussion below).

TABLE 2. Ground and excited state dipole moments of the PNA and DMPNA systems obtained from theoretical calculations

System	θ^a	ϕ^b	μ_g	μ_e	$\Delta\mu$
1	0	0	6.0	19.1	13.1
2	90	0	4.1	13.7	9.6
3	0	90	4.3	22.8	18.4
4	0	0	6.8	22.7	15.9
5	90	0	4.4	27.9	23.5
6	0	90	5.2	26.9	21.7

[a]Angle between the amino or *N,N*-dimethylamino group and the benzene ring.

[b]Angle between the nitro group and the benzene ring.

Theoretical results

Modified HMO calculations were carried out to obtain a theoretical explanation for the observed changes in dipole moments. Several other semiempirical SCF methods, such as MINDO/3 (18), MNDO (19), and AM1 (20), were also attempted, but none of them was successful in explaining the experimental results. All the above methods predict the -NO_2 group to be a mere spectator when it is out of the plane of the aromatic system. Such discrepancies in reproducing the experimental results, particularly for nitro-substituted aromatics, have been reported in the literature for these semiempirical methods (21).[1] Furthermore, due to the variational approach used in these SCF methods, which can only give the lowest energy state of a given symmetry, the excited state calculations are not valid for molecules having S_1 states belonging to totally symmetric representation, since the S_0 state is always totally symmetric for any closed shell system (22, 23). This has been found to be the case for the PNA and DMPNA systems, where the S_1 states in both cases belong to totally symmetric representation (A_1). All the above three methods show a slight *decrease* in dipole moment upon electronic excitation for both compounds **1** and **4**, and the first two methods suggest that an orthogonal conformation, where the nitro group and the aniline moiety are perpendicular to each other, is the most stable conformation in the ground state. These predictions are found not to be true experimentally (24). However, simple HMO type calculations, which are not subject to the above limitations, show a trend that

[1]Also, H. K. Sinha and K. Yates, unpublished results.

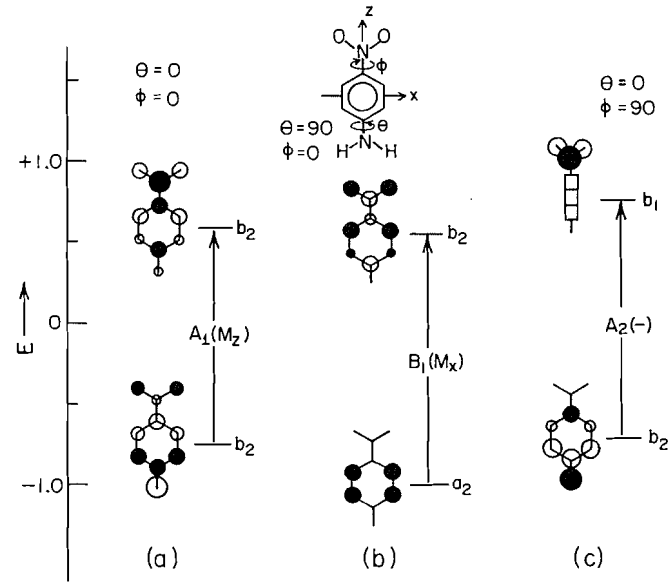


FIG. 3. Molecular orbital diagram of the PNA series; (a) all planar, (b) amino twisted, (c) nitro twisted.

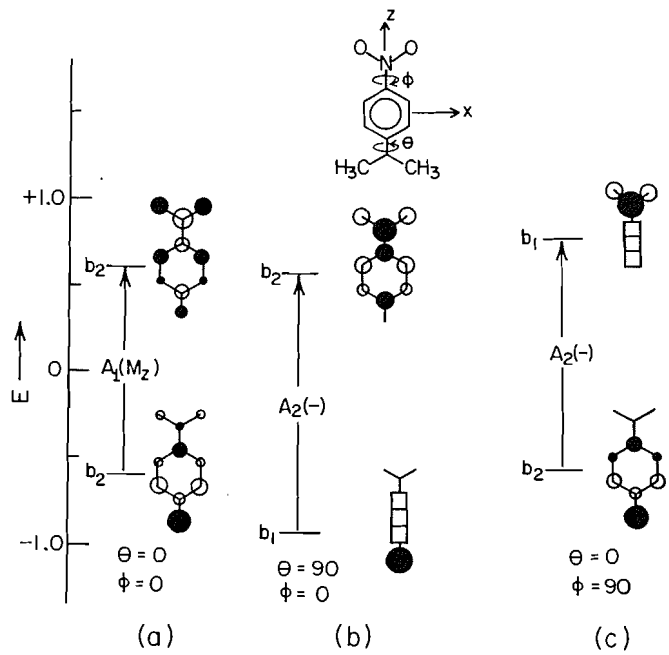


FIG. 4. Molecular orbital diagram of the DMPNA series; (a) all planar, (b) *N,N*-dimethylamino twisted, (c) nitro twisted.

is in fairly good agreement with the experimental results. Table 2 summarizes the theoretical results obtained from the HMO calculations.

Figures 3a and 3c show the MO diagram of planar and twisted PNA systems respectively. It is apparent that the difference in the charge transfer characteristics of the planar and twisted conformations arises mainly because of the specific localization of HOMO and LUMO upon twisting the nitro group. For example, the LUMO changes from a nitrobenzene type orbital in the planar form to a purely antibonding nitro group orbital in the perpendicular form. Therefore electronic excitation of twisted PNA, as in compound **3**, results in a complete electron transfer from the aniline group to the nitro group, producing a highly dipolar structure (μ_e calcd. = 22.8 D). On the other hand, on twisting the amino group out of plane, which cannot easily be achieved experimentally, produces merely a nitrobenzene type transition (Fig. 3b), with a μ_e (μ_e calcd. = 13.7 D) value similar to that observed in nitrobenzene (7*b*). In planar PNA, since the transition is an A_1 type transition (HOMO(b_2) → LUMO(b_2)), the transition should be M_z polarized, i.e., parallel to μ_g, which is along the *Z*-direction (see Fig. 3 for molecular coordinate axes). However, on twisting the nitro group out of plane, the HOMO(b_2) to LUMO(b_1) transition intensity falls to zero for the perfectly perpendicular form (in this π-electronic approximation), the transition being formally equivalent to a forbidden transition.

The theoretical results obtained for the DMPNA series are very different from those of the PNA series, discussed above. Because of the large difference in the ionization potentials of $-NH_2$ and $-N(CH_3)_2$, which is near 1.2 eV, in the planar form the HOMO becomes more localized on the *N,N*-dimethylamino group, whereas LUMO is a delocalized nitrobenzene type orbital (see Fig. 4a). The charge localization and the charge transfer on electronic excitation become more dramatic upon deconjugating the *N,N*-dimethylamino group from the rest of the aromatic system, as shown in Fig. 4b. However, when the *N,N*-dimethylamino group is perfectly orthogonal to the aromatic ring, the HOMO(b_1) to LUMO(b_2) transition is a forbidden transition. The $\Delta\mu$ calculated for this perpendicular form (23.5 D) is significantly higher than that for the planar configuration (15.9 D). This matches the results obtained from electric field measurements. The theoretical results obtained for the *N,N*-dimethylaminobenzonitrile system (in both planar and perpendicular form) by several π-electronic calculations are very similar to those observed for the DMPNA system, i.e., the excited state dipole moment of the perpendicular form is higher than the corresponding value for the planar form and the HOMO to LUMO transition becomes forbidden for the perfectly perpendicular configuration, where the *N,N*-dimethylamino group is perpendicular to the benzonitrile π-system (5, 25). In an analogous way, by twisting the nitro group by 90° and keeping the *N,N*-dimethylamino group in the plane of the benzene ring (Fig. 4c), as in compound **6**, HMO calculations indicate a change in dipole moment ($\Delta\mu$ = 21.7 D) that is nearly of the same magnitude as observed for compound **5**. In this case also, the HOMO(b_2) to LUMO(b_1) transition become forbidden for the perfectly perpendicular configuration. The calculated large dipole moment is again caused by the relative localization of the HOMO, which is a *N,N*-dimethylaniline type, and the LUMO, which is an antibonding nitro group orbital (see Fig. 4c). The calculated dipole moments for the DMPNA series are consistently higher than those observed experimentally.

Discussion

Recently we reported that in twisted nitrobenzene systems, where the nitro group is perpendicular to the aromatic benzene ring, the magnitude of charge transfer upon electronic excitation corresponds to nearly a full unit electron transfer from the benzene ring to the nitro group (7*b*). This creates a highly dipolar structure in the electronically excited state, as observed in nitromesitylene (μ_e = 21.6 D). The relative localization of the HOMO and LUMO, which is responsible for such a high degree of charge transfer, was evident from the theoretical and experimental results obtained for the model compounds. In this

Can. J. Chem. Downloaded from www.nrcresearchpress.com by 198.100.157.202 on 09/07/12
For personal use only.

Can. J. Chem. Downloaded from www.nrcresearchpress.com by 198.100.157.202 on 09/07/12
For personal use only.

paper we have extended the above work to various comformations of nitroaniline analogues to provide further support for the earlier results.

Compounds **1**, **4**, and the derivatives are some of the best known examples that show extensive charge transfer both in the ground and excited states (26, 27). This is partly due to the strong electron-withdrawing power of the $-NO_2$ group and also the strong electron-donating ability of the $-NH_2$ and $-NMe_2$ groups. In fact, $-NMe_2$ is by far a better electron donor than the $-NH_2$ group, which is evident from the large difference in their ionization potentials (1.2 eV). This has been directly verified experimentally by several spectroscopic methods, for example, from the direct determination of ground and excited state dipole moments by electro-optical methods, which reflect their charge transfer nature (27). Furthermore, these molecules are important in terms of their TICT behaviour, which cannot be investigated by the usual fluorescence techniques due to the reasons mentioned earlier. The electro-optical technique provides a unique method of establishing TICT character in such molecules. Since this method deals with the vertical excited states, the conformation of the molecule has to be modified prior to excitation, as done in these model molecules by substituting methyl groups at the *ortho* positions to either D or A.

The results obtained for compound **1** (μ_g = 5.5 D and μ_e = 13.7 D) show excellent agreement with those reported by Liptay (2*b*). Since compound **2** is identical to compound **1** as far as the planarity of the π-electron system is concerned, which is evident from its spectral behaviour as discussed earlier, the observed μ_g (5.8 D) and μ_e (13.8 D) values are similar to those of compound **1**. This indicates that they exhibit similar charge transfer characteristics both in the ground and excited states. However, in compound **3**, where the nitro group is nearly orthogonal to the aniline moiety, the excited state is extremely dipolar in nature. The observed μ_e of compound **3** is nearly twice as large as that of its planar analogue and corresponds to almost a full unit charge transfer from the D to A orbitals. These observations are similar to those reported for twisted nitrobenzene systems (7*b*), such as nitromesitylene. Even though the charge transfer interaction is diminished considerably in the ground state upon deconjugation of the π-system due to twisting of the C—NO_2 bond, it is enhanced dramatically in the excited state. This emphasizes the fact that *minimum overlap* of the D and A orbitals favours the maximum charge transfer interaction in the excited state for such systems.

The reason for such extensive charge transfer in the excited state of the twisted system, as in compound **3**, can be satisfactorily explained on the basis of MO diagrams, shown in Fig. 3. It is clear that for the planar system (compounds **1** and **2**), both HOMO and LUMO have mixed character. Therefore, because of delocalized charge distribution both in the ground and excited states, a moderate change in the dipole moments was observed upon electronic excitation. On the other hand, in the twisted system, as in compound **3**, the electronic excitation takes place from an orbital that is predominantly aniline type to an exclusively antibonding nitro orbital (see Fig. 3c), which results in complete charge separation with a large excited state dipole moment (22.6 D). This raises the possibility of the existence of a distinct TICT state for compound **3** and other similar compounds, particularly in polar solvents. Unfortunately, this prediction cannot be tested by other techniques because of the nonfluorescent nature of compound **3**, as pointed out earlier. The totally nonemissive nature of compound **3**, both at room temperature and low temperature, could be due to fast nonradiative processes from a low-lying, well-characterized TICT state. In all three cases, the transition polarization direction of the absorption band is along the direction of charge transfer, i.e., parallel to both μ_g and μ_e, which agrees with the predicted transition moment direction based on the symmetry properties of HOMO and LUMO except for compound **3**, where the transition is forbidden in the π-electron approximation.

The results obtained for compound **4**, which were also reported by Liptay (2*b*) from similar measurements, show excellent agreement (see Table 1). It is very clear from Table 1 that the DMPNA series behaves differently from the PNA series. Recently, in an attempt to analyze the TICT nature of compound **4**, Dobkowski *et al.* pointed out that TICT state formation is possible from the thermodynamic point of view (16). This was predicted on the basis of a linear correlation of the TICT fluorescence maxima with the difference of the oxidation potential of the donor and the reduction potential of the acceptor group, which has been found for several molecules showing TICT fluorescence. On the basis of the temperature dependence of the fluorescence spectra, they concluded that compound **4** does not relax to a TICT state. However, the fluorescence method adopted by them is not very conclusive because these compounds (**4**–**6**) are nonfluorescent at room temperature and very weakly fluorescent at low temperature (compound **6** is nonfluorescent even at low temperature), unlike other TICT emitting molecules such as the *N*,*N*-dimethylaminobenzonitrile system (5). However, the observation that has gone largely unnoticed in their experiments is the tremendously large Stokes shift observed for compound **5** in comparison to that for compound **4** at 100 K. For example, the Stokes shift observed for compound **4** is nearly 50 nm, whereas for compound **5** it is more than 125 nm. This large Stokes shift for **5** is in accord with our experimental observation that the excited state of **5** has considerably larger dipolar character than that of **4**. These observations clearly suggest that a distinct TICT state in the case of **4** is feasible, at least in polar solvents. However, the lack of TICT fluorescence in **4** may be caused by efficient nonradiative processes from the TICT state, such as intersystem crossing to T_1, which are very probable for such nitro compounds.

In compound **6**, where the $-NO_2$ group is twisted out of the plane of the benzene ring, the change in dipole moment on electronic excitation is not as large as that of compound **5**. In fact, for **6** the $\Delta\mu$ is at a minimum when compared with the other two conformations of the DMPNA series (see Table 1). This behaviour would be expected if the $-NO_2$ group orbitals are considered to be essentially not involved in the electronic transition process. In such a case the molecule will more or less resemble the parent *N*,*N*-dimethylaniline (DMA) in terms of its electronic transitions. In fact, the absorption spectral features of compound **6**, as described earlier, resemble as a whole those of DMA, supporting the above description. However, the calculated $\Delta\mu$ for **6** does not agree with the trend observed experimentally. This is primarily due to the fact that theoretically there is still significant interaction of the $-NO_2$ antibonding orbital in the LUMO of **6**, even if the $-NO_2$ group is out of the plane of the π-system, as shown in the MO diagram (Fig. 4c). Therefore, the HOMO to LUMO transition results in extensive charge transfer from the D to A orbitals, creating a large $\Delta\mu$. It should also be noted that the lowest energy transition in **6** becomes forbidden in the perfectly orthogonal configuration, as

TABLE 3. Expected dipole moment changes based on simple HOMO and LUMO descriptions

Compound	θ^a	ϕ^b	HOMO	LUMO	CT ($\Delta\mu$)
1, 2	0	0	Mainly anilino type	Mainly nitrobenzene type	Moderate (8.2 D)
3	0	90	Purely anilino type	Purely nitro type	Extensive (19.5 D)
4	0	0	Mainly *N,N*-dimethylamino type	Mainly nitrobenzene type	Moderate (6.2 D)
5	90	0	Purely *N,N*-dimethylamino type	Mainly nitrobenzene type	Extensive (10.7 D)
6	0	90	Mainly *N,N*-dimethylamino type	Mainly benzene type	Small (5.4 D)

[a,b]See footnotes of Table 2.

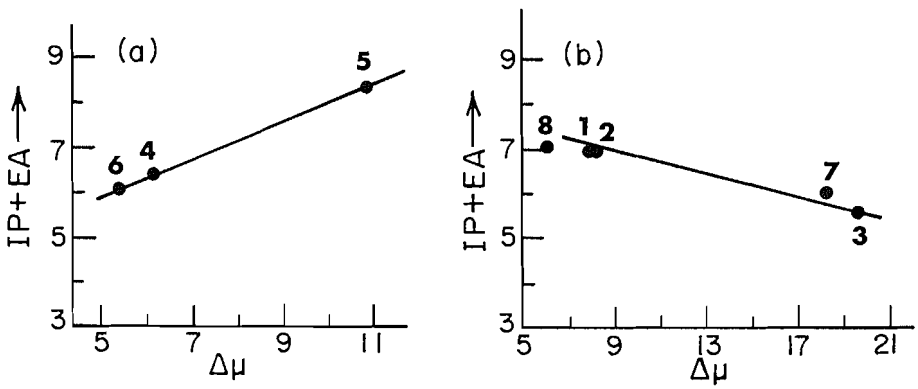


FIG. 5. Plot of IP + EA vs. $\Delta\mu$; (a) DMPNA series, (b) PNA series. The points corresponding to numbers **7** and **8** are, respectively, the values of nitromesitylene and nitrobenzene obtained from ref. 7*b*.

found in the case of compound **5**. On the other hand, the second transition, i.e., from HOMO to the second LUMO, exactly resembles the HOMO to LUMO transition expected for planar DMA. In fact, the calculated change in dipole moment ($\Delta\mu$ = 6.3 D) for planar DMA obtained from HMO calculations is very similar in magnitude to that of compound **6** (5.4 D) found experimentally. These observations strongly suggest that in **6**, the $-NO_2$ group acts merely as a spectator, and therefore is involved to a very small extent in the lowest energy electronic transition. Since compound **6** is also nonfluorescent even at low temperature, no conclusive explanation can be given regarding its TICT character. However, this experimental observation supports the fact that a twist of the acceptor ($-NO_2$) group in the DMPNA series does not introduce any TICT character in the parent molecule.

A very qualitative description based on the nature of the HOMO and LUMO, as shown in Table 3, can be used in explaining the observed changes in the dipole moments. In Fig. 5 the experimental values of the ionization potentials and electron affinities,[2] based on the description of HOMO and LUMO in Table 3, have been plotted against the observed change in the dipole moments. The good correlation observed for both the PNA and DMPNA series indicates that the above simple description is quite reasonable in explaining the charge transfer processes in the excited states of such systems. The two separate straight lines observed for the PNA and DMPNA series could be due to the large difference in the ionization potentials of the $-NH_2$ and $-NMe_2$ groups, which drastically changes the nature of the HOMO. These observations indicate that since ICT in the excited state is dependent on the nature of orbitals involved in the electronic transition, and since the ionization potential of the donor and the electron affinity of the acceptor decide specifically the localization of HOMO and LUMO in a typical $\pi\pi^*$ transition of such systems, a large change of ionization potential or electron affinity by twisting either the donor or acceptor group significantly changes the charge transfer character of the excited state. Therefore, the primary condition of planarity of the conjugated system, for maximum ICT, as observed generally for the ground state, is not a necessary condition for the excited state charge transfer process, supporting the minimum overlap rule for such systems.

[2]IP and EA values were taken from the CRC handbook of chemistry and physics, 1987.

Acknowledgement

The continued financial support of the Natural Sciences and Engineering Research Council of Canada (NSERC) is gratefully acknowledged.

1. (*a*) H. H. JAFFE and M. ORCHIN. Theory and application of ultraviolet spectroscopy. J. Wiley and Sons, New York. 1962; (*b*) H. SUZUKI. Electronic absorption spectra and geometry of organic molecules. Academic Press, New York. 1967; (*c*) V. I. MINKIN, O. A. OSIPOV, and YU. A. ZHDANOV. Dipole moments in organic chemistry. Plenum Press, New York. 1970.
2. (*a*) N. G. BAKHSHIEV, M. I. KNYAZHANSKII, V. I. MINKIN, O. A. OSIPOV, and G. V. SAIDOV. Russ. Chem. Rev. **38**, 740 (1969);

Can. J. Chem. Downloaded from www.nrcresearchpress.com by 198.100.157.202 on 09/07/12
For personal use only.

(*b*) W. LIPTAY. *In* Excited states. Vol. 1. *Edited by* E. C. Lim. Academic Press, New York. 1974. p. 129; (*c*) H. LABHART. Adv. Chem. Phys. **13**, 179 (1967).
3. (*a*) W. RETTIG. Angew. Chem. Int. Ed. Engl. **25**, 971 (1986); (*b*) E. LIPPERT, W. RETTIG, B. BONACIC-KOUTECKY, F. HEISEL, and J. A. MIEHE. Adv. Chem. Phys. **68**, 1 (1987).
4. Z. R. GRABOWSKI and DOBKOWSKI. Pure Appl. Chem. **55**, 245 (1983).
5. Z. R. GRABOWSKI, K. ROTKIEWICZ, A. SIEMIARCZUK, J. D. COWLEY, and W. BAUMANN. Nouv. J. Chim. **3**, 443 (1979).
6. Z. R. GRABOWSKI, K. ROTKIEWICZ, and A. J. SIEMIARCZUK. J. Luminesc. **18/19**, 420 (1979).
7. (*a*) H. K. SINHA, P. C. P. THOMSON, and K. YATES. Can. J. Chem. **68**, 1507 (1990); (*b*) H. K. SINHA and K. YATES. J. Chem. Phys. **93**, 7085 (1990); (*c*) W. LIPTAY, W. EBERLEIN, H. WEIDENBERG, and O. ELFLEIN. Ber. Bunsen-ges. Phys. Chem. **71**, 548 (1967); (*d*) W. BAUMANN. Ber. Bunsen-ges. Phys. Chem. **80**, 231 (1976); (*e*) R. MATHIES and A. C. ALBRECHT. J. Chem. Phys. **60**, 1420 (1974).
8. C. J. F. BÖTTHER. Theory of electric polarisation. Vols. 1 and 2. Elsevier, Amsterdam. 1973.
9. (*a*) N. A. KRIEBEL. Ph.D. Thesis, University of Zurich, Zurich (1974); (*b*) H. BISCHOFF, W. BAUMANN, N. DETZER, and K. ROTKIEWICZ. Chem. Phys. Lett. **116**, 180 (1985); (*c*) A. KRIEBEL and H. LABHART. Z. Phys. Chem. (Munich), **92**, 247 (1974).
10. W. A. DENNY, G. J. ATWELL, and B. C. BAGULY. J. Med. Chem. **26**, 1625 (1983).
11. K. IBBOTSON and J. KENNER. J. Chem. Soc. **123**, 1260 (1923).
12. B. M. WEPSTER. Recl. Trav. Chim. Pays-Bas, **76**, 357 (1957).
13. (*a*) V. I. VEDENEYEV, L. V. GURVICH, V. N. KONDRATYEV, V. A. MEDVEDEV, and V. L. FRANKEVICH. *In* Bond energies, ionisation potentials and electron affinities. Edward Arnold, London. 1966; (*b*) Tables of Interatomic Distances. Chem. Soc. Special Pub. No. 11 (1958); No. 18 (1968), Supplement.
14. A. STREITWEISER, JR. *In* Molecular orbital theory for organic chemists. J. Wiley and Sons, New York. 1961.
15. A. L. MCCLELLAN. *In* Tables of experimental dipole moments. W. H. Freeman Company, San Francisco. 1963.
16. J. DOBKOWSKI, J. HERBICH, J. WALUK, J. KOPUT, and W. KUHNLE. J. Luminesc. **44**, 149 (1989).
17. B. M. WEPSTER. Recl. Trav. Chim. Pays-Bas, **76**, 335 (1957).
18. R. C. BINGHAM, M. J. S. DEWAR, and D. H. LO. J. Am. Chem. Soc. **97**, 1285 (1975).
19. M. J. S. DEWAR and W. THIEL. J. Am. Chem. Soc. **99**, 4899 (1977).
20. M. J. S. DEWAR, F. J. ZOEBISCH, and J. J. P. STEWART. J. Am. Chem. Soc. **107**, 3902 (1985).
21. (*a*) L. P. DAVIS and R. M. GUIDRY. Aust. J. Chem. **32**, 1369 (1979); (*b*) E. J. PADMA MALER and K. JUG. J. Phys. Chem. **88**, 3508 (1984); (*c*) W. M. F. FABIAN. J. Comput. Chem. **9**, 368 (1968); (*d*) M. HEAD-GORDON and J. A. POPLE. Chem. Phys. Lett. **173**, 585 (1990).
22. M. A. BETHE and E. E. SALPETER. Quantum mechanics of one and two electron atoms. Academic Press, New York. 1957.
23. R. CARBO and O. GROPEN. Adv. Quantum Chem. **12**, 158 (1980).
24. J. TROTTER. Acta. Crystallogr. **12**, 884 (1959); Tetrahedron, **8**, 13 (1960).
25. D. J. COWLEY and A. H. PEOPLES. J. Chem. Soc. Chem. Commun. 352 (1977).
26. (*a*) O. S. KHALIL, C. J. SELISKAR, and S. P. MCGLYNN. J. Chem. Phys. **58**, 1607 (1973); (*b*) T. P. CARSEY, G. I. FINDLEY, and S. P. MCGLYNN. J. Am. Chem. Soc. **101**, 4502 (1979); (*c*) O. S. KHALIL, J. L. MEEKS, and S. P. MCGLYNN. J. Am. Chem. Soc. **95**, 5876 (1973); (*d*) B. F. LEVIN, C. G. BETHEA, C. D. THURMOND, R. T. LYNCH, and J. L. BERNSTEIN. J. Appl. Phys. **50**, 2523 (1979); (*e*) C. DANIEL and M. DUPIS. Chem. Phys. Lett. **171**, 209 (1990).
27. (*a*) H. LABHART. Tetrahedron, **19**, Suppl. 2, 223 (1963); (*b*) J. CZEKALLA and G. WICK. Z. Elektrochem. **65**, 727 (1961).

Can. J. Chem. Downloaded from www.nrcresearchpress.com by 198.100.157.202 on 09/07/12
For personal use only.

Stereoselectivity of C(3) methylation and aldol condensation of camphor and derivatives

J. H. HUTCHINSON, D. L. F. LI, T. MONEY,[1] AND M. PALME
Department of Chemistry, University of British Columbia, 2036 Main Mall, Vancouver, B.C., Canada V6T 1Y6

AND

M. R. AGHARAHIMI AND K. F. ALBIZATI
Department of Chemistry, Wayne State University, Detroit, MI 48202, U.S.A.

Received August 14, 1990

J. H. HUTCHINSON, D. L. F. LI, T. MONEY, M. PALME, M. R. AGHARAHIMI, and K. F. ALBIZATI. Can. J. Chem. **69**, 558 (1991).

The stereoselectivity of methylation and aldol condensation of camphor and derivatives is determined by the presence or absence of a C(7) *syn*-methyl group and (or) C(5) and C(6) *endo*-hydrogen atoms.

Key words: camphor, C(3) methylation, C(3) aldol.

J. H. HUTCHINSON, D. L. F. LI, T. MONEY, M. PALME, M. R. AGHARAHIMI et K. F. ALBIZATI. Can. J. Chem. **69**, 558 (1991).

En se basant sur la présence ou sur l'absence d'un groupement C(7) *syn*-méthyle et (ou) d'atomes d'hydrogène C(5) et C(6) *endo*, on a déterminé la stéréosélectivité des réactions de méthylation et aldoliques du camphre et de ses dérivés.

Mots clés : camphre, C(3) méthylation, C(3) aldol.

[Traduit par la rédaction]

C(3) methylation

The early literature (1–7) indicates that C(3) monomethylation of camphor (**1**) is readily accomplished, but the stereoselectivity of this process was not clearly established. Recent investigations (8, 9), however, have shown that sequential treatment of (+)-camphor (**1**) in THF with lithium diisopropylamide (1 mole equivalent) and methyl iodide (excess) at 0°C provides a product (~75% yield) that was shown by nmr (400 MHz) and capillary glc to be a mixture (~4:1) of 3-*exo*-methylcamphor (**2***a*) and 3-*endo*-methylcamphor (**2***b*) (Scheme 1). Subsequent treatment of this mixture with NaOMe in MeOH or with HCl and HOAc provides a mixture (~9:1) in which the major component is 3-*endo*-methylcamphor (**2***b*). The C(3) methylation of (+)-9-bromocamphor (**3**) (8, 9), (+)-9,10-dibromocamphor (**5**) (8), or (−)-4-methylcamphor (**7**) can be accomplished similarly and, in each case, nmr (400 MHz) evidence established that the ratio of *exo*-methyl to *endo*-methyl epimers was ~2:1 (Scheme 1). Subsequent equilibration with acid (HCl and HOAc) provided the corresponding 3-*endo*-methyl derivatives in 90–95% yield. Related to these observations is the fact that 6-methoxyepicamphor (**9**) can be converted exclusively to the *exo*-2-allyl derivative (**10**) (10). It has also been shown that camphor enol *tert*-butyldimethylsilyl ether (**11**) undergoes a Mukaiyama reaction to provide the *exo* product (**12**) (11) and that the related silyl ether (**13**) reacts with Eschenmoser's salt to yield a mixture (~6:1) of *exo* and *endo* products, **14***a* and **14***b* (12).

It has been suggested (8) that the unexpected preference of camphor and derivatives to undergo *exo* protonation, *exo* alkylation, or *exo* aldol condensation (see below) with carbonyl compounds could be due, *at least in part*, to the steric effect of the 5-*endo* hydrogen atom on the approach of electrophiles to the corresponding enolate ion. Support for this proposal has been provided by the fact that kinetic methylation of 5,6-dehydrocamphor (**15**) and 9-bromo-5,6-dehydrocamphor (**17**) provides mixtures (~12:1) in which the major products **16***a* and **18***a* are produced by *endo* methylation. It has also been shown that methylation of dehydro-10-norcamphor (**19**) and derivatives (**20–22**) (13*a–c*, 14) results in the almost exclusive formation of C(3)-*endo* methylated derivatives. Thus, in camphor and norcamphor compounds having a C(7) *syn*-methyl group and C(5) *endo*-hydrogen or substituents, kinetic *exo* methylation seems to be preferred, while in those compounds having a C(7) *syn*-methyl group and lacking a C(5) *endo* substituent (i.e., 5,6-dehydro derivatives) *endo* methylation is preferred. In compounds lacking a C(7) *syn*-methyl group (e.g., **23–25**), *exo* methylation occurs (15, 16) and the presence or absence of C(5) *endo*-hydrogen does not significantly affect the stereoselectivity of the reaction.

In contrast to the results described above, C(3) methylation of 3-methylcamphor (**2***a*,*b*) displays *endo* stereoselectivity (8). For example, addition of excess CD_3I to 3-methylcamphor enolate yields a product whose ^1H and ^2H nmr spectra indicate that it is a mixture (3.4:1) of 3-*exo*-methyl-3-*endo*-trideuteriomethylcamphor (**26***a*) and its C(3) epimer (**26***b*) (Scheme 2).

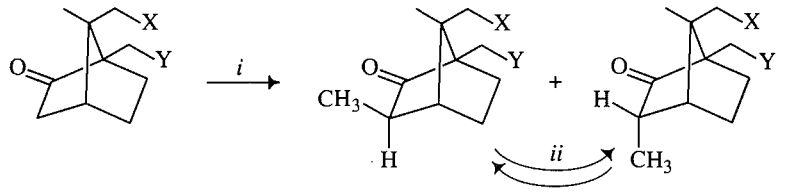
The striking difference in stereoselectivity between camphor enolate (**28**) (80% *exo* attack) and 3-methylcamphor enolate (**29**) (80% *endo* attack) can be explained by using the mechanism advanced by House and Umen (17) to explain preferential axial alkylation in substituted cyclohexanones. Thus, the enolate of 3-methylcamphor could be skewed (cf. **29**) to avoid eclipsing of the C(3) methyl group and the oxygen anion. The direction of this distortion would favour movement of the oxygen atom away from the C(10) methyl group and the C(3) methyl substituent to move up towards the C(3) hydrogen. The net result of this distortion would be to favour *endo* attack at the C(3) position.

Indirect support for the reasons advanced above to explain the stereoselective *exo* methylation of camphor (**1**) and *endo* methylation of 3-methylcamphor (**2***a*,*b*) was obtained by examining the stereoselectivity of methylation of 3,4-dimethylcamphor (**8***a*,*b*). In the enolate (**30**) derived from this compound, the downward movement of the C—O^- bond to avoid eclipsing with the C(3)—CH_3 bond would result in the corresponding upward movement of the C(3)—CH_3 bond. This would lead to increased torsional strain between the C(3)—CH_3

[1]Author to whom correspondence may be addressed.

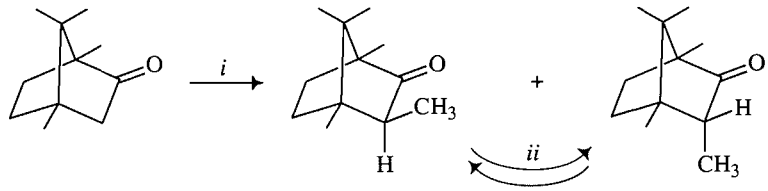
Printed in Canada / Imprimé au Canada

Can. J. Chem. Downloaded from www.nrcresearchpress.com by 198.100.157.202 on 09/07/12
For personal use only.

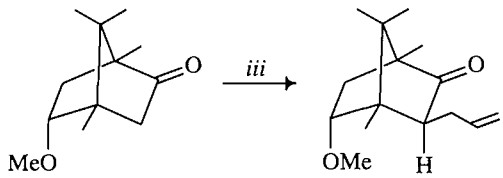


1 X = Y = H
3 X = Br, Y = H
5 X = Y = Br

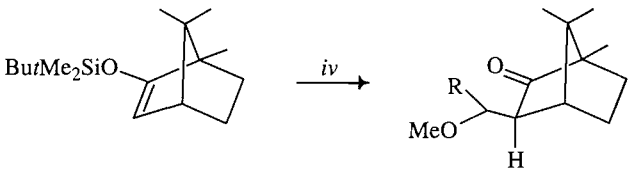
2*a* (X = Y = H) **2***b* (X = Y = H)
4*a* (X = Br, Y = H) **4***b* (X = Br, Y = H)
6*a* (X = Y = Br) **6***b* (X = Y = Br)



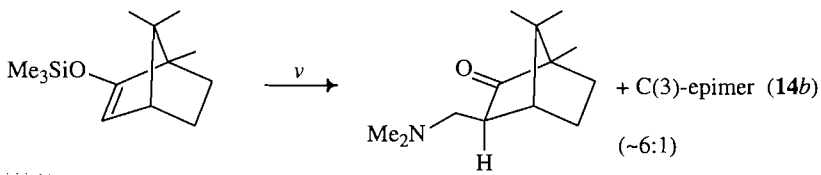
7 **8***a* **8***b*



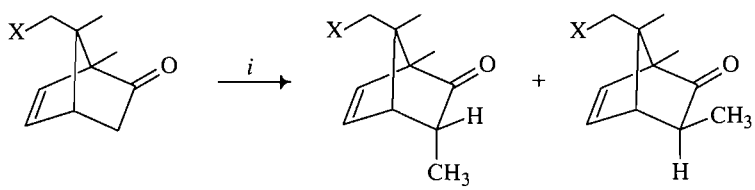
9 **10**



11 **12**



13 **14***a*



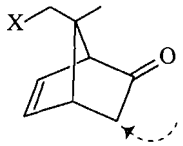
15 X = H
17 X = Br

16*a* **16***b*
18*a* **18***b*

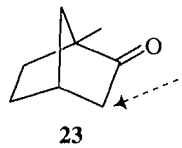
i: LDA/THF/0°C; MeI, 0°C; *ii*: HCl, HOAc, heat; *iii*: BuLi, THF, HMPA; $CH_2{=}CHCH_2I$; *iv*: $RCH(OMe)_2$, $TiCl_4$; *v*: $CH_2{=}\overset{+}{N}Me_2\ \ Cl^-$

SCHEME 1

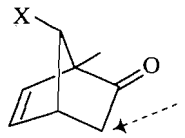
Can. J. Chem. Downloaded from www.nrcresearchpress.com by 198.100.157.202 on 09/07/12
For personal use only.



19 (X = H)
20 (X = CH_2OBn)
21 (X = $CH(CH_3)OTHP$)
22 (X = $(CH_2)_3OTHP$)

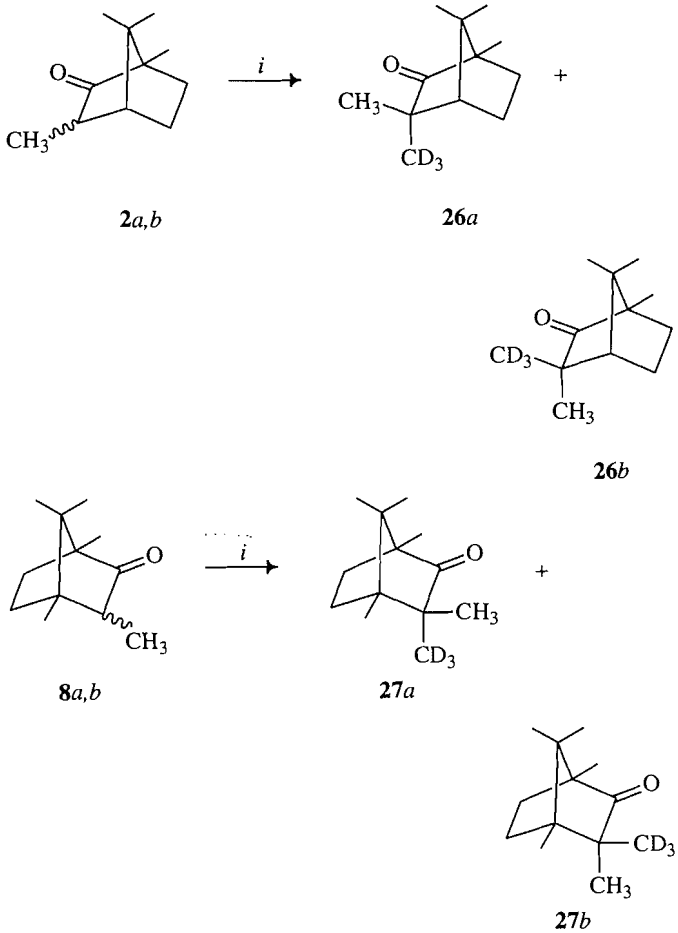


23



24 (X = CH_3)
25 (X = CH_2CH_2OBn)

and C(4)—CH_3 bonds and increased steric interaction between the C(3) and C(4) methyl groups. Therefore it is reasonable to expect that the balance of effects would result in less distortion of the enolate (**30**) of 3,4-dimethylcamphor (**8***a*,*b*) in the direction proposed for the enolate (**29**) derived from 3-methylcamphor (**2***a*,*b*). In the event, alkylation of 3,4-dimethylcamphor (**8***a*,*b*) with trideuteriomethyl iodide provided a mixture (~2:1) in which the major product (**27***a*) (Scheme 2) resulted from *endo* methylation of enolate **30**. Thus, in keeping with the prediction given above, 3,4-dimethylcamphor (**8***a*,*b*) undergoes *endo* methylation to a lesser extent than 3-methylcamphor (**2***a*,*b*). The initial assignment of structure to **27***a* and **27***b* was made by assuming that the nmr signals for the *exo* and *endo* methyl



2*a*,*b* **26***a* **26***b* **8***a*,*b* **27***a* **27***b*

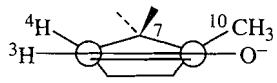
i: LDA, THF, 0°C; CD_3I, 0°C

SCHEME 2

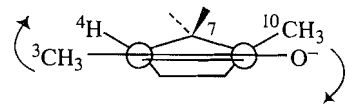
groups in **27***a* and **27***b* have the same relative relationship as those recorded for other C(3) epimeric pairs (cf. Scheme 1). These assignments were supported by nOe experiments; for example, irradiation at the C(8) methyl resonance (δ 0.76) led to enhancement of the signal at δ 1.05 (*exo*-3-methyl) and irradiation at the C(3) *endo*-methyl resonance (δ 0.97) resulted in enhancement of the signal at δ 1.69 (C(5) *endo*-hydrogen).

C(3) aldol condensation

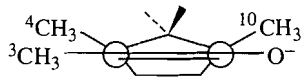
Aldol reactions of the enolates of camphor, 5,6-dehydrocamphor, and norcamphor exhibit the same selectivities as observed in the alkylations and are general phenomena.[2] Several aldehydes were allowed to react with the camphor



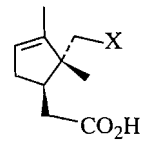
28



29

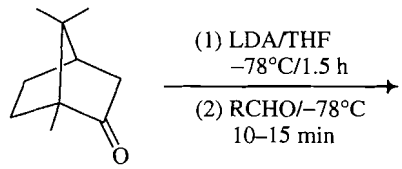


30



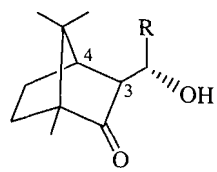
31 X = H
32 X = OH

enolate under standard aldol reaction conditions. The results are shown in Table 1. In every case, only two products were observed spectroscopically and confirmed by isolation using hplc on silica. The two products were the *exo-threo* adduct **33***a* (major) and the *endo-threo* adduct **33***b* (minor). No other

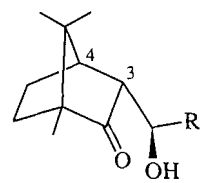


(1) LDA/THF
−78°C/1.5 h
(2) RCHO/−78°C
10–15 min

1



33*a*

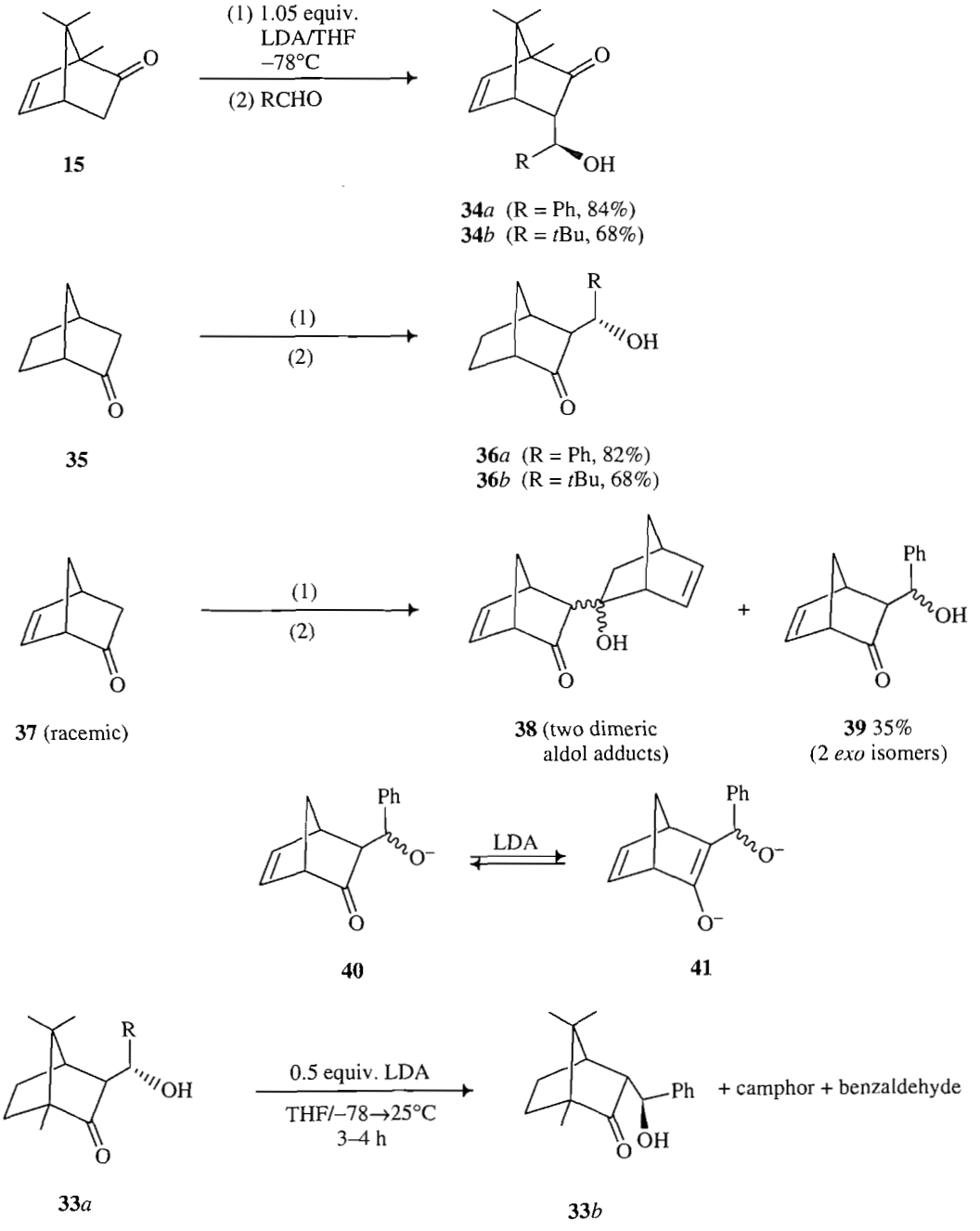


33*b*

adducts were observed under these conditions. This is consistent with the normally observed trend in which an *E*-enolate gives rise to predominantly *threo* adducts. This may indicate the occurrence of a closed (cyclic) transition state in these cases. Interestingly, when the reactions were run in THF containing 20–30% HMPA, no change in the product ratios was observed. A steric effect is noted in that the aldehydes with the two largest steric requirements (R = phenyl and *tert*-butyl) gave the highest *exo*/*endo* ratios. However, there is very little difference in *exo*/*endo* selectivity through the series where R = Me, Et, or *i*-Pr. Phenylacetaldehyde is exceptional since it shows the lowest *exo*/*endo* ratio (1.6:1) but is considerably larger than acetaldehyde or propionaldehyde. The stereochemistry of the adducts was assigned by analysis of ^1H nmr coupling constants

[2]Stereoselective aldol reactions were first observed with (+)-9-bromocamphor, cf. ref. 24.

Can. J. Chem. Downloaded from www.nrcresearchpress.com by 198.100.157.202 on 09/07/12
For personal use only.



SCHEME 3

involving the C3, C4, and carbinol hydrogens (25).[3] The identity of the cation had a negligible effect on stereoselectivity. When the camphor enolate was generated with either potassium or sodium hexamethyldisilazide at low temperature and treated with benzaldehyde, the same two adducts were formed in nearly the same ratio as was observed in the case of LDA deprotonation.

Aldol reaction of 5,6-dehydrocamphor (**15**) with PhCHO or *t*-BuCHO produces the *endo* adducts **34***a* and **34***b* (Scheme 3) in 84 and 78% yield respectively, along with <5% of *exo* adducts. In contrast, norcamphor provided only *exo* adducts **36***a* and **36***b* in 82 and 68% yield, respectively. No other aldol isomers were observed by ^{1}H nmr spectroscopy in the crude reaction products. We attempted the aldol reaction of bicyclo-[2.2.1]hept-5-en-2-one (**37**), but the reaction was complicated by a fast dimerization of **37**, providing two aldol dimers (**38**) as the major products and only a minor amount (no more than 35%) of a mixture of the two *exo* adducts (**39**) in approximately a 2:1 ratio (measured by ^{1}H nmr). This dimerization was observed previously by Minter.[4] We have shown in an unrelated project that the intermediate β-oxido ketone in aldol reactions can be deprotonated to give an aldolate dianion.[5] Since dimerization is a major factor in this system, it is likely that excess LDA will be present and can deprotonate **40** to **41**,

[3]For the use of nmr in assigning the configurations of aldol adducts, see ref. 25*a*; for the use of nmr in assigning the stereochemistry of bicyclo[2.2.1]heptanes, see ref. 25*b*.

[4]Professor David E. Minter. Private communication.

[5]Shawn Hitchcock. Unpublished results. See also ref. 26.

Can. J. Chem. Downloaded from www.nrcresearchpress.com by 198.100.157.202 on 09/07/12
For personal use only.

TABLE 1. Adduct ratios from the reaction of the camphor enolate with aldehydes

Aldehyde RCHO	Yield of adducts (%)[a]	*exo*/*endo* (**33***a*:**33***b*)[b]
R = Me	82	3.3/1.0
Et	64	3.2/1.0
i-Pr	63	3.1/1.0
t-Bu	80	7.6/1.0
Ph	85	11 /1.0
$PhCH_2$	91	1.6/1.0
2-Furyl	89	4.4/1.0

[a]Yields refer to isolated adduct mixtures ≥95% spectroscopically pure.
[b]Ratios determined by ^1H NMR integration.

equilibrating the α position. We are, therefore, reluctant to draw conclusions from this result.

To confirm that we were dealing with kinetically generated product mixtures, we treated the *exo-threo* adduct **33***a* (R = Ph) with 0.5 equiv. of LDA in THF at −78°C and allowed the reaction to warm to 0°C and to be held at this temperature for 3–4 h. Significant isomerization to the *endo* adduct **33***b* (R = Ph) was observed along with camphor and benzaldehyde resulting from retroaldol reaction (Scheme 3). Since *exo* → *endo* isomerization was observed under what appear to be equilibrating conditions, we conclude that the product mixtures under the standard conditions were determined kinetically. We did not, however, observe isomerization of adducts of **34***a* or **36***a* under these conditions.

In general, the stereoselectivity of C(3) alkylation and aldol condensation of bicyclo[2.2.1]heptan-2-one derivatives is associated with at least three factors, viz., (1) C(5) *endo*-hydrogen (or other substituents), which directs *exo*; (2) the C(7) *syn*-methyl group, which directs *endo*; and (3) enolate geometry in C(3) substituted compounds. The relative importance of these factors is presumably dependent on structural factors in the ketone substrate.

Experimental

Unless otherwise stated, the following are implied. Melting points (mp) were determined on a Kofler micro heating stage and are uncorrected. The capillary glc analysis was carried out on a Hewlett–Packard 5880A gas chromatograph employing a flame ionization detector and using a W.C.O.T. narrow bore (0.21 mm × 12 m) Carbowax 20 M column. Helium was used as the carrier gas. The 400 MHz ^1H nmr spectra were recorded on a Bruker WM-400 instrument. The 270 MHz ^1H nmr spectra were recorded on a 270 MHz instrument constructed from a Bruker console, a Nicolet computer model 293A with a Diablo disk, and a 270 MHz superconducting magnet supplied by Oxford Instruments. Signal positions are given in delta (δ) with tetramethylsilane (TMS) as an internal reference. Signal multiplicity and integrated areas are indicated in parentheses. The solvent used was deuteriochloroform. Infrared spectra were recorded on a Perkin–Elmer 137 spectrophotometer and optical rotations were measured using a Perkin–Elmer 141 polarimeter. Low resolution mass spectra were obtained using a Varian/MAT model CH_4B mass spectrometer and high resolution mass spectra using a Kratos MS50 instrument. Microanalyses were performed by Mr. P. Borda, Microanalytical Laboratory, University of British Columbia, Vancouver.

*(+)-5,6-Dehydrocamphor (**15**)*

(−)-6-*endo*-Bromocamphor (18, 19) (6.5 g, 0.028 mol), potassium hydroxide (7.89 g, 0.14 mol), dimethyl sulfoxide (280 mL), and water (40 mL) were stirred together at 120°C for 2 h. The solution was diluted with water, extracted with ether (3 × 300 mL), and the combined ether extracts washed with brine (3 × 100 mL), dried over anhydrous magnesium sulfate, and the solvent evaporated to give a yellow oil (2.2 g). Purification by column chromatography (silica gel; petroleum ether (30–60°C)/ether, 9:1) afforded a volatile white solid, (+)-5,6-dehydrocamphor (**15**) (2.0 g, 47%); $[\alpha]_D$ +756 (*c* 0.50, CH_2Cl_2) (lit. (20, 21) $[\alpha]_D$ −735 (*c* 1.0, EtOH)) for the enantiomer; ν_{max}: 1735 cm^{-1}; δ ($CDCl_3$, 400 MHz) (22): 0.91 (3H, s), 1.01 (3H, s), 1.07 (3H, s), 1.93 (1H, d, *J* = 16.5 Hz), 2.2 (1H, ddd, *J* = 16.5 Hz, 3.5 Hz, and 1.0 Hz), 2.68 (1H, br s), 5.58 (1H, br d, *J* = 5.5 Hz), 6.71 (1H, dd, *J* = 5.5 Hz and 3.0 Hz); *m/e* (relative intensity): 150 (M^+, 12), 93 (58), 85 (59), 71 (92), 69 (100). Exact Mass calcd. for $C_{10}H_{14}O$: 150.1045; found: 150.1049.

The aqueous phases were combined and acidified with 1 N hydrochloric acid, extracted with ether (3 × 300 mL), and the combined ether extracts washed with brine (3 × 100 mL) and dried over anhydrous magnesium sulfate. Removal of the solvent gave (−)-α-campholenic acid (**31**) (1.88 g, 40%); $[\alpha]_D$ −8.2 (*c* 2.25, CH_2Cl_2) (lit. (22) $[\alpha]_D$ −9.0 (*c* 1.1, $CHCl_3$); ν_{max} (film): 2950, 1710 cm^{-1}; δ ($CDCl_3$, 400 MHz): 0.80 (3H, s), 1.02 (3H, s), 1.62 (3H, br s), 1.94 (1H, m), 2.20–2.35 (2H, m), 2.40–2.52 (2H, m), 5.24 (1H, br s); *m/e* (relative intensity): 168 (M^+, 28), 153 (64), 135 (28), 108 (100), 107 (82), 93 (80), 91 (42).

*(−)-3-*endo*-Methyl-5,6-dehydrocamphor (**16**a)*

(+)-5,6-Dehydrocamphor (**15**) (2.0 g, 13.3 mmol) was added to a freshly prepared solution of lithium diisopropylamide (1.87 mL, 12.9 mmol) in dry THF (25 mL) at 0°C under argon and the enolate allowed to form over 0.5 h. Methyl iodide (4.0 mL, 65 mmol) was then added and the reaction stirred for a further 0.5 h before being quenched with 1 N hydrochloric acid. The mixture was extracted with ether (3 × 50 mL) and the combined ether extracts washed with brine (3 × 25 mL) and dried over anhydrous magnesium sulfate. Removal of the solvent yielded a pale yellow oil (2.0 g). Capillary glc analysis of the crude product indicated the ratio of 3-*endo*- (**16***a*) to 3-*exo*-methyl-5,6-dehydrocamphor (**16***b*) to be approximately 12:1.

Purification by column chromatography (silica gel; petroleum ether (30–60°C)/ether, 9:1) afforded starting material (0.21 g) and a mixture of 3-*endo*- and 3-*exo*-methyl-5,6-dehydrocamphor (1.68 g, 86% yield based on recovered starting material). The ^1H nmr (400 MHz) spectrum and capillary glc analysis showed the ratio of 3-*endo*- to 3-*exo*-methyl-5,6-dehydrocamphor to be approximately 12:1.

A mixture of 3-*endo*- and 3-*exo*-methyl-5,6-dehydrocamphor (**16***a*,*b*) (50 mg) was treated with a freshly prepared solution of potassium *tert*-butoxide (1.0 mL, 1.0 M) at 50°C for 12 h. The solution was diluted with water, extracted with ether (3 × 20 mL), and the combined ether extracts washed with brine (3 × 10 mL) and dried over anhydrous magnesium sulfate. Removal of the solvent yielded a pale yellow oil (48 mg, 96%). Capillary glc and the 400 MHz ^1H nmr spectrum indicated the presence of one epimer, 3-*endo*-methyl-5,6-dehydrocamphor (**16***a*). Low temperature crystallization (CO_2/acetone) from pentane provided pure (−)-3-*endo*-methyl-5,6-dehydrocamphor (**16***a*) as a colourless oil; $[\alpha]_D$ +676.0 (*c* 1.5, CH_2Cl_2); ν_{max} ($CHCl_3$): 1740 cm^{-1}; δ ($CDCl_3$, 400 MHz): 0.93 (3H, s), 1.01 (3H, s), 1.05 (3H, d, *J* = 7.3 Hz), 1.06 (3H, s), 2.41 (1H, dd, *J* = 7.0 Hz and 3.5 Hz), 2.54 (1H, t, *J* = 3.4 Hz), 5.53 (1H, d, *J* = 5.0 Hz), 6.51 (1H, dd, *J* = 5.0 Hz and 3.4 Hz); *m/e* (relative intensity): 164 (M^+, 8.3), 121 (28), 108 (64), 105 (19), 93 (100), 77 (28). Exact Mass calcd. for $C_{11}H_{16}O$: 164.1207; found: 164.1200. Anal. calcd. for $C_{11}H_{16}O$: C 80.44, H 9.82; found: C 80.60, H 9.75.

*(−)-9-Bromo-5,6-dehydrocamphor (**17**)*

(−)-6-*endo*-9-Dibromocamphor (3, 18) (423 mg, 1.36 mmol), potassium hydroxide (382 mg, 6.8 mmol), dimethyl sulfoxide (13 mL), and water (2 mL) were stirred at 70°C for 48 h. The solution was diluted with water, extracted with ether (3 × 100 mL), and the combined ether extracts washed with brine (3 × 50 mL), dried over anhydrous magnesium sulfate, and the solvent evaporated to give a yellow oil (136 mg). Purification by column chromatography (silica gel; petroleum ether (30–60°C)/ether, 25:1) gave (−)-9-bromo-5,6-dehydro-

Can. J. Chem. Downloaded from www.nrcresearchpress.com by 198.100.157.202 on 09/07/12
For personal use only.

Can. J. Chem. Downloaded from www.nrcresearchpress.com by 198.100.157.202 on 09/07/12
For personal use only.

camphor (**17**) (68.2 mg, 22%) as a white crystalline solid, mp 46.5–48.5° (sealed tube); $[\alpha]_D$ +377 (*c* 0.5, CH_2Cl_2); ν_{max} ($CHCl_3$): 1740 cm^{-1}; δ ($CDCl_3$, 400 MHz): 1.05 (3H, s), 1.08 (3H, d, *J* = 1 Hz), 2.01 (1H, d, *J* = 17 Hz), 2.22 (1H, ddd, *J* = 17 Hz, 3.5 Hz, and 1 Hz), 3.0 (1H, br s), 3.22 (1H, br d, *J* = 6 Hz), 6.49 (1H, dd, *J* = 6 Hz and 3 Hz); *m/e* (relative intensity): 230/228 (M^+, 2/2), 188/186 (19/19), 107 (100), 91 (29), 79 (21). Exact Mass calcd. for $C_{10}H_{13}OBr$: 230.0129/228.0150; found: 230.0135/228.0149. Anal. calcd. for $C_{10}H_{13}OBr$: C 52.42, H 4.72, Br 34.87; found: C 52.40, H 5.60, Br 34.77.

The aqueous phases were combined, acidified with 1 N hydrochloric acid, extracted with ether (3 × 100 mL), and the combined ether extracts washed with brine (3 × 50 mL). Removal of the dried solvent afforded a crude solid (130 mg), which was purified by column chromatography (silica gel: petroleum ether (30–60°C)/ether/acetic acid, 150:50:1) to give hydroxy-α-campholenic acid (**32**) as a white crystalline solid, mp 102–103.5°C; $[\alpha]_D$ −19.52 (*c* 0.21, CH_2Cl_2); ν_{max} ($CHCl_3$): 3000 (br), 1705 cm^{-1}; δ ($CDCl_3$, 400 MHz): 0.82 (3H, s), 1.65 (3H, br s), 1.97 (1H, m), 2.34 (1H, dd, *J* = 16 Hz and 9 Hz), 2.64 (1H, dd, *J* = 16 Hz and 5.5 Hz), 2.70 (1H, m), 3.42 (1H, d, *J* = 11 Hz), 3.54 (1H, d, *J* = 11 Hz), 5.41 (1H, br s); *m/e* (relative intensity): 184 (M^+, 0.01), 166 (17), 151 (32), 107 (59), 94 (100), 93 (80), 91 (63), 79 (95). Exact Mass calcd. for $C_{10}H_{16}O_3$: 184.1100; found: 184.1102. Anal. calcd. for $C_{10}H_{16}O_3$: C 65.19, H 8.75; found: C 65.01, H 8.70.

*(−)-9-Bromo-3-*endo*-methyl-5,6-dehydrocamphor (**18***a*)*

(−)-9-Bromo-5,6-dehydrocamphor (**17**) (380 mg, 1.66 mmol) was added to a freshly prepared solution of lithium diisopropylamide (1.58 mmol) in dry THF (5 mL) at 0°C under argon and the enolate allowed to form over 0.5 h. Methyl iodide (0.44 mL, 6.9 mmol) was then added and the reaction stirred for a further 0.5 h before being quenched with 1 N hydrochloric acid. The mixture was extracted with ether (3 × 50 mL) and the combined ether extracts washed with brine (3 × 25 mL) and dried over anhydrous magnesium sulfate. Removal of the solvent yielded a yellow oil (370 mg).

Purification by column chromatography (silica gel; petroleum ether (30–60°C)/ether, 8:1) afforded starting material (50 mg) and (−)-9-bromo-3-methyl-5,6-dehydrocamphor (290 mg, 82%) as a mixture of epimers. The 400 MHz ^1H nmr spectrum of this mixture indicated the ratio of 3-*endo*- to 3-*exo*-methyl epimers (**18***a* and **18***b*) to be ~14:1.

The mixture of (−)-9-bromo-3-*endo*- and (−)-9-bromo-3-*exo*-methyl-5,6-dehydrocamphor (30 mg) was treated with freshly prepared potassium *tert*-butoxide in *tert*-butanol (1.0 mL, 1.0 M) at 50°C for 12 h. The solution was diluted with water, extracted with ether (3 × 25 mL), and the combined ether extracts washed with brine (2 × 10 mL) and dried over anhydrous magnesium sulfate. Removal of the solvent afforded a pale yellow oil (28 mg). The 400 MHz ^1H nmr spectrum of the crude product indicated the presence of one epimer, (−)-9-bromo-3-*endo*-methyl-5,6-dehydrocamphor (**18***a*).

Low temperature crystallization (CO_2/acetone) from pentane provided pure (−)-9-bromo-3-*endo*-methyl-5,6-dehydrocamphor (**18***a*) as a white crystalline solid, mp 44–45°C; $[\alpha]_D$ +337 (*c* 1.23, CH_2Cl_2); ν_{max} ($CHCl_3$): 2980, 1740 cm^{-1}; δ ($CDCl_3$, 400 MHz): 1.04 (3H, s), 1.07 (3H, d, *J* = 7 Hz), 1.08 (3H, d, *J* = 2 Hz), 2.39 (1H, dq, *J* = 7 Hz and 3.5 Hz), 2.95 (1H, br s), 3.21 (1H, d, *J* = 10 Hz), 4.03 (1H, d, *J* = 10 Hz), 5.61 (1H, d, 6 Hz), 6.43 (1H, dd, *J* = 6 Hz and 3.2 Hz); *m/e* (relative intensity): 244/242 (M^+, 1.0/1.0), 188/186 (16/17), 135 (6.9), 121 (4.6), 107 (100), 91 (23), 79 (14). Exact Mass calcd. for $C_{11}H_{15}OBr$: 244.0286/242.0306; found: 244.0298/242.0308. Anal. calcd. for $C_{11}H_{17}OBr$: C 54.34, H 6.22, Br 32.86; found: C 54.54, H 6.28, Br 33.00.

*Alkylation of (−)-4-methylcamphor (**7**)*[6]

(−)-4-Methylcamphor (**7**) (23)[7] (4.32 g, 26.0 mmol) in dry THF (20 mL) was added to a freshly prepared solution of LDA in THF (30 mL) (derived from *n*-butyllithium (15.6 mL, 1.6 M in hexane) and diisopropylamine (3.5 mL, 25 mmol)) at 0°C under argon. After 30 min, methyl iodide (6.5 mL, 105 mmol) was added and the reaction mixture stirred for a further 30 min before being quenched with 1 M HCl solution. The reaction mixture was extracted with ether (3×) and the ether extracts were combined and washed with water (3×) and dried over anhydrous magnesium sulfate. Removal of the solvent yielded a light yellow solid (4.86 g). Capillary glc analysis (OV-101, 80°C) of the crude product indicated the ratio of *exo*- to *endo*-3,4-dimethylcamphor (**8***a* and **8***b*) was ~2:1.

Purification of the crude mixture by column chromatography (silica gel 230–400 mesh, elution with petroleum ether/ether, 98:2) afforded the starting material (**7**) (0.94 g) and a mixture of **8***a* and **8***b* (3.15 g, ~67%; 78% yield based on recovered starting material); ^1H nmr (400 MHz) and capillary glc analysis showed the ratio of **8***a* to **8***b* to be 2.0–2.5:1.

A sample of pure *exo*-3,4-dimethylcamphor (**8***a*) was obtained by chromatographing the above mixture using the same conditions. This provided **8***a* as a white crystalline solid, mp 140–141°C (sealed tube); ν_{max} ($CHCl_3$): 1720 cm^{-1}; δ ($CDCl_3$, 400 MHz): 0.70 (3H, s, C(9) methyl), 0.81 (3H, s, C(8) methyl), 0.92 (3H, s, C(10) methyl), 1.00 (3H, s, C(4) methyl), 1.08 (3H, d, *J* = 8 Hz, C(3) methyl), 1.33–1.49 (2H, m, C(5) and C(6) *endo* protons), 1.59 (1H, ddd, *J* = 12 Hz, 12 Hz, and 4 Hz, C(6) *exo* proton), 1.80 (1H, ddd, *J* = 12 Hz, 12 Hz, and 5 Hz, C(5) *exo* proton), 1.92 (1H, q, *J* = 7.5 Hz, C(8) proton); *m/e* (relative intensity): 180 (M^+, 10.3), 152 (4.3), 137 (26.6), 109 (26.9), 96 (31.7), 83 (100.0), 55 (56.4), 41 (78.8). Exact Mass calcd. for $C_{12}H_{20}O$: 180.1514; found: 180.1513. Anal. calcd. for $C_{12}H_{20}O$: C 79.94, H 11.18; found: C 79.68, H 11.21.

*endo-3,4-Dimethylcamphor (**8**b)*

A mixture of *exo*- and *endo*-3,4-dimethylcamphor (**8***a*,*b*) (0.25 g, 1.40 mmol) in glacial acetic acid/concentrated hydrochloric acid (2.0 mL, 9:1) was heated at 80°C for 6 h. The solution was cooled, diluted with water, extracted with ether (3×), and the ether extracts washed with saturated sodium bicarbonate solution (3×) and water (3×), and dried over anhydrous magnesium sulfate. Removal of the solvent yielded a white crystalline product (0.25 g, 100% yield); 400 MHz ^1H nmr and capillary glc analysis showed the ratio of *exo*- (**8***a*) to *endo*-3,4-dimethylcamphor (**8***b*) to be 1:19. Column chromatography (silica gel 230–400 mesh, elution with petroleum ether/ether, 99:1) yielded fractions containing pure **8***b* (monitored by capillary glc), which were combined and solvent evaporated to provide **8***b* as a white crystalline solid, mp 106–108°C (sealed tube); ν_{max} ($CHCl_3$): 1720 cm^{-1}; δ ($CDCl_3$, 400 MHz): 0.73 (3H, s, C(9) methyl), 0.88 (3H, s, C(8) methyl), 0.92 (3H, s, C(10) methyl), 0.97 (3H, s, C(4) methyl), 1.10 (3H, d, *J* = 8 Hz, C(3) methyl), 1.24 (1H, m, C(5) *endo* proton), 1.47 (1H, m, C(6) *endo* proton), 1.54–1.63 (2H, m, C(6) *exo* and C(5) *exo* protons), 2.08 (1H, dq, *J* = 7.5 Hz and 2 Hz, C(3) proton); *m/e* (relative intensity): 180 (M^+, 13.1), 152 (5.9), 137 (34.0), 109 (68.0), 96 (44.0), 83 (100.0), 55 (54.6), 41 (71.0). Exact Mass calcd. for $C_{12}H_{20}O$: 180.1514; found: 180.1520. Anal. calcd. for $C_{12}H_{20}O$: C 79.94, H 11.18; found: C 79.73, H 11.20.

*Methylation of 3,4-dimethylcamphor (**8**a,b)*

To a solution of lithium diisopropylamide in dry THF (prepared from diisopropylamine (0.31 mL, 2.2 mmol) and *n*-butyl lithium (1.5 M in THF, 1.5 mL) in dry THF (5 mL) at 0°C for 15 min) was added 3,4-dimethylcamphor (**8***a*,*b*) (0.4 g, 2.2 mmol) in dry THF (5 mL) and the mixture was stirred at 0°C for 20 min. Trideuteriomethyl iodide (0.56 mL, 8.8 mmol) (purified by passing through basic alumina) was added to this solution and after 30 min the reaction mixture was acidified with HCl (1 N). Extraction with ether and work-up in the usual way provided crude 3-trideuteriomethyl-3,4-dimethylcamphor (**26***a*,*b*) as a mixture of epimers. Column chromatography (SiO_2; elution with petroleum ether:ether, 98:2) provided the epimeric mixture **26***a*,*b* as a white crystalline solid; δ ($CDCl_3$, 400 MHz): 0.76 (3H, s, $C(8)H_3$), 0.88 (3H, s, $C(9)H_3$), 0.90 (3H, s, $C(10)H_3$), 0.93 (3H, s, $C(11)H_3$), 0.97 (1H, s, *endo*-3-methyl), 1.05 (2H, s, *exo*-3-methyl). The *exo*:*endo* ratio was ~2:1.

[6]The optical purity of (−)-4-methylcamphor was ~80% (cf. ref. 23*b*).

[7]See also ref. 1, p. 850; ref. 3, p. 233.

Can. J. Chem. Downloaded from www.nrcresearchpress.com by 198.100.157.202 on 09/07/12
For personal use only.

General procedure for the aldol reaction of camphor, norcamphor, and 5,6-dehydrocamphor with aldehydes

Lithium diisopropylamide (LDA) was prepared by reaction of diisopropylamine (1.00 mL, 7.0 mmol) with *n*-butyllithium (2.50 mL of a 2.5 M solution in hexane, 6.25 mmol) in 4 mL of dry THF at −78°C. The solution was stirred for 15 min and then a solution of camphor (0.91 g, 6.0 mmol) in dry THF (4 mL) was added dropwise (15 min). After the addition, the solution was stirred for 1.5 h (in the case of **15** and **37**, 2.5 h), treated with freshly distilled aldehyde (6.0 mmol), and stirred for an additional 15 min. The reaction was quenched at −78°C with a saturated aqueous solution of $NaHCO_3$ (50 mL). The cold bath was then removed and the mixture extracted with ether (3 × 50 mL). The combined organic layers were washed with saturated NaCl, dried over Na_2SO_4, and concentrated *in vacuo* to afford the adduct mixture.

Acetylation of an exo/endo *aldol adduct mixture*

A solution of triethylamine (13.9 mL, 100 mmol), acetic anhydride (4.7 mL, 50 mmol), and DMAP (0.122 g, 1.0 mmol) was cooled to −5°C. To this was added dropwise a solution (10 mL) of the *exo*:*endo* adduct mixture in CH_2Cl_2 (15 mL). The mixture was allowed to stir for 15 min and cold water (40 mL) was added. The aqueous layer was extracted with Et_2O (3 × 20 mL). The combined organic layers were washed with 5% HCl (2 × 20 mL), saturated aqueous $NaHCO_3$ (2 × 20 mL), water (3 × 30 mL), saturated aqueous NaCl, and then dried over anhydrous Na_2SO_4. Removal of the solvent *in vacuo* afforded a mixture of the *exo*:*endo* acetates.

General procedure for the isomerization of aldol adducts

Lithium diisopropylamide (LDA) was prepared by reaction of diisopropylamine (0.168 mL, 1.2 mmol) with *n*-butyllithium (0.419 mL of a 2.5 M solution in hexane, 1.05 mmol) in 4 mL of dry THF at −78°C. The solution was stirred for 15 min and a solution of a camphor aldol adduct (2.0 mmol in 4 mL of dry THF) was added. After the addition, the cold bath was removed and the solution was stirred for 3–4 h at room temperature. The reaction was then quenched with a saturated aqueous solution of $NaHCO_3$ (10 mL). The mixture was extracted with ether (3 × 10 mL) and the combined organic layers were washed with saturated aqueous NaCl, dried over Na_2SO_4, and concentrated *in vacuo* to afford the adduct mixture.

The isomeric aldol adducts or the derived acetates in all cases were separated cleanly by semi-preparative hplc on silica using hexane/ethyl acetate mixtures that varied from 90:10 to 65:35 depending on the mixture.

exo-threo *Adduct of camphor with pivalaldehyde (**33**a, R = t-Bu)*: ir (neat): 3487, 2956, 1720, 1478, 1393, 1362, 1104, 1084, 1055, 1015 cm^{-1}; ^1H nmr (300 MHz, $CDCl_3$), δ: 3.85 (t, *J* = 13.7 Hz, 1H), 3.36 (t, *J* = 6.5 Hz, 1H), 1.96 (m, 2H), 1.81 (d, *J* = 6 Hz, 1H), 1.66 (m, 1H), 1.48 (m, 1H), 1.36 (m, 1H), 0.94 (s, 3H), 0.92 (s, 3H), 0.89 (s, 3H), 0.87 (s, 9H); ^{13}C nmr (300 MHz, $CDCl_3$), δ: 223.6, 81.1, 57.4, 53.9, 49.6, 47.4, 26.6, 29.9, 27.9, 25.3, 20.2, 20.1, 9.0; ms *m/e* calcd. for $C_{15}H_{26}O_2$ + H: 239.2010; found: 239.2007.

endo-threo *Adduct of camphor with pivalaldehyde (**33**b, R = t-Bu)*: ir (neat): 3472, 2960, 1723, 1480, 1376, 1056, 1000 cm^{-1}; ^1H nmr (300 MHz, $CDCl_3$), δ: 3.91 (d, *J* = 5.4 Hz, 1H), 3.47 (t, *J* = 12, 6 Hz, 1H), 2.53 (m, *J* = 6, 1 Hz, 1H), 2.14 (t, *J* = 4 Hz, 1H), 1.78 (bm, 3H), 1.43 (m, 1H), 1.02 (s, 3H), 0.97 (s, 9H), 0.94 (s, 3H), 0.93 (s, 3H); ^{13}C nmr (300 MHz, $CDCl_3$), δ: 223.7, 59.3, 51.8, 48.7, 46.0, 36.0, 31.3, 26.0, 21.3, 19.7, 18.9, 9.4; ms *m/e* calcd. for $C_{15}H_{26}O_2$ − *tert*-butyl: 181.1228; found: 181.1232.

exo-threo *Adduct of camphor with benzaldehyde (**33**a, R = Ph)*: ir (neat): 3483, 3040, 2950, 1718, 1494, 1454, 1392, 1328, 1290, 1272, 1228, 1202, 1101, 1073, 1040, 1024, 914, 872.4 cm^{-1}; ^1H nmr (300 MHz, $CDCl_3$), δ: 7.22 (m, 5H), 4.79 (d, *J* = 10 Hz, 1H), 4.43 (s, 1H), 2.15 (d, *J* = 10 Hz, 1H), 1.77 (m, 1H), 1.62–1.39 (bm, 4H), 1.13 (m, 1H), 0.94 (s, 3H), 0.86 (s, 3H), 0.80 (s, 3H); ^{13}C nmr (300 MHz, $CDCl_3$), δ: 223.4, 142.3, 128.8, 128.3, 127.2, 76.8, 61.4, 58.7, 47.2, 46.1, 29.6, 29.4, 22.6, 20.7, 9.5; ms *m/e* calcd. for $C_{17}H_{23}O_2$: 258.1619; found: 258.1622.

endo-threo *Adduct of camphor with benzaldehyde (**33**b, R = Ph)*: ir (neat): 3484, 2959, 2925, 2871, 1721, 1454, 1411, 1197, 1034, 1000, 766, 699 cm^{-1}; ^1H nmr (300 MHz, $CDCl_3$), δ: 7.35 (m, 5H), 4.81 (d, *J* = 10 Hz, 1H), 4.46 (s, 1H), 2.73 (m, *J* = 11, 4.4, 1 Hz, 1H), 1.73 (m, 4H), 1.52 (m, 2H), 0.97 (s, 3H), 0.93 (s, 3H), 0.98 (s, 3H); ^{13}C nmr (300 MHz, $CDCl_3$), δ: 128.6, 128.5, 128.1, 126.8, 73.9, 59.8, 56.4, 45.9, 45.8, 31.5, 21.2, 19.6, 18.5, 9.4; ms *m/e* calcd. for $C_{17}H_{23}O_2$: 258.1619; found: 258.1621.

exo-threo *Adduct of camphor with acetaldehyde (**33**a, R = CH_3)*: ir (neat): 3508, 2964, 2908, 2861, 722, 1445, 1410, 369, 1326, 1295, 1121, 1070, 1035, 921 cm^{-1}; ^1H nmr (300 MHz, $CDCl_3$), δ: 4.20 (d, 1H), 4.03 (m, 1H), 2.05 (m, 1H), 1.94 (d, *J* = 4 Hz, 1H), 1.88 (d, *J* = 10 Hz, 1H), 1.68 (m, 1H), 1.54 (m, 1H), 1.42 (m, 1H), 1.20 (d, *J* = 6 Hz, 3H), 0.94 (s, 3H), 0.91 (s, 3H), 0.88 (s, 3H); ^{13}C nmr (300 MHz, $CDCl_3$), δ: 223.6, 69.6, 61.0, 57.7, 46.8, 45.9, 29.3, 28.9, 22.0, 21.6, 20.3, 8.9; ms *m/e* calcd. for $C_{12}H_{20}O_2$: 196.1463; found: 196.1459.

endo-threo *Adduct of camphor with acetaldehyde (**33**b, R = CH_3)*: ir (neat): 3511, 2964, 2873, 1721, 1484, 1445, 1412, 1372, 1292, 1228, 1090, 1046, 1005, 939, 913, 890, 861, 794 cm^{-1}; ^1H nmr (300 MHz, $CDCl_3$), δ: 3.94 (s, 1H), 3.86 (m, 1H), 2.26 (m, *J* = 4.5, 9 Hz, 1H), 2.09 (t, *J* = 4, 8 Hz, 1H), 1.79 (m, 2H), 1.40 (m, 2H), 0.15 (d, *J* = 6 Hz, 3H), 0.98 (s, 3H), 0.91 (s, 3H), 0.88 (s, 3H); ^{13}C nmr (300 MHz, $CDCl_3$), δ: 67.6, 59.1, 56.3, 45.9, 31.5, 20.8, 20.6, 19.6, 18.6, 9.3; ms *m/e* calcd. for $C_{12}H_{20}O_2$: 196.1464; found: 196.1462.

exo-threo *Adduct of camphor with phenylacetaldehyde (**33**a, R = CH_2Ph)*: ir (neat): 3489, 3061, 3027, 2960, 2874, 1719, 1603, 1495, 1453, 1406, 1372, 1326, 1295, 1105, 1081, 1048, 1027, 750, 700 cm^{-1}; ^1H nmr (300 MHz, $CDCl_3$), δ: 7.27 (m, 5H), 4.29 (s, 1H), 4.18 (m, *J* = 10, 6, 4 Hz, 1H), 2.95 (dd, *J* = 14, 4 Hz, 1H), 2.71 (dd, *J* = 14, 6.6 Hz, 1H), 2.01 (m, 2H), 1.89 (d, *J* = 10 Hz, 1H), 1.66 (m, 1H), 1.49 (m, 1H), 1.32 (m, 1H), 0.94 (s, 3H), 0.92 (s, 3H), 0.90 (s, 3H); ^{13}C nmr (300 MHz, $CDCl_3$), δ: 137.7, 129.8, 128.2, 126.4, 74.1, 58.1, 57.8, 46.9, 45.9, 42.1, 29.1, 28.9, 21.7, 20.4, 9.1; ms *m/e* calcd. for $C_{18}H_{24}O_2 - H_2O$: 254.1671; found: 254.1671.

endo-threo *Adduct of camphor with phenylacetaldehyde (**33**b, R = CH_2Ph) as its acetate*: ir (neat): 2859, 2872, 1738, 1490, 1453, 1371, 1234, 1143, 1067, 1028 cm^{-1}; ^1H nmr (300 MHz, $CDCl_3$), δ: 7.26 (m, 5H), 5.34 (m, *J* = 8, 4 Hz, 1H), 3.02 (m, *J* = 4 Hz, 1H), 2.80 (m, *J* = 8 Hz, 1H), 2.47 (m, 1H), 2.13 (t, *J* = 4 Hz, 1H), 2.01 (s, 3H), 1.87 (m, 1H), 1.74–1.51 (bm, 3H), 0.99 (s, 3H), 0.88 (s, 3H), 0.83 (s, 3H); ^{13}C nmr (300 MHz, $CDCl_3$), δ: 216.7, 136.8, 129.5, 128.4, 126.7, 72.2, 58.8, 50.7, 46.4, 45.5, 40.0, 30.0, 21.1, 19.4, 18.9, 9.5.

exo-threo *Adduct of camphor with isobutyraldehyde (**33**a, R = i-Pr) as its acetate*: ir (neat): 2963, 1741, 1466, 1389, 371, 1239, 1129, 1102, 1021, 939 cm^{-1}; ^1H nmr (300 MHz, $CDCl_3$), δ: 5.12 (dd, *J* = 2, 10.5 Hz, 1H), 2.05 (s, 3H), 1.93 (m, *J* = 2 Hz, 1H), 1.99–1.87 (bm, 3H), 1.57 (m, 1H), 1.37 (m, 2), 0.92 (s, 3H), 0.86 (s, 3H), 0.84 (d, *J* = 2 Hz, 6H), 0.82 (s, 3H); ^{13}C nmr (300 MHz, $CDCl_3$), δ: 218.3, 170.8, 76.2, 7.9, 54.9, 46.2, 45.9, 30.0, 29.6, 29.2, 21.5, 20.9, 20.2, 19.2, 15.0, 9.2; ms *m/e* calcd. for $C_{16}H_{26}O_3 - COCH_3$: 223.1697; found: 223.1701.

endo-threo *Adduct of camphor with isobutyraldehyde (**33**b, R = i-Pr) as its acetate*: ir (neat): 2962, 2875, 1740, 1486, 1467, 1390, 1371, 1323, 1239, 1185, 1130, 1102, 1021, 994, 939, 893 cm^{-1}; ^1H nmr (300 MHz, $CDCl_3$), δ: 5.03 (dd, *J* = 10 Hz, 1H), 2.41 (m, *J* = 10, 4 Hz, 1H), 2.06 (s, 3H), 1.98 (t, *J* = 4 Hz, 1H), 1.75 (m, 2H), 1.61 (m, 1H), 1.46 (m, 2H), 0.92 (s, 3H), 0.85 (m, 6H), 0.84 (s, 3H), 0.80 (s, 3H); ^{13}C nmr (300 MHz, $CDCl_3$), δ: 217.5, 170.9, 74.6, 58.6, 49.2, 46.0, 45.3, 30.0, 29.7, 21.2, 21.0, 19.3, 18.8, 14.8, 9.4; ms *m/e* calcd. for $C_{16}H_{26}O_3$ + H: 267.1960; found: 267.1955.

exo-threo *Adduct of camphor with propionaldehyde (**33**a, R = Et) as its acetate*: ir (neat): 2963, 2878, 1739, 1461, 1394, 1372, 1242,

Can. J. Chem. Downloaded from www.nrcresearchpress.com by 198.100.157.202 on 09/07/12
For personal use only.

1112, 1080, 1044, 1018, 965 cm^{-1}; ^1H nmr (300 MHz, C_6D_6), δ: 5.28 (m, 1H), 1.98 (s, 3H), 1.78 (d, J = 10.5 Hz, 1H), 1.56–1.39 (bm, 3H), 1.28–1.04 (bm, 3H), 0.84 (s, 3H), 0.81 (s, 3H), 0.78 (t, J = 7 Hz, 3H), 0.50 (s, 3H); ^{13}C nmr (300 MHz, $CDCl_3$), δ: 217.8, 170.9, 74.4, 58.0, 56.6, 46.4, 29.7, 29.3, 27.0, 21.5, 21.2, 20.3, 9.3, 8.9; ms m/e calcd. for $C_{15}H_{24}O_3$ − CH_3COOH: 192.1514; found: 192.1511.

endo-threo *Adduct of camphor with propionaldehyde (**33**b, R = i-Pr) as its acetate*: ir (neat): 2966, 2877, 1741, 1458, 1372, 1252, 1088, 1050, 1024, 966, 891 cm^{-1}; ^1H nmr (300 MHz, C_6D_6), δ: 5.21 (m, 1H), 2.24 (m, J = 9, 4 Hz, 1H), 1.95 (s, 3H), 1.49 (t, J = 4 Hz, 1H), 1.44–1.12 (bm, 6H), 0.81 (t, J = 7 Hz, 3H), 0.78 (s, 3H), 0.52 (s, 3H), 0.48 (s, 3H); ^{13}C nmr (300 MHz, $CDCl_3$), δ: 217.1, 171, 72.7, 58.7, 51.0, 56.3, 45.4, 30.1, 26.4, 21.2, 21.1, 19.4, 18.9, 9.5, 8.9; ms m/e calcd. for $C_{15}H_{24}O_3$ + H: 253.1803; found: 253.1809.

exo-threo *Adduct of camphor with 2-furaldehyde (**33**a, R = 2-furyl) as its acetate*: ir (neat): 2962, 2874, 1741, 1502, 1447, 1393, 1372, 1230, 1151, 1107, 1014, 964, 925, 884, 754 cm^{-1}; ^1H nmr (300 MHz, $CDCl_3$), δ: 7.39 (s, 1H), 6.32 (m, 1H), 6.16 (d, J = 11 Hz, 1H), 2.64 (d, J = 11 Hz, 1H), 2.09 (s, 3H), 1.97 (m, 1H), 1.62 (m, 1H), 1.27 (m, 4H), 0.99 (s, 3H), 0.89 (s, 3H), 0.86 (s, 3H); ^{13}C nmr (300 MHz, $CDCl_3$), δ: 216.7, 170.0, 151.5, 142.9, 110.2, 109.3, 68.0, 58.4, 54.7, 46.2, 46.3, 29.4, 29.0, 21.5, 21.0, 20.1, 9.3; ms m/e calcd. for $C_{16}H_{22}O_4$: 290.1518; found: 290.1522.

endo-threo *Adduct of camphor with 2-furaldehyde (**33**b, R = 2-furyl) as its acetate*: ir (neat): 2961, 2925, 1743, 1502, 1458, 1369, 1229, 1151, 1013, 966, 925, 745 cm^{-1}; ^1H nmr (300 MHz, $CDCl_3$), δ: 7.41 (s, 1H), 6.35 (m, 1H), 6.08 (d, J = 11 Hz, 1H), 3.06 (dd, J = 11, 4.5 Hz, 1H), 2.12 (s, 3H), 1.83 (m, 1H), 1.66 (m, 2H), 1.53 (m, 3H), 0.94 (s, 3H), 0.91 (s, 3H), 0.90 (s, 3H); ^{13}C nmr (300 MHz, $CDCl_3$), δ: 216.5, 170.2, 151.2, 142.9, 110.3, 109.2, 66.6, 50.0, 46.2, 45.3, 30.5, 21.2, 21.1, 19.5, 18.8, 9.5; ms m/e calcd. for $C_{17}H_{22}O_4$: 290.1518; found: 290.1520.

endo-threo *Adduct of 5,6-dehydrocamphor with benzaldehyde (**34**a)*: ir (neat): 3495, 3062, 3030, 2964, 2929, 2870, 1718, 1604, 1493, 1454, 1410, 1333, 1292, 1267, 1240, 1223, 1198, 1073, 1040, 1016, 920, 864, 786, 726, 700 cm^{-1}; ^1H nmr (300 MHz, $CDCl_3$), δ: 7.40–7.29 (m, 5H), 6.54 (d, J = 3 Hz, 1H), 5.67 (d, J = 5.5 Hz, 1H), 4.39 (d, J = 10 Hz, 1H), 4.29 (s, 1H), 2.67 (dd, J = 9, 3 Hz, 1H), 2.17 (s, 1H), 1.08 (s, 3H), 1.01 (s, 3H), 0.92 (s, 3H); ^{13}C nmr (300 MHz, $CDCl_3$), δ: 219.5, 141.3, 141.2, 133.3, 128.5, 128.0, 126.4, 78.8, 67.1, 60.4, 53.5, 51.4, 19.7, 18.6, 6.9; ms m/e calcd. for $C_{17}H_{21}O_2$: 256.1463; found: 256.1463.

exo-threo *Adduct of 5,6-dehydrocamphor with benzaldehyde (not shown)*: ir (neat): 3491, 3051, 3029, 2953, 2928, 2870, 1720, 1446, 1406, 1390, 1368, 1332, 1276, 1258, 1071, 1042, 1020, 996, 743, 701 cm^{-1}; ^1H nmr (300 MHz, $CDCl_3$), δ: 7.40–7.29 (m, 5H), 6.43 (m, J = 5.5, 3 Hz, 1H), 5.66 (d, J = 6 Hz, 1H), 4.97 (d, J = 10 Hz, 1H), 4.45 (s, 1H), 2.43 (d, J = 10 Hz, 1H), 2.33 (d, J = 3 Hz, 1H), 1.15 (s, 3H), 1.06 (s, 3H), 1.03 (s, 3H); ^{13}C nmr (300 MHz, $CDCl_3$), δ: 144.9, 134.3, 128.5, 128.0, 128.0, 126.7, 75.1, 66.4, 61.6, 54.6, 51.9, 21.9, 20.7, 7.1.

exo-threo *Adduct of 5,6-dehydrocamphor with pivalaldehyde (**34**b)*: ir (neat): 3483, 3065, 2959, 2871, 1716, 1482, 1468, 1447, 1413, 1380, 1362, 1312, 1291, 1242, 1212, 1182, 1083, 1053, 1032, 1012, 935, 884, 786, 730 cm^{-1}; ^1H nmr (300 MHz, $CDCl_3$), δ: 6.46 (dd, J = 6, 3 Hz, 1H), 5.58 (d, J = 5 Hz, 1H), 4.20 (d, J = 3 Hz, 1H), 3.04 (dd, J = 8, 2 Hz, 1H), 2.73 (t, J = 3 Hz, 1H), 2.42 (dd, J = 8, 3 Hz, 1H), 1.06 (s, 3H), 1.03 (s, 3H), 0.94 (s, 3H), 0.93 (s, 9H); ^{13}C nmr (300 MHz, $CDCl_3$), δ: 221.1, 141.4, 132.7, 82.6, 66.2, 60.1, 53.5, 48.0, 36.0, 26.1, 19.7, 18.9, 7.0; ms m/e calcd. for $C_{15}H_{24}O_2$: 236.1776; found: 236.1771.

exo-threo *Adduct of norcamphor with benzaldehyde (**36**a)*: ir (neat): 3503, 2960, 2876, 1728, 1457, 1395, 1327, 1194, 1078, 1045, 1006, 940, 862, 768, 707 cm^{-1}; ^1H nmr (300 MHz, $CDCl_3$), δ: 7.39–7.33 (m, 5H), 4.64 (d, J = 10 Hz, 1H), 4.09 (s, 1H), 2.72 (d, J = 4 Hz, 1H), 2.13 (d, J = 1 Hz, 1H), 2.06 (m, J = 10, 3 Hz, 2H), 1.79 (m, 2H), 1.57 (m, 2H), 1.37 (m, 1H); ^{13}C nmr (300 MHz, $CDCl_3$), δ: 220.8, 141.4, 128.5, 128.1, 126.8, 73.6, 59.5, 49.8, 37.6, 35.4, 28.0, 23.4; ms m/e calcd. for $C_{14}H_{16}O_2$: 216.1150; found: 216.1148.

exo-threo *Adduct of norcamphor with pivalaldehyde (**36**b)*: ir (neat): 3528, 2955, 2871, 1737, 1476, 1450, 1390, 1363, 1323, 1304, 1280, 1243, 1220, 1183, 1116, 1080, 1046, 1010, 996, 945, 899, 763, 744 cm^{-1}; ^1H nmr (300 MHz, $CDCl_3$), δ: 3.30 (m, J = 8 Hz, 1H), 2.90 (d, J = 8 Hz, 1H), 2.58 (d, J = 3 Hz, 1H), 2.49 (d, 1H), 2.10 (t, 1H), 1.83 (m, 3H), 1.51 (m, 3H), 0.93 (s, 9H); ^{13}C nmr (300 MHz, $CDCl_3$), δ: 221.2, 79.9, 55.0, 49.3, 42.2, 36.4, 35.0, 27.4, 25.6, 24.2; ms m/e calcd. for $C_{12}H_{20}O_2$: 196.1463; found: 196.1465.

Acknowledgments

This work was supported by NSERC, Ottawa, Canada, and by an Atlantic Richfield grant of Research Corporation. We wish to thank Professor David Minter for very helpful discussions.

1. E. Josephy and F. Radt (*Editors*). Elsevier's encyclopaedia of organic chemistry. Vol. 12A. Elsevier, Amsterdam. 1948.
2. J. L. Simonsen and L. N. Owen. The terpenes. Vol. II. 2nd ed. (rev). Cambridge University Press, London. 1957.
3. A. Pelter and S. H. Harper. *In* Rodd's chemistry and carbon compounds, Vol. IIc. *Edited by* S. Coffey. Elsevier, Amsterdam. 1969.
4. R. T. Brown. *In* Rodd's chemistry of carbon compounds. Suppl. Vol. IIc. *Edited by* M. F. Ansell. Elsevier, Amsterdam. 1974.
5. (*a*) W. F. Erman. Chemistry of monoterpenes. Part A. *Edited by* P. G. Gassmann. Marcel Dekker, New York. 1985; (*b*) Chemistry of monoterpenes. Part B. *Edited by* P. G. Gassmann. Marcel Dekker, New York. 1985.
6. H. Rupe and M. Lenzlinger. Helv. Chim. Acta, **18**, 255 (1935).
7. K. M. Baker and B. R. Davis. Tetrahedron, **24**, 1655 (1968).
8. (*a*) J. H. Hutchinson and T. Money. Can. J. Chem. **62**, 1899 (1984); (*b*) J. H. Hutchinson. Ph.D. Thesis, University of British Columbia, Vancouver (1985); (*c*) T. Money. Studies in natural product chemistry. Vol. 4. Stereoselective Syntheses (Part C). *Edited by* Atta-ur-Rahman. Elsevier, Amsterdam. 1989.
9. R. V. Stevens and D. S. Lawrence. Tetrahedron, **41**, 93 (1985).
10. H. Shibuya, H. Fujioka, A. Kajiwara, Y. Yamamoto, and I. Kitagawa. Tetrahedron, **30**, 1271 (1982).
11. K. Ishihara, H. Yamamoto, and C. H. Heathcock. Tetrahedron Lett. **30**, 1825 (1989).
12. (*a*) N. L. McClure, G.-Y. Dai, and H. S. Mosher. J. Org. Chem. **53**, 2617 (1988); (*b*) N. Holy, R. Fowler, E. Burnett, and R. Lorenz. Tetrahedron, **35**, 613 (1979).
13. (*a*) P. A. Grieco, T. Takigawa, and D. R. Moore. J. Am. Chem. Soc. **101**, 4380 (1979); (*b*) P. A. Grieco, G. F. Majetich, and Y. Ohfune. J. Am. Chem. Soc. **104**, 4226 (1982); (*c*) P. A. Grieco, Y. Ohfune, G. F. Majetich, and C.-L. J. Wang. J. Am. Chem. Soc. **104**, 4233 (1982).
14. B. M. Trost, P. R. Bernstein, and P. C. Funfschilling. J. Am. Chem. Soc. **101**, 4378 (1979).
15. (*a*) P. A. Grieco, Y. Ohfune, Y. Yokoyama, and W. Owens. J. Am. Chem. Soc. **101**, 4749 (1979); (*b*) P. A. Grieco, J. Inanaga, N.-H. Lin, and T. Yanami. J. Am. Chem. Soc. **104**, 5781 (1982).
16. E. J. Corey, R. Hartmann, and P. A. Vatakencherry. J. Am. Chem. Soc. **84**, 2611 (1962).
17. H. O. House and M. J. Umen. J. Org. Chem. **38**, 1000 (1973).
18. W. M. Dadson, J. H. Hutchinson, and T. Money. Can. J. Chem. **68**, 1821 (1990).
19. L. A. Heitaniemi and P. J. Malkonen. Dev. Biochem. **23**, 477 (1982); Chem. Abstr. **98**, 156960x (1983).

20. Y. ASAHINA, M. ISHIDATE, and T. TUKAMOTO. Chem. Ber. **69B**, 345 (1936); **69B**, 355 (1936); Chem. Abstr. **30**, 3804 (1936); **30**, 3805 (1936).
21. B. E. BAYS, R. C. COOKSON, and S. MACKENZIE. J. Chem. Soc. (B), 215 (1967).
22. H.-J. LIU and W. H. CHAN. Can. J. Chem. **60**, 1081 (1982).
23. (*a*) M. P. CAVA, R. L. LITTLE, and D. R. NAPIER. J. Am. Chem. Soc. **80**, 2257 (1958); (*b*) J. A. CLASE, D. L. F. LI, D. LO, and T. MONEY. Can. J. Chem. **68**, 1829 (1990).
24. L. RICHOU, V. VAILLANCOURT, D. J. FAULKNER, and K. F. ALBIZATI. J. Org. Chem. **54**, 4729 (1989).
25. (*a*) C. H. HEATHCOCK, M. C. PIRRUNG, and J. E. SOHN. J. Org. Chem. **44**, 4294 (1979); (*b*) J. L. MARSHALL and S. R. WALTER. J. Am. Chem. Soc. **96**, 6358 (1974).
26. V. A. MARTIN and K. F. ALBIZATI. J. Org. Chem. **53**, 5986 (1988).

Can. J. Chem. Downloaded from www.nrcresearchpress.com by 198.100.157.202 on 09/07/12
For personal use only.

Application of ^{59}Co NMR to the investigation of interactions between cobalt sepulchrate and various counterions

JOÃO SOTOMAYOR, HELENA SANTOS, AND FERNANDO PINA[1]

Faculdade de Ciências e Tecnologia, Universidade Nova de Lisboa, Quinta da Torre, 2825 Monte de Caparica, Portugal and Centro de Tecnologia Química e Biológica, Apartado 127, 2780 Oeiras, Portugal

Received July 6, 1990

JOÃO SOTOMAYOR, HELENA SANTOS, and FERNANDO PINA. Can. J. Chem. **69**, 567 (1991).

Association constants for the ion pairs formed between $[Co(Sep)]^{3+}$ and the anions fluoride, chloride, bromide, iodide, perchlorate, and oxalate were obtained from the chemical shifts of the ^{59}Co resonance that occur upon addition of such anions to solutions of the cobalt complex. The usefulness of ^{59}Co NMR to obtain formation constants, in order to calculate the "true" quantum yields for the ion pairs, is discussed.

Key words: association constant, cobalt sepulchrate, ion pair, ^{59}Co NMR, quantum yield.

JOÃO SOTOMAYOR, HELENA SANTOS et FERNANDO PINA. Can. J. Chem. **69**, 567 (1991).

Faisant appel aux déplacements chimiques observés dans les spectres RMN du ^{59}Co lors de l'addition de tels anions à des solutions du complexe de cobalt, on a déterminé les constantes d'association des paires d'ions qui se forment entre le $[Co(Sep)]^{3+}$ et les anions fluorure, chlorure, bromure, iodure, perchlorate et oxalate. On discute de l'utilité de la RMN du ^{59}Co pour la détermination des constantes de formation nécessaires pour calculer les «vrais» rendements quantiques des paires d'ions.

Mots clés : constante d'association, sépulchrate de cobalt, paire d'ions, RMN du ^{59}Co, rendement quantique.

[Traduit par la rédaction]

Introduction

Solutions of Co(III) complexes (for instance $Co(NH_3)_6^{3+}$ and $Co(en)_3^{3+}$ (en = ethylenodiamine)) and several reductive anions, such as I^-, exhibit deviations from additivity of their electronic absorption spectra due to the appearance of a new band, which has been ascribed to an ion pair charge transfer (IPCT) from the anion to the metal (1). We have reported a similar behaviour for the $Co(Sep)^{3+}$ complex (Sep = sepulchrate = 1,3,6,8,10,13,16,19-octaazabicyclo[6.6.6]eicosane) and the anions I^- (2), oxalate (3), and citrate (4). Irradiation in this "new band" causes the formation of photoproducts, a result that has been interpreted as due to the thermal evolution of the primary species, $Co(Sep)^{2+}$, and the oxidized anion, and that supports the previous identification of the IPCT band. It was also shown that the association constants for this kind of ion pair are not very high and, therefore, the assumption that all the complex is involved in the ion pair is not valid. As a consequence, to calculate the quantum yields for the irradiation in the IPCT band, based on the light absorbed by the ion pair, the so called "true" quantum yield, it is essential to evaluate their association constants.

Two important factors must be taken into account, regardless of the physical method that is selected to obtain the association constants of the ion pairs: (i) the influence of the "innocent" anions (i.e., anions that in principle do not cause any effect on the physical variable that is measured) that are used to keep the ionic strength constant; (ii) the presence of higher order ion pairs, such as $[Co(Sep)^{3+}(X^-)_2]^-$ and $[Co(Sep)^{3+}(X^-)_3]$ (X = anion).

Previously we used a spectrophotometric technique to determine the association constants of ion pairs (5). However, the results do not provide definite information about either the effect of the innocent anion or the formation of higher order ion pairs.

Laszlo and co-workers (6) have shown that ^{59}Co NMR is a sensitive probe for investigating ion pairing. In the present article, ion association is monitored by ^{59}Co NMR and the dependence of the ^{59}Co chemical shift upon addition of the counterion is investigated.

Experimental

$Co(Sep)Cl_3 \cdot H_2O$ was synthesized following the method of Sargeson and co-workers (7) as modified by Indelli.[2] All chemicals used in this preparation and in subsequent operations were of reagent grade.

NMR spectra were recorded using a Bruker CXP-300 spectrometer operating at 71.2 MHz for ^{59}Co. The spectral width was 20 000 Hz and 8192 points were used for data acquisition. The probe temperature was kept at 298 K using the standard VT unit of the Bruker spectrometer and at least 15 min were allowed for thermal equilibration of each sample. The spectra were run without spinning the NMR tube. A coaxial capillary containing D_2O was inserted into the 10 mm NMR tube, to provide a lock signal.

Aqueous solutions of several electrolytes (KF, KCl, KBr, KI, $NaClO_4$, $K_2C_2O_4$) with different concentrations and 5 mM cobalt sepulchrate were prepared. Spectra were recorded and shifts of the cobalt resonance were measured, relative to the $Co(Sep)^{3+}$ chloride salt solution spectrum.

All the electrolytes had potassium as the counterion, except perchlorate, for solubility reasons.

Results and discussion

Although addition of perchlorate, used to maintain a constant ionic strength, does not change the electronic absorption spectra of cobalt amino complexes, being regarded as the innocent anion, it gives rise to a chemical shift of the ^{59}Co NMR absorption band. For this reason all the experiments were performed at uncontrolled ionic strength.

Figure 1 shows the observed chemical shift of the ^{59}Co resonance of aqueous solutions containing 5×10^{-3} M $Co(Sep)^{3+}$ in the presence of the anions F^-, Cl^-, Br^-, I^-, ClO_4^-, and $C_2O_4^{2-}$. Sodium salts of the added anions show the same chemical shifts in the ^{59}Co resonance as the potassium analogues.

The simplest model to account for the observed resonance shift on the cobalt(III) complex, M, upon addition of anion, A,

[1]Author to whom correspondence may be addressed.

[2]A. Indelli, private communication.

Printed in Canada / Imprimé au Canada

Can. J. Chem. Downloaded from www.nrcresearchpress.com by 195.138.81.100 on 09/07/12
For personal use only.

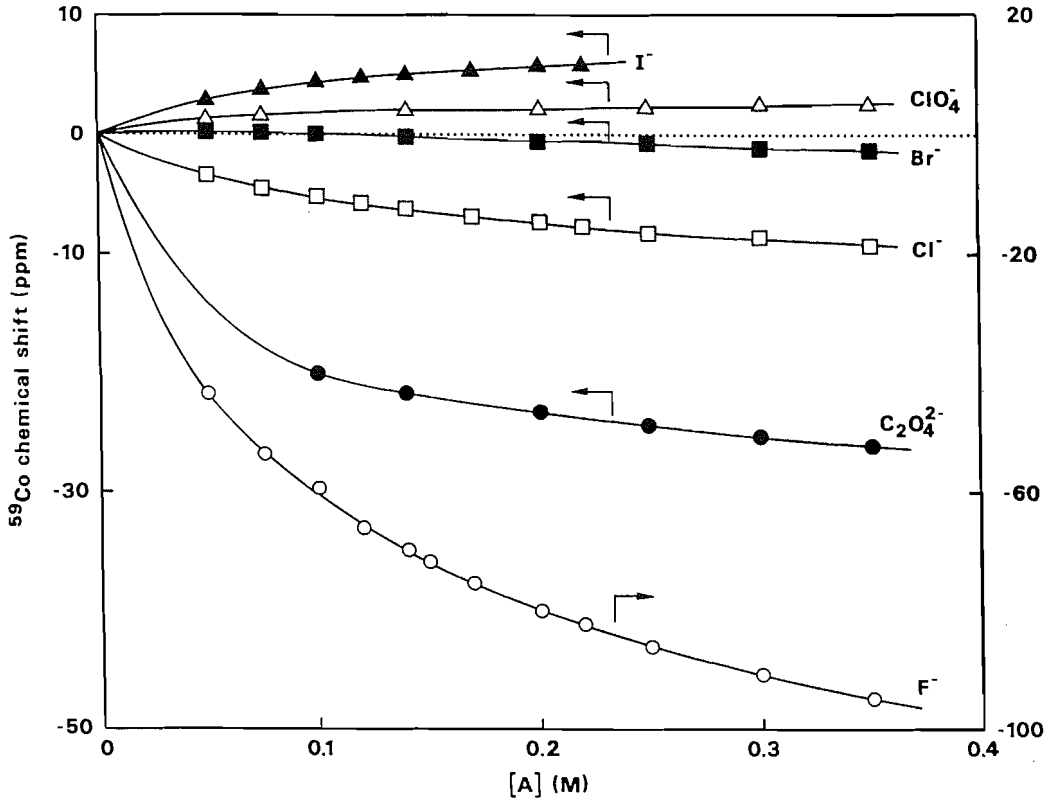


FIG. 1. ^{59}Co chemical shift of aqueous solutions containing 5×10^{-3} M $Co(Sep)^{3+}$ and various anions.

TABLE 1. Thermodynamic association constants calculated from ^{59}Co chemical shifts for the $Co(Sep)^{3+}$ ion paired with various anions, assuming 1:1 equilibrium

Anion	K_1^0	Δw_1(ppm)
F^-	35 ± 1	−123 ± 1
Cl^-	23 ± 1	−13.4 ± 0.2
Br^-	—	−0.5[a]
I^-	31 ± 1	9.1 ± 0.2
ClO_4^-	41 ± 2	3.10 ± 0.05
$C_2O_4^{2-}$	277 ± 68	−26.5 ± 0.2

[a]Innocent anion. Estimated value.

is demonstrated by considering equilibrium [1] and eq. [2]

[1] $M + A \rightleftharpoons MA$

$$[2] \quad K_1^0 = \frac{[MA]}{[M][A]} \frac{f_{MA}}{f_M f_A} = K_1 f_1$$

in which K_1^0 is the thermodynamic formation constant at infinite dilution, and f_i are the activity factors, calculated by the Davies type expression, valid up to 1 M (8).

$$[3] \quad \log f_i = -AZ_i^2\left(\frac{\sqrt{I}}{1 + Ba\sqrt{I}} - CI\right)$$

where $C = 0.3$ and the other parameters have the usual meaning.

Working on a large excess of A, eq. [4] is obtained:

$$[4] \quad W_{obs} - W_{obs(0)} = \frac{\Delta w_1 K_1^0 [A]_0}{f_1 + K_1^0 [A]_0}$$

where W_{obs} is the ^{59}Co NMR frequency upon addition of the anion $[A]_0$, to an initial concentration of metal complex $[M]_0$, $W_{obs(0)}$ is the resonance of the free complex, and $\Delta w_2 = w_1 - w_0$ is the difference between the adduct and the complex frequencies, respectively. This equation is formally equivalent to the one obtained for the spectrophotometric method, with the difference that the ^{59}Co NMR frequencies replace the molar absorptivities at the wavelength used. For this reason the known Benesi–Hildebrand approach (9) developed for the spectrophotometric method, slightly modified to account for the ionic strength changes, can also be used.

$$[5] \quad \frac{[A]_0}{W_{obs} - W_{obs(0)}} \times \frac{1}{f_1} = \frac{1}{K_1^0 \Delta w_1} + \frac{1}{\Delta w_1} \frac{[A]_0}{f_1}$$

A plot of $\dfrac{[A]_0}{W_{obs} - W_{obs(0)}} \times \dfrac{1}{f_1}$ versus $\dfrac{[A]_0}{f_1}$ will give a linear relation from which it is possible to obtain the thermodynamic formation constant, and the frequency of the resonance of the adduct. The results are summarized in Table 1. The values of the a parameter are 6 Å for the $Co(Sep)^{3+}$ and $[Co(Sep)^{3+}.X^{n-}]^{(3-n)+}$ ion pairs by comparing with similar cases (10), 3 Å for F^-, Cl^-, Br^-, and I^- (10*b*), 3.5 Å for ClO_4^-, and 4.5 Å for oxalate ion (10*a*). The errors presented for $(K_1^0, \Delta w_1)$ and $(K_1^0, \Delta \varepsilon_1)$ were obtained from the construction of the joint confidence region, for the plots of eq. [5] (11, 12).

If we consider a more complex model, adding one or two more equilibria in order to account for higher order adducts, a generalized Benesi–Hildebrand equation is obtained (5), eq. [8]:

[6] $MA + A \overset{K_2}{\rightleftharpoons} MA_2$

[7] $MA_2 + A \overset{K_3}{\rightleftharpoons} MA_3$

Can. J. Chem. Downloaded from www.nrcresearchpress.com by 195.138.81.100 on 09/07/12
For personal use only.

TABLE 2. Thermodynamic association constants by NMR and spectrophotometric methods, assuming 1:1 equilibrium

	Method			
	Spectrophotometric		NMR	
Anion	K_1^0	$\Delta\varepsilon_1^{max}$ (M^{-1} cm^{-1})	K_1^0	Δw_1 (ppm)
F^-	[a]	[a]	35 ± 1	−123 ± 1
Cl^-	21 ± 5	1054 ± 46	23 ± 1	−13.4 ± 0.2
Br^-	23 ± 1	1393 ± 7	[b]	[b]
I^-	22 ± 1	829 ± 28	31 ± 1	9.1 ± 0.2
ClO_4^-	[b]	[b]	41 ± 2	3.10 ± 0.05
$C_2O_4^{2-}$	597 ± 112	1005 ± 93	277 ± 68	−26.5 ± 0.2

[a]Not measurable.
[b]Innocent anion.

$$[8] \quad \frac{[A]_0}{W_{obs} - W_{obs(0)}} \times \frac{1}{f_1} = \frac{1}{K_1^0 \beta_1} + \frac{\beta_2}{\beta_1} \frac{[A]_0}{f_1}$$

where

$$[9] \quad \beta_1 = \Delta w_1 + \frac{K_2^0}{f_2} \Delta w_2 [A]_0 + \frac{K_2^0}{f_2} \frac{K_3^0}{f_3} \Delta w_3 [A]_0^2$$

$$[10] \quad \beta_2 = 1 + \frac{K_2^0}{f_2} [A]_0 + \frac{K_2^0}{f_2} \frac{K_3^0}{f_3} [A]_0^2$$

and $\Delta w_2 = w_2 - w_0$ and $\Delta w_3 = w_3 - w_0$ where w_2 and w_3 are the frequencies of the resonance of MA_2 and MA_3 adducts, respectively.

The ^{59}Co NMR chemical shifts reported in Fig. 1 become more markedly high field as the hydrogen bond ability of the various anions increases. This ability depends on the electronegativity of the anion placed near the cobalt ion, which will increase the shielding on the ^{59}Co nucleus. In fact, we observed a high field chemical shift in the order $F^- > Cl^- > Br^- > I^-$.

Similar results were described by Masuda *et al.* (13) for $Co(en)_3^{3+}$ and different anions, and were attributed in part to the deformation of the coordination sphere of the Co(III) ion.

As all NMR spectra are referred to the $Co(Sep)^{3+}$ chloride salt solution spectrum, what we define as the zero chemical shift includes the small interaction between the cobalt ion and the Cl^- (negligible because of the small concentration of the chloride) and the shielding of the water molecules in the solvation sphere. Therefore, Fig. 1 shows the competition for hydrogen bonding between the water molecules and the various anions. In the case of Br^-, this anion has an effect equivalent to the water and we observe almost zero chemical shift.

Fitting of eq. [8] for the simultaneous 1:1 and 1:2 equilibria gives a large uncertainty for the second constant, which indicates that the ^{59}Co NMR does not give any experimental evidence for the formation of higher order adducts.

The fact that equilibrium [1] gives good results in the NMR chemical shift method does not indicate that this equilibrium is the only one present in solution. The method is not sensitive enough to reveal the small deviations in the linearity of eq. [5] that would result from higher order ionic interactions.

Different values of the association constant for a given ion pair are usually obtained by independent physical methods, such as NMR and UV/VIS absorption (Table 2). For instance, ClO_4^- is either an innocent or an active anion depending on the method used to probe its behaviour.

The UV/VIS absorption technique is based on the observation of the IPCT, which results from the combination of the molecular orbitals (HOMO–LUMO) of the anion and the metal complex. This interaction is clearly at the shorter distance range, when compared with ^{59}Co NMR, where several longer distance interactions are expected to affect the chemical shift (6, 14).

In conclusion, the application of physical methods other than UV/VIS absorption, to calculate the association constants required for evaluation of the fraction of the light absorbed by the ion pair, is not useful. In fact, the ion pair is "defined" by the detection method, since different physical methods measure different association constants.

Acknowledgements

We are grateful to Professor A. V. Xavier for suggesting the use of ^{59}Co NMR, and to the Instituto Nacional de Investigação Científica for financial support.

1. V. BALZANI and V. CARASSITI. Photochemistry of coordination compounds. Academic Press, London. 1970.
2. F. PINA, M. CIANO, L. MOGGI, and V. BALZANI. Inorg. Chem. **24**, 844 (1985).
3. F. PINA, Q. G. MULAZZANI, M. VENTURI, M. CIANO, and V. BALZANI. Inorg. Chem. **24**, 848 (1985).
4. J. SOTOMAYOR, J. C. COSTA, Q. G. MULAZZANI, and F. PINA. J. Photochem. Photobiol. A, **49**, 195 (1989).
5. F. PINA, J. SOTOMAYOR, and L. MOGGI. J. Photochem. Photobiol. A. In press.
6. A. DEVILLE, P. LASZLO, and A. STOKIS. J. Am. Chem. Soc. **103**, 5991 (1981).
7. I. I. CREASER, R. J. GEUE, J. M. HARROWFIELD, A. J. HERLT, A. M. SARGESON, M. R. SNOW, and J. SPRINGBORG. J. Am. Chem. Soc. **104**, 6016 (1982).
8. C. W. DAVIES. Ion association. Butterworths, London. 1962.
9. H. A. BENESI and J. H. HILDEBRAND. J. Am. Chem. Soc. **71**, 2703 (1949).
10. (*a*) J. KIELLAND. J. Am. Chem. Soc. **59**, 1675 (1937); (*b*) N. TANAKA, Y. KOBAYASHI, and M. KAMADA. Bull. Chem. Soc. Jpn. **40**, 2839 (1967).
11. J. MANDEL and F. J. LINNIG. Anal. Chem. **29**, 743 (1957).
12. M. D. PATTENGILL and D. E. SANDS. J. Chem. Educ. **56**, 244 (1979).
13. Y. MASUDA and H. YAMATERA. J. Phys. Chem. **92**, 2067 (1988).
14. S. R. COHEN. J. Phys. Chem. **61**, 1670 (1957).

Can. J. Chem. Downloaded from www.nrcresearchpress.com by 195.138.81.100 on 09/07/12
For personal use only.

The synthesis of nor- and bisnorlupanes[1,2]

AMAL WAHHAB,[3] MARGARET OTTOSEN, AND FRANK W. BACHELOR
Department of Chemistry, The University of Calgary, Calgary, Alta., Canada T2N 1N4

Received July 6, 1990

AMAL WAHHAB, MARGARET OTTOSEN, and FRANK W. BACHELOR. Can. J. Chem. **69**, 570 (1991).

In the course of our studies on geochemical biomarkers we required a series of lupane standards. We report here an efficient synthesis of lupane (**1**) in three steps from betulin (**3**) in an overall yield of 47.2%. 17β(H)-28-Norlupane (**2**) was obtained in 90% purity employing Barton's method for the decarboxylation of 3-oxolupan-28-oic acid (**10**). 24,28-Bisnorlupane (**4**) and 24-norlupane (**5**) were obtained by a series of reactions involving formation of the oxime, the seconitrile, the epoxynitrile, ring closure, and finally a Wolff–Kishner reduction of the C3 carbonyl to the methylene. Also, to aid in the quantitative determination of these lupanes from oil shales and geological samples, 3-deuterolupane (**6**) and 2,3-dideuterolupane (**7**) were needed, and a method for their preparation is reported.

Key words: lupane, 24-norlupane, 28-norlupane, 24,28-bisnorlupane, 3-deuterolupane, 2,3-dideuterolupane.

AMAL WAHHAB, MARGARET OTTOSEN et FRANK W. BACHELOR. Can. J. Chem. **69**, 570 (1991).

Dans le cadre de nos études sur les biomarqueurs géochimiques, on a eu besoin d'une série de lupanes de référence. On rapporte ici une synthèse efficace du lupane (**1**) en trois étapes, à partir de la bétuline (**3**) et avec un rendement global de 47,2%. On a obtenu le 17β(H)-28-norlupane (**2**) à un état de pureté de 90% en appliquant la méthode de Barton à la décarboxylation de l'acide 3-oxolupan-28-oïque (**10**). On a obtenu les 24,28-bisnor- (**4**) et 24-nor- (**5**) lupanes par une série de réactions impliquant la formation de l'oxime, du séconitrile et de l'époxynitrile, une fermeture de cycle et finalement une réduction de Wolff–Kishner du carbonyle en C3 en un méthylène. De plus, afin d'aider à la détermination quantitative de ces lupanes dans les huiles de schistes et d'échantillons géologiques, on a aussi développé une méthode de préparation des 3-deutéro- (**6**) et 2,3-dideutéro- (**7**) lupanes.

Mots clés : lupane, 24-norlupane, 28-norlupane, 24,28-bisnorlupane, 3-deutérolupane, 2,3-dideutérolupane.

[Traduit par la rédaction]

Introduction

Pentacyclic triterpanes of the hopane series are known to be present as ubiquitous biological markers in nearly all sediments and crude oils (1–3). However, since the report of the identification of two isomeric C28-triterpanes of the lupane series in Tertiary sediments from West Greenland and the Gulf of Suez (4), interest in the lupanes has been growing. More recently, some isomeric C28-lupanes were found in the offshore Beaufort–MacKenzie Delta oils (5). Furthermore, a C29-triterpane, tentatively identified as 24-norlupane, was the almost exclusive constituent of the saturated cyclic hydrocarbons in Tertiary coal from the Beaufort–MacKenzie Delta.[4] This prompted a need for authentic samples of 28-nor-, 24-nor-, and 24,28-bisnorlupanes to compare with materials found in oil shales and other geological samples.

Lehn and Ourisson (7) have prepared lupane (**1**) starting from lupeol, by catalytic hydrogenation, oxidation with CrO_3, and finally Wolff–Kishner reduction in unreported yields. Rullkötter *et al.* (4) prepared 28-norlupane (**2**) starting from betulin (**3**) by acetylation followed by catalytic hydrogenation, saponification to dihydrobetulin, oxidation with *N*-bromosuccinimide, and Wolff–Kishner reduction to yield lupan-28-ol, which after photo-oxidation resulted in a mixture of 28-norlupenes. Column chromatographic separation and catalytic hydrogenation yielded a mixture of 17(αH) and 17(βH)-28-norlupanes.

To our knowledge, the syntheses of 24,28-bisnorlupane (**4**), 24-norlupane (**5**), 3-deuterolupane (**6**), and 2,3-dideuterolupane (**7**) have not been reported, but reports of either the isolation or identification of **4** and **5** in oil samples have been published (2–4).[5]

Betulin (**3**), commercially available, was the most logical choice for a starting material to prepare our target molecules. Schemes 1–4 depict our strategy for preparing compounds **1**, **2**, **4**, and **5**, and Schemes 5 and 6 outline that of compounds **6** and **7**.

Results and discussion

As outlined in Scheme 1, lupane **1** was prepared in three steps in an overall yield of 47.2% from **3**. Catalytic hydrogenation of **3** over 10% Pd/C in ethyl acetate gave dihydrobetulin **8** in 96% yield, mp 275–277°C (lit. (7) mp 278–280°C). Pyridinium chlorochromate oxidation of **8** in CH_2Cl_2 furnished the keto aldehyde **9** in 87.8% yield, mp 190–195°C (lit. (8) mp 196–198°C). The ^{13}C nmr of **9** showed the keto carbon at 217.7 ppm and the aldehydic carbon at 206.9 ppm. The Huang–Minlon modified Wolff–Kishner reduction (9) of **9** gave lupane in 56% yield, mp 186.5–188°C (lit. (7) mp 184–188°C). The ^1H and ^{13}C nmr spectra of **1** agreed well with reported data (10). The mass spectrum of **1** shows a molecular ion peak at m/z 412 and a base peak at m/z 191, which is a prominent and most characteristic fragment ion of lupanes and other triterpanes (11, 12).

An approach different from that of Rullkötter *et al.* (4) was taken to prepare 28-norlupane (**2**). Scheme 2 shows our strategy. Starting from **9**, a number of different oxidation procedures were tried, to oxidize the keto aldehyde **9** to the keto acid **10**. No reaction was observed with silver oxide (13) or calcium hypochlorite (14) and only moderate yields of **10** (46%) were obtained by prolonged reaction with CrO_3/pyridine (15).

[1]This work is taken in part from the M.Sc. thesis of M. Ottosen, University of Calgary, 1988.

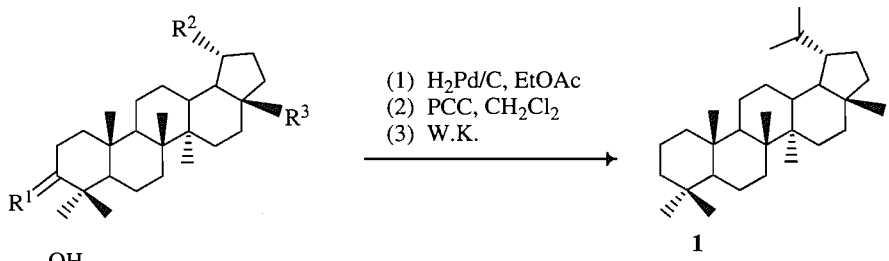
[2]Presented in part at the Symposium on Organic Synthesis, University of Melbourne, Australia, October, 1988.

[3]Author to whom correspondence may be addressed. Current address: University of Calgary, Department of Medical Biochemistry, 3330 Hospital Drive N.W., Calgary, Alta., Canada T2N 4N1.

[4]P. Brooks, Energy, Mines and Resources. Unpublished results.

[5]According to the numbering in lupane, see ref. 6, the methyl group removed is C24, hence it should be named 24,28-bisnorlupane instead of 23,28-bisnorlupane, as named by Rullkötter *et al.* (4).

Can. J. Chem. Downloaded from www.nrcresearchpress.com by 195.138.81.100 on 09/07/12
For personal use only.



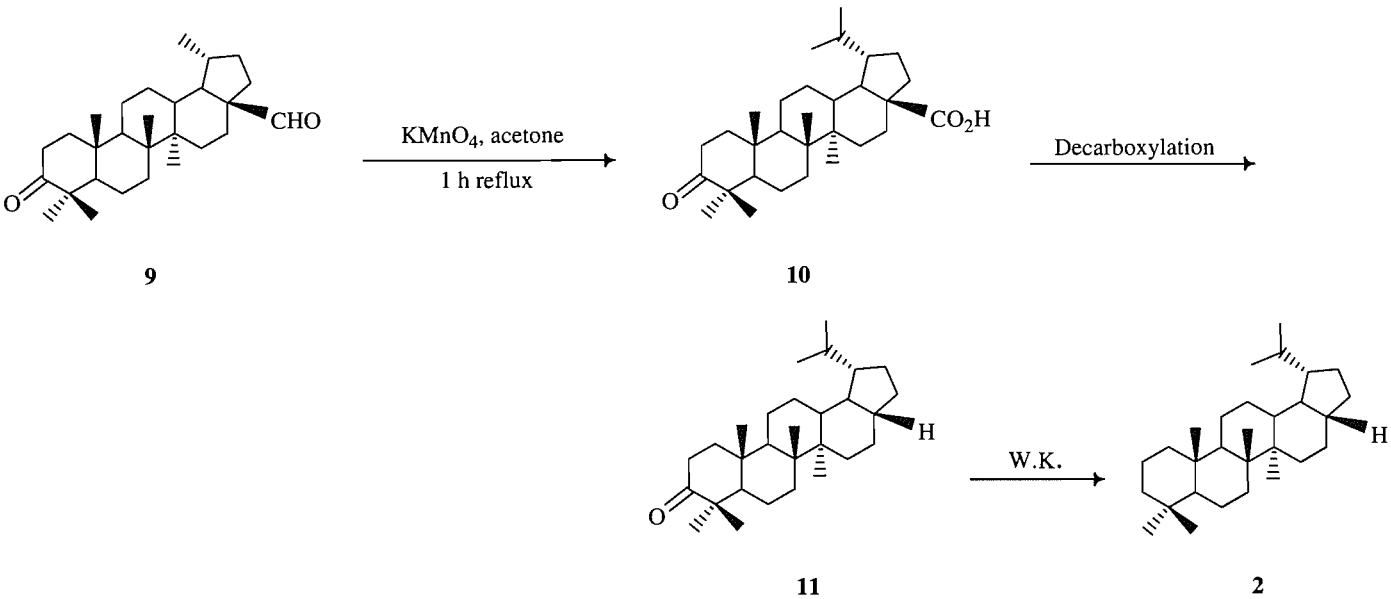
1

3: R^1 =  , $R^2 = C = CH_2$ (Me), $R^3 = CH_2OH$

8: R^1 =  , $R^2 = CH(CH_3)_2$, $R^3 = CH_2OH$

9: $R^1 = O$, $R^2 = CH(CH_3)_2$, $R^3 = CHO$

SCHEME 1



9 **10** **11** **2**

SCHEME 2

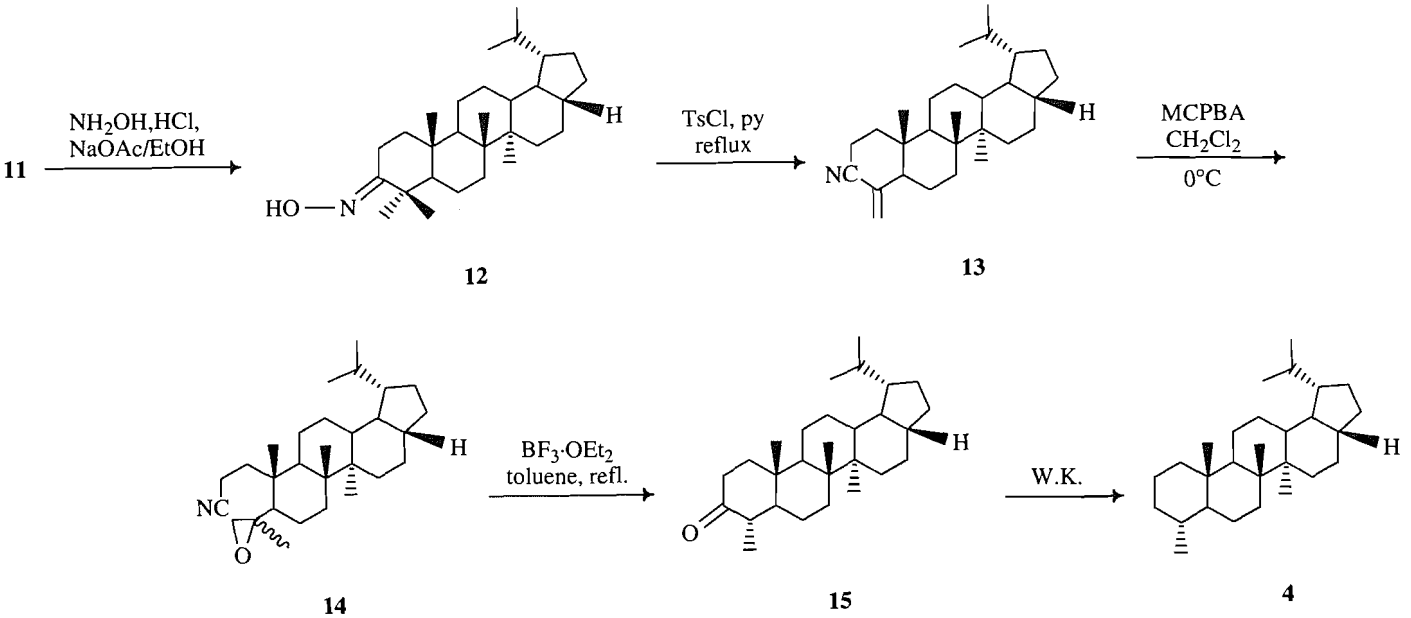
The most satisfactory results were obtained by refluxing **9** with $KMnO_4$ in acetone (16) for 1 h, giving crude **10** in 90% yield, mp 251–254°C (lit. (7) mp 258–260°C). The ^{13}C nmr spectrum of **10** showed the carboxylic acid carbon, C28, at 182.6 ppm, while betulinic acid shows the C28 signal at 178.9 ppm. Also, the C17 carbon appeared at 57.0 ppm while that in betulinic acid is reported at 56.3 ppm (17).

The critical step in the sequence to prepare **2** is the decarboxylation of **10**. The method of Crich *et al.* (18) was chosen, which involved the reaction of the acid chloride of **10** with *N*-hydroxypyridine-2-thione sodium salt in the presence of DMAP and *tert*-butyl mercaptan in benzene under reflux. 3-Oxo-28-norlupane (**11**) was obtained in 52% yield, but it was contaminated with $\Delta^{17,22}$-3-oxo-28-norlupene (10%), which was removed by chromatography on silica gel impregnated with 10% $AgNO_3$. The ir of **11** showed the carbonyl stretch at 1701 cm^{-1} and in the ^{13}C nmr spectrum C3 appeared at 218.37 ppm. The mass spectrum of **11** depicted the normal fragmentation of 3-oxolupanes, showing the molecular ion peak at m/z 412 and the base peak at m/z 205.

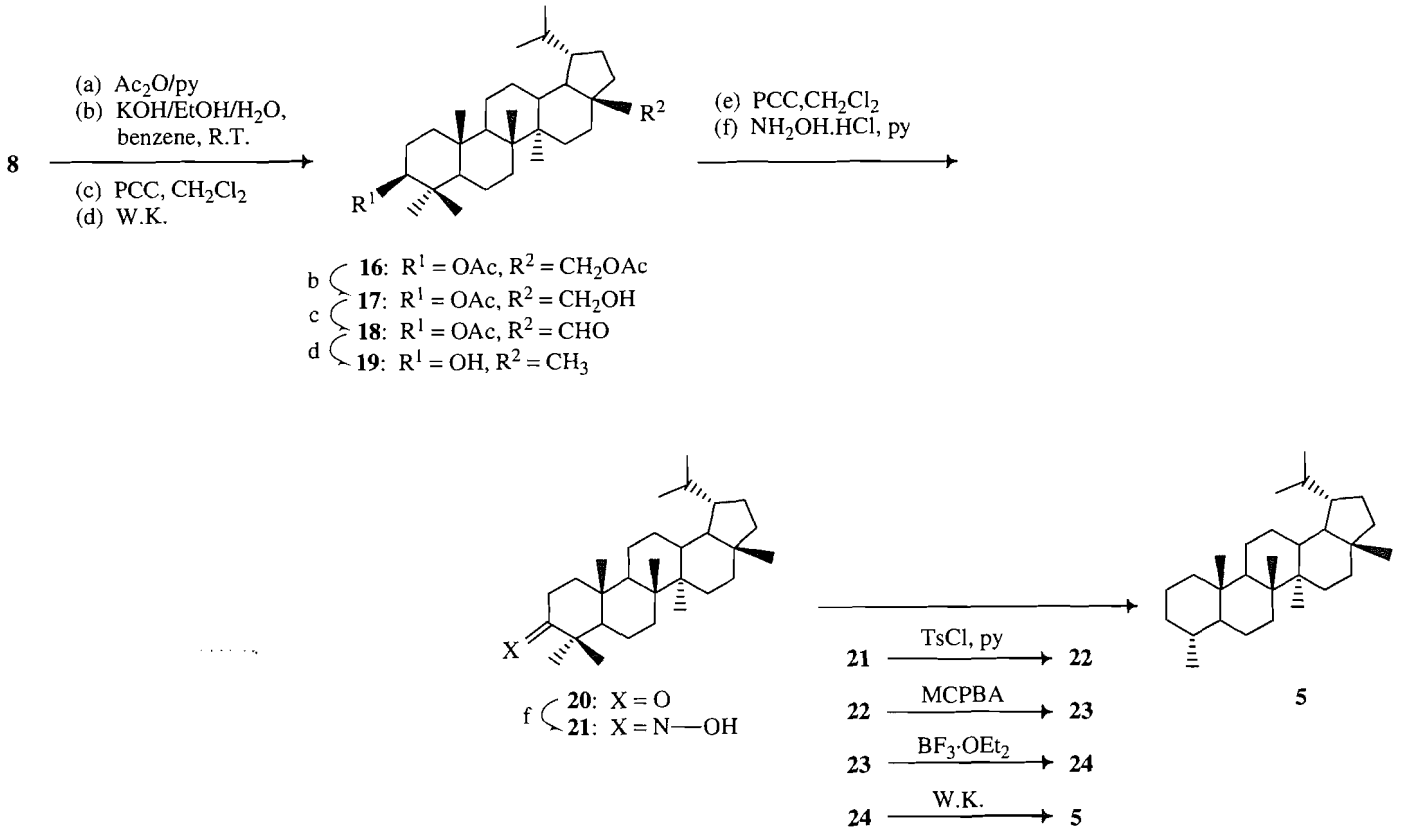
The final step in the synthesis of **2** was the Wolff–Kishner reduction of **11**. Applying the Huang–Minlon modification, **2** was obtained in 36.9% yield as a 9:1 mixture of two isomers, the major being the 17β(H) isomer and the minor the 17α(H) isomer, by comparison of their mass spectra from gc/ms with the results of Rullkötter *et al.* (4).

The second-order Beckmann rearrangement of the 3-oximino derivatives of 3-oxolupanes leading to unsaturated seconitriles was the key step in the preparation of 24,28-bisnorlupane (**4**) and 24-norlupane (**5**), as illustrated in Schemes 3 and 4. The reaction of 3-oxo-28-norlupane (**11**) with hydroxylamine hydrochloride according to the method of Valterová *et al.* (19) gave 3-oximino-28-norlupane (**12**) in 87% yield. Similarly, 3-oximinolupane (**21**) was prepared in 91% yield following the procedure of Klinot *et al.* (20). The Beckmann rearrangement of oximes **12** and **21** was carried out using *p*-toluenesulfonyl

Can. J. Chem. Downloaded from www.nrcresearchpress.com by 195.138.81.100 on 09/07/12
For personal use only.



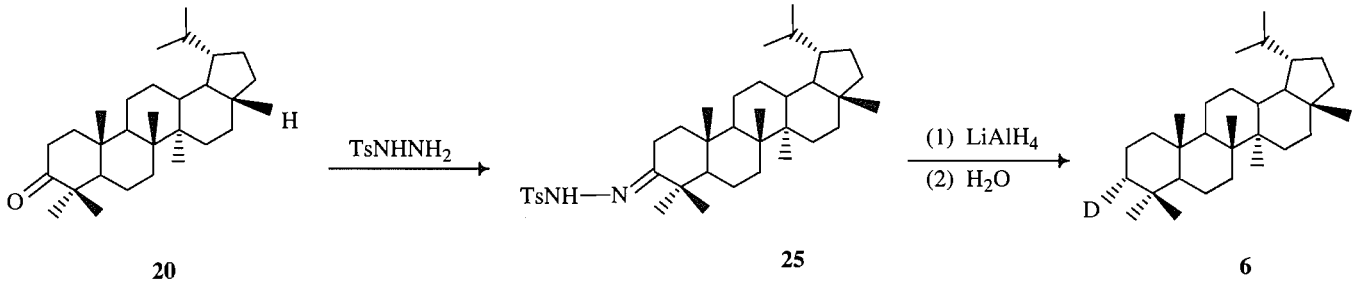
SCHEME 3



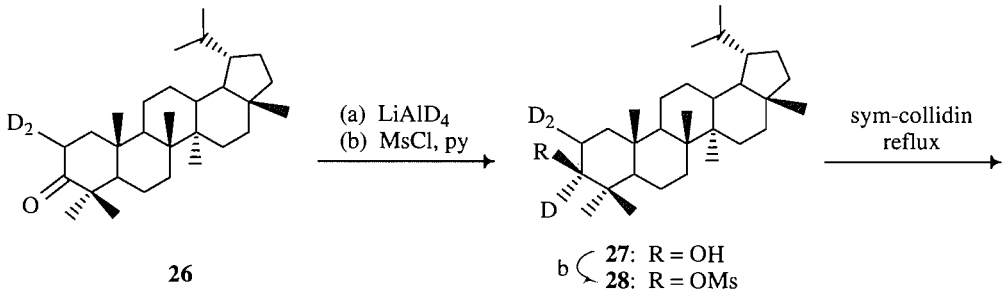
SCHEME 4

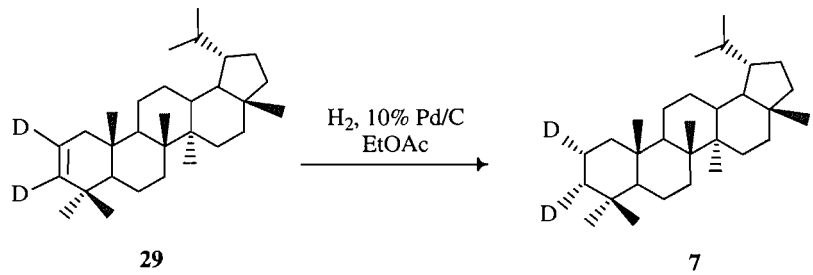
chloride in boiling pyridine as described by Klinot *et al.* (20). The pure seconitriles **13** and **22** were obtained in 67 and 57.9% yields respectively, after chromatography on basic alumina. In the infrared spectra, the nitrile stretch appeared at 2249 and 2242 cm^{-1}, and in the ^{13}C nmr spectra, the nitrile carbon appeared at 120.3 and 120.1 ppm (for **13** and **22** respectively). The vinyl methyl group in the ^1H nmr spectrum of **22** appeared at 1.74 ppm as a doublet (J = 0.5 Hz) showing long-range coupling with one of the terminal olefinic protons. Treatment of epoxynitrile **14** with $BF_3 \cdot Et_2O$ in dry toluene gave 24,28-bisnorlupan-3-one (**15**) in 63% yield. The carbonyl stretch of C3 appeared at 1708 cm^{-1}. Compound **15** was a mixture of isomers at C28, and hence the ^1H nmr spectrum was too complex to locate the methyl group at C4. Epoxynitrile **23**, when exposed to the same conditions as **14**, gave 24-norlupan-3-one (**24**) in 45.7% yield. From the ^1H nmr spectrum of **24**, the

Can. J. Chem. Downloaded from www.nrcresearchpress.com by 195.138.81.100 on 09/07/12
For personal use only.



SCHEME 5





SCHEME 6

compound appears to be a single epimer with the methyl group at C4 appearing as a doublet (J = 6.6 Hz) at 0.99 ppm. Pinhey and Cohen (21) reported that second-order Beckmann rearrangement of 3-hydroxyimino-4,4-dimethyl steroids followed by epoxidation to the epoxynitrile and cyclization with $BF_3 \cdot Et_2O$ yielded the 4α(CH_3)-3-ketones, which were not a mixture of C4 epimers. According to this, one would expect ketones **15** and **24** to be only the 4α(CH_3) epimers. The Wolff–Kishner reduction of **15** furnished 24,28-bisnorlupane (**4**) as a white waxy solid after chromatography on silica impregnated with 10% $AgNO_3$. The gc analysis of this compound showed it to be a mixture of three isomers. Attempts to separate these isomers by column chromatography failed. The major component (86.6%) was identified as 17β(H),4α(CH_3)-24,28-bisnorlupane by comparison of its mass spectrum with that reported by Rullkötter *et al.* (4). The second major component is thought to be the 17β(H),4β(CH_3) isomer, and the component of least abundance showed a more intense fragment in its mass spectrum at m/z 341 than that displayed by the 17β(H),4α(CH_3) isomer, and is comparable with the mass spectral data reported by Rullkötter *et al.* (4) for 17α(H),4α(CH_3)-24,28-bisnorlupane. Similarly, the Wolff–Kishner reduction of ketone **24** gave 24-norlupane (**5**) in 51.7% yield as a mixture of two epimers at C4. The major (86.4%) is thought to be the more stable 4α(CH_3) epimer, and the minor, the 4β(CH_3) epimer. In both **4** and **5**, epimerization at C4 is believed to have occurred under the Wolff–Kishner reduction conditions.

The monodeuterated lupane **6** was prepared in two steps starting from 3-oxolupane (**20**) as illustrated in Scheme 5. The reaction of **20** with tosylhydrazine and acetyl chloride in methanol gave 3-oxolupane tosylhydrazone (**25**) in 45% yield after chromatography. Reduction of **25** with excess $LiAlD_4$ in dry dioxane, and chromatography of the resulting product on silica impregnated with 10% $AgNO_3$, gave 3-deuterolupane (**6**), mp 188–189°C. The molecular ion peak in the mass spectrum of **6** appeared at m/z 413 and the base peak at mass 192, derived from the A/B rings, since the deuterium atom is in the A ring. The peak at m/z 191 is attributed to the D/E rings.

The preparation of 2,3-dideuterolupane (**7**), Scheme 6, proved to be more troublesome than anticipated. Most standard methods tried for the dideuteration of 3-oxolupane gave a mixture of both mono- and dideuteration products. However, dideuteration, 95%, was achieved by refluxing **20** with potassium carbonate in D_2O for 52 h, giving 2,2-dideutero-3-oxolupane (**26**) in 28.6% yield, contaminated with 5% of the monodeutero product. Reduction of **26** with $LiAlD_4$ followed by mesylation gave the 2,2,3-trideutero mesylate (**28**) in almost 60% yield from **26**. Elimination of mesylate **28** with *sym*-collidine at reflux gave crude 2,3-dideutero-2-lupene (**29**) in almost quantitative yield. The hydrogenation of crude **29** in ethyl acetate over 10% Pd/C was slow and required a large amount of catalyst. 2,3-Dideuterolupane (**7**) was obtained in 76.6% yield as a white waxy solid after 2 days of hydrogena-

Can. J. Chem. Downloaded from www.nrcresearchpress.com by 195.138.81.100 on 09/07/12
For personal use only.

tion. The mass spectrum of **7** showed a molecular ion peak at m/z 414 and a base peak at mass 193, derived from the A/B rings. The peak at mass 191 had the same intensity as that in the monodeuterolupane **6**, confirming its origin in the D/E rings.

Experimental

General

Infrared spectra were recorded on a Nicolet DX FT-IR spectrophotometer connected to a 5DX processor and a 7470A Hewlett Packard plotter. The spectra of solid samples were run as KBr discs, while those of liquids and semisolids were run as thin films on KBr plates. Mass spectra of pure solid samples were obtained on a Kratos MS80 (RFA) mass spectrometer at 70 eV. Gas chromatography/mass spectra were run on a VG 70-SQ mass spectrometer controlled by a 112505 data system at 70 eV. The gas chromatograph used was an HP model 5890 fitted with a J and W Scientific 30-m DB-5 capillary column. Elemental analyses were carried out on a Perkin Elmer 240b elemental analyser. Melting points are uncorrected and were taken on an Electrothermal melting point apparatus. The ^{1}H and ^{13}C nmr spectra were recorded either on a Varian XL200 spectrometer or a Bruker AC200 student model connected to an MP3200 Graphtec XY plotter, using $CDCl_3$ as both the solvent and the internal standard. Chemical shifts are listed in ppm.

Silica gel 230–400 or 60–200 mesh and basic alumina (activity II–III E. Merck aluminum oxide/90) were used for column chromatography. For the separation of unsaturated compounds, $AgNO_3$ (10–15%) impregnated alumina or silica was used. Merck DC Alufolien Kieselgel 60 F_{254} tlc plates were used, and visualization of the developed plates was achieved by dampening the plate, placing it in a tank containing SO_2Cl_2, and then drying it in an oven at 100°C.

*Hydrogenation of betulin **3** to dihydrobetulin **8***

Betulin (310 mg) in ethyl acetate (200 mL) was hydrogenated in a Parr hydrogenator over 10% Pd/C (200 mg) under 2 atm (1 atm = 101.3 kPa) of hydrogen for 2 h. After filtration of the catalyst and evaporation of the solvent, **8** was obtained in 96% yield, mp 275–277°C (lit. (7) mp 278–280°C); ^{1}H nmr ($CDCl_3$) δ: 3.79 (d, J = 10 Hz, 1H, C28-H), 3.31 (d, J = 11 Hz, 1H, C28-H), 3.21 (dd, J = 5.5 and 10 Hz, 1H, C3-H), 1.03 (s), 0.98 (s), 0.97 (s), 0.85 (d, J = 6.6 Hz), 0.84 (s), 0.77 (d, J = 6.7 Hz), 0.774 (s); ^{13}C nmr δ: 79.0 (C3), 60.6 (C28).

*3-Oxo-28-lupanal **9***

Dihydrobetulin **8** (1.0 g, 2.25 mmol) in CH_2Cl_2 (100 mL) was oxidized with PCC (1.45 g, 6.75 mmol) according to procedures in refs. 18 and 19. The keto aldehyde **9** was obtained in 87.8% yield, mp 190–195°C (lit. (8) mp 196–198°C); ^{13}C nmr δ: 217.7 (C3), 206.9 (C28), 59.9 (C17); ms m/z (%): 440 (14, M^+), 412 (8), 411 (18), 205 (50), 177 (36), 135 (45), 109 (57), 95 (68), 81 (85), 55 (100).

*Wolff–Kishner reduction of **9** to lupane*

Following the procedure of Matlin *et al.* (9), a mixture of crude **9** (400 mg, 0.9 mmol), dry diethylene glycol (40 mL), 85% hydrazine hydrate (0.72 mL), and KOH (0.98 g) was heated for 1 h under nitrogen at 100°. The temperature was raised to 200–210°C and maintained for 4 h. After cooling, the mixture was diluted with water and extracted with ether. The ether extracts were washed with water, 5% $NaHCO_3$, and water, then dried over anhydrous $MgSO_4$ and filtered. Removal of the solvent and chromatography over basic alumina, eluting with 9:5 hexane/ether, furnished lupane in 56% yield, mp 186.5–188°C (lit. (7) mp 184–185°C). Both ^{1}H and ^{13}C nmr spectra agreed well with the reported data (10).

*Oxidation of **9** to keto acid **10***

The keto aldehyde **9** (500 mg, 1.1 mmol) and $KMnO_4$ (1.33 g, 8.4 mmol) in acetone (70 mL) were refluxed for 1 h (16). The mixture was cooled, acidified with dilute H_2SO_4, and 5% $NaHSO_3$ was added until the brown color disappeared. The aqueous mixture was extracted with $CHCl_3$, washed with 5% $NaHCO_3$ and water, dried over anhydrous $MgSO_4$, filtered, and the solvent removed *in vacuo*. The crude product (89.5% yield) was chromatographed on silica, eluting with 95:5 $CHCl_3$/MeOH, to give **10** as fine white needles, mp 251–254°C (lit. (7) mp 258–260°C); ir ν_{max}: 1701, 1687 cm^{-1}; ^{1}H nmr δ: 1.08 (s), 1.03 (s), 0.97 (s), 0.94 (s), 0.87 (d, J = 6.8 Hz), 0.77 (d, J = 6.6 Hz); ^{13}C nmr δ: 218.1 (C3), 182.6 (C28), 57.0 (C17).

*Decarboxylation of **10***

A mixture of keto acid **10** (1.4 g, 0.31 mmol), oxalyl chloride (1.5 mL, 17.6 mmol), and DMF (3 drops) in benzene was stirred at room temperature for 2 h under nitrogen according to the procedure of Crich *et al.* (18). The crude acid chloride was obtained by evaporation of the solvent and was used in the decarboxylation step without purification. *N*-Hydroxypyridine-2-thione sodium salt (554 mg, 3.7 mmol), DMAP (36.6 mg, 0.3 mmol), and *tert*-butyl mercaptan (1.5 mL, 13.3 mmol) in dry benzene (30 mL) were refluxed under nitrogen for 5 min, then the acid chloride in dry benzene (15 mL) was added dropwise over 20 min to the refluxing solution. After 6 h reflux, the mixture was cooled and transferred to a separatory funnel, washed with water and with saturated NaCl solution, then dried over anhydrous $MgSO_4$, filtered, and the solvent removed *in vacuo*. The residue was chromatographed on silica, eluting with 9:5 hexane/ether, to give a semisolid that could be made to precipitate by adding cold methanol. 3-Oxo-28-norlupane **11** was obtained in 52% yield by rechromatography over silica gel impregnated with 10% $AgNO_3$ to remove the by-product, 3-oxonorlupene; ir ν_{max}: 1701 cm^{-1}; ^{1}H nmr ($CDCl_3$) δ: 2.48 (m, C2-H), 1.09 (s), 1.04 (s), 0.99 (s), 0.94 (s), 0.91 (s), 0.84 (d, J = 6.6 Hz), 0.82 (d, J = 6.6 Hz); ^{13}C nmr δ: 218.4 (C3); ms m/z (%): 412 (75, M^+), 369 (53), 206 (32), 205 (100), 177 (62), 135 (75), 81 (78).

*28-Norlupane **2***

The Wolff–Kishner reduction of **11** (170 mg, 0.4 mmol) with KOH (237 mg), diethylene glycol (20 mL), and 85% hydrazine hydrate (0.18 mL) was carried out as described for **9**. Chromatography of the crude product on basic alumina, eluting with 9:5 hexane/ether, gave 58.7 mg (36.9%) of a white waxy solid melting at 157–159°C. The gc–ms analysis showed the product to be composed of 2 isomers in a 9:1 ratio; ir (film) ν_{max}: 2952, 2868, 1455, 1384, 1082, 970 cm^{-1}; ^{1}H nmr ($CDCl_3$) δ: 0.96 (s), 0.91 (s), 0.85 (s), 0.83 (s), 0.82 (s), 0.80 (s); ms m/z (%): major isomer 17β(H), 90%: 398 (35, M^+), 383 (16), 355 (11), 260 (10), 217 (11), 192 (36), 191 (100), 177 (27), 109 (30), 95 (40); minor isomer 17α(H), 10%: 398 (44, M^+), 383 (10), 355 (12), 260 (25), 191 (100), 177 (43), 123 (45), 81 (60).

*3-Oximino-28-norlupane **12***

The method of Valterová *et al.* (19) was used to react **11** (800 mg, 1.9 mmol) with hydroxylamine·HCl (800 mg, 11.5 mmol) and pyridine (24 mL). After diluting with water, the mixture was extracted with chloroform and the organic layer was washed with 3 N HCl, 5% $NaHCO_3$, and water, and then dried over anhydrous $MgSO_4$, filtered, and the solvent removed under reduced pressure. Oxime **12** (720 mg, 87%) was used for the next step without further purification; ir ν_{max}: 3255, 2945, 2868, 1462, 1384, 1258, 1019, 927 cm^{-1}.

*3,4-Seconitrile **13***

The reaction of oxime **12** (690 mg, 1.6 mmol) with *p*-toluenesulfonyl chloride (2.30 g, 10 mmol) in pyridine (23 mL) for 6 h under nitrogen according to the procedure of Klinot *et al.* (20) gave **13** (435 mg, 67%) as a pale yellow solid after chromatography on basic alumina, eluting with benzene; ir ν_{max}: 2945, 2849, 2249, 1455, 1384, 1152, 1177, 808 cm^{-1}; ^{1}H nmr ($CDCl_3$) δ: 4.89 (m, 1H, =CH), 4.65 (m, 1H, =CH), 2.3 (m, 2H, -CH_2CN), 1.73 (d, J = 0.8 Hz, =CCH_3), 1.00 (s), 0.90 (s), 0.86 (s), 0.826 (s), 0.82 (d, J = 6.3 Hz); ^{13}C nmr δ: 147.1 (C4), 120.3 (CN), 114.0 (C24); ms m/z (%): 427 (2, M^+), 409 (14), 366 (17), 177 (31), 135 (62), 95 (71), 81 (93).

*Epoxynitrile **14***

To a solution of seconitrile **13** (470 mg, 1.1 mmol) in $CHCl_3$ at 0°C was added a precooled solution of *m*-chloroperbenzoic acid (376 mg, 2.2 mmol) in $CHCl_3$ (10 mL) according to the procedure of Valterová *et al.* (22). The reaction mixture was kept at 0°C in the dark for 67 h,

Can. J. Chem. Downloaded from www.nrcresearchpress.com by 195.138.81.100 on 09/07/12
For personal use only.

Can. J. Chem. Downloaded from www.nrcresearchpress.com by 195.138.81.100 on 09/07/12
For personal use only.

then washed with 5% KI, 5% $NaHSO_3$, 5% $NaHCO_3$, and water. The organic layer was dried over anhydrous $MgSO_4$, filtered, and the solvent removed under vacuum to yield epoxynitrile **14** (353 mg, 73% yield). An analytical sample was obtained by chromatography on basic alumina, eluting with 9:5 hexane/ether, mp 170–172°C; ir ν_{max}: 2952, 2249 (CN), 1455, 1384, 1265, 1152, 1089, 1019, 801, 519 cm^{-1}; ^1H nmr ($CDCl_3$) δ: 2.73 (d, J = 4.4 Hz, 1H, C-CH_2-O), 2.63 (d, J = 4.4 Hz, 1H, C-CH_2-O), 2.2 (m, -CH_2CN), 1.28 (s, 3H, O-C-Me), 0.98 (s), 0.96 (s), 0.85 (s), 0.82 (s), 0.81 (d, J = 6.3 Hz); ^{13}C nmr δ: 119.8 (CN). Anal. calcd. for $C_{29}H_{47}NO$: C 81.82, H 11.13, N 3.29%; found: 82.02, H 11.28, N 3.30%.

3-Oxo-24,28-bisnorlupane ***15***

Epoxynitrile **14** (184 mg, 0.4 mmol) was refluxed with BF_3-etherate (0.4 mL) in toluene (50 mL) for 6 h under nitrogen according to the procedure of Valterová *et al.* (22). The reaction mixture was cooled and diluted with ether, and the ether layer was separated and washed with 3 N HCl, 5% $NaHCO_3$, and water, then dried over anhydrous $MgSO_4$, filtered, and the solvents removed under vacuum. The residue was chromatographed on basic alumina, eluting with 9:5 hexane/ether, to give **15** (108 mg, 63% yield), mp 160–164°C; ir ν_{max} (film): 2938, 2868, 1708, 1455, 1384 cm^{-1}; ^{13}C nmr δ: 213.5 (C3); ms m/z (%): 398 (75, M^+), 355 (63), 306 (8), 263 (7), 192 (100), 191 (95), 135 (77), 109 (56), 95 (63), 81 (81). Exact Mass calcd. for $C_{28}H_{46}O$: 398.35508; found: 398.3586.

24,28-Bisnorlupane ***4***

3-Oxo-24,28-bisnorlupane **15** (400 mg, 1.0 mmol) was reacted with KOH (490 mg) and 85% hydrazine hydrate (0.36 mL) in diethylene glycol (40 mL) as described for **9**. Chromatography of the crude product on silica impregnated with 10% $AgNO_3$, eluting successively with hexane, 9:1 hexane/ether, and 9:2 hexane/ether, gave a white waxy solid melting at 104–111°C (82 mg), which was a mixture of isomers, as shown by gc–ms. Attempts to separate this mixture by chromatography on Kiesel gel silica – 5% $CaSO_4$, eluting with cyclohexane and with 9:1 cyclohexane/ether, were not successful; ir ν_{max} (film): 2938, 2868, 1448, 1384, 1216, 759 cm^{-1}. The ^1H nmr spectrum was too complex and not well resolved. Mass spectra of isomers are listed in order of their elution from gc, m/z (%): isomer 1, most likely 17β(H),4β(CH_3), 1.9%: 384 (27, M^+), 369 (21), 341 (17), 217 (8), 192 (22), 177 (100), 135 (32), 109 (33), 95 (42), 81 (40); isomer 2, possibly 17β(H),4α(CH_3), 86.6%: 384 (28, M^+), 369 (17), 341 (7), 192 (24), 177 (100), 149 (22), 135 (36), 109 (47), 95 (38), 81 (62); isomer 3, most likely 4α(CH_3),17α(H), 11.5%: 384 (30, M^+), 369 (13), 341 (5), 217 (7), 177 (100), 149 (13), 135 (12), 109 (23), 95 (28), 81 (26).

3,28-Diacetoxylupane ***16***

Dihydrobetulin **8** (1.14 g, 2.6 mmol) was heated with acetic anhydride (23 mL) and freshly distilled pyridine (57 mL) on a steam bath for 2 h, then stirred at ambient temperature overnight (23). The mixture was diluted with water and extracted with ether, and the organic layer was washed with 3 N HCl, 5% $NaHCO_3$, and water, dried over $MgSO_4$, filtered, and the solvent removed under vacuum. Recrystallization from CH_2Cl_2/MeOH or chromatography on basic alumina, eluting with 9:5 hexane/ether, gave **16** (1.1 g, 82%), mp 256–257°C (lit. (7) mp 256–259°C); ^1H nmr ($CDCl_3$) δ: 4.48 (dd, J = 5.8, 9.4 Hz, 1H, C3-H), 4.25 (d, J = 11.2 Hz, 1H, C28-H), 3.82 (d, J = 10.5 Hz, C28-H), 2.07 (s, 3H, CH_3CO), 2.05 (s, 3H, CH_3CO), 1.04 (s), 0.95 (s), 0.86 (s), 0.855 (s), 0.847 (s), 0.83 (s); 0.77 (d, J = 6.6 Hz, C20-Me_2); ^{13}C nmr δ: 171.6 (C=O), 171.0 (C=O), 80.9 (C3), 62.8 (C28), 21.6 (CH_3 on C28 acetate), 21.4 (CH_3 on C3 acetate).

3β-Acetoxy-28-lupanol ***17***

Partial hydrolysis of **16** (1.4 g, 2.6 mmol) with KOH (145 mg) in MeOH (10 mL) and benzene (26 mL) at room temperature was carried out according to the reported procedure of Protiva *et al.* (24). The progress of the reaction was followed by tlc. The mixture was diluted with ether and the organic layer was separated and washed with water, dried over anhydrous $MgSO_4$, filtered, and the solvent removed under vacuum. Chromatography of the residue on basic alumina, eluting with 9:3 hexane/ether, gave **17** (580 mg, 70%), mp 250.5–253.5°C. A small amount of dihydrobetulin **8** and **16** (37 mg) was also recovered; ir ν_{max}: 3445, 1736, 1226, 1026 cm^{-1}; ^1H nmr ($CDCl_3$) δ: 4.43 (m, 1H, C3-H), 4.08 (d, J = 7.1 Hz, 1H, C28-H), 3.72 (d, J = 10.9 Hz, 1H, C28-H), 2.05 (s, 3H, CH_3CO), 0.99 (s), 0.91 (s), 0.82 (s), 0.81 (s), 0.80 (s), 0.75 (s), 0.73 (d, J = 6.6 Hz); ^{13}C nmr δ: 171.1 (C=O), 81.0 (C3). Anal. calcd. for $C_{32}H_{54}O_3$: C 78.96, H 11.18; found: C 79.59, H 11.34%.

3β-Acetoxy-28-lupanal ***18***

Oxidation of monoacetate **17** (590 mg, 1.2 mmol) with PCC (376 mg, 1.8 mmol) in CH_2Cl_2 (40 mL) followed by chromatography on basic alumina, eluting with 9:3 hexane/ether, gave **18** (586 mg, 90%), mp 209–212°C; ir ν_{max}: 1736, 1708 cm^{-1}; ^1H nmr ($CDCl_3$) δ: 9.65 (s, 1H, CHO), 4.48 (m, 1H, C3-H), 2.06 (s, 3H, CH_3CO), 0.95 (s), 0.91 (s), 0.90 (s), 0.89 (s), 0.85 (s), 0.84 (s), 0.81 (s), 0.77 (s); ^{13}C nmr ($CDCl_3$) δ: 206.3 (C28), 170.1 (acetate carbonyl), 80.1 (C3).

Wolff–Kishner reduction of ***18***

The reaction of **18** (700 mg, 1.4 mmol) with KOH (860 mg) and 85% hydrazine hydrate (0.64 mL) in diethylene glycol (60 mL), as described for **9**, gave 3β-hydroxylupane **19** in 82% yield (503 mg) after chromatography on basic alumina, eluting with 9:5 hexane/ether, mp 207–208°C (lit. (25) mp 203–204°C).

3-Oxolupane ***20***

Oxidation of **19** (400 mg, 0.93 mmol) with PCC (300 mg, 1.4 mmol), as described for **8**, gave **20** in 88% yield (347 mg) after chromatography on basic alumina, eluting with 9:5 hexane/ether, mp 203.5–205.5°C (lit. (7) mp 209.5–210°C).

3-Oximinolupane ***21***

A mixture of 3-oxolupane **20** (210 mg, 0.49 mmol) and hydroxylamine hydrochloride (223 mg, 3.2 mmol) in pyridine (6.7 mL) was stirred at 100°C for 1 h, then at room temperature for 17 h according to the procedure of Klinot and co-workers (22). The reaction mixture was diluted with water and the precipitate was collected, washed with water, and air-dried overnight to give **21** in 91% yield (198 mg); ir ν_{max}: 3259 (HO-N), 1457, 1385, 945, 933 cm^{-1}.

Rearrangement of oxime ***21*** *to 3,4-seconitrile* ***22***

Oxime **21** (198 mg, 0.45 mmol) was reacted with tosyl chloride (0.66 g, 3.5 mmol) in pyridine (6.6 mL) as described for **12**. After chromatography on basic alumina, eluting with benzene, seconitrile **22** was obtained in 57.9% yield (110 mg); ir ν_{max}: 3072 (=CH_2), 2242 (CN), 1638 (C=C) cm^{-1}; ^1H nmr ($CDCl_3$) δ: 4.89 (bs, 1H, =CH), 4.66 (bs, 1H, =CH), 1.74 (d, J = 0.5 Hz, 3H, =C-CH_3), 1.10 (s), 0.96 (s), 0.87 (s), 0.86 (d, J = 6.7 Hz), 0.78 (s), 0.785 (d, J = 6.5 Hz); ^{13}C nmr δ: 147.0 (=C), 120.1 (CN), 113.9 (=CH_2). Exact Mass calcd. for $C_{30}H_{49}N$: 423.3865; found: 423.3863.

Epoxynitrile ***23***

The reaction of seconitrile **22** (110 mg, 0.26 mmol) in $CHCl_3$ (3 mL) with *m*-chloroperbenzoic acid (90 mg, 0.52 mmol) in $CHCl_3$ (3 mL) at 0°C was carried out as described for **13**. Chromatography of the crude product on basic alumina, eluting with 9:5 hexane/ether, gave epoxynitrile **23** in 61.3% yield (70 mg); IR ν_{max}: 2249 (CN) cm^{-1}; ^1H nmr δ: 2.71 (d, J = 4.4 Hz, 1H, epoxy proton), 2.62 (d, J = 4.1 Hz, 1H, epoxy proton), 2.18 (m, 2H, -CH_2CN), 1.26 (s, O-C-Me), 1.06 (s), 0.94 (s), 0.88 (s), 0.83 (d, J = 6.8 Hz), 0.75 (d, J = 6.7 Hz), 0.74 (s); ^{13}C nmr δ: 119.7 (CN), 57.9 (epoxy carbon), 55.4 (quaternary epoxy carbon).

3-Oxo-24-norlupane ***24***

The reaction of epoxynitrile **23** (70 mg, 0.16 mmol) in dry toluene (22 mL) with $BF_3 \cdot Et_2O$ (0.1 mL) for 3.5 h as described for **14** gave **24** in 45.7% yield (30 mg) after chromatography on basic alumina, eluting with 9:5 hexane/ether; ir ν_{max}: 1710 (C3=O) cm^{-1}; ^1H nmr ($CDCl_3$) δ: 1.1 (s), 1.04 (d, J = 0.6 Hz), 0.99 (d, J = 6.6 Hz, CO-CH-CH_3), 0.92 (d, J = 0.6 Hz), 0.84 (d, J = 6.8 Hz, CH-CH_3), 0.77 (s), 0.76 (d, J = 6.7 Hz, CH-CH_3); ^{13}C nmr δ: 213.7 (C3).

Can. J. Chem. Downloaded from www.nrcresearchpress.com by 195.138.81.100 on 09/07/12
For personal use only.

24-Norlupane ***5***

Compound **24** (30 mg, 0.07 mmol) was reacted with 98% hydrazine (4.8 mL) in *n*-butanol (30 mL) and diethylene glycol (30 mL) at 125°C for 2 h under nitrogen according to the procedure of van Dorsselaer *et al.* (26). Excess hydrazine and *n*-butanol were distilled off until the temperature reached 220°C. The reaction mixture was cooled and NaOH (0.69 g) was added, then the reaction temperature was raised to 220°C and maintained for 17 h. After cooling the reaction mixture, water was added, the product was extracted with hexane, and the hexane extracts were washed with water, dried over anhydrous $MgSO_4$, filtered, and the solvent removed under vacuum. Chromatography of the residue on alumina impregnated with 15% $AgNO_3$, eluting with hexane, gave 24-norlupane (**5**) in 51.7% yield (15 mg) as a mixture of 2 isomers in a ratio of 6.4:1; ^{1}H nmr ($CDCl_3$) δ: 1.06 (s), 0.94 (s), 0.846 (d, J = 6.9 Hz), 0.808 (d, J = 6.5 Hz), 0.778 (s), 0.769 (d, J = 7 Hz), 0.766 (s); ms m/z (%): major 4α (Me), 86.4%: 398 (23, M^+), 383 (20), 355 (15), 191 (34), 177 (100), 163 (41), 149 (27), 123 (62), 109 (44); minor 4β (Me), 13.6%: 398 (16, M^+), 383 (15), 355 (8), 274 (7), 259 (14), 231 (13), 191 (21), 177 (100), 163 (29), 149 (25), 123 (63), 109 (36). Exact Mass calcd. for $C_{29}H_{50}$: 398.3912; found: 398.3921.

3-Oxolupane tosylhydrazone ***25***

A mixture of 3-oxolupane **20** (100 mg, 0.28 mmol), tosylhydrazine (29) (120 mg, 0.6 mmol), and acetyl chloride (1 mL) in methanol (5 mL) was refluxed for 20 min, then water was added while the mixture was hot according to procedures in refs. 27 and 28. The mixture was cooled and the resulting precipitate filtered and vacuum-dried. Chromatography on basic alumina, eluting with 9:5 hexane/ether, gave **25** in 45% yield (50 mg), mp 169–171°C; ir ν_{max}: 3213, 1602 cm^{-1}; ^{1}H nmr ($CDCl_3$) δ: 7.84 (d, J = 8.2 Hz), 7.30 (d, J = 8.2 Hz), 2.42 (s, Me-C_6H_4), 1.08 (s), 1.03 (s), 0.94 (s), 0.89 (s), 0.86 (s), 0.82 (s), 0.78 (s), 0.77 (s), 0.75 (s).

3-Deuterolupane ***6***

A mixture of tosylhydrazone **25** (215 mg) and $LiAlD_4$ (227 mg) in freshly distilled dioxane (10 mL) was refluxed under nitrogen for 4 h (27, 30). After cooling the reaction mixture, excess $LiAlD_4$ was destroyed by careful addition of water and the product was extracted with ether. The ether extracts were washed with 5% $NaHCO_3$, water, dried over anhydrous $MgSO_4$, filtered, and the solvent removed *in vacuo*. Chromatography of the crude product on silica followed by recrystallization from MeOH and rechromatography on silica impregnated with 10% $AgNO_3$, eluting with 9:2 hexane/ether, gave 12 mg of 3-deuterolupane (**6**), mp 188–189°C; ms m/z (%): 413 (29, M^+), 398 (11), 370 (11), 259 (11), 231 (12), 205 (8), 193 (27), 192 (100), 191 (26), 177 (11), 123 (37), 95 (46), 81 (42), 69 (44), 55 (32).

Deuteration of 3-oxolupane ***20***

A mixture of 3-oxolupane **20** (611 mg, 0.4 mmol) and K_2CO_3 (6.25 mg) in D_2O (0.94 mL) was refluxed for 52 h according to the method of Fuhrer *et al.* (31). The mixture was saturated with NaCl and then extracted with ether, and the ether extracts were dried over anhydrous $MgSO_4$, filtered, and the solvent removed under vacuum to give 2,2-dideutero-3-oxolupane **26** in 28.6% yield (175 mg). The gc–ms analysis showed the material to be 95% dideutero and 5% monodeutero compound. Mass spectrum m/z (%): 428 (17, M^+), 427 (1.7), 385 (17), 207 (65), 163 (52), 123 (81), 95 (88), 69 (100).

Reduction of deuterated 3-oxolupane ***26***

The reduction of deuterated **26** (175 mg, 0.4 mmol) with $LiAlD_4$ as described for the reduction of **25** (32) gave 3-hydroxy-2,2,3-trideuterolupane (**27**) in 60.8% yield.

Preparation of 3-mesyloxy-2,2,3-trideuterolupane ***28***

Methanesulfonyl chloride (0.4 mL) was added to a solution of **27** (107 mg, 0.25 mmol) in pyridine (15 mL) at 0°C (32). After 3 h at 0°C, water was added and the mixture was extracted with ether. The ether extracts were washed with 3 N HCl, 5% $NaHCO_3$, and water, then dried over anhydrous $MgSO_4$, filtered, and the solvent removed under vacuum to give the crude mesylate **28** (164 mg); ^{1}H nmr ($CDCl_3$) δ: 3.02 (s, Me-SO_3), 1.03 (d, J = 4.4 Hz), 0.92 (s), 0.88 (s), 0.86 (s), 0.83 (s), 0.78 (s), 0.76 (s).

Elimination of mesylate ***28***

A mixture of crude **28** (164 mg, 0.3 mmol) in sym-collidine (1 mL) was refluxed for 5–6 h, then it was cooled, diluted with 3 N HCl, and extracted with ether (33). The ether extracts were washed with 3 N HCl, 5% $NaHCO_3$, and water, then dried over $MgSO_4$, filtered, and the solvent removed *in vacuo* to yield crude 2,3-dideuterolup-2-ene **29** (130 mg), which was used in the next step without purification.

Hydrogenation of ***29***

A mixture of **29** (130 mg), ethyl acetate (100 mL), and 10% Pd/C (150 mg) was shaken at room temperature for 2 days under 2 atm hydrogen in a Parr hydrogenator. Filtration of the catalyst and removal of the solvent under vacuum followed by chromatography on alumina, eluting with hexane, gave 2,3-dideuterolupane **7** (100 mg) in 76.6% yield as a white waxy solid, mp 129–148°C; ms m/z (%): 414 (36, M^+), 413 (1.5), 399 (17), 397 (1), 259 (14), 231 (13), 193 (100), 191 (20), 149 (18), 123 (37), 95 (46), 81 (37), 69 (33).

Acknowledgements

This work was funded by a DSS contract (no. 23294-8-0507/01-SG) under the auspices of the Institute of Sedimentary and Petroleum Geology, Energy, Mines and Resources, Canada.

1. A. Ensminger, A. van Dorsselaer, C. Spyckerelle, P. Albrecht, and G. Ourrison. *In* Adv. Org. Geochem. Proc. Int. Meet. 6th. Paris. 1973. p. 245.
2. A. van Dorsselaer, A. Ensminger, C. Spyckerelle, M. Dastillung, O. Sieskind, P. Arpino, P. Albrecht, G. Ourrison, P. W. Brooks, S. J. Gasbell, B. J. Kimble, R. P. Philip, J. R. Maxwell, and G. Eglinton. Tetrahedron Lett. 1343 (1974).
3. A. S. MacKenzie. Adv. Pet. Geochem. **1**, 115 (1984).
4. J. Rullkötter, D. Leythaeuser, and D. Wendisch. Geochim. Cosmochim. Acta, **46**, 2501 (1982).
5. P. Brooks. Org. Geochem. **10**, 401 (1985).
6. W. Ammann, R. Richarz, T. Wirthlin, and D. Wendisch. Org. Magn. Reson. **20**, 260 (1982).
7. J. M. Lehn and G. Ourisson. Bull. Soc. Chim. Fr. 1133 (1962).
8. N. P. Sahu, S. B. Mahato, and R. N. Chakravarti. J. Indian Chem. Soc. **1**, 771 (1973).
9. A. R. Maltin, C. F. George, S. Wolff, and W. A. Agosta. J. Am. Chem. Soc. **108**, 3385 (1986).
10. E. Wenkert, G. V. Baddeley, I. R. Burfitt, and L. N. Moreno. Org. Magn. Reson. **11**, 337 (1978).
11. H. Budzikiewicz, C. Djerassi, and D. H. Williams. Structural elucidation of natural products by mass spectrometry. Vol. II. Steroids, terpenoids, sugars and miscellaneous classes. Holden–Day, San Francisco, CA. 1964.
12. P. W. Brooks. Can. Soc. Pet. Geol. **34**, 490 (1986).
13. D. Garin. J. Org. Chem. **36**, 1697 (1971).
14. S. O. Nwaukwa and P. M. Keehn. Tetrahedron Lett. **23**, 3131 (1982).
15. G. Weeratunga, V. Kumar, M. U. S. Sultanbawa, and S. Balasubramaniam. J. Chem. Soc. Perkin Trans. 1, 2457 (1982).
16. A. A. L. Gunatilaka, N. D. P. Nanayakkara, and M. U. S. Sultanbawa. J. Chem. Soc. Perkin 1, 2459 (1983).
17. M. Scholichin, K. Yamasaki, R. Kasai, and O. Tanaka. Chem. Pharm. Bull. **28**, 1006 (1980).
18. D. Crich, D. H. R. Barton, and W. Motherwell. Tetrahedron, **41**, 3901 (1985).
19. I. Valterová, J. Klinot, and A. Vystrčil. Collect. Czech. Chem. Commun. **48**, 649 (1983).
20. J. Klinot, V. Šumanová, and A. Vystrčil. Collect. Czech. Chem. Commun. **37**, 603 (1972).

21. J. T. PINHEY, K. COHEN, and R. KAZLAUSKAS. J. Chem. Soc. Perkin Trans. 1, 2076 (1973).
22. I. VALTEROVÁ, J. KLINOT, and A. VYSTRČIL. Collect. Czech. Chem. Commun. **45**, 1964 (1980).
23. A. VYSTRČIL, E. STEJSKALOVÁ-VONDRASKOVÁ, and J. ČERNÝ. Collect. Czech. Chem. Commun. **24**, 3279 (1959).
24. J. PROTIVA, F. TURECEK, and A. VYSTRČIL. Collect. Czech. Chem. Commun. **42**, 140 (1977).
25. A. P. DANTANARAYANA, N. S. KUMAR, and M. U. S. SULTANBAWA. J. Chem. Soc. Perkin Trans. 1, 2717 (1981).
26. A. VAN DORSSELAER, P. ALBRECHT, and G. OURSSON. Bull. Soc. Chim. Fr. 165 (1977).
27. M. FISCHER, Z. PELAH, D. H. WILLIAMS, and C. DJERASSI. Chem. Ber. **98**, 3236 (1965).
28. G. W. KABALKA, R. HUTCHINS, N. R. NATALE, D. T. C. YANG, and V. BROACH. Org. Synth. **59**, 42 (1980).
29. D. TODD. Experimental organic chemistry. Prentice-Hall, Englewood Cliffs, NJ. 1979.
30. L. TÖKES, G. JONES, and C. DJERASSI. J. Am. Chem. Soc. **90**, 5465 (1968).
31. H. FUHRER, V. B. KARTHA, P. J. KRUGER, H. H. MANTSCH, and R. N. JONES. Chem. Rev. **72**, 439 (1972).
32. D. B. T. WIJERATNE, V. KUMAR, and M. U. S. SULTANBAWA. J. Chem. Soc. Perkin Trans. 1, 2724 (1981).
33. P. KOČOVSKÝ and V. ČERNÝ. Collect. Czech. Chem. Commun. **44**, 234 (1979).

Can. J. Chem. Downloaded from www.nrcresearchpress.com by 195.138.81.100 on 09/07/12
For personal use only.

Stereospecific synthesis, ^1H and ^{13}C NMR spectroscopy, and X-ray crystallographic studies of 6,6-dibromo-3α-cyano-2,2-dimethylpenam-(1*R*)-*S*-oxide

CLAUDIO J. SALOMON AND ORESTE A. MASCARETTI[1]

Instituto de Química Orgánica de Síntesis (CONICET-UNR), Facultad de Ciencias Bioquímicas y Farmaceúticas, Casilla de Correo 991, 2000 Rosario, Argentina

CHARLES E. STROUSE

Department of Chemistry and Biochemistry, UCLA, 405 Hilgard Ave., Los Angeles, CA 90024, U.S.A.

AND

G. PUNTE[1,2]

Departamento de Física, Facultad de Ciencias Exactas, Universidad Nacional de La Plata, C.C. 67, 1900 La Plata, Argentina

Received March 27, 1990[3]

CLAUDIO J. SALOMON, ORESTE A. MASCARETTI, CHARLES E. STROUSE, and G. PUNTE. Can. J. Chem. **69**, 578 (1991).

A stereospecific synthesis of 6,6-dibromo-3α-cyano-2,2-dimethylpenam-(1*R*)-*S*-oxide (**2**) is described. The X-ray single crystal investigation of this compound shows that it crystallizes in the monoclinic system, space group $P2_1$, with cell parameters $a = 6.194(1)$, $b = 9.363(1)$, $c = 9.869(1)$ Å, $\beta = 96.55(2)°$, $V = 568(1)$ Å^3, and two molecules per unit cell. The structure was solved, from low temperature data, by direct methods, and refined, by least-squares procedures, to a final $R = 3.17\%$, $R_w = 3.38\%$, for 1221 observed independent reflections. The sulfoxide configuration is *R*. The thiazolidine presents an envelope shape with the C(3) atom 0.56 Å above the other four members of the ring mean plane. Therefore, it exhibits the conformation with α-CH_3 pseudoequatorial and β-CH_3 and α-CN both pseudoaxial. This conformation is different from the one reported for other penicillin sulfoxide derivatives. The geometry of the β-lactam ring is typical of the fused bicyclic penam nucleus. The ring is non-planar. The N(4) atom displays a pyramidial arrangement. The examination of crystal packing shows that molecules along *a* are connected by a short C—H...O contact.

Reported single crystal studies showed two dominant conformations for the thiazolidine ring in the fused bicyclic penam nucleus: the C(3) or 2β-3α substituents both pseudoaxial, as found in **2**, and the S(1) or 2β-3α substituents both pseudoequatorial, adopted by most sulfoxides. Neither of these conformations can explain the nuclear Overhauser effect data. A conformation with the substituents C2-β-methyl-C3-α-H and C2-α-methyl-C3-α-CN fully eclipsed is in accordance with the experimental results in the solution. The ^1H nuclear magnetic resonance data reflect the influence of the magnetic anisotropy of the CN triple bond on the *gem*-dimethyl groups, particularly in relation with the geometrical features of the molecule. Comparison of ^{13}C nuclear magnetic resonance chemical shifts for **2** and its parent penicillin sulfide (**1**) indicates configurationally dependent substituent effects, the magnitude of which can be used for the stereochemical assignment of sulfoxide groups in this series.

Key words: penicillin sulfoxide derivatives, di-halogen penicillanates, stereospecific synthesis, NMR studies, absolute configuration determination.

CLAUDIO J. SALOMON, ORESTE A. MASCARETTI, CHARLES E. STROUSE et G. PUNTE. Can. J. Chem. **69**, 578 (1991).

On décrit une synthèse stéréospécifique du 6,6-dibromo-3α-cyano-2,2-diméthylpénam-(1*R*)-*S*-oxyde (**2**). Une étude par diffraction des rayons-X par un cristal unique de ce composé montre qu'il cristallise dans le système monoclinique, groupe d'espace $P2_1$, avec $a = 6,194(1)$, $b = 9,363(1)$ et $c = 9,869(1)$ Å, $\beta = 96,55(2)°$, $Z = 2$ et $V = 568(1)$ Å^3. On a déterminé la structure par des méthodes directes à l'aide de données obtenues à basse température et on l'a affinée par la méthode des moindres carrés (matrice complète) jusqu'à des valeurs de $R = 0,0317$ et $R_w = 0,0338$ pour 1221 réflexions indépendantes. La configuration du sulfoxyde est *R*. La thiazolidine se présente sous la forme d'une enveloppe dans laquelle l'atome C(3) se trouve à 0,56 Å au-dessus du plan moyen formé par les quatre autres atomes. Elle se présente donc dans le conformation avec le α-CH_3 en position pseudo-équatoriale alors que le β-CH_3 et le α-CN sont tous les deux en positions pseudo-axiales. Cette conformation diffère de celle rapportée pour d'autres dérivés sulfoxydes de la pénicilline. La géométrie du cycle β-lactame est typique de celles observées avec les noyaux pénames bicycliques condensés. Le noyau n'est pas plan. L'atomic N(4) présente un arrangement pyramidal. L'examen de l'empilement cristallin montre que les molécules de l'axe *a* sont reliées par un faible C—H...O.

Les études qui ont été effectuées antérieurement sur les structures cristallines ont démontré l'existance de deux conformations prédominantes pour le cycle thiazolidine condensé dans des noyaux pénames bicycliques : les substituants C(3) ou 2β,3α en positions pseudo-axiales, comme dans **2**, ou les substituants S(1) ou 2β,3α en positions pseudo-équatoriales, adoptées dans la plupart des sulfoxydes. Aucune de ces conformations ne peut expliquer les données d'effet Overhauser nucléaire. Pour les données expérimentales obtenues en solution, on doit faire intervenir une conformation complétement éclipsée des substituants C2-β-méthyl-C3-α-H et C2-α-méthyl-C3-α-CN. Les données de la RMN du ^1H reflètent l'influence de l'anisotropie magnétique de la triple liaison CN sur les groupements *gem*-diméthylés, particulièrement en relation avec les caractéristiques géométriques de la molécule. Une comparaision des déplacements chimiques, en RMN du ^{13}C, du composé **2** et du sulfure correspondant (**1**) suggère la présence d'effets de substituants qui dépendent de la configuration; leur amplitude peut être utilisée pour l'attribution stéréochimique de groupements sulfoxydes dans cette série.

Mots clés : derivés de pénicilline sulfoxyde, di-halogène pénicillanates, synthèse stéréospecifique, études RMN, détermination de la structure absolue.

[Traduit par la rédaction]

---

[1]Authors to whom correspondence should be addressed.

[2]Present address: Department of Physics and Astronomy, The Johns Hopkins University, Homewood Campus, Baltimore, MD 21218, U.S.A.

[3]Revision received November 9, 1990.

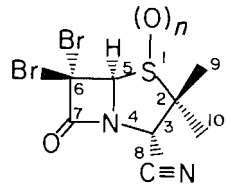
Can. J. Chem. Downloaded from www.nrcresearchpress.com by 198.100.157.202 on 09/07/12
For personal use only.

Can. J. Chem. Downloaded from www.nrcresearchpress.com by 198.100.157.202 on 09/07/12
For personal use only.

Introduction

There has been relatively little work reported on the conformation adopted by specific β-lactamase inhibitors in the solid state and in solution (1, 2). Greater attention has been directed to the study of the conformation of 6β-*N*-acylamino penicillins on the β-lactam binding proteins of bacteria for bacterial activities (3).

In recent years we have synthesized and examined with various techniques several penicillin derivatives (1, 4, 5). The aim of these investigations was to find the functional groups and conformations, the so-called topological and topographic patterns (6), essential for a good β-lactamase inhibitory activity. In the course of these comparative studies we became interested in introducing an oxygen atom at a specific site of the 6,6-dibromo-3α-cyano-2,2-dimethylpenam (**1**). Of special interest was the stereocontrolled access to (*R*)- and (*S*)-sulfoxides of dibromo derivatives like **2** and **3**, and also to their corresponding 6β- and



1 $n = 0$
2 $n = 1\alpha$ (*R*)
3 $n = 1\beta$ (*S*)

6α-bromo derivatives, to study the dependence of the ^{17}O and, particularly, the ^{33}S nmr parameters on the stereochemistry (7).

The conversion of penicillanates into the corresponding sulfoxides has been recently studied (for a recent review, see ref. 8). Conversion of sulfides into sulfoxides may be carried out by many oxidizing agents (for a review, see ref. 9). However, only a few of these permit oxidation to proceed in a selective manner with high yields under mild conditions (10).

Both 1α- (**2**) and 1β-6,6-dibromo-3α-cyano-2,2-dimethylpenam sulfoxide (**3**) have been observed in the mixture obtained when the parent penam sulfide (**1**) is treated with one equivalent of *m*-chloroperbenzoic acid (*m*-CPBA), in CH_2Cl_2 at 0°C for 12 h (1). We have now successfully used potassium hydrogen persulfate (11) (commercially sold as oxone),[4] in aqueous methanol as a selective oxidizing agent, for the synthesis of only one of the two sulfoxides expected.

An X-ray single crystal analysis of the synthesized compound (**2**) was performed in order to determine its absolute configuration.

The knowledge of the molecular geometry gathered by X-ray crystallography is essential in the study of the conformation–activity relationship and the mechanism of action of drugs. Notwithstanding, it has been proved to be important to ascertain by ^1H nmr studies the conformation of the molecule in solution (1, 12) as it can either be different from the solid state conformation, as we found to be the case for **2**, or the compound can be difficult to crystallize. A nuclear Overhauser effect study was therefore carried out to get information regarding the conformational nature of the thiazolidine ring of **2** in solution. In addition, ^{13}C nmr spectroscopy was applied to the study of the solution structures of **1** and **2**. This last technique has been reported effective for the study of sulfoxide configurations (1, 13, and, for a review, 14).

[4]Oxone contains 2 mol equiv. of $KHSO_5$, 1 mol equiv. of K_2SO_4, and 1 mol equiv. of $KHSO_4$, and was purchased from Aldrich Chemical Co.

Experimental

Routine ir spectra were obtained on a Beckman Acculab 8 spectrometer. The ^1H and ^{13}C nmr spectra were recorded on a Bruker WP 80 SY at 80.13 and 20.15 MHz; the chemical shifts are expressed in parts per million downfield from internal tetramethylsilane. Melting points were determined on a Kofler hot stage apparatus and are uncorrected. X-ray diffraction data were collected using a locally automated Picker Diffractometer.

4-Thia-1-azabicyclo[3.2.0]heptane-2-carbonitrile-6,6-dibromo-2,2-dimethyl-7-oxo [2S(2α,5α)][5] (**1**)

This compound was prepared from the corresponding 2-carboxamide as described in ref. 4. Mol. wt (hrms) calcd. for $C_8H_8Br_2N_2OS$: 337.8724; found: 337.8769.

4-Thia-1-azabicyclo[3.2.0]heptane-2-carbonitrile-6,6-dibromo-2,2-dimethyl-7-oxo-4-oxide (2S[2α,4α(R),5α]) (2)*

Compound **1** (2.00 g, 5.86 mmol) was dissolved in methanol (25 mL), the solution was cooled to 0°C, and a solution of oxone (containing 15.8 mmol of $KHSO_4$) in water (25 mL) was added. The resulting slurry was stirred for 24 h at room temperature, after which methanol was removed under reduced pressure, ethyl acetate (25 mL) added to the residue, and the layers separated. The aqueous layer was extracted with ethyl acetate (2 × 25 mL). The combined organic layers were washed with brine (2 × 20 mL), dried (Na_2SO_4), and concentrated. The resulting solid product was crystallized from chloroform to provide the pure α-sulfoxide **2** (1.350 g, 67.5%), mp 162–163°C; ir (KBr): 2225 (cyano), 1815 (β-lactam), and 1050 (SO) cm^{-1}; ^1H nmr ($CDCl_3$): 1.51 (s, 3H, 9-CH_3), 172 (s, 3H, 10-CH_3), 4.95 (s, 1H, C-3H), 5.32 (s, 1H, C-5H); cims *m/z*: 355, 357, 359 (MH^+) for $C_8H_8Br_2N_2O_2S$.[6]

A colorless parallelepiped-shaped crystal was used for the X-ray study. Crystal data are presented in Table 1. The unit cell parameters were obtained by least-squares refinement of the setting angles of 33 reflections ($8 < 2\theta < 21°$). Three standard reflections, measured every 100 reflections, showed only random intensity variations during data collection, max. 3.5%. Lorentz and polarization corrections were applied. An isotropic secondary extinction correction of the form $F' = F(1\text{-}CF^2/\sin\theta)$ was applied on F_c, refined *C* value: 7.7×10^{-4}. An absorption correction was done on I_o (15).

The structure was solved using direct methods, MULTAN80 (16). From the partial model obtained, all non-hydrogen atoms were located and refined from alternate difference Fourier and isotropic least-squares refinement cycles. The refinement was performed by full-matrix least squares based on *F*'s employing anisotropic thermal parameters. Quantity minimized: $\Sigma[w||F_o| - |F_c||]$. Hydrogens were stereochemically positioned (C—H = 1.08 Å); the H's bound to C(3) and C(5) atoms were refined, isotropically, with their thermal parameters fixed. The methyl hydrogens were refined with their positions riding on the bonded atoms and with overall temperature factor for each group.

The final refinement, converged to $R = 3.17$, $R_w = 3.38\%$, weighting scheme: $1.0709/\sigma^2$, where σ were based on counting statistics (no improvement could be seen with any other scheme). The biggest fluctuations of the electronic density were located near Br atoms. To establish the absolute configuration, an alternative refinement based on the mirror image of the molecule was performed to convergence. This led to $R = 4.02$, $R_w = 4.33$, and $R_g = 5.27\%$. Then, according to the Hamilton test (17), the non-inverted set of coordinates corresponds to the true configuration. Scattering factors for H and scattering factors and anomalous dispersion corrections for O, C, N, S, and Br were taken from SHELX76 (18).

[5]We used Systematic Chemical Abstracts names as headings for the title compound in the experimental section because they are the names most useful for literature searching, and non-systematic names in order to allow cross-reference correlations to the penicillins and penam nomenclature. For this naming and numbering see ref. 34.

[6]For this compound characteristic isotopic peaks were observed in the mass spectra.

Can. J. Chem. Downloaded from www.nrcresearchpress.com by 198.100.157.202 on 09/07/12
For personal use only.

TABLE 1. Summary of crystal data, intensity collection, and structure refinement

Composition	$Br_2SO_2N_2C_8H_8$
MW	356.05
$F(000)$	344
Crystal system	Monoclinic
Space group	$P2_1$
a, Å	6.194(1)
b, Å	9.363(1)
c, Å	9.869(1)
β, deg	96.55(2)
V, Å^3	6568(1)
Z	2
D_c, gm^{-3}	2.08
μ(MoKα), cm^{-1}	72.18
T, K	145
λ(MoKα), Å	0.71073
Crystal size, mm	0.16 × 0.14 × 0.30
Scan mode	θ–2θ
Scan speed, deg min^{-1}	6
$2\theta_{max}$	55.0
Index range	h: −8, 7; k: 0, 12; l: 0, 12
Number of measured reflections	1551
Number of observed reflections	1221
Acceptance criterion	$I > 3\sigma(I)$
Extreme values of transmission factor	0.32, 0.41
Number of variables	150
$R = \Sigma\|\|F_o\| - \|F_c\|\|/\Sigma F_o$ (18)	3.17
$R_w = \Sigma[\|\|F_o\| - \|F_c\|w^{1/2}]/\Sigma[F_o w^{1/2}]$(18)	3.38
$Rg = [\Sigma w\|\|F_o\| - \|F_c\|^2/\Sigma(F_o^2 w)]^{1/2}$ (17)	4.06
$S = \Sigma[w\|\|F_o\| - \|F_c\|^2]/)m - n)$	1.38
Maximum shift/esd	7×10^{-3}
Min. and max. of the residual electron density, e Å^{-3}	−0.55, 0.65

Calculations were carried out on VAX systems using the following programs: UCLA crystallographic computing package. (15), MULTAN80 (16), SHELX76 (18), ORTEP (19), and PLUTO (20).

Fractional atomic parameters with equivalent isotropic thermal parameters for the refined atoms are given in Table 2.[7] The numbering scheme is shown in a stereoscopic view of the molecule, Fig. 1. Table 3 shows intramolecular bond lengths and angles.

Results and discussion

Chemistry

The oxidation of 6,6-dibromo-3α-cyano-2,2-dimethylpenam (**1**) afforded the sulfoxide **2** in good yield as the pure (*R*) isomer. The oxidation occurred at the sterically more accessible α-face.

Description and discussion of the crystal structure

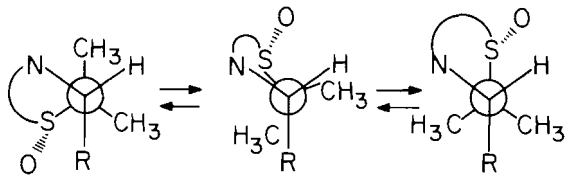
We have recently analyzed the X-ray crystal structure and solution conformation of several pivaloyloxymethyl 6,6-dihalo- and 6-halopenicillanates and their corresponding 1-oxides and 1,1-dioxides (1, 5). We found, in agreement with earlier reports on 6β-*N*-acylated penicillin derivatives (21, 22), that four of the five atoms of the puckered thiazolidine ring tend to be coplanar and can adopt one of two extreme conformations, I and II, described in the literature. I is illustrated by the Newman projection **4***a*. It is usually referred to as conformation C(3) (after Domiano *et al.* (22)). II is exemplified by the Newman

[7]Tables of structure factors, H-atom parameters, anisotropic thermal parameters, and best least-squares planes may be purchased from The Depository of Unpublished Data, Document Delivery, CISTI, National Research Council Canada, Ottawa, Canada K1A 0S2.

TABLE 2. Fractional positional parameters and equivalent isotropic thermal parameters (Å^2), esd's in parentheses; $B_{eq} = \frac{1}{3}\Sigma_i\Sigma_j \beta_{ij} a_i \cdot a_j$

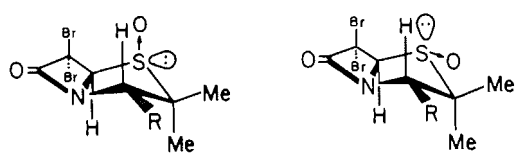
Atom	x/a	y/b	z/c	B_{eq}
S(1)	0.0013(2)	0.8492(2)	0.6627(2)	1.67(4)
Br(1)	0.2158(1)	1.1404	0.8471(1)	2.60(2)
Br(2)	0.1943(1)	0.9543(1)	1.1120(1)	2.88(2)
N(4)	0.3478(8)	0.7647(7)	0.8339(6)	1.7(2)
N(8)	0.2380(1)	0.4354(7)	0.6947(7)	2.5(2)
O(1)	−0.1489(7)	0.7246(6)	0.6439(5)	2.2(1)
O(8)	0.6498(8)	0.9105(6)	0.9108(5)	2.5(2)
C(2)	0.255(1)	0.7959(8)	0.5911(7)	1.6(2)
C(3)	0.3780(1)	0.6984(8)	0.7041(7)	1.5(2)
C(5)	0.132(1)	0.8288(8)	0.8408(7)	1.8(2)
C(6)	0.245(1)	0.9533(8)	0.9234(6)	1.7(2)
C(7)	0.463(1)	0.8807(7)	0.8965(7)	1.8(2)
C(8)	0.297(1)	0.5498(8)	0.7002(7)	1.8(2)
C(9)	0.386(1)	0.9277(8)	0.5688(7)	2.0(2)
C(10)	0.190(1)	0.7174(9)	0.4574(7)	2.2(2)
H(3)	0.53(1)	0.691(9)	0.690(7)	2.4
H(5)	0.03(1)	0.78(1)	0.888(7)	2.4

projection **4***c*. This is named conformation S(1) (22). An alternative identification, based on the relative position of the 2β-CH_3 and 3α-R substituents with respect to the thiazolidine ring, has been preferred by some crystallographers (see, e.g., refs. 23 and 24). Within this scheme, I is the 2β–3α pseudoaxial conformation and II is the 2β–3α pseudoequatorial conformation. I and II are interconvertible via the pseudo rotation associated with S(1)—C(2)—C(3)—N(4) torsion. In **2** the best plane (in the χ^2 sense) is defined by S(1), C(2), N(4), C(5); the C(3) atom is displaced from this plane by 0.560(7) Å *exo* to the



4*a* **4***b* **4***c*

nucleus. Therefore, as can be seen in Fig. 1, the five-membered ring exhibits a conformation close to the C(3) one with α-CH_3 pseudoequatorial and β-CH_3 and α-CN pseudoaxial. Endocyclic thiazolidine torsional angles and selected torsional angles involving C2 and C3 substituents are presented in Table 4. The conformation adopted by **2** is different from that reported for other penicillin sulfoxides such as phenoxymethyl penicillin-1β(1*S*)-sulfoxide (23), cloxacillin-1β(1*S*)-sulfoxide (24), pivaloyloxymethyl 6,6-dibromo penicillanate-1β(1*S*)-sulfoxide (**5**) (5), and methyl 6,6-dibromo penicillanate-1β(1*S*)-sulfoxide (**6**) (25). In compound **2** the value of the endocyclic bond angle at S(1), 92.0(3)°, though smaller than the expected value for the C(3) conformation, 96.1(2)° (3*d*), is higher than the values



R = $CO_2CH_2OCC(CH_3)_3$ R = CO_2CH_3

5 **6**

Can. J. Chem. Downloaded from www.nrcresearchpress.com by 198.100.157.202 on 09/07/12
For personal use only.

TABLE 3. Intramolecular bond distances (Å) and angles (°) and selected intermolecular distances (Å), esd's in parentheses

Br(1)—C(6)	1.907(7)
Br(2)—C(6)	1.923(6)
S(1)—O(1)	1.491(5)
S(1)—C(2)	1.863(7)
S(1)—C(5)	1.859(7)
O(8)—C(7)	1.183(9)
N(4)—C(3)	1.455(9)
N(4)—C(5)	1.474(9)
N(4)—C(7)	1.404(9)
C(2)—C(3)	1.57(1)
C(2)—C(9)	1.51(1)
C(2)—C(10)	1.52(1)
C(3)—C(8)	1.48(1)
C(3)—H(3)	0.97(8)
C(5)—C(6)	1.54(1)
C(5)—H(5)	0.94(8)
C(6)—C(7)	1.561(9)
C(8)—H(3)	1.97(8)
C(8)—N(8)	1.13(1)
C(2)—S(1)—O(1)	106.5(3)
C(2)—S(1)—C(5)	92.1(3)
O(1)—S(1)—C(5)	103.6(3)
S(1)—C(2)—C(10)	107.9(4)
S(1)—C(2)—C(9)	109.1(5)
S(1)—C(2)—C(3)	104.4(5)
C(10)—C(2)—C(9)	111.1(6)
C(10)—C(2)—C(3)	113.2(6)
C(9)—C(2)—C(3)	110.9(5)
N(4)—C(3)—C(8)	110.3(6)
N(4)—C(3)—C(2)	106.1(6)
C(8)—C(3)—C(2)	113.1(5)
C(8)—C(3)—H(3)	105(5)
N(4)—C(3)—H(3)	112(4)
H(3)—C(3)—C(2)	110(4)
C(3)—N(4)—C(7)	127.4(6)
C(3)—N(4)—C(5)	115.0(5)
C(7)—N(4)—C(5)	94.7(5)
S(1)—C(5)—N(4)	107.3(5)
S(1)—C(5)—C(6)	122.9(5)
N(4)—C(5)—C(6)	88.4(5)
N(4)—C(5)—H(5)	119(5)
S(1)—C(5)—H(5)	106(4)
H(5)—C(5)—C(6)	113(5)
C(7)—C(6)—C(5)	86.0(5)
C(7)—C(6)—Br(1)	112.2(5)
C(7)—C(6)—Br(2)	113.6(5)
C(5)—C(6)—Br(1)	117.9(5)
C(5)—C(6)—Br(2)	113.6(5)
Br(1)—C(6)—Br(2)	111.0(3)
N(4)—C(7)—O(8)	132.5(7)
N(4)—C(7)—C(6)	90.3(5)
O(8)—C(7)—C(6)	137.0(6)
C(3)—C(8)—N(8)	178.7(8)

found in **5**, 88.4(4)°, and in **6**, 89.1(3)°, as expected, since **5** and **6** show the S(1) conformation. The methyl group at C(10) is on the same side of the best thiazolidine ring as the CN substituent at C(3). The torsion angle C(10)—C(2)—C(3)—C(11) = −35.7(8)° and the C(10)—C(11) distance, 2.88(1) Å, indicate that these atoms present a nearly eclipsed conformation.

The geometry of the 2-azetidinone (β-lactam) ring in **2** is typical for the fused bicyclic penam nucleus. The ring is not

TABLE 4. Selected torsional angles involving thiazolidine ring and substituents (°), esd's in parentheses

C5—S1—C2—C3	26.8 (0.5)
S1—C2—C3—N4	−39.7 (0.6)
C3—N4—C5—S1	−16.7 (0.7)
C2—S1—C5—N4	−7.6 (0.5)
C5—N4—C3—C2	37.6 (0.7)
C5—S1—C2—C9	−91.6 (0.5)
C5—S1—C2—C10	147.4 (0.5)
S1—C2—C3—C8	81.3 (0.6)
O1—S1—C5—N4	100.0 (0.5)
C9—C2—C3—C8	−161.3 (0.6)
C10—C2—C3—N4	−156.7 (0.5)
C10—C2—C3—C8	−35.7 (0.8)
O1—S1—C2—C3	−78.1 (0.5)
O1—S1—C2—C9	163.5 (0.4)
O1—S1—C2—C10	42.6 (0.6)

planar; the N(4) atom shows a pyramidal arrangement, being out of the plane defined by its substituents. The value of the out-of-plane distance, 0.395(6) Å, and the sum of angles around N(4), 334.1°, compare well with the reported values for other penicillanates (21). The non-planarity of the 2-azetidinone ring can be assessed, as well, from the dihedral angle between the N(4)—C(5)—C(6) and N(4)—C(6)—C(7) planes, 7.4(2.0)°. Besides, it is found that the atoms N(4)—C(6)—C(7)—O(8) define a better plane than those forming the four-membered ring. The C(5) atom is displaced 0.178(7) Å on the same side of the mean four-membered ring plane as the sulfur atom.

Bond distances and angles within the nucleus, see Table 3, are in good agreement with those of other penicillin derivatives (21, 22).

The dihedral angle between the mean planes of the thiazolidine and 2-azetidinone rings, 117.5(3)°, is similar to that found in other C(3) penicillin derivatives (22).

The CN substituent geometry compares well with the geometry reported for CN groups bound to cyclic sp^3 carbon atoms (26).

The packing of the molecules in the crystal is shown in Fig. 2. Assuming as van der Waals radii for C, N, O, S, and Br atoms and for the CH_3 group, respectively, the values 1.6, 1.5, 1.4, 1.85, 1.95, and 2.0 Å, in agreement with Pauling (27), it has been found that some intermolecular distances are smaller than the sum of the corresponding van der Waals radii,[7] thus indicating that electrostatic interactions are contributing to the crystal structure stabilization. In particular the C(3)—H(3)....O(1) contact that is linking molecules along *a* may be considered as an H-bond, according to Taylor and Kennard (28), since C(3)....O(1) = 3.065(5) Å, H(3)...O(1) = 2.11(8) Å, and C(3)—H(3)—O(1) = 167(7)°. The existence of short C—H...O contacts, some of which can be described as hydrogen bonds according to Taylor and Kennard (28), has been recently reported by Verdilinde, Blaton, de Ranter, and Peeters from single crystal X-ray studies and CNDO/2 calculations performed on (1*S*,-5*R*,8*R*,9*R*)-2′-hydroxy-5,9-dimethyl-8,2-epoxyethano-6,7-benzomorphan hydrochloride (29). Taking account of the flexibility of the thiazolidine ring of the penam nucleus it can be assumed that the intermolecular interactions mentioned might force the conformation displayed by **2** in the solid state. This assumption is supported by molecular modelling studies of the nucleus (30, 31), which found energy barrier values of 0.5 and

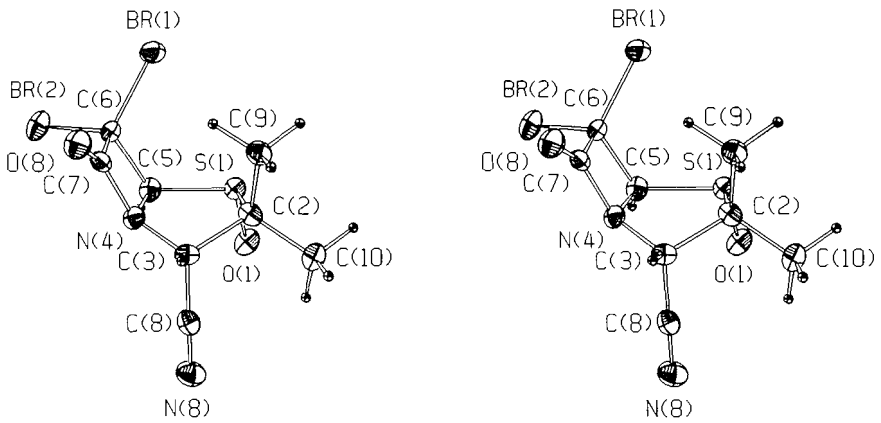


FIG. 1. Stereoscopic ORTEP drawing of the molecule, thermal ellipsoids 50%, showing non-hydrogen atoms labelling.

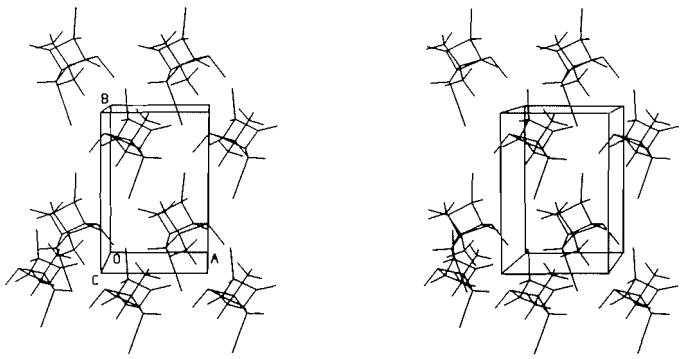


FIG. 2. Stereoscopic view of the molecular packing.

0.7 kcal respectively between conformers **4***a* and **4***c*, and by recent theoretical conformational analysis studies (32), which determined that global minima for various penicillins were 2.0–4.5 kcal/mol lower in energy than the corresponding crystal structure.

Spectroscopic data

Nuclear Overhauser effect

Results are presented in Table 5; they indicate an enhancement of 23.5% in the intensity of the H(3) resonance when the high-field methyl peak is saturated, whereas the enhancement of the H(5) resonance is negligible. Besides it can be seen that saturating the low-field methyl peak had no effect on the intensity of the H(3) and H(5) signals.

Neither of the two extreme conformations, C(3) or S(1), presented by the thiazolodine ring in the solid state can account for these experimental observations. Only in a conformation with the substituents C(2)-β-methyl-C(3)-βH and C(2)-α-methyl-C(3)-α-CN fully eclipsed, like **4***b*, can H(3) be relaxed by the 2β-methyl hydrogen. This would indicate that **2** in solution adopts a conformation different from that found in crystals.

Therefore, from single crystal and nOe data, it can be assumed that the thiazolidine ring in **2** is flexible enough to adopt whatever conformation may be energetically advantageous for the environment requirements. This is consistent with the reported theoretical conformational analysis studies (32), which predicted conformations of the methyl esters of penicillin G and bisnorpenicillin G in accord with the conformations observed in solution and suggested that neither penicillin V nor penicillin G retain their crystal structure in solution.

TABLE 5. Nuclear Overhauser effects in 6,6-dibromo-3α-cyano-2,2-dimethylpenam-1-oxide

Hydrogen irradiated	δ (ppm)[a]	Hydrogen observed	nOe (%)[b]
9-CH_3	1.51	H(3)	23.5
		H(5)	0.0
10-CH_3	1.72	H(3)	0.0
		H(5)	0.0

[a]Spectra recorded in $CDCl_3$ solution.
[b]Error limit 3%.

TABLE 6. ^{13}C Chemical shifts (δ^b) of 6,6-dibromo-3α-cyano-2,2-dimethylpenam (**1**) and its (1*R*)-sulfoxide (**2**)[a]

	1	**2**
C(2)	63.68	72.38
C(3)	59.43	56.27
C(5)	78.66	93.40
C(6)	57.94	46.90
C(7)	164.22	162.89
C(8)	114.11	113.65
C(9)	30.78	21.48
C(10)	25.63	17.59

[a]Spectra were recorded in DMSO solution.
[b]The δ values are in ppm, relative to Me_4Si.

^{13}C and ^1H nuclear magnetic resonance spectroscopy

Table 6 displays ^{13}C nmr spectral data for **1** and **2**. Figure 3 illustrates the observed changes in the chemical shifts on going from **1** to **2**. We have reported a similar pattern of changes for the series of pivaloyloxy methyl 6,6-dihalo- and 6-halopenicillanates and their corresponding (*R*)-sulfoxide (1). Clear and markedly different patterns in the shifts in resonance position on going from a sulfide to its β-sulfoxide or to its α-sulfoxide, which remain despite substantial alterations in the substitution at C(6), have been reported by Harrison and Hodge (13). Therefore, the ^{13}C nmr results presented here, together with the knowledge of the configuration and solution conformation of **2**

Can. J. Chem. Downloaded from www.nrcresearchpress.com by 198.100.157.202 on 09/07/12
For personal use only.

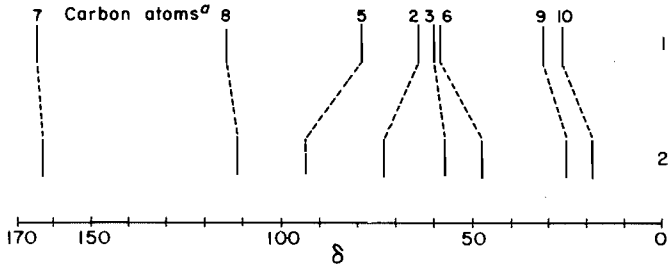


FIG. 3. Correlation for the process: penam sulfide (**1**) → (*R*)-sulfoxide (**2**). δ: ^{13}C chemical shift (parts per million from Me_4Si).

[a]Carbon numbering as in structures **1–3**, which are different from those shown in the chemical abstracts names in the heading.

provided by X-ray and nOe results, could be used to determine the penicillin sulfoxide configuration of mono- and dihalide derivatives of **1** from ^{13}C chemical shift data in solution.

The most remarkable feature of the ^1H nmr data is the strong magnetic anisotropy of the C≡N triple bond (33). The hydrogen atoms of the C(9) methyl group lie in the shielding region of the electron circulation induced by the magnetic field, that is, the magnetic anisotropy is negative. On the other hand, the hydrogen atoms of the C(10) methyl group are deshielded. This differential influence on the resonance of *gem*-methyl groups might be an important aid in the conformational analysis of the thiazolidine ring in the series 3α-cyano-2,2-dimethyl penam.

Acknowledgments

The authors thank CONICET (Consejo Nacional de Investigaciones Científicas y Técnicas de Argentina) and the Johns Hopkins University for financial support, Dr. E. G. Mata for skillful technical assistance, and Dr. M. G. Sierra for recording the nOe differential spectra and for helpful discussions.

1. D. U. BELIZONI, E. L. SETTI, and O. A. MASCARETTI. J. Chem. Res. (S), 176 (1988); (M), 1501 (1988).
2. (*a*) D. D. KEITH, J. TENGI, P. ROSSMAN, L. TODARO, and M. WEIGELE. Tetrahedron, **39**, 2445 (1983); (*b*) A. L. FINK, L. M. ELLERBY, and P. M. BASSETT. J. Am. Chem. Soc. **111**, 6871 (1989).
3. (*a*) D. B. BOYD. *In* Chemistry and biology of β-lactam antibiotics. Vol. 1. *Edited by* R. B. Morin and M. Gorman. Academic Press, New York. 1982. pp. 437–545; (*b*) N. C. COHEN. J. Med. Chem. **26**, 259 (1983); (*c*) D. B. BOYD, C. EIGENBROT, J. M. INDELICATO, M. J. MILLER, C. E. PASINI, and S. R. WOULFE. J. Med. Chem. **30**, 528 (1987); (*d*) P. C. BANPLAIN, J. B. NAGY, G. H. LAURENT, and F. V. DURANT. J. Med. Chem. **23**, 12 (1980); (*e*) S. WOLFE, K. YANG, and M. KHALIL. Can. J. Chem. **66**, 2733 (1988).
4. E. G. MATA, E. L. SETTI, O. A. MASCARETTI, S. B. BOGGIO, and O. A. ROVERI. J. Chem. Soc. Perkin Trans. 1, 1551 (1988).
5. (*a*) D. U. BELINZONI, O. A. MASCARETTI, P. M. ALZARI, G. PUNTE, C. FAERMAN, and A. PODJARNY. Can. J. Chem. **63**, 3177 (1985); (*b*) P. M. ALZARI, B. E. RIVERO, G. PUNTE, and A. E. RONCO. Acta Crystallogr. Sect. C: Cryst. Struct. Commun. **C42**, 1029 (1986); (*c*) P. M. ALZARI, A. E. RONCO, B. E. RIVERO, and G. PUNTE. Acta Crystallogr. Sect. C: Cryst. Struct. Commun. **C42**, 1032 (1986); (*d*) P. M. ALZARI, G. PUNTE, A. E. RONCO, and B. E. RIVERO. Acta Crystallogr. Sect. C: Cryst. Struct. Commun. **C42**, 1034 (1986); (*e*) G. PUNTE, B. E. RIVERO, and P. M. ALZARI. Acta Crystallogr. Sect. C: Cryst. Struct. Commun. **C42**, 1037 (1986).
6. P. GUND. *In* Progress in molecular and subcellular biology. Vol. 5. *Edited by* F. E. Hahn. Springer-Verlag, New York. 1977. p. 117.
7. H. DUDDECK, V. KOREK, D. ROSEMBAUM, and J. DRABOWICZ. Magn. Reson. Chem. **24**, 792 (1986), and references therein.
8. R. D. COOPER and G. A. KOPPEL. *In* Chemistry and biology of β-lactam antibiotics. Vol. 1. *Edited by* R. B. Morin and M. Gorman. Academic Press, New York. 1982. pp. 1–92.
9. (*a*) J. DRABOWICZ, P. KIELBASINSKI, and M. MIKOLAJCZYK. *In* The chemistry of sulphones and sulphoxides. *Edited by* S. Patai, Z. Rappoport, and C. J. M. Stirling. John Wiley, New York. 1988. pp. 233–378; (*b*) M. MADESCLAIRE. Tetrahedron, **42**, 5459 (1986).
10. R. G. MICETICH, R. SINGH, and C. C. SHAW. J. Org. Chem. **51**, 1811 (1986).
11. B. M. TROST and D. P. CURRAN. Tetrahedron Lett. **22**, 1287 (1981).
12. R. A. ARCHER, R. D. G. COOPER, P. V. DEMARCO, and L. R. F. JOHNSON. J. Chem. Soc. Chem. Commun. 1291 (1970).
13. C. T. HARRISON and P. HODGE. J. Chem. Soc. Perkin Trans. 1, 1772 (1976).
14. R. A. BELL and J. K. SAUNDERS. Top. Stereochem. **9**, 1 (1976).
15. C. STROUSE. UCLA crystallographic computing package. A system of program for crystal structure resolution. University of California at Los Angeles. U.S.A.
16. P. MAIN, S. J. FISKE, S. E. HULL, L. LESSINGER, G. GERMAIN, and M. M. WOOLFSON. MULTAN80. A system of computer programs for automatic solution of crystal structures from X-ray diffraction data. Universities of York, England, and Louvain-la-Neuve, Belgium. 1980.
17. W. C. HAMILTON. Acta Crystallogr. **18**, 502 (1965).
18. G. M. SHELDRICK. SHELX76. Program for crystal structure determination. Cambridge University, England. 1976.
19. C. K. JOHNSON. ORTEP. Report ORNL-3794. Oak Ridge National Laboratory, Tennessee. 1965.
20. W. D. S. MOTHERWELL and W. CLEGG. PLUTO. A program for plotting molecular and crystal structures. Cambridge University, England. 1978.
21. R. M. SWEET. *In* Cephalosporins and penicillins. *Edited by* E. H. Flynn. Academic Press, New York. 1972. pp. 280–309.
22. P. DOMIANO, M. NARDELLI, A. BALSAMO, B. MACCHIA, and F. MACCHIA. Acta Crystallogr. Sect. B: Struct. Crystallogr. Cryst. Chem. **B35**, 1363 (1979).
23. R. D. G. COOPER, P. V. DE MARCO, J. C. CHENG, and N. D. JONES. J. Am. Chem. Soc. **91**, 6 (1969); **91**, 1408 (1969).
24. P. C. BLANPAIN and F. DURANT. Cryst. Struct. Commun. **6**, 711 (1977).
25. O. M. PEETERS, N. M. BLATON, and C. J. DE RANTER. Cryst. Struct. Commun. **11**, 787 (1982).
26. D. DONATI, S. FUSI, and F. PONTICELLI. Acta Crystallogr. Sect. C: Cryst. Struct. Commun. **C45**, 317 (1989).
27. L. PAULING. The nature of the chemical bond. 3rd. ed. Cornell University Press, Ithaca, NY. 1960.
28. R. TAYLOR and O. KENNARD. J. Am. Chem. Soc. **104**, 5063 (1982).
29. C. L. VERDILINDE, N. M. BLATON, C. J. DE RANTER, and O. M. PEETERS. Acta Crystallogr. Sect. C: Cryst. Struct. Commun. **C45**, 799 (1989).
30. N. C. COHEN. J. Med. Chem. **26**, 259 (1983).
31. N. V. JOSHI, R. VIRUDACHALAM, and V. S. R. RAO. Curr. Sci. **47**, 933 (1978).
32. S. WOLFE, M. KHALIL, and D. F. WEAVER. Can. J. Chem. **66**, 2715 (1988).
33. L. M. JACKMAN and S. STERNBELL. Applications of nuclear magnetic resonance spectroscopy in organic chemistry. Pergamon Press, Oxford. 1969. pp. 92–94.
34. J. C. SHEEHAN, K. R. HÉNERY-LOGAN, and D. A. JOHNSON. J. Am. Chem. Soc. **75**, 3292 (1953).

Can. J. Chem. Downloaded from www.nrcresearchpress.com by 198.100.157.202 on 09/07/12
For personal use only.

Novel metal chelating chitosan derivative: attachment of iminodiacetate moieties via a hydrophilic spacer group

KEVIN R. HOLME[1] AND LAURANCE D. HALL[2]

Department of Chemistry, University of British Columbia, Vancouver, B.C., Canada V6T 1Y6

Received July 24, 1990

KEVIN R. HOLME and LAURANCE D. HALL. Can. J. Chem. **69**, 585 (1991).

Chitosan has been reductively N-alkylated with a 6-*O*-substituted galactose derivative bearing an iminodiacetate residue, to give a chitosan derivative having a hydrophilic branch and a metal chelating group. The Cu(II) binding capacity of the derivative was comparable to native chitosan, but showed better ion-exchange ability. The product was water soluble, giving viscous 1% aqueous solutions that showed decreased viscosity upon addition of Cu(II) ions.

Key words: chitosan, derivative, chelation, solubilization, viscosity.

KEVIN R. HOLME et LAURANCE D. HALL. Can. J. Chem. **69**, 585 (1991).

Dans le but d'obtenir un dérivé du chitosane portant une portion hydrophile et un groupement chélatant, on a procédé à une réduction N-alkylante du chitosane avec un dérivé 6-*O*-substitué du galactose portant une portion iminodiacétate. La capacité de chélation du Cu(II) de ce dérivé est semblable à celle du chitosane naturel; toutefois, il présente une meilleure habilité à l'échange ionique. Le produit est soluble dans l'eau et les solutions aqueuses à 1% sont visqueuses; ce résultat démontre que la viscosité diminue par addition d'ions Cu(II).

Mots clés : chitosane, dérivé, chélation, solubilisation, viscosité.

[Traduit par la rédaction]

Can. J. Chem. Downloaded from www.nrcresearchpress.com by 198.100.157.202 on 09/07/12
For personal use only.

Introduction

The amino polysaccharide chitosan, a β-(1-4)-linked 2-amino-2-deoxy-D-glucopyranose homopolymer, has attracted considerable attention as a result of its physical and chemical properties (1, 2). Chitosan has been modified in order to prepare controlled solubility derivatives (3, 4), metal sequestrants (5–7), drug carriers (8), and immobilization supports (ref. 2, pp. 443–444). Although our main efforts have been directed toward controlled solubility compounds (3, 4), we felt that our experience in chitosan modification could be exploited in the synthesis of metal chelating, controlled solubility conjugates.

Some metal chelating chitosan derivatives have been described, in which phthalaldehyde (5), salicaldehyde (6), and glyoxilic acid (7) were reductively alkylated to chitosan. The objective of this work was to incorporate controlled solubility features in conjunction with chelating properties to create a novel chitosan derivative. This was felt to be best accomplished by incorporating a hydrophilic spacer arm between the chitosan backbone and the desired chelating group. Previous work from this laboratory in which free sugars were coupled to chitosan to give acyclic hydrophilic branches (3) provided an ideal route to such a spacer group. Iminodiacetic acid, essentially one half of the well-known chelate ethylene diamine tetraacetic acid (EDTA), was chosen as an appropriate chelating functionality. The synthetic route to a precursor having the desired structural features, and its attachment to chitosan, will be discussed.

Results and discussion

Synthesis

By design, it was decided to prepare a compound that contained both an iminodiacetic acid functionality for metal chelation, and an aldehyde for coupling to chitosan. A carbohydrate-derived, hydrophilic spacer arm was chosen in order to enhance the solubility characteristics of the final product, and to act as a spacer arm. Scheme 1 outlines the synthesis of the ligand precursor **5**.

The epoxide **2** was prepared from 1,2:3,4-di-*O*-isopropylidene galactose (**1**), by reaction with epichlorohydrin in the presence of sodium hydride. Subsequent reaction of the epoxide with dimethyliminodiacetate (**3**) gave a 4:1 mixture of the dimethyliminodiacetate **4***a* and the morpholone **4***b*. Although cyclizations similar to that producing **4***b* have been observed in reactions of epoxides with amino acid esters (9), it appears to be more favourable for the diester compounds described here. Total conversion of the mixture to the morpholone **4***b* was easily achieved by distillation. Liquid chromatography on silica gel afforded some separation of the mixture, but it was determined that further cyclization occurred on the column. Base hydrolysis of the **4** mixture, and subsequent treatment with acid at 50°C, gave the free sugar derivative **5**.

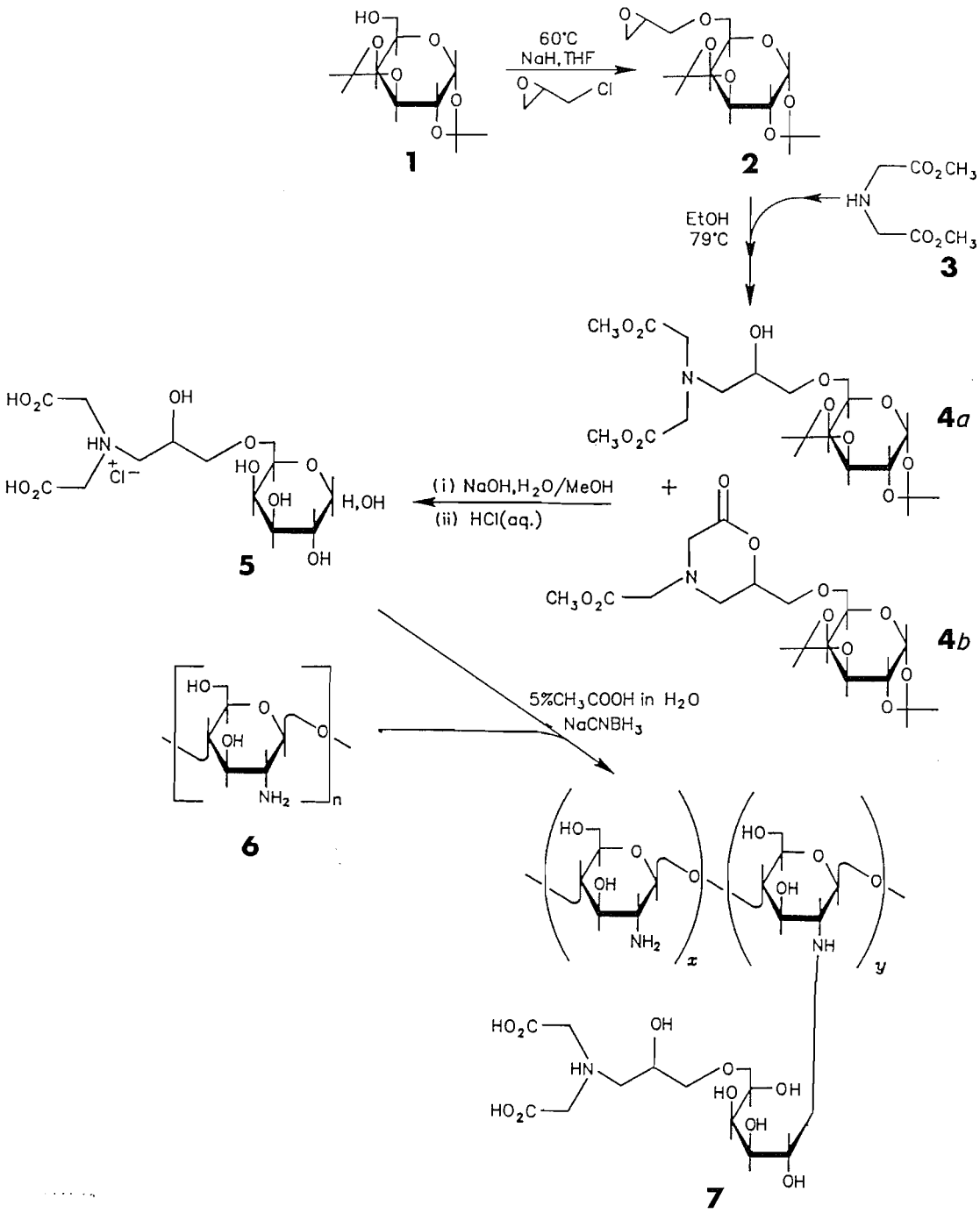
Compound **5** was coupled to chitosan via reductive amination (10), with sodium cyanoborohydride in 5% aqueous acetic acid, to give the derivative **7** at two levels of substitution (**7***a* and **7***b*). Control of the degree of substitution was achieved by varying the ratio of aldehyde to chitosan (A/C) as shown in Table 1. Derivative **7***a* was water soluble, giving a clear viscous solution at 5.0% (w/w) in distilled water. Compound **7***b*, on the other hand, gave an opaque gel at 5.0% (w/w) concentration and it retained much of its gelatinous nature at 1.0%.

Characterization

The solution state ^{13}C nmr spectrum of **7***a* was obtained, and resonances for the hydroxypropyl and iminodiacetate functionalities were easily discernible. Most of the carbohydrate resonances arising from the galactosyl branch were identifiable. The chitosan resonances, however, were very broad and assignment was difficult. Interestingly, the linewidth for C-1 of the chitosan backbone is of the order of 90 Hz, while the carbon resonances of C-6′ of the galactosyl group had a linewidth of 40 Hz, reflecting the relative mobilities of these portions of the molecule.

[1]Author to whom correspondence may be addressed. Current address: IBEX Technologies, 6100 Royalmount Ave., Montreal, Quebec, Canada H4P 2R2.

[2]Current address: Laboratory for Medicinal Chemistry, Level 4 Radiotherapeutic Center, Addenbrookes Hospital, Hills Road, Cambridge, England CB2 2QQ.



SCHEME 1

pH titration

The results for pH titrations of derivatives **7***a* and **7***b* gave inflection points corresponding to values of pK_a^1 2.1, pK_a^2 5.9, and p_i 3.9. These values are similar to those reported for *N*-carboxymethylchitosan (7), which contains similar functionalities. Some of the inflections are ill defined, probably because of the number of titratible groups present, and the insolubilization that occurs at pH values of approximately 10 and higher.

Copper (II) chelation

Table 1 summarizes the evaluation of copper(II) uptake of the derivatives **7***a* and **7***b*, and contrasts these with native lyophilized chitosan. The differential uptake of **7***a* and **7***b* reflects the higher degree of substitution (d.s.) value of **7***a*. The chelating capacity of native chitosan itself is 2.4 mmol/g and the percent uptake in terms of copper ions per residue corresponds to an average of 0.39. For the derivatives **7***a* and **7***b*, more than one ion binds per derivatized residue (i.e., uptake >100%), which indicates that additional binding to the backbone, over and above one equivalent binding per chelating branch, occurs in the derivative. The difference between the theoretical maximum (100%) expected for binding to the iminodiacetate moieties and the values determined for the derivatives is similar to the percent uptake of underivatized chitosan. This observation may indicate that two binding domains exist: specific chelation to the branch, and an apparently stronger nonspecific binding to functionalities

Can. J. Chem. Downloaded from www.nrcresearchpress.com by 198.100.157.202 on 09/07/12
For personal use only.

Can. J. Chem. Downloaded from www.nrcresearchpress.com by 198.100.157.202 on 09/07/12
For personal use only.

TABLE 1. Cu(II) chelating capacity for derivatives *7a* and *7b* contrasted with values obtained in parallel experiments for chitosan, and with literature values for chitosan

Sample	Degree of substitution (±0.05)	Cu (II) uptake[a] (mmol/g)	% Theoretical uptake[b]
7a	1.00	2.97	152
7a[c]	1.00	0.33	16.9
7b	0.50	2.45	87.5
Chitosan[d]		2.40	39.0
Chitosan[c,d]		1.15	18.5
Chitosan[e]		0.06	2.0
Chitosan[f]		3.12	51.0

[a]A 200 mg sample was dissolved or dispersed in ca. 15 mL of distilled water and treated with a 0.5 M Cu(II) acetate solution (15 mL), exhaustively dialysed, and freeze-dried.

[b]Based on the number of copper ions per GlcN residue.

[c]After saturation with Cu(II) these samples were dialysed for 3 days (3 × 250 mL) against water, 2 days against 0.1 M iminodiacetic acid solution, and finally, exhaustively with water, and freeze-dried.

[d]Precipitated, lyophilized chitosan.

[e]Chitosan flakes, ref. 6.

[f]Chitosan, ref. 1, p. 149.

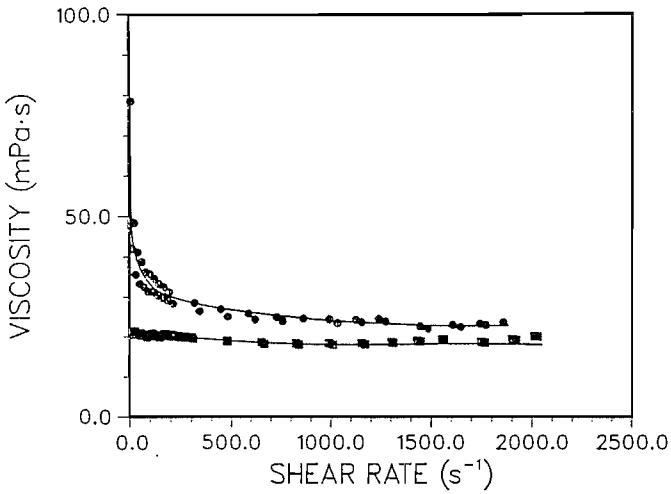


FIG. 1. Rheograms showing the steady shear flow behavior of derivative *7a*, at 1.0% w/w concentration in distilled water (●) and in 1.0 mM aqueous $CuSO_4$ (■), on linear coordinates.

on the polymer backbone. This point was further investigated by saturating both *7a* and chitosan with copper(II) ions, and then dialyzing the resulting chelates against 0.1 M iminodiacetic acid in distilled water for 48 h. The copper content of chitosan decreased by only half to 1.15 g/mmol or 18.5%, while most of the copper (89%) was removed from *7a*. Interestingly, the final percent copper contents of both *7a* and chitosan after dialysis were similar. The major limitation in making comparisons of this sort arises from the fact that the physical form of the polymer can be very important. This is illustrated in Table 1, which shows two very different values of copper(II) uptake for chitosan flakes (5) and lyophilized chitosan. It must also be noted that, in this study, the derivatives were dissolved prior to the addition of copper (II) acetate solution, while the lyophilized chitosan remained as a hydrated dispersion.

Viscometry

Compound *7a* formed viscous 1.0% (w/w) solutions, so it was of interest to evaluate its rheological properties. Also, it was felt that viscometry could offer some insight into the interaction of the polymer with copper(II) ions. The steady shear viscometric determinations are shown in Fig. 1 for 1.0% (w/w) solutions of *7a* in distilled water and in 1.0 mM aqueous copper-(II) sulfate. Interestingly, the viscosity of the solution containing copper ions is less than that for the distilled water solution. This is contrary to the known behaviour of other metal chelating polysaccharides, such as sodium alginate, which increase in viscosity or gel upon the addition of divalent metal ions such as calcium and copper (ref. 1, p. 149). This behaviour results from the crosslinking effect of the metal ions, something that is apparently not occurring in the samples described here. This leads us to believe that each branch or branched residue is a self-contained chelate for one copper ion. Thus, to satisfy the metal ion's ligand requirements, crosslinking is not necessary. The fact that the chelating results indicate >100% binding supports the conclusion that each branch chelates one ion.

Conclusion

We are gratified by the range of properties exhibited by this chitosan derivative as they reflect the success of a rational approach to tailoring the properties of polysaccharides. Thus, in accord with previous experience, the presence of the high level of N-substitution by a hydrophilic side chain resulted in a freely soluble derivative. Functional groups, in this case the chelating iminodiacetate, modifying the side chain offer access to additional properties. This encourages further research into the rational tailoring of chitosan for structure/property studies.

Experimental

General methods

All evaporations were performed under diminished pressure on a Buchi rotary evaporator. Melting points were determined using a Fischer–Johns melting point apparatus and are uncorrected. Infrared (ir) spectra were recorded on a Perkin–Elmer model 710B infrared spectrophotometer, and were calibrated using the 1601 cm^{-1} band of polystyrene film. Low resolution mass spectra (ms) were recorded on a Varian/MAT CH4B or Kratos/AEI MS 50 mass spectrometer. Analytical gas–liquid chromatography was performed on a Hewlett–Packard 5832A gas chromatograph with a 6 ft × 0.125 in. stainless steel column packed with 5% OV-17 on 80–100 mesh Chromosorb W (HP). Carbon, hydrogen, and nitrogen elemental microanalyses were performed by Mr. P. Borda, Microanalytical Laboratory, University of British Columbia. Copper microanalyses were done by Canadian Microanalytical Ltd., Vancouver, Canada. Analytical thin-layer chromatography (tlc) was done with 0.20 mm precoated aluminum back sheets of Silica Gel 60 F_{254} (E. Merck, Darmstadt, Germany). Solvent systems employed for tlc analyses were (A) ethyl acetate–hexane (3:2), (B) ethyl acetate–isopropanol–water (9:4:2). For detection of components, tlc sheets were sprayed with (a) 30% sulfuric acid in 95% ethanol followed by heating on a hot plate (for carbohydrates), or (b) 2.0% ammonium molybdate in 10% sulfuric acid – ethanol solvent, and subsequent heating on a hot plate. Flash liquid chromatography was performed using 230–400 mesh silica gel (Kieselgel 60, E. Merck, Darmstadt, Germany) according to the procedure of Still *et al.* (11).

Work-up and purification of reactions involving polysaccharides generally involved exhaustive dialysis (Spectrapor membrane tubing, M.W. cutoff 6000–8000) against distilled water, followed by freeze-drying. Polysaccharide samples were dried for 48 h at 70°C *in vacuo* (0.05 Torr; 1 Torr = 133.3 Pa) and stored in Schlenk tubes under nitrogen atmosphere prior to elemental microanalysis.

pH titration curves were determined on solutions of ~0.25 g of polysaccharide derivative in 0.1 N HCl (aq) solution (25.0 mL) with a pH meter. Copper chelation samples were prepared by dissolving the derivative (~200 mg) in distilled water (15 mL) and treating with 2.0 M copper(II) acetate (aq) solution (15 mL). After stirring for 24 h, the

Can. J. Chem. Downloaded from www.nrcresearchpress.com by 198.100.157.202 on 09/07/12
For personal use only.

suspensions were dialyzed against (1) distilled water exhaustively (6 × 1 L) or (2) distilled water for 3 days (3 × 1 L), 0.1 N iminodiacetic acid (250 mL) for 48 h, and then exhaustively with distilled water (6 × 1 L). The samples were freeze-dried and then dried *in vacuo* (70°C, 0.05 Torr).

^{1}H nuclear magnetic resonance: Proton nmr spectra were typically measured at 270 MHz using a home-built unit that comprised an Oxford Instruments 63.4 KG superconducting solenoid, a Nicolet model 1180 computer (32K), and a Bruker WP-60 console. Samples dissolved in deuterated chloroform were referenced relative to internal tetramethylsilane (TMS), those dissolved in deuterium oxide relative to internal sodium 3-trimethylsilylproprionate-2,2,3,3-d_4 (TSP).

^{13}C nuclear magnetic resonance: Proton-decoupled carbon-13 nmr spectra were recorded at 100.6 MHz on a Bruker WH-400 spectrometer, or at 75.5 MHz with a Varian XL-300 spectrometer. Spectra were typically obtained at temperatures of 305–310 K, unless otherwise specified. Polysaccharide samples were prepared directly in the 10 mm nmr tube to avoid handling of the viscous or gelatinous materials. Concentrations were typically 5% (w/w), unless further dilution was necessary for dissolution, in which case the concentrations are specified.

Materials

Boron trifluoride – methanol complex (50%), iminodiacetic acid, sodium cyanoborohydride, and sodium hydride (60% dispersion in oil) were obtained from Aldrich Chemical Co. Epichlorohydrin was from MC/B Chemical Co. and 1,2:3,4-di-*O*-isopropylidene-α-D-galactose was purchased from Koch–Light Laboratories. Chitosan (from crab shell, *N*-acetyl <5%) was supplied by Sigma Chemical Co.

Viscometry

For viscometry, sample solutions of 1.0% (w/w) concentration were prepared in distilled water (containing 5 ppm sodium benzoate as stabilizer) or in 0.1 mM copper(II) sulfate (aq) solution. Dissolution was aided by periodic mixing (Vortex–Genie) over a 24 h period. Entrapped air bubbles were removed by centrifugation for 30 min on a benchtop centrifuge. Viscometric measurements were performed with a rotational, controlled stress, rheometer (Visco-Elastic Analyzer, Sangamo Transucers, W. Sussex, England) with truncated cone and plate fixtures (diam. 50.0 mm, α 2.5°, gap 90 μm). A controlled temperature glycol bath under the plate provided temperature control. All measurements were recorded at 20.0 (±0.2)°C. The gap setting was zeroed with no sample present by lowering the cone fixture until contact was just made with the plate. The cone fixture was then raised ca. 2 mm to allow sample loading. A sample solution (~1.5 mL) was loaded into a syringe with an 18-gauge needle. The sample was then discharged onto the center of the plate, taking care to avoid the formation of air bubbles. The cone fixture was lowered onto the sample to the desired 90 μm gap setting. The sample was allowed to equilibrate to 20.0°C, as verified by measurement with a thermocouple. The sample was then stepped through a series of increasing torque settings, applied to the rotating cone fixture, typically from 0.1 to 60 G cm. For each torque setting, the resultant angular velocity (radians s^{-1}) was recorded on a strip chart, allowing the equilibrium value to be reached (usually within 30 s for the majority of samples). When either the maximum torque (60 G cm) or maximum angular velocity (100 radians s^{-1}) was approached, the torque was stepped through a similar decreasing series, and angular velocity was recorded. Duplicate measurements were performed on all samples. Three Newtonian standard oil samples were subjected to identical measurement, at all measured torque values, to calibrate the torque settings over the full range of observed viscosities. Shear stress (σ) is related to torque (T) according to eq. [1]:

$$[1] \quad \sigma = \frac{3T}{2\pi r^3}$$

where T is torque in dynes cm and r is radius; and shear rate ($\dot{\gamma}$) to angular velocity (ω) according to eq. [2]:

$$[2] \quad \dot{\gamma} = \frac{\omega}{\tan \alpha}$$

Substitution of values from cone geometry can provide shear stress and shear rate factors as seen in eqs. [3] and [4].

$$[3] \quad \sigma = 2996.7T \text{ (mPa)}$$

$$[4] \quad \dot{\gamma} = 22.92\omega \ (s^{-1})$$

Apparent viscosity will then be given by eq. [5]:

$$[5] \quad \eta = 130.76(T/\omega)$$

Corrected torque values (T_{corr}) were calculated from standard oil measurements by rearranging eq. [5] to give

$$[6] \quad T_{corr} = \frac{\eta_{oil}\omega}{130.76}$$

where η_{oil} is the known standard oil viscosity, and ω was the measured angular velocity. Corrected torque values and determined angular velocities provided shear stress, shear rates, and apparent viscosities from eqs. [3]–[5]. Rheograms of steady shear viscometric data were plotted on linear coordinates as apparent viscosity vs. shear rate.

Synthesis of chelating chitosan derivatives

Dimethyl iminodiacetate (iminodiacetic acid dimethylester) (3)

Iminodiacetic acid (5.15 g, 38.7 mmol) was stirred in anhydrous methanol (25 mL) to which was added 50% boron trifluoride–methanol complex (10 mL). The reaction mixture was refluxed for 9 h, cooled at room temperature, and poured into 150 mL of chloroform and 75 mL saturated sodium bicarbonate solution. Additional solid sodium bicarbonate was added until the aqueous layer was slightly basic (pH paper). The chloroform layer was separated, the aqueous layer was extracted twice more with chloroform (2 × 150 mL), and the chloroform extracts were combined. The chloroform solution was then dried over magnesium sulfate and filtered. Concentration gave 5.96 g (96%) of a liquid, which corresponded to the diester **3**. This material was one component by tlc analysis (R_f 0.27, solvent A); ir (film) ν_{max}: 1750 cm^{-1}; ^{1}H nmr (270 MHz, $CDCl_3$) δ: 2.07 (s, 1H, N*H*), 3.49 (s, 4H, -C*H*-), 3.74 (s, 6H, CO_2CH_3); ms, m/z (rel. intensity): 161 (15), 129 (6), 103 (7), 102 (94), 74 (37).

6-O-(2,3-Epoxypropyl)-1,2:3,4-di-O-isopropylidene -α-D-galactopyranose (2)

1,2:3,4-Di-*O*-isopropylidene-α-D-galactopyranose, **1** (10.00 g, 38.4 mmol), and epichlorohydrin (3.55 g, 38.4 mmol) were dissolved in anhydrous tetrahydrofuran THF, 100 mL). Sodium hydride (1.84 g, 60% oil dispersion, 46.1 mmol) was washed with three portions of hexane (10 mL) and added to the THF solution. The reaction mixture was refluxed for 9 h, and after dilution with methanol (2 mL) was cooled and poured into water (50 mL). The aqueous layer was extracted with three portions of ether (100 mL) and the combined ethereal extracts were washed twice with saturated brine solution (50 mL). The ether layer was dried with magnesium sulfate, filtered, and concentrated to give 11.40 g of a crude syrup. The tlc analysis (solvent A) of this material showed a major component at R_f 0.55 and minor components at lower R_f values. Flash liquid chromatography (2:1 ether–petroleum ether) afforded 6.88 (57%) of a white crystalline solid corresponding to diastereomeric **2**. Further processing of mixed fractions gave additional product; ir (KBr) ν_{max}: 1450 (CH deform), 1380 (-C(CH)$_2$ sym deform), 1250 (C—O epoxide) cm^{-1}; ^{1}H nmr (270 MHz, $CDCl_3$) δ: 1.34 (s, 6H, CH_3), 1.45 (s, 3H, CH_3), 1.54 (s, 3H, CH_3), 2.63 (m, 1H, *J* 5.5, 2.5 Hz, O-C*H*), 2.78 (t, 1H, *J* 5.5, 5.5 Hz, O-C*H*), 3.17 (m, 1H, -C*H*-C), 3.41, 3.49 (2dd, 1H, *J* 1.0, 5.5 Hz, H-1′aR,S), 3.59–3.83 (m, 3H, H-6a,6b, H-1bR,S), 3.98 (br t, 1H, *J* 5.5, 5.5 Hz, H-5), 4.24 (ddd, 1H, *J* 8.0, 2.0, 2.0 Hz, H-4), 4.30 (dd, 1H, *J* 5.5, 3.0 Hz, H-2), 4.57 (dd, 1H, *J* 8.0, 3.0 Hz, H-3), 5.52 (d, 1H, *J* 5.5 Hz, H-1); ms, m/e (rel. intensity): 316 (0.1), 301 (66), 258 (3), 243 (3), 229 (9). Anal. calcd. for $C_{15}H_{24}O_7$: C 56.95, H 7.65; found: C 56.95, H 7.78.

6-O-[2-Hydroxy-3-(methyliminodiacetate)propyl] - 1,2:3,4-di-O-isopropylidene-α-D-galactopyranose (4a and 4b)

6-*O*-(2,3-Epoxypropyl)-1,2:3,4-di-*O*-isopropylidene-α-D-galactopyranose (**2**, 2.00 g, 6.33 mmol) and dimethyliminodiaacetate (**3**, 1.00 g, 6.2 mmol) were dissolved in ethanol (50 mL) and refluxed for 8 h. The ethanol was removed and the resultant syrup dissolved in chlor-

oform (50 mL). The chloroform layer was washed with two portions (50 mL) of saturated brine, dried over magnesium sulfate, filtered, and concentrated to give 2.95 g of a syrup. The tlc analysis confirmed the absence of starting material and showed two major components (R_f 0.41, 0.34, solvent A). The glc analysis of the product showed one major peak (>95% peak area). The ^{1}H nmr spectrum of the syrup indicates a mixture of products **4***a* and **4***b* in a ratio of 2:1 respectively. After flash liquid chromatography purification, 2.45 g of a 1:4 mixture of **4***a* and **4***b* was obtained (86%). Early and late fractions from the chromatographic separation provided small quantities of pure **4***a* and **4***b*, respectively. Short path distillation (200°C, 0.05 Torr) gave 1.85 g of pure **4***b* by ^{1}H nmr spectroscopy. The glc analysis of this component gave one peak at the same retention time observed for the product mixture. **4***a*: ir (film) ν_{max}: 1755 (C=O ester), 3500 (OH) cm^{-1}; ^{1}H nmr (270 MHz, $CDCl_3$) δ: 1.33 (s, 6H, 2C*H*$_3$), 1.45 (s, 3H, C*H*$_3$), 1.54 (s, 3H, C*H*$_3$), 2.64 (ddd, 1H, *J* 12.5, 10.0, 2.0 Hz, -C*H*-N), 3.00 (dd, 1H, *J* 12.5, 2.0 Hz, -C*H*-N), 3.39–3.79 (m, 8H, H-6, H-6′, -C*H*$_2$O, 2 × -C*H*$_2$CO$_2$Me), 3.72 (s, 6H, 2CO$_2$C*H*$_3$), 3.83 (m, 1H, C*H*OH), 3.97 (br s, 1H, H-5), 4.25 (dd, 1H, *J* 8.0, 1.0 Hz, H-4), 4.33 (dd, 1H, *J* 5.0, 2.0 Hz, H-2), 4.61 (dd, 1H, *J* 8.0, 2.0 Hz, H-3), 5.54 (d, 1H, *J* 5.0 Hz, H-1). **4***b*: ir (film) ν_{max}: 1755 (C= ester, morpholone) cm^{-1}; ^{1}H nmr (270 MHz, $CDCl_3$) δ: 1.33 (s, 6H, 2C*H*$_3$), 1.44 (s, 3H, C*H*$_3$), 1.54 (s, 3H, C*H*$_3$), 2.86 (ddd, 1H, *J* 12.5, 10.0, 2.0 Hz, C*H*-N), 3.08 (dd, 1H, *J* 12.5, 2.0 Hz, -C*H*-N), 3.39 (s, 2H, -CH$_2$CO$_2$Me), 3.40–3.79 (m, 6H, H-6, H-6′, -C*H*$_2$CO$_2$Me, -C*H*$_2$O), 3.73 (s, 3H, C*H*$_3$), 3.97 (br t, 1H, *J* 5.0, 1.0 Hz, H-5), 4.25 (d, 1H, *J* 8.0, 1.0 Hz, H-4), 4.34 (dd, 1H, *J* 5.0, 2.0 Hz, H-2), 4.63 (dd, 1H, *J* 8.0, 2.0 Hz, H-3), 4.68 (m, 1H, C*H*OR), 5.54 (d, 1H, *J* 5.0 Hz, H-1). **4***a*, **4***b* mixture: ms, *m*/*z* (rel. intensity): 477 (5), 462 (10), 445 (2), 430 (6), 418 (30), 387 (12), 386 (14).

6-O-(2-Hydroxy-3-iminodiaceto-propyl)-D-galactose (5)

Compound **4** (2:1 mixture of **4***a* and **4***b*, 10.0 g, 21.4 mmol) was dissolved in 2 N sodium hydroxide in 9:1 methanol–water (100 mL). The reaction mixture was refluxed for 4 h and cooled in an ice bath. 6 N Hydrochloric acid (60 mL) was added to give a 1 N solution, which was then refluxed for 5 h. After cooling, the solution was filtered and the filtrate was concentrated to a volume of 10 mL. Ethanol (20 mL) was added and the mixture was cooled in ice, filtered, and concentrated. The residue was taken up in ethanol and precipitation was achieved by the addition of acetone. The gummy precipitate was taken up in ethanol and treated with decolourizing carbon, and the filtrate was treated with acetone to give a gummy precipitate. This material was a foamy hygroscopic solid (7.15 g, 86%) after drying *in vacuo* (25°C, 0.05 Torr) and consisted of a mixture of α and β 6-*O*-D-galactose isomers **5**; ^{13}C nmr (100.6 MHz, main isomer) δ (D_2O): 166.7 (COOH), 98 (C-1), 71.8, 71.2 (C-5,2), 69.3, 69.2 (CHOH), 67.9, 67.2 (C-3,4), 66.7 (C-6), 63.4 (CH_2O), 57.1, 57.2 (-CH_2NH), 54.3 (NHCH_2CO_2H).

6-O-[2-Hydroxy-3-(iminodiacetic acid hydrochloride) propyl]-D-galactitol (8)

Compound **5** (0.90 g, 2.3 mmol) was dissolved in 95% ethanol (10 mL) to which was added an aqueous solution of saturated sodium bicarbonate (2 mL). To this mixture, sodium borohydride (0.50 g, 13.2 mmol) was added and allowed to stir for 2 h at room temperature. The reaction was then acidified to pH 2 (pH paper) by dropwise addition of 6 N hydrochloric acid. The solution was filtered and the solvent removed. The residue was taken up in methanol and concentrated thrice more to remove borate salts. The residue was then dissolved in ethanol–methanol (1:1), and the resultant solution was filtered and precipitated with acetone to give 0.75 g (83%) of a foamy hydroscopic solid. Attempts to crystallize the diastereomeric mixture were unsuccessful; ^{13}C nmr (100.6 MHz) δ(D_2O): 167.3 (COOH), 71.7, 71.3, 69.1 (C-5,4,3,2), 68.8, 68.6 (CHOH), 67.3 (C-6), 63.3, 63.0 (CH_2O-), 62.0 (C-1), 56.37, 57.07, (CH_2NH), 54.1, 53.9 (NHCH_2CO_2H).

Chelating chitosan derivative (7)

(a) Chitosan (0.55 g, 3.4 mmol) was dissolved in 5% aqueous acetic acid (50 mL) and the galactose derivative **5** (2.0 g, 4.9 mmol) in 5% aqueous acetic acid (10 mL) was added to the resultant stirred solution. After 15 min, sodium cyanoborohydride (1.25 g, 20.0 mmol) in 5 mL of reaction solvent was added. After stirring for 24 h, the mixture was poured into a dialysis sac and dialyzed for 6 days (6 × 2 L) against distilled water and subsequently freeze-dried to give 1.62 g (84%) of a white fluffy solid; ^{13}C nmr (100.6 MHz) δ(D_2O): 168.6 (COOH), 98.4 (C-1′), 75.9 (C-4′), 73.2 (C-5′), 71.2, 71.1 (C-5,2), 68.9 (=CHOH), 67.9, 67.4 (C-3,2), 66.7 (C-6), 63.2 (-CH_2O-), 58.7 (-CH_2NH), 56.3 (NHCH_2CO_2H), 54.7 (C-1). Anal. calcd for $C_{19}H_{34}N_2O_{14}\cdot 1.56H_2O$: C 42.06, H 6.85, N 5.16; found: C 42.06, H 7.10, N 4.81.

(b) The procedure used for the preparation of **7***b* was as described for the preparation of **7***a*, with the exception that 1.00 g (2.45 mmol) of the galactose derivative **5** was used. The resultant yield was 1.16 g (63%) of a fluffy white solid. Anal. calcd. for $[(C_6H_{11}NO_4)_{0.50}\text{-}(C_{19}H_{34}N_2O_{14})_{0.50}]\cdot 1.1\ H_2O$: C 41.98, H 6.91, N 5.88; found: C 41.98, H 7.17, N 5.85.

1. R. A. A. MUZZARELLI. *In* Chitin. Pergamon Press, New York. 1977.
2. R. A. A. MUZZARELLI. *In* The polysaccharides. Vol. 3. *Edited by* G. O. Aspinal. Academic Press, New York. 1985. p. 417.
3. M. YALPANI and L. D. HALL. Macromolecules, **17**, 272 (1984).
4. L. D. HALL and K. R. HOLME. J. Chem. Soc. Chem. Commun. **3**, 217 (1986).
5. R. A. A. MUZZARELLI, F. TANFANI, S. MARIOTTI, and M. EMANUELLI. Carbohydr. Polym. **2**, 145 (1982).
6. L. D. HALL and M. YALPANI. Carbohydr. Res. **83**, C5 (1980).
7. R. A. A. MUZZARELLI, F. TANFANI, M. EMANUELLI, and S. MARIOTTI. Carbohydr. Res. **107**, 199 (1982).
8. S. HIRANO and Y. OHE. Carbohydr. Polym. **4**, 15 (1984).
9. K. JANKOWSKI and B. CASIMIR. Can. J. Chem. **45**, 2865 (1967).
10. R. F. BORCH, M. D. BERNSTEIN, and H. D. DURST. J. Am. Chem. Soc. **93**, 2897 (1971).
11. W. C. STILL, M. KAHN, and A. MITRA. J. Org. Chem. **43**, 2923 (1978).

Can. J. Chem. Downloaded from www.nrcresearchpress.com by 198.100.157.202 on 09/07/12
For personal use only.

Reactions of benzo[*b*]thiophene with some aqueous platinum metal species at elevated temperatures

PETER D. CLARK,[1] JAMES F. FAIT, COLIN G. JONES, AND MARTIN J. KIRK
Department of Chemistry, The University of Calgary, 2500 University Drive N.W., Calgary, Alta., Canada T2N 1N4

Received July 11, 1990

PETER D. CLARK, JAMES F. FAIT, COLIN G. JONES, and MARTIN J. KIRK. Can. J. Chem. **69**, 590 (1991).

The desulfurization of benzo[*b*]thiophene **1** with aqueous transition metal species in the presence of various hydrocarbons at elevated temperatures is described. Mechanistic studies have shown that treatment of **1** with solutions of $RuCl_3$ and other platinum metal species results in the formation of 2,3-dihydrobenzo[*b*]thiophene **2** and ethylbenzene **3** as major products. Metal coordinated species are probable intermediates in the formation of **2** and hydrocarbon products. **2** readily coordinates to $PdCl_2$ to form square-planar *trans*-dichlorobis(2,3-dihydrobenzo[*b*]thiophene) palladium(II), which decomposes to ethylbenzene at 300°C. The crystal structure of the complex was determined by a single crystal X-ray diffraction study. The complex crystallized in the monoclinic space group $C\,2/c$ with $Z = 8$ in a cell of dimensions $a = 23.057\ (3)$, $b = 9.711\ (1)$, $c = 15.227\ (2)$ Å and $\beta = 99.74(1)°$. The structure was solved by the Fourier method and was refined by full-matrix least-squares calculations to $R = 0.042$ for 2537 observed data with $I > 2.5\sigma(I)$.

Key words: benzo[*b*]thiophene, desulfurization, platinum metal species.

PETER D. CLARK, JAMES F. FAIT, COLIN G. JONES et MARTIN J. KIRK. Can. J. Chem. **69**, 590 (1991).

On décrit la désulfurisation du benzo[*b*]thiophène (**1**) réalisée à températures élevées, à l'aide de solutions aqueuses de dérivés de métaux de transition, en présence de divers hydrocarbures. Les études mécanistiques ont démontré que le traitement du composé **1** avec des solutions de $RuCl_3$ ou d'autres dérivés du platine conduit principalement à la formation du 2,3-dihydrobenzo[*b*]thiophène (**2**) et de l'éthylbenzène (**3**). Il est probable que les intermédiaires dans la formation des hydrocarbures et du produit **2** soient des espèces coordinées à des métaux. Le composé **2** se coordonne facilement avec le $PdCl_2$ pour former le *trans*-dichlorobis(2,3-dihydrobenzo[*b*]thiophène) palladium(II) plan carré qui se décompose en éthylbenzène par chauffage à 300°C. On a déterminé la structure cristalline par diffraction des rayons-X par un cristal unique. Les cristaux du complexe sont monocliniques, groupe d'espace $C\,2/c$, avec $a = 23{,}057(3)$, $b = 9{,}711(1)$ et $c = 15{,}227(2)$ Å, $\beta = 99{,}74(1)°$ et $Z = 8$. On a résolu la structure par la méthode de Fourier et on l'a affinée par la méthode des moindres carrés (matrice entière) jusqu'à une valeur de $R = 0{,}042$ pour 2537 réflexions avec $I > 2{,}5\sigma(I)$.

Mots clés : benzo[*b*]thiophène, désulfurisation, dérivés du platine.

[Traduit par la rédaction]

Introduction

Catalytic hydrodesulfurization of crude oil and bitumen is practiced widely by industry in order to produce low sulfur content transportation fuels (1), and is carried out industrially by passing the sulfur-containing oil over a γ-alumina-supported cobalt–molybdenum catalyst under hydrogen pressure (2). Catalysts based on the metal sulfides of ruthenium and osmium are known (3) to be much more active than commercial catalysts but, because of cost, they have not been used industrially.

The chemical mechanisms for catalytic hydrodesulfurization of simple compounds such as thiophene have been studied in detail (4, 5). However, despite the fact that benzothiophene **1**, its derivatives, and other condensed thiophenes are present in large quantities in many crude oils, mechanisms for their desulfurization are still open to debate (6, 7). It has been proposed (7) that **1** is activated to hydrogenation and desulfurization by coordination to active sites on the metal sulfide crystallites of the catalyst. The exact mode of the coordination is unknown but could occur through π-interactions centered either on the homocyclic or heterocyclic ring or, perhaps less likely, by a σ-interaction to the sulfur atom. Recently, Angelici and co-workers (7) prepared stable complexes of **1** based on rhodium, iridium, or ruthenium in which bonding to the metal takes place through a π-interaction centered on the homocyclic ring of the molecule. In contrast, complexes of **1** claimed to possess bonding interactions directly to the sulfur atom are very labile in the presence of coordinating solvents (8). Consequently, it is probable that initial coordination of **1** at catalyst surfaces involves π-interactions of the type described by Angelici.

Catalytic hydrodesulfurization of **1** under moderate conditions produces 2,3-dihydrobenzothiophene **2** and ethylbenzene **3** (9). The exact mechanisms leading to **2** and **3** are not known but it is clear that the mode of coordination of the molecule to the catalyst surface may change when **2** is formed since its sulfur atom is much more basic than either the sulfur or π-system of **1**. A plausible mechanism for the hydrodesulfurization of **1** is initial coordination via π-interaction to the homocyclic ring, hydrogenation of the 2,3-bond, and change to coordination via the sp^3 hybridized sulfur of **2** followed by hydrogenolysis of the C—S bonds to form **3** and H_2S.

We previously described studies on the desulfurization of thiophene and derivatives with aqueous metal species (10–12). This work showed that water is involved chemically, as ^{18}O-labelled oxygen from water was found in CO_2 formed during the desulfurizations. In this report we describe studies on the desulfurization of **1** to **2** and **3** using aqueous platinum metal species in the presence of alkanes but without molecular hydrogen. These conditions, although somewhat different from those encountered during heterogeneous catalytic hydrodesulfurization, provide metal and Brønsted acid sites and thus show similarity to conditions encountered during heterogeneous catalysis. Experiments using D_2O were conducted to help determine the mechanism of formation of **2** and **3**. In addition,

[1]Author to whom correspondence may be addressed.

Can. J. Chem. Downloaded from www.nrcresearchpress.com by 198.100.157.202 on 09/07/12
For personal use only.

Can. J. Chem. Downloaded from www.nrcresearchpress.com by 198.100.157.202 on 09/07/12
For personal use only.

complex formation between **2** and a palladium(II) species was investigated to determine if such complexes are intermediates in the desulfurization process.

Experimental

Materials

Benzothiophene **1** and platinum metal salts were obtained from the Aldrich Chemical Company and solvents were purchased from the Fisher Chemical Company. These reagents were used without further purification. **2** was prepared using the general method of Bordwell and McKellin (13).

Desulfurization experiments

1 (5.0 g, 37.3 mmol), a solution of a platinum metal chloride (3.73 mmol) in water (50 g, 2.77 M), and either hexadecane, isooctane, or tetrahydronaphthalene (220 mmol) were placed in a cap enclosure autoclave (internal volume 300 mL, fabricated from Hastelloy 276C) fitted with a Magnedrive stirrer assembly and internal cooling coil. The system was flushed with nitrogen and the stirred reaction mixture (stirring rate was 1000 rpm) was heated to the desired reaction temperature. Heat-up time to 370°C was approximately 60 min. At the conclusion of the experiment (see Tables 6 and 7 for further reaction parameters) the system was cooled to ambient conditions, the amount of produced gases was measured, and their composition was determined using standard gas chromatographic techniques. Liquid and solid products were recovered and the amount of **1** remaining and amounts of major products such as **2** and **3** were determined using gas chromatography. This analysis was conducted by injecting a sample of the liquid product onto a 10% FFAP CN Chromosorb column (3 mm × 2 m) using the following temperature program: 60°C, 2 min, 60–220°C at 10°C/min, and 220°C for 6 min. Helium carrier gas at a flow rate of 30 mL/min was used throughout the analysis; compounds were detected using a flame ionization detector and were quantified by reference to calibration samples.

GC–MS (30 m × 0.25 mm DB-5 column) was used to detect the presence of new compounds (other than **2** and **3**) in the liquid products. Most of these products were identified by reference to library spectra and unknowns were identified by analysis of their mass spectra. These products were not quantified, as in most cases they were present in small quantities. The following minor products were identified:

Benzothiophene/hexadecane experiments: C_5–C_{15} alkanes and alkenes (mostly linear compounds), alkylbenzothiophenes **4** (alkyl = C_1–C_3, position of substitution not determined).

Benzothiophene/isooctane experiments: Only compounds reported in Table 7 were detected in these experiments.

Benzothiophene/tetrahydronapthalene experiments: Naphthalene was the only other product detected in addition to those reported in Table 7.

trans-*Dichlorobis(2,3-dihydrobenzo[*b*]thiophene) palladium(II)*

2 (1.63 g, 12 mmol) was added to a stirred solution of palladium(II) chloride (0.89 g, 5 mmol) in 90% aqueous ethanol (50 mL) at 50°C. After 1 h, the deep red solid produced in the reaction was filtered off and was crystallized from ethanol/chloroform. Filtration and washing yielded deep red plates, 3.7 g, 83%, mp >250°C (dec.); IR, ν (cm^{-1}): 425 (m), 475 (m), 692 (m), 754 (s), 778 (s), 1264 (m) and 1440 (m). Anal. calcd. for $C_{16}H_{16}Cl_2PdS_2$: C 42.6, H 3.55, Cl 15.8, S 14.3; found: C 42.5, H 3.6, Cl 15.4, S, 14.5. Note: variable temperature NMR data are given in Tables 9 and 10; s, m, and w denote strong, medium, and weak absorptions.

X-ray structure determination of trans-*dichlorobis(2,3-dihydrobenzo-[*b*]thiophene) palladium(II)*

A suitable transparent block-shaped crystal was wedged in a Lindemann glass capillary and was mounted on an Enraf–Nonius CAD4 diffractometer. Unit cell parameters and their standard deviations were derived from the setting angles of 25 reflections in the range $8.84 < \theta < 18.02°$. Reduced cell calculations did not indicate any higher metric symmetry. Crystal and instrument stability were monitored throughout the measurement of 3 standard reflections every hour of X-ray exposure. There was no evidence of crystal decomposition. The net intensities of the data were corrected for reflection width, scale variation, and Lorentz and polarization effects. Variance $\sigma^2(I)$ was calculated based on counting statistics. Crystal data and experimental details are summarized in Table 1.

The structure was solved by placing palladium at the two centres of symmetry and expanding the structure by difference Fourier methods. All non-hydrogen atoms were located in difference maps after refining the scale and thermal parameters on the palladium. At this stage of the refinement all of the hydrogen atoms were located in difference Fourier maps. All non-hydrogen atoms were refined anisotropically with the hydrogen atoms included in the refinements at geometrically idealized positions with C—H bond lengths of 0.95 Å. Convergence was reached at $R = 0.042$. The final values of the refined positional parameters are compiled in Table 2. Selected bond distances, bond angles, and close contacts are summarized in Tables 3–5. Tables of hydrogen atom positions, thermal parameters, lists of bond angles and bond distances, and tables of F_o, F_c, and σF are available as supplementary material to this paper.[2] Neutral atom scattering factors were used with anomalous dispersion corrections applied (14). No corrections were made for extinctions.

All calculations were carried out on a VAX 11/780 computer using the XTAL software package (15).

NMR specta

Proton and carbon spectra were recorded on a Bruker AM-400 in deuterochloroform solution using solvent resonances as internal references. Probe temperatures were determined by reference to methanol and 1,2-dihydroxyethane chemical shift data.

Results and discussion

*Reactions of benzothiophene **1** with aqueous platinum species*

Table 6 summarizes data obtained from the reaction of **1** with aqueous platinum metal species and hexadecane at 370°C. Note that the amount of water used in these experiments ensured that liquid water was present at 370°C. One of the goals of these experiments was to determine the extent to which desulfurization of **1** occurred. Since the reactions were conducted in an autoclave fabricated from Hastelloy 276C (an alloy of nickel, cobalt, molybdenum, and other metals), the potential of the vessel walls to promote desulfurization had to be ascertained. Fortunately, this effect was minimal since very little reaction (0–5% consumption of **1**) occurred when **1** was heated at 370°C with water and a variety of hydrocarbons (see Tables 6 and 7). In addition, minimal decomposition (<1%) of the hydrocarbons was observed in these experiments.

When similar reactions were conducted with the addition of various water soluble platinum metal salts in the presence of hexadecane, significant desulfurization of **1** occurred. **2**, **3**, H_2S, and metal sulfides (identified by qualitative techniques but exact composition not determined) were the major products. Quantification of the organic products (**2** and **3**) was relatively straightforward (see experimental section) but accurate quantification of H_2S (either as the gas or as metal sulfides) was

[2]Supplementary tables of hydrogen atom parameters. non-hydrogen thermal parameters, dihedral angles, and observed and calculated structure factors have been deposited and may be purchased from the Depository of Unpublished Data, Document Delivery, CISTI, National Research Council Canada, Ottawa, Canada K1A 0S2.

Tables of hydrogen atom parameters and dihedral angles have also been deposited with the Cambridge Crystallographic Data Centre and can be obtained on request from The Director, Cambridge Crystallographic Data Centre, University Chemical Laboratory, Lensfield Road, Cambridge CB2 1EW, U.K.

Can. J. Chem. Downloaded from www.nrcresearchpress.com by 198.100.157.202 on 09/07/12
For personal use only.

TABLE 1. Crystallographic parameters for $PdCl_2$ $(C_8H_8S)_2$

Formula	$PdCl_2$ $(SC_8H_8)_2$
Cell dimensions a	23.057(3) Å
b	9.711(1) Å
c	15.227(2) Å
α	90.0°
β	99.74(1)°
γ	90.0°
Cell volume	3360.3(8) Å^3
D_c	1.778 g cm^{-3}
Crystal dimensions	0.2 × 0.2 × 0.1 mm^3
Space group	$C\,2/c$
λ	0.71069 MoKα graphite monochromometer
$\sin\theta/\lambda_{max}$	0.5941 Å^{-1}
Range h	0 27
k	0 11
l	−18 17
Total reflections	6349
Unique reflections	2950 R_{merg} 0.0217
Observed reflections	2537 2.5 σ(I) cut-off
Number of parameters refined	209
Least-squares function	$\Sigma\,(F_o - F_c)\,w$
$R = \dfrac{\Sigma\,(F_o - F_c}{\Sigma\,F_o}$	0.042
$R_w = \dfrac{\Sigma\,(F_o - F_c)\,w}{\Sigma\,F_o\,w} =$	0.031
$S = \left[\dfrac{\Sigma\,(F_o - F_c)\,w}{(m-n)}\right]^{1/2} =$	3.015
$w = 1/\sigma\,(F)^2$	

TABLE 2. Positional parameters and U_{eq} for the non-hydrogen atoms of $PdCl_2$ $(C_8H_8S)_2$

Atom	x	y	z	1000 U_{eq}
Pd(1)	0.25000	0.25000	0.50000	39.0
S(1)	0.27526(5)	0.0185(1)	0.50167(8)	40.4
C(11)	0.2119(2)	−0.0644(5)	0.4423(3)	34.7
C(12)	0.1765(2)	−0.1207(5)	0.4985(3)	40.7
C(13)	0.1254(2)	−0.1860(5)	0.4609(4)	53.8
C(14)	0.1103(2)	−0.1954(6)	0.3687(4)	59.0
C(15)	0.1459(3)	−0.1416(5)	0.3150(4)	55.3
C(16)	0.1977(2)	−0.0753(5)	0.3505(4)	46.7
C(17)	0.1984(2)	−0.0953(5)	0.5954(4)	50.3
C(18)	0.2637(2)	−0.0624(5)	0.6051(3)	48.2
Cl(1)	0.23776(7)	0.2579(1)	0.64668(9)	63.6
Pd(2)	0.50000	0.50000	0.00000	39.5
S(2)	0.46686(6)	0.6068(1)	0.11848(9)	42.2
C(21)	0.5158(2)	0.7490(5)	0.1423(3)	38.0
C(22)	0.4898(2)	0.8723(6)	0.1174(3)	50.0
C(23)	0.5234(3)	0.9904(6)	0.1334(4)	64.3
C(24)	0.5810(3)	0.9824(6)	0.1718(4)	66.8
C(25)	0.6065(2)	0.8574(6)	0.1972(4)	57.1
C(26)	0.5737(2)	0.7372(5)	0.1821(3)	46.7
C(27)	0.4260(3)	0.8652(6)	0.0737(4)	64.8
C(28)	0.4041(2)	0.7196(6)	0.0812(4)	61.6
Cl(2)	0.55341(7)	0.3636(2)	0.10629(9)	58.7

TABLE 3. Interatomic distances (Å) for $PdCl_2$ $(C_8H_8S)_2$[a]

Molecule 1			Molecule 2		
Pd(1)	Cl(1)	2.299(2)	Pd(2)	Cl(2)	2.284(1)
Pd(1)	S(1)	2.321(1)	Pd(2)	S(2)	2.320(1)
S(1)	C(11)	1.776(4)	S(2)	C(21)	1.782(5)
S(1)	C(18)	1.820(6)	S(2)	C(28)	1.826(6)
C(11)	C(12)	1.390(7)	C(21)	C(22)	1.364(7)
C(11)	C(16)	1.384(7)	C(21)	C(26)	1.373(6)
C(12)	C(13)	1.375(7)	C(22)	C(23)	1.383(8)
C(12)	C(17)	1.497(7)	C(22)	C(27)	1.510(8)
C(13)	C(14)	1.391(9)	C(23)	C(24)	1.359(8)
C(14)	C(15)	1.357(9)	C(24)	C(25)	1.374(8)
C(15)	C(16)	1.383(8)	C(25)	C(26)	1.388(8)
C(17)	C(18)	1.521(8)	C(27)	C(28)	1.512(9)

[a]Estimated standard deviations are given in parentheses.

impossible because of difficulties in recovering metal sulfide products adhering to the autoclave walls and in accounting for H_2S that might have reacted with autoclave components. $PtCl_4$ and $RuCl_3$ solutions caused most reaction (24 and 22% respectively). In addition to products derived from **1**, GS–MS studies indicated that a variety of alkanes and alkenes (C_1–C_{12}) were produced from the hexadecane. These analyses also revealed the presence of small amounts of alkyl-substituted (C_1–C_4) benzothiophenes **4** in the liquid phase product. Similar experiments were conducted in which **1** was heated with aqueous $RuCl_3$ and either isooctane or tetrahydronaphthalene (Table 7) at 370°C. As in experiments using hexadecane, **2** and **3** were the major products derived from **1**. However, significantly more of **1** was consumed than was observed with hexadecane (29% with isooctane and 37% for tetrahydronaphthalene). GC–MS analysis of the liquid products showed that a variety of small hydrocarbons were produced in the experiment using isooctane and that naphthalene was the major hydrocarbon product from the tetrahydronaphthalene experiment.

The question arises as to whether it is the aqueous form of the added metal species, or the metal sulfide formed during the reaction, that is responsible for the desulfurization of **1**. If the formed metal sulfide plays a major role in the desulfurization, complete consumption of **1** would be expected at longer reaction times. However, experiments using $RuCl_3$ over 8 h (Table 6) showed only slightly more reaction than experiments over 3 h (34% compared to 22%). Also, when ruthenium sulfide prepared by passing excess H_2S through aqueous $RuCl_3$ was used, in place of the aqueous salt, less reaction was observed (12% compared to 22%, Table 6). Thus, it can be concluded that the largely insoluble sulfides produced during the reaction do not promote desulfurization as efficiently as the water soluble materials.

*Mechanisms of reaction of benzothiophene **1** with aqueous metal species*

Determination of exact mechanisms is very difficult since none of the usual techniques lend themselves to detecting intermediates in autoclaves at high temperatures (370°C) and pressures (ca. 30 MPa) in what, after formation of metal sulfides, is a three-phase system. Also, the nature of solutions of platinum metal species at high temperatures has not been studied. Thus, although the data show that metal species are

TABLE 4. Bond angles (deg) for $PdCl_2(C_8H_8S)_2$[a]

Molecule 1				Molecule 2			
Cl1	Pd1	Cl1	180.0(1)	Cl2	Pd2	Cl2	180.0(2)
Cl1	Pd1	S1	84.63(5)	Cl2	Pd2	S2	94.75(5)
Cl1	Pd1	S1	95.37(5)	Cl2	Pd2	S2	85.25(5)
S1	Pd1	S1	180.0(2)	S2	Pd2	S2	180(0)
C11	S1	C18	90.9(2)	C21	S2	C28	92.3(2)
C11	S1	Pd1	104.5(2)	C21	S2	Pd2	103.0(2)
C18	S1	Pd1	110.7(2)	C28	S2	Pd2	112.0(2)
C12	C11	S1	112.5(3)	C22	C21	C26	123.0(5)
C16	C11	C12	121.9(4)	C22	C21	S2	112.9(3)
C16	C11	S1	125.6(4)	C26	C21	S2	124.1(4)
C11	C12	C17	114.0(4)	C21	C22	C23	118.1(5)
C13	C12	C11	118.4(5)	C21	C22	C27	115.7(5)
C13	C12	C17	127.5(5)	C23	C22	C27	126.2(5)
C12	C13	C14	120.0(5)	C24	C23	C22	120.4(6)
C15	C14	C13	120.7(5)	C23	C24	C25	120.7(6)
C14	C15	C16	120.9(5)	C24	C25	C26	120.1(5)
C15	C16	C11	118.1(5)	C21	C26	C25	117.6(5)
C12	C17	C18	107.1(5)	C22	C27	C28	108.7(5)
C17	C18	S1	107.1(3)	C27	C28	S2	109.1(4)
H13	C13	C12	120.0(6)	H23	C23	C22	119.8(6)
H13	C13	C14	120.0(5)	H23	C23	C24	119.8(6)
H14	C14	C13	119.7(6)	H24	C24	C23	119.6(6)
H14	C14	C15	119.7(6)	H24	C24	C25	119.7(6)
H15	C15	C14	119.5(6)	H25	C25	C24	119.9(6)
H15	C15	C16	119.6(6)	H25	C25	C26	120.0(6)
H16	C16	C11	120.9(5)	H26	C26	C21	121.2(5)
H16	C16	C15	120.9(5)	H26	C26	C25	121.2(5)
H171	C17	C12	110.1(4)	H271	C27	C22	109.7(5)
H171	C17	C18	110.0(4)	H271	C27	C28	109.7(6)
H171	C17	H172	109.5(6)	H271	C27	H272	109.5(6)
H172	C17	C12	110.1(4)	H272	C27	C22	109.6(6)
H172	C17	C18	110.0(5)	H272	C27	C28	109.7(5)
H181	C18	C17	110.1(5)	H281	C28	C27	109.6(6)
H181	C18	H182	109.5(5)	H281	C28	H282	109.5(5)
H181	C18	S1	110.1(4)	H281	C28	S2	109.6(5)
H182	C18	C17	110.0(5)	H282	C28	C27	109.5(5)
H182	C18	S1	110.0(4)	H282	C28	S2	109.5(5)

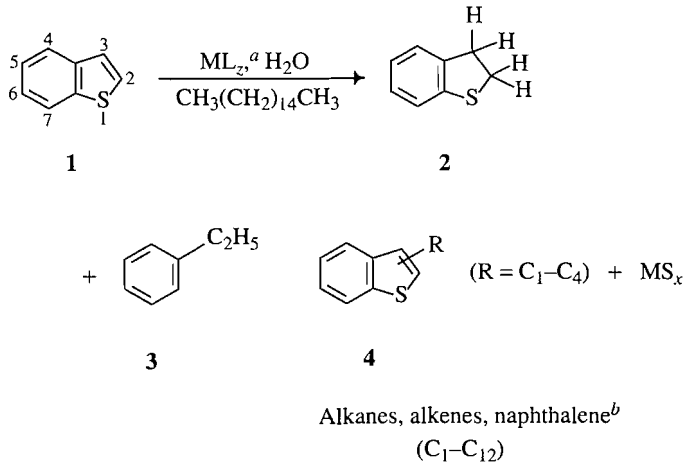
[a]Estimated standard deviations are given in parentheses.

TABLE 5. Contact distances for selected H and Cl atoms (Å)

Cl(1)	H(181)	2.654(2)
Cl(2)	H(15)	2.661(1)
Cl(2)	H(282)	2.699(2)
Cl(1)	H(16)	2.906(2)
Cl(2)	H(23)	2.998(2)
Cl(1)	H(171)	3.030(2)
Cl(2)	H(272)	3.163(2)
Cl(2)	H(26)	3.170(2)
Cl(1)	H(281)	3.321(2)

important in promoting desulfurization reactions, the exact nature of the reacting species is not known. However, any mechanism must account for the reaction pathways summarized in Scheme 1; i.e., the formation of ethylbenzene **3** from **1** via the dihydro intermediate **2** with participation of aqueous metal species. Also, any mechanism should account for the source of hydrogen needed to form **2** and to hydrogenolyse C—S bonds.

Since oxidation products of **1** were not observed in any significant amount, the water and hydrocarbons used in the



1 **2** **3** **4**

[a] L = H_2O or Cl

[b] Formed when tetrahydronaphthalene was used in place of hexadecane

SCHEME 1. Reaction pathways for the desulfurization of benzothiophene **1** with aqueous platinum metal species.

experiments (hexadecane, isooctane, and tetrahydronaphthalene) are the only possible sources of hydrogen. Evidence that the hydrocarbons supply some of the required hydrogen is given by the formation of alkenes and of naphthalene. The ability of tetrahydronaphthalene to donate hydrogen is well established (16) and, at high temperatures (>400°C), this usually occurs via a radical mechanism. It is not known if radicals are involved in hydrogen transfer in this work, but the formation of unsaturated hydrocarbons is clear evidence that the hydrocarbons provide some hydrogen. Aqueous solutions of platinum metal species are acidic (a 1 M solution of $RuCl_3$ has a pH of ca. 0.9) due to solvolysis of ligated water (for general discussion and further references, see ref. 17) and thus may promote protonation of the 2,3-bond of **1**. Protonation of **1** by moist $AlCl_3$ ($H^+AlCl_3OH^-$) is well known (18) and, if duplicated by the aqueous platinum metal species in this work, would produce benzothienyl carbocations that, in turn, could abstract hydrogen from hydrocarbons present in the reaction mixture. Such a mechanism explains the formation of alkenes from hexadecane (by standard β-scission chemistry) and the production of alkyl benzothiophenes (by electrophilic attack of carbocations resulting from β-scission on **1**). Admittedly, the same products could arise by radical mechanisms.

If protonation is the initial step in the reaction sequence, it could be argued that metal species are not required and that the same reactions would be promoted by mineral acids. However, experiments using sulfuric acid to generate a pH equivalent to that obtained in the experiments using $RuCl_3$ resulted in minimal reaction (Table 6). Thus, it appears that the ruthenium plays some role in the reaction sequence. This role likely involves formation of a coordination complex between **1** and the metal species. Initially, such a complex could be of the type described by Angelici (7) in which bonding occurs through the π-system on the carbocyclic ring of **1**. However, once saturation of the 2,3-bond occurs, coordination of the metal to the molecule should be via the sp^3 lone pair of electrons on sulfur, which become available as the sulfur is removed from participation in the aromatic system.

Once formed, **2** should form complexes with platinum metal species that could be intermediates in the formation of **3**. Although many thioether complexes have been prepared (19), none in-

Can. J. Chem. Downloaded from www.nrcresearchpress.com by 198.100.157.202 on 09/07/12
For personal use only.

TABLE 6. Reaction of benzo[*b*]thiophene with aqueous platinum metal species (370°C, 3 h, hexadecane)

	H_2O (pH 7)	H_2O (pH 1.2)	$PdCl_2$	$PtCl_4$	$RuCl_3$	$RuCl_3$[a]	RuS_x[b]
Benzothiophene consumed (mol%)	5	7	18	24	22	34	12
Products (mol% of reactant)							
Ethylbenzene	3	1	10	16	13	24	10
2,3-Dihydrobenzothiophene	2	6	8	8	9	10	2

[a]Data for a reaction carried out over 8 hs.
[b]Data for an experiment using preformed ruthenium sulfide.

TABLE 7. Reaction of benzo[*b*]thiophene with water and aqueous ruthenium trichloride in the presence of hexadecane, isooctane, or tetrahydronaphthalene (370°C, 3 h)[a]

	Hexadecane		Isooctane		Tetrahydronaphthalene	
	H_2O	$RuCl_3$	H_2O	$RuCl_3$	H_2O	$RuCl_3$
Benzothiophene consumed (mol%)	5	22	0	29	0	37
Products (mol% of benzothiophene)						
Ethylbenzene	3	13	0	24	0	28
2,3-Dihydrobenzothiophene	2	9	0	5	0	9

volving the 2,3-dihydrobenzothienyl ligand has been reported. To establish that complexes with this relatively bulky ligand can exist, **2** was reacted with $PdCl_2$. A deep red solid was quickly produced on mixing the reactants at 50°C. This compound (see later sections for full characterization) was determined to be a mononuclear, bisthioether *trans* square-planar complex in which the metal was bonded to the sulfur atom via the sp^3 lone electron pair of sulfur (see Fig. 1).

When this complex was heated at 300°C for 12 h with a 10 mole excess of water and either hexadecane or tetrahydronaphthalene, decomposition to **3**, **1**, and **2** and palladium sulfide took place. Most reaction occurred in the experiment using tetrahydronaphthalene (85%). In comparison, similar experiments with uncomplexed **2** and with no added palladium chloride did not produce **3**. These observations suggest that complexes of the type described above are intermediates in the formation of **3**. The hydrogen required to cleave the C—S bonds and form **3** could originate from either the hydrocarbon or from the aromatization of **2** to **1**. Presumably, the gain in resonance energy of stabilization for the formation of **1** is the driving force for this reaction.

The formation of alkenes and naphthalene from experiments using hexadecane and tetrahydronaphthalene established hydrogen transfer from these hydrocarbons. If the protonation mechanism suggested earlier is important, then one of the hydrogens in the dihydro product **2** should originate from water. To investigate this possibility, a series of experiments using D_2O were planned. Data from these experiments would be useful only if it could be established that H–D exchange between D_2O and **1** was insignificant at the reaction conditions used in the study. This seemed to be the case since in an experiment in which **1** and D_2O were heated at 370°C for 3 h only minimal D-incorporation was observed (Table 8, D-incorporation was calculated by analysis of mass spectra obtained from GC–MS studies). However, when **1** and D_2O were heated at 370°C in the presence of $RuCl_3$ either with or without hexadecane, unreacted **1** and the products **2** and **3** had undergone almost complete exchange (Table 8; it should be noted that the $RuCl_3$ used in these experiments contained normal water of hydration and thus complete deuteration is not possible). Earlier studies (20) showed that Ru(III) species promote exchange between D_2O and H_2O. This work shows that ruthenium species promote H–D exchange in unsaturated systems and, most likely, do so by coordination to the compounds undergoing exchange. Unfortunately, the rapid H–D exchange makes it impossible to determine whether protonation of the 2,3-bond of **1** plays any role in the desulfurization mechanism. However, based on known mechanisms (21) for H–D exchange of aromatic compounds in acidic media, one could argue that proton/deuteron addition is the mechanism of exchange in this system.

Another interesting result was that when **2** was reacted with D_2O and $RuCl_3$ under similar conditions, unreacted **2** showed minimal incorporation of deuterium whereas **1** and product **3** (formed in H-donor type reactions as discussed previously) were almost fully deuterated (Table 8). This result can be rationalized on the basis that coordination of ruthenium to **2** is necessary before H–D exchange can take place. Of course, when such coordination does take place, not only does H–D exchange occur, but desulfurization ensues and almost fully deuterated **3** is observed as the product. Interestingly, the degree of D-incorporation into the product **3** (7.7 D per molecule) is somewhat less than was observed for **3** formed in the experiment starting with benzothiophene **1** (9.4 D per molecule). This suggests that the dihydro protons already present in **2** are more difficult to exchange than the aromatic protons. Also, it should be noted that benzothiophene **1** formed from **2** had undergone considerable H–D exchange (5.0 D per molecule). As suggested

Can. J. Chem. Downloaded from www.nrcresearchpress.com by 198.100.157.202 on 09/07/12
For personal use only.

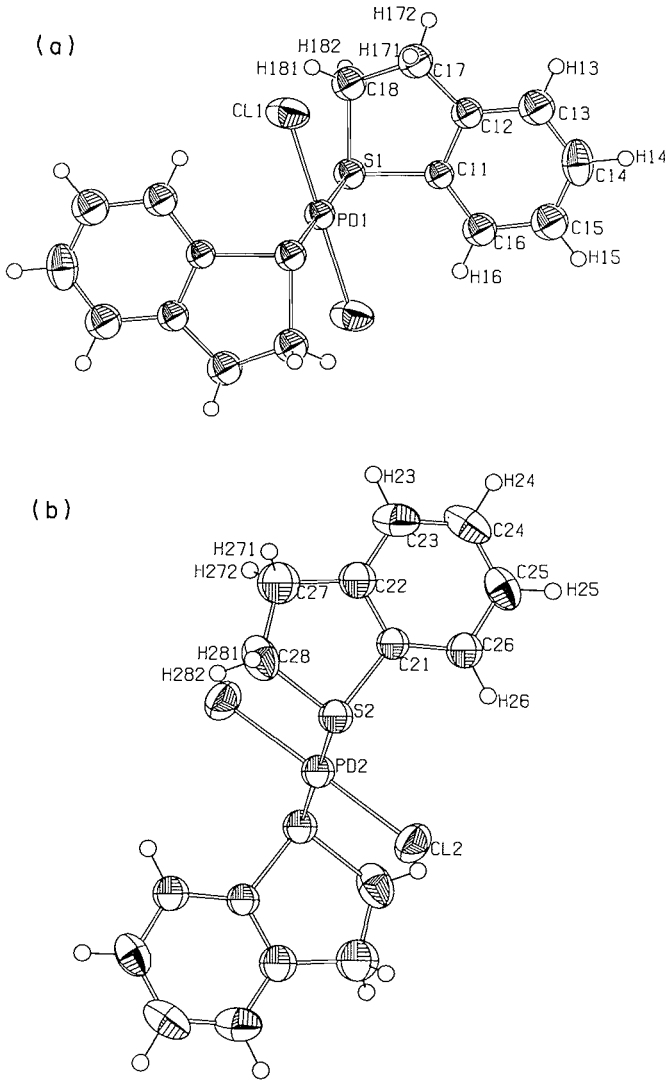


FIG. 1. (a) and (b) X-ray structures of bis-2,3-dihydrobenzo[*b*]-thienyl palladium dichloride.

earlier, **1** likely results from hydrogen donation from one molecule of the dihydro compound **2** to another undergoing desulfurization to **3**. It appears that the donor molecule must be activated towards H–D exchange during this process as it was shown that, in the absence of ruthenium species, **1** did not undergo H–D exchange (see Table 8).

X-ray study of trans-*dichlorobis(2,3-dihydrobenzo[*b*]-thiophene) palladium(II)*

Bond lengths, bond angles, and close contacts of atoms are compiled in Tables 3–5. Two discrete molecules were found in the unit cell and these structures are illustrated as ORTEP plots in Figs. 1a and 1b. The two molecules differ in a number of respects and each displays a variety of intramolecular and intermolecular hydrogen–chlorine contacts. Each molecule has a basic square-planar structure with like ligands *trans* to one another and Pd—S bond lengths of 2.320 (1) Å. This value is very close to the value obtained in other Pd–thioether complexes (2.30 Å, ref. 19) and only slightly shorter than the value obtained by summation of the Pauling radii (2.35 Å). The Cl—Pd—S bond angles of each molecule (Cl(1)—Pd(1)—S(1), 84.63, 95.37°, and Cl(2)—Pd(2)—S(2), 85.25, 94.75°) show that the chlorines are skewed towards the 2,3-dihydro portions

TABLE 8. Deuterium incorporation[a] during aqueous desulfurization of benzo[*b*]thiophene (BT) and 2,3-dihydro BT[b]

Reaction type	Products		
	BT	2,3-DihydroBT	Ethylbenzene
BT/D_2O	0.1	[c]	[c]
$BT/D_2O/RuCl_3$	3.9	7.8	9.4
$2,3\text{-DihydroBT}/D_2O$	[c]	0.2	[c]
$2,3\text{-DihydroBT}/D_2O/RuCl_3$	5.0	0.9	7.7
Maximum possible mass increase	6	8	10

[a]Data are average number of D per molecule calculated from mass spectra obtained from GC–MS studies. Experimental variation was ±0.2.

[b]All experiments were conducted at 370°C over 3 h using same reactant ratios as given in the experimental section.

[c]Either none, or very minimal quantities, of these products were formed.

of the sulfur ligands. The through-space close contacts between the chlorines and the dihydro hydrogens (Cl(1)—H(181), 2.654 Å and Cl(2)—H(282), 2.699 Å) suggest that interactions between these atoms control the conformation of the molecule. The slightly different C—S—C bond angles for each molecule (C(11)—S(1)—C(18), 90.9°, and C(21)—S(2)—C(28), 92.3°) are most likely a consequence of different Cl—H interactions in each species. Besides the intramolecular close contacts, there are close contacts between the chlorines and hydrogens of the two molecules in the unit cell. The most marked of these is the interaction between Cl(2) and H(15) (2.661 Å).

NMR spectra of trans-*dichlorobis(2,3-dihydrobenzo[*b*]-thiophene) palladium(II)*

The ^1H and ^{13}C NMR data for the Pd complex recorded at temperatures between 228 and 330 K are compiled in Table 9. ^1H NMR spectra of metal–thioether complexes are often complicated by inversion of the sulfur-containing ligand about the sulfur lone electron pairs. This phenomenon has been investigated by Abel *et al.* (22, 23). In this case, inversion of the benzothienyl ligands causes broad signals for the dihydro protons at temperatures above 273 K. These signals begin to coalesce and sharpen at 330 K. ^1H NMR spectra at 250 K show sharp signals for all protons, indicating that inversion of the ligands at this temperature is slow. These results are shown in Fig. 2. At most temperatures, one of the aromatic protons is observed as a doublet ($J = 7.9$ Hz; this value is typical of *ortho* couplings in these systems) well downfield (centered at 7.82 ppm at 273 K) of the other aromatic protons. This coupling pattern suggests that this signal is due to either H-4 or H-7 *ortho* coupled to either H-5 or H-6. It is very likely that this downfield signal is due to H-7 as a result of interaction with an adjacent chlorine. However, obtaining absolute evidence to assign H-4 or H-7 proved quite difficult.

At low temperatures, signals for the dihydro protons on C-2 and C-3 occur as four complex multiplets, each of which integrate as one proton (see Fig. 2). Potentially, irradiation of the proton resonances on C-3 could cause an enhancement of the signal for H-4 and thus allow an assignment of H-4 and H-7. A ^1H–^{13}C correlation experiment was conducted to determine the assignment of the dihydro protons at C-2 and C-3. These data showed that, at 228 K, the resonances centered at 3.0 and 4.0 ppm were associated with one carbon (either C-2 or C-3) and the resonances at 3.25 and at 3.58 ppm were associated with the other. Unfortunately, because of the large chemical shift

Can. J. Chem. Downloaded from www.nrcresearchpress.com by 198.100.157.202 on 09/07/12
For personal use only.

Can. J. Chem. Downloaded from www.nrcresearchpress.com by 198.100.157.202 on 09/07/12
For personal use only.

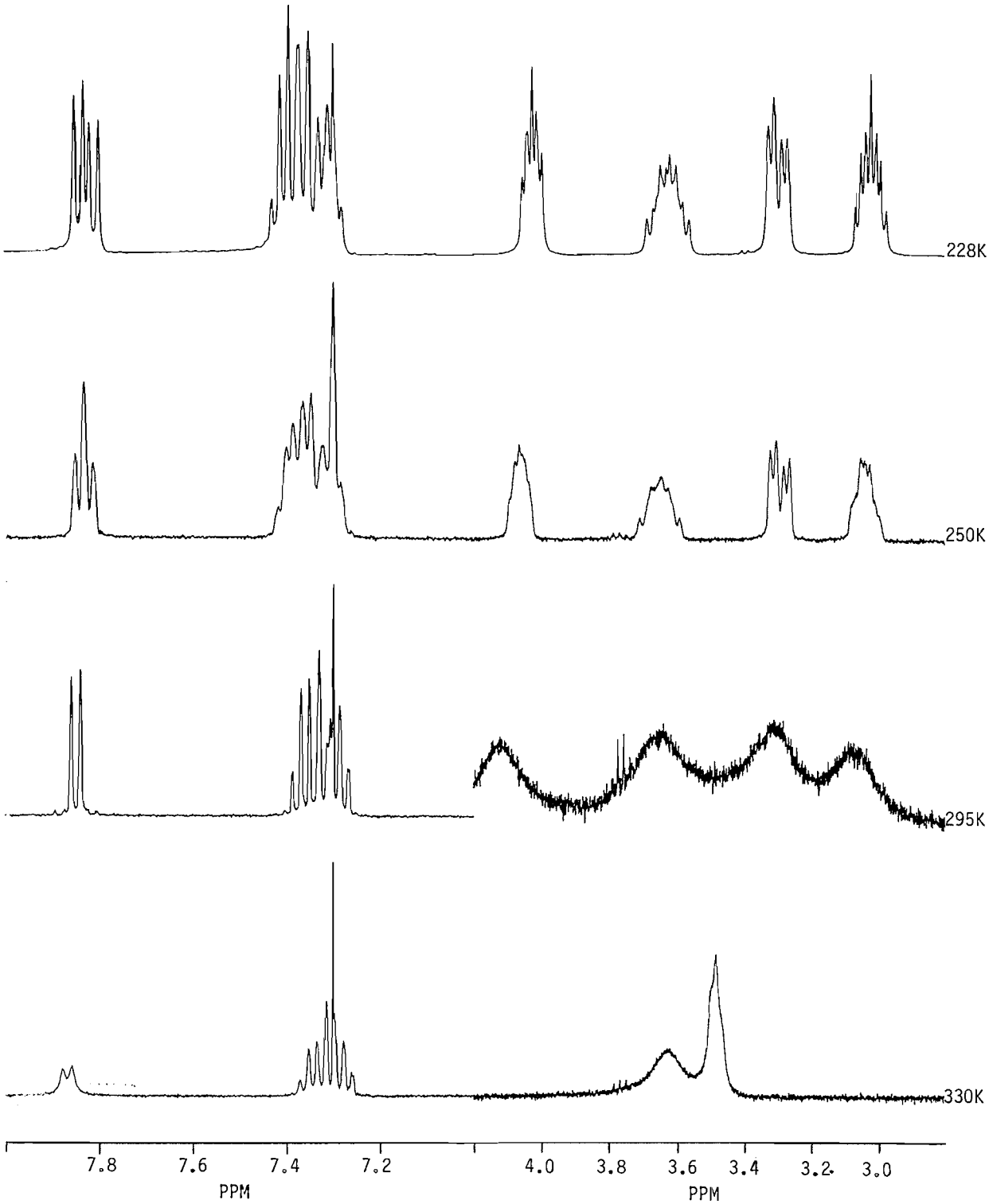


FIG. 2. Variable temperature ^{1}H NMR spectra of bis-2,3-dihydrobenzo[*b*]thienyl palladium dichloride.

differences of these proton resonances, nuclear Overhauser type experiments gave no clear assignment of H-4 and H-7. Other NMR techniques that could have resolved the assignment of H-4 and H-7, such as $^{13}C-^{13}C$ connectivity, proved impractical because of the insolubility of the complex.

Having exhausted the NMR spectroscopic techniques available to us for the assignment of H-4 and H-7, *trans*-dichlorobis-(2,3-dihydro-4-methylbenzo[*b*]thiophene) palladium(II) was synthesized. According to molecular models, the methyl substituent in this compound should have little effect on the overall geometry and the ^{1}H NMR spectrum should still show a downfield shift for H-7 because of close contact to the ligated chlorine. These predictions were borne out, as the ^{1}H NMR spectrum of the 4-methyl complex included an *ortho*-coupled doublet (J = 8 Hz) at 7.7 ppm. Full spectroscopic details and properties of the 4-methyl complex will be reported separately.

Having established that the signal at 7.8 ppm is most probably due to H-7, it is worthwhile to comment on the appearance of

TABLE 9. ^{1}H NMR spectal data for *trans*-dichlorobis(2,3-dihydrobenzo[*b*]thienyl) palladium (II)[a]

Assignment	Temperature						
	220	228	250	273	295	323	330
H-7[b]	7.86 7.84 7.82 7.80	7.81 7.79 7.78 7.76	7.82 7.80 7.78	7.83 7.81	7.83 7.81	7.85 7.83	7.85 7.83
H-4, H-5, H-6	7.43–7.28 (m)	7.39–7.26 (m)	7.38–7.25 (m)	7.38–7.25 (m)	7.36–7.24 (m)	7.34–7.23 (m)	7.34–7.23 (m)
H-3[c]	4.06–4.0 (m)	4.0–3.97 (m)	4.04 (m)	4.06 (m)	4.09 (brs)	3.45 (s)	3.45 (s)
H-2[c]	3.69–3.56 (m)	3.65–3.53 (m)	3.68–3.56 (m)	3.63 (m)	3.61 (brs)	3.58 (brs)	3.59 (brs)
H-2′[c]	3.33–3.27 (m)	3.29–3.23 (m)	3.29–3.23 (m)	3.29–3.23 (m)	3.25 (brs)	3.58 (brs)	3.59 (s)
H-3′[c]	3.07–2.96 (m)	3.03–2.94 (m)	3.02–2.99 (m)	3.06–3.01 (m)	3.04 (brs)	3.45 (s)	3.45 (s)

[a]In ppm relative to TMS.
[b]Observed as two doublets at low temperatures due to the presence of two non-equivalent invertomers (J_{ortho} = 7.9 Hz).
[c]Assignments may be reversed.

TABLE 10. ^{13}C NMR spectral data for *trans*-dichlorobis(2,3-dihydrobenzo[*b*]thienyl) palladium (II)[a]

Temperature	C-3a, C-7a		C-4, C-5, C-6, C-7				C-2, C-3	
298 K	142.7	133.6	129.0	127.9	127.6	125.3	36.4	35.6
210 K[b]	142.8 142.7	133.14 133.08	129.17 129.06	127.85	127.07 126.76	125.32	35.91 35.87	35.38

[a]In ppm relative to TMS; proton decoupled spectra.
[b]Two resonances were observed due to the presence of non-equivalent invertomers.

this resonance at low temperatures. At 250 K, the signal due to H-7 changed from the doublet observed at higher temperatures to a three-line resonance. At still lower temperatures further resolution of the signal occurred, so that at 228 K a pair of doublets was observed (each pair of lines separated by 7.9 Hz). The other resonances of the spectrum also changed as the temperature was lowered (see Fig. 2) although, because these signals occurred as complex multiplets, it was difficult to assign the exact changes. One explanation for these observations is that at 228 K the inversion of the benzothienyl ligands has ceased, and that each invertomer was observed.[3] Thus, the pairs of doublets centered at 7.8 ppm are simply the resonances of H-7 for each invertomer. Clearly, each invertomer must have a slightly different structure and, if this is the case, such differences should also be evident in a low temperature ^{13}C NMR spectrum. At 298 K, the proton decoupled ^{13}C spectrum is as expected (see Table 10). However, at 210 K, each of the eight lines observed at 298 K becomes split into two signals. When the same sample was warmed back to 298 K the normal eight-line spectrum was obtained. One further unusual feature of the ^{1}H spectra was that *meta* coupling of H-7 to H-5 could not be observed at any temperature. A possible explanation may be that the presence of two almost identical invertomers caused sufficient line broadening to wash out this small (ca. 2 Hz) coupling.

[3]One referee suggested that the spectra might be explained by the presence of rotamers.

The preceding data show that two structurally different invertomers are present in a solution of the complex but do not indicate what the differences are. This parallels the behaviour in the solid state. As for the structures found in the solid, the differences in solution may be controlled by interactions between hydrogens of the benzothienyl ligands and the chlorine substituents. Certainly, interactions between H-7 and chlorine in the complex must be quite significant, as uncomplexed 2,3-dihydrobenzothiophene has no signals downfield of 7.3 ppm in its ^{1}H NMR spectrum, whereas H-7 for the complexed ligand occurs at 7.8 ppm.

Conclusions

It has been demonstrated that benzothiophene **1** can be desulfurized using aqueous platinum metal species. The dihydro intermediate **2** is an important intermediate in the production of **3**. Experiments using D_2O suggest coordination of the metal species to **1** and **2** promotes the desulfurization reactions. The initial mode of coordination was not determined but σ-complexes via the sulfur atom of the 2,3-dihydro intermediate **2** are likely involved in the formation of **3**.

Acknowledgments

The authors wish to thank the Natural Sciences and Engineering Research Council of Canada and Alberta Sulphur Research Ltd., for financial support through an Industrial Research Professorship to P.D.C., and Masood Parvez for his helpful comments.

Can. J. Chem. Downloaded from www.nrcresearchpress.com by 198.100.157.202 on 09/07/12
For personal use only.

1. B. C. GATES, J. R. KATZER, and G. C. A. SCHUIT. Chemistry of catalytic processes. McGraw–Hill, New York. 1979.
2. F. E. MASSOTH. Adv. Catal. **27**, 265 (1978).
3. T. A. PECORARO and R. R. CHIANELLI. J. Catal. **67**, 430 (1981).
4. E. J. MARKEL, G. L. SCHRADER, N. N. SAUER, and R. J. ANGELICI. J. Catal. **116**, 11 (1989).
5. N. N. SAUER, E. J. MARKEL, G. L. SCHRADER, and R. J. ANGELICI. J. Catal. **117**, 295 (1989).
6. D. R. KILANOWSKI and B. C. GATES. J. Catal. **62**, 70 (1980).
7. S. L. HUCKETT, L. L. MILLER, R. A. JACOBSON, and R. J. ANGELICI. Organometallics, **7**, 686 (1988).
8. J. D. GOODRICH, P. N. NICKIAS, and J. P. SELEGUE. Chem. **26**, 3424 (1987).
9. P. GENESTE, P. AMBLARD, M. BONNET, and P. GRAFFIN. J. Catal. **61**, 115 (1980).
10. P. D. CLARK, N. I. DOWLING, K. L. LESAGE, and J. B. HYNE. Fuel, **66**, 1353 (1987); **66**, 1699 (1987).
11. P. D. CLARK, K. L. LESAGE, G. T. TSANG, and J. B. HYNE. Energy Fuels, **2**, 578 (1988).
12. P. D. CLARK, R. A. CLARKE, J. B . HYNE, and K. L. LESAGE. AOSTRA J. Res. **6**, 29 (1990).
13. F. G. BORDWELL and W. H. MCKELLIN. J. Am. Chem. Soc. **73**, 2251 (1951).
14. International tables for X-ray crystallography. Vol. 4. Kynoch Press, Birmingham, U.K. 1974.
15. S. R. HALL and J. M. STEWART (*Editors*). XTAL 2.2 user's manual. Universities of Western Australia and Maryland. 1987.
16. J. J. DE VLIEGER, A. P. G. KIEBOOM, and H. VAN BEKKUM. Fuel, **63**, 334 (1984).
17. F. A. COTTON and G. WILKINSON. Advanced inorganic chemistry. 4th ed. Wiley–Interscience, New York. 1980. pp. 66–67.
18. P. D. CLARK, K. CLARKE, D. F. EWING, and R. M. SCROWSTON. J. Chem. Soc. Perkin Trans. I, 677 (1980).
19. S. G. MURRAY and F. R. HARTLEY. Chem. Rev. **81**, 365 (1981).
20. J. HALPERN and B. R. JAMES. Can. J. Chem. **44**, 671 (1966).
21. N. H. WERSTIUK and G. TIMMINS. Can. J. Chem. **59**, 3218 (1981).
22. E. W. ABEL. Chem. Br. 148 (1990).
23. E. W. ABEL, K. G. ORRELL, K. B. QURESHI, and V. SIK. Polyhedron, **7**, 1321 (1988).

Can. J. Chem. Downloaded from www.nrcresearchpress.com by 198.100.157.202 on 09/07/12
For personal use only.

Kinetic and electrochemical analysis of Ni(II) reduction at the dropping mercury electrode in the presence of thiourea

ROSA M. VILLAMAÑÁN AND FERNANDO MATA-PÉREZ[1]

Departamento de Química-Física, Universidad de Valladolid, 47005 – Valladolid, Spain

Received May 1, 1990[2]

ROSA M. VILLAMAÑÁN and FERNANDO MATA-PÉREZ. Can. J. Chem. **69**, 599 (1991).

A study of the two polarographic prewaves of the Ni(II)–thiourea system has been made. The results were analysed by determining Koutecky's parameter from the ratio of the limiting current of the prewaves and the main wave. This parameter is considered an experimental rate constant and the influence of different variables on its value was analyzed. An electrochemical study of the prewaves was also made. Two formal mechanisms to explain both prewaves are proposed.

Key words: polarographic prewaves, electrochemical kinetics, reaction mechanisms.

ROSA M. VILLAMAÑÁN et FERNANDO MATA-PÉREZ. Can. J. Chem. **69**, 599 (1991).

On a réalisé une étude des deux pré-vagues polarographiques du système Ni(II)–thiourée. On a analysé les résultats en déterminant le paramètre de Koutecky à partir du rapport entre le courant limitant des pré-vagues et celui de la vague principale. On doit considérer ce paramètre comme une constante de vitesse expérimentale et on a analysé les effets de diverses variables. On a aussi réalisé une étude électrochimique des pré-vagues. On propose deux mécanismes formels qui expliquent l'apparition des deux pré-vagues.

Mots clés : pré-vagues polarographiques, cinétique électrochimique, mécanismes réactionnels.

[Traduit par la rédaction]

Introduction

In recent years, catalytic processes involving the discharge of metal ions in the presence of various additives have attracted the attention of chemists, and different experimental electrochemical techniques have been used to gain information about them. The most fruitful results have been obtained by means of polarography for several reasons (1). When Ni(II) ions are discharged on a dropping mercury electrode (DME) in aqueous solution, thiourea (Tu) exhibits a catalytic effect associated with the formation of electrochemically active species (1). We have shown (2), using different criteria, that the two prewaves observed in the polarograms exhibit a catalytic character, although the second prewave also has a small diffusive character.

Different papers (1–9) have appeared in the literature on the Ni(II)–Tu system, but only a schematic view of the mechanism has been given by refs. 1 and 4. In spite of its importance, the details on the formation of electrochemically active complexes responsible for the appearance of both prewaves are far from being clear. Thus we should first explore the characteristics of the kinetics of these discharges. From our experience with other systems (10, 11), we suggest that one can use Koutecky's parameter, x, as an experimental rate constant, implying that we employ a relaxation method. The study of the x-dependence of the different experimental variables is, in our opinion, a good way to understand the mechanism of this type of reaction. An electrochemical analysis of the prewaves is also made. Thus this paper is on a kinetic and electrochemical study of the Ni(II)–Tu system to enable us to improve the formulation of the reaction mechanisms responsible for the appearance of each prewave.

Experimental

Experimental conditions were optimized to resolve the two catalytic prewaves. Reagents used were Merck ($Ni(NO_3)_2$, Tu) and Panreac ($LiNO_3$, $NaNO_3$, KNO_3, $CsNO_3$, KOH, and HNO_3) of analytical grade.

The prewaves of Ni^{2+} ($1.3 \times 10^{-4} - 5.0 \times 10^{-4}$ mol dm^{-3}) were investigated in the presence of excess Tu ($3.4 \times 10^{-3} - 8.0 \times 10^{-2}$ mol dm^{-3}). An excess of electrolyte in the solutions was achieved by using KNO_3 ($LiNO_3$, $NaNO_3$, $CsNO_3$), at the time it provided a constant ionic strength conditions, I (0.1–0.5 mol dm^{-3}). Solutions were prepared from fresh twice distilled water. To avoid hydrolysis of Ni^{2+}, the pH of the solutions was maintained between 3.0 and 8.0. The acidity was adjusted to the desired values using very dilute solutions of HNO_3 and KOH. Oxygen in solutions was removed with a stream of purified nitrogen. The polarographic cell was thermostated from 293.15 to 304.15 K.

Polarographic measurements were made using a Radiometer-PO4g instrument equipped with a drop-life-timer unit. The drop life time was changed from 0.3 to 3.0 s, the blanking time is 80%. The sweeping rate was 0.4 V/min, and the voltage range between −0.3 and −0.6 V. Polarograms were recorded using a DME vs. the saturated calomel electrode (SCE), which was used as a reference electrode. Average currents were corrected for the residual current at given potentials.

Because of the sensitivity of catalytic prewaves to experimental conditions (12), heights of both first and second prewaves was recorded several times under a set of given conditions. The agreement between the experimental values was, in general, satisfactory and their average was taken.

Results

It seems reasonable to consider the appearance of a prewave as a special case of the irreversibility of the overall wave. Therefore we have taken the ratio $\bar{i}_k/\bar{i}_d$ ($\bar{i}_k$: limiting current for the first prewave, $\bar{i}_d$: limiting current for the main wave) and $\Sigma\bar{i}_k/\bar{i}_d$ ($\Sigma\bar{i}_k$: limiting current for the second prewave) as a function of $F(x)$ of the Koutecky's (13, 14) parameter x. Koutecky's tables contain a limited number of values for this parameter that are inadequate for our purpose. Our required x values were calculated using the following equation:

$$[1] \quad F(x) = (7\pi/12)^{1/2} \times \exp(7/12\, x^2)\, \mathrm{erfc}\, [(7/12)^{1/2}\, x]$$

In practice, values of $F(x)$ were determined experimentally and x values were obtained from eq. [1]. A similar equation has been used by different groups of researchers (15–18) and we have shown (2) that one can use this equation for determining parameter x for the present Ni(II)–Tu system. The meaning of this parameter depends on the rate-determining step of the

[1]Author to whom correspondence should be addressed.

[2]Revision received September 7, 1990.

Printed in Canada / Imprimé au Canada

Can. J. Chem. Downloaded from www.nrcresearchpress.com by 198.100.157.202 on 09/07/12
For personal use only.

Can. J. Chem. Downloaded from www.nrcresearchpress.com by 198.100.157.202 on 09/07/12
For personal use only.

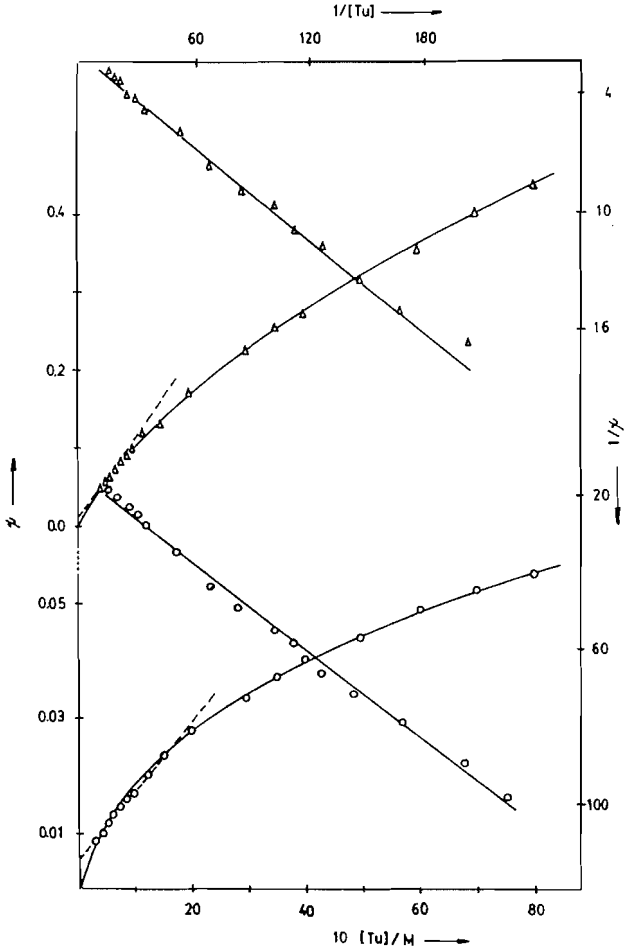


FIG. 1. Dependence of Koutecky's parameter x on the Tu concentration for the first prewave (○) and the second prewave (△). [Ni(II)] = 1.0×10^{-3} M; [Tu] = 5.0×10^{-3} M; [KNO_3] = 0.2 M; pH = 6.0.

mechanism, but in all cases x actually has all the characteristics of an experimental rate constant. The influence of different variables on this parameter has been analyzed to elucidate the reaction mechanism responsible of the appearance of each prewave.

The values of x obtained at different concentrations of Tu are given in Fig. 1. Analysis of these results leads to the following equations:

$$[2] \quad x_I = \frac{2.66[Tu]}{1 + 45.51[Tu]} \quad \text{and} \quad x_{II} = \frac{13.13[Tu]}{1 + 23.58[Tu]}$$

where I and II denote the first and second prewaves, respectively. Equations [2] have the formal structure of Langmuir's isotherm if it is assumed that Koutecky's parameter is proportional to the surface concentration of Tu. These equations are therefore evidence that both the first and second prewaves have a surface nature (5). Parsons and Symons (19) found that Tu adsorption can be expressed by a Frumkin isotherm. However, there is no unanimous view in the literature concerning the choice of isotherm for Tu. For example, Shopink *et al.* (20) described the adsorption of Tu in terms of Langmuir's isotherm. For [Tu] < 0.1 mol dm^{-3}, Lebedeva *et al.* (6) also found that the limiting current vs. [Tu] curve agrees better with Langmuir's isotherm than with Frumkin's isotherm. The causes of these disagreements have been discussed in detail (21). One

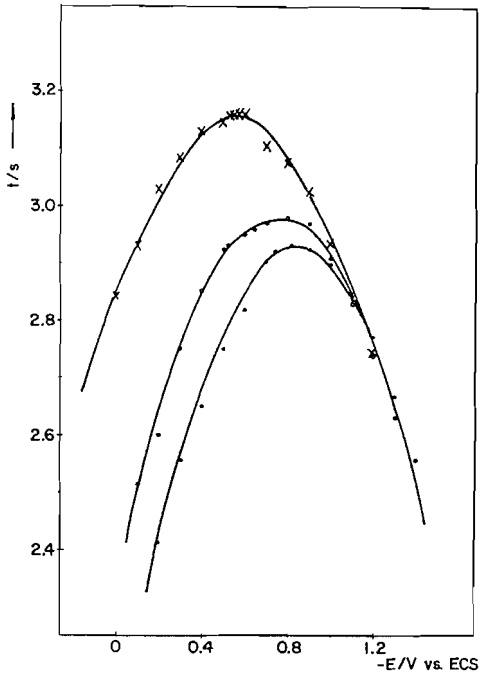


FIG. 2. Electrocapillary curves. (×): [KNO_3] = 0.2 M; (○): [KNO_3] = 0.2 M + [Tu] = 0.1 M; (●): [KNO_3] = 0.2 M + [Tu] = 0.1 M + [Ni(II)] = 0.001 M.

should note the sensitivity of the form of the isotherm to experimental conditions, in particular, to the drop formation time. This allows us to conclude that, under our experimental conditions, Langmuir's adsorption model is valid. In Fig. 1 the linear portion of the x vs. Tu concentration function remains valid if the reaction takes place partially or completely in the adsorption layer under the conditions of Henry's isotherm. The concentration interval where that occurs is greater for the first prewave than for the second. Let us examine the potential range where the prewaves are located. The first prewave is located ($E_{1/2} = -0.62 \pm 0.02$ V vs. SCE, t = 3 s) in the vicinity of the point of zero charge (p.z.c.) where the coverage of the DME surface by Tu is at a maximum. In contrast, the second prewave is located ($E_{1/2} = -0.83 \pm 0.02$ V vs. SCE, t = 3 s) in a potential range where that coverage is small. For comparative purposes the electrocapillary curves were obtained (Fig. 2), our results (p.z.c. values) are in good agreement with those found by Parsons and Symons (19). From radiotracer studies the adsorption equilibrium of Tu on iron was observed to take place within 5 min of the imposition of potentiostatic control (23). Hence one can consider that adsorption of Tu on the DME very quickly attains equilibrium conditions as the linear dependence of x vs. $t^{1/2}$ (Fig. 3) strongly suggests (24).

No changes were observed for the x values when the Ni(II) concentration was changed from 5.0×10^{-4} to 1.3×10^{-3} mol dm^{-3}.

In this work the range of pH is conditioned by both the protonation of Tu (which takes place (3) below pH = 1.0) and by the hydrolysis of Ni(II) ions; the latter being important for pH > 8.0. All experiments, however, were conducted in the range 3.0 < pH < 8.0. Under these conditions, the analytical Tu concentration equals, in practice, the concentration of the alkaline form of Tu, as one may deduce from the pK_a value reported for this compound (3). It is also possible to deduce that $1/[Tu]_s$ ($[Tu]_s$ = surface concentration of Tu) should be

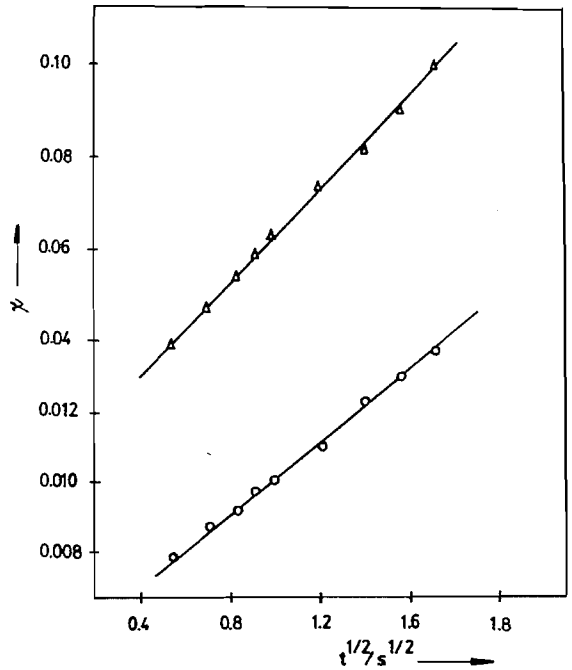


FIG. 3. Dependence of x on the drop life time for the first prewave (○) and the second prewave (△). [Ni(II)] = 1.0×10^{-3} M; [Tu] = 5.0×10^{-3} M; [KNO_3] = 0.2 M; pH = 6.0; T = 298.15 K.

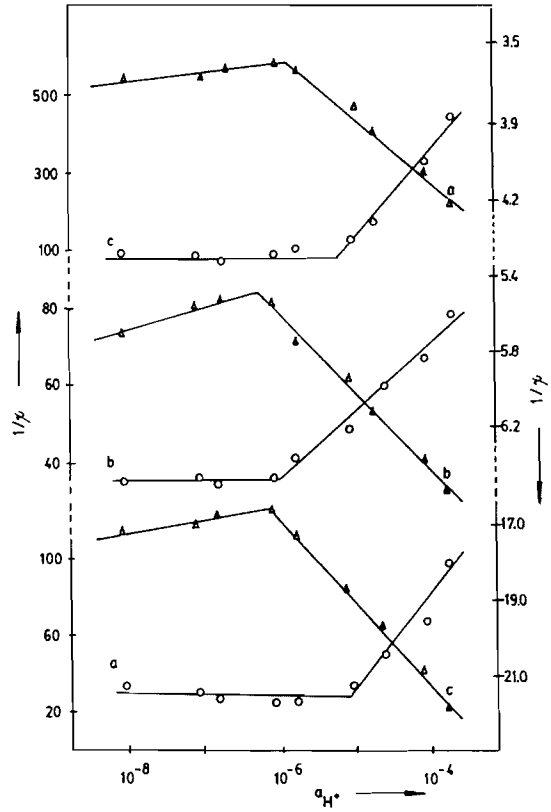


FIG. 4. Dependence of $1/x$ on proton activity for the first prewave (○) and the second prewave (△). [Ni(II)] = 1.0×10^{-3} M; [KNO_3] = 0.2 M; pH = 6.0; T = 298.15 K; [Tu]: (*a*) 4.0×10^{-2} M, (*b*) 2.0×10^{-2} M, (*c*) 5.0×10^{-3} M.

proportional to the activity, a_{H^+}. Hence, a plot of $1/x$ vs. a_{H^+} should be a straight line. However, this relation was not obtained (Fig. 4). A possible explanation is that the mechanisms which explain the appearance of both prewaves are preceded by an acid-catalyzed dehydration of $Ni(H_2O)_6^{2+}$ species (10, 11).

The dependence of x on the ionic strength (I) was also studied within the range 0.1 to 0.5 mol dm^{-3}, KNO_3 being the supporting electrolyte. A tentative fit of log x vs. $\sqrt{I}/(1+\sqrt{I})$ was made by using Guggenheim's correction (25) of the Debye–Hückel theory. In Table 1 the fit functions are given. There is no evidence of a kinetic salt effect for the reaction responsible for the first prewave. However, our results strongly suggest the existence of a kinetic salt effect for the reaction responsible for the second prewave. A high value of about −5 was found for the z_+z_- product. This number has to be taken with care because it could be the result of the limited validity of the Debye–Hückel–Guggenheim formula for interpreting the activity coefficients of reacting molecules and of the transition state. However, the unambiguous negative value of this product shows that the process responsible for the second prewave is partially controlled by a reaction between two species of opposite charge.

The double-layer effect (Ψ-effect) on the kinetics of this system was studied to determine the charge of the polarographic active compound (PAC) for both prewaves. In Fig. 5*a* plots of ln x vs. Ψ are given. The Ψ values were taken from Russell's tables (26) for the potential values (vs. SCE) of -0.65 ± 0.02 and -0.90 ± 0.02 V for the first and second prewaves, respectively. These potentials correspond to the limiting currents when serious interferences are not predicted (27). A charge of +1.35 was found for the polarographic active compound responsible for the second prewave. However, from our results no evidence for an Ψ-effect was found for the first prewave. This fact can be explained because the potential of −0.65 V is very close to the p.z.c. which is located (19) at about −0.58 V

TABLE 1. Dependence of Koutecky's parameter x on the ionic strength I [a]

I/mol dm^{-3}	First prewave[b]	Second prewave[c]
0.125	0.0127	0.096
0.150	0.0125	0.080
0.200	0.0111	0.060
0.250	0.0101	0.050
0.300	0.0093	0.040
0.350	0.0082	0.034
0.400	0.0076	0.029
0.500	0.0071	0.026

[a]Experimental conditions: [Ni(II)] = 1.0×10^{-3} M; [Tu] = 5.0×10^{-3} M; T = 298.15 K; pH = 6.0.
[b]Fit function: $\log x_I = -1.821 - 0.921I + 0.174I^{1/2}/(1 + I^{1/2})$, r_{xy} = 0.9959.
[c]Fit function: $\log x_{II} = 0.266 + 0.546I - 5.162I^{1/2}/(1 + I^{1/2})$, r_{xy} = 0.9962.

for similar conditions. Russell's table has also been used by other researchers (4, 5) for this system. However, the Ψ values of Russell's table were obtained for the mercury – aqueous NaF interface according to the Gouy–Chapman theory with the assumption of no specific adsorption of sodium or fluoride ions. For all these reasons, these values are only an approximation to the actual potentials on the outer Helmholtz plane for a given electrolyte (KNO_3) under our experimental conditions. Hence, the preceding conclusions on the Ψ effect have to be taken with caution.

It is well known (28) that an increase in the concentration

Can. J. Chem. Downloaded from www.nrcresearchpress.com by 198.100.157.202 on 09/07/12
For personal use only.

Can. J. Chem. Downloaded from www.nrcresearchpress.com by 198.100.157.202 on 09/07/12
For personal use only.

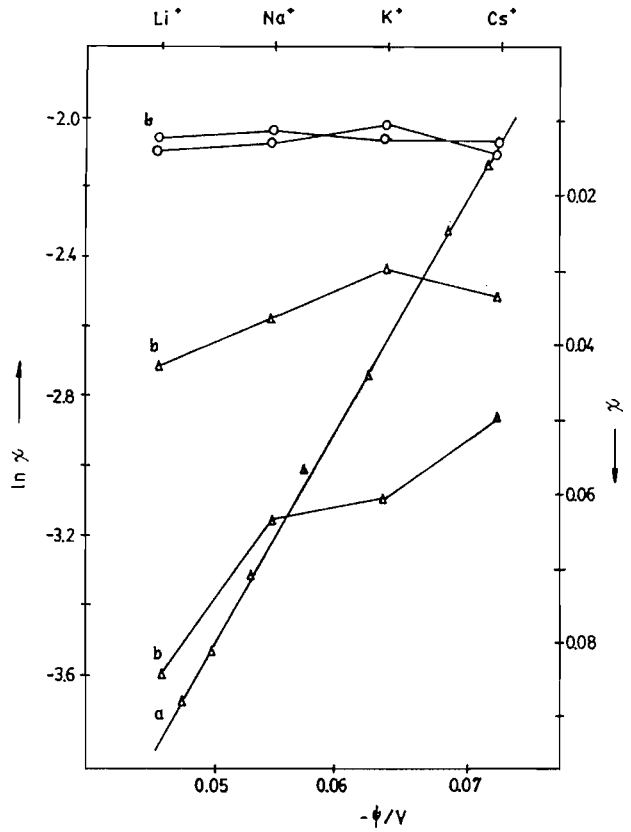


FIG. 5. Dependence of Koutecky's parameter x on the potential of the Helmholtz plane (a) for the second prewave (△), and on the cation nature (b) for the first prewave (○). [Ni(II)] = 1.0×10^{-3} M; [Tu] = 5.0×10^{-3} M; I = [XNO$_3$] = 0.2 M; pH = 6.0; T = 298.15 K.

of anions of the supporting electrolyte which are surface-active species gives rise to an increase in the limiting currents of the prewaves. Under our working conditions we have confirmed the adsorption of NO_3^- on the DME (22) using Langmuir's isotherm. The specific adsorption of this species is a factor that change the double-layer structure and, consequently, the potential on the outer Helmholtz plane. However, Parsons and Symons (19) found that the adsorption of NO_3^- species is reduced in the presence of Tu. Bockris *et al.* have shown (29) that the adsorption of NO_3^- is not important for $[NO_3^-] \leqslant 0.5$ mol dm^{-3}; so the adsorption of NO_3^- on the DME will have little effect on the magnitude of Koutecky's parameter. The only relevant role of anion of the supporting electrolyte appears to be conditioning the charge of the PAC (10, 11); this may be due to the association process of Ni^{2+} species with these anions in the surface layer (14). On the other hand, the effect of cation of the supporting electrolyte on the x values is only noticeable for the second prewave (Fig. 5b). This conclusion results from specific cation adsorption (3) because the second prewave is not located in the vicinity of p.z.c.

Our results on the effect of temperature on x allow us to determine both the activation enthalpy $\Delta H^{\neq}$ and the activation entropy $\Delta S^{\neq}$; these are given in Table 2. The existence of a compensation effect was confirmed, and the isokinetic temperature T_{iso} was determined.

$E_{1/2}$ values change with the drop life time, t. This is a sign that the electrode process is irreversible. Consequently the irreversibility of the polarographic curve was analyzed. Plots of $\ln \bar{i}/(\bar{i}_d - \bar{i})$ vs. $-E$ for different Tu concentrations are given

TABLE 2. Activation parameters[a]

10^3 [Tu]/mol dm^{-3}	$\Delta H^{\neq}$/kJ mol^{-1}	$-\Delta S^{\neq}$/J K^{-1} mol^{-1}
	1st prewave[c]	
5	51.46	115.06 (0.9965)[b]
20	35.15	162.34 (0.9958)
30	43.93	132.21 (0.9990)
40	53.14	98.74 (0.9990)
50	76.15	21.76 (0.9991)
60	94.14	−40.58 (0.9998)
	2nd prewave[d]	
5	57.32	82.42 (0.9998)
20	41.84	124.68 (0.9992)
30	32.22	154.81 (0.9998)
40	23.43	182.84 (0.9996)
50	32.64	151.04 (0.9998)
60	38.49	130.54 (0.9991)

[a]Experimental conditions: [Ni(II)] = 1.0×10^{-3} M; [KNO$_3$] = 0.2 M; pH = 6.0.
[b]Linear correlation coefficients.
[c]First prewave: T_{iso} = 228.0 K (r_{xy} = 0.9987).
[d]Second prewave: T_{iso} = 336.0 K (r_{xy} = 0.9961).

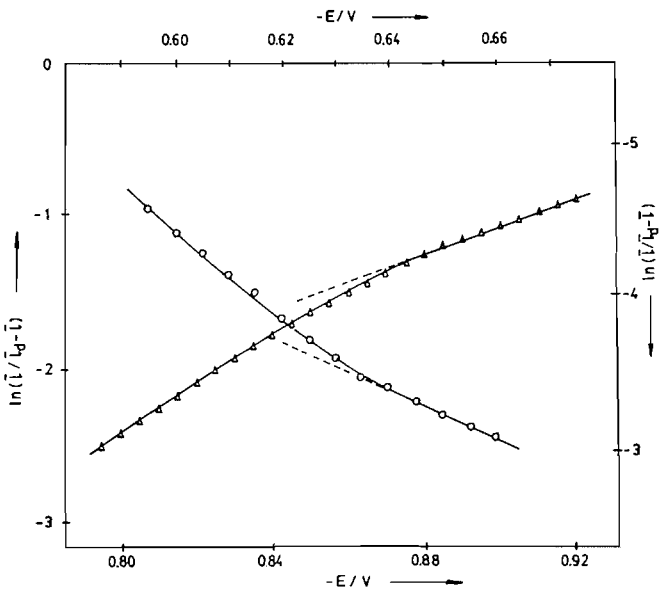


FIG. 6. Analysis of the irreversibility of the polarographic curve for the first prewave (○) and the second prewave (△). [Ni(II)] = 1.0×10^{-3} M; [Tu] = 5.0×10^{-3} M; [KNO$_3$] = 0.2 M; pH = 6.0; T = 298.15 K.

in Fig. 6. The hyperbolic profile is characteristic of a quasi-reversible process (30). Using Koryta's criterion (31), extrapolation of the first part of the plot gives $E_{1/2}$ for reversible conditions. From the slope of the same plot, we obtain the number of electrons, n, participating in the charge transfer process. Moreover, from the second part of the plot, both the transfer coefficient, α, and $E_{1/2}$ irreversible were obtained. Table 3 summarizes all these results.

The method described by Bard and Faulkner (32) was used to calculate the exchange current, i_0. It was thus verified that $\ln (\bar{i}_d - \bar{i})/\bar{i}$ vs. η (overpotential) are linear functions in the Tafel region under our experimental conditions (correlation coefficients >0.99). From the respective intercepts i_0 values

TABLE 3. Analysis of the irreversibility of the first prewave[a]

10^3 [Tu]/mol dm^{-3}	[KNO_3]/mol dm^{-3}	n	α	$-\Delta E_{1/2}$[b]/mV
5	0.125	0.97 (0.9966)[c]	0.34	237
	0.200	0.89 (0.9995)	0.36	230
	0.300	1.15 (0.9918)	0.37	191
	0.400	1.15 (0.9997)	0.35	222
20	0.125	1.05 (0.9981)	0.34	181
	0.200	1.19 (0.9948)	0.36	155
	0.400	1.03 (0.9992)	0.34	182
40	0.125	1.17 (0.9975)	0.35	154
	0.200	0.90 (0.9998)	0.38	190
	0.400	1.08 (0.9996)	0.33	182

[a]Experimental conditions: [Ni(II)] = 1.0×10^{-3} M; T = 298.15 K; pH = 6.0.
[b]$\Delta E_{1/2} = E_{1/2}^{irrev} - E_{1/2}^{rev}$.
[c]Linear correlation coefficients.

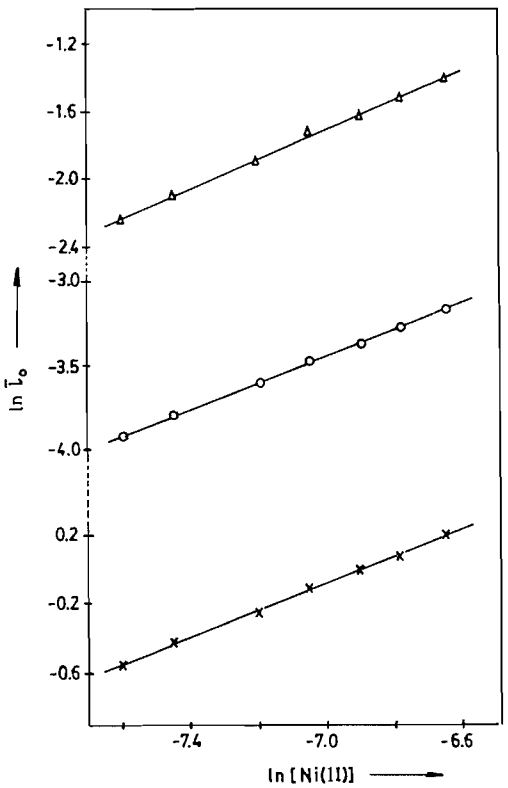


FIG. 7. Dependence of the exchange current on the Ni^{2+} concentration for the main wave (×), the first prewave (○), and the second prewave (△). [Ni(II)] = 1.0×10^{-3} M; [Tu] = 5.0×10^{-3} M; [KNO_3] = 0.2 M; pH = 6.0; T = 298.15 K.

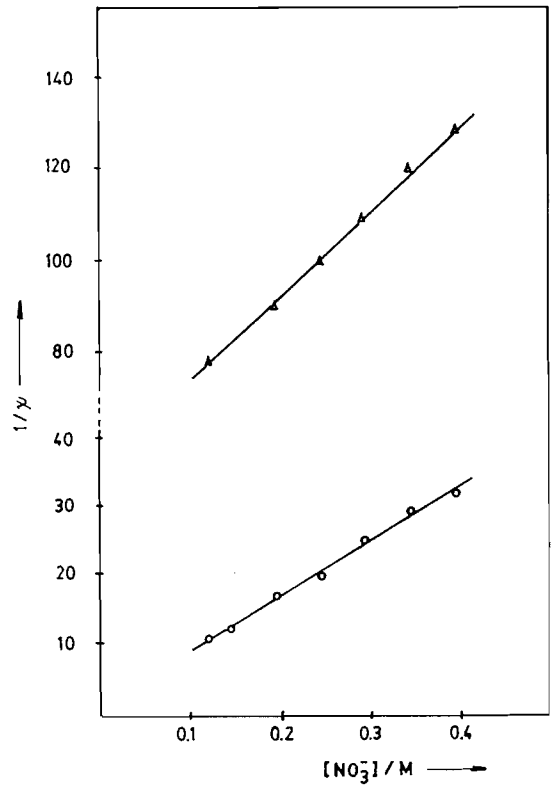


FIG. 8. Dependence of $1/x$ on the nitrate concentration for the first (○) and the second (△) prewaves. [Ni(II)] = 1.0×10^{-3} M; [Tu] = 5.0×10^{-3} M; [KNO_3] = 0.2 M; pH = 6.0; T = 298.15 K.

TABLE 4. Values of the stoichiometric number, ν[a]

10^3 [Ni(II)]/mol dm^{-3}	ν/n
0.59	1.02 (0.9999)[b]
0.88	0.91 (0.9994)
1.00	1.05 (0.9991)

[a]Experimental conditions: [Tu] = 5.0×10^{-3} M; T = 298.15 K; pH = 6.0.
[b]Linear correlation coefficients.

were obtained. Plots of ln i_0 vs. ln [Ni(II)] are linear (Fig. 7). The slopes are 1.0, an additional positive feature of the analysis.

In the region $\eta \rightarrow 0$ the stoichiometric number, ν, was determined from plots of η vs. $\bar{i}$. These plots yield $\nu = 1$, as Table 4 shows. However this analysis was only done for the first prewave, since η vs. $\bar{i}$ and i_0 are not sufficiently accurate for the second prewave.

Formal mechanism

The dependence of x on [Tu] shows that charge transfer is not (34) the rate-determining step for the reactions responsible for the appearance of the prewaves. On the contrary, the forms of eqs. [2] are consistent with the surface nature of both prewaves.

Can. J. Chem. Downloaded from www.nrcresearchpress.com by 198.100.157.202 on 09/07/12
For personal use only.

Moreover, the electrocapillary curves (Fig. 2), together with the dependence of both $\Sigma \bar{i}_k$ and x_{II} on the nature of the cation species of the supporting electrolyte (Fig. 5*b*), are additional proofs of our thesis.

Figure 4 confirms that the alkaline form of Tu is the adsorbed species on the DME. From FTIR studies (24) it has been proved that the sulfur atom is attracted to the electrode surface by strong chemical interaction forces and not through electrostatic interactions as proposed by Parsons and Symons (19). On the other hand, the NO_3^- species are also adsorbed on the DME (19, 29), and a competitive process exists between these ions and the Tu molecules. Figure 8 shows the existence of this co-adsorption phenomenon.

Pulse polarograms for Ni^{2+}/Tu system show three distinct signals at certain ligand concentrations (33). However no comprehensive constants are given for the formation of the corresponding polarographic active compounds that can explain these signals.

Although our interest is centered on the two prewaves, a few considerations on the processes responsible for the main wave are given. The formal mechanism explaining the appearance of the main wave consists (10, 11, 34, 35) of diffusion and dehydration (acid catalyzed) by partial loss of water molecules of the $Ni(H_2O)_6^{2+}$ species, and the discharge of $Ni(H_2O)_x^{2+}$ species on the DME:

$$[3]\quad [Ni(H_2O)_6^{2+}]_{BS} \xrightarrow[\text{Slow}]{\text{Diffusion}} [Ni(H_2O)_6^{2+}]_{DLL} \underset{\text{Fast}}{\overset{\text{Adsorption}}{\rightleftharpoons}} [Ni(H_2O)_6^{2+}]_{ES}$$

$$H^+ \downarrow \text{ Fast}$$

$$[4]\quad [Ni(H_2O)_x^{1+}]_{ES} \xleftarrow[\text{Main wave}]{1\ e^-} [Ni(H_2O)_x^{2+}]_{ES} + (6-x)H_2O$$

$$[5]\quad 2[Ni(H_2O)_x^{1+}]_{ES} \underset{}{\overset{\text{Fast}}{\rightleftharpoons}} [Ni(H_2O)_x^{2+}]_{ES} + Ni(Hg)$$

where BS is bulk solution, DLL is double layer limit, and ES is electrode surface.

The formulation of the discharge giving the Ni(I) species (reaction [4]) is in agreement with our preceding results (10, 11); it has also been postulated by other workers (35).

The mechanism which explains the origin of the first prewave is:

$$[6]\quad [Ni(H_2O)_x^{2+}]_{ES} + [Tu]_{ES} \xrightarrow{\text{Slow}} [Ni(H_2O)_{x-1}Tu^{2+}]_{ES} + H_2O$$

$$1\ e^- \downarrow \text{ First prewave}$$

$$[7]\quad [Ni(H_2O)_{x-1}{}^{1+}]_{ES} + Tu \leftarrow$$

The discharge is a one-electron step (Table 3), its stoichiometric number being $\nu = 1$. Aggarwal and Crow (36) have studied the electrochemical behaviour of the Ni^{2+} species at the DME for several complexing ligands. Heterocyclic ligands share a common feature that their reduction involves two electrons. This contrasts with the other systems (e.g. Ni^{2+}/Tu) for which the transfer of one electron is involved. Reduction of the complex $[Ni(H_2O)_xTu^{2+}]_{ES}$ produces unattached ligand molecules which can be adsorbed immediately on the electrode surface. The reaction of adsorbed aquo-ions $[Ni(H_2O)_x^{2+}]_{ES}$ with adsorbed Tu is slower than the electron transfer process. Thus, the surface nature of the first prewave is explained. Regeneration of Tu occurs (reaction [7]) and this implies a catalytic character for the first prewave as found for other systems (37–39).

No other ionic species are implied in this formulation. This is consistent with the absence of a kinetic salt effect for the reaction responsible for the first prewave. In this case, co-adsorption of the NO_3^- species appears to be kinetically irrelevant.

The appearance of the second prewave can be explained, in a similar manner, as follows:

$$[8]\quad [Ni(H_2O)_xTu^{2+}]_{ES} + [Tu]_{ES} \xrightarrow{\text{Slow}} [Ni(H_2O)_{x-1}Tu_2{}^{2+}]_{ES} + H_2O$$

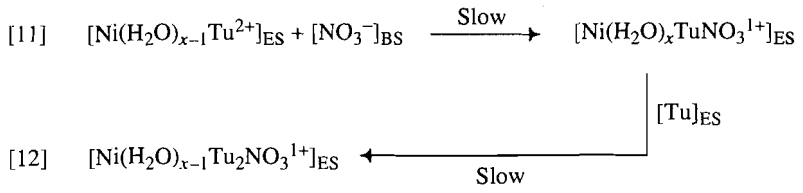
$$\text{I} \downarrow$$

$$[9]\quad [Ni(H_2O)_{x-1}Tu^{1+}]_{ES} + Tu \xleftarrow[\text{Second prewave}]{1\ e^-}$$

$$[10]\quad 2[Ni(H_2O)_{x-1}Tu^{1+}]_{ES} \underset{}{\overset{\text{Fast}}{\rightleftharpoons}} [Ni(H_2O)_{x-1}Tu^{2+}]_{ES} + Ni(Hg)$$

Can. J. Chem. Downloaded from www.nrcresearchpress.com by 198.100.157.202 on 09/07/12
For personal use only.

The experimental value of +1.35 for the electric charge of PAC I could be a consequence of the NO_3^- effect. The existence of the $Ni(H_2O)_xNO_3^{1+}$ species (39) has been confirmed. In this case, the existence of similar compounds seems to be unlikely from the dependence of x on the NO_3^- concentration. However, the kinetic salt effect for the reaction responsible for the second prewave points to the existence of a reaction where two species of opposite charges participate. On the other hand, the second prewave has a partial diffusive character. All these facts suggest that the PAC could be alternatively formulated as:



The NO_3^- species diffuses from the bulk solution to the electrode surface. Hence, the second prewave has a partial diffusive character. On the other hand, this alternative formulation for PAC reasonably explains the value of +1.35 found for its electric charge.

1. O. E. Ruvinskii and Ya. I. Tur'yan. Russ. J. Phys. Chem. **53**, 300 (1979).
2. R. M. Villamañán and F. Mata-Pérez. Unpublished results.
3. Ya. I. Tur'yan and O. E. Ruvinskii. Elektrokhimiya, **4**, 1446 (1968).
4. Ya. I. Tur'yan and O. E. Ruvinskii. J. Electroanal. Chem. **23**, 61 (1969).
5. O. E. Ruvinskii and Ya. I. Tur'yan. Elektrokhimiya, **7**, 732 (1971).
6. L. N. Lebedeva, A. Kh. Iskakova, and G. N. Babkin. Russ. J. Phys. Chem. **53**, 1498 (1979).
7. O. E. Ruvinskii and Ya. I. Tur'yan. Russ. J. Phys. Chem. **56**, 1702 (1981).
8. L. N. Lebedeva and G. N. Babkin. Russ. J. Phys. Chem. **53**, 303 (1979).
9. L. N. Lebedeva, A. Kh. Iskakova, and G. N. Babkin. Russ. J. Phys. Chem. **55**, 1704 (1981).
10. F. Mata and M. S. Crespo. Z. Phys. Chem. **260**, 1033 (1979).
11. F. Mata and M. S. Crespo. Z. Phys. Chem. **260**, 1042 (1979).
12. S. I. Sinyakova and V. F. Toropova. Advances in and prospects for the development of polarographic method. Shtiintsa, Kishinev, USSR. 1972. p. 117.
13. J. Weber and J. Koutecky. Coll. Czech. Chem. Commun. **20**, 980 (1955).
14. J. Koutecky and J. Cizet. Collect. Czech. Chem. Commun. **50**, 196 (1956); **21**, 836 (1956).
15. J. Caja, H. C. MacDonald Jr., E. Kirowa-Eisner, L. R. McCoy, and H. B. Mark Jr. J. Phys. Chem. **76**, 1170 (1972).
16. J. Koutecky and R. Brdicka. Collect. Czech. Chem. Commun. **18**, 597 (1953).
17. P. Delahay and J. E. Strassner. J. Am. Chem. Soc. **73**, 5219 (1951).
18. P. Delahay. New instrumental methods in electrochemistry. Interscience, New York. 1954. p. 417.
19. R. Parsons and P. C. Symons. Trans. Faraday Soc. **64**, 1077 (1968).
20. F. W. Shopink, M. Oudeman, K. W. Leu, and J. N. Helle. Trans. Faraday Soc. **56**, 415 (1960).
21. A. N. Frumkin and B. B. Damaskin. Modern aspects of electrochemistry. Mir, Moscow, USSR. 1967. pp. 179, 207.
22. R. M. Villamañán. Ph.D. Thesis. University of Valladolid, Valladolid, Spain. 1985.
23. J. O'M. Bockris, B. R. Scharifker, and J. L. Carbajal. Electrochim. Acta, **32**, 799 (1987).
24. R. L. McCoy and H. B. Mark. J. Phys. Chem. **73**, 953 (1969).
25. E. A. Guggenheim and J. C. Turgeon. Trans. Faraday Soc. **51**, 747 (1955).
26. C. D. Russell. J. Electroanal. Chem. **6**, 486 (1963).
27. L. R. McCoy, H. B. Mark, and L. Gierst. J. Phys. Chem. **72**, 4637 (1968).
28. L. Gierst, L. Vanderbergen, E. Nicolas, and A. Traboni. J. Electrochem. Soc. **113**, 1025 (1966).
29. H. Wroblowa, Z. Kovac, and J. O'M. Bockris. Trans. Faraday Soc. **51**, 747 (1955); **61**, 1523 (1965).
30. H. Matsuda and Y. Ayabe. Z. Elektrokhem. **63**, 1164 (1959).
31. J. Koryta. J. Electrochem. Acta, **6**, 67 (1962).
32. A. J. Bard and L. E. Faulkner. Electrochemical methods. John Wiley and Sons, New York. 1980. p. 110.
33. D. R. Crow. Electrochem. Acta, **29**, 1199 (1984).
34. J. Dandoy and L. Gierst. J. Electroanal. Chem. **2**, 836 (1961).
35. R. H. Sanborn and E. F. Orlemann. J. Am. Chem. Soc. **78**, 4852 (1956).
36. P. K. Aggarwal and D. R. Crow. Electrochem. Acta, **25**, 411 (1980).
37. D. R. Crow and M. E. Rose. Electrochem. Acta, **24**, 41 (1979).
38. H. B. Mark Jr. and C. N. Reilley. J. Electroanal. Chem. **4**, 189 (1962); J. Electroanal. Chem. **7**, 276 (1964); Anal. Chem. **35**, 195 (1963).
39. A. M. Bond. J. Phys. Chem. **75**, 2640 (1971).

Can. J. Chem. Downloaded from www.nrcresearchpress.com by 198.100.157.202 on 09/07/12
For personal use only.

Ionic dissociation in complexes of iodine with triphenylarsine and triphenylstibine

YING RU ZHANG, IRA SOLOMON, AND SEYMOUR ARONSON[1]
Department of Chemistry, City University of New York, Brooklyn College, Brooklyn, NY, U.S.A. 11210
Received, July 6, 1990

YING RU ZHANG, IRA SOLOMON, and SEYMOUR ARONSON. Can. J. Chem. **69**, 606 (1991).

An electrochemical technique has been employed to study the ionization of the iodine complexes of $(C_6H_5)_3As$, $(C_6H_5)_3Sb$, and pyridine. Several different ionization mechanisms are proposed depending on the chemical nature and concentration of the reactants. A new ionic complex, $(C_6H_5)_3MI_2^{2+}$ is postulated for the interaction of iodine with $(C_6H_5)_3As$ and $(C_6H_5)_3Sb$ at high iodine concentrations. Equilibrium constants have been calculated from the emf data for the various ionization steps.

Key words: triphenylarsine, triphenylstibine, iodine, complex formation, ionization.

YING RU ZHANG, IRA SOLOMON et SEYMOUR ARONSON. Can. J. Chem. **69**, 606 (1991).

On a utilisé une technique électrochimique pour étudier l'ionisation des complexes de l'iode avec le $(C_6H_5)_3As$, le $(C_6H_5)_3Sb$ et la pyridine. On propose plusieurs mécanismes d'ionisation suivant la nature chimique et la concentration des réactifs. À des concentrations élevées d'iode, on suggère l'implication d'un nouveau complexe ionique, $(C_6H_5)_3MI_2^{2+}$, pour l'interaction entre l'iode et le $(C_6H_5)_3As$ ou le $(C_6H_5)_3Sb$. En se basant sur les fem des diverses étapes d'ionisation, on a calculé les constantes d'équilibre.

Mots clés : triphénylarsine, triphénylstibine, iode, formation de complexes, ionisation.

[Traduit par la rédaction]

Introduction

Several investigators have studied the interaction of iodine with $(C_6H_5)_3As$ and $(C_6H_5)_3Sb$ in organic solution. The spectroscopic studies of Bhaskar *et al.* (1) and Bhat and Rao (2) in CCl_4 and $CHCl_3$ demonstrated that the outer complex, which forms initially $(C_6H_5)_3MI_2$, transforms slowly into the inner complex $(C_6H_5)_3MI^+I^-$, and in the presence of excess iodine, into $(C_6H_5)_3MI^+I_3^-$. The conductance measurements of Beveridge and co-workers (3, 4) in acetonitrile and Sahai *et al.* (5) in dioxane and tetrahydrofuran demonstrated that significant ionization of the complexes occurs.

In a previous paper (6), we have reported on a quantitative study of the ionization of the pyridine–iodine complex in pyridine and in 1,2-dichloroethane using an electrochemical technique involving I_3^- concentration cells. It was found that 25% of the complex is present in ionized form. The study was made at high concentration ratios of pyridine to iodine.

In the present work, we have applied the electrochemical technique to the ionization of the complexes formed between iodine and $(C_6H_5)_3As$, $(C_6H_5)_3Sb$, and pyridine in 1,2-dichloroethane primarily at high concentration ratios of iodine to organic molecule. Quantitative information has been obtained on the ionization reactions which occur in these systems.

Experimental

Triphenylarsine (Ph_3As), triphenylstibine (Ph_3Sb), and tetraethylammonium iodide (TEAI) were obtained in the highest commercial grades available from Aldrich Chemical Co. Spectrophotometric grades of pyridine (Py) and 1,2-dichloroethane (DCE) and A.C.S. reagent grade iodine (I_2) were also obtained from Aldrich. The iodine was resublimed and kept in a tightly closed container.

The electrochemical measurements were made in a 2-compartment "H" cell. Conductivity measurements were made using a standard conductivity cell. Details of the methods have been described previously (6).

All solutions were kept in sealed flasks, in the dark, between measurements. Data presented in this report were obtained on solutions which had reached equilibrium as determined by conductivity or electrochemical measurements.

The term "total concentration" used in connection with I_2, Ph_3As, Ph_3Sb, Py, and TEAI refers to the number of moles added to a liter of DCE solution. Dissociation and interaction in solution are not considered. The symbol used for total concentration is "c" as in $c(I_2)$ and $c(Ph_3As)$. The actual concentrations are shown in brackets as in $[I_3^-]$ and $[Ph_3AsI_2]$.

Reaction mechanisms

Many reaction sequences and ionization mechanisms were considered. Those presented here were found to be in best accord with the experimental data.

A. High iodine concentrations

The following reaction scheme was used for high concentration ratios of iodine to organic molecule in 1,2-dichloroethane.

[1] $R + I_2 \rightarrow RI_2$

[2] $RI_2 + I_2 \rightleftharpoons RI^+ + I_3^-$

[3] $RI^+ + 2I_2 \rightleftharpoons RI_2^{2+} + I_3^-$

We assume that the addition of tetraethylammonium iodide results quantitatively in the following reaction:

[4] $I_2 + TEAI \rightarrow I_3^- + TEAE^+$

where R in reaction [1] represents the organic molecule. We assume that reaction [1] proceeds completely to the right and that sufficient time has elapsed so that the complex present is the inner complex, RI^+I^-, which, for convenience, we write as RI_2. The extent to which reactions [2] and [3] proceed to the right depends on the nature of the organic molecule. A further assumption, that concentrations can be substituted for thermodynamic activities, permits us to write the following expressions for the equilibrium constants.

[5] $$K_2 = \frac{[RI^+][I_3^-]}{[RI_2][I_2]}$$

[6] $$K_3 = \frac{[RI_2^{2+}][I_3^-]}{[RI^+][I_2]^2}$$

Complexes of the form RI^+ have been proposed by many investigators. A new complex, RI_2^{2+}, is being proposed by us on the basis of the experimental data to be presented below.

For electrochemical cells of the type

[1] To whom correspondence should be addressed.

Printed in Canada / Imprimé au Canada

Can. J. Chem. Downloaded from www.nrcresearchpress.com by 198.100.157.202 on 09/07/12
For personal use only.

Can. J. Chem. Downloaded from www.nrcresearchpress.com by 198.100.157.202 on 09/07/12
For personal use only.

[7] Pt | R, I_2 || R, I_2, TEAI | Pt
(a) (b)

where the total concentrations of R and I_2 are the same on both sides of the cell, we propose the following virtual electrochemical reactions at the platinum electrodes.

[8] $3I_2(a) + 2e = 2I_3^-(a)$

[9] $2I_3^-(b) - 2e = 3I_2(b)$

The choice of electrode reactions is somewhat arbitrary. Species should be selected which are in reasonably high contration in the solution such as I_2 and I_3^-. The selection of a different pair of electrode reactions will give the same results if it is in accord with the equilibria specified in reactions [2] and [3].

The emf of such a cell is

$$[10] \quad E = -\frac{RT}{2F}\ln\frac{[I_3^-(a)]^2[I_2(b)]^3}{[I_3^-(b)]^2[I_2(a)]^3}$$

B. High concentrations of Ph_3As

The reaction scheme used for high concentration ratios of Ph_3As to I_2 is

[1] $R + I_2 \rightarrow RI_2$

[11] $RI_2 \rightleftharpoons RI^+ + I^-$

The expression for the equilibrium constant corresponding to reaction [11] is

$$[12] \quad K_{11} = \frac{[RI^+][I^-]}{[RI_2]}$$

For electrochemical cells of the type in [7] we propose the electrode reactions

[13] $RI^+(a) + 2e = R(a) + I^-(a)$

[14] $R(b) + I^-(b) - 2e = RI^+(b)$

The expression for the cell emf is

$$[15] \quad E = -\frac{RT}{2F}\ln\frac{[R(a)][I^-(a)][RI^+(b)]}{[R(b)][I^-(b)][RI^+(a)]}$$

The mathematical treatment used to obtain values for K_2, K_3, and K_{11} is discussed in the Appendix.

Results and discussion

A simple, approximate treatment can be performed using data at high iodine concentrations if the only equilibrium reaction of importance is reaction [2]. Such a treatment appears to be appropriate for the reaction between pyridine and iodine. If enough TEAI is added on side b of cell [7], the assumption can be made that reaction [2] is completely suppressed and that the concentration of I_3^- on side b is the total concentration of TEAI, c(TEAI), according to reaction [4]. An approximate form of eq. [10] can then be used.

$$[16] \quad E \approx -\frac{RT}{2F}\ln\frac{[I_3^-(a)]^2}{[I_3^-(b)]^2}$$

where $[I_3^-(a)]$ is the concentration of I_3^- for the intrinsic disociation of the complex according to reaction [2]. Therefore, in each experiment, a value for $[I_3^-(a)]$ can be calculated from the emf value and the value of c(TEAI) by substitution in reaction [16].

Data obtained for various iodine concentrations are shown in Table 1. The dissociation calculated using eq. [16] increases from 18% to 57% as we go from a $c(I_2)/c(Py)$ ratio of 25 to 200. The data in Table 1 do not yield a constant value for the equilibrium constant, K_2, below a $c(I_2)/c(Py)$ ratio of 100. The most probable reason for this is that the assumption that reaction [1] proceeds all the way to the right is not applicable at ratios lower than 100.

TABLE 1. Dependence of the ionic dissociation of the pyridine–iodine complex on the concentration of iodine; $c(Py) = 1.00 \times 10^{-3}$ M, $c(TEAI) = 3.00 \times 10^{-3}$ M

$c(I_2)/c(Py)$	Emf, mV	$[I_3^-]/c(Py)$
25	72.6	0.18
50	59.6	0.29
75	54.8	0.35
100	48.0	0.46
200	—	0.57*

*This value was calculated from the data in Table 2.

TABLE 2. Emf values for pyridine–iodine solutions at high iodine concentration*

$c(Py)$ $M \times 10^3$	$c(TEAI)$ $M \times 10^3$	Emf (mV) Experimental	Emf (mV) Calculated
2.00	0.400	7.5	6.7
2.00	1.00	11.6	11.1
2.00	1.40	15.5	15.1
2.00	2.00	25.2	25.8
1.00	0.400	10.9	10.7
1.00	1.00	21.5	22.3
1.00	1.40	26.1	28.2
1.00	2.00	31.5	35.4

*The total iodine concentration in all these measurements was 0.200 M. The equilibrium constants, K_2, used to calculate the emf values was 3.9×10^{-3}.

In Table 2 are emf data on the interaction between I_2 and Py which were used to calculate the equilibrium constant, K_2. Equations [2] and [5] and the treatment in Appendix A1 were used in this analysis. By computer calculation, using trial values of K_2 and successive approximation (see Appendix A1), a value of K_2 was selected which best fit the experimental emf data. The value selected was 3.9×10^{-3}. On the basis of the sensitivity of the calculated emf values to the choice of the equilibrium constant, the error in K_2 and the other equilibrium constants to be discussed is estimated to be within ±50%.

A check on the validity of the results presented in Tables 1 and 2 was made by comparing the electrical conductivity of a solution containing total concentrations of 2×10^{-1} M I_2 and 1×10^{-3} M TEAI with the conductivity of a solution with total concentrations of 2×10^{-1} M I_2 and 1×10^{-3} M Py. The conductivity values, 2.7×10^{-4} (ohm-cm)$^{-1}$ and 1.4×10^{-4} (ohm-cm)$^{-1}$, respectively, are shown in Table 3. The I_3^- concentrations for the two solutions are calculated to be 1×10^{-3} M and 0.57×10^{-3} M, respectively, on the basis of reactions [4] and [2]. If we make the crude assumption that the ionic conductivities of TEA^+ and PyI^+ are equal, the ratio of conductivities should equal the ratio of I_3^- concentrations. The conductivity ratio, 0.52, is in reasonable agreement with the concentration ratio, 0.57.

The above treatment for the pyridine–iodine system does not fit the data for the iodine complexes of Ph_3Sb and Ph_3As. An

Can. J. Chem. Downloaded from www.nrcresearchpress.com by 198.100.157.202 on 09/07/12
For personal use only.

TABLE 3. Conductivities of iodine solutions

Compound, R	c(R) M × 10^3	$c(I_2)$ M × 10^3	Conductivity $(ohm\text{-}cm)^{-1} \times 10^4$	$[I_3^-]$ M + 10^3
Py	1.00	200	1.4	0.57
TEAI	1.00	200	2.7	1.00
Ph_3Sb	1.00	100	3.2	1.19
TEAI	1.00	100	3.0	1.00
Ph_3As	1.50	150	3.9	1.92
TEAI	1.50	150	4.2	1.50
Ph_3As	500	1.00	0.30	0.12
TEAI	1.00	1.00	2.4	1.00

TABLE 4. Emf values for Ph_3Sb–iodine solutions at high iodine concentration*

c(Py) M × 10	c(TEAI) M × 10^3	Emf (mV) Experimental	Emf (mV) Calculated
1.20	0.200	4.4	3.4
1.20	0.500	8.0	7.9
1.20	0.700	10.6	10.5
1.20	1.00	13.9	14.1
1.00	0.200	4.1	3.6
1.00	0.500	8.3	8.3
1.00	0.700	10.9	11.1
1.00	1.00	14.8	14.8
0.800	0.200	4.2	3.8
0.800	0.500	8.7	8.8
0.800	0.700	11.9	11.7
0.800	1.00	15.5	15.5
0.500	0.200	5.0	4.3
0.500	0.500	11.4	9.6
0.500	0.700	14.3	12.7
0.500	1.00	17.8	16.8

*The total concentration of Ph_3Sb in all these measurements was 1.00×10^{-3} M. The equilibrium constant, K_3, used to calculate the emf values was $2.9 \times 10^{-2}\ M^{-1}$.

additional step, reaction [3], which postulated the existence of a new complex ion, RI_2^{2+}, was, therefore, invoked. The assumptions were made that reactions [1] and [2] proceed completely to the right and that the equilibrium process in reaction [3] is in operation.

In Tables 4 and 5 are emf data on the interaction between iodine and Ph_3Sb and Ph_3As which were used to calculate the equilibrium constant, K_3. Reactions [3] and [6] and the treatment in Appendix A2 were used in this analysis. The values of K_3 which best fit the data were $2.9 \times 10^{-2}\ M^{-1}$ and $3.8 \times 10^{-2}\ M^{-1}$, respectively, for Ph_3Sb and Ph_3As.

A comparison of conductivity data was again made as shown in Table 3. The I_3^- concentration values were calculated using the selected values of the equilibrium constant, K_3. The comparison is more complex than in the case of pyridine because of the presence of the two ionic species, Ph_3MI^+ and $Ph_3MI_2^{2+}$. The agreement between the conductivity ratios and the I_3^- concentration ratios is not as good as in the case of pyridine, especially for Ph_3As. The conductivity data do, at least qualitatively, support the assumption that the complexes are completely ionized.

TABLE 5. Emf values for Ph_3As–iodine solutions at high iodine concentration*

c(Py) M × 10	c(TEAI) M × 10^3	Emf (mV) Experimental	Emf (mV) Calculated
1.50	0.500	5.4	5.2
1.50	0.750	7.5	7.5
1.50	1.50	12.7	13.5
1.50	3.00	22.7	22.7
0.900	0.500	6.2	6.1
0.900	0.750	9.0	8.7
0.900	1.50	15.4	15.4
0.900	3.00	25.6	25.2
0.450	0.500	7.6	6.9
0.450	0.750	9.8	9.8
0.450	1.50	17.6	17.0
0.450	3.00	29.8	27.3

*The total concentration of Ph_3As in all these measurements was 1.50×10^{-3} M. The equilibrium constant, K_3, used to calculate the emf values was $3.8 \times 10^{-2}\ M^{-1}$.

TABLE 6. Emf values for Ph_3As–iodine solutions at high concentrations of Ph_3As*

$c(Ph_3As)$ M	$c(I_2)$ M × 10^3	c(TEAI) M × 10^3	Emf (mV) Experimental	Emf (mV) Calculated
0.500	1.00	0.600	36.5	36.7
0.500	1.00	0.900	48.6	46.0
0.500	1.00	1.80	64.1	63.0
0.500	1.00	3.00	75.0	75.9
0.350	0.500	1.00	58.1	57.1
0.350	0.500	2.00	73.3	74.5
0.350	0.500	3.00	82.6	84.8

*The equilibrium constant, K_{11}, used to calculate the emf values was 2.4×10^{-5} M.

Electrochemical data on the pyridine–iodine system at high ratios of pyridine to iodine were analyzed in a previous report (6) on the basis of the reaction which best fit the data

[17] $2PyI_2 \rightleftharpoons Py_2I^+ + I_3^-$

This reaction step does not appear to be useful in the case of the iodine complexes of Ph_3As and Ph_3Sb. In the case of Ph_3As, reactions [1] and [11] are in best agreement with the data. In the case of Ph_3Sb, the electrochemical data obtained could not be fitted with any simple mechanism and will not be discussed further.

For Ph_3As–I_2 solutions in DCE at concentration ratios of Ph_3As to I_2 of up to several hundred, reaction [2] occurs as well as reaction [11] as evidenced by the reddish-brown color of the solutions and the presence of I_3^- absorption bands in the UV–visible spectrum. At Ph_3As to I_2 concentration ratios of 500 and above, the solutions are colorless and no I_3^- is observed spectrophotometrically, indicating the absence of I_3^-.

Electrochemical data obtained on Ph_3As–I_2 solutions are shown in Table 6. Equations [11] and [12] and the treatment in Appendix B were used to obtain a value for the equilibrium constant, K_{11}. The value selected was 2.4×10^{-5} M. A comparison of conductivity data with an I_2–TEAI solution was

again made as shown in Table 3. The I_3^- concentration ratio, 0.13, is in good agreement with the conductivity ratio, 0.12.

We have observed that at high iodine concentrations Ph_3Sb and Ph_3As form the $Ph_3MI_2^{2+}$ ion as well as the Ph_3MI^+ ion whereas Py only forms the PyI^+ ion. Some factors that may play a roll in this difference of behavior are the differences in molecular geometry and ionization energy and the presence of empty *d* orbitals of fairly low energy in the arsenic and antimony atoms which can result in back-donation (7).

We have also observed that at high organic concentrations Ph_3As forms the I^- ion whereas Py forms the I_3^- ion (6). A probable reason for this difference is that the arsenic compound forms a stronger bond with iodine than the nitrogen compound. A reaction of the type

$$RI^+ + 2I^- \rightarrow R + I_3^-$$

is more likely to occur if the bond between the organic molecule and iodine is weaker.

Acknowledgment

This work was supported in part by the National Institute of General Medical Sciences MARC Program, Grant No. 5T 34 8078-06.

1. K. R. Bhaskar, S. N. Bhat, S. Singh, and C. N. R. Rao. J. Inorg. Nucl. Chem. **28**, 2060 (1966).
2. S. N. Bhat and C. N. R. Rao. J. Am. Chem. Soc. **88**, 3216 (1966).
3. A. D. Beveridge and G. S. Harris. J. Chem. Soc. 6076 (1964).
4. A. D. Beveridge, G. S. Harris, and F. Inglis. J. Chem. Soc. 520 (1966).
5. R. Sahai, P. C. Pande, and V. Singh. Ind. J. Chem. **18**A, 217 (1979).
6. S. Aronson, S. B. Wilensky, T. I. Yeh, D. Degraff, and G. M. Wieder. Can. J. Chem. **64**, 2060 (1986).
7. F. A. Cotton and G. Wilkinson. *In* Advanced inorganic chemistry. 4th ed., John Wiley and Sons, New York, NY. 1980. pp. 438–440.

Appendix. Mathematical treatment to obtain values for the equilibrium constants

A1. High iodine concentrations with reaction [2] as the relevant equilibrium reaction

In this case, eqs. [2] and [5] are the primary equations. For side a of [7] (no added TEAI), we have

$$[RI^+] = [I_3^-] = x$$
$$[RI_2] = c(R) - x$$
$$[I_2] = c(I_2) - c(R) - x$$

The expression for the equilibrium constant, K_2, in eq. [5] becomes

$$[18] \quad K_2 = \frac{x^2}{[c(R) - x][c(I_2) - c(R) - x]}$$

For side b of cell [7] (TEAI added), we have

$$[RI^+] = y$$
$$[I_3^-] = y + c(TEAI)$$
$$[RI_2] = c(R) - y$$
$$[I_2] = c(I_2) - y - c(TEAI) - c(R)$$

The expression for K_2 becomes

$$[19] \quad K_2 = \frac{y[y + c(TEAI)]}{[c(R) - y][c(I_2) - c(R) - y - c(TEAI)]}$$

The electrochemical equation [10] becomes

$$[20] \quad E = -\frac{RT}{F} \ln \frac{x[c(I_2) - y - c(TEAI) - c(R)]^{3/2}}{[y + c(TEAI)][c(I_2) - c(R) - x]^{3/2}}$$

The following algorithm was employed to calculate a value of K_2. An initial value of K_2 was used in the computer program to calculate x and y in eqs. [18] and [19]. A value of E was calculated in eq. [20] using these x and y values. The calculated E was compared to the experimental value of the emf. New values of K_2 were then employed until the calculated and experimental values of the emf were in agreement.

A2. High iodine concentrations with eq. [3] as the relevant equilibrium reaction

In this case, eqs. [3] and [6] are the primary equations. For side a of cell [7], we have

$$[RO_2^{2+}] = x$$
$$[I_3^-] = c(R) + x$$
$$[RI^+] = c(R) - x$$
$$[I_2] = c(I_2) - 2c(R) - 2x \approx c(I_2) - 2c(R)$$

The expression for the equilibrium constant, K_3, in eq. [6] becomes

$$[21] \quad K_3 = \frac{x[c(R) + x]}{[c(R) - x][c(I_2) - 2c(R)]^2}$$

For side b of cell [7], we have

$$[RI_2^{2+}] = y$$
$$[I_3^-] = c(R) + y + c(TEAI)$$
$$[RI^+] = c(R) - y$$
$$[I_2] = c(I_2) - 2c(R) - c(TEAI) - 2y \approx c(I_2) - 2c(R) - c(TEAI)$$

The expression for K_3 becomes

$$[22] \quad K_3 = \frac{y[c(R) + y + c(TEAI)]}{[c(R) - y][c(I_2) - 2c(R) - c(TEAI)]^2}$$

The electrochemical eq. [10] becomes

$$[23] \quad E = -\frac{RT}{F} \ln \frac{[c(R) + x][c(I_2) - 2c(R) - c(TEAI)]^{3/2}}{[c(R) + y + c(TEAI)][c(I_2) - 2c(R)]^{3/2}}$$

A computer program employing an algorithm similar to that described in Appendix A1 was used to calculate values of K_3 from eqs. [21], [22], and [23].

B. High Ph_3As concentrations with eq. [11] as the relevant equilibrium reaction

In this case, eqs. [11] and [12] are the primary equations. For side a of cell [7], we have

$$[I^-] = [RI^+] = x$$
$$[RI_2] = c(I_2) - x$$

The expression for the equilibrium constant, K_{11}, becomes

$$[24] \quad K_{11} = \frac{x^2}{c(I_2) - x}$$

For side b of cell [7], we have

Can. J. Chem. Downloaded from www.nrcresearchpress.com by 198.100.157.202 on 09/07/12
For personal use only.

$$[RI^+] = y$$

$$[I^-] = y + c(TEAI)$$

$$[RI_2] = c(I_2) - y$$

$$[R(a)] \approx [R(b)]$$

The expression for K_{11} becomes

$$[25] \quad K_{11} = \frac{[y + c(TEAI)]y}{c(I_2) - y}$$

The electrochemical equation [15] becomes

$$[26] \quad E = -\frac{RT}{2F} \ln \frac{y}{y + c(TEAI)}$$

A value for y is calculated from each experimental emf value. The equilibrium constant, K_{11}, is then calculated using eq. [25]. An average value of K_{11}, 2.4×10^{-5} M, was used in Table 6.

Can. J. Chem. Downloaded from www.nrcresearchpress.com by 198.100.157.202 on 09/07/12
For personal use only.

Recovery of silica from aqueous silicate solutions via trialkyl or tetraalkylammonium silicomolybdate[1]

A. S. W. DE FREITAS, A. W. MCCULLOCH, AND A. G. MCINNES
Institute for Marine Biosciences, National Research Council of Canada, 1411 Oxford Street, Halifax, N.S., Canada B3H 3Z1

Received August 17, 1990

A. S. W. DE FREITAS, A. W. MCCULLOCH, and A. G. MCINNES. Can. J. Chem. **69**, 611 (1991).

Reaction of aqueous silicate with ammonium molybdate at pH 1.5 affords the β form of silicomolybdic acid. The latter can be precipitated by the addition of a variety of quaternary ammonium salts. The precipitated silicomolybdate can then be decomposed to silica in a two-step combustion process (at 350 and 1000°C). Recoveries of Si are nearly complete, but the starting silicate solution must be made strongly basic prior to the reaction with molybdate. The overall process can be utilized for the recovery of silicon isotopes and as a method of silica purification.

Key words: silica, silicate, silicomolybdate, silicon-29.

A. S. W. DE FREITAS, A. W. MCCULLOCH et A. G. MCINNES. Can. J. Chem. **69**, 611 (1991).

La réaction d'un silicate aqueux avec du molybdate d'ammonium, à un pH de 1,5, conduit à la forme β de l'acide silicomolybdique. On peut le précipiter par addition de divers sels d'ammonium quaternaires. Utilisant un processus de combustion en deux étapes (à 350 et 1000°C), on peut alors décomposer le silicomolybdate précipité en silice. Les récupérations du Si sont pratiquement complètes; toutefois, on doit rendre la solution initiale de silicate très basique avant de la faire réagir avec le molybdate. On peut utiliser ce processus global pour récupérer des isotopes du silicium et pour purifier la silice.

Mots clés : silice, silicate, silicomolybdate, silicium-29.

[Traduit par la rédaction]

Introduction

During the course of a study of the processes involved in silicon biomineralization we conducted a number of biological experiments utilizing ^{28}Si- and ^{29}Si-labeled silica. Since these isotopes are both expensive and relatively difficult to obtain, we required a method to recover the material, typically from dilute aqueous solutions. An initial approach involving methylene chloride extraction of the tetrabutylammonium salt of the silicon–catechol complex was found to be inappropriate for recovery at low (20 ppm or below) Si concentrations.[2]

We now wish to report a successful procedure for removal and recovery of low concentrations of silicate, based on the formation of silicomolybdic acid and its precipitation from aqueous solution by the addition of appropriate organic counterions. Silica of high purity can then be recovered by stepwise combustion of the dried precipitate (1).

The interaction of silicate with molybdate is well-known and forms the basis of the traditional spectrophotometric determination of silicon (2–4), in which silicomolybdate is reduced and the products measured by colorimetric means. The reaction of silicate with ammonium molybdate produces a complex silicomolybdate of composition $H_4SiMo_{12}O_{40}$ (5). Two forms of the silicomolybdate may be obtained, depending on the pH of the reaction. At a pH of about 4 the α form is obtained, while the reaction at lower pH (1.5–2) yields the less stable β form, which has been shown to convert spontaneously to the α form (2, 4).

The silicomolybdate complex is water-soluble, but can be rendered less soluble by addition of a quaternary base. For example, the methyltricotylammonium derivative can be extracted from aqueous solution using chloroform (6). Addition of other bases such as quinoline causes precipitation of the complex, and this procedure has been used for analytical purposes (7–9). In the majority of our experiments we utilized readily available tetrabutylammonium bromide as the source of the organic counterion.

Results and discussion

The approach we have used to recover silicate from dilute aqueous environments consists of (*i*) formation of the β-silicomolybdate at pH 1.5, (*ii*) precipitation from solution as a tetrabutylammonium or analogous organic complex, and (*iii*) thermal decomposition of the complex to silica.

(i) Silicomolybdate formation

The stoichiometric requirements for the formation of $SiMo_{12}O_{40}^{4-}$ involve use of at least two molar equivalents of ammonium molybdate, $(NH_4)_6Mo_7O_{24}\cdot 4H_2O$, per mole of silicate. The following reaction parameters were found to be optimal: (*a*) addition of an excess (a total of 4 molar equivalents per Si); (*b*) immediate acidification to pH 1.5 using 2 N sulfuric acid (the formation of the β-silicomolybdate was indicated by the development of a bright yellow color); and (*c*) allowing the mixture to stand for at least 1 h at room temperature to ensure complete reaction.

(ii) Precipitation of tetraalkylammonium silicomolybdate

The second step of the procedure requires the addition of sufficient tetraalkylammonium halide to precipitate the silicomolybdate as $(R_4N)_4SiMo_{12}O_{40}$. The reaction of excess halide reagent with unreacted molybdate affords tetraalkylammonium molybdate, which co-precipitates. Such a co-precipitate may be of value as a carrier in the case of low Si concentrations, where the volume of precipitated silicomolybdate is small. We observed essentially quantitative precipitation when the concentration of Bu_4NBr was 12 molar equivalents per Si (i.e. 3 molar equivalents per molybdate). The precipitated solid was washed with 1 N nitric acid (to remove any adsorbed inorganic impurities) and with deionized water, and dried.

The completeness of the precipitation process was indicated by the fact that only trace levels of Si were observed in the reaction filtrate and washings.

[1]NRCC No. 31962.

[2]A. S. W. deFreitas, A. W. McCulloch, A. G. McInnes, A. Rogerson, and J. A. Walter. Unpublished work.

Can. J. Chem. Downloaded from www.nrcresearchpress.com by 198.100.157.202 on 09/07/12
For personal use only.

TABLE 1. Recovery of Si from basic and acidic media

Si concentration in substrate μg/100 mL	% Si recovery	
	From basic substrate	From acidified substrate
4000	97	59
2000	94	64
800	92	61
400	91	51
200	92	49

(iii) Recovery of silica from tetraalkylammonium silicomolybdate

Thermal degradation of the organic derivative was best conducted in a two-step combustion process. The solid was first heated to 350°C and this temperature maintained for 20 min. This served to break down the organic component (about 35% weight loss was observed) in a controlled fashion. The second stage of the combustion procedure involved raising the temperature to 1000°C, just below sintering temperature, and holding at that temperature for 1 h. Above 800°C molybdenum oxide sublimed. In a series of reactions involving original Si concentrations of 2–40 ppm the colorless silica residue represented an overall recovery (Table 1) of 90–95%.

Effect of pH

We observed that the Si recovery was dependent on the history of the starting silicate solution. When acidified silicate solutions were employed using the standard conditions outlined above, the observed silica recoveries were only 49–64% (Table 1). The availability of Si for reaction with molybdate is clearly pH-dependent. Thus, intended substrates should be made strongly basic prior to reaction with molybdate. Under such conditions the predominant orthosilicate species is available for reaction; in more acidic solutions the silicate is in equilibrium with a mixture of oligomeric species, the composition of which is pH- and concentration-dependent (10).

Alternative counterions

Although the majority of our reactions were conducted using tetrabutylammonium bromide as the source of the organic counterion, we have established that a variety of simpler and more economical alternatives may be employed with equal success. In principle any tetraalkylammonium salt containing C_1 to C_4 alkyl groups can be used. We have shown that good recoveries are obtained using tetramethylammonium bromide, tetraethylammonium bromide, and even triethylamine hydrochloride. Interestingly, triethylammonium molybdate is water-soluble, and in this case the precipitate is predominantly the silicomolybdate derivative (see Experimental).

Silica purification

Our procedure for silica recovery and purification has several advantages: (*1*) The precipitation of silicomolybdate is practically quantitative, even at relatively low Si concentrations, and can be accomplished using a wide variety of quaternary ammonium salts. (*2*) Most contaminants remain in aqueous solution and are removed by filtration, while others are removed by acid washing. (*3*) The organic component is eliminated by combustion at 350°C, and molybdenum oxide sublimes at 800–1000°C. (*4*) Although elements such as phosphorus and arsenic, which form isomorphous derivatives, $H_3PMo_{12}O_{40}$ and $H_3AsMo_{12}O_{40}$ (6), will also be precipitated under similar conditions, the oxides of these elements are much more volatile than silica and hence are removed during combustion. A potential problem exists in the case of germanium. With the use of a ^{68}Ge tracer we have shown that complete precipitation of the analogous germanomolybdate occurs under similar reaction conditions.

TABLE 2. Trace elements in biosilica before and after purification

Element	Concentration, μg/g			
	Neutron activation		ICP	
	Before	After*	Before	After*
Ag	100	ND	—	—
Al	1440	220	126	ND
Ba	100	ND	47	ND
Ca	880	ND	758	ND
Cu	—	—	229	ND
Fe	3330	1000	2071	53
Mg	1650	ND	1517	ND
Mn	55	20	109	10
P	—	—	2042	163
Pb	—	—	269	ND
Ti	470	ND	—	—
Zn	500	ND	385	ND

*ND = not detected.

As an example we have applied the overall process to a crude biogenic silica sample obtained from diatom biomass. Neutron activation analyses of the starting material and recovered product (Table 2) indicated large scale removal of many elements. Similar results were observed when the original and product silicas were fused with sodium carbonate and aqueous solutions of the fusion products analyzed by ICP (Table 2).

After we had completed this work, a similar approach, designed for desilicification of water, was reported in the patent literature (11). In that case the α-silicomolybdate or silicotungstate was formed at a pH below 3.9 and was then either precipitated by one of a variety of ways, such as addition of a cationic surfactant (e.g. hexadecyl pyridinium salt) or an organic base, or adsorbed on an anion exchanger (loaded with dihexadecyldimethylammonium ion) or extracted into an organic solvent (e.g. trioctylamine in kerosene).

Although more exhaustive experimentation is required to fully demonstrate the usefulness of our procedure to silica purification, it is eminently suited to the recovery of costly Si isotopes or the removal and concentration of small quantities of Si from aqueous solution. We have in fact applied the process to recover silica from isotopically enriched silicate solutions.

Experimental

Sodium metasilicate, $Na_2SiO_3 \cdot 5H_2O$, and ammonium molybdate, $(NH_4)_6Mo_7O_{24} \cdot 4H_2O$, were obtained from BDH. Anhydrous sodium carbonate was obtained from Merck. Germanium dioxide (99.999%), tetraethylammonium bromide (99+%), tetramethylammonium bromide (98%), tetrabutylammonium bromide (99%), and tetrabutylammonium hydrogen sulfate were obtained from Aldrich Chemical Co. Triethylamine hydrochloride was prepared from triethylamine and recrystallized from acetonitrile. The ^{68}Ge tracer (as the chloride) was obtained from New England Nuclear.

Deionized water obtained from a Milli-Q water purification system (Millipore) was used for preparation of aqueous solutions and for aqueous washings. For Si analysis, the pH of the analyte was adjusted to 8–9 prior to analysis using the procedure of Smith and Milne (3).

Can. J. Chem. Downloaded from www.nrcresearchpress.com by 198.100.157.202 on 09/07/12
For personal use only.

Can. J. Chem. Downloaded from www.nrcresearchpress.com by 198.100.157.202 on 09/07/12
For personal use only.

Procedure for optimal recovery of silica from dilute aqueous silicate solutions

(*a*) *Formation of silicomolybdate*

A solution of $Na_2SiO_3 \cdot 5H_2O$ (120.6 g, 0.00056 mol, 16 mg Si) in water (100 mL) was treated with ammonium molybdate (2.83 g, 0.00228 mol) in water (120 mL). The pH was adjusted to 1.5 with 2 N sulfuric acid (10.4 mL), and the reaction mixture stirred for 1 h at room temperature. A yellow color indicated formation of silicomolybdic acid.

(*b*) *Precipitation of tetrabutylammonium silicomolybdate*

The mixture from (*a*) was treated with a solution of tetrabutylammonium bromide (2.216 g, 0.00688 mol) in water (40 mL). This caused the precipitation of yellow tetrabutylammonium silicomolybdate. Colorless tetrabutylammonium molybdate was also formed as a result of reaction between the excess ammonium molybdate and tetrabutylammonium bromide, and co-precipitated. The mixture was allowed to stand overnight to ensure complete precipitation. The precipitated yellow solid was then filtered (the filtrate was colorless), washed successively with water (70 mL), 1 N nitric acid (3 × 30 mL), and water (4 × 30 mL), and then air-dried at 45°C. Total Si in the filtrate and washings, as measured by the spectrophotometric method, was only 50 μg.

(*c*) *Combustion of precipitate and recovery of silica*

The dry solid (3.1 g) from (*b*) was placed in a quartz or platinum boat and combusted in air. The temperature was first raised (30°/min) to 350°C and maintained at that temperature for 20 min, to eliminate the organic component and to produce a greyish solid residue. (Uncontrolled and violent decomposition of the material may occur if the temperature is raised too quickly to above 400°C). The combustion temperature was then increased (30°/min) from 350 to 1000°C and held at 1000°C for 60 min to allow complete volatilization of molybdenum oxide (>800°C), leaving a white silica residue (33.2 mg).

(*d*) *Analysis of residue*

The silica residue from (*c*) was fused with sodium carbonate prior to the determination of Si by the colorimetric molybdate method.

Tetrabutylammonium hydrogen sulfate could be substituted for the Bu_4NBr used in step (*b*).

Recoveries at various Si concentrations

(*a*) Aliquots (10, 5, 2, 1, and 0.5 mL) of a stock solution of Na_2SiO_3 (760 mg) in water (250 mL) were diluted to 100 mL to give substrate solutions containing 4000, 2000, 800, 400, and 200 μg (40–2 ppm) Si, respectively. Each aliquot was treated with a solution of ammonium molybdate (707 mg) in water (30 mL), acidified to pH 1.5 with 2 N sulfuric acid and stirred for 1 h. Each mixture was then treated with Bu_4NBr (554 mg) in water (10 mL) and allowed to stand for 24 h.

The resulting precipitate was recovered and combusted as described above, and the residue fused with sodium carbonate. The fusion product was dissolved in water and the solution analyzed for Si by the molybdate colorimetric method. The results are recorded in Table 1.

(*b*) A solution of $Na_2SiO_3 \cdot 5H_2O$ (1.52 g) in water (250 mL) was acidified to pH 2 with 2 N sulfuric acid and the volume made up to 500 mL with deionized water.

Aliquots (10, 5, 2, 1, and 0.5 mL) of this acidified silicate solution were diluted to 100 mL to give substrate solutions containing 4000, 2000, 800, 400, and 200 μg (40–2 ppm) Si, respectively. Each aliquot was processed as in (*a*) above. Si recovery data are given in Table 1.

Recoveries using different counterions

Solutions of $Na_2SiO_3 \cdot 5H_2O$ (121 mg) in water (100 mL) were treated with ammonium molybdate (2.83 g) in water (60 mL) and acidified to pH 1.5. After 1 h each mixture was treated with a solution of (*i*) tetramethylammonium bromide (1.058 g), (*ii*) tetraethylammonium bromide (1.444 g), or (*iii*) triethylamine hydrochloride (944 mg) in water (10 mL). The yellow precipitates were processed and combusted as before to yield residues of colorless silica (Table 2). Recoveries of Si were in the range 97–100%.

Purification of biogenic silica

Detergent-cleaned diatom biomass (about 1 g dry weight) was combusted at the non-sintering temperature of 800°C for 5 h to remove organic material. The resultant "biosilica" (250 mg) was fused with sodium carbonate (1 g) and the fused material dissolved in deionized water (150 mL). Spectrophotometric analysis showed a Si level of 716 μg/mL.

This solution (100 mL) was diluted with water (100 mL) and then treated with ammonium molybdate (14.14 g) in water (100 mL). The mixture was acidified to pH 1.5 with 2 N sulfuric acid (44 mL). After stirring for 1 h, a solution of Bu_4NBr (11.08 g) in water (50 mL) was added and the mixture stirred overnight at room temperature. The precipitate was filtered, washed with 0.5 N sulfuric acid (100 mL) and then water (300 mL), and finally dried at 50°C to give a solid (18.06 g).

The above solid (16.325 g) was combusted as before in a platinum crucible in small (ca. 1.7 g) portions, to give a solid residue (142 mg). Direct analyses of the original and product silica samples were performed by neutron activation. Inductively-coupled plasma (ICP) emission spectroscopic analyses were performed in each case after sodium carbonate fusion. The analytical results are recorded in Table 2.

Recovery of silicon-29 labelled silica

A colorless silica was obtained when a basic solution of products from ^{29}Si labelling experiments was submitted to the above recovery process.

Other products

(*i*) *Tetrabutylammonium molybdate*

The pH (5.0) of a solution of ammonium molybdate (2.47 g) in water (40 mL) was adjusted to 1.5 by the addition of 2 N sulfuric acid (2.7 mL). The mixture was stirred for 1 h and then treated with Bu_4NBr (3.87 g) in water (60 mL). After stirring overnight the precipitated solid was filtered, washed with water (15 mL) and dried at 45°C to give the product (3.68 g).

(*ii*) *Tetrabutylammonium germanomolybdate*

A solution of sodium germanate was prepared by dissolving GeO_2 (209 mg, 0.002 mol) in NaOH (160 mg) in water (40 mL). This was treated with ammonium molybdate (4.94 g, 0.004 mol) in water (60 mL) and the pH adjusted to 1.5 with 2 N sulfuric acid (9 mL). The mixture was then treated as in (*i*) above to give the product (6.62 g).

A similar experiment was conducted in the presence of a ^{68}Ge tracer. No ^{68}Ge was observed in the reaction filtrate, establishing the completeness of the precipitation process.

(*iii*) *Tetraethyl and triethylammonium molybdate*

The pH of each of two solutions of ammonium molybdate (1.414 g) in water (30 mL) was adjusted to 1.5 with 2 N sulfuric acid (8 mL), and the solutions then treated with (*a*) Et_4NBr (722 mg), or (*b*) Et_3NHCl (566 mg) in water (10 mL). The addition of water (100 mL) followed by shaking left most of the Et_4N molybdate precipitate undissolved, while the addition of only 50 mL caused dissolution of all of the Et_3N molybdate.

Acknowledgments

We gratefully acknowledge the excellent technical assistance of Margaret Flack and John van Ingen. We also thank Bill Hardstaff for ICP measurements, and Dr. J. Holzbecher of the Trace Analysis Research Centre, Dalhousie University, for neutron activation analyses.

1. A. S. W. DEFREITAS, A. W. MCCULLOCH, and A. G. MCINNES. U.S. Patent No. 4,885,149 (Dec. 5, 1989); Canadian application (525427) filed Dec. 16, 1986.
2. J. D. H. STRICKLAND. J. Am. Chem. Soc. **74**, 862 (1952); **74**, 868 (1952); **74**, 872 (1952); Chem. Ind. 393 (1950).
3. J. D. SMITH and P. D. MILNE. Anal. Chim. Acta, **123**, 263 (1981).
4. V. W. TRUESDALE and C. J. SMITH. Analyst, **100**, 203 (1975); **101**, 19 (1976).

5. H. ICHIDA, A. KOBAYASHI, and Y. SASAKI. Acta Crystallogr. Sect. B, B**36**, 1382 (1980).
6. H. AKAIWA, H. KAWAMOTO, and T. TAKENOUCHI. Nippon Kagaku Kaishi, 833 (1980); Chem. Abstr. **93**: 60360x.
7. M. M. PIRYUTKO, N. V. BENEDIKTOVA, and L. F. KORSAK. Steklo Keram. 30 (1981); Chem. Abstr. **95**: 143516v.
8. A. M. G. MACDONALD and F. H. VAN DER VOORT. Analyst, **93**, 65 (1968).
9. C. C. MILLER and R. A. CHALMERS. Analyst, **78**, 24 (1953).
10. R. K. ILER. The chemistry of silica. Solubility, polymerization, colloid and surface properties, and biochemistry. Wiley, New York. 1979.
11. K. HECKMAN and M. JONKE. German DE Patent No. 3,602,183; 27 May, 1987.

Can. J. Chem. Downloaded from www.nrcresearchpress.com by 198.100.157.202 on 09/07/12
For personal use only.

Rotational isomerism in fluorene derivatives. XX.[1] Conformational equilibria of 9-substituted 9-(*o*-methylthiomethylphenyl)- and 9-substituted 9-(*o*-methylsulfinylmethylphenyl)fluorenes

AKIKO NISHIDA, YOSHIFUMI AKAGAWA, SHINSUKE SHIRAKAWA, SHIZUO FUJISAKI, AND SHOJI KAJIGAESHI[2]
Department of Industrial Chemistry, Faculty of Engineering, Yamaguchi University, Tokiwadai, Ube, Japan 755

Received February 9, 1990[3]

AKIKO NISHIDA, YOSHIFUMI AKAGAWA, SHINSUKE SHIRAKAWA, SHIZUO FUJISAKI, and SHOJI KAJIGAESHI. Can. J. Chem. **69**, 615 (1991).

Several 9-substituted 9-(*o*-methylthiomethylphenyl)fluorenes and their oxidation products, 9-substituted 9-(*o*-methylsulfinylmethylphenyl)fluorenes, were prepared. Each equilibrium constant at room temperature or at low temperature was investigated and the conformational equilibria (*ap* ⇌ *sp*) of these compounds are discussed by comparing them with those of the corresponding 9-substituted 9-(*o*-methylthiophenyl)fluorenes and 9-substituted 9-(*o*-methylsulfinylphenyl)fluorenes in which the *o*-substituents were one CH_2 unit shorter than those of the title compounds. Kinetic data for the internal rotation of several compounds are also given.

Key words: conformational isomerism, restricted rotation, 9-arylfluorenes.

AKIKO NISHIDA, YOSHIFUMI AKAGAWA, SHINSUKE SHIRAKAWA, SHIZUO FUJISAKI et SHOJI KAJIGAESHI. Can. J. Chem. **69**, 615 (1991).

On a préparé plusieurs 9-(*o*-méthylthiométhylphényl)fluorènes substitués en position 9 ainsi que leurs produits d'oxydation, les 9-(*o*-méthylsulfinylméthylphényl)fluorènes substitués en position 9. On a étudié chacune des constantes d'équilibre, tant à la température ambiante qu'à basse température, et on discute des équilibres conformationnels (*ap* ⇌ *sp*) en les comparant à ceux des 9-(*o*-méthylthiométhylphényl)- et des 9-(*o*-méthylsulfinylméthylphényl)-fluorènes substitués en position 9 dans lesquels les *o*-substituants portaient une unité CH_2 de moins que ceux mentionnés dans le titre. On rapporte aussi les données cinétiques relatives à la rotation interne de plusieurs composés.

Mots clés : isomérie conformationnelle, rotation limitée, 9-arylfluorènes.

[Traduit par la rédaction]

Introduction

Because the barriers to rotation about the C(9)—C(Ar) bond in 9-arylfluorene derivatives are remarkably high, some interesting stereochemical studies have been carried out on these systems (2). In connection with 9-substituted 9-(*o*-substituted phenyl)fluorenes, we have investigated the effects of 9- or *o*-substituents on the restricted rotation and the conformational equilibria (*ap* ⇌ *sp*) (3) of these compounds by means of their ^{1}H NMR spectra (1, 4–12).

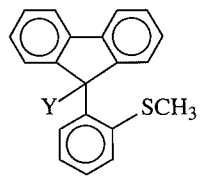
It turned out that the conformational equilibria of these compounds were affected by nonbonding intramolecular interactions (electronic attraction, repulsion, and steric effect, etc.) between the *o*-substituents and the 9-groups or the fluorene ring.

We recently investigated the restricted rotation about the C(9)—C(Ar) bonds in 9-substituted 9-(*o*-methylthiophenyl)-fluorenes (**1**) and their oxidation products, 9-substituted 9-(*o*-methylsulfinylphenyl)fluorenes (**2**) (8). In this paper, we wish to report on the syntheses of some 9-substituted 9-(*o*-methylthiomethylphenyl)fluorenes (**3**) and 9-substituted 9-(*o*-methylsulfinylmethylphenyl)fluorenes (**4**), and to discuss the conformational equilibria of these compounds compared with those of **1** and **2**. As well, we give the activation parameters determined by line-shape analyses of the signals of *o*-substituents in their dynamic ^{1}H NMR spectra (13).

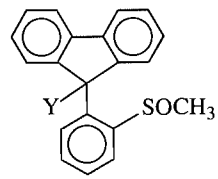
Results and discussion

Preparation of 9-substituted 9-(o-methylthiomethylphenyl)-fluorenes (3) and 9-substituted 9-(o-methylsulfinylmethyl-phenyl)fluorenes (4)

The compound, 9-(*o*-bromomethylphenyl)-9-fluorenol (**6**),



1



2

was prepared by the reaction of 9-(*o*-tolyl)-9-fluorenol (**5**) with NBS in carbon tetrachloride (7). The reaction of **6** with hydriodic acid in acetic acid gave 9-(*o*-iodomethylphenyl)-fluorene (**7**) (7). The reaction of an isothiouronium salt, which was obtained by treatment of **7** with thiourea in methanol, with aqueous sodium hydroxide followed by methylation with dimethyl sulfate, afforded 9-(*o*-methylthiomethylphenyl)-fluorene (**3***a*). The compound **3***a* was converted to 9-(*o*-methylsulfinylmethylphenyl)fluorene (**4***a*) by oxidation with nitric acid ($d = 1.38$). 9-Lithio-9-(*o*-methylthiomethylphenyl)fluorene (**8**) was prepared by the reaction of **3***a* with butyllithium in ether under a nitrogen atmosphere. Bubbling oxygen into the ethereal solution of **8** gave 9-(*o*-methylthiomethylphenyl)-9-fluorenol (**3***b*); then, **3***b* was oxidized by nitric acid to give 9-(*o*-methylsulfinylmethylphenyl)-9-fluorenol (**4***b*). 9-Methyl-9-(*o*-methylthiomethylphenyl)fluorene (**3***c*) was obtained from **8** and methyl iodide; then, **3***c* was converted into 9-methyl-9-(*o*-methylsulfinylmethylphenyl)fluorene (**4***c*) by oxidation with nitric acid.

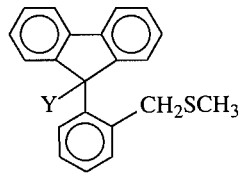
9-Acetyl- (**3***d*) and 9-benzoyl-9-(*o*-methylthiomethylphenyl)-fluorene (**3***e*) were obtained by treating the lithio compound **8** with acetic anhydride and benzoyl chloride, respectively. Then, **3***d* and **3***e* were treated with nitric acid to give 9-acetyl- (**4***d*) and 9-benzoyl-9-(*o*-methylsulfinylmethylphenyl)fluorene (**4***e*), respectively. 9-(*o*-Methylthiomethylphenyl)-9-fluorenecarboxylic acid (**3***f*) was prepared by the reaction of **8** with Dry Ice in ether.

[1]The preceding article in this series is ref. 1.
[2]Author to whom correspondence may be addressed.
[3]Revision received November 28, 1990.

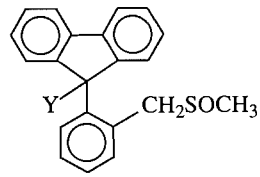
Printed in Canada / Imprimé au Canada

Can. J. Chem. Downloaded from www.nrcresearchpress.com by 198.100.157.202 on 09/07/12
For personal use only.

TABLE 1. Syntheses of 9-substituted 9-(*o*-methylthiomethylphenyl)fluorenes **3** and 9-substituted 9-(*o*-methylsulfinylmethylphenyl)fluorenes **4**



3



4

Compound	Y	Melting point (°C)	Yield (%)	Compound	Y	Melting point (°C)	Yield (%)
3*a*	H	72–74	77	**4***a*	H	148–150	75
3*b*	OH	124–126	29	**4***b*	OH	81–83	82
3*c*	CH_3	90–92	28	**4***c*	CH_3	137–139	48
3*d*	$COCH_3$	40–42	74	**4***d*	$COCH_3$	98–100	79
3*e*	COPh	56–58	71	**4***e*	COPh	154–155	63
3*f*	COOH	184–186	62				

TABLE 2. ^{1}H NMR and IR spectral data of **3** and **4** at room temperature

	^{1}H NMR ($CDCl_3$): δ (ppm)					
	o-Substituent					
Compound	CH_2	CH_3	6′-H	9-Substituent	Aromatics	IR(KBr) cm^{-1}
3*a*	*ap*: 2.48s(1)[a] *sp*: 4.10s(5)	1.30s(1)[a] 2.17s(5)	6.36d	4.96s(1) 5.56s(5)	6.7–7.8m	
3*b*	3.14br s	1.56br s	8.0br.s	2.76br s	7.1–7.8m	3340(OH)
3*c*	2.49s	1.28s	7.90d	1.74s	7.0–7.9m	
3*d*	3.22br s	1.76br s		1.94s	7.0–7.9m	1765(CO)
3*e*	3.68s	1.92s			6.8–8.3m	1660(CO)
3*f*	2.95br s	1.50br s			7.1–7.8m	2880(OH) 1690(CO)
4*a*	*ap*: 2.62d[b] (Ha)(1) 2.94d[b] (Hb)(1) *sp*: 4.30d[b] (Ha)(1.1) 4.44d[b] (Hb)(1.1)	1.60s(1) 2.54s(1.1)	6.36d	4.90s(1) 5.34s(1.1)	6.9–7.8m	1030(SO)
4*b*	3.4–5.2br s	2.3br s			6.9–7.9m	3200(OH) 1010(SO)
4*c*	2.76d[b] (Ha) 2.96d[b] (Hb)	1.78s	7.94d	1.78s	7.0–7.8m	1030(SO)
4*d*	2.98d[b] (Ha) 3.25d[b] (Hb)	1.82s		2.04s	7.2–8.0m	1700(CO) 1030(SO)
4*e*	3.22d[b] (Ha) 3.38d[b] (Hb)	1.90s			7.2–7.8m	1670(CO) 1040(SO)

[a]Approximate intensity ratios of a pair of the signals are given in parentheses.
[b]J = 13–15 Hz.

The melting points, yields, and spectral data (^{1}H NMR and IR) of these compounds **3** and **4** are shown in Tables 1 and 2.

Conformational equilibria of 3 and 4

Generally, two rotamers *ap* and *sp* of 9-(*o*-substituted phenyl)fluorenes are observed via their ^{1}H NMR spectra at room temperature or at low temperature, because of their high barriers to rotation about the C(9)—C(Ar) bond. In fact, as shown in Table 2, two signals (*ap* and *sp*) from the methylthiomethyl group of **3***a* and also from the methylsulfinylmethyl group of **4***a* are observed at room temperature. The isomerization process of **3***a* by the rotation about C(9)—C(Ar) bond is shown in Fig. 1.

As shown in Table 2, the methylene protons of the methylsulfinylmethyl groups in **4** give rise to two doublets in their ^{1}H NMR spectra at room temperature. These phenomena show that the sulfur atom of the methylsulfinyl group ($SOCH_3$) is a chiral center.

Since the predominant conformations of **3** and **4** (except **3***a* and **4***a*) were not elucidated on the basis of their ^{1}H NMR spectra at room temperature (see Table 2), dynamic NMR spectra of these compounds were measured. ^{1}H NMR data for the *o*-substituents in these compounds at low temperatures are shown in Table 3.

For compounds **3***c*, **4***c*, **4***d*, and **4***e*, the chemical shifts of

Can. J. Chem. Downloaded from www.nrcresearchpress.com by 198.100.157.202 on 09/07/12
For personal use only.

TABLE 3. ^{1}H NMR data of *o*-substituents in **3***b*–**3***f* and **4***b*–**4***e* at low temperature (δ, ppm; $CDCl_3$)

Compound		CHaHb	CH_3	Temperature (°C)
3*b*	*ap*:	2.65s(3.7)	1.26s(3.7)	−43
	sp:	4.48br s(1)	2.14s(1)	
3*c*		2.50s	1.30s	−50
3*d*	*ap*:	2.56br s	1.18s(1)	−57
	sp:	3.82 br d[a] (Ha), 3.94br d[a] (Hb)	2.36s(1.5)	
3*e*	*ap*:	2.80br s(1)	1.26br s(1)	−64
	sp:	4.06br s(2.1)	2.30br s(2.1)	
3*f*	*ap*:	2.60br s(2.6)	1.24br s(2.6)	−53
	sp:	4.30br s(1)	2.12br s(1)	
4*b*	*ap*:	2.98br s	1.74br s(1)	−48
	sp:	4.54br d[a] (Ha), 5.32br d[a] (Hb)	2.64br s(1.7)	
4*c*		2.88d[a] (Ha), 3.06d[a] (Hb)	1.80s	−50
4*d*		2.80br d[a] (Ha), 3.12br d[a] (Hb)	1.78br s	−62
4*e*		3.14br s	1.78br s	−57

[a] J = 13–15 Hz.

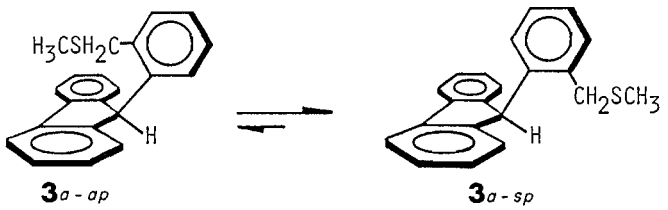


FIG. 1. Two rotamers of **3***a*.

their methyl and methylene protons are approximate, as are those for the methylthiomethyl proton of **3***a*–*ap* and the methylsulfinylmethyl proton of **4***a*–*ap*; these signals do not split even at −50 to −62°C (see Table 3). Thus, these results indicate that steric repulsion between the 9-substituents (CH_3, $COCH_3$, and COPh) and the *o*-substituents in **3***c*, **4***c*, **4***d*, and **4***e* makes the equilibria *ap* ⇌ *sp* shift exclusively to the *ap* form.

Two conformers *ap* and *sp* of **3***b*, **3***d*, **3***e*, **3***f*, and **4***b* were observed at low temperatures (see Table 3). Because compound **3***b* shows the equilibrium constant K as ap/sp = 3.7/1 at −43°C, the predominant conformer of **3***b* is the *ap* form. Thus, steric repulsion between the 9-hydroxyl and *o*-methylthiomethyl groups in the *sp* form may be larger than that between the fluorene nucleus and the *o*-methylthiomethyl group in the *ap* form, which controls the equilibrium of **3***a* ($K(ap/sp)$ = 1/5). On the contrary, however, the predominant conformer of **4***b* is the *sp* form ($K(ap/sp)$ = 1/1.7 at −48°C). We hypothesize that a dipole – lone pair electron attractive interaction between the methylsulfinylmethyl and hydroxyl groups exists in the *sp* form of **4***b*. We recently reported the same interaction between methylsulfinyl and hydroxyl groups in the *sp* form of 9-(*o*-methylsulfinylphenyl)-9-fluorenol **2***b* (8).

The predominant conformers of **3***d* and **3***e* at low temperature are the *sp* forms (**3***d*: $K(ap/sp)$ = 1/1.5, **3***e*: $K(ap/sp)$ = 1/2.1). We have recently shown that derivatives of 9-substituted 9-(*o*-methoxyphenyl)- (**9**) (5) and 9-(*o*-methylthiophenyl)-fluorenes (8), in which 9-substituents bear carbonyl groups such as $COCH_3$ and COPh, have an intramolecular attractive interaction between the carbonyl and the methoxyl or methylthio groups. Oki *et al.* have already shown that the same interaction exists in several 1,4-dimethoxy-9-(carbonylmethyl)triptycenes (**10**) (14) (Fig. 2). Thus, it is reasonable that a dipole – lone pair electron interaction between the carbonyl and methylthio groups in **3***d* and **3***e* makes the *sp* form more predominant.

It is particularly interesting that the methylene protons of the methylthiomethyl group in **3***d*-*sp* give rise to two doublets at low temperature (see Table 3). In the *sp* form of **3***d*, a dipole – unshared electron interaction between the carbonyl and methylthio groups, shown in Fig. 3, makes the sulfur atom a chiral center. Thus, the two protons of the methylene group may be revealed as diastereomeric protons. These phenomena have been observed for the *sp* form of 9-benzoyl-9-(*o*-methoxymethylphenyl)fluorene (**11***e*) at low temperature (7) as shown in Fig. 3.

In compound **3***f*, the predominant conformer is the *ap* form at low temperature ($K(ap/sp)$ = 2.6/1). Steric repulsion between the 9-carbonyl and *o*-methylthiomethyl groups in the *sp* form may control its equilibrium.

The rotational barriers about the C(9)—C(Ar) bonds in **3** and **4** were obtained by line-shape analyses of the methylthio and methylsulfinyl signals in their DNMR spectra. The results are tabulated, together with those for **1** and **2**, in Table 4.

From the values $K(ap/sp)$ in Table 4, it is noted that the equilibrium *ap* ⇌ *sp* in **3** and **4** (except for **3***c* and **4***c*) shifts predominantly to the *ap* form compared with the corresponding results for **1** and **2**, respectively. For example, in compounds **1***d*, **1***e*, **1***f*, **2***d*, and **2***e*, only the *sp* forms are detected, even at low temperature. However, in compounds **3***d*, **3***e*, **3***f*, **4***d*, and **4***e*, the *ap* forms are present along with the *sp* forms at low temperature. It seems that because the *o*-substituents in **3** or **4** are longer than the *o*-substituents of **1** or **2** because of one additional CH_2 moiety, the mobility of the *o*-substituents should increase. Thus, an attractive interaction between the *o*-substituents and 9-substituents (Y) of **3** or **4** may be reduced, in comparison with that of **1** or **2**.

Experimental

All melting points are uncorrected. The ^{1}H NMR spectra were recorded on a Jeol-MH-100 spectrometer with a Jeol model JES-VT-3 variable temperature controller. The chemical shifts are expressed in ppm, with tetramethylsilane as an internal standard. Dynamic NMR spectra were analyzed by using a modified version of the computer program DNMR 3 (13).

Can. J. Chem. Downloaded from www.nrcresearchpress.com by 198.100.157.202 on 09/07/12
For personal use only.

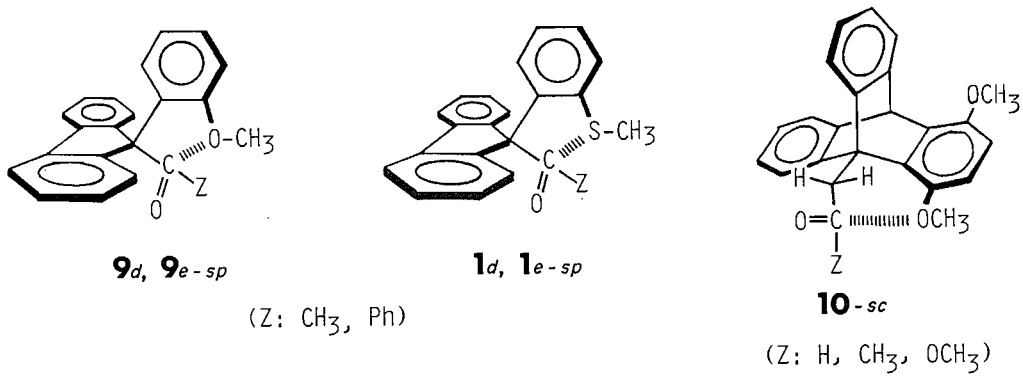


FIG. 2. Attractive interaction between carbonyl and OCH_3 or SCH_3.

TABLE 4. Activation free energies for rotation about C(9)—C(Ar) bonds and *ap*/*sp* ratios of **3**, **4**, **1**, and **2** at 25°C

			$\Delta G\neq$ (kcal[a] mol^{-1})				$\Delta G\neq$ (kcal mol^{-1})	
Y	Compound	$K(ap/sp)$	$ap \rightarrow sp$	$sp \rightarrow ap$	Compound	$K(ap/sp)$	$ap \rightarrow sp$	$sp \rightarrow ap$
H	**3***a*	1/5.0	16.2	17.1	**1***a*	1/14	—	—
OH	**3***b*	3.8/1	13.4	12.6	**1***b*	2.0/1[b]	14.3	14.0
CH_3	**3***c*	*ap* only	—	—	**1***c*	*ap* only	—	—
$COCH_3$	**3***d*	1/1.5[b]	—[c]	—[c]	**1***d*	*sp* only	—	—
COPh	**3***e*	1/2.1[b]	11.1	11.5	**1***e*	*sp* only	—	—
COOH	**3***f*	2.6/1[b]	13.5	12.9	**1***f*	*sp* only	—	—
H	**4***a*	1/1.1	18.0	18.0	**2***a*	1/1.5[b]	15.3	15.5
OH	**4***b*	1/1.7[b]	13.8	14.1	**2***b*	1/4.0[b]	13.5	14.3
CH_3	**4***c*	*ap* only	—	—	**2***c*	*ap* only	—	—
$COCH_3$	**4***d*	*ap* pre.[d]	—	—	**2***d*	*sp* only	—	—
COPh	**4***e*	*ap* pre.[d]	—	—	**2***e*	*sp* only	—	—

[a]1 cal = 4.18 J.
[b]*K* value was observed at low temperature.
[c]Because the 9-acetyl proton prevented the line-shape analysis of the methylthio signal in its DNMR spectrum, the activation parameter for rotation about the C(9)—C(Ar) single bond was not obtained.
[d]pre. = predominant.

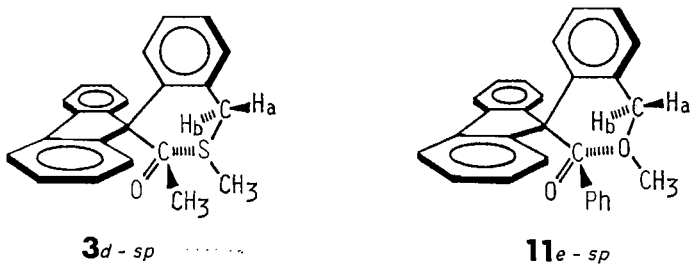


FIG. 3. Attractive interaction between carbonyl and CH_2OCH_3 or CH_2SCH_3.

9-(o-Methylthiomethylphenyl)fluorene (3a)

A solution of 9-(*o*-iodomethylphenyl)fluorene (**7**) (5 g, 13.1 mmol) and thiourea (1.3 g, 17.1 mmol) in methanol (40 mL) was refluxed for 5 h. After the solvent was distilled off, the isothiouronium salt obtained was dissolved in aqueous sodium hydroxide (10%) and the mixture was stirred for 30 min under a nitrogen atmosphere. Dimethyl sulfate (2.38 g, 19.7 mmol) was added dropwise to the above mixture and the precipitated solid was extracted with benzene. The benzene solution was washed with water, and then dried over $MgSO_4$. The solution was evaporated *in vacuo*, leaving a residue that was column-chromatographed on silica gel using carbon tetrachloride as eluent to give **3***a*; yield 3.06 g (77%); colorless crystals (from benzene–hexane); mp 72–74°C. Anal. calcd. for $C_{21}H_{18}S$: C 83.42, H 6.00%; found: C 83.35, H 6.03.

9-(o-Methylthiomethylphenyl)-9-fluorenol (3b)

9-Lithio-9-(*o*-methylthiomethylphenyl)fluorene (**8**) was prepared from the reaction of **3***a* (1 g, 3.3 mmol) in dry ether (30 mL) with a commercial solution of butyllithium in hexane (3.25 mL, containing 5 mmol of butyllithium) under a nitrogen atmosphere. Dry oxygen gas was bubbled into the above solution for 10 min. The reaction mixture was poured into water, and the organic layer was separated, washed with water, and dried over $MgSO_4$. The solution was evaporated *in vacuo*, leaving a residue that was column-chromatographed on silica gel using carbon tetrachloride as an eluent to give **3***b*; yield 0.3 g (29%); colorless needles; mp 124–126°C (from hexane). Anal. calcd. for $C_{21}H_{18}OS$: C 79.21, H 5.70; found: C 78.75, H 5.83.

9-Methyl-9-(o-methylthiomethylphenyl)fluorene (3c)

To a solution of **8** prepared from **3***a* (0.9 g, 3.0 mmol) in dry ether (40 mL) was added methyl iodide (0.68 g, 4.8 mmol) dropwise. The mixture was stirred for 30 min and was then poured into water. The organic layer was separated, washed with water, and dried over $MgSO_4$. The solution was evaporated *in vacuo*, leaving a residue that was column-chromatographed on silica gel using carbon tetrachloride as eluent to give **3***c*; yield 0.26 g (28%); colorless needles; mp 90–92°C (from benzene–hexane). Anal. calcd. for $C_{22}H_{20}S$: C 83.51, H 6.31; found: C 83.47, H 6.47.

9-Acetyl-9-(o-methylthiomethylphenyl)fluorene (3d)

To a solution of **8** prepared from **3***a* (0.6 g, 2.0 mmol) in ether was added a solution of acetic anhydride (2.7 mL, 2.6 mmol) in dry ether (20 mL) under cooling at −10°C; the mixture was stirred for 30 min and was then poured into water. The organic layer was worked up as

Can. J. Chem. Downloaded from www.nrcresearchpress.com by 198.100.157.202 on 09/07/12
For personal use only.

described for the preparation of **3***c*, to give **3***d* as colorless prisms; yield 0.51 g (74%); mp 42–44°C. Anal. calcd. for $C_{23}H_{30}OS$: C 80.19, H 5.85; found: C 79.72, H 5.96.

9-Benzoyl-9-(o-methylthiomethylphenyl)fluorene (3e)

Compound **8** prepared from **3***a* (2.0 g, 6.6 mmol) was reacted with benzoyl chloride (1.4 mL, 9.9 mmol) instead of acetic anhydride; the reaction mixture was worked up as described for the preparation of **3***d*, to give **3***e* as colorless prisms; yield 1.91 g (71%); mp 56–58°C. Anal. calcd. for $C_{28}H_{22}OS$: C 82.72, H 5.46; found: C 82.38, H 5.57.

9-(o-Methylthiomethylphenyl)-9-fluorenecarboxylic acid (3f)

A solution of compound **8** from **3***a* (0.61 g, 2.0 mmol) in ether was poured into crushed Dry Ice and stirred for 30 min. The mixture was poured into dilute HCl solution. The organic layer was worked up as described for the preparation of **3***c*, to give **3***f* as colorless needles; yield 0.43 g (62%); mp 184–186°C (from hexane). Anal. calcd. for $C_{22}H_{18}O_2S$: C 76.28, H 5.24; found: C 76.56, H 5.39.

9-Substituted 9-(o-methylsulfinylmethylphenyl)fluorenes (4a–4d)

9-(o-Methylsulfinylmethylphenyl)fluorene (4a)

To a solution of **3***a* (0.25 g, 0.79 mmol) in acetic acid (30 mL) was added nitric acid (d = 1.39, 0.5 mL) dropwise at 18°C with stirring. After being stirred at 15–18°C for 5 h, the reaction mixture was poured into cold water. The precipitated solid was extracted with benzene. The benzene solution was washed with a $NaHCO_3$ solution and water, and then dried over $MgSO_4$. The solvent was distilled off to obtain a residue that recrystallized from hexane–benzene (1:1) to give **4***a* as colorless prisms; yield 0.20 g (75%); mp 148–150°C. Anal. calcd. for $C_{21}H_{18}OS$: C 79.22, H 5.70; found: C 79.44, H 5.75.

9-(o-Methylsulfinylmethylphenyl)-9-fluorenol (4b)

Colorless prisms (from hexane–benzene 1:1), yield 82%; mp 81–83°C. Anal. calcd. for $C_{21}H_{18}O_2S$: C 75.42, H 5.42; found: C 75.83, H 5.36.

9-Methyl-9-(o-methylsulfinylmethylphenyl)fluorene (4c)

Colorless needles (from hexane), yield 48%; mp 137–139°C. Anal. calcd. for $C_{22}H_{20}OS$: C 79.49, H 6.06; found: C 79.34, H 5.99.

9-Acetyl-9-(o-methylsulfinylmethylphenyl)fluorene (4d)

Colorless prisms (from hexane–chloroform 1:1), yield 79%; mp 98–100°C. Anal. calcd. for $C_{23}H_{20}O_2S$: C 76.63, H 5.59; found: C 76.21, H 5.70.

9-Benzoyl-9-(o-methylsulfinylmethylphenyl)fluorene (4e)

Colorless prisms (from hexane–benzene 1:1), yield 64%; mp 154–155°C. Anal. calcd. for $C_{28}H_{22}O_2S$: C 79.59, H 5.25; found: C 79.59, H 5.25.

Acknowledgements

The authors wish to thank Professor Massashi Tashiro, Institute of Advanced Material Study, Kyushu University, for the elemental analyses.

1. A. Nishida, M. Takeshita, T. Harada, S. Fujisaki, and S. Kajigaeshi. Nippon Kagaku Kaishi, 945 (1990).
2. M. Ōki. Application of dynamic NMR spectroscopy to organic chemistry. VCH Publishers, Deerfield Beach, FL. 1985. p. 211.
3. IUPAC 1968 Tentative Rules, Sect. E: Fundamental Stereochemistry. J. Org. Chem. **35**, 2849 (1970).
4. A. Nishida, S. Watanabe, S. Fujisaki, H. Hara, and S. Kajigaeshi. Nippon Kagaku Kaishi, 1148 (1983).
5. A. Nishida, S. Shiwaku, S. Fujisaki, and S. Kajigaeshi. Nippon Kagaku Kaishi, 574 (1984).
6. A. Nishida, M. Takeshita, S. Fujisaki, and S. Kajigaeshi. Nippon Kagaku Kaishi, 1791 (1987).
7. A. Nishida, S. Shirakawa, S. Fujisaki, and S. Kajigaeshi. Kogakubu Kenkyu Hokoku (Yamaguchi Daigaku), **38**, 269 (1988).
8. A. Nishida, M. Takeshita, S. Fujisaki, and S. Kajigaeshi. Bull. Chem. Soc. Jpn. **61**, 1195 (1988).
9. A. Nishida, M. Takeshita, S. Fujisaki, and S. Kajigaeshi. Bull. Chem. Soc. Jpn. **61**, 3919 (1988).
10. A. Nishida, S. Shirakawa, T. Harada, S. Fujisaki, and S. Kajigaeshi. Tech. Rep. Yamaguchi Univ. **4**, 145 (1988).
11. A. Nishida, M. Takeshita, N. Kawano, S. Fujisaki, and S. Kajigaeshi. Bull. Chem. Soc. Jpn. **62**, 1093 (1989).
12. A. Nishida, S. Shirakawa, M. Yamamoto, S. Watanabe, S. Fujisaki, and S. Kajigaeshi. Bull. Chem. Soc. Jpn. **62**, 2093 (1989).
13. G. Binsch. J. Am. Chem. Soc. **91**, 1304 (1969).
14. M. Ōki, G. Izumi, G. Yamamoto, and N. Nakamura. Bull. Chem. Soc. Jpn. **55**, 159 (1982).

Can. J. Chem. Downloaded from www.nrcresearchpress.com by 198.100.157.202 on 09/07/12
For personal use only.

The proximate coupling constant, $^5J(H,CH_3)$, and the torsional mobility of the thiomethyl group in some thioanisole derivatives

TED SCHAEFER,[1] RUDY SEBASTIAN, SALMAN R. SALMAN, JAMES D. BALEJA, GLENN H. PENNER, and DAVID M. MCKINNON

Department of Chemistry, University of Manitoba, Winnipeg, Man., Canada R3T 2N2

Received September 17, 1990

TED SCHAEFER, RUDY SEBASTIAN, SALMAN R. SALMAN, JAMES D. BALEJA, GLENN H. PENNER, and DAVID M. MCKINNON. Can. J. Chem. **69**, 620 (1991).

The proximate coupling constants, ^5J, between *ortho* and methyl protons in thioanisole and 18 of its derivatives are discussed as conformational indicators. On the assumption that ^5J varies as $\cos^4\theta$, for $0° \leq \theta \leq 90°$, θ being the angle by which the methyl group twists out of the aromatic plane, ^5J for $\theta = 0°$ follows as -0.43 (2) Hz from the known internal barrier in thioanisole in solution. A measurement of ^5J in *meta*- or *para*-substituted thioanisole derivatives then yields an approximate value for the twofold barrier to rotation about the Csp^2—S bond. For derivatives containing an *ortho* substituent, ^5J yields an estimate of the torsion angle for the thiomethyl moiety. In some instances these angles are compared with those derived from long-range $^1H,^{13}C$ and $^{13}C,^{13}C$ coupling constants. The size of the *ortho* substituent appears to have only a small effect on the magnitude of ^5J. The major determinant of the latter appears to be the manner in which the substituent perturbs the mobile bond order of the Csp^2—S bond.

Key words: spin–spin coupling constants, thioanisole derivatives; ^1H NMR, thioanisole derivatives; conformations, thioanisole derivatives; conformations, torsional motion of SCH_3 group.

TED SCHAEFER, RUDY SEBASTIAN, SALMAN R. SALMAN, JAMES D. BALEJA, GLENN H. PENNER et DAVID M. MCKINNON. Can. J. Chem. **69**, 620 (1991).

On discute de l'utilité, comme indicateurs conformationnels, des constantes de couplage approximatives, ^5J, entre les protons *ortho* et ceux du méthyle du thioanisole et de 18 de ses dérivés. En faisant l'hypothèse que les valeurs de ^5J varient en fonction du $\cos^4\theta$, pour $0° \leq \theta \leq 90°$, où θ est l'angle entre le groupement méthyle et le plan du noyau aromatique, et en se basant sur la barrière interne connue du thioanisole en solution, ^5J pour $\theta = 0°$ est égal à $-0,143(2)$Hz. Une mesure de ^5J pour des dérivés du thioanisole substitués en *méta* ou en *para* fournit alors une valeur approximative de la barrière binaire à la rotation autour de la liaison Csp^2—S. Pour des dérivés contenant un substituant en *ortho*, la valeur de ^5J fournit une évaluation de l'angle de torsion de la portion thiométhyle. Dans quelques cas, on a pu comparer ces angles avec ceux dérivés des constantes de couplage à longue distance $^1H,^{13}C$ et $^{13}C,^{13}C$. La grosseur des substituants *ortho* ne semble avoir qu'une faible influence sur l'amplitude de ^5J. Le facteur déterminant de cette amplitude semble être la façon dont le substituant perturbe l'ordre de liaison mobile de la liaison Csp^2—S.

Mots clés : constantes de couplage spin–spin, dérivés du thioanisole; RMN ^1H, dérivés du thioanisole; conformations, dérivés du thioanisole; conformations, mouvement de torsion du groupe SCH_3.

[Traduit par le rédaction]

Introduction

While the conformational applications of the proximate proton–proton coupling constant over five formal bonds, $^5J(H,OCH_3)$, in anisole and its derivatives have been discussed in some detail (1–12), the analogous coupling constant, $^5J(H,SCH_3)$, in thioanisole has received relatively little attention.

An early experiment (13) implied the possible dependence of the magnitude of $^5J(H,SCH_3)$ on the size of the substituent, X, in 2-X-thioanisole derivatives. Presumably the bulky substituent forces a close approach of the methyl group to the *ortho* C—H bond in the ring, increasing the efficiency of a proximate (3, 9, 10, 14) or through-space coupling mechanism. By analogy to $^5J(H,OCH_3)$, such a mechanism would yield a negative $^5J(H,SCH_3)$. Indeed, this coupling constant was shown to be negative in 2,5-dichlorothioanisole (15), with a magnitude of $-0.352(9)$ Hz. This magnitude is twice as large as that reported (13) for 2-chlorothioanisole. It was suggested (8) that the *meta* substituent in 2,5-dichlorothioanisole could favor a more closely planar orientation of the SCH_3 group, as compared to 2-chlorothioanisole, thereby causing a larger coupling magnitude in the former compound. The barrier to rotation about the Csp^2—S bond in thioanisole is not large (16) and very likely 5–6 kJ/mol in solution (17, 18), in line with such a suggestion. Furthermore, it is known that $^5J(H,SCH_3)$ is not detectable when the SCH_3 is held in a plane perpendicular to that of the aromatic moiety (19), again implying its sensitive dependence on a proximate coupling mechanism.

In addition to the bulk of the *ortho* substituent, causing increased coplanarity of the thiomethyl group, the π acceptance or donation of the substituents should also play a role. Because the thiomethyl group is a π electron donor, a π electron acceptor placed *ortho* or *para* to it will increase the mobile bond order of, and therefore the internal barrier to rotation about, the Csp^2—S bond. The concomitant, larger, population of planar conformers at ambient temperatures entails a smaller average distance between the coupled protons in question and hence a larger magnitude of $^5J(H,SCH_3)$. A π electron-donating substituent, clearly, should cause a decrease in the magnitude of the coupling constant. The predictions about the perturbation of the internal barriers in thioanisole derivatives are borne out by deductions based on measurements of $^5J(^{13}C,^{13}C)$ and $^6J(H,^{13}C)$; these coupling constants involve a ^{13}C nucleus in the methyl group (17, 18). The change in the barrier caused by *meta* substituents can be rationalized with a perturbational approach to molecular orbital theory (20), as for the corresponding derivatives of thiophenol (21).

Because of the sensitivity of the magnitudes of proximate coupling constants to the separation between the atoms or bonds carrying the coupled nuclei (3, 9, 10, 14), the disentanglement

[1]Author to whom correspondence may be addressed.

Can. J. Chem. Downloaded from www.nrcresearchpress.com by 198.100.157.202 on 09/07/12
For personal use only.

Can. J. Chem. Downloaded from www.nrcresearchpress.com by 198.100.157.202 on 09/07/12
For personal use only.

TABLE 1. The ^{1}H nmr spectral parameters for 2-chlorothioanisole as a 2.0 mol% solution in acetone-d_6 at 300 K

Parameter	Value	Parameter	Value
$\nu(CH_3)$	750.387(1)[a,b]	$^5J_{36}$	0.349(1)
ν_3	2216.567(1)	^5J(H-6,CH_3)	−0.382(1)
ν_4	2145.946(1)	^6J(H-3,CH_3)[c]	0.063(1)
ν_5	2199.718(1)	^6J(H-5,CH_3)[c]	0.094(1)
ν_6	2189.031(1)	^7J(H-4,CH_3)[d]	−0.065(1)
$^3J_{34}$	7.962(1)	Calcd. transitions	260
$^3J_{45}$	7.423(1)	Assigned transitions	205
$^3J_{56}$	7.991(1)	No. of peaks	110
$^4J_{35}$	1.359(1)	Largest difference	0.014
$^4J_{46}$	1.490(1)	Root-mean-square deviation	0.004_7

[a]In Hz at 300.135_2 MHz to high frequency of internal tetramethylsilane, present at 0.5 mol%.
[b]Numbers in parentheses are standard deviations in the last significant figure.
[c]These coupling constants correlate with each other by 0.30.
[d]Correlates with $\nu(CH_3)$ by 0.15.

of steric or compressional from conjugational contributions to ^5J(H,SCH_3) can be beset with ambiguity. It turns out that, for many *ortho* substituents, the steric factor is not large, contrary to earlier reports.

Experimental

Those thioanisole derivatives not available commercially were obtained by methylation (22) of the commercial thiophenol derivative or were prepared from the corresponding commercial anilines by treatment of the aqueous diazonium hydrosulfate salt with cuprous methylmercaptide, as developed in this laboratory (23).

The ^{1}H nmr spectra were accumulated on a Varian HA100 or on Bruker WH 90 and AM 300 nmr spectrometers by methods described in detail previously (24, 25) and at probe temperatures ranging between 293 and 305 K. Tables 1 and 2 give conditions of solvents and concentrations. All sample tubes were, of course, degassed by at least four freeze–pump–thaw cycles and were flame-sealed.

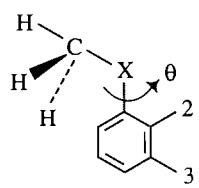
The ^{1}H nmr spectra were analyzed with the computer program NUMARIT (26), greatly modified by R. Sebastian.

Results and discussion

Table 1 reproduces, as an example of the spectral analytical results, the ^{1}H nmr spectral parameters for 2-chlorothioanisole in acetone-d_6 solution. Figure 1 displays the experimental and theoretical spectra for the methyl protons of this compound, illustrating the attainable spectral quality.

The value of $^5J(H,SCH_3)$ in planar thioanisole

As a proximate coupling constant, ^5J(H,SCH_3) is expected to be small in magnitude unless the *ortho* C—H bond is close to the methyl group. For anisole, X = O in **1**, the INDO MO FPT



1

computations (3) for ^5J(H-6, OCH_3) are closely proportional (4) to $\cos^4\theta$ for $0° \leq \theta \leq 60°$. Furthermore, ^5J(H-2,OCH_3) in **1** (X = O) appears to be inconsequential in size in this range of θ (3, 6, 7). By analogy, we shall assume that ^5J(H,SCH_3) ≡ ^5J behaves in a similar manner.[2] A value of ^5J at θ = 0° can be estimated as follows.

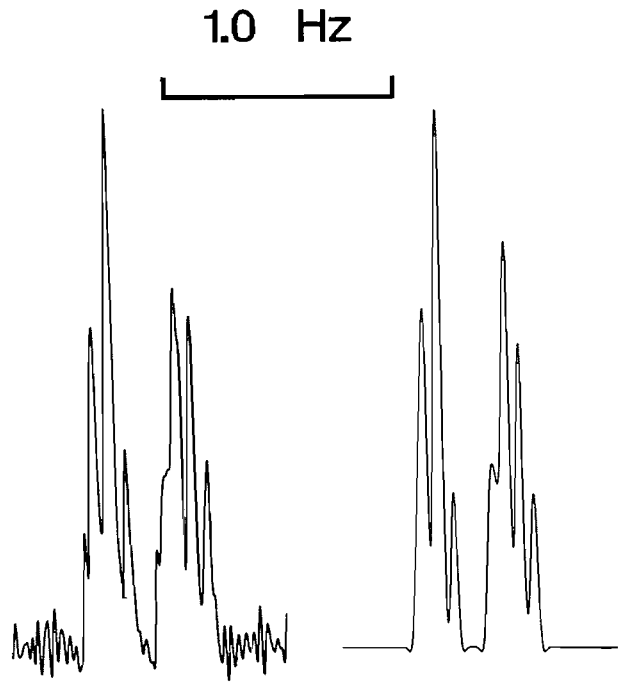


FIG. 1. The ^{1}H nmr spectrum of the methyl protons of 2-chlorothioanisole, as a 2.0 mol% solution in acetone-d_6 at 300 K and 300.135 MHz, is compared with the spectrum computed with the spectral parameters given in Table 1. The existence of coupling constants between the methyl protons and all four ring protons, together with the second-order nature of the ring proton spectrum, accounts for the appearance of the displayed peaks; none of the splittings is equal to a coupling constant.

For thioanisole in benzene-d_6 solution, ^5J(H,SCH_3) ≡ ^5J is −0.141 (0) Hz (27) and is −0.137 (0) Hz in acetone-d_6. Now, on the basis of $^6J(H,S^{13}CH_3)$ and $^5J(^{13}C,^{13}C)$ for thioanisole-α-^{13}C in benzene-d_6 (17) and acetone-d_6 (18) solutions, the twofold barrier to rotation about the Csp^2—S bond has been estimated to lie between 5.1 and 6.5 kJ/mol. That the barrier is predominantly twofold is attested by STO-3G MO computations on a series of *para*-substituted thioanisole derivatives (29), which find V_2 in thioanisole as 6.0(2) kJ/mol and V_4 as 0.4(2) kJ/mol. A classical calculation then yields the expectation value, $\langle\cos^4\theta\rangle$, as 0.64(3) at 300 K for the preceding range of twofold barriers. We have assumed that $^5J = {}^5J_0\langle\cos^4\theta\rangle$, where $^5J_0$ is the magnitude of ^5J at θ = 0°, this equation holding up to a θ of 60° and, trivially, up to 90° if ^5J is indeed a proximate coupling constant. Hence $^5J_0$ follows as $2J/\langle\cos^4\theta\rangle$, that is, as $2(-0.139(2))/0.64(3)$ or −0.43(2) Hz in thioanisole; the multiplier, 2, occurs because the conformation with θ = 0° has twofold degeneracy and ^5J is assumed to vanish for the remote *ortho* proton.

[2]For the STO 3G MO geometry (17) of planar thioanisole, ^5J is computed (unpublished work in this laboratory) as −0.59 Hz and is sensitive to the bond angles at sulfur, for example, as expected for a proximate coupling constant. However, there is a paucity of structural data for thioanisole compared to anisole (3) derivatives (the CSC bond angle is 102.6° for the STO-3G planar, but is apparently 105.6(7)° for the nonplanar, molecule according to electron diffraction data (28)). Accordingly, the empirical procedure in the text is probably more reliable.

Can. J. Chem. Downloaded from www.nrcresearchpress.com by 198.100.157.202 on 09/07/12
For personal use only.

TABLE 2. Values of $^5J(H,CH_3)$ and estimates of nonplanarity for some thioanisole derivatives

Compound	$-^5J(H,SCH_3)$(Hz)	arc cos$\langle\cos^4\theta\rangle^{1/4}$(deg)	arc sin$\langle\sin^2\theta\rangle^{1/2}$(deg)
1. Thioanisole	0.140(0),[a] 0.137(0)[b]	26(1)[l,m]	31(1),[c] 29(1)[d]
2. 4-NO_2	0.178(4)[b]	18(2)	17(1)[d]
3. 4-OCH_3	0.093(1)[e]	37(1)	36(3)[d]
4. 3,5-di-Cl	0.166(6)[b]	20(3)	23(2),[c] 21(1)[d]
5. 2-F	0.281(2)[e]	26(2)	34(1)[d]
6. 2-Cl	0.382(1)[f]	14(3)	—
7. 2-Br	0.387(2)[b]	13(3)	<14[d]
8. 2-I	0.394(1)[b]	12(3)	—
9. 2-Cl-5-Cl	0.35(2)[g]	18(3)	—
10. 2-Cl-4-NH_2	0.16(2)[h]	39(3)	—
11. 2,4,5-tri-Cl	0.412(1)[b]	8	—
12. 2-Br-5-Br	0.382(4)[i]	14(4)	—
13. 2-Br-4-F	0.347(2)[b]	18(2)	—
14. 2-OCH_3	0.24(2)[i]	30(3)	32(1)[d]
15. 2-CH_3-4-OH	0.20(2)[j]	34(3)	—
16. 2-CH_3-3-F	0.334(9)[b]	20(3)	—
17. 2-NH_2	<0.05[i]	>54	~65[d]
18. 2-OH	<0.03[g]	>60	~90[d]
19. 2-CHO	0.341(3)[k]	19(2)	—

[a]For a 2.0 mol% solution in benzene-d_6 (27).
[b]For a 2.4 mol% solution in acetone-d_6.
[c]From $^6J(H,^{13}CH_3)$ for a benzene-d_6 solution (17).
[d]From $^nJ(^{13}C,^{13}C)$, n = 3,4,5, in an acetone-d_6 solution (18).
[e]For a 5.0 mol% solution in acetone-d_6.
[f]See Table 1.
[g]5 mol% in CCl_4.
[h]3 mol% in $CDCl_3$.
[i]3 mol% in CCl_4.
[j]3 mol% in benzene-d_6.
[k]4 mol% in CCl_4. See ref. 33 for a discussion of the conformation of the carbonyl group.
[l]These angles follow from $2 \times {}^5J(H,CH_3) = -0.43(2)\langle\cos^4\theta\rangle$ for *ortho*-substituted derivatives. See text.
[m]It must be remembered that the torsion angles derived from arc cos $\langle\cos^4\theta\rangle^{1/4}$ and arc sin$\langle\sin^2\theta\rangle^{1/2}$ are the same only by coincidence. See text.

Some tests and applications of $^5J = -0.43(2)\langle\cos^4\theta\rangle$

For a vanishing barrier to rotation about the Csp^2—S bond, $\langle\cos^4\theta\rangle$ is 0.375, so that the minimum magnitude of ^5J in, say, a *para*-substituted thioanisole derivative is predicted as −0.081(4) Hz. If the conformation of minimum energy has $\theta \sim 90°$, and is very stable compared to kT, as in 2-hydroxythioanisole (19), then, according to the present formulation, ^5J should vanish, as it appears to do (19), unless another coupling mechanism is present. In 2-aminothioanisole it has been argued, on the basis of $^5J(^{13}C,^{13}C)$, that the S—C bond twists out of the aromatic plane by about 65° on average (18), a consequence of optimal hydrogen bonding between the N—H bond of the "bent" amino group and the 3p lone pair on the sulfur atom. For a 3 mol% solution of this molecule in CCl_4, our measurements imply ^5J as <0.05 Hz in magnitude, in line with a $\cos^4$ 65° of 0.03. In this situation, of course, one has $^5J = -0.43(2)\langle\cos^4\theta\rangle$ and the expectation value of $\cos^4\theta$ depends on the stability of the conformation with $\theta \sim 65°$. Nevertheless, the measurement is consistent with the $\cos^4\theta$ dependence of ^5J.

For 4-nitrothioanisole, the twofold barrier to rotation about the Csp^2—S bond has been assessed as 16.1 ± 1.5 kJ/mol in an acetone-d_6 solution (18). Hence $\langle\cos^4\theta\rangle$ at 300 K is 0.85(2). ^5J follows as $-0.43(2) \times 0.85(2)/2$ or −0.18(1) Hz; it is measured as (−)0.178(4) for a 2 mol% solution in acetone-d_6.

For 4-methoxythioanisole, the internal barrier appears (18) to be 0.7 ± 0.4 kJ/mol in acetone-d_6 solution; $\langle\cos^4\theta\rangle$ at 300 K is calculated as 0.41(2). ^5J follows as −0.09(1) Hz. It is measured as (−)0.093(1) Hz for a 5.0 mol% solution in acetone-d_6. Figure 2 displays the ^{1}H nmr spectrum of the thiomethyl protons under double resonance conditions and its caption describes the analytical procedure.

Again, the internal barrier in 3,5-dichlorothioanisole lies between 9.0 and 12.4 kJ/mol in acetone-d_6 solution (17, 18), corresponding to a $\langle\cos^4\theta\rangle$ of 0.77(3) at 300 K and hence a ^5J of $-0.16_5 \pm 0.015$ Hz. It is measured as −0.166(6) Hz in this solvent.

Because of its nature as a proximate interaction, ^5J in symmetrical *meta*- and *para*-substituted thioanisole derivatives is rather small in magnitude, being an average of a sizeable number and one which appears to be very small and assumed as zero. Consequently, very precise analyses of rather high resolution spectra (Fig. 1) are necessary if an estimate of the internal barrier is to follow from ^5J. Measurements of splittings in the ^{1}H nmr spectrum of the methyl protons do not necessarily yield ^5J, first because of the second-order nature of the ring proton spin system and, second, because the presence of coupling constants over six and seven formal bonds with other ring protons (Table 1) complicates the analysis.

However, if ^5J is extracted by an analysis of ^{1}H nmr spectra of sufficient quality, then it appears that reasonably accurate barriers to rotation about the Csp^2—S bond will follow.

Torsional mobility of the SCH_3 *group in thioanisole derivatives with one* ortho *substituent*

In 2-X-thioanisole derivatives, ^5J will be rather larger in magnitude, the remote *ortho* proton being absent. However, the

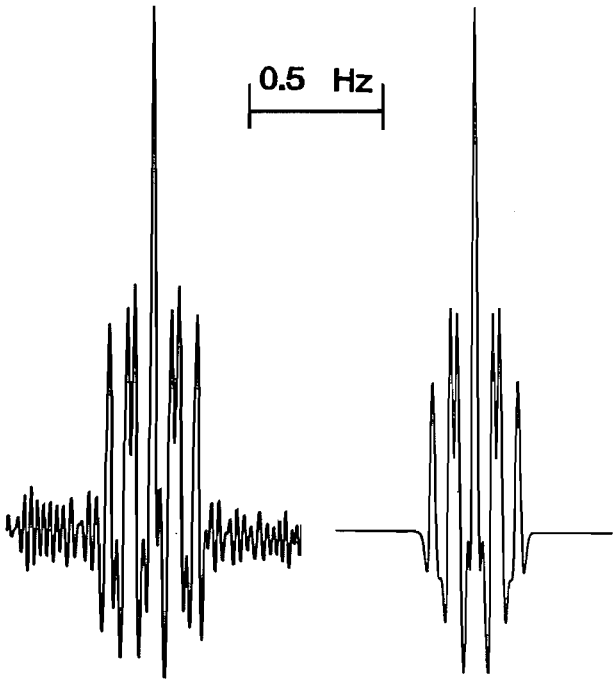
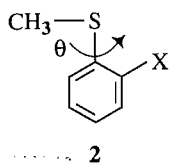


FIG. 2. The ^{1}H nmr spectrum of the thiomethyl protons is shown for a 5.0 mol% solution of 4-methoxythioanisole at 300 MHz and 300 K. $^5J(H,SCH_3)$ is $-0.093(1)$ Hz and $^6J(H,SCH_3)$ is 0.069(1) Hz, as obtained from a complete analysis of the spectrum in which the methoxy protons are decoupled. The simulated spectrum assumes a linewidth at half-height of 0.02 Hz and the experimental parameters used in resolution enhancement procedures on the free induction decay. The acquisition time of the latter is 60 s.

internal rotational potential is not easily determinable; presumably it will contain at least sizeable one- and twofold components, the former corresponding to the energy difference between the two planar conformers, the latter to the $3p\ldots\pi$ conjugation in the Csp^2—S bond. In the absence of reliable magnitudes for these components, recourse is had here to a comparison of estimates of the average out-of-plane motion of the SCH_3 group in the, at ambient temperatures, predominant conformer, **2**.



2

$^5J(^{13}C,^{13}C)$ yields an estimate (18) of $\langle\sin^2\theta\rangle$, whereas $^5J(H,SCH_3)$ indicates $\langle\cos^4\theta\rangle$ if X does not cause a significant compression of the CSC bond angle. For *some* of these expectation values, it happens that arc sin $\langle\sin^2\theta\rangle^{1/2}$ and arc cos $\langle\cos^4\theta\rangle^{1/4}$ are reasonable approximations to the expectation value of θ itself. For example, for a symmetrically substituted thioanisole and a V_2 of 16.0 kJ/mol, at 300 K one has $\langle\theta\rangle$ as 14°, arc sin $\langle\sin^2\theta\rangle^{1/2}$ as 17°, and arc cos $\langle\cos^4\theta\rangle^{1/4}$ as 16°, whereas for a V_2 of 8.0 kJ/mol, these angles are 22°, 26°, and 23°, respectively. As another example, in 2-bromothioanisole (18), $\langle\sin^2\theta\rangle$ is $<0.05_5$, corresponding to $<13.6°$ at 300 K for the torsion angle. $^5J(H,SCH_3)$ is $-0.387(2)$ Hz; hence $\langle\cos^4\theta\rangle$ is 0.90(4) and the arc cos value is 13 ± 3°. Table 2 gives some torsion angles derived in this fashion for a variety of thioanisole derivatives.

Conclusions

The coupling constants and approximate torsion angles, as defined in Table 2, lead to the following conclusions. First, π electron-donating (accepting) substituents in the *para* or *ortho* position decrease (increase) the mobile bond order of the Csp^2—S bond and cause smaller (larger) magnitudes of ^5J and the corresponding larger (smaller) torsion angles about this bond (entries 2, 3, 5, 14). Second, such substituents act in this manner in the *para* position also in the presence of *ortho* substituents (entries 10, 13, 15 in Table 2). Third, the compressional or steric perturbation of ^5J of an *ortho* substituent is not marked (entries 5, 6, 7, 8, 16), the rather lower magnitude of ^5J in 2-fluoroanisole arguably being due in some part to the π electron donation by fluorine (compare entries 7 and 13). Fourth, the dipole moments of 2-chloro- and of 2,4-dichlorothioanisole (30) should probably be reinterpreted in terms of the torsional angles in Table 2. Fifth, the value of -0.43 Hz in 2-nitrothioanisole (13) possibly indicates some steric compression of the thiomethyl group. This compression may, however, not be as large as implied by models because (31, 32) the nitro group twists out of the benzene plane in many *ortho* derivatives of nitrobenzene, thereby decreasing its effective size. Sixth, the steep dependence of ^5J on the torsion angle disallows the use of the latter for conformational deductions when, as in the 2-amino and 2-hydroxy derivatives, stereospecific intramolecular O—H...3*p* and N—H...3*p* hydrogen bonds cause very large out-of-plane torsion of the thiomethyl group (entries 17 and 18). Seventh, while ^5J is in principle available from a precise analysis of the ^{1}H nmr spectrum of a thioanisole derivative and is therefore a widely available conformational indicator, the less accessible $^6J(H,SCH_3)$ and $^nJ(^{13}C,^{13}C_3)$ are, of course, necessary for the di-*ortho*-substituted derivatives.

Acknowledgements

We are grateful to the National Sciences and Engineering Research Council of Canada for financial assistance.

1. R. W. CRECELY, K. W. MCCRACKEN, and J. H. GOLDSTEIN. Tetrahedron, **25**, 877 (1969).
2. H. A. GAUR, J. VRIEND, and W. G. B. HUYSMANS. Tetrahedron Lett. 199 (1969).
3. T. SCHAEFER and R. LAATIKAINEN. Can. J. Chem. **61**, 224 (1983).
4. T. SCHAEFER, S. R. SALMAN, T. A. WILDMAN, and G. H. PENNER. Can. J. Chem. **63**, 782 (1985), and references therein.
5. T. SCHAEFER and R. SEBASTIAN. J. Magn. Reson. **73**, 541 (1987), and references therein.
6. T. SCHAEFER and R. SEBASTIAN. Can. J. Chem. **67**, 1027 (1989).
7. T. SCHAEFER, R. SEBASTIAN, H. Y. LI, and T. QUACH. Can. J. Chem. **68**, 996 (1990).
8. R. H. CONTRERAS, M. A. NATIELLO, and G. E. SCUSERIA. Magn. Reson. Rev. **9**, 239 (1985).
9. D. G. DE KOWALEWSKI, R. H. CONTRERAS, A. R. ENGELMANN, J. C. FACELLI, and J. C. DURAN. Org. Magn. Reson. **17**, 199 (1981).
10. R. LAATIKAINEN. J. Magn. Reson. **52**, 293 (1983).
11. M. A. NATIELLO, R. H. CONTRERAS, J. C. FACELLI, and D. G. DE KOWALEWSKI. J. Phys. Chem. **87**, 2603 (1983).
12. T. SCHAEFER, H. D. GESSER, and J. B. ROWBOTHAM. Can. J. Chem. **54**, 2235 (1976).
13. L. LUNAZZI and D. MACCIANTELLI. Chem. Commun. 933 (1971).
14. J. HILTON and L. H. SUTCLIFFE. Prog. NMR Spectrosc. **10**, 27 (1975).

Can. J. Chem. Downloaded from www.nrcresearchpress.com by 198.100.157.202 on 09/07/12
For personal use only.

15. T. SCHAEFER, R. SEBASTIAN, and S. R. SALMAN. J. Magn. Reson. **46**, 325 (1982).
16. A. SCHWEIG and N. THON. Chem. Phys. Lett. **38**, 482 (1976).
17. T. SCHAEFER and J. D. BALEJA. Can. J. Chem. **64**, 1376 (1986).
18. T. SCHAEFER and G. H. PENNER. Can. J. Chem. **66**, 1229 (1988).
19. T. SCHAEFER, S. R. SALMAN, T. A. WILDMAN, and P. D. CLARK. Can. J. Chem. **60**, 342 (1982).
20. A. PROSS and L. RADOM. Prog. Phys. Org. Chem. **13**, 1 (1981).
21. T. SCHAEFER, J. D. BALEJA, and G. H. PENNER. Can. J. Chem. **63**, 2471 (1985).
22. L. F. FIESER and M. FIESER. Reagents in organic chemistry. J. Wiley & Sons, New York. 1967. p. 682.
23. J. D. BALEJA. Synth. Commun. **14**, 215 (1984).
24. T. SCHAEFER and R. SEBASTIAN. J. Magn. Reson. **41**, 395 (1980).
25. T. SCHAEFER, R. SEBASTIAN, and G. H. PENNER. Can. J. Chem. **63**, 2597 (1985).
26. J. S. MARTIN, A. R. QUIRT, and K. E. WORVILL. The NMR program library. Daresbury Laboratory, Daresbury, U.K.
27. T. SCHAEFER and J. D. BALEJA. J. Magn. Reson. **60**, 131 (1984).
28. N. M. ZARIPOV. Zh. Strukt. Khim. **17**, 741 (1976).
29. T. SCHAEFER and G. H. PENNER. J. Mol. Struct. (Theochem), **152**, 179 (1987).
30. H. LUMBROSO, J. CURÉ, and C. G. ANDRIEU. J. Mol. Struct. **43**, 87 (1978).
31. G. PUNTE, B. E. RIVERO, S. CERDEIRA, and N. S. NUDELMAN. Can. J. Chem. **68**, 298 (1990).
32. O. G. BATYUKHNOVA, N. I. SADOVA, Y. N. SEPHCHIKOV, L. V. VILKOV, and Y. A. PANKRUSHEV. J. Struct. Chem. Engl. Transl., **29**, 537 (1988).
33. T. SCHAEFER and R. SEBASTIAN. Can. J. Chem. **61**, 26 (1983).

Can. J. Chem. Downloaded from www.nrcresearchpress.com by 198.100.157.202 on 09/07/12
For personal use only.

Synthèse d'isoxazoles substitués en α de l'oxygène et d'isoxazoles substitués en α de l'azote et de l'oxygène par des chaînes alkyle ou alcényle

JEAN-CLAUDE CHERTON,[1] M. LANSON,[2] D. LADJAMA, N. LEFEBVRE, Z. VOSSOUGH et J-J. BASSELIER

Laboratoire de chimie organique structurale, Unité de recherche associée n° 455, Université P. et M. Curie, 4 Place Jussieu, 75252 Paris CEDEX 05, France

Reçu le 25 juillet 1990

JEAN-CLAUDE CHERTON, M. LANSON, D. LADJAMA, N. LEFEBVRE, Z. VOSSOUGH et J-J. BASSELIER. Can. J. Chem. **69**, 625 (1991).

Deux séries d'isoxazoles substitués par de longues chaînes alkyle ou alcényle en α de l'oxygène ou en α des deux hétéroatomes ont été élaborées. La métallation/alkylation régiosélective sur le méthyle α-O du 3,5-diméthyl isoxazole constitue une synthèse de choix d'«isoxazoles α-O» diversement substitués. Appliquée à des isoxazoles méthylés en α de l'oxygène présentant déjà une chaîne alcényle en α de l'azote, cette séquence constitue une synthèse univoque et originale de 3,5-dialcényles isoxazoles lorsque l'agent alkylant est un halogénure d'alcényle. La cycloaddition dipolaire-1,3 employant des dièmes terminaux comme dipolarophiles et des dipôles alcèniques constitue un autre accès satisfaisant à de tels dialcényles isoxazoles, bien qu'impliquant l'élimination du sous-produit di-isoxazoline préalablement à l'oxydation de l'isoxazoline intermédiaire. Enfin, pour les isoxazoles simplement 3,5-dialkylés, la cycloaddition entre un alcyne vrai et un dipôle alkylé reste la méthode la plus directe.

Mets clés : isoxazoles, chaînes latérales alcényle, métallation–alkylation, régiosélectivité.

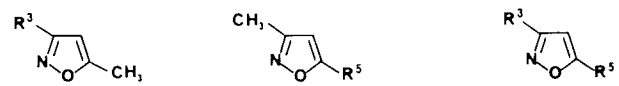
JEAN-CLAUDE CHERTON, M. LANSON, D. LADJAMA, N. LEFEBVRE, Z. VOSSOUGH, and J-J. BASSELIER. Can. J. Chem. **69**, 625 (1991).

Two series of isoxazoles substituted by long alkyl or alkenyl chains in the α position with respect to the oxygen atom or in the α position with respect to the two heteroatoms have been synthesized. Starting from 3,5-dimethylisoxazole, the regioselective metalation/alkylation on the α-O methyl group was a very convenient route to a large variety of "α-O substituted isoxazoles". When applied to α-O methylated isoxazoles bearing an α-N alkenyl chain the same method provides an original unequivocal approach to 3,5-dialkenyl isoxazoles. An alternative route to these compounds, despite the formation of di-isoxazoline as by-product and an additional step corresponding to the oxidation of the intermediate isoxazoline, is the 1,3-dipolar cycloaddition, by using terminal dienes as dipolarophiles with alkenyl dipoles. Nevertheless, the cycloaddition between monoalkylated alcynes and alkylated dipoles remains the most straightforward synthesis of 3,5-dialkyl isoxazoles.

Key words: isoxazoles, alkenyl side chains, metalation–alkylation, regioselectivity.

Can. J. Chem. Downloaded from www.nrcresearchpress.com by 198.100.157.202 on 09/07/12
For personal use only.

Nous nous intéressons dans la perspective de leurs propriétés pesticides (1) à des isoxazoles porteurs d'une ou de deux longues chaînes alkyles ou alcényles en α de l'azote ou (et) de l'oxygène (2). La synthèse des «isoxazoles α-N substitués» **1** constitue un cas bien particulier que nous avons précédemment abordé (3). Nous présentons maintenant celle des séries d'isoxazoles **2** substitués en α de l'oxygène et d'isoxazoles **3**, 3,5-disubstitués (cf. schéma 1).



Isoxazole α-N	Isoxazole α-O	Isoxazole 3,5 disubstitué
1 (2,3)	**2** (ce travail,2)	**3** (ce travail,2)

$R^3, R^5 = [CH_2]_m\text{-}{=}$ ou $[CH_2]_x\text{-}CH_3$

SCHÉMA 1. Isoxazoles substitués en α de l'oxygène et (ou) de l'azote par de longues chaînes alkyles ou alcényles.

Résultats et discussion

Nous avons employé deux grandes voies : soit des synthèses en ligne par métallation/alkylation de divers isoxazoles, soit des synthèses convergentes par cycloaddition dipolaire-1,3.

Introduction des chaînes latérales par métallation/alkylation de divers méthyl isoxazoles (voies A du schéma 2)

Nous avons mis à profit la régiosélectivité de la déprotonation des méthyles (ou méthylènes) α-O de divers isoxazoles[3] pour élaborer les séries d'isoxazoles **2** et **3**.

*Isoxazoles α-O substitués **2** à partir du diméthyl-3,5 isoxazole **4** (voie A_1)*

Nous avons procédé à une seule métallation/alkylation en opérant dans des conditions de contrôle thermodynamique (conditions (a) du schéma 2). En effet, lorsque la température est abaissée jusqu'à −105°C, on constate une compétition de la métallation des deux méthyles de l'isoxazole **4** (voie A_3 du schéma 2). L'addition ultérieure de différents électrophiles au milieu réactionnel maintenu à −78°C donne l'accès en bons rendements à des isoxazoles **2** portant des substituants très variés : chaînes alkyles, alcényles... (cf. tableau 1).

*Isoxazoles-3,5 disubstitués **3** par métallation/alkylation d'isoxazoles α-N **1** (voie A_2)*

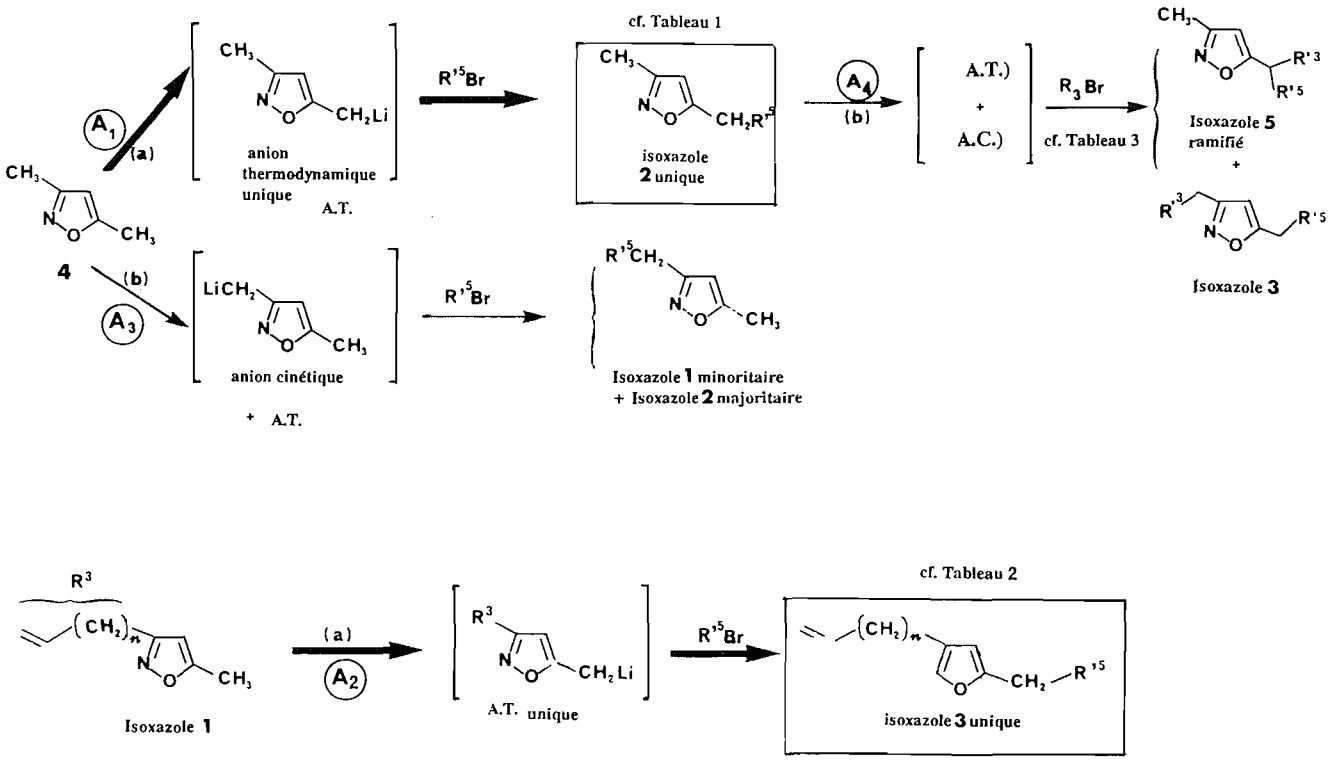
En utilisant encore les conditions de contrôle thermodynamique (conditions (a) du schéma 2), on observe aussi la régiosélectivité de la métallation/alkylation des isoxazoles α-N, (cf. schéma 2 et tableau 2). Le seul site réactionnel est alors le méthyle α-O. Cette stratégie montre que la série des isoxazoles α-N intéressante en elle-même (1–3) offre en outre des synthons permettant un accès original et univoque aux isoxazoles **3** et en particulier à des dialcényles-3,5 isoxazoles.

[1]Auteur à qui adresser toute correspondance.

[2]Partie de thèse soutenue à l'Université P. et M. Curie, Paris, 1987.

[3]L'étude théorique du diméthyl-3,5 isoxazole **4** a montré que la déprotonation par les bases du méthyl α-O est thermodynamiquement favorisée (4). Ces travaux dûs à Kashima *et al.* ont été confirmés par les résultats expérimentaux de Micetich (5) et de Brunelle (6) obtenus avec diverses bases comme le BuLi, le LDA et $NaNH_2$.

Printed in Canada / Imprimé au Canada



(a) Conditions de contrôle thermodynamique : 1 éq. de BuLi, −78°C (anion thermodynamique A.T.) voies A_1, A_2 univoques ⟶

(b) Conditions de contrôle cinétique : 1 éq. de BuLi, −105°C (anion cinétique A.C.) R'^3,R'^5 = $(CH_2)_m$-= ou $(CH_2)_x$-CH_3. Voies A_3 A_4 →

SCHÉMA 2. Synthèse d'isoxazoles-3,5 disubstitués **3** par métallation/alkylation du diméthyl-3,5 isoxazole **4** (voies A).

*Essai d'obtention d'isoxazoles **3** par métallation/alkylation d'isoxazoles **2** sous contrôle cinétique[4] (voie A_4)*

La métallation/alkylation de divers isoxazoles **2** réalisée dans des conditions de contrôle cinétique (conditions (b) du schéma 2, voie A_4 et tableau 3) conduit quel que soit l'électrophile ultérieurement employé à des mélanges : isoxazole **3** attendu et isoxazole ramifié **5** obtenu comme sous-produit. En combinant toutes les conditions favorables à un contrôle cinétique, nous avons amélioré la régiosélectivité sans toutefois atteindre 100% d'isoxazole **3** (tableau 3, essai 2 et partie expérimentale).

L'obtention d'isoxazoles **3** par une synthèse en ligne comme la métallation/alkylation implique donc pour être univoque de partir d'isoxazoles α-N **1** et non pas d'isoxazoles α-O **2**. Nous avons également examiné pour ces isoxazoles **3** des voies d'accès par synthèse convergente.

Synthèse convergente d'isoxazoles par cycloaddition dipolaire-1,3 (voies B)

Les cycloadditions dipolaires-1,3 sont en général appliquées à des dipolarophiles présentant un groupe aryle ou un groupe électroattracteur (groupe R^5 du schéma 3). Pour notre part, nous avons néanmoins tenté leur application au cas de dipôles et de dipolarophiles porteurs de groupes R^3 et R^5 alkyle ou alcényle pour accéder aux isoxazoles de type **3**.

*Synthèse d'isoxazoles-3,5 disubstitués **3** avec au moins une chaîne alcényle (voie B_1)*

L'emploi d'alcènes comme dipolarophiles[5] (7) conduit intermédiairement à des isoxazolines **9** dont l'oxydation fournit les isoxazoles correspondants **3** (8). Pour tenter la synthèse d'isoxazoles à groupe R^5 insaturé, nous avons appliqué cette stratégie au cas de l'octadiène-1,7 **7** utilisé comme dipolarophile.

Les dipôles nitrile-oxydes **6** à groupe alkyle ou alcényle sont générés *in situ* en raison de leur instabilité (9). Nous avons adopté la méthode de Mukaiyama et Hoshino (7) ou celle de Larsen et Torsell (10) consistant respectivement en la déshydratation de nitroalcanes primaires ou en la déshydrohalogénation de chloroaldoximes. Les di-isoxazolines **10**, sous-produits résultant de deux additions du dipôle sur le dipolarophile double, sont facilement éliminées du milieu réactionnel par filtration. Les isoxazolines **9** obtenues par distillation du filtrat sont aisément oxydées en isoxazoles correspondants par le bioxyde de manganèse activé (8), (cf. tableau 4). Cette méthode plus longue et moins efficace que la voie A_2 présente néanmoins l'intérêt de fournir les intermédiaires ou sous-produits **9** et **10** dont nous avons pu tester quelques propriétés biologiques (1).

[4]Selon Brunelle, la métallation/alkylation sur le méthyle α-N est rendu régiospécifique par l'emploi de bases encombrées comme le *sec*-BuLi ou le *tert*-BuLi (6).

[5]En revanche, l'emploi d'alcynes comme dipolarophiles ne convient pas pour la synthèse d'isoxazoles à groupe R^5 alcénique puisqu'il impliquerait la mise en oeuvre d'un synthon dipolarophile double (alcène/alcyne). On obtiendrait alors majoritairement une isoxazoline à terminaison alcyne (9).

Can. J. Chem. Downloaded from www.nrcresearchpress.com by 198.100.157.202 on 09/07/12
For personal use only.

TABLEAU 1. Synthèse d'isoxazoles α-O substitués **2** par métallation/alkylation du diméthyl-3,5 isoxazole (voie A_1 du schéma 2, conditions (a))

Nature de R^5 CH_2-R'^5	Electrophile Br R'^{5b} (Provenance)	Rdt(%)	Isoxazole **2**	Rdt(%)	(Torr)	Eb (°C)	Analyse calc. / tr. C	H	N	F
-$(CH_2)_2$-═ a	Bromure d'allyle[a]		a	80	(0,02)	38–39	70,04 70,00	8,08 8,26	10,21 10,30	
-$(CH_2)_3$-═ b	Bromobutène[a]		b	76	(0,7)	54	71,49 71,64	8,67 8,66	9,26 9,10	
-$(CH_2)_4$-═ c	Bromopentène (pentène 4-ol-1 (13))	60	c	65	(0,1)	68–70	72,66 72,74	9,15 9,23	8,47 8,42	
-$(CH_2)_5$-═ d	Bromohexène (hexène 5-ol-1 (13))	60	d	60	(0,07)	92	73,70 73,82	9,56 9,67	7,81 7,87	
-$(CH_2)_6$-═ e	Bromoheptène (heptènol (14))	32	e	60	(0,2)	65	74,57 74,50	9,91 9,73	7,25 7,12	
-$(CH_2)_7$-═ f	Bromooctène (octadiène (16))	17	f	50	(0,1)	126	75,31 75,21	10,21 10,18	6,75 6,77	
-$(CH_2)_8$-═ g	Bromononène (nonénol (14))	43	g	67	(0,5)	102	75,97 75,96	10,47 10,41	6,33 6,18	
-$(CH_2)_9$-═ h	Bromodécène (décénol)	93	h	95	(0,05)	113–114	76,54 76,57	10,70 10,81	5,95 5,99	
-$(CH_2)_{10}$-═ i	Bromo-undécène (undécénol)	52	i	50	(1)	154–156	77,06 77,04	10,91 11,09	5,62 5,56	
-$(CH_2)_{10}$-CH_3 j	Bromodécane[a]		j	76	(1)	142	75,89 75,90	11,46 11,39	5,90 5,72	
-$(CH_2)_7$-F k	Bromofluorohexane (1-6 fluorohexanol (17))	70	k	33	ccm prép. Eb non déterminé		66,30 66,42	9,10 9,02	7,03 6,90	9,53 9,40
-$(CH_2)_{11}$-F l	Bromofluorodécane (1-10 fluorodécanol (17))	80	l	89	(0,7)	150–152	70,55 70,35	10,26 10,67	5,48 5,26	7,44 7,26
-$(CH_2)_5$- m	Époxydation de **2***d*[c]	60	m	60	ccm prép. Eb non déterminé		67,66 67,50	8,77 8,89	7,17 7,21	
-$(CH_2)_9$-  n	Époxydation de **2***h*[c]	70	n	47	(0,3)	109	71,67 71,73	10,02 10,00	5,57 5,71	

[a]Commercial.
[b]Les bromolcènes sont obtenus par la méthode de Laforge (15) excepté le bromooctène préparé selon la référence 16.
[c]Le noyau isoxazole étant inerte vis à vis de l'acide métachloroperbenzoïque, on a époxydé les insaturations terminales des groupes R^5 des isoxazoles **2***d* et **2***h* selon la référence 18.

TABLEAU 2. Métallation/alkylation des isoxazoles α-N **1** sous contrôle thermodynamique (voie A_2 du schéma 2, conditions (a)

Isoxazole **1** R^{3a}	R^5 = -$CH_2R'^5$ (Electrophile R'^5Br)	Isoxazole **3**				Analyse calc. / tr. C	H	N
		3[a]	Rdt[b] (%)	(Torr)	Eb (°C)			
(b) CH_2═CH-$(CH_2)_3$-	(d) -$(CH_2)_5$-CH═CH_2	**3***db*	44	(0,03)	95	77,21 77,58	9,94 9,88	6,00 5,92
(g) CH_2═CH-$(CH_2)_8$-	(a) -$(CH_2)_2$-CH═CH_2	**3***ag*	42	(0,8)	78,11	10,41 78,20	5,36 10,77	5,20
(h) CH_2═CH-$(CH^+2)_9$	(a) -$(CH_2)_2$-CH═CH_2	**3***ah*	61	(0,8)	97	78,49 78,42	10,61 10,79	5,08 4,93

[a]Les notations pour les substituants R^3 et R^5 sont celles du tableau 1: on nomme d'abord R^5.
[b]Rendement en produit distillé. La rmn ^{1}H du mélange brut ne révèle pas de trace de l'isomère résultant d'une réaction sur le méthylène α-N.

Can. J. Chem. Downloaded from www.nrcresearchpress.com by 198.100.157.202 on 09/07/12
For personal use only.

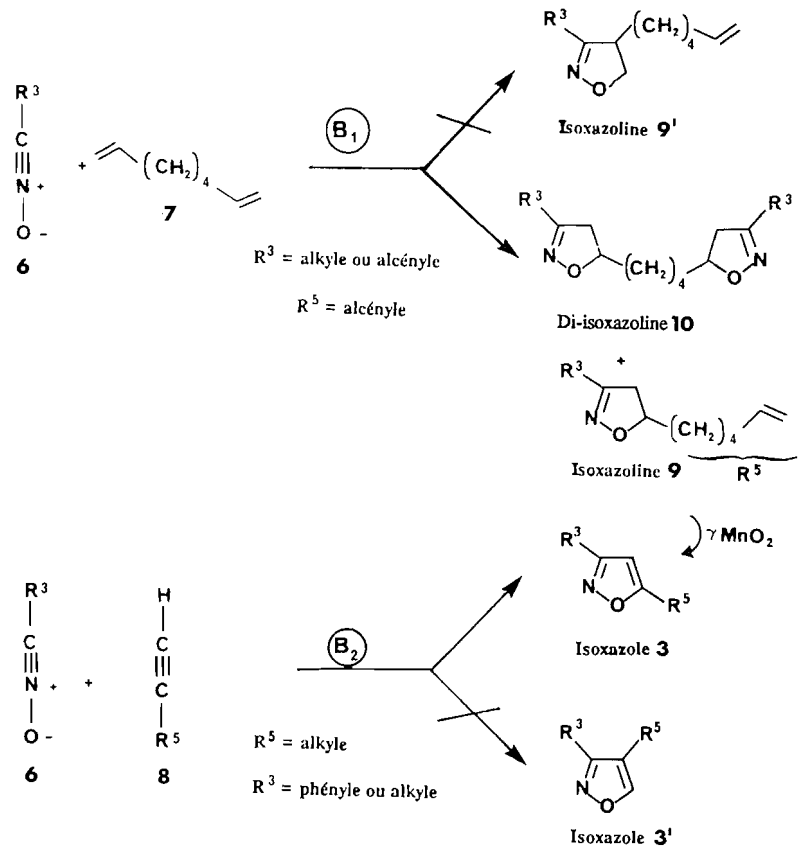


SCHÉMA 3. Synthèse d'isoxazoles-3,5 disubstitués par addition dipolaire-1,3 (voies B).

Synthèse de dialkyl-3,5 isoxazoles **3** *(voie B_2)*

L'addition dipolaire-1,3 d'un nitrile-oxyde sur un acétylénique conduit directement à un isoxazole (9). Cette voie nous a semblé particulièrement bien convenir pour une synthèse rapide et univoque d'isoxazoles-3,5 disubstitués **3** par deux chaînes alkyle, compte-tenu de la régiosélectivité de cyclisation[6] (9, 11) (schéma 3, voie B_2). Nous avons donc élaboré une série de dipôles-1,3 **6** à groupe R^3 saturé, la série des acétyléniques vrais **8** utilisés étant commerciale, à l'exception du dodécyne qui a été obtenu par homologation du bromodécane avec l'acétylure de sodium. Pour générer *in situ* les nitrile-oxydes **6** nous avons encore utilisé la méthode de Larsen et Torssell (10). Avec des rendements en produit purifié allant de 50 à 80% et la régiosélectivité déjà signalée pour d'autres substituants, les résultats montrent l'efficacité de cette voie pour la synthèse de dialkyl-3,5 isoxazoles **3** (cf. tableau 5).

Partie expérimentale

Les spectres d'absorption infrarouge ont été réalisés sur un appareil d'absorption infrarouge Pye Unicam modèle SP3-200, sous forme de film liquide entre pastilles de NaCl. Les bandes d'absorption sont exprimées en cm^{-1}. Les abréviations utilisées pour la description des bandes des spectres infrarouge sont les suivantes : l, large; F, forte; TF, très forte; m, moyenne; f, faible. Les spectres de rmn ^1H ont été effectués sur des appareils Bruker WP80, WM 250 et WM 500 dans le $CDCl_3$. Les déplacements chimiques sont exprimés en ppm par rapport au HMDS. Les abréviations suivantes sont employées : s, singulet; d, doublet; t, triplet; q, quadruplet; m, multiplet; M, massif. Les spectres de rmn ^1H et de rmn ^{13}C des isoxazoles **2** et **3** seront également présentés dans un article indépendant ainsi que les spectres de rmn ^{17}O et de rmn ^{15}N (12). Les spectres de masse ont été enregistrés par M^lle J. Mercier que nous remercions sur des spectrographes MS 30 et MS 50 sous impact électronique à 70 eV au centre de spectrochimie. Les pics sont exprimés en *m/z*, entre parenthèses figure leur intensité relative. Les analyses élémentaires ont été réalisées au service de microanalyse de l'Université Pierre et Marie Curie ou bien au service de microanalyse du CNRS à Vernaison. Le gel de silice Silicagel 60 PF_{254} (Merck) a été employé pour les ccm préparatives. Sauf précisions contraires les rendements indiqués sont calculés à partir des produits obtenus après distillation.

Introduction des chaînes latérales par métallation/alkylation de divers isoxazoles methylés (schéma 2, tableaux 1–3)

Synthèse des chaînes latérales

Le penténol et l'hexénol sont préparés selon la méthode de Brooks (13) et l'hepténol et le nonénol selon la méthode de Cahiez *et al.* (14). Les bromoalcènes sont obtenus par la méthode de Laforge *et al.* (15) à partir des alcools éthyléniques correspondants, excepté le bromo-7 octène-1 qui a été préparé à partir de l'octadiène-1,7 selon la référence 16. Les α-ω-bromofluoroalcanes sont synthétisés selon la méthode indirecte de Pattisson *et al.* (17) (monochloration des α,ω-diols puis fluoration du composé chloré intermédiaire par le fluorure de potassium).

Bromo-1 fluoro-6 hexane (71%), Eb_{30} = 117°C (litt. (17) Eb_{11} 67–68°C).

Bromo-1 fluoro-10 décane (80%), $Eb_{0,7}$ = 92°C (litt. (17) Eb_{11} 131°C).

Isoxazoles α-O substitués **2** *à partir du diméthyl-3,5 isoxazole* **4** *(voie A_1 du schéma 2, tableau 1)*

Ils sont obtenus à partir du diméthyl-3,5 isoxazole **4** en réalisant avec les différents électrophiles R'^5 Br du tableau 1 la métallation/alkylation dans des conditions de contrôle thermodynamique (conditions (a) du

[6]La cycloaddition d'un alcène ou d'un alcyne sur un dipôle se fait avec une remarquable régiosélectivité puisque des deux isomères possibles pour l'isoxazoline ou pour l'isoxazole, le seul composé 3,5-disubstitué est exclusivement obtenu.

Can. J. Chem. Downloaded from www.nrcresearchpress.com by 198.100.157.202 on 09/07/12
For personal use only.

TABLEAU 3. Métallation/alkylation d'isoxazoles α-O **2** sous contrôle cinétique (voie A_4 du Schéma 2)

		2ème Métallation/alkylation[a]					
Isoxazole α-O $R^5 = -CH_2-R'^5$	**2**	R'^3Br	Rdt global (%)	Isoxazole **3** Rdt(%) + Isoxazole **5** Rdt(%)	Analyse du mélange calc. / tr. C	H	N
Essai 1							
$-(CH_2)_2-=$	**2***a*	Br-CH_2-=	70	**3***aa*[b]	**5***aa*	74,54	8,53	7,90
a		(a)		34	66	74,90	8,41	7,83
Essai 2								
$-(CH_2)_2-=$	**2***a*	Br-CH_2-=	82	**3***aa*	**5***aa*			
a		(a)		79	21			
Essai 3								
$-(CH_2)_4-=$	**2***c*	Br-$(CH_2)_6$=	44	**3***cf*	**5***cf*	78,49	10,61	5,09
c		(f)		Eb 0,1 = 152	Eb 0,1 = 145	78,62	10,65	4,99
				52	48			
Essai 4								
$-(CH_2)_9-=$	**2***h*	Br-CH_2-=	55	**3***ha*	**5***ha*	78,49	10,61	5,08
h		(a)		Eb 0,1 = 151	Eb 0,1 = 146	78,40	10,83	4,89
				57	43			

[a]Conditions (b) : emploi de *sec*-BuLi, éther, −90°C, délai de 30 min entre les additions de lithien et d'électrophile pour tous les essais excépté pour l'essai 2 où l'on a utilisé le THF en opérant à −105°C et en supprimant le délai.

[b]Dosage par CPV capillaire pour la série *aa*. Séparation possible par distillation pour les séries *cf* et *ha*.

TABLEAU 4. Synthèse de divers mono- et di-alcényl isoxazoles **2** et **3** (voie B_1 du schéma 3)

R^{3a}	Isoxazoline **9**[b]	Rdt(%)	+ di-isoxazoline **10**[b]	Rdt(%)	Isoxazole[c]	Rdt(%)
CH_3-	**9***c*	56	+ **10***c*	5	**2***c*	85
=-$(CH_2)_8$- g	**9***cg*	52	+ **10***cg*	5	**3***cg*	80
=-$(CH_2)_7$- f	**9***cf*	48	+ **10***cf*	7	**3***cf*	80
C_2H_5- j	**9***cj*	47	+ **10***cj*	10	**3***cj*	85

[a]R^5 = c: $-(CH_2)_4-=$.

[b]Seules l'isoxazoline **9** et la di-isoxazoline **10** sont obtenues sans que l'on trouve trace de l'isoxazoline **9'** par rmn ^1H dans le mélange réactionnel.

[c]Pour les analyses et les caractéristiques physiques, cf. tableau 1 pour **2***c*, cf. tableau 2 pour **3***cg* et **3***cf* et cf. partie expérimentale pour **3***cj*.

schéma 2). Les solvants (THF, éther) employés lors des métallations sont distillés sur benzophénone et sodium et sous atmosphère inerte juste avant utilisation. Les réactions sont également effectuées sous atmosphère d'azote.

(Butène-3 yl)-5 méthyl-3 isoxazole **2**a. À une solution refroidie à −80°C de 15 cm^3 de diméthyl isoxazole **4** (0,156 mol) dans 250 cm^3 de THF on ajoute 95 cm^3 d'une solution 1,6 M de BuLi (0,152 mol). Après 30 min d'agitation à −70°C 16 cm^3 (0,184 mol) de bromure d'allyle sont ajoutés et l'agitation est poursuivie 1 nuit. Après neutralisation, lavage à l'eau, évaporation et distillation, on isole l'isoxazole **2***a* (0,12 mol, 16,93 g) (80%), $Eb_{0,5}$ 38–39°C; ir : 3080(f), 2920(F), 2850(F), 1640(m), 1610(F), 1495(f), 1450(F), 1370(f), 1000(m), 930(F), 800(m); uv (CH_3CN) λ_{max} en nm (log ε_{max}) : 229(2,01); rmn ^1H : 5,8(m, 2H), 5(m, 2H), 2,1(s, 3H), 2,5–2,1(m, 4H); masse : 137(M^+), 96(100), 82(45), 68(75), 55(65), 41(45).

En opérant à basse plus température (−105°C) toujours avec le bromure d'allyle comme électrophile (voie A_3 du Schéma 2), on a observé la formation d'un mélange du produit cinétique, l'isoxazole α-N **1***a*, et du produit thermodynamique, l'isoxazole α-O **2***a*. La rmn ^1H du mélange brut permet d'estimer les proportions 23 : 77 de ces deux isomères en se basant sur l'intégration des signaux méthyles respectifs à 2,3 et 2,1 ppm (2, 12).

Méthyl-3 (pentène-4 yl)-5 isoxazole **2**b (76%), $Eb_{0,7}$ 54°C; ir : 3080(f), 2920(F), 1640(m), 1610(F), 1495(f), 1450(F), 1370(f), 1000(m), 930(F), 800(m); rmn ^1H : 6,0–5,4(m, 2H), 5–4,6(m, 2H), 2,65(t, 8 Hz, 2H), 2,1(s, 3H), 2,4–1,4(m, 4H); masse : 151 (M^+), 110(50), 97(50), 82(40), 68(25), 50(100), 41(70).

(Hexène-5 yl)-5 méthyl-3 isoxazole **2**c (65%), $Eb_{0,1}$ 68–70°C; ir : 3080(f), 2930(F), 2850(F), 1640(m), 1600(F), 1490(f), 1440(m), 1420(F), 1000(m), 900(m), 800(f); uv (CH_3CN) λ_{max} en nm (log ε_{max}) : 229 (3,52); rmn ^1H : 6,1–5,4(m, 2H), 5–4,6(m, 2H), 2,6(t, 2H), 2,1(s, 3H), 2,0–1,5(m, 6H); masse : 165(M^+), 109(50), 92(40), 67(50), 55(60), 54(35), 41(100).

(Heptène-6 yl)-5 méthyl-3 isoxazole **2**d (56%), $Eb_{0,07}$ 92°C; ir : 2930(F), 1640(m), 1600(F), 1490(f), 1440(F), 1420(F), 1370(f), 1260(f), 1000(m), 910(F), 795(m); rmn ^1H : 6–5,4(m, 2H), 5,0–4,7(m, 2H), 2,6(t, 8 Hz, 2H), 2,2(s, 3H), 2,0–1,2(m, 6H); masse : 179(M^+), 97(65), 82(35), 55(100), 54(30), 41(95).

Méthyl-3 (octène-6 yl)-5 isoxazole **2**e (60%), $Eb_{0,2}$ 65°C; ir : 3080(f), 2940(F), 2860(m), 1640(m), 1600(F), 1495(f), 1450(m), 1420(m), 1380(f), 1000(m), 920(m), 800(m); rmn ^1H : 6,0–5,4(m, 2H), 5–4,7(m, 2H), 2,65(t, 7 Hz, 2H), 2,15(s, 3H), 2,1–1,0(m, 10H); masse : 193(M^+), 97(35), 82(30), 55(75), 54(30), 41(100).

Méthyl-3 (nonène-8 yl)-5 isoxazole **2**f (50%), $Eb_{0,1}$ 126°C; ir : 3080(f), 2920(F), 2850(F), 1630(m), 1600(F), 1490(f), 1420(F), 1370(f), 1000(m), 900(m), 790(m); rmn ^1H : 6,0–5,4 (m, 2H), 5–4,6(m, 2H), 2,8–2,4(t, 6 Hz, 2H), 2,1(s, 3H), 2,05–1(m, 12H); masse : 207(M^+), 110(75), 97(45), 82(30), 55(80), 43(30), 41(100).

(Decène-9 yl)-5 méthyl-3 isoxazole **2**g (67%), $Eb_{0,5}$ 102°C; ir : 1640(m), 1610(F), 1495(f), 1450(F), 1370(f), 1000(m), 930(F),

Can. J. Chem. Downloaded from www.nrcresearchpress.com by 198.100.157.202 on 09/07/12
For personal use only.

TABLEAU 5. Synthèse de dialkyl-3,5 isoxazoles **3** (voie B_2 du schéma 3)

		Isoxazole **3**[a]						
						Analyse {calc. / tr.		
$R^3$3	R^5		Rdt(%)	(Torr)	Eb(°C)	C	H	N
Phényle	Pentyle	a	79	(0,5)	120–122	78,10 78,23	7,96 7,89	6,50 6,26
Propyle	Pentyle	b	69	(0,5)	75–77	72,88 72,80	10,56 10,62	7,72 7,60
Propyle	Butyle	c	65	(0,1)	60–63	71,81 71,59	10,24 10,44	8,37 8,05
Décyle	Butyle	d	61	(0,5)	120–125	76,92 77,09	11,77 11,99	5,27 5,05
Décyle	Décyle	e	55	(0,5)	138–140	79,01 79,30	12,39 12,60	4,00 3,85
Hexyle	$CH_3(CH_2)_4CH(OH)$-	f	52	(0,5)	120	71,10 71,10	10,74 10,68	5,52 5,28
Hexyle	Hexyle	g	62	(0,5)	125	75,89 76,07	11,46 11,20	5,90 5,81

[a]Seul l'isoxazole **3** est obtenu sans que l'on puisse déceler par rmn ^{1}H de traces de son isomère **3'** dans le mélange réactionnel.

800(m); rmn ^{1}H : 6,0–5,4(m, 2H), 5–4,6(m, 2H), 2,6(t, 8 Hz, 2H), 2,2(s, 3H), 2,1–1,0(m, 14H); masse : 221(M^+), 110(48), 97(30), 55(64), 41(100).

Méthyl-3 (undécène-10 yl)-5 isoxazole **2**h (95%), $Eb_{0,05}$ 113–114°C; ir : 1640(m), 1610(F), 1495(f), 1450(F), 1370(f), 1000(m), 930(F), 800(m); uv (CH_3CN) λ_{max} en nm (log ε_{max}) : 229(3,17); rmn ^{1}H : 6,0–5,4(m, 2H), 5–4,6(m, 2H), 2,6(t, 8 Hz, 2H), 2,2(s, 3H), 2,1–1,0(m, 16H); masse : 235(M^+), 110(100), 97(45), 55(45), 41(40).

(Dodécène-11 yl)-5 méthyl-3 isoxazole 2i (50%), Eb, 154–156°C; ir : 2920(F), 2860(F), 1640(F), 1600(F), 1480(f), 1440(F), 1410(m), 1380(f), 990(m), 900(m), 780(m); rmn ^{1}H : 6,0–5,4(m, 2H), 5–4,6(m, 2H), 2,6(t, 8 Hz, 2H), 2,2(s, 3H), 2,1–1,0(m, 18H); masse : 249(M^+), 110(80), 97(75), 82(30), 55(95), 41(100).

Méthyl-3 undécyl-5 isoxazole **2**j (76%), Eb_1 142°C; ir : 2920(F), 2850(m), 1600(m), 1490(f), 1460(m), 1420(m), 370(f), 790(f); masse : 237(M^+), 110(100), 97(90), 55(80), 43(90), 41(90).

(Fluoro-7 heptyl)-5 méthyl-3 isoxazole **2**k (33%), Eb inconnu car purification par ccm préparative (silice, cyclohexane/AcOEt 80 : 20); ir : 2930(F), 2850(m), 1600(F), 1480(f), 1450(m), 1420(m), 1000(f), 890(f), 790(f); rmn ^{1}H : 5,7(s, 1H), 4,6(dt, J_{HH} = 6 Hz, J_{HF} = 57 Hz, 2H), 2,6(t, 7 = Hz, 2H), 2,15(s, 3H), 2,1–1,0(m, 10H); masse : 199(M^+), 110(40), 97(100), 55(70), 41(60).

(Fluoro-11 undécyl)-5 méthyl-3 isoxazole **2**l (89%), $Eb_{0,7}$ 150–152°C; ir : 2950(F), 2880(m), 1610(m), 1430(m), 1010(f), 900(F), 800(f); rmn ^{1}H : 5,7(s, 1H), 4,6(dt, J_{HH} = 6 Hz, J_{HF} = 57 Hz, 2H), 2,6(t, 7 Hz, 2H), 2,15(s, 3H), 2,1–1,0(m, 18H); masse : 255(M^+), 193(30), 110(90), 97(80), 55(90), 43(55), 41(100).

Pour obtenir les isoxazoles **2***m* et **2***n* à terminaison époxydiques, nous avons employé le méthode de Kishi (18) recourant à l'acide métachloroperbenzoique.

Méthyl-3 [(oxiranyl-2)-5 pentyl]-5 isoxazole **2**m (60%), Eb inconnu car isolé par ccm préparative (silice, cyclohexane/AcOEt 80 : 20); ir : 3040(f), 2930(f), 2860(m), 1600(F), 1480(f), 1420(m), 1420(f), 1370(f), 1260(m), 1000(m), 890(m), 800(m); rmn ^{1}H : 5,8(s, 1H), 2,9(m, 1H), 2,74(dd, 8 Hz, 1H), 2,73(t, 8 Hz, 2H), 2,45(dd, 1H), 2,25(s, 3H), 1,67–1,40(m, 8H).

Méthyl-3 [(oxiranyl-2)-9 nonyl]-5 isoxazole **2**n (47%), $Eb_{0,3}$ 109°C; ir : 2940(F), 2860(F), 1600(F), 1480(f), 1450(m), 1420(m), 1370(f), 1260(f), 1000(f), 900(f), 800(f); rmn ^{1}H : 5,8(s, 1H), 2,9(m, 1H), 2,74(dd, 1H), 2,73(t, 8 Hz, 2H), 2,45(dd, 1H), 2,25(s, 3H), 1,67–1,40(m, 16H); masse : 251(M^+), 110(100), 97(60), 96(30), 84(30), 55(60), 41(60).

Isoxazoles-3,5 disubstitués **3** *par métallation/alkylation d'isoxazoles α-N* **1** *(voie A_2 du schéma 2 et tableau 2)*

Comme pour les isoxazoles α-O, on utilise des conditions de contrôle thermodynamique (conditions (a), schéma 2).

(Heptène-6 yl)-5 (pentène-4 yl)-3 isoxazole **3**db (44%), $Eb_{0,03}$ 95°C; ir : 3140(f), 3080(m), 2940(TF), 2860(F), 1640(F), 1600(TF), 1480(m), 1440(F), 1425(F), 1350(f), 1000(f), 910(TF), 800(m); rmn ^{1}H : 5,80(m, 3H), 5(m, 4H), 2,80(m, 2H), 2,60(m, 2H), 1,7–2,10(M, 12H); masse : 233(M^+), 136(50), 81(30), 80(25), 55(60), 41(100).

(Butène-3 yl)-5 (decène-9 yl)-3 isoxazole **3**ag (42%), $Eb_{0,8}$ 97°C; ir : 3080(f), 2920(F), 2850(m), 1640(m), 1600(m), 1480(f), 1460(m), 1440(m), 1410(m), 990(f), 810(m), 780(m); rmn ^{1}H : 5,80(m, 3H), 5(m, 4H), 2,80(m, 2H), 2,60(m, 2H), 1,60–2,45(M, 16H); masse : 261(M^+), 137(30), 110(5), 97(10), 55(75), 43(30), (100).

(Butène-3 yl)-5 (undecène-10 yl)-3 isoxazole **3**ah (61%), $Eb_{0,8}$ 97°C; ir : 3080(f), 2920(F), 2850(F), 1650(m), 1600(F), 1480(f), 1440(m), 1420(m), 990(m), 910(F), 790(m); rmn ^{1}H : 5,80(m, 3H), 5(m, 4H), 2,80(m, 2H), 2,60(m, 2H), 1,60–2,40(M, 18H); masse : 275(M^+), 69(15), 67(15), 55(45), 44(100), 41(80).

Essai d'obtention d'isoxazoles **3** *par métallation/alkylation d'isoxazoles* **2** *sous contrôle cinétique (voie A_4, tableau 3)*

En combinant différents facteurs favorables à un contrôle cinétique (température de −105°C, base encombrée comme *sec*-BuLi, suppression du délai entre l'addition du lithien et celle de l'électrophile) lors de la métallation/alkylation des isoxazoles **2**, il a été possible d'augmenter la proportion d'isoxazole **3** sans toutefois atteindre la régiospécificité.

(Butène-3 yl)-3 (butène-3 yl)-5 isoxazole **3**aa. Selon les conditions opératoires le mélange brut analysé par cpv capillaire (colonne WCOT CP Sil 5, longueur 25 m, diamètre int. 0,23 mm avec un appareil Hewlett–Packard (5880 A), l'isomère **3***aa* servant d'étalon ayant été préparé de façon indépendante (2, 3)) contient des proportions très différentes de **3***aa* : 34 et 79% pour les essais 1 et 2.

(Butène-3 yl)-3 (undécène-10 yl)-5 isoxazole **3**ha. Le produit brut (55%), uv (CH_3CN) λ_{max} en nm (log ε_{max}) : 229(3,17); masse :

Can. J. Chem. Downloaded from www.nrcresearchpress.com by 198.100.157.202 on 09/07/12
For personal use only.

Can. J. Chem. Downloaded from www.nrcresearchpress.com by 198.100.157.202 on 09/07/12
For personal use only.

275(M^+), 69(15), 67(15), 55(45), 44(100), 41(80), étant en fait un mélange d'isoxazoles **3** et **5** séparables par distillation : **5***ha* (43%), $Eb_{0,1}$ 146°C; **3***ha* (57%), $Eb_{0,1}$ 151°C.

(Hexène-5 yl)-5 (nonène-8 yl)-3 isoxazole **3**cf. Le produit brut (44%), ir : 3140(f), 3100(m), 2940(F), 2880(F), 1650(m), 1610(F), 1490(f), 1470(m), 1430(F), 1000(m), 920(F), 800(m); masse : 275(M^+), 110(1), 96(1), 82(2), 69(5), 67(5), 55(15), 43(10), 42(10), 41(100), étant en fait un mélange d'isoxazoles **3** et **5** séparables par distillation : **5***cf* (48%), $Eb_{0,1}$ 145°C et **3***cf* (52%), $Eb_{0,1}$ 152°C.

Synthèse convergente par cycloaddition dipolaire-1,3 (voies B)

Synthèse d'isoxazoles-3,5 disubstitués **3** *avec un moins une chaine alcényle (voie B_1 : via les isoxazolines* **9***)*

Les isoxazolines-1,2 **9***c* et **9***cj* sont préparées selon la méthode de Mukaiyama et Hoshino (7) que nous avons tranposée en l'appliquant à l'octadiène comme dipolarophile alors que les isoxazolines **9***cg* et **9***cf* sont obtenues en utilisant la méthode de Larsen et Torssell (10) pour générer *in situ* le nitrile-oxyde.

(Héxène-5 yl)-5 méthyl-3 dihydro-4,5 isoxazoline **9**c. À un mélange d'isocyanate de phényle (0,1 mol) et d'octadiène (0,055 mol) dans 25 cm^3 de benzène anhydre, on ajoute goutte à goutte une solution de nitroéthane (0,055 mol) dans 15 cm^3 de benzène sec contenant 10 gouttes de triéthylamine. Après le démarrage de la réaction (avec dégagement de CO_2 et précipitation de diphénylurée), on agite 1 h puis porte à reflux une autre heure. Après refroidissement, la solution est lavée à l'eau, puis séchée. L'évaporation du solvant suivie d'un refroidissement 1 nuit à −15°C permet de séparer la di-isoxazoline **10***c* cristallisée (Fi 75°C) d'une huile contenant l'isoxazoline **9***c* brute. La distillation fournit 4,73 g (56%), $Eb_{0,3}$ 92–93°C; ir : 3080(f), 1725(m), 1640(m), 1600(f), 900(m); rmn ^1H : 5,75(m, 1H), 5(m, 2H), 4,5(m, 1H), 2,60–2,80(m, 2H), 2,0(m, 2H), 1,90(s, 3H), 1,30(m, 6H).

Éthyl-3 (héxène-5 yl)-5 dihydro-4,5 isoxazoline **9**cj (47%), $Eb_{0,5}$ 82–85°C; ir : 3080(f), 1640(m), 1620(f), 1600(f), 1000(m), 920(m); rmn ^1H : 5,80(m, 1H), 5,00(m, 2H), 4,55(m, 1H), 2,90(m, 1H), 2,60(m, 1H), 2,30(m, 2H), 2,00(2H), 1,30(m, 6H), 1,10(t, 3H).

(Décène-9 yl)-3 (hexène-5 yl)-5 dihydro-4,5 isoxazoline **9**cg. À une suspension de *N*-chlorosuccinimide (26 mmol, 3,46 g) dans 18 cm^3 de chloroforme on ajoute en une seule fois l'oxime de l'undécénal (26 mmol, 4,76 g) à 25°C. La chloration de l'oxime intervient en général après 10 min et se manifeste par la disparition de la suspension. On ajoute alors l'octadiène (32 mmol, 4,6 cm^3) et la température est portée à 40–50°C avant d'ajouter goutte à goutte en 30 min la triethylamine (28 mmol, 2,82 g) en solution dans 4 cm^3 de $CHCl_3$. Le mélange est lavé à l'eau, seché et concentré après avoir été agité 30 min. Du concentrat visqueux on sépare la di-isoxazoline **10***cg* brute précipitée par refroidissement (0,35 g, ~5%) d'une huile contenant l'isoxazoline **9***cg*. La distillation fournit 3,74 g (52%), $Eb_{0,1}$ 135–137°C; ir : 3080(f), 1720(m), 1640(m), 1000(m), 900(m); rmn ^1H : 5,90(m, 2H), 5,00(m, 4H), 4,5(m, 1H), 2,90(m, 1H), 2,45(m, 1H), 2,00(m, 2H), 2,25(m, 2H), 1,30(m, 20H).

(Heptène-6 yl)-3 (héxène-5 yl)-5 dihydro-4,5 isoxazoline **9**cf (48%), Eb_1 180–185°C; ir : 3080(f), 1720(m), 1640(m), 1600(f), 1000(m), 910(m); rmn ^1H : 5,90(m, 2H), 5,00(4H), 4,50(m, 1H), 2,90(m, 1H), 2,45(m, 1H), 2,25(m, 2H), 2,00(m, 2H), 1,30(m, 18H).

Les isoxazoles sont obtenus par oxydation par le MnO_2 activé selon la référence 7.

Méthyl-3 (héxène-5 yl)-5 isoxazole **3**c (85%), $Eb_{0,5}$ 102–105°C; ir : 3080(f), 1640(m), 1600(m), 910(m); rmn ^1H : 5,6–6(m, 1H), 5,8(s, 1H), 4,9–5,10(m, 2H), 2,75(t, 2H), 2,25(s, 3H), 2,30–2(m, 2H), 1,25–1,8(m, 4H).

(Décène-9 yl)-3 (hexène-5 yl)-5 isoxazole **3**cg (80%), $Eb_{0,1}$ 140–142°C; ir : 3080(f), 1640(f), 1600(f), 910(m); rmn ^1H : 6–5,60(m, 2H), 5,80(s, 1H), 5,2–4,9(m, 4H), 2,8–2,5(m, 4H), 2,5–1,75(m, 4H), 1,75–1(m, 16H).

(Nonène-8 yl)-3 (hexène-5 yl)-5 isoxazole **3**cf (80%), $Eb_{0,1}$ 135–136°C; ir : 3080(f), 1640(f), 1600(f), 910(m); rmn ^1H : 6–5,60(m, 2H), 5,80(s, 1H), 5,2–4,9(m, 4H), 2,8–2,5(m, 4H), 2,4–1,8(m, 4H), 1,5–1(m, 14H).

Éthyl-3 (héxène-5 yl)-5 isoxazole **3**cj (85%), $Eb_{0,5}$ 110–111°C; ir : 3080(f), 1640(m), 910(m); rmn ^1H : 6–5,5(m, 1H), 5,75(s, 1H), 5,10–4,9(m, 2H), 2,62(q, 2H), 2(m, 2H), 1,25–1,75(m, 6H), 1,20(t, 3H).

Synthèse de dialkyl-3,5 isoxazoles **3** *(voie B_2, emploi d'alcynes)*

Nous avons utilisé la méthode de Larsen et Torssell (10).

Pentyl-5 phényl-3 isoxazole **3**a (79%), $Eb_{0,5}$ 120–122°C; ir : 2960(F), 2940(F), 2880(m), 1600(F), 1490(m), 1470(F), 1430(F), 1380(m), 790(m); rmn ^1H : 7,7(m, 2H), 7,4(3H), 6,2(s, 1H), 2,75(t, 2H), 1,75(m, 2H), 1,30(m, 4H), 0,9(t, CH_3).

Pentyl-5 propyl-3 isoxazole **3**b (69%), $Eb_{0,5}$ 75–77°C; ir : 2960(F), 2940(F), 2880(m), 1600(F), 1490(m), 1470(F), 1430(F), 1380(m), 790(m); rmn ^1H : 5,80(s, 1H), 2,67(t, 2H), 2,57(t, 2H), 1,65(m, 4H), 1,32(m, 4H), 0,9(m, 6H).

Butyl-5 propyl-3 isoxazole **3**c (65%), $Eb_{0,1}$ 60–63°C; ir : 2960(F), 2940(m), 2880(f), 1600(F), 1490(f), 1460(f), 1430(m); rmn ^1H : 5,80(s, 1H), 2,67(t, 2H), 2,56(t, 2H), 1,70(m, 4H), 1,4(m, 2H), 0.90(m, 6H); masse : 167(M^+), 139(95), 110(10), 68(35), 57(30), 55(30), 43(70), 41(100).

Butyl-5 décyl-3 isoxazole **3**d (61%), $Eb_{0,5}$ 120–125°C; ir : 2960(F), 2940(m), 2880(f), 1600(F), 1470(m), 1430(m), 1000(f), 760(f); rmn ^1H : 5,80(s, 1H), 2,67(t, 2H), 2,57(t, 2H), 1,30(m, 20H), 0.90(m, 6H); masse : 265(M^+), 139(40), 57(40), 55(50), 43(70), 42(30), 41(100).

Didécyl-3,5 isoxazole **3**e (55%), $Eb_{0,5}$ 138–140°C; ir : 3020(f), 2920(TF), 2860(TF), 1600(m), 1470(m), 1220(F), 670(m); rmn ^1H : 5,80(s, 1H), 2,67(t, 2H), 2,56(t, 2H), 1,30(m, 32H), 0,90(m, 6H); masse : 349(M^+), 236(45), 110(45), 97(20), 57(30), 55(50), 43(100), 41(100).

Hexyl-3 (hydroxy-1 hexyl)-5 isoxazole **3**f (52%), $Eb_{0,5}$ 120°C; ir : 3380(large), 2980(F), 2940(TF), 2860(F), 1600(m), 1460(m), 1430(m); rmn ^1H : 6,25(s, 1H), 4,80(m, 1H), 3,60(1H, mobile), 2,60(m, 2H), 1,30(m, 16H), 0.90(m, 6H).

Dihexyl-3,5 isoxazole **3**g (62%), $Eb_{0,5}$ 125°C; ir : 2940(TF), 2860(F), 1600(F), 1480(m), 1460(m), 1430(m); rmn ^1H : 5,80(s, 1H), 2,67(t, 2H), 2,57(t, 2H), 1,30(m, 16H), 0,90(m, 6H); masse : 237(M^+), 167(45), 55(60), 44(45), 43(80), 41(100).

1. J. C. Cherton, D. Ladjama, N. Ronzani et M. Lanson. Analusis. Soumis. (1990).
2. M. Lanson. Thèse de Doctorat, Paris (1987).
3. J. C. Cherton, M. Lanson, D. Ladjama, Y. Guichon et J. J. Basselier. Can. J. Chem. **68**, 1271, (1990).
4. (*a*) C. Kashima, Y. Yamamoto, Y. Tsudo et Y. Omote. Bull. Chem. Soc. Jpn. **49**, 1047 (1976); (*b*) C. Kashima, Y. Yamamoto et Y. Tsudo. Heterocycles, **6**, 805 (1977).
5. R. G. Micetich. Can. J. Chem. **48**, 2006 (1970).
6. D. J. Brunelle. Tetrahedron Lett. **22**, 3699 (1981).
7. T. Mukaiyama et H. Hoshino. J. Am. Chem. Soc. **82**, 5339 (1960).
8. (*a*) A. Barco, S. Bennetti et G. P. Pollini. Synthesis, 837 (1977); (*b*) A. J. Fatiadi. Synthesis, 65 (1976).
9. (*a*) C. Grundmann. Synthesis, 65 (1976); (*b*) C. Grundmann et P. Grünanger. The Nitrile-Oxyde. Springer-Verlag, Berlin et New York. 1971.
10. K. E. Larsen et K. B. G. Torssell. Tetrahedron, **40**, 2985 (1984).
11. (*a*) B. J. Wakefield et D. J. Wright. J. Chem. Soc. 1165 (1970); (*b*) B. J. Wakefield. Adv. Heterocycl. Chem. **25**, 148 (1979); (*c*) A. Quilico. Chem. Heterocycl. Comp. **17**, 21 (1962); (*d*) R. Huisgen. Angew. Chem. **75**, 604 (1963); **75**, 742 (1963).
12. M. Lanson, J. C. Cherton, R. Sabbah et O. Convert. Magn. Reson. Chem. Soumis (1990).
13. L. A. Brooks. Org. Synth. Coll. Vol.III, 698 (1967).
14. G. Cahiez, A. Alexakis et J. F. Normant. Tetrahedron Lett. **33**, 3013 (1978).
15. F. B. Laforge, N. Green et W. A. Gersdorff. J. Am. Chem. Soc. **70**, 3709 (1948).
16. G. Stork. Pure Appl. Chem. **9**, 131, (1964).
17. F. L. M. Pattisson et W. C. Howell. J. Org. Chem. **21**, 739 (1956).
18. Y. Kishi. J. Chem. Soc. Chem. Commun. 64 (1972).

Ab initio molecular orbital calculations of the infrared spectra of hydrogen bonded complexes of water, ammonia, and hydroxylamine. Part 6. The infrared spectrum of the water–ammonia complex[1]

GEOFFREY ANDREW YEO AND THOMAS ANTHONY FORD[2]
Department of Chemistry, University of the Witwatersrand, Johannesburg, Wits 2050, South Africa

Received July 20, 1990

GEOFFREY ANDREW YEO and THOMAS ANTHONY FORD. Can. J. Chem. **69**, 632 (1991).

The molecular structure, interaction energy, and infrared spectrum of the linearly hydrogen bonded 1:1 molecular complex of water and ammonia have been predicted by means of a series of *ab initio* molecular orbital calculations, at the level of second order Møller–Plesset perturbation theory, using the 6-31G** basis set. The calculated wavenumbers and intensities have been compared with those calculated earlier for the respective monomers, and the wavenumber shifts and intensity changes rationalized in terms of the hydrogen bond interaction responsible for the stability of the complex.

The calculated hydrogen bond energy of the complex has been compared with those of the linear water and ammonia dimers, reported in a previous publication, and the relative strengths of interaction of the three aggregates have been rationalized on the basis of the electron donor/acceptor capacities of the respective monomer units.

Key words: *ab initio*, infrared spectrum, water, ammonia.

GEOFFREY ANDREW YEO et THOMAS ANTHONY FORD. Can. J. Chem. **69**, 632 (1991).

En se basant sur des calculs d'orbitales moléculaires *ab initio* au second niveau de perturbation de Møller–Plesset et utilisant un ensemble de base 6-31G**, on a fait des prédictions concernant la structure moléculaire, l'énergie d'interaction et le spectre infrarouge du complexe moléculaire 1:1 de l'eau et de l'ammoniac réunie par une liaison hydrogène linéaire. On a comparé les valeurs calculées pour les nombres d'onde et pour les intensités avec celles calculées antérieurement pour les monomères respectifs; on a rationalisé les déplacements dans les nombres d'onde et les changements dans les intensités en fonction de l'interaction de la liaison hydrogène responsable de la stabilité du complexe.

On a aussi comparé la valeur de l'énergie de la liaison hydrogène du complexe avec celles des dimères linéaire de l'eau et de l'ammoniac, rapportées dans une publication antérieure; on a rationalisé les forces relatives des interactions de ces trois agrégats en fonction des capacités des unités monomères respectives à agir comme donneur ou accepteur d'électrons.

Mots clés : *ab initio*, spectre infrarouge, eau, ammoniac.

[Traduit par la rédaction]

1. Introduction

The molecules water, ammonia, and hydroxylamine form an interesting series for a systematic study of hydrogen bonding. Water is a common electron acceptor (proton donor or Lewis acid) in hydrogen bonded structures, and ammonia is well-known as an electron donor (proton acceptor or Lewis base). Hydroxylamine is expected to show some characteristics of both types of interaction; it is capable of donating either a proton through its OH group, or the lone pair of electrons on its nitrogen atom. Hydrogen bonded structures containing hydroxylamine could also be envisaged in which proton donation occurs through the NH groups, or electron donation through the oxygen lone pairs, although such structures are expected to be far less likely.

We have initiated a study of the infrared spectra of the binary complexes of these three molecules, by means of matrix isolation spectroscopy and *ab initio* molecular orbital theory. We have reported the infrared spectra, in nitrogen and argon matrices, of the water and ammonia (1) and hydroxylamine (2) monomers and homodimers, and have predicted the spectra of the monomers (3, 4) and the water (1), ammonia (1, 5, 6), and hydroxylamine (7) dimers, at both the Hartree–Fock and Møller–Plesset levels of theory, using a variety of basis sets. We now turn our attention to the heterodimer formed between water and ammonia.

The structure of the water–ammonia complex in the gas phase has been studied by Herbine and Dyke (8), by means of molecular beam electron resonance (MBER), and by Millen and Mines (9), by infrared spectroscopy. The MBER results showed that the complex was essentially linearly hydrogen bonded, with an O...N separation of 298.3 pm, and with the ammonia C_3 symmetry axis having a vibrationally-averaged displacement of 23.1° from the O...N axis (8) (structures **I** and **II**, see Fig. 1). *Ab initio* theoretical calculations on this complex by Kerns and Allen (10), who examined a bifurcated (OH_2...NH_3) structure (**III**) at the RHF/4-31G level, concluded that this geometry was a saddle point, and not a genuine minimum, on the potential energy surface. Kerns and Allen also considered a cyclic, doubly hydrogen bonded heterodimer, but found that its structure collapsed on optimization to the linearly bonded OH...N structure (**I** or **II**) (10). Del Bene (11) studied the RHF/6-31G* structures of the bimolecular complexes of water with the hydrides of the first- and second-row atoms, including ammonia, and found that the complexes exhibit conventional hydrogen bonded structures with virtually linear hydrogen bonds and directed lone pairs of electrons. A similar conclusion was reached by Diercksen *et al.* (12), who examined the hypersurface of the water–ammonia complex at a number of different intermolecular geometries, using a basis set containing *d*-type polarization functions on the oxygen and nitrogen atoms and *p*-type functions on the hydrogen atoms. While this work was still in progress, Latajka and Scheiner (13) published a similar study to this one, in which the structure of the complex in configuration **II** was computed using a basis set obtained from 6-31G** by the addition of a diffuse *sp*-shell on the non-hydrogen centres, with electron correlation included to second order Møller–Plesset theory (MP2).

Nelander and Nord (14), in a matrix isolation infrared study

[1]Part of this work was presented at the 73rd Canadian Chemical Conference, Halifax, N.S., July 15–20, 1990.

[2]To whom correspondence should be addressed.

Printed in Canada / Imprimé au Canada

Can. J. Chem. Downloaded from www.nrcresearchpress.com by 198.100.157.202 on 09/07/12
For personal use only.

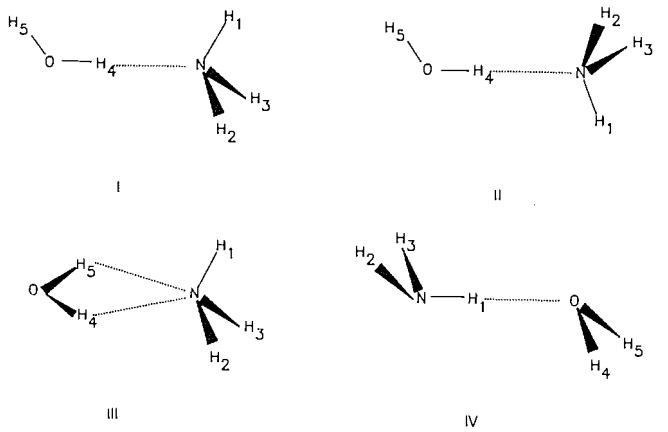


FIG. 1. Four possible structures for the water–ammonia complex (schematic).

using nitrogen and argon, and later Engdahl and Nelander (15) in neon and krypton matrices, have shown that the spectra in the region of the perturbed water fundamentals are consistent with a linear OH...N bonded structure (**I** or **II**). Our infrared spectra, obtained in both nitrogen and argon matrices (16), are in full agreement with those of Nelander *et al.* (14, 15).

In view of this earlier theoretical (10–13) and experimental (14, 15) evidence, we regarded the linear HOH...NH_3 hydrogen bonded geometries (**I** and **II**) to be the preferred structures of this complex, and used them as starting points for the geometry optimization, which is the first step in the *ab initio* prediction of vibrational spectra. Attempts to locate a minimum corresponding to the less probable linear $H_2NH...OH_2$ complex (structure **IV**), in which the electron donor and acceptor roles of the water and ammonia molecules were reversed, resulted in the starting structures invariably collapsing to the bifurcated $OH_2...N$ bonded geometry (**III**) proposed by Kerns and Allen (10). Accordingly, in addition to the computations on structures **I** and **II** we have performed some preliminary calculations, at lower levels of theory, on structure **III** as well.

2. Computational details

The computations on structures **I**, **II**, and **III** were performed using the GAUSSIAN-86 (17) and GAUSSIAN-88 (18) program packages on IBM 3083 and Convex C120 computers, respectively. The internally stored 6-31G** basis set was used (19, 20), and the calculations were carried out initially at the Hartree–Fock level of theory. In the light of these calculations, structure **III** was rejected as a plausible candidate for the correct structure, and the subsequent calculations, at the MP2 level (21), were limited to structures **I** and **II**. All molecular orbitals were included in the calculations. Total Berny geometry optimizations were employed, with the VERYTIGHT convergence criterion, subject to the conservation of C_s symmetry in each case. Dimerization energies were calculated, as reported earlier (6), and were corrected for basis set superposition error (BSSE) by the full counterpoise correction formula of Boys and Bernardi (22). The MASSAGE option of the programs was used for this phase of the computations (17, 18). The wavenumbers and infrared intensities were computed by means of the FREQ normal coordinate analysis option (17, 18).

3. Results

Ab initio calculations at the RHF/6-31G** level predict three stationary points on the potential energy surface of the hydrogen bonded water–ammonia complex, structures **I**, **II**, and **III**. The first of these configurations was obtained as a true minimum, and the second as a saddle point, with starting geometries in which ammonia was the electron donor. Starting geometries of type **IV**, with water as the electron donor, and with the symmetry constrained to C_s, invariably finally yielded the bifurcated structure **III**, with ammonia as the electron donor. At the MP2/6-31G** level, structure **II** was found to be the absolute minimum and structure **I** a transition state. A single, large negative eigenvalue calculated in the infrared spectrum of structure **III** at the RHF/6-31G** level indicated that this structure is also a transition state (23) (see later), confirming the findings of Kerns and Allen (10). Further analysis, at the MP2 level (21), was therefore confined to geometries **I** and **II**. The calculated geometries are presented in Table 1.

TABLE 1. Optimized geometrical parameters of the linear water–ammonia complexes, calculated at the MP2/6-31G** level of theory

Parameter	Structure **I**[a]	Structure **II**[a]
$r(NH_1)$/pm	101.2	101.2
$r(NH_2)$/pm	101.2	101.2
$r(N...H_4)$/pm	198.9	198.7
$r(OH_4)$/pm	97.2	97.2
$r(OH_5)$/pm	96.0	96.0
$\angle H_1NH_2$/deg	106.7	106.5
$\angle H_2NH_3$/deg	106.6	106.8
$\angle H_4...NH_1$/deg	121.7	102.4
$\angle H_4...NH_2$/deg	107.2	116.8
$\angle OH_4...N$/deg	175.7[b]	175.4[c]
$\angle H_4OH_5$/deg	103.9	103.9

[a]See Fig. 1.
[b]O *anti* to H_1.
[c]O *syn* to H_1.

TABLE 2. Dimerization energies and basis set superposition errors of the linear water–ammonia complex and of the linear water and ammonia dimers, calculated at the MP2/6-31G** level of theory

	Energy/kJ mol^{-1}		
Complex	ΔE (uncorrected)	BSSE	ΔE (corrected)
HOH...NH_3[a]	−33.5	6.6	−26.9
HOH...OH_2[b]	−29.8	10.2	−19.6
$H_2NH...NH_3$[b]	−17.8	5.3	−12.5

[a]Structure **II** (see Fig. 1).
[b]Reference 1.

The minimum energies corresponding to structures **I** and **II** were found to be −132.229315845 and −132.229309545 au (RHF) and −132.62211775 and −132.62213370 au (MP2), respectively. The uncorrected interaction energy, the BSSE and the difference for structure **II**, calculated at the MP2/6-31G** level, are collected in Table 2, and for purposes of comparison, the corresponding dimerization energies of the linear water and ammonia dimers, also derived at the MP2/6-31G** level (1), are included. The corresponding values for structure **I** are identical, within 100 J mol^{-1}.

The vibrational wavenumbers and intensities of the two linear OH...N bonded structures (**I** and **II**) were computed at the

Can. J. Chem. Downloaded from www.nrcresearchpress.com by 198.100.157.202 on 09/07/12
For personal use only.

TABLE 3. Predicted infrared spectrum of the linear water–ammonia complex (structure **II**), calculated at the MP2/6-31G** level of theory

Symmetry species	Mode	Approximate description[a]	Wavenumber /cm^{-1}	Intensity /km mol^{-1}
a'	ν_1	ν (OH) (free)	3989	53
	ν_2	ν (OH) (bonded)	3728	379
	ν_3	ν (NH) (64) + ν_s (NH_2) (33) (OP)	3721	15
	ν_4	ν_s (NH_2) (66) + ν (NH) (33) (IP)	3567	4.0
	ν_5	δ (HOH) (79) + δ (NH_2) (17) (OP)	1743	34
	ν_6	δ (NH_2) (74) + δ (HOH) (19) (IP)	1715	58
	ν_7	δ (NH_2) (65) + δ (NH) (33) (IP)	1158	149
	ν_8	δ (OH...N) (IM)	460	110
	ν_9	ν (H...N) (IM)	202	19
	ν_{10}	δ (HN...H) (54) + r (HOH) (24) (IM)	172	44
a''	ν_{11}	ν_a (NH_2)	3723	5.7
	ν_{12}	γ (HN...H) (58) + tw (NH_2) (42)	1724	20
	ν_{13}	γ (OH...N) (IM)	712	184
	ν_{14}	tw (NH_2) (76) + γ (OH...N) (13) (IM)	161	40
	ν_{15}	τ (HN...H) (IM)	30	77

[a]Numbers in parentheses indicate approximate percentage contributions to each normal mode (contributions > 10% only included). IP = in-phase, OP = out-of-phase, IM = intermolecular mode.

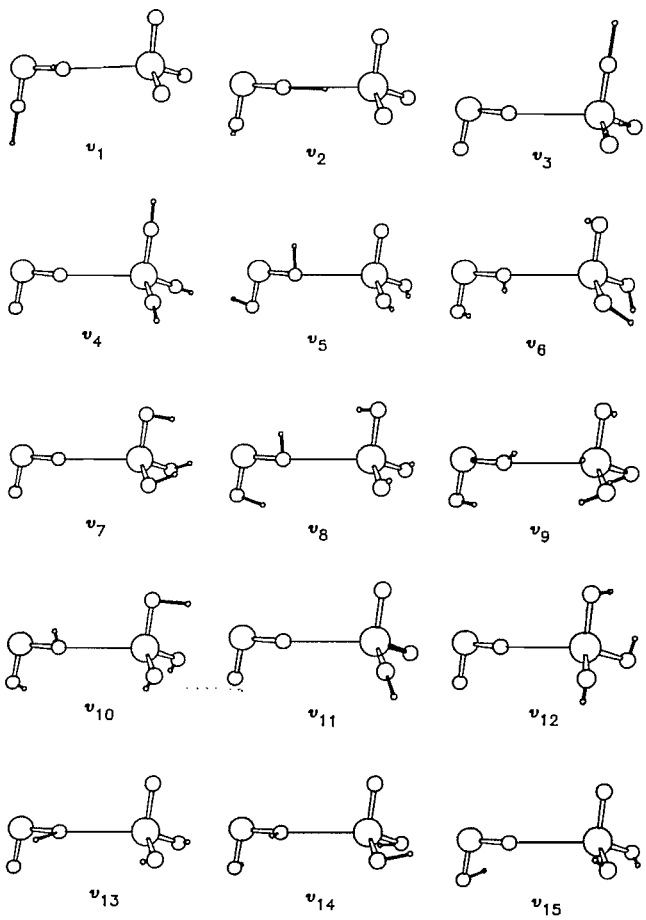


FIG. 2. Plots of the normal modes of vibration of the linear water–ammonia complex.

RHF/6-31G** and MP2/6-31G** levels, using the optimized geometries given in Table 1. At the lower level, no negative eigenvalues were predicted for structure **I**, while a single negative wavenumber was found for structure **II**. In contrast, calculations at the higher level yielded a single negative wavenumber for structure **I**, but no negative eigenvalues for structure **II**. This observation is consistent with the relative calculated minimum energies for the two structures at the two levels of theory, and the reversal of their relative stabilities at the MP2 compared with the RHF level. This confirms the implication of Table 2 that structures **I** and **II** are energetically very similar, and that prediction of the correct equilibrium structure is very sensitive to the level of theory employed. Apart from the negative eigenvalues, the calculated wavenumbers and intensities of both configurations, at both levels of theory, are very similar. Based on the calculations at the higher level of theory, however, structure **II** is predicted to be the preferred geometry. This is in agreement with other theoretical (10–13, 24–27) and experimental (8, 9, 14, 15) results. Thus the calculated wavenumbers and intensities of complex **II** only are presented in Table 3. Plots of the normal modes of vibration, which distribute between the irreducible representations a' and a'' according to

$$\Gamma_{vib} = 10a' + 5a''$$

are shown in Fig. 2.

4. Discussion

4.1. Molecular structures

A number of features are evident from the results of Table 1. The internal geometry of the water unit is the same in each case, remaining virtually unchanged from the calculated monomer geometry (1), except for the expected lengthening of the hydrogen bonded OH bond, whose length increases by 1.1 pm relative to the monomer value. Likewise, the geometries of the ammonia units are almost identical, with minimal changes in the bond angles only, compared with the monomer value (1). The local C_{3v} symmetry of the ammonia unit thus remains virtually intact. The hydrogen bond lengths, N...H_4, are also almost the same, differing by only 0.2 pm, and the hydrogen bonds deviate from linearity by less than 5° in each case, as measured by the value of the OH_4...N angle. The two angles H_4...NH_1 and H_4...NH_2 are quite different in the two isomers, however, and reference to Fig. 1 (structures **I** and **II**) shows that these are the angles which define the orientations of the ammonia molecules with respect to the N...H_4 hydrogen bond. In structure **I** hydrogen atoms H_1 and H_5 are in an eclipsed position and this,

Can. J. Chem. Downloaded from www.nrcresearchpress.com by 198.100.157.202 on 09/07/12
For personal use only.

Can. J. Chem. Downloaded from www.nrcresearchpress.com by 198.100.157.202 on 09/07/12
For personal use only.

together with a possible weak interaction between H_2 and H_3 and the lone pairs of electrons on the oxygen atom, has the effect of rotating the ammonia molecule into a position in which the $H_4 \ldots NH_1$ angle is 121.7°, rather than 112.7°, which would be the value of the angle if the C_3 axis were collinear with the $N \ldots H_4$ hydrogen bond. In structure **II** the H_2 and H_3 atoms are staggered with respect to H_5, and the H_1 atom interacts with the oxygen lone pairs such as to close the $H_4 \ldots NH_1$ angle to 102.4°.

The relative energies of structures **I** and **II** obtained at the MP2/6-31G** level, quoted above, indicate that structure **II** is the true minimum energy rotamer and **I** is a saddle point, separated from it by a barrier of only 42 J mol^{-1}. Del Bene has stated that the ammonia molecule is free to rotate about its own C_3 axis in the water–ammonia complex, this conclusion being based on calculations using the STO-3G basis set (25). The fact that structure **II** emerges only as a marginally preferred structure at the MP2/6-31G** level of theory supports this conclusion.

In the recent theoretical investigation of Latajka and Scheiner (13), the geometry was totally optimized at the RHF level of theory, using the augmented basis set referred to above, and the O...N distance only was then re-optimized at the MP2 level. The geometrical parameters found for structure **II** in this work are in good agreement with those of Latajka and Scheiner (13). The increase in the bonded OH bond length was computed to be 1.3 pm and the hydrogen bond was found to deviate from linearity by less than 5° (13). The O...N separation was calculated to be 294.2 pm, which compares with the value of 295.7 pm determined in this investigation. Moreover, the NH_3 unit was found to be tilted with respect to the O...N axis, with the pseudo C_3 axis following the bridging hydrogen atom H_4 (13), which is in agreement with the discussion above on the relative orientation of the NH_3 unit.

4.2. Dimerization energies

The interaction energies and BSSEs of the two linear water–ammonia structures, calculated at the MP2/6-31G** level, are virtually identical, and are shown in Table 2. For purposes of comparison, the same properties, calculated at the same level of theory, of the linear water and ammonia dimers (1), are also given. Calculations were also carried out at the RHF/6-31G** level on the bifurcated structure (**III**), and showed that this isomer is a much less stable configuration than structures **I** and **II** (corrected interaction energy 13.4 kJ mol^{-1} for **III**, compared with 31.4 kJ mol^{-1} for **I** and **II**). The hydrogen bond energy of 26.9 kJ mol^{-1} calculated here for structures **I** and **II** is in very good agreement with the most recently reported value of 26.6 kJ mol^{-1} obtained by Latajka and Scheiner (13). Del Bene has quoted a hydrogen bond enthalpy of 19.7 kJ mol^{-1} at the MP4/6-31+G(2*d*,2*p*) level, with corrections for zero-point and thermal vibrational contributions based on RHF/6-31G(*d*) wavenumbers (11). Millen and Mines (9) report a range of values from 24.7 to 43.5 kJ mol^{-1}, computed using a variety of basis sets, and our result accords well with those obtained using basis sets of comparable quality (12, 28). Comparing the hydrogen bond energy of the linear water–ammonia complex with those of the linear water and ammonia dimers (1), the observation that the interaction energy of $HOH \ldots NH_3$ is higher than that of $HOH \ldots OH_2$ is clearly due to the fact that ammonia is a stronger base than water, and the conclusion that the $HOH \ldots OH_2$ energy is higher than that of $H_2NH \ldots NH_3$ is rationalized by the fact that, although ammonia is a better proton acceptor than water, it is also a far poorer proton donor. Nelson *et al.*, in fact, have expressed doubts that ammonia is even capable of engaging in hydrogen bonds while acting as the proton donor (29).

4.3. Vibrational wavenumbers

In our previous discussion of the vibrational modes of the linear ammonia dimer (1, 5, 6), we pointed out that the intramolecular modes are almost completely localized in either the electron acceptor (EA) or the electron donor (ED) molecules and in essence are very similar to pure ammonia monomer vibrations. We also noted that, in the case of the linear water dimer (1), while the intramolecular modes of the ED are also virtually pure monomer vibrations, the OH-stretching vibrations of the EA are effectively decoupled by the interaction with the ED, which indicates that there is a much stronger hydrogen bonding interaction in $HOH \ldots OH_2$ compared with that in $H_2NH \ldots NH_3$ (see Table 2). This reasoning may also be extended to the linear water–ammonia complex. Modes ν_1 and ν_2 may be described as essentially free and bonded OH-stretching vibrations, respectively (see Table 3), since over 90% of each mode is localized in the individual bonds, compared with 80% in the EA of the linear water dimer. Modes ν_5 and ν_6, on the other hand, which are essentially the HOH-bending and NH_2-bending vibrations of the water and ammonia molecules, contain 17% and 19% contributions, respectively, from the appropriate group vibration of the partner monomer unit, a phenomenon which was not evident in either the linear water or ammonia dimers (1), and which also argues for a stronger interaction in the water–ammonia complex.

As was the case for the ED molecules in the linear water and ammonia dimers (1), the ammonia (ED) molecule in the water–ammonia complex is little perturbed by the presence of the water molecule. As noted above, its C_{3v} symmetry remains virtually intact, and a comparison of the percentage contributions of the motions of each atom in the intramolecular vibrations with those of the ammonia monomer shows that, except for the case of the ν_6 mode mentioned above, the forms of the vibrations are almost identical with their counterparts in the monomer.

The wavenumber shifts and intensity changes which occur on complex formation, expressed as the differences between the wavenumbers of the complex and of the corresponding modes of the relevant monomer, and the ratios of the complex to the relevant monomer band intensities, are shown in Table 4, along with the results of Latajka and Scheiner (13). Clearly, the largest wavenumber shifts in the complex are associated with the EA (water) molecule. The wavenumber of the non-bonded OH-stretching mode, ν_1, is red shifted by 45 cm^{-1}, which is a similar shift to that of the equivalent mode of the linear water dimer. The bonded OH-stretching mode (ν_2) wavenumber, however, is shifted to lower frequency by 167 cm^{-1}, which is more than double the shift calculated for the bonded OH-stretching mode of the water dimer. The complex HOH-bending mode, ν_5, is blue shifted by 60 cm^{-1} from the monomer value, a change which is also almost double that calculated for the water dimer. In contrast, the wavenumbers of the complex modes associated with the intramolecular modes of the ED (ammonia) molecule are changed very little from their monomer values, except for the bending vibration, ν_7, which is blue shifted by 36 cm^{-1} relative to the symmetric bending mode of the ammonia monomer.

Of the six intermolecular modes of the water–ammonia complex, the two modes identified as the in-plane and out-of-plane bendings of the hydrogen bond (ν_8 and ν_{13}) occur at the highest wavenumbers, and the more intense of these, ν_{13}, is

TABLE 4. Monomer-complex wavenumber shifts and intensity ratios of the linear water–ammonia complex, calculated at the MP2/6-31G** level of theory

Parent monomer	Parent monomer mode	Complex mode[a]	$\Delta\bar{\nu}/cm^{-1}$[b]		$A_{complex}/A_{monomer}$	
			This work	Ref. 13[c]	This work	Ref. 13[c]
H_2O	ν_3	ν_1	−45	−16	1.5	1.2
	ν_1	ν_2	−167	−103	87.6	14.0
	ν_2	ν_5	60	37	0.4	1.1
NH_3	ν_3	ν_{11}	2	4	17.1	1.9
		ν_3	0	−15	45.5	2.0
	ν_1	ν_4	3	1	17.4	2.5
	ν_4	ν_{12}	−4	0	1.3	0.5
		ν_6	−13	−2	3.7	0.8
	ν_2	ν_7	36	83	0.9	0.9

[a]See Table 3.
[b]$\Delta\bar{\nu} = \bar{\nu}_{complex} - \bar{\nu}_{monomer}$.
[c]RHF/augmented 6-31G**.

predicted to be the second most intense band in the spectrum (see Table 3). The two modes more closely associated with the ammonia molecule, ν_{10} and ν_{14}, occur at lower wavenumbers, consistent with the results obtained for other hydrogen bonded systems (13).

The predicted shifts in wavenumber undergone by the ammonia molecule on complexation are in general agreement with those calculated by Latajka and Scheiner at the SCF level (13), with some notable exceptions. For example, the blue shift of 36 cm^{-1} computed for the symmetric bending mode is less than half of that calculated by Latajka and Scheiner (13). In contrast, the computed wavenumber shifts experienced by the water molecule are all larger than those found by Latajka and Scheiner, although we are in agreement on the directions of the shifts. Also in contrast to the results of Latajka and Scheiner, our MP2/6-31G** calculations place the intermolecular hydrogen bond stretching mode, ν_9, at a higher wavenumber than the two modes, ν_{10} and ν_{14}, which they have described as the wagging vibrations of the proton acceptor molecule. Moreover, we predict that the torsional motion about the hydrogen bond, ν_{15}, will be a relatively intense band.

We shall be reporting the infrared spectra of this complex, in nitrogen and argon matrices, in the light of these theoretical predictions, in a forthcoming publication (16).

4.4. Infrared intensities

The familiar intensity enhancement which accompanies the red shift of the hydrogen bonded OH-stretching band on complex formation is also evident here, with an almost 90-fold increase over the monomer value (see Table 4). This again is double the 40-fold increase calculated for the corresponding mode of the EA molecule of the linear water dimer (1). The NH-stretching vibrations, ν_3, ν_4, and ν_{11}, all exhibit substantial intensity increases, which are all larger than the increases calculated for the corresponding modes (ν_1, ν_3, and ν_{12}) of the ED molecule of the linear ammonia dimer (1). It is interesting to note that the HOH-bending mode (ν_5), whose intensity decreases by a factor of 2.5 compared with its value in the water monomer, and the NH_2-bending mode, ν_6, which gains in intensity almost four-fold relative to the corresponding monomer mode, are the two modes of the water–ammonia complex in which there is considerable coupling between the vibrations of the two monomer units, and the intensity variations are thus due to the fact that there are contributions from both the EA and ED units to the total atomic displacements for each mode.

The relative intensity changes shown in Table 4, in particular those calculated for the bonded OH-stretching vibration of the water molecule, ν_2, and the NH-stretching modes of the ammonia molecule, ν_3, ν_4, and ν_{11}, are all considerably larger than those computed by Latajka and Scheiner (13). This is due to the relatively lower intensities calculated at the MP2/6-31G** level (1) for the corresponding monomer vibrations than at lower levels of theory (13). In particular, the ν_1 mode of the water monomer has a predicted intensity of 4.3 km mol^{-1} (MP2/6-31G**) (1), compared with 25 km mol^{-1} (RHF with the augmented 6-31G** basis set) (13). Similarly, the MP2/6-31G** intensities of the ν_1 and ν_3 modes of the ammonia monomer (1) are lower than the RHF/augmented 6-31G** values reported by Latajka and Scheiner (13). Nevertheless, the large increase in the intensity of the bonded OH-stretching band, and the increases in the NH-stretching band intensities on complex formation, are confirmed both by the present calculations and by those of Latajka and Scheiner (13).

The wavenumber shifts and intensity changes of the water and ammonia monomer modes, and the perturbations of the forms of those modes which are predicted to occur on formation of the water–ammonia complex, are consistent with those expected for a hydrogen bonded interaction (30). The larger wavenumber shifts and intensity enhancements, and the greater extent to which the normal modes of vibration of the water (EA) molecule in the complex are decoupled, compared with that of the EA molecule in the linear water dimer, are evidence that the hydrogen bond in the complex is stronger than that in the dimer, and this is supported by the higher calculated interaction energy reported in Table 2.

5. Acknowledgments

T.A.F. acknowledges the continuing financial support of the Foundation for Research Development, and G.A.Y. thanks the University of the Witwatersrand for the award of a Backeberg Scholarship.

1. G. A. YEO and T. A. FORD. Struct. Chem. In press.
2. G. A. YEO and T. A. FORD. J. Mol. Struct. **217**, 307 (1990).
3. G. A. YEO and T. A. FORD. J. Mol. Struct. **141**, 331 (1986).

Can. J. Chem. Downloaded from www.nrcresearchpress.com by 198.100.157.202 on 09/07/12
For personal use only.

4. G. A. YEO and T. A. FORD. J. Chem. Soc. Faraday Trans. **86**, 3057 (1990).
5. G. A. YEO and T. A. FORD. S. Afr. J. Chem. **39**, 243 (1986).
6. G. A. YEO and T. A. FORD. J. Mol. Struct. Theochem, **168**, 247 (1988).
7. G. A. YEO and T. A. FORD. J. Mol. Struct. Theochem, **200**, 507 (1989).
8. P. HERBINE and T. R. DYKE. J. Chem. Phys. **83**, 3768 (1985).
9. D. J. MILLEN and G. W. MINES. J. Chem. Soc. Faraday Trans. II, **73**, 369 (1977).
10. R. C. KERNS and L. C. ALLEN. J. Am. Chem. Soc. **100**, 6587 (1978).
11. J. E. DEL BENE. J. Phys. Chem. **92**, 2874 (1988).
12. G. H. F. DIERCKSEN, W. P. KRAMER, and W. VON NIESSEN. Theoret. Chim. Acta, **28**, 67 (1972).
13. Z. LATAJKA and S. SCHEINER. J. Phys. Chem. **94**, 217 (1990).
14. B. NELANDER and L. NORD. J. Phys. Chem. **86**, 4375 (1982).
15. A. ENGDAHL and B. NELANDER. J. Chem. Phys. **91**, 6604 (1989).
16. G. A. YEO and T. A. FORD. Spectrochim. Acta, Part A. In press.
17. M. J. FRISCH, J. S. BINKLEY, H. B. SCHLEGEL, K. RAGHAVACHARI, C. F. MELIUS, R. L. MARTIN, J. J. P. STEWART, F. W. BOBROWICZ, C. M. ROHLFING, L. R. KAHN, D. J. DEFREES, R. SEEGER, R. A. WHITESIDE, D. J. FOX, E. M. FLEUDER, and J. A. POPLE. GAUSSIAN-86, Carnegie-Mellon Quantum Chemistry Publishing Unit, Pittsburgh, PA 15213. 1984.
18. M. J. FRISCH, M. HEAD-GORDON, H. B. SCHLEGEL, K. RAGHAVACHARI, J. S. BINKLEY, C. GONZALEZ, D. J. DEFREES, D. J. FOX, R. A. WHITESIDE, R. SEEGER, C. F. MELIUS, J. BAKER, R. MARTIN, L. R. KAHN, J. J. P. STEWART, E. M. FLEUDER, S. TOPIOL, and J. A. POPLE. GAUSSIAN-88, Gaussian, Inc., Pittsburgh, PA 15213, 1988.
19. P. C. HARIHARAN and J. A. POPLE. Theoret. Chim. Acta, **28**, 213 (1973).
20. M. M. FRANCL, W. J. PIETRO, W. J. HEHRE, J. S. BINKLEY, M. S. GORDON, D. J. DEFREES, and J. A. POPLE. J. Chem. Phys. **77**, 3654 (1982).
21. C. MØLLER and M. S. PLESSET. Phys. Rev. **46**, 618 (1934).
22. S. F. BOYS and F. BERNARDI. Mol. Phys. **19**, 553 (1970).
23. J. W. MCIVER. Acc. Chem. Res. **7**, 72 (1974).
24. P. A. KOLLMAN and L. C. ALLEN. J. Am. Chem. Soc. **93**, 4991 (1971).
25. J. E. DEL BENE. J. Am. Chem. Soc. **95**, 5460 (1973).
26. H. UMEYAMA and K. MOROKUMA. J. Am. Chem. Soc. **99**, 1316 (1977).
27. G. KÖHLER and R. JANOSCHEK. J. Phys. Chem. **91**, 2051 (1987).
28. J. D. DILL, L. C. ALLEN, W. C. TOPP, and J. A. POPLE. J. Am. Chem. Soc. **97**, 7220 (1975).
29. D. D. NELSON, G. T. FRASER, and W. KLEMPERER. Science, **238**, 1670 (1987).
30. G. C. PIMENTEL and A. L. MCCLELLAN. The hydrogen bond. Freeman, San Francisco. 1960. pp. 70, 71.

Can. J. Chem. Downloaded from www.nrcresearchpress.com by 198.100.157.202 on 09/07/12
For personal use only.

Dimerization and continuous association including formation of cyclic dimers[1]

ALEXANDER APELBLAT
Department of Chemical Engineering, Ben Gurion University of the Negev, Beer Sheva, Israel
Received November 30, 1989[2]

A. APELBLAT. Can. J. Chem. **69**, 638 (1991).

New aspects of the theory of ideal associated mixtures related to a differentiation between formed cyclic and linear dimers are discussed. A mathematical analysis is presented for the dimerization model, $A + B + A_2$, the continuous association (Mecke–Kempter) model, $A + B + A_2 + A_3 + A_4 + \cdots$, both coupled with the cyclic dimer $\longrightarrow$ linear dimer transformation and for the unsymmetrical (mixed) dimer formation model, $A + B + A_2 + B_2 + AB$. Introduction of the standard reaction enthalpies and volumes associated with transformations of dimers leads to a considerable change in behavior and symmetry properties of the excess thermodynamic functions. In terms of the modified Mecke–Kempter model, a consistent representation of the excess Gibbs energy of mixing G^E, heat of mixing H^E, and excess molar volume V^E is reported for the acetic acid – water system at 298.15 K.

Key words: association, dimerization, linear dimers, cyclic dimers, hydrogen bonding, carboxylic acids, alcohols, aqueous solutions.

A. APELBLAT. Can. J. Chem. **69**, 638 (1991).

On discute de nouveaux aspects de la théorie des mélanges associés parfaits qui sont reliés à une différentiation entre la formation de dimères cycliques et linéaires. On présente une analyse mathématique du modèle de dimérisation, $A + B + A_2$, du modèle d'association continue (Mecke–Kempter), $A + B + A_2 + A_3 + A_4 + \cdots$, ainsi que deux modèles couplés avec la transformation du dimère cyclique $\longrightarrow$ dimère linéaire et finalement du modèle de formation du dimère asymétrique (mixte), $A + B + A_2 + B_2 + AB$. L'introduction des enthalpies standard de réaction et des volumes associés avec les transformations des dimères conduit à un changement important dans le comportement et les propriétés de symétrie des fonctions thermodynamiques en excès. Pour le système acide acétique/eau, à 298,15 K et utilisant le modèle de Mecke-Kempter modifié, on a obtenu une représentation cohérente de l'énergie de mélange de Gibbs en excès, G^E, de la chaleur de formation, H^E et du volume molaire en excès, V^E.

Mots clés : association, dimérisation, dimères linéaires, dimères cycliques, liaison hydrogène, acides carboxyliques, alcools, solutions aqueuses.

[Traduit par le Rédaction]

Introduction

Dimerization of carboxylic acids in both gaseous and liquid states is a well-established experimental fact (1–4). Usually, dimer formation is a decisive, but not exclusive reason for observed deviations from ideality in investigated systems. Besides contributions coming from the "physical" effects, the formation of higher associates is also postulated (5–8). A quantitative description of the systems with carboxylic acids always includes an assumption that the "chemical" contribution to the excess Gibbs energy of mixing is more important than the "physical" one. In a first approximation, the "chemical" contribution is frequently represented by the ideal associated solution model. Bearing the same number of introduced parameters, the advantage of this model lies in its simplicity.

Since the formation of dimers is not limited to the systems with carboxylic acids, but considered in many other systems, a general interest in a description of the monomer $\longrightarrow$ dimer equilibrium is therefore understandable. The most complete mathematical treatment for the dimerization reaction in an ideal associated solution approximation was given by Kehiaian and Sosnkowska-Kehiaian (9).

In this work, some new aspects related to the ideal associated solution model will be discussed. They resulted from a thermodynamic analysis recently performed in the carboxylic acid – water and carboxylic acid – carboxylic acid systems (10, 11). It was observed that experimental data of a different kind (vapor pressures, heats of mixing, and excess volumes) cannot be represented with the same set of equilibrium constants and standard reaction changes of the association reactions. In other words, there is a possibility to correlate these particular data with a molecular model, but it is difficult to obtain for this model a consistent description which includes all excess thermodynamic function G^E, H^E, S^E, and V^E. A typical example is the aqueous solutions of carboxylic acids, where the excess Gibbs energy of mixing G^E, and the excess molar volumes, V^E, derived from vapor pressure and density measurements can be reproduced using the Mecke–Kempter model with the same equilibrium constant (10).

The Mecke–Kempter model, originally developed for mixtures of alcohols in nonpolar solvents, represents the formation of hydrogen-bonded associates of different lengths (dimer, trimer, tetramer, etc.) with the same equilibrium constant in consecutive reactions. However, if the excess enthalpy, H^E, is considered to be a function of composition in the carboxylic acid – water system, the model predictions totally disagree with the experimental heats of mixing, not only with respect to the shape of the curves, but sometimes even with the sign of the thermal effect. To add to the difficulty in interpretation, most of the thermodynamic and spectroscopic data are available for dilute solutions of carboxylic acids, where there is almost no possibility to distinguish between descriptions based on the Mecke–Kempter and dimer formation models.

The self-association of carboxylic acids in water and the existence of higher than dimer associates are evidently linked

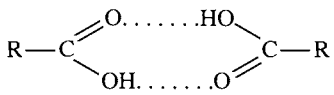
[1]This paper is dedicated to Professor Friedrich Kohler on the occasion of his 65th birthday.

[2]Revision received October 22, 1990.

Printed in Canada / Imprimé au Canada

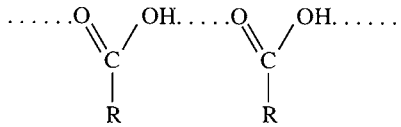
Can. J. Chem. Downloaded from www.nrcresearchpress.com by 198.100.157.202 on 09/07/12
For personal use only.

to the formation of two different types of dimers. The cyclic (closed) dimers are predominantly formed in pure acids or in mixtures with nonpolar solvents.



A

However, when a polar component (water) is added to the acid, only the linear (open) dimer is able to continue to form hydrogen-bonded chains



B

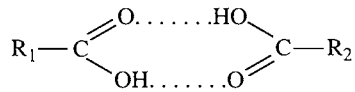
The linear dimers are formed with the nonpolar parts of molecules being in maximum contact with each other, minimizing their unfavorable contact with water (12). The cyclic and linear forms exist in different proportions in carboxylic acid – solvent mixtures. From the Raman, NMR, and ultrasonic absorption measurements it can be concluded that the presence of linear associates is significant even at low concentration of the acids (5, 6, 13, 14). In the case of alcohols, theoretical calculations and experimental results show that the linear dimer is more stable than the cyclic dimer (see, for example, Remko (15) and Brink and Glasser (16)).

In molecular association models, the excess Gibbs energy of mixing G^E depends on the total number of dimers in the system and a differentiation between the cyclic and linear dimers is not essential. This is evidently not true when the excess enthalpy of mixing H^E and the excess entropy of mixing S^E are considered, because the experimentally observed heat of mixing represents the over-all energetic balance associated with the monomer $\rightarrow$ dimer, cyclic dimer $\rightarrow$ linear dimer $\rightarrow$ higher polymers transformations.

The equality of equilibrium constants in the Mecke–Kempter continuous association model includes an assumption that the consecutive standard energy, enthalpy, entropy, and volume are proportional to the molecular size of associated molecules. However, a better agreement between theory and experiment is observed if two different constants are introduced, first a constant K_2 for dimer formation and second an equilibrium constant K for formation of higher associates with $K_2 < K$. Coggeshall and Saier (17) stated that in a linear polymer model of association, the energy released on forming a dimer is considerable smaller than the energy released on increasing the order of a higher polymer by one. The latter is almost independent of the degree of association for polymers larger than trimer. From the statistical mechanics of associated mixtures (18), the condition $K_2 < K$ as postulated by Coggeshall and Saier is related to a decrease in the number of possible orientations of associated molecules. During the formation of a dimer, two monomers lose their orientations, while in the case of higher associates, only one monomer loses its orientations when added to the already existing associate. On the basis of kinetic considerations, Ginell (19) showed that the Coggeshall-Saier modification of the Mecke–Kempter model represents a situation where all higher associates have the same number of modes of attachment and detachment of the monomer, except for the formation of dimers where the multiplicity (the number of ways in which each step can be taken) is different.

A quantitative description of the differentiation between linear and cyclic dimers requires the introduction of two equilibrium constants and the corresponding standard reaction changes. However, an almost original version of the Mecke–Kempter model with one equilibrium constant can be preserved if the cyclic dimer $\rightarrow$ linear dimer transformation is directly associated with the presence of polar molecules of solvent. For example, in the case of pure carboxylic acids, the existing dimers have a cyclic structure (**A**), but when a polar solvent is added, it changes its structure to a linear form (**B**) (one of two hydrogen bonds is broken). The simplest assumption about linear dimers is that they are formed in direct proportion to the number of solvent molecules. In this case, only one equilibrium constant is necessary, but the standard reaction changes (*e.g.*, the standard molar reaction enthalpy ΔH^0) are different for cyclic and linear dimers, In such modifications of the Mecke–Kempter or dimer formation models, the stoichiometry–concentration relations, the activity coefficients and the excess Gibbs energy of mixing remain the same as in original models. However, in the presentation of other excess thermodynamic functions we have more flexibility, We might be able to change the symmetry properties and to expect S-shaped (with double extrema) curves.

In binary mixtures of carboxylic acids we meet with the formation of symmetrical (structure **A**) cyclic dimers and asymmetrical (mixed) cyclic dimers, structure **C**.



C

There are only a few examples where the experimental data were described taking into account formation of mixed dimers (11, 20–23) and mathematically the mixed dimers formation model is far from being satisfactory.

To some extent, the formal theory of three types of ideal associated solution models are considered here. These include the dimer formation model, $A + B + A_2$, the Mecke–Kempter model, $A + B + A_2 + A_3 + A_4 + \cdots$, both linked to the cyclic dimer $\rightarrow$ linear dimer transformation, and the mixed dimers formation model, $A + B + A_2 + B_2 + AB$.

Dimerization reaction accompanied by a cyclic dimer $\rightarrow$ linear dimer transformation and the formation of unsymmetrical (mixed) dimers

If in a binary mixture, the nominal component 1 dimerizes, the species present in the mixture are monomers A and B and dimer A_2 (denoted by D). The actual mole fractions x_A, x_B, and x_D are related to the nominal mole fractions x_1 and x_2 in the following way:

$$[1] \qquad \begin{aligned} x_A &= x_1(1 + x_D) - 2x_D \\ x_B &= x_2(1 + x_D) \end{aligned}$$

In terms of the equilibrium constant K, the dimerization reaction, $2A \rightarrow A_2$, is expressed as

$$[2] \qquad K = \frac{x_D}{x_A^2}$$

Can. J. Chem. Downloaded from www.nrcresearchpress.com by 198.100.157.202 on 09/07/12
For personal use only.

where the mole fraction of the dimer is (9)

$$[3]\quad x_D = \left\{ \frac{x_1}{1+x_2} - \frac{\sqrt{1+4K_D x_1(1+x_2)}-1}{2K_D(1+x_2)^2} \right\}$$

The excess Gibbs energy of mixing is

$$[4]\quad G^E = RT\left\{ x_1 \ln\left[\frac{1}{x_A^0}\left((1+x_D) - \frac{2x_D}{x_1}\right)\right] + x_2 \ln(1+x_D)\right\}$$

where $x_A^0 = 1 - x_D^0$, is the mole fraction of the monomer A in the pure component 1

$$[5]\quad x_A^0 = \frac{\sqrt{1+4K_D}-1}{2K_D}$$

and

$$[6]\quad G^E = H^E - TS^E$$

where the excess enthalpy of mixing H^E, is given by

$$[7]\quad H^E = \Delta H^0 \left\{ \frac{x_D}{1+x_D} - \frac{x_1 x_D^0}{1+x_D^0} \right\}$$
$$\Delta H^0 = H^0_{A_2} - 2H^0_A$$

For any value of K and x_1, $H^E/\Delta H^0$ is always negative and since the standard molar enthalpy of the dimerization reaction, ΔH^0, is usually negative the heat of mixing (H^E) is expected to be positive. H^E has only one extremum (10) and for $K_D \rightarrow 0$ and $K_D \rightarrow \infty$, the heat of mixing of the monomers (A+B) and of the undissociated dimers (B+D) is zero.

Now, we will start to distinguish between cyclic and linear dimers. If x_D is the mole fraction of the total number of dimers (given by eq. [3]), then, as explained above, the mole fractions of the linear and cyclic forms are:

$$x_D(l) = x_D x_B = K_D x_A^2 x_B$$
$$[8]\quad x_D(c) = x_D(1-x_B)$$
$$= K_D x_A^2(x_A + x_D) = K_D x_A^3(1 + K_D x_A)$$

or

$$[9]\quad \frac{x_D(l)}{x_D(c)} = \frac{x_B}{1-x_B}$$

In this approach, the concentration of linear dimers is proportional to the concentration of the polar component in the mixture. The formation of linear dimers can be assumed to be two-step reaction. In the first step, an intermediate complex is formed between the cyclic dimer and the polar component and in the second step the short-living complex dissociates to giving the linear dimer. If eqs. [8] and [9] are treated as some kind of equilibrium expressions then the linear dimer has the same equilibrium constant at infinite dilution in B ($x_B \rightarrow 1$) as the cyclic dimer in pure A ($x_B \rightarrow 0$) and the cyclic dimer at infinite dilution in B obeys the equation for a trimeric equilibrium.[3] Cyclic dimers exist only in pure component 1, but with the addition of polar component 2, the number of cyclic dimers decreases and linear dimers gradually become the dominant

[3]I am indebted to a reviewer for this interpretation of eqs. [8] and [9].

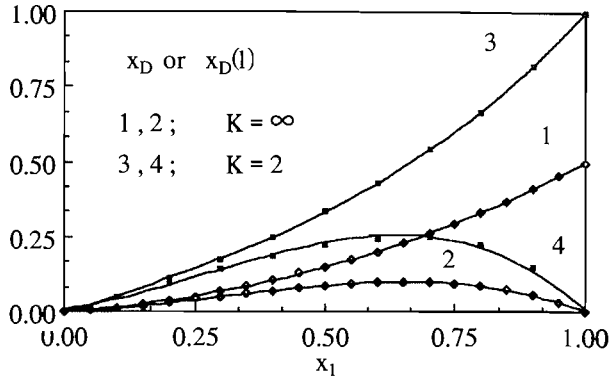


FIG. 1. Total mole fractions of dimers x_D (curves 1 and 3) and the mole fractions of linear dimers $x_D(l)$ (curves 2 and 4) as calculated for $K_D = 2$ and $K_D = \infty$.

form. This is illustrated in Fig. 1, where the mole fraction of the total (x_D) and the linear ($x_D(l)$) dimers are presented as a function of the mole fraction of the nominal (associating) component 1 for $K_D = 2$ and $K_D \rightarrow \infty$.

In the limiting case of complete dimerization ($K_D \rightarrow \infty$), the maximal values of x_D and $x_D(l)$ are

$$[10]\quad x_D^{max} = \frac{x_1}{1+x_2}$$
$$x_D^{max}(l) = \frac{2x_1x_2}{(1+x_2)^2}$$

For $0 < K_D < \infty$, the linear dimers have the maximum at $x = 2/3$, and

$$[11]\quad x_D^{max}(l) = \frac{1}{3}\left\{\left[\frac{\sqrt{1+q}-1}{q} - 1\right]^2 - \frac{1}{4}\right\} q = \frac{32K_D}{9}$$

The excess enthalpy of mixing H^E for the molecular model in question is given by a sum of two contributions $H^E(c)$ and $H^E(l)$ (dimerization reaction and cyclic dimer $\rightarrow$ linear dimer transformation). If the ratio of standard molar enthalpies of the transformation and dimerization reactions is introduced then H^E can be written in the form

$$[12]\quad H^E = \Delta H_D^0 \left\{ \frac{x_D(1+rx_D)}{1+x_D} - \frac{x_1 x_D^0}{1+x_D^0} \right\}$$
$$r = \Delta H_{tr}^0/\Delta H_D^0$$

where

$$[13]\quad \Delta H_D^0 = H^0_{A_2(c)} - 2H^0_A$$
$$\Delta H_{tr}^0 = H^0_{A_2(l)} - H^0_{A_2(c)}$$

In the case of complete dimerization, we have $H^E(c) = 0$ for $K_D \rightarrow \infty$ but $H^E(l) \neq 0$ and therefore

$$[14]\quad H^E(K_D \rightarrow \infty) = \Delta H_{tr}^0 \frac{x_1 x_2}{1+x_2}$$

with an extremum at $x^* = 2 - \sqrt{2}$, where

$$[15]\quad H^E(x^*, K_D \rightarrow \infty) = (\sqrt{2}-1)^2 \Delta H_{tr}^0$$

Can. J. Chem. Downloaded from www.nrcresearchpress.com by 198.100.157.202 on 09/07/12
For personal use only.

Can. J. Chem. Downloaded from www.nrcresearchpress.com by 198.100.157.202 on 09/07/12
For personal use only.

As explained above, the contribution coming from the formation of cyclic dimers $H^E(c)$ is positive, because usually $\Delta H_D^0 < 0$. The sign of the second term, $H^E(l)$, depends on the sign of ΔH_{tr}^0 and therefore the heat of mixing, H^E, can be negative, at least in part, only if $\Delta H_{tr}^0 < 0$. The S-shaped form of H^E can be expected if ΔH_D^0 and ΔH_{tr}^0 have the same sign (*i.e.*, r is positive).

Figure 2 presents a number of curves, $H^E/\Delta H_D^0 = f(x_1; r)$, which are calculated using the same dimerization constant, $K_D = 2$. The effect of K_D on $H^E/\Delta H_D^0 = f(x_1; K_D)$ for constant $r = 1$ is shown in Fig 3.

If the dimerization constant K_D is known independently from H^E (*e.g.*, from activity coefficients derived from vapor pressure measurements), the ratio of the standard enthalpies, r, can be determined from a knowledge of the experimental H^E curve and the location of composition, $x_1 = z$, at which $H^E(z) = 0$. Therefore

$$[16] \quad r = \frac{1}{(1-z)x_D}\left\{\frac{zx_D^0}{1+x_D^0} - \frac{x_D}{1+x_D}\right\}$$

where $x_D = f(K, z)$ is given by eq. [3].

The derivative of $H^E/\Delta H_D^0$ with respect to x_1 is

$$[17] \quad \frac{\partial(H^E/\Delta H_D^0)}{\partial x_1} = \left\{\left[rx_2 + \frac{1}{(1+x_D)^2}\right]\left(\frac{\partial x_D}{\partial x_1}\right) - rx_D - \frac{x_D^0}{1+x_D^0}\right\}\left(\frac{\partial x_D}{\partial x_1}\right) = \frac{2x_D(1+x_D)}{[x_1 + (1+x_2)x_D]}$$

Evidently, the extreme values of H^E are located at the compositions x_1 (min) and x_1 (max) where the derivative in eq. [16] is zero. Therefore, a numerical solution of simultaneous algebraic equations, $H^E(z) = 0$ and $\partial H^E/\partial x_1 = 0$ at x_1 (min) and x_1 (max), (eqs. [3], [16], and [17]) permits the evaluation of three parameters, $K_D, \Delta H_D^0$, and ΔH_{tr}^0 from the experimental H^E data. If the dimerization constant, K_D, is known and r is determined from the condition $H^E(z) = 0$ (eq. [16]), any other experimental point will give the value of ΔH_D^0 using eq. [12]. If the limiting slopes of the H^E curve at $x_1 \longrightarrow 0$ and $x_1 \longrightarrow 1$ are known with sufficient accuracy, $K_D, \Delta H_D^0$, and ΔH_{tr}^0 can be evaluated in a different way. From [17] we have

$$[18] \quad -\left(\frac{\partial H^E}{\partial x_1}\right)_{x_1=0} = \frac{\Delta H_D^0 x_D^0}{(1+x_D^0)} = a_0$$

$$\left(\frac{\partial H^E}{\partial x_1}\right)_{x_1=1} = \frac{\Delta H_D^0 x_D^0(1-x_D^0)}{(1+x_D^0)^2} + \Delta H_{tr}^0 x_D^0 = a_1$$

and therefore

$$[19] \quad r = \left\{\frac{(1+u)}{2u^2}\left[u\left(\frac{a_1}{a_0}\right) - 1\right]\right\}$$

$$u = \frac{1+x_D^0}{1-x_D^0} = \sqrt{1+4K_D}$$

Introducing [19] into [16] we have an algebraic equation which includes K_D as the only unknown parameter. Finally, ΔH_D^0 and ΔH_{tr}^0 can be calculated from the slopes a_0 and a_1 (eqs. [18]) by using the already determined value of the dimerization constant K_D. The same procedure can be applied to evaluation of $K_D, \Delta V_D^0$ and ΔV_{tr}^0 parameters when the excess molar volumes V^E are considered, because V^E are given by equations analogous to eqs. [12]–[19], but the standard molar reaction enthalpies should be replaced by the standard molar reaction volumes.

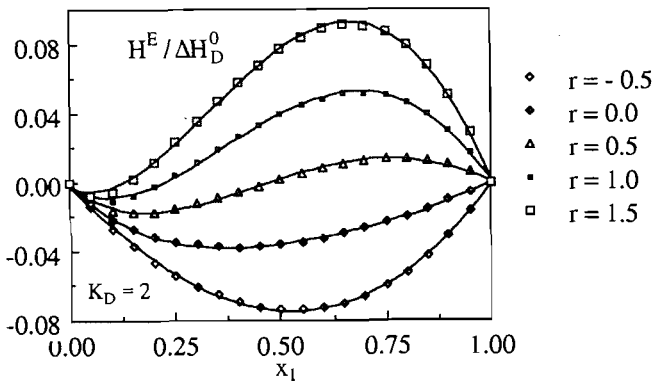


FIG. 2. Reduced excess molar enthalpies of mixing in the modified dimer formation model. Calculated for $K_D = 2$ and several values of r.

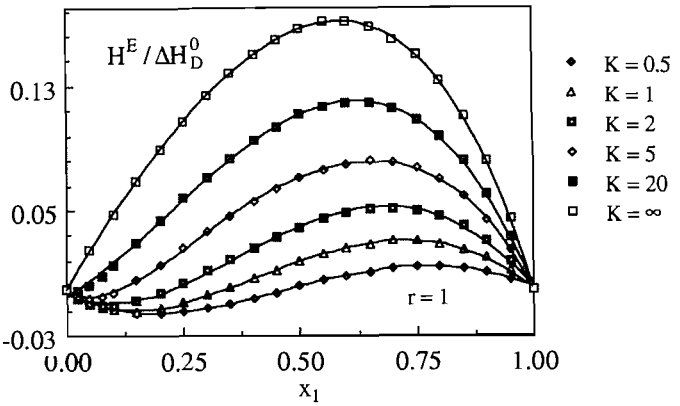


FIG. 3. Reduced excess molar enthalpies of mixing in the modified dimer formation model. Calculated for $r = 1$ and several values of K_D.

Dimers represented by structure **C** are expected to be present in systems where both nominal components are able to participate in dimerization reactions (*e.g.* in mixtures of carboxylic acids). Since only a few elements of the theory were studied in the literature (for details see Apelblat and Manzurola (11)), two cases of special interest (infinite dimerization constants and the pseudoideal behavior of mixtures) are discussed here. For an ideal association of the type $A + B + AB + A_2 + B_2$, we have

$$[20] \quad x_A + x_B + x_{AB} + x_{A_2} + x_{B_2} = 1$$

$$x_1 + x_2 = 1$$

and

$$[21] \quad K_1 = K_D(A_2) = \frac{x_{A_2}}{x_A^2}$$

$$K_2 = K_D(B_2) = \frac{x_{B_2}}{x_B^2}$$

$$K_{12} = K_D(AB) = \frac{x_{AB}}{x_A x_B}$$

where the actual and nominal mole fractions are related by:

$$[22]\quad \begin{aligned} x_A &= x_1(1 + x_{AB} + x_{A_2} + x_{B_2}) - 2x_{A_2} - x_{AB} \\ x_B &= x_2(1 + x_{AB} + x_{A_2} + x_{B_2}) - 2x_{B_2} - x_{AB} \end{aligned}$$

The mole fractions of monomers A and B in pure components 1 and 2 are

$$[23]\quad \begin{aligned} x_A^0 &= \frac{-1 + \sqrt{1 + 4K_1}}{2K_1} \\ x_B^0 &= \frac{-1 + \sqrt{1 + 4K_2}}{2K_2} \end{aligned}$$

with $x_A \leq x_A^0$ and $x_B \leq x_B^0$.

If the equilibrium constants of dimerization reactions are known, eqs. [20] and [21] lead to a fourth order algebraic equation which can be solved numerically to give the mole fractions of actual species as a function of x_1 or x_2.

For infinite dimerization constants ($x_A^0 = x_B^0 = 0$), if follows from [22] that

$$[24]\quad x_{AB} = 2(x_1 - x_{A_2}) = 2(x_2 - x_{B_2})$$

which is often expressed, basing on statistical arguments, as $x_{A_2} = x_1^2, x_{B_2} = x_2^2$, and $x_{AB} = 2x_1x_2$.

If the dimerization constants satisfy the condition (Gross and Wilson (28)):

$$[25]\quad (1 + 2K_{12})^2 = (1 + 4K_1)(1 + 4K_2)$$

the mixture A + B + A_2 + B_2 + AB obeys the Raoult law for any value of x_1. In this pseudoideal case we have $G^E = 0$ with $H^E = TS^E \neq 0$ and $V^E \neq 0$. For large equilibrium constants, K_{12} approaches its statistical value (Fowler and Guggenheim (29)):

$$[26]\quad K_{12}^2 = 4K_1K_2$$

This value of K_{12} satisfies eq. [25] only if the dimerization constants of symmetrical dimers K_1 and K_2 are equal (*i.e.*, $K_{12} = 2K_1 = 2K_2$).

The activity coefficients of the nominal components are

$$[27]\quad \begin{aligned} \gamma_1 &= \frac{x_A}{x_1x_A^0} \\ \gamma_2 &= \frac{x_B}{x_2x_B^0} \end{aligned}$$

With the exception of pseudoideal cases where $\gamma_1 = 1$ and $\gamma_2 = 1$ for any x_1, (eg. [25]), both activity coefficients are larger than unity and the excess Gibbs energy of mixing G^E is always positive reading its maximum at $x_1 = x^*$ where $\gamma_1 = \gamma_2 = \gamma^*$, *i.e.*

$$[28]\quad \frac{x_A}{x_B} = \frac{K_2x^*[\sqrt{1 + 4K_1} - 1]}{K_1(1 - x^*)[\sqrt{1 + 4K_2} - 1]}$$

From a knowledge of $x^*, G^E(x^*) = RT \ln \gamma^*$ and the limiting slopes

$$[29]\quad \begin{aligned} \left(\frac{\partial G^E}{\partial x_1}\right)_{x_1=0} &= RT \ln \gamma_1^\infty \\ \left(\frac{\partial G^E}{\partial x_1}\right)_{x_1=1} &= -RT \ln \gamma_2^\infty \end{aligned}$$

equilibrium constants can be evaluated because activity coefficients at infinite dilution are given by:

$$[30]\quad \begin{aligned} \gamma_1^\infty &= \frac{2K_1[1 + 4K_2 - \sqrt{1 + 4K_2}]}{(\sqrt{1 + 4K_1} - 1)[2K_2 + K_{12}(\sqrt{1 + 4K_2} - 1)]} \\ \gamma_2^\infty &= \frac{2K_2[1 + 4K_1 - \sqrt{1 + 4K_1}]}{(\sqrt{1 + 4K_2} - 1)[2K_1 + K_{12}(\sqrt{1 + 4K_1} - 1)]} \end{aligned}$$

Since K_{12} is difficult to determine independently, its value is usually replaced by [26] and this considerably simplifies the calculations.

The excess molar enthalpy of mixing H^E is a sum of three contributions:

$$[31]\quad \begin{aligned} H^E &= H^E(A_2) + H^E(B_2) + H^E(AB) \\ H^E(A_2) &= \Delta H_{A_2}^0 \left[\frac{x_{A_2}}{(2 - x_A - x_B)} - \frac{x_1(1 - x_A^0)}{(2 - x_A^0)}\right] \\ H^E(B_2) &= \Delta H_{B_2}^0 \left[\frac{x_{B_2}}{(2 - x_A - x_B)} - \frac{x_2(1 - x_B^0)}{(2 - x_B^0)}\right] \\ H^E(AB) &= \Delta H_{AB}^0 \frac{x_{AB}}{(2 - x_A - x_B)} \end{aligned}$$

where

$$[32]\quad \begin{aligned} \Delta H_{A_2}^0 &= H_{A_2}^0 - 2H_A^0 \\ \Delta H_{B_2}^0 &= H_{B_2}^0 - 2H_B^0 \\ \Delta H_{AB}^0 &= H_{AB}^0 - H_A^0 - H_B^0 \end{aligned}$$

A general analysis of eq. [31] is difficult, because the heat of mixing H^E, even if K_{12} is replaced by [26], depends on five adjustable parameters: two equilibrium constants and three standard molar reactions enthalpies. The sign of the first two terms is opposite to that of the standard enthalpies of dimerization reactions while the contribution coming from formation of mixed dimers has the same sign as the standard reaction enthalpy. However, for infinite dimerization constants, expressions [31] take a very simple form:

$$[33]\quad \begin{aligned} H^E &= \Delta H^0 x_1x_2/2 \\ \Delta H^0 &= 2H_{AB}^0 - H_{A_2}^0 - H_{B_2}^0 \end{aligned}$$

i.e., in this case, the excess molar enthalpy of mixing H^E is symmetrical with respect to composition. In pseudoideal mixtures, H^E is given by

$$[34]\quad \begin{aligned} H^E &= H^E(A_2) + H^E(B_2) + H^E(AB) \\ H^E(A_2) &= \Delta H_{A_2}^0 \left[\frac{x_1}{(2 - x_A - x_B)} - \frac{1}{(2 - x_A^0)}\right] \\ H^E(B_2) &= \Delta H_{B_2}^0 \left[\frac{x_2}{(2 - x_A - x_B)} - \frac{1}{(2 - x_B^0)}\right] \\ H^E(AB) &= \Delta H_{AB}^0 \frac{x_1x_2(2 - x_A^0 - x_B^0)}{(2 - x_A - x_B)} \end{aligned}$$

where $x_A = x_1x_A^0$ and $x_B = x_2x_B^0$ and x_A^0, x_B^0 are given by eq. [23].

If $K_{12} = 2K_1 = 2K_2$, then from [34] the heat of mixing is

Can. J. Chem. Downloaded from www.nrcresearchpress.com by 198.100.157.202 on 09/07/12
For personal use only.

$$[35]\quad H^E = \Delta H^0 \frac{x_1 x_2 (1 - x_A^0)}{(2 - x_A^0)}$$

and for infinite equilibrium constants, expressions in [34] and [35] are identical with [33].

In a general case, the derivative of H^E with respect to x_1 is given by a complex expression, but its limiting slope can be evaluated from

$$[36]\quad \left(\frac{\partial H^E}{\partial x_1}\right)_{x_1=0} = \Delta H^0_{AB} \frac{K_{12} x_B^0}{1 + K_{12} x_B^0} - \Delta H^0_{A_2} \frac{(1 - x_A^0)}{(2 - x_A^0)} - \frac{\Delta H^0_{B_2}}{(2 - x_B^0)} \left[\frac{(1 - x_B^0)}{1 + 2K_2 x_B^0} + \frac{K_{12} x_B^0 (1 - x_B^0)}{1 + K_{12} x_B^0}\right]$$

and

$$[37]\quad \left(\frac{\partial H^E}{\partial x_1}\right)_{x_1=1} = -\Delta H^0_{AB} \frac{K_{12} x_A^0}{1 + K_{12} x_A^0} + \Delta H^0_{B_2} \frac{(1 - x_B^0)}{(2 - x_B^0)} + \frac{\Delta H^0_{A_2}}{(2 - x_A^0)} \left[\frac{(1 - x_A^0)}{1 + 2K_1 x_A^0} + \frac{K_{12} x_A^0 (1 - x_A^0)}{1 + K_{12} x_A^0}\right]$$

These expressions take a simple form only for infinite equilibrium constants

$$[38]\quad \left(\frac{\partial H^E}{\partial x_1}\right)_{x_1=0} = -\left(\frac{\partial H^E}{\partial x_1}\right)_{x_1=1} = \frac{\Delta H^0}{2}$$

Excess molar volumes V^E are expressed by the same equations if the standard molar reaction enthalpies are replaced by the corresponding standard molar reaction volumes.

A large number of adjustable parameters and complexity of equations makes the mixed dimer formation rather difficult for a direct application. In the case of binary mixtures of carboxylic acids, the observed very small thermal effects (H^E is endothermic and symmetrical, Haase *et al.* (30, 31) and the absence of G^E, H^E, and V^E functions at the same temperature is an additional source of difficulties in the evaluation of these parameters. However, as has been shown in [11], the use of limiting expressions of the type [35], gives a reasonable representation of H^E and V^E functions in binary mixtures of carboxylic acids with the exception of the formic acid – acetic acid system. Mixing of formic acid with acetic acid is accompanied by contraction and expansion of the volume, but once again the overall effect is extremely small. The unusual form of V^E curve is probably associated with the presence of cyclic and linear dimers in the mixture. They can be included in the mixed dimers formation model in a similar way as previously (for example as in eq. [8]), but this procedure will introduce new parameters (one, two or even three standard molar reaction enthalpies) and increased complexity in model expressions. Evidently, such modification can only be justified if there is strong, experimental evidence on the importance of linear associates in the system.

The modified Mecke–Kempter models

If the association is not limited to the formation of dimers, but higher associates are also formed and the equilibrium constants of the consecutive reactions are independent of the degree of association

$$[39]\quad A + A_{n-1} \rightleftarrows A_n \qquad K_n = K^{n-1} \qquad n = 2, 3, 4, \ldots \infty$$

The continuous model ($A + B + A_2 + A_3 + A_4 + \cdots A_n + \cdots$) is called the Mecke–Kempter model. The model was modified by Coggeshall and Saier (1951) by introducing two equilibrium constants K_2 and K for $n > 2$. However, in both versions it is supposed that all associates have a linear form. The mathematical aspect of the ideal continuous association model was considered by Kehiaian (24, 25) and the most important results are presented here to provide a comparison between the different models. The material balance for the actually presented species is

$$[40]\quad x_A + x_B + \sum_{n=2}^{\infty} x_{A_n} = 1 \qquad x_{A_n} = K^{n-1} x_A^n$$

and the mole fractions of the monomers A and B are:

$$[41]\quad x_A = \frac{1}{(1 + K)} \left\{1 - \frac{2x_2}{1 + Q}\right\} \qquad x_B = \left\{1 - \frac{2x_1}{1 + Q}\right\} \qquad Q = \sqrt{1 + 4K x_1 x_2}$$

In the Mecke–Kempter model, the standard reaction enthalpies are assumed to be linearly related to the standard enthalpy of formation of one bond ΔH^0

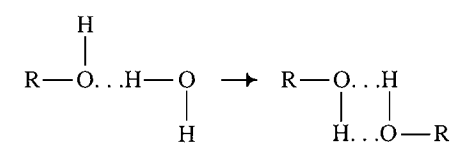
$$[42]\quad \Delta H_n^0 = (n - 1)\Delta H^0 \qquad \Delta H_n^0 = H^0_{A_n} - n H^0_A$$

and the excess molar enthalpy of mixing H^E is

$$[43]\quad H^E = \Delta H^0 \left\{\frac{1 - Q}{2(1 + K)}\right\}$$

H^E is symmetrical with respect to the composition and the function $H^E/\Delta H^0 = f(x_1; K)$ is always negative and becomes zero for $K \to 0$ and $K \to \infty$. Since usually $\Delta H^0 < 0$, H^E is maximum at equimolar mixtures.

A distinction between linear and cyclic dimers in the Mecke–Kempter model can be introduced in the same way as previously (eq. [8]). The addition of component 2 to the associating component 1 will create mixtures with the same final states (monomers of A and B, cyclic and linear dimers and higher linear associates of A). However, with regard to pure component A we have to distinguish between different situations. If it is assumed that in pure alcohols there exist only monomers and linear associates, then an addition of nonpolar B molecules will facilitate the formation of cyclic dimers, *i.e.*, we have the linear dimer → cyclic dimer transformation:



and therefore

Can. J. Chem. Downloaded from www.nrcresearchpress.com by 198.100.157.202 on 09/07/12
For personal use only.

$$[44]\quad \begin{aligned} x_D(c) &= x_D x_B = K x_A^2 x_B \\ x_D(l) &= x_D(1 - x_B) \end{aligned}$$

On the other hand, in pure carboxylic acids the existence of monomers, cyclic dimers, and higher linear associates or only monomers with cyclic dimers can be assumed. An addition of polar molecules B will support the cyclic dimer → linear dimer transformation and therefore:

$$[45]\quad \begin{aligned} x_D(l) &= x_D x_B = K x_A^2 x_B \\ x_D(c) &= x_D(1 - x_B) \end{aligned}$$

In the case of excess Gibbs energy of mixing G^E, there is essentially no difference between the cases described by eqs. [44] and [45] because the initial states of the species (monomer, dimers and higher associates) are the same. However, if only monomers and cyclic dimers are present in pure component 1, then this model differs from the classical Mecke–Kempter association model because here the higher linear associates come only from that part of cyclic dimers which is converted to the linear form. This case, being more complex, requires a separate treatment.

The excess molar enthalpy of mixing, H^E, for the continuous association coupled with the linear dimer → cyclic dimer transformation (eq. [44]) is given by:

$$[46]\quad H^E = \left\{ \Delta H^0 \frac{(1-Q)}{2(1+K)} + \Delta H^0_{tr} x_2 K \left[\frac{(x_1 - x_2 + Q)}{(1+K)(1+Q)} \right]^2 \right\}$$

$$\Delta H^0 = H^0_{A_n(l)} - H^0_{A_{n-1}(l)}$$

$$\Delta H^0_{tr} = H^0_{A_2(c)} - H^0_{A_2(l)}$$

where Q is defined in [41].

H^E is a rather complex function of x_1 and the parameters K and $r = \Delta H^0_{tr}/\Delta H^0$. For any x_1 and r, the function tends to zero for $K \to 0$ and $K \to \infty$. For positive values of r, the reduced excess molar enthalpy of mixing, $H^E/\Delta H^0$ is a sum of two terms which have opposite signs. To put the modified Mecke–Kempter and the dimer formation models on the same basis, $H^E/\Delta H^0 = f(x_1; r; K = 1)$ in Fig. 4 were calculated for mixtures having the same mole fraction of the monomer in pure component 1. In this case, the dimerization constant K_D (in Fig. 2, $K_D = 2$) is correlated to the Mecke–Kempter constant K as follows

$$[47]\quad K_D = K(K+1)$$

The effect of the equilibrium constant K for the same r is shown in Fig. 5 by plotting

$$H^E/\Delta H^0 = f(x_1; K; r = 4)$$

The evaluation of parameters $K, \Delta H^0$, and ΔH^0_{tr} in eq. [46] can be performed by a number of procedures, using for example the slopes of H^E.

$$\left(\frac{\partial H^E}{\partial x_1}\right)_{x_1=0} = \Delta H^0 \frac{K}{1+K}$$

$$[48]\quad \left(\frac{\partial H^E}{\partial x_1}\right)_{x_1=1} = \Delta H^0 \frac{K}{1+K} - \Delta H^0_{tr} \frac{K}{(1+K)^2}$$

$$\left(\frac{\partial H^E}{\partial x_1}\right)_{x_1=1/2} = \frac{\Delta H^0_{tr} K \sqrt{1+K}[2 - \sqrt{1+K}]}{[(1+K)(1+\sqrt{1+K})]^2}$$

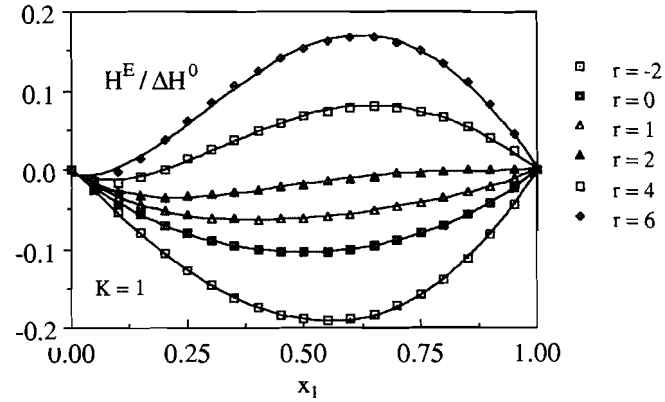


FIG. 4. Reduced excess molar enthalpies of mixing in the modified Mecke–Kempter model. Calculated for $K = 1$ and several values of r.

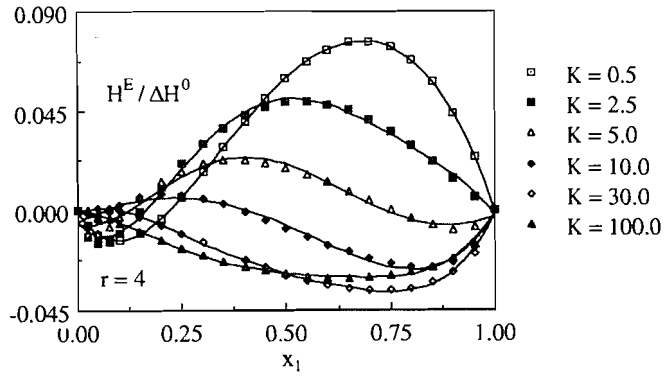


FIG. 5. Reduced excess molar enthalpies of mixing in the modified Mecke–Kempter model. Calculated for $r = 4$ and several values of K.

and the value of H^E at equimolar mixtures is

$$[49]\quad H^E\left(\frac{1}{2}\right) = \frac{\Delta H^0(1 - \sqrt{1+K})}{2(1+K)} + \frac{\Delta H^0_{tr} K \sqrt{1+K}}{2[(1+K)(1+\sqrt{1+K})]^2}$$

If the experiment H^E vanishes at some point, $x_1 = z$. For $H^E(z) = 0$, the ratio of standard reaction enthalpies is directly available from [46], if the equilibrium constant K is independently known.

When continuous association is coupled with the cyclic dimer → linear dimer transformation (eq. [45]), the excess molar enthalpy of mixing takes the form:

$$[50]\quad H^E = \left\{ \frac{\Delta H^0(1-Q)}{2(1+K)} + \frac{\Delta H^0_{tr} x_1 K}{(1-K)^2} \times \left[\frac{1}{1+K} - \frac{2x_2(x_1 - x_2 + Q)^2}{(x_2 - x_1 + Q)(1+Q)^2} \right] \right\}$$

$$\Delta H^0_{tr} = H^0_{A_2(l)} - H^0_{A_2(c)}$$

The reduced excess molar enthalpies of mixing, $H^E/\Delta H^0 = f(x_1; K; r)$ are plotted in Fig. 6, 7, and 8 to show the effect of the equilibrium constant K and the ratio of standard reaction enthalpies r on the behavior of H^E curves.

The parameters included in [50], $K, \Delta H^0$ and ΔH^0_{tr}, can be

Can. J. Chem. Downloaded from www.nrcresearchpress.com by 198.100.157.202 on 09/07/12
For personal use only.

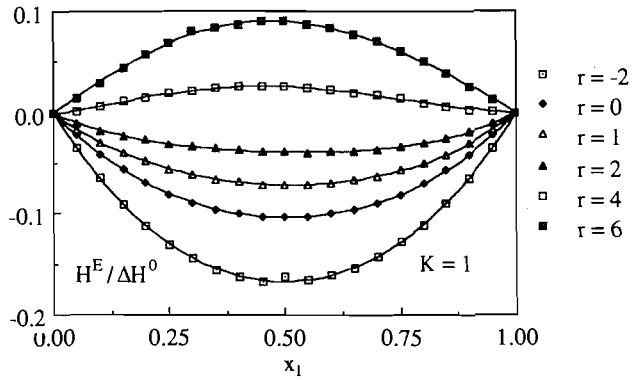


FIG. 6. Reduced excess molar enthalpies of mixing in the modified Mecke–Kempter model. Calculated for $K = 1$ and several values of r.

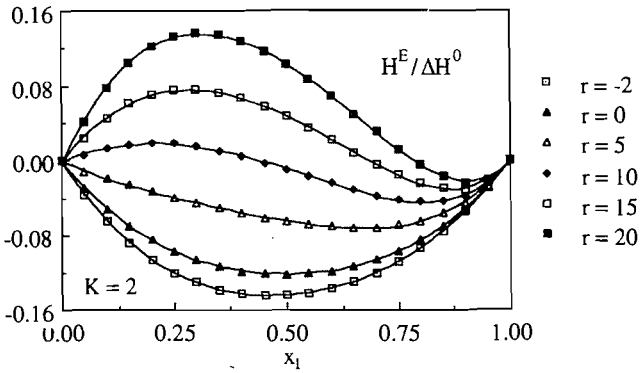


FIG. 7. Reduced excess molar enthalpies of mixing in the modified Mecke–Kempter model. Calculated for $K = 2$ and several values of r.

calculated from

$$\left(\frac{\partial H^E}{\partial x_1}\right)_{x_1=0} = -\Delta H^0 \frac{K}{1+K} + \Delta H^0_{tr} \frac{K}{(1+K)^3}$$

[51]
$$\left(\frac{\partial H^E}{\partial x_1}\right)_{x_1=1} = \Delta H^0 \frac{K}{1+K} - \Delta H^0_{tr} \frac{2K}{(1+K)^3}$$

$$\left(\frac{\partial H^E}{\partial x_1}\right)_{x_1=1/2} = \Delta H^0_{tr} \frac{K}{(1+K)^2} \cdots \times \left[\frac{1}{1+K} - \frac{1}{(1+\sqrt{1+K})^2}\right]$$

and

[52]
$$H^E\left(\frac{1}{2}\right) = \left\{\frac{\Delta H^0(1-\sqrt{1+K})}{2(1+K)} + \frac{\Delta H^0_{tr} K}{2(1+K)^2} \times \left[\frac{1}{1+K} - \frac{\sqrt{1+K}}{(1+\sqrt{1+K})^2}\right]\right\}$$

As can be seen in Fig. 4–8, the heat of mixing H^E (or V^E when ΔH^0 and ΔH^0_{tr} are replaced by the corresponding values of ΔV^0 and ΔV^0_{tr}) is always an asymmetrical function of composition in the modified Mecke–Kempter models ($r \neq 0$, eq. [46] or [50]). Depending on the chosen set of parameters, the function has one, two, or even three extrema (*e.g.* for $K = 1.40$ and $r = 4.98$, H^E calculated from [50] has two

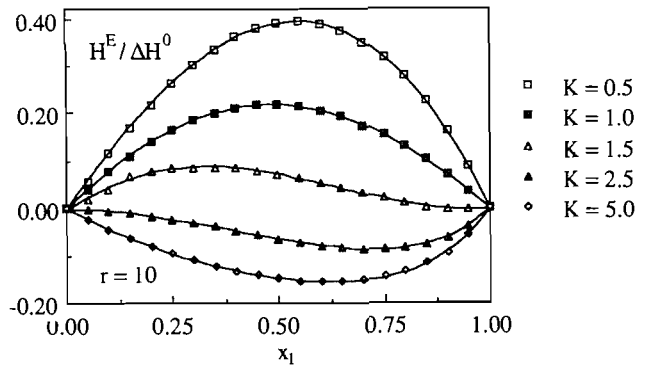


FIG. 8. Reduced excess molar enthalpies of mixing in the modified Mecke–Kempter model. Calculated for $r = 10$ and several values of K.

minima and one maximum). However, at finite concentrations, the first and second derivatives of H^E (or V^E) with respect to x_1 are given by complex algebraic expressions and therefore evaluation of the parameters from a knowledge of extremal properties of experimental H^E and V^E curves is rather difficult. Since G^E in both modified and classical Mecke–Kempter models is a symmetrical function of composition and experimental G^E curves are usually nearly symmetrical (in contrast to H^E curves), the equilibrium constant K can be derived from G^E values at equimolar mixtures (10):

[53]
$$G^E\left(\frac{1}{2}\right) = RT \ln\left[\frac{2\sqrt{1+K}}{1+\sqrt{1+K}}\right]$$

Evaluation of K from vapor pressure measurements (eq. [53]), permits a direct determination of other parameters from calorimetric measurements. We need heats of mixing at equimolar mixtures, $H^E(x_1 = 1/2)$, (eq. [49] or [42]) and one accurate value of the limiting slope of H^E (eq. [48] or [51]). Evidently, the ratio of standard reaction enthalpies r can be calculated from the condition $H^E(z) = 0$, if H^E as a function of composition changes its sign.

The acetic acid – water system

To illustrate the applicability of association models presented here, the acetic acid – water system at 298.15 K was chosen. In carboxylic acid – water mixtures, we have a complete set of the excess thermodynamic functions only for this system. Hansen *et al.* (26) measured vapor pressures in the system and expressed in the results in terms of activity coefficients. The excess Gibbs energy of mixing G^E is positive and almost symmetrical with respect to composition. Heats of mixing H^E (measured during the 1972–1977 period) were compiled by Christensen *et al.* (27). The form of H^E is strongly asymmetrical. In dilute aqueous solutions of acetic acid H^E is slightly negative and becomes positive with increasing acid concentration. The excess molar volumes V^E were determined in a number of works (for details see Apelbalt and Manzurola (10)). The experimental V^E curve is a nearly perfect symmetrical form (the minimal value is $V^E(x_1 = 1/2) = -1.16$ cm^3 mol^{-1}) and in very dilute solutions of the acid, V^E can be represented by:

[54]
$$V^E = -5.7548x_1 + 4.9285x_1^2$$

As has been demonstrated (10), predictions based on the formation of cyclic or open dimers are inconsistent with behavior

Can. J. Chem. Downloaded from www.nrcresearchpress.com by 198.100.157.202 on 09/07/12
For personal use only.

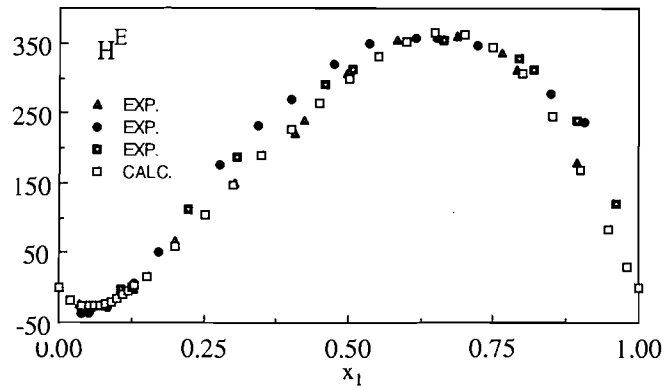


FIG. 9. Comparison between experimental and calculated values of H^E (J mol^{-1}) in the acetic acid – water system at 298.15 K (see text).

of the excess thermodynamic functions. On the other hand, the classical Mecke–Kempter model represents in a satisfactory way the excess Gibbs energy of mixing G^E and the excess molar volume V^E but is unable to predict the correct form of the excess molar enthalpy of mixing H^E. An adequate description of G^E and V^E is possible using the equilibrium $K = 1.40$ and the molar reaction volume, $\Delta V^0 = 10.14$ cm^3 mol^{-1}. Much against expectations, it was found that the continuous association coupled with the linear dimer $\rightarrow$ cyclic dimer transformation (eq. [44]) and not with the cyclic dimer $\rightarrow$ linear dimer transformation (eq. [45]) is suitable to represent G^E, H^E, and V^E functions in the acetic acid – water system. However, it should be mentioned that the initial state of the system is a mixture of linear associates (10, 12), and not the pure acetic acid where evidently the dimer is predominantly cyclic. Since both standard molar reaction enthalpies are endothermic and $\Delta G^0 < 0$, the standard entropy change ΔS^0 is positive and dominates the entropy – enthalpy relations. It seems the an increase in disorder results from a new arrangement of water molecules in the mixture, caused by the self-associated reaction of acetic acid. This indicates the importance of hydrated species which are completely excluded from our analysis. These species may facilitate the linear dimer $\rightarrow$ cyclic dimer transformation and not the opposite process, when water is added to acetic acid.

Introducing the equilibrium constant $K = 1.40$ into [46] and considering that H^E vanishes at about $x_1 = z = 0.125$, the ratio of standard reaction enthalpies is $r = 5.04$ and finally the standard enthalpies are $\Delta H^0_{tr} = 14.6$ kJ mol^{-1} and $\Delta H^0 = 2.9$ kJ mol^{-1}.

Using these parameters, the excess molar enthalpies of mixing H^E were calculated from [46] and compared with the calorimetric results compiled for the system by Christensen *et al.* (27). As can be seen in Fig. 9, there is quite a reasonable agreement between calculated and experimental results, especially a very satisfactory representation of a not-frequently observed form of H^E. In the case of V^E, it is possible to obtain an accurate value of the limiting slope of V^E at $x_1 = 0$ (eq. [54]) and compare it with [48]

$$[55] \quad \left(\frac{\partial V^E}{\partial x_1}\right)_{x_1=0} = -\Delta V^0 \frac{K}{1+K} = -5.7548$$

From [55], using the equilibrium constant $K = 1.40$, the standard reaction volume is $\Delta V^0 = 9.87$ cm^3 mol^{-1}. Introducing these parameters and the value of $V^E(x_1 = 1/2) = -1.16$ cm^3

TABLE 1. Excess molar volumes V^E (cm^3 mol^{-1}) in the acetic acid – water system at 298.15 K

x_1	$-V^E$ (exp.)	$-V^E (r = 0)$	$-V^E (r = -0.06935)$
0.00227	0.013	0.013	0.013
0.00368	0.021	0.022	0.021
0.00527	0.030	0.031	0.030
0.00753	0.042	0.044	0.043
0.00962	0.056	0.056	0.054
0.01130	0.061	0.065	0.063
0.01257	0.069	0.071	0.070
0.01400	0.076	0.080	0.078
0.01530	0.087	0.087	0.085
0.01590	0.089	0.091	0.088
0.01616	0.099	0.092	0.090
0.01858	0.10	0.10	0.10
0.02138	0.12	0.12	0.12
0.02194	0.12	0.12	0.12
0.02473	0.14	0.14	0.14
0.02500	0.14	0.14	0.14
0.02688	0.15	0.15	0.15
0.02964	0.16	0.16	0.16
0.02985	0.16	0.16	0.16
0.03220	0.18	0.18	0.17
0.03316	0.18	0.18	0.18
0.03456	0.19	0.19	0.19
0.0497	0.27	0.26	0.26
0.0697	0.36	0.35	0.35
0.0747	0.38	0.38	0.37
0.1141	0.54	0.53	0.52
0.1666	0.71	0.70	0.70
0.1961	0.79	0.79	0.78
0.2308	0.87	0.87	0.86
0.2683	0.94	0.95	0.94
0.3095	1.01	1.02	1.01
0.4118	1.12	1.13	1.13
0.5474	1.15	1.15	1.15
0.6294	1.11	1.10	1.10
0.7292	0.98	0.95	0.96
0.7731	0.89	0.86	0.86
0.8491	0.69	0.66	0.66
0.8749	0.61	0.61	0.57
0.9141	0.44	0.42	0.42
0.9237	0.41	0.38	0.38
0.9266	0.38	0.37	0.37
0.9141	0.44	0.42	0.42
0.9237	0.41	0.38	0.38
0.9266	0.38	0.37	0.37
0.9337	0.35	0.34	0.34
0.9360	0.37	0.33	0.33
0.9371	0.34	0.32	0.32
0.9360	0.37	0.33	0.33
0.9371	0.34	0.32	0.32
0.9488	0.30	0.27	0.27
0.9503	0.26	0.26	0.26
0.9575	0.24	0.23	0.23
0.9742	0.17	0.14	0.14
0.9769	0.14	0.13	0.13
0.9830	0.11	0.097	0.097
0.9841	0.13	0.091	0.091
0.9884	0.082	0.067	0.069
0.9904	0.072	0.056	0.056
0.9906	0.070	0.054	0.054
0.9927	0.060	0.042	0.043

Can. J. Chem. Downloaded from www.nrcresearchpress.com by 198.100.157.202 on 09/07/12
For personal use only.

mol^{-1} into [39] we have $\Delta V^0_{tr} = V^0_{A_2(c)} - V^0_{A_2(l)} = -0.684$ cm^3 mol^{-1}, *i.e.* as expected the molar volume of the linear dimer $V^0_{A_2(l)}$ is larger than that of the cyclic dimer $V^0_{A_2(c)}$.

Table 1 lists the calculated and experimental values (10) of V^E in the acetic acid – water system at 298.15 K. The calculations were performed using the classical Mecke–Kempter model ($K = 1.40$ and $\Delta V^0 = 10.14$ cm^3 mol^{-1}) and the modified Mecke–Kempter model ($K = 1.40, \Delta V^0 = 9.87$ cm^3 mol^{-1}, and $\Delta V^0_{tr} = -0.684$ cm^3 mol^{-1}, eq. [46]). As can be seen, both models reproduce values V^E nicely, but evidently an introduction of ΔV^0_{tr} to calculations slightly improves the agreement between the experimental and calculated results.

Thus, in terms of the modified Mecke–Kempter model, it is possible to present a consistent description of G^E, H^E, and V^E functions in the acetic acid – water system. Evidently, a successful description of the excess thermodynamic functions derived from different properties of the system (vapor pressures, heats of mixing, and densities) justifies the choice of molecular model, but without additional support (*e.g.* from spectroscopic measurements) the modified Mecke–Kempter model cannot be considered unique interpretation of experimental results. The excess molar enthalpy of mixing H^E can also be represented by the dimerization reaction coupled with the cyclic dimer $\rightarrow$ linear dimer transformation ($K_D = 3.30$ and $\Delta H^0_D = 4.1$ kJ mol^{-1}, $\Delta H^0_{tr} = 4.9$ kJ mol^{-1}), even better than by the modified Mecke–Kempter model, but such description is inconsistent with the behavior of the G^E and V^E functions.

1. G. Allen and E. F. Caldin. Q. Rev. Chem. Soc. **7**, 255 (1953).
2. A. L. Propov. Anhydrous acetic acid as nonaqueous solvent and other carboxylic acids. *In* The chemistry of nonaqueous solvents Vol. 3. *Edited by* J. J. Lagowsky. Academic Press, New York. 1970. pp. 241–332.
3. J. Chao and B. J. Zwolinski. J. Phys. Chem. Ref. Data, **7**, 363 (1978).
4. K. Marsh and F. Kohler. J. Mol. Liquids, **30**, 13 (1985).
5. P. Waldstein and L. A. Blatz. J. Phys. Chem. **71**, 2271 (1967).
6. M. A. Goldman and M. T. Emerson. J. Phys. Chem. **77**, 2295 (1973).
7. P. S. R. K. Rao and C. R. Rao. J. Phys. Chem. Jpn. **37**, 864 (1974).
8. P. Getta, M. Stockhausen and V. Wessels. Z. Phys. Chem N.F. **158**, 155 (1988).
9. H. Kehiaian and K. Sosnkowska-Kehiaian. Bull. Acad. Polon. Sci. Ser. Sci. Chem. **11**, 583 (1963); **11**, 591 (1963).
10. A. Apelblat and E. Manzurola. Fluid Phase Equilibr. **32**, 163 (1987).
11. A. Apelblat and E. Manzurola. Fluid Phase Equilibr. **38**, 273 (1987).
12. E. E. Schrier, M. Pottle, and H. A. Scheraga. J. Am. Chem. Soc. **86**, 3444 (1964).
13. R. D. Corsaro and G. Atkinson. J. Chem. Phys. **54**, 4090 (1971).
14. J. H. Clark and J. Emsley. J. Chem. Soc. 2154 (1973).
15. M. Remko. Z. Phys. Chem. N. F. **104**, 177 (1977).
16. G. Brink and L. Glasser. J. Phys. Chem. **82**, 1000 (1978).
17. N. D. Coggeshall and E. L. Saier. J. Am. Chem. Soc. **73**, 5414 (1951).
18. L. Sarolea-Mathot. Trans. Faraday Soc. **49**, 8 (1953).
19. R. Ginell. Association theory. The phases of matter and their transformations. Elsevier Sci. Publ. Co., Amterdam. 1979.
20. S. D. Christian. J. Phys. Chem. **61**, 1441 (1957).
21. H. E. Affsprung, S. D. Christian, and A. M. Melnick. Spectrochim. Acta, **20**, 285 (1964).
22. J. Sekine, M. Isayama, S. Yamaguchi, and H. Moriya. Bull. Chem. Soc. Jpn. **40**, 27 (1967).
23. Y. Fujii, Y. Kawachi, and M. Tanaka. J. Chem. Soc. Faraday Trans. 1, **77**, 63 (1981).
24. H. Kehiaian. Bull Acad. Polon. Sci. Ser. Chem. **12**, 497 (1964).
25. H. Kehiaian. Bull Acad. Polon. Sci. Ser. Chem. **12**, 567 (1964).
26. R. S. Hansen, F. A. Miller, and S. D. Christian. J. Phys. Chem. **59**, 391 (1955).
27. J. J. Christensen, R. W. Hanks and R. M. Izatt. Handbook of heats of mixing. J. Wiley and Sons, New York. 1982. pp. 1394–1397.
28. F. Gross and G. L. Wilson. Z. Phys. Chem. N. F., **41**, 304 (1964).
29. R. Fowler and E. A. Guggenheim. Statistical thermodynamics. Cambridge University Press, Cambridge, 1952. p. 167.
30. R. Haase, H. J. Jansen, K. Puder, and B. Winter. Z. Naturforsch. **38**A, 659 (1979).
31. R. Haase, H. J. Jansen, and B. Winter. Z. Naturforsch. **43**A, 1400 (1983).

Can. J. Chem. Downloaded from www.nrcresearchpress.com by 198.100.157.202 on 09/07/12
For personal use only.

The structure of the tetrachlorohydroxotellurate(IV) anion in $KTeCl_4(OH)\cdot 0.5H_2O$ and $KTeCl_4(OH)$

J. B. MILNE

Department of Chemistry, University of Ottawa, Ottawa, Ont., Canada K1N 6N5

AND

E. J. GABE AND C. BENSIMON

Chemistry Division, National Research Council, Ottawa, Ont., Canada K1A 0R9

Received July 26, 1990

J. B. MILNE, E. J. GABE, and C. BENSIMON. Can. J. Chem. **69**, 648 (1991).

Three compounds containing the tetrachlorohydroxotellurate(IV) anion, $\phi_4As[TeCl_4(OH)]\cdot H_2O$, $K[TeCl_4(OH)]\cdot 0.5H_2O$, and $K[TeCl_4(OH)]$, have been prepared. The crystal structure of $K[TeCl_4(OH)]\cdot 0.5H_2O$ has been determined. The structure contains isolated square pyramidal $TeCl_4(OH)^-$ anions with OH axial. Vibrational spectroscopy shows that $\phi_4As[TeCl_4(OH)]\cdot H_2O$ and $K[TeCl_4(OH)]\cdot 0.5H_2O$ both contain isolated anions but that, in $K[TeCl_4(OH)]$, the anion is polymerized with chloride bridging. The hydroxo group, like the fluoro group, acts to hinder coordination at the site *trans* to it on Te(IV).

Key words: tellurium(IV) complexes, chlorotellurate(IV), X-ray structure, vibrational spectroscopy.

J. B. MILNE, E. J. GABE et C. BENSIMON. Can. J. Chem. **69**, 648 (1991).

Trois composés, qui contiennent l'anion tetrachlorohydroxotellurate(IV), $\phi_4As[TeCl_4(OH)]\cdot H_2O$, $K[TeCl_4(OH)]\cdot 0.5H_2O$ et $K[TeCl_4(OH)]$, ont été préparés. La structure crystallographique de $K[TeCl_4(OH)]\cdot 0.5H_2O$ a été déterminée. La structure contient les anions $TeCl_4(OH)^-$ en forme d'une pyramide à base carré avec le groupe hydroxo, axial. Les spectres de vibration montrent que $\phi_4As[TeCl_4(OH)]\cdot H_2O$ et $K[TeCl_4(OH)]\cdot 0.5H_2O$ contiennent les anions isolés alors que l'anion dans $K[TeCl_4(OH)]$ est polymerisé avec les ponts de chlore. Le groupe hydroxo agit, comme le groupe fluoro, pour gêner le liaison *trans* à par rapport lui sur Te(IV).

Mots clés : complexes de tellure(IV), chlorotellurate(IV), structure par diffraction des rayons X, spectroscopie de vibration.

Introduction

The stereochemical activity of the non-bonded valence electron pair in Te(IV) species has been the subject of many studies. The non-bonded pair is inactive in the hexacoordinate anions, TeX_6^{2-} (X = Cl, Br, I), which all possess an essentially octahedral structure (1, 2), except in some cases where hydrogen bonding is important (3). The corresponding hexafluorotellurate(IV) anion is unknown (4, 5). The TeF_5^- ion is square pyramidal (6) and shows no tendency to form condensed ions or to bind a sixth ligand even when a possible ligand (Cl^-, H_2O) is present in the structure (4, 7). On the other hand, $TeCl_5^-$ and $TeBr_5^-$ ions exhibit a pronounced tendency either to polymerize (8–10) or to attach a sixth ligand to form TeX_6^{2-} or $TeX_5Y^{-(2-)}$ (11–13). Vibrational spectroscopy indicates that the isolated $TeCl_5^-$ ion exists in some cases where bulky cations are present (14).

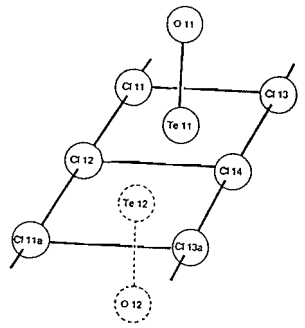
Raman studies have indicated that the hydrolysis of the $TeCl_6^{2-}$ ion does not yield $TeCl_5(OH)^{2-}$, as might be expected, but that the first equilibrium involves formation of the $TeCl_4(OH)^-$ ion (15). The crystal structure of $\phi_4As[TeCl_4O_2H_3]$ has been determined (16) but it was not possible to establish whether the tellurium-containing ion was an oxotellurate, $TeCl_4O^{2-}$, or a hydroxotellurate, $TeCl_4(OH)^-$. To establish the structure of the $TeCl_4(OH)^-$ anion and to provide a better understanding of the stereochemical effect of the non-bonded electron pair, a study of the salts containing this anion was carried out.

Experimental section

Materials and apparatus

Tellurium dioxide (Merck), hydrochloric acid (J. T. Baker), tetraphenylarsonium chloride (Merck), and potassium chloride (Fisher) were used directly in the preparation of the compounds.

Infrared spectra were measured with a Perkin–Elmer 283 spectrometer. Raman spectra were taken with a Jobin–Yvon RT 110 spectrometer, using 514.5 nm excitation from a Spectra Physics Ar ion laser. Samples were rotated. X-Ray powder patterns were determined with a calibrated Siemens powder diffractometer, using monochromatised Cu Kα radiation. Intensities were estimated visually.



Preparations

Preparation of $\phi_4As[TeCl_4O_2H_3]$ was by partial hydrolysis and crystallization of $[\phi_4As]_2TeCl_6$ (2) in 99% ethanol. *Anal.* calcd. for $\phi_4As[TeCl_4O_2H_3]$: Cl 20.62; found: Cl 20.38. The pale yellow crystals melted at 210–214°C, which compares with 211–213°C reported earlier (16). All of the X-ray diffraction reflexes observed in the powder diffraction pattern may be accounted for by the monoclinic unit cell reported earlier (16).

The $K[TeCl_4(OH)]\cdot 0.5H_2O$ was prepared from a stoichiometric mixture of 1:1:3 TeO_2/KCl/HCl (as concentrated HCl). This solution was concentrated to the point of crystallization by evaporation at 50°C or in a desiccator. The pale yellow product, which was very soluble in the solution, was filtered out, blotted dry, and stored in a desiccator over anhydrous calcium chloride. *Anal.* calcd. for $K[TeCl_4(OH)]\cdot 0.5H_2O$: Cl 42.39; found: 41.62. Attempts to prepare $K_2[TeCl_5(OH)]$ from 1:2:3 TeO_2/KCl/HCl solutions gave only $K[TeCl_4(OH)]\cdot 0.5H_2O$. The X-ray powder diffraction pattern for the compound was unique and showed no evidence of K_2TeCl_6 or TeO_2.

It was not possible to prepare other $TeCl_4(OH)^-$ salts by this

Can. J. Chem. Downloaded from www.nrcresearchpress.com by 198.100.157.202 on 09/07/12
For personal use only.

Can. J. Chem. Downloaded from www.nrcresearchpress.com by 198.100.157.202 on 09/07/12
For personal use only.

method. Using NaCl in place of KCl gave NaCl and TeO_2 upon evaporation; using Me_4NCl, NH_4Cl, and RbCl, gave the hexachlorotellurate(IV) and TeO_2. The Raman spectrum of the previously reported $Me_4NTeCl_4(OH)$ (15) can be interpreted in terms of a mixture of TeO_2 and $(Me_4N)_2TeCl_6$.

$KTeCl_4(OH)\cdot 0.5H_2O$ can be dehydrated at 50°C under high vacuum over a period of days. *Anal.* calcd. for $KTeCl_4(OH)\cdot 0.5H_2O$: H_2O 2.6; found by weight loss: H_2O 3.8. *Anal.* calcd. for $KTeCl_4(OH)$: Cl 43.56, Te 39.20; found: Cl 43.09, Te 38.96. This product was more yellow than its hydrate. $KTeCl_4(OH)\cdot 0.5H_2O$ also lost water when stored in a vacuum desiccator over phosphorus pentoxide.

Structure determination

Crystallographic data were collected for two crystals, both of which gave the same refinement. Final refinement was done with a crystal of dimensions 0.2 × 0.2 × 0.4 mm. Of the 2803 reflections measured, 2087 were unique. The crystals were monoclinic, space group $P2_1/c$, a = 9.2896(7) Å, b = 7.1503(7) Å, c = 24.3385(19) Å, β = 95.034(6), V = 1610.41(24) Å^3, Z = 8, calculated density: 2.743(6) g/cm^3. Throughout this work the estimated standard deviations are in parentheses and refer to the last digit printed. The diffraction intensities were collected on a Nonius diffractometer at 295 K with Mo Kα radiation, using θ/2θ scan technique, with profile analysis (17). The space group was determined from systematic absences. Unit cell parameters were obtained by least-squares refinement of the setting angles for 25 reflections with 2θ between 40 and 50°. Lorentz and polarization factors were applied. A Gaussian correction for absorption was made on the crystal (10 faces were measured). The minimum and maximum transmission factors were 0.10706 and 0.158889.

The structure was solved by direct methods and refined by full matrix least squares from 1891 reflections ($I_{net} > 2.5\sigma(I_{net})$) to a final R = 0.085 and R_w = 0.076 (significant reflections). There are two independent molecules in the asymmetric unit. One of the two telluriums is disordered between two positions with occupancies of 0.85 and 0.15. The occupancies of the two disordered telluriums were refined, using linked groups with complementary occupancies. The H atoms were not found because of the disorder. The highest peak (2.250 e/Å^3) in the last D-map is near tellurium 2.

All calculations were performed with the NRCVAX Structure Package (18). A list of the final structure factors is available as supplementary data from the author.[1]

Results and discussion

The solubility of the hexachloroplatinate(IV) salts in water decreases with cation size (19) and the tellurate(IV) salts exhibit parallel behaviour. For this reason, and because the tetrachlorohydroxotellurate(IV) salts are quite soluble, only mixtures of TeO_2 and M_2TeCl_6 were isolated from the 1:1:3 mixtures of TeO_2/MCl/HCl (MCl = RbCl, NH_4Cl, Me_4NCl) in aqueous solution, as shown by X-ray powder diffraction patterns. The relative solubilities are such that tetrachlorohydroxotellurate(IV) can be isolated only when KCl is used. The tetraphenylarsoniumtetrachlorohydroxotellurate(IV) is prepared by crystallization of the hexachlorotellurate(IV) from acetonitrile (16) or ethanol, containing a trace of water.

The crystal structure of $KTeCl_4(OH)\cdot 0.5H_2O$

The atomic positions for K, Te, Cl, and O atoms in $KTeCl_4(OH)\cdot 0.5H_2O$ are given in Table 1 and the temperature factors appear in Table 2. The interatomic distances and angles are listed in Table 3. The unit cell contains two types of $TeCl_4(OH)^-$ anion, one of which is disordered in the position of Te11[12] and O11[12]. The Te11[12] atoms occupy two possible sites along a double chain of Cl atoms as shown. The Te11 lie in alternate, approximately square planar sites, coordinated by four Cl atoms with O11 normal to the plane of chlorines. In the other occupancy, the Te12 lie in the other alternating square planar sites with O12 projecting to the opposite side of the plane from that of O11. Of these two Te and O positions 15% have one orientation (Te12/O12) and 85% (Te11/O11), the other. In Table 2 O12 has not been refined anisotropically, because of its low occupancy caused by the disorder. An ORTEP diagram of the asymmetric unit (1/4 of the unit cell), viewed along z, is given in Fig. 1. The orientation of the disordered ion with the greatest occupancy (Te11/O11) is shown. The structure consists of isolated square pyramidal $TeCl_4(OH)^-$ anions. There are four molecules of H_2O in the unit cell, which are not coordinated to Te(IV), but the oxygens of which lie at the van der Waals distance from K^+. The anion structure, which is consistent with that predicted by VSEPR theory (20), has the hydroxo oxygen in the axial position and all OTeCl angles less than 90° due to the repulsive effect of the stereochemically active non-bonded electron pair on tellurium. The TeCl bond distances are very similar to those observed for the equatorial chlorines in the isolated $TeCl_5^-$ ion (13). The mean TeCl distance is marginally shorter than that observed for the $TeCl_6^{2-}$ ion (2), reflecting the reduced negative charge as well as the repulsive influence of the $5s^2$ electron pair in the $TeCl_6^{2-}$ ion. The TeO distances (1.905, 1.908 Å) are marginally less than those normally observed (1.919–2.110 Å) (21, 22) for the Te(IV)—O bond but considerably greater than that reported by Collins and Webster (1.74 Å) (16).

TABLE 1. Atom positions

Atom	x/a	y/b	z/c	B_{iso}[a]
Te11	0.83533(24)	0.8380(3)	0.24302(7)	2.20(9)
Te12	0.8353(14)	0.6544(16)	0.2437(5)	3.2(5)
Te2	0.31872(15)	0.24815(25)	0.01032(5)	2.06(6)
Cl11	1.0101(8)	0.9866(9)	0.1804(3)	3.4(3)
Cl12	0.6818(6)	0.7387(11)	0.16044(21)	3.5(3)
Cl13	0.9825(8)	0.9848(9)	0.3242(3)	3.7(3)
Cl14	0.6447(7)	0.7434(11)	0.30348(22)	3.8(3)
Cl21	0.4505(8)	0.0053(9)	0.06967(24)	3.3(3)
Cl22	0.4468(8)	0.4962(9)	0.06938(24)	3.3(3)
Cl23	0.1622(8)	0.0027(9)	−0.03521(24)	3.1(3)
Cl24	0.1614(8)	0.4925(9)	−0.03586(24)	3.1(3)
O2	0.1797(15)	0.246(3)	0.0636(5)	3.6(7)
O11	0.7356(20)	1.0700(25)	0.2334(6)	3.0(9)
O12	0.735(12)	0.383(15)	0.243(4)	2.5(24)
K1	0.7135(6)	0.2537(10)	0.13346(19)	3.8(3)
K2	0.1375(6)	0.7486(11)	0.07916(19)	4.4(3)
O(H_2O)	0.3375(15)	0.765(3)	0.1819(5)	3.5(8)

[a] B_{iso} is the mean of the principal axes of the thermal ellipsoid.

Vibrational spectra

The Raman and IR spectra of the tetrachlorohydroxotellurate(IV) salts are given in Table 4. The anion bands of the two hydrate salts, $\phi_4As[TeCl_4(OH)]\cdot H_2O$ and $K[TeCl_4(OH)]\cdot 0.5H_2O$, show a close parallel. The frequency of the TeO stretching mode near 630 cm^{-1} confirms that both of these compounds contain hydroxo- and not oxo-tellurate(IV) anions. A TeO double bond stretch is expected to be above 800 cm^{-1}.

The skeletal bands have been assigned in square pyramidal symmetry (C_{4v}: $\Gamma_{vib} = 3A_1 + 2B_1 + B_2 + 3E$). The TeO ($\nu_1$) and [$TeCl_4$] in phase ($\nu_2$) stretching bands (both A_1 symmetry)

[1] Complete set of data may be purchased from the Depository of Unpublished Data, Document Delivery, CISTI, National Research Council Canada, Ottawa, Canada K1A 0S2.

TABLE 2. Anisotropic temperature factors, U_{ij} values ($\times 100$)[a]

Atom	U_{11}	U_{22}	U_{33}	U_{12}	U_{13}	U_{23}
Te11	4.02(13)	2.07(12)	2.22(9)	0.23(12)	−0.04(8)	−0.02(9)
Te12	2.6 (7)	2.3 (7)	6.7 (7)	−0.6 (7)	−3.2 (6)	−0.3 (7)
Te2	3.08(9)	2.02(8)	2.71(8)	0.05(9)	0.07(6)	−0.01(8)
Cl11	4.8 (5)	3.4 (4)	4.8 (4)	−0.5 (4)	1.3 (3)	−0.6 (3)
Cl12	4.1 (4)	5.2 (4)	3.7 (3)	0.2 (4)	−1.3 (3)	−1.0 (4)
Cl13	6.1 (6)	3.2 (4)	4.3 (4)	0.5 (4)	−1.8 (4)	−0.8 (3)
Cl14	4.6 (4)	5.3 (4)	4.6 (3)	−0.8 (5)	1.0 (3)	0.1 (4)
Cl21	5.6 (5)	3.0 (4)	3.6 (4)	0.8 (4)	−0.2 (3)	1.0 (3)
Cl22	5.8 (5)	2.8 (4)	3.9 (4)	−0.8 (4)	−0.5 (4)	−1.0 (3)
Cl23	4.4 (5)	3.5 (4)	3.9 (4)	−1.4 (4)	−0.2 (3)	−0.4 (3)
Cl24	4.6 (5)	3.4 (4)	3.7 (4)	1.2 (4)	−0.2 (3)	0.5 (3)
O2	3.5 (10)	6.7 (12)	3.6 (8)	−0.5 (12)	1.6 (7)	0.2 (10)
O11	5.4 (14)	3.1 (12)	2.6 (10)	2.1 (11)	−1.0 (9)	0.7 (9)
K1	5.9 (4)	4.4 (3)	4.0 (3)	−0.3 (4)	−1.2 (3)	0.8 (3)
K2	5.2 (4)	7.8 (4)	3.6 (3)	0.0 (5)	0.4 (3)	0.1 (4)
O(H_2O)	4.5 (10)	5.2 (11)	3.9 (8)	−0.9 (11)	1.5 (7)	2.4 (9)

[a]Anisotropic temperature factors are of the form $\exp[-2\pi^2(U_{11}h^2a^{*2} + U_{22}k^2b^{*2} + U_{33}l^2c^{*2} + 2U_{12}hka^*b^* \cos\gamma^* + 2U_{13}hla^*c^* \cos\beta^* + 2U_{23}klb^*c^* \cos\alpha^*)]$.

TABLE 3. Atomic distances (Å) and angles (deg)[a]

Atom pair	Distance	Atom pair	Distance
Te(11)–Cl(11)	2.554(7)	Cl(13)–K(1)	3.355(9)
Te(11)–Cl(12)	2.464(5)	Cl(13)–K(2)	3.285(9)
Te(11)–Cl(13)	2.530(6)	Cl(14)–K(1)	3.785(8)
Te(11)–Cl(14)	2.493(6)	Cl(23)–K(2)	3.396(9)
Te(11)–O(11)	1.905(17)	Cl(23)–K(2)	3.349(9)
Te(2)–Cl(21)	2.508(6)	Cl(24)–K(2)	3.358(9)
Te(2)–Cl(22)	2.516(6)	Cl(24)–K(2)	3.368(9)
Te(2)–Cl(23)	2.478(6)	Cl(21)–K(2)	3.464(10)
Te(2)–Cl(24)	2.483(6)	Cl(22)–K(1)	3.301(9)
Te(2)–O(2)	1.908(13)	Cl(21)–K(1)	3.297(9)
Cl(11)–K(1)	3.463(9)	Cl(22)–K(2)	3.419(10)
Cl(11)–K(2)	3.298(9)	Cl(23)–K(1)	3.301(9)
Cl(12)–K(1)	3.756(10)	Cl(24)–K(1)	3.282(9)
Cl(12)–K(1)	3.547(10)	O(11)–K(1)	2.759(16)
		K(2)–O(H_2O)	2.983(14)

Bonds	Angle	Bonds	Angle
Cl(11)—Te(11)—Cl(12)	89.18(22)	Cl(21)—Te(2)—Cl(22)	88.66(21)
Cl(11)—Te(11)—Cl(13)	88.01(23)	Cl(21)—Te(2)—Cl(23)	90.28(22)
Cl(11)—Te(11)—Cl(14)	170.7(3)	Cl(21)—Te(2)—Cl(24)	170.47(23)
Cl(11)—Te(11)—O(11)	83.9(6)	Cl(21)—Te(2)—O(2)	85.8(5)
Cl(12)—Te(11)—Cl(13)	172.20(24)	Cl(22)—Te(2)—Cl(23)	169.92(24)
Cl(12)—Te(11)—Cl(14)	90.75(21)	Cl(22)—Te(2)—Cl(24)	89.57(22)
Cl(12)—Te(11)—O(11)	84.9(5)	Cl(22)—Te(2)—O(2)	86.1(5)
Cl(13)—Te(11)—Cl(14)	90.84(23)	Cl(23)—Te(2)—Cl(24)	89.82(22)
Cl(13)—Te(11)—O(11)	87.6(5)	Cl(23)—Te(2)—O(2)	83.8(5)
Cl(14)—Te(11)—O(11)	86.8(6)	Cl(24)—Te(2)—O(2)	84.7(5)

[a]Estimated standard deviations refer to the last digits.

are readily identified by their intensity and frequency. The ν_2 mode is very close in frequency to that of the related stretch for ICl_4^- (23) and the $TeCl_5^-$ (14) anions. The remaining bands were assigned by comparison with the assignment for $SeCl_5^-$ (24) and $TeCl_5^-$ (14) except for the TeO wag, ν_8, which was assigned to the remaining band near 226 cm^{-1}. The non-skeletal modes are assigned by analogy with the IR and Raman spectra of $KTeF_4(OH)^-$ (25). The spectrum of tetrachlorohydroxotellurate(IV) in these compounds parallels spectra observed for 0.5 M TeO_2 in 7–9 M HCl solutions (15), 2.0–3.0 M TeO_2 in 12.29 M HCl solutions and 1:1:3 and 1:2:3 TeO_2/KCl/HCl (12.29 M) solutions. This parallel and the fact that only $KTeCl_4(OH)\cdot 0.5H_2O$ can be isolated from both 1:1:3 and 1:2:3 TeO_2/KCl/HCl solutions confirms that $TeCl_4(OH)^-$ and not $TeCl_5(OH)^{2-}$ is formed in these solutions.

The tetrachlorohydroxotellurate(IV) salts are readily de-

Can. J. Chem. Downloaded from www.nrcresearchpress.com by 198.100.157.202 on 09/07/12
For personal use only.

TABLE 4. The Raman and IR spectra of tetrachlorohydroxotellurate(IV)

$\phi_4As[TeCl_4(OH)]\cdot H_2O$ Raman[a]	$K[TeCl_4(OH)]\cdot 0.5H_2O$ Raman[b]	$K[TeCl_4(OH)]\cdot 0.5H_2O$ IR[b]	n-Bu_4NTeCl_5 Raman[c]	Mode No.	Description of mode (C_{4v})
—	38(3)	—			Lattice
—	48(0,sh)	—			
66(10)	69(2)	—	90	9(E)	δ ($TeCl_4$ out-of-plane)
—	102(1)	—	110	5(B_1)	δ_a ($TeCl_4$ out-of-plane)
144(4)	133(2)	—	133	3(A_1)	δ ($TeCl_4$ umbrella)
—	153(2)	—	168	6(B_2)	δ_s ($TeCl_4$ in plane)
—	—	226vs	85	8(E)	δ (TeO wag)
239(3)	251(2)	253vs	244	7(E)	ν_a ($TeCl_2$)
255(4)	268(3)	—	275	4(B_1)	ν_s ($TeCl_4$ out-of-phase)
287(8)	292(10)	285vs	251	2(A_1)	ν_s ($TeCl_4$ in phase)
628(1)	637(2)	628vs	362	1(A_1)	ν (TeO)

[a]Cation, H_2O and OH bands: 44(10), 91(8), 191(1), 255(2), 618(1), 676(1).
[b]H_2O and OH bands: Raman, 671(1) (δ_{OH} wag); IR, 458w,br, 562m,br (H_2O librations), 666s (δ_{OH} wag), 972w, 1042m, 1165m (δ_{TeOH} bend), 1605m (δ (H_2O), 2340w (2 × δ_{TeOH}), 3360m, 3460m, 3540m (δ_{OH} (H_2O, OH)).
[c]Reference 14.

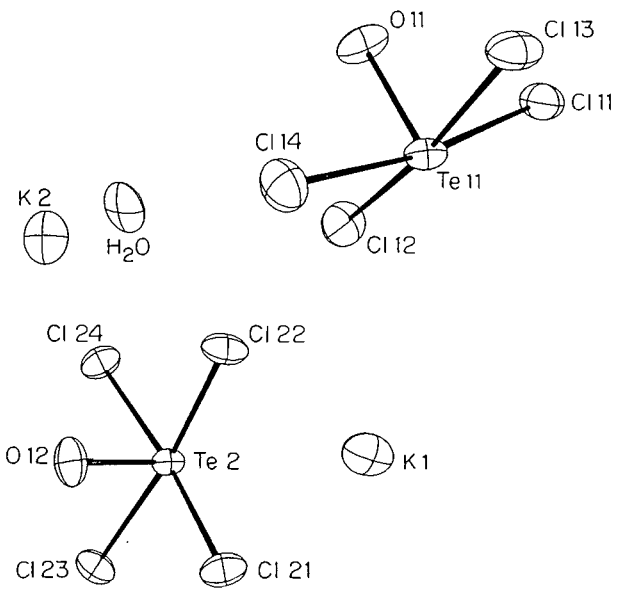


FIG. 1. ORTEP diagram of the asymmetric unit (1/4 of the unit cell), showing the two $TeCl_4(OH)^-$ ions. Of the two possibilities of the disordered anion (Te11[12] and O11[12]), the one with 85% occupancy is shown (Te11 and O11).

hydrated. Storage of $KTeCl_4(OH)\cdot 0.5H_2O$ in a vacuum desiccator over a period of weeks or dehydration under high vacuum at 50°C causes weight loss and the disappearance of the characteristic IR peak at 1605 cm^{-1} due to H_2O. Analysis shows the product to be $KTeCl_4(OH)$. The IR and Raman spectra are listed in Table 5. The appearance of a strong band near 355 cm^{-1}, accompanied by other changes, indicates that the structure of $TeCl_4(OH)^-$ in the dehydrated product is different from that in the hemihydrate. Decomposition to K_2TeCl_6 and TeO_2, according to

[1] $2KTeCl_4(OH)\cdot 0.5H_2O = K_2TeCl_6 + TeO_2 + 2HCl + H_2O$

does not fit the analysis or the observed spectra. Isomerization to an isolated trigonal bipyramidal $TeCl_4(OH)^-$ anion is unlikely in view of the tendency of Te(IV) halogen compounds to adopt structures based upon an octahedron. It has been shown that

TABLE 5. The Raman and IR spectra of $K[TeCl_4(OH)]$

Raman[a]	IR[a]	Description of mode
123(1)	—	δ ($TeCl_4$)
158(5)	—	ν ($TeCl_b$)[b]
187(2)	—	
240(2,sh)	250m	δ (TeO)
268(8)	—	ν ($TeCl_a$)[c]
292(10)	282m	
358(10)	353m	ν ($TeCl_t$)[d]
628(2)	622s	ν (TeO)

[a]H_2O and OH bands: Raman, 670(0); IR, 670 (δ_{OH} wag), 920m, 1030s, 1168w, 3362m, 3440m.
[b]Bridging Cl.
[c]Terminal Cl, out-of-plane.
[d]Terminal Cl, in plane.

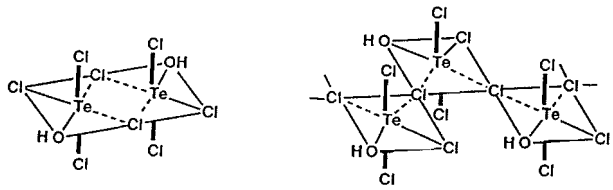
$TeCl_5^-$ and $TeBr_5^-$ form condensed anions via halogen bridges (8–10). Dehydration of $K[TeCl_4(OH)]\cdot 0.5H_2O$ probably leads to a related condensed anion.

[2] $2KTeCl_4(OH)\cdot 0.5H_2O = K_2[Te_2Cl_8(OH)_2] + H_2O$

[3] $nKTeCl_4(OH)\cdot 0.5H_2O = K_n[TeCl_4(OH)]_n + (n/2)H_2O$

This conclusion is supported by chemical analysis and the disappearance of the 1605 cm^{-1} band in the IR spectrum. The spectrum of the dehydrated product still exhibits the TeO stretching frequency near 630 cm^{-1} as well as the OH wag at 670 cm^{-1} and the TeOH bend at 1165 cm^{-1}, showing that the hydroxo group is still present. The small shifts in frequency from those of the same bands in the hydrates show that the group occupies a terminal, not a bridging, position. Since the position *trans* to the hydroxo group is vacant in the isolated $TeCl_4(OH)^-$ ion, it is likely that the Cl atoms with weaker Te—Cl bonds, the bridging Cl's, will occupy this *trans* position in the dehydrated form. It is not possible to establish the degree of condensation of the $[TeCl_4(OH)^-]$ units from the spectra. The $TeCl_5^-$ ion is found in both dimeric and polymeric forms (8, 10). Analogous $[TeCl_4(OH)^-]$ structures with terminal hydroxo groups *trans* to bridging chlorines may take the forms below.

Can. J. Chem. Downloaded from www.nrcresearchpress.com by 198.100.157.202 on 09/07/12
For personal use only.



Structures with a bridging Cl *trans* to two OH groups are not shown. These are unlikely, since such a coordination site would be unfavourable due to the *trans* repulsive effect of the OH groups. In the structures shown, each bridging Cl lies *trans* to only one OH group. The highest TeCl frequency observed near 355 cm^{-1} may be assigned to a mode involving the terminal Cl *trans* to the bridging Cl in these structures. The Cl *trans* to bridging Cl is expected to be more strongly bound than the axial Cl's *cis* to the bridging Cl's. A tentative assignment of the spectrum of $KTeCl_4(OH)$, which is independent of the degree of polymerisation, is given in Table 5.

Conclusion

A comparison of the ligand acceptor properties of the $TeCl_4(OH)^-$ and $TeCl_5^-$ ions shows important differences. The $TeCl_5^-$ ion exhibits a strong tendency to accept Cl^- ion forming $TeCl_6^{2-}$ and readily polymerizes to achieve hexacoordination. The $TeCl_4(OH)^-$ ion shows no tendency to accept Cl^- and form $TeCl_5(OH)^{2-}$ and exhibits a weaker tendency to polymerize or bind a sixth ligand to achieve hexacoordination. The hydrate water in $KTeCl_4(OH)\cdot 0.5H_2O$ is not even weakly coordinated to Te. Thus chloride and hydroxide ligands have differing effects on the ability of Te(IV) to bond to a ligand at the *trans* position. This "*trans*" effect has been reported for the $TeCl_3(O_2C_2H_4)^-$ ion (21), where the positions *trans* to the glycolate oxygens are either vacant or have a relatively weakly bonded Cl. The axial fluorine atom in the TeF_5^- ion and OH group in the $TeF_4(OH)^-$ ion (25) have the same effect on the *trans* position. Apparently the small size of the O and F ligands, compared to that of Cl and larger ligands, permits their close approach to the Te atom due to decreased interligand repulsions and consequent dominance or polarisation of the *p* orbital lying along this axis such that any *trans* ligand cannot bond to the Te atom effectively. The equatorial ligands of the TeF_5^- ion do not show this effect, since they can not approach the Te atom as closely as the axial F.

Acknowledgements

This work was supported by the Natural Sciences and Engineering Research Council of Canada and the NATO.

1. I. D. Brown. Can. J. Chem. **42**, 2758 (1964).
2. J. Milne, E. Philippot, and M. Maurin. Rev. Chim. Min. **21**, 749 (1984).
3. W. Abriel. Acta Crystallogr. B**42**, 449 (1986).
4. W. Abriel and A. duBois. Mat. Res. Bull. **21**, 1503 (1986).
5. R. J. Morris and K. C. Moss. J. Fluorine Chem. **13**, 551 (1979).
6. S. H. Mastin, R. R. Ryan, and L. B. Asprey. Inorg. Chem. **9**, 2100 (1970).
7. Yu. E. Gorbunova, S. A. Linde, V. I. Pakhomov, Yu. V. Kokunov, M. P. Gustyakova, and Yu. A. Buslaev. Koord. Khim. **10**, 340 (1984).
8. B. Krebs and V. Paulat. Angew. Chem. **85**, 662 (1973).
9. B. Krebs and K. Buescher. Z. Anorg. Allg. Chem. **463**, 56 (1980).
10. P. H. Collins and M. Webster. Acta Crystallogr. **28B**, 1260 (1972).
11. T. Schoenherr. Inorg. Chim. Acta, **144**, 151 (1988).
12. G. A. Ozin and A. Vander Voet. J. Mol. Struct. **13**, 435 (1972).
13. W. Hinrichs, D. Mandak, and G. Klar. Cryst. Struct. Commun. **11**, 1781 (1982).
14. T. Schoenherr. Z. Naturforsch. **43**b, 159 (1988).
15. (*a*) J. B. Milne and M. Mahadevan. Inorg. Chem. **23**, 268 (1984); (*b*) J. B. Milne. Can. J. Chem. In press.
16. P. H. Collins and M. Webster. J. Chem. Soc. Dalton, 1545 (1974).
17. D. F. Grant and E. J. Gabe. J. Appl. Crystallogr. **11**, 114 (1978).
18. E. J. Gabe, F. L. Lee, and Y. Lepage. J. Appl. Crystallogr. **22**, 384 (1989).
19. R. C. Weast (*Editor*). Handbook of chemistry and physics. Chemical Rubber Publishing Co., Cleveland, OH. 1970. Section B.
20. R. J. Gillespie. Molecular geometry. Van Nostrand Rheinhold Co., London. 1972.
21. O. Lindqvist. Acta Chem. Scand. **21**, 1473 (1967).
22. K. Buescher, S. Heuer, and B. Krebs. Z. Naturforsch. **36**b, 307 (1981).
23. W. B. Person, G. R. Anderson, J. M. Fordemwalt, H. Stammereich, and R. Forneris. J. Chem. Phys. **35**, 908 (1961).
24. P. Lahaie and J. Milne. Inorg. Chem. **18**, 632 (1979).
25. J. Milne and D. Moffett. Inorg. Chem. **13**, 2750 (1974).

Can. J. Chem. Downloaded from www.nrcresearchpress.com by 198.100.157.202 on 09/07/12
For personal use only.

Synthesis, electrochemistry, and ligand substitution reactions of conducting copolymer films of ruthenium polypyridine complexes and aromatic heterocycles

JOLANTA OCHMANSKA[1] AND PETER G. PICKUP[2]

Department of Chemistry, Memorial University of Newfoundland, St. John's, NFLD., Canada A1B 3X7

Received September 14, 1990

JOLANTA OCHMANSKA and PETER G. PICKUP. Can. J. Chem. **69**, 653 (1991).

Conducting films containing ruthenium complexes of the general formula $[Ru(2,2'\text{-bipyridine})_2(pmp)X]^{2+}$ (pmp = 3-(pyrrol-1-ylmethyl)pyridine, X = Cl^-, ClO_4^-, pmp, CH_3CN, or H_2O) have been prepared by copolymerization of the Ru complex monomer with pyrrole, 3-methylthiophene, 1-methyl-3-(pyrrol-1-ylmethyl)pyridinium(1+), or 2,2′-bithiophene. The immobilized complexes exhibit rapid and reversible electrochemistry in acetonitrile. The perchlorate and water ligands are rapidly substituted to give the acetonitrile complex, while the chloride ligand is replaced more slowly. In aqueous media, both the perchlorate complex and chloride yield an aqua complex. The substitution rate of the chloride ligand is again low but is enhanced by photolysis. No substitution reactions were observed for the acetonitrile or pmp ligands under a variety of conditions tested. Infrared spectroscopy and fast atom bombardment mass spectroscopy indicate that attempts to isolate $[Ru(bp)_2(pmp)(ClO_4)]^+$ as a solid in fact give the aqua complex. The perchlorate complex may also rearrange to the aqua complex in polymer films. Films containing the aqua complex were not useful for electrocatalytic oxidation because of the instability of the conducting polymer matrix at low pH and the inactivity of the complex at higher pH values.

Key words: polythiophene, polypyrrole, electropolymerization, metallopolymer.

JOLANTA OCHMANSKA et PETER G. PICKUP. Can. J. Chem. **69**, 653 (1991).

On a préparé des films conducteurs contenant des complexes de ruthénium de formule générale $[Ru(2,2'\text{-bipyridine})_2(pmp)X]^{2+}$ (pmp = 3-(pyrrol-1-ylméthyl)pyridine, X = Cl^-, ClO_4^-, pmp, CH_3CN, ou H_2O) par copolymérisation du monomére du complexe de Ru avec du pyrrole, du 3-méthylthiophène, du 1-méthyl-3-(pyrrol-1-ylméthyl)pyridinium(1+), ou du 2,2′-bithiophène. Dans l'acétronitrille, les complexes imobilisés présentent une électrochimie rapide et réversible. Les coordinats perchlorate et eau sont rapidement substitués pour donner le complexe acétonitrile; par ailleurs, le coordinat chlorure est remplacé plus lentement. En milieu aqueux, les complexes tant perchlorique que chlorure conduisent au complexe aqua. Encore une fois la vitesse de substitution du chlorure est faible; elles est toutefois augmentée par photolyse. Pour toutes les conditions étudiées, on n'a pas pu observer de réactions de substitution des coordinats acétonitrile ou pmp. La spectroscopie ir et la spectrométrie de masse par bombardement avec des atomes rapides indiquent que les tentatives d'isoler le complexe $[Ru(bp)_2(pmp)(ClO_4)]^+$ n'ont en fait fourni que la complexe aqua. Dans les films de polymères, le complexe perchlorique peut aussi se transformer en complexe aqua. Do à l'instabilité de la matrice du polymère conducteur aux bas pH et à l'inactivité du complexe à des valeurs plus élevées de pH, les films contenant le complexe aqua ne sont pas utiles pour l'oxydation électrocatalytique.

Mots clés : polythiophène, polypyrrole, électropolymérisation, métallopolymère.

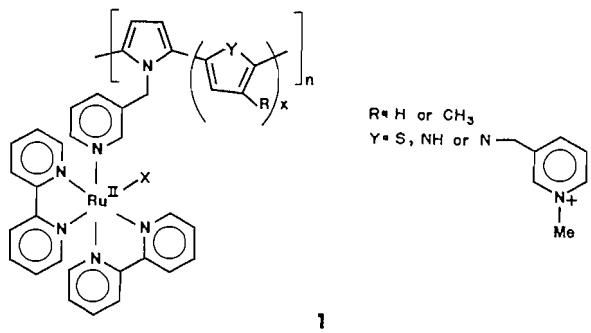
[Traduit par la rédaction]

Introduction

Pyrrole substituents have become very popular for facilitating electropolymerization of metal complexes (1). Since these metallopolymer films are most useful in electrocatalysis, it would be desirable if they also possess high electronic conductivity. This has been achieved by copolymerization of pyrrole-substituted complexes with unsubstituted pyrrole (2–5).

To further develop the synthetic chemistry of electronically conductive metallopolymers, we have prepared a number of copolymers (**I**) containing ruthenium polypyridine complexes of the general formula $[Ru(bp)_2(pmp)X]^{2+}$ (bp = 2,2′-bipyridine, pmp = 3-(pyrrol-1-ylmethyl)pyridine, X = Cl^-, ClO_4^-, pmp, H_2O, or CH_3CN). The above complexes have been copolymerized with pyrrole, 3-methylthiophene, 2,2′-bithophene, and/or 1-methyl-3-(pyrrol-1-ylmethyl)pyridinium(1+). The last pyrrole was chosen to enhance the hydrophilicity of the copolymer (6) while 3-methylthiophene and 2,2′-bithiophene were used to enhance its stability. The thermal and photolytic substitution reactions of the sixth ligand (X) in the copolymers have been investigated.

One of our main objectives was to develop synthetic routes to



I

conducting polymers containing an analogue of the versatile oxidation catalyst $[Ru(bp)_2(py)(H_2O)]^{2+}$ (py = pyridine) (7). This complex has previously been incorporated into polyvinylpyridine (8, 9) and Nafion (10) films.

Experimental

Electrochemistry

Electrochemical experiments were carried out in conventional three-compartment glass cells under an argon atmosphere at 23 ± 2°C. The working electrode was either a Pt disc sealed in glass (4.5×10^{-3} or 1.2×10^{-4} cm^2), or a glassy carbon disc (0.071 cm^2, Electrosynthesis Co., Inc.) sealed in epoxy (Lepage's). The counter electrode was a Pt wire and the reference electrode was either a saturated sodium chloride calomel electrode (SSCE) or a Ag/Ag^+ (0.1 M in CH_3CN) electrode which had a potential of 0.36 V vs. SSCE in CH_3CN. All

[1]Permanent address: Laboratory of Electroanalytical Chemistry, Department of Chemistry, Warsaw University, Pasteura 1, 02093, Warsaw, Poland.

[2]To whom correspondence should be addressed.

Can. J. Chem. Downloaded from www.nrcresearchpress.com by 198.100.157.202 on 09/07/12
For personal use only.

TABLE 1. Experimental conditions for the preparation of copolymer films

Heterocycle[a]	Ru complex[a]	Solvent + electrolyte	Potential (V vs. SSCE)	x^d
3-Methylthiophene (19 mM)	$[Ru(bp)_2(pmp)_2]^{2+}$ (4.5 mM)	$CH_3CN + Bu_4NClO_4$	0.50 to 1.60[c]	1
3-Methylthiophene (60 mM)	$[Ru(bp)_2(pmp)Cl]^+$ (9 mM)	$CH_3CN + Bu_4NClO_4$	1.65[b]	16
3-Methylthiophene (30 mM)	$[Ru(bp)_2(pmp)Cl]^+$ (4 mM)	$CH_3CN + Bu_4NClO_4$	0.40 to 1.70[c]	6
3-Methylthiophene (50 mM)	$[Ru(bp)_2(pmp)Cl]^+$ (10 mM)	Propylene carbonate + Bu_4NBF_4	1.65[b]	50
3-Methylthiophene (20 mM)	$[Ru(bp)_2(pmp)Cl]^+$ (5 mM)	$CH_3NO_2 + Bu_4NBF_4$	1.65[b]	35
$MPMP^+$ (30 mM)	$[Ru(bp)_2(pmp)Cl]^+$ (9 mM)	$CH_3CN + Bu_4NClO_4$	1.20[b]	~4
Pyrrole (1.7 mM)	$[Ru(bp)_2(pmp)(ClO_4)]^+$ (1.4 mM)	$CH_2Cl_2 + Bu_4NBF_4$	0.36 to 1.21[c]	~20
$MPMP^+$ (5 mM)	$[Ru(bp)_2(pmp)(ClO_4)]^+$ (1 mM)	$CH_2Cl_2 + Bu_4NBF_4$	1.11[b]	~20
Bithiophene (1.1 mM)	$[Ru(bp)_2(pmp)(CH_3CN)]^{2+}$ (1.6 mM)	$CH_3CN + Bu_4NClO_4$	0.36 to 1.48[c]	7

[a]$MPMP^+$ = 1-methyl-3-(pyrrol-1-ylmethyl)pyridinium(1+). The supporting electrolyte concentration was 0.1 M in all cases. Concentration in parentheses.
[b]Constant potential.
[c]Potential cycling at 100 mV/s.
[d]Heterocycle:[Ru complex] mole ratio in copolymer.

potentials are quoted with respect to the SSCE. The electrochemical instrumentation consisted of a HB-104 Hokuto Denko function generator, a HA-301 Hokuto Denko potentiostat/galvanostat, and a BBC SE780 X–Y recorder.

Spectroscopy

A Hitachi S570 scanning electron microscope operated at an accelerating voltage of 20 kV was used for X-ray emission spectroscopy (electron microprobe analysis). Emission spectra were collected using a Tracor Northern 5500 Energy Dispersive X-ray Analyzer equipped with a Microtrace 70152 silicon detector. Fast atom bombardment mass spectra of samples mixed with glycerol and *p*-toluene sulphonic acid were obtained using a VG Micromass 7070HS mass spectrometer. Infrared spectra were recorded using a Perkin-Elmer 283.

Synthesis of ruthenium complex monomers

$[Ru(bp)_2(pmp)Cl]PF_6$ (3) and **$[Ru(bp)_2(pmp)_2](ClO_4)_2$** (5) were prepared as previously described.

$[Ru(bp)_2(pmp)(ClO_4)]ClO_4$ was prepared following the literature procedure for $[Ru(bp)_2(py)(ClO_4)]ClO_4$ (11). Thus, $[Ru(bp)_2(pmp)_2](ClO_4)_2$ (100 mg) in dichloromethane (400 mL) was photolyzed until fully dissolved using a 150 W tungsten lamp (ca. 4 h). The volume was reduced to ca. 20 mL under reduced pressure and the product was precipitated with diethyl ether, collected by filtration, and dried in air (yield = 59%). The solid isolated this way appears to be $[Ru(bp)_2(pmp)(H_2O)](ClO_4)_2$ but produces $[Ru(bp)_2(pmp)(ClO_4)]^+$ in CH_2Cl_2 (see below).

$[Ru(bp)_2(pmp)(H_2O)](ClO_4)_2$ was prepared by the literature method for $[Ru(bp)_2(py)(H_2O)](ClO_4)_2$ (12).

$[Ru(bp)_2(pmp)(CH_3CN)]^{2+}$ was prepared *in situ* by dissolving $[Ru(bp)_2(pmp)(H_2O)](ClO_4)_2$ in acetonitrile.

Preparation of copolymer films

All copolymers were deposited as thin films on Pt or carbon electrodes by simultaneous electrochemical oxidation of an aromatic heterocyclic monomer (pyrrole, 3-methylthiophene, 2,2′-bithiophene or 1-methyl-3-(pyrrol-1-ylmethyl)pyridium(1+)) and a Ru complex ($[Ru(bp)_2(pmp)X]^{2+}$) in a non-aqueous solution containing 0.1 M supporting electrolyte. Typical preparation conditions, and approximate compositions of the resulting films are given in Table 1. Film compositions and thicknesses were routinely extimated by cyclic voltammetry as previously described (3, 5). A typical voltammogram of a (3-methylthiophene)$_x$$[Ru(bp)_2(pmp)_2]^{2+}$ copolymer film is shown in Fig. 1. The thiophene-to-Ru ratio of 6.7 (x) was obtained by dividing four times the charge under the poly(3-methylthiophene) oxidation wave (to 1.15 V) by the charge under the Ru reduction wave at 1.2 V (5). This assumes that oxidation of the poly(3-methylthiophene) backbone involves 0.25 electrons per thiophene unit.

Chemicals and solvents

Pyrrole (Aldrich) was purified on a dry alumina column. 1-Methyl-3-(pyrrol-1-ylmethyl)pyridinium tetrafluoroborate was prepared as previously described (13). 3-Methylthiophene (Aldrich) and 2,2′-bithiophene (Aldrich) were used as received. Bu_4NClO_4 (purum, Fluka) was precipitated from hot acetone with water, filtered, and dried under vacuum at 50°C for 10 h. Et_4NClO_4 (Fluka), Bu_4NBF_4 (Fluka), and other electrolytes were used as received. Acetonitrile (Aldrich, HPLC) was consecutively distilled from $KMnO_4 + Li_2CO_3$, P_4O_{10}, and CaH_2. Dichloromethane (Mallinckrodt, HPLC), propylene carbonate (Aldrich, Gold Label), nitromethane (Fisher, Spectranalyzed) were used as received.

Results and discussion

Characterization of Ru complexes

Characterization of the complexes and copolymers prepared in this work and the observation of ligand substitution reactions of the complexes in the copolymers rely on electrochemical data. The formal potentials ($E^{0\prime}$) of the Ru complex monomers are presented in Table 2. These are in good agreement with those previously reported for the pyridine analogues of these complexes (11) which are also included in Table 2. Clearly,

Can. J. Chem. Downloaded from www.nrcresearchpress.com by 198.100.157.202 on 09/07/12
For personal use only.

TABLE 2. Formal potentials from cyclic voltammetry of Ru complex monomers and their pyridine analogues

Complex	Solvent/electrolyte	Formal potential/V (vs. SSCE) L = pmp	L = pyridine
$[Ru(bp)_2(L)(H_2O)]^{3+/2+}$	1M NaOH(aq)	0.21	0.27[a]
$[Ru(bp)_2(L)Cl)]^{2+/+}$	CH_3CN + 0.1 M Bu_4NClO_4	0.78	0.76[a]
$[Ru(bp)_2(L)(H_2O)]^{3+/2+}$	CH_2Cl_2 + 0.1 M Bu_4NClO_4	1.10	
$[Ru(bp)_2(L)(ClO_4)]^{2+/+}$	CH_2Cl_2 + 0.1 M Bu_4NClO_4	1.12	1.09[b]
$[Ru(bp)_2(L)_2]^{3+/2+}$	CH_3CN + 0.1 M Bu_4NClO_4	1.25	1.29[b]
$[Ru(bp)_2(L)(CH_3CN)]^{3+/2+}$	CH_3CN + 0.1 M Bu_4NClO_4	1.29	1.35[b]

[a]Reference 10.
[b]Reference 11, in CH_3CN + 0.1 M Et_4NClO_4.

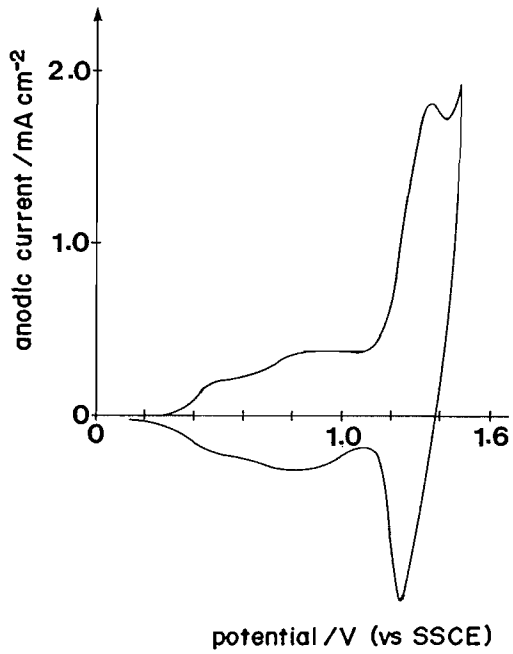


FIG. 1. Cyclic voltammogram at 10 mV/s of a (3-methylthiophene)$_7$–$[Ru(bp)_2(pmp)_2]^{2+}$ copolymer coated glassy carbon electrode in acetonitrile + 0.1 M Bu_4NClO_4.

formal potentials are acceptable for identifying most of the complexes used. The only difficulty arises in distinguishing between $[Ru(bp)_2(pmp)(ClO_4)]^+$ and $[Ru(bp)_2(pmp)(H_2O)]^{2+}$, since in this work we do not need to distinguish between $[Ru(bp)_2(pmp)(CH_3CN)]^{2+}$ and $[Ru(bp)_2(pmp)_2]^{2+}$. Infrared spectroscopy and fast atom bombardment mass spectroscopy were applied to this problem.

Infrared spectroscopy of $[Ru(bp)_2(pmp)(ClO_4)]ClO_4$ in CH_2Cl_2 revealed the bands at 1150 and 1015 cm^{-1} assigned to bound perchlorate for the pyridine analogue (11). The formal potential of this complex, from cyclic voltammetry in CH_2Cl_2, is also in agreement with that reported for the pyridine analogue (Table 2). However, fast atom bombardment mass spectroscopy of the solid isolated from CH_2Cl_2 revealed coordinated water but no evidence for perchlorate coordination. Peaks of similar intensity at m/z = 585, 431, and 414 were assigned to $[Ru(bp)_2]^{2+}[Me\text{-}4\text{-}C_6H_4SO_3]^-$, $[Ru(bp)_2(OH)]^+$, and $[Ru(bp)_2]^+$, respectively. No ions were observed at m/z = 671 ($[Ru(bp)_2(pmp)(ClO_4)]^+$), m/z = 513 ($[Ru(bp)_2(ClO_4)]^+$), m/z = 589 ($[Ru(bp)_2(pmp)(OH)]^+$), or m/z = 572 ($[Ru(bp)_2(pmp)]^+$). For comparison $[Ru(bp)_2(pmp)Cl]ClO_4$ produced peaks assigned to $[Ru(bp)_2(pmp)Cl]^+$ (m/z = 607, weak), $[Ru(bp)_2]^{2+}[Me\text{-}4\text{-}C_6H_4SO_3]^-$ (m/z = 585, weak), $[Ru(bp)_2Cl]^+$ (m/z = 449, strong), and $[Ru(bp)_2]^+$ (m/z = 414, strong). Infrared spectroscopy (Nujol mull) of the solid isolated from a CH_2Cl_2 solution of $[Ru(bp)_2(pmp)(ClO_4)]ClO_4$ was not significantly different from that of $[Ru(bp)_2(pmp)(H_2O)](ClO_4)_2$ and revealed no splitting of the perchlorate band at 1095 cm^{-1}. Both compounds exhibit broad bands in the 3000–3500 cm^{-1} region attributed to water. In CH_2Cl_2, the infrared spectrum of $[Ru(bp)_2(pmp)(H_2O)](ClO_4)_2$ revealed splitting of the perchlorate band similar to that observed for $[Ru(bp)_2(pmp)(ClO_4)]ClO_4$. Cyclic voltammetry indicated the same formal potential as for $[Ru(bp)_2(pmp)(ClO_4)]ClO_4$.

The above evidence indicates that the coordinated perchlorate complex was obtained in CH_2Cl_2. However, the solid isolated from this solution is the aqua complex, $[Ru(bp)_2(pmp)(H_2O)](ClO_4)_2$. Dissolution of the aqua complex in CH_2Cl_2 produces the perchlorate complex, as reported by Meyer and co-workers for the pyridine analogue (11).

Film synthesis

The compositions and quality of films resulting from the copolymerization of a pyrrole-substituted Ru complex and an aromatic heterocycle depend on many factors. These will be individually discussed and illustrated with specific examples.

Solvent

Acetonitrile was generally found to be the best solvent for incorporating Ru complexes into copolymer films. Propylene carbonate, nitromethane, and dichloromethane were also used but generally resulted in films with low Ru complex contents. This is illustrated by the data for (3-methylthiophene)$_x$–$[Ru(bp)_2(pmp)Cl]^+$ copolymers presented in Table 1. The films prepared from propylene carbonate and nitromethane contain only about a third as much Ru as the film prepared from acetonitrile under similar conditions. Bu_4NBF_4 was used as the electrolyte in propylene carbonate and nitromethane because copolymers could not be produced from these solvents when Bu_4NClO_4 was used. Bu_4NBF_4 was a satisfactory electrolyte for polymerization in acetonitrile.

Acetonitrile could not be used for the preparation of films containing $[Ru(bp)_2(pmp)(ClO_4)]^+$ or $[Ru(bp)_2(pmp)(H_2O)]^{2+}$ because of the rapid conversion of these complexes to $[Ru(bp)_2(pmp)(CH_3CN)]^{2+}$. Nor could films containing useful quantities of these complexes be prepared from propylene carbonate or nitromethane. Dichloromethane was found to be an acceptable

Can. J. Chem. Downloaded from www.nrcresearchpress.com by 198.100.157.202 on 09/07/12
For personal use only.

TABLE3. Experimental conditions for the preparation of (3-methylthiophene)$_x$–$[Ru(bp)_2(pmp)_2]^{2+}$ copolymer films (all data are for films deposited from acetonitrile + 0.1 M Bu_4NClO_4, onto 1.2×10^{-4} cm^2 Pt electrodes, by cycling the potential between 0.50 and 1.60 V at 100 mV/s)

3-Methylthiophene concentration/mM	$[Ru(bp)_2(pmp)_2](ClO_4)_2$ concentration/mM	Number of cycles	Film thickness /μm	x
44	0.5	10	1.1	34
44	0.5	15	1.8	56
44	0.9	9	0.5	16
44	2.2	4	0.6	10
44	2.2	10	1.9	12
32	2.3	4	0.5	6.1
32	2.3	12	1.6	6.9
19	2.3	5	0.5	4.4
19	2.3	13	1.1	3.0
19	4.5	4	0.6	0.9
19	4.5	6	0.9	1.2

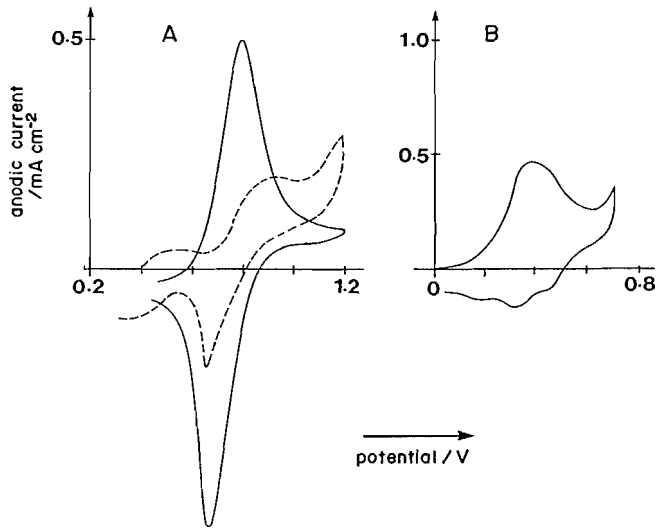


FIG. 2. (*A*) Cyclic voltammograms (100 mV/s) of 0.6 mM $[Ru(bp)_2(pmp)(ClO_4)]ClO_4$ in dichloromethane + 0.1 M Bu_4NClO_4 at a Pt electrode. The dashed curve is the first scan, while the solid curve was recorded after 650 s of potential cycling. Reference electrode Ag/Ag^+ (+0.36 V vs. SSCE). (*B*) Cyclic voltammogram (100 mV/s, vs. SSCE) of the electrode from *A* in 1 M $NaNO_3$(aq) + phosphate buffer at pH 7.

solvent from which to prepare copolymers of pyrrole or 1-methyl-3-(pyrrol-1-ylmethyl)pyridinium(1+) with $[Ru(bp)_2(pmp)(ClO_4)]^+$ (Table 1). However, $[Ru(bp)_2(pmp)(ClO_4)]^+$ failed to copolymerize with either 3-methylthiophene or 2,2′-bithiophene in dichloromethane. Oxidation of 3-methylthiophene, and hence polymerization, is blocked by a precipitate of $[Ru(III)(bp)_2(pmp)(ClO_4)](ClO_4)_2$ that rapidly forms on the electrode surface. Formation of this precipitated layer is demonstrated in Fig. 2*A*. The size of the Ru(III)/(Ru(II) voltammetric peaks of the complex increase with potential cycling, indicating that the complex is deposited on the electrode. After the potential scans depicted in Fig. 2*A* the electrode was visibly coated with an orange film of the complex and electrochemistry of the film could be observed in water (Fig. 2*B*). It is unlikely that this film is polymeric because it dissolves quite rapidly in acetonitrile. Copolymerization of $[Ru(bp)_2(pmp)(ClO_4)]^+$ with pyrrole or 1-methyl-3-(pyrrol-1-ylmethyl)pyridinium(1+) is not inhibited because these monomers polymerize at potentials below those required to rapidly form the blocking $[Ru(bp)_2(pmp)(ClO_4)](ClO_4)_2$ film. The copolymerization of 3-methylthiophene and $[Ru(bp)_2(pmp)(ClO_4)]^+$ does occur in nitromethane but only films with a low Ru complex content ($x > 50$) could be prepared.

Monomer ratio

As expected, the composition of all copolymers could be varied by changing the monomer ratio in the polymerization solution. This is demonstrated by the data for (3-methylthiophene)$_x$–$[Ru(bp)_2(pmp)_2]^{2+}$ copolymers presented in Table 3. Here the copolymer composition varies approximately linearly with monomer ratio over a wide range of compositions. The Ru complex is preferentially incorporated into the copolymer by a factor of about two. This is presumably the result of two pyrrole substituents on one Ru complex. This is supported by the fact that $[Ru(bp)_2(pmp)Cl]^+$, which has just one pyrrole substituent, is not preferentially incorporated into poly(3-methylthiophene) under similar conditions (Table 1). Copolymerization of the Ru complexes with pyrrole results in preferential incorporation of the unsubstituted polypyrrole which polymerizes at lower potentials than the pyrrole substituent of the complex (Table 1) (3).

Polymerization procedure and potential

All copolymers listed in Table 1 could be prepared under potentiostatic or potential cycling conditions. Generally, better reproductibility and more uniform coverage of the electrode were obtained with potential cycling. Film thicknesses could easily be controlled by the polymerization time or the number of cycles (Table 2). The optimum polymerization potentials (or upper potential limit for cycling) given in Table 1 are determined by the minimum potential required to produce satisfactory copolymer films and the potential at which oxidative deactivation of the copolymer becomes unacceptable. Within this range some control of composition is possible by varying the potential. The more easily polymerized monomer is favoured at lower potentials. This is particularly evident in the copolymerization of $[Ru(bp)_2(pmp)_2]^{2+}$ with 3-methylthiophene, where increasing the potential results in an increased thiophene:Ru ratio in the resulting film.

Monomer concentrations and residual water

The deposition of thiophene-based copolymers was inhibited by residual water in the polymerization solution. Reproduci-

Can. J. Chem. Downloaded from www.nrcresearchpress.com by 198.100.157.202 on 09/07/12
For personal use only.

bility and homogeneity of electrode coverage were enhanced by increasing the 3-methylthiophene concentration, presumably by increasing the monomer-to-residual water ratio. A minimum 3-methylthiophene concentration of 20 mM was found to be satisfactory. Increasing the Ru complex concentration generally made the copolymerization less reproducible. This problem appears to be related to water associated with the complex and can be alleviated by thoroughly drying the complex in a vacuum oven.

Determination of composition by X-ray emission spectroscopy

Copolymer compositions quoted in this and our previous work are based on electrochemical measurements. The determination of compositions in this way requires a separation of the Ru complex and polymer backbone components of a cyclic voltammogram (e.g. Fig. 1) (3, 5). In addition, the number of electrons (n) involved in the electrochemistry of the polymer backbone must be known. Estimation of the Ru complex content of pyrrole$_x$–$[Ru(bp)_2(pmp)Cl]^+$ copolymers by cyclic voltammetry has been validated by electronic absorption spectroscopy (3). However, estimation of the heterocycle content by cyclic voltammetry has not been tested for any heterocycle–[Ru complex] copolymer.

Ideally, an elemental analysis would be obtained for each film. However, a 1 μm polymer film on a 1 cm^2 electrode typically has a mass of ca. 0.2 mg. Conventional elemental microanalysis of such a film is obviously impractical. Thicker films could be used but their compositions may be different from the thin films studied by electrochemistry. X-Ray emission spectroscopy, however, is well suited to the study of the samples used in this work.

Unfortunately, H, C, N, and O could not be detected by X-ray emission spectroscopy. The analysis therefore focused on heavy atoms in the monomers and counterions (Ru, S, Cl, and P). Analysis is further complicated by the overlap of the Cl-K emission line and the Ru-L emission line when an energy dispersive detector is used. Perchlorate counterions were therefore replaced with PF_6^- by ion-exchange in acetonitrile. Figure 3 shows an X-ray emission spectrum of a typical (3-methylthiophene)$_x$–$[Ru(bp)_2(pmp)_2](PF_6)_2$ copolymer film on a glassy carbon electrode. The Ru-L, P-K, and S-K emissions are well resolved. Background-corrected peak areas were calculated by the data anlysis system (Standardless Quantitative Analysis). Standards were prepared by depositing 2–10 μg mixtures of $[Ru(bp)_3](PF_6)_2$ and tetraethylammonium *p*-toluenesulfonate on carbon electrodes by evaporating acetone solutions. Four standards with S:Ru mole ratios between 3 and 12 were each analyzed twice. A plot of S:Ru ratios calculated directly from peak areas for these standards against the actual mole ratios had a slope of 0.97 (±0.12) and an intercept of 0.33. The standard deviation about the regression was 1.1. Therefore the S:Ru ratios for copolymer films were calculated directly from peak areas with no corrections. Compositions of a number of copolymers determined this way are plotted against the electrochemically determined compositions in Fig. 4. There is significant scattering of the data because both analytical techniques are only semi-quantitative. However, for thiophene-to-Ru mole ratios below 8 the agreement is good. At higher thiophene contents electrochemically determined thiophene-to-Ru ratios are higher than those determined by X-ray emission spectroscopy. The values from the X-ray data are more likely to be incorrect because they do not reflect an increasing thiophene content of the polymer as the thiophene-to-Ru ratio in the

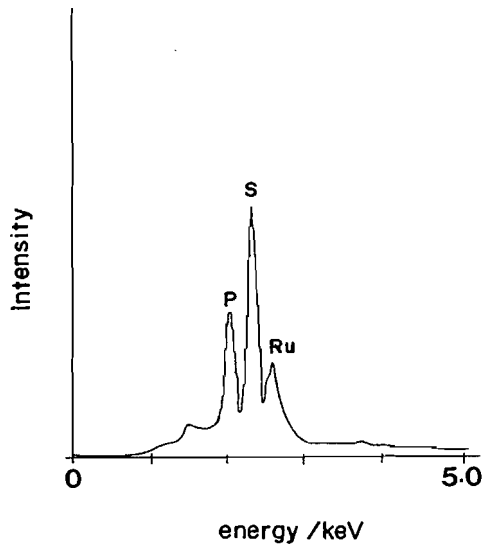


FIG. 3. X-Ray emission spectrum of a glassy carbon carbon electrode coated with a ca. 1.5 μm thick copolymer of 3-methylthiophene and $[Ru(bp)_2(pmp)_2](PF_6)_2$.

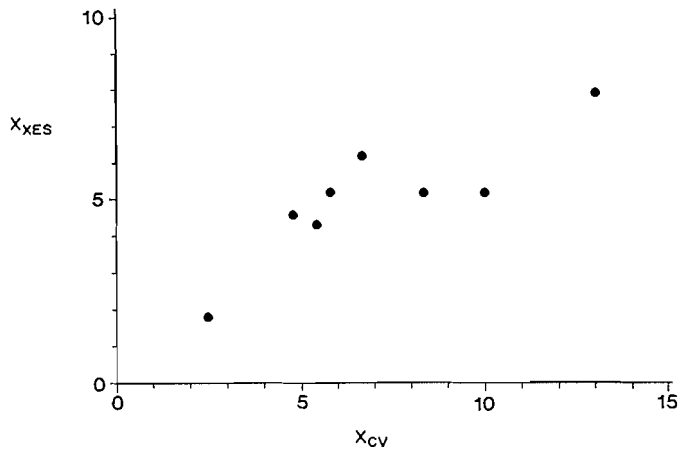


FIG. 4. Plot of thiophene-to-Ru ratios determined by X-ray emission spectroscopy (x_{XES}) against those determined by cyclic voltammetry (x_{CV}) for (3-methylthiophene)$_x$–$[Ru(bp)_2(pmp)_2](PF_6)_2$ copolymer films.

polymerization solution was increased. Further, the compositions from the X-ray data would require oxidation of the thiophene backbone of the copolymer to involve as few as two thiophene units per electron, which would be unusually low.

Electrochemistry and ligand substitution reactions of complexes in copolymers

$[Ru(bp)_2(pmp)Cl]^+$

Of the copolymers that could directly be prepared, (3-methylthiophene)$_x$–$[Ru(bp)_2(pmp)Cl]^+$ films offered the best precursors to electrocatalytic films containing $[Ru(bp)_2(pmp)(H_2O)]^{2+}$. Substitution of the chloride ligand by water has been shown to occur for an analogous complex immobilized in polyvinylpyridine (9, 14). This reaction is slow and incomplete under thermal conditions but facile under illumination (14).

Cyclic voltammograms of a (3-methylthiophene)$_8$–$[Ru(bp)_2(pmp)Cl]^+$ copolymer film in 1 M H_2SO_4(aq) before (—)and after (----) illumination with a 150 W tungsten lamp for 1 h are shown in Fig. 5*A*. After illumination, the peaks at $E^{0\prime} = 0.75$ V

Can. J. Chem. Downloaded from www.nrcresearchpress.com by 198.100.157.202 on 09/07/12
For personal use only.

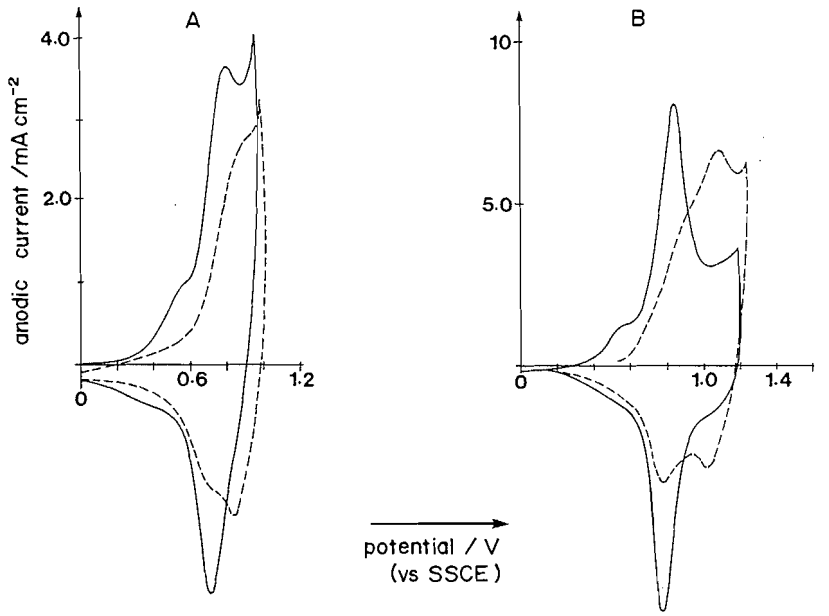


FIG. 5. (*A*) Cyclic voltammograms at 100 mV/s, in H_2SO_4(aq), of a Pt electrode coated with a copolymer of 3-methylthiophene and $[Ru(bp)_2(pmp)Cl]^+$. The solid line is the initial voltammogram, while the dashed line was recorded after ca. 1 h of photolysis in 1 M H_2SO_4. (*B*) Cyclic voltammograms of a similar electrode, in acetonitrile + 0.1 M Bu_4NBF_4, before (—) and after (---) ca. 1 h of photolysis in 1 M H_2SO_4(aq).

due to the chloro-complex had diminished and new peaks had appeared at $E^{0\prime} = 0.87$ V. This new formal potential can be assigned to the polymer-bound aqua complex, $[Ru(bp)_2(pmp)(H_2O)]^{2+}$, since it is close to the values observed for $[Ru(bp)_2(py)(H_2O)]^{2+}$ in 1 M $HClO_4$ (0.90 V) (11) and in polyvinylpyridine films (ca. 0.85 V) (14). The elctrochemistry of the polymer-bound aqua complex is more clearly observed in acetonitrile (Fig. 5*B*). From this voltammogram, the formal potential of the aqua complex in the polymer in acetonitrile is 1.08 V.[3] With potential cycling in the acetonitrile electrolyte, the waves due to the aqua complex were replaced by waves at $E^{0\prime} = 1.32$ V due to the acetonitrile complex.

Similar photosubstitution of the copolymer-bound chloro complex occurs in 1 M $HClO_4$(aq). The formal potentials of the chloro and aqua complexes are 0.59 and 0.79 V, respectively, in the 3-methylthiophene copolymer in this electrolyte solution. These potentials are similar to those reported for analogous complexes in polyvinylpyridine in 1 M $HClO_4$ (0.64 and 0.85 V) (14).

Substitution of the Cl^- ligand in (3-methylthiophene)$_x$–$[Ru(bp)_2(pmp)Cl]^+$ copolymers also occurs thermally in aqueous media but, as reported by Vos and co-workers (14) for $[Ru(bp)_2(py)Cl]^+$ in polyvinylpyridine, it is much slower than photosubstitution. This is demonstrated in Fig. 6. Immersion of the copolymer in 0.1 M $LiClO_4$(aq) for 15 h at room temperature resulted in only a partial decrease in the waves at $E^{0\prime} = 0.82$ V due to the chloro complex. New waves due to the aqua complex appeared at $E^{0\prime} = 1.12$ V. The difference of 40 mV between this formal potential and that obtained from Fig. 5*B* is too small to be regarded as significant. The voltammograms shown in Fig. 6 also exhibit small waves at $E^{0\prime} = 1.32$ V due to the acetonitrile complex which is formed from both the chloro and aqua complexes in acetonitrile (see below).

Thermal substitution of the Cl^- ligand of $[Ru(bp)_2(pmp)Cl]^+$ in copolymer films also occurs in acetonitrile. Figure 7 shows voltammograms of a (3-methylthiophene)$_9$–$[Ru(bp)_2(pmp)Cl]^+$ copolymer film in acetonitrile before (—) and after 1 h of heating at reflux in acetonitrile + 0.1 M $LiClO_4$ (---). The wave at $E^{0\prime} = 0.83$ V, due to the Cl complex, decreases and is replaced by a new wave at $E^{0\prime} = 1.34$ V, due to the acetonitrile complex. Interestingly, no substitution was observed under similar conditions in acetonitrile + 0.1 M Bu_4NClO_4. The latter result is most intriguing, indicating that Li^+ catalyzes the replacement of Cl^+ by CH_3CN.

The (3-methylthiophene)$_x$–$[Ru(bp)_2(pmp)H_2O]^{2+}$ copolymers prepared here did not prove to be useful for electrocatalysis because of the irreversible oxidation of the conducting backbone. As can be seen from the voltammograms shown in Fig. 5*A*, this occurs at potentials at which the electrocatalytic Ru aqua complex is oxidized. Poly(3-methylthiophene) was found to be a stable electrode material for the oxidation of [Ru(bp)(2,2′:6′,2″-terpyridine)$(H_2O)]^{2+}$ under basic conditions when the formal potential of the complex is much lower (15). However, the electrochemistry of the aqua complex in the copolymer film is suppressed in basic media. A similar phenomenon was reported for the aqua complex in polyvinylpyridine films (14). The more hydrophillic backbone of poly-[1-methyl-3-(pyrrol-1-ylmethyl)pyridium(1+)] was used to try to prevent this problem but irreversible oxidation of the resulting copolymers obscured any electrochemistry of the Ru aqua complex under all conditions tested.

$[Ru(bp)_2(pmp)(ClO_4)]^+$ and $[Ru(bp)_2(pmp)(H_2O)]^{2+}$

Copolymer films containing $[Ru(bp)_2(pmp)(ClO_4)]^+$ are attractive precursers to films containing the aqua complex because the perchlorate ligand is more easily replaced by water than is Cl^-. The infrared and mass spectroscopic data presented above for the perchlorate complex monomer suggest that substitution of perchlorate by adventitious water is likely to occur immediately upon removing the copolymer from the CH_2Cl_2 solution in which it is prepared. Evidence for this is

[3]Formal potentials in acetonitrile and water can not be directly compared because of junction potentials and solvent effects.

Can. J. Chem. Downloaded from www.nrcresearchpress.com by 198.100.157.202 on 09/07/12
For personal use only.

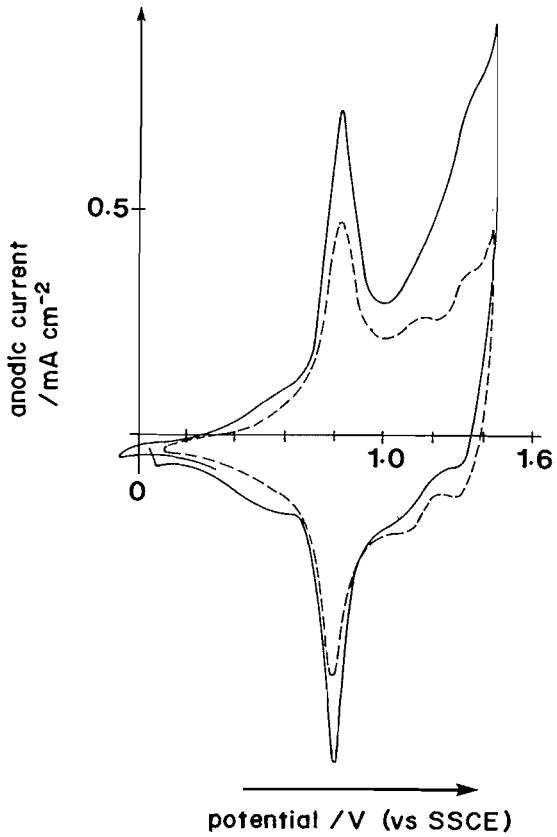


FIG. 6. Cyclic voltammograms at 100 mV/s, in acetonitrile + 0.1 M Bu_4NClO_4, of a Pt electrode coated with a copolymer of 3-methylthiophene and $[Ru(bp)_2(pmp)Cl]^+$. The solid line is the initial voltammogram, while the dashed line was recorded after ca. 15 h at room temperature in aqueous 0.1 M $LiClO_4$.

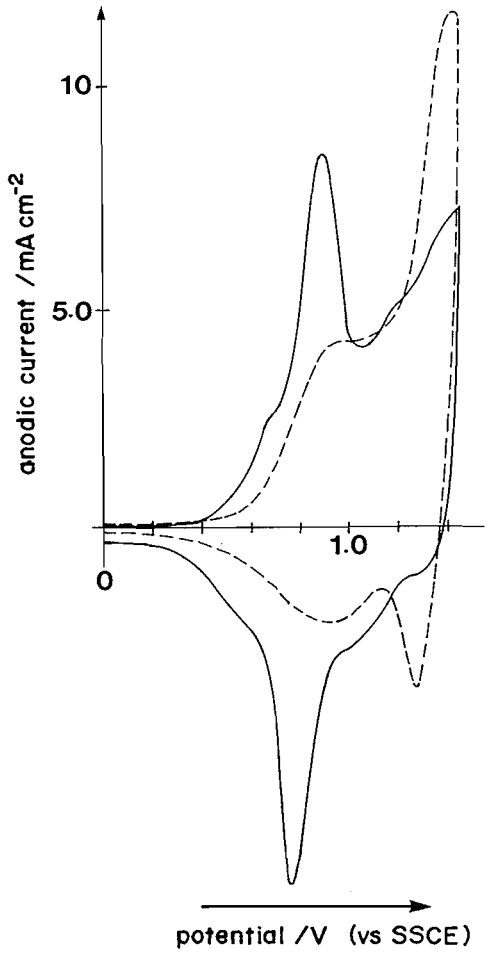


FIG. 7. Cyclic voltammograms at 100 mV/s, in acetonitrile + 0.1 M Bu_4NClO_4, of a Pt electrode coated with a copolymer of 3-methylthiophene and $[Ru(bp)_2(pmp)Cl]^+$. The solid line is the initial voltammogram, while the dashed line was recorded after ca. 1 h of heating at reflux in acetonitrile + 0.1 M $LiClO_4$.

presented in Fig. 8. Figure 8*A* shows cyclic voltammograms of a copolymer of pyrrole and $[Ru(bp)_2(pmp)(ClO_4)]^+$ in acetonitrile. The peaks at $E^{0\prime} = 1.13$ V could be due to either the perchlorate complex or the aqua complex. They decay rapidly and are replaced by peaks at $E^{0\prime} = 1.32$ V, characteristic of the acetonitrile complex, $[Ru(bp)_2(pmp)(CH_3CN)]^{2+}$. Figure 8*B* shows voltammograms of a similar film that had been soaked in aqueous KPF_6 overnight, to ensure substitution of the perchlorate ligand by water. These voltammograms are not significantly different from those in Fig. 8*A*, suggesting that both films contained the aqua complex. However, because of the similarity of the formal potentials of the perchlorate and aqua complexes (Table 2) we can not be sure that the voltammogram shown in Fig. 8*A* is not that of the perchlorate complex. No useful electrochemical data could be obtained for the pyrrole-based copolymers in aqueous media because electrochemical activity of the Ru complexes was obscured by irreversible oxidation of the polypyrrole.

The redox waves at $E^{0\prime} = 0.83$ V in Fig. 8*A* are due to $[Ru(bp)_2(pmp)(Cl)]^+$. This complex is present as an impurity in the $[Ru(bp)_2(pmp)(ClO_4)]^+$ polymerization solution and is preferentially incorporated into the copolymer film. Solid samples of "$[Ru(bp)_2(pmp)(ClO_4)]ClO_4$" slowly decompose to give $[Ru(bp)_2(pmp)(Cl)]^+$. Copolymers without this impurity can be prepared using freshly prepared $[Ru(bp)_2(pmp)(H_2O)](ClO_4)_2$.

The ligand substitution reactions of copolymers prepared from 1-methyl-3-(pyrrol-1-ylmethyl)pyridinium(1+) and $[Ru(bp)_2(pmp)(ClO_4)]^+$ are similar to those of the pyrrole-based films. Although this *N*-substituted polypyrrole is more stable to oxidation than polypyrrole, no voltammetric peaks due to the aqua complex could be observed in aqueous media.

$[Ru(bp)_2(pmp)(CH_3CN)]^{2+}$

The acetonitrile complex is remarkably stable in conducting copolymer films. Bithiophene$_x$–$[Ru(bp)_2(pmp)(CH_3CN)](ClO_4)_2$ copolymer films, immersed in either acetonitrile or dichloromethane containing Et_4NCl exhibited no voltammetric peaks due to formation of the chloro complex, even after more than 10 h at room temperature. A similar film exhibited no evidence of the formation of an aqua complex during 2 h of illumination in 1 M aqueous H_2SO_4.

$[Ru(bp)_2(pmp)_2](ClO_4)_2$

Photolysis of this complex in dichloromethane results in substitution of one of the pmp ligands by ClO_4^- (11). If this reaction could be reproduced in a conducting copolymer film it would be a usefuul route to make films containing the perchlorate complex and hence the aqua complex. However, 100 min of photolysis of a 3-methylthiophene$_x$–$[Ru(bp)_2(pmp)_2]^{2+}$ copolymer film on a Pt electrode in dichloromethane containing Bu_4NClO_4 produced no voltammetric evidence for the formation of the perchlorate complex. Similarly, photolysis in acetone + Et_4NCl resulted in no new voltammetric peaks due to the formation of the chloro complex.

Can. J. Chem. Downloaded from www.nrcresearchpress.com by 198.100.157.202 on 09/07/12
For personal use only.

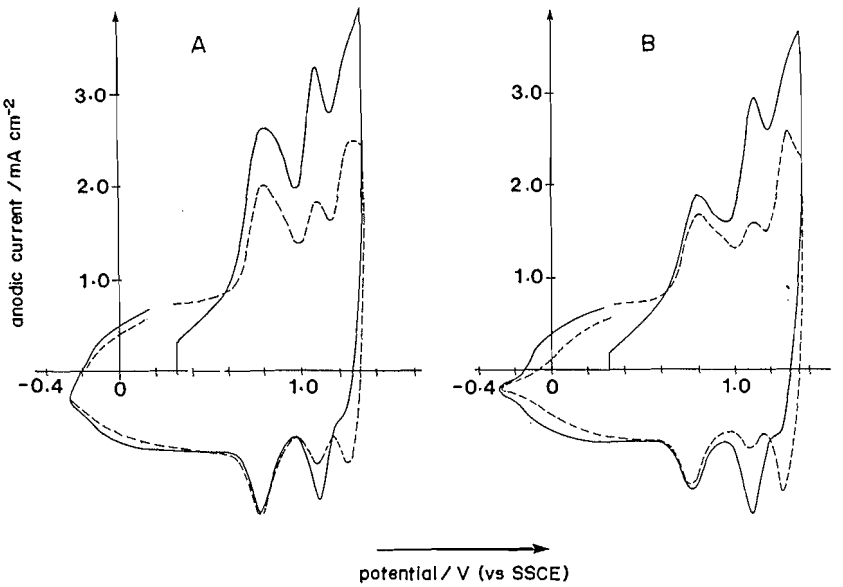


FIG. 8. Cyclic voltammograms at 100 mV/s, in acetonitrile + 0.1 M Bu_4NBF_4, of Pt electrodes coated with copolymers prepared from pyrrole and $[Ru(bp)_2(pmp)(ClO_4)](ClO_4)$ in CH_2Cl_2. The coated electrode for B was immersed in 0.1 M KPF_6(aq) at room temperature overnight before use. Solid lines are first scans while dashed lines as third (*A*) and fourth scans (*B*), respectively.

Kinetics

Ligand substitution reactions of the ruthenium complexes in the copolymer films studied in this work generally follow those observed in solution (11) and in polyvinylpyridine (9, 14). However, although no quantitative comparison has been made, it appears that these reactions are considerably slower than in solution. $[Ru(bp)_2(pmp)(CH_3CN)]^{2+}$ and $[Ru(bp)_2(pmp)_2)]^{2+}$ are particularly unreactive in the conducting copolymer films. Kinetic studies of these reactions may reveal important information about the chemical environment within the copolymers (16).

Acknowledgments

We gratefully acknowledge financial support from the Natural Sciences and Engineering Research Council of Canada (NSERC) and from Memorial University. We also thank Carolyn Emerson for assistance with X-ray emission spectroscopy, Brian Gregory and Marion Baggs for running the mass spectra, and Kenneth Seddon and Johannes Vos for helpful discussions of this work.

1. A. DERONZIER and J. MOUTET. Acc. Chem. Res. **22**, 249 (1989).
2. T. INAGAKI, M. HÜNTER, X. Q. YANG, T. A. SKOTHEIM, and Y. OKAMOTO. J. Chem. Soc. Chem. Commun. 126 (1988).
3. J. OCHMANSKA and P. G. PICKUP. J. Electroanal. Chem. **271**, 83 (1989).
4. C. ARMENGAUD, P. MOISY, F. BEDIOUI, J. DEVYNCK, and C. BIED-CHARRETON. J. Electroanal. Chem. **277**, 197 (1990).
5. J. OCHMANSKA and P. G. PICKUP. J. Electroanal. Chem. **297**, 197 (1991).
6. H. MAO and P. G. PICKUP. J. Phys. Chem. **93**, 6480 (1989).
7. B. A. MOYER, M. S. THOMPSON, and T. J. MEYER. J. Am. Chem. Soc. **102**, 2310 (1980).
8. G. J. SAMUELS and T. J. MEYER. J. Am. Chem. Soc. **103**, 307 (1981).
9. O. HAAS, M. KRIENS, and J. G. VOS. J. Am. Chem. Soc. **103**, 1318 (1981).
10. R. C. MCHATTON and F. C. ANSON. Inorg. Chem. **23**, 3935 (1984).
11. B. DURHAM, J. L. WALSH, C. L. CARTER, and T. J. MEYER. Inorg. Chem. **19**, 860 (1980).
12. B. A. MOYER and T. J. MEYER. Inorg. Chem. **20**, 436 (1981).
13. H. MAO and P. G. PICKUP. J. Electroanal. Chem. **265**, 127 (1989).
14. O. HAAS, H. R. ZUMBRUNNEN, and J. G. VOS. Electrichim. Acta, **30**, 1551 (1985).
15. K. J. TAKEUCHI, M. S. THOMPSON, D. W. PIPES, and T. J. MEYER. Inorg. Chem. **23**, 1845 (1984).
16. C. M. LIEBER, M. H. SCHMIDT, and N. S. LEWIS. J. Am. Chem. Soc. **108**, 6103 (1986).

Can. J. Chem. Downloaded from www.nrcresearchpress.com by 198.100.157.202 on 09/07/12
For personal use only.

Influence électronique et stérique du ligand tétraméthylcyclopentadiényle sur les propriétés physiques et sur la réactivité de complexes du titane et du zirconium

P. COURTOT, R. PICHON ET J. Y. SALAUN[1]

Unité associée au Centre national de la recherche scientifique, n° 322, Chimie, électrochimie et photochimie moléculaires, Université de Bretagne Occidentale, 29287 Brest CEDEX *France*

AND

L. TOUPET

Groupe de physique cristalline, Unité Associée au Centre national de la recherche scientifique, n° 804, Université de Rennes I, Campus de Beaulieu, 35042 Rennes CEDEX *France*

Reçu le 26 juillet 1990

P. COURTOT, R. PICHON, J. Y. SALAUN et L. TOUPET. Can. J. Chem. **69**, 661 (1991).

La préparation des composés de type $(C_5Me_4H)_2MR^1R^2$ (M = Ti, Zr) et $(C_5Me_4H)(C_5H_5)MR^1R^2$ (M = Ti) a été réalisée (R^1 = R^2 = Cl, CH_3, C_6H_5, *p*-$C_6H_4CH_3$, CO ; R^1 = Cl, R^2 = CH_3, C_6H_5, *p*-$C_6H_4CH_3$). Les caractéristiques RMN et IR de ces complexes montrent que le ligand C_5Me_4H induit une influence électronique beaucoup plus importante que le ligand C_5H_5 et très légèrement inférieure à celle de C_5Me_5. Une étude structurale réalisée sur le complexe $(C_5Me_4H)_2Zr(C_6H_5)Cl$ ainsi que l'examen des propriétés des composés $(C_5Me_4H)_2MR^1R^2$ (M = Ti, Zr ; R^1 = R^2 = C_6H_5, *p*-$C_6H_4CH_3$; R^1 = Cl, Br ; R^2 = C_6H_5, *p*-$C_6H_4CH_3$) en RMN dynamique ont également mis en évidence pour le ligand C_5Me_4H une influence intermédiaire entre celle de C_5H_5 et celle de C_5Me_5. Enfin, l'encombrement stérique ainsi que l'effet électronique du ligand C_5Me_4H ont été mis à profit pour induire, à l'aide du complexe $(C_5Me_4H)_2Ti(CH_3)_2$, des réactions d'isomérisation spécifiques de divers alcènes.

Mots clés : zirconium, titane, tétraméthylcyclopentadiényle, photoassistée, isomérisation, alcènes.

P. COURTOT, R. PICHON, J. Y. SALAUN, and L. TOUPET. Can. J. Chem. **69**, 661 (1991).

The complexes $(C_5Me_4H)_2MR^1R^2$ (M = Ti, Zr) and $(C_5Me_4H)(C_5H_5)MR^1R^2$ (M = Ti) have been prepared (R^1 = R^2 = Cl, CH_3, C_6H_5, *p*-$C_6H_4CH_3$, CO; R^1 = Cl, R^2 = CH_3, C_6H_5, *p*-$C_6H_4CH_3$). The NMR and IR spectra of these complexes indicate that C_5Me_4H exhibits an electron-donor effect more important than C_5H_5 and a little bit weaker than that of C_5Me_5. A structural investigation of the complex $(C_5Me_4H)_2Zr(C_6H_5)Cl$ and the study of the ^1H or ^{13}C dynamic NMR properties of the compounds $(C_5Me_4H)_2MR^1R^2$ (M = Ti, Zr; R^1 = R^2 = C_6H_5, *p*-$C_6H_4CH_3$; R^1 = Cl, Br, R^2 = C_6H_5, *p*-$C_6H_4CH_3$) show clearly that C_5Me_4H has a steric effect intermediate between C_5H_5 and C_5Me_5. The steric or electronic effects of C_5Me_4H have been used to induce specific isomerization reactions of various alkenes by using $(C_5Me_4H)_2Ti(CH_3)_2$ as catalyst.

Key words: zirconium, titanium, tetramethylcyclopentadienyl, photo-assisted, isomerization.

Introduction

Le remplacement d'un ligand cyclopentadiényle par un ligand pentaméthylcyclopentadiényle dans les dérivés de métallocènes conduit à augmenter la stabilité des complexes en raison de l'effet inductif et d'hyperconjugaison des groupements méthyle et d'un plus grand encombrement stérique autour du métal. L'effet inductif des méthyles modifie également les propriétés physiques et chimiques des complexes en augmentant la densité électronique du centre métallique. Nous avons voulu mettre en évidence l'influence électronique et stérique des groupements méthyle substituant les ligands cyclopentadiényle en réalisant la préparation et l'étude de dérivés du titanocène et du zirconocène possédant des ligands susceptibles de présenter des effets électroniques et stériques intermédiaires entre les complexes des séries $(C_5H_5)_2MR_2$ et $(C_5Me_5)_2MR_2$ déjà décrits dans la littérature. Pour réaliser ce travail, nous avons entrepris d'étudier les dérivés du titanocène et du zirconocène dont les ligands cyclopentadiényle sont substitués par quatre groupements méthyle : $(C_5Me_4H)_2MR^1R^2$.

Nous décrirons dans cet article la préparation des différents complexes dont nous commenterons les propriétés physiques les plus intéressantes. L'étude structurale de $(C_5Me_4H)_2Zr(C_6H_5)Cl$ sera ensuite détaillée ainsi que le comportement particulier en RMN dynamique des complexes substitués par un ou deux groupements aryle. Enfin, nous évoquerons les réactions spécifiques induites photochimiquement à l'aide du complexe $(C_5Me_4H)_2Ti(CH_3)_2$. Ce travail a fait l'objet de deux communications préliminaires (1, 2).

Résultats et discussion

Préparation des complexes

Le ligand C_5Me_4H a été obtenu par réduction de la tétraméthyl-2,3,4,5 cyclopentèn-2 one (3) par $LiAlH_4$ puis par déshydratation de l'alcool ainsi formé par l'acide *p*-toluène sulfonique en tétraméthyl-1,2,3,4 cyclopentadiène-1,3 (Rdt : 85%). Le sel de lithium de ce composé diénique (C_5Me_4HLi) est préparé à 0°C par échange avec le butyllithium. La condensation de deux équivalents de C_5Me_4HLi sur $TiCl_3$ ou $ZrCl_4$ selon des modes opératoires décrits dans la littérature pour la préparation de composés voisins porteurs des ligands C_5H_5 ou C_5Me_5 (4*a*, 4*b*, 5) conduit aux $(C_5Me_4H)_2TiCl_2$ et $(C_5Me_4H)_2ZrCl_2$. Lorsque le métal est le zirconium, seul le complexe biscyclopentadiénylé est obtenu (Rdt : 60%). Par contre, lorsque le métal est le titane, quelle que soit la quantité de sel de lithium utilisée, la formation d'au minimum 30% de $(C_5Me_4H)TiCl_3$ accompagne celle de $(C_5Me_4H)_2TiCl_2$. Ces deux complexes sont séparés par extractions successives à l'hexane.

Le composé $(C_5Me_4H)TiCl_3$ est obtenu exempt de $(C_5Me_4H)_2TiCl_2$ selon la méthode de Clark et coll. (6) (Rdt : 65%) en faisant réagir $C_5Me_4HSi(Me)_3$ sur $TiCl_4$. Le triméthylsilyl-5 tétraméthyl-1,2,3,4 cyclopentadiène-1,3 est lui-même préparé par réaction de C_5Me_4HLi sur $ClSi(Me)_3$ (Rdt : 77%).

La méthode choisie pour l'obtention du complexe «mixte» $(C_5Me_4H)(C_5H_5)TiCl_2$ est la réaction de C_5H_5Li sur

[1]Auteur à qui adresser toute correspondance.

Printed in Canada / Imprimé au Canada

Can. J. Chem. Downloaded from www.nrcresearchpress.com by 198.100.157.202 on 09/07/12
For personal use only.

TABLEAU 1. Caractéristiques RMN des complexes préparés (Cp′ = C_5Me_4H; Cp = C_5H_5)

Composés	RMN ^1H δ ppm $CDCl_3$	RMN ^{13}C δ ppm $CDCl_3$
$(C_5Me_4H)_2TiCl_2$	6,0(2H,s); 2,05(12H,s); 1,98(12H,s)	135,8(Cp′); 125,1(Cp′); 113,1(Cp′H) (d: 170 Hz; m: 3,8 Hz); 14,9(CH_3)(q: 127, 6Hz) 13,1(CH_3)(q: 127,8 Hz)
$(C_5Me_4H)TiCl_3$	6,7(1H,s); 2,45(6H,s); 2,40(6H,s)	139,18(Cp′); 137,97(Cp′); 124,38(Cp′H) (d: 175,2 Hz; m: 4,2 Hz); 16,45(CH_3) (q: 127,6 Hz); 14,07(CH_3)(q: 127,8 Hz)
$(C_5Me_4H)_2ZrCl_2$	5,8(2H,s); 2,01(12H,s); 1,96(12H,s)	129,7(s)(Cp′); 120,9(s)(Cp′); 110,0 (Cp′H)(d: 168,3 Hz; m: 3,9 Hz); 13,91(CH_3)(q: 127,6 Hz); 12,08(CH_3) (q: 127, 6Hz)
$(C_5Me_4H)(C_5H_5)TiCl_2$	6,4(5H,s); 6,13(1H,s); 2,10 (6H,s); 1,96(6H,s)	137,2(s)(Cp′); 126,5(s)(Cp′); 118,9(CpH) (d: 177 Hz; m: 6,5 Hz)(Cp); 115,2(C′pH)(d: 172 Hz; m: 4 Hz); 15,3(CH_3)(q: 127,5 Hz); 13,2(CH_3) (q: 128,5 Hz)
$(C_5Me_4H)_2Ti(CH_3)_2$	4,70(2H,s); 2,07(12H,s); 1,65 (12H,s); −0,90(6H,s)	124,7(Cp′); 118,1(Cp′), 108(Cp′H)(d: 167 Hz; m: 3,9 Hz); 47,0(CH_3-Ti)(q: 122, 2 Hz); 13,8(CH_3)(q: 126, 2 Hz); 12,2(CH_3)(q: 125, 8 Hz)
$(C_5Me_4H)_2Zr(CH_3)_2$	4,96(2H,s); 1,98(12H,s); 1,81(12H,s); −0,92(6H,s)	121,5(Cp′); 116,4(Cp′); 105,07(Cp′H)(d: 166 Hz); 34,23(CH_3-Zr)(q: 116,2 Hz); 13,28(CH_3) (q: 126, 6 Hz); 11,52(CH_3)(q: 126, 4 Hz)
$(C_5Me_4H)(C_5H_5)Ti(CH_3)_2$	6,15(5H,s); 5,12(1H,s); 2,00(6H,s); 1,80(6H,s); −0,50(6H,s)	123,4(Cp′); 119,2(Cp′); 113,3(Cp) (d 173 Hz m: 7 Hz); 110,5(Cp′H)(d: 169 Hz; m: 4 Hz); 45,5(CH_3-Ti)(q: 123 Hz); 14,1(CH_3)(q: 127 Hz); 11,95(CH_3)(q: 127 Hz)
$(C_5Me_4H)_2Ti(p\text{-}C_6H_4CH_3)_2$	7–6,4(8H,m), 5,2(2H,s); 2,22(6H,s), 1,87(12H,s); 1,50(12H,s)	195,4(C-Ti); 135,6(C_2 tolyle); 131,8(C_4 tolyle); 128,2(Cp′) 126,4(C_3 tolyle); 122,1(Cp′); 113,25(Cp′H); 21,0(CH_3 tolyle); 14,6(CH_3); 12,6(CH_3)
$(C_5Me_4H)(C_5H_5)Ti(p\text{-}C_6H_4CH_3)_2$	6,85–6,7(8H,m); 5,94(5H,s); 5,90(1H,s); 2,20(6H,s); 1,87(6H,s); 1,49(6H,s)	194,8(C-Ti); 135,3(C_2 ou C_3 tolyle); 132,3(C_4 tolyle); 129,4(Cp′); 126,6(C_2 ou C_3 tolyle); 124,8(Cp′); 120,4(Cp′H); 116,1(CpH); 20,9(CH_3 tolyle); 14,7 et 12,3(CH_3)
$(C_5Me_4H)_2Zr(C_6H_5)_2$	7,7–6,9(10H,m); 5,37(2H,s); 1,90(12H,s); 1,46(12H,s)	191,0(C-Zr); 135,9(C_2 phényle); 128,8 (C_4 phényle); 125,9(C_3 phényle); 123,9 (Cp′); 119,3(Cp′); 110,2(Cp′H); 13,78 (CH_3); 11,95(CH_3)
$(C_5Me_4H)_2Ti(CO)_2$[a]	4,12(2H,s); 1,65(24H,s)	265,6(CO); 111,2(Cp′); 106; 0(Cp′); 98,1(Cp′-H); 13,4(CH_3); 11,4(CH_3)
$(C_5Me_4H)_2Zr(CO)_2$[a]	4,56(2H,s); 1,80(12H,s); 1,71(12H,s)	274,15(CO); 109,1(Cp′); 106,0(Cp′); 96,9(Cp′-H); 13,1(CH_3); 11,25(CH_3)
$(C_5Me_4H)(C_5H_5)Ti(CO)_2$[a]	4,59(5H,s); 4,44(1H,s); 1,62(6H,s); 1,54(6H,s)	263(CO); 107(Cp′); 103(Cp′); 94,1(Cp) (d: 174 Hz; m: 6,5 Hz); 93,2(Cp′-H)(d: 169 Hz; m: 4 Hz); 13,7(CH_3)(q: 127 Hz); 11,50(CH_3) (q: 127 Hz)
$(C_5Me_4H)_2Ti(CH_3)Cl$	5,15(2H,s); 2,07(6H,s); 2,05(6H,s); 1,88(6H,s); 1,66(6H,s); −0,05(3H,s)	130,2(Cp′); 122,55(Cp′); 120,75(Cp′); 120,6(Cp′); 110,45(Cp′H)(d: 168,5 Hz; m: 3,9 Hz); 53,49(CH_3-Ti)(q: 126,4 Hz); 14,55 (CH_3)(q: 127 Hz); 13,94(CH_3)(q: 127 Hz); 12,96(CH_3)(q: 127 Hz); 12,17(CH_3)(q: 127 Hz)
$(C_5Me_4H)(C_5H_5)Ti(CH_3)Cl$	6,13(5H,s); 5,49(1H,s); 2,03 (3H,s); 2,01(3H,s); 1,87(3H,s); 1,83(3H,s); 0,40(3H,s)	128,7(Cp′); 128,6(Cp′); 122,55(Cp′); 122,4(Cp′); 122,7(Cp′)(d: 170 Hz); 115,5 (Cp)(d: 174 Hz; m: 6,5 Hz); 51,1(CH_3-Ti q: 127 Hz); 14,7(CH_3)(q: 127 Hz); 14,5(CH_3)(q: 127 Hz); 12,7(CH_3)(q: 127 Hz); 12,2(CH_3)(q: 127 Hz)

Can. J. Chem. Downloaded from www.nrcresearchpress.com by 198.100.157.202 on 09/07/12
For personal use only.

TABLEAU 1 (*suite et fin*)

Composés	RMN ^{1}H δ ppm $CDCl_3$	RMN ^{13}C δ ppm $CDCl_3$
$(C_5Me_4H)_2Ti(p\text{-}C_6H_4CH_3)Cl$	6,85–6,10(4H,m); 5,3(2H,s); 2,15(3H,s); 1,98(6H,s); 1,95 (6H,s); 1,77(6H,s); 1,51(6H,s)	198,4(C-Ti); 138,7 et 134,7(C_2 ou C_3 tolyle); 133,7(Cp′); 131,8(Cp′); 128,9 (Cp′); 128,55 et 126,91(C_2 ou C_3 tolyle); 123,6(C_4 tolyle); 123,4(Cp′); 112,7(Cp′-H); 20,85(CH_3 tolyle); 15,1 (CH_3); 14,35(CH_3); 13,15(CH_3); 12,95(CH_3)
$(C_5Me_4H)(C_5H_5)Ti(p\text{-}C_6H_4CH_3)Cl$	7,9–7,6(4H,m); 6,47(5H,s); 5,98(1H,s); 2,3(3H,s); 2,07 (3H,s); 2,01(3H,s); 1,9(3H,s); 1,63(3H,s)	197,2(C-Ti); 135,2 et 134,5(C_2 ou C_3 tolyle); 133,2(Cp′); 132,5(Cp′); 129,2 (C_2 ou C_3 tolyle); 128,9(Cp′); 127,6 (C_2 ou C_3 tolyle); 124,8(C_4 tolyle); 123,2(Cp′); 115,8(Cp); 112,5(Cp′-H); 20,9(CH_3 tolyle); 14,8(CH_3); 14,5(CH_3) 13,4(CH_3); 13,2(CH_3)
$(C_5Me_4H)_2Zr(C_6H_5)Cl$	7,24–6,90(5H,m); 5,47(2H,s); 2(3H,s); 1,99(6H,s); 1,83 (6H,s); 1,49(6H,s)	193,1(C-Ti); 136,9(C phényle); 128,0(Cp′); 126,6(C phényle); 124,8(Cp′); 124,3 (C phényle); 120,2(Cp′); 120,0(Cp′); 109,5(Cp′H); 13,9(CH_3); 13,5(CH_3); 12,0 (CH_3); 11,87(CH_3)
$(C_5Me_4H)_2Ti(p\text{-}C_6H_4CH_3)Br$	6,7–6(4H,m); 5,30(2H,s); 2,13(3H,s); 2,10(6H,s); 1,96 (6H,s); 1,77(6H,s); 1,60(6H,s)	195,4(C-Ti); 139,4; 134,4; 133,5; 131,7; 128,9; 128,5; 127,0; 123,9; 123,7; 112,7 (Cp′ + tolyle); 20,8(CH_3 tolyle); 15,3(CH_3); 14,35(CH_3); 13,7(CH_3); 13,3(CH_3)
$(C_5Me_4H)_2Ti(C_6H_5)_2$	7,35–6,5(10H,m); 5,10(2H,s); 1,80(12H,s); 1,39(12H,s)	199,2(C-Ti); 135,6(C_2 phényle); 128,7 (Cp′); 127,19(Cp′); 125,5(C_3 phényle); 122,9(C_4 phényle); 113,25(Cp′H); 14,55(CH_3); 12,4(CH_3)
$(C_5Me_4H)(C_5H_5)Ti(C_6H_5)_2$	7,25–6,85(10H,m); 5,98(5H,s); 5,93(1H,s); 1,90(6H,s); 1,51 (6H,s)	194,4(C-Ti); 135,3; 126,1; 125,0; 123,4; 123,15; 120,7; 116,2(phényle + Cp + Cp′); 14,7(CH_3); 12,3(CH_3)

[a]Dans C_6D_6 au lieu de $CDCl_3$.

$(C_5Me_4H)TiCl_3$ (Rdt : 80%). L'autre voie de synthèse possible : $(C_5H_5)TiCl_3$ + C_5Me_4HLi, conduit avec 67% de rendement à un mélange composé de 70% du produit désiré et de 30% de $(C_5H_5)_2TiCl_2$. Différents auteurs ont déjà rapporté dans la littérature de tels échanges de cycle. Cependant, ces échanges aboutissaient soit à l'élimination du cyclopentadiényle le plus petit stériquement et le moins électrodonneur (C_5H_5) soit à l'obtention en quantité équivalente de $(C_5H_5)_2TiCl_2$ et de $(C_5Me_5)_2TiCl_2$ (ref. 7 et références citées). Pour notre part nous n'avons pas pu mettre en évidence la formation de $(C_5Me_4H)_2TiCl_2$ dans le milieu réactionnel. Les différents mécanismes proposés dans la littérature ne semblent pas convenir pour expliquer nos résultats.

Les complexes dichlorés dont nous venons de décrire les préparations ont été utilisés comme composés de départ pour la synthèse de dérivés dialkylés, diarylés ou dicarbonylés. Les méthodes de préparation utilisées sont voisines de celles décrites pour l'obtention des analogues dicyclopentadiénylés ou bispentaméthylcyclopentadiénylés. Les dérivés diméthylés et diarylés sont obtenus avec des rendements variant de 50% (M = Zr, R = C_6H_5) à 80% (M = Ti, R = CH_3) par réaction à basse température (−80°C) du méthyl ou de l'aryl lithium sur les complexes dichlorés (*4b*, 8–11). De même les dérivés dicarbonylés sont préparés par réduction des complexes dichlorés par le magnésium activé en présence de chlorure mercurique sous atmosphère de CO (1 atm = 101,3 kPa) (12, 13), (rendements de 25 à 70%).

Les dérivés de type $(C_5Me_4H)_2MR^1R^2$ (M = Ti, Zr) ou $(C_5Me_4H)(C_5H_5)TiR^1R^2$ avec R^1 = Cl et R^2 = CH_3, C_6H_5 ou $p\text{-}C_6H_4CH_3$ sont obtenus quantitativement par addition d'un équivalent de HCl aux complexes $(C_5Me_4H)_2M(R^2)_2$ ou $(C_5Me_4H)(C_5H_5)Ti(R^2)_2$ en solution dans l'éther. L'addition d'un équivalent d'organolithien aux dérivés dichlorés conduit le plus souvent à l'obtention de mélanges composés du complexe dichloré de départ et des dérivés mono et dialkylés (ou arylés). Seul le complexe $(C_5Me_4H)_2Ti(p\text{-}C_6H_4CH_3)Br$ a été obtenu par addition de $p\text{-}CH_3C_6H_4MgBr$ au dérivé dichloré. Un suivi de la réaction par RMN ^{1}H nous a permis de mettre en évidence la formation intermédiaire de $(C_5Me_4H)_2Ti(p\text{-}C_6H_4CH_3)Cl$ (déjà préparé selon la méthode générale) qui subit à température ambiante un rapide échange chlore–brome.

Caractéristiques physiques des complexes de titane et de zirconium

Les caractéristiques RMN des composés préparés sont indiquées dans le tableau 1.

On peut noter que la dissymétrie au niveau du métal dans les complexes $(C_5Me_4H)_2MRCl$ ou $(C_5Me_4H)(C_5H_5)TiRCl$ se traduit en RMN ^{1}H par une différenciation des quatre méthyles des ligands C_5Me_4H. Ceci est particulièrement mis en évidence dans le deuxième type de complexes porteur d'un seul ligand C_5Me_4H alors que dans la première série de composés, les deux ligands C_5Me_4H sont équivalents. En RMN ^{13}C, les quatre méthyles sont également différents de même que les cinq car-

Can. J. Chem. Downloaded from www.nrcresearchpress.com by 198.100.157.202 on 09/07/12
For personal use only.

Can. J. Chem. Downloaded from www.nrcresearchpress.com by 198.100.157.202 on 09/07/12
For personal use only.

bones du cycle pentadiénique. Les ligands C_5H_5 sont vraisemblablement en rotation rapide. Les résultats RMN que nous avons obtenus (tableau 1) ne permettent pas d'affirmer qu'il en est de même pour les ligands C_5Me_4H. Bien que les intéractions stériques méthyle–méthyle entre deux C_5Me_4H ne soient pas négligeables (cf. étude structurale), les observations effectuées sur les complexes porteurs de ligands C_5Me_5 (rotation rapide) (4, 5, 7–9, 11) sont en faveur d'un comportement analogue de C_5Me_4H. Les spectres ^1H et ^{13}C des ligands aryle du complexe $(C_5Me_4H)_2Ti(p\text{-}C_6H_4CH_3)_2$ seront, à titre d'exemple, détaillés ultérieurement.

Evaluation par infrarouge de la densité électronique au niveau du métal

Une évaluation de la densité électronique induite au niveau du métal par les différents ligands peut être réalisée par l'étude des variations des fréquences des deux vibrations d'élongation de la liaison C≡O dans les deux modes A_1 et B_1. Un accroissement de la densité électronique sur le métal se traduit par une augmentation de la force de la liaison π en retour vers le ligand carbonylé. La liaison métal–carbone se trouve renforcée alors que la force de la liaison C≡O est diminuée. Ceci se traduit par une diminution des fréquences infrarouges ν_{CO} observées. Les valeurs des fréquences des ν_{CO} mesurées pour nos composés ainsi que celles décrites dans la littérature pour des composés voisins sont rapportées dans le tableau 2.

Nous observons tant pour les complexes du titane porteurs de deux cyclopentadiényles tétraméthylés que pour ceux du zirconium une diminution de la fréquence des ν_{CO} variant de 27 à 37 cm^{-1} par rapport aux complexes porteurs de cyclopentadiényles non substitués. Ces variations de fréquence sont très proches de celles observées lorsque les ligands cyclopentadiényle sont remplacés par des pentaméthylcyclopentadiényles (de 30 à 41 cm^{-1}) (13, 14). Le complexe $(C_5Me_4H)(C_5H_5)Ti(CO)_2$ porteur d'un seul groupement C_5Me_4H présente des abaissements de fréquence de 15 et 19 cm^{-1} voisins de ceux observés pour son homologue pentaméthylé (15).

Les ligands C_5Me_4H exerçent donc sur le centre métallique une influence électronique très voisine de celle engendrée par C_5Me_5.

Evaluation par RMN de la densité électronique du métal

L'évaluation de la densité électronique au niveau du métal peut également être établie sur les complexes porteurs d'un groupement méthyle directement lié à ce métal, par les fluctuations des valeurs des constantes de couplage $J_{^{13}C-H}$ de ce groupement méthyle. Cette constante de couplage sera d'autant plus grande que le caractère *s* de la liaison C—H sera important. Une faible densité électronique au niveau du métal augmente l'effet électroattracteur de ce dernier, elle va donc diminuer la nature *s* de la liaison métal–carbone et laisser plus de caractère *s* aux liaisons C—H, ce qui entraîne une forte constante de couplage. Une augmentation de la densité électronique sur le métal va, de ce fait, diminuer la constante de couplage mesurée sur le méthyle. L'évaluation de cette constante $J_{^{13}C-H}$ qui est une mesure relative de l'hybridation de la liaison M–CH_3 doit permettre de connaître la densité électronique du centre métallique.

Les valeurs que nous avons mesurées pour nos complexes ainsi que celles décrites dans la littérature pour des composés voisins, sont rapportées dans le tableau 3.

Les mesures que nous avons effectuées confirment les résultats obtenus par Grubbs et coll. (16); plus la densité électronique du métal est élevée, plus la constante de couplage $J_{^{13}C-H}$ est faible, Le remplacement de C_5H_5 par C_5Me_4H fait varier sa valeur de 1,4 Hz alors que cette variation est de 1,7 Hz pour C_5Me_5. La substitution du deuxième C_5H_5 entraîne une modification moins importante (0,7 Hz) du paramètre mesuré.

Il est vraisemblable que la faible valeur de cette seconde variation soit due à l'effet stérique occasionné par la présence des deux ligands cyclopentadiényle sur le métal. L'effet électroattracteur du chlore est montré par une forte diminution de $J_{^{13}C-H}$ (4,4 Hz) lors du remplacement de cet atome par un groupement méthyle.

Cette méthode d'évaluation de la densité électronique au niveau du centre métallique montre (comme la méthode infrarouge) que l'influence électronique du ligand C_5Me_4H est voisine de celle de C_5Me_5 et très différente de C_5H_5; cependant, l'effet stérique de ce ligand reste à estimer. Une étude en RMN dynamique des complexes aryles de type $(C_5Me_4H)_2M(aryle)X$ (M = Ti, Zr; aryle = C_6H_5, $p\text{-}C_6H_4CH_3$; X = aryle, Cl, Br) nous a permis de réaliser cette estimation.

Étude de l'influence stérique des ligands C_5Me_4H

Mise en évidence par RMN ^1H et ^{13}C d'une restriction à la rotation des ligands aryle

La figure 1 présente l'évolution en RMN ^1H (300.13 MHz) du spectre des protons aromatiques du complexe $(C_5Me_4H)_2Ti(p\text{-}C_6H_4CH_3)_2$ en fonction de la température.

À 223 K ses protons aromatiques se présentent sous forme de deux systèmes AB différents dont les déplacements chimiques déterminés par découplage de spin sont respectivement situés à 6,49; 6,51; 6,76 et 6,78 pour le premier AB et 6,78; 6,81; 6,87 et 6,90 ppm pour le second lorsque les spectres sont réalisés dans $CDCl_3$. L'existence de ces deux systèmes AB montre clairement l'inéquivalence des protons 2 et 6 d'une part et 3 et 5 d'autre part. Les deux groupements tolyle sont identiques. Cette non équivalence des couples de protons est plus clairement mise en évidence chez les complexes monoarylés, par exemple $(C_5Me_4H)_2Ti(p\text{-}C_6H_4CH_3)Cl$, qui présentent des spectres similaires dans la région des protons aromatiques. L'existence en

TABLEAU 2. Fréquences d'absorption (cm^{-1}) de la vibration ν_{CO} des complexes $Cp'_2M(CO)_2$ dans l'hexane (M = Ti, Zr)

Complexe	$\nu_{CO}(cm^{-1})$	Références
$(C_5H_5)_2Ti(CO)_2$	1977, 1899	13, 14
$(C_5Me_4H)_2Ti(CO)_2$	1946, 1862	Ce travail
$(C_5Me_5)_2Ti(CO)_2$	1940, 1858	13
$(C_5H_5)_2Zr(CO)_2$	1975, 1865	14
$(C_5Me_4H)_2Zr(CO)_2$	1948, 1854	Ce travail
$(C_5Me_5)_2Zr(CO)_2$	1945, 1852	13
$(C_5H_5)(C_5Me_4H)Ti(CO)_2$	1962, 1880	Ce travail
$(C_5H_5)(C_5Me_5)Ti(CO)_2$	1956, 1875	15

TABLEAU 3. Valeurs des constantes de couplage $J_{^{13}C-H}$ des groupements CH_3–M

Complexe	$J_{^{13}C-H}$(Hz)	Références
$(C_5H_5)_2Ti(CH_3)Cl$	128,9	16
$(C_5H_5)(C_5Me_4H)Ti(CH_3)Cl$	127,5	Ce travail
$(C_5H_5)(C_5Me_5)Ti(CH_3)Cl$	127,2	16
$(C_5Me_4H)_2Ti(CH_3)Cl$	127,0	Ce travail
$(C_5Me_5)_2Ti(CH_3)Cl$	126,5	16
$(C_5H_5)(C_5Me_4H)Ti(CH_3)_2$	123,1	Ce travail
$(C_5Me_4H)_2Ti(CH_3)_2$	122,2	Ce travail
$(C_5Me_4H)_2Zr(CH_3)_2$	116,2	Ce travail

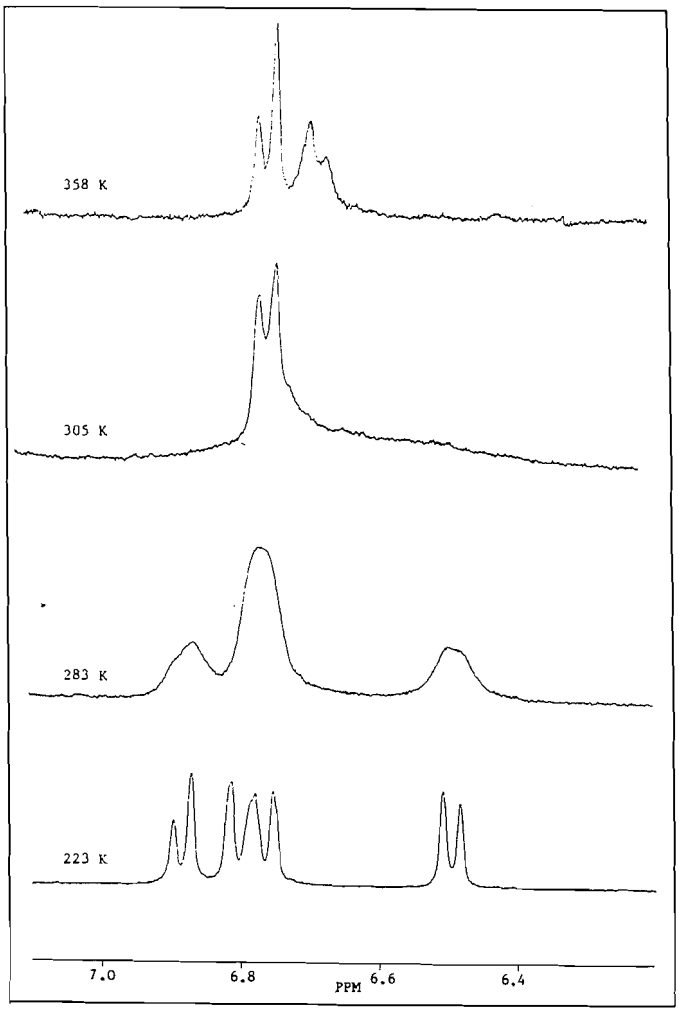


FIG. 1. Coalescence des signaux des protons aromatiques des groupements tolyle du complexe $(C_5Me_4H)_2Ti(p\text{-}C_6H_4CH_3)_2$ en solution dans $CDCl_3$.

RMN ^1H de ces deux systèmes AB indique sans ambiguïté qu'à 223 K, la rotation des ligands tolyle autour de la liaison carbone–métal s'effectue lentement par rapport à la détection RMN. Lorsque les spectres sont réalisés à température plus élevée, nous observons à 283 K la coalescence des signaux préalablement situés à 6,76; 6,78; 6,78 et 6,81 ppm (protons 3 et 5), puis apparaît à plus haute température un doublet centré à 6,79 ppm qui sera la partie A d'un nouveau système AB.

De même à 305 K, la coalescence des signaux situés à 6,49; 6,51; 6,87 et 6,90 ppm, lorsque le spectre est réalisé à basse température, est effective. Elle conduit lorsque la température s'élève à un nouveau doublet centré à 6,71 ppm (partie B du nouveau système AB). Les signaux situés vers 6,79 ont été attribués aux protons 3 et 5 car ces deux protons sont vraisemblablement les moins perturbés par les ligands cyclopentadiényle quelle que soit la position adoptée par le ligand aryle. Les protons 2 et 6 plus proches du centre métallique se sont vus attribuer les signaux les plus éloignés en RMN à 6,50 et 6,88 ppm.

Aux températures supérieures à 305 K, il y a équivalence des protons 2 et 6 d'une part et 3 et 5 d'autre part, ce qui indique une rotation rapide des ligands tolyle autour de la liaison carbone–métal.

En RMN ^{13}C, nous observons un phénomène analogue : à 223 K, les quatre carbones (2, 6, 3 et 5) des groupements aryle sont distincts à 136,83; 134,68; 126,46 et 126,33 ppm. La coalescence des deux derniers signaux se réalise à 273 K et celle des deux premiers à 294 K.

TABLEAU 4. Paramètres d'activation du complexe $(C_5Me_4H)_2Ti(p\text{-}C_6H_4CH_3)_2$

Mode de détermination RMN	$\Delta\nu$ (Hz)	T_c (K)	K_{T_c} (s^{-1})	$\Delta G^{0\neq}$ (kJ mol^{-1})
^1H	7,5	283	16,7	60,9 ± 4,0
^1H	111,55	305	256	60,7 ± 4,0
^{13}C	49,83	294	111	60,4 ± 4,0
^{13}C	3,05	273	6	62,2 ± 4,0

La température est sans effet sur les autres signaux ^1H ou ^{13}C du complexe.

La détermination des températures de coalescence a rendu possible l'évaluation des paramètres d'activation comme l'enthalpie libre d'activation $\Delta G^{0\neq}$ de la rotation des groupements tolyle autour de la liaison carbone–titane du complexe $(C_5Me_4H)_2Ti(p\text{-}C_6H_4CH_3)_2$. Les valeurs de $\Delta G^{0\neq}$ sont calculées par les relations :

$$\Delta G^{0\neq}\ (\text{kJ mol}^{-1}) = 1{,}914 \times 10^{-2} T_c(9{,}972 + \log T_c/(\delta\nu^2 + 6J^2_{AB})^{1/2})$$

pour les spectres protons (coalescences de deux AB) et par

$$\Delta G^{0\neq}(\text{kJ mol}^{-1}) = 1{,}914 \times 10^{-2} T_c(9{,}972 + log\ T_c/\delta\nu)$$

pour les spectres ^{13}C (17, 18). T_c = température de coalescence et $\delta\nu$ = écart en Hz entre les signaux en échange lent.

Les valeurs calculées pour les paramètres d'activation sont indiquées dans le tableau 4. Une bonne corrélation est observée entre les quatre mesures réalisées.

Nous avons mis en évidence ce phénomène de coalescence pour tous nos complexes mono ou bis arylés du titane ou du zirconium possédant deux C_5Me_4H. Les valeurs des énergies d'activation calculées pour ces complexes sont les suivantes : $(C_5Me_4H)_2Ti(p\text{-}C_6H_4CH_3)Cl$: 76,7 kJ mol^{-1}; $(C_5Me_4H)_2Ti(p\text{-}C_6H_4CH_3)Br$: 76,8 kJ mol^{-1}; $(C_5Me_4H)_2Zr(C_6H_5)Cl$: 84,9 kJ mol^{-1}.

Les études concernant des restrictions à la rotation de groupements autour d'une liaison métal–carbone sont peu nombreuses dans la littérature (ref. 19 et références incluses). Lappert *et al.* ont mis en évidence une gêne stérique engendrée par un groupement volumineux : $CH(SiMe_3)_2$ dans la série des complexes $(C_5H_4R)_2Zr[CH(SiMe_3)_2]Cl$ (20). À notre connaissance, un seul travail concerne un groupement aromatique; il a été réalisé sur les complexes $(C_5Me_5)RhX(PMe_3)(C_6H_4R)$ (19). Ces deux exemples présentent des valeurs élevées de barrière à la rotation autour de la liaison métal–carbone : $\Delta G^{0\neq}$ varie entre 60 et 65 kJ mol^{-1} pour la série du zirconium (20) et de 50 à 60 kJ mol^{-1} pour les complexes du rhodium (19). Les valeurs encore plus élevées que nous mettons en évidence pour nos complexes sont sans aucun doute induites par la gêne stérique due à la présence des deux ligands (C_5Me_4H) sur le centre métallique.

Lorsqu'un des deux ligands C_5Me_4H est remplacé par un groupement moins encombrant, le cyclopentadiényle non substitué, les complexes ne présentent plus de coalescence. Le ligand aryle, même à très basse température, est animé d'une vitesse de rotation rapide au regard de la détection RMN. Par contre, en raison d'un effet stérique plus important des ligands

Can. J. Chem. Downloaded from www.nrcresearchpress.com by 198.100.157.202 on 09/07/12
For personal use only.

C_5Me_5, le complexe $(C_5Me_5)_2Zr(C_6H_5)_2$ (11) ne présente pas de rotation des groupements phényle. (Ce complexe possède en effet en RMN ^{13}C quatre signaux différents pour les carbones 2, 3, 5 et 6 des ligands phényle.)

Cette étude en RMN dynamique nous a permis de confirmer que l'influence stérique engendrée par les ligands C_5Me_4H était intermédiaire entre les effets des ligands C_5H_5 et C_5Me_5. Une évaluation plus précise a pu être réalisée par une étude structurale radiocristallographique effectuée sur le complexe $(C_5Me_4H)_2Zr(C_6H_5)Cl$.

Étude radiocristallographique du complexe $(C_5Me_4H)_2Zr(C_6H_5)Cl$

Les cristaux ont été obtenus à −30°C dans l'hexane. Sur le tableau 5, nous avons indiqué les données cristallines ainsi que les paramètres d'acquisition de ces données. Les coordonnées des atomes (sauf hydrogènes) ainsi que les longueurs et les angles de liaison les plus représentatifs ont été rassemblés dans les tableaux 6, 7 et 8. Les figures 2 et 3 représentent les graphes ORTEP de la molécule. Les principales données structurales de composés voisins ont été reportées dans le tableau 9.[2]

L'atome de zirconium est au centre d'un tétraèdre déformé dont les angles sont de 99,0° (Cl—Zr—C19) et de 133,2° pour centroïde–Zr–centroïde. Afin de minimiser les interactions stériques, les deux ligands cyclopentadiényle sont décalés de 77° (figure 3) de façon analogue à la géométrie observée pour $Zr(C_4Me_4P)_2Cl_2$ (21). Les interactions stériques entre les deux ligands C_5Me_4H sont marquées par des distances Zr–centroïdes plus longues 2,240 et 2,347 Å et par un angle centroïde 1–Zr–centroïde 2 plus ouvert (133,2°) que dans les complexes porteurs de ligands cyclopentadiényle non substitués. Les distances moyennes entre l'atome de zirconium et les atomes de carbone des cyclopentadiényles (2,56 et 2,53 Å) sont supérieures à celles mesurées pour les complexes possédant des ligands C_5H_5 (2,52 Å) peu susceptibles de présenter de fortes interactions stériques. Il faut noter que les distances entre l'atome de zirconium et les carbones les moins encombrés des cyclopentadiényles sont les plus courtes (Zr—C_1 = 2,464 Å et Zr—C_{10} = 2,50 Å). De plus, les groupements méthyle des cyclopentadiényles sont, en regard du centre métallique, rejetés vers l'extérieur des plans des cyclopentadiényles. Les déviations par rapport à ces plans sont les suivantes : C_6 = 0,123 ; C_7 = 0,228 ; C_8 = 0,092 ; C_9 = 0,078 ; C_{15} = 0,187 ; C_{16} = 0,188; C_{17} = 0,061 ; C_{18} = 0,335. La longueur de la liaison Zr—Cl (2,443) est du même ordre de grandeur que celles mesurées dans d'autres complexes. Par contre, la valeur de l'angle Cl—Zr—C_{19} est anormalement élevée (99°) car généralement la présence de deux ligands cyclopentadiényle encombrés entraîne un resserrement de l'angle formé par le métal avec les deux autres substituants. Cette valeur est à rapprocher de celles observées pour les complexes $(C_5H_4CMe_3)_2ZrCl[CH(SiMe_3)_2]$ (26) et $(C_5H_5)_2Zr(C_6H_5)$-$[CH(SiMe_3)_2]$ (27) (98,2° et 100,4°). Elle résulte vraisemblablement de l'interaction stérique entre le phényle et le chlore. Cette interaction est également mise en évidence par l'angle de

TABLEAU 5. Paramètres cristallins et d'acquisition pour le complexe $(C_5Me_4H)_2Zr(C_6H_5)Cl$

Paramètre	Valeur
Formule	$C_{24}H_{31}ClZr$
Poids moléculaire	446,2
Système cristallin	Monoclinique
Groupe spatial	$P2_1/n$
a, Å	10,726 (4)
b, Å	14,724 (4)
c, Å	13,836(6)
β, degrés	96,07 (3)
V, Å^3	2173,0 (6)
Z	4
d(calc), g cm^{-3}	1,36
ν(MoKα), cm^{-1}	6,26
T^0, K	293
Taille du cristal, mm	0,15 × 0,10 × 0,10
Radiation, Å	α(MoKα) = 0,71069
Max. 2θ, deg	54
Scan	$w/2\theta = 1$
t_{max}(pour une mesure), s	60
Standards (toutes les 3600 s)	232, 243, 441
Variance des standards	±0,9%
Réflexions mesures	4175
Réflexions observées ($I \geq 2\sigma/I$)	3071
R_{INT}	0,011
R isotropique	0,084
R anisotropique	0,042
R final	0,028
RW	0,026
W	$1/\sigma(F_o)^2 = [\sigma^2(I) + (0{,}04\,F_o^2)^2]^{-1/2}$
Max. res. e.d. Å^{-3}	0,22

TABLEAU 6. Paramètres de positions et déviations standard estimées (entre parenthèses) pour les atomes (sauf hydrogènes) de $(C_5Me_4H)_2Zr(C_6H_5)Cl$

Atome	x	y	z	B (Å^2)
Zr	0,72990(2)	0,20297(2)	0,57171(2)	2,521(4)
Cl	0,56916(8)	0,13400(6)	0,45636(6)	4,72(2)
C1	0,9132(3)	0,1109(2)	0,6331(2)	3,80(6)
C2	0,9649(3)	0,1912(2)	0,5991(2)	3,51(6)
C3	0,9408(3)	0,1905(2)	0,4972(2)	3,48(6)
C4	0,8726(3)	0,1113(2)	0,4693(2)	2,89(6)
C5	0,8565(3)	0,0614(2)	0,5544(2)	3.97(7)
C6	1,0446(3)	0,2593(3)	0,6577(3)	5,45(9)
C7	0,9963(3)	0,2549(3)	0,4287(3)	5,36(8)
C8	0,8354(4)	0,0814(3)	0,3672(3)	6,6(1)
C9	0,7957(4)	−0,0308(3)	0,5580(4)	6,5(1)
C10	0,7141(3)	0,2973(3)	0,7202(2)	4,72(7)
C11	0,5988(3)	0,3103(2)	0,6647(2)	4,86(7)
C12	0,5356(3)	0,2271(3)	0,6611(2)	4,31(7)
C13	0,6130(3)	0,1630(2)	0,7151(2)	3,90(6)
C14	0,7217(3)	0,2084(3)	0,7547(2)	4,09(7)
C15	0,5504(4)	0,4010(3)	0,6291(4)	9,4(1)
C16	0,4030(4)	0,2126(5)	0,6192(3)	8,3(1)
C17	0,5771(4)	0,0669(3)	0,7348(3)	7,0(1)
C18	0,8159(4)	0,1754(4)	0,8348(3)	7,2(1)
C19	0,7522(3)	0,3378(2)	0,4940(2)	3,13(6)
C20	0,8184(3)	0,4146(2)	0,5299(2)	3,92(7)
C21	0,8301(3)	0,4914(2)	0,4739(3)	4,71(8)
C22	0,7769(4)	0,4946(2)	0,3797(3)	5,13(8)
C23	0,7112(4)	0,4209(3)	0,3416(3)	5,16(8)
C24	0,6987(3)	0,3444(2)	0,3980(2)	4,15(7)

[2]Les tableaux des longueurs de liaisons, des angles des liaisons, des paramètres de position, des paramètres généraux de déplacement et des valeurs de F_o et de F_c peuvent être obtenues du : Dépôt des données non publiées, Service de fourniture de documents, ICIST, Conseil national de recherches Canada, Ottawa Canada K1A 0S2.

On peut également se procurer les tableaux des longueurs et des angles des liaisons en s'adressant au Directeur, Cambridge Crystallographic Data Centre, University Chemical Laboratory, Lensfield Road, Cambridge CB2 1EW, Royaume-Uni.

Can. J. Chem. Downloaded from www.nrcresearchpress.com by 198.100.157.202 on 09/07/12
For personal use only.

TABLEAU 7. Distances interatomiques en angstrom

Atomes	Distance (Å)	Atomes	Distance (Å)
Zr—Cl	2,442(3)	C3—C7	1,507(5)
Zr—C1	2,464(4)	C4—C5	1,414(5)
Zr—C2	2,515(3)	C4—C8	1,493(5)
Zr—C3	2,590(4)	C5—C9	1,510(5)
Zr—C4	2,575(4)	C10—C11	1,398(4)
Zr—C5	2,512(3)	C10—C14	1,391(5)
Zr—C10	2,500(3)	C11—C12	1,397(5)
Zr—C11	2,552(3)	C11—C15	1,498(6)
Zr—C12	2,550(3)	C12—C13	1,416(5)
Zr—C13	2,663(4)	C12—C16	1,494(5)
Zr—C14	2,544(3)	C13—C14	1,404(4)
Zr—C19	2,291(2)	C13—C17	1,499(6)
Zr–Cent. 1	2,240	C14—C18	1,500(5)
Zr–Cent. 2	2,347	C19—C20	1,398(4)
C1—C2	1,408(5)	C19—C24	1,393(3)
C1—C5	1,395(4)	C20—C21	1,384(5)
C2—C3	1,406(4)	C21—C22	1,367(5)
C2—C6	1,499(5)	C22—C23	1,369(5)
C3—C4	1,408(4)	C23—C24	1,385(5)

TABLEAU 8. Table des angles de liaisons en degrés

Atomes	Angle (deg)	Atomes	Angle (deg)
ClZrC19	99,0(2)	C10C11C15	124,0(3)
Cent. 1 Zr Cent. 2	133,2	C12C11C15	128,3(3)
C2C1C5	109,5(3)	C11C12C13	108,1(3)
C1C2C3	106,9(3)	C11C12C16	125,3(4)
C1C2C6	127,1(3)	C13C12C16	126,2(4)
C3C2C6	125,5(3)	C12C13C14	107,7(3)
C2C3C4	108,4(3)	C12C13C17	125,3(3)
C2C3C7	125,7(3)	C14C13C17	126,6(3)
C4C3C7	125,2(3)	C10C14C13	107,3(3)
C3C4C5	107,9(3)	C10C14C18	124,7(3)
C3C4C8	125,6(3)	C13C14C18	126,9(4)
C5C4C8	126,2(3)	C20C19C24	115,2(3)
C1C5C4	107,3(3)	C19C20C21	122,3(3)
C1C5C9	126,8(3)	C20C21C22	120,6(3)
C4C5C9	125,9(3)	C21C22C23	119,1(3)
C11C10C14	109,5(3)	C22C23C24	120,3(3)
C10C11C12	107,3(3)	C23C24C19	122,6(3)

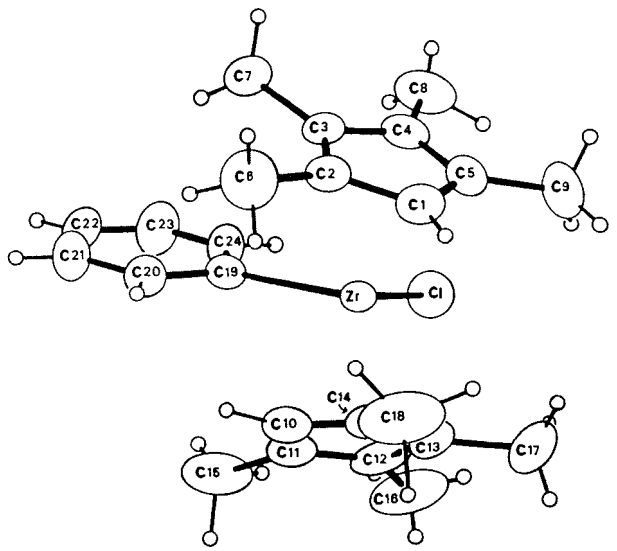


FIG. 2. Diagramme ORTEP de $(C_5Me_4H)_2Zr(C_6H_5)Cl$.

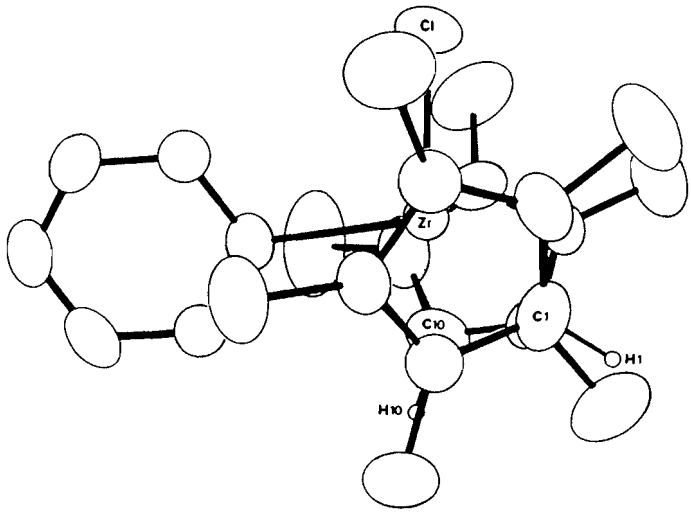


FIG. 3. Diagramme ORTEP de $(C_5Me_4H)_2Zr(C_6H_5)Cl$ vu selon le plan centroïde 1-Zr centroïde 2 (les hydrogènes des groupements méthyle et aryle ont été omis).

12° entre le plan formé par les atomes du phényle et celui contenant Cl, Zr et C_{19}.

Utilisation des propriétés particulières des complexes porteurs du ligand C_5Me_4H pour la réalisation de réactions catalytiques spécifiques : étude de l'isomérisation photoassistée d'oléfines

Nous avons tenté d'utiliser l'encombrement stérique mis en évidence dans nos complexes pour réaliser des réactions catalytiques stéréospécifiques. Nous nous sommes plus particulièrement intéressé aux isomérisations photoassistées et catalytiques thermiques d'oléfines initiées par les complexes du type $(C_5Me_4H)_2Ti(CH_3)_2$, $(C_5Me_4H)(C_5H_5)Ti(CH_3)_2$ et $(C_5H_5)_2Ti(p\text{-}C_6H_4CH_3)_2$. Une partie de cette étude concernant les résultats obtenus avec le complexe $(C_5Me_4H)_2Ti(CH_3)_2$ a fait l'objet d'une communication préliminaire (2).

La grande solubilité des complexes $(C_5Me_4H)_2Ti(CH_3)_2$ et $(C_5Me_4H)(C_5H_5)Ti(CH_3)_2$ dans les solvants hydrocarbonés, a permis d'effectuer les irradiations directement sur les solutions désoxygénées de ces complexes dans les oléfines (1 équivalent de complexe pour 400 équivalents d'oléfine) à l'aide d'un arc à vapeur de mercure Philips HPK 125 en filtrant les longueurs d'ondes inférieures à 310 nm.

Plusieurs types d'oléfines différant par la position de la double liaison, sa substitution et la position d'une ramification sur la chaîne hydrocarbonée ont été étudiés : pentène-1, hexène-1, octène-1, décène-1, pentènes-2 *E* et *Z*, hexènes-2 *E* et *Z*, hexènes-3 *E* et *Z*, octènes-2 *E* et *Z*, décènes-2 *E* et *Z*, décènes-5 *E* et *Z*, méthyl-2 pentène-1, méthyl-3 pentène-1 et méthyl-4 pentène-1.

Les irradiations des complexes $(C_5Me_4H)_2Ti(CH_3)_2$ et $(C_5Me_4H)(C_5H_5)Ti(CH_3)_2$ en présence d'oléfines à double liaison terminale et à chaîne aliphatique linéaire (pentène-1, hexène-1, octène-1, décène-1) conduisent à une réaction de migration sélective de la double liaison en position 2 sur la chaîne hydrocarbonée.

Ces isomérisations sont complètes après 3 h d'irradiation et dans tous les cas les mélanges obtenus contiennent 97% de l'isomère 2*E* (pentène-2*E*, hexène-2*E*, octène-2*E* ou décène-2*E*), 2% de l'isomère 2*Z* correspondant et 1% de l'oléfine

Can. J. Chem. Downloaded from www.nrcresearchpress.com by 198.100.157.202 on 09/07/12
For personal use only.

TABLEAU 9. Eléments structuraux de complexes du zirconium

Complexe	Zr—Ct (Å)	Zr—X (Å)	X—Zr—X (°)	Ct—Zr—Ct (°)	Référence
$(C_5H_5)_2ZrCl_2$	2,20	2,44	97	134	21
$(C_5H_5)_2ZrF_2$	2,21	1,98	96	127,8	22
$(C_5H_5)_2ZrI_2$	2,19	2,83	96	126,3	22
$(C_5H_5)(C_5Me_5)ZrCl_2$	2,21; 2,22	2,44	97,78	130	23
$(C_5H_4CH_2C_6H_5)_2ZrCl_2$	2,16	2,46	94	126	24
$(C_5H_4SiMe_3)_2ZrCl_2$	2,21	2,49	94	129	25
$(C_4Me_4P)_2ZrCl_2$		2,437	94,9	131,6	20
$(C_5H_4CMe_3)_2ZrCl[CH(SiMe_3)_2]$	2,26	2,452	98,2	128,1	26
$(C_5Me_4H)_2Zr(C_6H_5)Cl$	2,34 2,24	2,443	99	133,2	Ce travail

Ct : centroïde des cyclopentadiényles.

initiale. Aucun autre isomère possible tels que les hexènes-3 *E* ou *Z*, les octènes-3 ou -4, les décènes-3, -4, -5 n'est décelé en solution. Ces résultats mettent en évidence la grande stéréospécificité de la migration sigmatropique d'hydrogène induite chez les oléfines lors de l'irradiation de ces deux complexes.

Bien que nous n'ayons pas réussi à isoler les complexes responsables de ces réactions, l'étude des cinétiques de ces différentes isomérisations réalisées à l'aide du complexe $(C_5Me_4H)_2Ti(CH_3)_2$ apporte des éléments intéressants sur les processus mis en jeu au cours de ces irradiations.

Tout d'abord nous avons mis en évidence la présence d'une période d'induction au cours de laquelle les isomérisations des oléfines étudiées sont très faibles, 10–15% d'isomérisation en 1 h 40 min avec le complexe $(C_5Me_4H)_2Ti(CH_3)_2$, (cf. figure 4 : cinétique d'apparition des hexènes-2 lors de l'irradiation du complexe en présence d'hexène-1).

En suivant l'évolution des spectres de RPE des solutions irradiées, nous pouvons caractériser plusieurs espèces paramagnétiques de Ti(III) en solution. Dès le début des irradiations (30 s) on observe l'apparition d'un singulet large intense avec huit raies satellites (g = 1,979 et A(Ti) = 7,45 gauss). Le complexe de Ti(III) caractérisé par ce signal correspond très vraisemblablement à l'espèce $(C_5Me_4H)_2TiCH_3$ qui résulterait d'une coupure homolytique de la liaison Ti—CH_3. Ce type de réaction a été décrit dans la littérature pour d'autres complexes du titane, notamment par Samuel *et al.* (28) et constitue une réaction classique de la photochimie des complexes des métaux de transition (29–33).

En prolongeant les irradiations on voit ensuite apparaître progressivement deux autre signaux très larges (g = 1,992 et g = 1,973), le signal à champ faible devenant prépondérant. Il est intéressant de noter que la croissance de ce dernier signal correspond à l'accélération de la cinétique de l'isomérisation des oléfines.

Les caractéristiques RPE de ces complexes (g = 1,992 et ΔH = 6 gauss) étant très proches de celles des composés du type $(C_5H_5)_2Ti(\eta^3\text{-allyl})$ décrits dans la littérature (34–36), et bien que nous n'ayons pas réussi à le confirmer sans équivoque au cours des essais de synthèses que nous avons réalisé au laboratoire, nous pensons cependant que des complexes du type $(C_5Me_4H)_2Ti(\eta^3\text{-allyl})$ pourraient être impliqués dans une étape de ces réactions d'isomérisation d'oléfines.

L'étude des cinétiques permet également de montrer que ces réactions sont photoassistées et non photocatalytiques. L'excitation photochimique est nécessaire pour le déroulement de ces réactions à la température ordinaire, l'arrêt des irradiations

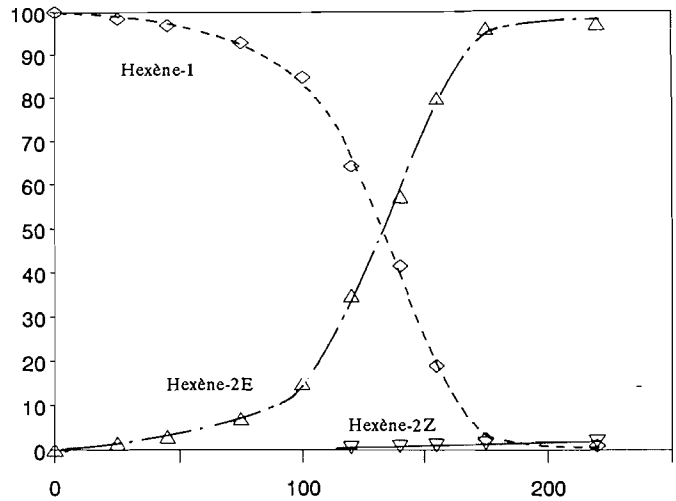


FIG. 4. Cinétique d'isomérisation photoassistée de l'hexène-1 initiée par le complexe $(C_5Me_4H)_2Ti(CH_3)_2$.

après 50% de transformation de l'oléfine initiale entraîne l'arrêt de l'isomérisation des oléfines. Les solutions peuvent être conservées une quinzaine d'heures à la température ordinaire, à l'abri de la lumière, sans évolution du mélange d'isomères. Par contre dès la reprise des irradiations l'isomérisation continue sans présenter de période d'induction.

Les irradiations des deux complexes $(C_5Me_4H)_2Ti(CH_3)_2$ et $(C_5Me_4H)(C_5H_5)Ti(CH_3)_2$ en présence d'oléfines α,β-disubstituées conduisent à une lente isomérisation *cis–trans* photoassistée de la double liaison carbone–carbone lorsque celle-ci se trouve en position 2 sur la chaîne hydrocarbonée, au delà de cette position nous n'observons pas de processus catalytique notable en solution. Ainsi quelle que soit la configuration de l'oléfine initiale (pentène-2, hexène-2 et décène-2 *E* ou *Z*) les irradiations aboutissent à des mélanges photostationnaires des deux isomères 2*E* et 2*Z* dans un rapport de concentration 80 : 20 en faveur de la configuration 2*E*, ceci après 35–40 h d'irradiation. Les essais réalisés en présence d'hexènes-3 ne donnent pas d'isomérisation notable même au cours d'irradiations prolongées (95% d'hexène-3*E* initial, 3% d'hexène-2*E*, 1% d'hexène-2*Z* et des traces d'hexène-3*Z* après 60 h).

À l'aide de ces résultats, en particulier la lenteur de l'isomérisation *cis–trans* de la double liaison en 2 sur la chaîne hydrocarbonée, nous mettons en évidence la stéréospécificité de la réaction de migration d'hydrogène. Elle conduit exclusivement au composé de configuration 2*E* à partir d'une oléfine à

Can. J. Chem. Downloaded from www.nrcresearchpress.com by 198.100.157.202 on 09/07/12
For personal use only.

Can. J. Chem. Downloaded from www.nrcresearchpress.com by 198.100.157.202 on 09/07/12
For personal use only.

double liaison terminale, les traces d'isomères de configuration 2*Z* présentes en solution à la disparition de l'oléfine initiale provenant d'une isomérisation *cis–trans* ultérieure de la double liaison carbone–carbone en 2.

Si le remplacement d'un ligand C_5Me_4H par un ligand C_5H_5 n'induit pas de perturbation appreciable de la réactivité du centre métallique vis-à-vis des oléfines précédentes, il n'en est pas de même lorsque les oléfines possèdent une chaîne ramifiée. En effet les méthyl-2 et méthyl-3 pentènes-1 qui ne sont pas isomérisés lors des irradiations en présence du complexe $(C_5Me_4H)_2Ti(CH_3)_2$ (moins de 5% après 30 h) s'isomérisent lentement en présence du complexe $(C_5Me_4H)(C_5H_5)Ti(CH_3)_2$ en méthyl-2 pentène-2 *E* et méthyl-3 pentène-2 *E* respectivement (environ 30 h d'irradiation). Par contre le méthyl-4 pentène-1 dont la ramification de la chaîne est plus éloignée de la double liaison terminale peut être isomérisé en méthyl-4 pentène-2 *E* par les deux complexes, (97% après 15 h d'irradiation avec $(C_5Me_4H)_2Ti(CH_3)_2$).

Ces résultats démontrent l'influence de la gêne stérique des ligands cyclopentadiényle au niveau du centre métallique et la sensibilité des réactions de migration d'hydrogène vis-à-vis de la position de la ramification sur la chaîne hydrocarbonée. Bien que les cinétiques soient nettement ralenties par les effets stériques des ligands d'une part, et de l'oléfine d'autre part, ces résultats confirment la sélectivité et la stéréospécificité de la réaction de migration d'hydrogène mises en évidence au cours des irradiations précédentes.

Le remplacement des deux ligands C_5Me_4H par des ligands C_5H_5 a été réalisé au cours de l'étude de la réactivité du complexe $(C_5H_5)_2Ti(p\text{-tolyl})_2$ en présence d'oléfines.

Bien que les conditions opératoires soient différentes compte tenu de la faible solubilité de ce complexe dans les oléfines, nous avons étudié les isomérisations sur des solutions d'un équivalent de complexe et de 40 équivalents d'oléfines dans le benzène ou le toluène.

Les irradiations en présence de pentène-1 ou d'hexène-1 conduisent à des mélanges photostationnaires de pentènes-2 *E* et *Z* ou d'hexènes-2 *E* et *Z* dans un rapport de concentration proche de 80 : 20 en faveur de la configuration *E*. Quel que soit l'avancement de la réaction, le rapport des concentrations des oléfines 2*E* sur les oléfines 2*Z* reste très proche de 80 : 20. Ces isomérisations bien qu'étant sélectives ne sont plus stéréospécifiques comme dans le cas des irradiations avec les deux complexes précédents. D'autre part ces réactions présentent également une période d'induction, mais elles sont ensuite extrêment rapides lorsque l'espèce active est générée.

Le remplacement des deux ligands C_5Me_4H par des ligands C_5H_5 modifie donc complètement la réactivité des complexes lors de leurs irradiations en présence d'oléfines. Ceci résulte très vraisemblablement de la modification de l'encombrement stérique de ces ligands mais également de la modification de la densité électronique un niveau du centre métallique.

Les isomérisations d'oléfines que nous venons de décrire peuvent être obtenues également par voie thermique à 130°C à l'aide de ces complexes (2).

Conclusion

L'étude des caractéristiques physiques des complexes du titane et du zirconium porteurs du ligand C_5Me_4H nous a permis d'évaluer l'influence électronique de ce ligand par rapport à celles de C_5H_5 et de C_5Me_5. Une étude radiocristallographique de $(C_5Me_4H)_2Zr(C_6H_5)Cl$ a mis en évidence les différentes contraintes stériques présentes dans cette molécule. Cet effet stérique du ligand C_5Me_4H, intermédiaire entre ceux présentés par C_5H_5 et C_5Me_5, a été évalué par une étude de RMN dynamique réalisée sur les complexes arylés. Ces composés, selon la température d'observation, présentent une restriction à la rotation du ligand aryle autour de la liaison métal – cycle aromatique. C'est la première fois, à notre connaissance, qu'une gêne stérique des ligands cyclopentadiényle a pu être ainsi démontrée et évaluée sur des complexes du titane et du zirconium. Enfin cet effet stérique a été utilisé pour réaliser à l'aide de certains de nos complexes des réactions spécifiques d'isomérisations photoassistées d'oléfines.

Partie expérimentale

La préparation des différents complexes a été réalisée sous argon en utilisant la technique des tubes de Schlenk. Les solvants sont séchés par distillation sous azote sur sodium–benzophénone (toluène, éther éthylique, THF), sur $LiAlH_4$ (hexane) ou sur hydrure de calcium (CH_2Cl_2); ils sont désoxygénés par cycles vide/argon avant utilisation.

Les spectres infrarouge ont été réalisés en solution dans l'hexane sur un spectrophotomètre Pye–Unicam SP2000. Les spectres de RMN ^1H et ^{13}C ont été effectués sur les spectromètres Jeol FX 100 ou Bruker A.C. 300 en solution dans $CDCl_3$ ou C_6D_6. Les spectres de masse ont été obtenus sur un appareil Hewlett–Packard 5995. Les spectres de RPE ont été tracés sur un appareil Jeol JES-FE2X. Les séparations en chromatographie en phase gazeuse ont été effectuées soit à l'aide d'un chromatographe Carlo–Erba 2300 muni d'une colonne remplie de 12 m de polypropylèneglycol à 30% sur Chromosorb P, soit sur un chromatographe Hewlett–Packard 5890 à colonne capillaire CPSIL greffée de 25 m. Les analyses chimiques ont été réalisées au centre de microanalyses du CNRS à Lyon.

Les données RMN indiquées au tableau 1 ne sont pas répétées en partie expérimentale.

Préparation du ligand $C_5(CH_3)_4H_2$

La tétraméthyl-2,3,4,5 cyclopentène-2 one obtenue par la méthode de Kohl et Jutzi (3) est réduite de façon classique par $LiAlH_4$ (37) et l'alcool ainsi obtenu est déshydraté à température ambiante par l'acide paratoluène sulfonique dans le benzène. Le rendement de la réaction est de 90% à partir de la cétone éthylénique. Le composé diénique est purifié par distillation ($Eb_{1\ Torr}$ = 24–26°C) (1 Torr = 133,3 Pa). RMN ^1H (δ ppm $CDCl_3$) : 1,78(s,6H); 1,90(s,6H); 2,72(m,2H).

Préparation de $C_5(CH_3)_4HLi$ ou C_5H_5Li

De façon classique, ces sels de lithium sont préparés par échanges avec le butyllithium. Les dienes sont dissous dans l'hexane à −10°C ; un équivalent de butyllithium est alors ajouté. Le milieu réactionnel est maintenu sous agitation pendant 18 h. Le précipité formé est filtré puis lavé deux fois à l'hexane (Rdt : 80%).

Préparation des complexes chlorés $(C_5Me_4H)_2MCl_2$: M = Ti,Zr et $(C_5Me_4H)TiCl_3$

$(C_5Me_4H)_2TiCl_2$ et $(C_5Me_4H)TiCl_3$

La préparation de ces composés est réalisée de façon analogue à celle décrite pour leurs homologues pentaméthylés (4, 5). À 28,16 g de C_5Me_4HLi (0,22 mol) en solution dans le THF on additionne soit 15,4 g (0,1 mol) soit 7,725 g (0,05 mol) de $TiCl_3$ solide. La solution devient rapidement noire; elle est portée 24 h à reflux du THF. Après refroidissement et évaporation du THF, le résidu est oxydé par une solution éther/hexane (50 : 50) saturée en HCl. Après évaporation du solvant, on obtient une poudre rouge composée des deux complexes dont les pourcentages varient selon la quantité de $TiCl_3$ ajoutée. Les deux composés sont séparés par extractions au soxhlet par de l'hexane saturé en HCl. Le composé le plus soluble $(C_5Me_4H)TiCl_3$ est obtenu après 5 h d'extraction, il contient 10% de $(C_5Me_4H)_2TiCl_2$. Il est purifié par recristallisation dans un mélange toluène/hexane pour donner de 4,1 à 13,7 g de $(C_5Me_4H)TiCl_3$ Rendements de 15 à 50%. SM, M^+ = 274. Anal. calc. : C 39.25; H 4,77; trouvé : C 39,10; H 4,75.

$(C_5Me_4H)_2TiCl_2$ est obtenu après une extraction ultérieure de 24 h et

Can. J. Chem. Downloaded from www.nrcresearchpress.com by 198.100.157.202 on 09/07/12
For personal use only.

recristallisé dans un mélange toluène/hexane. Rendements de 20 à 60% (7,2–21,6 g). SM, $M^+ = 360$. Anal. calc. : C 59,85; H 7,27; trouvé : C 59,75; H 7,21.

$(C_5Me_4H)_2ZrCl_2$

De façon analogue à l'obtention des complexes du titane ce composé est obtenu en faisant réagir 28,16 g de C_5Me_4HLi (0,22 mol) sur 23,3 g (0.1 mol) de $ZrCl_4$ dans le THF. La solution est maintenue 48 h à température ambiante puis le solvant est évaporé. Le résidu est extrait au toluène. Le résidu de cette extraction est lavé à l'hexane pour donner 60% (24,9 g) de complexe désiré (cristaux jaunes pâles). SM, $M^+ = 403$. Anal. calc. : C 53,44; H 6,49; trouvé : C 53,48; H 6,24.

Préparation spécifique de $(C_5Me_4H)TiCl_3$

Obtention de $C_5Me_4H\ SiMe_3$: À 16 g de tétraméthyl-1,2,3,4 cyclopentadiène-1,3 (0,13 mol) dissous dans 200 mL d'hexane, on ajoute, à 0°C, 0,13 mol de butyllithium puis 0,13 mol de tétraméthyl éthylène diamine (TMEDA). Le milieu réactionnel est maintenu sous agitation pendant 15 h à température ambiante puis le précipité jaune qui s'est formé est filtré et repris par 200 mL d'éther. On ajoute alors 0,13 mol de chlorotriméthyl silane avant de porter la réaction à reflux pendant 3 jours. Après refroidissement, le précipité de LiCl qui s'est formé est éliminé par filtration. La phase éthérée est lavée à l'eau, séchée sur sulfate de magnésium, puis le solvant est évaporé pour donner une huile jaune orangée qui sera utilisée sans purification ultérieure (19,5 g ; Rdt : 77%). RMN ^1H (δ ppm $CDCl_3$) : 2,86(s,1H); 1,97(s,6H); 1,86(s,6H); 0,01(s,9H). ^{13}C : 135,3; 133,08; 14,3; 11,23; 1,7.

Synthèse de $(C_5Me_4H)TiCl_3$: À 19,5 g de $TiCl_4$ ($1,03 \times 10^{-1}$ mol) en solution dans 150 mL d'hexane on additionne à 0°C 20 g ($1,03 \times 10^{-1}$ mol) de $C_5Me_4HSiMe_3$ L'agitation est maintenue 4.5 h à température ambiante. Le précipité brun qui s'est formé est filtré puis lavé à l'hexane. Il ne contient que le composé désiré (17 g ; Rdt : 60%).

$(C_5Me_4H)(C_5H_5)TiCl_2$

(a) $(C_5Me_4H)TiCl_3 + CpLi$: À 0,5 g de C_5H_5Li (8×10^{-3} mol) en solution à −20°C dans le THF on ajoute 2 g ($7,25 \times 10^{-3}$ mol) de $(C_5Me_4H)TiCl_3$ solide. La solution est ensuite maintenue pendant 30 min à la température ambiante. Après évaporation du solvant, le résidu rouge vif est lavé à l'hexane puis recristallisé dans un mélange toluène/hexane. On obtient 1,8 g de $(C_5Me_4H)(C_5H_5)TiCl_2$ (Rdt : 80%). SM, $M^+ = 304$. Anal. calc. : C 55,11; H 5,90; trouvé : C 55,05; H 6,00.

(b) $(C_5H_5)TiCl_3 + C_5Me_4HLi$: comme précédemment, 1 g (8×10^{-3} mol) de C_5Me_4HLi réagit sur 1,59 g ($7,25 \times 10^{-3}$ mol) de $(C_5H_5)TiCl_3$. Après lavage à l'hexane, on obtient 1,55 g (Rdt = 67%) de poudre cristalline composée à 70% du complexe désiré $(C_5Me_4H)(C_5H_5)TiCl_2$ et à 30% de $(C_5H_5)_2TiCl_2$. Nous ne sommes pas parvenus à séparer ces deux composés.

Préparation générale des complexes $(C_5Me_4H)_2MR_2$ et $(C_5Me_4H)(C_5H_5)TiR_2$: M = Ti, Zr; R = CH_3, C_6H_5, p-$C_6H_4CH_3$

À une suspension de $2,5 \times 10^{-3}$ mol de $(C_5Me_4H)_2MCl_2$ ou $(C_5Me_4H)(C_5H_5)TiCl_2$ dans 10 mL d'éther, on ajoute à −70°C 2,2 équivalents de R-Li en solution dans l'éther. On laisse le mélange réactionnel remonter à la température ambiante pendant 3 h lorsque M = Ti ou pendant 12 h lorsque M = Zr. La solution devient dans un premier temps limpide, puis lorsque M = Ti, elle prend une coloration jaune et on observe la formation d'un précipité de chlorure de lithium. L'excès d'alkyl ou d'aryllithium est neutralisé à −40°C par 30×10^{-3} mL de méthanol. L'éther est évaporé et le résidu est extrait par 3×10 mL d'hexane. Les complexes dialkylés ou diarylés sont recristallisés à − 70°C dans l'hexane.

$(C_5Me_4H)_2Ti(CH_3)_2$: Rendement : 80% cristaux jaunes d'or. SM, $M^+ = 320$. Anal. calc. : C 74,99; H 10,05; trouvé : C 74,80; H 9,95.

$(C_5Me_4H)_2Zr(CH_3)_2$: Rendement : 75% cristaux blancs. SM, $M^+ = 363$. Anal. calc. : C 66,06; H 8,86; trouvé : C 65,85; H 8,80.

$(C_5Me_4H)(C_5H_5)Ti(CH_3)_2$: Rendement : 60% cristaux jaunes d'or. SM, $M^+ = 264$. Anal. calc. : C 72,72; H 9,15; trouvé : C 72,87; H 9,22.

$(C_5Me_4H)_2Ti$(p-$C_6H_4CH_3)_2$: Rendement : 50% poudre orangée. SM : pas de pic correspondant au pic moléculaire du composé. Le premier pic détecté à 391 correspondant à $(C_5Me_4H)_2Ti(p$-$C_6H_4CH_3)^+$. Anal. calc. : C 81,35; H 8,52; trouvé : C 81,62; H 8,61.

$(C_5Me_4H)(C_5H_5)Ti$(p-$C_6H_4CH_3)_2$: Rendement : 50%. Poudre orangée. SM : pas de pic correspondant à la masse du composé. On observe $(C_5Me_4H)(C_5H_5)Ti(p$-$C_6H_4CH_3)^+$ à 325. Anal. calc. : C 80,76; H 7,74; trouvé : C 81,02; H 7,81.

$(C_5Me_4H)_2Ti(C_6H_5)_2$: Rendement 55%. Poudre orangée. SM : le premier pic observé correspond à $(C_5Me_4H)_2Ti(C_6H_5)^+$ à 367. Anal. calc. : C 81,07; H 8,16; trouvé : C 81,22; H 8,22.

$(C_5Me_4H)(C_5H_5)Ti(C_6H_5)_2$: Rendement 50%. Poudre orangée. SM : pic à 311 $(C_5Me_4H)(C_5H_5)Ti(C_6H_5)^+$. Anal. calc. : C 80,80; H 7,26; trouvé : C 80,50; H 7,27.

$(C_5Me_4H)_2Zr(C_6H_5)_2$: Rendement 50%. Cristaux blancs. Anal. calc. : C 73,87; H 7,43; trouvé : C 74,05; H 7,48.

Préparation des composés dicarbonylés

Méthode générale : $2,75 \times 10^{-3}$ mol de $(C_5Me_4H)_2M\ Cl_2$ (M = Ti, Zr) ou de $(C_5Me_4H)(C_5H_5)TiCl_2$ en solution dans 70 mL de THF sont traités par 334 mg ($1,375 \times 10^{-2}$ mol) de poudre de magnésium préalablement activée et par $2,75 \times 10^{-3}$ mol (750 mg) de $HgCl_2$. Le milieu réactionnel est maintenu sous forte agitation pendant 48 h sous une pression de 1,5 atm de CO. La solution sombre obtenue est filtrée (sur une petite colonne d'alumine neutre lorsque M = Ti) puis le solvant est évaporé. Le résidu est extrait trois fois par 20 mL d'hexane. Après filtration et concentration des filtrats, le composé désiré est obtenu par cristallisation à −50°C.

$(C_5Me_4H)_2Ti(CO)_2$: Rendement : 70%. Cristaux brun-rouge. Anal. calc. : C 69,36; H 7,56; trouvé : C 69,45; H 7,57.

$(C_5Me_4H)(C_5H_5)Ti(CO)_2$: Rendement 65%. Cristaux brun-rouge. Anal. calc. : C 66,22; H 6,25; trouvé : C 66,25; H 6,31.

$(C_5Me_4H)_2Zr(CO)_2$: Rendement 25%. Cristaux vert pâle. Anal. calc. : C 61,65; H 6,72; trouvé : C 61,78; H 6,75.

Préparation générale des complexes $(C_5Me_4H)_2MRCl$ ou $(C_5Me_4H)(C_5H_5)TiRCl$: M = Ti, Zr ; R = CH_3, p-$C_6H_4CH_3$, C_6H_5

À une solution de $3,75 \times 10^{-4}$ mol de $(C_5Me_4H)_2MR_2$ ou de $(C_5Me_4H)(C_5H_5)TiR_2$ dans 10 mL d'éther à −60°C, on ajoute 3.70×10^{-4} mol de HCl en solution éthérée préalablement dosée. On laisse revenir à température ambiante 30 min et l'éther est évaporé. Le résidu est repris à l'hexane, les différents extraits sont concentrés et le produit cristallise à −30°C dans ce solvant.

$(C_5Me_4H)_2Ti(CH_3)Cl$: Rendement quantitatif. Cristaux rouge-vif. SM : pic à 325 $(C_5Me_4H)_2TiCl^+$. Anal. calc. : C 66,96; H 8,56; trouvé : C 66,91; H 8,57.

$(C_5Me_4H)(C_5H_5)TiCH_3Cl$: Rendement quantitatif. Cristaux rouge vif. SM : pic à 269 $(C_5Me_4H)(C_5H_5)TiCl^+$. Anal. calc. : C 63,29; H 7,44; trouvé : C 63,32; H 7,44.

$(C_5Me_4H)_2ZrCH_3Cl$: Rendement quantitatif. Cristaux blancs. Anal. calc. : C 59,41; H 7,61; trouvé : C 59,28; H 7,55.

$(C_5Me_4H)_2Ti$(p-$C_6H_4CH_3)Cl$: Rendement 90%. Cristaux rouges. SM : pic à 325 $(C_5Me_4H)_2TiCl^+$. Anal. calc. : C 72,03; H 7,98; trouvé : 72,35; H 8,07.

$(C_5Me_4H)(C_5H_5)Ti$(p-$C_6H_4CH_3)Cl$: Rendement quantitatif. Cristaux rouges. Anal. calc. : C 69,91; H 6,98; trouvé : C 70,15; H 7,05.

$(C_5Me_4H)_2Zr(C_6H_5)Cl$: Rendement quantitatif. Cristaux blancs. Anal. calc. : C 64,61; H 7,00; trouvé : C 64,75; H 7,05.

Préparation de $(C_5Me_4H)_2Ti$(p-$C_6H_4CH_3)Br$: 100 mg de $(C_5Me_4H)_2TiCl_2$ ($2,77 \times 10^{-4}$ mol) sont dissous dans 10 mL d'éther. La solution est refroidie à −70°C et on ajoute 6×10^{-4} mol de p-$CH_3C_6H_4MgBr$ en solution dans l'éther. On laisse la température revenir à l'ambiante (2 h). L'excès de magnésien est neutralisé par addition de 30×10^{-3} mL de méthanol à −40°C. L'éther est évaporé et le résidu est extrait à l'hexane. Les extraits sont ensuite concentrés et le complexe est obtenu par cristallisation dans l'hexane à −40°C. Rendement 40%. Cristaux rouge-brun. SM : pic à 370 $(C_5Me_4H)_2TiBr^+$. Anal. calc. : C 65,09; H 7,21; trouvé : C 65,27; H 7,32.

Mise en évidence de la formation intermédiaire de $(C_5Me_4H)_2Ti(C_6H_4CH_3)Cl$: La réaction est réalisée comme la précédente. Lorsque la température atteint −20°C, l'excès de magnésien est neutralisé (−40°C). Le milieu réactionnel est ensuite traité comme précédem-

ment en prenant soin de ne pas dépasser −20°C. Le complexe $(C_5Me_4H)_2Ti(p\text{-}C_6H_4CH_3)Cl$ formé est identifié par comparaison avec le spectre de RMN ^1H d'un échantillon de ce produit préparé selon la méthode générale. Le complexe $(C_5Me_4H)_2Ti(p\text{-}C_6H_4CH_3)Cl$ représente 80% du mélange, $(C_5Me_4H)_2Ti(p\text{-}C_6H_4CH_3)Br$ 15% et $(C_5Me_4H)_2TiCl_2$ 5%.

Détermination de l'énergie libre d'activation

Les échantillons pour lesquels nous avons déterminé $\Delta G^{0\#}$ sont placés dans un tube de RMN en solution dans le toluène-d_8 ou dans $CDCl_3$. On fait varier la température jusqu'à ce que les spectres indiquent la coalescence des protons aromatiques *ortho* et *méta* (T_c) en ^1H ou, en ^{13}C, celle des carbones 2, 3, 5 et 6 des cycles aromatiques. La séparation entre les résonances des sites en échange est mesurée à la température la plus basse possible et est supposée être la même à la température de coalescence, $\delta\nu$ et T_c étant déterminés; $\Delta G^{0\#}$ est calculé comme indiqué en partie théorique.

Étude radiocristallographique de $(C_5Me_4H)_2Zr(C_6H_5)Cl$

Les cristaux nécessaires à une étude par diffraction de rayons X ont été obtenus à partir d'une solution diluée du complexe dans l'hexane à −30°C. Les mesures ont été effectuées sur un diffractomètre CAD-4 Enraf Nonius. Cristaux monocliniques, groupe spacial $P2_1/M$; a = 10,726 (4) Å; b = 14,724 (4) Å; c = 13,836 (6) Å, β = 96,07 (3)°; V = 2173,0 (6) Å^3, Z = 4; d(calc) = 1,62 g cm^3. La structure a été résolue par la méthode de Patterson et par différences de Fourier. Après affinage isotropique et anisotropique, les atomes d'hydrogène ont été localisés par différences de Fourier.

Irradiations des complexes en présence d'oléfines

Les irradiations des complexes $(C_5Me_4H)_2Ti(CH_3)_2$ et $(C_5Me_4H)(C_5H_5)Ti(CH_3)_2$ ont été réalisées d'une façon générale sur des solutions désoxygénées contenant un équivalent de complexe pour 400 équivalents d'oléfines placées dans des tubes de RMN scellés sous vide ou mises sous atmosphère d'argon. Ces solutions sont ensuite irradiées à l'aide d'un arc à vapeur de mercure de type Philips HPK 125 dont on filtre les longueurs d'ondes inférieures à 310 nm à l'aide d'une gaine en Pyrex. La température de la solution d'oléfine est maintenue à 18°C à l'aide d'une circulation d'eau. L'évolution du mélange réactionnel est suivi soit par RMN ^1H et ^{13}C soit par chromatographie en phase gazeuse.

Exemples de cinétiques d'irradiation des complexes $(C_5Me_4H)_2Ti(CH_3)_2$ et $(C_5Me_4H)(C_5H_5)Ti(CH_3)_2$ en présence d'oléfines

Isomérisation photoassistée de l'hexène-2 Z en hexène-2 E à l'aide du complexe $(C_5Me_4H)_2Ti(CH_3)_2$

Temps (h)	Hexène-2 *Z* (%)	Hexène2 *E* (%)	Hexène-1 (%)
0	100	0	0
4	100	Traces	0
10	96	4	0
20	64	36	Traces
29	39	61	Traces
39	20	79	1

Isomérisation photoassistée du méthyl-2 pentène-1 à l'aide du complexe $(C_5Me_4H)(C_5H_5)Ti(CH_3)_2$

Temps (h)	Me-2 pentène-1	Me-2 pentène-2
0	100	0
3	100	0
10	81.5	19.5
14	59	41
17	34.5	65.5
19	24.5	75.5
22	16	84
26	10	90
32	4	96

Isomérisation photoassistée du méthyl-4 pentène-1 à l'aide du complexe $(C_5Me_4H)_2Ti(CH_3)_2$

Temps (h)	Me-4 pentène-1 (%)	Me-4 pentène-2 *E* (%)	Me-4 pentène-2 *Z* (%)
0	100	0	0
3	98	2	0
7	84	16	0
10	48	52	Traces
13	11.5	88.5	Traces
15	2	97	1

Isomérisations thermiques des oléfines catalysées par les complexes $(C_5Me_4H)_2Ti(CH_3)_2$ et $(C_5Me_4H)(C_5H_5)Ti(CH_3)_2$

Les isomérisations catalytiques thermiques initiées par les deux complexes sont réalisées sur des solutions identiques à celles utilisées pour les isomérisations photoassistées précédentes. Elles sont placées également dans des tubes RMN scellés sous vide et chauffées à 130°C. L'évolution du mélange réactionnel peut être suivi par RMN ^1H et ^{13}C. Le dosage final des différents constituants des mélanges est réalisé comme précédemment par chromatographie en phase gazeuse.

1. P. Courtot, V. Labed, R. Pichon et J. Y. Salaun. J. Organomet. Chem., **359**, C9 (1989).
2. P. Courtot, R. Pichon, Y. Raoult et J. Y. Salaun. J. Organomet. Chem., **327**, C1 (1987).
3. F. X. Kohl et P. Jutzi. J. Organomet. Chem. **243**, 119 (1983).
4. (*a*) S. A. Cohen, P. R. Auburn et J. E. Bercaw. J. Am. Chem. Soc. **105**, 1136 (1983); (*b*) J. E. Bercaw, R. H. Marwich, L. G. Bell et H. H. Brintzinger. J. Am. Chem. Soc. **94**, 1219 (1972).
5. J. M. Manriquez, D. R. McAlister, E. Rosenberg, A. M. Shiller, K. L. Williamson, S. I. Chan et J. E. Bercaw. J. Am. Chem. Soc. **100**, 3078 (1978).
6. A. M. Cardoso, R. J. H. Clark et S. Moorhouse. J. Chem. Soc. Dalton Trans. 1152 (1980).
7. K. C. Ott, J. M. Deboer et R. H. Grubbs. Organometallics, **3**, 223 (1984).
8. J. X. McDermott, M. E. Wilson et G. M. Whitesides. J. Am. Chem. Soc. **98**, 6529 (1976).
9. E. Samuel et M. D. Rausch. J. Am. Chem. Soc. **95**, 6263 (1973).
10. L. Summers, R. H. Uloth et A. Holmes. J. Am. Chem. Soc. **77**, 3604 (1955).
11. L. E. Shock, C. P. Brock et T. J. Marks. Organometallics, **6**, 232 (1987).
12. B. Demerseman, G. Bouquet et M. Bigorgne. J. Organomet. Chem. **101**, C24 (1975).
13. D. Sikora, M. D. Rausch, R. D. Rogers et J. L. Atwood. J. Am. Chem. Soc. **103**, 1265 (1981).
14. J. L. Thomas et K. T. Brown. J. Organomet. Chem. **111**, 297 (1976).
15. B. Demerseman, R. Mahe et P. Dixneuf. J. Chem. Soc. Chem. Commun. 1394 (1984).
16. W. C. Finch, E. V. Anslyn et R. H. Grubbs. J. Am. Chem. Soc., **110**, 2406 (1988).
17. J. B. Lambert. Organic structural analysis. MacMillan, New-York. 1976. p. 116.
18. J. Sandström. Dynamic NMR spectroscopy. Academic Press, Londres. 1982. p. 96.
19. W. D. Jones et F. J. Feher. Inorg. Chem. **23**, 2376 (1984).
20. M. F. Lappert, P. I. Riley, P. I. W. Yarrow, J. L. Atwood, W. E. Hunter et M. J. Zaworotko. J. Chem. Soc. Dalton Trans. 815 (1981).
21. F. Nief, F. Mathey et L. Ricard. Organometallics, **7**, 921 (1988).
22. K. Prout, T. S. Cameron, R. A. Forder, S. R. Critchley, D. Benton et G. V. Rees. Acta. Crystallogr. Sect. B: Struct. Crystallogr. Cryst. Chem. **B30**, 2290 (1974).

Can. J. Chem. Downloaded from www.nrcresearchpress.com by 198.100.157.202 on 09/07/12
For personal use only.

23. M. A. BUSH et G. A. SIM. J. Chem. Soc. A, 2225 (1971).
24. R. D. ROGERS, M. M. BENNING, L. K. KURIHARA, K. J. MORIARTY et M. D. RAUSCH. J. Organomet. Chem. **293**, 51 (1985).
25. Y. DUSAUSOY, J. PROTAS, P. RENAUT, B. GAUTHERON et G. TAINTURIER. J. Organomet. Chem. **157**, 167 (1978).
26. A. ANTINOLO, M. F. LAPPERT, A. SINGH, C. J. WINTERBORN, L. M. ENGELHARDT, C. L. RASTON, A. H. WHITE, A. J. CARTY et N. C. TAYLOR. J. Chem. Soc. Dalton Trans. 1463 (1987).
27. J. JEFFERY, M. F. LAPPERT et N. T. LUONG-THI. J. Chem. Soc. Chem. Commun. 1081 (1978).
28. E. SAMUEL, P. MAILLARD et C. GIANNOTTI. J. Organomet. Chem. **142**, 289 (1977).
29. H. G. ALT et M. D. RAUSCH. J. Am. Chem. Soc. **96**, 5936 (1974).
30. M. PENG et C. H. BRUBAKER. Inorg. Chim. Acta, **26**, 231 (1978).
31. M. D. RAUSCH, W. H. BOON et H. G. ALT. J. Organomet. Chem. **141**, 299 (1977).
32. P. W. N. M. VAN LEEUWEN, H. VAN DER HEIJDEN, C. F. ROOREECK et J. H. G. FRIJNS. J. Organomet Chem. **209**, 169 (1981).
33. H. HUDSON, M. F. LAPPERT et R. PICHON. J. Chem. Soc. Chem. Commun. 374 (1983).
34. H. A. MARTIN et F. JELLINEK. J. Organomet. Chem. **8**, 115 (1967).
35. H. A. MARTIN et F. JELLINEK. J. Organomet. Chem. **12**, 149 (1967).
36. K. MACH, H. ANTROPIUSOVA, V. HANUS et F. TURECEK. J. Organomet. Chem. **269**, 39 (1984).
37. G. RIO et M. CHARIFI. Bull. Soc. Chim. Fr. 3593 (1970).

Can. J. Chem. Downloaded from www.nrcresearchpress.com by 198.100.157.202 on 09/07/12
For personal use only.

Structural studies of organoboron compounds. XLIV.[1] 2,3-Dihydro-3-hydroxy-2,2-tetramethylene-4*H*-benzoxazin-4-one and its difluoroboron chelate, 2,2-difluoro-4,4-tetramethylene-1,3,5-trioxa-3*a*-azonia-2-borata-2,3,4,5 -tetrahydro-1*H*-cyclopenta[*a*]naphthalene

WOLFGANG KLIEGEL AND MAHMOOD TAJERBASHI

Institut für Pharmazeutische Chemie der Technischen Universität Braunschweig, Beethovenstrasse 55,3300 Braunschweig, Bundesrepublik Deutschland

AND

STEVEN J. RETTIG AND JAMES TROTTER

Department of Chemistry, University of British Columbia, 2036 Main Mall, Vancouver, B.C., Canada V6T IZ1

Received August 10, 1990

WOLFGANG KLIEGEL, MAHMOOD TAJERBASHI, STEVEN J. RETTIG, and JAMES TROTTER. Can. J. Chem. **69**, 673 (1991).

The reaction of 2,3-dihydro-3-hydroxy-2,2-tetramethylene-4*H*-benzoxazin-4-one, **2**, and diethyl ether–boron trifluoride yields the difluoroboron chelate 2,2-difluoro-4,4-tetramethylene-1,3,5-trioxa-3*a*-azonia-2-borata-2,3,4,5-tetrahydro-1*H*-cyclopenta[*a*]naphthalene, **6**, in high yield. There are two crystal forms of **2**: **2***a*, triclinic, $P\bar{1}$, $a = 8.551(1)$, $b = 9.331(3)$, $c = 7.236(1)$ Å, $\alpha = 103.38(2)$, $\beta = 104.68(1)$, $\gamma = 80.37(2)°$, $Z = 2$, $\rho_c = 1.35$ g cm^{-3}, and **2***b*, monoclinic, $C2/c$, $a = 17.41(2)$, $b = 10.665(6)$, $c = 12.427(8)$ Å, $\beta = 115.74(5)°$, $Z = 8$, $\rho_c = 1.40$ g cm^{-3}. Crystals of **6** are monoclinic, $P2_1/c$, $a = 5.354(1)$, $b = 17.654(2)$, $c = 12.844(1)$ Å, $\beta = 100.11(2)°$, $Z = 4$, $\rho_c = 1.48$ g cm^{-3}. The structures were solved by direct methods and were refined by full-matrix least-squares procedures to final *R* values of 0.046, 0.046, and 0.041 for 1712, 1505, and 1675 reflections with $I \geq 3\sigma(I)$, respectively. In both forms of **2**, the structures consist of centrosymmetric O—H···O hydrogen-bonded dimers (O···O = 2.633(2) Å for **2***a* and 2.682(3) Å for **2***b*). The difluoroboron chelate **6** features a five-membered chelate ring planar within 0.068(2) Å, and bond lengths O—B = 1.504(3) and 1.516(3), F—B = 1.358(3) and 1.359(3) Å indicate weak binding of the ligand to the F_2B moiety.

Key words: organoboron compound, crystal structure, boron compound

WOLFGANG KLIEGEL, MAHMOOD TAJERBASHI, STEVEN J. RETTIG et JAMES TROTTER. Can. J. Chem. **69**, 673 (1991).

La réaction de la 2,3-dihydro-3-hydroxy-2,2-tétraméthylène-4*H*-benzoxazin-4-one, **2**, avec le complexe Et_2O/BF_3 fournit le chélate difluoroboré, 2,2-difluoro-4,4-tétraméthylène-1,3,5-trioxa-3*a*-azonia-2-borata-2,3,4,5-tétrahydro-1*H*-cyclopenta[*a*]-naphtalène, **6**, avec un excellent rendement. Il existe deux formes cristallines du produit **2**, soit **2***a*, triclinique, $P\bar{1}$, $a = 8{,}551(6)$, $b = 9{,}331(3)$ et $c = 7{,}236(1)$Å, $\alpha = 103{,}38(2)$, $\beta = 104{,}68(1)$ et $\lambda = 80{,}37(2)°$, $Z = 2$, $\rho_c = 1{,}35$ g cm^{-3} et **2***b*, monoclinique, $C2/c$, $a = 17{,}41(2)$, $b = 10{,}665(6)$ et $c = 12{,}427(8)$ Å, $\beta = 115{,}74(5)°$, $Z = 8$ et $\rho_c = 1{,}40$ g cm^{-3}. Les cristaux du produits **6** sont monocliniques, $P2_1/c$, $a = 5{,}354(1)$, $b = 17{,}654(2)$ et $c = 12{,}844(1)$ Å, $\beta = 100{,}11(2)°$, $Z = 4$ et $\rho_c = 1{,}48$ g cm^{-3}. On a déterminé les structures par des méthodes directes et on les a affinées par la méthode des moindres carrés (matrice complète) jusqu'à des valeurs finales de *R* de 0,046, 0,046 et 0,041 respectivement pour 1712, 1505 et 1675 réflexions avec $I \geq 3\sigma(I)$. Dans les deux formes du produit **2**, les structures se composent de dimères centrosymétriques réunis par des liaisons hydrogènes O—H···O (O···O = 2,633(2) Å pour **2***a* et 2,682(2) Å pour **2***b*). Le chélate difluoroboré **6** est caractérisé par un cycle à cinq chaînons, plan à 0,068(2) Å, dans lequel les longueurs des liaisons O—B = 1,504(3) et 1,516(3), F—B = 1,358(3) et 1,359(3) Å indiquent la présence d'une faible liaison entre le coordinat et la portion F_2B.

Mots clés : composé organoboré, structure cristalline, composé bore.

[Traduit par la rédaction]

Introduction

The synthesis of the diphenylboron chelate **3** via condensation of salicylohydroxamic acid, **1**, with cyclopentanone and subsequent reaction of the cyclocondensate **2** with oxybis-(diphenylborane) has been described in a previous report, along with the crystal and molecular structure of **3**(1).

In the course of this investigation we were interested in the reactivity of **2** towards the stronger Lewis acid BF_3 and also in the possible structural differences between the expected difluoroboron chelate **6** and the diphenylboron analog **3**. Thus we reacted **2** with boron trifluoride and obtained a crystalline product with the elemental analysis expected for the BF_2 chelate **6**. As for **3**, infrared and ^{1}H nmr data did not allow the exclusion of isomeric structures like **5**, **8**, **10**, or **12**, which, in part, have been discussed by analogy to the diphenylboron derivative **3**. An X-ray crystallographic analysis was undertaken in order to provide unambiguous proof of the structure **6**.

We also prepared single crystals of the hydroxamic acid with the assumed *O*,*N*-cycloacetal structure **2** in order to obtain data on the solid state structure of the free ligand. Formulae of the type **2** have generally been used for condensation products of salicylohydroxamic acid with aldehydes or ketones (2), but have never been proven. All subsequent reaction products, such as the chelates **3** and **6**, could also be the result of a rearrangement of possible educts like **4**, **7**, **9**, or **11** (which are isomers of **2**) during the reaction with the Lewis acid boron compound.

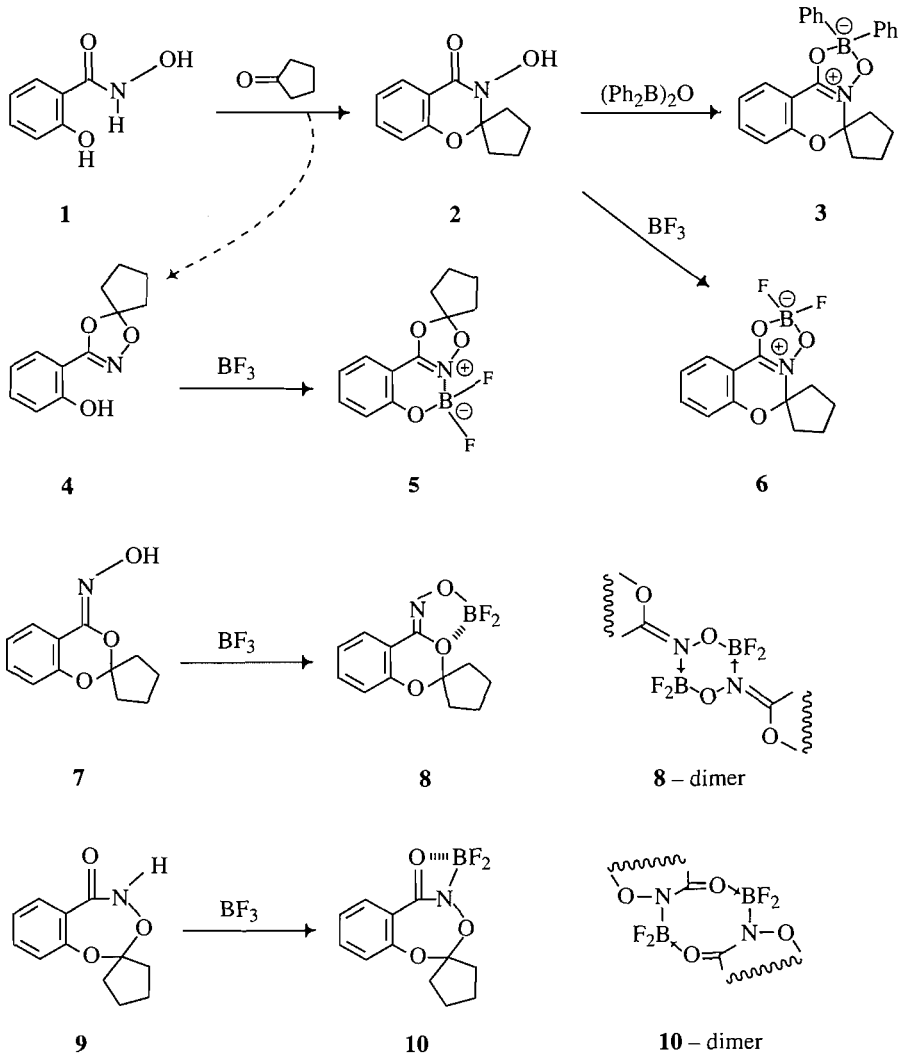
The five-membered cyclic *O*,*O*-acetal structure in **4** represents the well-known (3) 1,4,2-dioxazole ring system that can also be synthesized by condensation of hydroxamic acids with different carbonyl compounds (3*a*, 3*b*, 3*c*, 3*g*). The six- and seven-membered cyclic *O*,*O*-acetals, **7** and **9**, have not been reported in the literature, to the best of our knowledge. The 2*H*-1,3-oxazet *N*-oxide moiety of **11** (and of **12**) is an unknown type of heterocyclic *N*-oxide, and its formation seems unlikely under the applied reaction conditions. It is, however, reminiscent of the homologous dihydrooxazole *N*-oxide ring fragment

[1]Previous paper in this series: ref. 17.

Printed in Canada / Imprimé au Canada

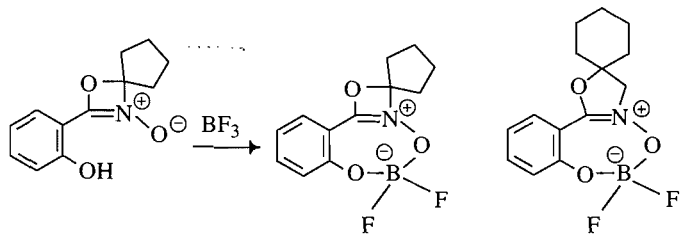
Can. J. Chem. Downloaded from www.nrcresearchpress.com by 198.100.157.202 on 09/07/12
For personal use only.

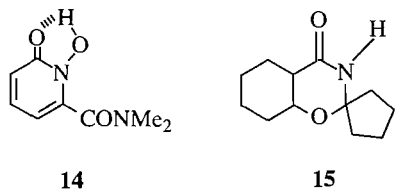
Can. J. Chem. Downloaded from www.nrcresearchpress.com by 198.100.157.202 on 09/07/12
For personal use only.



of **13**(4). For a definitive establishment of the hitherto postulated structure **2**, an X-ray analysis of this material has been performed.

A comparison of bond lengths in the free ligand **2** with those in the chelates **3** and **6** should give some indication of the influence of the different borenium ions, Ph_2B^+ and F_2B^+, on the bonding system of the hydroxamate and the *O*,*N*-acetal functions in these molecules.





Experimental

*2,3-Dihydro-3-hydroxy-2,2-tetramethylene-4*H*-benzoxazin-4-one, 2*

The compound was prepared according to our previous report (1). Crystals suitable for X-ray analysis were obtained by recrystallization from benzene/petroleum ether (**2***a*) or methanol (**2***b*).

*2,2-Difluoro-4,4-tetramethylene-1,3,5-trioxa-3*a*-azonia-2-borata-2,3,4,5-tetrahydro-1*H*-cyclopenta[a]naphthalene, 6*

2 (0.44 g, 2 mmol) was suspended in 30–50 mL diethylether. After addition of diethyl ether–boron trifluoride (0.57 g, 4 mmol) the suspension was refluxed for 30 min. The warm solution was filtered and the volume reduced by distillation of the solvent *in vacuo*, until only a few mL remained. Crystallization started during evaporation and was completed at room temperature. Yield: 0.49 g (91%), mp 125°C (from ether). *Anal.* calcd. for $C_{12}H_{12}BF_2NO_3$: C 53.97, H 4.53, N 5.24; found: C 54.03, H 4.60, N 5.22. Infrared (KBr): 1635 cm^{-1} (C=O/C=N). ^1H nmr (90 MHz, $CDCl_3$/TMS): δ (ppm) = 1.68–2.68 (m, —$(CH_2)_4$—), 6.94–7.78 (m, C_6H_4).

Crystals suitable for X-ray analysis were obtained by recrystallization from absolute diethylether.

X-ray crystallographic analyses of 2 and 6

Two crystalline modifications of the free ligand **2**, **2***a* and **2***b*, were analyzed. Crystallographic data for the three structures appear in Table 1. The final unit-cell parameters were obtained by least-squares on the setting angles for 25 reflections with 2θ = 35.9–40.2° for **2***a*, 16.2–19.2° for **2***b*, and 60.2–99.2° for **6**. The intensities of three standard reflections, measured every 150 reflections throughout the data collections, were essentially constant for all three compounds. The data were

TABLE 1. Crystallographic data[a]

Compound	**2***a*	**2***b*	**6**
Formula	$C_{12}H_{13}NO_3$	$C_{12}H_{13}NO_3$	$C_{12}H_{12}BF_2NO_3$
fw	219.24	219.24	267.04
Crystal size, mm	0.35 × 0.45 × 0.45	0.13 × 0.30 × 0.50	0.20 × 0.25 × 0.25
Crystal system	Triclinic	Monoclinic	Monoclinic
Space group	$P\bar{1}$	$C2/c$	$P2_1/c$
a, Å	8.551(1)	17.41(2)	5.354(1)
b, Å	9.331(3)	10.665(6)	17.654(2)
c, Å	7.236(1)	12.427(8)	12.844(1)
α, deg	103.38(2)	90	90
β, deg	104.68(1)	115.74(5)	100.11(2)
γ, deg	80.37(2)	90	90
V, Å^3	539.7(4)	2078(3)	1195.1(5)
Z	2	8	4
ρ_{calc}, g/cm^3	1.35	1.40	1.48
$F(000)$	232	928	552
Radiation	Mo	Mo	Cu
μ, cm^{-1}	0.91	0.95	10.40
Transmission factors			0.917–1.00
Scan type	ω–2θ	ω–2θ	ω–2θ
Scan range, deg in ω	1.30 + 0.35 tan θ	1.25 + 0.35 tan θ	1.00 + 0.30 tan θ
Scan speed, deg/min	32	16	32
Data collected	$+h, \pm k, \pm l$	$\pm h, +k, +l$	$+h, +k, \pm l$
$2\theta_{max}$, deg	55	55	150
Crystal decay	Negligible	Negligible	Negligible
Total no. of reflections	2627	2634	2739
No. of unique reflections	2475	2520	2468
R_{merge}	0.028	0.074	0.017
No. of reflcns with $I \geq 3\sigma(I)$	1712	1505	1675
No. of variables	198	198	223
R	0.046	0.046	0.041
R_w	0.061	0.062	0.051
gof	2.25	1.88	2.37
Max Δ/σ (final cycle)	0.01	0.01	0.09
Residual density e/Å^3	0.30	0.24	0.15

[a]Temperature 294 K, Rigaku AFC6S diffractometer, Mo $K_{\bar{\alpha}}$ (λ = 0.71069 Å) or Cu $K_{\bar{\alpha}}$ (λ = 1.54178 Å) radiation, graphite monochromator, takeoff angle 6.0°, aperture 6.0 × 6.0 mm at a distance of 285 mm from the crystal, stationary background counts at each end of the scan (scan/background time ratio 2:1), up to eight rescans, $\sigma^2(F^2) = [S^2(C + 4B) + (pF^2)^2]/Lp^2$ (S = scan rate, C = scan count, B = normalized background count, p = 0.045 for **2***a*, 0.050 for **2***b*, and 0.040 for **6**), function minimized $\Sigma w(|F_o| - |F_c|)^2$ where $w = 4F_o^2/\sigma^2(F_o^2)$, $R = \Sigma||F_o| - |F_c||/\Sigma|F_o|$, $R_w = (\Sigma w(|F_o| - |F_c|^2/\Sigma w|F_o|^2)^{1/2}$, and gof $= [\Sigma(|F_o| - |F_c|)^2/(m - n)]^{1/2}$. Values given for R, R_w, and gof are based on those reflections with $I \geq 3\sigma(I)$.

processed[2] and corrected for Lorentz and polarization effects, and in the case of **6**, absorption (empirical, based on azimuthal scans for four reflections).

The structure analyses of both the triclinic and monoclinic forms of **2** were initiated in the centrosymmetric space groups $P\bar{1}$ and $C2/c$, respectively, on the basis of E-statistics, the choices being confirmed by subsequent calculations. The structures were solved by direct methods, the coordinates of the non-hydrogen atoms being determined from E-maps and subsequent difference Fourier syntheses. The cyclopentane ring in compound **6** was found to be conformationally disordered. A twofold disordered model involving two ring carbon atoms was refined. Hydrogen atoms were refined with isotropic thermal parameters except for the disordered hydrogen atoms in **6** which were fixed in idealized positions (d_{C-H} = 0.98 Å, $B_H = 1.2B_{bonded\ atom}$). Neutral atom scattering factors and anomalous dispersion corrections for the non-hydrogen atoms were taken from the International tables for X-ray crystallography (5). Final atomic coordinates and equivalent isotropic thermal parameters, bond lengths, bond angles, and intra-annular torsion angles appear in Tables 2–5, respectively. Hydrogen atom parameters, anisotropic thermal parameters, bond lengths and angles involving hydrogen, general torsion angles, intermolecular contacts, least-squares planes, and measured and calculated structure factor amplitudes for the three structures are included as supplementary material.[3]

Results and discussion

The condensation product of salicylohydroxamic acid with cyclopentanone has the cyclic O,N-acetal structure **2** (Fig. 1) and belongs to the class of intramolecular N-alkylated cyclic hydroxamic acids (6). There is little structural information on this type of ligand in the literature. Besides an ORTEP diagram of 5-methoxy-6-methyl-1-hydroxy-2(1*H*)-pyridinone without further structural data (7) and some calculated bond lengths for 1-hydroxy-2(1*H*)-pyridinone (8), the only complete crystallog-

[2]TEXSAN/TEXRAY structure analysis package which includes versions of the following: MITHRIL, integrated direct methods, by C. J. Gilmore; DIRDIF, direct methods for difference structures, by P. T. Beurskens; ORFLS, full-matrix least-squares, and ORFFE, function and errors, by W. R. Busing, K. O. Martin, and H. A. Levy; ORTEP II, illustrations, by C. K. Johnson.

[3]Supplementary material mentioned in the text may be purchased from the Depository of Unpublished Data, Document Delivery, CISTI, National Research Council of Canada, Ottawa, Ont., Canada K1A 0S2.

Can. J. Chem. Downloaded from www.nrcresearchpress.com by 198.100.157.202 on 09/07/12
For personal use only.

Can. J. Chem. Downloaded from www.nrcresearchpress.com by 198.100.157.202 on 09/07/12
For personal use only.

TABLE 2. Final atomic coordinates (fractional) and B_{eq} (Å^2)*

Atom	x	y	z	B_{eq}
		2*a*		
O(1)	0.4062(1)	0.2679(1)	0.2386(2)	3.70(5)
O(2)	0.0017(1)	0.3178(2)	0.3190(2)	4.91(6)
O(3)	0.1720(2)	0.4208(1)	0.6774(2)	4.74(6)
N	0.1695(2)	0.3218(2)	0.3601(2)	3.70(6)
C(1)	0.2487(2)	0.2223(2)	0.2124(2)	3.40(6)
C(2)	0.2455(2)	0.3605(2)	0.5478(3)	3.46(6)
C(3)	0.4243(2)	0.3343(2)	0.5836(2)	3.24(6)
C(4)	0.5207(2)	0.3627(2)	0.7711(3)	4.04(7)
C(5)	0.6869(2)	0.3526(2)	0.7993(3)	4.57(8)
C(6)	0.7588(2)	0.3137(2)	0.6401(3)	4.44(8)
C(7)	0.6658(2)	0.2826(2)	0.4534(3)	4.02(7)
C(8)	0.4983(2)	0.2919(2)	0.4255(2)	3.21(6)
C(9)	0.1602(3)	0.2326(3)	0.0054(3)	4.55(9)
C(10)	0.2257(4)	0.0917(3)	−0.1161(3)	6.2(1)
C(11)	0.2661(3)	−0.0237(3)	0.0103(3)	5.2(1)
C(12)	0.2626(3)	0.0583(2)	0.2184(3)	4.24(8)
		2*b*		
O(1)	0.9970(1)	0.1226(2)	0.0884(1)	3.52(6)
O(2)	0.9598(1)	0.3230(2)	−0.1617(1)	3.42(6)
O(3)	1.1127(1)	0.2296(2)	−0.1159(1)	3.75(6)
N	0.9973(1)	0.2288(2)	−0.0758(1)	2.91(6)
C(1)	0.9670(1)	0.2339(2)	0.0183(2)	2.79(7)
C(2)	1.0797(1)	0.2045(2)	−0.0484(2)	2.85(8)
C(3)	1.1260(1)	0.1378(2)	0.0658(2)	2.87(8)
C(4)	1.2119(2)	0.1108(2)	0.1089(2)	3.54(9)
C(5)	1.2521(2)	0.0421(3)	0.2128(2)	4.2(1)
C(6)	1.2065(2)	0.0011(3)	0.2735(2)	4.2(1)
C(7)	1.1221(2)	0.0287(2)	0.2339(2)	3.7(1)
C(8)	1.0822(1)	0.0993(2)	0.1303(2)	3.00(8)
C(9)	0.8703(1)	0.2311(3)	−0.0316(2)	3.5(1)
C(10)	0.8508(2)	0.3173(2)	0.0506(2)	3.7(1)
C(11)	0.9155(2)	0.4210(3)	0.0796(3)	3.9(1)
C(12)	0.9964(1)	0.3539(2)	0.0954(2)	3.34(9)
		6		
F(1)	0.8511(2)	0.34546(8)	0.6888(1)	5.70(7)
F(2)	0.5535(3)	0.38442(9)	0.7798(1)	6.17(7)
O(1)	−0.1108(3)	0.26812(8)	0.4745(1)	4.28(6)
O(2)	0.4638(3)	0.27858(8)	0.6654(1)	4.79(6)
O(3)	0.4737(3)	0.40095(8)	0.5957(1)	4.40(6)
N	0.2769(3)	0.29313(9)	0.5799(1)	3.85(7)
C(1)	0.1172(4)	0.2320(1)	0.5268(2)	3.89(8)
C(2)	0.2926(4)	0.3607(1)	0.5426(2)	3.62(8)
C(3)	0.1115(4)	0.3837(1)	0.4521(2)	3.67(8)
C(4)	0.1209(4)	0.4532(1)	0.4013(2)	4.5(1)
C(5)	−0.0743(5)	0.4726(1)	0.3212(2)	5.1(1)
C(6)	−0.2776(5)	0.4241(1)	0.2930(2)	5.2(1)
C(7)	−0.2867(5)	0.3550(1)	0.3417(2)	4.7(1)
C(8)	−0.0911(4)	0.3347(1)	0.4214(2)	3.72(8)
C(9)	0.0416(6)	0.1744(1)	0.6032(2)	4.8(1)
C(10)†	0.006(2)	0.1018(8)	0.537(1)	5.3(4)
C(10A)†	0.081(4)	0.102(1)	0.559(2)	10.7(8)
C(11)†	0.230(4)	0.110(1)	0.475(2)	7.5(8)
C(11A)†	0.153(4)	0.106(1)	0.456(2)	5.5(4)
C(12)	0.2499(5)	0.1883(1)	0.4496(2)	4.8(1)
B	0.5984(5)	0.3531(2)	0.6883(2)	4.3(1)

*$B_{eq} = (8/3)\pi^2\Sigma\Sigma U_{ij}a_i^*a_j^*(\mathbf{a}_i\cdot\mathbf{a}_j)$.
†Site occupancy 0.50.

TABLE 3. Bond lengths (Å) with estimated standard deviations

Atom	Atom	Distance	Atom	Atom	Distance
		2*a*			
O(1)	C(8)	1.370(2)	C(3)	C(4)	1.389(3)
O(1)	C(1)	1.434(2)	C(3)	C(8)	1.392(2)
O(2)	N	1.395(2)	C(4)	C(5)	1.374(3)
O(3)	C(2)	1.236(2)	C(5)	C(6)	1.388(3)
N	C(2)	1.342(2)	C(6)	C(7)	1.376(3)
N	C(1)	1.470(2)	C(7)	C(8)	1.386(2)
C(1)	C(9)	1.514(3)	C(9)	C(10)	1.512(3)
C(1)	C(12)	1.525(3)	C(10)	C(11)	1.512(4)
C(2)	C(3)	1.473(2)	C(11)	C(12)	1.528(3)
		2*b*			
O(1)	C(8)	1.363(3)	C(3)	C(4)	1.383(4)
O(1)	C(1)	1.431(3)	C(3)	C(8)	1.386(3)
O(2)	N	1.404(2)	C(4)	C(5)	1.382(4)
O(3)	C(2)	1.233(3)	C(5)	C(6)	1.382(4)
N	C(2)	1.348(3)	C(6)	C(7)	1.364(4)
N	C(1)	1.477(3)	C(7)	C(8)	1.390(3)
C(1)	C(9)	1.521(4)	C(9)	C(10)	1.517(4)
C(1)	C(12)	1.547(3)	C(10)	C(11)	1.507(4)
C(2)	C(3)	1.476(3)	C(11)	C(12)	1.514(4)
		6			
F(1)	B	1.359(3)	C(3)	C(8)	1.390(3)
F(2)	B	1.358(3)	C(3)	C(4)	1.395(3)
O(1)	C(8)	1.372(2)	C(4)	C(5)	1.375(3)
O(1)	C(1)	1.435(3)	C(5)	C(6)	1.382(4)
O(2)	N	1.374(2)	C(6)	C(7)	1.376(4)
O(2)	B	1.504(3)	C(7)	C(8)	1.378(3)
O(3)	C(2)	1.295(2)	C(9)	C(10A)	1.43(2)
O(3)	B	1.516(3)	C(9)	C(10)	1.53(1)
N	C(2)	1.294(2)	C(10)	C(11)	1.56(3)
N	C(1)	1.469(2)	C(10A)	C(11A)	1.44(3)
C(1)	C(9)	1.516(3)	C(11)	C(12)	1.43(2)
C(1)	C(12)	1.527(3)	C(11A)	C(12)	1.55(2)
C(2)	C(3)	1.436(3)			

raphic characterization of a 1-hydroxy-2-pyridinone derivative is that reported (9) for compound **14**.

Both crystal forms of the free hydroxamic acid **2** contain centrosymmetric O—H···O hydrogen-bonded dimers (**2*a***: O(2)—H(1)···O(3)($-x$, $1-y$, $1-z$), O···H = 1.72(2) Å, O···O = 2.633(2) Å, O—H···O = 168(2)°; **2*b***: O(2)—H(1)···O(3)($2-x$, $-y$, $-1-z$), O···H = 1.80(3) Å, O···O = 2.682(3) Å, O—H···O = 164(3)°). Similar hydrogen-bonded dimers are present in the solid-state structure of free salicylohydroxamic acid (10). This is in contrast to the intramolecular hydrogen bond in **14**, the "chelated proton" being located from a difference Fourier synthesis (9). Nevertheless, an intramolecular hydrogen bond can be expected for compound **2** in non-polar solvents or in the gas phase, and is indirectly demonstrated by the replacement of the chelated proton by the borenium ions Ph_2B^+ (in compound **3**) or F_2B^+ (in compound **6**). Apart from the above-mentioned hydrogen bonds, all other intermolecular distances in both **2*a*** and **2*b*** correspond to normal van der Waals interactions.

The average C(2)—O and C(2)—N distances in the cyclocondensate **2** (1.235 and 1.346 Å) are shorter and longer, respectively, than the corresponding values of 1.258 and 1.316 Å reported for salicylohydroxamic acid **1** (10). There is more

TABLE 4. Bond angles (deg) with estimated standard deviations

Atom	Atom	Atom	Angle	Atom	Atom	Atom	Angle
			2a				
C(8)	O(1)	C(1)	116.5(1)	C(4)	C(3)	C(2)	121.3(1)
C(2)	N	O(2)	117.4(1)	C(8)	C(3)	C(2)	119.2(1)
C(2)	N	C(1)	123.3(1)	C(5)	C(4)	C(3)	120.2(2)
O(2)	N	C(1)	113.3(1)	C(4)	C(5)	C(6)	119.9(2)
O(1)	C(1)	N	107.4(1)	C(7)	C(6)	C(5)	120.8(2)
O(1)	C(1)	C(9)	106.2(1)	C(6)	C(7)	C(8)	119.1(2)
O(1)	C(1)	C(12)	110.8(1)	O(1)	C(8)	C(7)	118.6(1)
N	C(1)	C(9)	113.3(1)	O(1)	C(8)	C(3)	120.6(1)
N	C(1)	C(12)	114.2(1)	C(7)	C(8)	C(3)	120.7(2)
C(9)	C(1)	C(12)	104.7(2)	C(10)	C(9)	C(1)	103.9(2)
O(3)	C(2)	N	122.8(2)	C(9)	C(10)	C(11)	106.2(2)
O(3)	C(2)	C(3)	122.9(2)	C(10)	C(11)	C(12)	107.1(2)
N	C(2)	C(3)	114.2(1)	C(1)	C(12)	C(11)	105.1(2)
C(4)	C(3)	C(8)	119.3(2)				
			2b				
C(8)	O(1)	C(1)	115.6(2)	C(4)	C(3)	C(2)	121.3(2)
C(2)	N	O(2)	115.0(2)	C(8)	C(3)	C(2)	119.5(2)
C(2)	N	C(1)	121.0(2)	C(5)	C(4)	C(3)	119.7(2)
O(2)	N	C(1)	111.5(2)	C(4)	C(5)	C(6)	120.0(3)
O(1)	C(1)	N	106.8(2)	C(7)	C(6)	C(5)	121.3(3)
O(1)	C(1)	C(9)	106.2(2)	C(6)	C(7)	C(8)	118.5(2)
O(1)	C(1)	C(12)	112.0(2)	O(1)	C(8)	C(3)	120.3(2)
N	C(1)	C(9)	112.9(2)	O(1)	C(8)	C(7)	118.4(2)
N	C(1)	C(12)	112.7(2)	C(3)	C(8)	C(7)	121.1(2)
C(9)	C(1)	C(12)	106.1(2)	C(10)	C(9)	C(1)	104.2(2)
O(3)	C(2)	N	123.0(2)	C(11)	C(10)	C(9)	104.1(2)
O(3)	C(2)	C(3)	122.6(2)	C(10)	C(11)	C(12)	103.9(2)
N	C(2)	C(3)	114.3(2)	C(11)	C(12)	C(1)	105.8(2)
C(4)	C(3)	C(8)	119.3(2)				
			6				
C(8)	O(1)	C(1)	118.7(2)	C(7)	C(6)	C(5)	121.3(2)
N	O(2)	B	104.5(1)	C(6)	C(7)	C(8)	119.1(2)
C(2)	O(3)	B	107.1(2)	O(1)	C(8)	C(7)	118.6(2)
C(2)	N	O(2)	112.5(2)	O(1)	C(8)	C(3)	121.1(2)
C(2)	N	C(1)	125.2(2)	C(7)	C(8)	C(3)	120.1(2)
O(2)	N	C(1)	121.1(1)	C(10A)	C(9)	C(1)	105.5(8)
O(1)	C(1)	N	105.6(1)	C(1)	C(9)	C(10)	102.7(6)
O(1)	C(1)	C(9)	107.4(2)	C(11A)	C(10)	C(9)	110(1)
O(1)	C(1)	C(12)	112.0(2)	C(9)	C(10)	C(11)	100.1(9)
N	C(1)	C(9)	113.1(2)	C(9)	C(10A)	C(11A)	114(1)
N	C(1)	C(12)	111.9(2)	C(12)	C(11)	C(10)	107(2)
C(9)	C(1)	C(12)	106.8(2)	C(10A)	C(11A)	C(12)	104(1)
N	C(2)	O(3)	113.7(2)	C(11)	C(12)	C(1)	106(1)
N	C(2)	C(3)	118.8(2)	C(1)	C(12)	C(11A)	104(1)
O(3)	C(2)	C(3)	127.4(2)	F(2)	B	F(1)	111.3(2)
C(8)	C(3)	C(4)	120.4(2)	F(2)	B	O(2)	112.0(2)
C(8)	C(3)	C(2)	115.8(2)	F(2)	B	O(3)	109.4(2)
C(4)	C(3)	C(2)	123.5(2)	F(1)	B	O(2)	110.9(2)
C(5)	C(4)	C(3)	118.9(2)	F(1)	B	O(3)	111.1(2)
C(4)	C(5)	C(6)	120.2(2)	O(2)	B	O(3)	101.8(2)

withdrawal of electron density from the carbonyl group of salicylohydroxamic acid **1**, which is involved in a bifurcated hydrogen bond with an *N*-hydroxy group and the free phenolic OH group of neighboring molecules (10). The phenol function of **2** is blocked by *O*,*N*-acetalization and has no proton available for participation in intermolecular hydrogen-bonding. Thus the carbonyl group of **2** takes part in only one hydrogen bond to the hydroxamic acid group of a neighboring molecule, and retains more of its double bond character. The partial loss of double bond character of the carbonyl group in **1**, caused by donating into the bifurcated intermolecular hydrogen-bonding system present in crystalline **1**, should be even more pronounced in the boron chelates **3** and **6** which employ the carbonyl group as ligand for the electron-deficient borenium ions. Indeed, the lengthened C=O bonds of **3** and **6**, and the correspondingly shortened (carbonyl)C—N distances, suggest an increased elec-

Can. J. Chem. Downloaded from www.nrcresearchpress.com by 198.100.157.202 on 09/07/12
For personal use only.

Can. J. Chem. Downloaded from www.nrcresearchpress.com by 198.100.157.202 on 09/07/12
For personal use only.

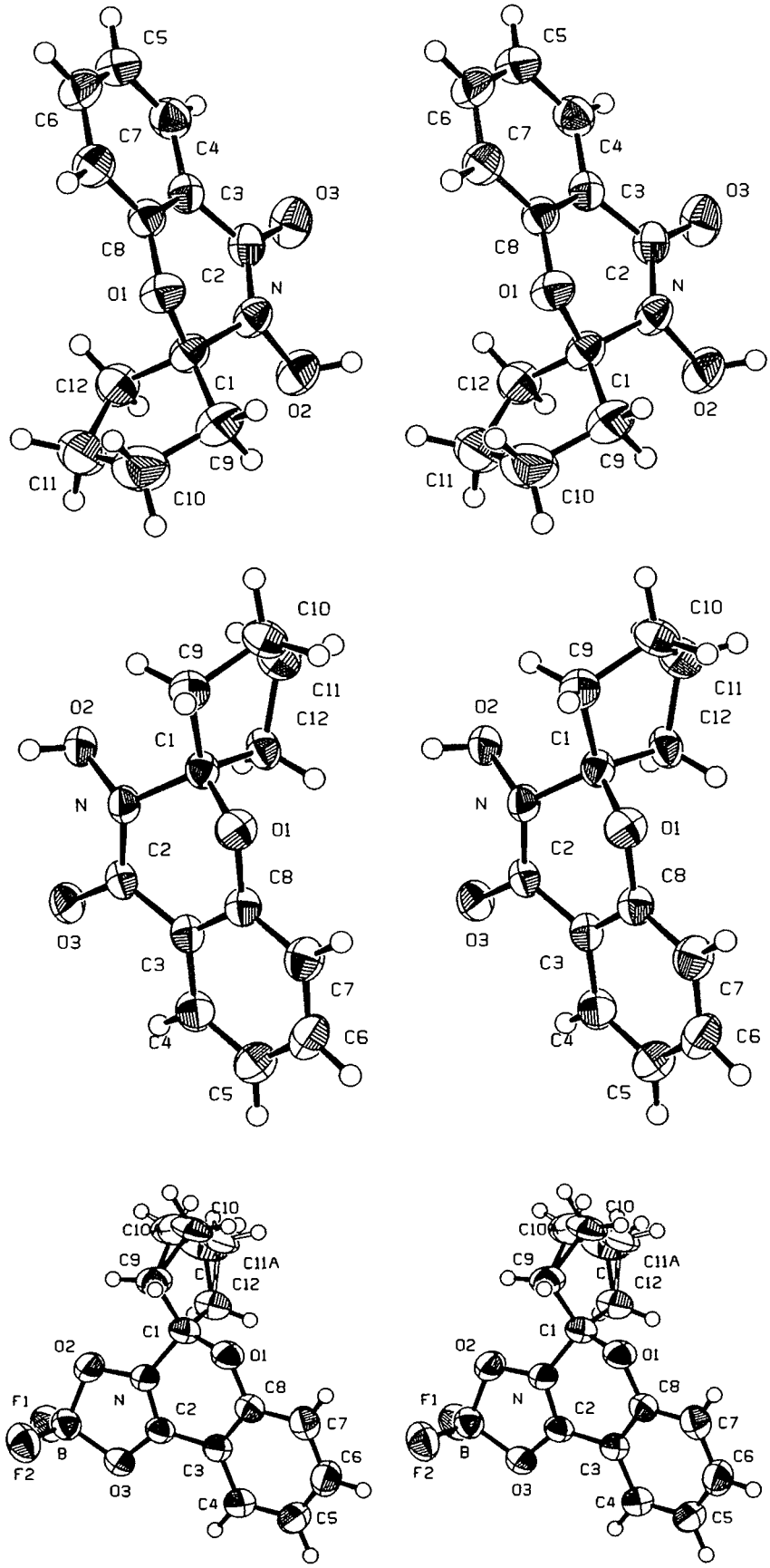


FIG. 1. Stereoviews of triclinic (top) and monoclinic **2** (middle) and **6** (bottom); 50% probability thermal ellipsoids are shown for the non-hydrogen atoms.

TABLE 5. Intra-annular torsion angles

Atoms	Value	
	2*a* (left) and **2***b* (right)	
O(1)—C(1)—N —C(2)	−44.9(2)	−49.8(2)
C(1)—N —C(2)—C(3)	17.8(2)	22.5(3)
N —C(2)—C(3)—C(8)	8.0(2)	4.0(3)
C(2)—C(3)—C(8)—O(1)	−3.0(2)	0.1(5)
C(3)—C(8)—O(1)—C(1)	−27.4(2)	−30.7(3)
C(8)—O(1)—C(1)—N	47.6(2)	51.9(2)
C(12)—C(1)—C(9)—C(10)	−36.8(2)	−19.8(2)
C(1)—C(9)—C(10)—C(11)	30.8(2)	36.9(3)
C(9)—C(10)—C(11)—C(12)	−13.2(3)	−39.7(3)
C(10)—C(11)—C(12)—C(1)	−9.5(2)	26.9(3)
C(11)—C(12)—C(1)—C(9)	28.5(2)	−4.3(2)
	6*	
O(1)—C(1)—N —C(2)	−36.5(3)	
C(1)—N —C(2)—C(3)	11.6(3)	
N —C(2)—C(3)—C(8)	9.4(3)	
C(2)—C(3)—C(8)—O(1)	−1.1(3)	
C(3)—C(8)—O(1)—C(1)	−28.2(3)	
C(8)—O(1)—C(1)—N	43.1(2)	
C(12)—C(1)—C(9)—C(10)	−28.3(6)	−11.0(8)
C(1)—C(9)—C(10)—C(11)	39(1)	−6(2)
C(9)—C(10)—C(11)—C(12)	−38(1)	19(2)
C(10)—C(11)—C(12)—C(1)	21(1)	−24(1)
C(11)—C(12)—C(1)—C(9)	4.8(8)	21.9(7)
O(2)—N —C(2)—O(3)	−2.4(2)	
N —C(2)—O(3)—B	−2.4(2)	
C(2)—O(3)—B —O(2)	5.6(2)	
O(3)—B —O(2)—N	−6.7(2)	
B —O(2)—N —C(2)	6.0(2)	

*Values for the two conformations of the disordered cyclopentane ring are given, those involving atoms C(10A) and C(11A) are on the right.

tron withdrawal out of the amide function accompanied by a more pronounced lone pair delocalization from the nitrogen atom towards the carbonyl group. The relatively small differences between the C=O and C—N bond distances in the boron chelates **3** and **6** reflect the higher Lewis acidity of the chelated borenium ion F_2B^+ in **6** relative to that of Ph_2B^+ in **3**. The C···O bond lengths increase from an average of 1.235 Å in **2**, 1.258 Å in **1** (10), 1.288 Å in **3** (1), to 1.295 Å in **6** while the amide C···N bond lengths decrease correspondingly: 1.346 (average), 1.316, 1.309, 1.294 Å. The π-bond orders of the C=O and C—N bonds have been estimated from plots of bond length vs. π-bond order (11): the C—O π-bond orders are 0.83, 0.70, 0.57, and 0.54 for **2**, **1**, **3**, and **6**, respectively, and the C—N π-bond orders are 0.53, 0.67, 0.72, and 0.79 for **2**, **1**, **3**, and **6**, respectively.

There is not much change in the bond lengths of the *O,N*-acetal grouping of the ligand **2** upon formation of the chelates **3** or **6**. The six-membered 1,3-oxazine heterocycle in the chelates **3** (1) and **6** have distorted "envelope" conformations. Compared to the less rigid tetrahydro-1,3-oxazin-4-one ring in compound **15** (12), the "semiplanar" skeleton of the dihydro-1,3-oxazin-4-one moiety in **2** shows slightly elongated bonds in the sterically less strained *O,N*-acetal fragment. The average C(1)—O and C(1)—N distances of 1.433 and 1.474 Å are slightly longer than the corresponding bond lengths of 1.417 and 1.469 Å in the saturated bicyclic system of **15** (12).

As discussed previously for the diphenylboron chelate **3** (1) an enhanced π-interaction between the hydroxamate system and the adjacent aryl group upon chelation can be observed by the shortening of the C(carbonyl)—C(aryl) bond of the ligand. The average C(2)—C(3) distance in **2** is 1.475 Å while the corresponding bond lengths in the diphenylboron chelate **3** and the difluoroboron chelate **6** are 1.438 and 1.436 Å, respectively. The B—O bonds of the difluoroborn chelate **6** (1.504 and 1.516 Å) are shorter by an average of 0.06 Å than those in the diphenylboron chelate **3** (1.558 and 1.578 Å) (1). This difference is similar to that observed for the difluoro- and diphenylboron chelates of *N*-methylacetohydroxamic acid (13, 14): about 0.05 Å. The mean F—B/mean O—B bond length ratio of 0.900 for **6** represents the weakest overall binding strength of the *O,O*-chelating ligand with respect to the "F_2B^+" moiety yet noted for a compound of this type having a five-membered chelate ring. These ratios range from 0.920 to 0.961 (mean 0.947) for other "F_2BO_2" compounds having five-membered chelate rings (13, 15, 16). The five-membered OBONC chelate ring in **6** has a flattened *B*-envelope conformation (Table 5) and is, in fact, planar to within 0.068(2) Å. The most significant intermolecular contact in the solid state structure of **6** corresponds to a weak C—H···O interaction: C(4)—H(1)···O(3)(1 − *x*,1 − *y*,1 − *z*), H···O = 2.45(3), C···O = 3.363(3) Å, and C—H···O = 151(2)°.

The free ligand, cyclic hydroxamic acid **2**, possesses a distinctly shorter C(2)—N amide bond (average 1.346 Å) than does the cyclic hydroxamic acid **14** (1.388 Å) which also has a six-membered ring skeleton (9). The difference between the C=O bonds in these two compounds is not very significant: average 1.235 Å in **2**, 1.241 Å in **14**. The N—O distance in **2** (average 1.398 Å) is longer by about 0.01 Å than that in **14** (1.387 Å) (9).

Acknowledgements

We thank the Natural Sciences and Engineering Research Council of Canada and the Fonds der Chemischen Industrie, Frankfurt am Main, for financial support.

1. W. KLIEGEL, M. TAJERBASHI, S. J. RETTIG, and J. TROTTER. Can. J. Chem. **68**, 69 (1990).
2. (*a*) D. B. REISNER and B. J. LUDWIG. J. Heterocycl. Chem. **6**, 953 (1969); (*b*) S. INAMASU and M. TSURUTA (YOSHITOMI PHARMACEUTICAL INDUSTRIES, LTD.). Japan. Patent 69 12,420 (5 June 1969), Chem. Abstr. **71**, 101869m (1969); (*c*) R. JUNG, J. Y. LE, F. WENGENMAYER, E. WOLF, and M. KRAMER. Biomed. Biochim. Acta, **44**, 485 (1985).
3. (*a*) O. EXNER. Coll. Czechoslov. Chem. Commun. **21**, 1500 (1956); (*b*) E. SCHMITZ and S. SCHRAMM. Chem. Ber. **100**, 2593 (1967); (*c*) H. NOHIRA, K. INOUE, H. HATTORI, T. OKAWA, and T. MUKAYAMA. Bull. Chem. Soc. Jpn. **40**, 664 (1967); (*d*) S. MORROCCHI, A. QUILICO, A. RICCA, and A. SELVA. Gazz. Chim. Ital. **98**, 891 (1968); (*e*) R. HUISGEN and W. MACK. Chem. Ber. **105**, 2805 (1972); (*f*) N. V. VASIL'EV, S. A. KHOKHLOVA, A. F. KOLOMIETS, and A. G. SOKOL'SKII. Zh. Org. Khim. **20**, 1983 (1984) (J. Org. Chem. USSR **20**, 1364 (1984)); (*g*) D. GEFFKEN. Arch. Pharm. (Weinheim) **318**, 895 (1985); (*h*) E. J. BREAUX. J. Heterocycl. Chem. **23**, 463 (1986); (*i*) D. MACKAY, E. G. NEELAND, and N. J. TAYLOR. J. Org. Chem. **51**, 2351 (1986).
4. W. KLIEGEL, M. TAJERBASHI, S. J. RETTIG, and J. TROTTER. Can. J. Chem. **66**, 2621 (1988).
5. International tables for X-ray crystallography. Kynoch Press: Birmingham, U.K. (present distributor Kluwer Academic Publishers: Dordrecht, The Netherlands), Vol. IV. 1974. pp. 99–102 and 149.

Can. J. Chem. Downloaded from www.nrcresearchpress.com by 198.100.157.202 on 09/07/12
For personal use only.

6. (*a*) R. T. COUTTS. Can. J. Pharm. Sci. **2**, 27 (1967); (*b*) J. B. BAPAT, D. ST. C. BLACK, and R. F. C. BROWN. Adv. Heterocycl. Chem. **10**, 199 (1969).
7. J. ITOH, S. AMANO, Y. OGAWA, Y. KODAMA, N. EZAKI, and Y. YAMADA. J. Antibiot. **33**, 377 (1980).
8. M. CIGNITTI, L. SOCCORSI, F. GATTA, and M. COTTA-RAMUSINO. Spectrochim. Acta, Sect. A, **41**, 1287 (1985).
9. R. C. SCARROW, P. E. RILEY, K. ABU-DARI, D. L. WHITE, and K. N. RAYMOND. Inorg. Chem. **24**, 954 (1985).
10. I. K. LARSEN. Acta Crystallogr. Sect. B, **34**, 962 (1978).
11. G. HÄFELINGER. Chem. Ber. **103**, 2941 (1970).
12. B. RIBAR, A. KAPOR, A. KALMAN, GY. ARGAY, F. FÜLÖP, and G. BERNATH. J. Mol. Struct. **192**, 125 (1989).
13. S. J. RETTIG, J. TROTTER, W. KLIEGEL, and D. NANNINGA. Can. J. Chem. **55**, 1 (1977).
14. S. J. RETTIG, J. TROTTER, W. KLIEGEL, and D. NANNINGA. Can. J. Chem. **56**, 1676 (1978).
15. C. M. LUKEHART and K. SRINIVASAN. J. Am. Chem. Soc. **103**, 4166 (1981).
16. P. G. LENHERT, C. M. LUKEHART, and K. SRINIVASAN. J. Am. Chem. Soc. **106**, 124 (1984).
17. W. KLIEGEL, G. LUBKOWITZ, S. J. RETTIG, and J. TROTTER. Can. J. Chem. **69**, 545 (1991).

Can. J. Chem. Downloaded from www.nrcresearchpress.com by 198.100.157.202 on 09/07/12
For personal use only.

Structural studies of organoboron compounds. XLV.[1] 5,5-Difluoro-2,2-pentamethylene-7,7-diphenyl-1,4,6-trioxa-3*a*-azonia-5-borata-2,3,4,5,6,7-hexahydroindene

WOLFGANG KLIEGEL AND UTE SCHUMACHER

Institut für Pharmazeutische Chemie der Technischen Universität Braunschweig, Beethovenstrasse 55, 3300 Braunschweig, Bundesrepublik Deutschland

AND

STEVEN J. RETTIG AND JAMES TROTTER

Department of Chemistry, University of British Columbia, 2036 Main Mall, Vancouver, B.C., Canada V6T 1Z1

Received August 10, 1990

WOLFGANG KLIEGEL, UTE SCHUMACHER, STEVEN J. RETTIG, and JAMES TROTTER. Can. J. Chem. **69**, 681 (1991).

The reaction of *N*,2-dihydroxy-*N*-(1-hydroxycyclohexyl)methyl-2,2-diphenylacetamide with dimethyl ether-boron trifluoride gives 5,5-difluoro-2,2-pentamethylene-7,7-diphenyl-1,4,6-trioxa-3*a*-azonia-5-borata-2,3,4,5,6,7-hexahydroindene in nearly quantitative yield. Crystals of the product are triclinic, $a = 9.4555(5)$, $b = 9.9813(6)$, $c = 10.5139(9)$ Å, $\alpha = 72.654(7)$, $\beta = 77.140(5)$, $\gamma = 88.542(6)°$, $Z = 2$, space group $P\bar{1}$. The structure was solved by direct methods and was refined by full-matrix least-squares procedures to $R = 0.044$ and $R_w = 0.060$ for 2971 reflections with $I \geq 3\sigma(I)$. The molecule has a six-membered difluoroboron chelate structure, confirming that the regioselective alkylation of *N*-substituted hydroxamic acids under non-basic conditions leads to imidate *N*-oxides in cases where intramolecular alkylation occurs. Bond lengths (corrected for libration): (N)O—B = 1.530(3), (C)O—B = 1.451(2), F—B = 1.389(3) and 1.379(3) Å indicate relatively strong binding of the BF_2^+ moiety by the *O*,*O*-chelating ligand.

Key words: organoboron compound, crystal structure, boron compound.

WOLFGANG KLIEGEL, UTE SCHUMACHER, STEVEN J. RETTIG et JAMES TROTTER. Can. J. Chem. **69**, 681 (1991).

La réaction du *N*,2-dihydroxy-*N*-(1-hydroxycyclohexyl)méthyl-2,2-diphénylacétamide avec le complexe $(CH_3)_2O/BF_3$ fournit le 5,5-difluoro-2,2-pentaméthylène-7,7-diphényl-1,4,6-trioxa-3*a*-azonia-5-borata-2,3,4,5,6,7-hexahydroindène avec un rendement pratiquement quantitatif. Les cristaux de ce produit sont tricliniques, groupe d'espace $P\bar{1}$, avec $a = 9{,}4555(5)$, $b = 9{,}9813(6)$ et $c = 10{,}5139(9)$ Å, $\alpha = 72{,}654(7)$, $\beta = 77{,}140(5)$ et $\gamma = 88{,}542(5)°$ et $Z = 2$. On a résolu la structure par des méthodes directes et on l'affinée par la méthode des moindres carrés jusqu'à des valeurs respectives de $R = 0{,}044$ et $R_w = 0{,}060$ pour 2971 réflexions avec $I \geq 3\sigma(I)$. La molécule comporte une structure à six chaînons impliquant une coordination du difluorure de bore; ces données confirment que, dans les cas où une alkylation intramoléculaire se produit, l'alkylation régiosélective des acides hydroxamiques *N*-substitués, dans des conditions qui ne sont pas basiques, conduit à des *N*-oxydes d'imidate. Les longueurs des liaisons (corrigées pour la libration): (N)O—B = 1,530(3), (C)O—B = 1,451(2), F—B = 1,389(3) et 1,379(3) Å indiquent la présence d'une liaison relativement forte de la portion BF_2^+ avec le coordinat *O*,*O*-chélatant.

Mots clés : composés organoborés, structure cristalline, composé boré.

[Traduit par la rédaction]

Introduction

The reaction of the bis(hydroxyalkyl) substituted hydroxamic acid **1** with boron trifluoride did not lead to the difluoroboron chelate **2** having the "normal" BF_2 hydroxamate structure that usually results from reactions of *N*-alkylhydroxamic acids with boron trifluoride (1), and which has been established by an X-ray crystallographic study of the simple prototype **3** (2). The crystalline compound obtained from the reaction of **1** with $BF_3 \cdot OMe_2$ produced spectra and elemental analyses showing not only HF elimination but also loss of H_2O. Neither infrared bands for O—H stretching vibrations nor OH-proton signals in the ^1H nmr spectra, both of which would arise from the hydroxyl groups of **2**, were observed. These data suggest an intra- or intermolecular condensation of **1** and difluoroboron chelate formation leading to structures such as **4**–**7**.

A possible intermediate **2** could form the cyclic ether **4** by intramolecular condensation and still feature the five-membered BF_2 hydroxamate chelate, similar to the cyclic ether compound **8** with an identical difluoroboron chelate ring portion within the molecule (3). Another intramolecular condensation reaction of **1** in the presence of BF_3 could give rise to the difluoroboron chelate **5** with the newly formed 2-oxazoline *N*-oxide moiety as one of the chelating ligands. A similar intramolecular cyclization of an *N*-(2-hydroxyalkyl) hydroxamic acid in the presence of BF_3, including the formation of a BF_2 chelate, has already been documented by the synthesis and structure analysis of the salicylohydroxamic acid derivative **9** (4). Less likely under the applied conditions of BF_3 catalysis is an intramolecular alkylation of the *N*-hydroxy group of **1** by the *N*-(2-hydroxyalkyl) residue giving the four-membered oxazetidine ring with subsequent (or concerted) formation of a BF_2^+ chelate (compound **6**). Also unlikely is the intermolecular condensation product **7** containing eight-membered boron chelate rings, although eight-membered boron chelate rings are known and have been structurally characterized (5) and the 1,4,2,5-dioxadiazine ring system is thought to exist in certain dimers of nitrile oxides (6). However, an EI mass spectrum of the isolated crystals displays a molecular ion peak consistent only with a monomer like **4**, **5**, or **6**. The fragmentation pattern does not allow for a definite assignment of one of these isomeric structures, nor do the infrared and ^1H nmr spectral data. An X-ray crystallographic analysis has been carried out in order to provide an unambiguous decision between the possible isomeric structures **4**–**6**.

Experimental

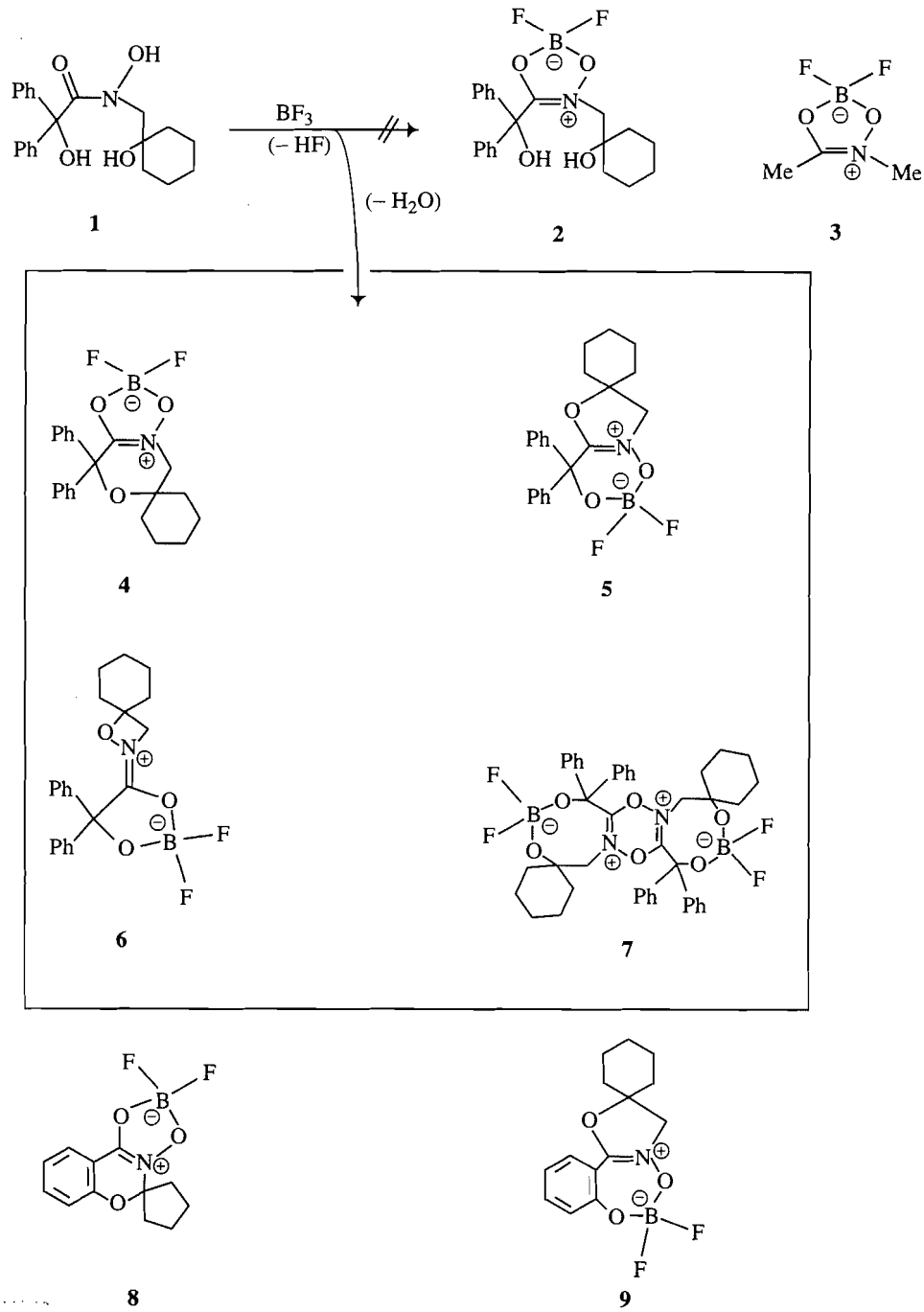
N,2-Dihydroxy-N-(1-hydroxycyclohexyl)methyl-2,2-diphenylacetamide, I

1-(Hydroxyaminomethyl)cyclohexanol (7) (4.35 g, 30 mmol) is

[1]Previous paper in this series: ref. 3.

Printed in Canada / Imprimé au Canada

Can. J. Chem. Downloaded from www.nrcresearchpress.com by 198.100.157.202 on 09/07/12
For personal use only.



Can. J. Chem. Downloaded from www.nrcresearchpress.com by 198.100.157.202 on 09/07/12
For personal use only.

reacted with ethyl oxalyl chloride (30 mmol) and phenylmagnesium bromide (225 mmol) according to literature methods (8). The product crystallizes from ether/petroleum ether. Yield: 4.47 g (42%). Colorless crystals. Melting point 124–126°C (from ether/petroleum ether). *Anal.* calcd. for $C_{21}H_{25}NO_4$: C 70.96, H 7.09, N 3.94; found: C 70.89, H 7.07, N 3.91. Infrared (KBr): 3400–3360, 3140 (O—H), 1615 cm^{-1} (C=O). ^1H nmr (90 MHz, $CDCl_3$/TMS): δ (ppm) = 1.47 (s, $(CH_2)_5$), 2.40 (s, broad, exchangeable, 2OH), 3.75 (s, N—CH_2), 5.40 (s, broad, exchangeable, OH), 7.13–7.60 (m, $2C_6H_5$).

5,5-Difluoro-2,2-pentamethylene-7,7-diphenyl-1,4,6-trioxa-3a-azonia-5-borata-2,3,4,5,6,7-hexahydroindene, 5

1 (1.07 g, 3 mmol) is dissolved in 30–40 mL toluene and, after addition of dimethyl ether–boron trifluoride (0.34 g, 3 mmol), refluxed for 30 min. The solvent is removed *in vacuo*, until the volume of the reaction mixture is reduced to 3–5 mL. Crystallization starts during cooling. Yield: 0.89 g (77%). Colorless crystals. Melting point 192–193°C (from toluene). *Anal.* calcd. for $C_{21}H_{22}BF_2NO_3$: C 65.48, H 5.76, N 3.64; found: C 65.57, H 5.74, N 3.60. Infrared (KBr): 1670 cm^{-1} (C=O/C=N). ^1H nmr (90 MHz, d_6-DMSO/TMS): δ (ppm) = 1.22–1.63, 1.67–2.00 (2 m, 3:2 $(CH_2)_5$), 4.33 (s, N—CH_2), 7.34 (s, 2 C_6H_5). Crystals suitable for X-ray analysis are obtained by recrystallization from toluene.

X-ray crystallographic analysis of 5

A crystal ca. 0.28 × 0.32 × 0.53 mm in size was mounted on a glass fiber. Unit-cell parameters were refined by least-squares on 2 sin θ/λ values for 25 reflections (2θ = 38.6–41.4°) measured on a diffractometer with Mo-K_α radiation ($\lambda_{K\alpha1}$ = 0.70930, $\lambda_{K\alpha2}$ = 0.71359 Å). Crystal data at 21°C are as follows

$C_{21}H_{22}BF_2NO_3$ fw = 385.22

TABLE 1. Final positional (fractional × 10^4) and isotropic thermal parameters ($U \times 10^3$ Å^2) with estimated standard deviations in parentheses

Atom	x	y	z	U_{eq}
F(1)	6644(2)	−1178(2)	3525(2)	99
F(2)	8323(2)	−1073(2)	1602(2)	92
O(1)	5980(1)	−622(1)	1439(1)	47
O(2)	7473(1)	978(1)	2004(1)	39
O(3)	3890(1)	2110(1)	2046(1)	37
N	4872(2)	211(1)	1743(2)	37
C(1)	6610(2)	2084(2)	1471(2)	29
C(2)	5082(2)	1466(2)	1750(2)	31
C(3)	2617(2)	1050(2)	2396(2)	36
C(4)	3353(2)	−230(2)	2054(2)	46
C(5)	1580(2)	1722(2)	1509(2)	46
C(6)	893(2)	2983(2)	1861(2)	51
C(7)	178(2)	2636(3)	3368(3)	58
C(8)	1270(2)	2050(3)	4235(2)	52
C(9)	1973(2)	775(2)	3904(2)	45
C(10)	6625(2)	3162(2)	2243(2)	29
C(11)	6100(2)	2731(2)	3654(2)	38
C(12)	6177(2)	3645(2)	4398(2)	46
C(13)	6767(2)	4985(2)	3758(2)	48
C(14)	7281(2)	5420(2)	2366(2)	46
C(15)	7211(2)	4508(2)	1604(2)	37
C(16)	7120(2)	2709(2)	−89(2)	30
C(17)	6221(2)	3536(2)	−857(2)	39
C(18)	6695(2)	4115(2)	−2254(2)	45
C(19)	8072(2)	3864(2)	−2901(2)	46
C(20)	8968(2)	3046(2)	−2149(2)	45
C(21)	8500(2)	2459(2)	−747(2)	37
B	7148(2)	−469(2)	2173(2)	43

Triclinic, a = 9.4555(5), b = 9.9813(6), c = 10.5139(9) Å, α = 72.654(7), β = 77.140(5), γ = 88.542(5)°, Z = 2, ρ_c = 1.387 Mg m^{-3}, $F(000)$ = 404, μ(Mo-K$_\alpha$) = 0.98 cm^{-1}. Absent reflections: none, space group $P\bar{1}$ (No. 2, reduced cell) from structure analysis.

Intensities were measured with graphite-monochromated Mo-K$_\alpha$ radiation on an Enraf-Nonius CAD4-F diffractometer. An ω–2θ scan at 1.2–10.0° min^{-1} over a range of (0.80 + 0.35 tan θ)° in ω (scan extended by 25% on each side for background measurement) was employed. Data were measured to 2θ = 55°. The intensities of three check reflections, measured every hour of X-ray exposure time throughout the data collection, showed only small random variations. The data were processed[2] and corrected for Lorentz and polarization effects. Of the 4232 independent reflections measured, 2971 (70.2%) had intensities greater than or equal to $3\sigma(I)$ above background where $\sigma^2(I) = [C + 2B + (0.040(C - B))^2]$ with C = scan count, B = normalized total background count.

The analysis was initiated in the centrosymmetric space group $P\bar{1}$ on the basis of the E-statistics, this choice being confirmed by the subsequent successful solution and refinement of the structure. The structure was solved by direct methods, the coordinates of all non-hydrogen atoms being determined from an E-map. The non-hydrogen atoms were refined with anisotropic thermal parameters and the hydrogen atoms were refined with isotropic thermal parameters. Scattering factors for all atoms and anomalous dispersion corrections for the non-hydrogen atoms were taken from ref. 9. The weighting scheme $w = 1/\sigma^2(F)$ gave uniform average values of $w(|F_o| - |F_c|)^2$ over ranges of both $|F_o|$ and sin θ/λ and was employed in the final stages of full-matrix least-squares refinement of 341 variables. Reflections with $I < 3\sigma(I)$ were not included in the refinement. Convergence was reached at R = 0.044 and R_w = 0.060 for 2971 reflections with $I \geq 3\sigma(I)$. The function minimized was $\Sigma w(|F_o| - |F_c|)^2$, $R = \Sigma||F_o| - |F_c||/\Sigma|F_o|$, $R_w = (\Sigma w(|F_o| - |F_c|)^2/\Sigma w|F_o|^2)^{1/2}$. On the final cycle of refinement the maximum parameter shift corresponded to 0.07σ. The mean error in an observation of unit weight was 2.13. The final difference map showed maximum fluctuations of −0.31 to +0.24 e Å^{-3}.

The thermal motion has been analyzed in terms of the TLS model (10). The rms error in the temperature factors U_{ij} (derived from the least-squares analysis) is 0.0009 Å^2. Five structural subunits were separately analyzed (rms ΔU_{ij} = 0.0013–0.0023 Å^2). The bond lengths have been corrected for liberation (10, 11) using shape parameters q^2 of 0.08 for all atoms. The final positional and (equivalent) isotropic thermal parameters for the non-hydrogen atoms appear in Table 1. Bond lengths (corrected and uncorrected) and angles are given in Tables 2 and 3 and intra-annular torsion angles in Table 4. Hydrogen atom parameters, anisotropic thermal parameters, bond lengths and angles involving hydrogen, torsion angles, and structure factors have been deposited.[3]

Results and discussion

As the structure analysis reveals, the intramolecular alkylation of **1** in the presence of BF_3 does not lead to the cyclic ether compound **4** having a BF_2 hydroxamate partial structure, but rather gives the 2-oxazoline *N*-oxide derivative **5** with a six-membered difluoroborn chelate ring (Fig. 1). This confirms the results of regioselective alkylation of *N*-substituted hydroxamic acids under non-basic conditions, leading to cyclic imidate *N*-oxides (4, 12) in the case of intramolecular alkylation or to acyclic imidate *N*-oxides (13) or thioimidate *N*-oxides (14) in the case of intermolecular alkylation.

The structure **5** contains a six-membered boron chelate ring analogous to the seven-membered chelate ring in compound **9**, which also has a cyclic imidate *N*-oxide oxygen atom serving as one of the donors of the bidentate ligand. The difference between these two compounds is found in the functionality of the second donor which is an alcoholate oxygen atom in **5** and a phenolate oxygen atom in **9**. To the best of our knowledge this is the first example of a six-membered boron chelate with this particular heterocyclic *B*,*N*-betaine structure. The formulation of **5** as an intramolecular iminium salt is justified by the extremely short C(2)—N bond[4] of the imidate *N*-oxide function: 1.281 Å, which is even shorter than the comparable C=N$^+$ bond in **9** (1.294 Å) (4), and also shorter than the C=N$^+$ bonds in the BF_2 hydroxamates **3** (1.289 Å) (2) and **8** (1.294 Å) (3). The π-bond order of the C(2)—N bond, estimated from bond length vs. π-bond order plots (15, 16), lies between 0.8 and 1.0 and is similar to that of C=N$^+$ bonds in boron complexes of oximes with bond lengths of 1.283 Å (17) and 1.287 Å (18).

In spite of the *O*-alkylation of the carbonyl oxygen atom O(3), the C(2)—O(3) bond shows some double bond character with a bond length of 1.310 Å. The estimated (16) π-bond order

[2]Computer programs used include locally written programs for data processing and locally modified versions of the following: MULTAN80, multisolution program by P. Main, S. J. Fiske, S. E. Hull, L. Lessinger, G. Germain, J. P. Declercq, and M. M. Woolfson; ORFLS, full-matrix least-squares, and ORFFE, functions and errors, by W. R. Busing, K. O. Martin, and H. A. Levy; FORDAP, Patterson and Fourier syntheses, by A. Zalkin; ORTEP II, illustrations, by C. K. Johnson.

[3]Supplementary material mentioned in the text may be purchased from the Depository of Unpublished Data, Document Delivery, CISTI, National Research Council of Canada, Ottawa, Ont., Canada K1A 0S2.

[4]Libration-corrected bond distances are employed throughout the discussion and are compared with similarly treated (10) bond lengths for other compounds in this series of papers and uncorrected distances otherwise.

Can. J. Chem. Downloaded from www.nrcresearchpress.com by 198.100.157.202 on 09/07/12
For personal use only.

TABLE 2. Bond lengths (Å) with estimated standard deviations in parentheses

Bond	Length		Bond	Length	
	Uncorr.	Corr.		Uncorr.	Corr.
F(1)—B	1.365(3)	1.389	C(5)—C(6)	1.507(3)	1.513
F(2)—B	1.357(3)	1.379	C(6)—C(7)	1.516(3)	1.524
O(1)—N	1.362(2)	1.367	C(7)—C(8)	1.519(3)	1.526
O(1)—B	1.515(3)	1.530	C(8)—C(9)	1.517(3)	1.522
O(2)—C(1)	1.410(2)	1.415	C(10)—C(11)	1.391(2)	1.399
O(2)—B	1.434(2)	1.451	C(10)—C(15)	1.378(2)	1.385
O(3)—C(2)	1.306(2)	1.310	C(11)—C(12)	1.380(3)	1.384
O(3)—C(3)	1.530(2)	1.536	C(12)—C(13)	1.374(3)	1.381
N—C(2)	1.276(2)	1.281	C(13)—C(14)	1.372(3)	1.379
N—C(4)	1.449(2)	1.452	C(14)—C(15)	1.392(3)	1.395
C(1)—C(2)	1.518(2)	1.522	C(16)—C(17)	1.388(2)	1.394
C(1)—C(10)	1.530(2)	1.534	C(16)—C(21)	1.389(2)	1.395
C(1)—C(16)	1.538(2)	1.541	C(17)—C(18)	1.381(3)	1.384
C(3)—C(4)	1.537(3)	1.542	C(18)—C(19)	1.383(3)	1.388
C(3)—C(5)	1.510(3)	1.518	C(19)—C(20)	1.373(3)	1.379
C(3)—C(9)	1.510(3)	1.519	C(20)—C(21)	1.386(3)	1.389

TABLE 3. Bond angles (deg) with estimated standard deviations in parentheses

Bonds	Angle (deg)	Bonds	Angle (deg)
N—O(1)—B	108.67(13)	C(7)—C(8)—C(9)	111.4(2)
C(1)—O(2)—B	123.53(13)	C(3)—C(9)—C(8)	112.7(2)
C(2)—O(3)—C(3)	107.41(12)	C(1)—C(10)—C(11)	118.26(14)
O(1)—N—C(2)	122.75(14)	C(1)—C(10)—C(15)	122.46(14)
O(1)—N—C(4)	123.34(14)	C(11)—C(10)—C(15)	119.2(2)
C(2)—N—C(4)	113.89(15)	C(10)—C(11)—C(12)	120.0(2)
O(2)—C(1)—C(2)	107.16(12)	C(11)—C(12)—C(13)	120.6(2)
O(2)—C(1)—C(10)	107.19(12)	C(12)—C(13)—C(14)	119.7(2)
O(2)—C(1)—C(16)	111.92(13)	C(13)—C(14)—C(15)	120.3(2)
C(2)—C(1)—C(10)	110.15(13)	C(10)—C(15)—C(14)	120.2(2)
C(2)—C(1)—C(16)	106.87(12)	C(1)—C(16)—C(17)	120.89(14)
C(10)—C(1)—C(16)	113.38(13)	C(1)—C(16)—C(21)	119.98(15)
O(3)—C(2)—N	114.12(14)	C(17)—C(16)—C(21)	119.1(2)
O(3)—C(2)—C(1)	125.20(14)	C(16)—C(17)—C(18)	120.6(2)
N—C(2)—C(1)	120.66(14)	C(17)—C(18)—C(19)	119.9(2)
O(3)—C(3)—C(4)	102.98(13)	C(18)—C(19)—C(20)	119.8(2)
O(3)—C(3)—C(5)	106.85(14)	C(19)—C(20)—C(21)	120.6(2)
O(3)—C(3)—C(9)	105.72(13)	C(16)—C(21)—C(20)	119.9(2)
C(4)—C(3)—C(5)	114.0(2)	F(1)—B—F(2)	111.6(2)
C(4)—C(3)—C(9)	113.0(2)	F(1)—B—O(1)	107.1(2)
C(5)—C(3)—C(9)	113.1(2)	F(1)—B—O(2)	110.3(2)
N—C(4)—C(3)	101.08(14)	F(2)—B—O(1)	105.1(2)
C(3)—C(5)—C(6)	112.5(2)	F(2)—B—O(2)	111.0(2)
C(5)—C(6)—C(7)	111.7(2)	O(1)—B—O(2)	111.52(15)
C(6)—C(7)—C(8)	110.5(2)		

between 0.4 and 0.5 indicates the participation of the C(2)—O(3) bond in the imidate π-bond system incorporating the adjacent C=N$^+$ bond. A similar situation has been noted for compounds of the type **9** (4). The C(3)—O(3) bond is very long (1.536 Å) compared to any other (sp^3)C—O bond lengths reported (19), and is also longer than the identical bond in compound **9** (1.512 Å) (4).

The boron atom has a slightly distorted tetrahedral geometry (see Table 3). The O—B bonds of **5** have the same average length of 1.491 Å as those in the seven-membered chelate **9** (4), but — as in **9** — they are markedly different from one another (by ~0.08 Å), B—ON = 1.530, B—OC = 1.451 Å. The distance between the *N*-oxide oxygen atom and the boron atom is longer than the distance between an alcoholate (or phenolate) oxygen atom and boron. This has also been noted for five- to seven-membered diphenylboron chelates of various *N*-oxides (4, 20–23). The B—F bond lengths in **5** (average 1.384 Å) are similar to those in **9** (average 1.387 Å), but distinctly longer than

Can. J. Chem. Downloaded from www.nrcresearchpress.com by 198.100.157.202 on 09/07/12
For personal use only.

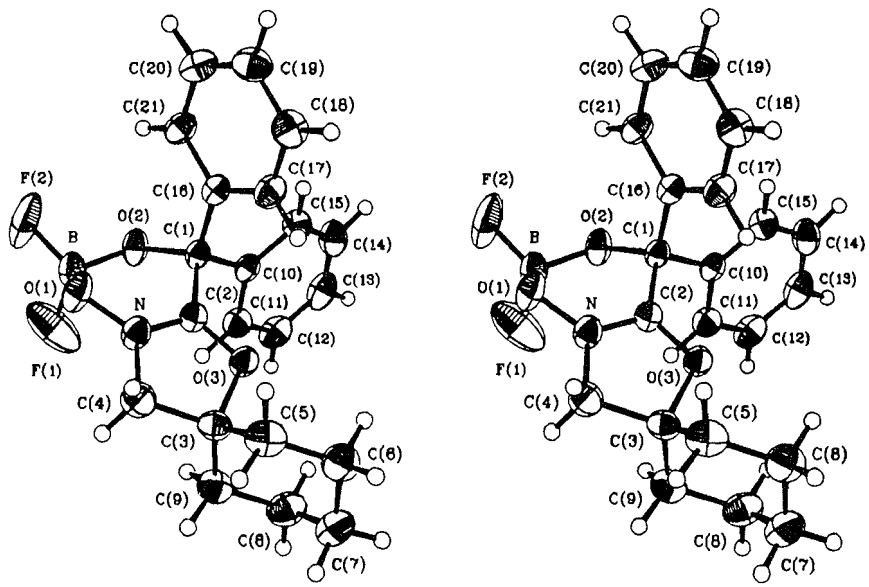


FIG. 1. Stereoview of **5**; 50% probability thermal ellipsoids are shown for the non-hydrogen atoms.

TABLE 4. Intra-annular torsion angles (deg) standard deviations in parentheses

Atom	Value (deg)
B—O(1)—N—C(2)	43.8(2)
O(1)—N—C(2)—C(1)	−2.5(2)
O(2)—C(1)—C(2)—N	−33.4(2)
B—O(2)—C(1)—C(2)	25.6(2)
C(1)—O(2)—B—O(1)	12.2(2)
N—O(1)—B—O(2)	−46.9(2)
C(9)—C(3)—C(5)—C(6)	49.7(2)
C(3)—C(5)—C(6)—C(7)	−53.5(2)
C(5)—C(6)—C(7)—C(8)	56.7(3)
C(6)—C(7)—C(8)—C(9)	−56.1(3)
C(7)—C(8)—C(9)—C(3)	52.8(2)
C(5)—C(3)—C(9)—C(8)	−49.4(2)
C(3)—O(3)—C(2)—N	4.3(2)
C(4)—N—C(2)—O(3)	0.4(2)
C(2)—N—C(4)—C(3)	−4.8(2)
O(3)—C(3)—C(4)—N	6.5(2)
C(2)—O(3)—C(3)—C(4)	−6.8(2)

those in the five-membered hydroxamate **8** (1.358 Å) and slightly longer than those in **3** (average 1.377 Å). The mean F—B/mean O—B bond length ratio of 0.929 for **5** is at the high end of the range 0.884–0.949 (average 0.915) observed for other "F_2BO_2" compounds having six-membered chelate rings (ref. 4 and references therein), indicating relatively strong binding of the difluoroborenium ion (F_2B^+) by the chelating ligand.

The six-membered BONCCO chelate ring has an O(1),C(1)-twist-boat conformation, flattened somewhat at the C(1) end. The five-membered oxazoline ring, fused to the N,C(2) side of the above-mentioned six-membered ring, has a flattened C(3)-envelope conformation. O(3) and C(4) of the oxazoline ring are in axial and equatorial positions with respect to the cyclohexane ring, which has a relatively undistorted chair conformation (see Table 4 for torsion angles). The phenyl substituents at C(1) are oriented nearly perpendicular to one another (dihedral angles between normals to the mean planes is 81.3°), the bond to the pseudo-axial substituent being slightly longer than the other (1.541(2) vs. 1.534(2) Å). The O(3)—C(2)—N—C(4) and C(1)—C(2)—N—O(1) groups are both approximately planar (all six of these atoms are coplanar to within 0.015(2) Å), the former being planar within experimental error as a result of the more extended π-system of the imidate function. The most significant intermolecular contact in the solid state of **5** corresponds to a weak C—H···F interaction: C(20)—H(20)···F(2)($2 - x, - y, - z$), H···F = 2.51(2) Å, C···F = 3.240(2) Å, C—H···F = 131(2)°.

Acknowledgements

We thank the Natural Sciences and Engineering Research Council of Canada and the Fonds der Chemischen Industrie, Frankfurt am Main, for financial support.

1. W. KLIEGEL and D. NANNINGA. Chem. Ber. **116**, 2616 (1983).
2. S. J. RETTIG, J. TROTTER, W. KLIEGEL, and D. NANNINGA. Can. J. Chem. **55**, 1 (1977).
3. W. KLIEGEL, M. TAJERBASHI, S. J. RETTIG, and J. TROTTER. Can. J. Chem. **69**, 673 (1991).
4. W. KLIEGEL, M. TAJERBASHI, S. J. RETTIG, and J. TROTTER. Can. J. Chem. **66**, 2621 (1988).
5. W. KLIEGEL, S. J. RETTIG, and J. TROTTER. Can. J. Chem. **66**, 1091 (1988).
6. K. B. G. TORSSELL. Nitrile oxides, nitrones, and nitronates in organic synthesis. VCH Publishers, New York. 1988. p. 55.
7. W. KLIEGEL and H. BECKER. Chem. Ber. **110**, 2067 (1977).
8. D. GEFFKEN and T. LAUTERBACH. Chemiker-Ztg. **109**, 192 (1985).
9. International tables for X-ray crystallography, Kynoch Press, Birmingham, U.K. (present distributor Kluwer Academic Publishers: Dordrecht, The Netherlands). Vol. IV. 1974. pp. 99–102 and 149.
10. V. SCHOMAKER and K. N. TRUEBLOOD. Acta Crystallogr. Sect. B, **24**, 63 (1968).
11. D. W. J. CRUICKSHANK. Acta Crystallogr. **9**, 747 (1956); **9**, 754 (1956); **14**, 896 (1961).

Can. J. Chem. Downloaded from www.nrcresearchpress.com by 198.100.157.202 on 09/07/12
For personal use only.

12. S. P. ASHBURN and R. M. COATES. J. Org. Chem. **49**, 3127 (1984); **50**, 3076 (1985).
13. J. A. WARSHAW, D. E. GALLIS, B. J. ACKEN, O. J. GONZALES, and D. R. CRIST. J. Org. Chem. **54**, 1736 (1989).
14. R. M. COATES and S. J. FIRSAN. J. Org. Chem. **51**, 5198 (1986).
15. L. M. TREFONAS, R. L. FLURRY, R. MAJESTE, E. A. MEYERS, and R. F. COPELAND. J. Am. Chem. Soc. **88**, 2145 (1966).
16. G. HÄFELINGER. Chem. Ber. **103**, 2941 (1970).
17. W. KLIEGEL, S. J. RETTIG, and J. TROTTER. Can. J. Chem. **62**, 1363 (1984).
18. S. J. RETTIG and J. TROTTER. Can. J. Chem. **61**, 206 (1983).
19. F. H. ALLEN, O. KENNARD, D. G. WATSON, L. BRAMER, A. G. ORPEN, and R. TAYLOR. J. Chem. Soc. Perkin II, S1 (1987).
20. S. J. RETTIG, J. TROTTER, and W. KLIEGEL. Can. J. Chem. **52**, 2531 (1974).
21. W. KLIEGEL, H.-W. MOTZKUS, S. J. RETTIG, and J. TROTTER. Can. J. Chem. **62**, 838 (1984).
22. W. KLIEGEL, U. LAUTERBACH, S. J. RETTIG, and J. TROTTER. Can. J. Chem. **65**, 1457 (1987).
23. E. EBELING, W. KLIEGEL, S. J. RETTIG, and J. TROTTER. Can. J. Chem. **67**, 933 (1989).

Can. J. Chem. Downloaded from www.nrcresearchpress.com by 198.100.157.202 on 09/07/12
For personal use only.

Crown ether complexes exhibiting unusual 1:2 macrocycle salt ratios: X-ray crystal structures of cyclohexano-15-crown-5·2LiOPh, cyclohexano-15-crown-5·2NaOPh, and 15-crown-5·2NaOPh

KIMBERLY A. WATSON AND SUZANNE FORTIER
Queen's University, Kingston, Ont., Canada K7L 3N6

AND

MICHAEL P. MURCHIE AND JOHN W. BOVENKAMP
Defence Research Establishment Ottawa, Ottawa, Ont., Canada K1A 0Z4

Received June 15, 1990

Can. J. Chem. Downloaded from www.nrcresearchpress.com by 198.100.157.202 on 09/07/12
For personal use only.

KIMBERLY A. WATSON, SUZANNE FORTIER, MICHAEL P. MURCHIE, and JOHN W. BOVENKAMP. Can. J. Chem. **69**, 687 (1991).

The crystal structures of three crown ether complexes (cyclohexano-15-crown-5·2LiOPh (**1**): $Li_2O_7C_{26}H_{36}$, M_r = 474.45, λ(CuKα)filt. = 1.5418 Å; cyclohexano-15-crown-5·2NaOPh (**2**): $Na_2O_7C_{26}H_{36}$, M_r = 504.54, λ(CuKα)filt. = 1.5418 Å; and 15-crown-5·2NaOPh (**3**): $Na_2O_7C_{22}H_{30}$, M_r = 452.46, λ(CuKα)mono. = 1.5418 Å) have been determined by X-ray diffraction at room temperature (T = 298 K). Complex **1** crystallizes in space group $P2_1/n$ with a = 15.032(5), b = 13.332(2), c = 13.533(3) Å, β = 106.28(2)°, V = 2603.2 Å^3, and Z = 4. Complex **2** crystallizes in space group $P2_1/n$ with a = 15.94(1), b = 12.194(7), c = 14.068(7) Å, β = 102.84(5)°, V = 2666.3 Å^3, and Z = 4. Complex **3** crystallizes in space group $P2_1/c$ with a = 12.451(3), b = 17.263(3), c = 12.659(6) Å, β = 115.74(3)°, V = 2450.8 Å^3, and Z = 4. The three structures were solved by direct methods and refined by full-matrix least-squares calculations to residuals, R, of 0.080, 0.069, and 0.081 for complexes **1**, **2**, and **3**, respectively. In each structure the macrocycle forms a 1:2 host–guest complex with the alkali metal. Each structure exhibits a dimer of the general form $(MAC{\cdot}2MOPh)_2$ where M = Li^+ and Na^+ for structures **1** and **2**, respectively, and MAC = cyclohexano-15-crown-5, while M = Na^+ and MAC = 15-crown-5 for structure **3**. In each case the two metals of the monomeric unit have different crystallographic and chemical environments. In structures **1** and **3** one alkali metal is coordinated to all five oxygens of the macrocycle and to one of the phenoxide oxygens, while the other alkali metal is coordinated to only one oxygen of the macrocycle and to three phenoxide oxygens. In structure **2**, one alkali metal is coordinated to only four of the five oxygens of the macrocycle and to two of the phenoxide oxygens, while the other alkali metal is coordinated to only one oxygen of the macrocycle and to three phenoxide oxygens (as in **1** and **3**).

Key words: crown ether, host–guest complexes, X-ray crystallography.

KIMBERLY A. WATSON, SUZANNE FORTIER, MICHAEL P. MURCHIE et JOHN W. BOVENKAMP. Can. J. Chem. **69**, 687 (1991).

Faisant appel à la diffraction des rayons-X à la température ambiante (T = 298 K), on a déterminé les structures cristallines de trois complexes d'éther-couronnes (cyclohexano-15-couronne-5·2LiOPh (**1**) : $Li_2O_7C_{26}H_{36}$, M_r = 474,45, λ(CuKα)filt. = 1,5418 Å; cyclohexano-15-couronne-5·2NaOPh (**2**) : $Na_2O_7C_{26}H_{36}$, M_r = 504,54, λ(CuKα)filt. = 1.5418 Å: 15-couronne-5·2NaOPh (**3**) : $Na_2O_7C_{22}H_{30}$, M_r = 452,46, λ(CuKα)mono. = 1,5418 Å). Le complexe **1** cristallise dans le groupe d'espace $P2_1/n$ avec a = 15,032(5), b = 13,332(2) et c = 13,533(3) Å, β = 106,28(2)°, V = 2603,2 Å^3 et Z = 4. Le complexe **2** cristallise dans le groupe d'espace $P2_1/n$ avec a = 15,94(1), b = 12,194(7) et c = 14,068(7) Å, β = 102,84(5)°, V = 2666,3 Å^3 et Z = 4. Le complexe **3** cristallise dans le groupe d'espace $P2_1/c$ avec a = 12,451(3), b = 17,263(3) et c = 12,659(6) Å, β = 115,74(3)°, V = 2450,8 Å^3 et Z = 4. On a résolu les trois structures par des méthodes directes et on les a affinées par la méthode des moindres carrés (matrice entière) jusqu'à des valeurs résiduelles de R de 0,080, 0,069 et 0,081 respectivement pour les complexes **1**, **2** et **3**. Dans chacune des structures, le macrocycle forme un complexe 1 : 2 hôte–invité avec le métal alcalin. Chaque structure comporte un dimère de la forme générale $(MAC{\cdot}2MOPh)_2$; pour les structures **1** et **2**, MAC = cyclohexano-15-couronne-5 et M = Li^+ et Na^+ respectivement alors que M = Na^+ et MAC = 15-couronne-5 pour la structure **3**. Dans chaque cas, les deux métaux de l'unité monomère sont dans des environnements cristallographiques et chimiques différents. Dans les structures **1** et **3**, un métal alcalin est coordiné aux cinq oxygènes du macrocycle et à un oxygène phénolique alors que l'autre métal alcalin est coordiné à un seul oxygène macrocyclique et à trois oxygènes phénoliques. Dans la structure **2**, un métal alcalin est coordiné à seulement quatre des cinq oxygènes du macrocycle et à deux oxygènes phénoliques alors que l'autre métal alcalin est coordiné à seulement un oxygène du macrocycle et à trois oxygènes phénoliques.

Mots clés : éther-couronne, complexes hôte–invité, diffraction des rayons-X.

[Traduit par la rédaction]

Introduction

The present paper reports the X-ray crystal structures of 1:2 host–guest complexes of cyclohexano-15-crown-5 with lithium and sodium phenoxides and of 15-crown-5 with sodium phenoxide. Over the last few years, we have studied several crown ether complexes that exhibit unusual host–guest ratios (1–3) and have shown that the resulting structural characteristics and stoichiometry were a result of concerted host, guest, anion, and solvent effects. The X-ray crystal structure analyses of many of these complexes have been reported (4–6). This paper is part of an investigation of the structural characteristics of these complexes.

There have been many alkali metal salt complexes of 15-crown-5 (7–10), cyclohexano-15-crown-5 (11), and benzo-15-crown-5 (12–14) synthesized and isolated. The X-ray crystal structures of several complexes of 15-crown-5 and of benzo-15-crown-5 have been determined; for example, 15-crown-5·X, where X = $NaSCN{\cdot}(1/2)H_2O$ (7), Na(ethyl acetoacetate) (8), and 2LiOPh (two polymorphs) (3), and benzo-15-crown-5·Y, where Y = $Li(pic){\cdot}2H_2O$ (15), Na(pic) (16), (1/2) (K(pic))

TABLE 1. Crystal data for complexes **1**, **2**, and **3**

Parameter	Complex 1	Complex 2	Complex 3
$F(000)$	1016	1072	960
Number of reflections used for the determination of unit cell parameters; 2θ range, deg	25; 24–42	25; 14–26	25; 14–30
Density (calcd.), g cm^{-3}	1.212	1.255	1.225
Number of measured reflections	2801	2857	2797
Number of observed reflections, $I \geq 3\sigma(I)$	1681	1420	1437
2θ range scanned, deg	0.5–50	0.5–50	0.5–50
Radiation used	Cu(Kα)filt.	Cu(Kα)filt.	Cu(Kα)mono.
μ, cm^{-1}	6.573	9.853	10.174
Crystal dimensions, mm	0.50 × 0.50 × 0.13	0.50 × 0.35 × 0.23	0.50 × 0.20 × 0.18
Isotropic secondary extinction coefficient, g	9.5197×10^{-7}	—	3.5936×10^{-7}
Final R; R_w	0.080; 0.103	0.064; 0.076	0.057; 0.070
Largest shift/error in final least-squares cycle, Δ/σ	0.00	0.00	0.01
Maximum and minimum residual electron density in final difference Fourier map, e Å^{-3}	0.426; −0.405	0.355; −0.382	0.550; −0.316
Standard deviation of an observation of unit weight	2.785	2.367	2.515

(17), and Cs(pic) (18) (where pic = 2,4,6,-trinitrophenolate). The stoichiometries of these systems have also been extensively discussed (19).

A search of the Cambridge Structural Database (20) for crystal structure analyses of 15-crown-5 with one cyclohexano substituent containing alkali metal salts revealed no such structures. Thus, this paper reports two of the first X-ray crystal structures of 1:2 host–guest complexes of cyclohexano-15-crown-5 with lithium and sodium phenoxides, complexes **1** and **2**, respectively. Also, the X-ray crystal structure results of a 1:2 complex of 15-crown-5 with sodium phenoxide, complex **3**, are reported and discussed.

Experimental

A standard method was used for the preparation of the three complexes in ethereal solvents. Using this method, 1 equivalent of the macrocycle was added to a solution containing 2 equivalents of the salt. Details of the syntheses of complexes **1**, **2**, and **3** have been reported in a previous publication (3).

The crystals used for the X-ray structure determinations were obtained from the following solutions: complex **1**, 0.084 g in 1,2-dimethoxyethane (5 mL); complex **2**, 0.098 g in tetrahydrofuran and hexane (11 mL/11 mL); and complex **3**, 0.085 g in tetrahydrofuran (5 mL). In all cases, the solutions were slowly (1–7 days) evaporated to dryness at room temperature in an argon atmosphere.

Data collection

Pertinent data about the crystals used and the measurement of diffraction intensities are summarized in Table 1. The crystals used in the diffraction experiments were mounted inside glass capillaries in a moisture-free environment. The intensity data were collected on an Enraf–Nonius CAD-4 diffractometer. In each case, intensities were collected by the $\omega/2\theta$ scanning procedure and three reflections were measured after every 7200 s of exposure time to check on the stability of the crystal. Evidence of crystal decay was detected only for complex **3**, with a total loss in intensity of 20.9%. A linear decay correction was applied to the data of complex **3** using the Enraf–Nonius SDP program DECAY (21); the maximum, minimum, and average corrections were 1.12414, 1.00009, and 1.06049, respectively. Data for all three complexes were corrected for Lorentz and polarization effects.

Structure and determination and refinement

All three structures were solved routinely by direct methods using

TABLE 2. Final fractional coordinates and equivalent isotropic temperature factors for **1** ($Li_2O_7C_{26}H_{36}$) with estimated standard deviations in parentheses

Atom	x	y	z	B_{eq}(Å^2)[a]
O1	0.0567(3)	−0.2102(4)	0.5753(4)	4.6
O4	−0.0105(4)	−0.3574(4)	0.4368(4)	6.5
O7	−0.1914(4)	−0.3773(5)	0.4080(4)	8.5
O10	−0.1992(3)	−0.3783(3)	0.6040(3)	3.8
O13	−0.0272(3)	−0.3265(4)	0.6884(4)	5.3
O20	−0.1430(3)	−0.1592(3)	0.5190(4)	3.9
O27	0.0172(3)	0.0268(3)	0.6011(3)	3.9
C2	0.1146(5)	−0.2502(7)	0.5197(7)	6.8
C3	0.0609(7)	−0.2982(8)	0.4238(7)	8.1
C5	−0.0614(6)	−0.4075(7)	0.3506(6)	6.6
C6	−0.1464(7)	−0.4439(8)	0.3672(8)	10.0
C8	−0.2751(6)	−0.4063(6)	0.4278(6)	5.2
C9	−0.2584(5)	−0.4468(6)	0.5335(6)	4.8
C11	−0.1563(5)	−0.4188(6)	0.7029(5)	4.1
C12	−0.0811(6)	−0.3473(6)	0.7577(6)	5.3
C14	0.0644(7)	−0.2912(9)	0.7300(7)	11.1
C15	0.0926(7)	−0.2198(9)	0.6797(7)	9.2
C16	−0.2246(6)	−0.4376(6)	0.7657(6)	5.7
C17	−0.2666(6)	−0.3401(7)	0.7918(6)	6.7
C18	−0.1925(7)	−0.2693(8)	0.8476(6)	7.9
C19	−0.1272(7)	−0.2458(7)	0.7824(7)	6.8
C21	−0.2226(5)	−0.1120(5)	0.4961(5)	3.6
C22	−0.2994(5)	−0.1521(6)	0.5236(6)	4.3
C23	−0.3838(5)	−0.1016(6)	0.5006(6)	5.0
C24	−0.3927(5)	−0.0101(7)	0.4494(6)	5.6
C25	−0.3196(5)	0.0303(6)	0.4245(6)	5.2
C26	−0.2355(5)	−0.0189(6)	0.4461(6)	4.2
C28	0.0341(5)	0.0563(5)	0.6970(5)	3.2
C29	−0.0187(5)	0.0211(6)	0.7610(6)	4.5
C30	−0.0026(5)	0.0531(7)	0.8605(5)	6.0
C31	0.0655(7)	0.1192(7)	0.9018(6)	7.1
C32	0.1218(6)	0.1562(6)	0.8428(7)	6.2
C33	0.1073(5)	0.1230(6)	0.7428(6)	4.6
Li1	−0.0356(8)	−0.082(1)	0.5201(9)	4.1
Li2	−0.1051(9)	−0.293(1)	0.539(1)	4.6

[a] $B_{eq} = (4/3)\Sigma_i\Sigma_j\beta_{ij}(a_i \cdot a_j)$.

Can. J. Chem. Downloaded from www.nrcresearchpress.com by 198.100.157.202 on 09/07/12
For personal use only.

Can. J. Chem. Downloaded from www.nrcresearchpress.com by 198.100.157.202 on 09/07/12
For personal use only.

TABLE 3. Final fractional coordinates and equivalent isotropic temperature factors for **2** ($Na_2O_7C_{26}H_{36}$) with estimated standard deviations in parentheses

Atom	x	y	z	B_{eq}(Å^2)[a]
O1	0.6765(3)	−0.1038(5)	0.5032(4)	5.2
O4	0.7397(4)	0.0518(5)	0.3810(4)	5.6
O7	0.7555(3)	0.2770(5)	0.4223(4)	5.4
O10	0.7473(3)	0.2715(4)	0.6155(4)	4.7
O13	0.7777(3)	0.0422(4)	0.6360(4)	4.8
O20	0.5453(4)	0.1979(5)	0.3781(4)	5.8
O27	0.4371(3)	−0.0773(5)	0.4142(4)	4.9
C2	0.6906(4)	−0.1295(9)	0.4074(6)	6.8
C3	0.7534(7)	−0.0603(9)	0.3756(8)	8.9
C5	0.8046(7)	0.1185(8)	0.3631(7)	8.0
C6	0.7923(7)	0.2250(9)	0.3495(7)	8.5
C8	0.8127(5)	0.3479(7)	0.4859(6)	5.2
C9	0.7667(6)	0.3691(7)	0.5704(6)	5.2
C11	0.8187(5)	0.2233(7)	0.6794(6)	5.0
C12	0.7935(6)	0.1173(7)	0.7149(6)	5.4
C14	0.7546(6)	−0.0627(7)	0.6631(6)	5.5
C15	0.7465(6)	−0.1385(8)	0.5799(7)	6.9
C16	0.6841(6)	0.4344(7)	0.5371(6)	5.6
C17	0.6992(7)	0.5416(8)	0.4908(7)	7.6
C18	0.7468(7)	0.5238(7)	0.4071(7)	7.7
C19	0.8266(7)	0.4555(8)	0.4386(7)	7.6
C21	0.5445(5)	0.2399(7)	0.2939(6)	4.6
C22	0.5519(6)	0.1768(8)	0.2145(6)	6.0
C23	0.5496(6)	0.2204(9)	0.1238(6)	7.0
C24	0.5351(6)	0.3316(9)	0.1080(6)	7.1
C25	0.5262(7)	0.3951(8)	0.1847(7)	7.0
C26	0.5294(6)	0.3514(7)	0.2756(6)	5.2
C28	0.4493(5)	−0.1400(7)	0.3418(5)	4.3
C29	0.4477(5)	−0.0974(8)	0.2484(6)	5.8
C30	0.4605(6)	−0.170(1)	0.1739(6)	7.8
C31	0.4801(6)	−0.2752(9)	0.1915(7)	7.0
C32	0.4849(7)	−0.3155(8)	0.2812(7)	7.1
C33	0.4698(5)	−0.2520(7)	0.3557(6)	4.9
Na1	0.5421(2)	−0.1033(3)	0.5531(2)	4.90
Na2	0.6638(2)	0.1393(3)	0.4962(2)	4.70

[a]$B_{eq} = (4/3)\Sigma_i\Sigma_j\beta_{ij}(a_i \cdot a_j)$.

TABLE 4. Final fractional coordinates and equivalent isotropic temperature factors for **3** ($Na_2O_7C_{22}H_{30}$) with estimated standard deviations in parentheses

Atom	x	y	z	B_{eq}(Å^2)[a]
O1	0.5844(5)	0.1303(4)	0.3459(5)	6.6
O4	0.8209(5)	0.1382(4)	0.3857(5)	5.8
O7	0.8597(5)	0.0735(4)	0.2087(5)	7.1
O10	0.6426(6)	0.1225(4)	0.0423(5)	8.2
O13	0.4656(6)	0.0922(4)	0.1077(6)	8.4
O16	0.6811(5)	−0.0430(3)	0.3314(4)	5.7
O23	0.3880(5)	−0.0200(4)	0.3835(5)	7.7
C2	0.6608(8)	0.1855(7)	0.4239(8)	8.1
C3	0.7878(8)	0.1440(6)	0.4804(7)	6.8
C5	0.9235(8)	0.0936(6)	0.4131(8)	7.0
C6	0.9569(9)	0.0996(7)	0.3142(9)	8.0
C8	0.851(1)	0.1077(7)	0.1041(9)	8.9
C9	0.728(1)	0.0892(7)	0.0072(8)	9.5
C11	0.525(1)	0.1145(7)	−0.0389(9)	9.9
C12	0.4451(9)	0.1462(7)	0.0191(9)	9.1
C14	0.403(1)	0.1097(8)	0.176(1)	10.0
C15	0.4707(8)	0.1627(7)	0.2752(9)	8.7
C17	0.7407(7)	−0.1082(5)	0.3489(7)	4.9(2)*
C18	0.8001(7)	−0.1262(5)	0.2800(7)	5.6(2)*
C19	0.8638(8)	−0.1966(6)	0.3016(8)	6.7(3)*
C20	0.8664(8)	−0.2471(7)	0.3856(8)	7.6(3)*
C21	0.8111(8)	−0.2282(6)	0.4527(8)	7.2(3)*
C22	0.7469(7)	−0.1612(6)	0.4355(7)	5.9(2)*
C24	0.2953(7)	−0.0578(6)	0.3116(7)	5.7(2)*
C25	0.3088(9)	−0.1352(7)	0.2977(9)	8.8(3)*
C26	0.215(1)	−0.1795(8)	0.231(1)	10.6(4)*
C27	0.1151(9)	−0.1521(7)	0.1712(9)	8.5(3)*
C28	0.084(1)	−0.0759(8)	0.172(1)	10.7(4)*
C29	0.1864(9)	−0.0226(7)	0.2491(9)	7.7(3)*
Na1	0.5783(3)	−0.0042(2)	0.4294(3)	6.2(1)
Na2	0.6749(3)	0.0639(2)	0.2286(3)	5.14(9)

*Atoms were refined isotropically.
[a]$B_{eq} = (4/3)\Sigma_i\Sigma_j\beta_{ij}(a_i \cdot a_j)$.

the program MULTAN80 (22). Difference Fourier syntheses were used to locate the positions of the hydrogen atoms.

Complex **1**: The positions of 30 hydrogen atoms were located in the difference Fourier map and the remaining 6 were calculated. The structure was refined by full-matrix least squares using all reflections with $I \geq 3\sigma(I)$. Anisotropic temperature factors were used for the non-hydrogen atoms. The hydrogen atoms were assigned isotropic temperature factors equal in magnitude to the equivalent isotropic temperature factors of their parent atoms. They were included in the calculations but they were not refined. The function minimized was $\Sigma w||F_o| - |F_c||^2$, where $w = 1/\sigma^2(|F_o|)$. A correction for isotropic secondary extinction effect was included in the refinement. The scattering factors were taken from Cromer and Waber (23). The fractional coordinates and equivalent isotropic temperature factors of the non-hydrogen atoms are presented in Table 2.

Complex **2**: The positions of 25 hydrogen atoms were located in the difference Fourier map and the remaining 11 were calculated. The refinement procedure was the same as that given previously for complex **1** with the following exception: the isotropic secondary extinction coefficient was not included in the calculations. The fractional coordinates and equivalent isotropic temperature factors of the non-hydrogen atoms are presented in Table 3.

Complex **3**: The positions of 25 hydrogen atoms were located in the difference Fourier map and the remaining 5 were calculated. The refinement procedure was the same as that given previously for complexes **1** and **2** with the following exception: anisotropic temperature factors were used for the non-hydrogen atoms except for the carbon atoms of the phenoxide moieties. The 12 carbon atoms of the phenoxide moieties were refined isotropically. The fractional coordinates and equivalent isotropic temperature factors of the non-hydrogen atoms are presented in Table 4.

All calculations were done on a PDP11/23 computer using the Enraf–Nonius SDP program package (21).[1]

Results

ORTEP (24) drawings of complex **1**, **2**, and **3**, showing the atom numbering scheme, are given in Figs. 1, 2, and 3, respectively. Alkali metal–oxygen bond distances and angles, for all three complexes, appear in Table 5; average and range of bond distances and angles of the macrocyclic rings, cyclohexano rings, and phenoxide rings, for all three complexes, are given in

[1]A complete set of tables of positional parameters, temperature factors, and observed and calculated structure factors may be purchased from the Depository of Unpublished Data, Document Delivery, CISTI, National Research Council Canada, Ottawa, Canada K1A 0S2.

Tables of positional parameters for each complex have also been deposited with the Cambridge Crystallographic Data Centre, and can be obtained on request from The Director, Cambridge Crystallographic Data Centre, University Chemical Laboratory, Lensfield Road, Cambridge, CB2 1EW, U.K.

Can. J. Chem. Downloaded from www.nrcresearchpress.com by 198.100.157.202 on 09/07/12
For personal use only.

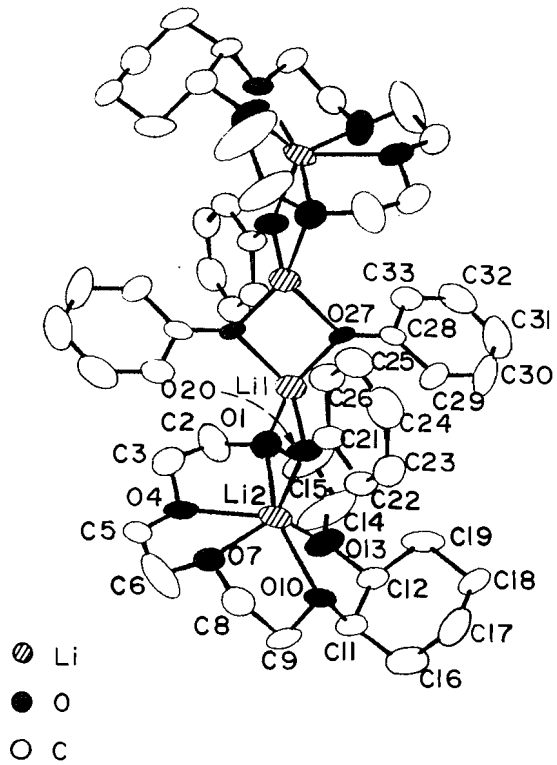


FIG. 1. ORTEP diagrams and atom numbering scheme for cyclohexano-15-crown-5·2LiOPh (**1**).

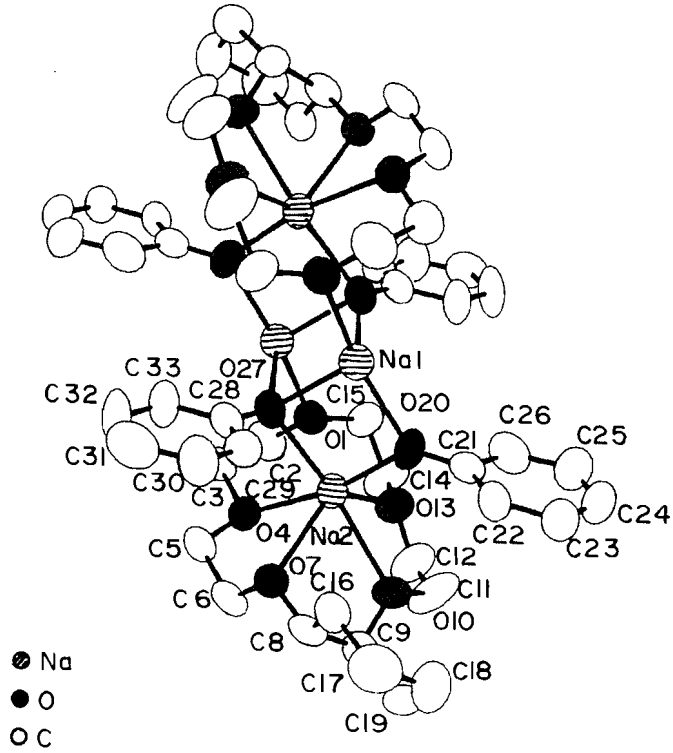


FIG. 2. ORTEP diagram and atom numbering scheme for cyclohexano-15-crown-5·2NaOPh (**2**).

Table 6; and macrocyclic ring torsion angles, for all three complexes, are presented in Table 7.

Host–guest interactions

Cyclohexano-15-crown-5·2LiOPh (1)

The structure may be described as an aggregate of four lithium phenoxide units complexed to two crown ethers. There is a center of symmetry in the dimer structure, easily located halfway between O27 and O27′. There are two different chemical environments for the lithium atoms of the monomeric unit. The coordination geometry of the two cations in complex **1** is very similar to that observed in the two polymorphs of 15-crown-5·2LiOPh (3). Li1 is coordinated to three phenoxide oxygens at an average distance of 1.89(3) Å and to only one crown ether oxygen at a distance of 2.194(9) Å. As can be seen in Fig. 1 and in the values of Table 5, the geometry around Li1 is that of a distorted tetrahedron. Li2 is coordinated to all five crown ether oxygens at an average distance of 2.3(2) Å and to only one phenoxide oxygen at a distance of 1.865(9) Å. The distances between the lithium ions and the phenoxide oxygens are all significantly shorter than those between the lithium ions and the crown oxygens, thus indicating stronger interactions between the lithium ions and the phenoxide oxygens of the aggregate. Li2 lies 0.63 Å out of the mean plane defined by the five crown ether oxygens. The average Li2–crown ether oxygen distance (2.3(2) Å) is longer than other lithium–crown ether oxygen distances found in the literature; however, we have found lithium–crown ether oxygen distances of similar length in other structures, for example 15-crown-5·2LiOPh (3), where the average lithium–crown ether oxygen distance was 2.3(1) Å. These observations provide further evidence of the strength of the lithium–phenoxide oxygen interactions. As a result, the $Li2^+$ ion is pulled out of the crown cavity with subsequent

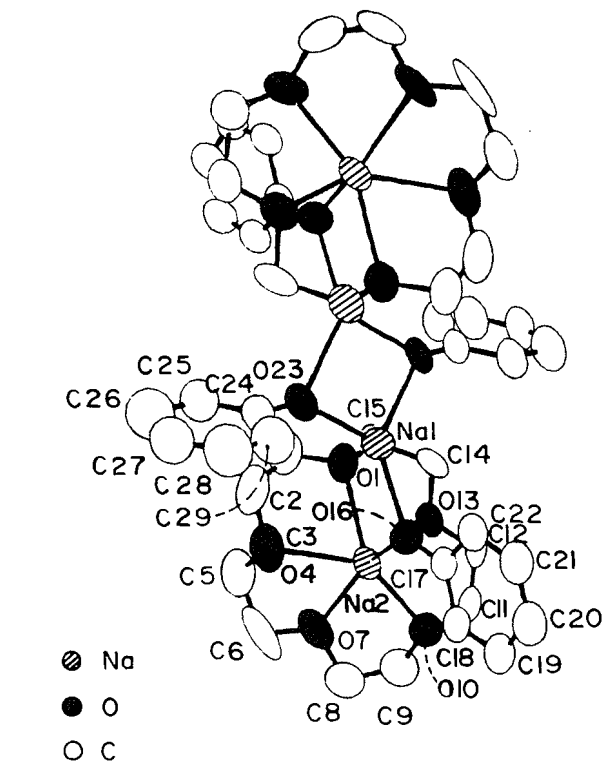


FIG. 3. ORTEP diagram and atom numbering scheme for 15-crown-5·2NaOPh (**3**).

TABLE 5. Oxygen – alkali metal bond lengths and angles for complexes **1**, **2**, and **3** with estimated standard deviations in parentheses[a]

Bonds	Length (Å)	Bonds	Angle (deg)
Complex **1** ($Li_2O_7C_{26}H_{36}$)			
Li1—O1	2.194(9)	O1—Li1—O20	92.1(4)
Li1—O20	1.910(8)	O1—Li1—O27	106.4(4)
Li1—O27	1.859(8)	O1—Li1—O27′	111.5(4)
Li1—O27′	1.888(8)	O20—Li1—O27	130.2(5)
Li2—O1	2.586(9)	O20—Li1—O27′	122.2(4)
Li2—O4	2.403(10)	O27—Li1—O27′	93.7(4)
Li2—O7	2.192(9)	O1—Li2—O4	65.6(3)
Li2—O10	2.186(9)	O1—Li2—O7	133.2(4)
Li2—O13	2.083(9)	O1—Li2—O10	145.6(4)
Li2—O20	1.865(9)	O1—Li2—O13	70.4(3)
		O1—Li2—O20	81.7(3)
		O4—Li2—O7	70.3(3)
		O4—Li2—O10	126.8(4)
		O4—Li2—O13	102.7(4)
		O4—Li2—O20	117.8(4)
		O7—Li2—O10	75.7(3)
		O7—Li2—O13	135.9(4)
		O7—Li2—O20	106.6(4)
		O10—Li2—O13	75.3(3)
		O10—Li2—O20	110.5(4)
		O13—Li2—O20	114.3(4)
Complex **2** ($Na_2O_7C_{26}H_{36}$)			
Na1—O1	2.399(5)	O1—Na1—O20	145.6(2)
Na1—O20	2.191(5)	O1—Na1—O27	106.3(2)
Na1—O27	2.295(4)	O1—Na1—O27′	87.8(2)
Na1—O27′	2.259(5)	O20—Na1—O27	91.9(2)
		O20—Na1—O27′	120.1(2)
Na2—O4	2.470(5)	O27—Na1—O27′	94.8(2)
Na2—O7	2.592(5)		
Na2—O10	2.490(5)		
Na2—O13	2.642(4)		
Na2—O20	2.333(5)		
Na2—O27	2.377(5)		
		O4—Na2—O7	67.3(2)
		O4—Na2—O10	117.1(2)
		O4—Na2—O13	86.5(2)
		O4—Na2—O20	95.9(2)
		O4—Na2—O27	134.3(2)
		O7—Na2—O10	65.5(2)
		O7—Na2—O13	103.5(2)
		O7—Na2—O20	87.5(2)
		O7—Na2—O27	158.1(2)
		O10—Na2—O13	67.2(1)
		O10—Na2—O20	120.6(2)
		O10—Na2—O27	99.9(2)
		O13—Na2—O20	168.8(2)
		O13—Na2—O27	84.1(2)
		O20—Na2—O27	86.5(2)
Complex **3** ($Na_2O_7C_{22}H_{30}$)			
Na1—O1	2.566(4)	O1—Na1—O16	84.9(1)
Na1—O16	2.240(3)	O1—Na1—O23	103.1(2)
Na1—O23	2.192(4)	O1—Na1—O23′	104.0(2)
Na1—O23′	2.250(4)	O16—Na1—O23	128.7(1)
Na2—O1	2.490(4)	O16—Na1—O23′	138.6(2)
Na2—O4	2.394(3)	O23—Na1—O23′	89.1(2)
Na2—O7	2.422(4)	O1—Na2—O4	69.1(1)
Na2—O10	2.430(4)	O1—Na2—O7	136.3(1)
Na2—O13	2.430(4)	O1—Na2—O10	117.4(2)
Na2—O16	2.232(3)	O1—Na2—O13	69.3(1)
		O1—Na2—O16	86.9(1)
		O4—Na2—O7	68.4(1)
		O4—Na2—O10	108.9(1)
		O4—Na2—O13	129.6(2)
		O4—Na2—O16	98.1(1)
		O7—Na2—O10	68.5(2)
		O7—Na2—O13	136.5(2)
		O7—Na2—O16	108.7(1)
		O10—Na2—O13	68.1(2)
		O10—Na2—O16	148.5(1)
		O13—Na2—O16	106.8(1)

TABLE 5. (*concluded*)

[a]The primed atoms are related to the unprimed atoms by the following symmetry operation: for **1**, $-x, -y, 1/2 - z$; for **2**, $-x, -y, -z$; for **3**, $1/2 - x, -y, 1/2 - z$.

lengthening of the Li2–crown ether oxygen distances. The lithium–phenoxide oxygen distances are consistent with previously reported literature values (ref. 3, and references therein).

The cyclohexano-15-crown-5·2LiOPh structure includes a $(Li^+O^-)_2$ four-membered ring similar to that reported for the two polymorphs of 15-crown-5·2LiOPh (3). In this case, the Li1—Li1′ distance is 2.56(2) Å compared to 2.55(1) and 2.58(1) Å found for the polymorphs **1***a* and **1***b* of 15-crown-5·2LiOPh. As shown in a previous publication (3), these distances are shorter than the Li—Li distance of 2.67 Å in Li2; however, other complexes with short lithium–lithium distances have been reported (13).

Cyclohexano-15-crown-5·2NaOPh (2)

As in structure **1**, structure **2** may be described as an aggregate of four sodium phenoxide units complexed to two crown ethers. Similarly, there is a center of symmetry in the dimer structure located halfway between O27 and O27′. The two sodium atoms of the monomeric unit have different chemical and crystallographic environments. Na1 is coordinated to three phenoxide oxygens at an average distance of 2.30(5) Å and to only one crown ether oxygen, O1, at a distance of 2.399(5) Å. Na2 appears to be coordinated to only four of the five crown ether oxygens, O4, O7, O10, and O13, with an average distance of 2.55(8) Å. The fifth crown ether oxygen, O1, is at a distance of 2.971(5) Å from Na2. In addition, Na2 is coordinated to two phenoxide oxygens at an average distance of 2.36(3) Å. Na2 lies 1.225(4) Å out of the mean plane defined by the five crown ether oxygens. As in complex **1**, the distances between the cations (in this case, sodium ions) and the phenoxide oxygens are consistently shorter than those between the cations and the crown ether oxygens. The average Na2–crown ether oxygen distance (2.55(8) Å) is consistent with other sodium–crown ether oxygen distances found in the literature. For example, the average sodium–crown ether oxygen distance is 2.54 Å for dibenzo-24-crown-8-bis(sodium *o*-nitrophenolate) (25), 2.40 and 2.77 Å for the 1:1 and 2:1 complexes of benzo-15-crown-5·Na[ClO_4], respectively (26), 2.83 Å for (benzo-15-crown-5)$_2$·Na[BPh_4] (26), 2.48 Å for dibenzo-30-crown-10·2Na[NCS] (27), 2.61 Å for the 1:1:1 complex of dicyclohexano-18-crown-6 (isomer A) with sodium phenoxide and phenol (4), 2.55 Å for dicyclohexano-18-crown-6·2NaOPH (5), 2.39(3) Å for benzo-15-crown-

Can. J. Chem. Downloaded from www.nrcresearchpress.com by 198.100.157.202 on 09/07/12
For personal use only.

TABLE 6. Average and range in the bond lengths (Å) and angles (deg) for the macrocyclic ring, cyclohexyl ring, and phenoxide rings of complexes **1**, **2**, and **3** with estimated standard deviations in parentheses

Complex **1** ($Li_2O_7C_{26}H_{36}$)			
Macrocyclic ring			
Average C—C	1.44(8)	Average C—O	1.40(3)
Range of C—C	1.308–1.505(7)	Range of C—O	1.327–1.435(6)
Average C—O—C	116.(2)	Average C—C—O	112.(3)
Range of C—O—C	113.1–118.8(5)	Range of C—C—O	106.6–120.9(5)
Cyclohexyl ring			
Average C—C	1.54(4)	Average C—C—C	111.(1)
Range of C—C	1.494–1.599(8)	Range of C—C—C	109.3–112.0(5)
Phenoxides			
O20—C21	1.309(5)	O27—C28	1.310(5)
O20—C21—C22	121.1(4)	O27—C28—C29	121.4(4)
O20—C21—C26	122.3(4)	O27—C28—C33	122.3(5)
Average C—C	1.39(2)	Average C—C—C	120.(2)
Range of C—C	1.347–1.415(7)	Range of C—C—C	116.2–121.7(5)
Complex **2** ($Na_2O_7C_{26}H_{36}$)			
Macrocyclic ring			
Average C—C	1.45(8)	Average C—O	1.42(2)
Range of C—C	1.321–1.551(9)	Range of C—O	1.383–1.450(7)
Average C—O—C	114.(1)	Average C—C—O	112.(5)
Range of C—O—C	112.4–115.9(5)	Range of C—C—O	103.8–120.8(6)
Cyclohexyl ring			
Average C—C	1.52(2)	Average C—C—C	112.(2)
Range of C—C	1.502–1.551(9)	Range of C—C—C	109.5–114.5(6)
Phenoxides			
O20—C21	1.289(7)	O27—C28	1.322(6)
O20—C21—C22	122.4(7)	O27—C28—C29	122.0(7)
O20—C21—C26	121.6(7)	O27—C28—C33	121.6(6)
Average C—C	1.38(3)	Average C—C—C	120.(2)
Range of C—C	1.335–1.417(9)	Range of C—C—C	115.8–123.1(7)
Complex **3** ($Na_2O_7C_{22}H_{30}$)			
Macrocyclic ring			
Average C—C	1.52(4)	Average C—O	1.42(2)
Range of C—C	1.484–1.586(8)	Range of C—O	1.397–1.442(6)
Average C—O—C	114.(2)	Average C—C—O	107.(3)
Range of C—O—C	111.0–115.3(5)	Range of C—C—O	102.9–112.2(5)
Phenoxides			
O16—C17	1.310(5)	O23—C24	1.287(6)
O16—C17—C18	121.0(5)	O23—C24—C25	122.9(7)
O16—C17—C22	121.9(5)	O23—C24—C29	120.4(6)
Average C—C	1.38(4)	Range of C—C—C	120.(2)
Range of C—C	1.25–1.42(7)	Range of C—C—C	117–124(2)

5·NaI·(H_2O) (28), 2.49(7) Å for the ethyl acetoacetate sodium enolate 15-crown-5 complex (8), and a range of 2.400(3)–2.501(3) Å was reported for the sodium–crown ether oxygen distances in benzo-15-crown-5·Na(picrate) (16).

The cyclohexano-15-crown-5·2NaOPh structure contains two different $(Na^+O^-)_2$ four-membered rings consisting of Na1—O27—Na1′—O27′ and Na1—O20—Na2—O27. The Na1—Na1′ distance is 3.081(5) Å and the Na1—Na2 distance is 3.721(3) Å. These distances are consistent with those found in the literature for other sodium–crown ether complexes. For

Can. J. Chem. Downloaded from www.nrcresearchpress.com by 198.100.157.202 on 09/07/12
For personal use only.

TABLE 7. Macrocyclic ring torsion angles for complexes **1**, **2**, and **3** with estimated standard deviations in parentheses

Bonds	Angle (deg)		
	Complex **1** ($Li_2O_7C_{26}H_{36}$)	Complex **2** ($Na_2O_7C_{26}H_{36}$)	Complex **3** ($Na_2O_7C_{22}H_{30}$)
O1—C2—C3—O4	−44.(1)	−52.(1)	68.4(9)
C2—C3—O4—C5	−177.8(7)	172.0(8)	−171.8(7)
C3—O4—C5—C6	−165.0(8)	168.1(9)	−173.3(8)
O4—C5—C6—O7	46.(1)	49.(1)	−58.(1)
C5—C6—O7—C8	−179.6(8)	110.1(9)	150.5(9)
C6—O7—C8—C9	91.0(9)	−166.3(7)	−165.9(9)
O7—C8—C9—O10	48.7(8)	56.3(8)	61.(1)
C8—C9—O10—C11	−163.2(6)	76.6(8)	177.0(9)
C9—O10—C11—C12	167.1(6)	−174.5(7)	174.3(9)
O10—C11—C12—O13	−49.8(7)	69.4(8)	−67.(1)
C11—C12—O13—C14	−158.2(7)	178.9(7)	178.9(9)
C12—O13—C14—C15	−139.3(9)	−175.2(7)	−87.(1)
O13—C14—C15—O1	−28.(1)	−64.9(9)	−56.(1)
C14—C15—O1—C2	−100.(1)	148.5(7)	166.7(9)
C15—O1—C2—C3	143.3(8)	−74.(1)	−171.2(8)

example, distances of 3.383 Å in dibenzo-24-crown-8-bis(sodium *o*-nitrophenolate) (25), 3.940 Å in dibenzo-30-crown-10·2Na[NCS] (27), and, 3.147 and 3.392 Å, respectively, for the Na1—Na1′ and Na1—Na2 in dicyclohexano-18-crown-6 (isomer A)·2NaOPh (5), have been reported.

15-Crown-5-·2NaOPh (3)

The structure is similar to that described previously for structure **2**, in that it consists of an aggregate of four sodium phenoxide units complexed to two crown ethers. Again, there is a center of symmetry, located halfway between O27 and O27′, and the two sodium atoms of the monomeric unit have different chemical environments. Na1 is coordinated to three phenoxide oxygens at an average distance of 2.23(4) Å and to only one crown ether oxygen at a distance of 2.566(4) Å. Na2 is coordinated to all five crown ether oxygens with an average distance of 2.43(4) Å and to only one phenoxide oxygen at a distance of 2.232(3) Å. Na2 lies 0.829(4) Å out of the mean plane defined by the five crown ether oxygens. The average Na2–crown ether oxygen distance of 2.43(4) Å is consistent with those found in the literature and cited previously. Again we see that the cation–phenoxide oxygen distances are shorter than the cation–crown ether oxygen distances, resulting, as observed previously, in the sodium cation being pulled out of the crown cavity with a subsequent lengthening of the Na–crown ether oxygen distances. These observations provide further evidence that the complexing abilities of 15-crown-5 (and cyclohexano-15-crown-5) are not sufficient to break up the alkali metal–phenoxide aggregates into contact ion pairs. In structure **3**, there is a $(Na^+O^-)_2$ four-membered ring consisting of Na1—O23—Na1′—O23′ and giving a Na1—Na1′ distance of 3.172(4) Å, consistent with a value of 3.147 Å reported for the Na—Na1′ distance in dicyclohexano-18-crown-6 (isomer A)·2NaOPh (5).

Host geometry and conformation

Cyclohexano-15-crown-5·2LiOPh (1)

A search of the Cambridge Structural Database (20) for crown ether complexes containing "cyclohexano-15-crown-5" revealed that none have been reported so far. The X-ray crystal structure determinations of complexes **1** and **2** appear to be the first ones containing this particular host.

The C—C bond lengths in the macrocycle show the characteristic shortening with an average value of 1.44(8) Å (see Table 6). The C—O bond lengths have an average value of 1.40(3) Å, and the C—C—O and C—O—C angles have average values of 112.(3)° and 116.(2)°, respectively.

The torsion angles about the O7—C8, C15—O1, and C15—C14 bonds deviate notably from the expected antiperiplanar and synclinal arrangements expected for C—O and C—C bonds, respectively. An unusually short bond distance of 1.308(8) Å for the C15—C14 bond is found and may coincide with the torsion angle deviation found in this region of the macrocycle. Indeed, there are several deviations from the expected torsion angles, particularly in the region of the C14—C15 bond of this complex. In addition, there appears to be an overall lessening of the torsion angles, about the C—C bonds, from the expected synclinal arrangement.

The cyclohexano ring adopts a chair conformation with an average torsion angle value of 57.(1)°. The conformation of the cyclohexano substituent in this complex is comparable to the conformation of the cyclohexano rings in the complexes with dicyclohexano-18-crown-6 as a ligand (5).

Cyclohexano-15-crown-5·2NaOPh (2)

The macrocycles in complexes **1** and **2** exhibit similar structural features. The C—C bond length, again, shows the characteristic shortening with an average value of 1.45(8) Å (see Table 6). The C—O bond lengths have an average value of 1.42(2) Å, and the C—C—O and C—O—C angles have average values of 112.(5)° and 114.(1)°. These values are consistent with those found in complex **1**.

Deviations, from an antiperiplanar arrangement, in the torsion angles about the C6—O7, C9—O10, and O1—C2 bonds are found in this complex. In addition, complex **2** exhibits an unusually short bond distance of 1.321(10) Å for the C5—C6 bond, similar to that found in complex **1**.

The cyclohexano ring adopts a chair conformation with an

Can. J. Chem. Downloaded from www.nrcresearchpress.com by 198.100.157.202 on 09/07/12
For personal use only.

Can. J. Chem. Downloaded from www.nrcresearchpress.com by 198.100.157.202 on 09/07/12
For personal use only.

average torsion angle value of 53.(3)°. This value is consistent with the literature values.

15-Crown-5·2NaOPh (3)

In complex **3** the values for the macrocyclic ring (see Table 6) are comparable to those found for the macrocyclic rings of the two polymorphs of 15-crown-5·2LiOPh (3). Small deviations can be accounted for on the basis of the differences in the size of the cations and the distortions in the macrocycle necessary for optimum coordination geometry of the respective cations. In complex **3**, the C—C bond lengths have an average value of 1.52(4) Å, a value larger than that observed for the two polymorphs of 15-crown-5·2LiOPh (3) (1.500(5) and 1.46(3) Å for **1***a* and **1***b*, respectively). This is also larger than the values given previously for complexes **1** and **2**. In the macrocycle of complex **3**, the C—O bond lengths have an average value of 1.42(2) Å, and the C—C—O and C—O—C angles have average values of 107.(3)° and 114.(2)°, respectively. The torsion angle values for complex **3** are those expected, with the exception of the torsion angle around the O13—C14 bond, which shows a slight deviation from an antiperiplanar arrangement. A similar deviation is also observed in the two polymorphic structures of 15-crown-5·2LiOPh (3).

Discussion

The present work completes the systematic study of 15-crown-5 and cyclohexano-15-crown-5 ethers with lithium and sodium phenoxide guests. In these complexes, it is observed that the competition for the cation between the hard anions and the macrocyclic ligand can give rise to unusual host–guest stoichiometries and unexpected structural characteristics.

In previous examples of 15-crown-5 complexes, 1:1 host–guest stoichiometries, with lithium and sodium cations, were usually observed. The 1:1 complexes were indeed expected to form on the basis of the ion–cavity size principle. The present work clearly shows the effect of solvent and anion on the resultant stoichiometry. The 1:2 ratios found in the present complexes are attributed to the tendency of alkali metal phenoxides to form aggregates in ethereal solvents. It is believed that the complexing abilities of these 15-crown-5 ethers are not sufficient to induce a separation of the solvated alkali metal – phenoxide aggregates to form contact ion pairs. However, effects due to the ion – cavity size relationship are still observed (see below).

A comparison of the torsion angle values of the two polymorphs of 15-crown-5·2LiOPh (3) and complex **3** shows some similarities; however, there are a few areas showing distortions from the expected synclinal and antiperiplanar geometries. Overall, the torsion angles observed for complex **3** are much closer to the expected values. This may be indicative of a better fit of the sodium cation in comparison to the distortions required for complexation of the smaller lithium cations by the 15-crown-5 host in the two polymorphic structures. A similar comparison of the torsion angle values for complexes **1** and **2** indicates that there are many deviations from the expected synclinal and antiperiplanar arrangements. In complex **1**, there appears to be an approximately 20° deviation in all the synclinal (C—C) torsion angles, with the largest deviation for the angle O13—C14—C15—O1. The largest deviation from an antiperiplanar arrangement appears on either side of these atoms, namely, between atoms C12—O13—C14—C15 and C14—C15—O1—C2. In the case of complex **2**, large deviations from an antiperiplanar arrangement are found for atoms C5—C6—O7—C8, C8—C9—O10—C11, and C15—O1—C2—C3, while only a small deviation from a synclinal arrangement is observed (for atoms O4—C5—C6—O7).

In this study, we have also observed the effect of a substituent on the resulting complexes. An examination of the average bond lengths and angles for the 15-crown-5 macrocycle, and for the cyclohexano-15-crown-5 macrocycles, indicates that there is very little difference between the two ligands; the differences in the average values are within the estimated standard deviations. However, a comparison of the ranges of both bond lengths and angles shows that adjacent to the cyclohexano substituents of complexes **1** and **2** the bond lengths are slightly shorter, and the angles, particularly the C—C—O angles, are marginally larger than similar values for complex **3**. These differences, however small, may therefore be due to the presence of the cyclohexano substituent in complexes **1** and **2**. The C—C bonds at the points of fusion are observed to be longer (C11—C12 = 1.505 Å in complex **1**, and C8—C9 = 1.551 Å in complex **2**), and the adjacent C—C bonds, namely, C14—C15 in complex **1** and C5—C6 in complex **2**, appear to be shorter, with values of 1.308 and 1.320 Å, respectively. The shortening of the C—C bonds in this region appears to accompany a small increase in the bond angles at O1—C15—C14 for complex **1**, and O4—C5—C6 for complex **2**, respectively.

An examination of the torsion angle values for the lithium complexes of 15-crown-5 (3) and cyclohexano-15-crown-5 (complex **1**) reveals many more deviations from the expected values for the latter macrocycle. More specifically, in complex **1**, deviations are observed in all the expected synclinal arrangements, as well as notable deviations in the C6—O7—C8—C9, C12—O13—C14—C15, C14—C15—O1—C2, and C15—O1—C2—C3 angles. Since the cation size, crown cavity size, coordination geometry, and relative bond strengths in each lithium complex are the same, the conformational differences observed in the macrocycles must be a result of the addition of the cyclohexano substituent. A similar comparison of complexes **2** and **3** gives rise to the same trend and leads to the same conclusion. In the 15-crown-5 macrocycle of complex **3** there are fewer deviations than in the cyclohexano-15-crown-5 macrocycle of complex **2**, the most notable being that observed for the C12—O13—C14—C15 angle. However, in the cyclohexano-15-crown-5 macrocycle, in complex **2**, many deviations from the expected torsion angle values are observed, namely, O4—C5—C6—O7, C5—C6—O7—C8, C8—C9—O10—C11, C14—C15—O1—C2, and C15—O1—C2—C3. Furthermore, the coordination geometry found in complex **2** is somewhat unusual. The Na2 cation, coordinated primarily to the crown ether, is also coordinated to two phenoxide oxygen atoms, whereas in complex **3** the Na2 cation is coordinated to only one phenoxide oxygen atom. Moreover, in complex **2** the Na2 cation is at an unusually long distance (2.971 Å) from O1 of the crown ether. Furthermore, the Na2 cation of complex **2** lies much further out of the mean plane defined by the crown ether oxygens than does the Na^+ cation in complex **3**. A possible explanation for the observed differences in the coordination geometries of complexes **2** and **3** is that distortion in the cyclohexano-15-crown-5 ring of complex **2**, arising from the cyclohexano substituent, causes the cation to be *pushed* out of the crown ring and, therefore, does not allow coordination of Na2 with O1. Consequently, O27 of the phenoxide moiety is able to come into contact with Na2 in complex **2**, while contact of Na2 with O23 in complex **3** is essentially *blocked* by the optimum coordination of Na2 with all five crown ether oxygens.

A comparison of the torsion angle values for various benzo-15-crown-5 complexes (16, 26, 28) indicates that generally the values are very similar. This is consistent with the assumption that 15-crown-5 and cyclohexano-15-crown-5 macrocycles will be more flexible than the benzo- or dibenzo-15-crown-5 macrocycles, analogous to the observation that the 18-crown-6 and dicyclohexano-18-crown-6 ligands are more flexible than the dibenzo-18-crown-6 ligand (29). Thus, the more flexible ligands are readily able to undergo changes in conformation in order to accommodate a guest. This is observed in the sodium phenoxide complex with dicyclohexano-18-crown-6 (isomer A), where the large flexible ligand adopts an irregular conformation in order to envelop the sodium guest (5).

In the present substituted and unsubstituted 15-crown-5 complexes, and in the dicyclohexano-18-crown-6 (isomer A)·2NaOPh complex (5), the formation of a phenoxide aggregate is the dominant effect, and the cations are found to be located out of the ideal nesting position of the host cavity. Similarly, in the dicyclohexano-18-crown-6 (isomer B)·2KOPh complex (5), the potassium ions are pulled out of the host cavity and a potassium phenoxide dimer is observed. In each case, the unusual 1:2 ratio is attributed to the tendency of the alkali metal phenoxides to form aggregates in ethereal solutions. However, the tendency to form aggregates in ethereal solutions does not preclude the possibility of obtaining an optimal host–guest coordination geometry. A case in point is the 1:2 host–guest complex of 18-crown-6 with lithium phenoxide, which exhibits strong lithium phenoxide aggregate formation in addition to an ideal host–guest geometry where both lithium cations lie in the cavity outlined by the 18-crown-6 (6). In this case, the cavity of the relatively large ligand can accommodate the two small guests and, therefore, the resultant 1:2 host–guest stoichiometry is not unexpected. Thus, the 18-crown-6·2LiOPh complex (6) provides an example of the balance and intricacy of these associated effects and, together with the results of this study, supports the idea that the stoichiometries and structural features of the crown ether complexes are indeed a result of concerted host, guest, anion, and solvent effects.

1. A. RODRIGUE, J. W. BOVENKAMP, B. V. LACROIX, R. A. B. BANNARD, and G. W. BUCHANAN. Can. J. Chem. **64**, 808 (1986).
2. A. RODRIGUE, J. W. BOVENKAMP, M. P. MURCHIE, G. W. BUCHANAN, and S. FORTIER. Can. J. Chem. **65**, 2551 (1987).
3. M. P. MURCHIE, J. W. BOVENKAMP, A. RODRIGUE, K. A. WATSON, and S. FORTIER. Can. J. Chem. **66**, 2515 (1988).
4. M. E. FRASER, S. FORTIER, M. K. MARKIEWICZ, A. RODRIGUE, and J. W. BOVENKAMP. Can. J. Chem. **65**, 2558 (1987).
5. M. E. FRASER, S. FORTIER, A. RODRIGUE, and J. W. BOVENKAMP. Can. J. Chem. **64**, 816 (1986).
6. K. A. WATSON, S. FORTIER, M. P. MURCHIE, J. W. BOVENKAMP, A. RODRIGUE, G. W. BUCHANAN, A. RODRIGUE, G. W. BUCHANAN, and C. I. RATCLIFFE. Can. J. Chem. **68**, 1201 (1990).
7. P. GROTH. Acta Chem. Scand. A, **35**, 721 (1981).
8. C. CAMBILLAU, G. BRAM, J. CORSET, and C. RICHE. Can. J. Chem. **60**, 2554 (1982).
9. A. I. GORBUNOV, A. P. STOROZHENKO, L. V. IVAKINA, B. M. BULYCHEV, and A. I. GUSEV. Dokl. Akad. Nauk SSSR, **285**, 129 (1985).
10. N. P. RATH and E. M. HOLT. J. Chem. Soc. Chem. Commun. 665 (1985).
11. C. J. PEDERSEN. J. Am. Chem. Soc. **89**, 7017 (1967).
12. N. S. POONIA and M. R. TRUTER. J. Chem. Soc. Dalton Trans. 2062 (1973).
13. N. S. POONIA. J. Am. Chem. Soc. **96**, 1012 (1974).
14. N. S. POONIA, P. BAGDI, and K. S. SIDHU. J. Inclusion Phenom. **4**, 43 (1986).
15. W. V. BHAGWAT, H. MANOHAR, and N. S. POONIA. Inorg. Nucl. Chem. Lett. **16**, 373 (1980).
16. D. L. WARD, A. I. POPOV, and N. S. POONIA. Acta Crystallogr. Sect. C: Cryst. Struct. Commun. C**40**, 238 (1984).
17. V. W. BHAGWAT, H. MANOHAR, and N. S. POONIA. Inorg. Nucl. Chem. Lett. **17**, 207 (1981).
18. K. VENKATASUBRAMANIAN, K. JOSHI, N. S. POONIA, W. R. MONTFORT, S. R. ERNST, and M. L. HACKERT. J. Inclusion Phenom. **3**, 453 (1985).
19. A. V. BAJAJ and N. POONIA. Coord. Chem. Rev. **87**, 55 (1988).
20. F. H. ALLEN, S. BELLARD, M. D. BRICE, B. A. CARTWRIGHT, A. DOUBLEDAY, H. HIGGS, T. HUMMELINK, B. G. HUMMELINK-PETERS, O. KENNARD, W. D. S. MOTHERWELL, J. R. RODGERS, and D. G. WATSON. Acta Crystallogr. Sect. B: Struct. Crystallogr. Cryst. Chem. **B35**, 2331 (1979).
21. Enraf–Nonius. Structure determination package. *Revised by* B. A. Frenz. Enraf–Nonius, Delft. 1979.
22. P. MAIN, S. J. FISKE, S. E. HULL, L. LESSINGER, G. GERMAIN, J.-P. DECLERCQ, and M. M. WOOLFSON. MULTAN80. A system of computer programs for the automatic solution of crystal structures from X-ray diffraction data. Univs. of York, England, and Louvain, Belgium. 1980.
23. D. T. CROMER and J. T. WABER. International tables for X-ray crystallography. Vol. IV. Kynoch Press, Birmingham. 1974.
24. C. K. JOHNSON. ORTEP. Report ORNL-3794, Oak Ridge National Laboratory. Tennessee. 1965.
25. D. L. HUGHES. J. Chem. Soc. Dalton Trans. 2374 (1975).
26. J. D. OWEN. J. Chem. Soc. Dalton Trans. 1066 (1980).
27. J. D. OWEN and M. R. TRUTER. J. Chem. Soc. Dalton Trans. 1831 (1979).
28. M. A. BUSH and M. R. TRUTER. J. Chem. Soc. Perkin Trans. 2, 341 (1972).
29. E. SHCHORI, J. J. GRODZINOSKI, and M. SHPORER. J. Am. Chem. Soc. **95**, 3842 (1973).

Can. J. Chem. Downloaded from www.nrcresearchpress.com by 198.100.157.202 on 09/07/12
For personal use only.

Tautomerism in ketomethyl quinolines. Part 3. 4-Ketomethylquinolines[1]

JOHN V. GREENHILL[2] AND HOSSEIN LOGHMANI-KHOUZANI
Pharmaceutical Chemistry, School of Pharmacy, University of Bradford, Bradford, West Yorkshire, BD7 1DP, England
AND
DEREK J. MAITLAND
Chemistry and Chemical Technology, University of Bradford, Bradford, West Yorkshire, BD7 1DP, England

Received June 25, 1990

JOHN V. GREENHILL, HOSSEIN LOGHMANI-KHOUZANI, and DEREK J. MAITLAND. Can. J. Chem. **69**, 696 (1991).

A series of 4-ketomethylquinolines has been prepared and their tautomerism investigated. The compounds were prepared from 4-methylquinoline deprotonated with lithium diisopropylamide or potassium ethoxide and treated with esters. Attempted deprotonation with *tert*-butyllithium or phenyllithium led to 2-substituted-4-methylquinolines. The simple alkyl or aryl 4-ketomethylquinolines exist essentially as the keto forms, but the quinoline-4-pyruvates are exclusively or substantially in the enol forms.

Key words: ketomethyl quinolines, pyruvates, tautomerism, enols.

JOHN V. GREENHILL, HOSSEIN LOGHMANI-KHOUZANI et DEREK J. MAITLAND. Can. J. Chem. **69**, 696 (1991).

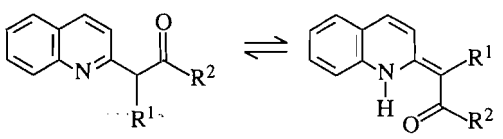
On a préparé une série de 4-cétométhylquinoléines et on a examiné leur tautomérie. On a préparé les produits à partir de la 4-méthylquinoléine déprotonée, à l'aide du diisopropylamide de lithium ou de l'éthylate de potassium, qui a été traitée par des esters. Des essais de déprotonation à l'aide du *tert*-butyllithium ou le phényllithium ont conduit à la formation de 4-méthylquinoléines substituées en position 2. Les 4-cétométhylquinoléines portant des groupements aryles ou alkyles simples existent essentiellement sous la forme cétonique; toutefois, les quinoléine-4-pyruvates existent exclusivement ou presque sous la forme énolique.

Mots clés : cétométhylquinoléines, pyruvates, tautomérie, enols.

[Traduit par la rédaction]

Introduction

We recently conducted detailed investigations into the tautomerism of 2-ketomethylquinolines (1), Scheme 1. By a combination of ir and nmr spectroscopy it was clearly shown that the enaminone form **B** was strongly favoured over the ketone form **A** for 2-ketomethylquinolines where R^1 = H, CN, or COOEt (R^2 = alkyl, aryl, CN, COOEt, etc.). For the compounds with R^1 = H, R^2 = Me, Et, *i*-Pr, or *t*-Bu, the tautomeric mixtures in chloroform had 12–20% of the ketone forms and signals for both forms **A** and **B** could clearly be seen in the ir and the ^{1}H, ^{13}C, and ^{15}N nmr spectra. The rest of the structures investigated showed only the enaminone signals. However, compounds of Scheme 1 where R^1 = Me or Br were found to be exclusively in the ketone form **A**.

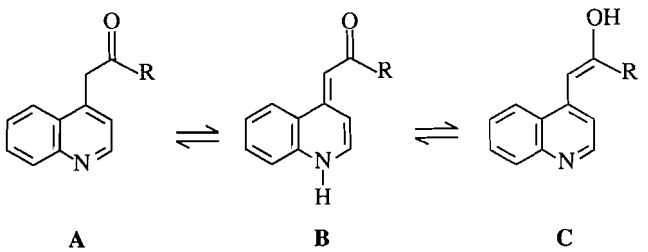


A **B**

SCHEME 1

We have now undertaken a study of 4-ketomethylquinolines by preparing and examining the compounds of Table 1. The few literature reports had reached differing conclusions regarding the tautomerism of compounds of this type. In principle, three forms are possible, Scheme 2.

It was claimed by Stock *et al.* (2) that the pyruvate **6** had 76%



A **B** **C**

SCHEME 2

of the enol form (**C**) after 20 min in methanol, which dropped to 22% at equilibrium (time unspecified). This investigation made use of bromine titration to determine the enol content, and intermolecular (O—H...N) hydrogen bonded stabilization was suggested to account for the enolic content of the mixture. In an nmr study of the same compound, Golankiewicz and Golankiewicz assigned a singlet, which appeared at δ 6.38 in both $CDCl_3$ and DMSO-d_6, to the vinyl proton of the enol form and in the absence of a methylene signal the pyruvate was concluded to be 100% enol (3). Mondelli and Merlini claimed to detect a small proportion of the dienaminone form (**B**) of this pyruvate (4). The 8-cyano derivative of compound **1** was claimed by Higishino *et al.* to be exclusively in the dienaminone form, based on the ir (1680 cm^{-1}) and 60 MHz nmr spectra (5). Compound **11** has recently been shown by Fukata *et al.*, using potentiometric titration, to have log K_T 1.78 in favour of the keto form (**A**) (6).

Synthesis

Compared with the 2-ketomethylquinolines, only a few 4-ketomethylquinolines have been reported (7). Those made from 4-methylquinoline and an ester usually required sodium diisopropylamide (SDA) as base (8), although compound **11** was obtained in good yield from methyl benzoate in the

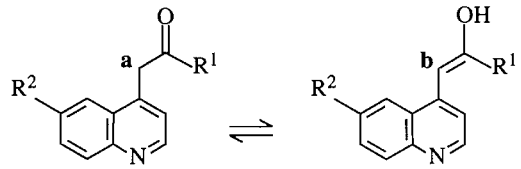
[1]For Part 2, see ref. 1.

[2]Author to whom correspondence may be addressed. New address: Department of Chemistry, University of Florida, Gainesville, FL 32611-2046, U.S.A.

Printed in Canada / Imprimé au Canada

Can. J. Chem. Downloaded from www.nrcresearchpress.com by 198.100.157.202 on 09/07/12
For personal use only.

TABLE 1. 4-Ketomethylquinolines and their tautomerism data



A C

No.	R^1	R^2	Chemical shift Ha (integral)	Hb (integral)	Ca	Cb	Infrared (cm^{-1})		Ratio A:C	Ref.
1	Me	H	4.14 (2H)	—	47.91	—	1714 (C=O)		100:0	8
2	Et	H	4.13 (2H)	—	46.69	—	1717 (C=O)	—	100:0	8
3	Pr^i	H	4.17 (2H)	—	44.48	—	1714 (C=O)	—	100:0	8
4	Bu^t	H	4.30 (2H)	—	40.21	—	1711 (C=O)	—	100:0	8
5	COOMe	H	4.76 (0.06H)	6.71 (0.97H)	41.87	[a]	2665 (O–H)	1632 (C=C)	3:97	
6	COOEt	H	4.73 (0.2H)	6.70 (0.90H)	44.37	100.97	2639 (O–H)	1631 (C=C)	10:90	11
7	COOEt	OMe	4.68 (0.38H)	6.68 (0.81H)	41.92	103.39	2619 (O–H)	[a]	19:81	
8	COOEt	COOMe	—	6.73 (1H)	—	79.07	2775 (O–H)	1635 (C=C)	0:100	
9	COOEt	COOEt	—	6.74 (1H)	—	94.39	2657 (O–H)	1639 (C=C)	0:100	
10	COOBu	H	[a]	7.12	42.49	99.24	2936 (O–H)	1626 (C=C)	18:82[b]	
11	Ph	H	4.75 (2H)	—	42.14	—	1691 (C=O)	—	100:0	6
12	2-Py	H	5.05 (2H)	—	40.79	—	1702 (C=O)	—	100:0	8

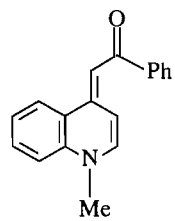
[a]Signal (band) not detected.
[b]Estimated from the ^{13}C nmr spectrum.

presence of sodium hydride (9). In our hands only **11** and the 2-pyridyl ketone **12** could be prepared by this technique.

Attempted use of *tert*-butyllithium or phenyllithium as ionizing bases with 4-methylquinoline, followed by a nitrile or an ester as the acylating agent, gave high yields of 2-*tert*-butyl-4-methylquinoline and 2-phenyl-4-methylquinoline respectively, see experimental section. No trace of any acylated product was detected. Attempted use of sodium hydride or N^1-*tert*-butyl-N^2,N^2,N^3,N^3-tetramethylguanidine (10) as base gave none of the required ketomethylquinolines; only starting materials were recovered. Finally, with lithium diisopropylamide (LDA), compounds **1**, **2**, **3**, and **4** were obtained in good yields. A literature report describes the preparation of ketone **3** from 4-methylquinoline and SDA followed by ethyl isobutyrate (8). The crude product was distilled and extracted with petroleum ether to give a soluble material, mp 45.5–46.6°C, and an insoluble product, mp 160–165°C. It was claimed that the low melting compound was the pure keto form and the high melting material was a mixture of the keto and enol forms. In our hands the same two products were obtained when LDA was substituted for SDA. The spectra of the low melting material showed it to be the required compound as a pure ketone, see experimental section. The nmr spectrum of the high melting material was as follows (δ $CDCl_3$): 1.28 (d), 1.52 (d), 2.94 (heptet), 3.45 (heptet), 4.55 (s), 7.86 (2H, m), 8.04 (2H, m), 8.85 (1H, d), 9.05 (1H, d), 9.40 (s, NH). We interpreted this to be a mixture of the required ketomethylquinoline hydrochloride and diisopropylamine hydrochloride (signals at δ 1.52, 3.45, and 9.4) in the proportions of 88:12. The mixture was dissolved in water, basified, and extracted with dichloromethane to give a further quantity of the low melting ketone.

The ethyl pyruvate **6** has been prepared from 4-methylquinoline and diethyl oxalate in the presence of potassium ethoxide (11). However, we found this compound to be only sparingly soluble in chloroform so that it was difficult to get good spectra for the study of its tautomerism. Therefore, the further pyruvates **5**, **7**, **8**, **9**, and **10** were prepared in the hope of finding more soluble examples. In this we were frustrated and had to rely on KBr discs for the ir spectra and prolonged acquisition times for the FT nmr spectra. The new compounds were prepared by the potassium ethoxide method except for the methyl ester **5**, which resulted from a transesterification of the ethyl ester **6** in methanol containing boron trifluoride.

To get an example of a fixed dienaminone, compound **13** was prepared from 1,4-dimethylquinolinium iodide by a Schotten–Baumann procedure (6).



13

Discussion

Aliphatic 4-ketomethylquinolines **1**, **2**, **3**, and **4** were clearly in the simple keto forms in chloroform with no trace of any other tautomers. They all had strong carbonyl bands in their ir spectra at about 1715 cm^{-1}. The ^1H nmr spectra showed two-proton singlets for the methylene groups between δ 4.1 and 4.3 and the ^{13}C spectra were characterized by methylene signals between δ 40 and 48 and by unconjugated carbonyl carbon signals in the δ 204—211 region. The uv spectra, Table 2, were closely similar to those of 4-methylquinoline.

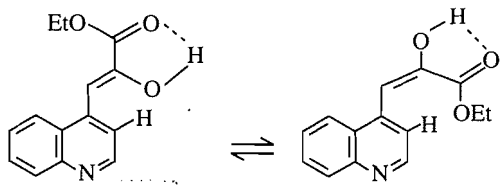
The pyruvic ester **9** proved to be in the enol tautomeric form. The ir spectrum showed a very broad, strong band centred at 2657 cm^{-1} for the hydrogen bonded enolic O–H stretch. A strong band at 1723 cm^{-1} represented both ester carbonyl groups and a medium band at 1639 cm^{-1} was in the range for enol C=C stretch. This was much weaker than the carbonyl

Can. J. Chem. Downloaded from www.nrcresearchpress.com by 198.100.157.202 on 09/07/12
For personal use only.

TABLE 2. Ultraviolet spectra (λ_{max} (ε) EtOH)

4-Methylquinoline			313 (3 800) 300 (4 200)	277 (6 300)	224 (26 000)
1			315 (3 300) 301 (4 100)	283 (5 200)	231 (13 900)
2			315 (3 100) 301 (3 800)	288 (4 500)	231 (13 000)
3			314 (3 400) 301 (3 900)	288 (4 400)	231 (13 800)
4			314 (2 800) 302 (3 500)	283 (4 600)	227 (23 000)
5	468 (25 700)	446 (18 700)	323 (8 000)	281 (7 200)	230 (20 300)
6	468 (17 600)	448 (14 300)	315 (6 300)		217 (20 000)
7	472 (9 800)	452sh (7 500)	350 (4 600) 324 (6 500)		234 (24 200)
9	479 (14 000)	453 (12 800)		285 (6 500)	242 (28 000)
10	468 (23 800)		315 (7 700)	281 (6 900)	228 (21 400)
11	466 (460)	442 (320)	314 (3 400) 300 (4 400)	280 (7 100)	232 (19 400)
12	479 (1 300)	452 (960)	330 (2 000) 314 (4 200)	271 (8 200)	227 (27 800)
13	474 (52 300)	452 (37 500)		279 (9 700)	230 (26 000)

stretching band of the dienaminone **13** at 1631 cm^{-1}. In the uv spectrum the compound showed strong peaks at 479 and 453 nm, consistent with the proposed extended conjugated system. The ^1H nmr spectrum showed signals for the enol, in particular a full one-proton singlet at δ 6.74 for the vinyl proton. In the ^{13}C spectrum there were the expected signals for the enol and the highest field signal was at δ 165.12 for an ester carbonyl carbon. By contrast, the dienaminone carbonyl carbon of compound **13** absorbed at δ 187.96. Neither nmr spectrum had any sign of a methylene signal from the keto form or any other indication of a second tautomer. Thus both simple ketone and dienaminone forms were ruled out and the compound shown to exist as the enol form. The very low O–H band in the ir spectrum and the fact that the simple ketones **1**, **2**, **3**, **4**, **11**, and **12** showed negligible amounts of their enol forms strongly suggest that the hydrogen bond in **9** is intramolecular, and the compound adopts one of the planar forms **14***a* or **14***b*. Of these we prefer form **14***a*



14*a* **14***b*

since the steric interaction between the C3-H and the ethoxy group of **14***b* would be expected to destabilize it. The mixed ester **8** was also 100% enol, but the other pyruvates **5**, **6**, and **7** were mixtures of keto and enol forms. The tautomeric ratios, calculated from the ^1H nmr spectra, are given in Table 1. For ester **10** a complex proton nmr spectrum indicated the presence of two forms, but it was not possible to identify positively signals on which the tautomeric ratio could be calculated. In the ^{13}C nmr spectrum it was not possible to see two full sets of signals, but the methylene group (δ 42.49) of the keto form and the vinyl carbon (δ 99.24) of the enol form were clearly visible. Their relative intensities in the DEPT spectrum indicated an approximate tautomeric ratio of 18:82.

The aromatic ketone **11** was, like the simple aliphatic compounds, essentially in the keto form. The ir and nmr spectra gave no indication of a second tautomer, but there were two small long-wavelength absorptions in the uv spectrum. The 2-pyridyl derivative **12** was prepared in the hope that the pyridine nitrogen would stabilize the enol form. However, its lone pair is not ideally orientated for intramolecular hydrogen bonding in the way that the oxygen lone pairs of the pyruvates are. Again, it did show two weak long-wavelength absorptions in the uv spectrum. However, neither compound gave any clear signals for a second form in either the ^1H or the ^{13}C nmr spectrum.

The ultraviolet spectra in aqueous solutions for four of the compounds are given in Table 3. The simple ketones, compounds **1** and **11**, showed spectra little changed between water and molar acid, as would be expected. The pyruvates **6** and **10** showed long-wavelength absorption in water similar to that seen in ethanol. Clearly the enolic forms exist in neutral aqueous solution. In acid all four compounds gave very similar spectra. Under these conditions the pyruvates revert to the ketone structures, perhaps because the carbonyl groups are stabilized by hydrogen bonding to the H_3O^+ molecules. It was interesting that all four compounds showed strong absorption at 388–406 nm in molar sodium hydroxide. These conditions must be sufficiently basic to induce deprotonation of the methylene group.

In comparing the structures of the 2-ketomethylquinolines with those of the present report it is clear that the *intra*-molecular hydrogen bond in the enaminone form, Scheme 1, is essential for its stabilization. The energy difference between the two forms of Scheme 1 must be small since the simple alkyl derivatives (R^1 = H, R^2 = alkyl) show significant proportions of the ketone forms in solution. The equivalent compounds of the 4-ketomethyl series, Scheme 2, have no comparable *intra*-molecular hydrogen bonding available and show only ketone structures.

In comparing the freely chloroform-soluble compounds **1**–**4**, **11**, and **12** (all 100% ketones) with the esters **5**–**10** there was the possibility that the DMSO-d_6, which had to be used to obtain the ester nmr spectra, had helped to stabilize the enol forms detected. Compound **1** was therefore re-run in DMSO-d_6, but

Can. J. Chem. Downloaded from www.nrcresearchpress.com by 198.100.157.202 on 09/07/12
For personal use only.

TABLE 3. Ultraviolet spectra in aqueous solutions (λ_{max} (ϵ))

1	H_2O		314 (4 400)	301 (4 700)	289 (4 800)	226 (30 600)
	M HCl		314 (8 200)			233 (31 700)
	M NaOH	388 (900)			264 (9 900)	225 (41 200)
6	H_2O	444 (18 600)			277 (6 300)	227 (20 700)
	M HCl		315 (7 800)			236 (35 800)
	M NaOH	388 (19 100)			263 (9 000)	218 (18 700)
10	H_2O	445 (17 200)	314 (5 000)		277 (6 400)	230 (25 900)
	M HCl		314 (9 900)			235 (42 500)
	M NaOH	390 (17 700)			265 (9 500)	223 (44 800)
11	H_2O		314 (6 200)	300 (7 000)	284 (8 600)	226 (42 200)
	M HCl		314 (10 200)			236 (40 800)
	M NaOH	406 (16 800)			257 (8 600)	223 (42 400)

neither the ^1H nor the ^{13}C spectrum was significantly different from the $CDCl_3$ spectrum (see experimental). The methyl (δ 2.29) and methylene (δ 4.38) proton signals were in an exact 3:2 ratio and there were no detectable signals for an enol form. Further evidence for the conclusions reached was provided by the uv spectra. The compounds of Scheme 1, which have been shown to be substantially enaminones in chloroform, had strong absorptions in ethanol and in water at 430–440 nm (for R^1 = H, R^2 = alkyl) or 450–460 nm (for R^1 = H, R^2 = aryl), establishing that the enaminone forms are dominant in these solvents also (14). Reference to Tables 2 and 3 shows that the alkyl 4-ketomethylquinolines **1**–**4** show no trace of long-wavelength absorption, and the aryl derivatives **11** and **12** have very low absorption in the 440–480 region.

It is reasonable to assume that other simple 4-ketomethylquinolines would exist as ketones, but that enol formation, giving a system conjugated to the quinoline ring, will always be a possibility where it can be stabilized by intramolecular hydrogen bonding. Whether any firm examples will be found in which dienaminone forms exist remains to be seen, but the loss of aromaticity in the heterocyclic ring cannot be compensated by hydrogen bonding as is the case with the enaminone forms of 2-ketomethylquinolines (1).

Experimental

The ir spectra were run on Perkin–Elmer 1700-X and 1720-X FT spectrophotometers. The 270 MHz ^1H and 67.8 MHz ^{13}C nmr (broad band decoupled and DEPT 135) spectra were run on a JEOL GX 270 spectrometer fitted with a 5 mm C/H probe. The uv spectra were obtained on a Perkin–Elmer Lambda 5 UV/VIS spectrophotometer and mass spectra on an AEI MS 902 spectrometer. Chromatography columns were prepared with Aldrich silica gel 70–230 mesh.

2-(1,1-Dimethylethyl)-4-methylquinoline

A solution of 4-methylquinoline (2.86 g, 0.02 mol) in dry ether (10 mL) was added dropwise to a solution of *tert*-butyllithium (11.76 mL of 1.7 M solution in pentane, 0.02 mol) in dry ether (20 mL) and stirred under nitrogen at room temperature for 1 h. Acetonitrile (5.0 g, 0.06 mol) in dry ether (10 mL) was added and stirring continued for a further 20 h. The product was washed with water and extracted with dilute hydrochloric acid. The aqueous extracts were neutralized with solid sodium carbonate and extracted with chloroform (2 × 50 mL). The chloroform solution was dried ($MgSO_4$) and the solvent removed to give *2-(1,1-dimethylethyl)-4-methylquinoline* as a colourless oil (3.4 g, 85%); ^1H nmr (δ $CDCl_3$); 1.46 (9H, s, 3 × CH_3), 2.67 (3H, s, CH_3), 7.34 (H, s), 7.47 (H, dt), 7.65 (H, dt), 7.93 (H, dd), 8.06 (H, dd); ^{13}C nmr (δ $CDCl_3$); 18.95 (CH_3), 30.10 (3 × CH_3), 37.88 (C), 118.87 (CH), 123.36 (CH), 125.36 (CH), 126.51 (C), 128.66 (CH), 129.91 (CH), 143.58 (C), 147.27 (C), 168.90 (C); *m/z* 199. It gave the *hydrochloride*, mp 225–226°C (from ethanol–ether). Anal. calcd. for $C_{14}H_{18}ClN$: C, 71.3, H 7.65, Cl 15.1, N 5.95%; found: C 71.2, H 7.5, Cl 15.2, N 5.9%.

4-Methyl-2-phenylquinoline was similarly prepared from 2-phenyllithium: 82%, mp 65°C (from methanol) (lit. (12) mp 67°C); ^1H nmr (δ $CDCl_3$, 60 MHz); 2.52 (3H, s, CH_3), 7.3–8.3 (10H, m, C_9H_5N + C_6H_5); *m/z* 219.

1-(4-Quinolyl)propan-2-one (1)

4-Methylquinoline (2.86 g, 0.02 mol) was added dropwise to a solution of lithium diisopropylamide (13.3 mL of a 1.3 M solution in cyclohexane, 0.02 mol) in THF (15 mL) with stirring under nitrogen at −78°C. After 20 min methyl acetate (1.5 g, 0.02 mol) was added and stirring continued for 30 min at −78°C. The mixture was allowed to warm to room temperature and stirred for a further 40 min. Water (2 mL) and ether (50 mL) were added, the cooled solution carefully acidified with hydrochloric acid, and the layers separated. The aqueous solution was treated with sodium hydroxide solution until nearly neutral and finally basified with solid sodium carbonate. The product was extracted with chloroform, dried ($MgSO_4$), the solvent evaporated, and the residue chromatographed on a silica column eluted with 1% methyl acetate in chloroform to give 1-(4-quinolyl)propan-2-one (1.37 g, 37%) mp 70–71°C (from petroleum ether 40–60) (lit. (8) mp 71.8–72.6°C); ir ($CHCl_3$): 1714(s), 1594(m), 1572(w), 1511(m) cm^{-1}; ^1H nmr (δ $CDCl_3$): 2.20 (3H, s, CH_3), 4.14 (2H, s, CH_2), 7.28 (H, d, C3-H, J = 4.40), 7.57 (H, t), 7.73 (H, t), 7.87 (H, d), 8.14 (H, d), 8.87 (H, d, C2-H, J = 4.39); ^1H nmr (δ DMSO-d_6): 2.29 (3H, s), 4.38 (2H, s), 7.39 (H, d, J = 4.29), 7.64 (H, t), 7.77 (H, t), 7.90 (H, d), 8.04 (H, d), 8.84 (H, d, J = 4.28); ^{13}C nmr (δ $CDCl_3$): 29.50 (CH_3), 47.91 (CH_2), 122.78 (CH), 123.62 (CH), 127.07 (CH), 127.54 (C), 129.50 (CH), 130.29 (CH), 140.43 (C), 148.42 (C), 150.16 (CH), 204.48 (C); ^{13}C nmr (δ DMSO-d_6): 30.24, 46.66, 123.56, 125.07, 126.90, 127.98, 129.60, 129.86, 141.96, 148.17, 150.53, 205.34; *m/z* 185.

The following were prepared similarly:

1-(4-Quinolyl)butan-2-one (2): 35%, bp 135–140°C (0.3 Torr; 1 Torr = 133.3 Pa) (lit. (8) bp 134–135°C (0.55 Torr)). Analytical sample purified via a silica column eluted with 1% ethyl acetate in chloroform; ir ($CHCl_3$): 1717 (s), 1593 (m), 1572 (w), 1511 (m) cm^{-1}; ^1H nmr (δ $CDCl_3$): 1.03 (3H, t, CH_3), 2.52 (2H, q, CH_2), 4.13 (2H, s, CH_2), 7.26 (H, d, C3-H, J = 4.39), 7.56 (H, t), 7.72 (H, t), 7.87 (H, d, J = 8.42), 8.14 (H, d, J = 8.42), 8.86 (H, d, C-2H, J = 4.39); ^{13}C nmr (δ $CDCl_3$): 7.70 (CH_3), 35.51 (CH_2), 46.69 (CH_2), 122.73 (CH), 123.70 (CH), 127.02 (CH), 127.60 (C), 129.47 (CH), 130.18 (CH), 140.73 (C), 148.34 (C), 150.08 (CH), 207.12 (C); *m/z* 199.

3-Methyl-1-(4-quinolyl)butan-2-one (3): 55%, bp 145°C (0.8 Torr) (lit. (8) bp 133–135°C (0.55 Torr)). The oil (2.1 g) was refluxed with petroleum ether 40–60, filtered, and the filtrate cooled in liquid nitrogen. The product was collected and chromatographed through a silica column eluted with 1% methyl acetate in chloroform to give the pure ketone (1.2 g), mp 43–44°C (lit. (8) mp 45.4–46.6°C); ir ($CHCl_3$); 1714 cm^{-1}; ^1H nmr (δ $CDCl_3$): 1.14 (6H, d, 2 × CH_3), 2.77 (H, heptet, CH), 4.17 (2H, s, CH_2), 7.23 (H, d, C3-H, J = 4.40), 7.54

Can. J. Chem. Downloaded from www.nrcresearchpress.com by 198.100.157.202 on 09/07/12
For personal use only.

Can. J. Chem. Downloaded from www.nrcresearchpress.com by 198.100.157.202 on 09/07/12
For personal use only.

(H, t), 7.68 (H, t), 7.82 (H, d), 8.13 (H, d), 8.84 (H, d, C2-H, J = 4.40); ^{13}C nmr (δ $CDCl_3$): 18.40 (CH_3), 40.48 (CH), 44.48 (CH_2), 122.76 (CH), 123.62 (CH), 126.86 (CH), 127.71 (C), 129.34 (CH), 130.17 (CH), 140.83 (C), 148.31 (C), 149.99 (CH, 210.20 (C); m/z 213. The petroleum ether insoluble residue (0.6 g) was dissolved in water, basified with dilute ammonium hydroxide, and extracted with dichloromethane. The extracts were dried ($MgSO_4$) and the solvent evaporated to give a residue identical (^{1}H nmr) with the pure ketone base prepared above.

3,3-Dimethyl-1-(4-quinolyl)butan-2-one (**4**): Purified through a silica column eluted with 1% ethanol in dichloromethane, 26.5%, mp 119–120°C (from petroleum ether 60–80) (lit. (8) mp 119–120°C); ir ($CHCl_3$): 1711 (s), 1596 (m), 1572 (w), 1512 (s) cm^{-1}; ^{1}H nmr (δ $CDCl_3$): 1.32 (9H, s, 3 × CH_3), 4.30 (2H, s, CH_2), 7.23 (H, d, C3-H, J = 4.40), 7.57 (H, t), 7.76 (2H, m), 8.20 (H, d, J = 8.43), 8.90 (H, d, C2-H, J = 4.40); ^{13}C nmr (δ $CDCl_3$): 26.65 (CH_3), 40.21 (CH_2), 45.07 (C), 122.84 (CH), 123.60 (CH), 126.94 (CH), 127.95 (C), 129.60 (CH), 129.64 (CH), 142.39 (C), 147.55 (C), 149.31 (CH, 211.01 (C); m/z 227.

Methyl 2-hydroxy-3-(4-quinolyl)propenoate (**5**)

A solution of ethyl 2-hydroxy-3-(4-quinolyl)propenoate (0.8 g) in 14% boron trifluoride – methanol complex (40 mL) was refluxed on a water bath for 12 h. Most of the solvent was removed and the residue basified with saturated potassium bicarbonate solution and extracted with chloroform (5 × 100 mL). The combined extract was dried ($MgSO_4$) and the solvent evaporated to give the methyl ester (0.6 g, 78%) mp 198–200°C (from pyridine); ir (KBr): 2665 (br s), 1727 (s), 1632 (m), 1601 (m), 1533 (vs), 1505 (vs) cm^{-1}; ^{1}H nmr (δ DMSO-d_6, 16°C): 3.77 (s, OCH_3), 3.86 (s, OCH_3, keto form), 4.76 (s, CH_2, keto form), 6.71 (s, =CH), 7.4–8.6 (6H, m, C_9H_6N), 12.40 (s, OH), ratio keto:enol 3:97; at 60°C the spectrum was the same, but the keto:enol ratio was 6:94; ^{13}C nmr (δ DMSO-d_6, 60°C): 41.87 (CH_2, keto form), 51.77 (OCH_3), 52.69 (OCH_3, keto form), 123.25, 123.53, 125.31, 126.43, 127.46, 129.12, 129.47, 131.00, 139.89, 147.86, 165.76 (C); it was not possible to identify the other carbon signals due to the low solubility; m/z 229. Anal. calcd. for $C_{13}H_{11}NO_3$: C 68.1, H 4.8, N 6.1%; found: C 67.9, H 4.85, N 6.15.

General method for the preparation of esters **6–10**

A solution of the appropriate oxalic acid diester (0.005) mol) in dry ether (10 mL) was added to potassium ethoxide (0.01 mol from potassium (0.4 g) and ethanol (1.8 mL) in dry ether (20 mL)). A solution of the 4-methylquinoline (0.005 mol) in dry ether (10 mL) was added dropwise and the mixture stirred for 3 days and allowed to stand for 4 days. The precipitate was collected rapidly and immediately added to dilute acetic acid (10 mL). After stirring for 2 h, the new precipitate was collected to give the required ester:

Ethyl 2-hydroxy-3-(4-quinolyl)propenoate (**6**): 70%, mp 192–194°C (from pyridine) (lit. (11) mp 196°C); ir (KBr): 2639 (br. s), 1716 (s), 1631 (m), 1602 (m), 1529 (s), 1505 (s) cm^{-1}; ^{1}H nmr (δ DMSO-d_6): 1.31 (t, CH_3), 4.24 (q, CH_2), 4.73 (s, CH_2, keto form), 6.70 (s, =CH), 7.4–8.5 (6H, m, C_9H_6N), keto:enol ratio 1:9; ^{1}H nmr (δ DMSO-d_6/TFA 1:2); 1.50 (t, CH_3), 4.52 (q, CH_2), 5.12 (s, CH_2, keto form), 7.45 (s, =CH), 8.0–9.0 (6H, m, C_9H_6N), keto:enol ratio 1:4; ^{13}C nmr (δ DMSO-d_6/TFA 1:2), strong signals (enol form); 14.14 (CH_3), 65.80 (CH_2), 100.97 (CH), 122.04 (CH), 122.19 (CH), 125.97 (CH), 128.11 (C), 131.53 (CH), 136.37 (CH), 139.12 (C), 143.61 (CH), 151.35 (C), 153.17 (C), 165.77 (C); weak signals (keto form): 14.02 (CH_3), 44.37 (CH_2), 65.63 (CH_2), 122.45 (CH), 125.22 (CH), 126.94 (CH), 130.26 (C), 132.27 (CH), 137.08 (CH), 138.99 (C), 144.48 (CH), 155.59 (C), 161.39 (C), 189.96 C); m/z 243.

Ethyl 2-hydroxy-3-(6-methoxy-4-quinolyl)propenoate (**7**): 49%, mp 188–190°C (from ethanol); ir (KBr): 2619 (br s), 1718 (s), 1606 (s), 1504 (vs), 1477 (vs) cm^{-1}; ^{1}H nmr (δ DMSO-d_6 70°C): 1.32 (3H, t, CH_3), 3.92 (3H, s, OCH_3), 4.27 (2H, q, CH_2), 4.68 (s, CH_2, keto form), 6.68 (s, =CH), 7.3–8.4 (5H, m, C_9H_5N), keto:enol ratio 19:81; ^{13}C nmr (δ DMSO-d_6 70°C): 13.71 (CH_3 keto form), 14.02 (CH_3), 41.92 (CH_2 keto form), 55.62 (OCH_3), 60.88 (CH_2), 62.07 (CH_2 keto form), 103.39 (CH), 121.24 (CH), 121.55 (CH), 122.64 (CH), 123.51 (CH), 124.38 (C), 128.52 (C), 131.08 (CH), 138.39 (C), 144.01 (C), 147.38 (CH), 157.06 (C), 157.59 (C), 160.47 (C), 165.20 (C), 190.56 (C=O keto form); clearly, two forms were present, but the other signals could not be distinguished because of low solubility; m/z 273. Anal. calcd. for $C_{15}H_{15}NO_4$: C 65.9, H 4.5, N 5.1%; found: C 65.8, H 4.55, N 5.0%.

Ethyl 2-hydroxy-3-(6-methoxycarbonyl-4-quinolyl)propenoate (**8**): 20%, mp 215–216°C (from methanol); ir (KBr): 2775 (br s), 1718 (s), 1635 (m), 1602 (w), 1538 (s), 1504 (s) cm^{-1}; ^{1}H nmr (δ DMSO-d_6 20°C); 1.37 (3H, t, CH_3), 3.78 (3H, s, OCH_3), 4.39 (2H, q, CH_2), 6.73 (H, s, =CH), 7.71 (H, d), 8.08 (H, br s), 8.19 (H, dd), 8.46 (H, d), 8.69 (H, s); ^{13}C nmr (δ DMSO-d_6 70°C): 14.11 (CH_3), 51.96 (OCH_3), 61.07 (CH_2), 79.07 (CH), 165.12 (C), 165.39 (C); due to low solubility only four aromatic carbons were clearly visible at 125.39, 126.32, 130.06, and 130.50; m/z 301. Anal. calcd. for $C_{16}H_{15}NO_5$: C 63.8, H 5.0, N 4.65%; found: C 63.5, H 5.1, N 4.55%.

Ethyl 2-hydroxy-3-(6-ethoxycarbonyl-4-quinolyl)propenoate (**9**): 76%, mp 210°C (from ethanol); ir (KBr): 2657 (br s), 1723 (s), 1639 (m), 1500 (vs), 1470 (vs) cm^{-1}; ^{1}H nmr (δ DMSO-d_6): 1.31 (3H, t, CH_3), 1.38 (3H, t, CH_3), 4.24 (2H, q, CH_2), 4.39 (2H, q, CH_2), 6.74 (H, s, =CH), 7.71 (H, d, J = 8.80), 8.07 (H, d), 8.18 (H, d, J = 8.79), 8.45 (H, d), 8.68 (H, s); ^{13}C nmr (δ DMSO-d_6): 13.98 (CH_3), 14.08 (CH_3), 60.76 (CH_2, 60.99 (CH_2), 94.39 (CH), 110.68 (CH), 121.59 (CH), 121.80 (C), 125.36 (CH), 126.08 (C), 130.26 (CH), 140.70 (CH), 142.74 (C), 147.96 (C), 148.02 (C), 165.12 (C), 170.36 (C); m/z 315. Anal. calcd. for $C_{17}H_{17}NO_5$: C 64.7, H 5.4, N 4.4%; found: C 64.3, H 5.3, N 4.0%.

Butyl 2-hydroxy-3-(4-quinolyl)propenoate (**10**): From dibutyl oxalate (13) (26.5%), mp 145°C (from ethanol); ir (KBr): 2936 (br s), 1722 (s), 1626 (m), 1591 (m), 1549 (m), 1500 (vs), 1468 (vs) cm^{-1}; ^{1}H nmr (δ $CDCl_3$): 0.93 (3H, t, CH_3), 1.44 (2H, m, CH_2), 1.76 (2H, m, CH_2), 4.31 (2H, t, OCH_2), 7.12 (s, =CH), 7.0–9.2 (m, Ar); ^{13}C nmr (δ $CDCl_3$): 13.71 (CH_3), 19.08 (CH_2), 30.51 (CH_2), 34.85 (CH_2), 42.49 (CH_2), 62.72 (CH_2), 65.77 (CH_2), 66.82 (CH_2), 99.24 (CH), 118.57 (CH), 123.60 (CH), 124.93 (CH), 127.35 (CH), 127.49 (CH), 130.04 (CH), 131.27 (CH), 152.80 (C), 163.21 (C), 165.30 (C), 169.36 (C); m/z 271. Anal. calcd. for $C_{16}H_{17}NO_3$: C 70.8, H 6.25, N 5.15%; found: C 70.5, H 6.45, N 5.15%.

1-Phenyl-2-(4-quinolyl)ethanone (**11**): By the literature method (6) (75%), mp 118–119°C (lit. (6) mp 116–117°C); ir ($CHCl_3$): 1691 (vs), 1597 (s), 1512 (s) cm^{-1}; ^{1}H nmr (δ $CDCl_3$): 4.75 (2H, s, CH_2), 7.27 (H, d, J = 4.40), 7.4–8.2 (9H, m, Ar), 8.86 (H, d, J = 4.40); ^{13}C nmr (δ $CDCl_3$): 42.14 (CH_2), 122.79 (CH), 123.62 (CH), 126.86 (CH), 127.70 (C), 128.44 (CH), 128.87 (CH), 129.31 (CH), 130.31 (CH), 133.71 (CH), 136.21 (C), 141.08 (C), 148.36 (C), 150.03 (CH), 195.98 (C); m/z 247.

1-(2-Pyridyl)-2-(4-quinolyl)ethanone (**12**): From ethyl 2-picolinate by the method for compound **11** (88%), mp 87–88°C (from petroleum ether 60–80) (lit. (8) mp 88.4–89.6°C); ir (KBr): 1702 cm^{-1} (s); ^{1}Hnmr (δ $CDCl_3$): 5.05 (CH_2), 7.4–8.3 (8H, m, Ar), 8.6–9.1 (2H, m, Ar); ^{13}C nmr (δ $CDCl_3$): 40.79 (CH_2), 122.43 (CH), 123.36 (CH), 124.16 (CH), 126.72 (CH), 127.70 (CH), 127.98 (C), 129.28 (CH), 130.01, 130.01 (CH), 137.19 (CH), 141.82 (C), 148.23 (C), 149.10 (CH), 149.91 (CH), 152.60 (C), 197.76 (C); m/z 248.

2-(1,4-Dihydro-1-methylquinilyliden-4-yl)-1-phenylethanone (**13**): Prepared by the literature method (6) (15.3%), mp 139–140°C (dec.) (lit. (6) mp 141–143°C (dec.)); ir ($CHCl_3$); 1631 (s), 1611 (w), 1597 (m), 1589 (m), 1567 (m), 1553 (m), 1520 (s), 1498 (vs), 1484 (vs), 1475 (vs) cm^{-1}; ^{1}H nmr (δ $CDCl_3$): 3.68 (3H, s, NCH_3), 6.87 (H, s, =CH), 7.0–8.6 (11H, m, Ar); ^{13}C nmr (δ $CDCl_3$): 40.65 (CH_3). 96.28 (CH), 107.42 (CH), 115.23 (CH), 123.27 (C), 123.95 (CH), 124.42 (CH), 127.32 (CH), 128.11 (CH), 130.25 (CH), 130.96 (CH), 138.88 (C), 139.29 (CH), 143.04 (C), 147.60 (C), 187.96 (C); m/z 261.

Acknowledgement

We are grateful for a grant from the Ministry of Higher Education, Iran, to H.L-K.

1. J. V. GREENHILL, H. LOGHMANI-KHOUZANI, and D. J. MAITLAND. J. Chem. Soc., Perkin Trans 1. In press.
2. A. M. STOCK, W. E. DONAHUE, and E. M. AMSTATZ. J. Org. Chem. **23**, 1840 (1958).
3. B. GOLANKIEWICZ and K. GOLANKIEWICZ. Bull. Acad. Polon. Sci. Ser. Sci. Chim. **14**, 199 (1966).
4. R. MONDELLI and L. MERLINI. Tetrahedron, **22**, 3253 (1966).
5. T. HIGISHINO, Y. NAGANO, and E. HAYASHI. Chem. Pharm. Bull. **21**, 1943 (1973).
6. G. FUKATA, C. O'BRIEN, and R. A. M. O'FERRALL. J. Chem. Soc. Perkin Trans 2, 792 (1979).
7. J. V. GREENHILL. *In* The chemistry of heterocyclic compounds; Quinolines. Part 3. *Edited by* G. Jones. John Wiley and Sons, Chichester. 1990. p. 248.
8. B. M. BAUM and R. LEVINE. J. Heterocycl. Chem. **3**, 272 (1966).
9. J. E. WOLF, D. E. PORTLOCK, and D. J. FEUERBACH. J. Org. Chem. **39**, 2006 (1974).
10. D. H. R. BARTON, J. D. ELLIOT, and S. D. GERO. J. Chem. Soc. Perkin Trans. 2, 2085 (1982).
11. N. J. LEONARD and J. H. BOYER. J. Am. Chem. Soc. **72**, 2980 (1950).
12. V. N. GOGTE, S. B. KULKARNI, and B. D. TILAK. Indian J. Chem. **15B**, 769 (1977).
13. J. KLOSA. Arch. Pharm. **285**, 364 (1952).
14. J. V. GREENHILL and H. LOGHMANI-KOUZANI. Spectrochim. Acta, **46A**, 803 (1990).

Can. J. Chem. Downloaded from www.nrcresearchpress.com by 198.100.157.202 on 09/07/12
For personal use only.

Poly(vinylbenzo macrocyclic polyethers). Synthesis and cation binding properties of 12-crown-4 derivatives

G. W. BUCHANAN[1] AND J. K. DENIKE

Ottawa–Carleton Chemistry Institute, Department of Chemistry, Carleton University, Ottawa, Ont., Canada K1S 5B6

Received August 20, 1990

G. W. BUCHANAN and J. K. DENIKE. Can. J. Chem. **69**, 702 (1991).

The synthesis of 4′-vinylbenzo-12-crown-4 ether is reported. Polymerization to relatively low molecular weight polymers can be accomplished with a free radical initiator. A copolymer with styrene can be prepared and the Li^+, Na^+, and K^+ binding properties of these polymers are compared to those of their monomeric analogs using salt distribution equilibria in water – methylene chloride. For all cations the homopolymer is found to extract the salts from the aqueous phase most effectively. The copolymer is slightly less effective than the homopolymer but more effective than either of the monomers by a factor of approximately 7, indicating that cooperative binding is likely. Na^+ is the most efficiently extracted cation, followed by K^+ and Li^+.

Key words: crown ether polymers, complexation properties.

G. W. BUCHANAN et J. K. DENIKE. Can. J. Chem. **69**, 702 (1991).

On a réalisé la synthèse de l'éther 4′-vinylbenzo-12-couronne-4. Sous l'influence d'une initiateur radicalaire, il est possible d'en faire une polymérisation qui conduit à des polymères de faibles poids moléculaires. On peut préparer un copolymère avec le styrène; utilisant l'équilibre de distribution des sels dans l'eau et le chlorure de méthylène, on a comparé les propriétés liantes de ces polymères avec le Li^+, le Na^+ et le K^+ à celles de leurs analogues monomères. Pour tous les cations, on a trouvé que l'homopolymère est le plus efficace pour extraire des sels de solutions aqueuses. Le copolymère est un peu moins efficace que l'homopolymère. Il est toutefois plus efficace que l'un ou l'autre des monomères par un facteur d'environ 7; ce résultat suggère qu'une liaison coopérative est probable. Le Na^+ est le cation qui peut être extrait le plus facilement, suivie par le K^+ et le Li^+.

Mots clés : polymères de l'éther-couronne, propriétés de complexation.

[Traduit par la rédaction]

Introduction

Polymers bearing pendant crown ethers have generated a substantial amount of interest. The early work (1) demonstrated, for 15-crown-5 and 18-crown-6 derivatives, that the 4′-vinylbenzo polymers were considerably more effective in binding cations than their monomeric analogs. Differences in binding between polymers and monomers arises from the possibility of cooperative binding between proximate crown ethers on the polymer chain, which also leads to facile binding of cations whose ionic radii exceed that of the individual crown ether cavities.

A number of potentially practical applications of such ionophoric polymers exist in the areas of thin film sensors, ion exchange membranes, ion selective electrodes, and solid electrolytes (2, 3). A major review of the work in this area is available (4).

The present study was undertaken in view of the current interest in the complexation of Li^+ by 12-crown-4 systems (5, 6) and the lack of information on binding properties of copolymeric species. Accordingly, we prepared 4′-vinylbenzo-12-crown-4, its homopolymer, and copolymer with styrene and compared the cation binding properties of these systems as well as of 12-crown-4 and benzo-12-crown-4 with Li^+, Na^+, and K^+. The synthetic scheme is such that facile ^{13}C incorporation into the vinyl group of these monomers is possible, a factor that will facilitate mobility studies of the polymers and their complexes via ^{13}C NMR spin lattice relaxation time measurements.

Discussion

The present synthetic scheme (Fig. 1) is a modification of the approach reported by Smid *et al.* (7) for 15-crown and 18-crown-6 systems with the exception of the use of the Wittig reaction for direct conversion of the formyl to the vinyl function. It is of interest to note that in the cyclization reaction to form the 12-membered ring, two other products were obtained, namely an uncyclized monoadduct and the 24-membered dimer, with structures as depicted in Fig. 2. The ratio of 12- to 24-membered crown ethers obtained in this reaction is approximately 3 to 1.

We chose to carry out the polymerization with a radical initiator as previously employed by Smid and co-workers (1) because of the simplicity of the reaction and the availability of the necessary reagents. The polymer chains are much shorter than those previously reported. We used 0.5% initiator by weight and obtained a polymer with a mean mass number of 3800. The weight is just over 10% of the values of those obtained by Smid even though we used less initiator by a factor of approximately 1.5. The polymerization properties of vinylbenzo-12-crown-4 are not expected to be significantly different from those of vinylbenzo-15-crown-5, and because the reaction time and temperature used were the same as those reported we must conclude that either our initiator was more active or that our degassing procedure was slightly less effective and that residual oxygen may also be acting as an initiator.

The identical procedure was carried out for the synthesis of the copolymer. ^1H NMR integration of the polymer obtained comparing the CH_2-O and aromatic reagents showed that both monomeric components were present in essentially equal amounts within the precision of the electronic integration ($\pm 3\%$).

We repeated Smid's procedure for the extraction of metal picrates to compare the binding efficiencies of both polymers with each of benzo-12-crown-4 and 12-crown-4 ether. Benzo-12-crown-4 was chosen over vinylbenzo-12-crown-4 because we felt that it would give a better indication of the extraction capabilities of the monomer, as vinylbenzo-12-crown-4 has an extended conjugation not found in the polymer.

In all cases polyvinylbenzo-12-crown-4 extracted the metal picrate with the highest efficiency (Figs. 3–5). At low concentrations, values for the copolymer were close but became

[1]Author to whom correspondence may be addressed.

Can. J. Chem. Downloaded from www.nrcresearchpress.com by 198.100.157.202 on 09/07/12
For personal use only.

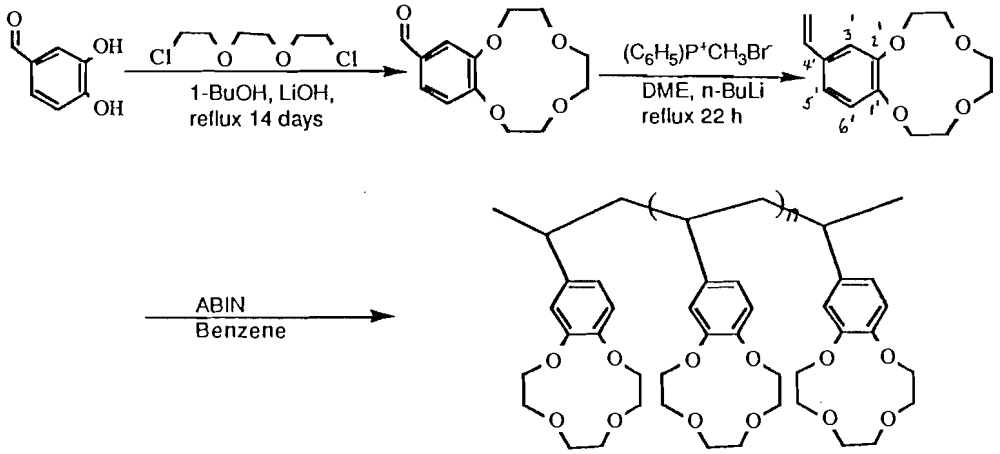


FIG. 1. Synthetic scheme for polyvinylbenzo-12-crown-4.

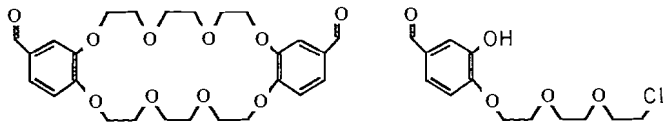


FIG. 2. Structures of the dimer and uncyclized monoadduct.

slightly lower as the concentrations increased. The values used to calculate the extraction efficiencies of the polymers are plotted as concentrations of crown ether units to concentration of picrate. If, however, the extraction efficiency was calculated on a basis of weight the homopolymer would be more efficient than the copolymer by an additional factor of 1.4, the ratio of molecular weight of repeating units. Both of the monomers were at least an order of magnitude less efficient than either of the polymers (Figs. 6–9). In all cases sodium extractions were the most efficient. This is consistent with the known stabilities of 12-crown-4 complexes (8). Lithium complexes of 12-crown-4 exhibit a 1:1 stoichiometry while analogous sodium complexes are 2:1. van Remoortere reported a complex of sodium chloride/12-crown-4 in which the sodium had a coordination number of eight binding to all eight crown ether oxygens (9). Potassium complexes are known to be less stable (8). Both of the polymers were also more than twice as effective when extracting potassium as when extracting lithium, supporting the idea of cooperative binding between adjacent crown ether moieties on the polymer chain. Of the monomers, benzo-12-crown-4 was the least effective. The benzo group increases the ridigity of the crown, thus reducing its binding capabilities relative to free 12-crown-4 ether.

Experimental

All ^{1}H NMR spectra were obtained on a Varian XL-200 200 MHz spectrometer using $CDCl_3$ as a solvent and TMS as an internal reference. ^{13}C NMR spectra were obtained at 50.3 MHz on a Varian XL 200 spectrometer using $CDCl_3$ as a solvent and TMS as an internal reference. The IR spectra were obtained on a Bomem Michelson-100 Fourier transform infrared spectrometer. The mass spectra were performed on a Finnigan VG 707E mass spectrometer.

3,4-Dihydroxybenzaldehyde was obtained from Aldrich. The ^{1}H NMR spectra indicated a high degree of impurity. Hence this material was recrystallized twice from three times its weight in water as suggested by Buck and Zimmerman (10), then judged to be pure by ^{1}H NMR; δ: 9.9 (1H, s, C*H*O), 8.7 (2H, s, O*H*), 7.4–6.9 (3H, m, aromatic *H*). ^{13}C NMR: 190.7 (*C*HO); 130.7, 115.9, 146.2, 152.1, 114.9, 125.3 (aromatic *C*) ppm.

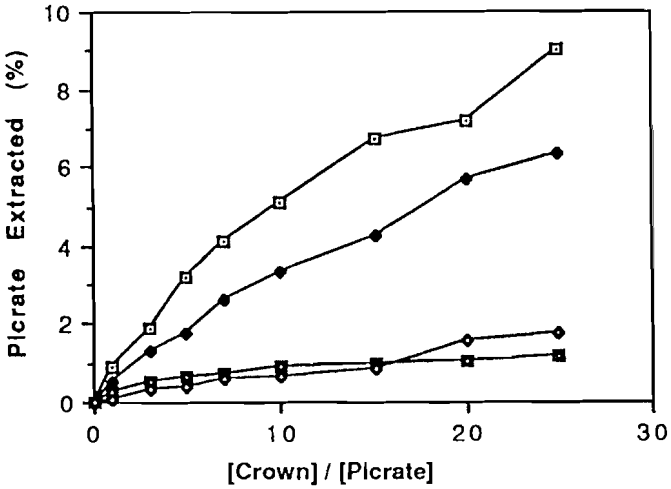


FIG. 3. Lithium extractions; ◘ PVB; ◆ COP; ■ B12C4; ◇ 12C4.

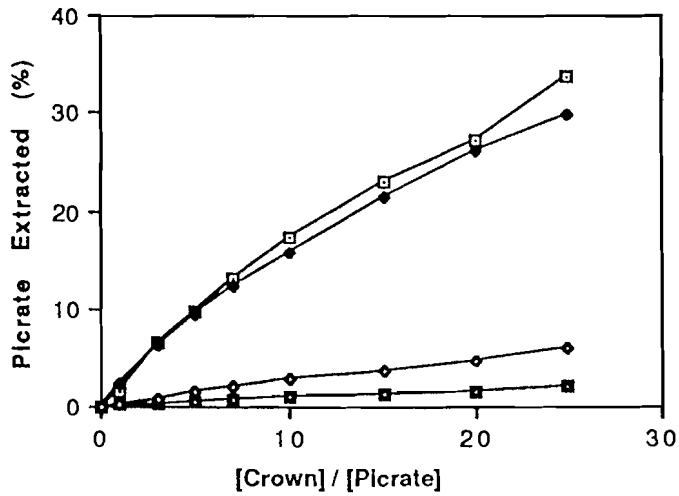


FIG. 4. Sodium extractions; ◘ PVB; ◆ COP; ■ B12C4; ◇ 12C4.

Synthesis of 4'-formylbenzo-12-crown-4

A 3-L, three-necked round bottom flask, equipped with a magnetic stirrer and reflux condenser, was charged with 1-butanol (2.0 L), 3,4-dihydroxybenzaldehyde (13.84 g, 0.10 mol), 1,8-dichloro-3,6-dioxaoctane (18.76 g, 0.10 mol), and lithium hydroxide (4.79 g, 0.20 mol) and the mixture was refluxed for 10 days. The solvent was removed by evaporation at reduced pressure and the resultant black

Can. J. Chem. Downloaded from www.nrcresearchpress.com by 198.100.157.202 on 09/07/12
For personal use only.

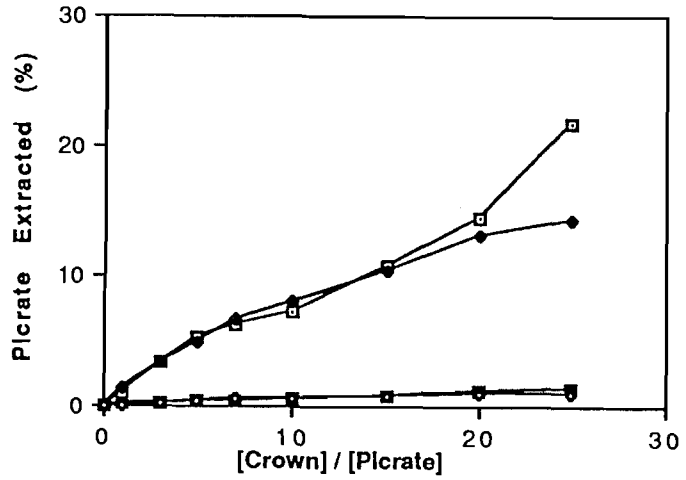


FIG. 5. Potassium extractions; ◘ PVB; ◆ COP; ■ B12C4; ◇ 12C4.

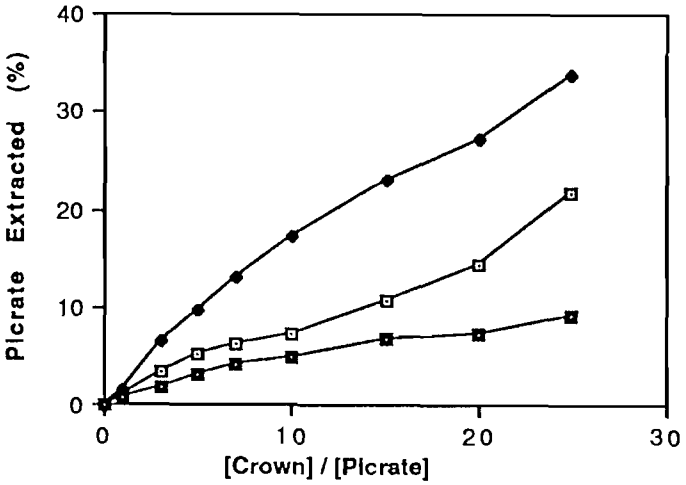


FIG. 6. Cation extractions with polyvinylbenzo-12-crown-4; ◘ K; ◆ Na; ■ Li.

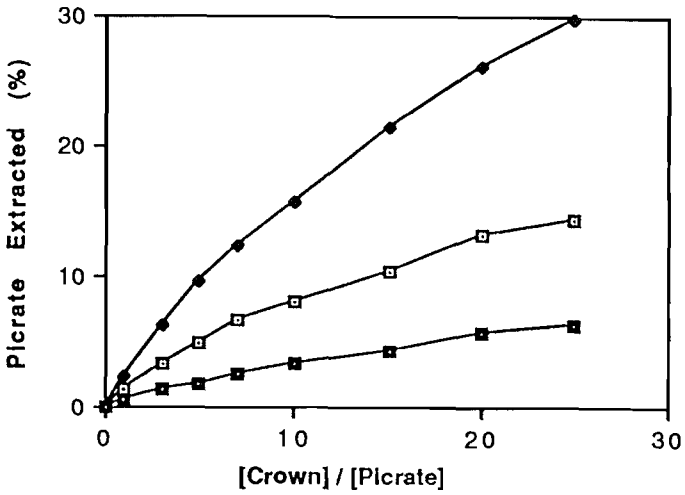


FIG. 7. Cation extractions with vinylbenzo-12-crown-4/styrene copolymer; ◘ K; ◆ Na; ■ Li.

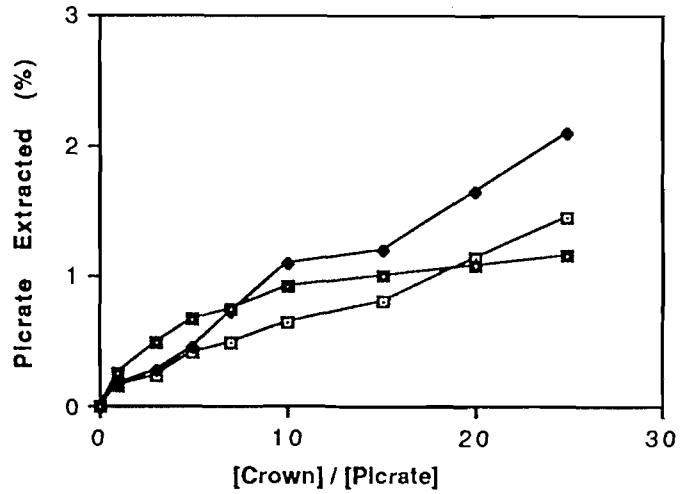


FIG. 8. Cation extractions with benzo-12-crown-4; ◘ K; ◆ Na; ■ Li.

slurry was dissolved in dichloromethane (500 mL). The water soluble salts were removed by filtration and subsequently washed with an additional 100 mL of dichloromethane. The combined organics were washed with HCl (1 M, 3 × 100 mL), water (3 × 100 mL), and saturated sodium chloride (1 × 100 mL), then dried over anhydrous sodium sulfate. The solvent was removed by evaporation at reduced pressure and the resultant black slurry was purified by column chromatography on silica gel (grade 923, 100–200 mesh) with 40% ethyl acetate in hexane as eluent. Three products, as well as starting material, were isolated. These were the desired product (recrystallized from ethyl acetate), its dimer, and the uncyclized mono adduct.

4′-Formylbenzo-12-crown-4: yield: 3.71 g, 14.72%; mp 81–82°C. IR: 1685.2 (CHO) cm^{-1}. ^1H NMR, δ: 9.84 (1H, s, C*H*O), 7.5–7.0 (3H, m, aromatic *H*), 4.38–3.79 (12H, m, CH_2). ^{13}C NMR: 190.6 (*C*HO); 156.5, 150.7, 131.1, 127.3, 118.2, 116.1 (aromatic *C*); 72.7, 71.3, 70.8, 70.7, 69.6, 69.4 (O-CH_2-CH_2-O). MS: M^+, 252; other peaks at 164, 149, 45. Anal. calcd. for $C_{13}H_{16}O_5$: C 61.90, H 6.39; found: C 61.66, H 6.64.

Dimer: yield: 0.63 g, 5.0%; mp 134–136°C. IR: 1685.2 (CHO) cm^{-1}. ^1H NMR, δ: 9.84 (1H, s, C*H*O), 7.5–7.0 (3H, m, aromatic *H*), 4.38–3.79 (12H, m, O-CH_2-CH_2-O). ^{13}C NMR: 190.8 (*C*HO); 154.1, 159.0, 130.1, 126.8, 111.7, 110.8 (aromatic *C*); 71.49, 71.40, 69.61, 69.44, 69.37, 69.30 (O-CH_2-CH_2-O). CIMS: M + 1, 505; other peaks at 149, 45.

Preparation of triphenylmethyl phosphonium bromide

The triphenylmethyl phosphonium bromide was prepared by the method outlined in Vogel (11). Yield: 44.98 g (98%); mp 231–233°C.

Preparation of 4′-vinylbenzo-12-crown-4

A dry 500-mL, three-necked round bottom flask, equipped with a magnetic stirrer, reflux condenser, and dropper funnel, was charged with 1,2-dimethoxyethane (60 mL) and triphenylmethyl phosphonium-bromide (6.32 g, 17.70 mmol). *n*-Butyllithium (1.6 M in hexane, 11.2 mL, 17.70 mmol) was added dropwise over a period of 10 min. The mixture turned orange and was stirred for an additional 90 min. 4′-Formylbenzo-12-crown-4 (2.98 g, 11.80 mmol) was dissolved in 100 mL of 1,2-dimethoxyethane and added dropwise over a period of 60 min. The resultant suspension was refluxed for 20 h, then cooled to room temperature. It was filtered and the filter cake was washed with ether (3 × 30 mL). The combined organics were washed with water (3 × 100 mL) followed by saturated sodium chloride (1 × 100 mL), then dried over anhydrous sodium sulfate and the solvent was removed by evaporation at reduced pressure. The resultant slurry was left at room temperature, causing triphenylphosphine oxide to crystallize out as colourless prisms. The remaining oil was purified by flash chromatography on silica gel (grade 923, 100–200 mesh) using 40% ethyl acetate in hexane as the solvent.

4′-Vinylbenzo-12-crown-4: yield 1.85 g, 62.6%. ^{13}C NMR, δ: 150.5 (C1′, C2′); 136.2 (vinyl methine); 132.5 (C4′); 121.1 (C5′);

Can. J. Chem. Downloaded from www.nrcresearchpress.com by 198.100.157.202 on 09/07/12
For personal use only.

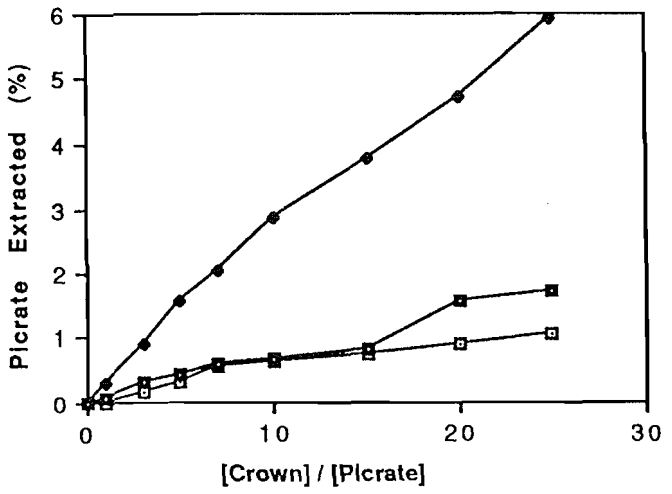


FIG. 9. Cation extractions with 12-crown-4; ◘ K; ◆ Na; ■ Li.

117.7 (C6′); 115.7 (C3′); 112.5 (vinyl methylene); 71.8, 71.6, 70.8, 70.1, 69.7 (relative intensity 2) (OCH_2-CH_2O). CIMS: M + 1, 251 (100%); other peaks at 164, 149, 45.

Polymerization of 4′-vinylbenzo-12-crown-4

4′-Vinylbenzo-12-crown-4 (1.00 g, 4.0 mmol) and azobis(isobutyronitrile) (AIBN) (0.0051 g), a radical initiator, were dissolved in benzene (60 mL) and degassed using a high vacuum and four freeze–pump–thaw cycles. The ampoule was sealed under vacuum and heated to 70°C for 48 h. The solution was then slowly added to approximately 20 times its volume of petroleum ether and the white precipitate was filtered off. The polymer was reprecipitated once again and dried under vacuum. The polymer had an M_n of 3800 and a M_w of 5500 as determined by gel permeation chromatography. Yield: 96%; mp 115–133°C. ^{1}H NMR, δ: 6.62–6.11 (3H, aromatic *H*), 4.2–3.6 (12H, O-CH_2-CH_2-O), 1.16–2 (3H, benzylic *CH*, CH_2). ^{13}C NMR: 149.9, 148.2, 140.2, 128.3, 121.7, 117.9 (aromatic *C*); 71.6–69.8 (O-CH_2-CH_2-O); 40.2 (benzylic *CH*, CH_2).

The copolymer was also prepared by the same procedure using equimolar quantities of 4′-vinylbenzo-12-crown-4 and styrene with the same ratio of initiator. The polymer had an M_n of 2700 and a M_w of 3500 as determined by gel permeation chromatography. Yield: 92%; mp 118–134°C. ^{13}C NMR (APT), δ: 152.2, 149.4, 147.6–144.8, 142.5–139.6 (quaternary aromatic); 127.9, 125.6, 121.7, 118.8 (tertiary aromatic); 71.6–69.8 (O-CH_2-CH_2-O); 40.5–40.1 (benzylic *CH*, CH_2).

Extractions

A metal hydroxide solution (0.01 M) containing a small amount of picric acid (7×10^{-5} M) was vigorously shaken with an equal volume of methylene chloride solution of the crown ether. Molar ratios of 0, 1, 3, 5, 7, 10, 20, and 25 of crown ether to picrate were employed. The layers were separated and filtered to remove cloudiness. The concentration of picrate was determined by visible spectroscopy using the extinction coefficients reported by Pedersen (12) (λ_m 357 nm, ε 1.5×10^4 in water, and λ_m 378 nm, ε 1.8×10^4 in CH_2Cl_2). The results are shown in Figs. 3–9.

Acknowledgements

We thank Dr. J. Roovers (NRC Ottawa) for the polymer molecular weight determinations. Continuing financial support from the Natural Sciences and Engineering Research Council of Canada is gratefully acknowledged.

1. S. KOPOLOW, T. E. HOGEN ESCH, and J. SMID. Macromolecules, **6**, 133 (1973).
2. J. M. GOLD, T. E. TEEGARDEN, K. M. MCCRANE, D. J. LUCA, P. A. FALCIGNO, C. C. CHEN, and T. W. SMITH. J. Am. Chem. Soc. **108**, 5827 (1986).
3. M. A. KAPLAN, E. A. RIETMAN, R. J. CAVA, L. K. HOLT, and E. A. CHANDROSS. Solid State Ionics, **25**, 37 (1987).
4. J. SMID and R. SINTA. Top. Curr. Chem. **121**, 105 (1983).
5. P. P. POWER. Acc. Chem. Res. **21**, 147 (1988).
6. G. W. BUCHANAN, R. A. KIRBY, and K. BOURQUE. Can. J. Chem. **67**, 449 (1989).
7. J. SMID, B. EL HAJ, T. MAJEWICZ, A. NONNI, and R. SINTA. Org. Prep. Proced. Int. **8**, 193 (1976).
8. F. A. L. ANET, J. KRANE, J. DALE, K. DAASVATN, and P. O. KRISTIANSES. Acta Chem. Scand. **27**, 3395 (1973).
9. F. P. VAN REMOORTERE and F. P. BOER. Inorg. Chem. **13**, 2071 (1974).
10. J. S. BUCK and F. J. ZIMMERMAN. Org. Synth. Coll. Vol. II, 549 (1943).
11. A. I. VOGEL. A textbook of practical organic chemistry. 4th ed. Longman, New York. 1979. p. 337.
12. C. J. PEDERSEN. Fed. Proc. **27**, 1305 (1968).

Can. J. Chem. Downloaded from www.nrcresearchpress.com by 198.100.157.202 on 09/07/12
For personal use only.

The rapid synthesis of organic compounds in microwave ovens. II

RICHARD N. GEDYE,[1] WERNER RANK, AND KENNETH C. WESTAWAY[1]
Chemistry Department, Laurentian University, Sudbury, Ont., Canada P3E 2C6

Received June 29, 1990

RICHARD N. GEDYE, WERNER RANK, and KENNETH C. WESTAWAY. Can. J. Chem. **69**, 706 (1991).

Using microwaves to carry out organic reactions does not significantly alter the product composition. The small changes in product composition that are observed when microwaves are used arise because the microwave reactions occur at higher temperatures than reflux reactions. The results demonstrate that ions in the reaction mixture alter the heating rate of the microwave reactions. Although scaling-up the reaction leads to a slightly lower rate of reaction (lower percentage yield), one still retains large rate enhancements.

Key words: microwave, synthesis, product composition, scale-up, ionic strength effects.

RICHARD N. GEDYE, WERNER RANK et KENNETH C. WESTAWAY. Can. J. Chem. **69**, 706 (1991).

L'utilisation de micro-ondes pour effectuer des réactions organiques ne modifie pas la composition des produits d'une façon importante. Les petits changements qui sont observés dans la composition des produits lorsqu'on utilise des micro-ondes proviennent du fait que les réactions effectuées sous l'influence de micro-ondes se produisent à des températures plus élevées que les réactions effectuées au reflux du solvant. Les résultats démontrent que les ions présents dans les milieux réactionnels influencent les taux de chauffage des réactions effectuées sous l'influence de micro-ondes. Les réactions sur de plus grandes quantités de substances condusient à des vitesses de réaction légèrement plus faibles (pourcentage de rendement inférieur); on observe toutefois des augmentations importantes des vitesses.

Mots clés : micro-onde, synthèse, composition des produits, reactions sur de plus grandes quantités, effets des ions.

[Traduit par la rédaction]

Introduction

Previous work has shown that organic reactions occur very much faster when carried out in sealed containers in a microwave oven than when they are done using conventional (reflux) techniques (1–4). In fact, rate enchancements of between 10 and 1200 were observed when a variety of organic reactions were carried out in sealed Teflon containers (2). However, it was not established whether the microwave technique only alters the rate of reaction or whether the microwaves influence the reaction pathways thereby leading to product compositions different from those obtained using conventional heating techniques. This issue is addressed in this report.

Results and discussion

Product composition in elimination–substitution reactions

The influence of microwave heating on product composition has been determined by examining the products from three different reactions. The first set of experiments studied the reactions of 1-bromooctane with (i) methoxide ion in methanol and (ii) with *tert*-butoxide ion in *tert*-butyl alcohol, eq. [1].

[1] $$CH_3(CH_2)_6CH_2Br + OR^- \longrightarrow CH_3(CH_2)_5CH{=}CH_2 + CH_3(CH_2)_6CH_2OR$$
$$(R = CH_3 \text{ and } (CH_3)_3C)$$

The ratios of the elimination/substitution products, expressed as the percent elimination product(s), obtained under normal reflux conditions were compared with those found when the reactions were done in a sealed Teflon container in the microwave oven.

The results in Table 1 indicate that neither reaction is affected significantly by a change in technique. Although more elimination product was obtained in the microwave oven experiments, the percent elimination in the methoxide ion reaction only changed from 2.4 to 4.4% when the reaction was carried out in the microwave oven rather than under reflux conditions.

[1]Authors to whom correspondence may be addressed.

TABLE 1. The product composition for the elimination–substitution reactions of 1-bromooctane and 2-bromooctane with alkoxide ion

Substrate	Base/solvent	% Alkene (reflux)[a]	% Alkene (microwave)[b]
1-Bromooctane	CH_3O^-/CH_3OH	2.4±0.4	4.4±0.1
1-Bromooctane	t-BuO^-/t-BuOH	5.3±0.1	14±4
2-Bromooctane	CH_3O^-/CH_3OH	70±5	67±1
2-Bromooctane	t-BuO^-/t-BuOH	100	100

[a]All the reflux reactions were heated for 1 h.

[b]The methoxide ion reactions were heated for between 45 s and 1.5 min at power level 7. The *tert*-butoxide ion reactions were heated for 10 min at power level 9.

The amount of elimination product was slightly higher when the base was changed from methoxide ion to *tert*-butoxide ion, Table 1. Again, changing the heating method did not markedly alter the amount of elimination product. The percent elimination increased from 5.3% under reflux conditions to 14% when the reaction was carried out in the microwave oven, i.e., the amount of substitution product only changes from 95% to 86%. Thus, from a synthetic point of view, the change in the product composition resulting from microwave irradiation is not significant.

This conclusion was corroborated by the product ratios from the reactions between 2-bromooctane and (i) methoxide ion in methanol and (ii) *tert*-butoxide ion in *tert*-butyl alcohol, eq. [2].

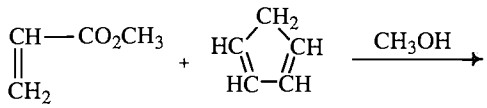
[2] $$CH_3(CH_2)_5CHBrCH_3 + OR^- \longrightarrow CH_3(CH_2)_5CH{=}CH_2 + CH_3(CH_2)_4CH{=}CHCH_3 + CH_3(CH_2)_5CHORCH_3$$
$$(R = CH_3 \text{ and } (CH_3)_3C)$$

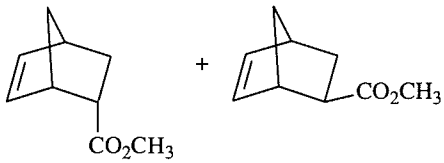
Although the amount of elimination was much higher from the secondary bromide as expected (5), changing the heating method from the microwave to the reflux technique did not significantly alter the product composition, Table 1. In fact, within experimental error, the percent elimination from both reactions was identical for the two heating methods.

Can. J. Chem. Downloaded from www.nrcresearchpress.com by 198.100.157.202 on 09/07/12
For personal use only.

Product composition in a Diels–Alder reaction

The conclusion based on the elimination/substitution ratios was tested further by determining the product composition of a Diels–Alder cycloaddition reaction between cyclopentadiene and methyl acrylate, eq. [3].

[3] 



This particular Diels–Alder reaction was chosen because (i) it had been studied at several different temperatures by Berson *et al.* and (ii) it showed the greatest change in product composition with temperature (6). The product ratios obtained in this investigation and by Berson *et al.* are presented in Table 2. Since the only products were the *endo* and *exo* adducts, the product composition can be reported as the percent *endo* product. The product compositions reported by Berson *et al.* (6) are, within the experimental error of the method, identical to those found in this study.

Again, from a synthetic point of view, the product composition observed with the microwave method is not significantly different from that found when heating with the conventional technique. In fact, the *endo* product in the microwave experiment only differs by 6% from the reflux results reported by Berson *et al.* Furthermore, when the temperature effect is taken into consideration, the change in the product composition is even smaller. The pressures found when various volumes of methanol were heated in sealed Teflon reaction vessels in the microwave oven suggest that the reaction mixture would have been at a temperature of approximately 110°C (7). If one accepts this temperature for the Diels–Alder reaction in the microwave experiment, the product composition is almost exactly what would be expected. The plot of the temperature versus percent *endo* adduct reported by Berson *et al.* (6) is effectively linear between 0 and 60°C, Fig. 1. If one assumes the relationship remains linear to 110°C, the product composition should be approximately 80% *endo* at this temperature. Since the product from the microwave reaction is 79% *endo*, it appears that the change in product composition is due to the change in the reaction temperature rather than to any special effects of the microwaves on the reaction.

The small change in the product composition that is observed in these reactions would be expected if the microwave heating technique only causes the reaction to occur at a higher temperature in the sealed Teflon container. If one increases the temperature, one increases the rate constant for the formation of both products. However, if measurable amounts of two products are obtained from competing reactions, their rate constants, and probably their $\Delta H^{\neq}$ (enthalpy of activation) values, are comparable. Since the change in the rate constant with temperature depends on the $\Delta H^{\neq}$ values for the competing reactions (8), a temperature increase should have only a small effect on the composition of the product. In fact, the rate constant for the reaction with the higher $\Delta H^{\neq}$ (the slower reaction) will increase slightly more with an increase in temperature. As a result, the yield of the minor component should increase when the reaction temperature is increased. This is observed in the Diels–Alder reaction. The percent *endo*, the major product in the reaction, is lower when the reaction is done at the higher temperature in the microwave oven. The same trend is observed in the 1-bromooctane reactions (Table 1). The percent elimination, the minor product in the elimination–substitution reaction, is greater in the microwave reactions with both the methoxide ion and the *tert*-butoxide ion. Thus, the concentration of the minor product increases in these three reactions when the reaction temperature increases.

In contrast, the percent elimination does not increase when 2-bromooctane is reacted with methoxide ion in the microwave oven (Table 1). The elimination/substitution ratio is only 2.3:1 in this reaction. This suggests that the $\Delta H^{\neq}$ values for the elimination and the substitution reactions are almost equal. If this is the case, the product ratio should not change noticeably with a change in reaction temperature.

The results of these investigations, although not exciting from a synthetic point of view, are important because they confirm that the microwaves do not alter the reaction but simply provide a much faster and more efficient (higher temperature) method of carrying out organic reactions. The changes in

TABLE 2. Product distribution in the Diels–Alder reaction between cyclopentadiene and methyl acrylate

Temperature (°C)	% *endo* classical (ref. 6)	% *endo* classical (observed)	% *endo* microwave (observed)
0	89.8	87.8	—
21	87.5	86.1	–
56	84.9	—	—
110[a]	—	—	79.0

[a]Temperature estimated from the pressures observed (7) when the same volume of methanol was heated in the sealed Teflon reaction vessels.

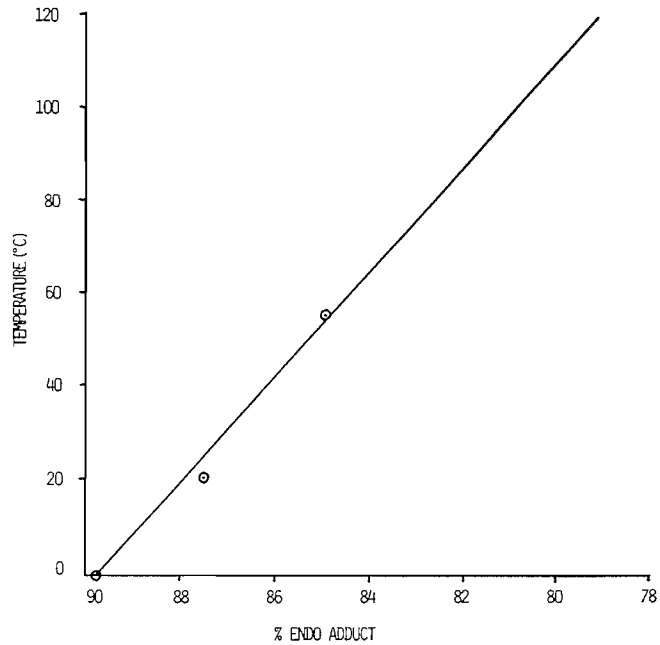


FIG. 1. Effect of temperature on the product composition of the Diels–Alder reaction.

Can. J. Chem. Downloaded from www.nrcresearchpress.com by 198.100.157.202 on 09/07/12
For personal use only.

product composition caused by the higher temperatures in the microwave oven are small because the $\Delta H^{\neq}$'s of the two competing reactions are undoubtedly close.

It is possible, however, that microwave reactions could have different products from reactions done using the conventional reflux technique. Since microwave heating markedly increases the reaction temperature, it is possible that the microwave reaction temperature could exceed the temperature (activation energy) required for a new reaction that was not possible at the lower reflux temperature. If this were the case, different products could be obtained in the microwave and the conventional reactions. In these instances, however, the amount of the new product should be small.

In fact, one instance of this phenomenon may have been found. Lubec *et al.* (9) reported that a small amount of the amino acids *trans*-3- and *trans*-4-hydroxyproline isomerize to the corresponding *cis* isomers when they are heated in a microwave oven. This isomerization does not occur when these *trans* amino acids are heated using conventional techniques. Although the reaction conditions for this experiment were not clear, the isomerization could have occurred because a higher reaction temperature was reached in the microwave oven. In any case, it is important to note that microwave heating would not be expected to change the product composition significantly from a synthetic point of view.

The effect of ions on the heating rate of microwave reactions

We have also discovered that adding ionic compounds, or compounds that generate ions in solution, affects the heating rates in microwave reactions. For example, adding sulfuric acid, sodium hydroxide, or sodium chloride to a reaction mixture leads to an increased heating rate relative to that found for solvent alone, Fig. 2. The faster heating rate found for ionic solutions is presumably observed because a new heating mechanism, ionic conductance, is added to the normal (dielectric) heating mechanism (10).

In addition, the change in the heating rate with a change in volume is different for the solvent alone and when the solvent contains ions. In water, the maximum heating rate is found when 15 mL of water is in the sealed Teflon reaction vessel (2). However, when ions are present in the reaction mixture, the maximum heating rate is observed when the reaction volume is 5 mL, the smallest volume investigated, Figs. 3 and 4. Ions in a solution increase the absorption of microwave energy through ionic conductance (10). If one assumes that an ionic solution absorbs all, or almost all, of the microwave energy, larger volumes heat up more slowly because the same amount of microwave energy heats a larger number of molecules.

The discovery that ions affect the heating rates obviously has implications when planning a microwave reaction. Since the heating rate is greater when ions are present, the maximum safe pressure may be reached much faster than one would expect from the heating profile of the solvent alone. To avoid the possibility of an explosion (2), it is important to know the heating characteristics of the reaction mixture before one begins an experiment.

Scaling-up microwave reactions

We have also explored scaling-up the microwave reactions. The approach has involved heating larger volumes of reaction mixtures in sealed Teflon containers connected to a pressure gauge. In these experiments the reaction mixture was heated at maximum power (750 watts) until the pressure reached approximately 70 psi, the maximum pressure that was considered to be

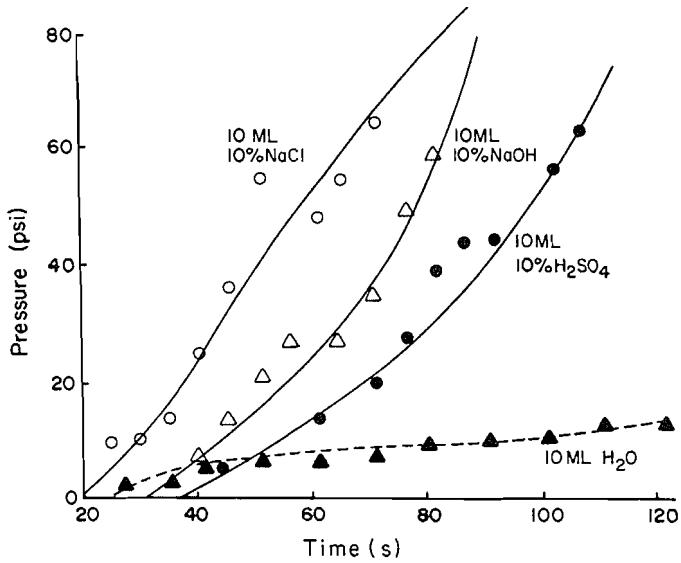


FIG. 2. The effect of the presence of ions in solution on the microwave heating rate in a 150-mL Savillex vessel.

safe (1 psi = 6.9 kPa). Then, the power setting was reduced to 2 or 3 (153 or 234 W) so that the pressure did not exceed a safe level. An alternative and equivalent programming technique is to operate the magnetron at full power for short periods to keep the pressure in the Teflon reaction vessel between 60 and 70 psi. Either programming technique allows the preparation of larger quantities of compounds while retaining the short reaction times and reducing the danger of an explosion.

Three reactions were investigated in the scaling-up experiments. These reactions were chosen because (i) they were relatively slow and (ii) the programming technique might be useful in driving them to completion. Two of the reactions, the hydrolysis of *N*-phenylbenzamide in 20% sulfuric acid, and the acid-catalyzed esterification of benzoic acid with 2-butanol, had ions in the reaction mixture. The third reaction, the hydrolysis of benzyl chloride, was done in water containing no ions.

Reactions with ions in the reaction mixture

In the acid-catalyzed hydrolysis of *N*-phenylbenzamide and in the acid-catalyzed esterification of benzoic acid, the yield obtained after identical reaction times (the rate of reaction), decreased as the reaction was scaled-up, Table 3. The percent yield decreased from 69 to 35% when the reaction volume was increased from 5 to 25 mL in the 8-min *N*-phenylbenzamide hydrolyses. This observation was confirmed by the fact that the yield (reaction rate) in the 16-min, 25-mL *N*-phenylbenzamide hydrolysis was lower than the yield in the 12-min, 10-mL hydrolysis reaction.

A similar trend was observed in the 8-min esterification reactions. The yield (rate) decreased from 53 to 42% when the reaction volume was increased from 10 to 30 mL. This decreased yield with increasing reaction volume is consistent with the heating rates observed when ions are present in solution, i.e., the greatest heating rate and fastest reaction (highest yield) were observed with the smallest (5 mL) reaction volume, Figs. 3 and 4.

It is important to note that although the rate of reaction decreased when the reactions were scaled-up, high rate enhancements were still observed. Rate enhancements of between 36 and 90 were observed in the scaled-up esterification and hydrolysis reactions.

Can. J. Chem. Downloaded from www.nrcresearchpress.com by 198.100.157.202 on 09/07/12
For personal use only.

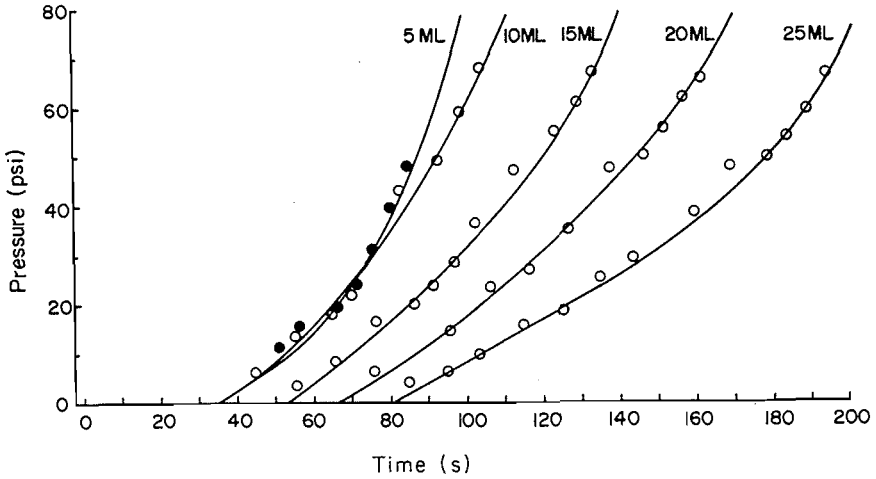


FIG. 3. Heating rates for various volumes of 10% sulfuric acid in a 150-mL Savillex vessel at 560 W in a microwave oven.

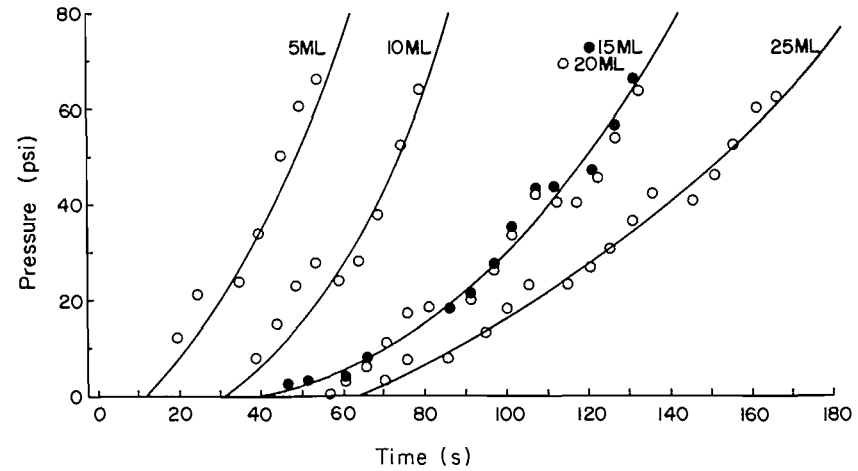


FIG. 4. Heating rates for various volumes of 10% sodium hydroxide in a 150-mL Savillex vessel at 560 W in a microwave oven.

TABLE 3. The reaction times, yields, and rate enhancements for different microwave reactions with programming

Weight reactant (g) / Volume solvent (mL)	Reaction time (min)	Yield (%)	Rate enhancement
Hydrolysis of *N*-phenylbenzamide			
0.5/5	8.0	69	—
1.0/10	8.0	47	—
2.5/25	8.0	35	—
1.0/10	12.0	74	90
2.5/25	16.0	52	68
Esterification of benzoic acid with 2-butanol			
1.3/10	8.0	53	—
2.6/20	8.0	49	36
3.9/30	8.0	42	—
3.9/30	30.0	70	—

Finally, programming was shown to be effective in increasing the yield. The yield in the *N*-phenylbenzamide hydrolysis reactions increased from 47 to 74% when the reaction time was increased from 8 to 12 min in the 10-mL experiments, and from 35 to 52% when the reaction time was increased from 8 to 16 min in the 25-mL experiments. Similarly, the yield increased from 42 to 70% in the esterification reaction when the reaction time was increased from 8 to 30 min in the 30-mL (the slowest) reaction.

Reactions with no ions in the reaction mixture

In the benzyl chloride hydrolysis in the absence of ions, the rate of reaction parallels the heating rate of the pure solvent, Table 4. The rate (yield/min) increases from 17%/min in the 3.0-min, 10-mL reaction to a maximum of 45%/min in the 2.0-min, 15-mL reaction. Then, the rate decreases slowly to a low of 9%/min as the reaction volume is increased to 50 mL. Thus the reaction rate is a maximum when the reaction volume is 15 mL, the volume of water for which the maximum heating rate was observed (2). This conclusion is confirmed by the fact that the rate enhancement and the heating rate (the time for the reaction mixture to reach a pressure of 60 psi is a minimum) are a maximum when the reaction volume is 15 mL.

Again, significant rate enhancements are observed at all

Can. J. Chem. Downloaded from www.nrcresearchpress.com by 198.100.157.202 on 09/07/12
For personal use only.

TABLE 4. The reaction times, yields, and rate enhancements for the hydrolysis of benzyl chloride with water

Weight reactant (g) / Volume solvent (mL)	Reaction time (min)	Yield (%)	Rate enhancement	Time to 60 psi (s)
0.50/10	3.0	50	—	—
0.75/15	2.0	89	20	57
1.0/20	3.0	95	10	73
1.25/25	3.0	96	9	71
1.5/30	3.0	97	11	75
2.5/40	3.0	66	7.6	100
3.5/50	5.0	44	—	106

reaction volumes when programming is used in microwave reactions. The rate enhancements range from 8 to 20 depending on the reaction volume.

Finally, it is worth noting that the amount of product is actually greater in the scaled-up experiments even though the reaction rate (percentage yield) decreases when the reactions are scaled-up. For example, a 44% yield of benzyl alcohol in a 50-mL benzyl chloride hydrolysis reaction corresponds to 1.32 g whereas a 95% yield in a 20-mL reaction is only 0.82 g.

Conclusion

This study has shown that microwaves do not significantly alter the product composition of a reaction. Rather, small changes in product composition arise because microwave reactions occur at higher temperatures than reflux reactions.

The presence of ions in the reaction mixture increases the heating rate of microwave reactions. Also when ions are present in solution, the maximum heating rate is observed at the smallest volume rather than at the intermediate (specific) volumes found for the solvent alone. Scaling-up the reaction leads to a slightly slower reaction rate and a lower percentage yield of product after the same reaction time. However, scaling-up is useful from a synthetic point of view because the larger reactions yield more product even though the percent yield is lower. Although the reaction rate is reduced when the reactions are scaled-up, large rate enhancements are still observed.

Experimental

Apparatus

The microwave oven used for this study was a domestic Toshiba model ER-8000 BTC with nine power settings, starting at 72 W and increasing by 81-W increments to 720 W. Unless otherwise stated, microwave reactions were carried out in 150-mL PFA Teflon containers manufactured by the Savillex Corporation (11).

Product analysis

The nmr spectra were recorded on a Varian T-60 nmr spectrometer. The ir spectra were recorded using sodium chloride discs on a Beckman Acculab I double beam spectrophotometer. The product compositions were determined with a Varian Aerograph model 90-P-3 gas chromatograph and a Varian CDS 111 integrator. A 3 m × 3 mm stainless steel column containing 7% SE-30 on 80/100 Chromosorb W was used at 124°C and a helium flow rate of 50 mL/min to determine the elimination–substitution product ratios. A 2 m × 3 mm Carbowax 1500 column was used at 105°C and a helium flow rate of 85 mL/min to determine the *endo*/*exo* ratio in the Diels–Alder reaction. The product ratios are the average of at least three analyses of the same reaction.

Pressure measurements

Pressure measurements were carried out by connecting the cap of a 150-mL Savillex Teflon bottle to a pressure gauge outside the microwave oven. The bottle was connected to the Union Carbide, 0–100 psi, pressure gauge by a 1/4 in. to 1/8 in. Swagelok reducing adapter, a 1/8 in. Teflon tube that passed through a small hole drilled in the back of the oven, and a Swagelok fitting. The pressure was recorded at regular intervals (usually every 30 s) for the duration of the heating period.

Safety precautions

Increasing the volume of the reaction mixture causes an increase in pressure and temperature that can lead to deformation and (or) explosion of the Teflon vessel. To ensure a safe experiment, one should either monitor the pressure and reduce the power level to maintain the pressure at a safe value, or keep the reaction time very short and the reaction volume to 10% of the volume of the container. When volatile solvents are used in sealed reaction vessels, power levels of greater than 560 W should be avoided, except for very short periods of time. Experiments in microwave ovens should be carried out in a fumehood.

Rate enhancements

The rate enhancement for comparable microwave and conventionally heated reactions, using identical concentrations of reactants, were calculated in the following manner:

$$\text{Rate enhancement} = (\text{conventional reaction time}/\text{microwave reaction time})$$

where the conventional reaction time and the microwave reaction time are for reactions taken to the same extent of completion.

Elimination–substitution reactions

General procedure

All of these reactions were carried out (a) under reflux conditions and (b) under microwave conditions using 1- or 2-bromooctane (1.0 g, 5 mmol) and 10.0 mL of 2 M sodium methoxide in methanol or 10.0 mL of 2 M sodium *tert*-butoxide in *tert*-butyl alcohol.

The reflux reactions were carried out for 1 h, whereas the heating conditions, i.e., the time and power level, for the microwave reactions varied because of the different volatilities and heating rates of the solvents. For example, the microwave reactions in methanol took much less time than those in *tert*-butyl alcohol because methanol absorbs microwave energy much more rapidly than *tert*-butyl alcohol.

In the microwave oven reactions, the reactants were mixed in the Teflon vessel, and the sealed vessel was placed in the microwave oven and heated at the appropriate power level for the specified time. The reaction vessel was left for 2 min to reduce the pressure. Then the vessel was removed from the oven and cooled in ice-water for 5 min. Water was added to the cooled reaction mixture and the products were extracted with ether. The combined ether layers were dried over anhydrous $MgSO_4$ and the ether solution was filtered and evaporated. These products were analysed by ir, and glc, and, in some cases, nmr. The spectroscopic and glc data for each reaction are as follows.

Reaction of 1-bromooctane with sodium methoxide in methanol

(a) Under reflux conditions: ir ν: 2970–2930, 1450 and 1115 (ether) cm^{-1}; nmr δ: 0.60 (t, 3H, $-CH_2CH_3$), 0.80–1.10 (m, 12H, $-CH_2-$), 2.80 (s, 3H, $-OCH_3$) overlapping with 2.90 (t, 2H, $-OCH_2-$) ppm; glc: 2 product peaks, retention times 2.0 min (2.4%, alkene) and 5.0 min (97.6%, ether).

(b) Under microwave conditions: This reaction was carried out in a 300-mL Berghof Teflon bottle for 1.5 min at power level 7 (560 W). The ir and nmr spectra of the products were identical to those from the reflux reaction; glc: 2 product peaks, retention times 2.0 min (4.4%, alkene) and 5.1 min (95.6%, ether).

Reaction of 1-bromooctane with sodium tert*-butoxide in* tert*-butyl alcohol*

(a) Under reflux conditions: ir ν: 3000–2880, 1465, 1360, 1200 (ether), and 910 (alkene, $=CH_2$) cm^{-1}; nmr δ: 0.62 (t, 3H, $-CH_2CH_3$), 0.98 (s, 9H, $-C(CH_3)_3$) superimposed on 0.95–1.03 (m, 10H, $-CH_2-$),

Can. J. Chem. Downloaded from www.nrcresearchpress.com by 198.100.157.202 on 09/07/12
For personal use only.

2.88 (t, 2H, -OCH_2-) ppm; glc: 2 product peaks, retention times 1.9 min (5.3%, alkene) and 10.0 min (94.7%, ether).

(b) Under microwave conditions: The reaction time was 10 min at power level 9 (720 W). The ir and nmr spectra of the product were identical to those found in the reflux reaction; glc: 2 product peaks, retention times 1.9 min (14%, alkene) and 9.8 min (86%, ether).

Reaction of 2-bromooctane with sodium methoxide in methanol

(a) Under reflux conditions: ir ν: 2960–2860, 1430, 1370, 1180 (ether), 960 (*trans* alkene), and 910 (alkene, $=CH_2$) cm^{-1}; glc: 2 product peaks, retention times 2.25 min (70%, alkene) and 4.29 min (30%, ether).

(b) Under microwave conditions: Reaction times varied between 45 s and 1 min at power level 7 (560 W). The ir spectrum of the product was identical to that found for the reflux reaction; glc: 2 product peaks, retention times 2.24 min (67%, alkene) and 4.23 min (33%, ether).

Reaction of 2-bromooctane with sodium tert*-butoxide in* tert*-butyl alcohol*

(a) Under reflux conditions: ir ν: 2980–2880, 1460, 1375, and 910 (alkene, $=CH_2$) cm^{-1}; glc: 1 product peak, retention time 2.19 min (100%, alkene).

(b) Under microwave conditions: The reaction time was 10 min at power level 9 (720 W). The ir spectrum of the product was identical to that found for the reflux reaction; glc: 1 product peak, retention time 2.15 min (100%, alkene).

Diels–Alder reaction of cyclopentadiene with methyl acrylate

(a) Conventional method

A mixture of methyl acrylate (1.0 mL) and freshly distilled cyclopentadiene (1.0 mL) in methanol (7.5 mL) was allowed to react at 0°C. Aliquots were removed at regular intervals over a 67 h period and analysed by glc to determine the product ratio of the *endo* and *exo* isomers. This procedure was repeated at 21°C.

(b) Microwave method

A mixture of methyl acrylate (1.0 mL) and freshly distilled cyclopentadiene (1.0 mL) in methanol (7.5 mL) was placed in a 150-mL Savillex Teflon vessel. The sealed vessel was heated in the microwave oven for 2.5 min at power level 7 (560 W). The vessel was allowed to stand for 30 s and then cooled in an ice-bath. The product was analysed by glc.

Hydrolysis of benzyl chloride

The specified amounts of benzyl chloride and water were mixed in a 150-mL Savillex Teflon vessel. The sealed vessel was placed in the microwave oven, connected to a pressure gauge outside the oven (see pressure measurements), and heated at full power (750 W) until the pressure reached 70 psi. The pressure was then maintained at 60–70 psi by operating the magnetron for short periods of time at the maximum power (750 W). After heating for the specified time, the vessel was left for 2 min to reduce the pressure and then removed from the oven and cooled in ice-water. Water (25 mL) was added to the product and the mixture extracted with three 20-mL portions of ether.

The yield of benzyl alcohol was determined by titrating the chloride ion in the aqueous phase with 0.10 M $AgNO_3$ using sodium chromate (0.125 M) as an indicator (12).

Hydrolysis of N*-phenylbenzamide*

The specified amounts of *N*-phenylbenzamide and a 20% H_2SO_4 solution were mixed in the 150-mL Teflon vessel, and heated for the specified time in the microwave oven using the method described in the previous experiment. After cooling, the reaction mixture was made basic with 20% sodium carbonate and the aniline and unchanged amide extracted with three 20-mL portions of chloroform. The aqueous layer was acidified with 20% H_2SO_4 and the benzoic acid extracted with three 20-mL portions of ether. The ether extracts were dried over anhydrous $MgSO_4$ and the benzoic acid isolated by evaporation of the ether.

Esterification of benzoic acid with 2-butanol

A mixture of the specified amounts of benzoic acid, 2-butanol, and 10 drops of concentrated H_2SO_4 per 10 mL of 2-butanol was mixed in a 150-mL Teflon vessel and heated for the specified time in the microwave oven using the method described above. After cooling, the mixture was made basic with 20% Na_2CO_3 and the ester extracted with three 20-mL portions of ether. The aqueous layer was acidified with 20% H_2SO_4 and the unreacted benzoic acid extracted with ether. Both ether extracts were dried over anhydrous $MgSO_4$ and the ester and benzoic acid isolated by evaporation of the ether.

Acknowledgements

The authors gratefully acknowledge the financial assistance provided by the Natural Sciences and Engineering Research Council of Canada, the Laurentian University Research Fund, and the Ontario Ministry of Energy. We would also like to thank Mr. Z. Lai, Mr. M. Blake, Ms. P. Harsora, Mr. T. Park, Ms. M. Skakoon, and Mr. D. Wunderlich for their assistance.

1. R. N. GEDYE, F. E. SMITH, K. C. WESTAWAY, H. ALI, L. BALDISERA, L. LABERGE, and J. ROUSELL. Tetrahedron Lett. **27**, 279 (1986).
2. R. N. GEDYE, F. E. SMITH, and K. C. WESTAWAY. Can. J. Chem. **66**, 17 (1988).
3. R. J. GIGUERE, T. L. BRAY, S. M. DUNCAN, and G. MAJETICH. Tetrahedron Lett. **27**, 4945 (1986).
4. R. J. GIGUERE. *In* Organic synthesis; theory and application. Vol. 1. *Edited by* T. Hudlicky. JAI Press Inc., Greenwich, CT. 1989. p. 103.
5. T. H. LOWRY and K. S. RICHARDSON. *In* Mechanism and theory in organic chemistry. 3rd ed. Harper and Row, New York. 1987. p. 616.
6. J. A. BERSON, Z. HAMLET, and W. A. MUELLER. J. Am. Chem. Soc. **84**, 297 (1962).
7. A. S. FOUST, L. A. WENZEL, C. W. CLUMP, L. MAUS, and L. B. ANDERSON. Principles of unit operations. 2nd ed. J. Wiley and Sons, New York. 1980. Appendix D. p. 728.
8. A. LIBERLES. *In* Introduction to theoretical organic chemistry. MacMillan, New York. 1968. p. 7.
9. G. LUBEC, C. WOLF, and B. BARTOSCH. Lancet, 1392 (1989).
10. E. D. NEAS and M. J. COLLINS. *In* Introduction to microwave sample preparation. *Edited by* H. M. Kingston and L. B. Jassie. American Chemical Society, Washington, DC. 1988. pp. 6–17.
11. Savillex Corporation, 5325 Hwy. 101, Minnetonka, MI. 55343, U.S.A.
12. D. A. SKOOG and D. M. WEST. *In* Fundamentals of analytical chemistry. 4th ed. Holt Rinehart and Winston, New York. 1982. p. 185.

Can. J. Chem. Downloaded from www.nrcresearchpress.com by 198.100.157.202 on 09/07/12
For personal use only.

Synthetic studies towards bruceantin. Part 1. Establishment of the carbon network

SULTAN DARVESH, ANDREW S. GRANT, DAVID I. MAGEE, AND ZDENEK VALENTA[1]
Department of Chemistry, University of New Brunswick, Fredericton, N.B., Canada E3B 6E2

Received September 20, 1990

SULTAN DARVESH, ANDREW S. GRANT, DAVID I. MAGEE, and ZDENEK VALENTA. Can. J. Chem. **69**, 712 (1991).

In a synthetic approach to the biologically active quassinoid bruceantin **1**, intermediate **47** was prepared, which contains all required C-atoms, rings A and B, and four of the 10 chiral centers of bruceantin. The possibilities for a convergent strategy were explored, in which a 5-carbon unit would be joined to a 15-carbon unit by three bonds. After the study of various alkylations and Michael additions needed for the key step, it was found that 3-iodo-1-trimethylsilyl-5-hexenyne **44** adds to the dianion of methyl ketone nitriles **3** and **13** chemo-, diastereo-, and enantioselectively.

Key words: bruceantin, quassinoids, alkylation, Michael addition.

SULTAN DARVESH, ANDREW S. GRANT, DAVID I. MAGEE et ZDENEK VALENTA. Can. J. Chem. **69**, 712 (1991).

Dans une approche à la synthèse de la quassinoïde brucéantine (**1**) biologiquement active, on a préparé l'intermédiaire **47** qui contient tous les atomes de carbone requis, les cycles A et B ainsi que quatre des 10 centres chiraux de la brucéantine. On a exploré les possibilités de stratégie convergente dans lesquelles une unité de cinq atomes de carbone serait reliée à une unité de 15 atomes de carbone par trois liaisons. Après avoir étudié diverses alkylations et additions de Michael requises pour l'étape clé, on a trouvé que le 3-iodo-1-triméthylsilyl-hexén-5-yne (**44**) s'additionne aux dianions des méthylcétone-nitriles **3** et **13** d'une façon chémo-, diastéréo- et énantio-sélective.

Mots clés : brucéantine, quassinoïdes, alkylation, addition de Michael.

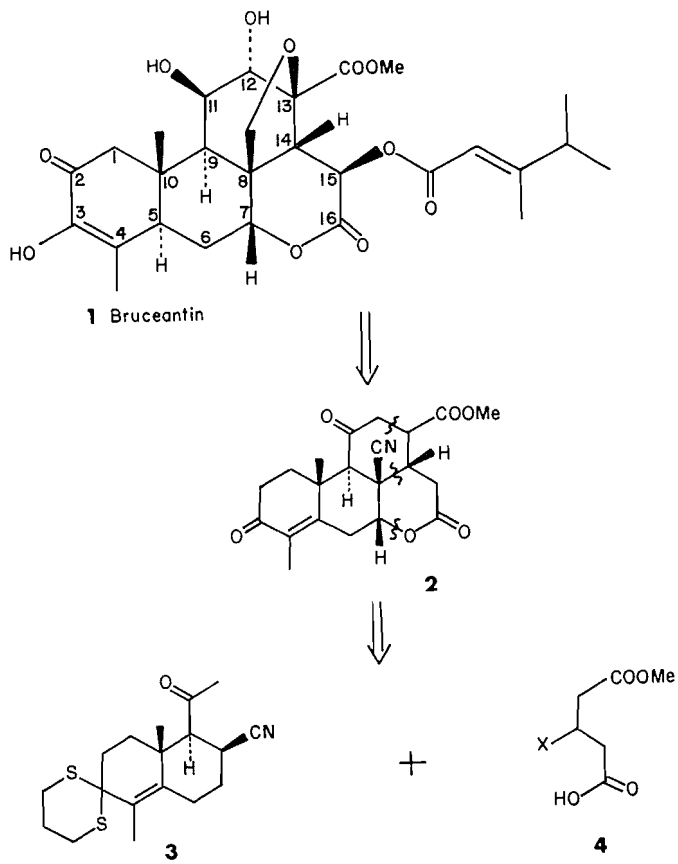
[Traduit par la rédaction]

Can. J. Chem. Downloaded from www.nrcresearchpress.com by 198.100.157.202 on 09/07/12
For personal use only.

The last two decades have seen the *Simaroubaceae* family of the plant kingdom make a prominent mark in natural product chemistry. The bitter substances produced in plants of this family, known as the quassinoids (1, 2), have received increased attention with the finding that some of them possess strong antileukemic activity in the murine lymphocytic leukemia P-388 test system, in addition to antimalarial, amebicidal, and antiviral activities.

The wealth of information gathered in the last two decades has shown what structural features are required for the antineoplastic activity exhibited by the quassinoids (3). An A-ring enone function, a C6 or a C15 ester function, and an oxymethylene bridge between C8 and C11 or C13 are essential for optimal activity. Due to this functional and stereochemical complexity, coupled with the potential use in cancer and other therapies, a considerable amount of synthetic activity has been expended towards these compounds (4). Four tetracyclic members of the C20 picrasane family have been synthesized, all in racemic form (5), and just recently an enantioselective synthesis has been reported for three others (4*a*). Finally, the synthesis of racemic 15-deoxybruceolide and a relay conversion of the naturally derived (−)-form of this compound into (−)-bruceantin **1** have been reported (4*h*). From the scarcity of completed syntheses, it is evident that much work is still required in this area, especially on the design of an efficient general synthesis. We wish to report in full our work on the synthesis of the natural quassinoid bruceantin **1**.

Bruceantin contains 10 asymmetric carbon atoms, of which six are at the junctions of the three carbon rings and the lactone ring. Our strategy, therefore, consisted first of the formation of the skeleton with the proper relative stereochemistry, followed by the subsequent incorporation of the functional groups with the desired configuration (Scheme 1). It appeared to us that disconnection at the lactone ether oxygen, at C8 and at C12, would present two "relatively simple" halves. This convergent strategy, we felt, held great promise since the connection of these two halves could be achieved in any one of several possible sequences (Fig. 1, where the three arrows point towards the potential electrophilic centers).



SCHEME 1

Results and discussion

Our synthetic route to bicyclic ketone **3**, depicted in Scheme 2, was initiated by the reaction of 2-methyl-1,3-cyclohexane dione with ethyl vinyl ketone under basic conditions to yield the Michael adduct **7**. This compound was then directly subjected,

[1]Author to whom correspondence may be addressed.

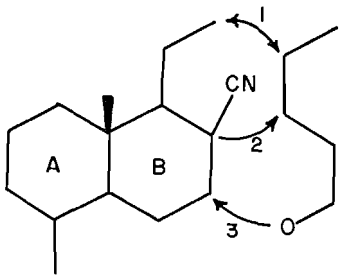
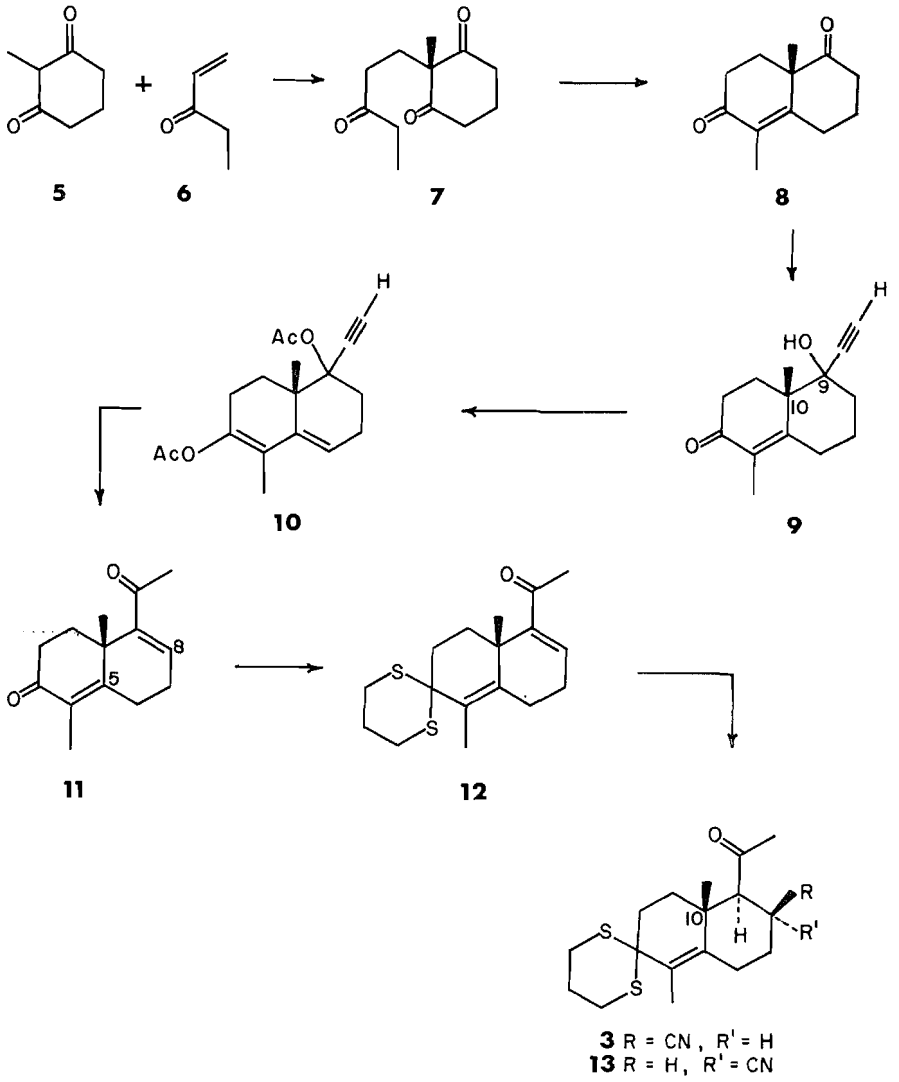


FIG. 1. Potential connecting points of the "two halves" for the synthesis of bruceantin.

without any purification, to pyrrolidine in refluxing benzene with azeotropic removal of water to furnish the enedione **8** in 67% overall yield (6). Ethynylation of **8** with lithium acetylide in liquid ammonia (*7a*) at −78°C proceeded smoothly and regioselectively to furnish the carbinol **9** in 71% yield. Treatment with acetic anhydride and a catalytic amount of *p*-toluenesulfonic acid (pTSA) (*7a*) resulted in clean conversion to the diacetate **10** in 94% yield. As Newman *et al.* (*7a*) found in a similar case, the transformation of the ethynyl carbinol to the diacetate became necessary due to the juxtaposition of the enone and the hydroxyl group in **9**. The acidic conditions and high temperatures required to produce the α,β-unsaturated acetyl group of **11** led to considerable destruction of the starting material when the direct **9** → **11** conversion was attempted. This was undoubtedly due to a reverse aldol process, which fragmented the C9—C10 bond. With the tertiary alcohol now protected, the Rupe rearrangement (*7a*, *7b*) proceeded as expected on treatment with refluxing formic acid (90%) for 2 h to produce the diene dione **11** in 70% yield as a crystalline solid. The remaining task was the installation of the nitrile at C8. We assumed that a regioselective hydrocyanation could be accomplished since C8 could be expected to be much less hindered than the corresponding C5 position. However, the best conditions found, sodium cyanide in dimethyl formamide (DMF) in the presence of sodium bicarbonate, led to a 1:1 mixture of regioisomers, and in only 40% conversion. To circumvent this problem, diene dione **11** was first treated with 1,3-propane dithiol and $BF_3 \cdot OEt_2$ in Et_2O to produce the protected enone **12** in 72% yield. Compound **12** then smoothly reacted with aqueous potassium cyanide in ammonium chloride buffered DMF to produce the epimeric nitriles **3** and **13** in a combined yield of 77%. The



SCHEME 2

Can. J. Chem. Downloaded from www.nrcresearchpress.com by 198.100.157.202 on 09/07/12
For personal use only.

Can. J. Chem. Downloaded from www.nrcresearchpress.com by 198.100.157.202 on 09/07/12
For personal use only.

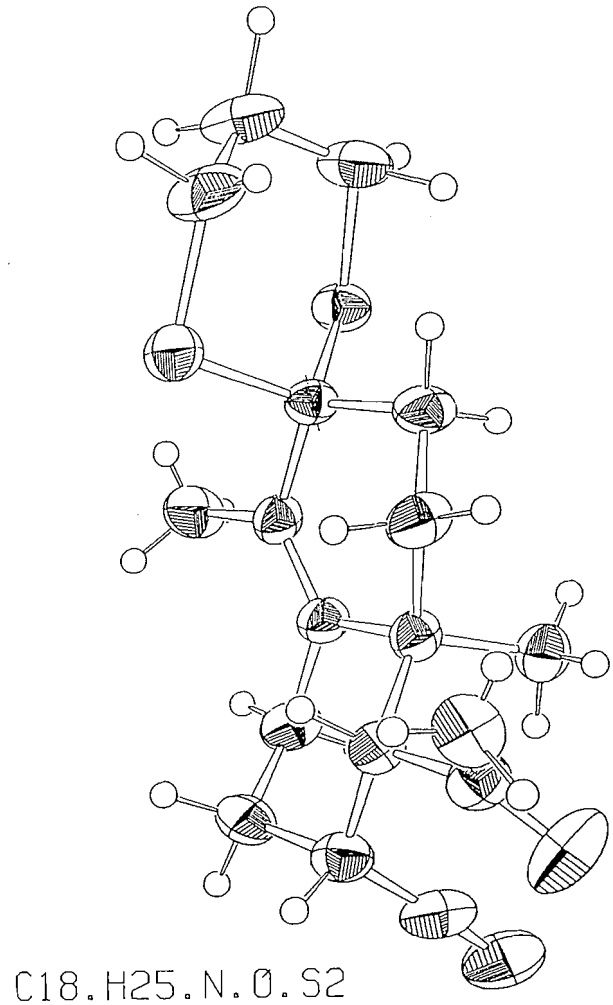


FIG. 2. X-ray structure of nitrile **3**.

typical ratio of nitriles was 5:1 in favor of **3**; however, there were instances when the other epimer predominated. The reasons for this variability are unclear.

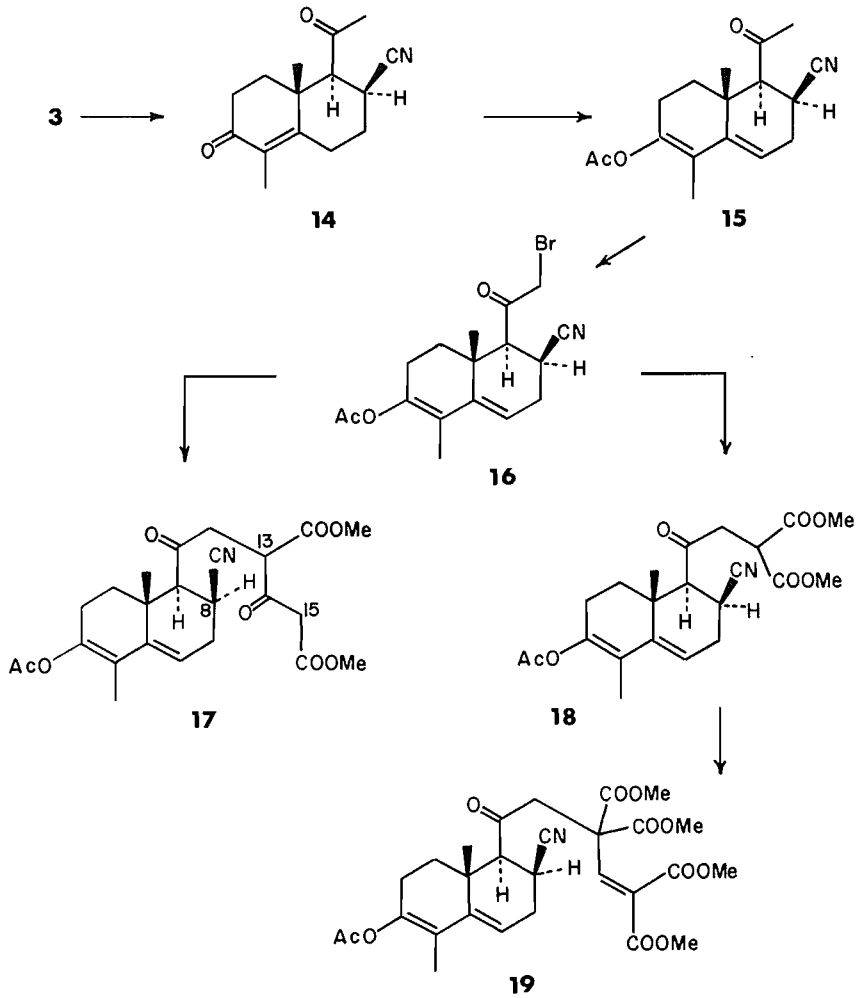
The structures of **3** and **13** were initially assigned as shown on ^{1}H NMR evidence. Epimer **3** showed a singlet at δ 1.47 for the C10 methyl group, while in **13** it appeared at δ 1.10. The difference in chemical shift was attributed to the fact that the C10 methyl group in **3** was deshielded by the nitrile. This assignment was later substantiated by single crystal X-ray crystallography (Fig. 2). From Fig. 2, it can be seen that the nitrile is in a quasi-axial position, while the acetyl group occupies the equatorial position. It was assumed, and later shown by chemical transformation, that both the acetyl group and the nitrile were equatorially disposed in nitrile **13**.

The next objective was to attach a suitable side chain, which would contain the remaining carbons required for the construction of the skeleton of bruceantin. Based on previous work done in these laboratories on the synthesis of 14β-hydroxysteroids (8), it was assumed that the best assembly sequence would be to form the C12—C13 bond first, followed by the C8—C14 bond (Fig. 1, arrows 1 and 2). In particular, this approach was expected to provide the desired stereochemistry at the quaternary C8 carbon.

Investigation of this strategy (Scheme 3) began by treating nitrile **3** with *N*-chlorosuccinimide and silver carbonate in aqueous acetonitrile (9) to give enone **14** in 80% yield. This was then simply protected as its dienol acetate **15** by treatment with acetic anhydride and a catalytic amount of hydrobromic acid (87% yield). Complete chemoselective bromination of C12 was accomplished with phenyl trimethyl ammonium perbromide (10) in tetrahydrofuran (THF) to give the unstable bromo ketone **16**. This bromo derivative became the pivotal point of further investigations in which C12 was used as an electrophilic center. Due to the instability of this compound, it was always used immediately after preparation. Bromide **16** was treated with the sodium salt of dimethyl acetone dicarboxylate to furnish diester **17** in 52% overall yield. Theoretically, this product could exist in eight different forms: the two diastereoisomers at C13, two geometrical isomers of the enol towards C12, and four isomers of the enol towards C15 (*E*/*Z* and diastereoisomers at C13). Three of these eight possible states were observed in the 200 MHz NMR spectrum, with the ratio of keto:enol forms being approximately 3:2. All the carbons required for the bruceantin skeleton were now present, and an aldol reaction between C8 and C14 would deliver the last crucial bond.

Before this aldol reaction could be accomplished, however, an obvious acidity problem had to be overcome. It was assumed that extending conjugation into ring B would give the C8 hydrogen an acidity comparable to those of H-atoms in the side chain. To meet this objective, direct bromination, via a variety of methods, was attempted on dienol acetate **17**, but only significant loss of starting material with no detection of the desired product was observed in all cases. These problems were attributed to the presumed high reactivity of the enol groups present in the side chain. All attempts to overcome these difficulties by conversion into a β-haloglutaconate or an enol acetate failed. Thus, unfortunately, compound **17** had to be discarded as a potential synthetic intermediate, in spite of its initially highly promising distribution of functional groups.

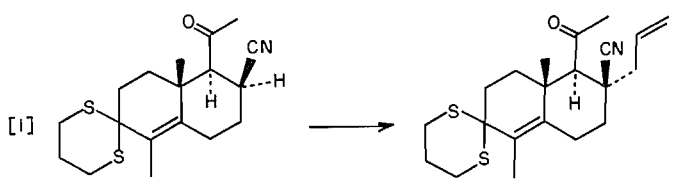
It was next attempted to remove the problem by incorporating a side chain that contained no acidic protons. Direct conversion of bromo acetate **16** to the malonyl adduct **18** proceeded uneventfully in 68% yield upon treatment with the sodium salt of dimethyl malonate. The sodium enolate of **18** was then quenched with chloromethylene malonate to yield the tetraester **19** in 75% yield. This compound now contained only the acidic protons at C9, C12, and C8, none in the added side chain. However, when tetraester **19** was treated with sodium hydroxide in the UV tube, it exhibited an unusual bathochromic shift to 400 nm. After inspection of the ^{1}H NMR spectrum, this shift was attributed to the rearranged product **20** (Scheme 4), presumably formed by addition of the C12 anion to the reactive Michael acceptor to form a cyclopropane intermediate, which subsequently reopened to give the more stable malonyl anion. It was also found that, in previous reactions, significant amounts of rearrangement product **20** were formed when, for the preparation of **19**, excess sodium hydride was used in the initial anion formation of **18**. All attempts to alleviate this problem failed; these included reduction of the C11 ketone with sodium borohydride, L-Selectride, or lithium borohydride and the extension of ring-A conjugation via bromination/dehydrobromination or selenation/elimination. However, when malonyl adduct **18** was treated with phenyl selenenyl chloride in benzene in the presence of silver trifluoroacetate (11), selenide **21** was produced in 70% yield as a single isomer (Scheme 5), the stereochemistry of which was not determined. Selenide **21** was then transformed into the tetraester **22** as before in a moderate 47% yield. Oxidation with *m*-chloroperbenzoic acid in methylene chloride then led, unfortunately, to the tertiary allylic alcohol **23** in 80% yield



SCHEME 3

via the [2,3]-sigmatropic rearrangement of the selenoxide (12). Clearly, the presence of the C3 keto group did not usefully slow down the allylic selenoxide rearrangement. Even though this rearrangement is an equilibrium reaction, prolonged treatment had no effect on the product distribution.

It now became clear that an efficient continuation of the synthesis required that the five additional carbon atoms and the method for joining them be kept relatively simple. While investigating other avenues, we became intrigued with the following serendipitous result; treatment of **3** with five equivalents of lithium diisopropyl amide in THF at −78°C, followed by excess allyl bromide, gave **24** as the sole product in 88% yield (eq. [1]).

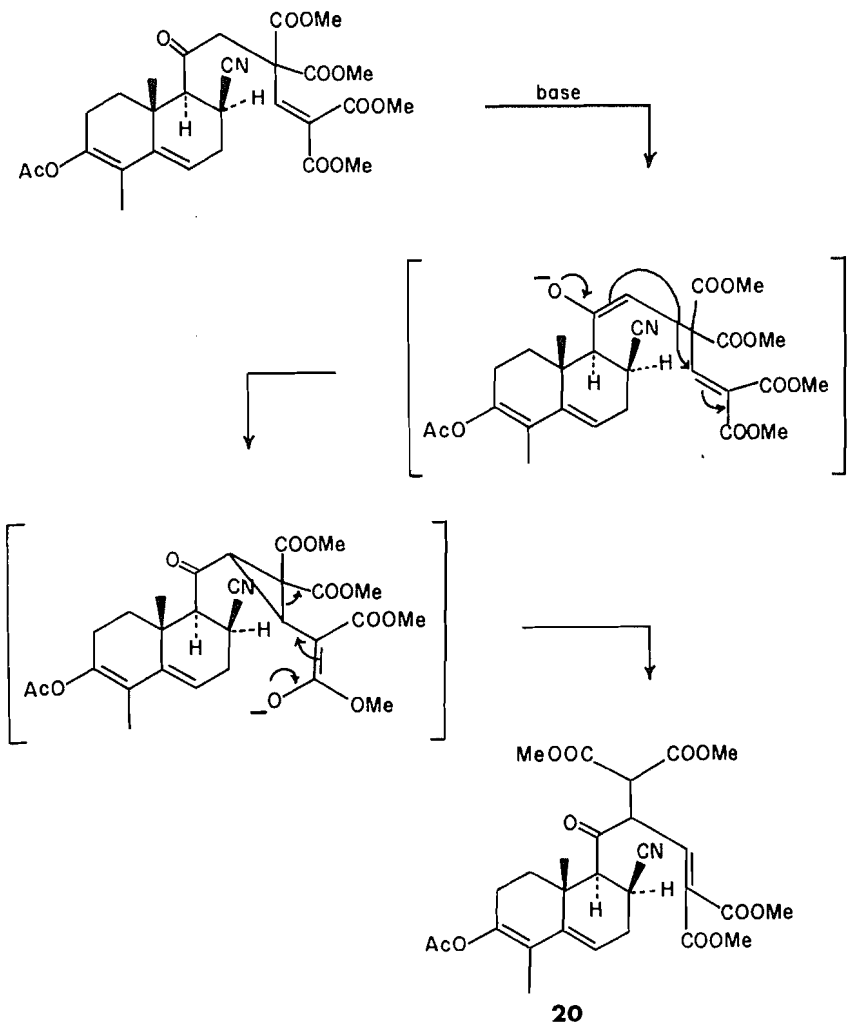


3 **24**

While it was not surprising that the alkylating agent approached the molecule at C8 exclusively from the α-face, it was indeed surprising that no alkylation was observed at the enolate carbon since we were undoubtedly dealing with a dianion. It must be assumed that the enolate anion alkylates very slowly, if at all, after the first alkylation occurs.

Utilization of this chemistry began with investigating the coupling of the dianion with several functionalized Michael acceptors (Table 1). Although two new asymmetric centers were created (three in the case of **33**, entry i), only one was of particular concern, C8; the C14 stereochemistry could be adjusted at a later stage. Several results listed in Table 1 are noteworthy. The reaction with ethylene malonate (entry a) gave the same chemo- and stereoselectivity at C8 as was observed for the alkylation with allyl bromide, but in poorer yield. Compound **26**, which was designed to incorporate the added oxygen functionality required in bruceantin, failed badly, even though it did give a product with the correct C8 stereochemistry. We concluded that the isopropylidene moiety of **26** was experiencing severe steric interactions with the decalin system, and that appropriate changes would overcome this. As seen in entry c, changing to an acetylene moiety did indeed improve the yield drastically; unfortunately, it also had a deleterious effect on the chemo- and stereoselectivity. The reason for the marked difference in reaction course is not at all evident, especially considering the fact that no reaction was observed for the di-*tert*-butyl derivative **28** (entry d). Other simple Michael acceptors were tried (entries e–h) but either no reaction or complex mixtures were obtained. The most interesting result was that with α-bromocrotonolactone (entry i). A single isomer was obtained in a reaction in which two new chiral centers were created by the Michael addition and a third one by enolate protonation. In

Can. J. Chem. Downloaded from www.nrcresearchpress.com by 198.100.157.202 on 09/07/12
For personal use only.



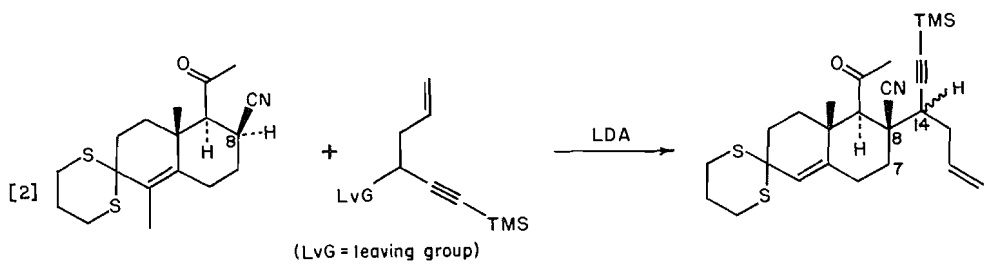
20

SCHEME 4

general, diastereoselective Michael reactions, in which two new chiral centers are generated, are not common. Reported cases include enamine and enolate additions to nitroolefins (13, 14).

The discouraging yields and selectivities in the Michael reactions forced us to consider "simple" alkyl halides, which would simulate the reactivity of allyl bromide but possess the required chain length and be functionalized enough to allow for further elaboration. After considerable experimentation, we decided to pursue haloenynes of type **38** as targets (eq. [2]). It should be noted that compounds **38** contain a chain of six carbons and that the double bond would therefore have to be cleaved at the appropriate time to give the desired chain length and terminal carboxylic acid functionality. Furthermore, the alkylation (eq. [2]) would only be efficient if, in addition to being chemoselective (attack at C8 rather than C12) and stereoselective at C8 (α-attack), it were also enantioselective (configuration at C14 of the product). Interestingly, however, *it should not matter which C14 diastereoisomer is formed*, as long as it is formed in high yield. Depending on the stereochemical outcome of the alkylation at C14, the acetylene would then be used either for the bond formation at C12 or at C7, while the other required bond (C7 or C12) would be formed using the allyl group. The C14 configuration of the alkylation product will thus dictate subsequent chemistry!

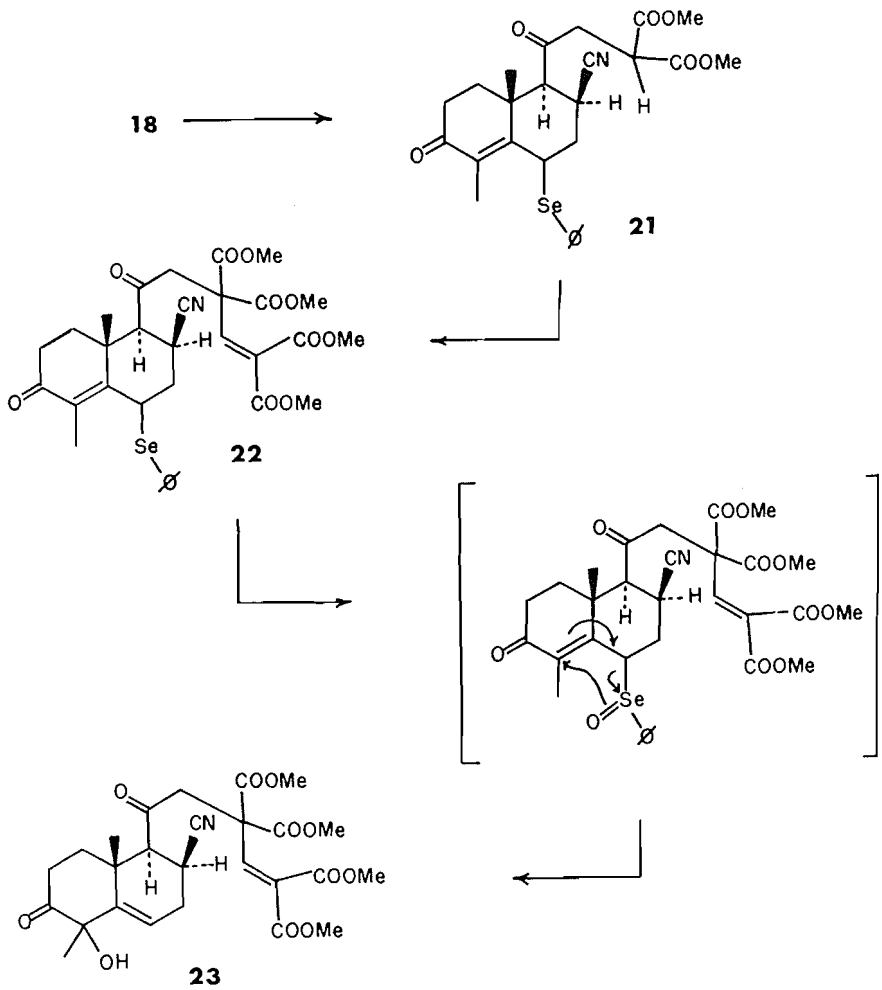
Our approach to the required compounds was initiated from the known aldehyde **39** (15), which was converted to propargylic alcohol **40** upon treatment with allyl magnesium bromide (Scheme 6). Mesylation under standard conditions gave **41**, which was then subjected to refluxing acetone with the appropriate potassium halide to give the corresponding chloride **42**,



38

Can. J. Chem. Downloaded from www.nrcresearchpress.com by 198.100.157.202 on 09/07/12
For personal use only.

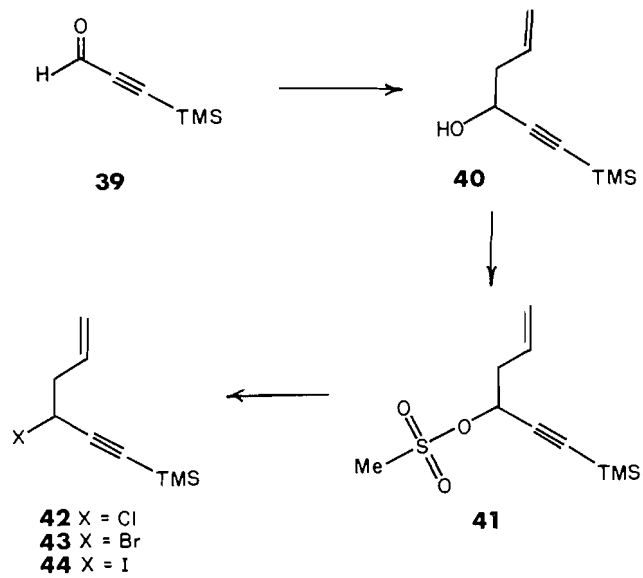
Can. J. Chem. Downloaded from www.nrcresearchpress.com by 198.100.157.202 on 09/07/12
For personal use only.



SCHEME 5

bromide **43**, and iodide **44** in 30–40% yield overall. With a convenient synthesis of these halides now in hand, the reactivity of each of them was investigated.

The dianions of nitriles **3** and **13** were generated by treatment with lithium pyrrolidide (LP)[2] in THF at −78°C for 2 h and then quenched with chloride **42** to give no alkylated product (Scheme 7). Upon recovery of the starting materials it was discovered that a significant quantity of the eliminated product **45** was obtained. This meant that the dianion, at least with this halide, acted as a base rather than a nucleophile. Treatment of the dianion, formed under identical conditions as before, with bromide **43** generated two new products, **46** and **47**, as a 1:1 mixture in 80% yield based on recovered starting material. These products arose from the two possible substitution pathways, namely S_N2 displacement to give **47** and S_N2' displacement to furnish **46**. Finally, treatment of the dianion with iodide **44** generated a single compound, **47**, in 95% yield and 50% conversion. Single crystal X-ray crystallography revealed that nitrile **47** possessed the correct C8 configuration and the indicated stereochemistry at C14 (Fig. 3). The enantioselectivity at C14 can possibly be explained by a transition state orientation of the two molecules indicated in Fig. 4. Placement of the acetylene under the decalin system and of the H-atom under the presumably strongly hindering ionic region would allow the more sterically demanding allyl



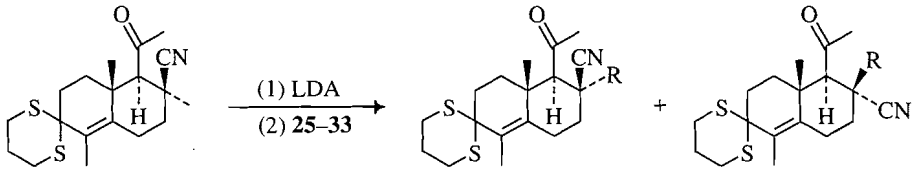
SCHEME 6

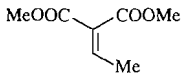
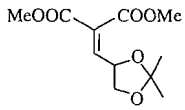
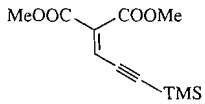
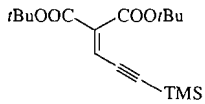
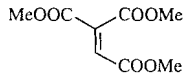
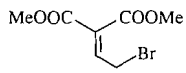
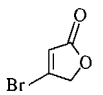
group to align itself away from the ring. This analysis not only rationalizes why the observed product is formed, but also why the process is so selective.[3]

[2]It was found that the nitriles could be used without separation when LP was used as a base instead of LDA. We have no evidence that LP or pyrrolidine reacted with the halides **42**–**44** under the reaction conditions used.

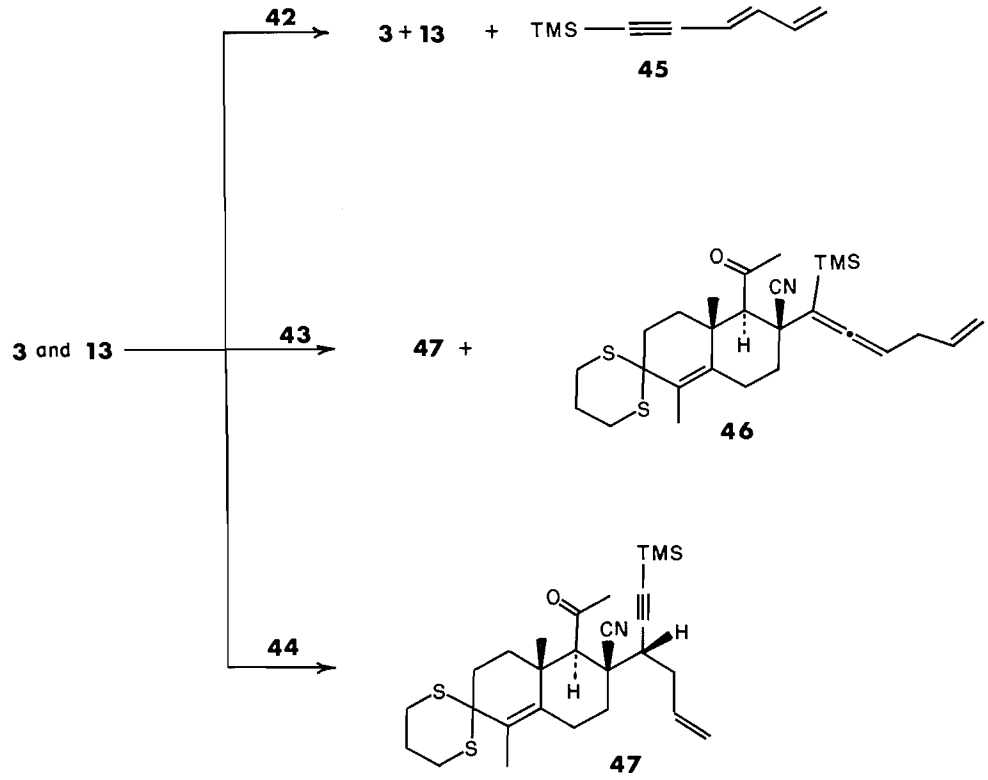
[3]The proposed transition state geometry (Fig. 4) finds some support in the fact that the conformation of the side chain in **47** as determined crystallographically is very similar.

TABLE 1. Michael additions



	Michael acceptor	34–37α product yield (α/β)	34–37β Ratio of stereoisomers (at C14-H of side chain; determined by ^{1}H NMR)
(a)	 **25**	**34** 49% (1/0)	2:1
(b)	 **26**	**35** 12% (1/0)	2:1
(c)	 **27**	**36** 77% (1/0) + C12 regioisomer	2:1
(d)	 **28**	No reaction	—
(e)	 **29**	Complex mixture	—
(f)	 **30**	Complex mixture	—
(g)	 **31**	No reaction	—
(h)	 **32**	No reaction	—
(i)	 **33**	**37** 20% (1/0)	Single isomer

Can. J. Chem. Downloaded from www.nrcresearchpress.com by 198.100.157.202 on 09/07/12
For personal use only.



SCHEME 7

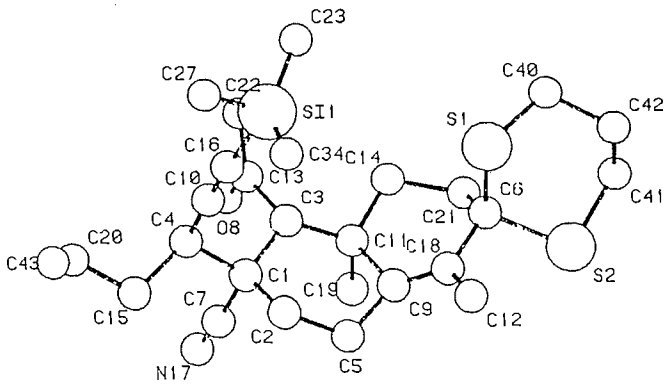


FIG. 3. X-ray structure of nitrile **47**.

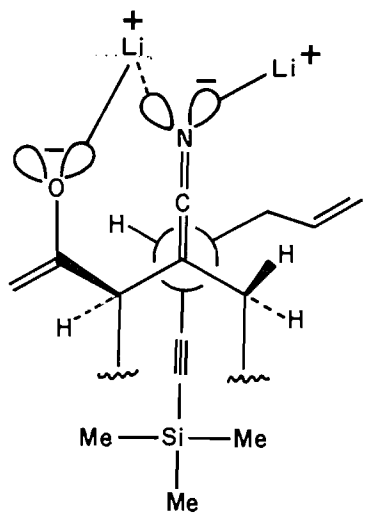


FIG. 4. Proposed transition state geometry of alkylation reaction.

Several attempts were made to improve the conversion of starting material. For example, HMPA was added (16), various concentrations of iodide **44** were used, and the temperature of the reaction was elevated, but no change was observed. This anomalous behavior has been observed in other alkylation systems (17). Regardless of the technical difficulties associated with only 50% conversion, the reaction was found to be high yielding, selective, and, most important, it provided the remaining carbon atoms required for the bruceantin skeleton in a simple yet differentiable form.

All compounds described here are racemic. Thus, in the alkylation reaction, each enantiomer of **3** (and **13**) selected the "fitting" enantiomer of racemic iodide **44**. Based on literature precedents (18), the formation of optically pure enedione **8** via an amino acid catalyzed aldol reaction of prochiral trione **7** will present no difficulties. It can then be anticipated that enantiomerically pure keto nitriles **3** and **13** thus prepared will react with only the fitting enantiomer of racemic iodide **44**. The nonreacting enantiomer of **44** will then either re-racemize by the action of the iodide ion generated in the alkylation reaction, or will be isolated and reconverted to the racemate in a separate reaction.

The next objective was to utilize alkylation product **47** for elaboration into compounds of type **2**. This work is reported in the following article.

Experimental section

Melting points were determined on a Kofler hot stage apparatus and are uncorrected. Infrared spectra (IR) were recorded on a Perkin–Elmer IR spectrophotometer model 717B using sodium chloride cells (0.5 mm) and are reported in wave numbers (cm^{-1}) with polystyrene as standard. Nuclear magnetic resonance (NMR) spectra were recorded on a Varian XL-200 (200 MHz) or a Varian T60 (60 MHz) spectrometer. Chemical shifts are reported in ppm (δ) downfield relative to tetramethylsilane as standard. Low resolution mass spectra were re-

Can. J. Chem. Downloaded from www.nrcresearchpress.com by 198.100.157.202 on 09/07/12
For personal use only.

corded on a Hitachi Perkin–Elmer RMU-6D spectrometer. High resolution mass spectra were recorded at the Mass Spectrometry Laboratory, Department of Chemistry, University of Alberta, Edmonton, Alberta. Elemental analyses were performed at Guelph Chemical Laboratories Ltd., Guelph, Ontario. Ultraviolet (UV) spectra were recorded on a Beckman spectrophotometer model 25, using quartz cells (4.5 mL capacity).

All reactions, unless otherwise specified, were run under an inert atmosphere of Ar or N_2, and reactions requiring anhydrous conditions were performed in a flame-dried or oven-dried (120°C) apparatus. Temperatures below room temperature refer to bath temperatures. Solvents and anhydrous reagents were dried according to established procedures by distillation under N_2 from an appropriate drying agent (19).

Analytical TLC was performed on E. Merck precoated silica gel plates (0.25 mm). Preparative TLC was performed on E. Merck precoated silica gel plates (1.0, 2.0 mm). Column chromatography was performed by the method of Still *et al.* (20) with E. Merck silica gel 60 (230–400 mesh).

Enedione 8

A solution of 100 g (0.79 mol) of 2-methyl-1,3-cyclohexanedione and 1.5 g (0.03 mol) of potassium hydroxide in 600 mL of anhydrous methanol was brought to reflux and 100 g (1.19 mol) of ethyl vinyl ketone was added dropwise over 1 h. The stirred solution was refluxed for an additional 3 h, and then the methanol was evaporated *in vacuo*. The residue was taken up in 400 mL of benzene and 5 mL (0.06 mol) of pyrrolidine was added. The solution was refluxed for 24 h with azeotropic removal of water. The dark reaction mixture was cooled and 200 mL of ether was added. The solution was washed once with 5% HCl, twice with brine, and then dried over anhydrous magnesium sulfate. The solvent was removed under reduced pressure to give a dark oil, which recrystallized from ether to give 76 g of solid. A further 26 g of compound was obtained after column chromatography of the mother liquor to give 102 g (67%) in total of enedione **8** (mp 46–48°C). IR ($CHCl_3$): 2950 (m), 2900 (m), 1720 (s), 1670 (s), 1610 (m), 1365 (m), 1340 (m), 1320 (m); NMR (200 MHz, $CDCl_3$): 3.0–2.0 (m, 9H), 1.83 (s, 3H), 1.83–1.7 (m, 1H), 1.43 (s, 3H); HRMS (EI) *m/e* (relative intensity): 192.1151 (M^+, 100).

Ethynylcarbinol 9

To a −78°C solution of 7.2 g (1.04 mol) of lithium metal in 2.5 L of ammonia, acetylene gas was bubbled in until the dark blue solution became colorless. To this was then added 100 g (0.51 mol) of **8** in 500 mL of anhydrous ether dropwise over 0.5 h. The reaction mixture was stirred for 1 h at −78°C and then carefully quenched with 600 mL of saturated ammonium chloride. After evaporation of the ammonia the aqueous phase was extracted with four 200-mL portions of chloroform. The combined organic phases were washed with water, brine, and then dried over anhydrous magnesium sulfate and filtered. Concentration of the filtrate gave a brown solid, which was recrystallized from ethanol to give 99.0 g (87%) of **9** (mp 135–138°C). IR ($CHCl_3$): 3610 (w), 3310 (m), 2950 (m), 1650 (s), 1610 (m), 1340 (m), 1310 (m); UV (95% ethanol): 251 nm (ϵ = 25 450); NMR (200 MHz, $CDCl_3$): 2.80–1.80 (m, 11H), 1.80 (s, 3H), 1.30 (s, 3H); HRMS (EI) *m/e* (relative intensity): 218.1308 (M^+, 100).

Dienol diacetate 10

A solution of 40.19 g (0.18 mol) of carbinol **9**, 3.0 g (0.016 mol) of *p*-toluenesulfonic acid, and 250 mL of acetic anhydride was stirred for 18 h. The reaction mixture was poured carefully into 500 mL of ice water, stirred for 1 h, and then filtered. The aqueous phase was extracted once with chloroform and combined with the solid obtained from the filtration. The combined organics were dried with anhydrous magnesium sulfate, filtered, and solvent evaporated under reduced pressure. The solid obtained was recrystallized from ethanol to give 51.0 g (92%) of diacetate **10** (mp 120–122°C). IR ($CHCl_3$): 3325 (s), 2950 (m), 1750 (s), 1740 (s), 1675 (m), 1370 (s), 1150 (s), 1095 (s); UV (95% ethanol): 235 nm (ϵ = 22 500); NMR (200 MHz, $CDCl_3$): 5.62 (t, J = 4 Hz, 1H), 2.93–2.78 (m, 1H), 2.54 (s, 1H), 2.18 (s, 3H), 2.06 (s, 3H), 1.65 (t, J = 1.5 Hz, 3H), 1.18 (s, 3H); HRMS (EI) *m/e* (relative intensity): 302.1523 (41).

Diene dione 11

A solution of 5 g (0.017 mol) of **10** in 20 mL of 88% formic acid was refluxed for 2 h. The formic acid was then removed under reduced pressure. The residue was taken up in 50 mL of ethyl acetate and washed with 5% $NaHCO_3$, water, and brine, dried with anhydrous $MgSO_4$, filtered, and solvent evaporated under reduced pressure. The solid was recrystallized from ether to give 2.45 g (68%) of diene dione **11** (mp 104–107°C). IR ($CHCl_3$): 2950 (w), 1660 (s), 1630 (m), 1370 (m); UV (95% ethanol): 240 nm (ϵ = 24 200); NMR (200 MHz, $CDCl_3$): 7.06–6.96 (m, 1H), 2.94–2.4 (m, 6H), 2.33 (s, 3H), 2.30–2.16 (m, 2H), 1.83 (s, 3H), 1.58 (s, 3H); HRMS (EI) *m/e* (relative intensity): 218.1308 (100).

Dithiane 12

A solution of 5 g (22.9 mmol) of **11** in 30 mL of anhydrous ether was cooled in an ice bath and 5 mL (40.7 mmol) of boron trifluoride etherate was added, followed by 3.5 mL (34.4 mmol) of 1,3-propane dithiol. The reaction mixture was stirred for 18 h and then poured carefully into 100 mL of 10% $NaHCO_3$. After separation of the layers the organic phase was washed with water and brine, dried with anhydrous $MgSO_4$, filtered, and evaporated *in vacuo*. The solid was recrystallized from ether to deliver 5.81 g (82%) of dithiane **12** (mp 148–150°C). IR ($CHCl_3$): 2920 (m), 1670 (s), 1360 (m); UV (95% ethanol): 230 nm (ϵ = 16 100), 209 nm (ϵ = 22 800); NMR (200 MHz, $CDCl_3$): 6.90–5.98 (m, 1H), 3.24–2.98 (m, 2H), 2.80–2.50 (m, 3H), 2.28 (s, 3H), 2.01 (s, 3H), 1.45 (s, 3H); HRMS (EI) *m/e* (relative intensity): 308.1270 (100).

Nitriles 3 and 13

A solution of 10 g (0.03 mol) of **12** in 100 mL of DMF was stirred until a uniform solution was obtained. Then a solution of 4.23 g (0.065 mol) of potassium cyanide and 2.68 g (0.05 mol) of ammonium chloride in 30 mL of water was added and the reaction mixture was heated at 80°C for 16 h. Upon cooling, 500 mL of water was added and the solution was thoroughly extracted with ethyl acetate (5 × 150 mL). The combined organic phases were washed with water, brine, dried over anhydrous $MgSO_4$, filtered, and evaporated under reduced pressure. Silica gel chromatography (4:1 hexane/ethyl acetate as eluant) gave 7.07 g of **3** and 1.28 g of **13** (77% combined yield). An analytical sample of each was obtained by recrystallization from ethyl acetate: **3** (mp 163–167°C, 192–197°C); IR ($CHCl_3$): 2950 (s), 2240 (m), 1720 (s), 1360 (s); NMR (200 MHz, $CDCl_3$): 3.18–2.96 (m, 3H), 2.78–2.50 (m, 5H), 2.29 (s, 3H), 1.98 (s, 3H), 1.96–1.56 (m, 4H), 1.48 (s, 3H); Anal. calcd. for $C_8H_{25}OS_2N$: C 64.43, H 7.51, N 4.17; found: C 64.50, H 7.52, N 4.19. **13** (mp 182–183°C); IR ($CHCl_3$): 2920 (m), 2240 (w), 1710 (s), 1350 (s); NMR (200 MHz, $CDCl_3$): 3.20–2.98 (m, 3H), 2.82–2.52 (m, 5H), 2.36 (s, 3H), 1.98 (s, 3H), 1.10 (s, 3H). Anal. calcd. for $C_8H_{25}OS_2N$: C 64.43, H 7.51, N 4.17; found: C 64.31, H 7.62, N 4.24.

Enone 14

A solution of 7.0 g (0.021 mol) of **3** in 100 mL of acetonitrile was treated with 6.98 g (0.052 mol) of *N*-chlorosuccinimide and 8.87 g (0.052 mol) of silver nitrate in 40 mL of 80% aqueous acetonitrile. The reaction mixture was stirred at room temperature for 2 h after which it was washed with saturated Na_2SO_3, saturated $NaHCO_3$, and brine. The organic solution was then dried over anhydrous $CaCl_2$ and filtered through Celite. The cake was thoroughly washed with methylene chloride/hexane (1:1), and the combined organic phases were evaporated under reduced pressure. Crystallization of the solid gave 4.1 g (80%) of **14** (mp 130–132°C). IR ($CHCl_3$): 2925 (m), 2240 (w), 1715 (s), 1660 (s), 1610 (m), 1360 (m); UV (95% ethanol): 246 nm (ϵ = 18 509); NMR (60 MHz, $CDCl_3$): 3.38–2.40 (m, 8H), 2.30 (s, 3H), 1.82 (s, 3H), 1.67 (s, 3H); MS (EI) *m/e* (relative intensity): 245 (M^+, 100).

Dienol acetate 15

A solution of 3.5 g (14.28 mmol) of **14** in 20 mL of acetic anhydride was treated with 0.5 mL of acetic anhydride/48% aqueous hydrobromic acid (3:2) and stirred for 16 h. The reaction mixture was then poured carefully into 100 mL of ice water and stirred for 1.5 h. The solidified product was taken up in chloroform and the aqueous phase was thoroughly extracted with chloroform (4 × 50 mL). The combined

Can. J. Chem. Downloaded from www.nrcresearchpress.com by 198.100.157.202 on 09/07/12
For personal use only.

Can. J. Chem. Downloaded from www.nrcresearchpress.com by 198.100.157.202 on 09/07/12
For personal use only.

organic phases were carefully washed with saturated $NaHCO_3$, water, and brine, and dried over anhydrous $CaCl_2$. Filtration and evaporation of solvent gave a brown solid, which was purified on silica gel chromatography (hexane/ethyl acetate 3:2 as eluant) to give 3.6 g (88%) of product. An analytical sample of **15** (125–127°C) was obtained by recrystallization from ethanol. IR ($CHCl_3$): 2910 (m), 2240 (w), 1740 (s), 1700 (s), 1665 (m), 1365 (s), 1350 (s); NMR (200 MHz, $CDCl_3$): 5.65 (t, J = 4 Hz, 1H), 3.22–3.1 (m, 1H), 2.77–2.42 (m, 4H), 2.36 (s, 3H), 2.20 (s, 3H), 1.68 (t, J = 2 Hz, 3H), 1.40 (s, 3H); MS (EI) m/e (relative intensity): 287 (M^+, 100).

Bromo dienol acetate ***16***

A solution of 200 mg (0.69 mmol) of **15** in 10 mL of anhydrous THF was treated with 260 mg (0.69 mmol) of phenyl trimethyl ammonium tribromide. The reaction mixture was stirred for 0.75 h and then poured into saturated $NaHCO_3$. The layers were separated and the aqueous phase was washed with two 5-mL portions of ether. The combined organic phase was washed several times with aqueous Na_2SO_3 until the aqueous phase was clear. Drying over anhydrous $CaCl_2$, filtering, and evaporation of solvent under reduced pressure gave 280 mg of a mixture of unstable bromide **16** and acetate **15**. This compound was always generated *in situ* for use in the next synthetic transformation. IR ($CHCl_3$): 2920 (m), 2240 (w), 1745 (s), 1720 (s), 1660 (m), 1370 (m), 1360 (m); NMR (60 MHz, $CDCl_3$): 5.75–5.52 (m, 1H), 4.0 (s, 2H), 2.20 (s, 3H), 1.68 (s, 3H), 1.45 (s, 3H); MS (EI) m/e: 367/365 (M^+).

Diester ***17***

A solution of **16**, prepared as described above, was treated directly with the sodium anion of dimethyl-1,3-acetone dicarboxylate, generated by stirring a solution of 50.1 mg (2.09 mmol) of sodium hydride with 0.31 mL (2.09 mmol) of dimethyl-1,3-acetone dicarboxylate for 1 h, followed by addition of 0.1 mL of HMPA. The reaction mixture was allowed to stir overnight and then poured into saturated aqueous NH_4Cl. The aqueous phase was extracted with ethyl acetate and the combined organic washings were dried over anhydrous $CaCl_2$, filtered, and solvent evaporated. Purification on 1 mm silica gel preparative TLC plates (hexane/ethyl acetate 1:1 as eluant) furnished 80 mg starting dienol acetate **15** and 100 mg (52%) of diester **17**. IR ($CHCl_3$): 2920 (m), 2240 (w), 1740 (s), 1730 (s), 1710 (s), 1660 (m), 1430 (m), 1360 (m), 1350 (m); UV (95% ethanol) 234 nm (ϵ = 15 643), (95% ethanol + 5% NaOH): 240 nm (ϵ = 14 107) (hydrolysis of enol acetate to enone), 280 nm (ϵ = 12 286) (enolate of β-keto ester); NMR (200 MHz, $CDCl_3$): 5.64 (t, J = 4 Hz, 1H), 4.72 and 4.74 (s, 1H), 4.38–4.32 (m, 1H), 3.78 (s, 6H), 3.26–3.06 (m, 3H), 2.18 (s, 3H), 1.68 (s, 3H), 1.36, 1.38, and 1.42 (s, 3H); MS (EI) m/s: 459 (M^+).

Malonyl dienol acetate ***18***

To a solution of **16** in 15 mL of THF was added the sodium anion of dimethyl malonate, prepared from 101 mg (4.2 mmol) of NaH and 0.48 mL (4.2 mmol) of dimethyl malonate in 15 mL of THF. The reaction mixture was stirred for 2 h and then quenched with 10 mL of saturated aqueous NH_4Cl. The layers were separated and the aqueous phase was washed with three 10-mL portions of ether. The combined extracts were dried over anhydrous $CaCl_2$, filtered, and evaporated under reduced pressure. The residue was purified on 1 mm silica gel preparative TLC plates (two developments with hexane/ethyl acetate 3:2 as eluant) to give 100 mg of dienol acetate **15** and 99 mg (68%) of malonyl adduct **18**. IR ($CHCl_3$): 2910 (w), 2240 (w), 1730 (s), 1740 (s), 1430 (m), 1415 (m), 1350 (m); NMR (200 MHz, $CDCl_3$): 5.57 (t, J = 4 Hz, 1H), 4.01 (t, J = 8 Hz, 1H), 3.73 (s, 6H), 3.2–3.06 (m, 3H), 2.8–2.28 (m, 6H), 2.20 (s, 3H), 1.67 (t, J = 2 Hz, 3H), 1.40 (s, 3H); MS (EI) m/e: 417 (M^+).

Tetraester ***19***

To a solution of 60 mg (0.14 mmol) of **18** in 10 mL of THF was added 10 mg (0.42 mmol) of sodium hydride. The reaction mixture was stirred for 1.5 h and then 30 mg (0.17 mmol) of dimethyl chloromethylene malonate was added and stirring continued for 0.5 h. The reaction mixture was diluted with 10 mL of ether and then poured carefully into water. The layers were separated and the organic phase was dried with anhydrous $CaCl_2$, filtered, and evaporated under reduced pressure. The residue was purified on 1 mm silica gel preparative TLC plates (hexane/ethyl acetate 3:2 as eluant) to deliver 56 mg (72%) of tetraester **19**. IR ($CHCl_3$): 2940 (m), 2840 (w), 2240 (w), 1730 (s), 1430 (m), 1365 (m); UV (95% ethanol): 231 nm (ϵ = 16 765), 235 nm (ϵ = 16 646), (95% ethanol, 5% NaOH), 400 nm (ϵ = 11 353), 390 nm (ϵ = 10 176); NMR (200 MHz, $CDCl_3$): 7.79 (s, 1H), 5.64 (t, J = 4 Hz, 1H), 3.82 (s, 3H), 3.79 (s, 3H), 3.76 (s, 3H), 3.74 (s, 3H), 3.22–3.10 (m, 2H), 2.80–2.26 (m, 4H), 2.16 (s, 3H), 1.67 (s, 3H), 1.34 (s, 3H); MS (EI) m/e: 459 (M^+).

Phenyl selenide ***21***

A solution of 100 mg (0.24 mmol) of **18** in 15 mL of benzene was treated with 50.5 mg (2.5 mmol) of phenyl selenyl chloride followed by 58.3 mg (2.5 mmol) of silver trifluoroacetate. The reaction mixture was stirred at room temperature for 6 h and then filtered through Celite. The cake was washed thoroughly with chloroform and the combined organic phases were evaporated under reduced pressure. Purification on silica gel preparative TLC plates (hexane/ethyl acetate 3:2 as eluant) gave 95 mg (75%) of selenide **21**. IR ($CHCl_3$): 2940 (w), 2240 (w), 1750 (s), 1730 (s), 1660 (s), 1600 (w), 1430 (m), 1355 (m); NMR (200 MHz, $CDCl_3$): 7.83–7.70 (m, 2H), 7.58–7.45 (m, 3H), 4.48 (t, J = 2 Hz, 1H), 4.08 (t, J = 8 Hz, 1H), 3.86 (s, 6H), 3.72 (dd, J = 12 Hz, J = 20 Hz, 2H), 3.27 (dd, J = 12 Hz, J = 6 Hz, 2H), 2.86–2.13 (m, 6H), 2.02 (s, 3H), 1.65 (s, 3H).

Tetraester phenyl selenide ***22***

A solution of 40 mg (0.08 mmol) of **21** and 10 mL of THF was treated with 3.6 mg (0.15 mmol) of sodium hydride for 1.5 h. To this was added 30 mg (0.17 mmol) of dimethyl chloromethylene malonate and the reaction mixture was stirred for an additional hour. The solution was filtered through a glass wool plug and diluted with 10 mL of ethyl acetate. After washing with water and brine, the organic phase was dried over anhydrous $CaCl_2$, filtered, and the solvent evaporated. The yellow oil obtained was purified on silica gel preparative TLC plates (hexane/ethyl acetate 3:2 as eluant) to deliver 25 mg (47%) of phenyl selenide tetramethylester **22**. IR ($CHCl_3$): 2940 (m), 2920 (m), 2240 (w), 1740 (s), 1665 (m), 1430 (m), 1355 (m); NMR (200 MHz, $CDCl_3$): 7.85 (s, 1H), 7.80–7.64 (m, 2H), 7.51–7.38 (m, 3H), 4.38 (t, J = 2 Hz, 1H), 3.82 (s, 3H), 3.80 (s, 6H), 3.78 (s, 3H), 2.74–2.29 (m, 6H), 1.94 (s, 3H), 1.52 (s, 3H).

Tertiary alcohol ***23***

A solution of 30 mg (0.045 mmol) of selenide **22** in 10 mL of THF was treated with 17.7 mg (0.09 mmol) of 85% mCPBA and stirred for 2 h. The reaction mixture was washed with saturated Na_2SO_3, $NaHCO_3$, water, and brine. After drying over anhydrous $CaCl_2$ and filtering, the solvent was evaporated under reduced pressure. Purification on silica gel preparative TLC plates (hexane/ethyl acetate 3:2) gave 19 mg (80%) of alcohol **23**. IR ($CHCl_3$): 2940 (m), 2920 (m), 2840 (m), 2240 (w), 1740 (s), 1720 (s), 1430 (m), 1360 (m); NMR (200 MHz, $CDCl_3$): 7.78 (s, 1H), 6.22 (t, J = 2 Hz, 1H), 3.83 (s, 3H), 3.80 (s, 9H), 3.22–3.13 (m, 1H), 3.0–2.86 (m, 1H), 2.74–1.99 (m, 7H), 1.66 (s, 3H), 1.58 (s, 3H).

General procedure for Michael reactions with the dianion: Generation of ***34***

A solution of LDA in 5 mL of dry THF (0.64 mmol, 3.2 equiv.) was cooled to −78°C and 100 mg (0.2 mmol) of **3** in 5 mL of dry THF was added via syringe over 2 min. The reaction was stirred at this temperature for 2 h at which time 60 mg (0.38 mmol) of dimethyl ethylidene malonate **25** in 0.5 mL of THF was added in one lot. After stirring for an additional 15 min at −78°C, the reaction mixture was poured into saturated NH_4Cl. The layers were separated and the aqueous phase was extracted with ethyl acetate. The combined extracts were washed with water and brine, dried over anhydrous $CaCl_2$, and filtered. The solvent was evaporated *in vacuo* and the resultant oil was chromatographed on silica gel preparative plates (hexane/ethyl acetate 3:2 as eluant) to deliver 70 mg (49%) of Michael adduct **34** as a 1:2 mixture of C14 diastereoisomers. IR ($CHCl_3$): 2960 (s), 2240 (w), 1750 (s), 1730 (s), 1440 (s), 1380 (m), 1360 (m); NMR (200 MHz, $CDCl_3$), major diastereomer: 3.78 (s, 6H), 3.19–2.96 (m, 3H), 2.83–2.48 (m, 6H), 2.36 (s, 3H), 2.0 (s, 3H), 1.44 (s, 3H), 1.32 (d, J = 8 Hz, 3H); minor diastereomer: 3.80 (s, 6H), 3.19–2.96 (m, 3H), 2.83–2.48 (m, 6H),

2.37 (s, 3H), 2.0 (s, 3H), 1.44 (s, 3H), 1.12 (d, J = 8 Hz, 3H); MS (EI) m/e: 493 (M^+).

Enyne alcohol ***40***

A suspension of 4.29 g (0.18 mol) of magnesium metal in 150 mL of dry ether was treated with 21.5 g (0.18 mol) of allyl bromide in 50 mL of ether. When the metal had been completely consumed, 8.87 g (0.07 mol) of aldehyde **39** in 30 mL of ether was added dropwise from a dropping funnel over 15 min. The reaction mixture was stirred for 2 h and then poured into cold 5% HCl. The layers were separated and the organic phase was washed with water and brine. After drying over anhydrous $MgSO_4$ and filtration, the solvent was evaporated under reduced pressure. Pure alcohol **40** (bp 48–50°C, 10 Torr (1 Torr = 133.3 Pa)) was obtained by vacuum distillation, 8.24 g (62%). IR ($CHCl_3$): 3600 (m), 2960 (m), 2180 (m), 1650 (m), 1390 (m), 1260 (m), 1030 (s); NMR (200 MHz, $CDCl_3$): 6.02–5.76 (m, 1H), 5.50–5.36 (m, 2H), 4.44 (t, J = 6 Hz, 1H), 2.49 (dd, J = 6 Hz, J = 7 Hz, 2H), 0.17 (s, 9H).

Mesylate ***41***

A solution of 4.35 g (0.026 mol) of alcohol **40** in 10 mL of dry DMF was cooled in an ice bath and treated with 4.04 g (0.031 mol) of 2,4,6-collidine and 3.52 g (0.031 mol) of methane sulfonyl chloride. The reaction mixture was allowed to warm to room temperature and stir for 3 h. It was then poured into ice water and diluted with 100 mL of hexane. The layers were separated and the organic phase was washed with saturated $NaHCO_3$, water, and brine. After drying over anhydrous $MgSO_4$ and filtration, the solvent was evaporated under reduced pressure. The crude mesylate **41** obtained, 6.2 g (96%), was used without further purification. IR ($CHCl_3$): 2940 (w), 2170 (w), 1640 (w), 1415 (w), 1360 (s), 1330 (m), 1180 (s); NMR (200 MHz, $CDCl_3$): 5.96–5.72 (m, 1H), 5.30–5.08 (m, 3H), 3.11 (s, 3H), 2.62 (dd, J = 6 Hz, J = 6 Hz, 2H), 0.18 (s, 9H).

General procedure for halide formation: Preparation of iodide ***44***

A solution of 6.2 g (0.025 mol) of mesylate in 100 mL of anhydrous acetone and 9 g (0.059 mol) of KI was refluxed for 12 h. Upon cooling and evaporation of solvent under reduced pressure the residue was taken up in 200 mL of hexane and 100 mL of water. The layers were separated and the organic phase was successively washed with water, $Na_2S_2O_3$, and brine, dried over anhydrous $MgSO_4$, filtered, and solvent evaporated under reduced pressure. The oil was distilled under vacuum (0.01 Torr) to yield 4.25 g (61%) of iodide **44** (bp 53–56°C). IR ($CHCl_3$): 2960 (s), 2920 (s), 2180 (s), 1680 (m), 1650 (s), 1630 (m), 1420 (s); NMR (200 MHz, $CDCl_3$): 5.96–5.73 (m, 1H), 5.29–5.10 (m, 2H), 4.53 (t, J = 7 Hz, 1H), 2.72 (dd, J = 7 Hz, J = 7 Hz, 2H), 0.16 (s, 9H).

Alkylated adduct ***47***

A solution of 0.057 mL (0.69 mmol) of pyrrolidine in 10 mL of dry THF was cooled to −78°C and 0.43 mL (0.69 mmol) of 1.5 M *n*BuLi in hexane was added via a syringe. After stirring for 15 min, 100 mg (0.3 mmol) of nitriles **3** and **13** in 1 mL of THF was added and stirring was continued for 2 h. Then 0.066 mL (0.3 mmol) of iodide **44** was added neat in one lot. Following stirring at −78°C for 1 h the reaction mixture was poured into saturated NH_4Cl. The layers were separated and the organic portion was washed with water and brine, dried over anhydrous $MgSO_4$, and filtered. After evaporation of solvent under reduced pressure, the oil was purified by silica gel chromatography (hexane/ethyl acetate 9:1 → 3:1 as eluant) to give 61 mg (95%) of alkylation product **47** and 56 mg of nitriles **3** and **13**. IR ($CHCl_3$): 2950 (s), 2880 (m), 2250 (w), 2180 (m), 1710 (s), 1650 (m), 1420 (m), 1360 (m); NMR (200 MHz, $CDCl_3$): 5.98–5.72 (m, 1H), 5.23–5.06 (m, 3H), 3.17 (s, 1H), 3.16–2.96 (m, 3H), 2.80–2.46 (m, 8H), 2.38 (s, 3H), 2.05 (s, 3H), 2.04–1.42 (m, 4H), 1.41 (s, 3H), 0.18 (s, 9H); MS (EI) m/e: 485 (M^+).

Acknowledgements

Support by the Natural Sciences and Engineering Research Council of Canada, Ottawa, in the form of operating grants and a fellowship to one of us (D.I.M.) is gratefully acknowledged. We thank Dr. Peter S. White of this department for the X-ray crystallographic determinations and Dr. Zarko Stojanac of this department for suggesting the strategic concept involving the formation of bonds 1 and 2 in Fig. 1.

1. J. POLONSKY. Fortschr. Chem. Org. Naturst. **30**, 101 (1973).
2. J. POLONSKY. Fortschr. Chem. Org. Naturst. **47**, 222 (1985).
3. (*a*) S. M. KUPCHAN, J. A. LACADIE, G. N. HOWIE, and B. R. SICKLES. J. Med. Chem. **19**, 1130 (1976); (*b*) M. E. WALL and W. C. WANI. J. Med. Chem. **21**, 1186 (1978).
4. (*a*) M. KIM, K. KAWADA, R. S. GROSS, and D. S. WATT. J. Org. Chem. **55**, 504 (1990); (*b*) P. A. GRIECO, R. P. NARGUND, and D. T. PARKER. J. Am. Chem. Soc. **111**, 6287 (1989); (*c*) T. K. M. SING, Y. TANG, and J. F. MALONE. J. Chem. Soc. Chem. Commun. 1294 (1989); (*d*) P. A. GRIECO, D. T. PARKER, P. GARNER, and S. SASAKI. Tetrahedron Lett. **30**, 3401 (1989); (*d*) M. KIM, K. KAWADA, and D. S. WATT. Synth. Commun. **19**, 2017 (1989); (*f*) K. KAWADA, M. KIM, and D. S. WATT. Org. Prep. Proced. Int. **21**, 521 (1989); (*g*) S. DARVESH, A. S. GRANT, D. I. MAGEE, and Z. VALENTA. Can. J. Chem. **67**, 2237 (1989), and references therein; (*h*) M. SASAKI, T. MURAE, and T. TAKAHASHI. J. Org. Chem. **55**, 528 (1990).
5. (*a*) P. A. GRIECO, S. FERRINO, and G. J. VIDARI. J. Am. Chem. Soc. **106**, 3539 (1984); (*b*) P. A. GRIECO, R. LIS, S. FERRINO, and J. Y. YAW. J. Org. Chem. **49**, 2342 (1984); (*c*) P. A. GRIECO, D. PARKER, and R. P. NARGUND. J. Am. Chem. Soc. **110**, 5568 (1988); (*d*) H. HIROTA, A. YOKOYAMA, K. MIYAJI, T. NAKAMURA, and T. TAKAHASHI. Tetrahedron Lett. **28**, 435 (1987).
6. A. B. MEKLER, S. RAMACHANDRAN, S. SWAMINATHAN, and M. S. NEWMAN. Org. Synth. **41**, 56 (1961).
7. (*a*) M. S. NEWMAN, S. RAMACHANDRAN, S. K. SANKARAPPA, and S. SWAMINATHAN. J. Org. Chem. **26**, 727 (1961); (*b*) H. RUPE and E. KAMBLI. Helv. Chim. Acta, **9**, 672 (1926).
8. (*a*) R. A. DANIEWSKI, P. S. WHITE, and Z. VALENTA. Can. J. Chem. **57**, 1397 (1979); (*b*) R. A. DANIEWSKI, Z. VALENTA, and P. S. WHITE. Bull. Pol. Acad. Sci. **32**, 29 (1984).
9. E. J. COREY and B. W. ERICKSON. J. Org. Chem. **36**, 3553 (1971).
10. A. MARQUET and J. JACQUES. Tetrahedron Lett. No. 9, 24 (1959).
11. H. J. REICH, J. M. RENGA, and I. L. REICH. J. Am. Chem. Soc. **97**, 5334 (1975).
12. D. L. J. CLIVE. Tetrahedron, **34**, 1039 (1978).
13. M. ZÜGER, T. WELLER, and D. SEEBACH. Helv. Chim. Acta, **63**, 2005 (1980).
14. D. SEEBACH and J. GOLINSKI. Helv. Chim. Acta, **64**, 1413 (1981).
15. (*a*) R. B. MILLER. Synth. Commun. **2**, 267 (1972); (*b*) T. R. BORONOEVA, N. N. BELYAEV, M. D. STADNICHUK, and A. A. PETROV. Zh. Obshch. Khim. **44**, 1949 (1973).
16. G. HELMCHEN, A. SELIM, D. DORSCH, and I. TAUFER. Tetrahedron Lett. **24**, 3213 (1983).
17. S. HANESSIAN, A. UGONLINI, D. DUBE, P. J. HODGES, and C. ANDRE. J. Am. Chem. Soc. **108**, 2776 (1986).
18. U. EDER, G. SAUER, and R. WIECHERT. Angew. Chem. Int. Ed. Engl. **10**, 496 (1971); Z. G. HAJOS and D. R. PARRISH. J. Org. Chem. **39**, 1615 (1974; J. GUTZWILLER, P. BUCHSCHACHER, and A. FURST. Synthesis, 167 (1977).
19. D. D. PERRIN and W. L. F. ARMAREGO. Purification of laboratory chemicals. 2nd ed. Pergamon Press, Toronto. 1980.
20. W. C. STILL, M. KAHN, and A. MITRA. J. Org. Chem. **43**, 2933 (1978).

Can. J. Chem. Downloaded from www.nrcresearchpress.com by 198.100.157.202 on 09/07/12
For personal use only.

Synthetic studies towards bruceantin. Part 2. The synthesis of a pentacyclic intermediate

SULTAN DARVESH, ANDREW S. GRANT, DAVID I. MAGEE, AND ZDENEK VALENTA[1]
Department of Chemistry, University of New Brunswick, Fredericton, N.B., Canada E3B 6E2

Received September 20, 1990

SULTAN DARVESH, ANDREW S. GRANT, DAVID I. MAGEE, and ZDENEK VALENTA. Can. J. Chem. **69**, 723 (1991).

In a synthetic approach to the quassinoid bruceantin (**2**), the key intermediate **8** obtained via alkylation of a dianion has been transformed into the pentacyclic intermediate **33** via an ABDC ring forming strategy. The key steps involved in this route are as follows: a unique acid catalyzed cyclization, **19** → **20**; an intramolecular Michael reaction, **24** → **28**; and an allyl sulfoxide [2,3]-sigmatropic rearrangement to introduce the axial C12 alcohol, **31** → **33**.

Key words: bruceantin, quassinoids, cyclization, sulfoxides, sigmatropic rearrangement.

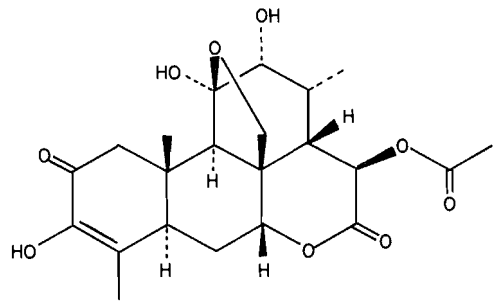
SULTAN DARVESH, ANDREW S. GRANT, DAVID I. MAGEE et ZDENEK VALENTA. Can. J. Chem. **69**, 723 (1991).

Dans une approche à la synthèse de la quassinoïde brucéantine (**2**), on a transformé l'intermédiaire clé (**8**), obtenu par alkylation d'un dianion, en intermédiaire pentacyclique **33** par le biais de la stratégie de formation des cycles ABDC. Les étapes clés impliquées dans cette voie sont : une cyclisation acido-catalysée unique de **19** en **20**, une réaction de Michael intramoléculaire de **24** en **28** et une transposition sigmatropique-[2,3] d'un sulfoxyde d'allyle pour introduire l'alcool axial en C12, **31** à **33**.

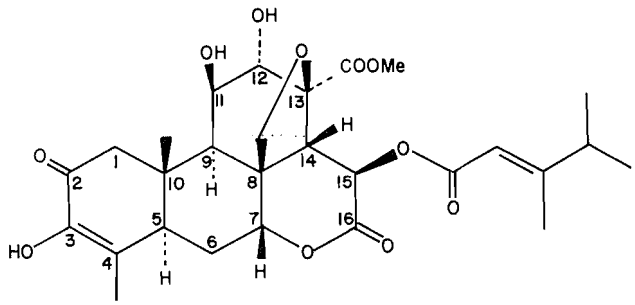
Mots clés : brucéantine, quassinoïde, cyclisation, sulfoxydes, transposition sigmatropique.

[Traduit par la rédaction]

Certain species of the *Simaroubaceae* family have traditionally been used as ingredients for the treatment of dysentery, amebiasis, and other ailments in folk medicine. However, increased attention developed with the report of antileukemic activity of holacanthone **1** (1–3). Since that report bruceantin **2**, a member of the same family, has undergone phase II testing

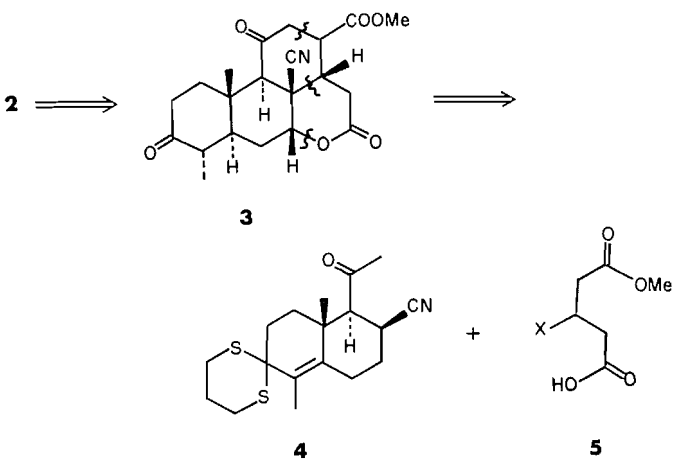


1 Holacanthone



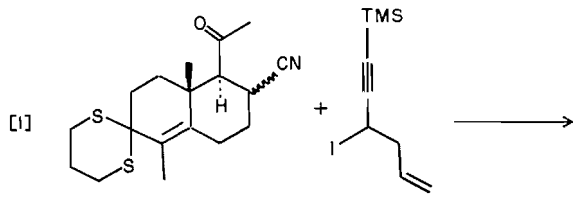
2 Bruceantin

in the United States (4). Due to this biological activity, as well as the fundamental complexity, these compounds have received considerable synthetic attention (5). In the preceding paper (6), we outlined a simple strategy, shown in Scheme 1, which should allow a rapid construction of the quassinoid skeleton, and described a convergent method for the preparation of intermediate **8**, which included the alkylation of the mixture

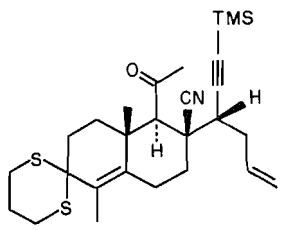


SCHEME 1

of C8-epimers **4** and **6** as the key step (eq. [1]). We now wish to report on the elaboration of this compound into a key pentacyclic intermediate that contains the complete bruceantin skeleton, as well as seven of its 10 chiral centers.



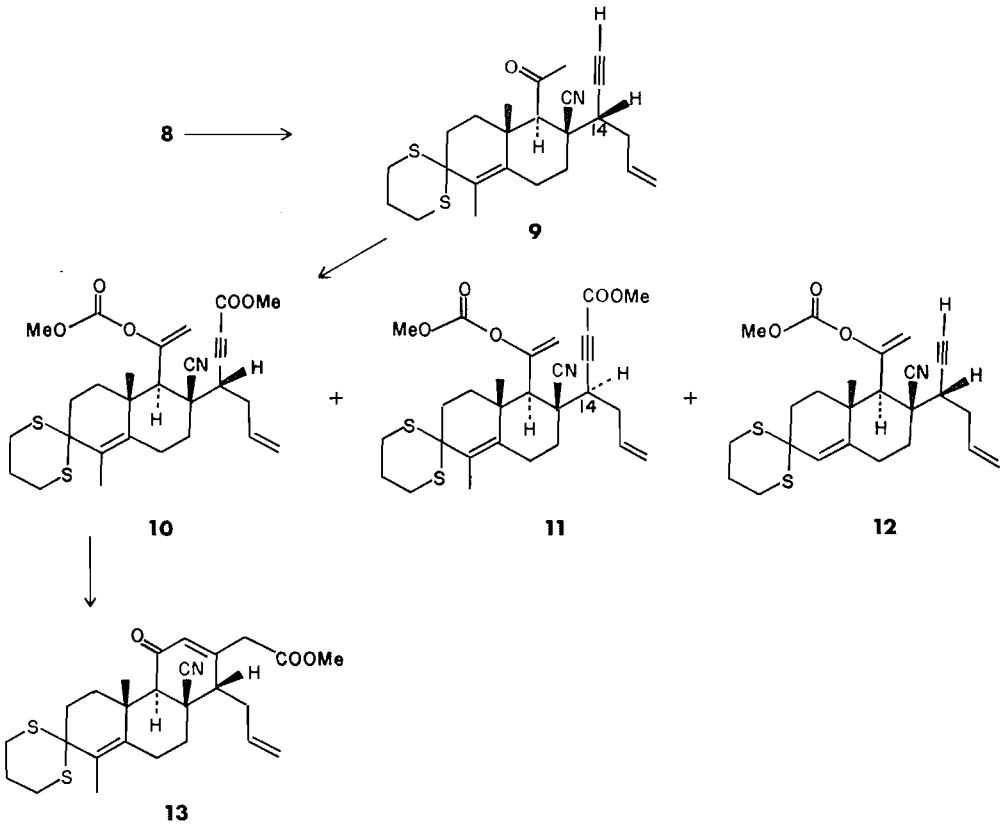
4 + **6** **7**



8

[1]Author to whom correspondence may be addressed.

Can. J. Chem. Downloaded from www.nrcresearchpress.com by 198.100.157.202 on 09/07/12
For personal use only.



SCHEME 2

Results and discussion

The transformation of intermediate **8** into a compound of type **3** requires that the acetylene functionality be used for the construction of ring C, and that the side-chain double bond be utilized for the formation of lactone ring D. Formation of ring C was envisaged as arising from a simple three-step protocol: deprotection of the acetylene, carbomethoxylation, and an intramolecular Michael reaction. Oxidative cleavage of the olefin would then furnish the carboxylic acid required for lactone formation.

Development of this strategy began with treatment of **8** with tetrabutylammonium fluoride (7) in tetrahydrofuran (THF) to give acetylene **9** in good yield (82%) (Scheme 2). Reaction of the dianion of **9** (*n*BuLi in THF at −78°C) with methyl chloroformate furnished **10**, **11**, and **12** in a 2:1:1 ratio and a 65% combined yield. Conversion of carbonate **10** into ester **13** then proceeded smoothly on treatment with sodium methoxide in THF (25% from **9**). Although the strategy worked, the low yield coupled with 25% epimerization at C14 made this route unattractive. Concerning the epimerization, examination of molecular models revealed that a facile proton shift was possible from C14 to the proximate enolate anion after carbomethoxylation of the acetylene, and that reprotonation of the C14 anion would then occur preferably from the α-side. Constructing ring D first would clearly remedy this problem since the C14 proton could no longer be aligned for the intramolecular proton transfer.

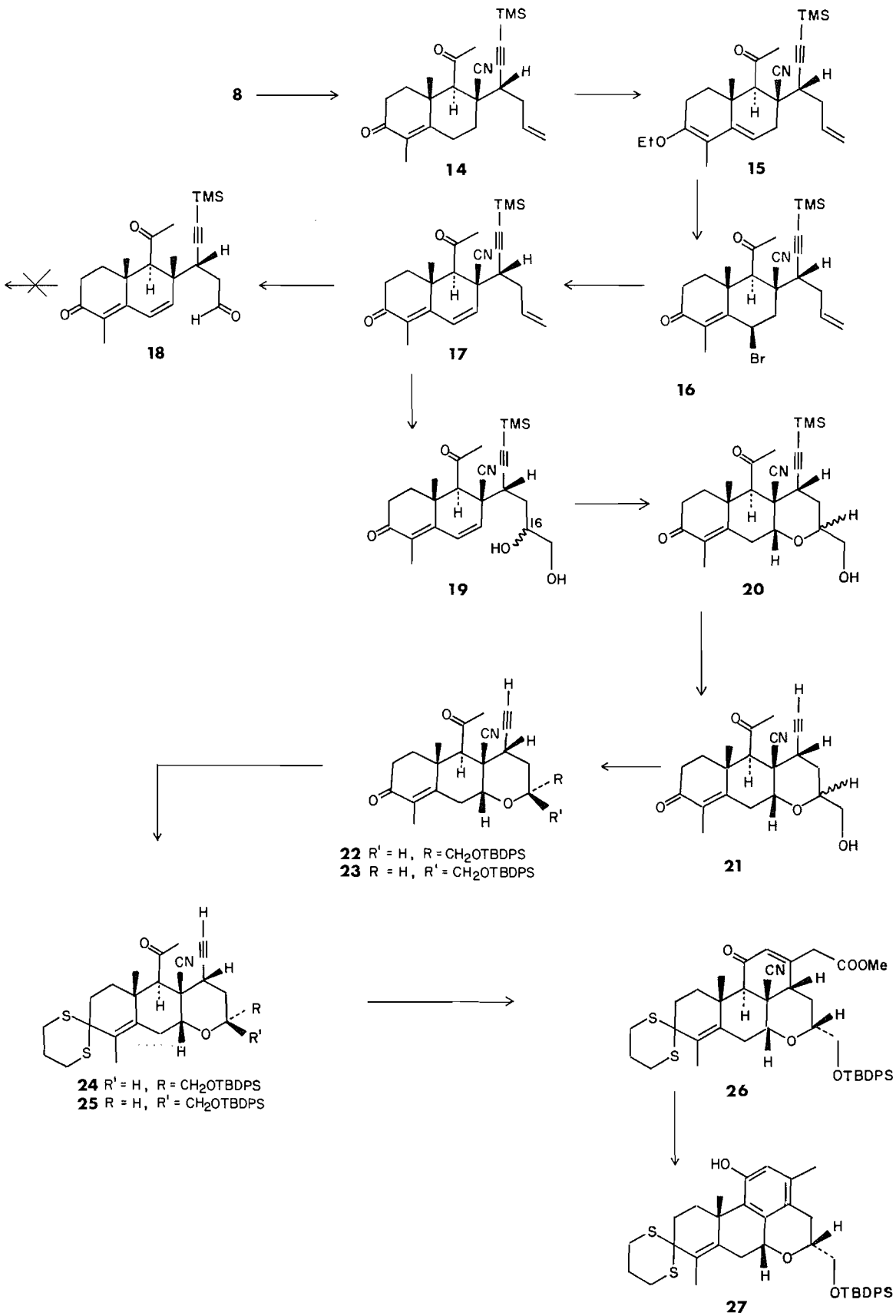
This modified route began with the extension of ring-A conjugation into ring B (Scheme 3). Deprotection of the C3 ketone with mercuric oxide (8) in aqueous THF with a catalytic amount of acid gave enone **14** in quantitative yield. Treatment of **14** with trimethyl orthoformate (9) and a catalytic amount of *p*-toluenesulfonic acid in benzene afforded dienol ether **15** (89%), which was brominated with pyridinium bromide perbromide (10) in aqueous THF to deliver **16** as a single isomer (88%). The exclusive formation of the isomer with an axial bromine at C6 can only be attributed to a strong stereoelectronic effect (11). Efficient dehydrobromination to **17** was then achieved with 1,5-diazabicyclo[4.3.0]non-5-ene (DBN) in THF (78%). It was found that a significant reduction in yield occurred when the base was not used in large excess and when reaction times exceeded 20 min.

Our next objective was the conversion of the side-chain alkene to a suitably oxygenated derivative. Oxidation of **17** with sodium periodate and a catalytic amount of osmium tetroxide (12) in aqueous ether afforded aldehyde **18** in 73% yield. However, all attempts to oxidize **18** efficiently to the acid failed (PCC, PDC, and MnO_2). Direct oxidation of the olefin to the acid also met with no success. Fortunately, a regioselective incorporation of the diol proceeded with ease, on treatment of **17** under the conditions described by Van Rheenan *et al.* (13), to produce **19** as a mixture of the two C16 epimers (see below) in 84% yield.[2]

Initial attempts to effect cyclization of ring D with a variety of acids proved fruitless. For example, **19** was inert to *p*-toluenesulfonic acid, boron trifluoride etherate, Amberlyst-15 (14), and perchloric acid. However, when **19** was heated with 1,3-propane diol in benzene with one-half equivalent of *p*-toluenesulfonic acid and azeotropic removal of water, 15% of enone **20** was obtained, along with 85% of recovered starting material. *There were no traces of any dioxolane compounds,*

[2]In contrast, an unmediated oxidation with osmium tetroxide alone gave a lower yield of **19** and by-products containing carbonyl groups in the side chain.

Can. J. Chem. Downloaded from www.nrcresearchpress.com by 198.100.157.202 on 09/07/12
For personal use only.



SCHEME 3

Can. J. Chem. Downloaded from www.nrcresearchpress.com by 198.100.157.202 on 09/07/12
For personal use only.

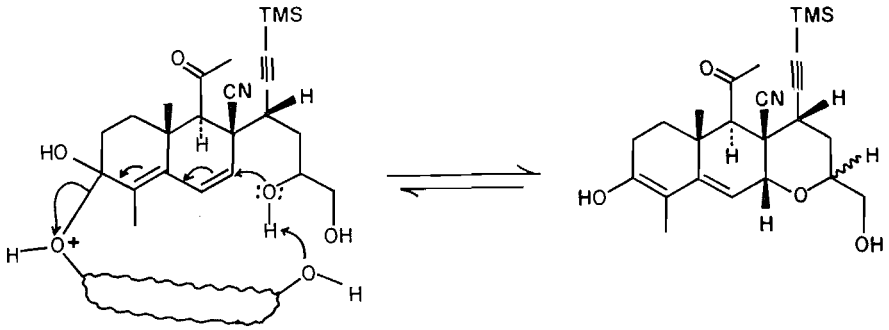


FIG. 1

and under prolonged heating only destruction of starting material was observed. The only difference from previous reaction conditions was the addition of 1,3-propane diol. Therefore, it was postulated that the reaction takes place on the surface of the propane diol[3] in a two-phase reaction (Fig. 1). In one possible interpretation, as part of the surface promotes formation of the oxonium ion at C3, another part of the surface abstracts a proton from the charged ether oxygen before reversion to the open form can occur. Subsequent protonation at C6 can then similarly take place on the surface of protonated propane diol. After considerable experimentation, it was found that **20** (mixture of C16 epimers) could be obtained in 90% yield, based on 20% recovered starting material, by treating diol **19** with 60 equivalents of 1,3-propane diol and 30 equivalents of *p*-toluenesulfonic acid in benzene at 40°C for 4 h. The ^{1}H NMR signal corresponding to C7-H in **20** (δ 4.21, t, J = 3 Hz) showed clearly that the ether O-atom had the desired axial configuration relative to ring B.

With rings A, B, and D now established, the final task was to incorporate ring C via our previous cyclization protocol. This began by deprotection of acetylene **20** with tetrabutylammonium chloride and potassium fluoride in acetonitrile (15) to deliver **21** in a quantitative yield. Protection of the primary alcohol in **21** with *tert*-butyldiphenylsilyl (TBDPS) chloride and imidazole in dimethylformamide (DMF) (16) then gave a 6:1 mixture of products **22** and **23** in 84% yield. These could be cleanly separated by silica gel chromatography, the ^{1}H NMR spectra showing the predominance of **22** containing the -CH_2OTBDPS group in an equatorial position. The C3 ketone of **22** and **23** was protected as its 1,3-propane dithiane with 1,3-propane dithiol in THF (1:1) at room temperature to provide **24** and **25** in 96 and 84% yield, respectively. The major isomer **24** was then subjected to dianion formation with lithium hexamethyl disilazide in THF at −30°C, followed by a dimethyl carbonate quench to deliver ester **26** in 75% yield. Unfortunately, all attempts to modify this intermediate failed. For example, **26** was inert to reducing agents such as diisobutylaluminum hydride and lithium triethoxyaluminum hydride. Furthermore, attempts at hydrolysis of the ester and decarboxylation under a variety of conditions only led to recovered starting material or to phenol **27**, which was presumably formed as a result of enolization between C9 and C11, followed by elimination of the nitrile and subsequent aromatization.

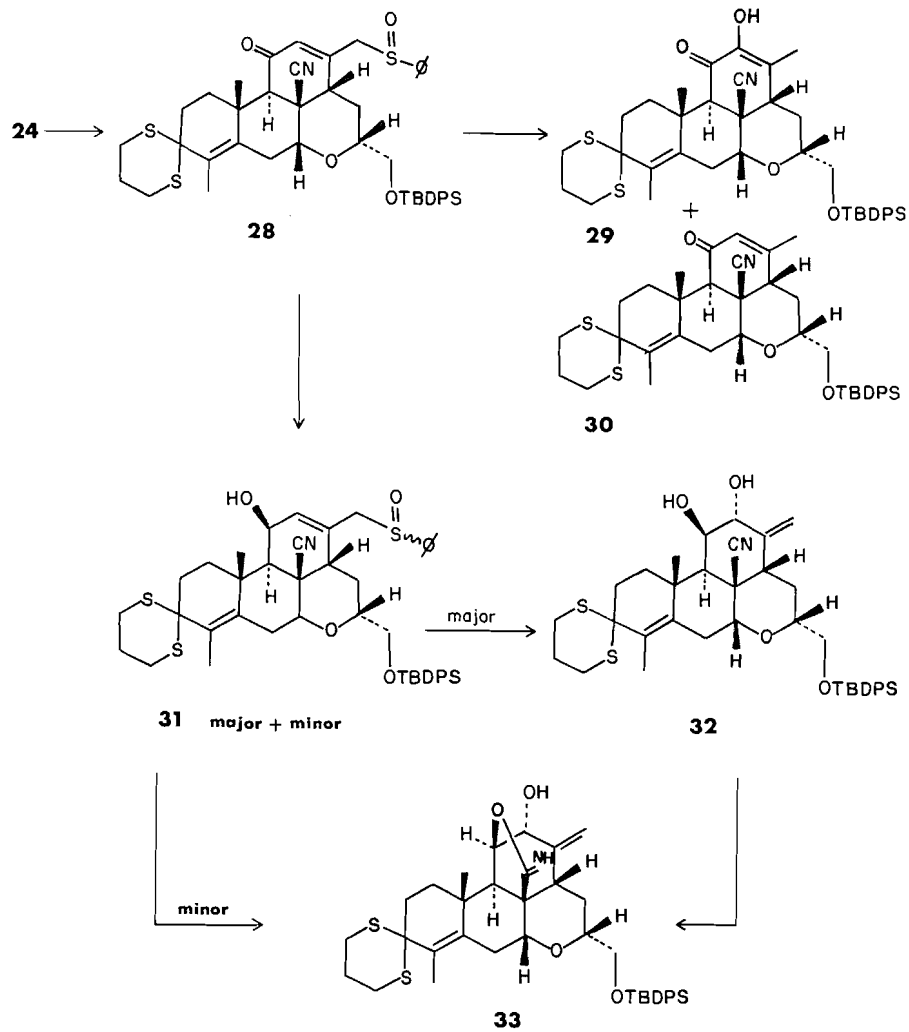
Since, in addition to the lack of desired reactivity, ester **26** clearly did not possess the features most suitable for the development of the complex ring-C functionality of bruceantin, we decided to modify the acetylene activation–cyclization strategy in a way that would satisfy two conditions: (1) The Michael addition should be accomplished without the introduction of an unwanted extra carbon. (2) An acetylene activating group should be used that could subsequently be modified and (or) manipulated to furnish the desired ring-C functionality. As a result, we chose to use an acetylenic sulfoxide, rather than a carbomethoxy acetylene, as the Michael acceptor. Implementation of this strategy again began with the conversion of **24** into the dianion, this time using *n*-butyllithium in THF at −78°C, followed by addition of isopropyl *p*-toluenesulfinate (17) at −78°C to give adduct **28** as an amorphous solid (81%, λ_{max} = 369 nm) (Scheme 4). Upon heating of **28** in methanol with 10 equivalents of sodium thiophenolate (18), diosphenol **29** and enone **30** were obtained in 25 and 50% yield respectively. Compound **29** was the product expected from a [2,3]-sigmatropic rearrangement followed by a base-catalyzed double bond migration, but the formation of **30** was unexpected and could only be rationalized by a reductive elimination process (eq. [2]). This type of reductive desulfurization was demonstrated recently by Theobald and Okamura (19). These results clearly indicated that the α,β-unsaturated ketone is not compatible as such with the [2,3]-sigmatropic rearrangement. However, this situation can be remedied by reducing the C11 ketone first.

After considerable experimentation, reduction was effected by treatment of **28** with lithium borohydride in THF/methanol (20) to give alcohol **31** as a 3:2 mixture of sulfoxide diastereoisomers in 77% yield. Separation of the isomers was achieved by careful silica gel chromatography to give **31 major** and **31 minor**; their stereochemistry was not determined. Compounds **31 major** and **31 minor** were then each treated with 10 equivalents of triethyl phosphite (18) in ethanol at 40°C for 5 days but only **31 major** rearranged to give diol **32** (75%). The minor isomer, even after a prolonged reaction time, gave only recovered starting material.

However, when **31 minor** was heated at 80°C for 48 h under identical conditions, a new compound assigned to be imino ether **33** was obtained in 75% yield. This initially caused some concern but it was found that **33** was also obtained as the sole product when **31 major** was heated at 80°C in the presence of 10 equivalents of triethyl phosphite, or when diol **32** was simply heated in ethanol at 80°C. This clearly demonstrated that the rearrangement of the two sulfoxide diastereomers was proceeding to give the same stereochemistry at C12, but at very different reaction rates. This must mean that one transition state involves more steric interactions than the other. Examination of molecular models showed that this can only be explained if the rearrangement proceeds from the α-face to deliver an

[3]It was observed that the 1,3-propane diol was insoluble in benzene and formed globules on reflux.

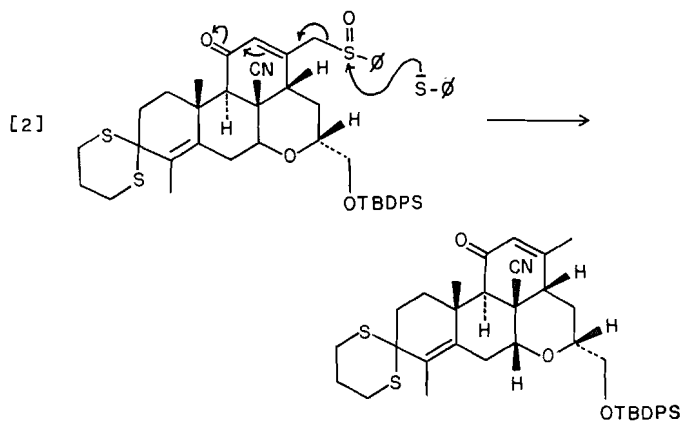
Can. J. Chem. Downloaded from www.nrcresearchpress.com by 198.100.157.202 on 09/07/12
For personal use only.



SCHEME 4

axial alcohol at C12 (Fig. 2). To reinforce this stereochemical assignment, a 10% nOe enhancement was observed at one of the vinyl protons when the C12 proton of **32** was irradiated.

The α (axial) assignment to the C12-OH group is also in agreement with a study reported by Hoffmann *et al.* (21). Using a simple cyclohexene whose conformation was anchored by a 4-*tert*-butyl group and whose position of the arylsulfoxy group relative to the cyclohexene was the same as in sulfoxide **31**, these authors concluded that there is a 6.2-fold preference for the formation of the axial (versus the equatorial) C—O bond



and that there is a 3.1-fold preference for an *exo* (aryl group away from the molecule) versus an *endo* (aryl group towards the molecule) transition state in that particular case. Thus, there is clearly a "six-membered ring bias" towards a quasi-axial attack of the cyclohexene via a quasi-chair conformation. However, in contrast to Hoffmann *et al.*, we have not detected a trace of the C12-β isomer on rearrangement of **31**, in spite of the fact that the sulfoxide of **31** may be involved in a 1,3-*cis* diaxial interaction with the C14—C15 bond when attacking from the α-side (see Fig. 2). Further experiments are required to establish whether the greater stereoselectivity in the case of **31** arises from a reduced conformational flexibility of the cyclohexene in **31** or whether the axial C11 hydroxyl group in **31** exerts a stereoelectronic effect favouring an antiperiplanar addition.

In conclusion, an efficient 19-step synthesis of a pentacyclic intermediate has been achieved in a 3.5% overall yield from 2-methylcyclohexane-1,3-dione and ethyl vinyl ketone. This intermediate, **33**, contains four of the five rings and seven of the 10 chiral centers of bruceantin. Its further synthetic manipulation and the general utility of the sequence **24** → **28** → **32** are currently under investigation.

Experimental section

Melting points were determined on a Kofler hot stage apparatus and are uncorrected. Infrared (IR) spectra were recorded on a Perkin–Elmer IR spectrophotometer model 717B using sodium chloride cells

Can. J. Chem. Downloaded from www.nrcresearchpress.com by 198.100.157.202 on 09/07/12
For personal use only.

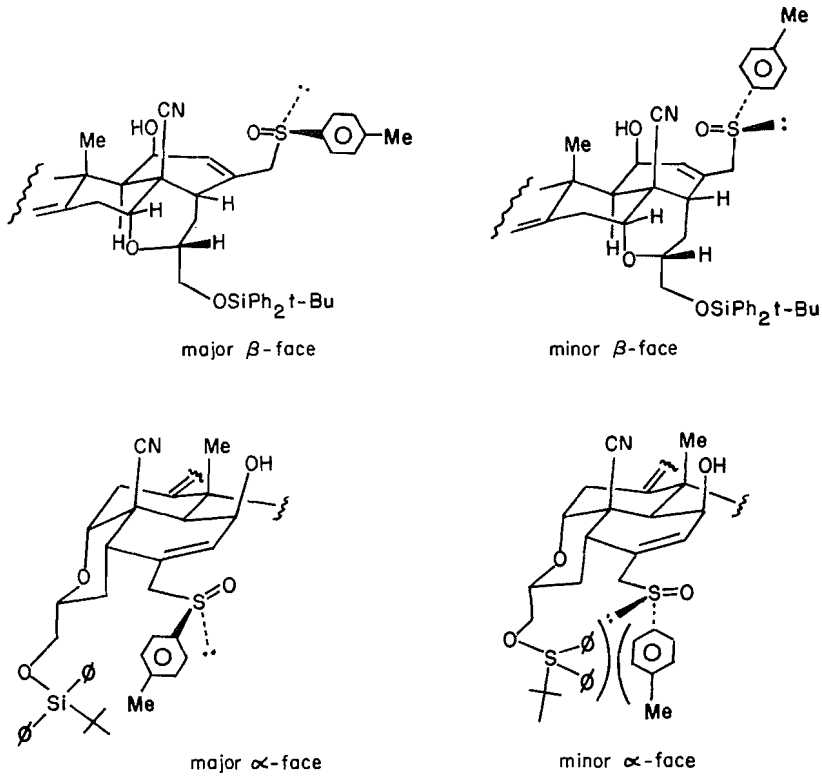


FIG. 2

(0.5 mm) and are reported in wave numbers (cm^{-1}) with polystyrene as standard. Nuclear magnetic resonance (NMR) spectra were recorded on a Varian XL-200 (200 MHz) spectrometer. Chemical shifts are reported in ppm (δ) downfield relative to tetramethylsilane as standard. High resolution mass spectra (HRMS) were recorded at the Mass Spectrometry Laboratory, Department of Chemistry, University of Alberta, Edmonton, Alberta. Ultraviolet (UV) spectra were recorded on a Beckman spectrophotometer model 25, using quartz cells (4.5 mL).

All reactions, unless otherwise specified, were run under an inert atmosphere of Ar or N_2, and reactions requiring anhydrous conditions were performed in a flame-dried or oven-dried (120°C) apparatus. Temperatures above or below room temperature refer to bath temperatures. All solvents used in the reaction flask were anhydrous, unless otherwise stated, and were dried according to established procedures by distillation under N_2 from an appropriate drying agent (22).

Analytical TLC was performed on E. Merck precoated silica gel plates (0.25 mm). Column chromatography was performed by the method of Still *et al.* (23) with E. Merck silica gel 60 (230–400 mesh).

Preparation of enone ***14***

A solution of 3.6 g (0.017 mol) of mercuric oxide, 120 mL of 0.5% H_2SO_4, and 200 mL of THF was heated to 40°C and 4.0 g (0.0082 mol) of **8** in 20 mL of THF was added. The reaction mixture was stirred at this temperature for 4 h, cooled, and filtered through Florisil. The filtrate was saturated with NaCl and extracted with ethyl acetate. The organic extract was washed with 10% $NaHCO_3$, water, and brine, and dried over anhydrous $MgSO_4$. After filtration and evaporation of solvent under reduced pressure, the solid was chromatographed on silica gel (hexane/ethyl acetate 4:1 as eluant) to give 3.26 g (100%) of enone **14**. An analytical sample of **14** (mp 158–159.5°C) was obtained by recrystallization from ether. IR ($CHCl_3$): 2950 (m), 2190 (w), 1720 (s), 1670 (s), 1610 (m), 1360 (m), 1320 (m); UV (95% ethanol): 243 nm (ε = 12 610); NMR (200 MHz, $CDCl_3$): 5.98–5.74 (m, 1H), 5.26–5.10 (m, 2H), 3.25 (s, 1H), 2.98–2.84 (m, 1H), 2.74–2.46 (m, 5H), 2.39 (s, 3H), 2.36–1.94 (m, 4H), 1.86 (s, 3H), 1.85–1.61 (m, 2H), 1.56 (s, 3H), 0.16 (s, 9H); HRMS (EI) *m/e* (relative intensity): 395.2277 (6.86).

Preparation of enol ether ***15***

A solution of 7.72 g (19.4 mmol) of **14** and 100 mL of dry benzene was treated with 6.47 mL (38.9 mmol) of triethylorthoformate and 0.7 g (4.07 mmol) of *p*-toluenesulfonic acid and stirred for 1 h. The reaction mixture was poured into saturated $NaHCO_3$ and the layers were separated. The organic portion was washed with water and brine, dried over anhydrous $MgSO_4$, filtered, and the solvent evaporated *in vacuo*. The yellow solid was purified by silica gel chromatography (hexane/ethyl acetate 6:1 as eluant) to yield 7.36 g (89%) of **17**. An analytical sample of **17** (mp 102–105°C) was obtained by recrystallization from ether/hexane. IR ($CHCl_3$): 2910 (s), 2240 (m), 2160 (m), 1710 (s), 1650 (s), 1380 (s), 1360 (s); UV (95% ethanol): 248 nm (ε = 10 582); NMR (200 MHz, $CDCl_3$): 5.96–5.74 (m, 1H), 5.47 (t, *J* = 4 Hz, 1H), 5.26–5.08 (m, 2H), 3.86 (q, *J* = 7 Hz, 2H), 3.28 (s, 1H), 2.86–2.46 (m, 4H), 2.40 (s, 3H), 2.39–2.06 (m, 3H), 1.96–1.84 (m, 1H), 1.81 (s, 3H), 1.78–1.56 (m, 1H), 1.36 (s, 3H), 1.29 (t, *J* = 7 Hz, 3H), 0.17 (s, 9H); HRMS (EI) *m/e* (relative intensity): 423.2604 (46.73).

Preparation of bromide ***16***

To a solution of 7.21 g (17 mmol) of enol ether **15** in 1.5 L of THF and 42 mL of water was added dropwise 5.97 g (18.7 mmol) of pyridinium bromide perbromide in 50 mL of THF over 5 min. Towards the end of the addition the solution became turbid, so an additional 25 mL of water was added. At the end of the addition the reaction mixture was stirred for 5 min. After the solution was washed with 10% $NaHCO_3$, water, and brine, it was dried over anhydrous $MgSO_4$, filtered, and evaporated under reduced pressure. Purification by silica gel chromatography (hexane/ethyl acetate 3:1 as eluant) furnished 7.07 g (88%) of **16**. An analytical sample of **16** (mp 134–137°C) was prepared by recrystallization from ether/hexane. IR ($CHCl_3$): 2970 (s), 2260 (w), 2190 (m), 1720 (s), 1680 (s), 1610 (m), 1360 (s), 1320 (s); UV (95% ethanol): 257 nm (ε = 15 083); NMR (200 MHz, $CDCl_3$): 5.90–5.70 (m, 1H), 5.40 (dd, *J* = 2 Hz, *J* = 2 Hz, 1H), 5.26–5.10 (m, 2H), 3.18 (s, 1H), 2.84–2.56 (m, 5H), 2.43 (s, 3H), 2.38–2.0 (m, 3H), 1.95 (s, 3H), 1.93 (s, 3H), 0.14 (s, 9H); HRMS (EI) *m/e* (relative intensity): 473.1395 (1.16).

Can. J. Chem. Downloaded from www.nrcresearchpress.com by 198.100.157.202 on 09/07/12
For personal use only.

Can. J. Chem. Downloaded from www.nrcresearchpress.com by 198.100.157.202 on 09/07/12
For personal use only.

Preparation of dienone ***17***

To a solution of 8.87 mL (71.7 mmol) of DBN and 100 mL of dry THF was added 6.83 g (14.4 mmol) of bromide **16** in 50 mL of THF via a dropping funnel over 10 min. After complete addition, the solution was stirred for 20 min and then quenched with 50 mL of saturated NH_4Cl. The layers were separated and the organic phase was washed with water and brine, dried over anhydrous $MgSO_4$, and filtered. After evaporation of solvent *in vacuo* and purification by silica gel chromatography (hexane/ethyl acetate 3:1 as eluant), 4.45 g (78%) of dienone **17** was obtained. An analytical sample of **17** (mp 167–168°C) was obtained by recrystallization from ether/hexane. IR ($CHCl_3$): 2970 (m), 2890 (m), 2250 (m), 2190 (m), 1720 (s), 1660 (s), 1630 (m), 1590 (m), 1360 (m), 1320 (m); UV (95% ethanol): 282 nm (ϵ = 17 300); NMR (200 MHz, $CDCl_3$): 6.85 (d, J = 10 Hz, 1H), 6.04 (d, J = 10 Hz, 1H), 6.02–5.82 (m, 1H), 5.36–5.17 (m, 2H), 3.53 (s, 1H), 2.88–2.44 (m, 5H), 2.42 (s, 3H), 1.93 (s, 3H), 1.57 (s, 3H), 0.17 (s, 9H); HRMS (EI) m/e (relative intensity): 393.2123 (8.18).

Preparation of diol ***19***

A mixture of 302 mL of *tert*-butanol, 38.2 mL of water, 114 mL of THF, 3.24 g (24 mmol) of *N*-methylmorpholine-*N*-oxide, and 8.59 g (21.8 mmol) of **18** was stirred until a homogenous solution was obtained, at which time 2 mL of a 4% (w/v) water solution of OsO_4 (0.3 mmol) was added and stirring continued for 18 h. To the solution was then added 2.2 g of Florisil and 1 g of $Na_2S_2O_4$; the solution was stirred for 5 min and then filtered through Celite. The solvent was evaporated under reduced pressure and the residue was taken up in ethyl acetate, washed with 5% HCl, water, and brine. After drying over anhydrous $MgSO_4$, filtration, and evaporation of solvent *in vacuo*, the solid was purified by silica gel chromatography (hexane/ethyl acetate 1:4 as eluant) to give 7.85 g (85%) of diol **19**. IR ($CHCl_3$): 3700–3300 (br, m), 2950 (s), 2250 (m), 2190 (m), 1720 (s), 1660 (s), 1630 (m), 1590 (m), 1380 (m), 1360 (s), 1330 (s); UV (95% ethanol): 278 nm (ϵ = 19 340); NMR (200 MHz, $CDCl_3$), major diastereomer: 6.81 (d, J = 10 Hz, 1H), 5.95 (d, J = 10 Hz, 1H), 4.05–3.92 (m, 1H), 3.84–3.40 (m, 3H), 3.08 (dd, J = 3 Hz, J = 12 Hz, 1H), 2.86–2.52 (m, 2H), 2.40 (s, 3H), 1.89 (s, 3H), 1.55 (s, 3H), 0.12 (s, 9H); minor diastereomer: 6.83 (d, J = 10 Hz, 1H), 5.97 (d, J = 10 Hz, 1H), 4.05–3.92 (m, 1H), 3.84–3.40 (m, 3H), 3.08 (dd, J = 3 Hz, J = 12 Hz, 1H), 2.86–2.52 (m, 2H), 2.40 (s, 3H), 1.89 (s, 3H), 1.55 (s, 3H), 0.14 (s, 9H); HRMS (EI) m/e (relative intensity): 427.2159 (1).

Preparation of enone ***20***

A solution of 300 mL of benzene, 21.4 mL (0.3 mol) of 1,3-propane diol, and 28.2 g (0.15 mol) of *p*-toluenesulfonic acid was brought to reflux for 2 h and the water was azeotropically removed via a Dean–Stark apparatus. The solution was cooled to 40°C and 2.11 g (0.005 mol) of diol **19** in 20 mL of dry benzene was added. The reaction mixture was rapidly stirred at this temperature for 4 h. The benzene was removed under reduced pressure and the residue was taken up in ethyl acetate and washed three times with saturated $NaHCO_3$, water, and brine. The organic phase was dried over anhydrous $MgSO_4$, filtered, and solvent evaporated. The solid was purified by silica gel chromatography (hexane/ethyl acetate 1:4 as eluant) to give 1.44 g (90%) of alcohol **20** and 0.5 g of starting material **19**. IR ($CHCl_3$): 3620 (m), 3600–3300 (br, m), 2950 (m), 2900 (m), 2260 (w), 2190 (w), 1720 (s), 1660 (s), 1620 (m), 1360 (s), 1320 (m); UV (95% ethanol): 245 nm (ϵ = 12 610); NMR (200 MHz, $CDCl_3$): 4.21 (t, J = 3 Hz, 1H), 4.16–3.86 (m, 3H), 3.78–3.52 (m, 2H), 3.36 (s, 1H), 3.36–2.72 (m, 5H), 2.44 (s, 3H), 1.81 (s, 3H), 1.60 (s, 3H), 0.18 (s, 9H); HRMS (EI) m/e (relative intensity): 427.2166 (12.82).

Preparation of acetylene ***21***

A solution of 5.3 g (0.012 mol) of enone **20** in 100 mL of dry CH_3CN was stirred with 11.8 g (0.042 mol) of tetrabutylammonium chloride and 5.61 g (0.097 mol) of potassium fluoride at room temperature for 0.5 h. The acetonitrile was evaporated under reduced pressure and the residue taken up in ethyl acetate and washed with saturated NH_4Cl, water, and brine. After drying over anhydrous $MgSO_4$ and filtering, the solvent was evaporated *in vacuo*. The solid obtained was purified by silica gel chromatography (hexane/ethyl acetate 1:2 as eluant) to give 4.4 g (100%) of acetylene **21**. IR ($CHCl_3$): 3320 (m), 2950 (m), 2880 (m), 2260 (w), 1720 (m), 1670 (s), 1625 (m), 1360 (m); UV (95% ethanol): 247 nm (ϵ = 12 739); NMR (200 MHz, $CDCl_3$): 3.93 (t, J = 4 Hz, 1H), 3.80–3.48 (m, 3H), 3.28–2.74 (m, 4H), 2.93 (s, 1H), 2.39 (d, J = 2.7 Hz, 1H), 1.18 (s, 3H), 1.59 (s, 3H); HRMS (EI) m/e (relative intensity): 355.1787 (96.25).

Preparation of silyl ethers ***22*** *and* ***23***

A solution of 4.40 g (0.012 mol) of acetylene **21** in 200 mL of dry DMF was stirred with 6.46 mL (0.025 mol) of *tert*-butyldiphenylsilyl chloride and 3.98 g (0.049 mol) of imidazole for 10 h at room temperature. The reaction mixture was poured into saturated NH_4Cl and diluted with 100 mL of benzene. The layers were separated and the organic phase was washed with water and brine, dried over anhydrous $MgSO_4$, filtered, and solvent evaporated under reduced pressure. Silica gel chromatography (hexane/ethyl acetate 7:3 as eluant) gave 5.31 g of **22** and 0.9 g of **23** (85% combined yield). An analytical sample of **22** (mp 199–200°C) and **23** (mp 207–208.5°C) was obtained by recrystallization from hexane/ethyl acetate. Major diastereomer **22**: IR ($CHCl_3$): 3310 (s), 2930 (s), 2860 (s), 2250 (w), 1720 (s), 1660 (s), 1620 (m), 1360 (s); UV (95% ethanol): 247 nm (ϵ = 13 260); NMR (200 MHz, $CDCl_3$): 7.74–7.34 (m, 10H), 3.88 (t, J = 3 Hz, 1H), 3.80–3.74 (m, 3H), 3.31 (s, 1H), 3.24–3.00 (m, 2H), 2.90–2.74 (m, 1H), 2.42 (s, 3H), 2.40 (d, J = 2 Hz, 1H), 1.84 (s, 3H), 1.61 (s, 3H), 1.03 (s, 9H); HRMS (EI) m/e (relative intensity): 536.2254 (M − C_4H_9, 100); minor diastereomer **23**: IR ($CHCl_3$): 3320 (m), 2940 (m), 2870 (m), 2260 (w), 1720 (m), 1670 (s), 1620 (s), 1360 (m); UV (95% ethanol): 247 nm (ϵ = 13 460); NMR (200 MHz, $CDCl_3$): 7.76–7.38 (m, 10H), 4.02 (t, J = 3 Hz, 1H), 4.01 (m, 1H), 3.92–3.80 (m, 2H), 3.31 (s, 1H), 3.31–3.20 (m, 1H), 2.96–2.60 (m, 2H), 2.44 (s, 3H), 2.35 (d, J = 2 Hz, 1H), 2.16–1.92 (m, 3H), 1.79 (s, 3H), 1.56 (s, 3H), 1.10 (s, 9H); HRMS (EI) m/e (relative intensity): 536.2267 (M − C_4H_9, 87.98).

Preparation of dithianes ***24*** *and* ***25***

A solution of 1.28 g (2.16 mmol) of ether **22** in 3 mL each of dry THF and Et_2O was treated with 4.0 mL (32.5 mmol) of $BF_3 \cdot OEt_2$ and 0.48 mL (4.77 mmol) of 1,3-propane dithiol at room temperature for 3 h. The reaction mixture was *carefully* poured into cold saturated $NaHCO_3$ and diluted with 50 mL of ethyl acetate. Separation of the layers and washing of the organic phase with water and brine, followed by drying over anhydrous $MgSO_4$, filtration, and evaporation of solvent under reduced pressure, gave a yellow solid. Purification by silica gel chromatography (hexane/ethyl acetate 3:1 as eluant) gave 1.42 g (96%) of dithiane **24**. An analytical sample of **24** (mp 180–183°C) was obtained by recrystallization from hexane/ether. IR ($CHCl_3$): 3310 (s), 2930 (s), 2860 (s), 2250 (w), 1720 (s), 1590 (w), 1420 (m), 1360 (s); NMR (200 MHz, $CDCl_3$): 7.76–7.36 (m, 10H), 3.80–3.44 (m, 3H), 3.75 (t, J = 3 Hz, 1H), 3.18–2.46 (m, 9H), 3.09 (s, 1H), 2.42 (s, 3H), 2.35 (d, J = 2 Hz, 1H), 2.28–1.72 (m, 7H), 2.00 (s, 3H), 1.48 (s, 3H), 1.08 (s, 9H); HRMS (EI) m/e (relative intensity): 683.2920 (39.45).

The same procedure was followed for the preparation of dithiane **25** (84%). An analytical sample of **25** (mp 196–198°C) was obtained by recrystallization from ether/hexane. IR ($CHCl_3$): 3320 (s), 2940 (s), 2860 (s), 2260 (m), 1710 (s), 1600 (m), 1420 (s), 1390 (m), 1360 (s), 1280 (s); NMR (200 MHz, $CDCl_3$): 7.78–7.38 (m, 10H), 4.12–3.99 (m, 1H), 3.89 (t, J = 3 Hz, 1H), 3.88–3.76 (m, 2H), 3.24–2.98 (m, 3H), 3.15 (s, 1H), 2.80–2.46 (m, 5H), 2.42 (s, 3H), 2.40–1.78 (m, 8H), 1.96 (s, 3H), 1.42 (s, 3H), 1.08 (s, 9H); HRMS (EI) m/e (relative intensity): 683.2906 (6.38).

Preparation of keto ester ***26***

A solution of 0.2 mL (0.98 mmol) of hexamethyldisilazine and 10 mL of dry THF was cooled to −30°C and 0.61 mL (0.98 mmol) of 1.6 M *n*BuLi in hexane was added dropwise via a syringe. The mixture was stirred for 15 min and then treated with acetylene **24** in 5 mL of dry

Can. J. Chem. Downloaded from www.nrcresearchpress.com by 198.100.157.202 on 09/07/12
For personal use only.

THF. After 2 h of stirring the temperature was lowered to −78°C and 0.018 mL (0.21 mmol) of dimethyl carbonate was added. The reaction mixture was maintained at this temperature for 4 h and then poured into saturated ammonium chloride. The layers were separated and the organic portion was washed with water and brine, dried over anhydrous $MgSO_4$, filtered, and solvent evaporated *in vacuo*. Purification by silica gel chromatography (hexane/ethyl acetate 3:1 as eluant) gave 92 mg (84%) of keto ester **26**. An analytical sample of **26** (mp 176–178°C) was obtained by recrystallization from ether/hexane. IR ($CHCl_3$): 2820 (s), 2850 (s), 2240 (w), 1740 (s), 1680 (s), 1640 (m), 1600 (w), 1430 (s), 1380 (m), 1360 (m), 1340 (m); UV (95% ethanol + 5% NaOH): 390 nm (ϵ = 60 975); NMR (200 MHz, $CDCl_3$): 7.78–7.36 (m, 10H), 6.00 (s, 1H), 3.87 (t, J = 3 Hz, 1H), 3.84–3.52 (m, 3H), 3.73 (s, 3H), 3.34–2.40 (m, 11H), 2.0 (s, 3H), 1.45 (s, 3H), 1.04 (s, 9H).

Preparation of keto sulfoxide 28

A solution of 500 mg (0.73 mmol) of acetylene **24** and 60 mL of dry THF was cooled to −78°C. To this via a syringe was added 0.88 mL (2.2 mmol) of 2.5 M *n*BuLi in hexane, and after 15 min 261 mg (1.32 mmol) of isopropoxy-*p*-toluenesulfinate in 1 mL of THF was added. The reaction mixture was warmed to room temperature gradually and stirred for 5 h. The solution was poured into saturated NH_4Cl and the layers were separated. The organic phase was washed with water and brine, dried over anhydrous $MgSO_4$, filtered, and solvent evaporated under reduced pressure. Purification by silica gel chromatography (hexane/ethyl acetate 1:1 as eluant) gave 490 mg (81%) of keto sulfoxide **28**. IR ($CHCl_3$): 2940 (s), 2860 (s), 2240 (w), 1685 (s), 1640 (m), 1605 (m), 1500 (m), 1470 (m), 1440 (m), 1385 (m), 1370 (m), 1350 (m), 1310 (m); UV (95% ethanol + 5% NaOH): 369 nm (ϵ = 30 400); NMR (200 MHz, $CDCl_3$): 7.78–7.32 (m, 14H), 5.61, 5.56 (C13-H from each sulfoxide diastereomer), 3.96–2.48 (m, 16H), 2.44 (s, 3H), 2.00 (s, 3H), 1.46 (s, 3H), 1.06 (s, 9H).

Preparation of diosphenol 29 and enone 30

A solution of 31 mg (0.037 mmol) of keto sulfoxide **28** and 5 mL of anhydrous methanol was treated with 0.62 mL (0.17 mmol) of 0.11 M sodium thiophenolate and refluxed for 60 h. After cooling, the methanol was evaporated under reduced pressure. The residue was taken up in 10 mL of ethyl acetate and washed with saturated NH_4Cl, water, and brine. Following drying over anhydrous $MgSO_4$ and filtration, the solvent was evaporated *in vacuo*. Purification by silica gel chromatography (hexane/ethyl acetate 85:15 as eluant) gave 7 mg of diosphenol **29** and 14 mg of enone **30** (79% combined yield). Diosphenol **29**: IR ($CHCl_3$): 3600–3300 (br, w), 2930 (s), 2860 (s), 2250 (w), 1720 (w), 1675 (s), 1645 (m), 1595 (w), 1420 (m), 1380 (m), 1360 (m), 1340 (m), 1300 (m); UV (95% ethanol): 276 nm; (95% ethanol + 5% NaOH): 324 nm; NMR (200 MHz, $CDCl_3$): 7.72–7.34 (m, 10H), 3.82 (t, J = 3 Hz, 1H), 3.79–3.42 (m, 3H), 3.20–2.82 (m, 3H), 2.76–2.42 (m, 8H), 1.99 (s, 3H), 1.96 (s, 3H), 1.45 (s, 3H), 1.04 (s, 9H).

Enone **30**: IR ($CHCl_3$): 2930 (s), 2240 (w), 1680 (s), 1640 (m), 1600 (m), 1470 (m), 1450 (m), 1430 (m), 1380 (m); UV (95% ethanol): 256 nm; NMR: 7.74–7.36 (m, 10H), 5.89 (s, 1H), 3.96–3.50 (m, 4H), 3.20–2.84 (m, 2H), 2.78–2.38 (m, 5H), 2.26–1.58 (m, 9H), 1.98 (s, 3H), 1.46 (s, 3H), 1.04 (s, 9H).

Preparation of hydroxy sulfoxides 31 major and 31 minor

A solution of 25 mL of dry THF, 2.5 mL of anhydrous methanol, and 26 mg (1.19 mmol) of lithium borohydride was stirred at room temperature for 20 min. Then 100 mg (0.12 mmol) of keto sulfoxide **28** in 1 mL of THF was added and stirring was continued for 10 min. The reaction mixture was diluted with 20 mL of reagent grade ether and 1 mL of 10% HCl. The mixture was then washed with 10% HCl, water, and brine. The organic layer was dried over anhydrous $MgSO_4$, filtered, and solvent evaporated under reduced pressure. Silica gel chromatography (hexane/ethyl acetate 1:1 as eluant) furnished 46 mg of **31 major** and 31 mg of **31 minor** (77% combined yield). **31 major**: IR ($CHCl_3$): 3580 (w), 3500–3200 (br m), 2930 (s), 2850 (s), 2240 (w), 1600 (w), 1470 (m), 1420 (m), 1365 (m); NMR (200 MHz, $CDCl_3$): 7.78–7.32 (m, 14H), 5.44 (d, J = 4 Hz, 1H), 4.35 (dd, J = 3 Hz, J = 4 Hz, 1H), 3.87 (t, J = 2 Hz, 1H), 3.80–3.24 (m, 5H), 3.22–2.50 (m, 8H), 2.44 (s, 3H), 1.98 (s, 3H), 1.66 (s, 3H), 1.05 (s, 9H).

31 minor: IR ($CHCl_3$): 3580 (w), 3540–3300 (br, w), 2930 (s), 2850 (s), 2230 (w), 1600 (w), 1500 (m), 1470 (m), 1430 (s), 1390 (m); NMR (200 MHz, $CDCl_3$): 7.74–7.32 (m, 14H), 5.44 (d, J = 4.5 Hz, 1H), 4.32 (dd, J = 3 Hz, J = 4.5 Hz, 1H), 3.88 (t, J = 3 Hz, 1H), 3.76–3.60 (m, 4H), 3.28–2.48 (m, 8H), 2.44 (s, 3H), 2.30–1.72 (m, 7H), 1.96 (s, 3H), 1.66 (s, 3H), 1.04 (s, 9H).

Preparation of diol 32

A solution of 19 mg (0.023 mmol) of **31 major** and 5 mL of anhydrous ethanol was heated at 40°C for 5 days with 0.039 mL (0.23 mmol) of triethyl phosphite. After cooling and evaporation of solvent the residue was purified by silica gel chromatography (hexane/ethyl acetate 1:1 as eluant) to give 12 mg (75%) of diol **32**. IR ($CHCl_3$): 3610 (m), 3550–3250 (br, w), 2920 (s), 2850 (s), 2240 (w), 1590 (w), 1420 (m), 1380 (m), 1360 (m); NMR (200 MHz, $CDCl_3$): 7.78–7.34 (m, 10H), 5.34 (s, 1H), 5.28 (s, 1H), 4.32 (dd, J = 3.5 Hz, J = 8 Hz, 1H), 4.21 (d, J = 3.5 Hz, 1H), 3.80 (t, J = 2 Hz, 1H), 3.76–3.40 (m, 3H), 3.22–2.02 (m, 12H), 1.98 (s, 3H), 2.58 (s, 3H), 1.05 (s, 9H).

Preparation of imino ether 33

A solution of 14 mg (0.017 mol) of **31 minor** and 5 mL of anhydrous ethanol was heated at 80°C for 48 h in the presence of 0.029 mL (0.17 mmol) of triethyl phosphite. After cooling, and evaporation of solvent *in vacuo*, the residue was purified by silica gel chromatography (hexane/ethyl acetate 1:1 as eluant) to deliver 9 mg (75%) of imino ether **33**.

The other sulfoxide diastereoisomer **31 major** can be subjected to the same conditions to give **33** (76%). IR ($CHCl_3$): 3280 (w), 2820 (s), 2850 (s), 1695 (s), 1600 (w), 1470 (m), 1430 (m), 1380 (m), 1360 (m); NMR (200 MHz, $CDCl_3$): 7.78–7.56 (m, 10H), 5.24 (s, 1H), 5.19 (s, 1H), 4.50 (d, J = 5 Hz, 1H), 4.41 (d, J = 5 Hz, 1H), 4.00 (t, J = 3 Hz, 1H), 3.80–3.46 (m, 3H), 3.18–2.94 (m, 2H), 2.80–2.00 (m, 11H), 1.93 (s, 3H), 1.90–1.55 (m, 3H), 1.07 (s, 3H), 1.04 (s, 9H).

Acknowledgements

The support of the Natural Sciences and Engineering Research Council of Canada, Ottawa, in the form of operating grants and a fellowship to one of us (D.I.M.) is gratefully acknowledged. We also thank the Terry Fox Grant Fund of New Brunswick for support. Mr. Larry A. Calhoun of this department kindly helped with certain NMR measurements and interpretations. We thank Professor E. Piers, University of British Columbia, for the suggestion that the exclusive formation of the axial alcohol during the sigmatropic rearrangement could be aided by a stereoelectronic effect.

1. M. E. Wall and M. C. Wani. J. Med. Chem. **21**, 1186 (1978).
2. M. E. Wall and M. C. Wani. 7th Int. Symp. Chem. Natl. Prod., Reja, U.S.S.R. Abstr. **E138**, 614 (1970).
3. R. Misra and R. C. Pandy. Antitumor compounds of natural origin: Chemistry and biochemistry. Vol. 2. CRC Press, Boca Raton, FL. 1981. p. 145.
4. Y. F. Liou, I. H. Hall, M. Okano, K. H. Lee, and S. G. Chaney. J. Pharm. Sci. **71**, 430 (1982).
5. (*a*) S. Darvesh, A. S. Grant, D. I. MaGee, and Z. Valenta. Can. J. Chem. **67**, 2237 (1989), and references therein; (*b*) K. Kawada, M. Kim, and D. S. Watt. Org. Prep. Proced. Int. **21**, 521 (1989), and references therein.
6. S. Darvesh, A. S. Grant, D. I. MaGee, and Z. Valenta. Can. J. Chem. **69**, 712 (1991).
7. E. J. Corey and B. B. Snider. J. Am. Chem. Soc. **94**, 2549 (1972).
8. E. J. Corey and B. W. Erickson. J. Org. Chem. **36**, 3553 (1971).

9. H. H. INHOFFEN. Chem. Ber. **84**, 361 (1951).
10. T. R. WILLIAMS and S. WAKEHAM. Anal. Chim. Acta, **52**, 152 (1970).
11. P. DESLONGCHAMPS. Stereoelectronic effects in organic chemistry. Pergamon Press, New York. 1983.
12. R. PAPPO, D. S. ALLEN, R. U. LEMIEUX, and W. S. JOHNSON. J. Org. Chem. **21**, 478 (1956).
13. V. VAN RHEENEN, R. C. KELLY, and D. Y. CHU. Tetrahedron Lett. 1973 (1976).
14. A. E. DANN, J. B. DAVIS, and M. J. NAGLER. J. Chem. Soc. Perkin Trans. 1, 158 (1978).
15. L. A. CARPINO and A. C. SAU. J. Chem. Soc. Chem. Commun. 514 (1979).
16. S. HANESSIAN and P. LAVALLEE. Can. J. Chem. **53**, 2975 (1975).
17. G. SOLLADIÉ. Synthesis, 185 (1981).
18. (*a*) D. A. EVANS and G. C. ANDREWS. Acc. Chem. Res. 7, 147 (1974); (*b*) D. A. EVANS, G. C. ANDREWS, T. T. FUJIMOTO, and D. WELLS. Tetrahedron Lett. 1385 (1973).
19. P. G. THEOBALD and W. H. OKAMURA. J. Org. Chem. **55**, 741 (1990).
20. (*a*) H. C. BROWN and S. NARASIMHAN. J. Org. Chem. **47**, 1604 (1982); (*b*) K. SOAI and A. OOKAWA. J. Org. Chem. **51**, 4000 (1986).
21. R. W. HOFFMANN, R. GERLACH, and S. GOLDMANN. Tetrahedron Lett. 2599 (1978).
22. D. D. PERRIN and W. L. F. ARMAREGO. Purification of laboratory chemicals. 2nd ed. Pergamon Press, Toronto. 1980.
23. W. C. STILL, M. KAHN, and A. MITRA. J. Org. Chem. **43**, 2923 (1978).

Can. J. Chem. Downloaded from www.nrcresearchpress.com by 198.100.157.202 on 09/07/12
For personal use only.

Gas-phase heteroaromatic substitution. 10.[1] Reaction of free phenylium ion with simple five-membered heteroarenes in the gaseous and liquid phase

ANTONELLO FILIPPI AND GIORGIO OCCHIUCCI
Istituto di Chimica Nucleare del CNR, Area della Ricerca di Roma, Rome, Italy
AND
MAURIZIO SPERANZA[2]
Dipartimento di Agrobiologia ed Agrochimica, Università della Tuscia, Viterbo, Italy

Received July 20, 1990

ANTONELLO FILIPPI, GIORGIO OCCHIUCCI, and MAURIZIO SPERANZA. Can. J. Chem. **69**, 732 (1991).

Phenylium ion, obtained from the spontaneous β decay of 1,4-ditritiobenzene, has been allowed to react with pyrrole, *N*-methylpyrrole, furan, and thiophene, in both the gaseous and liquid phases. The differences between the reactivity pattern of phenylium ion in the two environments can be essentially reduced to significant ion-neutral electrostatic interaction in the gas phase and to the much greater efficiency of collisional stabilization in the condensed phase, allowing a larger fraction of the excited ionic intermediates, from the highly exothermic attack of phenylium ion on the aromatic substrate, to survive dissociation and isomerization. The mechanism of the phenylation process and of the subsequent isomerization of the relevant ionic intermediates is discussed and the intrinsic substrate and positional selectivity of the phenylium ion evaluated. While the limited substrate discrimination of phenylium ion fully agrees with its well-known exceedingly high reactivity, its pronounced affinity toward the α carbons of the selected heteroarenes does not conform with the relatively "hard" character of the reactant, expected on the grounds of its STO-3G calculated LUMO energy. The conceivable occurrence of an intimate entropy-favored two-step addition mechanism, involving a preliminary single-electron transfer (SET) from the heteroaromatic substrate to the ionic electrophile, which is thermochemically allowed only for phenylium and methyl cations and prevented for other alkylating electrophiles, is discussed.

Key words: gas-phase ion chemistry, electrophilic heteroaromatic substitution, nuclear decay chemistry, phenylium ion, electron transfer.

ANTONELLO FILIPPI, GIORGIO OCCHIUCCI et MAURIZIO SPERANZA. Can. J. Chem. **69**, 732 (1991).

On a fait réagir l'ion phénylium, obtenu par une desintégration β spontanée du 1,4-ditritiobenzène, avec le pyrrole, le *N*-méthylpyrrole, le furane et le thiophène, tant en phase gazeuse que liquide. Les différences de comportement de l'ion phénylium observées entre les deux environnements peuvent être attribuées essentiellement à une interaction électrostatique ion-neutre importante en phase gazeuse et à une efficacité beaucoup plus grande de la stabilisation collisionnelle en phase condensée qui permettent à une fraction beaucoup plus grande des intermédiaires ioniques excités, provenant de l'attaque très exothermique de l'ion phénylium sur le substrat aromatique, de survivre à la dissociation et à l'isomérisation. On discute du mécanisme du processus de phénylation et de l'isomérisation subséquente des intermédiaires ioniques appropriés et on évalue le substrat intrinsèque et la sélectivité positionnelle de l'ion phénylium. Même si la discrimination limitée de l'ion phénylium par rapport aux substrats est en parfait accord avec son extrêmement grande réactivité bien connue, son affinité prononcés pour les carbones α des hétéroarènes choisie n'est pas conforme au caractère relativement « dur » du réactif auquel on s'attend sur la base de calculs STO-3G de l'énergie de son OM basse vacante. On discute de la possibilité d'existence d'un mécanisme d'addition intime en deux étapes, favorisé par l'entropie et impliquant un seul transfert préliminaire d'électron du substrat hétéroaromatique vers l'électrophile ionique qui, d'un point de vue thermochimique, n'est permis que pour les ions phénylium et méthyle et qui ne l'est pas pour tous les autres électrophiles alkylants.

Mots clés : chimie ionique en phase gazeuse, substitution hétéroaromatique électrophile, chimie de désintégration nucléaire, ion phénylium, transfert d'électron.

[Traduit par la rédaction]

Introduction

The general features of the electrophilic substitution on simple five-membered heteroaromatics by free alkylating electrophiles, such as CT_3^+ (2), $(CH_3)_2X^+X$ (X = F, Cl) (3), $C_2H_5^+$ (4), i-$C_3H_7^+$ (5), t-$C_4H_9^+$ (6), and $(CH_3)_3Si^+$ (1), in the dilute gas state have recently been investigated. It has been shown that the reactivity features of these alkylating carbocations toward the ring positions of selected heteroaromatic substrates, in particular pyrrole and *N*-methylpyrrole, can be linearly correlated with the electron distribution of the ionic reactants and, especially, with their LUMO energies (4), taken as a measure of their "hardness" character (7). Thus, "hard" electrophiles, such as t-$C_4H_9^+$, i-$C_3H_7^+$, $C_2H_5^+$, and $(CH_3)_2F^+$, are predominantly directed toward the ring positions of pyrroles with the highest net negative charge (the C_β and N centers), whereas the "soft" CT_3^+ cation attacks preferentially the C_α sites of the selected heteroarenes, characterized by the highest HOMO π-electron density (8). However, when the silylating electrophile $(CH_3)_3Si^+$ is included in the above linear correlation, an appreciable deviation is observed, reflecting a measured positional selectivity ($\log(\beta/\alpha) = 0.37$) that is lower than the one ($\log(\beta/\alpha) =$ ca. 1) expected on the grounds of its SCF STO-3G calculated LUMO energy ($\epsilon_L = -1.8$ eV) (1). Such an unexpectedly soft character of $(CH_3)_3Si^+$ is rationalized in terms of the larger $3p$ empty orbital of Si^+ if compared to the $2p$ orbitals of the C^+ center of carbocations, although other explanations related to the intimate nature of the energy profiles governing such reactions could not be a priori excluded (1).

The growing interest in the reactivity of heteroaromatic compounds in the gas phase, i.e., in the absence of the solvation and ion-pairing normally preventing related investigations in

[1]Reference 1 is Part 9.

[2]Author to whom correspondence may be addressed.

Printed in Canada / Imprimé au Canada

Can. J. Chem. Downloaded from www.nrcresearchpress.com by 198.100.157.202 on 09/07/12
For personal use only.

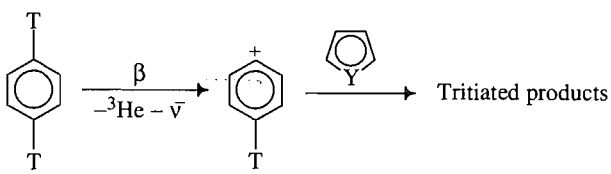
Can. J. Chem. Downloaded from www.nrcresearchpress.com by 198.100.157.202 on 09/07/12
For personal use only.

solution (9), calls for further work aimed at resolving the doubt introduced by the $(CH_3)_3Si^+$ electrophile, namely whether the Charge and Frontier Orbital Control Concept (8, 10) is adequate by itself to describe the intrinsic reactivity and selectivity properties of gaseous electrophiles toward five-membered heteroarenes.

To this purpose, the investigation is now extended to another category of ionic electrophiles, namely unsaturated carbocations, whose stable singlet configuration presents a nominally vacant orbital at the electron-deficient carbon that is orthogonal to a more or less polarized π system (11). As a response to π-electron polarization, the positively charged carbon center of unsaturated carbocations may acquire a certain carbenoid character and, therefore, exhibit reactivity properties that may largely differ from those of saturated carbocations. As the most representative members of this category, the phenylium ion $C_6H_5^+$ and two acylium ions, i.e., CH_3CO^+ and $C_6H_5CO^+$, are selected.

Such a choice arises primarily from the expected different extent of polarization of the π system orthogonal to the empty orbital of the above ions, owing to the presence of groups of largely different electronegativity adjacent to the electron-deficient carbon. In addition, the hybridization of the C^+ center of the selected electrophiles is also different, being pure *sp*-type in the acylium ions and distorted sp^2-type in the phenylium ion. Despite such differences, a recently advanced empirical hardness scale, based exclusively upon thermochemical arguments, ranks $C_6H_5^+$, $C_6H_5CO^+$, and CH_3CO^+ among the hardest ionic electrophiles known (10). Accordingly, all three reactants should exhibit a high selectivity toward the reaction centers of simple five-membered heteroaromatics with the highest net negative charge, irrespective of the electron distribution on the corresponding HOMOs. From a detailed analysis of this correspondence, it was hoped to define the domain of applicability of the Charge and Frontier Orbital Control Concept (8, 10) to heteroaromatic substitution by selected gaseous electrophiles and to ascertain whether more refined reactivity models are required.

This paper presents the results of a comparative study of the reactivity and the selectivity properties of free phenylium ion $C_6H_5^+$ toward pyrrole (**1**), *N*-methylpyrrole (**2**), furan (**3**), and thiophene (**4**), carried out both in the gaseous and in the condensed phase, using an ionic reactant from the β^- decay of a T atom in 1,4-T_2-benzene (eq. [1]). The decay technique

[1] 

Tritiated products

Y = NH (**1**); NMe (**2**); O (**3**); S (**4**)

affords a convenient means of introducing free cations of defined structure and concentration into any system of interest and to follow their reactions by radiotracer techniques (12). A comparative analysis of the reactivity and selectivity features of the acylating electrophiles, i.e., CH_3CO^+ and $C_6H_5CO^+$, toward the same substrates in the dilute gas state is left to the following paper.

Experimental section

Materials

The key substrate for the nuclear decay experiments, namely 1,4-T_2-benzene, was synthesized and purified according to described procedures (13). The heteroaromatic substrates and the gaseous additives used for the preparation of the decay mixtures were research grade chemicals from Fluka AG and Matheson Co., and were used without further purification. Not commercially available isomeric phenyl derivatives of **1**–**4**, used as carriers or as standards in the radio high-performance liquid chromatographic (radio-hplc) analysis, were prepared following well-established synthetic procedures (14). The identity of the synthesized products was checked by conventional IR and NMR spectroscopy.

Procedure

The gaseous samples were prepared by conventional vacuum techniques, introducing the 1,4-T_2-benzene mixture (ca. 1–2 mCi), diluted with inactive benzene to a specific activity of 86 mCi $mmol^{-1}$, into evacuated and carefully outgassed 100-mL Pyrex vessels containing a measured amount of the heteroaromatic substrate, together with O_2, used as a radical scavenger, and a powerful ion trap (NH_3 or NMe_3), when required. The vessels were than sealed off and stored in the dark, at room temperature, for ca. 6–8 months.

The liquid samples were prepared according to the following procedure: ca. 1 mCi of the 1,4-T_2-benzene mixture (specific activity: 86 mCi $mmol^{-1}$) was introduced into carefully evacuated and outgassed 0.5-mL Pyrex vials equipped with a long capillary arm closed by a fragile tip. Each vial was sealed off from the vacuum line, and its capillary arm was introduced into a cylindrical vessel containing at the bottom a layer of purified mercury and filled with ca. 1 mL of a 1:1 mixture of the heteroaromatic compound and benzene, used as a reference substrate. The fragile tip of the capillary arm was then broken under the level of the organic mixture, which was consequently forced into the evacuated vial. When only a small bubble of gas was left at the top of the vial, the capillary arm was lowered further into the mercury. In this way, the vial was entirely filled by the organic mixture, except for the lower portion of the capillary, where the mercury has risen, acting as a mobile seal. The vials were stored in the dark, at room temperature, for ca. 6–8 months.

After the storage period, the ampoules were opened and their content analyzed by the radio-hplc procedure. A Varian Vista 5500 high-pressure liquid chromatograph equipped with a 254-nm UV detector in series with a Berthold LB 503 HS flow liquid scintillation counter was used for the radio-hplc analyses.

The identity of the tritiated products was established by the coincidence of their retention volumes with those of authentic reference compounds on the following columns: (i) 25 cm × 5 mm Rosil C-18 HL from Alltech, Italy, using CH_3CN/H_2O = 1:1; (ii) 30 cm × 5 mm μBondapak from Waters, U.S.A., using CH_3CN/H_2O ranging from 42%:58% to 70%:30%. The absolute yields of the tritiated products correspond to the ratio of their activity to the activity of the labelled decay ions formed during the storage period in the reaction mixture from the β decay of 1,4-T_2-benzene.

Computational details

Standard quantum-mechanical calculations, with the GAUSSIAN 80 (15) set of programs, were performed in order to evaluate the STO-3G (16) SCF eigenvalues of the LUMOs of ground-state singlet phenylium ion and of its vibrationally excited form with the same regular hexagonal geometry of benzene. Geometry optimization of the ground-state ion was carried out in the C_{2v} symmetry framework. The LUMO energies for ground-state phenylium ion and for the vibrationally excited ion with the same geometry as the benzene precursor are −3.5 and −5.5 eV, respectively.

Results

Table 1 shows the absolute and relative yields of tritiated products recovered from the liquid decay samples, containing 1:1 mixtures of each selected heteroarene and benzene, used as competing substrate. The results concerning similar competition experiments, carried out in the gas phase in the pressure range 13–134 Torr (1 Torr = 133.3 Pa), are given in Table 2. Reaction conditions were chosen to span several orders of

TABLE 1. Tritiated products from the attack of phenylium ions on liquid heteroarenes

	System composition[a] (mmol)		Tritiated product distribution, %[b]				Apparent rate constant ratio k_S/k_R[c]	Total absolute yield, %[d]
								
1,Y = NH	3.1	3.1	67.6(81.2)	14.6(17.5)	1.1(1.3)	16.7	4.9	98.6
2,Y = NMe	3.1	3.1	81.4(88.1)	11.0(11.9)	—	7.6	12.0	96.7
3,Y = O	2.9	2.9	31.5(84.0)	6.0(16.0)	—	62.5	0.6	66.9
4,Y = S	2.7	2.7	47.8(77.3)	14.1(22.8)	—	38.1	1.6	72.1

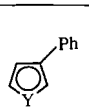
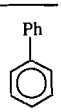
[a]All systems contained ca. 1 mCi of 1,4-ditritiobenzene.

[b]Ratio of the activity of each product to the combined activity of all products identified. Relative composition of phenylated heteroarenes given in parentheses. Each value is the average of several determinations, with an uncertainty level of ca. 5%.

[c]$k_S/k_R = \frac{[\text{Substrate products}]\,[\text{reference}]}{[\text{Reference products}]\,[\text{substrate}]}$; each value is the average of several determinations, with an uncertainty level of ca. 10%.

[d]Absolute yields expressed as the percent ratio of the total activity of all identified products to the activity originally contained in the nucleogenic phenylium ion.

TABLE 2. Tritiated products from the attack of phenylium ions on gaseous heteroarenes

	System composition[a] (Torr)			Tritiated product distribution, %[b]				Apparent rate constant ratio k_S/k_R[c]	Total absolute yield, %[d]
			Base						
1 NH	4.6	5.1	—	43.5(67.5)	20.0(31.0)	1.0(1.5)	35.6	2.0	89.2
1 NH	4.7	25.2	—	16.4(65.2)	8.3(33.2)	0.4(1.6)	74.9	1.8	93.6
1 NH	4.8	39.8	—	14.4(66.6)	6.3(29.1)	0.9(1.6)	78.3	2.3	97.8
1 NH	4.4	11.3	10(NH_3)	32.0(68.7)	13.2(28.3)	1.4(3.0)	53.4	2.2	30.7
1 NH	4.8	8.9	10(NMe_3)	38.6(72.5)	14.6(27.4)	1.1(2.0)	45.7	2.2	26.7
2 NMe	5.6	3.3	—	71.3(77.0)	21.3(23.0)	—	7.4	7.2	79.3
2 NMe	4.6	28.6	—	40.0(76.5)	12.3(23.5)	—	47.7	6.8	90.4
2 NMe	5.2	14.0	10(NMe_3)	54.4(75.0)	18.1(25.0)	—	27.5	7.1	30.4
3 O	18.7	3.4	—	4.2(73.1)	1.5(26.9)	—	94.3	0.01_1	8.9
3 O	88.0	42.1	—	1.3(73.5)	0.5(26.5)	—	98.3	0.00_8	47.0
3 O	8.5	32.9	—	0.0_7(70)	0.0_3(30)	—	99.9	0.00_4	86.1
3 O	110.0	3.0	10(NH_3)	20.0(88.3)	2.7(11.7)	—	77.3	0.00_8	7.6
3 O	12.0	4.5	10(NMe_3)	2.3(88.5)	0.3(11.5)	—	97.4	0.01_1	1.3
4 S	10.8	3.2	—	47.6(65.2)	25.4(34.8)	—	27.0	0.8	85.4
4 S	83.0	8.0	—	59.2(67.4)	28.6(32.6)	—	12.1	0.7	94.3
4 S	15.5	10.2	10(NMe_3)	42.4(70.3)	17.9(29.7)	—	39.7	1.0	24.6

[a]All systems contained ca. 1.2–2.2 mCi of 1,4-ditritiobenzene and 4 Torr of oxygen.

[b]See footnote *b* of Table 1.

[c]See footnote *c* of Table 1.

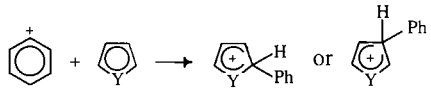
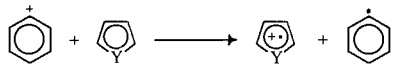
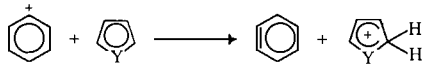
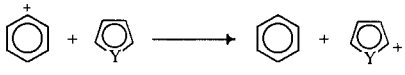
[d]See footnote *d* of Table 1.

magnitude for the relative concentrations of the two competing aromatic substrates. Occasionally, from ca. 8 to over 33 mol% of a powerful ion trap, such as NH_3 or NMe_3, was added to the mixtures. The absolute yields, defined by the ratio of the activity of the products to the total activity of the nucleogenic (nuclear-decay generated) *para*-T-phenylium precursor, can be calculated from the initial activity and the isotopic composition of tritiated benzene, the decay rate of tritium, the abundance (72%) of the phenylium ions among the decay fragments (17), and the absolute counting efficiency of the detector employed.

The overall absolute yields of the tritiated aromatic products from the liquid systems of Table 1 are quite close to the theoretical limit and are found to depend upon the nature of the heteroarene employed, increasing in the order: **3** (66.9%) < **4** (72.1%) < **2** (96.7%) < **1** 98.6%). Radio-chromatographic analyses showed that low-boiling fragmentation products account

Can. J. Chem. Downloaded from www.nrcresearchpress.com by 198.100.157.202 on 09/07/12
For personal use only.

TABLE 3. Energetics of several revelant reactions of tritiated phenylium ion on heterorenes[a]

Process	ΔH^0 (kcal/mol) Y = NH(**1**)	NMe(**2**)	O(**3**)	S(**4**)	C_2H_2[b]
[2]  **5α** **5β**	−91	−107	−77	−77	−76
[3]  **6**	−1	−7	+14	+15	+23
[4]  **7**	+4	−3	+19	+16	+30
[5]  **8**		Endothermic[c]			0

[a]The formation enthalpies of the ion and the neutrals used for these calculations have been taken from ref. 20. An estimate of the ΔH^0_f of **5** (Y = S) was obtained by assuming that the proton affinity of the *ipso* position of phenylthiophene is equal to that of thiophene, taken from ref. 20. The ΔH^0_f's of **5** (Y = NH, NMe, and O) were roughly estimated by assuming the same ΔH^0_f scale calculated for the corresponding methylated intermediates (ref. 2).

[b]Reference 18*c*.

[c]Estimated as due to the presumably higher strain energy of **8** relative to phenylium ion.

for only a very limited fraction of the missing activity (0–6%), the remainder being attributable to polymerization products. A similar trend is observed in the corresponding gaseous samples of Table 2. Here, the absolute yields of low-boiling products increase appreciably, especially in the case of furan **3**. However, if analysis is restricted to the absolute yields of the heteroaromatic products recovered under comparable conditions, a rather different trend emerges, increasing in the order **3** < **4** < **1** < **2** in the liquid samples (Table 1) and in the order **3** << **1** < **4** < **2** in the gaseous systems (Table 2). In general, while substantial amounts of phenylated derivatives of pyrrole **1**, *N*-methylpyrrole **2**, and thiophene **4** are invariably recovered from the decay samples under all conditions, those of the phenylated products from furan **3** are comparatively much lower, especially in the gas phase. In the gaseous samples, the absolute yields of the phenylated products appear to increase with the total system pressure and to decrease significantly (from 62 to 85%) by addition of ca. 30 mol% of a base (NH_3 or NMe_3). It is noteworthy that such a decrease is not accompanied by an appreciable change in the product pattern and in the apparent phenylation rate constant ratios k_S/k_R. Only a slight change in the relative distribution of the phenylated heteroarenes is observed, which, however, is always characterized by the predominance of the α-substituted isomer (65–88%).

Discussion

Nature of the reagent

The formation of *para*-T-phenylium cation from the decay of 1,4-T_2-benzene has been discussed in detail elsewhere (18). The phenylium ion, formed in its most stable singlet configuration for more than 72% of the decay events (17), is characterized by a certain excess of internal energy due *inter alia* to the relaxation from the regular hexagonal structure of its 1,4-T_2-benzene precursor to the vibrationally most stable distorted hexagonal geometry (19). In the extreme hypothesis of an overall adiabatic process for the formation of *para*-T-phenylium ion from the nuclear transition in 1,4-T_2-benzene, theoretical calculations set an upper limit of ca. 32 kcal mol^{-1} to the vibrational excitation energy of the decay phenylium ion (19).

Concerning the energetic β particle from the decay, it should be considered that the reaction conditions have been specifically selected to make negligible any contribution to the products of Tables 1 and 2 from β radiolytic processes. In fact, the very low activity employed in the experiments and concentrated in the molecules of 1,2-T_2-benzene, highly diluted into the systems ($<3 \times 10^{-7}$ mol%), makes the probability of β-particle induced processes, such as direct radiolysis of labeled benzene and (or) combination of reactive species from radiolysis of **1**–**4** with labeled benzene, vanishingly small. Furthermore, in the gaseous systems, wherein the 1,2-T_2-benzene concentration is higher (5×10^{-3} to 7×10^{-2} mol%) and thus the probability of secondary radiolytic processes is higher as well, the presence of an effective radical scavenger, such as O_2, is expected to cut off any conceivable thermal radical component to the products formation. Such circumstances, as well as the pronounced effect of the added bases on the absolute yields of the products of Table 2, allow one to conclude that singlet phenylium ion is the very major primary species responsible for the formation of the labeled products of Tables 1 and 2.

Several reaction channels are accessible to the tritiated phenylium ion in its attack on the heteroaromatic substrates **1**–**4** as well as on the reference benzene, as illustrated in Table 3, where the approximate ΔH^0 values for the relevant gas-phase processes are reported. The enthalpy changes have been

Can. J. Chem. Downloaded from www.nrcresearchpress.com by 198.100.157.202 on 09/07/12
For personal use only.

Can. J. Chem. Downloaded from www.nrcresearchpress.com by 198.100.157.202 on 09/07/12
For personal use only.

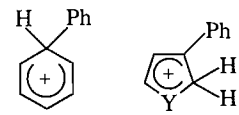
calculated from the ΔH^0_f value of gaseous phenylium ion in its vibrational ground state (269.3 kcal mol^{-1}) (20). If allowance is made for a certain excess of vibrational energy in the decay phenylium ion, the actual enthalpy changes of reactions [2]–[5] (Table 3) may be further lowered by up to 32 kcal mol^{-1}. Of course, the calculated ΔH^0 values of reactions [2]–[4] are much less cogent if referred to processes occurring in the liquid systems, where ion solvation might intervene. At any rate, the highly exothermic addition reacton [2] is recognized as the main source of the labelled phenylated products of Tables 1 and 2.

Conceivably, there are at least two "blind" (i.e., not leading to identifiable labeled products, other than the starting benzene) reaction channels, namely eqs. [3] and, perhaps, [5], which may be allowed on thermochemical grounds (Table 3) and may account for the activity loss observed, especially in the furan systems. However, reaction [3] would lead to the inactive molecular ion of the heteroarene **6** and to tritiated phenyl radical, whose contribution, if any, to the identified products is strongly depressed by the presence of the thermal radical trap O_2. Further evidence against occurrence of a free tritiated phenyl radical from path [3] as a significant source of phenylated products is provided by the equally high yields of labeled products recovered from pyrroles **1** and **2**, in view of the well-documented ability of radicals to efficiently abstract hydrogen atom from the methyl group of **2**, giving tritiated benzene and 1-pyrrolyl methyl radicals, a route that is not available for **1** (21). The high yields of phenylated products measured in both the gaseous and the liquid decay, except perhaps in the gaseous furan systems, rule out significant occurrence of the secondary processes [4] and [5] as well (Table 3). This conclusion is further supported by the absence of appreciable amounts of both tritiated **1–4**, obtained via eq. [4] from a largely "automerized" phenylium ion (18*a*,*b*) and tritiated 1,4-dihydro-1,4-epoxynaphthalene from Diels–Alder [$\pi 4s + \pi 2s$] cycloaddition of benzyne from eq. [4] to furan (22).

Reaction in the liquid phase

It is suggested that formation of the tritiated products listed in Table 1 from the decay of 1,2-T_2-benzene in liquid heteroarene/benzene mixtures occurs via the exothermic process [2] of Table 3, and the corresponding process [2] on the benzene competitor to produce the *ipso*-protonated biphenyl intermediate **9**. Following collisional stabilization, very effective in the liquid system, the primary intermediates **5** and **9** undergo deprotonation by a base to yield the observed phenylated derivatives. As to the nature of the base, it should be noted that deprotonation of both ground-state **5** and **9** by a single heteroarene molecule may be in most instances rather endothermic (18*c*, 20). However, the deprotonation process may occur, if excited **5** and **9** from the relevant highly exothermic formation process (eq. [2]) are involved. Besides, cooperative deprotonation by several molecules of heteroarene is likely to occur in the liquid, and even in the gaseous systems within an ionic cluster. Additional bases able to efficiently deprotonate the intermediates **5** and **9** can be generated by the passage of the highly energetic β particles through the liquid medium, which normally induces extensive fragmentation of inactive bulk molecules to yield highly reactive species. The efficiency of collisional stabilization of the excited intermediates **5** and **9** in the liquid systems is apparent from the exceedingly high absolute yields of phenylated products and from the absence of appreciable amounts of low-boiling fragmentation products, even in the case of furan **3** where the lowest product yield is measured. As pointed out in related studies (1–6, 23), the comparatively low absolute yield of products from furan **3** (ca. 25%) may be attributed, apart from possible fragmentation processes, to the typical bidentate nature of the substrate, where the *n*-electron pair of oxygen competes efficiently with the π system for the electrophile. Such a competition may increase the extent of processes consuming phenylium ion, such as formation of a stable oxonium ion or its ring opening to reactive species ending with polymeric products. Similar paths appear much less pronounced in the case of thiophene **4** and totally absent in the case of pyrroles **1** and **2**, as demonstrated by the much higher absolute yields of the corresponding phenylated derivatives (ca. 45% (**4**); ca. 82% (**1**); ca. 89% (**2**)).

The conceivable occurrence of fragmentation and, perhaps, isomerization of the intermediates **5** and **9** from the corresponding formation processes undoubtedly complicates the precise evaluation of the substrate and positional selectivity of the phenylium ion toward the selected substrates. However, in view of the large predominance of the phenylation channel [2], the present results (Table 1) point to the free phenylium ion as a rather selective electrophile, which is capable of discriminating between the heteroaromatic substrate and the reference benzene (k_S/k_R = 4.9 (**1**); 12.0 (**2**); 0.6 (**3**); 1.6 (**4**)). The positional selectivity deduced from the isomeric distribution of the phenylated heteroarenes must be regarded as a lower limit, because of the possible occurrence of isomerization of a minor fraction of the initially formed α-substituted intermediate **5**α to the more stable isomeric structure **10** (*vide infra*), already pointed out in related studies (1, 2).



9 **10**

The emerging picture is characterized by a pronounced preference of the phenylium ion for α-substitution on **1–4**, as shown by the isomeric composition of their phenylated derivatives (β/α = 0.22 (**1**); 0.13 (**2**); 0.19 (**3**); 0.29 (**4**)).

Reaction in the gas phase

In contrast with the efficiency of collisional deactivation and neutralization of the primary excited ionic intermediates **5** and **9**, observed in the liquid, the gas phase picture reflects partial isomerization and fragmentation processes affecting the primary excited adducts from attack of phenylium ion on the aromatic substrates. Such a trend is evidenced by the appreciable decrease of the absolute yields of the tritiated aromatic products recovered in the gaseous systems (Table 2), if compared to the liquid systems (Table 1), which is counterbalanced by a parallel increase in the yields of polymerization and fragmentation products. Furthermore, the apparent relative reactivity of the competing substrates toward the phenylation channel (k_S/k_R in Table 2) is significantly modified with respect to the liquid phase. In most cases, but especially in the case of furan **3**, this appears to be mainly due to a substantial decrease of the absolute yield of the phenylated heteroarene (<1.3% vs. 25%), which presumably is superimposed on the variation of intrinsic reactivity of the two competing substrates in the two phases. Finally, the composition of the isomeric phenylated heteroarenes of Table 2 is also appreciably different from the corresponding composition measured in the liquid phase (Table 1). In fact, although α substitution is always predominant, the

Can. J. Chem. Downloaded from www.nrcresearchpress.com by 198.100.157.202 on 09/07/12
For personal use only.

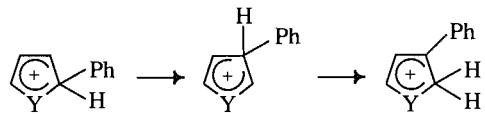
relative yields of the β-substituted isomers generally increase in the gas phase at the expense of the α-substituted isomers.

All such differences can be reasonably traced to the typical features of ionic processes in the gas phase at relatively low pressures. In these media, ion–molecule reactions are dominated by preliminary long-range electrostatic interactions, which lead to an encounter complex, characterized by a local energy minimum on the potential energy hypersurface, at a rate corresponding to the physical capture cross section. In agreement with the apparent k_S/k_R values of Table 2, classical theories predict similar rate coefficients for reactions involving a given ionic electrophile, such as phenylium ion, and molecules, such as the selected arenes, with comparable polarizability ($\alpha(A^3)$ = 7.94 (**1**); 7.23 (**3**); 9.00 (**4**); 10.39 (benzene) (24)) and dipole momentum (μ(Debye) = 1.84 (**1**); 2.12 (**2**); 0.66 (**3**); 0.55 (**4**) (9, 24)). Accordingly, a qualitative correspondence between the apparent k_S/k_R ratios and the α and μ values of each heteroarene is observed, except for furan **3**, whose exceedingly low k_S/k_R value (≤ 0.01) confirms the view, based on the liquid phase results, of extensive formation of stable oxonium ion or its ring opening to reactive species ending with polymeric products.

In the dilute gas state, the encounter complex, excited by the exothermicity of the ion–molecule electrostatic interactions, may either evolve to σ-bonded intermediates **5** or, alternatively, unimolecularly dissociate into the starting reactants. The branching ratio for these competing processes depends on the relative free energy activation barriers. In this view, the observation that the apparent rate constant ratios k_S/k_R are not affected by an over sixfold variation of the total pressure and by the presence of ca. 30 mol% of a powerful base points to a high efficiency for the conversion of the electrostatic complexes into the σ-bonded intermediates **5** relative to their back-dissociation to reactants.

In principle, σ-bonded intermediates **5**, excited by the exothermicity of their formation processes (Table 3), may rearrange themselves to give a thermodynamically more stable isomer before collisional quenching and neutralization. This may account for the small, but appreciable, increase in the relative yields of the β-substituted isomers recovered in the gaseous systems, whose formation is favored at low pressures and in the absence of added bases. It is, therefore, suggested that, after attack of phenylium ion on the gaseous aromatic compound occurring at the encounter rate, the ensuing electrostatic adduct efficiently evolves to the isomeric σ-bonded intermediates **5** and **9**. Their individual formation rates follow the inherent substrate and positional selectivity of the reactant, described by the k_S/k_R ratios and the relative distribution of the phenylated products, measured at the highest total system pressure and in the presence of a base, namely under conditions where fragmentation and isomerization processes are minimized. At low pressures and in the absence of bases, partial isomerization of the excited α-phenylated intermediates **5α** to the more stable structure **10**, via the β-phenylated isomers **5β** (eq. [6]), appreciably modifies the isomeric distribution of the phenylated products, recovered in the gaseous decay samples. The limited extent of isomerization, however, suggests that the α → β transfer of the phenyl group within **5α** is effectively contrasted by competing 1,2-shifts of the *ipso* hydrogen, leading to immediate quenching of the position of the phenyl group in the relevant intermediates.

The intrinsic directive properties of the selected heteroarenes **1–4** toward gas-phase phenylium ion attack confirm the

[6] 

5α **5β** **10**

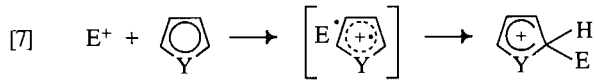
tendency of the substrate to direct the electrophile preferentially toward its C_α sites (β/α : 0.38 (**1**); 0.33 (**2**); 0.13 (**3**); 0.42 (**4**)), as already observed in the liquid phase.

Comparison with related gas-phase data

The gas phase reactivity order, expressed by the k_S/k_R ratios of Table 2, indicates that phenylium ion attacks the selected aromatic substrates at rates falling within the same order of magnitude. The result is in good agreement with the remarkably low discriminating ability of other gaseous alkylating electrophiles toward the same substrates (1–6). In contrast with its limited substrate discrimination, the phenylium ion exhibits a significant positional selectivity toward **1–4**, much like other ionic electrophiles (1–6).

The evident preference of the free phenylium ion for the α-positions of pyrroles **1** and **2**, observed in both gaseous (β/α : 0.38 (**1**); 0.33 (**2**)) and liquid phase (β/α : 0.22 (**1**); 0.13 (**2**)), conforms better to the site selectivity of a soft electrophile, e.g., CT_3^+ ($\epsilon_L = -6.4$ eV; β/α : 0.30 (**1**); 0.64 (**2**)) (2), rather than to that of typical hard alkylating species, such as bridged $C_2H_5^+$ ($\epsilon_L = -1.9$ eV; β/α : 7.7 (**1**), 4.3 (**2**)) (4); *i*-$C_3H_7^+$ ($\epsilon_L = -3.9$ eV; β/α : 3.5 (**1**), 1.6 (**2**)) (5); *t*-$C_4H_9^+$ ($\epsilon_L = -3.1$ eV; β/α : 3.4 (**1**), 1.1 (**2**)) (6); $(CH_3)_2F^+$ ($\epsilon_L = +1.8$ eV; β/α : 3.3 (**1**); 2.3 (**2**)) (3*a*); $(CH_3)_3Si^+$ ($\epsilon_L = -1.8$ eV; β/α : 2.3 (**1**); 3.0 (**2**)) (1). Accordingly, one is inclined to conclude that phenylium ion behaves as a typical soft electrophile toward pyrroles, although it exhibits a STO-3G calculated LUMO energy ranging between −3.5 eV (ground-state singlet configuration) to −5.5 eV (vibrationally excited singlet configuration), which would rather confer upon it a borderline character lying between that of the soft methyl cation and the very hard *i*-$C_3H_7^+$ ion. This peculiar behavior of a nucleogenic phenylium ion emerges as well from the significant deviation from the liner correlation between the site selectivity of gaseous ionic electrophiles toward **1** and their STO-3G calculated LUMO energy, proposed in previous papers of this series (Fig. 1) (1, 4).

Such outstanding discrepancy calls in question Klopman's Charge and Frontier Orbital Control Concept (8, 10) as a self-consistent reactivity model for the intrinsic behavior of gaseous electrophiles toward five-membered heteroarenes. Rather, rationalization of the peculiar reactivity and selectivity features of phenylium ion requires a more comprehensive reactivity model, accounting for the opposite site selectivity toward pyrroles (log(β/α) in Fig. 1) of methyl (2) and phenylium ions, on the one side, and all the remaining alkylating electrophiles studied (1, 3–6), on the other. A plausible rationale for the different behavior of the two families of reactants can be found in a possible difference in their intimate substitution mechanism. In particular, while *t*-$C_4H_9^+$, *i*-$C_3H_7^+$, $C_2H_5^+$, $(CH_3)_2F^+$, and $(CH_3)_3Si^+$ ions add to pyrroles via the classical two-electron S_E2 mechanism, methyl and phenylium ions may follow the alternative entropy-favored two-step mechanism shown in eq. [7], involving a preliminary single-electron transfer (SET)

[7] 

I **5α**

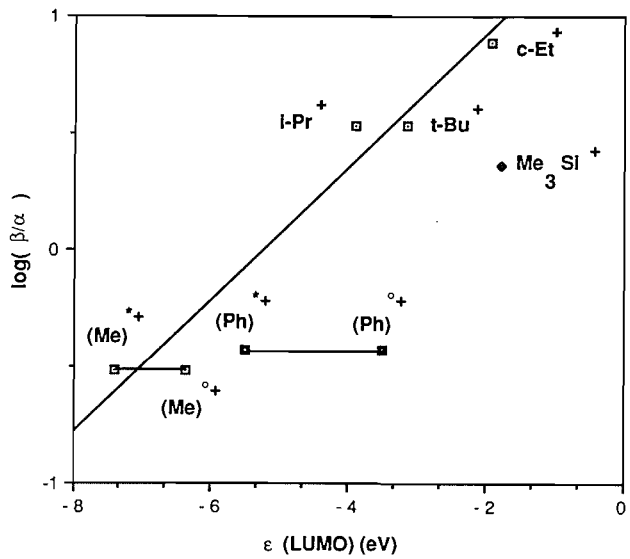


FIG. 1. Plot of site selectivity of ionic electrophiles toward the β and α carbons of pyrrole, expressed as log(β/α), as a function of SCF STO-3G calculated LUMO eigenvalues of the ionic electrophiles; (*) vibrationally excited; (°) ground state.

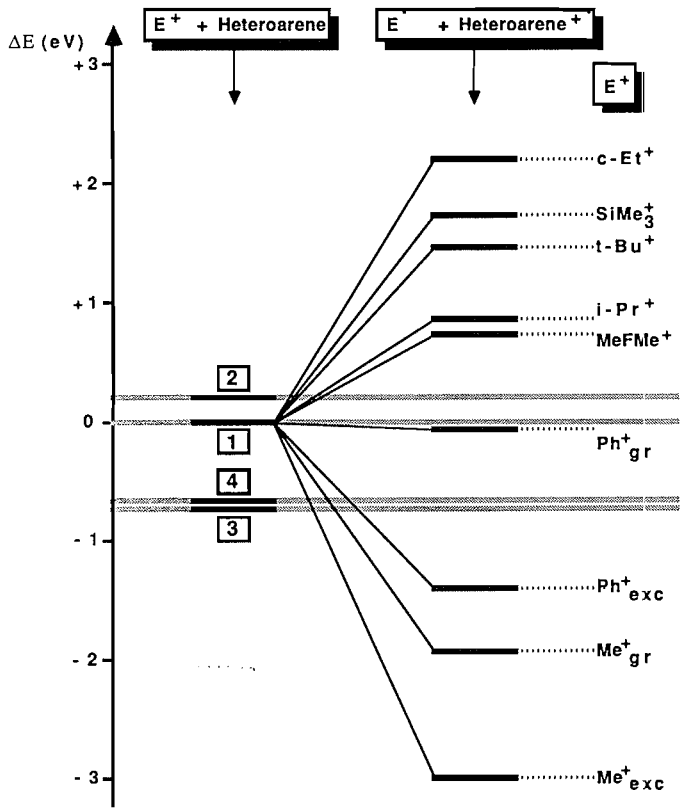


FIG. 2. Energetics of the vertical electron transfer from simple five-membered heteroarenes **1–4** to the electrophile E^+ (c-Et^+ = bridged ethyl cation; gr = ground state; exc = vibrationally excited). The relevant thermochemistry is equal to IP_v(heteroarene) + $EA_v(E^+)$. For electrophiles E^+ with the same geometry of ground state E·, IP_v(heteroarene) + $EA_v(E^+)$ is expressed by IP_v(heteroarene) − IP_v(E·). When, instead, the geometry of E^+ differs significantly from that of ground state E·, IP_v(heteroarene) + $EA_v(E^+)$ can be roughly expressed by IP_v(heteroarene) − IP_a(E·) (refs. 9, 10, 19, 20; see also ref. 28. If the E·/heteroarene$^{+\cdot}$ pair is considered electrostatically bonded in the encounter complex **I** of eq. [7], the energetics reported may be further lowered by several kcal mol^{-1} (ref. 29).

step yielding the two-body complex **I**. Under the conditions of the decay experiments, unimolecular disociation of **I** via eq. [3] (Table 3) is prevented by the rapid radical – radical ion recombination to give the σ-bonded intermediate **5**. This possibility is supported by inspection of Fig. 2, which visualizes the thermochemistry of the vertical SET step of sequence [7] for any given electrophile E^+. Accordingly, only for phenylium and methyl cations is the entropy-favored SET step accessible, leading to an encounter complex **I** (eq. [7]), wherein collapse between E· and the positions of the pyrrole molecular ion with the highest spin density, i.e., the C_α atoms (25), is mostly favored. The SET step of sequence [7] is highly endothermic (0.7–2.2 eV) for the other alkylating electrophiles, which therefore add directly to the most negatively charged centers of pyrroles, i.e., the C_β atoms, via the classical two-electron S_E2 mechanism (eq. [2] of Table 3). Conceivable occurrence of sequence [7] may justify the preferred α-substitution observed in the attack of phenylium and methyl cations on furan **3** and thiophene **4** as well, although such an explanation is not as exclusive as for pyrroles **1** and **2**. In other words, as proposed in related studies (1–6), predominant α-attack on **3** may find an alternative explanation in the presence of the negatively charged oxygen atom of the substrate, which is able to coordinate the electrophile, yielding an electrostatically bonded adduct, wherein subsequent attack on the adjacent C_α is favored by the proximity effect (26). The same effect may be operative in thiophene **4** as well, although to a much lesser extent, and may be superimposed on its normal α > β > S distribution of the net negative charge (27), which favors α substitution.

Conclusions

The results of the present study provide some information about the applicability of Klopman's Charge and Frontier Orbital Control Concept (8, 10) to the electrophilic attack of free ionic reactants on simple five-membered heteroarenes. In analogy with gas-phase heteroaromatic substitution by charged alkylating electrophiles, attack of nucleogenic phenylium ion on **1–4** is characterized by a limited substrate discrimination, which sharply contrasts with a remarkable positional selectivity both in the gaseous and liquid phase. Such a high selectivity is inferred from the kinetic predominance of the phenylium-ion attack on the α carbons of the selected heteroarenes. In pyrroles **1** and **2**, the preferred α phenylation does not correlate satisfactorily with the expected hard properties of a ground-state singlet phenylium ion (ϵ_L = −3.5 eV), nor with the expected borderline character of the vibrationally excited ion (ϵ_L = −5.5 eV).

Such a discrepancy seems to preclude the extension of Klopman's concept to phenylium ion and calls for some novel, more comprehensive, model for heteroaromatic reactivity in the gas phase. A plausible rationale for the diverging behavior of phenylium ion is based upon the possible occurrence of an entropy-favored two-step mechanism, involving preliminary single-electron transfer (SET) from the heteroarene to the electrophile prior to recombination of the ensuing radicals to the σ-bonded intermediate **5** (eq. [7]). The same sequence may, in principle, be operative in another strictly related process, i.e., methylation by free CT_3^+ of **1–4** (2), wherein a similar site discrimination is observed. A SET step in the alkylation of **1–4** by other alkylating electrophiles, i.e., $C_2H_5^+$, i-$C_3H_7^+$, t-$C_4H_9^+$, $(CH_3)_2F^+$, and $(CH_3)_3Si^+$, is made unlikely by unfavorable thermochemical constraints. Direct evidence for the predominant occurrence of a SET-induced energetically

Can. J. Chem. Downloaded from www.nrcresearchpress.com by 198.100.157.202 on 09/07/12
For personal use only.

allowed mechanism in a gas-phase electrophilic heteroaromatic substitution is presented in the following paper.

Acknowledgments

The authors wish to express their gratitude to Professor F. Cacace for his interest in the present work and to Dr. F. Grandinetti for performing the theoretical calculations. Acknowledgment is also due to the Ministero dell'Università e della Ricerca Scientifica e Tecnologica (MURST) and the Consiglio Nazionale delle Ricerche (CNR) of Italy for financial support.

1. M. E. Crestoni, S. Fornarini, and M. Speranza. J. Am. Chem. Soc. **112**, 6929 (1990).
2. G. Angelini, C. Sparapani, and M. Speranza. J. Am. Chem. Soc. **112**, 3060 (1990).
3. (*a*) G. Angelini, C. Sparapani, and M. Speranza. J. Am. Chem. Soc. **104**, 7084 (1982); (*b*) G. Angelini, G. Lilla and M. Speranza, **104**, 7091 (1982).
4. G. Laguzzi, R. Bucci, F. Grandinetti, and M. Speranza. J. Am. Chem. Soc. **112**, 3064 (1990).
5. G. Laguzzi and M. Speranza. J. Chem. Soc. Perkin Trans. 2, 857 (1987).
6. A. Margonelli and M. Speranza. J. Chem. Soc. Perkin Trans. 2, 1491 (1983).
7. (*a*) G. Klopman (*Editor*). Chemical reactivity and reaction paths. Wiley, New York. 1974; (*b*) K. N. Houk. Acc. Chem. Res. **8**, 361 (1975); (*c*) I. Fleming. Frontier orbitals and organic chemical reactions. Wiley, New York. 1976; (*d*) T. L. Ho. Hard and soft acids and bases principle in organic chemistry. Academic Press, New York. 1977.
8. (*a*) R. G. Pearson. Proc. Natl. Acad. Sci. U.S.A. **83**, 8440 (1986); (*b*) G. Klopman. J. Am. Chem. Soc. **90**, 223 (1968).
9. M. Speranza. Adv. Heterocycl. Chem. **40**, 25 (1986).
10. (*a*) R. G. Pearson. J. Am. Chem. Soc. **110**, 7684 (1988); (*b*) R. G. Pearson. J. Org. Chem. **54**, 1423 (1989).
11. P. J. Stang, Z. Rappoport, M. Hanack, and L. R. Subramanian. Vinyl cations. Academic Press, New York. 1979.
12. (*a*) F. Cacace and M. Speranza. Techniques for the study of ion molecule reactions. *Edited by* J. M. Farrar and W. Saunders, Jr. Wiley, New York. 1988; (*b*) F. Cacace. Adv. Phys. Org. Chem. **8**, 79 (1970).
13. G. Angelini, M. Speranza, A. L. Segre, and L. J. Altman. J. Org. Chem. **46**, 3291 (1980).
14. (*a*) G. Plancher and E. Ghigi. Gazz. Chim. Ital. **55**, 757 (1925); (*b*) T. Severin and C. Poehlmann. Chem. Ber. **110**, 491 (1977); (*c*) C. M. Camaggi, R. Leardini, M. Tiecco, and A. Tundo. J. Chem. Soc. B, 1251 (1969); (*d*) H. Wynberg. J. Am. Chem. Soc. **80**, 364 (1958); (*e*) C. M. Camaggi, R. Leardini, M. Tiecco, and A. Tundo. J. Chem. Soc. B, 1683 (1970); (*f*) H. Wynberg, H. van Driel, R. M. Kellogg, and J. Buter. J. Am. Chem. Soc. **89**, 3487 (1967).
15. J. S. Binkley, R. A. Whiteside, R. Krishnan, R. Seeger, D. J. DeFrees, H. B. Schlegel, S. Topiol, L. R. Khan, and J. A. Pople. QCPE, **13**, 406 (1981).
16. P. C. Hariharan and J. A. Pople. Theor. Chim. Acta, **28**, 213 (1973).
17. T. A. Carlson. J. Chem. Phys. **32**, 1234 (1960).
18. (*a*) G. Angelini, S. Fornarini, and M. Speranza. J. Am. Chem. Soc. **104**, 4773 (1982); (*b*) M. Speranza, Y. Keheyan, and G. Angelini. J. Am. Chem. Soc. **105**, 6377 (1984); (*c*) Y. Keheyan and M. Speranza. Helv. Chim. Acta, **68**, 2381 (1985); (*d*) S. Fornarini and M. Speranza. J. Chem. Soc. Perkin Trans. 2, 171 (1984); (*e*) S. Fornarini and M. Speranza. Can. J. Chem. **66**, 2506 (1988).
19. R.v.R. Schleyer, A. J. Kos, and K. Raghavachari. J. Chem. Soc. Chem. Commun. 1296 (1983).
20. S. G. Lias, J. E. Bartmess, J. F. Liebman, J. L. Holmes, R. D. Levin, and W. G. Mallard. J. Phys. Chem. Ref. Data, **17**, Suppl. 1 (1988).
21. R. A. Jones and G. P. Bean. The chemistry of pyrroles. Academic Press, London. 1977. Chap. 6.
22. (*a*) G. Wittig and L. Pohmer. Angew. Chem. **67**, 348 (1955); (*b*) M. S. Newman and R. Kanna. J. Org. Chem. **41**, 3356 (1976); (*c*) J. E. Anderson, R. W. Franck, and W. L. Mandella. J. Am. Chem. Soc. **94**, 4608 (1972).
23. G. Angelini, G. Laguzzi, C. Sparapani, and M. Speranza. J. Am. Chem. Soc. **106**, 37 (1984).
24. (*a*) T. Su and M. T. Bowers. *In* Gas-phase ion chemistry. *Edited by* M. T. Bowers. Academic Press, New York. 1979; (*b*) C. G. LeFevre, R. J. W. LeFevre, B. P. Rao, and M. R. Smith. J. Chem. Soc. 1188 (1959); (*c*) J. Schluyer, L. Blom, and D. W. van Krevelerf. Trans. Faraday Soc. **49**, 1391 (1953).
25. M. Shiotani, Y. Nagata, M. Tasaki, J. Sohma, and T. Shida. J. Phys. Chem. **87**, 1170 (1983).
26. F. Cacace and P. Giacomello. J. Chem. Soc. Perkin Trans. 2, 652 (1978).
27. (*a*) V. Gelius, B. Roos, and P. Siegbahn. Theor. Chim. Acta, **72**, 171 (1972); (*b*) F. Bernardi, A. Bottoni, and A. Mangini. Gazz. Chim. Ital. **101**, 55 (1977).
28. (*a*) F. A. Houle and J .L. Beauchamp. J. Am. Chem. Soc. **101**, 4067 (1979); (*b*) J. Bourdon, D. W. Davies, and G. del Condé. J. Chem. Soc. Perkin Trans. 2, 1193 (1976); (*c*) J .E. Williams, Jr., V. Buss, L. C. Allen, P.v.R. Schleyer, W. A. Lathan, W. J. Hehre, and J. A. Pople. J. Am. Chem. Soc. **93**, 6867 (1971); (*d*) M. W. Wong, J. Baker, R. H. Nobes, and L. Radom. J. Am. Chem. Soc. **109**, 2245 (1987).
29. P. Ausloos and S. G. Lias. J. Am. Chem. Soc. **102**, 3641 (1981).

Can. J. Chem. Downloaded from www.nrcresearchpress.com by 198.100.157.202 on 09/07/12
For personal use only.

Gas-phase heteroaromatic substitution. 11.[1] Electron transfer mechanism in the gas-phase acylation of simple five-membered heteroarenes

ANTONELLO FILIPPI, GIORGIO OCCHIUCCI, AND CINZIA SPARAPANI
Istituto di Chimica Nucleare del CNR, Area della Ricerca di Roma, Rome, Italy

AND

MAURIZIO SPERANZA[2]
Dipartimento di Agrobiologia ed Agrochimica, Università della Tuscia, Viterbo, Italy

Received July 20, 1990

ANTONELLO FILIPPI, GIORGIO OCCHIUCCI, CINZIA SPARAPANI, and MAURIZIO SPERANZA. Can. J. Chem. **69**, 740 (1991).

The results of a study of the gas-phase reactions of unsaturated carbocations, such as the CH_3CO^+ ion from γ-radiolysis of CH_3F/CO mixtures, and the $C_6H_4TCO^+$ ion from the β-decay of 1,4-ditritiobenzene in the presence of CO, with pyrrole, *N*-methylpyrrole, furan, and thiophene, are reported. In all systems investigated, acylated heteroarenes represent the predominant reaction products, accompanied by the methylated derivatives in the CH_3F/CO radiolytic mixtures, and by the phenylated ones in the 1,4-ditritiobenzene/CO decay samples. All substrates investigated are found to undergo predominant α substitution by both acetyl (88.6–98.4% (pyrrole); 90.8–98.7% (*N*-methylpyrrole); 97.2–98.9% (furan); 94.9–98.6% (thiophene)) and benzoyl cations (92.6–96.5% (pyrrole)) under all conditions. The predominant formation of the α-acylated pyrroles from both reactants (>88%), whose relative yields appear unaffected within the temperature interval from 303 to 383 K, indicates, in agreement with ancillary FT-ICR mass spectrometric evidence, that gas-phase acylation reactions toward simple five-membered heteroarenes proceed via a two-step substitution mechanism, involving a quasi-resonant single-electron transfer (SET) step followed by recombination of the ensuing radical – radical ion pair. By virtue of this entropy-favored mechanism, gaseous electrophiles with relatively high SCF STO-3G calculated LUMO energies such as CH_3CO^+ and $C_6H_4TCO^+$ are effectively oriented toward the "soft" C_α sites of the selected heteroarenes, at variance with Klopman's Charge and Frontier Orbital Control predictions. The behavior of gaseous acylating reactants toward simple heteroarenes is discussed and compared with that of other gaseous electrophiles, whose reactivity appears instead in qualitative agreement with Klopman's model.

Key words: gas-phase ion chemistry, electrophilic heteroaromatic substitution, nuclear decay and radiolysis, acylium ions, electron transfer.

ANTONELLO FILIPPI, GIORGIO OCCHIUCCI, CINZIA SPARAPANI et MAURIZIO SPERANZA. Can. J. Chem. **69**, 740 (1991).

On rapporte les résultats obtenus au cours d'une étude des réactions de carbocations insaturés, comme l'ion CH_3CO^+ obtenu par radiolyse γ de mélanges de CH_3F/CO et l'ion $C_6H_4TCO^+$ obtenu par désintégration β du 1,4-ditritiobenzène en présence de CO, avec le pyrrole, le *N*-méthylpyrrole, le furane et le thiophène. Dans tous les systèmes étudiés, les produits réactionnels prépondérants sont les hétéroarènes substitués; ils sont accompagnés des dérivés méthylés (dans les mélanges radiolytiques de CH_3/CO) et des dérivés phénylés (dans les échantillons provenant de la désintégration du 1,4-ditritiobenzène/CO). On a trouvé que, dans toutes les conditions, tous les substrats étudiés subissent principalement une substitution α par les cations acétyle (88,6–98,4% avec le pyrrole; 90,8–98,7% avec le *N*-méthylpyrrole; 97,2–98,9% avec le furane; 94,9–98,6% avec le thiophène) et benzoyle (92,6–96,5% avec le pyrrole). La formation prépondérante de pyrroles α-acylés à partir des deux réactifs (>88%), alors que leurs rendements relatifs ne semblent pas affectés dans l'intervalle de température allant de 303 à 383 K, suggère, en accord avec des données supplémentaires de spectrométrie de masse FT-ICR, que les réactions d'acylation en phase gazeuse d'hétéroarènes à cinq chaînons simples se produisent par un mécanisme de substitution en deux étapes impliquant une étape de transfert d'un seul électron quasi-résonant suivie d'une recombinaison de la paire de radical – ion radical qui s'en suit. En vertu de ce mécanisme favorisé par l'entropie, les électrophiles gazeux, comme le CH_3CO^+ et le $C_6H_4TCO^+$ dont les énergies d'OM basses vacantes calculées par des méthodes STO-3G auto-cohérentes sont élevées, sont de fait orientées vers les sites C_α «mous» des hétéroarènes choisis; ces résultats sont en opposition avec les prédictions du contrôle de la charge et des orbitales frontières de Klopman. On discute du comportement des réactifs gazeux acylants vis-à-vis des hétéroarènes simples et on le compare à celui d'autres électrophiles gazeux dont la réactivité semble plutôt se rapprocher qualitativement du modèle de Klopman.

Mots clés : chimie des ions en phase gazeuse, substitution hétéroaromatique électrophiles, désintégration nucléaire et radiolyse, ions acylium, transfert d'électron.

[Traduit par la rédaction]

Introduction

In previous papers of this series (1, 2), attention has been focussed on Klopman's Charge and Frontier Orbital Concept (3) as a general model for intrinsic heteroaromatic reactivity of gaseous ionic electrophiles. According to Klopman's model (3), kinetic studies on the reactivity of gaseous alkylating electrophiles, i.e., $t\text{-}C_4H_9^+$ (2*e*), $i\text{-}C_3H_7^+$ (2*d*), $C_2H_5^+$ (2*c*), and CH_3^+ (2*b*), toward simple five-membered heteroarenes allowed establishment of an approximately linear correlation between the "hardness" of the alkylating reactants, taken as a function of their SCF STO-3G calculated LUMO energy (4), and their positional selectivity toward pyrroles (log (β/α)). However, when a Si-centered, $(CH_3)_3Si^+$ (2*a*), or an unsaturated electrophile, $C_6H_5^+$ (1), is included in this correlation, an appreciable deviation from linearity is observed, reflecting an experimental positional selectivity (log (β/α)) that is appreciably different from that expected on the basis of their

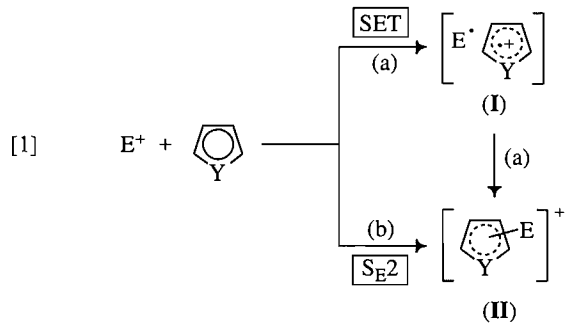
[1]Reference 1 is Part 10.

[2]Author to whom correspondence may be addressed.

Printed in Canada / Imprimé au Canada

Can. J. Chem. Downloaded from www.nrcresearchpress.com by 198.100.157.202 on 09/07/12
For personal use only.

calculated LUMO energies. Pronounced orbital control of orientation in the encounter complex, due to the comparatively large empty $3p$ orbital of Si in $(CH_3)_3Si^+$, is likely responsible for the relatively low log (β/α) value and thus for the relatively "soft" character of trimethylsilyl cation toward pyrroles ($2a$). The same factor cannot be operative in the phenylium ion $C_6H_5^+$, whose exceedingly high affinity for the α positions of pyrroles (log $(\beta/\alpha) = -0.42$ (pyrrole); -0.48 (*N*-methylpyrrole)) may be related to a conceivable change of the intimate substitution mechanism (eq. [1]). The two-step sequence [1a]



E = CH_3CO; C_6H_5CO
Y = NH (**1**); NMe (**2**); O (**3**); S (**4**)

was advanced, wherein the preliminary single-electron transfer (SET) step from the heteroarene to the electrophile is thermochemically allowed only for the α-oriented $C_6H_5^+$ and CH_3^+ electrophiles, and forbidden for the other β-directed alkylating species (1). In this view, the distinct preference of phenylium and methylium cations for the α-carbons of pyrroles arises directly from the favored radical – radical ion recombination in the intermediate adduct **I** (eq. [1a]) between phenyl or methyl radical and the positions of the heteroarene molecular ion with the highest spin density, i.e., the C_α atoms (5). Since the same SET step of sequence [1a] is energetically inaccessible to the other alkylating species investigated, these add to the heteroaromatic molecule via the classical two-electron S_E2 mechanism [1b] governed by electrostatic interactions in the encounter complex (2).

Although adoption of sequence [1a] for $C_6H_5^+$ (and CH_3^+) would satisfactorily account for the peculiar affinity of the electrophile for the α positions of pyrroles, no direct experimental evidence for its actual occurrence in the relevant systems is presently available. To gain further insight into the kinetic role of the proposed two-step mechanism [1a] in the gas-phase electrophilic attack of unsaturated cations on heteroarenes, we have now extended the investigation to the acylating electrophiles CH_3CO^+ and $C_6H_5CO^+$, which can be conveniently generated in the gas phase by γ-radiolysis (6) and nuclear decay (7) procedures. Both acylating ions exhibit rather unique features. On the one hand, they are ranked among the "hardest" ionic electrophiles known (8) and, therefore, they are expected to be oriented toward the ring positions of the heteroaromatic substrate with the highest net negative charge (e.g., the C_β's of pyrrole), if the classical S_E2 mechanism [1b] is operative (3, 4). On the other hand, these species can accept an electron from the heteroaromatic molecule via a very efficient quasi-resonant vertical transition (first step of eq. [1a]) (Fig. 1). In this case, a pronounced α substitution on the heteroaromatic ring would be actually observed, in spite of the "hard" character of the acylating reactants. By virtue of such a favorable combination of properties, it was hoped to provide firm indication of the kinetic role of thermochemically allowed SET processes in the gas-phase electrophilic attack of unsaturated carbocations on fundamental five-membered heteroarenes (eq. [1a]).

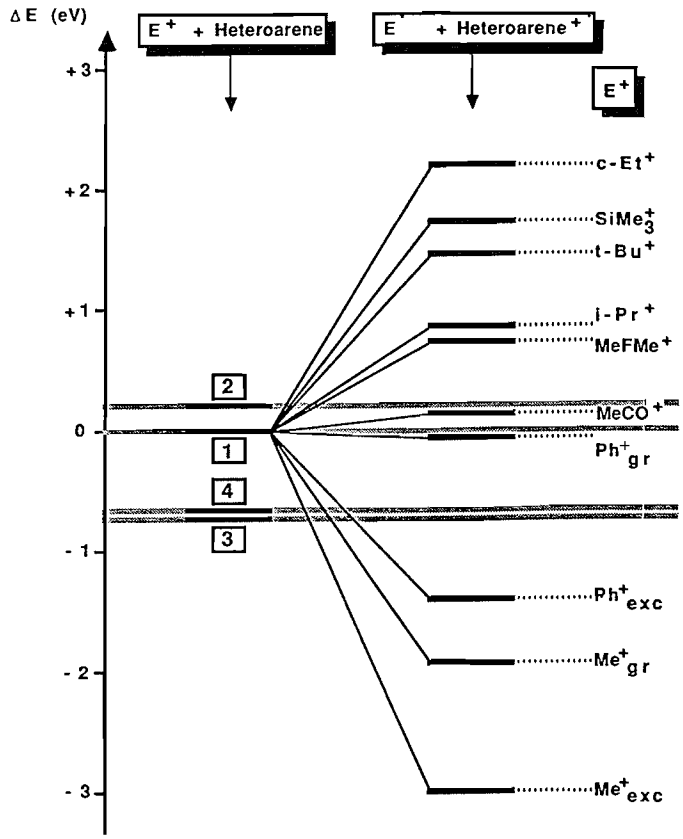


FIG. 1. Energetics of the vertical electron transfer from simple five-membered heteroarenes **1**–**4** to the electrophile E^+ (c-Et^+ = bridged ethyl cation; gr = ground state; exc = vibrationally excited). The relevant thermochemistry is equal to IP_v(heteroarene) + $EA_v(E^+)$. For electrophiles E^+ with the same geometry of ground-state E·, IP_v(heteroarene) + $EA_v(E^+)$ is expressed by IP_v(heteroarene) − IP_v(E·). When, instead, the geometry of E^+ significantly differs from that of ground-state E·, IP_v(heteroarene) + $EA_v(E^+)$ can be approximately expressed by IP_v(heteroarene) − IP_a(E·) (refs. 8 and footnote 5). If the E·/heteroarene$^{+\cdot}$ pair is considered electrostatically bonded in the encounter complex **I** of eq. [1a], the energetics reported may be further lowered by several kilocalories per mole (ref. 23).

Experimental section

Materials

1,4-Ditritiobenzene was prepared and purified according to described procedures (9) and diluted with benzene to a specific activity of 86 mCi mmol^{-1}. Methyl fluoride, carbon monoxide, oxygen, and trimethylamine were high-purity gases from Matheson Co., used without further purification. All the heteroaromatic substrates and the reference compounds used for the preparation of the reaction mixtures and their analysis were research grade chemicals from Fluka AG and were analyzed by gas chromatography (glc) and high-performance liquid chromatography (hplc) to check the absence of any acylated and alkylated products. Not commercially available isomeric acetylated, benzoylated, phenylated, and methylated derivatives of the selected heteroaromatic substrates, used as carriers or as standards in the chromatographic analyses, were prepared following well-established synthetic procedures (10). The identity of the synthesized products was checked by conventional ir, nmr, and glc – mass spectrometry (glc–ms).

Procedure

The gaseous mixtures for the radiolytic acetylation experiments were

Can. J. Chem. Downloaded from www.nrcresearchpress.com by 198.100.157.202 on 09/07/12
For personal use only.

prepared according to standard procedures using a greaseless vacuum line and were introduced into carefully evacuated and outgassed 135-mL Pyrex vessels. Typical experimental conditions were as follows: CH_3F/CO: 1:4; total pressure: 100–760 Torr (1 Torr = 133.3 Pa); heteroaromatic substrate: 1–2 Torr; O_2: 4 Torr; NMe_3: 0–17 Torr. The irradiations were carried out in a 220 Gammacell (Atomic Energy Canada Ltd.) to a total dose of 1×10^4 Gy at a dose rate of ca. 1×10^4 Gy h^{-1}, at a temperature of 30°C. A set of experiments with pyrrole as the substrate was carried out at temperatures ranging from 30 to 110°C.

The gaseous samples for the decay benzoylation experiments were prepared by introducing ca. 1 mCi of 1,4-ditritiobenzene into evacuated and carefully outgassed 100-mL Pyrex vessels containing a measured amount of pyrrole (ca. 4 Torr), together with CO (127–634 Torr), O_2 (4 Torr), used as a radical scavenger, and a powerful ion trap (NMe_3: 12.5 Torr) when required. The vessels were then sealed off and stored in the dark, at room temperature, for ca. 6–8 months. After the storage period, the ampoules were opened and their content analyzed by a radio-hplc procedure. A Varian Vista 5500 high-pressure liquid chromatograph, equipped with a 250 nm UV detector in series with a Berthold LB 503 HS flow scintillation counter, was used for the radio-hplc analyses.

The radiolytic samples were analyzed by glc and glc–ms using, respectively, Perkin–Elmer 8320 and Sigma 3 gas chromatographs, equipped with FID units, and a Hewlett–Packard model 5970B mass selective detector. To avoid selective losses of the products from both radiolytic and decay experiments by adsorption on the glass walls of the vessels, the analyses were carried out after washing the bulb walls with freshly purified toluene. The identity of the products was established by comparison of their retention volumes with those of authentic standards, as well as from their glc–ms spectra measured from the radiolytic runs. The amounts of the products formed were determined from the areas of the corresponding elution peaks using the internal standard calibration method.

The irradiated samples were analyzed on the following glc columns: (i) 1.5 m × 1/8 in. stainless steel column packed with 10% Bentone-34/6% diisodecylphthalate on Chromosorb W, operated between 110 and 120°C; (ii) 0.6 m × 1/8 in. stainless steel column packed with 5% SP1000/5% Bentone-34 on Chromosorb W, operated between 70 and 120°C; (iii) 2 m × 1/8 in. stainless steel column packed with KOH-treated activated carbon, operated between 100 and 190°C.

For the radio-hplc analysis of the decay samples, a 15 cm × 5 μm C-18 Violet column, eluted with H_2O/CH_3CN = 70%:30% was employed.

Fourier-transform (FT-ICR) mass spectrometry

The measurements were performed with a Nicolet FT-MS 1000 ICR spectrometer, equipped with a 2.54-cm cubic cell installed between the poles of a 2.0-T superconducting magnet. The pressure measurements (uncorrected) were obtained with a Granville–Philips 280 Bayard–Alpert ion gauge. Resolution was typically 1000 fwhh (full width half height) at m/e 100. The inlet system and the trapping cell were kept at room temperature, the ions being trapped within the cell by a differential voltage of ca. 1.0 V. Typical operating conditions were as follows: nominal electron energy: 12 eV; electron beam pulse time: 5 ms; emission current: 0.800 μA; total pressure: 5×10^{-7} Torr. The acetyl and benzoyl cations, conveniently generated by electron impact on acetone and acetophenone, respectively, were isolated from other ions by the triple-resonance technique, and their reactions with the heteroaromatic substrates were monitored by analyzing any daughter cations formed.

Computational details

Standard quantum-mechanical calculations, with the GAUSSIAN 80 (11) set of programs, were performed in order to evaluate the STO-3G (12) SCF eigenvalues of the LUMOs of acetyl and benzoyl cations. The optimized geometries of these ions were obtained at the SCF STO-3G level of theory by gradient-based techniques, C_{3v} point group symmetry framework being assumed for CH_3CO^+ and C_{2v} for $C_6H_5CO^+$. The LUMO energy of both CH_3CO^+ and $C_6H_5CO^+$ ions is −2.4 eV.

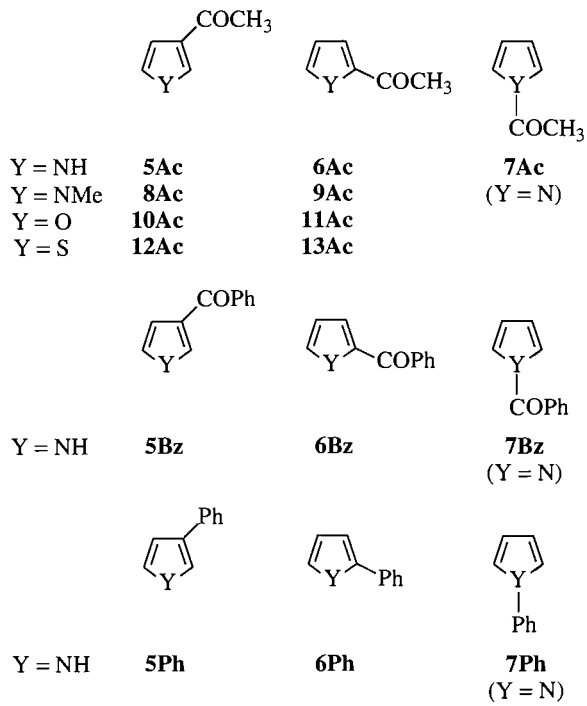


CHART 1

Results

Gas-phase attack of acetyl cation, generated by γ-radiolysis of CH_3F/CO mixtures in the presence of a thermal radical scavenger, such as O_2, on the selected heteroaromatic substrates **1–4** yields the corresponding acetylated derivatives, namely **5Ac–7Ac** from **1**, **8Ac** and **9Ac** from **2**, **10Ac** and **11Ac** from **3**, and **12Ac** and **13Ac** from **4** (Chart 1). Their absolute yields are expressed as the percent ratio between their G(M) values, i.e., the number of molecules M produced per 100 eV of energy absorbed by the gaseous mixtures, and the $G(CH_3CO^+)$ = ca. 2, estimated under comparable conditions from previous investigation (13). The results of these calculations, while largely approximate,[3] represent nevertheless an estimate of the relative efficiency order of the reaction channel leading to the acetylated products (69–84% (**1**); 44–74% (**2**); 10–24% (**3**); 13–40% (**4**)). The ionic character of the acetylation process is ensured by the presence of an effective thermal radical scavenger (O_2), contained in the gas at concentrations even higher than those of **1–4**, and confirmed by the dramatic decrease of the overall product yields caused by addition to the gaseous mixture of variable concentrations of the base NMe_3 (up to 91% (**1**); 89% (**2**); 80% (**3**); 77% (**4**), at ca. 2.0 mol% of NMe_3).

The isomeric distribution of the products from gas-phase acetylation of heteroarenes **1–4** has been measured under largely different experimental conditions. The results concerning pyrroles are illustrated in Tables 1 and 2 and Fig. 2.[4]

[3]There are considerable uncertainties as to the radiation dose actually absorbed by the gas and the precise value of $G(CH_3CO^+)$ and its dependence upon the mixture pressure. In addition, there are several reaction channels available to CH_3CO^+ ions following their attack on the heteroarene that represent only one of the nucleophiles present in the irradiated systems.

[4]For the sake of clarity, the relative distribution of methylated heteroarenes from the $(CH_3)_2F^+$ ion invariably accompanying formation of CH_3CO^+ from γ-radiolysis of CH_3F/CO mixtures (ref. 13) has not been included in Tables 1–4.

Can. J. Chem. Downloaded from www.nrcresearchpress.com by 198.100.157.202 on 09/07/12
For personal use only.

Can. J. Chem. Downloaded from www.nrcresearchpress.com by 198.100.157.202 on 09/07/12
For personal use only.

TABLE 1. Product yields from the γ-radiolysis of gaseous CH_3F/CO/pyrrole mixtures (30°C)

System composition (Torr)[a]				Isomeric distribution of acetylated products (%)[b]			Total absolute yield (%)[c]
CH_3F	CO	Pyrrole	NMe_3	α	β	N	
30	90	1.1	—	88.6	4.6	6.8	84
50	170	1.3	—	93.8	2.8	3.4	81
90	260	1.3	—	94.6	3.0	2.4	72
100	310	1.5	—	94.0	2.5	3.5	84
110	340	1.4	—	97.0	2.0	1.0	83
130	390	1.0	—	98.0	1.4	0.6	79
150	470	1.6	—	96.6	1.3	2.1	69
190	570	1.7	—	98.3	1.4	0.3	70
190	570	1.4	2	98.4	1.6	—	44
190	570	1.2	5	98.4	1.6	—	23
190	570	1.5	11	94.7	5.3	—	12
190	570	1.1	17	93.3	6.7	—	6

[a] O_2: 4 Torr. Radiation dose: 1×10^4 Gy; dose rate = 1×10^4 Gy h^{-1}.
[b] Uncertainty level: 10%.
[c] Total absolute yields estimated from the percent ratios between the overall G(M) values of products and the $G(CH_3CO^+)$ value equal to ca. 2, evaluated under the same conditions from previous investigations (refs. 13, 15).

TABLE 2. Product yields from the γ-radiolysis of gaseous CH_3F/CO/*N*-methylpyrrole mixtures (30°C)

System composition (Torr)[a]				Isomeric distribution of acetylated products (%)[b]		Total absolute yield (%)[c]
CH_3F	CO	*N*-Methylpyrrole	NMe_3	α	β	
30	90	1.0	—	97.8	2.2	74
50	170	1.5	—	97.6	2.4	72
90	260	1.3	—	97.6	2.4	73
100	310	1.7	—	97.0	3.0	64
110	340	1.4	—	98.0	2.0	53
130	390	1.4	—	96.7	3.3	49
150	470	1.3	—	92.8	7.2	47
190	570	1.2	—	90.8	9.2	50
190	570	1.9	2	95.2	4.8	28
190	570	1.7	5	96.7	3.3	14
190	570	1.5	10	96.6	3.4	8
190	570	1.9	15	98.7	1.3	5

[a] O_2: 4 Torr. Radiation dose: 1×10^4 Gy; dose rate: 1×10^4 Gy h^{-1}.
[b] Uncertainty level: 10%.
[c] Total absolute yields estimated from the percent ratios between the overall G(M) values of products and the $G(CH_3CO^+)$ value equal to ca. 2, evaluated under the same conditions from previous investigations (refs. 13, 15).

Inspection of Tables 1 and 2 and Fig. 2 reveals that α acetylation of pyrroles **1** and **2** predominates under all conditions (88.6–98.4% (**6Ac**); 90.8–98.7% (**9Ac**)). The relevant product distribution fluctuates within the uncertainty level (ca. 10%) of the measurements, in spite of large variations of the system pressure (100–760 Torr) (Tables 1 and 2) and the reaction temperature (30–110°C) (Fig. 2), and the addition of conspicuous amounts of the base NMe_3 to the reaction mixture (0–17 Torr) (Tables and 2).

Similar trends are observed for the relative yields of the

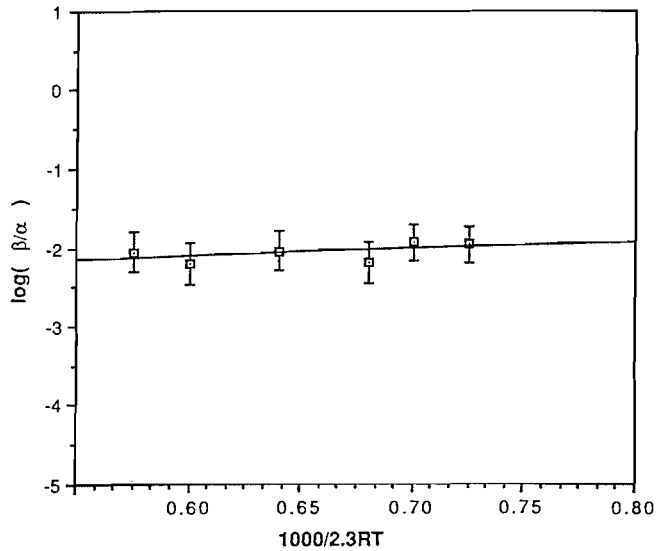


FIG. 2. Arrhenius plot for the competitive attack of CH_3CO^+ ion on the β and α positions of pyrrole **1** at 760 Torr. The vertical bars refer to the reproducibility of data from different irradiations carried out under identical conditions.

TABLE 3. Product yields from the γ-radiolysis of gaseous CH_3F/CO/furan mixtures (30°C)

System composition (Torr)[a]				Isomeric distributions of acetylated products (%)[b]		Total absolute yield (%)[c]
CH_3F	CO	Furan	NMe_3	α	β	
30	90	1.8	—	97.9	2.1	24
50	170	2.0	—	97.2	2.8	22
90	260	1.7	—	98.6	1.4	20
100	310	1.7	—	97.9	2.1	23
110	340	1.8	—	98.3	1.7	19
130	390	1.9	—	98.7	1.3	19
150	470	1.5	—	98.8	1.2	17
190	570	1.6	—	98.0	2.0	10
190	570	1.9	2	98.2	1.8	7
190	570	2.0	5	98.7	1.3	5
190	570	1.9	10	98.9	1.1	3
190	570	1.9	16	98.9	1.1	2

[a] O_2: 4 Torr. Radiation dose: 1×10^4 Gy; dose rate: 1×10^4 Gy h^{-1}.
[b] Uncertainty level: 10%.
[c] Total absolute yields estimated from the percent ratios between the overall G(M) values of products and the $G(CH_3CO^+)$ value equal to ca. 2, evaluated under the same conditions from previous investigations (refs. 13, 15).

acetylated derivatives of furan **3** (Table 3) and thiophene **4** (Table 4) as a function of the experimental conditions. Accordingly, the relative extent of α acetylation of these substrates remains around 97.2–98.9% (**11Ac** from **3**) and 94.9–98.6% (**13Ac** from **4**) within the entire interval of system pressures (100–760 Torr) and NMe_3 concentrations (0–16 Torr) investigated.

The features of the gas-phase attack of the acetyl cation on pyrrole **1** have been investigated as well at low pressures (5×10^{-7} Torr) in a FT-ICR ion source. Figure 3 shows the experimental results, which indicate that competing single-electron-transfer (SET) and proton-transfer (PT) processes take place. It should be noted that, while the measured bimolecular rate constant for the latter process ($k_{PT} = 7.8 \times 10^{-9}$ cm^3 mole-

TABLE 4. Product yields from the γ-radiolysis of gaseous CH_3F/CO/thiophene mixtures (30°C)

System composition (Torr)[a]				Isomeric distribution of acetylated products (%)[b]		Total absolute yield (%)[c]
CH_3F	CO	Thiophene	NMe_3	α	β	
30	90	1.8	—	95.1	4.9	40
50	170	2.0	—	94.9	5.1	38
90	260	1.3	—	95.6	4.4	33
100	310	2.0	—	95.5	4.5	30
110	340	2.0	—	95.0	5.0	23
130	390	1.7	—	95.7	4.3	17
150	470	1.3	—	96.8	3.2	14
190	570	1.8	—	95.8	4.2	13
190	570	1.9	2	97.2	2.8	9
190	570	2.0	5	97.7	2.3	6
190	570	1.5	10	98.6	1.4	4
190	570	1.9	15	98.4	1.6	3

[a] O_2: 4 Torr. Radiation dose: 1×10^4 Gy; dose rate: 1×10^4 Gy h^{-1}.
[b] Uncertainty level: 10%.
[c] Total absolute yields estimated from the percent ratios between the overall G(M) values of products and the $G(CH_3CO^+)$ value equal to ca. 2, evaluated under the same conditions from previous investigations (refs. 13, 15).

cule^{-1} s^{-1}) closely approaches the ADO calculated collision limit ($k_{ADO} = 8.0 \times 10^{-9}$ cm^3 molecule^{-1} s^{-1}) (14), that of the SET reaction exceeds such a limit by a factor of ca. 4 ($k_{SET} = 3.1 \times 10^{-8}$ cm^3 molecule^{-1} s^{-1}).

The yields of the labeled products from the decay of 1,4-ditritiobenzene in gaseous CO, containing minor amounts (0.7–3.4 mol%) of pyrrole **1**, are given in Table 5. In the absence of other nucleophiles, the combined yields of the pyrrole derivatives identified range from 30 to 79% of the activity of the nucleogenic (formed by nuclear decay) *para*-T-phenylium ions formed in the system, which represents the maximum activity theoretically incorporable in the products. The sharp decrease of the absolute yields of the heteroaromatic products (73–90%) from the systems containing NMe_3 (1.9 mol%) supports the ionic nature of their formation processes, since the amine is known to be an effective interceptor of gaseous cations.

The isomeric composition of benzoylpyrroles **5Bz–7Bz** of Table 5 closely reproduces that of their acetylated analogues **5Ac–7Ac** from the radiolytic experiments (Table 1). In fact, pyrrole **1** undergoes predominant benzoylation at its α positions under all conditions (92.6–96.5% (**6Bz**)). Labeled phenylpyrroles **5Ph–7Ph** accompany formation of the benzoyl derivatives of **1** in yields largely exceeding those expected on the grounds of the CO/pyrrole concentration ratios. The relative yields of labeled **5Ph–7Ph**, as well as their isomeric distribution, depend upon the composition of the gaseous mixture. In particular, a fivefold increase of the CO partial pressure causes a ca. threefold decrease of the relative yield of phenylpyrroles, while the **5Ph**:**6Ph** yield ratio changes from 32%:68% to 41%:59%. A noteworthy feature is that under no circumstances does substitution take place at the N center of **1**, in qualitative agreement with the acetylation results and with those of pyrrole phenylation reported in the preceding paper (1).

Discussion

Nature and properties of the acylating reagents

Detailed investigation (13, 15) of the γ-radiolysis and the related ion chemistry of gaseous CH_3F/CO mixtures indicates

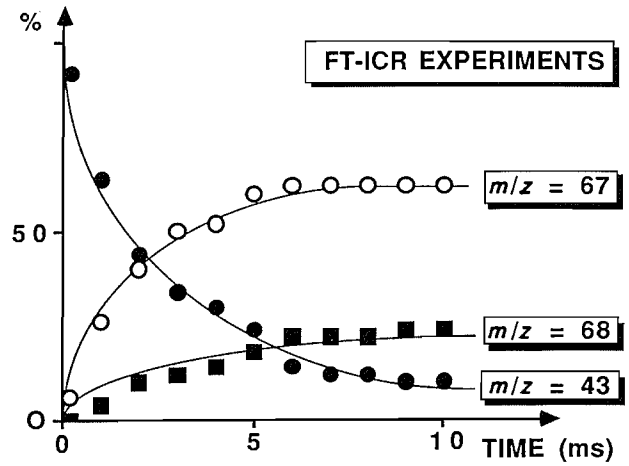
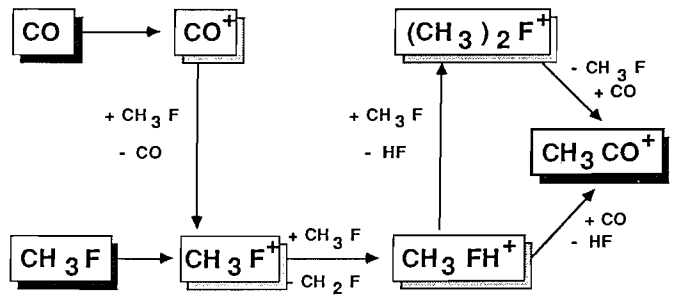


FIG. 3. Relative abundances of CH_3CO^+ (●), $C_4H_5N^{+\bullet}$ (○), and $C_4H_6N^+$ (■) ions as a function of time, observed in FT-ICR experiments of CH_3COCH_3/pyrrole **1** = 1:1 mixtures.



SCHEME 1

that, at CH_3F molar fractions ranging around 0.2, CH_3CO^+ represents the major ionic species formed, whose G(M) amounts to ca. 2.0 at 760 Torr total pressure. In agreement with the well-established reaction network given in Scheme 1 (16), γ-radiolysis of CH_3F/CO gaseous mixtures leads to the formation of CO^+ and CH_3F^+ as the most abundant primary species, which immediately react with CH_3F to yield eventually CH_3CO^+ and $(CH_3)_2F^+$. All individual steps of the reaction network of Scheme 1 are very efficient, as shown by related ICR kinetic studies (10). Thus, only a few collisions between the primary ionic species and the parent molecules are sufficient to establish stationary concentrations of CH_3CO^+ and $(CH_3)_2F^+$ ions, whose yield ratio depends on the system composition and reaches the maximum value at a CH_3F molar fraction equal to ca. 0.2.

Spontaneous nuclear decay in 1,4-ditritiobenzene (ca. 1 mCi), diluted in a large excess of CO (127–634 Torr), was used to generate free benzoyl cation $C_6H_4TCO^+$ in the gas phase (eq. [2]) (17).

Nuclear transition in 1,4-ditritiobenzene yields the daughter *para*-T-phenylium ion in its most singlet configuration (18) for more than 72% of the decay events (19). The primary daughter species is characterized by a certain excess of internal energy (<32 kcal mol^{-1}), due to the relaxation of its initial regular structure, reminiscent of that of the parent benzene, to the distorted hexagonal geometry of the ground-state singlet phenylium ion (20).

Nucleogenic phenylium ion is preferentially directed toward the O atom of CO in its first encounter with the bath gas (17), yielding **III** as the major primary adduct (eq. [2]). *Ab initio*

Can. J. Chem. Downloaded from www.nrcresearchpress.com by 198.100.157.202 on 09/07/12
For personal use only.

TABLE 5. Gas-phase reactions of decay-formed $PhCO^+$ ions with pyrrole (25°C)

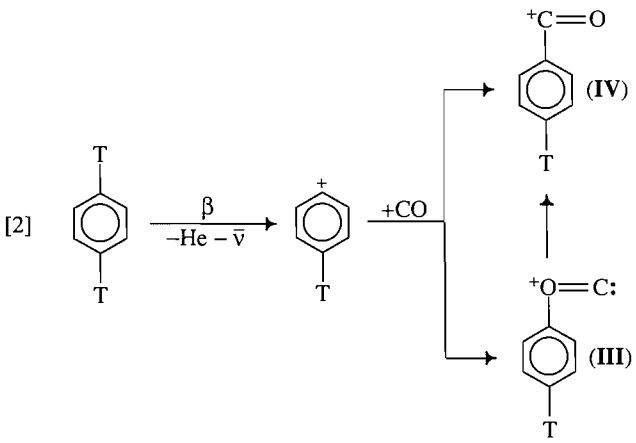
System composition (Torr)[a]		Relative activity of labeled products (%)[b]						Total absolute yield (%)[c]
CO	Pyrrole	**5Bz**	**6Bz**	**7Bz**	**5Ph**	**6Ph**	**7Ph**	
634	4.6	3.4(3.5)	92.9(96.5)	n.d.	1.5(41)	2.2(59)	n.d.	79
362	4.3	4.9(5.2)	89.4(94.8)	n.d.	2.1(37)	3.6(63)	n.d.	58
127	4.7	6.7(7.4)	83.9(92.6)	n.d.	3.0(32)	6.3(68)	n.d.	30
630	4.2[d]	2.9(3.5)	79.5(96.5)	n.d.	7.7(44)	9.9(56)	n.d.	8

[a]All systems contained ca. 1 mCi of 1,4-ditritiobenzene (specific activity: 86 mCi $mmol^{-1}$) and 4 Torr of oxygen.

[b]Ratio of the activity of each product to the combined activity of all heteroaromatic products. Relative composition of benzoylated (**5Bz**, **6Bz**) and phenylated (**5Ph**, **6Ph**) pyrroles given in parentheses. Each value is the average of several determinations, with an uncertainty level of ca. 5%.

[c]Absolute yields expressed as the percent ratio of the total activity of all identified products to the activity originally contained in the nucleogenic phenylium ion, precursor of the benzoyl cation. n.d. = below detection limit, ca. 0.2%.

[d]NMe_3: 12.5 Torr (ca. 1.9 mol%).



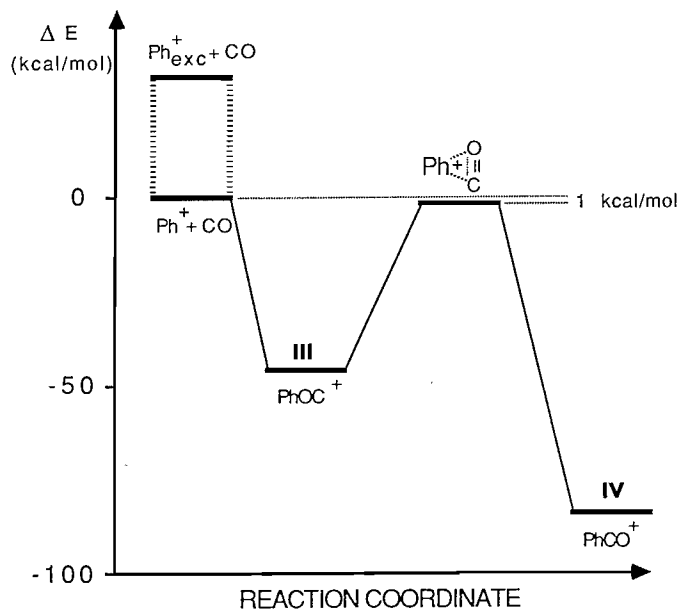


FIG. 4. Schematic energy profile for formation and rearrangement of $C_6H_5OC^+$ (**III**) and $C_6H_5CO^+$ (**IV**) from attack of $C_6H_5^+$ on CO.

calculations have been performed for the benzoyl cation **IV** and its isomer **III**, showing that the latter is less stable by 37.3 kcal mol^{-1} at the STO-3G level of calculation, while the calculated energy barrier for the **III** → **IV** isomerization along the reaction coordinate is very close (83.0 kcal mol^{-1}) to the energy required for the dissociation of **IV** into relaxed phenylium ion and CO (84.0 kcal mol^{-1}) (Fig. 4).[5] It follows that, in our decay systems, formation of benzoyl cation **IV** arises essentially from that restricted family of the primary intermediates **III** that, while sufficiently stabilized by collisional deactivation to escape back dissociation to phenylium and CO, still retain sufficient internal energy to overcome the activation barrier of the **III** → **IV** isomerization. The rather narrow energy window leading to isomerization explains the relative inefficiency of the benzoylation channel, in spite of the exceedingly high excess of CO relative to the heteroaromatic substrate in the corresponding nuclear decay systems. Most of the encounters between nucleogenic phenylium ion leads therefore to CO-solvated phenylium ion **III**, whose relative stationary distribution with respect to **IV** depends upon the efficiency of its collisional quenching and, thus, the partial pressure of CO. Ions **III** can generate the phenylated products of Table 5 by nucleophilic displacement of the CO moiety of **III** by the heteroaromatic substrate.

Although the energetics of the formation processes of both the radiolytic CH_3CO^+ ion (Scheme 1) ($-\Delta H^0$ = 23–46 kcal mol^{-1})[6] and the nucleogenic benzoyl cation (eq. [2]) ($-\Delta H^0$ = 68–100 kcal mol^{-1}) (21) are rather different, the large molar fraction of the bath gas(es) in both systems (>0.97), compared to the trace concentrations of the heteroaromatic substrate (molar fraction from ca. 2×10^{-3} to ca. 3×10^{-2}), ensures in both cases the efficient thermalization of the ionic acylating reactants by unreactive collisions with the bath gas(es) before their encounter with a heteroarene molecule. Moreover, the composition of the systems is such that undesired secondary processes, e.g., direct radiolysis of the heteroaromatic substrate or of its reaction products, can be safely neglected.

Rough thermochemical calculations, performed by using a heat of formation of 156 kcal mol^{-1} (21*b*) for CH_3CO^+ and of 175 kcal mol^{-1} (21*d*) for benzoyl cation, indicate that acylation of heteroarenes **1–4** by both ions is an energetically allowed

[5]F. Bernardi, F. Grandinetti, and A. Guarino, unpublished results.

[6]Thermochemical values for ions and neutrals taken from ref. 21.

Can. J. Chem. Downloaded from www.nrcresearchpress.com by 198.100.157.202 on 09/07/12
For personal use only.

Can. J. Chem. Downloaded from www.nrcresearchpress.com by 198.100.157.202 on 09/07/12
For personal use only.

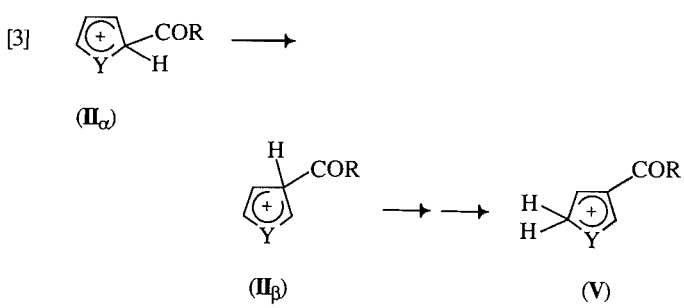
process,[7] which represents the predominant ionic pathway in the relevant samples, since other conceivable ionic processes are either energetically forbidden (e.g., hydride ion abstraction) or, although energetically allowed, kinetically insignificant (e.g., methyl and proton transfer) (*vide infra*) (22). This conclusion is corroborated by the substantial absolute yields of acylated products, recovered in both the radiolytic and the decay systems. Significant energy release is involved in the efficient addition on **1–4** of $(CH_3)_2F^+$ (*2f*), formed together with CH_3CO^+, and of **III**,[5] accompanying formation of **IV**.

The gas-phase acylation mechanism

In the framework of a classical S_E2 mechanism [1b] following Klopman's reactivity model (3), gas-phase attack of hard ionic electrophiles, such as acetyl and benzoyl cations (ε(LUMO) = −2.4 eV), on pyrroles **1** and **2** is expected to be predominantly governed by electrostatic interactions within the encounter pair and, therefore, directed mostly toward the carbon centers of the substrate with the highest net negative charge, i.e., the C_β atoms (1, 2). On the contrary, a conspicuous α substitution is *de facto* invariably observed in the gas-phase acylation of the selected heteroarenes by both electrophiles. This peculiar behavior is reflected in the large deviation of both acetyl and benzoyl cations from the linear correlation between the site selectivity of gaseous alkylating carbocations toward **1** and their STO-3G calculated LUMO energy, expected from Klopman's model (3) and verified in related studies (g and h in Fig. 5) (2). Such an outstanding discrepancy makes it opportune to inquire whether the unexpectedly large α acylation in **1–4** reflects indeed some peculiar reacting mode of the acylating electrophiles or, rather, a possible mechanistic changeover in the attack of alkylating (b–e in Fig. 5) and acylating carbocations (g and h in Fig. 5) on heteroarenes.

In fact, apart from the classical S_E2 pathway, a conceivable additional route to formation of acetyl derivatives of pyrroles **1** and **2** might involve the intermediacy of ketene, which may add to the heteroarene yielding its acetylated derivatives. Ketene, in fact, may arise from the exothermic proton transfer from CH_3CO^+ to pyrroles **1** ($-\Delta H^0$ = 10 kcal mol^{-1}) and **2** ($-\Delta H^0$ = 17 kcal mol^{-1}) (*21a,b*), a process that has been directly observed from FT-ICR experiments (Fig. 3). However, taking into account that, at the low pressures (5×10^{-7} Torr) prevailing in FT-ICR experiments, unimolecular fragmentation of the primary adduct **II** represents the main route for dissipating its excess energy, it is possible that a sizeable amount of the observed protonated pyrroles (*m/e* = 68) from CH_3CO^+ is due to back dissociation of **II** with a proton left to the most basic moiety, i.e., the pyrrole molecule (*21a,b*). Since back dissociation of **II** is hardly effective at the much higher pressures (up to 760 Torr) typical of the radiolytic and nuclear decay experiments, owing to the very rapid removal of the excess energy of **II** by collisional quenching with the bath gas(es), a question arises as to whether, at high pressures, direct proton loss from CH_3CO^+ to pyrroles and subsequent addition of the ensuing ketene to the heteroarene actually represents a significant route to its acetylated products. A first answer to this question arises from the FT-ICR results of Fig. 3, showing that in spite of the favorable experimental conditions proton transfer is only a minor path open to CH_3CO^+ in its attack on pyrroles, the major channel being direct charge exchange with the substrate. Furthermore, the complete correspondence between the isomeric distribution of the acylated pyrroles from both acetyl and benzoyl cations does not support the intermediacy of the corresponding ketene in their formation, proton transfer from benzoyl cation to **1** (or **2**) to give the relative ketene being energetically inaccessible.

Extensive intramolecular isomerization of the primary intermediates **II**, excited by the exothermicity of their formation processes (eq. [1b]), might in principle be responsible for the predominance of the α-substituted isomers among the acylated products. However, such a possibility can be safely ruled out in the light of the following considerations. Extensive isomerization within excited **II** is hardly consistent with the observation that the same isomeric distribution of products is measured at largely different ion lifetimes, namely at low pressure (100 Torr) in the absence of NMe_3 and at high pressure (760 Torr) in the presence of the base (15–17 Torr) (Tables 1–4). Nevertheless, such a discrepancy would be settled if one admits exceedingly rapid intramolecular acyl-group shifts within **II**, involving activation barriers so low as to make them very fast relative to the competing proton transfer within **II** as well as to NMe_3. This latter hypothesis contrasts strikingly with the very limited extent of isomerization of σ-intermediates from CH_3CO^+-ion attack on substituted arenes observed in related studies (13, *15b*). Moreover, negligible activation barriers for acyl-group shifts within excited **II** would mean that, under long-lived excited ion conditions (at low pressures and in the absence of NMe_3), the thermodynamic distribution of the acylated heteroarenium intermediates would be readily reached, irrespective of the initial composition of their primary precursors **II** (eq. [3]). As a consequence, under such conditions, predominance of the most stable heteroarenium isomer, i.e., the β-acylated intermediate **V**, and therefore of its neutral β-acylated product, would be expected, in contrast with the experimental evidence.

[3] 

In the light of the above considerations, it is legitimate to conclude that the exceedingly high yields of α-acylated heteroarenes, recovered in both the radiolytic CH_3CO^+ and decay $C_6H_4TCO^+$ systems, actually reproduce the predominant formation of their ionic primary precursors $\mathbf{II}_\alpha$ relative to their β-substituted isomers $\mathbf{II}_\beta$ (eq. [3]).

Concerning their detailed formation mechanism, the results of the FT-ICR experiments (Fig. 3) suggest exceedingly fast occurrence of a quasi-resonant SET event in the primary encounter complexes **I** (eq. [1a]), which, at the low pressures (5×10^{-7} Torr) prevailing in the FT-ICR ion source, ends up

[7]The ΔH^0 values for the CH_3CO^+ ion attack on **1–4** can be estimated as equal to ca. −32 (**1**), −48 (**2**), and −18 kcal mol^{-1} (**3** and **4**), by assuming that the proton affinity of the *ipso* position of an acetylated heteroarene is equal to that of the unsubstituted molecule, taken from ref. *21a*. Further support for exothermic acetylation of **1–4** is provided by the fact that CH_3CO^+ ion attack on the less activated methylbenzenes is still thermochemically allowed (ref. 13). The ΔH^0 values for the benzoyl cation attack on **1–4** are expected to be similar to those for acetylation.

Can. J. Chem. Downloaded from www.nrcresearchpress.com by 198.100.157.202 on 09/07/12
For personal use only.

with their unimolecular dissociation to E· and heteroarene $^{+\cdot}$. At the high pressures (100–760 Torr) typical of the radiolytic and nuclear decay experiments, where unimolecular fragmentation of ion-neutral complexes is efficiently prevented by collisional deactivation, the radical – radical ion pair in **I** is able to survive until recombination to produce the σ-bonded intermediates **II**.

Further evidence in favor of the two-step acylation mechanism [1a] is provided by analysis of the Arrhenius plot relative to gas-phase acetylation of pyrrole **1** by CH_3CO^+ (Fig. 2). The essential constancy of the site selectivity of CH_3CO^+ toward gaseous pyrrole **1** (log (β/α) ≃ −2.1 ± 0.1) within a wide temperature interval (80°) is only consistent with a CH_3CO^+ ion attack on the α and β positions of **1** governed by either negligible or very similar activation barriers ($\Delta E^* = E_\alpha^* - E_\beta^* = 0.6 \pm 0.8$ kcal mol^{-1}) and by largely different Arrhenius preexponential factors (log $(A_\beta/A_\alpha) = -2.4 \pm 0.6$). These conditions appear rather awkward if referred to a gas-phase acylation process following the classical S_E2 mechanism. It should be considered, in fact, that the hypothesis of largely different preexponential terms and, therefore, entropy factors in the attack of an ionic electrophile on isomeric unencumbered positions of a neutral molecule, such as **1**, appears unfounded. Furthermore, both acetyl and benzoyl cations are revealed as very selective, mild electrophiles toward arenes, displaying partial rate factors (up to 470) that are exceedingly high for the gas phase ion–molecule reaction standard (13, 15, 17). It follows that the hypothesis of negligible or equal activation barriers for S_E2 acylation of the differently activated positions of **1** is untenable as well. On the contrary, once extensive intramolecular rearrangements of primary **II** are excluded (*vide supra*), the experimental evidence of Fig. 2 can only be accounted for by a gas phase CH_3CO^+ acylation of **1** proceeding via the two-step mechanism [1a]. In fact, both the quasi-resonant SET step of eq. [1a] to yield **I** and the following recombination of the acyl radical and the pyrrole radical ion of **I** to yield **II** are expected to take place with negligible activation barriers, if any, irrespective of the particular position of the electron vacancy in the pyrrole radical ion. In the meantime, the probability of recombination between the acyl radical and each position of pyrrole radical ion in adduct **I** is determined by the largely uneven spin density distribution over the pyrrole$^{+\cdot}$ ring (5) and is reflected in the pronounced preexponential factor ratio arising from the Arrhenius plot of Fig. 2.

On the grounds of the above considerations, the experimental features of gas-phase attack of both acetyl and benzoyl cations on the selected heteroarenes conform to a simple two-step mechanistic model (eq. [1a]), involving a quasi-resonant SET step followed by radical – radical ion recombination, rather than to the classical S_E2 mechanism governing the gas-phase attack of alkylating carbocations on the same substrates (2). Such a mechanistic changeover causes dramatic differences in the relative isomeric distribution of the substitution intermediates **II** and, therefore, precludes extension of Klopman's concept (3) to gas-phase heteroaromatic acylation reactions.

Concerning the origin of the deviation of nucleogenic phenylium ion from the linear log (β/α) vs. ε (LUMO) correlation (*f** in Fig. 5) reported in the preceding paper (1), it should be considered that, if nucleogenic phenylium (1) (and methylium) (2*b*) cations follow the energetically allowed mechanism [1a] in much the same way as the acylating reactants, the same exceedingly high extent of α substitution in **1** would be observed, since it is essentially determined by the high spin density at the C_α's of the pyrrole radical ion (5). On the contrary, attack of nucleogenic phenylium (and methylium) cations on gaseous **1** is characterized by a site selectivity (log (β/α) = −0.42 (phenylium ion (1)); −0.51 (methylium ion (2*b*)) that diverges substantially from that of acetyl and benzoyl cations (log (β/α) < −1.1). Moreover, the relative distribution of the phenylated derivatives of **1**, recovered from the decay benzoylation samples under kinetically favored conditions (Table 5), appears significantly different (log (β/α) = −0.11) from that of direct pyrrole phenylation by nucleogenic phenylium ion (log (β/α) = −0.42) previously measured under comparable conditions (1). Such a marked selectivity difference can be accounted for by considering that, in the decay benzoylation systems, phenylpyrroles are generated from CO-solvated phenylium ion (**III**) (17). In this perspective, the higher log (β/α) values of phenylpyrroles recovered in the benzoylation mixtures are qualitatively consistent with the expected harder character of CO-solvated phenylium ion **III** relative to vibrationally excited phenylium ion (1). This conclusion lends support to the view that the deviation of nucleogenic phenylium ion from the linear correlation of Fig. 5 is likely due to factors related to the intimate nature of the relevant energy profile, rather than to a conceivable mechanism for its attack on pyrrole proceeding via a preliminary *exothermic* SET step (eq. [1a]).

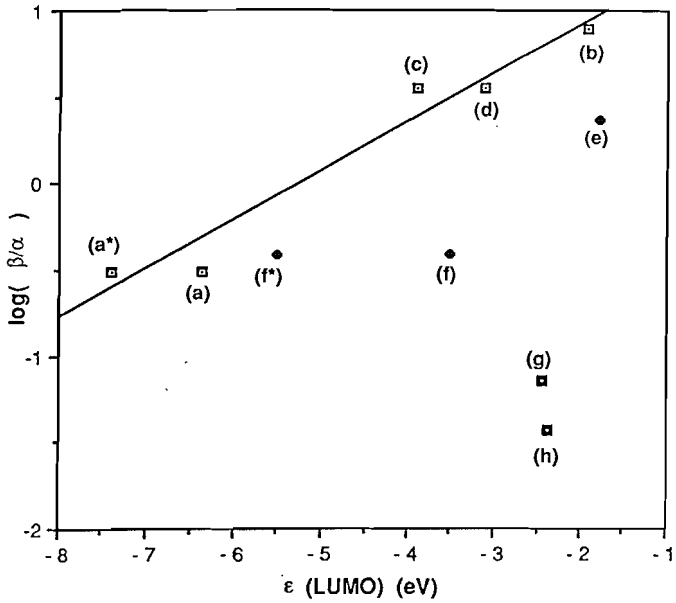


FIG. 5. Plot of site selectivity of ionic electrophiles toward the β and α carbons of pyrrole, expressed as log (β/α), as a function of SCF STO-3G calculated LUMO eigenvalues of the ionic electrophiles, (*) vibrationally excited: (a) CH_3^+; (b) proton-bridged $C_2H_5^+$; (c) *i*-$C_3H_7^+$; (d) *t*-$C_4H_9^+$; (e) $(CH_3)_3Si^+$; (f) $C_6H_5^+$; (g) CH_3CO^+; (h) $C_6H_5CO^+$.

In conclusion, the present acylation results answer the question of a possible mechanistic changeover in the gas-phase attack of carbocations on simple five-membered heteroarenes, providing firm evidence that electrophilic substitution generally proceeds via the classical S_E2 mechanism, except when an entropy-driven *quasi-resonant* single electron transfer (SET) from the substrate to the ionic electrophile is allowed, as for the CH_3CO^+ and $C_6H_5CO^+$ cations (respectively, g and h in Fig. 5). In spite of favorable entropy factors, a gas-phase SET process from the heteroarene to the ionic electrophile is

prevented when markedly *endothermic*, as for proton-bridged $C_2H_5^+$, *i*-$C_3H_7^+$, *t*-$C_4H_9^+$, and $(CH_3)_3Si^+$ (respectively, b, c, d, and e in Fig. 5). No definitive answer can, at the moment, be provided as regards the actual occurrence of an *exothermic* SET event between a heteroarene molecule and CH_3^+ or $C_6H_5^+$ ions (respectively, a and f in Fig. 5). More information on the efficiency of *exothermic* SET processes in electrophilic heteroaromatic substitutions in the gas phase will be given in a forthcoming paper. In general, when the gas-phase two-step sequence [1a] is inaccessible, gaseous ionic electrophiles react with heteroarenes via the classical S_E2 mechanism, qualitatively obeying Klopman's reactivity model (3), although several discrepancies are observed from the quantitative standpoint whose nature deserves further attention.

Acknowledgments

The authors wish to express their gratitude to Prof. F. Cacace for his interest in the present work and to Dr. F. Grandinetti for performing the theoretical calculations. Acknowledgment is due to the Ministero dell'Università e della Ricerca Scientifica e Tecnologica (MURST) and the Consiglio Nazionale delle Ricerche (CNR) of Italy for financial support. The collaboration of the Servizio FT-MS of the Area della Ricerca CNR di Roma is also acknowledged.

1. A. Filippi, G. Occhiucci, and M. Speranza. Can. J. Chem. **69**, 732 (1991).
2. (*a*) M. E. Crestoni, S. Fornarini, and M. Speranza. J. Am. Chem. Soc. **112**, 6929 (1990); (*b*) G. Angelini, C. Sparapani, and M. Speranza. J. Am. Chem. Soc. **112**, 3060 (1990); (*c*) G. Laguzzi, R. Bucci, F. Grandinetti, and M. Speranza. J. Am. Chem. Soc. **112**, 3064 (1990); (*d*) G. Laguzzi and M. Speranza. J. Chem. Soc. Perkin Trans. 2, 857 (1987); (*e*) A. Margonelli and M. Speranza. J. Chem. Soc. Perkin Trans. 2, 1491 (1983); (*f*) G. Angelini, C. Sparapani, and M. Speranza. J. Am. Chem. Soc. **104**, 7084 (1982); (*g*) G. Angelini, G. Lilla, and M. Speranza. J. Am. Chem. Soc. **104**, 7091 (1982).
3. (*a*) R. G. Pearson. Proc. Natl. Acad. Sci. U.S.A. **83**, 8440 (1986); (*b*) G. Klopman. J. Am. Chem. Soc. **90**, 223 (1968).
4. (*a*) G. Klopman. Chemical reactivity and reaction paths. Wiley, New York. 1974; (*b*) K. N. Houk. Acc. Chem. Res. **8**, 361 (1975); (*c*) I. Fleming. Frontier orbitals and organic chemical reactions. Wiley, New York. 1976; (*d*) T. L. Ho. Hard and soft acids and bases principle in organic chemistry. Academic Press, New York. 1977.
5. M. Shiotani, Y. Nagata, M. Tasaki, J. Sohma, and T. Shida. J. Phys. Chem. **87**, 1170 (1983).
6. (*a*) F. Cacace. Kinetics of ion–molecule reactions. *Edited by* P. Ausloos. Plenum, 1979; (*b*) F. Cacace. Radiat. Phys. Chem. **20**, 99 (1982); (*c*) M. Speranza. Gazz. Chim. Ital. **113**, 37 (1983); (*d*) F. Cacace. Structure, reactivity and thermochemistry of ions. *Edited by* P. Ausloos and S. G. Lias. Reidel, Dordrecht, The Netherlands. 1987; (*e*) F. Cacace. Acc. Chem. Res. **21**, 215 (1988).
7. (*a*) F. Cacace. Adv. Phys. Org. Chem. **8**, 79 (1970); (*b*) F. Cacace and M. Speranza. Techniques for the study of ion–molecule reactions. *Edited by* J. M. Farrar and W. Saunders, Jr. Wiley, New York. 1988; (*c*) F. Cacace. Science. In press.
8. R. G. Pearson. J. Am. Chem. Soc. **110**, 7684 (1988); (*b*) J. Org. Chem. **54**, 1423 (1989).
9. G. Angelini, M. Speranza, A. L. Segre, and L. J. Altman. J. Org. Chem. **46**, 3291 (1980).
10. (*a*) S. Gronowitz and G. Sorlin. Ark. Kemi, **19**, 515 (1962); (*b*) S. Gronowitz. Ark. Kemi, **12**, 533 (1958); (*c*) P. Linda and G. Marino. Ric. Sci. **37**, 424 (1967); (*d*) H. J. Anderson and C. W. Huang. Can. J. Chem. **45**, 900 (1967); (*e*) A. Pictet. Berichte, **37**, 2797 (1913); (*f*) M. Kakushima, P. Hamel, R. Frenette, and J. Rokach. J. Org. Chem. **48**, 3241 (1983); (*g*) P. S. Shell and G. P. Bean. J. Am. Chem. Soc. **84**, 4655 (1962); (*h*) R. L. Hinman and S. Theodoropulos. J. Org. Chem. **28**, 3052 (1963); (*i*) E. Sherman and E. D. Amstutz. J. Am. Chem. Soc. **72**, 2195 (1950); (*j*) R. B. Franklin, C. N. Statham, and M. R. Boyd. J. Labelled Compd. Radiopharm. **15**, 569 (1978); (*k*) G. Plancher and E. Chigi. Gazz. Chim. Ital. **55**, 757 (1925); (*l*) T. Severin and C. Poehlmann. Chem. Ber. **110**, 491 (1977); (*m*) C. M. Camaggi, R. Leardini, M. Tiecco, and A. Tundo. J. Chem. Soc. B, 1251 (1969); (*n*) H. Wynberg. J. Am. Chem. Soc. **80**, 364 (1958); (*o*) C. M. Camaggi, R. Leardini, M. Tiecco, and A. Tundo. J. Chem. Soc. B, 1683 (1970); (*p*) H. Wynberg, H. van Driel, R. M. Kellogg, and J. Buter. J. Am. Chem. Soc. **89**, 3487 (1967).
11. J. S. Binkley, R. A. Whiteside, R. Krishnan, R. Seeger, D. J. DeFrees, H. B. Schlegel, S. Topiol, L. R. Khan, and J. A. Pople. QCPE, **13**, 406 (1981).
12. P. C. Hariharan and J. A. Pople. Theor. Chim. Acta, **28**, 213 (1973).
13. M. Speranza and C. Sparapani. J. Am. Chem. Soc. **102**, 3120 (1980).
14. M. T. Bowers and T. Su. Interactions between ions and molecules. *Edited by* P. Ausloos. Plenum Press, New York. 1975.
15. (*a*) P. Giacomello and M. Speranza. J. Am. Chem. Soc. **99**, 7918 (1977); (*b*) M. Speranza and C. Sparapani. Radiochim. Acta, **28**, 87 (1981).
16. D. Holtz and J. L. Beauchamp. Nature (London), Phys. Sci. **231**, 204 (1971).
17. (*a*) G. Occhiucci, A. Patacchiola, C. Sparapani, and M. Speranza. J. Chem. Soc. Chem. Commun. 1269 (1982); (*b*) G. Occhiucci, M. Speranza, and F. Cacace. J. Chem. Soc. Chem. Commun. 723 (1984); (*c*) G. Occhiucci, F. Cacace, and M. Speranza. J. Am. Chem. Soc. **108**, 872 (1986).
18. (*a*) G. Angelini, S. Fornarini, and M. Speranza. J. Am. Chem. Soc. **104**, 4773 (1982); (*b*) M. Speranza, Y. Keheyan, and G. Angelini. J. Am. Chem. Soc. **106**, 6377 (1984); (*c*) Y. Keheyan and M. Speranza. Helv. Chim. Acta, **68**, 2381 (1985); (*d*) S. Fornarini and M. Speranza. J. Chem. Soc. Perkin Trans. 2, 171 (1984); (*e*) Can. J. Chem. **66**, 2506 (1988).
19. T. A. Carlson. J. Chem. Phys. **32**, 1234 (1960).
20. P. v. R. Schleyer, A. J. Kos, and K. Raghavachari. J. Chem. Soc. Chem. Commun. 1296 (1983).
21. (*a*) S. G. Lias, J. F. Liebman, and R. D. Levin. J. Phys. Chem. Ref. Data, **13**, 695 (1984); (*b*) S. G. Lias, J. E. Bartmess, J. F. Liebman, J. L. Holmes, R. D. Levin, and W. G. Mallard. J. Phys. Chem. Ref. Data, **17**, Suppl. 1 (1988); (*c*) J. K. Hovey and T. B. McMahon. J. Am. Chem. Soc. **108**, 528 (1986); (*d*) W. R. Davidson, S. Meza-Hojer, and P. Kebarle. Can. J. Chem. **57**, 3205 (1979).
22. R. C. Dunbar, M. M. Bursey, and D. A. Chatfield. Int. J. Mass Spectrom. Ion Phys. **13**, 195 (1974).
23. P. Ausloos and S. G. Lias. J. Am. Chem. Soc. **102**, 3641 (1981).

Can. J. Chem. Downloaded from www.nrcresearchpress.com by 198.100.157.202 on 09/07/12
For personal use only.

Study of the interactions between caesium bromide and kaolinite by photoacoustic and diffuse reflectance infrared spectroscopy

KIRK H. MICHAELIAN

Energy, Mines and Resources Canada, CANMET, Coal Research Laboratories, P.O. Bag 1280, Devon, Alta., Canada T0C 1E0

AND

SHMUEL YARIV AND AHMED NASSER

Department of Inorganic and Analytical Chemistry, The Hebrew University of Jerusalem, 91904 Jerusalem, Israel

Received July 17, 1990[1]

KIRK H. MICHAELIAN, SHMUEL YARIV, and AHMED NASSER. Can. J. Chem. **69**, 749 (1991).

The mechanochemical reactions between CsBr and kaolinite that occur during shaking, grinding at ambient atmosphere (air grinding), and grinding in the presence of a few drops of water (wet grinding), were investigated by photoacoustic and diffuse reflectance infrared spectroscopy and by thermal weight loss. An intercalation complex was formed by the wet grinding technique but not by mixing or air grinding. For comparison, the mechanochemical reactions of kaolinite with CsCl and CsI were also investigated. No complex of CsI was formed but CsCl gave an intercalation complex by air or wet grinding and, after an aging period of 3 months, also by mixing. A structure is suggested for the intercalation complex in which a water molecule coordinated to the large caesium cation donates one proton to an inner surface oxygen and another proton to the halide, while accepting a proton from an inner surface hydroxyl group.

Key words: kaolinite, infrared spectroscopy, intercalation.

KIRK H. MICHAELIAN, SHMUEL YARIV et AHMED NASSER. Can. J. Chem. **69**, 749 (1991).

Faisant appel à la spectroscopie infrarouge photoacoustique et de réflexion diffuse ainsi qu'à la perte thermique de poids, on a étudié les réactions mécanochimiques du CsBr et de la kaolinite qui se produisent par agitation (mélange), broyage dans un atmosphère ambiant (broyage à l'air) ainsi que par broyage en présence de quelques gouttes d'eau (broyage humide). Par la technique du broyage humide, il se forme un complexe d'intercalation; ce n'est pas le cas avec lors du mélange ou du broyage à l'air. Pour fins de comparaison, on a aussi examiné les propriétés mécanochimiques de la kaolinite avec le CsCl et le CsI. Il ne se forme pas de complexe avec le CsI; toutefois, avec le CsCl il se forme un complexe d'intercalation par broyage humide ou à l'air et, après une période de vieillissement de trois mois, aussi par mélange. On suggère une structure pour le complexe d'intercalation dans laquelle une molécule d'eau coordinée au volumineux cation de césium donne un proton à un oxygène de la surface interne et un autre proton à l'halogénure tout en acceptant un proton du groupement hydroxyle d'une surface interne.

Mots clés : kaolinite, le spectroscopie infrarouge, intercalation.

[Traduit par la rédaction]

Introduction

The grinding of a mineral of the kaolin sub-group with CsCl leads to its delamination and the formation of an intercalation complex in which CsCl, together with water adsorbed from the atmosphere, is located between the layers of the mineral (1–5). In this "intercalation complex" hydrogen bonds are formed between hydroxyl groups of the octahedral sheet of the kaolin-like layers and oxygens of sorbed water molecules, as well as between protons of sorbed water molecules and siloxane oxygens of the tetrahedral sheet. Both reactions, namely delamination and intercalation, occur during the grinding of the mineral with CsCl. However, the intercalation reaction associated with adsorption of water from the atmosphere is much slower than the delamination, and an aging period longer than a month is sometimes needed to complete the reaction.

Delamination of minerals of the kaolin sub-group has been proven from deuteration reactions (6). Washing of the intercalated minerals with D_2O resulted in the deuteration of inner surface hydroxyls of the minerals. In contrast, if the clay was not delaminated, only surface OH groups could be deuterated by this treatment. The formation of hydrogen bonds between OH groups of the octahedral sheet and sorbed water molecules, as well as between sorbed water molecules and basal siloxane oxygens of the tetrahedral sheet, was concluded from significant changes in the infrared spectra of the intercalated complexes.

The exact structure of the intercalation complex is not known. Yariv (1, 3, 6) suggested that the large Cs^+ ion, which may serve as a water "structure breaker", perturbs the ice-like structure of water clusters in the vicinity of the clay. The monomeric water molecules coordinated to Cs^+ are able to form hydrogen bonds to inner surfaces of kaolin-like layers by donating protons to basal oxygens and by accepting protons from inner surface hydroxyls. To obtain a better knowledge of the structure of the intercalation complex the study of intercalation of other salts and water is desirable.

In the present investigation mechanochemical reactions occurring during the grinding of kaolinite with CsBr were studied. In addition to the two techniques which were previously employed for the preparation of the intercalated CsCl complexes of kaolinite, shaking and dry grinding in ambient atmosphere (air grinding), both followed by aging, we studied possible intercalation in a wet technique. In this procedure a few drops of H_2O were added to the mixture from time to time during grinding in order to keep it moist. However, the mixture was never allowed to become too wet since this would prevent mechanochemical delamination.

Infrared spectroscopy is established as a reliable tool for the characterization of intercalation complexes (7, 8). The present study is concerned mainly with the infrared spectra obtained for the CsBr–kaolinite mixture after shaking or after air and wet grinding, supplemented by thermal weight loss. For comparison, the shaking and the air and wet grinding of CsCl– and

[1]Revision received December 3, 1990.

Can. J. Chem. Downloaded from www.nrcresearchpress.com by 198.100.157.202 on 09/07/12
For personal use only.

Can. J. Chem. Downloaded from www.nrcresearchpress.com by 198.100.157.202 on 09/07/12
For personal use only.

CsI–kaolinite mixtures were also investigated, and the spectra were compared to those of the equivalent CsBr–kaolinite mixtures.

In the previous studies on the mechanochemical interactions between alkali halides and kaolinite, conventional infrared absorption spectra were obtained after the samples were pressed into disks with alkali halides as matrices. Possible reactions between the mineral and the salt during the preparation of the disk may affect the recorded spectra, but this effect could not be accurately determined. In the present study we employed photoacoustic and diffuse reflectance FT-IR spectroscopy. These techniques yield spectra of powders without the requirement that they be pressed into disks. To avoid complications that might arise from further kaolinite/alkali halide interactions, the mixtures were investigated "as is", that is, they were not diluted in a nonabsorbing alkali halide matrix as is the customary practice in diffuse reflectance spectroscopy. Photoacoustic FT-IR spectra are commonly obtained for undiluted powders.

The results obtained by diffuse reflectance FT-IR spectroscopy are complementary to the photoacoustic study, with the advantage that one obtains higher signal-to-noise ratios in the former case. However, the diffuse reflectance spectra of the undiluted samples are not useful below 1000 cm^{-1} because the strong absorption by the lattice vibrations obscures all of the detail. Therefore, diffuse reflectance spectroscopy is used only for the study of the OH stretching region in the present work. The low frequency data reported are from the photoacoustic spectra.

Experimental

Materials

Natural jurassic kaolinite from Makhtesh Ramon, Israel (kindly donated by Dr. Shlomo Shoval from the Open Univesity of Tel Aviv) was manually ground using an agate mortar. The fraction passing an 80 mesh (0.177 mm) sieve was used. The IR spectrum of this sample shows a very weak absorption at 3601 cm^{-1}, originating from a very small degree of substitution of Fe for octahedral Al (9, 10). The sample contains ≈5% quartz but this mineral does not react with alkali halides. Caesium halides (Suprapur) were purchased from Merck.

Methods

Mixtures consisting of 500 mg kaolinite and 500 mg of a particular caesium halide were prepared by three different techniques. In the first, the components were thoroughly mixed in small test tubes by manual shaking for about 5 min. In the second technique, the mixtures were ground in a mechanical "Fisher" mortar grinder for 30 min at ambient atmosphere (air grinding). In the third technique the mixtures were ground mechanically for 60 min but 2–3 drops of water were added every 5 min in order to keep the mixture moist (wet grinding). In the latter case we took care that the mixture did not become too wet, so that the mechanochemical process would not be interrupted. For comparison, 1000 mg kaolinite were ground with no additives for 30 min in the same grinder. Mixtures prepared by the first two methods were aged for three months before determination of thermal weight loss or measurement of infrared spectra.

Thermal weight loss

Weight losses were determined for 200 mg of air-dried pure kaolinite (both ground and unground), and for 400 mg of the various CsCl-, CsBr-, and KBr-treated kaolinites. Samples were heated at 100, 150, and 200°C (24 h at each temperature), and at 250, 300, 350, 400, and 450°C (2.5 h).

Infrared measurements

Infrared spectra were obtained using a Bruker IFS 113v FT-IR spectrometer and two different sample accessories. Photoacoustic spectra were recorded with a Princeton Applied Research Corporation model 6003 cell and model 6005 preamplifier; the spectrometer was filled with nitrogen during the measurements. Diffuse reflectance spectra were recorded with a Harrick "praying mantis" attachment and a mercury cadmium telluride detector. The spectrometer was evacuated while the diffuse reflectance data were obtained. These reflectance spectra were later converted to pseudo-absorbance spectra and plotted in Kubelka-Munk units, even though that analysis is strictly applicable only for dilute samples. Hence the intensity scale for these spectra should be regarded as arbitrary.

Several photoacoustic spectra were also recorded using a Bruker IFS 88 spectrometer and an MTEC model 200 photoacoustic cell. The spectrometer was operated in the step-scan, or step-and-integrate, mode rather than the more conventional procedure in which the interferometer mirror moves rapidly and continuously (11). The intensity distributions in the step-scan spectra are slightly different from those in the rapid-scan spectra because of the lower modulation frequencies in the former case; this leads to a small degree of saturation of band intensities, and facilitates identification of weak bands in some situations.

Results

Thermal weight loss

Thermal weight losses of kaolinite treated with CsBr (mixed and air or wet ground) are shown in Table 1. For comparison, thermal weight losses of kaolinite ground for half an hour without any salt or together with CsCl (air and wet) and KBr (air) are also shown in the table. In the temperature ranges 0–250 and 250–450°C unground kaolinite lost 0.5 and 5.5% (not shown in Table 1), due to the removal of "free" water and partial dehydroxylation of the kaolinite, respectively. After grinding, kaolinite contains amorphous material and consequently much "free" water, losing 12.59 and 5.95%, respectively. Kaolinite mixed with CsBr lost 1.86 and 23.49%, respectively. According to Heller-Kallai (12) and Gabor *et al.* (13) the difference in the weight loss occurring during the dehydroxylation stage is in part due to the evolution of hydrogen halide which results from the following thermal hydrolysis:

$$2SiO_2 \cdot Al_2O_3 \cdot 2HOH + 2nCsBr \rightarrow 2SiO_2 \cdot Al_2O_3 \cdot nCs_2O + 2nHBr + (2 - n)HOH$$

On the clay surface a liberated water molecule associates with Br^- to form volatile HBr. The volatilization of HBr is responsible for great thermal weight losses of air ground kaolinite CsBr or KBr mixtures, especially at 400°C. A similar thermal hydrolysis occurs with alkali chlorides.

The thermal behaviour of the wet ground CsBr treated kaolinite shows some similarities to the wet ground CsCl treated kaolinite, but differs from that of the unground or ground kaolinite and from the other bromide-treated samples by losing much weight in the temperature range 150–350°C. This is probably due to the loss of intercalated water and, in part, the evolution of HBr which is formed in the interlayer. The loss at 400°C is much smaller than that found for mixed and air ground CsBr- or KBr-treated kaolinite, indicating the absence of a "free" CsBr phase due to the fact that the salt intercalated the clay.

Infrared studies

The effect of CsBr treatment on the IR spectrum of kaolinite

Figure 1 shows the infrared spectrum of untreated kaolinite (subjected only to the initial grinding to pass 80 mesh) and the spectra of CsBr treated kaolinites prepared by the following techniques: (*1*) air grinding, and (*2*) wet grinding. Band positions and assignments for the wet ground sample are summarized in Table 2. The spectra of kaolinite either mixed or air

TABLE 1. Percentage weight loss during the thermal treatment of kaolinite, air ground; kaolinite, air and wet ground with CsCl; kaolinite, mixed, air and wet ground with CsBr; and kaolinite, air ground with KBr (percentage losses for all mixtures are calculated on the basis of kaolinite).

	Kaolinite						
		CsCl mixture		CsBr mixture			KBr mixture,
T (°C)	Air ground	Air ground	Wet ground	Mixed	Air ground	Wet ground	air ground
100	7.64	1.70	6.70	≈0	1.50	7.64	1.45
150	1.85	0.30	3.70	0.30	0.75	3.34	≈0
200	1.30	1.00	2.65	0.96	1.46	4.04	0.95
250	1.80	0.20	3.00	0.60	1.40	5.24	0.75
0–250	12.59	3.20	16.05	1.86	5.11	20.26	3.15
300	≈0	0.25	0.60	≈0	0.25	1.85	0.20
350	1.25	1.90	2.20	4.52	5.11	9.33	1.45
400	3.25	8.31	2.85	14.03	12.12	4.94	15.66
450	1.45	1.75	1.30	4.94	3.50	2.50	8.25
250–450	5.95	12.21	6.95	23.49	20.98	18.62	25.56

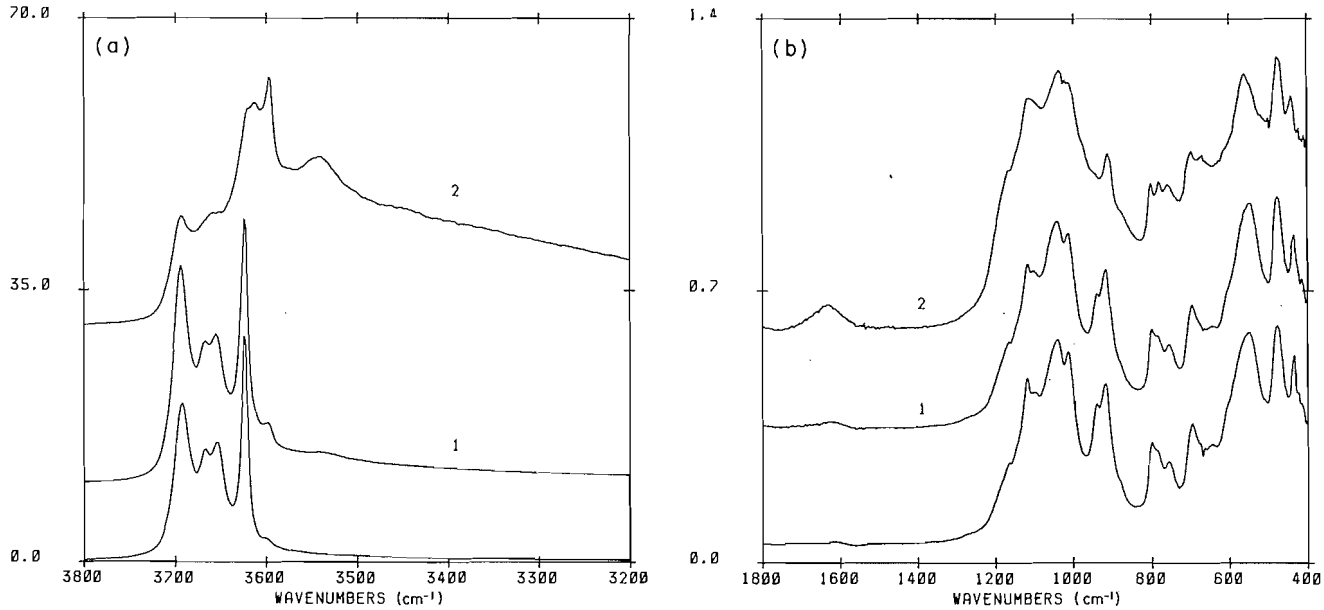


FIG. 1. (*a*) Diffuse reflectance FT-IR spectra of untreated kaolinite (lower curve) and of CsBr–kaolinite mixtures: (*1*) air ground and (*2*) wet ground. The intensity scale is arbitrary, and the curves are offset for clarity. (*b*) Photoacoustic FT-IR spectra of untreated kaolinite (lower curve) and of CsBr–kaolinite mixtures; identification of the samples is the same as in (*a*). Spectra have been ratioed against carbon black, rescaled and shifted in order to prevent overlap.

ground with CsBr are similar to those of unground kaolinite and of kaolinite which has been ground without additives, respectively. Aging of these samples has no effect on their spectra, implying that no intercalation complex was formed with CsBr in these techniques. On the other hand, the spectrum of the kaolinite/CsBr mixture ground under wet conditions shows similarities with that of CsCl treated kaolinite, indicating the intercalation of CsBr and H_2O (1–6). This is manifested by (*a*) diminution of the lattice OH stretching bands A, B, and C and the appearance of a new band A′, which is attributed to a perturbed OH stretching vibration and is characteristic for hydrogen bonded inner surface hydroxyls; (*b*) shifts of Al—OH and Al—O deformation vibrations to lower and higher frequencies, respectively; (*c*) shifts of the Si—O stretching and deformation vibrations; and (*d*) appearance of HOH stretching and bending vibrations which do not occur in the spectrum of untreated kaolinite (Table 2).

The weakening of bands A, B, and C and the appearance of band A′, as well as the shifts of the Al—OH deformation vibrations, indicate that hydrogen bonds are formed between adsorbed water molecules and inner surface hydroxyls; moreover, the shifts of the Si—O vibrations suggest that hydrogen bonds are formed between adsorbed water molecules and inner surface oxygens. However, if this spectrum is compared to

Can. J. Chem. Downloaded from www.nrcresearchpress.com by 198.100.157.202 on 09/07/12
For personal use only.

TABLE 2. Assignment of absorption bands (cm^{-1}) of kaolinite and its complexes with CsCl and CsBr[a]

Band assignment	Symbol	Natural clay	CsCl mixture: Mixed	CsCl mixture: Air ground	CsCl mixture: Wet ground	CsBr mixture, wet ground
AlO—H stretching	A	3692–3693	3690w	—	—	3693w
	Z	3686[b]	3672	3670	3672	
	B	3666–3668	—	—	—	3666vw
	C	3653–3655	—	—	—	3655vw
	D	3622–3624	3616s	3616m	3616sh	3620sh
FeO—H stretching		3601vw[c]	—	—	—	—
AlO—H stretching	A′	—	3601	3601	3599	3597
Intercalated HOH asym. stretching		—	3582	3582	3582	3612
Intercalated HOH sym. stretching		—	3522	3520	3508	3541
Intercalated HOH bending		—	—	—	1641	1630
Si—O stretching	E	1117	1113	1113	1111	1107
	P	1099	—	—	—	—
	F	1040	1038	1036	1030	1034
	G	1013	1015	1011	1009	1011
Al—OH deformation	H	939	941	—	—	—
	I	918	912	908	903	910
	J		781		779	781
	K	756	758	758	760	758
	L	694	690	690	690	697
Al—O deformation		552	563	567	565	561
Si—O deformation		476	476	474	471	473
		434	440	440	440	440

[a]s, m, w, vw, and sh denote strong, medium, weak, very weak, and shoulder, respectively.
[b]From step-scan photoacoustic spectrum (18).
[c]This band cannot be detected in the spectra of the mixtures because of overlap with other bands.

those obtained for CsCl-treated kaolinite, it is obvious that the degree of intercalation was smaller even than that of the aged mixed CsCl–kaolinite (see below). Consequently, bands A, B, and C, although relatively weak, are visible in the spectrum (curve *2*, Fig. 1) whereas band Z, which is located in the envelope of band A, cannot be detected. We tried to increase the period of wet grinding, but this resulted in the amorphisation of the kaolinite framework, as shown by broadening and disappearance of hydroxyl and lattice vibrations.

A band at 3582 cm^{-1} in the spectrum of CsCl-treated kaolinite was previously assigned by Yariv (6) as perturbed bands B and/or C. The 3582 cm^{-1} band does not appear in the spectrum of CsBr-treated kaolinite; instead, a band of similar shape occurs at 3612 cm^{-1}. It is therefore not plausible to assign this absorption either to perturbed band B or to band C.[2] A more satisfactory interpretation would be to assign this band to the asymmetric stretching vibration of HOH coordinated to CsBr, and the 3541 cm^{-1} band to the symmetric stretching vibration of HOH coordinated to this salt. Similarly, the 3582 and 3522 cm^{-1} bands in the spectra of CsCl-treated kaolinite should be assigned as the asymmetric and symmetric stretching vibrations, respectively, of HOH coordinated to CsCl.

Differences greater than 20 cm^{-1} in either the asymmetric or the symmetric stretching frequencies of HOH when CsCl is replaced by CsBr are indications of hydrogen bond formation between the coordinating water molecule and the coordinated halide. Data in the literature on hydrogen bond formation between halides other than F^- and proton donors is rare. However, neutron diffraction experiments for several heavy water electrolyte solutions at various concentrations recently established that the hydration geometry of a chloride is independent of the cation, and that a nearly linear Cl—D—O arrangement occurs with a Cl···O distance shorter than that expected for dipole interactions (14). The nearly linear geometry and the short Cl···O distance support the idea that hydrogen bonds exist between chloride ion and coordinating water molecules in aqueous solutions. Bromide is less electronegative and consequently less effective than chloride, forming weaker hydrogen bonds. The compound $Cs_3Br_3(H_3O^+)(HBr_2^-)$ provides an example in which a hydrogen bond involving Br^- occurs. The O—H···Br distance calculated from van der Waals radii of O and Br is 335 pm whereas the measured distance in this compound is only 304 pm (15).

The effect of CsCl treatment on the IR spectrum of kaolinite

Figure 2 shows the infrared spectra of CsCl-treated kaolinites prepared by the following three techniques: (*1*) mixing, (*2*) air grinding, and (*3*) wet grinding. Band positions are again summarized in Table 2. The mixtures were aged at ambient atmosphere for 3 months before recording the spectra. The appearance and intensity of the different absorption bands in the spectra of mixtures 1 and 2 depend on the aging period whereas the spectrum of mixture 3 hardly changes with time.

The spectra show that all three methods of treatment led to the formation of an intercalation complex. By comparing the three spectra of CsCl-treated kaolinite to the spectrum of the untreated

[2]Second derivative and curve-fitting calculations show that bands B and C occur near 3640 cm^{-1} in spectra of these complexes. These results will be described more fully in a separate publication.

Can. J. Chem. Downloaded from www.nrcresearchpress.com by 198.100.157.202 on 09/07/12
For personal use only.

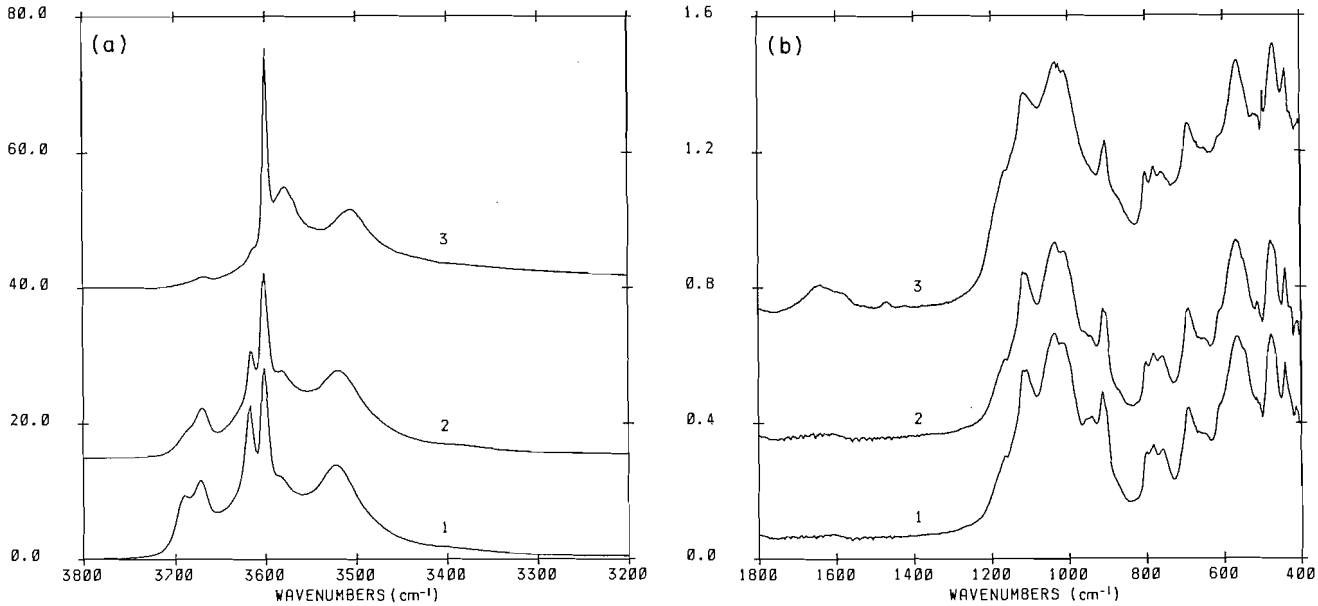


FIG. 2. (*a*) Diffuse reflectance FT-IR spectra of CsBr–kaolinite mixtures: (*1*) dry mixed, (*2*) air ground, and (*301*) *wet ground*. (*b*) Photoacoustic FT-IR spectra of CsBr–kaolinite mixtures; identification of the samples is the same as in (*a*). Plotting strategy is the same as in Fig. 1.

kaolinite, it is possible to follow the degree of intercalation. In the spectrum of sample 1 recorded after a period of 3 months, band A is very weak in comparison to its intensity in the spectrum of untreated kaolinite, but is still observed. The fact that unperturbed band A still occurs in the spectrum indicates that some of the inner surface hydroxyl planes did not react with water molecules. An OH band at about 3684 cm^{-1} (band Z) was previously observed by Michaelian (16) in the Raman spectrum of kaolinite and tentatively assigned as an uncoupled inner surface hydroxyl stretching. This assignment was supported in a separate infrared deuteration study (17). This band is not observed in the conventional IR spectrum of kaolinite because it is located in the envelope of band A. It is, however, observed in the step-scan photoacoustic spectrum of kaolinite (18). This band is clearly observed in the spectrum of aged mixture 1, after the diminution of band A.

In the diffuse reflectance spectrum of sample 2 band A is reduced to a barely identifiable shoulder. A curve-fitting analysis of this spectrum confirms that this band still exists, although with greatly reduced intensity. These data indicate that only very few of the hydroxyl inner surfaces did not react with adsorbed water.

In sample 3 delamination seems to be completed; the water band is broadened, shifted slightly to 3508 cm^{-1}, and its relative intensity is increased. Both kaolinite bands A and D are not observed in the diffuse reflectance spectrum. Based on deuteration studies, band D was assigned to an inner OH vibration (19). As such, it is expected that this band should not be affected by intercalation. The perturbation that is observed in the present study is probably due to the complete delamination of the kaolinite tactoid. The symmetry of a single alumino-silicate layer may be slightly altered relative to the symmetry of the layer in the tactoid, causing band D to become broad and shift slightly to a lower frequency. Since it is located in the envelope of band A′, it may be undetectable in the spectrum. It should be noted that the present spectrum of sample 3 is very similar to the spectrum obtained previously for CsCl-treated halloysite (4). It is therefore concluded that the wet grinding leads to complete delamination and intercalation of the kaolinite.

The three spectra of the CsCl-treated kaolinite show shifts of the lattice vibrations in comparison with the spectrum of the untreated kaolinite. Most of these shifts become progressively greater as the degree of intercalation increases. For example, several of the Si—O stretching and the Al—OH deformation vibrations (bands E, F, G, and I) shift gradually to lower frequencies from sample 1 through sample 2 to sample 3, whereas the Al—O deformation frequency displays the opposite trend. The latter shift may be real, but it may also be possible that it results from incomplete resolution of two vicinal maxima, one arising from the hydrogen bonded layer and one from the layer which did not react with the hydrated salt. In the latter case only sample 3 would yield the true spectrum of the intercalation complex.

The effect of CsI treatment on the IR spectrum of kaolinite

The spectra of kaolinites, either mixed or ground (air or wet) with CsI, are similar to that of kaolinite which has been ground without additives. The same spectrum is obtained even after an aging period of three months in the ambient atmosphere. This indicates that no intercalation complex was formed with CsI.

Discussion

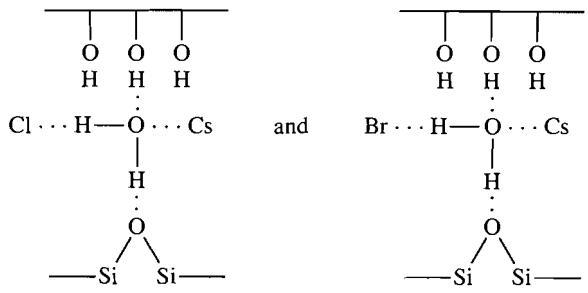
A system consisting of CsCl and kaolinite sorbs water from the atmosphere upon aging, forming an intercalation complex. If the mixture is ground, the formation of the complex is faster than when it is only shaken. If water is added during grinding, the intercalation complex is formed in situ. The present IR study showed that dry grinding of CsBr or CsI with kaolinite at ambient atmosphere did not result in any spectroscopic changes. This indicates that salt or water molecules from the atmosphere do not react with kaolinite to form an intercalation complex. Aging, which improves the intercalation in a CsCl–kaolinite system, does not help in the CsBr– or CsI– kaolinite systems. However, CsBr and water, but not CsI and water, formed a

Can. J. Chem. Downloaded from www.nrcresearchpress.com by 198.100.157.202 on 09/07/12
For personal use only.

kaolinite intercalation complex during wet grinding. It may be concluded that in the intercalation of kaolinite by caesium halide hydrates, the caesium halide salt as a whole is responsible for the intercalation, the activity of the salt decreasing with increasing size of the halide ion.

There are two possible reasons for this phenomenon: (*1*) I^- is too big and cannot penetrate into the interlayer space of the kaolinite, Br^- can penetrate only when forced to do so, whereas Cl^- is small enough to enter between the layers; (*2*) hydrogen bonds between sorbed water molecules and the anions are essential for the intercalation reaction. Such bonds, although weak, can be formed with Cl^-. They are very weak with Br^-, and still weaker and very rare with I^- (15). Our study shows that they are not formed at all in the CsI–kaolinite system. The varying strengths of these hydrogen bonds give rise to the differences which are observed between HOH absorption frequencies in the CsBr system as compared to the CsCl system (Table 2).

The shifts observed for the OH stretching and lattice vibrations in the spectra of the intercalation complexes as compared to the spectrum of untreated kaolinite, as well as the locations of the HOH vibrations in CsCl-and CsBr-treated kaolinite, lead us to suggest the following structures for the intercalaction complexes. A water molecule coordinated to the large Cs cation donates one proton to a siloxane oxygen and the other to the halide, while accepting a proton from an inner surface hydroxyl group:



Conclusions

Intercalation complexes of kaolinite are formed with CsCl or CsBr and water, but not with CsI. The CsBr complex is formed by grinding a mixture of CsBr and kaolinite in the presence of a few drops of water, whereas it is not necessary to add water during grinding with CsCl because water is sorbed from the atmosphere. However, in the presence of water the mechanochemical intercalation of CsCl is fast.

Acknowledgements

S. Y. and A. N. are grateful to the Internal Fund of the Hebrew University for financial support. The donation of the kaolinite sample by Dr. Shlomo Shoval is highly appreciated.

1. S. YARIV. Powder Technol. **12**, 131 (1975).
2. S. YARIV. Clays Clay Miner. **23**, 80 (1975).
3. S. YARIV. J. Chem. Soc. Faraday Trans. I, **71**, 674 (1975).
4. S. YARIV and S. SHOVAL. Clays Clay Miner. **24**, 253 (1976).
5. S. YARIV, E. MENDELOVICI, and R. VILLALBA. Proc. Seventh Intern. Conf. Therm. Anal. Kingston, Canada, 1982. *Edited by* Bernard Miller. **1**, 533 (1982).
6. S. YARIV. Intern. J. Trop. Agri. **4**, 310 (1986).
7. R. L. LEDOUX and J. L. WHITE. Clays Clay Miner. **13**, 289 (1964).
8. O. ANTON and P. G. ROUXHET. Clays Clay Miner. **25**, 259 (1977).
9. E. MENDELOVICI, S. YARIV, and R. VILLALBA. Clay Miner. **14**, 323 (1979).
10. E. MENDELOVICI, R. VILLALBA, and S. YARIV. Isr. J. Chem. **22**, 247 (1982).
11. K. H. MICHAELIAN. Appl. Spectrosc. **43**, 185 (1989).
12. L. HELLER-KALLAI. Clay Miner. **13**, 221 (1978).
13. M. GABOR, L. POEPPL, and E. KOEROES. Clays Clay Miner. **34**, 529 (1986).
14. D. HUGH POWELL, A. C. BARNES, J. E. ENDERBY, G. W. NEILSON, and P. S. SALMON. Faraday Discuss. Chem. Soc. **85**, 1 (1988).
15. N. N. GREENWOOD and A. EARNSHAW. Chemistry of the elements. Pergamon Press, Oxford. 1984. pp. 57–69.
16. K. H. MICHAELIAN. Can. J. Chem. **64**, 285 (1986).
17. K. H. MICHAELIAN, K. BUKKA, and D. N. S. PERMANN. Can. J. Chem. **65**, 1420 (1987).
18. K. H. MICHELIAN. Infrared Phys. **30**, 181 (1990).
19. P. G. ROUXHET, N. SAMUDACHEATA, H. JACOBS, and O. ANTON. Clay Miner. **12**, 171 (1977).

Can. J. Chem. Downloaded from www.nrcresearchpress.com by 198.100.157.202 on 09/07/12
For personal use only.

Internal standards in differential pulse anodic stripping voltammetry

ANGELO RANSIRIMAL FERNANDO AND BYRON KRATOCHVIL
Department of Chemistry, University of Alberta, Edmonton, Alta., Canada T6G 2G2

Received September 27, 1990

ANGELO RANSIRIMAL FERNANDO, and BYRON KRATOCHVIL. Can. J. Chem. **69**, 755 (1991).

The use of lead and cadmium as internal standards for each other in anodic stripping analysis was investigated. Although accuracy was not affected, precision was significantly improved. The surface active agents Triton-X 100 and starch affected the sensitivity of the anodic stripping procedure for lead and cadmium, leading to error if a calibration curve is used. Data for application of the procedure to the analysis of the marine biological reference material LUTS-1 and soil reference materials SO-2, SO-3, and SO-4 are provided.

Key words: internal standard, anodic stripping voltammetry, calibration curve, standard addition, lead determination, cadmium determination.

ANGELO RANSIRIMAL FERNANDO et BYRON KRATOCHVIL. Can. J. Chem. **69**, 755 (1991).

On a étudié la possibilité d'utiliser le plomb et le cadmium comme étalons internes réciproques lors de l'analyse par redissolution anodique. Même si l'exactitude n'est pas affectée, la précision est de beaucoup améliorée. Les agents tensioactifs, comme le Triton-X 100, affectent la sensibilité de la méthode par redissolution anodique pour le plomb et le cadmium; il en résulte qu'une erreur est introduite lorsqu'on utilise une courbe de calibration. On fournit des données concernant l'application de la méthode à l'analyse du LUTS-1, le produit de référence en biologie marine, et des matériaux de référence des sols, SO-2, SO-3 et SO-4.

Mots clés: étalon interne, voltammétrie par redissolution anodique, courbe de calibration, addition de référence, détermination du plomb, détermination du cadmium.

[Traduit par la rédaction]

Introduction

Although internal standards have been used in a variety of analytical techniques such as polarography to compensate for variations associated with poorly reproducible operations, their application in anodic stripping analysis was not described until 1988 by Pratt and Koch (1), who used indium as an internal standard along with a calibration curve for the quantification of several trace metals in water samples. While this approach has wide applicability under conditions where the background is constant for sample and standards, it is not so satisfactory when the background varies in composition. Voltammetric and potentiometric techniques require direct contact of the sample solution with the probe or the sensor and are more sensitive to matrix matching problems than many other methods.

Pratt and Koch (1) showed that use of an internal standard tends to eliminate random errors originating from the variations in mercury drop size and stirring. This work was to evaluate the merits of a combination of an internal standard and a standard addition procedure, using either lead or cadmium as analyte and the other as internal standard. The samples were biological materials and soils that had to be digested under conditions where the resulting solutions did not provide highly reproducible backgrounds.

Experimental

Instrumentation

A PAR model 303 stationary mercury drop electrode (SMDE) and a PAR Model 174A polarographic analyzer coupled to a MACSYM 150 (Analog Devices) microcomputer was used to perform all anodic stripping measurements. A detailed description of the instrument system appears elsewhere (2).

Reagents

Distilled deionized water was obtained from a Barnsted Bantam still. Lead and cadmium levels in acidified solutions (10^{-2} M HNO_3) were well below the detection limit (ca. 0.03 ppb) under the analytical conditions used.

Nitric and perchloric acids (ultra pure grade, Seastar Chemicals, Sidney, B.C., Canada) and sodium hydroxide (suprapure grade, Merck) were used as received.

An aqueous stock solution of KNO_3 was prepared from reagent grade salt and further purified by bulk electrolysis in a large volume cell with a mercury cathode. Triply distilled mercury was purified in a similar cell via anodic oxidation (2). Reagent grade potassium chloride, further purified by recrystallization and crystal adsorption, was used for the salt bridges (3). Reagent grade acetic acid was purified by isopiestic distillation (4–6). High purity nitrogen was passed through acidified vanadium(II) chloride/zinc amalgam scrubbers followed by aqueous washing towers to remove trace oxygen (7). All other chemicals were reagent grade.

Stock solutions (1000 ppm) of $Pb(NO_3)_2$ and $Cd(NO_3)_2$ (analytical grade) were used to prepare working standards.

Digestion of LUTS-1 samples

The marine biological reference material LUTS-1, obtained from the Marine Standards Analytical Program, Division of Chemistry, National Research Council of Canada, Ottawa, Canada, is a slurry obtained through mechanical homogenization of lobster hepatopancreas tissue. The bottles were sonicated for 30 min prior to opening and before removal of subsequent samples. Approximately 1-mL portions were pipetted directly from the bottles and weighed to ±0.01 mg on a Mettler H-51 semimicro balance into Savillex 60-mL Teflon PFA digestion vessels (Savillex Corp., Minnetonka, MN). After adding 3 mL of nitric acid, the vessels were closed and placed on a turntable in a microwave oven (Sears Kenmore, Model No. 88760) and heated for 2 min at 100% power followed by 10 min at 15% power. After cooling, the samples were transferred to 10-mL volumetric flasks and diluted to volume with water.

A 1-mL portion of this HNO_3 digested solution was placed in a Teflon PFA voltammetric cell (Princeton Applied Research GO 174) with 1 mL of $HClO_4$ and heated under cover (Teflon TFE cover plate) for 2 h at ca. 200°C. The covers were then removed and the solution was allowed to evaporate to dryness (2 to 3 h) at a temperature near 240°C. Heating was done on a sandbath covered with aluminum foil to prevent contamination and adherence of sand particles to the hot Teflon. The evaporation procedure was carried out in a stainless steel fumehood designed to handle perchloric fumes. (Caution: the usual precautions must be taken when working with hot concentrated $HClO_4$.)

Can. J. Chem. Downloaded from www.nrcresearchpress.com by 198.100.157.202 on 09/07/12
For personal use only.

Residue from the above procedure was dissolved in 5 mL of 0.01 M HNO_3 pipetted directly into the cell, a Teflon-coated stirbar was added, and the cell was placed in the electrode assembly for subsequent anodic stripping analysis.

Digestion of standard soils SO-2, SO-3, and SO-4

These reference materials, obtained from Canadian Reference Materials Project, Energy Mines and Resources Canada, were digested with nitric, perchloric, and hydrofluoric acids according to recommended procedures (2, 8). Briefly, 1-g portions, dried at 110°C overnight, were weighed into 100-mL Teflon beakers, heated with 20 mL of concentrated HNO_3 under cover for 30 min at 100 to 150°C, allowed to cool, then treated with 20 mL of concentrated $HClO_4$, followed by another 30 min of heating at 200 to 250°C. Subsequent cooling was followed by 20 mL of concentrated HF and 1-h heating under cover at 80°C. The resultant solution was evaporated to near dryness, dissolved in 25 mL of 1 M HNO_3, then diluted with water to 50 mL in a polypropylene volumetric flask.

Anodic stripping voltammetry

Anodic stripping analyses of LUTS-1 samples for cadmium were performed after adding 20 μL of 5 ppm Pb standard solution to 5-mL portions of the digestion solution. Since the final step of the digestion was performed in a voltammetric cell no sample transfer was needed.

Analyses of digested standard soil samples for lead were done in acetate buffer containing 0.1 M acetic acid and 0.1 M KNO_3 which was adjusted to pH 4 with sodium hyroxide. A 100-μL portion of the digested solution was added to 5 mL of the buffer solution in a voltammetric cell. To serve as internal standard 2 μL of 20 ppm Cd standard solution was added.

In all analyses a 5-min deaeration period was followed by a 2-min deposition step at −0.8 V vs. SCE. A differential pulse anodic scan was initiated after a 0.5-min equilibration. Measurement conditions were scan rate 5 mV/s, modulation 25 mV, and clock 1 s. Solutions were stirred magnetically during the deposition step. Three measurements were made on each solution.

Data aquisition and peak height evaluation was done using a Macsym 150 microcomputer and associated programs (2).

Results and discussion

In general the results obtained confirmed the findings of Pratt and Koch (1) with respect to precision of the anodic stripping determination. Data shown in Table 1 for a solution prepared using standard solutions of cadmium and lead illustrate this point. While relative standard deviations for individual peaks are around 7%, those for peak ratios drop to around 0.1%. This increase in precision stems from elimination or reduction of variations associated with stirring conditions and reproducibility of the mercury drops. Since a normal laboratory magnetic stirrer was used, reproducibility of stirring was the least controlled parameter in the system. In general, relative standard deviations of the order of 10% are typical (2) for ppb level determinations using anodic stripping voltammetry. Use of an internal standard, therefore, provides a considerable increase in the precision of the measurements. It is important, however, to realise that this improvement stems from the elimination of variability associated with parameters that cannot be readily controlled, rather than from inherent chemical or physical limitations.

Results obtained from analyses of digested LUTS-1 samples for cadmium using lead as an internal standard are listed in Table 2; those for analyses of standard soils SO-2, SO-3, and SO-4 appear in Tables 3, 4, and 5. These were obtained using at least two standard additions of either lead or cadmium. Additions were made directly into the cell with a micropipet. For LUTS-1 5 μL additions of a 20 ppm standard cadmium solution resulted in a 20 ppb change. For SO-2, SO-3, and SO-4, 5 μL additions of a 5 ppm standard lead solution increased the lead level in the solution by 5 ppb for each addition. The results given in Table 2 to 5 were calculated by procedures normally employed for standard addition calculations, using as the measured parameter either the direct peak height (μA) of the analyte or the ratio of the analyte peak height to that of the internal standard.

TABLE 1. Peak height and peak ratio data for analysis by anodic stripping of a solution containing 40 ppb cadmium and 20 ppb lead in 0.5 M KNO_3 and 0.01 M HNO_3

	Peak heights		Peak ratio
	Cd (μA)	Pb (μA)	Cd/Pb
	5.07	1.15	4.41
	4.58	1.04	4.40
	4.40	1.00	4.40
Mean	4.68	1.06	4.40
Std. dev.	0.35	0.08	0.004
RSD (%)	7.4	7.3	0.1

In all cases the use of an internal standard improves precision. It should be noted, however, that the accuracy of the determination when peak heights are used without the internal standard does not seem to be affected provided one acquires sufficient data. In general, triplicate measurements per sample tend to provide means that agree well between samples. Thus use of an internal standard improves precision markedly, but does not affect the accuracy of the overall procedure.

In trace analysis the definition of accuracy is affected by the width of the confidence interval. Improvement in the precision of an analysis has an important effect on the reliability of the determination. Therefore, even though in a statistical sense accuracy may not have been improved, the improvement in precision possible with an internal standard may significantly improve the reliability of a final result without requiring large numbers of analyses.

Table 6 shows results obtained for SO-4 analyses using a calibration curve obtained by adding appropriate amounts of a 5-ppm lead standard solution directly to 5 mL of 5 ppb cadmium in acetate buffer. Anodic stripping voltammograms obtained for these solutions were used to prepare two calibration curves, one of lead peak height vs. lead concentration and the other of the ratio of lead peak height/cadmium peak heights vs. lead concentration. The former calibration curve was used with peak height values obtained for soil SO-4 to calculate results reported under the "without internal standard" heading in Table 6. The lead/cadmium peak height ratios obtained for soil SO-4 with the latter calibration curve gave the values reporetd under the "with internal standard" heading. In this study the SO-4 solutions were also spiked to a level of 5 ppb with respect to cadmium.

It can be seen that agreement between the results obtained from standard additions and those obtained from calibration curves using peak size measurements is poor. This lack of agreement stems from the sensitivity of the direct method to the sample matrix; here a 100-μL aliquot of digested solution was added to 5 mL of acetate buffer. On the other hand, data from peak ratio measurements for the different sample matrices are in good agreement. Thus, when employing a calibration curve, use of an internal standard provides improved accuracy. In light of this result we consider the loss of accuracy in the analysis of

Can. J. Chem. Downloaded from www.nrcresearchpress.com by 198.100.157.202 on 09/07/12
For personal use only.

TABLE 2. Analysis of LUTS-1 for cadmium by anodic stripping analysis using lead as internal standard. The lead amount in each solution was increased to 20 ppb by addition of standard lead solution. Certified cadmium level in LUTS-1 is 2.12 ± 0.15 ppm

	From peak height			From peak ratio		
Sample	Cd content (ppm)	Std. dev.	RSD (%)	Cd content (ppm)	Std. dev.	RSD (%)
I	2.85	0.46	16	1.93	0.02	0.95
II	1.29	0.04	2.8	1.92	0.02	0.84
III	5.01	0.65	13	1.87	0.02	1.27
Mean	3.05			1.91		
Std. dev.	1.87			0.03		
RSD (%)	61			1.7		

TABLE 3. Anodic stripping data for soil reference material SO-2 (cadmium (5 ppb) was added to the analytical solution to serve as internal standard, certified lead level in SO-2 is 21 ± 4 ppm)

	From peak height			From peak ratio		
Sample	Pb content (ppm)	Std. dev.	RSD (%)	Pb content (ppm)	Std. dev.	RSD (%)
I	17.9	0.3	2	22.6	1.4	6
II	24.6	0.9	4	21.9	1.2	6
III	20.9	1.0	5	19.1	0.4	2
Mean	21.1			21.2		
Std. dev.	3			2		
RSD (%)	16			9		

TABLE 4. Anodic stripping data for soil reference material SO-3 (cadmium (5 ppb) was added to the analytical solution to serve as internal standard, certified lead level in SO-2 is 14 ± 3 ppm)

	From peak height			From peak ratio		
Sample	Pb content (ppm)	Std. dev.	RSD (%)	Pb content (ppm)	Std. dev.	RSD (%)
I	14.6	1.2	8	14.6	0.1	0.9
II	16.7	2.4	14	13.1	0.2	2
III	13.4	0.2	1	14.5	0.4	3
Mean	14.9			14.1		
Std. dev.	2			0.9		
RSD (%)	11			6		

SO-4 samples to stem from a process that affects equally either the deposition or the oxidation of lead and cadmium. Trace level organic compounds that adsorb on to the mercury surface can interfere. In any case an interference that selectively affects one of the metals will interfere with the use of a calibration curve approach, leading to a systematic error. Standard additions results will, however, still be valid.

To investigate the effect of organic adsorbents on the internal standard procedure, several experiments were carried out using acetate buffer solutions containing lead and cadmium in parts per billion levels, with and without added Triton X-100, a known surface active agent. Addition of Triton X-100 (in the form of a 0.06% (v/v) aqueous solution) in μL quantities to 5 mL of a solution containing Pb and Cd led to a decrease in peak height for both metals. Lead showed a linear decrease, but cadmium did not, which suggests that different forms of inhibiting actions are operating on these metals.

Under these conditions the ratios of the lead and cadmium signals varied significantly with concentrations of both metals and surfactant, confirming the earlier conclusion. Triton-X has been regarded as a neutral surface active agent in polarography, with an ability to form a uniform adsorbed organic layer upon the mercury surface. If the presence of adsorbed surfactant inhibited movement of both Cd and Pb between bulk solution

Can. J. Chem. Downloaded from www.nrcresearchpress.com by 198.100.157.202 on 09/07/12
For personal use only.

TABLE 5. Anodic stripping data for soil reference material SO-4 (cadmium (5 ppb) was added to the analytical solution to serve as internal standard, certified lead level in SO-4 is 16 ± 3 ppm)

	From peak height			From peak ratio		
Sample	Pb content (ppm)	Std. dev.	RSD (%)	Pb content (ppm)	Std. dev.	RSD (%)
I	18.2	0.8	5	15.3	0.2	1
II	15.9	2.2	14	13.6	0.2	2
III	10.0	1.6	15	15.2	0.2	1
Mean	14.7			14.7		
Std. dev.	4			1		
RSD (%)	29			7		

TABLE 6. Comparison of results obtained using a calibration curve with and without internal standard for determination of the lead content in the soil reference material SO-4 (cadmium (5 ppb) was added to the analytical solution to serve as internal standard, certified lead level in SO-4 is 16 ± 3 ppm)

	Without internal standard (peak ht.)		With internal standard (peak ratio)	
Sample	In solution (ppb)	In sample (ppm)	In solution (ppm)	In sample (ppb)
I	2.5	6.3	5.5	13.5
II	3.1	7.7	5.9	14.6
III	2.3	5.8	6.3	15.6
Mean		6.6		14.6
Std. dev.		1		1
RSD (%)		15		7

and the interfacial region to a similar extent, a constant Pb/Cd signal ratio with changing surfactant level should be observed. We observed, however, that the Pb/Cd signal ratio shows a complex dependence on the level of surfactant. Slower charge transfer kinetics exhibited by cadmium in aqueous media and possible potential dependence of the adsorption energy can be suggested as factors responsible for this observation. Similar results were observed upon addition of starch, though μL quantities of a 10% starch solution were needed to yield an observable change in signal level.

In light of these results the use of an internal standard/calibration curve approach with undigested environmental materials such as natural water may be affected by the presence of surface active macromolecules. On the other hand, the favorable results obtained for digested SO-4 soil samples indicate the applicability of this approach to samples that have been treated to destroy all potentially interfering macromolecules. Application of the standard addition procedure to peak heights obtained for a 9-ppb lead solution containing 2 μL of 0.06% Triton-X per 5 mL resulted in a value of 7.6 ± 0.5 ppb, while the same solution, using peak ratios with Cd as the internal standard, gave a value of 8.9 ± 0.1 ppb. This indiactes the merits of using an internal standard in a standard addition procedure.

In summary, we observe a significant improvement in precision in anodic stripping analytical data when an internal standard is employed. Whether use of this approach eliminates interferences to an extent sufficient to recommend replacement of standard addition procedures with a calibration curve depends on the nature of the sample matrix, but is likely to lead to improved results in many cases.

Acknowledgements

We thank Norine Motkosky for the microwave digestion of the LUTS-1 samples and Professor James Plambeck for providing the electroanalytical instrumentation. Financial support by the Natural Sciences and Engineering Research Council of Canada and the University of Alberta is gratefully acknowledged.

1. K. W. PRATT and W. F. KOCH. Anal. Chim. Acta, **215**, 21 (1988).
2. A. R. FERNANDO. Ph.D. Thesis, University of Alberta, Edmonton, Alta., Canada. 1988.
3. R. G. CLEM, G. LITTON, and L. D. ORNELAS. Anal. Chem. **45**, 1306 (1973).
4. A. MIZUIKE. Enrichment techniques for inorganic trace analysis. Springer Verlag, New York. 1983.
5. J. W. MITCHELL. Talanta, **29**, 993 (1982).
6. M. ZIEF and J. W. MITCHELL. Contamination control in chemical analysis. John Wiley and Sons, New York. 1985.
7. Application Note D-2. Deaeration.... why and how, Princeton Applied Research Corporation. 1980.
8. J. A. MCKEAGUE. Manual on soil sampling and methods of analysis. 2nd ed. Canadian Society of Soil Science. 1978.

Can. J. Chem. Downloaded from www.nrcresearchpress.com by 198.100.157.202 on 09/07/12
For personal use only.

COMMUNICATION

Bipolar charge carrier transport in amorphous molecular solid solution of arylamine and diphenoquinone derivatives

YASUHIRO YAMAGUCHI, TAKAHIRO FUJIYAMA, AND MASAAKI YOKOYAMA[1]

Chemical Process Engineering, Faculty of Engineering, Osaka University, Yamadaoka, Suita, Osaka 565, Japan

Received June 22, 1990[2]

YASUHIRO YAMAGUCHI, TAKAHIRO FUJIYAMA, and MASAAKI YOKOYAMA. Can. J. Chem. **69**, 759 (1991).

Amorphous molecular composites of *N,N,N',N'*-tetra(*m*-tolyl)-1,3-diaminobenzene as an electron donor and 3,5-dimethyl-3',5'-di-*tert*-butyl-4,4'-diphenoquinone as an electron acceptor have been found to be capable of transporting both hole and electron. Based on drift mobility measurements, it is demonstrated that the donor and acceptor components function independently as hole- and electron-hopping sites, respectively, with no electronic interaction between them.

Key words: bipolar charge transport, arylamine, diphenoquinone, molecular solid solution.

YASUHIRO YAMAGUCHI, TAKAHIRO FUJIYAMA et MASAAKI YOKOYAMA. Can. J. Chem. **69**, 759 (1991).

On a observé qu'un matériau composite moléculaire amorphe de *N,N,N',N'*-tétra(*m*-tolyl)-1,3-diaminobenzène agissant comme donneur d'électron et de 3,5-diméthyl-3',5'-di-*tert*-butyl-4,4'-diphénoquinone agissant comme accepteur d'électron peut transporter des trous ainsi que des électrons. Sur la base de mesures de la mobilité, on a démontré que les composantes donneur et accepteur respectivement agissent indépendamment comme sites de saut de trou et d'électron et qu'il n'existe aucune interaction électronique entre elles.

Mots clés : transfert de charge bipolaire, arylamine, diphénoquinone, solution solide moléculaire.

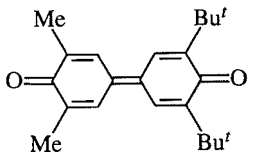
[Traduit par la rédaction]

Amorphous organic thin films have attracted much attention as a class of charge transport materials from both phenomenological and technological viewpoints. Most of such materials, however, are provided largely in the form of polymers or dispersions of transport-active molecules in inert polymeric binders, since generally low molecular weight organic compounds have no amorphous film forming capability. Only a few studies have been reported on charge transport in amorphous molecular solids (1–4). Amorphous molecular materials are not only important for the theoretical study of the transport mechanism, but are also very promising in a growing field of optoelectronics, where materials are required that permit easy film processibility by vacuum deposition or the solvent-cast technique.

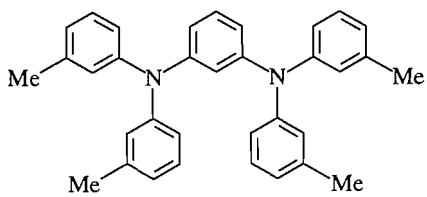
We present herein a novel class of amorphous molecular materials, i.e., solid solutions of *N,N,N',N'*-tetra(*m*-tolyl)-1,3-diaminobenzene (PDA) and 3,5-dimethyl-3',5'-di-*tert*-butyl-4,4'-diphenoquinone (MBDQ), which function as bipolar-charge (i.e., hole and electron) transport materials. We believe that the present work introduces the first molecular material in which both hole and electron mobilities have been measured in an amorphous state.

PDA was synthesized by the Ullmann condensation of 1,3-diaminobenzene and *m*-iodotoluene and purified by column chromatography on alumina and vacuum distillation (5). MBDQ, synthesized by the oxidative coupling of 2,6-dimethylphenol and 2,6-di-*tert*-butylphenol, was purified by column chromatography on silica gel and recrystallization from hexane (6).

Molecularly dispersed polymeric materials of charge-transporting small compounds are well known as the most successful class of functional organic materials. A large number of *hole* transport molecules that have high polymer compatibility have been reported and some of them form stable amorphous solids in



MBDQ



PDA

themselves (1–3). On the contrary, a limited number of *electron* transport molecules are known (4, 6–9) and, among these, 2,4,7-trinitro-9-fluorenone (TNF) is the only example whose electron mobility (although very unstable) has been measured in the amorphous solid (4).

Our previous studies revealed that PDA and MBDQ are capable of transporting hole and electron, respectively, in their polymeric dispersions (5, 6). PDA forms a stable amorphous state (3), but MBDQ itself does not. Fortunately, the mixture of PDA and MBDQ forms amorphous composite films from the solvent-cast method by the wired-bar technique. The amorphous films incorporating less than about 60 wt.% of MBDQ are relatively stable and show few signs of crystallization over several weeks at room temperature. Using differential scanning calorimetry, PDA and the composites were found to show a glass transition near 300 K. It is interesting that no charge transfer absorption appeared in the composite films, which is presumably because of no close contact due to the non-planarity of PDA and the presence of the bulky substituents in MBDQ.

[1]Author to whom correspondence may be addressed.

[2]Revision received December 19, 1990.

Printed in Canada / Imprimé au Canada

Can. J. Chem. Downloaded from www.nrcresearchpress.com by 198.100.157.202 on 09/07/12
For personal use only.

Can. J. Chem. Downloaded from www.nrcresearchpress.com by 198.100.157.202 on 09/07/12
For personal use only.

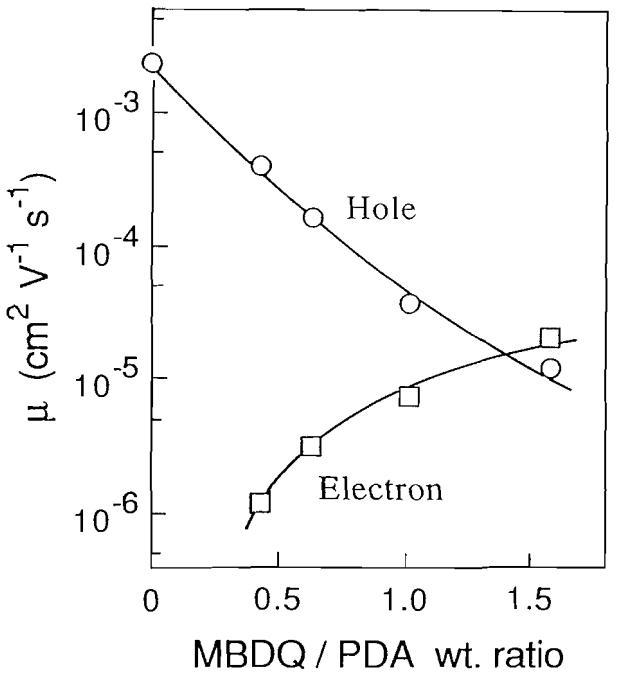


FIG. 1. The dependence on composition of the hole (○) and electron (□) mobilities in molecular composite films (thickness ~10 μm) of PDA and MBDQ; measured in a field of 5×10^5 V cm^{-1} at room temperature.

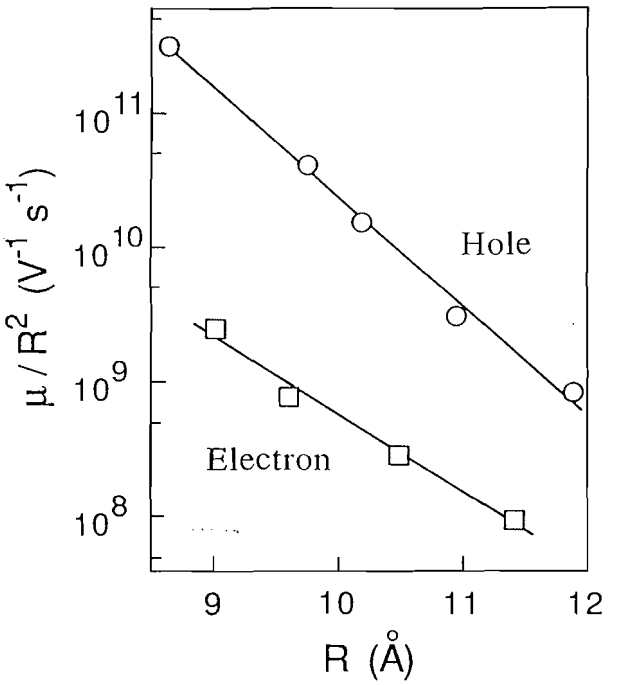


FIG. 2. The hole (○) and electron (□) mobilities as a function of the average intermolecular distance R of PDA and MBDQ, respectively. R for each component was calculated according to the equation $R = (M/NdC)^{1/3}$, where M is the molecular weight, N Avogadro's constant, d the density (1.2 g cm^{-3} for both), and C the fractional weight concentration.

As a result, PDA and MBDQ are each expected to function independently in the composite films. To our knowledge, MBDQ is the first electron-transporting electron acceptor that is compatible with hole-transporting electron donors, such as aromatic amine and hydrazone derivatives, with no or little charge transfer interaction.

The hole and electron transport properties of the amorphous composite films were examined by the standard time-of-flight method using a nitrogen gas laser pulse. Figure 1 shows the composition dependence of the hole and electron drift mobilities. The hole mobility increases, predominantly, with an increase in the PDA content and the electron mobility also increases with an increase in the MBDQ content. A composite film composed of ca. 40 wt.% PDA and 60 wt.% MBDQ exhibits almost the same hole and electron mobilities, which both exceed 10^{-5} cm^2 V^{-1} s^{-1} in an electric field of 5×10^5 V cm^{-1} at room temperature. These values are about 100 times as high as those of the charge transfer complex of poly(*N*-vinylcarbazole) (PVK) and TNF, a well-known bipolar charge transporting amorphous organic material (7). We believe that the high mobility of the present composite originates from no charge transfer interaction, as well as the excellent charge-transporting nature of both PDA and MBDQ, since it was reported that charge transfer complexation reduces charge-transporting ability in the PVK–TNF system (7). The variation of the mobilities with the composition gives important information about the nature of the transport mechanism. The strong dependence on composition of the mobilities shown in Fig. 1 suggests the intermolecular hopping mechanism through each component. For a hopping mechanism, the mobility μ can be expressed as

$$[1] \quad \mu/R^2 \propto \exp(-2R/R_0)$$

where R is the average intermolecular distance hopped and R_0 is a constant defined as the localization radius for a charge carrier (7). The data from Fig. 1 are replotted in Fig. 2 according to eq. [1]. Each plot for PDA and MBDQ gives a good fit to the form of eq. [1]. Moreover, the localization radii (1.1 and 1.5 Å) for hole and electron are approximately the same as those (1.3 and 1.5 Å) of PDA and MBDQ dispersed separately in polycarbonate.

From these results, we conclude that PDA and MBDQ function independently as hole- and electron-hopping sites, respectively, even in their molecular composite films. The details of bipolar charge transport properties in the amorphous solid solution, including the activation energy for hopping conduction, will be presented in a forthcoming paper.

1. W. D. GILL. Energy and charge transfer in organic semiconductors. *Edited by* K. Masuda and M. Silver. Plenum Press, New York. 1974. p. 137; H. KITAYAMA, M. YOKOYAMA, and H. MIKAWA. Mol. Cryst. Liq. Cryst. **69**, 257 (1981).
2. M. STOLKA, J. F. YANUS, and D. M. PAI. J. Phys. Chem. **88**, 4707 (1984).
3. K. YOKOYAMA, S. NOTSU, and M. YOKOYAMA. J. Chem. Soc. Chem. Commun. 805 (1990).
4. W. D. GILL. Amorphous and liquid semiconductors. *Edited by* J. Stuke and W. Brennig. Wiley and Son Inc., New York. 1973. p. 901.
5. M. YOKOYAMA. 30th Anniversary Conf. Soc. Electrophotography Jpn. May, 1988. Tokyo. Preprint.
6. Y. YAMAGUCHI, H. TANAKA, and M. YOKOYAMA. J. Chem. Soc. Chem. Commun. 222 (1990).
7. W. D. GILL. J. Appl. Phys. **43**, 5033 (1972).
8. B. S. ONG, B. KEOSHKERIAN, T. I. MARTIN, and G. K. HAMER. Can. J. Chem. **63**, 147 (1985).
9. R. O. LOUTFY, B. S. ONG, and J. TADROUS. J. Imaging Sci. **29**, 69 (1985).

072240018

Obtention de cyclopropanes *gem*-dicarboxylate par cyclocondensation de carbanions bromo- et chloromalonate sur des accepteurs de Michaël

JEAN-CHRISTOPHE LE MENN ET ANDRÉ TALLEC

Laboratoire d'électrochimie, Unité associée au Centre national de la recherche scientifique, n° 439, Université de Rennes, Campus de Beaulieu, F-35042 Rennes CEDEX, France

ET

JEAN SARRAZIN[1]

Laboratoire d'électrochimie et chimie analytique, Université des sciences et techniques du Languedoc, École nationale supérieure de chimie, 8 rue de l'École normale, F-34053 Montpellier CEDEX, France

Reçu le 27 août 1990

JEAN-CHRISTOPHE LE MENN, ANDRÉ TALLEC et JEAN SARRAZIN. Can. J. Chem. **69**, 761 (1991).

Des cyclopropanes *gem*-dicarboxylate sont préparés par réaction de cyclocondensation d'un carbanion chloro- ou bromomalonate sur des alcènes électrophiles. Le carbanion peut résulter de la déprotonation du monohalogénomalonate par du carbonate de potassium en suspension dans le THF; le chloromalonate conduit alors à de meilleurs rendements. L'influence de la nature et du nombre de substituants portés par l'alcène a été étudiée. Lorsque des réactions parasites (en particulier la protonation d'intermédiaires anioniques par le monohalogénomalonate) peuvent se produire, de meilleurs rendements sont obtenus en formant le carbanion par réduction électrochimique du dihalogénomalonate en présence d'alcène.

Mots clefs : halomalonates, cyclopropane *gem*-dicarboxylates, électroréduction.

JEAN-CHRISTOPHE LE MENN, ANDRÉ TALLEC, and JEAN SARRAZIN. Can. J. Chem. **69**, 761 (1991).

Cyclopropane *gem*-dicarboxylates are prepared through cyclocondensation of chloro or bromomalonate carbanion and electrophilic alkenes. The carbanion can be formed in THF by deprotonation of the monohalomalonates with powdered potassium carbonate; the chloromalonate always leads to better yields. The influence of the nature and the number of substituents on the alkene reactivity has been investigated. If side reactions (for instance protonation of anionic intermediates by halomalonate) can take place, better yields are obtained when the carbanion is generated by electroreduction of dihalomalonate in the presence of the Michael acceptor.

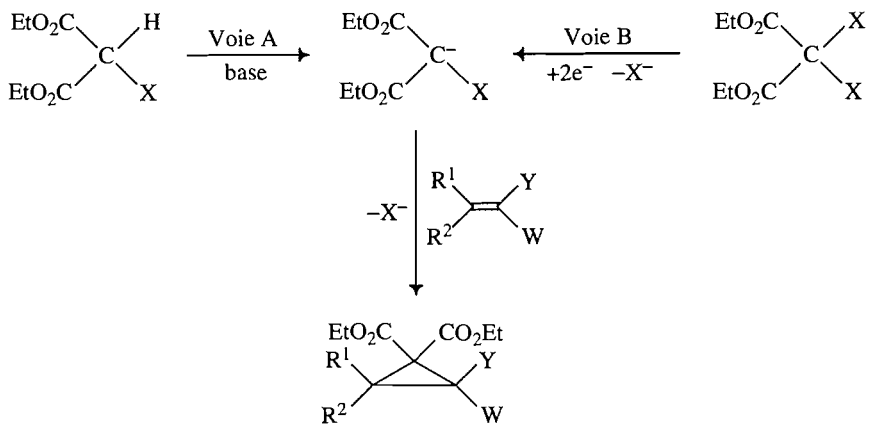
Key words: halomalonates, cyclopropane *gem*-dicarboxylates, electroreduction.

Introduction

Les cyclopropanes électrophiles et plus particulièrement les cyclopropanes *gem*-dicaboxylate sont des intermédiaires de synthèse intéressants. Sous l'action d'un nucléophile, ils sont susceptibles de subir une réaction d'ouverture du cycle, constituant souvent une étape-clé dans la synthèse de certains hétérocycles ou encore dans la chimie des stéroïdes; deux revues ont été consacrées à ce type d'application (1). Ainsi, récemment, des cyclopropanes *gem*-dicarboxylate, substituées par un groupement carbonyle, ont été utilisés pour la préparation de lactones bicycliques, précurseurs de produits d'intérêt pharmaceutique (2).

Les synthèses de ces cyclopropanes se sont développées selon deux approches : (i) soit par une réaction d'addition, sur un alcène *gem*-dicarboxylate, de réactifs variés : diazo-composés (3), anions nucléophiles (4), carbanions porteurs d'un groupe nucléofuge (5); (ii) soit à partir de dérivés du malonate : carbanion malonate (6), radical bromomalonate (7), carbanions halogénomalonate (8–11).

Cette dernière voie d'accès aux cyclopropanes *gem*-dicarboxylate met en jeu l'attaque nucléophile du carbanion sur un accepteur de Michaël (schéma 1) :



(X = Cl ou Br)

SCHÉMA 1

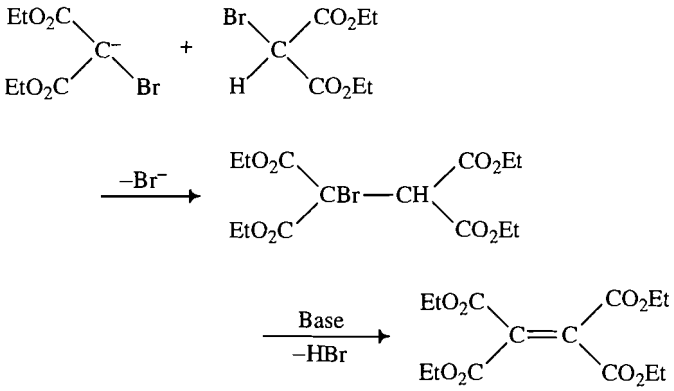
1. Auteur à qui adresser toute correspondance.

Printed in Canada / Imprimé au Canada

Can. J. Chem. Downloaded from www.nrcresearchpress.com by 198.100.157.202 on 09/07/12
For personal use only.

Can. J. Chem. Downloaded from www.nrcresearchpress.com by 198.100.157.202 on 09/07/12
For personal use only.

La réaction, réalisée par voie chimique (Voie A), a fait l'objet de travaux ponctuels (8–11), mais aucune étude systématique ne lui a été consacrée; de plus, elle n'a pratiquement été envisagée qu'à partir du carbanion bromomalonate, l'anion chloré n'ayant, à notre connaissance, donné lieu qu'à un essai préliminaire (8). En règle générale, les rendements obtenus à partir du bromomalonate ne sont pas très élevés, que la réaction soit conduite en milieu homogène (8), à l'aide de fluorures solides en suspension dans les réactifs liquides (6*d*) ou dans les conditions de catalyse de transfert de phase liquide–liquide (10); ces rendements limités résultent de l'existence d'une réaction, compétitive de la cyclocondensation, conduisant à l'éthylène tétracarboxylate :



Pour notre part, nous avons montré qu'il est possible de réaliser la cyclocondensation par voie électrochimique (Voie B) : le carbanion est formé par réduction biélectronique du dibromo- ou du dichloromalonate (12); cette étude a mis en évidence d'une part un effet de cation très prononcé sur le comportement de l'anion bromomalonate, d'autre part l'obtention de rendements plus élevés avec le carbanion chloré.

Ces résultats nous ont incités à rechercher des conditions optimales de formation du carbanion par déprotonation d'un halogénomalonate. Nous nous sommes orientés vers l'utilisation d'une base inorganique solide en suspension dans un solvant aprotique suffisamment volatil. Des essais préliminaires nous ont conduits à retenir le système K_2CO_3/THF.

Sur le plan synthétique, deux objectifs ont guidé notre démarche : (1) explorer la réactivité d'une gamme d'alcènes variés (les résultats sont rassemblés dans les tableaux 1 et 2); (2) exploiter la réactivité supérieure du carbanion chloré pour améliorer la sélectivité et le rendement de la réaction.

Enfin, lorsque des réactions secondaires de protonation d'intermédiaires anioniques par l'halogénomalonate ont été observées, nous avons utilisé la méthode électrochimique de formation du carbanion.

Résultats et discussion

1. Alcènes monoactivés

1.1 Limitations synthétiques de la méthode

Le tableau 1 regroupe les résultats obtenus par réaction mole à mole des halogénomalonates et des alcènes porteurs d'un seul groupement électroattracteur.

De l'examen de ce tableau, il ressort que les alcènes qui ne portent pas d'autre substituant (**1**–**3**) conduisent à d'excellents rendements en cyclopropane (**1***a*–**3***a*), et que la réaction est plus rapide avec le chloromalonate. Ces résultats sont comparables à ceux obtenus par voie électrochimique (12).

Les alcènes **4**–**9**, porteurs d'un substituant sur le carbone éthylénique en β du groupement activant, présentent des réactivités variées. Dans cette série, l'activation par le groupement attracteur croît dans l'ordre (8) : -CN< -COR< -CHO< $-NO_2$. D'autre part, la présence du second substituant sur la double liaison ralentit la réaction de cyclocondensation, l'effet du groupement aryle étant plus marqué que celui du groupement méthyle. Bien que les réactions ne soient pas toujours quantitatives, les rendements en cyclopropanes **4***a*–**8***a* observés sont nettement plus élevés que ceux obtenus avec les méthodes précédemment rapportées (8–10). Par ailleurs, le tableau 1 montre que le carbanion bromomalonate ne donne pas de cyclocondensation avec les alcènes **6**, **7** et **8** alors que le carbanion chloromalonate réagit avec ces accepteurs. La limite semble atteinte avec le cinnamonitrile **9** : après 10 h de chauffage à reflux avec le chloromalonate, celui-ci est récupéré quantitativement à côté de produits de condensation du malonate.

Avec les dérivés cycliques exométhyléniques **10**–**12**, on observe la formation des cyclopropanes spiranniques **10***a*–**12***a*. Cependant, la réaction n'est pas toujours sélective, ni quantitative.

Ces résultats montrent clairement la portée synthétique de la méthode et expliquent pourquoi nous n'avons pas envisagé la réaction d'un cinnamate d'alkyle, le pouvoir activant d'un groupement ester étant inférieur à celui d'un groupement nitrile.

1.2. Analyse des résultats

Alcènes 7 et 8. Ces deux accepteurs conduisent à environ 50% de cyclopropane lorsque la réaction est conduite pendant 10 h au reflux du THF, en présence d'un équivalent de chloromalonate (cf. schéma 1 : **7**, $R^1 = C_6H_5$, W = $COCH_3$; R^2 = Y = H; **8**, $R^1 = CH_3$, W = CN; R^2 = Y = H).

Lorsque la réaction est réalisée en utilisant deux équivalents de chloromalonate, on obtient un taux de conversion de l'alcène en cyclopropane de l'ordre de 80%. On notera l'intérêt de l'utilisation du chloromalonate; en particulier, le rendement obtenu en cyclopropane **7***a* est supérieur à celui que l'on peut atteindre à partir du magnésien du dibromomalonate (9*c*).

β-*Nitrostyrene* ***4***. L'action du bromomalonate conduit au cyclopropane **4***a* accompagné de produits de polymérisation de l'alcène. Avec le chloromalonate, on obtient uniquement l'adduit de Michaël correspondant **4***b*. Ceci peut être interprété par les réactions du schéma 2. Par suite de la présence du groupement nitro, le carbanion intermédiaire, résultant de l'addition du carbanion halogénomalonate sur le β-nitrostyrène, est très stabilisé et peu nucléophile; la cyclisation en cyclopropane ne s'observe qu'avec le bon nucléofuge Br^-. Dans le cas de l'intermédiaire chloré, la réaction de protonation par le chloromalonate est plus rapide.

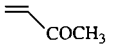
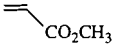
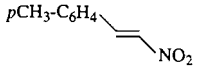
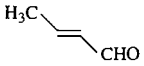
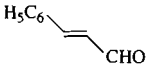
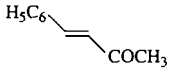
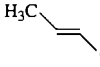
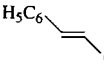
Alcènes formylés 5 et 6. Ces deux alcènes ont la particularité de posséder deux groupements électrophiles, susceptibles de réagir avec les anions halogénomalonate; des réactions d'époxydation du cyclopropane, formé dans un premier temps, ont été signalées dans le cas du crotonaldéhyde et de l'acroléine (10).

Le crotonaldéhyde **5** réagit avec les deux carbanions halogénomalonate formés dans le système K_2CO_3/THF.

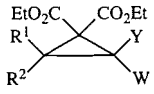
Avec le chloromalonate, il se forme un mélange de cyclopropane **5***a* et de produit **5***b* provenant d'une addition de Michaël. Le schéma 2 rend compte des réactions qui interviennent. La cyclisation du carbanion intermédiaire est plus rapide que dans le cas du β-nitrostyrène mais la réaction de protonation par le chloromalonate se produit avec une vitesse comparable.

Notons en outre que la durée de vie suffisamment importante du carbanion intermédiaire apparaît à l'analyse stéréochimique des produits : la réaction du crotonaldéhyde *trans* conduit à un

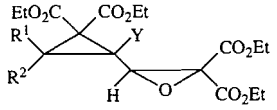
TABLEAU 1. Étude des alcènes monoactivés

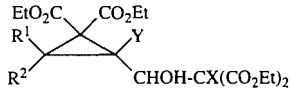
Alcène		Chloromalonate		Bromomalonate	
Formule	N°	Conditions[a]	Produits[b]	Conditions[a]	Produits[b]
	**1**	2 h; amb.	**1***a* (95%)	2 h; amb.	**1***a* (95%)
	**2**	2 h; amb.	**2***a* (95%)	6 h; amb.	**2***a* (95%)
	**3**	2 h; amb.	**3***a* (95%)	6 h; amb.	**3***a* (95%)
	**4**	6 h; amb.	**4***a* (73%)	6 h; amb.	**4***a* (55%) + polymères
	**5**	6 h; amb.	**5***a* (48%) **5***b* (48%)	6 h; amb.	**5***a* (80%) **5***c* (20%)
	**6**	48 h; amb.	**6***a* (25%) **6***d* (72%)		
	**7**	10 h; reflux	**7***a* (50%)		
	**8**	10 h; reflux	**8***a* (58%)		
	**9**		Pas de réaction		
	**10**	6 h; amb.	**10***a* (10%) **10***b* (85%)	10 h; amb.	**10***a* (75%)
	**11**	10 h; amb.	**11***a* (72%) **11***b* (25%)	10 h; amb.	**11***a* (85%)
	**12**	24 h; amb.	**12***a* (89%)	24 h; amb.	**12***a* (30%)

[a]*Conditions : durée (heures); température : amb., ambiante; reflux, reflux du THF.

a : 

b : $(EtO_2C)_2CX\text{-}CR^1R^2\text{-}CHYW$

c : 

d : 

mélange contenant 93% du cyclopropane *trans* et 7% d'isomère *cis* : une rotation partielle, non signalée dans les travaux antérieurs (8, 10), semble donc se produire au niveau de l'intermédiaire anionique.

La réaction de protonation n'est pas possible si l'on part du dichloromalonate (absence de donneur de protons) : effectivement, la réduction électrochimique du dichloromalonate, dans le système CH_3CN, CH_2Cl_2/Bu_4NBr conduit quantitativement au cyclopropane **5***a*.

Avec le bromomalonate, la cyclisation du carbanion intermédiaire du schéma 2 est plus rapide et il n'y a pas formation de l'adduit **5***b*. Cependant, comme cela a déjà été observé (8), il se produit partiellement une condensation du carbanion bromomalonate sur le groupement carbonyle du cyclopropane **5***a*, conduisant à l'époxycyclopropane **5***c* (schéma 3).

La réactivité élevée de ce groupe carbonyle est retrouvée lors de la réduction électrochimique du dibromomalonate dans le système CH_3CN, CH_2Cl_2/Bu_4NBr. Celle-ci conduit exclusivement à l'époxyde **5***c*, résultat semblable à celui obtenu dans les conditions de catalyse par transfert de phase (10).

Ainsi, le bromomalonate peut être mis en oeuvre pour réaliser sélectivement deux réactions avec le crotonaldéhyde **5** dans le

Can. J. Chem. Downloaded from www.nrcresearchpress.com by 198.100.157.202 on 09/07/12
For personal use only.

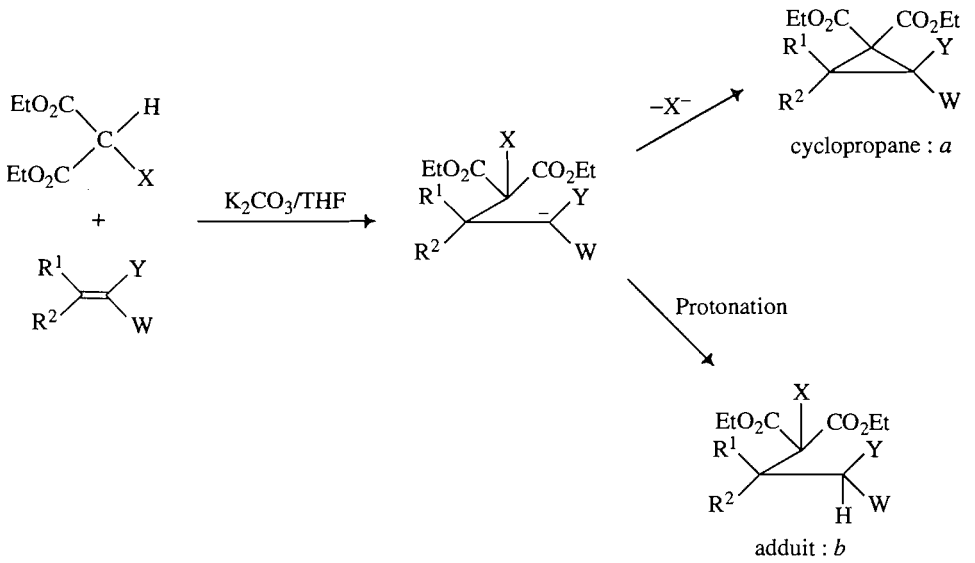


SCHÉMA 2. Compétition entre la protonation et la cyclisation de l'adduit intermédiaire.

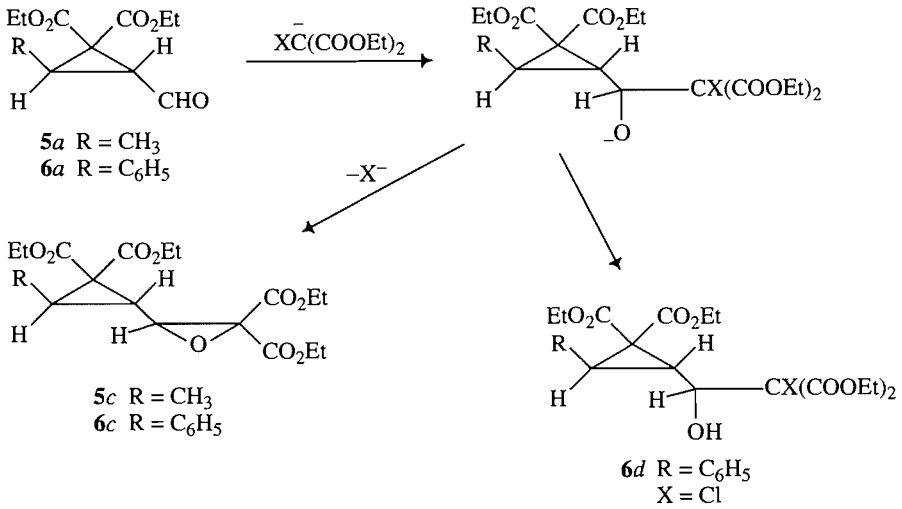


SCHÉMA 3

système K_2CO_3/THF : (i) en utilisant 0,5 équivalent d'alcène **5**, on obtient quantitativement l'époxyde **5***c*; (ii) en utilisant 5 équivalents d'alcène **5**, on obtient 95% de cyclopropane **5***a* après distillation.

Le cinnamaldehyde **6** ne réagit, dans le système K_2CO_3/THF, qu'avec le chloromalonate. Lorsque les réactifs sont introduits mole à mole, on obtient un mélange de cyclopropane **6***a* (25%) de stéréochimie *trans*, et d'halohydrine **6***d* (72%). Cette dernière résulte (schéma 3) de la protonation de l'anion intermédiaire, formé par addition du chloromalonate sur le carbonyle du cyclopropane **6***a*.

Cette protonation par le chloromalonate est donc plus rapide que la substitution nucléophile interne, avec élimination d'un chlorure, qui aurait conduit à l'époxycyclopropane correspondant **6***c*.

Il est cependant possible d'obtenir, avec un bon rendement, soit le cyclopropane **6***a*, soit l'halohydrine **6***d* dans le système K_2CO_3/THF : (i) la réaction d'un équivalent de carbanion chloromalonate sur 0,5 équivalent d'alcène **6** conduit quantitativement à l'halohydrine **6***d*; (ii) inversement, l'utilisation d'un excès d'alcène **6** (5 équivalents) fournit le cyclopropane **6***a*, qui n'avait pas encore été synthétisé par cette voie (3*b*), avec un rendement de 72% après distillation.

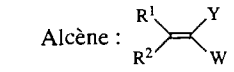
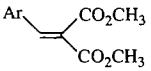
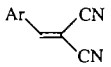
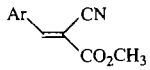
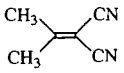
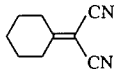
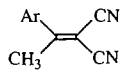
Si la réaction est réalisée mole à mole par voie électrochimique, en réduisant le dichloromalonate dans le système CH_3CN, CH_2Cl_2/Bu_4NBr ou bien le dibromomalonate dans le système $CH_3CN/LiBF_4$, on obtient un mélange de cyclopropane **6***a* (25%) et d'époxycyclopropane **6***c* (75%). En effet, la réaction est dans ces conditions effectuée en l'absence de donneurs de protons, ce qui permet à l'alcoolate intermédiaire de se cycliser en époxyde (schéma 3). Ainsi, lorsque l'électrolyse est réalisée en présence de 0,5 équivalent de cinnamaldéhyde **6**, on obtient quantitativement l'époxycyclopropane **6***c*.

*Alcènes **10**, **11** et **12***. Avec le bromomalonate, il y a formation des cyclopropanes spiranniques correspondants avec un rendement qui n'est limité que par la formation parasite d'éthylène tétracarboxylate.

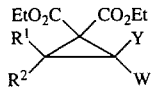
Avec le chloromalonate, seule la cétone **12** conduit uniquement au cyclopropane. Dans le cas des lactones **10** et **11**, l'addition du carbanion chloromalonate à la double liaison

Can. J. Chem. Downloaded from www.nrcresearchpress.com by 198.100.157.202 on 09/07/12
For personal use only.

TABLEAU 2. Étude des alcènes diactivés

Alcène : 		Chloromalonate		Bromomalonate	
Formule[a]	N°	Conditions[b]	Produits[c]	Conditions[b]	Produits[c]
	**13**	2 h; amb. 24 h; amb. 6 h; reflux	**13***a* (10%) **13***a* (60%) **13***a* (88%)	2 h; amb. 24 h; amb. 2 h; reflux	**13***a* (50%) **13***a* (36%) **13***a* (40%)
	**14**	2 h; amb. 6 h; amb.	**14***a* (88%) **14***a* (92%)	2 h; amb. 24 h; amb. 2 h; reflux	**14***a* (55%) **14***a* (92%) **14***a* (94%)
	**15**	10 h; amb.	**15***a* (92%)		
	**16**	48 h; amb.	**16***a* (70%) + polymères		
	**17**	48 h; amb.	**17***a* (76%) + polymères		
	**18**	48 h; amb.	**18***a* (10%) + polymères		

[a]Ar : pCH$_3$-C$_6$H$_4$–.
[b]Conditions : durée (heures); température : amb., ambiante; reflux, reflux du THF.
[c]Produits :

a : Cyclopropane. 

conduit à un intermédiaire anionique dont la cyclisation lente permet une protonation partielle en adduits de Michaël **10***b* et **11***b* par le chloromalonate (schéma 2).

Cependant, la formation de l'adduit de Michaël peut être évitée en formant le carbanion par réduction électrochimique du dichloromalonate dans le milieu CH_3CN, CH_2Cl_2/Bu_4NBr; on obtient alors sélectivement les cyclopropanes **10***a* et **11***a* avec des rendements respectifs de 81 et 79% après purification.

2. Alcènes diactivés

Les résultats sont regroupés dans le tableau 2.

Dans le cas des composés **13**–**15**, portant un seul substituant sur le carbone éthylénique en β des groupements activants, le seul produit de condensation obtenu est le cyclopropane.

L'effet du second groupement activant se manifeste puisque l'alcène dicyané **14** conduit en rendement quasi-quantitatif au cyclopropane **14***a* (en 6 h à la température ambiante avec le chloromalonate ou en 2 h au reflux du THF avec le bromomalonate) tandis que le cinnamonitrile **9** ne réagissait pas.

La réactivité du diester **13** est plus faible. En particulier, avec le bromomalonate, la réaction parasite de formation de l'éthylène tétracarboxylate devient prépondérante. Cette réaction compétitive ne se produit pas avec le chloromalonate qui fournit un excellent rendement en cyclopropane **13***a* après 6 h au reflux du THF.

Enfin, le cyanoester **15** présente une réactivité intermédiaire entre celles des deux alcènes précédents. On notera de plus que la réaction de cyclocondensation est alors stéréospécifique.

Compte tenu de la réactivité du composé **14**, les alcènes dicyanés **16**–**18** ont été choisis pour étudier l'influence de la disubstitution sur le carbone en β de la double liaison. Les réactions n'ont été réalisées qu'avec le chloromalonate.

Les rendements en cyclopropanes sont encore satisfaisants avec les alcènes **16** et **17**. Cependant, le milieu réactionnel se colore en noir et l'on constate une polymérisation partielle de l'alcène.

L'alcène **18** est très peu réactif : la polymérisation est importante et le rendement en cyclopropane **18***a* est limité à 10%. Divers essais de modification des conditions expérimentales n'ayant pas permis d'améliorer ce rendement, nous avons envisagé la formation du carbanion par voie électrochimique.

La réduction du dichloromalonate dans le système CH_3CN, CH_2Cl_2/Bu_4NBr ou du dichloromalonate dans le système $CH_3CN/LiBF_4$, en présence de l'alcène **18**, conduit encore à 10% de cyclopropane **18***a* et à des polymères; l'anion $(EtO_2C)_2CCl^-$, non complexé, ou même l'anion $(EtO_2C)_2CBr^-$ complexé par Li^+, sont donc suffisamment basiques pour induire la polymérisation.

Nous avons alors effectué la réduction du dichloromalonate dans le système $CH_3CN/LiBF_4$; il ne se produit plus de polymérisation (la solution ne noircit pas en cours d'électrolyse) mais on n'obtient toujours que 10% de cyclopropane **18***a* à côté d'une quantité importante de chloromalonate. La basicité de l'anion $(EtO_2C)_2CCl^-$, associé à Li^+, est suffisamment atténuée pour ne pas provoquer de polymérisation, mais la nucléophilie est également affaiblie et la réaction sur l'alcène devient trop lente.

Un dernier essai d'électrolyse a été réalisé dans le système $CH_3CN/NaBF_4$; le rendement en cyclopropane **18***a* est alors de 35%. Cependant, le chlorure de sodium, peu soluble dans

Can. J. Chem. Downloaded from www.nrcresearchpress.com by 198.100.157.202 on 09/07/12
For personal use only.

Can. J. Chem. Downloaded from www.nrcresearchpress.com by 198.100.157.202 on 09/07/12
For personal use only.

l'acétonitrile, précipite en masse à la moitié de l'électrolyse; la solution noircit si l'on poursuit l'électrolyse et il y a à nouveau formation de polymères. Cette expérience montre néanmoins que seule la méthode électrochimique permet de générer le carbanion, dans des conditions suffisamment douces, pour réaliser la cyclopropanation d'un alcène susceptible de se polymériser rapidement en milieu basique.

Conclusion

La mise au point d'une technique simple et performante de déprotonation des halogénomalonates d'éthyle, par l'utilisation du système biphasique solide–liquide K_2CO_3/THF, nous a permis de comparer la réactivité des carbanions chloro- et bromomalonate vis-à-vis d'alcènes électrophiles; en particulier, nous avons pu tirer pleinement partie de la réactivité plus favorable du carbanion chloré, dont le potentiel synthétique n'avait pas été exploité.

En règle générale, de bons rendements en cyclopropanes sont réalisés. Tel est le cas lorsque l'intermédiaire carbanionique, résultant de l'addition du carbanion halogénomalonate sur l'alcène, est suffisamment nucléophile; la cyclisation par substitution nucléophile intramoléculaire qui suit cette addition est alors assez rapide pour que l'on n'observe pas de protonation concurrente. Dans le cas contraire, la réduction électrochimique du dihalogénomalonate peut permettre l'obtention du cyclopropane attendu.

Partie expérimentale

1. Réactifs

Les chloro- et bromomalonate d'éthyle sont des produits commerciaux. Les dichloro- et dibromomalonate ont été synthétisés par réaction du malonate d'éthyle avec le dihalogène en milieu aqueux basique (13).

Les alcènes **1–3** et **5–9** sont des produits commerciaux. Les autres ont été synthétisés par réaction de Knoevenagel, selon des protocoles expérimentaux décrits dans la littérature : **4** (14), **10–12** (15), **13** (16) et **14–18** (17).

2. Mode opératoire

2.1 Électrochimique

Les électrolyses sont réalisées à intensité imposée, sous argon, à température ambiante dans une cellule à compartiments séparés. Le dichloromalonate est réduit sur une cathode en mercure et le dibromomalonate sur une cathode en platine. Le générateur est un appareil PAR EG&G modèle 362.

Le compartiment anodique, séparé du compartiment cathodique par un verre fritté, contient 20 mL de (CH_3CN/CH_2Cl_2 50 : 50; Bu_4NBr 0,1 M) ou 20 mL de (CH_3CN; Me_4NCl saturé). On y ajoute 1 mL de cyclohexène pour piéger le dihalogène formé.

Trois millimoles (3 mmol) du dihalogénomalonate et 3 mmol d'alcène sont dissous dans 30 mL de (CH_3CN/CH_2Cl_2 50 : 50; Bu_4NBr 0,1 M) ou de (CH_3CN; $LiBF_4$ 0,1 M) et la solution est électrolysée sous 20 mA pendant 8 h (2 F mol^{-1}). À la fin de l'électrolyse, le catholyte est évaporé; on ajoute alors 60 mL d'éther au résidu et on lave avec une solution de NaCl semi saturée (2 × 10 mL). La phase organique est séchée sur $MgSO_4$ et évaporée. Le résidu est ensuite distillé ou recristallisé.

2.2. Chimique

Trois millimoles (3 mmol) d'halogénomalonate et 3 mmol d'alcène sont dissous dans 5 mL de THF distillé. On ajoute 6 mmol de K_2CO_3 commercial finement broyé et la solution est maintenue sous bonne agitation pendant la durée et à la température indiquées. La réaction est suivie par chromatographie en couche mince sur silice, utilisant comme éluant : AcOEt/hexane 20 : 80. Les durées des expériences n'ont pas été optimisées.

À la fin de la réaction, on ajoute 15 mL de CH_2Cl_2. Les solides inorganiques sont filtrés, lavés avec 15 mL de CH_2Cl_2, et les solvants sont évaporés. Le résidu est purifié par distillation au moyen d'un four à boules ou par recristallisation.

3. Caractéristiques physico-chimiques et spectroscopiques des produits obtenus

Les produits de condensation ont été analysés par infra-rouge, RMN à 60 MHz, le cas échéant à 300 MHz; les masses molaires ont été déterminées par spectroscopie de masse.

Des microanalyses ont été réalisées sur les composés nouveaux à l'exception de l'adduit de Michaël **5***b*, qui n'a pu être obtenu sélectivement et dont l'intérêt synthétique est limité.

*2-Acétylcyclopropane-1,1-dicarboxylate de diéthyle (**1**a).* Eb : 80–90°C/1 Torr (10) (1 Torr = 133,3 Pa). RMN δ : 1,25 (3H, t, J = 7 Hz), 1,28 (3H, t, J = 7 Hz), 1,58 (1H, dd, J = 8 Hz, J = 4 Hz), 1,95 (1H, dd, J = 7 Hz, J = 4 Hz), 2,35 (3H, s), 2,83 (1H, dd, J = 8 Hz, J = 7 Hz), 4,17 (2H, q, J = 7 Hz), 4,22 (2H, q, J = 7 Hz).

*2-Cyanocyclopropane-1,1-dicarboxylate de diéthyle (**2**a).* Eb : 80–90°C/1 Torr (8). RMN δ : 1,32 (3H, t, J = 7 Hz), 1,35 (3H, t, J = 7 Hz), 1,7 (1H, dd, J = 9 Hz, J = 5 Hz), 2,03 (1H, dd, J = 7 Hz, J = 5 Hz), 2,48 (1H, dd, J = 9 Hz, J = 7 Hz), 4,23 (2H, q, J = 7 Hz), 4,33 (2H, q, J = 7 Hz).

*2-Méthoxycarbonylcyclopropane-1,1-dicarboxylate de diéthyle (**3**a).* Eb : 80–90°C/1 Torr. RMN δ : 1,28 (6H, t, J = 7 Hz), 1,65 (1H, dd, J = 5 Hz, J = 9 Hz), 1,93 (1H, dd, J = 7 Hz, J = 5 Hz), 2,58 (1H, dd, J = 9 Hz, J = 7 Hz), 3,73 (3H, s), 4,23 (4H, q, J = 7 Hz). Anal. calc. pour $C_{11}H_{16}O_6$: C 54,09; H 6,60; tr. : C 53,83; H 6,91.

trans-*2-Nitro-3-(4-méthylphényl)cyclopropane-1,1-dicarboxylate de diéthyle (**4**a).* Ce composé polymérise à la distillation; il est préférable de le purifier par chromatographie sur colonne de silice; éluant : AcOEt/hexane (20 : 80). Eb : 150–160°C/1 Torr. IR (CCl_4, cm^{-1}) : 1745 (C=O); 1560, 1370 (NO_2). RMN δ : 1 (3H, t, J = 7 Hz), 1,28 (3H, t, J = 7 Hz), 2,3 (3H, s), 4 (2H, q, J = 7 Hz), 4,13 (1H, d, J = 6 Hz), 4,27 (2H, q, J = 7 Hz), 5,33 (1H, d, J = 6 Hz), 7,1 (4H, s). Anal. calc. pour $C_{16}H_{19}NO_6$: C 59,81; H 5,96; N, 4,36; tr. : C 60,12; H 6,22; N 4,25.

*2-Chloro-2-éthoxycarbonyl-3-(4-méthylphenyl)nitrobutanoate d'éthyle (**4**b).* F : 110°C (AcOEt/hexane : 1 : 2). IR (KBr, cm^{-1}) :1780, 1750 (C=O); 1560, 1380 (NO_2). RMN δ : 1,1 (3H, t, J = 7 Hz), 1,27 (3H, t, J = 7 Hz), 2,27 (3H, s), 4,03 (2H, q, J = 7 Hz), 4,27 (2H, q, J = 7 Hz), 4,43–5,4 (3H, m), 7–7, 17 (4H, AB, J = 8 Hz). Masse calculée :357,0979; trouvée :357,0985. Anal. calc. pour $C_{16}H_{20}ClNO_6$: C 53,71; H 5,63; N, 3,91; tr. : C 54,18; H 5,64; N 3,87.

*2-Formyl-3-méthyl-cyclopropane-1,1-dicarboxylate de diéthyle (**5**a).* Eb : 90–100°C/1 Torr (10). RMN δ (300 MHz) : *trans* : 1,24 (3H, d, J = 6,1 Hz), 1,27 (3H, t, J = 7,1 Hz), 1,29 (3H, t, J = 7,1 Hz), 2,56 (1H, dq, J = 6,1 Hz, J = 7,1 Hz), 2,64 (1H, dd, J = 7,1 Hz, J = 4,9 Hz), 4,12–4,35 (4H, m), 9,26 (1H, d, J = 4,9 Hz), *cis* : 1,22–1,35 (6H, m), 1,43 (3H, d, J = 6,8 Hz), 2,27 (1H, dq, J = 6,8 Hz, J = 9,3 Hz), 2,47 (1H, dd, J = 9,3 Hz, J = 5,4 Hz), 4,12–4,35 (4H, m), 9, 52 (1H, d, J = 5,4 Hz).

*2-Chloro-2-éthoxycarbonyl-3-méthyl-4-formylbutanoate d'éthyle (**5**b).* Eb : 90–100°C/1 Torr. RMN δ : 1,1 (3H, d, J = 7 Hz), 1,1–1,5 (6H, m), 2,2–2,8 (2H, m), 3–3,4 (1H, m), 4–4,5 (4H, m), 9,68 (1H, m). Masse : (fragment :$(EtO_2C)_2CHCl$) calculée : 194,0346; trouvée : 194,0348.

*2-(2,2-Diéthoxycarbonyl-1,2-époxyéthyl)3-méthylcyclopropane-1,1-dicarboxylate de diéthyle (**5**c).* Eb : 150–160°C/1 Torr (10). RMN δ (deux isomères) : 1–1,5 (15H, m), 1,5–2,3 (2H, m), 3,23 (1H, d, J = 8 Hz), 3,45 (1H, d, J = 5 Hz), 4–4,5 (8H, m).

trans-*2-Formyl-3-phénylcyclopropane-1,1-dicarboxylate de diéthyle (**6**a).* Eb : 140–150°C/1 Torr. RMN δ : 0,9 (3H, t, J = 7 Hz), 1,3 (3H, t, J = 7 Hz), 3,37 (1H, dd, J = 8 Hz), 3,8 (1H, d, J = 8 Hz), 3,93 (2H, q, J = 7 Hz), 4,27 (2H, q, J = 7 Hz), 7,23 (5H, s), 9,43 (1H, d, J = 4 Hz). Anal. calc. pour $C_{16}H_{18}O_5$: C 66,20; H 6,25; tr. : C 66,39; H 6,11.

*2-(2,2-Diéthoxycarbonyl-1,2-époxyéthyl)-3-phénylcyclopropane-1,1-dicarboxylate de diéthyle (**6**c).* Purifié par chromatographie sur silice; éluant : AcOEt/hexane (30 : 70). RMN δ : 0,87 (3H, t, J = 7 Hz), 1,27 (3H, t, J = 7 Hz), 1,30 (3H, t, J = 7 Hz), 1,32 (3H, t, J = 7 Hz),

Can. J. Chem. Downloaded from www.nrcresearchpress.com by 198.100.157.202 on 09/07/12
For personal use only.

2,3–2,7 (1H, m), 3,3–3,6 (1H, m), 3,7–4,5 (9H, m), 7,13 (5H, s). Anal. calc. pour $C_{23}H_{28}O_9$: C 61,60; H 6,29; tr. : C 61,82; H 6,10.

*2 - (2 - Chloro - 2,2 - diéthoxycarbonyl - 1 - hydroxyéthyl) 3 - phénylcyclopropane-1,1-dicarboxylate de diéthyle (**6**d)*. F : 85–90°C (EtOH). IR (CCl_4, cm^{-1}) : 3600–3400 (OH); 1730 (C=O). RMN δ : 0,85 (3H, t, J = 7 Hz), 1,17 (3H, t, J = 7 Hz), 1,3 (6H, t, J = 7 Hz), 2,8–3,35 (2H, m), 3,6–4,45 (9H, m), 7,17 (5H, s). Anal. calc. pour $C_{23}H_{29}ClO_9$: C 56,97; H 6,03; Cl 7,31; tr. : C 56,84; H 6,09; Cl 7,49.

trans-*2-Acétyl-3-phénylcyclopropane-1,1-dicarboxylate de diéthyle (**7**a)*. Eb : 135–145°C/1 Torr (9*c*). RMN δ : 0,93 (3H, t, J = 7 Hz), 1,27 (3H, t, J = 7 Hz), 2,4 (3H, s), 3,4–3,63 (2H, AB, J = 7 Hz), 3,9 (2H, q, J = 7 Hz), 4,2 (2H, q, J = 7 Hz), 7,17 (5H, s).

*2-Cyano-3-méthylcyclopropane-1,1-dicarboxylate de diéthyle (**9**a)*. Eb : 90–100°C/1 Torr. RMN δ (deux isomères) : 1,2–1,5 (9H, m), 1,9–2,6 (2H, m), 4–4,5 (4H, m). Anal. calc. pour $C_{11}H_{15}NO_4$: C 58,66; H 6,71; N 6,22; tr. : C 57,98; H 6,64; N 5,29.

*1,1-Diéthoxycarbonyl-4-oxo-5-oxaspiro[2,4]heptane (**10**a)*. Eb : 130–140°C/1 Torr. IR (CCl_4, cm^{-1}) : 1780–1730 (C=O). RMN δ : 1,26 (3H, t, J = 7 Hz), 1,28 (3H, t, J = 7 Hz), 1,77–2,05 (2H, AB, J = 5 Hz), 2,4–2,7 (2H, m), 4–4,6 (6H, m). Anal. calc. pour $C_{12}H_{16}O_6$: C 56,24; H 6,29; tr. : C 56,51; H 6,49.

*2-(2-Chloro-2,2-diéthoxycarbonyléthyl)butyrolactone (**10**b)*. Eb : 140–150°C/1 Torr. IR (CCl_4, cm^{-1}) : 1780, 1750 (C=O). RMN δ : 1,3 (6H, t, J = 7 Hz), 1,7–3,2 (5H, m), 4,3 (4H, q, J = 7 Hz), 4–4,5 (2H, m).

*1,1-Diéthoxycarbonyl-4-oxo-5-oxaspiro[2,5]octane (**11**a)*. Eb : 135–145°C/1 Torr. IR (CCl_4, cm^{-1}) : 1730 (C=O). RMN δ : 1,23 (3H, t, J = 7 Hz), 1,27 (3H, t, J = 7 Hz), 1,63–1,2 (2H, AB, J = 5 Hz), 1,8–2,1 (2H, m), 4,12 (2H, q, J = 7 Hz), 4,20 (2H, q, J = 7 Hz), 4,3–4,6 (2H, m). Anal. calc. pour $C_{13}H_{18}O_6$: C 57,77; H 6,71; tr. : C 58,07; H 6,49.

*2-(2-Chloro-2,2-diéthoxycarbonyléthyl)valérolactone (**11**b)*. Eb : 145–155°C/1 Torr. IR (CCl_4, cm^{-1}) : 1740 (C=O). RMN δ : 1,28 (6H, t, J = 7 Hz), 1,5–3,3 (7H, m), 4,23 (4H, q, J = 7 Hz), 4,1–4,4 (2H, m).

*1,1-Diéthoxycarbonyl-4-oxospiro[2,6]nonane (**12**a)*. Eb : 115–125°C/1 Torr. IR (CCl_4, cm^{-1}) : 1745 (C=O). RMN δ : 1,27 (6H, t, J = 7 Hz), 1,47–2,50 (10H, m), 3,13 (2H, m), 4,27 (4H, q, J = 7 Hz). Anal. calc. pour $C_{15}H_{22}O_5$: C 63,81; H 7,85; tr. : C 63,71; H 7,83.

*2 - Diméthoxycarbonyl - 3 - (4 - méthylphényl)cyclopropane 1, 1 - dicarboxylate de diéthyle (**13**a)*. Eb : 170–180°C/1 Torr. RMN δ : 1,17 (3H, t, J = 7 Hz), 1,32 (3H, t, J = 7 Hz), 2,3 (3H, s), 3,67 (3H, s), 3,75 (1H, s), 3,83 (3H, s), 4,13 (2H, q, J = 7 Hz), 4,28 (2H, q, J = 7 Hz), 7,07–7,33 (4H, AB, J = 8 Hz). Anal. calc. pour $C_{20}H_{24}O_8$: C 61,22; H 6,16; tr. : C 61,49; H 6,34.

*2,2-Dicyano-3-(4-méthylphényl)cyclopropane-1,1-dicarboxylate de diéthyle (**14**a)*. F : 77°C (AcOEt/hexane : 1 : 2). RMN δ : 1,2 (3H, t, J = 7 Hz), 1,37 (3H, t, J = 7 Hz), 2,35 (3H, s), 3,9 (1H, s), 4,23 (2H, q, J = 7 Hz), 4,4 (2H, q, J = 7 Hz), 7,27 (4H, s). Anal. calc. pour $C_{18}H_{18}N_2O_4$: C 66,25; H 5,56; N 8,58; tr. : C 66,29; H 5,44; N 9,00.

E-*2-Cyano-méthoxycarbonyl-3-(4-méthylphényl)cyclopropane-1,1-dicarboxylate de diéthyle (**15**a)*. Eb : 175–185°C/1 Torr. RMN δ : 1,1 (3H, t, J = 7 Hz), 1,27 (3H, t, J = 7 Hz), 2,3 (3H, s), 3,86 (3H, s), 3,86 (1H, s), 4,1 (2H, q, J = 7 Hz), 4,23 (2H, q, J = 7 Hz), 7,06–7,23 (4H, AB, J = 8 Hz). Anal. calc. pour $C_{19}H_{21}NO_6$: C 63,50; H 5,89; N 3,90; tr. : C 62,92; H 5,95; N 3,86.

*2,2-Dicyano-3,3-diméthylcyclopropane-1,1-dicarboxylate de diéthyle (**16**a)*. Eb : 90–100°C/1 Torr. RMN δ : 1,33 (6H, t, J = 7 Hz), 1,57 (6H, s), 4,27 (4H, q, J = 7 Hz). Anal. calc. pour $C_{13}H_{16}N_2O_4$: C 59,08; H 6,10; N 10,60; tr. : C 58,48; H 6,08; N 10,87.

*1,1-Diéthoxycarbonyl-2,2-dicyanospiro[2,5]octane (**17**a)*. Eb : 130–140°C/1 Torr. RMN δ : 1,33 (6H, t, J = 7 Hz), 1,4–2 (10H, m), 4,26 (4H, q, J = 7 Hz). Anal. calc. pour $C_{16}H_{20}N_2O_4$: C 63,14; H 6,62; N 9,20; tr. : C 62,34; H 6,66; N 9,26.

*2, 2 - Dicyano - 3 - (4 - méthylphényl) - 3 - méthylcyclopropane - 1, 1 - dicarboxylate de diéthyle (**18**a)*. F : 122°C (AcOEt). RMN δ : 1,17 (3H, t, J = 7 Hz), 1,32 (3H, t, J = 7 Hz), 1,78 (3H, s), 2,33 (3H, s), 4,1 (2H, q, J = 7 Hz), 4,37 (2H, q, J = 7 Hz), 7,17 (4H, s). Anal. calc. pour $C_{19}H_{20}N_2O_4$: C 67,05; H 5,92; N 8,23; tr. : C 67,26; H 5,82; N 8,14.

1. (*a*) S. Danishefsky. Acc. Chem. Res. **12**, 66 (1979); (*b*) H. N. C. Wong, M. Y. Hon, C. W. Tse, Y. C. Yip, J. Tanko et T. Judlicky. Chem. Rev. **89**, 165 (1989).
2. M. Mladenova, F. Gaudemar-Bardone, N. Goasdoue et M. Gaudemar. Synthesis, 937 (1986).
3. (*a*) J. Martelli et R. Gree. J. Chem. Soc. Chem. Commun. 355 (1980); (*b*) H. Abdallah, R. Gree et R. Carrié. Can. J. Chem. **61**, 217 (1983); (*c*) H. Abdallah, R. Gree et R. Carrié. Tetrahedron Lett. **23**, 503 (1982).
4. (*a*) R. Verhe, N. De Kimpe, L. De Buyck, D. Courtheyn et N. Shamp. Synthesis, 531 (1978); (*b*) M. J. De Vos et A. Krief. Tetrahedron Lett. **21**, 1891 (1979); (*c*) R. Verhe, N. De Kimpe, L. De Buyck, D. Courtheyn, L. Van Caenegen et N. Shamp. Bull. Soc. Chim. Belg. **92**, 371 (1983).
5. (*a*) A. Krief et M. J. De Vos. Tetrahedron Lett. **26**, 6115 (1985); (*b*) G. Chaboteaux et A. Krief. Bull. Soc. Chim. Belg. **94**, 495 (1985); (*c*) A. Krief, L. Hevesi, G. Chaboteaux, P. Mathy, M. Sevrin et M. J. De Vos. J. Chem. Soc. Chem. Commun. 1693 (1985); (*d*) N. Ono, T. Yanai, I. Hamamoto, A. Kamimura et A. Kagi. J. Org. Chem. **50**, 2806 (1985).
6. (*a*) R. K. Singh et S. Danishefsky. J. Org. Chem. **40**, 2969 (1975); (*b*) J. Heiszman, I. Bitter, K. Harsanyi et L. Toke. Synthesis, 738 (1987); (*c*) F. Farina, M. C. Maestro, M. V. Martin et M. L. Soria. Tetrahedron, **43**, 4007 (1987); (*d*) M. Joucla et J. Le Brun. Tetrahedron Lett. **26**, 3001 (1985).
7. (*a*) N. Kawabata et M. Tanimoto. Tetrahedron. **36**, 3517 (1980); (*b*) N. Kawabata, S. Yanao et J. Yoshida. Bull. Chem. Soc. Jpn. **55**, 2687 (1982).
8. G. Bonavent, M. Causse, M. Guittard et R. Fraisse Jullien. Bull. Soc. Chim. Fr. 2462 (1964).
9. (*a*) F. Gaudemar-Bardone et M. Gaudemar. Bull. Soc. Chim. Fr. 3316 (1971); (*b*) Bull. Soc. Chim. Fr. 4188 (1971); (*c*) Bull. Soc. Chim. Fr. 3467 (1973).
10. J. M. McIntosh et H. Khalil. Can. J. Chem. **56**, 2134 (1978).
11. (*a*) N. I. Shtemenko, V. F. Kucherov et L. A. Yanovskaya. Izv. Akad. Nauk SSSR, Ser. Khim. 1444 (1978); Chem. Abstr. **89**, 108236 h (1978); (*b*) G. V. Kryshtal, N. I. Shtemenko et L. A. Yanovskaya. Izv. Akad. Nauk SSSR, Ser. Khim. 2420 (1980); Chem. Abstr. **94**, 46812 h (1981); (*c*) N. I. Shtemenko, G. V. Krishtal et L. A. Yanovskaya. Izv. Akad. Nauk SSSR, Ser. Khim. 445 (1981); Chem. Abstr. **95**, 24316 v (1981); (*d*) Z. Arnold, V. Kral, G. V. Kryshtal et L. A. Yanovskaya. Izv. Akad. Nauk SSSR, Ser. Khim 2162 (1983); Chem. Abstr. **100**, 34350 n (1984); (*e*) Z. Arnold, V. Kral, G. V. Kryshtal et L. A. Yanovskaya. Synthesis, 974 (1984).
12. J. C. Le Menn, J. Sarrazin et A. Tallec. Electrochim. Acta, **35**, 563 (1990).
13. D. A. Nicholson et V. Vaughn. J. Org. Chem. **36**, 1835 (1971).
14. E. Knoevenagel et L. Walter. Ber. **37**, 4502 (1904).
15. G. M. Ksander, J. E. McMurry et M. Johnson. J. Org. Chem. **42**, 1180 (1977).
16. C. F. H. Allen et F. W. Spangler. Org. Synth. Coll. Vol. III, 377 (1955).
17. F. Texier-Boullet et A. Foucaud. Tetrahedron Lett. **23**, 4927 (1982).

Chromodorane diterpenes from the tropical dorid nudibranch *Chromodoris cavae*

SANDRA A. MORRIS, E. DILIP DE SILVA, AND RAYMOND J. ANDERSEN[1]

Departments of Chemistry and Oceanography, University of British Columbia, Vancouver, B.C., Canada V6T 1Z1

Received November 14, 1990

SANDRA A. MORRIS, E. DILIP DE SILVA, and RAYMOND J. ANDERSEN. Can. J. Chem. **69**, 768 (1991).

Two novel diterpenoids, chromodorolides A (**1**) and B (**2**), have been isolated from skin extracts of the tropical dorid nudibranch *Chromodoris cavae*. Complete NMR assignments are presented for chromodorolide A (**1**). The structure of chromodorolide B (**2**) has been solved by spectroscopic analysis. Chromodorolides A (**1**) and B (**2**) are the first examples of diterpenoids with the highly rearranged chromodorane carbon skeleton.

Key words: nudibranch, diterpene, chromodorane, *Chromodoris*.

SANDRA A. MORRIS, E. DILIP DE SILVA et RAYMOND J. ANDERSEN. Can. J. Chem. **69**, 768 (1991).

On a isolé deux nouveaux diterpénoïdes, les chromodorolides A (**1**) et B (**2**), à partir des extraits de pelures de *Chromodoris cavae* tropicales. On présente des attributions complètes du spectre RMN du chromodorolide A (**1**). On a résolu la structure du chromodorolide B (**2**) par des analyses spectroscopiques. Les chromodorolides A (**1**) et B (**2**) sont les premiers exemples de diterpénoïdes comportant le squelette carboné chromodoragne fortement réarrangé.

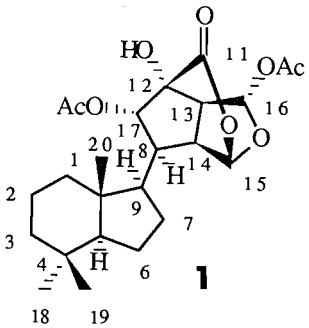
Mots clés : diterpène, chromodoragne, *Chlorodoris*.

[Traduit par la rédaction]

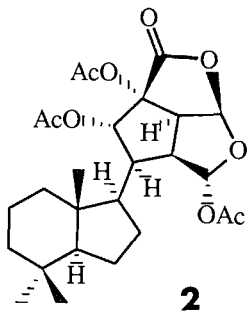
Can. J. Chem. Downloaded from www.nrcresearchpress.com by 198.100.157.202 on 09/07/12
For personal use only.

Introduction

It is well documented that many dorid nudibranchs employ secondary metabolites sequestered from sponges in their diets as defensive allomones to thwart predation (1–3). As part of our ongoing studies of molluscan chemical defenses (4–7), we have examined the tropical dorid nudibranch *Chromodoris cavae* for the presence of novel secondary metabolites. Skin extracts from specimens of *C. cavae* (90 individuals) collected in nearshore waters near Jaffna, Sri Lanka, in January 1989 yielded a single major metabolite, chromodorolide A (**1**), and traces of a companion metabolite. The structure of chromodorolide A (**1**) was solved by single crystal X-ray diffraction analysis (7). Chromodorolide A (**1**) represents the first example of a diterpenoid with the highly rearranged "chromodorane" carbon skeleton. Skin extracts of a second collection of *C. cavae* (January 1990; 54 individuals) once again yielded chromodorolide A (**1**) as the major component (7 mg), but fortunately they also yielded a reasonable quantity of the companion metabolite, chromodorolide B (**2**) (2 mg). We now wish to report the structure of chromodorolide B (**2**) and complete ^{1}H and ^{13}C NMR assignments for the previously reported metabolite, chromodorolide A (**1**).



1



2

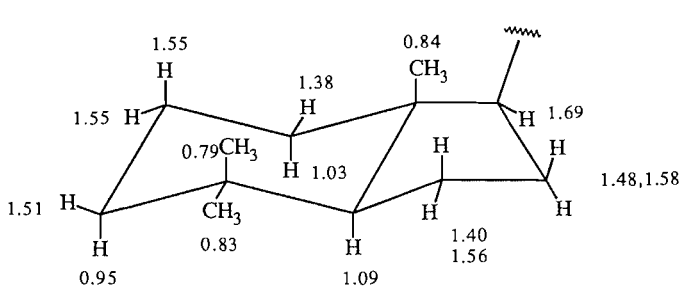
The details of the structure determination of chromodorolide A (**1**) by single crystal X-ray diffraction analysis have already been reported (7). A detailed analysis of the HMQC and COSY data for chromodorolide A (**1**) provided complete ^{1}H and ^{13}C NMR assignments for the molecule and these are presented in Table 1.

[1]Author to whom correspondence may be addressed.

Chromodorolide B (**2**) was isolated as an optically active colorless oil that gave a parent ion in the EIHRMS at m/z 492.2361 Da appropriate for a molecular formula of $C_{26}H_{36}O_9$ (ΔM, +0.2 mmu). Resonances at δ 170.2, 170.0, 169.2, and 169.1 (Table 1) in the ^{13}C NMR spectrum of **2** were assigned to four ester carbonyl carbons. The lack of ^{13}C NMR evidence for the presence of additional unsaturated functionalities indicated that chromodorolide B (**2**) had to be pentacyclic to satisfy the unsaturation number required by its molecular formula. Resonances at δ 2.04 (s,3H), 2.11 (s,3H), and 2.19 (s,3H) in the ^{1}H NMR spectrum of **2** were assigned to the methyl protons of three acetates. An intense IR band at 1751 cm^{-1} was assigned to the acetate carbonyl stretching vibrations and a second carbonyl stretching band, observed at 1812 cm^{-1}, suggested that the fourth ester functionality might be part of a small ring lactone.

Comparison of the ^{1}H and ^{13}C NMR data for chromodorolide B (**2**) with those for chromodorolide A (**1**) showed that the two molecules were closely related (Table 1). Thus, the $C_{12}H_{21}$ hydrocarbon fragment "**i**" found in chromodorolide A (**1**) could also be identified in chromodorolide B (**2**) by a detailed analysis of the data generated in COSY and HMQC experiments. The proton assignments for this fragment in **2** are shown on "**i**" and the observed COSY correlations are listed in Table 1. COSY correlations due to long range W coupling between the Me20 protons (δ 0.84) and the H1$_{ax}$ (δ 1.03) proton, and between the Me18 protons (δ 0.79) and the H3$_{ax}$ (δ 0.95), H5$_{ax}$ (δ 1.09), and Me19 (δ 0.83) protons (Table 1) provided crucial connectivities through the quaternary centers at C10 and C4.

The remaining fragment of chromodorolide B (**2**) had to have



Fragment "i"

TABLE 1. ^1H (400 MHz) and ^{13}C (75 and 125 MHz) NMR data for chromodorolides A(**1**) and B (**2**). Recorded in $CDCl_3$

Carbon no.	Chromodorolide A (**1**)		Chromodorolide B (**2**)			
	$^1H^a$	$^{13}C^b$	$^1H^a$	COSY correlations	nOe's^c	$^{13}C^b$
1_{ax}	1.03,dt(4.2,13.5)	41.1	1.03,dt(3.6,12.3)	$H1_{eq}$,H2,Me20		40.9
1_{eq}	1.40,m		1.38,m	$H1_{ax}$,H2		
2	1.50–1.52(2H),m	20.8	1.55(2H),m	$H1_{ax}$,$H1_{eq}$,$H3_{ax}$,$H3_{eq}$		21.1
3_{ax}	1.08,m	40.4	0.95,m	H2,$H3_{eq}$,Me18		39.1
3_{eq}	1.69,m		1.51,m	H2,$H3_{ax}$		
4		33.1	—			33.1
5	1.11,m	57.8	1.09,dd(6.6,13.1)	H6,H6',Me18		57.0
6	1.31,m	19.8	1.40,m	H5,H6',H7,H7'		19.9
6'	1.56,m		1.56,m	H5,H6,H7,H7'		
7	1.15,m	25.6	1.48,m	H6,H6',H7',H9		25.2
7'	1.76,m		1.58,m	H6,H6',H7,H9		
8	2.39,ddd(3.0,6.6,12.0)	44.6	2.57,ddd(7.9,11.6,12.1)	H9,H14,H17	H14,Me20	48.0
9	1.55,m	51.6	1.69,bdd(9.9,12.0)	H7,H7',H8		50.3
10		42.5	—			43.9
11		172.4*	—			169.1*
12		79.9	—			81.4
13	3.00,m	52.0	3.79,dd(6.1,8.9)	H14,H16	H16,H14	50.4
14	3.00,m	46.3	2.93,bt(8.2)	H8,H13,H15	H13,H8,H15	45.6
15	5.73,bt(2.1)	104.2	6.50,bs	H14	H17,H9,H14	97.8
16	6.30,s	95.5	6.08,d(6.1)	H13	H13	103.4
17	4.77,d(2.8)	78.8	5.30,d(11.6)	H8	H15	73.9
18	0.79,s	33.4	0.79,s	$H3_{ax}$,H5,Me19		33.4
19	0.80,s	20.8	0.83,s	Me18		21.0
20	0.82,s	13.6	0.84,s	$H1_{ax}$	Me18,H8	13.7
OAc	2.02,s	20.8: 168.8*	2.04,s			20.8: 169.2*
OAc	2.06,s	20.8: 170.0*	2.11,s			20.8: 170.0*
OAc			2.19,s			20.9: 170.2*

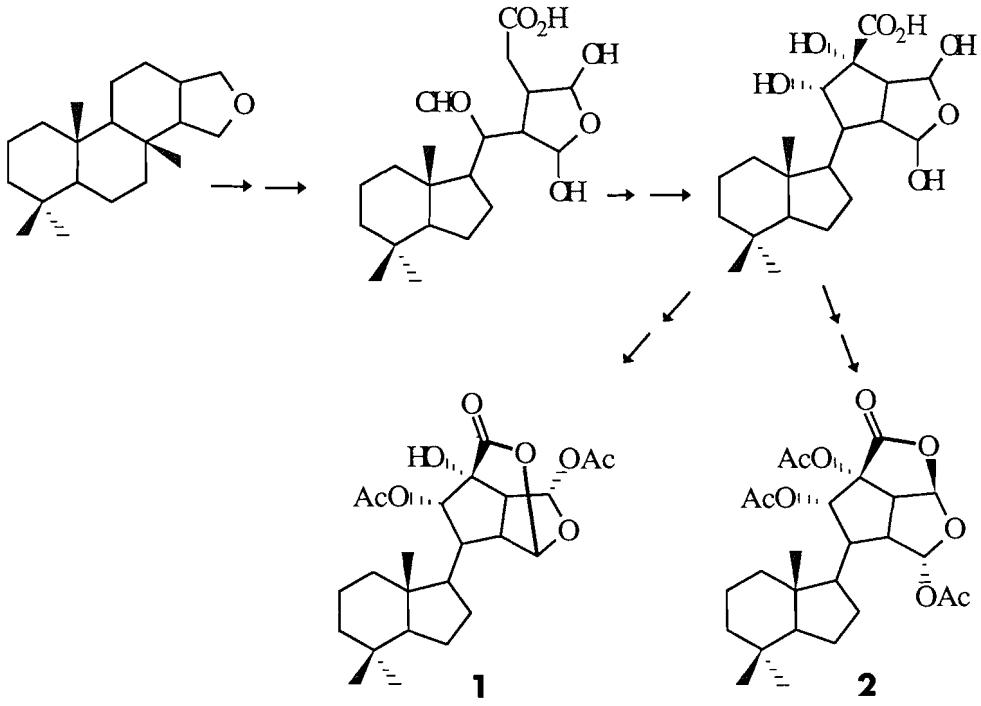
[a]Referenced to internal TMS.
[b]Referenced to solvent.
[c]Proton in "Carbon no." column irradiated.
*May be interchanged.

the elemental composition $C_{14}H_{15}O_9$, it had to be tricyclic, and it had to contain the acetate and lactone functinalities identified from the IR and ^{13}C NMR data. Resonances at δ 97.8 and 103.4 in the ^{13}C NMR spectrum of **2**, which were correlated in the HMQC spectrum to ^1H NMR resonances at δ 6.50 and 6.08 respectively, revealed that there were two acetal functionalities present in this fragment. COSY correlations connected the acetal methine resonance at δ 6.50 (H15) through two intervening methine resonances at δ 2.93 (H14) and 3.79 (H13) to the second acetal methine resonance at δ 6.08 (H16). The methine resonance at δ 2.93 (H14) showed an additional COSY correlation to a methine resonance at δ 2.57 (H8) that was in turn correlated to a deshielded methine resonance at δ 5.30 (H17) and to a resonance at δ 1.69, which had already been assigned to H9 of the hydrocarbon fragment (Table 1). The six-proton spin system elaborated above for the tricyclic fragment of chromodorolide B (**2**) corresponded exactly to the six-proton spin system (H8, H13, H14, H15, H16, and H17) present in the tricyclic fragment of chromodorolide A (**1**) (Table 1). In addition, with the exception of the resonances assigned to the acetate functionalities, the ^{13}C NMR resonances assigned to the tricyclic fragments of chromodorolides A (**1**) and B (**2**) also showed a direct one-to-one correspondence (i.e., C8 and C12 to C17: Table 1). We concluded, therefore, that chromodorolide B (**2**) also had the chromodorane skeleton with a bisacetal-oxolane ring fused 3,4 to a similarly functionalized cyclopentane ring (C8 and C12 to C17). Once we had reached this conclusion, it was apparent that there was a systematic difference in the relative chemical shifts of both the proton and carbon resonances assigned to C15 and C16 in the two metabolites.

In chromodorolide A (**1**), the most deshielded acetal proton resonance and the most shielded acetal carbon resonance were assigned via COSY and HMQC experiments to the acetal functionality that was bonded to the acetate (i.e., C16: ^1H, δ 6.30; ^{13}C, δ 95.5) and the most shielded acetal proton resonance and the most deshielded acetal carbon resonance were assigned to the acetal carbon bonded to the C11 δ-lactone carboxyl (i.e., C15: ^1H, δ 5.73; ^{13}C, δ 104.2) (Table 1). By analogy, the relative chemical shifts of the proton and carbon resonances assigned to the C15 and C16 acetal functionalities in chromodorolide B (**2**) (Table 1) indicated that the C15 acetal carbon was bonded to an acetate (^1H, δ 6.50; ^{13}C, δ 97.8) and that the C16 acetal carbon was bonded to the C11 lactone carboxyl (^1H, δ 6.08; ^{13}C, δ 103.4). The resulting tricyclic structure contained the γ-lactone that was suggested by the stretching band observed at 1812 cm^{-1} in the IR spectrum of **2**.

Placement of the two remaining acetate functionalities at C17 (^1H, δ 5.30: ^{13}C, δ 73.9) and C12 (^{13}C, δ 81.4), positions occupied in chromodorolide A (**1**) by acetate and tertiary hydroxyl functionalities respectively, was consistent with the

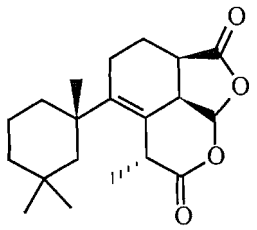
Can. J. Chem. Downloaded from www.nrcresearchpress.com by 198.100.157.202 on 09/07/12
For personal use only.



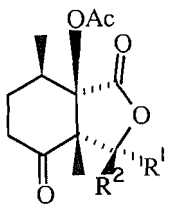
SCHEME 1

^1H and ^{13}C NMR data of chromodorolide B (**2**) (Table 1). Difference nOe experiments (Table 1) were in complete agreement with the proposed structure **2** for chromodorolide B and they defined the relative stereochemistry in the tricyclic fragment as shown. We have assumed that C8 and C9 in **2** have the same relative stereochemistries found in chromodorolide A (**1**) (7).

The rather high frequency of the stretching vibration for the γ-lactone carbonyl in **2** (1812 cm^{-1}) parallels the elevated stretching frequencies of the lactone carbonyl bands in chromodorolide A (**1**) (1770 cm^{-1}) (7) and cadlinolide A (**3**) (1789 and 1760 cm^{-1}) (8). Presumably the unusually high frequency in **2** is due to a combination of effects resulting from the attachment of the γ-lactone alkoxy oxygen to an acetal carbon (C16) and to the presence of an α-acetoxy functionality (attached to C12). The γ-lactones in the monoterpenes **4** and **5** isolated from *Nepeta tuberosa* also experience both of these effects and their carbonyl stretching freqencies are reported to be at 1810 and 1820 cm^{-1}, respectively (9).



3



4 $R^1 = OAc\ R^2 = H$

5 $R^2 = OAc\ R^1 = H$

Scheme 1 shows a proposed biogenetic pathway to the new chromodorane carbon skeleton found in chromodorolides A (**1**) and B (**2**). This proposal suggests that the chromodorane skeleton is formed from a spongian diterpenoid precursor by creation of a new carbon–carbon bond (C12—C17) subsequent to a series of degradation and rearrangement steps that generate the norrisane skeleton (10). Scheme 1 also illustrates that chromodorolides A (**1**) and B (**2**) represent alternate modes of cyclization of the C11 carboxyl group with the bisacetal-oxolane ring to generate a pair of densely functionalized heterocycles. Chromodorolide A (**1**) displays moderate cytotoxic (L1210 ED_{50} 20 μg/mL; P388 T/C 125% at 4 mg/kg) and antimicrobial (*Bacillus subtilis* MIC 60 μg/disc; *Rhizoctonia solani* MIC 60 μg/disc) activities. The limited quantity of chromodorolide B (**2**) that was available was not sufficient for biological testing.

Experimental

Extraction and purification procedure

Freshly collected animals were immediately immersed in methanol/dichloromethane (1:1) and stored in a freezer. At the time of work-up, the organic solvents were decanted from thawed samples and evaporated *in vacuo* to give an oily residue that was partitioned between water and dichloromethane. Fractionation of the dichloromethane soluble materials by sequential application of silica-gel flash chromatography (ethyl acetate/hexane 5:2) and normal phase HPLC (ethyl acetate/hexane 1:2) yielded pure metabolites.

Chromodorolide A (1): colorless needles (MeOH), mp 133–34°C; $[\alpha]_D$ −74° (*c* 0.1, CH_2Cl_2); IR (film) ν_{max}: 3461, 1770, 1748 (sh), 1220 cm^{-1}; ^1H NMR (Table 1); ^{13}C NMR (Table 1); EIHRMS, M^+ −HOAc, *m/z*: 390.2043 Da ($C_{22}H_{30}O_6$, ΔM +0.1 mmu); CIMS *m/z*: 468 ($M^+ + NH_4$).

Chromodorolide B (2): colorless oil; $[\alpha]_D$ −95° (*c* = 0.10, CH_2CL_2); IR (film) ν_{max}: 2917, 2846, 1812, 1751, 1368, 1214, 1096, 999, 964 cm^{-1}; ^1H NMR (benzene-d_6; 400 MHz), δ: 0.63 (s, 3H, H20), 0.68 (dd, *J* = 11.0, 7.0 Hz, 1H, H5), 0.81 (s, 3H, H18), 0.84 (s, 3H, H19), 0.90 (m, 1H, H1a), 1.00 (m, 1H, H3a), 1.14 (m, 1H, H6), 1.16 (m, 1H, H9), 1.37 (m, 1H, H6), 1.38 (m, 1H, H3b), 1.42 (m, 1H, H7), 1.43 (m, 1H, H1b), 1.44 (m, 1H, H7), 1.46 (m, 1H, H2), 1.50 (m, 1H, H2), 1.63 (s, 3H, $-OCOCH_3$), 1.66 (s, 3H, $-OCOCH_3$),

Can. J. Chem. Downloaded from www.nrcresearchpress.com by 198.100.157.202 on 09/07/12
For personal use only.

1.84 (s, 3H, $-OCOCH_3$), 2.51 (ddd, J = 12.2, 11.0, 7.0 Hz, 1H, H8), 2.62 (t, J = 8.7, 7.5 Hz, 1H, H14), 3.50 (dd, J = 8.8, 6.0 Hz, 1H, H13), 5.70 (d, J = 12.2 Hz, 1H, H17), 5.80 (d, J = 6.0 Hz, 1H, H16), 6.63 (br s, 1H, H15) ppm; ^{13}C NMR, see Table 1; LREIMS, m/z (relative intensity): 492 (<1), 477 (4), 432 (11), 417 (23), 285 (4), 165 (5), 163 (10), 138 (38), 123 (100), 122 (15), 109 (24), 95 (36), 82 (25), 69 (30); HREIMS, M^+ m/z: 492.2361 ($C_{26}H_{36}O_9$, ΔM +0.2 mmu).

Acknowledgements

The authors wish to thank Sandra Millen for identifying *C. cavae*. Financial support was provided by grants to R.J.A. from NSERC and the National Cancer Insitute of Canada. S.A.M. was supported by a NSERC Postgraduate Fellowship.

1. K. GUSTAFSON and R. J. ANDERSEN. Tetrahedron, **41**, 1101 (1985).
2. D. J. FAULKNER. *In* Biomedical importance of marine organisms. *Edited by* D. G. Fautin. California Academy of Sciences, San Francisco, CA. 1988. pp. 29–36.
3. P. KARUSO. *In* Bioorganic marine chemistry. Vol. 1. *Edited by* P. J. Scheuer. Springer Verlag, Berlin. 1987. pp. 31–60.
4. D. E. WILLIAMS and R. J. ANDERSEN. Can. J. Chem. **65**, 2244 (1987).
5. M. TISCHLER and R. J. ANDERSEN. Tetrahedron Lett. **42**, 5717 (1989).
6. E. D. DE SILVA and P. J. SCHEUER. Heterocycles, **17**, 167 (1982).
7. E. J. DUMDEI, E. D. DE SILVA, R. J. ANDERSEN, M. I. CHOUDHARY, and J. CLARDY. J. Am. Chem. Soc. **111**, 2712 (1989).
8. M. TISCHLER, R. J. ANDERSEN, M. I. CHOUDHARY, and J. CLARDY. J. Org. Chem. **56**, 42 (1991).
9. J. G. URONES, I. S. MARCOS, P. B. BARCALA, and A. M. LITHGOW-BERTELLONI. Phytochemistry, **27**, 1525 (1988).
10. J. E. HOCHLOWSKI, D. J. FAULKNER, G. K. MATSUMOTO, and J. CLARDY. J. Org. Chem. **48**, 1141 (1983).

Can. J. Chem. Downloaded from www.nrcresearchpress.com by 198.100.157.202 on 09/07/12
For personal use only.

Determination of the absolute stereochemistry of the fungal metabolite (*R*)-(−)-2-(4′-hydroxyphenyl)-2-hydroxyethanoic acid (pisolithin B)

YOULA S. TSANTRIZOS

Department of Chemistry, McGill University, Montréal, P.Q., Canada H3A 2K6

AND

KELVIN K. OGILVIE[1]

Vice President Academic and Department of Chemistry, Acadia University, Wolfville, N.S., Canada B0P 1X0

Received August 2, 1990

YOULA S. TSANTRIZOS and KELVIN K. OGILVIE. Can. J. Chem. **69**, 772 (1991).

The antifungal antibiotic pisolithin B (*p*-hydroxymandelic acid, 2-(4′-hydroxyphenyl)-2-hydroxyethanoic acid, **1***a*) was shown to have the absolute (*R*) configuration. The stereochemistry was established via comparison of its optical rotation to that of its synthetic (*R*) and (*S*) enantiomers. The synthetic samples were prepared by the stereospecific reduction of the prochiral α-keto acid, *p*-hydroxybenzoylformic acid (2-(4′-hydroxyphenyl)-2-oxoethanoic acid, **2***a*), with (*R*) or (*S*)-2,2′-dihydroxy-1,1′-binaphthyl lithium aluminum hydride (BINAL-H). The absolute configuration and enantiomeric purity of both products were determined using the ^{1}H NMR of their isobutyl esters in the presence of the chiral solvating agent (*R*)-(−)-2,2,2-trifluoro-1-(9-anthryl)ethanol.

Key words: pisolithin B, *p*-hydroxymandelic acid, antifungal, absolute configuration.

YOULA S. TSANTRIZOS et KELVIN K. OGILVIE. Can. J. Chem. **69**, 772 (1991).

On a démontré que la configuration absolue de l'antibiotique fongicide pisolithine B (acide *p*-hydroxymandélique, acide 2-(4′-hydroxyphényl)-2-hydroxyéthanoïque, **1***a*) est (*R*). On a établi cette stéréochimie par comparaison de sa rotation optique avec celle de ses énantiomères de synthèse (*R*) et (*S*). On a préparé les échantillons de synthèse sur une réduction stéréospécifique de l'acide cétonique prochiral, l'acide *p*-hydroxybenzoylformique (2-(4′-hydroxyphényl)-2-oxoéthanoïque, **2***a*), avec les hydrures (*R*) et (*S*) du 2,2′-dihydroxy-1,1′-binaphtyl lithium et aluminium (BINAL-H). On a déterminé les configurations absolues et les puretés énantiomériques de chacun des produits à l'aide de la RMN du ^{1}H de leurs esters isobutyliques en présence de l'agent de solvatation chiral (*R*)-(−)-2,2,2-trifluoro-1-(9-anthryl)éthanol.

Mots clés : pisolithine B, acide *p*-hydroxymandélique, fongicide, configuration absolue.

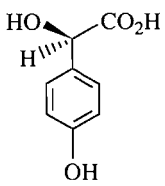
[Traduit par la rédaction]

Introduction

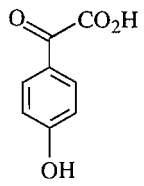
The antifungal antibiotic pisolithin B (*p*-hydroxymandelic acid, 2-(4′-hydroxyphenyl)-2-hydroxyethanoic acid, **1***a*) was isolated from the extracellular metabolite mixture of the mycorrhizal fungas *Pisolithus tinctorius* (Pers.) Coker & Couch (synonym to *P. arhizus* (Scop. pers Pers.) Rauschert) (1). This microorganism lives symbiotically on the roots of many plants and forest trees (2, 3) and is well known for is ability to promote its host's growth, especially in habitats characterized by poor environmental conditions and low fertility soils (4). The beneficial effects of *P. tinctorius* are attributed primarily to its large network of mycelia, which support the accumulation and transfer of minerals through the fungus to the host plants (5), and partly to its production of indoleacetic acid, cytokinin, and giberellin having phytohormonal activity (6).

Recently, the compounds *p*-hydroxybenzoylformic acid (2-(4′-hydroxyphenyl)-2-oxoethanoic acid, **2***a*) and *p*-hydroxymandelic acid (2-(4′-hydroxyphenyl)-2-hydroxyethanoic acid, **1***a*) were isolated from the culture media of *P. tinctorius* and they were given the trivial names pisolithin A and B respectively (1). Both compounds were shown to exhibit strong antifungal activity, causing hyphal lysis and inhibition of spore germination, against many phytopathogenic and dermatogenic fungi. Their production by *P. tinctorius* indicates an additional mechanism by which this microorganism aids in the development of its host plants, in that it provides protection to them against disease-causing fungi.

Racemic *p*-hydroxymandelic acid has been synthesized (7) and resolved by chiral stationary (8) and mobile (9) phase HPLC techniques, as well as by enzymatic methods (10). However, a facile approach to the synthesis of enantiomerically enriched samples is not yet available. Furthermore, the relationship between the optical rotation and absolute stereochemistry of each enantiomer has not been previously assigned. Hence, to determine the absolute stereochemistry of the optically active metabolite pisolithin B, a stereoselective synthesis of both the (*R*) and (*S*) enantiomers of this compound was carried out. ^{1}H NMR in the presence of a chiral shift reagent was used to determine the enantiomeric purity and absolute stereochemistry of the samples. The natural product and synthetic samples were subsequently utilized in a number of studies for the investigation of their antifungal activity. Preliminary results on their possible mode of action indicate that they possess metal-binding properties (ionophore type antibiotics), with the (*S*)-(+)-*p*-hydroxymandelic acid being the more potent antifungal agent of the two compounds (1).



Pisolithin B (**1***a*)



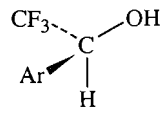
Pisolithin A (**2***a*)

Results and discussion

Chiral solvating agents are useful probes for obtaining stereochemical information through NMR experiments. Pirkle

[1]Author to whom correspondence may be addressed.

Can. J. Chem. Downloaded from www.nrcresearchpress.com by 198.100.157.202 on 09/07/12
For personal use only.

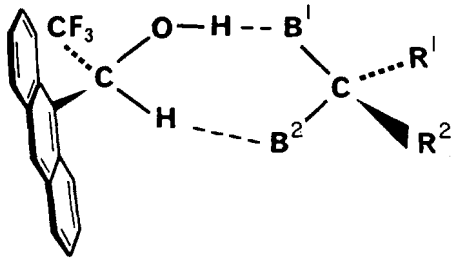


3

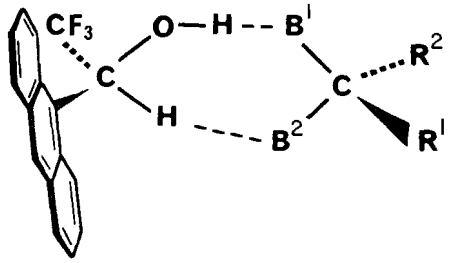
a, **Ar** = phenyl
b, **Ar** = 9-anthryl

et al. (11) have shown that chiral alcohols, of the general structure **3**, permit the direct determination of enantiomeric purity, and often allow correlations to be made regarding the absolute configuration of a compound.

These compounds were originally used to study the optical purity of chiral sulfoxides (11*a*), methyl esters of amino acids (11*b*), and the enantiomeric composition and absolute stereochemistry of chiral oxaziridines (11*c*, *d*). Their ability to hydrogen bond with two basic substituents of a compound (B^1 and B^2) leads to the formation of short-lived, chelate-like, diastereomeric complexes (**4** and **5**) (11*c*). It is expected that the



4



5

more basic substituent (B^1) will hydrogen bond preferentially to the hydroxyl proton of the solvating agent, where the less basic group will form a non-classical hydrogen bond with the acidic carbinyl hydrogen (11*c*). The inductive effects of the adjacent electron-withdrawing groups (trifluoromethyl, hydroxyl, 9-anthryl[2]) serve to render this hydrogen somewhat acidic so that it is able to participate in a dipole–dipole interaction (12). The magnetic field contributions of the aromatic electron cloud of the shift reagent induce nonequivalence to the substituents R^1 and R^2 in the two complexes **4** and **5**.

Application of this model to a suitable analogue of the natural product **1***a* (pisolithin B) would predict an upfield shift of the C-2 proton in the (*S*) enantiomer (but not in the (*R*)) upon chelation with the (*S*) enantiomer of the solvating agent, due to the location of that proton over the region of the diamagnetic

[2]Replacement of the phenyl group with 9-anthryl provides greater shielding ability, leading to a larger degree of nonequivalence.

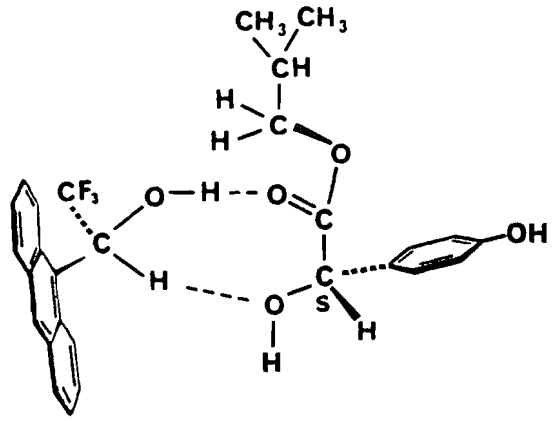
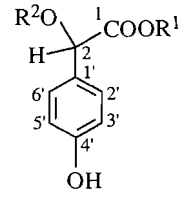


FIG. 1. Chelate complex of the (*S*) *p*-hydroxymandelate ester with the (*S*)-(+)-2,2,2-trifluoro-1-(9-anthryl)ethanol.

field of the aromatic ring (Fig. 1). Ideally, NMR experiments of this nature should be conducted in nonpolar solvents such as CCl_4 or C_6D_6. Any dipole–dipole interactions, other than those between the compound of interest and the shift reagent, would decrease the effectiveness of the latter. In an effort to obtain a nonpolar analogue of metabolite **1***a*, esters of the commercially available (racemic) *p*-hydroxymandelic acid were prepared. Since the methyl and ethyl esters were found to be practically insoluble in $CDCl_3$, the isobutyl ester (**1***b*) was synthesized along with a minor side product, compound **1***c*. The isobutyl ester was only moderately soluble in $CDCl_3$, hence it was expected that neither CCl_4 or C_6D_6 would be suitable solvents for these NMR experiments. Although $CDCl_3$ is not the ideal solvent for this work, since it can itself hydrogen bond to the shift reagent, moderate amounts of nonequivalence were observed, which were sufficient for the purpose of this investigation.

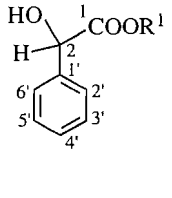
To verify the applicability of Pirkle's theory to metabolite **1***a*, the procedure was first tested on the closely related natural product mandelic acid (**6***a*). It was postulated that any observed ^1H NMR differences between optically pure (*R*) and (*S*) mandelic acid, in the presence of the solvating agent **3***b*, should be analogous to those expected for compound **1***a*.

Commercially available samples of optically pure (*R*) and (*S*) mandelic acid were converted to their respective isobutyl esters (**6***b*). The ^1H NMR of the enantiomerically pure esters **6***b* showed the C-2 hydroxyl as a doublet at 3.53 ppm, the two C-1″ protons as a multiplet at 3.93 ppm, and the C-2 proton as a doublet at 5.17 ppm. To a known enantiomeric mixture of compound **6***b* (*R*/*S* ~ 4:1), (*S*)-(+)-2,2,2-trifluoro-1-(9-anthryl)ethanol (**3***b*) was added in portions of 0.2 equivalents.



1

a, R^1 = H, R^2 = H
b, R^1 = isobutyl, R^2 = H
c, R^1 = R^2 = isobutyl
d, R^1 = CH_3, R^2 = H
e, R^1 = R^2 = CH_3



6

a, R = H
b, R = isobutyl

Can. J. Chem. Downloaded from www.nrcresearchpress.com by 198.100.157.202 on 09/07/12
For personal use only.

Can. J. Chem. Downloaded from www.nrcresearchpress.com by 198.100.157.202 on 09/07/12
For personal use only.

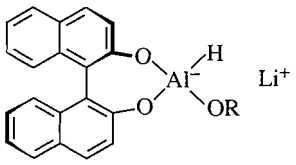
Fast proton exchange between the shift reagent and compound **6***b* caused the disappearance of coupling between C-2 H and C-2 OH at low concentrations of shift reagent. At ratios of 1:1, two singlet peaks were observed for the C-2 protons, with the lower intensity signal ((*S*) enantiomer) upfield from the higher intensity one ((*R*) enantiomer), and an integration of approximately 4:1 as was expected.

Optimum results were achieved at excess concentrations of solvating agent (1.5–2 equiv.). Under these conditions, coupling between the C-2 H and the C-2 OH was once again evident (Fig. 2: expansion of the spectral region of interest in the presence of the solvating agent), indicating maximum chelation through hydrogen bonding. These observations are consistent with those reported by Pirkle *et al.*, who noted that maximum nonequivalence was obtained at a two- to threefold excess of solvating agent to the compound of interest (13). Although the induced shift differences were very small (~0.014 ppm), the integration ratio of the two non-overlapping peaks of each doublet of the C-2 protons (peaks R and S in Fig. 2) were very close to the actual ratio of 4:1. Nonequivalence was also observed for the -COOCH_2- protons, where the downfield signal was assigned to the (*S*) enantiomers. This assignment was based on the speculation that deshielding of the -CH_2- protons (C-1″) of the (*S*) enantiomer could occur if these protons were placed close to the paramagnetic field of the 9-anthryl ring system and almost on the same plane. Molecular modeling calculations[3] suggested a distance of 3.97 Å between the C-1″ and the aromatic protons and showed them to be almost coplanar. Theoretical NMR calculations (14) predict that at such a distance, a downfield shift of about 0.2 ppm should be observed for the C-1″ protons of the (*S*) enantiomer, which was consistent with the shift observed. The greater sharpness of the C-1″ proton signal is most likely due to the absence of coupling with an exchangeable proton (Fig. 2).

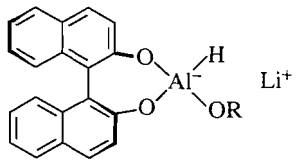
The experimental data for mandelic acid were in excellent agreement with the predictions made. Hence, the synthesis and subsequent determination of the absolute stereochemistry of the two enantiomers of pisolithin B (**1***a*) were attempted.

The ability of the solvating agent (*S*)-(+)-2,2,2-trifluoro-1-(9-anthryl)ethanol (**3***b*) to induce a useful degree of nonequivalence between the two enantiomers of ester **1***b* was confirmed through the ^{1}H NMR of a racemic mixture, which showed two equally intense signals for the C-2 proton ($\Delta\delta$ = 0.03 ppm). According to the model, the upfield signal corresponds to the (*S*) enantiomer and the downfield corresponds to the (*R*).

The simplest way to obtain *p*-hydroxymandelic acid in high enantiomeric purity would have been via stereospecific reduction of the easily obtainable α-keto acid or its ester analogue. The enantioselective reducing agents (*R*)- and (S)-2,2′-dihydroxy-1,1′-binaphthyl lithium aluminum hydride (BINAL-H, **7***a* and **7***b*) provide a useful method for the conversion of prochiral carbonyl compounds to either their (*R*) or (*S*) enantiomer.



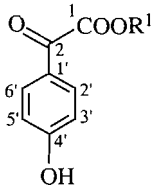
7*a*



7*b*

The preparation of these reagents was developed by Noyori *et al.* (15), who proposed that the reaction mechanism proceeds via a six-membered ring transition state in the chair conformation. The chirality of the product can be predicted by taking into consideration the steric and electronic effects that would give the most favorable energy for that particular transition state (Fig. 3). Hence, the reduction of the isobutyl ester **2***b* with the (*S*)-BINAL-H (**7***b*) should proceed via transition state **8** to give the (*R*) enantiomer of alcohol **1***a* (Fig. 3). In the transition state, the aromatic substituent is placed at the equatorial position in order to avoid electronic repulsion between the aromatic ring and the lone pair of electrons of the binaphthol oxygen. However, the 1,3-diaxial steric repulsion becomes increasingly significant as the bulkiness of the axial substituent increases, which leads to both low reactivity and low enantioselectivity (15).

Quantitative yields of the isobutyl *p*-hydroxybenzoylformate ester (**2***b*) were obtained by refluxing the free acid **2***a* in isobutyl alcohol containing catalytic amounts of *p*-toluenesulfonic acid. The esterification reaction was also attempted using the commercially available sodium salt of **2***a* as the starting material but this resulted in low yields of the desired product (due to a competing decarboxylation reaction leading to the formation of *p*-hydroxybenzaldehyde).



2

a, R = H
b, R = isobutyl

The BINAL-H reagents (16)[4] were prepared following Noyori's procedure (15), and used in threefold excess in an effort to reduce the isobutyl *p*-hydroxybenzoylformate ester (**2***b*) to the (*R*) and (*S*) enantiomers of alcohol **1***b*. When the (*S*)-BINAL-H reagent was reacted for 3.5 and 2 h with **2***b*, at −100°C and −78°C respectively, an insignificant amount of product was detected and most of the starting material was recovered. Noyori reported that the threefold excess of BINAL-H reagent is critical for the completion of these types of reactions in reasonable rates. Hence, taking into consideration that the phenolic proton will immediately be extracted by one equivalent of hydride, a fourfold equivalence of reducing agent to compound **2***b* was used. (The ionization of the phenol to the phenoxide ion was evident immediately upon addition of the

[3]Minimization of the conformational energies of compound **1***b*, using PCMODEL via MMX molecular mechanics, indicated that the *cis* ester (C-1″ *cis* to the carbonyl) was ~8 kcal lower in energy than the *trans*. Both compounds were first minimized separately and then minimized as a hydrogen-bonded complex. Only one hydrogen bond, between the C-1 carbonyl and the -OH group of the shift reagent, was allowed by this program; "hydrogen bonding" between the α-hydroxyl of **1***b* and the carbinyl hydrogen of the **3***b* solvating agent was not recognized. However, the two molecules were still placed close enough to give a distance of 3.97 Å between the C-1″ and the aromatic protons, and they were placed approximately on the same plane. The PCMODEL program was obtained from Serena Software, P.O. Box 3076, Bloomington, Indiana 47402-3076, USA.

[4]The optically pure binaphthol used was a generous gift of Dr. R. J. Kazlauskas.

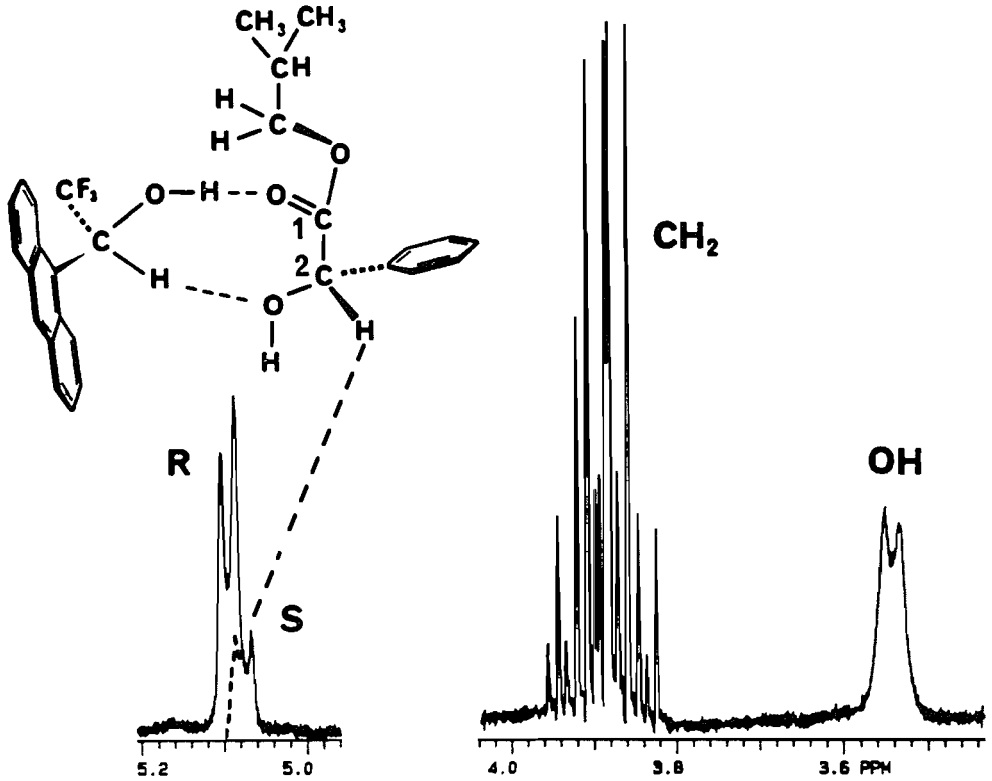


FIG. 2. ^{1}H NMR (300 MHz, $CDCl_3$) of chelate complex between **6***b* (*R*/*S* mixture of 4:1) and (*S*)-**3***b*.

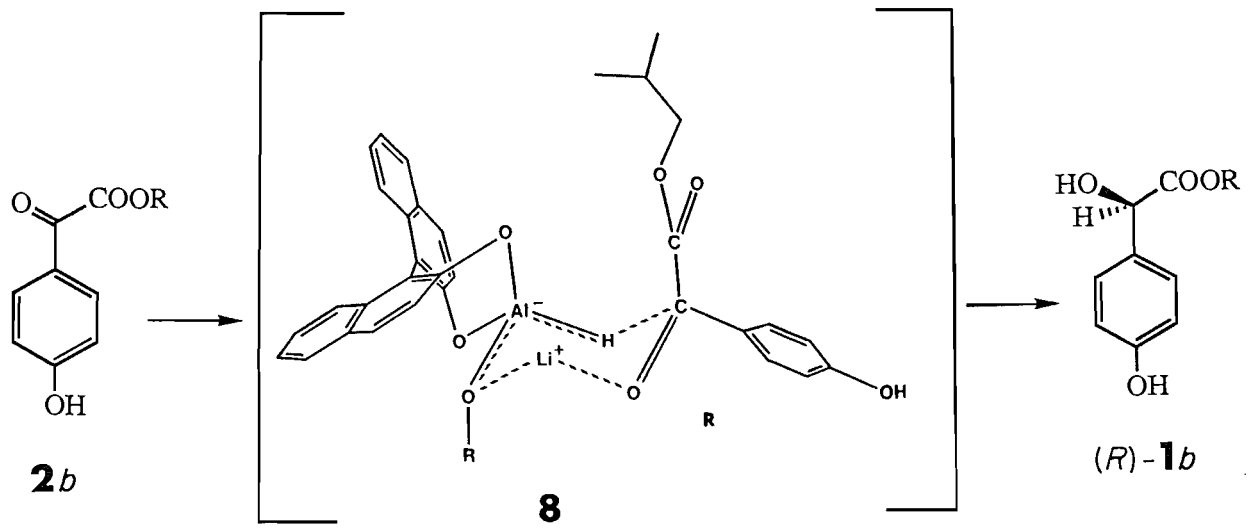
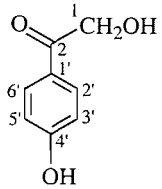


FIG. 3. (*S*)-BINAL-H reduction of *p*-hydroxybenzoylformate ester **2***b*.

substrate to the reagent by the change in colour of the reaction mixture from colourless to intense yellow.) Under these conditions and using (*S*)-BINAL-H, at −78°C for 2 h, the (*R*) enantiomer of compound **1***b* was formed at approximately 35% enantiomeric excess. In addition, the primary alcohol **9** was formed as a major side product; the isolated yields after column chromatography were 7% of **1***b*, 29% of **9**, and ~50% starting material.

Although a low degree of stereospecificity was obtained, the overall results were consistent with the proposed mechanism. It was speculated that a decrease of the %ee value could be caused either by the bulkiness of the isobutyl ester group, which would decrease the stability of the expected transition state **8**, or racemization of the chiral center (C-2) in the presence of base. The strongly basic conditions that result upon quenching of the



9

Can. J. Chem. Downloaded from www.nrcresearchpress.com by 198.100.157.202 on 09/07/12
For personal use only.

Can. J. Chem. Downloaded from www.nrcresearchpress.com by 198.100.157.202 on 09/07/12
For personal use only.

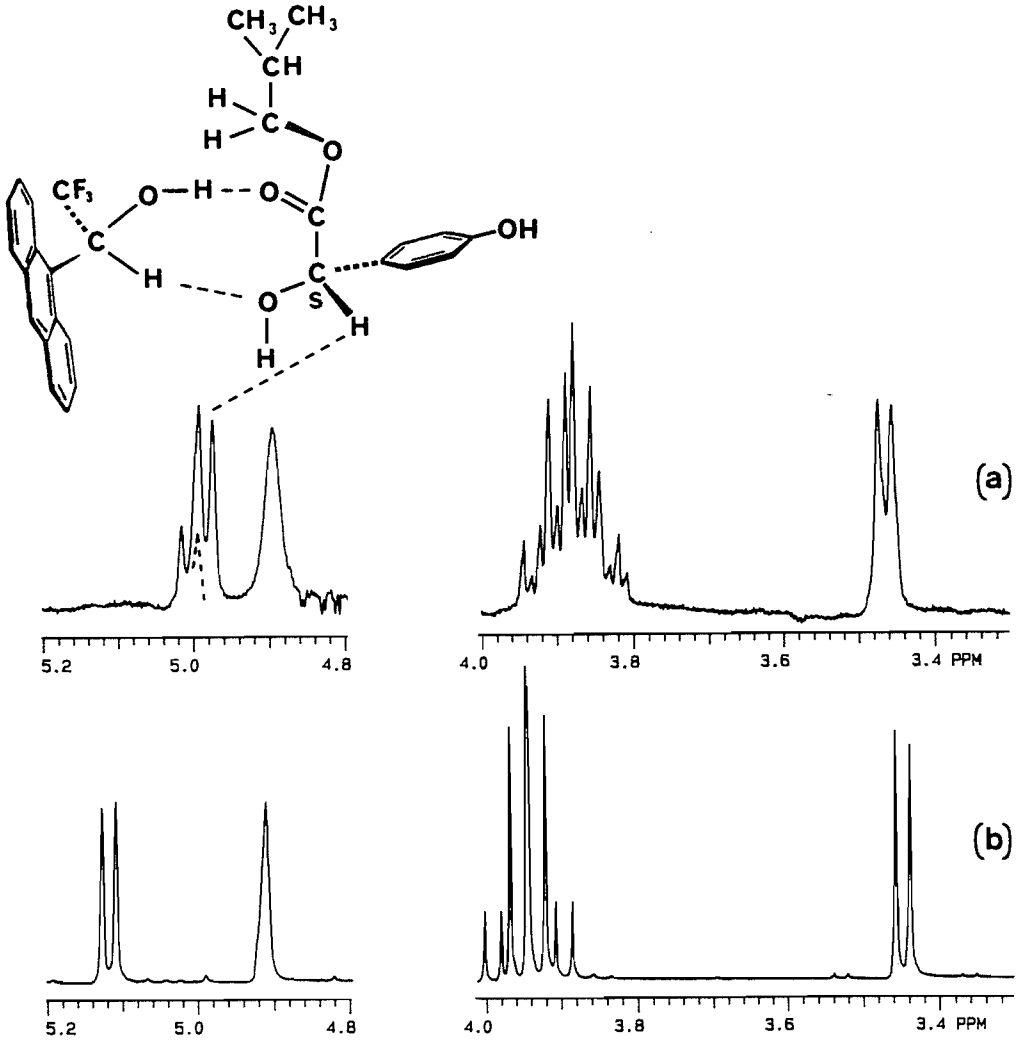


FIG. 4. ^{1}H NMR (300 MHz, $CDCl_3$) of compound (*S*)-**1***b*; (*a*) with solvating agent (*S*)-**3***b*; (*b*) pure.

excess hydride at the end of the reaction could cause not only racemization but low chemical yields due to possible hydrolysis of the ester. In an attempt to further investigate this reaction, the (*S*) enantiomer of **1***b* was synthesized, using the (*R*)-BINAL-H reagent, and quenching the reaction mixture with approximately 3 equivalents of glacial acetic acid. The pH of the reaction mixture was adjusted to about 6.5 before the temperature was allowed to rise above 0°C. After column chromatography, the desired (*S*) enantiomer of compound **1***b* was isolated in 15% yield, in addition to 10% of the primary alcohol (**9**) and more than 40% of unreacted starting material. The optical purity of **1***b* was determined to be 80% (*S*) to 20% (*R*) (60% ee) from its ^{1}H NMR in the presence of the chiral solvating agent (*S*)-**3***b* (Fig. 4a). The formation of the side product **9** clearly indicates the existence of competing reactions. Further investigation of this reaction would be required in order to determine conditions at which complete conversion of starting material to the desired product and better stereocontrol can be attained. However, the information thus far obtained was sufficient to permit the determination of the absolute configuration of the natural product pisolithin B (**1***a*).

Ester hydrolysis of the (*R*)- and (*S*)-**1***b* compounds was carried out with 3 equivalents of hydroxide base in dioxane. The reaction was almost complete after a period of 12 h at room temperature without racemization. (When the reaction was carried out in a solution of 50% dioxane/50% D_2O, deuterium exchange was not observed in the ^{1}H NMR of the carboxylic acid product.) Measurements of the optical rotation of natural pisolithin B along with both enantiomers of the synthetic material (Table 1) indicated that the metabolite has the absolute (*R*) stereochemistry. However, the [α] values obtained were not consistent, most likely due to autocatalysed racemization of the compound upon standing in solution at room temperature. This type of racemization was strongly suggested by the compound's inherent acidic nature and the decrease of its optical rotation value when left in aqueous solution at 23°C for a period of 24 h (refer to the values of the synthetic (*R*)-**1***b* in Table 1).[5]

Experimental

General methods

Ultraviolet spectra were recorded on a Hewlett Packard 8451A diode array spectrophotometer. Nuclear magnetic resonance spectra were

[5]The low measured optical rotation of the natural product pisolithin B ($\alpha = -0.029 \pm 0.002°$, $[\alpha] = -2.7°$, $c = 1.0$) indicates that this chiral metabolite of *Pisolithus tinctorius* slowly racemizes during isolation and purification. The rate of racemization would likely be greater in concentrated aqueous solutions of the pure compound ($pK_a = \sim 3.5$) than in the buffeted fungal medium (pH = ~5.5–6).

TABLE 1. Optical rotation properties of *p*-hydroxymandelic acid

Compound	[α]
Natural	−2.7°
Synthetic (*R*)-**1***b* (35% ee)[a]	−10.2° decreased to −6.1° after 24 h in aqueous solution at 23°C
Synthetic (*S*)-**1***b* (60% ee)[a]	+26.3°

[a]Products of BINAL-H reduction.

obtained at 20–22°C using Varian XL-200, XL-300, and Bruker 500 MHz instruments. ^{1}H and ^{13}C NMR chemical shifts are quoted in ppm and are referenced to the internal deuterated solvent downfield from tetramethylsilane (TMS). The samples used for D_2O ^{1}H NMR were first dissolved in ~1 mL of 99.8% D_2O and lyophilized twice before their data were recorded in 99.96% D_2O. All mass spectra were measured at the Biomedical Mass Spectrometry Unit, McGill University, unless otherwise indicated. The low resolution chemical ionization (NH_3) spectra were obtained using a HP 5980A spectrometer. FAB and high resolution chemical ionization spectra (NH_3) were obtained using a ZAB 2F HS instrument. Optical rotations were measured using a Jasco DIP-140 digital polarimeter.

Silica gel chromatography was performed on Merck Kieselgel 60 (230–400 mesh, no. 9385) using flash chromatography (17). Desalting of compounds was carried out on an ion exchange column packed with pre-swollen and washed Dowex 50W-X8 (H^+ form, 20–50 mesh) resin (J. T. Baker Chemical Co., Phillipsburg, NJ). All chromatographic solvents were fractionally distilled prior to use with the exception of acetic acid.

Sodium *p*-hydroxybenzoylformate, (*R*) and (*S*) mandelic acid, racemic *p*-hydroxymandelic acid, and the chiral solvating agents were obtained from Aldrich Chemical Co (Milwaukee, WI).

Synthesis of racemic methyl p-*hydroxymandelate (**1**d)*

A racemic mixture of *p*-hydroxymandelic acid (~1 g) was refluxed overnight in methanol (50 mL) in the presence of catalytic amounts of *p*-toluenesulfonic acid (~0.5 mg). Evaporation of the solvent gave a reddish oil containing the desired methyl ester (**1***d*) in ~50% yield, the minor product methyl 2-methoxy-*p*-hydroxymandelate (a red oil) in ~5% yield, and unreacted starting material. The mixture was separated by flash column chromatography using $EtOAc/CH_2Cl_2$ (1:1) as the eluting solvent.

(R/S)-*Methyl*-p-*hydroxymandelate* (**1**d): TLC: $EtOAc/CH_2Cl_2$ (1:1), R_f 0.38. ^{1}H NMR (200 MHz, $CDCl_3$) δ: 3.36 (d, J = 6.5 Hz, 1H, C-2 OH), 3.78 (s, 3H, $-CH_3$), 4.9 (bs, 1H, C-6 OH), 5.13 (d, J = 6.5 Hz, 1H, H2), 6.82 (d, J = 8.7 Hz, 2H, H5), 7.29 (d, J = 8.7 Hz, 2H, H4) ppm. MS (C.I.(NH_3), direct inlet, ~105°C), *m/z* (% relative intensity assignment): 200 (10.6, $M^+ + NH_3$), 182 (13, M^+), 165 (100, $M^+ - OH$), 123 (20.4, $M^+ - COOMe$).

(R/S) *Methyl 2-methoxy*-p-*hydroxymandelate* (**1**e): TLC: $EtOAc/CH_2Cl_2$ (1:1), R_f 0.52. ^{1}H NMR (200 MHz, $CDCl_3$) δ: 3.36 (s, 3H, C-8 CH_3), 3.70 (s, 3H, C-7 CH_3), 4.69 (s, 1H, H2), 4.84 (s, 1H, C-6 OH), 6.80 (d, J = 8.3 Hz, 2H, H5), 7.29 (*d*, J = 8.3 Hz, 2H, H4) ppm. MS (C.I. (NH_3), direct inlet, ~70°C), *m/z* (% relative intensity, assignment): 214 (4.7, $M^+ + NH_3$), 182 (18.0, $M^+ + NH_3 - MeOH$ or $M^+ + 1 - Me$), 165 (100.0, $M^+ - OMe$), 137 (61.9, $M^+ - COOMe$).

Synthesis of racemic isobutyl p-*hydroxymandelate (**1**b)*

A racemic mixture of *p*-hydroxymandelic acid (**1***a*, 1.02 g) was refluxed in isobutyl alcohol (75 mL) in the presence of catalytic amounts of *p*-toluenesulfonic acid (~0.5 mg) for 12 h. Evaporation of the solvent gave a reddish oil, which was a mixture of two products and some starting material. After flash column chromatography with pet. ether/EtOAc (3:1) compound **1***b* was isolated as the major product (40% yield after chromatography and recrystallization) and its 2-isobutyloxy derivative (**1***c*) as a minor side product (6% yield).

(R/S) *Isobutyl* p-*hydroxymandelate* (**1**b): TLC: pet. ether/EtOAc (3:1), R_f 0.18. ^{1}H NMR (200 MHz, $CDCl_3$) δ: 0.80 (2d, J = 7.6 Hz, 6H, 2 × CH_3), 1.86 (m, 1H, H8), 3.44 (d, J = 5.4 Hz, 1H, C-2 OH), 3.93 (m, 2H, H7), 4.94 (s, 1H, C-6 OH), 5.11 (d, J = 5.4 Hz, 1H, H2), 6.80 (d, J = 8.5 Hz, 2H, H5), 7.26 (d, J = 8.5 Hz, 2H, H4) ppm. ^{13}C NMR (300 MHz, $CDCl_3$) δ: 18.8 (C-9, C-10), 27.7 (C-8), 72.1 and 72.5 (C-7 and C-2), 115.5 (2C-4), 128.0 (2C-5), 130.5 (C-3), 155.9 (C-6), 174.0 (C-1) ppm. MS (C.I. (NH_3), direct inlet, ~60°C), *m/z* (% relative intensity, assignment): 242 (0.8, $M^+ + NH_3$), 224 (11.8, M^+), 207 (100, $M^+ - OH$), 123 ($M^+ - CO_2CH_2CHMe_2$).

(R/S) *Isobutyl 2-isobutyloxy*-p-*hydroxymandelate* (**1**c): TLC: pet. ether/EtOAc (3:1), R_f 0.53. ^{1}H NMR (200 MHz, $CDCl_3$) δ: 0.81 (d, J = 6.7 Hz, 6H, C-9 and C-10 2 × CH_3), 0.89 (dd, J = 6.7 and 2.2 Hz, 6H, C-13 and C-14 2 × CH_3), ~1.85 (m, 1H, H8), ~1.95 (m, 1H, H12), 3.23 (m, 2H, H11), 3.80 (m, 2H, H7), 4.77 (s, 1H, H2), 5.70 (s, 1H, C-6 OH), 6.78 (d, J = 8.7 Hz, 2H, H5), 7.28 (d, J = 8.7 Hz, 2H, H4) ppm. A number of selective decoupling experiments had to be carried out in order to correctly assign all proton signals as indicated. ^{13}C NMR (300 MHz, $CDCl_3$) δ: 18.9 (C-9 and C-10), 19.3 (C-13, C-14), 27.7 (C-12), 28.4 (C-8), 71.3 (C-11), 76.4 (C-7), 80.9 (C-2), 115.6 (2 × C-5), 128.3 (C-3), 128.6 (2 × C-4), 156.5 (C-6), 172.3 (C-1) ppm.

Synthesis of optically pure (R)-(−)-*isobutyl mandelate (**6**b)*

R-(−)-Mandelic acid (**6***a*, 1.0 g) was refluxed in isobutyl alcohol (~75 mL) in the presence of catalytic amounts of *p*-toluenesulfonic acid (~0.5 mg) for 12 h. Evaporation og the solvent followed by flash column chromatography with a solvent gradient of pet. ether/CH_2Cl_2 (1:1) to CH_2Cl_2 gave the (*R*)-(−)-isobutyl mandelate (**6***b*) as a clear liquid (which solidified under vacuum, mp 35–36°C) in quantitative yields. Using the same procedure the (*S*)-(+)-isobutyl mandelate was prepared from the (S)-(+)-mandelic acid.

(R)-(−)-*isobutyl mandelate ester* (**6**b): TLC: pet. ether/EtOAc (6:1), R_f 0.3–0.45. ^{1}H NMR (200 MHz, $CDCl_3$) δ: 0.80 (2d, J = 6.7 Hz, 6H, 2 × CH_3), 1.86 (m, 1H, H8), 3.53 (d, J = 4.8 Hz, 1H, C-2 OH), 3.93 (m, 2H, H7), 5.17 (d, J = 4.8 Hz, 1H, H2), 7.32–7.44 (m, 5H, aromatic) ppm.

Synthesis of isobutyl p-*hydroxybenzoylformate (**2**b)*

Commercially available sodium salt of *p*-hydroxybenzoylformic acid (**2***a*, 0.85 g) was refluxed in isobutyl alcohol (~40 mL) in the presence of catalytic amounts of *p*-toluenesulfonic acid (~0.5 mg) for 24 h. Evaporation of the solvent gave a purple-brown oil that, after flash column chromatography with CH_2Cl_2/EtOAc (10:0.5), was found to contain approximately an equal mixture of the desired product **2***b* (0.2 g, 20% yield), its decarboxylated analogue *p*-hydroxybenzaldehyde, and starting material. The reaction was repeated with the protonated form of the starting material in which case **2***b* was formed in nearly quantitative yields. The free acid was obtained by passing the salt through an ion exchange column (Dowex 50W-X8, H^+, 20–50 mesh) and removing the water on a lyophilizer.

p-*Hydroxybenzoylformic acid* (**2**a): IR (KBr): 3150–3380, 1735, 1654, 1608, 1586, 1443, 1400, 1252, 1173, 979, 855, 621 cm^{-1}. UV (0.1 M HCl, nm): max 296, min 226 and 206; (0.1 M NaOH, nm): max 334, min 240. ^{1}H NMR (500 MHz, DMSO) δ: 6.88 (dd, J = 8 and 0.9 Hz, 2H, H4), 7.75 (dd, J = 8 and 0.9 Hz, 2H, H5), 10.74 (s, 1H, -COO*H*) ppm. ^{13}C NMR *free acid* (300 MHz, DMSO + D_2O) δ: 116.0 (C-5), 123.3 (C-3), 132.3 (C-4), 163.8 (C-6), 166.8 (C-1), 187.0 (C-2) ppm. ^{13}C NMR *sodium salt* (300 MHz, DMSO) δ: 115.2 (C-5), 125.7 (C-3), 131.5 (C-4), 162.2 (C-6), 171 (br, C-1) 195 (br, C-2) ppm.

Isobutyl-p-*hydroxybenzoylformate* (**2**b): TLC CH_2Cl_2/EtOAc (10:0.5), R_f 0.40. ^{1}H NMR (200 MHz, $CDCl_3$) δ: 0.97 (d, J = 6.7 Hz, 6H, 2 × CH_3), 2.08 (m, 1H, H8), 4.15 (d, J = 6.7 Hz, 2H, H7), 6.95 (d, J = 9.0 Hz, 2H, H5), ~7.3 (br s, 1H, C-6 OH) and 7.93 (d, J = 9.0 Hz, 2H, H4) ppm. ^{13}C NMR (300 MHz, $CDCl_3$) δ: 19.0 (C-9 and C-10), 27.7 (C-8), 72.4 (C-7), 116.2 (2C-4), 125.0 (C-3), 133.2 (2C-5), 162.8 (C-6), 164.7 (C-1), and 185.6 (C-2) ppm.

Synthesis of optically active S-(+)-*isobutyl*-p-*hydroxymandelate ester* **1**b)

Isobutyl-*p*-hydroxybenzoylformate (**2***b*, 603 mg, 2.72 mmol), dissolved in dry THF (15 mL) was added dropwise to an (*R*)-(+)-BINAL-

Can. J. Chem. Downloaded from www.nrcresearchpress.com by 198.100.157.202 on 09/07/12
For personal use only.

H (11) reagent solution (4 equiv.) at −78°C over a period of 10–15 min. The reaction was stirred at −78°C for 3.5 h and quenched with 3 equivalents of glacial acetic acid (~0.5 mL, the excess hydride was estimated to be ~3 equiv.). EtOAc (100 mL) and H_2O (50 mL) were added, and the mixture was filtered through Celite and allowed to separate to room temperature. The EtOAc layer was removed; the aqueous layer was further adjusted to pH 6–7 and reextracted with EtOAc (3 × 50 mL). Flash column chromatography of the organic layer with pet. ether/EtOAc (3:1) afforded the (*S*) enantiomer of compound **1***b* (90 mg, 15% yield after chromatography) in ~60% enantiomeric purity (as determined by ^{1}H NMR), the side product alcohol **9** (40 mg, 10% yield), binaphthol, and unreacted starting material.

(S)-(+) *Isobutyl*-p-*hydroxymandelate* (**1***b*): TLC: pet. ether/EtOAc (3:1), R_f 0.18. $[\alpha]_D$ +26.3°. ^{1}H NMR and ^{13}C NMR were identical to the racemic **1***b* reported previously. However, in the presence of (*S*)-(+)-2,2,2-trifluoro-1-(9-anthryl)ethanol (1.5–2 equiv.) the proton spectra (300 MHz) clearly showed two sets of peaks for the C-2 proton; the (*S*) enantiomer upfield from the (*R*) with integration of S/R = ~4:1 (~60% ee).

2-(4-Hydroxyphenyl)-2-oxoethanol (**9**): TLC: pet. ether/EtOAc (3:1), R_f 0.08. ^{1}H NMR (200 MHz, acetone-d_6) δ: 4.79 (s, 2H, CH_2), 6.95 and 7.87 (dd, 4H, Ar) ppm, exchangeable protons were not seen. ^{13}C NMR (300 MHz, acetone-d_6) δ: 65.6 (C-1), 116.3 (2C-4), 127.1 (C-3), 131.1 (2C-5), 163.9 (C-6), and 198.6 (C-2) ppm. APT (D2 = 2 ms) NMR (300 MHz, acetone-d_6) δ: 127.1, 163.9, and 198.6 ppm. DEPT NMR (300 MHz, acetone-d_6) δ: 1CH_2 (65.6 ppm), 2CH (116.3, 131.1 ppm).

Hydrolysis of (R)-(−)-*isobutyl*-p-*hydroxymandelate ester* (**1***b*) *to* (R)-(−)-p-*hydroxymandelic acid* (**1***a*)

To a solution of ester (*R*)-**1***b* (60 mg, 0.27 mmol, 35% ee) in dioxane (3 mL), 2 equivalents of NaOH were added (1 M solution, 535 μL). The reaction was stirred at room temperature for 15 h, at which point 10 mL of H_2O was added and the pH adjusted to ~6.5 with 0.1 N HCl. The aqueous layer was extracted with EtOAc (3 × 15 mL) in order to remove unreacted starting material. The aqueous layer was evaporated to dryness under high vacuum at 40°C, redissolved in H_2O (~5 mL), and passed through an ion exchange resin (Dowex 50W-X9, H^+, 20–50 mesh) in order to remove Na^+. The free acid (*R*)-**1***a* was isolated in 90% yield (41 mg). Its optical rotation, $[\alpha]_D^{25}$ −10.2° (*c* = 0.98, H_2O), was compared to that of the natural product pisolithin B, $[\alpha]_D^{25}$ −2.7° (*c* = 1.0, H_2O). Although it was concluded that the metabolite must have the absolute (*R*) configuration, the values for the optical activity obtained were inaccurate; in solution, compound **1***a* is acidic enough to catalyze its own racemization.

Hydroylsis of (*S*)-**1***b* (60% ee), following exactly the same procedure, led to the isolation of the (*S*) enantiomer of pisolithin B, which showed an optical rotation $[\alpha]_D^{25}$ +26.3° (*c* = 0.16, H_2O).

(R)-(−)-p-*Hydroxymandelic acid* (**1***a*): UV (0.1 M HCl, nm); max 228, min 206 and 274; (0.1 M NaOH, nm): max 248, min 292. ^{1}H NMR (300 MHz, D_2O) δ: 5.0 (s, 1H, H2), 6.7 (d, *J* = 8.2 Hz, 2H, H5), 7.1 (d, *J* = 8.2 Hz, 2H, H4) ppm. ^{13}C NMR (300 MHz, DMSO + D_2O) δ: 74.4 (C-2), 117.3 (C-5), 130.4 (C-4), 132.3 (C-3), 157.5 (C-6), 178 (C-1) ppm. ^{252}Cf-plasma desorption MS (18): *electrosprayed sample*, *m/z*: 213.2 $(M^{2-} + H^+ + 2Na^+)^+$, 167.1 $(M^{2-} + H^+)^-$; *tridodecylmethylammonium chloride salt*, *m/z*: 167.1 $(M^{2-} + H^+)^-$, 869.9 $[(TDMA^+)(M^{2-} + H^+)_2^-]^-$, 1776.6 $[(TDMA^+)_3\ M^{2-}]$, 121.1 $(M^{2-} - HCO_2H)^-$.

Acknowledgments

We wish to thank Dr. J. André Fortin and Mr. Harry Kope, Forestry Department, Laval University, for carrying out the biological testing of pisolithin B and its synthetic enantiomer. We are also indebted to NSERC of Canada and FCAR of Quebec for financial support.

1. Y. S. Tsantrizos, H. H. Kope, J. A. Fortin, and K. K. Ogilvie. Phytochemistry. In press.
2. D. H. Marx. Can. J. Microbiol. **23**, 217 (1977).
3. (*a*) W. J. Brill. Sci. Am. 245, 199 (1981); (*b*) G. Gay, R. Rouillon, and G. Bruchet. Colloq. INRA 13(Mycorhizes. Partie Integr. Plante: Biol. Perspect. Util.), 163 (1982); (*c*) D. W. Greene, W. J. Manning, and D. R. Cooley. HortScience, **17**, 655 (1982).
4. J. W. Hendrix, C. Stevens Hunt, and D. M. Maronek. Can. J. Microbiol. **31**, 878 (1985).
5. P. Sihanonth and R. L. Todd. Ecol. Bull. **25** (Soil Org. Components Ecosyst.), 392 (1977).
6. I. Ho. Can. J. For. Res. **17**, 31 (1987).
7. (*a*) Beilstein's Handbuch der Organischen Chemie. Vol. 10, p. 410; (*b*) French Patent Application No. 2 495 137, June 4, 1982.
8. Y. Yuki, K. Saigo, H. Kimoto, K. Tachibana, and M. Hasegawa. J. Chromatogr. **400**, 65 (1987).
9. I. Benecke. J. Chromatogr. **291**, 155 (1984).
10. G. D. Hegeman, E. Y. Rosenberg, and G. L. Kenyon. Biochemistry, **9**, 4029 (1970).
11. (*a*) W. H. Pirkle and S. D. Beare. J. Am. Chem. Soc. **90**, 6250 (1968); (*b*) J. Am. Chem. Soc. **91**, 5150 (1969); (*c*) W. H. Pirkle and P. L. Rinaldi. J. Org. Chem. **42**, 3217 (1977); (*d*) J. Org. Chem. **43**, 4475 (1978).
12. A. Alerhand and P. v. R. Schleyer. J. Am. Chem. Soc. **85**, 1715 (1963).
13. W. H. Pirkle, S. D. Beare, and R. L. Muntz. Tetrahedron Lett., 2295 (1974).
14. C. E. Johnson, Jr. and F. A. Bovey. J. Chem. Phys. **29**, 1012 (1958).
15. (*a*) R. Noyori, Y. Tanimoto, and M. Nishizawa. J. Am. Chem. Soc. **106**, 6709 (1984); (*b*) R. Noyori, I. Tomino, M. Yamada, and M. Nishizawa. J. Am. Chem. Soc. **106**, 6717 (1984).
16. R. J. Kazlauskas. J. Am. Chem. Soc. **111**, 4953 (1989).
17. W. C. Still, M. Kahn, and A. Mitra. J. Org. Chem. **43**, 2923 (1978).
18. (*a*) C. J. McNeal and R. D. Macfarlane. Biochem. Biophys. Res. Commun. **139**, 18 (1986); (*b*) C. J. McNeal and R. D. Macfarlane. J. Am. Chem. Soc. **108**, 2132 (1986); (*c*) R. D. Macfarlane. Mass Spectrom. Rev. **4**, 421 (1985).

Can. J. Chem. Downloaded from www.nrcresearchpress.com by 198.100.157.202 on 09/07/12
For personal use only.

Free-radical based cycloalkanol synthesis and annulation from thioacetal precursors

VEEJENDRA YADAV AND ALEX G. FALLIS

The Ottawa–Carleton Chemistry Institute, Department of Chemistry, University of Ottawa, Ottawa, Ont., Canada K1N 6N5

Received June 27, 1990

VEEJENDRA YADAV and ALEX G. FALLIS. Can. J. Chem. **69**, 779 (1991).

A general procedure for the synthesis of diverse cyclopentanols via free-radical cyclization of unsaturated 1,3-oxathiolanes and 1,3-oxathiolan-5-ones is described. The scope of these reactions, including preliminary rate studies that indicate that the 1,3-oxathiolan-5-ones cyclize at a useful rate ($1.4 \times 10^6\ M^{-1}\ s^{-1}$ at 80°C), has been examined. This permits the rapid assembly, by intramolecular annulation, of various additional ring systems, including bicyclo[3.3.0]octanols, bicyclo[4.3.0]nonanols, and bicyclo[3.2.1]octanols for use in total synthesis.

Key words: radical cyclization, oxathiolanes, oxathiolanones.

VEEJENDRA YADAV et ALEX G. FALLIS. Can. J. Chem. **69**, 779 (1991).

On décrit une méthode générale de synthèse de divers cyclopentanols qui implique une cyclisation radicalaire de 1,3-oxathiolanes et de 1,3-oxathiolan-5-ones insaturés. On a étudié les possibilités de ces réactions, y compris des études préliminaires de leurs vitesses; elles indiquent que les 1,3-oxathiolan-5-ones se cyclisent à des vitesses utiles ($1,4 \times 10^6\ M^{-1}\ s^{-1}$, à 80°C). Cette procédure permet de faire un assemblage rapide, par annelation intramoléculaire, de divers systèmes cycliques additionnels, y compris les bicyclo[3.3.0]octanols, bicyclo[4.3.0]nonanols et bicyclo[3.2.1]octanols qui peuvent être utilisés dans des synthèses totales.

Mots clés : cyclisation radicalaire, oxathiolanes, oxathiolanones.

[Traduit par la rédaction]

Introduction

Over the past decade significant progress in the study and synthetic application of free-radical reactions to a variety of challenging targets has been achieved. Thus free-radical processes have evolved to join their counterparts, electrophilic, nucleophilic, and pericyclic reactions, in the arsenal of the synthetic organic chemist. This rapid, recent progress is summarized in several reviews (1–4). The established preference of 5-hexenyl radicals to form five-membered rings (5) allows rapid construction of complex systems, particularly cyclopentanoid natural products (6, 7). A liability inherent in classical radical precursors such as unsaturated organic halides is the net loss of the two functional groups that results. This severely limits, at an early stage in a synthetic sequence, the use of conventional radical cyclizations.

One potential solution to this problem is to employ α-heteroatom radical intermediates in the cyclization step in order to generate products that retain synthetically useful functionality for subsequent manipulation. At the outset of this study relatively few substituted systems of this type had been reported. The examples most studied concerned the intramolecular cyclization of α-nitrogen substituted radicals to olefins and the reductive cyclization of alkenyl ketones via radical anion intermediates (6*a*, 8). Representative examples of some of the oxygen related cases are summarized in Table 1 (9, 10). In addition to entry 4, Giese and Erfort have examined the conjugate addition of α-acetoxy radicals (9*d*) and more recently there have been reports of closely related systems (entries 5–8). However, in the case of entry 5 the method proved unsatisfactory with more complex examples and required high dilution when the α-*gem*-dimethyl functionality was absent (10*b*). In a different context, the cytotoxicity of the antitumor antibiotic bleomycin is believed to arise via an oxygen stabilized nucleotide radical intermediate, and thus there is added incentive to understand related species (11).

To employ the tin hydride mediated reductive cyclization procedure it is necessary to utilize a relatively reactive precursor in which hydrogen atom transfer from the stannane will be sufficiently slow so that ring closure may compete effectively. Beckwith and Pigou demonstrated that a methylthio substituent reacted so slowly with tributyltin radicals that they were unable to obtain accurate relative rate values (9*j*). This study established that for S_H2 attack by tributyltin radicals the relative order was I > Br > PhSe > Cl > PhS > MeS. In addition, it was noted that one of the important factors that affected the reactivity of RX with tributyltin radicals was the degree of stabilization of the product radical R·, particularly in the case of attack on sulfur. Nevertheless the kinetic data indicated that aryl sulfides were of borderline utility and were usually unsatisfactory for reactions involving alkyl radicals, although cyclizations from diphenyldithioacetals have been reported recently (8*k*).

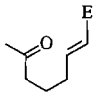
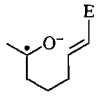
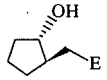
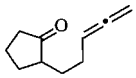
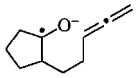
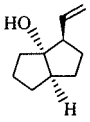
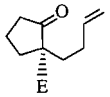
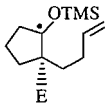
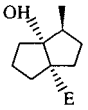
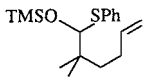
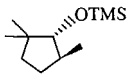
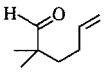
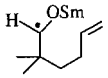
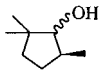
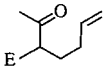
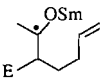
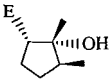
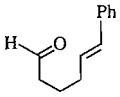
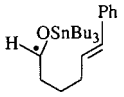
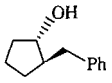
Several years ago Guiterrez *et al.* established that tri-*n*-butyltin hydride, plus azobis(isobutyronitrile) (AIBN) as initiator, was effective for desulfurization of dithioacetals and that this process involved a stepwise radical chain reaction (12). In the present context this demonstrated that sufficient strain will also assist the radical cleavage of alkyl sulfides. Consequently it appeared likely that quenching of a radical intermediate such as **2** (Scheme 1) would be slow relative to cyclization when a suitable unsaturated centre was also present in the thioacetal. We have demonstrated that this is indeed the case and wish to report the details for the ring closure of 5-hexenyl-1,3-thiolane (**1**) and related 1,3-oxathiolanes and 1,3-oxathiolan-5-ones to a variety of oxygenated cycloalkanes (13).

Results and discussion

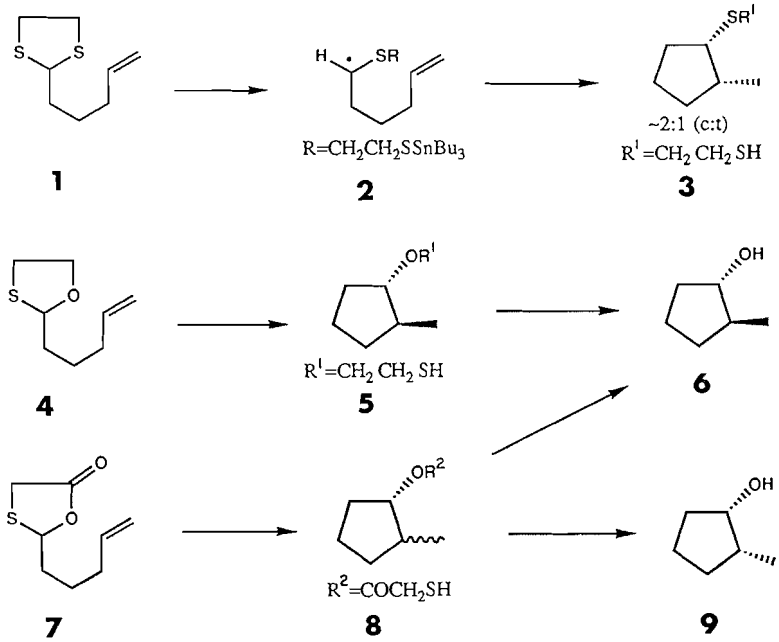
Treatment of **1** in refluxing benzene, to which tributyltin hydride and AIBN were added by syringe pump, resulted in 60% conversion to the cyclopentane **3** as a 2:1 *cis/trans* isomeric mixture (Scheme 1). Cyclization of the diphenyldithioacetal corresponding to **1** was recently reported to give a 35:65 *cis/trans* ratio (8*k*). Similar treatment of **4** afforded, after chromatography, a 60% isolated yield of the *trans* substituted system **5** as a single isomer. Ether cleavage was effected with boron trichloride (14) to provide *trans*-2-methylcyclopentanol (**5**) whose structure and stereochemistry were confirmed by comparison with an authentic sample prepared from cyclo-

Can. J. Chem. Downloaded from www.nrcresearchpress.com by 198.100.157.202 on 09/07/12
For personal use only.

TABLE 1. Reductive and free-radical cyclizations

Entry	Substrate[a]	Reagent(s)[b]	Intermediate	Product	Yield, %	Reference
1.		e^-			98	9*b*
2.		e^-		 1.4:1 (*t:c*)	70	9*g*
3.		e^- or $NaC_{10}H_8$			37 ~36	9*f*
4.		Zn TMSCl		 5:1 (*endo:exo*)	82	9*e*
5.		nBu_3SH AIBN		 ~2:1 (*t:c*)	73	10*b*
6.		SmI_2			Minor	10*b*
7.		SmI_2		 20:1 (*t:c*)	60	10*c*
8.		nBu_3SnH AIBN		 ~1:1 (*t:c*)	80	10*d*

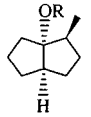
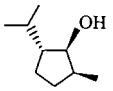
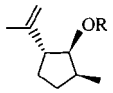
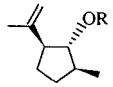
[a]E = CO_2CH_3.
[b]Electroreduction ≡ e^-.



SCHEME 1

Can. J. Chem. Downloaded from www.nrcresearchpress.com by 198.100.157.202 on 09/07/12
For personal use only.

TABLE 2. Selected nuclear magnetic resonance data for substituted cyclopentanes

Entry	Compound	CH_3		H-C-O	
		^{1}Hnmr	^{13}Cnmr	^{1}Hnmr	^{13}Cnmr
1.		0.98	19.3		
2.		1.07	15.1		
3.		0.99 (OH) 0.98	18.8 18.0	— 3.70	88.0 80.1
4.		1.02	13.5	4.06	76.0
5.		0.96 (OH) 0.97	14.4 13.3		
6.				3.87	78.1
7.		0.98	13.6	3.80	78.5
8.		0.98 (OH) 0.92	14.3 14.1	— 3.84	86.1 77.8
9.		1.01 (OH) 1.01	13.7 20.8	— 3.75	88.8 79.4

R = CH_2CH_2SH or H.

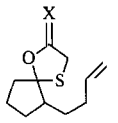
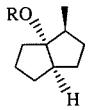
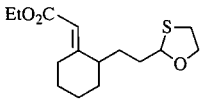
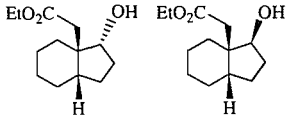
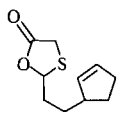
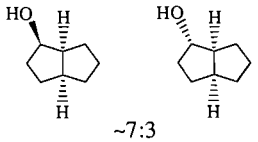
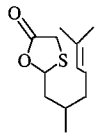
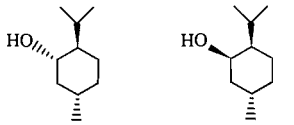
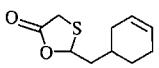
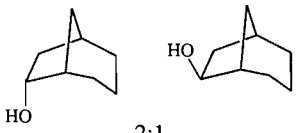
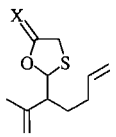
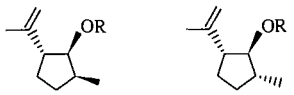
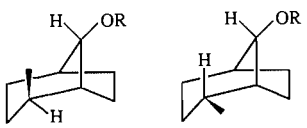
pentene oxide. Stereochemical assignments are often difficult in cyclopentanols compared to cyclohexanols, thus the key nmr data for several related 1,2-disubstituted cyclopentanes are summarized in Table 2. In the simplest systems a consistent trend was observed. The hydrogen signal for the *cis* methyl signal resonated at lower field than the *trans*. In contrast, in the ^{13}C nmr spectrum, as a consequence of the γ-*gauche* effect, the relative field positions were reversed and the *trans* methyl group appeared at lower field. Generally the signal for the proton on the carbon bearing oxygen in the *cis* series resonated at lower field than the *trans* isomer, while the opposite trend was evident for the relative positions of this carbon. These features facilitated the stereochemical assignments when both isomers were available, and was consistent with related observations (15*a*) that a *trans* relationship between vicinal hydrogens in cyclic systems caused a downfield shift for each of the carbon atoms involved. Additional useful compilations of several cyclopentane and quinane systems may be found in previous papers by others (15).

The cleavage of the ether side chain (-OCH_2CH_2SH) was sluggish in sterically demanding cases. Consequently the behaviour of 5-oxo-1,3-oxathiolanes was also investigated, and was shown to provide an even more useful route to cyclic systems in which the initial ester, such as **8**, was readily cleaved by base hydrolysis to afford the parent alcohols **6** and **9** in 74% yield as a 3:2 isomer mixture. The versatility of these approaches is reflected in several diverse examples that are summarized in Table 3.

The requisite heterocycles were prepared from the appropriate carbonyl compound in dioxane containing $ZnCl_2$ and 2-mercaptoethanol (16) or in refluxing benzene containing β-mercaptoacetic acid and *p*-toluenesulfonic acid as catalyst with azeotropic removal of water (17). The required substrates were synthesized, as illustrated briefly in Scheme 2, from commercially available starting materials. This involved alkylation, hydrolytic decarboxylation, and acetalation for **12** and **13**, while **16** was generated by alkylation of cyclohexanone followed by Horner–Wadsworth–Emmons olefination. The routes to **21** and **26** required lithium aluminum hydride reduction of the requisite carboxylic acids (18), bromination (Ph_3PBr_2), substitution (NaCN), reduction (diisobutylaluminum hydride), and acetalation. This sequence finds a close parallel in earlier work by Wilt, Massie, and Dabek (18*a*). Similarly, deconjugative alkylation of ethyl 3,3-dimethylacrylate with lithium diisopropyl amide (LDA) and 4-bromo-1-butene, lithium aluminum hydride reduction of the ester **27**, pyridinium chlorochromate oxidation, and protection of the aldehyde **29** afforded **30** and **31**.

Can. J. Chem. Downloaded from www.nrcresearchpress.com by 198.100.157.202 on 09/07/12
For personal use only.

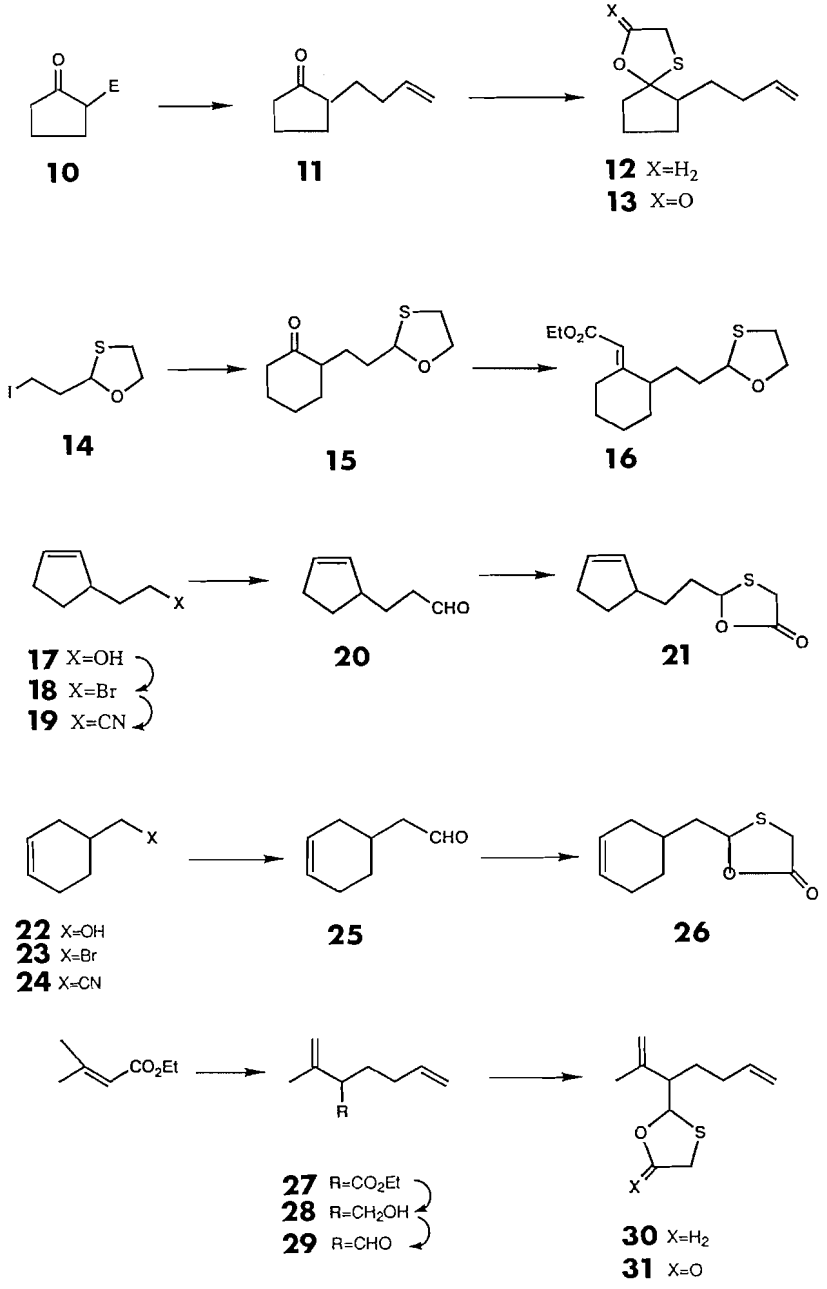
TABLE 3. Thioacetal cyclizations

Entry	Substrate	Product(s)	Yield
1.	 **12** X = H_2 **13** X = O	 **32** R = $(CH_2)_2SH$ **33** R = H	66% 93%
2.	 **16**	 **34** ~2:1 **35** R = $(CH_2)_3SH$	70%
3.	 **21**	 ~7:3 **36**	95%
4.	 **37**	 **38** ~1:1 **39**	80%
5.	 **26**	 **40** 2:1 **41**	81%
6.	 **30** X = H_2 **31** X = O	 65:35 R = $(CH_2)_3SH$ 80:10 **42** R = H **43**  **44** 8:2 **45**	

Examination of Table 3 reveals that these free-radical based cyclizations may be utilized for a variety of substitution patterns and ring systems. In a formal sense, this amounts to an intramolecular Grignard addition that is accomplished under neutral conditions. Indeed, direct intramolecular cyclization of halides onto carbonyl centres is usually difficult and requires the use of nickel complexes (19*a*), although samarium(II) iodide may be employed with iodo substituted β-keto esters or amides (19*b*). In addition, oxidation of the cyclized alcohol product to the ketone makes this two-step procedure equivalent to an acyl radical cyclization. This is a topic of considerable current interest (20), since in many circumstances the direct use of carbonyl systems is inhibited by decarbonylation.

For future synthetic applications several features may be

Can. J. Chem. Downloaded from www.nrcresearchpress.com by 198.100.157.202 on 09/07/12
For personal use only.



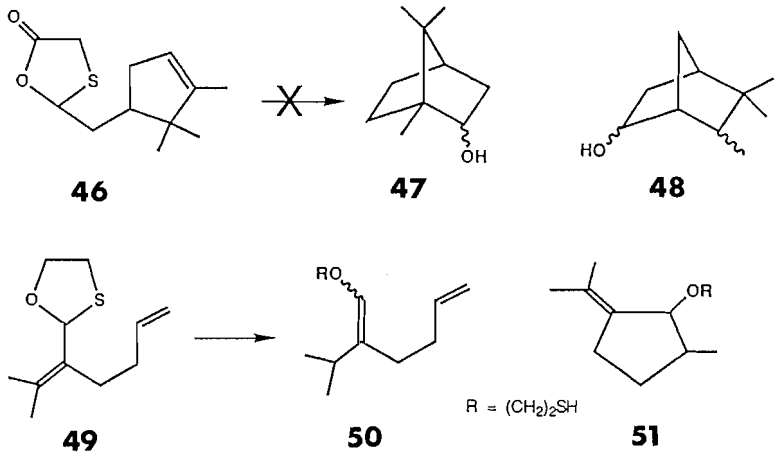
SCHEME 2

noted. These include the ease with which fused ring systems such as quinanes and hydrindanes bearing a variety of substitution patterns may be prepared (entries 1–3). Methyl substituted olefins such as **37** (prepared from citronellal) also reacted, providing menthol (**38**) and its epimer **39** in a 1:1 ratio via a 6-*exo-trig* ring closure. However, more sterically encumbered species such as the acetal **46** (Scheme 3) derived from α-campholenic aldehyde (21) failed to cyclize after carbon–sulfur bond cleavage. Neither of the bicyclic products **47** nor **48** were detected, although there is precedence for the formation of bicyclo[2.2.1]heptanes in simpler unsubstituted systems (18*a*). Cleavage of the carbon–sulfur bond in diene **49** (Scheme 3) afforded an allylic radical that could cyclize to **51**. However, this intermediate was insufficiently reactive and the major product was the enol ether **50**. Enol ethers of aldehydes are often difficult to prepare and thus this method for the generation of protected enols from conjugated acetals under neutral conditions should have further utility.

In principle, the cyclohexene **26** may cyclize via either a 5-*exo-trig* or 6-*exo-trig* pathway to generate the bicyclo[3.2.1]-octane and (or) bicyclo[2.2.2]octane skeletons. In practice, only the 6-bicyclo[3.2.1]octanols **40** and **41** were formed in a 70:30 *endo*/*exo* ratio accompanied by 12% of the non-cyclized product, 2-(3-cyclohexenyl)ethanol. An authentic sample of 2-bicyclo[2.2.2]octanol was prepared and shown to be both absent and different from **40** and **41**.

It was also of interest to examine the dienes **30** and **31**, which in principle are capable of tandem cyclization of the appropriate *cis* isomer to a bicyclo[2.2.1]heptane and (or) a bicyclo[3.2.1]octane nucleus. In the case of **30**, no bicyclic material was detected. In contrast, after cyclization and hydrolysis, four alcohols (**42**–**45**) were isolated from the reaction of **31**. The major cyclopentane component from both **30** and **31** had the isopropenyl and alcohol substituents in a *trans* orientation. The assignment was based on spectral data and comparison with related compounds including racemic (1*R**,2*R**,5*S**)-2-

Can. J. Chem. Downloaded from www.nrcresearchpress.com by 198.100.157.202 on 09/07/12
For personal use only.



46 47 48

49 50 51

SCHEME 3

methyl-5-isopropylcyclopentanol obtained by hydrogenation (Table 2, entry 7). The minor product from the initial ring closure was **43**. There was no evidence for a 5-*exo-trig* cyclization to a bicyclo[2.2.1]heptane system such as **52** (Scheme 4). The other products (10%) were the methyl epimers **44** and **45** from a 6-*endo-trig* ring closure. The major alcohol **44** (8%) contained an axial methyl group, as illustrated, with the hydroxyl function *anti*. A previous study has also observed this preference for *endo* closure to a bicyclo[3.2.1]octane when this choice is available (22). Thus both **26** and **31** provide a rapid preparation of the bicyclo[3.2.1]octane nucleus that is present in many terpenoid natural products. Unfortunately the yield in the latter case is rather low due to the requirement for *cis* substituents and the presence of the substituted double bond.

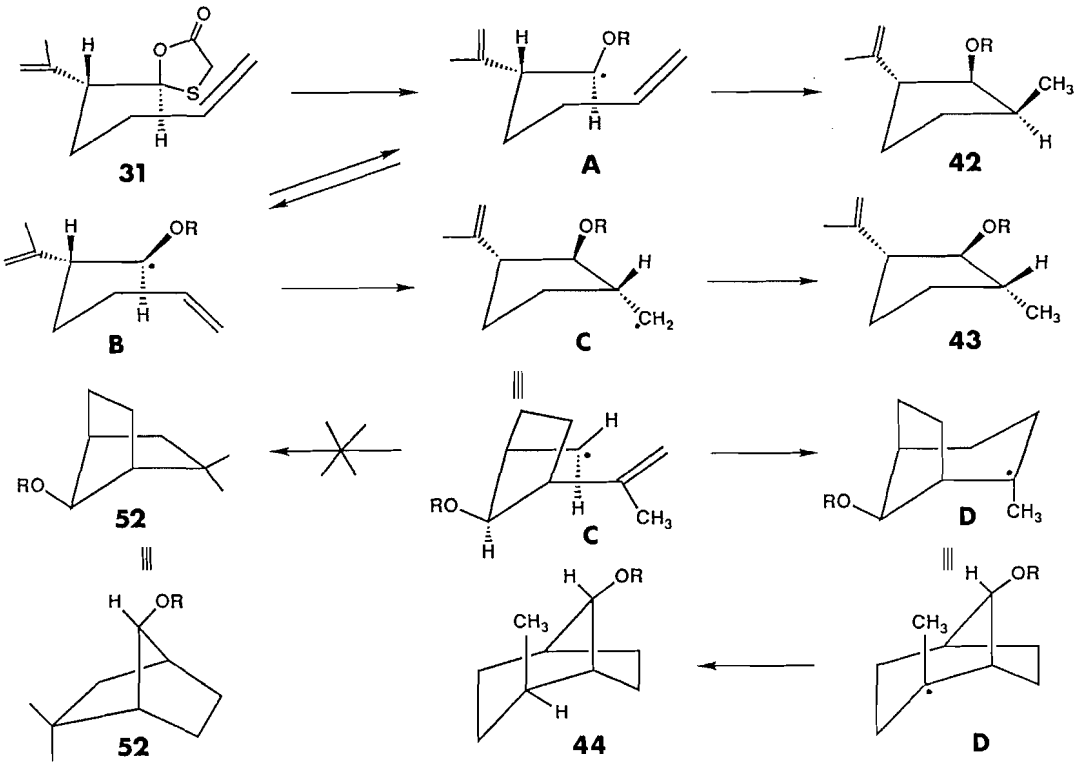
Studies of the stereochemistry of simple substituted 5-hexenyl radical cyclizations have allowed the formulation of guidelines to predict product stereochemistry. These are based on the assumption that the preferred transition state geometry resembles the most favorable cyclohexane chairlike conformation (23). Based on these studies, it has been established that, for simple monoalkyl substituted 5-hexenyl cyclizations, *cis* dialkylcyclopentanes predominate with 1- and 3-substituted systems. In contrast, *trans* products are formed preferentially when 2- and 4-substituted cyclopentanes are generated. The *cis* vs. *trans* selectivity is affected significantly by C4 substituents, a feature that has been used in synthesis (24). Less was known about the behaviour of C1, C2-disubstituted systems until recent investigations of highly functionalized carbohydrate derivatives revealed that these additional substituents may alter the expected 1,5 stereochemistry, and a boat conformation is often preferred (25). This led to exclusive 1,5-*trans* selectivity in highly functionalized systems. On the basis of theoretical calculations Spellmeyer and Houk (23*d*) estimated that the boatlike transition states lie only ~0.5 kcal/mol above the chairlike structures for these reactions. In the case of **30** and **31** the major product arose from an intermediate of type **A** (Scheme 4) with a chairlike conformation in which the substituents were equatorial. This species is in equilibrium with the boatlike radical **B**. Upon cyclization, intermediate **C** is generated, in which the carbon side chains bear a *cis* relationship. Approximately half of this material is quenched to give the minor isomer **43** while the rest cyclized further to form **D** and hence **44**. The preference for the *endo* vs. *exo* closure is apparent from inspection of **C**, since the 6-*endo-trig* cyclization involves both a less strained transition state and addition to the less substituted end of the double bond, as illustrated in Scheme 4.

As noted above, the oxathiolane **4** gave only the *trans* isomer **6**, while for the lactone **7** the *cis* isomer **9** was dominant. This difference reflects the faster cyclization rate for the oxathiolanone case, a consequence of the diminished stability of the intermediate radical due to an acyl rather than an ether substituent. Rapid cyclizations have an early transition state and give rise preferentially to 1,5-*cis* products. In contrast, eclipsing interactions become more important in longer lived intermediates as a consequence of the slower rate and later transition state, so that more 1,5-*trans* product is formed. Calculations indicated that the radical stabilization energies of monosubstituted methyl radicals were 2.38 kcal/mol ($\cdot CH_2OCOH$) and 5.30 kcal/mol ($\cdot CH_2OCH_3$), respectively (26). This order parallels the extent of delocalization of the unpaired electron in related radicals that is reflected by ESR hyperfine splitting constants (27) ($RCH_2OCH_2\cdot > RCO_2CH_2\cdot > RCH_2\cdot$). Intramolecular cyclization rates do not appear to have been determined previously for oxygen substituted radicals. In preliminary experiments,[1] which employed the radical clock based on the corresponding 5-hexenyl system (28), we established that the relative cyclization rate for **7** is approximately six times faster than for **4**. These values of $0.25 \times 10^6\ M^{-1}\ s^{-1}$ for **4** and $1.4 \times 10^6\ M^{-1}\ s^{-1}$ for **7** at 80°C may be compared to the corresponding k_c for 1-bromo-5-hexene at the same temperature, $1.5 \times 10^6\ M^{-1}\ s^{-1}$ (28). Thus the 1,3-oxathiolan-5-ones cyclize at a similar rate to 5-hexenyl cases, which will allow this oxygen containing system to be employed in a variety of synthetic endeavours.

To extend the versatility of these procedures, the use of allyl stannanes was also investigated (29). It was suspected that the allyl stannanes might be more reactive than simple monosubstituted alkenes, a result that was confirmed experimentally when either allyltri-*n*-butylstannane or methallyltri-*n*-butylstannane were employed with **4**, **7**, and **21** respectively. Allyl transfer worked efficiently but in each case the intermediate radical was trapped directly upon carbon–sulfur bond cleavage prior to cyclization to afford the 1,8-nonadiene product. Clearly, for this strategy to succeed, both a more rapid cyclization step and a slower trapping sequence will be required. Very recently, rate studies have demonstrated that the rate constant for the addition of cyclohexyl radicals to allyltriphenyl tin is $1 \times 10^5\ M^{-1}\ s^{-1}$

[1] M. Charron. Honours B.Sc. Thesis, University of Ottawa, Ottawa, Canada, April 1989. Rates were also measured at 58.5°C. The k_c values at 58.5°C were 0.12×10^6, 0.71×10^6, and $0.76 \times 10^{-6}\ M^{-1}\ s^{-1}$ for **4**, **7**, and 1-bromo-5-hexene respectively.

Can. J. Chem. Downloaded from www.nrcresearchpress.com by 198.100.157.202 on 09/07/12
For personal use only.



SCHEME 4

at 80°C (30). Thus allyltriphenylstannane is approximately 10 times less reactive than methyl acrylate, whereas 1-hexene is 10^3 less reactive than acrylate. Consequently substitution of at least one electron-withdrawing group will be required in compounds **4**, **7**, and the other examples so that the cyclization can compete with allyl transfer. Nevertheless, Keck and Tafesh (*10g*) conducted an effective cyclization – allyl transfer sequence with an unsaturated α-silyloxy phenylselenide.

In conclusion, thioacetals such as 1,3-oxathiolanes and 1,3-oxathiolan-5-ones are useful precursors of radical intermediates for intramolecular ring closure. This provides a facile route to both tertiary and secondary cyclic alcohols with a reasonable level of stereochemical control. The products retain synthetically useful functionality for subsequent manipulation, unlike conventional unsaturated organic halide precursors in which a net loss of two functional groups results. These features should facilitate the extended use of these methods in synthesis.

Experimental

Melting points were determined in capillary tubes with a Thomas–Hoover Uni-Melt apparatus, or on a Fisher–Johns melting point apparatus, and are uncorrected. Infrared (ir) spectra were recorded on a Perkin–Elmer 783 or 983G infrared spectrophotometer. Proton magnetic resonance spectra (^{1}H nmr) were measured in deuterochloroform at 60 MHz with a Varian model EM 360 spectrometer or at 200 MHz with a Varian Gemini spectrometer or at 300 MHz with a General Electric GN 300 or a Varian XL-300 spectrometer. Carbon magnetic resonance spectra (^{13}C nmr) were measured at 75 MHz with a General Electric GN 300 or a Varian XL-300 spectrometer. Chemical shifts are reported in ppm downfield from tetramethylsilane (δ scale) as an internal standard; the multiplicity, numbers of protons, and coupling constants are indicated in parentheses. Mass spectra were determined on a V.G. Micromass 7070 HS instrument using an ionization energy of 70 eV, or on a Hewlett Packard 5890A gas chromatograph 5970B mass selective detector equipped with a 12.5 m capillary column (0.2 mm i.d.) coated with cross-linked dimethyl silicone (0.33 μm). Flash column chromatography using E. Merck silica gel 60 (230–400 mesh) was employed for all column chromatography. Analytical thin-layer chromatography (tlc) was carried out on aluminum sheets precoated (0.2 mm layer thickness) with silica gel 60 F_{254} (E. Merck). The purity of all title compounds was judged to be ≥95% as determined by a combination of gc–ms, ^{1}H nmr, and ^{13}C nmr analysis.

Petroleum ether refers to a fraction with boiling range 30–60°C. Anhydrous diethyl ether (ether), tetrahydrofuran (THF), dimethoxyethane (DME), and dioxane were obtained by distillation from $LiAlH_4$ or potassium/benzophenone. Methanol and absolute ethanol were dried by distillation from magnesium. Dry hexamethylphosphoramide (HMPA), dimethylformamide (DMF), dimethyl sulfoxide (DMSO), and diisopropylamine were prepared by distillation from calcium hydride. Solutions in organic solvents were dried over anhydrous magnesium sulfate and stripped of solvent with a Büchi rotary evaporator connected to a water aspirator. Unless otherwise indicated, all reactions were conducted under an atmosphere of dry nitrogen.

Acetal preparation

2-(4-Pentenyl)-1,3-dithiolane (1)

5-Hexenal (1.19 g, 12.2 mmol) in $CHCl_3$ (5 mL) was added dropwise over 10 min to a chloroform solution (22 mL) containing ethane dithiol (1.15 g, 12.2 mmol), $BF_3 \cdot Et_2O$ (1.5 mL, 12.2 mmol), and glacial acetic acid (3 mL) maintained at −22°C with an external (solid CO_2/CCl_4) bath. Stirring was continued at −22°C for 30 min, at 0°C for 30 min, and 10% aqueous potassium hydroxide (50 mL) was then added with vigorous stirring. The aqueous layer was extracted with $CHCl_3$ (2 × 15 mL) and the combined chloroform extracts washed sequentially with 10% aqueous KOH, water, and brine, dried, filtered, and concentrated. The product was purified by chromatography (5% ethyl acetate/petroleum ether) to afford the dithioacetal **1**, 1.8 g (85%); ^{1}H nmr (60 MHz) δ: 1.4–2.4 (m, 6H), 3.2 (s, 4H, SCH_2CH_2S), 4.45 (t, 1H, J = 6 Hz, H-C(S)), 4.8–5.2 (m, 2H, H_2C=C), 5.4–6.2 (m, 1H, HC=C); ^{13}C nmr δ: 137.1, 115.5, 46.4, 34.3, 30.2, 30.0, 29.6, 25.7.

2-(4-Pentenyl)-1,3-oxathiolane (4) (Procedure based on ref. 16)

A dioxane solution (10 mL) containing 6-hexenal (1.47 g, 15 mmol) and 2-mercaptoethanol (1.40 g, 22 mmol, Aldrich) was cooled to 0°C with an external ice–water bath. Sodium sulfate (2 g) and freshly fused, powdered zinc chloride (2.05 g, 15 mmol) were added. After 10 min

Can. J. Chem. Downloaded from www.nrcresearchpress.com by 198.100.157.202 on 09/07/12
For personal use only.

Can. J. Chem. Downloaded from www.nrcresearchpress.com by 198.100.157.202 on 09/07/12
For personal use only.

the ice bath was removed and stirring was continued for a further 20 h at 22°C. The reaction mixture was diluted with water (20 mL) and extracted with ether (3 × 15 mL). The combined ether extracts were washed with water (3 × 10 mL), then with brine, dried, filtered, and concentrated. The product was purified by flash chromatography (10% ethyl acetate/petroleum ether) to give **4**, 1.66 g (70%); ^{1}H nmr δ: 1.44–1.62 (m, 2H, -CH_2-), 1.70–1.83 (m, 1H, CH_2-CH-O), 1.86–1.98 (m, 1H, CH_2-CH-O), 2.05–2.13 (m, 2H, CH_2-C=C), 2.98–3.03 (m, 2H, CH_2-S), 3.71–3.80 (m, 1H, O-CH_2), 4.28–4.35 (m, 1H, O-CH_2), 4.93–5.09 (m, 3H, H_2C=C, H-CO), 5.72–5.86 (m, 1H, HC=C); ^{13}C nmr δ: 138.2, 114.9, 86.8, 71.2, 35.8, 33.4, 32.6, 25.6. Exact Mass calcd. for $C_6H_{10}OS$ (M − C_2H_4): 130.0452; found: 130.0458.

The 1,3-oxathiolane-5-one acetals were prepared from the corresponding aldehyde in refluxing benzene containing β-mercaptoacetic acid and *p*-toluenesulfonic acid as catalyst with azeotropic removal of water according to the procedure of Satsumabayashi *et al.* (17).

2-(4-Pentenyl)-1,3-oxathiolan-5-one (7): ir (neat): 3090 (H-C=C), 1775 (C=O) cm^{-1}; ^{1}H nmr δ: 1.55 (m, 2H, CH_2), 1.90 (m, 2H, CH_2), 2.07 (m, 2H, CH_2), 3.63 (AB m, 2H, J = 16 Hz, S-CH_2-C=O), 4.95 (br s, 1H, HC=C), 5.02 (br d, 1H, J ~ 12 Hz, HC=C), 5.47 (t, 1H, J = 6.0 Hz, HC-S(O)), 5.75 (m, 1H, J = 12, 3.5 Hz, HC=C); ^{13}C nmr δ: 172.8, 137.6, 115.4, 82.1, 35.9, 32.8, 31.4, 23.9.

2-(2,6-Dimethyl-5-heptenyl)-1,3-oxathiolan-5-one (37): ^{1}H nmr δ: 0.92, 0.93 (d, 3H, J = 6.5 Hz, CH_3C, 2 diastereomers, ~1:1), 1.57 (s, 3H, CH_3C=C), 1.65 (s, 3H, CH_3C=C), 3.62 (2 AB m, 2H, J ~ 16 Hz, S-CH_2-C=O), 5.05 (t, 1H, J = 6.0 Hz, HC-S(O)), 5.53 (m, 1H, HC=C); ^{13}C nmr δ: 172.9, 131.7, 124.0, (2 diastereomers, ~1:1, 81.4, 80.8), (43.9, 42.4), 36.7, (31.6, 31.4), 29.5, 25.4, 25.0, (19.2, 19.0), 17.4.

2-(3-Buten-1-yl)-cyclopentanone (11)

A heterogeneous mixture of methyl-2-oxocyclopentylcarboxylate (5.68 g, 40 mmol, Aldrich), 4-bromo-1-butene (6.48 g, 48 mmol, Aldrich), K_2CO_3 (11 g, 80 mmol, ground to a fine powder before use), and sodium iodide (0.45 g, 3 mmol) was stirred vigorously under reflux in acetone (150 mL) for 48 h. The reaction mixture was filtered, concentrated, and a solution of hexamethylphosphoramide (HMPA)/water (9:1, 40 mL) and sodium iodide (60 mmol) added. The resulting solution was heated at 160° for 5 h. The reaction was cooled to room temperature, extracted with ether, the combined ether extracts washed with water, dried, filtered, and concentrated. The crude product was purified by flash chromatography (10% ethyl acetate/petroleum ether) to give ketone **11**, 2.26 g (50%); ^{1}H nmr (60 MHz) δ: 1.2–2.5 (m, 11H), 4.8–5.2 (m, 2H, H_2C=C), 5.4–6.2 (m, 1H, HC=C). Exact Mass calcd. for $C_9H_{14}O$: 138.1044; found: 138.1044.

5-(3-Buten-1-yl)-1,4-oxathiaspiro[4.4]nonane (12)

Prepared in 80% yield (0.317 g) after chromatography (20% ethyl acetate/petroleum ether); ^{1}H nmr (60 MHz) δ: 1.2–2.4 (m, 11H), 3.1–2.8 (m, 2H, CH_2-S), 3.6–4.4 (m, 2H, CH_2-O), 4.8–5.2 (m, 2H, H_2C=C), 5.4–6.2 (m, 1H, HC=C). Exact Mass calcd. for $C_{11}H_{18}OS$: 198.1077; found: 198.1080.

2-(2-Iodoethyl)-1,3-oxathiolane (14)

Dry sodium iodide (18.0 g, 120 mmol) was dissolved in acetonitrile (200 mL), followed by freshly distilled acrolein (5.60 g, 100 mmol) and chlorotrimethylsilane (15.4 mL, 120 mmol) (compare ref. 31). The reaction was stirred for 10 min and 2-mercaptoethanol (9.40 g, 120 mmol) was added. After a further 10 min the reaction was poured into aqueous 5% $NaHCO_3$ solution (100 mL) overlaid with pentane (300 mL). The organic phase was separated, washed with aqueous 5% $Na_2S_2O_3$ solution (100 mL), and repeatedly with brine (6 × 100 mL until a single organic phase was obtained). The organic phase was dried (K_2CO_3), filtered, and concentrated. The residue obtained was filtered through neutral alumina to provide the iodo-acetal **14**, 17.5 g (73%); ^{1}H nmr δ: 2.1–2.6 (m, 2H, CH_2-CH_2I), 2.8–3.4 (m, 4H, CH_2-I, CH_2-S), 3.6–4.1 (m, 1H, CH_2-O), 4.1–4.5 (m, 1H, CH_2-O), 5.2 (t, 1H, J = 6.5 Hz, H-C-O,S).

2-(2-(Oxocyclohexan-2-yl)ethyl)-1,3-oxathiolane (15)

A few drops of dimethyl sulfoxide (DMSO) were added to a THF (15 mL) suspension of KH (0.205 g, 5.1 mmol) maintained at 0°C with an external ice bath. A cold solution (0–5°C) of cyclohexanone (0.490 g, 5 mmol) in THF (5 mL) was added dropwise. After 10 min, a THF solution (5 mL) of iodide **14** (1.22 g, 5 mmol) was added. The resulting reaction mixture was stirred at 0°C for 30 min, warmed to 22°C, and stirred for a further 1 h. The reaction was quenched with saturated aqueous NH_4Cl solution, extracted with ether, dried, filtered, and concentrated. The product was purified by chromatography (20% ethyl acetate/petroleum ether) to give **15**, 0.640 g (60%); ^{1}H nmr (60 MHz) δ: 1.2–2.5 (m, 12H), 3.05 (m, 2H, CH_2S), 3.8 (m, 1H, CH_2O), 4.3 (m, 1H, CH_2O), 5.05 (t, 1H, J = 6 Hz, H-C-O,S); ^{13}C nmr δ: 212.8, 86.8, 71.3, 50.1, 41.8, 33.8, 32.4, 27.7, 26.0, 25.9, 24.7. Exact Mass calcd. for $C_{11}H_{18}O_2S$: 214.1026; found: 214.1028.

2-[(2-(2-Ethyl methylenecarboxylate)cyclohexyl)ethyl]-1,3-oxathiolane (16)

A suspension of NaH (0.09 g, 80% dispersion in oil, Aldrich) in THF (4 mL) was cooled to 0°C and a solution of triethyl phosphonoacetate (0.70 g, 3 mmol, Aldrich) in THF (4 mL) added dropwise. Approximately 10 min later, after hydrogen evolution had ceased, HMPA (0.8 mL) was added, followed by a THF solution (6 mL) of ketone **15** (0.321 g, 1.5 mmol). The ice bath was removed and the reaction stirred at 22°C for 48 h. The reaction was quenched with saturated aqueous NH_4Cl (10 mL), extracted with ether (3 × 10 mL), and the combined extracts washed with water and brine, dried, filtered, and concentrated. The product was purified by radial chromatography on silica gel (20% ethyl acetate/petroleum ether) to give **16**, 0.384 g (90%); ^{1}H nmr δ: 1.24 (t, 3H, J = 7 Hz, CH_3), 3.00 (m, 2H, H_2C-S), 3.75 (m, 1H, H_2C-O), 4.10 (m, 2H, H_2C-OC=O), 4.28 (m, 1H, H_2C-O), 5.03 (m, 1H, HC-S(O)), 5.55 (m, 1H, HC=C); ^{13}C nmr δ: 165.7, 114.5, 112.7, 86.9, 71.1, 60.0, 45.4, 34.1, 33.8, 32.5, 28.2, 27.4, 22.8, 20.4, 14.0. Exact Mass calcd. for $C_{15}H_{24}O_3S$: 284.1445; found: 284.1421.

2-(Cyclohexen-4-yl)methyl-1,3-oxathiolan-5-one (26)

An ether solution (20 mL) containing 3-cyclohexenyl-1-carboxylic acid (5.04 g, 40 mmol, Aldrich) was added dropwise to a stirred suspension of $LiAlH_4$ (3.0 g) in ether (40 mL) at 22°C (18*b*). The reaction was stirred at this temperature for 12 h, refluxed for 4 h, cooled to 0°C, and excess $LiAlH_4$ destroyed by dropwise addition of ethyl acetate and water. The reaction mixture was filtered, the precipitate washed with ether, and the combined filtrates were dried, filtered, and concentrated to give the alcohol **22**, 4.46 g (100%); ^{1}H nmr (60 MHz) δ: 1.2–2.3 (m, 7H), 2.4 (s, 1H, OH), 3.5 (bd, 2H, J ~ 5 Hz, CH_2-O), 5.65 (bs, 2H, HC=CH).

Bromine (7.03 g, 44 mmol) in benzene (15 mL) was added dropwise to a cold (external ice bath) mechanically stirred benzene solution (40 mL) containing triphenylphosphine (11.5 g, 44 mmol). After addition was complete, stirring was continued for a further 1 h at 22°C, pyridine (3.48 g, 44 mmol) was added, the reagent recooled to 0°C, and a benzene solution (15 mL) of the alcohol **22** (4.46 g, 40 mmol) was added dropwise. After this addition was complete, the ice bath was removed and stirring was continued for 6 h at 22°C. Petroleum ether was added (200 mL) and the mixture placed in the freezer at −20°C for 2 h. The precipitate was removed by filtration, washed thoroughly with petroleum ether, the filtrate concentrated, and the product purified by distillation (bp 68–70°C/12 Torr; 1 Torr = 133.3 Pa) to give the bromide **23**, 5.86 g (84%); ^{1}H nmr (60 MHz) δ: 1.2–2.4 (m, 7H), 3.40 (bd, 2H, J ~ 6 Hz, CH_2-Br), 5.65 (bs, 2H, HC=CH).

Sodium cyanide (3.73 g, 76 mmol) was added to a 90% aqueous ethanol solution (40 mL) containing the bromide **23** (6.64 g, 38 mmol) and the resulting suspension stirred under reflux for 16 h. The bulk of the ethanol was removed under reduced pressure, water was added, and the reaction extracted with ether. The combined ether extracts were washed with water and brine, dried, filtered, and concentrated. The product was purified by chromatography (10% ethyl acetate/petroleum ether) to give the nitrile **24**, 4.24 g (92%); ^{1}H nmr (60 MHz) δ: 1.2–2.5 (m, 9H), 5.65 (bs, 2H, HC=CH).

An *n*-hexane solution (60 mL) of the nitrile (0.605 g, 5 mmol) was cooled to −78°C with an external (solid CO_2/acetone) bath and a toluene solution of diisobutylaluminium hydride (6 mL, 6 mmol, 1.0 M, Aldrich) added dropwise over 15 min. After 30 min the cooling

Can. J. Chem. Downloaded from www.nrcresearchpress.com by 198.100.157.202 on 09/07/12
For personal use only.

bath was removed and stirring continued for a further 3 h. The reaction was quenched with saturated aqueous NH_4Cl (50 mL) and, 20 min later, 5% aqueous H_2SO_4 (20 mL) was added.

The reaction was extracted with ether, the combined ether extracts washed sequentially with 5% aqueous HCl, water, and brine, and dried, filtered, and concentrated carefully at 22°C to provide the aldehyde **25**, 0.62 (100%).

A benzene solution (20 mL) of mercaptoacetic acid (1.84 g, 20 mmol) was added to benzene (100 mL) and the aldehyde **25** (2.48 g, 20 mmol) in a flask equipped with a Soxhlet extractor containing a thimble packed with 4 Å molecular sieves. The bulk of the benzene was removed under reduced pressure, ether (100 mL) added, and the solution washed with saturated aqueous $NaHCO_3$ (2 × 30 mL), water (30 mL), and brine (30 mL), and dried, filtered, and concentrated. The product was purified by chromatography (10% ethyl acetate/petroleum ether) to give the acetal **26**, 1.73 g (44%, two diastereomers); ir (neat): 3030 (H-C=C), 1770 (C=O) cm^{-1}; ^1H nmr (300 MHz) δ: 1.22–1.29 (m, 1H), 1.63–2.20 (m, 8H), 3.60 (d, 2H, J = 16.6 Hz, CH_2-S), 5.52–5.63 (m, 3H, HC=CH, H-CO,S); ^{13}C nmr δ: 172.5, (126.7, 125.3 two diastereomers), (80.6, 80.5), 43.0, (31.4, 31.2), 31.0, 30.3, (28.3, 28.2), 24.4. Exact Mass calcd. for $C_6H_8O_2S$ (M − C_4H_6): 144.0245; found: 144.0216.

*2-(Cyclopenten-3-yl)ethyl-1,3-oxathiolan-5-one (**21**)*

A parallel series of reactions to those described above (18), commencing with 2-cyclopentene-1-acetic acid, were utilized to prepare **21** in 40% overall yield; ir (neat): 3025 (H-C=C), 1775 (C=O) cm^{-1}; ^1H nmr (60 MHz) δ: 1.2–3.0 (m, 9H), 3.7 (s, 2H, CH_2-S), 5.5 (t, 1H, J = 6 Hz, H-CO,S), 5.7 (m, 2H, HC=CH). Exact Mass calcd. for $C_{10}H_{14}O_2S$ − $C_2H_3O_2$: 139.0581; found: 139.0571.

*2-Isopropenyl-6-hexenal (**29**) and 2-methyl-3-formyl-2,6-heptadiene*

Lithium diisopropylamide (LDA), in THF (200 mL), prepared from *n*BuLi (45 mL, 2.7 M, hexane) and diisopropylamine (16.8 mL, 0.12 mol), was cooled to −78°C and HMPA (20.9 mL, 0.12 mol) added, followed by a THF solution (15 mL) containing ethyl 3,3-dimethylacrylate (12.8 g, 0.10 mol, Aldrich). After 15 min 4-bromo-1-butene (15 g, 0.11 mol) was added dropwise over 10 min, the reaction stirred at −78°C for 1 h, at 22°C for 5 h, and then quenched with saturated aqueous NH_4Cl (25 mL). Ether was added and the combined ether extracts (3 × 50 mL) were dried, filtered, and concentrated. The residue was redissolved in ether (150 mL), washed with water (4 × 25 mL) and then with brine (25 mL), dried, filtered, and concentrated and the product purified by distillation, bp 85–87°C/10 Torr, to give the diene-ester **27**, 14.6 g (80%); ^1H nmr (CCl_4, 60 MHz) δ: 1.1–1.4 (t, 3H, J = 7 Hz, -OCH_2CH_3), 1.7 (s, 3H, CH_3-C=C), 1.4–2.3 (m, 4H, CH_2-C=, CH_2-$CHCO_2Et$), 2.7–3.1 (t, 1H, J = 7 Hz, HC-CO_2Et), 3.8–4.3 (q, 2H, J = 7 Hz, CH_2-O), 4.7–5.2 (m, 4H, H_2C=C), 5.3–6.2 (m, 1H, H-C=).

An ether solution (50 mL) containing the diene-ester **27** (18.2 g, 0.1 mol) was added dropwise, over 30 min, to a stirred ether suspension (250 mL) of $LiAlH_4$ (1.9 g, 0.05 mol). The mixture was refluxed for 50 min after addition was complete. Excess hydride was destroyed by dropwise addition of ethyl acetate, then water (100 mL) was added and the organic layer separated. The aqueous fraction was extracted with ether (2 × 30 mL), and the combined extracts were washed with 10% aqueous H_2SO_4 (50 mL), 10% aqueous $NaHCO_3$ (50 mL), and brine (50 mL). These extracts were dried, filtered, concentrated, and the product was purified by distillation, bp 66–68°C/1.2 Torr, to give the alcohol **28**, 13.7 g (98%); ir (neat): 3360 (OH), 1645 (C=C) cm^{-1}; ^1H nmr δ: 1.2–2.5 (m, 5H), 1.7 (s, 3H, CH_3-C=C), 2.8–3.1 (t, 1H, J ~ 5 Hz, HO-CH_2), 3.2–3.5 (d, 2H, J ~ 6.5 Hz, CH_2-O), 4.7–5.2 (m, 4H, H_2C=C), 5.4–6.2 (m, 1H, H-C=C).

A dichloromethane solution (2 mL) of the alcohol **28** (0.140 g, 1 mmol) was added to a stirred dichloromethane suspension (3 mL) containing pyridinium chlorochromate (PCC) (0.324 g, 1.5 mmol) and NaOAc (0.017 g, 0.2 mmol). After 1.5 h the reaction appeared complete (tlc); ether (5 mL) was added and the suspension was filtered through silica gel. The residual dark gum was triturated with ether (2 × 5 mL), filtered, and concentrated to give 0.130 g of the aldehyde **29** and the conjugated isomer (non-conjugated/conjugated aldehydes, 5:1), which were separated by chromatography on silica gel (5% ethyl acetate/petroleum ether). For **29**: ^1H nmr δ: 1.2–2.4 (m, 4H, CH_2-CH_2), 1.7 (s, 3H, CH_3-C=), 2.7–3.1 (m, 1H, H-C-C=O), 4.6–5.2 (m, 4H, H_2C=C), 5.2–6.1 (m, 1H, H-C=C), 9.4 (d, 1H, H-C=O).

2-Methyl-3-formyl-2,6-heptadiene: ir (neat): 1670 (C=O), 1640 (C=C) cm^{-1}; ^1H nmr δ: 1.8–2.5 (m, 4H, CH_2-CH_2), 1.95 (s, 3H, CH_3-C=C), 2.2 (s, 3H, CH_3-C=C), 4.6–5.2 (m, 4H, H_2C=C), 5.4–6.1 (m, 1H, H-C=C), 10.0 (s, 1H, H-C=O).

General procedure for radical generation and cyclization

A solution of tributyltin hydride (1.5 mmol) and azobis(isobutyronitrile) (AIBN) (4 mol% with respect to *n*-Bu_3SnH) in dry benzene (9 mL) was added to a refluxing benzene solution (16 mL) containing the radical precursor (1.0 mmol) at a rate of 0.49 mL/h, using a syringe pump. Reflux was continued for a total reaction time of 24–30 h. Rigorous exclusion of oxygen was found to inhibit the cyclizations and thus they were conducted open to the atmosphere. The solvent was removed and the residue purified by flash chromatography on silica gel (eluting with 5–10% ethyl acetate/petroleum ether) to afford the cyclized products. Ester hydrolysis with 5% aqueous ethanolic sodium hydroxide gave the alcohol.

*1-Methyl-2-(1-oxa-4-mercaptobutyl)cyclopentane (**5**)*: ^1H nmr (300 MHz) δ: 0.99 (d, 3H, J = 6.5 Hz, CH_3C), 1.1–1.3 (m, 2H), 1.62 (m, 4H), 1.86 (m, 2H), 2.65 (m, 2H, H_2C-S), 3.4–3.55 (m, 3H, HC-O, H_2C-O); ^{13}C nmr δ: 88.0, 70.8, 39.8, 31.8, 31.0, 24.7, 22.0, 18.8.

trans-*2-Methylcyclopentanol (**6**) (ref. 32a)*: ^1H nmr (300 MHz) δ: 0.98 (d, 3H, J = 6.7 Hz, CH_3-C), 1.16 (m, 1H, H-CMe), 1.5–2.0 (m, 7H, CH_2's, HO), 3.69 (m, 1H, H-C-O); ^{13}C nmr δ: 80.1, 42.3, 31.4, 21.3, 18.0.

cis-*2-Methylcyclopentanol (**9**) (ref. 32)*: ^1H nmr (300 MHz) δ: 1.02 (d, 3H, J = 6.7 Hz, CH_3-C), 1.38 (m, 1H, H-CMe), 1.5–1.8 (m, 7H, CH_2's, HO), 4.06 (m, 1H, H-C-O); ^{13}C nmr δ: 76.0, 39.6, 34.4, 30.5, 21.9, 13.5.

trans-*2-Ethenylcyclopentanol (ref. 33)*: ^1H nmr (300 MHz) δ: 1.46 (m, 1H), 1.60 (m, 2H), 1.74 (m, 1H), 1.94 (m, 2H), 2.30 (m, 2H), 3.87 (m, 1H, HC-O), 5.04 (m, 2H, H_2C=C), 5.75 (m, 1H, H-C=C); ^{13}C nmr δ: 140.5, 114.8, 78.1, 52.6, 33.4, 29.4, 21.2.

cis-*1-(1-Oxa-4-mercaptobutyl)-2-*endo-*methylbicyclo[3.3.0]octane (**32**)*: ^1H nmr (300 MHz) δ: 0.96 (d, 3H, J = 6.8 Hz, CH_3-C), 1.1–1.4 (m, 5H), 1.5–1.7 (m, 6H), 2.05 (m, 1H), 2.33 (dd, 1H, J = 8.3, 8.6 Hz, HS), 2.64 (dd, 2H, J = 6.3, 8.3 Hz, H_2C-S), 3.48 (t, 2H, J = 6.3 Hz, H_2C-O); ^{13}C nmr δ: 97.5, 64.5, 47.2, 40.2, 34.5, 33.0, 32.6, 30.1, 25.8, 25.4, 14.4.

cis-*2-*endo-*Methylbicyclo[3.3.0]octan-1-ol (**33**)*: ^1H nmr (300 MHz) δ: 0.97 (d, 3H, J = 6.8 Hz, CH_3-C), 1.07 (m, 1H, H-C), 1.22 (m, 2H, CH_2), 1.50 (m, 2H, CH_2), 1.66 (m, 4H, CH_2, CH, HO), 1.86 (m, 2H, CH_2), 2.11 (m, 2H, CH_2); ^{13}C nmr δ: 92.8, 51.5, 45.5, 36.1, 35.0, 32.5, 29.9, 25.8, 13.3. Exact Mass calcd. for $C_9H_{16}O$: 140.1200; found: 140.1232.

1-(Ethyl ethanoate)-9-(1-oxa-4-mercaptobutyl)bicyclo[4.3.0]nonane: ^{13}C nmr (**35**:**34**, ~1:2) δ: 172.9, 172.4, 86.3, 85.5, 70.4, 71.4, 59.6, 59.9, 39.4, 39.2, 39.0, 38.6, 28.5, 27.6, 27.3, 27.0, 26.8, 26.6, 24.7, 24.3, 24.0, 23.2, 20.9, 20.7, 20.2, 14.2.

cis-*1-(Ethyl ethanoate)-9-*endo-*bicyclo[4.3.0]nonanol*: ^1H nmr (300 MHz) δ: 1.25 (t, 3H, J = 6.3 Hz, CH_3-CH_2), 2.53 (dd AB, 2H, J = 15 Hz, CH_2-C=O), 3.92 (s, 1H, HO), 4.15 (m, 2H, CH_2-O), 4.44 (d, 1H, J = 6 Hz, H-C-O); ^{13}C nmr δ: 174.7, 90.5, 81.9, 60.8, 42.0, 41.7, 29.0, 24.0, 23.1, 22.8, 21.0, 20.4, 14.1.

cis-*Bicyclo[3.3.0]octan-2-ol (**36**) (refs. 15c, 34)*: ^1H nmr (*endo*/*exo*, ~3:7) δ: 3.86 (m, 1H, H-C-O), 4.17 (m, 1H, H-C-O); ^{13}C nmr δ: 80.4, 75.6, 53.0, 47.7, 42.8, 42.1, 35.3, 34.7, 34.6, 34.4, 32.0, 30.7, 29.6, 28.2, 26.9.

*(1S,2R,5S)-2-Isopropyl-5-methylcyclohexanol (menthol) (**38**) (refs. 10g, 35)*: ^1H nmr (300 MHz) δ: 0.79 (d, 3H, J = 6.9 Hz, CH_3-C-H), 0.89 (d, 3H, J = 6.6 Hz, CH_3CMe), 0.91 (d, 3H, J = 6.6 Hz, CH_3-CMe), 3.39 (doubled quintet, 1H, J = 4.3, 10.2 Hz, H-C-O); ^{13}C nmr δ: 71.5, 50.2, 45.1, 34.6, 31.7, 25.9, 23.2, 22.3, 21.1, 16.2.

Can. J. Chem. Downloaded from www.nrcresearchpress.com by 198.100.157.202 on 09/07/12
For personal use only.

(1R,2R,5S)-2-Isopropyl-5-methylcyclohexanol (39) (refs. 10g, 35): ^{1}H nmr (300 MHz) δ: 0.80 (d, 3H, J = 6.3 Hz, CH_3-C-H), 0.85 (d, 3H, J = 6.7 Hz, CH_3CMe), 0.89 (d, 3H, J = 6.7 Hz, CH_3-CMe), 4.04 (b s, 1H, H-C-O); ^{13}C nmr δ: 68.1, 48.3, 43.0, 35.5, 29.6, 26.2, 24.6, 22.8, 21.6.

6-endo-Bicyclo[3.2.1]octanol (40) (ref. 36): ^{1}H nmr δ: 4.38 (apparent quintet, ddd, 1H, J ~ 4.7, 5.5 Hz, H-C-O); ^{13}C nmr δ: 75.3, 39.6, 38.2, 38.1, 34.5, 32.9, 27.1, 19.7.

6-exo-Bicyclo[3.2.1]octanol (41) (ref. 36): ^{1}H nmr δ: 4.15 (apparent d, 1H, J ~ 6 Hz, H-C-O); ^{13}C nmr δ: 76.6, 45.1, 41.6, 36.6, 36.2, 31.8, 30.2, 19.9.

(1R,2R*,5S*)-2-Methyl-5-isopropylcyclopentanol (ref. 37)*: ^{1}H nmr (300 MHz) δ: 0.86 (d, 3H, J = 6.4 Hz, CH_3-CMe), 0.95 (d, 3H, J = 6.5 Hz, CH_3CMe), 0.98 (d, 3H, J = 7 Hz, CH_3-CH), 1.15 (m, 1H, H-CMe), 1.30 (m, 2H, H-C, OH), 1.53 (m, 2H, CH_2), 1.66 (m, 1H, H-C), 1.80 (m, 2H, CH_2), 3.80 (dd, 1H, J = 3.4, 6.0 Hz, H-C-O); ^{13}C nmr δ: 78.5, 55.6, 39.2, 31.6, 31.4, 27.6, 21.5, 20.4, 13.5.

(1R,2R*,5S*)-2-Methyl-5-isopropenylcyclopentanol (42) (ref. 37)*: ^{1}H nmr (300 MHz) δ: 0.92 (d, 3H, J = 7.0 Hz, CH_3-C), 1.31 (m, 2H, CH_2), 1.67 (s, 3H, CH_3-C=C), 1.78 (m, 3H, CH_2, HO), 1.97 (m, 1H, J = 3.3, 7.0 Hz, H-CMe), 2.36 (m, 1H, H-C-C=C), 3.84 (t, 1H, J = 6.3 Hz, H-C-O), 4.70 (s, 2H, H_2C=C); ^{13}C nmr δ: 146.7, 110.0, 77.8, 54.1, 37.2, 30.7, 27.4, 20.6, 14.1. Exact Mass calcd. for $C_9H_{16}O$: 142.1357; found: 142.1362.

(1R,2R*,5S*)-2-Methyl-5-isopropenylcyclopentanol (43) (ref. 37)*: ^{1}H nmr (300 MHz) δ: 1.01 (d, 3H, J = 6.8 Hz, CH_3-C), 1.1–1.2 (m, 2H), 1.45 (d, 1H, J = 2.4 Hz, HO), 1.71 (m, 1H), 1.82 (s, 3H, CH_3-C=C), 2.07 (m, 2H), 2.50 (m, 1H, H-C-C=C), 3.75 (m, 1H, H-C-O), 4.86 (s, 1H, H-C=C), 5.02 (s, 1H, H-C=C); ^{13}C nmr δ: 144.6, 112.9, 79.4, 61.4, 41.7, 31.8, 27.0, 24.0, 20.8.

2-Methylbicyclo[3.2.1]octan-8-ol (44): ^{1}H nmr δ: 0.83 (d, 3H, J = 6.5 Hz, CH_3-C), 3.74 (s, 1H, H-C-O); acetate 0.75 (d, 3H, J = 6.6 Hz, CH_3-C), 1.94 (s, 3H, CH_3C=O), 4.61 (s, 1H, H-C-O); ^{13}C nmr (acetate) δ: 170.6, 85.3, 45.8, 38.8, 34.8, 30.3, 26.3, 25.8, 21.7, 21.4, 19.5.

2-Isopropyl-1-oxa(ethylmercapto)-1,5-hexadiene (50): ^{1}H nmr (300 MHz) δ: 1.00 (d, 6H, J = 7 Hz, *i*Pr), 1.56 (m, 1H, SH), 2.1 (m, 5H, allylic H), 2.7 (m, 2H, H_2C-S), 3.8 (t, 2H, J = 6 Hz, H_2C-O), 4.95 (m, 2H, H_2C=C), 5.83 (m, 2H, H-C=C, H-(O)C=C); ^{13}C nmr δ: 139.7, 139.5, 121.0, 114.0, 73.1, 33.0, 30.5, 25.9, 24.4, 22.0.

Acknowledgments

We are grateful to the Natural Sciences and Engineering Research Council of Canada and Merck Frost Canada Inc. for financial support of this research, to R. Capoor for nmr spectra, to Dr. Y.-F. Lu for additional spectroscopic measurements, and to a referee for helpful comments.

1. D. J. Hart. Science, **234**, 883 (1984).
2. B. Giese. Radicals in organic synthesis: formation of carbon–carbon bonds. Pergamon Press, New York, NY. 1986.
3. M. Ramaiah. Tetrahedron, **43**, 3541 (1987).
4. (*a*) D. P. Curran. Synthesis, 417 (1988); (*b*) Synthesis, 489 (1988).
5. A. L. J. Beckwith and C. H. Schiesser. Tetrahedron, **41**, 3925 (1985).
6. D. A. Burnett, J. Choi, D. J. Hart, and Y. Tsai. J. Am. Chem. Soc. **106**, 8201 (1986).
7. (*a*) D. P. Curran and M. Chen. Tetrahedron Lett. **26**, 4991 (1985); (*b*) D. P. Curran and D. M. Rakiewicz. Tetrahedron, **41**, 3943 (1985); (*c*) D. P. Curran and S. Kuo. J. Am. Chem. Soc. **108**, 1106 (1986).
8. (*a*) T. Kametani and T. Honda. Heterocycles, **19**, 1861 (1982); (*b*) M. D. Bachi, F. Frolow, and C. Hoornaert. J. Org. Chem. **48**, 1841 (1983); (*c*) D. J. Hart and Y.-M. Tsai. J. Am. Chem. Soc. **106**, 8209 (1984); (*d*) J. K. Choi and D. J. Hart. Tetrahedron, **41**, 3959 (1985); (*e*) A. Padwa, H. Nimmesgern, and G. S. K. Wong. J. Org. Chem. **50**, 5620 (1985); (*f*) A. L. J. Beckwith and D. R. Boate. Tetrahedron Lett. **26**, 1761 (1985); (*g*) M. D. Bachi, A. De Mesmaeker, and N. Stevenart-De Mesmaeker. Tetrahedron Lett. **28**, 2887 (1987). For α-sulfenyl radicals see (*h*) D. H. R. Barton, D. L. J. Clive, P. D. Magnus, and G. J. Smith. J. Chem. Soc. C, 2193 (1971); (*i*) H. Ishibashi, T. Sato, M. Irie, S. Harada, and M. Ikeda. Chem. Lett. 795 (1987); (*j*) H. Korth, R. Sustmann, K. S. Groninger, M. Leisung, and B. Giese. J. Org. Chem. **53**, 4364 (1988); (*k*) Y. M. Tsai, F. C. Chang, J. Huang, and C. L. Shiu. Tetrahedron Lett. **30**, 2121 (1989).
9. (*a*) G. Stork, S. Malhatra, H. Thompson, and G. Uchibayashi. J. Am. Chem. Soc. **87**, 1148 (1965); (*b*) T. Shono, I. Nishiguchi, H. Ohmizu, and M. Mitani. J. Am. Chem. Soc. **100**, 545 (1978); (*c*) S. K. Pradham, S. R. Kadam, J. N. Kolhe, T. V. Radhakrishnan, S. V. Sahani, and V. B. Thaker. J. Org. Chem. **46**, 2622 (1981); (*d*) B. Giese and U. Erfort. Chem. Ber. **116**, 1240 (1983); (*e*) E. J. Corey and S. G. Pyne. Tetrahedron Lett. **24**, 2821 (1983); (*f*) G. Pattenden and G. M. Robertson. Tetrahedron, **41**, 4001 (1985); (*g*) D. P. Fox, R. D. Little, and M. M. Baizer. J. Org. Chem. **50**, 2202 (1985); (*h*) T. Ikeda, S. Yue, and C. R. Hutchinson. J. Org. Chem. **50**, 5193 (1985); (*i*) D. Belotti, J. Cossy, J. P. Pete, and C. Portella. J. Org. Chem. **51**, 4196 (1986); (*j*) A. L. J. Beckwith and P. E. Pigou. Aust. J. Chem. **39**, 77 (1986).
10. (*a*) K. C. Nicolaou, D. G. McGarry, P. K. Sommers, C. A. Veale, and G. T. Furst. J. Am. Chem. Soc. **109**, 2504 (1987); (*b*) T. L. Fevig, R. L. Elliot, and D. P. Curran. J. Am. Chem. Soc. **110**, 5064 (1988); (*c*) G. A. Molander and C. Kenny. J. Am. Chem. Soc. **111**, 8236 (1989); (*d*) E. J. Enholm and G. Prasad. Tetrahedron Lett. **30**, 4939 (1989); (*e*) E. Kariv-Miller, H. Maeda, and F. Lombardo. J. Org. Chem. **54**, 4022 (1989); (*f*) G. E. Keck and A. M. Tafesh. 196th National Meeting of the American Chemical Society, Los Angeles, CA. September 25–30, 1988. Organic Abstract 55; (*g*) G. E. Keck and A. M. Tafesh. Synlett. 257 (1990).
11. (*a*) H. Umezawa, K. Maeda, T. Takeuchi, and Y. Okami. J. Antibiot. Ser. A, **19**, 200 (1966); (*b*) J. C. Wu, J. W. Kozarich, and J. Stubbe. J. Biochem. **24**, 7562 (1985); L. E. Rabow, J. Stubbe, and J. W. Kozarich. J. Am. Chem. Soc. **112**, 3196 (1990).
12. (*a*) C. G. Gutierrez, R. A. Stringham, T. Nitasaka, and K. G. Glasscock. J. Org. Chem. **45**, 3393 (1980); (*b*) C. G. Gutierrez and L. R. Summerhays. J. Org. Chem. **49**, 5206 (1984).
13. (*a*) V. K. Yadav and A. G. Fallis. Tetrahedron Lett. **29**, 897 (1988); (*b*) Tetrahedron Lett. **30**, 3283 (1989).
14. (*a*) S. Allen, T. G. Bonner, E. J. Bourne, and N. M. Saville. Chem. Ind. 630 (1958); (*b*) D. H. R. Barton, L. Bould, D. L. J. Clive, P. D. Magnus, and T. Hase. J. Chem. Soc. (C), 2204 (1971); (*c*) C. F. Carvalho and M. V. Sargent. J. Chem. Soc. Chem. Commun. 227 (1984); (*d*) D. A. Goff, R. N. Harris III, J. C. Bottaro, and C. D. Bedford. J. Org. Chem. **51**, 4711 (1986).
15. (*a*) J. K. Whitesell and M. A. Minton. J. Am. Chem. Soc. **109**, 225 (1987); (*b*) M. Christl, H. J. Reich, and J. D. Roberts. J. Am. Chem. Soc. **93**, 3463 (1971); (*c*) G. L. Lemiere, R. A. Dommisse, and F. C. Alderweireldt. Bull. Soc. Chim. Belg. **89**, 737 (1977); (*d*) J. K. Whitesell and R. S. Mathews. J. Org. Chem. **42**, 3878 (1977); (*e*) H.-J. Schneider, N. Nguyen-ba, and F. Thomas. Tetrahedron, **38**, 2327 (1982).
16. J. Romo, G. Rosenkrantz, and C. Djerassi. J. Am. Chem. Soc. **73**, 4961 (1951).
17. N. Satsumabayashi, S. Irioka, H. Kudo, T. Tsujimoto, and S. Motoki. Bull. Chem. Soc. Jpn. **45**, 913 (1972).
18. (*a*) J. W. Wilt, S. N. Massie, and R. B. Dabek. J. Org. Chem. **35**, 2803 (1970); (*b*) W. Oppolzer, S. Siles, R. L. Snowden,

B. H. BAKKER, and M. PETRZILKA. Tetrahedron, **41**, 3497 (1985).
19. (*a*) E. J. COREY and I. KUWAJIMA. J. Am. Chem. Soc. **92**, 395 (1970); (*b*) G. A. MOLANDER, J. B. ETTER, and P. W. ZINKE. J. Am. Chem. Soc. **109**, 453 (1987).
20. D. L. BOGER and R. J. MATHVINK. J. Am. Chem. Soc. **112**, 4003 (1990).
21. H.-J. LIU and W. H. CHEN. Can. J. Chem. **57**, 708 (1979); **60**, 1081 (1982).
22. A. L. J. BECKWITH and G. MOUD. J. Chem. Soc. Perkin Trans. 2, 1726 (1975).
23. (*a*) A. L. J. BECKWITH, C. J. EASTON, and A. K. SERELIS. J. Chem. Soc. Chem. Commun. 482 (1980); (*b*) A. L. J. BECKWITH, T. LAWRENCE, and A. K. SERELIS. J. Chem. Soc. Chem. Commun. 484 (1980); (*c*) A. L. J. BECKWITH and C. H. SCHIESSER. Tetrahedron, **41**, 3925 (1985); (*d*) D. C. SPELLMEYER and K. M. HOUK. J. Org. Chem. **52**, 959 (1987).
24. G. STORK, R. MOOK, JR., S. A. BILLER, and S. D. RYCHNOVSKY. J. Am. Chem. Soc. **105**, 3741 (1983).
25. T. V. RAJANBABU, T. FUKUNAGA, and G. S. REDDY. J. Am. Chem. Soc. **111**, 1759 (1989).
26. D. J. PASTO, R. KRASNANSKY, and C. ZERCHER. J. Org. Chem. **52**, 3062 (1987).
27. H. FISCHER. *In* Magnetic properties of free radicals. *Edited by* H. Fischer and K.-H. Hellwege. Landolt–Bornstein New Series 9b. 1977. p. 5.
28. (*a*) C. CHATGILIALOGLU, K. U. INGOLD, and J. C. SCAIANO. J. Am. Chem. Soc. **103**, 7739 (1981); (*b*) J. LUSZTYK, B. MAILLARD, S. DEYCARD, D. A. LINDSAY, and K. U. INGOLD. J. Org. Chem. **52**, 3509 (1987).
29. (*a*) G. E. KECK and J. B. YATES. J. Am. Chem. Soc. **104**, 5829 (1982); (*b*) G. E. KECK, E. J. ENHOLM, J. B. YATES, and M. R. WILEY. Tetrahedron, **41**, 4079 (1985).
30. D. P. CURRAN, P. A. VAN ELBURG, B. GIESE, and S. GILGES. Tetrahedron Lett. **31**, 2861 (1990).
31. G. L. LARSON and R. KLESSE. J. Org. Chem. **50**, 3627 (1985).
32. (*a*) P. CANONNE and M. BERNATCHEZ. J. Org. Chem. **52**, 4025 (1987); (*b*) H. C. BROWN and V. VARMA. J. Org. Chem. **39**, 1631 (1974).
33. L. S. HEGEDUS and J. M. MCKEARIN. J. Am. Chem. Soc. **104**, 2444 (1982).
34. (*a*) S. MURATA, M. SUZUKI, and R. NOYORI. Bull. Chem. Soc. Jpn. **55**, 247 (1982); (*b*) R. R. RAO, K. CHAKRABORTI, S. BHATTACHARYA, and A. RAO. Indian J. Chem. Sect. B, **22B**, 1122 (1983).
35. (*a*) E. L. ELIEL, M. H. GIANNI, T. H. WILLIAMS, and J. B. STOTHERS. Tetrahedron Lett. 741 (1962); (*b*) R. H. CRABTREE and M. W. DAVIS. J. Org. Chem. **51**, 2655 (1986).
36. C. A. GROB and U. ZUTTER. Tetrahedron Lett. **23**, 2849 (1982).
37. B. B. SNIDER, M. KARRAS, R. T. PRICE, and D. J. RODINI. J. Org. Chem. **47**, 4538 (1982).

Can. J. Chem. Downloaded from www.nrcresearchpress.com by 198.100.157.202 on 09/07/12
For personal use only.

On the reaction of *A*-nor-5α-cholestan-2-one with benzeneseleninic anhydride

JACEK W. MORZYCKI[1] AND JOLANTA OBIDZIŃSKA
Institute of Chemistry, University of Warsaw, Bialystok Branch, Al. 1-go Maja 11/4, 15-443 Bialystok, Poland

Received July 16, 1990

JACEK W. MORZYCKI and JOLANTA OBIDZIŃSKA. Can. J. Chem. **69**, 790 (1991).

A-Nor-5α-cholestan-2-one (**1**) was oxidized with BSA under various conditions. The stoichiometric reaction afforded diketones (**3** and **4**) and α-phenylseleno-ketone (**2**) while catalytic oxidation with the BSA/$PhIO_2$/*p*-TsOH system resulted in lactones (**7***a* and **7***b*) and anhydrides (**5** and **6**). The mechanism of these reactions is discussed.

Key words: benzeneseleninic anhydride, *A*-nor-5α-cholestan-2-one, catalytic oxidation.

JACEK W. MORZYCKI et JOLANTA OBIDZIŃSKA. Can. J. Chem. **69**, 790 (1991).

On a oxydé la *A*-nor-5α-cholestan-2-one (**1**) avec de l'ABS, sous diverses conditions. La réaction stoechiométrique conduit aux dicétones (**3** et **4**) et à l'α-phénylséléno-cétone (**2**) alors que l'oxydation catalytique par le système ABS/$PhIO_2$/*p*-TsOH conduit aux lactones (**7***a* et **7***b*) et aux anhydrides (**5** et **6**). On discute du mécanisme de ces réactions.

Mots clés : anhydride benzènesélénique, A-nor-5α-cholestan-2-one, oxydation catalytique.

[Traduit par la rédaction]

Introduction

It has previously been shown that benzeneseleninic anhydride (BSA) is an excellent reagent for dehydrogenation of ketones (1). Many biologically important steroidal cyclohexa-1,4-dien-3-ones can be obtained in high yields by dehydrogenation of the corresponding 3-oxo-steroids with BSA. Though having certain advantages over the commonly used methods employing dichlorodicyanoquinone, selenium dioxide, or bromination–dehydrobromination, the BSA method possesses two disadvantages. These are the need to use large amounts of toxic and expensive BSA, and the unwanted secondary reactions with benzeneselenenic acid or its anhydride formed in the elimination step. The development of a catalytic cycle (2, 3) based on immediate and efficient reoxidation of the reduced organoselenium species by iodoxybenzene (4, 5) obviated both these problems. Thus cyclic six-membered ketones are smoothly dehydrogenated in high yields using benzeneseleninic anhydride generated *in situ* by oxygen atom transfer from $PhIO_2$ to catalytic amounts of diphenyl diselenide. The five-membered ketones, however, are resistant (e.g., steroidal 17-ketones) to oxidation under the conditions commonly used for dehydrogenation of steroidal 3-ketones (2, 3). The examination of a reaction of *A*-nor-5α-cholestan-2-one (as a model five-membered ketone) with BSA under various conditions is the subject of this paper.

Results and discussion

It was proved that *A*-nor-5α-cholestan-2-one (**1**) is resistant to BSA in benzene at reflux. The reaction in boiling toluene is rather sluggish and gives a streak in TLC.

Further oxidations were carried out in refluxing chlorobenzene solutions. The reaction of **1** with two equivalents of BSA was quite fast and did not require acid catalysis. There were three main products of the oxidation (Scheme 1), which were separated by silica gel column chromatography: 1α-phenylseleno-*A*-nor-5α-cholestan-2-one (**2**), *A*-nor-5α-cholestane-1,2-dione (**3**), and *A*-nor-5α-cholest-3-en-1,2-dione (**4**). The structures of these products were determined on the basis of their ^1H NMR, IR, UV, and mass spectra (see Table 1 in Experimental). The data given in the literature (6) on the previously described compound **4** confirm the proposed structure. The relative yields of the isolated products **2**, **3**, and **4** were 28, 16, and 56%, respectively.

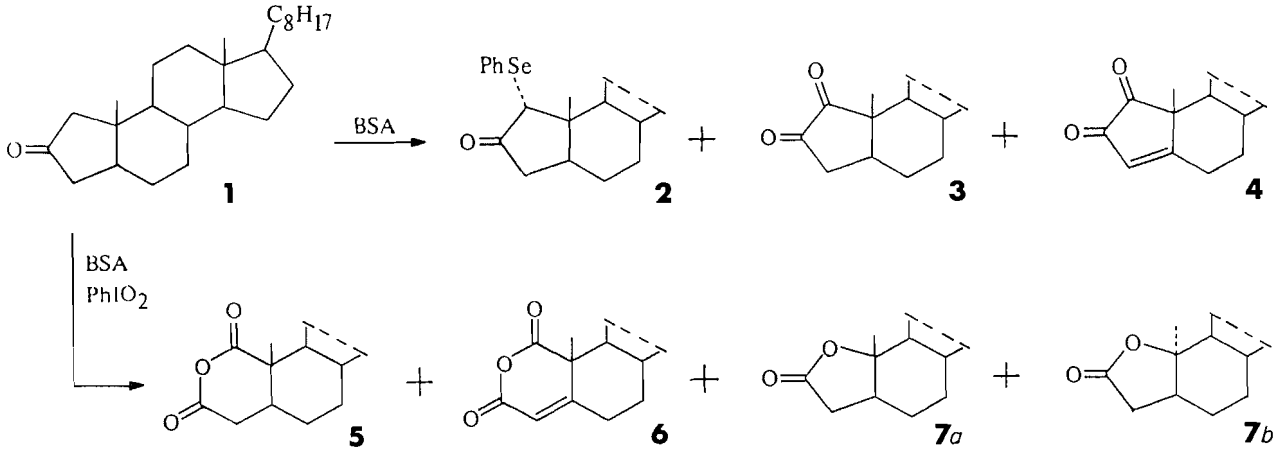
The oxidation of *A*-nor-5α-cholestan-2-one (**1**) was carried out once again using a diphenyl diselenide/iodoxybenzene system instead of BSA prepared in advance. To our surprise, completely different oxidation products were obtained than in the previous case. We also noted that the addition of *p*-toluenesulfonic acid in trace amounts leads to a faster rate of the reaction; probably for this reason the reaction is then cleaner. Strong acid activates both *A*-nor-5α-cholestan-2-one (facilitates enolization) and iodoxybenzene (protonation of the highly polarized iodine–oxygen bond reduces the kinetic activation energy barrier of oxidation). It was also found that the oxidation product distribution varies in the reactions with or without *p*-TsOH.

In a typical experiment, *A*-nor-5α-cholestan-2-one (**1**) was treated with an oxidizing mixture prepared from five equivalents of iodoxybenzene, diphenyl diselenide (0.1–0.3 equiv.), and traces of *p*-TsOH in chlorobenzene at reflux for 0.5–1 h. The main products of oxidation were identified as 1,3-seco-2-nor-5α-cholestane-1,3-dioic acid anhydride (**5**), 1,3-seco-2-nor-5α-cholest-4-en-1,3-dioic acid anhydride (**6**), and 10-hydroxy-3,10-seco-1,2-dinor-5α-cholestan-3-oic acid lactone (**7**). The last product proved to be a mixture (by ^1H NMR at 500 MHz) of 10*S* (the natural configuration) and 10*R* epimers (**7***a* and **7***b*) in a ratio 4:1. The epimeric mixture of lactones **7***a* and **7***b* can be separated by fractional crystallization from hexane (compound **7***a*) and then from acetone (compound **7***b*). The structures of the products were determined on the basis of their spectral properties (see Table 1 in Experimental), the relative yields of **5**, **6**, and **7** being 13, 24, and 63%, respectively. The oxidation of **1** carried out in the absence of *p*-TsOH afforded more of **5**, less of **6**, **7**, and a small amount of **4**.

The tentative mechanism of *A*-nor-5α-cholestan-2-one (**1**) oxidation with BSA is shown in Scheme 2. The favoured enolization of **1** is toward C-1 and this position is attacked in the first step of oxidation. It is known (7) that if carbon α to the carbonyl group is adjacent to the tertiary centre, α-hydroxylation with BSA takes place instead of dehydrogenation. However, under the reaction conditions (excess of the oxidizing agent, high temperature of the reaction) α-hydroxylation is followed by immediate further oxidation with BSA to α-diketone (**3**). This compound appeared to be a minor product of the reaction with

[1]Author to whom correspondence may be addressed.

Can. J. Chem. Downloaded from www.nrcresearchpress.com by 198.100.157.202 on 09/07/12
For personal use only.



SCHEME 1

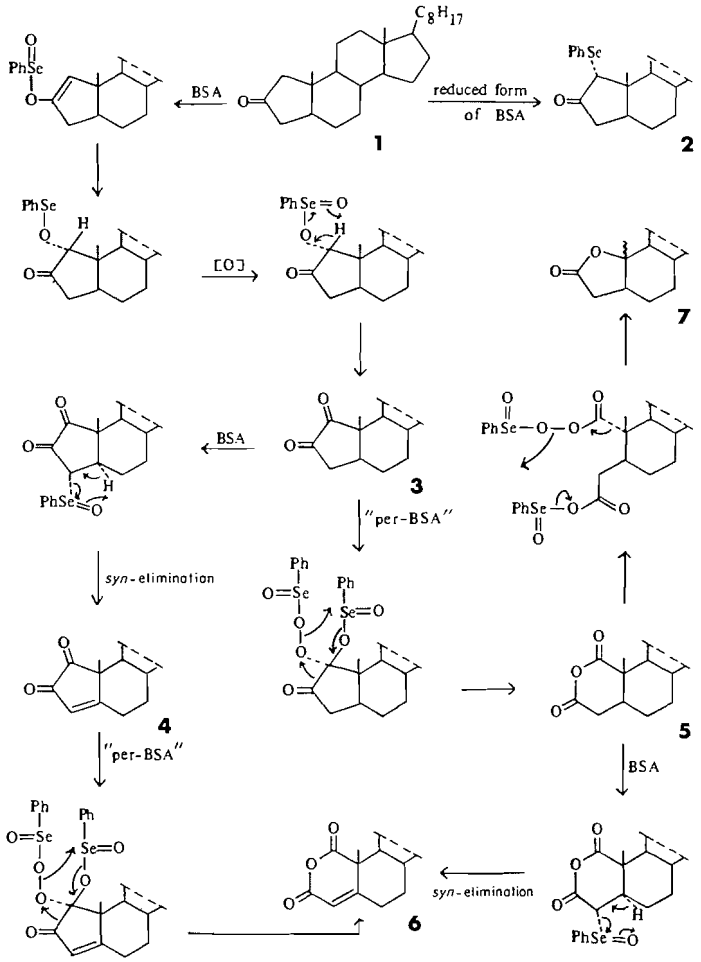
BSA alone but it was not present among the products of oxidation by the catalytic method. This is due to the high reactivity of this intermediate. In the stoichiometric reaction it is then dehydrogenated to the major product, *A*-nor-5α-cholest-3-en-1,2-dione (**4**). The third product of the oxidation, α-phenylselenoketone **2**, is formed from the reaction of **1** with a reduced form of BSA. Products of this type have never been obtained in catalytic BSA oxidations because all reduced forms of the anhydride are immediately reoxidized by iodoxybenzene. It was shown that both 1,2-dicarbonyl compounds **3** and **4** undergo further oxidation in the BSA/$PhIO_2$ system, under the reaction conditions, to the corresponding anhydrides **5** and **6**. Blank experiments proved that this transformation cannot be accomplished when using benzeneseleninic anhydride or iodoxybenzene separately. It is known (8) that α-diketones are oxidized to anhydrides with peroxycarboxylic acids. We assume that a certain peroxy species "per-BSA" is formed in a low concentration in the BSA/$PhIO_2$ system at 132°C. An alternative structure for per-BSA with Se(VI) may also be considered. All our attempts to isolate and identify this species failed. It is possible that the same per-BSA is responsible for further oxidation of anhydride **5** to the major product **7**. It was found in a separate experiment that **5** is a precursor of both lactones (**7***a* and **7***b*) and unsaturated anhydride **6**. Presumably a mixed anhydride is formed from **5** and per-BSA. This intermediate loses carbon dioxide to afford a carbocation at C-10. A similar mechanism has been proposed (9) for oxidation of 1,3-seco-2-nor-5α-cholestane-1,3-dioic acid to the same mixture of lactones with lead tetraacetate. The unsaturated anhydride **6** proved resistant to this type of transformation under the reaction conditions.

The following conclusions can be drawn from the experiments described:

1. The five-membered ketone **1** cannot be dehydrogenated with BSA (either by using stoichiometric amounts of BSA or by the catalytic method).

2. *A*-Nor-5α-cholestan-2-one (**1**) undergoes oxidation with BSA in both systems at 132°C but the reaction is not of any great practical importance.

3. The BSA/$PhIO_2$ (with or without *p*-TsOH) system is not always equal to BSA alone and special attention has to be paid to the reactions performed at a higher temperature. It is very likely that a highly reactive, more oxidated, species (per-BSA) is formed under these conditions.



SCHEME 2

Experimental

NMR spectra were taken with AM-500 Bruker and Gemini 200 Varian spectrometers using $CDCl_3$ solutions with TMS as an internal standard. Infrared spectra were recorded on a Specord 75 IR as CCl_4 solutions or as KBr pellets. Mass spectra were obtained at 110–120°C above ambient temperature at 70 eV with a LKB GCMS 2091 spectrometer. Ultraviolet absorption spectra were recorded in absolute ethanol with a Specord UV–VIS recording spectrometer. High-

Can. J. Chem. Downloaded from www.nrcresearchpress.com by 198.100.157.202 on 09/07/12
For personal use only.

Can. J. Chem. Downloaded from www.nrcresearchpress.com by 198.100.157.202 on 09/07/12
For personal use only.

TABLE 1. the ^{1}H NMR (δ, ppm), IR (ν_{max}, cm^{-1}), UV (λ_{max}, nm), and MS (m/z) data for the compounds **1–7**.

Compound no. (ref).	^{1}H NMR					IR	UV	MS
	H-1	H-3 (H-4 in **5** and **6**)	H-18	H-19	Others			
1 (10)	1.89 and 2.12 (2 × d, J = 16.8 Hz)	2.03 (dd, J_{gem} = 18.3 Hz, J_{vic} = 13.6 Hz) 2.16 (dd, J_{gem} = 18.3 Hz, J_{vic} = 8.5 Hz)	0.68	0.84	—	1773 (s)	—	372 (M^+, 44%), 217 ($M^+ - C_{11}H_{23}$, 100%)
2	3.37 (s)	1.98 (m) 2.46 (dd, J_{gem} = 18.3 Hz, J_{vic} = 7.7 Hz)	0.68	0.92	7.28 (m, *m*, *p*-ArH) 7.60 (m, *o*-ArH)	1733 (s)	220 and 260 (sh)	528[a] (M^+, 100%) 371 (M^+ − PhSe, 60%)
3	—	2.25 (dd, J_{gem} = 18.6 Hz, J_{vic} = 14.3 Hz) 2.45 (dd, J_{gem} = 18.6 Hz, J_{vic} = 6.9 Hz)	0.70	1.04	—	1752 (s), 1769 (m)	—	386[b] (M^+, 16%), 316 ($M^+ - C_3H_2O_2$, 100%) 358 (M^+ − CO, 13%), 330 ($M^+ - 2 \times$ CO, 19%)
4 (6)	—	6.57 (d, J = 1.2 Hz)	0.72	1.28	2.56 and 2.70 (2 × m, 6 − H)	1604 (m) 1722 (s), 1768 (m)	283 (ε = 3100)	384 (M^+, 8%) 356 (M^+ − CO, 100%)
5 (13)	—	2.53 and 2.75 (2 × m)	0.69	1.15	—	1759 (s), 1800 (m)	—	—
6[c]	—	5.94 (d, J = 1.0 Hz)	0.72	1.53	2.44 and 2.47 (2 × m, 6 − H)	1745 (s), 1782 (m)	231 (ε = 8100)	400 (M^+, 22%), 372 (M^+ − CO, 40%), 261 ($M^+ - C_7H_7O_3$, 100%)
7a (9)	—	2.37 (dd, J_{gem} = 16.6 Hz, J_{vic} = 7.3 Hz) 2.44 (dd, J_{gem} = 16.6 Hz, J_{vic} = 14.0 Hz)	0.68	1.21	—	1774 (s)	—	374 (M^+, 100%)
7b (9)	—	2.08 (m) 2.89 (dd, J_{gem} = 17.2 Hz, J_{vic} = 6.7 Hz)	0.69	1.35	—	1774 (s)	—	374 (M^+, 100%)

[a]Exact mass calcd. for $C_{32}H_{48}OSe$: 528.2870; found: 528.2872.
[b]Exact mass calcd. for $C_{26}H_{42}O_2$: 386.3185; found: 386.3187.
[c]Melting point 147–149°C; $[\alpha]_D^{20}$ −37.0° (*c* 0.4, $CHCl_3$). Anal calcd. for $C_{26}H_{40}O_3$: C 77.95, H 10.06; found: C 77.77, H 9.96.

pressure liquid chromatography was performed on a Laboratorni Pristroje Praha liquid chromatograph equipped with an LCD 2563 UV detector and a RIDK-102 differential refractometer unit. Column chromatography was performed on silica gel 70–230 or 230–400 mesh ASTM (Merck). Thin-layer chromatograms were developed on aluminium TLC sheets precoated with silica gel F_{254} and visualized with 50% sulfuric acid after heating. All solvents were dried and freshly distilled prior to use. The starting *A*-nor-5α-cholestan-2-one (**1**) was prepared analogously to the procedure described in ref. 10. Benzeneseleninic anhydride (BSA) was obtained (11) from diphenyl diselenide (Aldrich) by nitric acid oxidation followed by dehydration at 120°C. For preparation of iodoxybenzene a direct method (3), sodium hypochlorite oxidation of iodobenzene in acetic acid solution, was used (see also ref. 12).

Stoichiometric oxidation with BSA (typical procedure)

A solution of *A*-nor-5α-cholestan-2-one (372 mg, 1 mmol) and BSA (720 mg, 2 mmol) in chlorobenzene (15 mL) was refluxed under an argon atmosphere for 45 min. After cooling, the reaction mixture was filtered through a silica gel (70–230 mesh) column, washed with hexane to remove chlorobenzene, and then with benzene. The benzene fractions were combined, the solvent was evaporated under reduced pressure, and the residue was subjected to rechromatography (silica gel 230–400 mesh). Compounds **2**, **1** (starting material), **3**, and **4** were eluted consecutively with benzene–hexane mixtures.

Catalytic oxidation with BSA and iodoxybenzene (typical procedure)

The oxidizing mixture, consisting of diphenyl diselenide (78 mg, 0.25 mmol), iodoxybenzene (1180 mg, 5 mmol), and trace amounts of *p*-toluenesulfonic acid in chlorobenzene (20 mL), was intensively stirred and heated under reflux until the yellow colour disappeared (about 2 min; in the absence of *p*-TsOH, 10 min).

To the above mixture *A*-nor-5α-cholestan-2-one (372 mg, 1 mmol) was added, stirring was continued, and the reaction mixture was refluxed under an argon atmosphere for 45 min (in the absence of *p*-TsOH, for 1.5 h). After cooling, the reaction mixture was filtered through a silica gel (70–230 mesh) column, washed with hexane to remove chlorobenzene, and then with benzene. The benzene fractions were combined, the solvent was evaporated under reduced pressure, and the residue was subjected to rechromatography (silica gel 230–400 mesh). Compounds **5**, **1** (starting material), **6**, **7** (a mixture of C-10 epimers) were eluted consecutively with benzene–hexane mixtures (in the absence of *p*-TsOH after elution of **7**, a trace amount of compound **4** was also eluted with benzene).

Acknowledgements

We thank the Polish Ministry of Education for generous financial support.

1. D. H. R. Barton, D. J. Lester, and S. V. Ley. J. Chem. Soc. Perkin Trans. 1, 2209 (1980).
2. D. H. R. Barton, J. W. Morzycki, W. B. Motherwell, and S. V. Ley. J. Chem. Soc. Chem. Commun. 1044 (1981).
3. D. H. R. Barton, C. R. A. Godfrey, J. W. Morzycki, W. B. Motherwell, and S. V. Ley. J. Chem. Soc. Perkin Trans. 1, 1947 (1982).
4. D. F. Banks. Chem. Rev. **66**, 243 (1966).
5. D. H. R. Barton, C. R. A. Godfrey, J. W. Morzycki, W. B. Motherwell, and A. Stobie. Tetrahedron Lett. **23**, 957 (1982).
6. T. Kubota, K. Yoshida, F. Hayashi, and K. Takeda. Chem. Pharm. Bull. **13**, 50 (1965).
7. K. Yamakawa, T. Satoh, N. Ohba, and R. Sakaguchi. Chem. Lett. 763 (1979).
8. P. A. S. Smith. Molecular rearrangements. Vol. 1. *Edited by* P. de Mayo. Wiley–Interscience, New York. 1963. p. 568.
9. W. J. Rodewald and J. W. Szczepek. Rocz. Chem. **50**, 815 (1976).
10. R. M. Scribner. Organic reactions in steroids chemistry. Vol. 2. *Edited by* J. Fried and J. A. Edwards. Van Nostrand Reinhold, New York. 1972. Chap. 15. p. 408; A. Windaus and O. Dalmer. Ber. Dtsch. Chem. Ges. **53**, 162 (1919).
11. D. H. R. Barton, S. V. Ley, P. D. Magnus, and M. N. Rosenfeld. J. Chem. Soc. Perkin Trans. 1, 567 (1977).
12. M. W. Formo and J. R. Johnson. Org. Synth. Coll. Vol. **3**, 486 (1955).
13. G. Snatzke and B. Wessling. Liebigs Ann. Chem. 1028 (1979).

Can. J. Chem. Downloaded from www.nrcresearchpress.com by 198.100.157.202 on 09/07/12
For personal use only.

Chiral recognition in aqueous solutions at 25°C. A calorimetric study of the interaction between enantiomeric α-amino acids of different alkyl chain length

GIUSEPPINA CASTRONUOVO,[1] VITTORIO ELIA, AND MICHELA MAGLIULO
Department of Chemistry, University "Federico II" of Naples, Via Mezzocannone 4, 80134 Naples, Italy

Received January 10, 1990[2]

GIUSEPPINA CASTRONUOVO, VITTORIO ELIA, and MICHELA MAGLIULO. Can. J. Chem. **69**, 794 (1991).

Cross-homo- and cross-heterotactic enthalpic coefficients, $h_{x_Dy_D}$ or $h_{x_Ly_L}$ and $h_{x_Dy_L}$ respectively, were determined at 25°C, measuring the enthalpies of dilution of ternary aqueous solutions containing two different α-amino acids of the same or different chirality. Differences of about 200–300 J mol^{-2} kg between cross-homo- and cross-heterotactic coefficients were found, well beyond the experimental uncertainty. The role of the zwitterionic interaction, already proposed to explain the nature of chiral recognition, was strengthened.

Key words: α-amino acids, excess enthalpy, chiral recognition.

GIUSEPPINA CASTRONUOVO, VITTORIO ELIA et MICHELA MAGLIULO. Can. J. Chem. **69**, 794 (1991).

Opérant à 25°C et faisant appel à des mesures d'enthalpie de dilution de solutions aqueuses ternaires contenant deux acides α-aminés différents dont la chiralité est la même ou différente, on a déterminé les coefficients enthalpiques homo- et hétéro-tactiques croisés, respectivement $h_{x_Dy_D}$ ou $h_{x_Ly_L}$ et $h_{x_Dy_L}$. On a trouvé des différences d'environ 200–300 J mol^{-2} kg entre les coeffiients homo- et hétéro-tactiques croisés; ces différences sont beaucoup plus grandes que les incertitudes expérimentales. Le rôle de l'interaction zwitterionique, qui a déjà été proposé pour expliquer la nature de la reconnaissance chirale, est affirmé.

Mots clés : acides α-aminés, enthalpie en excès, reconnaissance chirale.

[Traduit par la rédaction]

Introduction

Differences in the thermodynamic properties of aqueous solutions containing two optically active solutes often cannot be distinguished. However, these differences in the excess properties, which depend on the interactions between solvated solutes (solute–solute interactions), must in principle be expected.

In recent years a number of papers have appeared concerning the possibility of demonstrating chiral recognition in aqueous solutions by means of calorimetric (1–6) or volumetric (7) techniques. Stereoselective interactions were identified for the first time for aqueous solutions of uncharged amide derivatives of some amino acids and dipeptides (3). Recently, the attractive interaction between the zwitterions present in aqueous solutions of α-amino-acids has been proposed as the main contribution to chiral recognition (1, 8). That is, the favourable electrostatic zwitterion–zwitterion interaction makes more probable one of the possible orientations responsible for chiral recognition in aqueous solutions. When the attractive interaction between the dipolar ions disappears, for instance for the protonation of the COO^- group, chiral recognition does not occur (8). Moreover, analysis of the enthalpic pairwise coefficients, by means of a group additivity approach (9), reveals a dramatic change in the prevailing mechanism of interaction when the electrostatic interactions are perturbed. The aim of the present work is to gain more information about the factors that determine chiral recognition, by studying the interactions, in aqueous solutions, between optically active α-amino acids bearing different alkyl chains (alanine, α-aminobutyric acid, valine, norvaline, leucine, isoleucine, norleucine). The pairwise interaction coefficients of the excess enthalpies are evaluated from the enthalpies of dilution of ternary solutions containing the same or different chiral forms of two different α-amino acids.

[1]Author to whom correspondence may be addressed.

[2]Revision received November 28, 1990.

Printed in Canada / Imprimé au Canada

Experimental

Materials and methods

Amino acids (Sigma) were of the highest purity commercially available. Tests of purity for these substances were extensively reported in a preceding paper (1). Solutions were prepared by weight using double distilled water. The heats of dilution were measured by means of an LKB standard flow microcalorimeter at 25°C. Details of the experimental procedure are reported in the literature (10–13).

Thermodynamic treatment

The excess enthalpy of a solution is defined as (14):

$$[1] \quad H^E = H - H_w^0 - \Sigma_x m_x \bar{H}_x^0$$

The symbols have the usual meaning: H is the total enthalpy referred to 1 kg of solvent, H_w^0 the standard enthalpy of 1 kg of solvent, $\bar{H}_x^0$ the limiting partial molal enthalpy of the solute x. H^E, as any thermodynamic property, can be expressed as a virial expansion of the molalities as follows:

$$[2] \quad H^E = \Sigma_x \Sigma_y h_{xy} m_x m_y + \text{higher terms}$$

The pairwise coefficients appearing in eq. [2] represent the enthalpic contribution to the free energy coefficient for pair and higher order interactions (14–17). They give information about all the variations of the thermodynamic function when two isolated molecules are brought together to interact (18). The enthalpies of dilution of a solution containing n solutes can be expressed as a function of the interaction coefficients and as a function of the excess enthalpies as follows:

$$[3] \quad \Delta H^{dil} \quad (\text{J/kg}) = H^E(\bar{m}\ ) - (m_x^f/m_x)\, H^E(\bar{m}^f) = \Sigma_x \Sigma_y h_{xy} m_x^f m_y^f - (m_x^f/m_y)\, \Sigma_x \Sigma_y h_{xy} m_x m_y + \ldots$$

where m_x, m_y,..., m_x^f, m_y^f..., are the molalities of each solute before and after the process of diluting the ternary solution and $\bar{m} = \Sigma_x m_x$, $m^f = \Sigma_x m_x^f$ are the osmolalities.

Can. J. Chem. Downloaded from www.nrcresearchpress.com by 198.100.157.202 on 09/07/12
For personal use only.

TABLE 1. Homo- and heterotactic enthalpic interaction coefficients[a] for amino acids in aqueous solutions at 25°C

	L-Ala/D-Ala	L-Aba/D-Aba	L-Val/D-Val	L-nVal/D-nVal	L-Leu/D-Leu	L-iLeu/D-iLeu	L-nLeu/D-nLeu
L-Ala	217(3)[b]	363(22)[c]		545(28)[c]			736(42)[c]
D-Ala	203(3)[b]	313(12)[c]		413(21)[c]			579(21)[c]
L-Abu		536(6)[b]		747(17)[c]			910(35)[c]
D-Abu		528(17)[b]		681(8)[c]			834(37)[c]
L-Val			848(10)[a]	913(37)[c]			1275(28)[c]
D-Val			790(9)[a]	820(34)[c]			1050(32)[c]
L-nVal				927(13)[b]	1386(27)[c]	1319(37)[c]	1274(44)[c]
D-nVal				971(27)[b]	1198(35)[c]	1200(42)[c]	1106(27)[c]
L-Leu					1269(9)[b]	1666(44)[c]	1529(42)[c]
D-Leu					1059(36)[b]	1528(39)[c]	1204(45)[c]
L-iLeu						1307(14)[b]	1581(19)[c]
D-iLeu						1161(34)[b]	1446(40)[c]
L-nLeu							1424(12)[b]
D-nLeu							1228(40)[b]

[a]Units: J mol^{-2} kg. Numbers in parentheses are the 68% confidence limits.
[b]The values for the self-coefficients are from ref. 1.
[c]This work.

Usually, an auxiliary function ΔH^{n}* (8) is used, which is the difference between the enthalpy of dilution of a solution containing n solutes and the sum of the enthalpies of dilution of the solutions containing each solute:

[4] $$\Delta H^{n}* = \Delta H^{\mathrm{dil}}(\bar{m}) - \Sigma \Delta H^{\mathrm{dil}}(m_x)$$

where $\bar{m}$ is the osmolality of the solutions. For a ternary solution, in the case where only pairwise coefficients are needed to obtain the best fit of the experimental data, the auxiliary function is given by:

[5] $$\Delta H^{**}(x,y) = \Delta H^{\mathrm{dil}}(x,y) - \Delta H^{\mathrm{dil}}(x) - \Delta H^{\mathrm{dil}}(y) = 2h_{xy}m_x^{\mathrm{f}}(m_y^{\mathrm{f}} - m_y)$$

For the sake of clarity, since the solutes used in the ternary solutions are different with respect to chirality, we are forced to introduce more complex symbols to define cross-coefficients. Thus, the interaction coefficient characterizing the ternary solution of a solute x in the D chiral form and of a solute y in the D chiral form, $h_{x_{\mathrm{D}}y_{\mathrm{D}}}$, will be defined as a cross-homotactic coefficient. The interaction coefficient between the two solutes x and y in different chiral sequence, $h_{x_{\mathrm{D}}y_{\mathrm{L}}}$, will be defined as a cross-heterotactic coefficient.

Results

The calorimetric experimental data, from which the enthalpic interaction coefficients are derived, have been deposited as supplementary material.[3]

In Table 1 the cross-homotactic and the cross-heterotactic coefficients, $h_{x_{\mathrm{D}}y_{\mathrm{D}}} = h_{x_{\mathrm{L}}y_{\mathrm{L}}}$, $h_{x_{\mathrm{D}}y_{\mathrm{L}}}$ respectively, are reported for all the α-amino acids studied, together with the values of the self- (homo and hetero) coefficients taken from the literature (1).

[3]Complete tables of the auxiliary function ΔH^{**} for the ternary solutions (each containing two different amino acids of the same or different chirality), along with the initial and final concentrations of each substance for every experiment, have been deposited, and may be purchased from: The Depository of Unpublished Data, Document Delivery, CISTI, National Research Council of Canada, Ottawa, Canada K1A OS2.

The self-homotactic coefficients ($h_{x_{\mathrm{D}}x_{\mathrm{D}}} = h_{x_{\mathrm{L}}x_{\mathrm{L}}}$) increase with increasing alkyl chain length, as do the self-heterotactic ones ($h_{x_{\mathrm{D}}x_{\mathrm{L}}} = h_{x_{\mathrm{L}}x_{\mathrm{D}}}$). For leucines the latter are smaller than the self-homotactic values, beyond the experimental uncertainty, thus indicating that chiral recognition occurs (1). The same happens for the cross-homotactic coefficients ($h_{x_{\mathrm{D}}y_{\mathrm{D}}}$), which are always higher than the corresponding cross-heterotactic ones ($h_{x_{\mathrm{D}}y_{\mathrm{L}}}$). In the case of the system norleucine/leucine, the difference between the cross-homo- and the cross-heterotactic coefficient reaches the highest value found in the literature (319 J mol^{-2} kg).

In Fig. 1, part A, the self- and cross-homotactic coefficients for the amino acids bearing linear alkyl chains are reported as a function of the half-sum of the aliphatic carbon atoms present on both molecules. A linear trend is obtained, as described by the following equation:

[6] $$h_{x_{\mathrm{D}}y_{\mathrm{D}}} = -798(61) + 445(18)\, n_{\mathrm{C}}$$

where $n_{\mathrm{C}} = 1/2\,(n_{\mathrm{C}}^{x} + n_{\mathrm{C}}^{y})$ and the figures in parentheses are the 68% confidence limits.

In the same figure, part B, the self- and cross-heterotactic coefficients are reported for the same linear α-amino acids against the same abscissa. Again a linear trend is obtained, whose equation is

[7] $$h_{x_{\mathrm{D}}y_{\mathrm{L}}} = -758(73) + 411(21)\, n_{\mathrm{C}}$$

It is worthwhile to emphasize that, for systems corresponding to the same abscissa (norvaline/aminobutyric acid and norleucine/alanine, norvaline/norvaline and norleucine/aminobutyric acid, aminobutyric acid/aminobutyric acid and norvaline/alanine), the coefficient is smaller for the system showing the greater difference between the length of the alkyl chains.

Discussion

The experimental data concerning dilute solutions can be rationalized using a simple model that postulates the overlap of the cospheres of solvated molecules (14) with subsequent release of the solvent to the bulk. This model qualitatively

Can. J. Chem. Downloaded from www.nrcresearchpress.com by 198.100.157.202 on 09/07/12
For personal use only.

Can. J. Chem. Downloaded from www.nrcresearchpress.com by 198.100.157.202 on 09/07/12
For personal use only.

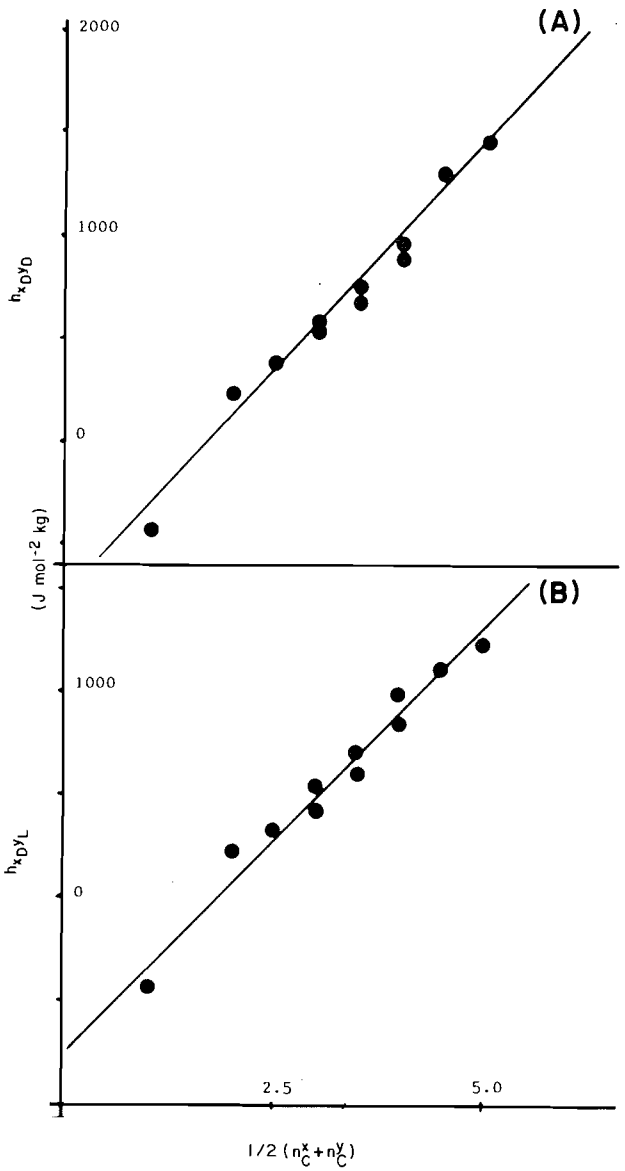


FIG 1. Self- and cross-homotactic (Part A) or self- and cross-heterotactic (Part B) enthalpic interaction coefficients vs. the half-sum of the number of aliphatic carbon atoms for α-amino acids bearing linear alkyl chains.

accounts for the sign, and to some extent for the magnitude, of the parameters that are used to characterize such "non-bonding" interactions, namely, the interaction coefficients of the virial expansion of the excess thermodynamic properties. More elaborate models have been proposed to gain a deeper insight into the interactions in these solutions. For instance, the Savage and Wood group additivity approach (SWAG) (9) considers the overall pairwise coefficient as due to additive contributions of the groups into which a molecule can be divided. However, if the SWAG approach is applied to positional isomers or stereoisomers, it obviously fails. This work, which continues a series of papers concerning enthalpic and volumetric differences between the pairwise coefficients of positional isomers (19–21), configurational isomers (22), and stereoisomers (1, 2, 4, 5, 7, 8), emphasizes that, for non-bonding interactions, preferred orientations of the interacting molecules play a major role.

For α-amino acids in aqueous solution at room temperature, hydrophobic interactions have been found to be negligible compared to the mixed interactions between zwitterions and alkyl chains (1, 8). This has been the main factor leading to the hypothesis that the most probable orientation is the one that allows the opposite charges of the zwitterions to interact. Inspection of molecular models shows that in this orientation both alkyl chains belong to the same half-space, when the two molecules are of the same chirality (cross- or self-homotactic interaction). Obviously, the opposite occurs for two molecules of different chirality (cross- or self-heterotactic interaction). The two different reciprocal positions of the alkyl chains in this orientation must play an important role in differentiating the interaction between stereoisomers. Also, the homotactic interaction coefficients are expected to be systematically larger than the heterotactic ones, because of the better juxtaposition of the hydrophobic alkyl chain cospheres for the homo interactions in this orientation. This is what actually happens (see Table 1). In fact, the cross-homotactic coefficients ($h_{x_D y_D}$) determined here are always larger than the corresponding cross-heterotactic ones ($h_{x_D y_L}$). It is important to point out that this orientation is not the only one that contributes to build up the pairwise coefficients or the difference between steroisomers, but it is the orientation that prevailingly contributes to chiral recognition.

As shown by the enthalpic (8) and volumetric (7) excess properties data, chiral recognition disappears when pure water is replaced by H_2O/HCl (1 M) mixed solvent. In the latter medium, the attractive dipolar interaction working in pure water is replaced by the +/+ repulsive interaction. Thus it seems that favourable interaction between zwitterions is needed for chiral recognition or, more generally, a "forced" orientation enhancing steric differences is necessary to detect chiral recognition in aqueous solutions or to make evident differences in excess enthalpies of aqueous solutions of positional, configurational, and stereo isomers. An analysis of the enthalpic data by means of the SWAG approach, restricted to homologous series of α-amino acids in water and in the mixed solvent (1 M, H_2O/HCl), indicates the changes in the interaction mechanism in the two solvents (8). However, this approach can give only qualitative indications, because the presence of a forced orientation is in contrast with the SWAG statistical principle. Then in the mixed solvent the absence of the "forced head–head" (+/−, +/− favourable interaction) orientation, substituted by the "side-on" (-COOH, -COOH and hydrophobic–hydrophobic interaction) orientation (19), could be the most significant process that cancels out the differences between stereoisomers. As reported in Fig. 1, the self- and cross-homotactic coefficients of the linear amino acids increase linearly with the half-sum of the number of the aliphatic carbon atoms present on both molecules. The linear dependence is a clear indication that the CH_2–CH_2 interaction is not cooperative. In fact, the trend should depend on the sum of both hydrophobic and mixed interactions, the first having a quadratic dependence on the number of aliphatic carbon atoms and the latter proportional to the number of carbon atoms. Probably the zwitterion–zwitterion interactions compete with the mixed and with the hydrophobic ones, so that the cooperativity of the hydrophobic interaction is attenuated. For α-amino acids in the HCl/H_2O mixed solvent, the hydrophobic interactions are instead found to prevail because of the disappearance of the favourable zwitterion–zwitterion interaction. In this case the homotactic coefficients show a quadratic dependence on the number of aliphatic carbon

atoms (8):

$$[8] \quad h_{x_D x_D} = -256(56) + 64(4)\, n_C^2$$

On the other hand, it has been found that for alkane-1,2-diols, a linear trend is obtained when the enthalpic self-coefficients are plotted against the third power of the number of aliphatic carbon atoms, thus indicating that the CH_2–CH_2 interaction is more than statistical. Therefore, in some way, it is a forced interaction and the CH_2–CHOH interaction is negligible. This and other considerations led to the hypothesis that there is a double simultaneous interaction between the hydroxyl groups that makes the interaction between the hydrophobic groups more effective (19, 20).

In conclusion, preferred orientations are likely to occur in aqueous solutions of substances bearing groups through which favourable interactions can be established. The preferred orientation makes different the behaviour of substances which, on the basis of the sign of the enthalpic coefficients, at first glance could have been considered as simply hydrophobic. Then α-amino acids in the mixed solvent behave as typical hydrophobic solutes, having coefficients proportional to the square of the number of aliphatic carbon atoms. For alkane-1,2-diols (19, 20), because of the presence of a side-on orientation, the interaction coefficients have instead a linear dependence on the third power of the number of aliphatic carbon atoms. In contrast, α-amino acids in water, as shown by the above discussion, behave in a complex manner (linear dependence of the coefficients on the first power of the number of carbon atoms), thus indicating that the interactions between the charges compete with the hydrophobic interactions.

Acknowledgments

This work was carried out with the financial support of the Italian Ministry of Public Education (MPI), Rome.

1. G. Barone, G. Castronuovo, P. Del Vecchio, V. Elia, and S. Puzziello. J. Solution Chem. **18**, 1105 (1989).
2. G. Barone, G. Castronuovo, V. Elia, and C. Giancola. J. Thermal Anal. **30**, 1367 (1985).
3. G. M. Blackburn, T. H. Lilley, and P. J. Milburn. J. Chem. Soc. Chem. Commun. 299 (1985).
4. G. Barone, G. Castronuovo, P. Del Vecchio, V. Elia, and C. Giancola. Thermochim. Acta, **122**, 105 (1987).
5. G. Barone, P. Cacace, G. Castronuovo, and V. Elia. J. Solution Chem. **13**, 625 (1984).
6. T. F. Wegrzin, I. D. Watson, and G. R. Hedwig. J. Solution Chem. **13**, 233 (1984).
7. S. Puzziello. Doctoral Thesis, University of Naples (1988).
8. G. Castronuovo, V. Elia, C. Giancola, and S. Puzziello. J. Solution Chem. **19**, 855 (1990).
9. J. J. Savage and R. H. Wood. J. Solution Chem. **5**, 731 (1976).
10. G. Barone, P. Cacace, G. Castronuovo, and V. Elia. J. Chem. Soc. Faraday Trans. 1, **77**, 1567 (1981).
11. G. Barone, P. Cacace, G. Castronuovo, and V. Elia. Can. J. Chem. **59**, 1257 (1981).
12. G. Barone, V. Elia, and R. Rizzo. J. Solution Chem. **12**, 11 (1983).
13. V. Abate, G. Barone, G. Castronuovo, V. Elia, and E. Rizzo. J. Solution Chem. **12**, 645 (1983).
14. H. L. Friedman and C. V. Krishman. J. Solution Chem. **2**, 119 (1973).
15. R. B. Cassel and R. H. Wood. J. Phys. Chem. **78**, 2465 (1974).
16. F. Franks, M. Pedley, and D. S. Reid. J. Chem. Soc. Faraday Trans. 1, **72**, 359 (1976).
17. J. E. Desnoyers, G. Perron, L. Avédikian, and J. P. Morel. J. Solution Chem. **5**, 631 (1976).
18. T. H. Lilley. *In* The chemistry and biochemistry of amino acids. *Edited by* G. C. Barret. Chapman and Hall-Methuen, London. 1984. Chap. 21.
19. C. Cascella, G. Castronuovo, V. Elia, R. Sartorio, and S. Wurzburger. J. Chem. Soc. Faraday Trans. **86**, 85 (1990).
20. S. Andini, G. Castronuovo, V. Elia, and L. Fasano. J. Chem. Soc. Faraday Trans. **86**, 3567 (1990).
21. G. Castronuovo, R. P. Dario, and V. Elia. Thermochim. Acta. In press.
22. G. Barone, B. Bove, G. Castronuovo, and V. Elia. J. Solution Chem. **10**,803 (1981).

Can. J. Chem. Downloaded from www.nrcresearchpress.com by 198.100.157.202 on 09/07/12
For personal use only.

Reactivity patterns of *N*-methylbenzhydroxamates. I. Studies of methyl transfer between *N*-methylbenzhydroxamates and arenesulfonates

KENNETH R. FOUNTAIN,[1] DANIEL P. FOUNTAIN, BERNICE MICHAELS, D. BRENTON MYERS, JON K. SALMON, DEAN A. VAN GALEN, AND PAT YU

Department of Chemistry, Northeast Missouri State University, Kirksville, MO 63501, U.S.A.

Received October 19, 1990

KENNETH R. FOUNTAIN, DANIEL P. FOUNTAIN, BERNICE MICHAELS, D. BRENTON MYERS, JON K. SALMON, DEAN A. VAN GALEN, and PAT YU. Can. J. Chem. **69**, 798 (1991).

The rates of methyl transfer between benzohydroxamates and sulfonates show large β_{nuc} values (ca. 0.8) indicating much charge transfer to the C atom, similar to the results of *N,N*-dialkylaminofluorene anions. A small α effect shows that even in methyl substrates, with certain leaving groups, the effect is displayed. Investigation of the β_{lg} shows that from the leaving group side of the reaction it is a normal S_N2 reaction. Correlation of the reactivity with computed gas phase ionization potentials shows that desolvation of anions is probably not important. These results suggest an α-effect model that explains the larger size of the effect at carbonyl groups in terms of greater solvation of the charge transferred to the O atom.

Key words: α effect, Brønsted plot, ionization potentials, cyclic voltammetry, β_{lg}, β_{nuc}, AMI, $E_{\frac{1}{2}}$.

KENNETH R. FOUNTAIN, DANIEL P. FOUNTAIN, BERNICE MICHAELS, D. BRENTON MYERS, JON K. SALMON, DEAN A. VAN GALEN et PAT YU. Can. J. Chem. **69**, 798 (1991).

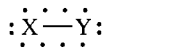
Les vitesses de transfert des groupements méthyles entre des benzohydroxamates et des sulfonates présentent des valeurs de β_{nuc} élevées (environ 0,8) qui indiquent un important transfert de charge vers l'atome de C, semblable à celui observé avec les anions *N,N*-dialkylaminofluorènes. Un faible effet α montre que, même avec des substrats méthyles de certains nucléofuges, on peut observer cet effet. Une étude du β_{lg} montre que, par rapport au groupement nucléofuge, il s'agit d'une réaction S_N2 normale. Une corrélation de la réactivité avec les potentiels d'ionisation en phase gazeuse calculés montre que la désolvatation des anions n'est probablement pas importante. Ces résultats suggèrent un modèle d'effet α qui explique l'importance plus grande de l'effet au niveau des groupements carbonyles en termes de plus grande solvatation de la charge qui est transférée à l'atome d'oxygène.

Mots clés : effet α, courbe de Brønsted, potentiels d'ionisation, voltamétrie cyclique, β_{lg}, β_{nuc}, AMI, $E_{\frac{1}{2}}$.

[Traduit par la rédaction]

Introduction

The α effect is displayed by nucleophiles having a lone pair of electrons on an atom neighboring the atom undergoing nucleophilic attack, such as **1**. The α effect is defined as an enhanced reactivity compared to nucleophiles of similar pK_a. The effect has been a source of much debate for several decades (1). It is strongest at unsaturated sites, such as the carbonyl group (lg, 13), but small α effects are also found at the benzylic group (2), and in displacement of *p*-nitrophenylsulfate ions from methyl groups by hydrazine and HO_2^- anion (3, 23).



1

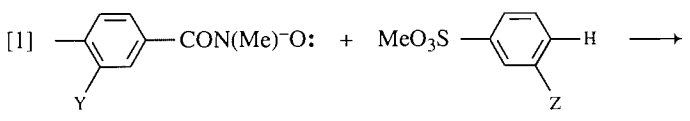
N-Methylbenzhydroxamate ions (G-NMBH), **2**, have long been known as α nucleophiles (1), but systematic studies to show the effect of structural variation on their reactivity are lacking. They are known to give α effects with *p*-nitrophenylacetate (PNPA) of ca. 45, or with 2,4-dinitrophenyltosylate of 145 (18, 22). The α effect in these cases was determined by comparison with phenols of pK_a similar to the G-NMBH acids. The α effect of G-NMBH anions toward benzyl bromide was smaller (= 13) (2). No study of the α effect of these nucleophiles in methyl transfers has yet appeared. Methyl transfer between substituted *N*-methylbenzhydroxamate ions (G-NMBH) and methyl arenesulfonates is the subject of this paper.



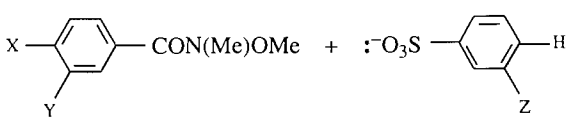
2

The reaction of G-NMBH ions with methylarenesulfonates is shown in reaction [1]. Our goals in studying this reaction are (a) to ascertain the differences in α-effect behavior between this reaction and the reactions with carbonyls and benzyl substrates; (b) to determine the existence of an α effect in this system; and (c) to interpret the findings in terms of current models of the S_N2 transition state (TS), which deal with the possibility of single electron transfer character (SET character) in transition state formation (4). Because so many factors have been advanced as reasons for the α effect (1), it is important to begin explanation from the simplest possible substrate system capable of structural variation in both the nucleophile and leaving group, and to sort out the factors involving these two groups. When the systems become increasingly more complex, as in the benzyl system, carbonyl systems, etc., additional factors can be analyzed as they enter the more complex substrate system. By means of this step-by-step approach, all of the factors usually cited for causes of the α effect can be explored experimentally.

In this study, reaction [1] is useful, even though the total range of reactivity of the G-NMBH anions is limited, because internal acid–base catalysis, such as found with benzhydroxamate ions, is eliminated (2). The data for the more complex



3 **4**



5 **6**

[1]Author to whom correspondence may be addressed.

Printed in Canada / Imprimé au Canada

Can. J. Chem. Downloaded from www.nrcresearchpress.com by 198.100.157.202 on 09/07/12
For personal use only.

Can. J. Chem. Downloaded from www.nrcresearchpress.com by 198.100.157.202 on 09/07/12
For personal use only.

carbon systems, carbonyl and benzyl, are already known, so the very simplest carbon system of this study can provide useful insight.

Results

Preparation of N-methylbenzhydroxamic acids and their sodium salts

The *N*-methylbenzhydroxamic acids (G-NMBHH) were made by known methods (5, 6) or by a method worked out by our group (see Experimental). All new compounds gave satisfactory (±0.4) microanalytical data. Each G-NMBHH was converted into its sodium salt (G-NMBHNa), structure **2**, by treating a methanol solution of the G-NMBHH with a stoichiometric amount of sodium methoxide in methanol. Removal of solvent on a rotary evaporator gave salts that were dihydrates. On careful heating, several salts decomposed nearly quantitatively to their anhydrous forms.[2]

Characterization of these G-NMBHH acids by gas chromatography – mass spectrometry (GC–MS) was interesting because the parent ions were very weak. The base peaks were all at m/e values corresponding to the amides, showing extrusion of O atoms. *o*-Alkylated G-NMBH display similar behavior (8, 9).

Preparation of methylarenesulfonates

The literature provided methods for synthesis of most of these (10). All new compounds were made in analogous reactions. All compounds gave acceptable analytical results.

Kinetic studies

Two types of kinetic studies were employed: following the disappearance of the methyl signals of the methyl *p*-methoxybenzenesulfonate (MPMBS) in the ^{1}H NMR as it reacted with the G-NMBH anion (G = substituting group), and competition reactions in which two substituted NMBH anions competed for a limited amount of MPMBS. Preliminary Brønsted plots (not shown) gave broken lines, suggesting that the more basic G-NMBH anions accept protons (deuterons) from the methanol-d_4. The more basic anions, beginning with NMBH anion itself, were then used in competition experiments. Comparison of k_{rel} with the known rate of *p*-NO_2NMBH determined the rate constants for the more basic anions. Table 1 summarizes the results.

Competition reactions determined the relative rates for methyl transfer to 4X,3Y-NMBH anions in water – 20% dioxane by adding 1.0 molar equivalent of MPMBS in 1,4-dioxane to 10.0 molar equivalents (each) of two different 4X,3Y-NMBH anions. The reaction mixtures were analyzed after 20 min by GC-MS. Experiments with authentic materials established that our integrator was linear in grams of material to ±3%. The relative rate constants are summarized in Table 2.

Determination of pK_a values

The most complete pK_a study of 4X,3Y-NMBHH in water is by Crumbliss and co-workers, who report (5) on four substituents ($\rho = 0.60$; $R = 0.91$). We determined two additional values under conditions similar to those of the Crumbliss group (11). Our results are combined with the values of Crumbliss in Table 3. Figure 1 shows the Hammett plot, which contains two extrapolated points from the following equation: $pK_a = -0.67\Sigma\sigma + 8.39$ ($R = 0.99$, excluding extrapolated values). From this equation the remaining values in water could be found, as shown in Table 3.

[2]This experiment was performed by Desert Analytics, Box 41838, Tucson, AZ 85717, U.S.A.

TABLE 1. Rate constants for methyl transfer to 4X,3Y-NMBH anions from *p*-methoxybenzenesulfonate at 29.5°C in methanol-d_4; ^{1}H NMR kinetics and competitions (reaction [1])

No.	X	Y	k_a (M^{-1} s^{-1})	$-\log k$
1.	H	H	0.064 (0.000)[b]	1.194
2.	NO_2	H	0.015 (0.000)	1.824
3.	Cl	H	0.041 (0.001)[b]	1.387
4.	CF_3	H	0.21 (0.001)	1.678
5.	Me	MeO	0.091 (0.000)[b]	1.041
6.	MeO	H	0.25 (0.01)[b]	0.602
7.	3,5-diNO_2		0.0050 (0.000)[b]	2.301
8.	Me	H	0.10 (0.001)[b]	1.000

[a]All values at least duplicated. Standard error in parentheses. Where (0.000) values occur they are the results of rounding to two significant figures.

[b]These values determined by direct competition with the *p*-NO_2NMBH anion.

TABLE 2. Relative rates of 4X,3Y-NMBH anions in 20% dioxane – 80% water

	Compound			
	X	Y	k_{rel}	log k_{rel}
1.	H	H	1.000	0.0000
2.	3-NO_2	5-NO_2	0.18 (0.005)	−0.7447
3.	Cl	H	0.89 (0.005)	−0.0531
4.	Cl	NO_2	0.40 (0.05)	−0.3980
5.	MeO	H	1.77 (0.07)	0.2480
6.	Me	MeO	1.63 (0.08)	0.2068

TABLE 3. pK_a values of 4X,3Y-NMBH-H in water and methanol at 25°C

Acid		pK_a	
X	Y	Water	MeOH
H	H	8.28[a]	12.38[b]
Cl	H	8.17[b]	12.04[c]
MeO	H	8.64[a]	12.80[b]
CF_3	H	8.06[b]	11.77[c]
No_2	H	7.91[a]	11.58[b]
Me	H	8.46[a]	12.45[c]
H	Me	8.52[b]	12.30[b]
Me	MeO	8.41[c]	12.32[c]
Cl	NO_2	7.78[c]	—
3,5-diNO_2		7.41[c]	10.80[b]

[a]Reference 1.
[b]Determined in this work.
[c]From the appropriate Hammett plot.

pK_a values of 4X,3Y-NMBH-H in anhydrous methanol were determined spectroscopically, using *p*-nitrophenol as an indicator (pK_a = 11.15, ref. 12*a*) for the more acidic (<12.5) 4X,3Y-NMBH-H compounds. Preliminary determinations of the least acidic 4X,3Y-NMBH-H compounds showed them to have pK_a's of ca. 13.5, using *p*-nitrophenyl as an indicator. This value puts them beyond the useful range of *p*-nitrophenol for accurate determinations, so *p*-bromothymol blue (pK_a = 12.4,

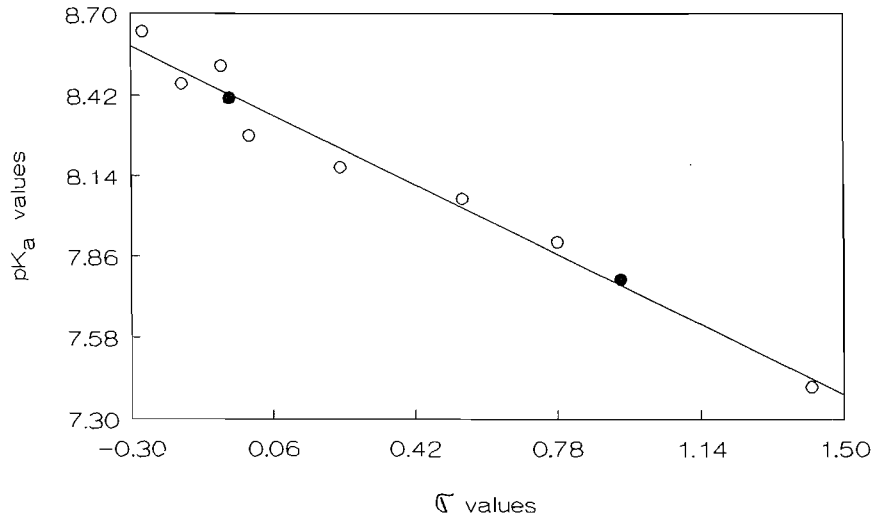


FIG. 1. Hammett plot of pK_a's of G-NMBH-H in water (2.0 M ionic strength) at 25°C (±0.1).

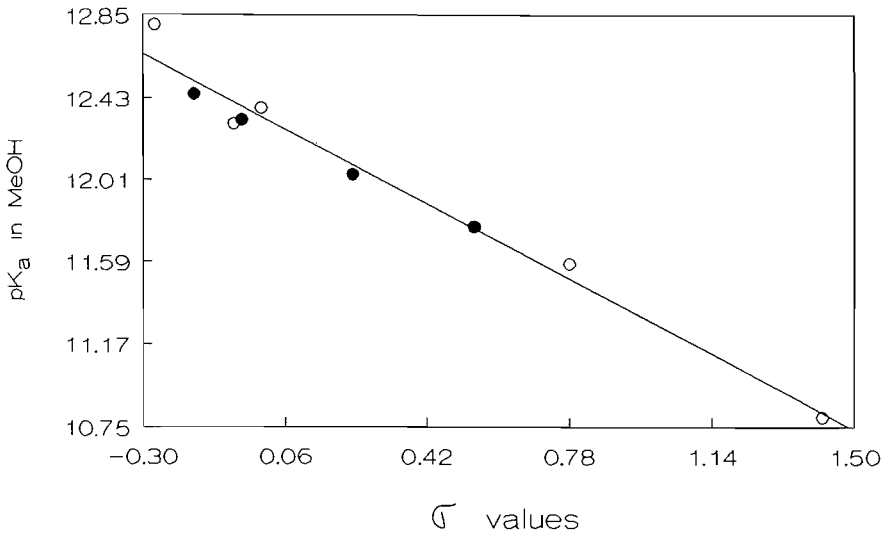


FIG. 2. Hammett plot of pK_a of G-NMBH-H in anhydrous methanol at 25°C (±0.1).

ref. 12*b*) was used. The pK_a values obtained, using eq. [2] (with the molarity quantities determined spectroscopically), are also shown in Table 3. Figure 2 gives the Hammett plot ($R = 0.98$) and shows the extrapolated values (used in making Brønsted plots) as filled circles. The correlation equation is $pK_a = -1.02\Sigma\sigma + 12.27$ ($\rho = -1.41$ in kcal/σ unit).

$$[2] \quad pK_{Ind} - pK_{Unkn} - \log\frac{[Unkn^-]}{[UnknH]} - \log\frac{[Ind]}{[IndH]}$$

Determination of the α effect

Competition reactions, as in the determination of relative rate constants, ensure consistency of methods. The G-NMBH-H acids were matched in pK_a by phenols.

Determining the expression of the α effect can be done in two ways: (1) finding an extra reactivity in the α nucleophile on a Brønsted plot (β_{nuc}), and (2) establishing the rate constant ratio of the α nucleophile and a normal nucleophile of matched pK_a (13, 14). We decided to obtain the expression for the α effect by direct competition of NMBH anions with pK_a matched phenols, *m*-nitrophenol (pK_a = 12.44) (15), and 3,4-dichlorophenol (pK_a = 12.93) (15) in MeOH. The result obtained is thus a minimum expression of the α effect for the NMBH anion because the pK_a's of the phenols are both slightly higher than those of the 4X,3Y-NMBH acids.

Competition reactions were run using a 10 molar equivalent excess of both the phenolate salt and the 4X,3Y-NMBH anion in 1.00 mL of methanol-d_4 containing excess MeO-d_3^-. One molar equivalent of methyl 4-methoxybenzenesulfonate was added, and the reaction mixture analyzed by GC–MS. Authentic materials supplied retention times and authentic MS results. The $k_{G\text{-}NMBH}/k_{m\text{-}NO_2phenolate}$ equals 3.50 ± 0.42. When a similar experiment using 3,4-dichlorophenolate was done with NMBH anions, $k_{NMBH}/k_{3,4\text{-}diCl\ phenolate} = 2.48 \pm 0.15$. These results are in line with Buncel's α-effect values for displacement of *p*-nitrophenylsulfate anions by HO_2^- ion.

Using phenolate anions as normal nucleophiles requires a set of phenolate ions with pK_a values matching those of the 4X,3Y-NMBH anions. Some of the substitutions cause resonance stabilization of the phenolates, thus perhaps lowering nucleophilic activity. Jencks deals with this issue (16) in a study of displacements by phenolates on 1-acetoxy-4-methoxy-

Can. J. Chem. Downloaded from www.nrcresearchpress.com by 198.100.157.202 on 09/07/12
For personal use only.

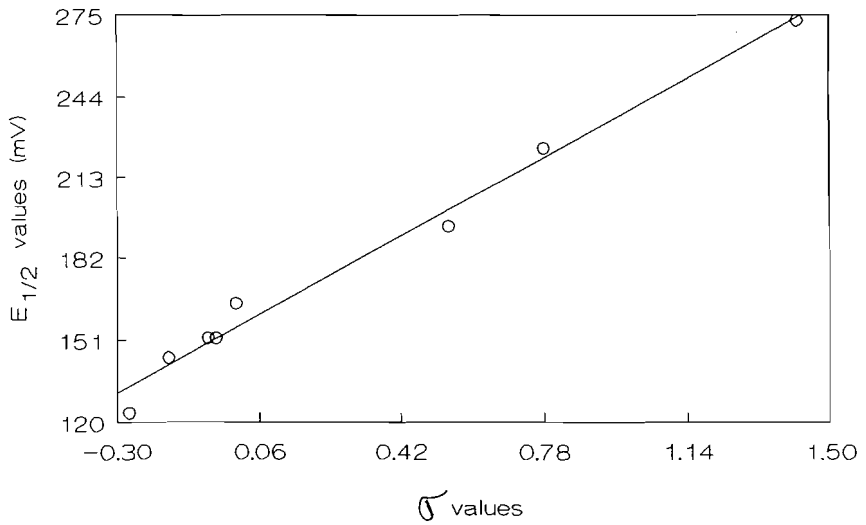


FIG. 3. Hammett plot of $E_{\frac{1}{2}}$ values of G-NMBH anions in anhydrous methanol at 25°C.

pyridinium perchlorate. By comparing reactivity of phenolate with that of the anions of fluorinated alcohols, he showed that there "was no evidence for a specific contribution of resonance delocalization in the phenolate ions to the β_{nuc} values or to the curvature of the Brønsted plot ..." Additionally, phenoxide ions have been the traditional nucleophiles for comparison with oxygen α nucleophiles (17, 18), which justifies our use of these anions.

Solvents play a great role in the expression of the α effect. Buncel and Um (14*a*) have shown that the α effect, comparing *p*-chlorophenylate with butane-2,3-dione monoximate ion (toward PNPA substrate) is 121 in 90 mol% DMSO and 96 in 100 mol% water. It was therefore interesting to see if an α effect existed in both solvent systems in the present study. The possibility of solvent isotope effects is implicit in this study, but these are expected to be small so will be neglected.

Determination of the α effect with NMBH anion (pK_a of NMBH-H = 8.28 in water) and *m*-nitrophenylate (pK_a of the phenol = 8.26 in water) in pure water was frustrated by the lack of solubility of the alkylation agent in water. Competition experiments in 20% dioxane – 80% water mixtures overcame this lack of solubility sufficiently to observe the α effect. The α effect found was 3.52 ± 0.42 for NMBHNa vs. *m*-nitrophenolate anion in water, and 4.81 ± 0.25 for NMBHNa vs. 3,5-dichlorophenolate in methanol. Interpretation of these numbers is not yet available, due to the effects of solvent composition on the α effect, as mentioned above. We are content to have shown the α effect in both solvents used in this study.

TABLE 4. Data for $E_{\frac{1}{2}}$ correlations in MeOH, 25°C

	G-NMBH, G	$E_{\frac{1}{2}}$ (mV)[a]
1.	4-CF_3	194.5
2.	4-MeO	123.5
3.	3,5-diNO_2	273.0
4.	4-NO_2	224.5
5.	H	165.0
6.	3-Me	152.0
7.	4-Me-3-MeO	152.0
8.	4-Me	144.5

[a]Versus an Ag/AgCl reference electrode.

TABLE 5. AMI computed IPs for correlation with Hammett constants

	G-NMBH, G	IP (eV)[a]
1.	H	2.54
2.	4-Cl	2.73
3.	4-Me-3-MeO	2.66
4.	3,5-diNO_2	3.49
5.	4-MeO	2.64
6.	4-Cl-3-NO_2	3.19

[a]AMI calculated by Koopman's theorem.

Determinations of $E_{\frac{1}{2}}$ *values of 4X,3Y-NMBHNa in methanol*

The oxidation potentials of a series of 4X,3Y-NMBHNa salts were determined in anhydrous methanol as outlined in the experimental section. The oxidations were reversible in methanol, but in water the $E_{\frac{1}{2}}$ values were not obtained, due to electrode fouling, or to slow, heterogeneous electron transfer.

The 4X,3Y-NMBH anions were oxidized at a freshly polished glassy carbon electrode. At slower scan rates, the radical resulting from NMBH anion oxidation undergoes significant chemical reaction on the time scale of the experiment, as evidenced by a relative decrease in the cathode peak for reduction of the radical. Thus, scan rates of at least 200 mV/s were employed for $E_{\frac{1}{2}}$ measurements. The values are listed in Table 4 and summarized as the Hammett plot in Fig. 3. The equation is $E_{\frac{1}{2}} = 83.18\Sigma\sigma + 155.96$ ($R = 0.99$; 8 points) ($\rho = 1.91$ kcal/σ unit).

Computations of AM1 IPs

Ionization potentials (IPs) were computed using QCMP no. 024 (Stewart's MOPAC, version 4.0) on a Zenith PC, using a CCG 032 coprocessor board (Denver, Colorado). Full minimization of geometry was obtained in each case, as shown by diagonalizing the Hessian matrix to find only positive and non-zero eigenvalues, showing that the geometries obtained were stationary states. The results are summarized in Table 5.

Can. J. Chem. Downloaded from www.nrcresearchpress.com by 198.100.157.202 on 09/07/12
For personal use only.

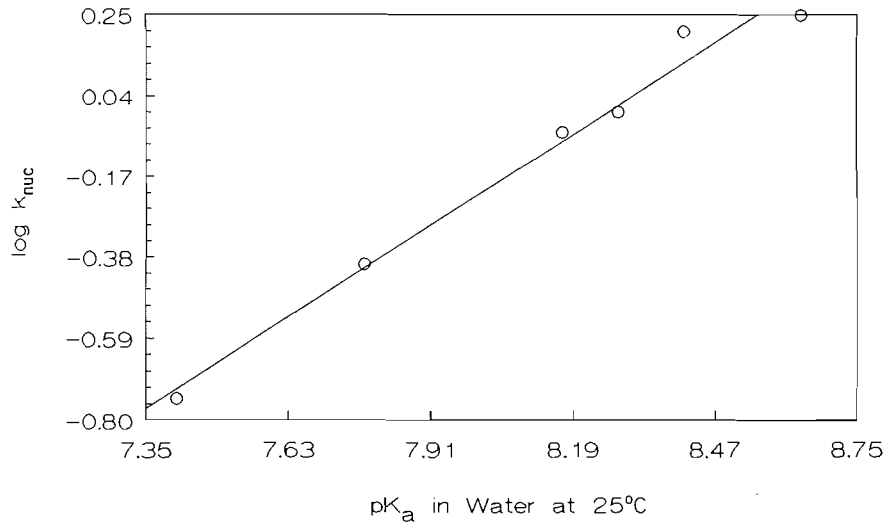


FIG. 4. Brønsted plot for reaction [1] in water at 25°C (±0.1) by competition reactions.

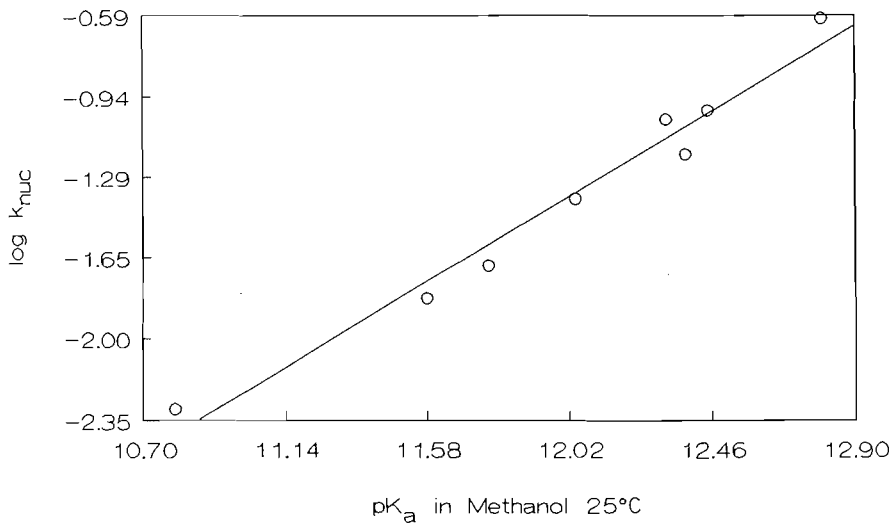


FIG. 5. Brønsted plot reaction [1] in methanol at 29.5°C (±0.5) by ^{1}H NMR and competition reactions.

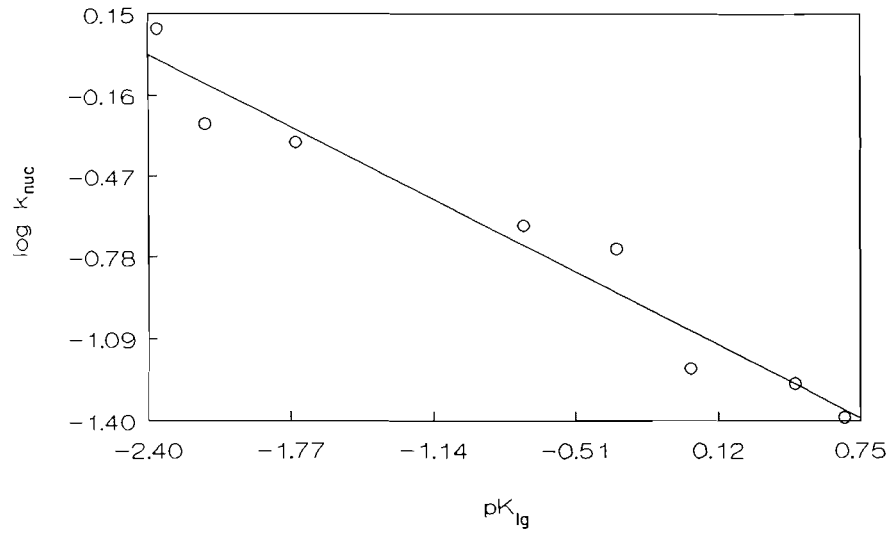


FIG. 6. Brønsted–Lewis plot for reaction [1] (X = Cl, Y = H) in methanol (W and Z varied) at 29.5°C (±0.5), ^{1}H NMR kinetics.

Can. J. Chem. Downloaded from www.nrcresearchpress.com by 198.100.157.202 on 09/07/12
For personal use only.

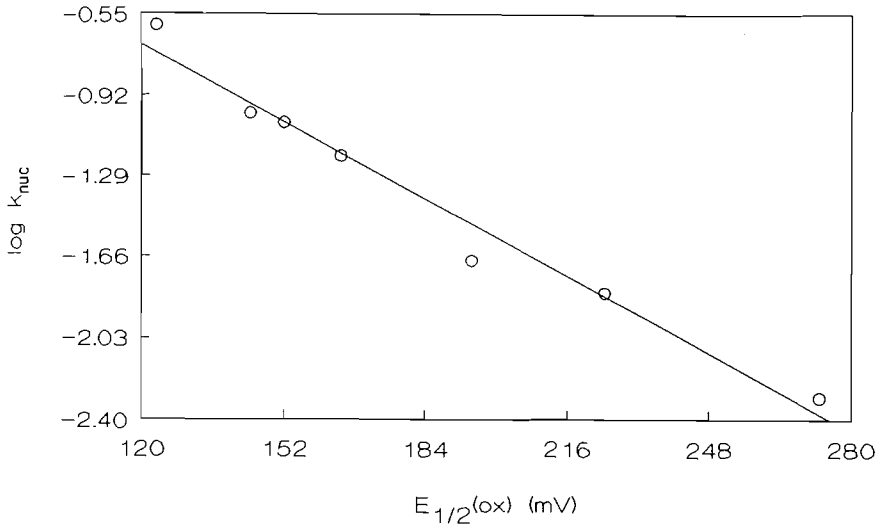


FIG. 7. Correlation of $E_{\frac{1}{2}}$ (ox) of G-NMBH anions with log k_{nuc} in methanol at 29.5° (±0.5).

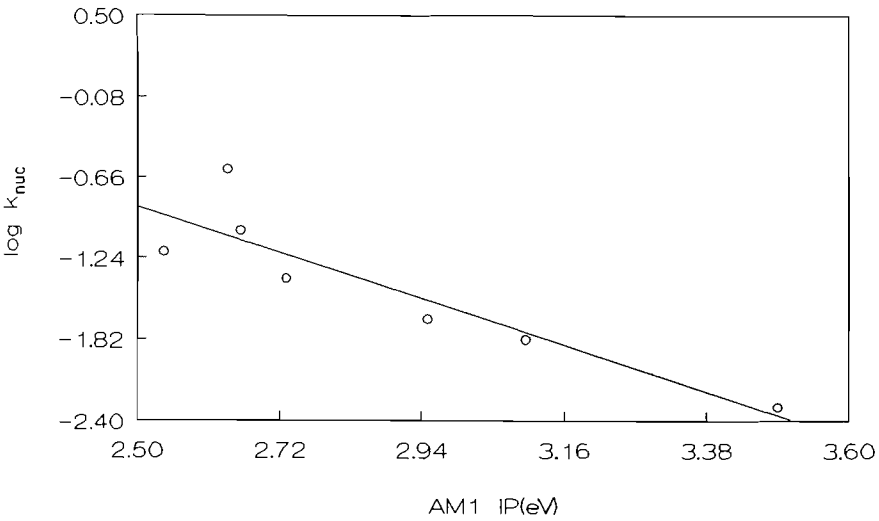


FIG. 8. Correlation of AM1 IPs G-NMBH anions with log k_{nuc} in methanol-d_4 at 29.5°C (±0.5).

Leaving group study

The rates of reaction [1] as a function of various arenesulfonate leaving groups were determined by NMR kinetics in the same manner as for methyl *p*-methoxybenzenesulfonate. The rate constants are summarized in Table 6 for *p*-ClNMBHNa.

The last column of Table 6 shows the pK_{lg} parameter developed by Hoffman and co-workers (19) from data on methyl transfers between arenesulfonate ions in sulfolane, by Lewis *et al.* (20). These parameters have been proven useful in classification of the degree of leaving of arene sulfonates in various nucleophilic reactions. They are used in the discussion section to examine reaction [1] from the leaving group side.

Correlations of data

The Brønsted plot of pK_a vs. log k_{nuc} for reaction [1] in water is presented in Fig. 4 and the correlation for methanol-d_4 in Fig. 5. The β_{nuc} values (slopes) of these plots are 0.84 and 0.86 (r = 0.98 and 0.97 respectively). Figure 6 shows the Brønsted–Lewis study, using the pK_{lg} values of Hoffman (19), as summarized in Table 6. The equation is log $k_{nuc} = -0.44\ pK_{lg} - 1.06$ (r = 0.98).

Correlations of log k_{nuc} with $E_{\frac{1}{2}}$ (ox) appear in Fig. 7 for the 4X,3Y-NMBH anions in methanol-d_4. The $E_{\frac{1}{2}}$ values also correlate with Hammett σ values, thus acting as a check on the ability to correlate the rate constants. The numbering follows Table 4.

AM1 IP values correlated with σ (plot not shown; R = 0.98): equation, IP = 0.58Σσ + 2.65. From this equation other IP values used in the following correlation could be obtained.

TABLE 6. Rate constants for reaction [11, X = Cl, in methanol-d_4 at 29.6°C

	Compounds				
	W	Z	k (M^{-1} min^{-1})[a]	log k	pK_{lg}
1.	H	H	0.063 (0.003)	−1.201	0.000
2.	Br	H	0.22 (0.02)	−0.658	−0.74
3.	Me	NO_2	0.46 (0.04)	−0.337	−1.75[b]
4.	NO_2	H	1.25 (0.17)	0.093	−2.36
5.	H	NO_2	0.54 (0.04)	−0.268	−2.15
6.	F	H	0.18 (0.01)	−0.745	−0.33
7.	Me	H	0.055 (0.001)	−1.260	0.46
8.	MeO	H	0.41 (0.001)	−1.387	0.68

[a]All values are from at least duplicate determinations.
[b]From a Hammett plot of the data of ref. 19*a*.

Can. J. Chem. Downloaded from www.nrcresearchpress.com by 198.100.157.202 on 09/07/12
For personal use only.

TABLE 7. Studies of the α effect for 4X,3Y-NMBH anions

Electrophilic substrate	β_{nuc}	α Effect	Solvent	References
p-Nitrophenyl acetate (PNPA)	0.23	45	12% v/v EtOH/H_2O	18, 22
2,4-dinitrophenyl tosylate	0.41	150	12% v/v EtOH/H_2O	18
Benzyl bromide	0.31	13	Water	2
Methylarene sulfonates	0.80	3.5–4.8	Water – 20% dioxane	This work
	0.86	2.5–3.5	Methanol-d_4	This work

AM1 gas phase ionization potentials are correlated with log k_{nuc} in Fig. 8. The omission of point 6 (4X = OMe, 3Y = H) gave improved correlation ($R = 0.95$). The large slopes show strong dependence on gas phase ionization potential. A similar correlation for the MNDO calculated IPs reported by Bugner (21) for the arenesulfonate leaving groups gave a good linear regression fit ($R = 0.96$, slope = −1.88; plot not shown). The point for the 4-MeO substituent was again considerably off the line.

A correlation of log k_{nuc} for reaction [1] (not shown) with the MNDO HOMO values calculated by Bugner (21) gave a good fit ($R = 0.96$). This plot is interesting because the MNDO calculations refer to gas phase only, and it shows that a gas phase parameter correlates with a solution phase measurement. This subject is discussed below.

Discussion

The correlations of kinetic data in this paper clearly show that methyl transfer to G-NMBH anions is unique in several aspects. First, the size of β_{nuc} both in water and in methanol-d_4 is large compared with the carbonyl and benzylic systems. Table 7 summarizes the available data.

Clearly the behavior of methyl transfer to the G-NMBH anions from arenesulfonates differs substantially from transfers of other groups to these hydroxamate anions. Also, the β_{nuc} values for water and methanol are very similar, showing a relative lack of solvent effects in this system. The α effect in the present work is consistent with the α effect for methyl transfers to HO_2^- from the *p*-nitrophenylsulfate ion (5.7–11.0) (23). The large β_{nuc} values are associated with very small α effects. We can estimate the β_{nuc} for the phenolate anions by using the known rate constants (Table 1) for 4X,3Y-NMBH anions and the values for the α effect with the substituted phenolate anions of similar basicity (this procedure followed the method of ref. 23). Equations [2] summarize the process. In water–dioxane the β_{nuc} was 0.30; in methanol-d_4 it was 0.31, showing essential agreement for the methylation of phenoxides by the methylating agents used in this study. These β_{nuc} values are the same order of magnitude as for other alkylating agents, where the β_{nuc} range is 0.16 for methylation by the methylsulfate anion ($MeOSO_3^-$) to 0.37 for butylation by butyl bromide (25).

$$[2a] \quad \alpha \text{ effect} = \frac{k_{4X,3Y\text{-NMBH}-}}{k_{G\text{-phenO}-}}$$

$$[2b] \quad \beta = \frac{\log k\text{G-PhenO}_1^- - \log k\text{G-PhenO}_2^-}{\Delta pK_a}$$

The result of larger values of β_{nuc} for transfers of methyl groups to 4X,3Y-NMBH anions is similar to that reported by Buncel *et al.* (23) for methyl transfer to HO_2^-. In that report the authors argued that an increased β_{nuc} showed that there was an anti-Hammond character in the behavior of the transition state (TS) (i.e., the TS was more covalently bound than for normal nucleophiles). The results of the present study could be interpreted in the same way.

TABLE 8. Summary of β_{lg}^{Me} of diverse mechanisms

System	β_{lg}	Type	References
MeO_3SAr	0.45	k_s	19, 27, 28
EtO_3SAR	0.45	k_s	27, 28
$AllylO_3SAr$	0.51	k_s	29
endo-2-Norbornyl-O_3SAr	0.56	k_s–k_c	28
exo-2-Norbornyl-O_3AR	0.57	k_Δ	28
CyclobutylO3SAr	0.55	k_Δ	31
2-AdamantylO_3Ar	0.57	k_Δ–k_c	30
2-(phenylthio)ethyl-O_3SAr	0.44	k_Δ	31

The concept of β_{lg}, based on the equilibrium constant values for transferring methyl groups between arenesulfonate anions (26), pioneered by Hoffman and Shankweiler (19*a*), was used to examine the extent of leaving group departure from the C atom. The essential idea of this method is that transfer of a proton between nucleophiles is not an adequate model for transfer of a methyl group. The ability to transfer a methyl group is ranked by the log of the equilibrium constant, pK_{lg}, between benzenesulfonate anion and a substituted benzenesulfonate anion. These pK_{lg} values have been used to map diverse systems of leaving group behavior. Table 8 shows a summary of the literature applications made (28). β_{lg}^{Me} is the slope of a plot of $-pK_{lg}$ vs. log k_{nuc} for methyl transfer. Its range is 0–1.0, showing no bond breaking to complete bond breaking.

The reason for presentation of these already published data is to attempt to locate the reaction type of our present system. The value of $\beta_{lg} = 0.44$ ($R = 0.98$) for our system means it resembles the leaving group portion of an ordinary S_N2 process. A k_Δ process, such as the 2-(phenylthio)-O_3SAr (neighboring group participation) could not be ruled out from these data alone. A referee pointed out a problem of interpreting the leaving group study using the β_{lg} values. This problem is discussed in the next few paragraphs.

Lewis[3] has reported a ρ value of 2.6 for the equilibrium constants for methyl transfer between arenesulfonate anions in sulfonate, on which the calculations of pK_{lg} depend. This ρ

[3]Lewis *et al.*, see ref. 17, Chap. 3.

Can. J. Chem. Downloaded from www.nrcresearchpress.com by 198.100.157.202 on 09/07/12
For personal use only.

Can. J. Chem. Downloaded from www.nrcresearchpress.com by 198.100.157.202 on 09/07/12
For personal use only.

value is nearly equal to that for ionization of benzoic acids in non-protic solvents (e.g., $\rho = 2.48$ in DMSO) (32). This ρ value will be solvent dependent, and should be ca. 1.3–1.6 in methanol (30). When corrected for the difference in ρ values in the two solvents the β_{lg} for G-NMBH anions would range from ca. 0.84 to 0.69. This range of β_{lg} values would show the NMBH anion methylation to be very tight from the nucleophile side and very loose from the leaving group side. This consideration also affects all the uses made of β_{lg} by McManus, Hoffman, *et al.* (19).

One might remark, since the studies of Hoffman, McMannus *et al.* have ranged over several previously well-established mechanistic types, without consideration of the differences in solvents, that the limitation due to solvent-dependent ρ values should be of no concern to us if all we are doing is comparing the present system with other well-known systems. It is possible, however, to finesse the consideration by calculating the ρ value for the *p*-Cl-NMBH anion reaction with the series of substituted methylarenesulfonates and comparing this value with known ρ values from the literature for other systems. From a Hammett correlation (not shown) this ρ value was determined as 1.29 ($\pm$0.07). The ρ values for comparison are as follows: for solvolysis of allylarenesulfonates in MeOH, 1.36 ($\pm$0.07), and in EtOH, 1.47 ($\pm$0.10); ethanolysis of methyl *p*- and *m*-nitrobenzenesulfonates at 70°C has $\rho = 1.32$ ($\pm$0.05) (30); for methanolysis of the same ester at 50°C, $\rho = 1.25$ ($\pm$0.04 (30). In contrast, methanolysis of 1-adamantyl esters had ρ values ranging from 1.82 to 1.65 (15–25°C) (30). (This treatment parallels Lewis' treatment in ref. 17, Chap. 3.)

We can conclude that the 4X,3Y-NMBH-methylarenesulfonate series resembles known systems that have a small amount of leaving group departure. Both β_{lg} and ρ considerations bear this out. An additional benefit is that the β_{lg} study parallels the ρ study (i.e., is valid for the present case). This statement is supported by observing that the ρ value correlates with the β_{lg} for the same reaction. Table 9 summarizes the data.

One can conclude that reaction [1], from the leaving group side, resembles an ordinary S_N2 reaction. From the nucleophile side the β_{nuc} of ca. 0.8 shows excessive bonding ($0.8 + 0.45 \approx 1.25$), which in turn suggests a very tight TS. What is the likely source of this excessive bond order?

The correlation of log rate constant with $E_{\frac{1}{2}}$ values assures us that the rate constants can be correlated, and that they probably have some claim of being accurate. The $E_{\frac{1}{2}}$ values also correlate with the pK_a values of the 4X,3Y-NMBH-H (not shown; $R = 0.98$). By itself this tells us little more than the Brønsted plots. The ionization potentials, discussed in the next paragraphs, help explain the results.

Correlation of the gas phase ionization potentials (IP), computed by the AM1 Hamiltonian in MOPAC (and diagonalization of the Hessian matrix to obtain only positive eigenvalues to ensure that each anion geometry was actually a stationary state), shows that single electron transfer character may be important in TS formation. There is no apparent reason why a gas phase computation should correlate with a solution phase measurement, particularly in protic media (38). This peculiarity of α nucleophiles was observed previously by us in cation–anion recombination chemistry (34), and by Bugner (21) for correlation of the IPs of the arenesulfonate ions (MNDO) with solution chemistry.[4]

[4]See ref. 36 for examples of the relationship between IP (gas) and IP (solution).

TABLE 9. Comparison of ρ values for leaving group studies with β_{lg} values

System	Nucleophile	Solvent	β_{lg}	ρ	References
MeO_3AR	EtOH	EtOH	0.45	1.32	19, 30
EtO_3SAr	EtOH	EtOH	0.44	1.30	19, 30
MeO_3SAr	MeOH	MeOH	—	1.32	30
MeO_3AR	4-ClNMBH	MeOH	0.44	1.29	This work

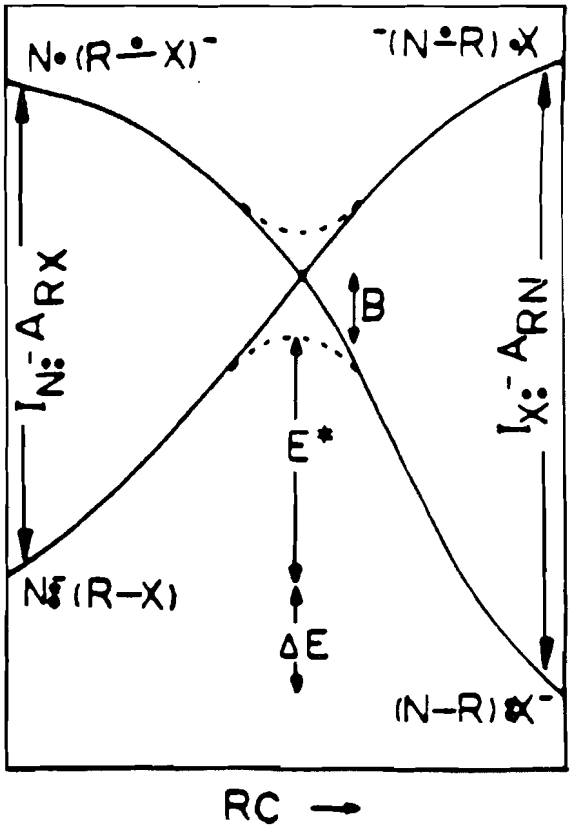
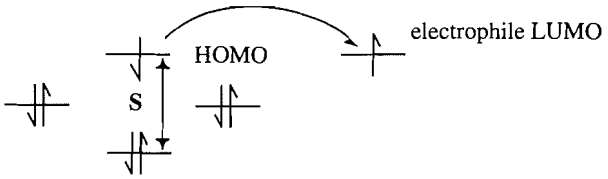


FIG. 9. Valence state configuration mixing model diagram.

Shaik's valence bond configurational mixing model (VBCM) of the S_N2 transition state (4) allows for direct inclusion of ionization potentials for both entering and leaving groups. Figure 9 summarizes the model. The transition state energy arises as a fraction of the energy gap between the ground state of the encounter complex of the nucleophile and the electrophile, and the excited state of the same complex. This excited complex has the same geometry as the ground state encounter complex. The gap is given by $I - A_{RX}$ where I is the ionization potential for the nucleophile, and A_{RX} is the electron affinity for the electrophile. As the energy of the upper state level falls and the energy of the lower state rises, the geometry of each state becomes distorted toward the geometry of its electronically corresponding partner on the diagram. At the TS the two states avoid crossing through quantum mixing of states, and the quantum hybrid representing the TS contains contributions describing transfer of a single electron, along with more conventional contributors. The degree of mixing of this single electron contribution into the TS is what is meant by "single electron transfer character," and the degree to which these



α-Nucleophiles configuration

SCHEME 1. Hoz model of the α effect.

single electron contributors mix into the TS hybrid governs how important single electron transfer characters is in TS formation.

The Hoz model (13*a*) for the α effect is summarized in Scheme 1 as a single electron transfer that contributes to an important degree to TS formation. This model shows that the α nucleophile easily transfers an electron to form a very stable radical, due to the orbital splitting retained after the single electron transfer has occurred. Thus, the mixing of a state resembling Scheme 1 into the TS involves a net stabilization of the TS because of mixing in this added stability. The α nucleophiles of this study are easily able to form radicals (35). It is therefore consistent that if one accepts the VBCM model for the S_N2 reaction and the Hoz model for the α effect, that the large β_{nuc} values should be interpreted as showing an increase of electronic transfer toward the C atom (large SET character).

The correlation of log k_{nuc} with a *gas phase* IP shows that desolvation of these α nucleophiles is perhaps not a strongly necessary process in TS formation. In Shaik's treatment of ionization potentials in nucleophilic activity (36) the ionization potentials all refer to the solvent phase. The facts that in simple cation–anion recombination (CAR) reactions the gas phase IPs of α nucleophiles correlated with N_+ values (35), and that in the present work a similar correlation also holds, show that desolvation of these nucleophiles is not important. If the SET character of the TS is important in TS formation for S_N2 reactions, and if the Hoz model is essentially correct in describing the α effect, then the data of this present study show that large β_{nuc} may be characteristic of reactions in which a large SET character in TS formation occurs.

In support of this view, Bordwell has reported (37) on the dual SET character – S_N2 behavior of 9-dialkylaminofluorenide ions. These ions, because they have the structure >C̈—N̈<, are also α nucleophiles. Their β_{nuc} values are all near 1.0 or larger. It would be a useful check if in this latter case a study of the S_N2 reactions from the leaving group side were also available.

Our basic contention is that these large β_{nuc} values, in the same systems where leaving group studies show essentially normal S_N2 behavior, are characteristic of reactions where a large SET character is present in TS formation. If this contention is tentatively accepted, several aspects of the α effect can be explained as outlined in the next few paragraphs.

The α effect is largest at carbonyls, followed by the benzylic position, then by methyl transfer. The α effect in mixtures of DMSO–water shows a dependence on solvent, with the greatest α effect coming at 50 mol% DMSO, comparing butane-2,3-dione monoximate anion with *p*-chlorophenoxide for attack at PNPA. When the structural environment around the C atom undergoing attack can carry away negative charge, e.g., for the carbonyl O atom, the α effect is largest and responds to solvent composition through easy solvation of the heteroatom (O) to give greater stability to the TS most able to transfer charge to the heteroatom. When the environment is less able to carry away negative charge, as in the benzylic case, solvation is harder for the TS because the delocalized charge is not so well solvated. In addition, the benzylic case probably involves a more open transition state in which greater carbocation character contributes, thus making both the attacking nucleophile and the leaving group more easily solvated than the C atom undergoing attack. Finally, in the methyl transfer case, apart from the leaving group, the only places into which charge can be dispersed are the H atoms on the C. These atoms are not particularly well solvated, nor are they very good at charge dispersal. The TSs here are tighter, so greater transfer of charge (greater β_{nuc}) will be observed. These ideas are corroborated in the literature in two ways. First, the bond lengths of the α nucleophiles, which have been studied by *ab initio* 4-31G computations (39*a*), are much shorter that those for normal nucleophiles. (The knowledge claimed in the thesis cited is that there is not much difference in geometries between α nucleophiles and normal nucleophiles, but in the geometries presented in the archives and in p. 114 of the thesis the Walden inversion has occurred at the TS for each α nucleophile, whereas the TSs for normal nucleophiles precede the inversion point). A case in point is that C—O bond length for OH displacing F^- is 1.973; the bond length for HOO^- displacing F^- is 1.815. Wiberg has calculated that alkoxide ions have shortened C—O bonds (implying greater bond order than in the corresponding alcohols) and greater charge on the H atoms (39*b*). The method he used was Bader's "atoms in molecules" theory in which bond critical points, where the electron density is a minimum, are related to bond lengths through the ratio of the distance between centers to the critical point. If electronegativities are equal, the critical point is midway between the atoms. If not, it is located closer to the more electronegative atom (7). There is a connection between this work and the present explanation as follows. The extra charge on the O atom of an alkoxide crudely models the additional charge on the O atom of the hydroxamate, which is due to greatly increased SET character in the TS, as in the Hoz model. (The -O—H group of the alcohol does not have this single extra negative charge.) The C—O bond increases bond order in response to this single (extra) charge in the alkoxide, and charge flows out to the H atoms. Because the O atom of the hydroxamate also contains extra negative charges (because of increased SET character in TS formation) it should also increase the bond order to the C atom undergoing nucleophilic attack. Secondly, Shi and Boyd (24), also using the Bader method, calculated at the post Hartree–Fock level (MP2, second-order Moller–Plesset perturbation level) that as charge flows toward C in an S_N2 reaction it is distributed to the H atoms. The α effect is thus much less in methyl transfer, though β_{nuc} increases, because solvation of the (now more negative) H atoms cannot include such features as H bonding. In fact, dipole–dipole bonding is not very good either.

The structural feature that distinguishes carbonyl compounds from the benzylic or methyl compounds is that excess charge easily delocalizes to the very electronegative O atom. This means that solvent stabilization of the TS (i.e., involving H bonding) is more important than with the other two cases.

The correlation of gas phase IPs of the arenesulfonates with reactivity shows that this closely related set of leaving groups in the same solvent is affected either to no extent at all, or, more likely, to the same extent by the solvent. Thus, only the gas phase IP component changes in the expression for solution phase IPs (29). One must then address the problem of solvating excess charge placed on the methyl group by the G-NMBH

Can. J. Chem. Downloaded from www.nrcresearchpress.com by 198.100.157.202 on 09/07/12
For personal use only.

TABLE 10. Analytical results for G-NMBH-H compounds

G-NMBH-H	Melting/ boiling point (°C)	Calculated			Found		
		C	H	N	C	H	N
p-Cl	118–120	51.77	4.35	7.55	52.04	4.27	7.72
p-NO_2	171–172	48.98	4.11	14.28	49.20	4.05	14.26
p-CF_3	124–126	49.12	3.57	6.14	49.32	3.68	6.39
3,5-DiNO_2	162–163	39.84	2.93	17.42	39.79	2.76	16.85
4-Me	121–123	61.57	6.79	7.09	61.55	6.71	7.18
3-MeO							
4-Cl	95.5–96.3	41.66	3.06	12.15	41.59	2.85	11.98
3-NO_2			Cl: 15.37			Cl:15.11	

anion. Solvating the relatively nonpolar C—H bonds is not connected with a substantial diminution of TS energy because these atoms cannot hold much charge. In this scheme, examination of the leaving group behavior in the benzylic case, where solvation of the leaving group is presumably more advanced due to cation-like contributions to the TS formation, may shed light on the general validity of this explanation of the α effect. Experiments of this type, using benzylarenesulfonates, are in progress in this laboratory.

Experimental

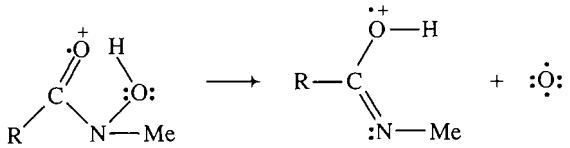
Spectroscopy

The ^{1}H NMR spectroscopy was performed on a Varian EM 360 or on a Varian XL 200 nmr spectrometer. Infrared spectroscopy was done on either a Beckman IR or a Nicolet FT IR spectrometer as KBr pellets or Nujol mulls. GC–MS determinations were made on a Hewlett–Packard GC 5890 with a 5970 series mass selective detector and a model 7946 computer work station (5). The column was a 12-m cross-linked methyl silicon gum capillary column, 0.2 mm × 0.33 μm film thickness.

Preparation of material

N-Methylbenzohydroxamic acids rearrange on heating to the *O*-acylated, thermodynamically controlled product (5*b*). However, Crumbliss and co-workers have detailed a good method for ensuring synthesis in good yield and high purity (5*a*), and some NMBH acids (NMBH-H) were made by this method. A simpler method that gave modest yields of great purity of the NMBH-H was developed as follows.

In a typical procedure, a 10.0 g (120 mmol) sample of *N*-methylhydroxylamine hydrochloride (Aldrich, 98% purity) was dissolved in 50 mL of water in an Erlenmeyer flask and neutralized with a 2.1-fold molar excess of solid sodium carbonate at ice-water bath temperature. *p*-Chlorobenzoyl chloride (20.95 g, 120 mmol) (Aldrich, 99% purity) was dissolved in sufficient *p*-dioxane (**CAUTION**: cancer suspect agent!) to give a 25% solution. This solution was added dropwise over 45 min with cooling and magnetic stirring. After an additional 3 h the precipitate was filtered (62% yield) to give 14.88 g of very pure material. Recrystallization from turbid acetone–water solutions, chilled in the refrigerator overnight, gave material that was 100% by GC–MS. The physical properties of the new G-NMBH-H appear in Table 10 with the microanalytical results. All compounds had ^{1}H NMR spectroscopy consistent with their structures. The GC–MS work displayed an interesting feature. At injection port temperatures above 260°C two peaks appeared in the GC trace of several G-NMBH-H. The second peak, at shorter retention time, was due to the corresponding *N*-methylbenzamide as shown by the MS. Lowering the inlet temperature to ca. 220–240°C gave a single peak of usually 100% purity (see ref. 5*a*). The MS of these peaks was always that of the corresponding amides. These compounds apparently extrude O easily, either by thermal excitation or by electron ionization. A cyclic transition state, leading to a distonic ion species, could account for this finding as shown below (8, 9). It is interesting that some *N*-phenylhydroxamic acids undergo a similar extrusion of O at 25°C in $CDCl_3$; see ref. 33.



Known compounds had physical properties consistent with literature values, and were analyzed by GC–MS to at least 98% purity.

Preparation of methylarenesulfonates was by literature methods (20), with analytical data given in Table 11.

Sodium salts of G-NMBH-H

Sodium salts were generated from the corresponding 4X,3Y-NMBH-H by dissolving the 4X,3Y-NMBH-H in methanol and adding an equivalent amount of standardized NaOMe in MeOH. Solvent removal or precipitation with ether gave the pure salts in dihydrated forms. IR examination of the air-dried salts showed substantial water content. This was confirmed by microanalysis (Desert Analytics). Table 12 represents typical results. First the salts were analyzed as received. Then, drying carefully under N_2 gave monohydrates; finally, the anhydrous salts were obtained by heating under N_2 for a longer period.

Similar results were obtained for other salts. The anhydrous salts readily acquired water on standing at ambient conditions. The hydration of these salts was extensive in each case, all forming dihydrates and losing water only after lengthy heating, sometimes with decomposition.

Kinetics

Kinetics were performed on the XL 200 by following the ^{1}H NMR signal of the methyl group of the methyl arenesulfonate at ca. 3.7 ppm. A 10.0 μL sample of dichloromethane was inserted in each kinetic run as an inert internal standard for measuring signal intensities. Samples of substrates and 4X,3Y-NMBH salts were weighed into calibrated pycnometers of 1.00 mL nominal volume, quickly diluted, and placed into the NMR magnet. Data were collected as an arrayed experiment, using the preacquisition delay (PAD) feature of the instrument. Temperature control was by the VT probe and was 29.5 ± 0.5°C. Typical data from a run appear in Table 13, and are plotted in Fig. 10.

A scalar for the I' signals was used. Scalar = I^0_{std}/I'_{std}. Each I' was multiplied by the scalar for that time and the $I - x$ column results. A factor relating the slope of the plot of $1/(I - x)$, Fig. 10, was used by equating the $I^0 = 207.403$ to the molar concentration. Here $M = 0.150$, so the factor is $207.304/0.150M = 1379.4\ M^{-1}$. The slope of Fig. 10 is 1.60×10^{-5}. The rate constant is $k = 1.60 \times 10^{-5} \times 1379.4 = 0.220\ M^{-1}\ min^{-1}$.

Kinetic runs were at least duplicated. No regression coefficient less than 0.98 was accepted. The results for all the runs are in the tables, with the error limits noted there.

Competition reactions

(a) The determinations of the rate constant of 3,5-diNO_2NMBH anion

The GC–MS of straightforward ^{1}H NMR kinetic determinations showed essentially no 3,5-diNO_2NMBH-OMe present, but instead a large amount of methyl 3,5-diNO_2benzoate-d_3 was found. Also the

Can. J. Chem. Downloaded from www.nrcresearchpress.com by 198.100.157.202 on 09/07/12
For personal use only.

TABLE 11. Microanalytical results for methylarenesulfonates

Substituent	Melting/boiling point (°C)	Calculated C	Calculated H	Calculated N	Calculated S	Found C	Found H	Found N	Found S
p-NO_2	—	38.71	6.45	6.45	14.76	38.59	3.12	6.12	14.47
4-Me 3-NO_2	61–62	41.55	3.92	6.06	13.87	41.61	3.87	6.12	13.58
p-MeO	(120/0.1 Torr)	47.51	4.98	—	15.85	47.50	5.00	—	15.94
m-NO_2	—	38.71	3.25	6.45	14.76	38.59	3.12	6.12	15.12
p-Br	59–60 (lit. 60)[a]								
p-Me	26 (lit. 27.5)[b]								
p-F	(70–72/0.15 Torr)	44.20	3.71 F: 9.99	—	16.86	44.19	3.71 F: 9.89	—	17.11
H	(103–106/1.1 Torr) (154/20 Torr)[c]								

[a]Beilstein II.[3] p. 57.
[b]Beilstein II. p. 99.
[c]Beilstein II. p. 20.

TABLE 12. Analytical results on selected dihydrated sodium G-NMBH salts

G	Calculated C	Calculated H	Calculated N	Found C	Found H	Found N
As received						
4-Me-3-MeO·$2H_2O$	47.41	6.37	5.53	46.28	6.69	5.17
After drying under $N_2$to monohydrated						
4-Me-3-MeO	51.10	5.99	5.96	53.19	5.67	5.92
4-NO_2·H_2O	40.69	3.84	11.86	40.86	3.46	11.26
After heating to 100°C under N_2 to anhydrous						
4-Me-3-MeO	55.30	5.57	6.45	54.90	5.67	6.31
4-NO_2	44.05	3.23	12.84	45.70	3.10	12.54

TABLE 13. Kinetic data for reaction [1] (X = Cl, Y = Z = H, W = MeO) in methanol-d_4 at 29.5°C (±0.5)

Time (min)	I std[a]	I'[b]	$I - x$[c]	$10^3/I - x$
0.0	129.739	207.304	207.304	4.824
60	114.560	144.010	163.091	6.132
120	111.716	120.011	139.372	7.175
180	111.298	102.612	119.614	8.360
240	111.056	91.899	116.705	8.569
300	112.025	82.879	95.984	10.418
360	113.844	78.813	89.816	11.114
420	114.558	70.822	80.207	12.468
480	117.478	68.636	75.799	13.193
540	114.459	63.791	72.307	13.830
600	116.031	61.632	68.913	14.511
660	116.371	56.470	62.960	15.884

[a]Intensity of the CH_2Cl_2 signal, as printed out at time t, by the instrument.
[b]The raw intensity of the OMe group of the methylarenesulfonate.
[c]Adjusted intensity at time t. (A referee pointed out that plotting the peaks as a fraction of the standard peak is an alternate method.)

kinetic results had apparent rate constants that were the largest of the entire 4X,3Y-NMBH group. The regularity of the other points in Fig. 5 indicates that this result is due to something other than the reaction we expected. This fact was confirmed when we performed competition experiments. The method used is outlined in ref. 10, and care was taken to ensure a ratio of at least 10:1 of both NMBH and 3,5-diNO_2NMBH anions. Thus, 209 mg (1.0 mmol) of NMBH anion (Na salt) and 299.0 mg (1.0 mmol) of sodium 3,5-diNO_2NMBH were dissolved in 1.0 mL of methanol-d_4 and 20.2 mg (0.1 mmol) of p-$MeOC_6H_4SO_3Me$ was added via preweighed microlitre syringe. After 15 min the reaction mixture was quenched with glacial acetic acid, and the mixture analyzed by GC–MS. Relative response factors for the compounds were determined by running known mixtures of authentic material. The response was within 3% of linear in grams.

The area ratio was related to the rate constant as follows:

$$[\text{NMBH-OMe}]/[3,5\text{-No}_2\text{NMBH-OMe}] = 26.884/7.167 = 3.75$$

When corrected for the MW ratio this is

$$k_{rel} = 3.75 \times 255.18/165.19 = 5.79$$

The rate constant was found by multiplying $0.029 \times 1/5.79 = 0.0050$; $\log k = -2.301$. (**Note**: These figures represent averages of duplicate runs. The $k_{avg.} = 0.0050 \pm 0.00045$). Only two significant figures were kept for all rate constants.

(b) Competition reactions of the most basic G-NMBH anions in excess base

The competition reaction experiments were set up as for the 3,5-diNO_2NMBH, except that Na methanol-d_4–methoxide-d_3 mixtures were used. Sufficient base was used (0.165 M) to ensure the deprotonation of the nucleophiles. Typically, relative rates were determined vs. p-NO_2NMBHNa, by dissolving the salt to be compared in the excess base mixture. (The MeONa-d_3 was made from NaH and methanol-d_4 in a glove box under argon.) The solutions were divided into two parts by syringe, and to each part was added an amount of methyl p-methoxybenzenesulfonate equal to 0.1 molar equivalent, as described for the 3,5-NO_2NMBHNa experiments. A typical result is given for 4-MeO-NMBHNa vs. NMBHNa.

Samples of 20.6 mg NMBHNa and 23.9 mg of 4-MeONMBHNa (0.1 mmol each) were weighed into two preweighed, dried vials. To each vial 1.00 mL of 0.165 M NaOMe-d_3 was added. The contents of the two vials were mixed thoroughly and divided into two portions. To each portion was added 0.005 mmol of methyl p-methoxybenzenesulfonate via a microlitre syringe. GC–MS gave peaks that could be identified by their MS, and by comparison with authentic material as described above for 3,5-diNO_2NMBH. The rate constants were computed as follows:

$$\frac{\text{Area ca. 9.973 min}}{\text{Area ca. 10.54 min}} = \frac{18.86}{96.19} = 0.196$$

$$k_{\text{NMBHNa}}/k_{p\text{-MeONMBHNa}} = 0.196 \times 195/165 = 0.232$$

The NMBHNa, in competition with p-NO_2NMBHNa, gave a rate

Can. J. Chem. Downloaded from www.nrcresearchpress.com by 198.100.157.202 on 09/07/12
For personal use only.

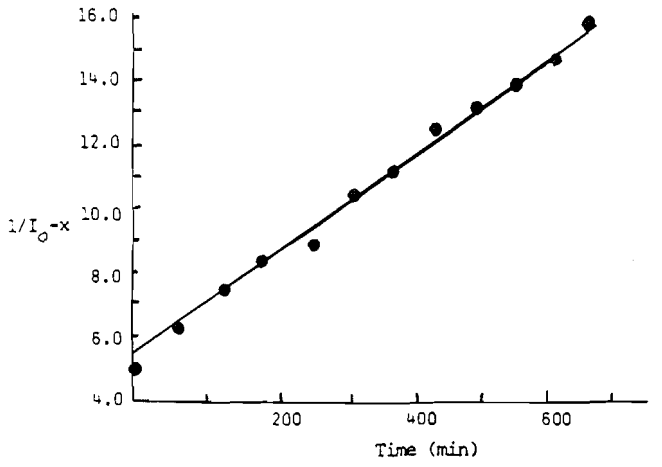


FIG. 10. Kinetic plot for *p*-ClNMBH anion reacting with methyl *p*-methoxybenzenesulfonate in methanol-d_4 at 29.5°C (±0.5).

constant of 0.0642 (±0.0002) and values determined by competition with NMBHNa were corrected to *p*-NO_2NMBHNa to give the results in Table 1.

Similarly the aqueous phase results were determined in 20% dioxane – 80% water. The salts were weighed into vials to 0.1 mg accuracy and each dissolved in 2.000 mL of the solution. The solutions were mixed and divided into two equal parts with a syringe. To each part was added 6.00 microlitres of alkylation agent (less than 0.1 mmolar equivalent in each case). After standing for an hour at 29.5°C (±0.1) in a circular bath (see below), the aqueous phase was extracted with 1.00 mL of methylene chloride and the aqueous layer removed with a pipette. Analysis by GC–MS was performed, and the GC peaks identified both by comparison of retention times with authentic samples and with their MS results. Table 2 summarizes the results.

Determination of pK_a values of 4X,3Y-NMBH

The p*K*a values of the 4X,3Y-NMBH-H indicated in Table 3 were determined by back titration of their sodium salts in solutions that were 2.0 M in KNO_3, using Nanopure water (Barnsted system). The titration was done in a jacketed cell at 25°C (±0.1) using a glass electrode and a standard Markson pH Meter (model 90). The temperature control was supplied by a Neslab–Endocal RTE-9 circulator. The sodium salts were titrated with standard HCl, and the pH–volume data plotted (ref. 10, p. 8).

The pK_a values in anhydrous methanol were determined by the overlapping indicator method,[5] using *p*-nitrophenol as the indicator (Aldrich Indicator Grade >99.99%). A sample determination is illustrated below.

The determination of the pK_a of 3,5-diNO_2NMBH-H is illustrated. A solution, 1.141×10^{-4} M in 3,5-diNO_2NMBH-H in anhydrous methanol, was treated with a 0.5000 equivalent amount of 0.0082 M NaOMe in anhydrous MeOH (distilled from Mg and I_2) to give a solution that was 5.705×10^{-5} M in salt and acid when diluted to 250.00 mL. The molar absorption values for 3,5-diNO_2NMBH and *p*-nitrophenolate were obtained from solutions of known concentration of the acids reacted with excess NaOMe/MeOH. They are $a_{3,5} = 1543.3$ (at 400 nm), and 4697.3 (at 300 nm); $a_{pNO_2} = 21\,502.2$ (400 nm) and 7025.2 (300 nm). The absorbance of this solution, when mixed with a similarly prepared solution, 5.655×10^{-5} M in *p*-nitrophenol and its anion in equal amounts, was 1.9062 (400 nm) and 0.4792 (300 nm). All determinations were made on a Beckman DU70, with all numerical values read digitally. Solution of the simultaneous equations relating the contributions of components at the indicated wavelengths gave concentrations of [*p*-NO_2-$C_6H_4O^-$] = 6.58×10^{-5} M and [3,5-diNO_2NMBH$^-$] = 8.65×10^{-5} M. From these values, and the known starting concentrations of the acids and salts, the concentrations of the conjugate acids could be calculated. Because each species present is a weak acid, the solution is highly buffered, and a_{H^+} is constant. Equation [2] therefore holds if the activity coefficients are 1.000, a reasonable assumption for these solutions. Computation of the pK_a follows from the known value of 11.15 for *p*-nitrophenol (see ref. 12*a*).

The pK_a of *p*-MeONMBH-H in anhydrous methanol was determined in the same way except that bromothymol blue (pK_a = 12.4) (see ref. 12*b*) was the indicator. The NMBH anions and conjugate acids are all known to follow Beer's law (40), see eq. [2].

Considerable overlapping of UV bands of the indicator and the 4X,3Y-NMBH anions occurred, but this handicap was overcome by using λ = 313 nm for the *p*-nitrophenyl, and λ = 390 nm for the conjugate base in excess 0.1 M NaOMe in MeOH. A region of absorbance was found for each 4X,3Y-NMBH anion used where the indicator did not absorb (except for 3,5-diNO_2NMBH-H, where a simultaneous equation had to be solved). Measurements were made in this region on the conjugate base of the 4X,3Y-NMBH-H in excess 0.1 M NaOMe in MeOH. The pK_a was computed from the known concentration of 4X,3Y-NMBH-H, the known concentration of the *p*-nitrophenyl and its measured anion concentration, and the measured 4X,3Y-NMBH anion concentration.

The results are displayed as a Hammett plot in Fig. 3. From this plot the pK_a values were obtained for those 4X,3Y-NMBH-Hs not having a region of absorbance free from overlap with the absorbance of the indicator. The Hammett plot for the pK_a values in anhydrous methanol is interesting because it shows that the solvent has a large effect on the sensitivity of the basicity of 4X,3Y-NMBH anions to the substituents on the ring. The ratio of values, MeOH/H_2O = 1.94, is close to the ratio of transfer of benzoic acid from water to methanol (=1.54) (41). The basicities of the 4X,3Y-NMBH anions become much more sensitive to substituents in the nonaqueous solvent, so their S_N2 reactivity is also expected to increase. There is a regular increase in basicity of 4X,3Y-NMBH anions as water content of the medium decreases. The ρ value in 80% methylcellusolve is 0.95 (40), which shows the same conclusion.

Determination of the α effect

This determination was performed in a manner similar to the competition reactions. A typical run is described.

A 20.9 mg (0.10 mmol) sample of NMBHNa was dissolved with 16.1 mg (0.10 mmol) of sodium *m*-nitrophenoxide (from NaOMe plus *m*-nitrophenol, Aldrich, 99% purity) in 1.0 mL of methanol-d_4. To this mixture was added 0.2 μL of *p*-MeO-$C_6H_4SO_3$Me. After 1 h the reaction was quenched with glacial acetic acid (subsequent work showed this step was unnecessary), and analyzed by GC–MS. The peak at 3.346 min has the MS of *m*-nitroanisole; that of 3.810 min was that of the NMBH-OMe. The product ratio was PR = 72.71/21.77 = 3.34; α effect = 3.34 × 153/165 = 3.10. Repetition gave a value of 3.94 for an average of 3.52 ± 0.42. Similar experiments with *p*-MeONMBHNa and 3,5-dichlorophenol gave an α effect of 4.81 ± 0.25 (two trials).

In an entirely analogous manner, the α effect for NMBHNa vs. sodium *m*-nitrophenoxide was determined in 80% H_2O – 20% dioxane. The value was 8.7 ± 1.2.

Determination of oxidation potentials, $E_{\frac{1}{2}}$

The oxidation potentials of 4X,3Y-NMBH anions were determined by cyclic voltammetry as follows: the sodium salts were dissolved in anhydrous methanol containing 0.1 M tetrabutylammonium perchlorate as the supporting electrolyte. Cyclic voltammetric experiments were performed using a model 273 PAR potentiostat/galvanostat with a PAR 175 universal programmer. Electronic IR compensation was used for all electrochemical experiments. A Nicolet model 310 digital storage oscilloscope was used to collect the potential–current data. A three-electrode cell configuration was used, with a glassy carbon working electrode, a silver/silver chloride reference electrode, and a Pt wire auxiliary electrode. At scan rates greater than 200 mV/s the reversibility is evidenced by the presence of a cathodic peak of approximately equal magnitude to the anodic peak. This cathodic peak corresponds to the reduction of the NMBH radical that is formed electrochemically on the anode scan. For many compounds, a relative

[5]A brief discussion of the principles of this method is given in ref. 38.

Can. J. Chem. Downloaded from www.nrcresearchpress.com by 198.100.157.202 on 09/07/12
For personal use only.

decrease in the cathodic peak is observed for scan rates less than ca. 200 mV/s, suggesting that the radical is undergoing a chemical reaction on these time scales. The results are collated in Table 4.

Determination of reactivity as a function of leaving group

The reactivity of *p*-ClNMBHNa in anhydrous methanol-d_4 was determined with several substituted methyl arenesulfonates in the same manner as outlined in this section for the study of various 4X,3Y-NMBHNa salts with methyl *p*-methoxybenzenesulfonate. The results are summarized in Table 6 and Fig. 6 of the results section.

Acknowledgments

We thank the Petroleum Research Fund, administered by the American Chemical Society, for support of this research. We also thank the Orscheln Foundation of Moberly Missouri for the purchase of the Hewlett–Packard GCMS with a computer work station.

1. (*a*) J. E. Dixon and T. S. Bruice. J. Am. Chem. Soc. **93**, 6592 (1971); (*b*) **93**, 3248 (1971); (*c*) W. P. Jencks and J. Carriulo. J. Am. Chem. Soc. **82**, 1778 (1960); (*d*) J. O. Edwards and R. G. Pearson. J. Am. Chem. Soc. **84**, 16 (1962); (*e*) G. Klopman, K. Tsuda, J. B. Louis, and R. E. Davis. Tetrahedron, **26**, 4569 (1970); (*f*) G. Klopman and R. C. Evans. Tetrahedron, **34**, 269 (1978); (*g*) N. J. Fina and J. O. Edwards. Int. J. Chem. Kinet. **5**, 1 (1973).
2. (*a*) J. D. Aubort and R. F. Hudson. Chem. Commun. 937 (1970); (*b*) Chem. Commun. 938 (1970); (*c*) Chem. Commun. 1378 (1970).
3. E. Buncel and C. Chuaqui. J. Org. Chem. **45**, 3621 (1980).
4. S. S. Shaik. Prog. Phys. Org. Chem. **15**, 197 (1985).
5. (*a*) C. P. Brink, L. L. Fish, and A. L. Crumbliss. J. Org. Chem. **50**, 2277 (1985); (*b*) W. B. Ankers, D. B. Bigley, R. F. Hudson, and J. C. Thurman. Tetrahedron Lett. 4539 (1969).
6. O. Exner and W. Simon. Collect. Czech. Chem. Commun. **30**, 4078 (1965), and references therein.
7. R. F. W. Bader. Acc. Chem. Res. **9**, 18 (1985).
8. R. G. Baughman, K. R. Fountain, D. P. Fountain, and A. M. Tappmeyer. J. Org. Chem. **54**, 5819 (1989).
9. S. A. Glover, A. Gassen, C. W. McCleland, and J. S. Scoonread. Tetrahedron, **43**, 2577 (1987).
10. N. S. Isaacs. Experiments in physical organic chemistry. Macmillan, London. 1969. p. 3.
11. C. P. Brink. Ph.D Thesis, Duke University, 1982.
12. (*a*) C. D. Ritchie and G. H. Megerle. J. Am. Chem. Soc. **89**, 1452 (1967); (*b*) B. W. Clare, D. Cook, E. C. F. Ko, Y. C. Moc, and A. J. Parker. J. Am. Chem. Soc. **88**, 1911 (1966).
13. (*a*) S. Hoz. J. Org. Chem. **47**, 3545 (1982); (*b*) S. Hoz and E. Buncel. Isr. J. Chem. **26**, 313 (1985).
14. (*a*) E. Buncel and I.-K. Um. J. Chem. Soc. Chem. Commun. 595 (1986); (*b*) M. Laloi-Diard, J.-F. Verchere, P. Gosselin, and F. Terrier. Tetrahedron Lett. **25**, 1267 (1984).
15. C. H. Rochester and B. Rossall. Trans. Faraday Soc. **65**, 1004 (1969).
16. W. P. Jencks, S. R. Brant, J. R. Gandler, G. Fendrich, and C. Nakamura. J. Am. Chem. Soc. **104**, 7045 (1982).
17. R. F. Hudson. *In* Nucleophilicity. *Edited by* J. M. Harris and S. P. McManus. American Chemical Society, Washington, DC. 1987.
18. M. Dessolin, M. Laloi-Diard, and M. Vilkas. Tetrahedron Lett. 2405 (1974).
19. (*a*) R. V. Hoffman and J. M. Shankweiler. J. Am. Chem. Soc. **108**, 5536 (1986); (*b*) S. P. McManus, M. R. Smith, J. M. Shankweiler, and R. V. Hoffman. J. Org. Chem. **53**, 141 (1988).
20. (*a*) E. S. Lewis and D. D. Hue. J. Am. Chem. Soc. **106**, 3392 (1984); (*b*) E. S. Lewis and S. Vanderpool. J. Am. Chem. Soc. **99**, 1946 (1977); (*c*) J. Am. Chem. Soc. **100**, 6421 (1978); (*d*) E. S. Lewis, S. Kukes, and C. D. Slater. J. Am. Chem. Soc. **102**, 1619 (1980); (*e*) E. S. Lewis, M. J. Smith, and J. J. Christie. J. Org. Chem. **48**, 2527 (1983).
21. D. E. Bugner. J. Org. Chem. **54**, 2580 (1989).
22. M. Dessolin and M. Laloi-Diard. Bull. Soc. Chim. Fr. 2946 (1971).
23. E. Buncel, H. Wilson, and C. Chuaqui. J. Am. Chem. Soc. **104**, 4896 (1982).
24. Z. Shi and R. J. Boyd. J. Am. Chem. Soc. **111**, 1575 (1989).
25. G. W. Klumpp. Reactivity in organic chemistry. Wiley–Interscience. New York. 1982. p. 182.
26. (*a*) D. S. Crumrine, J. M. Shankweiler, and R. V. Hoffman. J. Org. Chem. **51**, 5013 (1986); (*b*) R. V. Hoffman, R. A. Bartsch, and B. R. Cho. Acc. Chem. Res. **22**, 211 (1989).
27. R. E. Robertson. Can. J. Chem. **31**, 589 (1953).
28. S. P. McManus, M. R. Smith, J. M. Shankweiler, and R. V. Hoffman. J. Org. Chem. **53**, 141 (1988).
29. D. N. Kevill and T. J. Rissman. J. Org. Chem. **50**, 3062 (1985).
30. D. N. Kevill, K. C. Kalwyck, D. M. Shold, and C.-B. Kim. J. Am. Chem. Soc. **95**, 6022 (1973).
31. (*a*) S. P. McManus, M. R. Sedaghat-Herati, R. J. Cronise IV, N. Neamati-Mazraeh, and J. M. Harris. J. Org. Chem. **54**, 1911 (1989); (*b*) D. P. Roberts. J. Org. Chem. **37**, 1510 (1972).
32. I. M. Koltoff and M. K. Chantooni. J. Am. Chem. Soc. **93**, 3843 (1971).
33. A. Hasner, M. Ruse, H. E. Gottleib, and M. Cojocru. J. Chem. Soc. Perkin Trans. 1, 733 (1988).
34. K. R. Fountain and J. K. Salmon. Tetrahedron Lett. **29**, 5715 (1988).
35. (*a*) M. J. Perkins. *In* Chemistry and biology of hydroxamic acids. *Edited by* H. Kehl. Karger, New York. 1982. p. 29; (*b*) S. A. Hussain, A. H. Sharma, and M. J. Perkins. J. Chem. Soc. Chem. Commun. 289 (1979); (*c*) D. Griller and M. J. Perkins. J. Am. Chem. Soc. **102**, 1354 (1980).
36. S. S. Shaik. J. Org. Chem. **52**, 1563 (1987).
37. (*a*) F. G. Bordwell and A. H. Clemmens. J. Org. Chem. **46**, 1035 (1981); (*b*) F. G. Bordwell and J. A. Harrelson. J. Am. Chem. Soc. **109**, 8112 (1987).
38. C. H. Rochester. Acidity functions. Academic Press, New York. 1970. pp. 14–16.
39. (*a*) D. J. Mitchell. Ph.D Thesis, Queen's University, Kingston, Ont., 1981; (*b*) K. B. Wiberg. J. Am. Chem. Soc. **112**, 3379 (1990).
40. O. Exner and W. Simon. Collect. Czech. Chem. Commun. **30**, 4078 (1965).
41. R. W. Taft, Jr. and I. C. Lewis. J. Am. Chem. Soc. **81**, 5343 (1959).

Can. J. Chem. Downloaded from www.nrcresearchpress.com by 198.100.157.202 on 09/07/12
For personal use only.

Phosphoric amides. Part 11.[1] Intramolecular reactivity of phosphorotriamidates

SIEGELINDE BAUERMEISTER, AGNES M. MODRO, TOM A. MODRO,[2] AND ANDRZEJ ZWIERZAK[3]
Department of Chemistry, University of Pretoria, Pretoria 0002, South Africa

Received September 24, 1990

SIEGELINDE BAUERMEISTER, AGNES M. MODRO, TOM A. MODRO, and ANDRZEJ ZWIERZAK. Can. J. Chem. **69**, 811 (1991).

Five *N*-(2-chloroethyl)phosphorotriamidates, $(RNH)_2P(O)NHCH_2CH_2Cl$, have been synthesized, and their behavior under strongly basic conditions was studied. For *N*-alkyl derivatives (R = Me, $PhCH_2$), base-promoted intramolecular displacement of chloride yielded the *N*-phosphorylated aziridine, $(RNH)_2P(O)NC_2H_4$, as the exclusive cyclization product. For *N*-aryl derivatives (R = Ar), both the aziridine and the 1,3,2-diazaphospholidine, $RNHP(O)NHCH_2CH_2NR$, products could be obtained in comparable yields. The *N*-aromatic cyclic products are mutually interconvertible: 1,3,2-diazaphospholidines rearrange to the corresponding aziridines upon treatment with base, while bromide ions catalyze the reverse isomerization.

Key words: phosphoramidates acidity, *N*-phosphorylated aziridines – 1,3,2-diazaphospholidines isomerization, 1,3 vs. 1,5 cyclization.

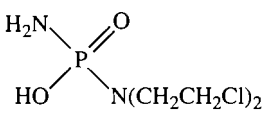
SIEGELINDE BAUERMEISTER, AGNES M. MODRO, TOM A. MODRO et ANDRZEJ ZWIERZAK. Can. J. Chem. **69**, 811 (1991).

On a réalisé la synthèse de cinq *N*-(2-chloroéthyl)phosphorotriamidates, $(RNH)_2P(O)NHCH_2CH_2Cl$, et on a étudié leur comportement dans des conditions fortement basiques. Pour les dérivés *N*-alkylés (R = Me, $PhCH_2$), le déplacement intramoléculaire du chlorure, catalysé par les bases, fournit l'aziridine *N*-phosphorylée, $(RNH)_2P(O)NC_2H_4$, comme seul produit de cyclisation. Pour les dérivés *N*-arylés (R = Ar), on peut obtenir avec des rendements comparables l'aziridine ainsi que la 1,3,2-diazaphospholidine, $RNHP(O)NHCH_2CH_2NR$. Les produits cycliques *N*-aromatiques sont mutuellement interconvertibles; les 1,3,2-diazaphospholidines se transposent en aziridines correspondantes par traitement avec des bases alors que les ions bromures catalysent l'isomérisation inverse.

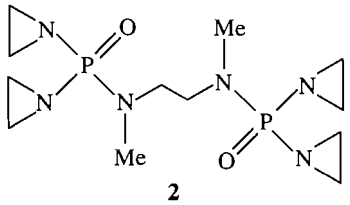
Mots clés : acidité de phosphoramidates, isomérisation aziridines *N*-phosphorylées – 1,3,2-diazaphospholidines, cyclisations 1,3 vs. 1,5.

[Traduit par la rédaction]

The phosphoramide mustard **1** is believed to be the active metabolite of the anti-tumor alkylating drug, cyclophosphamide, its cytotoxic action involving the cross-linking produced in cellular DNA (1). The alkylating reactivity of **1** is attributed to its intramolecular cyclization to the aziridinium ion, followed by the intermolecular reaction of that intermediate with a biological nucleophile (2). *N*-Phosphorylated aziridines (e.g., *aphamide* **2**) are known inhibitors of cell division, the property



1



2

responsible for their application as insect chemosterilants. Their sterilizing, as well as carcinogenic, action is again attributed to the alkylation of biological centers (3).

Intramolecular reactivity of a system of type **1** can, however, involve not only the 1,3 displacement of chloride ion (aziridinium ion formation), but also the 1,5 substitution in the NPNCCCl system, yielding the 1,3,2-diazaphospholidine product. Such cyclization was in fact postulated (4) and demonstrated (5) for the nonenzymatic hydrolysis of cyclophosphamide itself. Similarly, a compound like **2** may undergo a nucleophilic ring opening reaction not only with an external nucleophile, but via the attack of the endocyclic nitrogen, yielding the isomeric 1,3,2-diazaphospholidine skeleton. Such an intramolecular 1,5 opening of the aziridine ring was postulated (2) in the ^{31}P nmr spectroscopic study on the chemistry of phosphoramide mustard derivatives.

In this paper we report our results on the intramolecular reactivity of the *N*-(2-chloroethyl) substituted phosphorotriamidates **3**, in which the base-promoted cyclization via the nucleophilic displacement of chloride ion can lead directly to the aziridine **4** or 1,3,2-diazaphospholidine **5** derivatives (Scheme 1).

The proportion of the isomeric products **4** and **5** should be determined by the proportion of the respective conjugate bases **3'**, **3''**, and by the relative rates of the 1,3 and 1,5 cyclization steps. The first factor depends on the relative substituent effects of groups R and the 2-chloroethyl group on the acidity of the adjacent NH function. The second (kinetic) factor is more difficult to ascertain. Contrary to popular belief, the closure of three-membered rings is not necessarily favored over the formation of larger systems, and the k_3/k_5 ratio for different intramolecular reactions can vary from very high to very low values (6). The other problems addressed in this work relate to the structural effects and reaction conditions required for the base- or nucleophile-promoted mutual isomerization of products **4** and **5** via the respective anionic intermediates.

Results and discussion

Substrates **3** were prepared from phosphoryl chloride, according to eq. [1].

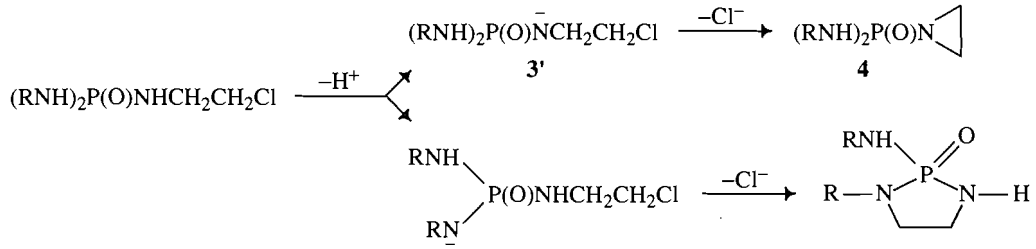
[1] $$P(O)Cl_3 \xrightarrow{ClCH_2CH_2NH_3^+Cl^-} ClCH_2CH_2NHP(O)Cl_2 \xrightarrow{4\ RNH_2} \mathbf{3}$$

The relative acidity of the NH functions in substrates **3** was assessed by examining the chemical shifts of the NH proton signals in the ^1H nmr spectra of those compounds. Although the relationship between the δ value of a proton and its acidity is only an approximate one (7), significant differences in the δ values found for the chemically non-equivalent NH groups in

[1]Preliminary communication: ref. 13.
[2]Author to whom correspondence may be addressed.
[3]On the leave from Technical University, Lodz, Poland.

Printed in Canada / Imprimé au Canada

Can. J. Chem. Downloaded from www.nrcresearchpress.com by 198.100.157.202 on 09/07/12
For personal use only.



3, *a*: R = Ph
b: R = 4-MeC_6H_4
c: R = 4-$MeOC_6H_4$
d: R = Me
e: R = CH_2Ph

SCHEME 1

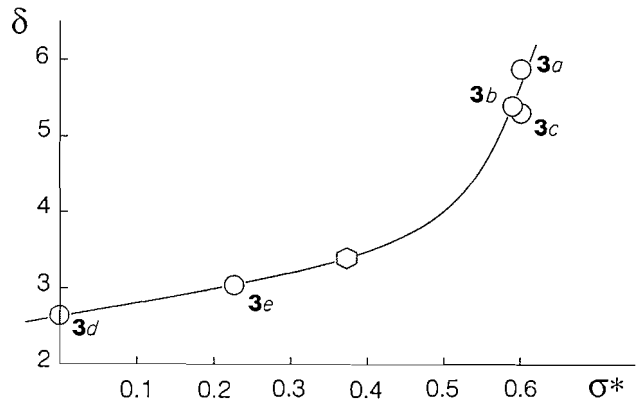


FIG. 1. δ_{NH} (ppm, $CDCl_3$, $c = 0.2$ M) vs. σ* for substrates **3**. ○: RHN: ⬡: average value for $HNCH_2CH_2Cl$ in **3***a–e*.

3 were used to determine the relative acidity order. Figure 1 shows the dependence of the shielding of the NH protons in **3** on Taft's polarity constants[4] of N substituents. The observed trend indicates that for the *N*-aromatic substrates, **3***a–c*, the conjugate base **3''**, and for **3***d,e*, the conjugate base **3'** should represent the major form of the deprotonated substrate. It was expected therefore that substrates **3***d,e* should yield aziridines **4**, *unless* the 1,3 ring closure in this system is much *slower* than the alternative 1,5 cyclization. For **3***a–c*, on the other hand, the diazaphospholidine **5** should be expected as the major product, *unless* the 1,3 cyclization is much *faster* than the direct cyclization of **3''** to **5**. We have found that when substrates **3***a–e* are treated with bases in the presence of phase-transfer catalyst (PTC, tetra-*n*-butylammonium bromide or bisulfate (9)),[5] they react smoothly according to Scheme 1 and the product composition depends on the substrate and the reaction conditions. For each **3** the reaction products were isolated in the pure state and characterized by nmr (^1H, ^{31}P) spectroscopy and elemental analyses. The results of cyclization of substrates **3** are given in Table 1.

For the *N*-alkyl substrates **3***d,e* the regioselectivity of the cyclization was complete; the corresponding *N*-phosphorylated aziridines **4** were the exclusive products, stable under reaction conditions. We confirmed this preference for the 1,3 cyclization of *N*-alkylphosphoroamidates on one additional example, i.e., diamidoester, *O*-methyl-*N*-methyl-*N'*-(2-chloroethyl)diamidophosphate **6**. Again, this substrate yielded, upon treatment with base, exclusively the aziridine **7** (eq. [2]), with no trace

[2] (MeO) (MeNH)P(O)$NHCH_2CH_2Cl$ —base→ **6**

(MeO) (MeNH)P(O)N **7**

of the corresponding 1,3,2-diazaphospholidine being formed (as demonstrated by comparison with an authentic sample). Although these results confirm the expected preferential (or exclusive) formation of **3'** (or the corresponding conjugate base of **6**) in the deprotonation step, they do not by themselves provide any conclusive information about the relative rates of the cyclization steps.

For the *N*-aromatic substrates **3***a–c* the results obtained are more complex. When the reactions were carried out in the presence of a small excess of the base (or for short periods), comparable quantities of both cyclization products, **4** and **5**, were formed. The formation of both products (which were isolated as pure compounds and were found to be stable under neutral conditions) demonstrates that for **3***a–c* the 1,5 cyclization can compete successfully with the 1,3 ring closure. When large excess of a base was used, and when reactions were carried out under more drastic conditions, the aziridine derivatives **4** were, however, formed as the exclusive products. It is clear therefore that those two types of compounds initially formed can undergo, under the reaction conditions, subsequent interconversion, finally yielding **4** as the sole reaction product. Those secondary reactions were then tested by investigating independently the effect of base (sodium hydride), and of tetrabutylammonium bromide on the individual cyclic products **4***a–e* and **5***a–e*, obtained either directly from the corresponding substrates **3** (**4***a–c*; **5***a–c*; **4***d,e*), or prepared by an independent route (**5***d,e*). This route involved formation of the 1,3,2-diazaphospholidine by the reaction of the corresponding *N*-substituted ethylenediamine with the *N*-substituted phosphoroamidodichloridate (eq. [3]).

With respect to the *N*-aromatic compounds, **4***a–c*, TBABr was found to catalyze their complete conversion to the 1,3,2-

[4]No proper parameters that describe ionization of the RNH function are available. The Taft's scale (in which σ* values could be found (8) for all N substituents) ignores the resonance effects, as can be seen from the upward curvature of the plot for the NAr substituents.

[5]Since sodium (or potassium) salts of **3** are insoluble in benzene (and other solvents tested), the addition of PTC was necessary for the reaction to proceed at reasonable rates.

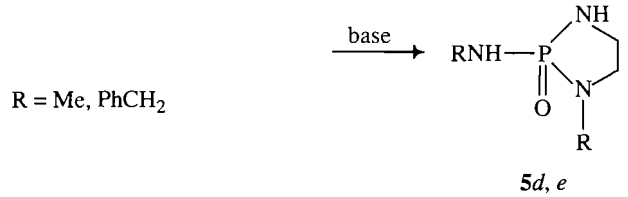
Can. J. Chem. Downloaded from www.nrcresearchpress.com by 198.100.157.202 on 09/07/12
For personal use only.

TABLE 1. Base-promoted cyclization of phosphorotriamidates **3** in benzene

Substrate	Reaction conditions	Conversion (%)	**4** (%)[a]	**5** (%)[a]
3*a*	NaH (2.0 equiv.), TBABr[b] (5 mol%), r.t., 15 min	100	53	47
	NaH (1.0 equiv.), TBABr (5 mol%), reflux, 5 h	88	67	21
	NaH (2.0 equiv.), TBABr (5 mol%), reflux, 8 h	100	100	
3*b*	NaH (1.1 equiv.), TBABr (10 mol%), reflux, 18 h	91	65	26
	$NaOH/K_2CO_3$ (4 equiv.), TBABr (10 mol%), reflux, 19 h	92	92	
	*t*BuOK (2.5 equiv.), TBABr (10 mol%), reflux, 18 h	93	92	1
3*c*	NaH (1.1 equiv.), TBABr (10 mol%), reflux, 5 h	85	48	37
	*t*BuOK (2.5 equiv.), TBABr (10 mol%), reflux, 18 h	100	100	
3*d*	NaH (1.1 equiv.), TBABr (10 mol%), 30–40°C, 6 h; r.t., 16 h	38	38	
	$NaOH/K_2CO_3$ (4 equiv.), TBAB[c] (10 mol%), r.t., 4.5 days	100	100	
3*e*	NaH (1.0 equiv.), TBABr (10 mol%), r.t., 20 h	97	97	
	NaH (1.1 equiv.), TBABr (10 mol%), r.t., 26 h	100	100	

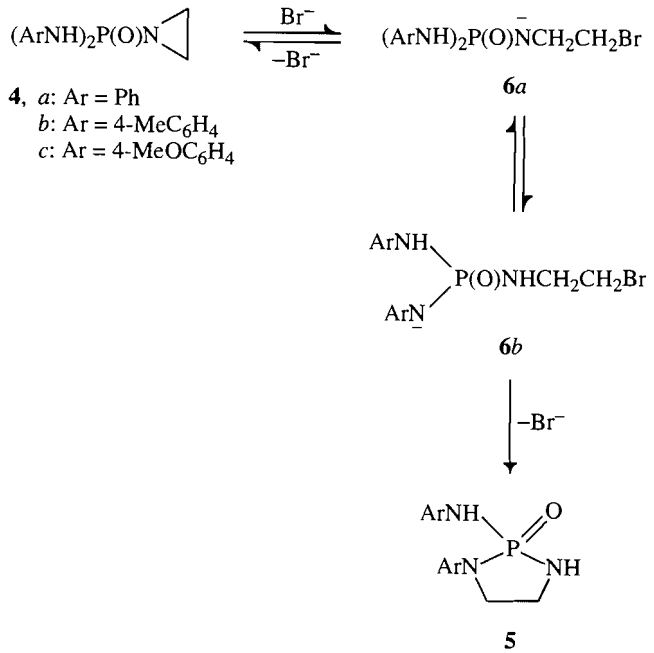
[a]**4**/**5** ratio determined by ^{31}P nmr spectroscopy.
[b]Tetra-*n*-butylammonium bromide.
[c]Tetra-*n*-butylammonium bisulfate.

[3] $RNH{-}P(O)Cl_2 + RNH{-}CH_2CH_2{-}NH_2$



5*d*, *e*

diazaphospholidine derivatives **5***a–c*. The reaction most likely proceeds via the nucleophilic opening of the aziridine ring, internal proton transfer, and the 1,5 ring closure (Scheme 2). When the reaction mixture was quenched with water, the ^{31}P nmr spectrum of the product always revealed, in addition to **5** (and, in some cases, unreacted **4**), small quantities of the product with the δ ^{31}P almost identical to that of the corresponding **3**. We assigned this signal to the conjugate acid of **6***a* (or **6***b*); thus we took it as evidence for the first step of the interconversion. The driving force for the **6***a* → **6***b* proton transfer should stem, of course, from the difference in the pK_a values of the NH groups of the ArNH and the $BrCH_2CH_2NH$ functions (*vide supra*). With **4***d* and **4***e*, although the bromide-induced opening of the aziridine ring (Scheme 2) should also take place, the subsequent proton transfer, prerequisite for the isomerization, is not favored by the pK_a difference of the respective NH groups. As a consequence, when **4***d*, **4***e* were treated with TBABr in benzene, they gave, even after prolonged heating under reflux, only minor (less than 10%) quantities of the corresponding **5**, the bulk of the substrate remaining unchanged.

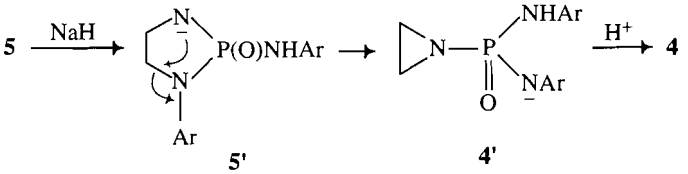


4, *a*: Ar = Ph
b: Ar = 4-MeC_6H_4
c: Ar = 4-$MeOC_6H_4$

SCHEME 2

With respect to the base, the situation is as follows. All *N*-phosphorylated aziridines **4***a–e* were stable upon prolonged treatment with sodium hydride. The absence of the isomerization results most likely from the reluctance of the conjugate base of **4** to undergo the intramolecular opening of the aziridine ring. Such a reaction, corresponding to the "5-*endo-tet*" cyclization process, should be disfavored on stereochemical grounds (10).

N,N'-Diaryl 1,3,2-diazaphospholidines **5***a–c* differ greatly in their reactivity under basic conditions from their *N*-alkyl (methyl, benzyl) analogues **5***d,e*. The former compounds, when heated in benzene solution in the presence of sodium hydride, undergo quantitative conversion to the corresponding isomeric products **4**. This interconversion, also responsible for the gradual disappearance of products **5**, initially formed by the base-promoted cyclization of **3***a–c*, can be explained by the following sequence (Scheme 3):



SCHEME 3

The **5'** → **4'** rearrangement illustrates the known (11) preference for the formation, if possible, of a three-membered ring. In this case, however, we observe a rather unusual example of a

Can. J. Chem. Downloaded from www.nrcresearchpress.com by 198.100.157.202 on 09/07/12
For personal use only.

"3-*exo-tet*" ring closure proceeding via the *syn* (and not, as in most cases, *anti*) orientation of the nucleophilic center (N^-) and the departing group (ArN^-). Both *N*-alkyl substrates **5***d*,*e* were found to be unaffected by sodium hydride, even after long periods of treatment. We explain this difference in stability by the difference in the structural conditions for the rearrangement of the conjugate base of **5** to the conjugate base of **4** (see Scheme 3). For **5***a*–*c*, the 1,3 ring closure is facilitated by the departure of a relatively good leaving group, i.e., the ArN anionic group. In the case of **5***d*,*e*, the rearrangement would involve the departure of a much poorer (more basic) leaving group, such as the RN^- group. It is worth noting that, in all substrates **5**, the parallel deprotonation of the exocyclic NH function could, in principle, also lead to a rearrangement process, but that pathway would again lead to the formation of a 1,3,2-diazaphospholidine system.

Experimental section

Solvents and commercially available substrates were purified by conventional methods immediately before use. The nmr spectra were recorded on a Bruker AC 300 MHz spectrometer in $CDCl_3$, and the chemical shift values are given relative to TMS (^1H) and trimethyl phosphate (^{31}P). For column chromatography Merck Kieselgel 60 (0.063–0.200 mm) was used as a stationary phase. The products were collected as homogeneous (according to tlc) fractions.

Substrates

N-*Benzylethylenediamine* was prepared from ethylenediamine (4 mol-equiv.) and benzyl bromide (1 mol-equiv.) by heating the mixture at reflux for 3 h. After washing with water and drying, pure product was obtained by distillation, 47% yield, bp 100°C (0.1 Torr; 1 Torr = 133.3 Pa); n_D^{20} 1.5417; ^1H nmr δ: 1.35 (3H, s, disappears in D_2O, NH), 2.61 (2H, t, J_{HH} 5.7 Hz, CH_2N), 2.73 (2H, t, J_{HH} 5.7 Hz, CH_2N), 3.73 (2H, s, CH_2Ph), 7.25 (5H, br s, Ph). Anal. calcd. for $C_9H_{14}N_2$: C 72.0, H 9.4, N 18.6; found: C 72.4, H 9.1, N 18.8%.

N-*Methylphosphoroamidodichloridate* was prepared from phosphoryl chloride and methylammonium chloride (12); 98% yield, purified by bulb-to-bulb distillation (oven temp. 110°C/0.2 Torr); n_D^{22} 1.4732; ^1H nmr δ: 2.72 (3H, d, J_{HP} 19.5 Hz, NMe), 5.07 (1H, br s, NH); ^{31}P nmr δ: 16.8.

N-*Benzylphosphoroamidodichloridate* was prepared in the same manner from phosphoryl chloride and benzylammonium chloride in almost quantitative yield (crude product); ^1H nmr δ: 4.25 (2H, d, J_{HP} 14.7 Hz, CH_2), 5.20 (1H, br s, NH), 7.31 (5H, br s, Ph); ^{31}P nmr δ: 13.6. The product was thermally unstable and could not be distilled without decomposition. It was therefore used for preparation of **5***e* without purification.

N-*(2-Chloroethyl)phosphoroamidodichloridate*

Phosphoryl chloride (3.9 mol-equiv.) and well-dried and finely powdered 2-chloroethylammonium chloride (1 mol-equiv.) were mixed and heated at reflux with exclusion of moisture for 16 h. The excess $POCl_3$ was distilled off and the residue was purified by distillation; 94% yield, bp 98–99°C (0.05 Torr); n_D^{25} 1.5031; ^1H nmr δ: 3.43 (2H, m, NCH_2), 3.64 (2H, t, J_{HH} 5.9 Hz, CH_2Cl), 5.04 (1H, br s, NH); ^{31}P nmr δ: 13.1.

Phosphorotriamidates 3; general procedure

A ca. 5 M solution of *N*-(2-chloroethyl)phosphoroamidodichloridate (1 mol-equiv.) in the appropriate solvent was added dropwise with stirring and cooling (−5 to 0°C) to the ca. 4 M solution of the required amine (4 mol-equiv.) in the same solvent. The mixture was then stirred at room temperature overnight, the amine hydrochloride was filtered off, and the organic solution was washed with water and dried ($MgSO_4$). After removal of the solvent the crude **3** was purified as indicated below.

3*a*: Prepared in $CHCl_3$, 93% yield. Purified by two crystallizations (benzene/$CHCl_3$ 1:1, followed by ethanol), mp 117–118°C; ^1H nmr δ: 3.33 (2H, m, NCH_2), 3.50 (2H, t, J_{HH} 5.5 Hz, CH_2Cl), 3.59 (1H, br s, $NHCH_2$), 5.71 (2H, d, J_{HP} 7.8 Hz, 2 × NHPh), 6.94 (2H, t, J_{HH} 7.2 Hz, H_{ortho}), 7.09 (3H, m, H_{meta}, H_{para}); ^{31}P nmr δ: 0.55. Anal. calcd. for $C_{14}H_{17}ClN_3OP$: C 54.3, H 5.5, N 13.6; found: C 54.5, H 5.4, N 13.5%.

3*b*: Prepared in ether, 67% yield. Purified by crystallization from ethanol/water; mp 154–155°C; ^1H nmr δ: 2.24 (6H, s, 2 × $ArCH_3$), 3.33 (3H, m, $NHCH_2$), 3.52 (2H, t, J_{HH} 5.4 Hz, CH_2Cl), 5.26 (2H, d, J_{HP} 6.9 Hz, 2 × NHAr), 6.94 (4H, d, J_{HH} 8.4 Hz, H_{meta}), 7.00 (4H, d, J_{HH} 8.4 Hz, H_{ortho}); ^{31}P nmr δ: 1.09. Anal. calcd. for $C_{16}H_{21}ClN_3OP$: C 56.9, H 6.3, N 12.4; found: C 56.7, H 6.1, N 12.4%.

3*c*: Prepared in $CHCl_3$, 45% yield. Purified by crystallization from ethanol; mp 150–150.5°C;. ^1H nmr δ: 3.30 (3H, m, $NHCH_2$), 3.50 (2H, t, J_{HH} 5.6 Hz, CH_2Cl), 3.72 (6H, s, 2 × OCH_3), 5.24 (2H, d, J_{HP} 7.7 Hz, NHAr), 6.74 (4H, d, J_{HH} 8.9 Hz, H_{meta}), 6.99 (4H, d, J_{HH} 8.9 Hz, H_{ortho}); ^{31}P nmr δ: 1.80. Anal. calcd. for $C_{16}H_{21}ClN_3O_3P$: C 52.0, H 5.7, N 11.4; found: C 51.9, H 5.5, N 11.3%.

3*d*: Prepared in benzene, 63% yield. Purified by column chromatography (ethanol); ^1H nmr δ: 2.55 (6H, d, J_{HP} 12.2 Hz, 2 × NCH_3), 2.60 (2H, br s, 2 × NHMe), 3.06 (1H, m, $NHCH_2$), 3.24 (2H, m, CH_2N), 3.58 (2H, t, J_{HH} 5.8 Hz, CH_2Cl); ^{31}P nmr δ: 16.85. Anal. calcd. for $C_4H_{13}ClN_3OP \cdot 2H_2O$: C 21.7, H 7.7, N 19.0; found: C 21.3, H 7.3, N 18.6%.

3*e*: Prepared in ether, 97% yield. Purified by crystallization from ether/cyclohexane; mp 63–64°C; ^1H nmr δ: 2.95 (3H, br s, 3 × NH), 3.21 (2H, m, NCH_2), 3.50 (2H, t, J_{HH} 5.5 Hz, CH_2Cl), 4.07 (4H, d of d, J_{HP} 10.1 Hz, J_{HH} 7.1 Hz, 2 × CH_2Ph), 7.28 (10H, br s, 2 × Ph); ^{31}P nmr δ: 13.36. Anal. calcd. for $C_{16}H_{21}ClN_3OP$: C 56.9, H 6.3, N 12.4; found: C 56.5, H 6.7, N 12.0%.

O-*Methyl*-N-*methyl*-N′-*(2-chloroethyl)phosphorodiamidate 6*

Dry methylamine was passed through the solution of *N*-(2-chloroethyl)phosphoroamidodichloridate (2.05 g, 0.010 mol) in dioxane (14 mL) with stirring and cooling (below 25°C). After the exothermic reaction subsided, 10 mL of dioxane was added, the mixture was filtered, the precipitate was washed with dioxane followed by chloroform, and the combined filtrates were concentrated under reduced pressure. Crude *N*-methyl-*N*′-(2-chloroethyl)diamidophosphorochloridate was obtained as colorless oil (1.73 g, 91%) and was used without further purification; ^1H nmr δ: 2.68 (3H, d, J_{HP} 10.1 Hz, NMe), 3.31–3.44 (2H, m, NCH_2), 3.45 (1H, br s, NH), 3.64 (2H, t, J_{HH} 5.6 Hz, CH_2Cl), 4.25 (1H, br s, NH); ^{31}P nmr δ: 20.7.

A solution of this product (1.7 g, 0.091 mol) in dry methanol (4 mL) was added dropwise at room temperature to the solution of one mol-equiv. of CH_3ONa in methanol (8 mL). The mixture was stirred for 20 h, filtered, and evaporated under reduced pressure. A small volume of chloroform was added, the suspension was filtered through a layer of anhydrous $MgSO_4$ and evaporated, yielding the crude product (1.39 g, 82%). Pure **6** was obtained by column chromatography ($CHCl_3$/acetone, 3:1) as a colorless oil; ^1H nmr δ: 2.52 (3H, d of d, J_{HP}, J_{HH} 12.3, 5.7 Hz, NMe), 2.90 (1H, br s, NH), 3.17 (2H, m, NCH_2), 3.29 (1H, br s, NH), 3.53 (2H, t, J_{HH} 5.8 Hz, CH_2Cl), 3.59 (3H, d, J_{HP} 11.2 Hz, OMe); ^{31}P nmr δ: 15.5. Anal. calcd. for $C_4H_{12}ClN_2O_2P$: C 25.7, H 6.5, N 15.0; found: C 25.3, H 6.4, N 14.9%.

Reactions of substrates 3 with bases

Base, followed by PTC, was added to a ca. 0.1 M solution of **3** in benzene, and the mixture was stirred vigorously with exclusion of moisture. The proportion of the reagents, the reaction time, and temperature are given in Table 1. The reaction was stopped when the ^{31}P nmr spectrum of a sample showed complete disappearance of **3**. After filtration, the solution was washed with small portions of water until neutral, dried ($MgSO_4$), evaporated, and the residue was identified and purified as described below. *N*-Phosphorylated aziridines **4**

Can. J. Chem. Downloaded from www.nrcresearchpress.com by 198.100.157.202 on 09/07/12
For personal use only.

Can. J. Chem. Downloaded from www.nrcresearchpress.com by 198.100.157.202 on 09/07/12
For personal use only.

were obtained by carrying out the reaction under conditions allowing for the exclusive formation of **4** (see Table 1, last entries for all substrates).

4*a* (2 mol-equiv. of NaH, 5 mol% TBABr, reflux, 8 h): 88% yield; purified by column chromatography (acetone/CH_2Cl_2, 2:1); mp 183–184°C; ^{1}H nmr δ: 2.30 (4H, d, J_{HP} 16.2 Hz, C_2H_4N), 5.48 (2H, d, J_{HP} 8.4 Hz, 2 × NHAr), 6.69–7.23 (10H, m, 2 × Ph); ^{31}P nmr δ: 12.1. Anal. calcd. for $C_{14}H_{16}N_3OP$: C 61.5, H 5.9, N 15.4; found: C 61.2, H 5.9, N 15.4%.

4*b* (4 mol-equiv. of 1:1 NaOH/K_2CO_3, 10 mol% TBABr, reflux, 19 h): 92% yield; purified by column chromatography (pet. ether); oil; ^{1}H nmr δ: 2.22 (6H, s, 2 × CH_3), 2.25 (4H, d, J_{HP} 11.4 Hz, C_2H_4N), 5.78 (2H, d, J_{HP} 8.7 Hz, 2 × NHAr), 6.95 (4H, d, J_{HH} 8.4 Hz, 2 × 2,6-H), 6.99 (4H, d, J_{HH} 8.4 Hz, 2 × 3,5-H); ^{31}P nmr δ: 12.8. Anal. calcd. for $C_{16}H_{20}N_3OP$: C 63.8, H 6.7, N 13.9; found: C 63.4, H 6.3, N 13.5%.

4*c* (2.5 mol-equiv. of *t*BuOK, 10 mol% TBABr, reflux, 18 h): 55% yield; purified by crystallization from $CHCl_3$/pet. ether (1:1); mp 47–51°C; ^{1}H nmr δ: 2.22 (4H, d, J_{HP} 15.6 Hz, C_2H_4N), 3.68 (6H, s, 2 × OCH_3), 5.80 (2H, d, J_{HP} 8.7 Hz, 2 × NHAr), 6.69 (4H, d, J_{HH} 8.8 Hz, 2 × 2,6-H), 7.00 (4H, d, J_{HH} 8.8 Hz, 2 × 3,5-H); ^{31}P nmr δ: 13.4. Anal. calcd. for $C_{16}H_{20}N_3O_3P$: C 57.7, H 6.1, N 12.6; found: C 57.3, H 6.2, N 12.2%.

4*d* (4 mol-equiv. of 1:1 NaOH/K_2CO_3, 10 mol% TBABr, room temp., 108 h): 37% yield. The compound was purified by filtering the benzene solution through a Celite/$MgSO_4$ layer and evaporating, affording a very hygroscopic oil; ^{1}H nmr δ: 2.02 (4H, d, J_{HP} 15.0 Hz, C_2H_4N), 2.48 (2H, br s, 2 × NH), 2.67 (6H, d of d, J_{HP}, J_{HH} 11.5, 5.4 Hz, 2 × NMe); ^{31}P nmr δ: 26.0.

4*e* (1.2 mol-equiv. of NaH, 10 mol% TBABr, room temp., 30 h): 85% yield. Purified by crystallization from benzene/pet. ether (1:1); mp 58–60°C; ^{1}H nmr δ: 2.04 (4H, d, J_{HP} 15.2 Hz, C_2H_4N), 3.01 (2H, m, 2 × NH), 4.13 (4H, 2 × d of d, J_{HP}, J_{HH} 9.2, 7.2 Hz, 2 × CH_2Ph), 7.29 (10H, br s, 2 × Ph); ^{31}P nmr δ: 22.9. Anal. calcd. for $C_{16}H_{20}N_3OP$: C 63.8, H 6.7, N 14.0; found: C 63.4, H 6.5, N 13.9%.

7: Substrate **6** (0.16 g, 8.6×10^{-4} mol) and NaH (9.4×10^{-4} mol) in benzene (5 mL) were stirred at room temperature for 96 h. Aqueous ethanol (1.5 mL) was added, the mixture was filtered through a layer of Celite/$MgSO_4$, washed with chloroform, and evaporated. Aziridine derivative **7** was obtained as a pale yellow oil in 65% yield; ^{1}H nmr δ: 2.03 (4H, d, J_{HP} 15.5 Hz, C_2H_4N), 2.60 (3H, d of d, J_{HP}, J_{HH} 11.4, 5.7 Hz, NMe), 3.00 (1H, br s, NH), 3.62 (3H, d, J_{HP} 11.0, OMe); ^{31}P nmr δ: 23.7. Anal. calcd. for $C_4H_{11}N_2O_2P \cdot H_2O$: C 28.6, H 7.8, N 16.7; found; C 28.7, H 7.3, N 16.5%.

1,3,2-Diazaphospholidines **5**

N-Aryl derivatives **5***a–c* were isolated by column chromatography from the mixtures obtained upon treatment of the corresponding substrates **3** with base (see Table 1, first entries for **3***a–c*).

5*a* (acetone/CH_2Cl_2, 2:1): 36% yield. Crystallized from $CHCl_3$/pet. ether (1:1); mp 203.5°C; ^{1}H nmr δ: 2.87 (1H, d, J_{HP} 10.5 Hz, *endo*-NH), 3.40–3.54 (1H, m) and 3.58–3.64 (3H, m) (CH_2CH_2), 5.43 (1H, d, J_{HP} 6.6 Hz, *exo*-NH), 6.82–6.97 (5H, m, Ph), 7.08–7.25 (5H, m, Ph); ^{31}P nmr δ: 13.1. Anal. calcd. for $C_{14}H_{16}N_3OP$: C 61.5, H 5.9, N 15.4; found: C 61.1, H 6.0, N 15.2%.

5*b* (acetone/CH_2Cl_2, 2:1): 26% yield. Crystallized from $CHCl_3$/acetone (1:1); mp 180–182°C; ^{1}H nmr δ: 2.20 (3H, s, Me), 2.23 (3H, s, Me), 2.85 (1H, br s, *endo*-NH), 3.34 (1H, m) and 3.65 (3H, m) (CH_2CH_2), 5.37 (1H, d, J_{HP} 6.6 Hz, *exo*-NH), 6.74 (2H, d, J_{HH} 8.1 Hz, 3,5-H of the *endo*-NAr), 6.94 (2H, d, J_{HH} 8.1 Hz, 2,6-H of the *endo*-NAr), 7.02 (2H, d, J_{HH} 8.6 Hz, 3′,5′-H of the *exo*-NAr), 7.08 (2H, d, J_{HH} 8.6 Hz, 2′,6′-H of the *exo*-NAr); ^{31}P nmr δ: 13.6. Anal. calcd. for $C_{16}H_{20}N_3OP$: C 63.8, H 6.7, N 13.9; found: C 63.4, H 6.2, N 13.5%.

5*c* (acetone/CH_2Cl_2, 1:1): 37% yield; mp 200–202°C; ^{1}H nmr δ: 2.73 (1H, d, J_{HP} 10.1 Hz, *endo*-NH), 3.36 (1H, m) and 3.56 (3H, m) (CH_2CH_2), 3.71 (3H, s, OMe), 3.74 (3H, s, OMe), 4.95 (1H, d, J_{HP} 7.5 Hz, *exo*-NH), 6.69 (2H, d, J_{HH} 8.8 Hz, 2,6-H of *endo*-NAr), 6.78 (2H, d, J_{HH} 8.4 Hz, 2′,6′-H of *exo*-NAr), 6.81 (2H, d, J_{HH} 8.4 Hz, 3′,5′-H of *exo*-NAr), 7.11 (2H, d, J_{HH} 8.8 Hz, 3,5-H of *endo*-NAr); ^{31}P nmr δ: 14.6. Anal. calcd. for $C_{16}H_{20}N_3O_3P$: C 57.6, H 6.0, N 12.6; found: C 57.2, H 6.1, N 12.4%.

N-Alkyl derivatives **5***d,e* were prepared as follows. A 0.3–0.5 M solution of the corresponding *N*-substituted ethylenediamine (1 mol-equiv.) and triethylamine (2 mol-equiv.) in dioxane/ether (3:1) was added dropwise with stirring and cooling at 0–5°C to the ca. 1 M solution of the corresponding *N*-substituted phosphoroamidodichloridate in the same solvent. After addition the mixture was stirred at room temperature overnight and filtered. For **5***d* the filtrate was saturated with dry gaseous ammonia, filtered again, and evaporated. Pure **5***d* was obtained as highly hygroscopic, colorless crystals in 11% yield; mp (sealed capillary) 75–78°C; ^{1}H nmr δ: 2.44 (3H, d of d, J_{HP}, J_{HH} 12.7, 5.5 Hz, *exo*-NMe), 2.54 (3H, d, J_{HP} 9.3 Hz, *endo*-NMe), 2.63 (2H, br s, 2 × NH), 2.98–3.37 (4H, m, CH_2CH_2); ^{31}P nmr δ: 27.6. Anal. calcd. for $C_4H_{12}N_3OP$: C 32.2, H 8.1, N 28.2; found: C 32.3, H 8.5, N 27.8%.

For **5***e* the filtrate was evaporated under reduced pressure and the residue was dissolved in benzene and washed three times with water. After drying and evaporating of solvent the crystalline product was obtained in 80% yield. Purified by crystallization from benzene/pet. ether (1:1); mp 101–103°C; ^{1}H nmr δ: 2.38 (1H, d, J_{HP} 7.8 Hz, NH), 2.75 (1H, br s, NH), 2.88–3.37 (4H, m, CH_2CH_2), 3.90–4.19 (4H, m, 2 × CH_2Ph), 7.10–7.45 (10H, m, 2 × Ph); ^{31}P nmr δ: 24.8. Anal. calcd. for $C_{16}H_{20}N_3OP$: C 63.8, H 6.7, N 14.0; found: C 63.4, H 6.5, N 13.9%.

O-Methyl-1-methyl-1,3,2-diazaphospholidine

Methylphosphorodichloridate (2.0 g, 0.013 mol) in dichloromethane (10 mL) was added dropwise with stirring and cooling at −5 to −10°C to the solution of *N*-methylethylenediamine (0.99 g, 0.013 mol) and triethylamine (2.72 g, 0.027 mol) in dichloromethane (25 mL). The mixture was then stirred at room temperature for 22 h and filtered. The residual triethylammonium chloride was removed from the filtrate by stirring it with solid NaOH/K_2CO_3 mixture, filtering, and evaporating under reduced pressure. The product was obtained as a viscous oil (0.82 g, 42%); ^{1}H nmr δ: 2.57 (3H, d, J_{HP} 9.5 Hz, NMe), 2.98 (1H, br s, NH), 3.10–3.38 (4H, m, CH_2CH_2), 3.58 (3H, d, J_{HP} 11.9 Hz, OMe); ^{31}P nmr δ: 27.2. The ^{31}P nmr spectrum showed absence of any other phosphorus containing products, and the ^{1}H nmr spectrum revealed only the presence of some residual triethylammonium chloride.

Interconversions of **4** *and* **5**

Individual compounds **4** or **5** were dissolved in benzene, the required amount of sodium hydride or TBABr was added, and the mixture was stirred at the temperature and for the duration identical to those applied to the corresponding substrates **3**. After filtration and evaporation of the solvent, the products were examined by nmr (^{1}H and ^{31}P) spectroscopy and identified by comparison with the spectra of the authentic samples.

Acknowledgement

The financial assistance of the University of Pretoria, the Foundation for Research Development (CSIR), and the National Cancer Association of South Africa is gratefully acknowledged.

1. W. J. STEC. *In* Organophosphorus chemistry. Vol. 13. The Royal Society of Chemistry, London. 1982. Chap. 8.
2. T. W. ENGLE, G. ZON, and W. EGAN. J. Med. Chem. **25**, 1347 (1982).
3. C. FEST and K. J. SCHMIDT. *In* The chemistry of organophosphorus pesticides. 2nd ed. Springer-Verlag, Berlin. 1982. Chap. 3.3.c.
4. O. M. FRIEDMAN, S. BIEN, and J. K. CHAKRABARTI. J. Am. Chem. Soc. **87**, 4978 (1965).

5. G. ZON, S. M. LUDEMAN, and W. EGAN. J. Am. Chem. Soc. **99**, 5785 (1977).
6. C. J. M. STIRLING. J. Chem. Educ. **50**, 844 (1973).
7. J. D. ROBERTS. *In* Nuclear magnetic resonance. McGraw–Hill, New York. 1959. Chap. 2.3.
8. (*a*) J. HINE. *In* Structural effects on equilibria in organic chemistry. Wiley–Interscience, New York. 1975. Chaps. 3–6; (*b*) D. D. PERRIN, B. DEMPSEY, and E. P. SERJEANT. *In* pK_a prediction for organic acids and bases. Chapman and Hall, London. 1981. Appendix A.1.
9. A. ZWIERZAK. Synthesis, 332 (1984).
10. P. DESLONGCHAMPS. *In* Stereoelectronic effects in organic chemistry. Pergamon Press, Oxford. 1983. Chap. 5.
11. G. STORK and J. F. COHEN. J. Am. Chem. Soc. **96**, 5270 (1974).
12. K. SASSE. *In* Organische Phosphorverbindungen. Vol. XII/2. G. Thieme Verlag, Stuttgart. 1964. p. 385.
13. S. BAUERMEISTER, A. M. MODRO, and T. A. MODRO. Tetrahedron Lett. **30**, 2141 (1989).

Can. J. Chem. Downloaded from www.nrcresearchpress.com by 198.100.157.202 on 09/07/12
For personal use only.

Carbohydrate protein interactions. Syntheses of agglutination inhibitors of wheat germ agglutinin by phase transfer catalysis

RENÉ ROY[1] AND FRANÇOIS D. TROPPER
Department of Chemistry, University of Ottawa, Ottawa, Ont., Canada K1N 6N5

Received November 1, 1990

RENÉ ROY and FRANÇOIS D. TROPPER. Can. J. Chem. **69**, 817 (1991).

Starting from chloride **1**, a series of *para*-substituted aryl 2-acetamido-2-deoxy-β-D-glucopyranosides were prepared using phase transfer catalysis conditions with tetrabutylammonium hydrogen sulfate in 1 M sodium hydroxide and methylene chloride at room temperature. Zemplén de-*O*-acetylation afforded the unprotected glycosides. Optimization of reaction conditions was evaluated. Several functional group manipulations were effected to widen the number and nature of the *para*-substituents.

Key words: phase transfer catalysis, aryl 2-acetamido-2-deoxy-β-D-glucopyranosides.

RENÉ ROY et FRANÇOIS D. TROPPER. Can. J. Chem. **69**, 817 (1991).

En utilisant le chlorure **1** comme produit de départ, une série 2-acetamido-2-deoxy-β-D-glucopyranosides d'aryles *para*-substitués ont été préparés en utilisant des conditions de catalyse par transfert de phase avec le bisulfate de tétrabutylammonium comme catalyseur dans l'hydroxyde de sodium 1 M et le chlorure de méthylène à la température de la pièce. Une de-*O*-acétylation de Zemplén a fourni les glycosides déprotégés. Les paramètres permettant d'optimiser les conditions de réactions ont été évalués. Quelques transformations de groupes fonctionnels ont été éffectuées afin d'élargir le nombre et la nature des substituants en position *para*.

Mots clés : catalyse par transfert de phase, aryle 2-acétamido-2-deoxy-β-D-glucopyranosides.

Introduction

Carbohydrate–protein interactions are of paramount importance in cellular recognition, in bacterial and viral colonization, and in tumor associated phenomena. We have been engaged in studies of the fundamental aspects of these interactions at the molecular level. The nature and the accessibilities of sugar moieties on native glycoproteins prompted us to synthesize a number of well-defined artificial glycoconjugates to be used as models in binding studies with lectins (1–4).

Of particular interest to the present study was the observation that *p*-nitrophenyl 2-acetamido-2-deoxy-β-D-glucopyranoside was a better inhibitor than the corresponding free monosaccharide in inhibition of agglutination of model glycoproteins with the lectin from wheat germ (wheat germ agglutinin, WGA) (5). The X-ray of WGA showed the presence of tyrosyl residues in the carbohydrate binding sites (5). To verify the possibility of charge transfer complex interactions between the electron-rich tyrosyl residues and the electron-poor aromatic glycosides, an efficient synthesis of aryl glycosides was required. Therefore, a series of aryl 2-acetamido-2-deoxy-β-D-glucopyranosides was synthesized to probe these potential electronic contributions and to evaluate their contributions to the relative binding energies with the lectin.

Phase transfer catalysis (PTC) has been recently applied to the syntheses of aryl glycosides (6–9). However, there was no application of this efficient procedure for the preparation of *O*-aryl 2-acetamido-2-deoxy-β-D-glucopyranosides until our own preliminary work (10). The most general method used so far was based on the reactions of the homologous sodium phenoxides in aqueous acetone (11, 12). In our hands this method was deemed unsatisfactory in terms of yields. The present work describes in full the efficient and stereospecific syntheses of this class of compounds using PTC conditions at room temperature with yield ranging from 66 to 93%.

Results and discussion

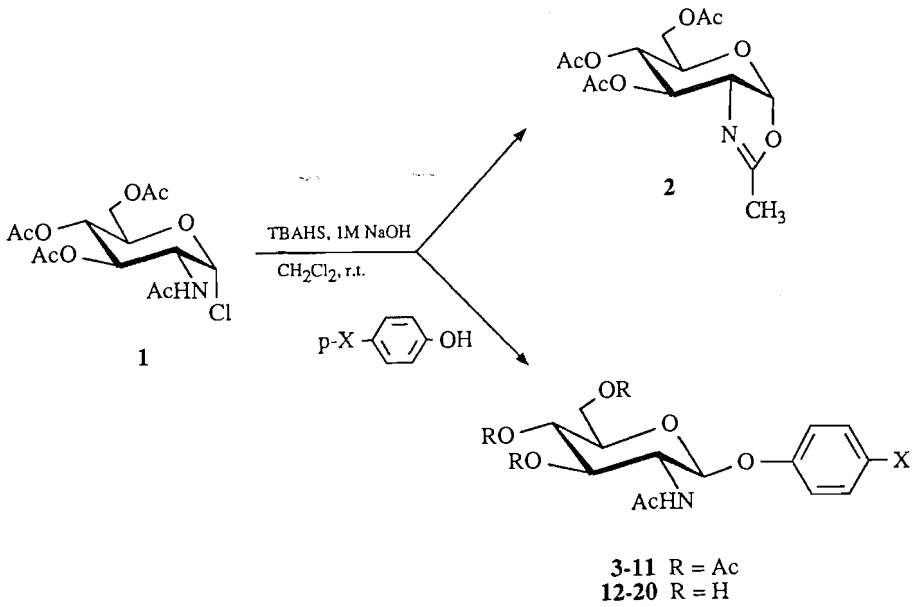
In continuation of our efforts (10, 13) to utilize phase transfer catalysis in glycoside syntheses of aryl 2-acetamido-2-deoxy-β-D-glucopyranosides, it was hypothesized that formation of the expected 2-methyl-(3,4,6-tri-*O*-acetyl-1,2-dideoxy-α-D-glucopyrano)-[2,1-*d*]-oxazoline **2** could be prevented if nucleophilic attack by the phenoxides at the anomeric center could occur at a faster rate than the attack by the catalyst counteranions. Nucleophilic attack by counteranions such as chlorides and bromides would lead to reactive β-glycosyl halides followed by anchimeric displacement by the neighboring acetamido group to give the oxazoline **2**. In this respect, it became obvious that non-nucleophilic and hydrophilic anions such as hydrogen sulfate would solve part of the problem. One should realize, however, that for each nucleophilic substitution by the phenoxide, there is one chloride anion released. Thus, nucleophilic competition at the anomeric center would still exist between the phenoxide and the chloride anions. To minimize this possibility, two equivalents of phenoxide were used throughout. Encouraged by the successful application of this technique to the synthesis of a glycosyl azide (14), we have investigated the effect of various catalysts and reaction conditions.

In the first set of experiments, the phenoxide was purposely omitted; the use of tetrabutylammonium bromide did provide a good yield of the expected oxazoline. This catalytic two-phase system is conceptually similar to the reaction conditions previously used by Lemieux and Driguez (15) for the synthesis of **2** in acetonitrile alone. The efficiency of a number of ammonium salts was then compared. Not surprisingly (16), the more hydrophobic tetrabutylammonium cation (TBA) was slightly more effective (~2 times faster) than the corresponding benzyltriethylammonium (BTEA) chloride or bromide in methylene chloride. With 0.2 molar equivalent (limiting conditions) of the catalyst over the phenoxide and TBA cations, the iodide anions gave more oxazoline than the bromides or the chlorides. These differences disappeared, however, under non-limiting conditions (1 equiv.) as shown in quantitative experiments using chloride, bromide, iodide, hydroxide, or hydrogen sulfate anions and TBA cations in methylene chloride (Scheme 1).

It was also observed that the reaction with phosphonium salts (17), such as ethyltriphenylphosphonium bromide, was faster

[1]Author to whom correspondence may be addressed.

Can. J. Chem. Downloaded from www.nrcresearchpress.com by 198.100.157.202 on 09/07/12
For personal use only.



SCHEME 1

than with the ammonium salt. However, irreversible formation of by-products, such as ethyl diphenylphosphine oxide[2] or ylide, consumed the catalyst and complicated the purification steps, thus rendering these catalysts inappropriate for the actual goals. When benzene was used as solvent in place of methylene chloride with TBA bromide, the reaction rate was found to be much slower, even under refluxing conditions.

The basicity of the aqueous phase was then examined. Molar sodium hydroxide gave faster reactions and therefore fewer by-products (oxazoline and hydrolysis) then 0.5 M (or less concentrated) NaOH and sodium carbonate or hydrogen carbonate. At a concentration of 2 M NaOH the reaction was even faster for most phenoxides. The concentration of the catalyst was also tested. With TBA bromide the reactions were faster with increasing concentrations (0.1–1 equiv.). The reactions did not proceed in the absence of the catalyst. At high concentration, fewer by-products were observed. The consumption of the chloride **1** was also faster under refluxing conditions but at the expense of more side reactions. The other products isolated were those having a hydrolyzed anomeric center, and partially de-*O*-acetylated phenyl glycosides. Transesterification by the phenoxides is postulated as a reaction pathway since acetylated phenols were isolated in a few instances. In view of the possibility of forming the glycosides **3–11** directly from the oxazoline **2**, the former was used under the optimum set of conditions described above. Treatment of the oxazoline **2** with *p*-hydroxybenzaldehyde and TBAHS (1 equiv.) and 1 M NaOH in methylene chloride at room temperature gave no glycoside, thus illustrating that the oxazoline was not an intermediate in the glycoside syntheses.

As shown in Table 1, the use of tetrabutylammonium hydrogen sulfate (TBAHS) in 1 M NaOH and methylene chloride at room temperature afforded good yields (66–93%) of the aryl 2-acetamido-2-deoxy-β-D-glucopyranosides **3–11** with a wide variety of *para* substituents as originally observed (10). The desired products could be purified from silica gel chromatography or by direct crystallization from the evaporated organic extracts. All the anomeric protons of the per-acetylated derivatives appeared between 5.03 and 5.55 ppm with vicinal coupling constants in accord with β-D(1,2-trans)-linkages ($J_{1,2}$ 8 Hz). The anomeric carbon signals appeared between 97.1 and 100.2 ppm with $^1J_{^{13}C\text{-}1,H\text{-}1}$ of 160 Hz, also consistent with β-linkage (axial H-1) (Table1) (18,19).

To widen the range and nature of the substituents, chemical transformations of the nitro and formyl groups were effected (Scheme 2). Thus, reduction of the *p*-nitro derivatives **9** or **18** under catalytic transfer hydrogenation (20) with 10% Pd/C and ammonium formate in methanol afforded the corresponding *p*-amino derivatives **21** and **22** in essentially quantitative yields. Usual *N*-acetylation (pyridine, acetic anhydride) of **21** afforded **23**, also in quantitative yield. Oxidation of the per-acetylated *p*-formylphenyl glycoside **10** with bromine in basic solutions of methanol according to Lichtenthaler *et al.* (21) gave directly the *p*-carbomethoxphenyl glycoside **25** in 55% yield. Reduction of the aldehyde **10** using sodium borohydride afforded the *p*-(hyroxymethyl)phenylglycoside **27** in quantitative yield.

Finally, Zemplén de-*O*-acetylation of all the per-acetylated derivates with sodium methoxide in methanol afforded excellent yields of the aryl 2-acetamido-2-deoxy-β-D-glucopyranosides **12–20, 22, 24, 28** (Table 2). Selected NMR signals are also indicated in Table 2.[3]

Experimental

General methods

Melting points were determined on a Gallenkamp apparatus and are uncorrected. The ^1H and ^{13}C NMR spectra were recorded on a Varian XL-300 or a Varian Gemini 200 at 300 and 200 MHz respectively for protons and at 75.4 and 50.3 MHz respectively for carbons. The proton chemical shifts (δ) are given relative to internal chloroform (7.24 ppm) for $CDCl_3$ solutions, to internal acetone (2.216 ppm) for D_2O solutions, and to DMSO (2.50 ppm) for DMSO-d_6 solutions. The carbon chemical shifts are given relative to deuterochloroform at 77.0 ppm, to internal acetone (31.1 ppm) for D_2O solutions, and to DMSO-d_6 (39.5 ppm).

The analyses were done as a first-order approximation. Optical rotations were measured on a Perkin Elmer 241 polarimeter and were run at 23–25°C for 0.5–1.0% solutions in chloroform unless otherwise

[2]Identified by MS and ^1H NMR spectroscopy, mp 122.6–123.8°C.

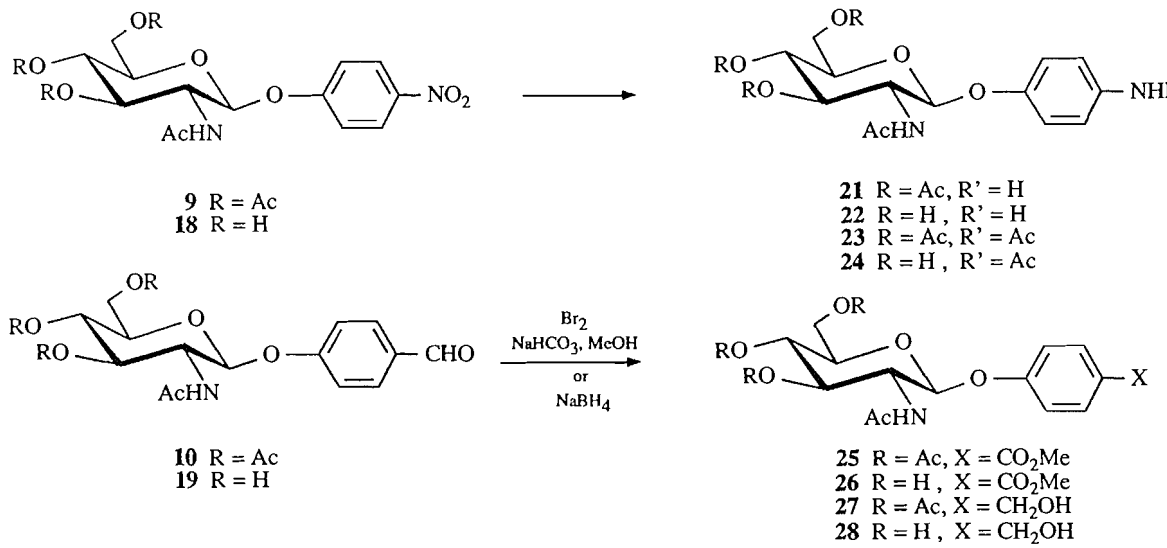
[3]Complete analyses of ^1H and ^{13}C NMR data can be found in refs. 18 and 19.

Can. J. Chem. Downloaded from www.nrcresearchpress.com by 198.100.157.202 on 09/07/12
For personal use only.

TABLE 1. Physical properties and selected NMR spectroscopic data of aryl 2-acetamido-3,4,6-tri-*O*-acetyl-2-deoxy-β-D-glucopyranosides

Compound, X	Yield (%)	Melting point (°C)	$[\alpha]_D$ ($CHCl_3$)	H-1[a] (ppm)	$J_{1,2}$ (Hz)	C-1[b] (ppm)	Formula	Elemental analyses: Calcd. (%) C	H	N	Found (%) C	H	N
3, H	93	203.5–204.6	−12.4	5.25	8.0	98.9	$C_{20}H_{25}NO_9$	56.73	5.95	3.31	56.54	6.07	3.65
4, Me	84	197.4–197.8	−10.9	5.18	8.2	99.3	$C_{21}H_{27}NO_9$	57.66	6.22	3.20	57.46	6.38	3.12
5, F	77	197.7–198.4	−12.7	5.18	8.3	99.7	$C_{20}H_{24}NO_9F$	54.42	5.48	3.17	53.88	5.51	3.44
6, Cl	66	212.6–213.5	−9.6	5.23	8.2	98.8	$C_{20}H_{24}NO_9Cl$	52.47	5.28	3.06	52.24	5.49	3.23
7, Br	88	228.3–228.8	−8.9	5.23	8.1	98.7	$C_{20}H_{24}NO_9Br$	47.82	4.82	2.79	47.65	4.73	2.79
8, I	83	252.3–252.9	−4.9	5.23	8.3	98.7	$C_{20}H_{24}NO_9I$	43.73	4.40	2.55	43.55	4.74	2.43
9, NO_2	73	237.4–238.4	−9.6	5.55	8.5	97.1	$C_{20}H_{24}N_2O_4$	51.28	5.16	5.98	51.15	5.11	6.05
10, CHO	67	226.8–227.6	−16.9	5.42	8.1	97.7	$C_{21}H_{25}NO_{10}$	55.87	5.58	3.10	55.99	5.51	2.96
11, CN	80	243.1–244.0	−29.4	5.43	8.1	97.5	$C_{21}H_{24}N_2O_9$	56.25	5.39	6.25	55.84	5.51	6.34
21, NH_2	98	174.2–175.4	−8.6	5.03	8.4	100.2	$C_{20}H_{26}N_2O_9$	54.79	5.98	6.39	54.72	6.22	6.20
23, NHAc	96	252.1–253.0	−13.2	5.05	8.4	99.2	$C_{22}H_{28}N_2O_{10}$	55.00	5.87	5.83	55.14	5.81	5.97
25, CO_2Me	55	213.6–214.1	−13.5	5.42	8.4	97.8	$C_{22}H_{27}NO_{11}$	54.89	5.65	2.91	55.00	5.74	3.01
27, CH_2OH	98	195.8–196.8	−9.0	5.24	8.3	99.1	$C_{21}H_{27}NO_{10}$	55.63	6.00	3.09	55.60	6.05	3.15

[a]Taken in $CDCl_3$ (25°C) at 200 MHz with $CHCl_3$ signal centered at 7.24 ppm.
[b]Taken in $CDCl_3$ (25°C) at 50.3 MHz with $CDCl_3$ signal centered at 70.0 ppm.



9 R = Ac
18 R = H

21 R = Ac, R' = H
22 R = H, R' = H
23 R = Ac, R' = Ac
24 R = H, R' = Ac

10 R = Ac
19 R = H

25 R = Ac, X = CO_2Me
26 R = H, X = CO_2Me
27 R = Ac, X = CH_2OH
28 R = H, X = CH_2OH

SCHEME 2

stated. Mass spectra were recorded on a VG 7070-E spectrometer. Elemental analyses were performed by Guelph Chemical Laboratories Ltd. (Guelph, Ont.) or M-H-W Laboratories (Phoenix, AZ). Thin-layer chromatography (TLC) was performed using silica gel 60-F254 plates and column chromatography on silica gel 60 (230–400 mesh, E. Merck No. 9385). The developed plates were sprayed or dipped with a solution of ceric sulfate (1%) and ammonium molybdate (2.5%) in 10% aqueous sulfuric acid and heated at ~150°C. All solvents and reagents used were reagent grade and, when required, further purifications were accomplished following published procedures (22). The chloride **1** was prepared according to Horton (23); the product was, however, usually contaminated. It was therefore purified by flash chromatography in ethyl acetate/hexane (1:1); on a large scale, up to 7 g could easily be purified, stored cold, and desiccated for 8 months without any decomposition.

Aryl2-acetamido-3,4,6-tri-O-acetyl-2-deoxy-β-D-glucopyranosides **3–11**

Typical procedure

Chloride **1** (0.28 mmol), tetrabutylammonium hydrogen sulfate or bromide (1 equiv.), and the phenols (2 equiv.) were vigorously stirred at room temperature in methylene chloride (1 mL) and 1 M sodium hydroxide (1 mL). The reactions were monitored by TLC ($CHCl_3$–EtOAc–*n*-ProH, 25:5:2, v/v/v). After complete consumption of the chloride **1** (30–45 min), the reaction mixtures were worked up by adding ethyl acetate (10 mL). The resulting organic phases were successively washed with 1 M NaOH (3 × 10 mL) followed by water (2 × 10 mL) and, finally, with saturated brine (10 mL). The dried organic phases (Na_2SO_4) were evaporated under reduced pressure. The resulting residues were purified by preparative TLC using the above eluent. The aryl glycosides were extracted from the silica gel using ethyl acetate and crystallized from ethanol to give **3–11** in 66–93% yields.

The above procedure could be efficiently accomplished on a large scale by direct crystallization of the residues obtained after the liquid–liquid extractions and evaporation of the organic phase. In the case of **9** (*p*-NO_2), the phenoxide was not entirely soluble in the two-phase mixture; gentle warming rendered it soluble. Previously known compounds (OAc and free OH) had physical constants (mp and $[\alpha]_D$) that generally agreed with those of the literature (11, 12, 24).

Can. J. Chem. Downloaded from www.nrcresearchpress.com by 198.100.157.202 on 09/07/12
For personal use only.

TABLE 2. Physical properties and selected NMR spectroscopic data of aryl 2-acetamido-2-deoxy-β-D-glucopyranosides

Compound, X	Melting point (°C)	$[\alpha]_D$[a]	H-1[b] (ppm)	C-1[c] (ppm)	Elemental analyses[d]					
						Calcd. (%)			Found (%)	
					Formula	C	H	N	C	H	N
12, H	240.9–241.3	−12.3	4.95	99.4	$C_{14}H_{19}NO_6$	56.78	6.68	4.73	56.56	6.44	4.71
13, Me	236.4–236.7	−5.3	4.86	99.7	$C_{15}H_{21}NO_6$	56.57	6.81	4.48	57.87	6.80	4.50
14, F	242.8–243.2	−14.8	4.85	99.9	$C_{14}H_{18}NO_6F$	51.16	5.72	4.23	53.33	5.75	4.44
15, Cl	249.5–250.1	−3.2	4.91	99.4	$C_{14}H_{18}NO_6Cl$	50.64	5.47	4.22	50.50	5.50	4.03
16, Br	243.9–244.5 (dec.)	+2.7	4.92	99.3	$C_{14}H_{18}NO_6Br$	44.56	4.68	3.78	44.70	4.82	3.72
17, I	249.2–249.6 (dec.)	+9.0	4.91	99.2	$C_{14}H_{18}NO_6I$	39.92	4.34	3.32	39.73	4.29	3.31
18, NO_2	206.2–206.7	−13.2	4.91	98.6	$C_{14}H_{18}N_2O_8$	49.11	5.17	8.10	49.12	5.30	8.18
19, CHO	195.0–195.5	−3.0	5.14	98.7	$C_{15}H_{19}NO_7$	55.50	5.81	4.45	55.38	5.89	4.31
20, CN	211.2–211.5	−4.3	5.07	98.5	$C_{15}H_{18}N_2O_6$	55.53	5.74	8.76	55.90	5.63	8.69
22, NH_2	227.5–228.6 (dec.)	+3.7	4.68	100.1	$C_{14}H_{20}NO_6$	53.84	6.45	8.97	52.75	6.65	8.75
24, NHAc	244.9–245.4 (dec.)	+2.2	4.47	99.8	$C_{16}H_{21}N_2O_7$	54.41	6.02	8.17	54.39	5.99	7.93
26, CO_2Me	230.2–230.6	−5.5	5.09	98.3	$C_{16}H_{21}NO_8$	54.17	6.13	4.02	54.08	5.96	3.94
28, CH_2OH	196.9–198.2	+2.4 (MeOH)	5.16	99.4	$C_{15}H_{21}NO_7$	55.16	6.47	4.15	55.04	6.47	4.28

[a]In DMSO at $c = 1.0 \pm 0.3$.
[b]At 200 MHz in DMSO-d_6, $J_{1,2} = 8.3 \pm 0.2$ Hz, ref. at 2.50 ppm with internal DMSO.
[c]Taken in DMSO-d_6 (25°C) at 50.3 MHz with DMSO signals centered at 39.49 ppm.
[d]Satisfactory microanalyses were also obtained for the halogens.

Zemplén de-O-acetylation to aryl 2-acetamido-2-deoxy-β-D-glucopyranosides

Two general methods were employed. These were based on the solubility properties of the acetylated glycosides. Method A was used for glycosides soluble or moderately soluble in methanol. These were de-*O*-acetylated in MeOH under standard conditions. The glycosides were dissolved in MeOH to which was added a catalytic amount of 1 M NaOMe in MeOH. The reaction mixtures were stirred for 1–2 h at room temperature with monitoring by TLC ($CHCl_3$–MeOH, 4:1). The sodium cations were removed with Amberlite IR-120 cationic resin (H^+). The solutions were filtered and evaporated to dryness. All the glycosides were obtained in almost quantitative yield by crystallization from ethanol or isopropanol. Method B: for glycosides that were not very soluble in MeOH, an equal volume of benzene was added as cosolvent. The solutions were then treated with 1 M NaOMe as above. The de-esterified glycosides progressively precipitated out of the solutions. Complete precipitation was ensured by adding an equal volume of hexane or ether. The solutions were cooled and the products filtered. They were always of analytical purity but were usually recrystallized from ethanol.

*Reduction of **9** to the acetylated* p-*aminophenylglucoside **21***

Compound **9** (176 mg, 0.376 mmol), 10% palladium on charcoal (15 mg), and ammonium formate (90 mg, 4 equiv.) were suspended in MeOH (20 mL). The solution was brought to a full boil for 2 min in a stopped round-bottom flask after which time TLC ($CHCl_3$–MeOH, 4:1) indicated complete reaction. The solution was filtered through Celite, which was rinsed with MeOH, and the solution evaporated to a white solid. Extraction of this residue with ethyl acetate washing with saturated sodium hydrogen carbonate (2 × 20 mL) and water (2 × 20 mL) gave pure **21** (160 mg, 97%) after the usual processing of the organic phase. An analytical sample of **21** was obtained by recrystallization from warm (not boiling) ethanol.

*Reduction of **18** to the free* p-*aminophenylglucoside **22***

Compound **18** (50 mg, 0.146 mmol) was refluxed for 10 min in MeOH (2.5 mL) containing ammonium formate (50 mg, 5.3 equiv.) and 10% palladium on charcoal (6 mg). Some ammonium formate sublimed in the condenser. The reaction was stopped when TLC (CH_3CN–acetone – 10% aq. HOAc, 5:3:1) indicated complete conversion of **18** (R_f 0.56) to **22** (R_f 0.35). Isolation by filtration and evaporation afforded pure **22** (44 mg, 98%).

p-N-*Acetamidophenyl 2-acetamido-3,4,6-tri*-O-*acetyl-2-deoxy-β-D-glucopyranoside **23***

The *p*-aminophenyl glycoside **21** (0.52 g, 1.164 mmol) was treated with pyridine (20 mL) and acetic anhydride (10 mL) for 1 h at room temperature. Methanol (10 mL) was then added to destroy the excess anhydride and after 45 min the solvents were evaporated to dryness with some coevaporation from toluene. Crystallization of the residue from ethanol gave **23** in 96% yield (2 crops, 531 mg).

p-*Carbomethoxphenyl 2-acetamido-3,4,6-tri*-O-*acetyl-2-deoxy-β-D-glucopyranoside **25***

To a solution of *p*-formylphenylglycoside **10** (350 mg, 0.776 mmol) and sodium hydrogen carbonate (800 mg) in MeOH (15 mL) was added bromine (300 μL). The reaction mixture was stirred at room temperature for 90 min, after which time TLC still indicated some starting aldehyde. Subjecting the reaction mixture to refluxing conditions or addition of excess bromine did not improve the situation. Ethyl acetate (40 mL) was added and the resulting organic phase was repeatedly washed with distilled water until the solution became clear. Usual processing of the organic phase (Na_2SO_4) and evaporation afforded a white solid. Purification by flash chromatography with ethyl acetate – hexane – 0.5% methanol (1:1) with change to 2:1 (v/v) gave pure **25** (206 mg, 55%). Crystallization from ethanol gave an analytical sample of **25**.

p-*(Hydroxymethyl)phenyl 2-acetamido-3,4,6-tri*-O-*acetyl-2-deoxy-β-D-glucopyranoside **27***

The *p*-formylphenylglycoside **10** (240 mg, 0.532 mmol) and sodium borohydride (15 mg, 0.395 mmol) were stirred at room temperature for 3 h in a mixture of ethanol (4 mL) and methylene chloride (2 mL). TLC in chloroform – ethyl acetate – *n*-propanol (25:5:2) showed complete reaction: R_f 0.39 (**10**), R_f 0.20 (**27**). Chloroform (20 mL) and 0.5 M HCl (20 mL) were added to the reaction mixture. The organic phase was washed with saturated sodium hydrogen carbonate (20 mL) followed by water (20 mL). The usual processing afforded **27** (240 mg, quant.) as a homogeneous white solid. An analytical sample was obtained from ethyl acetate–hexane.

Acknowledgements

We are grateful to NSERC for generous support of this work. Mr. F. D. Tropper also thanks NSERC for a graduate scholar-

Can. J. Chem. Downloaded from www.nrcresearchpress.com by 198.100.157.202 on 09/07/12
For personal use only.

ship. Finally, we acknowledge the contributions of Dr. C. Kazakoff for running the mass spectra and Ms. Cass Guthridge for preparing the manuscript.

1. R. Roy and F. D. Tropper. J. Chem. Soc. Chem. Commun. 1058 (1988).
2. R. Roy and F. D. Tropper. Glycoconjugate J. **5**, 203 (1988).
3. R. Roy and C. A. Laferrière. Can. J. Chem. **68**, 2045 (1990).
4. R. Roy and C. A. Laferrière. Carbohydr. Res. **177**, C1 (1988).
5. I. J. Goldstein and R. D. Poretz. *In* The lectins, properties, functions, and applications in biology and medicine. *Edited by* I. E. Liener, N. Sharon, and I. J. Goldstein. Academic Press, Orlando, Fl. 1986. pp. 209–214.
6. K. Brewster, J. M. Harrison, and T. D. Inch. Tetrahedron Lett. 5051 (1979).
7. D. Dess, H. P. Klein, D. V. Weinberg, R. J. Kaufman, and R. S. Sidhu. Synthesis, 883 (1981).
8. J. Bogusiak and W. Szeja. Pol. J. Chem. **59**, 293 (1985).
9. J. Rothermel and H. Faillard. Carbohydr. Res. **196**, 29 (1990).
10. R. Roy and F. D. Tropper. Synth. Commun. **20**, 2097 (1990).
11. D. H. Leeback, Biochem. Prep. **10**, 118 (1963).
12. F. Shafizadeh, M. H. Meshreki, and R. A. Susott. J. Org. Chem. **38**, 1190 (1973).
13. R. Roy, F. D. Tropper, A. Romanowska, M. Letellier, L. Cousineau, S. Meunier, and J. Boratynski. Glycoconjugate J. In press.
14. H. Kunz, H. Waldmann, and J. März. Liebigs Ann. Chem. 45 (1989).
15. R. U. Lemieux and H. Driguez. J. Am. Chem. Soc. **97**, 4063 (1975).
16. E. V. Dehmlow. Angew. Chem. Int. Ed. Engl. **16**, 493 (1977).
17. A. W. Herriott and D. Picker. J. Am. Chem. Soc. **97**, 2345 (1975).
18. R. Roy, F. D. Tropper, and A. J. Williams. Magn. Reson. Chem. In press.
19. R. Roy, F. D. Tropper, and A. J. Williams. Submitted.
20. S. Ram and R. E. Ehrenkaufer. Synthesis, 91 (1988).
21. F. W. Lichtenthaler, P. Jarglis, and K. Lorenz. Synthesis, 790 (1988).
22. D. D. Perrin, W. L. Armarego, and D. R. Perrin. *In* Purification of laboratory compounds. 2nd ed. Pergamon, London. 1980.
23. D. Horton. Methods Carbohydr. Chem. **6**, 282 (1972).
24. C. S. Jones and D. J. Kosman. J. Biol. Chem, **255**, 11861 (1980).

Can. J. Chem. Downloaded from www.nrcresearchpress.com by 198.100.157.202 on 09/07/12
For personal use only.

NMR studies of hydrocarbons solubilized in aqueous micellar solutions

RODERICK E. WASYLISHEN,[1] JAN C. T. KWAK, ZHISHENG GAO, ELISABETH VERPOORTE, J. BRUCE MACDONALD, AND ROSS M. DICKSON

Department of Chemistry, Dalhousie University, Halifax, N.S., Canada B3H 4J3

Received August 28, 1990

RODERICK E. WASYLISHEN, JAN C. T. KWAK, ZHISHENG GAO, ELISABETH VERPOORTE, J. BRUCE MACDONALD, and ROSS M. DICKSON. Can. J. Chem. **69**, 822 (1991).

Information concerning the solubilization of hydrocarbons in ionic surfactant micelles was obtained from ^2H NMR relaxation, ^1H NMR chemical shifts, and ^1H NMR paramagnetic relaxation measurements. The rotational motion of deuterated hydrocarbons, which is related to the micellar microviscosity at the location of the hydrocarbons, was probed by ^2H NMR relaxation. The relaxation data are interpreted using both the two-step and the single-step models, and the results are discussed in terms of the micellar microviscosity and the location of the hydrocarbons in micelles. The location of the hydrocarbons in micelles was further investigated by determining the aromatic ring current-induced ^1H chemical shifts along the surfactant alkyl chain and by comparing the ^1H spin-lattice relaxation enhancement of the hydrocarbons and the surfactant alkyl chain, induced by Mn^{2+} on the micellar surface. The hydrocarbons used include benzene, naphthalene, acenaphthalene, triphenylene, cyclohexane, cyclododecane, and *tert*-butylcyclohexane and the surfactants studied are hexadecyl-, tetradecyl-, and dodecyltrimethylammonium bromide; hexadecyl-, tetradecyl-, and dodecylpyridinium halide; and sodium dodecyl sulfate. The results indicate that the micellar microviscosity at the location of saturated hydrocarbons is approximately 5 cP for both the cationic and anionic micelles, whereas the micellar microviscosity at the location of unsaturated hydrocarbons is much higher. The unsaturated hydrocarbons are found to reside primarily near the surfactant headgroup in the cationic micelles, but are distributed evenly throughout the anionic SDS micelles. The saturated hydrocarbons appear to be located in the interior of the micelles.

Key words: NMR, relaxation, solubilization, surfactant, micelle.

RODERICK E. WASYLISHEN, JAN C. T. KWAK, ZHISHENG GAO, ELISABETH VERPOORTE, J. BRUCE MACDONALD et ROSS M. DICKSON. Can. J. Chem. **69**, 822 (1991).

Utilisant la relaxation RMN du ^2H, les déplacements chimiques en RMN du ^1H et des mesures de relaxation paramagnétique en RMN du ^1H, on a obtenu de l'information concernant la solubilisation d'hydrocarbures dans des micelles d'agents de surface ioniques. Pour étudier le mouvement de rotation des hydrocarbures deutérés qui est relié à la microviscosité micellaire au point de location des hydrocarbures, on a fait appel à la relaxation en RMN du ^2H. On a interprété les données de relaxation utilisant les modèles en une ainsi qu'en deux étapes et on discute des résultats en fonction de la microviscosité micellaire et de la position des hydrocarbures dans les micelles. On a réalisé une étude plus approfondie de l'influence de la position des hydrocarbures dans les micelles en déterminant les déplacements chimiques induits par le courant du noyau aromatique le long de la chaîne alkyle de l'agent de surface et en comparant les augmentations des relaxations spin-réseau du ^1H des hydrocarbures et de la chaîne alkyle de l'agent de surface qui sont induites par du Mn^{2+} sur la surface micellaire. Les hydrocarbures utilisés sont le benzène, le naphtalène, l'acénaphtalène, le triphénylène, le cyclohexane, le cyclododécane et le *tert*-butylcyclohexane alors que les agents de surface étudiés sont les bromures d'hexadécyl-, de tétradécyl- et dodécyl-triméthylammonium, les halogénures d'hexadécyl-, de tétradécyl- et de dodécylpyridinium et le dodécylsulfate de sodium. Les résultats indiquent que la microviscosité micellaire à la position des hydrocarbures saturés est égale à approximativement 5 cP pour les micelles tant cationiques qu'anioniques; par ailleurs, la microviscosité micellaire à la position des hydrocarbures insaturés est beaucoup plus élevée. On a trouvé que, dans les micelles cationiques, les hydrocarbures insaturés résident principalement près du groupe de tête de l'agent de surface; par ailleurs, dans les micelles de DSS, ils sont distribués d'une façon homogène. Il semble que les hydrocarbures saturés se situent à l'intérieur des micelles.

Mots clés : RMN, relaxation, solubilisation, agent de surface, micelle.

[Traduit par la rédaction]

Introduction

The presence of micelles in aqueous solution has a profound effect on the solubilization of some organic molecules that are normally insoluble or only sparingly soluble in water (1, 2). Micellar solubilization is of importance in many industrial processes such as detergency, emulsion polymerization, oil recovery, etc. (3, 4), and in a variety of fundamental research topics such as micellar modeling of biological membranes (5). The solubility of organic molecules in the micellar pseudophase is generally represented by the distribution coefficient between the micellar and aqueous phases. The distribution coefficients, which can be determined easily by use of the NMR paramagnetic relaxation method (6) or the NMR pulse gradient spin-echo self-diffusion method (7), are dependent on the structures of the solubilizate and the surfactant that constitute the micelles. In addition to the solubilization equilibrium, the microviscosity of the micellar interior and the location of the solubilizate within the micelles may also be important in many applications of micellar solubilization.

In recent years, the dynamic behavior of surfactant molecules in micelles has been investigated extensively by means of ^{13}C and ^2H NMR relaxation measurements on surfactant molecules (8–11); the NMR relaxation data are generally interpreted using the two-step model developed by Wennerström *et al.* (12). However, studies on the motion of solubilizates within the micelles are limited (13–16). In the absence of strong solute–solvent interactions the effective rotational correlation time, τ_c, of a solute molecule is related to the solvent viscosity, η, and the absolute temperature, T, by eq. [1] (17, 18):

$$[1] \quad \tau_c = C\eta/T + \tau_o$$

where C is a constant that can be measured experimentally or

[1]Author to whom correspondence may be addressed.

Can. J. Chem. Downloaded from www.nrcresearchpress.com by 198.100.157.202 on 09/07/12
For personal use only.

Can. J. Chem. Downloaded from www.nrcresearchpress.com by 198.100.157.202 on 09/07/12
For personal use only.

estimated using the hydrodynamic slip model. In hydrodynamic models, C is directly proportional to the volume of the solute molecule and τ_0 is a "free rotor" correlation time that is generally negligible compared to τ_c. Using this approach (eq. [1]), Stark *et al.* (14) studied nitrobenzene solubilized in hexadecyltrimethylammonium bromide (HTAB) and sodium dodecyl sulfate (SDS) micelles and deduced micellar microviscosities in the range 8–17 cP. Rotational correlation times of nitrobenzene were monitored using ^{13}C NMR relaxation data. Because of the rather poor inherent sensitivity of ^{13}C NMR spectroscopy, Stark *et al.* (14) used 100 mM solutions of nitrobenzene in 330 mM surfactant solutions. Such high concentrations of solubilizate may cause significant distortions in micellar structure since micelle size and shape are modified substantially by additives (19). From ^2H NMR studies, Eriksson *et al.* (13) concluded that the rotational diffusion of benzene and cyclohexane solubilized in HTAB and SDS is only 2 to 3 times slower than it is in the corresponding hydrocarbons, dodecane and hexadecane. Stilbs *et al.* (15) reported the results of a detailed ^2H NMR study of *trans*-decalin solubilized in several alkyltrimethylammonium halides and sodium alkyl sulfates. Their results indicate micellar microviscosities in the range of 3–10 cP. In contrast, fluorescence depolarization studies (20, 21) of 2-methylanthracene indicate much larger micellar microviscosities (17–50 cP). One study (22) reported a microviscosity of 670 cP for pyrene solubilized in aqueous solutions of sodium taurocholate. The dynamics of deuteriochloroform solubilized in rod-shaped alkylammonium chloride micelles was investigated recently by Canet *et al.* (16), using ^2H NMR relaxation.

Hydrocarbons can be solubilized either in the micellar interior or near the micellar surface, according to Mukerjee's "two-state" model (1). One of the most widely used methods for determining the location of aromatic hydrocarbons solubilized in micelles is to monitor the ring current shifts on the ^1H resonances of the surfactant alkyl chain (23–27). It is assumed that the observation of an aromatic ring current shift on a surfactant segment is evidence that on average the aromatic solubilizate is located in the vicinity of the surfactant segment. On the other hand, the absence of a ring current shift is taken to indicate a low aromatic solubilizate concentration in that region or an independent isotropic motion of the aromatic molecule and the surfactant segment (28). The solubilization site of hydrocarbons micelles has also been studied by measuring the ^1H spin–spin relaxation enhancement of the hydrocarbon molecules induced by paramagnetic probes located on the micellar surface (29). This enhancement is proportional to the inverse sixth power of the average distance between the protons and the paramagnetic ions on the micellar surface, if the interaction is purely dipolar. However, several assumptions were involved in the calculation, including the thickness of the micellar headgroup region (29). The locations of small aliphatic alcohols in micellar solutions have also been characterized recently by comparing the Mn^{2+}-induced relaxations of the alcohols in cationic and anionic surfactant systems (30).

In this paper, a combination of ^2H NMR relaxation, ^1H NMR chemical shifts, and ^1H NMR paramagnetic relaxation measurements is used to investigate the solubilization of a number of hydrocarbons in a series of ionic surfactant systems. Rotational motion of hydrocarbons in micelles is probed by ^2H NMR relaxation. The micellar microviscosity can be deduced from the rotational correlation time of the hydrocarbon. The dynamic behavior of hydrocarbons in micelles is related to their location. The effect of surfactant head group charge and alkyl chain length is also examined. Information concerning the location of hydrocarbons in micelles is obtained from aromatic ring current-induced ^1H shifts or from the comparison of Mn^{2+}-induced ^1H spin-lattice relaxation enhancements between the surfactant alkyl chain and the hydrocarbons. The hydrocarbons studied include benzene, naphthalene, acenaphthalene, triphenylene, cyclohexane, cyclododecane, and *tert*-butylcyclohexane and the surfactants used are *n*-alkyltrimethylammonium bromide (dodecyl-, tetradecyl-, and hexadecyl-), *n*-alkylpyridinium halide (dodecyl-, tetradecyl-, and hexadecyl-), and sodium dodecyl sulfate.

Theory

Deuterium NMR relaxation

For a spin $I = 1$ nucleus, such as deuterium, nuclear relaxation rates are given by (31):

$$[2] \quad R_1 = 1/T_1 = (3/10)\pi^2\chi_Q^2(1 + \eta^2/3)[J(\omega_0) + 4J(2\omega_0)]$$

and

$$[3] \quad R_2 = 1/T_2 = (3/10)\pi^2\chi_Q^2(1 + \eta^2/3)[(3/2)J(0) + (5/2)J(\omega_0) + J(2\omega_0)]$$

where R_1 and R_2 are the rates of spin-lattice and spin–spin relaxation respectively, χ_Q is the deuterium quadrupolar coupling constant, e^2qQ/h, η is the nuclear electric field gradient asymmetry parameter (less than 0.1 for the molecules in this study), and $J(\omega)$ is the spectral density function:

$$[4] \quad J(\omega) = \frac{\tau_c}{1 + (\omega_0\tau_c)^2}$$

ω_0 is the Larmor frequency ($\omega_0 = 2\pi\nu_0$) and τ_c is the rotational correlation time. For rotational diffusion, $\tau_c = (6D_r)^{-1}$ where D_r is the rotational diffusion constant. Plots of $\log_{10} T_1$ and $\log_{10} T_2$ vs. $\log_{10}\tau_c$ for $\nu_0 = 55.43$ MHz, and $\chi_Q = 190$ kHz are shown in Fig. 1 (the order parameter, S, equals zero).

The rate of spin-lattice relaxation is a maximum when $\omega_0\tau_c = 0.6158$. This corresponds to $T_1 = 2.2$ ms, $T_2 = 1.4$ ms, and $\tau_c = 1.7$ ns in Fig. 1 ($S = 0.0$). Under the so-called extreme narrowing condition, $\omega_0\tau_c \ll 1$, $J(0) = J(\omega_0) = J(2\omega_0) = \tau_c$, and

$$[5] \quad R_1 = R_2 = (3/2)\pi^2\chi_Q^2(1 + \eta^2/3)\tau_c$$

In the previously mentioned ^2H NMR study by Eriksson *et al.* (13), it was observed that $T_1 = T_2$ for benzene-d_6 in both SDS and HTAB solutions where the mole fraction of benzene in a benzene–HTAB mixture is 0.1. However, at higher benzene to HTAB mole ratios, $T_1 > T_2$. This was attributed to the formation of long, rod-shaped micelles in the presence of high concentrations of benzene. Under these conditions, Eriksson *et al.* (13) used the two-step model (12), which assumes two correlation times, one to describe rapid local motion and another to describe a slower motion over distances of the order of the dimensions of the micellar aggregates. It was further assumed that the spectral density function $J(\omega)$ is a sum of two Lorentz functions (9–13),

$$[6] \quad J(\omega) = S^2\frac{\tau_c^s}{1 + (\omega_0\tau_c^s)^2} + (1 - S^2)\frac{\tau_c^f}{1 + (\omega_0\tau_c^f)^2}$$

where τ_c^s and τ_c^f are rotational correlation times for the slow and fast motions and S is a local order parameter taken over

Can. J. Chem. Downloaded from www.nrcresearchpress.com by 198.100.157.202 on 09/07/12
For personal use only.

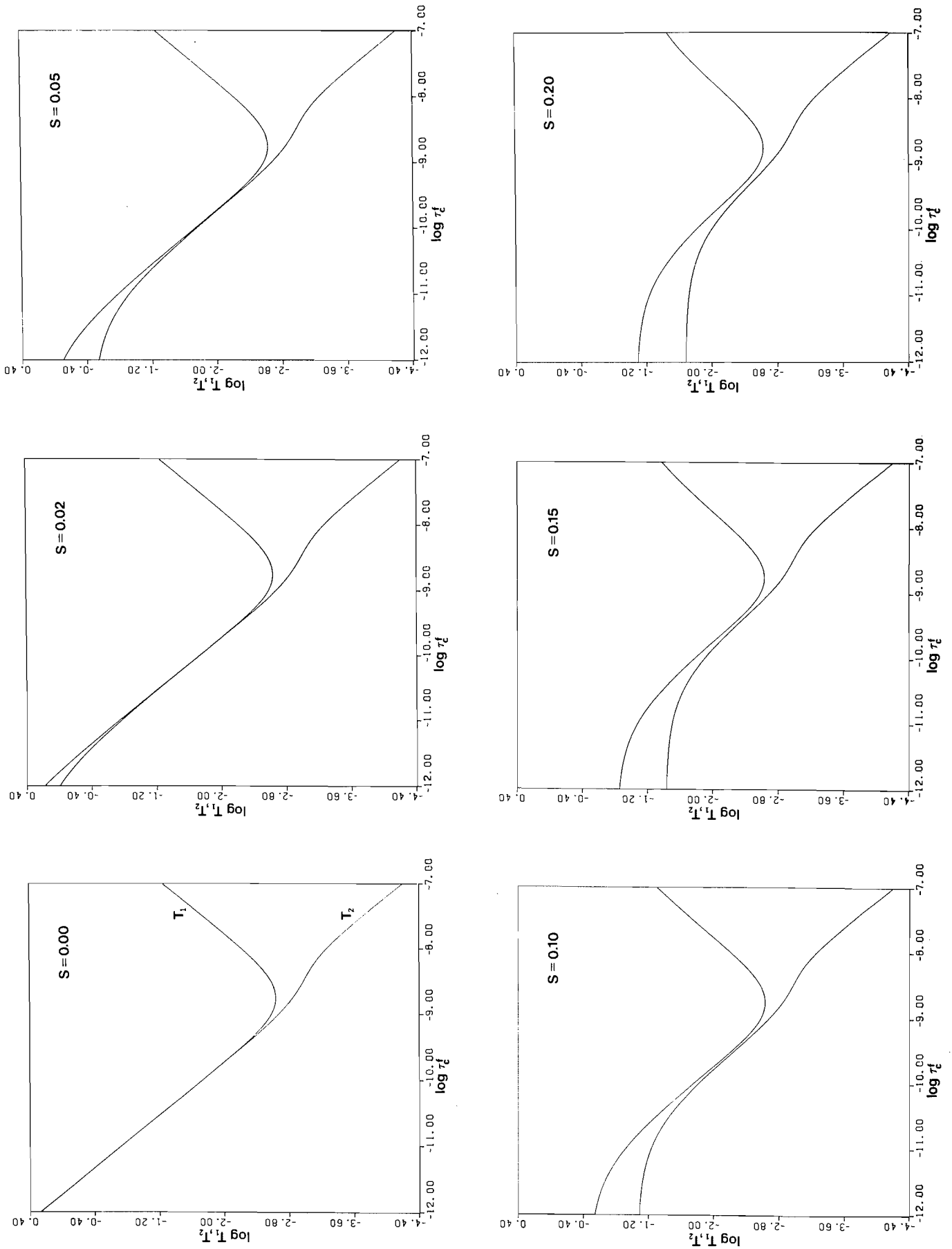


FIG. 1. $\log_{10} T_1$ and T_2 vs. $\log_{10} \tau_c^f$ at $\nu_0 = 55.43$ MHz, as a function of S. $\tau_c^s = 5$ ns.

Can. J. Chem. Downloaded from www.nrcresearchpress.com by 198.100.157.202 on 09/07/12
For personal use only.

times longer than τ_c^f, but shorter than τ_c^s. If the fast motion is sufficiently rapid to satisfy the extreme narrowing condition, $\omega_0\tau_c^f \ll 0$, eq. [6] becomes

$$[7] \quad J(\omega) = (1 - S^2)\tau_c^f + S^2\frac{\tau_c^s}{1 + (\omega_0\tau_c^s)^2}$$

Typical values of τ_c^s for surfactant micelles appear to be 1–10 ns (8–12), while values of τ_c^f and S will be dependent on the solubilizate. For example, for benzene-d_6 and cyclohexane-d_{12}, S values of approximately 0.08 and 0.01, respectively, have been reported (13). In the study of benzene-d_6 in HTAB, Eriksson and co-workers (13, 32) obtained S from ^2H quadrupolar splittings measured in the hexagonal liquid crystalline phase.

The difference between the two-step model and the single-step model can be illustrated in Figs. 1 and 2. It is important to recognize that if S is very small, the two-step model is essentially the same as the single-step model, and if S is significant, the two-step model predicts that: (i) $T_2 < T_1$ and (ii) both T_1 and T_2 are field dependent, since $\omega_0\tau_c$ may be comparable to or greater than 1. Figure 1 presents a plot of $\log_{10} T_1$ and $\log_{10} T_2$ vs. $\log_{10}\tau_c^f$ at 55.43 MHz since we carried out deuterium T_1 and T_2 measurements on several solubilizates at this frequency. The value of S was varied at 0.0, 0.02, 0.05, 0.10, 0.15, and 0.20, and the quadrupolar coupling constant and the slow motion correlation time were taken to be 190 kHz and 5 ns, respectively. From calculations using eqs. [2]–[6] with $\nu_0 = 55.43$ MHz, $\tau_c^s = 5$ ns, and $S = 0.1$, it is apparent that T_1 values in the range 5–50 ms will result in values of τ_c^f and τ_c (eq. [5]) that agree within 15% of one another. ^2H T_1 measurements have been carried out at both 15.36 MHz and 55.43 MHz, hence the plots of $\log_{10} T_1$ at these two frequencies vs. $\log_{10}\tau_c^f$ with $\tau_c^s = 1$ ns are given in Fig. 2.

In their study of *trans*-decalin-d_{18}, Stilbs *et al.* (15) found that T_1 and T_2 were equal within experimental error and that there is no field dependence of the rates of relaxation. This implies that the local order parameter, S, is small for *trans*-decalin-d_{18}.

The rotational correlation times (τ_c^f and τ_c^s) and the order parameter, S, can be calculated directly from eqs. [2], [3], and [7] if three or more than three independent relaxation data are obtained, e.g., in this study T_1 at 55.4 and 15.36 MHz and T_2 at 55.43 MHz were determined. Subtracting eq. [2] from eq. [3], and combining with eq. [7], one obtains

$$[8] \quad S^2 = (10/3)\pi^{-2}\chi_Q^{-2}\left[(3/2)\tau_c^s + \frac{(3/2)\tau_c^s}{1 + (\omega_0\tau_c^s)^2} - \frac{3\tau_c^s}{1 + (2\omega_0\tau_c^s)^2}\right]^{-1}(1/T_2 - 1/T_1)$$

$$[9] \quad \tau_c^f = (1/5)(1 - S^2)^{-1}\left[(10/3)\pi^{-2}\chi_Q^{-2}T_1^{-1} - \frac{S^2\tau_c^s}{1 + (\omega_0\tau_c^s)^2} - \frac{4S^2\tau_c^s}{1 + (2\omega_0\tau_c^s)^2}\right]$$

If τ_c^s is estimated (2–10 ns), S and τ_c^f can be calculated from T_1 and T_2 at 55.43 MHz using eqs. [8] and [9]. Also, by varying τ_c^s, many sets of τ_c^s, S, and τ_c^f can be obtained; however, only one set will give the same T_1 as that determined experimentally at 15.36 MHz.

Paramagnetic relaxation

In a solution containing paramagnetic transition metal ion complexes, the enhancement of the spin-lattice relaxation rate of a ligand nucleus is given (33, 34) by

$$[10] \quad R_{1p} = 1/T_1^p - 1/T_1^0 = \frac{P_M}{\tau_M + T_{1M}}$$

where T_1^p and T_1^0 are the measured relaxation rates in the presence and absence of paramagnetic species, respectively. P_M is the mole fraction of ligand in the bound state, τ_M the lifetime of the ligand in the complex, and T_{1M} the spin-lattice relaxation time of the ligand nuclei in the bound state. Equation [10] is valid provided the transition metal ion concentration is much lower than that of the ligand concentration. The complete expression for T_{1M} is given by the Solomon–Bloembergen–Morgan equation (35–37), which contains both the dipolar and the scalar terms. However, since in this paper Mn^{2+} is used as paramagnetic probe, only the dipolar term needs to be considered (38, 39).

$$[11] \quad 1/T_{1M} = (2/5)S(S + 1)\gamma_I^2\gamma_S^2\hbar^2 r_{IS}^{-6}\frac{\tau_R}{1 + (\omega_I\tau_R)^2}$$

Here S is the total electron spin, γ_I and γ_S the nuclear and electron magnetogyric ratios, ω_I the Larmor frequency of the nucleus I, r_{IS} the distance between the nuclear spin and the electron spin, and τ_R the correlation time for isotropic rotational motion of the complex. In the Mn^{2+}–alkylphosphate system, it has been found that R_{1p} decreases with increasing temperature, indicating $T_{1M} \gg \tau_M$ (39). Thus, R_{1p} is directly proportional to the inverse sixth power of the average distance between the Mn^{2+} on the surface and the nucleus in the micelles. It is reasonable to assume that this condition also holds for the Mn^{2+}–SDS system since the interaction between Mn^{2+} and SDS is much weaker than that between Mn^{2+} and alkyl phosphate (39). If the contributions of internal motion to the paramagnetic relaxation are the same for surfactant segments and the solubilizate (37), a comparison of the paramagnetic relaxation enhancement between the surfactant segments and the solubilizate can provide information on the location of the solubilizate inside the micelles.

Experimental

Materials and sample preparation

Dodecyl-, tetradecyl-, and hexadecyltrimethylammonium bromide (DTAB, TTAB, and HTAB) were obtained from Sigma Chemical Co. These products were purified by repeated recrystallization from acetone. Dodecylpyridinium chloride (DPC) and hexadecylpyridinium bromide (HPB) were obtained from Tokyo Kasei Kogyo Co. Ltd. and Eastman Kodak Co., respectively, and purified by repeated recrystallization from acetone and treatment with active carbon. Tetradecylpyridinium bromide (TPB) was synthesized by reacting 1-bromotetradecane (Eastman Kodak, purified by fractional distillation) with a small excess of pyridine (40). The reaction product was purified by extraction with diethyl ether followed by repeated recrystallization from acetone and treatment with active carbon. None of these products showed a minimum in surface tension, and cmc values were in good agreement with literature values (41). For sodium dodecyl sulfate we used both a commercial product (Aldrich, "99% pure"), and a highly purified sample prepared by reacting fractionally distilled 1-dodecanol (Eastman Kodak) with chlorosulfonic acid, followed by ether extraction and recrystallization (42). The NMR relaxation measurements of solubilized hydrocarbons reported here did not prove sensitive to the different degree of purity of these two

Can. J. Chem. Downloaded from www.nrcresearchpress.com by 198.100.157.202 on 09/07/12
For personal use only.

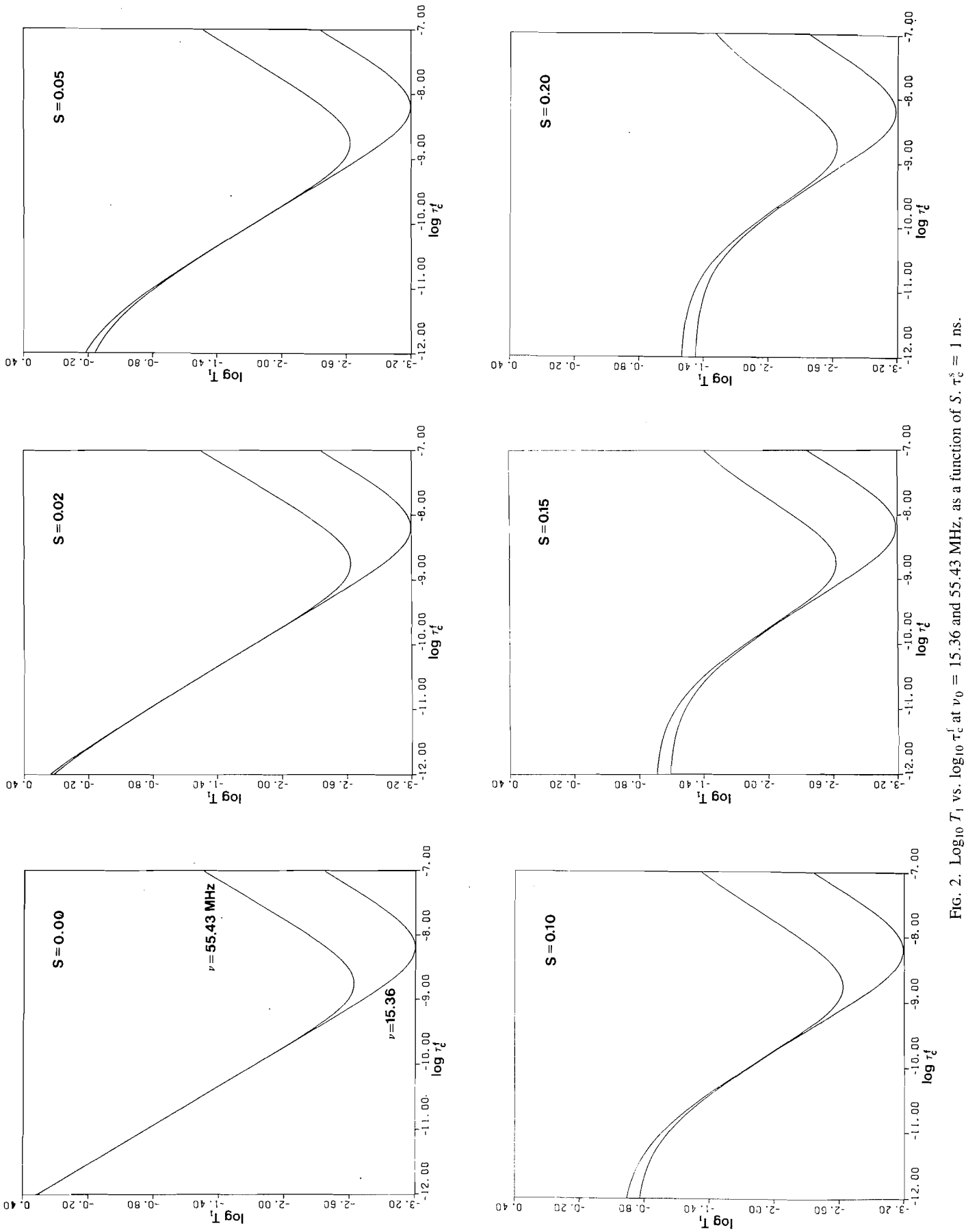


FIG. 2. $\text{Log}_{10}\, T_1$ vs. $\log_{10} \tau_c^f$ at $\nu_0 = 15.36$ and 55.43 MHz, as a function of S. $\tau_c^s = 1$ ns.

TABLE 1. Deuterium spin-lattice relaxation times for several hydrocarbons solubilized in alkyltrimethylammonium bromide surfactants, $C_nH_{2n+1}N(CH_3)_3^+Br^-$, at 55.43 MHz[a]

Solubilizate	Relaxation times (s) DTAB (n = 12) **I***a*	TTAB (n = 14) **I***b*	HTAB (n = 16) **I***c*
Benzene-d_6 (5 mM)	0.22	0.15	0.13
Naphthalene-d_8 (5 mM)	0.036	0.033	0.030
Acenaphthalene-d_{10} (5 mM)			
aromatic	—	0.027	0.027
aliphatic	—	0.026	0.021
Triphenylene-d_{12} (0.5 mM)	0.0113	0.0092	0.0075
Cyclohexane-d_{12} (5 mM)	0.44[b]	0.46[b]	0.45[b]
Cyclododecane-d_{24} (5 mM)	0.17	0.15	0.14

[a]All measurements carried out at 21 ± 2°C using a surfactant concentration of 50 mM unless otherwise indicated.
[b]Surfactant concentration 150 mM.

TABLE 2. Deuterium spin-lattice relaxation times for several hydrocarbons solubilized in alkylpyridinium halide surfactants at 55.43 MHz[a]

Solubilizate	Relaxation times (s) DPC (n = 12) **II***a*	TPB (n = 14) **II***b*	HPB (n = 16) **II***c*
Benzene-d_6 (5 mM) 21°C	0.23	0.15	—
35°C	0.43	0.24	0.22
Naphthalene-d_8 (5 mM)	0.048	0.038	0.032
Cyclododecane-d_{24} (5 mM)	0.15	—	—

[a]All measurements carried out at 21 ± 2°C using a surfactant concentration of 50 mM unless otherwise indicated.

Can. J. Chem. Downloaded from www.nrcresearchpress.com by 198.100.157.202 on 09/07/12
For personal use only.

samples. Surfactant solutions were prepared by weight using distilled and deionized water ($\kappa < 5 \times 10^{-7}$ ohm^{-1} cm^{-1}) for ^{2}H NMR experiments, and D_2O (99.8%) for ^{1}H NMR experiments, at a temperature well above the Kraft point. A weighed amount of hydrocarbon was added and the solution was shaken, normally for 24 h. In a number of cases the concentration of solubilized hydrocarbon was determined by UV spectroscopy. The result of the UV concentration determination was in good agreement with the calculated concentration.

NMR measurements

Deuterium NMR spectra were recorded at 55.427 MHz (B_0 = 8.48 T) using a Nicolet 360 NB spectrometer and at 15.36 MHz (B_0 = 2.35 T) using a Varian XL-100 spectrometer. Proton NMR chemical shift and relaxation measurements were carried out at 361.05 MHz on the Nicolet 360 NB spectrometer and the COSY spectrum was recorded at 500.13 MHz on a Bruker AMX 500 spectrometer. Spin-lattice relaxation times were measured using an inversion–recovery sequence in which alternate $\pi/2$ pulses are phase shifted by 180° (43) and a composite π pulse is used to compensate for imperfect B_1 homogeneity (44). All T_1 values were calculated from peak heights obtained at 12 or more different variable delays, using a nonlinear three-parameter least-squares fitting procedure (45) available on the Nicolet software (both instruments). Spin–spin relaxation times were measured by the Carr–Purcell–Meiboom–Gill method (46).

On any given sample, we believe that the deuterium relaxation times T_1 and T_2 are reproducible to ±5% and ±10%, respectively. Proton NMR chemical shifts were referred to the HOD residue (δ = 4.63 ppm) and typical errors in chemical shift measurements are 0.002 ppm. Error limits for proton T_1 values are less than 5%.

Results and discussion

Deuterium NMR relaxation

Deuterium spin-lattice relaxation times at 55.43 MHz for several hydrocarbons solubilized in alkyltrimethylammonium bromides, alkylpyridinium halides, and SDS micelles are given in Tables 1, 2, and 3, respectively. Deuterium T_1 and T_2 values determined at 55.43 MHz for benzene-d_6, naphthalene-d_8, cyclohexane-d_{12}, and cyclododecane-d_{24} solubilized in several different surfactant solutions are given in Table 4. Also, T_1 values for benzene-d_6, naphthalene-d_8, acenaphthalene-d_{10}, and cyclododecane-d_{24} solubilized in HTAB and SDS at two different resonant frequencies are compared in Table 5. First, we outline below how to obtain effective rotational correlation times for each of these solubilizates from the relaxation data in Tables 1–5.

As already mentioned in the theory section, the local order parameter, S, is small for saturated hydrocarbon solubilizates such as cyclohexane, *trans*-decalin, and cyclododecane, hence the single-step analysis and two-step model are essentially equivalent. This hypothesis is supported by the observation that for these solubilizates T_1 and T_2 are equal within experimental error (Table 4) and that the ^{2}H T_1 values for cyclododecane are independent of the frequencies used in this study (Table 5). Since χ_Q = 174 kHz in cyclohexane (47), τ_c for each of the saturated hydrocarbon solubilizates can be calculated by substitution into eq. [5] and the result is τ_c (ps) = $2.231/T_1$ (s).

Can. J. Chem. Downloaded from www.nrcresearchpress.com by 198.100.157.202 on 09/07/12
For personal use only.

TABLE 3. Deuterium spin-lattice relaxation times for several hydrocarbons solubilized in 50 mM sodium dodecyl sulfate at 55.43 MHz[a]

Solubilizate	T_1 (s)
Benzene-d_6 (5 mM)	0.49
Naphthalene-d_8 (5 mM) (average)	0.076
Acenaphthalene-d_{10} (5 mM) aromatic	0.062
aliphatic	0.045
Triphenylene-d_{12} (0.5 mM)	0.017
Cyclohexane-d_{12} (5 mM)	0.74
Cyclododecane-d_{24} (5 mM)	0.17

[a]All measurements carried out at 21 ± 2°C.

TABLE 4. Deuterium NMR spin-lattice relaxation times at 55.43 MHz

Solubilizate	Surfactant/solvent	T_1 (s)	T_2 (s)
Benzene-d_6	HTAB	0.13 s	0.095 s
	SDS	0.49	0.44
	Water	0.88	—
	n-Hexadecane	0.50	—
Naphthalene-d_8[a]	HTAB	0.028	0.019
	SDS	0.065	0.069
	n-Hexadecane	0.16	—
Cyclohexane-d_{12}	HTAB	0.45	0.37
	TTAB	0.46	0.42
	DTAB	0.44	0.39
	SDS	0.74	0.69
	n-Hexadecane	0.84	—
Cyclododecane-d_{24}	HTAB	0.14	0.12
	TTAB	0.15	0.14
	DTAB	0.17	0.15
	SDS	0.17	0.16
	n-Hexadecane	0.19	0.16
	n-Dodecane	0.28	0.24
	n-Hexane	0.63	0.63

[a]Data for H-2, H-3, H-6, and H-7.

In the case of the planar unsaturated hydrocarbons, the local order parameter is expected to be larger. For naphthalene in the cationic hexadecyltrimethylammonium surfactants we obtain $\tau_c^s = 9.0$ ns, $S = 0.10$, and $\tau_c^f = 62$ ps, using eqs. [2], [7], [8], and [9] ($\chi_Q = 193$ kHz (48, 49)), based on the two-step model. The correlation time for slow motion, τ_c^s, is in good agreement with that of hexadecyltrimethylammonium micelle in aqueous solution, $\tau_c^s = 7.6$ ns (50), obtained from ^{2}H relaxation data. We have also determined the order parameter of naphthalene in the hexadecyltrimethylammonium bromide hexagonal phase to be 0.12 from the ^{2}H powder pattern.[2] If the single-step model (eq. [5]) is used, we calculate $\tau_c = 60$ ps, very close to the τ_c^f (62 ps) from the two-step model. It is important to note that naphthalene has a T_1 value in the range 0.02–0.05 s in the cationic surfactant micelles, and that the single- and two-step models yield similar values for τ_c^f (see Figs. 1 and 2). A similar situation is expected for acenaphthalene in cationic alkyltrimethylammonium surfactant micelles.

For naphthalene in SDS, the T_1 and T_2 values at 55.43 MHz are the same within experimental error and no field dependence of T_1 is apparent (Tables 4 and 5). These comments also apply to acenaphthalene in SDS, and suggest that the effective order parameter, S, for naphthalene and acenaphthalene in SDS is much smaller than it is in the cationic surfactants.

Because of the low solubility of triphenylene in these surfactant systems, low signal-to-noise ratios at 15.36 MHz made it impossible to obtain reliable T_1 values at this frequency. However, the reliable high-field T_1 values in the range 0.0075–0.017 s suggest that τ_c values calculated using the single-step model will be in fair agreement with those obtained using the two-step model.

Benzene is rather a special case; it should be recognized that benzene has an appreciable solubility in the aqueous phase. In DTAB and SDS micellar solution, the fraction of benzene in the micellar phase has been determined to be 83% (6) and 85% (52), respectively, hence the corrected ^{2}H relaxation time of benzene in the micellar phase can be calculated. For benzene in HTAB micelles, we obtain $T_1 = 0.11$ s, $T_2 = 0.08$ s at 55.43 MHz, and $T_1 = 0.076$ s at 15.36 MHz. Based on the two-step model, τ_c^s, S, and τ_c^f are calculated to be 6.5 ns, 0.056, and 16 ps ($\chi_Q = 187$ kHz (32)), respectively. The order parameter for benzene in a HTAB hexagonal phase was determined by Eriksson and co-workers to be 0.084 (13, 32). The single-step model (eq. [5]) gives $\tau_c = 17$ ps for benzene in HTAB, in good agreement with the correlation time for fast motion in the two-step model. In the case of benzene in SDS, T_1 is independent of frequency and T_1 and T_2 at 55.43 MHz are equal within experimental error, indicating a small S value.

In Table 6 we have summarized the NMR rotational correlation times calculated using the single-step model (eq. [5]) for each of the solubilizates examined in this study. Values of τ_c for each solubilizate (concentration 5 mM) in *n*-hexane and *n*-hexadecane are also given. These values are probably accurate to better than ±10%.

Rotational correlation times for cyclohexane solubilized in the various micellar systems range from 3.0 to 5.1 ps. These values are not much longer than the rotational correlation time for cyclohexane in *n*-hexadecane, i.e., 2.7 ps. Similar comments apply to cyclododecane where τ_c values in the surfactant solutions are in the range 13–16 ps, while in *n*-hexadecane $\tau_c = 12$ ps. Since the viscosity of *n*-hexadecane is 3.34 cP (53), it can be concluded that the micellar viscosity at the location of cyclohexane and cyclododecane is approximately 5 cP for both cationic and anionic SDS micelles, in good agreement with the results of Stilbs *et al.* (15) for *trans*-decalin in micelles (3–10 cP).

Rotational correlation times of the planar unsaturated hydrocarbons are significantly longer in the alkyltrimethylammonium micelles than in SDS or in *n*-hexadecane. For example, for naphthalene solubilized in DTAB and SDS, $\tau_c = 50$ and 24 ps, respectively. The longer rotational correlation times in the cationic surfactant systems compared to SDS must be the result of different solubilization sites. The locations of hydrocarbons in micelles will be further characterized in the next two sections, using aromatic ring current-induced ^{1}H shift and paramagnetic relaxation enhancement methods.

Aromatic ring current-induced proton chemical shifts

^{1}H NMR spectra were recorded for 0.050 *m* HTAB, HPB, and SDS solutions containing 0–0.030 *m* benzene or 0–0.010 *m* naphthalene. The assignments of surfactant spectra were based on standard decoupling and two-dimensional (COSY) techniques. One typical example is shown in Fig. 3, which gives the ^{1}H spectra of 0.050 *m* HTAB in the absence and presence

[2]R. E. Wasylishen, unpublished results.

TABLE 5. Deuterium NMR spin-lattice relaxation times at 55.43 MHz and 15.36 MHz

Solubilizate[a]	Frequency (Hz)	Relaxation time (s) Surfactant HTAB	Surfactant SDS
Benzene-d_6	55.43	0.15 ± 0.02	0.49 ± 0.05
	15.36	0.09 ± 0.02	0.53 ± 0.05
Naphthalene-d_8	55.43	0.028 ± 0.004	0.09 ± 0.03
	15.36	0.020 ± 0.004	0.09 ± 0.03
Acenaphthalene-d_{10}			
aromatic	55.43	0.027 ± 0.003	0.062 ± 0.006
	15.36	0.020 ± 0.002	0.09 ± 0.03
aliphatic	55.43	0.021 ± 0.002	0.045 ± 0.004
	15.36	0.016 ± 0.002	—
Cyclododecane-d_{24}	55.43	0.14 ± 0.01	0.17 ± 0.01
	15.36	0.13 ± 0.01	0.17 ± 0.01

[a]Solubilizate 5 mM.
[b]Surfactant 50 mM.

TABLE 6. Effective rotational correlation times (in units of ps = 10^{-12} s) for hydrocarbons solubilized in several aqueous ionic micellar solutions[a]

Solubilizate	Correlation time (ps) DTAB	TTAB	HTAB
Benzene	10[b]	15[b]	17[b]
Naphthalene	50	55	60
Acenaphthalene	—	76	86
Triphenylene	160	200	240
Cyclohexane	5.1	4.8	4.9
Cyclododecane	13	15	16
	DPC	TPB	HPB
Benzene	9.7[b]	15[b]	—
Naphthalene	38	48	57
Cyclododecane	15	—	—
	SDS	*n*-Hexane[d]	*n*-Hexadecane[e]
Benzene	4.3[c]	0.97	3.6
Naphthalene	24	2.3	9.1
Acenaphthalene	39	—	—
Triphenylene	107	8.6	50
Cyclohexane	3.0	1.09	2.7
Cyclododecane	13	3.54	12

[a]Calculated using the data in Tables 1–3 and eq. [5] (single-step model).
[b]Calculated from the T_1 for benzene in the micellar phase, corrected according to the mole fraction of benzene in the cationic micelles (83%) (6).
[c]Calculated from the T_1 for benzene in the micellar phase, corrected according to the mole fraction of benzene in the SDS micelles (85%) (52).
[d]Viscosity: 0.326 cP (53).
[e]Viscosity: 3.34 cP (53).

of 0.010 *m* naphthalene. Upon the addition of naphthalene, the largest effect was observed for the chemical shift of the HTAB β-CH_2 proton resonance. The peaks corresponding to the γ-CH_2 group in HTAB (Fig. 3) were previously assigned to the methylene protons adjacent to the terminal methyl group of the alkyl chain in decyltrimethylammonium bromide by Jagannathan *et al.* (30). This latter assignment is inconsistent with the earlier work by Zachariasse *et al.* (54). Our decoupling spectra and COSY spectrum (Fig. 3c) of DTAB clearly show strong correlation between the β-CH_2 and the γ-CH_2 resonances and between the $(CH_2)_n$ and the ω-CH_3 resonances, providing full support to the assignment by Zachariasse *et al.* (54).

Figures 4, 5, and 6 illustrate the chemical shift changes along the surfactant methylene chains in 0.050 *m* HTAB, HPB, and SDS solutions when different amounts of benzene (0.005–0.030 *m*) are solubilized. For the cationic surfactants HTAB and HPB, the effects of benzene solubilization on the surfactant alkyl chain shifts are in the order β-CH_2 > γ-CH_2 > α-CH_2. Similar changes in chemical shift are not observed for $(CH_2)_n$ and ω-CH_3. In the case of the anionic surfactant SDS, the effects of benzene solubilization on the proton chemical shifts are in the order β-CH_2 ~ $(CH_2)_n$ > α-CH_2 ~ ω-CH_3. These results suggest that on average benzene molecules favour the headgroup region of the cationic surfactant micelles, but, in the anionic SDS surfactant micelles, benzene molecules are distributed more uniformly throughout the micelles.

When 0.010 *m* naphthalene is used as solubilizate, similar results are observed in the 0.050 *m* HTAB, HPB, and SDS systems, as shown in Fig. 7. Maximum chemical shift changes are observed for the β-CH_2 resonances in cationic surfactants HTAB and HPB. In the case of SDS micelles, the distribution of naphthalene is also more uniform.

These observations may clarify the result obtained in the previous section where the rotational correlation times of arenes are significantly longer in the alkyltrimethylammonium bromide micelles than in the anionic SDS micelles. The longer rotational correlation times for arenes in cationic micelles are reasonable if they are located near the headgroups, since it has been established that there is a gradient in the local motion along the surfactant hydrocarbon chain, with methylene groups near the headgroup moving more slowly than those in the micellar interior (8). The increase in rotational correlation time, with the cationic surfactant alkyl chain length, for any arene solubilizate (Table 6) is also evidence that solubilization occurs primarily near the surface of cationic surfactant micelles. Aromatic ring current-induced shifts of benzene in cationic HTAB and anionic SDS surfactant micelles were reported earlier by Fendler *et al.* (55). These authors also found that benzene is primarily located

Can. J. Chem. Downloaded from www.nrcresearchpress.com by 198.100.157.202 on 09/07/12
For personal use only.

Can. J. Chem. Downloaded from www.nrcresearchpress.com by 198.100.157.202 on 09/07/12
For personal use only.

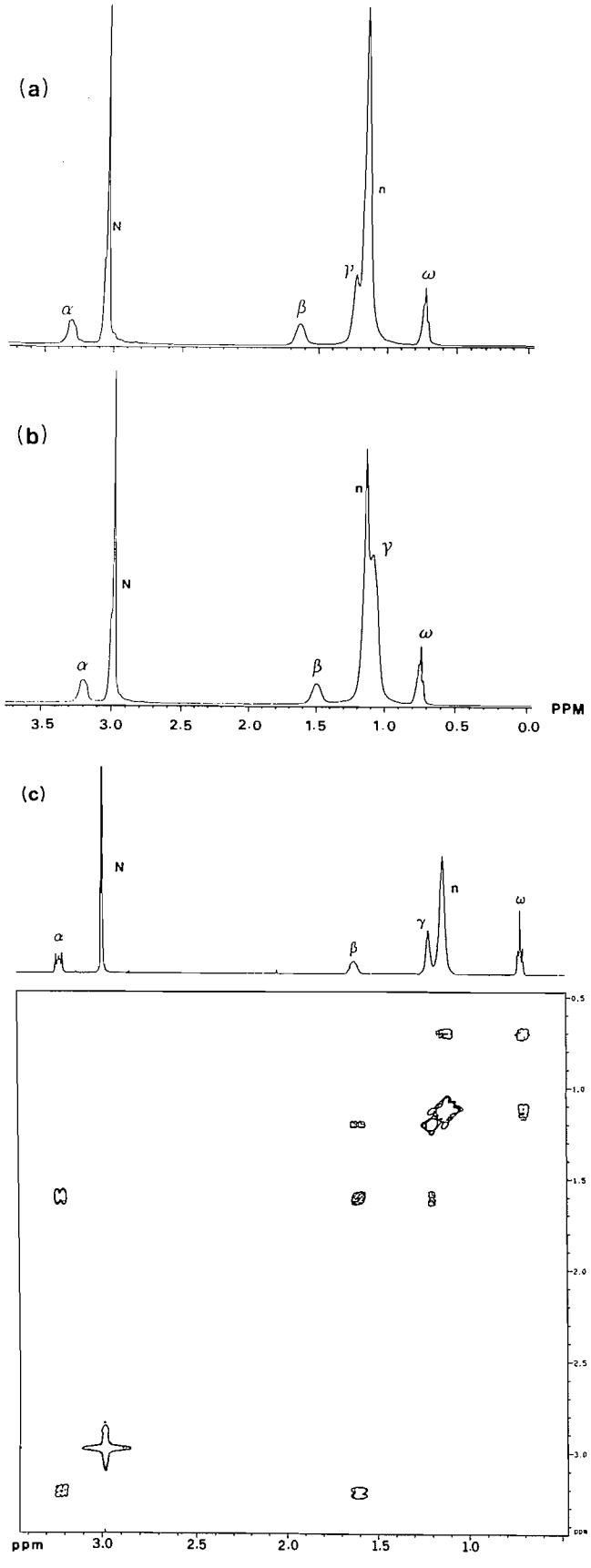


FIG. 3. Proton NMR spectra of (a) 0.050 *m* HTAB (360 MHz); (b) 0.050 *m* HTAB/0.010 *m* naphthalene (360 MHz); and (c) COSY spectrum of 0.050 *m* DTAB (500 MHz).

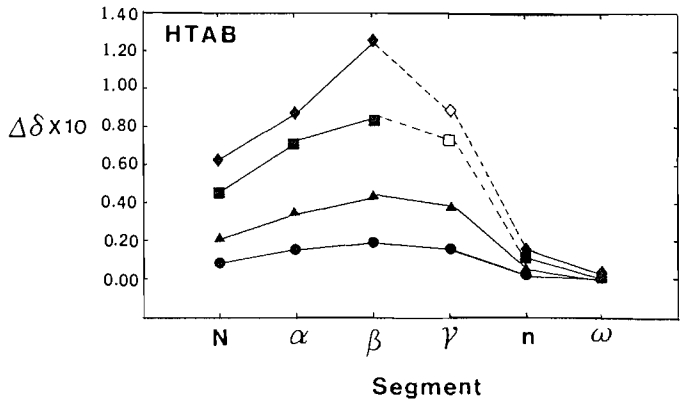


FIG. 4. Changes in proton chemical shifts (in ppm) of HTAB upon addition of benzene. $\Delta\delta = \delta$ (in HTAB) $- \delta$ (in HTAB/benzene). HTAB concentration 0.050 *m*; benzene: ● 0.005 *m*, ▲ 0.010 *m*, ■ 0.020 *m*, and ◆ 0.030 *m*. □ and ◇ denote the estimated values with errors ±0.02 ppm.

near the surface of HTAB micelles, but solubilized in the interior of the SDS micelles. However, our NMR results contradict the conclusion that benzene is solubilized in the core of the cationic DTAB micelles, drawn recently from UV spectrometry measurements (56).

^1H paramagnetic relaxation

The locations of both saturated and unsaturated hydrocarbons in micelles can be determined by comparing the ^1H NMR paramagnetic relaxation enhancement of the hydrocarbons induced by Mn^{2+} ions on the micellar surface with those of surfactant alkyl chain segments. As stated in the theory section, the relaxation enhancement is proportional to the inverse sixth power of the distance between the paramagnetic centre and the nucleus. If the hydrocarbon is located near the micellar surface, the relaxation enhancement of the hydrocarbon should be similar to that of the α-CH_2 group, while if it is located in the micellar interior, its relaxation enhancement should be similar to that of the ω-CH_3 group.

The ^1H spin-lattice relaxation enhancements of different SDS segments and of naphthalene in a SDS (0.050 *m*)/naphthalene (0.010 *m*)/Mn^{2+} (0.0002 *m*) system are given in Fig. 8. These enhancements are expressed in the ratio of R_{1p} of the protons of interest to those on the micellar surface, i.e., the α-CH_2 protons. Figure 8 indicates that the value of spin-lattice relaxation enhancement of naphthalene is between those of surfactant segments β-CH_2 and $(CH_2)_n$. The spin-lattice relaxation enhancements of different SDS segments and the *tert*-butyl group of *tert*-butylcyclohexane in SDS (0.050 *m*)/*tert*-butylcyclohexane (0.005 *m*)/Mn^{2+} (0.0002 *m*) system are presented in Fig. 9. The relaxation enhancement of the *tert*-butylcyclohexane is smaller than that of ω-CH_3.

The relaxation enhancement on the naphthalene can be easily understood. If the naphthalene molecules are evenly distributed in the SDS micelle, statistically most of them would be solubilized near the surface of the spherical micelles (57). On the other hand, it is surprising to find that saturated hydrocarbon *tert*-butylcyclohexane is located in the centre of SDS micelles. This finding may explain the fact that rotational correlation times for saturated hydrocarbons in SDS are much shorter than those of unsaturated hydrocarbons (Table 6), since the local motion increases from α-CH_2 to ω-CH_3 in the SDS hydrocarbon chain (58). However, it should be noted that the internal

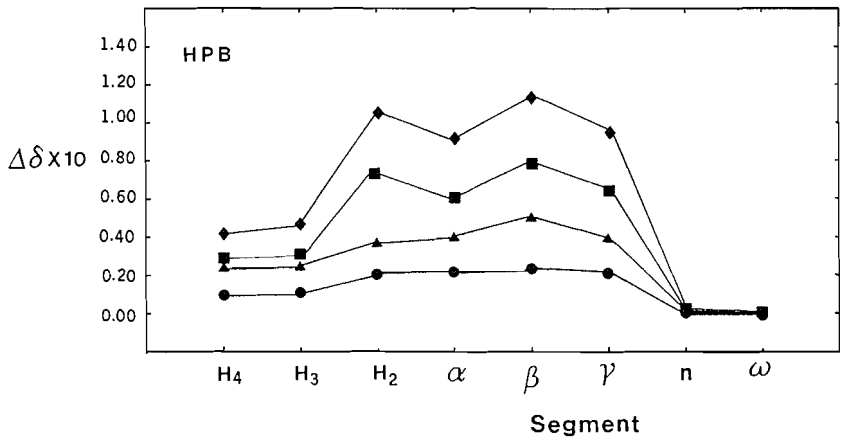


FIG. 5. Changes in proton chemical shifts (in ppm) of HPB upon addition of benzene. $\Delta\delta$ = δ (in HPB) − δ (in HPB/benzene). HPB concentration 0.050 *m*; benzene: ● 0.005 *m*, ▲ 0.010 *m*, ■ 0.020 *m*, and ◆ 0.030 *m*.

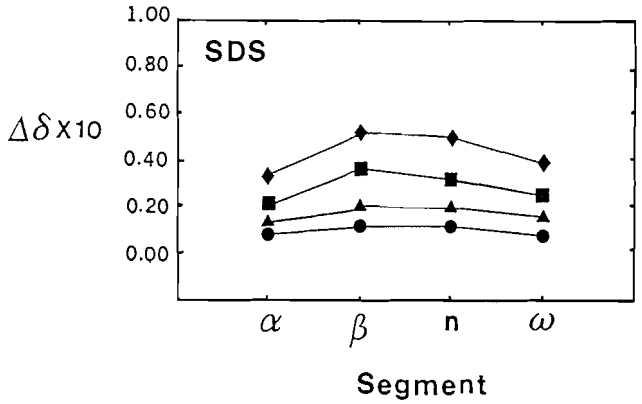


FIG. 6. Changes in proton chemical shifts (in ppm) of SDS upon addition of benzene. $\Delta\delta$ = δ (in SDS) − δ (in SDS/benzene). SDS concentration 0.050 *m*; benzene: ● 0.005 *m*, ▲ 0.010 *m*, ■ 0.020 *m*, and ◆ 0.030 *m*.

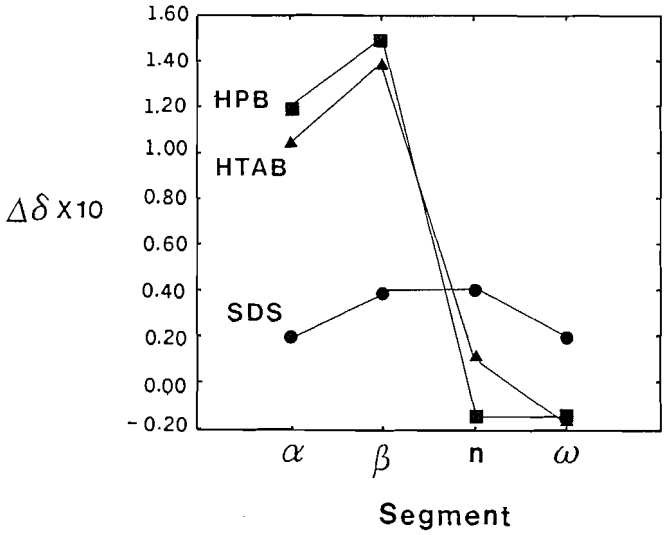


FIG. 7. Changes in proton chemical shifts (in ppm) of (▲) HTAB, (■) HPB, and (●) SDS upon addition of naphthalene $\Delta\delta$ = δ (in surfactant micelle) − δ (in surfactant micelle + naphthalene). Surfactant concentration 0.050 *m*, naphthalene 0.010 *m*.

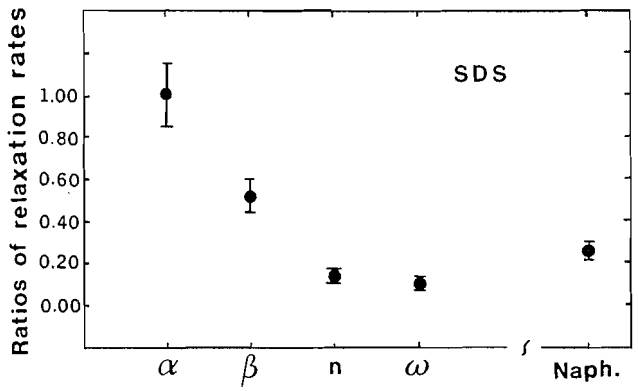


FIG. 8. Ratios of paramagnetic relaxation, R_{1p}/R^{α}_{1p}, in a 0.0002 *m* Mn^{2+}/0.010 *m* naphthalene/0.050 *m* SDS system.

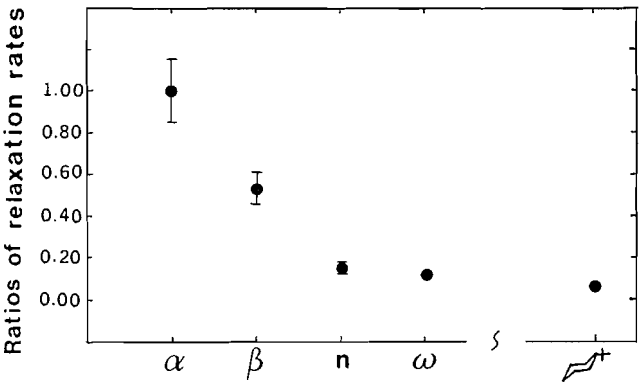


FIG. 9. Ratios of paramagnetic relaxation, R_{1p}/R^{α}_{1p}, in a 0.0002 *m* Mn^{2+}/0.005 *m* *tert*-butylcyclohexane/0.050 *m* SDS system.

motions of the hydrocarbon and the surfactant alkyl chain segment can also contribute to the paramagnetic relaxation enhancement (59), which may complicate the interpretation.

Summary

The solubilization of a number of hydrocarbons, saturated and unsaturated, in cationic *n*-alkyltrimethylammonium bromide, *n*-alkylpyridinium halide, and anionic SDS micelles was investigated by means of ^2H NMR relaxation, aromatic ring current-induced ^1H NMR shifts, and ^1H paramagnetic relaxa-

Can. J. Chem. Downloaded from www.nrcresearchpress.com by 198.100.157.202 on 09/07/12
For personal use only.

tion enhancement. For saturated hydrocarbons in all these micelles and for unsaturated hydrocarbons in SDS micelles, ^2H T_1 and T_2 values are equal within experimental error and independent of field strength, indicating insignificant local order parameters in these systems. Relaxation data of naphthalene and benzene in HTAB micelles were interpreted using both two-step and single-step models. The correlation times for fast motion obtained with the two-step model agree very well with the correlation times obtained with the single-step model using the data obtained at 55.43 MHz.

Rotational correlation times for saturated hydrocarbons (cyclohexane or cyclododecane) in all these micelles are close to those in *n*-hexadecane. The micellar viscosity at the sites where saturated hydrocarbons are solubilized can be estimated to be approximately equal to or slightly higher than the viscosity of *n*-hexadecane (3.34 cP). The rotational correlation times for unsaturated hydrocarbons (benzene, naphthalene, acenaphthalene, or triphenylene) in cationic surfactant micelles are significantly longer than those in *n*-hexadecane, which can be attributed to the fact that the unsaturated hydrocarbons are solubilized near the headgroups of the cationic surfactants.

The solubilization sites of benzene and naphthalene in HTAB, HPB, and SDS were further characterized by monitoring the aromatic ring current-induced ^1H chemical shifts. The results demonstrate that the unsaturated hydrocarbons are solubilized near the surface of cationic HTAB and HPB micelles, but are distributed evenly in anionic SDS micelles. Information concerning the location of naphthalene and *tert*-butylcyclohexane in anionic SDS micelles is also obtained from the ^1H spin-lattice relaxation enhancement induced by Mn^{2+} on the micellar surface. These data also indicate that naphthalene is solubilized uniformly throughout the SDS micelles, while *tert*-butylcyclohexane is primarily located in the centre of the micelles.

From the results presented it is clear why different probes give different micellar microviscosities. Aromatic hydrocarbons, including many fluorescence probes, generally indicate higher micellar microviscosities (51, 60), since they are primarily solubilized near the micellar surface (cationic surfactants), or evenly distributed throughout the micelle (anionic surfactants). On the other hand, saturated hydrocarbons are located in the micellar interior, hence probing the low microviscosity region.

Can. J. Chem. Downloaded from www.nrcresearchpress.com by 198.100.157.202 on 09/07/12
For personal use only.

Acknowledgements

We wish to thank Imperial Oil Limited (R.E.W.) and the Natural Sciences and Engineering Research Council of Canada for financial support. Also, we wish to thank Dr. O. Söderman, Dr. B. J. Forrest, and Dr. R. Stark for helpful comments, Dr. J. Walter for making available spectrometer time on the Varian XL-100 and the Bruker AMX 500 at the Atlantic Research Laboratory, National Research Council of Canada, and Daniel Allard for assistance in solution preparation. Finally, we appreciate the valuable comments of both referees.

1. P. MUKERJEE. *In* Solution chemistry of surfactants. Vol. 1. *Edited by* K. L. Mittal. Plenum Press, New York, NY. 1979. p. 153.
2. P. H. ELWORTHY, A. T. FLORENCE, and C. B. MACFARLANE. Solubilization by surface-active agents. Chapman and Hall Ltd., London. 1968.
3. D. R. KARSA (*Editor*). Industrial applications of surfactants. The Royal Society of Chemistry, Whitstable Litho Ltd., Kent. 1987.
4. D. MYERS. Surfactant science and technology. VCH, New York, NY. 1988.
5. J. H. FENDLER. Membrane mimetic chemistry. John Wiley & Sons, New York, NY. 1982.
6. Z. GAO, R. E. WASYLISHEN, and J. C. T. KWAK. J. Phys. Chem. **93**, 2190 (1989).
7. P. STILBS. J. Colloid Interface Sci. **80**, 608 (1981).
8. C. CHACHATY. Prog. Nucl. Magn. Reson. Spectrosc. **19**, 183 (1987).
9. H. WALDERHAUG, O. SÖDERMAN, and P. STILBS. J. Phys. Chem. **88**, 1655 (1984).
10. O. SÖDERMAN, G. CARLSTRÖM, U. OLSSON, and T. C. WONG. J. Chem. Soc. Faraday Trans. 1, **84**, 4475 (1988).
11. A. BELMAJDOUB, K. ELBAYED, J. BRONDEAU, D. CANET, I. RICO, and A. LATTES. J. Phys. Chem. **92**, 3569 (1988).
12. H. WENNERSTRÖM, B. LINDMAN, O. SÖDERMAN, T. DRAKENBERG, and J. B. ROSENHOLM. J. Am. Chem. Soc. **101**, 6860 (1979).
13. J. C. ERIKSSON, U. HENRIKSSON, T. KLASON, and L. ÖDBERG. *In* Solution behavior of surfactants. Vol. 2. *Edited by* K. L. Mittal and E. J. Fendler. Plenum Press, New York, NY. 1982. p. 907.
14. R. E. STARK, M. L. KASAKEVICH, and J. W. GRANGER. J. Phys. Chem. **86**, 335 (1982).
15. P. STILBS, H. WALDERHAUG, and B. LINDMAN. J. Phys. Chem. **87**, 4762 (1983).
16. D. CANET, T. TURKI, A. BELMAJDOUB, and B. DITER. J. Phys. Chem. **92**, 1219 (1988).
17. R. T. BOERÉ and R. G. KIDD. Annu. Rep. NMR Spectrosc. **13**, 319 (1982).
18. C. M. HU and R. ZWANZIG. J. Chem. Phys. **60**, 4354 (1974).
19. M. ALMGREN and S. SWARUP. J. Phys. Chem. **86**, 4212 (1982).
20. M. SHINITZKY, A.-C. DIANOUX, C. GITLER, and G. WEBER. Biochemistry. **10**, 2106 (1971).
21. L. A. SINGER. *In* Solution behavior of surfactants. Vol. 1. *Edited by* K. L. Mittal and E. J. Fendler. Plenum Press, New York, NY. 1982. p. 73.
22. M. CHEN, M. GRÄTZEL, and J. K. THOMAS. J. Am. Chem. Soc. **97**, 2052 (1975).
23. J. C. ERIKSSON and G. GILLBERG. Acta Chem. Scand. **20**, 2019 (1966).
24. J. ULMIUS, B. LINDMAN, G. LINDBLOM, and T. DRAKENBERG. J. Colloid Interface Sci. **65**, 88 (1978).
25. K. N. GANESH, P. MITRA, and D. BALASUBRAMANIAN. J. Phys. Chem. **86**, 4291 (1982).
26. C. A. BUNTON and C. P. COWELL. J. Colloid Interface Sci. **122**, 154 (1988).
27. T. HOSHINO and Y. IMAMURA. Bull. Chem. Soc. Jpn. **63**, 502 (1990).
28. P. STILBS. J. Colloid Interface Sci. **94**, 463 (1983).
29. K. K. FOX, I. D. ROBB, and R. SMITH. J. Chem. Soc. Faraday Trans. 1, **68**, 445 (1972).
30. N. R. JAGANNATHAN, K. VENKATESWARAN, F. G. HERRING, G. N. PATEY, and D. C. WALKER. J. Phys. Chem. **91**, 4553 (1987).
31. A. ABRAGAM. The principles of nuclear magnetism. Clarendon Press, Oxford. 1961. p. 313.
32. U. HENRIKSSON, T. KLASON, L. ÖDBERG, and J. C. ERIKSSON. Chem. Phys. Lett. **52**, 554 (1977).
33. T. J. SWIFT and R. E. CONNICK. J. Chem. Phys. **37**, 307 (1962).
34. Z. LUZ and S. MEIBOOM. J. Chem. Phys. **40**, 2686 (1964).
35. I. SOLOMON and N. BLOEMBERGEN. J. Chem. Phys. **25**, 261 (1956).
36. N. BLOEMBERGEN and L. O. MORGAN. J. Chem. Phys. **34**, 842 (1961).
37. J. KOWALEWSKI, L. NORDENSKIÖLD, N. BENETIS, and P.-O. WESTLUND. Prog. Nucl. Magn. Reson. Spectrosc. **17**, 141 (1985).
38. H. STERNLICHT, R. G. SHULMAN, and E. W. ANDERSON. J. Chem. Phys. **43**, 3123 (1965).
39. Y. CHEVALIER and C. CHACHATY. J. Am. Chem. Soc. **107**, 1102 (1985).

40. G. A. KNIGHT and B. D. SHAW. J. Chem. Soc. 682 (1938).
41. A. MALOVIKOVA, K. HAYAKAWA, and J. C. T. KWAK. *In* Relation between structure and performance of surfactants. *Edited by* M. J. Rosen. ACS Symp. Ser. **253**, 225 (1985).
42. K. HAYAKAWA and J. C. T. KWAK. J. Phys. Chem. **86**, 3866 (1982).
43. J. D. CUTNELL, H. E. BLEICH, and J. A. GLASEL. J. Magn. Reson. **21**, 43 (1976).
44. R. FREEMAN, S. P. KEMPSELL, and M. H. LEVITT. J. Magn. Reson. **38**, 453 (1980).
45. G. C. LEVY and I. R. PEAT. J. Magn. Reson. **18**, 500 (1975).
46. S. MEIBOOM and D. GILL. Rev. Sci. Instr. **29**, 688 (1958).
47. R. G. BARNES and J. W. BLOOM. J. Chem. Phys. **57**, 3082 (1972).
48. J. C. ROWELL, W. D. PHILLIPS, L. R. MELBY, and M. PANAR. J. Chem. Phys. **43**, 3442 (1965).
49. C. BREVARD and J. P. KINTZINGER. *In* NMR and the periodic table. *Edited by* R. K. Harris and B. E. Mann. Academic Press, New York, NY. 1978. p. 107.
50. O. SÖDERMAN, U. HENRIKSSON, and U. OLSSON. J. Phys. Chem. **91**, 116 (1987).
51. R. ZANA. *In* Surfactant solutions, new method of investigation. Surfactant Science Series, Vol. 22. *Edited by* R. Zana. Marcel Dekker, New York, NY. 1987. p. 241.
52. P. STILBS. J. Colloid Interface Sci. **87**, 385 (1982).
53. R. C. WEAST (*Editor*). CRC handbook of chemistry and physics. 64th ed. CRC Press Inc., Boca Raton, FL. 1983. p. F-41.
54. K. A. ZACHARIASSE, N. V. PHUC, and B. KOZANKIEWICZ. J. Phys. Chem. **85**, 2676 (1981).
55. E. J. FENDLER, C. L. DAY, and J. H. FENDLER. J. Phys. Chem. **76**, 1460 (1972).
56. K. KANDORI, R. J. MCGREEVY, R. S. SCHECHTER. J. Phys. Chem. **93**, 1506 (1989).
57. J. A. MARQUSSE and K. A. DILL. J. Chem. Phys. **85**, 434 (1986).
58. M. MONDUZZI, A. CEGLIE, B. LINDMAN, and O. SÖDERMAN. J. Colloid Interface Sci. **136**, 113 (1990).
59. P. L. WANG, J. H. LEE, S. M. HUANG, and L. P. HWANG. J. Magn. Reson. **73**, 277 (1987).
60. F. GRIESER and C. J. DRUMMOND. J. Phys. Chem. **92**, 5580 (1988).

Can. J. Chem. Downloaded from www.nrcresearchpress.com by 198.100.157.202 on 09/07/12
For personal use only.

A nitrogen-15 nuclear magnetic resonance study of the tetracycline antibiotics

RONALD D. CURTIS AND RODERICK E. WASYLISHEN[1]
Department of Chemistry, Dalhousie University, Halifax, N.S., Canada B3H 4J3

Received September 4, 1990

RONALD D. CURTIS and RODERICK E. WASYLISHEN. Can. J. Chem. **69**, 834 (1991).

Natural abundance ^{15}N NMR has been used to study several tetracycline antibiotics in the solid state and in solution. In the solid state, the ^{15}N chemical shifts of the tetracycline free bases are sensitive to the site of protonation in the "A" ring. A high frequency shift of 14 ppm is observed for the keto form of oxytetracycline (N protonated) relative to the enol form of oxytetracycline (O protonated). Comparison of ^{15}N chemical shifts in the solid and solution states indicates for the first time that the structural integrity (site of protonation and hence conformation) of the tetracyclines is maintained in $(CD_3)_2SO$ solutions. In addition, the solid state ^{15}N CP/MAS NMR spectra are sensitive to subtle conformational changes of the "A" ring amide substituent.

Key words: antibiotics, tetracyclines, ^{15}N NMR, molecular structure.

RONALD D. CURTIS et RODERICK E. WASYLISHEN. Can. J. Chem. **69**, 834 (1991).

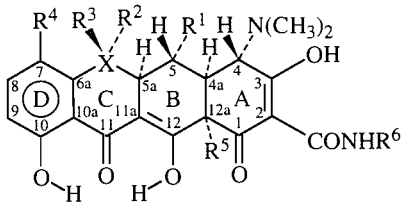
On a utilisé a RMN du ^{15}N en abondance naturelle pour étudier plusieurs tétracycline antibiotiques, à l'état solidé et en solution. À l'état solide, les déplacements chimiques du ^{15}N des tétracyclines sous la forme de bases libres sont sensibles aux sites de protonation dans le cycle « A ». On observe un déplacement de 14 ppm vers les hautes fréquences pour le forme cétonique de l'oxytétracycline (N protonée) par rapport à la forme énolique de l'oxytétracycline (O protonée). Une comparaison des déplacements chimiques du ^{15}N à l'état solidé et en solution indique pour la première fois que l'intégrité structurale (site de protonation ainsi que conformation) des tétracyclines est maintenue en solutions dans le $(CD_3)_2SO$. De plus, les spectres RMN du ^{15}N CP/MAS sont sensibles à des changements subtils de conformation du substituent amide du cycle « A ».

Mots clés : antibiotiques, tétracyclines, RMN du ^{15}N, structure moléculaire.

[Traduit par la rédaction]

Introduction

The tetracyclines, **1**, are an important family of antibiotics that are widely used in human and veterinary medicine (1–4). X-ray crystallographic studies of several tetracyclines have revealed that subtle changes in molecular structure can lead to dramatic changes in the overall conformation of the tetracycline (5–16). For example, X-ray diffraction results have indicated that the "A" ring of anhydrous oxytetracycline exists in a neutral "enol" form, **2**, whereas the dihydrate of oxytetracycline exists exclusively in the "keto" form, **3** (6). The principal differences between these two tautomers are the sites of protonation of the A ring, the conformation about the C_{4a}—C_{12a} bond axis, and the relative extent of intermolecular and intramolecular hydrogen bonding. OTC° has been shown to exist with a hydrogen atom bonded to O-3 and the *N,N*-dimethylamino nitrogen not protonated as in **2**, whereas OTC± is present as a zwitterion in the solid state with a hydrogen atom bonded to the *N,N*-dimethylamino group as in **3** (6). Conformational differences between OTC° and OTC± are primarily associated with the orientation of the A ring relative to the approximately planar B, C, and D rings. For OTC°, the A ring is flipped up and oriented at approximately 110° with respect to the B, C, and D rings. In this form, the $N(CH_3)_2$ group is directed above the B, C, and D plane and the dihedral angle, H—C_4— C_{4a}—H, is approxi-

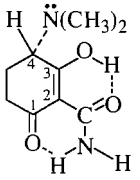


1

Generic name	X	R^1	R^2	R^3	R^4	R^5	R^6	Abbreviation
Tetracycline	C	H	CH_3	OH	H	OH	H	TC
Oxytetracycline	C	OH	CH_3	OH	H	OH	H	OTC
Chlortetracycline	C	H	CH_3	OH	Cl	OH	H	CTC
Demeclocycline	C	H	H	OH	Cl	OH	H	DEMTC
Doxycycline	C	OH	CH_3	H	H	OH	H	DOXYTC
Minocycline	C	H	H	H	$N(CH_3)_2$	OH	H	MINTC
Rolitetracycline	C	H	CH_3	OH	H	OH	$CH_2NC_4H_8$	ROLITC
Thiatetracycline	S	H	—	—	H	OH	H	6-STC
Diacetyloxy-tetracycline	C	$OCOCH_3$	CH_3	OH	H	$OCOCH_3$	H	DIAOTC

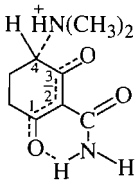
[1]Author to whom correspondence may be addressed.

Can. J. Chem. Downloaded from www.nrcresearchpress.com by 198.100.157.202 on 09/07/12
For personal use only.



OTC°

2

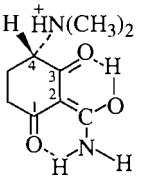


OTC±

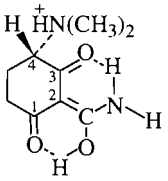
3

mately 170° (6). On the other hand, OTC± adopts a conformation such that the A ring is oriented approximately coplanar with the B, C, and D rings and the $^{+}N(CH_3)_2H$ group is situated below this plane. The dihedral angle, H—C_4—C_{4a}—H, in this case is approximately 74° (6). It has been postulated that both structural forms are important for the in vitro mechanism of activity (6). More specifically, the anhydrous free base, **2**, is most likely the predominant form found in hydrophobic regions such as the alkyl chains of membranes, whereas the hydrated tautomeric form, **3**, is the principal species present in hydrophilic regions such as blood plasma (6, 17).

The hydrochloride salts of most tetracyclines have the same basic overall conformation; however, the orientation of the amide substituent on the A ring can be either as in **4** or in **5** (10–15). The hydrochloride salt of DOXYTC crystallizes from aqueous ethanol with two crystallographically unique molecules per unit cell (13). One of the two nonequivalent molecules in DOXYTC·HCl exists with the A ring in conformation **4** while the other is in conformation **5** (13). The only other known example of this phenomenon for the tetracycline family is the observation of two different amide conformations for single crystals of OTC·HBr (15).



4



5

A previous investigation of several solid tetracyclines in this laboratory demonstrated the utility of high-resolution solid state ^{13}C CP/MAS NMR for distinguishing the enol and keto forms (**2** vs. **3**) of the tetracycline free bases (18). This method relied on the nature of the line shapes observed in ^{13}C CP/MAS NMR spectra for the carbon atoms that are directly bonded to a quadrupolar nitrogen nucleus (19, 20). There have been several ^{1}H and ^{13}C NMR studies of the tetracyclines in solution and these have been reviewed by Casy and co-workers (21). However, to date, no ^{15}N NMR data have been reported for the tetracycline antibiotics in either the solid or solution states. Given the inherent sensitivity of ^{15}N chemical shifts to changes in the local electronic environment (22), it was anticipated that this method would provide a sensitive probe of the site of protonation of the A ring of the tetracyclines. To this end, the solid tetracycline antibiotics indicated in **1** were examined by natural abundance ^{15}N CP/MAS solid state NMR. To determine if the structural integrity of the tetracyclines is maintained in solution, ^{15}N NMR spectra of several derivatives were investigated in $(CD_3)_2SO$ and pyridine-d_5 solutions for comparison with the results from the solid state.

Experimental

The hydrochloride salts of OTC, CTC, DEMTC, DOXYTC, and MINTC and the free base hydrates of TC and OTC were purchased from the Sigma Chemical Company. The hydrochloride salt of TC was purchased from the Aldrich Chemical Company. ROLITC·HCl was supplied by C. Marcotte of the Pharmaceutical Division of Hoechst Company in Montreal. The anhydrous form OTC° was prepared by azeotropic distillation of a toluene solution of OTC± (6). DIAOTC was prepared by the addition of acetic anhydride to a solution of OTC° in anhydrous dioxane (23). The 1:1 tetracycline urea adduct was precipitated from a saturated aqueous solution of urea by the addition of tetracycline hexahydrate (24). A sample of 6-STC·HCl was supplied by R. Kirchlechner of Merck Company in Darmstadt, West Germany. For completeness, additional solid samples of the hydrates of TC and OTC and the hydrochloride salt of DEMTC were all crystallized according to the methods outlined in their respective X-ray studies (5, 6*a*, 14). Purity of the prepared samples (i.e., OTC° and DIAOTC) was checked by the appearance of their respective solid state ^{13}C CP/MAS NMR spectra (18).

Nitrogen-15 CP/MAS NMR spectra of solid samples were recorded on a Bruker MSL-200 spectrometer operating at 20.30 MHz (B_0 = 4.7 T). The tetracycline samples (~500 mg) were ground into fine powder and packed into cylindrical rotors (7 mm o.d.) made from aluminum or zirconium oxide. Proton cross polarization (CP) to the ^{15}N nuclei was performed under the conditions of the Hartmann–Hahn match with ^{15}N and ^{1}H $\pi/2$ pulse widths of 3.5–5 μs and contact times of 3–5 ms. All NMR spectra were acquired with high-power decoupling and magic angle spinning (MAS) rates of 3–5 kHz. For the ^{15}N CP/MAS NMR experiments, approximately 5000 transients were required to obtain a S:N ratio of about 10:1. This was readily obtainable overnight with recycle times of 4–6 s. Prior to Fourier transformation, sensitivity enhancements corresponding to 20 Hz of line broadening were applied to the ^{15}N FIDs. For the dipolar dephasing NMR experiments (25), the decoupler was turned off prior to acquisition for approximately 60–100 μs. Nitrogen-15 CP/MAS NMR spectra are referenced with respect to NH_3(liq.)(293 K) at 0 ppm by setting the ammonium ion signal of doubly isotropically enriched $^{15}NH_4{}^{15}NO_3$ at 23.80 ppm.

Samples for ^{15}N solution state NMR were prepared as saturated solutions in $(CD_3)_2SO$ (ca. 1 M) or pyridine-d_5 just prior to obtaining the NMR spectra. Solution NMR spectra were recorded on a Nicolet-360 NMR spectrometer with ^{1}H and ^{15}N operating frequencies of 361.05 and 36.61 MHz, respectively. With the exception of OTC°, all ^{15}N spectra were acquired using the INEPT pulse sequence (26) with a delay time between ^{1}H $\pi/2$ and π pulses of 2.78 ms and a delay time for refocussing the ^{15}N signals of 2.25 ms. The ^{15}N NMR spectrum of OTC° in $(CD_3)_2SO$ was acquired using bilevel broadband decoupling and a delay of 30 s between acquisition of transients. The ^{15}N NMR spectrum of OTC° in pyridine-d_5 was acquired using a single pulse experiment without proton decoupling and a recycle time of 30 s. The ^{15}N $\pi/2$ pulse length was typically 60–65 μs. Signal averaging on the order of 5000–10 000 transients was employed for all samples. Line broadening of 15 Hz was applied to all FIDs prior to Fourier transformation. Solution ^{15}N NMR spectra were referenced with respect to liquid NH_3 (293 K) at 0 ppm by setting the observed ^{15}N chemical shift of external formamide at 112.3 ppm (27).

Results and discussion

The ^{15}N chemical shifts of several solid tetracycline antibiotics are given in Table 1. Since only two ^{15}N resonance signals were present (in most samples) for these compounds, assignment of the resonances was straightforward. Without exception, the high frequency resonance was assigned to the amide nitrogen.

The ^{15}N CP/MAS NMR spectra provided two distinct methods for distinguishing between the "enol", **2**, and zwitterionic "keto", **3**, tautomeric forms of the tetracycline free bases in the solid state. First, the ^{15}N chemical shift of the *N,N*-di-

Can. J. Chem. Downloaded from www.nrcresearchpress.com by 198.100.157.202 on 09/07/12
For personal use only.

Can. J. Chem. Downloaded from www.nrcresearchpress.com by 198.100.157.202 on 09/07/12
For personal use only.

TABLE 1. Nitrogen-15 chemical shifts of several tetracycline antibiotics. The values in parentheses indicate solution state measurements in $(CD_3)_2SO$

Compound	Nitrogen chemical shifts (δ/ppm)[a]		
	$^{15}N(CH_3)_2$	$CO^{15}NHR$	Other
TC·HCl	44.9 (46.1)	113.0 (111.6)	
TC±	41.8	107.5	
TC·UREA	43.4	107.2	81.9
OTC·HCl	43.5 (44.4)	113.3 (111.5)	
OT·HBr I	41.4	[b]	
II	45.7	111.6	
OTC±	41.6(*b*)	105.6 (108.9)	
OTC°	27.7 (25.3)† (22.3)[c]	109.5 (109.3)† (108.5[c])†	
CTC·HCl	45.3	113.1	
DEMTC·HCl	45.7	111.6	
DOXYTC·HCl I	41.4	105.5	
II	45.3	111.6	
MINTC·HCl	41.9	99.8	49.8
ROLITC·HCl	34.9	113.6	79.9
			74.8
6-STC·HCl	41.7	111.7	
DIAOTC	20.6	104.6	

[a]Estimated error in δ is ±0.5 ppm unless indicated otherwise.
[b]These signals were not observed in the ^{15}N NMR spectrum.
[c]Single pulse experiment in pyridine-d_5. $^1J(^{15}N, ^1H) = 91 \pm 5$ Hz for the A ring amide group.
†Estimated error, ±1.0 ppm.

methylamino nitrogen is expected to be sensitive to its presence in an amine or in an aminium ion. For example, in a solution NMR study of a series of 15 tertiary amines, the average ^{15}N chemical shift of the protonated amine was 12.8 ppm to high frequency (i.e., higher δ) of the free base (28, 29). Comparison of the ^{15}N NMR results for OTC± and OTC° in Table 1 indicates that the chemical shift of OTC± is 13.9 ppm to high frequency of the corresponding value for OTC°. The corresponding ^{15}N CP/MAS NMR spectra are shown in Figs. 1a and 1b for OTC± and OTC°, respectively. It should also be pointed out that the ^{15}N chemical shift of OTC° is similar to that observed for the *N,N*-dimethylamino nitrogen of DIAOTC ($\delta_{iso} = 20.6$ ppm). This is an important observation since it has been concluded from X-ray diffraction experiments that DIAOTC exists exclusively in the "enol" form (9).

The results obtained from the dipolar dephasing NMR experiments (25) on several of the tetracyclines **1**, provided an alternative method for studying the tautomeric state of the "A" ring in the solid state. The CP/MAS ^{15}N NMR spectrum obtained for OTC° using the dipolar dephasing pulse sequence is shown in Fig. 1c. Comparison with Figs. 1a and 1b indicates that there is no ^{15}N NMR signal observed for the amide nitrogen in the NMR spectrum of OTC° acquired with the dipolar dephasing pulse sequences. This is not surprising since this nitrogen is strongly dipolar coupled to the two directly bonded hydrogens; therefore, the corresponding signal dephases rapidly during the time the decoupler is off (25). Of greater significance, the ^{15}N NMR signal corresponding to the *N,N*-dimethylamino nitrogen of OTC° was still present in this NMR spectrum (Fig. 1c). Analogous results were obtained when a dipolar dephasing ^{15}N NMR experiment was performed on a sample of

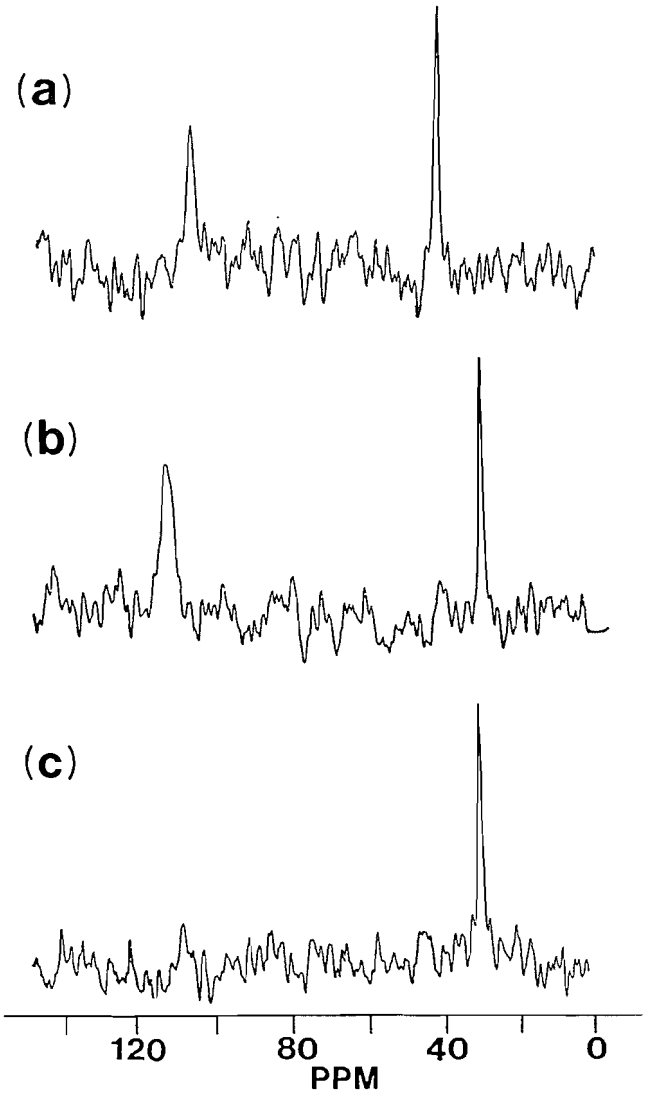


FIG. 1. Nitrogen-15 CP/MAS NMR spectra of solid samples of (a) oxytetracycline dihydrate, OTC±; (b) anhydrous oxytetracycline, OTC°; and (c) anhydrous oxytetracycline, OTC°, acquired with the dipolar dephasing pulse sequence using a delay time before acquisition of 65 μs.

DIAOTC indicating that both OTC° and DIAOTC exist exclusively in the neutral "enol" tautomeric form in the solid state.

The ^{15}N chemical shifts for TC·HCl, OTC·HCl, OTC±, and OTC° in $(CD_3)_2SO$ and pyridine-d_5 solutions are given in parentheses in Table 1. Preliminary ^{15}N solution NMR experiments were performed using the INEPT pulse sequence (26) without proton decoupling on samples of OTC·HCl dissolved in $(CD_3)_2SO$. This solvent was chosen since relatively concentrated solutions of OTC·HCl could be prepared (ca. 1 M) and because previous ^1H NMR experiments indicated that the conformational integrity of OTC·HCl is maintained when dissolved in this solvent (30). It is important to point out that the INEPT experiment is a polarization transfer technique that depends on the presence of a spin–spin coupling (J) between the nuclei involved (26). In this study, polarization transfer occurs from the directly bonded hydrogens to the nitrogen and therefore a $^1J(^{15}N, ^1H)$ coupling is essential for the INEPT NMR experiment to be applied successfully. Since no previous ^{15}N NMR investigations of the tetracyclines have been reported, a value for $^1J(^{15}N, ^1H)$ for the amide and protonated *N,N*-di-

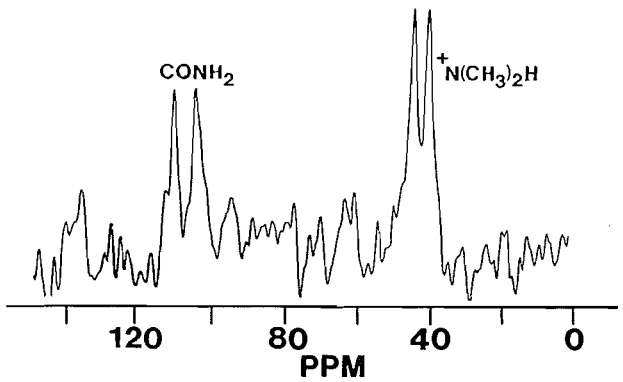


FIG. 2. A nitrogen-15 CP/MAS NMR spectrum of solid doxycycline hydrochloride, DOXYTC · HCl.

methylamino nitrogens was assumed to be similar to that reported for formamide (i.e., approximately 90 Hz) (21). This value for $^1J(^{15}N, ^1H)$ was then used to calculate the spin dephasing delay time ($J/4$) required for performing the INEPT NMR experiment (26). Subsequent acquisition of a ^{15}N NMR spectrum of OTC · HCl in $(CD_3)_2SO$ provided a proton coupled ^{15}N NMR spectrum. In this NMR spectrum, the amide resonance signal was a 1:0:−1 triplet with a $^1J(^{15}N, ^1H)$ of 95 ± 5 Hz whereas the low frequency signal for the *N,N*-dimethylamino resonance was observed as a 1:−1 doublet with a $^1J(^{15}N, ^1H)$ of 62 ± 5 Hz. The average of these two values was then used to calculate the spin dephasing delay for further ^{15}N NMR experiments performed with the INEPT sequence and proton decoupling.

Inspection of Table 1 indicates that the observed ^{15}N chemical shifts of the tetracyclines in solution are similar to the corresponding chemical shifts observed in the solid state. In addition, both TC · HCl and OTC · HCl exhibited a signal due to the *N,N*-dimethylamino nitrogen in their respective solution ^{15}N NMR spectrum. Since a resolvable spin–spin coupling between hydrogen and nitrogen is essential for the INEPT experiment to work (26), it can be concluded that TC · HCl and OTC · HCl exist exclusively with a protonated *N,N*-dimethylamino nitrogen in $(CD_3)_2SO$. More importantly, the low frequency resonance signal was not observed when a ^{15}N solution NMR spectrum of OTC± was acquired under experimental conditions identical to those for the hydrochloride salts. Based on this observation, it can be concluded that the *N,N*-dimethylamino nitrogen of OTC± in $(CD_3)_2SO$ does not have a resolvable $^1J(^{15}N, ^1H)$. This situation could result if the nitrogen were not protonated or if it were involved in rapid proton exchange. The ^{15}N NMR spectra of OTC° dissolved in $(CD_3)_2SO$ and pyridine-d_5 solutions were acquired with and without proton decoupling, respectively. For both samples, the ^{15}N NMR signal observed for the *N,N*-dimethylamino nitrogen was a single peak ($\nu_{1/2} \leq 6$ Hz).The observed ^{15}N chemical shifts for the *N,N*-dimethylamino nitrogen in $(CD_3)_2SO$ and pyridine-d_5, 25.3 ppm and 22.3 ppm, are in reasonable agreement with the corresponding value determined for OTC° in the solid state, 27.7 ppm. Thus, based on the similarity of ^{15}N chemical shifts in the solid and solution states and on the results from the INEPT experiments, it can be concluded that the structural integrity of the two tautomeric forms, **2** and **3**, is maintained in $(CD_3)_2SO$ and pyridine-d_5 solutions. In addition, the hydrochloride salts of TC and OTC also maintain their structural forms (i.e., with the *N,N*-dimethylamino nitrogen protonated) when dissolved in $(CD_3)_2SO$.

The ^{15}N CP/MAS NMR spectrum for a solid sample of DOXYTC · HCl is shown in Fig. 2. Two independent sets of isotropic resonances are apparent for the amide and protonated *N,N*-dimethylamino nitrogen of this sample. The observation of two sets of isotropic ^{15}N resonances is consistent with the reported X-ray diffraction results for this compound (13). The chemical shift difference observed for the dimethylamino nitrogen resonances was approximately 4 ppm, whereas for the amide nitrogen signals the chemical shift difference was approximately 6 ppm. For OTC · HBr, which also exists with two crystallographic nonequivalent forms (15), the ^{15}N chemical shifts of the *N,N*-dimethylamino nitrogens were also different by approximately 4 ppm. For this sample, the amide resonance signals were significantly broadened such that the ^{15}N chemical shifts could not be resolved. Several hydrochloride salts of the tetracycline family of antibiotics have been shown to exist in the solid state with only a single conformation of the amide substituent. For example, TC · HCl and OTC · HCl have been shown to exist in the solid state with the amide nitrogen oriented *cis* to the oxygen at C-1, **4**, (10, 11). On the other hand, DEMTC · HCl has been shown to exist in crystalline form with the opposite conformation of the amide substituent (i.e., amide nitrogen *trans* to O-1 as in **5**) (14). Although the ^{15}N chemical shifts of solid TC · HCl and OTC · HCl are approximately 1.4 ppm and 1.7 ppm to high frequency of the corresponding value for DEMTC · HCl (Table 1), the small range of ^{15}N chemical shifts for the amide nitrogen prevents any definitive assignment of the amide conformations in these systems.

Several other points regarding the solid state ^{15}N CP/MAS NMR spectra should be mentioned. The ^{15}N signal observed at 81.9 ppm for TC · UREA provides definitive evidence for the inclusion of the urea molecule in the crystalline solid. This value is similar to the ^{15}N chemical shift determined for a saturated solution of urea in H_2O/ethanol, 76 ppm (31). For MINTC · HCl, an additional resonance signal was observed at 48.9 ppm. This signal was assigned to the *N,N*-dimethylamino nitrogen attached at the C-7 position of the aromatic D ring. When a dipolar dephasing CP/MAS NMR spectrum of this compound was obtained, neither *N,N*-dimethylamino nitrogen exhibited a ^{15}N signal. This provided definitive evidence that both nitrogens are protonated in the solid state. Finally, the ^{15}N CP/MAS NMR spectrum of solid ROLITC · HCl consisted of single peaks for the *N,N*-dimethylamino and the amide nitrogens; however, a doublet (peak separation ~5 ppm) was observed for the nitrogen of the pyrrolidine ring. We have no explanation for this observation at this time.

Conclusions

Natural abundance ^{15}N CP/MAS NMR has proven to be a valuable method for studying the structural forms of the tetracycline free bases in the solid state. The inherent sensitivity of the ^{15}N chemical shifts to *N*-protonation and the conclusive evidence obtained with the dipolar dephasing experiments provide an even more sensitive probe of the structure of the "A" ring than previous ^{13}C CP/MAS NMR experiments (18). In addition, comparison of solid state ^{15}N chemical shifts with corresponding values in $(CD_3)_2SO$ and pyridine-d_5 solutions provides the first definitive evidence that the structural integrity of the tetracyclines is maintained in solution.

Acknowledgements

We wish to acknowledge the financial support of the Natural Sciences and Engineering Research Council of Canada (NSERC)

Can. J. Chem. Downloaded from www.nrcresearchpress.com by 198.100.157.202 on 09/07/12
For personal use only.

in the form of equipment and operating grants (R.E.W) and a postgraduate scholarship (R.D.C.). R.D.C. thanks Dalhousie University for a Killam postgraduate fellowship. We wish to thank Dr. M. McKinnon for his help in acquiring several preliminary CP/MAS NMR spectra. Dr. R. Kirchlechner of Merck Company in Darmstadt, West Germany, is acknowledged for sending a sample of thiatetracycline hydrochloride. We are grateful to C. Marcotte at Hoechst Company in Montreal for a sample of rolitetracycline hydrochloride. The technical assistance of Mr. Brian Millier and Mr. Stan Woodman in maintaining the Bruker MSL-200 is greatly appreciated. Finally, the comments of the referees are appreciated.

1. (*a*) S. C. STINSON. Chem. Eng. News, **64**, 33 (1986); (*b*) Chem. Eng. News, **64**, 51 (1987).
2. W. DÜRCKHEIMER. Angew. Chem. Int. Ed. Engl. **14**, 721 (1975).
3. J. J. HLAVKA and J. H. BOOTHE (*Editors*). The tetracyclines. Springer-Verlag, Heidelberg. 1985.
4. R. B. MARTIN. *In* Metal ions in biological systems. Vol. 19. *Edited by* H. Sigel. Marcel Dekker, New York. p. 19.
5. M. R. CAIRA, L. R. NASSIMBENI, and J. C. RUSSELL. Acta Crystallogr. Sect. B: Struct. Crystallogr. Cryst. Chem. **B33**, 1171 (1977).
6. (*a*) J. J. STEZOWSKI. J. Am. Chem. Soc. **98**, 6012 (1976); (*b*) R. Prewo and J. J. STEZOWSKI. J. Am. Chem. Soc. **99**, 1117 (1977).
7. G. J. PALENIK and M. MATHEW. J. Am. Chem. Soc. **100**, 4464 (1978).
8. (*a*) R. PREWO, J. J. STEZOWSKI, and R. KIRCHLECHNER. J. Am. Chem. Soc. **102**, 7021 (1980); (*b*) R. PREWO and J. J. STEZOWSKI. Tetrahedron Lett. **21**, 251 (1980).
9. R. B. VON DREELE and R. E. HUGHES. J. Am. Chem. Soc. **93**, 7290 (1971).
10. K. KAMIYA, M. ASAI, Y. WADA, and M. NISHIKAWA. Experientia, **27**, 363 (1971).
11. (*a*) Y. Takeuchi and M. J. BUERGER. Proc. Natl. Acad. Sci. U.S.A. **46**, 1366 (1960); (*b*) H. CID-DRESDNER. Z. Kristallogr. Kristallogeom. Kristallphys. Kristallchem. **121**, 170 (1965).
12. J. DONOHUE, J. D. DUNITZ, K. N. TRUEBLOOD, and M. S. WEBSTER. J. Am. Chem. Soc. **85**, 851 (1963).
13. J. J. STEZOWSKI. J. Am. Chem. Soc. **99**, 1122 (1977).
14. (*a*) G. J. PALENIK and M. MATHEW. Acta Crystallogr. Sect. A: Cryst. Phys. Diffr. Theor. Gen. Crystallogr. **A28**, S47 (1972); (*b*) G. J. PALENIK, M. MATHEW, and R. RESTINO. J. Am. Chem. Soc. **100**, 4458 (1978).
15. K. H. JOGUN and J. J. STEZOWSKI. Cryst. Struct. Commun. **5**, 381 (1976).
16. M. J. MARTELL and J. H. BOOTHE. J. Med. Chem. **10**, 44 (1967).
17. J. J. STEZOWSKI. Proceedings of the symposium on steric effects in biomolecules. Eger, Hungary. 1981, pp. 3–13.
18. S. MOOIBROEK and R. E. WASYLISHEN. Can. J. Chem. **65**, 357 (1987).
19. (*a*) J. G. HEXEM, M. H. FREY, and S. J. OPELLA. J. Am. Chem. Soc. **103**, 224 (1981); (*b*) S. J. OPELLA, J. G. HEXEM, M. H. FREY, and T. A. CROSS. Philos. Trans. R. Soc. London, A:**299**, 665 (1981); (*c*) J. G. HEXEM, M. H. FREY, and S. J. OPELLA. J. Chem. Phys. **77**, 3847 (1982); (*d*) J. G. HEXEM. Ph.D Thesis, University of Pennsylvania. 1982.
20. (*a*) A. C. OLIVIERI, L. FRYDMAN, and L. E. DIAZ. J. Magn. Reson. **75**, 50 (1987); (*b*) A. OLIVIERI, L. FRYDMAN, M. GRASSELLI, and L. DIAZ. Magn. Reson. Chem. **26**, 615 (1988).
21. (*a*) A. F. CASY and A. YASIN. J. Pharm. Biomed. Anal. **1**, 281 (1983); (*b*) J. Pharm. Biomed. Anal. **2**, 19 (1984); (*c*) S. K. BRANCH and A. F. CASY. *In* Prog. Med. Chem. Vol. 26. *Edited by* G. P. Ellis and G. B. West. Elsevier Science Publishers, Amsterdam. 1989. pp. 355–436.
22. (*a*) M. WITANOSKI, L. STEFANIK, and G. A. WEBB. *In* Annual Reports on NMR Spectroscopy: Nitrogen NMR spectroscopy. Vol. 18. *Edited by* G. A. Webb. Academic Press, London. 1986; (*b*) G. W. BUCHANAN. Tetrahedron, **45**, 581 (1989).
23. F. A. HOCHSTEIN, C. R. STEPHENS, L. H. CONOVER, P. P. REGNA, R. PASTERNACK, P. N. GORDON, F. J. PILGRIM, K. J. BRUNINGS, and R. B. WOODWARD. J. Am. Chem. Soc. **75**, 5455 (1953).
24. L. L. SMITH, S. A. MULLER, M. MARX, R. WINTERBOTTOM, and A. P. DOERSCHUK. J. Org. Chem. **23**, 721 (1958).
25. (*a*) M. ALLA and E. LIPPMAA. Chem. Phys. Lett. **37**, 260 (1976); (*b*) S. J. Opella and M. H. FREY. J. Am. Chem. Soc. **101**, 5854 (1979).
26. (*a*) G. A. MORRIS and R. FREEMAN. J. Am. Chem. Soc. **101**, 760 (1979); (*b*) G. A. MORRIS. J. Am. Chem. Soc. **102**, 428 (1980).
27. P. R. SRINIVASAN and R. L. LICHTER. J. Magn. Reson. **28**, 227 (1977).
28. G. C. LEVY and R. L. LICHTER. Nitrogen-15 nuclear magnetic resonance spectroscopy. John Wiley and Sons, New York. 1979.
29. R. O. DUTHALER and J. D. ROBERTS. J. Am. Chem. Soc. **100**, 3882 (1978).
30. J. GULBIS and G. W. EVERETT. Tetrahedron, **32**, 913 (1976).
31. M. L. MARTIN, M. FILLEUX-BLANCHARD, G. J. MARTIN, and G. A. WEBB. Org. Magn. Reson. **13**, 396 (1980).

Can. J. Chem. Downloaded from www.nrcresearchpress.com by 198.100.157.202 on 09/07/12
For personal use only.

The effect of *meta*- and *para*-methoxy substitution on the reactivity of the radical cations of arylalkenes and alkanes. Radical ions in photochemistry. Part 26[1]

DONALD R. ARNOLD,[2] XINYAO DU, AND KERSTIN M. HENSELEIT
Department of Chemistry, Dalhousie University, Halifax, N.S., Canada B3H 4J3

Received August 31, 1990

This paper is dedicated to Professor Paul de Mayo on the occasion of his 65th birthday

DONALD R. ARNOLD, XINYAO DU, and KERSTIN M. HENSELEIT. Can. J. Chem. **69**, 839 (1991).

The effect of *meta*- and *para*-methoxy substitution on the reactivity of some radical cations has been determined. The compounds chosen for study were 1-(3-methoxyphenyl)-1-phenylethylene (**7**), 1-(4-methoxyphenyl)-1-phenylethylene (**8**), 3-(3-methoxyphenyl)indene (**9**), 3-(4-methoxyphenyl)indene (**10**), methyl 2-(3-methoxyphenyl)-2-phenylethyl ether (**11**), methyl 2-(4-methoxyphenyl)-2-phenylethyl ether (**12**), *cis*- and *trans*-2-methoxy-1-(3-methoxyphenyl)indane (**13**), and *cis*- and *trans*-2-methoxy-1-(4-methoxyphenyl)indane (**14**). The radical cations of these compounds were generated by photosensitization (electron transfer) using 1,4-dicyanobenzene (**3**) as the electron acceptor. The three reactions studied were: (1) The addition of nucleophiles (methanol) to the radical cation of the arylalkenes, a reaction that yields the *anti*-Markovnikov addition product. (2) The carbon–carbon bond cleavage of radical cations, which yields products derived from the radical and carbocation fragments. (3) The deprotonation of the radical cation, a reaction that can be used to invert the configuration at a saturated carbon centre. The mechanisms of these reactions are discussed and the factors that need to be considered in order to predict reactivity are defined. Molecular orbital calculations (UHF/STO-3G) were carried out on the radical cations of the model compounds 3- and 4-vinylanisole and 3- and 4-methylanisole.

Key words: photochemistry, photosensitize (electron transfer), radical cation, radical.

DONALD R. ARNOLD, XINYAO DU et KERSTIN M. HENSELEIT. Can. J. Chem. **69**, 839 (1991).

On a déterminé l'effet de substituants en *méta* et en *para* sur la réactivité de quelques radicaux cations. Les composés choisis pour cette étude sont : les 1-(3-méthoxyphényl)-1-phényléthylène (**7**), 1-(4-méthoxyphényl)-1-phényléthylène (**8**), 3-(3-méthoxyphényl)indène (**9**), 3-(4-méthoxyphényl)indène (**10**), 1-méthoxy-2-(3-méthoxyphényl)-2-phényléthane (**11**), 1-méthoxy-2-(4-méthoxyphényl-2-phényléthane (**12**), les *cis*- et *trans*-2-méthoxy-1-(3-méthoxyphényl)indane (**13**) et les *cis*-et *trans*-2-méthoxy-1-(4-méthoxyphényl)indane (**14**). On a généré les cations radicaux de ces composés par photosensibilisation (transfert d'électron), en utilisant le 1,4-dicyanobenzène (**3**) comme accepteur d'électrons. Les trois réactions étudiées sont : (1) l'addition de nucléophiles (méthanol) aux cations radicaux des arylalcènes, une réaction qui conduit à un produit d'addition *anti*-Markovnikov; (2) le clivage de la liaison carbone–carbone des cations radicaux qui conduit à des produits qui dérivent des fragments radicalaires et carbocationiques et (3) la déprotonation des cations radicaux qui peut être utilisée pour inverser la configuration à un site carboné saturé. On discute des mécanismes de ces réactions et on définit les facteurs qu'il faut considérer afin de pouvoir prédire la réactivité. On a effectué des calculs d'orbitales moléculaires (UHF/ STO-3G) sur les cations radicaux des composés modèles, 3- et 4-vinylanisole et 3- et 4-méthylanisole.

Mots clés : photochimie, photosensibilisation (transfert d'électron), cation radical, radical.

[Traduit par la rédaction]

Introduction

Extensive studies over the past several years in the area of photosensitization (electron transfer) have greatly increased our understanding of the structure and fundamental behaviour of radical ions (2). One of the benefits to be derived from this knowledge is the discovery of new reactions that may become generally useful for organic synthesis. Three of these reactions are: (1) The addition of nucleophiles to the radical cations of arylalkenes, a reaction that yields the *anti*-Markovnikov addition product. (2) The carbon–carbon bond cleavage of radical cations, which yields products derived from the radical and carbocation fragments. (3) The deprotonation of the radical cation, a reaction that can be used to invert the configuration at a saturated carbon centre. Among the first examples of these reactions were: (reaction [1]) the photosensitized (electron transfer) addition of methanol to 1,1-diphenylethylene (**1**) (3); (reaction [2]) the subsequent cleavage of the radical cation of the product, methyl 2,2-diphenylethyl ether (**2**) (4); and (reaction [3]) the photosensitized (electron transfer) *trans* to *cis* isomerization of 2-methoxy-1-phenylindane (**6**) (5).[3] As useful as these reactions may become, the scope and limitations will have to be defined before they will even be considered during the initial planning of a synthesis strategy.

The mechanisms initially proposed for these reactions are shown in Schemes 1, 2, and 3. Subsequent study has generally supported these proposals (1, 6–8) and these mechanisms now provide a framework for the discussion of the scope of these reactions. While many questions remain to be answered, progress has been made to the point where several of the factors that can limit each reaction have been identified.

The purpose of this study was to determine the effect of *meta*- and *para*-methoxy substitution on these three reactions. The compounds chosen for study were 1-(3-methoxyphenyl)-1-phenylethylene (**7**), 1-(4-methoxyphenyl)-1-phenylethylene (**8**),

[1]The preceding publication in this series is ref. 1*a*.

[2]Author to whom correspondence may be addressed.

[3]Reactions [2] and [3] are both bond cleavage reactions; the first is a cleavage of a carbon–carbon bond and the second is cleavage of a carbon–hydrogen bond, that is, loss of a proton. While these reactions may compete with one another, it is unlikely that carbon–carbon bond cleavage will lead to isomerization under these conditions (7*c*,*d*); reaction of the carbocation with methanol (6 M) will be too rapid (9).

Can. J. Chem. Downloaded from www.nrcresearchpress.com by 198.100.157.202 on 09/07/12
For personal use only.

Can. J. Chem. Downloaded from www.nrcresearchpress.com by 198.100.157.202 on 09/07/12
For personal use only.

Reaction [1] (ref. 3)

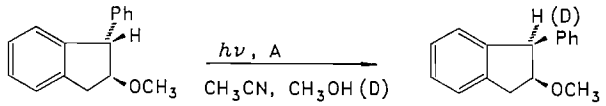
$$\underset{\mathbf{1}}{Ph_2C{=}CH_2} \xrightarrow[CH_3CN,\ CH_3OH]{h\nu,\ A} \underset{\mathbf{2}}{Ph_2CHCH_2OCH_3}$$

A = 1,4-dicyanobenzene (**3**, an electron accepting photosensitizer)

Reaction [2] (ref. 4)

$$\underset{\mathbf{2}}{Ph_2CHCH_2OCH_3} \xrightarrow[CH_3CN,\ CH_3OH]{h\nu,\ A} \underset{\mathbf{4}}{Ph_2CH_2} + \underset{\mathbf{5}}{CH_3OCH_2OCH_3}$$

Reaction [3] (ref. 5)



6 *trans* **6** *cis*

3-(3-methoxyphenyl)indene (**9**), and 3-(4-methoxyphenyl)indene (**10**) for reaction [1]; methyl 2-(3-methoxyphenyl)-2-phenylethyl ether (**11**) and methyl 2-(4-methoxyphenyl)-2-phenylethyl ether (**12**) for reaction [2]); and *cis*- and *trans*-2-methoxy-1-(3-methoxyphenyl)indane (**13**), and *cis*- and *trans*-2-methoxy-1-(4-methoxyphenyl)indane (**14**) for reaction [3].

Results

The required compounds were readily prepared by standard methods. The alkenes were obtained by dehydration of the alcohols, which were prepared by Grignard reactions. The ethers were prepared from the alkenes via the alcohols, by using the hydroboration, aqueous hydrogen peroxide oxidation, methylation sequence. The procedure shown in Scheme 4, for the preparation of 3-(4-methoxyphenyl)indene (**10**) and *trans*-2-methoxy-1-(4-methoxyphenyl)indane (**14**), is typical.

The irradiation conditions used for all of these reactions were similar to those used in the previous studies (3–5) so the results can be compared. Most of the irradiations were carried out in acetonitrile–methanol (3:1) solution, with 1,4-dicyanobenzene (**3**) added as a photosensitizer (electron acceptor), using the output of a 1-kW medium-pressure mercury vapour lamp filtered through Pyrex. The temperature of the photolysate generally was held at 10°C. Previous studies have shown that the carbon–carbon bond cleavage reaction (reaction [2]) can be thermally activated in some cases; therefore, when no cleavage was observed upon irradiation at 10°C, the irradiation was also attempted at 80°C. Progress of the reaction was followed by capillary column gas chromatography with mass selective detection (gc/ms).

The irradiation of 1-(3-methoxyphenyl)-1-phenylethylene (**7**) under the conditions used for reaction [1] gave an excellent yield (96%) of the *anti*-Markovnikov methanol addition product, methyl 2-(3-methoxyphenyl)-2-phenylethyl ether (**11**) (reaction [4]). In marked contrast, when 1-(4-methoxyphenyl)-1-phenylethylene (**8**) was irradiated under these conditions, the *anti*-Markovnikov addition product, methyl 2-(4-methoxyphenyl)-2-phenylethyl ether (**12**), was only a minor product (<5%). The major reaction (80%) led to a mixture of the stereoisomeric two-to-one (alkene/methanol) adducts **15**. This mixture was not fully characterized; **15** is relatively unstable. When the reaction mixture was allowed to stand for a period of days, under ambient conditions, *E*- and *Z*-1,4-di(4-methoxyphenyl)-1,4-diphenyl-1-butene (**16** *E* and *Z*) were isolated as

1. $A \xrightarrow{h\nu} A^*$
2. $A^* + Ph_2C{=}CH_2 \longrightarrow A^{\cdot-} + Ph_2C{=}CH_2^{\cdot+}$
3. $A^{\cdot-} + Ph_2C{=}CH_2^{\cdot+} \longrightarrow A + Ph_2C{=}CH_2$
4. $Ph_2C{=}CH_2^{\cdot+} + CH_3OH \longrightarrow Ph_2\dot{C}\text{-}CH_2OCH_3 + H^+$
5. $Ph_2\dot{C}\text{-}CH_2OCH_3 + A^{\cdot-} \longrightarrow Ph_2\bar{C}\text{-}CH_2OCH_3 + A$
6. $Ph_2\bar{C}\text{-}CH_2OCH_3 + H^+ \longrightarrow Ph_2CHCH_2OCH_3$

A = 1,4-dicyanobenzene (**3**, an electron-accepting photosensitizer)

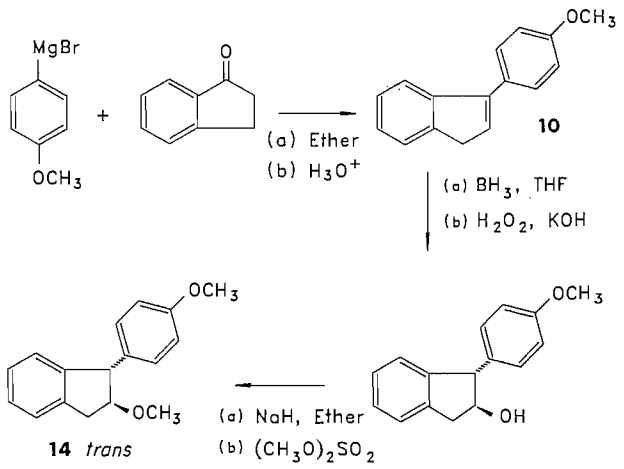
SCHEME 1. The mechanism for the photosensitized (electron transfer) nucleophilic (methanol) addition to arylalkenes.

1. $A \xrightarrow{h\nu} A^*$
2. $Ph_2CH\text{-}R + A^* \longrightarrow Ph_2CH\text{-}R^{\cdot+} + A^{\cdot-}$
3. $Ph_2CH\text{-}R^{\cdot+} + A^{\cdot-} \longrightarrow Ph_2CH\text{-}R + A$
4. $Ph_2CH\text{-}R^{\cdot+} \longrightarrow Ph_2CH^{\cdot} + R^+$
5. $R^+ + CH_3OH \longrightarrow R\text{-}OCH_3 + H^+$
6. $Ph_2CH^{\cdot} + A^{\cdot-} \longrightarrow Ph_2CH^- + A$
7. $Ph_2CH^- + CH_3OH \longrightarrow Ph_2CH_2 + CH_3O^-$

SCHEME 2. The mechanism for the photosensitized (electron transfer carbon–carbon bond cleavage.

1. $A \xrightarrow{h\nu} A^*$
2. $Ph_2CH\text{-}R + A^* \longrightarrow Ph_2CH\text{-}R^{\cdot+} + A^{\cdot-}$
3. $Ph_2CH\text{-}R^{\cdot+} + A^{\cdot-} \longrightarrow Ph_2CH\text{-}R + A$
4. $Ph_2CH\text{-}R^{\cdot+} \longrightarrow Ph_2C(\cdot)\text{-}R + H^+$
5. $Ph_2C(\cdot)\text{-}R + A^{\cdot-} \longrightarrow Ph_2C(-)\text{-}R + A$
6. $Ph_2C(-)\text{-}R + H^+ (D^+) \longrightarrow Ph_2CH\text{-}R\ (Ph_2CD\text{-}R)$

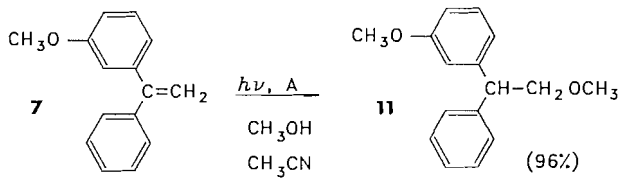
SCHEME 3. The mechanism for the photosensitized (electron transfer) isomerization involves deprotonation of the radical cation, reduction of the resulting radical to the anion, and reprotonation.



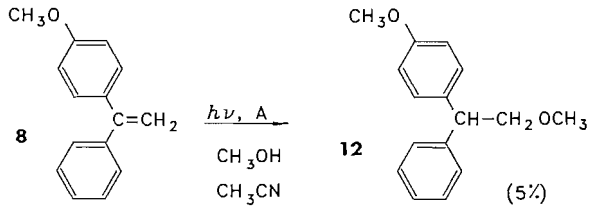
SCHEME 4

Can. J. Chem. Downloaded from www.nrcresearchpress.com by 198.100.157.202 on 09/07/12
For personal use only.

Reaction [4]



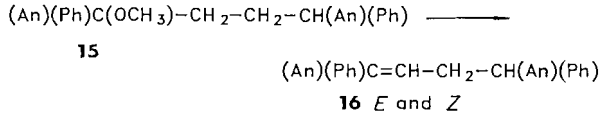
Reaction [5]



\+

(An)(Ph)C(OCH$_3$)–CH$_2$–CH$_2$–CH(An)(Ph)

15 (80%)



An = 4–methoxyphenyl
Ph = phenyl

the major products (reaction [5]). Examination of the ^{1}H nmr spectrum of the crude reaction mixture, immediately after the irradiation, indicates that **16** *E* and *Z* are initially only minor products.

The same pattern of reactivity was observed with the isomeric indenes. The 3-methoxyphenyl derivative **9** gave a mixture of the *cis*- and *trans-anti*-Markovnikov methanol adducts **13** (74%, *cis*/*trans* = 7:1), whereas little or no one-to-one adduct was obtained upon irradiation of the 4-methoxyphenyl derivative **10** (reactions [6] and [7]).

No reaction was observed when methyl 2-(3-methoxyphenyl)-2-phenylethyl ether (**11**) was subjected to the irradiation conditions (reaction [8]) that cause cleavage of the unsubstituted derivative (reaction [2]). There was also no reaction when this irradiation was carried out at the higher temperature (80°C). Furthermore, this ether was also stable to irradiation at 80°C when the solvent was acetonitrile–methanol-*O*-*d* (3:1); no deuterium was incorporated in **11** recovered after prolonged irradiation.

Again, with this reaction, the isomers behave differently. Irradiation of methyl 2-(4-methoxyphenyl)-2-phenylethyl ether (**12**) in the acetonitrile–methanol-*O*-*d* solution leads to relatively efficient deuterium incorporation at the bis-benzylic position (reaction [9]). No carbon–carbon bond cleavage was observed.

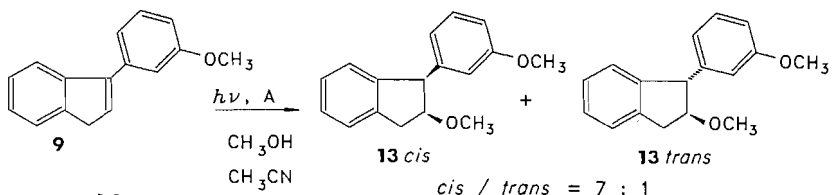
This pattern of reactivity is repeated in the indane series. No reaction (cleavage, isomerization, deuterium incorporation) was observed upon prolonged irradiation of *trans*-2-methoxy-1-(3-methoxyphenyl)indane (**13**) (reaction [10]). Analogous irradiation of *trans*-2-methoxy-1-(4-methoxyphenyl)indane (**14**) leads to relatively efficient isomerization to a mixture of the *cis* and *trans* isomers (reaction [11]). When the irradiation of **14** was carried out in the acetonitrile–methanol-*O*-*d* (3:1) solvent mixture, deuterium incorporation occurred at the bis-benzylic position.

The behaviour of the model compounds, 3- and 4-methylanisole (**17** and **18**), was also studied. The *meta* isomer **17** was relatively stable to irradiation in acetonitrile–methanol-d_4 (3:1) solution; a small amount of deuterium was incorporated in the recovered starting material after prolonged irradiation (reaction [12]). In marked contrast, deuterium was efficiently incorporated in the methyl group of the *para* isomer **18** under these conditions, and two other products were formed: 4-cyano-4′-methoxy-diphenylmethane (**19**) and 1,2-di(4-methoxyphenyl)-ethane (**20**) (reaction [13]). There was no evidence for exchange of the methoxy methyl group in either isomer.

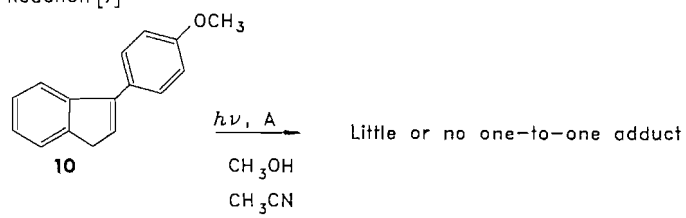
The oxidation potentials of the compounds of interest were determined by cyclic voltammetry. There was no evidence for reduction of the radical cation during the reverse cathodic sweep at a sweep rate of 100 mV s^{-1}. Therefore, the oxidation potentials were estimated to be 0.028 V less than the anodic peak potentials (10). These data, along with the oxidation potentials of several related compounds, are summarized in Table 1 (11).

The spin and charge density distribution on the radical cations of the model compounds: 3-vinylanisole (**21**), 4-vinylanisole (**22**), 3-methylanisole (**17**), and 4-methylanisole (**18**), were calculated. The *ab initio* molecular orbital calculations were carried out with Pople's Gaussian 86 series of programmes (12). The six carbons of the aromatic ring and the atoms directly attached were constrained to a plane; the remaining structural features were fully optimized at the UHF/STO-3G level. The spin density was taken as the square of the coefficient at the

Reaction [6]

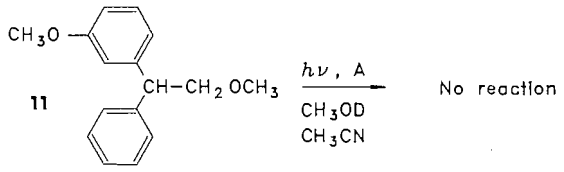


Reaction [7]

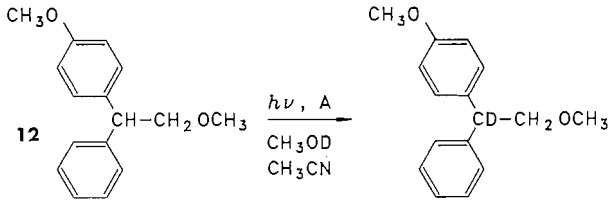


Can. J. Chem. Downloaded from www.nrcresearchpress.com by 198.100.157.202 on 09/07/12
For personal use only.

Reaction [8]



Reaction [9]



atomic p_z-orbital in the singly occupied molecular orbital (SOMO) and the charge distribution was calculated by Mulliken population analysis (13). The limitations of this method have been discussed (14). These data are summarized in Figs. 1 and 2.

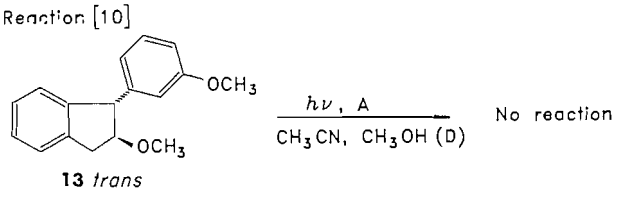
Structural assignments

The structures assigned to the starting materials and products rest primarily upon a thorough analysis of the ^1H and ^{13}C nmr spectra. There is an interesting difference in the ^1H nmr spectra of the 1-(3-methoxyphenyl)- and 1-(4)methoxyphenyl)-1-phenylethylenes (**7** and **8**). The 4-methoxyphenyl derivative shows the two vinyl protons as a distinct pair of doublets (δ 5.39 and 5.36, J = 1.26 Hz) (15), whereas, in the spectrum of the 3-methoxyphenyl derivative, the signals due to the vinyl protons are coincidentally equivalent (δ 5.44).

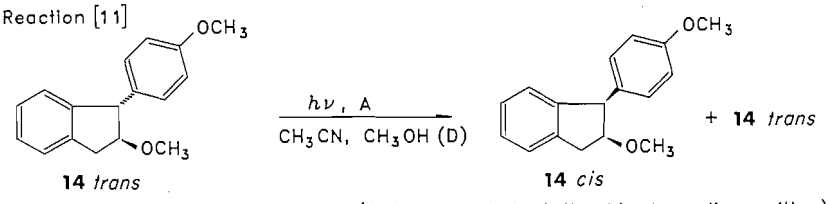
The stereochemical assignment of the *trans*-2-methoxy-1-(3-methoxyphenyl)indane and *trans*-2-methoxy-1-(4-methoxy phenyl)indane ethers (**13** *trans* and **14** *trans*) is firmly established by the regioselective *cis* addition during the hydroboration step (16). Knowing the stereochemistry of the *cis* and *trans* isomers of **13** and **14**, it is interesting to compare the magnitude of the vicinal coupling constants between the bis-benzylic proton (X) and the proton adjacent to the methoxy group (Y), both of which are part of ABXY patterns in the aliphatic region of the ^1H nmr spectra. In conformationally mobile cyclopentane rings, it is well known that there is no correlation between the magnitude of the vicinal proton coupling constant and configuration. On the other hand, when the rings cannot deviate appreciably from planarity, J_{cis} is larger than J_{trans}, as expected from the Karplus rule (17). These splitting patterns were analyzed with the aid of computer simulation, and the observed coupling constants (J_{XY}) are greater for the *trans* than for the *cis* isomer in both cases. The same pattern was observed in the case of the unsubstituted derivative (5); however, the differences are small: 2-methoxy-1-phenylindane (**6**) (J_{XY}: *trans* 6.3, *cis* 6.2 Hz), the 3-methoxyphenyl derivative (**13**) (J_{XY}: *trans* 6.31, *cis* 6.17 Hz), and the 4-methoxyphenyl derivative (**14**) (J_{XY}: *trans* 6.27, *cis* 6.20 Hz).

The major initial product (80%) from the irradiation of **8** (reaction [5]) was separated from the crude photolysate by dry-column flash chromatography. A tentative structural assignment, methyl 1,4-di(4-methoxyphenyl)-1,4-diphenyl-1-butyl ether (**15**), presumably a mixture of the diastereomers, was made on the basis of the ^1H nmr spectrum. In particular, the spectrum indicates the presence of three methoxy groups (δ 3.70, 3.68, and 2.93) and a low-field triplet signal (δ 3.74, J = 7.0 Hz), integrating for one hydrogen, attributed to the proton at the bis-benzylic position. This two-to-one adduct is readily converted to a mixture of the isomers of 1,4-di(4-methoxyphenyl)-1,4-diphenyl-1-butene (**16** *E* and *Z*) upon loss of methanol. The distinction between **16** *E* and *Z* was made on the basis of the difference in chemical shift of the vinyl protons; this proton resonates at lower field in the *E* isomer (15). The difference is small, δ 5.91 for **16***E* and δ 5.88 for **16***Z*, similar to the difference observed for the two vinyl protons in **8** (Δδ = 0.05 ppm).

Reaction [10]

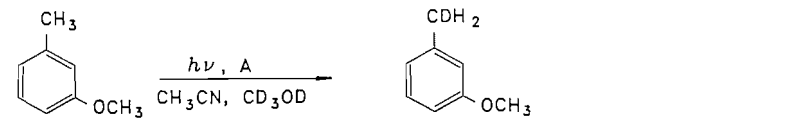


Reaction [11]



(D incorporated at the bis-benzylic position)

Reaction [12]



Relatively inefficient deuterium exchange

Can. J. Chem. Downloaded from www.nrcresearchpress.com by 198.100.157.202 on 09/07/12
For personal use only.

Reaction [13]

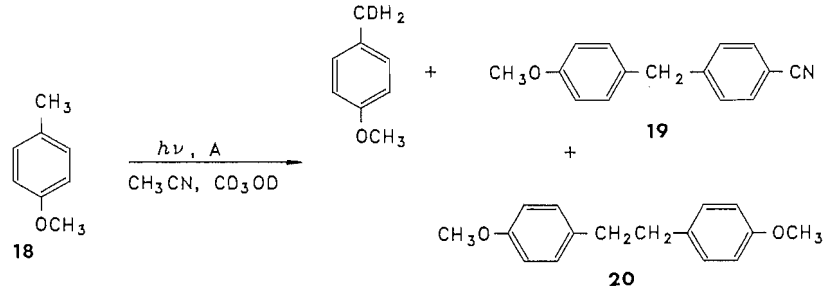


TABLE 1. The oxidation poential of several of the compounds of interest[a]

Compound	$E^{ox}_{1/2}$ (V)[b]
1,1-Diphenylethylene (**1**)	1.82[c]
1-(3-Methoxyphenyl)-1-phenylethylene (**7**)	1.53
1-(4-Methoxyphenyl)-1-phenylethylene (**8**)	1.32
3-Phenylindene	1.53
3-(3-Methoxyphenyl)indene (**9**)	1.44
3-(4-Methoxyphenyl)indene (**10**)	1.24
1,1-Diphenylethane	2.13[c]
Methyl 2.2-diphenylethyl ether (**2**)	2.15[c]
Methyl 2-(3-methoxyphenyl)-2-phenylethyl ether (**11**)	1.67
Methyl 2-(4-methoxyphenyl)-2-phenylethyl ether (**12**)	1.57
trans-2-Methoxy-1-phenylindane (**6***trans*)	2.01
trans-2-Methoxy-1-(3-methoxyphenyl)indane (**13***trans*)	1.64
trans-2-Methoxy-1-(4-methoxyphenyl)indane (**14***trans*)	1.62
Benzene	2.30[d]
Toluene	1.98[d]
Styrene	1.84[e]
Anisole	1.76[f]
3-Methylanisole (**17**)	1.77[g]
4-Methylanisole (**18**)	1.68[g]

[a]Measured by cyclic voltammetry at a sweep rate of 100 mV s^{-1}, in acetonitrile, 0.1 M tetraethylammonium perchlorate, with a saturated calomel electrode (sce).

[b]$E^{ox}_{1/2}$ ± 0.02 V; the anodic wave was irreversible. The oxidation potentials were taken as 0.028 V less than the anodic peak potential (ref. 10).

[c]Reference 4.

[d]Reference 11*a*.

[e]Reference 11*b*.

[f]Reference 11*c*.

[g]Reference 11*d*.

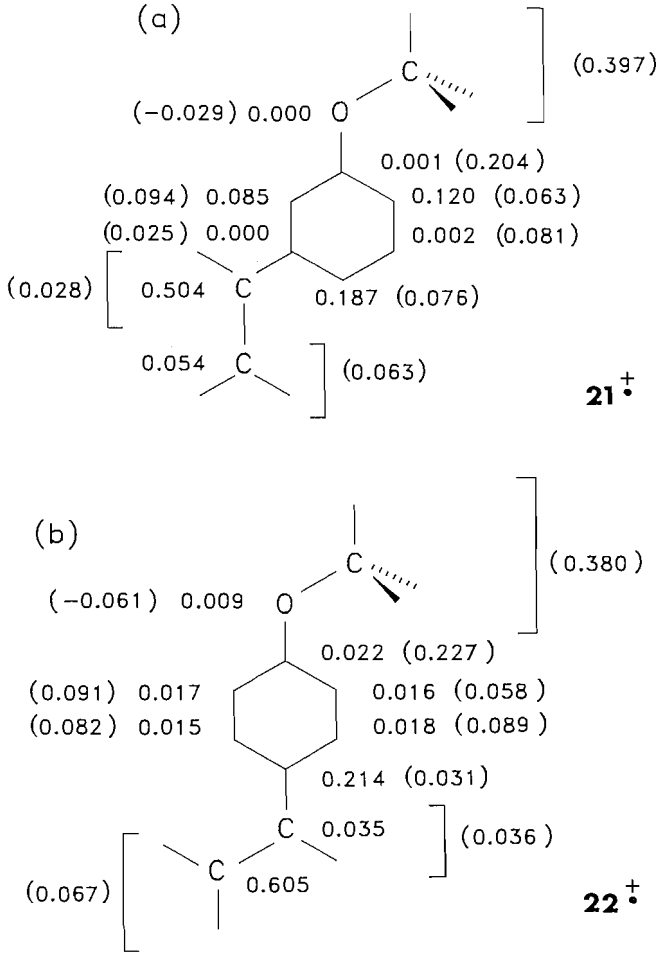


FIG. 1. Calculated spin and (charge) distribution on the radical cations: (a) 3-vinylanisole (**21**$^{+\cdot}$) and (b) 4-vinylanisole (**22**$^{+\cdot}$).

Discussion

The first three steps in the mechanisms (Schemes 1–3) proposed for all three of these reactions are the same. In each case the initial excitation is of the electron-accepting photosensitizer (A), 1,4-dicyanobenzene (**3**). The long-wavelength adsorption spectrum of **3** extends to wavelengths longer than 280 nm, the short wavelength cutoff of Pyrex glass. The arylalkenes and alkanes are essentially transparent in this region.

The energetics of the electron transfer process (step 2) can be calculated using the Weller equation (eq. [14]) where F is the Faraday constant, and the last term in the brackets takes into account the Columbic attraction between the radical cation and the radical anion at the encounter distance (18). The singlet excited state of 1,4-dicyanobenzene (**3**) will accept an electron at the diffusion-controlled rate from any prospective donor having an oxidation potential less than 2.4 V.[4] This includes all of the arylalkenes and alkanes studied here (Table 1). Previous work has shown that the fluorescence of **3** is quenched at essentially the diffusion-controlled rate by both 1,1-diphenylethylene (**1**) and by methyl 2,2-diphenylethyl ether (**2**) (4). The oxidation potentials of the methoxy derivatives, both *meta* and

[4]Electron transfer from the donor to the excited state of the acceptor will occur at the diffusion-controlled rate as long as it is exergonic by more than 12 kJ mol^{-1} (18). The singlet energy of 1,4-dicyanobenzene (**3**) ($E_{0,0}$ (A)) is 407.97 kJ mol^{-1} and the reduction potential ($E^{red}_{1/2}$ (A)) is −1.66 V (sce); the Coulombic attraction ($e/\epsilon\alpha$) is 0.06 eV in acetonitrile (4). All of the electrode potentials mentioned in this paper are referenced to the saturated calomel electrode (sce).

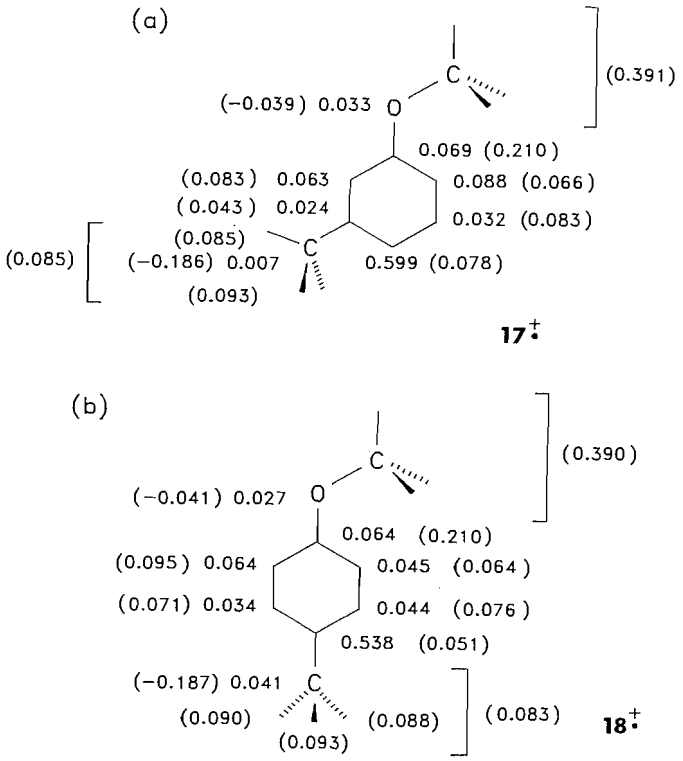


FIG. 2. Calculated spin and (charge) distribution on the radical cations: (a) 3-methylanisole ($17^{+\cdot}$) and (b) 4-methylanisole ($18^{+\cdot}$).

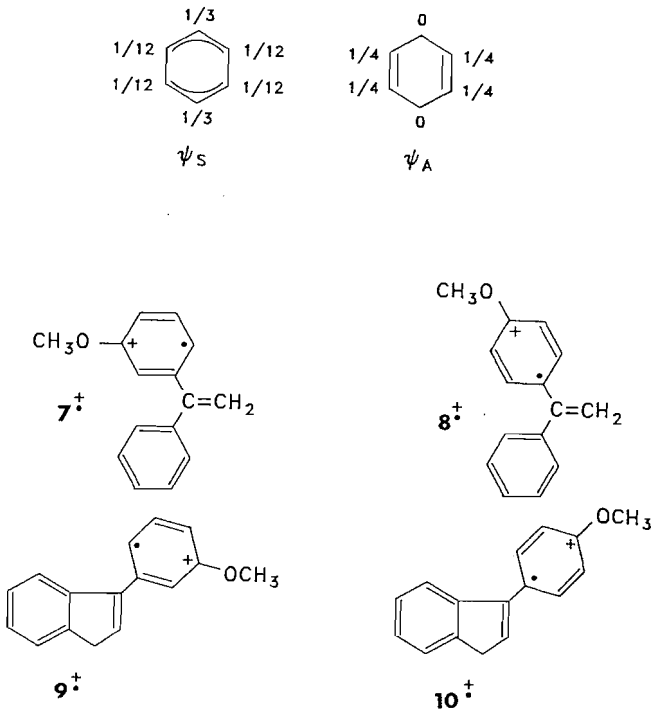


FIG. 3. The radical cation of benzene is a linear combination of the degenerate orbitals ψ_s and ψ_A. Spin and odd electron distribution.

para, are significantly lower (ca. 0.5 V less) than those of the unsubstituted compounds in all three series (Table 1); therefore, electron transfer (step 2) is even more favourable with these derivatives than it is with the unsubstituted analogues.

$$[14]\quad \Delta G_{et} = F[E^{ox}_{1/2}(D) - E^{red}_{1/2}(A) - e/\epsilon\alpha] - E_{0,0}(A)$$

$$[15]\quad \Delta G_{-et} = F(E^{red}_{1/2}(A) - E^{ox}_{1/2}(D))$$

Back-electron transfer from the radical anion of the electron acceptor to the radical cation of the donor within the radical ion pair (step 3) is the main competing deactivation pathway for all three reactions. The free-energy change for this process (ΔG_{-et}, eq. [15] is exergonic by 280 kJ mol^{-1} even in the least favourable case, that is, electron transfer from $3^{-\cdot}$ to $10^{+\cdot}$. This process is so exergonic that the rate falls within the Marcus inverted region (19). Back-electron transfer may be slower with the unsubstituted derivatives; methoxy substitution lowers the oxidation potential relative to the unsubstituted derivative in each series, so the process is less exergonic with the methoxy-substituted derivatives. Nevertheless, the rate of back-electron transfer has been measured in similar systems, and when the process is exergonic by 280 kJ mol^{-1}, the rate is ca. 10^8 s^{-1} (20). Step 3 is slow enough that diffusive separation of the radical ions from within the solvent cage, or reaction of the radical cation while still within the solvent cage, may compete.

The addition of nucleophiles to the radical cation of arylalkenes

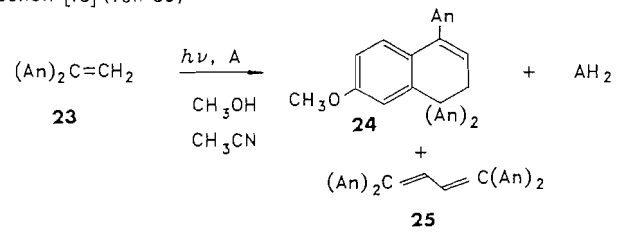
Step 4 in Scheme 1 involves the addition of the nucleophile methanol to the radical cation of the arylalkene. The singly occupied molecular orbital (SOMO) of the benzene radical cation is a linear combination of the degenerate symmetric and antisymmetric orbitals, ψ_s and ψ_A respectively (Fig. 3) (21). Substitution on benzene removes this degeneracy. Both the methoxy and the vinyl substituents stabilize adjacent positive charge and spin; the greatest influence is stabilization of the positive charge by interaction with the nonbonding pair of electrons on the methoxy group. This conclusion is supported by the relative oxidation potentials of benzene (2.30 V), styrene (1.84 V), and anisole (1.76 V) listed in Table 1. It seems likely that the SOMO of the *meta*- and *para*-methoxy substituted derivatives have the antisymmetric structures $7^{+\cdot}$ and $8^{+\cdot}$. The influence of the methoxy substituent in these structures provides the greatest delocalization (stabilization) of spin and charge. This simple empirical explanation of the effect of *meta*- and *para*-methoxy substitution is consistent with the quantum mechanical calculations of spin and charge density distribution.

The results of calculations carried out on the radical cations of the model compounds 3-vinylanisole (**21**) and 4-vinylanisole (**22**) are shown in Figs. 1a and 1b. In both cases, more than half of the positive charge density is associated with the methoxy group (the sum of the charge density on the *ipso* carbon, the oxygen, and the methyl group is 0.601 ($21^{+\cdot}$) and 0.607 ($22^{+\cdot}$)). There is little charge density on the terminal carbon of the alkene in either case (0.063 ($21^{+\cdot}$), 0.067 ($22^{+\cdot}$)). On the other hand, the spin density at the terminal carbon in the SOMO of the radical cation of 4-vinylanisole ($22^{+\cdot}$) (0.605) is significantly greater than that of 3-vinylanisole ($21^{+\cdot}$) (0.054).

The observed differences in the reactivity of **7** and **8** can now be explained: The rate of additon of a nucleophile (methanol) to the radical cation is dependent upon charge density. The addition to the terminal carbon of both $7^{+\cdot}$ and $8^{+\cdot}$ is slowed down by the methoxy substitution. The rate of addition of the radical cation to the neutral alkene depends upon the spin density on the terminal carbon in the SOMO. The spin density on the terminal carbon of the SOMO of $8^{+\cdot}$ is high relative to that of $7^{+\cdot}$. The addition of $8^{+\cdot}$ to the neutral molecule **8** is relatively fast. Therefore, with $7^{+\cdot}$, reaction with methanol is faster than reaction with the neutral molecule **7**; with $8^{+\cdot}$, relatively rapid reaction with the neutral molecule **8** effectively competes with reaction with methanol.

Can. J. Chem. Downloaded from www.nrcresearchpress.com by 198.100.157.202 on 09/07/12
For personal use only.

Reaction [16] (ref. 6e)



An = 4-methoxyphenyl
A = 9,10-dicyanoanthracene
AH_2 = 9,10-dihydro-9,10-dicyanoanthracene

The reactivity of the *para*-,*para'*-dimethoxy derivative analogous to **8**, 1,1-di(4-methoxyphenyl)ethylene (**23**), under conditions similar to those used for reaction [1], has been reported (6*e*). In this case the *anti*-Markovnikov methanol adduct was not observed; instead, the dimers **24** and **25** were obtained (reaction [16]. The rate of reaction of the radical cation $\mathbf{23}^{\ddagger}$ with methanol (Scheme 1, step 3) was estimated to be 10^7 $M^{-1}\,s^{-1}$, almost two orders of magnitude slower than reaction of $\mathbf{1}^{\ddagger}$ with methanol.

While the rate of reaction with methanol was significantly affected, the rate of addition of $\mathbf{23}^{\ddagger}$ to the neutral alkene **23** ($10^{10}\,M^{-1}\,s^{-1}$), on the way to dimer formation (**24** and **25**), was unaffected by the *para*-methoxy substitution (6*e*). The spin density on the terminal carbon of the SOMO of $\mathbf{23}^{\ddagger}$ is sufficient to maintain the rate of this reaction near the diffusion-controlled limit.

The rates of reaction of the analogous di(4-methoxyphenyl)-methyl, (4-methoxyphenyl)phenylmethyl, and diphenylmethyl cations with nucleophile (water) have been measured. While the effect of each additional substituent is not additive, each *para*-methoxy group significantly decreases the rate of reaction of the cation (9).

Methoxy substitution may also influence the electron transfer process involved in the reduction of the diarylalkyl radical by the radical anion of the electron acceptor (Scheme 1, step 5). The reduction potential of the radical must not be significantly greater (more negative) than that of the electron-accepting photosensitizer. These potentials are known or can be estimated (22). In the case of the parent system, the reduction potential of the 1,1-diphenylethyl radical is −1.34 V (22*a*) and the reduction potential of 1,4-dicyanobenzene (**3**) is −1.66 V (4); consequently, reduction of the diphenylethyl radical by the radical anion $\mathbf{3}^{\cdot-}$ is thermodynamically favourable. *para*-Methoxy substitution will make the radical harder to reduce; the reduction potential of the diphenylmethyl radical (−1.14 V) is 0.19 V less negative than that of the (4-methoxyphenyl)phenyl-methyl radical (−1.33 V) (22*b*). Assuming a similar incremental effect of a *para*-methoxy group in the diphenylethyl series, the reduction potential of the (4-methoxyphenyl)phenyl-ethyl radical will be ca. −1.5 V. *meta*-Methoxy substitution has less of an effect on the reduction potential of the radical; the reduction potential of the (3-methoxyphenyl)phenylmethyl radical (−1.16 V) is almost the same as that of the unsubstituted analogue (22*b*). Therefore reduction of the intermediate radical by the electron acceptor radical anion ($\mathbf{3}^{\cdot-}$) (step 5 in Scheme 1) will still be favourable when the radical is substituted by one *meta*- or *para*-methoxy group. Additional *para*-methoxy substitution, as in the di(4-methoxyphenyl)ethyl radical, may increase the reduction potential of the radical to the point that reduction to the anion by the 1,4-dicyanobenzene radical anion is endergonic.

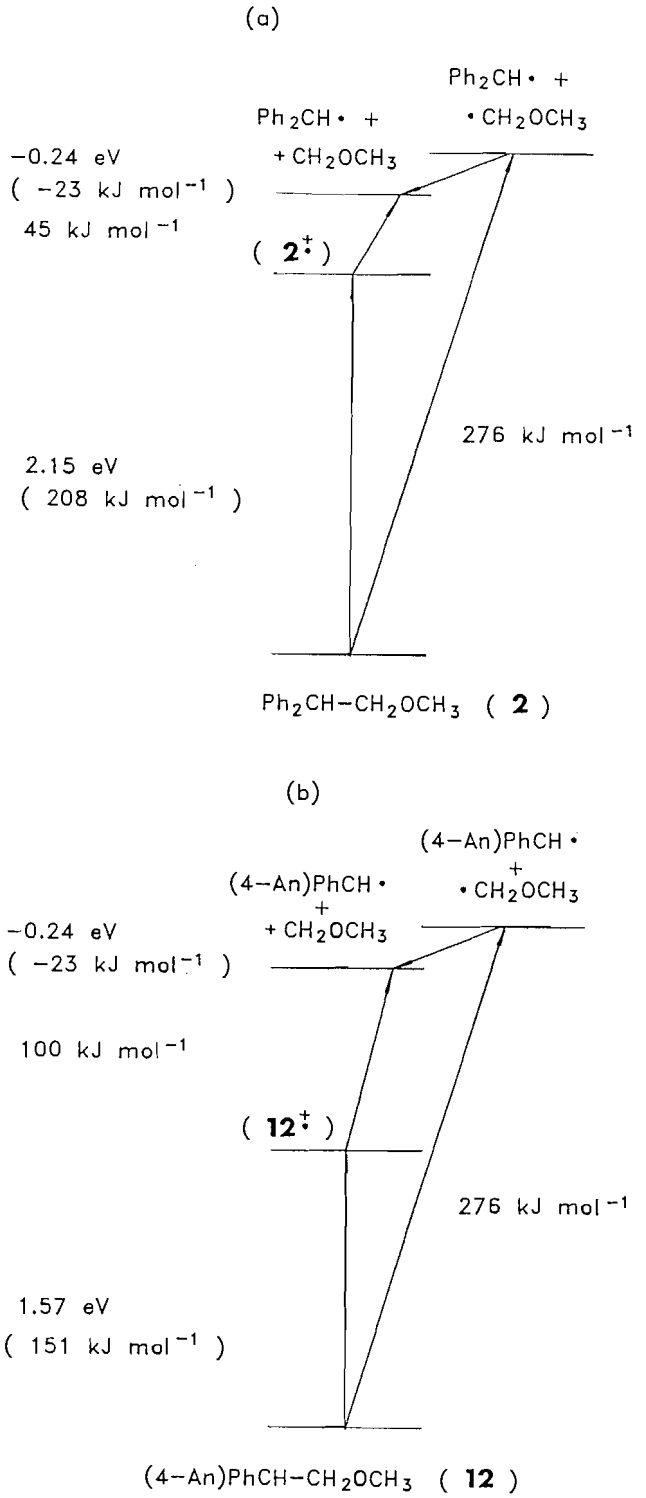


FIG. 4. Thermochemical cycles useful for estimating the bond dissociation energy of the radical cations of (a) methyl 2,2-diphenylethyl ether (**2**) and (b) methyl 2,2-(4-methoxyphenyl)ethyl ether (**12**).

The formation of **15** as the primary product in reaction [5] and the formation of the dimers **24** and **25** in reaction [16] can now be explained. The 1,4-radical cation that results from addition of $\mathbf{8}^{\ddagger}$ to **8** will react with methanol and the resulting radical will be reduced to the anion by $\mathbf{3}^{\cdot-}$; subsequent protonation of the anion yields **15**. Reaction of the 1,4-radical cation that results from addition of $\mathbf{23}^{\ddagger}$ to **23** with methanol will be slower and reduction of the radical by the anion radical of 9,10-dicyano-

Can. J. Chem. Downloaded from www.nrcresearchpress.com by 198.100.157.202 on 09/07/12
For personal use only.

Can. J. Chem. Downloaded from www.nrcresearchpress.com by 198.100.157.202 on 09/07/12
For personal use only.

anthracene ($E^{red}_{1/2} = -0.88$ V) is unfavourable; consequently, in this case cyclization and deprotonation of the 1,4-radical cation occurs instead of reaction with methanol or reduction of the radical to the anion.

Protonation of the anion by methanol (step 6) will be rapid and irreversible in every case.

The carbon–carbon bond cleavage of radical cations

The *meta*- and *para*-methoxy substituents may influence the crucial step in the proposed mechanism for reaction [2] (step 4, Scheme 2) in three (at least) ways: substitution will influence the energetics of the cleavage process; there is a required conformation of the SOMO relative to the vulnerable carbon–carbon bond that will be affected by substitution, and the electronic configuration of the SOMO will be important for this reaction, as it is for the addition reaction described above.

Consider first the thermodynamic requirements for cleavage. Previous studies have shown that the bond dissociation enthalpy of the carbon–carbon bond of the radical cation must be less than ca. 60 kJ mol^{-1} for cleavage to occur at a rate that is rapid enough to compete with deactivation by back-electron transfer (1, 7*a*). This bond dissociation energy (ΔH_C) can be estimated by consideration of the thermochemical cycle shown in Fig. 4, and represented by eq. [17] and [18] (1*b*).

$$[17]\quad \Delta H_C = \Delta H_{BDE} + F(E^{ox}_{1/2}(R\cdot) - E^{ox}_{1/2}(R{-}R)) - T(\Delta S(R{-}R) - \Delta S(R{-}R^{+}))$$

When $\Delta S(R{-}R) \approx \Delta S(R{-}R^{+})$:

$$[18]\quad \Delta H_C = \Delta H_{BDE} + F(E^{ox}_{1/2}(R\cdot) - E^{ox}_{1/2}(R{-}R))$$

Carbon–carbon bond cleavage of the radical cation yields the radical and carbocation fragments; the carbocation is associated with that fragment having the lower oxidation potential (1*b*). The oxidation potential of the diphenylmethyl radical (0.35 V) is significantly greater than that of the methoxymethyl radical (−0.24 V), so that when $\mathbf{2}^{\ddagger}$ cleaves, the methoxymethyl carbocation is formed. The oxidation potentials of the (3-methoxyphenyl)phenylmethyl radical (0.38 V) and the (4-methoxyphenyl)phenylmethyl radical (0.16 V) are also greater than that of the methoxymethyl radical (22*b*). Thus, cleavage of the radical cations $\mathbf{11}^{\ddagger}$ and $\mathbf{12}^{\ddagger}$ should also occur to give the methoxymethyl carbocation.

The bond dissociation enthalpy (ΔH_{BDE}) for the vulnerable bis-benzylic carbon–carbon bond of **2** has not been measured, but an estimate (276 kJ mol^{-1}) can be made from the known bond dissociation enthalpy of the corresponding bond in 1,1-diphenylethane, and some additional heat of formation data to assess the effect of the adjacent methoxy group (23).[5] The oxidation potential of **2** (Table 1) and the methoxymethyl radical (−0.24 V) are known (22). These data were used to construct the thermochemical cycle required for the calculation of the ΔH_C for **2** shown in Fig. 4a. The calculated value, ΔH_C = 45 kJ mol^{-1}, is well below the established threshold energy above which cleavage will not occur, and the observed reactivity of **2** is consistent. Methoxy substitution, both *meta* and *para*, will have a relatively small effect on the bond dissociation energy of the neutral molecules. While *para*-methoxy substitution will weaken the benzylic bond (i.e., stabilize the benzylic radical), *meta*-methoxy substitution will strengthen this bond; however, the effect is small (<4 kJ mol^{-1}) in both cases (24). On the other hand, the effect on the oxidation potential of these molecules is relatively large (Table 1). The combined influence of these factors, shown in Fig. 4b for **12**, is an increase in the bond dissociation enthalpy of the radical cation $\mathbf{12}^{\ddagger}$ (ΔH_C = 100 kJ mol^{-1}) to well above the threshold. Consequently, the observed lack of carbon–carbon bond cleavage upon photosensitized (electron transfer) irradiation of **11** and **12** (reactions [8] and [9]) can be explained on thermodynamic grounds.

While the lack of reactivity of the *meta* derivative **11** can be explained on the basis of energetics, the importance of the electronic configuration of the SOMO will become evident. The SOMOs of both **11** and **12** will have the ψ_A configuration (Fig. 3), which has considerable spin density at the position *para* to the methoxy group, and carbon–carbon bond cleavage of the radical cation $\mathbf{12}^{\ddagger}$ might occur. However, there is little spin density at the position *meta* to the methoxy group, and $\mathbf{11}^{\ddagger}$ might be unreactive for this reason, even if the energy requirement was met.

The results of the *ab initio* molecular orbital calculations on the radical cations of the model compounds 3-methylanisole (**17**) and 4-methylanisole (**18**), shown in Figs. 2a and 2b, lend support to this line of reasoning. More than half of the spin density is at the carbon *para* to the methoxy group in both isomers. There is much less spin and charge density at the carbon *meta* to the methoxy group.

The reactivity of the indane derivatives, **13** and **14**, is of particular interest. In the parent system, both *cis*- and *trans*-2-methoxy-1-phenylindane (**6**) are reported to undergo configurational isomerization under these conditions (reaction [3]), but there was no evidence for carbon–carbon bond cleavage in either case. The configurational isomerization was attributed to deprotonation of the radical cation followed by reduction of the resulting radical and reprotonation (Scheme 3). The explanation offered for the lack of carbon–carbon bond cleavage was that the SOMO in these molecules is largely associated with the fused aryl ring and is therefore held in a conformation orthogonal to the vulnerable bis-benzylic carbon–carbon bond. The oxidation potential of **6** is less than that of the acyclic analog **2**, consistent with this explanation.

Substitution by the electron-donating methoxy group in the *para* position of **14** lowers the energy of the SOMO associated with this unfused ring to the extent that it is below that of the fused ring. This shift in the site of the SOMO is evident from the lower oxidation potential of **14** (Table 1). Now the radical cation can attain a conformation that will allow overlap of the SOMO associated with the unfused ring with the vulnerable bis-benzylic carbon–carbon bond. Furthermore, the electronic configuration of the *para*-methoxy substituted ring will be ψ_A, which has considerable spin density at the *para* position, and cleavage could occur. The lack of carbon–carbon bond cleavage of $\mathbf{14}^{\ddagger}$ must be attributed to lack of sufficient energy as described above for the acyclic analog $\mathbf{12}^{\ddagger}$.

In the case of the *meta*-methoxy isomer, while the SOMO

[5]The carbon–carbon bond dissociation energy of ethane, calculated from the heats of formation of the methyl radical (147 kJ mol^{-1}) and ethane (−83.7 kJ mol^{-1}) is 377 kJ mol^{-1}. The carbon–carbon bond dissociation energy of ethyl methyl ether, calculated from the heat of formation of the methyl radical, the heat of formation of the methoxymethyl radical (−11.7 kJ mol^{-1}), and the heat of formation of ethyl methyl ether (−216 kJ mol^{-1}) is 351 kJ mol^{-1}. The methoxy group lowers the adjacent carbon–carbon bond dissociation energy in this case by 25.9 kJ mol^{-1}. The bond dissociation energy for the bis-benzylic carbon–carbon bond in 1,1-diphenylethane is 301 kJ mol^{-1}. If a methoxy group has the same effect on the bis-benzylic carbon–carbon bond of methyl 2,2-diphenylethyl ether (**2**), this bond dissociation energy will be 276 kJ mol^{-1}.

Can. J. Chem. Downloaded from www.nrcresearchpress.com by 198.100.157.202 on 09/07/12
For personal use only.

should again be associated largely with the unfused ring, the configuration of the SOMO (ψ_A) bears little spin or charge density at the position *meta* to the methoxy group. The radical cation **13**$^{+\cdot}$ has neither the required electronic configuration nor sufficient energy to cleave.

Step 6 of Scheme 2 involves reduction of the radical by the radical anion of the photosensitizer analogous to step 5 in Scheme 1. As was described above, the reduction potentials of the diphenylmethyl radical (−1.14 V), the (3-methoxyphenyl)-phenylmethyl radical (−1.16 V), and the (4-methoxyphenyl)-phenylmethyl radical (−1.33 V) are all well below that of 1,4-dicyanobenzene (−1.66 V), so, if cleavage had occurred, reduction of the radical would have been favourable in every case.

Deprotonation of the radical cation

The crucial step in the reaction that leads ultimately to incorporation of deuterium and to isomerization is deprotonation of the radical cation from the benzylic position (Scheme 3, step 4). The dramatic increase in acidity of the radical cation relative to that of the neutral molecule is well known (8, 25). The acidity of the bis-benzylic hydrogen of the radical cation of 1,1-diphenylethane, estimated from a thermochemical cycle (eq. [19] (25*a*)), is $pK_a = -14$; this is acidic enough for deprotonation to take place in acetonitrile–methanol (3:1).[6] Since *meta*- and *para*-methoxy substitution have a relatively small effect on the benzylic carbon–hydrogen bond dissociation energy (24), the major influence of methoxy substitution will result from the significant decrease in the oxidation potential of the molecule.

$$[19]\quad pK_{a(RH^{+\cdot})sol} = \frac{1}{2.303\,RT}(-FE^0_{RH} + \Delta G^0_{tr(H^+)sol} + \Delta G^0_{BDE(RH)g} - \Delta G^0_{f(H)g})$$

For compounds with similar carbon–hydrogen bond dissociation free energies, a decrease in the oxidation potential of 0.1 V corresponds to a decrease of 2 pK_a units in the acidity of the radical cation. Methoxy substitution (both *meta* and *para*) lowers the oxidation potential by ca. 0.5 V (Table 1); therefore, these derivatives are ca. 10 pK_a units less acidic than the unsubstituted analogues. Nevertheless, deprotonation from these radical cations, presumably with methanol acting as the base, may still be exergonic.

The radical cations of the *para*-methoxy derivatives, **12**, **14**, and the model compound **17**, undergo deprotonation as evidenced by deuterium incorporation and, in the case of **14**, isomerization (reactions [9], [11], and [13]). Deprotonation from the radical cations of these *para* derivatives must be rapid enough to compete with deactivation by back-electron transfer (Scheme 3, step 3). In contrast, the radical cations of the *meta*-methoxy derivatives, **11**, **13**, and **16**, are either stable or much less reactive under these conditions (reactions [8], [10], and [12]). The thermodynamic acidity of the *meta* and *para* derivatives is similar, the rate of deactivation by back-electron transfer is similar; therefore the difference in reactivity can be attributed to differences in the rate of deprotonation that can be explained in terms of the electronic configuration of the SOMO.

Figures 2a and 2b show the spin and charge distribution in the radical cations of the model compounds, 3-methylanisole (**17**) and 4-methylanisole (**18**). The SOMOs of both isomers have the ψ_A configuration. The total spin and charge and the spin and charge distribution on the individual atoms of the *meta*- and *para*-methyl groups are similar. The spin and charge are higher on the position *para* to the methoxy group in both isomers and loss of a proton from the *para*-methyl group should be favoured. The experimental observations are consistent. With the radical cations of the *meta*-methoxy derivatives **11**$^{+\cdot}$ and **13**$^{+\cdot}$, little or no deprotonation occurs. The radical cation of 3-methylanisole (**17**$^{+\cdot}$) does deprotonate, but less efficiently than does the *para* isomer.

The relatively efficient incorporation of deuterium in the *para*-methyl group of 4-methylanisole (**18**) is accompanied by the formation of two minor side products: 4-cyano-4′-methoxydiphenylmethane (**19**) and 1,2-di(4-methoxyphenyl)ethane (**20**). These products are indicative of the formation of the intermediate 4-methoxybenzyl radical. Coupling of this radical gives **20** and attack of this radical at the *ipso* position of the 1,4-dicyanobenzene radical anion (**3**$^{-\cdot}$), followed by loss of cyanide ion, leads to **19**.

More than half of the charge density in the radical cations **18**$^{+\cdot}$ and **19**$^{+\cdot}$ is associated with the methoxy group. There is significant charge on the carbon bearing the methoxy group. It is plausible that nucleophilic (methanol) attack occurs at this *ipso* position. However, there was no evidence for exchange of the methoxy-methyl group when the irradiation of either **18** or **19** was carried out under the usual conditions, but with acetonitrile–methanol-d_4 (3:1) as the solvent.

The difference in reactivity of the radical cations of *meta*- and *para*-substituted anisoles has been observed before. The side-chain oxidation, promoted either electrochemically or chemically (by cerium(IV) ammonium nitrate), of 5-substituted-1,2,3-trimethylbenzenes has been investigated, and the relative reactivity of the 2- and 1-methyl groups has been determined (27). Both reactions show similar substituent effects. The 2-methyl group is selectively attacked when the substituent is methoxy ($k_2/k_1 > 200$; no product of reaction at the 1-methyl was observed). This selectivity was similarly attributed to the electronic distribution in the radical cation, the key step in the reaction being deprotonation.

The oxidation of **17** and **18** with Co(III) (LiCl) has been studied (28). Products resulting from both side-chain oxidation and substitution in the ring were obtained upon oxidation of the *meta* isomer (substitution/side chain = 38%/3%). On the other hand, there was no substitution in the ring in the case of the *para* isomer (side-chain oxidation product, 65%).

Perspective

The scope and limitations of reactions of the type illustrated in reactions [1]–[3] can be defined by consideration of each step in the mechanistic schemes (Schemes 1–3). These are complex reactions. Several highly reactive species are involved. Frequently, the ultimate result of a particular irradiation will depend upon the ratios of several competing rapid processes. One of these processes will always be deactivation by back-electron transfer, in which case, no reaction will occur.

The explanations offered to explain the results depend upon thermochemical considerations, knowledge of the conforma-

[6]The acidity of the bis-benzylic hydrogen of the radical cation of 1,1-diphenylethane can be estimated from the bond dissociation free energy ($\Delta G^0_{BDE(RH)}$) and the standard oxidation potential (E^0_{RH}) using Method 1 (eq. [19]) described in 25*a*. The required data are $\Delta H_{BDE(RH)} = 339 \pm 8$ kJ mol^{-1} (26*a*); $\Delta S_{BDE(RH)} = 110 \pm 4$ J mol^{-1} (26*b*); so that $\Delta G^0_{BDE(RH)} = 316 \pm 25$ kJ mol^{-1}. $E^{ox}_{1/2} = 2.13$ V (vs. sce) (Table 1); accepting this value as an estimate of the standard oxidation potential, $E^0_{RH} = 2.37$ V (vs. standard hydrogen electrode); $\Delta G^0_{tr(H^+)CH_3CN} = 46.0$ kJ mol^{-1} (26*d*); $\Delta G^0_{f(H)g} = 203.2$ kJ mol^{-1} (26*c*).

tion of the reactant, and information concerning the electronic configuration and spin and charge distribution of the radical ions. While much remains to be done before the scope and limitations of these reactions will be defined, progress has been made. Clearly the effort to develop these reactions will continue — they are potentially useful.

Experimental

General information

The ^{1}H nmr spectra were recorded on a Varian Associates EM360L or a Nicolet narrow bore 360 MHz spectrometer and are reported in parts per million (δ) downfield from tetramethylsilane (TMS). The ^{13}C nmr spectra were recorded on the Nicolet spectrometer operating at 90 MHz. Infrared spectra were recorded on a Perkin Elmer 283B spectrometer and are reported in wavenumbers (ν) relative to the 1601.8 cm^{-1} absorption of polystyrene.

Irradiations were generally carried out through Pyrex using acetonitrile–methanol (3:1) as the solvent and 1,4-dicyanobenzene (**3**) as the electron-accepting photosensitizer. Irradiations at 10°C utilized a 1-kW medium-pressure mercury vapour lamp (CGE HR 1000 DX 36-15) with a quartz cooling jacket immersed in a constant temperature bath. A Hanovia 450-W medium-pressure mercury vapour lamp with a quartz cooling jacket was used for irradiations carried out at 80°C. The irridiation tubes were placed in a Pyrex vessel with a built-in cooling jacket that also serves as a short-wavelength (<280 nm) filter, connected to a circulating water bath (Julabo model F10V).

Progress of the irradiations was followed by gas chromatography (gc) on a Hewlett Packard 5890A instrument with a Hewlett Packard 5970 mass selective detector (ms) interfaced with a Hewlett Packard 9816 microcomputer. The column was 25 m × 0.2 mm, 5% phenyl methyl silicone on fused silica, with a film thickness of 0.25 μm. Quantitative gas chromatography was carried out on a Hewlett Packard 5890A gc fitted with an OV-1701 column (30 m × 0.26 mm, 0.25 μm film thickness) and a flame ionization detector (fid). The digital signal from the detector was transmitted to a Hewlett Packard 3392A integrator and acquired on a Commodore PC-II. A Varian Aerograph 1200 gc (column: 5 m × 0.53 mm, methyl silicone on fused silica) was also used for analyses. An Aerograph Autoprep A-700 gc using a 1.8 m × 1 cm aluminum column packed with 10% SE-30 on Chromosorb 60/80 NAW was used for isolating samples for analytical purposes. Preparative medium-pressure liquid chromatography (MPLC) was carried out using a 1 m × 2.5 cm column packed with TLC grade silica gel (Merck, without binder) at 14 psi helium (1 psi = 6.89 kPa). The columns were eluted with a solvent gradient, usually hexanes – methylene chloride, and the eluent was monitored by a UV spectrophotometer – fraction collector. Flash chromatography was performed by the method developed by W. C. Still (29) using 200–425 mesh silica gel (Mallinckrodt, 60 A or Baker 40).

Cyclic voltammetry was used to measure the oxidation potentials reported in Table 1. The apparatus has been described previously (30). The working electrode was a platinum sphere (1 mm), the counter electrode was a platinum wire, and a saturated calomel electrode was used as the reference. The electrolyte was tetraethylammonium perchlorate (0.1 M), the solvent was freshly distilled acetonitrile, and the concentration of substrate was approximately 1 mM. Since the cyclic voltammograms indicated that the oxidation processes were not reversible, the half-wave potentials could not be determined directly. The half-wave potential can be estimated as 0.028 V before the anodic peak potential (10).

Materials

Solvents were distilled prior to use. Acetonitrile (Fisher ACS grade) was distilled successively from sodium hydride and phosphorus pentoxide, passed through a column of basic alumina, then refluxed over calcium hydride for 24 h under a nitrogen atmosphere, and finally fractionally distilled. 1,4-Dicyanobenzene (Aldrich) was purified by treatment with decolorizing carbon (Norite) in methylene chloride, sublimation, and then recrystallization from 95% ethanol. Tetraethylammonium perchlorate (Aldrich) was recrystallized from 95% ethanol and then dried in a vacuum oven for 12 h at 80°C. 3-Methoxyacetophenone, 4-methoxyacetophenone, α-methoxyacetophenone, bromobenzene, 3-bromoanisole, 4-bromoanisole, indanone, and the borane–tetrahydrofuran complex were obtained from Aldrich Chemical Co., and were used without further purification.

1-(3-Methoxyphenyl)-1-phenylethylene (7)

This alkene (**7**) was prepared by dehydration of the alcohol formed by the Grignard reaction involving 3-methoxyacetophenone (7 g, 0.047 mol) and phenylmagnesium bromide from bromobenzene (7 g, 0.045 mol). The Grignard reaction mixture was worked up by pouring over cold, concentrated hydrochloric acid (6M). The product was extracted into ether. The ether extract was washed with saturated aqueous sodium bicarbonate and sodium chloride. The extract was then dried over magnesium sulphate, and the solvent was evaporated to give the alkene (**7**), which was purified by flash chromatography to a colourless oil. 1-(3-Methoxyphenyl)-1-phenylethylene (**7**) (6.7 g, 77%): ir (neat) ν: 3079 (w), 2951 (w), 2837 (w), 2362 (w), 1599 (m), 1575 (s), 1487 (s), 1429 (s), 1239 (s), 1047 (s), 896 (s), 775 (s), 685 (s); ^{1}H nmr (360 MHz, $CDCl_3$) δ: 7.34 (m, 9H), 5.44 (s, 2H), 3.74 (s, 3H); ^{13}C nmr ($CDCl_3$) δ: 159.43, 149.92, 142.94, 141.3, 129.05, 128.18, 128.09, 127.66, 120.84, 113.96, 113.16, 55.16.

1-(4-Methoxyphenyl)-1-phenylethylene (8)

A small amount of bromobenzene was added to a flask containing magnesium metal turnings (1.3 g, 0.058 mol) and an iodine crystal in ether (100 mL), and the reaction started immediately. A solution of bromobenzene (7.0 g, 0.045 mol) in ether (40 mL) was added slowly. Once the addition was complete, the reaction mixture was stirred at room temperature for 1 h. The mixture was then cooled to 0°C with an ice bath, and 4-methoxyacetophenone (7.0 g, 0.045 mol) in ether (40 mL) was added dropwise. This mixture was stirred for 24 h at room temperature, poured into a beaker of ice and concentrated hydrochloric acid, and extracted with ether. The ether extract was washed successively with saturated aqueous sodium bicarbonate and saturated aqueous sodium chloride, and then dried over magnesium sulphate. Evaporation of the solvent gave a light yellow solid, which was purified by flash chromatography, eluting with hexanes–ether (7:3), to give the alkene (**8**) as a colourless solid that was recrystallized from hexane (mp 74.7–75.0°C, 7.5 g, 80%); ir (KBr disc) ν: 3007 (w), 2937 (w), 2952 (w), 2835 (w), 1598 (s), 1600 (s), 1489 (s), 1286 (s), 1242 (s), 1110 (m), 1023 (s), 897 (s), 835 (s), 779 (s), 702 (s); ^{1}H nmr (360 MHz, $CDCl_3$) δ: 7.10 (m, 9H), 5.39 (d, 1H, J = 1.26 Hz), 5.35 (d, 1H, J = 1.26 Hz), 3.83 (s, 3H); ^{13}C nmr ($CDCl_3$) δ: 129.33, 128.26, 128.06, 127.58, 127.45, 113.45, 112.88, 77.32, 76.97, 76.62, 55.27.

3-(3-Methoxyphenyl)indene (9)

Additon of the Grignard reagent prepared from 3-bromoanisole (10.75 g, 0.058 mol) to indanone (6.7 g, 0.051 mol), followed by the strong hydrochloric acid work-up, gave 2-(3-methoxyphenyl)indene (**9**) (7.2 g, 73%); ir (neat) ν: 3062 (w), 2937 (w), 2837 (w), 1597 (m), 1577 (s), 1485 (s), 1475 (s), 1282 (s), 1231 (s), 1048 (s), 768 (s), 717 (s), 694 (s); ^{1}H nmr (60 MHz, $CDCl_3$) δ: 7.2 (m, 8H), 6.3 (s, 1H), 3.7 (s, 3H), 3.4 (s, 2H); ^{13}C nmr ($CDCl_3$) δ: 159.65, 144.99, 144.63, 143.69, 137.39, 130.89, 129.46, 126.06, 124.78, 123.99, 120.23, 120.05, 113.16, 112.95, 55.00, 38.03.

3-(4-Methoxyphenyl)indene (10)

To a flask containing magnesium metal turnings (1.4 g, 0.057 mol) and an iodine crystal, in anhydrous ether (50 mL), a small portion of 4-bromoanisole was added and the mixture was heated until the reaction started. A soluton of 4-bromoanisole (10.8 g, 0.058 mol) in ether (60 mL) was added slowly to the reaction mixture. When the addition was complete, the mixture was refluxed for 1 h, then cooled to room temperature, and a solution of indanone (6.7 g, 0.051 mol) in ether (60 mL) was added dropwise. This reaction mixture was refluxed for 1 h and was then stirred overnight at room temperature. The reaction mixture was poured onto a slurry of ice and concentrated hydrochloric acid; this mixture was then extracted with diethyl ether. The extract was washed with saturated aqueous sodium bicarbonate and with saturated aqueous sodium chloride, and then dried over magnesium sulphate.

Can. J. Chem. Downloaded from www.nrcresearchpress.com by 198.100.157.202 on 09/07/12
For personal use only.

Can. J. Chem. Downloaded from www.nrcresearchpress.com by 198.100.157.202 on 09/07/12
For personal use only.

The solvent was evaporated to give a dark yellow oil. By working up the reaction mixture with strong hydrochloric acid, the initally formed indanol was dehydrated directly to the indene. The crude product was purified by flash chromatography, eluting with hexanes, to give 3-(4-methoxyphenyl)indene (**10**) as a colourless low melting (54.8–55.8°C) solid (9.1 g, 0.041 mol, 80%); ir (KBr disc) ν: 3020 (w), 2958 (w), 2940 (w), 1613 (m), 1508 (s), 1460 (s), 1255 (s), 1239 (s), 1176 (s), 1025 (s), 835 (s), 772 (s), 757 (s), 716 (s); ^{1}H nmr (360 MHz, $CDCl_3$) δ: 7.58 (dm, 1H, J = 7.6 Hz), 7.54 (d, 2H, J = 8.83 Hz), 7.51 (dm, 1H, J = 7.6 Hz), 7.31 (tm, 1H, J = 7.6 Hz), 7.24 (td, 1H, J = 7.6, 1.2 Hz), 6.97 (d, 2H, J = 8.83 Hz), 6.49 (t, 1H, J = 2.2 Hz), 3.83 (s, 3H), 3.47 (d, 2H, J = 2.2 Hz); ^{13}C nmr ($CDCl_3$) δ: 159.2, 144.7, 144.5, 144.1, 129.7 (two carbons), 129.0, 128.8, 126.0, 124.7, 124.0 (two carbons), 120.2, 114.0, 55.3, 38.0; ms, m/z (relative intensity): 222 (100), 207 (46), 179 (25), 178 (43).

*Methyl 2-(3-methoxyphenyl)-2-phenylethyl ether (**11**)*

1-(3-Methoxyphenyl)-1-phenylethylene (**7**) (1.0 g, 5 mmol) and 1,4-dicyanobenzene (**3**) (0.041 g, 0.32 mmol) were dissolved in acetonitrile–methanol (3:1) (30 mL) and irradiated through Pyrex. After 6 h irradiation, essentially all of the alkene had been converted to the *anti*-Markovnikov methanol addition product (**11**); 1,4-dicyanobenzene (**3**) was unchanged. The solvent was evaporated and the resulting yellow residue was purified by flash chromatography using hexanes–ether (7:3) as the eluent. The ether (**11**) was obtained, in good yield, as a colourless oil (1.1 g, 96%); ir (neat) ν: 3095 (w), 3054 (w), 3032 (w), 2932 (m), 2896 (m), 2876 (m), 2836 (m), 1600 (s), 1582 (s), 1491 (s), 1450 (s), 1258 (s), 1148 (m), 1115 (s), 1140 (m), 694 (s); ^{1}H nmr (360 MHz, $CDCl_3$) δ: 7.02 (m, 9H), 4.28 (t, 1H, J = 7.36 Hz), 3.91 (d, 2H, J = 7.36 Hz), 3.77 (s, 3H), 3.37 (s, 3H); ^{13}C nmr ($CDCl_3$) δ: 143.64, 141.87, 129.35, 120.37, 77.205, 75.89, 58.91, 55.09, 50.99. Exact Mass calcd. for $C_{16}H_{18}O_2$: 242.1307; found: 242.1304.

*Methyl 2-(4-methoxyphenyl)-2-phenylethyl ether (**12**)*

Attempts to make the ether **12**, by the photosenstized (electron transfer) addition of methanol to the alkene (**8**) were unsuccessful. Two alternative methods were used.

Method 1

To a flask containing 1-(4-methoxyphenyl)-1-phenylethylene (**8**) (2.62 g, 0.0125 mol), a tetrahydrofuran solution of the boron hydride–tetrahydrofuran complex (13.5 mL of 1.0 M, 0.013 mol) was added slowly and the reaction was stirred overnight. The reaction mixture was poured into water (50 mL) and an aqueous solution of sodium hydroxide and hydrogen peroxide (15 mL of 6 M NaOH in 20 mL of 30% H_2O_2) was added dropwise. This mixture was stirred for 2 h at room temperature. The product was extracted into ether and washed with saturated aqueous solutions of ammonium chloride and sodium chloride (Rochelle salt was added to help break up the emulsion that formed). The ether layer was dried over magnesium sulphate and the solvent was evaporated. 2-(4-Methoxyphenyl)2-phenyl-1-ethanol (2.6 g, 93%) was obtained as a colourless oil. This alcohol was used in the next step, without further purification; ^{1}H nmr (360 MHz, $CDCl_3$) δ: 7.20 (m, 9H), 4.07 (s, 1H), 4.04 (s, 2H), 3.70 (s, 3H).

The alcohol described above (2.6 g, 0.011 mol) was added to a suspension of sodium hydride (4.2 g, 0.199 mol) in ether (60 mL) and the mixture was stirred, under nitrogen, for 1 h. Dimethyl sulphate (4.3 mL, 0.046 mol) was added and the mixture was heated under reflux for 20 h. The work-up involved pouring the reaction mixture into saturated aqueous ammonium chloride, and separating the ether layer, which was then stirred over an aqueous ammonium hydroxide solution. The ether extract was washed with water and saturated aqueous sodium chloride and then dried over magnesium sulphate. Evaporation of the solvent gave the crude product, which was purified by flash chromatography, eluting with hexanes–ether (3:1), to give methyl 2-(4-methoxyphenyl)-2-phenylethyl ether (**12**) as a colourless oil (2.5 g, 93%); ir (neat) ν: 3050 (w), 3036 (w), 2934 (w), 2836 (w), 1610 (m), 1510 (s), 1490 (m), 1448 (m), 1246 (s), 1172 (m), 1116 (m), 1102 (m), 1030 (m), 692 (m); ^{1}H nmr (360 MHz, $CDCl_3$) δ: 7.02 (m, 9H), 4.21 (t, 1H, J = 7.25 Hz), 3.84 (d, 2H, J = 7.25 Hz), 3.67 (s, 3H), 3.31 (s, 3H)); ^{13}C nmr ($CDCl_3$) δ: 158.10, 142.39, 134.23, 129.03, 128.39, 113.83, 77.34, 58.87, 55.18, 50.11. Exact Mass calcd. for $C_{16}H_{18}O_2$: 242.1307; found: 242.1302.

Method 2

A small amount of 4-bromoanisole was added to a flask fitted with an overhead mechanical stirrer and containing magnesium metal turnings (1.4 g, 0.061 mol), an iodine crystal, and ether (60 mL). The mixture was heated until the reaction started. An ether solution of 4-bromoanisole (10 g, 0.054 mol in 40 mL) was added slowly, then the mixture was heated under reflux for 1 h, cooled, and a solution of α-methoxyacetophenone (7.6 g, 0.051 mol) in ether (60 mL) was added dropwise. The resulting mixture was refluxed 1 h and was then allowed to stir overnight at room temperature. The reaction mixture was poured into a beaker of ice and hydrochloric acid (6 M). The organic layer was separated, washed with saturated aqueous sodium bicarbonate and saturated aqueous sodium chloride, dried over magnesium sulphate, and the solvent was evaporated. The resulting yellow oil was chromatographed over silica gel, eluting with a hexanes–ether gradient. 2-Methoxy-1-(4-methoxyphenyl)-1-phenylethanol (8.2 g, 68%) was obtained as a colourless oil. This alcohol was used in the next step without further purification.

To a flask containing aluminium trichloride (9.0 g, 0.093 mol) in ether (100 mL), lithium aluminium hydride (1.7 g, 0.045 mol) was added slowly and the mixture was allowed to stir at room temperature for 1 h. To this complex, a solution of 2-methoxy-1-(4-methoxyphenyl)-1-phenylethanol (4.2 g, 0.027 mol) in ether (60 mL) was added dropwise. This reaction was refluxed for 24 h, cooled to room temperature, and was then poured into aqueous sodium hydroxide (6.0 M, 100 mL) and extracted with ether. The ether extract was washed successively with water and saturated aqueous sodium chloride, and was then dried over magnesium sulphate. The solvent was evaporated to give methyl 2-(4-methoxyphenyl)-2-phenylethyl ether (**12**), a yellow oil (3.2 g, 69%), which has been described above.

*The photosensitized (electron transfer) irradiation of 1-(4-methoxyphenyl)-1-phenylethylene (**8**) in acetonitrile–methanol*

A solution of 1-(4-methoxyphenyl)-1-phenylethylene (**8**) (1.28 g, 6.1 mmol) and 1,4-dicyanobenzene (**3**) (0.65 g, 5.1 mmol) in acetonitrile–methanol (3:1) (122 mL) was irradiated, through Pyrex, with the 1-kW mercury vapour lamp for 72 h. Analysis (gc/ms) indicated that reaction was complete, **8** was consumed, and that the *anti*- Markovnikov additon product (**12**) of methanol to the alkene was a minor (<5%) product. The structure of **12** was established by comparison (gc/ms, retention time, and mass spectral fragmentation pattern) with an authentic sample; ms, m/z (relative intensity): 242 (4.9), 197 (100; $C_{14}H_{13}O$), 182 (9.4), 165 (13.0), 153 (18.9), 91 (3.1), 77 (4.7).

The solvent was evaporated and the crude reaction mixture was separated from unreacted **3** by dry-column flash chromatography using ethyl acetate (6%) in hexane as the eluent. A colourless oil (80%), giving one peak in the gc/ms, was obtained in the early fractions. The assigned structure (**15**), a mixture of the diastereomers, was based upon the ^{1}H and ^{13}C nmr and mass spectra. The ^{1}H nmr spectrum of the two diastereomers were indistinguishable; ^{1}H nmr (360 MHz, $CDCl_3$) δ: 7.28–7.00 (m, 14H), 6.77–6.73 (two overlapping doublets, 4H, J = 8 Hz), 3.74 (t, 1H, J = 7.99 Hz, coupled to the proton at 1.95–1.76 ppm), 3.698 (s, 3H), 3.684 (s, 3H), 2.93 (s, 3H), 2.28–2.14 (m, 2H), 1.95–1.76 (m, 2H). The proton decoupled ^{13}C nmr spectrum showed pairs of peaks for some of the carbons indicative of two diastereomers; ^{13}C nmr ($CDCl_3$) δ: 158.05 (s), 157.73 (s), 145.65 (s), 145.40 (s), 137.39 (s), 137.13 (s),128.59 (d), 128.30 (d), 128.09 (d), 127.74 (d), 127.59 (d), 126.72 (d), 126.38 (d), 125.92 (d), 113.68 (d), 113.07 (d), 81.99 (s), 55.13 (q), 50.56 (d), 49.86 (q), 33.47 (t), 28.83 (t); ms, m/z (relative intensity): 422 (0.8), 421 (0.4), 420 (0.9), 419 (1.3), 418 (3.1), 227 (16.1; $C_{15}H_{15}O_2$), 223 (69.2), 210 (16.1), 197 (100; $C_{14}H_{13}O$), 165 (10.6), 153 (9.1), 115 (21.0), 91 (8.7), 77 (2.6).

This initial product (**15**) is unstable; loss of methanol occurs when the sample is stored over a period of days at room temperature. The final product is a mixture (ca. 1:1) of *Z*- and *E*-1,4-di(4-methoxy-

Can. J. Chem. Downloaded from www.nrcresearchpress.com by 198.100.157.202 on 09/07/12
For personal use only.

phenyl)-1,4-diphenyl-1-butene (**16** *Z* and *E*). These isomers were separated by gc/ms and were partially separated upon medium-pressure column chromatography (MPLC) using a solvent gradient of toluene – ethyl acetate. **16***Z*, colourless crystals from hexane – methylene chloride, mp 115.4–115.6°C; ir (KBr disc) ν: 3046 (m), 3016 (m), 2986 (w), 2946–2886 (s), 2828 (s), 1603 (vs),1583 (m), 1503 (vs), 1460 (s), 1441 (s), 1303 (s), 1283 (s), 1244 (vs), 1173 (vs), 1156 (s), 1030 (vs), 815 (vs), 775 (s), 755 (s), 695 (vs); ^{1}H nmr (360 MHz, $CDCl_3$) δ: 7.34–6.97 (m, 14H), 6.77 (d, 2H, J = 8.43 Hz), 6.71 (d, 2H, J = 8.63 Hz), 5.88 (t, 1H, J = 7.15 Hz), 4.01 (t, 1H, J = 7.9 Hz), 3.70 (s, 3H), 3.69 (s, 3H), 2.80 (t, 2H, J = 7.59); ^{13}C nmr ($CDCl_3$) δ: 158.69 (s), 157.91 (s), 144.82 (s),142.03 (s), 140.34 (s), 136.58 (s), 135.42 (s), 129.80 (d), 128.94 (d), 128.28 (d), 128.10 (d), 127.93 (d), 126.86 (d), 126.23 (d), 126.02 (d), 113.73 (d), 113.58 (d), 113.39 (d), 55.30 (q), 50.92 (d), 36.01 (t). The mass spectra of the *E* and *Z* isomers were essentially the same: ms, m/z (relative intensity): 422 (0.1), 421 (0.4), 420 (0.9), 419 (0.8), 418 (1.8), 223 (62.1), 197 (100; $C_{14}H_{13}O$), 165 (12.5), 153 (9.8), 115 (23.4), 91 (6.5), 77 (1.6). Anal. calcd. for $C_{30}H_{28}O_2$: C 85.68, H 6.71; found: C 85.51, H 6.76. **16***E* was not completely separated from the *Z* isomer by MPLC; ^{1}H nmr (360 MHz, $CDCl_3$) δ: 5.91 (t, 1H, J = 7.07 Hz), 4.04 (t, 1H, J = 7.53 Hz), 3.76 (overlapping singlets, 6H), 2.85 (t, 2H, J = 7.52).

*The photosensitized (electron transfer) irradiation of 1-(4-methoxyphenyl)-1-phenylethylene (**8**) in acetonitrile – deuterated methanol*

The irradiation of **8** was carried out as described above except the solvent was acetonitrile–methanol-*O*-*d* (3:1). Under these conditions the base peak in the mass spectrum of **12**, **15**, and **16** *Z* and *E* was m/z = 198 ($C_{14}H_{12}DO$), instead of 197. This is consistent with the incorporation of one deuterium atom at the bis-benzylic position of these products. When methanol-d_4 was used in the solvent mixture instead of methanol, the large peak in the mass spectrum of **15** at m/z = 227 was replaced by one at 230 ($C_{15}H_{12}D_3O_2$) indicating the incorporation of the deuterated methoxy group.

cis-*(and* trans-*)2-Methoxy-1-(3-methoxyphenyl)indane (**13**)*

These *meta*-methoxy isomers were prepared by the methods described above for the analogous acyclic analogue (**11**).

Method 1

The *trans* isomer was obtained by the Grignard reaction, hydroboration, oxidation, methylation sequence.

Hydroboration of the indene (**9**) (9.1 g, 0.041 mol) with boron–tetrahydrofuran (40 mL) followed by oxidative work-up, as described above for the preparation of **11**, gave *trans*-1-(3-methoxyphenyl)-2-indanol (3.84 g, 50%), which was used in the next step without further purification.

Methylation of *trans*-1-(3-methoxyphenyl)2-indanol (3.8 g, 0.016 mol) by the NaH, dimethyl sulphate procedure gave *trans*-2-methoxy-1-(3-methoxyphenyl)indane (**13***trans*) (3.2 g, 79%); ir (neat) ν: 3080 (w), 3010 (w), 2920 (m), 2816 (m), 1600 (s), 1582 (s), 1484 (s), 1456 (s), 1434 (m), 1256 (s), 1246 (m), 1110 (s), 1096 (m), 1046 (m), 736 (s); ^{1}H nmr (360 MHz, C_6D_6) δ: 6.95 (m, 8H), 4.39 (d, 1H, J = 6.31 Hz), 4.09 (ddd, 1H, J = 6.31, 6.52, 6.84 Hz), 3.33 (s, 3H), 3.11 (dd, 1H, J = 6.84, 15.70 Hz), 3.10 (s, 3H), 2.89 (dd, 1H, J = 6.52, 15.70 Hz); ^{13}C nmr (C_6D_6) δ: 160.05, 145.36, 140.87, 129.78, 126.54, 125.57, 124.80, 121.14, 114.82, 112.26, 90.85, 58.40, 57.18, 54.71, 38.15.

Method 2

Irradiation of 3-(3-methoxyphenyl)indene (**9**) in acetonitrile–methanol gave a mixture of the *cis* and *trans anti*-Markovnikov methanol addition products (**13** *cis* and *trans*).

A solution of 3-(3-methoxyphenyl)indene (**9**) (0.70 g, 0.3 mmol), and 1,4-dicyanobenzene (**3**) (0.58 g, 0.5 mmol) in acetonitrile–methanol (3:1) (20 mL) was irradiated, through Pyrex, with the 1-kW mercury vapour lamp for 36 h. Analysis (gc/ms) indicated that reaction was complete, with formation of the *anti*-Markovnikov addition products of methanol to the alkene. Both the *cis* and *trans* isomers were formed (*cis*/*trans* = 7:3). The solvent was evaporated and the products were separated by MPLC (74% combined yield). *cis*-2-Methoxy-1-(3-methoxyphenyl)indane (**13***cis*): ^{1}H nmr (360 MHz, C_6D_6) δ: 7.02 (m, 8H), 4.27 (d, 1H, J = 6.17 Hz), 3.98 (ddd, 1H, J = 6.02, 6.17, 4.27 Hz), 3.38 (s, 3H), 3.12 (dd, 1H, J = 15.90, 4.27 Hz), 2.95 (s, 3H), 2.91 (dd, 1H, J = 15.90, 6.03 Hz); ^{13}C nmr (C_6D_6) δ: 160.05, 144.6, 141.2, 129.02, 126.54, 125.59, 124.79, 121.18, 114.80, 112.29, 90.88, 58.42, 57.19, 54.67, 38.15. Anal. calcd. for (**13***cis*) $C_{17}H_{18}O_2$: C 80.28, H 7.13; found: C 80.63, H 7.25.

trans-*2-Methoxy-1-(4-methoxyphenyl)indane (**14**trans)*

Key steps in this synthetic sequence involve the hydroboration of the indene (**10**) followed by oxidation to the *trans*-indanol and methylation. This reaction sequence yields exclusively the *trans* isomer (**14***trans*) (Scheme 4).

A solution of the borane–tetrahydrofuran complex in tetrahydrofuran (1.0 M, 40 mL, 0.040 mol) was added through a gas-tight syringe, to a flask containing 3-(4-methoxyphenyl)indene (**10**) (9.1 g, 0.041 mol) under nitrogen. This mixture was refluxed for 18 h and was then poured into water (50 mL). The reaction was cooled in ice and a solution of sodium hydroxide (6.0 M, 30 mL) and hydrogen peroxide (30%, 25 mL) was added dropwise. The reaction mixture was stirred at room temperature for 1 h and was then extracted with diethyl ether. The extract was washed successively with water, saturated aqueous ammonium chloride, and saturated aqueous sodium chloride, and was then dried over magnesium sulphate. Evaporation of the solvent gave *trans*-1-(4-methoxyphenyl)-2-indanol, which was purified by recrystallization from 95% ethanol to colourless needles, mp 109.2–109.8°C (9.0 g, 90%); ^{1}H nmr (360 MHz, $CDCl_3$) δ: 7.26–7.12 (m, 3H), 7.10 (d, 2H, J = 8.71 Hz), 6.92 (d, 1H, J = 7.30 Hz), 6.87 (d, 2H, J = 8.71 Hz), 4.43 (ddd, 1H, J = 6.86, 6.94, 7.46 Hz), 4.11 (d, 1H, J = 6.94 Hz), 3.79 (s, 3H), 3.28 (dd, 1H, J = 15.52, 6.86 Hz), 2.93 (dd, 1H, J = 15.52, 7.46 Hz. 2.14 (s, (OH), 1H); ^{13}C nmr ($CDCl_3$) δ: 158.7, 143.9, 140.3, 133.8, 129.4 (two carbons), 127.2, 127.0, 125.2, 124.6, 114.2 (two carbons), 82.3, 59.5, 55.3, 40.1.

A solution of *trans*-1-(4-methoxyphenyl)-2-indanol (7.18 g, 0.030 mol) in diethyl ether was added slowly to a suspension of NaH (7.2 g, 0.300 mol) in ether (60 mL), which was then stirred at room temperature for 1 h. Dimethyl sulphate (11.3 g, 0.090 mol) was added to the mixture, which was then heated under reflux for 24 h. The reaction mixture was then poured onto an ice–concentrated hydrochloric acid mixture. The product was extracted into ether, which was then stirred over aqueous ammonia for 2 h to remove excess dimethyl sulphate. The ether layer was successively washed with water and saturated aqueous sodium chloride, and was then dried over magnesium sulphate. The solvent was evaporated to give a yellow oil (7.5 g). This crude product was chromatographed over silica gel, eluting with a hexane–ether gradient, to give *trans*--2-methoxy-1-(4-methoxyphenyl)indane (**14***trans*) (5.3 g, 73%) as a colourless oil; ir (neat) ν: 3004 (w), 3000 (w), 2916 (m), 2901 (m), 2816 (m), 1610 (m), 1510 (s), 1456 (m), 1300 (w), 1246 (s), 1175 (m), 1110 (m), 1030 (m), 740 (m); ^{1}H nmr (300 MHz, $CDCl_3$) δ: 7.26–7.14 (m, 3H), 7.10 (d, 2H, J = 8.60 Hz), 6.91 (d, 1H, J = 7.17 Hz), 6.86 (d, 2H, J = 8.60 Hz), 4.27 (d, 1H, J = 6.27 Hz), 4.12 (ddd, 1H, J = 6.27, 6.42, 6.71 Hz), 3.80 (s, 3H), 3.35 (s, 3H), 3.33 (dd, 1H, J = 15.73, 6.71 Hz), 2.93 (dd, 1H, J = 15.73, 6.42 Hz); ^{13}C nmr (C_6D_6) δ: 158.98, 144.94, 140.80, 135.64, 129.80, 128.26, 128.00, 127.73, 127.25, 125.52, 124.80, 114.32, 91.14, 57.48, 57.25, 54.79, 38.09. Anal. calcd. for (**14***trans*) $C_{17}H_{18}O_2$: C 80.28, H 7.13; found: C 80.06, H 7.13.

*cis-2-Methoxy-1-(4-methoxyphenyl)indane (**14** cis)*

3-(4-Methoxyphenyl)indene (**10**) was stable to photosensitized (electron transfer) irradiation in acetonitrile–methanol. *cis*-2-Methoxy-1-(4-methoxyphenyl)indane (**14***cis*) was isolated from the irradiation mixture following the photosensitized (electron transfer) isomerization of *trans*-2-methoxy-(4-methoxyphenyl)indane (**14***trans*).

A solution of *trans*-2-methoxy-(4-methoxyphenyl)indane (**14***trans*) (0.4 g, 1.6 mmol) and 1,4-dicyanobenzene (**3**) (0.15 g, 1.2 mmol) in acetonitrile–methanol (3:1) (30 mL) was irradiated at 10°C through Pyrex with a 1-kW mercury vapour lamp. Progess of the reaction was followed by gc/ms. After 12 h of irradiation the gc/ms indicated that

Can. J. Chem. Downloaded from www.nrcresearchpress.com by 198.100.157.202 on 09/07/12
For personal use only.

14*cis* had formed; **14***cis* / **14***trans* (4:6). The solvent was evaporated and the products were separated by MPLC using a hexanes–ether gradient. cis-2-Methoxy-1-(4-methoxyphenyl)indane (**14***cis*): ^{1}H nmr (300 MHz, $CDCl_3$) δ: 7.29 (d, 1H, J = 6.91 Hz), 7.23–7.13 (m, 2H), 7.09 (d, 2H, J = 8.7 Hz), 7.04 (d, 1H, J = 7.20 Hz), 6.84 (d, 2H, J = 8.7 Hz), 4.42 (d, 1H, J = 6.2 Hz), 4.23 (ddd, 1H, J = 6.20, 5.84, 4.83 Hz), 3.79 (s, 3H), 3.16 (dd, 1H, J = 15.98, 5.84 Hz), 3.13 (s, 3H), 3.09 (dd, 1H, J = 15.98, 4.83 Hz); ^{13}C nmr ($CDCl_3$) δ: 158.3, 144.7, 140.9, 131.3, 130.7, 126.9, 126.8, 125.2, 124.7, 113.4, 85.0, 57.7, 55.1, 54.5, 37.8.

*The photosensitized (electron transfer) irradiation of 3-(4-methoxyphenyl)indene (**10**) in acetonitrile–methanol*

An acetonitrile–methanol (3:1) (30 mL) solution of **10** (200 mg, 0.90 mmol) and **3** (40 mg, 0.31 mmol) was irradiated, under the conditions described above, for 40 h. Analysis (gc/ms) of the photolysate indicated that neither **14***cis* nor **14***trans* was formed.

*The photosensitized (electron transfer) irradiation of methyl 2-(3-methoxyphenyl)-2-phenylethyl ether (**11**) in acetonitrile–methanol*-O-d

An acetonitrile–methanol-*O-d* (3:1) (30 mL) solution of **11** (200 mg, 0.83 mmol) and **3** (70 mg, 0.55 mmol) was irradiated, under the conditions described above, for 50 h. Analysis (gc/ms) of the photolysate indicated that no reaction had occurred.

*The photosensitized (electron transfer) irradiation of methyl 2-(4-methoxyphenyl)-2-phenylethyl ether (**12**) in acetonitrile–methanol*-O-d

An acetonitrile–methanol-*O-d* (3:1) (30 mL) soluton of **12** (700 mg, 2.9 mmol) and **3** (200 mg, 1.6 mmol) was irradiated, under the conditions described above, for 8 h. Analysis (gc/ms) of the photolysate indicated that ca. 70% of one deuterium was incorporated at the bis-benzylic position.

The photosensitized (electron transfer) irradiation of trans-*3-methoxy-2-(3-methoxyphenyl)indane (**13**) in acetonitrile–methanol*-O-d

An acetonitrile–methanol-*O-d* (3:1) (25 L) soluton of **13** (586 mg, 2.3 mmol) and **3** (160 mg, 125 mmol) was irradiated, under the conditions described above, for 100 h. Analysis (gc/ms) of the photolysate indicated that no reaction had occurred.

The photosensitized (electron transfer) irradiation of trans-*2-methoxy-1-(4-methoxyphenyl)indane (**14**trans) in acetonitrile–methanol*-O-d

A solution of *trans*-2-methoxy-1-(4-methoxyphenyl)indane (**14***trans*) (20 mg, 0.078 mmol) and 1,4-dicyanobenzene (**3**) (2.7 mg, 0.0215 mmol) in acetonitrile–methanol-*O-d* (3:1, 2 mL), in a Pyrex tube, was irradiated at 10°C with the 1-kW mercury vapour lamp. Progress of the reaction was followed by gc/ms. The increase in the abundance of the M + 1, M + 2, and M + 3 peaks in the mass spectrum was monitored using the selected ion monitor acquisition mode. The contribution due to naturally occurring ^{13}C was subtracted and the relative abundance of each peak was used to calculate the percent deuterium incorporation. After 100 h of irradiation, deuterium (48% of one deuterium) was incorporated in the *trans* isomer and in the *cis* isomer (100% of one deuterium). The *trans* isomer was isolated; the ^{1}H nmr spectrum showed that the original quartet-like coupling pattern at 4.12 ppm had partly become a triplet-like pattern. Integration indicates that 12.8% deuterium incorporation had occurred at 4.27 ppm (carbon 1, the bis-benzylic position), 31.0% at 3.33 ppm, and 8.5% at 2.93 ppm (carbon 3, the mono-benzylic positions). The ^{1}H nmr spectrum of the *cis* isomer showed that the doublet at 4.42 ppm and the quartet-like pattern at 4.23 ppm had disappeared; a triplet-like pattern appeared at 4.23 ppm (proton on carbon 2).

*The photosensitized (electron transfer) irradiation of 3-methylanisole (**17**) in acetonitrile–methanol*-O-d

A solution of 3-methylanisole (**17**) (50 mg, 0.41 mmol) and 1,4-dicyanobenzene (**3**) (30 mg, 0.23 mmol) in acetonitrile–methanol-*O-d* (3:1, 4 mL), in a Pyrex tube, was irradiated at 10°C with the 1-kW mercury vapour lamp. Progress of the reaction was followed by gc/ms as described above and, after 170 h, 3% of one deuterium atom was incorporated. No other products were detected (gc/ms).

*The photosensitized (electron transfer) irradiation of 4-methylanisole (**18**) in acetonitrile–methanol*-O-d

A solution of 4-methylanisole (**18**) (60 mg, 0.49 mmol) and 1,4-dicyanobenzene (**3**) (30 mg, 0.23 mmol) in acetonitrile–methanol-*O-d* (3:1, 5 mL), in a Pyrex tube, was irradiated at 10°C with the 1-kW mercury vapour lamp. Progress of the reaction was followed by gc/ms as described above and, after 170 h, 8% of one deuterium atom was incorporated. There were minor products detected (gc/ms). Two of these were identified as 4-cyano-4′-methoxydiphenylmethane (**19**) and 1,2-di(4-methoxyphenyl)ethane (**20**) by comparison (gc/ms, retention time, mass spectral fragmentation pattern, and ^{1}H nmr spectra) with anthentic samples. The ^{1}H nmr spectrum of the recovered starting material indicated that the deuterium (6%) was incorporated in the *para*-methyl group.

Acknowledgements

This work was supported by a grant from the Natural Sciences and Engineering Research Council of Canada. We thank Dr. D. L. Hooper at the Atlantic Regional Magnetic Resonance Centre at Dalhousie University for the 360 MHz nmr spectra and for help in the preparation of the manuscript. Mr. B. Millier developed the software that interfaces the gas chromatograph (gc/fid) and the integrator to the PC. We also thank Dr. R. K. Boyd and Mr. D. J. Embree at the Atlantic Regional Laboratories of the National Research Council of Canada for the mass spectra run on the ZAB-E spectrometer.

1. (*a*) L. J. Lamont and D. R. Arnold. Can. J. Chem. **68**, 390 (1990); (*b*) R. Popielarz and D. R. Arnold. J. Am. Chem. Soc. **111**, 3068 (1990).
2. (*a*) S. L. Mattes and S. Farid. *In* Organic photochemistry. Vol. 6. *Edited by* A. Padwa. Marcel Dekker, New York. 1983. p. 233; (*b*) P. S. Mariano and J. L. Stavinoha. *In* Synthetic organic photochemistry. *Edited by* W. M. Horspool. Plenum Press, New York. 1984. p. 145; (*c*) J. Mattay. Synthesis, 233 (1989); (*d*) M. A. Fox and M. Chanon (*Editors*). Photoinduced electron transfer. Part A. Elsevier, Amsterdam. 1988.
3. R. A. Neunteufel and D. R. Arnold. J. Am. Chem. Soc. **95**, 4080 (1973).
4. D. R. Arnold and A. J. Maroulis. J. Am. Chem. Soc. **98**, 5931 (1976).
5. D. R. Arnold, B. J. Fahie, L. J. Lamont, J. Wierzchowski, and K. M. Young. Can. J. Chem. **65**, 2734 (1987).
6. (*a*) D. R. Arnold, R. M. Borg, and A. Albini. J. Chem. Soc. Chem. Commun. 138 (1981); (*b*) Y. Shigemitsu and D. R. Arnold. J. Chem. Soc. Chem. Commun. 407 (1975); (*c*) A. J. Maroulis, Y. Shigemitsu, and D. R. Arnold. J. Am. Chem. Soc. **100**, 535 (1978); (*d*) A. J. Maroulis and D. R. Arnold. Synthesis, 819 (1979); (*e*) S. L. Mattes and S. Farid. J. Am. Chem. Soc. **108**, 7356 (1986); (*f*) C. Pac, A. Nakasone, and H. Sakurai. J. Am. Chem. Soc. **99**, 5806 (1977); (*g*) T. Ansanuma, T. Gotoh, A. Tsuchida, M. Yamamoto, and Y. Nishijima. J. Chem. Soc. Chem. Commun. 485 (1977); (*h*) T. Majima, C. Pac, A. Nakasone, and H. Sakurai. J. Am. Chem. Soc. **103**, 4499 (1981).
7. (*a*) A. Okamoto, M. S. Snow, and D. R. Arnold. Tetrahedron, **42**, 6175 (1986); (*b*) A. Okamoto and D. R. Arnold. Can. J. Chem. **63**, 2340 (1985); (*c*) L. W. Reichel, G. W. Griffin, A. J. Muller, P. K. Das, and S. N. Ege. Can. J. Chem. **62**, 424 (1984); (*d*) H. F. Davis, P. K. Das, L. W. Reichel, and G. W. Griffin. J. Am. Chem. Soc. **106**, 6968 (1984).
8. (*a*) D. R. Arnold, L. J. Lamont, and A. L. Perrott. Can. J. Chem. **69**, 225 (1991); (*b*) A. Sulpizio, A. Albini, N. d'Alessandro, E. Fassani, and S. Pietra. J. Am. Chem. Soc.

111, 5773 (1989); (*c*) A. ALBINI, E. FASANI, and E. MONTESSORO. Z. Naturforsch. B: Chem. Sci. **39**, 1401 (1984).
9. R. A. MCCLELLAND, V. M. KANAGASABAPATHY, N. S. BANAIT, and S. STEENKEN. J. Am. Chem. Soc. **111**, 3966 (1989).
10. R. S. NICHOLSON and I. SHAIN. Anal. Chem. **36**, 706 (1964); **37**, 178 (1965).
11. (*a*) E. S. PYSH and N. C. YANG. J. Am. Chem. Soc. **85**, 2124 (1963); (*b*) W. C. NECKAM, G. R. DIMELER, and M. M. DESMOND. J. Electrochem. Soc. **111**, 1190 (1964); (*c*) A. ZWEIG, W. G. HODGSON, and W. H. JURA. J. Am. Chem. Soc. **86**, 4124 (1964); (*d*) S. FUKUZUMI and J. K. KOCHI. J. Am. Chem. Soc. **103**, 7240 (1981).
12. M. J. FRISCH, J. S. BINKLEY, H. B. SCHEGEL, K. RAGHAVACHARI, C. F. MELIUS, R. L. MARTIN, J. J. P. STEWART, F. W. BOBROWICZ, C. M. ROHLFING, L. R. KAHN, D. J. DEFREES, R. SEEGER, R. A. WHITESIDE, D. J. FOX, E. M. FLEUDER, and J. A. POPLE. Gaussian 86. Release H; Carnegie Mellon University: Pittsburg, PA. 1984.
13. R. S. MULLIKEN. J. Chem. Phys. **23**, 1833 (1955).
14. W. J. HEHRE, L. RADOM, P. V. R. SCHLEYER, and J. A. POPLE. *Ab initio* Molecular orbital theory. Wiley, New York. 1986.
15. (*a*) Y.-T. TAO and W. H. SAUNDERS, JR. J. Am. Chem. Soc. **105**, 3183 (1983); (*b*) B. R. DOHNER and W. H. SAUNDERS, JR. J. Am. Chem. Soc. **108**, 245 (1986).
16. (*a*) G. W. KABALKA and N. S. BOWMAN. J. Org. Chem. **38**, 1607 (1973); (*b*) H .C. BROWN and G. ZWEIFEL. J. Am. Chem. Soc. **83**, 2544 (1961).
17. L. M. JACKMAN and S. STERNHELL. Applications of nuclear magnetic resonance spectroscopy in organic chemistry. Pergamon Press, Toronto. 1969. Chap. 4-2.
18. D. REHM and A. WELLER. Isr. J. Chem. **8**, 259 (1970).
19. R. A. MARCUS. Discuss. Faraday Soc. **29**, 21 (1960).
20. I. R. GOULD, D. EGE, S. L. MATTES, and S. FARID. J. Am. Chem. Soc. **109**, 3794 (1987).
21. (*a*) K. W. BOWERS. *In* Radical ions. *Edited by* E. T. Kaiser and L. Kevan. Interscience, New York. 1968. Chap. 5; (*b*) A. CARRINGTON. Q. Rev. Chem. Soc. **17**, 67 (1963).
22. (*a*) D. D. M. WAYNER, D. J. MCPHEE, and D. GRILLER. J. Am. Chem. Soc. **110**, 132 (1988); (*b*) B. A. SIM, P. H. MILNE, D. GRILLER, and D. D. M. WAYNER. J. Am. Chem. Soc. **112**, 6635 (1990); (*c*) B. A. SIM, D. GRILLER, and D. D. M. WAYNER. J. Am. Chem. Soc. **111**, 754 (1989).
23. (*a*) J. B. PEDLEY, R. D. NAYLOR, and S. P. KIRBY. Thermochemical data of organic compounds. 2nd ed. Chapman and Hall, London. 1986; (*b*) O. DOBIS and S. W. BENSON. Int. J. Chem. Kinet. **19**, 691 (1987); (*c*) D. F. MCMILLEN and D. M. GOLDEN. Annu. Rev. Phys. Chem. **33**, 493 (1982).
24. (*a*) D. R. ARNOLD. Substituent effects in radical chemistry. *Edited by* H. G. Viehe *et al.* D. Reidel, Dordrecht. 1986; (*b*) A. M. DE P. NICHOLAS and D. R. ARNOLD. Can. J. Chem. **64**, 270 (1986); (*c*) W. P. NEUMANN, A. PENENORY, U. STEWEN, and M. LEHNIG. J. Am. Chem. Soc. **111**, 5845 (1989).
25. (*a*) A. M. DE P. NICHOLAS and D. R. ARNOLD. Can. J. Chem. **60**, 2165 (1982); (*b*) C. J. SCHLESENER, C. AMATORE, and J. K. KOCHI. J. Am. Chem. Soc. **106**, 7472 (1984); (*c*) F. G. Bordwell and M. J. BAUSCH. **108**, 2473 (1986).
26. (*a*) S. E. STEIN. ACS Symposium Ser. **169**, 97 (1981); (*b*) S. W. BENSON. Thermochemical kinetics. 2nd ed. Wiley–Interscience, New York. 1976; (*c*) CODATA Bulletin No. 28, ICSU CODADA, Paris 1978. J. Chem. Thermodyn. **10**, 903 (1978); (*d*) B. G. COX, G. R. HEDWIG, A. J. PARKER, and D. W. WATTS. Aust. J. Chem. **27**, 477 (1974).
27. E. BACIOCCHI, A. D. CORT, L. EBERSON, L. MANDOLINI, and C. ROL. J. Org. Chem. **51**, 4544 (1986).
28. E. I. HEIBA, R. M. DESSAU, and W. J. KOEHL, JR. J. Am. Chem. Soc. **91**, 6830 (1969).
29. W. C. STILL, M. KAHN, and A. MITRA. J. Org. Chem. **43**, 2925 (1978).
30. D. D. M. WAYNER and D. R. ARNOLD. Can. J. Chem. **63**, 871 (1985).

Can. J. Chem. Downloaded from www.nrcresearchpress.com by 198.100.157.202 on 09/07/12
For personal use only.

Total synthesis of *d,l*-quassin

NADA STOJANAC AND ZDENEK VALENTA[1]

Department of Chemistry, University of New Brunswick, Bag Service no. 45222, Fredericton, N.B., Canada E3B 6E2

Received November 12, 1990

NADA STOJANAC and ZDENEK VALENTA. Can. J. Chem. **69**, 853 (1991).

The completion of the total synthesis of *d,l*-quassin **1** is described. Key steps are a facile intramolecular acylation of a protected cyanohydrin carbanion (**4** → **5**), a selective deprotonation with trioctyl methyl ammonium hydroxide leading to the removal of HCN from **8**, and the unusual sequence **5** → **12** in which the ring C enol ether of **5** is converted selectively into ring C diosphenol of **12**.

Key words: quassin, synthesis, selective base, diosphenols, acylation.

NADA STOJANAC et ZDENEK VALENTA. Can. J. Chem. **69**, 853 (1991).

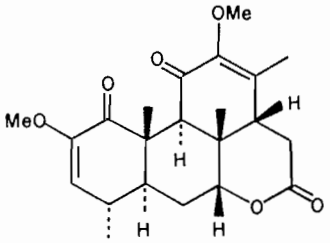
On décrit le parachèvement de la synthèse totale de la *d,l*-quassine (**1**). Les étapes clés sont une acylation intramoléculaire facile d'un carbanion de cyanohydrine protégée (**4** → **5**), une déprotonation sélective avec l'hydroxyde de trioctylméthylammonium conduisant à l'enlèvement du HCN du produit **8** et la séquence inhabituelle de **5** → **12** au cours de laquelle le cycle C de l'éther énolique **5** est transformé sélectivement en cycle diosphénol C du produit **12**.

Mots clés : quassine, synthèse, base sélective, diosphénols, acylation.

[Traduit par la rédaction]

Introduction

We wish to report the completion of the total synthesis of *d,l*-quassin **1**, a mild insecticide of *Quassia amara* (1), by a 13-step sequence from the previously reported ester hemiacetal **2**[2] (2) by a strategy that includes the use of a highly selective base and an unusual regioselective introduction of the two diosphenol groupings.[3]



1

To facilitate the cyclization of ring A in **2**, we have chosen the attack of a nucleophilic C(1) upon the unencumbered primary ester group (see arrow in **2**), The required nitrile **4** was prepared from **2** in four steps (see Scheme 1). For a good yield, it proved essential to perform the hemiacetal acetylation and C(14)-OH dehydration in two steps. The hydrogenation of the 14,15-olefin proceeded exclusively from the convex side. Throughout the sequence **2** → **4**, including the -OAc → -CN exchange (4), a mixture of C(1) epimers was formed and was used without separation (^{1}H nmr ($CDCl_3$) singlets in **2** at δ 5.45 and 5.32, in **3** at δ 6.28 and 6.15, and in **4** at δ 4.86 and 4.74). Lithium pyrrolidide (rather than one of the standard hindered bases) was then used for cyclization of epimeric mixture **4**[4] to **5**, because it alone completely deprotonated both epimers at low temperature. No amide formation (by base attack of the ester group) occurred under the reaction conditions.

Compound **5**, mp 188–190°C, containing all four rings of quassin, was then oxidized to epoxy lactone **6**, mp 254–256°C (^{1}H nmr ($CDCl_3$) C7-H δ 4.31, t, $w/2$ = 6 Hz) via the isolable epoxy diketone.[5] Triol **8**, mp 208–210°C (^{1}H nmr (acetone-d_6) C(12)-H δ 3.78, d, J = 12.61 Hz) was then produced from **6** in two steps. Only pyridinium *p*-toluenesulfonate (5) gave a quantitative yield of allyl alcohol **7**, mp 257–260°C (^{1}H nmr (acetone-d_6) C(12)-H δ 4.81, d, J = 2.50 Hz) in the **6** → **7** conversion.

The four nonepimerizable chiral centers of quassin (C(5), C(7), C(8), and C(10)) and the epimerizable center C(14) all have the desired relative configuration in triol **8**. It could furthermore be anticipated, based on previous deuteration experiments (1*d*) that the axial β-methyl group at C(4) in **8** as well as the H-atom to be introduced at C(9) would adopt the thermodynamically favoured quassin configuration on equilibration at an appropriate later stage. Thus, since triol **8** is at the same oxidation level as quassin, it only remained to eliminate HCN in **8** and subsequently to dehydrate (C(9)-OH) via an 11, 12-enol or enolate. These proved to be exceptionally delicate operations.

Treatment of **8** with not more than 1 mol equivalent of trioctyl methyl ammonium (TOMA) hydroxide[6] gave diosphenol **9**, mp 248–252°C (^{1}H nmr ($CDCl_3$) C(3)-H δ 6.06, d, J = 5.71 Hz; C(12)-H δ 3.50, d, J = 12.70 Hz) in good yield. However, an excess of TOMA hydroxide irreversibly rearranged

[1]Author to whom correspondence may be addressed.

[2]**2** was obtained in 13 steps from 2,6-dimethyl-1,4-benzoquinone and 1,3-dimethyl-6-(1′-acetoxyethyl)-1,3-cyclohexadiene. The ^{1}H nmr spectrum of **2** indicated an equilibrium mixture of the two diastereomeric hemiacetals and a small amount of the keto aldehyde.

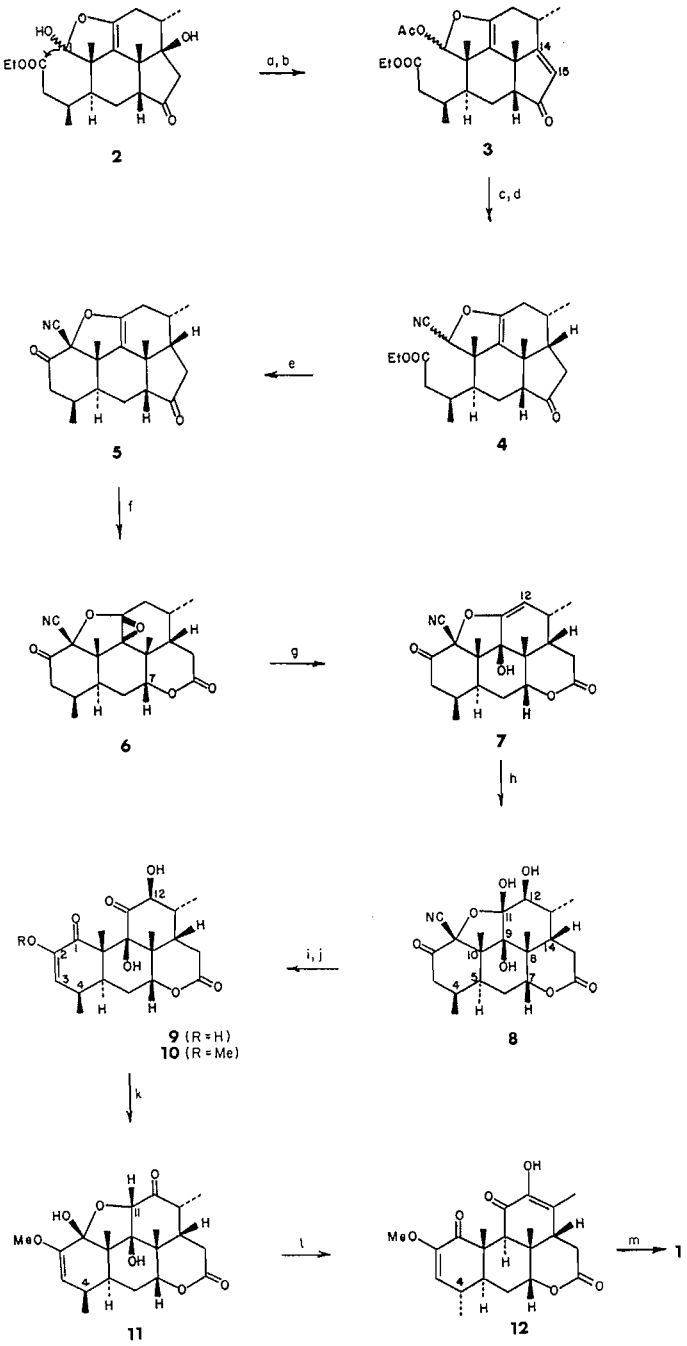
[3]Quassin has previously been synthesized by Grieco and co-workers (3*a*) and by Watt and co-workers (3*b*). The strategies used by these two laboratories are fundamentally different from the approach reported here.

[4]The two pure epimers of **4** could be prepared by $NaBH_4$ reduction of the 5-membered ketone in **4**, separation of the two alcohols on silica, and reoxidation.

[5]Only a small amount (5–8%) of the epoxy bislactone, formed by the oxidation of both keto groups in **5**, was isolated.

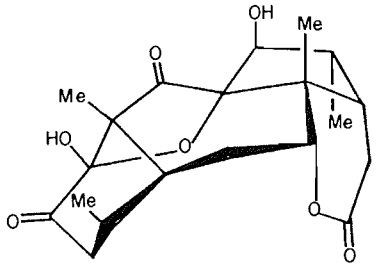
[6]This was prepared from TOMA chloride (Aliquat 336, Aldrich Chem. Co.) by repeated passage through basic ion-exchange resin Amberlite IRA-400 (OH) (Aldrich Chem. Co.), which was extensively washed with methanol before the exchange.

Can. J. Chem. Downloaded from www.nrcresearchpress.com by 198.100.157.202 on 09/07/12
For personal use only.



(a) Ac_2O, NaOAc, C_6H_6, reflux, 30–45 min (tlc monitored), yield >90%; (b) Ac_2O, Py, 100°C, 3 days (tlc monitored), yield >80%; (c) H_2/PtO_2, EtOH, room temp., yield quantitative; (d) $(CH_3)_3SiCN$, $BF_3.Et_2O$, CH_3NO_2, room temp., 6 h (tlc monitored), yield 66% chromatographed; (e) LiC_4H_8N, THF, −78°C, 30 min – 1 h (tlc monitored), yield 68–79% chromatographed; (f) MCPBA, $NaHCO_3$ + Na_2CO_3, CH_2Cl_2, room temp., 3–5 days (tlc monitored), yield 40–50% chromatographed; (g) PPTS, CH_2Cl_2 + $CHCl_3$ (1:1), reflux, 2–3 days (tlc monitored), yield >95%; (h) OsO_4, C_6H_6, Py cat, room temp., 5–7 days (tlc monitored), yield 50–60% chromatographed; (i) TOMA hydroxide, C_6H_6–H_2O (1:1), 80°C, 10 min or 50°C, 1 h (tlc monitored), yield 60–80% chromatographed; (j) CH_2N_2, Et_2O, MeOH, 5°C, 5–7 days (tlc monitored), yield 55–60% chromatographed; (k) Bi_2O_3, HOAc, 100°C, 10–12 h (tlc monitored), yield >95%; (l) DBN, C_6H_6, reflux, 7 h (tlc monitored), yield 79%; (m) $(CH_3)_2SO_4$, NaOH aq. (2 N), room temp., 25 h, yield 71% chromatographed.

SCHEME 1

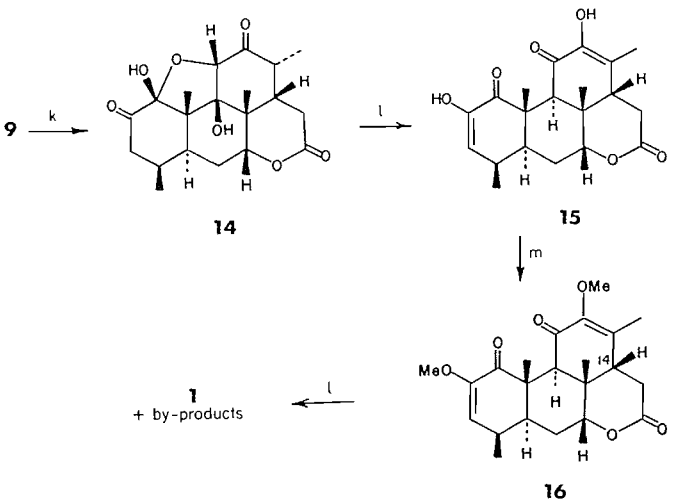


13

the initially formed **9** to **13**.[7] The required dehydration eliminating the C(9)-OH group could therefore not be achieved under basic conditions at this stage.

Compound **9** was first methylated with diazomethane in ether, to give **10**, mp 201–203°C (^{1}H nmr ($CDCl_3$) C(3)-H δ 5.77, d, J = 5.71 Hz; C(2)-OCH_3 δ 3.65, s; C(12)-H δ 3.50, d, J = 12.77 Hz). Treatment of **10** with Bi_2O_3 in hot acetic acid (6) then effected the desirable ketol rearrangement **10** → **11**, mp 196–198°C (^{1}H nmr ($CDCl_3$) C(11)-H δ 5.07, s; C(3)-H δ 4.80, d, J = 5.08 Hz, C(2)-OCH_3 δ 3.57, s) rather than the expected C(12)-oxidation.[8]

Dehydration and C(4)-epimerization were now achieved in a one-pot reaction of **11** with DBN in boiling benzene,[9] to give norquassin **12** (^{1}H nmr ($CDCl_3$) C(3)-H δ 5.29, d, J = 2.22 Hz; C(2)-OCH_3 δ 3.57, s; C(9)-H δ 3.08, s; C(13)-CH_3 δ 1.87, s).[10] Methylation (7) of **12** provided synthetic *d,l*-quassin **1**, mp 187–188°C (^{1}H nmr ($CDCl_3$) C(3)-H δ 5.29, d, J = 2.57 Hz; C(7)-H δ 4.26, t, $w/2$ = 6 Hz; C(12)-OCH_3 δ 3.65, s; C(2)-OCH_3 δ 3.57, s; C(9)-H δ 2.97, s; C(13)-CH_3 δ 1.86, s; C(10)-CH_3/C(8)-CH_3 δ 1.54/1.18, s; C(4)-CH_3 δ 1.10, d, J = 6.91 Hz).



(l) DBN, C_6H_6, reflux, 3.30 h (tlc monitored), yield 80%; (m) $(CH_3)_2SO_4$, NaOH aq. (2 N), room temp., 47 h, yield 52% chromatographed.

SCHEME 2

[7]Small amounts of **13** were produced even when not more than 1 mol equivalent of TOMA hydroxide was used. Thus, this base does effect the **9** → **13** rearrangement, but fortunately the rearrangement rate is slower than that of HCN elimination.

[8]No reaction took place without Bi_2O_3 under these conditions!

[9]The intermediate 4-epinorquassin could be isolated by running the reaction at higher dilution.

[10]The ^{1}H nmr spectrum of norquassin **12** proved identical to that of the compound prepared by partial demethylation of quassin with BBr_3.

Can. J. Chem. Downloaded from www.nrcresearchpress.com by 198.100.157.202 on 09/07/12
For personal use only.

It proved essential to have the ring A diosphenol methylated and the ring C diosphenol nonmethylated during the C(4)-epimerization. Thus, when 4-epiquassin **16** (Scheme 2), mp 217–219°C (^{1}H nmr ($CDCl_3$) C(3)-H δ 5.46, d, J = 4.84 Hz; C(12)-OCH_3 δ 3.64, s; C(2)-OCH_3 δ 3.59, s; C(9)-H δ 2.91, s; C(13)-CH_3 δ 1.85, s) prepared by double methylation of 4-epibisnorquassin **15** (**9** → **14** → **15** → **16**) was reacted with DBN in boiling benzene, only a low yield of quassin was obtained. 14-Epiquassin (isoquassin (1*c*, 1*e*)) and desmethoxylated ring C, D, dienones were formed as by-products. The ring C diosphenolate thus acted as a "protecting group" for C(14)-H during the above successful **11** → **12** transformation.

Of the five (formal) carbonyl groups of quassin, only that at C(1) was produced by the oxidation of a secondary OH group and, with the exception of the CN auxiliary in compounds **4**–**8**, no carbonyl group was protected in the course of this synthesis.

Acknowledgements

Support in the form of Natural Sciences and Engineering Research Council operating grants is gratefully acknowledged.

1. (*a*) E. P. CLARK. J. Am. Chem. Soc. **59**, 927, 2511 (1937); (*b*) E. LONDON, A. ROBERTSON, and H. WORTHINGTON. J. Chem. Soc. 3431 (1950); (*c*) K. R. HANSON, D. B. G. JAQUISS, J. A. LAMBERTON, A. ROBERTSON, and W. E. SAVIGE. J. Chem. Soc. 4238 (1954); (*d*) Z. VALENTA, S. PAPADOPOULOS, and C. PODESVA. Tetrahedron, **15**, 100 (1961); (*e*) Z. VALENTA, A. H. GRAY, D. E. ORR, S. PAPADOPOULOS, and C. PODESVA. Tetrahedron, **18**, 1433 (1962); (*f*) J. POLONSKY. Fortschr. Chem. Org. Naturst. **30**, 101 (1973); (*g*) J. POLONSKY. Prog. Chem. Org. Nat. Prod. **47**, 221 (1985).
2. N. STOJANAC, Z. STOJANAC, P. S. WHITE, and Z. VALENTA. Can. J. Chem. **57**, 3346 (1979).
3. (*a*) G. VIDARI, S. FERRINO, and P. A. GRIECO. J. Am. Chem. Soc. **106**, 3539 (1984); (*b*) M. KIM, K. KAWADA, R. S. GROSS, and D. S. WATT. J. Org. Chem. **55**, 504 (1990).
4. F. G. DE LAS HERAS and P. FERNANDEZ-RESA. J. Chem. Soc. Perkin Trans. 1, 903 (1982).
5. M. MIYASHITA, A. YOSHIKOSHI, and P. A. GRIECO. J. Org. Chem. **42**, 3772 (1977).
6. (*a*) D. J. CRAM and N. L. ALLINGER. J. Am. Chem. Soc. **78**, 2518 (1956); (*b*) W. RIGBY. J. Chem. Soc. 793 (1951).
7. T. MURAE, T. TSUYUKI, T. IKEDA, T. NISHIHAMA, S. MASUDA, and T. TAKAHASHI. Tetrahedron, **27**, 1545 (1971).

Can. J. Chem. Downloaded from www.nrcresearchpress.com by 198.100.157.202 on 09/07/12
For personal use only.

Synthetic conversion of bryostatin 2 to bryostatin 1 and related bryopyrans[1]

GEORGE R. PETTIT,[2] DIPANJAN SENGUPTA, AND CHERRY L. HERALD
Cancer Research Institute and Department of Chemistry, Arizona State University, Tempe, AZ 85287-1604, U.S.A.

AND

NANCY A. SHARKEY AND PETER M. BLUMBERG
Molecular Mechanisms of Tumor Promotion Section, LCCTP, National Cancer Institute, Bethesda, MD 20892, U.S.A.

Received August 22, 1990

GEORGE R. PETTIT, DIPANJAN SENGUPTA, CHERRY L. HERALD, NANCY A. SHARKEY, and PETER M. BLUMBERG. Can. J. Chem. **69**, 856 (1991).

Bryostatin 2 (**1***a*) has been converted to bryostatin 1 (**1***e*) and bryostatin 12 (**1***i*) by a selective protection and deprotection involving the C-26 hydroxyl group. The new bryostatins **1***g*, **1***k*, and **1***m* were also prepared starting from bryostatin 2. The C-7 substituents of natural bryostatins 4 and 5 were revised from isovalerate → pivalate employing comparative ^{1}H and ^{13}C NMR studies of the semi-synthetic bryostatins **1***k* and **1***m* and the natural products.

Key words: bryostatin 2 → 1, selective conversion, bryostatins 4 and 5, pivalates.

GEORGE R. PETTIT, DIPANJAN SENGUPTA, CHERRY L. HERALD, NANCY A. SHARKEY et PETER M. BLUMBERG. Can. J. Chem. **69**, 856 (1991).

On a transformé la bryostatine 2 (**1***a*) en bryostatine 1 (**1***e*) et en bryostatine 12 (**1***i*) grâce à une protection et une déprotection sélective impliquant le groupement hydroxyle en C-26. On a aussi préparé les bryostatines **1***g*, **1***k* et **1***m* à partir de la bryostatine 2. En se basant sur des études comparatives de RMN du ^{1}H et du ^{13}C, effectuées sur les bryostatines semi-synthétiques **1***k* et **1***m* et sur les produits naturels, on propose une révision de la nature de substituants en position C-7 des bryostatines 4 et 5 d'isovalérate à pivalate.

Mots clés : bryostatine, conversion sélective, bryostatines 4 et 5, pivalates.

[Traduit par la rédaction]

The marine Bryozoan *Bugula neritina* has been found to contain a series of biologically and chemically exciting constituents now known as the bryostatins (2*a*–*g*). Other interesting biosynthetic products of the Phylum Bryozoa such as the β-lactam bearing chartellines have recently been isolated from *Chartella papyracea* (3). Bryostatin 1 (**1***e*) has been found to profoundly affect protein kinase C at picomolar concentrations (4*a*). Uniquely among protein kinase C modulators, whereas bryostatin 1 activates protein kinase C in vitro, it antagonizes phorbol ester responses in many biological systems (4*b*) and is deficient in tumor promoting activity (4*c*,*d*). Bryostatin 1 has powerful immunopotentiating activities (4*e*,*f*). The ability of bryostatin 1 to initiate cytotoxic T lymphocyte development (4*f*), and to induce production of interleukin-2 (4*f*,*g*) and growth of normal bone marrow cells (4*h*), combined with its strong *anti*tumor (4*i*) promoter and antineoplastic effects resulted in its selection for clinical development by the U.S. National Cancer Institute. To increase significantly the availability of bryostatin 1 (**1***e*) it became very important to convert bryostatin 2 (**1***a*), which was also obtained from *Bugula neritina* in nearly equal amounts, to bryostatin 1 in an efficient and selective way. Realization of this objective was accomplished as follows.

The bryostatin hydroxyl groups at C-3, C-9, and C-19 were earlier found (2*b*) to resist acetylation (under mild conditions), presumably due to intramolecular hydrogen bonding, while the C-7 and C-26 hydroxyl groups were readily acetylated (2*b*,*g*). Thus, synthetic conversion was undertaken by methods utilizing selective protection of the C-26 hydroxyl group. The steric environment of the two hydroxyl groups (viz. C-7 and C-26) suggested that a bulky silyl ether[3] would offer an attractive possibility.

Application of *tert*-butyldimethylsilyl chloride (6) was found very effective for selective protection of the bryostatin 2 C-26 hydroxyl group. Bryostatin 2 (**1***a*) was allowed to react (7) at room temperature with excess *tert*-butyldimethylsilyl (TBDMS) chloride in the presence of 4-(*N*,*N*-dimethyl)aminopyridine (and triethylamine in dimethylformamide) to produce 26-*tert*-butyldimethylsilyl ether **1***b* and bryostatin 2 7,26-di-*tert*-butyldimethylsilyl ether **1***c*. The disilyl ether was reconverted to bryostatin 2 employing 48% hydrofluoric acid – acetonitrile (1:20) (8). The yield of monosilyl ether **1***b* was 71% on the basis of total recovered bryostatin 2. Treatment of the C-26 silyl ether with acetic anhydride – pyridine (room temperature) gave acetate **1***d*. The C-26 hydroxyl was regenerated using 48% hydrofluoric acid – acetonitrile (1:20 at 0–5°C). The product was isolated in 80% overall yield (from **1***a*) by silica gel column chromatography and found to be identical with natural bryostatin 1 (**1***e*).

The high resolution SP-SIMS spectrum of bryostatin **1***e* displayed *m*/*z* 911 $(M + Li)^+$ and 927 $(M + Na)^+$ corresponding to the molecular formula $C_{47}H_{68}O_{17}$. The ^{1}H NMR spectrum revealed an acetate chemical shift at δ 2.04, the C-7 proton signal at δ 5.14 (dd, J = 12, 4.9 Hz), and the three-proton doublet of the C-27 methyl at δ 1.23 (J = 6.5 Hz). The significant downfield shift of the C-7 proton from δ 3.95 (**1***a*, **1***b*) to δ 5.14 (**1***e*) further confirmed acetylation at the C-7 hydroxyl group.

Selective protection of the C-26 hydroxyl group in bryostatin 2 allowed us to selectively introduce other groups at C-7.

[1]Part 192 of Antineoplastic Agents. For part 191 see ref. 1.

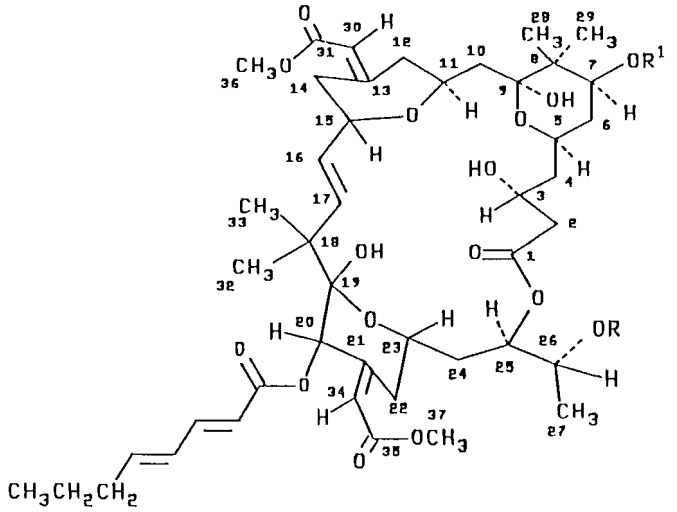
[2]Author to whom correspondence may be addressed.

[3]For review see Use of organosilicon reagents as protective groups in organic synthesis, ref. 5.

Printed in Canada / Imprimé au Canada

Can. J. Chem. Downloaded from www.nrcresearchpress.com by 198.100.157.202 on 09/07/12
For personal use only.

Can. J. Chem. Downloaded from www.nrcresearchpress.com by 198.100.157.202 on 09/07/12
For personal use only.



1, *a* R = R^1 = H, bryostatin 2
b R = TBDMS, R^1 = H
c R = R^1 = TBDMS
d R = TBDMS, R^1 = -$COCH_3$
e R = H, R^1 = -$COCH_3$, bryostatin 1
f R = TBDMS, R^1 = -$COCH_2CH_3$
g R = H, R^1 = -$COCH_2CH_3$
h R = TBDMS, R^1 = -$COCH_2CH_2CH_3$
i R = H, R^1 = -$COCH_2CH_2CH_3$, bryostatin 12
j R = TBDMS, R^1 = -$COCH_2CH(CH_3)_2$
k R = H, R^1 = -$COCH_2CH(CH_3)_2$
l R = TBDMS, R^1 = -$COC(CH_3)_3$
m R = H, R^1 = -$COC(CH_3)_3$

Treatment of 26-*tert*-butyldimethylsilyl ether **1***b* with butyric anhydride and pyridine, followed by deprotection, led to bryostatin 2 7-butyrate (**1***i*) identical to bryostatin 12 (**1***i*). Bryostatin 2 7-propionate (**1***g*) was obtained in an analogous manner.

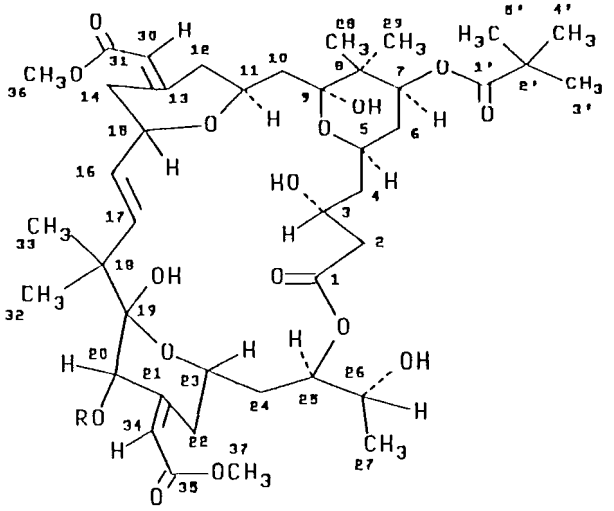
Conversion of bryostatin 2 to bryostatin 2 7-isovalerate (**1***k*) and bryostatin 2 7-pivalate (**1***m*) provided convincing support for the revision[4] of C-7 substituents in bryostatins 4 (**2***a*) (2*d*) and **5** (**2***b*) (2*e*). Esterification of bryostatin 2 26-OTBDMS (**1***b*) with isovaleric acid in the presence of dicyclohexylcarbodiimide and 4-pyrrolidinopyridine (10) in methylene chloride provided ester **1***j*. The TBDMS protecting group was removed to afford the new bryostatin **1***k*. Treatment of bryostatin 2 26-OTBDMS (**1***b*) with pivalic anhydride and 4-(*N*,*N*-dimethyl)aminopyridine (50–55°C) (for a review, see ref. 11) in methylene chloride provided bryostatin 2 26-OTBDMS-7-pivalate (**1***l*). Removal of the protecting group afforded bryostatin 2 7-pivalate (**1***m*) in 42% overall yield from **1***b*. The ^{1}H NMR spectrum of bryostatin **1***m* showed a strong singlet for the pivalate unit at δ 1.17 (Table 1) and a multiplet for the C-7 proton at δ 5.08 (dd, J = 11.8, 4.8 Hz), whereas bryostatin **1***k* showed a doublet at δ 0.93 (J = 6.3 Hz, Table 1) for the isovalerate unit.

The isovalerate → pivalate revision was further supported by the ^{13}C NMR spectra of natural bryostatins 4 and 5 (Table 2).

[4]In 1988, during another reisolation of bryostatins 4 and 5, recharacterization employing high-field NMR techniques suggested possible presence of a pivalate ester at C-7. The realization of this minor modification at C-7 was made possible by newer NMR techniques and these structural changes have already been entered in a contribution by Pettit *et al.* (9).

Comparison of the ^{1}H and ^{13}C NMR spectra of natural bryostatins 4 and 5 with those of the semi-synthetic bryostatins **1***m* and **1***k* confirmed the C-7 pivalate substitution. The strong singlet at δ 1.17 in the ^{1}H NMR spectrum of semi-synthetic bryostatin **1***m* (Table 1) was nearly identical to the singlet at δ 1.16 and δ 1.19 of natural bryostatins 4 and 5, respectively. Moreover, the bryostatin **1***m* gave rise to ^{13}C chemical shifts at δ 177.99 (C-1′), 39.01 (C-2′), and 27.14 (C-3′, -4′, and -5′, Table 2), in close agreement with the ^{13}C NMR shifts displayed by the C-7 substituents of natural bryostatins 4 and 5. The proton spectrum of bryostatin **1***k* showed a doublet due to two methyl groups at δ 0.93 (J = 6.3 Hz) (Table 1) and the ^{13}C NMR spectrum gave evidence of C-1′ at δ 172.81, C-2′ at δ 43.75, C-3′ at δ 24.93, and C-4′ and -5′ at δ 22.35 (Table 2), thereby substantiating that bryostatins 4 (**2***a*) and 5 (**2***b*) contain the unusual pivalate ester group at C-7 (2*d*,*e*, 9).

In initial biochemical characterization, the binding affinities of bryostatins **1***g*, **1***k*, and **1***m* for protein kinase C were determined by competition of [^{3}H]bryostatin 4 binding as described previously for bryostatins 1–10 (4*i*). The assay conditions involve reconstitution of protein kinase C in Triton X-100/phosphatidylserine. Although these conditions give



2, *a* R = -$COCH_2CH_2CH_3$, bryostatin 4
1″ 2″ 3″ 4″

b R = -$COCH_3$, bryostatin 5
1″ 2″

significantly lower affinity than found for the enzyme reconstituted under the more physiological conditions of phospholipid alone, they permit quantification under equilibrium conditions. The K_i values for bryostatins **1***g*, **1***k*, and **1***m* were 1.7 ± 0.5, 0.74 ± 0.23, and 0.73 ± 0.17 nM (mean ± range, n = 2 experiments) respectively. Similar values were thus observed for the isovalerate and pivalate esters, with slightly less activity for the propionate ester **1***g* and the acetate ester (bryostatin 1, K_i = 1.4 ± 0.2 nM, 4*i*).

The strategy for selective reaction at the C-7 hydroxyl group of bryostatin 2 with protection and deprotection of the more reactive C-26 hydroxyl now opens a useful pathway to a variety of new bryostatins (12). In time, that will allow further study of the structure/activity relationships among this fascinating group of marine animal antineoplastic constituents.

TABLE 1. Bryostatin ^{1}H NMR (400 MHz) chemical shift assignments in deuteriochloroform solution[a]

	Bryostatin **1***g*			Bryostatin **1***k*			Bryostatin **1***m*		
H	δ	Multiplicity	$J_{H,H}$ (Hz)	δ	Multiplicity	$J_{H,H}$ (Hz)	δ	Multiplicity	$J_{H,H}$ (Hz)
2	2.45	m		2.45	m		2.45	m	
3	4.16	m		4.17	m		4.17	m	
4	2.01, 1.56	m		2.06, 1.58	m		2.05, 1.58	m	
5	4.22	d	12	4.22	d	12	4.21	d	11.4
6	1.45, 1.75	m		1.44, 1.71	m		1.43, 1.71	m	
7	5.14	dd	11.8, 4.8	5.14	dd	11.8, 4.7	5.08	dd	11.8, 4.8
10	2.06, 2.15	m		2.07, 2.17	m		2.07, 2.14	m	
11	3.79	m		3.78	m		3.78	m	
12	2.06, 3.64	m		2.07, 3.63	m		2.06, 3.63	m	
14	1.86, 3.62	m		1.93, 3.63	m		1.89, 3.63	m	
15	4.04	dt	8.5, 2	4.03	m		4.04	m	
16	5.30	dd	15.8, 8.5	5.30	dd	15.7, 8.4	5.30	dd	15.7, 8.4
17	5.79	d	15.8	5.78	d	15.7	5.77	d	15.7
20	5.16	s		5.18	s		5.19	s	
22	2.08	m		2.09	m		2.09	m	
	1.66	d	15.1	1.67	d	15.2	1.64	d	15.1
23	4.01	m		4.01	m		4.00	m	
24	1.92, 2.06	m		1.91, 2.07	m		1.92, 2.07	m	
25	5.14	m		5.15	m		5.17	m	
26	3.79	m		3.80	m		3.80	m	
27	1.23	d	6.6	1.22	d	6.4	1.22	d	7.0
28[b]	0.93	s		0.92	s		0.93	s	
29[b]	0.99	s		0.99	s		0.99	s	
30	5.67	s		5.66	s		5.67	s	
32[c]	1.14	s		1.14	s		1.13	s	
33[c]	1.08	s		0.99	s		0.99	s	
34	6.00	d	1.5	5.99	d	1.5	5.99	d	1.5
36	3.69	s		3.69	s		3.68	s	
37	3.65	s		3.65	s		3.64	s	
2′	2.31	q	6.8	2.16	m		1.17	s	
3′	1.12	t	7.6	~1.9–2.0	m				
4′, 5′				0.93	d	6.3	1.17	s	
2″	5.80	d	15.4	5.80	d	15.2	5.80	d	15.2
3″	7.25	m		7.26	m		7.25	m	
4″	6.16	dd	8.5, 2.4	6.16	dd	8.5, 2.6	6.15	dd	8.2, 2.4
5″	6.16	dd	4.9, 1.5	6.16	dd	4.8, 1.5	6.16	dd	4.9, 1.5
6″	2.15	m		2.15	m		2.14	m	
7″	1.45	m		1.45	m		1.45	m	
8″	0.91	t	7.2	0.91	t	7.4	0.90	t	7.4

[a]Residual $CHCl_3$ as internal reference (7.25 ppm).
[b]Chemical shift values are interchangeable.
[c]Chemical shift values are interchangeable.

Can. J. Chem. Downloaded from www.nrcresearchpress.com by 198.100.157.202 on 09/07/12
For personal use only.

Experimental section

General procedures

Solvent solutions from reaction mixtures washed with water were dried over anhydrous sodium sulfate. All chromatographic solvents were redistilled. Silica gel (E. Merck, Darmstadt, 70–230 mesh) was employed for column chromatography and silica gel GHLF uniplates (Analtech, Inc., Newark, DE) were used for thin-layer chromatography (TLC). The TLC plates were viewed with UV light and developed with anisaldehyde – sulfuric acid spray reagent followed by heating. The NMR spectra were measured using a Bruker AM-400 instrument with deuteriochloroform employed as solvent. All high and low resolution fast atom bombardment (FAB) mass spectra (13) were recorded using a Kratos MS-50 mass spectrometer (Mid West Center for Mass Spectrometry, University of Nebraska, Lincoln, NE).

*Bryostatin 2 26-*tert*-butyldimethylsilyl ether (**1***b*). General procedure*

The following procedure for silyation, acylation, and desilyation was repeated in analogous fashion for each bryostatin interconversion. A solution of bryostatin 2 (**1***a*, 50 mg), 4-(*N*,*N*-dimethyl)aminopyridine (15 mg), *tert*-butyldimethylsilyl chloride (40 mg), and triethylamine (20 μL) in dimethylformamide (2 mL) was stirred at room temperature (under argon) for 22 h. The reaction mixture was diluted with ice water, stirred for 10 min, and extracted with methylene chloride. The organic phase was washed with saturated aqueous sodium bicarbonate, followed by water, dried, and solvent evaporated under reduced pressure. The residue was purified by column chromatography on silica gel (1:1 hexane – ethyl acetate) to afford silyl ether **1***b* (21.8 mg), bryostatin 2 7,26-di-*tert*-butyldimethylsilyl ether **1***c* (21.4 mg), and bryostatin 2 (5.5 mg). The silyl protecting groups in **1***c* were removed with 48% hydrofluoric acid – acetonitrile (1:20, 10 mL). The reaction mixture was stirred at 0–5°C (1.5 h), diluted with water, and extracted with methylene chloride. The chlorocarbon phase was washed with saturated aqueous sodium bicarbonate followed by water, and dried. The residue (from solvent removal at reduced pressure) was separated by silica gel column chromatography (1:1 hexane – ethyl acetate) to afford 17.2 mg of bryostatin 2. On the basis of total recovered bryostatin 2, the yield of monosilyl ether **1***b* was 71%. The 400 MHz ^{1}H NMR spectrum of silyl ether **1***b* displayed significant

TABLE 2. Bryostatin ^{13}C NMR chemical shift assignments in deuteriochloroform solution

C	Bryostatin 4 (**2***a*)	Bryostatin 5 (**2***b*)	Bryostatin **1***k*	Bryostatin **1***m*
1	172.21	172.31	172.15	172.11
2	42.14	42.14	42.35	42.37
3	65.45	65.50	65.79	65.79
4	39.94	39.89	39.98	39.86
5	68.46	68.46	68.46	68.46
6	33.19	33.17	33.35	33.16
7	72.68	72.60	72.43	72.23
8	41.20	41.19	40.93	41.17
9	101.72	101.75	101.79	101.76
10	44.13	44.11	44.09	44.08
11	64.70	64.69	64.68	64.68
12	31.21	31.17	31.27	31.28
13	157.25	157.09	156.42	156.41
14	36.47	36.40	36.32	36.31
15	78.88	78.92	79.12	79.12
16	129.67	129.67	129.39	129.38
17	138.96	138.91	139.26	139.27
18	44.73	44.75	44.89	44.89
19	98.83	98.71	98.99	98.99
20	74.25	74.39	74.03	74.03
21	151.84	151.68	151.96	151.97
22	41.86	41.86	41.97	41.94
23	71.44	71.43	71.46	71.45
24	35.81	35.79	35.84	35.83
25	73.56	73.61	73.65	73.61
26	70.01	70.02	70.13	70.10
27	19.60	19.66	19.79	19.78
28	19.76	19.81	19.79	19.78
29	20.99	21.00	21.07	21.01
30	113.96	114.05	114.45	114.46
31	166.70	166.72	166.68	166.68
32	16.91	16.92	16.88	16.89
33	24.57	24.58	24.57	24.57
34	119.58	119.67	119.56	119.57
35	166.97	166.96	167.00	167.01
36, 37	51.03	51.02, 51.10	51.04	51.05
1′	178.33	178.27	172.81	177.99
2′	39.01	39.01	43.75	39.01
3′	27.07	27.09	24.93	27.14
4′, 5′	27.07	27.09	22.35	27.14
1″	171.98	169.32	165.58	165.58
2″	36.47	21.43	118.60	118.59
3″	18.16		146.35	146.33
4″	13.57		128.36	128.37
5″			145.49	145.50
6″			35.04	35.05
7″			21.85	21.02
8″			13.67	13.68

Can. J. Chem. Downloaded from www.nrcresearchpress.com by 198.100.157.202 on 09/07/12
For personal use only.

chemical shifts at δ 0.07 (s, 3H), 0.11 (s, 3H), 0.90 (s, 9H), 1.08 (d, 3H, J = 5.6 Hz), 3.65 (s, 3H), 3.68 (s, 3H), 3.73 (m, 1H), and 3.95 (m, 1H).

*Conversion of bryostatin 2 26-*tert*-butyldimethylsilyl ether (**1**b) to bryostatin 1 (**1**e)*

A solution of bryostatin 2 26-*tert*-butyldimethylsilyl ether (**1***b*, 1.6 mg) in acetic anhydride (100 μL) and pyridine (150 μL) was stirred for 18 h (room temperature), diluted with methanol, and stirred for an additional 30 min. Solvent was removed (reduced pressure) and the residue was chromatographed on a column of silica gel (1:1 hexane – ethyl acetate) to afford 1.2 mg (72%) of acetate **1***d*. The product (**1***d*) was subjected to desilylation by treating with 48% hydrofluoric acid – acetonitrile (1:20, 100 μL). The reaction mixture was stirred at 0–5°C (1.5 h), diluted with water, and extracted with methylene chloride. The organic phase was washed with saturated aqueous sodium bicarbonate, water, and dried. After solvent removal (reduced pressure) the residue was purified by silica gel column chromatography (1:1 hexane – ethyl acetate) to afford bryostatin 1 (**1***e*, 0.8 g, 80%), identical with the natural product (by comparison with TLC, analytical HPLC, SP-SIMS (13), and ^1H NMR).

*Conversion of bryostatin 2 26-*tert*-butyldimethylsilyl ether (**1**b) to bryostatin 2 7-propionate (**1**g)*

Bryostatin 2 26-*tert*-butyldimethylsilyl ether (**1***b*, 2 mg) was treated with propionic anhydride (100 μL) – pyridine (130 μL) and stirred for 18 h at room temperature. The product was purified as described directly above to afford **1***f* (2.0 mg, 95%). Desilylation and purification as described above afforded bryostatin **1***g* (1.5 mg, 88%): for ^1H NMR data see Table 1.

*Conversion of bryostatin 2 26-*tert*-butyldimethylsilyl ether (**1**b) to bryostatin 12 (**1**i)*

Bryostatin 2 26-*tert*-butyldimethylsilyl ether (**1***b*, 2.7 mg) was esterified (20 h) with butyric anhydride (100 μL) in pyridine (120 μL) employing the same procedure as utilized above to provide ester **1***h* (1.9 mg, 73%). Desilylation (150 μL of the 1:20 48% hydrofluoric acid – acetonitrile) as described above gave bryostatin 12 (**1***i*, 0.8 mg, 47%), identical to the natural product (by comparison with TLC, SP-SIMS (13), and ^{1}H NMR spectra.

*Conversion of bryostatin 2 26-*tert*-butyldimethylsilyl ether (**1**b) to bryostatin 2 7-isovalerate (**1**k)*

A solution of isovaleric acid (5 μL), *N,N*-dicyclohexylcarbodiimide (10 mg), bryostatin 2 26-*tert*-butyldimethylsilyl ether (**1***b*, 4.6 mg), and 4-pyrrolidinopyridine (1.3 mg) in methylene chloride (150 μL) was stirred at room temperature for 5 h (under argon). The *N,N*-dicyclohexylurea was removed by filtration, and the filtrate was concentrated (reduced pressure). The residue was separated by column chromatography on silica gel (1:1 hexane – ethyl acetate) to afford isovalerate **1***j* (4.5 mg, 90%). Removal of the silyl group as summarized above (cf., **1***e*, 150 μL of the 1:20 reagent) afforded bryostatin 2 7-isovalerate (**1***k*, 2.2 mg, 55%); FAB-MS (DTT/DTE as matrix), *m/z*: 969 $[M + Na]^+$ for $C_{50}H_{72}O_{16}Na$ (20% of base peak), and 911 $[M + H - 2H_2O]^+$ as base peak; for the ^{1}H and ^{13}C NMR data refer to Tables 1 and 2.

*Conversion of bryostatin 2 26-*tert*-butyldimethylsilyl ether (**1**b) to bryostatin 2 7-pivalate (**1**m)*

To a solution of bryostatin 2 26-*tert*-butyldimethylsilyl ether (6.9 mg) in methylene chloride (150 μL) were added 4-(*N,N*-dimethyl)aminopyridine (45 mg) and pivalic anhydride (40 mg). The reaction mixture was stirred at 52–55°C for 4 h (under argon) followed by addition of methanol at room temperature. The residue obtained following solvent removal was separated by column chromatography on silica gel (1:1 hexane – ethyl acetate) to afford pivalate **1***l* (5.7 mg, 76%). Desilylation was performed as described earlier to afford bryostatin **1***m* (2.8 mg, 56%): FAB-MS (3-NBA LiI as matrix), *m/z*: 969 $[M + Na]^+$ for $C_{50}H_{72}O_{16}Na$ (10% of base peak), 953 $[M + Li]^+$ for $C_{50}H_{72}O_{16}Li$ as base peak; for the ^{1}H and ^{13}C NMR data consult Tables 1 and 2.

Acknowledgments

Very necessary financial assistance was provided by Eleanor W. Libby, the Waddell Foundation (Donald Ware), the Fannie E. Rippel Foundation, The Robert B. Dalton Endowment Fund, the Arizona Disease Control Research Commission, the National Cooperative Drug Discovery Group Grant AI 25696-02-03, NIAID, the Outstanding Investigator Grant CA 44344-01A1 awarded by the Division of Cancer Treatment, National Cancer Institute, DHHS, and by the U.S. Army Medical Research and Development Command under Grant No. DAMD-17-89-Z-9021. For other assistance we are pleased to thank Drs. D. L. Doubek and D. E. Schaufelberger, the National Science Foundation Regional Instrumentation Facility in Nebraska (Grant CHE 8620177), and NSF NMR equipment grant (CHE-8409644).

1. M. B. Lilly, C. Thompkins, C. Brown, G. R. Pettit, and A. S. Kraft. Cancer Res. **50**, 5520 (1990).
2. (*a*) G. R. Pettit, C. L. Herald, D. L. Doubek, and D. L. Herald. J. Am. Chem. Soc. **104**, 6846 (1982); (*b*) G. R. Pettit, C. L. Herald, Y. Kamano, D. Gust, and R. Aoyagi. J. Nat. Prod. **46**, 528 (1983); (*c*) G. R. Pettit, C. L. Herald, and Y. Kamano. J. Org. Chem. **48**, 5354 (1983); (*d*) G. R. Pettit, Y. Kamano, C. L. Herald, and M. Tozawa. J. Am. Chem. Soc. **106**, 6768 (1984); (*e*) G. R. Pettit, Y. Kamano, C. L. Herald, and M. Tozawa. Can. J. Chem. **63**, 1204 (1985); (*f*) G. R. Pettit, Y. Kamano, and C. L. Herald. J. Org. Chem. **52**, 2848 (1987); (*g*) G. R. Pettit, J. E. Leet, C. L. Herald, Y. Kamano, F. E. Boettner, L. Baczynskyj, and R. A. Nieman. J. Org. Chem. **52**, 2854 (1987).
3. (*a*) P. H. Nielsen, U. Anthoni, and C. Christophersen. Acta Chem. Scand. **B42**, 489 (1988); (*b*) C. Christophersen. Acta Chem. Scand. **B39**, 517 (1985).
4. (*a*) D. J. deVries, C. L. Herald, G. R. Pettit, and P. M. Blumberg. Biochem. Pharmacol. **37**, 4069 (1988); (*b*) P. M. Blumberg. Cancer Res. **48**, 1 (1988); (*c*) H. Hennings, P. M. Blumberg, G. R. Pettit, C. L. Herald, R. Shores, and S. H. Yuspa. Carcinogenesis, **8**, 1343 (1987); (*d*) M. Gschwendt, G. Fürstenberger, S. Rose-John, M. Rogers, W. Kittstein, G. R. Pettit, C. L. Herald, and F. Marks. Carcinogenesis, **9**, 555 (1988); (*e*) A. D. Hess, M. K. Silanskis, A. H. Esa, G. R. Pettit, and W. S. May. J. Immunol. **141**, 3263 (1988); (*f*) G. Trenn, G. R. Pettit, H. Takayama, J. Hu-Li, and M. V. Sitkovsky. J. Immunol. **140**, 433 (1988); (*g*) H. Mohr, G. R. Pettit, and A. Plessing-Menze. Immunobiology, **175**, 420 (1987); (*h*) W. S. May, S. J. Sharkis, A. H. Esa, V. Gebbia, A. S. Kraft, G. R. Pettit, and L. L. Sensenbrenner. Proc. Natl. Acad. Sci. U.S.A. **84**, 8483 (1987); (*i*) P. A. Wender, C. M. Cribbs, K. F. Koehler, N. A. Sharkey, C. L. Herald, Y. Kamano, G. R. Pettit, and P. M. Blumberg. Proc. Natl. Acad. Sci. U.S.A. **85**, 7197 (1988).
5. M. Lalonde and T. H. Chan. Synthesis, 817 (1985).
6. E. J. Corey and A. Venkateswarlu. J. Am. Chem. Soc. **94**, 6190 (1972).
7. P. J. Kocienski, D. A. S. Street, C. Yeates, and S. F. Cambell. J. Chem. Soc. Perkin Trans. 1, 2189 (1987).
8. F. E. Ziegler, A. Nangia, and G. Schulte. Tetrahedron Lett. 1669 (1988).
9. G. R. Pettit, Y. Kamano, D. Schaufelberger, C. L. Herald, P. M. Blumberg, and S. W. May. J. Liq. Chromatogr. **12**, 553 (1989).
10. A. Hassner and V. Alexanian. Tetrahedron Lett. 4475 (1978).
11. (*a*) E. F. V. Scriven. Chem. Soc. Rev. **12**, 129 (1983); (*b*) G. Holfe, W. Steglich, and H. Vorbruggen. Angew. Chem. Int. Ed. Engl. **17**, 569 (1978).
12. G. R. Pettit, D. L. Herald, F. Gao, D. Sengupta, and C. L. Herald. J. Org. Chem. **56**, 1337 (1991).
13. (*a*) C. W. Holzapfel, G. R. Pettit, and G. M. Cragg. J. Nat. Prod. **46**, 917 (1983); (*b*) J. Nat. Prod. **48**, 513 (1985).

Can. J. Chem. Downloaded from www.nrcresearchpress.com by 198.100.157.202 on 09/07/12
For personal use only.

Comparison of chemical and electrochemical reduction of cyanamides: an example of cathodic decyanation

MICHEL CARIOU[1] AND JACQUES SIMONET

Laboratoire d'électrochimie, Équipe de recherche associée au Centre national de la recherche scientifique, N° 439, Université de Rennes 1, Campus de Beaulieu, 35042 Rennes CEDEX, France

Received October 17, 1990

MICHEL CARIOU and JACQUES SIMONET. Can. J. Chem. **69**, 861 (1991).

Most disubstituted cyanamides exhibit a very low cathodic activity and are therefore difficult to reduce. However, the cathodic cleavage of diarylcyanamides can be carried out directly and leads to the corresponding diarylamine; the action of sodium causes the same cleavage. Alkylarylcyanamides display no cathodic step, but can be reduced indirectly by redox catalysis; this allows the determination of the standard potential corresponding to the first electron transfer. The macroscale electrolysis, in the presence of the catalyst, leads to the alkylarylamine by cleavage, whereas the action of sodium gives mainly a cyanoguanidine. Dialkylcyanamides are electroreducible neither directly, nor indirectly, whereas by action of sodium they trimerize almost quantitatively into triazines.

Key words: cyanamide, decyanation, electroreduction, redox catalysis.

MICHEL CARIOU et JACQUES SIMONET. Can. J. Chem. **69**, 861 (1991).

La plupart des cyanamides disubstitués présentent une très faible activité cathodique et, par conséquent, se réduisent difficilement. Cependant, la coupure cathodique des diarylcyanamides peut être effectuée directement et conduit à la diarylamine correspondante; l'action du sodium provoque la même coupure. Les alkylarylcyanamides ne présentent pas de pic cathodique, mais peuvent être réduits indirectement par catalyse rédox; cela permet alors la détermination du potential standard correspondant au premier transfert d'électron. L'électrolyse préparative, en présence du catalyseur, conduit à l'alkylarylamine par coupure, alors que l'action du sodium donne principalement une cyanoguanidine. Les dialkylcyanamides ne sont électroréductibles ni directement, ni indirectement, alors que par action du sodium ils se trimérisent presque quantitativement en triazines.

Mots clés : cyanamide, décyanation, électroréduction, catalyse rédox.

[Traduit par la rédaction]

Can. J. Chem. Downloaded from www.nrcresearchpress.com by 198.100.157.202 on 09/07/12
For personal use only.

Introduction

The cathodic cleavage of the C—N bond is not current at all in electrochemistry. The only reported reactions (1) concern the degradation of ammonium salts under electron transfer. The cleavage of those onium salts was also carried out indirectly (2). On the contrary, the reduction of amines (even activated ones such as benzylic and allylic amines) has never been observed, nor even suggested. This lack of reactivity is probably due to the donating effect of the electron-rich amino group. We want to report here the behaviour of cyanamides of general formula:

RR'N—CN

1 *a* R = R' = Me
b R = R' = Ph
c R = Me, R' = Ph

Results and discussion

1. *Action of alkali metals*

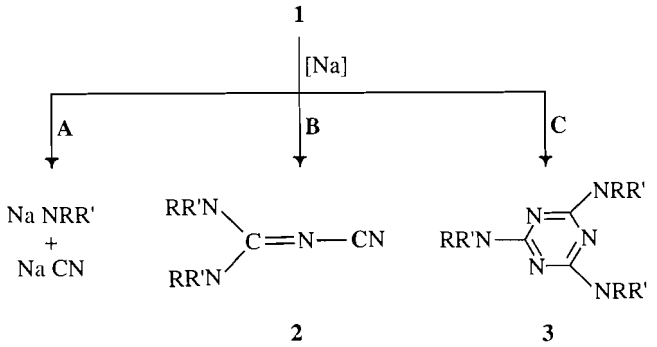
In search of new organic solvents usable in lithium batteries, we observed in our laboratory (3) for the first time the almost complete trimerization of *N*-cyanopyrrolidine, a disubstituted cyanamide, on mere storage over lithium shavings for about 12 h. This preliminary observation led us to study the action of alkali metals on several disubstituted cyanamides **1**; sodium (in dispersion) is the best metal for this study, because it is more reactive than lithium and less hazardous than potassium (4).

The action of sodium on cyanamides **1** gives rise to three types of reactions according to the nature of R and R':

A. Cleavage into cyanide and dialkylamide, when R and R' are aromatic (R = R' = Ph: **1***b*) or simply bulky (R = R' = *i*Pr).

B. Formation of cyanoguanidines **2**, when R = Me and R' = Ph: **1***c*.

C. Trimerization into 2,4,6-tris(*N*,*N*-dialkylamino)-1,3,5-triazines **3**, only when R = R' = alkyl, as in the case of **1***a*:



These chemical reactions with sodium may occur under electron transfer catalysis. Consequently, it was of interest to test the cathodic behaviour of molecules of type **1**, in order to compare chemical and electrochemical reactivities and also, possibly, to elucidate mechanisms.

2. *Cyclic voltammetry*

The three model cyanamides **1** were tested with a mercury microelectrode as a working electrode and the $Ag/AgI/I^-$ 0.1 M system as a reference electrode; the electrolyte was a solution of 0.1 M tetraethylammonium perchlorate in dimethylformamide dried over molecular sieves (4 Å).

Cyanamide ***1***b

Only **1***b* exhibits a voltammetric step, located at very negative potential values: $E_p = -2.13$ V (Fig. 1). The step is irreversible and corresponds to a one-electron reaction; the monoelectronic character was checked by comparison with the voltammogram of naphthalene. **1***b* does not exhibit any redox catalysis: no indirect reduction by the stilbene radical anion formed at E^0 =

[1]Author to whom correspondence may be addressed.

Printed in Canada / Imprimé au Canada

Can. J. Chem. Downloaded from www.nrcresearchpress.com by 198.100.157.202 on 09/07/12
For personal use only.

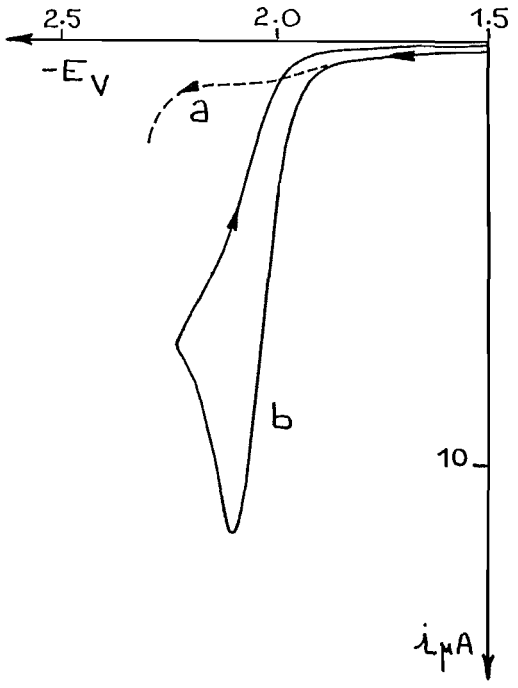


FIG. 1. Voltammetries of cyanamide **1***b*. Electrolyte: DMF–TEAP 0.1 M. Hg microelectrode. Reference: Ag/AgI/I^- 0.1 M system. Sweep rate: 0.1 V s^{-1}. Curve a: background response. Curve b: in the presence of 2.5×10^{-3} M of **1***b*.

−1.67 V, while a kind of catalysis is visible at the level of the second step ($E = -1.95$ V), which is, however, fully irreversible.

Actually, one can expect a redox catalysis phenomenon for cyanamides by analogy with the classical case of alkyl halides where the C—X bond, able to cleave after an electron transfer, is comparable to the N—CN bond of cyanamides (see below).

*Cyanamide 1*c

Cyanamide **1***c*, less activated than **1***b*, does not display any cathodic step. However, here the use of redox catalysis allows us to observe a catalytic current for **1***c*, with mediators (Ar) such as naphthalene (Fig. 2) and biphenyl. The theory defined for electrochemical–chemical (EC) systems can completely apply (5). Results fit in nicely with a monoelectronic reduction of **1***c*; this is analogous to what is observed with **1***b*.

The kinetically limiting process is the electron transfer rate from the catalyst radical anion $Ar^{\cdot-}$ to substrate **1***c*. Catalytic efficiency increases with catalyst concentration, which is what we observed by varying this concentration while maintaining constant the excess factor γ (ratio of cyanamide to catalyst concentration: $\gamma = C^0_{1c}/C^0_{Ar}$).

The values found for the electron exchange rate constant in solution are as follows: $k_1 = 265$ s^{-1} with the naphthalene anion, $k_1 = 1960$ s^{-1} with the biphenyl anion. Comparison of the high rate of the cleavage process for **1***c* with the absence of redox catalysis for **1***b* leads us to think that, with more conjugated structures, the rate of cleavage of the radical anion is much slower. By using the method developed by Savéant and co-workers (5), these values of k_1 permit access to the standard potential of cyanamide **1***c* despite the absence of a cathodic peak:

$$E^0_{Ar} - E^0_{1c} = 0.058 \log k_2/k_1$$

$$E^0_{1c} = E^0_{Ar} + 0.058 \log k_1 - 0.58$$

(since k_2 (diffusion) = 10^{10} M^{-1} s^{-1} for dimethylformamide,

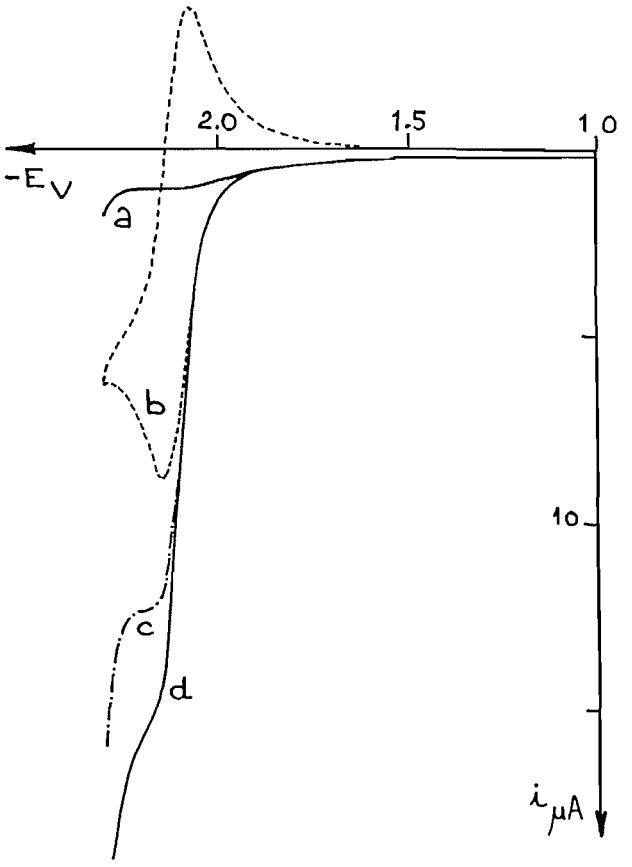


FIG. 2. Redox catalysis relative to cyanamide **1***c* in the presence of naphthalene as an electron carrier. Electrolyte: DMF–TEAP 0.1 M. Hg microelectrode. Reference Ag/AgI/I^- 0.1 M system. Sweep rate: 0.1 V s^{-1}. Curve a: background response. Curve b: naphthalene voltammetric response, $c = 2.5 \times 10^{-3}$ M. Curve c: preceding solution containing **1***c*, $c = 5 \times 10^{-3}$ M. Curve d: solution b containing **1***c*, $c = 7.5 \times 10^{-3}$ M.

the solvent used for the voltammetry studies). With naphthalene as a mediator: $E^0_{1c} = -1.94$ V + 0.058 log 265 − 0.58 = −2.38 V; and with biphenyl as a mediator: $E^0_{1c} = -2.00$ V + 0.058 log 1960 − 0.58 = −2.39 V. So the average standard potential of cyanamide **1***c*: $E^0 = -2.385$ V vs. Ag/AgI/I^- 0.1 M, lies at the level of the accessible limit of the electrolyte.

*Cyanamide 1*a

Despite numerous attempts utilizing mediators with very negative standard potentials (*trans*-stilbene, biphenyl, naphthalene, acenaphthene), in the case of dialkylcyanamide **1***a* no indirect reduction was observed.

3. *Macroscale electroreductions: comparison with the action of sodium*

*Cyanamide 1*b

We observed previously that **1***b* exhibits a one-electron step in cyclic voltammetry. However, in macroscale electroreduction, the electricity consumption is close to 1.8 F mol^{-1}, with almost quantitative formation of diphenylamine (92%):

$$Ph_2N{-}CN \xrightarrow[e^-]{\text{Hg, DMF–TEAP, –2.10 V}} (Ph_2N{-}CN)^{\cdot-} \xrightarrow{-NC^-} Ph_2N^{\cdot} \xrightarrow[\text{slow}]{e^-,\ H^+} Ph_2NH$$

Can. J. Chem. Downloaded from www.nrcresearchpress.com by 198.100.157.202 on 09/07/12
For personal use only.

This means that the monoelectronic first step is the kinetically limiting process, while the second electron transfer is slow. Note that, in the case of diphenylcyanamide **1***b*, the results of preparative electroreduction and action of sodium are exactly the same: cleavage of the C—N single bond.

Cyanamide ***1***c

The indirect preparative electroreduction of methylphenylcyanamide **1***c* exhibits the same cleavage reaction, also with an electricity consumption of 2 F mol^{-1} and quantitative formation of N-methylaniline. The mechanism and conclusions are the same as in the case of **1***b*:

$$\mathrm{PhMeN{-}CN} \xrightarrow[e^-]{\text{Hg, DMF–TEAP, –2.00 V}} (\mathrm{PhMeN{-}CN})^{\cdot-} \xrightarrow{-NC^-} \mathrm{PhMeN^{\cdot}} \xrightarrow[\text{slow}]{e^-,\,H^+} \mathrm{PhMeNH}$$

This electroreduction gives a result different from the action of sodium on cyanamide **1***c*: beside 19% of *N*-methylaniline, 61% of cyanoguanidine **2***c* was isolated. Anderson *et al.* (6) also obtained this cyanoguanidine, by reacting PhMeN—CN with Ph Li (yield: 58%) or with PhMeN Li (75%). From their results and observations, the following mechanism can be proposed:

$$\mathbf{1}c \xrightarrow{Na} \mathbf{1}c^{\cdot-}\,Na^+ \longrightarrow NaCN + \mathrm{PhMeN^{\cdot}} \xrightarrow{Na} \mathrm{PhMeN^-}\,Na^+$$

$$\xrightarrow{\mathbf{1}c} \begin{matrix}\mathrm{PhMeN}\\ \mathrm{PhMeN}\end{matrix}\!\!>\!C{=}N^-\,Na^+$$

$$\xrightarrow{\mathbf{1}c} \begin{matrix}\mathrm{PhMeN}\\ \mathrm{PhMeN}\end{matrix}\!\!>\!C{=}N{-}CN + \mathrm{PhMeN^-}\,Na^+$$

2*c*

At the start, the formation of a catalytic quantity of $PhMeN^-$ is sufficient, since it is continually regenerated. But one can also suggest a mechanism in which radical anion $\mathbf{1}c^{\cdot-}$ adds directly, without prior cleavage, to cyanamide **1***c*; it is therefore a simple coupling reaction catalyzed by sodium:

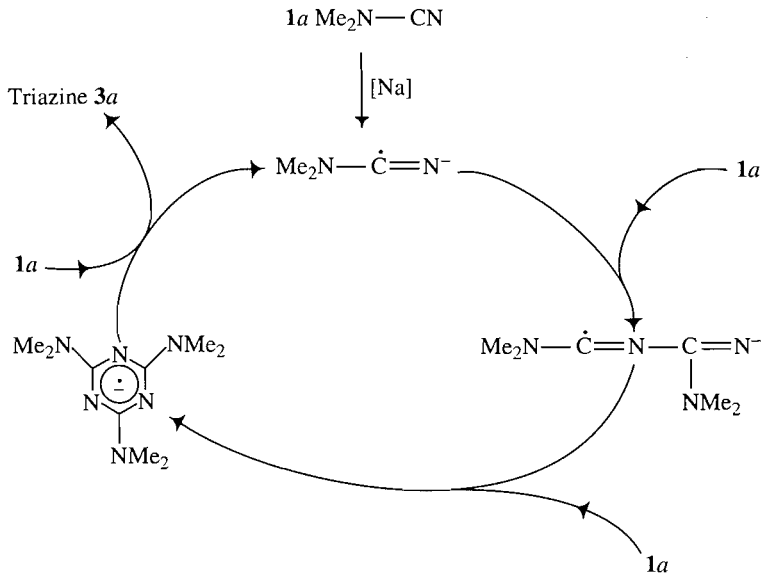
$$\mathbf{1}c^{\cdot-} \xrightarrow{\mathbf{1}c} \mathbf{2}c^{\cdot-} \xrightarrow{\mathbf{1}c} \mathbf{2}c + \mathbf{1}c^{\cdot-}$$

However, in cyclic voltammetry, when cyanamide **1***c* is added to the radical anion of cyanoguanidine **2***c* (formed at −1.60 V versus Ag/AgI/I^- 0.1 M, on a mercury microelectrode in DMF–TEAP), there is no redox catalysis; this is not surprising, because the potential gap is high ($E^0_{1c} - E^\circ_{2c} = 0.8$ V).

Cyanamide ***1***a

Considering the propensity of dialkylcyanamides **1** to trimerize into triazines **3** under the action of sodium, we attempted the electrochemical trimerization (cathodic induction of electron transfer) of cyanamide **1***a*. Despite many and various attempts, at constant current intensity, the formation of triazine **3***a* was never observed by the following procedures: reduction by quaternary ammonium amalgam, according to experimental conditions defined previously (7), in DMF–TEAP; electroreduction at a glassy carbon cathode in $MeCN–Bu_4NBF_4$; redox catalysis on mercury pool, in DMF-TEAP, in the presence of acenaphthene; electroreduction in toluene–$(C_6H_{13})_4N\ ClO_4$ (it was impossible to exceed 2 mA in intensity). Therefore, it appears clear that electron transfer does not occur under extreme electrochemical conditions.

However, in the presence of a catalytic amount of sodium (less than 5%), dimethylcyanamide **1***a* was converted into triazine **3***a* in almost quantitative yield, very likely according to a catalytic cycle initiated by a monoelectronic transfer, where the anion radical of **3***a* is the reducing species of **1***a* ($E^0_{1a} > E^0_{3a}$):



This is quite different from the mechanism proposed previously (see ref. 6, p. 2316) for the same trimerization carried out in the presence of phenyllithium (yield of triazine **3***a*: 14%).

Thus, the behaviour of cyanamides towards reducing species on the one hand, and a metallic cathode on the other hand, can be dramatically changed as a function of experimental conditions. The reason why electrochemical dimerization (of cyanamide **1***c* into cyanoguanidine **2***c*) and electrochemical trimerization (of cyanamide **1***a* into triazine **3***a*) failed could be the radically different experimental conditions; the action of sod-

ium was carried out in toluene, a nonpolar solvent, whereas electroreductions were performed in polar solvents such as dimethylformamide and acetonitrile where radical anions, if formed, are strongly solvated and therefore far less reactive.

Experimental

N,N-dimethylcyanamide **1***a* was a commercial product.

Preparation of N-*methyl*-N-*phenyl-cyanamide* **1**c *(8, 9)*

To an ice-cold mixture of magnesium carbonate (6.95 g), ether (80 mL), water (9 mL), and cyanogen bromide (25 g) was added, dropwise, over 40 min with stirring, *N*-methylaniline (25.25 mL). At the end of the addition, the ice bath was removed and stirring was maintained for 1 h. Then the mixture was extracted with 150 mL of ether, washed several times with water, and dried over K_2CO_3. After the usual work-up, distillation gave 22.2 g (72%) of methylphenylcyanamide **1***c*: bp 140°C (16 Torr; 1 Torr = 133.3 Pa); mp 28°C; IR (KBr) ν (CN): 2225; NMR ($CDCl_3$), δ: 3.30 (s, 3H, Me), 6.96–7.00 (m, 5H, Ph).

Preparation of N,N-*diphenylcyanamide* **1**b *(10)*

A mixture of magnesium carbonate (6.95 g), acetonitrile (80 mL), water (9 mL), cyanogen bromide (25 g), and diphenylamine (39.44 g) was refluxed for 12 days; after cooling, it was extracted with 250 mL of ether, washed several times with water, and dried over K_2CO_3. The usual work-up, followed by careful distillation, allowed us to isolate 24.7 g (54%) of diphenylcyanamide **1***b*: bp 185–195°C (16 Torr); mp 74°C (cylcohexane) IR (KBr) ν (CN): 2250; NMR ($CDCl_3$), δ: 7.10–7.65 (m, Ph).

Chemical cleavage of diphenylcyanamide **1**b

A mixture of 0.25 g of sodium (dispersion) and 2.0 g of diphenylcyanamide **1***b* in 50 mL of toluene was warmed at 80°C for 10 h, with stirring; then 200 mL of dichloromethane was added, the organic layer was washed several times with water, and dried over K_2CO_3; after the usual work-up, 1.40 g of diphenylamine was obtained (identified by its melting point, IR spectrum and TLC). The presence of cyanide in the aqueous layer was proven by the Prussian blue precipitate test.

Electrochemical cleavage of diphenylcyanamide **1**b

In a three-compartment H-shaped cell, 5 mmol (0.97 g) of diphenylcyanamide **1***b* in 65 mL of DMF–TEAP 0.1 M were electrolyzed, on a mercury pool (A = 15 cm^2) at −2.10 V (vs. Ag/AgI/I^- 0.1 M) for 24 h. The electricity consumption was 1.8 F mol^{-1}. The catholyte was diluted with 300 mL of ether, washed several times with water, and dried over K_2CO_3. After the usual work-up, 0.78 g (92%) of diphenylamine was isolated and identified as above. The presence of cyanide in the aqueous layer was also proven as above.

Indirect cathodic cleavage of methylphenylcyanamide **1**c*, in the presence of naphthalene as a redox catalyst*

In a three-compartment H-shaped cell, 5 mmol (0.661 g) of methylphenylcyanamide **1***c* in 65 mL of DMF–TEAP 0.1 M, together with 1 mmol (0.128 g) of naphthalene, were electrolyzed, on a mercury pool (A = 15 cm^2) at −2.0 V (vs. Ag/AgI/I^- 0.1 M) for 48 h. The electricity consumption was about 2 F mol^{-1}. The catholyte was diluted with 300 mL of ether, washed several times with water, and dried over K_2CO_3. After the usual work-up, 0.56 g of oil was obtained, identified by TLC, IR, and NMR spectroscopy as *N*-methylaniline contaminated with a little naphthalene; NMR ($CDCl_3$), δ: 2.77 (s, 3H, Me), 3.50 (dome, 1H, NH). The presence of cyanide in the aqueous layer was proven by the Prussian blue precipitate test.

Reaction of sodium with methylphenylcyanamide **1**c*: preparation of 2-cyano-1,3-dimethyl-1,3-diphenyl-guanidine* **2**c

A mixture of 0.40 g of sodium (dispersion) and 3.60 g of methylphenylcyanamide **1***c* in 50 mL of toluene was stirred, at room temperature, for 24 h; then 200 mL of dichloromethane was added, the organic layer was washed several times with water, and dried over K_2CO_3; after the usual work-up, 3.4 g of a mixture of oil and crystals was obtained, which after crystallization in 11 mL of ethanol allowed us to isolate a first crop of 1.0 g of cyanoguanidine **2***c*. Purification of the filtrate by silica gel column chromatography with CH_2Cl_2–MeOH 98:2 as an eluent gave a further amount of 1.1 g of cyanoguanidine **2***c* (overall yield 61%) and 0.55 g of *N*-methylaniline (19%): mp 128°C (ethanol) (lit. (6) mp 126°C); IR (KBr) ν (CN): 2180; NMR ($CDCl_3$), δ: 3.38 (s, 6H, Me), 6.65–6.90 (m, 4H, Ph), and 6.97–7.35 (m, 6H, Ph).

Reaction of sodium with dimethylcyanamide **1**a*: preparation of 2,4,6-tris(*N,N-*dimethylamino)-1,3,5-triazine* **3**a

A mixture of 0.40 g of sodium (dispersion) and 8.1 mL (0.1 mol) of dimethylcyanamide **1***a* in 80 mL of toluene was stirred at room temperature for 3 h. Then the sodium was filtered off on glasswool; the solution was diluted with 70 mL of ether, washed several times with water, and dried over K_2CO_3. After the usual work-up, 6.6 g (94%) of crude crystals of triazine **3***a* were obtained; recrystallization from 55 mL of ethanol allowed us to isolate 5.3 g (74%) of colorless needles; mp 176°C (lit. (6) mp 173°C); IR (KBr) ν (triazine): 1500, 1390; NMR ($CDCl_3$), δ: 3.13 (s, NMe_2).

1. L. Horner. *In* Organic electrochemistry. 2nd ed. *Edited by* M. M. Baizer and H. Lund. M. Dekker, New York. 1983. p. 729.
2. P. Martigny and J. Simonet. J. Electroanal. Chem. **101**, 275 (1989).
3. S. Guibert, M. Cariou, and J. Simonet. Bull. Soc. Chim. Fr. 924 (1989).
4. K. El Hobbi. Thèse de l'Université de Rennes 1, 1989.
5. (*a*) C. P. Andrieux, J. M. Dumas-Bouchiat, and J. M. Savéant. J. Electroanal. Chem. **87**, 55 (1978); (*b*) J. Electroanal. Chem. **113**, 1 (1980); (*c*) C. P. Andrieux, C. Blocman, J. M. Dumas-Bouchiat, F. M'Halla, and J. M. Savéant. J. Electroanal. Chem. **113**, 19 (1980); (*d*) C. P. Andrieux, C. Blocman, J. M. Dumas-Bouchiat, and J. M. Savéant. J. Am. Chem. Soc. **101**, 3431 (1979).
6. H. J. Anderson, N. C. Wang, and E. T. P. Jwili. Can. J. Chem. **49**, 2315 (1971).
7. E. Kariv-Miller, R. I. Pacut, and G. K. Lehman. Organic electroreductions at very negative potentials. *In* Topics in current chemistry. no. 148. Electrochemistry III. Springer-Verlag, Berlin. (1988). pp. 97–130.
8. T. N. Birkinshaw, D. W. Gillon, S. A. Harkin, G. D. Meakins, and M. D. Tirel. J. Chem. Soc. Perkin Trans. 1, **2**, 147 (1984).
9. O. Wallach. Chem. Ber. **32**, 1873 (1899).
10. J. R. Robinson and W. H. Brown. Can. J. Chem. **29**, 1069 (1951).

Can. J. Chem. Downloaded from www.nrcresearchpress.com by 198.100.157.202 on 09/07/12
For personal use only.

Theoretical calculations of chemical interactions. VII.[1] SCF-MO conformational studies of substituted 2′-hydroxychalcones

NORMA SBARBATI NUDELMAN[2]

Departamento Química Orgánica, Facultad de Ciencias Exactas y Naturales, Universidad de Buenos Aires, Pab. II, P. 3, Ciudad Universitaria, 1428 Buenos Aires, Argentina

AND

JORGE JAVIER P. FURLONG

Cátedra de Química Física II, Facultad de Química, Bioquímica y Farmacia, Universidad Nacional de San Luis, San Luis, Argentina

Received October 6, 1990

NORMA SBARBATI NUDELMAN and JORGE JAVIER P. FURLONG. Can. J. Chem. **69**, 865 (1991).

INDO calculations have been performed on substituted 2′-hydroxychalcones. The results show that the intramolecularly hydrogen-bonded *trans-s-cis* conformation is the most stable. The calculations assist in assignment of NMR signals and interpretation of kinetic determinations. The calculated energy of the intramolecular hydrogen bond is compared with IR data when available and with experimentally determined heats of formation of the chalconates. Regarding the isomerization to flavanones, calculations of the ring A rotation in the chalconates show that it is exergonic; on the contrary, complete rotation of the styryl system encounters a strong barrier. MNDO calculations on this process show similar trends. These results indicate that this last rotation is involved in the slow step, which is consistent with kinetic determinations.

Key words: chemical interactions, theoretical calculations, substituted hydroxychalcones, flavanones.

NORMA SBARBATI NUDELMAN et JORGE JAVIER P. FURLONG. Can. J. Chem. **69**, 865 (1991).

On a effectué des calculs INDO sur des 2′-hydroxychalcones substituées. Les résultats montrent que la conformation *trans-s-cis* avec liaison hydrogène intramoléculaire est la plus stable. Des calculs aident à l'attribution des signaux RMN et à l'interprétation des données cinétiques. Lorsqu'elles sont disponibles, on a comparé les énergies calculées pour la liaison hydrogène intramoléculaire avec les données IR et avec les chaleurs de formation des chalconates déterminée expérimentalement. En ce qui a trait à l'isomérisation en flavanones, les calculs relatifs à la rotation du cycle A des chalconates démontrent que cette réaction est exergonique; au contraire, la rotation complète du système styryle est soumise à une forte barrière. Des calculs MNDO sur ce processus suggèrent les mêmes tendances. Ces résultats indiquent que cette dernière rotation est impliquée dans l'étape lente, ce qui est en accord avec les déterminations cinétiques.

Mots clés : calculs théoriques des reactions chimiques, hydroxychalcones substituées, flavanones.

[Traduit par la rédaction]

Introduction

There are no experimental studies on the conformation of 2′-hydroxychalcones, **1**, and in previous kinetic studies on their conversion into flavanone (2, 3) the conformation is not defined. The importance of the stereochemistry in discussion of chemical reactivity is being widely recognized and nowadays considerable efforts are being devoted to the evaluation of the preferred molecular conformations (4–6). ^{1}H and ^{13}C NMR spectroscopy (4*a*, 7) and, more recently, MO calculations (4*b*, 5, 6, 8) have been successfully used in the elucidation of conformational preferences as well as in the evaluation of energy and entropy barriers.

In our kinetic studies (9, 10) on the mechanism of cyclization of substituted 2′-hydroxychalcones, assumptions were made about the preferred substrate conformations (mainly suggested by NMR determinations (9)), and some internal rotations were proposed to be involved in the rate-determining step (10). Since such conformational changes are not amenable to experimental determination and, curiously, some recent papers presume different substrate conformations (11, 12), the purpose of the present work was to study those points by SCF MO calculations.

Results and discussion

Method of calculation

The molecules under study are of a moderately large size, rendering an *ab initio* MO analysis too expensive. Turning our attention to semiempirical methods, several points are worthy of mention. Buemi *et al.* (13) reported that the MINDO/3 method is unable to differentiate between the *cis* and *trans* conformations of the methoxy moiety in 4-methoxy-2-nitroaniline. Using the PCILO method, problems have been met with optimization of the geometry (14). Although some shortcomings of CNDO/2 and INDO-like methods in describing conjugative effects are documented (15), they have been successful in showing relative stabilities and optimized geometries (6, 16). MNDO gives good heats of formation and relative reactivities but its weakness in accounting for hydrogen bonds is well known (ref. 1, and references therein). The INDO method was thus preferred for the purpose of this work: in some cases MNDO (1) calculations were also carried out and the results given for both methods were compared. Calculations were performed using the INDO method (17) with 3*d* orbitals included (18). The standard program was modified to an extended basis of maximum 99 atomic orbitals; consistency with experimental results, where data exist, gave us confidence in the method. The starting geometries were calculated using standard bond lengths and angles except for the following bonds: $C_{\alpha,\beta}$—H (19), C_{Ar}—O^-, C4—N, N—O, and ONO (20), for which optimized values of structurally related compounds were used.

Substrate conformation. Intramolecular hydrogen bonding

There has been considerable progress in theoretical and conceptual studies of hydrogen-bonded systems. In our previous kinetic studies (9) we proposed that compound **1** exists in

[1]Part VI. See ref. 1.

[2]Author to whom correspondence may be addressed.

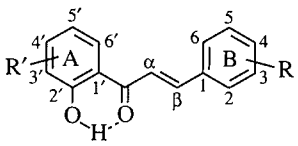
Can. J. Chem. Downloaded from www.nrcresearchpress.com by 198.100.157.202 on 09/07/12
For personal use only.

TABLE 1. Energy differences for several conformers of 2′-hydroxychalcone as a function of the O—H bond length and the COH bond angle[a]

Conformer	$d_{O—H}$, Å	COH angle, degrees								
		120	118	114	112	110	108	106	104	102
Structure[b]	0.97	12.8	11.9	105.1						
with	1.00							4.2	3.1	
intramolecular	1.05		4.3	2.2	1.3	0.7	0.3	0	0	0.3
H-bond	1.10			3.9	2.8			0.6	0.4	
	1.15			9.2						
Structure[c,d]	0.97	6.7								
without	1.00					1.5				
intramolecular	1.05			0.3	0.1	0	0.1	0.3		
H-bond	1.10					3.9		4.0		

[a]In kcal mol^{-1}, with respect to the most stable conformer.
[b]Minimum energy conformer: d = 1.07 Å, ∠COH = 105°.
[c]All the COH angles are negative (no intramolecular hydrogen bond).
[d]Minimum energy conformer: d = 1.03 Å, ∠COH = −110°.

the *trans-s-cis* conformation shown, suitable for the establishment of an intramolecular hydrogen bond. This was also suggested by analysis of IR data (21, 22) and by a Pariser–Parr–Pople (CNDO/S) calculation (23). In contrast, in recent papers (2, 3, 11, 12) the phenolic moiety is assumed to be in a conformation that does not allow the intramolecular H-bond. It was then of interest to investigate the degree of stabilization that could be achieved through the interaction involved in the hydrogen bond establishment.



1

2 R = 4-NO_2 R′ = H
3 R = H R′ = H
4 R = 3-O^- R′ = H
5 R = 4-O^- R′ = H
6 R = H R′ = 4′-O^-

The search for the minimum energy structure in this case was performed by varying the C2′OH angle and the O—H length, d. Similarly, the most stable conformer with no hydrogen bond interaction was calculated by considering the 2′OH group rotated 180°. The results for 2′-hydroxychalcone are gathered in Table 1; they are given as the excess in total energy (in kcal mol^{-1}) with respect to the minimun energy conformer in each case, calculated from the plots of energy as functions of d and of the C2′OH (not shown). The difference in energy between the most stable conformers (d = 1.07 Å, C2′OH = 105°, and d = 1.03 Å, C2′OH = −110°, for the structures that are bonded and those that are not, respectively) is 13.7 kcal/mol, indicating the stabilizing effect of the intramolecular hydrogen bond. The calculated value compares satisfactorily with the experimental value (10.2 kcal/mol^{-1}) obtained by Shigorin (21) by IR determinations. The calculated dipolar moment, μ = 4.5 D, for the minimum energy conformer, is fairly close to the μ = 3.94 D found in dioxane solution (24). On the contrary, the MNDO results are not consistent with experimental data. In fact, when INDO geometries were allowed to optimize (OH length and C2′OH angle) by the MNDO procedure, not only the energies (the structure that is not H-bonded is 6 kcal/mol^{-1} more stable), but also the final values of the parameters (d = 0.94 Å, C2′OH = 121°, and d = 0.95 Å, C2′OH = −113°, for the structures with and without H-bonds, respectively) are not reasonable. As mentioned before, MNDO does not account for the H-bond stabilization.

Substituent effects on the H-bond strength were evaluated by similar calculations performed with substituted chalcones **2–6**, for which experimental data are not available. Geometry optimization was carried out by allowing variations in the O—H length and in C2′OH; the calculated values were plotted for each substituted chalcone as was done with **3**. The results are gathered in Table 2. Substituents on ring B have a strong influence on the strength of the H-bond since they only affect the electron density on the carbonyl group. It can be observed in Table 2 that electron-withdrawing groups reduce the strength whereas electron-attracting groups increase it. Comparison of the oxyanion group effect for the 4 and the 4′-positions reinforces this conclusion. The oxyanion in the 4′-position (chalcone **6**), negatively affects the charge distribution on the phenolic group, thus slightly weakens the H-bond. Considering the structure that is not H-bonded, there is an additional stabilization provided by the interaction between the O—H and 4′-O^-. Its magnitude was calculated from the difference between the total energy of the monoanion of resorcinol with the same values of O—H and COH and the energy of the minimum energy conformer of resorcinol (d = 1.07 Å, COH = 104°). This energy difference (0.65 kcal mol^{-1}) could be added to the calculated value in Table 2 for a best estimation.

From the above data it is clear that in all cases the H-bonded structure is preferred. The heat of formation of each 2′-oxyanion was determined experimentally (Table 2) and an acceptable qualitative correlation was found between these and the calculated H-bond energies (the stronger the H-bond, the higher the heat of formation of the corresponding chalconate). The only exception is compound **6**.

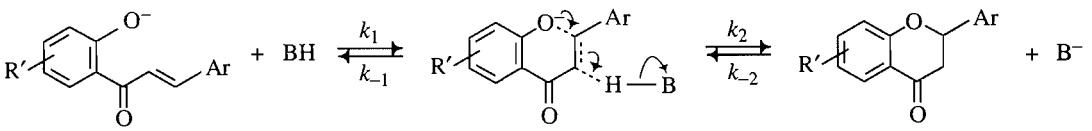
The atomic populations for both minimum energy conformers were calculated in each case, and also the atomic population involved in the intramolecular hydrogen bond, which is given in the last column of Table 2. It can be observed that there is good correlation of these data with the energy of the H-bond for the different compounds gathered in the table and also with the experimental ΔG; even compound **6** correlates well, which gives us confidence in the correction suggested.

Can. J. Chem. Downloaded from www.nrcresearchpress.com by 198.100.157.202 on 09/07/12
For personal use only.

TABLE 2. Minimum energy conformers of substituted 2′-hydroxychalcones with and without intramolecular hydrogen bond. Heats of formation of the chalconates and atomic population of the intramolecular hydrogen bond

Substituted chalcone	∠2′OH	d_{O-H}, Å	$d_{H\cdots O}$, Å	ΔE,[a] kcal mol^{-1}	ΔG,[b] kcal mol^{-1}	Intramolecular H-bond atomic population
2	106° −110°	1.07 1.04	1.51 —	13.3	−5.69	0.0696
3	105° −110°	1.07 1.04	1.50 —	13.7	−5.36	0.0745
4[c]	104° −110°	1.07 1.04	1.49 —	16.6	−5.18	0.0780
5	104° −110°	1.08 1.04	1.48 —	18.1	−4.71	0.0978
6	104° −109°	1.07 1.05	1.49 —	13.25 (±0.65)	−0.72	0.0730

[a]Calculated H-bond energy.
[b]Heat of formation of 2′-chalconates determined from the pre-equilibrium constant (H-bond rupture and proton abstraction), which is the ratio of second-order rate constants at relatively low[3] and high pH (10).
[c]Average values for both possible substitutions (3-O$^-$ and 5-O$^-$).



SCHEME 1

In conclusion, taking into account all the above considerations, the H-bonded *trans-s-cis* conformation seems to be preferred in all the 2′-hydroxychalcones studied, and this conformation should be taken into account in mechanistic and spectroscopic studies on these compounds.

Internal rotations in the 2′-hydroxychalcone

In the mechanism we propose for cyclization in alkaline solution (9, 10) the H-bond is broken, the 2′–OH is converted into the oxyanion, and two internal rotations are needed: (a) rotation of ring A and (b) rotation about the single bond, which changes the *trans-s-cis* into the *trans-s-trans* conformer (Scheme 1).

INDO calculations of the rotation of ring A show that there is no rotational barrier. In fact, when ring A was allowed to rotate in steps of 30° from 0° to 180° in the 2′-chalconate the total energy steadily diminishes (Table 3). The total energy change involved in the rotation is −9.03 kcal mol^{-1}.

Figure 1 shows the charge distribution calculated for the 2′-chalconate in the new conformation (the values corresponding to the conformation shown by **1** are given in parentheses). It is clear from the values that the rupture of the H-bond and rotation of ring A produce a $+0.072e$ change in the H_α charge, which is responsible for the δ 0.35 downfield shift observed in the ^{1}H NMR spectrum for the H_α signal. Also, the change in the H_β charge distribution explains the observed NMR shift (0.25 upfield). These results confirm previous assignments of NMR signals (9).

Once ring A has rotated, a second rotation is needed in order to attain the required conformation for cyclization (see Scheme 1). Table 3 shows INDO calculations of the energy change for the *trans-s-cis* into the *trans-s-trans* 2′-chalconate. Sieiro *et al.* (25) found that the CNDO/2 method fails to predict the right values when the rotation axis is a delocalized bond. It is probable that something similar may occur with the INDO method due to the underestimation of the loss in π interaction. Nevertheless, although the absolute values of Table 3 likely do not represent the real data, it is clear that they show a minimum for a rotation angle close to 90° and then strong repulsive interaction in the last steps of the rotation (rotation angle >160°, where steric interactions between O$^-$ and H_β should be important). For the case of the vinyl-butadienyl-ketone rotation (26), a single energy minimum was found in the potential

TABLE 3. INDO calculations on internal rotations in 2′-chalconates

	Rotation angle, degrees	ΔE, kcal mol^{-1}
Rotation of ring A	30	−1.44
	90	−2.63
	150	−8.33
	180	−9.03
Rotation of the styryl system	30	−2.3
	60	−6.0
	90	−8.5
	120	−2.3
	150	2.8
	160	109

[3]J. J. P. Furlong and N. S. Nudelman. J. Phys. Org. Chem. Submitted.

Can. J. Chem. Downloaded from www.nrcresearchpress.com by 198.100.157.202 on 09/07/12
For personal use only.

TABLE 4. MNDO calculations on the styryl system rotation in 2′-chalconate

Rotation angle, degrees	ΔE, kcal mol^{-1}	Interaction distances, Å		Net atomic charges, 10^3e				
		2′-O...H_α	2′-O...H_β	Carbonyl oxygen	Carbonyl carbon	C_α	C_β	2′-O
0	—	1.69	4.60	−401	336	−99	−87	−590
30	−5.8	1.87	4.45	−401	335	−53	−97	−598
60	−13.9	2.28	3.99	−398	337	−4	−108	−579
90	−13.6	2.74	3.27	−399	341	−13	−79	−572
120	−1.1	3.13	2.34	−402	350	−115	42	−584
150	69.2	3.39	1.27	−421	370	−402	72	−505

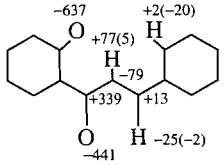


FIG. 1. Charge distribution ($10^{-3}e$) for the 2′-chalconate. Net atomic charges calculated for the minimum energy conformer of 2′-hydroxychalcone are shown in parentheses.

energy curve calculated by the CNDO/2 method. The same occurs in the present calculations; the minimum is reached when the styryl moiety is located perpendicular to the plane of the benzoyl system (Table 3).

The MNDO calculations shown in Table 4, although giving different ΔE values, show a similar trend, which leads to the same conclusions. An energy minimum is observed for a rotation angle of about 75° (estimated by the intercept of the curves in the energy vs. angle plot), and a strong barrier is encountered for a more advanced rotation (>150°). It can be observed in the table that for an intermediate rotation angle of around 120° there is no energy barrier, the distance 2′O...H_β is reasonable, and the distribution of net atomic charges favours the occurrence of the proposed mechanism (see Scheme 1).

In fact, both methods of calculation show that complete rotation of the styryl system encounters a strong barrier and it is unlikely to occur without some additional assistance.

In previous papers (9, 10) we proposed that complete rotation into the *trans-s-trans* conformation occurs in concert with proton addition to the C_α and phenoxide attack at the C_β. The proposal was based on the finding of general acid catalysis (9) and of huge isotope effects (10). The two concerted additions mentioned change the hybridization of the C_α and C_β in the transition state and contribute to diminishing the energy barrier as suggested by Tables 3 and 4. Data from both tables indicate that rotation to the *trans-s-trans* conformation takes place in the rate-determining step. This proposal finds strong support in the present results. In fact, the high electron density on C_α and the electron deficiency on C_β shown in Table 4, after enough rotation of the styryl system has occurred, tend to promote the reactions of the second step depicted in Scheme 1.

Conclusions

INDO calculations performed on several 2′-hydroxychalcones indicate the preferred conformation in each case and allow an estimate of the strength of the intramolecular hydrogen bond in the different minimum energy conformers. The calculated energies compare satisfactorily with experimental values when available, which gives us confidence in the method. Internal rotation of ring A and of the styryl system were also calculated: the first was found to occur spontaneously, while the second encounters a strong barrier in the last steps. MNDO calculations on this process show similar trends. These results are wholly consistent with previous proposals that the chalcones exist originally in the *trans-s-cis* conformation and cyclization to flavanones involves concerted rotation through the CO—C_α bond and annulation in the slow step. MNDO calculations afford strong support to the proposed mechanism for this step, but they do not account for the H-bond stabilization in the 2′OH-chalcone.

Acknowledgments

We are indebted to the National Research Council (CONICET) for financial support. Calculations were performed on an IBM 370 computer through the courtesy of IBM Buenos Aires. The generous help of Dr. D. Palleros and Dr. M. Estrada is also gratefully acknowledged.

1. D. PEREZ and N. S. NUDELMAN. J. Chem. Soc. Perkin Trans. 2, 931 (1989).
2. K. B. OLD and L. MAIN. J. Chem. Soc. Perkin Trans. 2, 1309 (1982).
3. S. K. DAVID, L. MAIN, and K. B. OLD. J. Chem. Soc. Perkin Trans. 2, 1367 (1981).
4. (*a*) P. W. RABIDEAU, J. L. MOONEY, and J. N. HARDIN. J. Org. Chem. **50**, 5737 (1985); (*b*) M. TAKASURA, H. NAKAI, and M. SHIRO. J. Chem. Soc. Perkin Trans. 2, 1969 (1986).
5. J. WIORKIEWICZ-KUCZERA and A. RABCZENKO. J. Chem. Soc. Perkin Trans. 2, 785 (1985); 437 (1986).
6. N. S. NUDELMAN and D. R. PALLEROS. J. Chem. Soc. Perkin Trans. 2, 805 (1985).
7. (*a*) J. A. GERLT and V. YOUNGBLOOD. J. Am. Chem. Soc. **102**, 7433 (1980); (*b*) N. S. NUDELMAN and S. CERDEIRA. Magn. Reson. Chem. **24**, 507 (1986); (*c*) R. J. ABRAHAM, H. A. BERGEN, and D. J. CHADWICK. Tetrahedron, **38**, 3271 (1982).
8. Z. SLANINA. Theor. Chim. Acta, **69**, 135 (1986).
9. J. J. P. FURLONG and N. S. NUDELMAN. J. Chem. Soc. Perkin Trans. 2, 633 (1985).
10. J. J. P. FURLONG and N. S. NUDELMAN. J. Chem. Soc. Perkin Trans. 2, 1213 (1988).
11. G. PANDEY, A. KHRISHNA, and G. KUMARASWAMY. Tetrahedron Lett. 4615 (1987).
12. Z. SANICONIS and I. TABAKOVIC. Tetrahedron Lett. 407 (1986).
13. G. BUEMI, A. RANDINO, and F. ZUCCARELLO. J. Mol. Struct. Theochem. **76**, 113 (1981).
14. P. NAGY, A. I. KISS, and A. LOPATA. J. Mol. Struct. Theochem. **86**, 41 (1981).
15. J. TYRREL, R. B. WEINSTOCK, and F. WEINHOLD. Int. J. Quantum Chem. **19**, 781 (1981).
16. N. S. NUDELMAN and P. MACCORMACK. Tetrahedron, **40**, 4227 (1984).
17. QCPE, Indiana University, Bloomington, IN, U.S.A.

Can. J. Chem. Downloaded from www.nrcresearchpress.com by 198.100.157.202 on 09/07/12
For personal use only.

18. V. GALASSO. Z. Naturforsch. Teil A, **28**, 1951 (1973).
19. J. A. POPLE and M. GORDON. J. Am. Chem. Soc. **89**, 4253 (1967).
20. N. S. NUDELMAN. An. Asoc. Quim. Argent. **68**, 95 (1980).
21. D. N. SHIGORIN. The hydrogen bond. Izd. Nauka, Moscow. 1964; V. D. ORLOV, I. A. BOROVOI, and V. F. LAVRUSHIN. Zh. Obshch. Khim. **43**, 642 (1973).
22. E. R. DAVID, G. B. SZABO, M. RAKOSI, and G. LITKEI. Acta Chim. Acad. Sci. Hung. **94**, 57 (1977).
23. A. GROULLIER, P. THOMASSERY, H. PACHECO, C. DECORET, and B. TINLAND. Bull. Soc. Chim. Fr. 3454 (1973).
24. V. D. ORLOV, I. A. BOROVOI, V. N. TISCHENKO, and V. F. LAVRUSHIN. Zh. Obshch. Khim. **46**, 2746 (1976).
25. C. SIEIRO, P. GONZALEZ-DIAZ, and Y. G. SMEYERS. J. Mol. Struct. **24**, 345 (1975).
26. Z. DINYA, A. I. KISS, and G. PONGOR. Acta Chim. Acad. Sci. Hung. **98**, 37 (1978).

Can. J. Chem. Downloaded from www.nrcresearchpress.com by 198.100.157.202 on 09/07/12
For personal use only.

Thermodynamic treatment of multicomponent fused salt solutions: common anion reactive systems approximation

S. N. FLENGAS
Department of Metallurgy and Materials Science, University of Toronto, Toronto, Ont., Canada M5S 1A4
Received July 8, 1990

S. N. FLENGAS. Can. J. Chem. **69**, 870 (1991).

From a modified F.F.G. (1) thermodynamic cycle, equations have been developed from which the molar and partial molar excess thermodynamic properties of j-component molten salt solutions may be predicted from binary data.

The theory is applicable to reactive molten salt systems and particularly to charge asymmetric fused salt solutions with common anions.

It is shown that for a system having $j+1$ components, such as MX_q–AX–BX$\cdots$ $\cdots$JX, any molar or partial molar property of mixing for MX_q, may be calculated from available data on corresponding j-binary systems, such as MX_q–AX, MX_q–BX, and $\cdots MX_q$–JX.

The equations are of the general form,

$$\underset{(\text{in } j+1 \text{ component system})}{\Delta Z_{MX_q}} = \frac{X_2}{1-X_1}(\Delta Z_{MX_q})_{MX_q\text{–AX}} + \frac{X_3}{1-X_1}(\Delta Z_{MX_q})_{MX_q\text{–BX}} + \cdots + \frac{X_j}{1-X_1}(\Delta Z_{MX_q})_{MX_q\text{–JX}}$$

The latter is applicable only when the multicomponent and the binary solutions have the same MX_q content and same temperature.

The theoretical expressions have been found to predict quite well available data on ternary and quarternary systems.

New composition parameters for expressing the compositions in quarternary and quinary systems have been established.

Key words: molten salt solutions, multicomponent systems, ternary systems, quarternary systems, quinary systems.

S. N. FLENGAS. Can. J. Chem. **69**, 870 (1991).

Utilisant un cycle thermodynamique F.F.G. modifié, on a développé des équations à l'aide desquelles on peut prédire, à partir de données binaires, les propriétés thermodynamiques molaires et molaires partielles en excès de solutions de sels fondus à j-composantes.

On peut appliquer la théorie à des systèmes de sels réactifs et, en particulier, àdes solutions de sels fondus chargés d'anions communs.

On a démontré que — pour un système comportant $j+1$ composantes, comme MX_q–AX–BX$\cdots$ $\cdots$JX — on peut calculer toutes les propriétés molaires et molaires partielles de mélange de MX_q à partir des j systèmes binaires correspondants, comme MX_q–AX, MX_q–BX et $\cdots MX_q$–JX.

Les équations sont de la forme générale,

$$\underset{(\text{in } j+1 \text{ component system})}{\Delta Z_{MX_q}} = \frac{X_2}{1-X_1}(\Delta Z_{MX_q})_{MX_q\text{–AX}} + \frac{X_3}{1-X_1}(\Delta Z_{MX_q})_{MX_q\text{–BX}} + \cdots + \frac{X_j}{1-X_1}(\Delta Z_{MX_q})_{MX_q\text{–JX}}$$

La dernière n'est applicable que lorsque le multicomposant et les solutions binaires contiennent le même MX_q et qu'ils sont à la même température.

On a trouvé des expressions théoriques qui permettent de prédire assez bien les données disponibles des systèmes ternaires et quaternaires.

On a établi de nouveaux paramètres de composition pour exprimer les compositions dans des systèmes quaternaires et quinaires.

Mots clés: solutions de sels fondus, multicomposant systèmes, systèmes ternaires, systèmes quarternaires, systèmes quinaires.

[Traduit par la revue]

Introduction

The thermodynamic properties of binary fused salt solutions have been the object of several systematic investigations and extensive compilations of thermodynamic data are available.

However, similar information for ternary solutions is very limited and for quarternary systems there is hardly any information at all. Yet systems of industrial and of metallurgical importance are usually multicomponent, and the application of thermodynamics to the calculation of equilibria and to the efficiency of chemical reactions is usually restricted by the lack of the appropriate experimental data.

Regarding binary systems, an activity isotherm is usually obtained from about five experimental measurements. In a ternary system, the Gibbs isothermal surface may be covered with about 25 separate experiments on activities, and, for a quarternary system a minimum of about 200 experiments are needed in order to cover adequately the entire composition range. It is evident that the large number of experiments required have discouraged researchers from undertaking the systematic investigation of multicomponent systems.

Because of the shortage of experimental data, there is considerable theoretical and practical interest in the establishment of expressions from which the thermodynamic properties of ternary and quarternary molten salt systems may be predicted from available data on the corresponding binary solutions.

For ternary metallic solutions several such equations have been proposed. These include the analytical expressions by Kohler (2), Bonnier and Caboz (3), and Muggianu *et al.* (4), and those derived by Alcock and Richardson (5), and Toop (6).

Can. J. Chem. Downloaded from www.nrcresearchpress.com by 198.100.157.202 on 09/07/12
For personal use only.

Can. J. Chem. Downloaded from www.nrcresearchpress.com by 198.100.157.202 on 09/07/12
For personal use only.

The relative merits of each of these expressions have been compared by Spencer *et al.* (7), Ansara (8), and Hillert (9).

In general, these expressions include terms representing the thermodynamic properties of the three binary component systems and differ mainly in the kind of composition parameters used and in the composition path to be followed within the ternary isothermal composition surface.

Saboungi and Blander (10) have extended the Conformal Ionic Solution theory to additive ternary molten salt solutions. However, the derived expressions were rather complex, and, even for mixtures of monovalent salts, they required fourth order terms. Their applicability to a large number of ternary charge asymmetric systems has not been demonstrated.

The thermodynamic properties of charge asymmetric molten salt solutions are of considerable theoretical and practical interest, as they are characterized by very low activity values and by highly exothermic enthalpies of mixing. This behaviour is usually interpreted as indicating strong interactions between the ionic specie in solution, and to the formation of complex species. To interpret such systems Pelton and Thompson (11) have proposed a Discrete Complex Anion Model which has been applied to systems such as binary $MgCl_2$-containing systems and to the system $MgCl_2$–NaCl–$CaCl_2$ (12).

In previous publications from this laboratory (13–17) a "hybrid" regular solution model representing the combination of a reaction mechanism followed by the regular mixing of the products of reaction, has been applied to the derivation of equations which allow the calculation of the thermodynamic properties of ternary and quarternary charge asymmetric fused salt solutions from the properties of the component binary systems. However, this model was based on the assumption that all complex-forming reactions proceeded to completion and the thermodynamic requirement of equilibrium between specie in solution was not considered.

In the present publication, equations relating thermodynamic properties of multicomponent, common anion charge asymmetric fused salt solutions to the properties of the component binary system, are derived using a modified form of the F.F.G. thermodynamic cycle (1) which is ideally suited to mixed equilibria. The theoretical treatment makes use of well established thermodynamic relationships and is applicable to systems in which all chemical reactions reach equilibrium.

For the treatment it is necessary to consider solutions that contain at least one charge asymmetric component, MX_q, as in the system, MX_q–AX–BX–$\cdots$ JX in which the components AX and BX etc. are acting as ligand donors for reactions like,

$$[1] \qquad MX_q + rAX \rightarrow A_rMX_{q+r}$$

An exact knowledge of the type or the stoichiometry of the complex specie formed is not required for the derivation of the thermodynamic relationships.

Thermodynamic treatment of multicomponent molten salt solutions

For the thermodynamic treatment a $j + 1$ component, common anion and charge asymmetric molten salt system, like the solution of MX_q–AX–BX$\cdots$JX, will be considered.

The derivation is based on a modified form of a thermodynamic cycle for successive reactions first proposed by Flood, Förland, and Grojtheim (1). The steps considered are given in Table 1.

The cycle consists of chemical reactions [*a*], [*b*] $\cdots$ [*j*] and of two mixing reactions [1] and [2]. Standard states are chosen as the pure molten salts at all temperatures. Mole numbers are taken as,

$$n_2 + n_3 + \cdots + n_j = 1$$

and the summation,

$$n_2MX_q + n_3MX_q + \cdots + n_jMX_q$$

represent 1 g. mol of pure molten MX_q. Through addition of reactions in the sequence [*a*] + [*b*] + $\cdots$ + [*j*] − [1] + [2], the overall reaction of MX_q with a mixed melt is obtained as reaction [3]. Reaction [3] may be taken as "standard" if the two solutions $[(AX)_{n_2}\cdot(BX)_{n_3}\cdots(JX)_{n_j}]$, and $[(A_rMX_{q+r})_{n_2}\cdot(B_rMX_{q+r})_{n_3}\cdots(J_rMX_{q+r})_{n_j}]$, are chosen as the "standard states" for the mixed system containing all species at their equilibrium compositions.

In Table 1 the "standard free energy" for reaction [3] is given by eq. [4] and it defines the mixed equilibrium constant K_M, as in eq. [5]. The "standard state" for MX_q is still the state of pure molten MX_q at all temperatures. For the other compounds JX and J_rMX_{q+r} etc., their standard states, respectively, are the above mentioned "mixed" solutions (Appendix 1).

From the well known relationships, [4] and [5*a*] in Table 1, eq. [5] may be written in terms of the partial molar free energies of mixing, $\overline{\Delta G_i}$, and is given as eq. [6]. The latter may be simplified through conversion of the standard states using eqs. [7] and [8], which are derived in Appendix 1.

From eqs. [3], [4], [6], [7], [8] and Appendix 1, eq. [9] is readily derived. In the latter the quantities $\overline{\Delta G}''_{JX}$ and $\overline{\Delta G}''_{J_rMX_{q+r}}$ represent partial molar Gibbs free energies of mixing; expressed with respect to pure molten JX and pure molten J_rMX_{q+r} as standard states, respectively, where J stands for A, B, $\cdots$ J.

Considering reactions [*a*], [*b*], [*c*] $\cdots$ [*j*] in Table 1, the equilibrium constant for a *j*-type reaction may be written in terms of activities as,

$$[j\text{-}1] \qquad k_j = \frac{a_{J_rMX_{q+r}}}{a_{MX_q}\cdot a_{JX}^{n_j}}$$

Following the same general method, as for the derivation of eq. 9 in Table 1, it is readily shown that for a binary system,

$$[j\text{-}2] \qquad \underset{(MX_q\text{–}JX)}{\overline{\Delta G}_{MX_q}} = \Delta G_j^0 - r\overline{\Delta G}''_{JX} + \overline{\Delta G}''_{J_rMX_{q+r}}$$

In this equation $\overline{\Delta G}''_{JX}$ and $\overline{\Delta G}''_{J_rMX_{q+r}}$ refer to the binary solution JX–MX_q at equilibrium. Standard states of reference are the pure molten salts.

From Table 1 equations similar to [*j*-2] may be derived for all the other complex forming reactions in binary solutions and are designated, respectively, as [*a*-2], [*b*-2], etc.

Considering solutions representing the same mole fraction for MX_q, it will be assumed that the partial molar Gibbs free energies of mixing for pairs like AX–A_rMX_{q+r}, BX–B_rMX_{q+r}, $\cdots$ JX–J_rMX_{q+r}, in the multicomponent system, have approximatley the same values as in the corresponding binary solutions.

The combination of eq. [9] with equations like [*a*-2], [*b*-2] $\cdots$ [*J*-2], yields eq. [10]. Also, by introducing eq. [11], the final expression [12] relating Gibbs free energies of mixing of multicomponent to binary systems is obtained.

TABLE 1. Equilibria in mixed systems

Equation	*Chemical reactions*	*Gibbs free energy*
[*a*]	$n_2\mathrm{MX}_{q(l)} + n_2 r\mathrm{AX}_{(l)} = n_2 A_r\mathrm{MX}_{q+r(l)}$	$n_2\Delta G^0_a$
[*b*]	$n_3\mathrm{MX}_{q(l)} + n_3 r\mathrm{BX}_{(l)} = n_3 B_r\mathrm{MX}_{q+r(l)}$	$n_3\Delta G^0_b$
[*j*]	$n_j\mathrm{MX}_{q(l)} + n_j r\mathrm{JX}_{(l)} = n_j \mathrm{J}_r\mathrm{MX}_{q+r(l)}$	$n_j\Delta G^0_j$
	Mixing reactions	
[1]	$n_2 r\mathrm{AX}_{(l)} + n_3 r\mathrm{BX}_{(l)} + \cdots n_j r\mathrm{JX}_{(l)} = r[(\mathrm{AX})_{n_2}\cdot(\mathrm{BX})_{n_3}\cdots(\mathrm{JX})_{n_j}]_{\text{solution}}$	$r\Delta G_{\mathrm{M}}$
[2]	$n_2\mathrm{A}_r\mathrm{MX}_{q+r(l)} + n_3\mathrm{B}_r\mathrm{MX}_{q+r(l)} + \cdots n_j\mathrm{J}_r\mathrm{MX}_{q+r(l)}$ $= [(\mathrm{A}_r\mathrm{MX}_{q+r})_{n_2}\cdot(\mathrm{B}_r\mathrm{MX}_{q+r})_{n_3}\cdots(\mathrm{J}_r\mathrm{MX}_{q+r})_{n_j}]_{\text{solution}}$	ΔG_{M}

where $n_2 + n_3 + \cdots n_j = 1$

From eqs [*a*] + [*b*] + $\cdots$ [*j*] − [1] + [2]

[3] $$\mathrm{MX}_{q(l)} + r[(\mathrm{AX})_{n_2}\cdot(\mathrm{BX})_{n_3}\cdots(\mathrm{JX})_{n_j}]_{\text{solution}} = [(\mathrm{A}_r\mathrm{MX}_{q+r})_{n_2}\cdot(\mathrm{B}_r\mathrm{MX}_{q+r})_{n_3}\cdots(\mathrm{J}_r\mathrm{MX}_{q+r})_{n_j}]_{\text{solution}}$$ (standard state reaction)

[4] $$\Delta G^0_{\mathrm{R,M}} = n_2\Delta G^0_a + n_3\Delta G^0_b + \cdots n_j\Delta G^0_j - r\Delta G_{\mathrm{M}(1)} + \Delta G_{\mathrm{M}(2)} = -RT\ln K_{\mathrm{M}}$$

[5] $$\mathrm{K_M} = \frac{a^{n_2}_{\mathrm{A}_r\mathrm{MX}_{q+r}}\cdot a^{n_3}_{\mathrm{B}_r\mathrm{MX}_{q+r}}\cdots a^{n_j}_{\mathrm{J}_r\mathrm{MX}_{q+r}}}{a^{n_2 r}_{\mathrm{AX}}\cdot a^{n_3 r}_{\mathrm{BX}}\cdots a^{n_j r}_{\mathrm{JX}}\cdot a_{\mathrm{MX}_q}}.$$

Standard states: for MX_q, the standard state is the pure molten MX_q; for $\mathrm{A}_r\mathrm{MX}_{q+r}$, $\mathrm{B}_r\mathrm{MX}_{q+r}$, $\cdots\mathrm{J}_r\mathrm{MX}_{q+r}$, the standard state is the solution $[(\mathrm{A}_r\mathrm{MX}_{q+r})_{n_2}\cdot(\mathrm{B}_r\mathrm{MX}_{q+r})_{n_3}\cdots(\mathrm{J}_r\mathrm{MX}_{q+r})_{n_j}]$; for AX, BX, $\cdots$ JX, the standard state is the solution $[(\mathrm{AX})_{n_2}, (\mathrm{BX})_{n_3}, \cdots(\mathrm{JX})_{n_j}]$.

[5*a*] From $\overline{\Delta G}_i = RT\ln a_i$

[6] $$\overline{\Delta G}_{\mathrm{MX}_q} = \Delta G^0_{R(\mathrm{M})} + \sum_{n_2}^{n_j} n_j\,\Delta G_{\mathrm{J}_r\mathrm{MX}_{q+r}} - \sum_{n_2}^{n_j} n_j\,\Delta G_{\mathrm{JX}}$$ $$(\mathrm{J} = \mathrm{A}, \mathrm{B}\cdots, \mathrm{J}\ \text{and}\ j = a, b, \cdots j)$$

	For the mixed system at a given composition (solutions as standard states)		In mixed system with respect to pure molten JX or $\mathrm{J}_r\mathrm{MX}_{q+r}$ as standard states		In solutions having compositions,* (*a*) $(\mathrm{AX})_{n_2}\cdot(\mathrm{BX})_{n_3}\cdots(\mathrm{JX})_{n_j}$ and (*b*) $(\mathrm{A}_r\mathrm{MX}_{q+r})_{n_2}\cdot(\mathrm{B}_r\mathrm{MX}_{q+r})_{n_3}\cdots(\mathrm{J}_r\mathrm{MX}_{q+r})_{n_j}$
[7]	$\overline{\Delta G}_{\mathrm{JX}}$	=	$\overline{\Delta G}''_{\mathrm{JX}}$	−	$\overline{\Delta G}'_{\mathrm{AX}}$
[8]	$\overline{\Delta G}_{\mathrm{J}_r\mathrm{MX}_{q+r}}$	=	$\overline{\Delta G}''_{\mathrm{J}_r\mathrm{MX}_{q+r}}$	−	$\overline{\Delta G}'_{\mathrm{J}_r\mathrm{MX}_{q+r}}$

* pure molten JX and $\mathrm{J}_r\mathrm{MX}_{q+r}$ as standard states

From [3], [4], [6], [7], [8], in a $n_j + 1$ component system,

[9] $$\begin{aligned}\overline{\Delta G}_{\mathrm{MX}_q} = {} & n_2\left[\Delta G^0_{\mathrm{R}(a)} - r\overline{\Delta G}''_{\mathrm{AX}} + \overline{\Delta G}''_{\mathrm{A}_r\mathrm{MX}_{q+r}}\right] + \\ & + n_3\left[\Delta G^0_{\mathrm{R}(b)} - r\overline{\Delta G}''_{\mathrm{BX}} + \overline{\Delta G}''_{\mathrm{B}_r\mathrm{MX}_{q+r}}\right] + \cdots \\ & + n_j\left[\Delta G^0_{\mathrm{R}(j)} - r\overline{\Delta G}''_{\mathrm{JX}} + \overline{\Delta G}''_{\mathrm{J}_r\mathrm{MX}_{q+r}}\right]\end{aligned}$$

For binary solutions having the same X_{MX_q}, in $n_j + 1$ component system, from eq. [9].

[10] $$\overline{\Delta G}_{\mathrm{MX}_{q(y)}} = n_2\left(\overline{\Delta G}''_{\mathrm{MX}_q}\right)_{\mathrm{MX}_q-\mathrm{AX}_{(y)}} + n_3\left(\overline{\Delta G}''_{\mathrm{MX}_q}\right)_{\mathrm{MX}_q-\mathrm{BX}_{(y)}} + \cdots n_j\left(\overline{\Delta G}''_{\mathrm{MX}_q}\right)_{\mathrm{MX}_q-\mathrm{JX}_{(y)}}$$

Can. J. Chem. Downloaded from www.nrcresearchpress.com by 198.100.157.202 on 09/07/12
For personal use only.

TABLE 1. (*concluded*)

Equation	*Chemical reactions*	*Gibbs free energy*

Also

[11] $$n_j = \frac{n_j/\sum n}{n_2 + n_3 + \cdots n_j/\sum n} = \frac{X_j}{X_2 + X_3 + \cdots X_j}$$

where X's are mole fractions.

In $n_j + 1$ component system

[12] $$\overline{\Delta G}_{MX_{q(y)}} = \frac{X_2}{X_2 + X_3 + \cdots X_j} (\overline{\Delta G}''_{MX_q})_{MX_q\text{–}AX(y)} + \frac{X_3}{X_2 + X_3 + \cdots X_j} (\overline{\Delta G}''_{MX_q})_{MX_q\text{–}BX(y)} + \cdots \frac{X_j}{X_2 + X_3 + \cdots X_j} (\overline{\Delta G}''_{MX_q})_{MX_q\text{–}JX(y)}$$

where MX_q–JX are binary systems

This expression allows the calculation of the activities of MX_q in a multicomponent system, from their values in the component binary systems, when the mole fraction of MX_q is the same throughout.

From the well known van't Hoff expression

[13] $$\left[\frac{d(\overline{\Delta G}_i)}{d\left(\frac{1}{T}\right)}\right]_{P,X_i} = \left[\frac{\overline{\Delta H}_i}{R}\right]_{\text{at same } X_i}$$

it is readily seen that partial molar enthalpies of mixing are also expressed by equations similar to eq. [12] in Table 1.

In general it may be shown that any molar or partial molar solution property for MX_q in a multicomponent system may be written as:

[14] $$\underset{(1,2\cdots J+1)}{\Delta Z_{MX_q}} = \frac{X_2}{1 - X_1} (\Delta Z_{MX_q})_{1,2} + \frac{X_3}{1 - X_1} (\Delta Z_{MX_q})_{1,3} + \cdots \frac{X_j}{1 - X_1} (\Delta Z_{MX_q})_{1,j}$$

where X_{MX_q} and temperature are the same for the multicomponent as for the binary mixtures.

The assumptions that the Gibbs partial molar free energies of mixing for components like JX and J_rMX_{q+r}, are "frozen" at their levels in the binary solutions for compositions representing the same MX_q content, have important structural and theoretical implications. They can only be valid if the cations A^+, B^+, and J^+ are randomly distributed and when short range interactions of the next neighbour type, like in a sequence A^+ X^- M^{q+}, are significant.

Ternary charge asymmetric fused salt solutions

The composition of a ternary system is usually represented by points within a Gibbs equilateral triangle. Pure components are situated at the corners, as shown in Fig. 1.

Any composition point P is found by drawing through P lines parallel to each of the three sides. The complement of the distance from each corner to the respective line through P gives the amount of the particular component. If the composition variable is the mole fraction, then the values thus calculated must satisfy the relationship

[15] $$X_1 + X_2 + X_3 = 1$$

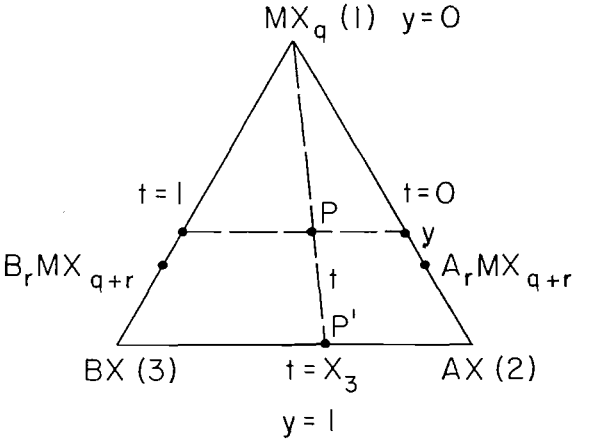


FIG. 1. Composition paths in a ternary system $t = X_3/(X_2 + X_3)$ and $y = 1 - X$.

where 1, 2, and 3 are components MX_q, AX, and BX, respectively.

A tie-line from 1 to the 2,3 binary represents compositions for which,

[16] $$t' = \frac{X_2}{X_3} = \text{constant}$$

but since t' goes to inifinity as X_2 goes to zero, it is more convenient to define

[17] $$t = \frac{X_3}{X_2 + X_3}$$

which varies from 0 and 1.

At constant X_i, the parameter y is defined as $y = 1 - X_1$. In the binary 1–2, $t = 0$, and in the binary 1–3, $t = 1$. For pure component 1, $y = 0$, and for all values of t in the 2–3 binary $y = 1$.

It is also readily calculated that

[19] $$X_1 = 1 - y$$

[20] $$X_2 = y(1 - t)$$

[21] $$X_3 = ty$$

from eqs. [12] and [5a] in Table 1, and eqs. [19], [20], [21],

Can. J. Chem. Downloaded from www.nrcresearchpress.com by 198.100.157.202 on 09/07/12
For personal use only.

the corresponding expressions for the activities and for the other molar and partial molar properties in ternary solutions are derived, respectively, as,

$$[22] \quad a_{MX_{q(1,2,3)_y}} = a^{(1-t)}_{MX_{q(1,2)_y}} \cdot a^{t}_{MX_{q(1,3)_y}}$$

and as,

$$[23] \quad \Delta Z_{MX_{q(1,2,3)_y}} = (1-t)\Delta Z_{MX_{q(1,2)_y}} + t\Delta Z_{MX_{q(1,3)_y}}$$

where 1,2 and 1,3 refer to the binary systems, AX–MX_q and BX–MX_q, respectively. ΔZ could represent molar volumes, enthalpies, or Gibbs free energies of mixing.

Quarternary charge asymmetric fused salt solutions

Compositions in a quarternary system are represented (18) by points within the volume of an equilateral tetrahedron, as shown in Fig. 2. The four vertices correspond to the pure components MX_q, AX, BX, and DX, and the edges represent the six binary systems MX_q–AX, MX_q–BX, MX_q–DX, AX–BX, BX–DX, and DX–AX.

The triangular faces represent the four ternary systems MX_q–AX–BX, MX_q–AX–DX, MX_q–BX–DX, and AX–BX–DX.

It is a property of all equilateral tetrahedra that lines originating from any internal point P, drawn parallel to the four different faces, have a total length equal to one edge, and each of these segments may be taken to define the mole fraction of a particular component occupying an apex.

In view of the complexity of such three-dimensional plots, useful composition paths have been defined mathematically, and the composition parameters, y, t, and S have been defined in terms of mole fractions by the following expressions (17):

$$[24] \quad y = 1 - X_1$$

where $1.0 > y > 0$

$$[25] \quad t = \frac{X_4}{X_3 + X_4}$$

where $1.0 > t > 0, t = 1$ along the MX_q–DX binary, and $t = 0$ along the MX_q–BX binary.

$$[26] \quad S = \frac{X_2}{X_2 + X_3 + X_4}$$

where $0 > S > 1, S = 1$ along the MX_q–AX binary and $S = 0$ for all compositions in the ternary MX_q–BX–DX.

Considering Fig. 2, in which MX_q is placed at the apex of the tetrahedron, constant "t" represents the pseudo-quarternary composition surface LMN. All compositions along that surface have in common the constant ratio of $X_4/(X_3 + X_4)$.

Also, constant "y" represents compositions along a pseudo-ternary surface parallel to the base of the equilateral tetrahedron having a constant X_{MX_q} content.

The intersection of the planes, t and y, defines the line "S".

The relationship between primary mole fractions and the composition parameters y, t, and S, is readily found as,

$$[27] \quad X_1 = X_{MX_q} = 1 - y$$

$$[28] \quad X_3 = y(1-t)(1-S)$$

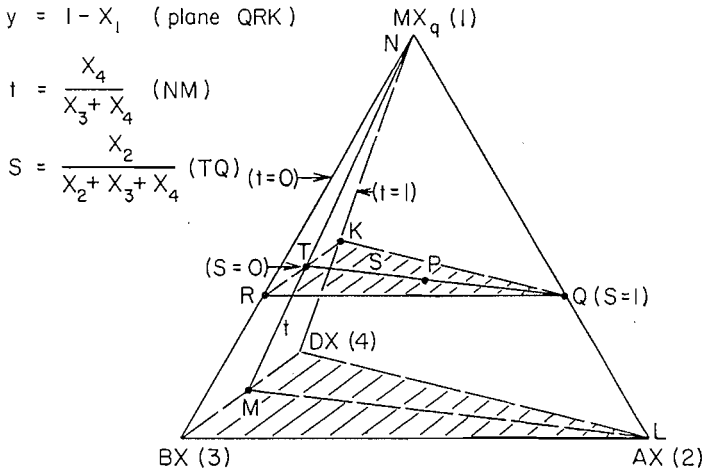


FIG. 2. Isothermal composition diagram in a quarternary system represented by an equilateral tetrahedron; t, y, S are composition parameters. Equilateral triangle QRK represents a section of the quarternary having the same MCl_q content.

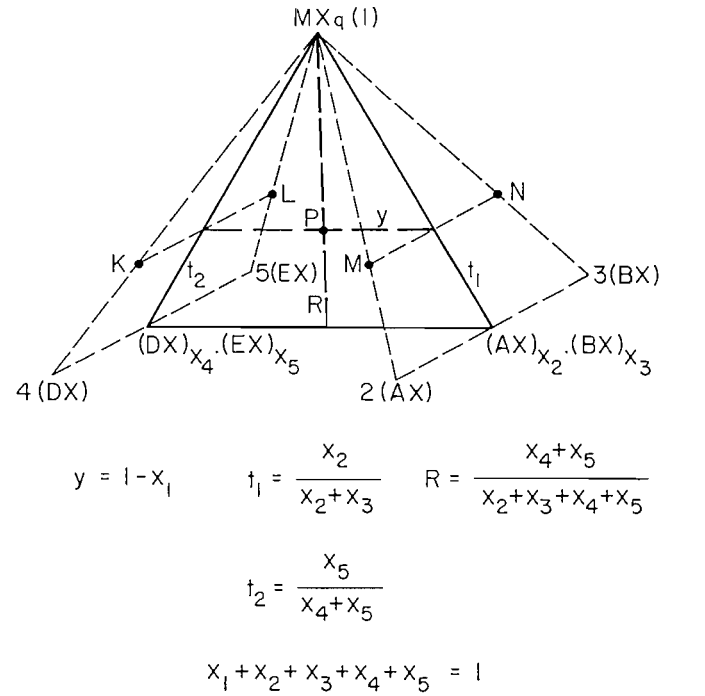


FIG. 3. Representation of compositions in a quinary system; y, t_1, t_2, R are composition parameters.

$$[29] \quad X_2 = ys$$

$$[30] \quad X_4 = ty(1-S)$$

Considering the S path QT, within the quarternary tetrahedron shown in Fig. 2, all compositions along QT have the same X_{MX_q} content and the same ratio of DX to BX. However, as S changes from 0 (point T) to 1 (point Q), the amount of AX in the quarternary changes in proportion to S (eg. [26]) and the value of any thermodynamic property measured along the S-composition path should reflect the reactivity of AX towards MX_q. In this melt, the ratio of DX/BX remains con-

Can. J. Chem. Downloaded from www.nrcresearchpress.com by 198.100.157.202 on 09/07/12
For personal use only.

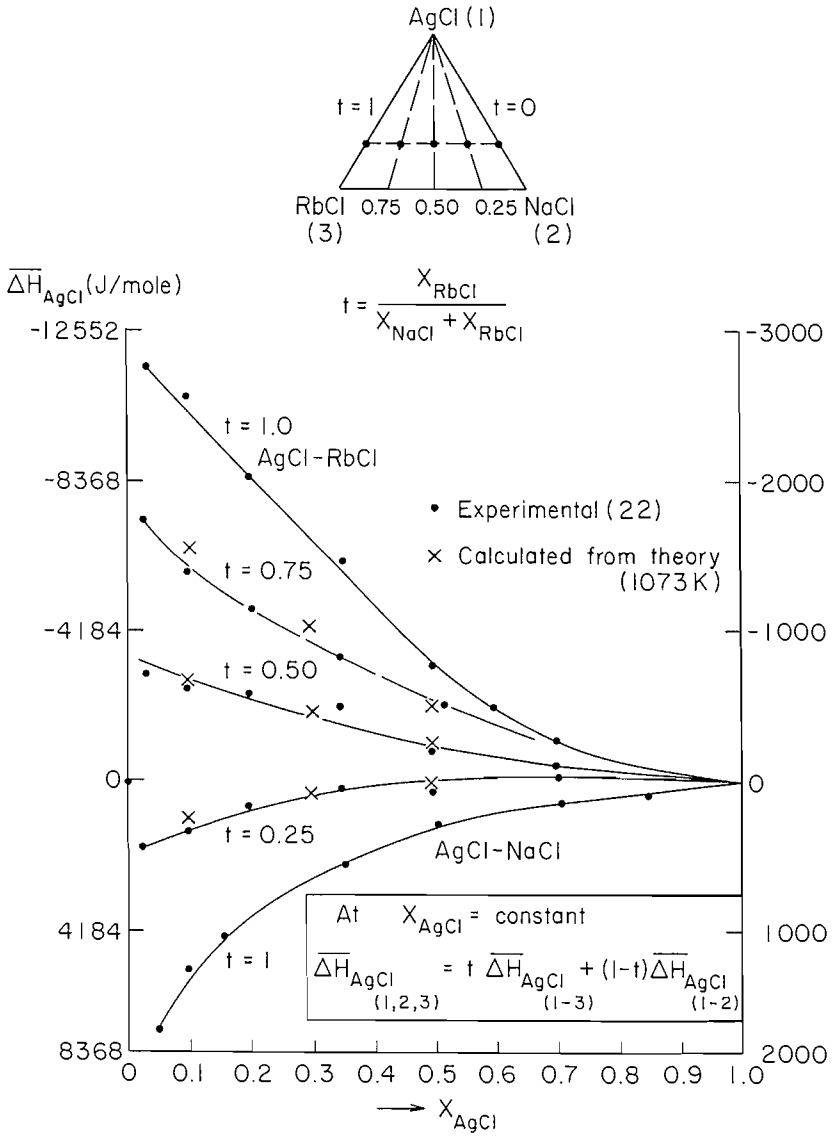


FIG. 4. Comparison between calorimetric and electrochemical data in the system NaCl–RbCl–AgCl.

stant, but the absolute amounts of these two components decrease as they are replaced by AX.

It follows that the y, S, and t parameters proposed in this paper define quarternary composition paths along which it is possible to follow the relative contributions of the various salt components to the magnitude of the thermodynamic properties of the solutions.

When expressions [27]–[30] are applied to the general expressions [12] and [5a], the corresponding equations for a quarternary system are derived as,

$$[31] \qquad a_{MX_{q(1,2,3,4)_y}} = a^{S}_{MX_{q(1,2)_y}} \cdot a^{(1-S)(1-t)}_{MX_{q(1,3)_y}} \cdot a^{t(1-S)}_{MX_{q(1,4)_y}}$$

and

$$[32] \qquad \Delta Z_{MX_{q(1,2,3,4)_y}} = S\Delta Z_{MX_{q(1,2)_y}} + (1-S)\left[t\Delta Z_{MX_{q(1,4)_y}} + (1-t)\Delta Z_{MX_{q(1,3)_y}}\right]$$

Extension of the theory to quinary molten salt solutions

For a five component system there is no simple geometric method for the graphic representation of the composition. In general, a $j+1$ component system requires plots in J dimensions (18, 19).

For the purpose of this treatment the composition of a five component system is represented on the surface of a Gibbs equilateral triangle in which the apex is occupied by the reactive molten MCl_q component and the other two vertices are occupied by solutions having fixed ratios of ligand donors (5), as in Fig. 3.

For the system MX_q–AX–BX–DX–EX having the mole fraction composition defined by x_1, x_2, x_3, x_4, and x_5, respectively, the composition parameters are defined as,

$$[33] \qquad y = 1 - x_1$$

$$[34] \qquad t_1 = \frac{x_3}{x_2 + x_3}$$

Can. J. Chem. Downloaded from www.nrcresearchpress.com by 198.100.157.202 on 09/07/12
For personal use only.

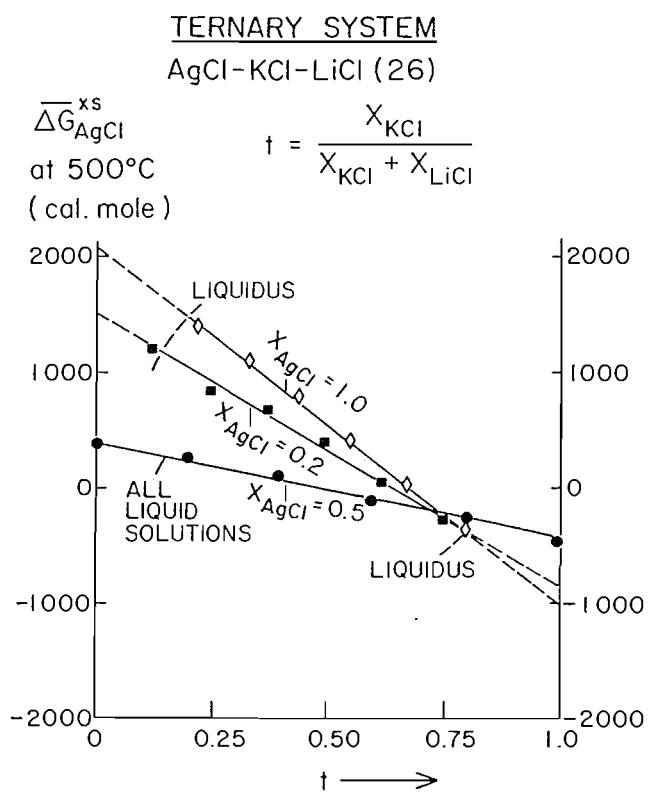


FIG. 5. Plots of $\overline{\Delta G}^{XS}_{AgCl}$ versus t for the ternary system AgCl–KCl–LiCl (26). Points are experimental. Straight lines have been calculated from eq. [23].

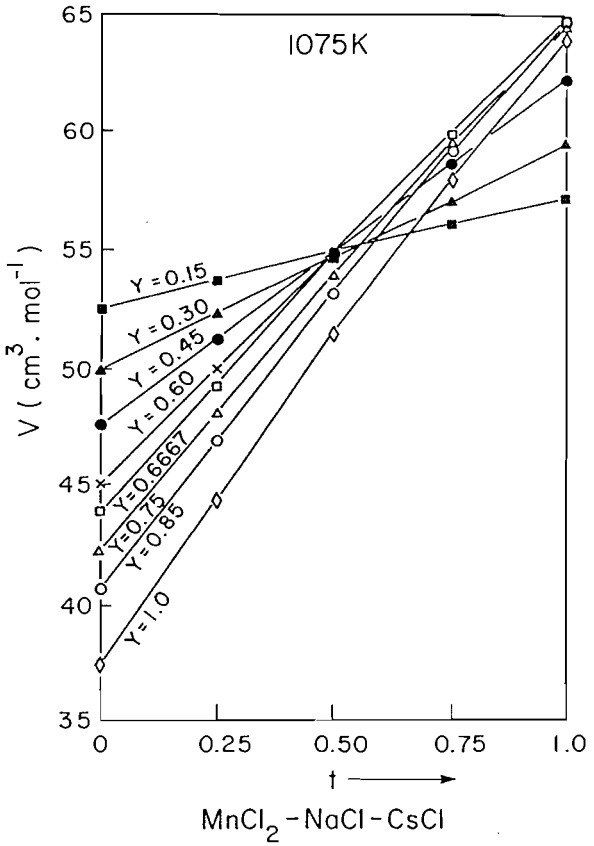


FIG. 6. Plots of the molar volumes V versus t for various y values in the ternary system $MnCl_2$–NaCl–CsCl (23) calculated from eq. [23].

[35] $$t_2 = \frac{x_5}{x_4 + x_5}$$

[36] $$R = \frac{x_2 + x_3}{x_2 + x_3 + x_4 + x_5}$$

The relationship between conventional mole fractions and the above composition parameters are readily derived as

[37] $$x_1 = 1 - y$$

[38] $$x_2 = yR(1 - t_1)$$

[39] $$x_3 = yRt_1$$

[40] $$x_4 = (1 - t_2)(1 - R)y$$

[41] $$x_5 = t_2(1 - R)y$$

Through introduction of eqs. [37]–[41], into eqs. [12] and [5a], the quinary system expressions are derived as,

[42] $$a_{\underset{(\text{In quinary})_y}{MX_q}} = a^{R(1-t_1)}_{MX_{q(1,2)_y}} \cdot a^{Rt_1}_{MX_{q(1,3)_y}} \cdot a^{(1-R)(1-t_2)}_{MX_{q(1,4)_y}} \cdot a^{(1-R)t_2}_{MX_{q(1,5)_y}}$$

Similarly,

[43] $$\Delta Z_{MX_{q(\text{quinary})_y}}$$

$$= (1 - R)\left[t_2 \Delta Z_{MX_{q(1,5)_y}} + (1 - t_2)\Delta Z_{MX_{q(1,4)_y}}\right]$$

$$+ R\left[t_1 \Delta Z_{MX_{q(1,3)_y}} + (1 - t_1)\Delta Z_{MX_{q(1,2)_y}}\right]$$

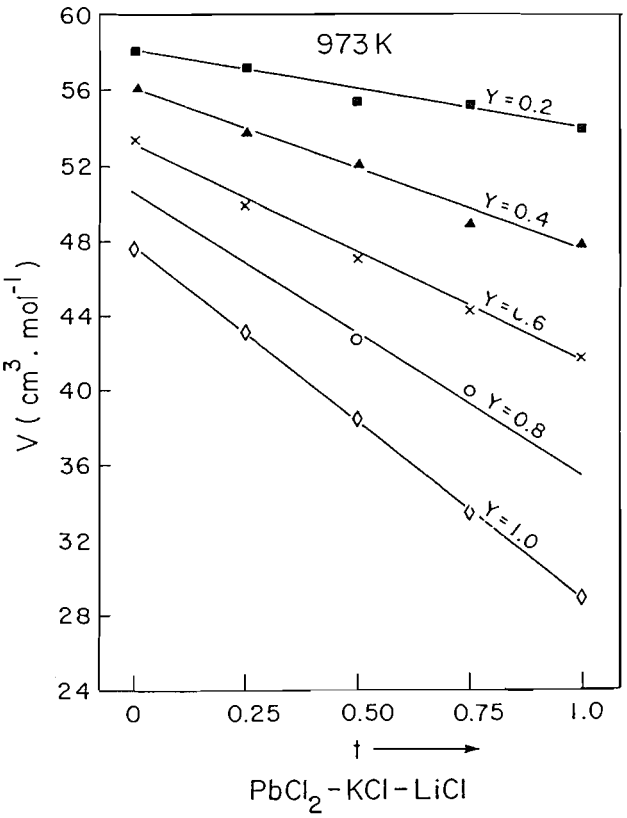


FIG. 7. Plots of the molar volumes versus t for various y values in the ternary system $PbCl_2$–LiCl–KCl (27). Points are experimental. Straight lines have been calculated from eq. [23].

Can. J. Chem. Downloaded from www.nrcresearchpress.com by 198.100.157.202 on 09/07/12
For personal use only.

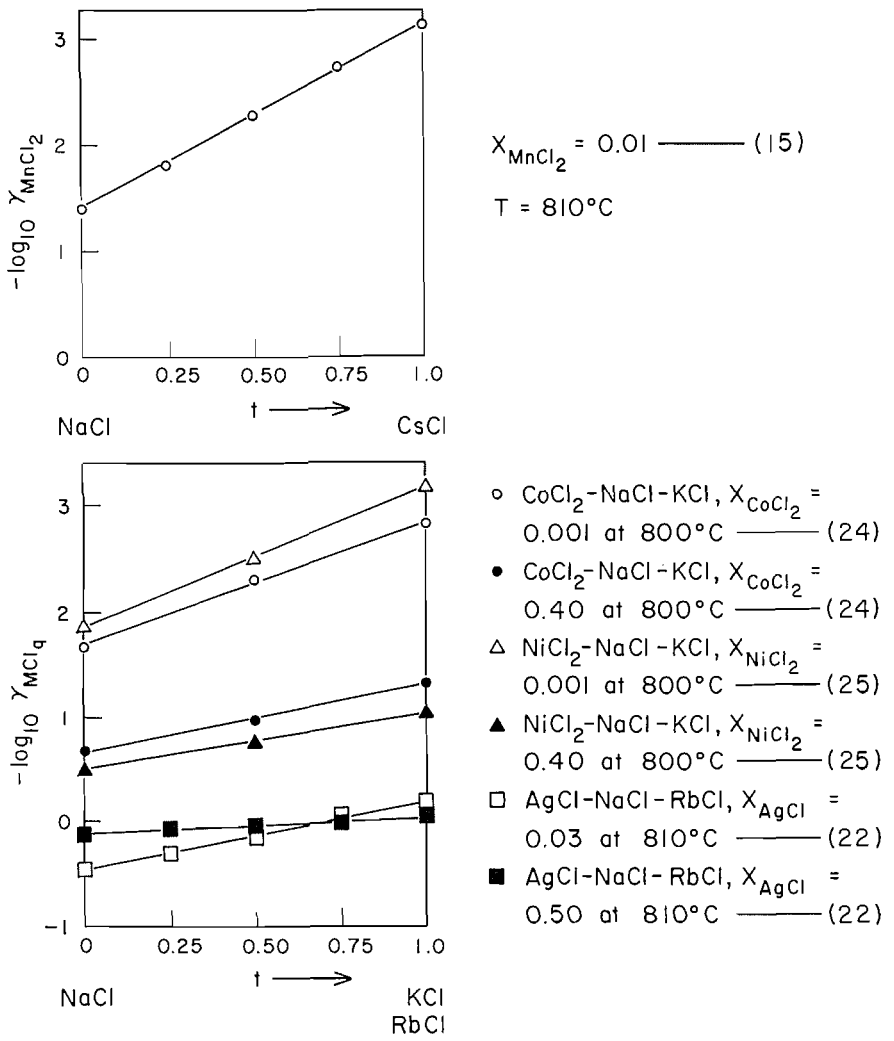


FIG. 8. log γ_{MCl_q} plotted as function of t for various systems. Points are experimental while straight lines have been calculated from eq. [22] expressed in terms of activity coefficients.

Limiting values for the y, t_1, t_2 and R terms are $y = 1$ for pure MX_q, $y = 0$ in the quarternary AX–BX–DX–EX, $t_1 = 1$ in pure AX, $t_1 = 0$ in pure BX, $t_2 = 1$ in pure EX, $t_2 = 0$ in pure DX, $R = 0$ in AX–BX binary, and $R = 1$ in DX–EX binary.

Equation [43] implies that the partial molar free energies of mixing for the reactive M_q component are linear functions of R, when y has a common value for the binary and the quinary solutions and t_1 and t_2 are fixed to represent given ratios.

Agreement with experimental evidence

There is overwhelming evidence for the validity of the expressions [22], [23], for "reactive" or charge asymmetric ternary systems, for which there is reliable information on the corresponding binaries.

Table 2 lists some of the ternary systems for which agreement between theory and experimental values is excellent.

For example, the binary systems AgCl–NaCl and AgCl–CsCl have been investigated by the emf method (31) and by calorimetry (32, 33). Enthalpy of mixing information on the binary NaCl–CsCl is also available (34) and the electrochemical and the calorimetric data are in very good agreement. The ternary system AgCl–NaCl–CsCl has been investigated by the emf method (21) and the comparison between experimental and calculated excess free energies of mixing is excellent.

The binary systems AgCl–NaCl and AgCl–RbCl have been investigated in this laboratory (31) and by Kleppa and associates (32, 33) calorimetrically.

These data indicate that the NaCl–AgCl system exhibits exothermic enthalpies of mixing, while the RbCl–AgCl system mixes endothermically and should be described as a "reactive system". The ternary system AgCl–NaCl–RbCl has also been investigated by the emf method in this laboratory (22) and, as shown in Fig. 4, there is excellent agreement between experimental and calculated molar enthalpies of mixing over the entire composition range.

Plots of $\overline{\Delta G}^{XS}_{AgCl}$ versus t for the system AgCl–KCl–LiCl investigated by Gruner and Thompson (26), shown in Fig. 5, are also linear, indicating the compliance of this system with eq. [22].

The $MnCl_2$ – alkali chloride systems are of interest as they demonstrate negative deviations from ideality, which increase dramatically from the $MnCl_2$–NaCl to the $MnCl_2$–CsCl binary.

For these systems the agreement between the calorimetric (34) and the electrochemical (35) enthalpies of mixing is very good. For the ternary $MnCl_2$–NaCl–CsCl (23) molar volumes calculated from the corresponding expression

$$[44] \qquad V^{\text{ternary}}_{1,2,3} = (1-t)V_{(1,2)_y} + tV_{(1,3)_y}$$

Can. J. Chem. Downloaded from www.nrcresearchpress.com by 198.100.157.202 on 09/07/12
For personal use only.

Can. J. Chem. Downloaded from www.nrcresearchpress.com by 198.100.157.202 on 09/07/12
For personal use only.

TABLE 2. List of ternary and quarternary fused salt solutions which are in agreement with the present thermodynamic treatment of the "Reactive Systems Approximation"

Ternary system	Method/property	T (°C)	Authors
AgCl–NaCl–KCl	EMF/γ_{AgCl}	650–850	Flengas and Ingraham (20)
AgCl–NaCl–KCl	EMF/ΔG_{AgCl}	650–850	Guion, Blander, Hengstenberg, and Hagemark (21)
AgCl–NaCl–CsCl	EMF/$\overline{\Delta G}_{ACl}$	700–850	Guion, Blander, and Hagemark (21)
AgCl–NaCl–RbCl	EMF/γ_{AgCl} $\overline{\Delta H}_{AgCl}$	500–900	Pelton and Flengas (22)
$MnCl_2$–NaCl–CsCl	EMF/activities	700–900	Sadoway and Flengas (15)
$MnCl_2$–NaCl–CsCl	Molar volumes (V_m) (density)	550–1050	Carmichael and Flengas (23)
$MnCl_2$–NaCl–CsCl	Electrical conductivities	510–1054	Carmichael and Flengas (23)
$NiCl_2$–NaCl–KCl $\left(\frac{1}{1}\right)$	EMF/γ_{NiCl_2}	700–900	Hamby and Scott (24)
$CoCl_2$–NaCl–KCl $\left(\frac{1}{1}\right)$	EMF/γ_{CoCl_2}	650–900	Hamby and Scott (25)
AgCl–KCl–LiCl	EMF/$\overline{\Delta G}^{XS}_{AgCl}$	500	Gruner and Thompson (26)
NaCl–$CaCl_2$–$MgCl_2$	EMF/ΔH_M	700–850	Karakaya and Thompson (12)
$PbCl_2$–LiCl–KCl	Molar volumes (V_M) (density)	700	Gutierrez and Toguri (27)
$PbCl_2$–LiCl–KCl$\left(\frac{1}{1}\right)$	EMF/$\overline{\Delta G}_{PbCl_2}$	750	Takahashi (28)
$MgCl_2$–NaCl–KCl$\left(\frac{1}{1}\right)$	EMF/$\overline{\Delta G}_{MgCl_2}$	800	Neil, Clark, and Wiswall (29)
$AlCl_3$–NaCl–CsCl	EMF/$\gamma^H_{AlCl_3}$	850	Tumidajski and Flengas (30)
$AlCl_3$–KCl–CsCl	EMF/$\gamma^H_{AlCl_3}$	850	Tumidajski and Flengas (30)

Quarternary system	Method/property	T (°C)	Authors
$MnCl_2$–NaCl–KCl–CsCl	EMF/$(E - E^0)$	650–850	Pickles and Flengas (17)

are shown in Fig. 6, and indicate excellent agreement with the experimental data.

Molar volumes for the system $PbCl_2$–LiCl–KCl, measured by Gutierrez and Toguri (27) and shown in Fig. 7, are in excellent agreement with calculated values from binary data using eq. [23].

Figure 8 demonstrates the validity of eq. [22] in a number of ternary systems.

Agreement between experimental and calculated partial molar free energies of mixing is also found for the systems $MgCl_2$–NaCl–KCl and $PbCl_2$–LiCl–KCl, as shown in Fig. 9.

The recently reported NaCl–$CaCl_2$–$MnCl_2$ system is of interest as it represents a ternary containing two ligand acceptors, e.g. $CaCl_2$ and $MgCl_2$, and NaCl as the single ligand donor.

If $t = X_{MgCl_2}/(X_{CaCl_2} + X_{MgCl_2})$ and NaCl is placed at the apex of the Gibbs triangle, the calculated and experimental enthalpies of mixing shown in Table 3 are in good agreement with theory, considering that the ternary Gibbs–Duhem had been used for the calculation of the activities for the three components (12)

Similar agreement between experimental data and theory is demonstrated by all the systems given in Table 2.

Regarding quarternary systems, the only system which has been systematically investigated by the emf method is the system $MnCl_2$–NaCl–KCl–CsCl (17).

From available data on binary systems (35), the theoretical plot of $\overline{\Delta G}_{MnCl_2}$ as a function of S for a number of t values

TABLE 3. Integral enthalpies of mixing in the system NaCl–$MgCl_2$–$CaCl_2$ (26) for $t = X_{CaCl_2}/(X_{CaCl_2} + X_{MgCl_2})$ and $y = 1 - X_{NaCl}$

		ΔH_M (J/mol)	
y	t	Experimental*	Theoretical†
0.40	0.50	−5 820	−5 820
0.60	0.67	−4 064	−4 574
0.62	0.20	−5 864	−6 032
0.75	0.33	−3 448	(−4 034)
0.77	0.10	−4 397	−4 290
0.80	0.75	−1 700	(−2 515)
0.85	0.18	−2 509	−2 748

*From ternary Gibbs–Duhem integration (12). Only the a_{MgCl_2} in the ternary was measured electrochemically.

†From calorimetric data on the binary systems NaCl–$MgCl_2$ and NaCl–$CaCl_2$.

[32] $\Delta H_{M(1,2,3)} = (1 - t)\ \underset{(NaCl-CaCl_2)}{\Delta H_M} + t\ \underset{(NaCl-CaCl_2)}{\Delta H_M}$

which cover entire y-planes within the quarternary, has been calculated from eq. [31].

Figures 10*a*, 10*b*, 10*c*, and 10*d* show the actual comparison between experimental (17) and calculated values of $\overline{\Delta G}_{MnCl_2}$ for four different y compositions.

It is seen that all compositions along a constant y-plane,

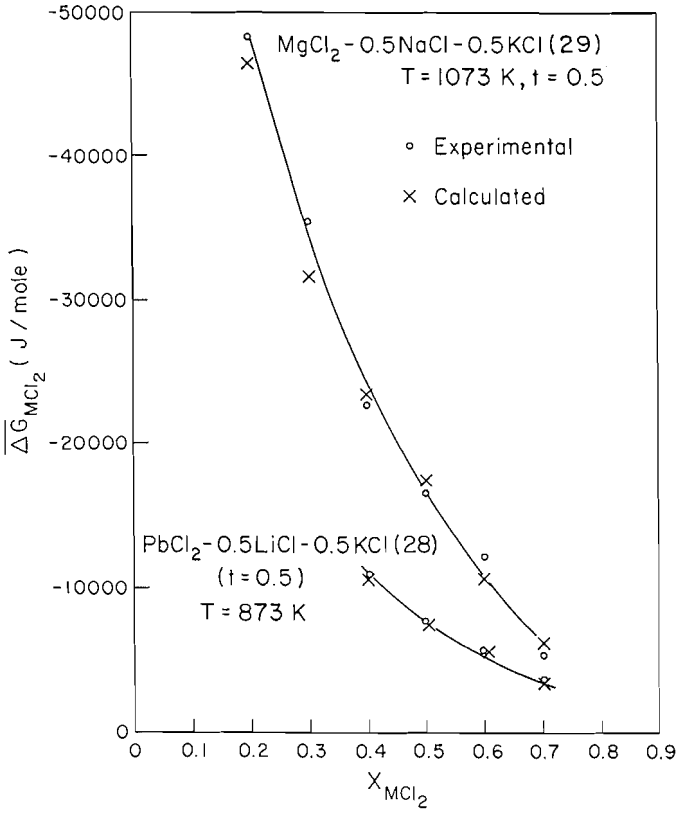


FIG. 9. Plots of $\overline{\Delta G}_{MCl_2}$ versus X_{MCl_2} for $t = 0.5$ for the systems $PbCl_2$–LiCl–KCl (28) and $MgCl_2$–NaCl–KCl (29).

which are obtained when t is changed from 0 to 1, are represented by a family of curves which are terminated in the three component binary systems, as shown on the graph.

Equations [31] and [32] are applicable only if the ligand acceptor component $MnCl_2$ is placed at the apex of the tetrahedron, while the three ligand donors, namely NaCl, KCl, and CsCl, are located at the three remaining vertices.

In a recent publication (38) from this laboratory "formal" formation potentials in the dilute solutions of the binary systems $CoCl_2$–ACl, $NiCl_2$–ACl, $FeCl_2$–ACl, $FeCl_3$–ACl, $CrCl_2$–ACl, $CrCl_3$–ACl, CuCl–ACl, $CuCl_2$–ACl, and $ThCl_4$–ACl where A was respectively NaCl, KCl, or CsCl, were investigated by emf measurements. Also, "formal" potentials were measured in the corresponding ternary systems in which the solvents were respectively the equimolar mixtures NaCl–KCl, NaCl–CsCl and KCl–CsCl.

In all cases it was shown that the "formal" formation potentials of the ternary systems were in good agreement to within 2 to 5% with values calculated from the theoretical expression,

$$[45] \qquad E^0_{f(1,2,3)} = (1-t)E^0_{f(1,2)_y} - tE^0_{f(1,3)_y}$$

which is equivalent to eq. [32] written for an excess partial molar free energy.

Standard "formal" potentials, E^0_f, are related to the usual "standard" potentials, E^0_s, by the well-known relationship

$$[46] \qquad E^0_f = E^0_s - \frac{RT}{ZF} \ln \gamma_n$$

where γ_n is the Henrian activity coefficient for a salt in solution. In such dilute solutions the formation of a complex species and its coordination is expected to have reached a limiting value and a complex should remain unchanged over the entire "Henrian" concentration range.

Therefore, dilute solutions ought to be ideally suited for investigating relationships between multicomponent and their component binary systems.

Conclusions

It has been shown that the thermodynamic properties of non-ideal and non-regular charge asymmetric fused salt systems may be predicted from data on the component binary systems, along isothermal composition paths representing a constant content of the charge asymmetric or reactive component MX_q.

Although the derivation of eqs. [22] and [23] for ternary systems, [31] and [32] for quarternary systems, and [42] and [43] for quinary systems, have been based on assumptions that complexes are formed, such assumptions are not really necessary. Any kind of internal reactivity should satisfy the theoretical treatment and the derived expressions should be applicable.

Regarding quarternary systems, the introduction of the composition parameters y, t, and S serves in the planning of experiments and in reducing the large numbers of compositions to be studied in order to adequately characterize a quarternary system. The use of these composition parameters makes it possible to plot thermodynamic data along well-defined composition paths and to identify the effects of competing interactions on a charge asymmetric cation. For example, the different complexing effects of CsCl or KCl on $MnCl_2$ become evident as the quarternary solutions become richer in CsCl or KCl, respectively.

The successful application of eqs. [22], [23], [31], and [32] to non-ideal charge asymmetric fused-salt solutions indicates that in ternary, quarternary, and possibly even in higher order systems, reactions within the binary solutions account for most of the internal reactivity which is responsible for deviations from ideality.

In quarternary systems which may deviate from eq. [31] or [32], plots such as Figs. 10*a*, 10*b*, 10*c*, and 10*d* are useful in that they display the thermodynamic data in a systematic way. For example, isoactivity paths are readily obtained, and activity plots covering an entire S-composition surface are readily constructed.

Regarding five component systems, an experimental verification of the derived expressions could not be made at this time, because of the lack of the appropriate experimental data. However, in systems for which the ternary and the quarternary approximations have been found to be applicable, it is reasonable to expect that the corresponding five component systems should also approximately obey eqs. [42] and [43].

The present treatment takes into account that reacting systems reach equilibrium and it should not be described as a "model". The formulation of specific complex species is not required except in a most general way. Equation [9] is derived on the basis of a rigorous thermodynamic cycle and the generic eq. [10] is justified on the assumptions that the partial molar properties for the alkali chlorides and for the complex compounds are "frozen" at their levels in the corresponding binary solutions at same MCl_q content. Such assumptions are expected to be valid only if short range coulombic interactions are truly significant and if the cations A, B, ⋯, J are randomly distributed in the multicomponent mixed melt.

Although an exact knowledge of the structure of complexes is not necessary for the thermodynamic treatment, there are certain indirect indications regarding their probable configu-

Can. J. Chem. Downloaded from www.nrcresearchpress.com by 198.100.157.202 on 09/07/12
For personal use only.

Can. J. Chem. Downloaded from www.nrcresearchpress.com by 198.100.157.202 on 09/07/12
For personal use only.

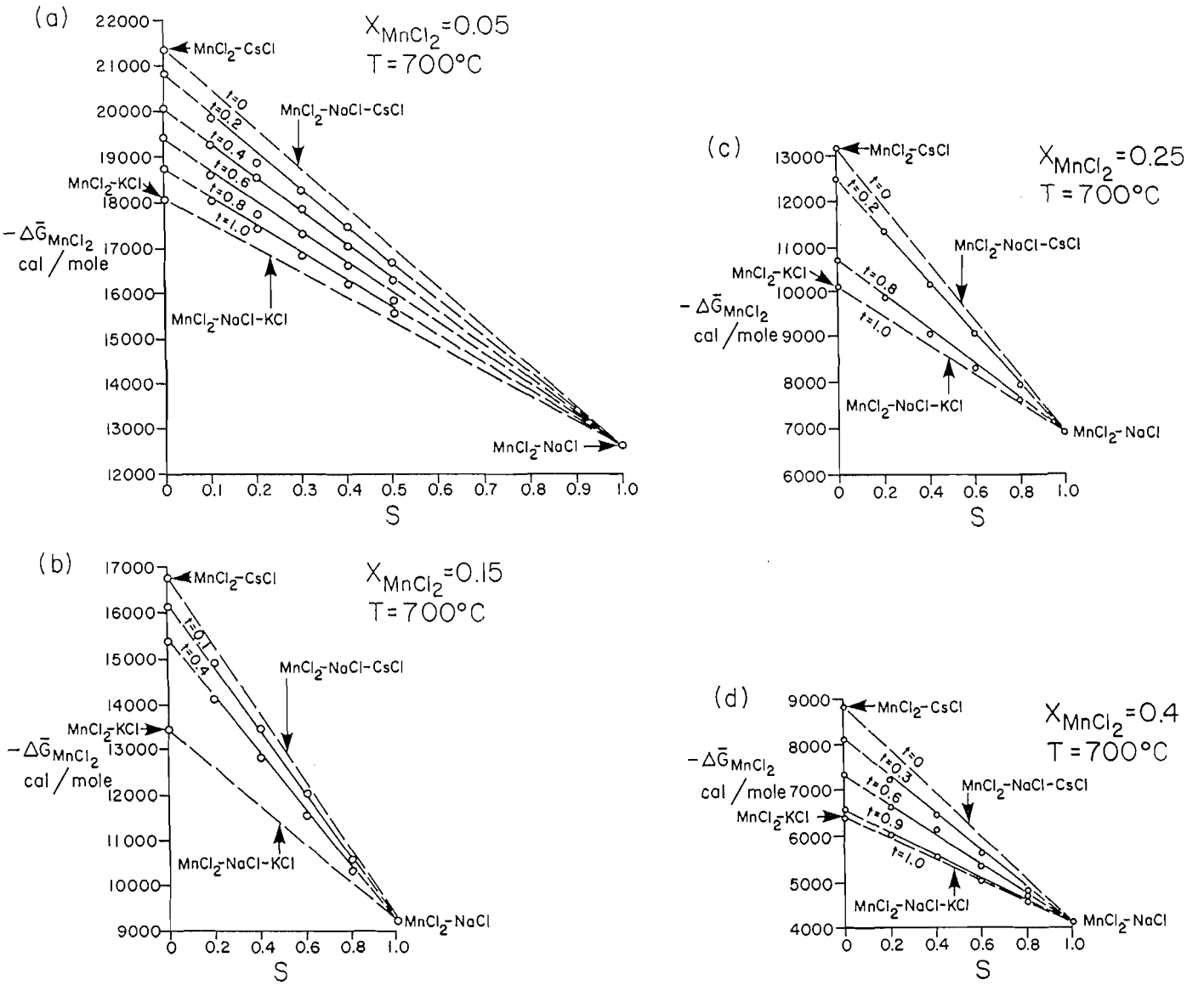


FIG. 10 (a–d). Excess partial molar free energies of mixing for the quarternary system $MnCl_2$–NaCl–KCl–CsCl (17) as functions of s and for various t values. Points are experimental. Straight lines are theoretical.

ration. For example, structural evidence (39) as well as measurements of electrical conductivities and molar volumes (23) suggest that solutions of $MnCl_2$ in alkali chloride melts appear to contain tetrahedrally coordinated complexes of the type $MnCl_4^{2-}$. Similarly, thermodynamic evidence indicates that the solutions of $ZrCl_4$, $HfCl_4$, $NbCl_5$, and $TaCl_5$ (36, 37) in alkali chlorides contain octahedrally coordinated complexes of the type MCl_6^{2-} or MCl_6^-. In all these systems, the negative deviations from ideality increase as the size of the alkali metal cation increases as in the sequence LiCl–NaCl–KCl–RbCl–CsCl (36, 37).

These trends reflect the effects of competing interactions between the M^{q+} and alkali metal cations for the same Cl^- anions, in which the alkali chloride acts as a ligand donor and the reactive metal chloride MCl_q is the ligand acceptor. Alkali metal cations like Li^+, because of their small ionic radius are strongly attracted to their chloride anions and effectively the LiCl salt is less "dissociated" than other alkali metal chlorides containing larger cations like K^+, Rb^+, or Cs^+. The difference in the strength of the complexes which are formed when a reactive metal chloride MCl_q is mixed with either of the alkali chlorides ACl or BCl should be reflected by the difference in the bond distances in configurations of the type M—Cl—A or M—Cl—B.

Summary

(A) For a multicomponent system MX_q–M_2AX–$n_3BX\cdots n_jJX$ where $n_2 + n_3 + \cdots + n_j = 1$, $X_2 + X_3 + \cdots + X_j = 1 - X_1$,

[S-1] $$\Delta Z_{MX_q} = \frac{X_2}{1-X_1}\left(\Delta Z_{MX_q}\right)_{AX\text{-}MX_q} + \frac{X_3}{1-X_1}\left(\Delta Z_{MX_q}\right)_{BX\text{-}MX_q} + \cdots + \frac{X_j}{1-X_1}\left(\Delta Z_{MX_q}\right)_{JX\text{-}MX_q}$$

for X_{MX_q} values which are the same in the binary and in the multicomponent systems.
ΔZ is any partial or molar solution property.

(*B*) For a ternary system MX_q–n_2AX–n_3BX

$$y = 1 - X_{MX_q} = 1 - X_1 \qquad \overline{\Delta H}_{MX_{q(y)}} = (1-t)\overline{\Delta H}_{MX_{q(1,2)(y)}} + \overline{\Delta H}_{MX_{q(1,3)(y)}} \qquad \text{[S-2]}$$

$$t = \frac{X_3}{X_2 + X_3} \qquad (1,2,3)$$

or

$$X_1 = 1 - y \qquad a_{MX_{q(1,2,3)(y)}} = \left(a^{1-t}_{MX_q}\right)_{1,2(y)} \left(a_{MX_q}\right)^{t}_{1,3(y)} \qquad \text{[S-3]}$$

$$X_2 = y(1-t)$$

$$X_3 = ty$$

For a quarternary system MX_q–n_2AX–n_3BX–n_4CX

$$y = 1 - X_1 \qquad \overline{\Delta H}_{MX_{q(y)}} = S\left(\overline{\Delta H}_{MX_q}\right)_{1,2(y)} + (1-S)\left[t\left(\overline{\Delta H}_{MX_q}\right)_{1,4(y)} + (1-t)\left(\overline{\Delta H}_{MX_q}\right)_{1,3(y)}\right] \qquad \text{[S-4]}$$

$$t = \frac{X_4}{X_3 + X_4} \qquad (1,2,3,4)$$

$$S = \frac{X_2}{X_2 + X_3 + X_4}$$

or

$$X_1 = 1 - y \qquad a_{MX_{q(y)}} = a^{S}_{MX_{q(1,2)(y)}} \cdot a^{(1-S)(1-t)}_{MX_{q(1,3)(y)}} \cdot a^{t(1-S)}_{MX_{q(1,4)(y)}} \qquad \text{[S-5]}$$

$$X_2 = yS$$

$$X_3 = y(1-t)(1-S) \qquad (1,2,3,4)$$

$$X_4 = yt(1-S)$$

For a quinary system MX_q–n_2AX–n_3BX–n_4CX–n_5DX

$$y = 1 - X_1 \qquad \overline{\Delta H}_{MX_{q(y)}} = (1-R)\left[t_2\left(\overline{\Delta H}_{MX_q}\right)_{1,5(y)} + (1-t_2)\left(\overline{\Delta H}_{MX_q}\right)_{1,4(y)}\right] + \qquad \text{[S-6]}$$

$$t_1 = \frac{X_3}{X_2 + X_3} \qquad (1,2,3,4,5)$$

$$t_2 = \frac{X_5}{X_4 + X_5} \qquad R\left[t_1\left(\overline{\Delta H}_{MX_q}\right)_{1,3(y)} + (1-t_1)\left(\overline{\Delta H}_{MX_q}\right)_{1,2(y)}\right]$$

$$R = \frac{X_2 + X_3}{X_2 + X_3 + X_4 + X_5}$$

or

$$X_1 = 1 - y \qquad a_{MX_q(y)} = a^{R(1-t_1)}_{MX_{q(1,2)(y)}} \cdot a^{Rt_1}_{MX_{q(1,3)(y)}} \cdot a^{(1-R)(1-t_2)}_{MX_{q(1,4)(y)}} \cdot a^{(1-R)t_2}_{MX_{q(1,5)(y)}} \qquad \text{[S-7]}$$

$$X_2 = y(1-t_1)R$$

$$X_3 = yRt_1$$

$$X_4 = y(1-t_2)(1-R) \qquad X_{MX_q} = \text{Common}$$

$$X_5 = yt_2(1-R)$$

1. H. Flood, T. Forland, and K. Grojtheim. The correlation between activity and composition in mixtures of fused salts. *In* The physical chemistry of melts. Institution of Mining and Metallurgy, London. 1953.
2. F. Kohler. Monatsch. Chem. **91**, 738 (1960).
3. E. Bonnier and R. Caboz. C.R. Acad. Sci. **250**, 527 (1960).
4. Y. M. Muggianu, M. Gambino, and J. P. Bros. J. Chim. Phys. **72**, 83 (1975).
5. C. B. Alcock and F. D. Richardson. Acta Met. **6**, 305 (1958).
6. G. W. Toop. Trans. TMS-AIME, **233**, 850 (1965).
7. P. J. Spencer, F. H. Hayes, and O. Kubaschewski. Rev. Chim. Miner. **9**, 13 (1972).
8. I. Ansara. Metallurgical chemistry. Proc. Sympos. Brunel Univ. and NPL, (1971); HMSO, 403 (1972).
9. M. Hillert. Calphad, **4**, 1 (1980).
10. M. L. Saboungi and M. Blander. J. Chem. Phys. **63**, 1 (1975); **63**, 212 (1975).
11. A. D. Pelton and W. T. Thompson. Can. J. Chem. **48**, 1585 (1970).
12. I. Karakaya and W. T. Thompson. Can. Metall. Q. **25**, 307 (1986).
13. S. N. Flengas and A. S. Kucharski. Can. J. Chem. **49**, 3971 (1971).
14. S. N. Flengas and J. M. Skeaff. Can. J. Chem. **50**, 1345 (1972).
15. D. R. Sadoway and S. N. Flengas. J. Electrochem. Soc. **122**, 515 (1975).
16. S. N. Flengas and D. R. Sadoway. Proc. of the 3rd International Symposium on Molten Salts. *Edited by* G. Manantov, M. Blander, and G. P. Smith. 1981 pp. 68–94.
17. C. A. Pickles and S. N. Flengas. J. Electrochem. Soc. **131**, 2 (1984); **131**, 69 (1984).

Can. J. Chem. Downloaded from www.nrcresearchpress.com by 198.100.157.202 on 09/07/12
For personal use only.

18. A. PRINCE. Alloy phase equilibria. Elsevier, New York. 1966.
19. L. S. PALATNIK and A. I. LANDA. Phase equilibria in multicomponent systems. Holt, Rinehart and Winston, New York, London. 1961. *Translated by* Scripta Technical.
20. S. N. FLENGAS and T. R. INGRAHAM. J. Electrochem. Soc. **106**, 714 (1959).
21. J. GUION, M. BLANDER, D. HENGSTENBERG, and K. HAGEMARK. J. Phys. Chem. **72**, 2086 (1968).
22. A. D. PELTON and S. N. FLENGAS. J. Electrochem. Soc. **118**, 1307 (1971).
23. N. R. CARMICHAEL and S. N. FLENGAS. J. Electrochem. Soc. **128**, 2098 (1979); **126**, 2104 (1979).
24. D. C. HAMBY and A. SCOTT. J. Electrochem. Soc. **115**, 704 (1968).
25. D. C. HAMBY and A. SCOTT. J. Electrochem. Soc. **117**, 319 (1970).
26. A. C. GRUNER and W. T. THOMPSON. Can. J. Chem. **53**, 1084 (1975).
27. A. GUTIERREZ and J. M. TOGURI. J. Chem. Eng. **27**, 109 (1982).
28. M. TAKAHSHI. J. Electrochem. Soc. Jpn. **25**, 432 (1957).
29. D. E. NEIL, H. M. CLARK, and R. H. WISWALL. J. Chem. Eng. Data, **10**, 2 (1965).
30. P. J. TUMIDAJSKI and S. N. FLENGAS. Can. J. Chem. **63**, 1080 (1985).
31. A. D. PELTON and S. N. FLENGAS. J. Electrochem. Soc. **117**, 1130 (1970).
32. P. DANTZER and O. J. KLEPPA. J. Chim. Phys. Phys.-Chim. Biol. **71**(2), 216 (1974).
33. L. S. HERSH and O. J. KLEPPA. J. Chem. Phys. **42**, 1309 (1965).
34. G. N. PAPATHEODOROU and O. J. KLEPPA. J. Inorg. Nucl. Chem. **5**, 1249 (1971).
35. A. S. KUCHARSKI and S. N. FLENGAS. J. Electrochem. Soc. **119**, 1170 (1972).
36. R. L. LISTER and S. N. FLENGAS. Can. J. Chem. **43**, 2947 (1965).
37. D. R. SADOWAY and S. N. FLENGAS. Can. J. Chem. **56**, 2538 (1978).
38. P. J. TUMIDAJSKI and S. N. FLENGAS. Potential measurements of reactive metal chlorides in alkali halide solutions. *In* Proceedings 7th International Symposium on Molten Salts. Montreal, May 1990; J. Electrochem. Soc. **137**, 2717 (1990).
39. K. TANEMOTO and T. NAKAMURA. Chem. Lett. **351**, 356 (1975).

Appendix 1. Standard state conversion

Considering reaction [3] at equilibrium, the "overall" mixed system contains species such as MX_q, AX,$\cdots$JX and $A_rMX_{q+r}, \cdots J_rMX_{q+r}$, at their equilibrium concentrations which are determined by the condition that $\Delta G_R = 0$.

Reaction [3] could also be taken as "standard", if the solutions

$$[(AX)_{n_2} \cdot (BX)_{n_2} \cdots (JX)_{n_j}]$$

and

$$[(A_rMX_{q+r})_{n_2} \cdot (B_rMX_{q+r})_{n_3} \cdots (J_rMX_{q+r})_{n_j}]$$

where

$$n_2 + n_3 + \cdots + n_j = 1$$

are taken as the "standard states" in the "overall mixed" system which contains all of the above species.

For components AX, BX, $\cdots$ JX in this "overall mixed" melt, the standard state is the solution of fixed composition given as $[(AX)_{n_2} \cdot (BX)_{n_3} \cdots (JX)_{n_j}]$, at all temperatures.

Similarly, the standard state for either A_rMX_{q+r}, $B_rMX_{q+r}, \cdots$ and J_rMX_{q+r}, is the solution containing n_2 moles, A_rMX_{q+r}, n_3 moles B_rMX_{q+r}, and $\cdots n_j$ moles J_rMX_{q+r}. The terms $r\Delta G_{m(1)}$ and $\Delta G_{M(2)}$ in eq. [4] of Table 2 are readily eliminated during the conversion of the standard states to those representing the pure liquids at same temperatures. $\overline{\Delta G}_{MX_q}$ represents the partial molar Gibbs free energy of mixing for pure molten MX_q, as before.

Activities are defined by relationships like

$$[A\text{-}1] \qquad a_{JX\ (\text{in "mixed" melt})} = \frac{(P_A) \text{ over "mixed" melt}}{(P_A^1) \text{ over "standard" solution } [(AX)_{n_2} \cdot (BX)_{n_3} \cdots (JX)_{n_j}]}$$

and

$$[A\text{-}2] \qquad a_{J_rMX_{q+r}\ (\text{in "mixed" melt})} = \frac{(P_{J_rMX_{q+r}}) \text{ over "mixed" melt}}{(P^1_{J_rMX_{q+r}}) \text{ over "standard" solution } [(A_rMX_{q+r}) \cdots (J_rMX_{q+r})]}$$

For conversion purposes Gibbs free energies will be defined as follows: $\bar{G}_{JX}$ = for JX in the "overall" mixed system at the equilibrium composition (reaction [3] at equilibrium); G^0_{JX} = for pure molten JX; and $\bar{G}'_{JX}$ for JX in the "standard" solution $[(AX)_{n_2} \cdot (BX)_{n_3} \cdots (JX)_{n_j}]$.

Gibbs free energies of mixing may be expressed in terms of the two different standard states given. These are

$$[A\text{-}3] \qquad \overline{\Delta G}''_{JX\ (\text{in "mixed" system})} = \bar{G}_{JX} - G^0_{JX}$$

$$[A\text{-}4] \qquad \overline{\Delta G}'_{JX\ (\text{in "standard" solution})} = \bar{G}'_{JX} - G^0_{JX}$$

Can. J. Chem. Downloaded from www.nrcresearchpress.com by 198.100.157.202 on 09/07/12
For personal use only.

and,

[A-5] $$\underset{\text{(in "mixed" system)}}{\overline{\Delta G}_{JX}} = \bar{G}_{JX} - \bar{G}'_{JX}$$

From eqs. [A-3], [A-4], and [A-5],

[A-6] $$\overline{\Delta G}_{JX} = \overline{\Delta G}''_{JX} - \overline{\Delta G}'_{JX}$$

Similarly, considering the standard states for pure molten J_rMX_{q+r} as $G^0_{J_rMX_{q+r}}$ and of J_rMX_{q+r} in the standard solution $(A_rMX_{q+r})_{n_2} \cdot (B_rMX_{q+r})_{n_3} \cdots (J_rMX_{q+r})_{n_j}$ as $\overline{G}'_{J_rMX_{q+r}}$, it is possible to relate the partial molar Gibbs free energy of mixing for J_rMX_{q+r}, by the expression

[A-7] $$\overline{\Delta G}_{J_rMX_{q+r}} = \underset{\text{[A-5]}}{\overline{\Delta G}''_{J_rMX_{q+r}}} - \overline{\Delta G}'_{J_rMX_{q+r}}$$

where $\overline{\Delta G}''_{J_rMX_{q+r}}$ is the Gibbs free energy of mixing for J_rMX_{q+r} with respect to the state of J_rMX_{q+r} in the "standard" solution.

Equations [A-6] and [A-7] in this appendix are also listed as eqs. [7] and [8] in Table 1.

Can. J. Chem. Downloaded from www.nrcresearchpress.com by 198.100.157.202 on 09/07/12
For personal use only.

Solvent structure effects on solvated electron reactions with ions in 2-butanol/water mixed solvents

SEDIGALLAGE A. PEIRIS AND GORDON R. FREEMAN
Chemistry Department, University of Alberta, Edmonton, Alta., Canada T6G 2G2

Received November 27, 1990

SEDIGALLAGE A. PEIRIS and GORDON R. FREEMAN. Can. J. Chem. **69**, 884 (1991).

The Smoluchowski–Debye–Stokes–Einstein equation for the rate constant k_2 of a bimolecular reaction between charged or polar species

$$k_2 = \kappa RTfr_r/1.5\eta r_d$$

was used to evaluate effects of bulk solvent properties on reaction rates of solvated electrons with $NO_{3,s}^-$, H_s^+, Tl_s^+, Cu_s^{2+}, and Al_s^{3+} in 2-butanol/water mixed solvents. To explain detailed effects it was necessary to consider more specific behavior of the solvent. Rate constants k_2, activation energies E_2, and pre-exponential factors A_2 of these reactions vary with the composition of 2-butanol/water mixtures. The values of E_2 were in general similar to activation energies of ionic conductance $E_{\Lambda 0}$ of the solutions, except for much higher values of E_2 of (e_s^- + $NO_{3,s}^-$) in alcohol-rich solvents and of (e_s^- + Al_s^{3+}) in pure water solvent. The solvent apparently participates chemically in the $NO_{3,s}^-$ reaction, and the Al_s^{3+} reaction is multistep. Rate constant and conductance measurements of thallium acetate solutions in 2-butanol containing zero and 10 mol% water were complicated by the formation of ion clusters larger than pairs.

Key words: alcohol/water mixed solvents, ions, reaction kinetics, solvated kinetics, solvated electron, solvent effects.

SEDIGALLAGE A. PEIRIS et GORDON R. FREEMAN. Can. J. Chem. **69**, 884 (1991).

On a utilisé l'équation de Smoluchowski–Debye–Stokes–Einstein

$$k_2 = \kappa RTfr_r/1.5\eta r_d$$

pour la constante de vitesse k_2 d'une réaction entre des espèces chargées ou polaires pour évaluer les effets des propriétés globales du solvant sur les vitesses de réaction des électrons solvatés avec des $NO_{3,s}^-$, H_s^+, Tl_s^+, Cu_s^{2+} et Al_s^{3+} dans des solvants mixtes de 2-butanol/eau. Pour offrir une explication détaillée des effets, il est nécessaire de considérer un comportement plus spécifique du solvant. Les constantes de vitesses, k_2, les énergies d'activation, E_2, et les facteurs pré-exponentiels, A_2, de ces réactions varient avec la composition des mélanges de 2-butanol/eau. Les valeurs de E_2 sont généralement similaires aux énergies d'activation de la conductance ionique $E_{\Lambda 0}$ des solutions; les seules exceptions sont les valeurs beaucoup plus élevées observées pour les valeurs de E_2 de (e_s^- + $NO_{3,s}^-$) dans les solvants riches en alcool et de (e_s^- + Al_s^{3+}) dans l'eau pure. Apparemment, le solvant participe chimiquement à la réaction du $NO_{3,s}^-$ alors que la réaction du Al_s^{3+} se ferait en plusieurs étapes. Les mesures de constante de vitesse et de conductance de solutions d'acétate de thallium dans du butanol contenant de zéro à 10 mol% d'eau sont compliquées par la formation d'agrégats ioniques plus gros que des paires.

Mots clés : solvants mixtes alcool/eau, ions, cinétiques de réactions, électron solvaté, effets de solvants.

[Traduit par la rédaction]

Introduction

This article is a continuation of the study of solvent structure effects on solvated electron reactions in alcohol/water mixed solvents (1–4). Alcohol/water mixtures are good systems to study the effects of solvent structure on solvated electron reactivity because varying the composition of the mixture results in strong variations in the solvent structure, as reflected in physical properties such as viscosity (5) and dielectric relaxation time (6).

In this article we report solvent composition effects on the rates of (e_s^- + $NO_{3,s}^-$), (e_s^- + Tl_s^+), (e_s^-, Cu_s^{2+}), and (e_s^- + Al_s^{3+}) in 2-butanol/water mixed solvents. The subscript "s" is used on the ions to emphasize the fact that the solvating molecules influence the reaction.

Experimental

2-Butanol was obtained from Aldrich Chemical Co. (99+%, spectroscopic grade, gold label). It was dried for two weeks on Davison Molecular Sieves 3 Å and then treated for one day under UHP argon (Liquid Carbonic Canada Ltd.) with sodium borohydride (~2 g/L) at ~330 K. The alcohol was then fractionally distilled under argon through an 80 × 2.3 cm column packed with glass helices, discarding the first 20% and last 40%. The water content of the collected 40%, measured by Karl-Fisher titration, was 0.1 mol%. The solvated electron half-life after a 100 ns pulse of 1.9 MeV electrons (~3 J/kg, 2×10^{16} eV/g) at 298 K was about 4 μs.

Water was purified in a Barstead Nanopure II ion exchange system. The solvated electron half-life after a 100 ns pulse of radiation was 20 μs.

Lithium nitrate (99.999%, Aldrich, gold label), thallium acetate (96%, BDH Chemicals Ltd.), Copper(II) perchlorate (Aldrich reagent grade), aluminium(III) perchlorate (98%, Aldrich Chemical Co.), and perchloric acid (70%, Fisher Scientific Co.) were used as received. The salts were stored in a vacuum desiccator that contained fresh P_2O_5 powder.

Techniques

Methods of sample preparation from solid solutes were as described in ref. 7. Perchloric acid samples were made by measuring 70% perchloric acid solution with a glass pipet to prepare 50 mol/m^3 stock solutions, and then diluting as previously described.

Methods of irradiation, dosimetry, and optical measurement were similar to those described in ref. 8.

The first-order decay rate constants k_{obs} of e_s^- were calculated from the half-lives $t_{1/2}$. The computer calculated $t_{1/2}$ values as a function of time along each absorbance decay trace (~50 points/cm) and plotted the half-life curve together with the optical absorbance decay trace. A horizontal $t_{1/2}$ line ($t_{1/2}$ independent of time) showed that the decay was first-order.

Electrical conductance measurements were as described in ref. 9.

Can. J. Chem. Downloaded from www.nrcresearchpress.com by 198.100.157.202 on 09/07/12
For personal use only.

Can. J. Chem. Downloaded from www.nrcresearchpress.com by 198.100.157.202 on 09/07/12
For personal use only.

Dissolved CO_2 was removed from the conductance cell by bubbling UHP argon through the solution, then the cell was sealed with Parafilm. A small amount of chemical reaction sometimes occurred at the higher temperatures, detected by drift of the conductance. In these cases a fresh sample was used for each measurement.

Values of viscosities were obtained from ref. 10. Values of relative permittivities were obtained from refs. 11 and 12.

Results and discussion

The second-order rate constant k_2 were obtained as described in ref. 4*a*.

Water and 2-butanol were only miscible in the composition regions 0–66 mol% water and 97–100 mol% water.

Diffusion and reaction

The rate constants data were analyzed according to the modified Arrhenius equation (4),

$$[1] \quad k_2/f = A_2 \exp(-E_2/RT)$$

where E_2 is the overall energy of activation of the reaction and A_2 is the pre-exponential factor. The factor f reflects the effect of the electrostatic interaction between the reactants on their probability of attaining the closeness of approach r_r at which reaction occurs (13):

$$[2] \quad f = \frac{U(r_r)}{k_B T}[\exp(U(r_r)/k_B T) - 1]^{-1}$$

where $U(r_r)$ is the interaction energy of the reactants at distance r_r, k_B is Boltzmann's constant, and T is the temperature. When the reactants repel each other $U(r_r)$ is positive and the value of f is <1. For attraction $U(r_r)$ is negative and f is >1.

For the interaction of e_s^- with a solute of charge $z\xi$, $U(r_r)$ is given by

$$[3] \quad U(r_r) = -z\xi^2/4\pi\epsilon_0\epsilon r_r$$

where $-\xi$ is the charge on the electron, ϵ_0 is the permittivity of vacuum, and ϵ is the relative permittivity of the solvent between the electron and the ion. The value of r_r is larger than the van der Waals diameter of a water molecule (0.28 nm), so short range interactions are ignored and the static value of ϵ is used. The value of ϵr_r is chosen somewhat arbitrarily, so if a value of ϵ less than the static value were preferred, it would be used with a larger r_r.

For the interaction of e_s^- with a neutral, polar solute molecule S,

$$[4] \quad U(r_r) = -M\xi \cos\theta/4\pi\epsilon_0\epsilon r_r^2$$

where M is the dipole moment of S and θ is the angle of approach of e^- to the dipole axis of S.

In Figs. 1 and 2 values of f are plotted for nitrobenzene and for ions of different z and appropriate values of r_r (2), for a range of values of ϵ and T. The value of ϵ of each solvent at each T used in the experiments was obtained by interpolation of data in refs. 11 and 12.

Each value of k_2 was divided by the value of f at the corresponding values of (ϵ, T, r_r) to remove the simple coulombic effect from k_2.

The rate constants for the reactions of e_s^- with the counter ions perchlorate, acetate, and lithium are less than 10^3 m^3/mol s in water (14). Therefore, the observed rate constants are due to $NO_{3,s}^-$, H_s^+, Tl_s^+, Cu_s^{2+}, and Al_s^{3+}. Arrhenius plots of log (k_2/f) against T^{-1} are shown for $NO_{3,s}^-$ in Fig. 3*A*, for H_s^+ in Fig. 4*A*,

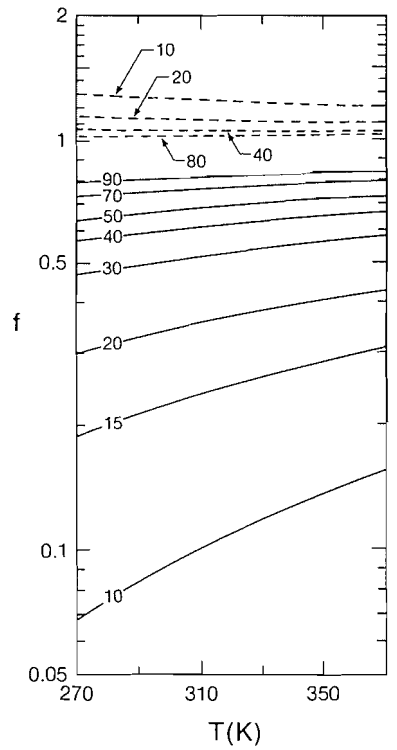


FIG. 1. Temperature dependence of the Debye factor f at different values of dielectric permittivity ϵ. ---, nitrobenzene, using r_r = 1.0 nm, θ = 0 rad, and $M = 1.4 \times 10^{-29}$ C m in eq. [4]. —, NO_3^-, using r_r = 1.5 nm in eq. [3]. Values of ϵ are indicated.

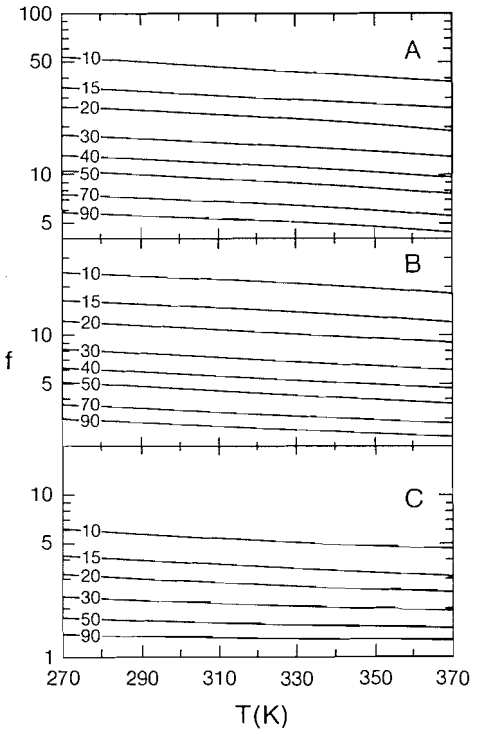


FIG. 2. Temperature dependence of the Debye factor f at different values of dielectric permittivity ϵ in eq. [3]. *A*: z = +3, using r_r = 0.35 nm. *B*: z = +2, using r_r = 0.5 nm. *C*: z = +1, using r_r = 1.0 nm.

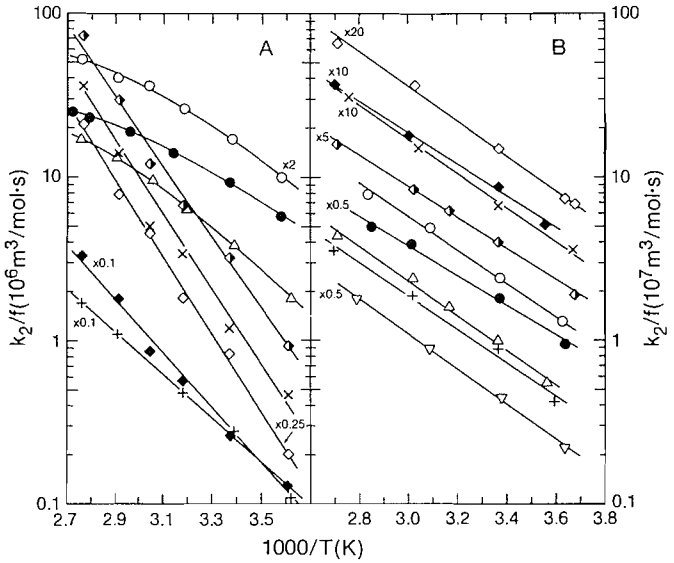


FIG. 3. Arrhenius plots of $k_2(e_s^- + NO_{3,s}^-)/f$ (*A*) and $k_2(e_s^-$ + nitrobenzene)/f (*B*) in 2-butanol/water mixed solvents. Symbols representing mol% water are given in Table 1, except: △, (*A*, 66; *B*, 68); +, (*A*, 51; *B*, 50); ◆, (*A*, 34; *B*, 35).

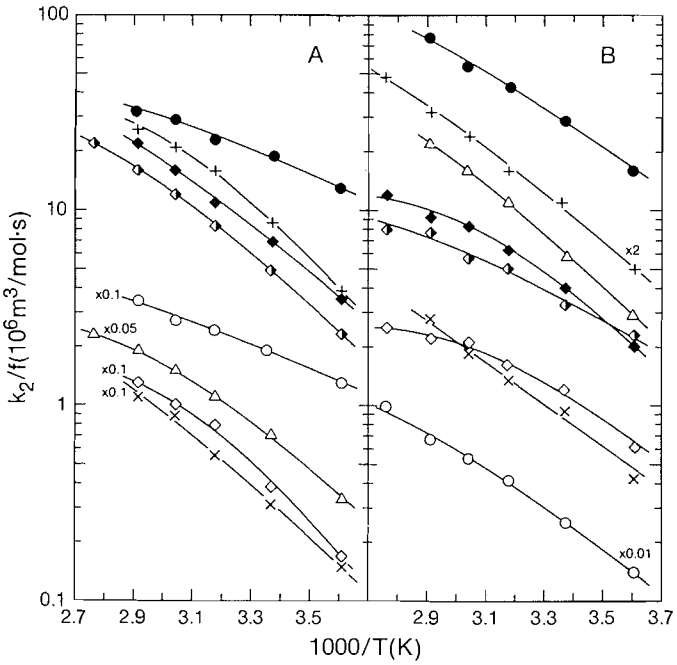


FIG. 4. Arrhenius plots of $k_2(e_s^- + H_s^+)/f(A)$ and $k_2(e_s^- + Tl_s^+)/f$ (*B*) in 2-butanol/water mixed solvents. Symbols representing mol% water are given in Table 1, except △, 66; +, 51; ◆, 34.

for Tl_s^+ in Fig. 4*B*, for Cu_s^{2+} in Fig. 5*A*, and for Al_s^{3+} in Fig. 5*B*. The mol% of water represented by the symbols in these figures are shown in Table 1.

The reaction of e_s^- with nitrobenzene is nearly diffusion controlled (7, 15) and we use it as a reference (4*a*). Arrhenius plots of k_2/f for nitrobenzene are given in Fig. 3*B*, using k_2 values from ref. 16.

For a diffusion controlled reaction E_2 is essentially that for the mutual diffusion of e_s^- and S, which encounter each other

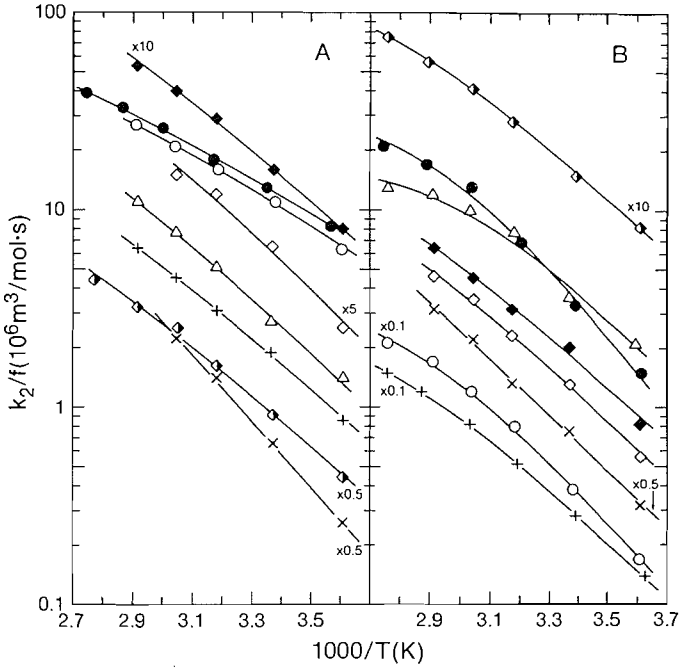


FIG. 5. Arrhenius plots of $k_2(e_s^- + Cu_s^{2+})/f$ (*A*) and $k_2(e_s^- + Al_s^{3+})/f(B)$ in 2-butanol/water mixed solvents. Symbols representing mol% water are given in Table 1, except: △, 66; +, (*A*, 52; *B*, 51); ◆, 34.

TABLE 1. Symbols in Figs. 3–5, representing mol% of water in 2-butanol

Symbol	% H_2O	Symbol	% H_2O	Symbol	% H_2O
×	0	◆	34–35	△	66–68
◇	10	+	50–52	○	97
◈	20	▽	64	●	100

at random,

[5′] $e_s^- + S \rightarrow (e_s^-, S)$

and react,

[5″] $(e_s^-, S) \rightarrow$ products

In slow reactions most encounter pairs diffuse apart again,

[−5′] $(e_s^-, S) \rightarrow e_s^- + S$

in which case the measured E_2 is mainly the activation energy of reaction [5″]. The values of E_2 for nitrobenzene do not vary greatly with solvent composition (Fig. 6*A*), and are similar to E_η for viscosity (Fig. 7).

For the reaction of $(e_s^- + NO_{3,s}^-)$ the values of E_2 in the water-rich solvents are similar to those for nitrobenzene. However, in the alcohol-rich solvents E_2 increases with alcohol content (Fig. 6*A*). The value of E_2 in pure 2-butanol is about three times that in pure water. The value of A_2 increases along with E_2 (Fig. 6*B*) in such a way that the value of k_2/f for $e_s^- + NO_{3,s}^-$ at 298 K is independent of water content at <60 mol% water (Fig. 8). The strong variations of E_2 and A_2 indicate that the alcohol participates chemically in the $e_s^- + NO_{3,s}^-$ reaction; details of the participation are not yet known (4*a*).

On the water-rich side of the solvent immiscibility gap the values of k_2/f for $(e_s^- + NO_{3,s}^-)$ are larger (Fig. 8), due to the

Can. J. Chem. Downloaded from www.nrcresearchpress.com by 198.100.157.202 on 09/07/12
For personal use only.

Can. J. Chem. Downloaded from www.nrcresearchpress.com by 198.100.157.202 on 09/07/12
For personal use only.

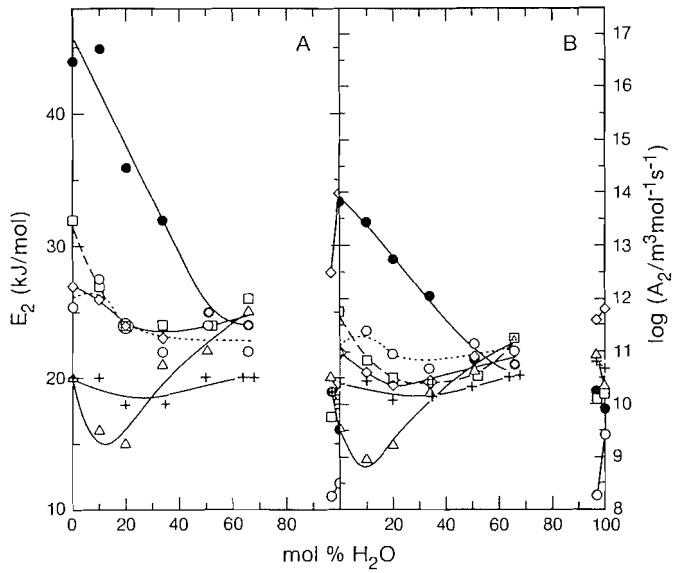


FIG. 6. Solvent composition dependence of the activation energies E_2 (A) and log A_2 (B) near 298 K in 2-butanol/water mixed solvents. ◇, Al_s^{3+}; □, Cu_s^{2+}; △, Tl_s^+; ○, H_s^+; +, nitrobenzene; ●, $NO_{3,s}^-$.

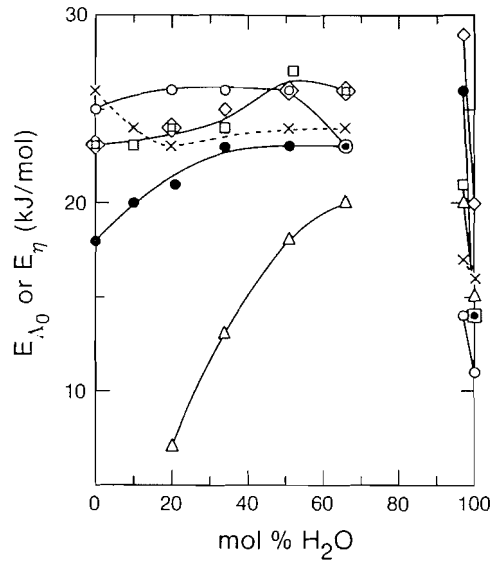


FIG. 7. Solvent composition dependence of the activation energies $E_{\Lambda 0}$ of the molar conductances of the salts and of solvent shear viscosity, E_η, near 298 K. ◇, $Al(ClO_4)_3$; □, $Cu(ClO_4)_2$; △, TlAc; ○, $HClO_4$; ●, $LiNO_3$. ×, E_η.

lower viscosity of the liquid (Table 2) and the consequently higher diffusion coefficients.

The values of k_2/f for the cation reactions differ by factors up to ten (Fig. 8), but the solvent dependences of k_2/f do not reflect those of the corresponding values of E_2 and log A_2 (Fig. 6). The most remarkable observation is that, while in pure alcohol solvent the values of E_2 and log A_2 for the reactions of the anions and cations differ greatly, the values in the mixed solvent near 60 mol% water are similar, then separate differently in pure water solvent (Fig. 6 and ref. 4). At the present early stage of investigation of solvent effects we can only say that this peculiarity points to an unexpected influence of solvent on reaction rates.

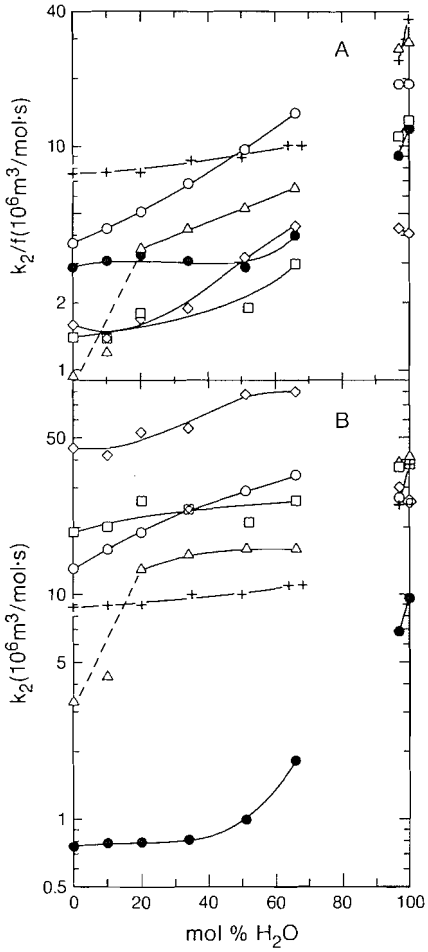


FIG. 8. Solvent composition dependence of $k_2/f(A)$ and $k_2(B)$ at 298 K. Symbols as in Fig. 6.

Values of the activation energy of diffusion of e_s^- in the mixed solvents are not known, but the activation energy of conductance $E_{\Lambda 0}$ of the reactant salt gives a rough idea of E_2 that might be expected for a diffusion controlled reaction (4*b*). Plots of $E_{\Lambda 0}$ against solvent composition are shown in Fig. 7. There are many significant differences between the values of $E_{\Lambda 0}$ and E_2 (Fig. 6), which cannot yet be interpreted.

Values of the reaction rate parameters are summarized in Tables 2 and 3.

Effect of solvent viscosity

The Smoluchowski–Debye–Stokes–Einstein equation for the rate constant k_2 of a bimolecular reaction between charged or polar species is given by (16)

$$[6] \qquad k_2 = \kappa RTfr_r/1.5\eta r_d$$

where κ = probability that a reactant encounter-pair will react, η = solvent viscosity (kg/m s), and r_d and r_r are the effective radii for mutual diffusion and reaction, respectively. Rearrangement of [6] gives the dimensionless ratio of reaction parameters $\kappa r_r/r_d$, which is a sort of reaction efficiency parameter:

$$[7] \qquad \kappa r_r/r_d = k_2\eta/5.5fT$$

where the constant 5.5 (J/mol K) represents $R/1.5$. The values of this ratio at 298 K for nitrobenzene are about three times those for $NO_{3,s}^-$ in all these solvents (Fig. 9*A*). In the pure alcohol

TABLE 2. Rate parameters for the reaction of solvated electrons with solutes in 2-butanol/water mixtures

X_w[a]	ϵ[b]	η[c] (10^{-3} Pa s)	k_2[d] (10^7 m^3/mol s)	k_2/f[d] (10^7 m^3/mol s)	E_2[e,f] (kJ/mol)	log A_2[f] (A_2 in m^3/mol s)	E_η[g] (kJ/mol)
				$NO_{3,s}^-$[h]			
1.00	78.5	0.89	0.96	1.2	16	9.91	16
0.97	70.0	1.45	0.68	0.91	19	10.25	17
0.66	26.0	3.32	0.18	0.40	24	10.76	24
0.51	20.0	3.06	0.098	0.29	25	10.86	24
0.34	16.7	2.85	0.080	0.31	32	12.06	
0.20	15.8	2.75	0.078	0.33	36	12.74	23
0.10	15.8	2.78	0.077	0.31	45	13.45	24
0.00	15.8	3.05	0.075	0.29	44	13.83	26
				Nitrobenzene[i]			
1.00	78.5	0.89	3.8	3.7	18	10.68	
0.97	70.0	1.45	2.5	2.4	19	10.80	
0.68	27.4	3.38	1.1	1.0	20	10.55	
0.64	25.2	3.28	1.1	1.0	20	10.53	
0.50	19.6	3.10	1.0	0.89	20	10.33	
0.35	16.8	2.85	1.0	0.87	18	10.13	
0.20	15.8	2.75	0.90	0.77	18	10.07	
0.10	15.8	2.78	0.89	0.77	20	10.46	
0.00	15.8	3.05	0.88	0.76	20	10.39	

[a]Mole fraction water.
[b]Static dielectric permittivity at 298 K.
[c]Viscosity at 298 K.
[d]At 298 K.
[e]Near 298 K.
[f]From Arrhenius plots of k_2/f.
[g]Arrhenius temperature coefficient for shear viscosity.
[h]$NO_{3,s}^-$ concentrations 0.03–0.5 mol/m^3.
[i]Nitrobenzene concentrations 0.01–0.09 mol/m^3.

Can. J. Chem. Downloaded from www.nrcresearchpress.com by 198.100.157.202 on 09/07/12
For personal use only.

solvents the values of $\kappa r_r/r_d$ for $e_s^- + NO_{3,s}^-$ at 298 K are 5.3 in 2-butanol, 2.7 in 2-propanol, ~1.7 in *tert*-butanol, and 0.25 in 1-propanol. The values in the propanols were calculated from data in ref. 4*a*, and that in *tert*-butanol was estimated from data in ref. 2 ($k_2 \approx 1 \times 10^5$ m^3/mol s, $r_r \approx 1.5$ nm, $f \approx 0.16$, $\epsilon = 12.5$, $\eta = 4.45 \times 10^{-3}$ Pa s). The variation of $k_2(e_s^- + NO_{3,s}^-)$ with water content in *tert*-butanol (Fig. 4 of ref. 2, note that ◇ represents NO_3^- and ■ represents CrO_4^{2-}) is similar to that in 1-propanol (Fig. 7*A* of ref. 4*a*), and these are quite different from the behavior in the two secondary alcohols (Fig. 7*A* of ref. 4*a* and the present Fig. 8*B*). The secondary alcohols participate more readily in the $e_s^- + NO_{3,s}^-$ reaction than do the primary and tertiary alcohols. The secondary alcohols possess a relatively reactive C—H group that the primary and tertiary alcohols lack, so perhaps this enters the overall reaction.

In the 2-butanol/water solvents the relative values of $\kappa r_r/r_d$ for the different cations change with solvent composition (Fig. 9*A*). The lower values of the ratio for Cu_s^{2+} and Al_s^{3+} are attributed to difficulty in forming the relatively unstable Cu_s^+ and Al_s^{2+} ions from e_s^- and Cu_s^{2+} and Al_s^{3+}, respectively (4*b*). In aqueous solution the Cu_s^+ ion is unstable with respect to Cu_s^{2+} and Cu. The equilibrium

[8] $$2Cu_s^+ \rightleftharpoons Cu_s^{2+} + Cu_s$$

lies far to the right, and compounds of Cu(I) are covalent (17). Compounds of Al(II) are not known. The overall reaction with Al_s^{3+} might be either

[9] $$Al_s^{3+} + e_s^- \rightarrow (AlOH)_s^{2+} + H_s$$

or

[10] $$3Al_s^{3+} + 3e_s^- \rightarrow 3Al_s^{2+} \rightarrow\rightarrow Al_s^0 + 2Al_s^{3+}$$

In support of reaction [9], the equilibrium constant for the hydrolysis of Fe_s^{3+}

[11] $$Fe_s^{3+} \rightleftharpoons (FeOH)_s^{2+} + H_s^+$$

increases eight times when 40 mol% methanol is added to pure water solvent (18). It does not change much when more alcohol is added. We measured pH values of solutions of $Al(ClO_4)_3$ in pure water and in 32 mol% 1-propanol in water.

[12] $$Al_s^{3+} \rightleftharpoons (AlOH)_s^{2+} + H_s^+$$

The equilibrium constant calculated from these pH values increased twenty times ($K = 9.2 \times 10^{-3}$ mol/m^3 to 0.19 mol/m^3) when 32 mol% 1-propanol was added to the water. Apparently dissociation reactions of type [12] increase when alcohol is added to aqueous solution. This could explain why the overall rate constant for e_s^- reaction in the Al_s^{3+} solutions increases abnormally, relative to those of other positive ions, when alcohol is added to pure water solvent (4*b*). The effective concentration of the reactant is larger because of the presence of both $(AlOH)_s^{2+}$ and H_s^+.

Comparison with ionic conductivities

The diffusion coefficients D_i of the reacting species are related to their molar conductivities λ_i (C m^2/V s mol), so the solvent dependence of $k_2/fT[(\lambda_i/z_i^2) + \lambda_e]$ indicates the solvent dependence of the effective reaction radius κr_r (4*a*):

TABLE 3. Rate parameters for the reaction of solvated electrons with solutes in 2-butanol/water mixtures

X_w[a]	ϵ[b]	η[c] (10^{-3} Pa s)	k_2[d] (10^7 m^3/mol s)	k_2/f[d] (10^7 m^3/mol s)	E_2[e,f] (kJ/mol)	log A_2[f] (A_2 in m^3/mol s)
			H_s^+[g]			
1.00	78.5	0.89	2.6	1.9	12	9.42
0.97	70.0	1.45	2.7	1.9	11	8.27
0.66	26.0	3.32	3.4	1.4	22	11.00
0.51	20.0	3.06	2.9	0.97	24	11.15
0.34	16.7	2.85	2.4	0.69	22	10.67
0.20	15.8	2.74	1.9	0.51	24	10.95
0.10	15.8	2.78	1.6	0.43	27	11.39
0.00	15.8	3.05	1.3	0.37	25	10.97
			Tl_s^+[h]			
1.00	78.5	0.89	4.1	2.9	19	10.34
0.97	70.0	1.45	3.8	2.7	20	10.92
0.66	26.0	3.32	1.6	0.65	25	11.24
0.51	20.0	3.06	1.6	0.53	22	10.63
0.34	16.7	2.85	1.5	0.43	21	10.20
0.20	15.8	2.74	1.3	0.35	15	9.19
0.10	15.8	2.78	0.43	0.12	16	8.95
0.00	15.8	3.05	0.33	0.094	20	9.50
			Cu_s^{2+}[i]			
1.00	78.5	0.89	3.9	1.3	18	10.20
0.97	70.0	1.45	3.7	1.1	17	10.09
0.66	26.0	3.32	2.6	0.30	26	11.00
0.52	20.2	3.08	2.1	0.19	24	10.52
0.34	16.7	2.85	2.4	0.18	24	10.41
0.20	15.8	2.74	2.6	0.18	24	10.50
0.10	15.8	2.78	2.0	0.14	27	10.83
0.00	15.8	3.05	1.9	0.14	32	11.76
			Al_s^{3+}[j]			
1.00	78.5	0.89	2.5	0.41	34	11.79
0.97	70.0	1.45	3.0	0.43	28	11.60
0.66	26.0	3.32	8.0	0.44	24	10.76
0.51	20.0	3.06	7.8	0.32	25	10.91
0.34	16.7	2.85	5.5	0.19	23	10.38
0.20	15.8	2.74	5.3	0.17	24	10.36
0.10	15.8	2.78	4.2	0.14	26	10.60
0.00	15.8	3.05	4.5	0.16	27	10.95

[a–f]As in Table 2.
[g]H_s^+ concentrations 0.01–0.12 mol/m^3.
[h]Tl_s^+ concentrations 4–54 mmol/m^3.
[i]Cu_s^{2+} concentrations 5–54 mmol/m^3.
[j]Al_s^{3+} concentrations 2–24 mmol/m^3.

Can. J. Chem. Downloaded from www.nrcresearchpress.com by 198.100.157.202 on 09/07/12
For personal use only.

[13] $\kappa r_r = 1.48 \times 10^{-16} k_2/fT[(\lambda_i/z_i^2) + \lambda_e]$

where λ_e is the molar conductivity of e_s^- and the units of 1.48×10^{-16} are C K/sr V ion. Note that r_r has units m/entity sr. The entity is the pair of reactants, where one is considered to be at the center of a sphere and the other is approaching it at a particular solid angle. The reaction probability κ is averaged over all angles (4πsr) of approach.

In alcohol-rich solvents the plots of specific conductance against concentration for $LiNO_3$ were sublinear, which indicates ion pair formation:

[14] $Li_s^+ + NO_{3,s}^- \rightleftharpoons (Li_s^+, NO_{3,s}^-)$

Association constants of [14] were estimated from the curved plots at different temperatures; by comparison of various individual cation and anion mobilities in water (19) the ionic conductivities in these solvents were assumed to be $\lambda(NO_{3,s}^-) \approx 2\lambda(Li_s^+)$. The equation for the association constant K is

[15] $K = x/(a - x)^2$

where x is the amount of association of Li_s^+ and $NO_{3,s}^-$, and the total concentrations are a. Then the conductance C of the solution is given by

[16] $C = 3\lambda_{Li^+}(a - x)$

where λ_{Li^+} is the molar conductance of Li_s^+; $C_0(Li_s^+ + NO_{3,s}^-) \approx (3\lambda_{Li^+}a)$ is the value of C at $x = 0$. Arrhenius plots of

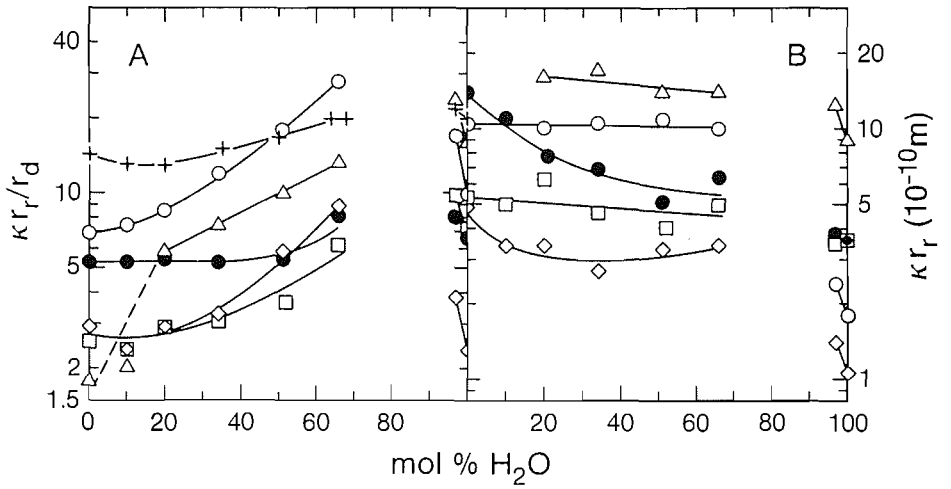


FIG. 9. Solvent composition dependence of $\kappa r_r/r_d$ (*A*) and κr_r (*B*) at 298 K. Symbols as in Fig. 6.

the estimated association constants are given in Fig. 10. The association constants increase with increasing temperature, due to the concomitant decrease of permittivity. The amount of association in the solutions used for rate constant measurements at these water concentrations varied from 53% (at 343 K in pure 2-butanol) to 3% (at 277 K in 20 mol% water).

Ion association also occurred in the thallium acetate solutions at zero and 10 mol% water. The value of the association constant K at 298 K was roughly 3000 m^3/mol in pure 2-butanol and 200 m^3/mol at 10 mol% water. However, the conductances of solutions in the thallium acetate concentration range 0.02–0.4 mol/m^3 were not sufficiently sublinear to be explained by simple ion pairing:

[17] $\quad Tl_s^+ + Ac_s^- \rightleftharpoons [Tl_s^+, Ac_s^-]$

It appears that larger, charged clusters formed at higher salt concentrations:

[18] $\quad [Tl_s^+, Ac_s^-] + Tl_s^+ \rightleftharpoons [2Tl_s^+, Ac_s^-]$

[19] $\quad [Tl_s^+, Ac_s^-] + Ac_s^- \rightleftharpoons [Tl_s^+, 2Ac_s^-]$

and so on.

The formation of larger clusters is probably the cause of the low apparent values of k_2 in the pure 2-butanol and 10 mol% water solvents (Fig. 8*B*).

The solvent dependence of the molar conductivities Λ_0 of the salts and the acid at 298 K are shown in Fig. 11.

In pure water at 298 K the ratios of the λ's of e_s^- (18): $NO_{3,s}^-$:H_s^+:Tl_s^+:Cu_s^{2+}:Al_s^{3+} (20) are 4.7:1.9:9.1:2.0:3.0:4.9, so the diffusion coefficients ($\propto \lambda_i/z_i^2$) are in the ratios 4.7:1.9:9.1:2.0:0.8:0.5. Thus diffusion of e_s^- dominates the relative motion of each reactant pair except for that with H_s^+. The values of the individual ionic conductivities in the mixed solvents are not known, so we have to use approximations. In water the ratio $[\lambda(e_s^-) + \lambda(NO_{3,s}^-)]/\Lambda_0(Li_s^+ + NO_{3,s}^-) = 2.3$, $[\lambda(e_s^-) + \lambda(H_s^+)]/\Lambda_0(H_s^+ + ClO_{4,s}^-) = 1.3$, $[\lambda(e_s^-) + \lambda(Tl_s^+)]/\Lambda_0(Tl_s^+ + Ac_s^-) = 2.2$, $[\lambda(e_s^-) + 0.25\lambda(Cu_s^{2+})]/(1/2)\Lambda_0(Cu_s^{2+} + 2ClO_{4,s}^-) = 1.6$, and $[\lambda(e_s^-) + 0.11\lambda(Al_s^{3+})]/(1/3)\Lambda_0(Al_s^{3+} + 3ClO_{4,s}^-) = 1.5$. This ratio for Li_2CrO_4 (4) is $[\lambda(e_s^-) + 0.25\lambda(CrO_{4,s}^{2-})]/(1/2)\Lambda_0(2Li_s^+ + CrO_{4,s}^{2-}) = 1.8$. Thus eq. [13] can be approximated as

[20] $\quad \kappa r_r \approx 1 \times 10^{-16} z_i k_2/fT\Lambda_0$

where z_i is the number of charges on the reactant ion.

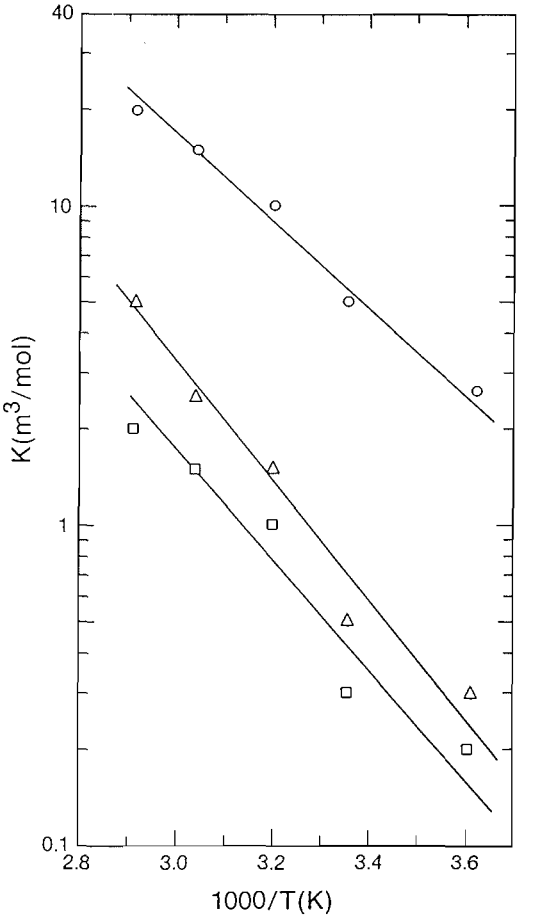


FIG. 10. Arrhenius plots of the association constant of Li_s^+ and $NO_{3,s}^-$ ions in 2-butanol/water mixtures. Mol% water: ○, 0; △, 10; □, 20. $\Delta H = 30 \pm 5$ kJ/mol.

The approximate values of κr_r obtained from eq. [20] are plotted against solvent composition in Fig. 9*B*. The shapes of the curves are somewhat different from those in Fig. 9*A* partly because the effective radii for diffusion r_d are solvent dependent, and partly because $\lambda(e_s^-)$ probably has a somewhat different solvent composition dependence than does $\lambda(Li_s^+)$ or $\lambda(ClO_{4,s}^-)$.

Can. J. Chem. Downloaded from www.nrcresearchpress.com by 198.100.157.202 on 09/07/12
For personal use only.

Can. J. Chem. Downloaded from www.nrcresearchpress.com by 198.100.157.202 on 09/07/12
For personal use only.

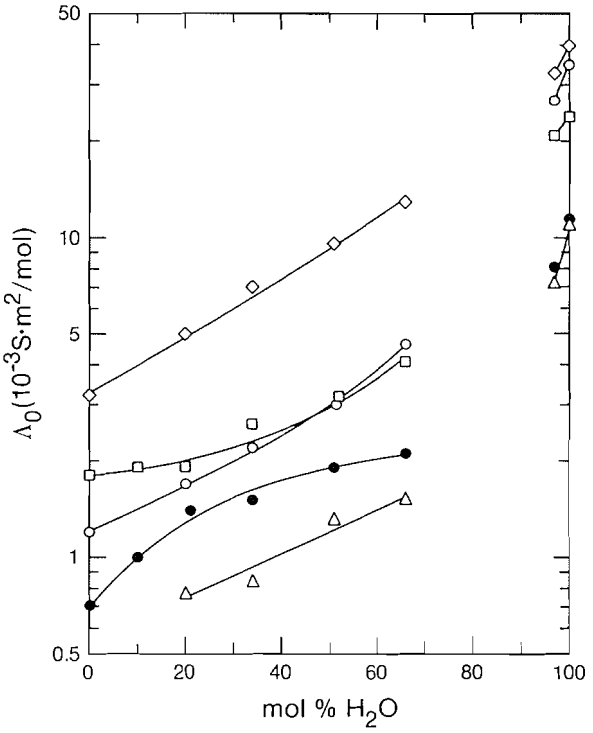


FIG. 11. Solvent composition dependence of molar conductivities of ions in 2-butanol/water at 298 K. ◇, $Al(ClO_4)_3$; □, $Cu(ClO_4)_2$; △, TlAc; ○, $HClO_4$; ●, $LiNO_3$.

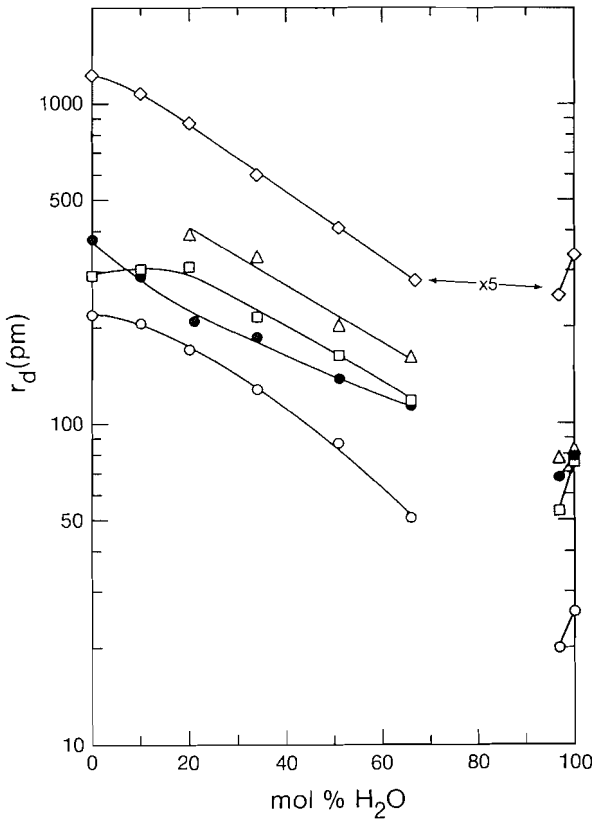


FIG. 12. 2-Butanol/water composition dependence of the effective radius for mutual diffusion of: ◇, $Al^{3+} + ClO_4^-$; □, $Cu^{2+} + ClO_4^-$; △, $Tl^+ + Ac^-$; ○, $H^+ + ClO_4^-$; ●, $Li^+ + NO_3^-$.

The Stokes radius r_d for mutual diffusion of the ions is given by (4*a*):

$$[21] \quad r_d = 8.2 \times 10^{-16} \Big/ \eta \left(\frac{\lambda_+}{z_+^2} + \frac{\lambda_-}{z_-^2} \right)$$

where 8.2×10^{-16} has units C^2/mol ion sr. Note that r_d also has units of (m/entity sr), and that the viscous force is assumed to be exerted over the surfaces of spherical ions, $4\pi r_{d+}^2$ and $4\pi r_{d-}^2$. Furthermore, $r_d^{-1} = r_{d+}^{-1} + r_{d-}^{-1}$, so r_d emphasizes the more mobile ion. Separate values of λ_+ and λ_- in the mixed solvents are not available, so values of r_d cannot be calculated from molar conductivities when $z_+ \neq z_-$. In pure water the values of $[(\lambda_+/z_+^2) + \lambda_-] = 9.6$ and 8.8 (10^{-3} S m^2/mol) for Cu_s^{2+} and Al_s^{3+} perchlorates at 298 K, respectively (4*b*). These values are a bit closer to the values of $\Lambda_0(\text{salt})/z_+$, 12.4 and 13.0 ($10^{-3}$ S m^2/mol), than to those of $\Lambda_0(\text{salt})/z_+^2$, 6.2 and 4.3 ($10^{-3}$ S m^2/mol), respectively. We therefore estimated r_d for the Cu_s^{2+} and Al_s^{3+} salt solutions from

$$[22] \quad r_d \approx 8 \times 10^{-16} z_+ / \eta \Lambda_0$$

Values of r_d estimated from eq. [22] are plotted in Fig. 12. With the exception of 100% to 97 mol% water the values of r_d increase with alcohol content of the solvent. The increase of r_d is attributed to solvation of the ions by alcohol molecules, which are larger than water molecules. The values of r_d in 2-butanol solutions are also larger than those in 1-propanol and 2-propanol solutions (4). The ratio of molar volumes alcohol/water at 298 K are 4.2 for 1-propanol, 4.3 for 2-propanol, and 5.2 for 2-butanol (21).

The apparent decrease in r_d when a few mol% of alcohol are added to water might indicate that the microscopic viscosity of the solvent in the vicinity of the ions is smaller than the bulk viscosity; the ions remain in the disordered water. This would explain the maxima in $\kappa r_r/r_d$ at ~90 mol% water in the propanol solvents (4*b*).

It should be mentioned that for the Li_s^+, $CrO_{4,s}^{2-}$ solutions (4*a*), the required value of $[\lambda_+ + (\lambda_-/z_-^2)] = 8.2 \times 10^{-3}$ S m^2/mol in water is closer to $\Lambda_0(\text{salt})/z_-^2 = 6.2 \times 10^{-3}$ S m^2/mol than to $\Lambda_0(\text{salt})/z_- = 12.4 \times 10^{-3}$ S m^2/mol, so in that case we estimated r_d from

$$[23] \quad r_d \approx 8 \times 10^{-16} z_-^2 / \eta \Lambda_0$$

This work points to the need of renewed interest in electrolyte solutions.

Conclusions

The reactivity of solvated electrons with solutes is determined not only by the electron affinity of the solute, but also by electron–solvent, solute–solvent, and solvent–solvent (solvent structure) interactions. The solvent structure affects the diffusion rates of the reactants as well as the solvation energies of the reactants, transition state, and products.

For (e_s^- + $NO_{3,s}^-$) the solvent apparently participates chemically in the reaction. The activation energy E_2 and the pre-exponential factor A_2 of (e_s^- + $NO_{3,s}^-$) decrease greatly as water is added to 2-butanol solvent.

The effective reaction radii κr_r for (e_s^- + Cu_s^{2+}) and (e_s^- + Al_s^{3+}) are relatively low because of the difficulty of forming the relatively unstable Cu_s^+ and Al_s^{2+} from reactions of e_s^- with Cu_s^{2+} and Al_s^{3+}, respectively. In pure water the value of κr_r for (e_s^- + H_s^+) is low because of relative difficulty of the reaction sequence $e_s^- + H_s^+ \rightarrow [H_3O]_s \rightarrow H_s + H_2O_s$.

Acknowledgements

We thank the Natural Sciences and Engineering Research Council for financial assistance, and the personnel of the Radiation Research Centre for aid with the electronics and for maintaining the equipment.

1. Y. MAHAM and G. R. FREEMAN. J. Phys. Chem. **92**, 1506 (1988).
2. P. C. SENANAYAKE and G. R. FREEMAN. J. Phys. Chem. **92**, 5142 (1988).
3. C. C. LAI and G. R. FREEMAN. J. Phys. Chem. **94**, 302 (1990); **94**, 4891 (1990).
4. A. P. SEDIGALLAGE and G. R. FREEMAN. (*a*) Can. J. Phys. **68**, 940 (1990); (*b*) Can. J. Chem. **69**, 157 (1991).
5. P. C. SENANAYAKE, N. GEE, and G. R. FREEMAN. Can. J. Chem. **65**, 2441 (1987).
6. D. BERTOLINI, M. CASSETTARI, and G. SALVETTI. J. Chem. Phys. **78**, 365 (1983).
7. Y. MAHAM and G. R. FREEMAN. J. Phys. Chem. **89**, 4347 (1985).
8. G. L. BOLTON and G. R. FREEMAN. J. Am. Chem. Soc. **98**, 6825 (1985).
9. C. C. LAI. Ph.D. thesis. University of Alberta, Edmonton, Alta. 1989.
10. J. TIMMERMANS. Physico-chemical constants of binary mixtures. Vol. 4. Wiley-Interscience, New York. 1960.
11. Y. Y. AKHADOV. Dielectric properties of binary solutions. Pergamon Press, Oxford. 1981.
12. W. DANNHAUSER and L. W. BAHE. J. Chem. Phys. **40**, 3058 (1964).
13. P. DEBYE. Trans. Electrochem. Soc. **82**, 265 (1942).
14. M. ANBAR, M. BAMBENEK, and A. B. ROSS. NSRDS-NBS **43**, US Govt. Printing Office, Washington, D.C. 1973.
15. Y. MAHAM and G. R. FREEMAN. Can. J. Chem. **66**, 1706 (1988).
16. P. C. SENANAYAKE and G. R. FREEMAN. J. Chem. Phys. **87**, 7007 (1987).
17. R. S. BOIKESS and E. EDELSON. Chemical principles. 3rd ed. Harper and Row, New York. 1985. p. 796.
18. W. WADA and Y. KOBAYASHI. Bull. Chem. Soc. Jpn. **48**, 2451 (1975).
19. K. H. SCHMIDT. Int. J. Radiat. Phys. Chem. **4**, 439 (1972).
20. D. DOBOS. Electrochemical data. Elsevier, Amsterdam. 1975.
21. R. W. GALLANT. Physical properties of hydrocarbons. Vol. 1. Gulf Publishing Co., Houston, TX. 1968.

Can. J. Chem. Downloaded from www.nrcresearchpress.com by 198.100.157.202 on 09/07/12
For personal use only.

1-*n*-Propyl- and 1-*n*-butyl-3-hydroxy-2-methyl-4-pyridinone complexes of group 13 (IIIA) metal ions

LINDA SIMPSON, STEVEN J. RETTIG, JAMES TROTTER,[1] AND CHRIS ORVIG[1]

Department of Chemistry, University of British Columbia, 2036 Main Mall, Vancouver, B.C., Canada V6T 1Z1

Received October 22, 1990

LINDA SIMPSON, STEVEN J. RETTIG, JAMES TROTTER, and CHRIS ORVIG. Can. J. Chem. **69**, 893 (1991).

The aluminum, gallium, and indium tris(ligand) complexes of 3-hydroxy-2-methyl-1-*n*-propyl-4-pyridinone and 1-*n*-butyl-3-hydroxy-2-methyl-4-pyridinone have been prepared and characterized. All six compounds were prepared in a one-pot synthesis from maltol, *n*-propyl-, or *n*-butylamine and an appropriate metal(III) salt, and were completely characterized (IR, FAB-MS, ^{1}H NMR, ^{27}Al NMR, elemental analysis). Three of the six complexes were studied by single-crystal X-ray diffraction and were found to form trihydrates, unlike their 1-methyl and 1-ethyl analogues, which formed dodecahydrates. The *n*-butylpyridinone complex $Al(C_{10}H_{14}NO_2)_3\cdot 3H_2O$ ($Al(nbp)_3\cdot 3H_2O$) and *n*-propylpyridinone complexes $Al(C_9H_{12}NO_2)_3\cdot 3H_2O$ ($Al(npp)_3\cdot 3H_2O$), and $Ga(C_9H_{12}NO_2)_3\cdot 3H_2O$ ($Ga(npp)_3\cdot 3H_2O$) were essentially isostructural, crystallizing in the space group $P\bar{3}$ with the following crystal parameters for $Al(nbp)_3\cdot 3H_2O$ ($Al(npp)_3\cdot 3H_2O$, $Ga(npp)_3\cdot 3H_2O$): a = 15.885(1) (15.328(1), 15.367(2)) Å, c = 7.280(8) (7.231(2), 7.256(2)) Å, Z = 2. The data were refined by using 1280 (1377, 1802) reflections with $I > 3\sigma(I)$ to R and R_w values of 0.047 (0.057, 0.055) and 0.061 (0.077, 0.081), respectively. They form *fac* geometries with infinite chains of hydrogen bonds parallel to the c axis similar to those found in the 1-methyl and 1-ethyl complexes. They lack the hexagonal channels of water molecules which characterized the dodecahydrates and are therefore not exoclathrates.

Key words: metal complexes, hydroxypyridinone ligands, exoclathrate, hydrogen bonding, crystal structures.

LINDA SIMPSON, STEVEN J. RETTIG, JAMES TROTTER et CHRIS ORVIG. Can. J. Chem. **69**, 893 (1991).

On a préparé et caractérisé les complexes tricoordinés de l'aluminium, du gallium et de l'indium avec la 3-hydroxy-2-méthyl-1-*n*-propyl-pyridin-4-one et la 1-*n*-butyl-3-hydroxy-2-méthyl-pyridin-4-one. On a préparé les six composés par des synthèses "bouillabaisses" impliquant le maltol, les *n*-propyl- ou *n*-butyl-amines et le sel métallique(III) approprié et on les a caractérisés complètement par ir, sm-bar, rmn du ^{1}H, rmn du ^{27}Al et analyse élémentaire. On a examiné trois des six complexes par diffraction des rayons-X par des cristaux uniques et on a trouvé qu'ils forment des trihydrates alors que leurs analogues 1-méthyle et 1-éthyle forment des dodécahydrates. Le complexe de la *n*-butylpyridinone, $Al(C_{10}H_{14}NO_2)_3\cdot 3H_2O$ ($Al(nbp)_3\cdot 3H_2O$) et les complexes de la *n*-propylpyridinone, $Al(C_9H_{12}NO_2)_3\cdot 3H_2O$ ($Al(npp)_3\cdot 3H_2O$) et $Ga(C_9H_{12}NO_2)_3\cdot 3H_2O$ ($Ga(npp)_3\cdot 3H_2O$) sont essentiellement isostructuraux et ils cristallisent dans le groupe d'espace $P\bar{3}$ avec a = 15,885(1) (15,328(1) et 15,367(2)) Å et c = 7,280(8), 7,231(2) et 7,256(2) Å respectivement pour $Al(nbp)_3\cdot 3H_2O$ ($Al(npp)_3\cdot 3H_2O$ et $Ga(npp)_3\cdot 3H_2O$) : dans tous les cas Z = 2. On a affiné les données à l'aide de 1280, 1377 et 1802 réflexions avec $I > 3\sigma(I)$, jusqu'à des valeurs de R et R_w de 0,047, 0,057 et 0,055 et 0,061, 0,077 et 0,081 respectivement. Comme leurs analogues 1-méthyle et 1-éthyle, ils existent dans des géométries *fac* avec des chaînes infinies de liaisons hydrogènes parallèles à l'axe c. Ils ne comportent pas de canaux hexagonaux de molécules d'eau qui caractérisent les dodécahydrates ; ils ne sont donc pas des exoclathrates.

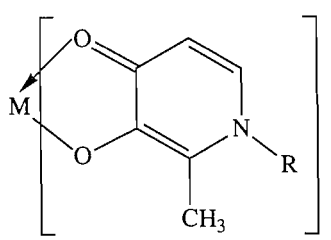
Mots clés : complexes métalliques, ligands hydroxypyridinone, exoclathrate, liaisons hydrogènes, structures cristallines.

[Traduit par la rédaction]

Introduction

The coordination chemistry of group 13 (IIIA) metals is of great interest because of their varied biological effects. Aluminum (1) has been implicated in the etiology of certain diseases and isotopes of gallium (2,3) and indium (3) are used in the diagnosis of disease. Research in these laboratories has focussed on the development of ligands which will bind effectively to these metals, both *in vitro* and *in vivo*. In the course of this work, a series of pyridinonato metal complexes with unexpected and novel crystallographic properties was discovered (4–8).

N-Substituted-3-hydroxy-2-methyl-4-pyridinones, initially chosen for their efficiency in binding group 13 metal ions (9, 10), formed tris(ligand)metal(III) dodecahydrate complexes when the *N*-substituent was methyl or ethyl (the complexes $M(dpp)_3$ and $M(mepp)_3$) (4–8). These crystallized in a manner unknown amongst inorganic hydrates; unusual hydrogen bonding was observed in the solid state. Single crystal X-ray diffraction revealed that water molecules formed hydrogen bonded hexagonal channels, which were in turn linked by other water molecules to the oxygen atoms which chelate the metal atom. This extensive network bears a closer resemblance to one of the crystalline forms of ice (I_h) (11) than to the typical structure of inorganic hydrates.



3

M = Al, Ga, In

R = H,	$M(mpp)_3$
R = CH_3	$M(dpp)_3$
R = C_2H_5	$M(mepp)_3$
R = *n*-C_3H_7	$M(npp)_3$
R = *n*-C_4H_9	$M(nbp)_3$
R = *n*-C_6H_{13}	$M(mhpp)_3$

Increasing the size of the metal atom (12) in these $ML_3\cdot 12H_2O$ complexes from aluminum (effective six-coordinate ionic radius, r = 0.535 Å) to gallium (r = 0.620 Å) to indium (r = 0.800 Å) seemed to have little effect upon the intricate hydrogen bonding network (5, 6). Also, increasing the size of the nitrogen substituent R from methyl to ethyl left intact the extensive hexagonal water channel network exoclathrate (8). The work described in this contribution was undertaken in order to probe the steric limitations of these unusual structures. It was hypothesized that an *n*-propyl group as the nitrogen substituent might form an exoclathrate, but that perhaps the lattice would not accommodate a more sterically demanding *n*-butyl group, and hence a different structure would be found. The synthesis, characterization, and X-ray crystallographic

[1]Authors to whom correspondence should be addressed.

Can. J. Chem. Downloaded from www.nrcresearchpress.com by 198.100.157.202 on 09/07/12
For personal use only.

Can. J. Chem. Downloaded from www.nrcresearchpress.com by 198.100.157.202 on 09/07/12
For personal use only.

studies of the tris(3-hydroxy-2-methyl-4-pyridinonato)-metal(III) complexes with an *n*-propyl or *n*-butyl group as the nitrogen substituent are described.

Experimental

All chemicals were reagent grade, were used without further purification, and were received from the following chemical companies: amines and maltol (Sigma); $AlCl_3 \cdot 6H_2O$ (Anachemia); $Ga(NO_3)_3 \cdot 9H_2O$ (Johnson Matthey); $In(NO_3)_3 \cdot 5H_2O$ (Alfa). Melting points were measured with a Mel-Temp apparatus and are uncorrected. The reaction conditions, based on a one-pot synthesis (13), were the same for aluminum, gallium, and indium with any given ligand. Preparative details are given for the aluminum complexes; only reactant concentrations and yields are given for the corresponding gallium and indium complexes. All yields are based on metal complex trihydrates. Elemental analyses were performed by Mr. Peter Borda of this department on samples of anhydrates prepared from the hydrates by drying in vacuo at 80°C for 24 to 48 h (5). The pyrone conversion reaction was monitored by thin layer chromatography (TLC) on silica gel plates eluted with 5% methanol in methylene chloride. Optimum yields were obtained after 3 days. Infrared spectra were recorded on a PE 783 spectrophotometer and were referenced to polystyrene. For the Ga complexes, FAB-MS peaks were in the natural isotopic ratio of 3:2 ^{69}Ga to ^{71}Ga. ^1H NMR spectra were referenced to TMS. ^{27}Al NMR spectra were referenced to $Al(H_2O)^{3+}$.

*Tris(3-hydroxy-2-methyl-1-*n*-propyl-4-pyridinonato)aluminum(III)*, $Al(npp)_3$. $AlCl_3 \cdot 6H_2O$ (1.68 g, 6.95 mmol) and maltol (2.62 g, 20.7 mmol) were dissolved in distilled deionized water (50 mL). *n*-Propylamine (10.0 mL, 121 mmol) was added and the reaction mixture was stirred under nitrogen for 3 days, during which time a precipitate formed. The suspension was filtered, and recrystallization of the solid from hot water yielded a pale yellow–orange solid. This solid was then dissolved in a small volume of hot water and the volume reduced to 10 mL by heating at 70°C. This suspension was filtered while still hot, to give a pale yellow–orange coloured product. The yield was 2.59 g (64%), mp 300°C (dec). Infrared (cm^{-1}, KBr disk): 1610, 1560, 1520, 1495 ($\nu_{C=O}$ and ν_{ring}); 720, 580 (b), 470 (ν_{Al-O}). FAB-MS (*m/z*): 884 ± 1 ($M_2L_5^+$) (14), 526 (HML_3^+), 359 (ML_2^+). ^1H NMR (δ at 400 MHz in $CDCl_3$, atom numbering as in Fig. 1): 0.94 (t, 3H, C(9)H_3), 1.74 (sextet, 2H, C(8)H_2), 2.44 (s, 3H, C(1)H_3), 3.83 (t, 2H, C(7)H_2), 6.54 (d, 1H, C(5)H), 7.06 (d, 1H, C(6)H). ^{27}Al NMR ($CDCl_3$): 37 ppm ($W_{1/2}$ = 730 Hz). *Anal.* calcd for $C_{27}H_{36}AlN_3O_6$: C 61.70, H 6.90, N 8.00; found: C 62.00, H 7.01, N 7.97.

*Tris(3-hydroxy-2-methyl-1-*n*-propyl-4-pyridinonato)gallium(III)*, $Ga(npp)_3$. $Ga(NO_3)_3 \cdot 9H_2O$ (1.00 g, 2.39 mmol), maltol (0.91 g, 7.22 mmol), and *n*-propylamine (5.0 mL, 60.8 mmol) were used in water (50 mL). The yield was 1.17 g (78%), mp 290°C (dec). Infrared (cm^{-1}, KBr disk): 1600, 1550, 1510, 1485 ($\nu_{C=O}$ and ν_{ring}); 710, 570 (b), 410 (b), (ν_{Ga-O}). FAB-MS (*m/z*): 971 ± 2 ($M_2L_5^+$), 568, 570 (HML_3^+), 401, 403 (ML_2^+), 236 (ML^+). ^1H NMR (δ at 400 MHz in $CDCl_3$): 0.95 (t, 3H, C(9)H_3), 1.73 (sextet, 2H, C(8)H_2), 2.41 (s, 3H, C(1)H_3), 3.83 (t, 2H, C(7)H_2), 6.47 (d, 1H, C(5)H), 7.07 (d, 1H, C(6)H). *Anal.* calcd. for $C_{27}H_{36}GaN_3O_6$: C 57.06 H 6.38, N 7.39; found: C 57.17, H 6.44, N 7.52.

*Tris(3-hydroxy-2-methyl-1-*n*-propyl-4-pyridinonato)indium(III)*, $In(npp)_3$. $In(NO_3)_3 \cdot 5H_2O$ (1.00 g, 2.55 mmol), maltol (1.00 g, 7.93 mmol), and *n*-propylamine (5.0 mL, 60.8 mmol) were used in water (50 mL). The yield was 1.30 g (76%), mp 280°C (dec.). Infrared (cm^{-1}, KBr disk): 1600, 1540, 1500, 1485 ($\nu_{C=O}$ and ν_{ring}); 705, 555, <300 (ν_{In-O}). FAB-MS (*m/z*): 1062 ± 2 ($M_2L_5^+$), 614 (HML_3^+), 447 (ML_2^+), 281 (ML^+). ^1H NMR (δ at 400 MHz in $CDCl_3$): 0.91 (t, 3H, C(9)H_3), 1.71 (sextet, 2H, C(8)H_2), 2.46 (s, 3H, C(1)H_3), 3.84 (t, 2H, C(7)H_2), 6.53 (d, 1H, C(5)H), 7.06 (d, 1H, C(6)H). *Anal.* calcd. for $C_{27}H_{36}InN_3O_6$: C 52.87, H 5.92, N 6.85; found: C 52.45, H 5.85, N 6.70.

*Tris(1-*n*-butyl-3-hydroxy-2-methyl-4-pyridinonato)aluminum(III)*, $Al(nbp)_3$. $AlCl_3 \cdot 6H_2O$ (1.68 g, 6.96 mmol) and maltol (2.66 g, 21.1 mmol) were dissolved in distilled deionized water (50 mL). *n*-Butylamine (13.0 mL, 130 mmol) was added and the reaction mixture was stirred under nitrogen for 3 days, during which time a precipitate formed. The suspension was filtered, and recrystallization of the solid from hot water yielded a beige solid. This solid was then dissolved in a small volume of hot water and the volume reduced to 10 mL by heating at 70°C. This suspension was filtered while still hot, to give a beige coloured product. The yield was 2.37 g (55%), mp 180°C (dec.). Infrared (cm^{-1}, KBr disk): 1610, 1560, 1520, 1490 ($\nu_{C=O}$ and ν_{ring}); 720, 590 (b), 470 (b), (ν_{Al-O}). FAB-MS (*m/z*): 954 ± 1 ($M_2L_5^+$), 568 (HML_3^+), 387 (ML_2^+). ^1H NMR (δ at 400 MHz in $CDCl_3$): 0.96 (t, 3H, C(10)H_3), 1.37 (sextet, 2H, C(9)H_2), 1.69 (q, 2H, C(8)H_2), 2.44 (s, 3H, C(1)H_3), 3.86 (t, 2H, C(7)H_2), 6.48 (d, 1H, C(5)H), 7.07 (d, 1H, C(6)H). ^{27}Al NMR ($CDCl_3$): 37 ppm ($W_{1/2}$ = 920 Hz). *Anal.* calcd. for $C_{30}H_{42}AlN_3O_6$: C 63.48, H 7.46, N 7.40; found: C 63.41, H 7.55, N 7.51.

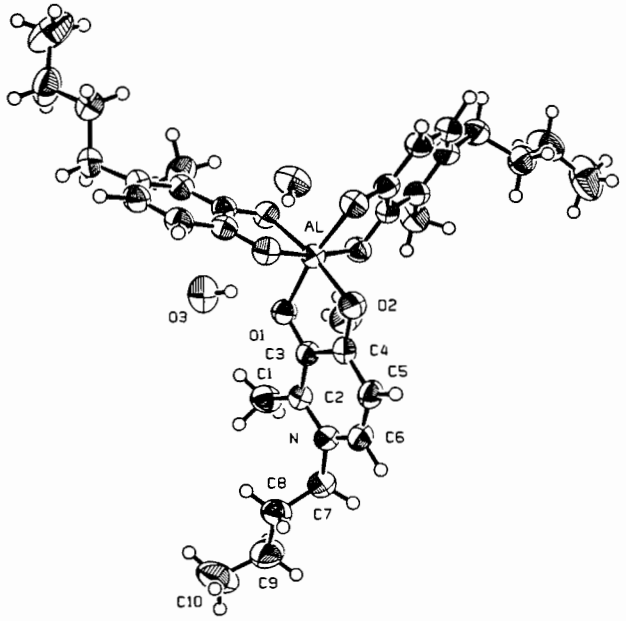


FIG. 1. ORTEP view of the $Al(nbp)_3 \cdot 3H_2O$ unit down the *c* axis.

*Tris(1-*n*-butyl-3-hydroxy-2-methyl-4-pyridinonato)gallium(III)*, $Ga(nbp)_3$. $Ga(NO_3)_3 \cdot 9H_2O$ (1.03 g, 2.47 mmol), maltol (0.93 g, 7.38 mmol), and *n*-butylamine (5.0 mL, 50 mmol) were used in water (50 mL). The yield was 1.19 g (73%), mp 170°C (dec). Infrared (cm^{-1}, KBr disk): 1605, 1550, 1510, 1485 ($\nu_{C=O}$ and ν_{ring}); 7.15, 570 (b), 410 (b), (ν_{Ga-O}). FAB-MS (*m/z*): 1040 ± 2 ($M_2L_5^+$), 610, 612 (HML_3^+), 429, 431 (ML_2^+), 250 (ML^+). ^1H NMR (δ at 400 MHz in $CDCl_3$): 0.96 (t, 3H, C(10)H_3), 1.36 (sextet, 2H, C(9)H_2), 1.69 (q, 2H, C(8)H_2), 2.44 (s, 3H, C(1)H_3), 3.86 (t, 2H, C(7)H_2), 6.53 (d, 1H, C(5)H), 7.06 (d, 1H, C(6)H). *Anal.* calcd. for $C_{30}H_{42}GaN_3O_6 \cdot 0.5H_2O$: C 58.17, H 7.00, N 6.78; found: C 57.93, H 6.84, N 6.45.

*Tris(1-*n*-butyl-3-hydroxy-2-methyl-4-pyridinonato)indium(III)*, $In(nbp)_3$. $In(NO_3)_3 \cdot 5H_2O$ (1.01 g, 2.59 mmol), maltol (1.09 g, 8.67 mmol), and *n*-butylamine (5.0 mL, 50 mmol) were used in water (50 mL). The yield was 1.60 g (87%), mp 255°C (dec). Infrared (cm^{-1}, KBr disk): 1600, 1540, 1500, 1490 ($\nu_{C=O}$ and ν_{ring}); 705, 555 (b), <300 (ν_{In-O}). FAB-MS (*m/z*): 1129 ± 2 ($M_2L_5^+$), 656 (HML_3^+), 475 (ML_2^+), 295 (ML^+). ^1H NMR spectrum (δ at 400 MHz in $CDCl_3$): 0.94 (t, 3H, C(10)H_3), 1.33 (sextet, 2H, C(9)H_2), 1.67 (q, 2H, C(8)H_2), 2.47 (s, 3H, C(1)H_3), 3.87 (t, 2H, C(7)H_2), 6.54 (d, 1H, C(5)H), 7.06 (d, 1H, C(6)H). *Anal.* calcd. for $C_{30}H_{42}InN_3O_6 \cdot 1.5H_2O$: C 52.79, H 6.64, N 6.16; found: C 52.91, H 6.37, N 6.11.

X-ray crystallographic analyses

Crystallographic data for $Al(nbp)_3 \cdot 3H_2O$, $Al(npp)_3 \cdot 3H_2O$, and $Ga(npp)_3 \cdot 3H_2O$ appear in Table 1. Data were collected in the unique volume of reciprocal space. Three standard reflections were selected on the basis of good intensity and spatial distribution from the reflections used to determine the orientation matrix. Their intensity and orientation

TABLE 1. Crystallographic data[a] for $Al(nbp)_3 \cdot 3H_2O$, $Al(npp)_3 \cdot 3H_2O$, and $Ga(npp)_3 \cdot 3H_2O$

Parameter	Value		
	$Al(nbp)_3 \cdot 3H_2O$	$Al(npp)_3 \cdot 3H_2O$	$Ga(npp)_3 \cdot 3H_2O$
Formula	$C_{30}H_{48}AlN_3O_9$	$C_{27}H_{42}AlN_3O_9$	$C_{27}H_{42}GaN_3O_9$
fw	621.7	525.6	622.36
Crystal system	Trigonal	Trigonal	Trigonal
Space group	$P\bar{3}$	$P\bar{3}$	$P\bar{3}$
a, Å	15.885 (1)	15.328 (1)	15.367 (2)
c, Å	7.280 (8)	7.231 (2)	7.256 (2)
V, Å^3	1591.0 (2)	1471.3 (4)	1484.0 (7)
Z	2	2	2
ρ_{calcd}, g cm^{-3}	1.30	1.19	1.39
$F(000)$	668	560	656
μ (Cu-K_α) (cm^{-1})	9.98	9.25	17.02
Crystal dimensions (mm)	0.15 × 0.15 × 0.30	0.15 × 0.15 × 0.40	0.25 × 0.25 × 0.50
Transmission factors	0.84–1.00	0.84–1.00	0.80–1.00
Scan range, deg in ω	0.94 + 0.30 tan θ	0.89 + 0.30 tan θ	0.80 + 0.20 tan θ
Scan speed, deg/min	8	32	32
$2\theta_{max}$ (deg)	156.5	155.1	155.3
Unique reflections	1994	2032	2032
Reflctns with $I \geq 3\ \sigma(I)$	1280	1377	1802
Number of variables	195	165	158
R	0.047	0.057	0.055
R_w	0.061	0.077	0.081
Max Δ/σ (final cycle)	0.01	0.01	0.01
Residual density, e/Å^3	0.15	0.44	0.66
p	0.05	0.05	0.04

[a]Temperature 21°C, Cu-K_α radiation (λ_{K_α} = 1.54178 Å), graphite-monochromated, ω–2θ scan, Rigaku AFC6S diffractometer, caclulations performed on a VAX-based TEXRAY system (Molecular Structure Corp.), $R = \Sigma||F_o| - |F_c||/\Sigma|F_o|$, $R_w = (\Sigma w(|F_o| - |F_c|)^2/\Sigma w F_o^2)^{1/2}$, $w = 4F_o^2/\sigma^2(F_o^2)$, $\sigma^2(F_o^2) = [S^2(C + R^2B) + (pF_o^2)^2]/L_p^2$ where S = scan rate, C, = peak count, R = scan time/background time, B = background count, L_p = Lorentz-polarization factor, p = p-factor, function minimized: $\Sigma w(|F_o| - |F_c|)^2$.

indicated that there was not any significant crystal decay or crystal movement.[2] The intensities of three standard reflections were essentially constant throughout data collections. The data were corrected for Lorentz and polarization effects, the space group ($P\bar{3}$, #147) was indicated by the E-statistics, the transmission factors for absorption correction were calculated, and the absorption correction was applied after data processing.

A three dimensional Patterson map was used to locate the metal atom (Al or Ga). The positions of all other non-hydrogen atoms were obtained from subsequent electron density difference Fourier maps. In all three structures, all hydrogen atoms were located and their positions and isotropic thermal parameters were refined. In the solution of the $Al(npp)_3 \cdot 3H_2O$ structure, the three hydrogen atoms on the methyl carbon of the n-propyl substituent were placed in calculated positions and their isotropic thermal parameters were fixed.

Further refinement of all parameters, including anisotropic temperature factors for all non-hydrogen atoms, was done by full-matrix least-squares methods and minimized with the function $\Sigma w(|F_o| - |F_c|)^2$. Neutral atom scattering factors were taken from ref. 15*a*. Anomalous disperson effects were included in F_{calcd} (16); the values for $\Delta f'$ and $\Delta f''$ were those of Cromer (ref. 15*b*). A correction for secondary extinction (17) was applied to $Al(nbp)_3 \cdot 3H_2O$ (coefficient = 0.29804 × 10^{-5}) as well as to $Ga(npp)_3 \cdot 3H_2O$ (coefficient = 0.47472 × 10^{-5}). Refinement was terminated when the maximum shift/error was less than 0.015 and there was only a small peak of residual electron density (Table 1).

[2]TEXSAN/TEXRAY structure analysis package was used. This includes versions of the following: DIRDIF, direct methods for difference structures, by P. T. Beurskens; ORFLS, full-matrix least-squares, and ORFFE, function and errors, by W. R. Busing, K. O. Martin, and H. A. Levy; ORTEP II, illustrations, by C. K. Johnson.

Atomic positional parameters and equivalent isotropic thermal parameters are given in Table 2. Selected bond distances, angles, and hydrogen-bonding data are given in Tables 3, 4, and 5, respectively. Anisotropic thermal parameters, intramolecular bond lengths and angles involving hydrogen, least squares planes, and torsion angles for the three compounds are included as supplementary material as are tables of observed and calculated structure factor amplitudes for each of the three compounds.[3]

Results and discussion

The one-pot reaction which was originally successful with methylamine (13) and ethylamine (13) also works with n-propylamine, and n-butylamine. Attempts to synthesize the i-propylamine and t-butylamine analogues of the tris(3-hydroxy-2-methyl-4-pyridinone)metal(III) complexes were unsuccessful, however. Several solvent systems were tried, but tris(maltolato)metal(III) products (14) were isolated. The basicities of all six of these amines are comparable (pK_a about 10.6 (18)) so steric bulk at nitrogen likely determines the yield; each of the successful syntheses involves a linear primary amine. Steric factors must retard the conversion reaction with branched amines. An extensive study on the conversion reaction for the uncomplexed ligands concluded that more basic and less hindered amines gave the greatest yields of 4-pyridinones (19).

The first crystal suitable for crystallographic analysis formed from a dilute aqueous solution of the $Al(nbp)_3$ complex. The

[3]These may be purchased from the Depository of Unpublished Data, Document Delivery, CISTI, National Research Council of Canada, Ottawa, Ont., Canada, K1A 0S2.

Can. J. Chem. Downloaded from www.nrcresearchpress.com by 198.100.157.202 on 09/07/12
For personal use only.

Can. J. Chem. Downloaded from www.nrcresearchpress.com by 198.100.157.202 on 09/07/12
For personal use only.

TABLE 2. Final atomic positional and equivalent isotropic thermal parameters, B_{eq} for $Al(nbp)_3 \cdot 3H_2O$, $Al(npp)_3 \cdot 3H_2O$, and $Ga(npp)_3 \cdot 3H_2O$ with estimated standard deviations in parentheses

Atom	x	y	z	B_{eq} (Å^2)
	$Al(nbp)_3 \cdot 3H_2O$, $C_{30}H_{48}AlN_3O_9$			
Al	2/3	1/3	0.4392(2)	3.40(3)
O(1)	0.7076(1)	0.2623(1)	0.5879(2)	3.95(6)
O(2)	0.6149(1)	0.2204(1)	0.2844(3)	4.15(7)
O(3)	0.8294(2)	0.3628(2)	0.9260(4)	6.4(1)
N	0.6335(2)	0.0074(2)	0.5549(3)	4.20(8)
C(1)	0.7207(3)	0.1205(3)	0.8141(5)	5.3(1)
C(2)	0.6750(2)	0.0995(2)	0.6287(4)	3.9(1)
C(3)	0.6705(2)	0.1714(2)	0.5300(4)	3.58(8)
C(4)	0.6216(2)	0.1498(2)	0.3593(4)	3.77(9)
C(5)	0.5829(2)	0.0559(2)	0.2876(4)	4.2(1)
C(6)	0.5904(2)	−0.0128(2)	0.3895(5)	4.5(1)
C(7)	0.6316(2)	−0.0738(2)	0.6582(5)	5.0(1)
C(8)	0.7274(3)	−0.0723(3)	0.6464(6)	5.4(1)
C(9)	0.7323(4)	−0.1439(3)	0.7751(8)	7.4(2)
C(10)	0.8327(6)	−0.1321(6)	0.787(1)	10.0(3)
H(1B)	0.722(4)	0.189(4)	0.820(7)	9(1)
H(1C)	0.684(4)	0.078(4)	0.911(8)	11(2)
H(1A)	0.777(5)	0.105(5)	0.815(8)	12(2)
H(3B)	0.782(4)	0.341(4)	0.848(8)	9(2)
H(3A)	0.812(4)	0.368(4)	1.04(1)	11(2)
H(5)	0.552(2)	0.040(2)	0.167(4)	4.4(6)
H(6)	0.557(3)	−0.085(3)	0.354(5)	5.6(8)
H(7A)	0.609(2)	−0.072(2)	0.786(5)	5.2(7)
H(7B)	0.578(2)	−0.133(2)	0.599(4)	4.4(6)
H(8B)	0.784(3)	−0.006(2)	0.673(5)	5.6(8)
H(8A)	0.735(3)	−0.091(3)	0.497(5)	7(1)
H(9A)	0.711(4)	−0.135(3)	0.921(6)	9(1)
H(9B)	0.677(4)	−0.210(4)	0.749(7)	10(1)
H(10C)	0.825(5)	−0.193(4)	0.83(1)	12(2)
H(10B)	0.884(5)	−0.063(5)	0.84(1)	14(2)
H(10A)	0.856(5)	−0.135(5)	0.64(1)	16(3)
	$Al(npp)_3 \cdot 3H_2O$, $C_{27}H_{42}AlN_3O_9$			
Al	2/3	1/3	0.4608(2)	3.56(4)
O(1)	0.7114(2)	0.2623(1)	0.6107(3)	3.89(8)
O(2)	0.6149(2)	0.2160(2)	0.3055(3)	4.12(8)
O(3)	0.8386(2)	0.3702(2)	0.9450(4)	5.9(1)
N	0.6426(2)	0.0005(2)	0.5795(4)	4.2(1)
C(1)	0.7317(4)	0.1194(4)	0.8388(6)	5.2(2)
C(2)	0.6841(2)	0.0964(2)	0.6538(4)	4.0(1)
C(3)	0.6751(2)	0.1683(2)	0.5529(4)	3.6(1)
C(4)	0.6241(2)	0.1442(2)	0.3817(4)	3.7(1)
C(5)	0.5871(2)	0.0477(2)	0.3104(5)	4.1(1)
C(6)	0.5980(2)	−0.0216(2)	0.4135(5)	4.4(1)
C(7)	0.6499(3)	−0.0792(3)	0.6805(7)	5.1(2)
C(8)	0.7524(4)	−0.0716(4)	0.6436(7)	6.6(2)
C(9)	0.7753(4)	−0.1320(4)	0.7753(8)	8.3(3)
H(1A)	0.699(3)	0.081(4)	0.931(7)	7(1)
H(1B)	0.795(4)	0.131(4)	0.829(7)	11(2)
H(1C)	0.745(4)	0.184(5)	0.886(7)	10(1)
H(3A)	0.811(3)	0.375(3)	1.059(6)	7(1)
H(3B)	0.798(4)	0.352(4)	0.856(8)	9(2)
H(5)	0.550(2)	0.026(2)	0.191(4)	4.0(7)
H(6)	0.575(3)	−0.089(3)	0.381(5)	6(1)
H(7A)	0.643(3)	−0.071(3)	0.815(6)	5.2(9)
H(7B)	0.590(3)	−0.144(3)	0.625(5)	5.4(8)
H(8A)	0.760(3)	−0.083(3)	0.518(6)	7(1)
H(8B)	0.814(4)	−0.008(4)	0.693(6)	8(1)
H(9A)	0.7196	−0.2019	0.7755	10.0
H(9B)	0.8375	−0.1304	0.7373	10.0
H(9C)	0.7839	−0.1037	0.8999	10.0

TABLE 2 (*concluded*)

Atom	x	y	z	B_{eq} (Å^2)
	$Ga(npp)_3 \cdot 3H_2O$, $C_{27}H_{42}GaN_3O_9$			
Ga	2/3	1/3	0.46383(7)	3.31(2)
O1	0.7113(2)	0.2583(2)	0.6189(3)	3.70(7)
O2	0.6156(2)	0.2115(2)	0.3034(3)	3.93(7)
O3	0.5274(3)	0.1592(2)	0.9470(4)	5.8(1)
N	0.6419(2)	−0.0026(2)	0.5847(4)	4.0(1)
C1	0.7287(4)	0.1148(3)	0.8429(6)	5.0(1)
C2	0.6816(2)	0.0922(2)	0.6579(4)	3.7(1)
C3	0.6744(2)	0.1645(2)	0.5586(4)	3.4(1)
C4	0.6242(2)	0.1409(2)	0.3843(4)	3.5(1)
C5	0.5879(2)	0.0446(2)	0.3140(4)	4.0(1)
C6	0.5971(2)	−0.0247(3)	0.4154(5)	4.2(1)
C7	0.6502(3)	−0.0819(3)	0.6827(6)	5.0(1)
C8	0.7522(4)	−0.0740(4)	0.6463(7)	6.7(2)
C9	0.7769(5)	−0.1324(5)	0.7728(9)	8.1(3)
H1A	0.731(5)	0.163(5)	0.898(8)	10(2)
H1B	0.774(4)	0.106(3)	0.842(6)	6(1)
H1C	0.695(3)	0.074(3)	0.940(6)	5(1)
H3A	0.557(3)	0.176(3)	1.024(6)	5(1)
H3B	0.541(4)	0.199(4)	0.858(7)	7(1)
H5	0.559(3)	0.026(3)	0.195(6)	5.0(9)
H6	0.571(2)	−0.088(3)	0.371(4)	3.7(7)
H7A	0.609(4)	−0.130(3)	0.630(6)	7(1)
H7B	0.636(3)	−0.076(3)	0.800(5)	4.0(8)
H8A	0.7517	−0.0976	0.5207	8.1
H8B	0.8044	−0.0032	0.6567	8.1
H9A	0.7815	−0.1072	0.8986	9.7
H9B	0.8415	−0.1258	0.7374	9.7
H9C	0.7243	−0.2032	0.7672	9.7

TABLE 3. Selected bond lengths (Å) for $Al(nbp)_3 \cdot 3H_2O$, $Al(npp)_3 \cdot 3H_2O$, and $Ga(npp)_3 \cdot 3H_2O$ with estimated standard deviations in parentheses

Bond	Length (Å)		
	$Al(nbp)_3 \cdot 3H_2O$	$Al(npp)_3 \cdot 3H_2O$	$Ga(npp)_3 \cdot 3H_2O$
M —O(1)	1.898(2)	1.887(2)	1.965(2)
M —O(2)	1.921(2)	1.921(2)	2.002(2)
O(1)—C(3)	1.326(3)	1.326(3)	1.332(3)
O(2)—C(4)	1.298(3)	1.301(4)	1.297(4)
N —C(2)	1.378(3)	1.385(4)	1.374(4)
N —C(6)	1.342(4)	1.339(5)	1.365(4)
N —C(7)	1.481(4)	1.475(4)	1.471(4)
C(1)—C(2)	1.489(4)	1.480(5)	1.482(5)
C(2)—C(3)	1.382(4)	1.385(4)	1.375(4)
C(3)—C(4)	1.414(4)	1.411(4)	1.430(4)
C(4)—C(5)	1.400(4)	1.392(4)	1.391(4)
C(5)—C(6)	1.372(5)	1.375(5)	1.360(5)
C(7)—C(8)	1.513(5)	1.540(6)	1.533(6)
C(8)—C(9)	1.505(5)	1.488(6)	1.460(6)
C(9)—C(10)	1.511(9)		

unit cell parameters indicated that the exoclathrate water network had been perturbed by the larger butyl group. The complex crystallized in the same space group as the exoclathrates, $P\bar{3}$; however, the length of the *a* axis (15.885 (1) Å) was almost 1 Å shorter than the corresponding axis for the N—CH_3 $Al(dpp)_3$ complex (16.600(2) Å (4, 5)). The empirical formula proved to be $Al(nbp)_3 \cdot 3H_2O$, a trihydrate. X-ray quality crystals of both $Al(npp)_3$ and $Ga(npp)_3$ were subsequently produced from dilute

TABLE 4. Selected bond angles (deg) for $Al(nbp)_3 \cdot 3H_2O$, $Al(npp)_3 \cdot 3H_2O$, and $Ga(npp)_3 \cdot 3H_2O$ with estimated standard deviations in parentheses

Bonds	Angle (deg)		
	$Al(nbp)_3 \cdot 3H_2O$	$Al(npp)_3 \cdot 3H_2O$	$Ga(npp)_3 \cdot 3H_2O$
O(1)—M—O(2)	83.83(9)	83.74(9)	82.72(9)
O(1)—M—O(1)′	90.7(1)	90.5(1)	90.45(8)
O(1)—M—O(2)′	97.14(9)	97.27(9)	98.39(9)
O(2)—M—O(1)′*trans*	170.49(7)	171.06(9)	168.84(8)
O(2)—M—O(2)′	89.1(1)	89.5(1)	89.62(9)
M—O(1)—C(3)	111.6(2)	111.8(2)	111.2(2)
M—O(2)—C(4)	112.3(2)	112.1(2)	111.3(2)
C(2)—N—C(6)	121.3(2)	121.4(3)	120.9(3)
C(2)—N—C(7)	121.2(3)	120.2(3)	121.0(3)
C(6)—N—C(7)	117.5(3)	118.4(3)	118.1(3)
N—C(2)—C(1)	120.9(3)	120.9(3)	120.3(3)
N—C(2)—C(3)	118.7(3)	117.7(3)	118.8(3)
C(1)—C(2)—C(3)	120.4(3)	121.3(3)	120.8(3)
O(1)—C(3)—C(2)	123.8(2)	122.9(3)	122.7(3)
O(1)—C(3)—C(4)	115.8(2)	116.0(3)	116.7(2)
C(2)—C(3)—C(4)	120.4(2)	121.1(3)	120.6(3)
O(2)—C(4)—C(3)	115.6(2)	115.5(3)	117.1(3)
O(2)—C(4)—C(5)	125.6(2)	125.7(3)	124.7(3)
C(3)—C(4)—C(5)	118.8(2)	118.8(3)	118.2(3)
C(4)—C(5)—C(6)	118.6(3)	118.6(3)	119.4(3)
N—C(6)—C(5)	122.1(3)	122.3(3)	121.9(3)
N—C(7)—C(8)	112.1(3)	110.4(3)	111.0(3)
C(7)—C(8)—C(9)	112.6(4)	113.0(4)	114.4(4)
C(8)—C(9)—C(10)	113.0(5)		

TABLE 5. Hydrogen-bonding distances and angles for $Al(nbp)_3 \cdot 3H_2O$, $Al(npp)_3 \cdot 3H_2O$, and $Ga(npp)_3 \cdot 3H_2O$ with estimated standard deviations in parentheses

Complex	Bond (Å)			Angle (deg)
	O···O	O—H	H···O	O—H···O
$Al(nbp)_3 \cdot 3H_2O$	O3···O2 2.844(4)	O3—H3A 0.88(7)	H3A···O2 1.97(7)	O3—H3A···O2 176(6)
	O3···O1 3.044(4)	O3—H3B 0.85(5)	H3B···O1 2.25(5)	O3—H3B···O1 152(5)
$Al(npp)_3 \cdot 3H_2O$	O3···O2 2.839(4)	O3—H3A 0.94(5)	H3A···O2 1.91(5)	O3—H3A···O2 168(4)
	O3···O1 3.026(4)	O3—H3B 0.84(5)	H3B···O1 2.23(6)	O3—H3B···O1 158(5)
$Ga(npp)_3 \cdot 3H_2O$	O3···O2 2.843(4)	O3—H3A 0.68(4)	H3A···O2 2.17(4)	O3—H3A···O2 166(5)
	O3···O1 3.019(4)	O3—H3B 0.84(5)	H3B···O1 2.19(5)	O3—H3B···O1 170(5)

aqueous solutions and these too were trihydrates $M(npp)_3 \cdot 3H_2O$. This suggested that the steric requirements of the exoclathrate structure were greater than originally expected; addition of a single methylene unit to the alkyl nitrogen substituent was sufficient to completely disrupt the water network. The three compounds were isostructural (the $Al(nbp)_3 \cdot 3H_2O$ complex with one more methylene group in the nitrogen substituent than the other two complexes). The structures can therefore be discussed concurrently.

The crystallographically imposed symmetry ($Z = 2$ in $P\bar{3}$) of the *fac* isomer results in an asymmetric unit consisting of 1/3 of a metal ion, one ligand, and one water molecule (Fig. 1). Although the water molecule does not coordinate the metal atom, hydrogen bonding interactions with the chelating oxygen atoms do make an important contribution to the lattice. The threefold symmetry about the central metal atom is common to all of the tris(*N*-substituted-3-hydroxy-2-methyl-4-pyridinonato)metal(III) complexes, including the exoclathrates (4–8).

Can. J. Chem. Downloaded from www.nrcresearchpress.com by 198.100.157.202 on 09/07/12
For personal use only.

Can. J. Chem. Downloaded from www.nrcresearchpress.com by 198.100.157.202 on 09/07/12
For personal use only.

Comparisons of these three new structures with the exoclathrates can be made since the atomic labelling system for the trihydrates is consistent with the labelling for the exoclathrates.

Distortions from true octahedral geometry around the metal atom are evinced by the metal–oxygen bond lengths and oxygen–metal–oxygen bond angles (Tables 3 and 4). The M—O(1) bond lengths are consistently shorter than the M—O(2) bond lengths. Not surprisingly, despite partial delocalization of the carbonyl formal double bond at O(2), the deprotonated 3-hydroxy oxygen atom O(1) tends to form a stronger bond with the central metal atom.

Examination of the packing arrangement (which will be discussed in detail later) reveals that the distance between these *fac* tris-ligand metal units is largely determined by the single water molecule O(3) of the asymmetric unit. Hydrogen bonds to this water molecule join the chelating oxygen atom O(1) in one unit cell to a second chelating oxygen atom O(2) in a neighbouring unit cell. This hydrogen bonding network parallels the *c* axis (the C_3 or 3 axis). The lengths of these hydrogen bonds do not vary significantly among the three structures (Table 5), indicating that the tris-ligand metal complex must distort in order to be accommodated by the pocket in the hydrogen bonding network. Similar but stronger distortions are observed in the exoclathrate complexes, in which the hydrogen bonds are shorter and more numerous: compare *c* for $Al(npp)_3 \cdot 3H_2O$ (7.231(2) Å) with that for $Al(mepp)_3 \cdot 12H_2O$ (6.827(1) Å) (5). There is a compression along the 3 axis, a twisting of the chelate plane, and further distortion from true octahedral geometry.

The compression along the 3 axis is seen in the compressed O(1)—M—O(2) bond angles; they are significantly less than 90° (Table 4). Among these three complexes, this compression is greatest for $Ga(npp)_3 \cdot 3H_2O$, where the O(1)—M—O(2) bond angle reaches a minimum value of 82.72 (9)°. Comparison with the exoclathrate structures shows that this O(1)—M—O(2) bond angle is smaller only in $In(dpp)_3 \cdot 12H_2O$ (77.87(6)°) (6). The decrease in the O(1)—M—O(2) bond angle is accompanied by a related increase in the exocyclic O(1)—M—O(2)′ bond angle. This increase is accordingly greater for the Ga complex than for the two Al complexes (Table 4). The exocyclic O(1)—M—O(1)′ and O(2)—M—O(2)′ bond angles are close to the ideal values (90 ± 1°).

Chelation causes a compression in the interior angles of the chelate ring. Although the free ligands with *n*-propyl or *n*-butyl substituents were not synthesized, the structures of Hmpp (N—H) and Hdpp (N—CH_3) (20), as well as Hmepp (8) are known. The O(1)—C(3)—C(4) and O(2)—C(4)—C(3) angles in these uncomplexed ligands are within 1.3° of 120° (Table 4) but have decreased in both the Al and Ga complexes to ~115.7° (Table 4). These O—C—C bond angles are similar to the analogous angles in the exoclathrate structures.

The increased size of the metal ion is accompanied by a reduction in chelate ring strain, as evidenced by the degree of compression of the O—C—C bond angles. By this criterion, Ga best fits the npp^- anion, as it causes the least deviation from the free ligand values. The planarity of the chelate rings C(3)—O(1)—M—O(2)—C(4) varies in the opposite direction. Deviation from planarity of this chelate ring is greatest for the $Ga(npp)_3$ complex, in which the mean deviation from the plane is 0.051 Å, compared with 0.044 Å for $Al(npp)_3$ and 0.047 Å for $Al(nbp)_3$.

This buckling of the chelate ring, as well as the compression along the C_3 axis, actually increases directly with the ionic radius of the metal center. The effective six-coordinate ionic radius of gallium is 0.620 Å, while that of aluminum is 0.535 Å (12). The increased buckling of the chelate ring (mean deviation from the chelate plane), as well as the compression along the 3 axis (compression of the O(1)—M—O(2) bond angle), in the Ga complex is due to its larger ionic radius. Indium has an effective six-coordinate ionic radius of 0.800 Å, thus $In(dpp)_3 \cdot 12H_2O$ complex has a smaller O(1)—M—O(2) bond angle than its Ga analogue.

The delocalization in the C—O bonds is directly related to the difference between the O(1)—C(3) and O(2)—C(4) bond lengths. This difference is 0.025 Å for $Al(npp)_3 \cdot 3H_2O$, 0.028 Å for $Al(nbp)_3 \cdot 3H_2O$, and 0.035 Å for $Ga(npp)_3 \cdot 3H_2O$, indicating that the delocalization in the C—O bonds is slightly greater in the Al complexes than in the Ga complex (Table 3). The extent of delocalization is clearly seen by comparing bond lengths with the related dihydroxy ligands, the catechols. The average C—O distance (calculated from a number of different metal complexes) is 1.36 Å for the catecholate anion and 1.29 Å for the delocalized semiquinone radical anion (21). The O(1)—C(3) bonds are significantly shorter (mean bond length = 1.328(7) Å) than the catecholate bond, and the O(2)—C(4) bonds are the same length (mean bond length = 1.299(6) Å) as the semiquinone bond (within the estimated standard deviation). The same trend was observed for the exoclathrate complexes.

In each complex the pyridinone ring is slightly nonplanar, the distortion being toward an N—C(4) boat for all three structures. The maximum deviation from the mean plane is 0.019(3) Å for each of the trihydrate structures. There are no significant differences in the ring bond lengths between $Al(nbp)_3 \cdot 3H_2O$, $Al(npp)_3 \cdot 3H_2O$, and $Ga(npp)_3 \cdot 3H_2O$ (Table 3). There are also no significant differences in the ring bond angles between the three complexes (Table 4). These ring bond lengths and bond angles are comparable to those found in the exoclathrate structures, indicating that there is no significant difference in double bond delocalization within the ring between these structures.

Crystal packing forces, which favour the minimum energy lattice, are similar for all three trihydrates. $Al(nbp)_3 \cdot 3H_2O$, $Al(npp)_3 \cdot 3H_2O$, and $Ga(npp)_3 \cdot 3H_2O$ all crystallize in the trigonal space group $P\bar{3}$. This is the same space group found for the exoclathrates, which means that the trihydrates are isomorphous with the dodecahydrates.

There are two tris-ligand metal units in the unit cell, and three lattice water molecules per metal complex molecule. Figure 2 shows a view of the packing of the unit cell of $Al(nbp)_3 \cdot 3H_2O$. $Al(npp)_3 \cdot 3H_2O$ and $Ga(npp)_3 \cdot 3H_2O$ pack similarly, the only difference being one less methylene group in the nitrogen substituent. The ligand contains non-polar hydrophobic *N*-substituents (*n*-propyl or *n*-butyl). The complexes crystallized such that hydrophobic layers of *N*-substituted pyridinone rings alternated with hydrophilic layers of water molecules.

The packing of these tris-ligand metal units is different from that of the previous exoclathrate structures. An important feature of the exoclathrate unit cell is the neat tucking of the hydrophobic ring substituents (the methyl and ethyl groups) into the center core of the unit cell, with the hexagonal water channels at each corner. The C(2) methyl substituents in the exoclathrates are not nearly as crowded toward the center of the unit cell as they may at first appear, one of these methyl groups points up the *c* axis, while the other points down (as they do in Fig. 2 as well). The hydrophobic ligands are completely enclosed by the ubiquitous water molecules in the exoclathrate. In the trihydrates, Fig. 2 reveals that there are no hexagonal water channels at the corners of the unit cell.

Can. J. Chem. Downloaded from www.nrcresearchpress.com by 198.100.157.202 on 09/07/12
For personal use only.

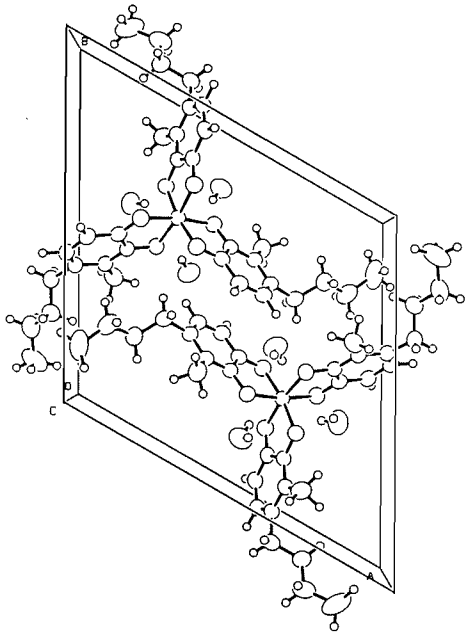


FIG. 2. ORTEP view of the unit cell packing in $Al(nbp)_3 \cdot 3H_2O$ down the *c* axis.

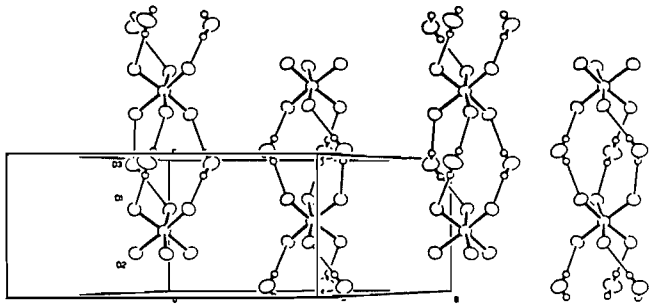


FIG. 3. ORTEP view of the hydrogen bonding network in $M(npp)_3 \cdot 3H_2O$ down the *a* axis; only the MO_6 octahedral coordination sphere and water O and H atoms are included (thick lines denote covalent bonds, thin lines denote hydrogen bonds).

The space between the hydrophobic ligand and the hydrophilic water fence in the exoclathrate appeared sufficient to accommodate one more methylene group. This is not the case, and the single extra methylene group of the *n*-propyl substituent precludes the formation of the extensive hexagonal water channels of the exoclathrates, resulting in a more conventional hydrogen bonding network. Despite the reduced number of water molecules in the unit cell, hydrogen bonding does increase the crystal lattice stability. The water molecules form an important hydrogen bonding network with the oxygen atoms which chelate the metal atom of the trihydrate crystal. Table 5 summarizes the bond distances and angles involved in this network. The oxygen atoms which chelate the metal atom in the trihydrate have no hydrogen atoms directly attached to them so they are hydrogen atom acceptors. The oxygen atoms of the water molecules are hydrogen atom donors.

The hydrogen bonding in the trihydrates is weaker than in the exoclathrates. In the trihydrates, the H···O and O···O distances are longer than in the exoclathrates. Comparison of the hydrogen bond distances and angles in Table 5 shows that there are

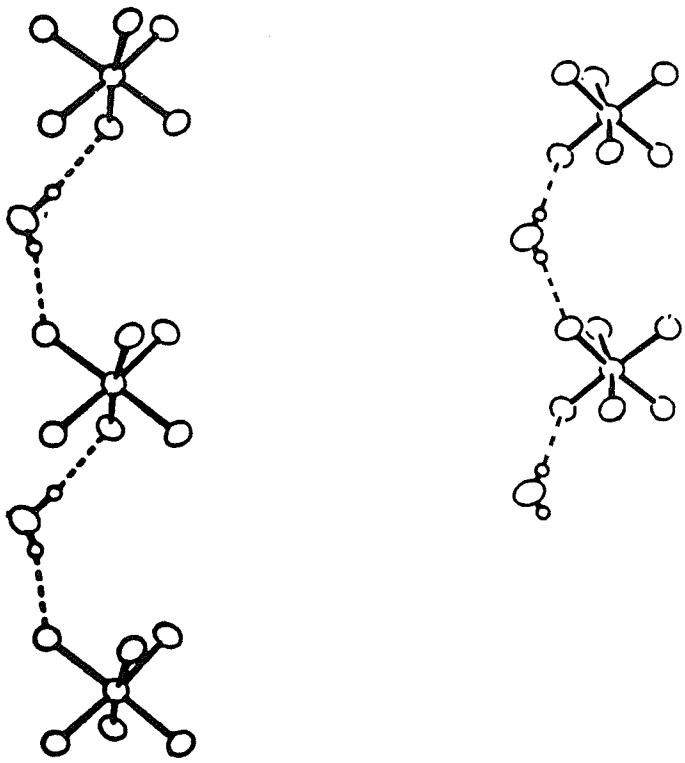


FIG. 4. ORTEP view of a part of the hydrogen bonding network of waters in $M(mepp)_3 \cdot 12H_2O$ (on the left, from ref. 8) and $M(npp)_3 \cdot 3H_2O$ (right). This view down the *a* axis shows the infinite chains of hydrogen bonds which occur down the *c* axis in both the exoclathrates and the trihydrates. Solid lines denote covalent bonds, while dashed lines denote hydrogen bonds.

no significant differences in the water network among the three trihydrate structures. The weaker hydrogen bonding is not surprising; in the trihydrates two or the three oxygen atoms involved in the water network are chelating a metal atom. A weak hydrogen bond, however, has an enthalpy of ca. 20 kJ mol^{-1}, so that even the less intricate hydrogen bonding network observed in the trihydrate structures will result in substantial stabilization of the lattice.

This (less unconventional) network is built up of water molecules which hydrogen bond chelating oxygen atoms in neighbouring unit cells. An ORTEP view of this network is given in Fig. 3. These water molecules form an infinite chain down the *c* axis. They join the hydroxy O(1) in one ligand to the carbonyl oxygen O(2) of a ligand rotated by 120° and translated by one unit cell. The O···H and O···O distances vary from 1.9 to 2.25 Å and from 2.84 to 3.04 Å respectively (Table 5). The chelating carbonyl O(2) consistently forms shorter and hence stronger O···H bonds than the chelating hydroxy O(1). This may reflect the delocalization of the formal double bond of the carbonyl C(4)—O(2). It is also consistent with the fact that O(1) forms stronger bonds with the metal atom than O(2) (M—O(1) is shorter than M—O(2)).

The structural differences between the trihydrates and the dodecahydrates are exaggerated by the increased complexity of the water network in the latter. The extended hydrogen bonding network of the exoclathrate can be reduced to that shown in Fig. 4 by removal of the hexagonal water rings (O(4), O(5)), as well as the bridging water molecules to which they are directly attached (O(6)). The hydrogen bonding network is thus simplified to an infinite chain down the *c* axis. The similarity to

the infinite chain of hydrogen bonded water molecules of the trihydrate structures is striking; in Fig. 4, comparison of the simplified exoclathrate and the trihydrate structures shows that in the former the essential features of the trihydrate are reproduced intact. In fact, all of these structures are isostructural, except that the exoclathrates have more hydrogen bonds to (and including) the hexagonal water channels to accommodate. Very recently, van der Helm and collaborators reported (22) at a conference the structures of the trihydrate complexes $M(mepp)_3 \cdot 3H_2O$ where M = Al, Ga, Fe; as reported, they are isostructural with the trihydrates reported here. These are a direct link to the exoclathrates since they involve one of the ligands characteristic of the exoclathrates *without* the dodecahydrate structure. We have been unable to prepare any hydrates of $M(dpp)_3$ or $M(mepp)_3$ except the dodecahydrates.

The tris(3-hydroxy-2-methyl-4-pyridinonato)metal complex could not distort sufficiently to allow the *N*–*n*-propyl substituent to be accommodated within the rigid hydrogen bonded exoclathrate lattice. The perturbation of the complicated, energetically favoured water network of the exoclathrates resulted in the retention of the infinite chain of hydrogen bonds down the *c* axis. The interactions between the larger tris-ligand metal molecules appear to take precedence over those between the smaller water molecules, and this helps to explain why the hydrogen bonding seen in the trihydrate structures is more conventional for inorganic hydrates.

Acknowledgement

We thank the NSERC of Canada and the U.S. Public Health Service (National Cancer Institute CA 48964) for operating grants.

1. P. O. Ganrot. Environ. Health Perspect. **65**, 363 (1986).
2. M. A. Green and M. J. Welch. Nucl. Med. Biol. **16**, 435 (1989).
3. R. L. Hayes and K. F. Hübner. Metal Ions Biol. Syst. **16**, 279 (1983).
4. W. O. Nelson, S. J. Rettig, and C. Orvig. J. Am. Chem. Soc. **109**, 4121 (1987).
5. W. O. Nelson, T. B. Karpishin, S. J. Rettig, and C. Orvig. Inorg. Chem. **27**, 1045 (1988).
6. C. A. Matsuba, W. O. Nelson, S. J. Rettig, and C. Orvig. Inorg. Chem. **27**, 3935 (1988).
7. J. Charalambous, A. Dodd, M. McPartlin, S. O. C. Matondo, N. D. Pathirana, and H. R. Powell. Polyhedron, **7**, 2235 (1988).
8. W. O. Nelson, S. J. Rettig, and C. Orvig. Inorg. Chem. **28**, 3153 (1989).
9. D. J. Clevette, D. M. Lyster, W. O. Nelson, T. Rihela, G. A. Webb, and C. Orvig. Inorg. Chem. **29**, 667 (1990).
10. D. J. Clevette and C. Orvig. Polyhedron, **9**, 151 (1990).
11. D. W. Peterson and H. A. Levy. Acta. Crystallogr. **10**, 70 (1957).
12. R. D. Shannon. Acta Crystallogr. A**32**, 751 (1976).
13. Z. Zhang, T. L. T. Hui, and C. Orvig. Can. J. Chem. **67**, 1708 (1989).
14. M. M. Finnegan, T. G. Lutz, W. O. Nelson, A. Smith, and C. Orvig. Inorg. Chem. **26**, 2171 (1987).
15. International tables for X-ray crystallography. Vol. IV. Kynoch press, Birmingham, UK. 1974. (Present distributer D. Reidel; Dordrecht, the Netherlands). (*a*) Table 2.2A; (*b*) Table 2.3.1.
16. J. A. Ibers and W. C. Hamilton. Acta Crystallogr. **17**, 781 (1964).
17. G. H. Stout and L. H. Jensen. X-ray structure determination: a practical guide. MacMillan, New York, NY. 1968. p. 411.
18. S. Patai. The chemistry of the amino group. Wiley, New York, NY. 1968. p. 174.
19. K. Heyns and G. Vogelsang. Chem. Ber. **87**, 1377 (1954).
20. W. O. Nelson, T. B. Karpishin, S. J. Rettig, and C. Orvig. Can. J. Chem. **66**, 123 (1988).
21. C. G. Pierpont and R. M. Buchanan. Coord. Chem. Rev. **38**, 45 (1981).
22. G. Xiao, D. van der Helm, R. C. Hider, and P. Dobbin. 40th Anniversary Meeting of the American Crystallographic Association, New Orleans, LA, April 1990. Abstract PL07.

Can. J. Chem. Downloaded from www.nrcresearchpress.com by 198.100.157.202 on 09/07/12
For personal use only.

Vibrational spectra of two new organic semiconductors: tetrathiafulvalene (TTF) and tetramethyltetraselenafulvalene (TMTSF) salts of paranitrophenylmalononitrile (PNMA)[1]

K. D. TRUONG AND A. D. BANDRAUK
Département de chimie, Université de Sherbrooke, Sherbrooke, Qué., Canada J1K 2R1

J. ZAUHAR
Collège Militaire Royal, St-Jean, Qué., Canada

AND

C. CARLONE
Département de Physique, Université de Sherbrooke, Sherbrooke, Qué., Canada J1K 2R1

Received May 22, 1990[2]

K. D. TRUONG, A. D. BANDRAUK, J. ZAUHAR, and C. CARLONE. Can. J. Chem. **69**, 901 (1991).

Two new complexes of stoichiometry 2:1 are reported for the donors tetrathiafulvalene (TTF) and tetramethyltetraselenafulvalene (TMTSF) with the acceptor paranitrophenylmalononitrile (PNPMA). Both compounds are semiconductors with a resistivity of about $4 \times 10^{-4}\ \Omega$ m for $(TMTSF)_2PNPMA$ and $0.58\ \Omega$ m for $(TTF)_2PNPMA$. The larger conductivity of the first complex can be attributed to the disorder of the PNPMA anions. Vibrational spectra were obtained by FTIR and Raman spectroscopy, in order to determine the degree of charge transfer in these systems. Both complexes have the electron distribution $(D^{+0.4})_2A^{-0.8}$. As a result the donors D stack in tetramerized units and exhibit vibronic activation of certain symmetric monomer modes, thus indicating the presence of strong electron–vibrational interactions in the donor stacks.

Key words: TTF and TMTSF salts, charge transfer complexes, IR and Raman spectra, degree of charge transfer, paranitrophenylmalononitrile (PNPMA).

K. D. TRUONG, A. D. BANDRAUK, J. ZAUHAR et C. CARLONE. Can. J. Chem. **69**, 901 (1991).

On a observé deux nouveaux complexes de stoechiométrie 2:1 pour les donneurs tétrathiafulvalène (TTF) et tétraméthyltétrasélénafulvalène (TMTSF) avec l'accepteur *p*-nitrophénylmalononitrile (PNPMA). Les deux composés sont des semiconducteurs dont la résistance est d'environ $4 \times 10^{-4}\ \Omega$ m pour le $(TMTSF)_2PNPMA$ et $0{,}58\ \Omega$ m pour le $(TTF)_2PNPMA$. On peut attribuer la conductivité plus grande du premier complexe au désordre des anions PNPMA. Les spectres de vibration ont été déterminés par IR-TF et par spectroscopie Raman pour évaluer le degré de transfert de charge dans ces systèmes. Les deux complexes ont une distribution électronique $(D^{+0,4})_2A^{-0,8}$. Il en résulte que les donneurs D s'entassent dans des unités tétramères et présentent de l'activation vibronique de certains modes monomères symétriques qui indiquent la présence de fortes interactions électron-vibrationnelle dans les entassements de donneurs.

Mots clés : sels de TTF et de TMTSF, complexes de transfert de charge; spectres IR et Raman, degré de transfert de charge, *p*-nitrophénylmalononitrile (PNPMA).

[Traduit par la rédaction]

Introduction

The organic conducting salts of tetramethyltetraselenafulvalene (TMTSF) of the type $(TMTSF)_2X$, called Bechgaard salts, have attracted great attention due to the discovery of superconductivity in these systems below 10 K, the rich variety of electronic and magnetic ground states depending on the anion present, the temperature, and the pressure (1–5). In such compounds one finds in the presence of nonsymmetric *inorganic* anions a high temperature metallic state which extends down in temperature to 100 K below which an anion ordering transition is observed.

In the previous work we investigated the influence of nonsymmetric organic anions on the conductivity of TMTSF and TTF salts (TTF = tetrathiafulvalene) (6). For that purpose we synthesized paranitrophenylmalononitrile (PNMA), an organic planar acceptor similar to the well known donor tetracyanoquinodimethane (TCNQ), except that one malononitrile group is replaced with a nitro group (see Fig. 1). Complexation with TTF and TMTSF results in complexes of stoichiometry D_2A, where D is the donor and A the acceptor. The donors form linear chains of tetramers (Fig. 1). In the TTF compound, the anions are ordered and form sheets perpendicular to the stacks, with an inversion center between pairs of anions. In the TMTSF compound, the donor stacking is similar but the anions are highly disordered (7). Both compounds are semiconductors with a room temperature resistivity of about $4 \times 10^{-4}\ \Omega$ m for $(TMTSF)_2PNPMA$ and $0.58\ \Omega$ m for the TTF salt. The much higher conductivity of the TMSTF was thus attributed to the random distribution of the anions (6).

In the TTF salt, the ordered distribution of the PNPMA ions creates an effective periodic perturbation on the electronic band of the conducting electrons in the donor chain. Assuming an oxidation state $D^{+1/2}$, the electronic band is 3/4 full. Thus any perturbation with a period 4a, i.e., four times the lattice spacing between the donors, will introduce a Peierls gap in the electronic spectrum, and the system will become semiconducting (8). As seen from Fig. 1, both the tetramerization of the TTF donor stack and the periodicity of the PNPMA anions produce such perturbations of periodicity 4a. In the TMSF compound, only the donor stacking is present; no ordering of the anions is found. In the present work, we report IR and Raman spectra of both the ordered and disordered compounds in order to establish the corresponding charge transfer states. We also present a simple model of electron–vibration couplings in the cation tetramers

[1]Contribution from le Groupe de Recherche sur les Semiconducteurs et Diélectriques, Faculté des Sciences, Université de Sherbrooke.

[2]Revision received December 27, 1990.

Can. J. Chem. Downloaded from www.nrcresearchpress.com by 198.100.157.202 on 09/07/12
For personal use only.

Can. J. Chem. Downloaded from www.nrcresearchpress.com by 198.100.157.202 on 09/07/12
For personal use only.

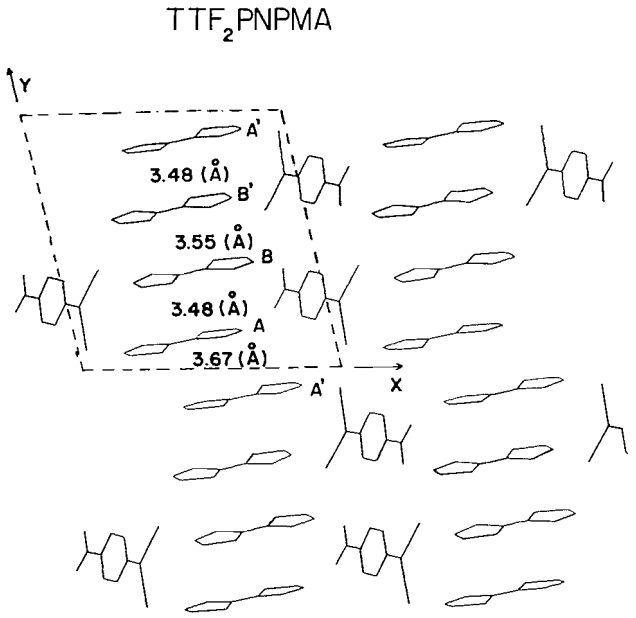


FIG. 1. Projection along (stacking) y axis of the sample $(TTF)_2$-PNPMA.

in terms of a tetramer molecular orbital description, i.e., a delocalized model, in order to explain the splittings observed in the spectra.

Experimental details

Single crystals of these complexes were prepared and described elsewhere (7). Chemical analysis showed 2:1 stoichiometry. Raman spectra were taken using a Jobin Yvon spectrometer equipped with holographic gratings and photon counting electronics. The excitation source was argon and krypton ion lasers operating with a power lower than 5 mW to avoid sample damage. Infrared absorption spectra were obtained using a FTIR spectrometer BOMEM model DA3; a cooled detector of Ge doped with Cu was used in the frequency range 400 to 4000 cm^{-1}. All infrared measurements were made on powder and low temperature spectra were obtained by thermally anchoring the sample to a controlled cold finger. The temperature was measured with Au–Chromel thermocouples with an accuracy of ± 3 K.

Electron-A_g mode coupling in a tetramer

The crystal structure of TTF_2PNPMA is triclinic (6). The separation along the TTF chains is not regular, but can be described as tetrameric, with quasiisolated tetramers ABBA. The AB, BB, and AA distances are respectively 3.48, 3.55, and 3.67 Å (Fig. 1). We will assume as a first approximation that we have a perfect tetramer AAAA and examine the possible electronic couplings to symmetric modes. In a dimer, it is well known that A_g modes of ions appear unchanged in frequency in the Raman spectrum, whereas these same modes can appear in the IR spectrum but are considerably shifted in frequency due to the interaction of the electron transfer with the A_g modes of the two molecules of the dimer (9–13).

We take a Hückel-type Hamiltonian for the electrons in the tetramer, including a first order coupling of electrons to a single symmetric vibration mode on each site. Such a model has been considered previously in the strong electron correlation limit, i.e., a valence bond model (Heitler London or Hubbard) (14). In the present case we shall examine the weak correlation limit for which a delocalized molecular orbital model is appropriate as in the dimer case (9–13). Our starting Hamiltonian neglecting electron correlation is therefore:

$$[1] \quad H_e = -t \sum_{i=1}^{3} [C_i^+ C_{i+1} + C_{i+1}^+ C_i]$$

$$[2] \quad H_{ev} = \sum_{i=1}^{4} Q_i C_i^+ C_i$$

$$[3] \quad H_V = \frac{1}{2\gamma^2} \sum_{i=1}^{4} (Q_i^2 + \omega_0^2 Q_i^2)$$

$C_i^+(C_i)$ is the creation (annihilation) operator for electron occupation of a molecular orbital on site i; t is the transfer (hopping integral) between two neighbouring site orbitals; $Q_i = \gamma q_i$, where q_i is a vibrational normal mode of a molecule at site i of frequency ω_0; $\gamma = \partial\epsilon/\partial q_i$ is the change in energy of a site molecular orbital due to change in the bond length of the mode q_i by the electron population $C_i^+ C_i$. γ is *nonzero* only for symmetric (A_g) modes. This interaction produces a change in the equilibrium bond length only, i.e., there is no frequency change from this linear perturbation (9–13). The last equation [3] represents the vibrational energy of the four independent site modes of frequency ω_0.

Diagonalization of the electronic energy, i.e. eq. [2] is achieved in terms of the *delocalized orbitals* for the tetramer which are linear combinations of the site molecular orbitals. Such a delocalized representation is obtained from the unitary transformation

$$[4] \quad C_i' = UC_i; \quad U = \begin{bmatrix} a & b & b & a \\ b & a & -a & -b \\ b & -a & -a & b \\ a & -b & b & -a \end{bmatrix}$$

where $a = 0.3718$, $b = 0.6015$ for a tetramer (15). Defining the new Hamiltonian $H' = U^+ H U$ in this delocalized basis, we obtain the following Hamiltonian matrix after transforming $H_e + H_{ev}$ (eqs. [2] and [3]), and defining dimer modes,

$$[5] \quad \begin{aligned} Q_{1g} &= Q_1 + Q_4, & Q_{2g} &= Q_2 + Q_3 \\ Q_{1u} &= Q_1 - Q_4, & Q_{2u} &= Q_2 - Q_3 \end{aligned}$$

$$[6] \quad H' = \begin{pmatrix} a^2Q_{1g} + b^2Q_{2g} + \epsilon_1 & ab(Q_{1u} + Q_{2u}) & ab(Q_{1g} - Q_{2g}) & a^2Q_{1u} - b^2Q_{2u} \\ ab(Q_{1u} + Q_{2u}) & a^2Q_{1g} + b^2Q_{2g} + \epsilon_2 & b^2Q_{1u} - a^2Q_{2u} & ab(Q_{1g} - Q_{2g}) \\ ab(Q_{1g} - Q_{2g}) & b^2Q_{1u} - a^2Q_{2u} & a^2Q_{1g} + b^2Q_{2g} + \epsilon_3 & ab(Q_{1u} + Q_{2u}) \\ a^2Q_{1u} - b^2Q_{2u} & ab(Q_{1g} - Q_{2g}) & ab(Q_{1u} + Q_{2u}) & a^2Q_{1g} + b^2Q_{2g} + \epsilon_4 \end{pmatrix}$$

TABLE 1. Infrared vibrational frequencies of $PNPMA^0$, $TMTSF^+$, $(TMTSF)_2PNPMA$, K^+PNPMA^-, TTF^+, and $(TTF)_2PNPMA$

$PNPMA^0$	$TMTSF^+$	$(TMTSF)_2PNPMA$			K^+PNPMA^-	TTF^+	$(TTF)_2PNPMA$		
ω (cm^{-1})	(20)	295 K	15 K	Assignment		(19)	295 K	15 K	Assignment
	1070		1067	TMTSF $b_{1u}\nu_{31}$		1068	1091	1091	TTF $b_{1u}\nu_{15}$
		1106	1106	TMTSF		1075	1096	1094	TTF
			1123	PNPMA	1117		1108	1110	PNPMA
		1184	1184	PNPMA	1189		1184	1185	PNPMA
							1249	1247	TTF
		1272	1270	PNPMA	1301	1237	1263	1264	TTF
1317							1269	1269	TTF
1347							1322	1348	$(TTF)_2^+$ $A_g\nu_3$
1361		1371	1366	PNPMA		1368		1357	$(TTF)_2^+$ $A_g\nu_3$
	1386		1385	TMTSF CH_3sym					
		1397	1389	TMTSF					
	1434	1424	1428	TMTSF CH_3asym		1416	1427	1429	TTF b_{1u}
							1458	1459	TTF
	1515	1519	1519	TMTSF $b_{1u}\nu_{28}$		1509	1504	1511	TTF
							1519	1519	TTF
1528		1581	1581	PNPMA	1597		1580	1582	PNPMA C=NO_2

where $\epsilon_1 = -1.618t$, $\epsilon_2 = -0.618t$, $\epsilon_3 = +0.618t$, $\epsilon_4 = +1.618t$.

We now examine two limit cases. The first case, $t \ll \langle Q_i \rangle$ would correspond to strong electron–vibrational coupling. In such a limit, taking $a = b = 1/2$ gives four *independent* vibrational normal modes for the tetramer:

[7] $$Q_{1g} + Q_{2g}, \quad Q_{1u} + Q_{2u}, \quad Q_{1g} - Q_{2g}, \quad Q_{1u} - Q_{2u}$$

Clearly, from the new Hamiltonian [6] one sees that the totally symmetric tetramer mode ($Q_{1g} + Q_{2g}$) would uncouple completely from the electron motion. Thus in the limit of large electron–vibrational coupling, this Raman-active, totally symmetric mode would undergo *no* frequency change as in the case of dimers. By symmetry, the second and fourth modes in eq. [7] are IR-active whereas the third would be Raman-active. All three would undergo frequency changes since they couple different electronic states.

The case $t \gg \langle Q_i \rangle$ is the limit which applies to our system, since new electronic bands appear below 600 nm in the visible spectrum of the complexes which cannot be ascribed to isolated molecular transitions (Fig. 2). Equation [6] shows that the four dimer modes described in eq. [5] have their frequency shifted from ω_0 as they are all involved in nondiagonal electronic couplings. Especially noteworthy is the fact that Q_{1g}, the in-phase vibration of the two outer molecules, and Q_{2g}, the in-phase vibration of the two inner molecules, produce the same bond length changes in all four energy levels of the tetramer. These bond length changes produce no frequency shifts.

We now apply second order perturbation theory to obtain the frequency shifts of each dimer mode in the tetramers. Thus for Q_{1g} and Q_{2g}, we obtain the effective potentials,

[8] $$V_g = \frac{(ab)^2}{\epsilon_1 - \epsilon_3}(Q_{1g}^2 + Q_{2g}^2) = \left(\frac{-0.02}{t}\right)(Q_{1g}^2 + Q_{2g}^2)$$

The frequency change $\Delta\omega_g = -0.02\gamma^2/t$, obtained by expanding to first order with respect to γ^2/t, is therefore *identical* for these two dimer modes, i.e. Q_{1g} and Q_{2g}, whose in-phase collective vibration is Raman active. Similar calculations for the other tetramer modes give

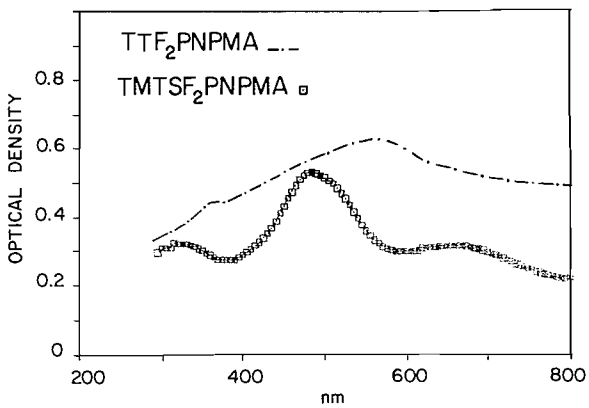


FIG. 2. Ultraviolet and visible absorption spectra of $(TMTSF)_2$-PNPMA and $(TTF)_2PNPMA$.

[9] $$\Delta\omega(Q_{1u}) = \frac{-0.05\gamma^2}{t}; \qquad \Delta\omega(Q_{2u}) = \frac{-0.1\gamma^2}{t}$$

for the two collective combinations, of out-of-phase IR-active dimer modes.

In conclusion, we have shown that one should expect in the spectra of tetramer stacks of ions, the following correlation: appearance of A_g modes in the Raman spectra at lower frequencies than the monomer ion; A_g modes in the IR spectrum are also displaced to lower frequencies but now split in two due to the two different collective dimer vibrations, Q_{1u} and Q_{2u} (eq. [5]). The ratios of the frequency shifts should occur in the order

[10] $$\Delta\omega_g{:}\Delta\omega_{1u}{:}\Delta\omega_{2u} = 1{:}2.5{:}5$$

Hence one expects A_g modes to appear as doublets in the IR but as single lines in the Raman. The IR lines should undergo larger frequency shifts than the Raman lines.

The present model assumes weak electron correlation, i.e., an independent particle model, so that optical properties depend on the delocalized tetramer molecular orbitals C' (eq. [4]). Another limiting model is the strong electronic correlation

Can. J. Chem. Downloaded from www.nrcresearchpress.com by 198.100.157.202 on 09/07/12
For personal use only.

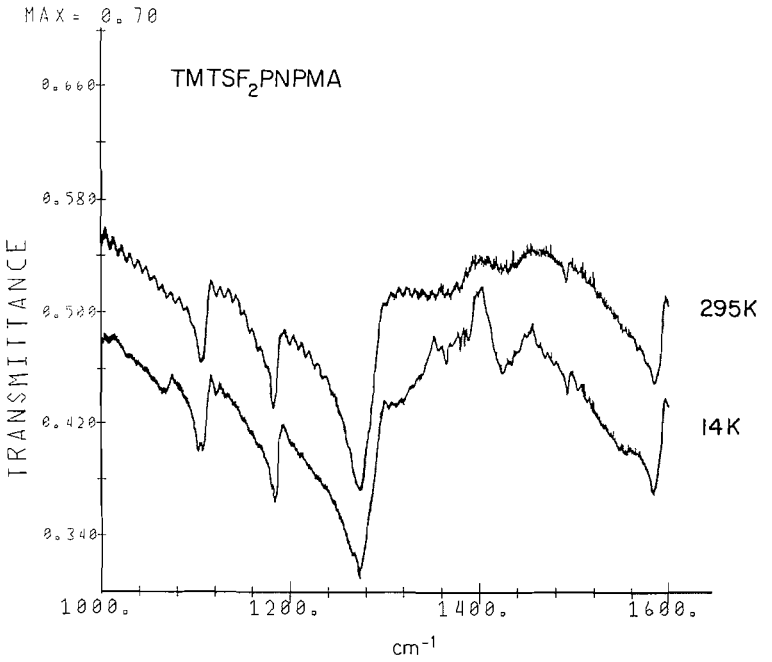


FIG. 3. Infrared spectra of $(TMTSF)_2PNPMA$ at 295 and 14 K.

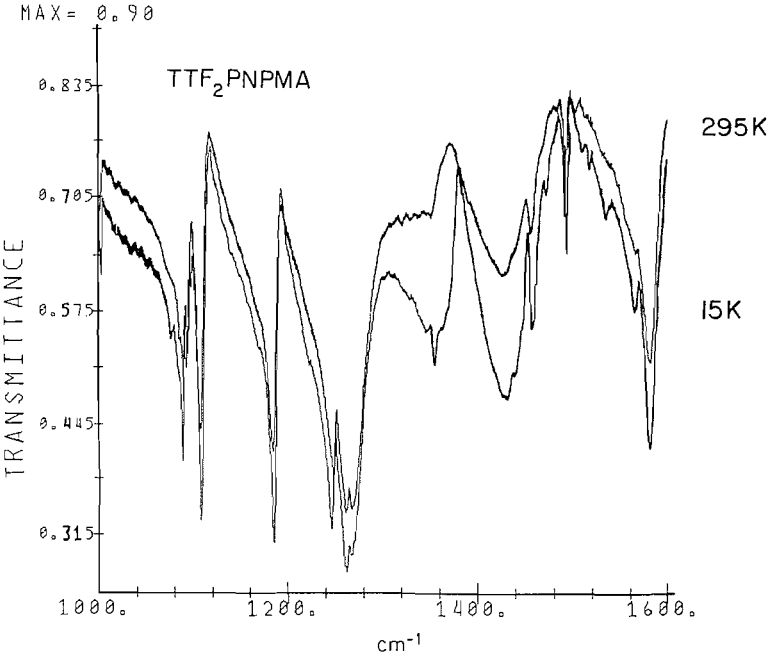


FIG. 4. Infrared spectra of $(TTF)_2PNPMA$ at 295 and 15 K.

valence bond model (Heitler–London or Hubbard), where the description is in terms of monomer, i.e., localized configurations (14). Such a localized model also predicts fine structure in the IR-active A_g modes but no analysis of the Raman-active modes has yet been performed in this strong correlation limit.

Results and discussions

Infrared absorption spectra of $(TMTSF)_2PNPMA$, $(TTF)_2$-PNPMA are presented in Figs. 3 and 4, respectively. Some large bands are observed between 1000 and 1600 cm^{-1} in both complexes. The infrared spectra of the neutral compounds $TMTSF^0$, TTF^0, and $PNPMA^5$ (Fig. 5) exhibit only sharp bands in that region. Broad bands are indicative of strong interaction between conduction electrons and molecular vibrations (9–13). In Table 1 we report the IR vibrational frequencies of $(TMTSF)_2PNPMA$, $(TTF)_2PNPMA$, and the individual ions. A detailed comparison of these frequencies permits us to determine the degree of charge transfer by establishing a pairwise correspondence between vibrational modes of the neutral, e.g., $PNPMA^0$ and the corresponding anion as in

Can. J. Chem. Downloaded from www.nrcresearchpress.com by 198.100.157.202 on 09/07/12
For personal use only.

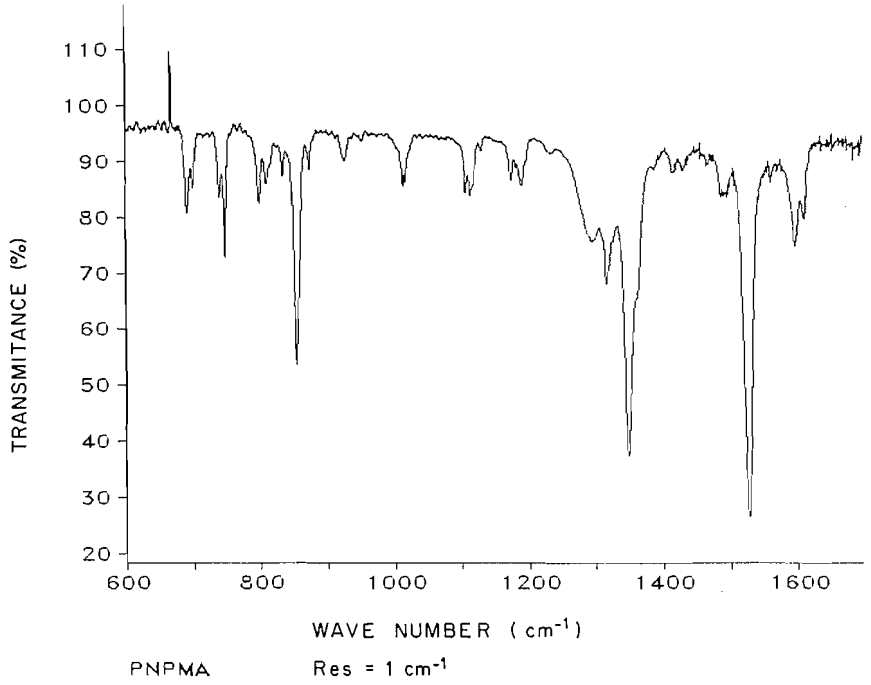


FIG. 5. Infrared spectrum of PNPMA at 295 K.

TABLE 2. Infrared vibrational frequency of C—NO_2 mode and degree of charge transfer ρ at 295 K

Species	ω (cm^{-1})	Δω	ρ
$PNPMA^0$	1528	0	0
K^+PNMA^-	1597	69	1
$(TMTSF)_2PNPMA$	1581	53	−0.8
$(TTF)_2PNPMA$	1580	52	−0.8

TABLE 3. Raman vibrational frequency of C=C mode in TMTSF and TTF and the degree of charge transfer ρ in $(TMTSF)_2PNPMA$ and $(TTF)_2PNPMA$ at 295 K

Species	ω (cm^{-1})	Δω	ρ
$TMTSF^0$	1539	0	0
$TMTSF^+$	1399	140	1
$(TMTSF)_2PNPMA$	1490	49	+0.4
$(TTF)^0$	1518	0	0
TTF^+	1420	98	1
$(TTF)_2PNPMA$	1479	39	+0.4

K^+PNPMA^-. The concept of ionization frequency shifts (Δν) linear with charge transfer is well established and has been applied to many electron donor as well as acceptor molecules. It can be used when the effective molecular configuration symmetry is retained upon ionization as in our complexes (16–18).

An estimate of the degree of charge ρ is best obtained from molecular vibrational frequencies which display the highest ionization shift. Comparing the neutral compound $PNPMA^0$ to the anion $PNPMA^-$, the frequency of the vibrational mode C—NO_2 is increased from 1528 to 1597 cm^{-1} (Table 2). We utilised the frequency shift of this vibrational mode to evaluate the partial charge on PNPMA in our complexes and the results are reported in Table 2. The degree of charge transfer is partial for the anion, i.e. (−0.8) for $(TMTSF)_2PNPMA$ and also for $(TTF)_2PNPMA$. It remains almost unchanged at 14 K. The most important new feature in going to lower temperatures is the growth of peaks in the region from 1350 to 1430 cm^{-1}. These can be attributed to A_g modes of the cations activated by the coupling of the conduction electrons to intramolecular vibrational modes (9–13). The mode at 1357 cm^{-1} of $(TTF)_2PNPMA$ is characterized as the vibronic intensity enhancement of the A_g ν_3 modes of the $(TTF^+)_2$ dimer observed previously in solution (19). The splitting of these bands at 1348, 1357 cm^{-1} can be explained by the presence of TTF tetramer inferred from X-ray data (Fig. 1) and the corresponding model described in the previous section.

To determine the degree of charge on the donors, Raman spectra are preferable since the excitation by Ar^+ and Kr^+ lasers produces Raman intensities which display a resonance character (Figs. 6, 7), thus allowing us to identify the C=C ν_3 vibrations. Furthermore, as shown in the previous section, Raman-active modes should show no splittings from the electron–vibration couplings inherent in these systems. From the neutral compound $TMTSF^0$ to the cation, the frequency of the C=C mode is shifted from 1539 to 1399 cm^{-1} (Table 3). We utilise the maximum frequency shift of this vibrational mode to estimate the charge on TMTSF in $(TMTSF)_2PNPMA$. The same approach was used to evaluate ρ of $(TTF)_2PNPMA$, and the results are reported in Table 3. Again the degree of charge transfer is partial (+0.4) for both $(TMTSF)_2PNPMA$ and $(TTF)_2PNPMA$.

In conclusion, we note that the fundamental difference between A_g modes in stacked dimers as opposed to tetramers in organic conductors is that in the former the frequency of A_g monomer modes remains unperturbed in the Raman spectra due to electron–vibration couplings. This enables one to use these

Can. J. Chem. Downloaded from www.nrcresearchpress.com by 198.100.157.202 on 09/07/12
For personal use only.

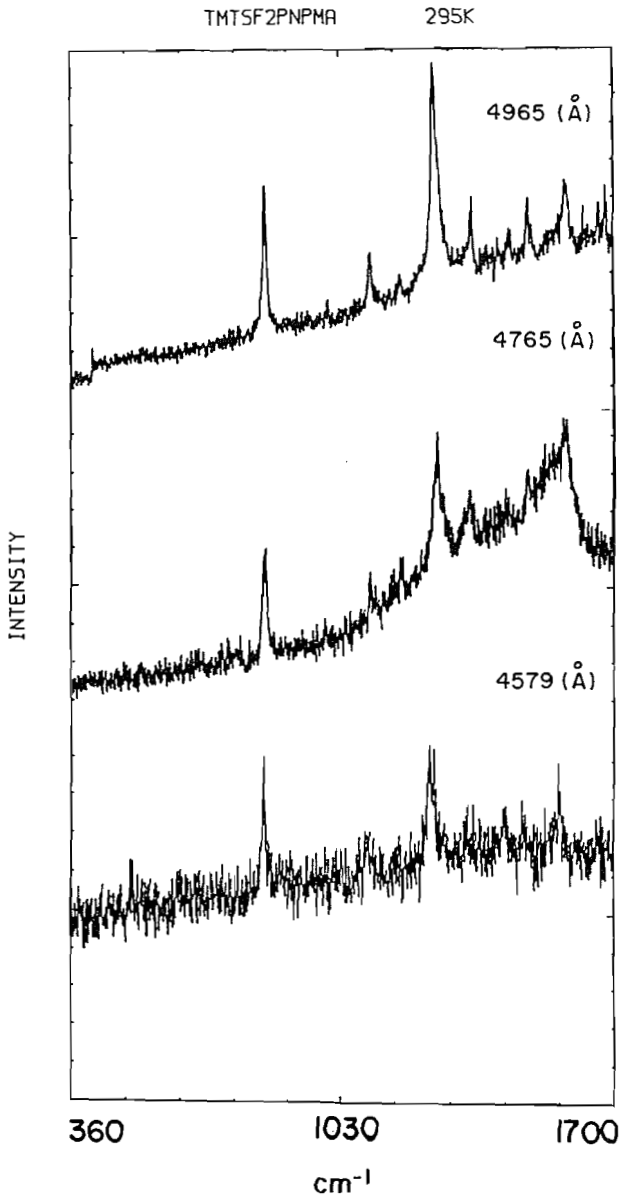


FIG. 6. Raman spectra of $(TMTSF)_2PNPMA$.

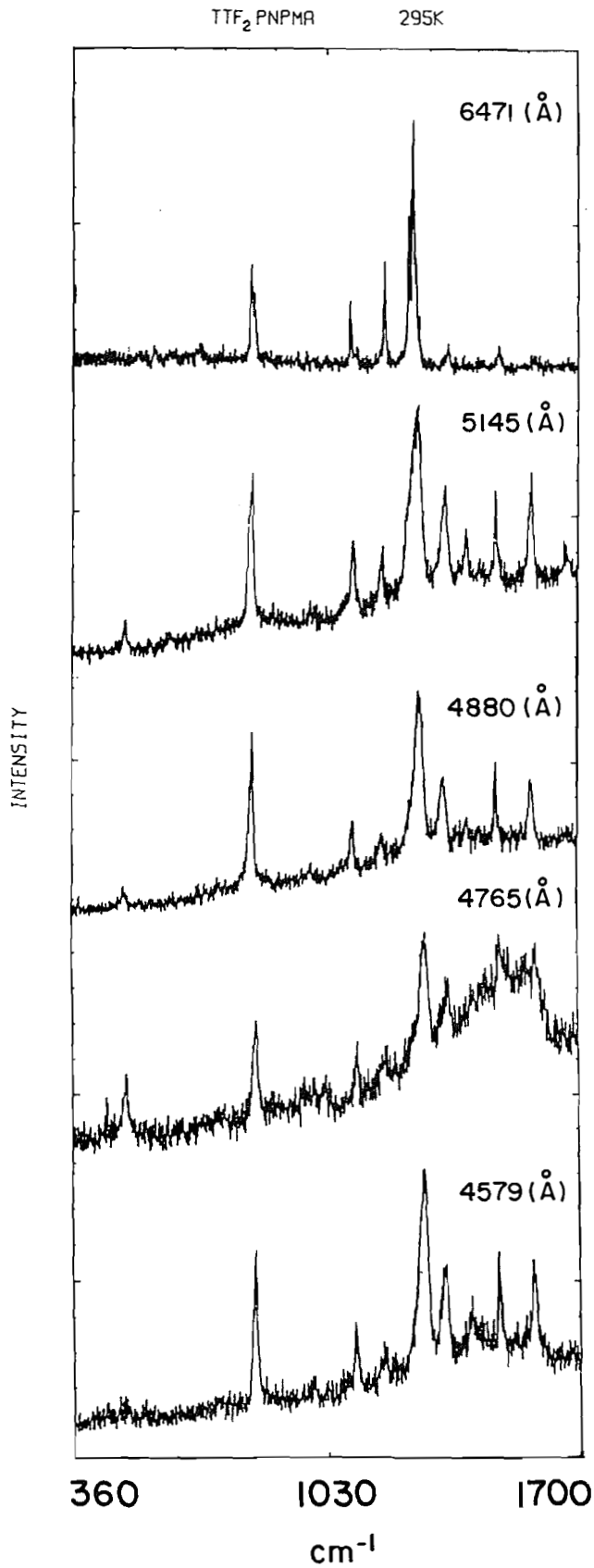


FIG. 7. Raman spectra of $(TTF)_2PNPMA$.

spectra as useful tools to measure the degree of charge transfer in the stacks. In the case of tetramers, our single model, eqs. [1]–[3] showed that now the A_g modes appear in the Raman spectrum slightly downshifted in frequency with respect to the isolated monomer as a result of the electron–vibrational coupling in the stack. However, the A_g mode lines remain single lines as opposed to the IR active combinations of these same A_g modes which undergo larger frequency shifts and further generally appear as doublets (see Table 1).

We have used therefore the frequency shifts of IR modes of the acceptor PNPMA, to established its degree of charge transfer as it appears as isolated monomers in the crystal (Fig. 1) and hence is not expected to undergo electron–vibrational coupling. For the donors TTF and TMTSF, the most reliable estimates of degree of charge transfer from frequency shifts of A_g modes was obtained from the Raman spectrum, since we have shown by our model, it is the Raman lines which undergo the smallest electron–vibrational coupling effects as well as

Can. J. Chem. Downloaded from www.nrcresearchpress.com by 198.100.157.202 on 09/07/12
For personal use only.

no splittings of the individual lines. Thus both charge transfer estimates, i.e. from the IR frequencies of the acceptor and the Raman spectra of the donors, were found to agree remarkably well. We conclude therefore that both semiconductors can be described by the stoichiometric and electronic formula $(D^{+0.4})_2A^{-0.8}$. This is consistent with a tetrameric stacking of the donors, since $D^{+1/2}$ linear chains are known to undergo Peierls tetramerization as a result of the electron–vibrational couplings which are also responsible for the frequency shifts and IR activation of A_g modes. As a consequence, Peierls systems are usually known to undergo metal–semiconductor transitions (8). Both compounds reported here exhibited normal semiconducting behaviour between 77 and 400 K and no phase transition was found from conductivity measurements in this temperature range (6). The metal–semiconducting transition probably occurs at higher temperatures than 400 K.

Acknowledgments

This research was financed by the Research and Development Branch of the Department of National Defence (DND) under contract 8SD85-00313.

1. K. Bechgaard, C. S. Jacobsen, K. Mortensen, H. J. Pedersen, and N. Thorup. Solid Stat. Commun. **33**, 1119 (1980).
2. D. Jerome, A. Mazaud, M. Ribault, and K. Bechgaard. J. Phys. Lett. **41**, L95 (1980).
3. M. M. Walsh, Jr., F. Wudl, G. A. Thomas, D. Nalewajek, J. J. Hauser, Pa. A. Lee, and T. Poehler. Phys. Rev. Lett. **45**, 829 (1980).
4. C. S. Jacobsen, H. J. Pedersen, K. Mortensen, G. Rindorf, N. Thorup, J. B. Torrance, and K. Bechgaard. J. Phys. **C15**, 2651 (1982).
5. S. S. P. Parkin, D. Jerome, and K. Bechgaard. Mol. Crys. Liq. Crys. **79**, 213 (1982).
6. K. D. Truong, A. D. Bandrauk, J. Zauhar, and M. Aubin. Synth. Metals, **27**, B439 (1988).
7. A. W. Hanson. Private communication.
8. J. B. Torrance. Acc. Chem. Res. **12**, 79 (1979).
9. M. J. Rice. Solid State Commun. **31**, 93 (1979).
10. M. J. Rice, V. M. Yartsev, and C. S. Jacobsen. Phys. Rev. **B21**, 3437 (1980).
11. A. D. Bandrauk, K. D. Truong, and S. Jandl. Can. J. Chem. **60**, 1881 (1982).
12. A. D. Bandrauk, K. D. Truong, and K. Ishii. J. Phys. Chem. **89**, 434 (1985); **89**, 1478 (1985).
13. A. D. Bandrauk. *In* Low-dimensional conductors and superconductors. *Edited by* D. Jerome and L. Caron. NATO ASI vol. B155. Plenum Press, New York, NY. 1987. pp. 295–306.
14. V. M. Yartsev. Phys. Stat. Sol. (b) **126**, 501 (1984).
15. R. L. Furry. Quantum chemistry. Prentice Hall, NJ, USA. 1983.
16. S. Matsuzaki, R. Kuwata, and K. Toyoda. Solid State Commun. **33**, 403 (1980).
17. J. S. Chappell, A. N. Bloch, W. A. Bryden, M. Maxfield, T. O. Paehler, and D. D. Cowan. J. Am. Chem. Soc. **103**, 2442 (1981).
18. M. Takumoto, N. Koshizuka, H. Anzai, and T. Ishizuro. J. Phys. Soc. Jpn. **51**, 332 (1982).
19. R. Bozio, I. Zanon, A. Girlando, and C. Pecile. J. Chem. Phys. **71**, 2282 (1979).
20. M. Meneghetti, R. Bozio, I. Zanon, C. Pecile, C. Ricotta, and M. Zanetti. J. Chem. Phys. **80**, 6210 (1984).

Can. J. Chem. Downloaded from www.nrcresearchpress.com by 198.100.157.202 on 09/07/12
For personal use only.

Experimental and theoretical conformer distributions of 3-methylbenzaldehyde

TED SCHAEFER,[1] KERRY J. COX, AND RUDY SEBASTIAN
Department of Chemistry, University of Manitoba, Winnipeg, Man., Canada R3T 2N2
Received, November 5, 1990

TED SCHAEFER, KERRY J. COX, and RUDY SEBASTIAN. Can. J. Chem. **69**, 908 (1991).

The long-range coupling constants between the aldehydic and ring protons of 3-methylbenzaldehyde, in CS_2/C_6D_{12} and acetone-d_6 solutions, imply an equilibrium constant, $K(O\text{-}cis/O\text{-}trans)$ of 1.07(4) in both solvents at 300 K. The small preference for the *O-cis* conformer in both solutions suggests that the *O-cis* conformer is also the more abundant in the vapor, indicating a reassignment of recently reported electronic bands in this state. Geometry-optimized molecular orbital computations, using the AM1, STO-3G, and 6-31G bases, confirm the slightly lower energy of the free *O-cis* conformer. The ^6J(H,CHO) of +0.015(1) Hz for the acetone solution has the correct sign and magnitude implied by a recent simple model for this coupling constant. Other long-range coupling constants are also discussed in terms of their mechanisms.

Key words: conformations, 3MB; NMR, 3MB; spin–spin coupling constants, 3MB; MO computations, 3MB.

TED SCHAEFER, KERRY J. COX et RUDY SEBASTIAN. Can. J. Chem. **69**, 908 (1991).

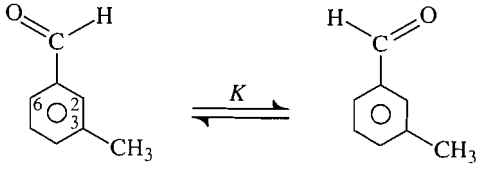
Les constantes de couplage à longue distance entre le proton aldéhydique et les protons du cycle du 3-méthylbenzaldéhyde, dans des solutions de CS_2/C_6D_{12} et d'acétone-d_6, impliquent que la constante d'équilibre, $K(O\text{-}cis/O\text{-}trans)$, est égale à 1,07(4) dans chacune des solutions suggère que le conformère *O-cis* est aussi le plus abondant en phase gazeuse et qu'il est nécessaire de réattribuer des bandes observées récemment dans cet état. Des calculs d'orbitales moléculaires avec géométrie optimisée, réalisés à l'aide de bases AM1, STO-3G et 6-31G, confirment que l'énergie du conformère *O-cis* libre est légèrement plus faible. Sur la base d'un modèle récent pour cette constante de couplage, le signe et l'amplitude de la ^6J(H,CHO), +0,0015(1) Hz, pour la solution dans l'acétone, sont corrects. On discute aussi d'autres constantes de couplage à longue distance en fonction de leurs mécanismes.

Mot clés : conformations, 3MB; RMN, 3MB; constantes de couplage spin–spin, 3MB; calculs d'OM, 3MB.

[Traduit par la rédaction]

Introduction

A recent discussion (1) of the phosphorescence excitation spectrum of jet-cooled 3-methylbenzaldehyde (3MB) tentatively assumes that the *O-trans* conformer in the ground electronic state is somewhat more abundant than the *O-cis* conformer ($K < 1$). The reported values of K range from 11 for the vapor at 368 K (2), based on torsional frequencies, to 1.22 for a 0.5 M solution in $CHCl_2F/CCl_2F_2$ at 123 K (3), as assessed from the ^{13}C nmr spectrum of the distinct conformers. An early ^1H nmr spectrum of 3MB in acetone solution at ambient temperature (4) gave K as ≥ 2.3, as indicated by the long-range coupling constant, ^5J(H,CHO), between the aldehydic and *meta* ring proton.



O-trans *O-cis*

Now, a methyl group is certainly a weak perturber (1) of the benzaldehyde moiety and intuition suggests that K must be little different from unity and relatively insensitive to environment. Precise measurements of ^5J(H,CHO) are possible with modern instruments and this coupling constant is a good indicator of K (5). Such measurements are reported here for 3MB in the nonpolar CS_2/C_6D_{12} solvent mixture as well as in the polar solvent acetone-d_6. In addition, molecular orbital computations of the conformational energies of the free molecule allow a comparison with those derived from ^5J(H,CHO). It appears that the *O-cis* is only slightly more abundant than the *O-trans* conformer, roughly independent of solvent.

[1]Author to whom correspondence may be addressed.

Experimental

Dilute solutions of 3MB in CS_2/C_6D_{12} and acetone-d_6 (see Table 1 for details) were filtered into 5-mm o.d. nmr sample tubes. These were degassed by five freeze–pump–thaw cycles and were then flame-sealed under vacuum. The ^1H nmr spectra were acquired on an AM 300 Bruker spectrometer in a manner described in detail (6) previously; see also the caption to Fig. 1. The spectra were acquired with and without decoupling of the methyl protons and were analyzed with the computer program NUMARIT (7), as extensively altered by R. Sebastian. The ensuing chemical shifts and coupling constants can be found in Table 1. Figure 1 displays the aldehydic proton spectrum, illustrating the spectral quality attainable with due care.

AM1 (8) and *ab initio* molecular orbital calculations, employing STO-3G (9) and 6-31 G (10) basis sets, of the conformational energies of 3 MB were performed on an Amdahl 5870 system with the program GAUSSIAN 86 (11). Optimization procedures allowed all bond angles and lengths to vary for a given conformation with the constraint, however, that the aromatic moiety remain planar.

Results and discussion

Table 1 contains the spectral parameters for 3MB in a polar and a nonpolar medium. It can be seen that, even at 300 MHz, the ring protons are strongly coupled in the sense that the chemical shift differences for certain pairs are quite small; for example, H-4 and H-5 have less than a 3 Hz difference in their shifts in the CS_2/C_6D_{12} solution. In consequence, certain spectral parameters correlate relatively strongly (footnotes to Table 1) and the precision of analysis for the nonpolar solution is lower than desirable. Nevertheless, some reliable conformational information can be extracted.

The cis–trans *equilibrium*

Because the barrier to rotation about the Csp^2—Csp^2 bond in 3MB is at least 30 kJ/mol (3) in solution and is most likely (12) very near 20 kJ/mol in the vapor, a discussion in terms of planar conformers (the methyl groups, of course, rotate almost freely)

Can. J. Chem. Downloaded from www.nrcresearchpress.com by 198.100.157.202 on 09/07/12
For personal use only.

TABLE 1. The ^{1}H nmr spectral parameters for 3-methylbenzaldehyde in CS_2/C_6D_{12}[a] and acetone-d_6[b] solutions at 330 K

Parameter	CS_2/C_6D_{12}	Acetone-d_6	Parameter	CS_2/C_6D_{12}	Acetone-d_6
$\upsilon(CH_3)$	719.395(1)[c,d]	725.826(0)	^4J(H-6,CHO)	−0.147(2)	−0.164(1)
υ(CHO)	2959.953	3002.151(0)	^5J(H,CHO)	0.413(3)	0.418(1)
υ_2	2266.184(1)	2315.605(1)	^6J(H,CHO)	0.024(3)[j]	0.015(1)
υ_4	2198.025(4)[e]	2253.310(2)[h]	^4J(H-2,CH_3)	−0.741(1)	−0.739(1)
υ_5	2195.199(4)[f]	2242.420(1)[i]	^4J(H-4,CH_3)	−0.697(2)	−0.718(1)
υ_6	2263.799(1)	2314.101(1)	^5J(H,CH_3)	0.325(2)	0.343(1)
$^3J_{45}$	7.498(3)	7.565(2)	^6J(H,CH_3)	−0.588(1)	−0.601(1)
$^3J_{56}$	7.616(7)	7.626(2)	^6J(CHO,CH_3)	−0.006(1)	—
$^4J_{26}$	1.631(2)	1.645(1)	Transitions calcd.	653[k]	653
$^4J_{24}$	1.863(3)	1.871(1)	Peaks	98	98
$^4J_{46}$	1.191(7)[g]	1.205(2)	Assigned transitions	405	371
$^5J_{25}$	0.573(3)	0.572(2)	Largest difference	0.022	0.020
^4J(H-2,CHO)	−0.160(2)	−0.162(1)	Root-mean-square deviation	0.010	0.005

[a]4.0 mol% in CS_2, containing also 10 mol% of C_6D_{12} and 0.5 mol% of TMS.
[b]4.0 mol% in acetone-d_6, containing 0.5 mol% of TMS.
[c]In Hz at 300.135$_2$ MHz to high frequency of internal TMS, the proton numbering scheme having H-2 between CHO at position 1 and CH_3 at position 3.
[d]Standard deviations in the last significant figure are given in parentheses.
[e]Correlates by 0.880 With υ_5 and by 0.695 with $^3J_{56}$.
[f]Correlates with $^4J_{46}$ by 0.770 and with $^3J_{56}$ by 0.693.
[g]Correlates with $^3J_{56}$ by 0.894.
[h]Correlates by 0.632 with υ_5 and by 0.762 with $^3J_{45}$.
[i]Correlates by 0.690 with $^3J_{45}$.
[j]Correlates by 0.657 with ^5J(H, CHO).
[k]Many degenerate transitions occur in the methyl proton spectral region.

is a good approximation at ambient temperatures; even at 368 K, RT is only about 3 kJ/mol.

In benzaldehye, ^5J(H,CHO) ≡ ^5J is 0.431(2) and 0.430(1) Hz in CS_2/C_6D_{12} and acetone-d_6 solutions, respectively (13). As discussed previously (5), ^5J, as a σ-electron coupling constant in the effectively planar conformers (the essentially zero coupling constant between the aldehydic and methyl protons in 3MB confirms this conclusion), vanishes in the *O-cis* conformer above. Hence, because the methyl group lies far from the coupling pathway in 3MB and is also a weakly perturbing substituent, one has ^5J(H,CHO) in the *O-trans* conformer as 0.861(4) Hz in either solution (even in 2-fluorobenzaldehyde, the sum of the two ^5J values is 0.869(2) and 0.850(2) Hz in the nonpolar and polar solvent systems, respectively (5), indicating a small perturbation by the much stronger perturber placed closer to the coupling fragment). For 3MB, ^5J is 0.413(3) and 0.418(1) Hz in CS_2/C_6D_{12} and acetone-d_6, respectively, implying a K of 1.07(4) in both solutions. The error estimate follows from an average ^5J of 0.415(5) Hz in the two solutions and the estimate of 0.861(4) Hz for ^5J in the *O-trans* conformer.

The inference is drawn of a conformational equilibrium insensitive to solvent polarity. It is possible that the K of 1.22 obtained from peak intensities in the ^{13}C nmr spectrum of 3MB at 123 K is in good agreement with the present result. If the entropy difference between the conformers vanishes in all solvents, then the free energy difference of 170 ± 100 J/mol at 300 K implies a K of 1.18 (12) at 123 K. If, indeed, K is independent of solvent, then the *O-cis* conformer is also very likely slightly the more abundant in the vapor, suggesting the opposite of the assignment in ref. 1. It is therefore of interest to have a molecular orbital result for the relative stability of the conformers of 3MB.

Molecular orbital computations

Table 2 presents AM1, STO-3G, and 6-31G MO energies for the *O-cis* and *O-trans* conformers of 3MB, together with the energies of each conformer as influenced by two orientations of the methyl group, one with a C—H bond in the aromatic plane and pointing towards the other substituent, the other with this C—H bond pointing away from the aldehydic group. The upshot is that the total energy of the *O-cis* conformer is 120, 160, and 490 J/mol lower than that of the *O-trans* conformer at the AM1, STO-3G, and 6-31G levels of molecular orbital theory, respectively. Naively, ignoring zero point energy differences, for example, these energy differences imply a K of 1.03, 1.07, and 1.22 at 300 K. At these levels of molecular orbital theory, therefore, it appears that the *O-cis* will be more abundant than the *O-trans* conformer at the temperature of the jet-cooled vapor.

Figure 2 displays the 6-31G structures of the most stable *O-cis* and *O-trans* conformers. These may well be useful to molecular spectroscopists. The figure caption also provides some useful statements.

The dipole moment of 3MB in benzene solution (19) at 298 K is 2.93 D (from which it was concluded that only the *O-cis* conformer is present). This number lies between the *ab initio* estimates in Table 2. The mean of these estimates, weighted by the abundances measured in CS_2/C_6D_{12} and acetone-d_6 solutions above, yields a dipole moment of 3.07 D. Alternatively, addition of 0.9 D to each of the STO-3G values similarly yields a dipole moment of 2.94 D, reflecting the underestimate and

Can. J. Chem. Downloaded from www.nrcresearchpress.com by 198.100.157.202 on 09/07/12
For personal use only.

Can. J. Chem. Downloaded from www.nrcresearchpress.com by 198.100.157.202 on 09/07/12
For personal use only.

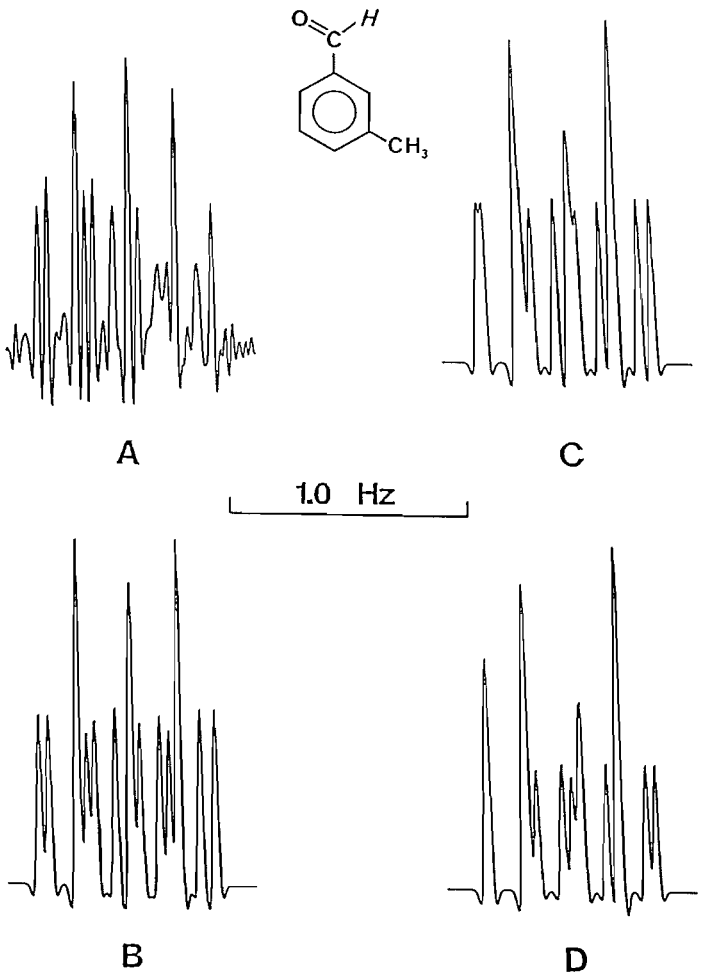


FIG. 1. In A the ^{1}H nmr spectrum at 300 MHz of the aldehydic proton of 3-methylbenzaldehyde, as a 4.0 mol% solution in acetone-d_6, is displayed under conditions in which the methyl protons are decoupled (the methyl protons are coupled by less than 0.01 Hz to the aldehydic proton in the single resonance spectrum). The spectrum in A extends over 0.8 Hz, the acquisition time for each of 32 free induction decays was 54.6 s, the digital resolution was better than 0.005 Hz/point, the probe temperature was 300 K, and considerable resolution enhancement was applied before Fourier transformation, causing some intensity distortion. In B the simulated spectrum uses the spectral parameters from Table 1 and has ^6J(H-4,CHO) as +0.015 Hz. In C the simulated spectrum has ^6J(H-4,CHO) as −0.015 Hz and in D it is taken as zero. The spectrum is sensitive to the sign and magnitude of this coupling constant because of the strongly second-order nature of the ring proton spectrum. A model mentioned in the text demands that ^6J(H-4,CHO) be positive.

TABLE 2. AM1, STO-3G and 6-31G MO energies, and dipole moments of four conformers of 3-methylbenzaldehyde

Conformer	Relative energy[a]/dipole moment[b]		
	AM1	STO-3G	6-31G
O-cis, CH-*cis*	0.000/1.15	0.000/1.92[c]	0.000/3.96[d]
O-cis, CH-*trans*	0.006/1.13	0.117/1.87	0.301/3.86
O-trans, CH-*cis*	0.110/1.26	0.195/2.20	0.572/4.33
O-trans, CH-*trans*	0.150/1.26	0.242/2.18	0.716/4.29

[a]In kJ/mol.
[b]In debye.
[c]Total energy is −377.705 294 au.
[d]Total energy is −382.319 590 au.

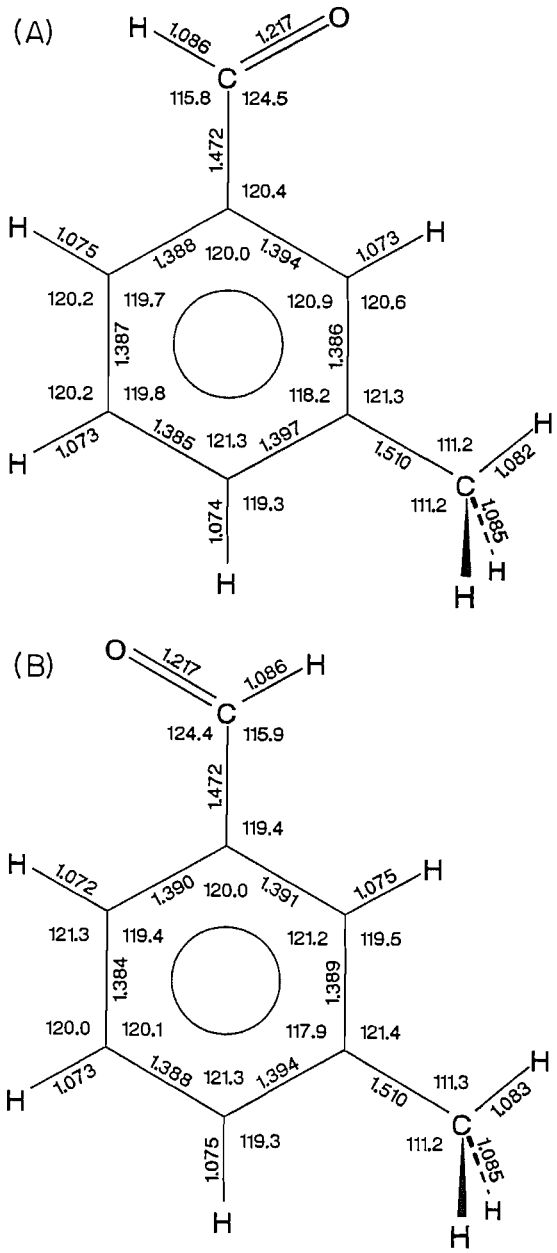


FIG. 2. The most stable 6-31G structures of the *O-cis* and *O-trans* (B) conformers of 3-methylbenzaldehyde are presented. The computed internal angles, averaged over the two conformations of the methyl group, are reproduced very closely by addition of the empirical angular substituent parameters (20) for the CH_3 and COOH groups (CHO not being listed). There is no obvious structural detail suggestive of why the *O-cis* is of slightly lower energy than the *O-trans* conformer, except perhaps that, in the former, the C=O bond lies *trans* to the shorter *ortho* C—C bond; it has been argued (21) that an energetic advantage arises from such an orientation.

overestimate, respectively, of the dipole moment of benzaldehyde by the STO-3G and 6-31G bases.

The coupling constants, $^4J(H, CHO) = {}^4J$ *and* $^6J(H, CHO) = {}^6J$

In benzaldehyde, ^4J is −0.16 Hz (13) and, as discussed previously (13, 14), is a composite of contributions of positive σ- and negative π-electrons. Furthermore (13), an electronegative substituent in the *meta* position polarizes the σ electrons at the neighbouring *ortho* position, causing an increase in the σ-electron component of ^4J. For the most electronegative substituent, fluorine, ^4J(H-2,CHO) vanishes, the two compo-

Can. J. Chem. Downloaded from www.nrcresearchpress.com by 198.100.157.202 on 09/07/12
For personal use only.

nents having cancelled each other (5). The polarization is of interest also because the greater stability of the *O-cis* conformer in 3-fluorobenzaldehyde has been attributed (3) to an attractive interaction between the C═O and the (polarized) *ortho* C—H bond. For 3MB in acetone-d_6 solution, the two ^4J values are indistinguishable from the ^4J of benzaldehyde in the same solvent (Table 1), as expected for a negligible polarization by the methyl substituent. In CS_2 solution, ^4J is -0.15 Hz in benzaldehyde, not very different from the values quoted for 3MB; the general precision of the analysis for this solution is inferior to that for the polar solution.

^6J is $+0.01_5$ Hz for 3MB in acetone-d_6 solution (see Fig. 1). A simple model (13), involving an ionic valence bond structure, predicts ^6J as $+0.012$ Hz in 3MB. The apparent ^6J of $+0.024(3)$ Hz in CS_2/C_6D_{12}, however, cannot be discounted entirely even though, in our opinion, the spectral quality and complexity suggests its relative unreliability. Again, ^6J in 3,5-dimethylbenzaldehyde (13) was not observed; the model implies it as $+0.017$ Hz. It must be noted that, in this molecule, the symmetry of the spin system is high, unlike that in 3MB in which the sign and magnitude of ^6J for the acetone-d_6 solution is manifested, not as a direct splitting, but via the asymmetry of a tightly coupled spectrum (see Fig. 1).

It is concluded that the most reliable of the ^6J results, under discussion here, is in agreement with the model in question.

The long-range methyl proton coupling constants

$^4J(H,CH_3)$ is a predominantly $\sigma-\pi$ coupling constant, containing also a σ-electron component (15). Its magnitude is also sensitive to the bond order of the intervening aromatic C—C bond (16, 17), rising in magnitude as the bond order increases. In toluene, $^4J(H,CH_3)$ is $-0.702(1)$ Hz in a CS_2/C_6D_{12} solvent mixture (18). For the same solvent, ^4J(H-4,CH_3) is $-0.697(2)$ Hz for 3MB and ^4J(H-2,CH_3) is $-0.741(1)$ Hz. These numbers imply a larger bond order of the C(2)—C(3) than of the C(3)—C(4) bond, consistent with an obvious resonance structure. The 6-31G geometries in Fig. 2 do not support this interpretation, judging by the relevant computed C—C bond lengths. Hence the larger magnitude of ^4J(H-2,CH_3) may arise, not from the π-electron contribution, but from an increased σ-electron component induced by the carbonyl group attached *ortho* to H-2.

In toluene, the $^5J(H,CH_3)$ of $0.329(1)$ Hz does not differ significantly from the $0.324(2)$ Hz of 3MB in CS_2/C_6D_{12} but is somewhat smaller than the $0.343(1)$ Hz in the acetone-d_6 solution; presumably because the substituent lies far from the coupling pathway, it does not perturb to any extent either the $\sigma-\pi$ or σ-electron contributions (18) to $^5J(H,CH_3)$.

$^6J(H,CH_3)$ in toluene is $-0.602(2)$ Hz (18) and is relatively insensitive to intrinsic substituent perturbations. For 3MB, ^6J is $-0.601(1)$ Hz in the acetone-d_6, but $-0.588(1)$ Hz in the nonpolar solution.

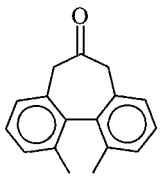
Acknowledgments

We thank the Natural Sciences and Engineering Research Council of Canada for financial assistance.

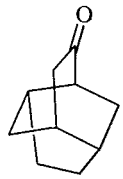
1. S. YAMAMOTO, T. EBATA, and M. ITO. J. Phys. Chem. **94**, 5786 (1990).
2. F. A. MILLER, W. G. FATELEY, and R. E. WITKOWSKI. Spectrochim. Acta, Part A, **23**, 891 (1967).
3. T. DRAKENBERG, R. JOST, and J. M. SOMMER. J. Chem. Soc. Perkin Trans. 2, 1682 (1975).
4. G. J. KARABATSOS and F. M. VANE. J. Am. Chem. Soc. **85**, 3886 (1963).
5. T. SCHAEFER and C. S. TAKEUCHI. Can. J. Chem. **68**, 339 (1990), and references therein.
6. T. SCHAEFER, J. PEELING, and R. SEBASTIAN. Can. J. Chem. **63**, 3219 (1985).
7. J. S. MARTIN, A. R. QUIRT, and K. E. WORVILL. The nmr program library. Daresbury Laboratory, Daresbury, U.K.
8. M. J. S. DEWAR, E. J. ZOEBISCH, E. F. HEALY, and J. J. P. STEWART. J. Am. Chem. Soc. **107**, 3902 (1985).
9. W. J. HEHRE, R. DITCHFIELD, R. F. STEWART, and J. A. POPLE. J. Chem. Phys. **52**, 2796 (1970).
10. W. H. HEHRE, R. DITCHFIELD, and J. A. POPLE. J. Chem. Phys. **56**, 2257 (1972).
11. M. J. FRISCH, J. S. BINKLEY, H. B. SCHLEGEL, K. RAGHAVACHARI, C. F. MELIUS, R. L. MARTIN, J. J. P. STEWARD, F. W. BOBROWICZ, D. F. ROHLFING, L. R. KAHN, D. J. DEFREES, R. SEEGER, R. A. WHITESIDE, D. J. FOX, E. M. FLUDER,, and J. A. POPLE. Carnegie–Mellon Quantum Publishing Unit, Pittsburgh, PA. 1984.
12. G. H. PENNER, P. GEORGE, and C. W. BOCK. J. Mol. Struct. (Theochem), **152**, 201 (1987), and references therein.
13. T. SCHAEFER and C. S. TAKEUCHI. Can. J. Chem. **67**, 827 (1989).
14. I. R. PEAT and W. F. REYNOLDS. Can. J. Chem. **52**, 2403 (1974).
15. M. BARFIELD, C. J. FALLICK, K. HATA, S. STERNHELL, and P. W. WESTERMAN. J. Am. Chem. Soc. **105**, 2178 (1983).
16. M. BARFIELD, M. J. COLLINS, J. E. GREADY, S. STERNHELL, and C. W. TANSEY. J. Am. Chem. Soc. **111**, 4285 (1989).
17. J. E. GREADY, K. HATA, S. STERNHELL, and C. W. TANSEY. Aust. J. Chem. **43**, 593 (1990).
18. T. SCHAEFER, R. SEBASTIAN, and G. H. PENNER. Can. J. Chem. **63**, 2597 (1985).
19. H. LUMBROSO and C. G. ANDRIEU. Bull. Soc. Chim. Fr. 1575 (1973).
20. A. DOMENICANO and P. MURRAY-RUST. Tetrahedron Lett. 2283 (1979).
21. L. I. KRUSE, C. W. DEBROSSE, and C. H. KRUSE. J. Am. Chem. Soc. **107**, 5435 (1985).

John R. Jones, David A. Wickenden, Carel W. Funke, and Frans M. Kaspersen. Kinetics of the detritiation of [10,10-^{3}H] mianserin and related compounds in highly basic media. Can. J. Chem. **68**, 1818 (1990).

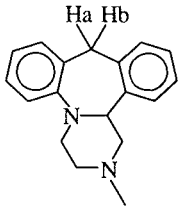
The chemical structures **1** to **5** were inadvertently omitted from the paper. They are as follows:



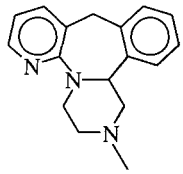
1



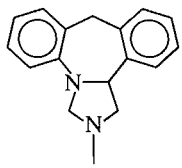
2



3



4



5

Can. J. Chem. Downloaded from www.nrcresearchpress.com by 198.100.157.202 on 09/07/12
For personal use only.

Conformation and dynamics in solution of an *N*-quaternarized benzophenone derivative: a molecule active as UV filter

CECILIA ANSELMI, MARISANNA CENTINI, MIRELLA SCOTTON, AND ALESSANDRO SEGA[1]

Istituto di Chimica Organica, Piano dei Mantellini, 44, 53100 Siena, Italy

Received August 16, 1990

CECILIA ANSELMI, MARISANNA CENTINI, MIRELLA SCOTTON, and ALESSANDRO SEGA. Can. J. Chem. **69**, 913 (1991).

The dynamics and conformation of *N,N*-dimethyl-*N*-[3-(benzoyl-4-phenoxy)]-*N*-*n*-dodecylammonium bromide, **1**, have been established in two solvents ($CDCl_3$ and DMSO-d_6) by the use of ^{13}C spin-lattice relaxation rates, non-selective and selective proton spin-lattice relaxation rates, and ^1H–{^1H} nuclear Overhauser enhancement (nOe) experiments. The data obtained are consistent with two main mean conformations for compound **1**: a "linear" conformation in $CDCl_3$ and a folded conformation in DMSO-d_6 where the alkyl chain forms a loop toward the aromatic moiety.

Key words: UV filter, carbon and proton relaxation rates, nuclear Overhauser enhancement experiments, solvent dependent conformations.

CECILIA ANSELMI, MARISANNA CENTINI, MIRELLA SCOTTON et ALESSANDRO SEGA. Can. J. Chem. **69**, 913 (1991).

Faisant appel aux vitesses de relaxation spin-réseau du ^{13}C, à des vitesses de relaxation spin-réseau du ^1H sélectives ainsi que non-sélectives et à des expériences d'eOn ^1H–{^1H}, on a déterminé les dynamiques et la conformation du bromure de *N,N*-diméthyl-*N*-[3-(benzoyl-4-phénoxy)]-*N*-*n*-dodécylammonium, **1**, dans deux solvants ($CDCl_3$ et DMSO-d_6). Les données obtenues suggèrent l'existence de deux conformations principales pour le composé **1** : une conformation «linéaire» dans le $CDCl_3$ et une conformation repliée dans le DMSO-d_6 dans laquelle la chaîne alkyle forme une boucle avec la portion aromatique.

Mots clés : filtre UV, vitesses de relaxation du ^{13}C et du ^1H, expériences d'effet Overhauser nucléaire, conformations qui dépendent du solvant.

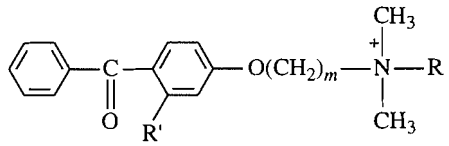
[Traduit par la rédaction]

Introduction

Research into the synthesis of molecules active as sunscreens has become of great importance (1, 2). These molecules, besides having a high protective efficacy, must also have (i) the capacity of adhering to and of being retained by the keratin of the skin, thus resisting removal by bathing and perspiration (a property known as substantivity (3)) and (ii) a very low toxicity.

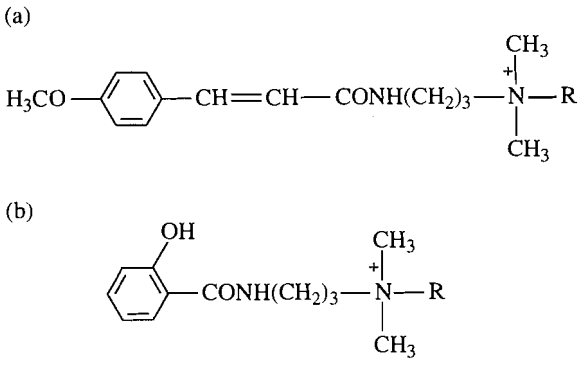
In our study aimed at identifying new sunscreens (4–8), we synthesized a series of *N*-quaternarized benzophenone derivatives (see Fig. 1). In this series, however, maximum substantivity was reached by the *n*-C12 derivative; this was accompanied by the highest level of antibacterial activity (9). These results are compatible with those obtained for the *N*-quaternarized derivatives of cinnamic and salicylic acids (10) (see Fig. 2): the *n*-C12 derivative shows the highest degree of antibacterial activity and substantivity. On the other hand, it is well known that several anionic or cationic detergents containing the *n*-C12 alkyl chain are the most efficient agents for detergency–adsorption–denaturation–permeability–irritation interactions (11). Garcia Dominguez *et al.* put forward an interesting rationalization of this "odd" behaviour of *n*-C12 detergents in their interaction with keratinic proteins (11). They maintained that the success of this mechanism is due to the fact that the *n*-C12 alkyl chain is able to adopt a coiled structure: in this way the surface/volume ratio of the molecule is reduced to a minimum. It is likely that this is of great importance when the adsorbed molecule migrates inside the protein structure.

Significant analogies appear to exist between this mechanism and that of the antibacterial activity of quaternary cationic detergents proposed by other authors (12). From these studies, it would appear that the substantivity of an *N*-quaternarized sunscreen for a keratinic substrate might not be unconnected with an antibacterial action, concomitant damage to the cell membrane and contents, and skin irritation phenomena.



R' = H, OH
R = *n*-C_{12}, *n*-C_{14}, *n*-C_{16}, *n*-C_{18}
m = 2,3

FIG. 1. *N*-Quaternarized benzophenone derivatives.



R = C_2, *n*-C_8, *n*-C_{12}, *n*-C_{16}

FIG. 2. *N*-Quaternarized derivatives of (a) cinnamic and (b) salicylic acids.

However, compound **1** shows a lower antibacterial activity than the corresponding *n*-C12 derivatives of cinnamic and salicylic acids. Therefore it is very likely that, with appropriate modification of the molecular structure, antibacterial activity can be minimized or eliminated without reducing the high degree of substantivity. Our study was designed to investigate the dynamics and conformation of compound **1** in solution (see

[1]Author to whom correspondence may be addressed.

Printed in Canada / Imprimé au Canada

Can. J. Chem. Downloaded from www.nrcresearchpress.com by 198.100.157.202 on 09/07/12
For personal use only.

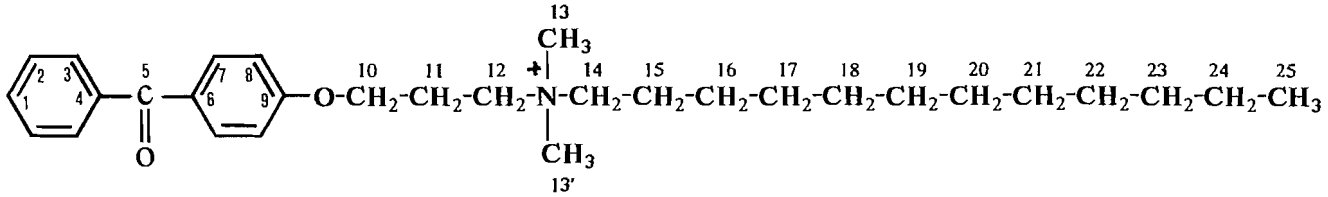


FIG. 3. *N,N*-Dimethyl-*N*-[3-(benzoyl-4-phenoxy)propyl]-*N*-*n*-dodecylammonium bromide. The numbering system is that used throughout the text.

Fig. 3), as we consider this to be the initial step in analysing the behaviour of these molecules.

It is recognised that the environment in which the molecule – keratinic protein interaction takes place plays a fundamental role in the conformation of the molecule; taking this into consideration, this study was carried out using two solvents that differ widely in their properties: $CDCl_3$ and DMSO-d_6.

Results and discussion

^1H and ^{13}C assignments were made on the basis of semi-empirical methods (13*a*,*b*), reference to data in the literature (13*a*), and ^{13}C–{^1H} nuclear Overhauser enhancements (nOe's).

Dynamics and conformation of compound ***1***

(a) In $CDCl_3$

^{13}C chemical shifts and relaxation rates (R_1) of compound **1** in $CDCl_3$ are shown in Table 1.

It is known that ^{13}C R_1 ($R_1 = 1/T_1$), relaxation rates, are almost exclusively determined by dipolar interactions with directly bonded or nearby protons, thus allowing suitable delineations of the molecular dynamics (13*c*, 14). The motional features of aromatic carbons were considered first since they have fewer degrees of freedom than side-chain carbons.

For ring A, the relaxation rate of C1 was faster than those of the other carbon atoms, suggesting that C1–C4 is the main rotation axis for this aromatic ring. The relaxation rates of C2 and C3 were very similar, such that an anisotropic model consisting of rotational reorientation around the main rotation axis with some degree of internal motion could be applied (15) (eq. [1] with $A = 0.25(3\cos^2\alpha - 1)^2$, $B = 3(\sin^2\alpha\cos^2\alpha)$, and $C = 0.75(\sin^4\alpha)$).

$$[1]\quad \frac{1}{nT_1} = \frac{\hbar^2\gamma_H^2\gamma_C^2}{r_{CH}^6}\tau_c A\left\{A + B\frac{3\tau_g A}{3\tau_g A + \tau_c A} + C\frac{6\tau_g A}{6\tau_g A + \tau_c A}\right\}$$

In eq. [1], $\tau_c A$ is the main rotation correlation time, $\tau_g A$ is the correlation time for librational motions of aromatic ring A, r_{CH} is the length of the C—H bond, n is the number of protons attached to the carbon under consideration, and α is the angle between the main rotation axis and the C–H vector. The main correlation time, $\tau_c A$, can be calculated by considering the relaxation rate R_1 ($= 1/T_1$) of C1: since the C1–H1 vector lies on the main axis, eq. [2] can be applied.

$$[2]\quad \frac{1}{nT_1} = \frac{\hbar^2\gamma_H^2\gamma_C^2}{r_{CH}^6}\tau_c$$

This holds for a pure dipole–dipole relaxation mechanism within the extreme narrowing region (16). As all protonated carbons exhibit maximum ^{13}C–{^1H} nuclear Overhauser effects,

TABLE 1. ^{13}C chemical shifts[a] and spin-lattice relaxation rates for compound **1** (0.1 mol dm^{-3} in $CDCl_3$, T = 298 K)

	Chemical shift (ppm)	R_1 (s^{-1})
C5	195.5	0.12±0.01
C9	161.6	0.21±0.01
C4	137.9	0.09±0.01
C7	132.5	2.35±0.09
C1	132.1	2.00±0.12
C6	130.7	0.15±0.01
C3	129.7	1.13±0.02
C2	128.2	1.15±0.03
C8	114.1	2.42±0.08
C10	64.5	5.49±0.23
C14	64.4	5.62±0.33
C12	61.1	5.88±0.29
C13,13′	51.5	4.81±0.13
C23	31.8	0.44±0.02
C20,21	29.5	0.87±0.02
C19	29.4	1.24±0.04
C17,18	29.35	1.51±0.07
C22	29.3	0.69±0.03
C16	26.2	3.11±0.11
C11	23.1	5.75±0.31
C15	22.7	4.29±0.28
C24	22.6	0.35±0.02
C25	14.1	0.26±0.01

[a]Measured downfield from internal TMS.
[b](±) Figures denote approximate 95% confidence limits of the exponential regression analysis.

eq. [2] was used to extract $\tau_c A$, and $\tau_g A$ was then obtained by applying eq. [1] (see Table 2).

The same analysis holds for ring B: the relaxation rates of C7 and C8 are very close to each other and the main rotation axis is C6–C9, as would be expected for a *para*-disubstituted benzene. Thus the same anisotropic model can be applied.

However, it is impossible to calculate $\tau_c B$, the main correlation time of ring B, from the relaxation rates of carbon atoms. Here it is necessary to use proton relaxation rates; indeed the H7–H8 vector is parallel to the main axis C6–C9, and by taking advantage of double selective and selective relaxation rates we can write eq. [3] (see later for a discussion on proton relaxation rates):

$$[3]\quad R_{7,8}^7 - R_s^7 = \sigma_{7,8} = \frac{1}{2}\frac{\hbar^2\gamma_H^4}{r_{7,8}^6}\tau_c B$$

where $r_{7,8}$ is the H7–H8 interproton distance (it has been determined from neutron scattering data: $r_{7,8}$ = 2.45 Å (17)).

Then, from eq. [3] we obtained $\tau_c B = 1.52 \times 10^{-10}$ s and, again applying eq. [1], the corresponding correlation time for

Can. J. Chem. Downloaded from www.nrcresearchpress.com by 198.100.157.202 on 09/07/12
For personal use only.

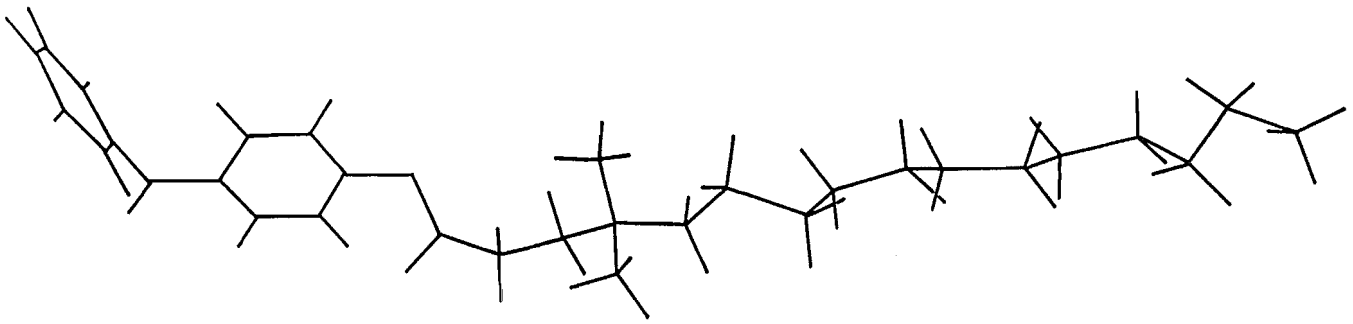


FIG. 4. Projection of the Dreiding model of the "most probable" conformation of compound **1** in 0.1 M $CDCl_3$ solution as inferred from NMR experiments.

TABLE 2. Correlation times ($\times 10^{-10}$ s) of carbon atoms of compound **1** (0.1 mol dm^{-3} in $CDCl_3$ and in DMSO-d_6, T = 298 K)

	$CDCl_3$	DMSO-d_6
τ_cA	0.98	1.03
τ_gA	0.25	0.36
τ_cB	1.52	1.14
τ_gB	0.84	1.12
τ_c10	1.35	1.07
τ_c11	1.41	1.03
τ_c12	1.45	1.54
τ_c13	0.79	0.63
τ_c13′	0.79	0.74
τ_c14	1.38	1.76
τ_c15	1.06	1.07
τ_c16	0.76	0.68
τ_c17	0.37	0.48
τ_c18	0.37	0.40
τ_c19	0.30	0.35
τ_c20	0.21	0.26
τ_c21	0.21	0.26
τ_c22	0.17	0.20
τ_c23	0.11	0.12
τ_c24	0.087	0.089
τ_c25	0.043	0.044

[a]See the text for discussion.

librational motions was calculated, $\tau_g B = 0.84 \times 10^{-10}$ s. The correlation times of side-chain carbons were evaluated from eq. [2] (see Table 2).

The analysis of correlation times reveals three main considerations: (i) the motion of the aromatic rings is dephased as a consequence of great internal freedom; (ii) the correlation times from C10 to C14 have values very close to each other and to τ_cB; (iii) from τ_c15 onwards the correlation times steadily decrease: segmental motion takes place.

These facts strongly suggest the presence of a main rotation axis parallel or nearly parallel to the C6–C9 axis and passing through the quaternary nitrogen atom; the carbon skeleton from C10 to C14 should develop on and along this axis as depicted in Fig. 4. This conclusion, and the presence of segmental motion from C15 onwards, brings about the broad picture of a "linear" main mean conformation for **1** in $CDCl_3$.

To examine the conformation(s) of compound **1** more closely, we then made use of proton relaxation rates and the homonuclear $^1H-\{^1H\}$ nuclear Overhauser effect.

TABLE 3. ^1H chemical shifts[a] for compound **1** (0.1 mol dm^{-1} in $CDCl_3$ and in DMSO-d_6, T = 298 K)

	Chemical shift (ppm)	
	$CDCl_3$	DMSO-d_6
H25	0.87	0.83
H16–24	1.24	1.22
H15	1.72	1.63
H11	2.35	2.19
H13	3.46	3.08
H14	3.52	3.30
H12	3.89	3.48
H10	4.23	4.18
H8	6.95	7.09
H2	7.47	7.55
H1	7.54	7.66
H3	7.77	7.68
H7	7.81	7.76

[a]Measured downfield from internal TMS.

TABLE 4. Non-selective (R_{ns}) (s^{-1}), mono-selective (R_s) (s^{-1}), and double-selective (R_{ds}) (s^{-1}) spin-lattice relaxation rates for selected protons of compound **1** (0.1 M $CDCl_3$ and DMSO-d_6 solutions)

	$CDCl_3$	DMSO-d_6
R_{ns}^7	1.09	1.12
R_s^7	0.76	0.79
$R_{7,8}^7$	0.96	0.94
R_{ns}^8	1.67	1.85
R_s^8	1.18	1.28
R_{ns}^7/R_s^7	1.44	1.42
R_{ns}^8/R_s^8	1.42	1.44

^1H chemical shifts in 0.1 M $CDCl_3$ and DMSO-d_6 solutions are summarized in Table 3.

Non-selective (R_{ns}^i), mono-selective (R_s^i), and double-selective (R_{ds}^{in}) proton spin-lattice relaxation rates of selected protons of compound **1** are shown in Table 4.

The measurement of ^1H non-selective, mono-selective, and double-selective spin-lattice relaxation rates has been suggested as a suitable aid to conformational studies in solution (18–20).

Can. J. Chem. Downloaded from www.nrcresearchpress.com by 198.100.157.202 on 09/07/12
For personal use only.

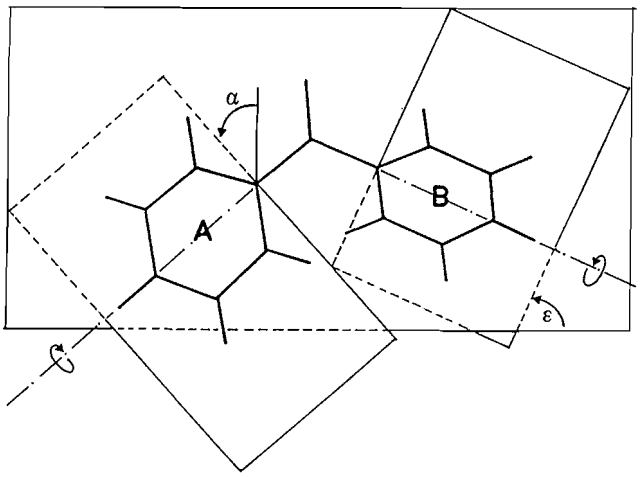


FIG. 5. Conformation of the benzophenone moiety.

In fact, the ratio (R^i_{ns}/R^i_s) for any proton i allows evaluation of the extent to which pairwise dipole–dipole interactions provide the relaxation mechanism (the ratio is 1.5 for a purely dipolar mechanism).

In the limit of 100% contribution from the ^1H–^1H dipole–dipole relaxation mechanism, eqs. [4]–[6] can be given:

$$[4] \quad R^i_{ns} = \sum_{i \neq j} \rho_{ij} + \sum_{i \neq j} \sigma_{ij}$$

$$[5] \quad R^i_s = \sum_{i \neq j} \rho_{ij}$$

$$[6] \quad R^{in}_{ds} = \sum_{i \neq j} \rho_{ij} + \sigma_{in}$$

where ρ_{ij} and σ_{ij} are the direct- and cross-relaxation rates respectively for any proton pair (eqs. [7] and [8]) (21) where r_{ij} is the interproton distance, ω is the proton Larmor frequency, and τ_c is the motional correlation time.

$$[7] \quad \rho_{ij} = \frac{1}{10}\frac{\hbar^2\gamma_H^4}{r_{ij}^6}\left\{\frac{3\tau_c}{1+(\omega\tau_c)^2} + \frac{6\tau_c}{1+(2\omega\tau_c)^2} + \tau_c\right\}$$

$$[8] \quad \sigma_{ij} = \frac{1}{10}\frac{\hbar^2\gamma_H^4}{r_{ij}^6}\left\{\frac{6\tau_c}{1+(2\omega\tau_c)^2} - \tau_c\right\}$$

It is evident from eqs. [5] and [6] that eq. [9] holds,

$$[9] \quad R^{in}_{ds} - R^i_s = \sigma_{in} = \frac{1}{10}\frac{\hbar^2\gamma_H^4}{r_{in}^6}\left\{\frac{6\tau_c}{1+(2\omega\tau_c)^2} - \tau_c\right\}$$

which, in the limit of the extreme narrowing region, reduces to eq. [10]:

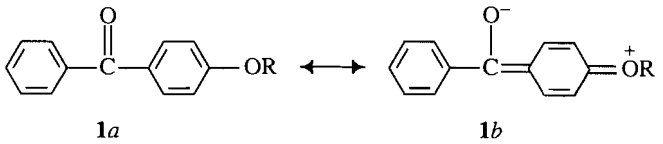
$$[10] \quad \sigma_{in} = \frac{1}{2}\frac{\hbar^2\gamma_H^4}{r_{in}^6}\tau_c$$

Then the measurement of double-selective and mono-selective proton spin-lattice relaxation rates allows determination of proton–proton distances if τ_c is known from other sources (or vice versa as was applied formerly in eq. [3]). It is also possible to calculate the distance between the H3 and H7 protons; indeed:

$$[11] \quad R^7_{ns} - R^7_s = \sigma_{7,3} + \sigma_{7,8}$$

$$[12] \quad R^7_{7,8} - R^7_s = \sigma_{7,8}$$

$$[13] \quad \sigma_{7,3} = (R^7_{ns} - R^7_s) - (R^7_{7,8} - R^7_s)$$



1*a* 1*b*

FIG. 6. Mesomeric forms of substituted benzophenones.

and, then, from eq. [10], using $\tau_c B = 1.52 \times 10^{-10}$ s we obtained $r_{7,3} = 2.6$ Å. This distance alone is insufficient to define the conformation of the benzophenone moiety (see Fig. 5). One of the angles (α or ε) must also be specified. It is well known that benzophenone cannot be coplanar ($\alpha = \varepsilon = 0°$) due to the steric repulsion between *ortho* protons (22, 23). The values of these two angles were calculated using various techniques (24*a*–*d*) and the most reliable values are $\alpha = \pm 30°$ and $\varepsilon = \pm 30°$ (for this geometry $r_{3,7} = 2.4$ Å).

The presence of a *para* substituent does not at first seem to influence the conformation of benzophenone as do *ortho* and *meta* substituents (25); however, in *para*-substituted benzophenones, it has been demonstrated that the chemical shift of the C4 carbon atom correlates with the F and R substituent constants in a reversed manner (26) (F is the field/inductive constant and R is the resonance constant) (27). The observations on *para*-substituted benzophenones show that C4 is not in direct conjugation with the *para* substituent and the situation can be described by the mesomeric forms **1***a* and **1***b* (see Fig. 6). Then, in the real structure, the carbonyl group should be nearly coplanar with ring B, at which point the $r_{3,7}$ distance allows the calculation of $\alpha = \pm 74°$.

From proton relaxation data of the H8 proton it is also possible to calculate the mean distance between the H8 and H10 protons ($\bar{r}_{8,10}$):

$$[14] \quad R^8_{ns} - R^8_s = \sigma_{8,7} + \sigma_{8,10}$$

$$[15] \quad \sigma_{8,10} = (R^8_{ns} - R^8_s) - (R^8_{7,8} - R^8_s)$$

from which, using $\tau_c B = 1.52 \times 10^{-10}$ s, $r_{8,10} = 2.3$ Å.

To investigate the possible main conformation(s) of the alkyl chain we made use of the homonuclear Overhauser effect.

The origins of the ^1H–$\{^1H\}$ nOe have been extensively investigated and a comprehensive review published (21). We did not find any non-trivial nOe effect; the measurements were also repeated in a 0.01 M solution without any significant results: only trivial nOe's were observed.

These data confirm the presence of a "linear" main mean conformation for **1** in $CDCl_3$ solution: the main rotation axis is as previously defined and, in addition, the segmental motion of the alkyl chain takes place along this axis; this does not exclude the possibility of folding, but stable main conformation(s) with extensive folding of the alkyl chain must definitely be ruled out.

(b) In 0.1 M DMSO-d_6

^{13}C chemical shifts and relaxation rates (R_1) of compound **1** in DMSO-d_6 are shown in Table 5.

It is important to note that in this solvent C1 and C7 carbon atoms have the same chemical shift (134.05 ppm); the corresponding relaxation rate ($R_1 = 2.04$) is very close to the relaxation rate of C8 ($R_1 = 2.08$), as is to be expected. On the other hand, analysis of the spectra of the inversion–recovery sequence for the determination of T_1 shows that the resonance at 134.05 ppm behaves as a single line. In a recent paper (28) on the dynamics of *para*-substituted benzophenones, where the *para* substituents are *n*-alkyloxy groups (n = 8, 11, 13) or *n*-alkyl and ω-alkenyl esters of *para*-benzophenone carboxylic

Can. J. Chem. Downloaded from www.nrcresearchpress.com by 198.100.157.202 on 09/07/12
For personal use only.

Can. J. Chem. Downloaded from www.nrcresearchpress.com by 198.100.157.202 on 09/07/12
For personal use only.

TABLE 5. ^{13}C chemical shifts[a] and spin-lattice relaxation rates for compound **1** (0.1 mol dm^{-3} in DMSO-d_6, T = 298 K)

	Chemical shift (ppm)	R_1 (s^{-1})
C5	196.30	0.11±0.01
C9	163.75	0.19±0.01
C4	139.66	0.09±0.01
C1,7	134.05	2.04±0.06
C6	131.66	0.16±0.01
C3	131.10	1.03±0.02
C2	130.36	1.01±0.02
C8	116.38	2.08±0.06
C10	67.04	4.35±0.21
C14	65.02	7.14±0.24
C12	62.17	6.25±0.28
C13	52.20	3.85±0.19
C13′	52.16	4.54±0.23
C23	33.17	0.49±0.02
C20,21	30.90	1.05±0.05
C19	30.84	1.41±0.07
C18	30.72	1.61±0.06
C22	30.58	0.80±0.04
C17	30.40	1.96±0.11
C16	27.68	2.78±0.12
C11	24.08	4.17±0.23
C24	23.97	0.36±0.02
C15	23.64	4.35±0.20
C25	15.81	0.27±0.01

[a]Measured downfield from internal TMS.
[b](±) Figures denote approximate 95% confidence limits of the exponential regression analysis.

TABLE 6. Nuclear Overhauser enhancements[a] for selected proton resonances of compound **1** (0.1 and 0.01 mol dm^{-3} in DMSO-d_6, T = 298 K)

		Enhancement	
Proton irradiated	Proton observed	0.1 M	0.01 M
H15	H12	0.050	0.046
H25	H7	0.064	0.057

[a]Errors in the nOe's were evaluated at ±10%.

acid, it appears that the relaxation rate of C1 is always very close to or equal to those of C7 and C8 (this is also true for the 0.1 M solution of **1** in $CDCl_3$). For this reason, we consider R = 2.04 to be the relaxation rate of C1 as well.

The same arguments as those developed for the delineation of the dynamics of **1** in $CDCl_3$ were used, and the application of eqs. [1] and [2] yielded all the τ_c and τ_g values (see Table 2).

Analysis of the correlation times revealed the following: (i) τ_gB is practically equal to τ_cB (1.12×10^{-10} s and 1.14×10^{-10} s respectively): internal librational motions for ring B are absent; also τ_cA (1.03×10^{-10} s) is close to τ_cB, so internal motions of the benzophenone moiety as a whole are severely restricted; (ii) τ_c10 and τ_c11 have values close to τ_cA and τ_cB, suggesting that this part of the chain reorients jointly with the benzophenone moiety; the methylene carbon atoms directly bonded to the quaternary nitrogen atoms, C12 and C14, show the longest τ_c in the molecule, corresponding to the slowest motions; (iii) from C15 onwards, segmental motion takes place.

Points (i) and (ii) are in striking contrast with the situation

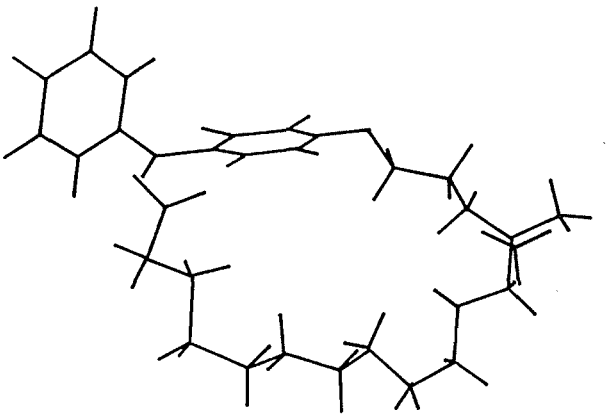


FIG. 7. Projection of the Dreiding model of the "most probable" conformation of compound **1** in 0.1 M DMSO-d_6 solution as inferred from NMR experiments.

outlined in $CDCl_3$: these differences are probably a consequence of the different main mean conformation(s) presented by **1** in the two solvents.

Once again possible further information on the conformation can be obtained using proton relaxation rates and the ^1H–{^1H} nuclear Overhauser effect. (For ^1H chemical shifts and coupling constants see Table 3.)

From proton relaxation rates, the interproton distances $r_{3,7}$ = 2.4 Å and $r_{8,10}$ = 2.1 Å were extracted; the same rationale as applied before permitted the evaluation of $\alpha = \pm 60°$. The geometry of the benzophenone moiety changes slightly on passing from $CDCl_3$ to DMSO.

Surprising results were obtained from the nOe's: neat nuclear Overhauser effects are present between H12 and H15 and between H7 and H25 (see Table 6). These same effects are present with practically the same values in a 0.01 M solution: thus they are intramolecular effects.

These nOe's are consistent with a folded conformation where the alkyl chain forms a loop toward the aromatic ring B (see Fig. 7). This main conformation as deduced from nOe's is consistent with the corresponding dynamic situation: (i) in the folded conformation the molecule adopts an ellipsoidal shape; the main axis of the ellipsoid (which passes near or through the nitrogen atom) is very probably the main rotation axis; (ii) the presence of the alkyl chain in the proximity of the aromatic moiety has little influence on its main conformation, but it greatly affects its local motions: indeed, it competes with the aromatic moiety for the same spatial region; as a consequence, internal motions in the benzophenone moiety are severely restricted (above all, those of ring B).

We maintain that this drastic change in the main mean conformation in the two solvents could be brought about by three main factors: (i) the ion–dipole interactions between the quaternary nitrogen atom and DMSO that slow down the corresponding motions (29); (ii) the more-or-less central location of the nitrogen atom in the molecule; and (iii) the lyophobic environment created by DMSO, which leads the alkyl chain and the benzophenone moiety to expose the least possible surface area to the solvent. (The latter is accomplished by adopting a folded conformation in which the two frameworks converge upon each other.)

This change in the main mean conformation in the two solvents either masked or eliminated any evidence of a coiled structure, i.e., the type of conformation associated with antimicrobial activity, toxicity, and irritation of the skin.

However, it is possible that the molecule adopts its main mean conformations in response to environmental changes: a property which could be correlated with its antimicrobial activity.

Experimental

The compound under investigation was synthesized as already described (9). Solutions were made in 99.8% DMSO-d_6 and 99.8% $CDCl_3$ and were carefully deoxygenated. NMR measurements were carried out with a Varian XL-200 Fourier transform spectrometer. Chemical shifts were referred to internal TMS. Spin-lattice relaxation rates were measured using the inversion–recovery pulse sequence; 4 and 100 FIDs were collected for ^1H and ^{13}C T_1 measurements respectively. The relaxation rate was calculated with a three-parameter exponential regression analysis of the recovery curves of longitudinal magnetization components.

Selective and double-selective relaxation rates were measured using inversion–recovery pulse sequences where the π pulse was given by the proton decoupler at selected frequencies at low power for relatively long times (30). A typical setting for a selective π pulse was 20 db power attenuation and 20 ms pulse width. The selective rate was measured (31) in the initial slope approximation by considering only the first part of the recovery curve; ^{13}C–$\{^1H\}$ and ^1H–$\{^1H\}$ nOe's were measured with gated decoupling techniques using nOe difference pulse sequences.

Acknowledgments

This research was funded by the Italian Ministry of Public Instruction (40%) and by the National Research Council (CNR, Progetto Strategico).

1. N. A. Shaath. Cosmet. Toiletries, **102**, 21 (1987).
2. C. Fox. Cosmet. Toiletries, **102**, 41 (1987).
3. E. D. Goddard. Cosmet. Toiletries, **102**, 71 (1987).
4. C. Anselmi, A. Camparini, and M. Scotton. J. Heterocycl. Chem. **20**, 687 (1983).
5. M. Checchi, M. F. Saettone, B. Giannaccini, B. Pach, and C. Anselmi. Cosmet. Toiletries, Ed. Int. 35 (1986).
6. G. Adembri, C. Anselmi, A. Camparini, M. F. Saettone, and M. Scotton. C.N.R. Patent Appl. 47509/A 86 (1986).
7. G. Adembri, C. Alderigi, C. Anselmi, B. Giannaccini, M. G. Rossetti, M. F. Saettone, and M. Scotton. C.N.R. Patent Appl. 48245/A 88 (1988).
8. G. Adembri, C. Anselmi, A. Camparini, M. G. Rossetti, and M. Scotton. J. Heterocycl. Chem. **25**, 1019 (1988).
9. M. F. Saettone, C. Alderigi, B. Giannaccini, C. Anselmi, M. G. Rossetti, M. Scotton, and R. Cerini. Int. J. Cosmet. Sci. **10**, 99 (1988).
10. M. F. Saettone, B. Giannaccini, C. Morganti, A. Persi, and C. Cipriani. Int. J. Cosmet. Sci. **8**, 9 (1986).
11. J. Garcia Dominguez, J. L. Parra, M^A R. Infante, C. M. Pelejero, F. Balaguer, and T. Sastre. J. Soc. Cosmet. Chem. **28**, 165 (1977).
12. D. W. Blois and J. Swarbrick. J. Pharm. Sci. **61**, 393 (1972).
13. (*a*) L. B. Alemany. Magn. Reson. Chem. **27**, 1065 (1989); (*b*) B. Shoulders and S. C. Welch. J. Chem. Educ. **64**, 915 (1987); (*c*) F. W. Werlhi. *In* Topics in carbon-13 NMR spectroscopy. Vol. 2. *Edited by* G. C. Levy. Wiley, New York. 1976. p. 343.
14. J. R. Lyerla, Jr. and G. C. Levy. *In* Topics in carbon-13 NMR spectroscopy. Vol. 1. *Edited by* G. C. Levy. Wiley, New York. 1974. p. 74.
15. A. Allerhand, D. Doddrell, and R. Komoroski. J. Chem. Phys. **55**, 189 (1971).
16. F. W. Wehrli and T. Wirthlin. Interpretation of carbon-13 NMR spectra. Heyden, London. 1980.
17. M. N. Frey, T. F. Koetzle, M. S. Lehmann, and W. C. Hamilton. J. Chem. Phys. **58**, 2547 (1973).
18. C. W. M. Grant, L. D. Hall, and C. M. Preston. J. Am. Chem. Soc. **95**, 7742 (1973).
19. L. D. Hall. Chem. Soc. Rev. **4**, 401 (1975).
20. L. D. Hall, K. F. Wong, and H. D. W. Hill. J. Chem. Soc. Chem. Commun. 951 (1979).
21. J. H. Noggle and R. E. Shirmer. The nuclear Overhauser effect. Academic Press, New York. 1971.
22. E. B. Fleischer, N. Sung, and S. Hawkinson. J. Phys. Chem. **12**, 4311 (1968).
23. G. M. Lobanova. Crystallographia, **13**, 984 (1968).
24. (*a*) E. J. Moriconi, W. F. O'Connor, and W. F. Forbes. J. Am. Chem. Soc. **82**, 5454 (1960); (*b*) G. W. Buchanan, G. Montaudo, and P. Finocchiaro. Can. J. Chem. **52**, 597 (1974); (*c*) G. Pfister-Guillozo, M. Grimaud, and J. Deschamps. Bull. Soc. Chim. Fr. 1203 (1969); (*d*) M. Grimaud, M. Loudet, R. Royer, and G. Pfister-Guillozo. Bull. Soc. Chim. Fr. 1161 (1974); 1176 (1974); 1189 (1974); 1935 (1974); 1976 (1974); 1983 (1974).
25. M. Grimaud and G. Pfister-Guillozo. Org. Magn. Reson. **7**, 386 (1975).
26. A. W. Frahm and H. F. Hambloch. Org. Magn. Reson. **14**, 444 (1980).
27. C. G. Swain and E. C. Lufton, Jr. J. Am. Chem. Soc. **90**, 4328 (1968).
28. P. Dais. Magn. Reson. Chem. **27**, 161 (1989).
29. G. C. Levy, A. D. Godwin, J. M. Hewitt, and C. Sutcliffe. J. Magn. Reson. **29**, 553 (1978).
30. G. Valensin, G. Sabatini, and E. Tiezzi. *In* Advanced magnetic resonance techniques in systems of high molecular complexity. *Edited by* N. Niccolai and G. Valensin. Birkanser, Boston. 1986. p. 69.
31. R. Freeman, H. D. Hill, B. L. Tomlinson, and L. D. Hall. J. Chem. Phys. **61**, 4466 (1974).

Can. J. Chem. Downloaded from www.nrcresearchpress.com by 198.100.157.202 on 09/07/12
For personal use only.

C—H...O=C and C—H...H—C interactions in the side chains of 2-isopropylbenzaldehyde. A negative $^5J(CHO,CH(CH_3)_2)$

TED SCHAEFER[1] AND KERRY J. COX
Department of Chemistry, University of Manitoba, Winnipeg, Man., Canada R3T 2N2

Received October 1, 1990

TED SCHAEFER and KERRY J. COX. Can. J. Chem. **69**, 919 (1991).

The ^1H nuclear magnetic resonance spectra of 2-isopropylbenzaldehyde in CS_2/C_6D_{12} and acetone-d_6 solutions provide the chemical shifts and coupling constants of all the protons. The long-range coupling constants involving the side-chain protons yield certain sums of the populations of the four putatively planar conformations. The *o-anti* conformers have a fractional population of 0.55(3) in the polar and of 0.49(3) in the nonpolar solvent. The conformers in which the methine C—H bond lies *cis* to the aldehyde group have a fractional population of 0.83(3) in both solutions. The close approach of the methine and aldehydic hydrogen atoms in one conformer is indicated by a negative proximate coupling constant between their protons of −0.39(1) Hz. The chemical shifts of the ring and of the side-chain protons are consistent with the conformer populations deduced from the long-range coupling constants and also with the indications that the side chains do not, on average, deviate from "coplanarity" with the ring by much more or less than in the parent compounds. The C—H...H—C and C—H...O=C interactions in the *o-syn* and *o-anti* conformers are most likely repulsive and of very similar magnitude and lead to a significant deshielding of the protons in these moieties. Molecular orbital computations are also reported and are an aid in estimating the populations of the individual conformers. The STO-3G MO structures have H...H and H...O distances well below the sums of the van der Waals radii of hydrogen and oxygen atoms in the conformers with the methine C—H bond placed *cis* to the aldehyde group, yet these are computed to be by far the most abundant by the STO-3G as well as by AM1 algorithms.

Key words: 2-isopropylbenzaldehyde, conformations of; 2-isopropylbenzaldehyde, proximate spin–spin coupling constants in; MO calculations, STO-3G, and AM1 on 2-isopropylbenzaldehyde, ^1H NMR and long-range spin–spin coupling constants in 2-isopropylbenzaldehyde.

TED SCHAEFER et KERRY J. COX. Can. J. Chem. **69**, 919 (1991).

Les spectres en résonance magnétique nucléaire du ^1H du 2-isopropylbenzaldéhyde dans des solutions de CS_2/C_6H_{12} et d'acétone-d_6 permettent de déterminer les déplacements chimiques et les constantes de couplage de tous les protons. Les constantes de couplage à longue distance impliquant les protons de la chaîne latérale fournissent certaines sommes de populations des quatre conformations putativement planaires. Les populations fractionnaires des conformères *o-anti* sont respectivement de 0,55(3) et de 0,49(3) dans les solvants polaire et non-polaire. Les populations fractionnaires des conformères dans lesquels la liaison C—H méthine est *cis* par rapport au groupement aldéhydique sont égales à 0,83(3) dans les deux solvants. Le grand rapprochement des atomes d'hydrogène méthinique et aldéhydique dans un conformère se reflète par une constante de couplage de proximité négative (−0,39(1) Hz) entre leurs protons. Les déplacements chimiques des protons du cycle et de la chaîne latérale sont en accord avec les populations de conformères déduites à partir des constantes de couplage à longue distance ainsi qu'avec les indications à l'effet que, en moyenne, les chaînes latérales ne dévient pas plus de la «coplanéité» avec le cycle que les composés parents. Les interactions C—H...H—C et C—H...O=C dans les conformères *o-syn* et *o-anti* sont probablement répulsives et d'amplitudes très semblables et elles conduisent à un déblindage important des protons de ces portions. On a aussi effectué des calculs d'orbitales moléculaires qui sont utiles pour évaluer les populations des conformères individuels. Dans les structures des OM STO-3G, les distances H...H et H...O sont beaucoup plus faibles que les sommes des rayons de van der Waals des atomes d'hydrogène et d'oxygène dans les conformères où la liaison méthine C—H est *cis* par rapport au groupement aldéhydique; il n'en reste pas moins que, d'après des calculs avec une base STO-3G ainsi qu'avec des algorithmes AM1, ces structures sont les plus abondantes.

Mots clés : 2-isopropylbenzaldéhyde, conformations; 2-isopropylbenzaldéhyde, constantes de couplage de proximité; calculs OM, STO-3G, AM1, 2-isopropylbenzaldéhyde; RMN ^1H et constantes de couplage à longue distance, 2-isopropylbenzaldéhyde.

[Traduit par la rédaction]

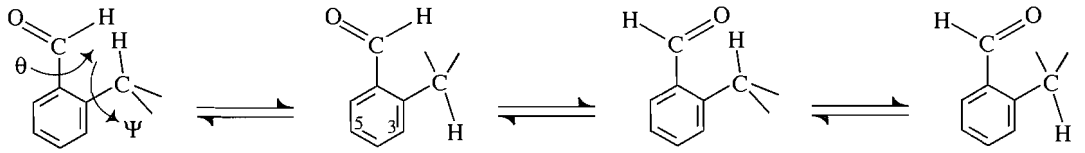
Introduction

There is considerable evidence, extracted mainly from crystallographic data bases in recent years (1), for the existence of intermolecular hydrogen bonding by C—H bonds. Such hydrogen bonds, defined in terms of close contacts, involve slightly acidic C—H bonds found in acetylenic, ethylenic, and sometimes in alkanic groupings. The latter normally contain one or more electronegative substituents attached to the carbon atom of the C—H bond. However, there exist recent reports of inter- and intramolecular hydrogen bonds formed by C—H bonds of methyl groups and the oxygen atoms in water or ether linkages (2, 3). Infrared spectra of intermolecular C—H hydrogen bonds formed in host matrices are also abundant (4).

It is perhaps not always clear that a short contact arises from the formation of a C—H..X hydrogen bond, caused predominantly by electrostatic attraction (1), it being conceivable that the intermolecular contact is determined by other crystal packing forces or possibly by repulsive intramolecular interactions in a molecule. For example, for the crystal of 2,4,6-trinitrotoluene (5) an intramolecular C—H...O bond is deduced from an H...O distance of 2.39 Å, a distance of less than 2.70 Å being sometimes taken as indicative of a hydrogen bond (6, 7), and is apparently confirmed (8) by infrared and nmr spectra in solution. However, the nitro groups placed *ortho* to the methyl substituent are twisted substantially out of the aromatic plane. One might surmise that repulsion between the substituents causes this twist and that the short H...O contacts are therefore a consequence of an energetic compromise between repulsion,

[1]Author to whom correspondence may be addressed.

Can. J. Chem. Downloaded from www.nrcresearchpress.com by 198.100.157.202 on 09/07/12
For personal use only.



1 θ = 0 Ψ = 0 2 3 4

which causes the twist, and the conjugationally driven tendency to coplanarity of the nitro groups; the internal barrier to rotation in nitrobenzene is 13.6 kJ/mol or perhaps somewhat lower (9).

The capacity of the methine C—H bond of the isopropyl group as a proton donor in a hydrogen bond is probably very little different from that of a C—H bond in a methyl group. The carbonyl group, however, is an excellent acceptor in a hydrogen bond. Suppose that the carbonyl group is constrained to one or two orientations in a molecule, as in benzaldehyde, for example, in which the internal rotational barrier in solution is greater than 30 kJ/mol (10). The barrier is large compared to thermal energies at 300 K, so that a planar conformation is a good approximation in the description of the molecule. By way of contrast, the barrier to rotation about the C_{sp^2}—C_{sp^3} bond in isopropylbenzene in solution is very likely less than 10 kJ/mol (11). Hence, in 2-isopropylbenzaldehyde, where a six-membered-ring intramolecular C—H...O=C hydrogen bond, analogous to the strong one (12, 13) in the 2-hydroxy derivative, is conceivable (such bonds forming in preference to intermolecular ones (14)), a high stability of such a bond should be evinced by a preponderant population of **3**.

Alternatively, repulsive interactions in **3** and **1** might be relieved by twists about the C_{sp^2}—C_{sp^3} bond rather than about the exocyclic C_{sp^2}—C_{sp^2} bond (the idealized planar conformers, **1**–**4**, are understood to be those in which the C_{sp^3}—C_{sp^3} bonds are staggered about the aromatic C—H(3) bond in **1** and **3** and C—H or C=O bonds of the aldehyde group in **2** and **4**). The anticipated, repulsive C—H...H—C forces in **1**, models indicating an H,H distance of less than 2 Å, would favor **3**, given that congestion in **2** and **4** renders small their populations.

Now, long-range coupling constants between aldehydic and ring protons in benzaldehyde and its derivatives (15, 16) and between benzylic and ring protons in isopropylbenzene (11) are stereospecific. Those over five formal bonds are closely related to the populations of **1**–**4**, while those over six bonds are a measure of the out-of-plane motion of the side chains (deviations of θ and ψ from zero in **1**, for example). Accordingly, analyses of the ^{1}H nmr spectra in a nonpolar as well as in a polar solvent should provide information about the populations of **1**–**4** and about their solvent dependence. Such analyses are reported here. A by-product of the latter is the detection of a negative coupling constant between the aldehydic and methine protons, very likely a proximate interaction, providing evidence for a close approach of these protons in **1**. In addition, some molecular computations of the relative energies and of the geometries of the four conformers represent an attempt at gauging attraction or repulsive forces between the side-chain moieties.

Experimental

The 2-isopropylbenzaldehyde was prepared (17) as follows. To 6.1 mmol of 2-bromoisopropylbenzene (Lancaster) in 25 mL of diethyl ether under nitrogen was added 14.3 mmol of lithium. The formation of aryl-lithium intermediate was aided by immersing the vessel in an ultrasound bath for 2 h at room temperature. Still under nitrogen, 6.1 mmol of *N,N*-dimethylformamide was added and the reaction proceeded, with stirring, for 30 min. The reaction was quenched with an excess of aqueous NH_4Cl (saturated). The mixture was shaken with 25 mL of diethyl ether. The ether layer was dried over $MgSO_4$ and evaporated. The product was purified on a silica gel column with hexane as a solvent. The yield was ca. 40%.

Solutions of 2-isopropylbenzaldehyde in CS_2/C_6D_{12}/TMS and acetone-d_6/TMS solvent mixtures (see Table 1 for details) were filtered into 5-mm o.d. nmr sample tubes. These were degassed by four cycles of the freeze–pump–thaw procedures and then flame-sealed to yield symmetrical closures.

The ^{1}H nmr spectra were accumulated on a Bruker AM300 spectrometer at a probe temperature of 300 K. Figure 1 displays the spectrum of the aldehydic proton in acetone-d_6 solution; the caption gives the acquisition conditions. The figure also illustrates an experiment (18) designed to determine the sign of $^5J(CHO,CH(CH_3)_2)$.

The ^{1}H nmr spectra were analyzed with the computer program NUMARIT (19), extensively reworked by R. Sebastian in this laboratory. The spectral parameters appear in Table 1, together with analytical conditions.

STO-3G MO (20) and AM1 (21) computations employed the program GAUSSIAN 86 (22) on an Amdahl 5870 computer. All bond angles and lengths were optimized with the constraint that the carbon and hydrogen atoms of the benzene moiety remain in a plane. CNDO/2 and INDO MO FPT (23, 24) computations of spin–spin coupling constants utilized the STO-3G geometries.

Results and discussion

The populations, $p_1 + p_2$ *(o-anti) and* $p_3 + p_4$ *(o-syn)*

The available evidence (12, 25) strongly suggests that ^5J(H,CHO) in benzaldehyde and its derivatives is highly stereospecific; ^5J(H-3,CHO) ≡ $^5J_3$ in **1**, for example, is implied as vanishing whereas ^5J(H-5,CHO) ≡ $^5J_5$ is large. If this is so, then $p_1 + p_2$ follows from the coupling constants in Table 1 as $^5J_5/(^5J_3 + {}^5J_5)$ or 0.58 in acetone-d_6 and as 0.52 in CS_2/C_6D_{12}; hence $p_3 + p_4$, the sum of the fractional populations of **3** and **4**, the *o-cis* conformers, is 0.42 and 0.48, respectively. The higher population of the *o-anti* conformers in the more polar solvent is consistent (26) with their higher computed dipole moments at the STO-3G level of *ab initio* molecular orbital theory (see below).

This treatment assumes that the all-*trans* ^5J_t, that is, ^5J(H,CHO) in **1** and **3**, is not perturbed by the isopropyl substituent. In that event, $^5J_5 + {}^5J_3$ should be the same as in benzaldehyde, where this sum is 0.860(2) Hz in acetone-d_6 and 0.862(4) in CS_2/C_6D_{12} (25); in 2-fluorobenzaldehyde, for example, $^5J_3 + {}^5J_5$ does not deviate from these sums by more than 0.01 Hz (16). However, in 2-isopropylbenzaldehyde the sums are about 0.05 Hz smaller than in benzaldehyde, implying that the limiting values of ^5J_t need not be the same in the *o-syn* and *o-anti* conformers. Defining $^5J_{3,t}$ and $^5J_{5,t}$ as these values and the populations of the *o-syn* conformers, say, in the two solutions as the other two unknowns, one obtains four equations. These yield $^5J_{5,t}$ as 0.895 Hz and $^5J_{3,t}$ as 0.723 Hz, and $p_1 + p_2$ as 0.53 and 0.47 in acetone-d_6 and CS_2/C_6D_{12}, respectively. $^5J_{3,t}$ is much less than its value in benzaldehyde

Can. J. Chem. Downloaded from www.nrcresearchpress.com by 198.100.157.202 on 09/07/12
For personal use only.

TABLE 1. The ^{1}H nmr spectral parameters for 2-isopropylbenzaldehyde at 300 K in CS_2/C_6D_{12} and acetone-d_6 solutions

Parameter	CS_2/C_6D_{12}[a]	Acetone-d_6[b]	Parameter	CS_2/C_6D_{12}[a]	Acetone-d_6
ν(CHO)	3059.957(1)[c]	3112.755(1)	^4J(H,CHO)	−0.273(1)	−0.264(1)
ν(CH)	1185.5	1214.0	^5J(H-3,CHO)	0.383(1)	0.341(1)
ν(CH_3)	378.2[e]	385.1[e]			
ν_3	2208.959(1)	2262.350(1)	^5J(H-5,CHO)	0.421(1)	0.473(1)
ν_4	2230.121(1)	2281.980(1)	^6J(H-4,CHO)	−0.014(1)	−0.017(1)
ν_5	2175.037(1)	2218.858(1)	^5J(H-4,CH)	0.500(1)	0.503(1)
ν_6	2300.599(1)	2349.096(1)	^5J(H-6,CH)	0.167(1)	0.168(1)
$^3J_{34}$	7.877(1)	7.905(1)[f]	^6J(H-5,CH)	−0.265(1)	−0.252(1)
$^3J_{45}$	7.326(1)	7.340(1)	^5J(CHO,CH)	−0.376(1)	−0.388(1)[d]
$^3J_{56}$	7.687(1)	7.721(1)	Transitions calcd.	192	192
$^4J_{35}$	1.191(1)	1.179(1)	Observed peaks	127	122
$^4J_{46}$	1.546(1)	1.545(1)	Transitions assigned	137	138
$^5J_{36}$	0.503(1)	0.515(1)	Largest difference	0.007	0.006
^4J(H,CH)	−0.559(1)	−0.555(1)	Root-mean-square error	0.002_5	0.002

[a] 4.0 mol% in CS_2, containing also 10 mol% of C_6D_{12} and 0.5 mol% TMS.
[b] 4.0 mol% in acetone-d_6 with 0.5 mol% TMS.
[c] In Hz at 300.135_2 MHz to high frequency of internal TMS. Numbers in parentheses are the standard deviations in the last significant figure.
[d] From the double resonance sign determination (Fig. 1).
[e] ^3J(CH,CH_3) is 6.86 Hz in both solutions and ^5J(H-3,CH_3) is ±0.10(2) Hz.
[f] The commonly larger coupling constants between ring protons in the more polar solvent for benzene derivatives is fairly general (11, 25) and is not an artefact of the analyses.

and reminiscent of the 0.623(4) Hz in salicylaldehyde in which ^5J(H-5,CHO) vanishes, the molecule existing as one conformer (12). The unprecedented perturbation of ^5J(H-3,CHO) in salicylaldehyde may well be a consequence of the perturbation of the carbonyl group orbitals during formation of the relatively strong hydrogen bond (it is known (27) that the $2p_z$ orbital on oxygen plays a significant role in the transmission of nuclear spin state information). The apparently somewhat smaller reduction of $^5J_{3,t}$ in the *o-syn* conformers of 2-isopropylbenzaldehyde suggests that the C—H...O=C interaction also causes a decrease in ^5J(H,CHO). This result does not establish this interaction as attractive; repulsion might also decrease the coupling magnitude. CNDO/2 and INDO MO FPT computations on the STO-3G structures yield $^5J_{3,t}$ in **3** as 0.1 Hz smaller in magnitude than $^5J_{5,t}$ in **1**, in qualitative agreement with the deduction above.

However this may be, it is probably safe to conclude that $p_1 + p_2$ is $0.55_5 \pm 0.02_5$ in acetone-d_6 and $0.49_5 \pm 0.025$ in CS_2/C_6D_{12} solutions at 300 K. These numbers are the averages of the two sets of estimates above and the errors easily encompass the small uncertainties in the measured coupling constants.

The o-syn and o-anti *populations in the vapor by extrapolation*

The populations of the *o-syn* and *o-anti* conformers above correspond to free energy differences at 300 K of −0.55 ± 0.25 kJ/mol in acetone-d_6, favoring *o-anti*, and 0.05 ± 0.25 kJ/mol in CS_2/C_6D_{12}. Because the *o-anti* conformers are more polar than the *o-syn* (see below), the reaction field model (26) predicts a stabilization of the former in acetone-d_6. Furthermore, empirically (see p. 562 of ref. 26) it is found that the stabilization of the more polar form by CS_2 relative to the vapor is approximately that by acetone-d_6 relative to CS_2. Hence an estimate of the stability of the conformers in the vapor follows as 0.65 ± 0.35 kJ/mol in the free energy difference, *o-syn* favored, corresponding to an equilibrium constant of 1.28 ± 0.15.

If the free energy difference in the acetone-d_6 solution is equated to the enthalpy difference, then the *o-syn* population at 113 K is 0.36 ± 0.06. At about this temperature in a CHF_2Cl solution, concentration not given (17), this population, based on the ^{1}H nmr spectrum at 100 MHz of the aldehyde proton, is reported as 0.15. Given the different solvent, the possibility of small entropy differences between the conformers, and the possibility of some error in the measurements at low temperatures (compare, for example, the substantial differences in the estimates of the populations of the conformational isomers of 2-methylbenzaldehyde obtained by ^{13}C and ^{1}H nmr measurements at low temperatures (17, 28)), the disagreement is very likely only apparent.

The populations, $p_1 + p_3$, *and* $p_2 + p_4$

These populations are retrievable from ^5J(H-4,CH) ≡ $^5J_4$ and ^5J(H-6,CH) ≡ $^5J_6$, treated as follows. These coupling constants contain a σ−π component, proportional to $\langle \sin^2 \psi \rangle$, see **1**; this expectation value is given by ^6J(H-5,CH)/$^6J_{90}$ where $^6J_{90}$ is ^6J when the methine C—H is twisted out of the aromatic plane by 90° and is −1.12 Hz (11). Hence $\langle \sin^2 \psi \rangle$ is −0.259(7)/−1.12 or 0.231(6). Proceeding as before (11), the σ−π components of $^5J_4$ and $^5J_6$ are 0.073(2) Hz. The σ components are obtained by subtraction of this number from the $^5J_4$ and $^5J_6$ values in Table 2, to yield 0.428(4) and 0.095(3) Hz, respectively. Hence $p_1 + p_3$ follows as 0.428(4)/0.523(7) or 0.82(2), implying that $p_2 + p_4$, the population of the conformers in which the methyl groups lie near the aldehyde moiety, is 0.18(2).

Again, however, $^5J_4 + {}^5J_6$, at 0.669(2) Hz, is larger than in isopropylbenzene (11), where this sum is 0.591(5) Hz in the same solvents. Because $^6J_5$ is effectively the same in the two compounds, the difference must be attributed to an increase in either $^5J_4^{\sigma}$ or $^5J_6^{\sigma}$ in the derivative. The CNDO/2 and INDO MO FPT computations, using the optimized STO-3G MO geometries, imply that $^5J_4^{\sigma}$ is larger than $^5J_6^{\sigma}$ by 0.1 Hz. Therefore, attribution of 0.428(4) + 0.078(7) = 0.506(11) Hz

Can. J. Chem. Downloaded from www.nrcresearchpress.com by 198.100.157.202 on 09/07/12
For personal use only.

Can. J. Chem. Downloaded from www.nrcresearchpress.com by 198.100.157.202 on 09/07/12
For personal use only.

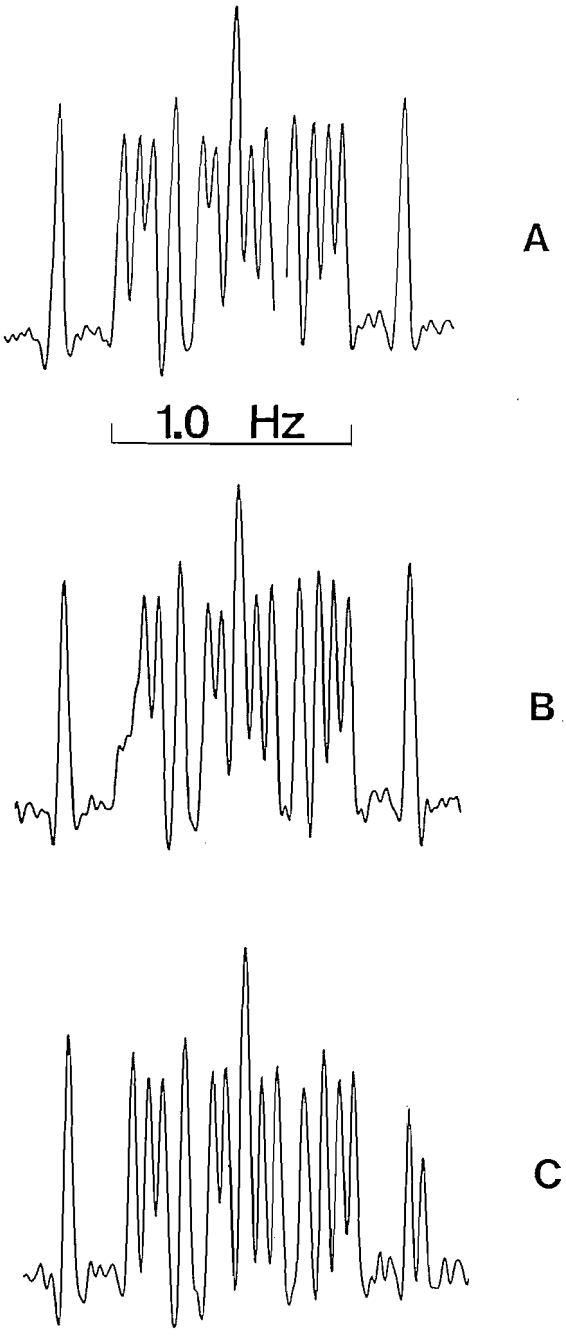


FIG. 1. In A the ^{1}H nmr spectrum of the aldehydic proton of 2-isopropylbenzaldehyde is shown for a 4.0 mol% solution in acetone-d_6 at 300 K, as controlled by the Bruker variable temperature device. The spectrum, obtained from 16 decays, occupies just over 1.4 Hz. The acquisition time per free induction decay is 41 s, the digital resolution is 0.006 Hz/point, and resolution enhancement (lb = −0.13 and gb = 0.60) has been applied before Fourier transformation. In B the same spectrum is shown under conditions in which a weak second radiofrequency field is applied to the peak at highest frequency in the multiplet due to H-5. For that peak the spin states of the ring protons coupled to H-5 are all positive, using the convention that positive spin states of coupled protons give rise to peaks at high frequency in the spectrum under observation; the spin state of the methine proton is negative, however, given that ^6J(H-5,CH) is negative because it is a $\sigma-\pi$ coupling constant (11). Together with the known (12) signs of ^4J(H,CHO), negative, and of ^5J(H,CHO), positive, it follows that the second peak from the left in A should be perturbed if ^5J(CH,CHO) is negative. This is observed to be the case (the J values in Table 1 can be used to construct the aldehyde spectrum and each peak can be labelled with the proton spin states of the other nuclei). In C the aldehydic proton spectrum is that for which a peak in the H-5 region is again being weakly irradiated by a second radiofrequency field; this time the spin states of H-4, H-6, and the methine proton are positive, but that of H-3 is negative. Accordingly, the peak at lowest frequency in A represents a transition with an energy level in common with the irradiated transition in the H-5 region if ^5J(CH,CHO) < 0. The result in C confirms the result in B.

TABLE 2. Dipole moments and relative energies of planar conformers **1–4** from geometry-optimized STO 3G and AM1 MO computations

	Energy[a]				Dipole moment	
Conformer	STO-3G	p_i^g	AM1	p_i^g	STO-3G	AM1
1[c]	4.107	0.16	0	0.63	2.068	0.778
2[d]	11.291	0.01	5.297	0.08	2.071	1.209
3[e]	0	0.81	1.953	0.29	1.637	1.032
4[f]	9.197	0.02	14.647	0.00	1.720	1.032

[a]In kJ/mol.
[b]In debye.
[c]Proximate C—H bonds in the side chains (see text), an *o-anti* conformer.
[d]Proximate C—H bond and CH_3 groups in the side chains.
[e]Proximate C=O and C—H bonds in the side chains, an *o-syn* conformer.
[f]Proximate C=O bond and CH_3 groups in the side chains.
[g]The fractional populations at 300 K based on a Boltzmann weighting.

to $^5J_4^\sigma$ and 0.095(3) Hz to $^5J_6^\sigma$, results in a $p_2 + p_4$ of 0.16(1); 0.078 Hz is the difference between 0.669(2) and 0.591(5) Hz above.

It appears that $p_1 + p_3 = 0.83(3)$ and $p_2 + p_4 = 0.17(3)$, independent of solvent. In view of the change in $p_1 + p_2$ induced by the more polar solvent, attributed to the higher dipole moment of the *o-anti* conformer in the previous section, this independence suggests that C=O...H—C and C—H...H—C repulsions in the side chains, or attractions, are nearly the same in magnitude. Furthermore, these interactions are relatively strongly favored over those of CHO with the methyl groups, the latter presumably being staggered about the C—H or C=O bonds of the aldehydic group.

That **2** and **4** have low populations is also suggested by the (probably proximate) coupling constants between the *ortho* ring protons and the methyl protons. In isopropylbenzene (11) the magnitude is ±0.04(1) Hz, whereas in the present compound ^5J(H-3,CH_3) is ±0.10(2) Hz. If this coupling constant is mediated by direct interactions, then it is expected to have a sizeable magnitude in only **1** and **3**. Comparison of the two magnitudes implies their consistency with a low population of **2** and of **4**.

Confirmation of the populational differences was also sought in STO-3G MO and AM1 computations, amenable to reasonable computing times.

*The theoretical relative energies of **1–4***

Presented in Table 2, the relative energies and dipole moments of the four planar conformers of 2-isopropylbenzaldehyde display large differences between the *ab initio* and semiempirical results. Populations in this table, derived from a simple exponential weighting, emphasize the disparity between the predictions for p_1 and p_3. However, there is agreement insofar as p_2 and p_4 are calculated as small at 300 K in the vapor and p_4 is computed as 0.02 and 0.00 by the two methods. In solution, the (more realistic) STO-3G dipole moments suggest

Can. J. Chem. Downloaded from www.nrcresearchpress.com by 198.100.157.202 on 09/07/12
For personal use only.

that p_2 is additionally favored over p_4, the latter having the smaller dipole. The relative instability of **4**, in which the C=O bond bisects the CH_3—C—CH_3 bond angle, is understandable in terms of repulsion between the proximate bonds. With the C—H bonds of the methyl groups staggered about the neighbouring linkages, implying the usual parallel C—H arrangements of the methyl moieties, the C—H...O distances can be as small as 1.6 Å, clearly a strongly destabilizing situation.

Some insight into the relative computed stabilities of **1**–**4** can be had from computations of the relative energies of the analogous conformers of 2-methylbenzaldehyde. Geometry optimization with the STO-3G basis set, but keeping the nuclei of the aromatic moiety in a plane, yields the relative energies of **1**–**4** as 7.41, 1.22, 3.70, and 0.00 kJ/mol, respectively. In other words, conformers analogous to **2** and **4** are now the stable ones, implying also that C—H...H—C and C—H...O=C interactions in **1** and **3** of 2-isopropylbenzaldehyde are repulsive but less so than are the C—H,$(CH_3)_2$ and C=O,$(CH_3)_2$ interactions in **1** and **3** of this compound.

The STO-3G basis indicates an attractive C—H...O=C arrangement *relative* to C—H...H—C in both molecules. AM1 computations indicate the opposite, the latter being 1.48 kJ/mol more favorable in the methyl and 1.95 kJ/mol in the isopropyl derivative. Similar remarks apply to the energies of **2** and **4** for both molecules: AM1 favors H,H over H,O interactions whereas the STO-3G basis does the opposite. The experimental data above, extrapolated to the vapor phase for 2-isopropylbenzaldehyde, are consistent with a small bias towards C—H...O=C arrangement for the isolated molecules, qualitatively favoring the STO-3G MO computations.

The STO-3G computations on **1** and **3** allowed θ and ψ to vary (see **1**); however, the twists about the exocyclic bonds did not exceed 0.2° during the minimization procedures, implying the local stability of the planar conformers. That the aldehyde group does not deviate substantially from the aromatic plane, at least in solution, is indicated by the apparent ^6J(H,CHO) of −0.015(3) Hz (Table 1). This coupling constant was not manifested by a detectable splitting in the ^{1}H nmr spectra, but is a result of the least-squares fits of the Hamiltonian to the spectra. ^6J(H,CHO) has a value near −0.33 Hz when θ is 90° (27) and varies as $\sin^2\theta$. Hence the expectation value of the latter and, by implication, that of θ, is small in **1** and **3**, the predominant conformers at 300 K. According to these computations, the repulsion between the side chains in **1** and **3** is insufficient to yield a local barrier to their planarity. However, STO-3G MO methods rather overestimate the barrier to rotation about the exocyclic bond in isopropylbenzene (11) but not in benzaldehyde. Accordingly, it is an approximation to speak of planar **1** and **3**, although the long-range coupling constants suggest no greater an average twist about the C_{sp^2}—C_{sp^3} bond in the present molecule than in isopropylbenzene.[2]

The repulsive nature of the C—H...H—C and C—H...O=C interactions in **1** and **3** is implied by their STO-3G structures in Fig. 2. The figure caption elaborates on this matter.

Finally, were the theoretical populations of *one* of the less abundant **2** and **4** in Table 2 roughly correct, then the experimental data would yield reliable values of the populations of the other three conformers. This conundrum is discussed next.

[2]A referee states that molecular mechanics calculations on **1** and **3** suggest "substantial out-of-plane twisting of the methine C—H bond". Accordingly, the STO-3G results should be taken as tentative.

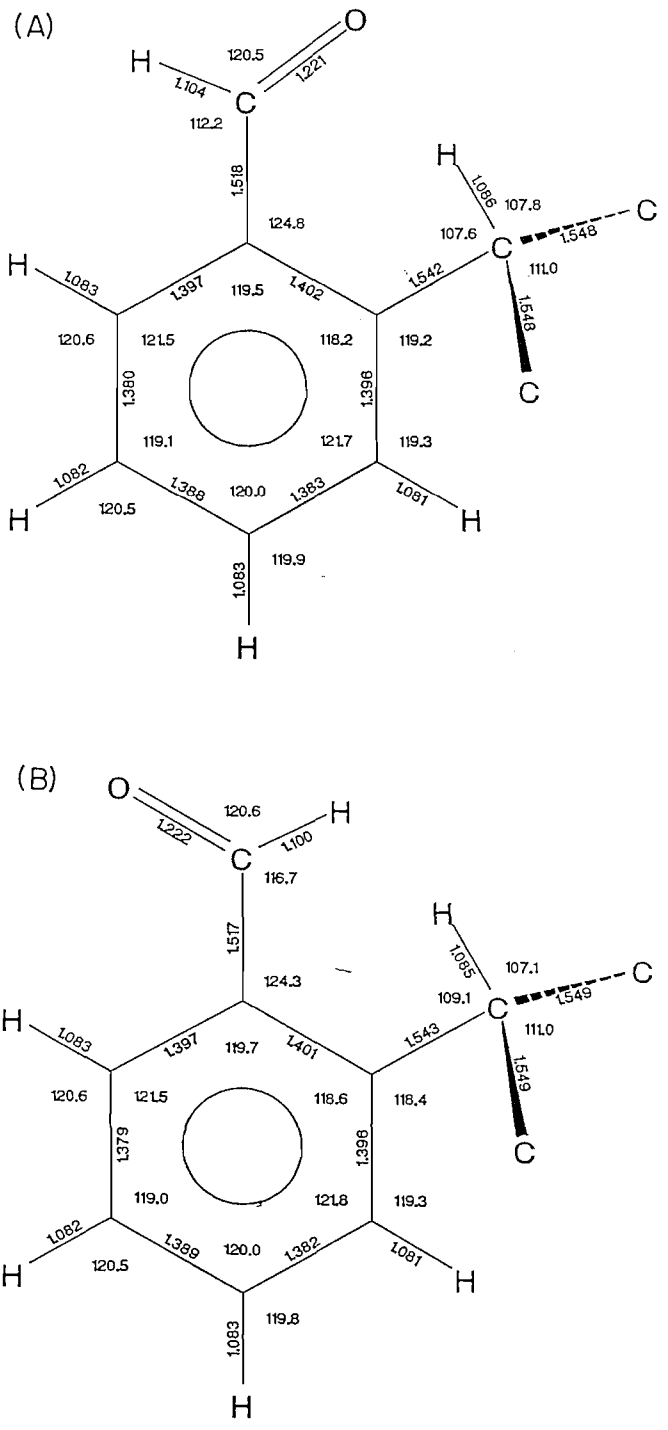


FIG. 2. The STO-3G structures of the planar conformers, (A) **1** and (B) **3**, are shown. The total energy of the *o-syn* conformer is −454.859 792 au, the relative energies of other conformers being given in Table 2. Compared with the structures of benzaldehyde (37) and isopropylbenzene (11), the C(O)C(1)C(2) and C(1)C(2)C(CH_3) bond angles suggest repulsion between the side chains; they bend away from each other in both conformers. Nevertheless, the computations imply that these structures represent local energy minima in that there is not a barrier to planarity. The energy of the process, 2-isopropylbenzaldehyde + benzene → isopropylbenzene + benzaldehyde (the isodesmic reaction (38)) is −14.6 kJ/mol for **1**, indicating an unfavorable substituent interaction, and is −10.5 kJ/mol for **3**. For salicylaldehyde, a similar procedure, using a 6-31G basis (13) gives +23.8 kJ/mol. The present STO-3G structures of **1** and **3** can serve as a starting point for computations with larger basis sets.

TABLE 3. Experimental populations of the planar conformers of 2-isopropylbenzaldehyde at 300 K

Conformer(s)	Acetone-d_6	CS_2/C_6D_{12}	Vapor
$(p_1 + p_2)^a$	$0.55_5 \pm 0.025$	$0.49_5 \pm 0.025$	0.43 ± 0.08
$(p_3 + p_4)^b$	$0.44_5 \pm 0.025$	$0.50_5 \pm 0.025$	0.57 ± 0.08
$(p_1 + p_3)^c$	0.83(3)	0.83(3)	0.83(3)
$(p_2 + p_4)^d$	0.17(3)	0.17(3)	0.17(3)
p_2^e	$0.08^{+0.11_5}_{-0.08_5}$	0.08_5	0.08_5
p_4	0.08_5	0.08_5	0.08_5
p_1^f	$0.47^{+0.14}_{-0.11}$	0.41	0.35 ± 0.2
p_3	0.36	0.42	0.48 ± 0.2

[a]The *o-anti* conformers.
[b]The *o-syn* conformers.
[c]The methine C—H bond lies *cis* to the aldehyde group.
[d]The methine C—H bond lies *trans* to the aldehyde group.
[e]The uncertainties in p_2 and p_4 are all the same and as given in one instance.
[f]The uncertainties in p_1 and p_3 are all as given in one instance.

Limits of the individual populations of ***1–4***

Table 3 contains a variety of populational estimates, including the sums of *o-anti* and *o-syn* populations as well as the population sums of conformers in which the methine C—H bond lies *cis* or *trans* to the aldehyde group. These sums, as derived from the long-range coupling constants, could imply a somewhat larger *o-syn* than *o-anti* population in the vapor phase. The reverse occurs in the polar solvent, attributable to the higher dipole moments (Table 2) of the *o-anti* conformers. By way of contrast, the population of the conformers with a *cis* orientation of the methine C—H bond is apparently independent of solvent polarity, presumably because these conformers are very much more stable than those with a *trans* orientation of this bond.

Unfortunately, the present experimental and theoretical approaches do not allow a reliable decision as to the relative individual populations of these two conformers. Accordingly, it can only be stated that p_2 and p_4 are each $0.08^{+0.11_5}_{-0.08_5}$ in both solvents and probably also in the vapor phase at 300 K. In consequence, any estimates of p_1 and p_3, the conformers in which the methine C—H bond closely approaches the C—H or C=O bond of the aldehyde group, carry a large uncertainty. It does appear reasonable, however (last two rows of Table 3), that the C=O...H...C interaction is less repulsive in the free molecule than is the C—H...H...C interaction in the side chains. In the polar solvent, the larger dipole moment of p_1 causes the stabilization of p_1, carrying the C—H...H—C arrangement.

The chemical shifts of the side-chain protons

Table 4 presents the chemical shifts of the side-chain protons in benzaldehyde, isopropylbenzene, and their 1,2 and 1,4 derivatives. Comparison of the shifts in the parent compounds with those in the 1,4 derivative gives an indication of the shift changes caused by long-range interactions. These changes are relatively small compared to those which occur in the 1,2 derivative for the aldehydic and methine protons.

Taking the 1,4 derivative as a reference, the shielding of the aldehydic proton in the 1,2 derivative decreases by 0.35 ppm in CS_2/C_6D_{12} and by 0.38 ppm in acetone-d_6. Attribution of the deshielding to the presence of the *o-anti* conformer, in which intense mean-square electric fields due to the close approach of the various vibrating C—H bonds (29, 30) are the cause of the lower screening of the aldehydic proton, allows a rough estimate of its chemical shift in this conformer. Use of the populations of the *o-syn* and *o-anti* conformers deduced in previous sections and assignment of δ(CHO) of the *o-syn* conformer as that in the 1,4 derivative, entails a δ(CHO) in the *o-anti* conformer of 10.67(4) in acetone-d_6 and of 10.54(4) in CS_2/C_6D_{12}. Then it follows that the difference in chemical shifts between the *o-anti* and *o-syn* conformers is 0.68(4) and 0.69(4) ppm in the two solutions. If δ(CHO) values for benzaldehyde are instead used as those of the *o-anti* conformers in the two solutions, the difference becomes 0.56(4) in both solvents. At 113 K, the chemical shift difference is observed (17) as 0.55 ppm for a solution of unknown concentration in CHF_2Cl. The present discussion can be taken as confirmation of the, at that time, equivocal assignment (17) of the deshielded peak to the *o-anti* conformer.

Turning to the methine proton, the same approach yields δ(CH) in **1** + **3** as 4.26(5) in acetone-d_6 and 4.16(5) in CS_2/C_6D_{12} solutions. Hence the methine proton is deshielded by about 1.2_5 ppm in either solution when the methine bond is oriented *cis* to the aldehydic functionality. The lower screening is no doubt a composite of electric field, magnetic anisotropy, and intramolecular van der Waals perturbations (30–32). These are impossible to assess quantitatively. The deshielding is consistent with a close approach of the methine C—H bond to the C—H and C=O bonds in **1** and **3**, which together have a fractional population of 0.83(3) in both solutions. Given the deshielding of the aldehyde proton in **1**, which is not greatly different in population from **3**, it is possible that the C—H...H—C interaction in **1** also acts to lower the screening of the methine proton by, say, about 0.6(1) ppm. In that event, the C=O...H—C interaction in **3** deshields the methine proton by about 0.6(1) ppm. It is possible, but improbable, that this represents a shift due to formation of a weak hydrogen bond, such bonds evincing a decrease in screening of the proton in the bond. In our opinion, a large part of the descreening in **3** arises from other sources.

That the shielding of the methine proton in **1** and **3** is much the same is consistent with the experiments at 113 K (17), in which distinct methine peaks are not observed for the conformers displaying different aldehydic proton signals.

Finally, the effective constancy of δ(CH_3) in the 1,2 and 1,4 derivatives in Table 4 is most easily interpreted as due to the low populations of **2** and **4**, particularly of the latter, and in line with the discussion in previous sections.

The chemical shifts of the ring protons

Based on the chemical shifts of isopropylbenzene (11), benzaldehyde (25), and benzene (33) in CS_2 solution at 300 K, an additivity scheme implies that, in 2-isopropylbenzaldehyde, 7.300, 7.441, 7.243, and 7.675 are δ_3–δ_6, in that order. The measured values are 7.360, 7.430, 7.247, and 7.665. Allowing for small differences in concentration of the various compounds, it is noteworthy that only δ_3 demonstrates a significant deviation. The H-3 protons are deshielded by 0.06 ppm, relative to the shielding expected from additivity, interpretable as caused by intramolecular van der Waals forces of the methyl groups in the large populations of **1** and **3**. If $p_1 + p_3$ were 0.5 instead of 0.83(3), then the deviation of δ_3 would presumably be less than 0.01 ppm. The very similar populations of the *o-syn* and *o-anti* conformers in CS_2/C_6D_{12}, equal to within experimental error, probably account for the insignificant deviations of δ_4–δ_6, particularly the latter. These shifts also imply that the side chains do not deviate from planarity by much more or

Can. J. Chem. Downloaded from www.nrcresearchpress.com by 198.100.157.202 on 09/07/12
For personal use only.

TABLE 4. The chemical shifts of aldehydic and alkyl protons in some benzene derivatives at 300 K

Compound	δ(CHO)		δ(CH)		δ(CH_3)	
	CS_2	Acetone-d_6	CS_2	Acetone-d_6	CS_2	Acetone-d_6
C_6H_5CHO[a]	9.918	10.054	—	—	—	—
$C_6H_5C(CH_3)_2$[b]	—	—	2.811	2.889	1.219	1.225
1-CHO-4-$CH(CH_3)_2$[c]	9.849	9.992	2.925	3.014	1.267	1.270
1-CHO-2-$CH(CH_3)_2$[d]	10.195	10.371	3.950	4.045	1.260	1.283

[a]As a 4.0 mol% solution containing also 10 mol% of C_6D_{12} and 0.5 mol% of TMS or as a 4.0 mol% solution in acetone-d_6 containing also 0.5 mol% of TMS.
[b]As 2.5 mol% solutions in the solvent mixtures above.
[c]As 3.6 mol% in the CS_2/C_6D_{12}/TMS and 4.0 mol% in the acetone-d_6/TMS mixture.
[d]4.0 mol% solutions in the solvent mixtures above.

Can. J. Chem. Downloaded from www.nrcresearchpress.com by 198.100.157.202 on 09/07/12
For personal use only.

less than in the parent compounds; a considerably increased nonplanarity of the carbonyl group of the derivative, for example, should surely manifest itself by nonadditivity of δ_4 and δ_6. Accordingly, the suggestion (17) that the lower barrier to rotation of the aldehydic group in 2-isopropylbenzaldehyde arises from its nonplanarity in the rotational ground state, needs reexamination. Those long-range coupling constants sensitive to θ and ψ (see **1**) also indicate the validity of the above interpretation of δ_4–δ_6.

The proximate coupling constant, $^5J(CHO,CH(CH_3)_2)$

The use of the STO-3G MO geometries of the planar conformers in CNDO/2 and INDO MO FPT computations of $^5J(CHO,CH(CH_3)_2) \equiv {}^5J_p$, gave rise to −0.30 Hz for **1**, in which the C—H bonds are proximate. Of course, ^5J_p is very sensitive to the interatomic distance (34, 35), the contact contribution to the coupling constant depending on the overlap of orbitals on the atoms or bonds carrying the coupled nuclei (36), so that the present result is taken as confirmation of the proximate mechanism of ^5J_p, determined as −0.376(1) Hz in CS_2/C_6D_{12} and as −0.388(1) Hz in acetone-d_6 solution. The slightly larger magnitude in the latter is consistent with the larger *o-trans* population in this solvent. Similar computations for the other conformers yielded small, positive, ^5J_p values; these may or may not be artefacts of the parameterization but agree with the idea that a close C—H...H—C approach of bonds in the side chains is accompanied by a negative coupling constant.

Because ^5J_p is very likely sizeable only in **1** and because $p_1 < 0.5$ in both solutions, it follows that its magnitude in this conformer is likely near 1 Hz. For obvious reasons, ^5J_p cannot at present be used to deduce p_1.

It is interesting that no evidence exists in the ^{1}H nmr spectra for spin–spin coupling between the aldehydic and methyl protons. Were there such evidence, (no doubt) it would have been taken as an indication of the existence of **2**, in which the methyl groups lie rather near the C—H bond of the aldehyde group.

Conclusion

The experimental data suggest that C—H...H—C and C=O...H—C interactions in the side chains of 2-isopropylbenzaldehyde are roughly isoenergetic. Consideration of the STO-3G MO structures in Fig. 2, in which the H...H and H...O distances are 1.92 and 2.05 Å and hence markedly below the sum of the van der Waals radii of the hydrogen and oxygen atoms of 1.2 and 1.4 Å, respectively, implies repulsive interactions for these bond arrangements. Hence there is no evidence for an intramolecular C=O...H—C hydrogen bond, although the H...O distance, if met in a crystal, likely would be taken as evidence for a hydrogen bond. It would be of interest to have an assignment of the stretching frequencies of the aldehydic and methine C—H bonds in this molecule, together with a comparison of these frequencies in the parent molecules.

Acknowledgements

We thank the Natural Sciences and Engineering Research Council of Canada for a grant in aid of research. The referees are thanked for helpful criticism.

1. G. R. DESIRAJU. J. Chem. Soc. Chem. Commun. 454 (1990), and references therein.
2. P. SEILER and J. D. DUNITZ. Helv. Chim. Acta, **72**, 1125 (1989).
3. M. ŌKI, N. TAKIGUCHI, S. TOYOTA, G. YAMAMOTO, and S. MURATA. Bull. Chem. Soc. Jpn. **61**, 4295 (1988).
4. M.-L. H. JENG and B. S. AULT. J. Phys. Chem. **93**, 5426 (1989); **94**, 4851 (1990), and references therein.
5. W. R. CARPER, L. P. DAVIS, and M. W. EXTINE. J. Phys. Chem. **86**, 459 (1982).
6. R. TAYLOR and O. KENNARD. J. Am. Chem. Soc. **104**, 5036 (1982).
7. G. A. JEFFREY, J. R. RUBLE, L. M. WINGERT, J. H. YATES, and R. K. MCMULLAN. J. Am. Chem. Soc. **107**, 6227 (1985).
8. W. R. CARPER, S. R. BOSCO, and J. J. P. STEWART. Spectrochim. Acta, **42**, Part A, 461 (1986).
9. T. CORRELL, N. W. LARSEN, and T. PEDERSEN. J. Mol. Struct. **65**, 43 (1980).
10. F. A. L. ANET and M. AHMAD. J. Am. Chem. Soc. **86**, 119 (1964).
11. T. SCHAEFER, R. SEBASTIAN, and G. H. PENNER. Can. J. Chem. **66**, 1495 (1988).
12. T. SCHAEFER, R. SEBASTIAN, R. LAATIKAINEN, and S. R. SALMAN. Can. J. Chem. **62**, 326 (1984), and references therein.
13. P. GEORGE, C. W. BOCK, and M. TRACHTMAN. J. Mol. Struct. (Theochem), **133**, 11 (1985).
14. M. C. ETTER. Acc. Chem. Res. **23**, 120 (1990).
15. G. J. KARABATSOS and F. M. VANE. J. Am. Chem. Soc. **85**, 3886 (1963).
16. T. SCHAEFER and C. S. TAKEUCHI. Can. J. Chem. **68**, 339 (1990).
17. L. LUNAZZI, A. TICCA, D. MACCIANTELLI, and G. SPUNTA. J. Chem. Soc. Perkin Trans. 2, 1121 (1976).
18. R. FREEMAN and W. A. ANDERSON. J. Chem. Phys. **37**, 2053 (1962).
19. J. S. MARTIN, A. R. QUIRT, and K. E. WORVILL. The NMR program library. Daresbury Laboratory, Daresbury, U.K.

20. W. J. HEHRE, R. DITCHFIELD, R. F. STEWART, and J. A. POPLE. J. Chem. Phys. **52**, 2769 (1970).
21. M. J. S. DEWAR, E. J. ZOEBISCH, E. F. HEALY, and J. J. P. STEWART. J. Am. Chem. Soc. **107**, 3902 (1985).
22. M. J. FRISCH, J. S. BINKLEY, H. B. SCHLEGEL, K. RAGHAVACHARI, C. F. MELIUS, R. L. MARTIN, J. J. P. STEWARD, F. W. BOBROWICZ, D. F. ROHLFING, L. R. KAHN, D. J. DEFREES, R. SEEGER, R. A. WHITESIDE, D. J. FOX, E. M. FLUDER, and J. A. POPLE. Carnegie–Mellon Quantum Publishing Unit, Pittsburgh, PA. 1984.
23. J. A. POPLE, J. W. MCIVER, and N. S. OSTLUND. J. Chem. Phys. **49**, 2965 (1968).
24. P. DOBOSH and N. S. OSTLUND. QCPE, **11**, 281 (1975).
25. T. SCHAEFER and C. S. TAKEUCHI. Can. J. Chem. **67**, 827 (1989).
26. R. J. ABRAHAM and E. BRETSCHNEIDER. *In* Internal rotation in molecules. *Edited by* N. J. Orville-Thomas. J. Wiley and Sons, New York. 1974. Chap. 13.
27. T. SCHAEFER, J. PEELING, G. H. PENNER, A. LEMIRE, and R. LAATIKAINEN. Can. J. Chem. **64**, 1859 (1986).
28. T. DRAKENBERG, R. JOST, and J. M. SOMMER. J. Chem. Soc. Perkin Trans. 2, 1682 (1975).
29. W. T. RAYNES, A. D. BUCKINGHAM, and H. J. BERNSTEIN. J. Chem. Phys. **36**, 3481 (1962).
30. R. F. ZÜRCHER. Prog. Nucl. Magn. Reson. Spectrosc. **2**, 205 (1967).
31. H. GÜNTHER. NMR spectroscopy. Wiley, New York. 1980. pp. 73–77.
32. R. K. HARRIS. NMR spectroscopy. Pitman Books, London. 1983. pp. 193–196.
33. T. SCHAEFER, R. SEBASTIAN, and G. H. PENNER. Can. J. Chem. **63**, 2597 (1985).
34. J. HILTON and L. H. SUTCLIFFE. Prog. Nucl. Magn. Reson. Spectrosc. **10**, 27 (1975).
35. R. H. CONTRERAS, M. A. NATIELLO, and G. E. SCUSERIA. Magn. Reson. Rev. **9**, 239 (1985).
36. M. C. RUIZ DE AZUA, A. C. DIZ, C. G. GIRIBET, R. H. CONTRERAS, and I. D. RAE. Int. J. Quant. Chem. **S20**, 585 (1986), and references therein.
37. G. H. PENNER, P. GEORGE, and C. W. BOCK. J. Mol. Struct. (Theochem), **152**, 201 (1987).
38. W. J. HEHRE, L. RADOM, P. V. R. SCHLEYER, and J. A. POPLE. *Ab initio* molecular orbital theory. Wiley, New York. 1986. pp. 271, 272, and 360–362.

Can. J. Chem. Downloaded from www.nrcresearchpress.com by 198.100.157.202 on 09/07/12
For personal use only.

Molecular orbital and ^1H nuclear magnetic resonance studies of the inversion potentials of thianthrene and thioxanthene

TED SCHAEFER,[1] RUDY SEBASTIAN, AND CHRISTIAN BEAULIEU[2]
Department of Chemistry, University of Manitoba, Winnipeg, Man., Canada R3T 2N2

Received October 10, 1990

TED SCHAEFER, RUDY SEBASTIAN, and CHRISTIAN BEAULIEU. Can. J. Chem. **69**, 927 (1991).

The inversion potentials, obtained from STO-3G, STO-3G(*), 3-21G, 3-21G(*), and 4-31G basis sets, are reported for thianthrene and thioxanthene, molecules in which both or only one of the methylene groups have been replaced by sulfur in 9,10-dihydroanthracene. Comparison with the available experimental data suggests that the split-valence bases lead to an overestimate, possibly by about 10 kJ/mol, of the inversion barrier in the crystal, whereas the STO-3G and STO-3G* basis sets underestimate this barrier. It appears that the inversion barrier for thianthrene is much lower in solution than in the crystal. The long-range coupling constants between the methylene and ring protons for thioxanthene in solution are consistent with an inversion barrier somewhat smaller than those obtained with the split-valence bases but rather larger than those predicted with the STO-3G basis set. The bond lengths and angles in the equilibrium structures of the two molecules, as computed with the 3-21G(*) basis, agree reasonably well with those in their crystals, except that the theoretical folding angles are smaller than measured. These discrepancies become less marked when expectation values are calculated from the theoretical inversion potentials at finite temperatures.

Key words: MO calculations, inversion potentials of thianthrene and thioxanthene; ^1H NMR, thioxanthene; spin–spin coupling constants, long range, in thioxanthene.

TED SCHAEFER, RUDY SEBASTIAN et CHRISTIAN BEAULIEU. Can. J. Chem. **69**, 927 (1991).

Utilisant des ensembles STO-3G, STO-3G(*), 3-21G, 3-21G(*) et 4-31G, on a calculé les potentiels d'inversion du thianthrène et du thioxanthène, des molécules dans lesquelles l'un ou les deux groupements méthylènes du 9,10-dihydroanthracène ont été remplacés par des soufres. Une comparaison des résultats des calculs avec les données expérimentales disponibles suggère que les ensembles à valence partagée conduisent à des surévaluations, pouvant aller jusqu'à 10 kJ/mol, de la barrière à l'inversion dans le cristal; par ailleurs, les ensembles STO-3G et STO-3G(*) sous-évaluent cette barrière. Il semble que la barrière à l'inversion du thianthrène est beaucoup plus faible en solution que dans le cristal. Les constantes de couplage à longue distance entre le méthylène et les protons du cycle du thioxanthène en solution sont en accord avec une barrière d'inversion inférieure à celles obtenues avec les ensembles à valence partagée, mais plus élevée que celles prédites par l'ensemble STO-3G. Les longueurs des liaisons et les angles dans les structures en équilibre des deux molécules, telles que calculées avec un ensemble 3-21G(*), sont en bon accord avec celles observées dans les cristaux; toutefois, les angles théorique de repliement sont plus faibles que ceux mesurés. Ces différences deviennent moins marquées lorsque les valeurs attendues sont calculées à partir des potentiels théoriques d'inversion à des températures finies.

Mots clés : calculs d'OM, potentiels d'inversion du thianthrène et du thioxanthène; RMN ^1H, thioxanthène; constantes du couplage à longue distance du thioxanthène.

[Traduit par la rédaction]

Introduction

Geometry-optimized STO-3G and 4-31G molecular orbital computations give 8.6 and 7.8 kJ/mol, respectively, for the inversion barrier in 9,10-dihydroanthracene, compatible with the available experimental data (1). The folding angle is computed as very near 141° in the boat form, as compared to 144.7° in the crystal (2). Replacement of both methylene groups by sulfur atoms, to give thianthrene, entails a folding angle of 128° (3, 4), or 127.14(3)° at 163 K and 128.09(5)° (5) in the crystal; both angles are reasonably compatible with electron diffraction data for the vapor (6). In benzene solution, the dipole moment and Kerr constant of thianthrene suggest a folding angle of approximately 142° (7). The inversion barrier, opposing the formation of a planar molecule with a folding angle of 180°, ranges from 15 ± 3 kJ/mol (enthalpy of activation) in a polymer matrix, as derived from dielectric loss measurements (8), to 26 kJ/mol (9), estimated from approximate molecular mechanics calculations in connection with dielectric loss studies in a benzene solution at 293 K. For the free molecule, presumably at 400 K (6), inversion barriers as low as 16.7 or as high as 29.2 kJ/mol could be fit to the radial distribution curve in the electron diffraction experiments; the folding angle is 128–130°. In contrast to the results for the solid and vapor, the analyses of the nmr spectra of thianthrene in nematic solvents imply a folding angle of 141.6(2)° in one anisotropic solvent (10) at 307 K and 140.6(4)° in another (11) at 308 K; the folding angle was 139.8(7)° for the 2,7-dichloro derivative (11). No large-amplitude motion was assumed in the derivation of these angles, implying the assumption of an inversion barrier large compared to thermal energies. A recent molecular mechanics calculation (12) has the folding angle as 130° for a boat form of C_{2v} symmetry and the inversion barrier as 19.2 kJ/mol, rather lower than the 25–29 kJ/mol in an early calculation combining Hückel molecular orbitals with estimates of strain and σ-bond deformation energies (13). One has the peculiar conclusion that, in solution, the molecule is less puckered by about 10° than in either the vapor or solid state. In contrast, dibenzo-*p*-dioxin is planar in the solid state and puckered in solution (14).

Turning to thioxanthene, in which one of the methylene groups of 9,10-dihydroanthracene is replaced by a sulfur atom, the folding angle in the crystal is 135.3(1)° and the intermolecular separations are larger than the van der Waals contact distances (15). This indication, that crystal packing forces do not appreciably deform the molecule, is supported by the folding angle of 135 ± 8° estimated from molar Kerr contants at 298 K in CCl_4 and C_6H_6 solutions (16). Such a degree of pucker is consistent with the magneto-optical rotation of thioxanthene

[1]Author to whom correspondence may be addressed.
[2]Undergraduate research participant, 1989.

Can. J. Chem. Downloaded from www.nrcresearchpress.com by 198.100.157.202 on 09/07/12
For personal use only.

TABLE 1. Relative energies and dipole moments of thianthrene as a function of the folding angle, θ, computed with various basis sets

	STO-3G		STO-3G(*)		3-21G		3-21G(*)		4-31G	
θ/deg	E^a	μ^b	E	μ	E	μ	E	μ	E	μ
180	9.73	0.00	5.99	0.00	31.26	0.00	31.52	0.00	31.47	0.00
170	9.01_5	0.13	5.49	0.01	29.58	0.50	29.75	0.43	29.70	0.43
160	6.98	0.27	4.07	0.00	24.71	1.01	24.61	0.85	24.61	0.88
150	4.03	0.42	2.09	0.03	17.24	1.51	16.79	1.28	16.91	1.32
140	1.10	0.60	0.34	0.07	8.62	1.99	7.88	1.70	8.16	1.75
134.8_4	—	—	0.00	0.11	—	—	—	—	1.30	2.14
132.0_2	0.00	0.74	—	—	—	—	—	—	—	
130	0.10	0.78	0.42	0.14	1.62	2.42	1.06	2.07	—	—
125.2_4	—	—	—	—	—	—	0.00	2.22	—	—
124.5_8	—	—	—	—	—	—	—	—	0.00	2.33
123.8_2	—	—	—	—	0.00	2.65	—	—	—	—
120	4.85	0.94	5.59	0.21	0.77	2.77	1.62	2.37	1.17	2.46
110	22.16	1.03	22.40	0.22	12.40	3.01	16.90	2.56	14.70	2.68
100	63.16	1.02	62.19	0.12	44.43	3.16	55.91	2.66	50.59	2.82

[a]In kJ/mol, E(minimum) being −1239.872 667 (STO-3G), −1239.956 170 (STO-3G(*)), −1247.632 741 (3-21G), −1247.849 646 (3-21G(*)), and −1252.525 371 (4-31G) au.
[b]In debye.

Can. J. Chem. Downloaded from www.nrcresearchpress.com by 198.100.157.202 on 09/07/12
For personal use only.

in $CHCl_3$ solution at 293 K (17). The dipole moment at 303 K in C_6H_6 and the ^1H nmr chemical shift of the methylene protons in $CDCl_3$ at 309 K are apparently interpretable in terms of a planar or a rapidly inverting, nonplanar, molecule (18). No evidence for slow inversion on the nmr time scale (presumably indicated by a difference in the chemical shifts of the methylene protons in the puckered conformation of thioxanthene) was found at 193 K, the lowest temperature for which suitable solvents could be found (18).

In the present report, long-range coupling constants between the methylene and ring protons are discussed in terms of the degree of pucker of thioxanthene and in terms of *ab initio* molecular orbital computations meant to provide not only the folding angle for the free molecule but also the barrier to inversion. Similar computations are given for thianthrene and these may be compared to inversion barriers provided by the other theoretical methods discussed above. A comparison between theoretical and experimental structures is also presented.

Experimental

Thioxanthene (K & K Laboratories) was prepared for ^1H nmr studies as 4 mol% solutions in CS_2/C_6D_{12}/TMS and C_6D_6/TMS solvent mixtures (Table 1). These solutions were filtered into 5-mm o.d. nmr sample tubes, were degassed by five cycles of the freeze–pump–thaw technique, and were then flame-sealed. The ^1H nmr spectra were obtained on a Bruker AM300 nmr spectrometer in a manner previously described in detail (19).

Ab initio molecular orbital computations utilized an Amdahl 5870 system and employed the program GAUSSIAN 86 (20) with various basis sets (21). For thianthrene, the geometry-optimization procedure allowed all bond angles and lengths to vary, with the constraint, however, that the molecule retain C_{2v} symmetry in the folded form. For thioxanthene, the constraints included a mirror plane containing the sulfur atom and the carbon atom of the methylene group, as well as planarity of the two aromatic fragments. Computations were performed for as many as nine values of the folding angle (see below).

Results and discussion

Molecular orbital computations

(i) Thianthrene

Table 1 presents the relative computed energies of thianthrene as a function of the folding angle, θ. The structures of planar and folded thianthrene are given in Fig. 1, as calculated with the basis set, 3-21G(*). The bond lengths and angles involving heavy atoms agree very closely with the most recent X-ray determination (5), if averages of the various experimental values are compared with the parameters in Fig. 1(a). Comparison of the planar structure, Fig. 1(b), with the equilibrium geometry implies that bond angle distortion, mainly at sites in the heterocyclic ring, accounts for much of the instability of the planar form. The expectation value, $\langle\theta\rangle$, of the folding angle at 300 K is computed as 126.3°, not far from the 127.1° found in the crystal at 163 K (5).

This comparison raises the question of the inversion potential appropriate to various states of the molecule. The theoretical potentials for the free molecule from the various basis sets are written in the form of eq. [1]

$$[1]\quad V(\phi)/\text{kJ mol}^{-1} = A\phi^2 + B\phi^4 + C\exp(D\phi^2)$$

where $\phi = \theta - 180°$, and are as shown.

Basis	$A/10^{-2}$	$B/10^{-6}$	C	$D/10^{-4}$
STO-3G	−1.20(3)	0.80(10)	9.97(23)	3.71(6)
STO-3G(*)	−0.84(3)	0.66(8)	6.17(19)	4.18(12)
3-21G	−2.64(3)	1.54(23)	31.62(32)	2.44(9)
3-21G(*)	−2.81(4)	1.83(23)	31.97(40)	2.53(10)
4-31G	−2.73(3)	1.69(22)	31.81(32)	2.49(9)

The errors are given for a 95% confidence interval, Fig. 2, illustrating the fit to the computed energies for the 4-31G basis. The split-valence basis sets yield an inversion barrier near 31 kJ/mol, while the STO-3G and STO-3G(*) bases predict a barrier rather less than 10 kJ/mol in magnitude (see also Table 1).

The temperature-dependent folding angle in the crystal indicates "butterfly" motion even at 163 K; the four outermost carbon atoms still have the largest thermal parameters (5) at this temperature. The values of $\langle\theta\rangle$ were computed at three temperatures with the potentials in eq. [1] and are shown

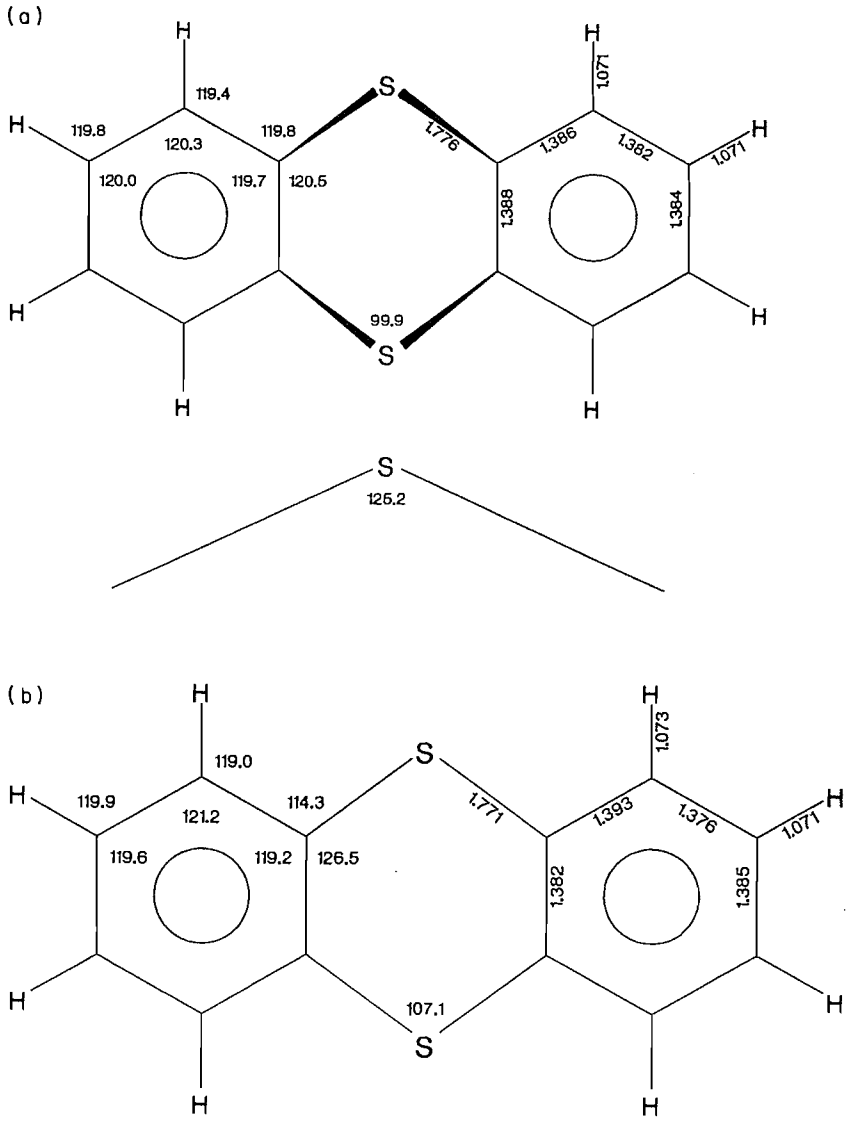


FIG. 1. The equilibrium 3-21G(*) structure of thianthrene is shown in (a), the computation having assumed C_{2v} symmetry. There is rather good agreement with the latest X-ray structure (5). In (b) the computed planar geometry suggests, by comparison with that in (a), that bond angle distortions in the central ring are the primary cause of its instability.

together with literature values for the folding angle. Differences

Basis/method	$\langle\theta\rangle_{163}$/degree	$\langle\theta\rangle_{300}$	$\langle\theta\rangle_{400}$
STO-3G	134.5	136.4	137.9
STO-3G*	138.5	141.2	142.6
3-21G	124.3	124.8	125.2
3-21G(*)	126.0	126.4	126.8
4-31G	125.2	125.7	126.1
Crystal (5)	127.14(3)	128.09(5)	—
Nematic (10, 11)	—	141.1(5)	—
Benzene (7)	—	142.0	—
Vapor (6)	—	—	129(1)

in the theoretical barriers have also been noted for 1,4-dithiin (the aromatic moieties in thianthrene are replaced by C=C bonds). For this molecule, the minimal basis set (12, 22) is assessed as underestimating the inversion barrier, whereas the split-valence bases, including 3-21G(*) and 6-31G* (using 3-21G(*) optimized geometries), are felt (22) to overestimate the barrier.

These comparisons suggest that the inversion barrier in thianthrene lies somewhere between those from the STO-3G and split-valence bases given in Table 1, possibly a value not far from the 15 ± 3 kJ/mol estimated from the dielectric loss measurements on a polymer matrix (8) or the 19.2 kJ/mol obtained by molecular mechanics (12). The much larger folding angle obtained in anisotropic (10, 11) or isotropic (7) solutions of thianthrene is most simply interpreted as a consequence of a lower inversion barrier in these intermolecular environments. It may be noted that $\langle\theta\rangle$ at 300 K is given as 141.2° by the low STO-3G(*) inversion potential, very near the average, 141.1°, of the angles obtained in two anisotropic solutions near 307 K. It would be of interest to apply the various theoretical potentials above to the dipolar nmr parameters (10, 11) and to the electron diffraction patterns.

It may also be noted that STO-3G MO calculations on thioanisole (23) give the barrier to rotation about the C_{sp^2}—S bond as 6.2 kJ/mol, not far from the 5.5(4) kJ/mol found for a benzene solution.

Finally, it is to be noted that the accuracy of a computed equilibrium geometry does not necessarily imply a corresponding accuracy in the internal barrier computed with the same

Can. J. Chem. Downloaded from www.nrcresearchpress.com by 198.100.157.202 on 09/07/12
For personal use only.

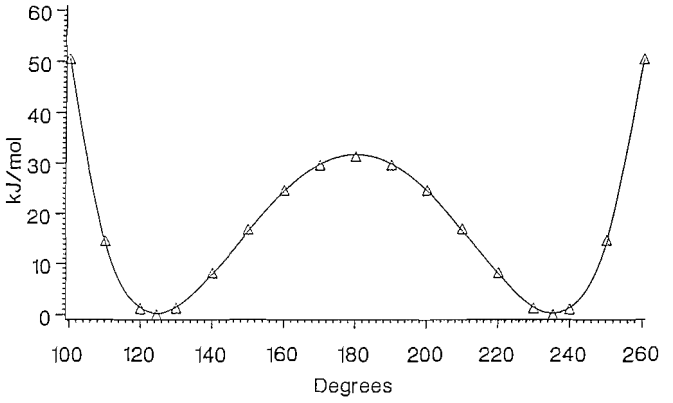


FIG. 2. The inversion potential of thianthrene is shown, as computed with the basis set, 4-31G. The triangles give the computed relative energies, whereas the solid curve represents eq. [1] of the text, an analytical form for the inversion potential.

basis set. For example, the internal barrier in benzaldehyde is best given by the minimal basis set, when compared to split-valence bases as large as 6-31G* (24), whereas the equilibrium geometry is better reproduced by the larger bases. Thus, while the 3-21G equilibrium structure for thianthrene (Fig. 1(a)) is rather close to the experimental structure in the crystal (5), it does not follow that the inversion potential is correct.

The dipole moment of thianthrene is 1.42 D in benzene at both 298 and 323 K (7, 25). Clearly, the minimal basis set underestimates, while the split-valence bases overestimate, its magnitude. The mean of the STO-3G and 3-21G(*) or 4-31G values, at their respective equilibrium geometries (Table 1), is within 0.1 D of experiment. The overestimates are typical for compounds containing sulfur (26).

(ii) Thioxanthene

The computed energies of thioxanthene appear in Table 2 as a function of the folding angle for the bases, STO-3G, STO-3G(*), and 4-31G. The folding angles at equilibrium (see footnote in Table 2) for those computed with the basis sets 3-21G and 3-21G(*) are, on average, computed as 4.6° larger than in thianthrene; the 4-31G basis has this number as 6.3°. In the crystal, this difference in angle is near 7° (5, 15). Figure 3 displays the equilibrium structure computed with the 3-21G(*) basis set. The bond lengths and angles in the central ring appear to agree with those deduced (15) from X-ray diffraction patterns to within experimental error. The folding angle is, however, some 5° less than that in the crystal. Probably by coincidence, the STO-3G basis has a folding angle, 136.6° at equilibrium, rather closer to the 135.3(1)° derived for the crystal. Of course, the expectation value of the angle will depend on temperature and on the inversion potential.

The terms of eq. [1] are shown for the various basis sets, appropriate to thioxanthene,[3] as are the (classical) average

Basis	$A/10^{-2}$	$B/10^{-6}$	C	$D/10^{-4}$	$\langle\theta\rangle_{300}$/deg
STO-3G	−1.36(2)	0.46(17)	9.60(8)	4.89(10)	140.2
STO-3G(*)	−1.20(4)	1.30(18)	7.60(22)	4.64(11)	143.4
4-31G	−2.51(6)	1.25(43)	22.79(4)	3.54(15)	132.2

folding angles at 300 K derived from these potentials. These averages all lie within the 135 ± 8° estimated from Kerr constants in CCl_4 and C_6H_6 solutions at 298 K (16). In the next section, the long-range proton–proton coupling constants are discussed with a view to a narrowing of the range of the folding angle appropriate to solutions.

Rather as for thianthrene, the mean of the computed dipole moments of the equilibrium structures at the STO-3G and 4-31G level of *ab initio* molecular orbital theory, being 1.25 D (Table 2), effectively coincides with the 1.25 D reported for CCl_4 and C_6H_6 solutions (16).

The ^1H nmr parameters for thioxanthene

(i) Spectral analysis

The ^1H nmr spectra were analyzed with the computer program NUMARIT (27), as extensively modified by R. Sebastian. The plethora of closely spaced peaks in the methylene proton region, caused by long-range coupling constants to eight ring protons, precluded assignments of computed to measured transitions in this region. The small range of chemical shifts in the ring proton region had the consequence that large correlations existed between many spectral parameters obtained from the analyses.

This fact very likely accounts for differences between coupling constants within the ring as deduced for the two solutions. For example, $^3J_{34}$ is correlated by 0.72 with ν_3 in the C_6D_6 solution; hence its value of 7.447(7) Hz is much less reliable than the 7.410(3) Hz obtained for the CS_2 solution in Table 3. Similar statements could be made about other coupling constants among ring protons. Fortunately, the coupling constants between the methylene and ring protons did not suffer significantly from such correlations. It is these which are of use in the conformational analysis of thioxanthene.

(ii) The long-range methylene proton coupling constants

In toluene (19), $^6J(H,CH_3)$ is −0.602(2) Hz and is proportional to $\langle\sin^2\psi\rangle$, where ψ is the angle by which the α C—H bond twists out of the benzene plane. Hence $^6J_{90}$, the value of $^6J(H,CH_3)$ when ψ is 90°, is −1.204(4) Hz because the internal barrier is very low and therefore $\langle\sin^2\psi\rangle$ is 0.5. The latter value holds as long as the methyl group reorients about the C_{sp^2}—C_{sp^3} bond in a time short compared to J^{-1}, where J is long-range coupling constant over six bonds for *any* value of ψ: the methyl group has threefold symmetry.

The magnitude of $^6J_{90}$ depends on the electronegativity of the α substituent, E_x. In benzyl fluoride, $^6J_{90}$ is −0.94 Hz (28), and is assessed as −1.16 Hz in ethyl benzene (29). The available E_x scales all have the phenyl as more electronegative than the methyl group (30). The assumption of a linear relationship between $^6J_{90}$ and E_x, together with the comparisons of

[3]A referee comments that the planar conformation of thioxanthene is not necessarily the transition state for inversion; a force constant analysis, using computing times unavailable to us, is necessary for such a characterization.

Can. J. Chem. Downloaded from www.nrcresearchpress.com by 198.100.157.202 on 09/07/12
For personal use only.

TABLE 2. Relative energies and dipole moments of thioxanthene computed with various basis sets as a function of the folding angle, θ

	STO-3G		STO-3G(*)		4-31G			
θ/deg	$E^{a,c}$	μ	E	μ	E	μ	ψ(H_a)/deg[b]	ψ(H_b)/deg[b]
180	9.53	0.76	7.38	0.23	22.42	1.82	56.86	−56.86
170	8.70	0.76	6.68	0.24	20.95	1.81	66.97	−46.81
160	6.35	0.75	4.71	0.26	16.66	1.80	77.33	−36.65
150	3.06	0.74	2.05	0.27	10.16	1.79	88.04	−26.41
140	0.34	0.73	0.14	0.28	3.25	1.77	98.92	−16.50
138.4_2	—	—	0.00	0.28	—	—	—	—
136.6_1	0.00	0.73	—	—	—	—	—	—
130.8_6	—	—	—	—	0.00	1.77	108.57	−8.47
130	1.50	0.72	2.18	0.28	0.06	1.77	109.32	−7.87
120	12.78	0.69	14.29	0.27	7.90	1.77	118.31	−1.61
110	43.99	0.63	46.29	0.26	36.36	1.77	125.65	2.14

[a]In kJ/mol, E(minimum) being −885.272 474 (STO-3G), −885.313 804 (STO-3G*), and −894.463 688 (4-31G) au.

[b]The angles by which the methylene C—H bonds are twisted out of the aromatic planes.

[c]For the 3-21G basis, the planar molecule (θ = 180°) is 23.70 kJ/mol less stable than that with a θ of 128.8_4°, which has a total energy of −890.912 424 au. For the 3-21G(*) basis set, these numbers are 21.64 kJ/mol, 130.0_4°, and −891.020 026 au.

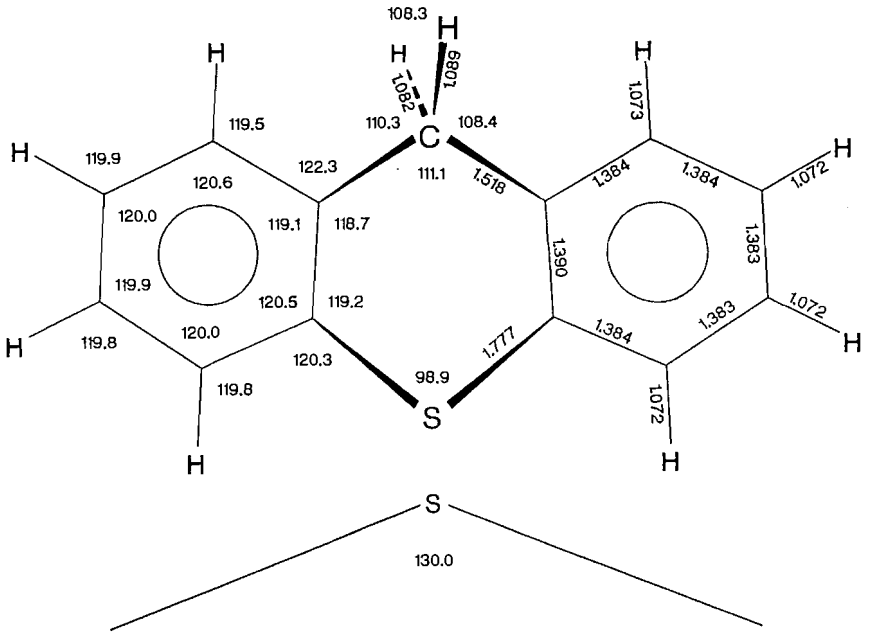


FIG. 3. The 3-21G(*) structure of thioxanthene is displayed, the agreement with the geometry in the crystal being rather good in that the CSC and CC(H_2)C angles agree to within experimental error. However, the folding angle is some 5° less than in the crystal, reminiscent of a similar discrepancy between split-valence bases and experiment for 9,10-dihydroanthracene (1) where, again, other bond lengths and angles show good agreement between experiment and theory. Of course, the expectation value of the folding angle depends on the temperature and on the inversion potential and will be higher than the equilibrium value (see text).

E_x (30), yields $^6J_{90}$ as −1.13(2) Hz for thioxanthene. The immediate and trivial consequence is that the molecule cannot be planar in solution. Planarity implies a ψ near 60°, a $\sin^2\psi$ near 0.75, and hence a $^6J(H,CH_2)$ near −0.85 Hz; the measured value is −0.551(3) Hz in both solvents (Table 3). In fact, at 300 K the value of $\langle\sin^2\psi\rangle$ is −0.551(3)/−1.13(2) or 0.49(1).

The theoretical inversion potentials for thioxanthene, applied to the ψ values for the methylene C—H bonds in Table 2 (shown only for the 4-31G geometries because they are very similar for the geometries obtained from all the basis sets), yield $\langle\sin^2\psi\rangle$ as shown.

Method	$\langle\sin^2\psi\rangle_{300}$	$\langle\sin^2(\psi/2)\rangle_{300}$
STO-3G	0.529	0.302
STO-3G(*)	0.547	0.295
4-31G	0.470	0.328
$^6J(H,CH_2)$	0.49(1)	0.32(4)

Can. J. Chem. Downloaded from www.nrcresearchpress.com by 198.100.157.202 on 09/07/12
For personal use only.

TABLE 3. The ^{1}H nmr spectral parameters for thioxanthene at 300 K

Parameter	Value		Parameter	Value	
	CS_2[a]	C_6D_6[b]		CS_2[a]	C_6D_6[b]
$\nu(CH_2)$[c]	1113.92[e]	1055.25	$^5J_{25}$	0.506(2)	0.520(3)
ν_2[d]	2142.541(1)	2082.893(3)	$^4J(H,CH_2)$	−0.823(2)	−0.825(3)
ν_3	2117.571(2)	2079.801(3)	$^5J(H\text{-}3,CH_2)$	0.272(4)	0.281(4)
ν_4	2111.978(2)	2064.894(1)	$^5J(H\text{-}5,CH_2)$	0.411(2)	0.418(2)
ν_5	2182.686(1)	2191.169(1)	$^6J(H,CH_2)$	−0.551(3)	−0.550(2)
$^3J_{23}$	7.566(3)	7.558(3)	Calcd. transitions	184	173
$^3J_{34}$	7.410(3)	7.447(7)	Peaks observed	96[f]	115[f]
$^3J_{45}$	7.743(3)	7.766(2)	Assigned transitions	92[f]	83[f]
$^4J_{24}$	1.400(3)	1.400(7)	Largest difference	0.016	0.019
$^4J_{35}$	1.265(3)	1.252(4)	Root-mean-square deviation	0.007[g]	0.007[g]

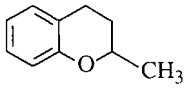
[a]As a 4.0 mol% solution in CS_2 containing also 10 mol% of C_6D_{12} and 0.5 mol% of TMS.
[b]As a 4.2 mol% solution in C_6D_6 containing 0.5 mol% TMS.
[c]In Hz at 300.135_2 MHz to high frequency of internal TMS.
[d]H-2 is placed *ortho* to the methylene group.
[e]Not included in the iterative analysis.
[f]In the aromatic proton region only.
[g]Significant correlations exist between spectral parameters (see text).

Can. J. Chem. Downloaded from www.nrcresearchpress.com by 198.100.157.202 on 09/07/12
For personal use only.

It appears that the inversion potential is computed as somewhat high with the basis, 4-31G, and, by implication, with the 3-21G and 3-21G(*) bases (footnote in Table 2). The STO-3G and STO-3G(*) bases seem to yield too small an inversion barrier.

The long-range coupling constant, $^5J(H,CH_3)$, in toluene has been written (19) as $^5J/Hz = {}^5J^{\pi}\sin^2\psi + {}^5J^{\sigma}\sin^2(\psi/2)$, where $^5J^{\pi}$ is 0.336 Hz and $^5J^{\sigma}$ is 0.322 Hz. $^5J^{\pi}$ in thioxanthene should scale in the same way as $^6J_{90}$ but $^5J^{\sigma}$ is not known for this compound. However, if $\sin^2(\psi/2)$ applies to $^5J(H\text{-}2,CH_2)$, then $1 - \sin^2(\psi/2)$ is appropriate to $^5J(H\text{-}5,CH_2)$. The two coupling constants are 0.276(8) and 0.414(6) Hz, respectively, where the averages for the two solutions are quoted. The quantities $^5J^{\sigma}$ and $\langle\sin^2(\psi/2)\rangle$ then follow as 0.384(26) Hz and 0.32(4) at 300 K. Because of the large uncertainties in $^5J(H,CH_2)$ it can be said only that this value of $\langle\sin^2(\psi/2)\rangle$ is consistent with the conformational deductions from $^6J(H,CH_2)$.

In toluene (19), $^4J(H,CH_3)$ obeys the equation (31): $^4J/Hz = -1.08\langle\sin^2\psi\rangle - 0.32\langle\cos^2\psi\rangle$. Applied to thioxanthene, this relationship has $^4J(H,CH_2)$ as −0.69(1) Hz because $\langle\sin^2\psi\rangle = 0.49(1)$. The measured number is −0.824(3) Hz. However, for $\psi < 90°$, this relationship appears (31) to underestimate the magnitude of ^4J for some molecules. In one of these, **1**, a ψ of



1

45° corresponds to a ^4J of −0.84 Hz, for example, and $\sin^2 45°$ is, of course, 0.5. Hence, apart from other considerations, such as the appropriate bond order of the intervening aromatic C—C bond (32), ^4J in thioxanthene cannot be taken as evidence against the conformational indications based on $^6J(H,CH_2)$.

Acknowledgments

We are grateful to the Natural Sciences and Engineering Research Council of Canada for financial assistance.

1. T. SCHAEFER and R. SEBASTIAN. J. Mol. Struct. (Theochem), **153**, 55 (1987), and references therein.
2. F. H. HERBSTEIN, M. KAPON, and G. M. REISNER. Acta Crystallogr. Sect. B: Struct. Sci. **B42**, 181 (1986).
3. H. LYNTON and E. G. COX. J. Chem. Soc. London, 4886 (1956).
4. I. ROWE and B. POST. Acta Crystallogr. **11**, 372 (1958).
5. S. B. LARSON, S. H. SIMONSEN, G. E. MARTIN, K. SMITH, and S. PUIG-TORRES. Acta Crystallogr. Part C: Cryst. Struct. Commun. **C40**, 103 (1984).
6. K. L. GALLAHER and S. H. BAUER. J. Chem. Soc. Faraday Trans. 2, **71**, 1173 (1975).
7. M. J. ARONEY, R. J. LEFÈVRE, and J. D. SAXBY. J. Chem. Soc. London, 571 (1965).
8. M. DAVIES and J. SWAIN. Trans. Faraday Soc. **67**, 1637 (1971).
9. Y. KOGA, H. TAKAHASHI, and K. HIGASI. Bull. Chem. Soc. Jpn. **46**, 3359 (1973).
10. H. FUJIWARA, A. KAWAMURA, T. TOKAGI, and T. SASAKI. J. Am. Chem. Soc. **105**, 125 (1983).
11. G. FRONZA, E. RAGG, and G. RONSISVALLE. J. Chem. Soc. Perkin Trans. 2, 1209 (1982).
12. J. KAO, C. EYERMANN, E. SOUTHWICK, and D. LEISTER. J. Am. Chem. Soc. **107**, 5323 (1985).
13. A. K. CHANDRA. Tetrahedron, **19**, 471 (1963).
14. T. SCHAEFER and R. SEBASTIAN. J. Mol. Struct. (Theochem), **204**, 41 (1990), and references therein.
15. J. A. GILLEAN, D. W. PHELPS, and A. W. CORDES. Acta Crystallogr. Sect. B: Struct. Crystallogr. Cryst. Chem. **B29**, 2296 (1973).
16. M. ARONEY, G. M. HOSKINS, and R. J. W. LE FEVRE. J. Chem. Soc. London, Part B, 980 (1969).
17. P. CANSELIER and P. CASSOUX. J. Mol. Struct. **39**, 301 (1977).
18. Z. AIZENSHTAT, E. KLEIN, H. WEILER-FEILCHENFELD, and E. D. BERGMANN. Isr. J. Chem. **10**, 753 (1972).
19. T. SCHAEFER, R. SEBASTIAN, and G. H. PENNER. Can. J. Chem. **63**, 2597 (1985).
20. M. J. FRISCH, J. S. BINKLEY, H. B. SCHLEGEL, K. RAGHAVACHARI, C. F. MELIUS, R. L. MARTIN, J. J. P. STEWARD, F. W. BOBROWICZ, C. F. ROHLFING, L. R. KAHN, D. J. DEFREES, R. SEEGER, R. A. WHITESIDE, D. J. FOX, E. M. FLUDER, and J. A. POPLE. Carnegie–Mellon Quantum Publishing Unit, Pittsburgh, PA. 1984.
21. W. J. HEHRE, L. RADOM, P. V. R. SCHLEYER, and J. A. POPLE. *Ab initio* molecular orbital theory. J. Wiley and Sons, New York. 1986.
22. S. SAEBO, L. RADOM, and G. L. D. RITCHIE. J. Mol. Struct. (Theochem), **108**, 59 (1984).
23. T. SCHAEFER and J. D. BALEJA. Can. J. Chem. **64**, 1376 (1986).
24. G. H. PENNER, P. GEORGE, and C. W. BOCK. J. Mol. Struct. (Theochem), **152**, 201 (1987).

25. W. S. WALLS and C. P. SMYTH. J. Chem. Phys. **1**, 337 (1933).
26. W. J. PIETRO, M. M. FRANCL, W. J. HEHRE, D. J. DEFREES, J. A. POPLE, and J. S. BINKLEY. J. Am. Chem. Soc. **104**, 5039 (1982).
27. J. S. MARTIN, A. R. QUIRT, and K. E. WORVILLE. The NMR program library. Daresbury Laboratory, Daresbury, U.K.
28. T. SCHAEFER, C. BEAULIEU, R. SEBASTIAN, and G. H. PENNER. Can. J. Chem. **68**, 581 (1990).
29. T. SCHAEFER, G. H. PENNER, and R. SEBASTIAN. Can. J. Chem. **65**, 873 (1987).
30. S. G. BRATSCH. J. Chem. Educ. **62**, 101 (1985).
31. M. BARFIELD, C. J. FALLICK, K. HATA, S. STERNHELL, and P. W. WESTERMAN. J. Am. Chem. Soc. **105**, 2178 (1983).
32. M. BARFIELD, M. J. COLLINS, J. E. GREADY, S. STERNHELL, and C. W. TANSEY. J. Am. Chem. Soc. **111**, 4285 (1989).

Can. J. Chem. Downloaded from www.nrcresearchpress.com by 198.100.157.202 on 09/07/12
For personal use only.

Thiol esters in organic synthesis. XVI.[1] Formation of α,β-unsaturated thiol esters via a Wadsworth–Emmons process

HSING-JANG LIU, PATRICIA A. ROSE, AND DOUG J. SASAKI
Department of Chemistry, The University of Alberta, Edmonton, Alta., Canada T6G 2G2

Received November 9, 1990

HSING-JANG LIU, PATRICIA A. ROSE, and DOUG J. SASAKI. Can. J. Chem. **69**, 934 (1991).

α,β-Unsaturated thiol esters could be readily prepared via a Wadsworth–Emmons reaction using diethyl alkylthiocarbonylmethylphosphonate, which proved to be superior in reactivity to the corresponding Wittig reagent.

Key words: α, β-unsaturated thiol esters, Wadsworth–Emmons reaction.

HSING-JANG LIU, PATRICIA A. ROSE et DOUG J. SASAKI. Can. J. Chem. **69**, 934 (1991).

On peut facilement préparer les esters de thiols α,β-insaturés en faisant appel à une réaction de Wadsworth–Emmons utilisant l'alkylthiocarbonylméthylphosphonate de diéthyle dont la réactivité est supérieure à celle du réactif de Wittig correspondant.

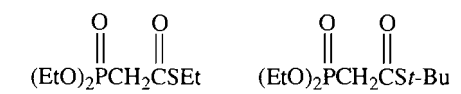
Mots clés : esters de thiols α, β-insaturés, réaction du Wadsworth–Emmons.

[Traduit par la rédaction]

Can. J. Chem. Downloaded from www.nrcresearchpress.com by 198.100.157.202 on 09/07/12
For personal use only.

Thiol esters are stable acid derivatives and yet highly versatile synthetic intermediates. Their increased utility in synthesis has attracted extensive efforts in developing new methods of preparation.[2] Several years ago, Keck *et al.* reported the preparation of α,β-unsaturated thiol esters using ethylthiocarbonylmethylenetriphenylphosphorane (2). This Wittig reagent was shown to react with aldehydes with high stereoselectivity (2), and has been applied to the synthesis of (+)-colletodiol (3). However, no report has appeared regarding its reaction with ketones. In our hands, attempted reaction of this reagent with 4-*tert*-butylcyclohexanone and 6-undecanone failed completely even after extended reaction time at temperatures greater than 60°C. Herein we wish to report the use of diethyl alkylthiocarbonylmethylphosphonate to facilitate the preparation of α,β-unsaturated thiol esters. This Wadsworth–Emmons reagent shows a greater propensity to react with carbonyl compounds.

Both ethyl (**1**, bp 114–116°C/0.6 Torr; 1 Torr = 133.3 Pa) and *tert*-butyl phosphonates (**2**, bp 147–149°C/3.6 Torr) were examined. These compounds were readily prepared in ca. 90% yield by treatment of the corresponding α-bromo thiolacetate with triethyl phosphite (4, 5) in refluxing benzene overnight, followed by distillation. These reagents were found to readily undergo reactions with aldehydes and ketones. A typical reaction sequence involved generating the anion by dropwise addition of a solution of the phosphonate ester (1.1 equiv.) in tetrahydrofuran to a stirred suspension of sodium hydride (1.1 equiv.) under argon at 0°C. The reaction mixture was stirred until bubbling ceased (~10 min) and then the carbonyl compound (1 equiv.) was added. The resulting solution was warmed to room temperature and allowed to react until completion as indicated by thin-layer chromatography (silica gel).



1 **2**

The procedure is apparently general. A number of carbonyl compounds were examined and the results are compiled in Table 1. Both reagents, **1** and **2**, showed comparable reactivity. As expected, aldehydes were found to react with the reagents more rapidly then ketones (1–2 h vs. ~16 h). A single stereoisomer (*trans*) was obtained from all the aldehydes examined (Entries 7–10). This stereoselectivity compares favorably with that observed previously using the Wittig reagent (2). The principle difference between the two types of reagents, however, lies in their reactivity towards carbonyl compounds. With the Wittig reagent, the reaction towards aldehydes requires more than 12 h at ~60°C (2). With the phosphonates, the reaction readily occurred at room temperature in less than 2 h (Entries 7–10). A more profound difference was observed for ketones. While the Wittig reagent failed to react (*vide supra*), phosphonates **1** and **2** reacted with ketones smoothly to give the expected condensation products in greater than 80% yield (Entries 1–3, 5, and 6). As the only exception, the reaction of **2** and 4-*tert*-butylcyclohexanone (Entry 4) gave a substantial amount of the β,γ-unsaturated thiol ester, apparently as a result of the concomitant migration of the double bond.

In conclusion, phosphonates **1** and **2** proved to be considerably more reactive towards carbonyl compounds than the corresponding Wittig reagent. Their reaction with aldehydes and ketones provides a general procedure for the preparation of synthetically useful α,β-unsaturated thiol esters.

Experimental

General

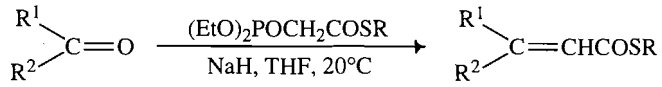
The ir spectra were determined using a Nicolet 7199 FTIR or Nicolet MX-1 FTIR spectrometer and, except where otherwise stated, were obtained as a $CHCl_3$ cast. High resolution mass spectra (hrms) were obtained using a Kratos AE1 MS50 high resolution mass spectrometer. Elemental analyses were determined by the microanalytical laboratory of this department. The ^{1}Hmr spectra were obtained as $CDCl_3$ solutions using the following spectrometers: Bruker WH-200 (200 MHz) and Bruker AM-400 (400 MHz). Flash chromatography was performed according to the procedure of Still *et al.* (6) using silica gel (Merck) of 230–400 mesh. All solvents were distilled prior to chromatography. Thin-layer chromatography was performed on Merck aluminum-backed plates precoated with silica gel 60 GF_{254}. All reactions were run under an argon atmosphere. Tetrahydrofuran (THF) was distilled from a blue solution of sodium benzophenone ketyl under an argon atmosphere. Methylene chloride and benzene were distilled over calcium hydride. Bromoacetyl bromide was purchased from Aldrich Chemical Company, Inc. *S-tert*-Butyl bromoacetate was prepared directly from acetic acid according to the procedure[3] of Luo of this laboratory.

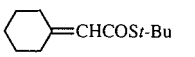
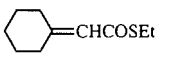
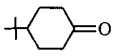
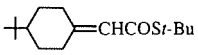
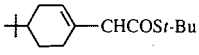
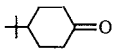
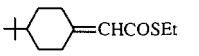
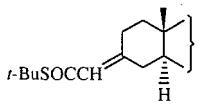
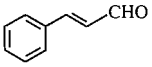
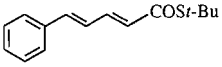
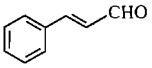
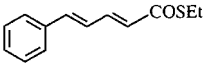
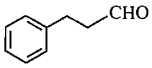
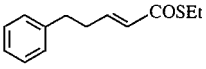
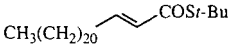
[1]For part XV of this series, see ref. 1.

[2]A review article on the preparation and synthetic applications of thiol esters is being prepared by us.

[3]This procedure will soon be published.

TABLE 1. Preparation of α,β-unsaturated thiol esters



Entry	Carbonyl compound	Phosphonate	Time (h)	Product(s)	Isolated % yield
1		**2**	23	 **3**	85
2		**1**	19	 **4**	87
3		**1**	17	 **5**	80
4		**2**	20	 **6**  **7** **6/7** = 5:2	82
5		**1**	16	 **8**	92
6	5α-cholestan-3-one	**2**	18	 **9** (*E*/*Z* isomers, 1:1)	80
7		**2**	1	 **10**	76
8		**1**	1	 **11**	72
9		**1**	1	 **12**	83
10	$CH_3(CH_2)_{20}CHO$	**2**	1.5	 **13**	92

Diethyl ethylthiocarbonylmethylphosphonate (1)

Bromoacetyl bromide (0.87 mL, 10 mmol) was dissolved in 20 mL of CH_2Cl_2 and cooled to 0°C. Ethyl mercaptan (0.74 mL, 10 mmol) dissolved in 5 mL of CH_2Cl_2 was added dropwise. After addition, the solution was warmed to room temperature and left to stir overnight. The resulting solution was washed with a 5% sodium carbonate solution (2 × 25 mL), water (2 × 25 mL), and brine (25 mL). The combined organic layers were dried over magnesium sulfate, filtered, and concentrated. This afforded ~2 g of *S*-ethyl bromoacetate, which was used without purification. The Wadsworth–Emmons reagent was then formed by mixing triethyl phosphite (1.72 mL, 10 mmol) with the bromoacetate thus obtained in 10 mL of benzene at room temperature, followed by heating to reflux with stirring for 24 h. Distillation under reduced pressure (114–116°C/0.6 Torr) afforded the desired product **1** in 91% yield (2.19 g); ir: 1684 (C=O) cm^{-1}; ^{1}Hmr (200 MHz) δ: 4.16 (dq, $J = J' = 7.5$ Hz, 4H, -OCH_2), 3.20 (d, $J = 21$ Hz, 2H, -PCH_2),

Can. J. Chem. Downloaded from www.nrcresearchpress.com by 198.100.157.202 on 09/07/12
For personal use only.

Can. J. Chem. Downloaded from www.nrcresearchpress.com by 198.100.157.202 on 09/07/12
For personal use only.

2.92 (q, J = 7 Hz, 2H, -SCH_2CH$_3$), 1.34 (t, J = 7.5 Hz, 6H, -OCH$_2$CH_3), 1.26 (t, J = 7 Hz, 3H, -SCH$_2$CH_3); hrms M$^+$: 240.0582 (calcd. for $C_8H_{17}PO_4S$: 240.0585).

Diethyl tert-*butylthiocarbonylmethylphosphonate (2)*

A solution of *S-tert*-butyl bromoacetate (28.4 g, 0.135 mol) and triethyl phosphite (23.3 mL, 0.135 mol) was heated to reflux with stirring for 24 h. Distillation under reduced pressure (147–149°C/3.6 Torr) afforded the desired product **2** in 89% yield (31.1 g); ir: 1679 (C=O) cm^{-1}; ^{1}Hmr (400 MHz) δ: 4.15 (dq, J = J' = 7.5 Hz, 4H, -OCH_2), 3.13 (d, J = 21 Hz, 2H, -PCH_2), 1.47 (S, 9H, -C(CH_3)$_3$), 1.30 (t, J = 7.5 Hz, 6H, -OCH$_2$CH_3); hrms M$^+$: 268.0898 (calcd. for $C_{10}H_{21}PO_4S$: 268.0898).

General procedure for forming the α,β-*unsaturated thiol esters*

All reactions were carried out using the general procedure illustrated below with cyclohexanone and reagent **2**. The time required for each reaction is to be found in Table 1.

To a dried 50-mL three-necked flask containing 1 mL of THF was added sodium hydride (42 mg, 60% dispersion in oil, 1.1 mmol). This was cooled to 0°C, with stirring, and the Wadsworth–Emmons reagent **2** (287 mg, 1.1 mmol) in 0.5 mL of THF was slowly added. The mixture was stirred until bubbling ceased (~10 min), indicating complete formation of the anion. Freshly distilled cyclohexanone (1.0 mmol, 111 mg) in 0.5 mL of THF was added and the reaction mixture was slowly warmed to room temperature and stirred overnight. The solution was quenched with 10 mL of 1M HCl, extracted into CH_2Cl_2 (3 × 20 mL), and the combined organic extracts washed with 20 mL of brine, dried over magnesium sulfate, filtered, and concentrated. Flash chromatography (20% ether/petroleum ether) produced 186 mg (86%) of compound **3** as an amorphous solid; ir: 1664 (C=O), 1623 (C=C) cm^{-1}; ^{1}Hmr (200 MHz) δ: 5.84 (t, J = 1Hz, 1H, =CH), 2.78 (m, 2H, =CCH_2), 2.14 (m, 2H, =CCH_2), 1.62 (m, 6H, -CH_2CH_2CH_2), 1.47 (s, 9H, -C(CH_3)$_3$); hrms M$^+$: 212.1221 (calcd. for $C_{12}H_{20}OS$: 212.1235).

The thiol esters **4**–**13** showed the following spectral data. Compound **4**; ir: 1668 (C=O), 1624 (C=C) cm^{-1}; ^{1}Hmr (200 MHz) δ: 5.86 (s, 1H, =CH), 2.89 (q, J = 7 Hz, 2H, -CH_2CH$_3$), 2.78 (m, 2H, =CCH_2), 2.14 (m, 2H, =CCH_2), 1.62 (m, 6H, -CH_2CH_2CH_2), 1.28 (t, J = 7 Hz, 3H, -CH$_2$CH_3); hrms M$^+$: 184.0921 (calcd. for $C_{10}H_{16}OS$: 184.0922). Anal. calcd. for $C_{10}H_{16}OS$: C 65.17, H 8.75, S 17.40; found: C 65.04, H 8.96, S 17.28.

Compound **5**; ir: 1667 (C=O), 1626 (C=C) cm^{-1}; ^{1}Hmr (200 MHz) δ: 6.10 (t, J = 2 Hz, 1H, =CH), 2.90 (q, J = 7 Hz, 2H, -CH_2CH$_3$), 2.74 (m, 2H, =CCH_2), 2.38 (m, 2H, =CCH_2), 1.70 (m, 4H, -CH_2CH_2), 1.25 (t, J = 7 Hz, 3H, -CH$_2$CH_3); hrms M$^+$: 170.0765 (calcd. for $C_9H_{14}OS$: 170.0765).

Compounds **6** and **7** were isolated as an inseparable mixture of α,β and β,γ isomers (2:1 ratio). The mixture showed the following spectral data; ir: 1680 (sh, C=O), 1667 (unsaturated thiol ester C=O), 1625 (C=C) cm^{-1}; hrms M$^+$: 268.1858 (calcd. for $C_{16}H_{28}OS$: 268.1861). The ^{1}Hmr (400 MHz) spectrum showed the following signals for the major isomer **6**: δ: 5.51 (m, 1H, -C=CHCOSR), 3.65 (m, 2H, =CCH_2), 2.20 (t, J = 6 Hz, 2H, =CCH_2), 0.87 (s, 18H, -C(CH_3)$_3$). The minor isomer **7** showed the following peaks in the ^{1}Hmr (400 MHz) spectrum: δ: 5.35 (tt, J = 2, J' = 7 Hz, 1H, -CH=CCH$_2$CO), 4.15 (br d, J = 7 Hz, 2H, -CH_2CO), 0.85 (s, 9H, -C(CH_3)$_3$), 0.83 (s, 9H, -C(CH_3)$_3$).

Compound **8**; ir: 1671 (C=O), 1627 (C=C) cm^{-1}; ^{1}Hmr (200 MHz) δ: 5.86 (s, 1H, =CH), 3.80 (m, 1H, =CCHH), 2.88 (q, J = 7 Hz, 2H, -SCH_2CH$_3$), 2.20 (m, 2H, =CCH_2), 1.90 (m, 3H), 1.25 (t, J = 7 Hz, 3H, -SCH$_2$CH_3 overlapping with m, 3H), 0.84 (s, 9H, -C(CH_3)$_3$); hrms M$^+$: 240.1539 (calcd. for $C_{14}H_{24}OS$: 240.1548). Anal. calcd. for $C_{14}H_{24}OS$: C 69.95, H 10.06, S 13.34; found: C 70.10, H 10.16, S 13.23.

Compound **9** was an inseparable mixture of *E* and *Z* isomers present in a 1:1 ratio; ir: 1667 (C=O), 1622 (C=C) cm^{-1}; ^{1}Hmr (400 MHz) δ: 5.80 (s, 0.5H, =CH), 5.82 (s, 0.5H, =CH), 1.50 (s, 9H, -C(CH_3)$_3$), 0.95 (s, 3H, -CH_3), 0.90 (d, J = 6 Hz, 3H, -CHCH_3), 0.86 (d, J = 6 Hz, 3H, -CH(CH_3)$_2$), 0.84 (d, J = 6 Hz, 3H, -CH(CH_3)$_2$), 0.65 (s, 3H, -CH_3); hrms M$^+$: 500.4050 (calcd. for $C_{33}H_{56}OS$: 500.4052.

Compound **10**; ir (CH_2Cl_2 cast): 1662 (C=O), 1621 (C=C) cm^{-1}; ^{1}Hmr (200 MHz) δ: 7.2–7.5 (m, 6H, C_6H_5 and -CH=), 6.85 (d, J = 15 Hz, 1H, Ar-CH=), 6.80 (dd, J = 15, J' = 10 Hz, 1H, Ar-CH=CH-), 6.20 (d, J = 15 Hz, 1H, =CH-CO), 1.52 (s, 9H, -C(CH_3)$_3$); hrms M$^+$: 246.1078 (calcd. for $C_{15}H_{18}OS$: 246.1078).

Compound **11**; ir: 1668 (C=O), 1659 (C=C) cm^{-1}; ^{1}Hmr (200 MHz) δ: 7.4 (m, 6H, C_6H_5 and -CH=), 6.96 (d, J = 15 Hz, 1H, Ar-CH=), 6.80 (dd, J = 15, J' = 10 Hz, 1H, Ar-CH=CH-), 6.28 (d, J = 15 Hz, 1H, =CH-CO), 2.98 (q, J = 7 Hz, 2H, -SCH_2CH$_3$), 1.28 (t, J = 7 Hz, 3H, -SCH$_2$CH_3); hrms M$^+$: 218.0766 (calcd. for $C_{13}H_{14}OS$: 218.0765).

Compound **12**; ir: 1672 (C=O), 1632 (C=C) cm^{-1}; ^{1}Hmr (200 MHz) δ: 7.3 (m, 5H, C_6H_5), 6.94 (dt, J = 15.5, J' = 6.5 Hz, 1H, -CH=CHCO), 6.15 (dt, J = 15.5, 1.5 Hz, 1H, =CHCO), 2.95 (q, J = 7 Hz, 2H, -SCH_2CH$_3$), 2.78 (m, 2H, Ar-CH_2), 2.48 (m, 2H, -CH_2CH=), 1.26 (t, J = 7 Hz, 3H, -SCH$_2$CH_3); hrms M$^+$: 220.0923 (calcd. for $C_{13}H_{16}OS$: 220.0922).

Compound **13**; ir: 1672 (C=O), 1631 (C=C) cm^{-1}; ^{1}Hmr (400 MHz) δ: 6.84 (dt, J = 15, J' = 7 Hz, 1H, -CH=), 6.02 (dt, J = 15, J' = 1.5 Hz, 1H, =CH-CO), 2.16 (dq, J = 7, J' = 1.5 Hz, 2H, -CH_2CH=), 1.50 (s, 9H, -C(CH_3)$_3$), 1.3 (m, 38H), 0.88 (vt, J = 7 Hz, 3H, -CH_3); hrms M$^+$: 438.3889 (calcd. for $C_{28}H_{54}OS$: 438.3895).

Acknowledgements

We are grateful to the Natural Sciences and Engineering Research Council of Canada and the University of Alberta for financial support, and to the Province of Alberta for a Fellowship for P.R.

1. H. J. Liu and W. Luo. Synth. Commun. **19**, 387 (1989).
2. G. E. Keck, E. P. Boden, and S. A. Mabury. J. Org. Chem. **50**, 709 (1985).
3. G. E. Keck, E. P. Boden, and M. R. Wiley. J. Org. Chem. **54**, 896 (1989).
4. A. E. Arbuzov and A. F. Razumov. J. Russ. Phys. Chem. Soc. **61**, 623 (1929).
5. W. S. Wadsworth, Jr. and W. D. Emmons. J. Am. Chem. Soc. **83**, 1733 (1961).
6. W. C. Still, M. Kahn, and A. Mitra. J. Org. Chem. **43**, 2923 (1978).

Substitution reactions of benzethonium chloride with ion associates of bromocresol green – quinine and bromophenol blue – quinine in dichloromethane

ALBERTO HERNANDEZ GAINZA[1] AND ROY IKEMEFULA KONYEASO

Departamento de Química Física, Facultad de Farmacia, Campus de Cartuja, Universidad de Granada, 18027 Granada, Spain

Received August 29, 1990

ALBERTO HERNANDEZ GAINZA and ROY IKEMEFULA KONYEASO. Can. J. Chem. **69**, 937 (1991).

An excess concentration of base quinine (Q) reacts with a sulphonphthalein diacidic dye XH_2, (bromocresol green, $BCGH_2$, or bromophenol blue, $BPBH_2$) in dichloromethane solution to form an ion associate ($X^{2-}(QH^+)_2$) of stoichiometry 1:2 (dye:amine). Benzethonium chloride (ClB) reacts with the 1:2 ion associate to form an ion associate (QH^+, X^{2-}, B^+) and quinine hydrochloride $ClQH^+$. This substitution reaction is a chemical equilibrium with formation constants of 1.50 ± 0.67, 1.61 ± 0.54, 1.07 ± 0.29, 1.04 ± 0.20, and 0.84 ± 0.26 for BCG and 1.86 ± 0.59, 1.47 ± 0.23, 1.40 ± 0.65, 1.13 ± 0.37, and 1.11 ± 0.27 for BPB at 283.16, 288.16, 293.16, 298.16, and 303.16 K respectively. The thermodynamic parameters determined by van't Hoff's equation are $\Delta H^0 = -21.766 \pm 7.482$ kJ mol^{-1}, $\Delta S^0 = -73 \pm 51$ J mol^{-1} K^{-1}, and $\Delta G^0 = -1.134 \pm 0.972$ kJ mol^{-1} for BCG and $\Delta H^0 = -18.678 \pm 7.482$ kJ mol^{-1}, $\Delta S^0 = -61 \pm 26$ J mol^{-1} K^{-1}, $\Delta G^0 = -0.916 \pm 0.401$ kJ mol^{-1} for BPB (ΔG^0 at 293.16 K; and ΔH^0 and ΔS^0 determined in the range 283–303 K).

Key words: bromocresol green – quinine–benzethonium, ion associate mixture, bromophenol blue – quinine–benzethonium, equilibrium constants, thermodynamic parameters.

ALBERTO HERNANDEZ GAINZA et ROY IKEMEFULA KONYEASO. Can. J. Chem. **69**, 937 (1991).

Les colorants diacides sulphonphtaléiniques, XH_2 (le vert de bromocrésol, BCG, et le bleu de bromophénol, BPB) réagissent avec des concentrations élevées de la quinine base, Q, dans le chlorure de méthylène en formant des paires d'ions de stoechiométrie 1 : 2 (colorant : quinine). Le chlorure de benzéthonium, ClB, réagit avec le paire d'ions 1 : 2 en formant des ions associés (QH^+, X^{2+}, B^+) et du chlorohydrate de quinine. On a démontré l'existence d'un équilibre chimique entre la paire ionique 1 : 2 et les ions associés et on a calculé les constantes d'équilibre correspondant à la formation des ions associés (QH^+, BCG^{2-}, B^+) et (QH^+, BPB^{2-}, B^+) qui sont respectivement égales à 1,50 ± 0,67, 1,61 ± 0,54, 1,07 ± 0,29, 1,04 ± 0,20 et 0,84 ± 0,26; et 1,86 ± 0,59, 1,47 ± 0,23, 1,40 ± 0,65, 1,13 ± 0,37 et 1,11 ± 0,27 à 283,16, 288,16, 293,16, 298,16 et 303,16 K. Les paramètres thermodynamiques correspondant à la formation des (QH^+, BCG^{2-}, B^+) et (QH^+, BPB^{2-}, B^+) sont respectivement : $\Delta H^0 = -21,766 \pm 7,482$ kJ mol^{-1}, $\Delta S^0 = -73 \pm 51$ J mol^{-1} K^{-1} et $\Delta G^0 = -1,134 \pm 0,972$ kJ mol^{-1} (à 293,16 K); et $\Delta H^0 = -18,678 \pm 7,482$ kJ mol^{-1}, $\Delta S^0 = -61 \pm 26$ J mol^{-1} K^{-1}, $\Delta G^0 = -0,916 \pm 0,401$ kJ mol^{-1} à 293,16 K (ΔH^0 et ΔS^0 déterminés en faisant la moyenne de la relation de van't Hoff dans un intervale de 283–303 K).

Mots clés : vert de bromocrésol – quinine–benzéthonium, mélange d'ions associés, bleu de bromophénol – quinine–benzéthonium, constantes d'équilibre, paramètres thermodynamiques.

Introduction

Sakai proposed a new method for the analysis of various quaternary ammonium ions (B) by extraction of ion associates mixed with bromocresol green (BCG) and quinine (Q) (1) or bromophenol blue (BPB) and quinine (2). Sakai's method was empirical and the nature of the ion associate mixture dye–quinine – ammonium ion was suggested but was not proved (1, 2). This new method of analysis is of great interest since it is specific and the methods of analysis based on the extraction of ion pairs are not specific (3–8). These unspecific methods have been widely proposed for the analysis of amines of pharmacological interest. The extraction of ion-associate mixtures could make possible the specificity of these methods of analysis, which are very important in pharmaceutical analytical chemistry. However, there is no information about the formation and stability of ion-associate mixtures.

In this paper, we obtained the ion-associate mixtures of BCG–Q–benzethonium and BPB–Q–benzethonium only in a dichloromethane medium. These reactions were performed only in organic medium, making possible the determination of the stoichiometry and stability of the ion-associate mixtures obtained. The stoichiometry of these ion associates could not be determined in a two-phase system, this being the reason why its existence could not be proved (1, 2).

Firstly, to obtain the dye–Q–benzethonium ion-associate mixture it is necessary to generate the dye–Q_2 ion associate in dichloromethane solution by neutralization of the dye with an excess of quinine base. In previous work, the neutralization reactions of the two protons of BCG and BPB dyes with quinine base and its hydrochloride salt (9), ajmaline and homatropine base (10), and atropine and tropine (11), in dichloromethane, have been studied. These studies showed that in an excess of amine base, given the low dielectric constant of the organic solvent, the stabilization of the dye with the amines is produced by formation of a dye–(amine)$_2$ ion associate, that is to say $X^{2-}(amineH^+)_2$. Therefore, the dye is present in negative, divalent form, as indicated by the scheme of reactions 1 and 2 in ref. 10 (or also reactions [3] and [4] in this paper).

In dichloromethane, the formation of the ion-associate mixture, dye–quinine–benzethonium, $X^{2-}QH^+B^+$, in strong excess of quinine base is established to be

$$[1] \quad X^{2-}(QH^+)_2 + ClB \rightleftharpoons X^{2-}QH^+B^+ + ClQH$$

where $X^{2-}(QH^+)_2$ is the ion associate obtained by the reaction of Q with the sulphonphthalein dye (the formation of $X^{2-}(QH^+)_2$ is complete in a strong excess of Q); ClB, benzethonium chloride; and ClQH, quinine hydrochloride. The existence of this reaction in dichloromethane is demonstrated in this paper. Furthermore the equilibrium constants, K, and the molar extinction coefficients of the ion-associate mixture, ε', of the reaction have been calculated. These have been determined through a procedure of iterative calculation proposed in this paper, which makes possible the determination of K, ε', and their corresponding errors. This procedure is similar to that

[1]Author to whom correspondence may be addressed.

Can. J. Chem. Downloaded from www.nrcresearchpress.com by 198.100.157.202 on 09/07/12
For personal use only.

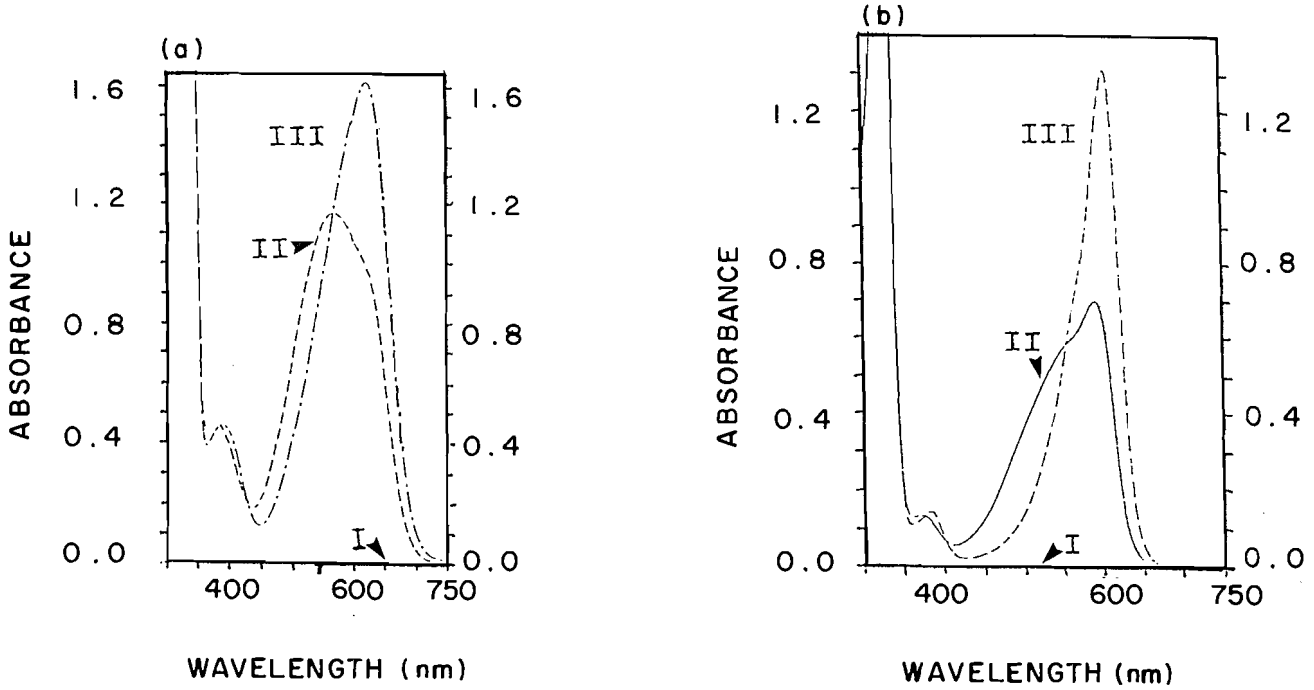


FIG. 1. (a) Dichloromethane solutions of I: benzethonium chloride 8×10^{-5} M; II: bromocresol green 4×10^{-5} M and quinine 4×10^{-3} M; III: (II) with benzethonium chloride 4×10^{-5} M. Temperature = 283 K. (b) Dichloromethane solutions of I: benzethonium chloride 2×10^{-5} M; II: bromophenol blue 2×10^{-5} M and quinine 4×10^{-4} M; III: (II) with benzethonium chloride 2×10^{-5} M. Temperature = 283 K.

Can. J. Chem. Downloaded from www.nrcresearchpress.com by 198.100.157.202 on 09/07/12
For personal use only.

proposed by Rosseinsky and Kellawi (12) for addition reactions, whereas this method solves substitution reactions. The proposed method reduces to a minimum the square of the residuals using the Gauss procedure (13) with analytical derivation and the best values for K and ε' are obtained. The equilibrium constants have been calculated at various temperatures and the thermodynamic parameters have been determined by the van't Hoff equation.

The absorption spectra of BCG–Q–B and BPB–Q–B are identical to the spectra in the organic phase of the products obtained by Sakai (1, 2), which indicates that these are ion-associate mixtures.

Experimental part

Instruments and reagents

The spectrophotometric measurements were carried out with a Perkin–Elmer Lambda 5 spectrophotometer, using a Selecta Tectron thermostat with ±0.5°C accuracy, 1 cm quartz cells with Teflon stoppers, and an Amstrad PC1512SD microcomputer. Dichloromethane: Probus HPLC, with water content less than 0.02%. Anhydrous quinine base (Q): Sigma. Bromocresol green (BCG) and bromophenol blue (BPB): Merck. All solid reagents were of analytical grade and were stored in a desiccator with phosphorus pentoxide and used without previous purification. All dichloromethane solutions were used immediately after preparation.

Absorption spectra and stoichiometric balance

When a solution containing dye (BCG or BPB) and excess quinine base (Q) in dichloromethane (the $X^{2-}(QH^+)_2$ species is generated immediately, X can be BCG or BPB) is mixed with another which contains benzethonium chloride (ClB), a new absorption spectrum is observed with maximum wavelengths of absorption at 630 nm for BCG and 605 nm for BPB. This new spectrum suggests the existence of a new compound in the solution ($X^{2-}QH^+B^+$ in eq. [1], X can be BCG or BPB). The spectra of $X^{2-}(QH^+)_2$, $X^{2-}QH^+B^+$, and ClB in dichloromethane are shown in Figs. 1a and 1b. Figure 2 shows the effect of the concentrations of Q and ClB, in a mixture dye–Q–benzethonium with a constant concentration of dye, on the absorption spectrum.

The stoichiometry of these reactions has been determined using Job's method (14). The experimental data are shown in Tables 1 and 2. Since the reagent $X^{2-}(QH^+)_2$ shows some absorption at the same wavelength as that of the maximum absorption of the $X^{2-}QH^+B^+$ product (Figs. 1a and 1b), the law of Lambert–Beer can be expressed here as $A' = A_m - A_0 = x\{\varepsilon_{x^{2-}QH^+B^+} - \varepsilon_{x^{2-}(QH^+)_2} = x\varepsilon'$ (for derivation of this see Appendix). A_m is the experimental absorbance of the system given by eq. [1]; A_0 is the absorbance due to the $(X^{2-}(QH^+)_2)$ ion associate, this being equal to the total (or initial) dye concentration, a, in the experiment multiplied by the molar absorptivity of the $X^{2-}(QH^+)_2$ species ($A_0 = \varepsilon_{x^{2-}(QH^+)_2} \cdot a$). A is equally the absorbance found in a previous identical experiment where the species ClB was excluded; x is the concentration of the product of the reaction, $\varepsilon_{x^{2-}QH^+B^+}$ its molar extinction coefficient, and $\varepsilon_{x^{2-}(QH^+)_2}$ the molar extinction coefficient of the 1:2 ion associate ($X^{2-}(QH^+)_2$). The difference between $\varepsilon_{x^{2-}QH^+B^+}$ and $\varepsilon_{x^{2-}(QH^+)_2}$ is the ε' value. The value of the extinction coefficient of $X^{2-}(QH^+)_2$ has been determined using a solution of dye–quinine with an excess of quinine. The values of A' are shown in the last column of Tables 1 and 2. The stoichiometry of the reaction is always 1:1, according to Job's method, after subtracting the absorbance, A_0, due to the ion associate 1:2 (Tables 1 and 2). Supplementary information about the subject discussed in this section can be consulted in ref. 15.

Determination of the equilibrium constants

Figure 3 shows superposed absorption spectra of a solution containing BCG with excess Q to which increasing amounts of benzethonium chloride (ClB) are added. These spectra show various isosbestic points, which suggest the existence of a chemical equilibrium between the 1:2 ion associate and the new product ($X^{2-}QH^+B^+$). Similar spectra to those of Fig. 3 have been obtained for BPB. To determine the equilibrium constants and the molar extinction coefficients of the product, a series of solutions in dichloromethane containing mixtures of dye–Q (in excess quinine) and benzethonium chloride with the sum of the concentrations constant were prepared. The experimental data for BCG are shown in Table 3. These data correspond to the values of

Can. J. Chem. Downloaded from www.nrcresearchpress.com by 198.100.157.202 on 09/07/12
For personal use only.

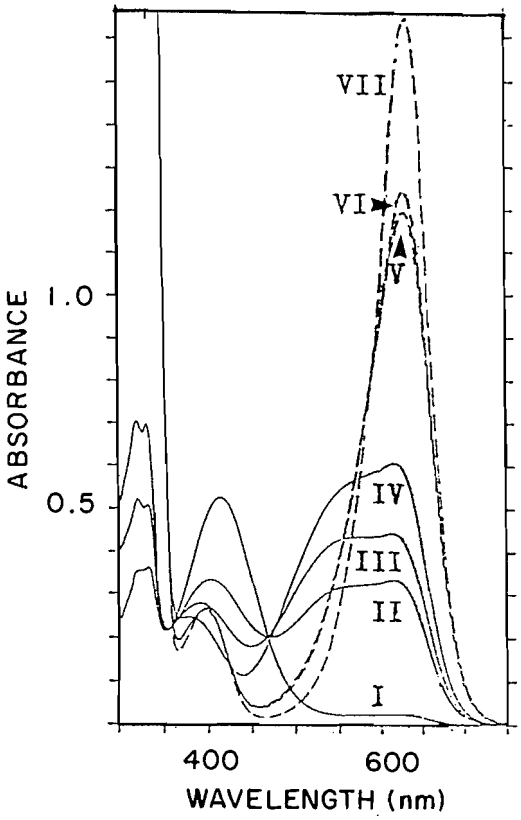


FIG. 2. UV–VIS absorption spectra in dichloromethane at 293 K of I: bromocresol green (BCG) 2×10^{-5} M, quinine (Q), 2×10^{-5} M, and benzethonium chloride (ClB) 4×10^{-6} M; II: BCG 2×10^{-5} M, Q 5×10^{-5} M and ClB 4×10^{-6} M; III: BCG 2×10^{-5} M, Q 10^{-4} M, and ClB 4×10^{-6} M; IV: BCG 2×10^{-5} M, Q 3×10^{-4} M, and ClB 4×10^{-4} M; V: BCG 2×10^{-5} M, Q 3×10^{-4} M, and ClB 8×10^{-5} M; VI: BCG 2×10^{-5} M, Q 3×10^{-4} M, and ClB 9×10^{-5} M; VII: BCG 2×10^{-5} M, Q 3×10^{-4} M, and ClB 10^{-2} M.

TABLE 1. The difference, $A' = A_m - A_0$, between the experimental absorbance, A_m, and the absorbance due to the 1:2 ion associate, A_0, at 630 nm for different mole ratios using Job's method. The sum of the concentrations of BCG and ClB is constant ([BCG] + [ClB] = 4×10^{-5} M); temperature = 283 K; [Q] = 100 [BCG]

[BCG–Q] × 10^5	[ClB] × 10^5	Mole ratio	A_m	$A_m - A_0$
0.333	3.667	0.0833	0.177	0.119
0.667	3.333	0.1668	0.327	0.229
1.333	2.667	0.3333	0.599	0.333
1.600	2.400	0.4000	0.689	0.441
2.000	2.000	0.5000	0.792	0.482
2.400	1.600	0.6000	0.823	0.451
2.667	1.333	0.6668	0.779	0.366
3.333	0.667	0.8325	0.710	0.194
3.667	0.333	0.9168	0.728	0.160

A' and they have been obtained for various temperatures in order to determine the thermodynamic parameters of the reaction.

The equilibrium constant for reaction [1] is given by the following expression:

$$[2] \quad K = \frac{[X^{2-}QH^+B^+][ClQH^+]}{[X^{2-}(QH^+)_2][ClB]} = \frac{x^2}{(a-x)(b-x)}$$

where a and b are the initial (or total) concentrations of the dye (BCG or BPB) and benzethonium bromide (ClB) and x represents the concentrations of the products in the equilibrium (corresponding to eq. [1]). The procedure for calculation of the equilibrium constant, K, will be discussed subsequently.

TABLE 2. The difference, $A' = A_m - A_0$, between the experimental absorbance, A_m, and the absorbance due to the 1:2 ion associate, A_0, at 630 nm for different mole ratios using Job's method. The sum of the concentrations of BPB and ClB is constant ([BPB] + [ClB] = 4×10^{-5} M); temperature = 283 K; [Q] = 20 [BPB]

[BPB–Q] × 10^6	[ClBt] × 10^6	Mole ratio	A_m	$A_m - A_0$
3.33	36.67	0.0833	0.276	0.171
6.67	33.33	0.1668	0.535	0.325
13.33	26.67	0.3333	1.023	0.603
20.00	20.00	0.5000	1.320	0.690
26.67	13.33	0.6668	1.367	0.527
33.33	6.67	0.8325	1.297	0.247
36.67	3.33	0.9168	1.250	0.095

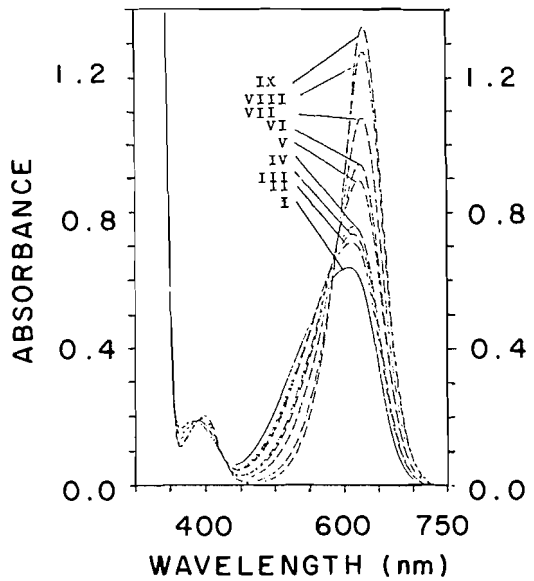


FIG. 3. UV–VIS absorption spectra in dichloromethane at 293 K of I: bromocresol green (BCG) 2×10^{-5} M and quinine (Q) 2×10^{-3} M; II: (I) with benzethonium chloride (ClB) 1.87×10^{-6} M; III: (I) with ClB 2.28×10^{-5} M; IV: (I) with ClB 2.34×10^{-5} M; V: (I) with ClB 3.13×10^{-5} M; VI: (I) with ClB 3.46×10^{-5} M; VII: (I) with ClB 5.04×10^{-5} M; VIII: (I) with ClB 1.34×10^{-4} M; IX: (I) with ClB 3.37×10^{-4} M.

Discussion

Tables 1 and 2 suggest a clear 1:1 stoichiometry for the product formed with each of the dyes. Accordingly, the reaction that takes place in the solution has to be reaction [1].

This is true only when Q is present in the solution in strong excess. With a slight excess of Q the stoichiometry is not clear. This is due to the fact that Q neutralizes the two protons of the dye generating the 1:1 and 1:2 ion associates by the following reactions (9–11):

$$[3] \quad XH_2 + Q \rightleftharpoons XH^-QH^+$$

$$[4] \quad XH^-QH^+ + Q \rightleftharpoons X^{2-}(QH^+)_2$$

where XH_2 is the free dye and XH^-QH^+ the 1:1 ion associate.

TABLE 3. Differences in absorbance values, at 630 nm, between solutions of initial concentrations of bromocresol green – quinine with benzethonium chloride, A_m, and the absorbance due to the 1:2 ion associate (BCG–Q), A_0, at different temperatures

			$A_m - A_0$				
[BCG] × 10^6	[Q] × 10^4	[ClBt] × 10^6	10°C	15°C	20°C	25°C	30°C
1.67	1.67	7.83	0.077	0.076	0.076	0.073	0.073
3.33	3.33	7.67	0.145	0.138	0.134	0.133	0.132
5.00	5.00	7.50	0.203	0.259	0.192	0.193	0.189
6.67	6.67	7.33	0.260	0.260	0.262	0.251	0.255
13.33	13.33	6.67	0.458	0.457	0.446	0.448	0.445
20.00	20.00	6.00	0.639	0.638	0.617	0.599	0.595
26.67	26.67	5.33	0.846	0.785	0.739	0.722	0.720
33.33	33.33	4.67	0.852	0.858	0.802	0.792	0.756
40.00	40.00	4.00	0.901	0.892	0.837	0.820	0.801
1.67	1.67	7.83	0.077	0.076	0.076	0.073	0.073
3.33	3.33	7.67	0.145	0.138	0.134	0.133	0.132
5.00	5.00	7.50	0.203	0.259	0.192	0.193	0.189
6.67	6.67	7.33	0.260	0.260	0.262	0.251	0.255
13.33	13.33	6.67	0.458	0.457	0.446	0.448	0.445
20.00	20.00	6.00	0.639	0.638	0.617	0.599	0.595
26.67	26.67	5.33	0.846	0.785	0.739	0.722	0.720
33.33	33.33	4.67	0.852	0.858	0.802	0.792	0.756
40.00	40.00	4.00	0.901	0.892	0.837	0.820	0.801
1.67	1.67	7.83	0.077	0.076	0.076	0.073	0.073
3.33	3.33	7.67	0.145	0.138	0.134	0.133	0.132
5.00	5.00	7.50	0.203	0.259	0.192	0.193	0.189
6.67	6.67	7.33	0.260	0.260	0.262	0.251	0.255
13.33	13.33	6.67	0.458	0.457	0.446	0.448	0.445
20.00	20.00	6.00	0.639	0.638	0.617	0.599	0.595
26.67	26.67	5.33	0.846	0.785	0.739	0.722	0.720
33.33	33.33	4.67	0.852	0.858	0.802	0.792	0.756
40.00	40.00	4.00	0.901	0.892	0.837	0.820	0.801

Can. J. Chem. Downloaded from www.nrcresearchpress.com by 198.100.157.202 on 09/07/12
For personal use only.

The XH^-QH^+ ion associate shows a maximum at approximately 415 nm and the $X^{2-}(QH^+)_2$ at 550 and 590 nm for BCG and BPB, respectively (ref. 9, and Fig. 2 for BCG). The formation of XH^-QH^+ is quantitative from the spectrophotometric point of view (therefore reaction [3] is not taking place in the solution) while that of the 1:2 ion associate is clearly a chemical equilibrium that is displaced towards the formation of this last compound with an increase in the concentration of the alkaloid base or a decrease in temperature (9–11). Therefore, in a slight excess of Q reactions [1] and [4] are present in the solution, which explains an uncertain stoichiometry under these conditions.

The simultaneous existence of reactions [1] and [4] in solution can be seen in Fig. 2 where a dye–Q–benzethonium mixture with constant concentration of dye increases its absorption intensity (at 630 nm for BCG and 605 nm for BPB) when the concentration of Q, dye, or both at the same time increases. This suggests that reactions [1] and [4] are chemical equilibria. The fact that reaction [1] is in equilibrium will be demonstrated subsequently.

Consequently, a dye–Q–benzethonium mixture in a slight excess of Q generates in solution three absorbing species XH^-QH^+, $X^{2-}(QH^+)_2$, and $X^{2-}QH^+B^+$ (lines II, III, and IV in Fig. 2); Fig. 2 demonstrates a case where absorption spectra with an isosbestic point are due to three absorbing species. On the other hand, in an excess of Q only the last two species are present (Fig. 3). This has been confirmed by Coleman's method (16), as can be seen in Figs. 4a and 4b.

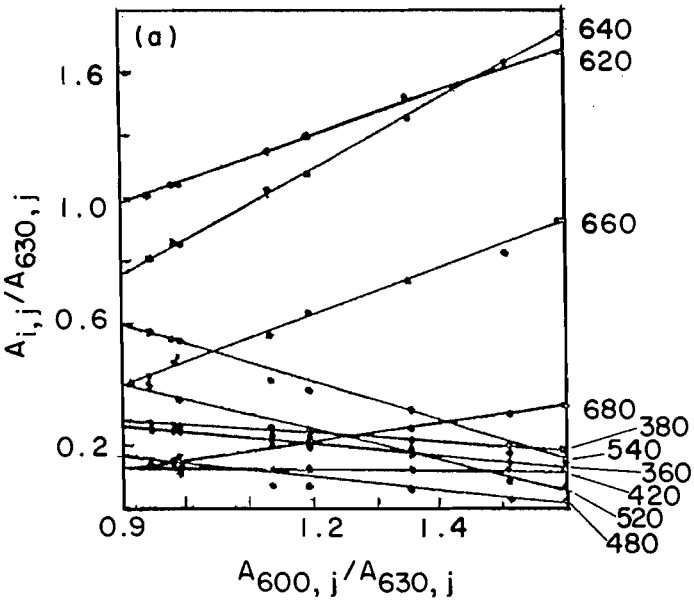
The equilibrium constants at 293 K for reaction [4] are, respectively, 25 751 ± 2822 L mol^{-1} for BCG and 183 486 ± 61 775 L mol^{-1} for BPB in dichloromethane (9–11). Therefore, with a concentration of Q at least 100 times higher than that of BCG and 20 times higher than that of BPB, reaction [4] is totally displaced to the right. In this way it is guaranteed that reaction [4] is not taking place in the solution and therefore reaction [1] can be easily studied. A higher excess of Q does not affect the absorption measurements. This indicates that the excess concentration of Q is not important in the substitution reaction, a logical result since Q does not take part in reaction [1].

The previous discussion justifies that all experiments were carried out in a sufficient excess of Q to complete reaction [4].

The isosbestic points in Fig. 3 indicate the chemical equilibrium suggested in reaction [1]. Furthermore, Coleman's method (16) confirms the existence of two absorbing species (Fig. 4a) under the experimental conditions in Fig. 3 and also agrees with the condition that the sum of the concentrations of the two species is constant (Fig. 4b). Most spectrophotometric methods so far published are valid for addition reactions but this reaction is a substitution process. For this reason, we are proposing a procedure that permits the simultaneous calculation of the equilibrium constant, K, and the molar absorptivity, ε' ($\varepsilon' = \varepsilon_{x^{2-}QH^+B^+} - \varepsilon_{x^{2-}(QH^+)_2}$, obtained from data in Table 3. The relationship between the absorbance, A', of each solution, K, and ε' is given by the following equation:

$$[5] \quad \frac{ab}{A'^2} = \frac{a+b}{\varepsilon' A'} - \frac{1}{\varepsilon'^2(1-K^{-1})}$$

which is obtained by substituting A'/ε' for x in eq. [2]. The graphic plot of ab/A'^2 against $(a+b)/A'$ permits the



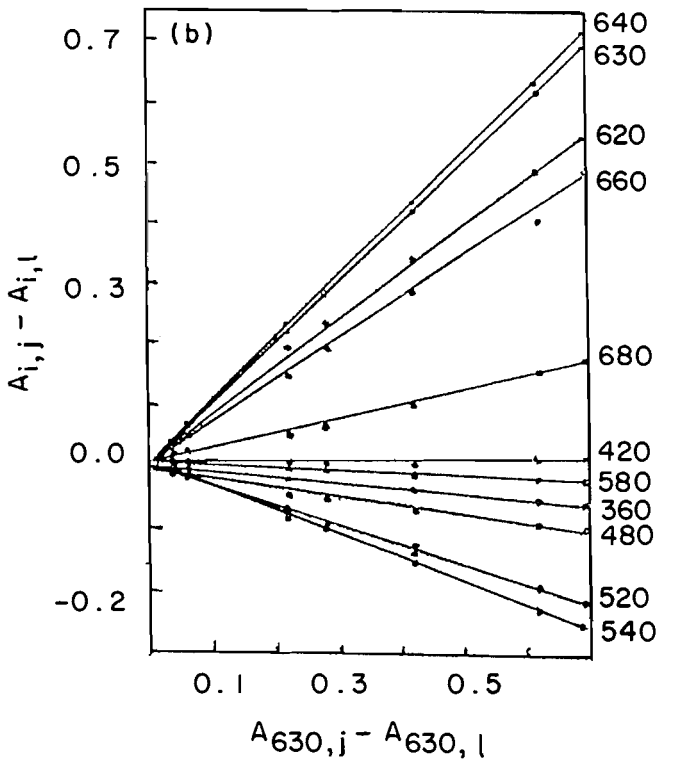


FIG. 4. (a) Coleman's test for two species for the ion associate BCG–Q–B with excess of quinine, using data obtained from Fig. 3. The numbers on the right side of the graph represent the wavelength for each line. (b) Coleman's test for two species with the sum of concentrations constant for the ion associate BCG–Q–B with excess quinine, using data obtained from Fig. 3. The numbers on the right side of the graph represent the wavelengths for each line.

determination of K and ε' from the values of the ordinate and the slope obtained by the least-squares method. An example of this plot for BCG is shown in Fig. 5. In order to refine K and ε' and determine their corresponding errors, an iterative method similar to that of Rosseinsky and Kellawi (12), adapted to processes of type A + B $\rightleftharpoons$ C + D, has been proposed. This method begins with the values of K and ε' obtained from the graphic method already described. A computer program in

TABLE 4. K and ε' parameters at 605 nm determined by Rosseinsky's method, confidence intervals for a 0.95 probability, root-mean-squared deviation (r.m.s.d.), and the values for r^2 obtained for the ion associate dye–Q–ClB

T (K)	K (mol^{-1})	ε' ($mol^{-1}\,cm^{-1}$)	r.m.s.d.	r^2
		BPB–Q–ClB		
283.16	1.86 ± 0.59	62994 ± 3264	0.006	0.998
288.16	1.47 ± 0.23	63958 ± 1900	0.003	0.999
293.16	1.40 ± 0.65	62395 ± 4932	0.008	0.999
298.16	1.13 ± 0.37	63906 ± 4000	0.006	0.999
303.16	1.11 ± 0.27	62822 ± 3107	0.004	0.999
		BCG–Q–ClB		
283.16	1.50 ± 0.67	40265 ± 3002	0.011	0.998
288.16	1.61 ± 0.54	39729 ± 2304	0.008	0.994
293.16	1.07 ± 0.29	40781 ± 2218	0.007	0.998
298.16	1.04 ± 0.20	40299 ± 1650	0.005	0.998
303.16	0.84 ± 0.26	41447 ± 2780	0.008	0.998

GWBASIC has been written to perform all these calculations. The program has been checked with synthetic absorbance data, obtaining an exact reproduction of the expected values of K and ε'. In the same way it was checked with synthetic data affected with random errors. The program reproduced the values of K and ε' expected, which were better than those obtained from the graphic method from Fig. 5.

The program gives the values of K and ε' with their respective confidence intervals with a 95% confidence level, root-mean-square deviation (r.m.s.d.) of the experimental absorbance values, and the values of the linear determination coefficient (r^2) obtained by the least-squares method. One additional advantage of the refinement procedure is that it eliminates experimental data with dispersion greater than 2 × (r.m.s.d.). In Table 4 the values obtained for BCG and BPB reagents are given. The values of r^2 obtained, which are close to 1, and the r.m.s.d. about the instrumental error suggest that reaction [1] is taking place in the solution. Another important result is that ε' is almost constant at different temperatures. The values from Table 4 indicate that the equilibrium constant K diminishes with an increase in temperature, making possible the determination of the thermodynamic parameters using van't Hoff's equation (17). The thermodynamic parameters have been obtained by plotting log $K \times \varepsilon'$ against $1/T$. Since the product of $K \times \varepsilon'$ is more exact than K, a more exact result for ΔH^0 and ΔS^0 is obtained (18, 19). The values of ΔS^0 and ΔH^0 obtained using least-squares methods are shown in Table 5 with their respective confidence intervals, for a confidence level of 95% from the Student "t"-test (20). An example of the alternative method to van't Hoff's plot is shown in Fig. 6.

As shown in Table 5, since the ΔH^0 values are negative, the reaction is exothermic; these ΔH^0 values are of the same sign but smaller than those of the neutralization reactions to form 1:2 ion associates (reaction [4]) in dichloromethane (9–11). The ΔS^0 values of the reactions are negative, which is considered to reflect the evidence that the degree of freedom of the system decreases, perhaps due to a stronger solvation sphere about the products of the reaction. These ΔS^0 values are also of the same sign but smaller than those of the neutralization reactions to form 1:2 ion associates (reaction [4]) in dichloromethane. The ΔG^0 values are close to zero and their confidence intervals suggest that they can either be negative or positive. Thus, a

Can. J. Chem. Downloaded from www.nrcresearchpress.com by 198.100.157.202 on 09/07/12
For personal use only.

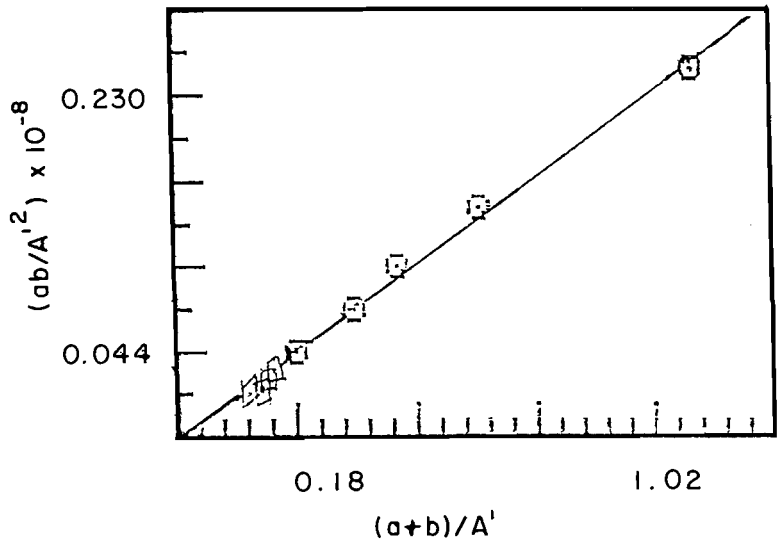


FIG. 5. Determination of the equilibrium constants using the data from Table 3 for the substitution reaction BCG–Q–B. Temperature = 283 K.

TABLE 5. Thermodynamic parameters ΔH^0, ΔS^0, ΔG^0, with their respective confidence intervals for a 0.95 probability, and linear determination coefficient, r^2, obtained using the alternative plot for the ion associate dye–Q–ClB

T (K)	ΔH^0 (kJ mol^{-1})	ΔS^0 (J mol^{-1} K^{-1})	ΔG^0 (kJ mol^{-1})	r^2
		BPB–Q–ClB		
283.16	−18.678 ± 7.482	−61 ± 26	−1.463 ± 0.894	0.955
288.16	−18.678 ± 7.482	−61 ± 26	−0.916 ± 0.401	0.955
293.16	−18.678 ± 7.482	−61 ± 26	−0.821 ± 1.536	0.955
298.16	−18.678 ± 7.482	−61 ± 26	−0.297 ± 0.974	0.955
303.16	−18.678 ± 7.482	−61 ± 26	−0.261 ± 0.710	0.955
		BCG–Q–ClB		
283.16	−21.766 ± 14.970	−73 ± 51	−0.958 ± 1.397	0.877
288.16	−21.766 ± 14.970	−73 ± 51	−1.134 ± 0.972	0.877
293.16	−21.766 ± 14.970	−73 ± 51	−0.174 ± 0.764	0.877
298.16	−21.766 ± 14.970	−73 ± 51	−0.101 ± 0.537	0.877
303.16	−21.766 ± 14.970	−73 ± 51	0.445 ± 0.957	0.877

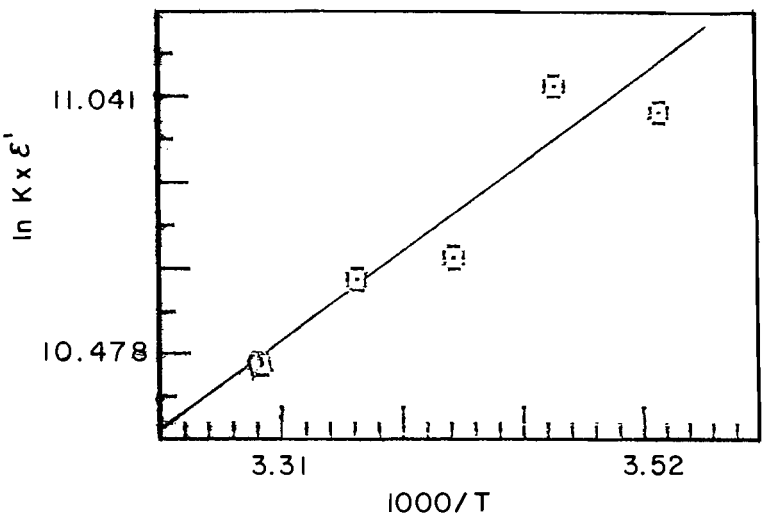


FIG. 6. Graph using the alternative method for the ion associate BCG–Q–B.

Can. J. Chem. Downloaded from www.nrcresearchpress.com by 198.100.157.202 on 09/07/12
For personal use only.

Can. J. Chem. Downloaded from www.nrcresearchpress.com by 198.100.157.202 on 09/07/12
For personal use only.

mixture of the reagents in their normal states might not give a spontaneous reaction. Since at high temperature the K values decrease, this would be more probable.

Conclusions

Causing the ion associate 1:2 (dye–Q) to react with benzethonium chloride in dichloromethane permits determination of the stoichiometry, equilibrium constants, and thermodynamic magnitudes of a reaction of great analytical importance. The reaction is established as an exchange of ions where QH^+ is replaced with B^+ in a clear chemical equilibrium with equilibrium constants that agree with the van't Hoff equation. The values of the equilibrium constants indicate a reaction that is displaced towards the formation of the products and that this reaction can be favoured by reducing the temperature. The molar absorptivity of the ion associate dye–Q – ammonium ion is, by far, much greater than that corresponding to the ion associate dye–Q_2, which is also important from the analytical point of view.

1. T. Sakai. Analyst, **108**, 608 (1983).
2. T. Sakai. Anal. Chim. Acta, **147**, 331 (1983).
3. G. Schill and M. Marsh. Sven. Farm. Tidskr. **67**, 385 (1963).
4. G. Schill. Acta Pharm. Suec. **2**, 13 (1965).
5. A. Hernández, P. Gutierrez, and J. Thomas. An. Real Acad. Farm. **50**, 115 (1984).
6. L. G. Chatten and K. O. Okamura. J. Pharm. Sci. **62**, 1318 (1973).
7. R. Modin and G. Schil. Talanta, **22**, 1017 (1975).
8. F. Matsui and W. W. French. J. Pharm. Sci. **60**, 287 (1961).
9. M. T. Quintela. Ph.D. Thesis, University of Granada, 1985.
10. A. Hernández. Can. J. Chem. **65**, 1279 (1987).
11. A. Hernández and J. M. Alvarez. An. Quim. **84**, 141 (1984).
12. D. R. Rosseinsky and H. Kellawi. J. Chem. Soc. (A), 1207 (1969).
13. F. Gaizer. Magy. Kem. Foly. **83**, 250 (1977).
14. P. Job. Ann. Chem. **9**, 113 (1928).
15. T. Sakai. Bunseki Kagaku, **37**, 174 (1988).
16. J. S. Coleman, L. P. Varga, and S. H. Mastin. Inorg. Chem. **9**, 1015 (1970).
17. W. E. Wentworth, W. Hirsch, and E. J. Chen. J. Phys. Chem. **71**, 281 (1967).
18. I. Hanazaki. J. Phys. Chem. **76**, 1982 (1972).
19. P. Farrel and P. Ngo. J. Phys. Chem. **77**, 2545 (1973).
20. V. K. Roatgi. An introduction to probability theory and mathematical statistics. John Wiley and Sons, New York. 1976. Chap. 2. p. 100.

Appendix

For the system A + B $\rightleftharpoons$ C + D, in equilibrium (corresponding to eq. [1]), the concentrations of the four species are $a - x$, $b - x$, x, and x respectively. In the system mentioned species A and C are exclusively absorbent. Reagent A shows some degree of absorption at the same wavelength for which reagent C exhibits the maximal absorbance. Therefore, the absorbance, A_m, of the system at peak wavelength of C for unit path length would be:

$$[6] \quad A_m = \varepsilon_A(a - x) + \varepsilon_C x = \varepsilon_A a + (\varepsilon_C - \varepsilon_A)x = A_0 + \varepsilon' x$$

where a and b are the initial concentrations of A and B; ε_A, ε_C, and ε' are the molar absorptivities of A, C, and the difference between the two, $\varepsilon_C - \varepsilon_A$, respectively; A_0 is the absorbance found in a previous identical experiment where species B was excluded, and x represents the concentration of C and D in equilibrium. If the difference, $A_m - A_0$, is represented by A', Beer's Law can be expressed as

$$[7] \quad A' = \varepsilon' x = \varepsilon' f(K,a,b)$$

The A' value depends on the ε' and x and therefore on K, a, and b. The quadratic solution for $x = f(K,a,b)$ from eq. [2] would be:

$$[8] \quad x = \frac{1}{2}\left\{\frac{a+b}{1-K^{-1}} \pm \sqrt{\left(\frac{a+b}{1-K^{-1}}\right)^2 - \frac{4ab}{1-K^{-1}}}\right\}$$

Differentiation of eq. [7] with respect to the parameters required, K and ε', yields:

$$[9] \quad \left(\frac{dA'}{dK^{-1}}\right)_{\varepsilon'} = \frac{\varepsilon'}{2}\left\{\frac{a+b}{(1-K^{-1})^2} \pm \frac{\dfrac{(a+b)^2}{(1-K^{-1})^3} - \dfrac{2ab}{(1-K^{-1})^2}}{\sqrt{\left(\dfrac{a+b}{1-K^{-1}}\right)^2 - \dfrac{4ab}{1-K^{-1}}}}\right\}$$

$$[10] \quad \left(\frac{dA'}{d\varepsilon'}\right)_K = x$$

If K is greater than 1 the positive sign is used in the equations while if $K < 1$ then it takes the negative sign. If $K = 1$ then $(dA/dK^{-1})_{\varepsilon'} = 0$ and $x = ab/(a + b)$. The partial derivatives of K^{-1} are calculated instead of those of K, just for algebraic convenience (12).

We require that K^{-1} and ε' fulfill these conditions:

$$[11] \quad \frac{d}{dK^{-1}}\Sigma(Ac - A')^2 = 0 \quad \text{and} \quad \frac{d}{d\varepsilon'}\Sigma(Ac - A')^2 = 0$$

Starting with initial values of K^{-1} and ε' obtained using the graphic method (eq. [5]), we can write the value of A_c, to be substituted in the eq. [11] in terms of a truncated Taylor series that involves corrections ΔK^{-1} and $\Delta\varepsilon'$ to K^{-1} and ε':

$$[12] \quad A_c = A_{c_i} + \Delta K^{-1}(dA/dK^{-1})_{\varepsilon'} + \Delta\varepsilon'(dA/d\varepsilon')_K$$

We now calculate ΔK^{-1} and $\Delta\varepsilon'$ from the normal equations derived from the conditions in eq. [11] described above. The A_{c_i} is calculated from the initial K^{-1} and ε' values. Solutions of the simultaneous equations for ΔK^{-1} and $\Delta\varepsilon'$ are the first-order corrections to the initial values of K^{-1} and ε'. The new improved values are then taken as trial values, and the procedure is repeated until convergence is obtained. The parameters in the final cycle ($\Delta K^{-1}/K^{-1} < 0.000002$ and $\Delta\varepsilon'/\varepsilon' < 0.000002$) are then the best-fitting values. The values obtained using the graphic method (eq. [5]) are suitable as initial values of K^{-1} and ε' since they are very close to the real values, and therefore within the convergence domain of this iterative method. The root-mean-square deviation (r.m.s.d.) is given by

$$[13] \quad \text{r.m.s.d.} = \{(\Delta A)^2/n\}^{0.5}$$

To carry out all these calculations, a computer program in GWBASIC was designed. This program uses the values of a, b, and A' to calculate all the results. The program also calculates the linear determination coefficient, r^2, obtained by the graphic method, and the root-mean-square deviation, r.m.s.d., the last being calculated by eq. [13] in the final cycle. Moreover, the

program eliminates those experimental data with values of $A_c - A' > 2 \times$ r.m.s.d. (A_c is the absorbance calculated with the values of K and ε' selected after a series of iterations). The inadequate points are eliminated one by one, and each time one value is eliminated, the calculation procedure is repeated so that the error does not affect the selected values of K and ε'. Finally, the standard deviations, $\gamma_K - 1$ and $\gamma_{\varepsilon'}$, are obtained from Rosseinsky's equations (12). The confidence intervals at the 0.95 level are calculated by Tchevicheff inequalities.[2]

[2]See ref. 20, Chap. 12, pp. 506–519.

Can. J. Chem. Downloaded from www.nrcresearchpress.com by 198.100.157.202 on 09/07/12
For personal use only.

Thermodynamic and kinetic acidities of *N*-(substituted benzyl) 4-phenylacetylpyridinium cations in aqueous solution

JOHN W. BUNTING AND P. PHILIPPE AUBIN[1]

Department of Chemistry, University of Toronto, Toronto, Ont., Canada M5S 1A1

Received December 20, 1990

JOHN W. BUNTING and P. PHILIPPE AUBIN. Can. J. Chem. **69**, 945 (1991).

The pK_a values for the deprotonation of a series of eight 1-(X-benzyl)-4-phenylacetylpyridinium cations (**6**) have been measured in aqueous solutions of ionic strength 0.1 at 25°C: pK_a = $-0.18\sigma + 8.91$. The pseudo-first-order rate constants for deprotonation of these carbon acids have been measured over the range pH = 11–13, and have been found to display kinetic saturation effects that are consistent with the addition of hydroxide ion to the carbonyl group (pK_z) as the product of kinetic control upon basification of neutral aqueous solutions of these pyridinium cations, with the subsequent transformation of this anionic hydrate to the thermodynamically more stable enolate conjugate base. Analysis of the pH–rate profiles gives substituent effects upon pK_z ($\rho = -0.19$) and upon the second-order rate constant (k_{OH} ($\rho = 0.09$)) for deprotonation of **6** by hydroxide ion.

Key words: carbon acids, deprotonation, pK_a, kinetics, substituent effects.

JOHN W. BUNTING et P. PHILIPPE AUBIN. Can. J. Chem. **69**, 945 (1991).

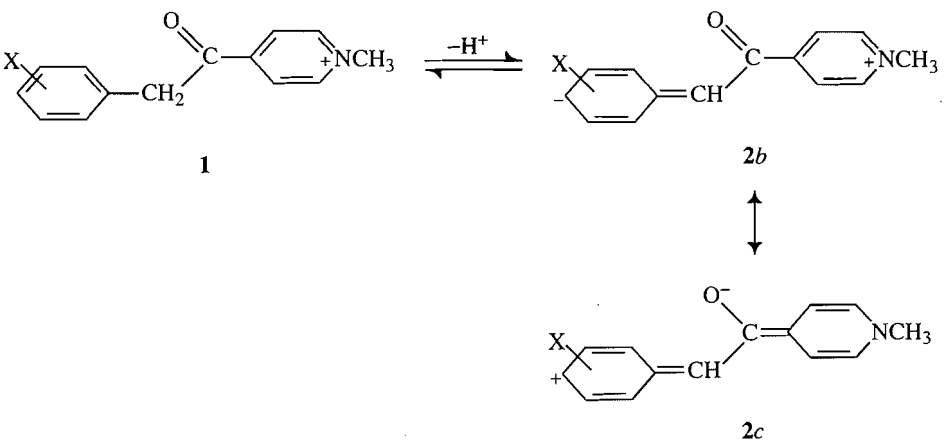
Opérant en solutions aqueuses de force ionique 0,1, à 25°C, on a mesuré les valeurs de pK_a pour la déprotonation d'une série de huit cations 1-(X-benzyl)-4-phénylacétylpyridinium (**6**): pK_a = $-0{,}18\sigma + 8{,}91$. On a aussi mesuré les constantes de vitesse de pseudo-premier ordre pour la déprotonation de ces acides carbonés à des pH allant de 11 à 13 et on a observé qu'elles présentent des effets de saturation cinétique qui sont en accord avec l'addition d'un ion hydroxyde sur le groupe carbonyle (pK_z) conduisant au produit de contrôle cinétique lors de la basification de solutions aqueuses neutres de ces cations pyridinium avec une transformation subséquents de cet hydrate anionique vers l'énolate conjugué, thermodynamiquement plus stable. Une analyse des profiles du pH vs. vitesse permet de déterminer les effets de substituant sur pK_z ($\rho = -0{,}19$) et sur la constante de vitesse de réaction du deuxième ordre (k_{OH} ($\rho = 0{,}09$)) pour la déprotonation des acides **6** par l'ion hydroxyde.

Mots clés : acides carbonés, déprotonation, pK_a, cinétique, effets de substituant.

[Traduit par la rédaction]

The isomeric ketones **1** (pK_a = 9.02 for X = H (1)) and **3** (pK_a = 7.66 for X = H (2)) readily undergo deprotonation in aqueous solution to form their enolate conjugate bases (**2** and **4**, respectively). In previous studies, we explored the influence of substituents in the phenyl ring of each of **1** and **3** upon both the thermodynamic and kinetic acidities of these ketones, and derived Brønsted slopes for these reactions (1–4). These investigations have been instrumental in the development of a useful empirical modification to the Marcus relationship as it is applied to the study of rate–equilibrium relationships for the deprotonation of carbon acids (1, 2, 4, 5).

The relatively high acidities of the ketones **1** and **3** can be traced to the resonance stabilization provided by the contributors **2***a*–**2***c* and **4***a*–**4***c*, respectively, to the electronic structures

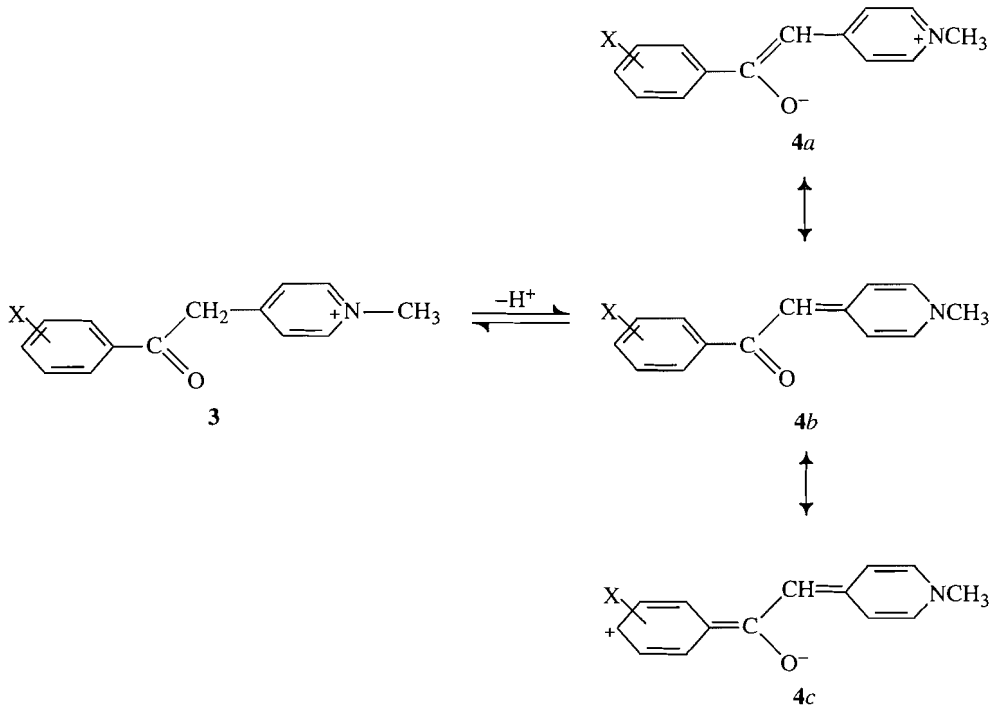


1 **2***a* **2***b* **2***c*

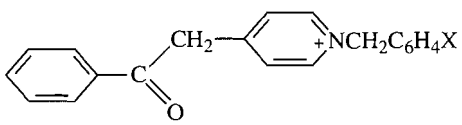
[1]Recipient of a 1990 NSERC Summer Bursary for Undergraduate Research.

Can. J. Chem. Downloaded from www.nrcresearchpress.com by 198.100.157.202 on 09/07/12
For personal use only.

Can. J. Chem. Downloaded from www.nrcresearchpress.com by 198.100.157.202 on 09/07/12
For personal use only.

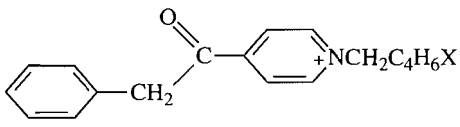


of the enolate conjugate bases. Each of **2** (λ_{max} = 446 nm for X = H (1)) and **4** (λ_{max} = 405 nm for X = H (2)) displays a long wavelength electronic absorption maximum that is consistent with a highly delocalized electronic structure. The importance of such resonance contributors is also apparent from the influence of substituents upon the acidities of these ketones. We have reported substituent effects for ring substituents (X) upon the pK_a values of both **1** (ρ = 1.29 (1)) and **3** (ρ = 1.38 (2)), and have also probed the importance of **4***b* and **4***c* through substituent effects upon the pK_a values of the *N*-(substituted benzyl) pyridinium cations, **5**, for which ρ = 0.47 was obtained (2).



5

We did not previously explore substituent effects upon the *N*-(substituted benzyl) 4-phenylacetylpyridinium cations (**6**), and the thermodynamic and kinetic acidities of this latter series of ketones are the subjects of the current work.



6

Experimental

Materials

4-Phenylacetylpyridine was available from an earlier study (1). The bromide salt of each *N*-(X-benzyl) 4-phenylacetylpyridinium cation (**6**·Br^-) was prepared by refluxing 4-phenylacetylpyridine with a slight excess of the appropriate X-substituted benzyl bromide in ethanolic solution overnight. Removal of the solvent on the rotary evaporator gave an oil that solidified upon stirring with anhydrous diethyl ether. The crude product was recrystallized from hexanol and characterized by ^{1}H NMR spectroscopy in trifluoroacetic acid solution.

pK_a *values*

All pK_a values were measured spectrophotometrically at 445 nm as described previously (1), in buffered aqueous solutions at ionic strength 0.1 and 25°C.

Kinetic studies

All rate data were obtained by mixing an aqueous solution of each **6**·Br^- with aqueous potassium hydroxide solutions of ionic strength 0.2 (KOH + KCl) in the Durrum–Gibson stopped-flow spectrophotometer at 25°C to give a final ionic strength of 0.1. The formation of the enolate conjugage base was monitored via the time dependence of the absorbance at 445 nm. All data collection and numerical analyses were performed as described in earlier work from this laboratory (1).

Results

In aqueous solutions, the cationic ketones, **6**, display pH-dependent electronic absorption spectra, which are very similar to those previously described (1) for the corresponding *N*-methyl cations (**1**). For all **6**, enolate formation in aqueous base is accompanied by the development of an absorbance maximum near 445 nm; this maximum is essentially independent of the X-substituent in the *N*-benzyl unit. The pH dependence of the absorbance at constant wavelength in the vicinity of this maximum accurately describes an acid titration. The pK_a values listed in Table 1 were obtained for a series of eight X-substituted **6** at 25°C.

The rates of formation of the conjugate base species from **6** are readily measured when neutral aqueous solutions of **6** are mixed with aqueous KOH/KCl solutions in the stopped-flow spectrophotometer. These reactions proved to be cleanly first order in [**6**], and the pseudo-first-order rate constants (k_{obs}) were evaluated over the range pH = 11–13 at ionic strength 0.1 and 25°C. Typical pH dependences for k_{obs} for the deprotonation of **6** are shown in Fig. 1. These pH–rate profiles display a similar kinetic saturation effect to that previously found (1) for the *N*-methyl cations, **1**. Scheme 1, in which **1** (or **6**) is represented as the carbon acid (CH), was shown to be consistent with this kinetic saturation phenomenon.

This scheme requires that a species Z, identified as the hydroxide adduct of the carbonyl group (*gem* diol anion), **7**, be the

TABLE 1. pK_a values and rate parameters for deprotonation of **6** in aqueous solution[a]

X	pK_a	$k_{OH}(M^{-1}\,s^{-1})$	pK_z
4-CH_3	8.83(±0.03)	682(±18)	11.79(±0.01)
H	8.80(±0.02)	721(±23)	11.77(±0.02)
4-Br	8.77(±0.02)	720(±40)	11.74(±0.03)
3-Cl	8.76(±0.02)	703(±24)	11.70(±0.02)
3-CN	8.69(±0.01)	773(±13)	11.69(±0.01)
4-CN	8.66(±0.01)	793(±35)	11.65(±0.02)
3-NO_2	8.68(±0.03)	875(±59)	11.61(±0.03)
4-NO_2	8.68(±0.02)	[b]	[b]
1(X = H)[c]	9.02	801	11.81

[a]At 25°C, ionic strength 0.1; k_{OH} and pK_z are defined in Scheme 1.
[b]Not measured.
[c]Data from ref. 1.

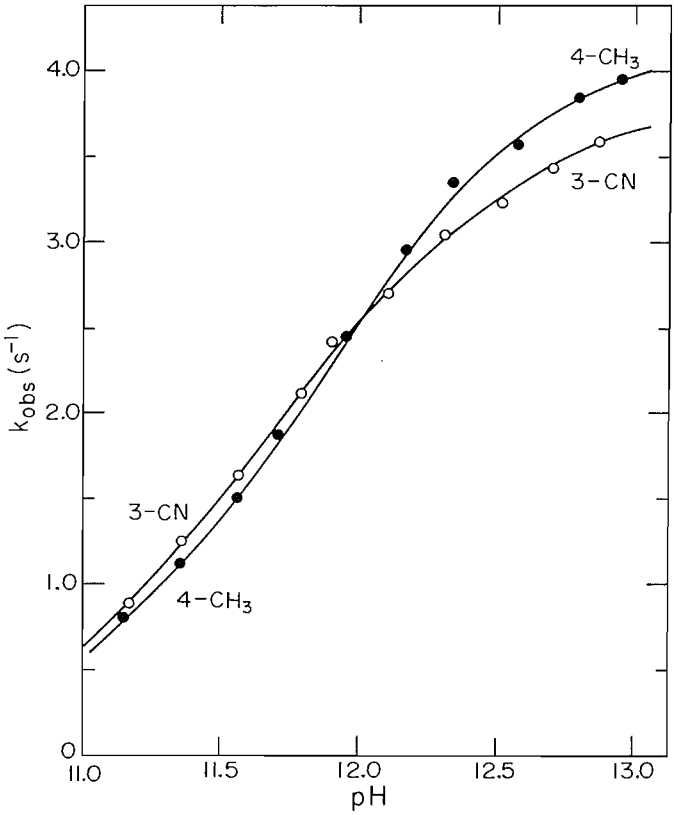
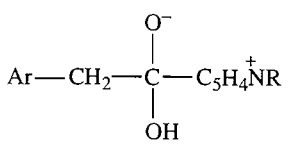


FIG. 1. The pH dependence of the pseudo-first-order rate constant (k_{obs}) for deprotonation of **6**:X = 4-CH_3 and **6**:X = 3-CN in aqueous solutions of ionic strength 0.1 at 25°C. Curves are calculated using eq. [1] and the appropriate parameters from Table 1.

kinetically controlled product upon mixing a neutral aqueous solution of **1** (or **6**) with aqueous base. Formation of **7** is complete within the mixing time of the stopped-flow instrument, and this species then subsequently isomerizes into the enolate conjugate base of **1**, which is the product of thermodynamic control in these reactions.



7

$$H^+ + Z^- \underset{}{\overset{K_Z}{\rightleftharpoons}} CH \overset{k_{OH}[^-OH]}{\rightleftharpoons} C^- + H_2O$$

SCHEME 1

Kinetic analysis of Scheme 1 leads to eq. [1], and the parameters, k_{OH} and pK_z, can be obtained upon fitting eq. [1] to the pH profiles of Fig. 1. Values for these two parameters, which were obtained via such an analysis for each of the cations **6**, are included in Table 1.

[1] $k_{obs} = k_{OH}[^-OH]/(1 + K_z[^-OH]/K_w)$

Discussion

The thermodynamic acidities of the *N*-benzyl ketones (**6**) indicate that they are slightly more acidic than the corresponding *N*-methyl ketone (**1**:X = H) (Table 1). A slightly greater, but still modest, increase in acidity from the *N*-methyl to the *N*-benzyl derivative was observed for **3** (X = H) and its *N*-benzyl analog (Table 2). There is a somewhat larger increase in acidity associated with *N*-benzyl substitution in comparisons of methylammonium and benzylammonium cations (Table 2).

Substituent effects upon the thermodynamic acidities of **6** in Table 1 are defined by the Hammett correlation:

[2] $pK_a = -0.18(\pm0.02)\,\sigma + 8.81(\pm0.01)$

The Hammett $\rho = 0.18$ in eq. [2] is considerably smaller than that found for any of the other cationic acids in Table 2. If one uses $\rho = 1.14$ for the tertiary benzyldimethylammonium cations as a reference, then $\rho = 0.18$ from eq. [2] indicates only a small fractional decrease in the effective charge upon the cationic nitrogen atom in **6** upon enolate formation. This result suggests a limited contribution from resonance contributors such as the *N*-benzyl analog of **2***c* to the electronic structure of the conjugate base, although the electronic absorption spectrum (λ_{max} = 445 nm) of this species is only readily rationalized in valence bond terms via a contribution from **2***c* to the electronic structure of the resonance stablized enolate species. The ρ values of Table 2 certainly indicate that **2***c* is far less important as a contributor to the electronic structure of the enolate conjugate base of 4-phenylacetylpyridinium cations than are **4***b* and **4***c* to the enolate conjugate base of the 4-phenacylpyridinium cations.

The pH–rate profiles of Fig. 1 for the deprotonation of **6** are identical to those analyzed previously (1) in terms of Scheme 1 for the corresponding *N*-methyl cation (**1**:X = H). Although the *N*-benzyl cations (**6**) are slightly stronger acids than their *N*-methyl analog (**1**:X = H), the kinetic acidity of **6**:X = H (as k_{OH}) is slightly lower than that of the *N*-methyl derivative (Table 1). Although the weak substituent dependence of k_{OH} leads to some experimental scatter in the data in Table 1, the general overall trend of parallel increases in the kinetic and thermodynamic acidities for substituted **6** in Table 1 seems to be well established. The substituent dependences on the kinetic parameters in Table 1 are described by the Hammett correlations of eqs. [3] and [4] and the Brønsted relationship of eq. [5].

[3] $\log k_{OH} = 0.09(\pm0.03)\,\sigma + 2.84(\pm0.01)$

[4] $pK_z = -0.19(\pm0.02)\,\sigma + 11.77(\pm0.01)$

[5] $\log k_{OH} = -0.48(\pm0.13)\,pK_a + 7.14(\pm1.16)$

The experimental uncertainty in the small ρ value in eq. [3] translates into an appreciable uncertainty in the Brønsted α value of eq. [5]. Within the limits imposed by this uncertainty, it

Can. J. Chem. Downloaded from www.nrcresearchpress.com by 198.100.157.202 on 09/07/12
For personal use only.

TABLE 2. Acidities of *N*-methyl and *N*-benzyl cations in aqueous solution

Cation	pK_a R = CH_3	pK_a R = $C_6H_5CH_2$	ΔpK_a	$\rho(K_a)$ R = $XC_6H_4CH_2$
$C_6H_5CH_2COC_5H_4\overset{+}{N}R$	9.02(**1**:X = H)	8.80(**6**:X = H)	0.22	0.18
$C_6H_5COCH_2C_5H_4\overset{+}{N}R$	7.66	7.28	0.38	0.47[a]
$R\overset{+}{N}H(CH_3)_2$	9.76[b]	8.93[b]	0.83	1.14[c]
$R\overset{+}{N}H_3$	10.62[b]	9.34[b]	1.28	1.06[d]

[a]All data from ref. 2.
[b]Reference 6.
[c]Reference 7.
[d]Reference 8.

TABLE 3. Substituent (X) effects upon rate and equilibrium constants for deprotonation of pyridinium ketones

X-substituted ketone	$\rho(K_a)$	$\rho(k_{OH})$	α
3[a]	1.38	0.62	0.45
6[b]	0.18	0.09	0.48
1[c]	1.29	0.98	0.76
5[a]	0.47	0.16	0.35

[a]Data from ref. 2.
[b]From the current investigation.
[c]Data from ref. 1.

seems that the Brønsted $\alpha = 0.48$ for **6** is quite similar to the previously reported (2) $\alpha = 0.45$ for substituent effects upon the deprotonation of **3**. The X-substituents in **3** and **6** both probe the electron density delocalization through the carbonyl group into an aromatic ring in the rate-determining transition state species for hydroxide ion catalyzed deprotonation. The similarity in the α values for **3** and **6** indicates that rate–equilibrium comparisons of substituent effects are independent of whether this carbonyl substituent is a phenyl ring or a pyridinium ring.

This result constrasts with the previously reported α values for **1** and **5** (Table 3) in which the substituent effects in the pendant ring on the enolate α-carbon atom indicate a dramatic discrepancy in Brønsted α values for substitution in a phenyl and in a pyridinium ring, and represent a dramatic difference in substituent effects upon the stabilization of the transition state and product species in these two closely related systems. The imbalanced transition state electronic effects that we noted previously (2) from the different α values for **3** and **5** have a direct analogy in the different α values that are now also apparent for **1** and **6** (Table 3).

Probably the most unexpected feature of the current experimental data lies in the similarity of the Hammett ρ values in eqs. [2] and [4]. We had originally assumed that pK_z would be similar for the *N*-methyl and *N*-benzyl derivatives, and essentially independent of the X-substituents in **6**. Since there is no apparent resonance interaction between the carbonyl group and the cationic nitrogen atom of the pyridinium ring of **6**, substituent effects in the *N*-benzyl unit of **6** appear to be quite remote from the carbonyl group that undergoes nucleophilic addition to give the hydrated anionic species in **7**. The only simple explanation for $\rho = 0.19$ for pK_z appears to be in terms of a variation of the effective charge on the cationic nitrogen atom with the X-substituent in the benzylic group, and the transmission of this charge variation to the carbonyl group via bond polarization effects.

Acknowledgement

We appreciate the continued support of this work by the Natural Sciences and Engineering Research Council of Canada.

1. J. W. BUNTING and D. STEFANIDIS. J. Am. Chem. Soc. **110**, 4008 (1988).
2. D. STEFANIDIS and J. W. BUNTING. J. Am. Chem. Soc. **112**, 3163 (1990).
3. J. W. BUNTING and D. STEFANIDIS. J. Am. Chem. Soc. **112**, 779 (1990).
4. D. STEFANIDIS and J. W. BUNTING. J. Am. Chem. Soc. **113**, 991 (1991).
5. J. W. BUNTING and D. STEFANIDIS. J. Am. Chem. Soc. **111**, 5834 (1989).
6. H. K. HALL, JR. J. Am. Chem. Soc. **79**, 5441 (1957).
7. D. H. ROSENBLATT, L. A. HULL, D. C. DELUCA, G. T. DAVIS, R. C. WEGLEIN, and H. K. R. WILLIAMS. J. Am. Chem. Soc. **89**, 1158 (1967).
8. L. F. BLACKWELL, A. FISCHER, I. J. MILLER, R. D. TOPSOM, and J. VAUGHN. J. Chem. Soc. 3588 (1964).

Can. J. Chem. Downloaded from www.nrcresearchpress.com by 198.100.157.202 on 09/07/12
For personal use only.

A versatile synthetic route to the anti-implantation agent, yuehchukene, and its analogues

JAMES P. KUTNEY,[1] FRANCISCO J. LOPEZ, SHYH-PYNG HUANG, HIROSHI KUROBE, ROBERT FLOGAUS, KRYSTYNA PIOTROWSKA, and STEVEN J. RETTIG

Department of Chemistry, University of British Columbia, 2036 Main Mall, Vancouver, B.C., Canada V6T 1Y6

Received August 22, 1990

JAMES P. KUTNEY, FRANCISCO J. LOPEZ, SHYH-PYNG HUANG, HIROSHI KUROBE, ROBERT FLOGAUS, KRYSTYNA PIOTROWSKA and STEVEN J. RETTIG. Can. J. Chem. **69**, 949 (1991).

A detailed study directed toward the development of a versatile synthetic route to the interesting dimeric natural product yuehchukene (**1**) and its epimer, 6a-*epi*-yuehchukene (**2**), has been completed. Due to the anti-implantation activity associated with **1**, it was important to provide a synthetic strategy not only to **1**, but to a family of yuehchukene analogues that, hopefully, would reveal superior chemical stability and (or) elevated biological activity. The experiments described herein and which utilize the readily available and inexpensive isophorone (**6**) satisfy these requirements.

Key words: yuehchukene synthesis, yuehchukene analogues, anti-implantation activity.

JAMES P. KUTNEY, FRANCISCO J. LOPEZ, SHYH-PYNG HUANG, HIROSHI KUROBE, ROBERT FLOGAUS, KRYSTYNA PIOTROWSKA et STEVEN J. RETTIG. Can. J. Chem. **69**, 949 (1991).

On a réalisé une étude détaillée entreprise dans le but de développer une voie de synthèse versatile du yuehchukène (**1**) et de son épimère, le 6a-*épi*-yuehchukène (**2**), des produits naturels dimères intéressants. Compte tenu de l'activité anti-implantation associée au composé **1**, il était important de proposer une stratégie de synthèse qui ne conduirait pas seulement à **1**, mais à une famille d'analogues du yuehchukène qui pourraient éventuellement posséder une stabilité chimique supérieure et (ou) une activité biologique plus grande. Les expériences décrites dans ce travail, qui utilisent l'isophorone (**6**) (un produit facilement disponible et peu coûteux) comme produit de départ, satisfont à ces critères.

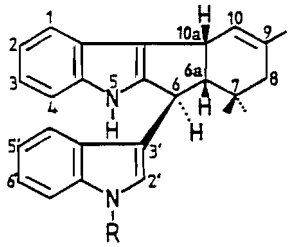
Mots clés : synthèse du yuehchukène, analogue du yuehchukène, activité anti-implantation.

[Traduit par la rédaction]

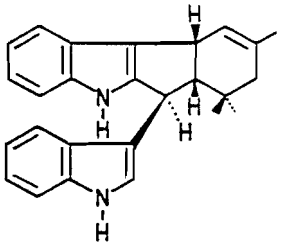
Can. J. Chem. Downloaded from www.nrcresearchpress.com by 198.100.157.202 on 09/07/12
For personal use only.

The genus *Murraya*, of the plant family *Rutacaea*, occurs throughout tropical and sub-tropical east Asia, from China and India in the north through to New Caledonia and northeastern Australia in the south. Chemically, *Murraya* species are characterized by the occurrence of carbazole, furoquinoline, and acridone alkaloids (1–4), coumarins (5, 6), and flavanoids (7). Yuehchukene (**1**), a novel type of dimeric indole natural product, was recently isolated in racemic form, in trace quantities (<18 ppm), from the roots of *M. paniculata* (8). Its name derives from the word yueh-chu, which is the name of the plant in Chinese.

Owing to the low yield of **1**, a survey of other *Murraya* species was carried out (2, 9) but the problem of low yield persisted.

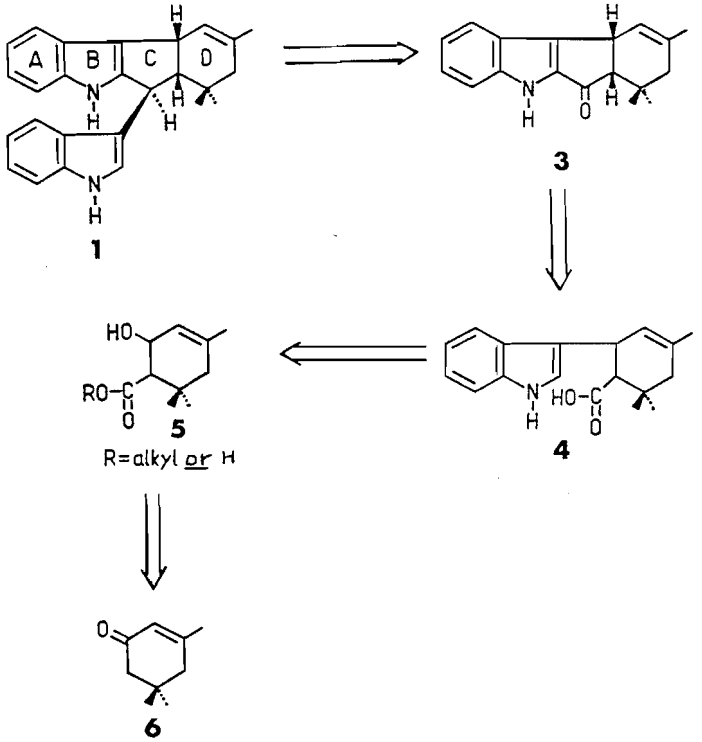


1



2

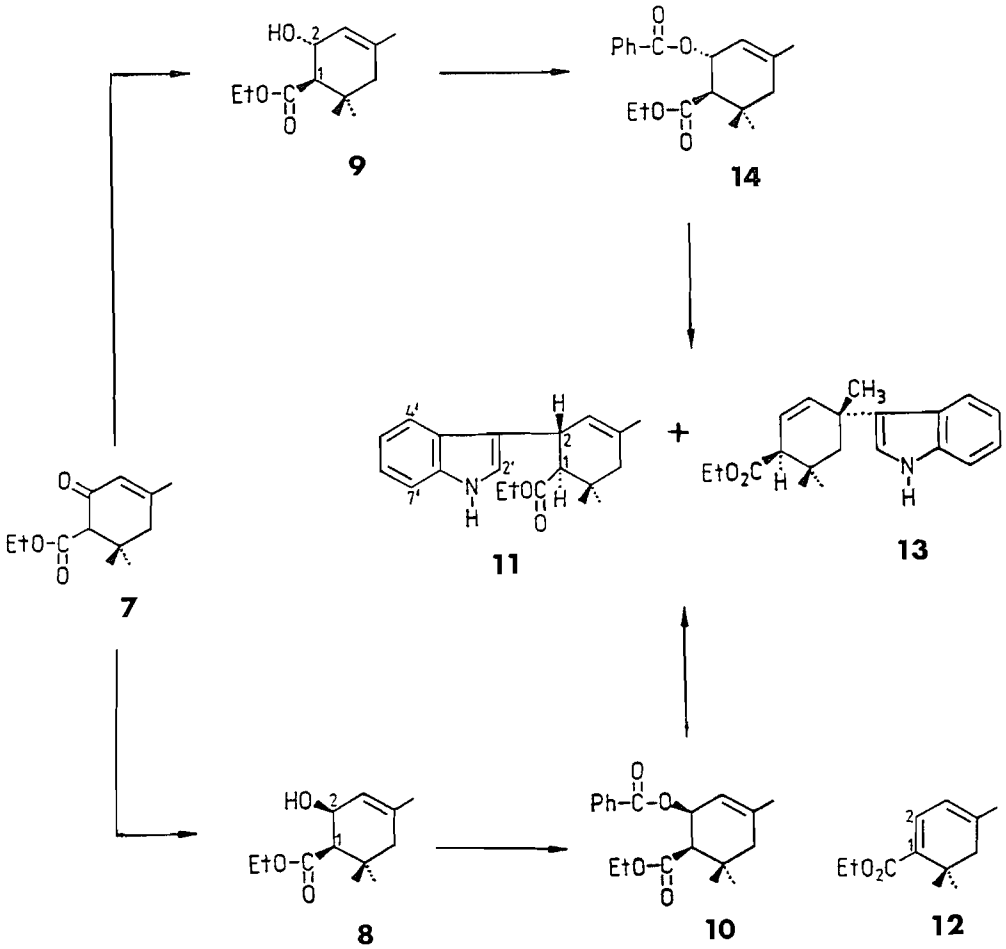
The most interesting feature about yuehchukene is its biological activity. Crude extracts of *M. paniculata* have been used in China as an astringent and antidysenteric (10–12). They also showed strong cardiac depressant and antispasmodic activity (13) but the most interesting results came from the studies of Kong *et al.* (8, 11, 14, 15), which revealed that **1** possessed strong anti-implantation activity in rats. To fully exploit the pharmacological potential of this molecular system, it was considered appropriate to develop a versatile stereoselective synthetic route that, in addition to **1**, would also allow preparation of closely related analogues. The present study describes results that satisfy these objectives. A preliminary account of a portion of this study has appeared (16).



SCHEME 1. Retrosynthetic analysis for the synthesis of yuehchukene (**1**) and its analogues.

A retrosynthetic analysis was planned according to Scheme 1. The assembly of the target molecule was strategically envisaged so as to facilitate the required variations for the preparation of

[1]Author to whom correspondence may be addressed.



SCHEME 2. Conversion of keto-ester **7** to indole intermediates **11** and **13**.

desired analogues. Thus, for instance, the indole groups could be differently substituted or, even more interestingly, the protons at C-6a and C-10a in ketone **3** could have an *anti* relationship to produce a *trans* junction of rings C and D, thus providing the isomer, 6a-*epi*-yuehchukene (**2**). This strategy also has the advantage of starting from commercially inexpensive isophorone (**6**).

The initial studies were performed with the known keto-ester (**7**), available via condensation of mesityl oxide and ethyl acetoacetate (17), since it was envisaged (see later) that **7** could be subsequently available from **6** (Scheme 2). The keto-ester **7** was reduced with sodium borohydride in methanol to give *cis*-hydroxyester **8** in 71% yield and the epimeric alcohol **9** in 23% yield. The stereochemistry at C-1 and C-2 in these isomers was readily available from the ^{1}H NMR spectra (see Experimental).

The next transformation required an activation of the hydroxyl group of **8** to facilitate its displacement by the indole moiety (see Scheme 1). Treatment of hydroxyester **8** with *p*-toluenesulfonyl chloride in the presence of various bases (DMAP, pyridine, Et_3N) gave the undesired product **12** as a result of overall elimination of water. Fortunately, the desired activation of the hydroxyl group could be achieved by treatment of **8** with benzoyl chloride and DMAP (18) in dichloromethane at 5°C to obtain the allylic benzoate **10** as an oil (85% yield).

Having in hand **10**, the nucleophilic substitution of the benzoate group was attempted by utilizing indolylmagnesium iodide in ether at 5°C. The desired indole-ester **11** was obtained in 42% yield along with the isomer **13** (31%).

The indole-ester **11** revealed particularly informative spectra and its structure was readily available from spectral analysis. The IR spectrum shows the characteristic sharp absorption band of N-H at 3480 cm^{-1} and the intense band of the carbonyl group at 1730 cm^{-1}. The mass spectrum reveals the molecular ion and the base peak at m/z 311. Finally, the ^{1}H NMR spectrum shows the proton at C-1 at 2.67 ppm as a doublet with a J value of 12 Hz due to the coupling with the proton at C-2, which in turn appears at 3.90 ppm as a multiplet. Irradiation of the latter signal simplified the doublet at 2.67 ppm to a singlet. Owing to the large coupling constant between these two protons (12 Hz), the *trans* stereochemistry was assigned. The proton at C-2′ appears at 6.99 ppm as a doublet with a J value of 3.2 Hz due to the coupling with the N-H proton, which appears at 7.92 ppm as a broad signal. The coupling was again corroborated by double resonance experiments. The signals of the other aromatic protons are sufficiently resolved so that assignments could also be made (see Experimental).

The product **13** was characterized mainly by ^{1}H NMR spectroscopy. Its IR spectrum shows the bands corresponding to N-H and C=O at 3480 and 1730 cm^{-1}. The ^{1}H NMR spectrum displays the vinylic protons as two pairs of doublet of doublets at 5.79 (J = 10 and 4 Hz) and 6.05 ppm (J = 10 and 2 Hz) being both coupled with the proton at C-1, which appears at 2.95 ppm as a doublet of doublets (J = 4 and 2 Hz). These assignments were corroborated by double resonance experiments. The stereochemistry shown in **13** was assigned later by correlation with another intermediate, the indole-acid **32** (Scheme 4) discussed later.

Following similar transformations to those described above,

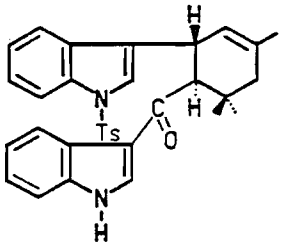
Can. J. Chem. Downloaded from www.nrcresearchpress.com by 198.100.157.202 on 09/07/12
For personal use only.

Can. J. Chem. Downloaded from www.nrcresearchpress.com by 198.100.157.202 on 09/07/12
For personal use only.

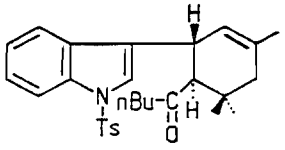
the minor *trans*-hydroxyester **9** (Scheme 2) was transformed to *trans*-benzoate **14** and, in turn, to the compounds **11** and **13** with practically the same yields and same ratio of **11**/**13** as obtained with **8** as starting material. Therefore, it seems that a carbocation intermediate or a similar species is involved in the overall conversion of **10** and **14** to the final products. An alternative rationale could involve **12** as an intermediate followed by 1,4- and 1,6-conjugate addition of the Grignard reagent.

The next step required the hydrolysis of **11** to the corresponding acid in accord with the retrosynthetic analysis (see **4**, Scheme 1). Unfortunately, treatment of **11** with either aqueous sodium hydroxide in refluxing ethanol or trimethylsilyl iodide in refluxing acetonitrile (19) did not afford the desired product; the starting material was recovered unchanged and direct cyclization of **11** to **3** also failed.

An alternative route to the yuehchukene system from ester **11** could involve initial attachment of the other indole unit and then subsequent cyclization. For this purpose, **11** was converted to its *N*-tosyl derivative and the latter was reacted with indolylmagnesium iodide in an effort to obtain the ketone **15** but only unreacted **11** was recovered even though similar reaction of **11** with *n*-butyllithium did afford the expected product **16**.



15

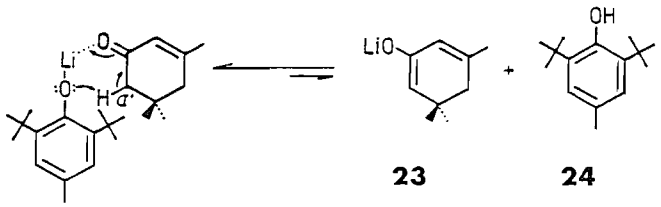


16

In view of the above, reconsideration of the synthetic strategy in terms of the corresponding acid **5** (Scheme 1) was made. The hydroxyester **8** could be hydrolyzed to the corresponding acid **18** (NaOH, room temperature, 5 days, 75% yield) but the low yield (16%) in the original preparation of **7** according to the literature procedure (17) demanded a superior synthetic route to **17**. A solution to this objective is now provided (Scheme 3).

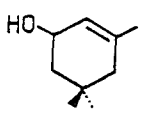
The readily available and inexpensive isophorone (**6**), when treated with lithium 2,6-di-*tert*-butyl-4-methylphenoxide and carbon dioxide gas in diethyl ether at room temperature (20), gave keto-acid **17**. This product turned out to be too unstable for isolation after the acidic work-up of the reaction mixture, so reduction with sodium borohydride was performed *in situ* on the salt **19** to give, upon acidification, *cis*-hydroxy acid **18** in 46% overall yield. Small quantities (about 5%) of the corresponding *trans*-hydroxy acid **21** were also obtained. Since the remainder was recovered isophorone **6**, the effective yield in the overall conversion from **6** to **18** was 90%.

Several aspects of this transformation are worthy of comment. First of all, this appears to be the first case of a kinetic carboxylation of an α,β-unsaturated ketone under these mild conditions, although carboxylation of simple ketones with these reagents has been reported (20). Perhaps the reason that such a mild base (pK_a of conjugated acid = 12.3) (21) was capable of abstracting the α′ proton ($pK_a \simeq 20$) (**22** → **23** + **24**) is, in part, due to the complex-induced proximity effect (CIPE) (22), which refers to the chelation of the metal (lithium, in this case) to the carbonyl oxygen making the α′ proton more acidic and, at the same time, placing the base closer to the same proton. The reason for using such a bulky base was to prevent its carboxylation under the conditions of the reaction (20).

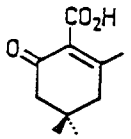


22 **23** **24**

The fact that isophorone (**6**), and *not* alcohol **25**, was recovered from the "one-pot" double transformation suggests that the carboxylation step was complete, thereby giving the products **19** and **20**. Sodium borohydride reacted only with **19** to give **18** while **20** decomposed back to **6** during the acidic work-up of the reaction mixture.



25

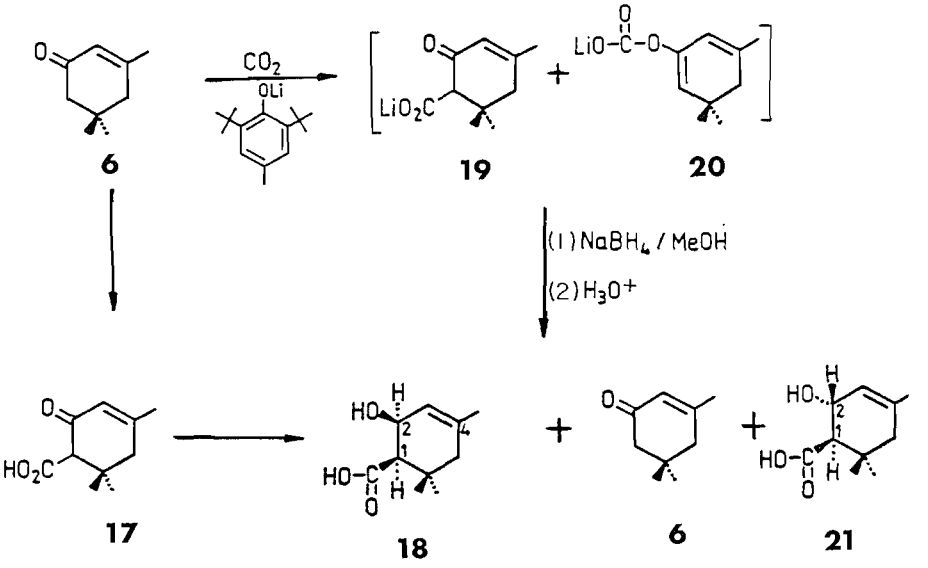


26

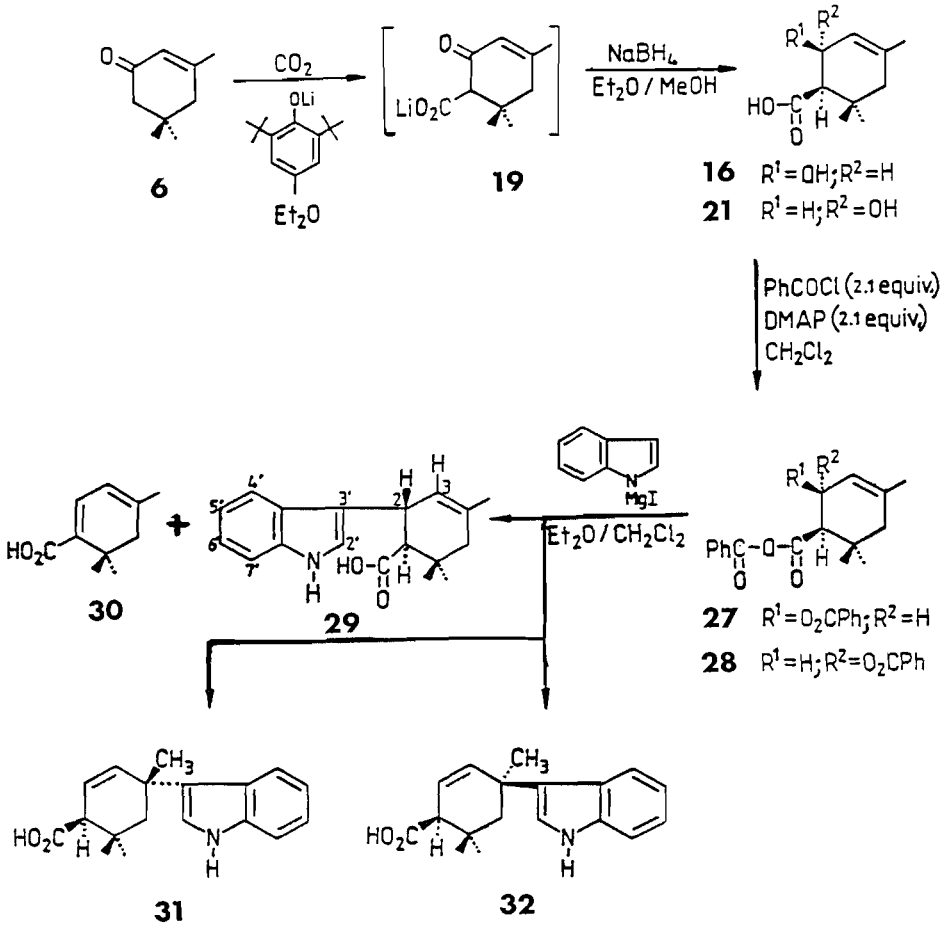
It should be noted that direct carboxylation with methylmagnesium carbonate[2] or bromomagnesium ureide – carbon dioxide adducts (24) affords mainly the undesired acid **26**.

The next step was the activation of the hydroxyl functionality in **18** in order to provide a good leaving group for subsequent nucleophilic displacement (Scheme 4). Thus, treatment of **18** with 2.1 equivalents of benzoyl chloride and DMAP in dichloromethane at 5°C furnished the unstable ester-anhydride **27**, which was obtained as a crude liquid and was not further purified. Treatment of **27** with indolylmagnesium iodide from 5 to 25°C gave rise to the long-desired indole-acid **29** (40% yield) as colorless crystals (mp 173–174°C). Careful purification of the crude mixture also gave by-products **30** (15%), **31** (26%), and **32** (3%). The structure and stereochemistry of **29** could be readily assigned from a detailed analysis of its spectroscopic properties. Apart from the mass spectrum, which provided the correct molecular ion (*m*/*z* 283), the ^{1}H NMR spectrum was particularly informative. The *gem*-dimethyl group protons appear as singlets at 1.08 and 1.14 ppm and the protons of the vinylic methyl group at 1.71 as a broad singlet. The AB system corresponding to the protons at C-5 appears at 1.76 and 2.15 ppm with a *J* value of 16 Hz. The hydrogen at C-2 appears at 3.93 ppm as a doublet with a *J* value of 10 Hz caused by the *trans* coupling with the proton at C-1, which appears at 2.71 ppm as a doublet. These assignments were corroborated by double resonance experiments. Thus, irradiation of the proton at C-2 causes the proton at C-1 to become a singlet, and irradiation of the proton at C-1 changes the signal of the proton at C-2 from doublet to singlet. The vinylic proton appears at 5.47 ppm as a broad singlet. The protons at C-2 and C-3 show only a small coupling to each other since a molecular model of **29** reveals that the dihedral angle between them is nearly 90°C. The proton at position 2′ of the indole moiety appears at 6.94 ppm as a doublet with a small *J* value of 2 Hz because of its coupling to the proton on the nitrogen atom (7.77 ppm), the latter also corroborated by decoupling experiments. The signals of the other aromatic protons were also identified. These assignments were based on nOe-difference and double resonance experiments. Irradiation at the N-H proton resonance enhances both the signal at 6.94

[2]J. P. Kutney and H. Kurobe. Unpublished results.



SCHEME 3. Conversion of isophorone (**6**) to hydroxy acids **18** and **21**.



SCHEME 4. Overall sequence from isophorone (**6**) to indole intermediates **29**, **31**, and **32**.

ppm and the doublet at 7.33 ppm. Since the signal at 6.94 ppm had already been assigned to the aromatic proton at C-2′, the signal at 7.33 ppm must correspond to the proton at C-7′, and this was confirmed by a second nOe experiment. Irradiation at 5.47 ppm, which is the signal corresponding to the vinylic proton, increases the signals of only two aromatic protons: the signal at 6.94 ppm (proton at C-2′) and the doublet at 7.62 ppm. As can be seen from models, the only aromatic protons that are in proximity with the vinylic proton when the C-2—C-3′ bond is rotated are those at C-2′ and C-4′. Therefore, the doublet at 7.62 ppm was assigned to the proton at C-4′. The knowledge of the chemical shifts of the protons at C-4′ and C-7′ permitted the assignment of the signals of the protons at C-5′ and C-6′ by double resonance experiments. Thus, decoupling of the proton at C-4′ simplified only the signal at 7.08 ppm to a doublet. Therefore, the signal at 7.08 ppm (doublet of doublets, $J = 8,8$

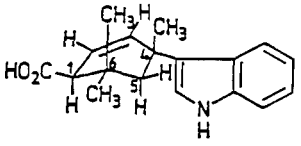
Can. J. Chem. Downloaded from www.nrcresearchpress.com by 198.100.157.202 on 09/07/12
For personal use only.

Can. J. Chem. Downloaded from www.nrcresearchpress.com by 198.100.157.202 on 09/07/12
For personal use only.

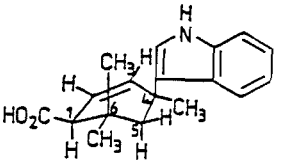
Hz, in the normal spectrum) corresponds to the proton at C-5′ and the signal at 7.17 ppm (doublet of doublets, J = 8,8 Hz) is assigned to the proton at C-6′.

The by-product diene **30**, obviously the result of base-catalyzed elimination, is readily characterized from its IR (3200–2800 and 1679 cm^{-1}) and typical homoannular diene UV absorption (λ_{max} 290 nm) spectra.

The isomeric nature of the interesting by-product indole-acids **31** and **32** was shown by the identical molecular ion peaks (m/z 283) in their mass spectra and their similarity in the ^1H NMR spectra. The stereochemistry of both compounds was determined on the basis of nOe-difference experiments. As a result of these experiments, the 3-dimensional structures of the main conformers of **31** and **32** are shown in **31A** and **32A**.



31A



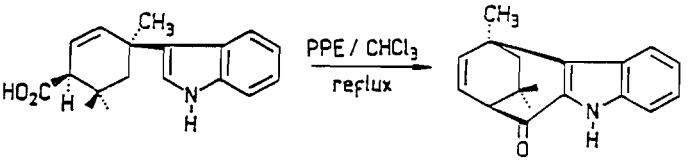
32A

The stereochemistry of **31** was determined as follows. Irradiation of the singlet due to the protons of the methyl group at C-4 (1.58 ppm) enhances the singlet due to the β-methyl group at C-6 (1.10 ppm) and the signals due to the vinylic proton at C-3 (6.06 ppm) and the β-proton at C-5 (1.99 ppm). Irradiation of the signal due to the other methyl group at C-6, namely, the α-methyl (0.95 ppm), enhances the signal of the axial proton at C-1 and both doublets due to the protons at C-5 (1.99 and 2.25 ppm). Finally, irradiation of the signal due to the proton at C-1 enhances the signal corresponding to the protons of the α-methyl at C-6 (but not the signal due to the β-methyl), the doublet of the α-proton at C-5 (2.25 ppm), and the signal of the vinylic proton at C-2. Therefore, these results indicate that the methyl group at C-4 has an *anti* relationship to the proton at C-1 in **31**. The stereochemistry of **32**, which could also be determined from the same results, was confirmed by the following experiments. Irradiation at 0.60 ppm, which is the signal due to one of the methyl groups at C-6, enhances both the doublet of the proton at C-2′ (6.92 ppm) and the doublet of the β-proton at C-5 (2.52 ppm). Therefore, the singlet at 0.60 ppm was assigned to the β-methyl group. Irradiation of the signal due to the other methyl group (1.13 ppm) namely, the α-methyl at C-6, enhances the signal of the axial proton at C-1 (3.02 ppm) and both doublets due to the protons at C-5 (1.73 and 2.52 ppm). Finally, irradiation of the signal of the proton at C-1 enhances both the singlet due to the α-methyl group at C-6 and the doublet due to the α-proton at C-5 (1.73 ppm). Therefore, the structure of **32** was confirmed to be as shown in **32A**.

The indole-acid **31** was transformed into the ester **13** discussed earlier (Scheme 2) under the neutral conditions of ethanol, triphenylphosphine, and diethylazodicarboxylate (25). The above NMR data were therefore also utilized to assign the structure and stereochemistry to ester **13**.

Additional quantities of the crucial intermediate **29** could be obtained when the *trans* benzoate **28**, obtained from esterification of the hydroxy acid **21** (Scheme 4), was treated with indolylmagnesium iodide. The reaction mixture with the same product ratio as obtained with the *cis* isomer **27** was obtained. This result again suggests a carbocationic intermediate is involved in the conversion to **29**, **31**, and **32**. Thus for preparative purposes, the mixture of alcohols **18** and **21** is directly converted to **27** and **28** and the latter, without isolation, is treated with the Grignard reagent to afford **29**, **31**, and **32**.

With indole-acid **29** on hand, the strategy outlined in Scheme 1 (**4** → **3**) was again considered. Intramolecular cyclization of **29** with either polyphosphoric acid (26) or polyphosphoric ester (PPE) (27) met with failure even though the indole-acid **32** underwent facile cyclization with PPE in chloroform to afford ketone **33** in 55% yield. The structure proof of **33** is presented later in this discussion.



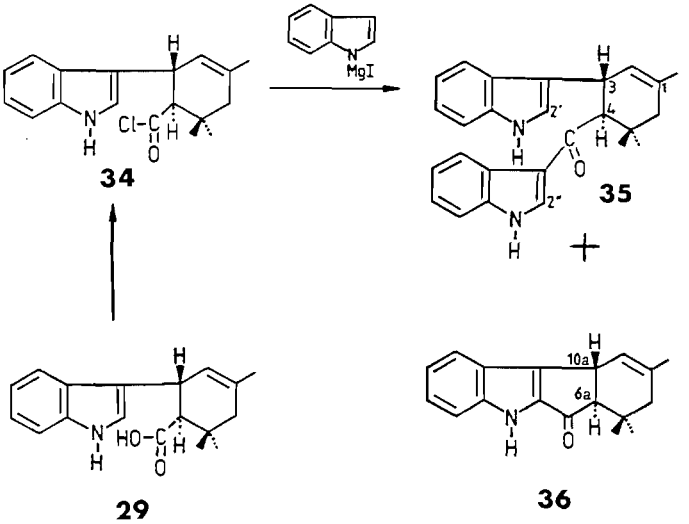
32 **33**

Conversion of **29** into the corresponding acid chloride **34** and attempts to achieve an intramolecular Friedel–Crafts acylation under conditions ($ZnCl_2$, nitrobenzene) reported for acylation at position 2 of 3-substituted indoles (28) also failed.

On the other hand, reaction of **34** with indolylmagnesium iodide under careful conditions (initially at −50°C and then at −5°C) afforded the expected product **35** (18% yield) and, somewhat surprisingly, the previously desired ketone **36** (25% yield) (Scheme 5).

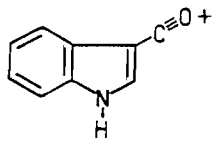
The most pertinent features in the mass spectrum of **35** are the molecular ion (m/z 382) and the base peak at m/z 144 corresponding to the fragment ion **a**. The ^1H NMR spectrum displays at 3.54 ppm the proton at C-4 as a doublet with a J value of 10 Hz, revealing a *trans* stereochemical relationship with the proton at C-3, which appears as a multiplet at 4.14 ppm. Also, integration of the aromatic proton region shows the presence of two indole systems with the proton at C-2′ appearing at 6.85 ppm as a doublet (J = 2 Hz) and the N-H protons at 7.59 and 7.98 ppm as broad signals. The proton at C-2″ appears downfield of 7.0 ppm due to the presence of the carbonyl group at the position 3″.

The IR spectrum of the crystalline ketone **36** (mp 129–131°C) shows the N-H absorption at 3464 cm^{-1} and the conjugated carbonyl group at 1683 cm^{-1}. The mass spectrum displays the molecular ion at m/z 265 and the base peak at m/z 250 due to the easy loss of a methyl radical. The ^1H NMR spectrum shows the N-H proton at 8.73 ppm and, most importantly, no aromatic



34 **35** **29** **36**

SCHEME 5. Conversion of indole-acid **29** to the ketones **35** and **36**



a

signals upfield of 7.0 ppm, thereby confirming the absence of the aromatic proton at C-2′ in the heterocyclic ring. Finally, the *trans* relationship between the protons at carbons 6a and 10a was assigned by X-ray diffraction analysis of the molecule. The results are presented in Fig. 1.

Efforts to increase the yield of **36** are summarized in Table 1. Careful monitoring revealed that the reaction only occurs at a temperature of −15°C or higher, giving both products in about the same ratio (expts. 1 and 2). When acid chloride **34** was added into indolylmagnesium iodide (expts. 1–4) there was a tendency to give a higher ratio of products **35**/**36** as the equivalents of the Grignard reagent were increased. On the other hand, when the addition was reversed (expts. 5–7), the yield of ketone **36** could be improved as the length of time for the addition of indolylmagnesium iodide was increased from 3 to 8 h. Therefore, it appears from these results that the abstraction of a proton from the nitrogen atom is faster than the addition of indolylmagnesium iodide to the carbonyl group, but the intramolecular cyclization is slow. When there is an excess of the Grignard reagent, compound **35** is predominantly formed (expt. 3). On the other hand, the ratio **36**/**35** is maximum when acid chloride **34** is maintained in excess (expts. 6 and 7).

Since ketone **36** was apparently formed by the behaviour of indolylmagnesium iodide acting as a base, attempts were made to increase even further the yield of **36** by utilizing a hindered base (LDA). Table 2 shows the results. Addition of 1.2 equivalents of LDA at −15°C gave only 15% of ketone **36** along with recovered indole-acid **29** (expt. 1). Increasing both the amount of LDA (to 2.5 equivalents) and the length of time for its addition (to 7 h, expt. 3) raised the yield by a factor of 2, although this was still low. On the other hand, increasing the temperature to 20°C did not give any **36** but rather the next expected intermediate, *cis*-ketone **37** (Scheme 6). Since the yield of both **37** and **29** was almost the same as the yield of **36** and **29** when the conditions of the reaction were the same (except for the temperature) (expts. 3 and 4), it seems that no further cyclization took place on warming but only the epimerization of **36** occurred. Furthermore, in a separate experiment, *trans*-ketone **36** was epimerized to *cis*-ketone **37** (85% yield) in the presence of LDA (−15 to 20°C) (Scheme 6).

The spectroscopic characteristics of crystalline *cis*-ketone **37** are, as expected, quite similar (but not identical) to those of *trans*-ketone **36**. Perhaps most noteworthy is that the coupling constant between the protons at carbons 6a and 10a in the ^{1}H NMR spectra of both compounds is the same (6 Hz). The most pronounced difference is their melting points: 129–131°C for **36** and 220–223°C for **37**.

In attempting to optimize the yield of the epimerization reaction, it was found that sodium methoxide in refluxing THF–MeOH gives the thermodynamically more stable *cis*-ketone **37** in quantitative yield.

In summary, the indole-acid **29**, via the routes outlined in Schemes 5 and 6, affords a potentially attractive entry into *both* the natural yuehchukene (**1**) and unnatural 6a-*epi*-yuehchukene (**2**) series.

The overall strategy (**3** → **1**, Scheme 1) in attaching the second indole unit onto the carbonyl function of the *trans*-

TABLE 1.

Expt.	Equiv. of Grignard	Temperature (°C)	Length of addition of Grignard[a] (h)	Yield (%) 36	35
1	3.5	−50 to 5	—	25	18
2	5.0	−50 to 5	—	23	20
3	20.0	−50 to 5	—	08	40
4	3.5	−50 to 15	—	24	17
5	3.5	−15 to 20	3.0	29	16
6	3.5	−15 to 20	8.0	46	14
7	3.5	−15 to 20	14.0	46	19

[a]Acid chloride was added into Grignard, expts. 1–4, in 0.5 h.

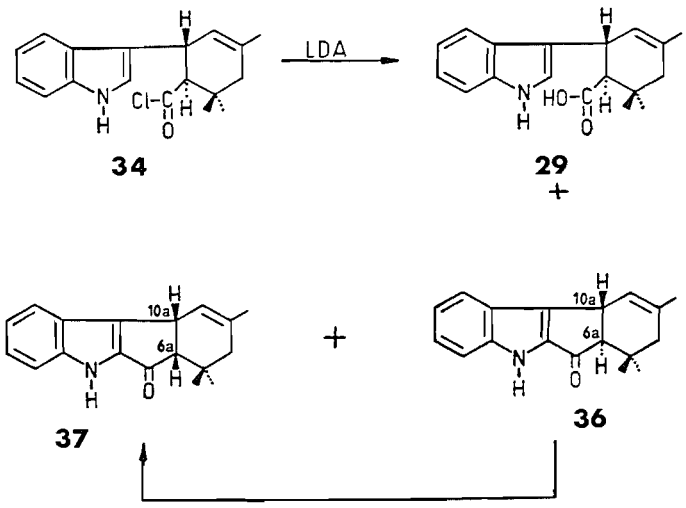
TABLE 2.

Expt.	Equiv. of of LDA	Temperature (°C)	Length of addition of LDA (h)	Yield (%) 29	36	37
1	1.2	−15	0.3	50	15	—
2	2.0	−15	0.3	43	20	—
3	2.5	−15	7.0	27	30	—
4	2.5	−15 to 20	7.0	26	—	27

ketone **36** and, thereby, an entry into the natural series was now considered. The successful route to **1** is outlined in Scheme 7.

Mild hydride reduction ($NaBH_4$/MeOH) was unsuccessful in the conversion **37** → **38** but, fortunately, the more reactive reagent $LiAlH_4$ did reduce the ketone functionality to give alcohol **38** as the main product (65% yield), along with the epimeric alcohol **39** as a minor component (35%). Lithium tri-*sec*-butylborohydride (L-Selectride) (29) gave, as expected, only alcohol **38** but, unfortunately, in lower yield (50%).

The ^{1}H NMR spectrum of **38** displays, at 5.06 ppm, the signal of the hydrogen at C-6 as a broad signal, which becomes a distinct doublet (J = 6 Hz) only after exchange of the O-H proton with D_2O. This latter result shows that the proton at C-6 is coupled with both the O-H proton and the proton at C-6a. The O-H proton appears at 2.6–2.7 ppm and overlaps with the signals of the vinylic methyl group and one of the protons at C-8. On the other hand, the ^{1}H NMR spectrum of **39** shows the signal



SCHEME 6. Conversion of acid chloride **34** to the ketones **36** and **37**.

Can. J. Chem. Downloaded from www.nrcresearchpress.com by 198.100.157.202 on 09/07/12
For personal use only.

Can. J. Chem. Downloaded from www.nrcresearchpress.com by 198.100.157.202 on 09/07/12
For personal use only.

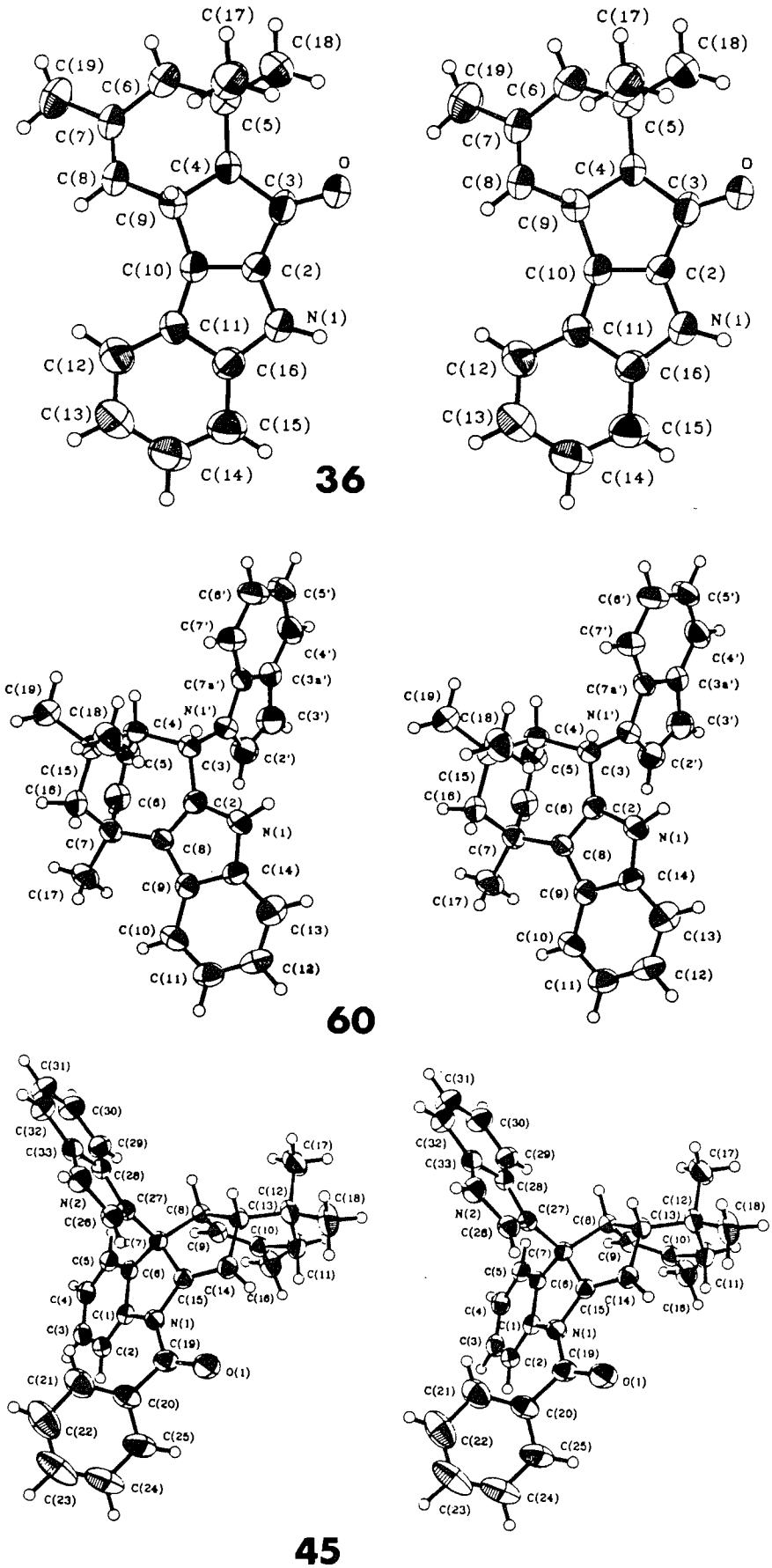
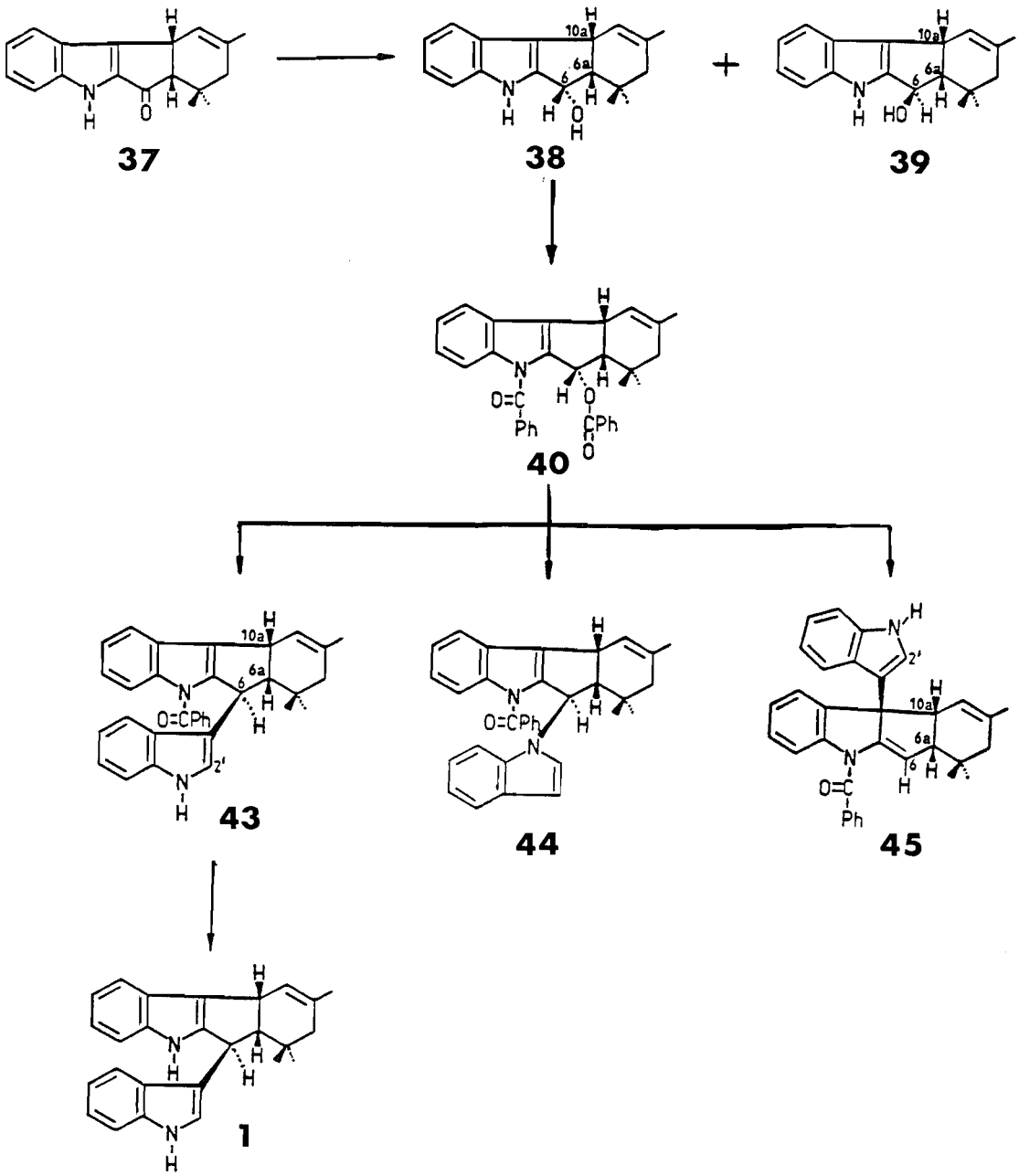


FIG. 1. Stereoviews of **36** (top), **60** (middle), and **45** (bottom) showing crystallographic atom numbering schemes;[5] 50% probability thermal ellipsoids are shown for the non-hydrogen atoms. Both structures contain equal numbers of both enantiomers, those depicted above being chosen at random.

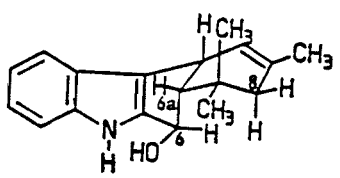
Can. J. Chem. Downloaded from www.nrcresearchpress.com by 198.100.157.202 on 09/07/12
For personal use only.



SCHEME 7. The synthesis of yuehchukene (**1**) and related analogues from ketone **37**.

of the proton at C-6, at 5.12 ppm as a doublet (J = 6 Hz) due to coupling with only the proton at C-6a, thus revealing no coupling with the O-H proton.

The distinction between the two alcohols was established by nOe-difference experiments performed with alcohol **39**. Thus, irradiation at the signal of the proton at C-6 did not affect the signal of the proton at C-6a but did show an effect on the signals of the protons of the methyl groups at C-7 and one of the protons at C-8. The conformational structure of **39**, shown as **39A**, shows the proximity between protons at C-6 and C-8. Therefore

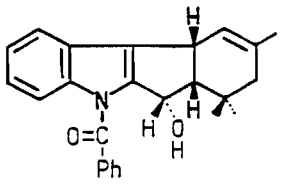


39A

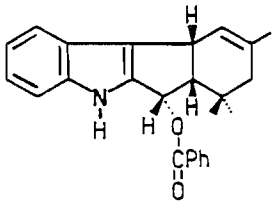
the hydroxyl group in **39** bears a *cis* relationship to the proton at C-6a.

The next transformation involved a dibenzoylation of **38** using 4 equivalents of benzoyl chloride, 1.2 equivalents of DMAP, and 4 equivalents of triethylamine (18) in dichloromethane, to give rise to compound **40** as white crystals (76% yield). Its structure and stereochemistry were readily ascertained from the informative spectroscopic data (see Experimental). Addition of only one equivalent of benzoyl chloride to alcohol **38** gave rise to the chemoselective formation of compound **41** (and not **42**).

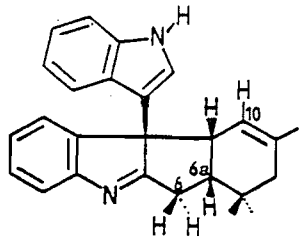
To complete the synthetic route, nucleophilic displacement of the benzoate group in **40** was appropriate. Reaction of **40** with indolylmagnesium iodide in ether–dichloromethane solution at 5°C afforded the expected benzoylyuehchukene (**43**) as a white foam (40% yield) but, in addition, two other isomeric compounds subsequently assigned the structures **44** (18% yield) and **45** (30% yield) (Scheme 7).



41



42



46

Benzoylyuehchukene (**43**) was characterized by IR, MS, and ^{1}H NMR spectroscopy. The IR spectrum reveals the N-H and carbonyl absorptions at 3480 and 1681 cm^{-1}, respectively. The mass spectrum shows the molecular ion at m/z 470 and the base peak at m/z 105 corresponding to the relatively stable cation PhC≡O$^+$. The ^{1}H NMR spectrum shows the proton at C-6 at 4.12 ppm as a doublet with a J value of 4 Hz. As expected, this chemical shift is at consideraly higher field than that of the starting benzoate **40** (6.39 ppm). The N-H proton appears at 7.73 ppm as a broad signal and the signal of the hydrogen at C-2′ of the heterocyclic ring of the newly incorporated indole appears at 6.15 ppm as a doublet with a J value of 2 Hz. This latter assignment was corroborated by decoupling the signal corresponding to the proton on the nitrogen atom, with the resulting collapse of the doublet at 6.15 ppm into a singlet. Finally, the structural assignment was firmly established when **43** was treated with sodium methoxide in methanol at 5°C to afford (±)-yuechchukene (**1**) in 90% yield. The synthetic material was identical with the racemic natural product isolated from the plant.

Compound **44**, formed by N-alkylation rather than C-alkylation, reveals in its IR spectrum the typical amide absorption at 1685 cm^{-1} and the mass spectrum displays the molecular ion at m/z 470, the base peak at 105, and an intense peak (relative intensity = 50%) at 354, not observed in **43** and due to the facile loss of indole from the molecular ion. The ^{1}H NMR spectrum shows the proton at C-6 at 5.53 ppm as a broad signal. The proton at C-2′ appears at 6.29 ppm as a doublet with a J value of 3.5 Hz. The result shows the coupling of the latter with the proton at C-3′, appearing at 6.48 ppm as a doublet with the same J value. Double resonance experiments confirm this assignment.

The stereochemistry at C-6 in **44** was assigned on the basis of nOe experiments. Thus, irradiation of the signal due to the proton at C-6a (2.85 ppm) shows enhancement of both the signal of the proton at C-10a (4.08 ppm) and the signal of the proton at C-2′ (6.29 ppm) but it does not affect the signal due to the proton at C-6 (5.53 ppm). Also, irradiation of the signal due to the proton at C-6 does not affect the proton at C-10a, but only the aromatic protons at C-2′ and possibly at C-7′. Therefore, the newly incorporated indole moiety was assigned to be in a *cis* relationship with the proton at C-6a.

The unexpected compound **45** was characterized by IR, MS, ^{1}H NMR, and X-ray analysis (Fig. 1).

Since deprotection of **44** affords a new analogue of yuehchukene, which is one of the objectives of this project, that transformation was also carried out. Thus, treatment of **44** with sodium methoxide in methanol gave compound **46** in 97% yield. During this conversion, there was concomitant migration of the double bond to the more stable imine form. The IR spectrum of this unstable yellowish oil shows the N-H absorption at 3477 cm^{-1} and the mass spectrum displays the molecular ion as the base peak at m/z 366. The ^{1}H NMR spectrum shows the protons at C-6 and at C-6a as an ABC system. The C-6 protons appear at 2.29 ppm (doublet of doublets, J = 8, 18 Hz) and 2.83 ppm (doublet of doublets, J = 10, 18 Hz) while C-6a appears at 2.64 (multiplet). These assignments were corroborated by double resonance experiments. When the signal at 2.64 ppm was decoupled, both C-6 signals became doublets, showing that only *geminal* coupling exists with these protons. Also, the spectrum shows only one vinylic proton signal (4.72 ppm) (and not two as in **45**) corresponding to C-10, thereby establishing the proposed migration of the double bond to form the imine structure.

As noted earlier, the main objective of this study was to develop a versatile synthetic route that would afford not only an approach to the natural product but *also* to new analogues, which may portray similar efficacy as contraceptive agents but with lower toxicity, when evaluated in the pharmacological screening program.

With the above results in hand (Scheme 7), it was natural to consider the corresponding *trans*-ketone **36** so as to complete the synthesis of 6a-*epi*-yuehchukene (**2**). Unfortunately the corresponding intermediates in this series revealed a high degree of instability and low yields in the conversions so new chemistry had to be developed.

Although reduction of **36** ($LiAlH_4$, ether, 5°C) (Scheme 8) did afford the desired alcohol **47** (R = R′ = H′) in 90% yield, the subsequent conversion to the dibenzoyl derivative **47** (R = R′ = COPh) for further elaboration to the *epi*-yuehchukene system (compare **40** → **43**, Scheme 7), met with little success. Treatment of **47** (R = R′ = H) with various concentrations of benzoyl chloride afforded a low yield (15%) of the *O*-benzoyl derivative **47** (R = COPh; R′ = H) and extensive decomposition. The desired dibenzoyl derivative was never obtained.

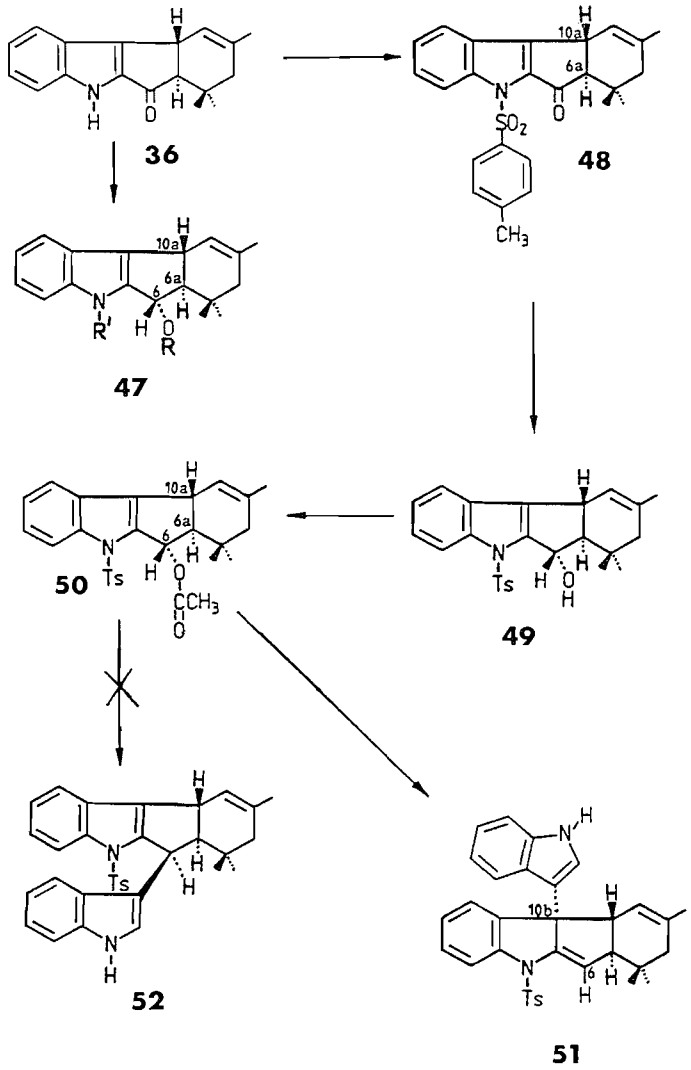
To increase the stability of the intermediates, it was decided to protect the indole ring at an earlier stage of the synthetic route. The first choice was the *p*-toluenesulfonyl functionality since this group was expected to decrease the reactivity of the indole unit because of its electron-withdrawing properties.

Ketone **36** was converted to its tosyl derivative **48** in 90% yield by using *p*-toluenesulfonyl chloride in the presence of sodium hydride (Scheme 8). Reduction of **48** proceeded smoothly to the alcohol **49** (90% yield).

The stereochemistry at C-6 in **49** was assigned on the basis of nOe-difference experiments. Irradiation of the signal due to the proton at C-10a (3.38 ppm) enhances the signal of the proton at C-6 (5.27 ppm). This experiment also served to assign the β-methyl group at C-7 (1.05 ppm). Irradiation of the protons of this β-methyl group enhances both the signal of the proton at C-6 and that of the proton at C-10a, but shows no effect on the signal due to the proton at C-6a (2.42 ppm). Therefore, the stereochemistry at C-6 was assigned to have the O-H group and the proton at C-6a in a *cis*-relationship.

Treatment of alcohol **49** with acetic anhydride and DMAP in CH_2Cl_2 at room temperature gave acetate **50** in 75% yield. The use of acetic anhydride, instead of benzoyl chloride as used in the previous study, was an attempt to increase further the stability of the ester.

Can. J. Chem. Downloaded from www.nrcresearchpress.com by 198.100.157.202 on 09/07/12
For personal use only.



SCHEME 8. Conversion of ketone **36** to indoline **51**.

The next transformation in the sequence involved nucleophilic displacement of the acetate group by indolylmagnesium iodide. Unfortunately, the expected derivative of 6a-*epi*-yuehchukene (**52**, Scheme 8) could not be observed. Instead, the isomer **51** was obtained in 40% yield and characterized by the usual spectroscopic data (see Experimental).

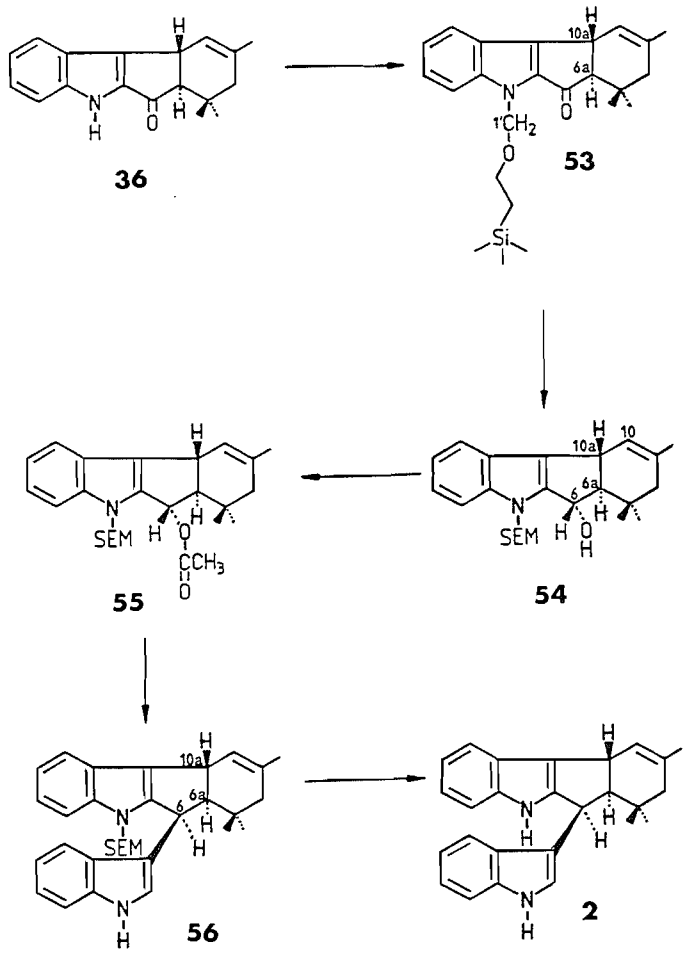
It thus appears that, in this reaction, the approach of indolylmagnesium iodide to the C-6 carbon atom is considerably hindered by the axial methyl at C-7 and also, perhaps, by the bulky tosyl group. On the basis of this result, it was thought that perhaps the approach of the nucleophile might be easier with a less bulky protecting group on the indole system. Trimethylsilylethoxymethyl chloride (SEM-Cl) was chosen as another alternative to protect the indole moiety. SEM-Cl has not been previously utilized for the protection of the indole system, although it is usually employed to protect alcohols (30). However, it has been used for the protection of the pyrrole group (31) and it was felt that its applicaction in this study might prove fruitful. It was also anticipated that the introduction of this protecting group should increase the reactivity of the indole functionality when compared with the tosyl group. Scheme 9 summarizes the successful route.

Treatment of *trans*-ketone **36** with 1.5 equivalents of SEM-Cl in the presence of sodium hydride funished compound **53**. This unstable product was usually used *in situ* for the next reaction, but in one study it was isolated in a pure form (93% yield) to be characterized by IR, MS, and ^{1}H NMR spectroscopy. The infrared spectrum displays the absorption of the carbonyl group at 1695 cm^{-1} while the mass spectrum reveals the molecular ion at m/z 395 and the base peak at m/z 73 corresponding to the ratio $(CH_3)_3Si^+$. The ^{1}H NMR spectrum displays, at −0.1 ppm, a singlet that integrates for 9 protons and is due to the trimethylsilyl group; at 0.86 ppm, a multiplet corresponding to the protons of the methylene carbon bonded to the silicon; at 3.52 ppm, another multiplet due to the adjacent methylene carbon; and at 5.61 and 5.69 ppm, an AB system, with a coupling constant of 11.5 Hz, corresponding to the diastereotopic protons of the methylene carbon attached to the nitrogen atom.

That neither **36** nor **53** epimerized at C-6a, during the reaction conditions employed, was proved by obtaining a different product from the corresponding *cis*-ketone **37**, namely, compound **57**. In fact, the amount of sodium hydride was critical for the exclusive formation of **53**, especially with THF as the solvent. Any excess of sodium hydride in the conversion of **36** to **53** led to variable quantities of **57** as a by-product.

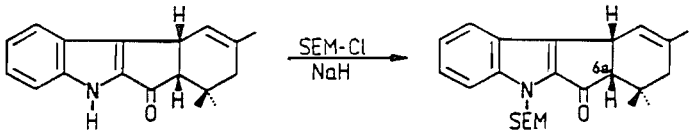
Treatment of ketone **53** in a pure form, or *in situ*, with $LiAlH_4$ at 5°C, or with DIBAL at −78°C (32), gave **54** as a single alcohol in 80–85% yield (67% overall for the one-pot reaction from **36** to **54**). The product, isolated as an oil, was then subjected to the usual spectroscopic measurements.

The stereochemistry at C-6 was again established on the basis of nOe-difference experiments. Irradiation of the signal due to



SCHEME 9. The synthesis of 6a-*epi*-yuehchukene (**2**) from ketone **36**.

Can. J. Chem. Downloaded from www.nrcresearchpress.com by 198.100.157.202 on 09/07/12
For personal use only.

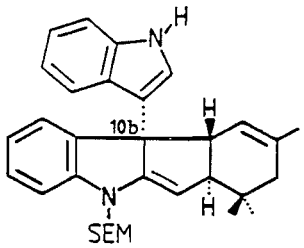


37 57

the proton at C-6 (5.12 ppm) enhances the signal of the proton at C-10a (3.41 ppm). Also, irradiation of the β-methyl at C-7 (1.03 ppm), which was assigned by irradiation of the signal due to the proton at C-10a, enhances both the signal of the proton at C-6 and that of the proton at C-10a, but not the one at C-6a. Therefore, the O-H group and the proton at C-6a were assigned to be in a *cis* relationship.

Treatment of alcohol **54** with an excess of acetic anhydride, DMAP, and triethylamine in dichloromethane at 20°C gave the corresponding acetate **55** (86% yield) as a colorless oil.

In the next step, the crucial displacement of the acetate group by indolylmagnesium iodide was attempted. Fortunately, treatment of acetate **55** with this reagent in ether–dichloromethane at 5°C furnished SEM-6a-*epi*-yuehchukene (**56**) as a white foam after isolation, and in 36% yield. Although this yield is apparently low, it might be considered quite satisfactory, firstly, because the other routes could not give the desired product and, secondly, because the newly incorporated indole still bears the strong 1,3 diaxial-like interaction with the β-methyl at C-7. The isomeric product **58**, in which the indole group is attached to the C-10b, was not observed in this case.



58

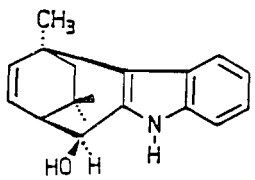
The structure of SEM-6a-*epi*-yuehchukene (**56**), including its stereochemistry, was characterized by IR, MS, and mainly ^{1}H NMR spectroscopy. The IR spectrum shows the N-H band at 3414 cm^{-1} and the mass spectrum gives the correct molecular ion at *m/z* 496. The ^{1}H NMR spectrum shows the proton at C-6 at 4.78 ppm, as a doublet, with a *J* value of 6 Hz because of its coupling with the proton at C-6a (2.70 ppm, dd, J = 11, 6 Hz). This analysis was corroborated by double resonance experiments. The β-methyl group at C-7 (assigned by nOe experiments, *vide supra*) appears as a broad singlet with the usual chemical shift of 0.34 ppm. The magnetic anisotropic effects of the newly incorporated indole group are probably the cause of this shielding.

The nOe-difference experiments provided the important data to establish the stereochemistry at C-6. Thus, irradiation of the signal due to the proton at C-6 enhances the signal of the proton at C-6a (2.70 ppm) but not the signal of the proton at C-10a (4.06 ppm). Also, irradiation of the signal due to the α-methyl group (1.13 ppm) (assigned by the enhancement of the β-methyl group when irradiating the signal due to the proton at C-10a) enhances both the signal of the proton at C-6a and the signal due to the proton at C-6. Therefore, the protons at C-6a and C-6 were assigned to bear a *cis* relationship.

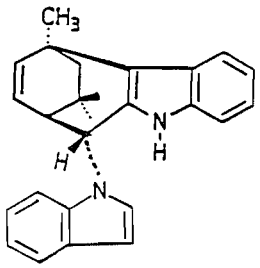
Finally, the total synthesis of 6a-*epi*-yuehchukene (**2**) was accomplished by treatment of **56** with tetra-*n*-butylammonium fluoride in THF–HMPA at 40°C for 1 day to give **2** as a white foam (89% yield). Both the solvent and the reaction temperature were critical for the success of this reaction. Without HMPA, the reaction is much slower and apparently decomposition starts to take place. At 25–30°C there is no reaction and above 45°C decomposition of the reactant and (or) the product is a serious problem. On the other hand, deprotection of the indole system using lithium tetrafluoroborate in acetonitrile (33) led only to decomposition of **56**.

The IR spectrum of **2** displays the N-H absorption at 3400 cm^{-1}, the mass spectrum the molecular ion at *m/z* 366, and in the ^{1}H NMR spectrum the protons at each nitrogen atom appear at different chemical shifts. One of these broad signals appears at 8.89 ppm while the other is present at 9.10 ppm.

More recently, experiments designed to complete the structure elucidation of ketone **33**, mentioned earlier, were completed. Ketone **33**, upon reduction with lithium aluminum hydride, afforded alcohol **59** isolated as an oil. The latter was then converted to the corresponding benzoate, which, without purification, was treated directly with an ethereal solution of indolylmagnesium iodide. The resulting crystalline product, obtained by the expected nucleophilic displacement of the benzoate group, was subjected to X-ray analysis, which provided the structural assignment **60** to this compound (Fig. 1). On the basis of this assignment, it is clear that the structures of **59** and **33** are firmly established.



59



60

In spite of numerous frustrations and unanticipated difficulties in what appeared initially to be a rather straightforward series of objectives, the routes described are sufficiently versatile to provide a series of novel analogues of yuehchukene for appropriate biological screening within the anti-implantation area. It should be emphasized that many of the difficulties encountered are clearly due to the high chemical reactivity and (or) instability of the indolic intermediates. Unfortunately, the compounds are often unstable to air, acidic reagents, and (or) in various solvents normally employed in obtaining the spectral data. The natural product yuehchukene, for example, as well as its isomer **2**, are highly unstable unless kept in the cold under an inert atmosphere, and a similar situation prevails with a number of the intermediates obtained. In fact, it should be noted that yuehchukene instability is presenting a considerable problem in formulation studies involving extensive tests in animals. It is hoped that some of the intermediates, for example, the *N*-benzoyl derivative of natural yuehchukene (**43**) or the SEM derivative of 6a-*epi*-yuehchukene (**56**), which are more stable, will prove to be active in the anti-implantation screening tests.

Can. J. Chem. Downloaded from www.nrcresearchpress.com by 198.100.157.202 on 09/07/12
For personal use only.

Can. J. Chem. Downloaded from www.nrcresearchpress.com by 198.100.157.202 on 09/07/12
For personal use only.

Yuehchukene (**1**) has previously been synthesized in low yield by acid-induced dimerization of 3-isoprenylindole (35, 36) and via a different route (37). Neither study offers the versatility to prepare a "family" of yuehchukene analogues provided in the present study.

Experimental

Melting points were determined on a Nalge melting point apparatus and were uncorrected. The infrared spectra were recorded on Perkin–Elmer 710B and 1710 (Fourier transform IR) spectrometers either in chloroform solution (using sodium chloride cells of 0.1 mm path length) or as a neat liquid film. The ultraviolet spectra were recorded on a Cary 15 spectrometer, the extinction coefficients (log ε_{max}) are given in parentheses, and the wavelength(s) of the maxima in nanometers. The mass spectra were recorded on AEI-MS-9 (low resolution) or Kratos-MS-50 (high resolution) spectrometers. The ^{1}H NMR spectra were recorded on either Bruker WH-400 or Varian XL-300 spectrometers unless otherwise stated, in $CDCl_3$ solution, and the chemical shifts are reported in ppm relative to tetramethylsilane (internal standard). The optical rotations were recorded on a Perkin–Elmer 141 automatic polarimeter in a 10-cm cell at ambient temperature using the solvent and concentrations (g/100 mL) indicated in parentheses following the recorded rotation values. The elemental analyses were determined by Mr. P. Borda, Microanalytical Laboratory, The University of British Columbia. The X-ray diffraction analysis were performed by Dr. S. Rettig on a Rigaku AFC6 diffractometer. Column chromatography (34) was performed using 230–400 mesh silica gel supplied by E. Merck Co. Gas–liquid chromatography was performed on a Hewlett Packard model 5890 gas chromatograph, using a flame ionization detector and a 25 m × 0.21 mm fused silica capillary column: DB1701.

Ethyl 2β-hydroxy-4,6,6-trimethylcyclohex-3-ene-1β-carboxylate **8** *and ethyl 2α-hydroxy-4,6,6-trimethylcyclohex- 3-ene-1β-carboxylate* **9**

To a solution of keto-ester **7** (500 mg, 2.38 mmol) in methanol (10 mL) at room temperature under nitrogen, sodium borohydride (74 mg, 2.40 mmol) was added. The reaction mixture was stirred at room temperature for 2 h. Water (3 mL) and ammonium chloride (3 mL, sat. aq.) were added, and methanol was evaporated *in vacuo*. The residue was extracted with ether (3×, 10 mL) and the organic solution was washed with water (15 mL), brine (15 mL), dried over sodium sulfate, filtered, and concentrated *in vacuo* to yield a yellow oil. Purification by flash chromatography using hexanes/ether (7:3, v/v) gave *cis*-hydroxyester **8** (358 mg, 71%) and *trans*-hydroxyester **9** (116 mg, 23%) as colorless liquids. *cis*-Hydroxyester **8**: IR ν_{max} ($CHCl_3$): 3450, 2920, 1740 cm^{-1}. ^{1}H NMR (80 MHz) δ: 1.15 (3H, s, C6-CH_3), 1.22 (3H, s, C6-CH_3), 1.42 (3H, t, J = 7, C2′-H), 1.66 (1H, d, J = 17, C5-H), 1.72 (3H, brs, C4-CH_3), 2.07 (1H, d, J = 17, C5-H), 2.34 (1H, brs, O-H), 2.65 (1H, d, J = 6, Cl-H), 4.12 (2H, q, J = 7, Cl′-H), 4.40 (1H, m, C2-H), 5.42 (1H, brs, C3-H). MS *m/z*: 212 (M$^+$), 197, 194, 83. High resolution mass measurement, calcd. for $C_{12}H_{20}O_3$: 212.1412; found: 212.1408. Anal. calcd. for $C_{12}H_{20}O_3$: C 67.88, H 9.50; found: 67.73, H 9.48.

trans-Hydroxyester **9**: IR ν_{max} ($CHCl_3$): 3400, 2960, 1725 cm^{-1}. ^{1}H NMR (80 MHz) δ: 1.00 (3H, s, C6-CH_3), 1.05 (3H, s, C6-H), 1.30 (3H, t, J = 6, C2′-H), 1.59 (1H, d, J = 17, C5-H), 1.60 (1H, brs, O-H), 1.70 (3H, brs, C4-CH_3), 2.02 (1H, d, J = 17, C5-H), 2.25 (1H, d, J = 10, Cl-H), 4.20 (2H, d, J = 6, Cl′-H), 4.54 (1H, m, C2-H), 5.42 (1H, brs, C3-H). MS *m/z*: 212 (M$^+$), 197, 194, 121. High resolution mass measurement, calcd. for $C_{12}H_{20}O_3$: 212.1412; found: 212.1410. Anal. calcd. for $C_{12}H_{20}O_3$: C 67.88, H 9.50; found: C 67.66, H 9.62.

Ethyl 2β-benzoxy-4,6,6-trimethylcyclohex-3-ene-1β-carboxylate **10**

To a solution of hydroxyester **8** (300 mg, 1.43 mmol) and dimethylaminopyridine (DMAP, 189 mg, 1.54 mmol) in methylene dichloride (10 mL) at 5°C under nitrogen was added benzoyl chloride (0.18 mL, 1.54 mmol). The reaction mixture was stirred at 5°C for 3 h and then poured into water (10 mL) and the layers were separated. The aqueous phase was extracted with methylene dichloride (10 mL twice) and the combined organic phases were dried over sodium sulfate, filtered, and evaporated *in vacuo* to give a pale yellow oil. This crude product was purified by flash chromatography using hexanes/ether (9:1, v/v) to afford benzoate **10** (380 mg, 85%) as a colorless oil: IR ν_{max} ($CHCl_3$): 2975, 1725, 1610 cm^{-1}. ^{1}H NMR δ: 1.05 (3H, t, J = 6, C2′-H), 1.11 (3H, s, C6-CH_3), 1.15 (3H, s, C6-CH_3), 1.73 (1H, d, J = 18, C5-H), 1.76 (3H, brs, C4-CH_3), 2.26 (1H, d, J = 18, C5-H), 2.87 (1H, d, J = 6.7, Cl-H), 4.01 (2H, q, J = 6, Cl′-H), 5.51 (1H, brs, C3-H), 5.80 (1H, m, C2-H), 7.40 (2H, dd, J = 7.6, 7.6, C3″ and C5″-H), 7.53 (1H, tt, J = 7.6, 1.3, C4″-H), 8.10 (2H, dd, J = 7.6, 1.3, C2″ and C6″-H). MS *m/z*: 316 (M$^+$), 211, 194, 105. High resolution mass measurement, calcd. for $C_{19}H_{24}O_4$: 316.1675; found: 316.1667. Anal. calcd. for $C_{19}H_{24}O_4$: C 72.11, H 7.65; found: C 71.81, H 7.82.

Ethyl 2α-benzoxy-4,6,6-trimethylcyclohex-3-ene-1β-carboxylate **14**

Following the same conditions as above, *trans*-hydroxyester **9** (105 mg, 0.50 mmol) gave *trans*-benoate **14** (128 mg, 82%): IR ν_{max} ($CHCl_3$): 2980, 1730, 1710, 1605 cm^{-1}. ^{1}H NMR δ: 1.08 (3H, s, C6-CH_3), 1.09 (3H, s, C6-CH_3) 1.18 (3H, t, J = 7, C2′-H), 1.71 (3H, brs, C4-CH_3), 1.77 (1H, d, J = 18, C5-H), 2.09 (1H, d, J = 18, C5-H), 2.70 (1H, d, J = 10, C1-H), 4.13 (2H, q, J = 7, C1′-H), 5.52 (1H, brs, C3-H), 5.83 (1H, brd, J = 10, C2-H), 7.39 (2H, dd, J = 8, 8, C3″ and C5″-H), 7.52 (1H, t, J = 8, C4″-H), 8.00 (2H, d, J = 8, C2″-H and C6″-H). MS *m/z*: 316 (M$^+$), 271, 211, 165, 105. High resolution mass measurement, calcd. for $C_{19}H_{24}O_4$: 316.1675; found: 316.1662. Anal. calcd. for $C_{19}H_{24}O_4$: C 72.11, H 7.65; found: C 71.88, H 7.80.

Ethyl 2α-(3-indoyl)-4,6,6-trimethylcyclohex-3-ene-1β-carboxylates **11** *and* **13**

To a suspension of magnesium (116 mg, 4.80 mmol) in dry ether (5 mL) at room temperature under nitrogen, was added methyl iodide (0.3 mL, 4.80 mmol) dropwise. After stirring for 30 min, a solution of indole (590 mg, 5.10 mmol) in dry ether (5 mL) was added at 5°C. The mixture was stirred for 1 h at room temperature, then dichloromethane (3.5 mL) was added to bring the complex into solution. This freshly prepared solution of indolylmagnesium iodide (about 4.80 mmol) was added dropwise to a solution of benzoate **10** (500 mg, 1.61 mmol) in dry ether (10 mL) at 5°C. The reaction mixture was stirred for 2 h at 5°C and for 1 h at room temperature, and then decomposed with ammonium chloride (5 mL, sat. aq.). The layers were separated and the aqueous phase was extracted with dichloromethane (3×, 10 mL). The combined organic phases were washed with water (30 mL), brine (30 mL), dried over sodium sulfate, filtered, and evaporated *in vacuo* to yield a brown residue. Purification by flash chromatography using hexanes/ether (8:2, v/v) gave indole-ester **11** (206 mg, 42%) and with further elution the isomer **13** (158 mg, 31%) as pale yellow liquids. Indole-ester **11**: UV λ_{max} (log ε) (MeOH): 224 (4.50), 280 (3.78) nm. IR ν_{max} ($CHCl_3$): 3480, 2960, 1730 cm^{-1}. ^{1}H NMR δ: 0.99 (3H, t, J = 8, C2′-H), 1.03 (3H, s, C6-CH_3), 1.14 (3H, s, C6-CH_3), 1.73 (3H, brs, CR-CH_3), 1.74 (1H, d, J = 16, C5-H), 2.15 (1H, d, J = 16, C5-H), 2.67 (1H, d, J = 12, C1-H), 3.90 (1H, m, C2-H), 3.90 (2H, q, J = 8, C1′-H), 5.48 (1H, brs, C3-H), 6.99 (1H, d, J = 3.2, C2″-H), 7.06 (1H, dd, J = 8, 8, C5″-H), 7.15 (1H, dd, J = 8, 8, C6″-H), 7.31 (1H, d, J = 8, C7″-H), 7.61 (1H, d, J = 8, C4″-H), 7.92 (1H, brs, N-H). MS *m/z*: 311 (M$^+$), 296, 238, 222. High resolution mass measurement, calcd. for $C_{20}H_{25}NO_2$: 311.1885; found: 311.1879. Anal. calcd. for $C_{20}H_{25}NO_2$: C 77.14, H 8.09, N. 4.50; found: C 76.99, H 8.26, N 4.60.

Indole-ester **13**: UV λ_{max} (log ε) (MeOH): 225 (4.53), 283 (3.71) nm. IR ν_{max} ($CHCl_3$): 3480, 2980, 1730, 1635 cm^{-1}. ^{1}H NMR (80 MHz) δ: 0.75 (3H, s, C6-CH_3), 1.00 (3H, s, C6-CH_3), 1.27 (3H, t, J = 6, C2′-H), 1.58 (3H, s, C4-CH_3), 1.95 (1H, d, J = 14, C5-H), 2.25 (1H, d, J = 14, C5-H), 2.95 (1H, dd, J = 4, 2, C1-H), 4.20 (2H, q, J = 6, C1′-H), 5.79 (1H, dd, J = 10, 4, C2 or C3-H), 6.05 (1H, dd, J = 10, 2, C2 or C3-H), 6.95 (1H, d, J = 2.5, C2″-H), 7.06 (1H, dd, J = 8, 8, Ar-H), 7.15 (1H, dd, J = 8, 8, Ar-H), 7.23 (1H, d, J = 8, C7″-H), 7.74 (1H, d, J = 8, C4″-H), 7.93 (1H, brs, N-H). MS *m/z*: 311 (M$^+$), 296, 238, 117. High resolution mass measurement, calcd. for $C_{20}H_{25}NO_2$: 311.1885; found: 311.1880. Anal. calcd. for $C_{20}H_{25}NO_2$: C 77.14, H 8.09, N 4.50; found: C 76.96, H 8.22, N 4.39.

Can. J. Chem. Downloaded from www.nrcresearchpress.com by 198.100.157.202 on 09/07/12
For personal use only.

2β-Hydroxy-4,6,6-trimethylcyclohex-3-ene-1β-carboxylic acid **18** *and 2α-hydroxy-4,6,6-trimethylcyclohex-3-ene-1β-carboxylic acid* **21**

To a solution of 2,6-di-*tert*-butyl-4-methylphenol (231.8 g, 1.05 mmol) in dry ether (2.75 L) at −78°C under nitrogen was added dropwise a solution of *n*-butyllithium (0.625 L, 1.0 mol, 1.6 M in hexane). The suspension of white solid was warmed to room temperature and carbon dioxide gas was passed through the mixture for 10–12 min. A solution of isophorone **6** (50.05 mL, 0.33 mol) in dry ether (0.23 L) was then added with the precipitate dissolving completely. CO_2 was bubbled through the solution until no more absorption occurred. A positive pressure of CO_2 was then installed by connecting CO_2-filled balloons to the reaction flask. The stirring was continued for 4 days at room temperature. The reaction mixture was then cooled to 0°C, the balloons were removed, and a nitrogen flow was connected. To the lithium salt of the β-keto-acid **19** was added sodium borohydride (11.4 g, 0.37 mol) in methanol (0.5L) in three portions. After 2.5 h of stirring at 0°C, additional sodium borohydride (11.4 g, 0.37 mol) in methanol (0.5L) was added. The ice bath was removed and the stirring was continued for 3 h. The solvent was evaporated *in vacuo* and the residue was dissolved in ether (1.2 L) and water (1 L). After separating the layers, the aqueous phase was washed with ether (2×, 0.5 L) and acidified very carefully with HCl (10% aq.) to pH 5.5 at 5°C. Extraction with ethyl acetate (3×, 300 mL) followed by drying over sodium sulfate, filtration, and evaporation *in vacuo* gave a crude pale yellow solid. Crystallization from ether/hexane furnished *cis*-hydroxy acid **18** (28 g, 46%) as colorless crystals. Crystallization of the evaporated mother liquor with chloroform yielded *trans*-hydroxy acid **21** (2.5 g, 4%). *cis*-Hydroxy acid **18**: mp 115–118°C (ether/hexane). IR ν_{max} ($CHCl_3$): 3350–2500, 3010, 2970, 1718 cm^{-1}. ^1H NMR δ: 1.05 (3H, s, C6-CH_3), 1.15 (3H, s, C6-CH_3), 1.70 (1H, d, J = 17.5, C5-H), 1.73 (3H, brs, C4-CH_3), 2.07 (1H, d, J = 17.5, C5-H), 2.69 (1H, d, J = 6, C1-H), 4.45 (1H, brs, C2-H), 5.45 (1H, brs, C3-H). MS *m/z*: 184 (M^+), 166, 151, 121, 83. High resolution mass measurement, calcd. for $C_{10}H_{16}O_3$: 184.1100; found: 184.1099. Anal. calcd. for $C_{10}H_{16}O_3$: C 65.19, H 8.75; found: C 65.45, H 8.65.

trans-Hydroxy acid ***21***: mp 186–188°C ($CHCl_3$). IR ν_{max} (KBr): 3375, 3200–2300, 2950, 1710, 1635 cm^{-1}. ^1H NMR δ: 0.98 (3H, s, C6-CH_3), 1.08 (3H, s, C6-CH_3), 1.64 (1H, d, J = 17, C5-H), 1.69 (3H, brs, C4-CH_3), 2.01 (1H, d, J = 17, C5-H), 2.24 (1H, d, J = 10, C1-H), 4.48 (1H, m, C2-H), 5.41 (1H, brs, C3-H), MS *m/z*: 184 (M^+), 166, 151, 83. High resolution mass measurement, calcd. for $C_{10}H_{16}O_3$: 184.1100; found: 184.1102. Anal. calcd. for $C_{10}H_{16}O_3$: C 65.19, H 8.75; found: C 64.89, H 8.66.

2β-Benzoxy-4,6,6-trimethylcyclohex-3-ene-1β-carboxylic benzoic anhydride **27**

To a suspension of hydroxy acid **18** (20 g, 0.109 mol) in methylene dichloride (450 mL) was added dimethylaminopyridine (28 g, 0.228 mol) at room temperature. The mixture was stirred 10 min, then was cooled to 0–5°C under nitrogen. Benzoyl chloride (26.5 mol, 0.228 mol) was added and the stirring was continued for 4.5 h at 0–5°C. An aliquot (0.5 mL) was taken from the reaction mixture and was determined by GC to contain 72% product with no hydroxy acid. The reaction mixture was poured into water (200 mL), and the layers were separated. The aqueous phase was extracted with methylene dichloride (2×, 100 mL) and the combined organic phases were dried over sodium sulfate, filtered, and evaporated *in vacuo* to give **27** as a yellow oil that was used without further purification for the next reaction.

Compound **27**: IR ν_{max} ($CHCl_3$): 2960, 1795, and 1725 cm^{-1}. ^1H NMR δ: 1.22 (3H, s, C6-CH_3), 1.31 (3H, s, C6-CH_3), 1.78 (3H, brs, C4-CH_3), 1.80 (1H, d, J = 17, C5-H), 2.30 (1H, d, J = 17, C5-H), 3.10 (1H, d, J = 6, C1-H), 5.58 (1H, m, C3-H), 5.82–6.05 (1H, m, C2-H), 7.17–8.30 (10H, m, Ar-H).

2α-(3-Indolyl)-4,6,6-trimethylcyclohex-3-ene-1β-carboxylic acid **29**

To a suspension of magnesium (10.6 g, 0.44 mol) in dry ether (212 mL) at room temperature under nitrogen was added dropwise a solution of methyl iodide (27.2 mL, 0.44 mol) in dry ether (81.5 mL). After stirring for 30 min a solution of indole (54.4 g, 0.47 mol) in dry ether (330 mL) was added at 5°C. The mixture was stirred for 1 h at room temperature, then dichloromethane (213 mL) was added to bring the complex into solution. This freshly prepared solution of indolylmagnesium iodide (about 0.44 mol) was added dropwise to a solution of the crude benzoate **27** (38 g) in dry ether (203 mL) at 5°C. The reaction mixture was stirred for 2 h at 5°C, for 1 h at room temperature, and then decomposed with ammonium chloride (700 mL, sat. aq.). The layers were separated and the aqueous phase was extracted with ethyl acetate (3×, 200 mL). The combined organic layers were washed with water (800 mL), brine (800 mL), dried over sodium sulfate, filtered, and evaporated *in vacuo*. The residue was dissolved in ether (500 mL) and 3-benzoylindole was separated by filtration. The resulting solution was extracted with sodium hydroxide solution (3×, 150 mL, 5% aq.) and the combined aqueous layers were cooled to below 10°C and acidified with hydrochloric acid (10% aq.) to pH 5. Extraction with ethyl acetate (3×, 300 mL) followed by washings with water (400 mL), and brine (400 mL), drying over sodium sulfate, and evaporation *in vacuo* yielded a crude foam (20 g). Purification by flash chromatography using hexanes/ethyl acetate (7:3, v/v) gave a mixture (14.36 g) of indole-acid **29** and compound **31** in a ratio 6:4 in favor of indole-acid **29** (i.e., 40% yield) as determined by ^1H NMR. Compounds **32** (0.64 g, 3%) and **30** (1.9 g, 15%) were also obtained from the column. Further purification of the mixture of **29** and **31** by flash chromatography using chloroform/hexanes (6.5:3.5, v/v) afforded indole-acid **29** (6.5 g, 30%), although always accompanied by some decomposition. Since there is no detriment to the yield of the next step in using the mixture of products, this last purification was usually avoided.

Indole-acid **29**: mp 173–174°C (ether–hexane). UV λ_{max} (log ε) (MeOH): 222 (4.51), 282 (3.76) nm. IR ν_{max} : 3480, 3400–2450, 3020, 2980, 1710, 1630 cm^{-1}. ^1H NMR δ: 1.08 (3H, s, C6-CH_3), 1.14 (3H, s, C6-CH_3), 1.71 (3H, brs, C4-CH_3), 1.76 (1H, d, J = 16, C5-H), 2.15 (1H, d, J = 16, C5-H), 2.71 (1H, d, J = 10, C1-H), 3.93 (1H, brd, J = 10, C2-H), 5.47 (1H, brs, C3-H), 6.94 (1H, d, J = 2, C2′-H), 7.08 (1H, dd, J = 8, 8, C5′-H), 7.17 (1H, dd, J = 8, 8, C6′-H), 7.33 (1H, d, J = 8, C7′H), 7.62 (1H, d, J = 8, C4′-H), 7.77 (1H, bs, N-H). MS *m/z*: 283 (M^+), 222, 182, 168. High resolution mass measurement, calcd. for $C_{18}H_{21}NO_2$: 283.1572; found: 283.1573. Anal. calcd. for $C_{18}H_{21}NO_2$: C 76.30, H 7.47, N 4.94; found: C 76.49, H 7.42, N 4.90.

Compound **31**: UV λ_{max} (log ε) (MeOH): 222 (4.49), 281 (3.79) nm. IR ν_{max} ($CHCl_3$): 3500–2450, 3400, 3025, 2940, 1700, 1660 cm^{-1}. ^1H NMR δ: 0.95 (3H, s, C6-CH_3), 1.10 (3H, s, C6-CH_3), 1.58 (3H, s, C4-CH_3), 1.99 (1H, d, J = 16, C5-H), 2.25 (1H, d, J = 16, C5-H), 3.02 (1H, dd, J = 3, 2, C1-H), 5.85 (1H, dd, J = 10, 3, C2-H), 6.06 (1H, dd, J = 10, 2, C3-H), 6.94 (1H, d, J = 2, C2′-H), 7.10 (1H, ddd, J = 8, 8, 1.5, Ar-H), 7.18 (1H, ddd, J = 8, 8, 1.5, Ar-H), 7.36 (1H, d, J = 8, C7′-H), 7.74 (1H, d, J = 8, C4′-H), 7.89 (1H, brs, N-H). MS *m/z*: 283 (M^+), 268, 222, 117. High resolution mass measurement, calcd. for $C_{18}H_{21}NO_2$: 283.1572; found: 283.1574. Anal. calcd. for $C_{18}H_{21}NO_2$: C 76.30, H 7.47, N 4.94; found: C 76.50, H 7.52, N 4.83.

Compound **32**: UV λ_{max} (log ε) (MeOH): 223 (4.54), 283 (3.70) nm. IR ν_{max} ($CHCl_3$): 3400, 3400–2700, 3029, 2962, 1700, 1660 cm^{-1}. ^1H NMR δ: 0.60 (3H, s, C6-CH_3), 1.13 (3H, s, C6-CH_3), 1.51 (3H, brs, C4-CH_3), 1.73 (1H, d, J = 14, C5-H), 2.52 (1H, dd, J = 14, 1, C5-H), 3.02 (1H, m, C1-H), 5.82 (1H, dd, J = 10, 2, C2-H), 6.13 (1H, ddd, J = 10, 2, 1, C3-H), 6.92 (1H, d, J = 2, C2′-H), 7.10 (1H, ddd, J = 7.5, 7.5, 1, Ar-H), 7.18 (1H, ddd, J = 7.5, 7.5, 1, Ar-H), 7.36 (1H, d, J = 7.5, C7′H), 7.82 (1H, d, J = 7.5, C4′-H), 7.90 (1H, brs, N-H). MS *m/z*: 283 (M^+), 268, 117. High resolution mass measurement, calcd. for $C_{18}H_{21}NO_2$: 283.1572; found: 283.1574.

Compound **30**: mp 115–117°C (ether/hexane). UV λ_{max} (log ε) (MeOH): 290 (4.1) nm. IR ν_{max} ($CHCl_3$): 3200–2800, 3048, 2959, 1680, 1642 cm^{-1}. ^1H NMR δ: 1.20 (6H, s, C6-CH_3), 1.85 (3H, brs, C4-CH_3), 2.13 (2H, s, C5-H), 5.81 (1H, dq, J = 6.5, 1.2, C3-H), 7.00 (1H, d, J = 6.5, C2-H). MS *m/z*: 166 (M^+), 151, 107. High resolution mass measurement, calcd. for $C_{10}H_{14}O_2$: 166.0994; found: 166.0995. Anal. calcd. for $C_{10}H_{14}O_2$: C 72.26, H 8.49; found: C 72.33, H 8.40.

6-Oxo-7,7-9-trimethyl-5,6,6aα,7,8,10aβ-hexahydroindeno-[2,1-b]indole **36**

Method A

To a solution of indole-acid **29** (450 mg, 1.6 mmol) in benzene (10

Can. J. Chem. Downloaded from www.nrcresearchpress.com by 198.100.157.202 on 09/07/12
For personal use only.

mL) at 0°C under nitrogen was added oxalyl chloride (0.21 mL, 2.4 mmol). After stirring for 24 h at room temperature, the solvent was removed *in vacuo* to give a dark residue, which was diluted with dry benzene (5 mL) and, again, the solvent was removed *in vacuo*. The acid chloride **34** was then dissolved in ether (10 mL) and a solution of indolylmagnesium iodide (3.5 equiv., prepared as described above, see experiment on compound **29**) in ether (8 mL), and dichloromethane (3.1 mL) was added dropwise for 8 h at −15°C under nitrogen. The reaction mixture was stirred for 14 h at room temperature, followed by quenching with ammonium chloride (10 mL, sat. aq.) and extraction with dichloromethane (3×, 10 mL). The organic phase was washed with sodium bicarbonate (10 mL, sat. aq.) and brine (10 mL), dried over sodium sulfate, filtered, and concentrated *in vacuo* to yield a dark oil. This crude product was purified by flash chromatography using hexanes/ether (8.5:1.5, v/v) to give *trans*-ketone **60** (194 mg, 46% overall) as a pale yellow powder. Further elution using hexanes/ether (6.5:3.5, v/v) furnished **35** (85 mg, 14%) as a yellowish foam.

Method B

To a solution of the acid chloride **34** (prepared from indole-acid **29** (198 mg, 0.7 mmol) as in Method A), in dry tetrahydrofuran (4 mL) at −15°C under nitrogen, was added dropwise a solution of lithium diisopropylamide in tetrahydrofuran prepared from diisopropylamine (0.25 mL, 1.75 mmol) for 7 h. After this time, the reaction mixture was further stirred for 1.5 h at −15°C and then quenched by the addition of ice (about 1 g) and ammonium chloride (2 mL, sat. aq.). After extraction with ethyl acetate (3×, 10 mL), the organic phase was washed with water/brine (10 mL, 1:1, v/v), brine (10 mL), dried over sodium sulfate, filtered, and evaporated *in vacuo* to yield a brown oil. Purification by flash chromatography using hexanes/ether (8.5:1.5, v/v) afforded pure *trans*-ketone **36** (55.6 mg, 30%). Further elution using hexanes/ether (6:4, v/v) recovered indole-acid **29** (53 mg, 27%).

trans-Ketone **36**: mp 129–131°C (acetone/hexane). UV λ_{max} (log ε) (MeOH): 232 (4.26), 307 (4.23) nm. IR ν_{max} ($CHCl_3$): 3464, 3040, 2960, 1683, 1625 cm^{-1}. ^1H NMR δ: 1.14 (3H, s, C7-CH_3), 1.47 (3H, s, C7-CH_3), 1.75 (3H, brs, C9-CH_3), 1.97 (1H, d, J = 18, C8-H), 2.07 (1H, d, J = 18, C8-H), 2.84 (1H, d, J = 6, C6a-H), 3.99 (1H, m, C10a-H), 6.24 (1H, brs, C10-H), 7.18 (1H, ddd, J = 8, 8, 1, Ar-H), 7.35 (1H, ddd, J = 8, 8, 1, Ar-H), 7.44 (1H, d, J = 8, Ar-H), 7.80 (1H, d, J = 8, Ar-H), 8.73 (1H, brs, N-H). MS m/z: 265 (M^+), 250, 222. High resolution mass measurement, calcd. for $C_{18}H_{19}NO$: 265.1466: found: 265.1466. Anal. calcd. for $C_{18}H_{19}NO$: C 81.48, H 7.22, N 5.28; found: C 81.16, H 7.09, N 5.23.

Compound **35**: UV λ_{max} (log ε) (MeOH): 219 (4.56) nm. IR ν_{max} ($CHCl_3$): 3465, 3025, 2960, 1637 cm^{-1}. ^1H NMR δ: 0.93 (3H, s, C5-CH_3), 1.27 (3H, s, C5-CH_3), 1.79 (1H, d, J = 18, C6-H), 1.80 (3H, brs, C1-CH_3), 2.30 (1H, d, J = 18, C6-H), 3.54 (1H, d, J = 10, C4-H), 4.14 (1H, m, C3-H), 5.59 (1H, brs, C2-H), 6.85 (1H, d, J = 2, C2′-H), 7.05–7.14 (3H, m, Ar-H), 7.15–7.24 (4H, m, Ar-H), 7.59 (1H, brs, N-H), 7.74 (1H, d, J = 8, Ar-H), 7.98 (1H, brs, N-H), 8.40 (1H, d, J = 8, Ar-H). MS m/z: 382 (M^+), 238, 144. High resolution mass measurement, calcd. for $C_{26}H_{26}N_2O$: 382.2044; found: 382.2042.

6-Oxo-7,7,9-trimethyl-5,6,6aβ,7, 8,10Aβ-hexahydroindeno-[2,1-b]indole **37**

Method A

To a solution of *trans*-ketone **36** (430 mg, 1.6 mmol) in dry tetrahydrofuran (6 mL) and dry methanol (15 mL) at room temperature under nitrogen was added sodium methoxide (10 mL, 0.03 M in methanol). The reaction mixture was refluxed for 1 h, cooled to room temperature, and then water (2 mL) and ammonium chloride (5 mL, sat. aq.) were added. The organic solvent was evaporated *in vacuo* and the resulting residue was extracted with methylene chloride. The organic phase was washed with water (10 mL), brine (10 mL), dried over Na_2SO_4, filtered, and evaporated *in vacuo* to yield a yellow solid. Recrystallization of this powder from acetone/hexane gave pure *cis*-ketone **37** (426 mg, 99%) as pale yellow crystals.

Method B

To a solution of *trans*-ketone **36** (24.6 mg, 0.093 mmol) in dry tetrahydrofuran (3 mL) at −15°C under nitrogen was added dropwise a solution of lithium diisopropylamide in tetrahydrofuran (prepared from diisopropylamine (0.03 mL, 0.21 mmol)). The reaction was warmed to room temperature and stirred for 2.5 h. Ice (about 0.5 g) and ammonium chloride (4 mL, sat. aq.) were added, followed by extraction with ethyl acetate (3×, 5 mL). The organic phase was washed with water/brine (7 mL, 1:1, v/v), brine (7 mL), dried over sodium sulfate, filtered, and evaporated *in vacuo* to yield a yellow solid. Crystallization from hexane/acetone furnished *cis*-ketone **24** (21 mg, 85%) as pale yellow crystals.

Method C

To a solution of acid chloride **34** (prepared from indole-acid **29** (281.5 mg, 0.99 mmol)) in dry tetrahydrofuran (5.6 mL) at −15°C under nitrogen was added dropwise a solution of lithium diisopropylamide in tetrahydrofuran (prepared from diisopropylamine (0.35 mL, 2.48 mmol)) for 7 h. After completion of the addition, the reaction mixture was allowed to reach room temperature. After stirring for 14 h, ice (about 1 g) and ammonium chloride (10 mL, sat. aq.) were added, followed by extraction with ethyl acetate (3×, 10 mL). The organic phase was washed with water/brine (10 mL, 1:1 v/v), brine (10 mL), dried over sodium sulfate, filtered, and evaporated *in vacuo* to yield a brown oil. Purification by flash chromatography using hexanes/ether (8.5:1.5, v/v) furnished *cis*-ketone **37** (71.2 mg, 27%) and further elution using hexanes/ether (6:4, v/v) returned indole-acid **29** (73.2 mg, 26%).

cis-Ketone **37**: mp 220–223°C (acetone/hexane). UV λ_{max} (log ε) (MeOH): 227 (4.29), 302 (4.25) nm. IR ν_{max} ($CHCl_3$): 3464, 3021, 2831, 1676, 1620 cm^{-1}. ^1H NMR δ: 0.92 (3H, s, C7-CH_3), 1.27 (3H, s, C7-CH_3), 1.69 (3H, brs, C9-CH_3), 1.76 (1H, d, J = 16.5, C8-H), 1.96 (1H, d, J = 16.5, C8-H), 2.89 (1H, d, J = 6, C6a-H), 4.05 (1H, m, C10a-H), 5.90 (1H, brs, C10-H), 7.18 (1H, ddd, J = 9, 8, 1.5, Ar-H), 7.36 (1H, ddd, J = 10, 9, 1.5, Ar-H), 7.48 (1H, dd, J = 10, 1.5, Ar-H), 7.79 (1H, dd, J = 8, 1.5, Ar-H), 9.75 (1H, brs, N-H). MS m/z: 265 (M^+), 250, 222. High resolution mass measurement, calcd. for $C_{18}H_{19}NO$: 265.1466; found: 265.1473. Anal. calcd. for $C_{18}H_{19}NO$: C81.48, H 7.22, N 5.28; found: C 81.19, H 7.10, N 5.10.

6α-Hydroxy-7,7,9-trimethyl-5,6α,6aβ-7,8,10aβ-hexahydroindeno-[2,1-b]indole **38** *and 6β-hydroxy-7,7,9-trimethyl-5,6α,6aβ-7,8,10aβ-hexahydroindeno[2,1-b]indole* **39**

Method A

To a solution of *cis*-ketone **37** (1.02 g, 3.85 mmol) in dry THF (40 mL) at 0°C under nitrogen was added lithium aluminum hydride (about 0.14 g, 4.0 mmol). After stirring for 1 h at 0.5°C and 1 h at room temperature, wet ether (15 mL, sat. aq.), sodium hydroxide (30 mL, 15% aq.), and water (10 mL) were slowly added. The mixture was extracted with ether (5×, 15 mL) and the organic phase was washed with water/brine (100 mL, 1:1, v/v), brine (50 mL), dried over magnesium sulfate, filtered, and evaporated *in vacuo* to yield a yellow solid. Purification by flash chromatography using hexanes/ether (8.5:1.5, v/v) afforded pure crystals of alcohol **38** (1.27 g, 65%) and further elution with hexanes/ether (7.5:2.5, v/v) afforded alcohol **39** (0.68 g, 35%) as a crystalline solid.

Method B

To a solution of L-selectride (0.24 mL, 0.24 mmol, 1 M in tetrahydrofuran) at −78°C under nitrogen was added a solution of *cis*-ketone **37** (21.7 mg, 0.08 mmol) in dry tetrahydrofuran (1.5 mL). The reaction mixture was stirred for 1 h at −78°C, 2 h at 0°C, and 1 h at room temperature. The reaction was then cooled to 0°C and a further portion of L-selectride (0.24 mL, 0.24 mmol, 1 M in tetrahydrofuran) was added. After stirring at room temperature overnight, water (0.1 mL), sodium hydroxide (0.3 mL, 3 M), and H_2O_2 (0.22 mL, 30% aq.) were added at 0°C. The mixture was stirred for 2 h at room temperature and then diluted with dichloromethane (5 mL). The aqueous layer was treated with excess of solid sodium chloride and extracted with dichloromethane (3×, 5 mL). The combined organic phases were washed with water (10 mL), brine (10 mL), dried over sodium sulfate, filtered, and evaporated *in vacuo* to yield a yellow oil. Purification by flash chromatography using hexanes/ether (8.5:1.5, v/v) gave unreacted *cis*-ketone **37** (8 mg, 36%), and alcohol **38** (11 mg, 50.3%).

Can. J. Chem. Downloaded from www.nrcresearchpress.com by 198.100.157.202 on 09/07/12
For personal use only.

Alcohol **38**: mp 159–162°C (ether/hexane). UV λ_{max} (log ε) (MeOH): 224 (4.50), 282 (3.85) nm. IR ν_{max} ($CHCl_3$): 3571, 3470, 3250, 2958, 1669 cm^{-1}. ^1H NMR δ: 1.12 (3H, s, C7-CH_3), 1.34 (3H, s, C7-CH_3), 1.63 (3H, brs, C9-CH_3), 1.70 (1H, d, J = 16.6, C8-H), 2.44 (2H, m, C6a-H and C8-H), 2.65 (1H, brs, O-H), 3.72 (1H, m, C10a-H), 5.06 (1H, m, C6-H), 5.75 (1H, brs, C10-H), 7.10–7.30 (2H, m, C2-H and C3-H), 7.38 (1H, d, J = 7, C4-H), 7.64 (1H, d, J = 7, C1-H), 8.17 (1H, brs, N-H). MS m/z: 267 (M^+), 249, 234, 219. High resolution mass measurement, calcd. for $C_{18}H_{21}NO$: 267.1623; found: 267.1629. Anal. calcd. for $C_{18}H_{21}NO$: C 80.86, H 7.92, N 5.24; found: C 80.50, H 8.18, N 4.96.

Alcohol **39**: mp 149–150°C (ether/hexane). UV λ_{max} (log ε) (MeOH): 227 (4.48), 282 (3.88) nm. IR ν_{max} ($CHCl_3$): 3587, 3470, 3350, 3019, 2961 cm^{-1}. ^1H NMR δ: 1.06 (3H, s, C7-CH_3), 1.18 (3H, s, C8-CH_3), 1.56 (3H, brs, C9-CH_3), 1.60 (1H, d, J = 17, C8-H), 2.02 (1H, d, J = 17, C8-H), 2.03 (1H, brs, O-H), 2.37 (1H, dd, J = 6.6, 6.6, C6a-H), 3.86 (1H, m, C10a-H), 5.12 (1H, d, J = 6.6, C6-H), 5.56 (1H, brs, C10-H), 7.11 (1H, dd, J = 7.3, 7.3, Ar-H), 7.15 (1H, dd, J = 7.3, 7.3, Ar-H), 7.27 (1H, d, J = 7.3, C4-H), 7.55 (1H, d, J = 7.3, C1-H), 8.18 (1H, brs, N-H), MS m/z: 267 (M^+), 249, 234, 219. High resolution mass measurement, calcd. for $C_{18}H_{21}NO$: 267.1623; found: 267.1616.

5-Benzoyl-6α-benzoxy-7,7,9-trimethyl-5, 6α-6aβ,7,8,10aβ-hexahydroindeno[2,1-b]indole ***40***

To a solution of alcohol **38** (697 mg, 2.61 mmol), dimethyl aminopyridine (382 mg, 3.13 mmol), and triethylamine (7 mL) in dichloromethane (57 mL) at room temperature under nitrogen was added benzoyl chloride (1.21 mL, 10.44 mmol). After 1 day at reflux, the reaction mixture was cooled to room temperature and water (30 mL) was added. The organic phase was washed with sodium bicarbonate (30 mL, 10% aq.), water (30 mL), dried over sodium sulfate, filtered, and evaporated *in vacuo* to yield a pale yellow foam. Purification by flash chromatography using hexanes/ethyl acetate (9.3:0.7, v/v) gave **40** (942 mg, 76%) as white crystals.

Compound **40**: mp 171–174°C (ether/hexane). UV λ_{max} (log ε) (MeOH): 225 (4.27), 260 (4.02) nm. IR ν_{max} ($CHCl_3$): 3010, 2959, 1718, 1684, 1603 cm^{-1}. ^1H NMR δ: 1.03 (3H, s, C7-CH_3), 1.12 (3H, s, C7-CH_3), 1.54 (1H, d, J = 17, C8-H), 1.67 (3H, brs, C9-CH_3), 2.09 (1H, d, J = 17, C8-H), 2.74 (1H, dd, J = 5.5, 5.5, C6a-H), 3.84 (1H, m, C10a-H), 5.73 (1H, brs, C10-H), 6.40 (1H, d, J = 5.5, C6-H), 7.20–7.80 (14H, m, Ar-H). MS m/z: 475 (M^+), 353, 338, 105. High resolution mass measurement, calcd. for $C_{32}H_{29}NO_3$: 475.2147; found: 475.2145. Anal. calcd. for $C_{32}H_{29}NO_3$: C 80.82, H 6.15, N 2.94; found: C 80.80, H 6.13, N 2.89.

5-Benzoyl-6β-(3-indolyl)-7,7,9-trimethyl -5,6β,6aβ,7,8,10aβ-hexahydroindeno[2,1-b]indole ***43***

To a solution of indolylmagnesium iodide (for preparation, see experiment on compound **29**), in dry ether (1.8 mL) and dry dichloromethane (0.5 mL) at 0–5°C under nitrogen, was added dropwise a solution of benzoate **40** (169 mg, 0.35 mmol) in dry ether (1.2 mL) and dry dichloromethane (0.8 mL). After stirring for 2 h at 0–5°C and 3 h at room temperature, water (1 mL) and ammonium chloride (4 mL, sat. aq.) were added, followed by extraction with dichloromethane (2×, 10 mL). The organic phase was washed with water (10 mL), brine (10 mL), dried over sodium sulfate, filtered, and evaporated *in vacuo* to yield a brown oil. Purification by flash chromatography using hexanes/ether (8:2, v/v) furnished, in order of increasing polarity, the N-substituted compound **44** (29 mg, 18%), as an oil, benzoylyuehchukene **43** (66.1 mg, 40%) as a foam, and indoline **45** (50.7 mg, 30%) as white crystals.

Benzoylyuehchukene **43**: UV λ_{max} (MeOH): 226, 263 nm. IR ν_{max} (film): 3481, 3020, 2961, 1681, 1603 cm^{-1}. ^1H NMR δ: 0.88 (3H, s, C7-CH_3), 1.05 (3H, s, C7-CH_3), 1.72 (3H, brs, C9-CH_3), 1.76 (1H, d, J = 16, C8-H), 1.95 (1H, d, J = 16, C8-H), 2.74 (1H, dd, J = 7, 4, C6a-H), 3.95 (1H, m, C10a-H), 4.12 (1H, brd, J = 4, C6-H), 5.86 (1H, brs, C10-H), 6.15 (1H, d, J = 2.5, C2′-H), 6.82–6.92 (2H, m, Ar-H), 7.03–7.10 (1H, m, Ar-H), 7.12–7.35 (7H, m, Ar-H), 7.44 (1H, m, Ar-H), 7.61 (1H, d, J = 8, Ar-H), 7.72 (1H, brs, N-H), 7.82 (1H, d, J = 8, Ar-H). MS m/z: 470 (M^+), 455, 365, 105. High resolution mass measurement, calcd. for $C_{33}H_{30}N_2O$: 470.2357; found: 470.2353.

Compound **44**: UV λ_{max} (log ε) (MeOH): 207 (5.71), 253 (4.37) nm. IR ν_{max} (film): 3010, 2959, 1685, 1603 cm^{-1}. ^1H NMR δ: 0.85 (3H, s, C7-CH_3), 1.08 (3H, s, C7-CH_3), 1.73 (3H, s, C9-CH_3), 1.82 (1H, d, J = 16.5, C8-H), 1.98 (1H, d, J = 16.5, C8-H), 2.85 (1H, m, C6a-H), 4.08 (1H, m, C10a-H), 5.53 (1H, m, C6-H), 5.84 (1H, brs, C10-H), 6.92 (1H, d, J = 3.5, C2′-H), 6.48 (1H, d, J = 3.5, C3′-H), 6.69 (1H, d, J = 8, C7′-H), 6.93 (1H, dd, J = 7, 7, Ar-H), 6.98 (1H, ddd, J = 8, 8, 1.5, Ar-H), 7.11–7.29 (5H, m, Ar-H), 7.32 (1H, ddd, J = 8, 8, 1.5, Ar-H), 7.41–7.52 (2H, m, Ar-H), 7.61 (1H, m, Ar-H), 7.68 (1H, d, J = 8, C1-H). MS m/z: 470 (M^+), 354, 105. High resolution mass measurement, calcd. for $C_{33}H_{30}N_2O$: 470.2357; found: 470.2355. Anal. calcd. for $C_{33}H_{30}N_2O$: C 84.22, H 6.43, N 5.96; found: C 84.06, H 6.20, N 6.12.

Indoline **45**: mp 250–252°C (acetone/hexane). UV λ_{max} (log ε) (MeOH): 224 (4.66), 282 (4.23) nm. IR ν_{max} ($CHCl_3$): 3477, 3009, 2960, 1650 160 cm^{-1}. ^1H NMR δ: 0.78 (3H, s, C7-CH_3), 1.40 (1H, d, J = 17, C8-H), 1.56 (3H, brs, C9-CH_3), 1.81 (1H, d, J = 17, C8-H), 2.72 (1H, brd, J = 5, C6a-H), 3.64 (1H, m, C10a-H), 5.11 (1H, brs, C6-H or C10-H), 5.36 (1H, brs, C6-H or C10-H), 6.97–7.05 (2H, m, Ar-H), 7.15 (1H, d, J = 2.5, C2′-H), 7.12–7.24 (2H, m, Ar-H), 7.23–7.32 (1H, m, Ar-H), 7.34 (1H, dd, J = 7.5, 1, Ar-H), 7.42 (2H, dd, J = 8, 8, Ar-H), 7.51 (1H, brdd, J = 8, 8, Ar-H), 7.58 (3H, m, Ar-H), 7.91 (1H, d, J = 8, Ar-H), 7.97 (1H, brs, N-H). MS m/z: 470 (M^+), 365, 105. High resolution mass measurement, calcd. for $C_{33}H_{30}N_2O$: 470.2357; found: 470.2354. Anal. calcd. for $C_{33}H_{30}N_2O$: C 84.22, H 6.43, N 5.96; found: C 84.15, H 6.44, N 5.84.

Yuehchukene ***1***

To a solution of benzoylyuehchukene **43** (200 mg, 0.43 mmol) in dry methanol (5 mL) at 5°C under nitrogen, was added sodium methoxide (freshly prepared from sodium (about 23 mg, 1 mmol) and methanol (4 mL)). After stirring at 5°C for 4 h, water (1 mL) and ammonium chloride (3 mL, sat. aq.) were added. The organic solvent was evaporated *in vacuo* and the residue was extracted with ethyl acetate (4×, 5 mL). The organic phase was washed with water (5 mL), brine (5 mL), dried over sodium sulfate, filtered, and evaporated *in vacuo* to yield a brown oil. This crude product was purified by flash chromatography using hexanes/ether (8.5:1.5, v/v) to give the synthetic yuehchukene **1** (140.3 mg, 90%) as a white foam.

Yuehchukene **1**: UV λ_{max} (MeOH): 225, 283. IR ν_{max} ($CHCl_3$): 3400, 2955, 1618 cm^{-1}: ^1H NMR δ: 0.86 (3H, s, C7-CH_3), 1.10 (3H, s, C7-CH_3), 1.63 (1H, d, J = 17, C8-H), 1.66 (3H, brs, C9-CH_3), 2.28 (1H, d, J = 17, C8-H), 3.15 (1H, dd, J = 8.5, 8.5, C6A-H), 4.02 (1H, m, C10a), 4.56 (1H, d, J = 8.5), 5.70 (1H, brs, C10-H), 6.98–7.12 (5H, m, Ar-H), 7.38 (1H, d, J = 8, Ar-H), 7.44 (1H, d, J = 8, Ar-H), 7.48 (1H, brs, N-H), 7.57 (1H, d, J = 8, Ar-H), 8.00 (1H, brs, N-H). MS m/z: 366 (M^+), 351, 254. High resolution mass measurement, calcd. for $C_{26}H_{26}N_2$: 366.2095; found: 366.2096.

Samples of synthetic **1** and natural **1** were compared by TLC, NMR, and IR spectra, and shown to be identical.

6α-Hydroxy-7,7,9-trimethyl-5,6α,6aα7,8, 10aβ-hexahydroindeno-[2,1-b]indole ***47***

To a suspension of lithium aluminum hydride (about 29 mg, 2 mmol) in tetrahydrofuran (1 mL) at 0°C under nitrogen was added a solution of *trans*-ketone **36** (212 mg, 0.80 mmol) in tetrahydrofuran (2 mL). After stirring for 2 h at 0°C, the reaction was quenched with wet ether (0.5 mL, sat. aq.), sodium hydroxide (0.5 mL, 15% aq.), and water (1 mL). After filtration through Celite, the filtrate was evaporated *in vacuo* to give a residue that was diluted with ether (5 mL). This ethereal solution was washed with brine (5 mL), dried over sodium sulfate, filtered, and evaporated *in vacuo*. The crude product was purified by flash chromatography using hexanes/ether (8:2, v/v) to give alcohol **47** (192 mg, 90%).

Alcohol **47**: UV λ_{max} (log ε) (MeOH): 223 (4.49), 282 (4.07) nm. IR ν_{max} ($CHCl_3$): 3685, 3466, 3020, 1621 cm^{-1}. ^1H NMR δ: 1.06 (3H, s, C7-CH_3), 1.24 (3H, s, C7-CH_3), 1.60 (1H, brs, O-H), 1.71 (3H, brs, C9-CH_3), 1.84 (1H, d, J = 18, C8-H), 2.04 (1H, d, J = 18, C8-H), 2.18 (1H, dd, J = 8.5, 8.5, C6a-H), 3.45–3.56 (1H, m, C10a), 5.08

(1H, d, J = 8.5, C6-H), 6.15 (1H, brs, C10-H), 7.09 (1H, ddd, J = 8, 8, 1.5, Ar-H), 7.13 (1H, ddd, J = 8, 8, 1.5, Ar-H), 7.33 (1H, dd, J = 8, 1.5, Ar-H), 7.62 (1H, dd, J = 8, 1.5, Ar-H), 8.10 (1H, brs, N-H). MS m/z: 267 (M^+), 249, 234, 117. High resolution mass measurement, calcd. for $C_{18}H_{21}NO$: 267.1623; found: 267.1623.

*6-Oxo-5-(*p*-toluenesulfonyl)-7,7,9-trimethyl-5,6,6aα,7,8,10aβ-hexahydroindeno[2,1-b]indole* **48**

To a solution of *trans*-ketone **36** (600 mg, 2.26 mmol) in dichloromethane (5 mL) at 0°C under nitrogen was added sodium hydride (90 mg, 2.3 mmol, 60% dispersion in oil). After stirring for 10 min at room temperature, *p*-toluenesulfonyl chloride (450 mg, 2.4 mmol) was added to the reaction mixture at 0°C. The reaction was stirred for 2 h at room temperature, then quenched with ammonium chloride (5 mL, sat. aq.), and diluted with dichloromethane (5 mL). The organic phase was washed with brine (5 mL), dried over sodium hydroxide, filtered, and evaporated *in vacuo* to yield a yellow solid. Purification by flash chromatography using hexanes/ether (9:1, v/v) furnished tosyl-ketone **48** (853 mg, 90%) as pale yellow crystals.

Tosyl-ketone **48**: mp 123–124°C (acetone/hexane). UV λ_{max} (log ε) (MeOH): 297 (4.21), 243 (4.23), 222 (4.28) nm. IR ν_{max} ($CHCl_3$): 3032, 2959, 1713, 1605, 1381, 1123 cm^{-1}. ^1H NMR δ: 1.08 (3H, s, C7-CH_3), 1.44 (3H, s, C7-CH_3), 1.71 (3H, brs, C9-CH_3), 1.92 (1H, d, J = 18, C8-H), 2.04 (1H, d, J = 18, C8-H), 2.36 (3H, s, Ar-CH_3), 2.81 (1H, d, J = 8, C6a-H), 3.77–3.84 (1H, m, C10a), 6.12 (1H, brs, C10-H), 7.25 (2H, d, J = 8, C3′-H and C5′-H), 7.33 (1H, dd, J = 8, 8, Ar-H), 7.50 (1H, dd, J = 8, 8, Ar-H), 7.74 (1H, d, J = 8, Ar-H), 8.04 (2H, d, J = 8, C2′-H and C6′-H), 8.28 (1H, d, J = 8, Ar-H). MS m/z: 419 (M^+), 404, 263, 248. High resolution mass measurement, calcd. for $C_{25}H_{25}NO_3S$: 419.1555; found: 419.1556. Anal. calcd. for $C_{25}H_{25}NO_3S$: C 71.57, H 6.01, N 3.34; found: C 71.23, H 6.09, N 3.44.

*6α-Hydroxy-5-(*p*-toluenesulfonyl)-7,7,9-trimethyl-5,6α,6aα,7,8,-10aβ-hexahydroindeno[2,1-b]indole* **49**

To a suspension of lithium aluminum hydride (about 72 mg, 2 mmol) in tetrahydrofuran (2 mL) at 0°C under nitrogen was added a solution of tosyl ketone **48** (800 mg, 1.91 mmol) in tetrahydrofuran (4 mL). After stirring for 2 h at 0°C, the reaction was quenched with wet ether (1 mL, sat. aq.), sodium hydroxide (1 mL, 15% aq.), and water (2 mL). After filtration through Celite, the filtrate was evaporated *in vacuo* to give a residue that was diluted with ether (10 mL). This ethereal solution was washed with brine (10 mL), dried over sodium sulfate, filtered, and evaporated *in vacuo*. The crude product was purified by flash chromatography using hexanes/ether (8.5:1.5, v/v) to give alcohol **49** (691 mg, 86%) as colorless needles.

Alcohol **49**: mp 118–119°C (ether/hexane). UV λ_{max} (log ε) (MeOH): 222 (4.43), 258 (4.40) nm. IR ν_{max} 3563, 3010, 2962, 1599, 1381, 1123 cm^{-1}. ^1H NMR δ: 1.05 (3H, s, C7-βCH$_3$), 1.28 (3H, s, C7-αCH$_3$), 1.70 (3H, brs, C9-H), 1.88 (1H, d, J = 17.5, C8-H), 2.09 (1H, d, J = 17.5, C8-H), 2.33 (3H, s, Ar-CH_3), 2.42 (1H, dd, J = 10, 8.5, C6a-H), 3.38 (1H, m, C10a), 4.10 (1H, d, J = 2, O-H), 5.27 (1H, ddd, J = 8.5, 2, 2, C6-H), 6.04 (1H, brs, C10-H), 7.19–7.34 (4H, m, Ar-H), 7.54 (1H, d, J = 7, C1-H), 7.84 (2H, d, J = 9, C2′-H and C6′-H), 7.91 (1H, dd, J = 8, 1.5, C4-H). MS m/z: 421 (M^+), 406, 251, 91. High resolution mass measurement, calcd. for $C_{25}H_{27}NO_3S$: 421.1711; found: 421.1715. Anal. calcd. for $C_{25}H_{27}NO_3S$: C 71.23, H 6.46, N 3.32; found: C 71.20, H 6.47, N 3.46.

*6α-Acetoxy-5-(*p*-toluenesulfonyl)-7,7,9-trimethyl-5,6α,6aα,7,8,10aβ-hexahydroindeno[2,1-b]indole* **50**

To a solution of alcohol **49** (100 mg, 0.24 mmol) and *N,N*-dimethylaminopyridine (37 mg, 0.31 mmol) in dichloromethane (5 mL) at room temperature was added acetic anhydride (0.027 mL, 0.29 mmol). The reaction mixture was stirred for 3 days at room temperature, then diluted with dichloromethane (5 mL) and washed with water (10 mL). The organic phase was washed with brine (10 mL), dried over sodium sulfate, filtered, and evaporated *in vacuo* to yield a yellow foam. This crude product was purified by flash chromatography using hexanes/ether (8:2, v/v) to obtain acetate **50** (82.5 mg, 75%) as a white foam.

Acetate **50**: UV λ_{max} (log ε) (MeOH): 221 (4.41), 257 (4.21) nm. IR ν_{max} ($CHCl_3$): 3019, 2960, 1739, 1599, 1373, 1170 cm^{-1}. ^1H NMR δ: 1.07 (3H, s, C7-CH_3), 1.09 (3H, s, C7-CH_3), 1.71 (3H, brs, C9-CH_3), 1.86 (1H, d, J = 17, C8-H), 2.04 (1H, d, J = 17, C8-H), 2.15 (3H, s, O=C-CH_3), 2.33 (3H, s, Ar-CH_3), 2.53 (1H, dd, J = 10, 9, C6a-H), 3.37–3.45 (1H, m, C10a-H), 6.05 (1H, brs, C10-H), 6.67 (1H, dd, J = 9, 2.5, C6-H), 7.20–7.32 (4H, m, Ar-H), 7.54 (1H, d, J = 8, C1-H), 7.81 (2H, d, J = 8, C2′-H and C6′-H), 8.04 (1H, d, J = 8, C4′-H). MS m/z: 463 (M^+), 403, 388, 308, 248. High resolution mass measurement, calcd. for $C_{27}H_{29}NO_4S$: 463.1817; found: 463.1818. Anal. calcd. for $C_{27}H_{29}NO_4S$: C 69.96, H 6.30, N 3.02; found: C 69.56, H 6.32, N 2.88.

*10bα-(3-Indolyl)-5-(*p*-toluenesulfonyl)-7,7,9-trimethyl-5,6aα,-7,8,10aβ,10bα-hexahydroindeno[2,1-b]indole* **51**

To a solution of indolymagnesium iodide in dry ether (12 mL) and dichloromethane (4 mL) at 0–5°C under nitrogen was added a solution of acetate **50** (540 mg, 1.17 mmol) in ether (7 mL). After stirring for 17 h at 5°C, the reaction mixture was quenched with ammonium chloride (8 mL, sat. aq.) and extracted with dichoromethane (3×, 8 mL). The organic phase was washed with water (8 mL), brine (8 mL), dried over sodium sulfate, and evaporated *in vacuo* to yield a brown oil. Purification by flash chromatography using hexanes/ether (7:3, v/v) gave compound **51** (250 mg, 41%) as a white powder.

Compound **51**: mp 207–208°C (acetone/hexanes). UV λ_{max} (log ε) (MeOH): 226 (4.73), 270 (4.08) nm. IR ν_{max} ($CHCl_3$): 3470, 2960, 1650, 1370, 1170 cm^{-1}. ^1H NMR δ: 0.71 (3H, s, C7-CH_3), 1.06 (3H, s, C7-CH_3), 1.54 (3H, brs, C9-CH_3), 1.63 (1H, d, J = 17, C8-H), 1.79 (1H, d, J = 17, C8-H), 2.33 (3H, s, Ar-CH_3), 2.76 (2H, m, C6a-H and C10a-H), 5.87 (1H, brs, C6-H or C10-H), 5.94 (1H, brs, C6-H or C10-H), 6.97–7.30 (8H, m, Ar-H), 7.25 (1H, d, J = 8, Ar-H), 7.59 (1H, d, J = 8, Ar-H), 7.65 (1H, d, J = 8, Ar-H), 7.76 (2H, d, J = C2′-H and C6′-H), 7.90 (1H, brs, N-H). MS m/z: 520 (M^+), 403, 388, 365. High resolution mass measurement, calcd. for $C_{33}H_{32}N_2O_2S$: 520.2184; found: 520.2179

6-Oxo-7,7,9-trimethyl-5-trimethylsilylethoxymethyl-5,6,6aα,7,8,-10aβ-hexahydroindeno-[2,1-b]indole **53**

To a solution of *trans*-ketone **36** (31 mg, 0.12 mmol) in dichloromethane (4 mL) at 0°C under nitrogen was added sodium hydride (4.5 mg, 0.15 mmol, 80% dispersion in oil). After stirring at 0°C for 1 h, 2-(trimethylsilyl)ethoxymethyl chloride (SEM-Cl), (0.03 mL, 0.175 mmol) was added and the stirring was continued for 40 min. Water (2 mL) and ammonium chloride (4 mL, sat. aq.) were added and the mixture was extracted with dichloromethane (3×, 4 mL). The organic phase was washed with water (6 mL), brine (6 mL), dried over sodium sulfate, filtered, and evaporated *in vacuo* to yield a yellow liquid. The product was immediately purified by flash chromatography using hexanes/ether (9.7:0.3, v/v) to obtain *trans*-SEM-ketone **53** (43 mg, 93%) as a yellow oil. This product turned out to be very unstable so it was usually utilized without purification for the next reaction. IR ν_{max} (film): 2954, 1695, 1615 cm^{-1}. ^1H NMR δ: −0.1 (9H, s, Si-$(CH_3)_3$), 0.86 (2H, m, C4′-H), 1.10 (3H, s, C7-CH_3), 1.42 (3H, s, C7-CH_3), 1.72 (3H, brs, C9-CH_3), 1.93 (1H, d, J = 17, C8-H), 2.03 (1H, d, J = 17, C8-H), 2.79 (1H, d, J = 7, C6a-H), 3.52 (2H, m, C3′-H), 3.94 (1H, m, C10a), 5.61 (1H, d, J = 11.5, C1′-H), 5.69 (1H, d, J = 11.5, C1′-H), 6.23 (1H, brs, C10-H), 7.19 (1H, dd, J = 8, 8, Ar-H), 7.36 (1H, dd, J = 8, 8, Ar-H), 7.53 (1H, d, J = 8, Ar-H), 7.77 (1H, d, J = 8, Ar-H). MS m/z: 395 (M^+), 73.

6α-Hydroxy-7,7,9-trimethyl-5-trimethylsilylethoxymethyl-5,6α,-6aβ,7,8,10aβ-hexadroindeno[2,1-b]indole **54**

Method A

To a solution of SEM-*trans*-ketone **53** (29.4 mg, 0.074 mmol) in dry toluene (2.5 mL) at −78°C under nitrogen was added diisobutylaluminium hydride (DIBAL) (0.11 mL, 0.11 mmol, 1 M in hexane). After stirring for 1 h at −78°C, solid ammonium chloride (about 20 mg) was added. The temperature was raised to 0°C, then water (2 mL) and ammonium chloride (5 mL, sat. aq.) were added. Careful extraction with ether (4×, 5 mL) followed by washing with brine (15 mL), drying

Can. J. Chem. Downloaded from www.nrcresearchpress.com by 198.100.157.202 on 09/07/12
For personal use only.

Can. J. Chem. Downloaded from www.nrcresearchpress.com by 198.100.157.202 on 09/07/12
For personal use only.

over sodium sulfate, filtration, and evaporation *in vacuo* yielded a yellow oil, which was purified by flash chromatography using hexanes/ether (8:2, v/v) to give alcohol **54** (19.4 mg, 80% based on recovered ketone) and unreacted **53** (5.2 mg).

Method B

To a suspension of sodium hydride (13.6 mg, 0.45 mmol, 80% dispersion in oil) (prewashed twice with dry ether (1 mL) in dry tetrahydrofuran (1 mL) at 0°C under nitrogen), was added *trans*-ketone **36** (100 mg, 0.38 mmol) in dry tetrahydrofuran (1.5 mL). After stirring for 40 min, SEM-Cl (0.073 mL, 0.415 mmol) was added and the reaction stirred for 2.5 h at 0°C. Lithium aluminium hydride (about 36 mg, 1 mmol) was then added and, after 30 min at the same temperature, the reaction was quenched with ice (about 0.5 g), and sodium hydroxide (4 mL, 15% aq.). Exhaustive extraction with ether (5×, 5 mL) followed by washing with water/brine (10 mL, 1:1, v/v), brine (10 mL), drying over sodium sulfate, filtration, and evaporation *in vacuo* yielded a yellow oil. Purification by flash chromatography using hexanes/ether (8:2, v/v) furnished pure alcohol **54** (100.2 mg, 67% overall). UV λ_{max} (log ε) (MeOH): 230 (4.44), 280 (3.89) nm. IR ν_{max} (film): 3440, 2960, 1660 cm^{-1}. ^1H NMR δ: −0.07 (9H, s, $Si(CH_3)_3$), 0.81–0.90 (2H, m, C4′-H), 1.03 (3H, s, C7-βCH_3), 1.21 (3H, s, C7-αCH_3), 1.70 (3H, brs, C9-CH_3), 1.84 (1H, d, J = 17, C8-H), 2.03 (1H, d, J = 17, C8-H), 2.10 (1H, dd, J = 9, 9, C6a-H), 3.30 (1H, d, J = 9, Hz, O-H), 3.41 (1H, m, C10a-H), 3.46–3.58 (2H, m, C3′-H), 5.12 (1H, ddd, J = 9, 9, 2, C6-H), 5.41 (1H, d, J = 11, C1′-H), 5.58 (1H, d, J = 11, C1′-H), 6.15 (1H, brs, C10-H), 7.06 (1H, ddd, J = 8, 8, 1.5, Ar-H), 7.13 (1H, ddd, J = 8, 8, 1.5, Ar-H), 7.44 (1H, d, 8, C4-H), 7.57 (1H, d, J = 8, C1-H). MS m/z: 397 (M^+), 379, 73. High resolution mass measurement, calcd. for $C_{24}H_{35}NO_2Si$: 397.2437; found: 397.2443. Anal. calcd. for $C_{24}H_{35}NO_2Si$: C 72.50, H 8.87, N 3.52; found: C 73.00, H 9.00, N 3.24.

6α-Acetoxy-7,7,9-trimethyl-5-trimethylsilylethoxymethyl-5,6α,5aα,7,8,10aβ-hexahydroindeno[2-1-b]indole ***55***

Method A

To a solution of alcohol **54** (46.5 mg, 0.12 mmol) and *N*,*N*-dimethylaminopyridine (DMAP) (21.4 mg, 0.18 mmol) in dichloromethane (1.5 mL) at 0–5°C under nitrogen were added acetic anhydride (0.094 mL, 1 mmol) and triethylamine (0.147 mL, 1.05 mmol). The reaction mixture was stirred for 2 h at room temperature, then water (5 mL) and dichloromethane (5 mL) were added and the layers separated. The organic phase was washed with brine (5 mL), dried over sodium sulfate, filtered, and evaporated *in vacuo* to yield a yellow oil. This crude product was purified by flash chromatography using hexanes/ether (9.5:0.5, v/v) to obtain acetate **55** (44 mg, 86%) as a colorless oil.

Method B

To a suspension of sodium hydride (37.3 mg, 1.24 mmol, 80% dispersion in oil) (prewashed twice with dry ether (1 mL) in dry tetrahydrofuran (2 mL)) at 0°C under nitrogen was added *trans*-ketone **36** (300 mg, 1.13 mmol) in dry tetrahydrofuran (3 mL). The mixture was stirred for 40 min at 0°C, then 2-(trimethylsilyl)ethoxymethyl chloride (SEM-Cl) (0.22 mL, 1.24 mmol) was added. Stirring was continued at 0°C for 2.5 h and then the reaction mixture was cooled to −15°C. Diisobutylaluminum hydride (DIBAL) (2.26 mL, 2.26 mmol, 1 M in hexane) was added and after 1 h at −15°C acetic anhydride (0.32 mL, 3.4 mmol) was added dropwise. After stirring for 16 h at 0°C the reaction mixture was poured into sodium bicarbonate (10 mL, sat. aq.), followed by extraction with ether (3×, 10 mL). The organic phase was washed with brine (20 mL), dried over sodium sulfate, filtered, and evaporated *in vacuo* to yield a dark oil. This crude product was purified by flash chromatography using hexanes/ether (9.5:0.5 v/v) to obtain acetate **55** (250.1 mg, 50.3% overall).

Acetate **55**: UV λ_{max} (log ε) (MeOH): 227 (4.49), 280 (3.94) nm. IR ν_{max} (film): 2955, 1737, 1659 cm^{-1}. ^1H NMR (CD_3CN) δ: −0.09 (9H, s, Si-$(CH_3)_3$), 0.77–0.90 (2H, m, C4′-H), 1.04 (6H, s, C7-CH_3), 1.71 (3H, brs, C9-CH_3), 1.87 (1H, d, J = 17, C8-H), 2.04 (1H, d, J = 17, C8-H), 2.11 (3H, s, O=C-CH_3), 2.50 (1H, dd, J = 10, 10, C6a-H), 3.43 (2H, dd, J = 9, 9, C3′-H), 3.50 (1H, m, C10a), 5.29 (1H, d, J = 11, C1′-H), 5.33 (1H, d, J = 11, C1′-H), 6.18 (1H, brs, C10-H), 6.43 (1H, d, J = 10, C6-H), 7.10 (1H, brdd, J = 8, 8, Ar-H), 7.18 (1H, brdd, J = 8, 8, Ar-H), 7.46 (1H, d, J = 8, C4-H), 7.62 (1H, d, J = 8, C1-H). MS m/z: 439 (M^+), 379, 75, 73. High resolution mass measurement, calcd. for $C_{26}H_{37}NO_3Si$: 439.2542; found: 439.2549.

6β-(3-Indolyl)-7,7,9-trimethyl-5-trimethysilylethoxymethyl-5,6β,6aα,7,8,10aβ-hexahydroindeno[2,1-b]indole ***56***

To a solution of indolylmagnesium iodide (prepared as above) in dry ether (5.5 mL) and dichloromethane (1.6 mL) at 0–5°C under nitrogen was added a solution of acetate **55** (492 mg, 1.12 mmol) in dry ether (3.7 mL). The reaction mixture was stirred for 2.5 h at 0–5°C, then water (3 mL) and ammonium chloride (5 mL, sat. aq.) were added. After extraction with ether (2×, 10 mL), the organic phase was washed with sodium bicarbonate (10 mL, sat. aq.), brine (10 mL), dried over sodium sulfate, filtered, and evaporated *in vacuo* to yield a brown viscous oil. This crude product was purified by flash chromatography using hexanes/ethyl acetate (96.5:3.5, v/v) to furnish SEM-*trans*-yuehchukene **56** (201 mg, 36%) as a pale yellow foam. UV λ_{max} (log ε) (MeOH): 223 (4.7), 280 (4.14) nm. IR ν_{max} (film): 3414, 3055, 2952, 1657 cm^{-1}. ^1H NMR (CD_3CN) δ: −0.16 (9H, s, $Si(CH_3)_3$), 0.34 (3H, brs, C7-βCH_3), 0.44–0.73 (2H, m, C4′-H), 1.13 (3H, m, C7-α-CH_3), 1.67 (1H, d, J = 17, C8-H), 1.70 (3H, s, CH_3), 2.05 (1H, d, J = 17, C8-H), 2.70 (1H, dd, J = 11, 6, C6a-H), 3.05–3.32 (2H, m, C3′-H), 4.06 (1H, m, C10a-H), 4.78 (1H, d, J = 6, C6-H), 4.98 (1H, brd, J = 11, C1′-H), 5.19 (1H, d, J = 11, C1′-H), 6.25 (1H, brs, C10-H), 6.30–7.85 (9H, m, Ar-H), 9.15 (1H, brs, N-H). MS m/z: 496 (M^+), 481, 75. High resolution mass measurement, calcd. for $C_{32}H_{40}N_2OSi$: 496.2909; found: 496.2908. Anal. calcd. for $C_{32}H_{40}N_2OSi$: C 77.37, H 8.12, N 5.64; found: C 77.10, H 8.21, N 5.40.

6a-epi-*Yuehchukene* ***2***

To a solution of SEM-*trans*-yuehchukene **56** (46 mg, 0.093 mmol) in dry tetrahydrofuran (1 mL) at room temperature under nitrogen were added tetra-*n*-butylammonium fluoride (1.85 mL, 1.85 mmol, 1 M in tetrahydrofuran) and hexamethylphosphoramide (HMPA) (0.7 mL). The temperature was increased to 40–45°C and the reaction mixture was maintained at this condition for 1 day. Then a further portion of tetra-*n*-butylammonium fluoride (1 mL, 1 mmol, 1 M in the tetrahydrofuran) and hexamethylphosphoramide (0.6 mL) was added and the stirring at 40–45°C was continued for another day. Water (2 mL) and ammonium chloride (5 mL, sat. aq.) were added and the mixture was extracted with ether (3×, 6 mL). The organic phase was washed with brine, dried over sodium sulfate, filtered, and evaporated *in vacuo* to yield a yellow oil. This crude product was purified by flash chromatography using hexanes/ether (9:1, v/v) to obtain *trans*-yuehchukene **2** (30.2 mg, 89%) as a white foam. UV λ_{max} (log ε) (MeOH): 324 (4.63), 280 (4.03) nm. IR ν_{max} (film): 3400, 2920, 1655 cm^{-1}. ^1H NMR (CD_3CN) δ: 0.32 (3H, s, C7-βCH_3), 1.15 (3H, s, C7-αCH_3), 1.67 (1H, d, J = 17, C8-H), 1.69 (3H, s, C9-CH_3), 2.05 (1H, d, J = 17, C8-H), 2.69 (1H, dd, J = 10, 7, C6a-H), 4.01 (1H, brd, J = 10, C10a-H), 4.70 (1H, d, J = 7, C6-H), 6.26 (1H, brs, C10-H), 6.70–7.17 (6H, m, Ar-H), 7.29 (1H, dd, J = 7, 3, Ar-H), 7.34 (1H, d, J = 8, Ar-H), 7.66 (1H, brd, J = 8, Ar-H), 8.89 (1H, brs, N-H), 9.10 (1H, brs, N-H). MS m/z: 366 (M^+), 351, 142. High resolution mass measurement, calcd. for $C_{26}H_{26}N_2$: 366.2095; found: 366.2090.

10α-Methyl-6-oxo-5,6,7β,10β-tetrahydro-7β, 10β-(1-1-dimethylethano)-cyclohept[b]indole ***33***

To a solution of indole-acid **28** (400 mg, 1.41 mmol) in dry chloroform (70 mL) at room temperature under nitrogen was added polyphosphate ester (PPE) (1.5 mL). The reaction mixture was refluxed for 1 h, followed by cooling and addition of water (20 mL). The organic phase was then washed with sodium bicarbonate (25 mL, sat. aq.), water (25 mL), brine (25 mL), dried over sodium sulfate, filtered, and evaporated *in vacuo* to yield a viscous oil. The crude product was purified on a short silica gel column using hexanes/ether (8.5:1.5, v/v) to give pure ketone **33** (190 mg, 55%) as colorless prisms. UV λ_{max} (log ε) (MeOH): 237 (4.33), 314 (4.32) nm. IR λ_{max} (KBr): 3300, 3060, 2960, 1620, 1601 cm^{-1}. ^1H NMR δ: 1.00 (3H, s,

C1′-CH_3), 1.18 (3H, s, C1′-CH_3), 1.63 (1H, d, J = 15, C2′-H), 1.97 (3H, s, C10-CH_3), 2.01 (1H, d, J = 15, C2′-H), 3.29 (1H, d, J = 7, C7-H), 6.18 (1H, dd, J = 8, 7, C8-H), 6.45 (1H, d, J = 8, C9-H), 7.10 (1H, dd, J = 8, 6, Ar-H), 7.29 (1H, dd, J = 8, 6, Ar-H), 7.38 (1H, d, J = 8, Ar-H), 8.04 (1H, d, J = 8, Ar-H), 8.86 (1H, brs, N-H). MS m/z: 265 (M^+), 250, 237, 209, 181. High resolution mass measurement, calcd. for $C_{18}H_{19}NO$: 265.1466; found: 265.1465. Anal. calcd. for $C_{18}H_{19}NO$: C 81.48, H 7.22, N 5.28; found: C 81.39, H 7.40, N 5.24.

6α-Hydroxy-10-α methyl 5,6,7β,10β-tetrahydro-7β,10β-(1,1-dimethylethano)-cyclohept[b]indole ***59***

To a suspension of lithium aluminium hydride (29 mg, 0.76 mmol) in 5 mL of tetrahydrofuran at −40°C, the cooled solution of ketone **33** (200 mg, 0.75 mmol) in 5 mL tetrahydrofuran was added. The reaction was stirred for 1 h at −40°C. Then the reaction mixture was quenched with 1 mL of H_2O, warmed up to room temperature, diluted with water, and extracted with dichloromethane. The organic layer was dried with sodium sulfate, evaporated to dryness, and purified on a silica gel column using hexane/ether (8.5:1.5, v/v) to give unreacted ketone **33** (23 mg, 12%) and one alcohol **59** (142 mg, 71%). ^{1}H NMR δ: 1.06 (3H, s), 1.17 (3H, s), 1.55 (1H, d, J = 15), 1.08 (3H, s), 2.23 (1H, bs), 2.42 (1H, dd, J = 3, 6), 4.96 (1H, s), 6.18 (1H, dd, J = 6, 8), 6.26 (1H, d, J = 8), 7.02 (1H, dd, J = 6, 8), 7.09 (1H, dd, J = 6, 8), 7.31 (1H, d, J = 8), 7.87 (1H, *d*, J = 8), 8.42 (1H, b). MS m/z: 267 (M^+) (100%), 252, 234. High resolution mass measurement, calcd. for $C_{18}H_{21}NO$: 267.1623; found: 267.1620.

6β-(N-Indolyl)-10α-methyl-5,6,7β,10β-tetrahydro-7β,10β-(1,1-dimethylethano)-cyclohept[b]indole ***60***

To a solution of alcohol **59** (140 mg, 0.522 mmol), dimethylaminopyridine (77 mg, 0.626 mmol), and triethylamine (1.4 mL) in dichloromethane (12 mL) at room temperature under nitrogen was added benzoyl chloride (0.25 mL, 2.1 mmol). After 18 h of reflux, the reaction mixture was cooled to room temperature and water (30 mL) was added. The organic phase was washed with sodium bicarbonate (10% aq.) and water, dried over sodium sulfate, filtered, and evaporated to dryness to yield crude benzoate of the alcohol **59**. Then, without futher purification, the crude benzoate was dissolved in a mixture of dry ethyl ether (2 mL) and dichloromethane (1 mL), and added dropwise to a solution of indolylmagnesium iodide (for preparation, see Experimental for compound **29**) in a mixture of ethyl ether (3 mL) and dichloromethane (1 mL). After stirring for 2 h at 0–5°C and 2 h at room temperature, water (2 mL) and ammonium chloride (6 mL, sat. aq.) were added, followed by extraction with dichloromethane (3 × 10 mL). The organic phase was washed with water (15 mL), brine (15 mL), dried over sodium sulfate, filtered, and evaporated to yield a brown oil. Flash chromatography on silica gel employing hexanes/ether (8:2) as eluent gave 124 mg (64.5%, calcd. based on alcohol **59**) of the compound **60**, as white crystals; mp 124–124.5°C. ^{1}H NMR δ: 1.11 (3H, s), 1.30 (3H, s), 1.54 (1H, d, J = 12), 1.92 (3H, s), 2.05 (1H, d, J = 12), 2.73 (1H, dd, J = 8, 4), 5.57 (1H, dd, J = 8, 8), 5.99 (1H, d, J = 4), 6.31 (1H, d, J = 8), 6.34 (1H, d, J = 4), 6.64 (1H, d, J = 4), 7.0–7.3 (5H, m), 7.42 (1H, d, J = 8), 7.59 (1H, d, J = 6), 7.7 (1H, s, b), 7.93 (1H, d, J = 8). MS m/z: 366 (M^+), 250, 194. High resolution mass measurement, calcd. for $C_{26}H_{26}N_2$: 366.2096; found: 366.2107.

Acknowledgements

Financial aid from the World Health Organization and the Natural Sciences and Engineering Research Council of Canada is gratefully acknowledged. We are grateful to Professor Y. C. Kong, Chinese University of Hong Kong, for an authentic sample of racemic natural yuehchukene.

1. Y. C. Kong, K. F. Cheng, K. H. Ng, P. P. But, Q. Li, S. X. Yu, H. T. Chang, R. C. Cambie, T. Konoshita, W. S. Kan, and P. G. Waterman. Biochem. Syst. Ecol. **14**: 491 (1986).
2. G. A. Cordell. Introduction to alkaloids—a biogenetic approach. Wiley–Interscience, New York. 1981. p. 614.
3. M. T. Faurel, J. Gleye, C. Moulis, and I. Fourasti. Plant. Med. Phytother. **12**, 207 (1978).
4. I. Mester. *In* Chemistry and chemical taxonomy of the rutales. *Edited by* P. G. Waterman and M. F. Grundon. Academic, London. 1983. p. 31.
5. P. G. Waterman. *In* Chemistry and chemical taxonomy of the rutales. *Edited by* P. G. Waterman and M. F. Grundon. Academic, London. 1983. p. 377.
6. A. I. Gray. *In* Chemistry and chemical taxonomy of the rutales. *Edited by* P. G. Waterman and M. F. Grundon. Academic, London. 1983. p. 97.
7. J. B. Harborne. *In* Chemistry and chemical taxonomy of the rutales. *Edited by* P. G. Waterman and M. F. Grundon. Academic, London. 1983. p. 147.
8. Y. C. Kong, K. F. Cheng, R. C. Cambie, and P. G. Waterman. J. Chem. Soc. Chem. Commun. 47 (1985).
9. Y. C. Kong, K. H. Ng, P. P. But, Q. Li, S. X. Yu, H. T. Zhang, K. F. Cheng, D. D. Soejarlo, N. S. Kan, and P. G. Waterman. J. Ethnopharmacol. **15**, 195 (1986).
10. Y. C. Kong, G. K. Ng, C. K. Wat, and P. P. But. Int. J. Crude Drug Res. **24**, 167 (1986).
11. Y. C. Kong, G. K. Ng, C. K. Wat, A. Wong, I. F. Lau, K. F. Cheng, P. P. But, and H. T. Chang. Planta Med. 304 (1985).
12. I. M. Perry. Medicinal plants of Southeast Asia. MIT Press, 1980.
13. R. L. Khosa, S. P. Sen, and S. N. Dixit. Indian J. Pharm. **32**, 65 (1970).
14. Y. C. Kong, J. X. Xie, and P. P. But. J. Ethnopharmacol. **15**, 1 (1986).
15. Y. C. Kong, C. N. Lam, K. F. Cheng, and T. C. W. Mak. Struct. Chem. **4**, 30 (1985).
16. J. P. Kutney, F. J. Lopez, S. P. Huang, and H. Kurobe. Heterocycles, **28**, 565 (1989).
17. J. D. Surmatis, A. Walser, J. Gibas, and R. Thommen. J. Org. Chem. **35**, 1053 (1970).
18. E. F. V. Scriven. Chem. Soc. Rev. **12**, 129 (1983).
19. G. A. Olah and J. Narang. Tetrahedron, **32**, 2225 (1982).
20. E. J. Corey and R. H. K. Chen. J. Org. Chem. **38**, 4086 (1973).
21. L. A. Cohen and W. M. Jones. J. Am. Chem. Soc. **85**, 3397 (1963).
22. P. Beak and A. I. Meyers. Acc. Chem. Res. **19**, 356 (1986).
23. International tables for X-ray crystallography. Vol. IV. Kynoch Press, Birmingham, U.K. (Present distributor Kluwer Academic Publishers, Dordrecht, The Netherlands). 1974. pp. 99–102 and 149.
24. H. Sakuray, A. Shirihata, and A. Hosomi. Tetrahedron Lett. **21**, 1967 (1980).
25. O. Mitsunobu. Synthesis, 1 (1981).
26. F. E. Ziegler and G. B. Bennett. J. Am. Chem. Soc. **93**, 5930 (1971).
27. T. Imanishi, A. Nakai, N. Yagi, and M. Hanacka. Chem. Pharm. Bull. **29**, 901 (1981).
28. Y. Langlois and P. Potier. Tetrahedron, **31**, 423 (1975).
29. J. Krishnamurthy and H. C. Brown. J. Am. Chem. Soc. **94**, 7159 (1972).
30. B. H. Lipshutz and J. J. Pegram. Tetrahedron Lett. **21**, 3343 (1980).
31. M. P. Edwards, S. V. Ley, S. J. Lister, B. D. Palmer, and D. J. Williams. J. Org. Chem. **49**, 3503 (1984).
32. E. Winterfeldt. Synthesis, 617 (1975).
33. B. H. Lipshutz, J. J. Pegram, and M. C. Morey. Tetrahedron Lett. **22**, 4603 (1981).
34. W. C. Still, M. Kahn, and A. Mitra. J. Org. Chem. **43**, 2923 (1978).
35. K. F. Cheng, Y. C. Kong, and T. Y. Chan. Chem. Commun. 48 (1985).

Can. J. Chem. Downloaded from www.nrcresearchpress.com by 198.100.157.202 on 09/07/12
For personal use only.

TABLE 3. Crystallographic data[a]

Compound	**36**	**60**·½ CH_2Cl_2	**45**·C_3H_6O
Formula	$C_{18}H_{19}NO$	$C_{26.5}H_{27}ClN_2$	$C_{36}H_{36}N_2O_2$
FW	265.35	408.97	528.69
Crystal size, mm	0.05 × 0.19 × 0.25	0.25 × 0.25 × 0.42	0.22 × 0.35 × 0.56
Crystal system	Triclinic	Orthorhombic	Monoclinic
Space group	$P\bar{1}$	$Fdd2$	$P2_1/n$
a, Å	8.2249(9)	19.242(1)	9.5050(3)
b, Å	12.845(1)	56.193(3)	21.9825(9)
c, Å	7.8662(8)	8.1466(5)	14.0170(4)
α, deg	85.58(1)	90	90
β, deg	113.207(8)	90	94.981(4)
γ, deg	107.076(9)	90	90
V, Å^3	731.2(1)	8808(1)	2917.7(2)
Z	2	16	4
ρ_{calc}, g/cm^3	1.205	1.234	1.204
$F(000)$	284	3472	1128
$\mu/(CuK_\alpha)$, cm^{-1}	5.43	16.36	5.44
Transmission factors		0.587–0.714	0.787–0.891
Scan type	ω–2θ	ω–2θ	ω–2θ
Scan range, deg in ω	0.85 + 0.14 tan θ	0.55 + 0.14 tan θ	0.70 + 0.14 tan θ
Scan speed, deg/min	1.3–10.0	0.9–10.0	1.1–10.0
Data collected	$\pm h, +k, \pm l$	$\pm h, +k, \pm l$	$\pm h, +k, \pm l$
$2\theta_{max}$, deg	150	150	150
Cryst. decay	Negligible	Negligible	Negligible
No. of unique reflections	3004	2430	5986
No. of reflections with $I \geq n\sigma(I)$	911 (n = 2)	1342 (n = 3)	4290 (n = 3)
No. of variables	181	264	482
R	0.054	0.062	0.043
R_w	0.048	0.070	0.051
gof	1.62	2.39	0.96
Max Δ/σ (final cycle)	0.002	0.28	0.30
Residual density e/Å^3	−0.22 to +0.36	−0.26 to +0.91	−0.20 to +0.28

[a]Temperature 294 K, Enraf–Nonius CAD4-F diffractometer, Cu-K_α radiation ($\lambda(K_{\alpha 1})$ = 1.54056, $\lambda(K_{\alpha 2})$ = 1.54439 Å), nickel filter, takeoff angle 3.0°, aperture (4.0 × 2.0) + 1.0 tan θ mm at a distance of 173 mm from the crystal, scan extended by 25% on each side for background measurement, $\sigma^2(I) = [C + 2B + (0.040(C - B))^2]$ with C = scan count, B = normalized total background count, function minimized $\Sigma w(|F_o| - |F_c|)^2$ where $w = 4F_o^2/\sigma^2(F_o^2)$, $R = \Sigma||F_o| - |F_c||/\Sigma|F_o|$, $R_w = (\Sigma w(|F_o| - |F_c|)^2/\Sigma w|F_o|^2]^{1/2}$, and gof = $[\Sigma(|F_o| - |F_c|)^2/(m-n)]^{1/2}$. Values given for R, R_w, and gof are based on those reflections with $I \geq n\sigma(I)$.

36. E. WENKERT, E. C. ANGELL, V. F. FERREIRA, E. L. MICHELOTTI, S. R. PIETTRE, J. H. SHEU, and C. S. SWINDELL. J. Org. Chem. **51**, 2343 (1986).
37. J. BERGMAN and L. VENEMALM. Tetrahedron Lett. **29**, 2993 (1988).

Appendix

X-ray crystallographic analyses of **36**, **60**·½ CH_2Cl_2, *and* **45**·C_3H_6O

Crystallographic data for the three compounds appear in Table 3. The final unit-cell parameters were obtained by least squares on the setting angles for 25 reflections with 2θ = 32.3–50.4° for **36**, 40.1–88.0° for **60**, and 80.2–94.0° for **45**. The intensities of three standard reflections, measured every hour of X-ray exposure time throughout the data collections, remained essentially constant for all three compounds. The data were processed[3] and corrected for Lorentz and polarization effects, and absorption for **60**·½CH_2Cl_2 and **45**·C_3H_6O (analytical method).

The structure analysis of **36** was initiated in the centrosymmetric space group $P\bar{1}$ on the basis of E-statistics, the choice being confirmed by subsequent calculations. The structures were solved by direct methods, the coordinates of the non-hydrogen atoms being determined from E-maps and subsequent difference Fourier syntheses. The asymmetric unit of **60** contains one half of a dichloromethane solvate molecule (situated on a crystallographic twofold rotation axis), and the asymmetric unit of **45** contains an acetone solvate molecule. All non-hydrogen atoms (except for the carbon atom of the dichloromethane molecule in **60**·½CH_2Cl_2) were refined with anisotropic thermal parameters. Hydrogen atoms were fixed in idealized positions (C(sp^2)—H = 0.97, C(sp^3)—H = 0.98, N—H = 0.92 Å, $U_H \propto U_{bonded\ atom}$) except for **45**·$C_3H_6O$ where all hydrogen atoms except those associated with the acetone molecule were refined with isotropic thermal parameters. Neutral atom scattering factors and anomalous dispersion corrections for the non-hydrogen atoms were taken from the International Tables for X-ray Crystallography (23). A parallel refinement of the structure of **60**·½CH_2Cl_2 having the opposite polarity gave slightly higher residuals, the R_w factor ratio being 1.005. Final atomic coordinates and equivalent isotropic thermal parameters

[3]Computer programs used include locally written programs for data processing and locally modified versions of the following: MULTAN80, multisolution program by P. Main, S. J. Fiske, S. E. Hull, L. Lessinger, G. Germain, J. P. Declercq, and M. M. Woolfson; ORFLS, full-matrix least-squares, and ORFFE, function and errors, by W. R. Busing, K. O. Martin, and H. A. Levy; FORDAP, Patterson and Fourier syntheses, by A. Zalkin; ORTEP II, illustrations, by C. K. Johnson.

Can. J. Chem. Downloaded from www.nrcresearchpress.com by 198.100.157.202 on 09/07/12
For personal use only.

Can. J. Chem. Downloaded from www.nrcresearchpress.com by 198.100.157.202 on 09/07/12
For personal use only.

TABLE 4. Final position (fractional × 10^4, Cl and **45** × 10^5) and isotropic thermal parameters ($U \times 10^3$ Å^2) with estimated standard deviations in parentheses

Atom	*x*	*y*	*z*	U_{eq}/U_{iso}
		36		
O	7944(5)	−1570(3)	9787(5)	72
N(1)	8806(5)	404(3)	7210(5)	63
C(2)	7509(7)	−598(4)	6957(7)	51
C(3)	7088(7)	−1462(4)	8146(7)	54
C(4)	5321(6)	−2256(4)	6831(6)	50
C(5)	4626(7)	−3452(4)	7186(6)	54
C(6)	2749(7)	−3903(4)	5558(7)	72
C(7)	2440(7)	−3419(4)	3682(7)	63
C(8)	3646(7)	−2547(4)	3410(6)	60
C(9)	5449(7)	−2059(4)	4923(6)	55
C(10)	6560(6)	−885(4)	5130(7)	51
C(11)	7266(6)	−34(4)	4132(7)	53
C(12)	6927(7)	120(5)	2261(7)	70
C(13)	7947(8)	1051(5)	1771(7)	74
C(14)	9295(8)	1839(5)	3124(9)	78
C(15)	9684(7)	1712(5)	4979(9)	71
C(16)	8649(7)	762(4)	5472(8)	56
C(17)	5977(8)	−4069(4)	7240(7)	79
C(18)	4365(7)	−3591(4)	9010(7)	79
C(19)	637(8)	−3953(5)	2178(7)	100
		60		
Cl	3242(6)	2471(1)	909(15)	334
N(1)	5040(3)	2295(1)	3408	47
N(1′)	4417(3)	1804(1)	2950(11)	44
C(2)	5362(4)	2091(1)	2848(12)	41
C(3)	5122(3)	1854(1)	3463(13)	42
C(4)	5632(4)	1651(1)	2975(13)	44
C(5)	5605(4)	1621(1)	1150(14)	55
C(6)	5956(4)	1776(1)	278(13)	51
C(7)	6392(3)	1969(1)	1065(12)	43
C(8)	5902(3)	2149(1)	1833(13)	39
C(9)	5915(4)	2410(1)	1797(13)	41
C(10)	6336(4)	2583(1)	1011(13)	51
C(11)	6202(4)	2821(1)	1329(14)	54
C(12)	5661(5)	2892(1)	2291(15)	56
C(13)	5226(4)	2733(1)	3043(13)	58
C(14)	5367(4)	2490(1)	2779(12)	44
C(15)	6379(4)	1680(1)	3613(14)	52
C(16)	6809(3)	1845(1)	2424(14)	52
C(17)	6889(4)	2072(1)	−183(14)	63
C(18)	6382(4)	1782(2)	5406(15)	67
C(19)	6713(4)	1434(1)	3644(15)	70
C(2′)	4099(4)	1873(2)	1531(15)	63
C(3′)	3470(4)	1769(2)	1403(16)	69
C(3a′)	3370(4)	1622(1)	2806(14)	49
C(4′)	2843(4)	1473(2)	3361(15)	62
C(5′)	2935(4)	1353(1)	4838(16)	61
C(6′)	3533(5)	1379(1)	5736(14)	62
C(7′)	4075(4)	1527(1)	5212(14)	52
C(7a′)	3978(4)	1647(1)	3743(13)	42
C(s)	2500	2500	−333(93)	290(22)
		45		
O(1)	65798(19)	19109(8)	53527(12)	64
N(1)	52267(17)	13169(8)	43325(11)	36
N(2)	33115(20)	21329(9)	13944(14)	47
C(1)	43926(19)	7743(9)	41672(14)	33
C(2)	35945(21)	4714(10)	47966(15)	38
C(3)	30057(21)	−848(10)	45124(16)	41
C(4)	32036(21)	−3288(10)	36268(16)	42
C(5)	40042(21)	−182(10)	29964(15)	37
C(6)	46082(19)	5327(8)	32671(13)	32
C(7)	55266(19)	9739(9)	27523(13)	31
C(8)	69054(20)	7685(9)	23070(14)	34
C(9)	74821(21)	1810(9)	27238(14)	37
C(10)	87640(22)	1059(10)	31654(15)	40
C(11)	98017(23)	6207(11)	32831(19)	48
C(12)	94944(21)	11387(10)	25690(16)	44
C(13)	79195(20)	13132(9)	25536(15)	37
C(14)	74525(22)	15359(10)	34997(15)	39
C(15)	61599(19)	13384(9)	35944(13)	33
C(16)	92445(30)	−4934(12)	35854(23)	56
C(17)	98113(31)	9328(16)	15630(21)	61
C(18)	104447(29)	16819(14)	28613(27)	64
C(19)	54489(24)	16575(10)	51581(15)	43
C(20)	42433(26)	17511(10)	57496(17)	48
C(21)	29102(31)	18833(13)	53345(24)	66
C(22)	18542(43)	20358(15)	59198(34)	88
C(23)	21288(52)	20347(14)	68999(33)	92
C(24)	34365(50)	18986(16)	73036(82)	84
C(25)	45146(37)	17645(13)	67390(20)	65
C(26)	41653(22)	19430(10)	21789(16)	40
C(27)	45936(20)	13611(9)	20535(13)	34
C(28)	39466(20)	11693(10)	11326(14)	38
C(29)	39375(25)	6296(11)	6057(16)	47
C(30)	31616(29)	6030(14)	−2760(18)	60
C(31)	24045(29)	11053(15)	−6398(19)	63
C(32)	23826(26)	16403(14)	−1436(18)	56
C(33)	31578(22)	16678(10)	7466(15)	43
O(2))	32408(56)	33502(19)	30111(32)	210
C(34)	29392(56)	36405(23)	36647(31)	111
C(35)	35960(48)	42373(23)	38698(29)	115
C(36)	17811(69)	34679(28)	42737(40)	162

(U_{eq} = 1/3 trace of diagonalized *U*), bond lengths, and bond angles appear in Tables 2–4, respectively. Hydrogen atom parameters, anisotropic thermal parameters, torsion angles, and measured and calculated structure factor amplitudes for the three structures are provided as supplementary material.[4]

Discussion of crystal structures

The crystal structure of compound **36** consists of centrosymmetric hydrogen-bonded dimers (N(1)—H(N)···O(2-*x*,-*y*,2-*z*), H···O = 2.00, N···O = 2.864(5) Å, N—H···O = 157°). The junction between the cyclohexene and cyclopentanone rings (at C(4)—C(8)) is *trans* (see Fig. 1).[5] The indole moiety is planar to within 0.030(7) Å. The five-membered C(2–4),C(9–10) ring has a slightly distorted C(4)-envelope conformation, and the C(4–9) cyclohexene ring has a semiplanar conformation with C(4) displaced from the approximate plane of the other five

[4]Supplementary material mentioned in the text may be purchased from: The Depository of Unpublished Data, Document Delivery, CISTI, National Research Council Canada, Ottawa, Canada K1A 0R6.

Tables of hydrogen atom coordinates, and of bond lengths and angles involving hydrogen atoms, have also been deposited with the Cambridge Crystallographic Data Centre and can be obtained on request from The Director, Cambridge Crystallographic Data Centre, University Chemical Laboratory, Lensfield Road, Cambridge CB2 1EW, U.K.

[5]The crystallographic atom numbering shown in Fig. 1, which differs from that shown in schemes above, is employed in this section. Atom labels in Tables 4–7 correspond to those in Fig. 1.

TABLE 5. Bond lengths (Å) with estimated standard deviations in parentheses

Bond	Length (Å)	Bond	Length (Å)
		36	
O—C(3)	1.223(5)	C(7)—C(8)	1.328(6)
N(1)—C(2)	1.380(5)	C(7)—C(19)	1.490(6)
N(1)—C(16)	1.377(5)	C(8)—C(9)	1.481(6)
C(2)—C(3)	1.448(6)	C(9)—C(10)	1.500(6)
C(2)—C(10)	1.356(5)	C(10)—C(11)	1.416(6)
C(3)—C(4)	1.528(6)	C(11)—C(12)	1.395(6)
C(4)—C(5)	1.520(6)	C(11)—C(16)	1.411(6)
C(4)—C(9)	1.543(6)	C(12)—C(13)	1.372(6)
C(5)—C(6)	1.548(6)	C(13)—C(14)	1.402(7)
C(5)—C(17)	1.532(7)	C(14)—C(15)	1.373(6)
C(5)—C(18)	1.522(6)	C(15)—C(16)	1.394(6)
C(6)—C(7)	1.512(6)		
		60	
Cl—C(s)	1.76(4)	C(9)—C(10)	1.419(10)
N(1)—C(2)	1.382(8)	C(9)—C(14)	1.397(10)
N(1)—C(14)	1.361(8)	C(10)—C(11)	1.386(10)
N(1′)—C(3)	1.448(9)	C(11)—C(12)	1.362(11)
N(1′)—C(2′)	1.364(11)	C(12)—C(13)	1.370(11)
N(1′)—C(7a′)	1.381(9)	C(13)—C(14)	1.407(10)
C(2)—C(3))	1.493(9)	C(15)—C(16)	1.574(11)
C(2)—C(8))	1.368(9)	C(15)—C(18)	1.568(14)
C(3)—C(4)	1.557(10)	C(15)—C(19)	1.527(10)
C(4)—C(5)	1.497(12)	C(2′)—C(3′)	1.348(11)
C(4)—C(15)	1.538(11)	C(3′)—C(3a′)	1.421(12)
C(5)—C(6)	1.313(10)	C(3a′)—C(4′)	1.393(11)
C(6)—C(7)	1.512(10)	C(3a′)—C(7a′)	1.403(10)
C(7)—C(8)	1.520(10)	C(4′)—C(5′)	1.389(13)
C(7)—C(16)	1.534(11)	C(5′)—C(6′)	1.372(12)
C(7)—C(17)	1.511(10)	C(6′)—C(7′)	1.399(11)
C(8)—C(9)	1.468(10)	C(7′)—C(7a′)	1.387(10)
		45	
O(1)—C(19)	1.220(3)	C(12)—C(17)	1.536(3)
N(1)—C(1)	1.440(2)	C(12)—C(18)	1.531(3)
N(1)—C(15)	1.421(2)	C(13)—C(14)	1.516(3)
N(1)—C(19)	1.379(2)	C(14)—C(15)	1.321(3)
N(2)—C(26)	1.374(3)	C(19)—C(20)	1.486(3)
N(2)—C(33)	1.367(3)	C(20)—C(21)	1.379(4)
C(1)—C(2)	1.383(3)	C(20)—C(25)	1.389(4)
C(1)—C(6)	1.400(3)	C(21)—C(22)	1.391(4)
C(2)—C(3)	1.388(3)	C(22)—C(23)	1.376(5)
C(3)—C(4)	1.380(3)	C(23)—C(24)	1.354(5)
C(4)—C(5)	1.394(3)	C(24)—C(25)	1.380(4)
C(5)—C(6)	1.379(3)	C(26)—C(27)	1.359(3)
C(6)—C(7)	1.527(3)	C(27)—C(28)	1.444(3)
C(7)—C(8)	1.566(3)	C(28)—C(29)	1.397(3)
C(7)—C(15)	1.508(2)	C(28)—C(33)	1.409(3)
C(7)—C(27)	1.523(3)	C(29)—C(30)	1.384(3)
C(8)—C(9)	1.501(3)	C(30)—C(31)	1.391(4)
C(8)—C(13)	1.557(3)	C(31)—C(32)	1.367(4)
C(9)—C(10)	1.328(3)	C(32)—C(33)	1.394(3)
C(10)—C(11)	1.501(3)	O(2)—C(34)	1.172(5)
C(10)—C(16)	1.498(3)	C(34)—C(35)	1.470(6)
C(11)—C(12)	1.527(3)	C(34)—C(36)	1.499(7)
C(12)—C(13)	1.544(3)		

atoms of the ring (see Table 7). There is evidence of considerable steric strain at the junction of the two five-membered rings. The (N(1),C(3)]C(2)—C(10)[C(4),C(11)) grouping is significantly non-planar (maximum deviation from the mean plane is 0.091(6) Å) and there is substantial angular distortion about both C(2) and C(10) (see Table 6). The short C(2)—C(3) distance of 1.448 Å is indicative of conjugation between the indole and carbonyl groups, while the C(3)—C(4) bond of 1.528 Å is long for a $C(sp^2)$—$C(sp^3)$ single bond. The detailed molecular geometry reflects both steric and electronic effects but is generally as expected.

Compound **60** crystallizes as a hemi-dichloromethane solvate with the CH_2Cl_2 molecule situated on a crystallographic C_2 axis. The crystal structure consists of well-separated molecules of **60** and CH_2Cl_2, the shortest intermolecular distances between non-hydrogen atoms being N(1)···C(11)($1 - x$, $1/2 - y$, $1/2 + z$) = 3.44(1) Å. The molecule **60** consists of a substituted indolo[2,3-*b*]bicyclo[3.2.2]non-6-ene ring system (Fig. 1). The indole moiety fused to the bicyclic system is planar within 0.03(1) Å, and both the 1-indolyl substituent at C(3) and the C(4)–C(5)═C(6)–C(7) group are planar within experimental error. As expected, there is less strain at the junction between the fused indole moiety and the seven-membered ring(s) of the bicyclo[3.2.2.] nonene system in **60** than at the corresponding junction between two five-membered rings in **36**. Bond lengths and angles (Tables 3 and 4) are generally as expected, with steric lengthening of some bonds between substituted atoms (e.g., C(3)—C(4) = 1.557, C(7)—C(8) = 1.520, C(15)—C(16) = 1.574, and C(15)—C(18) = 1.568 Å).

The solid state structure of **45**·Me_2CO consists of molecules of **45** linked into infinite chains by N—H···O hydrogen bonds (N(2)—H(N2)···O(1)($x - 1/2$, $1/2 - y$,$z - 1/2$), H···O = 2.25(3), N···O = 2.974(2) Å, N—H···O = 144(2)°) and well-separated acetone solvate molecules. The junction between the cyclopentene and cyclohexene rings (at C(8)—C(13)) is *cis* (see Fig. 1). Within the central system of four fused rings, the five-membered heterocyclic ring has a distorted C(15)-envelope conformation, the cyclopentene ring has a C(8)-envelope conformation, the cyclohexene ring has a semiplanar conformation with C(12) displaced from the approximate plane of the other five ring atoms, and the C(1–6) aromatic ring is planar within experimental error. The 3-indolyl substituent at C(7) and the phenyl group at C(19) are planar to within 0.014(2) Å and experimental error, respectively. The geometry about N(1) is nearly planar, the bond lengths involving this atom being consistent with interactions of N(1) with the three adjacent π-systems (the C(1–6) aromatic ring, the carbonyl group, and the C(14)═C(15) double bond). The angle between normals to the N(1) coordination group and the C(19)-carbonyl group mean planes (usually near zero for amides) is 29°. A weak intramolecular C—H···O interaction may be at least partially responsible for this (C(14)—H(14)···O, H···O = 2.51(2), C···O = 2.913(3) Å, C—H···O = 107(2)°). The C(20–25) phenyl ring is twisted 43° out of the plane of the carbonyl group. Strain in the fused ring system is indicated by a 0.140(2) Å deviation of N(1) from the C(1–6) mean plane, a significant non-planarity about the C(14)═C(15) double bond, and the lengthening of several intra-annular bonds (C(6)—C(7) = 1.527, C(7)—C(8) = 1.566, C(8)—C(13) = 1.557, and C(12)-C(13) = 1.544 Å). Remaining aspects of the molecular geometry (Tables 5–7) are as expected.

Can. J. Chem. Downloaded from www.nrcresearchpress.com by 198.100.157.202 on 09/07/12
For personal use only.

TABLE 6. Bond angles (deg) with estimated standard deviations in parentheses

Bonds	Angle (deg)	Bonds	Angle (deg)
	36		
C(2)—N(1)—C(16)	106.6(4)	C(8)—C(7)—C(19)	122.3(5)
N(1)—C(2)—C(3)	135.5(5)	C(7)—C(8)—C(9)	120.7(4)
N(1)—C(2)—C(10)	110.9(4)	C(4)—C(9)—C(8)	111.0(4)
C(3)—C(2)—C(10)	113.1(4)	C(4)—C(9)—C(10)	102.0(4)
O—C(3)—C(2)	129.6(5)	C(8)—C(9)—C(10)	125.7(4)
O—C(3)—C(4)	127.3(5)	C(2)—C(10)—C(9)	109.0(4)
C(2)—C(3)—C(4)	103.1(4)	C(2)—C(10)—C(11)	107.4(4)
C(3)—C(4)—C(5)	124.4(4)	C(9)—C(10)—C(11)	141.9(5)
C(3)—C(4)—C(9)	103.7(4)	C(10)—C(11)—C(12)	134.3(5)
C(5)—C(4)—C(9)	113.8(4)	C(10)—C(11)—C(16)	106.0(5)
C(4)—C(5)—C(6)	105.9(4)	C(12)—C(11)—C(16)	119.7(5)
C(4)—C(5)—C17)	110.7(4)	C(11)—C(12)—C(13)	118.8(5)
C(4)—C(5)—C(18)	111.4(4)	C(12)—C(13)—C(14)	120.6(5)
C(6)—C(5)—C(17)	110.4(4)	C(13)—C(14)—C(15)	122.3(5)
C(6)—C(5)—C(18)	109.8(4)	C14)—C(15)—C(16)	116.9(5)
C(17)—C(5)—C(18)	108.6(4)	N(1)—C(16)—C(11)	109.1(5)
C(5)—C(6)—C(7)	119.2(4)	N(1)—C(16)—C(15)	129.1(5)
C(6)—C(7)—C(8)	122.5(4)	C(11)—C(16)—C(15)	121.7(5)
C(6)—C(7)—C(19)	115.1(5)		
	60		
C(2)—N(1)—C(14)	109.6(6)	C(9)—C(10)—C(11)	118.1(7)
C(3)—N(1′)—C(2′)	127.5(7)	C(10)—C(11)—C(12)	122.1(7)
C(3)—N(1′)—C(7a′)	124.3(7)	C(11)—C(12)—C(13)	122.2(7)
C(2′)—N(1′)—C(7a′)	107.6(6)	C(12)—C(13)—C(14)	116.6(8)
N(1)—C(2)—C(3)	119.3(6)	N(1)—C(14)—C(9)	107.9(6)
N(1)—C(2)—C(8)	109.9(6)	N(1)—C(14)—C(13)	129.2(7)
C(3)—C(2)—C(8)	130.6(6)	C(9)—C(14)—C(13)	122.8(7)
N(1′)—C(3)—C(2)	111.5(6)	C(4)—C(15)—C(16)	110.3(7)
N(1′)—C(3)—C(4)	111.9(6)	C(4)—C(15)—C(18)	110.9(7)
C(2)—C(3)—C(4)	111.9(6)	C(4)—C(15)—C(19)	107.5(7)
C(3)—C(4)—C(5)	108.4(7)	C(16)—C(15)—C(18)	111.0(7)
C(3)—C(4)—C(15)	115.1(6)	C(16)—C(15)—C(19)	108.8(6)
C(5)—C(4)—C(15)	112.3(7)	C(18)—C(15)—C(19)	108.2(7)
C(4)—C(5)—C(6)	116.3(8)	C(7)—C(16)—C(15)	115.8(6)
C(5)—C(6)—C(7)	122.1(7)	N(1′)—C(2′)—C(3′)	110.2(8)
C(6)—C(7)—C(8)	107.9(5)	C(2′)—C(3′)—C(3a′)	108.0(8)
C(6)—C(7)—C(16)	105.8(6)	C(3′)—C(3a′)—C(4′)	135.1(8)
C(6)—C(7)—C(17)	109.9(7)	C(3′)—C(3a′)—C(7a′)	105.6(7)
C(8)—C(7)—C(16)	109.3(6)	C(4′)—C(3a′)—C(7a′)	119.3(8)
C(8)—C(7)—C(17)	114.4(6)	C(3a′)—C(4′)—C(5′)	118.7(8)
C(16)—C(7)—C(17)	109.2(6)	C(4′)—C(5′)—C(6′)	121.1(7)
C(2)—C(8)—C(7)	124.1(6)	C(5′)—C(6′)—C(7′)	121.7(8)
C(2)—C(8)—C(9)	105.3(6)	C(6′)—C(7′)—C(7a′)	116.9(8)
C(7)—C(8)—C(9)	130.5(6)	N(1′)—C(7a′)—C(3a′)	108.6(7)
C(8)—C(9)—C(10)	134.7(7)	N(1′)—C(7a′)—C(7′)	129.2(7)
C(8)—C(9)—C(14)	107.2(7)	C(3a′)—C(7a′)—C(7′)	122.3(7)
C(10)—C(9)—C(14)	118.1(7)	Cl—C(s)—Cl*	110(4)
	45		
C(1)—N(1)—C(15)	106.27(15)	C(8)—C(13)—C(14)	102.7(2)
C(1)—N(1)—C(19)	128.8(2)	C(12)—C(13)—C(14)	115.2(2)
C(15)—N(1)—C(19)	122.2(2)	C(13)—C(14)—C(15)	109.1(2)
C(26)—N(2)—C(33)	109.0(2)	N(1)—C(15)—C(7)	108.68(15)
N(1)—C(1)—C(2)	128.4(2)	N(1)—C(15)—C(14)	136.8(2)
N(1)—C(1)—C(6)	109.7(2)	C(7)—C(15)—C(14)	114.1(2)
C(2)—C(1)—C(6)	121.5(2)	O(1)—C(19)—N(1)	120.2(2)
C(1)—C(2)—C(3)	118.1(2)	O(1)—C(19)—C(20)	121.3(2)
C(2)—C(3)—C(4)	121.1(2)	N(1)—C(19)—C(20)	118.3(2)
C(3)—C(4)—C(5)	120.3(2)	C(19)—C(20)—C(21)	121.3(2)
C(4)—C(5)—C(6)	119.5(2)	C(19)—C(20)—C(25)	118.3(2)
C(1)—C(6)—C(5)	119.4(2)	C(21)—C(20)—C(25)	120.1(3)
C(1)—C(6)—C(7)	108.6(2)	C(20)—C(21)—C(22)	119.1(3)

Can. J. Chem. Downloaded from www.nrcresearchpress.com by 198.100.157.202 on 09/07/12
For personal use only.

TABLE 6 (*concluded*)

Bonds	Angle (deg)	Bonds	Angle (deg)
C(5)—C(6)—C(7)	132.0(2)	C(21)—C(22)—C(23)	120.3(4)
C(6)—C(7)—C(8)	122.5(2)	C(22)—C(23)—C(24)	120.4(3)
C(6)—C(7)—C(15)	99.98(15)	C(23)—C(24)—C(25)	120.5(4)
C(6)—C(7)—C(27)	109.51(15)	C(20)—C(25)—C(24)	119.6(4)
C(8)—C(7)—C(15)	100.03(15)	N(2)—C(26)—C(27)	110.2(2)
C(8)—C(7)—C(27)	111.44(15)	C(7)—C(27)—C(26)	127.4(2)
C(15)—C(7)—C(27)	112.1(2)	C(7)—C(27)—C(28)	126.2(2)
C(7)—C(8)—C(9)	112.5(2)	C(26)—C(27)—C(28)	106.3(2)
C(7)—C(8)—C(13)	102.31(15)	C(27)—C(28)—C(29)	134.7(2)
C(9)—C(8)—C(13)	112.1(2)	C(27)—C(28)—C(33)	106.7(2)
C(8)—C(9)—C(10)	125.3(2)	C(29)—C(28)—C(33)	118.6(2)
C(9)—C(10)—C(11)	121.7(2)	C(28)—C(29)—C(30)	119.1(2)
C(9)—C(10)—C(16)	121.9(2)	C(29)—C(30)—C(31)	120.8(3)
C(11)—C(10)—C(16)	116.4(2)	C(30)—C(31)—C(32)	121.8(2)
C(10)—C(11)—C(12)	113.8(2)	C(31)—C(32)—C(33)	117.5(2)
C(11)—C(12)—C(13)	108.9(2)	N(2)—C(33)—C(28)	107.7(2)
C(11)—C(12)—C(17)	109.9(2)	N(2)—C(33)—C(32)	130.2(2)
C(11)—C(12)—C(18)	109.3(2)	C(28)—C(33)—C(32)	122.1(2)
C(13)—C(12)—C(17)	109.1(2)	O(2)—C(34)—C(35)	120.7(6)
C(13)—C(12)—C(18)	111.0(2)	O(2)—C(34)—C(36)	123.3(6)
C(17)—C(12)—C(18)	108.5(2)	C(35)—C(34)—C(36)	115.8(4)
C(8)—C(13)—C(12)	113.1(2)		

TABLE 7. Intra-annular torsion angles (deg) with standard deviations in parentheses

Atoms	Value (deg)
36	
C(10)—C(2)—C(3)—C(4)	−15.2(6)
C(2)—C(3)—C(4)—C(9)	27.2(5)
C(3)—C(4)—C(9)—C(10)	−29.1(5)
C(4)—C(9)—C(10)—C(2)	21.0(5)
C(3)—C(2)—C(10)—C(9)	−4.0(6)
C(9)—C(4)—C(5)—C(6)	−55.5(5)
C(4)—C(5)—C(6)—C(7)	30.9(6)
C(5)—C(6)—C(7)—C(8)	−6.9(8)
C(6)—C(7)—C(8)—C(9)	5.3(8)
C(7)—C(8)—C(9)—C(4)	−28.8(7)
C(5)—C(4)—C(9)—C(8)	56.7(5)
60	
C(8)—C(2)—C(3)—C(4)	6.9(11)
C(2)—C(3)—C(4)—C(5)	−67.4(8)
C(3)—C(4)—C(5)—C(6)	78.7(9)
C(4)—C(5)—C(6)—C(7)	2.9(12)
C(3)—C(2)—C(8)—C(7)	0.8(12)
C(5)—C(6)—C(7)—C(8)	−71.1(9)
C(6)—C(7)—C(8)—C(2)	49.8(10)
C(8)—C(2)—C(3)—C(4)	6.9(11)
C(2)—C(3)—C(4)—C(15)	59.3(9)
C(3)—C(4)—C(15)—C(16)	−83.9(8)
C(4)—C(15)—C(16)—C(7)	8.5(9)
C(8)—C(7)—C(16)—C(15)	67.0(8)
C(16)—C(7)—C(8)—C(2)	−64.8(9)
C(3)—C(2)—C(8)—C(7)	0.8(12)

TABLE 7 (*concluded*)

Atoms	Value (deg)
C(15)—C(4)—C(5)—C(6)	−49.6(10)
C(4)—C(5)—C(6)—C(7)	2.9(12)
C(5)—C(6)—C(7)—C(16)	45.8(9)
C(6)—C(7)—C(16)—C(15)	−48.9(8)
C(4)—C(15)—C(16)—C7)	8.5(9)
C(5)—C(4)—C(15)—C(16)	40.7(9)
45	
C(15)—N(1)—C(1)—C(6)	−10.8(2)
N(1)—C(1)—C(6)—C(7)	−6.0(2)
C(1)—C(6)—C(7)—C(15)	19.0(2)
C(6)—C(7)—C(15)—N(1)	−25.9(2)
C(1)—N(1)—C(15)—C(7)	23.7(2)
C(15)—C(7)—C(8)—C(13)	−31.9(2)
C(7)—C(8)—C(13)—C(14)	32.1(2)
C(8)—C(13)—C(14)—C(15)	−20.0(2)
C(13)—C(14)—C(15)—C(7)	−1.4(2)
C(8)—C(7)—C(15)—C(14)	21.9(2)
C(13)—C(8)—C(9)—C(10)	−6.9(3)
C(8)—C(9)—C(10)—C(11)	−0.7(3)
C(9)—C(10)—C(11)—C(12)	−21.3(3)
C(10)—C(11)—C(12)—C(13)	48.6(3)
C(11)—C(12)—C(13)—C(8)	−56.8(2)
C(9)—C(8)—C(13)—C(12)	36.1(2)

Can. J. Chem. Downloaded from www.nrcresearchpress.com by 198.100.157.202 on 09/07/12
For personal use only.

^{13}C nuclear magnetic resonance spectra of 3,6-disubstituted pyridazines[1,2]

GOTTFRIED HEINISCH AND WOLFGANG HOLZER[3]

Institute of Pharmaceutical Chemistry, University of Vienna, Währinger Strasse 10, A-1090 Vienna, Austria

Received October 24, 1990

GOTTFRIED HEINISCH and WOLFGANG HOLZER. Can. J. Chem. **69**, 972 (1991).

The ^{13}C nuclear magnetic resonance spectra of 17 3,6-disubstituted pyridazine derivatives have been systematically analyzed. Chemical shifts and various $^{13}C,^{1}H$ coupling constants are reported. Attempts were made to correlate these data with results obtained from semiempirical molecular orbital calculations as well as with substituent electronegativities and Taft's substituent constants σ_I and σ_R^0.

Key words: 3,6-disubstituted pyridazines, ^{13}C NMR spectroscopy, $^{13}C,^{1}H$ spin coupling constants.

GOTTFRIED HEINISCH et WOLFGANG HOLZER. Can. J. Chem. **69**, 972 (1991).

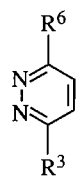
On a fait des analyses systématiques des spectres de résonance magnétique nucléaire du ^{13}C de 17 pyridazines disubstituées en 3 et 6. On décrit les déplacements chimiques des carbones et quelques constantes de couplage entre ^{13}C et ^{1}H. On a essayé de trouver des corrélations entre ces résultats et les calculs semi-empiriques des orbitales moléculaire, les électronegativités des groupes substitués et les constants Taft σ_I et σ_R^0.

Mots clés : pyridazines 3,6-disubstituées, spectroscopie RMN du ^{13}C, constantes de couplage de spin $^{13}C,^{1}H$.

Introduction

Pyridazine derivatives continue to attract considerable attention due to a wide variety of interesting pharmacological activities observed (3). Most of the bioactive compounds so far investigated are characterized by a 3,6-substitution pattern and thus for their synthesis simple 3,6-disubstituted pyridazines of type **2**–**18** usually serve as appropriate starting materials. Many of these compounds were prepared several decades ago and only in some cases are there reports on selected ^{13}C nmr data (4–7), which, however, were obtained using different solvents and acquisition parameters. So far, a systematic investigation of ^{13}C chemical shifts and $^{13}C,^{1}H$ coupling constants of 3,6-disubstituted pyridazines has not been performed.

Here we report on the analysis of the ^{13}C nmr spectra of 17 simple 3,6-disubstitution products (**2**–**18**). Moreover, we attempt to correlate the data obtained with results derived from MO calculations (AM1) as well as with substituent electronegativities and Taft's substituent constants σ_I and σ_R^0.



Compound no.	R^3	R^6	Compound no.	R^3	R^6
1	H	H	**10**	Cl	Me
2	Cl	Cl	**11**	Cl	COOH
3	Br	Br	**12**	Cl	COOEt
4	I	I	**13**	Br	Me
5	OMe	OMe	**14**	Me	CN
6	C≡CPh	C≡CPh	**15**	Me	COMe
7	COPh	COPh	**16**	OH	OH
8	Cl	I	**17**	Cl	OH
9	Cl	OMe	**18**	OH	Me

[1]Counts as 53rd communication on pyridazines; for part 52 see ref. 1.

[2]Presented as part of a communication at the 2nd International Symposium on the Chemistry and Pharmacology of Pyridazines, Vienna, Austria, July 1990 (see also ref. 2).

[3]Author to whom correspondence may be addressed.

Experimental

General

All nmr spectra were recorded in 5 mm sample tubes from DMSO-d_6 solutions (approximately 1 M) at 30°C on a Bruker AM 400 WB (operating frequency for ^{1}H: 400.14 MHz, for ^{13}C: 100.63 MHz) and (or) a Bruker AC 80 spectrometer (operating frequency for ^{1}H: 80.13 MHz, for ^{13}C: 20.15 MHz), both equipped with Aspect 3000 computers and standard software. The centre of the solvent peak was used as an internal standard, which was related to tetramethylsilane with 2.49 ppm for ^{1}H and 39.50 ppm for ^{13}C, respectively. ^{13}C chemical shifts were determined using the *J*-modulated spin-echo technique (8) with a decoupler switch-off delay of 6.9 ms for an average $^{1}J(^{13}C,^{1}H)$ coupling constant of 145 Hz and a relaxation delay of 6 s. According to the acquisition parameters used, the digital resolution here was 0.9 Hz/data point. ^{1}H-coupled ^{13}C nmr spectra with digital resolutions from 0.1 to 0.2 Hz/data point (acquisition times 5–10 s, spectral window and number of data points adjusted to obtain the desired digital resolution, pulse angle 51°, relaxation delay 6 s) were obtained using the gated decoupling mode. Heteronuclear decoupling experiments were carried out with single frequency CW irradiation of the appropriate proton resonance lines. ^{1}H chemical shifts and H,H coupling constants (needed for spin simulation) were derived from high-precision proton nmr spectra (digital resolution 0.1 Hz/data point) using exactly the same (concentrated) samples as for the acquisition of the coupled carbon spectra. Iterative analysis of all ^{1}H and ^{13}C nmr spectra was carried out with Bruker's PANIC spin-simulation program (a version of the well-known LAOCOON program); rms errors smaller than 0.05 Hz were obtained.

The ir spectra were recorded on a Jasco IRA-1 spectrophotometer. Mass spectra were obtained on a Varian MAT 311A instrument (70 eV), glc/ms analyses were performed on a Hewlett Packard 5890A/5970B-MSD (70 eV).

Melting points were determined with a Reichert–Kofler hot-stage microscope and are uncorrected.

MO calculations were carried out using the semiempirical AM1 method (9) as implemented in the AMPAC program package (10). All geometries were completely optimized without making any assumptions.

Materials

Pyridazine (**1**), 3,6-dichloropyridazine (**2**), 3-chloro-6-methoxypyridazine (**9**), 3,6-dihydroxypyridazine (**16**), 3-chloro-6-hydroxypyridazine = 6-chloro-3(2*H*)-pyridazinone (**17**), and 3-hydroxy-6-methylpyridazine = 6-methyl-3(2*H*)-pyridazinone (**18**) are commercially available (Aldrich). The following compounds were prepared according to reported procedures: **3** (11), **4** (12), **7**,[4] **10** (13), **11** (14), **12** (15), **13** (16), **14** (17), **15** (18).

[4]G. Heinisch and W. Holzer, manuscript in preparation.

Printed in Canada / Imprimé au Canada

Can. J. Chem. Downloaded from www.nrcresearchpress.com by 198.100.157.202 on 09/07/12
For personal use only.

Can. J. Chem. Downloaded from www.nrcresearchpress.com by 198.100.157.202 on 09/07/12
For personal use only.

TABLE 1. ^{13}C chemical shifts of 3,6-disubstituted pyridazines (DMSO-d_6 solutions)

Compound no.	R^3	R^6	^{13}C chemical shifts (δ, ppm) C-3	C-4	C-5	C-6	Other C	References
1	H	H	151.75 (0.00)[a]	126.66 (0.00)	126.66 (0.00)	151.75 (0.00)	—	19, 20, 21, 4, 5
2	Cl	Cl	155.73 (3.98)	131.56 (4.90)	131.56 (4.90)	155.73 (3.98)	—	4, 5
3	Br	Br	147.78 (−3.97)	134.33 (7.67)	134.33 (7.67)	147.78 (−3.97)	—	—
4	I	I	126.55 (−25.20)	138.13 (11.47)	138.13 (11.47)	126.55 (−25.20)	—	—
5	OMe	OMe	161.64 (9.89)	121.21 (−5.45)	121.21 (−5.45)	161.64 (9.89)	53.90 (OCH_3)	5
6	C≡CPh	C≡CPh	145.26 (−6.49)	129.64 (2.98)	129.64 (2.98)	145.26 (−6.49)	131.86 (Ph-2,6), 130.11 (Ph-4), 128.92 (Ph-3,5), 120.53 (Ph-1), 94.46 and 86.03 (—C≡C—)	—
7	COPh	COPh	158.08 (6.33)	128.60 (1.94)	128.60 (1.94)	158.08 (6.33)	191.55 (CO), 135.02 (Ph-1), 133.84 (Ph-4), 130.91 (Ph-2,6), 128.41 (Ph-3,5)	—
8	Cl	I	156.37 (4.62)	129.78 (3.12)	139.84 (13.18)	125.39 (−26.36)	—	—
9	Cl	OMe	150.54 (−1.21)	131.28 (4.62)	120.51 (−6.15)	164.36 (12.61)	54.68 (OCH_3)	5
10	Cl	Me	154.16 (2.41)	128.12 (1.46)	130.21 (3.55)	159.70 (7.95)	20.85 (CH_3)	—
11	Cl	COOH	158.21 (6.46)	129.48 (2.82)	130.53 (3.87)	151.55 (−0.20)	164.16 (CO)	—
12	Cl	COOEt	158.46 (6.71)	129.64 (2.98)	130.63 (3.97)	151.00 (−0.75)	162.80 (CO), 62.10 (OCH_2), 13.90 (CH_3)	—
13	Br	Me	145.82 (−5.93)	131.33 (5.27)	129.96 (3.30)	159.86 (8.11)	20.91 (CH_3)	—
14	Me	CN	162.51 (10.76)	127.48 (0.82)	130.87 (4.21)	137.31 (−14.44)	116.17 (CN), 21.98 (CH_3)	—
15	Me	COMe	162.60 (10.85)	127.85 (1.19)	124.13 (−2.53)	153.98 (2.23)	197.98 (CO), 25.56 ($COCH_3$), 21.79 (CH_3)	—
16[b]	OH	OH	156.49 (4.74)	130.53 (3.87)	130.53 (3.87)	156.49 (4.74)	—	6
17[b]	Cl	OH	137.44 (−14.31)	134.67 (8.01)	132.57 (5.91)	159.69 (7.94)	—	—
18[b]	OH	Me	160.36 (8.61)	129.53 (2.87)	134.76 (8.10)	144.29 (−7.46)	20.03 (CH_3)	7

[a]Values in parentheses represent differences in chemical shifts compared to the relevant carbon atom in pyridazine.
[b]Compounds **16–18** show a dynamic behaviour (tautomerism with oxo forms, see references) and care should be taken when comparing their data with those of compounds **1–15**.

TABLE 2. ^{1}H chemical shifts of 3,6-disubstituted pyridazines (DMSO-d_6 solutions)

Compound no.	R^3	R^6	^{1}H chemical shifts (δ, ppm) H-4	H-5	Other H	References
1	H	H	7.68	7.68	9.23 (H-3,6)	25–27
2	Cl	Cl	7.98	7.98	—	25
3	Br	Br	7.99	7.99	—	—
4	I	I	7.83	7.83	—	—
5	OMe	OMe	7.14	7.14	3.92 (OCH_3)	28
6	C≡CPh	C≡CPh	8.00	8.00	7.70–7.68 (Ph-2,6), 7.55–7.48 (Ph-3,4,5)	—
7	COPh	COPh	8.42	8.42	8.17–8.02 (Ph-2,6), 7.86–7.48 (Ph-3,4,5)	—
8	Cl	I	8.18	7.65	—	—
9	Cl	OMe	7.71	7.26	3.98 (OCH_3)	25
10	Cl	Me	7.74	7.64	2.57 (CH_3)	25
11	Cl	COOH	8.01	8.17	11.95 (OH)	—
12	Cl	COOEt	8.10	8.23	4.41 (CH_2), 1.35 (CH_3)	—
13	Br	Me	7.88	7.55	2.57 (CH_3)	—
14	Me	CN	7.82	8.17	2.71 (CH_3)	—
15	Me	COMe	7.70	7.93	2.70 (CH_3), 2.67 ($COCH_3$)	—
16	OH	OH	6.91	6.91	11.41 (OH)	6, 28–30
17	Cl	OH	7.42	6.93	13.09 (OH)	—
18	OH	Me	6.77	7.25	11.50 (OH), 2.17 (CH_3)	31

The ^{1}H and ^{13}C nmr data for 3-chloro-6-iodopyridazine (**8**) (ms (*m/z*, %): 240, 242 (M^+, 100, 33), 152 (10), 127 (16), 85 (33); high-resolution ms: calcd. for M^+ (C_4H_2ClI): 239.895; found: 239.8947 ± 0.0024) were acquired from a sample contaminated with minor amounts of **2** (according to glc/ms analysis). This mixture was obtained following the procedure for the synthesis of 3,6-diiodopyridazine as given in ref. 12 (treatment of 3,6-dichloropyridazine (**2**) with NaI/HI in dry acetone) and subsequent column chromatography (silica gel, eluent: dichloromethane).

3,6-Di(phenylethinyl)pyridazine (6)

To a mixture of 500 mg (1.51 mmol) of 3,6-diiodopyridazine (**4**) (12) and 329 mg (3.22 mmol) of phenylacetylene in 10 mL of dry triethylamine, dimethyl sulfoxide was added dropwise until a clear solution was obtained. Then 22 mg (31 μmol) of bis(triphenylphosphine)palladium(II)chloride and 4 mg of copper(I) iodide were added and the mixture was stirred under Ar for 2 days. After removal of the solvents under reduced pressure, the residue was extracted several times with dichloromethane. The combined organic layers were washed with water, dried over anhydrous sodium sulfate, and evaporated. The remaining brown solid was subjected to column chromatography (silica gel, eluent: dichloromethane). Recrystallization from ethanol afforded 258 mg (61%) of straw-yellow crystals, mp 180–186°C (dec.); ir(KBr): 2220 (C≡C) cm^{-1}; ms (*m/z*, %): 280 (M^+, 37), 252 (26), 127 (11), 126 (100); high-resolution ms: calcd. for M^+ ($C_{20}H_{12}N_2$): 280.100; found: 280.1008 ± 0.003. For ^{1}H and ^{13}C nmr data see Tables 1, 2, and 4. Anal. calcd. for $C_{20}H_{12}N_2 \cdot 0.2H_2O$: C 84.60, H 4.40, N 9.87; found: C 84.70, H 4.56, N 10.14.

Results and discussion

^{13}C chemical shifts

In Table 1, chemical shift data of the parent pyridazine (**1**) and of the 3,6-disubstituted pyridazines **2**–**18** are given. The spectra were recorded from DMSO-d_6 solutions in order to achieve sufficient solubility for all compounds. Assignments of the chemical shifts of the ring carbon atoms were made using the *J*-modulated spin-echo sequence (8) to separate quaternary carbon atoms from those with attached protons.

Based on the chemical shifts for C-3 (C-6) in symmetrically disubstituted pyridazines **2**, **3**, **4**, **5**, and **16**, discrimination between C-3 and C-6 resonances of unsymmetrical pyridazine derivatives **8**–**13** and **17** could be achieved unambiguously. With compounds **14** and **18** the resonances of those carbon atoms bearing the methyl substituent could be assigned simply by taking into account the ^2J coupling between the side-chain protons and the ring carbon atom (see Table 4). A comparison of the chemical shifts (in DMSO-d_6) of the C-3 atoms in 3-methylpyridazine (159.69 ppm) and methyl 3-pyridazinyl ketone (155.55 ppm)[4] enabled us to also assign the resonances of C-3 and C-6 in compound **15**.

For most of the compounds under investigation in the present study, the ^{1}H chemical shifts were reported previously (compare refs. in Table 2; for reviews see refs. 22–24). The proton nmr data obtained using the same solutions as employed for recording the ^{13}C nmr spectra are summarized in Table 2. Selective heteronuclear decoupling experiments irradiating unambiguously assigned ^{1}H nmr lines finally enabled us to distinguish between the C-4 and C-5 resonances in all unsymmetrically 3,6-disubstituted compounds under investigation. In addition, with compounds **10**, **13**–**15**, and **18** bearing a methyl substituent, the assignments made could be confirmed on the basis of the $^3J(C,CH_3)$ coupling constant (see Table 4).

The observed substituent effects (Table 1) were found to follow general trends as known from the benzene or especially from the 2-pyridine series (32–34). Only with compounds **16**–**18** is the situation complicated due to hydroxypyridazine–pyridazinone tautomerism (6, 29, 31, 35). As found with compounds **10**–**12**, **14**, and **15**, the chemical shifts calculated by assuming the additivity of substituent effects (32) are in very good agreement with those observed. Ethyl 6-chloro-3-pyridazinecarboxylate (**12**) may serve as an illustrative example (see Fig. 1).

Since Spiesecke and Schneider (36), in 1961, reported a linear correlation between ^{13}C chemical shifts and local π-electronic densities for monocyclic $(4n + 2)$ π electron systems, the applicability of this relationship has been intensively investigated. Correlations of total charge densities (obtained from semiempirical MO calculations) and ^{13}C chemical shift values have also been attempted in the azine series (20, 37–42). Although in some cases close correlations were obtained, more recent reports (43) indicate that the results depend highly on the

Can. J. Chem. Downloaded from www.nrcresearchpress.com by 198.100.157.202 on 09/07/12
For personal use only.

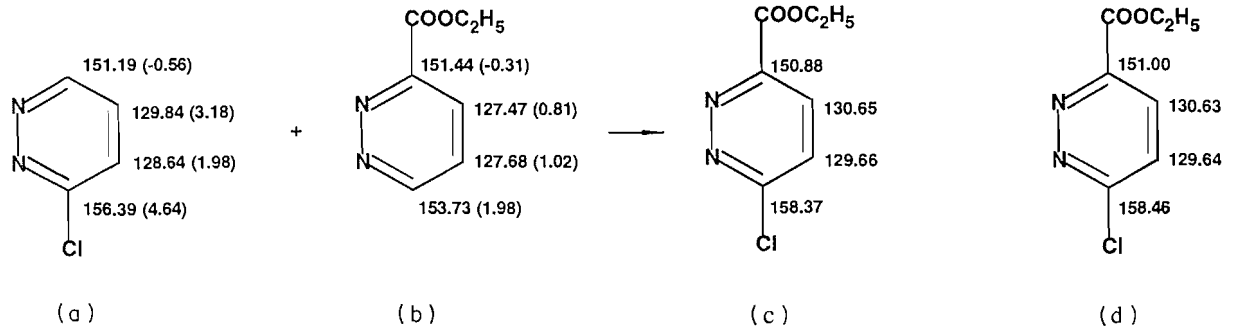


FIG. 1. Additivity of substituent effects in ethyl 6-chloro-3-pyridazinecarboxylate (**12**). (a) ^{13}C chemical shifts (substituent chemical shifts, SCS) of 3-chloropyridazine in DMSO-d_6.[4] (b) ^{13}C chemical shifts (substituent chemical shifts, SCS) of ethyl 3-pyridazinecarboxylate in DMSO-d_6.[4] (c) Calculated ^{13}C chemical shifts for **12** obtained after adding the SCS values of (a) and (b) to the chemical shift values of pyridazine. (d) Observed chemical shifts of **12**.

TABLE 3. Total charge densities ($\sigma + \pi$) of compounds **1–5**, **8–10**, and **13** calculated by the AM1 method

Compound no.	Pyridazine carbon atoms			
	C-3	C-4	C-5	C-6
1	4.1399	4.1359	4.1359	4.1399
2	4.0862	4.1201	4.1201	4.0862
3	4.1772	4.1082	4.1082	4.1772
4	4.2674	4.1044	4.1044	4.2674
5	3.9724	4.1258	4.1258	3.9724
8	4.0685	4.1341	4.0907	4.2857
9	4.1216	4.0964	4.1521	3.9372
10	4.0920	4.1237	4.1339	4.0763
13	4.1948	4.1024	4.1432	4.0639

MO method used. With compounds **1–5**, **8–10**, and **13**, an attempt to correlate the chemical shifts of the pyridazine carbon atoms with total charge densities (Table 3) obtained from AM1 calculations (9) met with a poor result (correlation coefficient when all carbon atoms are taken into consideration: −0.6120, slope of the correlation line: −118.67 ppm/electron).

Coupling constants

The coupling constants of the parent pyridazine and of 3,6-disubstituted derivatives **2–18** are summarized in Table 4.

All $^{13}C,^{1}H$ coupling constants follow from spin simulations (as mentioned in the experimental part) using X-approximation. Couplings over one and three bonds were assumed to be positive. In a few selected cases relative signs of coupling constants were determined via SPT or INDOR experiments. With the symmetrically substituted pyridazines **2–7** the vicinal H-4,H-5 coupling constants were derived from the ^{13}C satellite spectra. In these compounds the resonances of C-3 (C-6) were treated as parts of AA'X spin systems (X = ^{13}C), whereas the C-4 (C-5) lines were considered as parts of ABX systems due to a ^{13}C isotope effect (ca. 0.9 Hz upfield shift at 400 MHz spectrometer frequency) on the proton directly attached to the carbon-13.

In all unsymmetrically substituted compounds the carbon resonance lines were analyzed as parts of separate ABX three-spin systems or, in cases where additional couplings to methyl protons were observed, as ABY_3X systems (X = ^{13}C).

$^{1}J(^{13}C,^{1}H)$

The values of the one-bond carbon-proton coupling constants for C-4 and C-5 range from 165 to 180 Hz. A two-parameter correlation btween $^{1}J(^{13}C,^{1}H)$ and Taft's substituent constants

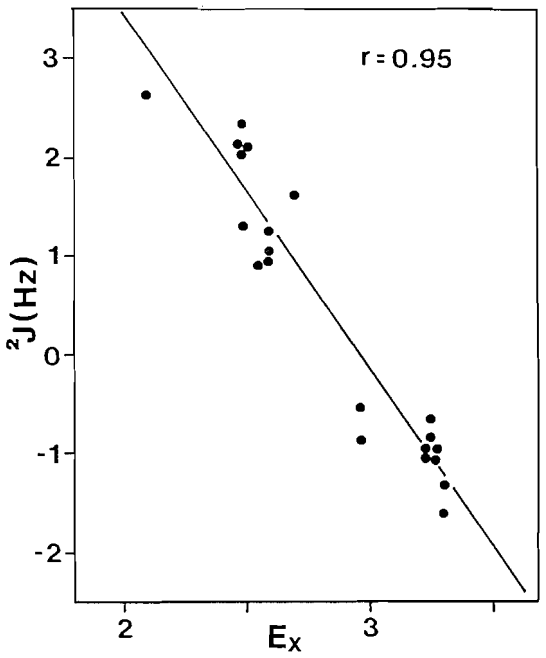


FIG. 2. Dependence of the geminal coupling constants C-3,H-4 and C-6,H-5 on the electronegativity E_x[5] of the substituents attached to the coupled carbon atom in pyridazines **1–5**, **8–15**.

σ_I and σ_R^0, as successfully applied in the benzene series (44), was attempted with symmetrical pyridazines **1–5**, **7**, and **16**, leading to the equation $^{1}J(^{13}C,^{1}H) = 168.40 + 28.44\sigma_I + 13.58\sigma_R^0$ and a satisfactory correlation ($r = 0.96$); values for σ_I and σ_R^0 were taken from refs. 45 and 46.

$^{2}J(^{13}C,^{1}H)$

The two-bond coupling constants C-3,H-4 or C-6,H-5, respectively, in the pyridazine derivatives studied have values ranging from −1.9 Hz to 2.7 Hz. It is well documented in the literature (refs. 32, pp. 470–472, and 44) that in benzoid compounds or heterocyclic aromatic systems $^{2}J(C,H)$ of the substituted carbon atom becomes more positive when the electronegativity of the substituent decreases. This trend is also observed with pyridazines **1–5** and **8–15** as shown in Fig. 2. As anticipated, the geminal coupling constants C-4,H-5 and C-5,H-4

[5] E_x values taken from refs. 47–49 (H: 2.10, Cl: 3.25, Br: 2.96, I: 2.60, OMe: 3.31, Me: 2.50, COOH: 2.60, COOEt: 2.55, CN: 2.50, COMe: 2.70).

Can. J. Chem. Downloaded from www.nrcresearchpress.com by 198.100.157.202 on 09/07/12
For personal use only.

Can. J. Chem. Downloaded from www.nrcresearchpress.com by 198.100.157.202 on 09/07/12
For personal use only.

TABLE 4. ^{1}H,^{1}H and ^{13}C,^{1}H spin coupling constants in 3,6-disubstituted pyridazines (DMSO-d_6 solutions)

Compound no.	R^3	R^6	Spin coupling constants (Hz)										References
			H4,H5	C3,H4	C3,H5	C4,H4	C4,H5	C5,H5	C5,H4	C6,H5	C6,H4	Other ^{13}C,^{1}H coupling constants	
1	H	H	8.29	2.65[a]	5.97[a]	169.67	0.02	169.67	0.02	2.65	5.97	C3,H3: 182.45; C3,H6: −1.52; C4,H3: 6.52; C4,H6: 5.24	5, 19, 21
2	Cl	Cl	9.02[b]	−0.99	8.71	179.86	0.10	179.86	0.10	−0.99	8.71	—	5
3	Br	Br	8.97[b]	−0.47	8.58	180.26	0.05	180.26	0.05	−0.47	8.58	—	—
4	I	I	8.77[b]	1.25	7.16	178.18[c]	0.43[c]	178.18[c]	0.43[c]	1.25	7.16	—	—
5	OMe	OMe	9.20[b]	−1.61	8.67	170.91	−0.35	170.91	−0.35	−1.61	8.67	OCH_3: 146.19; C3,OCH_3: 3.53	5
6	C≡CPh	C≡CPh	8.79[b]	2.32	6.18	174.41[c]	0.44[c]	174.41[c]	0.44[c]	2.32	6.18	[d]	—
7	COPh	COPh	8.65[b]	1.43	6.06	174.88[c]	0.43[c]	174.88[c]	0.43[c]	1.43	6.06	[d]	—
8	Cl	I	8.90	−1.03	8.77	179.09	0.25[c]	178.79[c]	−0.10	1.05	7.58	—	—
9	Cl	OMe	9.23	−0.61	9.04	176.63	−0.15	173.93	−0.15	−1.29	8.16	OCH_3: 147.07; C6,OCH_3: 3.50	5
10	Cl	Me	8.82	−1.00	8.99	176.50[c]	0.57[c]	170.76	−0.34	2.12	5.99	CH_3: 128.47; C3,CH_3: 0.77[e]; C5,CH_3: 3.72; C6,CH_3: 6.55[e]	—
11	Cl	COOH	8.87	−0.84	8.87	179.41	0.30	175.47	−0.17	0.95	6.00	[d]	—
12	Cl	COOEt	8.90	−0.83	8.76	179.81[c]	0.70[c]	175.84	0.05	0.87	6.69	—	—
13	Br	Me	8.80	−0.89	8.81	177.12	0.46	170.79[c]	−0.32[c]	2.10	6.15	CH_3: 128.47; C5,CH_3: 3.71; C6,CH_3: 6.45; CH_3,H5: 2.08	—
14	Me	CN	8.66[f]	2.11	5.79	172.77	−0.27	176.11	0.69	1.30	7.23	C3,CH_3: 6.55[e]; C4,CH_3: 3.86; C6,CH_3: 0.78[e]; CN,H5: 3.14	—
15	Me	COMe	8.62[g]	2.40	6.13	169.89	0.13	171.30	0.32	1.66	5.83	C3,3-CH_3: 6.48[e]; C4,3-CH_3: 3.78	—
16[h]	OH	OH	9.81[a]	[d]	[d]	169.13[c]	0.57[c]	169.13[c]	0.57[c]	[d]	[d]	—	—
17[h]	Cl	OH	9.85	−0.18	11.98	174.76	0.15	173.30	−1.00	−1.91	8.71	—	—
18[h]	OH	Me	9.65[i]	−1.65	8.83	169.86	0.22	165.26	−0.12	2.50	7.94	CH_3: 128.13; C6,CH_3: 6.82[e]; C5,CH_3: 3.54	7

[a]Assignments of ^2J(C-3,H-4) and ^3J(C-3,H-5) as given in ref. 21 have to be revised (see footnote 4).
[b]Obtained from the ^{13}C satellite spectrum.
[c]Because of collapsing lines the accuracy of the spin simulation is somewhat reduced.
[d]Not determined unequivocally.
[e]Signs not determined.
[f]^4J(H4,CH_3): 0.50[e] Hz.
[g]^4J(H4,CH_3): 0.44[e] Hz; ^5J(H5, $COCH_3$): 0.35[e] Hz.
[h]Compare footnote *b* in Table 1.
[i]^4J(H4,OH): 0.33[e] Hz.

(ranging from −1.0 Hz to 0.7 Hz) are only slightly affected by the electronegativity of a substituent attached to C-3 or C-6.

$^3J(^{13}C,^1H)$

The three-bond coupling constants C-3,H-5 and C-6,H-4 have values of 5.4–12.0 Hz and again there is a marked dependence on the electronegativity of the substituent attached to the coupled carbon atom. As expected, a parallel trend is observed with the vicinal coupling constants H-4,H-5 in 3,6-disubstituted pyridazines **2**–**18** (compare Table 4).

Acknowledgements

The authors thank Mr. T. Huber for preparing compounds **7** and **17**. Our thanks are also due to the "Fonds zur Förderung der Wissenschaftlichen Forschung" for providing technical equipment (projects P6260C and P6537C).

1. N. Haider, G. Heinisch, and G. Kemetmüller. J. Heterocycl. Chem. **27**, 1645 (1990).
2. G. Heinisch and W. Holzer. Sci. Pharm. **58**, 213 (1990).
3. G. Heinisch and H. Frank. Prog. Med. Chem. **27**, 1 (1990).
4. T. Tsujimoto, T. Nomura, M. Iifuru, and Y. Sasaki. Chem. Pharm. Bull. **27**, 1169 (1979).
5. D. E. Klinge, H. C. van der Plas, and A. van Veldhuizen. Recl. Trav. Chim. Pays-Bas, **95**, 21 (1976).
6. H. P. Fritz, F. H. Köhler, and B. Lippert. Chem. Ber. **106**, 2918 (1973).
7. H. McNab. J. Chem. Soc. Perkin Trans. 1, 1203 (1983).
8. C. Le Cocq and J.-Y. Lallemand. J. Chem. Soc. Chem. Commun. 150 (1981).
9. M. J. S. Dewar, E. G. Zoebisch, E. F. Healy, and J. J. P. Stewart. J. Am. Chem. Soc. **107**, 3902 (1985).
10. M. J. S. Dewar. Quantum Chemistry Program Exchange (QCPE); Program No. 506 (AMPAC).
11. E. A. Steck, R. P. Brundage, and L. T. Fletcher. J. Am. Chem. Soc. **76**, 3225 (1954).
12. P. Coad, R. A. Coad, S. Clough, J. Hyepock, R. Salisbury, and C. Wilkins. J. Org. Chem. **28**, 218 (1963).
13. W. G. Overend and L. F. Wiggins. J. Chem. Soc. 239 (1947).
14. G. Rosseels. Bull. Soc. Chim. Belg. **75**, 5 (1966).
15. Chimie et atomistique. Brit. Pat. 856,409 (Dec. 14, 1960); Chem. Abstr. **55**, 13459a (1961).
16. C. Grundmann. Chem. Ber. **81**, 1 (1948).
17. W. Dostal and G. Heinisch. Heterocycles, **24**, 793 (1986).
18. J. Easmon. Ph.D. Thesis, University of Vienna, Vienna, Austria (1989).
19. P. C. Lauterbur. J. Chem. Phys. **43**, 360 (1965).
20. R. J. Pugmire and D. M. Grant. J. Am. Chem. Soc. **90**, 697 (1968).
21. F. J. Weigert, J. Husar, and J. D. Roberts. J. Org. Chem. **38**, 1313 (1973).
22. A. G. Lenhert and R. N. Castle. Chem. Heterocycl. Compd. **28**, 1 (1973).
23. M. Tisler and B. Stanovnik. Adv. Heterocycl. Chem. **24**, 363 (1979).
24. M. Tisler and B. Stanovnik. *In* Comprehensive heterocyclic chemistry. Vol. 3. *Edited by* A. R. Katritzky and C. W. Rees. Pergamon Press, Oxford. 1984. p. 1.
25. K. Tori and M. Ogata. Chem. Pharm. Bull. **12**, 272 (1964).
26. J. A. Elvidge and P. D. Ralph. J. Chem. Soc. B, 249 (1966).
27. V. M. S. Gil and A. J. L. Pinto. Mol. Phys. **16**, 623 (1969).
28. A. R. Katritzky and I. Pojarlieff. J. Chem. Soc. B, 873 (1968).
29. O. Ohashi, M. Mashima, and M. Kubo. Can. J. Chem. **42**, 970 (1964).
30. H. Rubinstein, J. E. Skarbek, and H. Feuer. J. Org. Chem. **36**, 3372 (1971).
31. G. B. Barlin and M. D. Fenn. Aust. J. Chem. **32**, 2297 (1979).
32. H.-O. Kalinowski, S. Berger, and S. Braun. ^{13}C-NMR-Spektroskopie. Georg Thieme Verlag, Stuttgart/New York. 1984. pp. 283–370.
33. E. Breitmaier and W. Voelter. Carbon-13 NMR spectroscopy. 3rd ed. VCH, Weinheim/New York. 1987. pp. 254–293.
34. D. F. Ewing. Org. Magn. Reson. **12**, 499 (1979).
35. A. R. Katritzky and A. J. Waring. J. Chem. Soc. 1523 (1964).
36. H. Spieseke and W. G. Schneider. Tetrahedron Lett. 468 (1961).
37. R. J. Pugmire, D. M. Grant, M. J. Robins, and R. K. Robins. J. Am. Chem. Soc. **91**, 6381 (1969).
38. T. Tokuhiro and G. Fraenkel. J. Am. Chem. Soc. **91**, 5005 (1969).
39. R. J. Pugmire, M. J. Robins, D. M. Grant, and R. K. Robins. J. Am. Chem. Soc. **93**, 1887 (1971).
40. T. Tsujimoto, C. Kobayashi, T. Nomura, M. Iifuru, and Y. Sasaki. Chem. Pharm. Bull. **27**, 2105 (1979).
41. G. W. H. Cheeseman, C. J. Turner, and D. J. Brown. Org. Magn. Reson. **12**, 212 (1979).
42. M. Matsuo, S. Matsumoto, T. Kurihara, Y. Akita, T. Watanabe, and A. Ohta. Org. Magn. Reson. **13**, 172 (1980).
43. H. Baumann and H. Olsen. Helv. Chim. Acta, **63**, 2202 (1980).
44. L. Ernst, V. Wray, V. A. Chertkov, and N. M. Sergeyev. J. Magn. Reson. **25**, 123 (1977).
45. J. Bromilow, R. T. C. Brownlee, V. O. Lopez, and R. W. Taft. J. Org. Chem. **44**, 4766 (1979).
46. O. Exner. *In* Correlation analysis in chemistry: recent advances. *Edited by* J. Shorter and N. B. Chapman. Plenum Press, New York. 1978. p. 439.
47. P. Laszlo and P. von Rague-Schleyer. J. Am. Chem. Soc. **85**, 2709 (1963).
48. K. L. Williamson, C. A. Lanford, and C. A. Nicholson. J. Am. Chem. Soc. **86**, 762 (1964).
49. T. Schaefer and H. M. Hutton. Can. J. Chem. **45**, 3153 (1967).

Can. J. Chem. Downloaded from www.nrcresearchpress.com by 198.100.157.202 on 09/07/12
For personal use only.

Reactions of the super-electrophile, 2-(2′,4′-dinitrophenyl)-4,6-dinitrobenzotriazole 1-oxide, with methoxide and *tert*-butoxide: basicity and steric hindrance as factors in σ-complex formation versus nucleophilic displacement[1,2]

JULIAN M. DUST[3]
Department of Chemistry, Sir Wilfred Grenfell College, Corner Brook, Nfld., Canada A2H 6P9
AND
ERWIN BUNCEL[3]
Department of Chemistry, Queen's University, Kingston, Ont., Canada K7L 3N6

Received July 4, 1990[4]

JULIAN M. DUST and ERWIN BUNCEL. Can. J. Chem. **69**, 978 (1991).

The course of the reactions of methoxide and *tert*-butoxide with 2-(2′,4′-dinitrophenyl)-4,6-dinitrobenzotriazole 1-oxide (**4**) clearly shows that the C-7 electrophilic site is significantly more reactive than the C-1′ site of the substrate. The reaction pathways of these alkoxides, which differ in basicity (as a measure of nucleophilicity) and steric bulk, were followed by 400 MHz ^{1}H nuclear magnetic resonance spectroscopy. While both alkoxides lead to immediate formation of the respective C-7 anionic σ-adducts, a greater percentage of C-7 adduct formation occurs with methoxide as attacking nucleophile. Reaction with excess alkoxide results in attack at C-1′ being observed, as well. This leads to formation of metastable C-1′ σ-adducts, whose rapid decomposition results in formation of 2,4-dinitrophenyl ethers and the dinitrobenzotriazole 1-oxyanion in an overall nucleophilic displacement reaction. Under these excess conditions, methoxide also causes a faster rate of displacement than does *tert*-butoxide as nucleophile. These results are discussed on the basis of the basicity of the nucleophiles, the relative electrophilicity of the positions in the substrate (C-7 versus C-1′), the steric hindrance involved in attack and in the resultant C-7 and C-1′ complexes, and in terms of an activation energy/reaction coordinate profile comparing the pathways for attack at the two electrophilic sites.

Key words: anionic σ-complexes, super-electrophiles, aromatic nucleophilic substitution (S_N Ar).

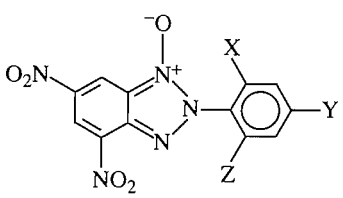
JULIAN M. DUST et ERWIN BUNCEL. Can. J. Chem. **69**, 978 (1991).

La nature des produits des réactions des ions méthylate et *tert*-butylate avec le 1-oxyde du 2-(2′,4′-dinitrophényl)-4,6-dinitrobenzotriazole (**4**) montre clairement que le site électrophile C-7 de ce substrate est beaucoup plus réactif que le site C-1′. Les voies réactionnelles de ces alcoolates, qui diffèrent tant par leur basicité (qui est une mesure de leur caractère nucléophile) que par leur encombrement stérique, ont été examinées par le biais de la résonance magnétique nucléaire du ^{1}H à 400 MHz. Alors que les deux alcoolates conduisent à la formation d'intermédiaires des adduits-σ anioniques en C-7, le pourcentage de formation d'adduit en C-7 est plus grand lorsque le méthylate agit comme nucléophile. Les réactions avec un excès d'alcoolate conduisent aussi à une attaque en position C-1′. Ceci donne lieu à la formation d'adduits-σ C-1′ métastables dont la décomposition rapide conduit à la formation d'éthers du 2,4-dinitrophénol et du 1-oxyanion du dinitrobenzotriazole provenant d'une réaction globale de substitution nucléophile. Lorsque les bases sont en excès, la vitesse de réaction du méthylate est aussi plus rapide que celle observés avec le *tert*-butylate. On discute de ces résultats en fonction de la basicité des nucléophiles, du caractère électrophile relatif des diverses positions du substrat (C-7 vs. C-1′), de l'empêchement stérique impliqué dans l'attaque et dans les complexes C-7 et C-1′ qui en résultent ainsi qu'en fonction d'un profil de l'énergie d'activation/coordonnées de la réaction permettant de comparer les diverses voies réactionnelles sur les deux sites électrophiles.

Mots clés : complexes-σ anioniques, super-électrophiles, substitution aromatique nucléophile (S_N Ar).

[Traduit par la rédaction]

We have been engaged in the study of the novel anionic σ-complexes (1) formed through the reactions of nucleophiles with the super-electrophile 2-nitroaryl-4,6-dinitrobenzotriazole 1-oxide series, **1**, **4**, and **5**, containing one or more electron-withdrawing NO_2 groups in the *N*-aryl moiety (2–5).

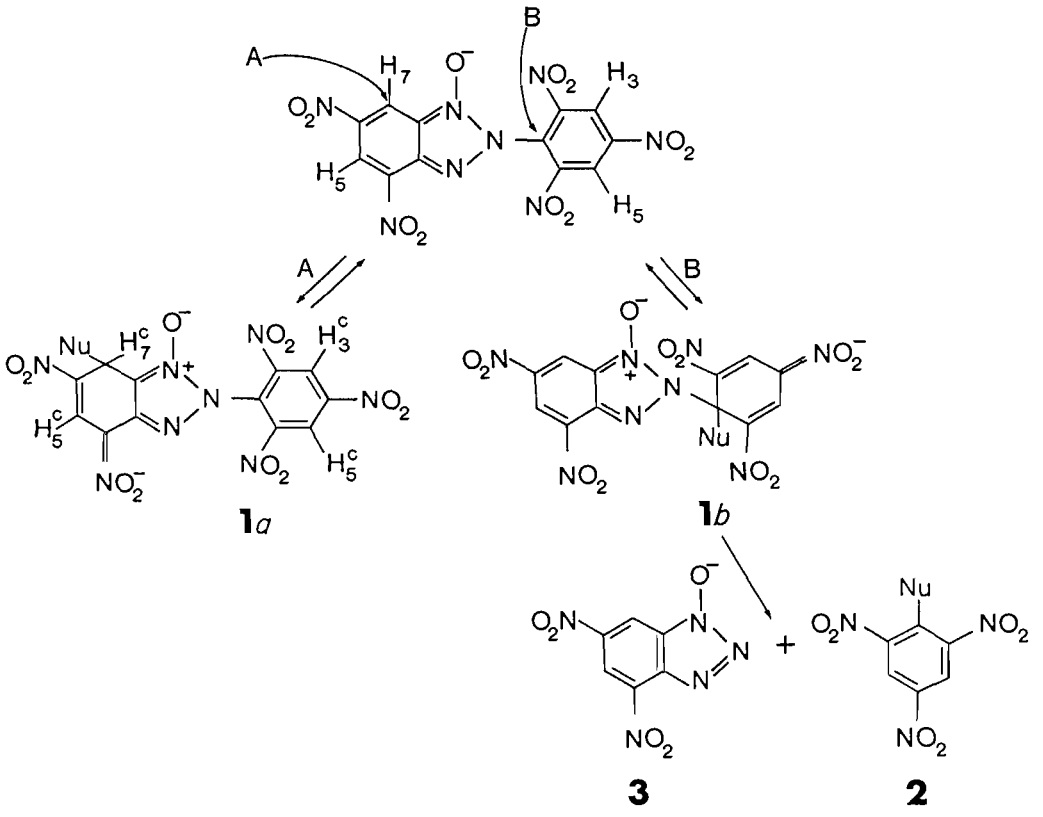


1 X = Y = Z = NO_2
4 Z = H, Y = Z = NO_2
5 X = Z = H, Y = NO_2

It has become clear that this family of electron-deficient heteroaromatic compounds have two sites available for reaction with nucleophiles, as illustrated on Scheme 1 for 2-(picryl)-4,6-dinitrobenzotriazole 1-oxide (Pi-DNBT, **1**): at C-7 of the benzotriazole 1-oxide moiety to yield a C-7 adduct, **1***a* (Path A), which is usually spectrally observable, and at C-1′ of the 2-nitroaryl ring to yield the displacement product, **2**, and the dinitrobenzotriazole 1-oxyanion, $DNBT^-$, as the anionic nucleofuge (**3**), via the metastable C-1′ adduct, **1***b* (Path B). For example, MeO^- reacts with **1** in accord with Scheme 1, but in the reaction of PhO^- as an ambident nucleophile, the C-7 adduct (formed via either oxygen or carbon centres) is not observed; only O-attack at the C-1′ position, accompanied by N-2:C-1′ bond scission, is found (2–4). With the other two members of the series, 2-(2′,4′-dinitrophenyl)-4,6-dinitrobenzotriazole 1-oxide (DNP-DNBT, **4**) and 2-(4′-nitrophenyl)-4,6-dinitrobenzotriazole 1-oxide (NP-DNBT, **5**), reaction with PhO^- showed marked differences from the behaviour found in the reaction with **1**. In these systems, C-7 adducts formed by the reaction of the *para* and *ortho* PhO^- carbon centres were observable, as well as the displacement products of O-centred attack at C-1′ of

[1]Part 8 in a series on Heteroaromatic super-electrophiles. For Part 7, see ref. 5.
[2] This is also paper 45 on Anionic σ-complexes.
[3]Authors to whom correspondence may be addressed.
[4]Revision received January 10, 1991.

Can. J. Chem. Downloaded from www.nrcresearchpress.com by 198.100.157.202 on 09/07/12
For personal use only.



SCHEME 1

the substrates, namely, the respective nitroaryl ether and **3** (5). The phenoxide carbon adducts of **4** and **5** were both formed in a 2:1 (*ortho*:*para*) ratio.

We had previously considered **1** to be a super-electrophile (6) of reactivity intermediate between that of the normal electrophile, 1,3,5-trinitrobenzene (TNB) (7, 8), and the super-electrophile, 4,6-dinitrobenzofuroxan (DNBF) (6, 9, 10), on the basis of its relative electrophilicity towards ethanethiol (2). The observation of the C-7 phenoxide C-adducts of **4** and **5** (in a statistical 2:1 *ortho*:*para* ratio) is a function not only of the high electrophilicity of the C-7 site but also of the decreased ratio of N-2:C-1′ bond cleavage exhibited by **4** and **5** as compared to **1**. This, in turn, is the result of the progressive decrease in electron-withdrawing power of the 2-nitroaryl ring that accompanies the decrease in the number of NO_2 groups attached to this ring. Thus, the C-7 site of all of the 2-nitroaryl-4,6-dinitrobenzotriazole 1-oxides is super-electrophilic, while the C-1′ site of these compounds displays conventional electrophilicity.

Interestingly, nmr spectral evidence was also found in the reaction of **4** with PhO^- for formation of a C-7 DNP-DNBT·OH^- adduct, **4***a*, generated from traces of water in the solvent (5).

Prompted by the interesting and variable behaviour found with PhO^- as compared to MeO^- (with **1** as substrate), and by **4** as compared to **1** (with PhO^- as ambident nucleophile), we have now extended our study to the reactions of **4** with two model alkoxides, ROK (R = CH_3 and $(CH_3)_3C$). These alkoxides represent a significant modulation in nucleophilicity as well as in steric bulk. Assuming, as an initial approximation, the common correlation of basicity and nucleophilicity (11), *tert*-butoxide (*t*-BuO^-) would be expected to exhibit enhanced nucleophilicity compared to methoxide (MeO^-) (12) in tandem with increased steric hindrance about the nucleophilic centre, based upon E_s, Taft's steric substituent constant (13).

The results we report herein will be discussed in terms of selectivity considerations and an activation energy/reaction coordinate profile. These approaches to the description of the various processes have proved useful in related systems (3–5).

Results

The reactions of **4** with the alkoxides (MeOK, *t*-BuOK) were monitored by 400 MHz ^1H nmr spectroscopy. Coupling constants (Hz) and chemical shifts (ppm) for all observed adducts are listed in Table 1. Integrals support the assignments made. Concentrations of these adducts could be determined at any given time by comparison of the integrals of these species to that for the singlet of 1,4-dibromobenzene (DBB) present in the reaction mixture in a known quantity (5). Spectral parameters are reported in Table 1.

Generally, reaction of **4** involves formation of: (a) the C-7 DNP-DNBT·OR^- adducts, **4***b* and **4***d*, (b) the products of N-2:C-1′ bond rupture formed through the unobserved C-1′ adducts, **4***c* and **4***e*, and (c) the C-7 DNP-DNBT·OH^- adduct, **4***a*. Furthermore, displacement of nitrite yields aromatic compounds that contain only a single NO_2 group. However, the presence of any or all of these products is dependent upon the concentration regime followed. Hence, the reactions of **4** were undertaken under several concentration regimes: equimolar and excess (2 and (or) 3 equivalents of ROK).

The alkoxides were prepared as high concentration solutions (1.4–4 M), by dissolution of metallic potassium in the parent alcohol. In this way the % ROH present in the $(CD_3)_2SO$ solvent never exceeded 10 mol% (in the 3 equivalent case) and was commonly less than 4 mol%. Reaction was initiated by injection of the appropriate amount of ROK (in ROH) into the nmr tube.

Reaction of 4 with MeOK

The initial spectrum (4 min) in the reaction of 1 equivalent of MeO^- with **4** (initial concentrations: ca. 0.023 M) contains

Can. J. Chem. Downloaded from www.nrcresearchpress.com by 198.100.157.202 on 09/07/12
For personal use only.

TABLE 1. The ^{1}H nmr spectral characteristics of the C-7 DNP-DNBT·OR$^-$ adducts (**4***a*, **4***b*, **4***d*)[a]

Substrate	Nucleophile	Chemical shifts, ppm (J = Hz)					
		H_7^c	H_5^c	$H_{6'}^c$	$H_{5'}^c$	$H_{3'}^c$	OR
1[a]	MeO^-	6.042 (s)	8.761 (s)		9.302 (s)	9.302 (s)	3.256 (s, CH_3)
4	MeO^-	5.959 (d, 0.60)	8.762 (d, 0.60)	8.186 (d, 8.82)	8.782[b] (d, 2.20)	8.905 (d, 2.20)	3.293 (s, CH_3)
4	t-BuO^-	5.955 (s)	8.675 (s)	8.133 (d, 8.79)	8.760, 8.740 (d, d, 8.79 2.35)	8.885 (d, 2.35)	[c]
4	OH^-[d]	5.9[e] (br, s)	8.672 (br, s)	8.135 (d, 9.0)			6.080 (d, 9.0, OH)[e]

[a]The spectral characteristics of the C-7 Pi-DNBT·OMe$^-$ adduct (**1***a*, Nu = MeO) are included for comparison; ref. 4.
[b]Other doublet obscured by the doublet due to H_5^c of **4***b*.
[c]Obscured by parent alcohol and (or) alkoxide resonances.
[d]Spectral parameters assigned by comparison to literature (see footnote 5).
[e]Not fully resolved.

signals for the substrate, although these are diminished in intensity and broadened. We have previously attributed such broadness to the intervention of parallel free-radical (electron-transfer) reactions that are not involved in the main reaction pathway (5). Peaks for the C-7 DNP-DNBT·OMe$^-$ adduct, **4***b*, are noted at 3.293 (s, OCH_3), 5.959 (s, H_7^c), 8.186 (d, $H_{6'}^c$, J = 8.82), 8.762 (s, H_5^c), 8.782 (d, $H_{5'}^c$, J = 2.20), and 8.905 (d, $H_{3'}^c$, J = 2.20). In some well-tuned spectra the signals of the benzotriazole 1-oxide moiety, H_5^c and H_7^c, appear as doublets (J = 0.60). Note that the resonances attributable to H_5^c, should appear as a doublet of doublets (*ortho* and *meta* coupling) but only a doublet (*meta* coupling) can be observed; the remainder of the set of signals is partly obscured by the H_5^c singlet of **4***b* at 8.762.

No signals are seen under these conditions that can be assigned to the products of N-2:C-1′ bond scission via the C-1′ adducts, **4***c*; i.e., **3** and **6***a* are not visible.

At longer times or when the initial spectrum was acquired later (ca. 7 min) the foregoing peaks are joined by another partial set: ca. 5.9 (mostly obscured), 6.080 (d, 1H, J ca. 9), 8.135 (d, 1H, J ca. 9), and 8.672 (s, br, 1H). These signals are ascribable, in turn, to H_7^c, OH, $H_{6'}^c$, and H_5^c of the C-7 DNP-DNBT·OH$^-$ adduct, **4***a*. The remaining resonances are presumably hidden by the more intense signals for **4***b* or the broad signals due to **4**. The assignment of **4***a* can be made with certainty due to separate experiments with **4** and OH^-.[5] The longer time required for appearance of these signals is no doubt a result of the relatively low concentration of OH^- in the system.

Necessary to the assignment of both **4***a* and **4***b* is the observation that the peaks due to these adducts disappear upon injection of trifluoroacetic acid (TFA). Simultaneously, the resonances due to **4** revert to almost their original intensity. This behaviour is in accord with the assignment of both **4***a* and **4***b* to oxygen-centred adducts since O-adducts are generally acid labile (ref. 1, pp. 454–457, and ref. 15), including those formed by substrates such as **1**, **4**, and **5** (2–5).

Addition of an excess of MeOK (3 equiv.) to an nmr tube (concentration of **4**: 0.022 M) results in the disappearance of the peaks due to **4** and concomitant appearance of the signals assignable to **4***b*. The resonances due to **4***a* are not observed although small peaks due to the cleavage products can be seen, notably the doublets at the anionic nucleofuge, **3**, at 8.725 and 8.720 (H_7 and H_5, J = 2.00).

[5]E. Buncel and R. A. Manderville. Unpublished data.

All peaks derived from the C-1′ adducts, **4***c*, intensify with time. At 3.5 h the peaks of 2,4-dinitroanisole (DNA, **6***a*) are clearly visible at 4.073 (s, OCH_3), 7.593 (d, H_6, J = 9.33), 8.533 and 8.509 (d, d, H_5, J = 9.33, 2.70); this assignment is verified by comparison with the spectrum of authentic DNA. The H_3 signal of DNA is buried beneath peaks due to **3**. Also at this time the spectrum has sharpened enough to permit a determination of the concentration of **4***b*: 0.020 M, i.e., **4***b* is formed in ca. 90% yield under these conditions.

Even so, other minor peaks can be discerned at 3.970 (s, 3H), 3.258 (s, 3H), 7.563 and 7.541 (d, d, J = 8.91, 2.71, partially obscured), 7.796 (d, 1H, J = 2.71), and 7.843 (d, 1H, J = 8.91). These peaks are consistent with the 1,2,4-trisubstituted benzene structure of 1,4-dimethoxy-2-nitrobenzene (DMN), where the signals at 3.258 and 3.970 are ascribable to the C-4 and C-1 methoxyls, respectively, and the peaks located at 7.563 and 7.541, 7.796, and 7.843 are due to H_5, H_3, and H_6, in turn.

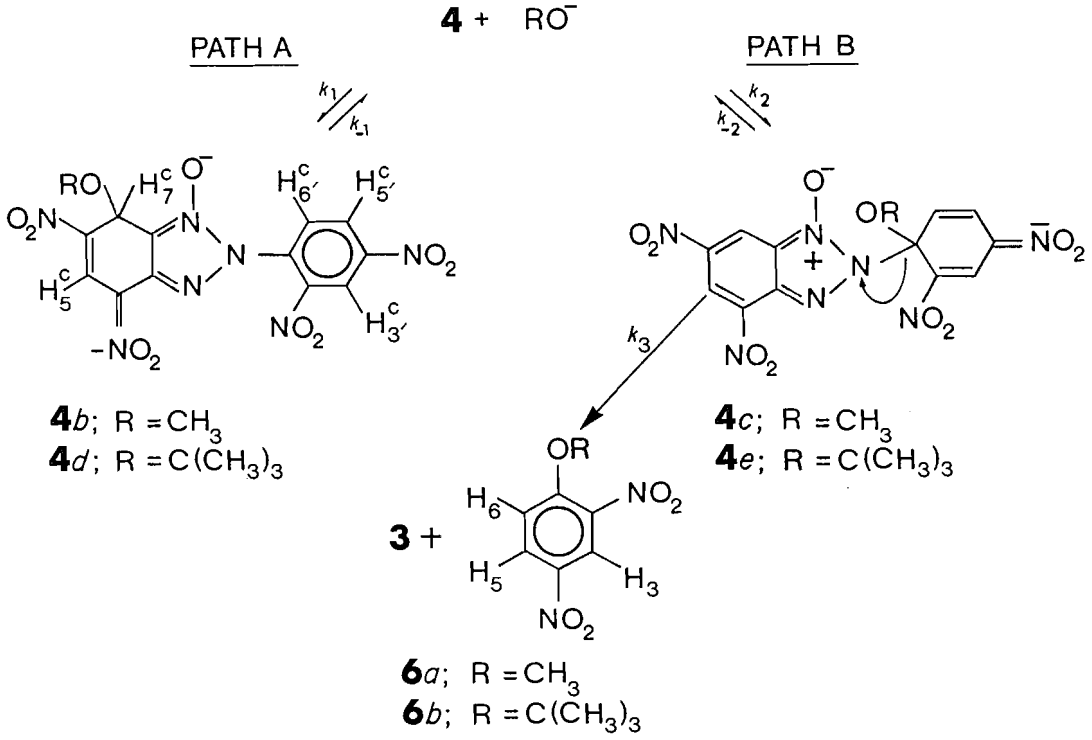
The C-7 DNP-DNBT·OMe$^-$ adduct, **4***b*, is persistent under these conditions and declines in intensity slowly over the course of 57 h. During this time the peaks due to both **6***a* and DMN correspondingly increase in intensity, as do those due to the leaving group, **3**. Neither 2,4-dinitrophenol (or the derived aryloxide) nor the 1,1 DNA·OMe$^-$ adduct (17) appear at any time in the spectrum. The final spectrum does not contain any signals due to **4***a*.

Reaction of **4** *with* t-*BuOK*

As in the previous experiment, the spectrum obtained immediately after mixing the reagents (5 min) is broad and contains diminished peaks for **4**, under these equimolar conditions. The peaks can only be assigned with surety when the signals sharpen and resolve with time (ca. 1 h). The resonances attributable to the C-7 DNP-DNBT·OBut^- adduct, **4***d*, are as follows: 5.995 (s, H_7^c), 8.133 (d, $H_{6'}^c$, J = 8.79), 8.675 (s, H_5^c), 8.760 (d, d, $H_{5'}^c$, J = 8.79, 2.35), and 8.885 (d, $H_{3'}^c$, J = 2.35).

While **4***a* may be found in this reaction system, the evidence consists solely of one doublet at 6.072 (J = 7.55), which can be assigned tentatively to the OH of **4***a*.[5] The other resonances of **4***a* occur in the vicinity of the intense band attributed to **4***d* (Scheme 2). Significantly, not only the peaks of **4***d* disappear upon acidification but the doublet of the putative C-7 hydroxide adduct, **4***a*, as well, accompanied by intensification of the residual resonances of **4**. These observations are consistent with the assignment of **4***d* to an O-adduct since such adducts are acid-reversible (refs. 1, pp. 454–457, and 15).

Can. J. Chem. Downloaded from www.nrcresearchpress.com by 198.100.157.202 on 09/07/12
For personal use only.



SCHEME 2

As in the reaction of MeO^-, no scission products derived from the C-1′ adduct, **4***e*, are noted during the period of monitoring (ca. 2 h). In contrast, a black viscous solution, devoid of interpretable peaks, results upon addition of 3 equivalents of *t*-BuOK to an nmr tube that contains **4**.

With 2 equivalents of the nucleophile the resonances due to **4** disappear completely and the peaks for **4***d* appear. Signals for **3** and the *tert*-butyl 2,4-dinitrophenyl ether **6***b* (8.159 (d, H_6, J = 8.89), 8.794 and 8.817 (d, d, H_5, J = 8.89, 2.51), and 8.920 (d, H_3, J = 2.51; *tert*-butyl singlet obscured)) are observed in the initial spectrum, but those due to **4***a* are not seen.

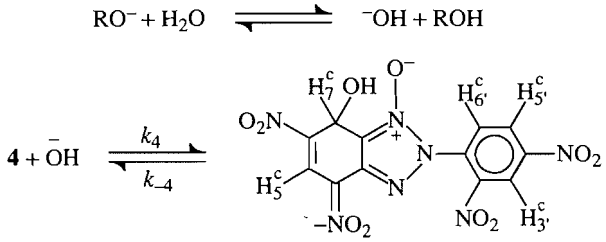
Even though the products of N-2:C-1′ bond rupture are recorded in the initial spectrum, the process of conversion of all of **4***d* into **3** and **6***b* is slow. In this regard, only **3** and a set of peaks indicative of a 1,2,4-trisubstituted benzene remain in the spectrum *acquired after 9 days*. These peaks correspond to the 2,4-dinitrophenoxide ion (generated in a control experiment by addition of a little KOH in H_2O to a $(CD_3)_2SO$ solution of the phenol): at 6.306 (d, H_6, J = 9.80), 7.779 and 7.758 (d, d, H_5, J = 9.80, 2.48), and at 8.591 (d, H_3, J = 2.48).

Unlike the other system studied, the DNP-DNBT/*t*-BuO^- reaction mixture does not appear to contain products ascribable to nitrite loss.

Discussion

Reaction pathways

There are interesting gradations in behaviour in the reactions of nucleophiles with the series of substrates **1**, **4**, and **5**. Whereas reaction of the alkoxides (MeO^-, *t*-BuO^-) at the C-7 position of **4** leads to formation of observable C-7 adducts, **4***b* and **4***d*, respectively, in a manner strictly comparable to the reaction of MeO^- with **1** via Path A (Scheme 1), these adducts are significantly more persistent than the analogous C-7 species formed by **1**, i.e., **1***a* (3, 4). This would appear to be a reflection of the overall decreased favourability of Path B for **4** relative to **1**, which coincides with removal of an electron-withdrawing nitro group from the 2-nitroaryl ring (5). This overwhelms the



4*a*

decreased favourability of Path A that might be expected as a result of decreasing the inductive electron-withdrawing power of the 2-nitroaryl moiety as it impinges on the remote C-7 position.

Interestingly, there is evidence for formation of **4***a*, the C-7 hydroxide adduct, in these systems. We have not noted comparable adduct formation in the related Pi-DNBT (2–4) or NP-DNBT (5) reaction systems. While this might be construed as indicative of an especial enhanced electrophilicity of the C-7 position of **4** as compared to **1** or **5**, it is more likely due to the relative concentration of nucleophile as compared to adventitious water present in the systems, as well as the relative basicities of the nucleophiles studied thus far.

With **1** as the substrate there is also the potential for reaction of the initially formed picryl ether with the nucleophile, particularly in those reactions where the nucleophile is present in excess. Picryl ethers react with alkoxides to form 1,1 and 1,3 isomeric adducts or either isomer alone (18, 19). In contrast the 2,4-dinitrophenyl ethers, generated through rupture of the N-2:C-1′ bond in the transient C-1′ adducts (**4***c* and **4***e*), do not appreciably react further with alkoxide under the reaction conditions to give observable adducts of **6***a* (or **6***b*) even when the alkoxide is initially present in excess.

The resultant 2,4-dinitrophenyl ethers, **6***a* (or **6***b*) (Scheme 2), do undergo further reaction, however. In the case of the *tert*-butyl 2,4-dinitrophenyl ether, **6***b*, reaction occurs at longer

Can. J. Chem. Downloaded from www.nrcresearchpress.com by 198.100.157.202 on 09/07/12
For personal use only.

Can. J. Chem. Downloaded from www.nrcresearchpress.com by 198.100.157.202 on 09/07/12
For personal use only.

times to give rise to the 2,4-dinitrophenoxide ion, presumably via an elimination process involving *t*-BuO^-, OH^-, etc. Attack of OH^- directly on **4** to yield the hydroxide analog of **4***c* is less likely since it specifically requires OH^-, which is present in the DNP-DNBT/*t*-BuO^- system only in low concentration. (The C-7 hydroxide adduct, **4***a*, if present, is present below the limit of detection.) Further, nitrite displacement products may form in both DNP-DNBT/RO^- systems studied, although there is only compelling spectral evidence in the DNP-DNBT/MeO^- reaction. In this regard, it is likely that nitrite loss is only significant with MeOK as nucleophile.

Overall, then, the reaction pathways available to **4** in reaction with ROK are (a) attack at C-7 to give rise to persistent C-7 alkoxide adducts, **4***b* (or **4***d*) (and a minority of the C-7 hydroxide adduct, **4***a*) and (b) slow attack at C-1′ to give rise to unobserved C-1′ adducts, **4***c* (or **4***e*), which rapidly decay via N-2:C-1′ bond scission to form the appropriate 2,4-dinitrophenyl alkyl ether (**6***a* or **6***b*) and **3**, the anionic nucleofuge. These pathways are illustrated in Scheme 2.

Mechanism of nitrite loss

Loss of nitro groups from 1-X-2,4-dinitrobenzenes is well known (20) and also occurs in other related nitroarene systems (21, 22); nitro group displacement from an aromatic ring may even compete with S_NAr substitution in appropriate cases (23). Single electron transfer to an initially formed anionic σ-adduct to yield a radical (from which the nitro group is lost) has also been invoked as the central step in nitrite loss in a comparable system (24).

In the present study several observations are germane to determination of a possible mechanism. In considering the DNP-DNBT/MeO^- system, it is noteworthy that DMN, the nitrite displacement product, is seen only in conjunction with DNA, **6***a*, the immediate N-2:C-1′ scission product, and that DMN is not observed at all in the 1-equivalent experiment where **6***a* is also absent. Moreover, nitrite displacement from **4** prior to N-2:C-1′ bond rupture would yield a new substrate for which there is no nmr spectroscopic evidence. DMN may, therefore, derive from **6***a*. It is also significant that the nmr spectrum is sharp and well resolved even during the progressive increase in DMN concentration; nmr spectra are usually broadened even by low concentrations of paramagnetic species such as radicals (25, 26). Consequently, we favour a non-radical mechanism (in view of the sharpness of the nmr spectra), a mechanism that involves **6***a* as a possible precursor (27).

Kinetic description of pathways

With the exception of the mechanism for nitrite loss, Paths A and B (Scheme 2) essentially govern the reactivity of **4**. In consideration of Path A processes, the present evidence is in agreement with and emphasizes our previous assessment (5) that **4** is a super-electrophile that contains a C-7 centre of reactivity intermediate between comparable positions in TNB and DNBF (2–5). Consequently, immediately upon mixing, **4** is converted into the C-7 Meisenheimer adducts (**4***a*, **4***b*, and **4***d*), which decompose slowly. If OH^- and the alkoxides, MeO^- and *t*-BuO^-, were present in comparable and constant concentrations in the respective systems, the rate of disappearance of **4** would be described by:

$$[1] \quad -d[\mathbf{4}]/dt = k_1[\mathbf{4}][RO^-] + k_4[\mathbf{4}][OH^-] - k_{-1}[\text{C-7}] - k_{-4}[\mathbf{4}\text{a}]$$

where [C-7] refers to the concentration of the C-7 adducts, **4***b* or **4***d*. The derivation of eq. [1] further assumes that Path B does not intervene appreciably (*vide infra*). This would be a valid assumption only for the earliest portion of the equimolar experiments. Carried to its logical limit, observation of the system close to the time of mixing would yield simplified kinetic behaviour, where the reverse rate constants (k_{-1} and k_{-4}) could be ignored.

$$[2] \quad -d[\mathbf{4}]/dt = k_1[\mathbf{4}][RO^-] + k_4[\mathbf{4}][OH^-]$$

Equation [2] has the form of competitive second-order kinetic expressions (28) and, under the conditions outlined, could be used to evaluate the reactivity of each alkoxide towards the C-7 electrophilic centre, relative to hydroxide attack, i.e., give an estimate of the magnitude of k_1 as compared to k_4. It should be pointed out that the nmr experiment in DMSO-rich solvent may be a sufficiently fast observational technique to permit the application of eq. [2] to analysis of the RO^- systems. The related super-electrophile, DNBF, forms adducts with MeO^- and OH^- with equilibrium constants (K_{eq}) of the order of 10^{10} in the respective parent solvents (i.e., MeOH and H_2O) (29). While K_{eq} may be expected to be smaller for **4** than for DNBF (2–6), at the same time it is well recognised that for a given adduct the equilibrium constant for formation increases significantly with addition of DMSO to hydroxylic solvent; the increase in K_{eq} is the result primarily of an increase in the magnitude of the forward rate coefficient ($K_{eq} = k_f/k_r$) combined with a smaller decrease in the magnitude of the reverse rate coefficient (29). Thus, in the DMSO-rich solvent used in the present study, both k_1 and k_4 might be expected to be much greater than the corresponding constants for decomposition of the complexes back to **4** (i.e., k_{-1} and k_{-4}) and eq. [2] would be a reasonable kinetic description of the Path A part of the reaction in the period shortly after mixing.

Ideally, comparison of the initial concentrations of **4***a* relative to **4***d* or **4***b* would provide an assessment of the nucleophilicity of OH^- and RO^- towards the C-7 position of **4**. However, this analysis is hampered by the non-comparable initial concentrations of hydroxide ion and by the general broadness of the initial nmr spectra, which limits the accuracy of the determination of initial concentrations of the C-7 adducts.

If we consider Path B, the reaction of **4** with alkoxide to give the C-1′ adducts, **4***c* (or **4***e*) (Scheme 2), the inability to observe the C-1′ adducts in this or related reactions (2–5) suggests that the process of N-2:C-1′ bond scission is facile. This is also in agreement with the anticipated leaving group ability of **3**, a

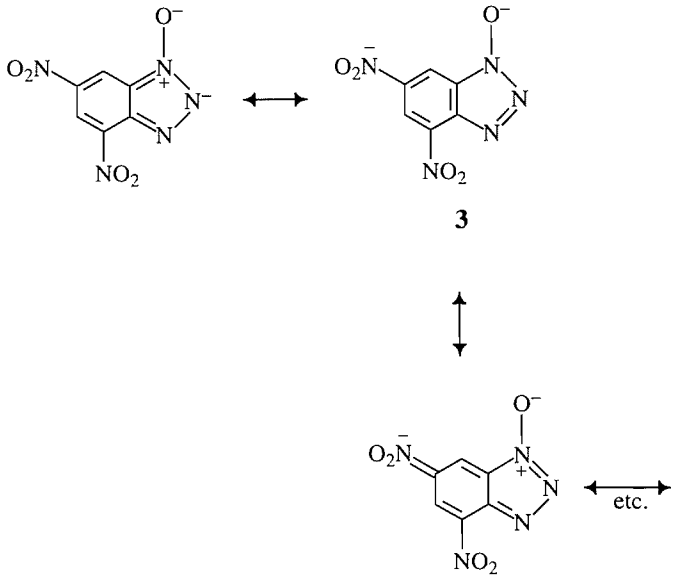


TABLE 2. The extent of formation of the C-7 DNP-DNBT·OR$^-$ adducts

Alkoxide; adduct	Time, min	% C-7 OR$^-$	% C-7 OH$^-$	% C-7[a]	pK_a^b	E_s^c
MeO$^-$; **4***b*	62	83.5	5.7	89.2	29.0	0.0
t-BuO$^-$; **4***d*	67	27.6	9.2	36.8	32.5	−1.47

[a]Determined from comparison of the signals due to the adducts to the singlet of 1,4-dibromobenzene. Total of all C-7 adducts formed.
[b]pK_a of the parent alcohol in DMSO; ref. 12.
[c]Reference 13.

delocalized anion, as well as the steric congestion that is presumed to exist about the N-2:C-1′ bond in the C-1′ adduct. In consequence, we can expect that the rate constant associated with decomposition of the C-1′ adduct, k_3, is likely much larger than k_2, the rate constant assigned to formation of the C-1′ adduct; k_2 would likely be the rate-determining coefficient, since the C-1′ adduct once formed would presumably decompose to the displacement product, **6***a* (or **6***b*) and **3**, more readily than to starting material, **4**. In fact, the very slow rate of decomposition of C-7 adducts, **4***b* and **4***d*, indicates that in the early part of the reaction, shortly after mixing, Path B does not affect Path A.

Two general cases then arise from the later part of the reaction. First, the concentration of OH$^-$ may be significantly lower than that of either alkoxide. This appears to be reasonable in that **4***a* is seen only at longer times in both systems (>7 min after mixing) under equimolar conditions. The kinetic expression for the disappearance of the C-7 adducts is

$$[3] \quad -\mathrm{d[C\text{-}7]}/\mathrm{d}t = k_{-1}[\mathrm{C\text{-}7}] - k_1[\mathbf{4}][\mathrm{RO}^-]$$

where RO$^-$ represents either alkoxide.

If we further assume a steady-state concentration of the substrate, **4**, and rearrange to isolate the [**4**][RO$^-$] term, substitution into eq. [3] leads to

$$[4] \quad -\mathrm{d[C\text{-}7]}/\mathrm{d}t = (k_{-1}k_2)/(k_1 + k_2)[\mathrm{C\text{-}7}] + (k_1k_{-4})/(k_1 + k_2)[\mathbf{4}\mathrm{a}]$$

In the second case, the equilibrium between **4** and OH$^-$ might be ignored entirely. This appears to be a valid assumption in the reactions of **4** with an excess of alkoxide where **4***a* is not observed in the nmr experiments. In this case, the term involving **4***a* in eq. [4] can be removed and the equation simplifies to

$$[5] \quad -\mathrm{d[C\text{-}7]}/\mathrm{d}t = (k_{-1}k_2)/(k_1 + k_2)[\mathrm{C\text{-}7}] = k_{\mathrm{obs}}[\mathrm{C\text{-}7}]$$

Equations [1]–[5] also lack a term to account for OH$^-$ attack at C-1′ since the final product of such a reaction, 2,4-dinitrophenol (or the aryloxide), is only found in the DNP-DNBT/*t*-BuO$^-$ system where it likely arises from an elimination reaction involving the initially formed 2,4-dinitrophenyl *tert*-butyl ether, **6***b*.

In evaluating eq. [5] it is clear that both k_1 and k_{-1}, the rate constants that combine to give the equilibrium constant, K_1 (which governs the intrinsic stability of the C-7 alkoxide adducts), are important. Nor is it possible *a priori* to determine the trend in K_1 that would arise as the nucleophile is varied, since pK_a (as a measure of nucleophilicity) (12) and steric hindrance (13) run counter to each other in the series studied.

If attack at C-7 and C-1′ can be viewed as independent events then an estimate for k_{obs} should, theoretically, be obtained from the values for the individual rate constants for reaction of model systems. The rate constant for C-1′ attack could be estimated from the S_NAr reaction of 2,4-dinitrophenylimidazole or 2,4-dinitrophenylbenzpyrazole as suitable models. However, these data are not available from the literature. Moreover, simpler compounds such as 2,4-dinitrophenylpiperidine apparently undergo hydrolysis (as a model for alkoxide attack) via a displacement process involving a C-3 (or C-5) hydroxide adduct rather than the initial substrate (30). The central intermediate in this reaction is not the C-1 adduct, corresponding to **4***c* or **4***e* in Scheme 2, but a C-1,3,3 dianionic adduct. There is no nmr spectral evidence for a C-1,1,3 dianionic adduct or the precursor C-3′ (or C-5′) adduct(s) in the present study.

Similarly, an appropriate model for reaction at C-7 is lacking. DNBF is clearly more electrophilic than **4**, while TNB is less electrophilic than **4**, but we do not, as yet, have a quantitative measure for the reactivity of **4** relative to other electrophiles.

Further implications of eq. [5] will be examined below.

Selectivity considerations

The reactions of the 2-nitroaryl-4,6-dinitrobenzotriazole 1-oxides have proven to be amenable to analysis on the basis of qualitative selectivity arguments (3, 5). Selectivity (*S*) has been defined as the ratio of the forward rate constants for formation of the C-7 as compared to the C-1′ adduct, under selective equimolar conditions, i.e., $S = k_1/k_2$.

While the percentage of **4***b* (or **4***d*) formed reflects the stability (K_1) of the particular C-7 DNP-DNBT·OR$^-$ adduct and not just the relative tendency for RO$^-$ to react at the C-7 position, the ratio of the percentages of the two adducts formed (%C-7/%C-1′ = %C-7/%**3**) might serve as a guide to selectivity. This approach is modified by two general considerations. To the extent that reaction of OH$^-$ at C-7 of **4** prevents the reaction of RO$^-$ at that position, the percentage of **4***b* (or **4***d*) formed will be unduly low. More significantly, at the earliest moment at which the percentage of **4***b* (or **4***d*) can be accurately ascertained, **3** or **6***a* (or **6***b*), i.e., **4***c* (or **4***e*), are not observed. The cleavage reaction is very slow under 1 equivalent conditions. We have previously found the rate of cleavage to be slow in the DNP-DNBT/PhO$^-$ system as compared to the rate of cleavage in the reaction of **1** with PhO$^-$(5).

As Table 2 shows, the percentage of **4***b* formed at 62 min is 83.5% but the percentage of **4***d* formed at 67 min declines to 27.6%. This notable 3-fold decline in the percentage of the C-7 adduct produced would not be modified even if the percentages of **4***a* formed were *included* as a correction to the percentages of C-7 adducts found (Table 2). Clearly, attack at C-7 by *t*-BuO$^-$ is less favourable than attack by MeO$^-$. Other evidence from the related Pi-DNBT/MeO$^-$ and *t*-BuO$^-$ systems agrees with this assessment (31).

On the other hand, the excess nucleophile experiments offer some evidence about attack at C-1′ of **4**. Thus, with 3 equivalents of MeO$^-$, the scission reaction is observed to be complete within 56 h whereas with 2 equivalents of *t*-BuO$^-$ the comparable reaction *requires over 9 days*. These results suggest that the percentages of C-1′ adduct formed and, consequently, the mag-

Can. J. Chem. Downloaded from www.nrcresearchpress.com by 198.100.157.202 on 09/07/12
For personal use only.

nitudes of k_2, decrease as the nucleophile is changed from MeO^- to t-BuO^-. In fact, there has been a 4-fold increase in the time taken for completion of the cleavage reaction and, hence, a 4-fold decrease in the reactivity of t-BuO^- towards C-1′ as compared to that of MeO^-.

Assuming the trend in reactivity of the nucleophiles towards C-1′ is preserved under the equimolar conditions, the combined results indicate that although k_1 declines for t-BuO^- as compared to MeO^-, k_2 declines to an even greater extent for t-BuO^-. Therefore, $S_{t\text{-BuO}^-}$ ($= k_1/k_2$) is greater than S_{MeO^-}. The less reactive nucleophile, t-BuO^-, has been the more selective; it reacts more readily at the C-7 position than at the C-1′ position, even relative to MeO^-.

In summary, in the equimolar nucleophile systems, t-BuO^- is more selective than MeO^-, although a higher percentage of the C-7 adduct is formed with MeO^- in comparison to t-BuO^-. It is apparent that attack at both C-7 and C-1′ positions is dominated by steric effects rather than by nucleophilicity, assuming pK_a (in DMSO) is a suitable measure of nucleophilicity. It is noteworthy that in a kinetic and equilibrium study of the reaction of a series of alkoxides (in the parent alcohols) with 1,3,5-trinitrobenzene Norris and Gan found that both the forward rate constants (k_f) and the equilibrium constant (K) for formation of the TNB·OBu-t^- adduct were smaller than the related constants for the addition of MeO^- to TNB to form the analogous complex (32). Ignoring any ion-pairing effects (33, 34), this constitutes further support for the view that selectivity in these electron-deficient systems is governed by steric factors.

Significantly, attack at C-1′ has not advanced appreciably at the moment of first observation of the systems, whereas the C-7 site is readily attacked by both RO^- and OH^-. Without doubt the C-7 position of **4** is super electrophilic compared to the C-1′ site.

Comparative energy profile

Kinetic eq. [5] adequately describes these reaction systems under the conditions of excess alkoxide or where formation and decomposition of **4***a* may be ignored. Since **4***a* may only serve as a reservoir for **4**, its formation and decomposition are peripheral to the overall course of the reactions. Therefore, eq. [5] will be taken as the appropriate description of the reaction systems.

Equation [5] can be rendered in the form of a comparative energy–reaction coordinate diagram. It is a prerequisite of the application of reactivity–selectivity arguments that the reactions should be described by the same energy profile (35, 36).

Figure 1 compares attack at the C-7 position (left-hand branch; Path A, Scheme 2) with attack at the C-1′ position (right-hand branch; Path B) as a function of the variation of the alkoxide. The Path A profile consists of the activation barriers associated with formation of **4***b* and **4***d*; the barrier for **4***b* is shown as lower than that for **4***d*, as a reflection of the expected steric hindrance to attack at C-7 for t-BuO^- as compared to MeO^-. This forward barrier corresponds to the rate constant k_1, for both alkoxides. By similar reasoning, **4***d* is presumed to be less stable than **4***b*; the tendency for t-BuO^- to leave from the C-7 adduct should be greater than for MeO^-, again on steric grounds. These qualitative considerations are derived from the observed selectivities for the alkoxides (*vide supra*), as well as our conclusion that the observed selectivity is a function primarily of steric factors.

The activation barriers associated with Path A are shown as lower than those of Path B, consistent with the super-electrophilicity of the C-7 position (2–5). In accord with the

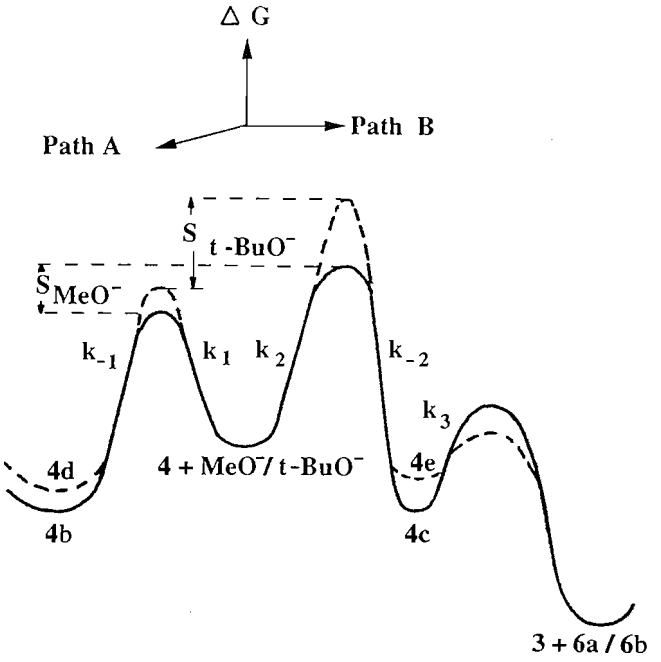


FIG. 1. Attack at C-7 of **4** is shown on the left-hand branch of the energy profile (Path A, Scheme 2) by MeO^- (solid line) and by t-BuO^- (dashed line). The right-hand branch represents attack at C-1′ of **4** (Path B) leading to formation of C-1′ adducts (**4***c* or **4***e*) as metastable intermediates. The selectivity, S, for the two nucleophiles is shown as the energy gap between the respective k_1 and k_2 activation barrier heights.

observed rates of disappearance of **4***b* (or **4***d*) when excess (2 or 3 equiv.) alkoxide was used, the initial barrier (k_2) for C-1′ attack (right-hand branch, Fig. 1) is shown as being significantly higher for t-BuO^- than for MeO^-. Conversely, congestion in the C-1′ adduct (**4***e* versus **4***c*) would presumably provide a driving force for decomposition of the C-1′ DNP-DNBT·OBu-t^- adduct to products (**3** and **6***b* versus **3** and **6***a*) relative to the C-1′ DNP-DNBT·OMe^- adduct. This is shown in the diagram (Fig. 1) as a reduced kinetic barrier for decomposition, i.e., k_3 is larger for **4***e* than for **4***c*.

The final products, the 2,4-dinitrophenyl ethers (**6***a* and **6***b*) and **3** are irreversibly formed and are stable. Since **3** is common to each of the alkoxide systems and since there is no spectral evidence to suggest a significant difference in stabilities of the ethers, the final state for each system is shown as having virtually the same energy. Similarly, Fig. 1 assumes that the initial states (**4** and MeO^- versus **4** and t-BuO^-) are of approximately the same energy. These simplifications permit a clear comparison of the energetics involved in these reactions and, on these grounds, might be justified. More importantly, the comparative energy profile also clearly shows that selectivity in these systems arises from the energy difference between the respective activation barriers for k_1 and k_2. This is illustrated in Fig. 1 by labelling the k_1 versus k_2 energy gap as $S_{t\text{-BuO}^-}$ or S_{MeO^-}. It is apparent from the diagram, then, that $S_{t\text{-BuO}^-}$ is greater than S_{MeO^-} even though the absolute energy barriers for MeO^- attack at either C-7 or C-1′ are individually lower than those for t-BuO^- attack at either of these sites. The energy gap that favours C-7 over C-1′ attack, however, is greater for t-BuO^- than for MeO^-. This is the source of the observed selectivity.

Finally, the comparative energy profile emphasizes that the C-7 position is the super-electrophilic site and is generally

Can. J. Chem. Downloaded from www.nrcresearchpress.com by 198.100.157.202 on 09/07/12
For personal use only.

TABLE 3. The nmr assignment of protons in substrates **1**, **4**, and **5**, and in 4,6-dinitrobenzofuroxan (DNBF)

			2-*N*-(Nitroaryl) ring protons			
Substrate	H_5	H_7	$H_{2'}$	$H_{3'}$	$H_{5'}$	$H_{6'}$
1	9.089 (d, J = 1.90)	9.454 (d, J = 1.90)	—	9.485 (s)	9.485 (s)	—
4	9.091 (d, J = 1.90)	9.363 (d, J = 1.90)	—	9.072 (d, J = 2.30)	8.950 (d, d, J = 8.71, 2.30)	8.368 (d, J = 8.71)
5	9.059 (d, J = 1.90)	9.293 (d, J = 1.90)	8.489 (d, J = 9.18)	8.591 (d, J = 9.18)	8.591 (d, J = 9.18)	8.489 (d, J = 9.18)
DNBF	8.949 (d, J = 1.9)	9.273[a] (d, J = 1.9)				

[a]Reference 16.

favoured over the C-1′ site for nucleophilic attack in this system.

Conclusions

The present study clearly demonstrates the preference for attack by alkoxide nucleophiles at C-7 of 2-(2′,4′-dinitrophenyl)-4,6-dinitrobenzotriazole 1-oxide, **4**. In the reaction of **4** with MeO^- and *t*-BuO^-, the C-7 adducts, **4***b* and **4***d*, are more stable than the C-1′ adducts, **4***c* and **4***e*, respectively, since the latter possess a good leaving group, namely, the delocalized dinitrobenzotriazole 1-oxyanion, **3**. Reaction of **4** at the normal electrophilic position, C-1′, has been found to be quite slow, especially in comparison with attack at C-1′ of **1**.

The alkoxides exhibit significant selectivity, under equimolar conditions, in attack at the C-7 position over attack at the C-1′ site; a greater percentage of C-7 adduct formed with MeO^- than with *t*-BuO^-. Under excess alkoxide conditions, MeO^- also proved to be more reactive towards the C-1′ site than was *t*-BuO^-. The combined results show that *t*-BuO^-, the less reactive alkoxide, is the more selective in its preference for attack at the C-7 site. Reaction at both C-7 and C-1′ positions is controlled to a greater extent by steric hindrance (E_s) than by basicity (as a measure of nucleophilicity) of the attacking alkoxide.

The reactivity of **4** both as a normal and as a supernucleophile has been summarized with the aid of a comparative energy profile.

Experimental

Materials and equipment

$(CD_3)_2SO$ (Merck) was dried thrice sequentially with 4A molecular sieves prior to use. 1,4-Dibromobenzene (DBB, Eastman) was recrystallized twice from ethanol and dried *in vacuo* (<133.3 Pa). The purification of materials used and the method of preparation of **4** have been described in detail previously (5). Methanol (HPLC grade, Caledon) was purified by refluxing with and distillation from Mg turnings (37) and *tert*-butyl alcohol (HPLC grade, Caledon) was purified by similar treatment with CaH_2 (38). The respective alkoxides (MeOK, ca. 4 M; *t*-BuOK, ca. 1.4 M) were prepared from freshly cut potassium metal and the dry alcohol in a nitrogen-filled dry box. TRIS (tris(hydroxymethyl)aminomethane, Aldrich) was dried but otherwise used without purification. The ROK solutions were standardized against standard HCl, which had been previously standardized against weighed quantities of TRIS (39). 2,4-Dinitroanisole (DNA, **6***a*) was prepared by reaction of 2,4-dinitrochlorobenzene (Eastman) and MeOK in MeOH. Yield: 57%, mp 94–95°C (lit. (14) 94.5–95.5°C). The melting points were determined with a Thomas–Hoover melting point apparatus and are uncorrected.

The ^1H nmr experiments were carried out on a Bruker AM-400 spectrometer, operating at 400 MHz. Wilmad PP-507 nmr tubes were used in all experiments. Care was taken in assuring the cleanliness of the tubes; these were typically washed with acetone (2×), followed by MeOH (3×), followed by drying in an oven at ca. 90°C (12 h minimum), followed by thorough rinsing with CCl_4 (3–5×) and a final drying cycle at ca. 90°C. The routine adjustment of the spectrometer has been given before (5). All stock solutions and the nmr tubes were capped with rubber septa and all tubes were swept out with N_2 prior to the injection of reactants. All tubes were injected with a known volume of a stock DBB solution in $(CD_3)_2SO$ (0.1047 g, 0.443 M in 1.0 mL), which acted as an internal integration standard. CD_3COCD_2H served as the chemical shift standard (2.500 ppm relative to TMS).

*The ^1H nmr spectral characteristics of the substrates **1**, **4**, and **5***

Exact assignment of the peak positions for H_5 and H_7 in the substrates has only become possible recently. It previously appeared, on consideration of the proximity of the protons to the various nitro groups, that the doublet of **1** found at 9.454 should be assigned to H_7 and the doublet at 9.089 to H_5 of the substrate. However, the similarities in chemical shift for the full dinitrobenzotriazole 1-oxide series (**1**, **4**, and **5**) suggested that the reverse assignment held, i.e., that all of the substrate doublets that appear at ca. 9.1 be ascribed to H_5 of the substrates. The rationale here is that H_5 is more remote from the 2-nitroaryl ring and would be expected, on this basis, to be similar in chemical shift throughout the series. Moreover, the chemical shifts of the peaks of DNBF have recently been unambiguously assigned through isotopic labelled experiments (16). In $(CD_3)_2SO$ the H_5 doublet is found upfield of that for H_7; the H_5 doublet is located close to 9.0 ppm (16). The new assignments for H_5 and H_7 of the substrates, **1**, **4**, and **5**, are in agreement with the revised assignments for DNBF, a structurally related compound. Table 3 (below) lists the full spectral characteristics of the substrates; it supersedes any previous assignments of ^1H nmr parameters for this family (2–5).

*A representative nmr experiment: **4** and equimolar MeOK*

The DNP-DNBT stock solution (0.1329 M) was prepared by dissolution of a weighed quantity of **4** (0.2601 g; 6.649×10^{-5} mol) in $(CD_3)_2SO$ (0.50 mL). The initial spectrum was obtained from a sample consisting of $(CD_3)_2SO$ (400 μL), **4** (85 μL), and DBB (5 μL for a concentration of 4.52×10^{-3} M). The purity of the starting material having been confirmed by the first spectrum, 1 equivalent of MeOK (4 μL of 2.991 M MeOK in MeOH for a final concentration of MeOK of 0.0242 M and of **4** of 0.0229 M, a ratio of 1.06:1) was injected into the nmr tube. The FID (32 transients) was collected within 4 min of mixing the reagents. In later spectra 64–128 transients per FID sufficed to obtain the spectra reported herein. Spectra were recorded at various intervals, typically in rapid succession initially and then with greater periods between acquisitions.

Spectra were plotted from 4200 to 0 Hz and replotted from 3850 to 2050 Hz at a higher peak amplitude. Computer printouts of the chemi-

Can. J. Chem. Downloaded from www.nrcresearchpress.com by 198.100.157.202 on 09/07/12
For personal use only.

cal shifts (5 places) were obtained. The spectra were integrated and the integrals supported the assignments reported.

Acknowledgements

Support of this research in the form of grants from the Natural Sciences and Engineering Research Council of Canada (E.B.) is gratefully acknowledged. We thank R. A. Manderville for his assistance in interpreting the nmr characteristics of the substrates. We acknowledge helpful discussions with Professors R. Y. Moir, I. Onyido, and J. Hirst.

1. E. Buncel, M. R. Crampton, M. J. Strauss, and F. Terrier. Electron deficient aromatic and heteroaromatic-based interactions. The chemistry of anionic sigma complexes. Elsevier, Amsterdam. 1984.
2. R. A. Renfrow, M. J. Strauss, S. Cohen, and E. Buncel. Aust. J. Chem. **36**, 1843 (1983).
3. E. Buncel, R. A. Renfrow, and M. J. Strauss. J. Org. Chem. **52**, 488 (1987).
4. E. Buncel, J. M. Dust, K. T. Park, R. A. Renfrow, and M. J. Strauss. *In* Nucleophilicity. *Edited by* J. M. Harris and S. P. McManus. Adv. Chem. Ser. **215**, 369 (1987).
5. E. Buncel and J. M. Dust. Can. J. Chem. **66**, 1712 (1988).
6. (*a*) M. J. Strauss, A. DeFusco, and F. Terrier. Tetrahedron Lett. **22**, 1945 (1981); (*b*) F. Terrier, F. Millot, and W. P. Norris. J. Am. Chem. Soc. **98**, 5888 (1976).
7. (*a*) E. Buncel and J. G. K. Webb. J. Am. Chem. Soc. **95**, 8470 (1973); (*b*) E. Buncel, A. Jonczyk, and J. G. K. Webb. Can. J. Chem. **53**, 3761 (1975); (*c*) E. Buncel, R. Y. Moir, A. R. Norris, and A. P. Chatrousse. Can. J. Chem. **59**, 2470 (1981); (*d*) E. Buncel, S. K. Murarka, and A. R. Norris. Can. J. Chem. **62**, 534 (1984).
8. (*a*) E. Buncel and J. G. K. Webb. Can. J. Chem. **52**, 630 (1974); (*b*) E. Buncel and W. Eggiman. J. Am. Chem. Soc. **99**, 5958 (1977); (*c*) E. Buncel, C. Innis, and I. Onyido. J. Org. Chem. **51**, 3680 (1986).
9. W. P. Norris, R. J. Spear, and R. W. Read. Aust. J. Chem. **36**, 297 (1983).
10. (*a*) F. Terrier, A. P. Chatrousse, and F. Millot. J. Org. Chem. **45**, 2666 (1980); (*b*) C. Deicha and F. Terrier. J. Chem. Res. S, 312 (1981).
11. F. G. Bordwell, T. A. Cripe, and D. L. Hughes. *In* Nucleophilicity. *Edited by* J. M. Harris and S. P. McManus. Adv. Chem. Ser. **215**, 137 (1987).
12. W. N. Olmstead, Z. Margolin, and F. G. Bordwell. J. Org. Chem. **45**, 3295 (1980).
13. T. H. Lowry and R. S. Richardson. Mechanism and theory in organic chemistry. Harper and Row, New York. 1981. p. 126, pp. 137–140.
14. R. C. Weast and M. J. Astle (*Editors*). Handbook of chemistry and physics. 62nd ed. CRC Press, Boca Raton, FL. 1981. C-99.
15. E. Buncel and W. Eggiman. Can. J. Chem. **54**, 2436 (1976).
16. F. Terrier, J. C. Halle, P. MacCormack, and M. J. Pouet. Can. J. Chem. **67**, 503 (1989).
17. W. E. Byrne, E. J. Fendler, J. H. Fendler, and G. E. Griffin. J. Org. Chem. **32**, 2506 (1967).
18. (*a*) K. T. Servis. J. Am. Chem. Soc. **87**, 5495 (1964); (*b*) J. Am. Chem. Soc. **89**, 1508 (1967).
19. (*a*) A. Cooney and M. R. Crampton. J. Chem. Soc. Perkin Trans. 2, 1973 (1984); (*b*) A. R. Norris. Can. J. Chem. **45**, 2703 (1967); (*c*) E. Buncel, A. R. Norris, and W. Proudlock. Can. J. Chem. **46**, 2759 (1968).
20. C. A. Lobry de Bruyn. Recl. Trav. Chim. Pays-Bas, **9**, 208 (1890).
21. R. Rverdin. Org. Synth. 7, 28 (1927).
22. (*a*) V. Gold and C. H. Rochester. Proc. Chem. Soc. 403 (1960); (*b*) J. Chem. Soc. 1687 (1964); (*c*) J. Chem. Soc. 1692 (1964).
23. M. W. Logue and B. H. Han. J. Org. Chem. **46**, 1638 (1981).
24. H. M. Relles, D. S. Johnson, and J. S. Manello. J. Am. Chem. Soc. **99**, 6677 (1977).
25. P. Laszlo and P. Stang. Organic spectroscopy: Principles and applications. Harper and Row, New York. 1971. p. 71.
26. V. F. Starichenko, V. A. Ryabinin, and S. M. Shein. Zh. Strukt. Khim. **15**, 138 (1974).
27. J. Miller. Nucleophilic aromatic substitution. Elsevier, Amsterdam. 1968.
28. A. A. Frost and R. G. Pearson. Kinetics and mechanism. Wiley, New York. 1953. pp. 147–154.
29. F. Terrier. Chem. Rev. **82**, 77 (1982).
30. E. B. de Vargas, R. H. de Rossi, and A. V. Veglia. J. Org. Chem. **51**, 1976 (1986).
31. J. M. Dust. Ph.D. Thesis. Queen's University, Kingston, Ontario. 1987. p. 329.
32. A. R. Norris and L. H. Gan. Can. J. Chem. **49**, 2490 (1971).
33. A. D. AlAruri and M. R. Crampton. J. Chem. Soc. Perkin Trans. 2, 807 (1981).
34. S. Sekiguchi, T. Aizawa, and N. Tomoto. J. Org. Chem. **49**, 93 (1981).
35. E. Buncel and H. Wilson. J. Chem. Educ. **64**, 475 (1987).
36. E. Buncel, C. Chuaqui, and H. Wilson. J. Org. Chem. **45**, 3621 (1980).
37. A. I. Vogel. A textbook of practical organic chemistry. Longmans, London. 1948. p. 168.
38. D. D. Perrin, W. L. F. Armarego, and D. R. Perrin. Purification of laboratory chemicals. 2nd ed. Pergamon, Oxford. 1980.
39. T. H. Whitehead. J. Chem. Educ. **36**, 297 (1959).

Can. J. Chem. Downloaded from www.nrcresearchpress.com by 198.100.157.202 on 09/07/12
For personal use only.

Hexachlorotellurate(IV) hydrolysis equilibria in hydrochloric acid. Measurement by Raman and ^{125}Te NMR spectroscopy and a reconsideration of earlier spectrophotometric results

J. B. MILNE
Department of Chemistry, University of Ottawa, Ottawa, Canada K1N 6N5
Received November 9, 1990

J. B. MILNE. Can. J. Chem. **69**, 987 (1991).

Solutions of TeO_2 (0.001 M) in HCl over a range of concentrations are shown to contain $TeCl_2(OH)_2$ in addition to $TeCl_6^{2-}$ and $TeCl_4(OH)^-$. The hydrolysis constants for $TeCl_6^{2-}$ and $TeCl_4(OH)^-$ have been determined from a reconsideration of earlier UV-visible spectrophotometric results (1)

$$TeCl_6^{2-} + H_2O = TeCl_4(OH)^- + HCl + Cl^-$$
$$K_1 = 3.78\ (\pm\ 0.01) \times 10^4\ M^3$$
$$TeCl_4(OH)^- + H_2O = TeCl_2(OH)_2 + HCl + Cl^-$$
$$K_2 = 456\ (\pm\ 24)\ M^3$$

The hydrolysis constants have also been determined by quantitative Raman spectroscopy ($K_1 = 2.21\ (\pm\ 0.16) \times 10^4\ M^3$; $K_2 = 442 \pm 57\ M^3$). The agreement between K_2 determined by the two methods is good but K_1 from spectrophotometry is much larger than that from Raman studies. This disagreement is attributed to ion-pairing which will be significant at the concentration at which the Raman measurements were made ($c(TeO_2) = 0.50$ M). The hydrolysis constant for $TeCl_6^{2-}$ was also determined from the ^{125}Te NMR spectra of TeO_2/HCl solutions, which consisted of one signal, indicating rapid Te exchange between all species. The hydrolysis constant, determined in this way ($K_1 = 1.92\ (\pm\ 0.07) \times 10^4\ M^3$) was also low compared to that determined from spectrophotometry.

Key words: solution, equilibria, tellurium, hydrochloric acid, Raman spectroscopy, ^{125}Te NMR spectroscopy, UV–visible spectrophotometry.

J. B. MILNE. Can. J. Chem. **69**, 987 (1991).

Il est montré que les solutions de TeO_2 (0,001 M) dans l'HCl contiennent $TeCl_2(OH)_2$ en plus de $TeCl_6^{2-}$ et $TeCl_4(OH)^-$. On a réexamine les résultats spectrophotométriques rapportés plus tôt (1) et à partir de ces données on a déterminé des ceux les constantes d'hydrolyse de $TeCl_6^{2-}$ et $TeCl_4(OH)^-$.

$$TeCl_6^{2-} + H_2O = TeCl_4(OH)^- + HCl + Cl^-$$
$$K_1 = 3{,}78\ (\pm\ 0{,}01) \times 10^4\ M^3$$
$$TeCl_4(OH)^- + H_2O = TeCl_2(OH)_2 + HCl + Cl^-$$
$$K_2 = 456\ (\pm\ 24)\ M^3$$

Les constantes d'hydrolyse ont été aussi determinées en faisant appel à la spectroscopie Raman quantitative ($K_1 = 2{,}21\ (\pm\ 0{,}16) \times 10^4\ M^3$; $K_2 = 442 \pm 57\ M^3$). L'accord entre le K_2 evalué par les deux méthodes est bon, mais le K_1 évalué par le spectrophotométrie est plus grand que celvi évalué par la spectroscopie Raman. Ce désaccord est attribué à la formation de paires d'ions qui sont importantes aux concentrations utilisées pour mésurer les spectres Raman ($c(TeO_2) = 0{,}5$ M). La constante d'hydrolyse de $TeCl_6^{2-}$ a aussi été évaluée en faisant appel à la spectroscopie RMN du ^{125}Te sur des solutions de TeO_2 dans le HCl. Les spectres montrent une seule bande qui indique l'échange rapide de Te. La constante d'hydrolyse, évaluée par la spectroscopie RMN ($K_1 = 1{,}92\ (\pm\ 0{,}07) \times 10^4\ M^3$) est aussi basse comparée à celle évaluée par la spectrophotométrie.

Mots clés: solution, équilibres, tellure, acide chlorohydrique, spectroscopie Raman, spectroscopie de RMN de ^{125}Te, spectroscopie électronique.

Introduction

A previous study of the equilibria, involving chlorotellurate(IV) species formed in hydrochloric acid, showed that besides hexachlorotellurate(IV), $TeCl_6^{2-}$, two other chlorotellurates were formed depending on HCl concentration, tetrachlorotellurate(IV), $TeCl_4(OH)^-$, and another species thought to be a monochlorotellurate(IV) (1). The $TeCl_6^{2-}$ hydrolysis constant for the formation of the $TeCl_4(OH)^-$ ion could not be evaluated and this was attributed to a significant variation in the activity coefficient factor over the range of HCl concentration studied. A reconsideration of this problem is occasioned by the successful treatment of equilibria involving Se(IV) species in hydrohalic acids (2, 3). This represents an extension of previous work concerning the complexes of tellurium (4).

Experimental section

Solutions were prepared from TeO_2 (Aldrich) and hydrochloric acid (J. T. Baker). Spectrophotometric measurements were made on a Varian DMS 90 UV–visible spectrophotometer, using 1 mm path length quartz cells. Quantitative Raman measurements were made as described earlier (5). Standard perchloric acid solution spectra were run before and after each TeO_2/HCl solution spectrum. The normalization assumption was that the 925 cm^{-1} band in 1 M perchloric acid has an area intensity of 6.45 cm^2. Spectra were run at 25 ± 0.1°C. The ^{125}Te NMR spectra were measured with a Varian XL-300 spectrometer operating at 94.745 MHz. All shifts were measured by sample replacement, using 1 M $Te(OH)_6$ in D_2O as standard. The signal of this standard is 712 ppm less shielded than dimethyl tellurium (6). Signal drift was negligible in the time required for the measurements. The HCl and water activites were taken from refs. 8 and 9.

Can. J. Chem. Downloaded from www.nrcresearchpress.com by 198.100.157.202 on 09/07/12
For personal use only.

TABLE 1. Spectrophotometric measurements and final calculated results for solutions of TeO_2 (10^{-3} M) in hydrochloric acid

c_{HCl} (M)	A_{375}[a] obsd	A_{295}[a] obsd	10^5 $[TeCl_6^{2-}]$	10^4 $[TeCl_4(OH)^-]$	10^5 $[TeCl_2(OH)_2]$	A_{375} calcd	A_{295} calcd
10.0	2.82	11.29	98.4	0.164	—	2.78	11.16
8.5	2.57	10.56	90.6	0.935	0.012	2.57	10.52
8.0	2.35	9.92	82.6	1.74	0.044	2.35	9.86
7.5	1.99	8.78	69.6	3.03	0.159	2.00	8.78
7.0	1.59	7.52	53.0	4.65	0.493	1.56	7.40
6.5	1.14	6.02	34.3	6.43	1.45	1.06	5.84
6.0	0.75	4.80	20.5	7.61	3.40	0.69	4.66
5.5	0.45	3.67	13.2	8.08	5.95	0.49	3.98
5.0	0.29	2.96	4.37	7.86	17.1	0.23	2.93
4.5	—	2.29	1.74	6.71	31.2	—	2.31
4.0	—	1.69	0.566	4.88	50.7	—	1.66
3.75	—	1.38	0.305	3.91	60.6	—	1.35
3.5	—	1.04	0.151	2.96	70.2	—	1.06
3.25	—	0.77	0.069	2.12	78.8	—	0.81
3.0	—	0.58	0.030	1.45	85.5	—	0.61
2.5	—	0.38	0.005	0.611	93.9	—	0.37

[a]Corrected for HCl background.

TABLE 2. Spectrophotometric results and initial estimates for solutions of 0.001 M TeO_2 in moderately concentrated HCl (c_{HCl} = 6.5–10.0 M)

c_{HCl} (M)	A_{375}[a]	10^4 $[TeCl_6^{2-}]$ (initial estimate)[b]	10^4 $[TeCl_4OH^-]$ (initial estimates)[b]	$a(HCl)$[c]	a_w[d]
10.0	2.82	10.00	0.0	280	0.273
8.5	2.57	9.113	0.887	128	0.380
8.0	2.35	8.333	1.667	97.4	0.422
7.5	1.99	7.057	2.943	73.5	0.466
7.0	1.59	5.638	4.362	56.0	0.510
6.5	1.14	4.043	5.957	41.5	0.555

[a]Corrected for HCl background.
[b]See Table 4.
[c]Reference 9.
[d]Reference 8.

Results and discussion

Spectrophotometry

Previous work (1) showed that the first hydrolysis step for the $TeCl_6^{2-}$ ion in 7–9 M hydrochloric acid solution is to the $TeCl_4(OH)^-$ ion. This is governed by the equilibrium constant,

$$[1] \quad K_1 = \frac{[TeCl_4(OH)^-][Cl^-]a(HCl)^2}{[TeCl_6^{2-}]a(H_2O)} \frac{y(TeCl_4(OH)^-)y(Cl^-)}{y(TeCl_6^{2-})}$$

The $y(X)$ represents the molar activity coefficient of X. It should be noted that $a(HCl)$ represents the mean molar ionic activity and not the overall activity for hydrochloric acid and, therefore, must be squared in eq. [1]. This was not done in the previous TeO_2/HCl work (1) and explains why K_1 could not be calculated. The identification of the second hydrolysis species will also be affected by this correction. New spectrophotometric measurements have been made and the absorbances at 375 and 295 nm for 0.001 M TeO_2 solutions in 2.5–10.0 M HCl solutions are listed in Table 1.

Moderate HCl concentrations (6.5–10.0 M)

From the extinction coefficient for $TeCl_6^{2-}$, $\epsilon_{375}(TeCl_6^{2-})$ (= 2820 mol^{-1} L cm^{-1}),[1] the concentration of $TeCl_6^{2-}$ may be calculated and that of $TeCl_4(OH)^-$, determined by difference (1). The concentrations of these ions are given in Table 2. The activity coefficient factor is essentially unity as calculated from the Debye–Hückel equation (8). From eq. [1], a plot of log $\{[TeCl_6^{2-}]/\{[TeCl_4(OH)^-][Cl^-]\}\}$ against log $\{a(HCl)/\sqrt{a(H_2O)}\}$ should give a straight line of slope 2 and intercept log K_1. Such a plot is shown in Fig. 1. The limiting slope is 2.0 and from the intercept, the first estimate of K_1 is 3.47 (± 0.01) × 10^4 M^3.

Low HCl concentrations (2.5–4.5 M)

From K_1, it may be shown that 3% or less of the total Te(IV) concentration (0.001 M) is present as $TeCl_6^{2-}$ at HCl concentrations of 4.5 M or less. A comparison of the change in absorbance at 295 and 375 nm with changing c(HCl) (6.5–10.0 M) shows that both the $TeCl_6^{2-}$ and $TeCl_4(OH)^-$ ions absorb at 295 nm. In the range of c(HCl) from 2.5 to 4.5 M, the shoulder at 295 nm is a prominent feature of the spectra due to the

[1]The absorbances and extinction coefficients reported previously (1) were for a 1 mm path length and are therefore one tenth of the values given here.

Can. J. Chem. Downloaded from www.nrcresearchpress.com by 198.100.157.202 on 09/07/12
For personal use only.

TABLE 3. Spectrophotometric results and initial concentration estimates for solutions of 0.001 M TeO_2 in HCl at low concentrations (2.50–4.50 M)

c_{HCl} (M)	A_{295}[a]	10^6 $[TeCl_6^{2-}]$ (M)	10^4 $[TeCl_4OH^-]$ (M)	10^4 $[TeCl_2(OH)_2]$ (M)	$a(HCl)$[c]	$a(H_2O)$[d]	K_2[b] (M^3)
4.50	2.29	18.60	6.60	3.22	12.6	0.730	478
4.00	1.69	6.30	4.98	4.96	9.18	0.768	437
3.75	1.38	3.41	4.02	5.95	7.87	0.788	437
3.50	1.04	1.61	2.90	7.09	6.67	0.809	470
3.25	0.77	0.704	1.99	8.00	5.59	0.828	492
3.00	0.58	0.300	1.35	8.65	4.67	0.847	496
2.50	0.38	0.056	0.66	9.34	3.23	0.879	420

[a]Corrected for HCl background.
[b]K_2 = 461 (± 23) M^3.
[c]Reference 9.
[d]Reference 8.

presence of $TeCl_4(OH)^-$. The absorbances at 295 nm for c(HCl) in the range 2.5 to 5.0 M are given in Table 3. As c(HCl) decreases, the absorbance at 295 nm, A_{295}, decreases, reflecting the decreasing concentration of $TeCl_4(OH)^-$, which is in equilibrium with a third Te(IV) species. A preliminary calculation of formation constants for various possible Te(IV) species, which could arise from hydrolysis of $TeCl_4(OH)^-$ (ignoring $[TeCl_6^{2-}]$) revealed that the constant varied least over the 2.5–4.5 M HCl range for the formation of a dichlorotellurate(IV). Species considered for this preliminary treatment were $TeCl_3O^-$, $TeCl_3(OH)$, $TeCl_2O$, $TeCl_2O(OH)^-$, $TeCl_2(OH)_2$, $TeCl_2(OH)_3^-$, $TeCl_2O_2^{2-}$, $TeClO_2^-$, $TeClO(OH)$, and $TeClO(OH)_2^-$. Equilibria involving more highly aquated species with the same Te/Cl ratio would differ little in the dependence on c(HCl) from those considered. The best preliminary fit to the data was found for $TeCl_2(OH)_2$ (K_2 = 328 (± 34) M^3).

The Raman spectra of solutions of TeO_2 in hydrochloric acid (1) indicate the presence of two Te(IV) species, $TeCl_6^{2-}$ and $TeCl_4(OH)^-$, at moderate HCl concentrations and a third species formed at low c(HCl) ($c(TeO_2)$ = 0.5 M; c(HCl) = 3–5 M). This third species exhibits a TeCl stretching band at 280 cm^{-1} and a broad TeO stretching band at 685 cm^{-1}, which is characteristic of TeO single bonding (7) and is consistent with the formation of $TeCl_2(OH)_2$. Other Te(IV) species such as $TeCl_2O$ and $TeCl_2O(OH)^-$ are not consistent with the Raman spectra. Neither of these latter two species, nor the $TeCl_2(OH)_3^-$ anion, fits the spectrophotometric data as well as $TeCl_2(OH)_2$.

A more accurate calculation of K_2 from the spectrophotometric results is obtained if the contribution of $TeCl_6^{2-}$, which is present in low concentration but has a high extinction coefficient at 295 nm, is allowed for. The calculation is made from the expression for K_1 (eq. [1]), that for K_2,

$$[2]\quad K_2 = \frac{[TeCl_2(OH)_2][Cl^-]a(HCl)^2}{[TeCl_4(OH)^-]a(H_2O)} \frac{y(TeCl_2(OH)_2)y(Cl^-)}{y(TeCl_4(OH)^-)}$$

the mass balance, and the expression for total absorbance

$$[3]\quad A_{295} = \epsilon_{295}(TeCl_6^{2-})[TeCl_6^{2-}] + \epsilon_{295}(TeCl_4(OH)^-)[TeCl_4(OH)^-] + \epsilon_{295}(TeCl_2(OH)_2)[TeCl_2(OH)_2]$$

The value of $\epsilon_{295}(TeCl_6^{2-})$, determined from the absorbance of the 10 M HCl solution in Table 1, is 11290 mol^{-1} L cm^{-1} and that of $\epsilon_{295}(TeCl_4(OH)^-)$, as calculated from the absorbance of the 8.0 and 8.5 M HCl solutions in Table 1, where interference from $TeCl_2(OH)_2$ would be least, is 3065 (± 5) mol^{-1} L cm^{-1}. The equilibrium constant, K_2, was determined by choosing the value of $\epsilon_{295}(TeCl_2(OH)_2)$, which gave the minimum variation in K_2 for all c_{HCl} from 2.5 to 4.5 M. The activity coefficient factor was assumed to be unity. The choice of $\epsilon_{295}(TeCl_2(OH)_2)$ = 190 mol^{-1} L cm^{-1} gave the values listed in Table 3 for which K_2 = 461 ± 23 M^3.

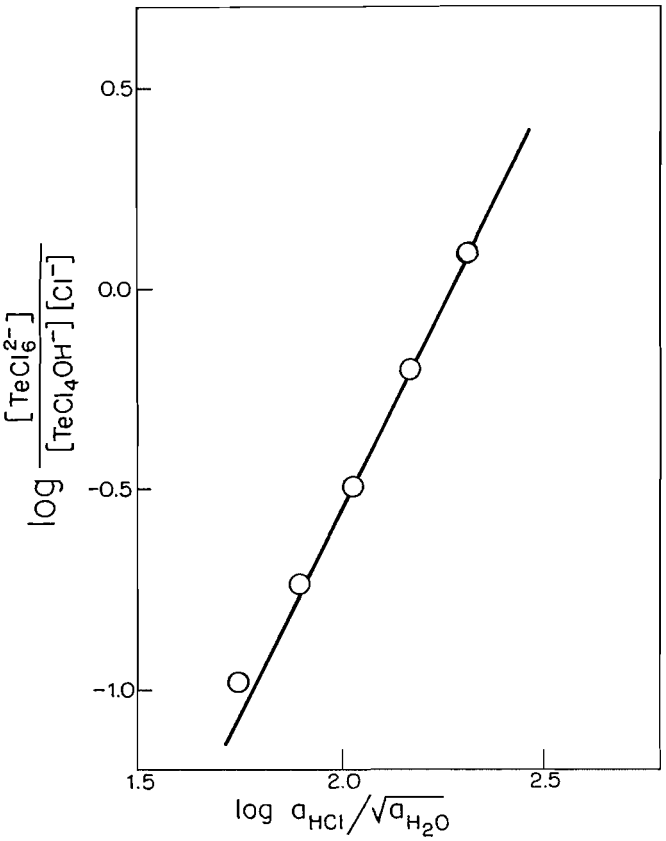


FIG. 1. Plot for the evaluation of K_1 from spectrophotometric results (see text).

To achieve an optimum fit to the observed absorbances over the entire HCl concentration range, it was necessary to allow for a small absorbance at 375 nm due to the $TeCl_4(OH)^-$ ion. From A_{375} at c_{HCl} = 5.0 and 6.0 M, $\epsilon_{375}(TeCl_4(OH)^-)$ was estimated

Can. J. Chem. Downloaded from www.nrcresearchpress.com by 198.100.157.202 on 09/07/12
For personal use only.

TABLE 4. Normalized scattering intensities for the TeO stretching modes at 650 cm^{-1}[a]

c_{HCl}	i_{650-90}[b] (cm^2)	$10^{-4}K_1$[c] (M^3)	K_2[d] (M^3)	$[TeCl_6^{2-}]$	$[TeCl_4OH^-]$	$[TeCl_2(OH)_2]$
10.0	0.53	1.93	—	0.45	0.051	—
9.0	1.78	2.54	—	0.33	0.17	—
8.0	3.22	2.18	—	0.19	0.31	—
7.0	4.44	2.20	—	0.073	0.43	—
6.0	6.34	—	553	0.017	0.33	0.16
5.0	7.60	—	414	0.003	0.21	0.29
4.0	8.85	—	446	—	0.065	0.43
3.0	9.28	—	356	—	0.014	0.49

[a] $c(TeO_2) = 0.50$ M.
[b] Estimated precision = ±3%.
[c] $K_1 = 2.21 (\pm 0.16) \times 10^4$ M^3.
[d] $K_2 = 442 (\pm 57)$ M^3.

to be 140 ± 57 mol^{-1} L cm^{-1}. A new plot of the moderate HCl concentration data with this correction gave a slope of 2.0 and $K_1 = 3.78 (\pm 0.01) \times 10^4$ mol L^{-1}. Recalculation with the low c_{HCl} data, using this value of K_1, gives the best value for $K_2 = 456 \pm 24$ M^3 at $\epsilon_{295}(TeCl_2(OH)_2) = 190$ mol^{-1} L cm^{-1}.

From K_1, K_2, and the extinction coefficients, the concentrations of all Te(IV) species at various c_{HCl} and A_{295} and A_{375} can be calculated. These are listed in Table 1. Agreement between calculated and observed absorbances is good and equilibria in solutions of TeO_2 in HCl are best described in terms of the species $TeCl_6^{2-}$. $TeCl_4(OH)^-$, and $TeCl_2(OH)_2$.

Raman spectroscopic determination of K_1 *and* K_2

The Raman spectra of solutions of 0.5 M TeO_2 in hydrochloric acid of various concentrations have been reported earlier (1). Normalized scattering intensities for the TeO stretching modes of $TeCl_2(OH)_2$ and $TeCl_4(OH)^-$ ion at 650–90 cm^{-1} over a range of c_{HCl} (3.0–10.0 M) are listed in Table 4. The hydrolysis constant, K_1, may be evaluated from the data for 7.0–10.0 M HCl solutions, using the mass balance equations for Te(IV) and HCl, the expression for K_1 (eq. [1]), the charge balance, and the scattering intensity relation,

$$[4] \quad [TeCl_4(OH)^-] = i_{650}/I_{650}(TeCl_4(OH)^-)$$

where i_{650} represents the measured normalized scattering intensity at 650 cm^{-1} and $I_{650}(TeCl_4(OH)^-)$, the molar scattering intensity. The constant, K_1, can be evaluated by choosing $I_{650}(TeCl_4(OH)^-)$, which gives the smallest variation in K_1 for the solutions measured. However, the values of the activities of HCl and H_2O to be used in eq. [1] must be considered first. The use of a(HCl) and a_w which correspond to actual HCl concentration, would ignore the effect of the acids $(H^+)_2TeCl_6^{2-}$ and $H^+TeCl_4(OH)^-$, which is substantial due to the relatively large concentrations of these species, unlike in the case of the spectrophotometric measurements. Since it is the H^+ ion, which has the largest effect on these activities, a(HCl) and a_w, corresponding to $[H^+]$, and not to $[Cl^-]$, were used in the calculations. This assumes, effectively, that $y(HCl) = y(HTeCl_4(OH)) = 2y(H_2TeCl_6)$. A choice of 10.4 cm^2 M^{-1} for $I_{650}(TeCl_4(OH)^-)$ gave the best K_1 (= 2.21 (± 0.169) × 10^4 M^3). The uncertainty represents the range of variation of K_1 for the four HCl concentrations considered. The precision on the area intensity measurements (±3%) produces a precision on K_1 of ±10%.

From this Raman value for K_1, the expressions for the equilibrium constants (eqs. [1] and [2]), the mass balance for Te(IV) and chloride, the charge balance and the expression for the area intensity,

$$[5] \quad i_{650-90} = 10.4[TeCl_4(OH)^-] + I_{650-90}(TeCl_2(OH)_2)[TeCl_2(OH)_2]$$

K_2 may also be calculated. Various values of $I_{650-90}(TeCl_2(OH)_2)$ were chosen in increments of 0.1 cm^2 M^{-1} over the range 15–20 cm^2 M^{-1} and K_2 was calculated by an iterative process for each of the c_{HCl} from 3.0 to 6.0 M measured. The minimum variation was found with $I_{650-90}(TeCl_2(OH)_2) = 18.8$ cm^2 M^{-1} for which $K_2 = 442 (\pm 57)$ M^3. As before, the a(HCl) and $a(H_2O)$ correponding to $[H^+]$, and not to $[Cl^-]$ were used in the iterative process. The precision on the measurement of area intensities for the calculation of K_2 leads to greater uncertainty limits for this equilibrium constant (±40%) than in the case of K_1 (±10%).

Nevertheless, the agreement between K_2, calculated from UV–visible spectrophotometry, and K_2, from Raman spectroscopy is good. However, K_1 from Raman spectrometry (2.21 × 10^4 M^3) is substantially lower than that measured by spectrophotometry (3.78 × 10^4 M^3). This difference may be the result of ion pairing of H_3O^+ and $TeCl_6^{2-}$, which would be more important at the high Te(IV) concentrations used for the Raman spectra. The effect of ion pairing on the magnitude of ionic dissociation constants as determined by low and high concentration methods has been observed in other systems (10, 11). The effect of such ion-pairing on K_2 will be less significant, since uninegative anions appear as both reactant (Cl^-) and product ($TeCl_4(OH)^-$) in this case.

^{125}Te NMR measurement of K_1

The ^{125}Te NMR spectra of solutions of TeO_2 in HCl consist of a single resonance, indicating rapid exchange between all Te(IV) species present. Cooling of the solutions to −49°C (10.0 M solutions) and −69°C (7.0 M solutions) caused the signal to broaden and shift towards increased shielding but separation into individual signals for $TeCl_6^{2-}$, $TeCl_4(OH)^-$, or $TeCl_2(OH)_2$ did not occur. The rapid exchange of Te(IV) in these solutions is understandable where coordinately unsaturated species such as $TeCl_4(OH)^-$ and $TeCl_2(OH)_2$ may form ligand-bridged intermediates but the exchange involving $TeCl_6^{2-}$ is more problematic unless seven coordination occurs. A more attractive mechanism

Can. J. Chem. Downloaded from www.nrcresearchpress.com by 198.100.157.202 on 09/07/12
For personal use only.

TABLE 5. ^{125}Te nuclear magnetic resonance results

Solution	Chemical shift[a] (ppm)
$(n\text{-}Bu_4N)_2TeCl_6$ in $(CD_3)_2CO$[b]	1329
$(n\text{-}Bu_4N)_2TeCl_6$ in CH_3CN (0.16 M)	1336.2
$KTeCl_4OH$ in H_2O (4.03 M)	1511.0
$HTeCl_4OH$ in H_2O (2.97 M)	1505.9
0.484 M TeO_2 in 10.0 M HCl	1383.4
0.380 M TeO_2 in 10.0 M HCl	1379.7
0.290 M TeO_2 in 10.0 M HCl	1377.7
0.196 M TeO_2 in 10.0 M HCl	1376.6
0.499 M TeO_2 in 7.0 M HCl	1467.1
0.381 M TeO_2 in 7.0 M HCl	1457.0
0.292 M TeO_2 in 7.0 M HCl	1449.1
0.191 M TeO_2 in 7.0 M HCl	1438.8

[a]Shifts are referred to $(CH_3)_2Te$ as calculated from $(Me_2Te) = (Te(OH)_6) + 712$ ppm.
[b]Reference 6, p. 412.

TABLE 6. Hydrolysis constants, K_1, determined from ^{125}Te data[a] for 7 M HCl solutions[b]

$c(TeO_2)$	K_1 (M^3)
0.191	2.04(±0.02)
0.292	1.90(±0.02)
0.381	1.79(±0.01)
0.499	1.94(±0.01)

[a]Table 5.
[b]$\delta(TeCl_6^{2-}) = 1375 \pm 0.5$; $\delta(TeCl_4OH^-) = 1484$; $K_1 = 1.92 (\pm 0.07)$ M^3.

would involve the presence of a small concentration of $TeCl_5^-$ ion, which could form bridged structures with six coordination as intermediates like the known structures, $(TeCl_4(OH))_2^{2-}$ (4) and $Te_2Cl_{10}^{2-}$ (12). Such intermediates would probably go undetected by the methods used in this work. The chemical shifts of various solutions studied are given in Table 5. The solutions in 10.0 M HCl contain predominantly $TeCl_6^{2-}$ ion, while those in 7.0 M HCl have mainly $TeCl_4(OH)^-$ present. The chemical shifts for the 10.0 M HCl solutions lie close to that reported for $TeCl_6^{2-}$ in acetone (6) and, in acetonitrile (Table 5). The chemical shift for $TeCl_6^{2-}$ in HCl is estimated by extrapolation of the 10.0 M HCl data to zero $c(TeO_2)$ where the contribution of $TeCl_4(OH)^-$ is negligible. The shift for $TeCl_6^{2-}$ is found to be 1375.5 ± 0.5 ppm. The concentration of $TeCl_6^{2-}$ and $TeCl_4(OH)^-$ in the 7.0 M HCl solutions, where $[TeCl_6^{2-}]$ and $[TeCl_4(OH)^-]$ are present at comparable concentrations, may be calculated from the mass balance for Te(IV) and the observed chemical shifts, using the equation

$$[6] \quad \delta = \frac{\delta(TeCl_6^{2-})[TeCl_6^{2-}] + \delta(TeCl_4(OH)^-)[TeCl_4(OH)^-]}{c(TeO_2)}$$

The constant, K_1, may then be calculated with the same assumptions about a(HCl) and a_w and the activity coefficient factor used for the Raman work. The $TeCl_4(OH)^-$ ion in HCl solution is expected, on the grounds of nuclear screening, to be less shielded than the $TeCl_6^{2-}$ ion and the chemical shift is expected to be near that observed for the highly concentrated solutions of stoichiometry corresponding to that for $TeCl_4(OH)^-$ in water, i.e. near 1500 ppm. Using the extrapolated value for the shift for $TeCl_6^{2-}$, various $\delta(TeCl_4(OH)^-)$ were chosen to find the value for minimum variation in K_1 as calculated from [1], [6], and the mass and charge balance equations. The optimum value for $\delta(TeCl_4(OH)^-)$ was found to be 1484 ppm for a $\delta(TeCl_6^{2-})$ of either 1375 or 1376 ppm, which gave $K_1 = 1.92 (\pm 0.07) \times 10^4$ M^3. The individual calculated K_1 for each TeO_2 concentration are given in Table 6. This value is close to that calculated from Raman spectroscopy and is lower than K_1 determined by spectrophotometry. As in the case of the Raman measurements, the high TeO_2 concentrations used for the ^{125}Te NMR measurements favours ion pair formation, especially of the dianion, $TeCl_6^{2-}$, and this is the likely cause of the low value of K_1. It should be noted that the chemical shifts of the individual Te(IV) ions will change with their concentration but this effect will be small compared to that resulting from the shift in equilibrium.

Conclusion

Solutions of TeO_2 in hydrochloric acid contain three Te(IV) species, $TeCl_6^{2-}$, $TeCl_4(OH)^-$, and $TeCl_2(OH)_2$. For comparable haloacid concentrations, halo-coordination of Te(IV) is greater for chloride than for fluoride (*7d*). While the $TeX_4(OH)^-$ anion is formed in both cases, there is no evidence for formation of large concentrations of $TeCl_5^-$ in HCl solutions although TeF_5^- is the most highly halo-coordinated ion in the HF solutions.

These results show the expected trend in the acid dissociation of the various chlorotellurate(IV) acids,

$$H_2TeCl_6 > HTeCl_4(OH) > TeCl_2(OH)_2$$

showing that increasing chloro coordination gives stronger protonic acids.

Comparison with Se(IV) behaviour (2, 5) reveals the tendency towards higher coordination by water for the heavier chalcogen species of equal halide-to-chalcogen ratio. The three coordinate $SeOCl_2$ is formed in SeO_2/HCl solutions, while four coordinate $TeCl_2(OH)_2$ is formed in TeO_2/HCl solutions. Furthermore, for comparable hydrochloric acid concentrations, Te(IV) is more highly halocoordinated than Se(IV).

Hydrolysis constants determined for $TeCl_6^{2-}$ (K_1) by a low concentration method (spectrophotometry) and two high concentration methods (Raman and ^{125}Te nmr spectrometry) differ by a factor of about 2 in magnitude with K_1, determined by spectrophotometry, lying higher. The difference may be accounted for by the more favourable ion pair formation of the $TeCl_6^{2-}$ ion compared to the $TeCl_4(OH)^-$ ion. A similar argument has been applied to account for the dependence of acid dissociation constants on the concentration range of the method of measurement used (10, 11).

Acknowledgement

The Natural Sciences and Engineering Research Council is thanked for past support.

1. J. MILNE and M. MAHADEVAN. Inorg. Chem. **23**, 268 (1984).
2. J. MILNE. Can. J. Chem. **65**, 316 (1987).
3. J. MILNE and P. LAHAIE. Inorg. Chem. **24**, 840 (1985).
4. J. MILNE, C. BENSIMON, and E. GABE. Can. J. Chem. In press.

Can. J. Chem. Downloaded from www.nrcresearchpress.com by 198.100.157.202 on 09/07/12
For personal use only.

5. J. MILNE and P. LAHAIE. Inorg. Chem. **18**, 3180 (1979).
6. C. RODGER, N. SHEPPARD, H. C. E. MCFARLANE, and W. MCFARLANE. *In* NMR and the Periodic Table. *Edited by* R. K. Harris and B. Mann. Academic Press, New York. 1979. p. 413
7. (*a*) J. MILNE and P. LAHAIE. Spectrochim. Acta, **39**A, 555 (1983); (*b*) J. MILNE and P. LAHAIE. Inorg. Chem. **18**, 632 (1979); (*c*) J. B. MILNE and D. MOFFETT. Inorg. Chem. **12**, 2240 (1973); (*d*) J. B. MILNE and D. MOFFETT. Inorg. Chem. **13**, 2750 (1974).
8. R. A. ROBINSON and R. H. STOKES. Electrolyte solutions. 2nd ed. Butterworths, London. 1959. Appendix 8.10.
9. M. RANDALL and L. E. YOUNG. J. Am. Chem. Soc. **50**, 1002 (1928).
10. A. K. COVINGTON, J. G. FREEMAN, and T. H. LILLEY. J. Phys. Chem. **74**, 3773 (1970).
11. J. B. MILNE and T. J. PARKER. J. Soln. Chem. **10**, 479 (1981).
12. B. KREBS and V. PAULAT. Angew. Chem. **85**, 662 (1973).

Can. J. Chem. Downloaded from www.nrcresearchpress.com by 198.100.157.202 on 09/07/12
For personal use only.

The structure of the CCl_n^- (n = 1–4) anions and electronic affinities of the corresponding neutrals

G. L. GUTSEV[1] AND TOM ZIEGLER[2]

Chemistry Department, The University of Calgary, 2500 University Drive N.W., Calgary, Alta., Canada T2N 1N4

Received October 10, 1990

G. L. GUTSEV and TOM ZIEGLER. Can. J. Chem. **69**, 993 (1991).

Electronic and geometrical structures for the ground states of the singly charged anions CCl_n^-, n = 1–4, and Cl_m^-, m = 2, 3, as well as the corresponding neutral species have been studied by Approximate Density Functional Theory (DFT). A full geometry optimization has been carried out on both anionic and neutral species. Vertical and adiabatic electron affinities were evaluated for the neutral species along with an estimate of the first ionization potential (FIP) for the anions. A discussion is given of the different dissociation channels for CCl_4^-. It follows from the present set of calculations that the anion CCl_4^- is non-rigid with a global minima corresponding to an elongated tetrahedron of C_{3v} symmetry.

Key words: Density Function Theory, electronic affinities.

G. L. GUTSEV et TOM ZIEGLER. Can. J. Chem. **69**, 993 (1991).

Faisant appel à la théorie des fonctions de densités approximatives, on a étudié les structures électroniques et géométriques des états fondamentaux des anions monochargés CCl_n^-, n = 1–4, et Cl_m^-, m = 2, 3, ainsi que des espèces neutres correspondantes. On a réalisé un optimisation sur la géométrie complète sur les espèces tant anioniques que neutres. On a évalué les affinités électroniques tant verticales qu'adiabatiques des espèces neutres et on a évalué le premier potentiel d'ionisation (PPI) dans anions. On présente une discussion de diverses voies de dissociation du CCl_4^-. Il ressort de cet ensemble de calculs que l'anion CCl_4^- n'est pas rigide et qu'il possède un minima global correspondant à la symétrie C_{3v} d'un tétraèdre allongé.

Mots clés : la théorie des fonctions de densités, affinités électroniques.

[Traduit par la rédaction]

1. Introduction

Many complex molecules possess a large cross section for electron attachment at quite low energies. This property has recently found applications in several areas of technology. The CCl_4 molecule is one of the most extensively studied species of this kind along with other halogen substituted methanes (1–8) and SF_6. Much of the experimental data on electron attachment is obtained from collision experiments with a beam of electrons (reaction [1]), alkali atoms (in the ground or excited states (reaction [2]), or some simple anions (9) (reaction [3]).

[1] $e^- + AB \dashrightarrow AB^{-*} \dashrightarrow A^- + B$

[2] $M + AB \dashrightarrow M^+ + (AB)^-$

[3] $M^- + AB \dashrightarrow M + AB^{-*} \dashrightarrow A^- + B$

The beam experiments afford in general cross sections and rate constants for the processes given above. The formation of the parent CCl_4^- anions seems to be sensitive to the nature of the beam experiment. Thus, the anion is formed with relatively low cross section in collision experiments involving potassium atoms (10) (reaction [2]). On the other hand, the anion is not detected (8) in collision experiments involving electron beams (reaction [1]).

The interpretation of the beam experiments has been hampered by a lack of information on the molecular parameters of CCl_4^- as well as the fragments formed on dissociation. The geometrical structure of CCl_4 has been studied extensively by experiments (11–19) as well as theory (20). The only geometrical information on CCl_4^- comes from an *ab initio* study (21) carried out with a minimal STO-3G basis, which is known to be insufficient (22) for negatively charged species. As for the possible fragments formed from CCl_4^- on dissociation, the neutral species such as Cl, Cl_2, CCl, Cl_3, CCl_3 have been the subject of a great number of investigations (see, e.g., refs. 23–25), and referenes therein). The data on the corresponding anions are, on the other hand, scarce.

The CCl_4^- anion was observed for the first time as early as 1953 (26–28) and the adiabatic electron affinity (EA_{ad}) of the parent CCl_4 molecule was first determined by magnetron techniques (29–31) to be equal to 2.06 eV. Dispert and Lacmann (10) confirmed this value by estimating EA_{ad} of CCl_4 as 2.0 ± 0.2 eV from potassium atom beam experiments according to reaction [2]. Dispert and Lacmann implied further from their experiment that the C—Cl distance in CCl_4^- should be as long as 2.18 Å, which is to be compared to the experimental C—Cl bond distance of 1.77 Å for CCl_4. The estimate of R(C—Cl) by Dispert and Lacmann was based on the assumption that CCl_4^- is tetrahedral. However, ESR experiments on CCl_4^- (21, 32), CBr_4^- (33), and SiH_4^- (34) seem to indicate a distorted tetrahedron of C_{3v} symmetry. It should be mentioned that the sulphur hexafluoride anion (35) appears to retain (36) the O_h symmetry of the SF_6 parent molecule.

The objectives of the present theoretical work have been to explore the potential energy surface of the CCl_4^- anion, to estimate the electron affinity of the parent CCl_4 molecule, and to probe the possible dissociation channels for the CCl_4^- anion. We have, in order to meet the latter objective, optimized the structures of CCl, CCl_2, CCl_3, Cl_2, Cl_3, as well as the corresponding anions. This family of compounds has not been previously the subject of a uniform theoretical study based on a single computational method.

Our theoretical approach will be based on the approximate Density Functional Theory. This theory has been applied extensively to transition metals. However, applications to main-group molecules are rather limited. We would like, in the present study, to demonstrate that the approximate Density Functional Theory provides rather accurate geometrical parameters as well as reasonable estimates of electron affinities for main-group molecules.

[1]On leave from Institute of Chemical Physics of the USSR Academy of Sciences, Chernogolovka, Moscow Region 142432, USSR.

[2]To whom correspondence should be addressed.

Can. J. Chem. Downloaded from www.nrcresearchpress.com by 198.100.157.202 on 09/07/12
For personal use only.

Can. J. Chem. Downloaded from www.nrcresearchpress.com by 198.100.157.202 on 09/07/12
For personal use only.

2. Computational details

All calculations were based on the simple Hartree–Fock–Slater (HFS) or Xα method (37) due to Slater. We have utilized the vectorized version of the HFS-LCAO program system developed by Baerends *et al.* (38, 39) and vectorized by Ravenek (39*b*). The numerical integration procedure applied in the calculations was developed by Becke (40). The geometry optimization procedure was based on the method developed by Versluis and Ziegler (41). All structures were determined at the HFS level of theory with a uniform exchange parameter, α_{ex}, of 0.7. The electronic configurations of the molecular systems were described by an uncontracted triple-ζ STO basis set (42) (ζ_{2s_C} = 1.28, 2.10, and 4.60; ζ_{2p_C} = 0.82, 1.48, and 2.94; $\zeta_{3s_{Cl}}$ = 1.6, 2.3, and 3.3; $\zeta_{3p_{Cl}}$ = 1.2, 2.05, and 2.85) augmented by two 3*d* functions on carbon (ζ_{3d_C} = 3.0 and 1.5) and chlorine ($\zeta_{3d_{Cl}}$ = 3.0 and 1.5). Our basis is of the composition recommended by Baker *et al.* (35) for negative ions. Their recommendation was based on an extensive series of *ab initio* calculations on electron affinities and emphasised the needed for diffuse basis functions. The 1*s*, 2*s*, and 2*p* electrons on Cl and the 1*s* electrons on C were assigned to the core and treated by the frozen-core approximation (38). A set of auxillary (43) *s*, *p*, *d*, *f*, and *g* STO functions, centred on all nuclei, was used to fit the molecular density and present Coulomb and exchange potentials accurately in each SCF cycle.

Electron affinities and bond energies were calculated by augmenting the HFS method (α_{ex} = 2/3) with the local correlation corrections due to Stoll *et al.* (44) in the parametrization by Vosko, Wilk, and Nusair (VWN) (45) as well as Becke's (46) non-local exchange corrections. The correlation correction (Stoll) was included self-consistently whereas Becke's correction was added as a perturbation based on the density from a HFS + Stoll SCF-calculation. The correlation correction by Stoll (44) as well as the exchange correction by Becke (46) eliminate the so-called self-interaction present in the original Local Density Approximation (LDA) due to Gunnarsson (37). It is also important to note that Becke's exchange correction ensures the correct asymptotic behaviour of the exchange potential $V_{ex}(r)$ when r is large (46). The extended version of the LDA method, which we shall refer to as LSD/NL, has been shown to afford metal–ligand and metal–metal bond energies of nearly chemical accuracy (± 5 kcal mol^{-1}) in calculations on metal carbonyls (47), binuclear metal complexes (48), alkyl and hydride complexes (49), as well as complexes containing M—L bonds for a number of different ligands (50). More than 50 molecular structures optimized by the HFS method have been compared with experiment (41). The agreement between experiment and theory is in most cases excellent. However, only four of the optimized structures were anions.

3. Computational results

CCl_4^-

We find for CCl_4^- that the optimized structure of lowest energy corresponds to an elongated tetrahedron, **1***a*, of C_{3v} symmetry. The axial C—Cl distance of 2.58 Å is seen to be elongated considerably compared to the calculated C—Cl distance of the neutral CCl_4 molecule, **1***b*, with R(C—Cl) = 1.77 Å. Three other local minima were located at slightly higher energies. The first, **1***c*, corresponds to a compressed tetrahedron with three long equatorial bonds of R(C—Cl) = 1.975 Å. It resembles closely the structure optimized by Bonazolla *et al.* (21) and is calculated to be 6.93 kcal higher in energy than **1***a*. A second structure, **1***d*, has a tetrahedral geometry with all four bonds stretched at R(C—Cl) = 1.926 Å and an energy of 6.69 kcal above **1***a*. We have finally located the structure **1***e* of C_{2v} symmetry with one pair of elongated bonds at R(C—Cl) = 2.08 Å and an open Cl—C—Cl angle of 117.5°. This structure is calculated to be 6.48 kcal mol^{-1} above **1***a* in energy.

The CCl_4^- anion in the tetrahedral conformation, **1***d*, can interconvert along the normal modes to the other structures (**1***a*, **1***c*, and **1***e*) with a negligible barrier of less than 2 kcal mol^{-1} on top of the thermodynamical energy difference between **1***d* and any of the structures **1***a*, **1***c*, and **1***e*. Thus the anion is essentially a non-rigid molecule according to our calculations. The fluxional behaviour of CCl_4^- is related to the fact that the unpaired electron occupies a strongly anti-bonding orbital which is distributed over different centers in the various conformations. The anti-bonding orbital for the most stable structure, **1***a*, is concentrated between the axial ligand Cl_a and carbon, **2**. Thus the odd electron resides in this case in the elongated axial bond. Each of the structures (**1***a*, **1***c–e*) can be seen as a channel for the decomposition of CCl_4^- with **1***a* representing a fragmentation of CCl_4^- into CCl_3 and Cl^-. We shall later return to this point. It is interesting that the optimized Cl_{ax}—C—Cl_{eq} angle in **1***a* still is close to tetrahedral. The angle will eventually increase as the C—Cl_{ax} bond is stretched to the CCl_3 + Cl^- dissociation. The structure of CCl_3 will be discussed later.

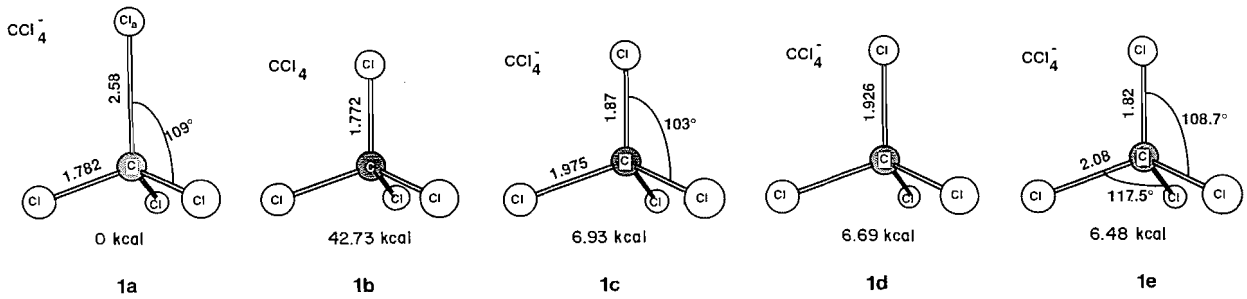
There are only indirect experimental data on the structure of CCl_4^-. Dispert *et al.* (10) inferred from their potassium atom beam experiment a C—Cl distance of 2.18 Å by assuming CCl_4^- to have a tetrahedral structure. This distance is somewhat longer than the 1.93 Å calculated in the present study for the tetrahedral conformation, **1***d*, of CCl_4^-. The ESR experiments by Bonazolla *et al.* (21) indicate clearly that CCl_4^- has a structure of C_{3v} symmetry with either an elongated, **1***a*, or compressed, **1***c*, tetrahedron. Our calculations point to the elongated structure, **1***a*, as the more stable; whereas Bonazolla *et al.* (21), based on an *ab initio* HF calculation with a minimal basis set, found CCl_4^- to have the structure of a compressed tetrahedron, **1***c*. It would be of interest to redo the *ab initio* study with the same extensive basis set as employed in our DFT calculations. Our calculated C—Cl bond distance of 1.772 Å for CCl_4 compares well with the experimental value of 1.769 Å (12*a*) and the calculated average bond energy $\bar{D}$(C—Cl) of 3.0 eV for CCl_4 is also in line with the experimental value of 3.3 eV.

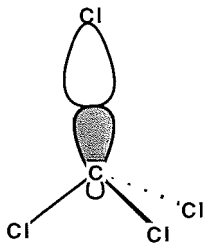
Table 1 presents calculations on the vertical (EA_{vert}) and adiabatic (EA_{ad}) electron affinities of CCl_4 as well as the first ionization potential (FIP) of CCl_4^-. FIP can also be viewed as EA_{vert} of CCl_4 at the equilibrium geometry of the anion CCl_4^-. Our calculated values are in reasonable agreement with experimental findings. The large observed (Table 1) difference between the vertical and adiabatic electron affinity of CCl_4 is in line with the substantial difference in geometry between CCl_4, **1***b*, and CCl_4^-, **1***a*.

CCl^-

Results from calculations on the neutral radical CCl and the anion CCl^- are presented in Table 2. For CCl, there are experimental data on the bond length (53) and the dissociation energy (51–53). Our theoretical bond length is very close to the experimental value whereas the theoretical bond energy differs by 0.5 eV from the observed value (Table 2). We expect part of the deviation to be due to experimental uncertainties.

Experimental data are not available for CCl^-. The additional electron enters into an anti-bonding 2π orbital. It is thus not surprising that CCl^- is calculated to have a long R(C—Cl) bond





2

distance of 1.91 Å and a modest bond dissociation energy of 1.56 eV (Table 2). It is interesting to note that the bond length and dissociation energy calculated for CCl^- in this work are in very close agreement with the highest levels of theory (MP4SDTQ) in a recent publication (54) where results from several *ab initio* methods were compared, Table 2.

CCl_2^-

Dihalocarbenes are important constituents in several organic and organometallic compounds. This class of extremely reactive intermediates has been studied extensively by theoretical (55–57) as well as experimental (58–60) techniques. Of particular interest has been the energy separation between the singlet $^1A_1$ ($a_1^2 b_1^0$) and the triplet $^3B_1$ ($a_1^1 b_1^1$) states (61–64) as well as their geometrical structures (65). It is well established that CCl_2 has a singlet ground state. However, only a rough experimental estimate of 31 ± 10 kcal mol^{-1} (63) is available for the singlet–triplet separation. Further, geometrical parameters are only known experimentally for the singlet (65). Our calculated singlet structure, **3***a*, is quite close to that obtained in the recent experimental (65) study by Fujitake and Hirota, Table 3. We calculate (Table 3) that the triplet, **3***b*, has a wider angle and a shorter C—Cl bond than the singlet, **3***a*. This trend, which can be explained readily from simple perturbational molecular orbital considerations (PMO), was also found in the theoretical study by Bauschlicher *et al.* (56), Table 3. Triplet–singlet separations obtained by *ab initio* methods for carbenes are quite sensitive to the extent of correlation included in the calculations. Hartree–Fock (56) affords only 0.1 kcal mol^{-1} for CCl_2 whereas GVB (56), Table 3, gives 13.5 kcal mol^{-1}. The most extensive *ab initio* calculation to date on CCl_2 applied the CCCl method by Goddard and Carter (63). The CCCl calculation afforded a separation of 25.9 kcal mol^{-1} (Table 3), which is close to our estimate of 23.7 kcal mol^{-1} and the rough experimental estimate of 31 ± 10 kcal mol^{-1}.

The CCl_2^- anion appears not to have been studied by *ab initio* methods. We calculate the anion to possess two states with an energy below that of a free electron and the neutral parent molecule in its $^1A_1$ ground state, **3***a*. The calculated ground state is of $^2B_1$ ($a_1^2 b_1^1$) symmetry. Its optimized geometry, **3***c*, is quite similar to the structure recently deduced by Murray *et al.* (66) from IR spectroscopy. Murray *et al.* (66) deduced a C—Cl bond distance of 1.91 Å and a bond angle of 103°. The second state, of $^2A_1$ ($a_1^1 b_1^2$) symmetry, **3***d*, has a wide Cl—C—Cl angle of 164° and a considerably stretched C—Cl bond of 2.18 Å. Murray *et al.* (66) have also determined EA_{ad} for CCl_2. Their experimental

TABLE 1. Vertical[a,b] (EA_{vert}) and adiabatic (EA_{ad}) electron affinities for CCl_n and Cl_m as well as the first ionization potential (FIP) for CCl_n^- and Cl_m^-

Species	EA_{ad}[e] (eV)	EA_{vert}[f] (eV)	FIP (eV)
CCl_4	1.65 (2.06)[c]	−0.49 (−1.0 ± .2)[d]	2.07
CCl_3	2.36 (>2.10)[g]	0.05	2.68
CCl_2	1.61 (1.60)[h]	0.38	1.67
CCl	0.93	0.25	1.16
Cl_2	3.05 (2.5)[i]	3.06	3.92
Cl_3	4.34 (4.6–5.1)[j]	3.85	4.41
Cl	3.28 (3.6)[k]		
C	0.97 (1.26)[k]		

[a]Experimental numbers in parentheses.
[b]All energy calculations were based on the LSD/NL method.
[c]Reference 6.
[d]Reference 30.
[e]Corresponding to the difference in energy between the neutral CCl_n molecule in its optimized conformation of lowest energy and the CCl_n^- anion in its optimized conformation of lowest energy.
[f]With respect to the ground state conformation of the neutral CCl_n molecule.
[g]The most recent experimental value from ref. 73. Other experimental values are >1.9, see ref. 74, >1.45, see ref. 75.
[h]Reference 66.
[i]Reference 82.
[j]Reference 88.
[k]Reference 89.

TABLE 2. Dissociation energies[a] (eV) and bond lengths (Å) for the CCl molecule ($^2\Pi$, $3\sigma^2 2\pi^1$) and CCl^- anion ($^3\Sigma$, $3\sigma^2 2\pi^2$)

Species	*R*(C—Cl)	*D*(C—Cl)
CCl	1.642 (1.645)[b]	3.87 (3.34)[c]
CCl^-	1.907	1.56[d]
CCl^-[e]	1.87	1.69[d]

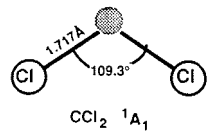
[a]Experimental data in parentheses.
[b]Experimental data for *R*(C—Cl), see ref. 53.
[c]Experimental data for bond energy *D*(C—Cl), see ref. 52.
[d]Dissociation energy for $CCl \rightarrow C + Cl^-$.
[e]From MP4SDTQ ab initio calculations, see ref. 54.

Can. J. Chem. Downloaded from www.nrcresearchpress.com by 198.100.157.202 on 09/07/12
For personal use only.

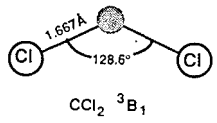
TABLE 3. Geometries[a] and singlet–triplet splittings (kcal mol^{-1}) for CCl_2

Molecule	R(C—Cl)	∠ClCCl	$\Delta E(^3B_1 - {}^1A_1)$	Method
CCl_2 ($^1A_1$)	1.717 (1.716)[b]	109.3′ (109.2°)[b]	23.7 (31 ± 11)[c]	LSD/NL
CCl_2 ($^3B_1$)	1.667	128.9°		LSD/NL
CCl_2 ($^1A_1$)	1.756	109.4°	13.5	GVB[d]
CCl_2 ($^3B_1$)	1.730	125.5°		GVB[d]
CCl_2			25.9	CCCI[e]

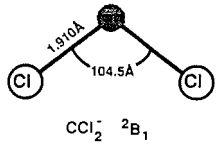
[a]Experimental values in parentheses.
[b]Experimental structure from ref. 65.
[c]Experimental estimate from ref. 63.
[d]Theoretical calculations from ref. 56.
[e]Theoretical calculations from ref. 63.



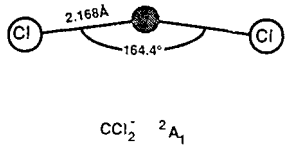
3a



3b



3c



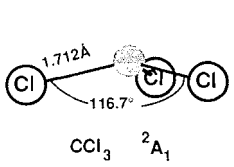
3d

value of 1.60 eV is in excellent agreement with our theoretical estimate of 1.61 Ev, Table 1.

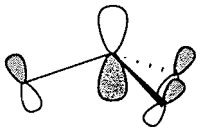
CCl_3^-

We find the CCl_3 molecule to have a trigonal pyramidal equilibrium structure of C_{3v} symmetry, **4***a*, with a $^2A_1$ ground state where the unpaired electron is residing in a π^* orbital, **4***b*, with an a_1' designation. The geometry of CCl_3 has been investigated by *ab initio* methods (67–70) as well as ESR (71, 72) and vibrational spectroscopy (70). All studies point to a trigonal bipyramidal structure of C_{3v} symmetry. The most recent structural information comes from the work by Hudgens *et al.* (70) in which they deduce a Cl—C—Cl angle of 116.7° from IR spectroscopy and a C—Cl distance of 1.7142 Å from an *ab initio* calculation at the UHF/6-31G* level of theory. Both numbers are in close agreement with our findings, **4***a*.

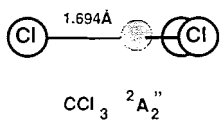
The inversion of **4***a* through the trigonal planar transition state, **4***c*, was calculated to have a barrier of 2.541 kcal mol^{-1}. The best experimental estimate (70) gives 1.3 kcal mol^{-1}.



4a



4b



4c

Earlier experimental studies (10, 29–31) on the electron affinity of CCl_3 gave a low value for EA_{ad} of 1.3 eV. The more recent estimates (73–75) are somewhat higher at around 2 eV

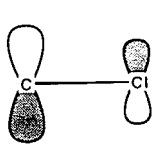
TABLE 4. Bond distances[c] (Å) and bond energies (eV) for Cl_2 and Cl_3 as well as their anions

Molecule	R(Cl—Cl)	D(Cl—Cl)
Cl_2	1.993 (1.988)[b]	2.02 (2.5)[c]
Cl_2^-	2.696 (2.65)[d]	1.78 (1.26)[b]
Cl_3 ($^2\Pi_u$)	2.179	0.45
Cl_3 ($^2A_1$)	2.159[e]	0.47
Cl_3^- ($^1\Sigma_g$)	2.317	1.73[f]
		1.97[g]

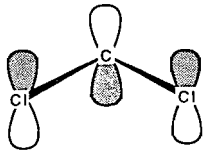
[a]Experimental values in parentheses.
[b]Reference 90.
[c]Reference 91.
[d]Rough-estimate based on Morse potential curve fitting techniques, see refs. 76, 77.
[e]Cl—Cl—Cl angle 153.6°.
[f]For the process $Cl_3^- \rightarrow Cl_2 + Cl^-$.
[g]For the process $Cl_3^- Cl_2^- + Cl$.

(Table 1). Our calculated value at 2.36 eV is close to the most recent experimental estimate (74) of 1.9 ± 0.2 eV (Table 1).

We calculate an increase in the electron affinities through the series CCl_n $n = 1, 3$ as well as a decrease in FIP in CCl_n^-, $n = 1, 3$ (Table 1). The HOMO's of CCl_n^- (n = 1–3) are for all three anions essentially a π^* orbital represented by **5***a*, **5***b*, and **4***b* for CCl, CCl_2^-, and CCl_3, respectively. The calculated trends can be rationalized by observing that the excess electron density achieves a favorable increase in delocalization through the series **5***a* (CCl^-), **5***b* (CCl_2^-), and **4***b* (CCl_3^-). The CCl_4 molecule does not fit into the series since CCl_4^- has a σ^* type HOMO, **2**, rather than a HOMO with π^* character. The excess electron density in CCl_4^- achieves some delocalization on account of the substantially stretched C—Cl bond with R(C—Cl) = 2.58 Å. The calculated values for EA_{ad}, EA_{vert}, and FIP fall between those of CCl_3 and CCl_2, (Table 1).



5a



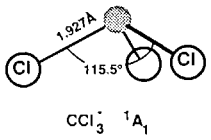
5b

The CCl_3^- anion appears not to have been studied previously by experimental or theoretical techniques. We find the CCl_3^- anion to have a $^1A_1$ (a'^2) ground state with a trigonal pyramidal structure, **6***a*, of C_{3v} symmetry where the C—Cl bond has been stretched to 1.93 Å. The inversion through the transition state, **6***b*, has a substantial barrier of 27 kcal mol^{-1}.

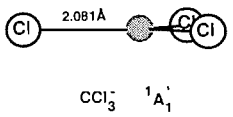
Can. J. Chem. Downloaded from www.nrcresearchpress.com by 198.100.157.202 on 09/07/12
For personal use only.

TABLE 5. Dissociation energies (eV) for CCl_n^-

Process	D(C—Cl)	Process	D_1(C—Cl)
$CCl_4^- \rightarrow CCl_3 + Cl^-$	0.70	$CCl_4^- \rightarrow CCl_3^- + Cl$	1.58
$CCl_3^- \rightarrow CCl_2 + Cl^-$	1.29	$CCl_3^- \rightarrow CCl_2^- + Cl$	2.92
$CCl_2^- \rightarrow CCl + Cl^-$	1.41	$CCl_2^- \rightarrow CCl^- + Cl$	3.72
$CCl^- \rightarrow C + Cl^-$	1.56	$CCl^- \rightarrow C^- + Cl$	3.84



6a

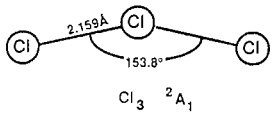


6b

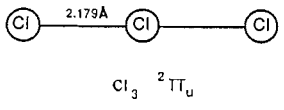
Cl_2^- and Cl_3^-

Calculated bond distances and bond energies for Cl_2 and Cl_3 as well as their anions are compared in Table 4 with experimental data, where available. The theoretical values compare reasonably well with experiment for Cl_2 and Cl_2^- (Table 4). The experimental bond distance for Cl_2^- ($\sim$ 2.65 Å) is a rough estimate (76, 77) based on a Morse potential curve fitting technique. Bond distances calculated by the HFS method are usually on the short side and our value of 2.69 Å, Table 5, might well be a lower bound. It should be noted that a recent *ab initio* study (78) found R(C—Cl) = 2.65 Å. There have been several experimental (10, 79–82) and a few theoretical (78) studies on the electron affinity of Cl_2. Our calculated value of 3.0 eV for EA_{ad} is somewhat higher than the favoured value of 2.5 eV (Table 1).

The Cl_3 radical was calculated to have two nearly degenerate states. The first has a linear structure, **7***b*, with a $^2\Pi_u$ ($3\sigma_g^2 2\pi_u^3$) electronic state whereas the second, which is calculated to be 0.5 kcal mol^{-1} lower in energy has a bent structure, **7***a*, with a $^2A_1$ ($3\sigma_g^1 2\pi_u^4 = 5a_1^2 2b_1^2 4a_1^2$) electronic state. The near degeneracy between the two states parallels a similar degeneracy between $3\sigma_g$ and $2\pi_u$ as discussed by Sannigrahi and Peyerimhoff (83, 84). These authors obtained structures quite similar to ours. However, the bent structure, **7***a*, is, according to their MRD-Cl calculations 7 kcal mol^{-1} more stable than the linear structure, **7***b*. Experimental data are not available on the structure of Cl_3 radical.

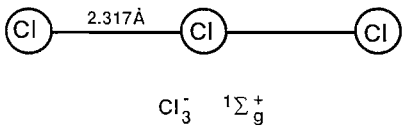


7a



7b

We find the Cl_3^- anion to have a linear structure with a $^1\Sigma_g$ ($3\sigma_g^2 2\pi_u^3$) ground state and a Cl—Cl bond distance of 2.32 Å, **8**. Earlier calculations carried out within the HF method without (85) or with pseudopotentials (86) have predicted somewhat larger bond lengths (2.54–2.41 Å) for this anion. However, the bond distances calculated recently by the MRD-Cl (84) and



8

TABLE 6. Dissociation channels for CCl_4

Channel	Dissociation energy (eV) Calculated	Observed[a]
$CCl_4^- \rightarrow CCl_3 + Cl^-$	0.70	1.4
$CCl_2 + Cl_2^-$	1.13	3.8
$CCl_3^- + Cl$	1.58	3.6
$CCl + Cl_3^-$	2.25	—
$CCl_2^- + Cl_2$	2.57	4.4

[a]Semiquantitative estimates from the energy loss spectrum, see ref. 6.

DVM-X_α (87) methods of 2.34 and 2.35 Å, respectively, are quite close to our estimate. The calculated energies for the dissociation of Cl_3^- into $Cl_2 + Cl^-$ (1.73 eV) and $Cl_2^- + Cl$ (1.97 eV), Table 4, are quite close to the theoretical estimates of Tasker *et al.* (86) with 1.69 and 1.57 eV, respectively.

We find the adiabatic electron affinity of Cl_3 to be 4.5 eV, which is close to the range (4.6–5.1 eV) of experimental values (Table 1). We note that EA_{ad} and EA_{vert} for Cl_3 and FIP for Cl_3^- are calculated to be larger than the corresponding values in the dichloro systems (Table 1). This is not surprising since the excess electron density is better able to delocalize in Cl_3^- compared to Cl_2^-. We have for the sake of completeness included the calculated electron affinities of the carbon and chlorine atoms in Table 1.

Dissociation channels for CCl_4^- and bond dissociation energies for CCl_n (n = 1,4)

We find that the dissociation channel of lowest energy for CCl_n^- in all cases (n = 1, 4) corresponds to the process

[4] $CCl_n^- \rightarrow CCl_{n-1} + Cl^-$

The dissociation energy for reaction [4] is given in Table 5 for n = 1, 4. It follows that all the anions, CCl_n- (n = 1, 4), are stable with respect to the corresponding fragments CCl_{n-1} and Cl^-. The dissociation of CCl_n^- into CCl_{n-1}^- and Cl requires substantially more energy (Table 5), in accordance with the fact that Cl has a larger electron affinity than any of the CCl_n^- species (Table 5).

Lacmann *et al.* (6) have carried out collision experiments with CCl_4 and a beam of potassium atoms. The CCl_4^- anions formed according to reaction [2] will fragment due to the excess energy transferred from the potassium atoms during the collision. Lacmann *et al.* (6) were able to deduce a rough estimate of the energies for the different dissociation channels based on the energy loss spectrum. The estimates, which likely are rough upper bounds, are compared to calculated dissociation energies in Table 6. We have, in our calculations, considered all channels with a dissociation energy below 3 eV. There is a general agreement between theory and experiment as to the nature of the

Can. J. Chem. Downloaded from www.nrcresearchpress.com by 198.100.157.202 on 09/07/12
For personal use only.

low-energy dissociation channels. However, the experimental estimates for the dissociation energies are most likely too high.

4. Concluding remarks

We have investigated the molecular and electronic structure of CCl_n^- ($n = 1, 4$) and Cl_m^- ($m = 2, 3$) as well as the parent neutral molecules using the approximate Density Functional Theory. We find a good agreement between observed and calculated structures for the neutrals, where experimental data are available. The structures of the anions have not been investigated by diffraction techniques and our calculations constitute the first extensive investigation on CCl_4^-, CCl_3^-, and CCl_2^-. The CCl_4^- anion was found to be non-rigid with several structures of similar energies (**1***a*, **1***c*–**1***e*) connected by low barrier paths. The global minima was calculated to have the structure of an elongated tetrahedron, **1***a*.

The calculated adiabatic affinities are, in general, in good agreement with experiment. We find for the series CCl_3, CCl_2, CCl as well as Cl_3, Cl_2, an increse in EA_{ad} with the number of Cl atoms. All members of the series accommodate the additional electron in a π-type orbital delocalized over all centers and the rise in EA_{ad} with the number of chlorine atoms stems from an increasing ability to delocalize the excess change.

The CCl_n anions were found to be stable with respect to dissociation into smaller fragments. The decomposition channel of lowest energy was in all cases calculated to be represented by

$$CCl_n^- \rightarrow CCl_{n-1} + Cl^-$$

A more detailed analysis was further provided for the decomposition of CCl_4^- in which all dissociation channels with an energy below 3 eV were identified as

[a] $CCl_4^- \rightarrow CCl_3 + Cl^- + 0.70$ eV

[b] $CCl_4^- \rightarrow CCl_2 + Cl_2^- + 1.13$ eV

[c] $CCl_4^- \rightarrow CCl_3^- + Cl + 1.58$ eV

[d] $CCl_4^- \rightarrow CCl + Cl_3^- + 2.25$ eV

[e] $CCl_4^- \rightarrow CCl_2^- + Cl_2 + 2.57$ eV

These are essentially the dissociation channels observed experimentally in beam experiments with potassium atoms. Our dissociation energies are considerably lower than the experimental estimates. However, these estimates are most likely upper bounds of the actual values.

We have in the present investigation made use of the LDA/NL method. It is shown elsewhere (92), for a larger sample of molecules, that this method affords better estimates of EA_{ad} than HFS and LDA. In fact, the calculated electron affinities are as accurate as the best available *ab initio* methods in which a substantial part of the electron correlation is taken into account. The success of the LDA/NL method compared to the HFS and LDA schemes stems in large measure from the elimination of the spurious self-interaction terms present in HFS and LDA. The non-local exchange correction due to Becke was introduced in the present work as a perturbation, without taking into account the SCF effects. We have found in a recent investigation (93) that the change in density induced by Becke's non-local correction is negligible and we expect this to be the case for the anions studied here.

Acknowledgments

This investigation was supported by the Natural Sciences and Engineering Research Council of Canada (NSERC). We acknowledge an international collaboration grant from NSERC to G.L.G. We thank the University of Calgary for access to their Cyber-205 facilities.

1. W. E. Wentworth, R. George, and H. Keith. J. Chem. Phys. **51**, 1791 (1969).
2. A. A. Christodoulides and L. G. Christophorou. J. Chem. Phys. **54**, 4691 (1971); L. G. Christophorou. Atomic and molecular radiation physics. Wiley–Interscience, New York, 1971.
3. F. J. Davis, R. N. Compton, and D. R. Nelson. J. Chem. Phys. **59**, 2324 (1973).
4. D. Spence and G. J. Schultz. J. Chem. Phys. **58**, 1800 (1973).
5. H.-U. Scheunemann, E. Illenberger, and H. Baumgärtel. Ber. Bunsenges. Phys. Chem., **84**, 580 (1980).
6. K. Lacmann, M. J. P. Maneira, A. M. C. Moutinho, and U. Weigmann. J. Chem. Phys. **78**, 1767 (1983).
7. C. W. Walter, K. A. Smith, and F. B. Dunning. J. Chem. Phys. **90**, 1652 (1989).
8. T. Oster, A. Kühn, and E. Illenberger. Int. J. Mass Spectrom. Ion Processes, **89**, 1 (1989).
9. L. G. Christoforou. (*Editors*). Electron-molecule interactions and their applications. Academic Press. New York. 1984.
10. H. Dispert and K. Lacmann. Int. J. Mass Spectrom. Ion Phys., **28**, 49 (1978).
11. L. O. Brockway. Acta Crystallogr. **7**, 682 (1954).
12. L. S. Bartell, L. O. Brockway, and R. H. Scheunemann. J. Chem. Phys. **23**, 1854 (1955).
13. Y. Morino, Y. Nakamura, and T. Iijuma. J. Chem. Phys. **32**, 643 (1960).
14. S. Cohen, K. Powers, and R. Rudman. Acta Crystallogr. Sect. B: Struct. Crystallogr. Cryst. Chem. **35**, 1670 (1969).
15. J. C. Whitehead, D. R. Hardin, and R. Grice. Mol. Phys. **23**, 787 (1972).
16. G. Reichelt, J.-U. Weidner, and H. W. Zimmerman. Ber. Bunsenges. Phys. Chem., **78**, 1050 (1974).
17. A. H. Narten. J. Chem. Phys. **65**, 573 (1976).
18. J. B. Van Tricht. J. Chem. Phys. **66**, 85 (1977).
19. J. R. Granada, G. W. Stanton, J. H. Clarke, and J. C. Dore. Mol. Phys. **37**, 1297 (1979).
20. S. S. Choi, R. J. Boyd, and O. Knop. Can. J. Chem. **66**, 2465 (1988).
21. L. Bonazzola, . P. Michaut, and J. Roncin. Chem. Phys. Lett. **153**, 52 (1988).
22. R. S. Mulliken and W. C. Ermler. Polyatomic molecules. Results of *ab initio* calculations. Academic Press, New York. 1981.
23. W. Kirmse. Carbene chemistry. Academic Press, New York. 1971.
24. R. A. Moss and M. Jones, Jr. (*Editors*). Carbenes. Wiley Interscience, New York. 1982.
25. E. R. Davidson. *In* Diradicals. *Edited by* W. T. Borden. Wiley Interscience, New York. 1982.
26. H. O. Pritchard. Chem. Rev. **52**, 529 (1953).
27. W. M. Hickam and D. Berg. J. Chem. Phys. **29**, 517 (1958).
28. J. S. Buchel'nicova. Usp.fiz.nauk, **65**, 351 (1958); Sov. Phys. JETP, **8**, 783 (1959).
29. A. F. Gaines, J. Kay, and F. M. Page. Trans. Faraday Soc. **62**, 874 (1966).
30. F. M. Page and G. C. Goode. Negative ions and magnetron. Wiley Interscience, London, 1969.
31. J. L. Franclin and P. W. Harland. Ann. Rev. Phys. Chem. **25**, 485 (1974).
32. W. E. Wentworth and W. Ristau. J. Phys. Chem. **73**, 2129 (1969).
33. J. A. Connor, J. P. Day, and R. M. Turner. J. Chem. Soc. Chem. Commun. 578 (1973).
34. A. Hasegawa, S. Uchimura, and M. Hayashi. J. Magn. Reson. **38**, 391 (1980).

Can. J. Chem. Downloaded from www.nrcresearchpress.com by 198.100.157.202 on 09/07/12
For personal use only.

Can. J. Chem. Downloaded from www.nrcresearchpress.com by 198.100.157.202 on 09/07/12
For personal use only.

35. P. J. HAY. J. Chem. Phys. **76**, 502 (1982); R. TANG and J. CALLAWAY. J. Chem. Phys. **84**, 6854 (1986); M. KLOBUKOWSKI, Z. BARANDIARAN, L. SEIJO, and S. HUZINAGA. J. Chem. Phys. **85**, 1637 (1987); E. MIYOSHI, Y. SAKAI, and S. MIYOSHI. J. Chem. Phys. **88**, 1470 (1988); J. BAKER, R. H. NOBES, and L. RADOM. J. Comp. Chem. **7**, 349 (1986).
36. E. P. GRIMSRUD, S. CHOWDHURY, and P. KEBARLE. J. Chem. Phys. **83**, 1059 (1985).
37. J. C. SLATER. Phys. Rev. **81**, 385 (1951); O. GUNNARSSON and I. LUNDQUIST. Phys. Rev. B**13**, 4274 (1976).
38. E. J. BAERENDS, D. E. ELLIS, and P. ROS. Chem. Phys. **2**, 41 (1973).
39. (*a*) E. J. BAERENDS. Ph.D. Thesis. Vrije Universiteit, Amsterdam. 1975; (*b*) W. RAVENEK. *In* Algorithms and applications on vector and parallel computers. *Edited by* H. J. J. Riele, Th. J. Dekker and H. A. van de Vorst. Elsevier, Amsterdam, 1987.
40. A. D. BECKE. J. Chem. Phys. **88**, 2547 (1988).
41. L. VERSLUIS and T. ZIEGLER. J. Chem. Phys. **88**, 322 (1988).
42. (*a*) G. J. SNIJDERS, E. J. BAERENDS and P. VERNOIJS. At. Nucl. Data. Tables **26**, 483 (1982); (*b*) P. VERNOIJS, G. J. SNIJDERS, and E. J. BAERENDS. Slater type basis functions for the whole periodic system. Internal report, Free University of Amsterdam, The Netherlands, 1981.
43. J. KRIJN and E. J. BAERENDS. Fit functions in the HFS-method. Internal Report (in Dutch), Free University of Amsterdam, The Netherlands. 1984.
44. H. STOLL, C. M. E. PAVLIDOU, and H. PREUSS. Theor. Chim. Acta, **49**, 143 (1978); H. STOLL, E. GOLKA, and H. PREUSS. Theor. Chim. Acta, **55**, 29 (1980).
45. S. H. VOSKO, L. WILK, and M. NUSAIR. Can. J. Phys. **58**, 1200 (1980).
46. A. BECKE. J. Chem. Phys. **84**, 4524 (1986); **88**, 1053 (1988).
47. T. ZIEGLER, V. TSCHINKE, and C. URSENBACK. J. Am. Chem. Soc. **109**, 4825 (1987).
48. T. ZIEGLER, V. TSCHINKE, and A. BECKE. Polyhedron, **6**, 685 (1987).
49. (*a*) T. ZIEGLER, V. TSCHINKE, and A. BECKE. J. Am. Chem. Soc. **109**, 1351 (1987); (*b*) T. ZIEGLER, W. CHENG, E. J. BAERENDS, and W. RAVENEK. Inorg. Chem. **27**, 3458 (1988); (*c*) T. ZIEGLER, V. TSCHINKE, E. J. BAERENDS, G. J. SNIJDERS, and W. RAVENEK. J. Phys. Chem. **93**, 3050 (1989).
50. T. ZIEGLER, V. TSCHINKE, L. VERSLUIS, E. J. BAERENDS, and W. RAVENEK. Polyhedron, **7**, 1625 (1988).
51. M. E. JACOX and D. E. MULLIGAN. J. Chem. Phys. **53**, 2688 (1970).
52. R. D. GORDON and G. W. KING. Can. J. Phyc., **39**, 252 (1961).
53. R. D. VERMA and R. S. MULLIKEN. J. Mol. Spectrosc. **6**, 419 (1961).
54. K. A. PETERSON and R. C. WOODS. J. Chem. Phys. **93**, 1876 (1990).
55. R. HOFFMAN, G. D. ZEISS, and G. W. VAN DINE. J. Am. Chem. Soc. **90**, 1485 (1968).
56. C. W. BAUSCHLICHER, JR., H. F. SHAEFER, III, and P. S. BAGUS. J. Am. Chem. Soc. **99**, 7106 (1977).
57. M. T. NGUEN, M. C. KERRINS, A. F. HEGARTY, and N. J. FITZPATRICK. Chem. Phys. Lett. **117**, 295 (1985).
58. L. ANDREWS. J. Chem. Phys. **48**, 979 (1968).
59. D. E. MILLIGAN and M. E. JACOX. J. Chem. Phys. **47**, 703 (1967).
60. D. E. TEVAULT and L. ANDREWS. J. Mol. Spectrosc. **54**, 110 (1975).
61. T. K. HA, H.-U. GREMLICH, and R. E. BÜHLER. Chem. Phys. Lett. **65**, 16 (1979).
62. E. A. CARTER and W. A. GODDARD, III. J. Phys. Chem. **91**, 4651 (1987); J. Chem. Phys., **88**, 1752 (1988).
63. E. A. CARTER and W. A. GODDARD, III. J. Phys. Chem. **90**, 998 (1986).
64. P. H. MUELLER, N. G. RONDAN, K. N. HOUK, J. F. HARRISON, D. HOOPER, B. H. WILLEN, and J. F. LIEBMAN. J. Am. Chem. Soc. **103**, 5049 (1981).
65. M. FUJITAKE and E. HIROTA. J. Chem. Phys. **91**, 3426 (1989).
66. K. K. MURRAY, D. G. LEOPOLD, T. M. MILLER, and W. C. LINEBERGER. J. Chem. Phys., **89**, 5442 (1988).
67. J. MOC, Z. LATAJKA, and H. RATAJCZAK. Z. Phys., D**4**, 185 (1986).
68. B. T. LUKE, G. H. LOEW, and A. D. MCLEAN. I. Am Chem. Soc. **109**, 1307 (1987).
69. J. MOC, J. M. RUDZINSKI, Z. LATAJKA, and H. RATAJCZAK. Chem. Phys. Lett. **168**, 79 (1990).
70. J. W. HUDGENS, R. D. JOHNSON, III, B. T. TSAI, and S. A. KAFAFI. J. Am. Chem. Soc. **112**, 5763 (1990).
71. G. MAAS, A. K. MALTSEV, and J. L. MARGRAVE. J. Inorg. Nucl. Chem. **35**, 1945 (1973).
72. L. ANDREWS. J. Chem. Phys. **48**, 972 (1968).
73. R. K. CURRAN. J. Chem. Phys. **34**, 2007 (1961).
74. H.-U. SCHEUNEMANN, E. ILLENBERGER, and H. BAUMGÄRTEL. Chem. Phys. **37**, 21 (1979).
75. D. K. BOHME, E. LEE-RUFF, and L. B. YOUNG. J. Am. Chem. Soc. **94**, 5153 (1972).
76. W. B. PEARSON. J. Chem. Phys. **38**, 109 (1963); M. M. HUBERS, A. W. KLEYN, and J. LOS. Chem. Phys. **17**, 303 (1976); J. A. AJALA, W. E. WENTWORTH, and E. C. M. CHEN. J. Phys. Chem. **85**, 768 (1981).
77. E. C. M. CHEN and W. E. WENTWORTH. J. Phys. Chem. **89**, 4099 (1985).
78. M. T. NGUEN and T.-K. HA. Chem. Phys. Lett. **136**, 413 (1987).
79. J. J. DECORPO and J. L. FRANKLIN. J. Chem. Phys. **54**, 1885 (1971); K. LACMANN and D. R. HERSCHBACK. Chem. Phys. Lett. **6**, 106 (1970); D. B. DUNKIN, F. C. FEHSENFELD, and E. E. FERGUSON. Chem. Phys. Lett. **15**, 257 (1972); S. Y. TANG, C. B. LEFFERT, E. W. ROTHE, and G. P. RECK. J. Chem. Phys. **62**, 132 (1975); H. DISPERT and K. LACMANN. Chem. Phys. Lett. **47**, 533 (1977).
80. A. P. W. BAEDE. Physica, **59**, 541 (1972).
81. B. M. HUGHES, C. LIFTSHITZ, and T. O. TIENAN. J. Chem. Phys. **59**, 3162 (1973).
82. B. M. SMIRNOV. Negative Ions. Moscow, Atomizdat. 1978 (in Russian).
83. A. B. SANNIGRAHI and S. D. PEYERIMHOFF. Int. J. Quantum Chem. **30**, 413 (1986).
84. A. B. SANNIGRAHI and S. D. PEYERIMHOFF. Chem. Phys. Lett. **141**, 49 (1987).
85. E. F. RIEDEL and R. D. WILLET. Theor. Chim. Acta, **42**, 237 (1976).
86. P. W. TASKER. Mol. Phys. **33**, 511 (1977), P. W. TASKER, G. G. BALINT-KURTI, and R. N. DIXON. Mol. Phys. **32**, 1651 (1976).
87. G. L. GUTSEV. Russian J. Struct. Chem. **30**, 41 (1989).
88. K. H. BOWEN, G. W. LIESENGANG, R. A. SANDERS, and D. R. HERSCHBACH. J. Phys. Chem. **87**, 557 (1983).
89. H. HOTOP and W. C. LINEBERGER. J. Phys. Chem. Ref. Data, **14**, 731 (1985).
90. K. P. HUBER and G. HERZBERG. Molecular spectra and molecular structure, IV. Constants of diatomic molecules. Van Nostrand Reinhold, New York. 1979.
91. G. LIAS, J. F LIEBMAN, and R. D. LEVIN. J. Phys. Chem. Ref. Data, **13**, 695 (1984).
92. T. ZIEGLER and G. L. GUTSEV. J. Comp Chem. To be published.
93. L. FAN and T. ZIEGLER. J. Chem. Phys. To be published.

Ab initio studies of isocyanatoborane and difluoroisocyanatoborane; bent or linear BNCO chains?

SUSAN ELLIS, EDWARD G. LIVINGSTONE, AND NICHOLAS P. C. WESTWOOD[1]

Guelph–Waterloo Centre for Graduate Work in Chemistry, Department of Chemistry and Biochemistry, University of Guelph, Guleph, Ont., Canada N1G 2W1

Received November 17, 1990

SUSAN ELLIS, EDWARD G. LIVINGSTONE, and NICHOLAS P. C. WESTWOOD. Can. J. Chem. **69**, 1000 (1991).

Ab initio calculating at the 3-21G, 6-31G*, 6-31G**, 6-311G*, and 6-311G** Hartree–Fock levels, have been performed on the unknown H_2BNCO and F_2BNCO molecules in order to establish the geometries of these isoelectronic propadienone analogues. For H_2BNCO the double split valence basis sets lead to linear BNCO chains, whereas *either* a triple split valence basis set, *or* the inclusion of correlation to second order (MP2/6-31G*) gives *trans*-bent structures. These have angles at nitrogen of 153.6° (6-311G*) or 149.9° (MP2/6-31G*), with the potential surface for angle bending extremely flat, and 0.5 kJ mol^{-1} (6-311G*) or 1.12 kJ mol^{-1} (MP2/6-31G*) separating the C_{2v} and C_s structures. For the bent structures there is a small *trans*-bend (4–6°) at the carbon atom. The F_2BNCO molecule is also linear at the 3-21G level, but is, however, already *trans*-bent (145.6° at nitrogen, 175.9° at carbon) at the 6-31G* Hartree–Fock level; 1.47 kJ mol^{-1} separates the bent and linear structures. The triple split valence basis set 6-311G* leads to a further decrease in the angle at nitrogen (141.0°), and a similar NCO angle (175.9°), with the bent structure favoured by 3.85 kJ mol^{-1}. MP2/6-31G* calculations give a minimum with an angle at nitrogen of 140.2°, and a bent-linear energy difference of 3.58 kJ mol^{-1}.

Key words: *ab initio* calculations, isocyanatoboranes, structures, quasilinearity, propadienone analogues.

SUSAN ELLIS, EDWARD G. LIVINGSTONE et NICHOLAS P. C. WESTWOOD. Can. J. Chem. **69**, 1000 (1991).

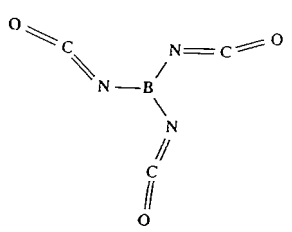
Dans le but d'établir les géométries des molécules inconnues H_2BNCO et F_2BNCO, analogues isoélectroniques de la propadiénone, on a effectué des calculs *ab initio* aux niveaux 3-21G, 6-31G*, 6-31G**, 6-311G* et 6-311G** de Hartree–Fock. Dans le cas de H_2BNCO, les ensembles de base à valence doublement partagée conduisent à des chaînes linéaires de BNCO alors que l'ensemble de base à valence triplement partagés *ou* l'inclusion d'une corrélation aux calculs du deuxième ordre (MP2/6-31G*) conduisent à des structures *trans*-déformées dans lesquelles les angles à l'azote sont de 153,6° (6-311G*) ou 149,9° (MP2/6-31G*), la surface de potentiel pour la déformation de l'angle est extrêmement plane alors que 0,5 (6-311G*) ou 1,12 kJ $mole^{-1}$ (MP2/6-31G*) séparent les structures C_{2v} et C_s. Pour les structures déformées, il y a une légère déformation-*trans* (4–6°) au niveau du carbone. La molécule de F_2BNCO est aussi linéaire au niveau 3-21G; elle possède toutefois déjà une déformation-*trans* (145,6° à l'azote et 175,9° au carbone) au niveau 6-31G* de Hartree–Fock alors que 1,47 kJ $mole^{-1}$ séparent les structures linéaires et déformées. L'ensemble de base 6-311G* à valence triplement partagée abaisse encore plus l'angle à l'azote (141,0°) alors que l'angle NCO est semblable (175,9°) et que la structure déformée est favorisée par 3,85 kJ mol^{-1}. Des calculs au niveau MP2/6-31G* fournissent un minimum pour un angle à l'azote de 140,2° et une différence d'énergie de 3,58 kJ mol^{-1} entre les formes linéaires et déformées.

Mots clés : calculs *ab initio*, isocyanatoboranes, structures, quasilinéarité, analogues de la propadiénone.

[Traduit par la rédaction]

Introduction

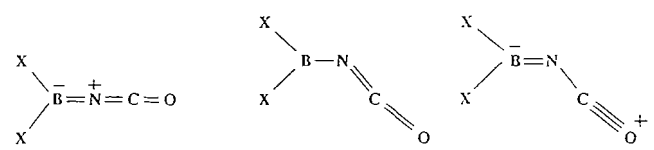
Recent experimental studies on the ultraviolet photoelectron spectra (UPS) of chloroisocyanatoboranes, $Cl_xB(NCO)_{3-x}$ (1), coupled with semiempirical MNDO calculations, have posed the question of non-linearity or linearity in the BNCO chain(s). It was shown that successive isocyanation of BCl_3 leads, ultimately, to a C_{3h} manx-like $B(NCO)_3$ structure (**1**) with individual BN bonds weaker than those in $BCl(NCO)_2$, or BCl_2NCO, and substantial bends at nitrogen (estimated from MNDO calculations to be 47.3° off-axis). Analysis of the gas phase infrared spectra of this molecule and the chloro- derivatives is underway to confirm the structures (2).



1

Of particular relevance to the geometries of monoisocyanato-substituted haloboranes is the competition between structures of the type, where a feature that determines the structure is the extent of $p\pi$ donation from X to the vacant $p\pi$ orbital on boron (possibly mediated by σ effects) making that centre less accessible for electron donation from nitrogen, and thereby reducing the likelihood of the linear structure (**2**).

UPS studies (1) cannot distinguish between linear (**2**) and bent (**3**, **4**) structures when X = Cl, due to the insensitivity of the



2 **3** **4**

calculated orbital energies to such energetically small structural changes; semiempirical MNDO results favor a bent (142.6° at nitrogen) Cl_2BNCO molecule by 6.7 kJ mol^{-1}. It has, however, been claimed (from infrared studies in solution) (3) that Cl_2BNCO has a co-linear BNCO group, and so this must remain an open question, particularly since the corresponding Me_2BNCO molecule, previously found by solution infrared to

[1]To whom correspondence should be addressed.

Can. J. Chem. Downloaded from www.nrcresearchpress.com by 198.100.157.202 on 09/07/12
For personal use only.

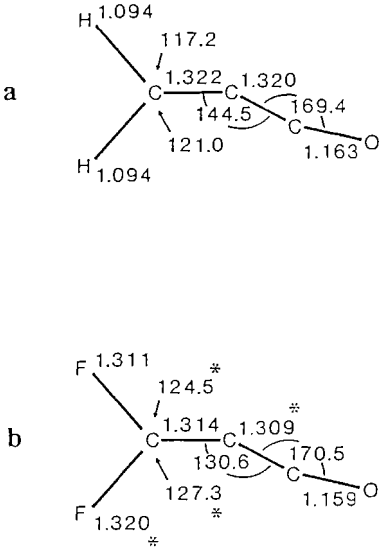


FIG. 1. r_0, or partial r_0 structures for (*a*) H_2CCCO[8] and (*b*) F_2CCCO (12); bond lengths in Å, angles in degrees. Parameters marked with an asterisk were constrained during the structural determination.

have a linear BNCO group (4), has now been shown by electron diffraction to be bent at nitrogen (5). It is also clear that a substituent such as hydrogen, that does not compete for the vacant $p\pi$ orbital on boron, may tend to favor a more linear structure.

In this study we have performed *ab initio* calculations at the Hartree–Fock (HF) level, with basis sets up to the triple split valence 6-311G** [6-311G (*d*,*p*)] level, and with the inclusion of correlation to second order at the 6-31G* level (MP2/6-31G*), in order to investigate the question of linearity or non-linearity in the BNCO chain of the possible synthetic targets, H_2BNCO and F_2BNCO. These molecules are of especial interest in view of the UPS work (1), and are more computationally tractable than the already observed chloro-species. In addition, they are the isoelectronic analogues of the corresponding propadienone molecules, H_2CCCO and F_2CCCO, which have (especially in the former case) been subjected to a great deal of structural scrutiny, both by experiment (6–12) and theory (13–17). The parent propadienone molecule has been shown by microwave spectroscopy to be *trans*-bent (C_s) with a bond angle at C_2 of 144.5°. Interestingly, single configuration HF calculations with reasonably large basis sets up to 6-311G(*df*,*p*) fail to arrive at this structure (refs. 13, 15, and unpublished observations in ref. 7) preferring the linear C_{2v} form. Only with the introduction of correlation do experiment and theory closely agree, this being one of the first instances in which high level HF results predict the incorrect gross structure. The F_2CCCO molecule, recently generated (10, 11), has been shown to be *trans*-bent even at the HF 6-31G* level (angle $C_1C_2C_3$ = 132.8°), although a lower level of theory, 3-21G, leads to a linear structure. The microwave spectrum of this molecule was reported recently (12), confirming the *trans*-bent C_s structure of the higher level calculation. The experimental r_0 structures of both of these molecules are shown in Fig. 1.

The intention, therefore, is to investigate the H- and F-substituted isoelectronic boron–nitrogen analogues with a view to establishing the basis set and correlation dependencies of their molecular structures, and the influence of boron substituents on the BNC angle. In addition, since F_2BNCO has been suggested as an intermediate in the reaction of silyl isocyanate with boron trifluoride (18), it is a reasonable synthetic target, whereas the unsubstituted species, H_2BNCO, is likely to be more difficult to generate due to the propensity of monosubstituted boranes to disproportionate.

TABLE 1. Total energies (au) at various levels of theory for H_2BNCO

Level	Symmetry	Energy
3-21G	C_{2v}	−191.97272
6-31G*	C_{2v}	−193.05935
6-31G**	C_{2v}	−193.06127
6-311G*	C_{2v}	−193.10462
6-311G*	C_s	−193.10482
6-311G**	C_{2v}	−193.10720
6-311G**	C_s	−193.10742
MP2/6-31G*	C_{2v}	−193.60215
MP2/6-31G*	C_s	−193.60257

TABLE 2. Total energies (au) at various levels of theory for F_2BNCO

Level	Symmetry	Energy
3-21G	C_{2v}	−388.79492
6-31G*	C_{2v}	−390.92629
6-31G*	C_s	−390.92685
6-311G*	C_{2v}	−391.02554
6-311G*	C_s	−391.02701
MP2/6-31G*	C_{2v}	−391.81222
MP2/6-31G*	C_s	−391.81359

Computational methods

The geometric structures of H_2BNCO and F_2BNCO were fully optimized by means of analytic gradient procedures, using Gaussian 86 employing RHF wavefunctions with a variety of split valence plus polarization basis sets at the Hartree–Fock level, *viz.*, 3-21G, 6-31G*, 6-31G**, 6-311G*, and 6-311G**. Optimized structures for stationary points, both minima and transition states, were checked by frequency calculations, for respectively, zero and one negative hessian eigenvalue. Geometry optimization was also performed with the inclusion of some electron correlation (Møller–Plessett perturbation theory to second (MP2) order). The best energies are thus MP2/6-31G*. All calculations were performed using Gaussian 86 (19) on an IBM-3081K computer at the University of Guelph.

Results

The final structures for H_2BNCO and F_2BNCO at the different levels of theory are shown in Figs. 2 (*a*)–(*e*) and 3(*a*)–(*d*) in order of improving total energy. These energies (au) at the HF and post-HF levels are given in Tables 1 and 2.

Discussion

H_2BNCO

A perusal of the relevant literature reveals some previous calculations for H_2BNCO which, at the STO-3G and 4-31G levels, established the planarity of the molecules, the resulting optimization to linear BNCO chains, and the preference for isocyanate over cyanate structures (20).

Can. J. Chem. Downloaded from www.nrcresearchpress.com by 198.100.157.202 on 09/07/12
For personal use only.

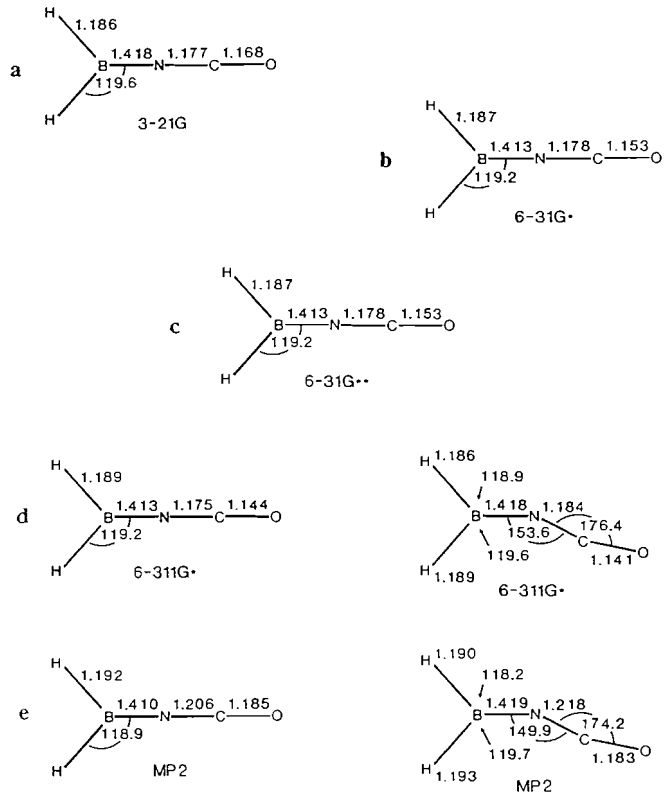


FIG. 2. Optimized structures for H_2BNCO at various levels of theory: (*a*) 3-21G; (*b*) 6-31G*; (*c*) 6-31G**; (*d*) 6-311G*; (*e*) MP2/6-31G*. In the latter two cases the linear (TS) and bent (minimum) structures are shown.

Starting at the 3-21G level, this molecule is predicted to have a linear BNCO chain (Fig. 2*a*) and, typical for this level of calculation on isocyanates, the NC and CO bond lengths are relatively close (21). With the 6-31G* basis, the largest routinely used at the HF level, a linear chain structure for H_2BNCO is also predicted (Fig. 2*b*) with a shortening of the CO bond. This result therefore parallels that for the isoelectronic H_2CCCO molecule, which also adopts a linear heavy atom structure at the 6-31G* HF-SCF level (13, 15). Such a result is not unexpected in the sense that the vacant $p\pi$ orbital on boron can accept π donation from nitrogen with no competition from the hydrogen substituents. This in turn provides an extended π electron system (**2**), leading to linearity in the BNCO chain, and a calculated (6-31G*) BN bond length of 1.413 Å, shorter than that predicted in H_3NBH_3 (1.689 Å) (22) and larger than that predicted in H_2NBH_2 (1.389 Å) (23) at the same level of theory. Polarization functions on the hydrogen atoms lead to no change in the calculated structure (Fig. 2*c*).

In a routine study the optimized geometry at the 6-31G* level would be used for a series of single point calculations involving electron correlation via perturbation theory, *e.g.* MP3/6-31G*//6-31G*. However, the history of propadienone is such that geometry optimization, with correlation included, was necessary to achieve a structure of the proper point group (C_s) (15). Keeping this in mind, structure optimization for H_2BNCO was carried out at the MP2 level with the 6-31G* basis set. The resulting optimized structure (Fig. 2*e*) has a *trans*-bent BNCO chain with a BNC angle of 149.9°, and an NCO angle of 174.2°. The linear structure is now a transition state to inversion at nitrogen. Thus it appears that H_2BNCO behaves with *ab initio* theory in a similar fashion to its isoelectronic carbon analogue, H_2CCCO.

The bent structure of H_2CCCO was interpreted from CAS SCF calculations (16) as being due to a mixing of the ground state with an excited state consisting of a double excitation into the $14a'$ virtual orbital, a low-lying σ level. The electron densities on the individual atoms indicated that the structure could be explained qualitatively through the importance of a resonance structure $H_2C{=}C^-{-}C{\equiv}O^+$, where the negative charge on the central carbon atom acts as a lone pair. In the H_2BNCO molecule, the in-plane lone pair on nitrogen can act in the same way to cause bending, leading to a lengthening of the B—N bond as predicted by the valence bond structure, (**3**). A comparison of the C_{2v} and C_s structures at the MP2/6-31G* level (Fig. 2*e*) shows this effect, and also indicates that upon bending, the NC bond lengthens and the CO bond shortens, a result similar to that seen for C_2C_3 and C_3O in H_2CCCO (15). These results indicate that an excited state of the form **4** may be contributing to the ground state (compare H_2CCCO) to give an unsymmetrical conformation. Since the two molecules are isoelectronic, it is possibly the same σ orbital (*viz.*, $14a'$ (C_s) or $4b_2$ (C_{2v})) that is involved in both cases. This could be confirmed by carrying out a limited configuration interaction (CI) calculation on H_2BNCO; such a calculation was not performed due to computational constraints. However, a representation of the low lying $4b_2/14a'$ orbital in the C_{2v}/C_s structures (where the HOMO is $3b_2/12a'$) is shown in Fig. 4; bending will stabilize this molecular orbital by decreasing the antibonding NC interaction, and introducing an electronic population transfer on the heavy atoms from 2*p* to 2*s*.

At this point it was decided to return to the HF level and carry out calculations using the less common triple split valence 6-311G* and 6-311G** basis sets. Interestingly, when either of these basis sets are used, the optimum structure is also *trans*-bent (Fig. 2*d*), and approaches the structure obtained when correlation is included. Thus the additional flexibility of the triple split valence basis set[2] is sufficient to cause the molecule to bend, a structural change that is not commonly observed for this kind of modification in the basis set. It should be noted that using 6-311G** with polarization functions on the hydrogen atoms has a negligible effect (not shown) on the 6-311G* structure.[3] The computed bent structure at the 6-311G* level does have some essential features that distinguish it from the MP2/6-31G* structure (Fig. 2*e*) in that all the bonds are shorter, particularly the NC and CO bonds (by *ca.* 0.02–0.04 Å), and there is a reduction in the off-axis angle. Such increases in bond lengths are typical for MP2 results, and more specifically, the NC and CO bond lengths in isocyanates calculated at this level have been observed to be overestimated by 0.01–0.02 Å when compared to experiment (21). Computational results at similar levels of theory for the F_2CCCO molecule (below), where there is an experimental structure for comparison, reach essentially the same conclusions.

Whether one considers the MP2/6-31G* or the HF 6-311G* structure, what is clear is that the energy difference between structures with bent (minima), or linear (transition states)

[2]Reference 24*a*. We note that recently this basis set has been described as being not a true valence triple-zeta basis set, but rather of double-zeta quality in *s* space (24*b*).

[3]However, this may not be true at the correlated level, but computational resources prohibited use of the preferable MP2/6-311G** calculations.

Can. J. Chem. Downloaded from www.nrcresearchpress.com by 198.100.157.202 on 09/07/12
For personal use only.

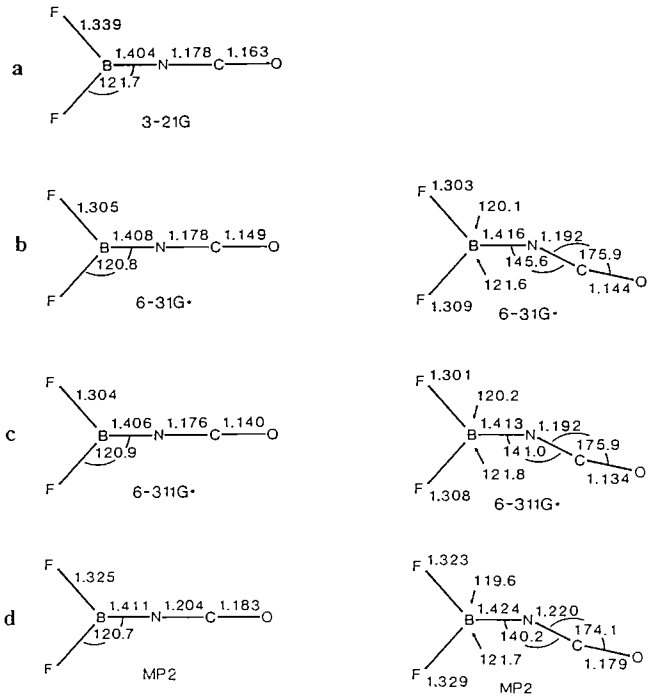


FIG. 3. Optimized structures for F_2BNCO at various levels of theory: (*a*) 3-21G; (*b*) 6-31G*; (*c*) 6-311G*; (*d*) MP2/6-31G*. In the latter three cases the linear (TS) and bent (minimum) structures are shown.

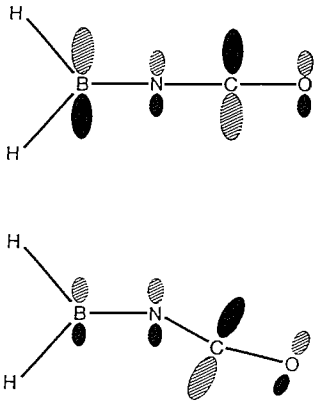


FIG. 4. Schematic of the $4b_2/14a'$ unoccupied molecular orbital of H_2BNCO in both linear and bent configurations; *s* character is not shown.

BNCO chains is very small. At the 6-311G* level the energy difference is 0.53 kJ mol^{-1}, and at the optimized MP2/6-31G* level, 1.12 kJ mol^{-1}. These values indicate a very flat potential surface with a low barrier to inversion at nitrogen, and from previous experience with H_2CCCO this barrier is likely to decrease (indeed it approximately halves) (15) at the higher MP3/6-31G* level, with a corresponding small decrease in the off-axis angle. The lowest calculated vibrational frequency (harmonic, unscaled) of the bent structure occurs at 82 cm^{-1}, 0.99 kJ mol^{-1} (6-311G*), or 106 cm^{-1}, 1.27 kJ mol^{-1} (MP2/6-31G*), and is associated with the in-plane BNC bending coordinate of b_2 symmetry, ν_{12}. Given that the harmonic approach fails for a double minimum potential (25), no significance should be attached to these numbers; they simply indicate the likelihood of a quasilinear molecule. Clearly, higher levels of theory beyond the single determinant framework are required to fully describe the bending potential in this molecule (26), and clarify the lack, or presence, of a double well.

We should reiterate that the lowest level of theory at which H_2BNCO bends, *viz.*, HF 6-311G*, the H_2CCCO molecule remains quite linear. Indeed, it is reported to remain linear up to the 6-311G (*df,p*) level (unpublished observations in ref. 7), although it is entirely feasible that additional polarization functions may cause it to bend at the HF level. When H_2CCCO does bend, at comparable levels of theory to those reported here for H_2BNCO, *viz.*, MP2/6-31G*, the linear-bent energy difference (estimated from Fig. 1 in ref. 15 to be 8.6 kJ mol^{-1}) is substantially greater than for the boron isocyanate analogue, and the angle at C_2 (136°) is calculated to be much smaller.

F_2BNCO

At the HF 3-21G level the optimized structure is linear (Fig. 3*a*), and can be compared with H_2BNCO at the same level (Fig. 2*a*). An interesting feature, which persists for the linear structure at higher levels of theory, is the reduction in the BN bond length upon replacing H by F, an effect analogous to that when F is placed adjacent to a multiple CC bond (27, 28). This is true also for F_2CCCO and H_2CCCO (Fig. 1), and can be ascribed to a stronger σ CC (or BN) bond, associated with an increased polarity of this bond. When the basis set is increased in size to 6-31G*, the optimized structure (Fig. 3*b*) is *trans*-bent with a BNC angle of 145.6°, an NCO angle of 175.9°, and a bent/linear energy difference of 1.47 kJ mol^{-1}. Thus the difluoro-derivative does not require a HF triple split valence basis set, or the inclusion of correlation, to make it bend, and this can be attributed to the competition for the boron $p\pi$ orbital imposed by the fluorine atoms, thereby limiting the ability of boron to accept electrons from nitrogen, leading to a dominance of resonance forms **3** and **4** over form **2**.

Even though correlation was not needed to achieve the bent structure for F_2BNCO, the difference between the C_{2v} and C_s structures is still very small. At the larger triple split valence 6-311G* level the bent structure (Fig. 3*c*, BNC angle now 141.0°) is only 3.85 kJ mol^{-1} lower in energy than the linear structure. A comparison of the optimized bent structures at the 6-31G* and 6-311G* levels indicates an increased bend at N, and concomitant decreases in the BN and CO bond lengths at the higher level of theory. To put this in perspective with regard to structural predictions, we have performed triple split valence 6-311G* calculations on F_2CCCO, and can confirm that this leads to an even better geometry; the $C_1C_2C_3$ angle is now 131.7° (experiment 130.6°) (12) compared to 132.8° calculated at the 6-31G* level (10).

Inclusion of correlation (Fig. 3*d*) follows the pattern observed for H_2BNCO, *viz.*, an increase in all bond lengths especially the NC and CO bonds (see ref. 21 for similar effects), and a decrease in the angle at nitrogen, although in this case the reduction from the 6-311G* value is only 0.8°, and the energy difference hardly changes (3.58 kJ mol^{-1}). Thus the effect of correlation on the angle is not as marked as in the H_2BNCO case, reflecting the fact that correlation in this case is not so critical in achieving the bent structure.

The first vibrational level of bent F_2BNCO, corresponding to the BNC in-plane bending frequency, is calculated (harmonic, unscaled) at 85 cm^{-1}, 1.02 kJ mol^{-1} (6-311G*) or 81 cm^{-1}, 0.97 kJ mol^{-1} (MP2/6-31G*), below the calculated barrier to inversion. Again these values must be taken *cum grano salis*, especially since this molecule may possess large amplitude vibra-

Can. J. Chem. Downloaded from www.nrcresearchpress.com by 198.100.157.202 on 09/07/12
For personal use only.

Can. J. Chem. Downloaded from www.nrcresearchpress.com by 198.100.157.202 on 09/07/12
For personal use only.

tional motion, with the feasibility of tunneling through the barrier, primarily from excited vibrational states. For what it's worth the out-of-plane frequency is calculated to be only 7–8 cm^{-1} higher, and so internal rotation may be a competitive process to in-plane inversion.

We note that fluorine substitution on H_2BNCO leads to a calculated increase in the off-axis angle of 12.6°, which follows closely the experimentally observed increase of 13.9° in this angle for the replacement of H by F in H_2CCCO (Fig. 1*a* and 1*b*) (8, 12). In addition, when compared to its isoelectronic carbon analogue, difluoropropadienone (Fig. 1*b*), F_2BNCO (Fig. 3*d*) is predicted to be significantly less bent (approximately 10° at the 6-311G* level), reflecting the fact that these substituted boron isocyanates have a greater tendency towards a linear BNCO structure, despite the fact that most isocyanates (except H_3SiNCO) have a distinctly off-axis substituent. A possible rationale for this observation, alluded to earlier, may be found in the effect of excited state contributions, which have not been evaluated in this study.

Conclusions

Ab initio calculations are reported for the propadienone analogue, H_2BNCO and the difluoro-derivative F_2BNCO. At reasonably high levels of theory (up to 6-31G**) the parent H_2BNCO molecule remains linear, until the introduction of a triple split valence basis set, *or* the inclusion of correlation (MP2/6-31G*), which both lead to a *trans*-bent structure. The linear-bent energy difference is extremely small, 0.53 kJ mol^{-1} (6-311G*), and 1.12 kJ mol^{-1} (MP2/6-31G*); in the 6-311G* case so small that ZPVE corrections can essentially cancel the difference, due to the non-inclusion of the negative frequency in the transition state. In addition to an analogy with the H_2CCCO case, we note that a similar conclusion regarding the influence of correlation on bending was reached recently for the isoelectronic molecule, H_2CCNN (29). In our work, the effect of the triple split valence basis set on the BNC angle is interesting; additional polarization functions on a double split valence basis set, *e.g.* 6-31G** clearly have no effect at all, as expected for simply a refinement of the hydrogen space. This implies that a somewhat more flexible and economical double valence basis set may be sufficient to cause bending in molecules of this type.

The difluoro-substituted F_2BNCO molecule is also predicted linear with a small basis set (3-21G), but is *trans*-bent at *both* the HF 6-31G*, and 6-311G* levels, with a correspondingly larger energy difference between the linear and bent forms, *e.g.*, 3.85 kJ mol^{-1}, at the 6-311G* level. The MP2/6-31G* calculation leads to a similar result, implying that in this case the HF level calculations with reasonable basis sets are sufficient to describe the structure.

The trends in the calculated structures between the H_2BNCO and F_2BNCO molecules track those features observed in the experimental structures for the analogous H_2CCCO and F_2CCCO molecules, although the propadienone analogues are significantly more bent, and have greater linear-bent energy differences. This study of the substituted boron isocyanates indicates that there are very subtle electronic effects pertaining to the question of linearity versus non-linearity in X_2BNCO molecules. Thus calculations at the HF 6-31G* level show BNC angles of 180° (X = H) 180° (X = CH_3) (5), 155.2° (X = Cl) (2), and 145.6° (X = F). Note that where X = CH_3, the recently reported experimental structure gives a BNC angle of 153.8°. The introduction of correlation can, as we have seen, affect these results, but the indicate is that π-donating substitutents tend to favor the bent structures **3** and **4**. Indeed, the earlier semiempirical work on the CL_2BNCO, $ClB(NCO)_2$, and $B(NCO)_3$ molecules (1) indicated a trend toward increasing bends at nitrogen due to the greater π-donating ability of the NCO donor. Subsequent to this theoretical study we can report that we have now generated the novel difluoro-molecule, F_2BNCO, and have investigated it by both UPS and FTIR (30). Computed Koopmans' orbital energies, and vibrational frequencies calculated during this study have proven useful for identification, and confirm the isocyanate formulation. Thus, the ν_{as} NCO and ν_s NCO modes are calculated (6-311G* and MP2/6-31G*) at 2514/2418 and 1694/1585 cm^{-1}, respectively, and are observed at 2330 and 1540 cm^{-1}. Partial corrections for anharmonic effects would substantially improve the correspondence between experiment and theory. Experiments involving microwave spectroscopy have also been initiated on this species, in order to investigate the question of linearity/non-linearity, although we would make the final remark that the computed dipole moment is extremely small (<0.1 D).

Acknowledgements

N.P.C.W. thanks the Natural Sciences and Engineering Research Council of Canada for grants in support of this research. We thank Drs. Harmony and Oberhammer for preprints of their work on, respectively, F_2CCCO and $(Me)_2BNCO$.

1. M. Alaee, P. Hofstra, C. Kirby, and N. P. C. Westwood. J. Chem. Soc. Dalton Trans. 1569 (1990).
2. M. Alaee, S. Ellis, E. G. Livingstone, and N. P. C. Westwood. To be published.
3. H. Mongeot, H. R. Atchekzai, M. Fouassier, and M. T. Forel. J. Mol. Struct. **62**, 35 (1980).
4. J. Goubeau and H. Grabner. Chem. Ber. **93**, 1379 (1960).
5. R. Hausser-Wallis, H. Oberhammer, W. Einholz, and P. O. Paetzold. Inorg. Chem. **29**, 3286 (1990).
6. G. L. Blackman, R. D. Brown, R. F. C. Brown, F. W. Eastwood, and G. L. McMullen. J. Mol. Spectrosc. **68**, 488 (1977).
7. R. D. Brown, P. D. Godfrey, R. Champion, and D. McNaughton. J. Am. Chem. Soc. **103**, 5711 (1981) (see also erratum, J. Am. Chem. Soc. **104**, 6167 (1982)).
8. R. D. Brown, R. Champion, P. S. Elmes, and P. D. Godfrey. J. Am. Chem. Soc. **107**, 4109 (1985).
9. O. L. Chapman, M. D. Miller, and S. M. Pitzenberger. J. Am. Chem. Soc. **109**, 6867 (1987).
10. J. C. Brahms and W. P. Dailey. J. Am. Chem. Soc. **111**, 3071 (1989).
11. J. C. Brahms and W. P. Dailey. J. Am. Chem. Soc. **111**, 8940 (1989).
12. H. S. Tam, M. D. Harmony, J. C. Brahms, and W. P. Dailey. J. Mol. Struct. **223**, 217 (1990).
13. L. Radom. Aust. J. Chem. **31**, 1 (1978).
14. A. Kormornicki, C. E. Dykstra, M. A. Vincent, and L. Radom. J. Am. Chem. Soc. **103**, 1652 (1981).
15. L. Farnell and L. Radom. Chem. Phys. Lett. **91**, 373 (1982).
16. R. D. Brown and R. G. Dittman. Chem. Phys. **83**, 77 (1984).
17. P. R. Taylor. J. Comput. Chem. **5**, 589 (1983).
18. E. A. V. Ebsworth and M. J. Mays. J. Chem. Soc. 4844 (1962).
19. M. J. Frisch, J. S. Binkley, H. B. Schlegel, K. Raghavachari, R. Martin, J. J. P. Stewart, D. DeFrees, R. Seeger, R. Whiteside, D. Fox, E. Fluder, and J. A. Pople. GAUSSIAN 86, Release C. Department of Chemistry, Carnegie-Mellon University, Pittsburgh, PA. 1986.
20. D. Poppinger and L. Radom. J. Am. Chem. Soc. **100**, 3674 (1978).
21. H-G. Mack and H. Oberhammer. Chem. Phys. Lett. **157**, 436 (1989).

22. J. S. BINKLEY and L. R. THORNE. J. Chem. Phys. **79**, 2932 (1983).
23. R. A. WHITESIDE, M. J. FRISCH, and J. A. POPLE (*Editors*). The Carnegie-Mellon Quantum Chemistry Archive. 3rd ed. Carnegie-Mellon University, Pittsburgh, PA. 1983.
24. (*a*) R. KRISHNAN, J. S. BINKLEY, R. SEEGER, and J. A. POPLE. J. Chem. Phys. **72**, 650 (1980); (*b*) R. S. GREV and H. F. SCHAEFER. J. Chem. Phys. **91**, 7305 (1989).
25. P. CARSKY, V. SPIRKO, B. A. HESS, and L. J. SCHAAD. J. Phys. Chem. **94**, 5493 (1990).
26. J. H. TELES, G. MAIER, B. A. HESS, L. J. SCHAAD, M. WINNEWISSER, and B. P. WINNEWISSER. Chem. Ber. **122**, 753 (1989).
27. J. L. CARLOS, R. R. KARL, and S. H. BAUER. J. Chem. Soc. Faraday Soc. Trans. 2, **70**, 177 (1974).
28. D. A. DIXON, T. FUKUNAGA, and B. E. SMART. J. Am. Chem. Soc. **108**, 1585 (1986).
29. M. A. MURCKO, S. K. POLLACK, and P. M. LAHTI. J. Am. Chem. Soc. **110**, 364 (1988).
30. A. ALAEE, E. G. LIVINGSTONE, and N. P. C. WESTWOOD. To be published.

Can. J. Chem. Downloaded from www.nrcresearchpress.com by 198.100.157.202 on 09/07/12
For personal use only.

Excess molar volumes and excess viscosities of *n*-butylamine + 1,4-dioxane + carbon tetrachloride system at 298.15 K[1]

INÉS L. ACEVEDO, GRACIELA C. PEDROSA, AND MIGUEL KATZ[2]

Cátedra de Fisicoquímica, Instituto de Ingeniería Química, Facultad de Ciencias Exactas y Tecnología, Universidad N. de Tucumán, Avda. Independencia 1800, S. M. de Tucumán (4000), R. Argentina

Received May 14, 1990

INÉS L. ACEVEDO, GRACIELA C. PEDROSA, and MIGUEL KATZ. Can. J. Chem. **69**, 1006 (1991).

Densities and viscosities were determined for the *n*-butylamine + 1,4-dioxane + carbon tetrachloride system at 298.15 K. Molar excess volumes and excess viscosities were calculated from the experimental results. Analytical expressions can be used to predict these excess properties from binary data, the empirical correlation of Cibulka being the best for this system.

Key words: density; mixture of *n*-butylamine + 1,4-dioxane + carbon tetrachloride; viscosity, mixture of *n*-butylamine + 1,4-dioxane + carbon tetrachloride; excess properties of ternary mixture.

INÉS L. ACEVEDO, GRACIELA C. PEDROSA et MIGUEL KATZ. Can. J. Chem. **69**, 1006 (1991).

Opérant à 298,15 K, on a déterminé les densités et les viscosités du système *n*-butylamine + 1,4-dioxane + tétrachlorure de carbone. Utilisant les données expérimentales, on a calculé les volumes molaires en excès ainsi que les viscosités en excès. On peut utiliser des expressions analytiques pour prédire ces propriétés en excès à partir de données binaires; la corrélation empirique de Cibulka est la meilleure pour ce système.

Mots clés : densité; viscosité; mélange *n*-butylamine + 1,4-dioxane + tétrachlorure de carbone; propriétés en excès du mélange ternaire.

[Traduit par la Rédaction]

Introduction

Data of excess volumes and excess viscosities are known for a number of binary liquid mixtures of non-electrolytes and they can be found in several articles. On the other hand, experimental data on excess volumes, densities, on viscosities of mixtures with more than two components are rather rare in the literature. It is therefore interesting to estimate excess volumes and excess viscosities of mixtures with more than two components from binary data.

Data for ternary systems can be found in the works of Redlich and Kister (1), Scatchard and co-workers (2), Tsao and Smith (3), Mathieson and Tynne (4), Kohler (5), Toop (6), Rastogi *et al.* (7), Radojković *et al.* (8), Jacob and Fitzner (9), Cibulka (10), Bertrand *et al.* (11), Nagata (12–14), and Singh *et al.* (15).

This work is to determine the molar excess volumes (V^E) and excess viscosities (η^E) for the *n*-butylamine (BA) + 1,4-dioxane (D) + carbon tetrachloride (CT) system at 298.15 K, and for the three corresponding binary systems, and to consider some empirical correlations assuming that interactions in a ternary mixture are closely dependent on the interactions of the constituents of the binary mixtures.

Experimental

The methods used in our laboratory have been described previously (16, 17). Densities were determined with a digital densimeter AP, model DMA 45. All weighings were made on a H315 Mettler balance.

A thermostatically controlled bath (constant to 0.01°C) was used. Temperatures were read from calibrated thermometers. Calibration was done with air and doubly distilled water, with an error of ± 0.1 kg m^{-3}.

Viscosities of the pure liquids and the mixtures were determined with a Cannon-Fenske viscosimeter calibrated with doubly distilled water and benzene. Kinetic energy corrections were applied to the viscosity data. The estimated error was ± 0.005 mPa s.

[1]Presented at the VII Congreso Argentino de Fisicoquimica, Cordoba, Argentina, 1991.

[2]To whom correspondence should be addressed.

TABLE 1. Properties characterizing the pure compounts at 298.15 K

	$\rho \times 10^{-3}$ (kg m^{-3})		η (mPa s)	
Substance	Exp.	Lit.	Exp.	Lit.
n-Butylamine	0.7328	0.73308[a]	0.474	0.470[c]
1,4-Dioxane	1.0283	1.02687[b]	1.181	1.204[b]
Carbon tetrachloride	1.5844	1.58439[d]	0.905	0.909[d]

[a]Reference 19.
[b]Reference 20.
[c]Reference 21.
[d]Reference 22.

Materials and solutions

n-Butylamine (BA), Riedel de Häen (puriss.) was dried over potassium hydroxide pellets for 3 days, refluxed for 2 h, and fractionally distilled (18). 1,4-Dioxane (D), Fluka (puriss.) was distilled over sodium at reduced pressure and the middle fraction collected. Carbon tetrachloride (CT), Merck (puriss.) was used without purification.

Mixtures were prepared by mixing weighed amounts of the pure liquids. Caution was taken to prevent evaporation.

Results and discussion

The experimental results for the pure liquids are reported in Table 1 together with literature values for comparison.

Densities and viscosities of the binary mixtures can be calculated from the experimental data, with mole fraction from the following equation:

$$[1] \quad P = x_i P_i + x_j P_j + x_i x_j \sum_{\substack{k=0 \\ i<j}}^{n} a_k (x_i - x_j)^k$$

where P_i and P_j are properties of the pure components. Table 2 shows the values of the coefficients a_k as well as their standard deviations, calculated by the method of least squares with a VAX 11/780 computer.

Can. J. Chem. Downloaded from www.nrcresearchpress.com by 198.100.157.202 on 09/07/12
For personal use only.

TABLE 2. Coefficients a_k for eq. [1] and standard deviations for the binary systems at 298.15 K (BA = (1); D = (2); CT = (3))

Parameter	a_0	a_1	a_2	a_3	a_4	σ
		System (1) + (2)				
$\rho \times 10^{-3}$ (kg m^{-3})	−0.0512	0.0049	−0.0007	—	—	3×10^{-5}
η (mPa s)	−0.672	0.297	−0.149	—	—	7×10^{-4}
		System (2) + (3)				
$\rho \times 10^{-3}$ (kg m^{-3})	0.08767	−0.00035	−0.004132	—	—	1×10^{-4}
η (mPa s)	−0.672	0.10942	−0.03383	−0.00546	−0.049165	4×10^{-4}
		System (1) + (3)				
$\rho \times 10^{-3}$ (kg m^{-3})	0.000808	−0.000159	−0.001169	—	—	3×10^{-5}
η (mPa s)	−0.000114	0.00199	—	—	—	2×10^{-4}

TABLE 3. Coefficients a_k for eq. [2] and standard deviations for the binary systems at 298.15 K

Parameter	a_0	a_1	a_2	a_3	a_4	σ
		System (1) + (2)				
$V^E \times 10^6$ (m^3 mol^{-1})	0.641	−0.054	0.187	0.254	−0.364	4×10^{-3}
η^E (mPa s)	−0.353	0.248	−0.140	—	—	9×10^{-4}
		System (2) + (3)				
$V^E \times 10^6$ (m^3 mol^{-1})	−1.235	0.218	−0.020	−0.340	0.580	3×10^{-3}
η^E (mPa s)	0.5036	0.112	−0.035	−0.011	−0.047	4×10^{-4}
		System (1) + (3)				
$V^E \times 10^6$ (m^3 mol^{-1})	−2.060	−0.770	−0.190	—	—	3×10^{-3}
η^E (mPa s)	0.146	−0.016	—	—	—	4×10^{-4}

The excess function of a binary system can be represented by a Redlich–Kister form of the type:

$$[2] \quad X^E = x_i x_j \sum_{k=0}^{n} a_k (x_i - x_j)^k$$

where X^E represents V^E or η^E, x_i and x_j are the mole fractions of components i and j, and a_k the polynomial coefficients. The methods of least squares were used to determine the values of the coefficients. In each case, the optimum number of coefficients was ascertained from an examination of the standard error of the estimate with n:

$$[3] \quad \sigma = [\sum (X^E_{obs} - X^E_{cal})^2/(n_{obs} - n)]^{1/2}$$

The values adopted for the coefficients and the standard error of estimates associated with the use of eq. [3] are summarized in Table 3.

Figure 1 shows the experimental values of V^E and η^E for the three systems. The continuous curves were calculated from eq. [2] using these values for the coefficients.

For the systems BA(1) + D(2) and BA(1) + CT(2) there are no values in the literature. For D(1) + CT(2) values of V^E are found in refs. 23 and 24. These authors work at temperatures different from ours and our results are closer to those of Adya *et al.* (24).

The experimental values of densities and viscosities of the ternary system are obtained by adding the third component to a constant relation of the other two. Molar excess volume is calculated with the following equation:

$$[4] \quad V^E = x_1 M_1(\rho^{-1} - \rho_1^{-1}) + x_2 M_2(\rho^{-1} - \rho_2^{-1}) + x_3 M_3(\rho^{-1} - \rho_3^{-1})$$

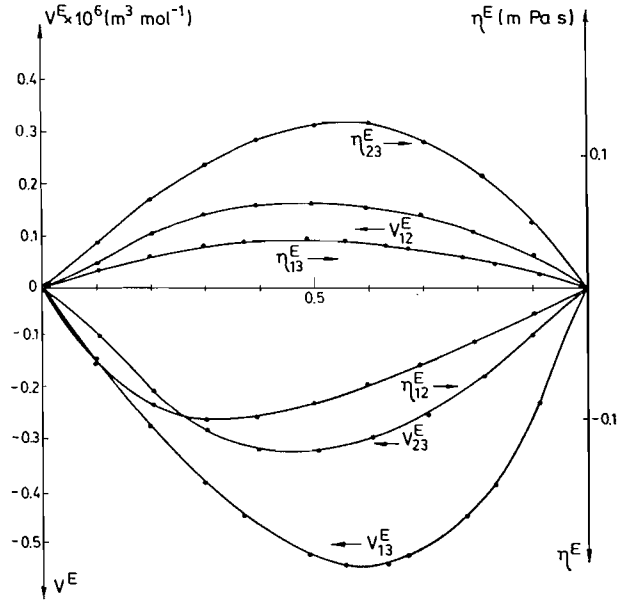


FIG. 1. Excess molar volumes and excess viscosities for binary systems at 298.15 K. Experimental results ····; continuous curves were calculated from eq. [2].

where M_1, M_2, and M_3 are the molecular weights of the components, ρ_1, ρ_2, and ρ_3 are the densities of the pure components, and ρ the density of the mixture.

The excess viscosity is defined by the following equation:

$$[5] \quad \eta^E = \eta - \exp(x_1 \ln \eta_1 + x_2 \ln \eta_2 + x_3 \ln \eta_3)$$

where η, η_1, η_2, and η_3 are the viscosities of the mixture and the

Can. J. Chem. Downloaded from www.nrcresearchpress.com by 198.100.157.202 on 09/07/12
For personal use only.

Can. J. Chem. Downloaded from www.nrcresearchpress.com by 198.100.157.202 on 09/07/12
For personal use only.

pure components, where a logarithmic additivity law is assumed for ideal mixtures.

Table 4 shows the experimental values of densities and viscosities at different mole fractions.

Figures 2 and 3 show the experimental constant values of V^E_{123} and η^E_{123}.

If interaction in a ternary system $i + j + k$ is assumed to be closely dependent on the interactions of the constituents $i + j$, $j + k$, and $i + k$ mixtures, it should be possible to evaluate excess properties for ternary mixtures of non-electrolytes, when the corresponding properties for the binary $i + j$, $j + k$, and $i + k$ mixtures are known.

Redlich and Kister (1) proposed an equation in terms of mole fractions for the excess Gibbs free energy of a ternary mixture with the general form:

$$[6]\quad G^E_{123} = x_1x_2\sum_{\nu=0}^{r}(G_\nu)_{12}(x_1 - x_2)^\nu + x_1x_3\sum_{\nu=0}^{r}(G_\nu)_{13}(x_1 - x_3)^\nu + x_2x_3\sum_{\nu=0}^{r}(G_\nu)_{23}(x_2 - x_3)^\nu$$

and recommended the same general form for the excess enthalpy and volume.

Scatchard and co-workers (2) suggested an alternate form in the case of one polar component (component 1) mixed with two nonpolar components:

$$[7]\quad G^E_{123} = x_1x_2\sum_{\nu=0}^{r}(G_\nu)_{12}(2x_1 - 1)^\nu + x_1x_3\sum_{\nu=0}^{r}(G_\nu)_{13}(2x_1 - 1)^\nu + x_2x_3\sum_{\nu=0}^{r}(G_\nu)_{23}(x_2 - x_3)^\nu$$

Tsao and Smith (3) proposed an equation for predicting the excess enthalpy of a ternary system. For excess volume, this equation is:

$$[8]\quad V^E_{123} = \left(\frac{x_2}{1 - x_1}\right)V^E_{12} + \left(\frac{x_3}{1 - x_1}\right)V^E_{13} + (1 - x_1)V^E_{23}$$

in which V^E_{ij} refers to the excess volume for the binary mixtures at compositions x^0_i, x^0_j such that $x^0_i = x_i$ for the 1,2 and 1,3 binary systems, and $x^0_2 = x_2/(x_2 + x_3)$ for the 2,3 binary system.

This equation, like eq. [7], is asymmetrical and requires specification of some criteria for identifying component 1.

Mathieson and Tynne (4) proposed an equation which is intermediate between eqs. [6] and [7], using the following form for enthalpies:

$$[9]\quad H^E_{123} = x_1x_2\sum_{\nu=0}^{r}(H_\nu)_{12}\left(\frac{x_1 - x_2 - x_3}{2}\right)^\nu + x_1x_3\sum_{\nu=0}^{r}(H_\nu)_{12}\left(\frac{x_1 - x_3 - x_2}{2}\right)^\nu + x_2x_3\sum_{\nu=0}^{r}(H_\nu)_{23}(x_2 - x_3)$$

TABLE 4. Densities and viscosities for the *n*-butylamine (1) + 1,4-dioxane (2) + carbon tetrachloride (3) system at 298.15 K

x_1	x_2	x_3	$\rho \times 10^{-3}$ (kg m^{-3})	η (mPa s)
0.4279	0.1336	0.4385	1.1485	0.736
0.3481	0.2952	0.3567	1.1285	0.801
0.2529	0.4879	0.2592	1.1032	0.890
0.1621	0.6719	0.1660	1.0774	0.983
0.1150	0.7671	0.1179	1.0634	1.036
0.0559	0.8868	0.0573	1.0454	1.108
0.1692	0.1414	0.6894	1.3692	0.884
0.1393	0.2931	0.5676	1.3156	0.949
0.1046	0.4694	0.4280	1.2495	1.024
0.0709	0.6405	0.2886	1.1818	1.091
0.0463	0.7649	0.1888	1.1305	1.132
0.0222	0.8875	0.0903	1.0777	1.164
0.2854	0.1265	0.5881	1.2759	0.810
0.2313	0.2921	0.4766	1.2341	0.879
0.1813	0.4452	0.3735	1.1932	0.947
0.1491	0.5493	0.3070	1.1658	0.991
0.0885	0.7293	0.1822	1.1120	1.072
0.0412	0.8739	0.0849	1.0679	1.135
0.5913	0.1498	0.2589	0.9972	0.652
0.4867	0.3002	0.2131	1.0023	0.713
0.3753	0.4603	0.1644	1.0079	0.786
0.2823	0.5941	0.1236	1.0123	0.859
0.1722	0.7524	0.0754	1.0177	0.962
0.0786	0.8870	0.0344	1.0234	1.071
0.0872	0.1362	0.7766	1.4430	0.937
0.1892	0.1210	0.6898	1.3623	0.868
0.3185	0.1017	0.5798	1.2604	0.790
0.4463	0.0826	0.4711	1.1604	0.722
0.5900	0.0612	0.3488	1.0484	0.650
0.6484	0.0525	0.2991	1.0030	0.622
0.0912	0.3144	0.5944	1.3469	0.995
0.1830	0.2826	0.5344	1.2922	0.911
0.3295	0.2319	0.4386	1.1803	0.806
0.4516	0.1897	0.3587	1.0966	0.729
0.5842	0.1438	0.2720	1.0068	0.656
0.7795	0.0763	0.1442	0.8766	0.562
0.1200	0.5819	0.2981	1.1705	1.027
0.2024	0.5274	0.2702	1.1264	0.938
0.4387	0.3711	0.1902	1.0036	0.743
0.6477	0.2329	0.1194	0.8995	0.619
0.6992	0.1989	0.1019	0.8745	0.593
0.8637	0.0901	0.0462	0.7956	0.520
0.1095	0.7947	0.0958	1.0514	1.042
0.2452	0.6736	0.0812	0.9975	0.885
0.3698	0.5624	0.0678	0.9499	0.769
0.5350	0.4150	0.0500	0.8890	0.660
0.7064	0.2620	0.0316	0.8288	0.576
0.9154	0.0755	0.0091	0.7596	0.499

Kohler (5) proposed an equation for a ternary system of the following form:

$$[10]\quad V^E_{123} = (x_1 + x_2)^2V^E_{12} + (x_1 + x_3)^2V^E_{13} + (x_2 + x_3)^2V^E_{23}$$

Kohler's equation is symmetrical in that all three binary systems are treated identically. In this equation, V^E_{ij} refers to the excess volume of x^0_i, x^0_j in the binary mixtures, using

$$[11]\quad x^0_i = 1 - x^0_j = x_i/(x_i + x_j)$$

Toop (6) developed an equation for the excess Gibbs energy of mixing quite similar to that suggested previously by Tsao and Smith for excess enthalpies.

Rastogi *et al.* (7) suggested a form for predicting the excess

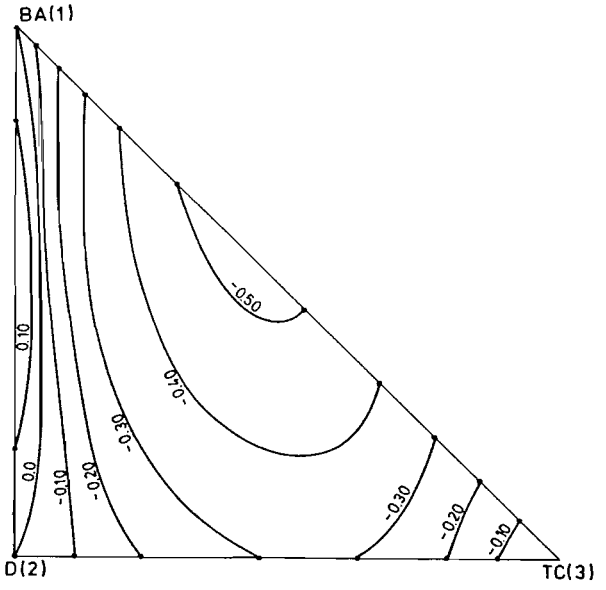


FIG. 2. Lines of constant excess molar volumes V^E ($\times 10^6$ m^3 mol^{-1}) for *n*-butylamine (1) + 1,4-dioxane (2) + carbon tetrachloride (3) system at 298.15 K.

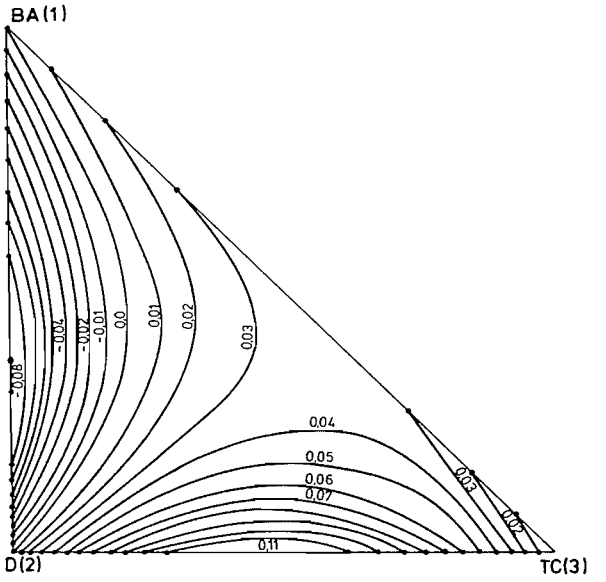


FIG. 3 Lines of constant excess viscosities η^E (mPa s) for *n*-butylamine (1) + 1,4-dioxane (2) + carbon tetrachloride (3) system at 298.15 K.

volume of a ternary system, similar to eq. [10].

$$[12]\quad V^E_{123} = \tfrac{1}{2}[(x_1 + x_2)V^E_{12} + (x_1 + x_3)V^E_{13} + (x_2 + x_3)V^E_{23}]$$

This expression is inappropriate for describing the system near infinite dilution.

Radojković *et al.* (8) considered an expression proposed by Redlich and Kister for excess Gibbs free energy. For excess molar volume:

$$[13]\quad V^E_{123} = V^E_{12*} + V^E_{23*} + V^E_{13*}$$

where V^E_{12*}, V^E_{23*}, and V^E_{13*} represent the excess molar volumes with x_1, x_2, and x_3 mole fractions in the ternary system calculated with eq. [2], using the coefficients in Table 3.

Jacob and Fitzner (9) suggested an equation for estimating the

TABLE 5. Standard deviations for *n*-butylamine (1) + 1,4-dioxane (2) × carbon tetrachloride (3) system at 298.15 K

Equation	$\sigma(V^E) \times 10^6$ (m^3 mol^{-1})	$\sigma(\eta^E)$ (mPa s)
[8]	0.07	0.03
[10]	0.11	0.02
[13]	0.10	0.02
[14]	0.10	0.02
[16][a]	0.03	0.01
[19][a]	0.06	0.02

[a]These equations contain three adjustable parameters.

properties of a ternary solution based on the binary data at composition nearest the ternary composition, using the following form for excess molar volume:

$$[14]\quad V^E_{123} = \frac{x_1x_2V^E_{12}}{\left(x_1 + \frac{x_3}{2}\right)\left(x_2 + \frac{x_3}{2}\right)} + \frac{x_1x_3V^E_{13}}{\left(x_1 + \frac{x_2}{2}\right)\left(x_3 + \frac{x_2}{2}\right)} + \frac{x_2x_3V^E_{23}}{\left(x_2 + \frac{x_1}{2}\right)\left(x_3 + \frac{x_1}{2}\right)}$$

so that for binary system at composition x_i^0, x_j^0:

$$[15]\quad x_i - x_j = x_i^0 - x_j^0$$

Cibulka (10) proposed the following equation:

$$[16]\quad V^E_{123} = V^E_{12*} + V^E_{13*} + V^E_{23*} + x_1x_2x_3(A + Bx_1 + Cx_2)$$

where A, B, and C are parameters calculated from experimental data.

Bertrand *et al.* (11) presents the following equation for an excess property in a multicomponen system:

$$[17]\quad Z^E_{123} = (x_1 + x_2)(f_1 + f_2)(Z^E_{12})^* + (x_1 + x_3)(f_1 + f_3)(Z^E_{13})^* + (x_2 + x_3)(f_2 + f_3)(Z^E_{23})^*$$

in which Z represents any extensive thermodynamic property described in terms of interaction parameters A_0 and the weighting factor f_i relates to the composition of the system. The superscript * represents a composition of a binary system which would be formed if all the third component is removed, so that for the $i - j$ system:

$$[18]\quad x_i^* = 1 - x_j^* = x_i/(x_i + x_j)$$

Nagata (12–14) has proposed more complex equations for the excess enthalpy of a ternary system of one alcohol + two hydrocarbons, taking association of the components into account.

Finally, Singh *et al.* (15) proposed an equation of the following form:

$$[19]\quad V^E_{123} = V^E_{12*} + V^E_{13*} + V^E_{23*} + x_1x_2x_3[A + Bx_1(x_2 - x_3) + Cx_1^2(x_2 - x_3)^2]$$

where A, B, and C are parameters characteristic of the mixtures evaluated by the method of least squares using a standard deviation defined in eq. [3].

We have used eqs. [8], [10], [13], [14], [16], and [19] to calculate excess molar volumes and excess viscosities in our system.

Can. J. Chem. Downloaded from www.nrcresearchpress.com by 198.100.157.202 on 09/07/12
For personal use only.

The parameters obtained for V^E_{123} in Cibulka's equation are $A = 8.7571$; $B = -24.6172$; $C = -13.7019$. For η^E_{123} the parameters are $A = -2.4474$; $B = 5.3179$; and $C = 1.1798$.

The parameters obtained for V^E_{123} in the equation of Singh *et al.* are $A = -3.3083$; $B = -18.7442$; and $C = -81.6366$. For η^E_{123} the parameters are $A = -0.4753$; $B = 1.6449$; and $C = 19.6837$.

Table 5 shows the standard deviations for the excess volumes and viscosities calculated by using some of the equations previously mentioned for a ternary system.

Equation [16] shows the best agreement with the experimental data. Only eqs. [16] and [19] contain three adjustable parameters while the others include only experimental data for the corresponding binary mixtures. There is no preferred way of knowing which method will provide the best prediction for a given system. The last two methods use parameters which are obtained from experimental data. The fact that so many empirical equations have been developed suggests that no single equation can describe all types of available systems.

Acknowledgments

The present work was financed by a CONICET (PID Program) and a CIUNT research grant. We are grateful to Ing. Mario R. Cesca for assistance in computer programming.

1. O. Redlich and A. T. Kister. Ind. Eng. Chem. **40**, 345 (1948).
2. G. Scatchard, L. B. Tickner, J. R. Goates, and E. R. McCartney. J. Am. Chem. Soc. **74**, 3721 (1952).
3. C. C. Tsao and J. M. Smith. Chem. Eng. Prog. Symp. **49**, 107 (1953).
4. A. R. Mathieson and J. C. J. Tynne. J. Chem. Soc. 3713 (1956).
5. F. Kohler. Monatsch. Chem. **91**, 738 (1960).
6. G. W. Toop. Trans. TMS-AIME, **233**, 850 (1965).
7. R. P. Rastogi, J. Nath, and S. S. Das. J. Chem. Eng. Data, **22**, 249 (1977).
8. N. Radojkovič, A. Tasič, D. Grozdanič, B. Diordievič, and M. Malič. J. Chem. Thermodyn. **9**, 349 (1977).
9. K. J. Jacob and K. Fitzner. Thermochim. Acta, **18**, 197 (1977).
10. I. Cibulka. Coll. Czech. Chem. Commun. **47**, 1414 (1982).
11. G. L. Bertrand, W. E. Acree Jr., and T. E. Burchfield. J. Sol. Chem. **12**, 327 (1983).
12. I. Nagata. Fluid Phase Equilib. **1**, 211 (1977).
13. I. Nagata. J. Chem. Eng. Data, **20**, 110 (1975).
14. I. Nagata. J. Chem. Eng. Data, **22**, 249 (1977).
15. P. P. Singh, R. K. Nigam, S. P. Sharma, and S. Aggarwal. Fluid Phase Equilibr. **18**, 222 (1984).
16. I. L. Acevedo, M. A. Postigo, and M. Katz. Can. J. Chem. **66**, 367 (1988).
17. G. C. Pedrosa, J. A. Salas, and M. Katz. Phys. Chem. **21**, 207 (1990).
18. M. Sreenivasulu and P. R. Naidu. J. Chem. Thermodyn. **10**, 731 (1978).
19. M. K. Dultachoudhury and H. B. Mathur. J. Chem. Eng. Data, **19**, 145 (1974).
20. A. Weissberger (*Editor*). Technique of organic chemistry. Vol. 7. Organic solvents. 2nd ed. Interscience Publishers, New York. 1955.
21. R. C. Reid, J. M. Prausnitz, and T. K. Sherwood. The properties of gases and liquids. 3rd ed. McGraw-Hill Book Co., New York. 1977.
22. J. I. Riddick, N. B. Bunger, and T. Sakano. Organic solvents. 4th ed. J. Wiley and Sons, New York. 1986.
23. P. R. Naidu and V. R. Krishnan. J. Chem. Soc. Faraday Trans. 1347 (1964).
24. A. K. Adya, B. S. Mahl, and P. P. Singh. Thermochim. Acta, **9**, 318 (1974).

Can. J. Chem. Downloaded from www.nrcresearchpress.com by 198.100.157.202 on 09/07/12
For personal use only.

The synthesis of 3*H*-naphthol[1,8-*bc*]thiophene derivatives

PETER D. CLARK,[1] NICHOLAS M. IRVINE, AND PRATIBHA SARKAR
Department of Chemistry, The University of Calgary, 2500 University Drive N.W., Calgary, Alta., Canada T2N 1N4

Received November 9, 1990

PETER D. CLARK, NICHOLAS M. IRVINE, and PRATIBHA SARKAR. Can. J. Chem. **69**, 1011 (1991).

Methods for the synthesis of keto derivatives of the little studied naphtho[1,8-*bc*]thiophene system have been developed. Using the readily available benzothiophene derivative 6,7-dihydrobenzo[*b*]thiophen-4(5*H*)-one **4**, a 3-keto-naphtho-[1,8-*bc*]thiophene **14** was synthesized by a tin(IV) chloride catalyzed cyclization of the acid chloride derivative of the saturated acid **13***b*. The bicyclic ketone **4** was also used to prepare the keto-sulfoxide **7**, which was cyclized to the 4-keto-naphtho-[1,8-*bc*]thiophene system **9** in a Pummerer-type rearrangement.

Key words: synthesis, organosulfur, naphtho[1,8-*bc*]thiophenones.

PETER D. CLARK, NICHOLAS M. IRVINE et PRATIBHA SARKAR. Can. J. Chem. **69**, 1011 (1991).

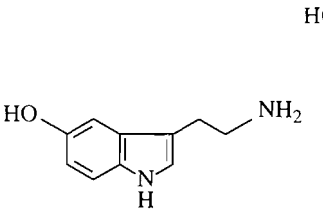
On a mis au point des méthodes de synthétiser les dérivés cétoniques du système naphto[1,8-*bc*]thiophène qui n'a pas été très étudié jusqu'à maintenant. Utilisant comme produit de départ la 6,7-dihydrobenzo[*b*]thiophén-4(5*H*)-one (**4**), un dérivé benzothiophène facilement disponible, on a réalisé la synthèse de la naphto[1,8-*bc*]thiophén-3-one (**14**) en faisant appel à une cyclisation, catalysée par la chlorure d'étain (IV), du chlorure d'acide de l'acide saturé **13***b*. On a utilisé la cétone bicyclique **4** pour préparer ie céto-sulfoxyde **7** qui, par une cyclisation impliquant une transposition du type de Pummerer, conduit au système naphto[1,8-*bc*]thiophón-4-one, **9**.

Mots clés : synthèse, organosulfure, naphto[1,8-*bc*]thiophénones.

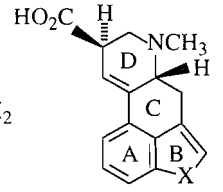
[Traduit par la rédaction]

Introduction

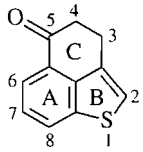
Compounds and alkaloids containing the indole nucleus have a wide spectrum of pharmacological activity (1–4). Perhaps the best known examples of these compounds are the natural transmitter 5-hydroxytryptamine **1** (5) and derivatives of the ergoline ring system such as lysergic acid **2***a* (for a general review, see ref. 6). Replacement of the indole nitrogen by sulfur is known (7) to change the pharmacological action of **1** and related compounds and, in some cases, to produce isosteres with useful biological properties (8). Several workers have attempted to prepare the sulfur analogues of ergolines **2***b* but, to our knowledge, none have been successful (9–12). This paper describes the synthesis of naphtho[1,8-*bc*]thiophene derivatives, which should be useful intermediates in the preparation of thia-ergolines **2***b*.



1



2*a* = NH
2*b* = S



3

Very few derivatives of the naphtho[1,8-*bc*]thiophene system have been reported (9–11, 13–15). Most of the syntheses described have been in connection with development of routes of the preparation of thia-ergolines. Considerable effort (9, 10) was put into developing syntheses and the chemistry of the tricyclic ketone **3** as it was expected to be a useful intermediate in constructing ring D of thia-ergoline systems. Unfortunately, this (and related compounds) isomerizes readily to naphthalene derivatives in which the A and C rings become the aromatic nucleus (10). This problem may be overcome by working with derivatives in the early stages of the synthesis in which the A ring is saturated since these compounds would show little tendency to be involved in aromatization processes involving the C ring. Consequently, we have designed syntheses of the novel tricyclic ketones **9** and **14** and report on their preparation here.

Experimental

Melting points were determined using a Thiele tube apparatus containing silicon oil and were uncorrected. The IR spectra were recorded on a Nicolet 5DX spectrometer as neat liquids, thin films, or KBr discs. The ^1H and ^{13}C NMR spectra were recorded on a Bruker ACE 200 or a Bruker AM 400 spectrometer, at 200 and 400 MHz respectively, in $CDCl_3$ solution with either tetramethylsilane or chloroform as the internal standard. Assignments for ^{13}C spectra were made (where possible) on the basis of DEPT, 2D correlation experiments,[2] and chemical shift data. MS and GCMS were recorded on a Hewlett Packard 5970/5890 spectrometer. Elemental analyses were obtained from Canadian Microanalytical Service Ltd., B.C. Column chromatography was performed on Merck silica gel, grade 60, 230–400 mesh. Reagents were obtained from the Aldrich Chemical Company and, unless stated otherwise, were used without purification. Solvents were purified according to procedures described in ref. 16.

*6,7-Dihydro-5*H*-benzo[*b*]thiophen-4-one* **4**

This ketone was prepared either from thiophene or from 2-cyclohexen-1-one using methods described previously (17–20). Both methods are reliable although the preparation from 2-cyclohexen-1-one (20) is preferred for large-scale work.

Preparation of the ene-acetates **5**a *and* **5**b

These compounds were prepared by the following modifications of the literature method (21).

A solution of triethyl phosphonoacetate (22.4 g, 100 mmol) in dry tetrahydrofuran (100 mL) was added dropwise over 45 min to a suspension of sodium hydride (60% in oil, 3.7 g, 90 mmol) in dry tetrahydrofuran (100 mL) under an argon atmosphere. The resulting clear yellow solution was heated under reflux for 15 min and a solution of the ketone **4** (10.0 g, 66 mmol) in tetrahydrofuran (100 mL) was added in one portion. After 36 h at reflux, the resulting orange solution was cooled

[1]Author to whom correspondence may be addressed.

[2]Copies of the homo- and heteronuclear shift correlation spectra for **9** and **14** may be purchased from The Depository of Unpublished Data, Document Delivery, CISTI, National Research Council Canada, Ottawa, Canada K1A 0S2.

Can. J. Chem. Downloaded from www.nrcresearchpress.com by 198.100.157.202 on 09/07/12
For personal use only.

Can. J. Chem. Downloaded from www.nrcresearchpress.com by 198.100.157.202 on 09/07/12
For personal use only.

and was added to water (300 mL). Organic material was recovered by extraction into dichloromethane (3 × 250 mL). The organic extracts were washed with water (3 × 100 mL), dried ($MgSO_4$), and evaporated. The residual tan colored oil was chromatographed on silica (5% ethyl acetate in hexanes) to remove residual phosphorus compounds and was distilled at reduced pressure to yield a colorless liquid (14.17 g, 97%; bp 105–125°C at 0.05 Torr (1 Torr = 133.3 Pa)). ^{1}H NMR[a] indicated that the product was a 63:37 mixture of *E* and *Z* isomers **5***a* and **5***b*; IR (ν_{max}, neat): 3107, 2933, 1706, 1612, 1174, 1150, and 1049 cm^{-1}; ^{1}H NMR, *E* isomer,[b] δ: 7.20 (d, *J* = 5.4 Hz, -C*H*=CH-), 7.06 (d, *J* = 5.4 Hz, -CH=C*H*), 6.11 (t, *J* = 1.7 Hz, -C=C*H*), 4.19 (q, -C*H*$_2$-CH$_3$), 3.20–3.05 (m, -C*H*$_2$-C=CH-), 2.89 (t, *J* = 6.1 Hz, -C*H*$_2$-S-), 1.95 (m, -CH$_2$-C*H*$_2$-CH$_2$-), 1.31 (t, -CH$_2$-C*H*$_3$); *Z* isomer,[c] δ: 7.81 (d, *J* = 5.5 Hz, -C*H*=CH-), 7.02 (d, *J* = 5.5 Hz, -CH=C*H*-), 5.65 (br, s -C=C*H*-), 4.18 (q, -C*H*$_2$-CH$_3$), 2.93 (t, -C*H*$_2$C=-CH-), 2.50–2.40 (m, -C*H*$_2$-S-), 1.96 (m, -CH$_2$-C*H*$_2$-CH$_2$-), 1.28 (t, -CH$_2$C*H*$_3$); ^{13}C NMR, *E* isomer, δ: 167.17 (*C*=O), 150.32, 144.73, and 134.71 (quaternary C), 123.24, 122.51, and 110.31 (-*C*H=CX), 59.42 (-OC*H*$_2$CH$_3$), 26.18, 25.29, and 23.53 (*C*H$_2$), 14.25 (OCH$_2$*C*H$_2$CH$_3$); Z isomer[c]: 166.45 (*C*=O), 146.81, 145.45, and 132.49 (quaternary C), 128.55, 120.88, and 112.03 (-*C*H=CX), 59.76 (-OC*H*$_2$CH$_3$), 35.51, 25.86, and 24.14 (*C*H$_2$), 14.15 (OCH$_2$*C*H$_3$). Anal. calcd. for $C_{12}H_{14}O_2S$: C 64.84, H 6.35, S 14.42%; found: C 65.22, H 6.55; S, 14.53%.

[a]Determined by integration of vinylic protons in the ^{1}H NMR of the crude reaction mixture.

[b]Remaining isomer after hydrogenation with Wilkinson's catalyst; see Discussion.

[c]Obtained by analysis of spectra for mixture of isomers.

*4′-(4,5,6,7-Tetrahydrobenzo[*b*]thienyl) ethyl ethanoate* **6**

A solution of the ene-acetates **5***a* and **5***b* (20 g, 90 mmol) in toluene (700 mL) was stirred with 10% Pd on charcoal (4.5 g) for 24 h under a hydrogen atmosphere. The mixture was filtered through Celite and the crude product was recovered by evaporation of the solvent. Traces of unhydrogenated material were separated by flash chromatography on silica (5% ethyl acetate in hexanes) and the product was obtained as a colorless liquid (17.75 g, 88%) by distillation (bp 85–92°C at 0.05 Torr); IR (ν_{max}, neat): 2934, 1733, and 1175 cm^{-1}; ^{1}H NMR, δ: 7.01 (d, *J* = 5.2 Hz, -C*H*=CH-), 6.79 (d, *J* = 5.2 Hz, -CH=C*H*-), 4.16 (q, -OC*H*$_2$CH$_3$), 3.35–3.15 (m, -CH$_2$C*H*CH$_2$-), 2.74 (t, -C*H*$_2$-S-), 2.69 and 2.38 (each dd, -CH-C*H*$_2$CO-), 2.05–1.65 and 1.65–1.45 (m, -C*H*$_2$C*H*$_2$-), 1.26 (t, -OCH$_2$C*H*$_3$); ^{13}C NMR, δ: 172.35 (*C*=O), 137.37 and 136.21 (quaternary carbons), 126.13 and 121.73 (-*C*H=*C*H-), 60.11 (-OCH$_2$CH$_3$), 40.84, 28.61, 24.89, and 21.26 (four CH$_2$), 32.48 (-CH-). Anal. calcd. for $C_{12}H_{16}O_2S$: C 64.25, H 7.19, S 14.29%; found: C 64.00, H 7.04, S 14.31%.

Preparation of the keto-sulfoxide **7**

Dimethyl sulfoxide, freshly distilled from calcium hydride (30 mL, 420 mmol), was added dropwise to a stirred solution of *n*-butyllithium (36 mL of a 1.6 M solution in hexane, 58 mmol) in dry tetrahydrofuran (30 mL) at 0°C under an argon atmosphere. A solution of the ester **6** (5.0 g, 22.3 mmol) in dry tetrahydrofuran (10 mL) was added to the resulting cream colored slurry and the reaction mixture was allowed to warm to room temperature. The orange solution produced was added to water and the mixture was extracted with dichloromethane (3 × 150 mL). The organic extracts were washed with saturated sodium bicarbonate (2 × 100 mL) and with water (3 × 100 mL), dried ($MgSO_4$), and evaporated. The light brown residue was chromatographed on silica (ethyl acetate) to yield a light brown solid (4.8 g, 84%), which was a mixture of diastereomers of **7**. An analytically pure sample of the minor diastereomer was obtained as white crystals, mp 75–77°C, on crystallization from hexanes; IR (ν_{max}, neat): 2930, 1710, and 1035 cm^{-1}; ^{1}H NMR, δ: 7.03 (d, *J* = 5.3 Hz, -C*H*=CH-), 6.75 (d, *J* = 5.3 Hz, -CH=C*H*-), 3.90–3.60 (2 × q,[a] -COC*H*$_2$SO-), 3.45–3.25 (m, -CH$_2$C*H*CH$_2$-), 2.68, 2.66[a] (s, -SOC*H*$_3$), 3.02–2.65 and 2.05–1.40 (unres. m, methylene protons); ^{13}C NMR, δ: 201.39 (*C*=O), 136.95, 136.42 (quaternary carbons), 126.16, 121.94 (-*C*H=*C*H-), 64.55 [63.94][b] (*C*OCH$_2$SO), [51.7] 51.51 (*C*HCH$_2$CO), 39.03 [38.78] (SO*C*H$_3$), 30.81 (CH$_2$*C*HCH$_2$), 28.68, 24.76, and 21.18 (3CH$_2$ in six-membered ring). Anal. calcd. for $C_{12}H_{16}O_2S_2$: C 56.22, H 6.29, S 25.01%; found: C 55.86, H 6.21, S 24.87%.

[a]Signals due to diastereomers.

[b]Values for the minor diastereomer given in square brackets.

*3-Methylthio-4,5,5a,6,7,8-hexahydro-3*H*-naphtho[1,8-*bc*]thiophen-4-one* **8**

A solution of *p*-toluenesulfonic acid monohydrate (3.71 g, 19.5 mmol) in 1.2 L of chloroform (distilled from P_2O_5 to remove ethanol) was heated under reflux for 3 h with removal of water via a Dean Stark trap. The sulfoxide **7** (2.5 g, 9.75 mmol) in chloroform (150 mL) was added and resulting orange-brown solution was heated under reflux for 15 min. The cooled reaction mixture was poured into saturated sodium bicarbonate (500 mL) and the organic layer was washed with bicarbonate (500 mL) and with water (2 × 500 mL), and then dried ($MgSO_4$). Evaporation of the chloroform gave a brown oil, which was purified by column chromatography on silica (10% ethyl acetate in hexanes). The pale yellow oil obtained (1.1 g, 47%) was used immediately as it darkened quickly on standing and decomposed on attempted distillation. Spectroscopic analysis indicated that **8** was formed as a mixture of diastereomers; IR (ν_{max}, neat): 3096, 2923, 1704, 1603, and 1435 cm^{-1}; ^{1}H NMR[a], δ: [7.11] 7.00 (s, -C*H*=C-), 4.20 [4.16] (s, -C*H*SCH$_3$-), 3.40–2.65 (unres. m, 5H), [2.15] 2.13 (s, -SCH$_3$), 2.20–1.10 (unres. m, 4H).

[a]Integration of signals at 7.0 and 2.1 ppm suggested that the product was a 2:1 mixture of diastereomers; values for the minor isomer are shown in square brackets.

*4,5,5a,6,7,8-Hexahydro-3*H*-naphtho[1,8-*bc*]thiophen-4-one* **9**

W-2 Raney nickel (ca. 6 g) was added to a solution of the methylthio ether **8** (1.3 g, 5.5 mmol) in acetone (100 mL) and the mixture was stirred at room temperature for 5 h. The catalyst was removed by filtration through Celite and the crude product was obtained by evaporation of the solvent. Column chromatography on silica (10% ethyl acetate in hexanes) yielded a pale orange solid that crystallized from hexane (charcoal) to yield off-white plates (0.44 g, 43%); mp 60–63°C; IR (ν_{max}, Nujol): 3095, 2930, 1712, 1446, 1393, 1325, 1228, and 1173 cm^{-1}; ^{1}H NMR (400 MHz),[a] δ: 6.79 (d, *J* = 0.9 Hz, -C*H*=C-), 3.59 (d, *J* = 21.0 Hz, 1H of =C-C*H*$_2$-CO), 3.47 (dd, *J* = 21 and 0.9 Hz, 1H of =C-C*H*$_2$CO), 3.05–2.85 (m, -CH$_2$C*H*CH$_2$-), 2.90–2.60 (m, C*H*$_2$S and 1 proton of CHC*H*$_2$CO), 2.20–2.10 (m, 1 proton of CHC*H*$_2$CO, 1 proton of CHC*H*$_2$CH$_2$, and 1 proton of CH$_2$C*H*$_2$CH$_2$S), 1.95–1.80 (m, 1 proton of CH$_2$C*H*$_2$CH$_2$S), and 1.4–1.25 (m, 1 proton of CHC*H*$_2$CH$_2$); ^{13}C NMR, δ: 209.0 (*C*=O), 135.63, 134.86, and 132.71 (quaternary carbons), 116.64 (*C*H=C-), 46.14 (-CHCH$_2$CO), 41.15 (=CCH$_2$CO), 32.22 (-C*H*-), 29.84 (CH$_2$*C*H$_2$CH), 24.64 (SC*C*H$_2$), and 23.45 (CH$_2$CH$_2$CH$_2$). Anal. calcd. for $C_{11}H_{12}OS$: C 68.72, H 6.29, S 16.67%; found: C 68.28, H 6.19, 17.04%.

[a]Assignments were made on the basis of proton–proton and proton–carbon correlation experiments.

*4-Methoxymethylene-6,7-dihydro-5*H*-benzo[*b*]thiophene* **10**a, **10**b

Phenyllithium (22 mL of a 2 M solution in cyclohexane–ether, 44 mmol) was added dropwise to a suspension of (methoxymethyl)-triphenylphosphonium chloride (**22**) (17.14 g, 50 mmol) in dry ether (100 mL) at 0°C under an argon atmosphere. After stirring the resulting red mixture for 15 min, the temperature was lowered to −65°C and a solution of the ketone **4** (3.04 g, 20 mmol) in anhydrous ether was added over 5 min. The reaction mixture was allowed to warm to room temperature, stirred vigorously for 5 h, and then poured into cold water (100 mL). The ether layer was collected and the aqueous layer was extracted with ether (3 × 25 mL). The combined organic extracts were washed with saturated sodium chloride solution, dried ($MgSO_4$), and evaporated. Column chromatography of the residue on silica (0–2% ethyl acetate in hexanes) gave a mixture (TLC, NMR) of the *E* and *Z* enol ethers **10***a* and **10***b*, which was distilled to yield a colorless liquid (2.7 g, 75%; bp 72–75°C at 0.03 Torr); IR (ν_{max}, neat): 2932, 2832, 1661, 1452, 1223, 1157, and 1124 cm^{-1}; ^{1}H NMR, δ: 7.58[a] (d, *J* = 5.3 Hz, -C*H*=CH-), 7.05–6.94 (unres. m, thiophenic H), 6.45[b] (t, *J* = 1.6 Hz, -C=C*H*OCH$_3$), 5.88[a] (t, *J* = 1.2 Hz, -C=C*H*OCH$_3$), 3.66 (s,

Can. J. Chem. Downloaded from www.nrcresearchpress.com by 198.100.157.202 on 09/07/12
For personal use only.

-OCH_3), 2.88–2.75 (m, -CH_2CH_2S-), 2.50–2.44[b] (m, -CH_2CH_2C=), 2.30–2.24[a] (m, -CH_2CH_2C=), 1.95–1.79 (m, -$CH_2CH_2CH_2$-); ms *m/e*: 180 (89).

NOTE: *a* and *b* refer to signals for the *Z* and *E* isomers respectively (see discussion).

*4'-(4,5,6,7-Tetrahydrobenzo[*b*]thienyl) methanal* ***11***

6 M Aqueous hydrochloric acid (6 mL) was added to a solution of the enol ethers **10***a* and **10***b* (8.06 g, 45 mmol) in tetrahydrofuran (100 mL) under argon and the mixture was heated under reflux for 15 h. A further 4 mL of the 6 M acid was added and the solution refluxed for an extra 2 h. The reaction mixture was cooled, evaporated to a small volume, and quenched with water (100 mL). The mixture was extracted with dichloromethane (4 × 20 mL) and the organic extracts were washed with saturated sodium bicarbonate (2 × 10 mL), brine (1 × 50 mL), dried ($MgSO_4$), and evaporated to yield **11** as a pale yellow oil[a] (7.80 g); IR (ν_{max}, neat): 2937, 2858, 2717, and 1725 cm^{-1}; ^{1}H NMR, δ: 9.66 (d, *J* = 2.2 Hz, -*CH*O), 7.15 and 6.88 (each d, *J* = 5.2 Hz, -*CH*=*CH*-), 3.54 (m, -CH_2*CH*CHO), 2.8 (t, -SCH_2CH_2-), 2.21–1.81 (m, -CH_2CH_2-); ^{13}C NMR, δ: 200.68 (-*C*HO), 138.23 and 129.06 (quaternary C), 126.4 and 122.5 (-*C*H=*C*H-), 48.75 (-*C*HCHO), 24.47, 22.57, and 21.19 (3 × CH_2); ms *m/e*: 166. The aldehyde was characterized as a 2,4-dinitrophenylhydrazone derivative, which crystallized from ethyl acetate as orange crystals, mp 210–213°C. Anal. calcd. for $C_{15}H_{14}N_4O_4S$: C 52.02, H 4.07, N 16.18, S 9.26%; found: C 51.51, H 4.16, N 15.94, S 9.24%.

[a]This product decomposed rapidly unless stored at low temperatures under an inert atmosphere, and was used directly in the next stage.

E-*3-(4'-(4,5,6,7-Tetrahydrobenzo[*b*]thienyl)) ethyl propenoate* ***12***

A solution of triethyl phosphonoacetate (16.08 g, 71.8 mmol) in dry tetrahydrofuran (100 mL) was added dropwise to a suspension of sodium hydride (60% in oil, 2.88 g, 72 mmol) in tetrahydrofuran (100 mL) under an argon atmosphere. The mixture was cooled to −60°C and a solution of the aldehyde **11** in tetrahydrofuran (100 mL) was added over a period of 10 min. The reaction mixture was allowed to warm to room temperature and was stirred for 1.5 h. Solvent was removed by rotary evaporation, the residue was quenched with water (100 mL), and the resulting mixture was extracted with dichloromethane (4 × 20 mL). Evaporation of the washed (brine, 1 × 50 mL) and dried ($MgSO_4$) extracts yielded an oil that was distilled (bp 116–119°C at 0.03 Torr) to give **12** as a clear liquid (9.50 g, 90% from **10***a* and **10***b*); IR (ν_{max}, neat): 2936, 1718, and 1652 cm^{-1}; ^{1}H NMR, δ: 7.05 (d, *J* = 5.2 Hz, S-*CH*=CH-), 7.0 (dd, -CHC*H*=CHCO$_2$-), 6.73 (d, *J* = 5.2 Hz, SCH=C*H*-), 5.79 (dd, *J* = 15.6 and 1.2 Hz, -CHCH=C*H*CO$_2$-), 4.18 (q, -OCH_2CH_3), 3.56 (m, -CH_2*CH*(C=)CH=), 2.78 (t, SCH_2CH_2-), 1.70–1.90 (m, -$CH_2CH_2CH_2$CH-), 1.29 (t, -OCH_2CH_3); ^{13}C NMR, δ: 166.64 (-*C*O$_2CH_2CH_3$), 151.49 (=*C*HCO$_2CH_2CH_3$), 136.87 and 134.59 (quaternary C), 127.28, 122.02, and 121.54 (thiophenic *C*H and remaining olefinic C), 60.23 (-OCH_2CH_3), 39.1 (-CH_2CH(C=)CH=), 28.64, 24.90, and 21.16 (3 × CH_2), 14.24 (-OCH_2CH_3); ms *m/e*: 236 (M^+). Anal. calcd. for $C_{13}H_{16}O_2S$: C 66.07, H 6.83, S 13.57%; found: C 66.01, H 6.72, S 12.95%.

*3-(4'-(4,5,6,7-Tetrahydrobenzo[*b*]thienyl)) ethyl propionate* ***13***a

Tris(triphenylphosphine)rhodium(I) chloride (0.86 g, 9.3 mmol) was added to benzene (270 mL) that had been presaturated with hydrogen. After stirring the resulting orange solution for 15 min, a solution of the ester **12** (8.72 g, 36.6 mmol) in benzene (30 mL) was added and the reaction mixture was stirred under a hydrogen atmosphere for 50 h at 20°C. After removal of solvent, the residue was purified by flash chromatography on silica (5% ethyl acetate in hexanes) and the oil obtained was distilled (bp 117–121°C at 0.07 Torr), yielding **13***a* as a clear liquid (8.62 g, 98%); IR (ν_{max}, neat): 2933, 1733, and 1174 cm^{-1}; ^{1}H NMR, δ: 7.03 and 6.86 (two d, *J* = 5.1 Hz, SC*H*=C*H*-), 4.13 (q, -OCH_2CH_3), 2.75 (t, -SCH_2CH_2-), 2.37 (dd, -$CH_2CH_2CO_2$-), 2.12 (m, -CH_2*CH*CH_2-), 1.98–1.22 (m, 3 × CH_2); ^{13}C NMR, δ: 173.73 (-*C*O$_2$-), 138.38 and 136.11 (quaternary C), 126.59 and 121.61 (-*C*H=*C*H-), 60.26 (-CH_2*C*O$_2$-), 35.01 (-CH_2*C*HCH_2-), 31.89, 30.73, 27.79, 25.10, and 21.59 (5 × CH_2), 14.21 (-O$_2CH_2CH_3$); ms *m/e*: 238 (M^+). Anal. calcd. for $C_{13}H_{18}O_2S$: C 65.51, H 7.61, S 13.43%; found: C 65.74, H 7.64, S 13.12%.

*3-(4'-(4,5,6,7-Tetrahydrobenzo[*b*]thienyl))propanoic acid* ***13***b

A mixture of the ester **13***a* (6.96 g, 29 mmol) and 1:1 absolute ethanol and 20% aqueous sodium hydroxide solution (140 mL) was heated under reflux for 2 h. The cooled reaction mixture was extracted with dichloromethane (2 × 20 mL), acidified with concentrated hydrochloric acid, and extracted with dichloromethane (3 × 20 mL). Evaporation of the washed (water) and dried ($MgSO_4$) extracts gave a solid residue that was recrystallized as pale yellow plates (5.26 g, 86%), mp 78–80°C from aqueous ethanol; IR (ν_{max}, KBr): 3000 (br) and 1704 cm^{-1}; ^{1}H NMR, δ: 10.10 (br s, -O*H*), 7.05 and 6.86 (two, d, *J* = 5.2 Hz, -SC*H*=C*H*-), 2.76 (t, -SCH_2CH_2-), 2.43 (dd, -$CH_2CH_2CO_2$H), 2.12 (m, -CH_2*CH*CH_2-), 2.0–1.41 (m, 3 × CH_2); ^{13}C NMR, δ: 180.13 (-*C*O$_2$H), 138.17 and 136.25 (quaternary C), 126.49 and 121.49 (-SC*H*=C*H*-), 34.97 (-CH_2*C*HCH_2-), 31.59, 30.47, 27.86, 25.10, and 21.65 (5 × CH_2); ms *m/e*: 210. Anal. calcd. for $C_{11}H_{14}O_2S$: C 62.83, H 6.71, S 15.22%; found: C 63.22, H 6.79, S 14.95%.

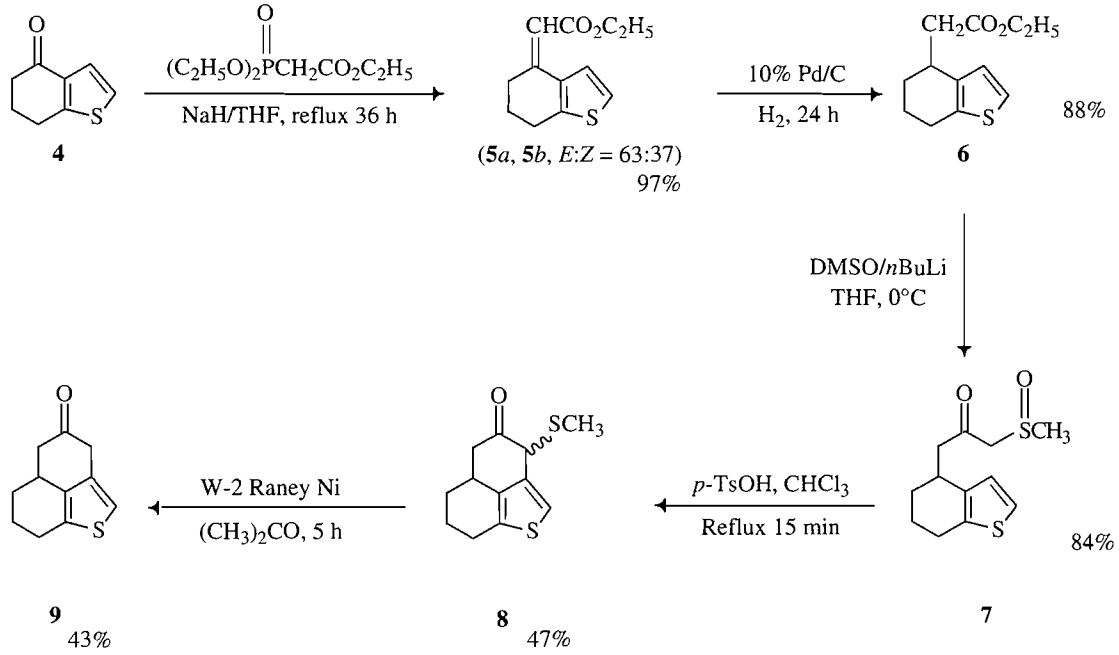
*4,5,5a,6,7,8-Hexahydro-3*H*-naphtho[1,8-*bc*]thiophen-3-one* ***14***

A solution of the acid **13***b* (1.05 g, 5 mmol) in dichloromethane (10 mL) was gently heated under reflux with thionyl chloride (1.19 g, 10 mmol) and pyridine (25 μL) under argon for 3 h. The mixture was concentrated by rotary evaporation and the crude acid chloride (IR 1798 cm^{-1}) was dissolved in carbon disulfide (5 mL). Under argon, the solution was cooled to 0°C, and tin tetrachloride (0.70 mL, 6 mmol) in carbon disulfide (15 mL) was added dropwise over 10 min. After carefully stirring the dark green mixture for 20 min at this temperature, it was heated under reflux for 2.5 h. The contents were cooled, evaporated to near dryness, and taken up into chloroform (50 mL). Ice (20 g) and hydrochloric acid (3 mL) were added, the organic layer was separated off, and the aqueous layer extracted with chloroform (3 × 10 mL). Organic extracts were combined, washed with brine (25 mL), dried ($MgSO_4$), evaporated down, and the residue was purified by flash column chromatography on silica (20% ethyl acetate in hexanes) to yield 0.74 g (77%) of **14** as a yellow solid. Recrystallization from hexanes produced pale yellow needles; mp 67–68°C; IR (ν_{max}, KBr): 3082, 2903, and 1681 cm^{-1}; ^{1}H NMR (400 MHz), δ: 7.92 (C*H*=C), 2.95–2.84 (dd, 1 proton of SCCH*H*$_2$), 2.80–2.62 (m, 1 proton of CH_2CO, 1 proton of SCCH_2 and CH_2*CH*CH_2), 2.55–2.44 (td, 1 proton of *CH*$_2$CO), 2.20–2.02 (m, 1 proton of $CH_2CH_2CH_2$, 1 proton of CHCH_2CH_2CO, and 1 proton of CHC$H_2CH_2CH_2$), 1.92–1.80 (m, 1 proton of $CH_2CH_2CH_2$), 1.66–1.52 (qd, 1 proton of CHCH_2CH_2CO), and 1.36–1.20 (m, 1 proton of CHC$H_2CH_2CH_2$); ^{13}C NMR, δ: 194.39 (-*C*=O-), 140.95, 136.01, and 135.92 (quaternary C), 128.02 (-SC*H*=), 40.12 (-CH_2CO-), 35.66 (-CH_2C*H*CH_2-), 31.08 (CH*C*H$_2CH_2$CO), 29.02 (CH*C*H$_2CH_2CH_2$), 24.15 (SC*C*H$_2$), and 23.36 (CH_2*C*H$_2CH_2$); ms *m/e*: 192 (M^+). Anal. calcd. for $C_{11}H_{12}OS$: C 68.71, H 6.29, S 16.68%; found: C 68.87, H 6.17, S 16.99%.

Results and discussion

*4,5,5a,6,7,8-Hexahydro-3*H*-naphtho[1,8-*bc*]thiophen-4-one* ***9***

Synthesis of the naphthol[1,8-*bc*-]thiophenones requires benzo[*b*]thiophene compounds functionalized at the 3- and 4-positions. The bicyclic ketone **4** satisfies this requirement if both the carbonyl and the aromatic centres are viewed as substituents, and is readily available from either thiophene or from 2-cyclohexen-1-one (17–20). Our general strategy was to introduce a side chain at the 4-position, incorporating the carbonyl group of the target ketone and containing a functional group that could be cyclized onto the thiophene ring in an electrophilic process. This approach avoids using direct oxidation procedures to introduce the carbonyl group that could also oxidize the thiophenic sulfur.



SCHEME 1. Synthesis of 4,5,5a,6,7,8,-hexahydro-3*H*-naphtho[1,8-*bc*]thiophe-4-one.

Functionalization of the bicyclic ketone **4** at the 4-position using Wittig chemistry afforded the unsaturated ester **5** as a mixture of *E* and *Z* isomers (67:33) in almost quantitative yield. The reaction mixutre was readily analysed using ^{1}H NMR spectroscopy because the proximity of the ester function to the thiophenic proton H-3 in the *Z* isomer caused a considerable downfield shift of the resonance for H-3. The *E* to *Z* ratio was dependent on the base used to form the ylid; butyllithium produced the 67:33 *E*/*Z* mixture, and sodium hydride and potassium *tert*-butoxide produced 63:37 and 56:44 mixtures respectively. Various solvents and other reaction conditions were tried but it was not possible to produce either isomer as a major product.

A key step in the overall synthesis was the reduction of the double bond in **5** to produce the saturated ester **6**. Thiophenic compounds are difficult to reduce using conventional heterogeneous catalysts because of catalyst poisoning caused by adsorption of the sulfur to the active sites (23). In addition, high activity catalysts can desulfurize thiophenic systems. In general, homogeneous hydrogenation catalysts such as Wilkinson's catalyst are less susceptible to poisoning by aromatic sulfur compounds but often will not saturate hindered double bonds (24). In this case, hydrogenation using Wilkinson's catalyst resulted in rapid reduction of the *Z* isomer of **5** but left the *E* isomer, containing the more hindered double bond, unreduced. Since the *Z* isomer was the minor product of the Wittig reaction, this approach to the saturated ester **6** was not practical. After consideration of a number of other hydrogenation catalysts, it was found that both isomers of **5** were reduced quite conveniently (24 h, 88% yield) employing a standard Pd-on-carbon catalyst in a somewhat larger compound/catalyst ratio (5:1) than is usual.

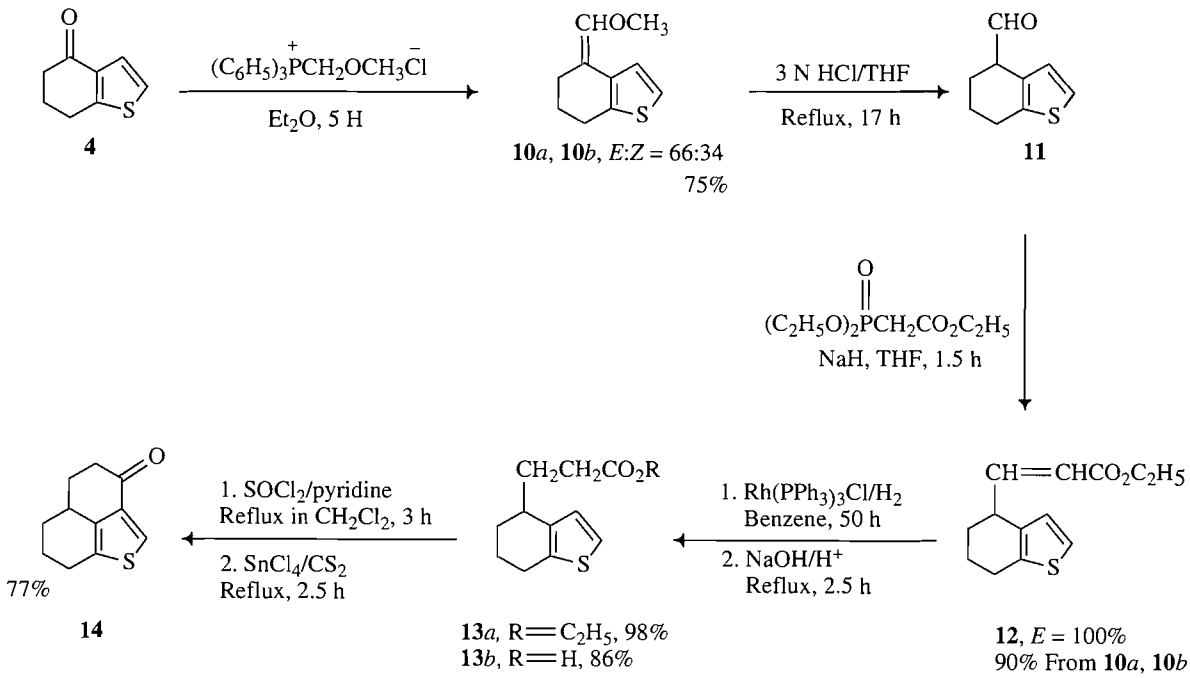
Reaction of the saturated ester **6** with the lithium anion of dimethyl sulfoxide gave a good yield (85%) of the keto-sulfoxide **7** as a mixture of diastereoisomers. Treatment of **7** under acidic conditions resulted in a Pummerer-type rearrangement and cyclization to the keto-sulfide **8**. Raney nickel treatment of this product under mild conditions removed the thioether sulfur to give the desired tricyclic ketone **9** without desulfurization of the thiophenic ring. Despite the moderate yield for the cyclization, this synthesis has the advantage of introducing a carbonyl substituent directly into the 4-position of the naphtho[1,8-*bc*]thiophene ring system.

Clear evidence that the tricyclic product had been obtained was given by the observation of only one thiophenic proton in the ^{1}H NMR spectrum. Spectra recorded at 400 MHz showed that the signal for the thiophenic proton of **9** was a doublet (J = 0.9 Hz). Two of the lines of the quartet representing the signal for the methylene sandwiched between the carbonyl and the thiophene ring showed the same small coupling, and double irradiation experiments confirmed that the thiophenic proton was coupled to one of the protons of the methylene group at the 3-position. This coupling is similar to those observed in alkylaromatics (25). Using chemical shift arguments and shift correlation spectra[2] it was possible to assign all of the signals in the ^{1}H NMR spectrum of **9**. Perhaps the most interesting feature of this spectrum is the large difference in chemical shift for the methylene protons at C-6 (1.3 and 2.15 ppm). Examination of molecular models of **9** shows that one possible conformation of the B and C rings results in close contact between C-6 and the carbonyl group at C-4, thus explaining why one of the protons at C-6 is deshielded.

*4,5,5a,6,7,8-Hexahydro-3*H*-naphtho[1,8-*bc*]thiophen-3-one* ***14***

It should be possible to synthesize the 3-keto-substituted naphthothiophene **14** by cyclization of the acid chloride derivative of the carboxylic acid **13***b* under Friedel–Crafts-type conditions. Introduction of the appropriate substituent to the 4-position of the bicyclic ketone **4** was accomplished in three basic stages. Firstly, **4** was converted to the aldehyde derivative **11** by reaction with (methoxymethyl)triphenylphosphonium chloride and hydrolysis of the resultant mixture of enol ethers **10***a* and **10***b*. A satisfactory analysis for the enol ethers could not be

Can. J. Chem. Downloaded from www.nrcresearchpress.com by 198.100.157.202 on 09/07/12
For personal use only.



SCHEME 2. Synthesis of 4,5,5a,6,7,8,-hexahydro-3*H*-naphtho[1,8-*bc*]thiophen-3-one.

obtained. The enol ethers were formed as an *E*/*Z* mixture that hydrolyzed readily to the aldehyde **11**. Extension of the 4-substituent by two carbons and introduction of an ester functional group was accomplished by reaction of the aldehyde with triethyl phosphonoacetate under standard Wittig conditions in an overall yield of 90% from the enol ether mixture. This reaction yielded the unsaturated ester **12** as a single isomer, which was assigned as the *E* isomer on the basis of the value of the coupling constant for the olefinic protons (J = 15.6 Hz). Also, the observation that the resonance due to the thiophenic proton on C-3 had not been shifted appreciably (as might have been expected if the ester group was in close proximity, as it would be in the *Z* isomer and as was observed for the *Z* isomer of **5**) supports the conclusion that **12** was formed as the *E* isomer.

Saturation of the double bond in **12** using palladium-on-carbon was very slow and difficult to force to completion unless large quantities of catalyst were used. However, reduction using Wilkinson's catalyst, although slow, gave an almost quantitative yield of the saturated ester **13**. This reduction and the reduction of the *Z* isomer of **5** indicate the general utility of Wilkinson's catalyst for reducing double bonds in thiophene derivatives as long as the double bond is relatively unhindered. Standard chemistry involving saponification of **13***a*, conversion of the resulting carboxylic acid **13***b* to its acid chloride, and treatment of the acid chloride with $SnCl_4$ gave the 3-keto naphthothiophene **14** in an overall yield of 77%. It was difficult to maintain this yield for large-scale preparations (>2 g).

^{1}H NMR spectra of **14** confirmed that cyclization had taken place, as only one uncoupled singlet was observed in the aromatic region. The rest of the ^{1}H NMR spectrum of **14** was complex although a reasonable assignment was possible using shift correlation spectra[2] and from chemical shift arguments. Interestingly, as was observed in the ^{1}H NMR spectra of **9**, the signals for the two protons on C-6 occur at quite different chemical shifts, one being considerably more downfield than would be expected (2.08 and 1.28 ppm). Inspection of molecular models indicates that when overlap of the carbonyl substituent and the π-system of the thiophene ring is maximized, one of the protons on C-6 is in close contact with the carbonyl group and thus is shifted downfield.

Acknowledgments

The authors gratefully acknowledge financial support from the Natural Sciences and Engineering Research Council of Canada and Alberta Sulphur Research Limited, Calgary.

1. W. A. JACOBS and R. G. GOULD, JR. J. Biol. Chem. **120**, 141 (1937).
2. A. STOLL and A. HOFMANN. Alkaloids, **8**, 727 (1965).
3. M. E. JARUK. *In* The pharmacalogical basis of therapeutics. 4th ed. *Edited by* L. S. Goodman and A. Gilman. Macmillan, New York. 1970. p. 194.
4. E. CAMPAIGNE and D. R. KNAPP. J. Pharm. Sci. **60**, 809 (1971).
5. M. PANCIULACCI, G. GRANCHI, and F. SICUTERI. Headache, **16**, 226 (1976).
6. S. GARATTINI and P. A. SHORE (*Editors*). Adv. Pharmacol. **6A** and **6B** (1968).
7. R. M. PINDER, D. M. GREEN, and P. B. J. THOMPSON. J. Med. Chem. **14**, 626 (1971).
8. E. CAMPAIGNE, D. R. KNAPP, E. S. NEISS, and T. R. BOSIN. Adv. Drug Res. **5**, 1 (1970).
9. E. CAMPAIGNE and D. R. KNAPP. J. Heterocycl. Chem. **7**, 107 (1970).
10. J. CYMERMAN-CRAIG and S. D. HURT. J. Org. Chem. **44**, 1113 (1979).
11. D. G. HAWTHORNE and Q. N. PORTER. Aust. J. Chem. **19**, 1909 (1966).
12. N. R. BELLER. Ph.D. Thesis, University of New Mexico, 1976.
13. R. NEIDLEIN and H. SEEL. Angew. Chem. Int. Ed. Engl. **15**, 775 (1976).
14. R. NEIDLEIN and G. HUMBURG. Liebigs Ann. Chem. 904 (1977).
15. R. NEIDLEIN and G. HUMBURG. Chem. Ber. **112**, 349 (1979).
16. Vogel's textbook of practical organic chemistry. 5th ed. *Revised and edited by* B. S. Furniss, A. J. Hannaford, P. W. G. Smith, and A. R. Tatchell. Longman Scientific and Technical, U.K. 1989.
17. D. MACDOWELL and T. GREENWOOD. J. Heterocycl. Chem. **2**, 44 (1965).

Can. J. Chem. Downloaded from www.nrcresearchpress.com by 198.100.157.202 on 09/07/12
For personal use only.

18. L. F. FIESER and R. G. KENNELLY. J. Am. Chem. Soc. **57**, 1611 (1935).
19. R. P. NAPIER, H. A. KAUFMAN, P. R. DRISCOLL, L. A. GLICK, C-C. CHU, and H. M. FOSTER. J. Heterocycl. **7**, 393 (1970).
20. R. NAPIER and C-C. CHU. INT. J. SULFUR CHEM. A, **1**, 62 (1971).
21. I. R. TREHAN, G. L. KAD, S. RANI, and R. BALA. Indian J. Chem. Sect. B, **24B**, 659 (1985).
22. S. G. LEVINE. J. Am. Chem. Soc. **80**, 1650 (1958).
23. Y. L. GOL'DFARB, S. Z. TAITS, and L. I. BELEN'KII. Tetrahedron, **19**, 1851 (1963).
24. F. H. JARDINE. Prog. Inorg. Chem. **28**, 63 (1981).
25. C. H. YODER and C. D. SCHAEFFER, JR. Introduction to multinuclear NMR. Benjamin/Cummings, Menlo Park, CA. 1987. p. 157.

Can. J. Chem. Downloaded from www.nrcresearchpress.com by 198.100.157.202 on 09/07/12
For personal use only.

Isotope effects in nucleophilic substitution reactions. VIII. The effect of the form of the reacting nucleophile on the transition state structure of an S_N2 reaction

YAO-REN FANG AND KENNETH CHARLES WESTAWAY[1]
Chemistry Department, Laurentian University, Sudbury, Ont., Canada P3E 2C6

Received August 27, 1990

YAO-REN FANG and KENNETH CHARLES WESTAWAY. Can. J. Chem. **69**, 1017 (1991).

A spectroscopic investigation indicated that lithium thiophenoxide exists as a contact ion pair complex in dry diglyme whereas the other alkali metal thiophenoxides exist as a solvent-separated ion pair complex in diglyme. The addition of small amounts of water converts the lithium thiophenoxide contact ion pair complex into a solvent-separated ion pair complex. A smaller secondary α-deuterium kinetic isotope effect and a larger Hammett ρ value are observed when the nucleophile is the contact ion pair complex in the S_N2 reaction between *n*-butyl chloride and thiophenoxide ion in diglyme. This indicates that the transition state for the contact ion pair complex reaction is tighter with a shorter nucleophile–α-carbon bond than the transition state for the solvent-separated ion pair complex reaction. The secondary α-deuterium kinetic isotope effects for the free ion and the solvent-separated ion pair complex reactions between sodium thiophenoxide and *n*-butyl chloride in DMF suggest that the loosest transition state is found when the nucleophile is the free ion.

Key words: transition state, S_N2, isotope, deuterium, Hammett ρ.

YAO-REN FANG et KENNETH CHARLES WESTAWAY. Can. J. Chem. **69**, 1017 (1991).

Une étude spectroscopique indique que, dans le diglyme sec, le thiophénolate de lithium existe sous la forme d'une paire d'ions de contact; dans le même solvant, les autres thiophénolates de métaux alcalins existent sous la forme d'une paire d'ions séparés par le solvant. L'addition de faibles quantités d'eau transforme la paire d'ions de contact du thiophénolate de sodium en une paire d'ions séparés par le solvant. Pour les réactions S_N2 entre le chlorure de butyle et l'ion thiophénolate effectuées dans le diglyme, l'effet isotopique secondaire α du deutérium est plus faible et la valeur ρ de Hammett est plus grande lorsque le nucléophile est une paire d'ions de contact. Ce résultat indique que l'état de transition de la réaction impliquant la paire d'ions de contact est plus compact, avec une liaison carbone α–nucléophile plus courte, que l'état de transition de la réaction avec la paire d'ions séparés par le solvant. Les effets isotopiques cinétiques secondaires des deutérium en α, observés pour les réactions des ions libres et des paires d'ions séparés par le solvant du thiophénolate de sodium avec le chlorure de butyle dans le DMF suggèrent que l'état de transition le plus lâche est celui impliquant l'ion libre.

Mots clés : état de transition, S_N2, isotope, deutérium, ρ de Hammett.

[Traduit par la rédaction]

Introduction

Conductivity measurements, ultraviolet (uv) spectroscopy, and experiments with crown ethers have shown that alkali metal thiophenoxides can exist in different forms in organic solvents (1–3). At low concentrations, alkali metal thiophenoxides exist as free ions in methanol, DMF, and DMSO. At higher concentrations, that depend on the solvent, these salts exist as solvent-separated ion pair complexes, eq. [1].

[1] $$xM^+ + x^-SC_6H5 \rightleftarrows [M^+ (solvent)_y{}^-SC_6H_5]_x$$

Sodium thiophenoxide exists as a solvent-separated ion pair complex at all concentrations in the much less polar solvent, diglyme (1).

Buncel *et al.* (4, 5) used a spectroscopic test to determine whether an ion pair exists in solution as a contact ion pair or as a solvent-separated ion pair. The test involves determining how changing the metal ion in an ion pair affects the absorption maximum in the uv spectrum. When the alkali metal ion is changed in a contact ion pair, the electron density on the nucleophilic atom (the chromophore) is altered and the absorption maximum of the ion pair spectrum changes. If the ion pair is a solvent-separated ion pair, the metal ion is separated from the nucleophilic atom and changing the metal ion does not alter significantly the electron density on the nucleophilic atom. As a result, the absorption maximum for the ion pair does not change significantly when the metal ion of the ion pair is altered.

With one exception (lithium thiophenoxide in diglyme), the absorption maximum of the uv spectrum of alkali metal thiophenoxide ion pair complexes in methanol, in DMF, in DMSO, and in diglyme does not change significantly, Table 1, when the alkali metal ion is altered (1). Thus, the spectroscopic technique used by Buncel *et al.* to identify the structure of ion pairs indicates that all of the ion pair complexes, except for the lithium thiophenoxide in diglyme, are solvent separated (1–3). The large change that is found in the absorption maximum when lithium is substituted for sodium in the alkali metal thiophenoxide ion pair complex in diglyme indicates that the form of the lithium thiophenoxide ion pair complex is different from that of the other alkali metal ion pair complexes and suggests that the lithium thiophenoxide exists as a contact ion pair complex in diglyme.

We are unable to explain why the absorption maximum for the contact ion pair complex is greater than that found for the solvent-separated ion pair complex. It is worth noting, however, that the change observed in the absorption maximum when the solvent-separated ion pair complex is converted into the contact

TABLE 1. The absorption maxima for the lithium, sodium and cesium thiophenoxide ion pair complexes in DMSO, DMF, CH_3OH, and diglyme at 20°C

	λ_{max} (nm)			
Salt	DMSO	DMF	CH_3OH	Diglyme
$Li^+ {}^-SC_6H_5$	305	308	266	325
$Na^+ {}^-SC_6H_5$	305	308	267	302
$Cs^+ {}^-SC_6H_5$	305	307	267	306

[1]Author to whom correspondence may be addressed.

Can. J. Chem. Downloaded from www.nrcresearchpress.com by 198.100.157.202 on 09/07/12
For personal use only.

ion pair complex (λ_{max} increases from 304 nm to 325 nm) is in the same direction as the change found when the free ion is converted into the solvent-separated ion pair complex, i.e., λ_{max} increases from 235 nm for the free ion to 267 nm for the solvent-separated ion pair complex in methanol and from approximately 280 nm for the free ion to 305 nm and 308 nm for the solvent-separated ion pair complex in DMSO and DMF, respectively (1). Thus, the absorption maximum always moves to longer wavelengths as the interaction with the cation increases.

Secondary α-deuterium kinetic isotope effects and Hammett ρ values have been measured for the solvent-separated (sodium and potassium) and the contact (lithium) ion pair complex reactions to determine how the form of the reacting nucleophile affects the transition state structure of the S_N2 reaction between *n*-butyl chloride and thiophenoxide ion in diglyme, eq. [2].

$$[2]\quad \left.\begin{array}{l}[M^+\ {}^-SC_6H_5]_x \\ \text{or} \\ [M^+(\text{solvent})_y\ {}^-SC_6H_5]_x\end{array}\right] + CH_3CH_2CH_2CL_2Cl \longrightarrow$$

$$CH_3CH_2CH_2CL_2SC_6H_5 + M^+ + Cl^-$$

$$L = H, D$$

Results and discussion

The secondary α-deuterium kinetic isotope effects found for the S_N2 reactions (2, 6) between *n*-butyl chloride and the solvent-separated (sodium thiophenoxide) ion pair complex and the contact (lithium thiophenoxide) ion pair complex are shown in Table 2. The secondary α-deuterium kinetic isotope effect of 1.07 found for the contact (lithium thiophenoxide) ion pair complex reaction in diglyme at 20°C is significantly lower than that found when the nucleophilic reagent is the solvent-separated (sodium thiophenoxide) ion pair complex (k_H/k_D = 1.14). Thus, it appears that the form of the reacting nucleophile has a marked effect on the magnitude of the secondary α-deuterium kinetic isotope effect and transition state structure.

Small amounts of a more solvating solvent, water, were added to the dry diglyme used in the lithium thiophenoxide contact ion pair complex experiments in an effort to convert the contact ion pair complex into the solvent-separated ion pair complex and confirm that the different secondary α-deuterium kinetic isotope effect was, indeed, due to a change in the form of the reacting nucleophile. The results in Table 3, and Fig. 1, show that this is possible. When small amounts of water are added to the dry diglyme, the secondary α-deuterium kinetic isotope effect initially remains constant. However, when the amount of water is increased from 2.0 to 3.0%, the isotope effect jumps from 1.07 to 1.12. Increasing the amount of water to 4.0% leads to a further increase in the isotope effect, i.e., to 1.13, a secondary α-deuterium kinetic isotope effect that is within experimental error of the isotope effect found when the solvent-separated sodium thiophenoxide ion pair complex is the reactant, Table 2. Increasing the amount of water in the solvent still further, i.e., to 7.5%, does not alter the secondary α-deuterium kinetic isotope effect of the lithium thiophenoxide reaction.

The ability to change the secondary α-deuterium kinetic isotope effect for the lithium thiophenoxide contact ion pair complex reaction from 1.07 to 1.14, the isotope effect for the reaction of the solvent-separated (sodium thiophenoxide) ion pair complex, by adding water is strong evidence that the change in secondary α-deuterium kinetic isotope effect is due to a change in the form of the reacting nucleophile rather than to a change in the cation. The contact ion pair complex is presumably converted into the solvent-separated ion pair complex because water is a more ionizing solvent than diglyme and solvates the ions in the ion pair complex more strongly.

The secondary α-deuterium kinetic isotope effect for the reaction of a different solvent-separated ion pair complex, potassium thiophenoxide, was measured in an effort to confirm that the change in the isotope effect was due to a change in the form of the reacting nucleophile and not to a change from the lithium to the sodium cation. The secondary α-deuterium kinetic isotope effect for the reaction with the solvent-separated potassium thiophenoxide ion pair complex is 1.13, Table 2. In fact, the isotope effects for all the reactions of the solvent-separated ion pair complexes are identical within experimental error. Thus, the different (smaller) secondary α-deuterium kinetic isotope effect is only found when lithium thiophenoxide is used in dry or almost dry diglyme and the uv spectrum indicates

TABLE 2. The secondary α-deuterium kinetic isotope effects for the S_N2 reactions between *n*-butyl chloride and the solvent-separated and contact ion pair complexes of alkali metal thiophenoxides in diglyme at 20°C

Salt/ solvent	$k_H \times 10^3$ (L mol^{-1} s^{-1})	$k_D \times 10^3$ (L mol^{-1} s^{-1})	$(k_H/k_D)_\alpha$
Contact ion pair complex			
$Li^+\ {}^-SC_6H_5$/ dry diglyme	2.607 ± 0.05[a]	2.436 ± 0.042[a]	1.070 ± 0.028[b]
Solvent-separated ion pair complex			
$Na^+\ {}^-SC_6H_5$/ dry diglyme	5.627 ± 0.087	4.927 ± 0.031	1.142 ± 0.019
$Li^+\ {}^-SC_6H_5$ 4% aqueous diglyme	1.184 ± 0.002	1.046 ± 0.002	1.131 ± 0.002
$K^+\ {}^-SC_6H_5$ 0.5% aqueous diglyme	12.75 ± 0.007	11.30 ± 0.002	1.128 ± 0.007

[a]Standard deviation from at least three kinetic runs.
[b]The error is $1/k_D[(\Delta k_H)^2 + (k_H/k_D)^2 \times (\Delta k_D)^2]^{1/2}$ where Δk_H and Δk_D are the standard deviations for the rate constants for the undeuterated and deuterated substrates, respectively (1).

TABLE 3. The secondary α-deuterium kinetic isotope effects for the S_N2 reaction between *n*-butyl chloride and lithium thiophenoxide in various mixtures of aqueous diglyme at 20°C

Percent water	$k_H \times 10^3$ L mol^{-1} s^{-1}	$k_D \times 10^3$ L mol^{-1} s^{-1}	$(k_H/k_D)_\alpha$
None	2.607 ± 0.050[a]	2.436 ± 0.042[a]	1.070 ± 0.028[b]
0.5	2.029 ± 0.016	1.880 ± 0.013	1.079 ± 0.0113
1.0	1.670 ± 0.0059	1.544 ± 0.007	1.082 ± 0.0089
2.0	1.338 ± 0.011	1.247 ± 0.009	1.073 ± 0.012
3.0	1.215 ± 0.007	1.0835 ± 0.0018	1.121 ± 0.007
4.0	1.1836 ± 0.0016	1.0464 ± 0.0017	1.131 ± 0.002
7.5	0.91503 ± 0.00017	0.80946 ± 0.0004	1.130 ± 0.006

[a]Standard deviation from at least three kinetic runs.
[b]The error is $1/k_D[(\Delta k_H)^2 + (k_H/k_D)^2 \times (\Delta k_D)^2]^{1/2}$ where Δk_H and Δk_D are the standard deviations for the rate constants for the undeuterated and deuterated substrates, respectively (1).

Can. J. Chem. Downloaded from www.nrcresearchpress.com by 198.100.157.202 on 09/07/12
For personal use only.

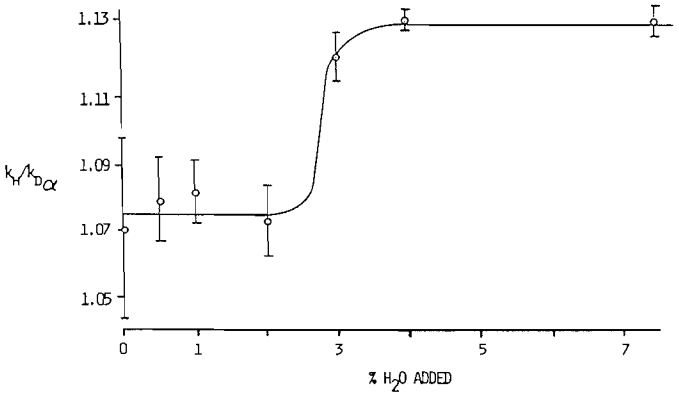


FIG. 1. The secondary α-deuterium kinetic isotope effect versus the percent water added to dry diglyme in the S_N2 reaction between *n*-butyl chloride and the lithium thiophenoxide ion pair complexes.

that the form of the reacting nucleophile is different, i.e., the contact ion pair complex.

Form of reacting nucleophile and transition state structure

Once it had been established that different secondary α-deuterium kinetic isotope effects were found for the contact ion pair complex and the solvent-separated ion pair complex reactions, it was interesting to determine how the form of the reacting nucleophile affected the structure of the S_N2 transition state.

Secondary α-deuterium kinetic isotope effects and Hammett ρ values can be used to elucidate the structure of the transition states in the S_N2 reactions (7, 8). The initial state for the secondary α-deuterium kinetic isotope effect in both the contact ion pair complex and the solvent-separated ion pair complex reactions is the same, i.e., *n*-butyl chloride. Thus, the very different secondary α-deuterium kinetic isotope effects observed for the solvent-separated and contact ion pair complex reactions in diglyme require that the transition states for these two S_N2 reactions be significantly different. One might worry that changing the solvent from 1% aqueous diglyme to 4% aqueous diglyme would affect the magnitude of the secondary α-deuterium kinetic isotope effect because the partially formed chloride ion in the transition state could be more strongly solvated by hydrogen bonding to the extra H_2O molecules present when the reaction was done in 4% aqueous diglyme. This change in solvent would not affect the magnitude of the secondary α-deuterium kinetic isotope effect significantly, however. Theoretical calculations of the secondary α-deuterium kinetic isotope effect in the S_N2 reaction between benzyl chloride and an alkoxide ion (9) indicate that solvating the developing chloride ion with three hydrogen bonds to H_2O only changes the isotope effect by 0.0002. Since adding three hydrogen bonds (altering the reduced mass of the developing chloride ion) has a negligible effect on the secondary α-deuterium kinetic isotope effect, the different isotope effects observed in 1% and 4% aqueous diglyme must be due to a change in transition state structure. The magnitude of the secondary α-deuterium kinetic isotope effect is primarily dependant on the C_α–H(D) out-of-plane bending vibrations and, therefore, on the steric crowding around the C_α—H(D) bonds in the S_N2 transition state (7, 8, 10). In fact, the C_α–H(D) out-of-plane bending vibrations will be of higher energy (the secondary α-deuterium kinetic isotope effect will be smaller) when the α-carbon–nucleophile and α-carbon–leaving group bonds are short in the transition state (8). Applying this rationale to the experimental isotope effects in the two reactions indicates that the contact ion pair complex transition state must be tighter, with shorter nucleophile–α-carbon and (or) α-carbon–leaving group bonds than the solvent-separated ion pair complex transition state.

The tighter S_N2 transition state for the reaction with the contact ion pair complex seems probable because the small lithium cation has a large charge density and will tie up (reduce) the electron density on the sulfur atom of the nucleophile. This, in turn, would mean that the sulfur nucleophile would have to come closer to the α-carbon before it disturbed the α-carbon–chlorine bond sufficiently to cause reaction. If this occurred, the transition state would have a shorter S---C_α bond and, presumably, a tighter transition state. The smaller secondary α-deuterium kinetic isotope effect that is observed is consistent with this hypothesis.

Hammett ρ values were determined for the S_N2 reactions between *n*-butyl chloride and *para*-substituted lithium thiophenoxides in 1% and in 4% aqueous diglyme where the nucleophile is the contact ion pair complex and the solvent-separated ion pair complex, respectively. These ρ values were measured in an attempt (i) to determine the structure of the S_N2 transition states in more detail and (ii) to determine if the length of the sulfur–α-carbon bond is indeed shorter in the contact ion pair complex transition state. The Hammett ρ value of −1.39 found in the contact ion pair complex reaction is much larger than the ρ value of −0.56 found for the solvent-separated ion pair complex reaction, Table 4. Negative ρ values are found in both reactions because the sulfur of the nucleophile becomes less negative when the reactants are converted into the transition state. The addition of water to the solvent would be expected to alter the magnitude of the Hammett ρ value. If this effect were significant, it could alter the conclusions drawn about the relative lengths of the sulfur–α-carbon transition state bonds in 1 and 4% aqueous diglyme. However, the most aqueous solvent only contains 4% water rather than 1% water and the rate constants are only slightly (from 6% to 2.7 times) different in the two solvents. In contrast, the rate constant in a protic solvent (MeOH) is more than 100 times smaller than the rate constant in diglyme (1, 6). As a result, the effect of the change in solvent on the magnitude of the ρ value should be reasonably small. Since the change in the ρ value with the change from 1% water to 4% water is large, i.e., the ρ value is 2.5 times larger in the case where the nucleophile is the solvent-separated ion pair complex, it is probably safe to conclude that the change in ρ is related to a change in transition state structure.[2] If this is the case, the larger ρ value in the contact ion pair complex reaction indicates that more charge density has been lost from the sulfur atom in going

[2]A referee suggested that the Hammett ρ value could be affected by the change in solvent in another way. He proposed that the interaction between the nucleophile and the developing chloride ion in the transition state would be greater when the developing chloride ion is not solvated with hydrogen-bonded water molecules. If this interaction were different, the ρ value in 4 and 1% aqueous diglyme would be different because of a change in solvent rather than a change in transition state structure. However, it is not clear whether the interaction between the negative sulfur and the negative chloride ion would affect the magnitude of the ρ value. Presumably, the nucleophile would interact much more strongly with the partially positively charged α-carbon than with the leaving group. As a result, the proposed effect should be small. Since the ρ value in 1% aqueous diglyme is 2.5 times that in 4% aqueous diglyme, it seems probable that the sulfur–α-carbon bond is shorter in the transition state of the contact ion pair reaction.

Can. J. Chem. Downloaded from www.nrcresearchpress.com by 198.100.157.202 on 09/07/12
For personal use only.

TABLE 4. The rate constants and Hammett ρ values for the S_N2 reactions between *n*-butyl chloride and the solvent-separated and contact ion pair complexes of *para*-substituted lithium thiophenoxides in 1% and 4% aqueous diglyme, respectively, at 20°C

para Substituent	$k \times 10^3$ (L mol^{-1} s^{-1}) 1% Aqueous diglyme	$k \times 10^3$ (L mol^{-1} s^{-1}) 4% Aqueous diglyme
CH_3O-	4.711 ± 0.015	1.7726 ± 0.0005
CH_3-	3.4050 ± 0.0098	1.4917 ± 0.0036
H-	1.6702 ± 0.0059	1.1836 ± 0.0016
Cl-	0.9821 ± 0.0009	0.9245 ± 0.0018
Hammett ρ	−1.39 ± 0.13	−0.559 ± 0.04
Correlation	0.991	0.995

TABLE 5. The secondary α-deuterium kinetic isotope effects and Hammett ρ values for the S_N2 reactions between *n*-butyl chloride and the sodium thiophenoxide solvent-separated ion pair complex and the free thiophenoxide ion in DMF at 20°C

Form of reacting nucleophile	$(k_H/k_D)_\alpha$	ρ
Solvent-separated ion pair complex	1.085 ± 0.011[a]	−1.93 ± 0.09[b]
Free ion	1.129 ± 0.010[a,c]	−2.05 ± 0.08[b,c]

[a]The error is $1/k_D[(\Delta k_H)^2 + (k_H/k_D)^2) \times (\Delta k_D)^2]^{1/2}$ where Δk_H and Δk_D are the standard deviations for the rate constants for the undeuterated and deuterated substrates, respectively (1).

[b]The correlation coefficients for the least-squares lines were 0.998.

[c]The original data is in ref. 1.

from the reactant to the contact ion pair complex transition state. Since the charge on the sulfur atom is reduced when the bond forms, the contact ion pair complex transition state must have the most S---C_α bond formation in the transition state, i.e., the shortest S---C_α transition state bond. The Hammett ρ values are consistent with the proposed hypothesis because they suggest that the contact ion pair complex reaction has the shortest sulfur–α-carbon transition state bond.

Thus, the secondary α-deuterium kinetic isotope effects and Hammett ρ values for the contact and the solvent-separated ion pair complex reactions in diglyme indicate that the S_N2 transition state is tighter, with at least a shorter S---C_α transition state bond when the nucleophile is the contact ion pair complex. To date, we have not been able to determine the chlorine kinetic isotope effect for these reactions. As a result, we do not know how the α-carbon–chlorine bond differs in the contact ion and solvent-separated ion pair complex transition states.

The same general trend is observed when the cation is removed and the nucleophile is changed from a solvent-separated ion pair complex to a free ion. A comparison of the secondary α-deuterium kinetic isotope effects for the solvent-separated ion pair complex and the free ion S_N2 reactions between sodium thiophenoxide and *n*-butyl chloride in DMF, Table 5, shows that the smaller isotope effect (k_H/k_D = 1.085 for the solvent-separated ion pair complex reaction versus k_H/k_D = 1.129 for the free ion reaction) is found in the reaction with the solvent-separated ion pair complex. Thus, it appears that the solvent-separated ion pair complex transition state is tighter and has shorter nucleophile–α-carbon and (or) α-carbon–leaving group bonds than the free ion transition state. Again, this seems reasonable because the cation in the solvent-separated ion pair complex should still reduce the electron density on the sulfur atom. If this occurs, the sulfur would have to come closer to the α-carbon to initiate the reaction and a tighter transition state should be found.

The secondary α-deuterium kinetic isotope effects for the solvent-separated ion pair complex and the free ion reactions in DMF lead one to conclude that the S_N2 transition state is tighter for the solvent-separated ion pair complex reaction than for the free ion reaction. However, the Hammett ρ values for the free ion and the solvent-separated ion pair complex reactions, Table 5, are, within experimental error, the same. This is opposite to the trend found in the contact and solvent-separated ion pair complex reactions.

An alternative explanation of the Hammett ρ values is that the S---C_α transition state bond is slightly shorter in the solvent-separated ion pair complex reaction but that the ρ value is misleading. The charge on the sulfur atom changes from −1.00 to 0 in the free ion reaction. The sodium ion in the solvent-separated ion pair complex would reduce the negative charge on the sulfur in the ion pair complex so the total change in charge on the sulfur atom in the reaction will be less than 1.00. As a result, the magnitude of the Hammett ρ value for the free ion reaction would be expected to be larger than that for the solvent-separated ion pair complex reaction given the same S---C_α transition state bond length. If this were the case, the identical ρ values in the solvent-separated ion pair complex and free ion reactions would really mean that the S---C_α bond is shorter in the reaction where the nucleophile is the solvent-separated ion pair complex.

However the Hammett ρ values should be interpreted, the secondary α-deuterium kinetic isotope effects indicate that the S_N2 transition states are tighter with shorter α-carbon–nucleophile and (or) α-carbon–leaving group bonds when the nucleophile is the solvent-separated ion pair complex. It does appear, however, that the difference between the S---C_α bond lengths in the free ion and the solvent-separated ion pair complex reaction are probably small. This is not surprising because one would expect that the difference in the length of the S---C_α transition state bond between the solvent-separated ion pair complex and the free ion reactions would be smaller than that between the contact ion pair complex and the solvent-separated ion pair complex reactions, i.e., when the cation is closer to the nucleophilic atom.

Conclusion

This study has shown that the secondary α-deuterium kinetic isotope effects and transition state structures are very different when the form of the reacting nucleophile is changed from a free ion to a solvent-separated ion pair complex to a contact ion pair complex. The contact ion pair complex transition state is tighter, with shorter nucleophile–α-carbon and (or) α-carbon–leaving group bonds, than the solvent-separated ion pair complex transition state. The same trend is found when the solvent-separated ion pair complex transition state is compared with the free ion transition state. The Hammett ρ values (i) indicate that the nucleophile–α-carbon bond is significantly shorter in the contact ion pair transition state than in the solvent-separated ion pair transition state and (ii) suggest that the nucleophile–α-carbon bonds in the solvent-separated ion pair and the free ion transition states are similar. The tighter transition states found when the cation is closer to the nucleophilic atom may arise because the nucleophile has to approach the α-carbon more closely before sufficient electron density is available to rupture the C—Cl bond and cause reaction.

Can. J. Chem. Downloaded from www.nrcresearchpress.com by 198.100.157.202 on 09/07/12
For personal use only.

Experimental

Preparation of reagents

Diglyme

Two litres of spectroscopic grade diglyme were purified by stirring with 50 g of ferrous sulfate dihydrate and 50 g of potassium hydroxide for 2 h at room temperature. After the solvent had been filtered, it was distilled at atmospheric pressure. The fraction boiling between 160 and 162°C was collected and dried over sodium metal for 8 h before use.

Butyl chloride

The preparation of the undeuterated and deuterated substrates is described elsewhere (1).

Kinetic measurements

The concentration of the unreacted thiophenoxide ion was determined by titrating 1 mL aliquots of the reaction mixture electrochemically with a standard silver nitrate solution (1, 11). The substrate concentration varied from 1.6 to 2.7 $\times$ 10^{-2} M and the alkali metal thiophenoxide (nucleophile) concentration ranged from 3.6 to 6.6 $\times$ 10^{-3} M in these experiments. The rate constants were obtained from the slope of the normal second-order plot (12). The reactions were followed to between 50 and 75% of completion. Good second-order plots, linear up to at least 75% of completion, were found for all the reactions. The correlation coefficients of the least-squares line for individual rate constants varied from 0.998 to 0.9999. Over 90% of the reactions had a correlation coefficient greater than 0.999.

Can. J. Chem. Downloaded from www.nrcresearchpress.com by 198.100.157.202 on 09/07/12
For personal use only.

Acknowledgement

The authors gratefully acknowledge the financial support provided by the Natural Sciences and Engineering Research Council of Canada.

1. K. C. WESTWAY and Z. G. LAI. Can. J. Chem. **66**, 1263 (1988).
2. Z. G. LAI and K. C. WESTAWAY. Can. J. Chem. **67**, 21 (1989).
3. K. C. WESTAWAY and Z. G. LAI. Can. J. Chem. **67**, 345 (1989).
4. E. BUNCEL, B. C. MENON, and J. P. COLPA. Can. J. Chem. **57**, 999 (1979).
5. E. BUNCEL and B. MENON. J. Org. Chem. **44**, 317 (1979).
6. D. G. GRACZYK, J. W. TAYLOR, and C. R. TURNQUIST. J. Am. Chem. Soc. **100**, 7333 (1978).
7. K. C. WESTAWAY and Z. WASZCZYLO. Can. J. Chem. **60**, 2500 (1979).
8. K. C. WESTAWAY and S. F. ALI. Can. J. Chem. **57**, 1354 (1979).
9. D. M. BRUBAKER. Ph.D. Thesis, University of Arkansas, Fayetteville, AR. 1978.
10. V. J. SHINER, JR., M. W. RAPP, E. A. HALEVI, and M. WOLFSBERG. J. Am. Chem. Soc. **90**, 7171 (1968).
11. D. G. GRACZYK and J. W. TAYLOR. J. Am. Chem. Soc. **96**, 3255 (1974).
12. K. J. LAIDLER. *In* Chemical kinetics. 2nd ed. McGraw–Hill, Toronto. 1965. p. 9.

Negative hyperconjugation in hexachloro-3-cyclopentenylaminosulphenyl halides: Preparation and X-ray structure of C_5Cl_6NSBr and synthesis of $C_5Cl_6NS^+AsF_6^-$

ALLEN APBLETT, TRISTRAM CHIVERS,[1] JAMES F. FAIT, AND RAINER VOLLMERHAUS
Department of Chemistry, The University of Calgary, Calgary, Alta., Canada T2N 1N4

Received November 12, 1990

ALLEN APBLETT, TRISTRAM CHIVERS, JAMES F. FAIT, and RAINER VOLLMERHAUS. Can. J. Chem. **69**, 1022 (1991).

The reaction of hexachlorocyclopentadiene with $(NSCl)_3$ at 65°C in the absence of a solvent produced hexachloro-3-cyclopentenylidenaminosulfenyl chloride, C_5Cl_6NSCl, in good yield. The derivatives C_5Cl_6NSX (X = Br, I, C_5Cl_6N, NPr_2^i, Ph) were prepared by treatment of C_5Cl_6NSCl with Me_3SiBr, Me_3SiI, Ph_3Sb, $^iPr_2NH$, and Ph_2Hg, respectively. The crystal structure of C_5Cl_6NSBr was determined by X-ray crystallography. Crystals of C_5Cl_6NSBr are triclinic, space group $P\bar{1}$ with $a = 9.626(2)$, $b = 9.810(2)$, $c = 13.736(2)$ Å, $\alpha = 79.68(1)$, $\beta = 88.62(1)$, $\gamma = 74.73(1)°$, $Z = 4$, final R and R_w values were 0.075 and 0.063, respectively, for 4850 unique observed reflections. The >C═NSBr moiety adopts a *syn* conformation and there are two different molecules of C_5Cl_6NSBr in the asymmetric units. The bond lengths are d(C═N) = 1.278(8) and 1.253(8), d(N—S) = 1.560(6) and 1.569(6), and d(S—Br) = 2.229(2) and 2.235(2) Å. The bond angles at nitrogen are 146.7(4) and 148.6(4) and those at sulfur are 116.8(2) and 116.5(2)°. The unusual geometry of the <C═NSBr moiety is explained in terms of negative hyperconjugation ($n_N \rightarrow \sigma_{SBr}^*$). A variable temperature ^{13}C NMR of C_5Cl_6NSCl provides evidence for a fluxional process ($\Delta G^*_{298} = 68.1 \pm 1.2$ kJ mol^{-1}) in solution. The dark purple compound $C_5Cl_6NS^+AsF_6^-$ was synthesized from the reaction of C_5Cl_6NSCl and $AgAsF_6$ in SO_2.

Key words: hexachloro-3-cyclopentenylidenamino sulfides, crystal structure, hexachloro-3-cyclopentenylidenaminosulfenyl bromide.

ALLEN APBLETT, TRISTRAM CHIVERS, JAMES F. FAIT et RAINER VOLLMERHAUS. Can. J. Chem. **69**, 1022 (1991).

La réaction de l'hexachlorocyclopentadiène avec le $(NSCl)_3$, à 65°C, en l'absence de solvant, conduit au chlorure d'hexachloro-3-cyclopenténylidènaminosulfényle, C_5Cl_6NSCl, avec un bon rendement. On a préparé les dérives C_5Cl_5NBX (X = Br, I, C_5Cl_6N, $NiPr_2^i$, Ph) par réaction du C_5Cl_6NSCl avec le Me_3SiBr, le Me_3SiI, le Ph_3Sb, la $^iPr_2NH$ et le Ph_2Hg, respectivement. On a déterminé la structure cristalline du C_5Cl_6NSBr par cristallographie des rayons-X. Les cristaux du C_5Cl_6NSBr sont tricliniques, groupe d'espace $P\bar{1}$, avec $a = 9{,}626(2)$, $b = 9{,}810(2)$ et $c = 13{,}736(2)$ Å, $\alpha = 79{,}68(1)$, $\beta = 88{,}62(1)$ et $\gamma = 74{,}73(1)°$, $Z = 4$, valeurs respectives de $R = 0{,}075$ et $R_N = 0{,}063$ pour 4850 réflexions observées. La portion >C═NSBr adopte une conformation *syn* et il existe deux molécules différentes de C_5Cl_6NSBr dans chaque unité asymétrique. Les longueurs des liaisons sont: d(C═N) = 1,278(8) et 1.253(8), d(N—S) = 1,560(6) et 1,569(6) et d(S—Br) = 2,229(2) et 2,235(2) Å. Les angles de liaison au niveau de l'azote sont 146,7(4) et 148,6(4)° alors que ceux au niveau du soufre sont de 116,8(2) et 116,5(2)°. On explique le géométrie inhabituelle de la portion >C═NSBr en fonction d'une hyperconjugaison négative ($n_N \rightarrow \sigma_{SBr}^*$). Les spectres rmn du ^{13}C du C_5Cl_6NSCl, mesurés à basse température, suggèrent qu'il existe une processus de fluxion ($\Delta G^{\ddagger}_{298} = 68{,}1 \pm 1.2$ kJ mol^{-1}) en solution. On a synthétisé le composé violet, $C_5Cl_6NS^+AsF_6^-$, par réaction du C_5Cl_6NSCl avec le $AgAsF_6$, dans le SO_2.

Mots clés : disulfures d'hexachloro-3-cyclopenténylidènamino; structure cristalline; bromure d'hexachloro-3-cyclopenténylidènaminosulfényle.

[Traduit par la rédaction]

Introduction

As part of our investigations of the utility of $(NSCl)_3$ as a reagent in sulfur–nitrogen (S–N) chemistry (1–3), we found that hexachlorocyclopentadiene reacts with $(NSCl)_3$ in the absence of a solvent to give high yields of C_5Cl_6NSCl (4). While our work was in progress Haas and Mischo reported the preparation of C_5Cl_6NSCl by a similar method (5). They also determined the X-ray crystal structures of C_5Cl_6NSX (X = Cl, CF_3) and observed some remarkable differences in the structural parameters of the >C═NSX moiety in these two derivatives that were ascribed to p_π–d_π interactions in the case of the chloride (5).

In this paper we report those aspects of our work that complement the findings of Haas and Mischo (5). These include (*a*) the X-ray crystal structure of C_5Cl_6NSBr, (*b*) the preparation and characterization of the novel purple cation $C_5Cl_6NS^+AsF_6^-$ and some new derivatives of the type C_5Cl_6NSX (X = I, NPr_2^i, Ph) and (*c*) the fluxional behaviour of C_5Cl_6NSCl as determined by variable temperature ^{13}C nmr studies. An explanation of the geometrical features of C_5Cl_6NSX compounds that is significantly different from that of Haas and Mischo (5) is also presented.

[1] To whom correspondence should be addressed.

Experimental

Reagents and general procedures

All experimental procedures were performed under an atmosphere of dry nitrogen. Solvents were dried by heating at reflux with the appropriate drying agent and then distilled before use.

The following reagents were commercial products used as received: hexachlorocyclopentadiene (MCB), trimethylsilyl bromide and trimethylsilyl iodide (Petrarch), di(isopropyl)amine (Aldrich), diphenylmercury (Aldrich), triphenylantimony (Kodak). $(NSCl)_3$ was prepared from $S_3N_2Cl_2$ by the method described in ref. 2. $AgAsF_6$ was prepared from silver powder and arsenic pentafluoride (Ozark-Mahoning) in SO_2 (6).

Instrumentation

Infrared spectra were recorded as Nujol or Fluorolube mulls on CsI or polyethylene windows. The 4000–400 cm^{-1} range was recorded on a Nicolet DX-5 FTIR spectrometer while spectra in the 400–200 cm^{-1} region were obtained on a Perkin Elmer 457 grating infrared spectrometer. Mass spectra were obtained with a Kratos MS80 RFA instrument operating at 70 eV. ^{13}C nmr spctra were recorded on either a Bruker ACE 200 or, for variable temperature experiments, a Bruker AM 400 spectrometer. Chemical shifts are reported relative to Me_4Si in $CDCl_3$. ^{14}N nmr spectra were run on a Bruker AM 400 spectrometer and chemical shifts are reported relative to $MeNO_2$ (6). Ultraviolet–visible spectra were measured by use of a Cary 219 spectrophotometer.

Melting points were obtained in nitrogen-filled sealed capillaries.

Can. J. Chem. Downloaded from www.nrcresearchpress.com by 198.100.157.202 on 09/07/12
For personal use only.

Can. J. Chem. Downloaded from www.nrcresearchpress.com by 198.100.157.202 on 09/07/12
For personal use only.

Chemical analyses were performed by the Analytical Services Division of the Department of Chemistry, The University of Calgary, and by Canadian Microanalytical Service, New Westminster, B.C.

Preparation of C_5Cl_6NSCl

A mixture of $(NSCl)_3$ (1.95 g, 8.0 mmol) and hexachlorocyclopentadiene (6.50 g, 23.8 mmol) was heated at 65°C in a Schlenk tube for 48 h. The dark red reaction mixture was extracted with *n*-hexane (4 × 25 mL). Solvent was removed under vacuum and the residue was sublimed at 30°C/0.1 torr to give pale yellow crystals of C_5Cl_6NSCl (4.0 g, 10.3 mmol), which was recrystallized from CH_2Cl_2, mp 69°C (lit. (5): 68°C). *Anal.* calcd. for C_6Cl_7NS: C 16.95, N 3.95; found: C 16.63, N. 3.72. The infrared spectrum was in excellent agreement with that reported in the literature (5). ^{14}N nmr ($CDCl_3$) δ: −81.5 (cf. lit. δ(^{15}N) −81.0) (5).

Preparation of C_5Cl_6NSBr

A mixture of C_5Cl_6NSCl (0.35 g, 1.0 mmol) and Me_3SiBr (0.16 g, 1.1 mmol) in hexane (3 mL) was stirred at 23°C for 4 h. Removal of solvent under vacuum produced C_5Cl_6NSBr (0.38 g, 0.96 mmol) as a yellow solid. An analytically pure sample (mp 74°C) was obtained by recrystallization from *n*-hexane. *Anal.* calcd. for C_5BrCl_6NS: C 15.06, N 3.51; found: C 15.02, N 3.47. Infrared (cm^{-1}): 1646 (s), 1608 (s), 1206 (s), 1034 (s), 810 (vs), 692 (s), 637 (s), 583 (s), 419 (s), 355 (s). ^{14}N nmr ($CDCl_3$) δ: −75.0.

Preparation of $C_5Cl_6NS^+AsF_6^-$

A mixture of C_5Cl_6NSCl (0.50 g, 1.41 mmol) and $AgAsF_6$ (0.418 g, 1.41 mmol) was transferred to one arm of a two-bulb vessel under an atmosphere of dry N_2. Liquid SO_2 (25 mL) was condensed onto this mixture at −78°C to give an intensely purple solution. After 16 h the precipitate of AgCl (0.16 g, 1.12 mmol) was separated by filtration. Some of the AgCl adhered to the frit and could not be recovered. Removal of the SO_2 under vacuum produced dark purple crystals of $C_5Cl_6NS^+AsF_6^-$ (0.70 g, 1.38 mmol). An analytical sample was obtained by recrystallization from an SO_2–$CFCl_3$ mixture. *Anal.* calcd. for $C_5AsCl_6F_6NS$: C 11.83, Cl 41.89, N 2.76, S 6.31; found: C 10.98, Cl 41.65, N 2.53, S 5.35. Infrared (cm^{-1}): 1750 (m), 1581 (m), 1561 (m), 1259 (s), 1164 (s), 1063 (m), 1041 (sh), 860 (m), 836 (s), 811 (vs), 702 (vs, ν_3 AsF_6^-), 658 (m), 639 (m), 439 (m). Ultraviolet–visible (CH_2Cl_2): λ_{max} 562 nm.

Preparation of C_5Cl_6NSI

A cold solution of trimethylsilyl iodide (0.58 g, 2.9 mmol) in *n*-hexane (15 mL) was added to a solution of C_5Cl_6NSCl (1.0 g, 2.8 mmol) in *n*-hexane (15 mL) at −78°C. The solution became red immediately. After 1 h solvent was removed under vacuum and the brown solid was recrystallized from *n*-hexane at −20°C to give red crystals of C_5Cl_6NSI (0.50 g, 1.1 mmol). *Anal.* calcd. for C_5Cl_5INS: C 13.47, N 3.14; found: C 13.84, N 3.06. Infrared (cm^{-1}): 1617 (m), 1208 (vs), 1154 (m), 982 (m), 824 (s), 809 (vs), 653 (m), 636 (vs), 595 (s), 581 (m). ^{14}N nmr ($CDCl_3$) δ: −78.9.

Preparation of C_5Cl_6NSPh

1,2-Dichloroethane (30 mL) was added to a mixture of C_5Cl_6NSCl (1.0 g, 2.8 mmol) and Ph_2Hg (1.0 g, 2.8 mmol) and the solution was heated at reflux for 2 days. Solvent was removed under vacuum and the solid residue was extracted with CCl_4 (25 mL) to give an insoluble white solid identified as PhHgCl (0.44 g, 1.4 mmol) by infrared spectroscopy. Solvent was removed under vacuum and the residue was sublimed at 100°C/0.1 torr. The sublimate (0.67 g) was dissolved in CCl_4 (25 mL) and PhHgCl (0.08 g, 0.25 mmol) was separated by filtration. At 0°C the CCl_4 solution produced yellow crystals of C_5Cl_6NSPh (0.59 g, 1.5 mmol) mp 64°C. *Anal.* calcd. for $C_{11}H_5Cl_6NS$: C 33.37, H 1.27, N 3.54; found: C 33.17, H 1.45, N 4.14. Infrared (cm^{-1}): 1623 (s), 1577 (m), 1229 (s), 1209 (vs), 1158 (m), 811 (vs), 751 (s), 737 (vs), 725 (s), 702 (m), 687 (m), 662 (m), 595 (m).

Preparation of $C_5Cl_6NSNPr_2^i$

A mixture of C_5Cl_6NSCl (1.0 g, 2.8 mmol) and di(isopropyl)amine (0.57 g, 5.6 mmol) in CH_2Cl_2 (25 mL) was stirred at 23°C for 16 h. Solvent was removed under vacuum and the residue was treated with *n*-pentane (30 mL) to give a white precipitate (0.83 g) which was subsequently removed by filtration. At 0°C the filtrate yielded colourless crystals of $C_5Cl_6NSNPr_2^i$, (0.74 g, 1.7 mmol) mp 94°C. *Anal.* calcd. for $C_{11}H_{14}Cl_6N_2S$: C 31.53, H 3.37, N 6.69; found: C 31.44, H 3.47, N 6.91. Infrared (cm^{-1}): 1621 (m), 1206 (s), 1171 (m), 1158 (m), 1123 (m), 1094 (m), 971 (m), 812 (vs), 635 (s), 597 (s). ^1H nmr ($CDCl_3$) δ: 1.30 (d), 3.57 (septet).

Preparation of $C_5Cl_6NSNC_5Cl_6$

A solution of C_5Cl_6NSCl (0.89 g, 2.5 mmol) and Ph_3Sb (0.44 g, 1.25 mmol) in CH_2Cl_2 (3 mL) was stirred at 23°C for 4 days to give pale yellow crystals of $C_5Cl_6NSNC_5Cl_6$ (0.70 g, 1.2 mmol), mp 260°C (lit. (5): 263°C), which were isolated by filtration. *Anal.* calcd. for $C_{10}Cl_{12}N_2S$: C 19.81, N 4.62; found: C 19.92, N 4.54. The infrared spectrum was in good agreement with the values reported in the literature (5). δ(^{14}N) ($CDCl_3$)−83.8.

X-ray analysis of C_5Cl_6NSBr

A suitable transparent yellow plate was glued on a glass fibre, and mounted on an Enraf-Nonius CAD4 diffractometer. Unit cell parameters and their standard deviations were derived from the setting angles of 25 reflections in the range $7.40° < \theta < 14.31°$. Reduced cell calculations did not indicate any higher metric symmetry. Crystal and instrumental instability were monitored through the measurement of three standard reflections every 1 h of X-ray exposure time; there was no indication of crystal decomposition. The net intensities of the data were corrected for reflection width, scale variation, Lorentz, and polarization effects. Variance $\sigma^2(I)$ was calculated based on counting statistics. Crystal data are compiled in Table 1.

TABLE 1. Crystal data for C_5Cl_6NSBr

Formula	C_5Cl_6NSBr
M_w	398.744
System	Triclinic
Space group	$P\bar{1}$
a (Å)	9.626(2)
b (Å)	9.810(2)
c (Å)	13.736(2)
α (deg)	79.68(1)
β (deg)	88.62(1)
γ (deg)	74.73(1)
V (Å^3)	1230.69
Z	4
λ (MoK_α) (Å)	0.71069 (graphite monochromator)
Crystal size (mm)	0.32 × 0.56 × 0.15
Temperature (K)	298
D_c(g cm^{-3})	2.152
μ (cm^{-1})	46.06
Unique reflections	7164
Observed reflections	4850 ($I \geq 2.0\ \sigma$ (I))
F(000)	760
R	0.075
R_w	0.063

The bromine positions were located in an *E* map with phases derived from symbolic addition (7). The remaining atoms were located in difference maps after refining the scale and thermal parameters. The data were corrected for absorption using DIFABS (8) after isotropic refinement. All atoms were refined anisotropically using full-matrix least-squares calculations minimizing the function $\Sigma w(|F_o| - |F_c|)^2$, where $w = {}^1/_{\sigma^2}(F_o)$. Final agreement factors, $R = \Sigma||F_o| - |F_c||/\Sigma|F_o|$ and $R_w = [\Sigma w(|F_o| - |F_c|)^2/\Sigma wF_o^2]^{1/2}$ were 0.075 and 0.063, respectively. A difference Fourier map calculated at the conclusion of refinements was essentially featureless. The final fractional coordinates of the two crystallographically independent molecules present in the asymmetric unit are presented in Table 2. Thermal parameters and F_o/F_c lists are available on request from the Depository of Unpublished

Can. J. Chem. Downloaded from www.nrcresearchpress.com by 198.100.157.202 on 09/07/12
For personal use only.

TABLE 2. Atom coordinates for C_5Cl_6NSBr

Atom	X	Y	Z	1000 U_{eq}[a]
Br(1)	0.29124(9)	0.60955(8)	0.11815(5)	65.5
S(1)	0.3105(2)	0.5910(2)	−0.0413(1)	50.0
N(1)	0.2907(5)	0.4500(5)	−0.0694(3)	40.8
C(11)	0.2665(6)	0.3277(6)	−0.0389(4)	32.5
C(12)	0.2613(6)	0.2294(6)	−0.1112(4)	36.9
C(13)	0.2248(6)	0.1046(6)	−0.0471(4)	41.8
C(14)	0.2123(6)	0.1187(6)	0.0469(4)	37.0
C(15)	0.2370(6)	0.2579(6)	0.0630(4)	34.6
Cl(11)	0.1299(2)	0.3128(2)	−0.2075(1)	62.9
Cl(12)	0.2062(2)	−0.0373(2)	−0.0961(1)	65.9
Cl(13)	0.0813(2)	0.3626(2)	0.1131(1)	48.9
Cl(14)	0.4319(2)	0.1749(2)	−0.1667(1)	64.9
Cl(15)	0.3872(2)	0.2249(2)	0.1451(1)	49.0
Cl(16)	0.1742(2)	0.0007(2)	0.1420(1)	59.4
Br(2)	0.16610(8)	0.44852(8)	0.35636(5)	62.4
S(2)	0.2130(2)	0.4139(2)	0.5189(1)	59.8
N(2)	0.2369(5)	0.5454(5)	0.5601(3)	46.2
C(21)	0.2458(6)	0.6726(6)	0.5434(4)	38.2
C(22)	0.2364(6)	0.7774(6)	0.4477(4)	36.2
C(23)	0.2657(7)	0.9045(6)	0.4791(4)	43.9
C(24)	0.2879(6)	0.8865(6)	0.5762(4)	41.4
C(25)	0.2743(6)	0.7428(6)	0.6279(4)	40.2
Cl(21)	0.1289(2)	0.7633(2)	0.7107(1)	59.9
Cl(22)	0.0620(2)	0.8233(2)	0.3897(1)	59.9
Cl(23)	0.3684(2)	0.7086(2)	0.3640(1)	62.5
Cl(24)	0.4347(2)	0.6433(2)	0.6949(1)	65.3
Cl(25)	0.3243(2)	1.0069(2)	0.6397(1)	67.5
Cl(26)	0.2679(2)	1.0548(2)	0.3960(1)	75.1

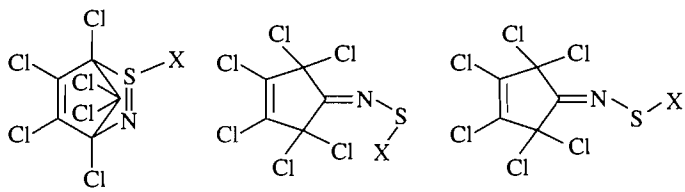
[a] $U_{eq} = \frac{1}{3}\Sigma U_{ij}a^*_i a^*_j \alpha_i \cdot \alpha_j$.

Data.[2] Neutral atom scattering factors were used with anomalous dispersion corrections applied (9). No corrections for extinction were made. All calculations were carried out on a Zenith 386 running UNIX V.3 at the University of Calgary with the program package XTAL (10).

Results and discussion

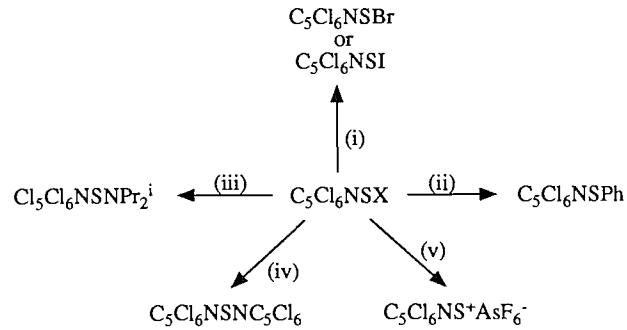
Preparation of C_5Cl_6NSX derivatives

The monomers NSF (11) and NSCl (12) undergo [2 + 4] cycloaddition reactions with hexafluorobutadiene to give six-membered rings. It was anticipated that NSCl would react with hexachlorocyclopentadiene in a similar manner to give **1**. Monomeric thiazyl chloride, generated from $(NSCl)_3$, does indeed react with C_5Cl_6 at 65°C in the absence of a solvent to give excellent yields of a 1:1 adduct. Haas and Mischo have demonstrated by X-ray crystallography that this adduct is **2***a* (X = Cl) and they have presented a plausible mechanism for the formation of **2***a* that involves a [2 + 1] addition of NSCl (acting as a nitrene) to one double bond of C_5Cl_6 as the initial step (5).



1 **2***a* **2***b*

[2]A complete set of supplementary material, comprising structure factors, final atomic positional parameters, final thermal parameters, and interatomic distances, and angles may be purchased from the Depository of Unpublished Data, Document Delivery, CISTI, National Research Council of Canada, Ottawa, Canada K1A 0S2.



SCHEME 1. Preparation of C_5Cl_6NSX derivatives and $C_5Cl_6NS^+AsF_6^-$. (*i*) Me_3SiY (Y = Br or I), (*ii*) Ph_2Hg, (*iii*) 2^iPr_2NH, (*iv*) Ph_3Sb, (*v*) $AgAsF_6$.

This high yield synthesis of C_5Cl_6NSCl provides an opportunity to investigate simple substitution reactions involving the S—Cl bond. The results of such reactions are summarized in Scheme 1. Halogen exchange occurs readily at room temperature upon treatment of C_5Cl_6NSCl with the appropriate trimethylsilyl halide to give C_5Cl_6NSBr or C_5Cl_6NSI. The latter is a rare example of a thermally stable compound of the type RSI (13). The derivatives C_5Cl_6NSPh and $C_5Cl_6NSNPr_2^i$ are also obtained in good yields by the routes indicated in Scheme 1. The reduction of C_5Cl_6NSCl with Ph_3Sb produced $C_5Cl_6NSNC_5Cl_6$ rather than the corresponding disulfide.

The new hexachloro-3-cyclopentenylsulphenyl derivatives were characterized by elemental analyses, ^{13}C (see Table 6) and ^{14}N nmr, mass and infrared spectroscopy, and by X-ray crystallography in the case of C_5Cl_6NSBr. All derivatives showed a weak parent ion in the mass spectrum and the cleavage of the S—X bond as the major fragmentation process. The ^{14}N chemical shifts were observed in the range −75 to −85 ppm (relative to $MeNO_2(l)$). The infrared spectra of the series C_5Cl_6NSX (X = Cl, Br, I) show bands at *ca.* 1205, 810, 635, and 590 cm^{-1} characteristic of the C_5Cl_6NS moiety. An intense band at 452 cm^{-1} in the infrared spectrum of C_5Cl_6NSCl is replaced by a strong absorption at 355 cm^{-1} for C_5Cl_6NSBr. These bands are tentatively assigned to ν(S—Cl) and ν(S—Br), respectively.

Crystal structure of C_5Cl_6NSBr

The structure of C_5Cl_6NSBr is shown in Fig. 1, which depicts the two independent molecules in the asymmetric unit together with the atomic numbering scheme. The bond lengths and bond angles for the two C_5Cl_6NSBr molecules are given in Tables 3 and 4, respectively, and the structural parameters for the >C=NSX moiety in C_5Cl_6NSX (X = CF_3, Cl, Br) are compared in Table 5. The structures of C_5Cl_6NSBr and C_5Cl_6NSCl are very similar and they exhibit remarkable differences compared to that of $C_5Cl_6NSCF_3$. The most obvious difference is that the CF_3 derivative adopts a *anti* conformation **2***b* with respect to the S—N bond whereas the halides (X = Cl, Br) have the *syn* structure **2***a*. In addition, both C_5Cl_6NSBr and C_5Cl_6NSCl have short S—N bond distances of 1.56–1.57 Å and large angles of *ca.* 147° and *ca.* 116° at nitrogen and sulphur, respectively. The corresponding values of *d*(S—N) = 1.667 Å, < CNS = 124.3°, and <NSCF_3 = 94.9° for the CF_3 derivative are typical for a divalent sulfur compound (cf. *d*(S—N) = 1.675(2) Å, < CNS = 122.4(2) and 121.5(2)°, and <NSN = 94.7(1)° for $Ph_2CNSNCPh_2$ (14)). The S—Cl distance of 2.055 Å for C_5Cl_6NSCl and the average value of 2.233 Å for *d*(S—Br) in C_5Cl_6NSBr are slightly longer than the sum of covalent radii

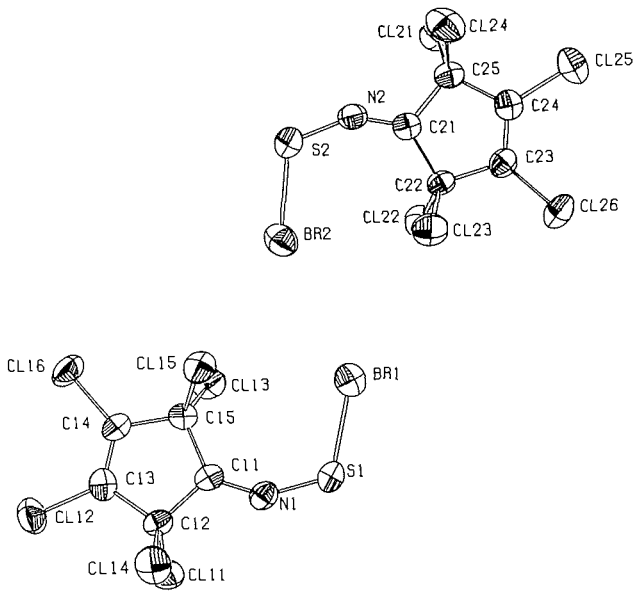


FIG. 1. ORTEP plots (50% probability ellipsoids) and atomic numbering scheme for the two different molecules of C_5Cl_6NSBr in the asymmetric unit.

(2.03 Å for S—Cl and 2.18 Å for S—Br (15)). The value of d(C=N) falls in the range 1.25–1.28 Å typical for a double bond (16) and does not show significant differences among the three derivatives.

Thus both C_5Cl_6NSCl and C_5Cl_6NSBr exhibit normal C=N bond lengths, short S—N bond lengths, anomalously large bond angles at N and S, and a *syn* geometry for the =CNSX unit. Any bonding model must explain all these structural features. In the case of C_5Cl_6NSCl, Haas and Mischo account for these observations in terms of "dative p_π–d_π interaction between the sp^2 hybridized nitrogen as donor and sulfur as acceptor" (5). We suggest that the unusual geometry of the =CNSX (X = Cl, Br) moiety is the result of *negative hyperconjugation* ($n_N \rightarrow \sigma_{SX}^*$) (17, 18). This interaction involves donation from the in-plane non-bonding orbital on N to the antibonding σ orbital of the sulfur–halogen bond. It is bonding with respect to the S—N bond and will be enhanced (better overlap) by wider angles at N and/or S. The C=N bond would not be significantly affected by this interaction, but the partial occupancy of the σ^*_{SX} orbital would be expected to result in a longer than single S—X bond as observed. Negative hyperconjugation cannot occur for *anti* structures of type **2***b* since the n_N and σ^*_{SX} orbitals are not favourably disposed for overlap in this geometry.

The structural features of C_5Cl_6NSX (X = Cl, Br) are reminiscent of those found for salts of the $ClSNSCl^+$ cation for which < SNS = *ca.* 150°, < NSCl = *ca.* 111°, and d(S—N) = *ca.* 1.53 Å (19). A natural bond order analysis of this cation at the 3-21G(*) level using the experimental geometry showed that the nitrogen in-plane lone pairs have 87% *p* character and donate 0.15e to σ_{SCl}^* orbital, of which only 0.018e$^-$ go into sulphur d orbitals (18). The positive charge presumably contributes to the shorter S—N and S—Cl (*ca.* 1.99 Å (19)) bond lengths in $ClSNSNCl^+$ compared to the corresponding values in C_5Cl_6NSCl.

^{13}C nmr spectra and fluxional behaviour of C_5Cl_6NSX derivatives

The ^{13}C nmr data for C_5Cl_6NSX derivatives are given in Table 6. Although two of the derivatives (X = CF_3, NC_5Cl_6) exhibit five reasonances consistent with the static structure **2***a* or **2***b*, the majority (X = Cl, Br, I, Ph, NPr^i_2, NSO and SCF_3) show three signals at room temperature indicating the equivalence of the pairs of carbon atoms C_b/C_c and C_d/C_e on the nmr time scale. The chemical shifts for C_b/C_c and C_d/C_e fall within the narrow ranges 78–85 and 135–143 ppm, respectively. The chemical shift of C_a is more sensitive to the nature of X with values from 140 to 174 ppm.

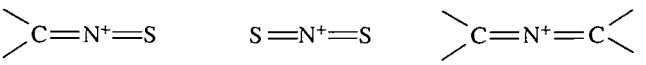
TABLE 3. Bond lengths (Å)

1		2	
Bond	Length	Bond	Length
Br(1)—S(1)	2.229(2)	Br(2)—S(2)	2.235(2)
S(1)—N(1)	1.560(6)	S(2)—N(2)	1.569(6)
N(1)—C(11)	1.278(8)	N(2)—C(21)	1.253(8)
C(11)—C(15)	1.499(7)	C(21)—C(22)	1.505(7)
C(11)—C(12)	1.514(8)	C(21)—C(25)	1.516(9)
C(12)—C(13)	1.492(8)	C(22)—C(23)	1.484(9)
C(12)—Cl(11)	1.779(5)	C(22)—Cl(23)	1.775(6)
C(12)—Cl(14)	1.785(6)	C(22)—Cl(22)	1.787(6)
C(13)—C(14)	1.321(8)	C(23)—C(24)	1.328(8)
C(13)—Cl(12)	1.702(7)	C(23)—Cl(26)	1.701(6)
C(14)—C(15)	1.501(9)	C(24)—C(25)	1.498(8)
C(14)—Cl(16)	1.685(6)	C(24)—Cl(25)	1.698(7)
C(15)—Cl(13)	1.780(5)	C(25)—Cl(24)	1.771(5)
C(15)—Cl(15)	1.780(6)	C(25)—Cl(21)	1.775(6)

A variable temperature ^{13}C nmr study revealed fluxional behaviour for C_5Cl_6NSCl. At −50°C, the ^{13}C nmr spectrum exhibits five resonances as expected for structure **2***a* (see Table 6). Upon warming the solution the resonances for C_d and C_e broaden and collapse symmetrically to give a singlet at 135.2 ppm while the chemical shift of C_a is independent of temperature. This change is reversible and can be explained in terms of a fluxional process. Since the addition of hexachlorocyclopentadiene to a solution of C_5Cl_6NSCl in $CDCl_3$ does not alter the position of the ^{13}C nmr signals of C_5Cl_6NSCl, a dissociative mechanism can be ruled out. The coalescence temperature is *ca.* 30°C, which corresponds to an interconversion barrier of 68.1 ± 1.2 kJ mol^{-1}. The observed fluxional behaviour can be explained either by rotation about the S—N bond or inversion at the nitrogen centre. For comparison, the rotational barrier for $ClSNH_2$ has been calculated to be 66.5 kJ mol^{-1} (18) while experimental values for *N,N*-dialkyl substituted compounds are in the range 60.7–64.9 kJ mol^{-1} (20). The inversion process would be facilitated by the negative hyperconjugative effect but it is not possible to distinguish between these two processes on the basis of the available data.

Preparation of $C_5Cl_6NS^+AsF_6^-$

Haas and Mischo reported the observation of a transient blue colour in the reaction of C_5Cl_6NSCl with $SbCl_5$ in SO_2 to give $C_5Cl_6NSNC_5Cl_6$ in 62% yield (5). We were intrigued by the possibility that the blue species is $C_5Cl_6NS^+$, which would represent the first example of a hybrid, **3**, of the well known NS_2^+ cation, **4**, (21) and the hypothetical cations, **5**, which are only known as transient species (22).



3 **4** **5**

Can. J. Chem. Downloaded from www.nrcresearchpress.com by 198.100.157.202 on 09/07/12
For personal use only.

Can. J. Chem. Downloaded from www.nrcresearchpress.com by 198.100.157.202 on 09/07/12
For personal use only.

TABLE 4. Bond angles (deg)

1		2	
Bonds	Angle	Bonds	Angle
N(1)—S(1)—Br(1)	116.8(2)	N(2)—S(2)—Br(2)	116.5(2)
C(11)—N(1)—S(1)	146.7(4)	C(21)—N(2)—S(2)	148.6(4)
N(1)—C(11)—C(15)	130.5(5)	N(2)—C(21)—C(22)	130.8(6)
N(1)—C(11)—C(12)	120.2(5)	N(2)—C(21)—C(25)	120.2(5)
C(15)—C(11)—C(12)	109.3(5)	C(22)—C(21)—C(25)	109.1(5)
C(13)—C(12)—C(11)	102.8(4)	C(23)—C(22)—C(21)	103.2(5)
C(13)—C(12)—Cl(11)	111.9(4)	C(23)—C(22)—Cl(23)	110.4(4)
C(13)—C(12)—Cl(14)	110.8(4)	C(23)—C(22)—Cl(22)	110.7(4)
C(11)—C(12)—Cl(11)	112.1(3)	C(21)—C(22)—Cl(23)	111.4(4)
C(11)—C(12)—Cl(14)	111.0(4)	C(21)—C(22)—Cl(22)	111.8(4)
Cl(11)—C(12)—Cl(14)	108.2(3)	Cl(23)—C(22)—Cl(22)	109.2(3)
C(14)—C(13)—C(12)	112.7(6)	C(24)—C(23)—C(22)	112.9(5)
C(14)—C(13)—Cl(12)	126.7(5)	C(24)—C(23)—Cl(26)	125.5(5)
C(12)—C(13)—Cl(12)	120.5(4)	C(22)—C(23)—Cl(26)	121.6(4)
C(13)—C(14)—C(15)	111.9(5)	C(23)—C(24)—C(25)	111.7(6)
C(13)—C(14)—Cl(16)	127.1(5)	C(23)—C(24)—Cl(25)	126.8(5)
C(15)—C(14)—Cl(16)	121.0(4)	C(25)—C(24)—Cl(25)	121.5(4)
C(11)—C(15)—C(14)	103.2(5)	C(24)—C(25)—C(21)	103.0(4)
C(11)—C(15)—Cl(13)	111.9(3)	C(24)—C(25)—Cl(24)	111.1(5)
C(11)—C(15)—Cl(15)	111.4(4)	C(24)—C(25)—Cl(21)	110.5(4)
C(14)—C(15)—Cl(13)	110.4(4)	C(21)—C(25)—Cl(24)	111.6(4)
C(14)—C(15)—Cl(15)	110.3(3)	C(21)—C(25)—Cl(21)	111.5(4)
Cl(13)—C(15)—Cl(15)	109.4(3)	Cl(24)—C(25)—Cl(21)	109.0(3)

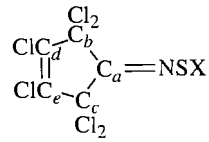
TABLE 5. Comparison of structural parameters for C_5Cl_6NSX derivatives

Bond distance (Å) or bond angle (deg)	Value for X =			
	CF_3[a]	Cl[a]	Br(1)[b]	Br(2)[b]
d(S—X)	1.798(7)	2.055(25)	2.229(2)	2.235(2)
d(S—N)	1.667(5)	1.561(19)	1.560(6)	1.569(6)
d(C—N)	1.255(7)	1.262(15)	1.278(8)	1.253(8)
∠ CNS	124.3(4)	147.2(7)	146.7(4)	148.6(4)
∠ NSX	94.9(3)	114.9(2)	116.8(2)	116.5(2)

[a]Taken from ref. 5.
[b]This work.

The reaction of C_5Cl_6NSCl with $Ag^+AsF_6^-$ in SO_2 produced $C_5Cl_6NS^+AsF_6^-$ as very moisture-sensitive, dark purple crystals in almost quantitative yield. This salt was characterized by elemental analyses (C, Cl, N, and S), ^{13}C and ^{14}N nmr spectroscopy, infrared and uv–visible spectroscopy. The infrared spectrum shows the expected absence of the band at 452 cm^{-1}, attributed to ν(S—Cl) in C_5Cl_6NSCl, and a very strong absorption at 703 cm^{-1} due to $\nu_3(AsF_6^-)$. There are substantial differences in the frequencies and intensities of the ir bands of the cation compared to those of neutral C_5Cl_6NSX compounds, but the very strong band at 810 cm^{-1} is a prominent feature in the ir spectrum of $C_5Cl_6NS^+AsF_6^-$. The visible spectrum exhibits an absorption at 562 nm in CH_2Cl_2, but this salt decomposes rapidly in solvents other than SO_2 so that an accurate extinction coefficient could be obtained. Attempts to obtain crystals of $C_5Cl_6NS^+AsF_6^-$ suitable for an X-ray structural determination or to prepare $C_5Cl_6NS^+$ salts with other anions, e.g. $SbCl_6^-$, $AlCl_4^-$, have been unsuccessful.

TABLE 6. ^{13}C nmr parameters for C_5Cl_5NSX derivatives



X	δ[a]				
	C_a	C_b	C_c	C_d	C_e
Cl[b]	142.3	78.4	78.4	135.4	135.4
Cl[c]	142.3	79.6	76.3	135.8	134.6
Br	142.7	78.3	78.3	135.8	135.8
I	174.0	79.8	79.8	138.2	138.2
Ph	147.5	77.8	77.8	137.6	137.6
NPr_2^i	139.8	80.2	80.2	137.5	137.5
NC_5Cl_6	152.0	79.5	78.4	142.2	136.1
CF_3[d]	158.9	85.0	82.2	142.4	140.4
NSO[d]	151.7	83.8	83.8	141.5	141.5
SCF_3[d]	154.9	79.0	79.0	137.1	137.1

[a]Chemical shifts in $CDCl_3$ at 25°C. The assignments for the inequivalent carbon atoms of the pairs C_a, C_b and C_d, C_e are arbitrary.
[b]Lit.: 143.2 (C=N), 136.0 (C—Cl), 82.0 and 80.0 (CCl_2) (5).
[c]At −50°C.
[d]Data taken from ref. 5.

Conclusions

The structural features of hexachloro-3-cyclopentenylaminosulphenyl halides, C_5Cl_6NSX (X = Cl, Br), can be explained in terms of the negative hyperconjugation effect. Variable temperature ^{13}C nmr studies of C_5Cl_6NSCl reveal a fluxional process that probably involves inversion at nitrogen. The dark purple salt, $C_5Cl_6NS^+AsF_6^-$, is readily obtained by the reaction of

C_5Cl_6NSCl with $AgAsF_6$ in SO_2. The preparation and structural determination of other examples of the hybrid cation R_2CNS^+ are being pursued.

Acknowledgements

The financial support of the NSERC (Canada) in the form of operating and infrastructure grants, a postgraduate scholarship to A.A., and an undergraduate summer research award to R.V. is gratefully acknowledged. We also wish to thank Professor A. Haas (University of Bochum) for helpful correspondence and a copy of the thesis of T. Mischo, Professor A. Rauk (University of Calgary) for fruitful discussions of negative hyperconjugation, and Dr. R. Yamdagni for the variable temperature nmr measurements.

1. A. APBLETT and T. CHIVERS. J. Chem. Soc. Chem. Commun. 1889 (1987). Can. J. Chem. **68**, 650 (1990).
2. A. APBLETT and T. CHIVERS. J. Chem. Soc. Chem. Commun. 96 (1989). Phosphorus, Sulfur and Silicon **41**, 439 (1989). Inorg. Chem. **28**, 4544 (1989).
3. A. APBLETT, T. CHIVERS, and J. F. FAIT. J. Chem. Soc. Chem. Commun. 1596 (1989); A. APBLETT, T. CHIVERS, and J. F. FAIT. Inorg. Chem. **29**, 1643 (1990).
4. A. APBLETT. Ph.D. Thesis, The University of Calgary, Calgary, Alta. March 1989.
5. A. HAAS and T. MISCHO. Chimia, **41**, 344 (1987). Can. J. Chem. **67**, 1902 (1989).
6. A. APBLETT, A. J. BANISTER, D. BIRON, A. G. KENDRICK, J. PASSMORE, M. SCHRIVER, and M. STOJANAC. Inorg. Chem. **25**, 4451 (1986).
7. H. SCHENK and S. R. HALL. "SIMPEL", XTAL2.4 User's Manual. *Edited by* S. R. Hall and J. M. Stewart. Universities of Western Australia and Maryland. 1988.
8. N. WALKER and D. STEWART. Program DIFABS, Acta Crystallogr. **A39**, 158 (1983).
9. International tables for X-ray crystallography. Vol. 4, Kynoch Press, Birmingham. 1974.
10. S. R. HALL and J. M. STEWART 1988. (*Editors*). XTAL2.4 User's Manual. Universities of Western Australia and Maryland.
11. W. BLUDSSUS and R. MEWS. J. Chem. Soc. Chem. Commun. 35 (1979).
12. J. PASSMORE and M. J. SCHRIVER. Inorg. Chem. **27**, 2749 (1988).
13. R. MINKWITZ, R. LEKIES, D. LENNHOFF, J. SAWATZKI, J. KADEL, and H. OBERHAMMER. Inorg. Chem. **29**, 2587 (1990) and references therein.
14. M.-T. AVERBUCH-POUCHOT, A. DURIF, A. J. BANISTER, J. A. DURRANT, and J. HALFPENNY. J. Chem. Soc. Dalton Trans. 221 (1982).
15. L. PAULING. *In* The nature of the chemical bond. 3rd ed. Cornell Univ. Press, New York. 1960. p. 225.
16. D. J. CRAM and G. S. HAMMOND. *In* Organic chemistry. McGraw-Hill, New York. 1959. p. 112.
17. A. E. REED and P. VON R. SCHLEYER. J. Am. Chem. Soc. **112**, 1434 (1990) and references therein.
18. A. E. REED and P. VON R. SCHLEYER. Inorg. Chem. **27**, 3969 (1988).
19. O. GLEMSER, E. KINDLER, B. KREBS, R. MEWS, F.-M. SCHNEPEL, and J. WEGENER. Z. Naturforsch. **35**b, 657 (1980).
20. M. RABAN and D. KOST. Tetrahedron, **40**, 3345 (1984); L. CRAINE and M. RABAN. Chem. Rev. **89**, 689 (1989).
21. R. FAGGIANI, R. J. GILLESPIE, C. J. L. LOCK, and J. D. TYRER. Inorg. Chem. **17**, 2975 (1978).
22. P. G. GASSMANN and D. K. DYGOS. J. Am. Chem. Soc. **91**, 1543 (1969).

Can. J. Chem. Downloaded from www.nrcresearchpress.com by 198.100.157.202 on 09/07/12
For personal use only.

Densities and viscosities of binary and ternary liquid mixtures at 25°C[1]

TEJRAJ M. AMINABHAVI,[2] SHRIKANT S. JOSHI, AND RAMACHANDRA H. BALUNDGI
Department of Chemistry, Karnatak University, Dharwad-580 003, India

AND

SHYAM S. SHUKLA
Department of Chemistry, Lamar University, Beaumont, TX 77710, U.S.A.

Received February 7, 1990[3]

TEJRAJ M. AMINABHAVI, SHRIKANT S. JOSHI, RAMACHANDRA H. BALUNDGI, and SHYAM S. SHUKLA. Can. J. Chem. **69**, 1028 (1991).

Densities and viscosities of ten binary and four ternary mixtures containing bromoform, bromobenzene, chlorobenzene, toluene, mesitylene, and dimethylformamide at 25°C have been measured over the whole range of mixture compositions. Excess molar volumes, apparent values of excess molar viscosities, and Gibbs energy of activation of flow have been calculated for these mixtures. The calculated results have been fitted to a linear regression equation to estimate the parameters and the standard deviation between the calculated and the experimental data.

Key words: ternary systems, excess quantities, bromoform, density, viscosity.

TEJRAJ M. AMINABHAVI, SHRIKANT S. JOSHI, RAMACHANDRA H. BALUNDGI et SHYAM S. SHUKLA. Can. J. Chem. **69**, 1028 (1991).

Opérant à 25°C et sur l'ensemble des mélanges de composition, on a mesuré les densités et les viscosités de dix mélanges binaires et de quatre mélanges ternaires contenant du bromoforme, du bromobenzène, du chlorobenzène, du toluène, du mésitylène et du diméthylformamide. Pour chacun de ces mélanges, on a calculé les volumes molaires en excès, les valeurs apparentes des viscosités molaires en excès et l'enthalpie libre d'activation d'écoulement. On a ajusté les résultats calculés à une équation de régression linéaire afin d'évaluer les paramètres et les écarts types entre les données expérimentales et calculées.

Mots clés : systèmes ternaires, quantités en excès, bromoforme, densité, viscosité.

[Traduit par la rédaction]

Introduction

Theoretical predictions of excess molar volumes of nonideal binary liquid mixtures have been satisfactory in explaining the sign and magnitude in terms of the extent of interactions between mixing components (1, 2). For ternary mixtures, the predictive approach is more complex and thus empirical methods based on experimental binary data have to be used (3, 4). However, if significant interactions among the liquids occur, considerable errors may be introduced if we attempt to express the excess molar volumes of ternary systems in terms of binary contributions. The study of transport properties of liquid mixtures, on the other hand, is also informative as it gives an insight into the intermolecular forces and the microscopic structure of liquids (5).

Previous work on binary systems has suggested that correlations of molecular order in addition to donor–acceptor type interactions play a significant role in studying the excess molar volumes of mixtures of bromoform with aromatic liquids (6–8). A search of the literature on ternary mixtures suggests the availability of several empirical relations used to calculate the excess volume (9–19). In this paper, we report the experimental densities and viscosities of ten binary and four ternary mixtures comprising bromoform, mesitylene, chlorobenzene, bromobenzene, dimethylformamide (DMF), and toluene. The density data were used to calculate the binary and ternary excess molar volumes and these results were analyzed in terms of the empirical ternary relations. The viscosity data were also used to predict the apparent values of excess molar viscosity and excess molar Gibbs energy of activation of flow.

Experimental

Materials

Bromoform (Thomas Baker, Bombay) was obtained in its highest purity grade (>99 mol% as claimed by the manufacturer) and was thus not purified further. The reagent grade solvents, namely, chlorobenzene, bromobenzene, DMF, toluene, and mesitylene were purified before use (20, 21). The physical properties of the pure liquids are in close agreement with the literature results. The purity of the solvents as tested by gas chromatography exceeded more than 99 mol%. Mixtures were prepared by weighing on a Mettler balance with a precision of 1×10^{-4} g.

Methods

Densities were determined with a single stem pycnometer having a bulb volume of about 10 cm^3 and a capillary of 1 mm internal diameter. Viscosities were determined with a Cannon–Fenske viscometer, size 100, calibrated with double distilled water and benzene. The details of the procedures have been described earlier (6–8). The pycnometer and viscometer were suspended vertically for sufficient time in a constant temperature bath maintained within ±0.01°C. The temperatures were read with certified thermometers. Densities and viscosities determined are accurate to ±0.0001 and ±0.003 units respectively. Densities (ρ) and viscosities (η) of the binary and ternary mixtures, over the entire scale of mole fractions at 25°C, have been measured.[4]

Results and discussion

Following our earlier suggestions (22), the excess molar volumes of binary mixtures, $V^E_{m,B}$, have been calculated from density data as

$$[1] \quad V^E_{m,B} = \left[\left(\sum_{i=1}^{2} M_i x_i\right) \Big/ \rho\right] - \sum_{i=1}^{2} (M_i x_i / \rho_i)$$

[1]Taken from Ph.D. thesis of S.S.J. submitted to Karnatak University, 1989.

[2]Author to whom correspondence may be addressed.

[3]Revision received December 20, 1990.

[4]All numerical data may be purchased from the Depository of Unpublished Data, Document Delivery, CISTI, National Research Council Canada, Ottawa, Canada K1A 0S2.

Printed in Canada / Imprimé au Canada

Can. J. Chem. Downloaded from www.nrcresearchpress.com by 198.100.157.202 on 09/07/12
For personal use only.

TABLE 1. Estimated coefficients and standard errors of excess molar volumes ($V^E_{m,B}$, $m^3\ mol^{-1}$, eq. [2]) of binary mixtures at 25°C

System		$A_B^{(0)} \times 10^6$	$A_B^{(1)} \times 10^6$	$A_B^{(2)} \times 10^6$	$A_B^{(3)} \times 10^6$	$\sigma \times 10^6$
I.	Mesitylene (1) + bromoform (2)	3.27	−0.97	−3.72	7.79	0.18
II.	Bromobenzene (1) + bromoform (2)	−0.03	−0.12	−0.36	0.26	0.01
III.	Chlorobenzene (1) + bromoform (2)	0.11	0.08	0.35	−0.45	0.02
IV.	Bromobenzene (1) + mesitylene (2)	0.33	−0.18	0.05	0.98	0.02
V.	Mesitylene (1) + chlorobenzene (2)	0.41	−0.34	−0.18	0.54	0.02
VI.	DMF (1) + chlorobenzene (2)	−0.90	−0.20	−0.13	0.08	0.02
VII.	Bromobenzene (1) + chlorobenzene (2)	0.17	0.72	0.48	−0.85	0.03
VIII.	Chlorobenzene (1) + toluene (2)	−0.37	−0.07	0.41	0.48	0.02
IX.	Bromobenzene (1) + DMF (2)	−0.87	−0.23	−0.45	0.25	0.02
X.	DMF (1) + toluene (2)	−0.47	−0.13	−0.03	0.15	0.01

where M_i, x_i, and ρ_i represent the molar mass, mole fraction, and density of the ith component of the mixture, respectively; ρ refers to density of binary mixture. These results are further fitted to a Redlich–Kister–type formula (23).

$$[2] \quad V^E_{m,B} = x_1 x_2 \sum_{i=0}^{n} A_B^{(i)} (x_2 - x_1)^i$$

By using a nonlinear regression analysis (Marquardt algorithm) we have estimated the binary parameters $A_B^{(i)}$ of eq. [2]. In each case, the optimum number of coefficients was ascertained from an examination of the variation of the standard error (σ) of the estimate with:

$$[3] \quad \sigma = [\Sigma (X^E_{obs} - X^E_{cal})^2/(n - P)]^{1/2}$$

where n is the total number of data points and P is the number of coefficients considered ($P = 4$ in the present calculation). The estimated parameters and the standard deviations between the computed and observed values of $V^E_{m,B}$ are given in Table 1.

The plots of $V^E_{m,B}$ versus x_1 for all the systems at 25°C are shown in Fig. 1 together with the lines for the standard errors. The estimated error in $V^E_{m,B}$ varies in the range (2–5) × $10^{-8}\ m^3\ mol^{-1}$. The magnitude of the various binary mixtures follow the sequence: DMF + toluene < DMF + chlorobenzene < bromobenzene + DMF < chlorobenzene + toluene < bromobenzene + bromoform < bromobenzene + chlorobenzene ≃ bromobenzene + mesitylene < chlorobenzene + bromoform < mesitylene + chlorobenzene < mesitylene + bromoform.

To extend the discussion to ternary mixtures, it is legitimate to write the ternary excess molar volume, $V^E_{m,T}$ as

$$[4] \quad V^E_{m,T} = \left[\left(\sum_{i=1}^{3} M_i x_i \right) \Big/ \rho \right] - \sum_{i=1}^{3} (M_i x_i / \rho_i)$$

Here, ρ refers to density of the ternary mixture. Analogously, $V^E_{m,T}$ can also be measured directly from dilatometry (14). However, $V^E_{m,T}$ has been calculated from consideration of $V^E_{m,B}$ data of the binaries making up the ternary mixture. This approach has led to the development of several empirical relations to predict $V^E_{m,T}$ data. The popular ones among these are as follows:

Rastogi *et al.* model (4)

$$[5] \quad V^E_{m,T} = 0.5[(x_1 + x_2)V^E_{12} + (x_1 + x_3)V^E_{13} + (x_2 + x_3)V^E_{23}]$$

Radojkovic *et al.* model (9)

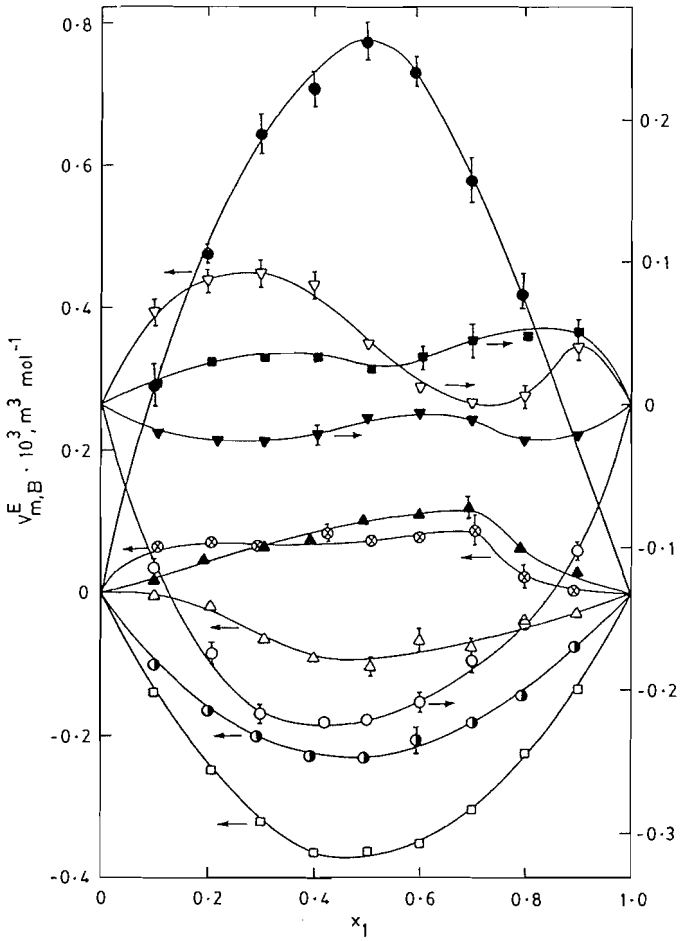


FIG. 1. Dependence of excess molar volume ($V^E_{m,B}$) on mole fraction (x_1) of binary mixtures at 25°C. Symbols: (○) bromobenzene(1) + DMF(2); (□) DMF(1) + toluene(2); (△) chlorobenzene(1) + toluene(2); (◑) DMF(1) + chlorobenzene(2); (●) mesitylene(1) + bromoform(2); (▲) mesitylene(1) + chlorobenzene(2); (⊗) bromobenzene(1) + mesitylene(2); (▽) bromobenzene(1) + chlorobenzene(2); (■) chlorobenzene(1) + bromoform(2); (▼) bromobenzene(1) + bromoform(2).

$$[6] \quad V^E_{m,T} = V^E_{12} + V^E_{23} + V^E_{13}$$

Kohler model (12)

$$[7] \quad V^E_{m,T} = (x_1 + x_2)^2 V^E_{12} + (x_1 + x_3)^2 V^E_{13} + (x_2 + x_3)^2 V^E_{23}$$

Jacob and Fitzner model (13)

Can. J. Chem. Downloaded from www.nrcresearchpress.com by 198.100.157.202 on 09/07/12
For personal use only.

TABLE 2. Estimated coefficients and standard errors of excess molar volumes ($V^E_{m,T}$, $m^3\ mol^{-1}$, eq. [12]) of ternary mixtures at 25°C

System	$A_T^{(0)} \times 10^6$	$A_T^{(1)} \times 10^6$	$A_T^{(2)} \times 10^6$	$A_T^{(3)} \times 10^6$	$\sigma \times 10^6$
A. Bromoform (1) + mesitylene (2) + chlorobenzene (3)	0.87	−6.58	7.92	18.31	0.08
B. Chlorobenzene (1) + DMF (2) + toluene (3)	0.16	−8.51	5.40	42.20	0.05
C. Bromoform (1) + mesitylene (2) + bromobenzene (3)	12.35	25.06	−0.29	−16.57	0.01
D. Chlorobenzene (1) + DMF (2) + bromobenzene (3)	0.16	1.83	−0.82	3.73	0.03

[8] $$V^E_{m,T} = 4\left[\frac{x_1x_2V^E_{12}}{(2x_1 + x_3)(2x_2 + x_3)} + \frac{x_1x_3V^E_{13}}{(2x_1 + x_2)(2x_3 + x_2)} + \frac{x_2x_3V^E_{23}}{(2x_2 + x_1)(2x_3 + x_1)}\right]$$

Tsao and Smith model (11)

[9] $$V^E_{m,T} = \left(\frac{x_2}{1 - x_1}\right)V^E_{12} + \left(\frac{x_3}{1 - x_1}\right)V^E_{13} + (1 - x_1)V^E_{23}$$

Sanchez and Lacombe (24, 25) also developed a theory to calculate excess quantities of ternary mixtures. Following this approach, we propose to compute $V^E_{m,T}$ from binary interactions obtained from $V^E_{m,B}$ data. The total volume $V^E_{m,T}$ of a ternary mixture can be expressed as

[10] $$V_{m,T} = \sum_{i=1}^{3} V_i x_i + \Delta V_{12} + \Delta V_{23} + \Delta V_{13} + \Delta V_{m,T}$$

where the various ΔV terms representing the changes in volume are given in terms of molar volumes of the respective binary mixtures. So eq. [10] becomes

[11] $$V_{m,T} = \sum_{i=1}^{3} V_i x_i + x_1x_2 \sum_{n=0}^{3} A_{12}^{(n)}(x_1 - x_2)^n + x_2x_3 \sum_{n=0}^{3} A_{23}^{(n)}(x_2 - x_3)^n + x_1x_3 \sum_{n=0}^{3} A_{13}^{(n)}(x_1 - x_3)^n + x_1x_2x_3 \sum_{n=0}^{3} A_T^{(n)}(x_2 - x_3)^n x_1^n$$

since the difference, $\left[V_{m,T} - \sum_{i=1}^{3} V_i x_i\right]$, represents $V^E_{m,T}$, which is obtained from the experimental density data and has been fitted to the following relationship:

[12] $$V^E_{m,T} - x_1x_2 \sum_{n=0}^{3} A_{12}^{(n)}(x_1 - x_2)^n - x_2x_3 \sum_{n=0}^{3} A_{23}^{(n)}(x_2 - x_3)^n - x_1x_3 \sum_{n=0}^{3} A_{13}^{(n)}(x_1 - x_3)^n = x_1x_2x_3 \sum_{n=0}^{3} A_T^{(n)}(x_2 - x_3)^n x_1^n$$

where $A_T^{(n)}$ represents the ternary interaction parameter. The various binary terms (as estimated from $V^E_{m,B}$ data) given in Table 1 are used along with $V^E_{m,T}$ estimated by eq. [4] to evaluate the ternary coefficients $A_T^{(n)}$ from eq. [12]. These data are included in Table 2. A detailed analysis of the various theoretical relations is summarized in Tables 2 and 3.

The apparent values of excess molar viscosity η^E and excess molar Gibbs energy of activation of flow ΔG^{*E}, for binary and

TABLE 3. Standard errors (σ) in estimating excess molar volumes ($V^E_{m,T}$, $m^3\ mol^{-1}$) of ternary mixtures at 25°C

Relation	$\sigma \times 10^6$ For systems[a] A	B	C	D
Rastogi *et al.* (eq. [5])	0.083	0.085	0.102	0.039
Radojkovic *et al.* (eq. [6])	0.055	0.051	0.078	0.078
Kohler (eq. [7])	0.054	0.080	0.067	0.036
Jacob and Fitzer (eq. [8])	0.055	0.074	0.067	0.037
Tsao and Smith (eq. [9])	0.057	0.067	0.077	0.035
Present work (eq. [12])	0.077	0.051	0.012	0.029

[a]A, B, C, and D refer to ternary mixtures given in Table 2.

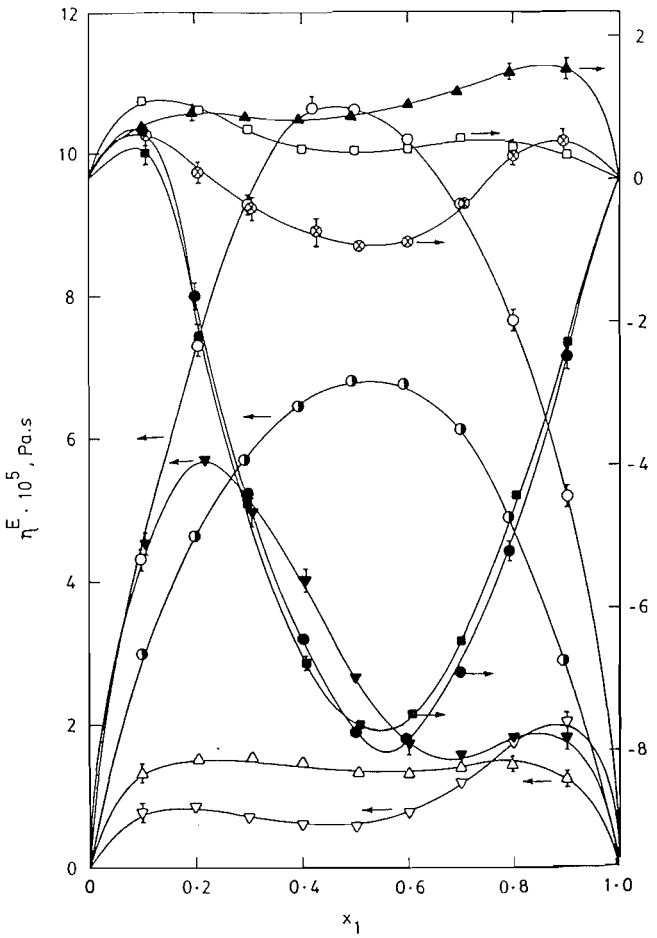


FIG. 2. Dependence of excess molar viscosity (η^E) on mole fraction (x_1) at 25°C. Symbols have the same meanings as in Fig. 1.

Can. J. Chem. Downloaded from www.nrcresearchpress.com by 198.100.157.202 on 09/07/12
For personal use only.

TABLE 4. Estimated coefficients and standard errors of excess molar viscosity (η^E, Pa s, eq. [13]) and excess molar Gibbs energy of activation of flow (ΔG^{*E}, J mol^{-1}, eq. [14]) for binary mixtures at 25°C

System[a]	Property	$A_B^{(0)}$	$A_B^{(1)}$	$A_B^{(2)}$	$A_B^{(3)}$	σ
I	$\eta^E \times 10^3$	−0.31	0.13	0.28	0.11	0.003
	ΔG^{*E}	1171.52	0.00	418.40	334.72	12.552
II	$\eta^E \times 10^3$	0.10	0.23	0.36	−0.07	0.006
	ΔG^{*E}	669.44	251.04	543.92	−292.88	8.368
III	$\eta^E \times 10^3$	−0.31	0.08	0.30	0.16	0.003
	ΔG^{*E}	502.08	125.52	502.08	0.00	4.184
IV	$\eta^E \times 10^3$	−0.04	0.02	0.16	−0.08	0.004
	ΔG^{*E}	292.88	41.84	460.24	−41.84	12.552
V	$\eta^E \times 10^3$	0.03	−0.02	0.14	−0.04	0.002
	ΔG^{*E}	251.04	−41.84	502.08	−167.36	8.368
VI	$\eta^E \times 10^3$	0.27	−0.03	0.07	0.06	0.001
	ΔG^{*E}	878.64	−83.68	251.04	209.20	4.184
VII	$\eta^E \times 10^3$	0.02	−0.01	0.19	−0.11	0.003
	ΔG^{*E}	209.20	0.00	502.08	209.20	8.368
VIII	$\eta^E \times 10^3$	0.05	0.01	0.13	−0.02	0.002
	ΔG^{*E}	334.72	83.68	502.08	41.84	4.184
IX	$\eta^E \times 10^3$	0.42	0.03	0.14	−0.16	0.003
	ΔG^{*E}	1255.20	209.20	376.56	−292.88	8.368
X	$\eta^E \times 10^3$	0.01	−0.01	0.09	0.09	0.001
	ΔG^{*E}	334.72	0.00	376.56	418.40	4.184

[a]Systems I–X refer to binary mixtures given in Table 1.

TABLE 5. Estimated coefficients and standard errors of excess molar viscosity (η_T^E, Pa s, of eqs. [13] and [15]) and excess molar Gibbs energy of activation of flow (ΔG_T^{*E}, J mol^{-1}, of eq. [14]) for ternary mixtures at 25°C

System[a]	Property	$A_T^{(0)}$	$A_T^{(1)}$	$A_T^{(2)}$	$A_T^{(3)}$	σ
A	$\eta_T^E \times 10^3$, eq. [13]	−2.56	−1.53	−2.60	4.68	0.02
	ΔG^{*E}, eq. [14]	6903.60	8744.56	7112.80	14183.76	83.68
	$\eta_T^E \times 10^3$, eq. [15]	2.45	2.88	−0.61	−6.43	0.04
B	$\eta_T^E \times 10^3$, eq. [13]	1.25	2.67	2.36	−3.25	0.01
	ΔG^{*E}, eq. [14]	41.84	7322.00	12300.96	−10543.68	41.84
	$\eta_T^E \times 10^3$, eq. [15]	1.51	2.41	3.08	−3.05	0.01
C	$\eta_T^E \times 10^3$, eq. [13]	−1.42	−2.23	−1.42	−0.79	0.01
	ΔG^{*E}, eq. [14]	6736.24	6736.24	10920.24	−11254.96	83.68
	$\eta_T^E \times 10^3$, eq. [15]	2.68	2.75	0.18	−9.37	0.04
D	$\eta_T^E \times 10^3$, eq. [13]	−2.26	7.09	28.17	−15.05	0.10
	ΔG^{*E}, eq. [14]	−6652.56	21756.80	87445.60	−43639.12	334.72
	$\eta_T^E \times 10^3$, eq. [15]	−1.98	6.73	28.84	−14.95	0.10

[a]A, B, C, and D refer to ternary mixtures given in Table 2.

ternary mixtures, were calculated (26–28) as:

$$[13] \quad \eta^E = \eta_m - \sum_{i=1}^{n} (\eta_i x_i)$$

$$[14] \quad \Delta G^{*E} = RT\left[\ln \eta_m V_m - \sum_{i=1}^{n} x_i \ln \eta_i V_i\right]$$

Quite often an exponential relation was also used to calculate η^E of the mixtures.

$$[15] \quad \eta^E = \eta_m - \exp\left(\sum_{i=1}^{n} x_i \ln \eta_i\right)$$

The computed values of η^E and ΔG^{*E} from eqs. [13] and [14] for binary mixtures have been fitted to eq. [2] to estimate the coefficients that are included in Table 4.

The results of η^E at 25°C calculated from eq. [13] along with the errors as indicated by the solid vertical lines are displayed in Fig. 2 for all the binary mixtures. The error analyses indicate that η^E results vary in the range of (2–4) × 10^7 Pa s. The results for ΔG^{*E} at 25°C are plotted in Fig. 3. The errors involved in the computation of ΔG^{*E} are estimated to be, at the most, around ± (2–3) J mol^{-1}. The magnitude of ΔG^{*E} for the various binary mixtures follows the sequence: bromobenzene + DMF > mesitylene + bromoform > DMF + chlorobenzene > bromo-

Can. J. Chem. Downloaded from www.nrcresearchpress.com by 198.100.157.202 on 09/07/12
For personal use only.

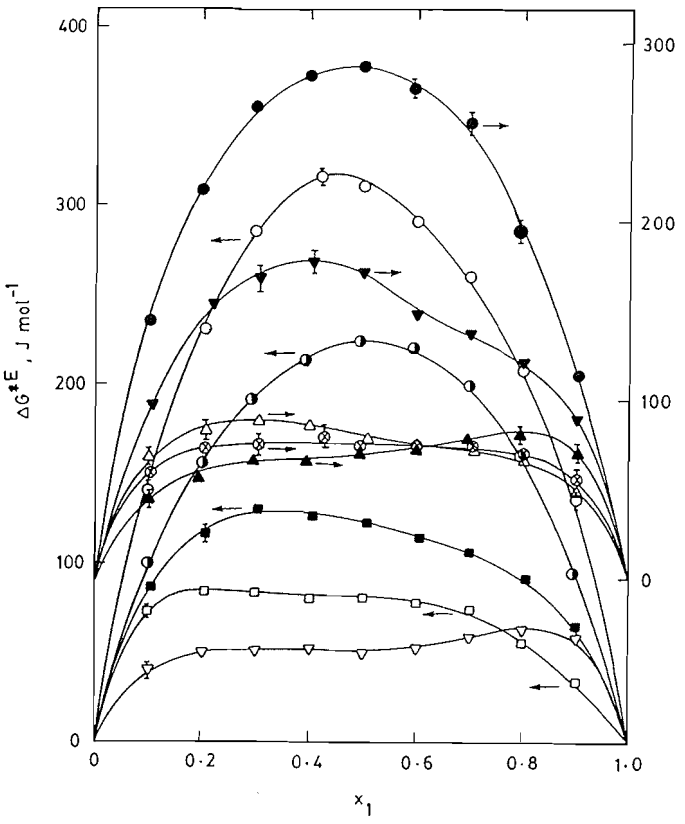


FIG. 3. Dependence of excess molar Gibbs energy of activation of flow (ΔG^{*E}) on mole fraction (x_1) at 25°C. Symbols have the same meanings as in Fig. 1.

benzene + bromoform > chlorobenzene + bromoform > DMF + toluene > chlorobenzene + toluene > bromobenzene + mesitylene > mesitylene + chlorobenzene > bromobenzene + chlorobenzene.

The ternary viscosity data have also been analysed in terms of eqs. [13]–[15] and these data are fitted to the following empirical relation:

$$[16] \quad X^E = x_1x_2x_3\left[\sum_{i=0}^{n} A_T^{(i)}(x_2 - x_3)^i x_1^i\right]$$

where X^E refers to η^E as calculated from eqs. [13] and [15] and ΔG^{*E} from eq. [14]. The estimated coefficients and the standard deviations are compiled in Table 5. The η^E as calculated from eq. [13] appears to be better than that given by eq. [15].

Acknowledgements

We thank the University Grants Commission (major grant: F-12-55/88-SR-III) New Delhi, India, and the Robert A. Welch Foundation, Houston, Texas, for the financial support of this study. We also thank Professor Keith C. Hansen, Chairman, Chemistry Department, Lamar University, Beaumont, Texas, U.S.A., for his interest in this research.

1. J. S. ROWLINSON. Liquid and liquid mixtures. 2nd ed. Butterworth, London. 1969.
2. I. PRIGOGINE. Molecular theories of solutions. North Holland Publishing, Amsterdam. 1957.
3. I. L. ACEVEDO, M. A. POSTIGO, and M. KATZ. Can. J. Chem. **66**, 367 (1988).
4. R. P. RASTOGI, J. NATH, and S. S. DAS. J. Chem. Eng. Data, **22**, 249 (1977).
5. T. M. AMINABHAVI and P. MUNK. J. Phys. Chem. **84**, 442 (1980).
6. T. M. AMINABHAVI, L. S. MANJESHWAR, and R. H. BALUNDGI. Indian J. Chem. **25A**, 465 (1986).
7. L. S. MANJESHWAR and T. M. AMINABHAVI. J. Chem. Eng. Data, **33**, 184 (1988).
8. T. M. AMINABHAVI, L. S. MANJESHWAR, S. S. JOSHI, R. H. BALUNDGI, and S. B. HALLIGUDI. Indian J. Chem. **27A**, 721 (1988).
9. N. RADOJKOVIC, A. TASIC, D. GROZDANIC, B. DJORDJEVIC, and M. MALIC. J. Chem. Thermodyn. **9**, 349 (1977).
10. R. P. SINGH, R. K. NIGAM, S. P. SHARMA, and S. AGGARWAL. Fluid Phase Equilib. **18**, 333 (1984).
11. C. C. TSAO and J. M. SMITH. Chem. Eng. Prog. Symp. No. 7, 107 (1957).
12. F. KOHLER. Monatsh. Chem. **91**, 738 (1960).
13. K. T. JACOB and K. FITZNER. Thermochim. Acta, **18**, 197 (1977).
14. P. P. SINGH and S. P. SHARMA. J. Chem. Eng. Data, **30**, 477 (1985).
15. J. O. TRIDAY and P. RODRIGUEZ. J. Chem. Eng. Data, **30**, 112 (1985).
16. M. J. MUSSCHE and L. A. VERHOEYE. J. Chem. Eng. Data, **20**, 46 (1975).
17. E. L. HERIC and C. D. POSEY. J. Chem. Eng. Data, **12**, 40 (1967).
18. E. L. HERIC and C. D. POSEY. J. Chem. Eng. Data, **10**, 340 (1965).
19. G. R. NAIDU and P. R. NAIDU. J. Chem. Eng. Data, **26**, 197 (1981).
20. A. WEISSBERGER. Techniques of organic chemistry; organic solvents. Vol. 7. Interscience, New York. 1959.
21. J. TIMMERMANS. Physico-chemical constants of pure organic compounds. Vols. 1 and 2. Elsevier, Amsterdam. 1950 and 1965, respectively.
22. S. S. JOSHI, T. M. AMINABHAVI, and S. S. SHUKLA. Can. J. Chem. **68**, 251 (1990).
23. O. REDLICH and A. T. KISTER. Ind. Eng. Chem. **40**, 345 (1948).
24. I. C. SANCHEZ and R. H. LACOMBE. J. Phys. Chem. **80**, 2352 (1976).
25. R. H. LACOMBE and I. C. SANCHEZ. J. Phys. Chem. **80**, 2568 (1976).
26. S. L. OSWAL. Indian J. Technol. **26**, 389 (1988).
27. J. SHAH, M. N. VAKHARIA, M. V. PANDYA, G. D. TALELE, K. G. PATHAK, P. P. PALSANAWALA, and S. L. OSWAL. Indian J. Technol. **26**, 383 (1988).
28. S. L. OSWAL. Can. J. Chem. **66**, 111 (1988).

Can. J. Chem. Downloaded from www.nrcresearchpress.com by 198.100.157.202 on 09/07/12
For personal use only.

Synthetic transformations of cyclopropyl annulated dihydroisoquinolines[1]

IVAN LANTOS[2] AND HARALAMBOS E. KATERINOPOULOS[3]

Department of Synthetic Chemistry, Chemical R&D, SmithKline Beecham Pharmaceuticals, Philadelphia, PA 19101, U.S.A.

Received December 17, 1990

IVAN LANTOS and HARALAMBOS E. KATERINOPOULOS. Can. J. Chem. **69**, 1033 (1991).

Isomeric 3-cyano-3-methyl-2-acetyl-cycloprop[*c*]isoquinolines, **5** and **6**, were prepared by alkylation and cyclopropanation of Reissert compounds and their reactions under basic conditions were examined. Both compounds, under the influence of methoxide, yielded isoquinoline derived products resulting from cleavage of the peripheral C—C bond. The results are postulated to derive from attack of the methoxide on the acyl carbonyl, forming a tetrahedral adduct that undergoes ring opening.

Key words: cyclopropanation, ring opening, tetrahedral complex, pyramidalization.

IVAN LANTOS et HARALAMBOS E. KATERINOPOULOS. Can. J. Chem. **69**, 1033 (1991).

On a préparé les 3-cyano-3-méthyl-2-acétyl-cycloprop[*c*]isoquinoléines isomères, **5** et **6**, par alkylation et cyclopropanation de composés de Reissert et on a étudié leurs réactions dans des conditions basiques. Sous l'influence du méthylate, les deux composés fournissent des produits dérivés de l'isoquinoléine par clivage de la liaison C—C périphérique. On suppose que les produits obtenus sont le résultat d'une attaque du méthylate sur le groupe carbonyle de l'acétyle conduisant à un adduit tétraédrique qui subit ensuite une ouverture de cycle.

Mots clés : cyclopropanation, ouverture de cycle, complexe tétraédrique, pyramidalisation.

[Traduit par la rédaction]

Introduction

As the continuation of our previous work dealing with the ring expansion reactions of the dihydrocycloprop[*c*]isoquinoline heterocyclic system (1), we desired to prepare disubstituted analogs having *gem* substituents of different steric sizes in the 3-position. It appeared to us that the methyl and cyano groups were especially advantageous in this context not only on account of their ready accessibility by synthesis but also because of the potential to obtain both stereoisomers. In this report we detail the successful preparation of these desired isomeric 3-methyl-3-cyano compounds **5** and **6** together with the discovery that under basic conditions these compounds undergo a novel ring opening reaction previously not observed within this heterocyclic system. The reactivity of these compounds under thermal conditions will be described in a separate report.

Results

The successful strategy leading to the preparation of isomers **5** and **6** was based on the cyclopropanation of the Reissert adducts of isoquinoline (2). Treatment of the methylated Reissert adduct **4** with dibromocarbene (3) afforded **5** in moderate yield as shown in Scheme 1.

The relative stereochemical assignment was originally based on the known tendency of the carbenoid species to enter the molecule *anti* to the more bulky group, in this instance the methyl group. This stereochemical assignment was later confirmed by nOe experiments and by a single crystal X-ray structural determination. To prepare the isomer with the inverted substitution pattern in the 3-position, the alkylation–cyclopropanation sequence was reversed. Thus cyclopropanation of the base-sensitive Reissert adduct **2** was readily accomplished with the Seyferth reagent (4) and the resultant compound **3** was alkylated with NaH/MeI. The success of this latter reaction is noteworthy, since the cyclopropyl group is potentially sensitive to the incipient carbanion in the benzylic position. The stereochemical assignment of **3** is based on the assumption that the cyclopropyl moiety enters opposite to the 1-substituent, in this case the cyano group. Assignment of **6** rests on nOe spectral comparison with isomer **5**. Irradiation of the C-3 methyl of **5** gave significant enhancements of the aromatic proton at C-4, and the cyclopropyl proton at C-1a. In contrast, irradiation of the C-3 methyl protons of **6** gave no noticeable nOe of the C-1a cyclopropyl proton signal, although it did show an enhancement of the signal due to the proton at C-4.

If the stereochemical assignment of **3** is correct, then the introduction of the methyl group *syn* to the cyclopropyl unit in **6** is worthy of note since it occurs with retention of configuration. This is in contrast to our previous findings that the incoming molecule always enters *anti* to the existing more bulky substituent in the molecule. The results would indicate that deprotonation from the *syn* face results in a carbanion that, in accordance with the *gauche* (5) effect, being α to a nitrogen, retains some sp^3-like character and its stereochemical integrity upon treatment with electrophiles.

Having isomers **5** and **6** in hand allowed us to examine their reactivity under conditions that previously resulted in ring expansion. Disappointingly, we found the thermally induced reactions extremely sluggish and these results will be reported in a future communication. Much greater reactivity was observed, however, when compounds **5** and **6** were treated with NaOMe in refluxing methanol. The formation of three products, which were isolated after 6 h of reaction time, was observed almost immediately.

Based on spectroscopic and X-ray data, these proved to be the 1-methyl-4-dimethoxymethylisoquinoline (**8**) and the isomeric compounds **9** and **10** (R = CH_3). They were obtained, in product ratios of 1:3:1 and 7:1:1, from **5** and **6** respectively. Assignment of the structure of **9** (R = CH_3) is based on X-ray single crystal data, while that of **10** (R = CH_3) is supported by ^{1}H NMR. The stereochemical disposition of the methoxy group in **10** is supported by the nOe (approx. 10%) between the protons of the methyl group at C-3 and on the methoxy group. Such interactions were not observed between the respective groups in **9**. Clearly all three compounds result from a cyclo-

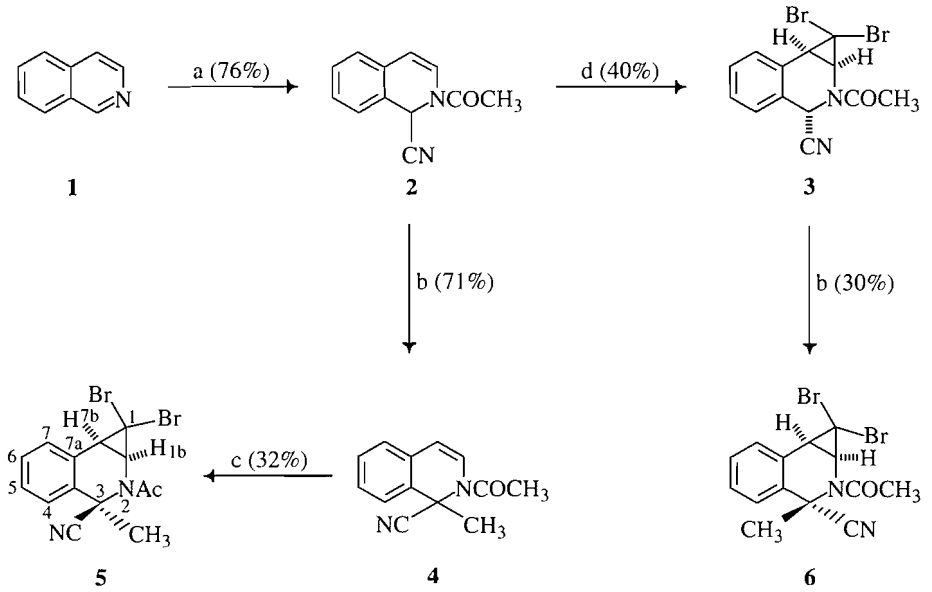
[1]Dedicated to the memory of Professor David Ginsburg, Technion, Israel.

[2]Author to whom correspondence may be addressed.

[3]SmithKline Beecham postdoctoral fellow. Current address: University of Crete, Department of Chemistry, P.O. Box 1470, Iraklion, 71110 Crete, Greece.

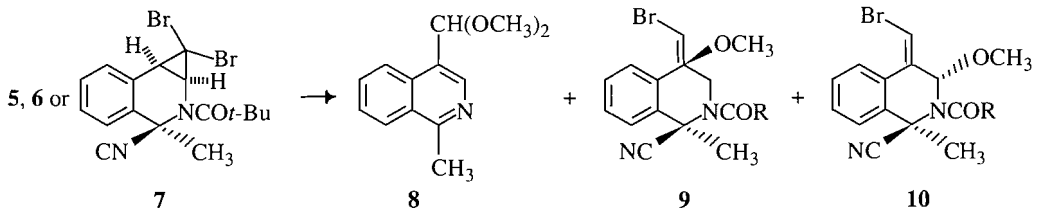
Printed in Canada / Imprimé au Canada

Can. J. Chem. Downloaded from www.nrcresearchpress.com by 198.100.157.202 on 09/07/12
For personal use only.



Reagents: a, AcCl/KCN; b, NaH/CH_3I/DMF; c, $CHBr_3$/$BnEt_3NCl$/NaOH; d, $PhHgCBr_3$/toluene

SCHEME 1



SCHEME 2

propyl fragmentation process wherein the peripheral C—C bond is cleaved in preference to the central bond. It could be demonstrated by further NaOMe treatment that **8** can be derived from **9** and **10** under the reaction conditions. Furthermore, interconversion of **9** and **10** under similar conditions could also be shown.

To examine the steric effect of the acyl substituent on the reaction, pivaloyl compound **7** was also prepared and treated with NaOMe in methanol. No change in the starting material was observed at room temperature, but a slow reaction resulting in the formation of **9** and **10** (R = *t*-butyl) was observed at reflux temperature.

Discussion

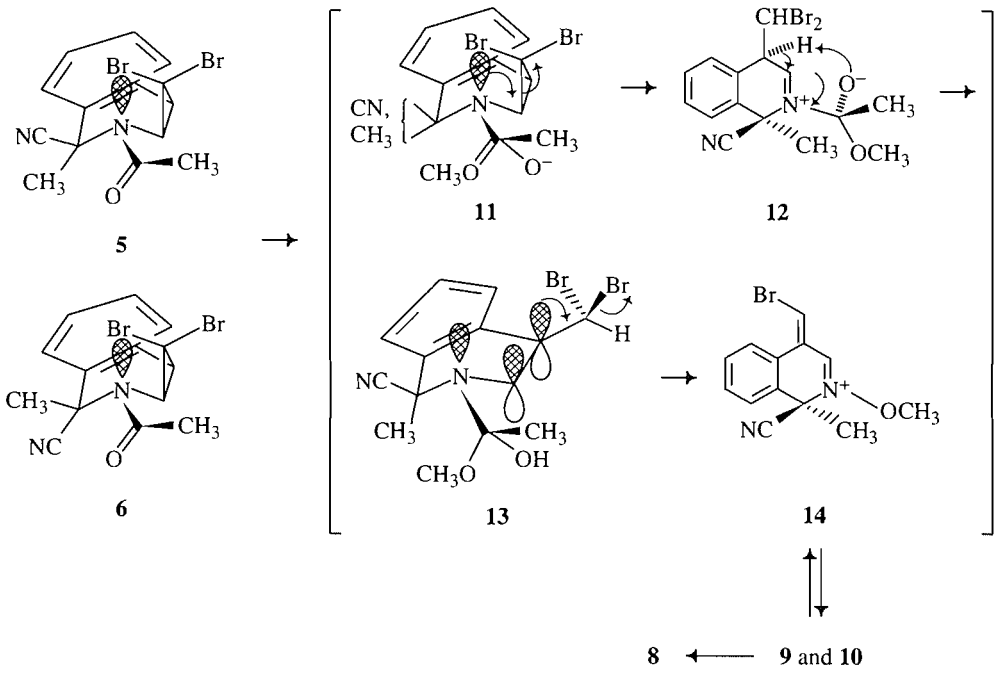
In attempting to arrive at a mechanistic interpretation for the foregoing reaction we considered the following observations: (1) the methoxide appears to be essential for the reaction yet the acetyl (acyl) group remains on the substrate after ring opening; (2) the same two products **9** and **10** are derived from both substrates **5** and **6** although in different amounts; furthermore **9**, the product where the methoxy group is *trans* to the methyl, is obtained in higher yield; and (3) the pivaloyl derivative yielded products of similar structure although displayed less reactivity, reacting only at elevated temperature.

We believe that most or all of these observations can be accommodated by a reaction mechanism involving the cascade of intermediates shown in Scheme 3. Observation 2 is consistent with the penultimate intermediacy of imminium species such as **14**, which can add methoxide from either side of the molecule. Based on steric arguments, this addition will preferentially take place from the side *anti* to the methyl, forming **9** (R = CH_3, *t*-Bu). It is attractive to postulate that **14** arises from intermediate **13**, which, having the least unfavourable 1,3 allylic interactions (6), will eliminate bromide to form the *trans* isomer only.

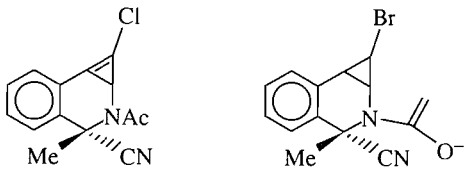
It is more difficult to interpret the role of the methoxide (observation 1) and the mechanism of formation of intermediate **12**. Base-induced cleavage of dihalocyclopropane carbocyclic systems has been previously noted by several authors (7) and the primary formation of cyclopropene-like intermediates (i.e., **15**) has been postulated.

It is unlikely that such intermediates would be involved in our case since their formation would not be greatly retarded by the presence of the bulky pivaloyl group in a position that is quite distant from the reaction center (observation 3) as it is in compound **7**. A second possibility requires formation of the enol **16** and cyclopropyl cleavage proceeding from this species. Again, the fact that the pivaloyl compound undergoes the same type of reaction excludes such an intermediate. The two mechanisms that would allow a satisfactory interpretation of the results appear not to be distinguishable by the data. They are (a) nucleophilic attack of the methoxide at C-1a, or (b) methoxide addition to the acyl carbonyl and formation of a tetrahedral adduct such as **11**, as the species actually suffering the ring cleavage. Based on the known propensity (8) of cyclopropyl compounds to undergo electrophilic ring cleavages, we current-

Can. J. Chem. Downloaded from www.nrcresearchpress.com by 198.100.157.202 on 09/07/12
For personal use only.



SCHEME 3



15 16

ly favour the latter mechanism for the reaction. The consequence of such adduct formation would be the pyramidalization of the nitrogen and this intermediate could undergo spontaneous opening of the cyclopropyl moiety to afford **12**. To gain additional support for this mechanistic proposal we have constructed the most likely conformers of such a tetrahedral adduct using MacroModel 2.5 (9) employing MM2.[4] The dihedral angle between the peripheral breaking bond and the lone pair of nitrogen was determined. It was found that pyramidalization of nitrogen results in significant changes in the molecular geometry with dihedral angles of 2.7° and 3.8° developing for the lone pair of electrons on the nitrogen and the peripheral bond of the cyclopropyl group in compounds **5** and **6** respectively. Such very small angles indicate an almost perfect alignment of the free electron pair with the peripheral bond of the cyclopropyl ring and it may be that such orbital interaction is the reason for the facile formation of 2-substituted isoquinolines rather than the desired 2-benzazepines. The severe steric crowding present in adducts **12** and **13** may lead to a geometry that, according to stereoelectronic considerations (10), would favour expulsion of the methoxide and thus retention of the acetyl (acyl) groups.

One additional comment must be made concerning the chemical behavior of this heterocyclic system. In spite of numerous attempts at conformational calculations, we have thus far been unable to explain the large differences in the reaction profiles between the unsubstituted compounds (which readily undergo ring expansion to benzazepines) and the compounds having 3-substituents (base-promoted reactions of which are detailed in this report). Studies to answer these mechanistic questions are ongoing.

[4]We used MM2 (ref. 11) as implemented by the MacroModel (9).

Experimental

General

Melting points were determined in open capillary tubes on a Thomas–Hoover melting point apparatus and are uncorrected. IR spectra were obtained as liquid films or in Nujol on a Perkin–Elmer 283 spectrophotometer and are expressed as reciprocal centimeters. ^{1}H NMR spectra were obtained in $CDCl_3$ solutions on a Bruker AM 250 MHz spectrometer and are expressed in parts per million downfield from TMS as internal reference. Mass spectra were recorded on a Hewlett Packard 5790 GC/MS or a Finnigan 3625 mass spectrometer.

2-Acetyl-1-methyl-1,2-dihydroisoquinaldonitrile (4)

To a solution of the Reissert compound **2** (2) (4.95 g, 0.025 mol) and methyl iodide (3.9 g, 0.028 mol) in DMF (100 mL) was added sodium hydride (0.66 g, 0.028 mol) over 1 h with cooling. The solution was stirred for 2 h at room temperature, diluted with ether, washed with water and brine, dried over magnesium sulfate, filtered, and the solvent was removed *in vacuo* to yield the crude product. This was treated with hexane to give 4.87 g (92%) of crystalline **4**; mp 73.5–74.5°C (lit. (2) mp 95–96.5°C). IR ν_{max}: 2230, 1685, 1640, 1315, 1265; ^{1}H NMR: 7.65–7.61 (m, 1H), 7.31–7.27 (m, 2H) 7.04–7.03 (m, 1H), 6.54 (d, J = 7.5 Hz, 1H), 5.77 (d, J = 7.5 Hz, 1H), 2.32 (s, 3H), 1.88 (s, 3H); mass spectrum, *m/e*: 212.

anti-*2-Acetyl-1,1-dibromo-3-methyl-1a,2,3,7b-tetrahydro-1H-cycloprop[c]isoquinaldonitrile (5)*

To a solution of **4** (1.5 g, 0.0071 mol) and benzyltriethyl ammonium chloride (1.0 g, 0.004 mol) in bromoform (20 mL) was added a 40% aqueous sodium hydroxide solution (20 mL) over 30 min with cooling. The solution was allowed to reach room temperature and was stirred overnight. It was diluted with ether, washed with water and brine, dried over magnesium sulfate, filtered, and the solvent was removed *in vacuo* to give a yellow residue that was purified by chromatography over silica gel using 1:1 ether–petroleum ether as eluent. Evaporation of the solvent afforded pure product **5** (860 mg, 31.5%), mp 191–193°C. IR ν_{max}: 2260, 1660, 1300, 1190; ^{1}H NMR: 7.74–7.40 (m, 1H) 7.46–7.39 (m, 3H), 4.02 (d, J = 10 Hz, 1H), 3.27 (d, J = 10 Hz, 1H), 1.82 (s, 3H), 1.51 (s, 3H); mass spectrum, *m/e*: 382. X-ray structural data available on request.

Can. J. Chem. Downloaded from www.nrcresearchpress.com by 198.100.157.202 on 09/07/12
For personal use only.

Can. J. Chem. Downloaded from www.nrcresearchpress.com by 198.100.157.202 on 09/07/12
For personal use only.

Reaction of anti-*2-acetyl-1,1-dibromo-3-methyl-1a,2,3,7b-tetrahydro-1*H*-cycloprop[c]iso quinaldonitrile (5) with sodium methoxide in methanol at room temperature*

A solution of **5** (670 mg, 0.0017 mol) and sodium methoxide (470 mg, 0.008 mol) in methanol (10 mL) was stirred at room temperature for 100 h. The solvent was removed *in vacuo* and the residue was rapidly passed through a silica gel column using 70% ether in petroleum ether as eluent to give 92 mg (14%) of starting material, 179 mg (32%) of compound **9**, 99 mg (17%) of compound **10**, and 30 mg (8%) of compound **8**, characterized by the following spectral analysis. **8**: IR ν_{max}: 2920, 1665, 1285, 1125; ^{1}H NMR: 8.53 (s, 1H), 8.32 (dd, J = 7.6 and 0.8 Hz, 1H), 8.17 (dd, J = 6.4 and 0.9 Hz, 1H), 7.74 (td, J = 5.6 and 1.4 Hz, 1H), 7.63 (td, J = 5.6 and 1.4 Hz, 1H), 5.8 (s, 1H), 3.40 (s, 3H), 3.00 (s, 3H); mass spectrum, *m/e* 217. Anal. calcd. for $C_{13}H_{15}NO_2$: C 71.87, H 6.96, N 6.45; found: C 71.65, H 7.18, N 6.47. **9**: IR ν_{max}: 2240, 1680, 1390, 1310, 1070; ^{1}H NMR: 8.02 (dd, J = 7.4 and 1.6 Hz, 1H), 7.82 (dd, J = 6.95 and 1.45 Hz, 1H), 7.52–7.43 (m, 2H), 6.74 (s, 1H), 5.29 (br s, 1H), 3.15 (s, 3H), 2.39 (s, 3H), 1.87 (s, 3H); mass spectrum, *m/e*: 334. Anal. calcd. for $C_{15}H_{14}N_2O_2Br$: C 53.91, H 4.22, 8.38; found: C 53.81, H 4.59, N 8.38. X-Ray structural data available on request. **10**: IR ν_{max}: 2240, 1680, 1395, 1310, 1065; ^{1}H NMR: 8.18 (dd, J = 6.2 and 1.4 Hz, 1H), 7.66 (dd, J = 6.0 and 1.8 Hz, 1H), 7.53–7.44 (m, 2H), 6.71 (s, 1H), 5.42 (br s, 1H), 3.21 (s, 3H), 2.38 (s, 3H), 2.13 (s, 3H); mass spectrum, *m/e*: 334. Anal. calcd. for $C_{15}H_{14}N_2O_2Br$: C 53.91, H 4.22, N 8.38; found: C 54.22, H 4.55, N 8.52.

Reaction of anti-*2-acetyl-1,1-dibromo-3-methyl-1a,2,3,7b-tetrahydro-1*H*-cycloprop[c]isoquinaldonitrile (5) with sodium methoxide in methanol at reflux temperature*

A solution of **5** (0.100 g, 0.25 mmol) and sodium methoxide (0.068 g, 1.2 mmol) in dry methanol (5 mL) was heated under reflux for 6 h). The solution was treated as described above to give **9**, 37 mg (39%), **10**, 11 mg (11.4%), and **8**, 8 mg (15%).

*Preparation of 2-acetyl-1,1-dibromo-1a,2,3,7b-tetrahydro-1*H*-cycloprop[c] -isoquinaldonitrile (3)*

A solution of **2** (0.99 g, 0.005 mol) and phenyltribromomethyl mercury (2.64 g, 0.005 mol) in toluene (50 mL) was heated at 80°C for 2.5 h. The precipitated phenylmercuric chloride was removed by filtration and the solvent was removed *in vacuo*. The residue was crystallized from ether–hexane to yield 745 mg (40%) of pure **3**, mp 174–175°C. IR ν_{max}(Nujol): 2260, 1695, 1340, 810, 580; ^{1}H NMR: 7.59–7.27 (m, 4H), 6.19 (s, 1H), 3.90 (d, J = 9.3 Hz, 1H), 3.37 (d, J = 9.3 Hz, 1H), 2.39 (s, 3H); mass spectrum, *m/e*: 368. Anal. calcd. for $C_{13}H_{10}N_2OBr_2$: C 42.19, H 2.72, N 7.57; found: C 43.08, H 2.83, N 7.91.

syn-*2-Acetyl-1,1-dibromo-3-methyl-1a,2,3,7b-tetrahydro-1*H*-cycloprop[c] isoquinaldonitrile (6)*

Compound **3** (1.38 g, 0.004 mol) was dissolved in DMF (40 mL) and the solution was cooled to −30°C. Sodium hydride (0.090 g, 0.004 mol) was added in one portion, and the suspension was stirred for 1 min. Methyl iodide (0.57 g, 0.004 mol) was added and the reaction was allowed to reach room temperature over 2 h. It was then diluted with ether, washed with water and brine, dried over anhydrous magnesium sulfate, filtered, and the solvent was removed *in vacuo* to yield the crude **6**, which was purified by chromatography over silica gel (50% ether in pet. ether). Evaporation of the solvent yielded 630 mg of the oily product **6** (45%), mp 150–151°C. IR ν_{max}: 2255, 1690, 1315, 780, 590; ^{1}H NMR: 7.51–7.39 (m, 4H), 3.77 (d, J = 10.2 Hz, 1H), 3.26 (d, J = 10.2 Hz, 1H), 2.41 (s, 3H), 2.20 (s, 3H); mass spectrum, *m/e*: 382.

Reaction of syn-*2-acetyl-1,1-dibromo-3-methyl-1a,2,3,7b-tetrahydro-1*H*-cycloprop[c] isoquinaldonitrile (6) with sodium methoxide in methanol at reflux temperature*

A solution of **6** (0.192 g, 0.5 mmol) and sodium methoxide (0.135 g, 2.5 mmol) in methanol (5 mL) was heated under reflux for 6 h. The GC/MS spectrum of the reaction indicated the formation of **8**:**9**:**10** in the 7:1:1 ratio.

Preparation of 2-[(1,1,1-trimethyl)acetyl]-1,2-dihydroisoquinaldonitrile

To a mixture of isoquinoline (64.5 g, 0.5 mol) and potassium cyanide (97.5 g, 1.5 mol) in methylene chloride (625 mL) and water (250 mL) was added 1,1,1-trimethyl acetyl chloride (120.6 g, 1.0 mol) at 0°C, over a 1 h period with vigorous stirring. The reaction was stirred at room temperature for 24 h, diluted with methylene chloride, and washed in a sequential order with water, dilute hydrochloric acid, water, dilute sodium hydroxide, water, and brine. The organic layer was separated, dried over anhydrous magnesium sulfate, and the solvent was removed to give a brown residue. This residue was purified by flash chromatography on silica gel using 50% ether in petroleum ether as eluent; 700 mg (1%) of the product was obtained, mp 110–111°C; 17.23 g (27%) of isoquinoline was also isolated. IR ν_{max}: 2215, 1655, 1620, 1170, 770; ^{1}H NMR: 7.37–7.27 (m, 3H), 7.20 (d, J = 6.2 Hz, 1H), 7.06 (d, J = 7.8 Hz, 1H), 6.59 (s, 1H), 6.09 (d, J = 7.8 Hz, 1H), 1.25 (s, 9H); mass spectrum, *m/e*: 240. Anal. calcd. for $C_{15}H_{16}N_2O$: C 74.97, H 6.71, N 11.66; found: C 75.45, H 6.75, N 11.81.

2-[(1,1,1-Trimethyl)acetyl]-1-methyl-1,2-dihydroisoquinaldonitrile

To a solution of 2-[(1,1,1-trimethyl)acetyl]-1,2-dihydroisoquinaldonitrile (0.7 g, 3.0 mmol) and methyl iodide (0.47 g, 3.3 mmol) in dimethylformamide (6 mL) was added sodium hydride (60% oil, 0.13 g, 3.3 mmol), and the product was isolated according to the procedure for the preparation of **4**. The product yield was 615 mg (81%), mp 109–109.5°C. IR ν_{max}: 1745, 1675, 1500, 780; ^{1}H NMR: 7.69–7.64 (m, 1H), 7.30–7.27 (m, 2H), 7.07–7.03 (m, 1H), 6.81 (d, J = 8.1 Hz, 1H), 5.77 (d, J = 8.1 Hz, 1H) 1.84 (s, 3H), 1.39 (s, 9H); mass spectrum, *m/e*: 254. Anal. calcd. for $C_{16}H_{18}N_2O$: C 75.56, H 7.13, N 11.01; found: C 75.55, H 7.11, N 10.63.

anti-*2-[(1,1,1-trimethyl)acetyl]-1,1-dibromo-3-methyl-1a,2,3,7b-tetrahydro-1*H*-cycloprop[c]isoquinaldonitrile (7)*

A mixture of the methyl-quinaldonitrile prepared in the previous experiment (0.51 g, 2.0 mmol) and benzyl triethylammonium chloride (0.25 g, 1.1 mmol) in bromoform (4.0 mL) was treated with 40% sodium hydroxide solution (4.0 mL) at room temperature for 24 h and the product was isolated as described for the preparation of **5**. The product was crystallized from ether, affording 105 mg (12.4%), mp 177–178°C. IR ν_{max}: 3100, 2243, 1662, 766; ^{1}H NMR: 7.7 (d, J = 6.7 Hz, 1H), 7.46–7.39 (m, 3H), 4.03 (d, J = 10.2 Hz, 1H), 3.27 (d, J = 10.2 Hz, 1H), 1.82 (s, 3H) 1.51 (s, 9H); mass spectrum, *m/e*: 424. Anal. calcd. for $C_{17}H_{18}N_2OBr_2$: C 47.91, H 4.26, N 6.57; found: C 48.50, H 4.39, N 6.67.

Reaction of anti-*2-[(1,1,1-trimethyl)acetyl]-1,1-dibromo-3-methyl-1a,2,3,7b-tetrahydro-1*H*-cycloprop[c]isoquinaldonitrile with sodium methoxide in methanol at reflux temperature*

To a solution of **7** (25 mg, 0.06 mmol) in methanol (3 mL) was added sodium methoxide (16 mg, 0.3 mmol) and the reaction was stirred at ambient temperature for 73 h. GC/MS and TLC monitoring indicated the presence of only starting material. The solution was then heated under reflux and after 4 h the GC/MS assay indicated the presence of **9** and **10** (R = *t*-butyl) and of the acetal **8** in a 7.5:5.8:1 ratio. The solvent was removed *in vacuo* and the products were separated on a 60F-254 silica gel analytical plate using 2% acetone in toluene as eluent to give **9**, 3.6 mg (16%), and **10**, 3.4 mg (15%). Spectral data: **9**: IR ν_{max}: 1663; ^{1}H NMR: 8.10 (d, J = 7.6 Hz, 1H), 7.81 (d, J = 7.6 Hz, 1H), 7.55 (d, J = 7.6 Hz, 1H), 7.49 (d, J = 7.6 Hz, 1H), 6.69 (s, 1H), 5.64 (s, 1H), 3.04 (s, 3H), 2.12 (s, 3H), 1.40 (9H, s, 9H); mass spectrum, *m/e*: 376; **10**: IR ν_{max}: 2237, 1663, 1066; ^{1}H NMR: 8.22 (d, J = 7.6 Hz, 1H), 7.67 (d, J = 7.6 Hz, 1H), 7.52 (d, J = 7.8 Hz, 1H), 7.46 (d, J = 7.8 Hz, 1H), 6.67 (s, 1H), 5.74 (s, 1H), 3.04 (s, 3H), 2.11 (s, 3H), 1.25 (s, 9H); mass spectrum, *m/e*: 376.

Acknowledgements

The authors wish to express their indebtedness to Ms. Edith Reich of the Analytical Chemistry Department for the elemental analyses, to Mr. Lewis Killmer of the Analytical Chemistry

Department for mass spectral analyses, and to Dr. Drake Eggleston of the Physical and Structural Chemistry Department for the X-ray structural determinations.

1. (*a*) I. LANTOS, B. BHATTACHARJEE, and D. S. EGGLESTON. J. Org. Chem. **51**, 4147 (1986); (*b*) C. PERCHONOCK, I. LANTOS, J. A. FINKELSTEIN, and K. G. HOLDEN. J. Org. Chem. **45**, 1950 (1980).
2. H. W. GIBSON. J. Heterocycl. Chem., **7**, 1169 (1970).
3. P. WEYERSTAHL. *In* The chemistry of functional groups: dihalocyclopropanes. *Edited by* S. Patai and Z. Rappoport. Wiley, U.K. 1983. Suppl. D.
4. (*a*) D. SEYFERTH, J. M. BURLITCH, and J. K. HEEREN. J. Org. Chem. **27**, 1491 (1962); (*b*) D. SEYFERTH. Acc. Chem. Res. **5**, 65 (1972).
5. S. WOLFE. Acc. Chem. Res. **5**, 102 (1972).
6. F. JOHNSON. Chem. Rev. **68**, 375 (1968).
7. (*a*) C. W. REES and C. E. SMITHEN. Adv. Heterocycl. Chem. **3**, 57 (1964); (*b*) A. R. BROWNE and B. HALTON. Tetrahedron, **33**, 345 (1977); (*c*) W. E. BILLUPS and L. E. REED. Tetrahedron Lett. **34**, 2239 (1977); (*d*) J. ARCT and B. MIGAJ. Tetrahedron Lett. **37**, 953 (1980); (*e*) J. M. CONIA. Pure Appl. Chem. **43**, 317 (1975).
8. (*a*) A. DE MEIJERE. Angew. Chem. Int. Ed. Engl. **18**, 809 (1979); (*b*) N. Y. LUKINA. Russ. Chem. Rev. **31**, 419 (1962).
9. F. MOHAMADI, N. G. J. RICHARDS, W. C. GUIDA, R. LISKAMP, M. LIPTON, C. CAUFIELD, G. CHANG, and W. C. STILL. Macro-Model 2.5: Department of Chemistry, Columbia University, New York, NY.
10. P. DESLONGCHAMPS. Stereoelectronic effects in organic chemistry. Pergamon Press, New York. 1983.
11. N. ALLINGER. J. Am. Chem. Soc. **99**, 8127 (1977).

Can. J. Chem. Downloaded from www.nrcresearchpress.com by 198.100.157.202 on 09/07/12
For personal use only.

A. McAuley, S. Subramanian, and T. W. Whitcombe. Synthesis and crystal structure of an octahedral nickel(II) complex derived from pentaerythrityl tetraamine. Can. J. Chem. **67**, 1650 (1989).

Page 1653, Table 2, x/a for O(1) should read -1995.

Can. J. Chem. Downloaded from www.nrcresearchpress.com by 198.100.157.202 on 09/07/12
For personal use only.

The conformational distribution of 2-cyanobenzaldehyde and 3-cyanobenzaldehyde in solution and in the vapor

TED SCHAEFER,[1] KERRY J. COX, AND RUDY SEBASTIAN
Department of Chemistry, University of Manitoba, Winnipeg, Man., Canada R3T 2N2

Received August 9, 1990

TED SCHAEFER, KERRY J. COX, and RUDY SEBASTIAN. Can. J. Chem. **69**, 1039 (1991).

The ^{1}H nuclear magnetic resonance spectra of 2-cyanobenzaldehyde (2CNB) and 3-cyanobenzaldehyde (3CNB) in CS_2/C_6D_{12} and acetone-d_6 solutions at 300 K yield precise stereospecific long-range proton–proton coupling constants. These are used to establish the conformational population of the *o-cis* and *o-trans* conformers of these relatively polar molecules. For example, the fractional *o-cis* population of 2CNB changes from 0.12(4) in CS_2/C_6D_{12} to 0.46(6) in acetone-d_6, whereas that of 3CNB is 0.48(2) in both solvents. Extrapolation to the vapor phase, using a dielectric model, implies a negligible concentration of the *o-cis* conformer of 2CNB and a roughly 50% abundance of each conformer of 3CNB. Computations at various levels of molecular orbital theory provide estimates of the rotational barrier of the aldehyde moiety and confirm the planar structure of each conformer. The geometries of three conformers are given as obtained from the 6-31G MO basis and may be useful to molecular spectroscopists. Theoretical and experimental dipole moments are interpolated to yield estimates of their magnitudes for the four planar conformers. Somewhat less precise ^{1}H nmr spectral parameters (than for the above solutions) are also obtained for dilute solutions in benzene-d_6 at 300 K. The conformational distributions based on these parameters are compared with their only other measurement, based on dipolar moments in benzene at 298 K. Good agreement between the results of the two methods is found for 3CNB but not for 2CNB. It is suggested that specific interactions occur between benzene solvent and solute molecules, particularly for 3CNB, for which these interactions stabilize the conformer having a low dipole moment. Remarkable changes in the intraring proton–proton coupling constants occur in going from CS_2/C_6D_{12} to acetone-d_6 solution.

Key words: 2- and 3-cyanobenzaldehyde (2CNB and 3CNB): ^{1}H NMR, conformations, long-range spin–spin coupling constants, MO computations.

TED SCHAEFER, KERRY J. COX et RUDY SEBASTIAN. Can. J. Chem. **69**, 1039 (1991).

Les spectres de résonance magnétique nucléaire du ^{1}H du 2-cyanobenzaldéhyde (2CNB) et du 3-cyanobenzaldéhyde (3CNB), mesurées à 300 K, dans des solutions dans le CS_2/C_6D_{12} et dans l'acétone-d_6, fournissent des constantes de couplage proton–proton à longue distance très précise. On les a utilisées pour déterminer les populations conformationnelles des conformères *o-cis* et *o-trans* de ces molécules relativement polaires. Par exemple, la fraction de la population *o-cis* du 2CNB varie de 0,12(4) dans le CS_2/C_6D_{12} à 0,46(6) dans l'acétone-d_4; par ailleurs, celle du 3CNB est égale à 0,48(2) dans les deux solvants. Une extrapolation jusqu'à la phase vapeur, utilisant un modèle diélectrique, suggère que la concentration du conformère *o-cis* du 2CNB est alors négligeable, mais que celle du 3CNB est approximativement égale à 50%. Des calculs à divers niveaux de la théorie des orbitales moléculaires fournissent des évaluations de la barrière à la rotation de la portion aldéhydique et confirment la structure planaire de chaque conformère. Les géométries de trois conformères ont été évaluées sur la base d'OM 6-31G; elles pourraient être utiles aux spectroscopistes moléculaires. On a interpolé les moments dipolaires théoriques et expérimentaux pour obtenir des évaluations de leurs amplitudes pour les quatre conformères. On a aussi déterminé des paramètre spectraux (moins précis que ceux obtenus plus haut) de la rmn du ^{1}H, à 300 K, pour des solutions diluées dans le benzène-d_6. On compare les distributions conformationnelles déterminées à l'aide de ces paramètres avec celles obtenues à l'aide de leur seule autre mesure basée sur les moments dipolaires dans le benzène, à 298 K. Pour le 3CNB, on a observé un bon accord entre les résultats de ces deux méthodes; ce n'est toutefois pas le cas avec le 2CNB. On suggère que des interactions spécifiques se produisent entre les molécules du solvant (benzène) et du soluté, particulièrement avec le 3CNB, pour lequel ces interactions stabiliseraient le conformère de faible moment dipolaire. Il se produit des changements remarquables dans les constantes de couplage proton–proton intracycliques lorsqu'on passe des solutions dans le CS_2/C_6D_{12} à celles dans l'acétone-d_6.

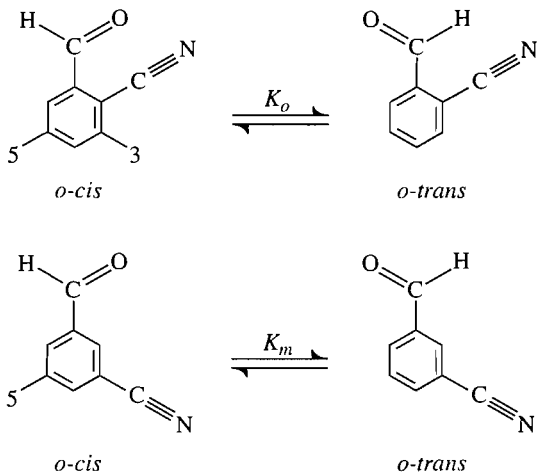
Mots clés : 2- et 3-cyanobenzaldéhyde (2CNB et 3CNB) : RMN ^{1}H, conformations, constantes de couplage proton–proton à longue distance, calculs d'OM.

[Traduit par la rédaction]

Introduction

The spin–spin coupling constant between the aldehydic and *meta* protons in benzaldehyde and its derivatives is stereospecific (1), is apparently a pure σ electron mediated interaction for effectively planar molecules (2), and, when measured with precision, is perhaps the most sensitive indicator available for the *cis–trans* equilibria for *ortho* and *meta* substituted benzaldehydes in solution (3). The detailed discussion of ^5J(H-*m*, CHO) in 2- and 3-fluorobenzaldehyde (3) may be consulted for a comparison with other techniques for this purpose.

In the present report, this coupling constant is used to find the conformational equilibria for 2-cyanobenzaldehyde (2CNB) and 3-cyanobenzaldehyde (3CNB) as solutions in a nonpolar CS_2/C_6D_{12} solvent mixture as well as in the polar solvent,



[1]Author to whom correspondence may be addressed.

Can. J. Chem. Downloaded from www.nrcresearchpress.com by 84.41.108.74 on 09/07/12
For personal use only.

TABLE 1. The ^{1}H nmr spectral data for 2-cyanobenzaldehyde and 3-cyanobenzaldehyde at 300 K

Parameter	Compound			
	2CNB (CS_2)[a]	2CNB (acetone)[b]	3CNB (CS_2)[c]	3CNB (acetone)[b]
ν(CHO)	3099.799[d]	3083.554	2965.010	3036.289
ν_2	—	—	2370.223	2493.900
ν_3	2320.561	2400.530	—	—
ν_4	2304.404	2375.044	2299.370	2430.330
ν_5	2312.081	2387.770	2208.984	2356.567
ν_6	2399.714	2439.262	2317.614	2474.964
$^3J_{34}$	7.709(2)[e]	7.703	—	—
$^3J_{45}$	7.520	7.602	7.929	7.735
$^3J_{56}$	7.847	7.797	7.617	7.820
$^4J_{24}$	—	—	2.054	1.701
$^4J_{26}$	—	—	1.497	1.623
$^4J_{35}$	1.229(2)	1.206	—	—
$^4J_{46}$	1.340(2)	1.307	1.103	1.211
$^5J_{25}$	—	—	0.447	0.642
$^5J_{36}$	0.588	0.562	—	—
^4J(2,CHO)	—	—	−0.087	−0.072
^4J(6,CHO)	−0.099	−0.130	−0.133	−0.115
^5J(3,CHO)	0.098	0.378	—	—
^5J(5,CHO)	0.796	0.480	0.454	0.451
^6J(4,CHO)	−0.010(2)[f]	−0.009[g]	0.000[h]	−0.001[i]
Calcd. transitions	100	92	80	80
Assigned transitions	72	72	74	73
Peaks observed	66	73	59	62
Largest difference	0.008	0.005	0.002	0.002
Root-mean-square deviation	0.003	0.002	0.001	0.001

[a]A saturated solution in CS_2, being considerably less than 2 mol% in 2CNB, containing also 10 mol% of C_6D_{12}, and 0.5 mol% of TMS.
[b]4.0 mol% in acetone-d_6, containing also 0.5 mol% of TMS.
[c]4.0 mol% in CS_2, containing also 10 mol% of C_6D_{12} and 0.5 mol% of TMS.
[d]The ^{1}H nmr chemical shifts are in Hz at 300.135_2 MHz to high frequency of internal TMS.
[e]Standard deviations in the last significant figure are all less than or equal to 0.001, except for those given in parentheses.
[f]Simulations with various values imply that $-0.020 < {}^6J(4,CHO) < 0.000$ Hz.
[g]Appears to be negative or, possibly, zero, by simulation; see Fig. 1.
[h]Simulations suggest $-0.015 < {}^6J(4,CHO) < 0.020$ Hz.
[i]Again, spectral simulations imply that $-0.010 < {}^6J(4,CHO) < 0.010$ Hz.

Can. J. Chem. Downloaded from www.nrcresearchpress.com by 84.41.108.74 on 09/07/12
For personal use only.

acetone-d_6. Rough estimates are made for these equilibria in the vapor phase on the basis of a dielectric model and of some molecular orbital calculations. It turns out that the equilibrium for 2CNB is remarkably solvent dependent, compared to other *ortho* substituted benzaldehydes; that for 3CNB is much less dependent on solvent. The only previous work on these equilibria appears to be a study of the dipole moments in benzene solution (4); this solvent is chosen because of the low solubility of these compounds in CCl_4. It is concluded that 2CNB exists predominantly, perhaps exclusively, in the *o-trans* form whereas the *o-cis* conformer of 3CNB is present to the extent of 35 ± 2% at 298 K (4).

Experimental

2CNB from TCI and 3CNB from Aldrich were dissolved as dilute solutions (see Table 1 for details) in CS_2/C_6D_{12}/TMS and acetone-d_6/TMS solvent mixtures. These solutions were filtered into 5 mm o.d. nmr sample tubes, which were degassed by five freeze–pump–thaw cycles and were flame-sealed at the pump stage of the last cycle. The ^{1}H nmr spectra were acquired on a Bruker AM 300 spectrometer at a probe temperature of 300 K and in a manner previously described in detail (5). The digital resolution was at least 0.006 Hz/pt, acquisition times for the 32 or more free induction decays were 41–60 s. Line and Gaussian broadening parameters, typically −0.1 and 0.6, respectively, were applied to the decays before Fourier transformation. Care was taken to establish a persistently homogeneous external magnetic field; manual shimming on the TMS signal was necessary for this purpose. Some ^{1}H nmr spectra of 2CNB and 3CNB were also obtained for solutions in benzene-d_6.

Molecular orbital calculations were performed with the computer program Gaussian 86 (6), details of which can be found at appropriate places in the discussion to follow. The computations employed an Amdahl 5870 system.

Results and discussion

Spectral analyses

The ^{1}H nmr spectra of 2CNB and 3CNB were analyzed with the computer program NUMARIT (7), extensively modified by R. Sebastian in this laboratory. Table 1 contains the chemical shifts and proton–proton coupling constants obtained from the analyses. Figure 1 displays the aldehydic proton spectrum of 2CNB in acetone-d_6 solution, together with some theoretical simulations described in the figure caption.

The conformational equilibria of 2CNB and 3CNB in CS_2/C_6D_{12} and acetone-d_6 solutions

As stated above, ^5J(H, CHO) ≡ ^5J is stereospecific. In benzaldehyde, ^5J is 0.431(2) and 0.430(1) Hz in CS_2/C_6D_{12} and acetone-d_6, respectively (2). As discussed in detail previously (3), all the available evidence implies that ^5J vanishes for a conformation such as *o-cis* in 3CNB and that it has its maximum value for the *o-trans* orientation. The barrier to rotation about

Can. J. Chem. Downloaded from www.nrcresearchpress.com by 84.41.108.74 on 09/07/12
For personal use only.

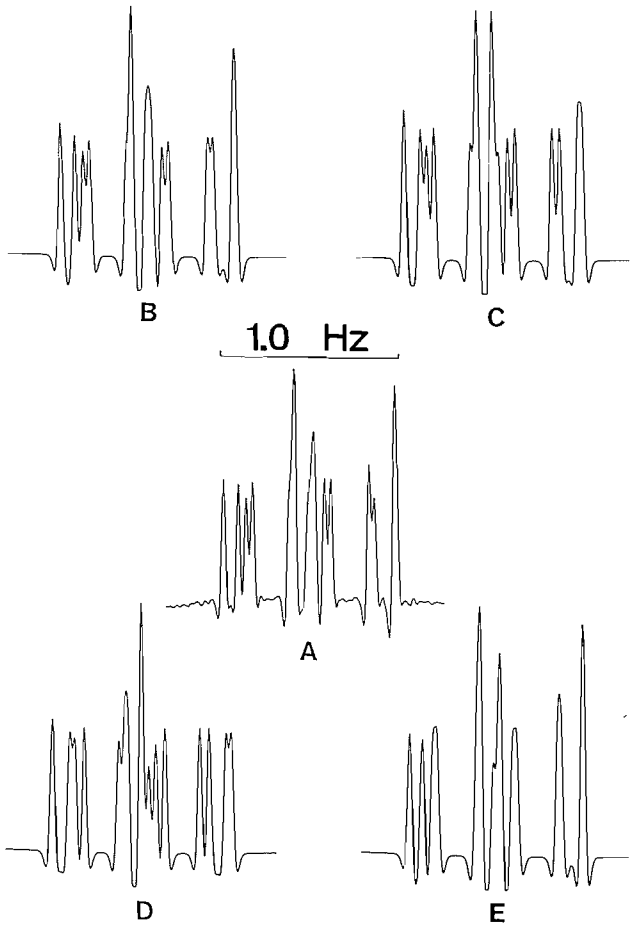


FIG. 1. In A the aldehydic ^{1}H nmr spectrum of a 4 mol% solution of 2CNB in acetone-d_6 is displayed. The width at half-height of single peaks, after some resolution enhancement, is near 0.03 Hz. In B the computed spectrum employs the chemical shifts and coupling constants in Table 1; in particular, ^6J(H-4,CHO) is −0.009 Hz. The agreement between the calculated and measured spectra is not exact, but is rather better than for the theoretical spectrum in C, which assumes ^6J(H-4,CHO) as 0.000 Hz, or for that in D, which is based on +0.010 Hz for this coupling constant. In E the simulated spectrum has ^6J(H-4,CHO) as −0.020 Hz.

the exocyclic Csp^2—Csp^2 bond for benzaldehyde is about 30 kJ/mol, so that a discussion in terms of planar conformations is a good approximation at ambient temperatures. Accordingly, for benzaldehyde one may write $^5J_3 \equiv {}^5J$(H-3, CHO) = 0.861(3) Hz for a conformer analogous to *o-cis* in 3CNB, and that $^5J_5 \equiv {}^5J$(H-5,CHO) vanishes.

In 3CNB, ^5J is essentially the same, or 0.452(3) Hz, in both solvents of Table 1. If the maximum in ^5J is independent of the cyano substituent then the fractional population of the *o-trans* form follows as 0.452(3)/0.861(3) or 0.52(1); K_m is therefore 1.08(4) at 300 K and the free energy difference favoring the *o-trans* form is 0.2(1) kJ/mol. That a ring substituent, not directly bonded to a carbon atom in the coupling pathway, does not significantly perturb ^5J is suggested, for example, by the effective identity of ^5J in benzaldehyde (2) and its 4-fluoro derivative (unpublished work in this laboratory). Even if the ring substituent is placed adjacent to the coupling path, it appears at first that large perturbations of ^5J do not occur.

Thus, for 2CNB in acetone-d_6 solution, the sum of the ^5J values is 0.858(2) Hz, compared to 0.860(2) for benzaldehyde (2). K_m follows as 1.27(3) and, at 300 K, the free energy of the *o-trans* is 0.60(5) kJ/mol lower than that of the *o-cis* conformer. In CS_2 solution, however, the two ^5J values sum to 0.894(2) Hz, substantially higher than the 0.862(2) Hz for benzaldehyde (2). If the extrema in $^5J_3$ and $^5J_5$ are both taken as 0.894(2) Hz, then K_o follows as 8.2(2), the fractional population of the *cis* conformer being 0.11 and the free energy difference between the conformers, 5.2(1) kJ/mol at 300 K. The, in our experience, rather large deviation of the sum of the ^5J values from its value in benzaldehyde is somewhat unsettling. An attempt at an assessment of the indicated intrinsic substituent effect on ^5J goes as follows. Define $^5J_{3,c}$ and $^5J_{5,t}$ as the ^5J numbers in the *o-cis* and *o-trans* forms of 2CNB; the other two, antizigzag, ^5J values vanish. Hence, for the two solutions, there exist four equations in four unknowns. These are the fractional populations of, say, the *trans* forms and $^5J_{3,c}$ and $^5J_{5,t}$, assumed to be independent of solvent. $^5J_{5,t}$ and $^5J_{3,c}$ follow as 0.907 Hz and 0.803 Hz, respectively, and the fractional population of the *trans* form as 0.88 in the CS_2/C_6D_{12} mixture and as 0.53 in the acetone-d_6 solution. Hence K_o is 7.2 in the former and 1.13 in the latter solution, corresponding to free energy advantages of 4.9 and 0.3 kJ/mol, respectively. Comparison of these magnitudes with those derived above suggests an uncertainty of 0.3 kJ/mol in the derived energy differences. In the light of a referee's remarks, the discussion in the following sections doubles this uncertainty and takes the free energy differences as $0.4_5 \pm 0.6$ and $5.0_5 \pm 0.6$ kJ/mol in the polar and nonpolar media, respectively.

It is interesting that $^5J_{5,t}$ is implied as larger than in benzaldehyde by about 0.05 Hz or 6%. True, in the *o-trans* conformer of 2CNB the very polar cyano group (the dipole moment of cyanobenzene is 4.0 D(8) compared, for example, to 1.4 D for fluorobenzene) lies parallel to the C—H bond of the aldehydic moiety and its dipolar field will act to polarize it in the sense C^-—H^+. This polarization is demonstrated by the chemical shift of the aldehydic proton (Table 1) in CS_2 solution and will be discussed below. An indication of the change in ^5J caused by such a perturbation of the charge distribution was sought from CNDO/2 and INDO MO FPT (9, 10) computations, done for the optimized STO 3G geometries. Indeed, $^5J_{5,t}$ was calculated as 0.926 Hz and $^5H_{3,c}$ as 0.842 Hz, with the CNDO/2 parametrization, in qualitative support of the treatment above. ^5J_t in benzaldehyde is calculated as 0.90 Hz and ^5J_c as 0.02 Hz. The two conformers are highly polar, the dipole moments being estimated in a later section as 6.2 and 4.5 D for the *o-cis* and *o-trans*, respectively. Hence a significant perturbation of the charge distribution in the aldehydic moiety by internal fields is perhaps feasible, leading to the implied perturbations in the extrema of ^5J. Of course, the apparent agreement between the above model and the computations may be coincidental. In any event, the uncertainty introduced into the populational distribution by such perturbations is reasonably small in solution. Extrapolation to the vapor will tend to amplify this uncertainty. Fortunately, as seen next, the bias in favor of the *o-trans* conformer of 2CNB in the vapor at ambient temperatures is very large indeed.

The conformer distribution in the vapor by extrapolation

(i) 2-Cyanobenzaldehyde

To a first approximation in the reaction field model of medium effects on conformational equilibria (11), the more polar conformer is stabilized relative to the less polar conformer

Can. J. Chem. Downloaded from www.nrcresearchpress.com by 84.41.108.74 on 09/07/12
For personal use only.

in a medium of dielectric constant, ϵ, greater than unity; the stabilization energy is proportional to $(\epsilon - 1)/(2\epsilon + 1) \equiv x$. The dipole moment of the *o-cis* conformer of 2CNB is clearly higher than that of the other conformer, so that the increased population of the former in the more polar solvent, acetone-d_6, is expected. A quantitative calculation of the stabilization energies requires the dipole moments of the conformers, which must be estimated or computed. Furthermore, in second order the electric quadrupole moment of each conformer must be known in order to find the quadrupolar contributions to the energy of interaction with the dielectric medium; these contributions are also proportional to x. Additional interactions are also considered on occasion (11). The model has been rather successful in accounting for the relative conformer energies of polar cyclic and acyclic polar alkane derivatives in various solvents (11). With polar aromatic systems, our own experience (12) is that quantitative reproduction of relative conformer energies in solution is difficult, perhaps because of errors in the estimation of dipole and quadrupole moments; the squares of these quantities enter into the computations of stabilization energies.

However, empirically it is found (11) that the change in the energy difference between conformers on going from acetone to CS_2 as a solvent is close to that in going from CS_2 solution to the vapor (see eq. 13.18 and p. 562 of ref. 11 for a rationalization of this finding). Because the reaction field model yields free energy differences between conformers (13, 14) and because these are $0.4_5 \pm 0.6$ and $5.0_5 \pm 0.6$ kJ/mol for 2CNB in CS_2 and acetone-d_6 solutions, respectively, this procedure implies a free energy difference of $9.6_5 \pm 1.2$ kJ/mol in the vapor at 300 K, *o-trans* favored. Alternatively, if x is taken as 0.25 for the CS_2/C_6D_{12} solvent mixture and as 0.46 for the acetone solution, an extrapolation of an assumed linear relationship between the free energy difference and x (eq. 13.18 of ref. 11, examined in detail) yields the free energy difference as 10.9 ± 1.2 kJ/mol at 300 K. It appears that a reasonable, semiempirical, estimate is 10.3 ± 2.4 kJ/mol at 300 K. It follows that the fractional population of the *o-trans* conformer of 2CNB in the vapor at 300 K is 0.98(2). Accordingly, measurements on the vapor at ambient temperatures are predicted to involve the *o-trans* form almost exclusively.

(ii) 3-Cyanobenzaldehyde

This molecule presents an example of a molecule whose conformational distribution is independent of polarity of the two solvents, even though the dipole moments of the two conformers differ substantially (see below). If the constituent dipoles are sufficiently far apart (p. 507 of ref. 11), then the reaction field model becomes inappropriate and, at least for 3CNB, the orientation of the local aldehyde dipole, relative to that of a local dipole centered at the cyano group, is effectively unaltered by the surrounding medium (an accidental cancellation of dipolar and quadrupolar stabilization energies such as to leave the conformational distribution unaltered in the two solvents cannot be ruled out, however). The free energy difference between the two conformers is 0.2(2) kJ/mol at 300 K, where the apparent error has again been doubled. Accordingly, in the vapor the *o-trans* form will be probably slightly the more abundant and measurements at ambient temperatures will involve both conformers. It is of interest how molecular orbital computations for the free molecules compare with experiment and such computations are discussed below.

Conformational populations in benzene-d_6 solution

It is known (11) that, in the reaction field model of solvent perturbations of conformational energies, benzene often behaves *as if* it had a much higher dielectric constant than its static value of 2.3. Perusal of the available data (11) suggests that the effective dielectric constant varies from solute to solute and that it can be as low as 4.3 or even as high as 35, with 7.5 being a more common value. Specific interactions with the polar solute molecules are indicated by these observations. Because the dipole moments of 2CNB and 3CNB were measured in benzene solution (4), it is of interest to have an independent measure of their conformational behaviour in this solvent.

Although very nearly first order in appearance, the ^{1}H nmr spectra of 2CNB and 3CNB were not of the quality normally attainable (see, for example, Fig. 1) and their analysis gave data of rather lower precision than those reported for other solvents in Table 1. Hence the spectral parameters are not tabulated here.

However, for a <1.3 mol% solution of 2CNB in benzene-d_6, ^5J(H-3,CHO) is 0.210 ± 0.007 Hz and ^5J(H-5,CHO) is 0.654 ± 0.004 Hz. Their sum is 0.864 ± 0.011 Hz, the same as for 2CNB in acetone-d_6 solution, to within experimental error, or for benzaldehyde in acetone-d_6 solution (3). As before, the population of the *o-trans* conformer follows as 0.74(4) at 300 K, and the free energy difference between the conformers as 2.6 ± 0.6 kJ/mol. In terms of the reaction field model, the benzene-d_6 solvent behaves as if its dielectric constant were about 5 in this instance. The populational distribution is intermediate to those established for CS_2/C_6D_{12} and acetone-d_6 solutions and rather different from that estimated from the dipole moment (see below).

For a 4.0 mol% solution of 3CNB in benzene-d_6, ^5J(H-5, CHO) is 0.542 ± 0.002 Hz. It follows that the fractional population of the *o-trans* form has increased to 0.63(2) from the 0.52(2) measured for both of the other solvents. In any event, the free energy difference of 1.3 ± 0.2 kJ/mol between the conformers at 300 K agrees rather well with that of 1.5 ± 0.2 kJ/mol obtained from the dipole moment measurement (4), to be discussed further below.

Molecular orbital computations of conformational energies, dipole moments, and internal rotational barriers

It is known (15) that *ab initio* molecular orbital computations with a minimal basis set reproduce the internal rotational potential in benzaldehyde much more faithfully than those with split valence bases such as 6-31G and 6-31G*. Accordingly, the internal rotational potentials in 2CNB and 3CNB were computed with the basis STO-3G (16). Experience teaches that geometries of the planar conformers, however, are more reliably obtained from the 6-31G basis (17, 18). Such geometries are probably of interest in future investigations by molecular spectroscopy and hence were calculated here. Again, computed dipole moments vary from method to method and basis to basis (19). Some semiempirical orbital approaches yield dipole moments of benzene derivatives in rather good agreement with experiment (2, 20). Therefore, dipole moments were also computed by CNDO/2, INDO, and AM1 MO methods. As a matter of curiosity, the AM1 (21) method was also used to compute the internal rotational potential in 3CNB.

(i) Internal barrier and relative energies

Table 2 contains the results of the computations of the internal rotational potentials. The STO-3G energies of 2CNB are fit, to within a standard deviation of 0.03 kJ/mol, by eq. [1]:

$$[1]\quad V(\theta)/\text{kJ mol}^{-1} = 4.31 \sin^2(\theta/2) + 20.37 \sin^2\theta - 0.08 \sin^2(3\theta/2) - 0.80 \sin^2 2\theta - 0.15 \sin^2 3\theta - 0.02 \sin^2 4\theta$$

except that the energy at $\theta = 15°$ is overestimated by

TABLE 2. STO-3G and AM1 MO energies of 2-cyanobenzaldehyde and 3-cyanobenzaldehyde

	Relative energy[c]/kJ mol^{-1}		
		3CNB	
θ/degrees	2CNB STO-3G	STO-3G	AM1
0[a]	0.00[b,e]	0.00[d,e]	0.00
15	0.88	1.46	0.67
30	4.52	5.58	2.60
45	9.88	11.50	5.41
60	15.67	17.72	8.34
75	20.27	22.40	10.50
90	22.33	24.13	11.29
105	21.39	22.48	10.58
120	17.87	17.97	8.56
135	12.98	11.95	5.81
150	8.36	6.12	3.18
165	5.25	1.95	1.38
180	4.19	0.46	0.76

[a]θ = 0 corresponds to the *o-trans* conformer.
[b]The total energy is −429.671 389 au.
[c]Geometry optimization allowed all bond angles and lengths to vary, with the constraint, however, that the carbon and hydrogen atoms of the benzene moiety remained in a plane.
[d]The total energy is −429.672 768 au.
[e]Equations [1] and [2] of the text reproduce these energies by Fourier series.

0.26 kJ/mol by this expression. The *o-trans* conformer corresponds to θ = 0°. The height of the barrier at θ = 90°, relative to θ = 0° (the *o-trans* barrier), is computed as 2.0 kJ/mol lower than in benzaldehyde (15). The only internal barriers known for 2-X-benzaldehydes are those measured for X = alkyl, by dynamic nmr (22, 23). For X = CH_3, the barrier is 3.6 kJ/mol (22) lower than for benzaldehyde in the same solvent system. The lower barrier is attributed to steric destabilization of the planar conformers. In 2CNB, the *o-cis* barrier is computed as 6.1 kJ/mol lower than in benzaldehyde, presumably due to destabilization of the *o-cis* conformer by dipole–dipole repulsion of the two dipoles and by a decrease of the Csp^2—Csp^2 mobile bond order caused by the cyano group that competes with the carbonyl group for π electrons. This competition could also account for the barrier decrease computed for the *o-trans* conformer. Measurement of the internal barrier in 2CNB by dynamic nmr would require the use of a rather polar solvent because otherwise very little of the *o-cis* conformer would exist at the requisite low temperatures (see the previous section). This measurement would be of interest because 2CNB is the only 2-X-benzaldehyde with a polar X for which a large population of the *o-cis* conformer exists, even in a polar solvent. Thus, a solution of 2-fluorobenzaldehyde in acetone-d_6 contains the *o-cis* conformer only to the extent of 15% (3).

The relative STO-3G MO energies of 3CNB in Table 2 are fit by eq. [2] with a standard deviation

$$[2]\quad V(\theta)/\text{kJ mol}^{-1} = 0.5\sin^2(\theta/2) + 23.8\sin^2\theta - 0.1\sin^2(3\theta/2) - 0.4\sin^2 2\theta$$

of 0.1 kJ/mol. The barrier at 90° for the more stable *o-trans* form, defined by θ = 0°, is essentially that computed for benzaldehyde (15), as is the fourfold component, in $\sin^2 2\theta$. In this instance, the *meta* substituent has a minor influence on the predominantly conjugative barrier to rotation of the carbonyl group, a result expected on the basis of simple resonance structures.

The internal barrier computed for 3CNB by AM1, at about 11.3 kJ/mol in Table 2, is much too low, as are the dipole moments of the planar conformers (see below).

However, the AM1 value of 0.76 kJ/mol favoring the *o-trans* over the *o-cis* conformer is in qualitative agreement with the other molecular orbital and experimental results in Table 3. The ^{5}J values in CS_2 and acetone solutions imply a slightly greater abundance of the *o-trans* conformer, in best agreement with the INDO MO calculations but also close to the predictions from the STO 3G MO computations (see the last column in Table 3). 3CNB therefore behaves qualitatively differently from 3-F-benzaldehyde, in which the *o-cis* conformer predominates both at 300 K (3) and 123 K (23); at the latter temperature it is also true for X = Cl, Br, CH_3 (23), but not at 300 K according to unpublished work in this laboratory. The explanation (23) advanced for this preference is that the inductive effect of the substituent causes polarization of the C^-—H^+ bond at position 2 in the indicated sense, thereby stabilizing the *o-cis* form by electrostatic interaction with the C^+=O^- bond.

The computed energy differences between the conformers of free 2CNB range from 0.3 kJ/mol to 14.7 kJ/mol in Table 3. The extrapolated value of 10.3 ± 2.4 kJ/mol, based on solution data, lies roughly midway between the STO-3G and 6-31G results. The latter basis suggests very small amounts of the *o-cis* conformer in the vapor phase at 300 K, in best agreement with the extrapolated population of 2 ± 2%.

For 3CNB all the theoretical computations have the *o-trans* form as most abundant, the range of p_t at 300 K being 0.53–0.61. The 6-31G basis now has the largest deviation from the extrapolated value of 0.52(2).

(ii) Dipole moments

Table 3 presents theoretical dipole moments of the planar conformers of 2CNB and 3CNB; estimates based on group moments (4) are also reproduced there. A lack of solubility in CCl_4 dictated the measurement of the dipole moments in benzene solution at 298 K(4). The authors (4) are aware of the peculiarity of benzene as a dielectric medium. In Table 3, the value of 0.92 for the fractional population, p_t, of the *o-trans* conformer of 2CNB in benzene is calculated from the measured dipole moment and the group moments. It should be noted that the authors (4) realize the uncertainty of their predicted dipole moments, arising from the proximity of the polar substituents, and conclude only that the *o-trans* form is strongly favoured.

Consider now the conformer populations of 2CNB in benzene-d_6 as deduced from ^5J(H,CHO). These populations, together with the dipole moments of the conformers estimated from group moments, imply a dipole moment of 5.3 D for 2CNB in benzene solution; the measured value is 4.9 D (4). Therefore at least one of the estimated dipole moments of the individual conformers is presumably too large.

Again, the dipole moments of the conformers, as given by the STO-3G basis, imply a dipole moment of 4.0 D in benzene solution. Therefore, at least one of the theoretical dipole moments must be underestimated. The minimal basis set underestimates (24) the dipole moments of benzaldehyde and cyanobenzene by 1.08 and about 0.5 D, respectively, so that this conclusion is expected. If, arbitrarily, the STO-3G values are increased by 1.0 D, then, together with the populations given by ^5J(H,CHO), the dipole moment of 2CNB in benzene at 300 K is calculated as 4.95(4) D, precisely as measured. According to a previous section, only the *o-trans* conformer is likely to occur in the vapor at ambient temperatures; it is tempting to predict that a dipole moment of 6.2 D will be observed.

Can. J. Chem. Downloaded from www.nrcresearchpress.com by 84.41.108.74 on 09/07/12
For personal use only.

TABLE 3. Relative conformational energies, populations, and dipole moments of 2-cyanobenzaldehyde and 3-cyanobenzaldehyde

Method	*o-cis*	*o-trans*	C_6H_6	$E_c - E_t$	P_t
2-Cyanobenzaldehyde					
μ/C_6H_6[a]	6.89[a]	4.74[a]	4.94[a]	6.1[b]	0.92
$^5J/C_6D_6$	—	—	(5.3)[g]	2.6(3)	0.74(4)
$^5J/CS_2$	—	—	—	$5.0_5 \pm 0.6$[c]	0.88(4)
^5J/acetone	—	—	—	$0.4_5 \pm 0.6$[c]	0.54(6)
Vapor/extrap	—	—	—	10.3 ± 2.4[d]	0.98(2)
STO-3G MO	5.16	3.50	(4.0)[f]	4.19[e]	0.84
6-31 G	7.87	5.21	(6.0)[f]	14.71[e]	0.99_5
CNDO/2	5.46	4.22	(4.5)[f]	1.42	0.64
INDO	5.51	3.54	(4.1)[f]	0.32	0.53
3-Cyanobenzaldehyde					
μ/C_6H_6[a]	5.31[a]	1.75[a]	3.45[a]	1.5(2)[b]	0.65(2)
$^5J/C_6D_6$	—	—	(3.5)[g]	1.3(2)	0.63(2)
$^5J/CS_2$	—	—	—	0.2(2)[c]	0.52(2)
^5J/acetone	—	—	—	0.2(2)[c]	0.52(2)
Vapor/extrap	—	—	—	0.2(2)[d]	0.52(2)
STO-3G MO	4.32	1.97	(3.1)[f]	0.46[e]	0.55
6-31 G	6.36	1.93	(4.2)[f]	1.12	0.61
CNDO/2	4.42	1.08	(2.8)[f]	0.35	0.54
INDO	4.41	1.15	(2.8)[f]	0.29	0.53

[a]Dipole moment, μ, in Debye, measured in benzene at 298 K (4); the dipole moments of the two conformers are estimated from group dipoles (4).

[b]The free energy difference in kJ/mol at 298 K, calculated from the fractional population, p_t, of the *o-trans* conformer; p_t follows from the measured dipole moment of 4.94 D and the estimated conformer moments.

[c]The free energy difference between the *o-cis* and *o-trans* conformers at 300 K, as deduced from ^5J(H,CHO) by methods described in the text.

[d]The free energy difference in the vapor at 300 K, obtained by extrapolation of solution data on the basis of a dielectric model discussed in the text.

[e]The energy differences between conformers, obtained from the molecular orbital computations, are assumed to be free energy differences in the calculation of p_t at 300 K.

[f]The dipole moments in parentheses are those calculated for a benzene solution in which the computed dipole moments in the same row are used and the conformer populations are those implied by ^5J(H,CHO). Of course, the predicted dipole moment follows from $\mu^2 = p_t\mu_t^2 + (1 - p_t)\mu_c^2$.

[g]Calculated with the dipole moments of the conformers as estimated from the group moments in the row above and from the value of p_t obtained from ^5J(H,CHO).

Can. J. Chem. Downloaded from www.nrcresearchpress.com by 84.41.108.74 on 09/07/12
For personal use only.

Turning to 3CNB, the good agreement between the population distributions in benzene, based on ^5J(H,CHO) and group dipole moments, suggests the reliability of the latter. Again, the theoretical dipole moments of the conformers are in general too low, especially those from the AM1 computations.

The 6.31 G structures

Figures 2 and 3 reproduce the 6-31G geometries of the *o-trans* conformer of 2CNB and of the two conformers of 2CNB. These are the three conformers predicted to occur in the vapor near ambient temperatures. The structures may well be useful to molecular spectroscopists. See the figure captions for structural comments.

The other spectral parameters

(i) The ^1H nmr chemical shifts

Ordinarily, the protons of polar benzene derivatives are deshielded in passing from nonpolar to polar environments, a result mainly due to the reaction field induced in the solvent (27). In Table 1, the chemical shifts of all the protons in 3CNB, including that in the side chain, are an example of this phenomenon; the aldehydic proton is deshielded by 0.24 ppm in the acetone-d_6 relative to the CS_2/C_6D_{12} solution. In 2CNB, however, the shielding of the aldehydic proton is reversed and is 0.05 ppm higher in the acetone-d_6 solution. Almost certainly, it is the local electric field of the cyano group (28) which is responsible, the population of the *o-trans* conformer being so much larger in the nonpolar solvent; this deshielding must outweigh the anticipated shielding caused by the magnetic anisotropy of the C≡N grouping (29).

In benzene-d_6 solution, the protons are all screened relative to the CS_2 solution, as expected on the basis of the diamagnetic anisotropy of the benzene molecule (30, 31). The average of this screening is 0.86 ppm for the ring protons of 2CNB and is 0.62 ppm for those of 3CNB. The ratio of 1:4 for these numbers is the same as the ratio of the dipole moments of these compounds in benzene (Table 3). This result is qualitatively consistent with the dipole induced-dipole model for the aromatic solvent induced shift or ASIS (32, 33). However, the ASIS for the individual ring protons does not provide evidence for preferred association of the benzene molecule with the most polar site of the solute molecules (the largest ASIS occurs for H-4 in 2CNB and H-5 in 3CNB) and hence their values are not quoted here or discussed further. A dipole induced-dipole model would presumably predict stabilization of the more polar conformer by benzene; this occurs for 2CNB, but the opposite is true for 3CNB.

(ii) The intraring $^nJ(H,H)$

It is a general result in this laboratory that ^nJ(H,H) in benzene

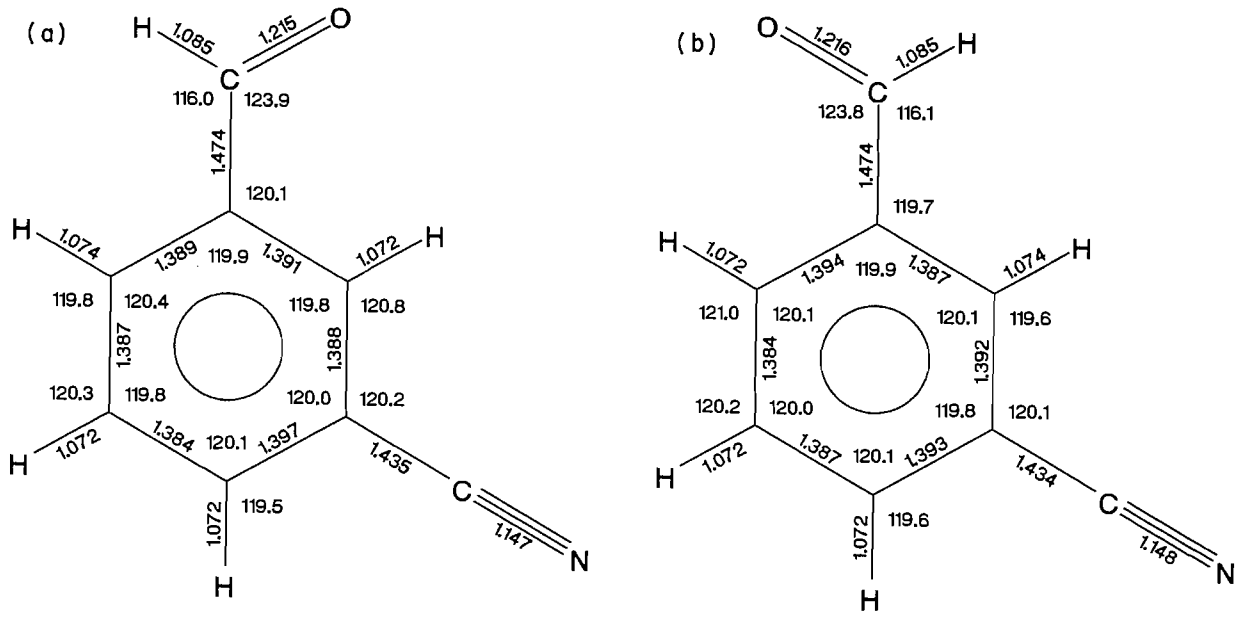


FIG. 2. The 6-31G structures of the (a) *o-cis* and (b) *o-trans* planar conformers of 3-cyanobenzaldehyde are displayed. Comparison with the 6-31G structures of the parent compounds (25) shows that the present internal ring angles are derivable additively from the parent compounds. The presence of the aldehyde group does not significantly alter the geometry at the cyano site (the converse is not true). At this level of theory, the experimental structure of cyanobenzene (26) is therefore to be used for the local site geometry. The total energies are −434.983 722 au for the *o-trans* and −434.983 295 au for the *o-cis* conformer.

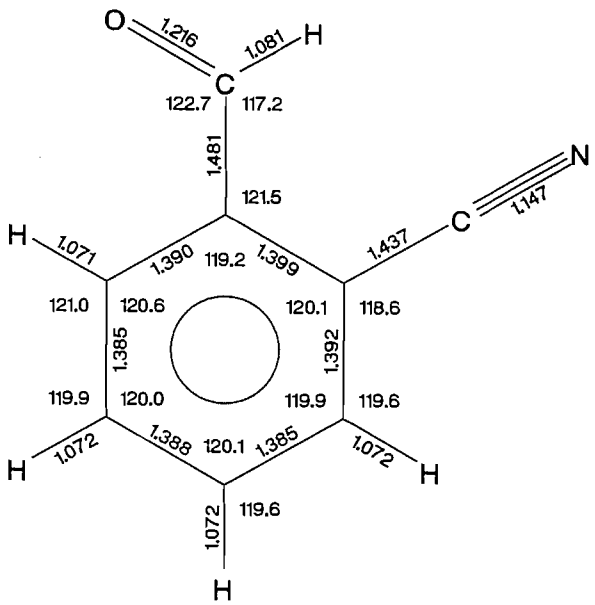


FIG. 3. The planar geometry of the *o-trans* conformer of 2-cyanobenzaldehyde, as given by the 6-31G basis, is shown and is predicted to be the conformer observable at ambient and lower temperatures. Its total energy is −434.980 755 au. The internal bond angles are no longer given by an additivity scheme (see Fig. 2). The local geometry at the substitution sites indicates repulsive forces between the substituents (compare the geometry with that in Fig. 2(b)).

derivatives are larger in acetone-d_6 than in CS_2/C_6D_{12} solutions. For nonpolar solutes such as isopropylbenzene, for example (34), the differences amount to 0.02 Hz or less, increasing to as much as 0.03 Hz for some ^nJ(H,H) in a polar solute such as benzaldehyde (2) or even 0.06 Hz for $^3J_{45}$ in 3-fluorobenzaldehyde (3). The striking result in Table 1 is that ^nJ(H,H) can differ by as much as 0.35 Hz in the two solvents. Furthermore, a given ^nJ(H,H) in 2CNB or 3CNB may be larger or smaller in acetone-d_6 than in CS_2/C_6D_{12}. The solvent dependence of ^nJ(H,H) in cyanobenzene is unknown. It is noted that $^4J_{24}$ in 3CNB, that is, the coupling constant across the site of substitution by the cyano group, as well as $^5J_{25}$, undergo the largest relative change; the former decreases by 0.35 Hz in the polar solvent and the latter increases by 0.20 Hz, or almost 50% of its value in CS_2/C_6D_{12}. This unprecedented and unexpected (35) behaviour is possibly related to a solvent dependent polarization of the aromatic π orbitals by the polar cyano group.[2] Thus, ^5J(H,H) is dominated by a $\sigma-\pi$ electron coupling mechanism (37) and displays the largest proportional change. The conformational behaviour of 3CNB is independent of the two solvents in Table 1, so that, unlike 2CNB, the variation in ^nJ(H,H) is not due to orientational changes in the carbonyl dipole.

(iii) ^{4}J*(H,CHO) and* ^{6}J*(H,CHO)*

^4J(H,CHO) in Table 1 can be understood in a manner previously discussed for other benzaldehyde derivatives (2). The values will not be discussed in detail, except to note that, for example, ^4J(H-2,CHO) has a smaller magnitude than ^4J(H-6,CHO) because the electrognegative cyano group polarizes the electron framework at C-2, with the consequence that the positive σ electron contribution to ^4J(H-2,CHO) is increased and partially cancels the negative π electron component.

^6J(H,CHO) in benzaldehyde has not been detected (2). Its value in some *meta* substituted benzaldehyde derivatives

[2]A recent computation (36) on vinyl cyanide shows that an electric field comparable in magnitude to the reaction field in acetone solution causes a redistribution of σ and π charges in the vinyl group; the π electrons follow the field while the σ electrons tend to counterbalance this movement. Measurements of ^nJ(H,H) in cyanobenzene and the appropriate cyanotoluenes as a function of solvent should prove informative. Certain long-range $^{n+1}J(H,CH_3)$ are good indicators of the π electron contributions to the corresponding ^nJ(H,H).

Can. J. Chem. Downloaded from www.nrcresearchpress.com by 84.41.108.74 on 09/07/12
For personal use only.

follows (2) the relationship: ${}^6J/\text{Hz} = 0.007 - 0.127\,\Sigma\sigma_{R,ST}$, where $\sigma_{R,ST}$ are the so-called standard resonance substituent constants for *meta* substituents (38). This constant for a cyano group is 0.01, so that ${}^6J$ in 3CNB is predicted as +0.006 Hz. This coupling is not detectable in the ^{1}H nmr spectrum, but is consistent with the spectral simulations described in the footnotes to Table 1.

The quantity, $\sigma_{R,ST}$, is a measure of the charge transfer between ring and substituent (16) and is not available for *ortho* substituents. However, if the value of the *para* substituent constant, +0.19 for the cyano group, is used in the relationship above, then ${}^6J$ in 2CNB is anticipated as −0.017 Hz. It appears (Table 1 and Fig. 1) that ${}^6J$ is very likely negative in this compound, but not larger than 0.02 Hz in magnitude. Large deviations from planarity of the aldehydic group are also contraindicated by this small magnitude (39), in agreement with the molecular orbital computations in a previous section.

Acknowledgments

We are grateful to the Natural Sciences and Engineering Research Council of Canada for financial assistance.

1. G. J. Karabatsos and F. M. Vane. J. Am. Chem. Soc. **85**, 3886 (1963).
2. T. Schaefer and C. S. Takeuchi. Can. J. Chem. **67**, 827 (1989).
3. T. Schaefer and C. S. Takeuchi. Can. J. Chem. **68**, 339 (1990).
4. E. A. W. Bruce, G. L. D. Ritchie, and A. J. Williams. Aust. J. Chem. **27**, 1809 (1974).
5. T. Schaefer, R. Sebastian, and G. H. Penner. Can. J. Chem. **63**, 2597 (1985).
6. M. J. Frisch, J. S. Binkley, H. B. Schlegel, K. Raghavachari, C. F. Melius, R. L. Martin, J. J. P. Steward, F. W. Bobrowicz, D. F. Rohlfing, L. R. Kahn, D. J. Defrees, R. Seeger, R. A. Whiteside, D. J. Fox, E. M. Fluder, and J. A. Pople. Carnegie-Mellon Quantum Publishing Unit, Pittsburgh, PA. 1984.
7. J. S. Martin, A. R. Quirt, and K. E. Worvill. The NMR program library. Daresbury Laboratory, Daresbury, U.K.
8. A. L. McClellan. Tables of experimental dipole moments. Freeman and Co., San Francisco, CA. 1963. p. 233.
9. J. A. Pople, J. W. McIver, and N. S. Ostlund. J. Chem. Phys. **49**, 2965 (1968).
10. P. Dobosh and N. S. Ostlund. QCPE, **11**, 281 (1975).
11. R. J. Abraham and E. Bretschneider. *In* Internal rotation in molecules. *Edited by* W. J. Orville-Thomas. J. Wiley & Sons, New York, NY. 1974. Chap. 13.
12. W. Danchura, T. Schaefer, J. B. Rowbotham, and D. J. Wood. Can. J. Chem. **52**, 3986 (1974).
13. J. J. Maura Ramos, L. Dumont, M. L. Stein, and J. Reisse. J. Am. Chem. Soc. **102**, 4150 (1980).
14. A. Y. Meyer. J. Mol. Struct. **195**, 147 (1989).
15. G. H. Penner, P. George, and C. W. Bock. J. Mol. Struct. (Theochem), **152**, 201 (1987).
16. W. J. Hehre, R. Ditchfield, R. F. Stewart, and J. A. Pople. J. Chem. Phys. **52**, 2769 (1970).
17. W. H. Hehre, R. Ditchfield, and J. A. Pople. J. Chem. Phys. **56**, 2257 (1972).
18. W. J. Hehre, L. Radom, P. v. R. Schleyer, and J. A. Pople. *Ab initio* molecular orbital theory. J. Wiley & Sons, New York, NY. 1986.
19. S. Marriott, A. Silvestro, and R. D. Topsom. J. Chem. Soc. Perkin Trans. **2**, 457 (1988), and references therein.
20. J. A. Pople and D. L. Beveridge. Approximate molecular orbital theory. McGraw–Hill, New York, NY. 1970.
21. M. J. S. Dewar, E. J. Zoebisch, E. F. Healy, and J. J. P. Stewart. J. Am. Chem. Soc. **107**, 3902 (1985).
22. L. Lunazzi, A. Ticca, D. Macciantelli, and G. Spunta. J. Chem. Soc. Perkin Trans. **2**, 1121 (1976).
23. T. Drakenberg, R. Jost, and J. M. Sommer. J. Chem. Soc. Perkin Trans. **2**, 1682 (1975).
24. W. J. Hehre, L. Radom, and J. A. Pople. J. Am. Chem. Soc. **94**, 1496 (1972).
25. C. W. Bock, M. Trachtman, and P. George. J. Mol. Struct. (Theochem), **122**, 155 (1985).
26. G. Portalone, A. Domenicano, G. Schultz, and I. Hargittai. J. Mol. Struct. **97**, 160 (1987).
27. A. D. Buckingham, T. Schaefer, and W. G. Schneider. J. Chem. Phys. **32**, 1227 (1960).
28. A. D. Buckingham. Can. J. Chem. **38**, 300 (1960).
29. R. F. Zurcher. Prog. NMR Spectrosc. **2**, 205 (1967).
30. P. Laszlo. Prog. NMR Spectrosc. **3**, 231 (1967), and references therein.
31. R. Wasylishen, T. Schaefer, and R. Schwenk. Can. J. Chem. **48**, 2885 (1970).
32. W. G. Schneider. J. Phys. Chem. **66**, 2653 (1962).
33. T. L. Brown and K. Stark. J. Phys. Chem. **69**, 2679 (1965).
34. T. Schaefer, R. Sebastian, and G. H. Penner. Can. J. Chem. **66**, 1495 (1988).
35. M. Barfield and M. Johnston. Chem. Rev. **73**, 53 (1973).
36. M. Raynaud, C. Reynaud, Y. Ellinger, G. Hennico, and J. Delhalle. Chem. Phys. **142**, 191 (1990).
37. R. Wasylishen and T. Schaefer. Can. J. Chem. **49**, 94 (1970), and references therein.
38. G. F. Fadhil and M. Godfrey. J. Chem. Soc. Perkin Trans. **2**, 133 (1988).
39. T. Schaefer, J. Peeling, G. H. Penner, A. Lemire, and R. Laatikainen. Can. J. Chem. **64**, 1859 (1986).

Can. J. Chem. Downloaded from www.nrcresearchpress.com by 84.41.108.74 on 09/07/12
For personal use only.

Long-range $^1H,^{19}F$ and $^{13}C,^{19}F$ coupling constants and molecular orbital computations as indicators of internal motion in $C_6H_5OCF_3$ and its 4-fluoro derivative

TED SCHAEFER,[1] GLENN H. PENNER,[2] RUDY SEBASTIAN, JAMES PEELING, AND CHRISTIAN BEAULIEU
Department of Chemistry, University of Manitoba, Winnipeg, Man., Canada R3T 2N2

Received October 16, 1990

TED SCHAEFER, GLENN H. PENNER, RUDY SEBASTIAN, JAMES PEELING, and CHRISTIAN BEAULIEU. Can. J. Chem. **69**, 1047 (1991).

Internal rotational potentials for rotation about the Csp^2—O bond in $C_6H_5OCF_3$ and its 4-fluoro derivative are computed at the STO-3G and 3-12G levels of molecular orbital theory. As for anisole, the perpendicular conformer is calculated as least stable for $C_6H_5OCF_3$ but the height of the internal barrier is considerably lower than in anisole. The 4-fluoro substituent reduces the twofold component significantly, indicating reduced $p...\pi$ conjugation, but does not much change the values of the higher terms in the theoretical potentials. The internal potentials are rather flat with minima between about 30° and 45°, these angles measuring the twist away from planarity. The ^1H, ^{13}C, and ^{19}F nuclear magnetic resonance spectra in polar and nonpolar solution yield long-range coupling constants, $^nJ(^1H,^{19}F)$ and $^nJ(^{13}C,^{19}F)$. These parameters are qualitatively consistent with relatively low barriers to rotation about the Csp^2—O bonds in these molecules and with only a small dependence on solvent polarity.

Key words: $C_6H_5OCF_3$ and 4-F-$C_6H_4OCF_3$: ^1H NMR, ^{19}F NMR, conformations, MO computations.

TED SCHAEFER, GLENN H. PENNER, RUDY SEBASTIAN, JAMES PEELING et CHRISTIAN BEAULIEU. Can. J. Chem. **69**, 1047 (1991).

Opérant aux niveau STO-3G et 3-21G, on a calculé les potentiels rotationnels internes pour la rotation autour de la liaison Csp^2—O du $C_6H_5OCF_3$ et de son dérivé 4-fluoré. Comme dans le cas de l'anisole, on a calculé que le conformère perpendiculaire est le moins stable pour le $C_6H_5OCF_3$; toutefois, la hauteur à la barrière interne est beaucoup plus faible qu'avec l'ainsole. Le groupe 4-fluoro réduit considérablement la composante binaire, ce qui indique que la conjugaison $p...\pi$ est réduite; il ne provoque toutefois pas de changements dans les valeurs des termes supérieurs des potentiels théoriques. Les potentiels internes sont plutôt plats, avec des minima à des déviations d'environ 30° et 45° par rapport à la planéité. Les spectres de résonance magnétique nucléaire du ^1H, du ^{13}C et du ^{19}F, dans des solvants polaires en non polaires, fournissent les constantes de couplage à longue distance, $^nJ(^1H,^{19}F)$ et $^nJ(^{13}C,^{19}F)$. Ces paramètres sont qualitativement en accord avec les barrières à la rotation autour de ces liaisons Csp^2—O qui sont relativement basses dans ces molécules et qui ne présentent qu'une faible dépendance sur la polarité du solvant.

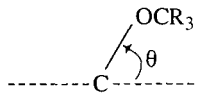
Mots clés : $C_6H_5OCF_3$ et 4-F-$C_6H_4OCF_3$: RMN ^1H, RMN ^{19}F, conformations, calculs d'OM.

[Traduit par la rédaction]

Introduction

Compared to the extensive experimental and theoretical work on the nature of the motion about the Csp—O bond in anisole (1, 2), that on trifluoromethoxybenzene is sparse. Allusive evidence comes from the Hammett σ constants (3–7), these being positive for the OCF_3 and negative for the OCH_3 group. The inductive σ constants of OCF_3 and OCH_3 are 0.55 and about 0.3, respectively, the larger value for OCF_3 being intuitively sensible, considering the electronegativity of fluorine (8); the mesomeric constants are about −0.2 and −0.44, respectively (8). Again, the delocalization constants (5) are reported as −0.16 and −0.55 for OCF_3 and OCH_3. Insofar as a major component of the barrier to rotation about the Csp^2—O bond in anisole originates (1) in $p-\pi$ conjugation, causing partial double-bond character, the numbers above imply a lower barrier in $C_6H_5OCF_3$ than in $C_6H_5OCH_3$. The proton chemical shifts of the *para* protons in these compounds, to be discussed below, also imply minimal $p-\pi$ conjugation in the fluorinated compound.

It appears that the only direct approach to the conformational properties of the OCF_3 group has been an investigation (9) of the dipolar couplings in ^1H and ^{19}F nmr spectra of the 4-fluoro and 4-iodo derivatives as solutions in a liquid crystalline solvent. For anisole, the planar conformer, with θ = 0 in **1**, is the most stable. For 4-F-$C_6H_4OCF_3$, the dipolar couplings between ^1H and ^{19}F can be fit (9) with a range of shapes of the internal rotational potential about the Csp^2—O bond, $V(\theta)$. Strongly favored planar or perpendicular (θ = 90°) conformers, those with internal barriers large compared to thermal energies at 300 K, can be rejected (9). However, the fits do not distinguish firmly between a pure twofold potential, with a minimum at θ = 90° and a maximum at θ = 0°, and one with an additional fourfold term, with a maximum at θ = 45°. Nevertheless, it is clear that the perpendicular is lower in energy than the planar conformer of 4-F-$C_6H_4OCF_3$. Because the fluorine substituent is a π electron donor and because the conjugation of the OCF_3 group with the aromatic π electron system is indicated as weak by the σ constants, it seems possible that the parent compound has a preferred planar conformation and that the 4-fluoro derivative does not. This possibility depends on the magnitude of the mobile bond order in the parent compound and on its perturbation by the 4-fluoro substituent. For example, the relatively weakly conjugative SH group in thiophenol has its barrier to internal rotation reduced almost to zero by such a perturbation (10).



1

R = H
R = F

Another potential source of information about the internal mobility in $C_6H_5OCF_3$ in solution are the long-range spin–spin coupling constants involving the ^{13}C and ^{19}F nuclei in the side

[1]Author to whom correspondence may be addressed.

[2]Present address: Department of Chemistry and Biochemistry, University of Guelph, Guelph, Ontario.

Can. J. Chem. Downloaded from www.nrcresearchpress.com by 84.41.108.74 on 09/07/12
For personal use only.

Can. J. Chem. Downloaded from www.nrcresearchpress.com by 84.41.108.74 on 09/07/12
For personal use only.

chain and the ^1H and ^{13}C nuclei in the aromatic moiety. Taking anisole as an analogy, the proximate coupling constant, $^5J(H,OCH_3)$, between the *ortho* and methyl protons is very sensitive to θ in **1**, as are $^6J(H,OCH_3)$ and $^6J(F,OCH_3)$, the σ–π coupling constants over six bonds (11–13). It is therefore of interest to obtain some analogous long-range coupling constants for $C_6H_5OCF_3$ and its 4-fluoro derivative in an attempt at their use in the conformational analysis of the OCF_3 group. These are reported here. Because CNDO/2 and INDO MO FPT computations (14) can provide useful qualitative information about the angle dependence of long-range coupling constants, such computations are also performed.

In addition, STO-3G (15) and 3-21G (16) MO computations of the internal barrier to rotation about the Csp^2—O bond are described.

Experimental

Dilute solutions of $C_6H_5OCF_3$ and 4-F-$C_6H_4OCF_3$ in acetone-d_6 and CS_2/C_6D_{12} (see Tables 3 and 4 for details) were filtered into 5 mm o.d. nmr sample tubes. These were degassed by four cycles of the freeze–pump–thaw procedure and were then flame-sealed under vacuum. The ^1H, ^{13}C, and ^{19}F nmr spectra were acquired on Bruker WH 90 and AM 300 spectrometers at probe temperatures of 300 K by standard procedures (17–19). The ^1H and ^{19}F nmr spectra were analyzed with the computer program NUMARIT (20), as reworked by R. Sebastian.

CNDO/2 and INDO MO FPT calculations (21) of coupling constants on the molecules above used the STO-3G MO geometries for the various conformations. The STO-3G and 3-21G MO computations employed GAUSSIAN 86 (22) on an Amdahl 5870. At each conformation all bond angles and lengths were optimized, with the proviso, however, that the nuclei of the aromatic moiety remain in a plane.

Results and discussion

The theoretical conformational energies

Table 1 contains the relative energies of the conformations defined by intervals of 15° in the angle of rotation, θ, about the Csp^2—O bonds in $C_6H_5OCF_3$ and its 4-fluoro derivative. These energies can be reproduced by the potentials described in Table 2.

(a) $C_6H_5OCF_3$

Noting that a vanishing θ refers to the planar conformer (see **1**), the data from the minimal basis set can be usefully compared with similar data for anisole (23). In this molecule, the twofold component, V_2, in $\sin^2\theta$, is 5.8 (2) kJ/mol while V_4 and V_6 are 2.4 (2) and −0.6 (2) kJ/mol, respectively. V_2 is directly related (1) to electronic interactions, most simply denoted as of π conjugative origin. At the STO-3G level of theory, in $C_6H_5OCF_3$ the twofold term has therefore decreased by 4.1 (2) kJ/mol, indicating much weaker conjugation across the Csp^2—O bond than in anisole. Although the gas phase barrier in anisole is not known, it must be emphasized that larger bases (1, 2, 24), including electron correlation (but without geometry optimization during the MP2 procedures (1, 2)), imply a V_2 of 9–10 kJ/mol. The substantial V_4 indicated by the minimal basis set for anisole is substantiated at higher levels of MO theory (1, 2, 10), its magnitude being much less sensitive to the basis than is V_2, and is likely (1) to be steric in origin. For $C_6H_5OCF_3$, on the other hand, V_4 is negative (of opposite sign to V_2) and an order of magnitude smaller than for anisole. It is not surprising that the CH_3 and CF_3 groups are thereby implied to be distinct in their interactions with the *ortho* C—H bond. What may be unexpected are the very similar V_6 terms in the STO-3G potentials for anisole and $C_6H_5OCF_3$; for the former molecule the 6-31G basis also has V_6 as −0.54 (5) kJ/mol. The implied consequence is that, unlike anisole, in which all the *ab initio* profiles (1) have an almost flat potential between 50° and 90° and a rapid rise between 0° and 50° for θ, the internal rotational potential for $C_6H_5OCF_3$ has a flat appearance between θ = 0° and about 40° and rises rapidly at larger θ values.

TABLE 1. STO-3G and 3-21G MO energies of some geometry-optimized conformations of $C_6H_5OCF_3$ and 4-F-$C_6H_4OCF_3$

	Relative energy (kJ/mol)			
	$C_6H_5OCF_3$		4-F-$C_6H_4OCF_3$	
θ/deg	STO-3G	3-21G	STO-3G	3-21G
0	0.000	0.000	0.000	0.000
15	−0.028	−0.189	−0.103	−0.158
29.9_8	−0.049[a]	—	—	—
30	−0.040	−0.555	−0.359	−0.892
31.2_7	—	—	−0.394[c]	—
40.1_0	—	−0.672[b]	—	—
45	0.436	−0.643	−0.217	−1.276
47.1_1	—	—	—	−1.285[d]
60	1.219	−0.087	0.202	−1.285
75	1.451	1.273	0.122	0.165
90	1.262	2.355	−0.227	1.182

[a]The total energy is −632.716 247 au.
[b]The total energy is −637.684 897 au.
[c]The total energy is −730.174 946 au.
[d]The total energy is −736.006 727 au.

Because 3-21G computations on anisole (1) mimic 6-31G* energies reasonably well, the less computationally expensive basis was employed also for $C_6H_5OCF_3$ in an attempt at verification of the relatively low internal barrier. The twofold term of the 3-21G potential is very little different from that at the STO-3G level, but the positive V_6 means that the barrier height, at 2.3 kJ/mol, is 1 kJ/mol higher than that predicted by STO-3G. Also, V_4 is much larger in magnitude for the split valence basis. Nevertheless, the expectation value of θ is very similar for the two bases, being 39.2° and 39.8° at 300K with the minimal and the split-valence basis sets, respectively. Figure 1 illustrates the computed potentials and Fig. 2 the 3-21G geometry for the planar molecule; the caption of the latter discusses the changes in exocyclic bond angles during the internal rotaion.

(b) 4-F-$C_6H_4OCF_3$

As expected from a π electron donor, the STO-3G potential for 4-F-$C_6H_4OCF_3$ suggests a decrease of V_2 in the presence of the fluorine substituent. The decrease of 1.45 kJ/mol, to 0.24 kJ/mol, is roughly that (23) computed for the corresponding anisole species with this basis set. The higher terms are insensitive to the 4-fluoro substituent, implying their origin in interactions local to the substituent, as distinct from the delocalization implied by 2*p*...π conjugative phenomena responsible for the twofold term.

The 3-21G potential implies a decrease in V_2 of 1.2 kJ/mol relative to the parent molecule and, again, the higher terms are unchanged from those for the latter. However, whereas the STO-3G potential implies that the perpendicular conformer of 4-F-$C_6H_4OCF_3$ is 0.2 kJ/mol more stable than the planar, that from the split-valence basis gives the perpendicular conformer as less stable by 1.1 kJ/mol. The conformer of minimum energy has a θ near 47° (Table 1) while the minimal basis predicts 31.3°. Of course, both barriers are calculated as less than *RT* at 300 K, so that all angles, θ, are appreciably represented in the ensemble

TABLE 2. The components of the computed internal rotational potentials, $V(\theta)$, for $C_6H_5OCF_3$ and 4-F-$C_6H_4OCF_3$

	$C_6H_5OCF_3$			4-FC_6H_4-OCF_3	
V_n[a]	STO-3G		3-21G	STO-3G	3-21G
V_2	1.693(4)[b]	5.8(2)[c]	1.80(4)	0.241(7)	0.59(5)
V_4	−0.215(4)	2.4(2)	−1.79(4)	−0.134(7)	−1.82(5)
V_6	−0.423(4)	−0.6(2)	0.48(4)	−0.459(7)	0.51(5)
V_8	0.156(4)	—	−0.18(4)	0.169(7)	−0.14(5)
V_{12}	0.016(4)	—	—	0.126(7)	—

[a]In kJ/mol, θ being zero for a conformation in which the carbon atom of the side chain lies in the aromatic plane. The multipliers of V_n are, respectively, $\sin^2(n/2)\theta$.

[b]Numbers in parentheses are the standard errors in the fit to the relative energies given in Table 1.

[c]This column refers to the STO-3G data for anisole (23).

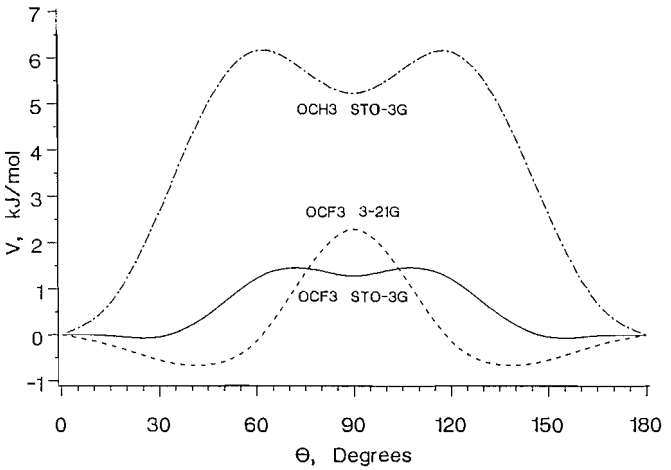


FIG. 1. The 3-21G and STO-3G MO potentials for rotation about the Csp^2—O bond in $C_6H_5OCF_3$ are compared with the STO-3G MO potential for $C_6H_5OCH_3$. Analytical expressions for these curves are given in the text, as are relative energies at intervals of 15° in the twist angle, θ. A θ of 0° defines a planar comformer, that in which the carbon atom of the side chain lies in the aromatic plane. The twofold term in the potential, indicative of $p...\pi$ conjugation, is smaller in $C_6H_5OCF_3$ and the fourfold term is negative, unlike its positive value in $C_6H_5OCH_3$.

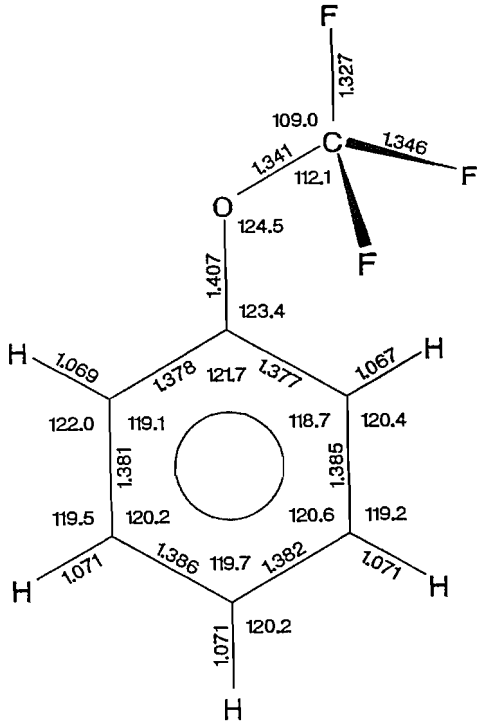


FIG. 2. The 3-21G geometry of the planar conformer of $C_6H_5OCF_3$ is displayed. It can serve as a starting point for higher level computations and may also be useful to molecular spectroscopists. Of some interest are the variations in the exocyclic bond angles during rotation about the Csp^2—O bond. These go as follows for the 3-21G (STO-3G) computations. At θ = 0°, for the planar conformer, ∠C(2)C(1)O is 123.4 (125.8) and becomes 119.0 (120.0) at θ = 90°. In a similar fashion, ∠C(1)OC varies from 124.5(116.5) to 120.2(112.1) as θ increases from 0 to 90°. In other words, rather like anisole (1), steric strain is indicated for the planar conformer. Furthermore, as θ increases from zero the CF_3 group twists by as much as 17° (STO-3G) or 6.5° (3-21G) in such a way as to minimize CF,CH contacts (the maximum twist occurs near θ = 45°); the twist vanishes again for the perpendicular conformer. At the 3-21G level for anisole (1), the maximum twist angle is about 14°. Of course, unlike $C_6H_5OCF_3$, V_2 and V_4 have the same sign in anisole.

at this temperature. This point is emphasized by $\langle\sin^2\theta\rangle$, computed as 0.488 and 0.480 at 300 K by the STO-3G and 3-21G bases, respectively. A $\langle\sin^2\theta\rangle$ of 0.5 corresponds to unhindered motion about the Csp^2—O bond.

By way of contrast, the potentials derived from intramolecular dipolar coupling constants for this compound in a nematic solvent can be written as $V(\theta)/\text{kJ mol}^{-1} = -13.5\sin^2\theta$ or $V(\theta)/\text{kJ mol}^{-1} = -1.8\sin^2\theta - 14.1\sin^2 2\theta$, the latter producing a slighter better fit (9). Both potentials have the perpendicular conformer as most stable, and yield $\langle\sin^2\theta\rangle$ as 0.885 and 0.656 at 300 K. Comparison with the MO potentials (Tables 1 and 2) would indicate a large solvent dependence of the internal rotational potential. The next section describes the information about the internal motion available from spin–spin coupling constants in CS_2/C_6D_{12} and acetone-d_6 solutions.

Long-range spin–spin coupling constants

(a) $^{5,6,7}J(H,CF_3)$ and $^7J(F,CF_3)$

The normal INDO MO FPT computations of long-range coupling constants between nuclei in the side chain and those in the aromatic moiety are known to reproduce their conformational dependence qualitatively. The magnitudes are not normally reproduced correctly, although certain computed H,H coupling constants happen nearly to coincide with experiment (25, 26). One exception to the general qualitative agreement between theoretical and experimental data is the proximate coupling constant, $^5J(F,CH_3)$, in a derivative of 2-fluoroanisole (27). It is

Can. J. Chem. Downloaded from www.nrcresearchpress.com by 84.41.108.74 on 09/07/12
For personal use only.

TABLE 3. The ^1H and ^{19}F nmr spectral parameters for $C_6H_5OCF_3$ in CS_2/C_6D_{12}[a] and acetone-d_6[b] solutions at 300 K

Parameter	CS_2/C_6D_{12}	Acetone-d_6	Parameter	CS_2/C_6D_{12}	Acetone-d_6
$\nu(CF_3)$	29139.60[c]	—	$^5J_{25}$	0.453	0.461(1)
ν_2	2133.806(1)[d]	2198.111(1)	$^5J(H,CF_3)$	1.027(1)	1.038(1)
ν_3	2190.824(1)	2253.017(1)	$^6J(H,CF_3)$	0.050(1)	−0.008(1)[f]
ν_4	2161.526(1)	2219.318(1)	$^7J(H,CF_3)$	0.138(1)	0.133(2)
$^3J_{23}$	8.280(1)	8.310(1)	Calcd. transitions	384[g]	384
$^3J_{34}$	7.484(1)	7.499(1)	Assigned transitions	336	270
$^4J_{26}$	2.588(1)[e]	2.642(1)	Peaks	142	—
$^4J_{24}$	1.091(1)	1.077(1)	Largest difference	0.016	0.022
$^4J_{35}$	1.746(1)	1.753(1)	Root-mean-square deviation	0.002	0.008

[a]For a 5.0 mol% solution in CS_2, containing also 10 mol% of C_6D_{12}, 0.5 mol% of TMS, and 0.25 mol% of C_6F_6.
[b]For a 4.0 mol% solution in acetone-d_6, containing also 0.5 mol% of C_6F_6.
[c]Not optimized; in Hz at 282.364 MHz to high frequency of internal C_6F_6.
[d]In Hz at 300.135_2 MHz to high frequency of internal TMS; numbers in parentheses are the standard deviations in the last significant figure.
[e]$^4J_{26}$ and $^5J_{25}$ are correlated by 0.409.
[f]No spectral evidence for this coupling constant, the quality of the spectrum in acetone-d_6 solution being inferior to that of the spectrum in CS_2/C_6D_{12} solution.
[g]Excludes 128 for the CF_3 group.

TABLE 4. The ^1H and ^{19}F nmr spectral parameters for 4-F-$C_6H_4OCF_3$ in CS_2/C_6D_{12}[a] and acetone-d_6[b] solutions at 300 K

Parameter	CS_2/C_6D_{12}	Acetone-d_6	Parameters	CS_2/C_6D_{12}	Acetone-d_6
$\nu(CF_3)$	28963.50[c]	29766.792(1)	$^5J_{25}$	0.345(1)	0.346(1)
ν_2	2130.024(1)[d]	2217.235(1)	$^5J(H,CF_3)$	0.938(1)	+0.950(1)[e]
ν_3	2092.920(1)	2182.139(1)	$^6J(H,CF_3)$	0.016(1)	+0.015(1)[e]
ν_4	13561.727(1)[c]	13642.895(1)	$^7J(F,CF_3)$	0.207(1)	+0.207(1)[e]
$^3J_{23}$	8.997(1)	9.054(1)	Calcd. transitions	384[f]	512
$^3J_{34}$	7.685(1)	8.202(1)	Assigned transitions	273	396
$^4J_{26}$	3.127(1)	3.192(1)	Peaks	145	—
$^4J_{24}$	4.344(1)	4.395(1)	Largest difference	0.014	0.021
$^4J_{35}$	3.038(1)	3.125(1)	Root-mean-square deviation	0.005	0.008

[a]5.0 mol% in the $CS_2/C_6D_{12}/TMS/C_6F_6$ solvent mixture described in Table 2.
[b]5.7 mol% in the acetone-d_6/TMS/C_6F_6 solvent mixture in Table 2.
[c]In Hz at 282.364 MHz to high frequency of internal C_6F_6, the quoted numbers coming from the output of the least-squares analysis.
[d]In Hz at 300.135_2 MHz to high frequency of internal TMS.
[e]Signs determined as described in the caption to Fig. 3.
[f]Excludes 128 transitions for the CF_3 group.

positive, but calculated as negative, for the most likely orientations of the methoxy group.

A similar discrepancy occurs for $^5J(H,CF_3)$ in $C_6H_5OCF_3$ and 4-F-$C_6H_4OCF_3$ (see Tables 3 and 4 and Fig. 3). In the former, $^5J(H,CF_3)$ is 1.04 Hz in acetone-d_6 solution. INDO MO FPT results for the STO-3G MO geometries are that $^5J(H,CF_3)$ is −0.75 Hz at $\theta = 0°$ in the *cis* orientation, increasing in magnitude to −1.22 Hz at $\theta = 45°$ and becoming 0.01 Hz at $\theta = 90°$. The theoretical numbers imply a proximate mechanism for the coupling constant in the sense that $^5J(H,CF_3)$ is computed as very small for the *ortho* proton *trans* to the CF_3 group in the conformations above and, at $\theta = 90°$, the computed coupling constant essentially vanishes because of the distance between the atoms carrying the coupled nuclei. The sign discrepancy means that the computed numbers cannot be used in a quantitative assessment of the conformational behaviour of the OCF_3 group, except insofar as the large magnitude of $^5J(H,CF_3)$ in either solution is not consistent with a stability of the perpendicular conformer large compared to *RT* at 300 K. For 4-F-$C_6H_4OCF_3$, $^5J(H,CF_3)$ is +0.95 Hz in acetone-d_6 and 0.94 Hz in CS_2/C_6D_{12} so that dramatic changes in the conformational distribution, caused by the 4-fluoro substituent, are contraindicated. Qualitatively, the smaller magnitude of $^5J(H,CF_3)$ is expected if θ values nearer 90° become more probable in the presence of the fluorine substituent, just as qualitatively predicted by the MO potentials in Table 2.

Turning to $^6J(H,CF_3)$, it is certainly finite and positive in 4-F-$C_6H_4OCF_3$ (see caption to Fig. 3), but only 0.01_5 Hz in magnitude. It is computed as 0.11 Hz between $\theta = 0°$ and 45° and then as 0.05 Hz between $\theta = 60°$ and 90°. It is impossible to derive the conformational behaviour from $^6J(H,CF_3)$.

Similar remarks apply to $^7J(F,CF_3)$ and $^7J(H,CF_3)$. The former is measured as +0.20 Hz and is computed as 0.19 ± 0.03 Hz for all angles. The latter is measured as ±0.13 Hz and is computed as 0.17 Hz at $\theta = 0°$, as 0.12 Hz at 45°, and as 0.00 Hz at $\theta = 90°$. While the measured value is consistent with higher probabilities for conformations with low θ values, the computed $^7J(H,CF_3)$ being 0.15 Hz at the conformation of lowest energy near 30°, it is clearly unwise to draw quantitative conformational conclusions except, again, to note that theory implies a vanishing $^7J(H,CF_3)$ if the perpendicular conformer is exclusively present.

(a) $^nJ(C,F)$

One computed *J* with a simple conformational dependence is ^6J(4-F,C) in 4-F-$C_6H_4OCF_3$. It varies, in Hz, as $0.90 \sin^2\theta$.

Can. J. Chem. Downloaded from www.nrcresearchpress.com by 84.41.108.74 on 09/07/12
For personal use only.

Can. J. Chem. Downloaded from www.nrcresearchpress.com by 84.41.108.74 on 09/07/12
For personal use only.

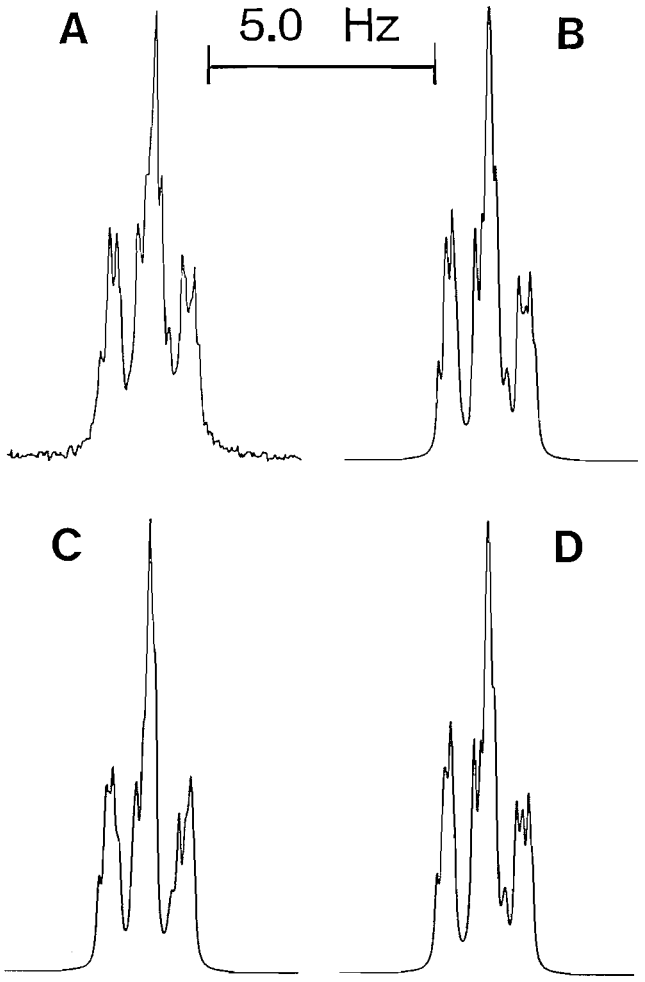


FIG. 3. In A is displayed the ^{19}F nmr spectrum at 84.7 MHz of the CF_3 group of 4-F-$C_6H_4OCF_3$ as a dilute solution in acetone-d_6; no resolution enhancement has been applied. The simulated spectra use the properly scaled spectral parameters obtained from the ^1H and ^{19}F nmr spectra at 300.1 and 282.4 MHz, respectively, acquired on an AM300 spectrometer (same sample). The tightly coupled proton spin system at the lower spectrometer frequency allows the direct determination of the signs of $^5J(H,CF_3)$, $^6J(H,CF_3)$, and $^7J(F,CF_3)$. This information is contained in the appearance of all the spectral regions but is here illustrated only for that of the CF_3 group. In B the simulated spectrum has a linewidth at half-height of 0.10 Hz and ^5J, ^6J, and ^7J are 0.950, 0.015, and 0.207 Hz, respectively, as given in Table 3. In C, ^5J is taken as negative because of the INDO MO FPT results (see text). The disagreement with experiment is apparent, as it is for all other sign combinations of the three coupling constants. In D, ^6J is taken as zero and the other two J's are positive. A ^6J of -0.015 Hz produces severe disagreement with experiment. The signs, of course, are relative to those of the coupling constants within the ring.

This is the angle dependence expected from a $\sigma-\pi$ mechanism (13, 25) and is also found for the analogous (13, 17, 28) coupling constants in 4-fluorophenyl-X-CH_3 (X = O,S,CH_2), for example. What is also common to the INDO MO FPT computations for such molecules is the underestimation of the coefficient of $\sin^2\theta$, that is, of $^6J_{90}$.

Thus, for 4-fluoroanisole, $^6J_{90}$ is computed as 0.7 Hz, the experimental value obtained from appropriate 2,6-disubstituted derivatives being 1.48 Hz (13). For X = CH_2, the underestimate is only 0.5 Hz, but substitution of hydrogen by an electronegative substituent on the methyl group causes a significant increase in the theoretical $^6J_{90}$ (17). Hence the increase in $^6J_{90}$ on passing from 4-F-$C_6H_4OCH_3$ to 4-F-$C_6H_4OCF_3$ is as anticipated. If the former molecule is taken as a reference, then the $^6J_{90}$ for the latter may be estimated[3] as 0.90 (1.48/0.7) or 1.90 Hz. In that event the measured value of ^6J(4-F,C), 1.00 Hz (Table 5), for 4-F-$C_6H_4OCH_3$ in acetone-d_6 solution yields $\langle\sin^2\theta\rangle$ as 0.526 at 300 K. The STO-3G potential gives $\langle\sin^2\theta\rangle$ as 0.488, while that from 3-21G yields 0.480. The potentials deduced for the molecule in the liquid crystal environment (9) entail $\langle\sin^2\theta\rangle$ values of 0.885 or 0.656. The larger of these numbers implies $^6J_{90}$ as 1.13 Hz, that is, 1.00/0.885 Hz. This magnitude is much too small, as judged by our experience with INDO MO FPT calculations for coupling constants of this kind. The $\langle\sin^2\theta\rangle$ of 0.885 comes from the purely twofold potential, unlikely in view of the *ab initio* computations. The value of 0.656 cannot be dismissed as easily. It implies a $^6J_{90}$ of 1.52 Hz, effectively the same as the 1.48 Hz found experimentally (13) for 4-fluoroanisole. However, the adjusted theory indicates a larger $^6J_{90}$ in the OCF_3 molecule, physically sensible because the fluorine atoms bonded to the carbon atom cause contraction of its *s* orbitals and thereby enhance the contact contribution to ^6J; alternatively, the electronegative fluorine substituents cause increased *s*-character at the coupled carbon atom (29). The molecular orbital calculations imply a $^6J_{90}$ of about 2.05 Hz. It is possible, of course, that the solvent alters the internal rotational potential although the coupling constants in Tables 3–5 imply only minor changes in the potential on passing from a nonpolar to a polar solvent environment.

Turning to $^nJ(C,CF_3)$, the INDO MO FPT values, using the STO-3G geometries, can be summarized and compared with experiments as follows. ^3J is calculated as 2.36 Hz at $\theta = 0°$ for $C_6H_5OCF_3$ and decreases to 1.70 Hz at 60°, after which it again increases to 2.02 Hz at $\theta = 90°$; the same trend occurs for the 4-fluoro derivative, but the computed values are 0.04–0.11 Hz larger. Comparison with the measured values of 1.8–1.9 Hz for the parent compound and 2.05 (3) Hz for the derivative (Table 5) suggests that the theoretical values are compatible with observation, but that they cannot at present be used to derive an internal rotational potential.

^4J, as averaged for C-2 and C-6, is calculated to drop slowly from 0.86 Hz at 0° to 0.69 Hz at 45° and then more rapidly to -0.13 Hz at $\theta = 90°$ for $C_6H_5OCF_3$; for the 4-fluoro derivative, the magnitudes are about 0.05 Hz larger between 0° and 60°. The values of 0.9–1.0 Hz in Table 5 are then consistent with a relatively low population of the perpendicular conformers or those closely approximating to them. This consistency is similar to that implied by the molecular orbital computations as well as by a number of the other coupling constants discussed above. It also suggests that the simple twofold potential, based on dipolar couplings, is quantitatively incorrect because it strongly favors large θ values. On the other hand, ^4J is roughly consistent with the alternative potential based on the dipolar couplings in a nematic solvent (9).

Again, ^5J, averaged for C-3 and C-5, is computed as 0.23 Hz at $\theta = 0°$, dropping off to 0.07 Hz at 45° and then, between 60° and 90°, remains at -0.05 Hz for $C_6H_5OCF_3$; for the 4-fluoro compound, the computed numbers between 0° and 45° are about 0.3 Hz larger. The measured ^5J for the latter, at 0.31 Hz, is perhaps somewhat larger than the 0.26 Hz for the parent com-

[3]It is apparently beyond our resources to synthesize, say, the 2,6-dibromo-4-fluoro derivative of $C_6H_5OCF_3$; this compound might give an experimental estimate of $^6J_{90}$.

TABLE 5. The ^{13}C nmr chemical shifts and $^nJ(C,F)^a$ for $C_6H_5OCF_3$ and 4-F-$C_6H_4OCF_3$

Parameter	$C_6H_5OCF_3$ CS_2/C_6D_{12}	$C_6H_5OCF_3$ Acetone-d_6	Parameter	4-F-$C_6H_4OCF_3$ Acetone-d_6[e]
ν_α	120.41[d]	121.49	^1J[f]	−244.75
ν_1	149.34	150.05	^2J	24.08
ν_2	120.81	121.84	^3J	8.91
ν_3	129.64	131.04	^4J	2.92
ν_4	126.55	128.16	^6J	1.00(2)
^1J	−257.27 (256.9)[g]	−255.09		−255.41
^3J	1.84 (2.0)	1.88		2.05
^4J	0.97 (0.9)	0.92		1.00
^5J	0.27	0.26		0.31
^6J	<0.1	<0.1		<0.1

[a]With a precision of 0.03 Hz or better.
[b]As in Table 1, footnote *a*.
[c]As in Table 1, footnote *b*.
[d]Obtained by dividing the frequency relative to that of TMS by 75.469.
[e]Ca, 30 vol.% in acetone-d_6.
[f]These are coupling constants for F-4.
[g]Numbers in parentheses are for 50% solutions in $CDCl_3$ at 295–297 K (31).

pound (Table 4). These numbers are qualitatively consistent with the molecular orbital potentials for $C_6H_5OCF_3$, which imply that the conformations with θ less than about 60° are more heavily populated than those with larger angles.

Finally, $^6J(C,CF_3)$ is calculated to vary little as θ changes, increasing slowly from 0.01 Hz at 0° to about 0.12 Hz for θ greater than 60°. The nonobservation of this coupling constant (Table 4) is therefore not a surprise.

The ring proton chemical shifts

For anisole, as a 2.5 mol% solution in CS_2/C_6D_{12} at 300 K (12), δ_o,δ_m, and δ_p are 6.729, 7.122, and 6.786, respectively. δ_H for benzene in such a solution is 7.218 (31), so that the larger screening by 0.432 ppm of the *para* protons is consistent with π electron donation (see references in ref. 31) by the methoxy group. δ_o, δ_m, and δ_p for $C_6H_5OCF_3$, for 5.0 mol% solution in the same solvent and at the same temperature, are 7.109, 7.299, and 7.202, respectively. Dilution shifts for anisole at least (32), in CCl_4, are negligible for purposes of the present comparison; it is most probable that the dilution shift for $C_6H_5OCF_3$ is less than 0.005 ppm between 5.0 and 2.5 mol%. Hence, the δ_H of benzene and δ_p of $C_6H_5OCF_3$ are essentially equal, implying that the OCF_3 group is a weak π electron donor. Qualitatively, a low barrier to rotation about the Csp^2—O bond in $C_6H_5OCF_3$ is therefore inferable, insofar as the barrier arises from p–π conjugation.

In $CDCl_3$, δ(C-4) of $C_6H_5OCF_3$ is smaller than that of benzene by 1.8 (30) whereas for anisole this number is 7.8, again consistent with a much lower delocalization of π electrons by the OCF_3 group. Some donative p–π conjugation is indicated, however, consistent with the planar conformer as the more stable relative to the perpendicular, and as computed by the molecular orbital methods above.

Conclusions

As expected intuitively, the molecular orbital computations predict a lower barrier to internal rotation about the Csp^2—O bond in $C_6H_5OCF_3$ than in anisole, $C_6H_5OCH_3$. The perpendicular conformer is still the least stable, theoretically, as is also indicated qualitatively by the long-range spin–spin coupling constants measured in CS_2 and acetone-d_6 solutions. The experimental data are consistent with at most a small dependence of the internal rotational potential on solvent polarity. Again as expected, the computations on 4-F-$C_6H_4OCF_3$ predict a further reduction of the internal barrier, probably caused by π electron donation from the substituent. Qualitatively, the long-range coupling constants are again consistent with a very low barrier in both solvents. These results suggest that of two possible internal rotational potentials, derived from intramolecular dipolar coupling constants for 4-F-$C_6H_4OCF_3$ in a liquid crystalline solvent, the purely twofold is probably incorrect. The other, having the perpendicular as 1.8 kJ/mol more stable than the planar conformer, cannot be rejected on the basis of the long-range indirect coupling constants.

NOTE ADDED IN PROOF: We have also studied $C_6H_5OCF_3$ and 4-F-$C_6H_4OCF_3$ with geometry-optimized 6-31G computations; the internal potentials (in kJ/mol) are $-2.652(3)\ \sin^2\theta + 0.928(3)\ \sin^2 2\theta - 0.180(3)\ \sin^2 3\theta$ and $-3.628(3)\ \sin^2\theta + 0.984(3)\ \sin^2 2\theta - 0.190(3)\ \sin^2 3\theta$, respectively. At 300 K, $\langle\sin^2\theta\rangle$ values are 0.641 and 0.687. The perpendicular conformers are now the most stable, with relatively small barriers to internal rotation; the mean out-of-plane angles are 56° and 59° at 300 K.

Acknowledgments

This work was supported by the Natural Sciences and Engineering Research Council of Canada. We thank the referees for constructive criticism.

1. D. C. SPELLMEYER, P. D. J. GROOTENHUIS, M. D. MILLER, L. F. KUYPER, and P. A. KOLLMAN. J. Phys. Chem. **94**, 4483 (1990), and references therein.
2. M. A. VINCENT and I. H. HILLIER. Chem. Phys. **140**, 35 (1990).
3. D. R. EATON and W. A. SHEPPARD. J. Am. Chem. Soc. **85**, 1310 (1963).
4. P. J. WAGNER and M. J. THOMAS. J. Org. Chem. **46**, 5431 (1981).
5. M. CHARTON. Prog. Phys. Org. Chem. **16**, 287 (1987).
6. L. M. YAGUPOLSKII. J. Fluorine Chem. **36**, 1 (1987).
7. R. W. TAFT. J. Phys. Chem. **64**, 1805 (1960).
8. O. EXNER. *In* Correlation analysis in chemistry. *Edited by* N. B. Chapman and J. Shorter. Plenum Press, New York. 1978. p. 517.

Can. J. Chem. Downloaded from www.nrcresearchpress.com by 84.41.108.74 on 09/07/12
For personal use only.

9. M. BARNES, J. W. EMSLEY, T. J. HORNE, G. M. WARMS, G. CELEBRE, and M. LONGERI. J. Chem. Soc. Perkin Trans. 2, 1807 (1989).
10. T. SCHAEFER, T. A. WILDMAN, and R. SEBASTIAN. Can. J. Chem. **60**, 1924 (1982).
11. T. SCHAEFER and R. LAATIKAINEN. Can. J. Chem. **61**, 224 (1983).
12. T. SCHAEFER and R. SEBASTIAN. J. Magn. Reson. **73**, 541 (1987), and references therein.
13. T. SCHAEFER, R. LAATIKAINEN, T. A. WILDMAN, J. PEELING, G. H. PENNER, J. BALEJA, and K. MARAT. Can. J. Chem. **62**, 1592 (1984).
14. J. A. POPLE, J. W. MCIVER, and N. S. OSTLUND. J. Chem. Phys. **49**, 2965 (1968).
15. W. K. HEHRE, R. DITCHFIELD, and J. A. POPLE. J. Chem. Phys. **52**, 2769 (1970).
16. J. S. BINKLEY, J. A. POPLE and W. J. HEHRE. J. Am. Chem. Soc. **102**, 939 (1980).
17. T. SCHAEFER, J. PEELING, G. H. PENNER, A. LEMIRE, and R. SEBASTIAN. Can. J. Chem. **63**, 24 (1985).
18. T. SCHAEFER and R. SEBASTIAN. J. Magn. Reson. **41**, 395 (1980).
19. T. SCHAEFER, J. PEELING, and R. SEBASTIAN. Can. J. Chem. **63**, 3219 (1985).
20. J. S. MARTIN, A. R. QUIRT, and K. E. WORVILL. The NMR program library. Daresbury Laboratory, Daresbury, U.K.
21. P. DOBOSH and N. S. OSTLUND. QCPE, **11**, 281 (1975).
22. M. J. FRISCH, J. S. BINKLEY, H. B. SCHLEGEL, K. RAGHAVACHARI, C. F. MELIUS, R. L. MARTIN, J. J. P. STEWARD, F. W. BOBROWICZ, C. F. ROHLFING, L. R. KAHN, D. J. DEFREES, R. SEEGER, R. A. WHITESIDE, D. J. FOX, E. M. FLUDER, and J. A. POPLE. Carnegie-Mellon Quantum Publishing Unit, Pittsburgh, PA. 1984.
23. T. SCHAEFER and G. H. PENNER. J. Mol. Struct. (Theochem), **152**, 179 (1987).
24. T. SCHAEFER and R. SEBASTIAN. Can. J. Chem. **67**, 1148 (1989).
25. R. WASYLISHEN and T. SCHAEFER. Can. J. Chem. **50**, 1852 (1972).
26. T. SCHAEFER and R. LAATIKAINEN. Can. J. Chem. **61**, 224 (1983).
27. T. A. WILDMAN. Ph.D. thesis. University of Manitoba, Winnipeg, MB. 1982.
28. T. SCHAEFER and J. D. BALEJA. Can. J. Chem. **64**, 1376 (1986).
29. K. D. SUMMERHAYS and G. E. MACIEL. J. Am. Chem. Soc. **94**, 8348 (1972).
30. R. A. NEWMARK, J. R. HILL, and G. V. D. TIERS. Magn. Reson. Chem. **26**, 612 (1988).
31. T. SCHAEFER, R. SEBASTIAN, and G. H. PENNER. Can. J. Chem. **63**, 2597 (1985).
32. K. HAYAMIZU and O. YAMAMOTO. J. Mol. Spectrosc. **28**, 89 (1968).

Can. J. Chem. Downloaded from www.nrcresearchpress.com by 84.41.108.74 on 09/07/12
For personal use only.

Selenium-77 and phosphorus-31 nuclear spin relaxation in tri-(*tert*-butyl) phosphine selenide

GLENN H. PENNER

Guelph–Waterloo Centre for Graduate Work in Chemistry, University of Guelph, Guelph, Ont., Canada N1G 2W1

Received October 24, 1990

GLENN H. PENNER. Can. J. Chem. **69**, 1054 (1991).

Selenium-77 and phosphorus-31 spin-lattice relaxation times are reported for tri-*tert*-butylphosphine selenide in chloroform-*d*, at 303 K and at several different magnetic field strengths. At moderate fields the ^{31}P–^{1}H dipole–dipole, spin-rotation, and chemical shift anisotropy mechanisms contribute significantly towards the ^{31}P T_1. At high fields chemical shift anisotropy dominates. The selenium-77 nuclear spin relaxes almost exclusively by spin rotation at low to moderate fields and the chemical shift anisotropy contribution only becomes significant at very high fields. This is due to an unusually small ^{77}Se CSA. The contribution due to ^{31}P–^{77}Se dipole–dipole interactions is small but significant.

Key words: ^{77}Se NMR, NMR relaxation, phosphine selenide.

GLENN H. PENNER. Can. J. Chem. **69**, 1054 (1991).

On a déterminé les temps de relaxation spin réseau du sélénium-77 et du phosphore-31 pour le sélénure de tri-*tert*-butylphosphine, dans le chloroforme-*d*, à 303 K et à diverses forces du champ magnétique. À des champs modérés, les mécanismes de dipôle–dipôle ^{31}P–^{1}H, de rotation de spin et d'anisotropie de déplacement chimique contribuent d'une façon importante à la valeur T_1 du ^{31}P. Aux champs plus élevés, l'anisotropie domine. Aux champs allant de faibles à modérés, la relaxation du spin nucléaire du sélénium-77 se fait presqu'exclusivement par une rotation de spin; la contribution de l'anisotropie du déplacement chimique ne devient importante qu'à des champs très élevés. Ce résultat est attribuable à une ADC du ^{77}Se inhabituellement faible. La contribution attribuable aux interactions dipôle–dipôle ^{31}P–^{77}Se est faible mais significative.

Mots clés : RMN ^{77}Se, relaxation de RMN, sélénures de phosphine.

[Traduit par la rédaction]

Introduction

Phosphorus-31 nuclear spin relaxation in organophosphorus compounds has been the subject of a number of studies (1). Two such studies on phosphine oxides have appeared recently (2, 3). Phosphorus-31 T_1 values have been reported for only one phosphine selenide (2). Investigations of ^{77}Se nuclear spin relaxation have been relatively rare (4–8). Selenium-77 T_1 values have been measured for the C=Se moiety (8) in a number of organoselenium compounds and a large contribution from chemical shift anisotropy was reported. Recently Pulkkinen, Jokisaari, and Kowalewski have reported the ^{77}Se spin-lattice relaxation in carbon diselenide at several fields (9). No investigation of the P=Se moiety has been reported. To study ^{31}P and ^{77}Se relaxation in the P=Se group, tri-*tert*-butylphosphine selenide, **1**, was chosen. Solid ^{77}Se and ^{31}P powder spectra of **1** have been measured[1] and provide values for the chemical shift anisotropies. Compound **1** is stable and relatively easy to synthesize (11).

$$((CH_3)_3C)_3P{=}Se$$

1

In general, when the extreme narrowing condition applies, the rate of spin-lattice relaxation for ^{31}P or ^{77}Se in **1** should consist of several contributions.

$$[1]\quad \frac{1}{T_1} = R_1 = R_1(\mathrm{DD},{}^{1}\mathrm{H}) + R_1(\mathrm{SR}) + R_1(\mathrm{CSA}) + R_1(\mathrm{DD,X})$$

The contribution from the dipole–dipole interaction between the ^{31}P or ^{77}Se nucleus (A) and the protons (H) is given by

$$[2]\quad R_1(\mathrm{DD},{}^{1}\mathrm{H}) = \frac{\gamma_H^2\gamma_A^2\hbar^2\tau_c}{r^6}$$

where γ is the magnetogyric ratio, r is the average A—H internuclear distance, and τ_c is the correlation time for molecular tumbling in solution. The $R_1(\mathrm{DD},{}^{1}\mathrm{H})$ term related to the nuclear Overhauser enhancement, η, by eq. [3].

$$[3]\quad \frac{R_1}{R_1,(\mathrm{DD},{}^{1}\mathrm{H})} = \frac{\eta_{max}}{\eta}$$

The spin-rotation contribution, $R_1(\mathrm{SR})$, is given as

$$[4]\quad R_1(\mathrm{SR}) = \frac{2IkTC^2}{3\hbar^2}\tau_J$$

where I is the moment of inertia, T is the temperature, C^2 is the square of the trace of the spin rotation tensor, and τ_J is the angular momentum correlation time. For a molecule undergoing small-step diffusion, τ_J and τ_c are related by the Hubbard equation,

$$[5]\quad \tau_c\tau_J = \frac{I}{6kT}$$

The chemical shift anisotropy contribution is given by

$$[6]\quad R_1(\mathrm{CSA}) = \frac{2}{15}\gamma_A^2B_0^2(\Delta\sigma)^2\tau_c$$

where B_0 is the magnetic field strength and $\Delta\sigma$ is the chemical shift anisotropy.

A dipolar coupling between the ^{31}P and ^{77}Se nuclei may also contribute towards the relaxation rate:

$$[7]\quad R_1(\mathrm{DD,X}) = \frac{\gamma_{Se}^2\gamma_P^2\hbar^2}{r^6}\tau_c$$

where r is the P—Se bond length.

[1] R. E. Wasylishen, G. H. Penner, and T. Allman. Unpublished results.

Can. J. Chem. Downloaded from www.nrcresearchpress.com by 84.41.108.74 on 09/07/12
For personal use only.

Experimental

Commercial tri-*tert*-butylphosphine (Alfa Products) was stirred under nitrogen with excess selenium powder in dry toluene for 3 days. After filtering the excess selenium the toluene was evaporated, leaving tri-*tert*-butylphosphine selenide as light yellow crystals. The solid was recrystallized from pentane. The product was shown to be pure by ^{1}H, ^{13}C, ^{31}P, and ^{77}Se NMR spectroscopy (11).

Samples of 0.5 M **1** in $CDCl_3$ were prepared in 5 mm and 10 mm NMR tubes. After degassing by three freeze–pump–thaw cycles the tubes were vacuum sealed.

Spectra were acquired at 303 K on Bruker AC-200, Bruker AM-250, Bruker AM-300, Bruker AM-500, and Varian UNITY-600 NMR spectrometers. Relaxation time measurements employed the inversion–recovery pulse sequence with 7–10 delay values (depending on available spectrometer time) with a relaxation delay of 5 times the T_1. The resulting points were fit to the equation

$$[8] \quad M = A + B \exp(-\tau/T_1)$$

using the NLIN program of the SAS/STAT software package (12). Computations were performed on an IBM 3081-K mainframe computer.

Results and discussion

Contributions towards ^{31}P spin-lattice relaxation

Spin-lattice relaxation times for the center-band and ^{77}Se satellites are collected in Table 1. A linear regression yields eq. [9]. The ^{31}P solid powder spectrum has been measured,[1] yielding a $\Delta\delta$ value of 129 ppm. A rotational correlation time of 19.4 ps is obtained from the slope of eq. [9].

$$[9] \quad R_1 = (4.63 \pm 0.43) \times 10^{-2} + [(5.06 \pm 0.47) \times 10^{-4}]B_0^2$$

The maximum ^{1}H–^{31}P nuclear Overhauser enhancement, η_{max}, is 1.234. At 4.7 T (AC-200) and 303 K η is 0.486. Substitution of these values into eq. [3] yields a ^{1}H–^{31}P dipole–dipole contribution, $R_1(DD,^{1}H)$, of 0.023. This value and τ_c yields, via eq. [2], an average phosphorus–hydrogen internuclear distance of 2.1 Å.

The contribution of $R_1(DD,^{77}Se)$ can be calculated using eq. [7] and a P=Se bond length of 2.09 Å, the average of 12 values obtained from X-ray diffraction studies (13); the standard deviation is 0.02 Å. The calculated value of $R_1(DD,^{77}Se)$ is $(8 \pm 1) \times 10^{-4}$ s^{-1}. This relaxation mechanism should only affect the ^{77}Se satellites of the ^{31}P spectrum. The rather small calculated contribution of the ^{77}Se–^{31}P dipole–dipole mechanism is in accord with the nearly equal T_1 values for both the ^{31}P center band and ^{77}Se side bands. An exception to this is the observation at 11.74 T (AM-500), where the T_1 values for both ^{77}Se side bands are longer than for the center band. The T_1 values for the side bands may be different than those for the center band under various conditions. A ^{77}Se–^{31}P dipole–dipole contribution can be ruled out as this mechanism is independent of field under extreme narrowing conditions. Cross relaxation between the dipole–dipole and CSA mechanisms is field dependent (10, 14), but if this were the case the center-band T_1 value would be midway between the values for the side bands; this is not observed at 11.74 T. An instrumental reason for the observed difference in T_1 values may be non-uniform excitation of all resonances. Since the transmitter frequency is very near the center band (and the 90° pulse is calibrated using the center-band resonance), an insufficient excitation of the side-band resonances may be considered, although this seems rather unlikely since the 90° pulse in all experiments was less than 30 μs, which should be sufficiently short for uniform excitation of the 1000-Hz spectral region of interest.

TABLE 1. ^{77}Se and ^{31}P T_1 values for 0.5 M tri-*tert*-butyl phosphine selenide in $CDCl_3$

	Field (T)	T_1(s)
^{31}P[a]	4.70	17.1(17.7, 17.2)
	5.87	14.5(14.4, 14.3)
	7.05	14.6(15.2, 13.8)
	11.74	9.52(13.5, 11.8)
	14.09	6.51(6.68, 6.41)
^{77}Se[b]	4.70	74.6 73.8
	11.74	66 66

[a]Relaxation times for ^{77}Se side bands in parentheses.
[b]First T_1 entry is for highest frequency resonance.

TABLE 2. Contribution towards ^{31}P and ^{77}Se spin-lattice relaxation rates in tri-*tert*-butyl phosphine selenide[a]

	^{31}P	^{77}Se
$R_1(DD,^{1}H)$	0.0230	0.0000
$R_1(CSA)$	$(5.06 \times 10^{-4})B_0^2$	$(1.38 \times 10^{-5})B_0^2$
$R_1(SR)$	0.0225	0.0125
$R_1(DD, X)$	0.0008	0.0008

[a]Relaxation rates in s^{-1}; B_0 is the magnetic field strength in tesla.

The remaining contribution towards the ^{31}P relaxation rate is attributed to R_1 (SR), the spin-rotation mechanism. Subtracting $R_1(DD,^{1}H)$ and $R_1(DD,X)$ from the intercept in eq. [9] yields $R_1(SR) = 0.0225$ s^{-1}.

The various contributions towards the ^{31}P nuclear spin-lattice relaxation rate in the tri-*tert*-butylphosphine selenide are summarized in Table 2.

Contributions towards ^{77}Se spin-lattice relaxation

The selenium-77 T_1 values, measured at 4.7 and 11.74 T, are included in Table 1. Selenium-77 solid-state experiments on **1** yield a $\Delta\delta$ value of 34.7 ppm.[1] The field dependence of the ^{77}Se relaxation rate is given by eq. [10].

$$[10] \quad R_1 = 1.33 \times 10^{-2} + (1.38 \times 10^{-5})B_0^2$$

The slope yields a rotational correlation time of 32 ps. Considering the uncertainty in the two T_1 measurements (estimated to be about 10%) and the rather small slope in eq. [10], the τ_c value of 19.4 ps as derived from the ^{31}P data is the more reliable number.

No proton nOe was observed for ^{77}Se. Therefore the term $R_1(DD,^{1}H)$ can be neglected. The ^{31}P–^{77}Se dipole–dipole contribution $R_1(DD,^{31}P)$ is equal to the value previously calculated for $R_1(DD,^{77}Se)$. Although small, this contribution is not negligible. Assuming no cross-correlation effects, this term will equally affect the two resonances of the doublet (due to J coupling to ^{31}P).

If there are no other contributions to the ^{77}Se relaxation rate, the spin-rotation contribution, $R_1(SR)$, is obtained by subtracting $R_1(DD,^{31}P)$ from the intercept of eq. [10]. This leaves an $R_1(SR)$ value of 0.0125 s^{-1}. The contributions towards ^{77}Se spin-lattice relaxation in tri-*tert*-butylphosphine selenide are summarized in Table 2.

The ratios of the slopes, m(P) and m(Se), of eq. [9] and [10]

Can. J. Chem. Downloaded from www.nrcresearchpress.com by 84.41.108.74 on 09/07/12
For personal use only.

should obey the relationships given in eq. [11].

$$[11]\quad \frac{\gamma(\mathrm{Se})\Delta\sigma(\mathrm{Se})}{\gamma(\mathrm{P})\Delta\sigma(\mathrm{P})} = \sqrt{\frac{m(\mathrm{Se})}{m(\mathrm{P})}}$$

Experimentally, we find that

$$[12]\quad \frac{\gamma(\mathrm{Se})\Delta\sigma(\mathrm{Se})}{\gamma(\mathrm{P})\Delta\sigma(\mathrm{P})} = 0.127$$

and

$$[13]\quad \sqrt{\frac{m(\mathrm{Se})}{m(\mathrm{P})}} = 0.165$$

Equations [12] and [13] are in fair agreement. If the ratio of slopes is adjusted to take into account that 19.4 ps is the much more reliable correlation time, eq. [13] yields a value of 0.129, which is in excellent agreement with eq. [12]. The ratio of the intercepts of eqs. [9] and [10], which are both reliable numbers, is equal to the ratio of the squares of the spin rotation constants:

$$[14]\quad \frac{C^2(\mathrm{Se})}{C^2(\mathrm{P})} = 0.555$$

Conclusion

In this study ^{77}Se and ^{31}P longitudinal relaxation times were measured for tri-*tert*-butylphosphine selenide in chloroform-*d* at 303 K and at several different magnetic field strengths. At moderate fields the ^{31}P–^{1}H dipole–dipole, spin-rotation, and chemical shift anisotropy mechanisms contribute significantly towards the ^{31}P T_1. At high fields (>400 MHz) chemical shift anisotropy dominates. The ^{77}Se nuclear spin relaxes almost exclusively by spin rotation. The chemical shift anisotropy contribution only becomes significant at very high fields (>500 MHz). This is due to an unusually small ^{77}Se CSA. The ^{31}P–^{77}Se dipole–dipole contribution accounts for 5–6% of the ^{77}Se relaxation rate at fields attainable with present NMR spectrometers.

Acknowledgements

Spectra were acquired at the NMR centres of McMaster University and the University of Waterloo. Bruker Spectrospin Canada and Varian Associates are also thanked for generous allocations of spectrometer time. The financial assistance of NSERC is gratefully acknowledged.

1. K. R. DIXON. *In* Multinuclear NMR. *Edited by* J. Mason. Plenum Press, New York. 1987.
2. M. I. M. WAZEER. Spectrochim. Acta, **45A**, 1257 (1989).
3. *(a)* P. RUBINI and H. EL ALAOUI EL ABDALLAOUI. J. Chim. Phys. **87**, 345 (1990); *(b)* P. RUBINI and H. EL ALAOUI EL ABDALLAOUI. J. Chim. Phys. **87**, 355 (1990).
4. W. H. DAWSON and J. D. ODOM. J. Am. Chem. Soc. **99**, 8352 (1977).
5. J. D. ODOM, W. H. DAWSON, and P. D. ELLIS. J. Am. Chem. Soc. **101**, 5815 (1979).
6. O. A. GANSOW, W. D. VERNON, and J. J. DECHTER. J. Magn. Reson. **32**, 19 (1978).
7. W-H. PAN and J. P. FACKLER, JR. J. Am. Chem. Soc. **100**, 5783 (1978).
8. T. C. WONG, T. T. ANG, F. S. GUZIEC, JR., and C. A. MOUSTAKIS. J. Magn. Reson. **57**, 463 (1984).
9. A. PULKKINEN, J. JOKISAARI, and J. KOWALEWSKI. J. Magn. Reson. **85**, 388 (1989).
10. T. L. FARRAR and R. A. QUINTERO-ARCAYA. J. Phys. Chem. **91**, 3224 (1987).
11. W-W. DUMONT. Z. Naturforsch. **408**, 1453 (1985).
12. SAS Institute Inc. SAS Users Guide: Basics, Version 5 Edition. SAS Institute Inc., Cary, NC. 1985.
13. F. H. ALLEN, O. KENNARD, D. G. WATSON, L. BRAMMER, A. G. ORPEN, and R. TAYLOR. J. Chem. Soc. Perkin Trans. 2, S1 (1987).
14. H. SHIMIZU. J. Chem. Phys. **40**, 3357 (1964).

Can. J. Chem. Downloaded from www.nrcresearchpress.com by 84.41.108.74 on 09/07/12
For personal use only.

Rate of the OH + C_6H_6 + He reaction in the fall-off range by discharge flow and OH resonance fluorescence

A. GOUMRI, J. F. PAUWELS, AND P. DEVOLDER

Laboratoire de Cinétique et Chimie de la Combustion URA CNRS 876, Université des Sciences et Techniques de Lille, Flandres-Artois, 59655 Villeneuve D'ASCQ Cedex, France

Received October 24, 1990

A. GOUMRI, J. F. PAUWELS, and P. DEVOLDER. Can. J. Chem. **69**, 1057 (1991).

The rate constant k_1 of the reaction

$$OH + C_6H_6(+ He) \longrightarrow \text{products } (+ He)$$

has been investigated by discharge flow resonance fluorescence of OH in the fall-off pressure range. From systematic measurements at five pressures between 0.5 and 9.5 torr, the Troe parameters k_0 and k_∞ (with $F_c = 0.6$) have been derived at two temperatures: room temperature and 353 K. For room temperature, (297 ± 3) K, these parameters are $k_0 = (1.7 \pm 0.5) \times 10^{-29}$ cm^6 molecule^{-2} s^{-1}, $k_\infty = (10 \pm 2) \times 10^{-13}$ cm^3 molecule^{-1} s^{-1}. Our experimental results are consistent with addition as the dominant path, in agreement with flash photolysis investigations and with the existence of a fast reaction with NO_2 of the (OH—benzene) radical adduct. A numerical simulation shows that this latter reaction should have a rate constant of $(4 \pm 2) \times 10^{-11}$ cm^3 molecule^{-1} s^{-1} at 353 K.

Key words: gas phase kinetics, discharge flow, resonance fluorescence, reaction of OH with benzene, tropospheric chemistry.

A. GOUMRI, J. F. PAUWELS et P. DEVOLDER. Can. J. Chem. **69**, 1057 (1991).

Opérant dans la région de la diminution de la pression et utilisant la fluorescence de resonance OH par la technique de l'écoulement continue, on a déterminé la constante de vitesse k_1 de la réaction

$$OH + C_6H_6(+ He) \longrightarrow \text{produits } (+ He)$$

A partir de mesures systématiques effectuées à cinq pressions différentes, entre 0,5 et 9,5 torr, on a déduit les paramètres de Troe, k_0 et k_∞ (avec $F_c = 0,6$), à deux températures : à la température ambiante et à 353 K. Pour la première, (297 ± 3) K, ces paramètres sont : $k_0 = (1,7 \pm 0,5) \times 10^{-29}$ cm^6 molecule^{-2} s^{-1} et $k_\infty = (10 \pm 2) \times 10^{-13}$ cm^3 molecule^{-1} s^{-1}. Nos données expérimentales sont en accord avec un mécanisme impliquant une addition comme voie principale; cette conclusion est en accord avec les résultats de la photolyse éclair et avec le fait que le NO_2 réagit rapidement avec l'adduit radicalaire (OH—benzène). Une simulation numérique montre que cette dernière réaction devrait avoir une vitesse de réaction de $(4 \pm 2) \times 10^{-11}$ cm^3 molecule^{-1} s^{-1}, à 353 K.

Mots clés : cinétique en phase gazeuse, fluorescence de résonance, réaction de OH avec le benzène, chimie de la troposphère, technique de l'écoulement continue.

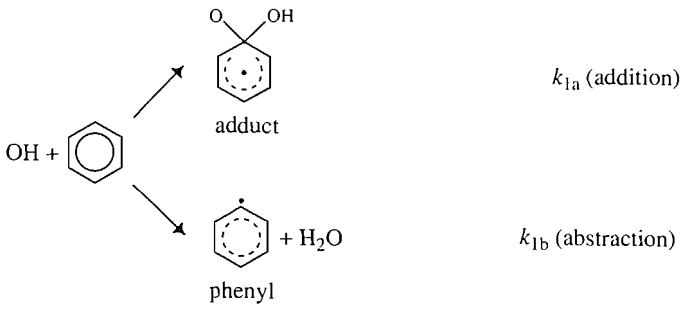
[Traduit par le rédaction]

Introduction

Aromatic hydrocarbons produced by car engines are important pollutants of the urban atmosphere (1); they are suspected to play an important role in the mechanism of photochemical smog, mainly via intermediates or end products of their trophospheric oxidation (nitroaromatics, cresols, ring opening products, ...) (1, 2). Benzene and its methylated derivatives (toluene, xylenes) are the most abundant trophospheric aromatic hydrocarbons (1, 2).

At room temperature, gas phase trophospheric oxidation of these aromatics is initiated by an attack by the OH radical (1–3) with a major contribution from the addition route.

For benzene, the abstraction route leads to a phenyl radical whereas the addition route gives a conjugated adduct radical, the hydroxycyclohexadienyl radical:



k_{1a} (addition)

k_{1b} (abstraction)

At higher temperatures ($T > 500$ K), direct (4) or end product (5) investigations are explained assuming the abstraction route is the dominant process.

This OH—benzene adduct radical has been directly observed by Zellner *et al.* (6) by long path absorption in the UV range. A geometry of this radical adduct has been proposed by Sloane and Brudzynski (7). The various subsequent steps of tropospheric oxidation have been discussed thoroughly by Atkinson *et al.* in a series of reviews (3) and by others (2). The measurements of the rate constant $k_1 = (k_{1a} + k_{1b})$ by absolute techniques have been the subject of various investigations. To clarify the following bibliographic discussion, let us classify these investigations into three categories: (i) measurements of k_1 at room temperature above 10 torr (i.e., in the high pressure limiting range), (*ii*) variable temperature measurements of k_1, (*iii*) variable pressure measurements of k_1 in the fall-off range (below 10 torr).

(i) Room temperature measurements in the high pressure range (4a, 8–12)

All measurements of k_1 at room temperature in the 25–760 torr pressure range have been performed with the same technique: flash (or laser) photolysis technique with the detection of OH by resonance fluorescence. There is satisfactory agreement between the various authors; from their data it is apparent that above ~25 torr (helium or argon), k_1 is already in the high

Printed in Canada / Imprimé au Canada

Can. J. Chem. Downloaded from www.nrcresearchpress.com by 84.41.108.74 on 09/07/12
For personal use only.

Can. J. Chem. Downloaded from www.nrcresearchpress.com by 84.41.108.74 on 09/07/12
For personal use only.

pressure regime, with an average value of

$$k_1 = (11 \pm 2) \times 10^{-13} \text{ cm}^3 \text{ molecule}^{-1} \text{ s}^{-1}$$

(ii) Variable temperature measurements (4, 8b, 9–11)

Variable temperature measurements have also been achieved by the flash photolysis technique. They fall in two temperature ranges, low temperature (i.e. below 400 ~ 450 K) and high temperature (up to 1000 K). From their observation of non-exponential OH decays (i.e. ln [OH] is non-linear versus reaction time in reactant pseudo-first order conditions) in the temperature range 320 ~ 400 K, a few authors (4*a*, 9–11) suggest a contribution from the unimolecular decay of the adduct radical:

$$C_6H_6OH \rightarrow C_6H_6 + OH \qquad k_{-1a}$$

This suggestion has been checked by Zetzsch *et al.* (8*b*, 13) on a quantitative basis: these authors were able to derive the variation of k_{-1a} versus temperature (up to 353 K):

[1] $$k_{-1a} = 3 \times 10^{12} \exp(-8200/T) \text{ s}^{-1}$$

However, in contrast to room temperature results, the measured values of k_1 are not in good agreement in this intermediate range (around 400 K), ranging from 1.93×10^{-13} cm^3 molecule^{-1} s^{-1} (11) to $4 \sim 5 \times 10^{-13}$ cm^3 molecule^{-1} s^{-1} (9). This poor agreement is probably connected with the increasing onset of reaction [−1*a*]. At much higher temperatures (above 450 ~ 500 K), the reaction rate k_1 exhibits smaller values (i.e., below that at room temperature) and typical activation energy characteristic of abstraction reactions (4); the contribution of the addition route is considered to become negigible at these high temperatures due to the quickly established equilibrium:

$$OH + C_6H_6 \text{ (+M)} \rightleftarrows C_6H_6OH \text{ (+M)}$$

From their high temperature measurements, Tully *et al.* (4*a*) and Madronich and Felder (4*b*) can thus derive the following abstraction reaction rates (cm^3 molecule^{-1} s^{-1}):

[2] $$k_{1b} = 2.4 \times 10^{-11} \exp(-2260/T) \qquad (4a)$$

[3] $$k_{1b} = 3.5 \times 10^{-11} \exp(-2300/T) \qquad (4b)$$

(iii) Variable pressure measurements of k_1

In the fall-off range of k_1, below 20 ~ 25 torr, only three measurements have been reported: with the flash photolysis resonance fluorescence technique, Zellner *et al.* (9) and Zetzsch *et al.* (8*b*) both use argon as the diluent gas, with a large scatter of experimental data (Fig. 1) and the investigation of Baulch *et al.* (14) uses the same technique as ours (discharge flow resonance fluorescence).

The results of these three investigations are gathered in Fig. 1. It is obvious that the agreement is bad.

Our present measurements at room temperature have been performed to precise the pressure dependence of k_1 and to derive the Troe parameters k_0 and k_∞ (15). It is also interesting to compare the present results with those of Baulch *et al.* (14) who used the same technique and with the results of our previous investigation (16*a*) of the rate constant of the (OH + tolueme → products) reaction under the same conditions. Furthermore, we have chosen to investigate the temperature behavior of k_1 in the range 293–383 K for the following reasons: (*i*) OH additions on aromatic rings usually exhibit low (positive or negative) temperature coefficients (10) and (*ii*)

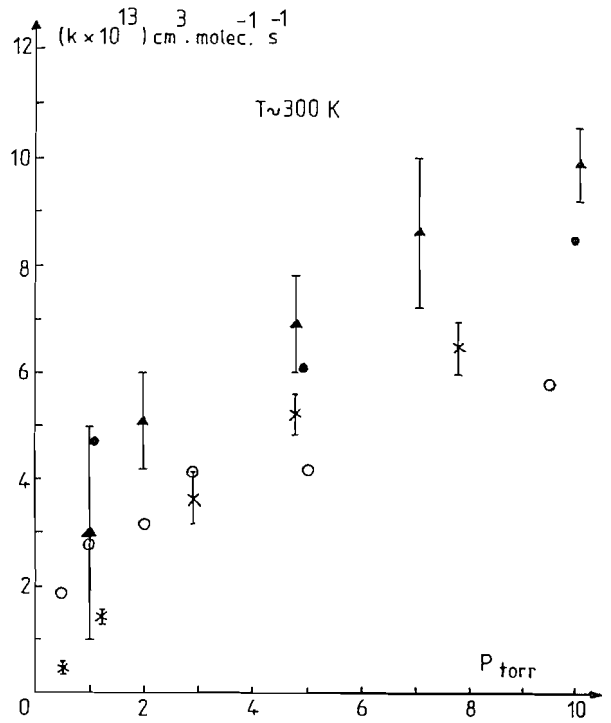


FIG. 1. Comparison of the measurements of k_1, versus pressure in the fall-off range: ▲, ref. 8; ●, ref. 9; ×, ref. 14; ○, this work.

as mentioned above, a few authors report the observation of non-exponential OH decay plots around 353 K. The latter observation needs further investigation.

Experimental

The experimental set up for OH resonance fluorescence and detection by photon counting has been descibed elsewhere (16*b*). Only some specific details of the present experiments are presented below.

The flow rate of benzene from degassed liquid is measured by diverting the pure benzene vapor flow (downstream the needle valve) from the flow tube to an evacuated calibrated reservoir and measuring the rate of pressure increase with an absolute capacitive gauge (0–10 torr). Other flow rates (He, H_2/He, NO_2/He) are regulated by flow controllers periodically checked by absolute techniques (wet testmeter or $\Delta P/\Delta t$ method). The flow tube pressure is measured at the fluorescence cell with an absolute 0–10 torr capacitive manometer. The pressure gradient (Poiseuille law) is taken into account to compute a mean corrected pressure P_c:

[4] $$P_c = P_{obs} + (\Delta P/\Delta z)\Delta z \text{ with } \Delta P/\Delta z = 5.9\ 10^{-3}\ \mu v/r^2$$

where μ = helium viscosity, v = flow velocity, r = tube radii. A systematic upstream correction of $\Delta z = 30$ cm, corresponding to the center of most OH decay curves, is applied.

For most experiments, OH radicals have been generated by the classical O atom transfer reaction:

$$H + NO_2 \rightarrow OH + NO$$

$$k = 1.3 \times 10^{-10} \text{ cm}^3 \text{ molecule}^{-1} \text{ s}^{-1}$$

All these experiments have been performed with a large excess of initial NO_2 concentrations over initial H concentrations ([OH] ~ 5 to 10×10^{11} molecules cm^{-3}, [NO_2] ~ 5 to 50×10^{12} molecules cm^{-3}) because we noticed a decrease of the slope of the OH decay plot at lower NO_2 concentrations [NO_2] < 2×10^{12}); provided the use of these large NO_2 concentrations, the OH decay plots were insensitive to NO_2 concentrations.

It is well known that the main drawback of the flow tube technique

Can. J. Chem. Downloaded from www.nrcresearchpress.com by 84.41.108.74 on 09/07/12
For personal use only.

is the uncontrolled influence of wall reactions on the overall kinetics. Concerning the aromatics or related compounds, a few authors have already mentioned the presence of unstable signals; Bonanno *et al.* (ref. 17: O + benzene by ESR and mass spectrometry) report the existence of a steady slow decay of the oxygen atom concentration; also, Knutti and Buhler (ref. 18: H + benzene by mass spectrometry with a Teflon coating), mention the existence of very long stabilization times for benzene signals. On the contrary, these difficulties are not mentioned by a few other authors; for example, neither by Tappe *et al.* (ref. 19: O + various aromatics by mass spectrometry in a clean quartz reactor), Kim *et al.* (ref. 20: H + benzene by ESR and mass spectrometry in a boric acid coated tube), nor Hoyermann *et al.* (ref. 21: H + benzene by mass spectrometry with a quartz tube cleaned with HF). However, a very recent flow tube study of the kinetics of NH_2 with toluene has stressed the importance of the coating of the flow tube (22).

As a consequence, we have paid particular attention to the choice of the flow tube coating. Preliminary experiments with the thick Teflon flow tube used previously (16*b*) gave high and irreproducible values of k_1, larger than the value observed at 760 torr by flash photolysis techniques. We faced a similar situation during our previous experiments devoted to the measurements of the (OH + toluene → products) reaction rate (16*a*). These inconsistencies, already noticed by Le Bras *et al.* in their study of OH + thiophene (23) reaction, led us not to use Teflon. In contrast, coating with widespread halocarbon waxes (24) (either the 12-00 or 15-00 waxes), gave stable and reproducible signals, with low values of k_1 typical of the low pressure range of a fall-off behavior. Also the observed variation of k_1 with pressure (see below) can be fitted with a Troe-type fall-off curve consistent with high pressure measurements (100 to 760 torr) of k_1. This was also true for our previous measurements devoted to (OH + toluene → products) reaction rate measurements (16*a*) with which the present results appear to be self-consistent. We have thus performed all our measurements with the flow tube and the injector coated with halocarbon waxes.

A few experiments have also been performed to measure the rate constant of OH with C_6D_6:

$$OH + C_6D_6 + He \rightarrow \text{products} \qquad k_1'$$

in the following experimental conditions: 1 torr, 353 K. For that purpose, taking into account the very close vapor pressures of C_6H_6 and C_6D_6 (25), a specific experimental protocol is followed to measure the ratio k_1/k_1': a known flow rate of C_6H_6 is first established and the curve ln [OH] versus reaction distance is plotted; then, with all other experimental parameters remaining unchanged, the reservoir of C_6H_6 is changed for a reservoir of C_6D_6. The ratio of the pseudo-first order rate constants is thus a direct measure of k_1/k_1'. Within experimental uncertainty, we find

$$k_1/k_1' = (1 \pm 0.1) \text{ (at 353 K, 1 torr).}$$

Results and discussion

Systematic measurements of k_1 have been performed at two temperatures, room temperature (297 ± 3) K and 353 K; and five pressures (torr): 0.5, 1, 2, 3, 4, ~9.

A few experiments at intermediate temperatures and pressures have been performed to confirm the tendencies established by systematic measurements. The results of the systematic measurements are gathered in Table 1. A few OH decay plots corresponding to variable benzene concentrations are presented in Fig. 2. A few resulting pseudo-first order plots for varying temperature or helium pressure are presented in Fig. 3. Finally, the variation of k_1 as a function of pressure between 0.5 and 9 torr is presented in Figs. 4 (~300 K) and 5 (353 K).

Figures 4 and 5 show that, at both temperatures, the variation of k_1 with pressure exhibits a clear behavior of fall-off

TABLE 1. Averaged values of the rate constant k_1 (in 10^{-13} cm^3 molecule^{-1} s^{-1}) as a function of pressure for two temperatures; to characterize the scatter, the uncertainty is arbitrarily taken as the largest difference k_1 (average) − k_1 (experiment); the number of different experiments in parentheses

P	k_1	
torr	353 K	(297 ± 3) K
0.5	1.25 ± 0.8 (4)	1.93 ± 0.6 (2)
1	1.82 ± 0.7 (6)	2.7 ± 0.7 (4)
2	2.4 ± 0.5 (2)	3.15 ± 0.5 (2)
3	2.25 ± 1 (4)	4.1 ± 0.7 (2)
5	3.92 ± 1 (3)	4.1 ± 0.7 (2)
9	4.65 ± 1 (2)	5.7 ± 1 (3)

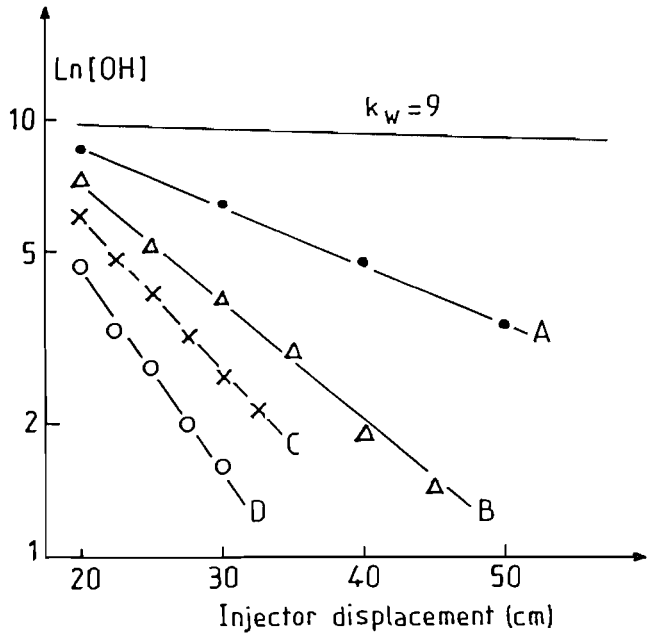


FIG. 2. Examples of a few OH decay plots (ln [OH] versus reaction distance) at 300 K and 1 torr; flow velocity = 1660 cm s^{-1}. Notations as follows: benzene concentration (in 10^{13} molecules cm^{-3}) first order decay rate constant (s^{-1}): *A*, 12.7–55; *B*, 26.9–106; *C*, 38.7–143; *D*, 52.2–182.

range. Moreover, over the whole pressure range covered by the experiments, k_1 exhibits a negative temperature dependency (Table 1), this corresponds to a "negative" activation energy ranging from −0.9 kcal mol^{-1} (at ~9 torr) to −2 kcal mol^{-1} (at 1 torr). These slight negative activation energies are in agreement with the results of Wallington *et al.* (11) and Zetzsch and co-workers (36) but in contrast to literature data by Perry *et al.* (10), Tully *et al.* (4*a*), and Lorenz and Zellner (9).

Derivation of Troe parameters

All our available experimental observations: (*i*) existence of a fall-off behavior, (*ii*) absence of isotope effect, and (*iii*) existence of a slightly negative temperature dependence, suggest that the addition channel (association reaction) should be the dominant one among the following possible channels:
Additional channel, i.e., formation of the stabilized adduct rad-

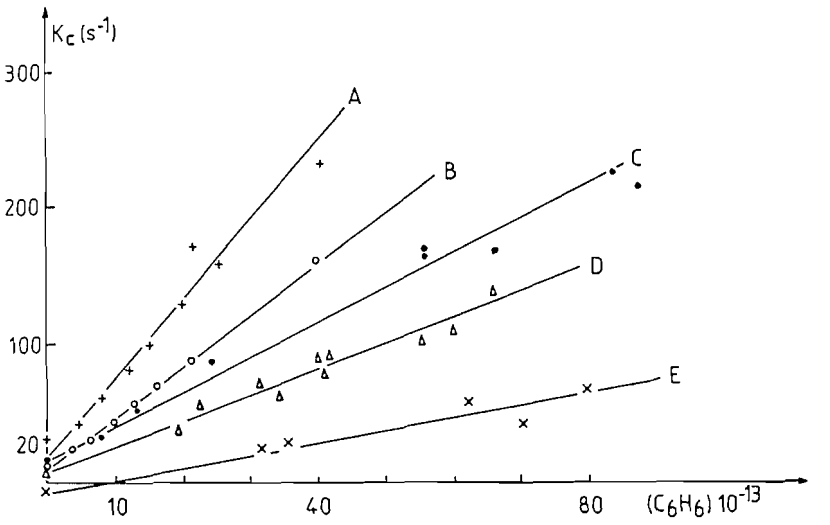


FIG. 3. First-order rate constants versus C_6H_6 concentrations for a few experiments: *A* (297 K, 9.6 torr), *B* (353 K, 4 torr), *C* (328 K, 2 torr), *D* (353 K, 1 torr), *E* (353 K, 0.5 torr).

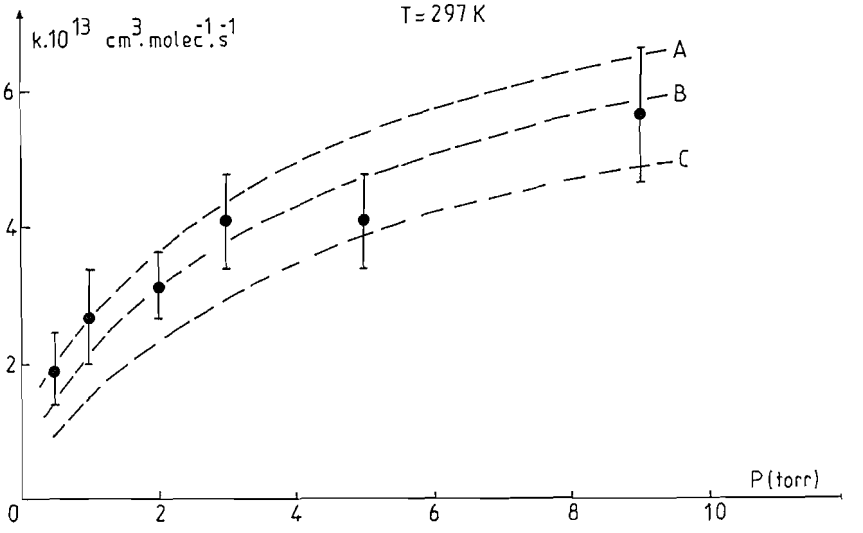


FIG. 4. Experimental results (×) at 297 K. The dotted lines correspond to three Troe theoretical curves with $k_\infty = 10^{-12}$ cm^3 molecule^{-1} s^{-1} and variable k_0 (in 10^{-29} cm^6 molecule^{-1} s^{-1}): *A* ($k_0 = 2.5$), *B* ($k_0 = 1.7$) best fit, *C* ($k_0 = 1$).

ical is

$$OH + C_6H_6\ (+M) \rightleftarrows C_6H_6OH^{\cdot} + (M) \qquad k_{1a},\ k_{-1a}$$

Abstraction channel, i.e. formation of phenyl radical is

$$OH + C_6H_6 \rightarrow C_6H_5^{\cdot} + H_2O \qquad k_{1b}$$

Formation of phenol is

$$OH + C_6H_6 \rightarrow C_6H_5OH + H \qquad k_{1c}$$

Formation of the phenoxy radical is

$$OH + C_6H_6 \rightarrow C_6H_5O^{\cdot} + H_2 \qquad k_{1d}$$

The suggestion ($k_{1a} \gg k_{1b}$, k_{1c}, k_{1d}) is also supported by (*i*) the available thermodynamic data and (*ii*) an extrapolation of the high temperature measurements of k_{1b} to the low temperature range.

(i) Thermochemical data

Figure 6 gathers the known thermochemical data for channels [1*a*] to [1*d*] extracted from reviews (26, 27) or articles by Zetzsch *et al.* (8*b*, *c*) and Manion and Louw (28). Inspection of Fig. 6 shows that the addition channel should be dominant at low temperature.

(ii) Extrapolated data

The extrapolated values of k_{1b} from both high temperature studies (4*a*, *b*)

$$297\ K \cdot k_{1b} = 0.13 \text{ or } 0.16 \times 10^{-13}\ cm^3\ molecule^{-1}\ s^{-1}$$

$$353\ K \cdot k_{1b} = 0.4 \text{ or } 0.52 \times 10^{-13}\ cm^3\ molecule^{-1}\ s^{-1}$$

also confirm the low contribution of the abstraction channel at low temperature (although such a large extrapolated temperature range may be questionable).

The above discussion allows us to compute the Troe parameters k_0 and k_∞ for an association reaction from a fit of our experimental data (k_1 versus pressure) to the following theoretical curve (15):

Can. J. Chem. Downloaded from www.nrcresearchpress.com by 84.41.108.74 on 09/07/12
For personal use only.

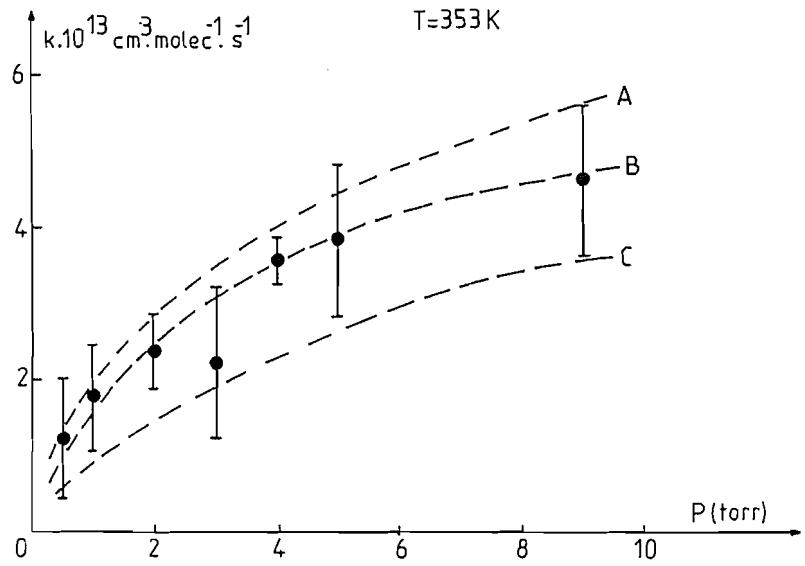


FIG. 5. Experimental results (×) at 353 K. The dotted lines correspond to three Troe theoretical curves with $k_\infty = 10^{-12}$ cm^3 molecule^{-1} s^{-1} and variable k_0 (in 10^{-29} cm^6 molecule^{-2} s^{-1}): *A* ($k_0 = 1.5$), *B* ($k_0 = 1$) best fit, *C* ($k_0 = 0.5$).

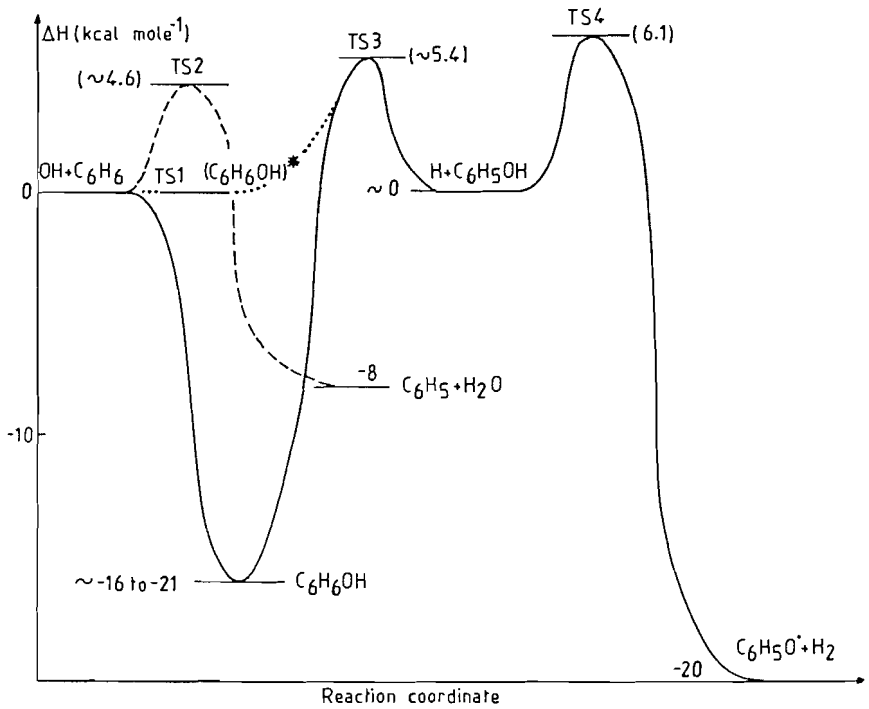


FIG. 6. Probable reaction enthalpies and activation energies of a few reaction paths in the (OH + benzene → products) reaction system.

[5] $$\log k = \log [k_0/(1 + k_0/k_\infty)] + \log \{0.6/\{1 + [\log(k_0/k_\infty)]^2\}\}$$

The following values are derived:
At (297 ± 3) K

$$k_0 = (1.7 \pm 0.5) \times 10^{-29} \text{ cm}^6 \text{ molecule}^{-2} \text{ s}^{-1}$$

$$k_\infty = (10 \pm 2) \times 10^{-13} \text{ cm}^3 \text{ molecule}^{-1} \text{ s}^{-1}$$

At 353 K

$$k_0 = (1 \pm 0.2) \times 10^{-29} \text{ cm}^6 \text{ molecule}^{-2} \text{ s}^{-1}$$

$$k_\infty = (10 \pm 1) \times 10^{-13} \text{ cm}^3 \text{ molecule}^{-1} \text{ s}^{-1}$$

The corresponding theoretical (predicted) Troe curves are plotted as lines *B* in Figs. 4 and 5 together with experimental data. As a whole, the agreement is good. From our values of k_0 and k_∞ at room temperature, it is possible to derive the value of the rate constant at atmospheric pressure: 9.3×10^{-13} cm^3 molecule^{-1} s^{-1}, which is in reasonable agreement with direct measurements or extrapolations of flash photolysis experiments.

Can. J. Chem. Downloaded from www.nrcresearchpress.com by 84.41.108.74 on 09/07/12
For personal use only.

Can. J. Chem. Downloaded from www.nrcresearchpress.com by 84.41.108.74 on 09/07/12
For personal use only.

It is interesting to compare our room temperature values of k_0 and k_∞ with those of other authors. With the standard broadening factor $F_c = 0.6$, Zetzsch *et al.* find (in argon) (8*b*):

$$k_0 = 3.02 \times 10^{-29} \text{ cm}^6 \text{ molecule}^{-2} \text{ s}^{-1}$$

$$k_\infty = 1.3 \times 10^{-12} \text{ cm}^3 \text{ molecule}^{-1} \text{ s}^{-1}$$

With the same fixed value of k_∞ as Zetzsch, Baulch *et al.* (14) compute from a best fit:

$$F_c = 1.1 \qquad k_0 = 4.4 \times 10^{-30} \text{ cm}^6 \text{ molecule}^{-2} \text{ s}^{-1}$$

Since this value of F_c is considered too large, they also compute another k_0 adopting the standard $F_c = 0.6$: $k_0 = 1.36 \times 10^{-29}$ cm^6 molecule^{-2} s^{-1} (14). However, this latter set of parameters exhibits a bad agreement between prediction and experiment, especially at low pressures (below 2 torr). A comparison of the experimental results from both discharge flow experiments (ref. 14 and this work) is plotted in Fig. 7 together with the two best fitted curves according to expression [5].

Role of adduct secondary reactions

As mentioned in the Experimental section, the measurements of k_1 have been purposely performed using large NO_2 concentrations, in the 10^{13} molecules cm^{-3} range, to avoid OH regeneration via reaction [−1a]; this is connected to the expected role of NO_2 as an adduct scavenger:

$$C_6H_6OH + NO_2 \rightarrow \text{products} \qquad k_4$$

since large values of k_4 have been measured (6, 13); two measurements of k_4 are available, one by Zellner *et al.* (6): $k_4 = 0.85 \times 10^{-11}$ cm^3 molecule^{-1} s^{-1}, the other by Zetzsch *et al.* (13): $k_4 = 2.7 \times 10^{-11}$ cm^3 molecule^{-1} s^{-1}, both at room temperature.

However, to assess the correctness of our measurements and to evaluate k_4, we have performed a series of experiments and the corresponding simulations with a single variable parameter: the NO_2 concentration. An example of such measurements (at 1 torr and 353 K) is presented in Fig. 8. It appears that when $[NO_2]$ decreases from 10^{14} molecules cm^{-3} to ~0 (excess hydrogen atoms), the slope of the OH decay also decreases; a few experiments performed with the NO_2 free method (29) (i.e. when OH is formed by $F + H_2O \rightarrow HF + OH$) are also in agrement with the experiments at low NO_2 concentrations.

The corresponding simulations are based on the following mechanism: Approach to the equilibrium

$$OH + C_6H_6 + (M) \rightleftarrows \text{products} (+M) \qquad k_{1a,-1a}$$

Wall reactions

$$OH \rightarrow \text{products} \qquad k_w$$

$$\text{adduct} \rightarrow \text{products} \qquad k_w'$$

Adduct reactions

$$\text{Adduct} + NO_2 \rightarrow \text{products} \qquad k_4$$

$$\text{Adduct} + NO \rightarrow \text{products} \qquad k_4'$$

Reactant concentrations (C_6H_6, NO_2, NO, OH) and rate constants k_{1a} and k_w are from this work. Other rate constants are chosen as described below:

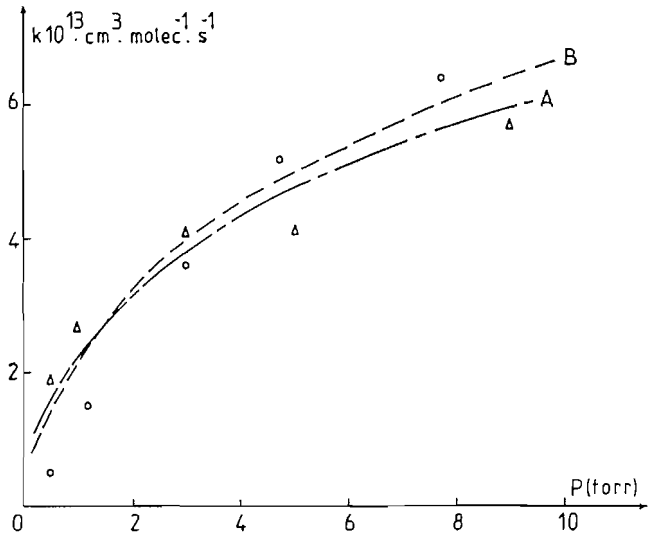


FIG. 7. Comparison of experimental and fitted curves from both discharge flow experiments (ref. 14, and this work). Experimental data: ○, ref. 14; △, this work. Troe fits: *A* (this work), *B* (ref. 14: $k_0 = 1.36 \times 10^{-29}$ cm^6 molecule^{-2} s^{-1}, $k_\infty = 1.4 \times 10^{-13}$ cm^3 molecule^{-1} s^{-1}).

(*i*) From the Arrhenius plot established by Zetzsch *et al.* (13) at 100 torr, k_{-1a} increases from ~5 s^{-1} at room temperature to ~300 s^{-1} at 353 K. However, these values of the reverse reaction constant rate are measured in the high pressure range of the fall-off curve (i.e. when k_{1a} and k_{-1a} approach their high pressure limiting values). To deduce the reduced value of k_{-1a} valid at our experimental pressure (1 torr), we have simply computed the following reducing factor from our data concerning the forward reaction: k_{1a} (1 torr)/$k_{1\infty}$; we can thus derive the values of k_{-1a} (at 1 torr) of ~1 s^{-1} at 297 K and ~40 s^{-1} at 353 K. Though the room temperature value of k_{-1a} is entirely negligible, this is no longer true at 353 K.

(*ii*) The value of $k_4' = 0$ remeasured recently after extensive purification of NO has been preferred (13).

(*iii*) The two last rate constants: $k_w' = (60 \pm 20)$ s^{-1} and $k_4 = (4 \pm 2) \times 10^{-11}$ cm^3 molecule^{-1} s^{-1} have been estimated from a fit of computed OH decay plots such as presented in Fig. 8; it is worth mentioning that this value of adduct wall recombination ($k_w' = 60$ s^{-1}) is a typical of one for benzyl-type radicals presently studied in the same flow tube (30) or for other adduct radicals (31). A few simulated OH decay curves (at 353 K, 1 torr) are presented in Fig. 8 for varying NO_2 concentrations: the first milliseconds, which reflect the approach to equilibrium, cannot be compared to the experiments since they correspond to the reaction distance between the oven and the center of the fluorescence cell; the end part of the curves is almost strictly exponential with a decay rate constant depending mainly of $[NO_2]$.

The agreement between simulations and experiments (at 353 K) is acceptable. The same kind of behavior has been observed during our previous work devoted to the (OH + toluene → adduct) investigations (16a); also, this is in agreement with the quantitative measurements of Zetzsch *et al.* (8).

It is also worth mentioning that our observations and simulations are quite similar to those presented by the system OH + $CS_2 \rightleftarrows$ adduct in the presence of an adduct reaction with O_2 (32, 33).

On the contrary, at room temperature, due to a much lower value of k_{-1a}, the contribution of reaction [−1a] is negligible

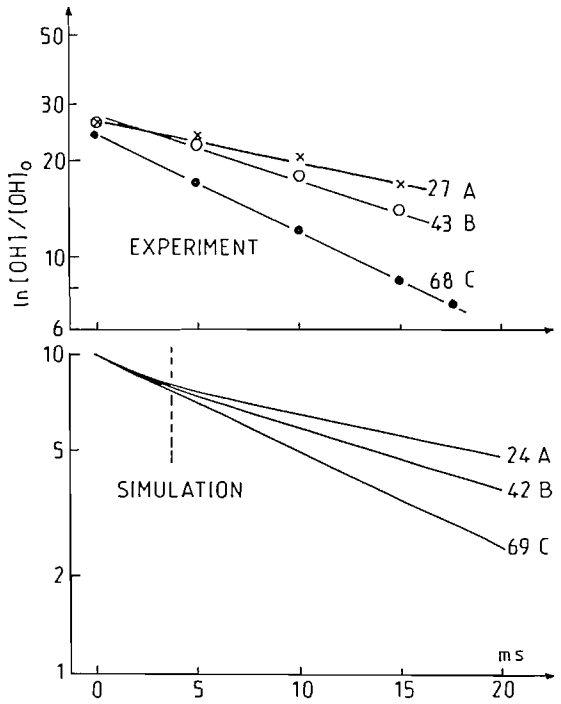


FIG. 8. Examples of experimental (up) and computed (down) OH decay plots. *Experimental data* (concentrations in molecules cm^{-3}): $P = 1$ torr, $T = 353$ K, $[OH] = 6 \times 10^{11}$. Curve *A*: $[C_6H_6] = 3.92 \times 10^{14}$, $[NO_2] = 4.5 \times 10^{13}$; curve *B*: $[C_6H_6] = 3.41 \times 10^{14}$, $[NO_2] = 1.7 \times 10^{12}$; curve *C*: $[C_6H_6] = 2.76 \times 10^{14}$, $[NO_2] = 0$. The numbers on the curves correspond to the measured decay rate (in s^{-1}) *Parameters of the simulation* (see text): concentrations as above, $k_{-1a} = 1.8 \times 10^{-13}$ cm^3 molecule^{-1} s^{-1}, $k_{-1a} = 40\ s^{-1}$, $k_w = 0$, $k_w' = 60\ s^{-1}$, $k_4 = 4 \times 10^{-11}$ cm^3 molecule^{-1} s^{-1}, $k_4' = 0$. The first 4 ms (left of dotted line), which correspond to the approach to equilibrium, are not observable (see text); the numbers of the curves correspond to the final exponential decay rate (s^{-1}).

within our reaction times (<40 ms). As shown by Baulch *et al.* (14), even in the absence of NO_2 (excess [H]), the contribution of reaction [−1a] is negligible. Our experiments confirm these expectations.

To conclude, the (fortunate) existence of a high reaction rate: adduct + NO_2 → products, together with our large NO_2 concentrations, explains our apparent discrepancy with flash photolysis non-exponential decays at 353 K.

At room temperature, our experimental results are in reasonable agreement with those of Baulch *et al.* (14), except in the low pressure range (below 2 torr) where we observe larger values. Though such a disagreement is not unusual, the use of excess [H] (over $[NO_2]$) by these authors (D. L. Baulch, private communication), in contrast to our experimental conditions, is one apparent difference. Thus, we tentatively assign the lower rate constants observed in ref. 14 to OH regeneration via the following reaction of the adduct with H atoms:

$$H + C_6H_6OH \rightarrow C_6H_7 + OH$$

Such a reaction is expected to be extremely fast by analogy with the two following closely related reactions of H atoms, which exhibit collision rates: (*i*) with the OH–ethene adduct (ref. 34: $k = 10^{-10}$ cm^3 molecule^{-1} s^{-1}, (*ii*) with the benzyl radical (ref. 35: $k = 5.5 \times 10^{-10}$ cm^3 molecule^{-1} s^{-1}), which is a conjugated radical with very similar spectroscopic properties to cyclohexadienyl type radicals.

Conclusion

The rate of the reaction OH + C_6H_6 + He → products has been investigated by discharge flow resonance fluorescence. From systematic measurements at two temperatures (297 ± 3 and 353 K) in the fall-off range velow 10 torr, the following Troe parameters have been derived (with $F_c = 0.6$):
At (297 ± 3) K

$$k_0 = (1.7 \pm 0.5) \times 10^{-29} \text{ cm}^6 \text{ molecule}^{-2} \text{ s}^{-1}$$

$$k_\infty = (10 \pm 2) \times 10^{-13} \text{ cm}^3 \text{ molecule}^{-1} \text{ s}^{-1}$$

At 353 K

$$k_0 = (1 \pm 0.2) \times 10^{-29} \text{ cm}^6 \text{ molecule}^{-2} \text{ s}^{-1}$$

$$k_\infty = (10 \pm 1) \times 10^{-13} \text{ cm}^3 \text{ molecule}^{-1} \text{ s}^{-1}$$

In agreement with flash photolysis investigations and literature data our results are consistent with the formation of a radical adduct (OH–benzene adduct) as the primary reaction step. At 353 K, the influence of the NO_2 concentration can be rationalized on the basis of a fast reaction with NO_2 of this OH–benzene adduct ($(4 \pm 2) \times 10^{-11}$ cm^3 molecule^{-1} s^{-1}), in good agreement with the recent results of Zetzsch *et al.* (36).

Acknowledgements

We thank D. L. Baulch (University of Leeds, U.K.) for a few discussions and C. Zetzsch and co-workers for both communication and discussion of their recent results (36).

1. (*a*) J. Arey, B. Zielinska, R. Atkinson, and S. M. Aschmann. Int. J. Chem. Kinet. **21**, 775 (1989); (*b*) R. Atkinson and S. M. Aschmann. Int. J. Chem. Kinet. **21**, 355 (1989); (*c*) R. Atkinson, S. M. Aschmann, J. Arey, and W. P. L. Carter. Int. J. Chem. Kinet. **21**, 801 (1989).
2. (*a*) J. A. Leone and J. H. Seinfeld. Int. J. Chem. Kinet. **16**, 159 (1984); (*b*) M. W. Gery, D. L. Fox, H. E. Jeffries, L. Stockburger, and W. S. Weathers. Int. J. Chem. Kinet. **17**, 931 (1985).
3. (*a*) R. Atkinson and A. C. Lloyd. J. Phys. Chem. Ref. data, 13, no. 2 (1984); (*b*) R. Atkinson. Chem. Rev. **86**, 69 (1986); (*c*) R. Atkinson. J. Phys. Chem. Ref. Data, Monograph 1 (1989).
4. (*a*) F. P. Tully, A. R. Ravishankara, R. L. Thompson, J. M. Nicovich, R. C. Shah, N. M. Kreutter and P. H. Wine. J. Phys. Chem. **85**, 2262 (1981); (*b*) S. Madronich and W. Felder. J. Phys. Chem. **89**, 3556 (1985).
5. P. Mulder and R. Louw. (*a*) Recl. Trav. Chem. Pays-Bas, **103**, 282 (1984); (*b*) Int. J. Chem. Kinet. **20**, 577 (1988).
6. R. Zellner, B. Fritz, and M. Preidel. Chem. Phys. Lett. **121**, 412 (1985).
7. T. M. Sloane and R. J. Brudzynski. J. Chem. Phys. **72**, 4394 (1980).
8. (*a*) A. Wahner and C. Zetzsch. J. Phys. Chem. **87**, 4954 (1983); (*b*) F. Witte, E. Urbanik, and C. Zetzsch. J. Phys. Chem. **90**, 3251 (1986); (*c*) F. Witte. Dessertation. Bochum. 1987.
9. R. Zellner and K. Lorentz. Ber. Bunsenges Phys. Chem. **87**, 629 (1983).
10. R. A. Perry, R. Atkinson, and J. N. Pitts Jr. J. Phys. Chem. **81**, 296 (1977).
11. T. J. Wallington, D. M. Neuman, and M. J. Kurylo. Int. J. Chem. Kinet. **19**, 725 (1987).
12. D. D. Davies, W. Bollinger, and S. Fischer. J. Phys. Chem. **79**, 293 (1975).
13. C. Zetzsch, R. Koch, M. Siese, F. Witte, and P. Devolder. Proc. 5th European Symposium on Physicochemical behaviour of atmospheric pollutants. Reidel Publ. Co., Dordrecht. (1989).

Can. J. Chem. Downloaded from www.nrcresearchpress.com by 84.41.108.74 on 09/07/12
For personal use only.

14. D. L. BAULCH, I. M. CAMPBELL, and S. M. SAUNDERS. J. Chem. Soc. Faraday Trans. II, **84**, 377 (1988).
15. J. TROE. J. Phys. Chem. **83**, 114 (1979).
16. (*a*) N. BOURMADA, M. CARLIER, J-F. PAUWELS, and P. DEVOLDER. J. Chim. Phys. **85**, 881 (1988); (*b*) P. DEVOLDER, M. CARLIER, J. F. PAWELS, and L. R. SOCHET. Chem. Phys. Lett. **111**, 94, (1984).
17. R. A. BONANNO, P. KIM, J-H. LEE, and R. B. TIMMONS. J. Chem. Phys. **57**, 1377 (1972).
18. R. KNUTTI and R. E. BUHLER. Chem. Phys. **7**, 229 (1975).
19. M. TAPPE, V. SSCHLIEPHAKE, and H. GG WAGNER. Z. Phys. Chem. **162**, 129 (1989).
20. M. KIM, J-H. LEE, R. J. BONANNO, and R. B. TIMMONS. J. Chem. Phys. **59**, 4593 (1973).
21. K. HOYERMANN, A. W. PREUSS, and H. GG WAGNER. Ber. Bunsenges Phys. Chem. **79**, 156 (1975).
22. W. HACK, H. KURZSKE, H. ROUVEIROLLES, and H. GG WAGNER. Ber. Bunsenges Phys. Chem. **90**, 1210 (1986).
23. D. MARTIN, J-L. JOURDAIN, and G. LEBRAS. Int. J. Chem. Kinet. **17**, 1247 (1985).
24. KMZ Chemicals, Leatherhead, U.K.
25. Handbook of physics and chemistry. The Chemical Rubber Co.
26. S. W. BENSON. Thermochemical kinetics. 2nd ed. John Wiley and Sons. 1976.
27. D. F. MCMILLEN and D. M. GOLDEN. Ann. Rev. Phys. Chem. **33**, 493 (1982).
28. J. A. MANION and R. LOUW. J. Phys. Chem. **93**, 3563 (1989).
29. L. F. KEYSER. J. Phys. Chem. **85**, 3667 (1981).
30. A. GOUMRI, J. F. PAUWELS, J. P. SAWERYSYN, and P. DEVOLDER. Chem. Phys. Lett. **171**, 303 (1990).
31. D. MARTIN, J. L. JOURDAIN, and G. LE BRAS. J. Phys. Chem. **90**, 4143, (1986).
32. A. J. HYNES, P. H. WINE, and J. M. NICOVICH. J. Phys. Chem. **92**, 3846 (1988).
33. T. P. MURRELLS, E. R. LOVEJOY, and A. R. RAVISHANKARA. J. Phys. Chem. **94**, 2381 (1990).
34. M. BARTELS, K. HOYERMANN, and R. SIEVERT. Proceedings of the 19th Symposium on Combustion, 1982. p. 61.
35. M. BARTELS, J. EDELBUTTEL-EINHAUSS, and K. HOYERMAN. Proceedings of the 22nd Symp. Combustion, Seattle, 1988. p. 1041.
36. R. KNISPEL, R. KOCH, M. SIESE, and C. ZETZSCH. Ber. Busenges Phys. Chem. In press.

Can. J. Chem. Downloaded from www.nrcresearchpress.com by 84.41.108.74 on 09/07/12
For personal use only.

Excess partial molar enthalpies in the water-rich region of the isobutyric acid – water system

WILLIAM W. Y. SIU, TERRANCE Y. H. WONG, LISA C. F. CHAO, AND YOSHIKATA KOGA[1]
Department of Chemistry, The University of British Columbia, Vancouver, B.C., Canada V6T 1Y6

Received June 19, 1990[2]

WILLIAM W. Y. SIU, TERRANCE Y. H. WONG, LISA C. F. CHAO, and YOSHIKATA KOGA. Can. J. Chem. **69**, 1065 (1991).

The excess partial molar enthalpies of isobutyric acid (IBA), H_m^E(IBA), and those of H_2O, $H_m^E(H_2O)$, were measured in aqueous solutions of IBA. The temperature dependence of H_m^E(IBA) at the infinite dilution suggested that the structure enhancement of the solvent H_2O by IBA is weaker than those by *tert*-butanol (TBA) or 2-butoxyethanol (BE). The concentration dependence of H_m^E(IBA), and that of the enthalpic IBA–IBA interaction, $N\{\partial H_m^E(\text{IBA})/\partial n_B\}$, shows that there are two distinct mixing schemes bounded at about $x_B = 0.03$, before reaching the two phase separation. Namely, the IBA–IBA interaction is repulsive below this boundary, while above this boundary it becomes attractive leading eventually to phase separation at a higher concentration. The transition between the two schemes is associated with a peak(negative) anomally in the fourth derivative of the free energy, $N^2\{\partial^2 H_m^E(\text{IBA})/\partial n_B^2\}$.

Key words: excess partial molar enthalpies, isobutyric acid – water, transition in mixing scheme.

WILLIAM W. Y. SIU, TERRANCE Y. H. WONG, LISA C. F. CHAO et YOSHIKATA KOGA. Can. J. Chem. **69**, 1065 (1991).

On a mesuré les enthalpies molaires partielles en excès de l'acide isobutyrique (AIB), H_m^E(AIB), et de l'eau, $H_m^E(H_2O)$, dans des solutions aqueuses d'AIB. La relation entre la température et la valeur de H_m^E(AIB), à dilution infinie, suggère que l'augmentation de la structure du solvant (H_2O) par l'AIB est plus faible que celle provoquée par le *tert*-butanol (ATB) ou par le 2-butoxyéthanol (BE). La relation entre la concentration et la valeur de H_m^E(AIB) ainsi que l'interaction enthalpique AIB–AIB, $N\{\partial H_m^E)\text{AIB})/\partial n_B\}$, démontre que, près de $x_B = 0{,}03$, il existe deux schéma distincts de mélange avant d'atteindre la séparation en deux phases. Au-dessous de la frontière, l'interaction AIB–AIB est répulsive alors qu'au dessus de cette frontière elle devient attractive pour conduire éventuellement à une séparation de phase à une concentration plus élevée. La transition entre les deux schémas est associée à un pic (négatif) anormal dans la quatrième dérivée de l'énergie libre, $N^2\{\partial^2 H_m^E(\text{AIB})/\partial n_B^2\}$.

Mots clés : enthalpies molaires partielles en excès, acide isobutyrique – eau, transition dans le schéma de mélange.
[Traduit par la rédaction]

Can. J. Chem. Downloaded from www.nrcresearchpress.com by 84.22.46.98 on 09/08/12
For personal use only.

Introduction

We have been directly measuring the excess partial molar enthalpies of aqueous solutions of non-electrolytes (1–6). Such data have provided more direct information on solute–solvent and solute–solute interactions in terms of enthalpy. As part of such continuing efforts, we report the results in the water-rich region of aqueous isobutyric acid (IBA) solutions. The IBA–H_2O system has been an object of various studies (7–12) on its static and dynamic properties near the upper critical solution temperature (UCST). As for thermal measurements, the excess (integral) molar enthalpies, H_m^E, were determined at 27.00°C (13). The data points, however, were spaced out in concentration. Graphical differentiation was therefore not applicable in calculating the partial molar enthalpies, H_m^E(i) (i = IBA or H_2O).

Experimental

The excess partial molar enthalpies, H_m^E(i) (i = IBA or H_2O) were measured by an LKB 8700 Bromma Precision Calorimeter. We used the titration method, the details of which were described elsewhere (3). The only modification is that a Brinkman Dispensette was used instead of a glass burette. Isobutyric acid of Aldrich, 99 + %, Gold Label, was used without further purification. Analytical gas chromatography showed that the actual purity was 99.74%. We also determined the phase separation point visually for six solutions. About 15 mL of a solution was stirred magnetically and was cooled in a water bath at a rate of 0.03 to 0.04°C per minute. The temperature of the water bath was measured by the same glass thermometer used in the thermal measurement. This thermometer had been previously calibrated to ±0.01°C at the ice point and the incongruent melting point of $Na_2SO_4 \cdot 10H_2O$ (38.38°C). The calibration was checked satisfactorily at 20.09°C with the vapour pressure of H_2O.

[1]To whom correspondence should be addressed.
[2]Revision received January 31, 1991.

Results and discussion

The values of H_m^E(i) (i = IBA or H_2O) are listed in Table 1 and plotted in Fig. 1. The uncertainty for H_m^E(IBA) is estimated to be ±0.05 kJ mol^{-1} and that for $H_m^E(H_2O)$, ±0.03 kJ mol^{-1}. The values of the excess (integral) molar enthalpies, H_m^E, are evaluated and plotted in Fig. 2. Since the values of $H_m^E(H_2O)$ are not measured as closely spaced in concentration as those of H_m^E(IBA), a smooth curve is drawn between the points by taking into account of the Gibbs–Duhem relation,

$$(1 - x_B)\{\partial H_m^E(H_2O)/\partial x_B\} + x_B\{\partial H_m^E(\text{IBA})/\partial x_B\} = 0$$

The values of $H_m^E(H_2O)$ on the smooth curve were then used to calculate H_m^E as

$$H_m^E = (1 - x_B)H_m^E(H_2O) + x_B H_m^E(\text{IBA}).$$

The uncertainty in H_m^E is estimated to be ±0.03 kJ mol^{-1}. As shown in Fig. 2, comparison with existing data (13) appears reasonable.

It is surprising that although the sign of H_m^E(IBA) at the infinite dilution is negative, its absolute value is very small in comparison with those for *tert*-butanol (TBA) (1, 3), −17.4 kJ mol^{-1}, and 2-butoxyethanol (BE) (5, 6), −17.0 kJ mol^{-1}. As in the case of TBA and BE, it is likely that IBA molecules also enhance the structure of H_2O. That is to say, the value of H_m^E(IBA) at $X_B = 0$ should consist of an enthalpy gain due to the enhancement of the hydrogen bond network of H_2O and an enthalpy change of an IBA molecule due to breaking bonds from the surrounding IBA molecules in pure liquid followed by forming bonds with the nearest H_2O molecules. The former value for TBA was estimated to be about −10 kJ mol^{-1}. If this value applies to IBA, then the latter effect should be about +8 kJ mol^{-1}, resulting in a measured value of −2 kJ mol^{-1} for

Can. J. Chem. Downloaded from www.nrcresearchpress.com by 84.22.46.98 on 09/08/12
For personal use only.

TABLE 1. Excess partial molar enthalpies

IBA in IBA/H_2O system at 25°C		H_2O in IBA/H_2O system at 27°C	
X_B	H_m^E(IBA) (kJ mol^{-1})	X_B	H_m^E(H_2O) (kJ mol^{-1})
0.00357	−1.20	0.00638	−0.01
0.00593	−0.78	0.00645	−0.02
0.00829	−0.37	0.00652	−0.01
0.01063	0.02	0.00660	−0.01
0.01297	0.45	0.00668	−0.02
0.01529	0.84	0.01171	−0.07
0.01990	1.56	0.01185	−0.08
0.02219	1.97	0.01199	−0.09
0.02447	2.30	0.01973	−0.08
0.02673	2.58	0.01996	−0.09
0.02899	2.72	0.02019	−0.10
0.03376	3.14	0.05281	−0.14
0.03617	3.21	0.05353	−0.12
0.03858	3.24	0.05426	−0.13
0.04429	3.20	0.09911	0.006
0.04679	3.14	0.1007	0.01
0.05177	3.04	0.1024	0.01
0.05274	2.99	0.1559	0.04
0.05423	2.97	0.1586	0.05
0.05506	2.94	0.1615	0.05

IBA in IBA/H_2O system at 27°C			
X_B	H_m^E(IBA) (kJ mol^{-1})	X_B	H_m^E(H_2O) (kJ mol^{-1})
0.00344	−1.06	0.07933	3.07
0.00572	−0.68	0.08131	3.09
0.00799	−0.27	0.08203	3.07
0.01251	0.49	0.08384	3.05
0.01475	0.89	0.08785	3.02
0.01698	1.33	0.09051	3.01
0.01920	1.70	0.09316	3.01
0.02237	2.25	0.09578	3.01
0.02445	2.59	0.1010	3.03
0.02652	2.82	0.1036	3.02
0.02858	3.04	0.1061	3.00
0.03596	3.38	0.1087	3.00
0.03833	3.42	0.1143	3.06
0.04070	3.37	0.1171	3.06
0.04305	3.38	0.1200	3.04
0.04772	3.38	0.1228	3.06
0.05003	3.33	0.1284	3.02
0.05234	3.35	0.1311	3.01
0.05430	3.40	0.1339	3.04
0.05464	3.34	0.1366	3.01
0.05715	3.35	0.1425	3.00
0.05998	3.27	0.1454	2.96
0.06559	3.21	0.1484	2.98
0.06837	3.13	0.1514	2.95
0.07114	3.13	0.1572	2.89
0.07662	3.10	0.1601	2.90
0.07876	3.15	0.1630	2.90

H_m^E(IBA, $x_B = 0$). Since the heats of vapourization are 46.0 kJ mol^{-1} for IBA and 40.7 kJ mol^{-1} for H_2O, the value of +8 kJ mol^{-1} may not be unreasonable as an estimate for an IBA molecule to break out of the pure IBA environment and to form new bonds with the nearest H_2O molecules. However, for the structure enhancement of H_2O due to IBA to be of the same magnitude as for the case of TBA, the value of the excess partial molar heat capacity of IBA, $C_p^E(\text{IBA}) = \partial H_m^E(\text{IBA})/\partial T$, appears too small. Namely, at $x_B = 0$,

$$\Delta H_m^E(\text{IBA})/\Delta T = (-1.55 + 1.70) \times 10^3/(27.0 - 25.0) \approx 75 \text{ J K}^{-1} \text{ mol}^{-1}$$

in comparison with 280 J K^{-1} mol^{-1} for C_p^E(TBA). The latter value was attributed to breaking the enhanced hydrogen bond network on heating. Thus, we conclude that the degree of the structure enhancement of H_2O by IBA is not as large as that by TBA, or BE.

The derivative,

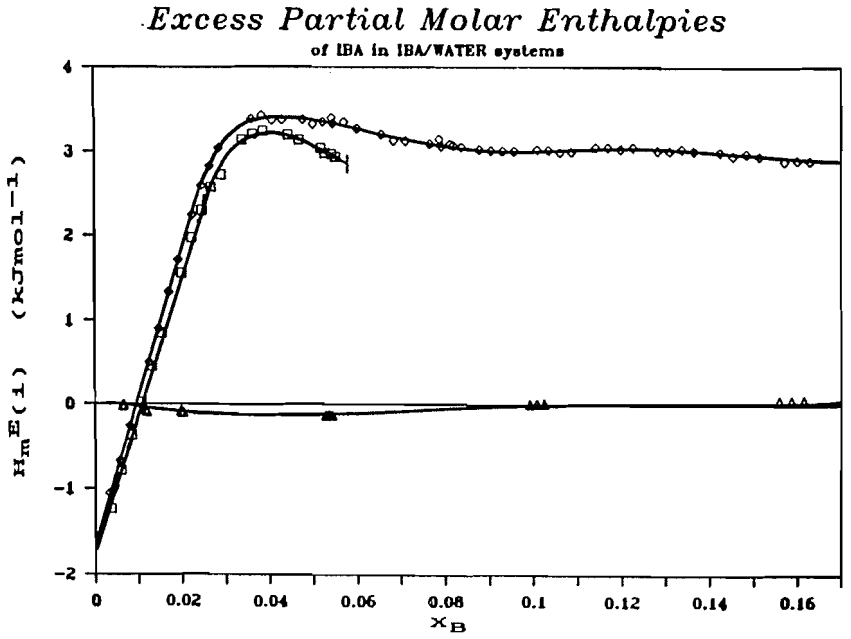


FIG. 1. Plot of excess partial molar enthalpy, $H_m^E(i)$ (i = BE or H_2O), versus x_B: □, i = IBA, 25.00°C; ◇, i = IBA, 27.00°C; △, i = H_2O, 27.00°C.

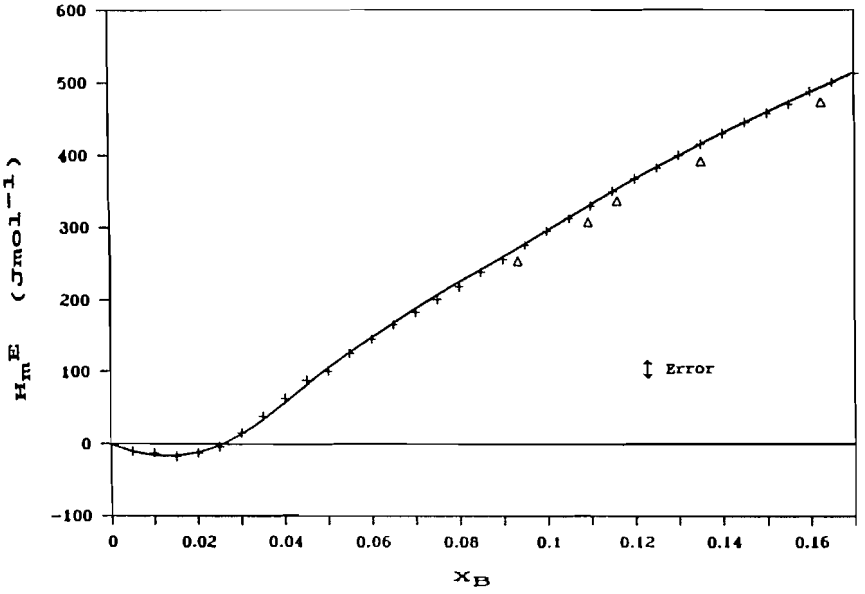


FIG. 2. The excess (integral) molar enthalpies, H_m^E, at 27.00°C: +, this work; △, ref. 13.

$$N\{\partial H_m^E(\text{IBA})/\partial n_B\} = (1 - X_B)\{\partial H_m^E(\text{IBA})/\partial X_B\}$$

are shown in Fig. 3*a*. As has been discussed elsewhere (3, 5, 6, 14–16), this derivative is a measure of IBA–IBA interaction in terms of enthalpy. Figure 3*a* indicates that the enthalpic IBA–IBA interaction is repulsive and stays constant up to $X_B \approx 0.02$. Even at the lowest concentration of measurement, $X_B \approx 0.003$ (one IBA in 300 H_2O molecules), an IBA molecule feels the presence of other IBA in a repulsive manner. This suggests that the IBA–IBA interaction is of a long range nature. Such a long range interaction may be operative via the hydrogen bond network of the solvent water. Indeed, it has been suggested that the portion of the hydrogen bond intact in liquid H_2O is above the percolation threshold (17–19). Thus, on average, a molecule of H_2O is connected to others in the entire bulk via hydrogen bonds.

For the range, $X_B > 0.03$, the enthalpic IBA–IBA interaction becomes attractive and stays constant until the system hits the two phase separation, at $x_B = 0.058$ and 25.00°C. The fact that the derivative of H_m^E(IBA) is negative near the UCST is a natural consequence of the stability criterion (22, 23). The stability criterion for a binary system, $(\partial^2 G_m/\partial x_B^2) \geq 0$, leads to $(\partial^2 H_m^E/\partial x_B^2) \leq 0$ near the UCST. Note that

$$(\partial H_m^E(\text{IBA})/\partial x_B) = (1 - x_B)(\partial^2 H_m^E/\partial x_B^2)$$

At 27.00°C, about 0.3°C above the highest UCST reported in literature (8), the values of H_m^E(IBA) appear to become constant in the range $0.09 < x_B < 0.12$, very close to the UCST. Indeed, a recent analysis, using a scaling law, of the cyclohexane–methanol system suggested $(\partial^2 H_m^E/\partial x_B^2) = 0$ at the critical point (24). While the uncertainty prevents the unequi-

Can. J. Chem. Downloaded from www.nrcresearchpress.com by 84.22.46.98 on 09/08/12
For personal use only.

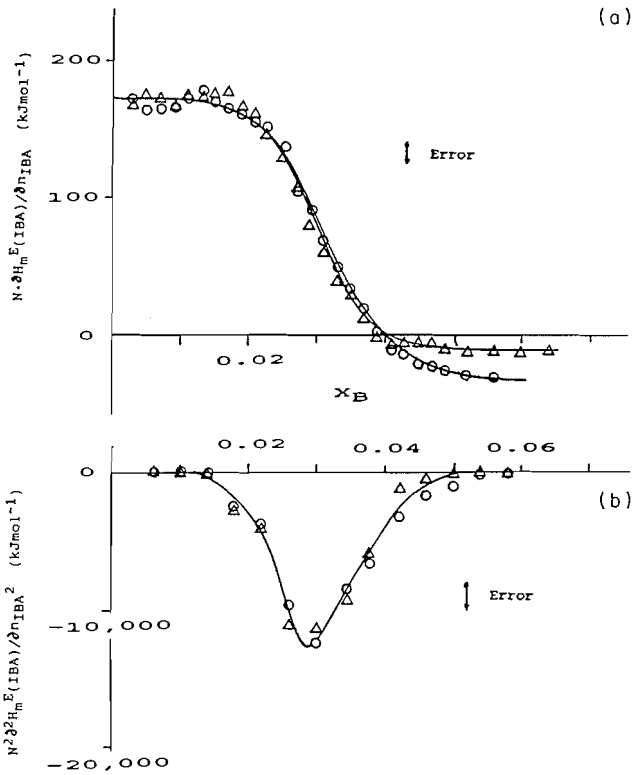


FIG. 3. (*a*) The enthalpic IBA–IBA interaction,

$$N\{\partial H_m^E(\text{IBA})/\partial n_B\}$$

○, 25.00°C; △, 27.00°C.

(*b*) The fourth derivative,

$$N^2\{\partial^2 H_m^E(\text{IBA})/\partial n_B^2\}$$

○, 25.00°C; △, 27.00°C.

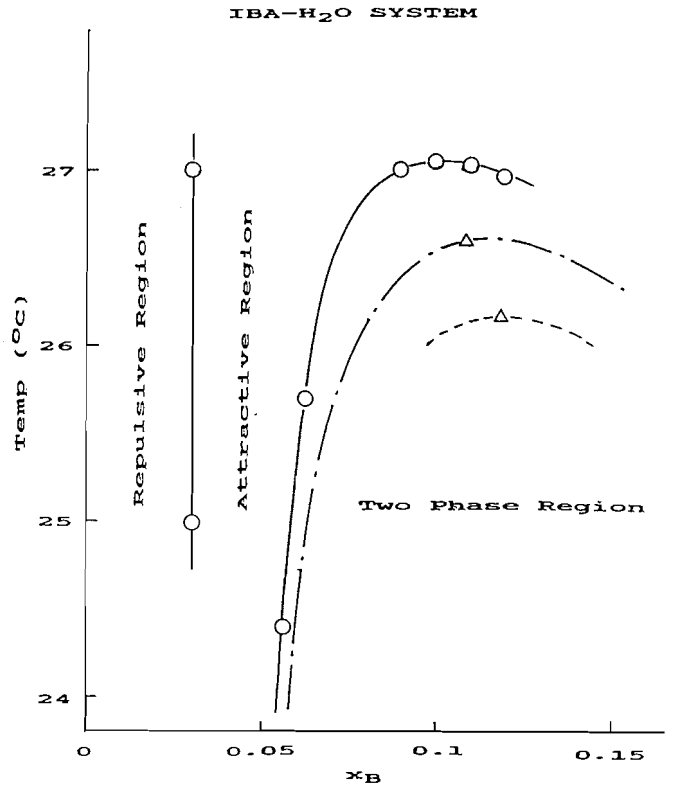


FIG. 4. Mixing scheme/phase diagram: ○, —, this work; ·····, ref. 8; -----, ref. 21; △, reported critical points.

vocal conclusion that the derivative of H_m^E(IBA) with respect to x_B is indeed zero, it was suggested by a referee to check the UCST for the present particular solutions. This suggestion was appropriate since impurities tend to alter the critical point as shown in a detailed study on the triethylamine–H_2O system (20).

The observed phase separation points, together with some literature values, are shown in Fig. 4 (8, 21). Since our method is based on visual observation in a cooling mode, the determined phase separation points may be lower bound values. In particular, for x_B = 0.0965, 0.1082, and 0.1183, i.e. near the presumed critical point, the effect of critical opalescence was so strong that the transition point was hard to pin-point. Furthermore, there should also be the effect of critical slowing-down present. Therefore, these three points must indeed be lower bound estimates. It is not our purpose to focus on the critical point and the possible effects of the various impurities. It suffices to note that for the present particular solutions the system is in two phase in the range $0.09 < x_B < 0.12$ at 27.00°C. Thus the values of H_m^E(IBA) appear to stay constant as shown in Fig. 1.

Our main focus is the transition in mixing scheme. The IBA–IBA interaction changes from a repulsive to an attractive mode at about x_B = 0.03. This crossover, however, does not seem as drastic as those for TBA (3, 14, 15) and BE (5, 6, 16). In other works, the enthalpic solute–solute interaction,

$$N\{\partial H_m^E(\text{IBA})/\partial n_B\}$$

the third derivative of the free energy, does not show any anomaly in contrast to the TBA and BE cases. Rather, the derivative once more with respect to n_B, $N^2\{\partial^2 H_m^E(\text{IBA})/\partial n_B^2\}$, the fourth derivative, shows a peak (negative) anomaly as shown in Fig. 3*b*. Thus the crossover from low concentration to high concentration mixing scheme in the IBA–H_2O system is qualitatively more subtle than those in the TBA–H_2O (3, 14, 15) and BE–H_2O (5, 6, 16) systems. This must be related to the apparent weakness of the effect of the solvent IBA on the structure of H_2O as discussed above. This boundary for the transition in mixing scheme is shown in Fig. 4.

While a more detailed and conclusive discussion must await the data of the excess partial molar entropies, S_m^E(i) (i = IBA or H_2O), it is safe to say that there are two mixing schemes present bounded at about x_B = 0.03 below the two phase separation.

Acknowledgements

We would like to thank Dr. D. H. Dolphin for the use of the LKB calorimeter. We also thank John Lai for helping us with use of various softwares. This research was supported by the Natural Sciences and Engineering Research Council of Canada, in the form of an operating grant to Y.K. and a University Undergraduate Student Research Award to W.W.Y.S. T.Y.H.W. thanks the Governments of Canada and British Columbia for the Award of Challenge 89 and Work Study Programme. We are grateful to a reviewer for the suggestion noted above.

1. Y. KOGA. Can. J. Chem. **64**, 206 (1986).
2. Y. KOGA. J. Chem. Thermodyn. **19**, 571 (1987).
3. Y. KOGA. Can. J. Chem. **66**, 1187 (1988).
4. Y. KOGA. Can. J. Chem. **66**, 3171 (1988).
5. W. SIU and Y. KOGA. Can. J. Chem. **67**, 671 (1989).
6. Y. KOGA, W. W. Y. SIU, and T. Y. H. WONG. J. Phys. Chem. **94**, 3879 (1990).
7. M. ARATONO and K. MOTOMURA. Bull. Chem. Soc. Jpn. **58**, 1853 (1985).

Can. J. Chem. Downloaded from www.nrcresearchpress.com by 84.22.46.98 on 09/08/12
For personal use only.

8. M. ARATONO and K. MOTOMURA. Bull. Chem. Soc. Jpn. **58**, 3205 (1985).
9. N. EASWAR, M. JOSHUA, J. V. MAKER, and W. I. GOLDBERG. Physica, **118A**, 268 (1983).
10. F. P. HARMISCH and D. WOERMANN. Ber. Bunsenges. Phys. Chem. **91**, 811 (1981).
11. J. C. NIEUWONDT and J. V. SENGERS. J. Chem. Phys. **90**, 457 (1989).
12. R. F. BERG and M. R. MOLDOVER. J. Chem. Phys. **89**, 3694 (1988).
13. D. V. FENBY, J. R. KHURMA, Z. S. KOONER, and R. F. SMITH. Aust. J. Chem. **36**, 215 (1983).
14. Y. KOGA, T. Y. H. WONG, and W. W. Y. SIU. Thermochim. Acta, **169**, 27 (1990).
15. Y. KOGA, W. W. Y. SIU, and T. Y. H. WONG. J. Phys. Chem. **94**, 7700 (1990).
16. Y. KOGA. J. Phys. Chem. In press.
17. H. E. STANLEY and J. TEIXEIRA. J. Chem. Phys. **73**, 3404 (1980).
18. H. E. STANLEY, R. L. BLUMBERG, and A. GEIGER. Phys. Rev. **B28**, 1626 (1983).
19. R. L. BLUMBERG, H. E. STANLEY, A. GEIGER, and P. MAUSBACH. J. Chem. Phys. **80**, 5230 (1984).
20. B. J. HALES, G. L. BERTRAND and L. G. HEPLER. J. Phys. Chem. **70**, 3970 (1966).
21. T. S. VENKATARAMAN and L. M. NARDUCCI. J. Phys. **C10**, 2849 (1977).
22. I. PRIGOGINE and R. Defay. *In* Chemical thermodynamics. *Translated by* D. H. Everett. Longmans, London, 1965, p. 284.
23. G. MORRISON. J. Phys. Chem. **78**, 4790 (1983).
24. M. B. EWING, K. A. JOHNSON and M. L. MCGLASHAN. J. Chem. Thermodyn. **18**, 979 (1986).

Can. J. Chem. Downloaded from www.nrcresearchpress.com by 84.22.46.98 on 09/08/12
For personal use only.

Vibrational and electronic spectra of new liposoluble metalloporphyrins in a nonpolar noncoordinating solvent

MICHEL RINGUET,[1] DENIS GIRARD, AND CAMILLE CHAPADOS

Département de Chimie-biologie, Université du Québec à Trois-Rivières, Trois-Rivières, Qué., Canada G9A 5H7

Received September 5, 1990[2]

MICHEL RINGUET, DENIS GIRARD, and CAMILLE CHAPADOS. Can. J. Chem. **69**, 1070 (1991).

A new liposoluble porphyrin, 2,7,12,17-tetrahexyl-3,8,13,18-tetramethylporphin (THTMP), and its complexes with divalent (Mg, Co, Ni, Cu, Zn, Cd, Hg) and trivalent (Mn, Fe) metals have been synthesized. The electronic, infrared, and far-infrared spectra of these compounds were obtained in the same nonpolar, noncoordinating solvent, CCl_4. After comparison with the experimental data and the results of normal coordinate analyses from the literature, the assignment of the vibrational bands of THTMP and its complexes is made. Some correlations between the shifts of the metal sensitive bands in the diffferent regions and the structural characteristics of the porphyrin complexes are reported. Some emphasis is made on the magnesium complex in relation to chlorophyll.

Key words: Metalloporphyrin, porphyrin, infrared spectroscopy, far-infrared spectroscopy, electronic spectroscopy, nitrogen–metal bond, covalent radius, reduced mass.

MICHEL RINGUET, DENIS GIRARD et CAMILLE CHAPADOS. Can. J. Chem. **69**, 1070 (1991).

On présente la synthèse d'une nouvelle porphyrine liposoluble, la tétrahexyl-2,7,12,17 tétraméthyl-3,8,13,18 porphine (THTMP), et de ses complexes de métaux bivalents (Mg, Co, Ni, Cu, Zn, Cd, Hg) et trivalents (Mn, Fe). On a obtenu les spectres électroniques, dans l'infrarouge et dans l'infrarouge lointain, de ces substances en solution dans un même solvant non polaire et non coordonnant, le CCl_4. Les bandes vibrationnelles sont attribuées à la suite de comparaisons avec les spectres et les résultats d'analyses de coordonnées normales déjà publiés. On établit des corrélations entre les déplacements des bandes influencées par le métal dans les différentes régions spectrales et diverses caractéristiques physicochimiques des métalloporphyrines. On porte une attention particulière aux spectres de la porphyrine de magnésium en regard des spectres de la chlorophylle.

Mots clés : métalloporphyrine, porphyrine, spectroscopie infrarouge, spectroscopie dans l'infrarouge lointain, spectroscopie électronique, liaison azote–métal, rayon covalent, masse réduite.

Introduction

The studies of the absorption spectra shown by natural porphyrin–type pigments like the chlorophylls, heme, and their derivatives have led to a better understanding of the nature of the electronic transitions in these chromophores (1, 2). Studies on synthetic metalloporphyrins allowed a theoretical explanation of typical (3) and atypical (4) absorption spectra. Systematic experiments with a series of metalloporphyrins were done to determine the influence of the metal on the electronic structure of these pigments (5–7).

The Raman spectroscopy of the metalloporphyrins is an active field mostly because resonance Raman (RR) is facilitated by the availability of lasers whose emission wavelength coincide with the absorption bands of the metalloporphyrins (8, 9).

Infrared spectroscopy of the porphyrins is also studied intensively. Spectra of natural (10) and synthetic (11–17) metalloporphyrins were obtained which led to the assignment of almost all the 24 infrared active vibrational bands (18 E_u in-plane and 6 A_{2u} out-of-plane skeletal modes) of the porphin ring. Correlations between selected vibrational bands and various properties of the complexes were reported (18).

Normal coordinate analyses (9, 14, 19–22) on isotopic compounds have confirmed unequivocal assignment of most of the bands while the other bands have contradictory assignment. Willems and Bocian (23), in a RR study of nickel–formyldeuteroporphyrin, showed the difficulty of choosing the right assignment.

Unequivocal attribution of the ir bands of metalloporphyrins is complicated by the intense coupling between different vibrational modes and because the data reported so far were collected with porphyrins of different symmetry and in different media. Moreover, in the RR studies, excitation beams at different wavelengths give spectra with different intensity profile (22*b*). The crystal polymorphism, shown by metalloporphyrins of small-size metal ion such as Ni^{2+} and perhaps Co^{2+}, brings additional complication to the spectra which, according to Alden *et al.*, may have resulted in false interpretation of the normal coordinate analyses (24).

To solve the problem of comparing the data given by nonidentical substrates, numerous works were done on octaethylporphin (OEP) and its metal complexes. However, these compounds are not very soluble in nonpolar, noncoordinating solvent. KBr matrices, which were used in almost all previous ir studies, showed some interaction between the matrice and the porphyrin. The Nujol mull technique, used to obtain the far-infrared spectra, showed aggregation. The results obtained with these techniques could be misleading and, indeed, Katz *et al.* showed that the infrared spectra of chlorophyll, a Mg–porphyrin type compound, were strongly dependent on the aggregation states (25). These authors noticed that the spectra of porphyrins in solution, although difficult to obtain, gave sharper bands than with solids. These observations were verified in our laboratories (26).

The purpose of this work is to report (*1*) the synthesis of metalloporphyrin complexes soluble in nonpolar organic solvent and (2) their spectroscopic data obtained over a broad spectral range (visible, infrared, and far-infrared regions) in CCl_4 solutions. The use of the same noncoordinating solvent facilitates the comparison of the displacements of the bands in different spectral regions which the other studies could not do.

To achieve this goal, we synthesized a new liposoluble porphyrin, 2,7,12,17-tetrahexyl-3,8,13,18-tetramethylporphin (THTMP). This porphyrin has eight peripheral pyrrole carbons bonded to alkyl groups in a four-fold symmetry arrangement. These structural characteristics allow comparison with similar

[1]To whom correspondence should be addressed.

[2]Revision received February 5, 1991.

Can. J. Chem. Downloaded from www.nrcresearchpress.com by 198.100.157.202 on 09/07/12
For personal use only.

Can. J. Chem. Downloaded from www.nrcresearchpress.com by 198.100.157.202 on 09/07/12
For personal use only.

natural porphyrins. THTMP was complexed with the bivalent cations of Co, Ni, Cu, Zn, Cd, and Hg to obtain two series in the periodic table, one within a period and the other within a group. The Mg complex was synthesized in order that we may compare its spectra with those of chlorophyll. The trivalent complexes of Mn and Fe, as chlorides, were made to complement the series with substrates giving atypical absorption spectra. Visible (300–700 nm), infrared (4000–500 cm^{-1}), and far-infrared (500–62 cm^{-1}) absorption spectra of solutions of these metalloporphyrins in CCl_4 were obtained and critically compared with the spectra of similar complexes found in the literature. The metal-sensitive bands are identified and the shifts of these bands are related to structural and chemical parameters of the complexes. This study complements our previous work on the aggregation and ionization states of surfactant porphyrins (27, 28).

Experimental

Synthesis

THTMP was made by a modified version of the method of Smith and Bisset for the synthesis of alkyl-substituted porphyrins (29).

2-Carboxybenzyl-3,5-dimethyl-4-hexylpyrrole

A mixture of 1-iodohexane (10 g), 2,4-pentanedione (7.1 g), and potassium carbonate (10 g) in dry acetone (10 mL) was refluxed under nitrogen for 24 h. Filtration of the reaction mixture and distillation under reduced pressure gave 3-hexyl-2,4-pentanedione (5.2 g, 60%).

A solution of sodium nitrite (8.5 g) in water (20 mL) was slowly added to a stirred solution of benzylacetoacetate (20 mL) in glacial acetic acid (40 mL), maintained below 10°C. The mixture was left in the dark and under nitrogen for 12 h, extracted with ether and evaporated to give benzylacetoacetate-oxime (22 g, 86%).

A mixture of 3-hexyl-2,4-pentanedione (3.0 mL) and benzylacetoacetate-oxime (12.0 mL) in glacial acetic acid (20 mL) was heated at 70°C and zinc powder (1.4 g) was slowly added. The solution was heated to boiling for 1 h, cooled, and poured over ice. The product was collected by filtration and recrystallized in methanol to give 2-carboxybenzyl-3,5-dimethyl-4-hexylpyrrole (1.35 g, 60%), mp 61–62°C; ν_{KBr}: 3320, 3045, 2960, 2920, 2850, 1670, 1585, 1500, 1265, 1085; ^1H $\partial(CDCl_3)$: 0.85 (t, 3H, CH_3CH_2—), 1.28 (m, 8H, 4 CH_2), 2.13 (s, 3H, CH_3-5), 2.27 (s, 3H, CH_3-3), 5.27 (s, 2H, CH_2—benzyl), 5.33 (s, 5H, arom.). *Anal.* calcd for $C_{20}H_{27}NO_2$: C 76.64, H 8.68, N 4.47; found: C 76.39, H 8.56, N 4.57.

2,7,12,17-Tetrahexyl-3,8,13,18-tetramethylporphin (THTMP)

2-Carboxybenzyl-3,5-dimethyl-4-hexylpyrrole (2.5 g) was dissolved in tetrahydrofuran (50 mL) and triethylamine (0.05 mL). Pd (10%) on charcoal (250 mg) was added to the solution which was hydrogenated at 162 kPa for 1 h. The mixture was filtrated over celite and evaporated under reduced pressure. The resulting oil was dissolved in glacial acetic acid (6.5 mL) and bromine (1.6 mL) was added dropwise. The mixture was stirred for 15 h. The sample was evaporated under reduced pressure, diluted with toluene, evaporated, diluted with cold ether, and filtrated. The orange solid obtained (dipyrromethenes) was dissolved in boiling formic acid (8.5 mL) and refluxed for 3 h. After cooling, the reaction mixture was diluted with water and extracted with chloroform. The extract was washed with water and with a saturated sodium bicarbonate solution, dried, and evaporated. The residue was column chromatographed on deactivated silica gel to afford THTMP which was recrystallized from $CHCl_3$:CH_3OH (355 mg, 25%), mp 132–133°C; ν_{KBr}: 3310, 2951, 2924, 2866, 2852, 1674, 1465, 1458, 678; ^1H $\partial(CDCl_3)$: −3.88 (s, 2H, NH), 1.1 (t, 12H, 4 CH_3-6′), 2.30 (t, 8H, 4 CH_2-2′), 3.52 (s, 12H, 4 CH_3-3,8,13,18), 3.79 (t, 8H, 4 CH_2-1′), 9.88 (s, 4H, meso). *Anal.* calcd. for $C_{48}H_{70}N_4$: C 81.99, H 10.04, N 7.97, found: C 81.71, H 10.22, N 7.54.

The metal complexes were prepared using four different methods. (*1*) The complexes of Mn, Fe, Co, Ni, Cu, and Zn were obtained by incorporating the metals from the corresponding salts ($MnCl_2$, $FeSO_4$, $Co(OAc)_2$, $Ni(OAc)_2$, $Cu(OAc)_2$, $Zn(OAc)_2$) by the acetate method (30). The Mn and Fe complexes were treated with air and HCl to allow oxidation and formation of chlorides. (*2*) The Mg complex was obtained by the reaction of propioxymagnesium bromide on THTMP at 70–75°C (31). (*3*) The Cd complex was obtained by refluxing a mixture of $Cd(OAc)_2$ and THTMP in benzene:DMF 3:4 for 5 h. (*4*) The Hg complex was obtained by refluxing $Hg(OAc)_2$ and THTMP in pyridine for 2 h. MgTHTMP was chromatographed on basic alumina. The other samples were recrystallized in the solvent systems indicated below. All the samples were dried in a vacuum dessicator over $CaCl_2$. From THTMP, the yields are MgTHTMP, 56%; MnTHTMPCl, 97%; FeTHTMPCl, 98%; CoTHTMP, 95%; NiTHTMP, 95%; CuTHTMP, 98%; ZnTHTMP, 85%; CdTHTMP, 70%; HgTHTMP, 35%.

Elemental analyses were made by Guelph Chemical Lab., Guelph, Ont., and showed that the substances were pure and anhydrous. MgTHTMP, mp 155–157°C. *Anal.* calcd. for $C_{48}H_{68}N_4Mg$: C 79.75, H 9.60, N 7.68; found: C 79.48, H 9.45, N 7.72. MnTHTMPCl, recrystallized from $CHCl_3$: ligroin, mp 265–268°C. *Anal.* Calcd for $C_{48}H_{68}N_4MnCl$: C 72.84, H 8.66, N 7.08; found: C 72.53, H 8.99, N 7.11. FeTHTMPCl, recrystallized from CH_2Cl_2:CH_3OH, mp 239–242°C. *Anal.* calcd for $C_{48}H_{68}N_4FeCl$: C 72.76, H 8.65, N 7.07; found: C 73.10, H 8.71, N 7.02. CoTHTMP, recrystallized from CH_2Cl_2:CH_3OH, mp 178–180°C. *Anal.* calcd. for $C_{48}H_{68}N_4Co$: C 75.86, H 9.02, N 7.37; found: C 75.38, H 8.98, N 7.57. NiTHTMP, recrystallized from CH_2Cl_2:CH_3OH, mp 115–116°C. *Anal.* calcd. for $C_{48}H_{68}N_4Ni$: C 76.00, H 9.03, N 7.38; found: C 76.16, H 9.31, N 6.94. CuTHTMP, recrystallized from CH_2Cl_2:CH_3OH, mp 180–182°C. *Anal.* calcd. for $C_{48}H_{68}N_4Cu$: C 75.40, H 8.96, N 7.33; found: C 75.56, H 8.89, N 7.02. ZnTHTMP, recrystallized from CH_2Cl_2:ligroin, mp 196–197°C. *Anal.* calcd. for $C_{48}H_{68}N_4Zn$: C 75.22, H 8.94, N 7.31; found: C 75.54, H 9.05, N 7.03. CdTHTMP, recrystallized from CH_2Cl_2:CH_3OH, mp 170–173°C. *Anal.* calcd. for $C_{48}H_{68}N_4Cd$: C 70.87, H 8.43, N 6.89; found: C 70.59, H 8.83, N 6.59. HgTHTMP, recrystallized from ether, mp 184–187°C. *Anal.* calcd. for $C_{48}H_{68}N_4Hg$: C 63.94, H 7.60, N 6.21; found: C 63.64, H 7.88, N 6.17.

Spectrum recording

The absorption spectra were obtained from solutions of the porphyrins in spectrograde CCl_4 (Anachemia Chemicals; water <0.01%) at a concentration of 1×10^{-5} M. The spectra were recorded on a Perkin-Elmer IF553 spectrophotometer with a resolution of 1 nm. Two spectra were recorded for each sample; the spectral data were transferred to a computer (Cyber 174, from Control Data Co.) where the averages of the original spectra were made to give the figures in this paper. Spectra of 1×10^{-2} M solutions were also obtained; these were identical to the ones obtained with the 1×10^{-5} M solutions.

The vibrational spectra were obtained in the same solvent at a concentration of 1×10^{-2} M. KBr cells of 1 mm pathlength were used in the 4000–400 cm^{-1} region and high-density polyethylene cells of 5 mm pathlength were used in the 400–62 cm^{-1} region. The spectra were recorded on a Perkin-Elmer model 180 spectrophotometer with a resolution of 2 cm^{-1} in the 4000–400 cm^{-1} region and of 3 cm^{-1} in the 400–62 cm^{-1} region. The calibration was made with water vapor, ammonia, and carbon dioxide. The precision of the bands was better than 1 cm^{-1}. Compensation of the solvent bands was excellent except in two regions: 810–730 and 325–300 cm^{-1}. Three spectra were recorded for each sample, except for CoTHTMP whose spectrum varied with time. The averaging of the spectra, calibration and subtraction of the background were made with the Cyber 174 computer to give the figures presented in this paper.

The product–moment correlation coefficients (r) were obtained from standard statistical calculation of regression analysis (32). All data were plotted to ensure that a straight-line relationship had not been wrongly deduced.

Results and discussion

Synthesis

THTMP was obtained with an overall yield of 8% from the reagents 2,4-pentanedione and benzylacetoacetate. This result

Can. J. Chem. Downloaded from www.nrcresearchpress.com by 198.100.157.202 on 09/07/12
For personal use only.

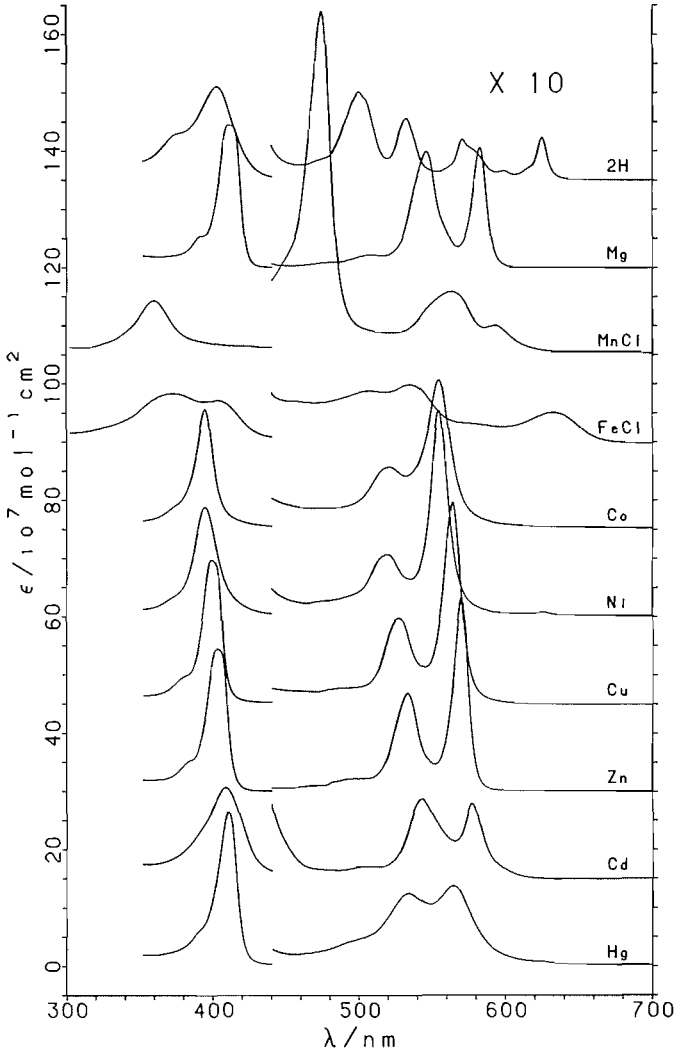


FIG. 1. Electronic spectra of THTMP and its metal complexes. Note the change of scale at 450 nm.

is comparable to the 4% overall yield obtained by Smith and Bisset (29) for some other hydrocarbon-soluble porphyrins. THTMP and its metal complexes were both crystalline and liposoluble (up to 1×10^{-2} M solution in CCl_4), which were the general characteristics required for the spectroscopic studies of pure compounds.

Spectroscopy

The UV–visible, infrared, and far-infrared spectra of free base THTMP and its metal complexes with Mg^{2+}, Mn^{3+}, Fe^{3+}, Co^{2+}, Ni^{2+}, Cu^{2+}, Zn^{2+}, Cd^{2+}, and Hg^{2+} are shown in Figs. 1, 2, and 3, respectively. The structural formula of the metal complexes of THTMP and OEP (OEP = 2,3,7,8,12,13,17,18-octaethylporphin), including the symbols used to identify the carbon atoms of the porphin ring and the side-chains, are given in Fig. 4.

Within the series (Co, Ni, Cu, and Zn) of normal absorption spectra (1), the spectral shifts of the Soret, B(0,0), and the visible Q(0,0) and Q(1,0) bands of THTMP complexes are similar to those normally observed for porphyrins (33). For the ir work, the principal vibrational absorption bands with their assignments for THTMP and its metal complexes are given in Table 1. The assignments given in this table are based on experimental studies (10, 12) and normal coordinate analyses (9, 21, 22) made on similar porphyrins. For some unequivocally assigned bands, a difference of 5 to 10 cm^{-1} is often found between the positions observed for THTMP and its metal complexes and those reported for OEP and its complexes. These shifts are mostly due to a mass effect by the substituents since the shifts caused by solvents are less than 3 cm^{-1}. For some other bands, the differences between our data and those in the literature are greater than 10 cm^{-1}. In the following, we look closely at these bands. We will also identify the regions of the spectrum which are significantly modified by a change of the complexed metal.

Infrared region

The in-plane N—H deformation mode of the free base should be observed near 1220 cm^{-1} (20*a*). However, an intense C_m—H deformation band is found in this region which prevents the observation of the N—H band. In the spectrum of PP (PP = protoporphyrin IX dimethylester) (10), a band is observed at 1418 cm^{-1} and a similar one is observed at 1412 cm^{-1} for OEP (12). These bands as well as the band observed at 1407 cm^{-1} in the spectrum of THTMP (Fig. 2, Table 1) disappear in the corresponding metalloporphyrins. The transformation of the ir active modes of the free base into degenerate e_u modes in metalloporphyrins could be the cause of the disappearance of these bands.

A strong band observed at 1146 cm^{-1} was assigned by Ogoshi *et al.* (12) to the C_b—H and C_m—H out-of-plane deformations coupled with C_a—C_m stretching. Gladkov and Solovyov assigned this band to C_b—C_{let} coupled with C_b—C_a, C_a—N, and side-chain vibrations (20*b*, 21). This band, which is not metal dependant, is also observed in the spectrum of THTMP (Fig. 2, Table 1) which has no C_b—H group. These observations support the assignment of this band to the C_b—C_{1hex} stretching mode.

Only one C_m—H stretching band should be observed for the metalloporphyrins in the 3200 to 3000 cm^{-1} region (9, 22, 24). However, for the THTMP complexes, two or three bands are observed near 3210, 3170, and 3060 cm^{-1}. The position and intensity of these bands are sensitive to a change of metal. According to normal coordinate analyses (19*b*, 21, 22*b*), the lower frequency band should be assigned to the C_m—H stretching mode. The other bands are combination bands.

The band in the 1689–1674 cm^{-1} region is found too high to be assigned to the C=C, C=N stretching vibrations (9, 19*b*). Indeed, this band is assigned to a harmonic of the metal-sensitive C_m—H deformation band observed in the 844–836 cm^{-1} region. The bands assigned to the C=C, C=N, E_u skeletal modes of the porphyrins are situated between 1630 and 1400 cm^{-1} (19*b*, 22*b*). The bands observed at 1610 and 1505 cm^{-1} for THTMP are assigned to the vibrations of these groups. Some other components of these vibrations are possibly burried under the strong 1460 cm^{-1} C—H deformation bands. Because of symmetry modification, the 1610 and 1505 cm^{-1} bands almost disappear in the spectra of the metal complexes of THTMP.

Abe *et al.* assigned the band observed in the 1111–1104 cm^{-1} region to C_b—C_{let} and C_b—C_a stretching vibrations of OEP (19). On the contrary, Spiro *et al.* (9), Li *et al.* (22) and Gladkov and Solovyov (21) assigned this band to C_b—C_{let}—H and C_{let}—C_{2et}—H deformation modes coupled with C_a—N stretching of OEP. However, the spectra of the unsubstituted porphin and its metal complexes do not show a band in this region (14, 20, 22a).

Can. J. Chem. Downloaded from www.nrcresearchpress.com by 198.100.157.202 on 09/07/12
For personal use only.

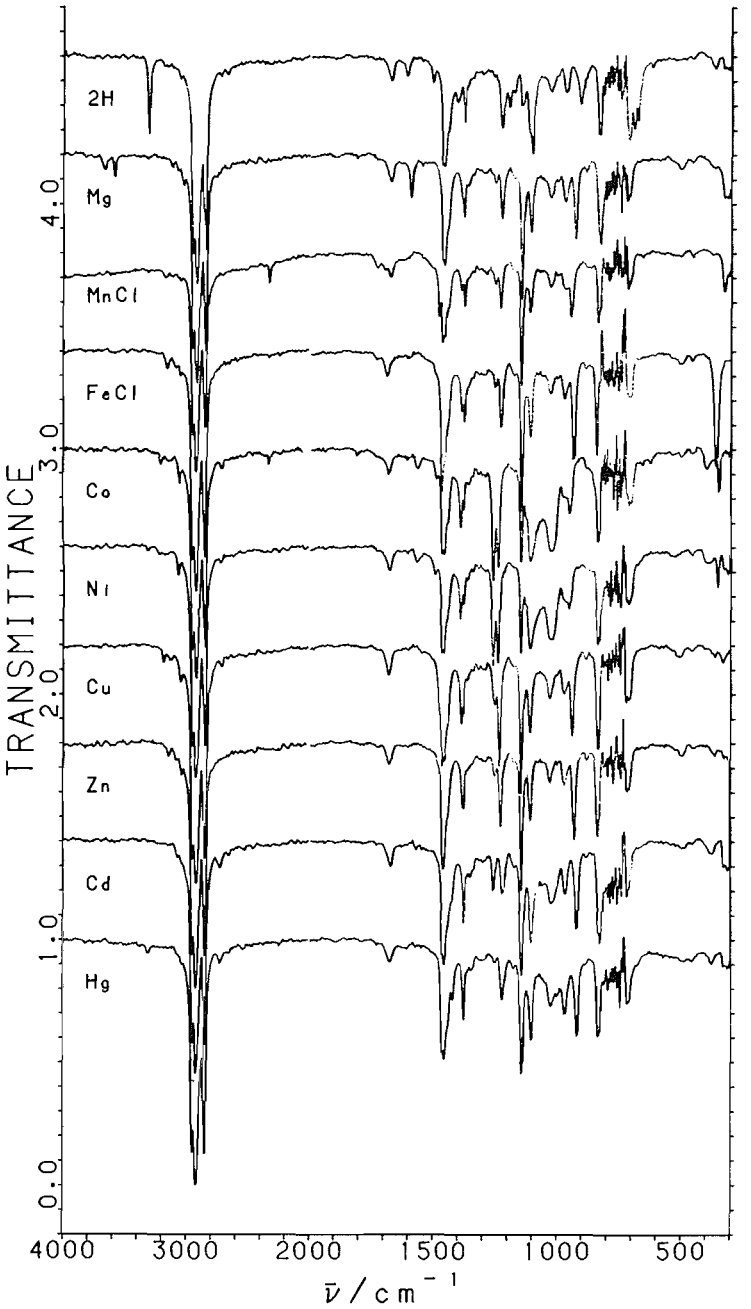


FIG. 2. Infrared spectra of THTMP and its metal complexes. The strong absorption by CCl_4 obscures the 810–730 cm^{-1} region.

Accordingly, the band near 1108 cm^{-1} cannot be assigned to pure C_b—C_a and C_a—N stretching vibrations. Since the position of the band is too high for C—C—H out-of-plane deformations, the bands found in the 1111–1104 cm^{-1} region are assigned to stretch vibrations of C_b—C_{1hex}, C_b—C_{1me}, and C—C of the side-chains.

Far-infrared region

Few data are available in the far-infrared region for the porphyrins. Moreover, the assignment of the N–metal vibrations in heme proteins and chlorophylls are not completely resolved (9, 34, 35). Therefore, there is a need for a study of simpler metalloporphyrins in the far-infrared (22*c*).

The metal-sensitive bands of THTMP complexes are observed in the 402–364, 354–192, and 226–101 cm^{-1} regions. Following the literature (9, 19*b*, 22*c*), the bands in the 354–192 cm^{-1} region are assigned to the N—metal out-of-plane stretch coupled with an out-of-plane deformation mode of the ring. Indeed, the band observed at 354 cm^{-1} for NiTHTMP corresponds to the position (351 cm^{-1}) calculated for the A_{2u} mode of NiOEP (9, 22*c*). The Mn—Cl and Fe—Cl stretching modes of the trivalent metal complexes are observed at 333 and 363 cm^{-1}, respectively. The assignments of the far-infrared bands will be discussed below where the spectra of the synthetic and the natural porphyrins are compared.

The bands observed in the 402–364 cm^{-1} region have not been definitely assigned in the literature. The intensities of these bands vary considerably with the metal. Since the intensity of

Can. J. Chem. Downloaded from www.nrcresearchpress.com by 198.100.157.202 on 09/07/12
For personal use only.

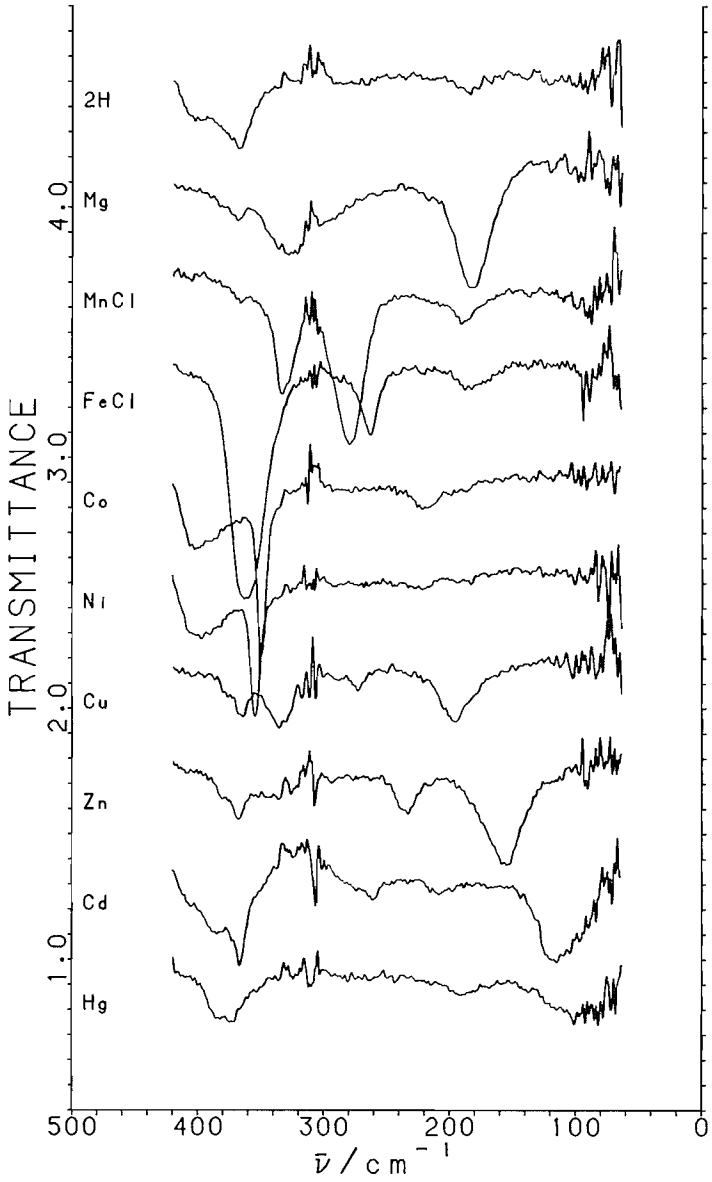


FIG. 3. Far-infrared spectra of THTMP and its metal complexes. The strong absorption by CCl_4 obscures the 325–300 cm^{-1} region.

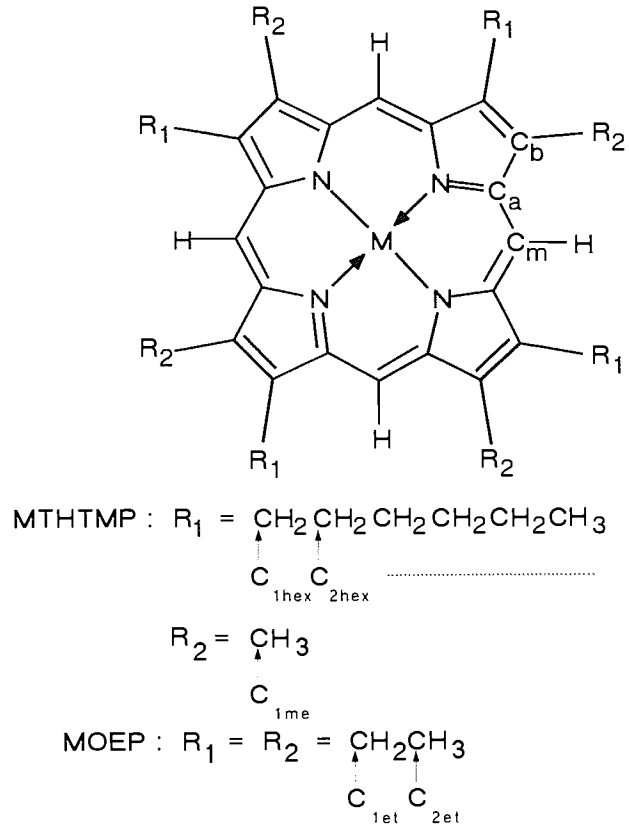


FIG. 4. Structural formulae of the metal complexes of THTMP and OEP with symbol identification of carbons.

the ir bands are related to a variation in the dipole moment derivatives and since only the central metal is varied in the porphyrins studied, the central metal affects the dipole moment derivative related to these far-infrared bands. Further studies are needed to understand this relationship.

Band shift/parameter correlations

Some correlations have been made between electronic and structural properties of metalloporphyrins and the positions of specific bands of their resonance Raman and their electronic spectra (6, 7, 12–14, 16, 31, 36–41). Similar relationships are observed between spectral shifts of ir bands and the following structural parameters: (*a*) the strength of the N—metal bond (13, 14); (*b*) the number of *d* electrons on the metal (16); (*c*) the center-to-nitrogen distance or core size (7, 35, 39–41); (*d*) the stability of the complexes (38); (*e*) the spectral shifts in the UV–vis region (7, 12, 42). The correlation factors between the ir displacement and the parameters mentioned are seldom greater than 0.9 even when the series of complexes are restricted to the ones formed with the elements of one single group or with the elements of a period in the periodic table. None of these correlations were made with far-infrared bands.

The correlations that we present here refer to the metal complexes of THTMP which show a typical electronic spectrum: Mg-, Co-, Ni-, Cu-, Zn-, Cd-, and HgTHTMP. Table 2 lists the structural characteristics and the positions of the absorption bands that are correlated. The most significant correlation factors are listed in Table 3.

Shelnutt and Ondrias (7) have shown that linear relationships are lost when porphyrins with different axial ligation state are studied. Accordingly, all the spectra presented here were obtained in CCl_4, a noncoordinating solvent, to prevent the axial ligation of the metal with the solvent. One exception is MgTHTMP which is highly hygroscopic and complexes with the few water molecules present in the CCl_4 solvent (43).

The correlation patterns obtained between the spectral shifts in the different spectral regions and the molar reduced mass of the N—metal bond are shown in Fig. 5. The correlation factors from the linear regression equation are very good ($r > 0.95$) for two series of complexes: the series of the metal complexes of the same group (Zn, Cd, Hg) (Table 3.A4) and the series of the metal complexes of the same period (Co, Ni, Cu, Zn) (Table 3.A3). However, the slopes of the regression lines for these two series are different so that the correlation factor becomes less significant when the set of six complexes is considered (Table 3.A2). When the Mg complex is added to the list, the correlation is completely lost (Table 3.A1). This is understandable because the Mg complex is more ionic than the other complexes and water is axially ligated to the Mg.

A correlation is found between the reduced mass of N—metal

Can. J. Chem. Downloaded from www.nrcresearchpress.com by 198.100.157.202 on 09/07/12
For personal use only.

TABLE 1: Positions (cm^{-1}) of the ir bands of THTMP and its metal complexes.

THTMP	Mg	MnCl	FeCl	Co	Ni	Cu	Zn	Cd	Hg	Assignment
	3665w									ν_{as} (OH) (H_2O)
	3587w									ν_{s} (OH) (H_2O)
3310m										ν (NH)
				3209w	3217vw					
3187vw		3172vw			3174vw	3185w				
3157w			3159w				3146w			
	3119w	3120vw		3141w		3129vw				
	3073w		3083vw				3082vw	3077w		
3057w		3053vw	3050vw	3058vw	3065w	3045w	3066w	3044vw	3052vw	ν (C_mH)
	3029w								3030vw	
2951s	2951s	2951s	2952s	2951s	2952s	2951s	2951s	2951s	2951s	ν_{as} (CH_3)
2924s	2923s	2924s	2925s	2923s	2923s	2922s	2923s	2923s	2922s	ν_{as} (CH_2)
2866s	2865s	2865s	2865s	2865s	2864s	2865s	2865s	2865s	2865s	ν_{s} (CH_3)
2852s	2851s	2851s	2853s	2852s	2852s	2852s	2852s	2851s	2851s	ν_{s} (CH_2)
		2337w		2337vw						ν_{as} (CO_2)
		1732w	1730vw							
		1700w								
		1693w								
1674m	1674m	1688m	1689m	1682m	1678m	1680m	1681m	1675m	1676m	2(π(C_mH))
1610w										ν (C_b-C_b)
	1594m									δ (H_2O)
				1562w	1570w					ν (C_b-C_b), ν (C_b-C_{1hex})
1505m										ν (C_a-C_m)
		1480m		1488w	1484w					ν' (C_a-C_m), ν' (C_a-C_b)
1465s	1465s	1466s	1467s	1466s	1465s	1466s	1465s	1465s	1465s	δ_{as} (CH_3)
1458s	1457s	1456s	1457s	1456s	1457s	1457s	1461s	1456s	1456s	δ_{s} (CH_2)
									1422m	
1407m										
		1390m	1388m	1390m	1391m	1387m	1383m			ν (C_a-N), δ (C_a-C_m)
1378m	1378m	1378m	1377m	1378m	1378m	1378m	1378m	1378m	1378m	δ_{s} (CH_3)
1257vw	1252w	1252w	1252w	1259s	1259s	1254m	1253m	1260m	1252w	δ (ring)
1227m	1226m	1231m	1230m	1239s	1239s	1234s	1230m	1223m	1222m	δ (C_mH)
1146m	1146s	1147s	1145s	1146s	1146s	1146s	1147s	1144s	1142s	ν (C_bC_{1hex})
1104s	1108m	1111m	1110m	1109s	1110s	1111m	1110m	1105s	1104s	ν (C_bC_{1hex}) ν (C_bC_{1me})
1027m	1027m	1031m	1029m	1022bs	1025bs	1031m	1030m	1021bm	1025m	δ (ring) ν (C_bC_b)
968m	971m	969m	974m	968bm	968bm	974m	973m	970m	969m	ν (C_aC_m) ν (C_aN)
908m	930s	947s	936s	951m	954m	941s	933s	923s	920s	δ (ring)
834s	833s	838s	844s	837s	837s	838s	838s	834s	836s	π (C_mH)
830s	829s	830s	830s	830s	829s	829s	830sh	828s	829s	δ ($C_bC_{1hex}H$) δ ($C_bC_{1me}H$)
715s	721m	718m	711m	711m	721m	722m	720m	722m	717m	π (ring) ν (C_b-C_{1hex})
695m	712m	713sh	705m	704m	713m	715m	710m	714sh	710sh	π (ring) δ (C_bC_aN)
678m										π (NH)
402bm										
							383w	385bm	383bm	
368bm	368bw	366bw		402bm	397bm	364m	368m	367m	373bm	π (NM) δ (C_bC_aN) ν (C_bC_a)
						335bm				δ (C_b-C_{1hex})
						330bm				
		333s	363s							ν (MX)
								261bw		
	328bm	279s	262m	349s	354s	272w	234bm	208bm	192bvw	π (ring) π (C_m-H)
184bw										π (C_bC_aN)
	182m	191bm	188bw	220bw	226bvw	198bm	156bm	117bm	101bw	π (NMN) δ (ring)

Rel. int.: s, strong; m, medium; w, weak; vw, very weak; sh, shoulder; bs, broad and strong; bm, broad and medium; bw, broad and weak; bvw, broad and very weak

TABLE 2. Data used in the correlations*

Metal	μ	E_N	r_{cov}	Band positions (cm^{-1}) B(0,0)	Q(1,0)	Q(0,0)	a	b	c	d
Mg	8.89	1.31	1.36	24213	18315	17153	182	328	930	1226
Co	11.32	1.88	1.16	25316	19231	18018	220	349	951	1239
Ni	11.31	1.91	1.15	25381	19268	18018	226	354	954	1239
Cu	11.48	1.90	1.17	24938	18975	17730	198	272	941	1234
Zn	11.54	1.65	1.25	24876	18762	17544	156	234	933	1230
Cd	12.46	1.69	1.48	24450	18416	17331	117	208	923	1223
Hg	13.09	2.00	1.49	24390	18762	17730	101	191	920	1222

*μ, molar reduced mass of the N—metal bond of the MTHTMP complexes; E_N, electronegativity (Pauling); r_{cov}, covalent radius of the metal in Å; a, b, c, and d, ir position of the metal sensitive bands (see texts).

TABLE 3. Correlation factors between sets of data*

		1	2	3	4
	Data sets	All bivalent complexes (Mg → Hg)	For a period and a group (Co → Hg)	For a period (Co → Zn)	For a group (Zn → Hg)
A	μ/B(0,0)	0.09	−0.91	−0.99	−0.95
	μ/Q(1,0)	0.23	−0.69	−0.99	−0.11
	μ/Q(0,0)	0.38	−0.50	−0.99	−0.37
	μ/a	−0.55	−0.92	−0.95	−0.99
	μ/b	−0.68	−0.82	−1.00	−1.00
	μ/c	−0.28	−0.89	−0.99	−0.98
	μ/d	−0.22	−0.92	−0.99	−0.96
B	E_N/Q(1,0)	0.47	0.11	−0.99	0.41
C	r_{cov}/B(0,0)	−0.87	−0.94	−0.77	−1.00
	r_{cov}/Q(1,0)	−0.78	−0.84	−0.91	−0.47
	r_{cov}/Q(0,0)	−0.63	−0.68	−0.89	0.00
	r_{cov}/a	−0.92	−0.96	−0.97	−0.97
	r_{cov}/b	−0.73	−0.86	−0.86	−0.93
	r_{cov}/c	−0.94	−0.93	−0.90	−0.98
	r_{cov}/d	−0.96	−0.96	−0.91	−1.00
D	B(0,0)/a	0.75	0.97	0.89	0.99
	B(0,0)/b	0.57	0.97	0.98	0.96
	B(0,0)/c	0.92	0.99	0.97	0.99
	B(0,0)/d	0.94	0.99	0.95	1.00
E	Q(1,0)/a	0.65	0.89	0.98	0.23
	Q(1,0)/b	0.48	0.91	0.99	0.12
	Q(1,0)/c	0.83	0.91	1.00	0.30
	Q(1,0)/d	0.86	0.91	1.00	0.40
F	Q(0,0)/a	0.50	0.76	0.97	−0.25
	Q(0,0)/b	0.36	0.83	1.00	−0.36
	Q(0,0)/c	0.72	0.80	0.99	−0.18
	Q(0,0)/d	0.75	0.79	1.00	−0.08
G	a/b	0.93	0.96	0.95	0.99
	a/c	0.95	0.99	0.97	1.00
	a/d	0.93	0.99	0.98	0.99
	b/c	0.84	0.99	0.99	0.98
	b/d	0.79	0.97	0.99	0.96
	c/d	0.99	0.99	0.99	0.99

*See Table 2 for captions.

Can. J. Chem. Downloaded from www.nrcresearchpress.com by 198.100.157.202 on 09/07/12
For personal use only.

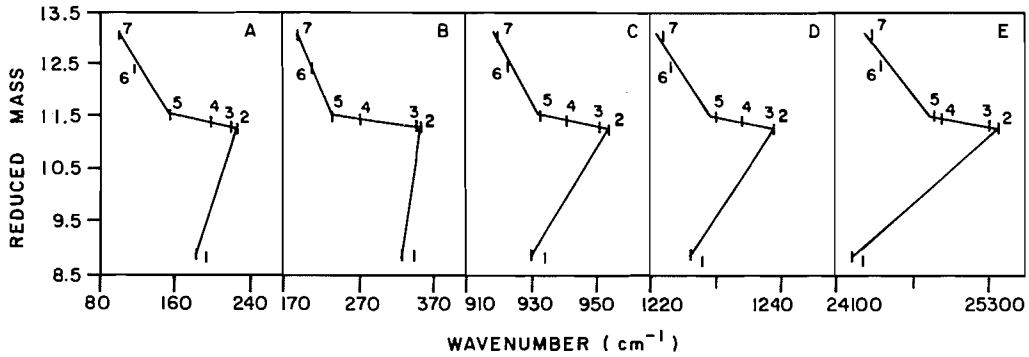


FIG. 5. Correlation curves between the reduced mass of the N–metal bond and the shift of absorption bands of THTMP metal complexes. *A*: band a, 101–226 cm^{-1}; *B*: band b, 349–192 cm^{-1}; *C*: band c, 954–920 cm^{-1}; *D*: band d, 1239–1222 cm^{-1}; *E*: B(0,0) band (Soret), 25381–24213 cm^{-1}. *1*: Mg; *2*: Ni; *3*: Co; *4*: Cu; *5*: Zn; *6*: Cd; *7*: Hg.

bond and the band situated in the 954–920 cm^{-1} region (Table 3.A). This observation supports the assignment of this band to a pyrrole ring mode involving the metal.

The relation between the B(0,0) (Soret) band and the reduced mass of the N—metal bond is given in Fig. 5*E*. The pattern in this figure is similar to the others (Fig. 5*A–D*) which show the correlation patterns of the metal-sensitive bands in the infrared and far-infrared regions. This is surprising since no direct relationship between the reduced mass of the N—metal bond and the electronic transition which give rise to the B(0,0) band has been established so far. However, within these series, an increase of the reduced mass corresponds to an increase of π-bonding between the metal and the porphyrinato ligand, this being due either to a greater number of *d* electrons on the metal, among a period, or to more polarizable *d* orbitals, among a group.

The spectral shifts of the Q(1,0) band are the only ones that correlate well with the electronegativity of the complexed metals, and only for the elements within a period (Table 3.B). This direct relationship has already been reported for other metalloporphyrins (7, 36, 38). Indeed, this correlation has led to the use of the position of the Q(1,0) band to evaluate the covalency of the N—metal bond (7). Our results confirm the general applicability of this relationship which states that a porphyrin complex of a metal of lower electronegativity shows its Q(1,0) band at higher wavelength.

The metals studied have high electronegativity. Therefore the covalent N—metal bonding prevails and the covalent radius of the metals gives an appropriate measure of their sizes. Indeed, a relation is observed between the spectral shifts and the covalent radii of the metals (Table 3.C). The four bands in the infrared and far-infrared regions give fair to good correlations, even when the Mg complex is included in the series. The covalent radius is indicative of the ability of a metal to fit into the porphin N_4-cavity and to form a linear metal—N—metal arrangement. This should reflect directly on the a, b, and c bands. The d band is assigned to an in-plane deformation of the C_m—H bond. Its sensitivity to the metal could be related to the modification of the force constants of the methine bridge when complexation is made with metals of different sizes (17, 24).

The position of the B(0,0) band of all the complexes (Table 3.C1) and the position of the visible Q(1,0) and Q(0,0) bands for the complexes containing an element in the same period (Table 3.C3) correlate with the covalent radii of the metals. This good correlation may be due to two factors (7, 12). The first one is the ruffling of the ring, which modifies the A_{2u}—π orbitals of the ring and therefore causes a change in the electronic ground state of the porphyrin. The second factor is an increased d_{metal}–$2p_{ring}$ orbital interaction which is due to more *d* electrons or to a greater polarizability of the *d* orbitals of the metal.

The similar dependence of the vibrational and electronic absorptions on various structural characteristics, added to the fact that the shifts of the most metal-sensitive bands of the vibrational spectra are not directly related to the reduced mass of the N—metal bond, demonstrates that the shifts of all these bands, even the vibrational ones, are related to an electronic rather than to a mass effect. A conclusion similar to this one has been reached by Owens and O'Connor in their study on hemes (2) and by Gladkov and Solovyov on OEP and other porphyrins (44).

The dependence of the various shifts of the selected bands on electronic effects is supported by the observation that the shift of the B(0,0) band correlates with the shifts of the four vibrational bands for the series of bivalent complexes (Table 3.D). However, the shifts of the bands in the visible region correlate with the shifts of the vibrational bands only for the complexes of the metals in the same period (Table 3.E–F). In this case, the change in the size of the valence orbitals might affect the vibrational and the electronic transitions in a different way. The shifts of the four bands in the infrared and far-infrared regions correlate one with the other (Table 3.G) and hence these shifts are due to similar effects which are mostly electronic.

Far-infrared spectroscopy of natural porphyrins

The far-infrared spectrum of MgTHTMP is of special interest because it can be compared with the spectra of chlorophyll in different aggregation states. Katz *et al.* have observed a band at 306–312 cm^{-1} for an aggregated species of chlorophyll in which the N—Mg bond is modified by an interaction of the magnesium atom with the carbonyl group of another chlorophyll molecule (25). The nonaggregated chlorophyll, produced by dissolving the pigments in a solvent system containing electron-donating molecules (MeOH and pyridine), gives two bands, one at 292 and the other at 195 cm^{-1} (25). However, in this nonaggregated species, the magnesium atom must interact with the solvent as an axial ligand. Thus, these bands are not related to an isolated N—Mg—N group.

The aggregation states and the external ligation of other natural porphyrins (heme proteins) are also of great interest (9). The magnesium derivative of protoporphyrin-IX in Nujol

Can. J. Chem. Downloaded from www.nrcresearchpress.com by 198.100.157.202 on 09/07/12
For personal use only.

absorbs at 342, 319, and 189 cm^{-1}; Mg—hematoporphyrin-IX absorbs at 337, 261, 217, and 189 cm^{-1} (10). These compounds have carboxyl oxygens on their side-chains which can interact with the central magnesium. MgOEP in Nujol absorbs at 336, 214, and 129 cm^{-1} (12). For MgTHTMP in CCl_4, which, as we have shown before (43), axially ligates water molecules present in the solvent, we observe two bands situated at 328 and 182 cm^{-1} (Fig. 3). Assuming that the side-chains do not have a great influence on the symmetry of the Mg—porphyrin ring (7), the band found in the 195–180 cm^{-1} region could be assigned to the N—Mg vibration of the nonaggregated species associated with an axial ligand. Indeed MgOEP in Nujol, which is aggregated but not axially ligated, does not show this band (12). This complex shows a band situated at 214 cm^{-1} which is also found in the Mg–hematoporphyrin spectrum at 217 cm^{-1}. Accordingly, the hematoporphyrin samples would be made of both the axially ligated (band at 189 cm^{-1}) and nonligated (band at 217 cm^{-1}) species. A band corresponding to the nonligated species in the nonaggregated chlorophyll spectrum has yet to be observed. Such a band would be useful to establish the nature of the displacement observed in the spectrum of the ligated species.

Conclusion

The spectra of a new series of liposoluble metalloporphyrin complexes are presented over a very broad spectral range in a nonpolar, noncoordinating solvent. These data are helpful to make the assignment of the vibrational bands of metalloporphyrins, with special interest in the spectra of the natural porphyrins. Significant correlations are found between the shifts of metal sensitive bands and structural parameters.

Some bands in the far-infrared region are observed at positions close to the ones that had been calculated with normal coordinate analyses (9, 19*b*, 22). However, the shift of these bands do not correlate with the reduced mass of the N—metal bond and therefore these bands cannot be assigned to pure vibrational modes of the N—metal bond. This confirms the conclusion of Abe that there is a need for more studies in the far-infrared region for such compounds (19*b*). The intensities of the bands in this region vary greatly with the metal. In the other regions, no variation of this magnitude is observed. Further studies are needed to determine the nature of the variation observed in the far-infrared.

Some anomalies were observed during the course of this work. The high hygroscopicity of MgTHTMP in CCl_4, as shown by the associated water bands at 3665, 3587, and 1594 cm^{-1}, disappears in the solid sample. This peculiar behavior, which has some implications in the comprehension of the aggregation of chlorophyll, is discussed elsewhere in this journal (43). CoTHTMP in CCl_4 is decomposed. The transformation of this complex, as followed by visible and infrared spectroscopies, induces the formation of CO_2 molecules (45). Work is in progress to identify the cause of the instability of CoTHTMP in CCl_4.

Acknowledgements

This work was supported in part by the Fonds FCAR of the Province of Québec and in part by the Natural Sciences and Engineering Council of Canada. Denis Girard received a scholarship from the Fonds FCAR of the Province of Québec. We thank Michel Trudel for the computer treatment of the data.

1. M. Gouterman. *In* The porphyrins. vol. 3. *Edited by* D. Dolphin. Academic Press, New York. 1978. Chap. 1.
2. J. W. Owens and C. J. O'Connor. Coord. Chem. Rev. **84**, 1 (1988).
3. M. Gouterman. J. Mol. Spectrosc. **6**, 138 (1961).
4. M. Gouterman, L. K. Hanson, G. E. Khalil, and W. R. Leenstra. J. Chem. Phys. **62**, 2343 (1975).
5. A. H. Corwin, A. B. Chivvis, R. W. Poor, D. G. Whitten, and E. W. Baker. J. Am. Chem. Soc. **90**, 6577 (1968).
6. A. Antipas and M. Gouterman. J. Am. Chem. Soc. **105**, 4896 (1983).
7. J. A. Shelnutt and M. R. Ondrias. Inor. Chem. **23**, 1175 (1984).
8. R. H. Felton and N.-T. Yu. *In* The porphyrins. Vol. 3. *Edited by* D. Dolphin. Academic Press, New York. 1978. Chap. 3.
9. T. G. Spiro, R. S. Czernuszewicz, and X.-Y. Li. Coord. Chem. Rev. **100**, 541 (1990).
10. L. J. Boucher and J. J. Katz. J. Am. Chem. Soc. **89**, 1340 (1967).
11. H. Burger, K. Burczyk, and J. H. Fuhrhop. Tetrahedron, **27**, 3257 (1971).
12. H. Ogoshi, N. Masai, Z. Yoshida, J. Takemoto, and K. Nakamoto. Bull. Chem. Soc. Jpn. **44**, 49 (1971).
13. H. Ogoshi and Z. Yochida. Bull. Chem. Soc. Jpn. **44**, 1722 (1971).
14. H. Ogoshi, Y. Saito, and K. Nakamoto. J. Chem. Phys. **57**, 4194 (1972).
15. H. Ogoshi, E. Watanabe, Z. Yoshida, J. R. Kincaid, and K. Nakamoto. J. Am. Chem. Soc. **95**, 2845 (1973).
16. J. R. Kincaid and K. Nakamoto. J. Inorg. Nucl. Chem. **37**, 85 (1975).
17. J. R. Kincaid, M. W. Urban, T. Watanabe, and K. Nakamoto. J. Phys. Chem. **87**, 3096 (1983).
18. H. Burger. *In* Porphyrins and metalloporphyrins. *Edited by* K. M. Smith. Elsevier, Amsterdam. 1975. Chap. 11.
19. (*a*) M. Abe, T. Kitagawa, and Y. Kyogoka. J. Chem. Phys. **69**, 4526 (1978); (*b*) M. Abe. *In* Spectroscopy of biological systems. *Edited by* R. J. H. Clark and R. E. Hester. John Wiley and Sons, New York. 1986. Chap. 7.
20. L. L. Gladkov and K. N. Solovyov. Spectrochim. Acta, (*a*) **41A**, 1437 (1985); (*b*) **41A**, 1442 (1985).
21. L. L. Gladkov and K. N. Solovyov. Spectrochim. Acta, **42A**, 1 (1986).
22. (*a*) X.-Y. Li, R. S. Czernuszewicz, J. R. Kincaid, Y. O. Su, and T. G. Spiro. J. Phys. Chem. **94**, 31 (1990); (*b*) X.-Y. Li, R. S. Czernuszewicz, J. R. Kincaid, P. Stein, and T. G. Spiro. J. Phys. Chem. **94**, 47 (1990); (*c*) X.-Y. Li, R. S. Czernuszewicz, J. R. Kincaid, and T. G. Spiro. J. Am. Chem. Soc. **111**, 7012 (1989).
23. D. L. Willems and D. F. Bocian. J. Phys. Chem. **89**, 234 (1985).
24. R. G. Alden, B. A. Crawford, R. Doolen, M. R. Ondrias, and J. A. Shelnutt. J. Am. Chem. Soc. **111**, 2070 (1989).
25. J. J. Katz, R. C. Dougherty, and L. J. Boucher. *In* The chlorophylls. *Edited by* L. P. Vernon and G. R. Seely. Academic Press, New York. 1966. Chap. 7.
26. C. Chapados and R. M. Leblanc. Biophys. Chem. **17**, 211 (1983).
27. M. Ringuet and J. Gagnon. Can. J. Chem. **63**, 2420 (1985).
28. M. Ringuet, J. Gagnon, and R. M. Leblanc. Langmuir, **2**, 700 (1986).
29. K. M. Smith and M. F. Bisset. J. Org. Chem. **44**, 2077 (1979).
30. J. H. Fuhrhop and K. M. Smith. *In* Porphyrins and metalloporphyrins. *Edited by* K. M. Smith. Elsevier, Amsterdam. 1975. p. 798.
31. I. H. Fisher, W. Neumann, and A. Treibs. Justus Liebigs Ann. Chem. **494**, 225 (1932).

Can. J. Chem. Downloaded from www.nrcresearchpress.com by 198.100.157.202 on 09/07/12
For personal use only.

32. J. C. MILLER and J. N. MILLER. Statistics for analytical chemistry. Ellis Horwood, Chichester. 1984. Chap. 4.
33. J. W. BUCHLER. *In* Porphyrins and metalloporphyrins. *Edited by* K. M. Smith. Elsevier, Amsterdam. 1975. Chap. 5.
34. H. LEE, T. KITAGAWA, M. ABE, R. K. PANDEY, H.-K. LEUNG, and K. M. SMITH. J. Mol. Struct. **146**, 329 (1986).
35. M. TASUMI and M. FUJIWARA. *In* Spectroscopy of inorganic-based materials. *Edited by* R. J. H. Clark and R. E. Hester. John Wiley and Sons, New York. 1987. Chap. 6.
36. M. GOUTERMAN. J. Chem. Phys. **30**, 1139 (1959).
37. J. B. ALLISON and R. S. BECKER. J. Phys. Chem. **67**, 2675 (1963).
38. J. A. SHELNUTT. J. Am. Chem. Soc. **105**, 774 (1983).
39. L. D. SPAULDING, C. C. CHANG, N.-T. YU, and R. H. FELTON. J. Am. Chem. Soc. **97**, 2517 (1975).
40. J. D. STONG, T. G. SPIRO, R. J. KUBASKA, and S. I. SHUPACK. J. Raman Spectrosc. **9**, 312 (1980).
41. M. FUJIWARA and M. TASUMI. J. Phys. Chem. **90**, 5646 (1986).
42. T. KITAGAWA, H. OGOSHI, E. WATANABE, and Z. YOSHIDA. J. Phys. Chem. **79**, 2629 (1975).
43. C. CHAPADOS, D. GIRARD, and M. RINGUET. Can. J. Chem. **66**, 273 (1988).
44. L. L. GLADKOV and K. N. SOLOVYOV. Teor. Eksp. Khim. **16**, 705, (1980).
45. D. GIRARD. M.Sc. Thesis, Université du Québec. 1986. pp. 91–95.

Can. J. Chem. Downloaded from www.nrcresearchpress.com by 198.100.157.202 on 09/07/12
For personal use only.

The crystal structure of the "White Salt" trisilver(I) amidoselenate-3-ammonia-2-water $[Ag(NH_3)_2]Ag_2SeO_3N \cdot 3NH_3 \cdot 2H_2O$

ZDIRAD ŽÁK[1] AND ANTONÍN RŮŽIČKA

Department of Inorganic Chemistry, Masaryk University, Kotlářská 2, 611 37 Brno, Czechoslovakia

AND

TADEUSZ GŁOWIAK

Institute of Chemistry, University of Wrocław, F. Joliot-Curie 14, 50-383 Wrocław, Poland

Received July 26, 1990

ZDIRAD ŽÁK, ANTONÍN RŮŽIČKA, and TADEUSZ GŁOWIAK. Can. J. Chem. **69**, 1080 (1991).

Trisilver(I) amidoselenate-3-ammonia-2-water, $Ag_3SeO_3N \cdot 3NH_3 \cdot 2H_2O$, M_r = 551.70, is orthorhombic, space group $P2_12_12_1$ with a = 11.864(3), b = 14.550(3), c = 6.433(2) Å, Z = 4, D_m = 3.25, D_x = 3.30 Mg m^{-3}, radiation MoK$\bar{\alpha}$, λ = 0.71069 Å, μ = 8.62 mm^{-1}, $F(000)$ = 1024, T = 295 K. The structure was solved by direct methods and refined to R = 0.036 for 1759 observed reflections. In the structure, only two independent Ag atoms are directly bonded to the N(Se) atom of the amidoselenic group ($NSeO_3$) and these groups are joined by Ag into an infinite polymeric chain via [—N(Se)—Ag] bridges. The third Ag atom is present as a complex cation $[Ag(NH_3)_2]^+$. Each silver atom is coordinated by two N atoms: Ag(1) by N(Se) and a NH_3 molecule, Ag(2) by two N(Se) atoms, and Ag(3) by two NH_3 molecules. Important blood lengths are Ag(1)—N(Se), NH_3 2.111 and 2.110(8); Ag(2)—N(Se), N(Se^i) 2.106 and 2.096(7); and Ag(3)—NH_3, NH_3 2.115 and 2.150(10); N(Se)—Se 1.727(8); and Se—O 1.641, 1.647, and 1.639(7) Å.

Key words: Silver amidoselenate, silver–nitrogen bond, nitrogen–selenium bond.

ZDIRAD ŽÁK, ANTONÍN RŮŽIČKA, and TADEUSZ GŁOWIAK. Can. J. Chem. **69**, 1080 (1991).

L'amidosélenate d'argent $Ag_3SeO_3N \cdot 3NH_3 \cdot 2H_2O$ est orthorhombique groupe spatial $P2_12_12_1$ avec a = 11,864(3) b = 14,550(3) et c = 6,433(2) Å, Z = 4, D_m = 3,25, D_x = 3,30 Mg m^{-3}, radiation MoK$\bar{\alpha}$, λ = 0,71069 Å, μ = 8,62 mm^{-1}, $F(000)$, = 1024, T = 295 K. La structure a été résolue par les méthodes directes et affinée à un résidu de R = 0,036 utilisant 1759 réflections uniques observées. Dans la structure, seulement deux atomes d'argent indépendantes sont liés directement à l'atome d'azote N(Se) de la groupe amidosélénique ($NSeO_3$) et cettes groupes sont liées par Ag dans une chaîne polymérique infinie via les ponts [—N(Se)—Ag]. Le troisième atome d'argent est dans la forme du cation complex $[Ag(NH_3)_2]^+$. Chaque atome d'argent est coordiné par deux atomes d'azote: Ag(1) par N(Se) et par la molécule d'ammoniaque, Ag(2) par deux N(Se) atomes et Ag(3) par deux molécules d'ammoniaque. Les longueurs de liaison importantes sont: Ag(1)—N(Se), NH_3 2,111 et 2,110(8); Ag(2)—N(Se), N(Se^i) 2,106 et 2,096(7); Ag(3)—NH_3, NH_3 2,115 et 2,150(10); N(Se)—Se 1,727(8) et Se—O 1,641, 1,647 et 1,639 Å.

Mots clés : amidosélénate d'argent, liaison argent–azote, liaison azote–sélénium.

Introduction

By the reaction of $SeO_3NH_2^-$ ions with an excess of $AgNO_3$ in dilute water solutions of NH_3 and/or NaOH an amorphous orange–red precipitate of Ag_3SeO_3N is produced (1, 2):

$$SeO_3NH_2^- + 3Ag^+ + 2OH^- = Ag_3SeO_3N + 2H_2O$$

Two crystalline modifications of trisilver amidoselenate are known and can be distinguished by their X-ray powder diffraction patterns and IR spectra. The deep-red α-modification (the "red salt") is formed when the amorphous precipitate is boiled in the mother liquor for a few minutes, the light-red β-modification results if the precipitate is allowed to stay in the mother liquor at room temperature for some time (2, 3). The crystal structure of the "red salt" has already been determined (4, 5). Both α and β modifications dissolve easily in dilute water solution (1%) of ammonia and after a few hours of standing at room temperature, colourless needles of the "white salt" $Ag_3SeO_3N \cdot 3NH_3 \cdot 2H_2O$ crystallize from the solution. This salt is non-explosive and by the action of water it decomposes slowly to the β-modification of Ag_3SeO_3N (2).

A sulfur analogue of the "white salt", $Ag_3SO_3N \cdot 3NH_3 \cdot 2H_2O$, has been known for a long time (6) and its structure has recently been determined (7).

To understand the bonding in selenium(VI)–nitrogen compounds and to compare the structures of $Ag_3SeO_3N \cdot 3NH_3 \cdot 2H_2O$ and $Ag_3SO_3N \cdot 3NH_3 \cdot 2H_2O$, we have undertaken the X-ray structure determintion of the "white salt", the results of which comprise this article.

TABLE 1. Final atomic parameters of non-hydrogen atoms (× 10^4) and their esd's in parentheses

Atom	x	y	z	B_{eq} (Å^2)
Ag(1)	4446(05)	1138(05)	7780(1)	2.3(1)
Ag(2)	2490(06)	−13(05)	5607(1)	2.1(1)
Ag(3)	4623(07)	1006(06)	2783(1)	3.3(2)
Se	1842(07)	1876(05)	8041(1)	1.6(1)
O(1)	2434(6)	2738(4)	9271(10)	2.7(4)
O(2)	1608(7)	2195(5)	5622(10)	2.9(4)
O(3)	624(6)	1668(6)	9144(10)	2.9(5)
O(W1)	3124(8)	4302(6)	7096(20)	5.7(8)
O(W2)	387(9)	1035(7)	3139(20)	4.9(8)
N(Se)	2696(6)	915(5)	8092(10)	1.9(4)
N(1)	3765(7)	2276(6)	3012(15)	2.9(5)
N(2)	5762(9)	−145(7)	2591(20)	4.0(7)
N(3)	6205(7)	1295(5)	7456(10)	2.6(6)

*$B_{eq} = \frac{1}{3}(B_{11} + B_{22} + B_{33})$.

Experimental

The suitable crystals for X-ray work were prepared as described (1, 2). The experimental density was obtained by pycnometry in decahy-

[1]To whom correspondence should be addressed.

Printed in Canada / Imprimé au Canada

Can. J. Chem. Downloaded from www.nrcresearchpress.com by 84.41.108.74 on 09/07/12
For personal use only.

TABLE 2. Bond lengths (Å) and bond angles (deg) with esd's in parentheses

Bond	Distance	Bonds	Angle
Ag(1)—N(Se)	2.111(8)	N(Se)—Ag(1)—N(3)	177.4(3)
Ag(2)–N(Se)	2.106(7)	N(Se)—Ag(2^i)—N(Se^i)	178.7(3)
Ag(2^i)—N(Se)	2.096(7)	N(1)—Ag(3)—N(2)	170.0(4)
Ag(1)—N(3)	2.110(8)	Ag(1)—N(Se)—Ag(2)	98.1(3)
Ag(3)—N(1)	2.115(10)	Ag(1)—N(Se)—Ag(2^i)	105.8(3)
Ag(3)—N(2)	2.150(10)	Ag(2)—N(Se)—Ag(2^i)	99.9(3)
Se—N(Se)	1.727(8)	Ag(1)—N(Se)—Se	116.8(3)
Se—O(1)	1.640(7)	Ag(2)—N(Se)—Se	115.9(3)
Se—O(2)	1.649(7)	Ag(2^i)—N(Se)—Se	117.3(3)
Se—O(3)	1.637(7)	O(1)—Se—O(2)	108.2(4)
		O(1)—Se—O(3)	108.1(4)
Symmetry code:		O(2)—Se—O(3)	108.1(4)
(i) $0.5 - x; -y; 0.5 + z$		O(1)—Se—N(Se)	111.1(4)
		O(2)—Se—N(Se)	110.1(4)
		O(3)—Se—N(Se)	111.1(4)

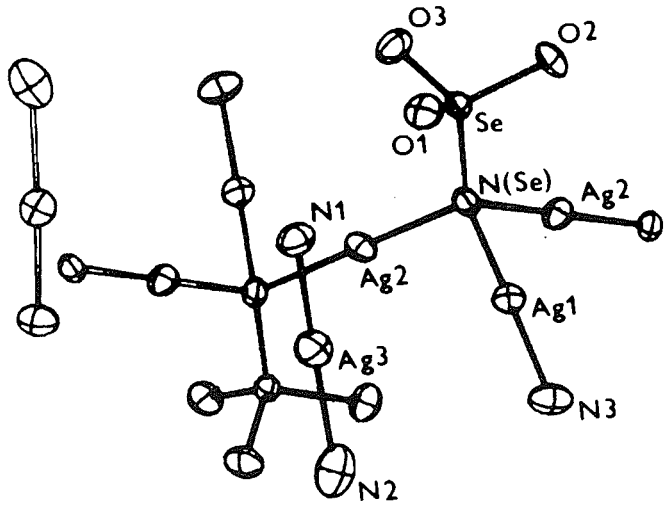


FIG. 1. A part of the structure showing the [—Ag—N(Se)—] chains. Water molecules and hydrogen atoms of ammonia molecules are omitted for clarity.

dronaphtalene. Preliminary lattice parameters and the space group were determined from Weissenberg and precession photographs. Final parameters were refined from 15 reflections $21° < 2\theta < 33°$, collected on a Syntex $P2_1$ diffractometer. Basic crystallographic data are summarized in the abstract.

The intensities of 2404 independent reflections were collected by the θ–2θ scan technique up to $2\theta = 66°$, $0 < h < 16$, $0 < k < 22$, $0 < l < 9$. The intensities were corrected for Lorentz-polarization and absorption effects. The absorption correction was calculated using program DIFABS from Syntex XTL program system. The minimum and maximum values of the absorption were 0.854 and 1.451, respectively. The stability of the crystal was checked by measuring two standard refections after every 50 measured but no significant decrease in their intensities was detected. From the total of 2404 reflections measured, 1759 with $I > 4\sigma(I)$ were taken for the structure solution and refinement.

The structure was solved by direct methods, the heavy atoms, silver and selenium, were located from the E-map. The electron density map based on the positions of the heavy atoms revealed the rest of the structure, except hydrogen atoms. These were placed according to possible H bonds 1.0 Å from the atoms to which they are bonded and assigned an arbitrary isotropic temperature factor of 6.0 Å^2. The refinement was performed by a full-matrix least-squares method on $|F_o|$ with weights $w = 1/(\sigma^2 + k|F_o|^2)$ with k empirically set to 0.002. Non-hydrogen atoms were refined anisotropically, hydrogen atoms were not refined. A secondary extinction correction according to Darwin (8), with an extinction parameter g set to 2.307×10^{-6}, was applied to the strongest reflections. The absolute configuration of the structure was determined from two simultaneous runs of least-squares refinement with the structure and its enantiomorph. The model which yielded a significantly lower value of R was accepted as the correct configuration. The refinement was stopped when the average shift of the parameters was less than 0.05. The final R and R_w values are 0.036 and 0.014 respectively. $R_w = [\Sigma w_i(|F_o| - |F_c|)^2/\Sigma w_i|F_o|^2]^{1/2}$, $S = 0.972$. For the atoms Ag and Se anomalous dispersion was taken into account. The programs used were SHELX 86 for the structure solution (9), Syntex XTL program system for absorption correction and the electron density map calculations (10), a part of UNIBOX program system for bond and angles calculations and for a secondary extinction correction (11), ORFLS least-squares program (12), and the figures were drawn by ORTEP (13). The atomic scattering factors of neutral atoms were those of Cromer and Mann (14), anomalous dispersion correction was from the International tables (15). The atomic parameters of non-hydrogen atoms including B_{eq} are given in Table 1. The lists of the atomic parameters of hydrogen atoms, anisotropic temperature factors of non-hydrogen atoms, and observed and calculated structure factors have been deposited, and are available from the Depository of Unpublished Data.[2]

Results and Discussion

The "white salt" $Ag_3SeO_3N \cdot 3NH_3 \cdot 2H_2O$ is formed by polymeric chains via [—Ag—N—] bridges and is isostructural with its sulfur analogue, $Ag_3SO_3N \cdot 3NH_3 \cdot 2H_2O$ (7). A part of the structure is shown in Fig. 1. Unlike the "red salt" Ag_3SeO_3N (4, 5) where all three Ag atoms are bonded to the N atom and its polymeric network created by [—Ag—N—Se—O—] chains, in the "white salt" only two independent Ag atoms, namely Ag(1) and Ag(2), are directly bonded to the N(Se) atom of the amidoselenic group ($NSeO_3$) and these groups are joined by Ag(2) into an infinite simple polymeric chain $[—Ag(2)—N(Se)—]_n$. The third Ag(3) atom is in the form of a complex cation $[Ag(NH_3)_2]^+$. No matter how closely are the "red" and "white" salts related from a chemical point of view, there seems to be a significant difference in the Ag—N and Se—N bond character in these compounds. The bonding in the "red salt" is thoroughly

[2]A complete set of the structure factor table, atomic parameters of hydrogen atoms, and anisotropic temperature factors may be purchased from the Depository of Unpublished Data, Document Delivery, CISTI, National Research Council of Canada, Ottawa, Canada K1A 0S2.

Can. J. Chem. Downloaded from www.nrcresearchpress.com by 84.41.108.74 on 09/07/12
For personal use only.

TABLE 3. Comparison of the structures of the "red" and "white" salts; distances and angles are partly averaged

Bond	Distance (Å)	
	Ag_3SeO_3N	$Ag_3SeO_3N \cdot 3NH_3 \cdot 2H_2O$
Ag—NH_3		2.13(2)
Ag—N(Se)	2.164(8)	2.104(8)
Ag—O	2.23(1)	
Se—N(Se)	1.70(2)	1.727(8)
Se—O	1.651(8)	1.642(7)

Bonds	Angle (deg)	
	Ag_3SeO_3N	$Ag_3SeO_3N \cdot 3NH_3 \cdot 2H_2O$
Ag—N(Se)—Ag	107.3(6)	101(4)
N(Se)—Se—O	112.9(4)	110.8(4)
O—Se—O	105.8(5)	108.2(4)

Bonds	Torsion angle (deg)	
	Ag_3SeO_3N	$Ag_3SeO_3N \cdot 3NH_3 \cdot 2H_2O$
Ag(1)—N(Se)—Se—O(1)		−38.2(3)
Ag(2)—N(Se)—Se—O(2)	11.1	−33.3(3)
Ag(2^i)—N(Se)—Se—O(3)		−31.4(3)

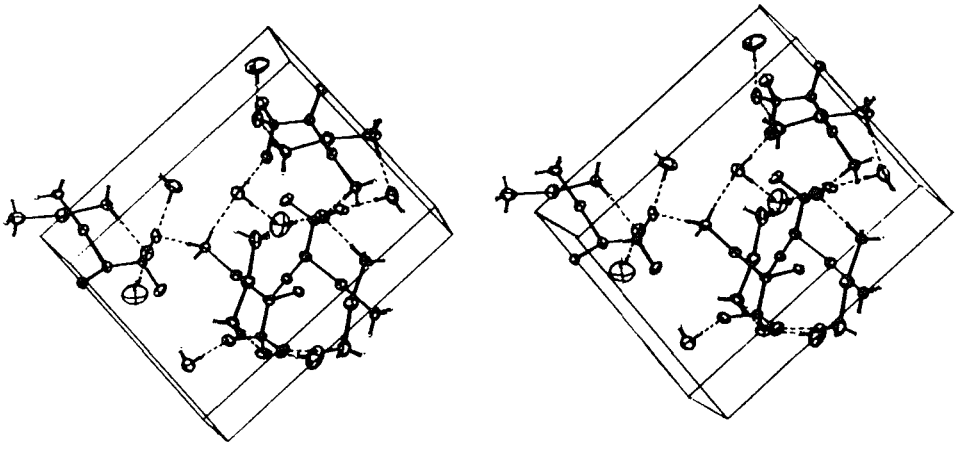


FIG. 2. A stereoview of the packing of the unit cell with possible hydrogen bonds.

studied by Kocman and Szymański (5). While in the "red salt" a partially ionic character of the Ag—N bond and a substantial π-bond contribution to Se—N bond is supposed, a rather high covalency of the Ag—N bond in the "white salt" is compensated by a decrease in π-bond contribution to the Se—N bond as follows from the mutual comparison of their bond lengths and valency angles (Tables 2 and 3). However, there is no significant change in the character of Se—O bonds, their lengths conform to values commonly encountered in selenates (16).

The Ag—N distances range from 2.096(7) to 2.150(10) Å, the longest belonging to the $[Ag(NH_3)_2]^+$ cation, and are comparable with those found in other related structures: 2.16–2.22(2) Å in $Ag_3SO_3N \cdot H_2O$ (17) and 2.08–2.17(2) Å in $Ag_3SO_3N \cdot 3NH_3 \cdot 2H_2O$ (7). Each Ag atom is coordinated approximately linearly by two N atoms: Ag(1) by N(Se) and $N(3)H_3$; Ag(2) by N(Se) and $N(Se^i)$; and Ag(3) by $N(1)H_3$ and $N(2)H_3 \cdot N(Se)$ and Se atoms are coordinated tetrahedrally as expected: N(Se) by 3Ag + Se, Se by N(se) + 3O and the entity $[Ag_3NSeO_3]$ has approximately a C_{3v} point symmetry. The Se—O and Ag—N bonds are staggered by approximately 34° (Table 3). The molecules of ammonia, besides the coordination of Ag atoms and water form hydrogen bonds towards the O atoms of the ($NSeO_3$) group and water molecules. Because the H atoms were placed linearly toward the possible acceptors, a proper discussion of the H bonds cannot be made. Their average length is 2.03 Å with minimum and maximum values of 1.80 and 2.47 Å, respectively. A stereoscopic drawing of the packing of the unit cell including possible H bonds is in Fig. 2.

Acknowledgements

The authors are indebted to Dr. V. Kocman of Domtar Research Centre, Senneville, Quebec, Canada for providing a

Can. J. Chem. Downloaded from www.nrcresearchpress.com by 84.41.108.74 on 09/07/12
For personal use only.

preprint of ref. 5 and for many valuable discussions. T.G. acknowledges the grant from the Polish Ministry of Science and Higher Education Projekt No. CPBP 01.12.

1. K. DOSTÁL and A. RŮŽIČKA. Z. Chem. **2**, 88 (1962).
2. K. DOSTÁL and A. RŮŽIČKA. Z. anorg. allg. Chem. **337**, 325 (1965).
3. R. PAETZOLD, K. DOSTÁL and A. RŮŽIČKA. Z. anorg. allg. Chem. **348**, 1 (1966).
4. J. K. FAWCETT, V. KOCMAN, S. C. NYBURG, and R. J. O'BRIEN. Chem. Commun. 1198 (1968).
5. V. KOCMAN and J. T. SZYMAŃSKI. Can. J. Chem. **90**, 1606 (1990).
6. L CHAUMETON and C. R. HEBD. Séances Acad. Sci. **202**, 1783 (1936).
7. F. BELAJ, CH. KRATKY, E. NACHBAUR, and A. POPITSCH. Monatsh. Chem. **118**, 349 (1987).
8. G. H. STOUT and L. H. JENSEN. *In* X-ray structure determination. A practical guide. The Macmillan Co., New York, NY. 1968. pp. 409–412.
9. G. M. SHELDRICK. SHELX 86. Program for crystal structure solution, University of Göttingen, BRD. 1986.
10. XTL structure determination system. Syntex Analytical Instruments, Cupertino, California, U.S.A. 1971.
11. Z. ŽÁK. UN I BOX. A system of programs for the determination of crystal structures. Postgraduate thesis, Technical University of Brno. 1977.
12. W. R. BUSING, K. O. MARTIN, and H. A. LEVY. ORFLS. Report ORNL-TM-305. Oak Ridge National Laboratory, TN, 1962.
13. C. K. JOHNSON. ORTEP. Report ORNL-3794. Oak Ridge National Laboratory, TN, 1965.
14. D. T. CROMER and J. B. MANN. Acta Crystallogr. A**24**, 321 (1968).
15. J. A. IBERS and W. C. HAMILTON (*Editors*). International tables for X-ray crystallography. Vol. IV. Kynoch Press, Birmingham, England.
16. I. D. BROWN, M. C. BROWN, and F. C. HAWTHORNE (*Editors*). BIDICS (Bond index to the determination of inorganic crystal structures). Institute for Materials Research, McMaster University, Hamilton, Ont. 1969–1981.
17. F. BELAJ, CH. KRATKY, E. NACHBAUR, and A. POPITSCH. Monatsh. Chem. **118**, 947 (1987).

Can. J. Chem. Downloaded from www.nrcresearchpress.com by 84.41.108.74 on 09/07/12
For personal use only.

Comparaison des approches empirique et chimiométrique dans la modélisation des effets de solvant. Cas des propriétés spectrales en RMN, IR et UV–visible

ABDELOUAHED AUHMANI ET HASSANE BITAR[1]

Département de chimie, Faculté des sciences, Université Cadi Ayyad, B.P. S 15, Marrakech, Maroc

ROGER PHAN TAN LUU

Laboratoire de prospective réactionnelle et d'analyse de l'information, Centre Universitaire de St Jérôme, Université d'Aix-Marseille III, 13397 Marseille CEDEX 13, France

ET

LAURA BARRIOS

Centro de calculo, Consejo Superior de Investigaciones Científicas, C/Rosario Pino 19, E-28006, Madrid, Espagne

Reçu le 4 janvier 1991

ABDELOUAHED AUHMANI, HASSANE BITAR, ROGER PHAN TAN LUU et LAURA BARRIOS. Can. J. Chem. **69**, 1084 (1991).

La comparaison des résultats des approches empiriques et chimiométriques dans la modélisation de l'effet de solvant sur un ensemble de propriétés spectrales en RMN, IR et UV–visible, est abordée dans cet article. Les solvants sont caractérisés dans un premier temps par les échelles π^*, α et β qui décrivent respectivement la polarité–polarisabilité, l'acidité et la basicité par liaison hydrogène, et les 17 les plus informatifs possibles ont été choisis, tout en ayant des ensembles de paramètres orthogonaux. Nous avons essayé de rationaliser les effets observés sur les propriétés étudiées en utilisant des modèles empiriques linéaires simples faisant intervenir π^*, α et β de Kamlet, Taft, Abboud; E_T^N de Reichardt et A et B de Swain. Par ailleurs, une analyse en composantes principales est appliquée à ces effets et sur l'ensemble des propriétés que nous avons étudiées; il apparaît que la qualité des corrélations obtenues est en général satisfaisante et comparable à celle permise par l'approche empirique.

Mots clés : effet de solvant, approche empirique, approche chimiométrique.

ABDELOUAHED AUHMANI, HASSANE BITAR, ROGER PHAN TAN LUU, and LAURA BARRIOS. Can. J. Chem. **69**, 1084 (1991).

In this paper, we review a comparison of the empirical and chemiometrical approaches to the modelization of the effects of solvent on a number of NMR, IR and UV–visible spectral properties. The solvents have first been characterized by the π^*, α and β scales, which describe respectively the polarity–polarisability, the acidity, and the basicity by hydrogen bond; the 17 most representative, with orthogonal parameters, have been chosen. An attempt has been made to rationalize the observed effects on the observed properties by using simple linear empirical models like the π^*, α, and β parameters of Kamlet, Taft, and Abboud; E_T^N of Reichardt; and A and B of Swain. Furthermore, an analysis of the main components has been applied to these effects and to the properties examined; it appears that the quality of the correlations obtained is generally satisfactory and can be compared to the quality that can be observed with the empirical approach.

Key words: solvent effect, empirical approach, chemiometrical approach.

[Journal translation]

Introduction

La sensibilité des propriétés spectrales des solutés en RMN, IR, RPE et UV–visible à leur environnement moléculaire, a été souvent utilisée dans les études quantitatives des effets de solvant (1–10).

Afin de quantifier et de rationaliser ces effets, deux approches ont été adoptées : (i) l'approche empirique qui a donnée lieu à des échelles de solvant et dont on peut citer : π^*, α et β de Taft, Abboud et Kamlet (1, 11, 12); E_T de Reichardt (8); A et B de Swain *et al.* (13) et les paramètres de Koppel et Pal'm (14); (ii) l'approche chimiométrique appliquée par Sjöström et Wold (15), qui permet de définir une ou plusieurs composantes utilisées pour quantifier l'effet du milieu.

Le problème fondamental se pose lors de la comparaison des méthodes empirique et chimiométrique, car les ensembles de paramètres de la première ne sont pas en général parfaitement orthogonaux. Ceci a donné lieu à une importante controverse entre les partisans de chacune des deux approches qui s'est traduite par un échange d'articles très vifs entre Kamlet et coll. (16) d'un côté et Wold et coll. (15, 17) de l'autre.

Nous nous sommes proposés de comparer les résultats des échelles empiriques où, pris globalement, les paramètres ne sont pas parfaitement orthogonaux, avec ceux de l'analyse en composantes principales (18, 19) où, par construction, les différentes composantes le sont.

Pour ce faire, nous avons choisi et étudié un ensemble de propriétés sensibles à l'effet de solvant. En prenant comme référence les paramètres empiriques π^*, α et β, nous avons choisi à l'aide des méthodes de construction des matrices d'expériences optimales,[2,3] un ensemble de 17 solvants les plus informatifs possibles et ayant des ensembles de paramètres π^*, α et β orthogonaux.[4]

Les effets observés sur les propriétés étudiées ont été analysés d'une part au moyen des paramètres empiriques et d'autre part au moyen de l'analyse en composantes principales faite à l'aide du programme BMDP (20).

Partie expérimentale

Les solvants ainsi que les solutés, produits commerciaux, ont été purifiés par des méthodes standards (21).

1. Auteur à qui adresser toute correspondance.

2. Le choix a été fait à l'aide du programme NEMROD mis au point par R. Phan Tan Luu et D. Mathieu, L.P.R.A.I., Centre Universitaire de St Jérôme, U. d'Aix Marseille III, France.

3. D. Mathieu, Thèse, Marseille, 1981.

4. Les corrélations sont : entre π^* et β : $r^2 = 0{,}001$; entre π^* et α : $r^2 = 0{,}052$; entre α et β : $r^2 = 0{,}028$.

Printed in Canada / Imprimé au Canada

Can. J. Chem. Downloaded from www.nrcresearchpress.com by 198.100.157.202 on 09/07/12
For personal use only.

Can. J. Chem. Downloaded from www.nrcresearchpress.com by 198.100.157.202 on 09/07/12
For personal use only.

TABLEAU 1. Solvants sélectionnés et leurs paramètres (π^*, β et α),[a] (E_T), (A et B)

N°	Solvant	π^*	β	α	E_T^N	A	B
1	Cyclohexane (C_6H_{12})	0,00	0,00	0,00	0,006	0,02	0,06
2	Triéthylamine (TEA)	0,14	0,71	0,00	0,043	0,08	0,19
3	Tri-*n*-butylamine (TBA)	0,16	0,62	0,00	0,043	—[b]	—[b]
4	Tetrachlorure de carbone (CCl_4)	0,28	0,00	0,00	0,052	0,09	0,34
5	Carbonate de diéthyle (DEC)	0,45	0,40	0,00	0,194	—[b]	—[b]
6	Toluène ($PhCH_3$)	0,54	0,11	0,00	0,099	0,13	0,54
7	Acétonitrile (CH_3CN)	0,75	0,31	0,19	0,460	0,37	0,86
8	Diméthyl-2,6 pyridine (DMP)	0,80	0,76	0,00	0,191	0,18	0,81
9	Dichlorométhane (CH_2Cl_2)	0,82	0,00	0,30	0,309	0,33	0,80
10	Diméthylsulfoxyde (DMSO)	1,00	0,76	0,00	0,444	0,34	1,08
11	Nitrobenzène ($PhNO_2$)	1,01	0,39	0,00	0,324	0,29	0,86
12	Tertiobutanol (*t*-BuOH)	0,41	1,01	0,68	0,389	0,45	0,50
13	*n*-Butanol (*n*-BuOH)	0,47	0,88	0,79	0,602	0,61	0,43
14	Méthanol (MeOH)	0,60	0,62	0,93	0,762	0,75	0,50
15	Ethylène glycol ($(CH_3OH)_2$)	0,92	0,52	0,90	0,790	0,78	0,84
16	Trifluoro-2,2,2 éthanol (TFE)	0,73	0,10	1,51	0,898	—[b]	—[b]
17	Hexafluoroisopropanol (HFIP)	0,65	0,00	1,96	1,068	—[b]	—[b]

[a]Les paramètres π^*, β et α utilisés dans les corrélations, ont été codés selon :

$\pi^*_{codé} = (\pi^* - 0{,}505)/0{,}505$ $\beta_{codé} = (\beta - 0{,}505)/0{,}505$ $\alpha_{codé} = (\alpha - 0{,}980)/0{,}980$

[b]Valeurs non mesurées.

Les spectres de RMN ont été obtenus à 36°C sur un appareil Varian FT 80A dans des tubes de 10 mm de diamètre. Les concentrations de solutés sont les plus faibles possibles et varient entre 0,05 et 0,1 M. Le composé deutéré (D_2O) nécessaire au verrouillage du champs magnétique est contenu dans un tube coaxiale de 5 mm. Tous les spectres ont été obtenus en découplage complet des protons et en abondances naturelles. En RMN du ^{13}C (20 MHz) le nombre d'accumulations varie de 2×10^3 à 3×10^4 avec un temps d'acquisition de 2 s. La largeur spectrale est de 4000 Hz, la résolution est de 0,05 ppm et la reproductibilité des déplacements chimiques (D.C.) est de 0,01 à 0,02 ppm. Les spectres du ^{31}P (32,023 MHz) sont enregistrés dans les mêmes conditions avec une largeur spectrale de 5000 Hz et un nombre d'accumulations variant de 5×10^2 à 5×10^3.

Les spectres UV–visible ont été enregistrés sur un appareil Cary 219; la température (25°C) a été maintenue constante à l'aide d'un thermostat Lauda K2R, les concentrations variant entre 3×10^{-5} et 5×10^{-5} M.

Les spectres IR ont été enregistrés sur un appareil Nicolet 20SX à 25°C, la concentration variant entre 10^{-3} et 10^{-5} M. Les cuves utilisées ont une épaisseur de 14 à 15 μm.

Résultats et discussion

Les solvants sélectionnés ainsi que les valeurs des paramètres empiriques (π^*, α et β), (E_T^N) et (A et B) sont regroupés dans le tableau 1.

Les propriétés que nous avons choisies sont :

1. Les signaux de RMN du ^{13}C des carbone des solutés suivants : méthylphénylsulfoxyde (A), tropone (B), pyridine (C), 4-picoline (D), *N,N*-diméthylamino-4 pyridine (E), acétyl-4 pyridine (F), cyano-4 pyridine (G), chlorobenzène (H), α,α,α-trifluorotoluène (I), tropolone (J), diméthylsulfoxyde (K) (Fig. 1).

Les D.C. sont mesurés par rapport au signal du carbone en position *méta* de l'α,α,α-trifluorotoluène utilisé comme référence interne, en suivant la méthode de Taft et coll. (1, 2).

2. Le signal de RMN du ^{31}P du phosphate de triméthyle (L) est mesuré par rapport à celui du phosphite de triisopropyle; le signal de l'oxyde de triphénylphosphine (M) est donné relativement à celui de la triphénylphosphine. Ces références sont également internes.

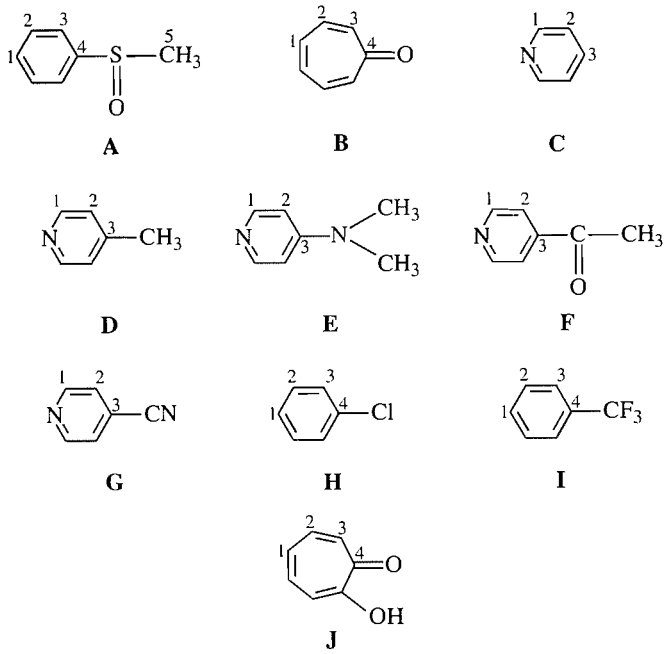


FIG. 1. Solutés étudiés en spectroscopie de RMN du ^{13}C.

3. Les fréquences des vibrations d'élongation : ν_{CO} de CF_3COOMe (N), CCl_3COOMe (O), CH_3COCH_3 (P), $HCONMe_2$ (R); ν_{CN} de $CH_3CH_2CH_2CN$ (Q) et ν_{SO} de CH_3SOCH_3 (K).

4. Les nombres d'onde au maximum d'absorption UV–visible ν_{max} de : nitro-4 aniline (S), *N*-méthylnitro-4 aniline (T), *N,N*-diméthylnitro-4 aniline (U), *N,N*-diéthylnitro-4 aniline (V), nitro-4 phénol (W), nitro-4 anisole (X), dinitro-3,4 phénol (Y) et β-carotène (Z).

Les résultats expérimentaux sont donnés dans les tableaux 1–6 du document complémentaire.[5]

5. Ce document peut être acheté de : Dépôt des données non publiées, service de fourniture de documents, ICIST, Conseil national de recherches Canada, Ottawa, Canada K1A 0S2.

TABLEAU 2. Résultats des corrélations empiriques et chimiométrique pour les propriétés étudiées en RMN

		π^*, α, β		E_T^N		A, B		F_1, F_2, F_3	
Soluté	P	r^2	ETE	r^2	ETE	r^2	ETE	r^2	ETE
A	δC1	0,987(0,981)	0,117(0,068)	0,782	0,424	0,898	0,150	0,987	1,167
	δC2	0,960(0,871)	0,083(0,077)	0,611	0,242	0,745	0,102	0,954	0,088
	δC3	0,920(0,846)	0,109(0,116)	0,277	0,308	0,752	0,140	0,929	0,103
	δC4	0,982(0,955)	0,340(0,386)	0,950	0,530	0,962	0,334	0,993	0,213
	δC5	0,900(0,802)	0,411(0,388)	0,914	0,351	0,877	0,290	0,953	0,279
B	δC1	0,984(0,961)	0,196(0,187)	0,902	0,448	0,959	0,183	0,993	0,125
	δC2	0,985(0,976)	0,284(0,269)	0,957	0,451	0,979	0,235	0,980	0,327
	δC3	0,734(0,834)	0,355(0,312)	0,446	0,504	0,831	0,299	0,774	0,346
	δC4	0,986(0,975)	0,219(0,201)	0,901	0,549	0,930	0,321	0,963	0,362
C	δC1	0,950(0,912)	0,228(0,221)	0,934	0,245	0,913	0,208	0,983	0,134
	δC2	0,978(0,956)	0,096(0,098)	0,861	0,224	0,913	0,131	0,970	0,112
	δC3	0,992(0,984)	0,122(0,122)	0,918	0,372	0,971	0,158	0,994	0,107
D	δC1	0,919(0,932)	0,380(0,210)	0,871	0,447	0,938	0,190	0,965	0,251
	δC2	0,974(0,958)	0,110(0,086)	0,797	0,286	0,888	0,134	0,977	0,104
	δC3	0,973(0,987)	0,400(0,156)	0,857	0,862	0,982	0,175	0,988	0,265
E	δC1	0,933(0,933)	0,376(0,283)	0,873	0,478	0,936	0,261	0,961	0,288
	δC2	0,685(0,589)	0,115(0,110)	0,057	0,184	0,619	0,101	0,736	0,105
	δC3	0,938(0,877)	0,313(0,188)	0,627	0,718	0,830	0,211	0,962	0,247
F	δC1	0,960(0,924)	0,128(0,128)	0,949	0,134	0,948	0,101	0,990	0,063
	δC2	0,981(0,947)	0,093(0,108)	0,741	0,316	0,870	0,162	0,979	0,096
	δC3	0,970(0,959)	0,123(0,112)	0,592	0,438	0,941	0,127	0,955	0,156
G	δC1	0,909(0,809)	0,165(0,154)	0,882	0,174	0,886	0,112	0,961	0,107
	δC2	0,976(0,943)	0,103(0,100)	0,819	0,262	0,899	0,126	0,984	0,082
	δC3	0,431(0,575)	0,580(0,458)	0,004	0,715	0,651	0,394	0,496	0,546
H	δC1	0,880(0,921)	0,042(0,026)	0,534	0,077	0,804	0,039	0,930	0,032
	δC2	0,781(0,820)	0,151(0,149)	0,220	0,265	0,867	0,122	0,872	0,115
	δC3	0,826(0,883)	0,034(0,021)	0,376	0,061	0,717	0,032	0,926	0,022
	δC4	0,843(0,855)	0,279(0,302)	0,200	0,587	0,888	0,252	0,907	0,215
I	$\delta(C_m - C_o)$	0,943(0,956)	0,086(0,081)	0,206	0,292	0,902	0,115	0,933	0,091
	$\delta(C_p - C_o)$	0,943(0,962)	0,119(0,109)	0,212	0,410	0,927	0,144	0,949	0,111
	$\delta(C_p - C_m)$	0,749(0,826)	0,081(0,080)	0,166	0,138	0,802	0,081	0,799	0,073
J	δC1	0,965(0,904)	0,292(0,312)	0,831	0,591	0,852	0,366	0,972	0,261
	δC2	0,960(0,872)	0,240(0,269)	0,789	0,505	0,820	0,301	0,965	0,223
	δC3	0,967(0,936)	0,203(0,205)	0,839	0,412	0,830	0,315	0,971	0,189
	δC4	0,197(0,303)	0,895(0,957)	0,011	0,913	0,072	1,041	0,195	0,895
K	δC	0,919(0,858)	0,324(0,329)	0,955	0,225	0,922	0,232	0,942	0,275
L	δP	0,944(0,904)	0,370(0,323)	0,785	0,652	0,824	0,416	0,940	0,371
M	δP	0,987(0,977)	0,582(0,663)	0,926	1,300	0,977	0,613	0,989	0,532

NOTE : Les valeurs entre parenthèses sont obtenues pour les mêmes solvants que ceux pour lesquels les paramètres *A* et *B* sont connus.

Pour interpréter les effets observés sur chacune de ces propriétés, nous leurs avons appliquées des analyses empiriques et chimiométriques.

1. Approche empirique

Les effets observés ont été reliés aux paramètres empiriques à l'aide des modèles linéaires simples suivants :

$$[1] \quad P = P_0 + a_1\pi^* + a_2\beta + a_3\alpha$$

$$[2] \quad P = P_0 + bE_T^N$$

$$[3] \quad P = P_0 + c_1A + c_2B$$

Ces modèles ont été appliqués à chacune des propriétés étudiées et les résultats obtenus (coefficient de corrélation (r^2) et écart type de l'estimation (ETE)) sont regroupés dans les tableaux 2 et 3.

Les paramètres π^* tabulés ont été utilisés «naïvement», c'est à dire sans introduire le terme correctif dδ, dit de «polarisabilité» que l'on doit utiliser pour décrire le comportement des solvants aromatiques et polychlorés (11, 12). Son emploi aurait, bien entendu, amélioré la qualité des correlations.

L'analyse de ces résultats montre que les paramètres π^*, α et β donne des corrélations qui sont en général plus satisfaisantes. En effet, les coefficients de corrélation obtenus à l'aide de l'équation [2] sont nettement inférieurs à ceux de l'équation [1]; ceci est confirmé par les valeurs de l'écart type de l'estimation. On peut attribuer ceci au fait que le paramètre E_T est un mélange de polarité et d'acidité par liaison hydrogène (L.H.) (1); par la suite la contribution de la basicité n'est pas représentée.

En utilisant les paramètres *A* et *B*, nous remarquons que pour certains solutés, la corrélation est comparable à celle de l'équation [1], alors que pour d'autre et en particulier pour les donneurs de L.H., il apparait clairement que π^*, α et β donnent des résultats nettement meilleurs. Ceci est en accord avec les travaux de Abboud et coll. (22) qui ont analysé *A* et *B* et montré qu'ils sont liés entre eux lorsque les solvants donneurs de L.H. sont exclus de la corrélation.

Nous devons signaler que l'application des modèles plus

Can. J. Chem. Downloaded from www.nrcresearchpress.com by 198.100.157.202 on 09/07/12
For personal use only.

TABLEAU 3. Résultats des corrélations empiriques et chimiométrique pour les propriétés étudiées en IR et en UV–visible

		π^*, α, β		E_T^N		A, B		F_1, F_2, F_3	
Soluté	P	r^2	ETE	r^2	ETE	r^2	ETE	r^2	ETE
N	ν_{CO}	0,946(0,994)	1,222(0,243)	0,604	3,071	0,661	1,731	0,986	0,621
O	ν_{CO}	0,930(0,862)	1,575(1,307)	0,609	3,279	0,630	2,027	0,960	1,126
P	ν_{CO}	0,959(0,960)	1,242(1,031)	0,925	1,546	0,971	0,835	0,971	1,038
R	ν_{CO}	0,972(0,950)	2,362(2,503)	0,921	3,621	0,966	1,947	0,976	2,172
K	ν_{SO}	0,935(0,954)	7,682(6,355)	0,866	10,166	0,915	8,192	0,965	5,639
Q	ν_{CH}	0,994(0,991)	0,449(0,381)	0,538	4,054	0,923	1,078	0,992	0,592
S	ν_{max}	0,984(0,990)	0,218(0,202)	0,449	1,186	0,732	0,989	0,974	0,275
T	ν_{max}	0,963(0,984)	0,297(0,192)	0,752	0,713	0,865	0,530	0,971	0,265
U	ν_{max}	0,954(0,976)	0,328(0,202)	0,767	0,684	0,988	0,133	0,984	0,191
V	ν_{max}	0,959(0,990)	0,303(0,124)	0,779	0,655	0,986	0,139	0,986	0,178
W	ν_{max}	0,895(0,969)	0,369(0,241)	0,271	0,899	0,559	0,856	0,812	0,493
X	ν_{max}	0,950(0,969)	0,214(0,151)	0,673	0,505	0,973	0,133	0,976	0,148
Y	ν_{max}	0,963(0,969)	0,380(0,396)	0,407	1,352	0,757	1,031	0,927	0,530
Z	ν_{max}	0,745(0,691)	0,192(0,186)	0,198	0,315	0,641	0,189	0,693	0,211
E_T		0,953(0,907)	2,500(3,233)			0,974	1,613	0,968	0,214

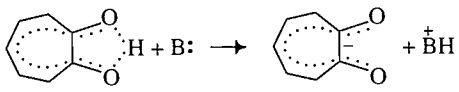
NOTE : Pour les valeurs entre parenthèses, cf. note du tableau 2.

complexes, faisant intervenir des termes carrés et d'interaction en π^* et β, n'a pas apportée d'améliorations significatives au niveau des corrélations. Nous limitons donc notre discussion aux résultats obtenus à partir de l'équation [1].[6]

L'analyse de ces résultats montre qu'ils sont en accord avec l'intuition chimique. En effet, l'application de l'équation [1] aux D.C. mesurés pour les solutés A–G a montré que la principale contribution aux effets observés est due à l'acidité par L.H. et, dans une proportion moindre, à la polarité–polarisabilité alors que la basicité ne participe pas à ces effets. Ceci est en accord avec la nature de ces solutés qui sont de bons accepteurs de L.H. et qui ont des moments dipolaires assez significatifs.

Pour les solutés H et I, les interactions dipolaires sont prédominantes et donc un seul paramètre à savoir, π^*, a été suffisant pour décrire les effets observés; les autres paramètres ont souvent des coefficients non significatifs.

Dans le cas de la tropolone (J), les effets de solvant sur les D.C. mesurés sont globalement moins importants que ceux de la tropone, ceci à condition de ne pas tenir compte des effets dus à la triéthylamine et à la tri-*n*-butylamine qui sont fortement basiques et qui peuvent conduire à une déprotonation de la fonction «phénol».



Les variations importantes obtenues dans ces deux solvants confirment cette hypothèse. En excluant ces deux valeurs, l'équation [1] a montré que la contribution de la basicité par L.H. est négligeable, ceci est dû à une L.H. intramoléculaire plus forte que celle qu'aurait ce soluté avec le solvant.

En RMN du ^{31}P, l'équation [1] montre que les effets observés sur les solutés L et M sont dus principalement aux effets d'association par L.H. et, à un degré moindre, aux interactions dipolaires. Le rapport a_3/a_1 montre l'importante contribution de α : a_3/a_1 (L) = 2,83 et a_3/a_1 (M) = 4,47.

6. Les résultats complets des corrélations selon l'équation [1] sont donnés dans les tableaux 7–10 du document complémentaire.

Les effets observés sur les fréquences de vibration IR des solutés N–Q et K, sont assez bien décrits à l'aide de l'équation [1]. Les principales contributions sont dues à π^* et α et sont en accord avec les caractères fortement dipolaire et accepteur de L.H. de ces solutés.

La modélisation avec π^*, α et β de l'effet du milieu sur les nombres d'onde au maximum d'absorption ν_{max}, est assez satisfaisante et permet une interprétation physique raisonnable des valeurs des différents coefficients. En effet pour la nitro-4 aniline (S), le nitro-4 phénol (W) et le dinitro-3,4 phénol (Y), ce sont principalement les effets de dipolarité et de basicité du solvant qui prédominent. Ceci est illustré par les valeurs assez importantes des coefficients a_1 et a_2 de l'équation [1] :

$$a_1(S) = -1{,}582 \pm 0{,}054 \quad a_2(S) = -1{,}379 \pm 0{,}043$$
$$a_1(W) = -0{,}869 \pm 0{,}092 \quad a_2(W) = -1{,}034 \pm 0{,}073$$
$$a_1(Y) = -1{,}732 \pm 0{,}126 \quad a_2(Y) = -1{,}353 \pm 0{,}098$$

La contribution de la basicité par L.H. diminue en passant de la nitro-4 aniline à son dérivé *N*-méthylé et elle n'est plus significative pour X = NMe_2, NEt_2 et OMe. Pour ces trois derniers, nous avons noté leur sensibilité particulière à π^*, sans sous-estimer celle de α et qui peut être expliquée par le comportement accepteur de L.H. du groupement nitro ainsi que par la nature du substituant X.

Nous avons analysé par ailleurs les valeurs de E_T des 17 solvants sélectionnés, à l'aide de π^*, α et β, et le résultat obtenu à montré l'importante contribution de l'acidité par L.H. à cette échelle.

2. Approche chimiométrique

Nous avons appliqué l'analyse multivariée et en particulier l'analyse en composantes principales pour rationaliser les multiples effets observés sur chacune des propriétés étudiés.

Une analyse déscriptive préalable de toutes les données expérimentales confirme que cet ensemble des mesures suit une distribution normale. Certaines valeurs qu'on n'a pas pû mesurées, ont été calculées à l'aide de l'équation [1]. Par ailleurs, les propriétés peu sensibles à l'effet du milieu et celles qui mettent en jeu un mécanisme de solvatation particulier, ont

Can. J. Chem. Downloaded from www.nrcresearchpress.com by 198.100.157.202 on 09/07/12
For personal use only.

été exclues de cette analyse. Ces propriétés sont : les D.C. δC2 et δC3 du soluté A; δC3 de B; δC1 et δC2 de E; δC2 et δC3 de F, δC3 de G; δC2 de H; les D.C. de J; ν_{max} de Y et celle de Z.

Dans un premier temps, nous avons réparti les différentes propriétés en trois sous-ensembles : 25 propriétés de RMN dans le premier, 6 propriétés IR dans le deuxième et 7 propriétés UV–visible dans le troisième. Pour décrire un minimum de 95% de la variance, la méthode d'analyse en composantes principales a donné trois facteurs pour chacun de ces trois sous-ensembles.

L'application de l'analyse en composantes principales à toutes les propriétés regroupées dans le même ensemble, a donné également trois facteurs qui décrivent 95% de la variance. Les valeurs de ces facteurs pour chacun des solvants séléctionnés sont données dans le tableau 4.

Ces facteurs ont été utilisés pour modéliser, selon l'équation [4], l'effet de solvant sur les différentes propriétés étudiées.

$$[4] \quad P = P_0 + f_1F_1 + f_2F_2 + f_3F_3$$

Les résultats des corrélations (tableaux 2, 3) sont assez satisfaisants et de qualité comparable à celle permise par l'analyse empirique.

Nous avons établi aussi une bonne corrélation pour chacun des trois sous-ensembles, en utilisant les facteurs propres à chacun d'entre eux. Cependant, le fait d'étendre cette analyse en utilisant les facteurs d'une famille pour décrire les effets d'une autre, donne des résultats nettement moins satisfaisants que ceux de la même famille.

On a tenté de relier les facteurs obtenus à partir de toutes les propriétés regroupées, aux paramètres π*, α et β et nous avons obtenu les équations suivantes :

$$[5] \quad F_1 = (0{,}603 \pm 0{,}034) - (0{,}519 \pm 0{,}047)\pi^* + (0{,}421 \pm 0{,}041)\beta + (1{,}691 \pm 0{,}023)\alpha$$
$$r^2 = 0{,}991 \qquad \text{ETE} = 0{,}108$$

$$[6] \quad F_2 = (2{,}129 \pm 0{,}065) - (2{,}719 \pm 0{,}089)\pi^* - (1{,}462 \pm 0{,}078)\beta + (0{,}104 \pm 0{,}045)\alpha$$
$$r^2 = 0{,}965 \qquad \text{ETE} = 0{,}207$$

$$[7] \quad F_3 = (-1{,}089 \pm 0{,}112) - (1{,}769 \pm 0{,}155)\pi^* - (2{,}351 \pm 0{,}136)\beta + (0{,}043 \pm 0{,}078)\alpha$$
$$r^2 = 0{,}900 \qquad \text{ETE} = 0{,}358$$

Ces régressions montrent qu'aucun de ces facteurs ne décrit à lui seul une propriété physique du solvant. En effet, on note pour F_1 une nette contribution de α alors que celles de π* et β sont moins importantes tout en restant non négligeables. D'autre part, F_2 ainsi que F_3 sont particulièrement sensibles à π* et β. Il s'en suit qu'il est difficile d'attribuer un sens physique à ces facteurs et par la suite aux coefficients f_i de l'équation [4]. Ceci limite l'interprétation physique des effets observés sur les propriétés étudiées, ce qui n'est pas le cas pour l'approche empirique.

Nous devons signaler aussi que dans les corrélations avec F_1, F_2 et F_3, aucune des contributions de ces facteurs n'est négligeable. Un modèle à un ou à deux facteurs s'avère en général insuffisant.

La méthode d'analyse en composantes principales permet cependant une prévision pour une famille de propriétés, meilleure que celle donnée par l'analyse empirique; mais, les facteurs obtenus ne peuvent pas être étendus à d'autres familles. Ceci est par contre possible dans l'approche empirique qui permet une comparaison des effets sur des familles de propriétés différentes.

TABLEAU 4. Valeurs des facteurs F_1, F_2 et F_3 pour les solvants utilisés

N°	Solvant	F_1	F_2	F_3
1	Cyclohexane	−0,670	2,010	−0,071
2	Triéthylamine	−0,361	0,744	1,452
3	Tri-*n*-butylamine	−0,620	0,822	0,809
4	Tetrachlorure de carbone	−0,578	1,520	−0,325
5	Carbonate de diéthyle	−0,537	0,283	0,038
6	Toluène	−0,874	0,425	−0,606
7	Acétonitrile	−0,569	−0,666	−0,667
8	Diméthyl-2,6 pyridine	−0,808	−0,774	−0,003
9	Dichlorométhane	−0,527	−0,068	−0,938
10	Diméthylsulfoxyde	−0,761	−1,955	−0,410
11	Nitrobenzène	−0,930	−0,874	−0,858
12	Tertiobutanol	0,807	−0,280	1,697
13	*n*-Butanol	0,919	−0,452	1,664
14	Méthanol	0,998	−0,413	1,014
15	Ethylène glycol	0,614	−1,250	−0,074
16	Trifluoro-2,2,2 éthanol	1,451	0,256	−1,097
17	Hexafluoroisopropanol	2,445	0,669	−1,627

Par ailleurs, l'approche empirique comme l'approche chimiométrique présentent des limitations chaque fois que la propriété étudiée fait intervenir un mécanisme de solvatation particulier. Ceci permet de dire que les deux méthodes «n'ignorent pas» les mécanismes physiques. Nous pouvons citer comme exemple le cas de la β-carotène (Z) pour laquelle l'application de l'approche empirique comme celle de l'analyse chimiométrique, donne des corrélations non satisfaisantes. Ceci est dû au fait que l'effet observé sur le maximum d'absorption de ce soluté, est énergétiquement modeste et dépend surtout des phénomènes de dispersion. En effet, une meilleure corrélation (éq. [8]) est obtenue en utilisant l'échelle π_2^* d'Abe (23) dépendant de l'indice de refraction n_D :

$$[8] \quad \nu_{max}(Z) = (23{,}51 \pm 0{,}08) - (1{,}530 \pm 0{,}076)\pi_2^*$$
$$r^2 = 0{,}900 \qquad \text{ETE} = 0{,}116$$

où

$$\pi_2^* = -1{,}137 + 1{,}098(n_D)^2$$

Conclusion

Nous avons essayé de comparer les résultats des approches empiriques et chimiométriques dans l'étude de l'effet de solvant sur un ensemble de propriétés spectrales en RMN, IR et UV–visible.

Les solvants ont été paramétrisés par les échelles π*, α et β et les 17 solvants les plus informatifs possibles ont été selectionnés à l'aide des méthodes de construction des matrices d'expériences optimales.

L'application des modèles empiriques linéaires simples faisant intervenir (π*, α et β), (E_T^N) et (A et B), a montré que les paramètres π*, α et β donnent généralement les meilleurs résultats.

D'une façon plus générale, nos résultats montrent que :

1. Lorsque les effets du milieu sur des propriétés physiques des solutés peuvent être décrits sous forme de combinaisons linéaires de trois variables explicatives mutuellement orthogonales (mesurant respectivement la polarité–polarisabilité, l'acidité et la basicité par L.H. du solvant) la qualité de la

Can. J. Chem. Downloaded from www.nrcresearchpress.com by 198.100.157.202 on 09/07/12
For personal use only.

description est tout à fait comparable à celle obtenue au moyen d'une analyse en composantes principales à trois vecteurs (un maximum de trois vecteurs justifiant au moins 95% de la variance). On peut passer, évidement, d'une description à l'autre au moyen d'une transformation unitaire (rotation dans l'espace R^3).

2. Lorsque les propriétés considérées montrent une faible sensibilité aux facteurs physiques ci-dessus, la méthode empirique échoue, en même temps que l'approche chimiométrique basée sur des composantes principales construites à l'aide des propriétés sensibles à ces facteurs.

Dès lors, il semble que dans un grand nombre de cas, le conflit entre les partisans de ces deux approches n'a pas de raison d'être.

Remerciements

Nous remercions vivement les professeurs J.-L. M. Abboud (C.S.I.C., Madrid), M. H. Abraham (University of Surrey, Royaume Uni), J. Elguero (C.S.I.C., Madrid) et C. Laurence (Faculté des sciences de Nantes) pour leurs fructueuses discussions et pour avoir lu le mauscrit. Nous remercions également G. Mille (Centre de spectroscopie moléculaire Université d'Aix-Marseille III) pour la réalisation des spectres IR.

1. M. J. KAMLET, J.-L. M. ABBOUD et R. W. TAFT. Prog. Phys. Org. Chem. **13**, 485 (1981).
2. B. CHAWLA, S. K. POLLACK, C. B. LEBRILLA, M. J. KAMLET et R. W. TAFT. J. Am. Chem. Soc. **103**, 6924 (1981).
3. J.-L. M. ABBOUD, A. AUHMANI, H. BITAR, M. EL MOUHTADI, J. MARTIN et M. RICO. J. Am. Chem. Soc. **109**, 1332 (1987).
4. M. J. KAMLET et R. W. TAFT. J. Am. Chem. Soc. **98**, 377 (1976).
5. (*a*) C. LAURENCE, P. NICOLET et C. REICHARDT. Bull. Soc. Chim. Fr. 125 (1987); (*b*) Bull. Soc. Chim. Fr. 1001 (1987).
6. E. BUNCEL et S. RAJAGOPAL. J. Org. Chem. **54**, 798 (1989).
7. (*a*) L. S. PRABHUMERASHI et S. S. KUNTE. Spectrochim. Acta, **42A**, 435 (1986); (*b*) Spectrochim. Acta, **44A**, 213 (1988).
8. C. REICHARDT. *Dans* Solvent and solvent effects in organic chemistry. Verlag Chemie, Weinheim, Allemagne. 1988.
9. M. BERTHELOT, G. GRABOWSKI et C. LAURENCE. Spectrochim. Acta, **41A**, 657 (1985).
10. M. C. R. SYMONS et G. EATON. J. Chem. Soc. Faraday Trans. 1, **81**, 1963 (1985).
11. (*a*) M. J. KAMLET, J.-L. M. ABBOUD, M. H. ABRAHAM et R. W. TAFT. J. Org. Chem. **48**, 2877 (1983); (*b*) M. J. KAMLET, J.-L. M. ABBOUD et R. W. TAFT. J. Am. Chem. Soc. **99**, 6027 (1977).
12. (*a*) R. W. TAFT et M. J. KAMLET. J. Am. Chem. Soc. **98**, 2886 (1976); (*b*) M. J. KAMLET et R. W. TAFT. J. Chem. Soc. Perkin Trans. 2, 349 (1979); (*c*) R. W. TAFT, J.-L. M. ABBOUD, M. J. KAMLET et M. H. ABRAHAM. J. Solution Chem. **14**, 153 (1985).
13. C. G. SWAIN, M. S. SWAIN, A. L. POWELL et S. ALUNNI. J. Am. Chem. Soc. **105**, 502 (1983).
14. I. A. KOPPEL et Y. A. PAL'M. *Dans* Advances in linear free energy relationships. *Éditeurs* : N. B. Chapman et J. Shorter. Plenum Press, London. 1972. Chap. V.
15. (*a*) M. SJÖSTROM et S. WOLD. J. Chem. Soc. Perkin Trans. 2, 104 (1981); (*b*) Acta. Chem. Scand. **B35**, 537 (1981).
16. (*a*) M. J. KAMLET et R. W. TAFT. Acta. Chem. Scand. **B39**, 611 (1985); (*b*) M. J. KAMLET, R. M. DOHERTY, G. R. FAMINI et R. W. TAFT. Acta. Chem. Scand. **B41**, 589 (1987).
17. S. WOLD et M. SJÖSTROM. Acta. Chem. Scand. **B40**, 270 (1986).
18. E. R. MALINOWSKI et D. G. HOWERY. *Dans* Factor analysis in chemistry. Wiley, New York. 1980.
19. D. L. MASSART et L. KAUFMAN. *Dans* The interpretation of analytical chemical data by the use of cluster analysis. Wiley, New York. 1983.
20. W. J. DIXON (*Rédacteur en chef*). Programme BMDP, version 1988, University of California.
21. J. A. RIDDIK et W. B. BUNGER. *Dans* Organic solvents. Vol. II, 3e éd. Wiley–Interscience, New York. 1970.
22. R. W. TAFT, J.-L. M. ABBOUD et M. J. KAMLET. J. Org. Chem. **49**, 2001 (1984).
23. T. ABE. Bull. Chem. Soc. Jpn. **63**, 2328 (1990).

Can. J. Chem. Downloaded from www.nrcresearchpress.com by 198.100.157.202 on 09/07/12
For personal use only.

Analysis of reactive ion transport in weakly ionized gas mixtures

KOICHI IINUMA
Department of Nuclear Engineering, Tohoku University, Sendai 980, Japan

Received May 15, 1990[1]

KOICHI IINUMA. Can. J. Chem. **69**, 1090 (1991).

A new formulation for the analysis of low density multiple-ion swarms drifting, diffusing, and inter-reacting in a neutral gas is proposed on a transport theory basis. A set of coupled three-dimensional transport equations for an arbitrary number of ion species, which governs the number densities of the ion swarms as functions of time and position coordinates, is exactly solved using a Fourier transform in a matrix representation. A picture of dynamic equilibrium state for hypothetical four ion swarms in a neutral gas is numerically obtained. Also, experimental data of transport coefficients and reaction rates for (Li^+, $Li^+ \cdot N_2$, $Li^+ \cdot 2N_2$)flN_2 system are examined in a complete reversible cyclic reaction scheme and compared with a Green's function method. The initial and boundary conditions, the analysis in gas mixtures, and the inelastic process associated with the present formulation are briefly discussed.

Key words: ion swarm, cluster ion, transport equation, ion–molecule reaction.

KOICHI IINUMA. Can. J. Chem. **69**, 1090 (1991).

Sur la base d'une théorie des transports, on propose une nouvelle formulation pour l'analyse d'essaims d'ions multiples de faible densité qui dérivent, diffusent et inter-agissent dans un gaz neutre. Utilisant une transformation de Fourier dans une représentation matricielle, on a résolu d'une façon exacte un ensemble d'équations de transport tridimensionnel couplées, pour un nombre arbitraire d'espèces ioniques, qui gouvernent le nombre décrivant les densités d'ions par essaim en fonction du temps et des coordonnées de position. On obtient un représentation numérique de l'état d'équilibre dynamique pour des essaims hypothétiques de quatre ions dans un gaz neutre. On a aussi examiné les données expérimentales pour les coefficients de transport et les vitesses de réaction du système (Li^+, $Li^+ \cdot N_2$, $Li^+ \cdot 2N_2$)/N_2 dans un schéma réactionnel cyclique complètement réversible et on les compare avec une méthode de la fonction de Green. On discute brièvement des conditions initiales et limites, de l'analyse des mélanges gazeux et des processus inélastiques associés avec la présente formulation.

Mots clés : essaim ionique, agrégat ionique, équation de transport, réaction ion–molécule.

[Traduit par la rédaction]

Introduction

The space–time dependence of concentrations of multiple chemical species in an ambient medium is generally governed by the competition between their transport processes and a complex reaction scheme composed of a series of elementary reactions. A set of coupled transport equations (diffusion equations), which involve a number of appropriate kinetic coefficients (transport coefficients and reaction rates), control the dynamic process of those inter-converting species irrespective of the chemical system being in gas, liquid or solid phase. This paper deals with the derivation of a general solution of an arbitrary number of coupled transport equations with respect to the same number of chemical concentrations, which are functions of time and position coordinates, within a framework of linear process. The "linear process" means that each transport equation is formed by a linear function in the concentrations of species of present interest, in which we are considering the non-equilibrium behaviour of multiple species dilutely dispersed in a large excess of other constituents considered at equilibrium. The particles of the dilute species are often referred to as "test particles". With this assumption, only (test particle)–moderator collisions need be considered. With the neglect of (test particle)–(test particle) collisions, the kinetic equations are (by definition) linear (pseudo-first order process). Even in this model, however, we can exactly treat the (test particle)–moderator reactions as multi-body processes (higher-order reactions). For this kind of nonthermal linear process it is possible to treat all the kinetic coefficients as functions of more general energy parameters than the temperature of surroundings. In usual transport analysis, the mean relative translational energy between each test particle and a surrounding molecule is employed as a basic energy parameter.

The experimental and theoretical study on reactive ion transport phenomena, which has a history of almost one hundred years, has been developed mainly in two research fields, gaseous electronics (1) and radiation chemistry (2), although there were somewhat different concerns between them on their early research stages. Namely, "non-reactive" transport process of charged particles in gases seemed to be a primary research subject in gaseous electronics, while time-dependence of the concentrations of chemical products was believed to provide the most useful information on the complex scheme of radiolysis in radiation chemistry, except for a few outstanding works on nonhomogeneous phenomena in tracks and spurs (2). Basically, the general solution of a set of coupled transport equations enables us to analyze this kind of time-dependent nonhomogeneous phenomena in a unified manner. In this paper we will concentrate our attention on the derivation of a general analysis for the reactive ion transport process in a neutral gas.

In usual ion swarm experiments, an external electric field (drift field, E) exerts a constant continuous force on each ion and causes the ions to flow through the gas at a certain drift velocity and diffusion rate. Moreover, other types of ions may be created by collisions of the initial ions with surrounding molecules with the proper reaction rates. The drift velocity, diffusion coefficient, and reaction rate are characteristic of the particular ion–gas combination, field strength, gas number density, and gas temperature. A transport equation involves the three kinetic coefficients and is applicable to all swarm experiments amenable to a hydrodynamic description in both thermal ($E = 0$) and nonthermal systems.

The transport coefficients of non-reactive mixtures are simple to measure because the experimental analysis of this system has been well established, and theory provides additional support for the observed results (3). In fact, many transport coefficients for various ion–molecule combinations are now available

[1]Revision received January 22, 1991.

Printed in Canada / Imprimé au Canada

Can. J. Chem. Downloaded from www.nrcresearchpress.com by 84.41.108.74 on 09/07/12
For personal use only.

Can. J. Chem. Downloaded from www.nrcresearchpress.com by 84.41.108.74 on 09/07/12
For personal use only.

(4–6); they have been determined experimentally with a variety of sophisticated apparatus (3). However, when the simple transport phenomena are accompanied by a mutually inter-reacting scheme characteristic of multiple-ion swarms, the analytical treatment of the system will become more difficult mathematically, because the dynamical behaviour of all ion swarms requires the solution of a set of coupled transport equations. A great deal of effort has been devoted to solve the coupled equations since the mid-1950s (3). Gatland got a one noticeable full solution using Green's function method. There is an excellent review on this method and its theoretical and experimental backgrounds (7). Although its mathematical formulation, including the treatment of the boundary effects, is clear, the required "summing up" of the complicated histories of interconverting ions may limit its practical applicability for reaction schemes involving more than three ion swarms.

So far, appropriately simplified coupled equations have usually been set up and solved for the analysis of many inter-reacting systems. It is well known that a series of definitive experiments for higher-order clustering reactions were carried out by Kebarle and co-workers at the University of Alberta using several high-pressure mass spectrometers (8). By selecting experimental conditions where the diffusive effect was almost negligible, they determined scores of reaction rates for several consecutive reaction sequences from fairly simplified coupled rate equations in thermal systems (9). In addition to these thermal reaction data, a lot of data on reaction rates for bimolecular and termolecular ion–molecule reactions in nonthermal systems have been obtained by a number of groups (10, 11).

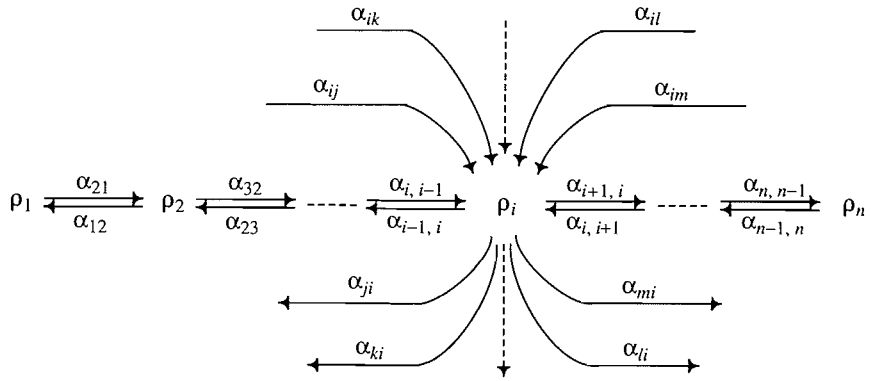
While reaction rates determined under conditions in which diffusion is neglected are useful, one would like a flexible method for probing reaction kinetics under conditions which include multiple species, diffusion, and field-driven drift. Recent growing interest in cluster ions and ion–molecule reactions in both fundamental and applied fields (12–15) has encouraged us to attempt a general formulation for the analysis of this kind of nonhomogeneous phenomena. The following section provides mathematical details on its derivation based on the drift tube experiment.

General formulation

Drift tube technique is a standard time-of-flight method for swarm experiments, where a pulse of charged particles travels through the gas under the influence of an external electric field supplied in a cylindrical tube. In a linear process (a process where all interactions between ions can be ignored), the drift velocity of each ion swarm is directly related to the mean translational energy between the ion and the neutral molecule by well known Wannier's formula (3). The mobility, diffusion coefficient, and reaction frequencies of the ion swarm are, in general, functions of the translational energy, kinetic theory of which from a "molecular" viewpoint has a long and brilliant history, and the reader can refer to several treatises for the subjects (3, 16–18).

The general inter-reacting scheme for n-ion swarms is depicted as follows:

[1]



where ρ_i is the number density of ith species ($i = 1, 2, \cdots\cdots, n$), and α_{ij} is the reaction frequency per ion, from species j to i. A commonly used chemical reaction rate, k_{ij}, is defined by the relation

$$[2] \qquad \alpha_{ij} = k_{ij}N^p$$

where N is the gas number density, and p is the order of reaction with respect to gas molecules.

The set of coupled transport equations for [1] becomes

$$[3] \qquad \frac{\partial \rho_i}{\partial t} = \nabla\cdot(\mathbf{D}_i\cdot\nabla\rho_i) - v_{di}\cdot\nabla\rho_i + R_i\rho_i + \sum_{k\neq i}^{n}\alpha_{ik}\rho_k$$

where

$$[4] \qquad R_i = -\sum_{j\neq i}^{n}\alpha_{ji}$$

The symbols $\mathbf{D}_i$ and v_{di} refer to the diffusion tensor and drift velocity of ith species, respectively. The derivation of eq. [3] and following mathematical formalization basically originated from Whealton–Woo's analysis for a ρ_1 ‰ ρ_2 system (19, 20) and Gatland's review (7). By introducing a cylindrical coordinate, we separate the solution into a radial part ($R_m(r)$) and an axialfltime part ($Z_{im}(z,t)$) as

$$[5] \qquad \rho_i(\boldsymbol{r},t) = \sum_{m=1}^{\infty} a_{im}R_m(r)Z_{im}(z,t)$$

where a_{im} are constants to be determined from the initial conditions. The separate transport equations, which are consistent with the boundary conditions and the assumption of diagonal diffusion tensors, are

$$[6] \qquad \frac{d^2R_m(r)}{dr^2} + \frac{1}{r}\frac{dR_m(r)}{dr} + \frac{\beta_m^2}{r_0^2}R_m(r) = 0$$

$$[7]\qquad \frac{\partial Z_{im}(z,t)}{\partial t} = D_{zi}\frac{\partial^2 Z_{im}(z,t)}{\partial z^2} - v_{di}\frac{\partial Z_{im}(z,t)}{\partial z} + \left(R_i - \frac{\beta_m^2}{r_0^2}D_{ri}\right)Z_{im}(z,t) + \sum_{k\neq i}^{n}\alpha_{ik}Z_{km}(z,t)$$

where β_m is the mth root of the zeroth-order Bessel function, and r_0 is the drift-tube radius. D_{zi} and D_{ri} are, respectively, longitudinal and transverse diffusion coefficients of the ith species. A solution to eq. [6] is

$$[8]\qquad R_m(r) = J_0(\beta_m r/r_0)$$

More precise treatment on the radial part, involving the initial radial distribution of the ion swarm, was given by Whealton and Woo (19, 20). Equation [7] is transformed from the axis coordinate (z) to the frequency (ω) by using a Fourier transform. A set of resulting ordinary differential equations is solved with respect to time, and formally unified into a simple matrix form as

$$[9]\qquad \mathfrak{Z}(\omega,t) = \exp(\mathbf{A}t)\,\mathfrak{Z}(\omega,0)$$

where $\mathfrak{Z}(\omega,t)$ and $\mathfrak{Z}(\omega,0)$ are n-component column vectors composed of the Fourier transformed solutions and initial conditions, respectively. An explicit form of the operator matrix $\mathbf{A}$ is

$$[10]\qquad \mathbf{A} = \begin{pmatrix} T_1, \alpha_{12}, \alpha_{13}, \cdots, \alpha_{1i}, \cdots, \alpha_{1n} \\ \alpha_{21}, T_2, \alpha_{23}, \\ \alpha_{31}, \alpha_{32}, T_3, \\ \vdots \quad \ddots \quad , \alpha_{i-1,i} \quad \vdots \\ \alpha_{i1}, \cdots, \alpha_{i,i-1}, T_i, \alpha_{i,i+1}, \cdots, \alpha_{in} \\ \quad , \alpha_{i+1,i} \quad \ddots \\ \vdots \quad \vdots \quad \vdots \quad T_{n-1}, \alpha_{n-1,n} \\ \alpha_{n1}, \cdots, \alpha_{ni}, \cdots, \alpha_{n,n-1}, T_n \end{pmatrix}$$

with

$$[11]\qquad T_i = -D_{zi}\omega^2 - iv_{di}\omega + R_i - (\beta_m/r_0)^2 D_{ri}$$

where i refers to the imaginary unit.

In chemical kinetics, the matrix algebra is a standard and conventional mathematical technique to solve the coupled rate equations (21), which may stem from the non-equilibrium theory of reaction developed by Zwolinski and Eyring (22). Unfortunately, the following theoretical progress for this useful method seems to be limited to the analysis of only time-dependent phenomena, and the method has never been combined with a Fourier transform technique on space coordinates until recently (see ref. 7, p. 426).

With the help of matrix algebra and the residue theorem in complex analysis, we obtain the explicit form of each element of the solution [9] as follows:

$$[12]\qquad \mathfrak{Z}_{im}(\omega,t) = -\sum_{j=1}^{n}\left\{\Delta_i(\lambda_j)\exp(\lambda_j t)\Big/\sum_{k=1}^{n}\Delta_{kk}(\lambda_j)\right\}$$

where λ_j is the jth root ($j = 1, 2, \cdots, n$) of the characteristic equation of matrix $\mathbf{A}$

$$[13]\qquad |\mathbf{A} - \lambda\mathbf{E}| = 0$$

where $\mathbf{E}$ is the unit matrix. $\Delta_i(\lambda)$ is denoted by the following nth order determinant

$$[14]\qquad \Delta_i(\lambda) = \begin{vmatrix} & & & (i\text{th column}) & \\ T_1 - \lambda, & \alpha_{12}, \cdots, -\partial_1(\omega,0), \cdots, & \alpha_{1n} \\ \alpha_{21}, & T_2 - \lambda, \cdots, -\partial_2(\omega,0), \cdots, & \alpha_{2n} \\ \vdots & \vdots & \vdots & \vdots & \vdots \\ \alpha_{n1}, & \alpha_{n2}, \cdots, -\partial_n(\omega,0), \cdots, & T_n - \lambda \end{vmatrix}$$

$\Delta_{kk}(\lambda)$ is the cofactor of the (k,k) element in the determinant (13). The solution of eq. [7] as a function of z and t is represented in integral form as

$$[15]\qquad Z_{im}(z,t) = \frac{1}{2\pi}\int_{-\infty}^{\infty}\mathfrak{Z}_{im}(\omega,t)\exp(i\omega z)\,d\omega$$

By substituting [8] and [15] back into [5], we obtain the final solution of the number density of the ith ion swarm for reaction sequence [1]. The solution [15] can basically be represented by an infinite sum of the Weber function (or the parabolic cylinder function). However, appropriate direct quadrature techniques to the real part of the integrand in [15] are recommended for practical analysis because of insufficient convergence of the expansion solution. While [5] is composed of an infinite sum in m, only the first few terms are necessary to adequately describe the most realistic initial conditions.

A rather important result in the limit of $z, r_0 \to \infty$ can be derived from [12]. As the drift length becomes much longer, the ratio of the integrals of the number densities with respect to time asymptotically converges to the following relation,

$$[16]\qquad \lim_{\substack{z\to\infty \\ r_0\to\infty}}\int_0^{\infty}\rho_1 dt : \lim_{\substack{z\to\infty \\ r_0\to\infty}}\int_0^{\infty}\rho_2 dt : \cdots : \lim_{\substack{z\to\infty \\ r_0\to\infty}}\int_0^{\infty}\rho_i dt : \cdots : \lim_{\substack{z\to\infty \\ r_0\to\infty}}\int_0^{\infty}\rho_n dt = |S_1| : |S_2| : \cdots : |S_i| : \cdots : |S_n|$$

with

$$[17]\qquad S_i = -\begin{vmatrix} & & & (i\text{th column}) & \\ R_1, & \alpha_{12}, \cdots, -C_1, \cdots, & \alpha_{1n} \\ \alpha_{21}, & R_2, \cdots, -C_2, \cdots, & \alpha_{2n} \\ \vdots & \vdots & \vdots & \vdots & \vdots \\ \alpha_{k1}, & \alpha_{k2}, \cdots, -C_k, \cdots, & \alpha_{kn} \\ \vdots & \vdots & \vdots & \vdots & \vdots \\ \alpha_{n1}, & \alpha_{n2}, \cdots, -C_n, \cdots, & R_n \end{vmatrix}$$

where C_k refers to an initial input of the kth species. This formula is substantial in the dynamic equilibrium state of reaction scheme [1], and holds exactly regardless of the initial conditions (even C_k's themselves). This is a natural consequence of the particle conservation law applied to a closed reactive system [1].

Numerical analysis of four-ion swarms

The analysis of four-ion swarms is a suitable subject to test the workability of present formulation. It may give us more general insight to the entire dynamic process, including the initial, transition, and dynamic equilibrium state, for the reactive ion transport involving more than five ion swarms. In fact, recent *in situ* ion composition measurements in atmospheric ion chemistry are going to reveal that scores of positive and negative ions take part in the complex reaction scheme of the earth's atmosphere (23, 24). Unfortunately, the number of measured transport coefficients and reaction rates for these compositions are still not quite satisfactory, and no complete

Can. J. Chem. Downloaded from www.nrcresearchpress.com by 84.41.108.74 on 09/07/12
For personal use only.

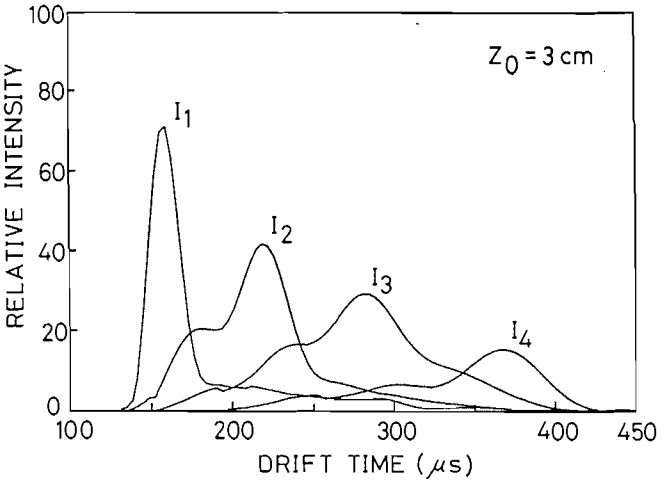


FIG. 1. Arrival time spectra of inter-reacting four ion species in a neutral gas. The abscissa is divided into 100 channels, numerical calculation is carried out for each channel. The drift length is 3 cm.

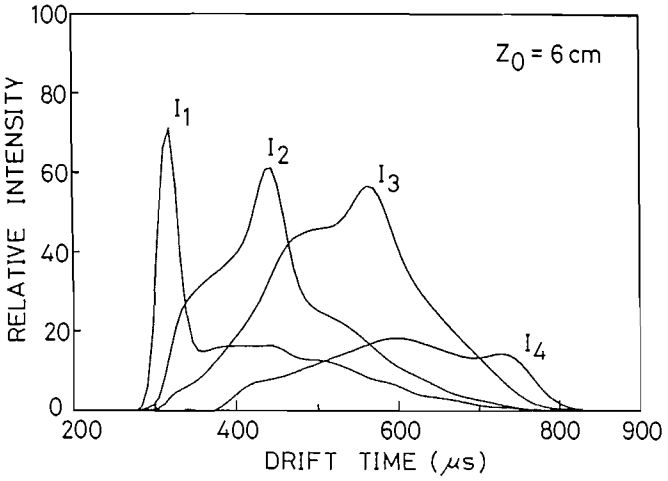


FIG. 2. Same as Fig. 1, with drift length of 6 cm.

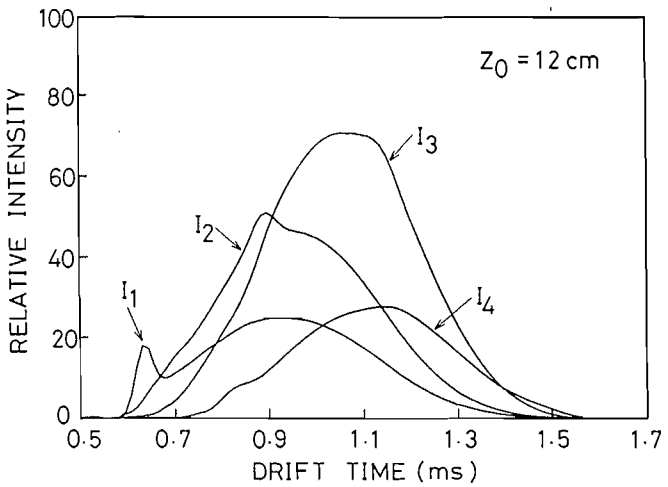


FIG. 3. Same as Fig. 1, with drift length of 12 cm.

set of kinetic coefficients for four ion swarms is available at the present time. We will therefore adopt a model composed of partly hypothetical four-ion swarms, roughly derived from the preliminary experiments carried out in our laboratory for the Na^+/HCl combination. While the system may have a complex scheme because of HCl's relatively large dipole moment, all reaction frequencies are still hypothetical.

The reaction scheme of four ion swarms comprises, in general, twelve elementary reactions. Now, we will represent [12] in a more tractable form as

$$[18] \qquad \Im_{im}(\omega,t) = \sum_{j=1}^{4} g_i(\lambda_j) \exp(\lambda_j t)/f(\lambda_j) \qquad (i = 1, 2, 3, 4)$$

The explicit forms of $g_i(\lambda)$ and $f(\lambda_j)$ are given in Appendix along with those of two and three ion swarms. In drift-tube experiments, one is usually interested in the ion–current profile with respect to drift time at the collector (arrival time spectrum), which is

$$[19] \qquad I_i(z_0,t) = 2\pi \int_0^{r_c} \left(-D_{zi} \frac{\partial \rho_i}{\partial z} + v_{di}\rho_i \right) r\,dr$$

where z_0 and r_c are the drift length and radius of the collector, respectively. Details of the present numerical calculation of [19] are as follows.

We employed four $\delta(z)$ functions as the initial conditions, the ratio of the number densities was set to be $\rho_1:\rho_2:\rho_3:\rho_4 = 10:5:3:6$. This ratio is absolutely not related to the real system at all. The differentiation of ρ_i with respect to z was carried out by using a numerical differential method. Because the integrand in [15] is an even function in ω, we changed the integral variable from ω to x as $\omega = -\log x$. The integral region ranging from $1 \mathrm{G} x \mathrm{G} 10^{-6}$ was employed, and a simple quadrature technique was applied to obtain four arrival time spectra at appropriate drift length and duration time. Four roots of the characteristic equation [13] were calculated from a standard formula for quartic equation of complex variables. Small oscillations of the solutions near the base line were occasionally observed. These were partly averaged. This kind of numerical instability, however, may easily be eliminated by employing more elaborate numerical techniques for an inverse Fourier transform than the present simple quadrature. Numerically obtained four arrival time spectra at five different drift lengths are shown in Figs. 1 to 5. Their transport coefficients and the twelve reaction frequencies are listed in Tables 1 and 2, respectively.

By carefully observing these five figures, we can find that the space–time evolution of the ion swarms is roughly classified into three phases, the initial phase, the non-equilibrium phase, and the dynamic equilibrium phase.

The initial phase (Fig. 1) corresponds to a primary step in the evolution, where we can separate the current profile of each arrival time spectrum into two component currents, the initial component and the product component. Relatively large and dominant component arises from the initially injected ions, an original Gaussian shape of which is well preserved during the transport process, and it may give us the most accurate information of its transport coefficients in the three phases. This component is accompanied by the small product component current(s) at its leading edge and/or trailing edge. This feature is helpful to us to estimate qualitatively (and sometimes quantitatively) which elementary reactions are taking place in the system. Each product component generally comprises several subcomponent ions, each arising from an elementary

Can. J. Chem. Downloaded from www.nrcresearchpress.com by 84.41.108.74 on 09/07/12
For personal use only.

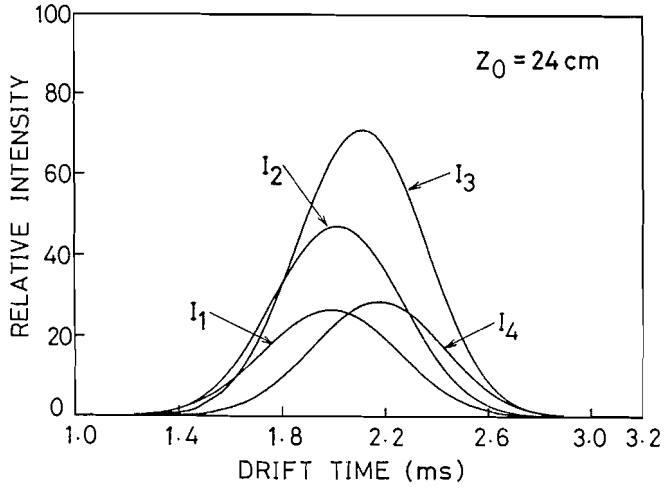


FIG. 4. Same as Fig. 1, with drift length of 24 cm. The ratio of the integrated number densities, which are directly obtained from these spectra by using a numerical quadrature, is $\rho_1:\rho_2:\rho_3:\rho_4$ = 1.000:2.404:4.551:2.448.

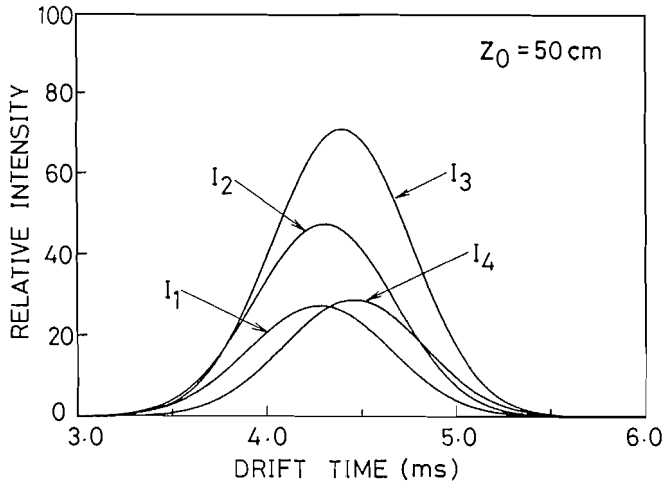


FIG. 5. Same as Fig. 4, with drift length of 50 cm. The ratio is $\rho_1:\rho_2:\rho_3:\rho_4$ = 1.000:2.405:4.555:2.454.

reaction of different original ions. Needless to say, all the product ions in the subcomponents are same species. These subcomponents can often be observed stepwise on the superimposed current profile of product ions (Fig. 1). By examining the relative positions between the steps and peaks of the initially injected components, we can roughly estimate the number of elementary reactions.

The non-equilibrium phase corresponds to an intermediate step in the evolution (Figs. 2 and 3), where the transport and reactive processes operate competitively and the current profiles of all arrival time spectra are subject to dramatic changes. While we can still find the traces of initially injected ions in each arrival time spectrum, these ions are destined to be buried in rapidly growing produced ions due to several reactions. It is almost impossible to determine the diffusion coefficients and drift velocities of all ion species from these spectra in a straightforward manner. However, one noteworthy point in Fig. 2 is that we cannot observe any remarkable reactive component ions at the leading edge of profile I_1, nor at the trailing edge of I_4. This means that the present reactive system is a closed

TABLE 1. Drift velocities, longitudinal diffusion coefficients, and transverse diffusion coefficients for four ion species

Parameter	Value			
	ρ_1	ρ_2	ρ_3	ρ_4
v_d (cm/s)	1.89×10^4	1.34×10^4	1.05×10^4	8.0×10^3
D_z (cm^2/s)	86.6	57.5	42.2	35.0
D_r (cm^2/s)	77.2	52.8	39.8	33.0

TABLE 2. The reaction frequencies (s^{-1}) from jth species to ith species

i \ j	1	2	3	4
1	—	600	750	500
2	5000	—	870	560
3	800	3000	—	2500
4	260	700	1500	—

system in which only four ion species take part in the reaction scheme.

The dynamic equilibrium phase (Figs. 4 and 5) is the final step in the evolution. This apparently placid phase may be the most important phase from both theoretical and practical standpoints. A rather surprising fact is that all the ion swarms lose their initial individuality and seem to be drifting and diffusing with almost the same transport coefficients. These well-featured profiles may give us hope that we can easily determine the transport coefficients of each ion swarms from them. However, the most dominant process in this phase is the inter-reacting process between four ion species, where any direct information on the transport coefficients must be hidden almost completely into the spurious Gaussian profiles made up of several reactive component currents. Nevertheless, relation [16] holds exactly in this phase. The ratio calculated from [16] and [17] for the present system is $I_1:I_2:I_3:I_4$ = 1:2.40:4.53:2.45, which agrees well with both ratios obtained from the current profiles in Figs. 4 and 5 by using the direct numerical quadrature. The number density of each ion swarm was obtained from the current profile by dividing it with its drift velocity, by assuming that the diffusive component in [19] is almost negligible. That this assumption is reasonable is discussed later. Moreover, the practical importance of [16] is to be emphasized again, because the ratio is independent of initial conditions, diffusion coefficients, and drift velocities of all ion swarms, suggesting that we can derive several relations between the reaction frequencies from experimentally measured arrival time spectra. If certain reactions are significant in the system, the measured ratio may give us a group of considerably reliable reaction frequency data within the limit of experimental difficulties, even when the drift length of the apparatus is rather short. Unfortunately, [16] is not defined by each reaction frequency but by groups of mutually multiplied reaction frequencies. In real experimental analysis, however, elimination of the improbable reactions will make the relation mathematically far too simplistic.

While the above numerical calculations, based on a "hypothetical" transport/reactive system for four ion swarms, have

Can. J. Chem. Downloaded from www.nrcresearchpress.com by 84.41.108.74 on 09/07/12
For personal use only.

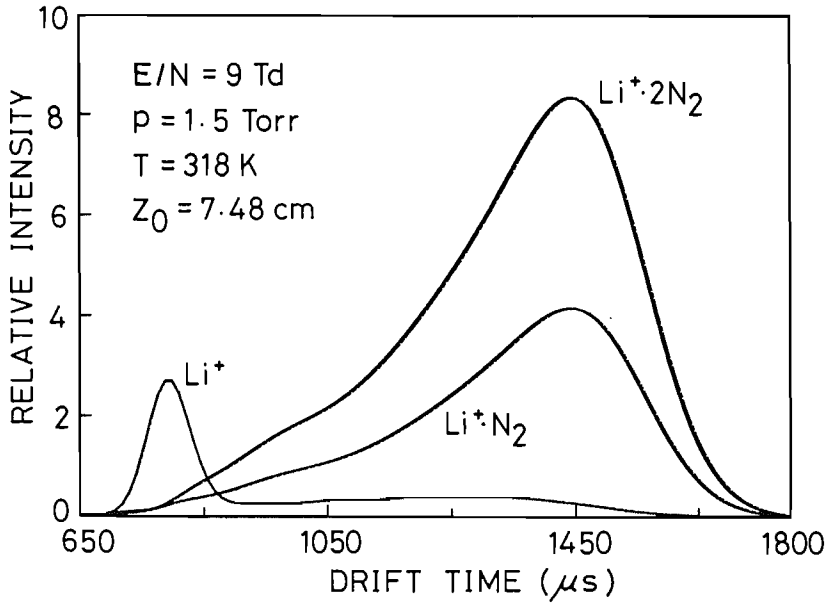


FIG. 6. Arrival time spectra of Li^+, $Li^+ \cdot N_2$, and $Li^+ \cdot 2N_2$ ions in nitrogen. $v_{d1} = 9.358 \times 10^3$, $v_{d2} = 4.933 \times 10^3$, $v_{d3} = 4.740 \times 10^3$ cm/s. $D_{z1} = D_{r1} = 62.55$, $D_{z2} = D_{r2} = 49.46$, $D_{z3} = D_{r3} = 47.52$ cm^2/s. Suffix 1, 2, and 3 correspond to Li^+, $Li^+ \cdot N_2$, and $Li^+ \cdot 2N_2$, respectively. $\alpha_{21} = 4150$, $\alpha_{12} = 320$, $\alpha_{32} = 45650$, $\alpha_{23} = 21860$, $\alpha_{13} = \alpha_{31} = 0$/s. Solid curves are obtained from the exact current eq. [19]. Dot–dashed curves are calculated by the drift component in [19].

been carried out to test the mathematical consistency and physical and chemical soundness of the present formulation, the results may hold in more general cases. Firstly, the three phases mentioned above exist in any transport/reactive process of multiple ion swarms in gases. Secondly, as time goes on, the space–time behaviour of the ion swarms apparently changes as a transport-dominant process to a reaction-dominant process. Thirdly, as the non-equilibrium phase nears its end, all ion swarms seem to be aggregating in appearance, drifting, and diffusing with almost the same transport coefficients, their current profiles becoming very Gaussian. Fourthly, the dynamic equilibrium phase gives us an indisputable information on the reaction frequencies. Finally, the accuracy and sensitivity of the measured kinetic coefficients strongly depend on the phase chosen for the ion swarms in the dynamic process.

Application to experimental analysis

Now, we will prove that the present formulation can justifiably be applied to real systems. Gatland *et al.* extensively analyzed a reactive ion transport process of Li^+, $Li^+ \cdot N_2$, and $Li^+ \cdot 2N_2$ (cluster) ions in N_2 by using a well-known Georgia Tech drift-tube mass spectrometer. They determined the mobilities, diffusion coefficients, and four reaction rates of the above ion species as functions of E/N (the ratio of the electric field strength to the neutral gas number density) (25). The Green's function method (7) was used to analyze the experimental arrival time spectra. We will treat the same system in a reversible cyclic reaction scheme by using the present formulation. The reaction scheme is depicted as

$$[20] \quad Li^+ \underset{\alpha_{12}}{\overset{\alpha_{21}}{\rightleftharpoons}} Li^+ \cdot N_2 \underset{\alpha_{23}}{\overset{\alpha_{32}}{\rightleftharpoons}} Li^+ \cdot 2N_2, \qquad \alpha_{13}, \ \alpha_{31}$$

At first, we reproduce three arrival time spectra obtained by Gatland *et al.* at 9 Td (units of E/N; 1 Td = 10^{-17} V cm^2). In our calculation, two reaction frequencies, α_{13} and α_{31}, were temporarily set to be zero, at this time the other kinetic coefficients were directly derived from their experimental data. We introduced a Gaussian-type initial condition only for Li^+ ions. This includes two adjustable parameters, steepness factor and shift factor. A method of their determination is discussed later. The effect of diffusive component in [19] to the ion–current profile was checked.

Three arrival time spectra calculated from [19] and those from only drift term in it are shown in Fig. 6. Two groups of results almost overlapped each other, indicating that the diffusive component is, in this case, negligibly small compared to the drift component. However, simple disposal of the diffusive component may occasionally give rise to a rather serious experimental error in the kinetic coefficients under certain experimental conditions, where the arrival time spectrum is often drastically deformed in the short distance of drift length. The truncation effect for the infinite sums in m of [5] also proved to be negligible after testing a few terms. This is generally true in the usual drift-tube analysis.

For the present formulation, a standard procedure of experimental analysis is as follows. Firstly, we determine the detection efficiency for each ion species from the preliminary experiments. Secondly, we measure two groups of arrival time spectra, those in initial phase and those in dynamic equilibrium phase. Thirdly, the ion–current profiles are to be divided by their own detection efficiencies, and a set of new spectra are reconstructed in both phases. Fourthly, by using the initial-phase spectra we determine the drift velocity and longitudinal diffusion coefficient of each ion swarm, and roughly estimate several reaction frequencies from the areas of current profiles. The drift-tube apparatus with movable ion source is strongly recommended; we obtain several arrival time spectra of different ion source positions with such apparatus. The set of spectra

Can. J. Chem. Downloaded from www.nrcresearchpress.com by 84.41.108.74 on 09/07/12
For personal use only.

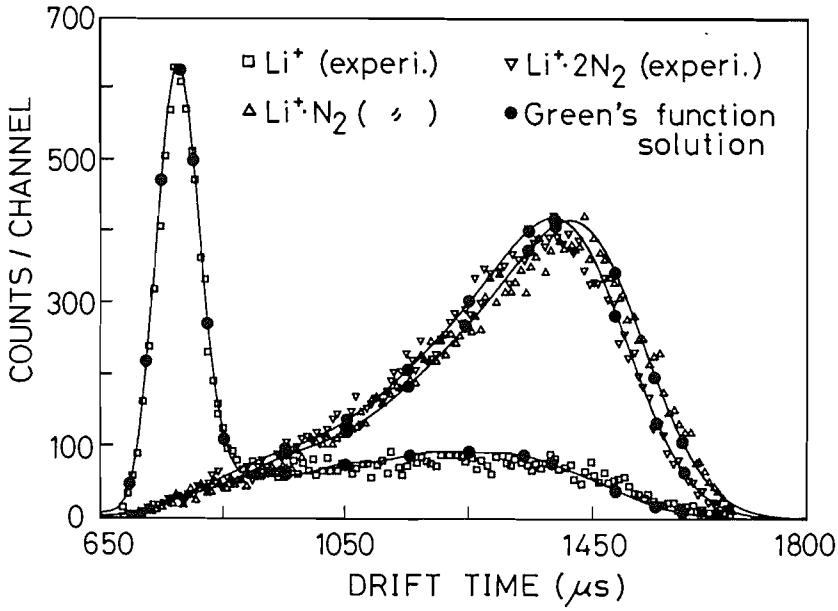


FIG. 7. A comparison of modified theoretical arrival time spectra with Green's function solutions and experimental data. The ratio of detection efficiencies is $I_1:I_2:I_3 = 1.00:0.44:0.22$. Experimental conditions and kinetic parameters for calculations are the same as in Fig. 6.

is useful in more accurate measurement of the above kinetic coefficients. Moreover, with the help of initial-phase spectra we can determine the two adjustable parameters involved in the initial condition from the set of initially injected spectra. The Gaussian-type initial condition is represented by a function, $F(r)\exp[-a(z-b)^2]$. $F(r)$ is a radial distribution of the initial condition, by which a_{im} in [5] can be evaluated using the orthogonality of Bessel functions. The steepness factor, a, is estimated from the full widths at half the maxima of the initially injected profiles at several distinct ion source positions. The shift factor, b, is closely connected to the end effects (3) arising at the ion source or the detector end of the apparatus, which is therefore estimated from the extrapolation length yielded by a standard experimental procedure for determining the drift velocity (3). Fifthly, we determine the ratio of reaction frequencies, [16], from the areas of the spectra measured in the dynamic equilibrium phase, by which we can re-examine the accuracy of the roughly estimated reaction frequencies and the pertinence of assumed number of elementary reactions. Finally, we substitute all these kinetic coefficients back into the appropriate number of solutions and reproduce the space–time behavior of the multiple-ion swarms. Any additional correction of these parameters must be iteratively carried out in the above procedure.

Three arrival time spectra of Li^+, $Li^+\cdot N_2$, and $Li^+\cdot 2N_2$ ions, involving a little surmise upon the magnitudes of detection efficiencies, are shown in Fig. 7 along with the experimental data and the Green's function solutions obtained by Gatland *et al.* (25). The experimental data were read off from their original figure by using our small digitizer, the reading error of which was estimated to be no worse than 0.5% for all data. The agreement between the present spectra and their solutions, which also were read off by the digitizer, seems to be excellent.

Now we examine the effect of non-neighbor reaction, α_{13} in [20], how much deformation arises in the original three spectra. Gatland *et al.* already pointed out the possibility of a α_{13} reaction. However, α_{31} reaction can be reasonably ruled out because the probability of four-body reaction is negligibly small at the pressure range (0.5–1.5 Torr) selected in their experiments. We therefore ignore this reaction. By examining the pressure dependence of a long tail in the Li^+ spectrum, they concluded that both reactions could be ignored. The present formulation is directly applicable to analyze this problem, and may give us more precise information to confirm their conclusion.

Three groups of arrival time spectra for three different reactive conditions are shown in Fig. 8. We are concerned with the source of the Li^+ ions produced in the long tail of the Li^+ spectrum; $Li^+\cdot N_2$ ions (α_{12} reaction), or $Li^+\cdot 2N_2$ ions (α_{13} reaction), or both ion species. Figure 8 shows that the deformation of the Li^+ spectrum arisen from the product ions is restricted only to its long tail area, and we cannot observe any remarkable difference in the deformation of initially injected component between three reaction schemes. The ions in the tail seem to be simply partitioned into α_{13}- and α_{12}-reaction products. The area of tail of No. 3 is almost twice as large as that of No. 1. These numerical results may support their claim that the Li^+ ions in the tail of the Li^+ spectrum are produced mainly by the α_{12} reaction. If we adopt other combinations of reaction frequencies, the ratio of initially injected area to tail area may disagree with that from experimentally obtained Li^+ spectrum. However, if the assumed detection efficiencies for the $Li^+\cdot N_2$ and $Li^+\cdot 2N_2$ ions are rather doubtful, the situation will become appreciably different.

We will now discuss briefly the analysis of the two ion swarms. Since this is the simplest reactive ion transport involving only two reaction rates and six transport coefficients, two ion swarms have been extensively analyzed by many researchers (3). Most of the methods, however, were limited to the analyses of rather specified ion/molecule (or electron/molecule) combinations in specified experimental conditions, except for the Green's function method. The present formulation may become another useful and more tractable method to treat the two ion swarm phenomena in a general manner. Furthermore, it is to be noted that the present method can easily be extended to treat more general transport coefficients like

Can. J. Chem. Downloaded from www.nrcresearchpress.com by 84.41.108.74 on 09/07/12
For personal use only.

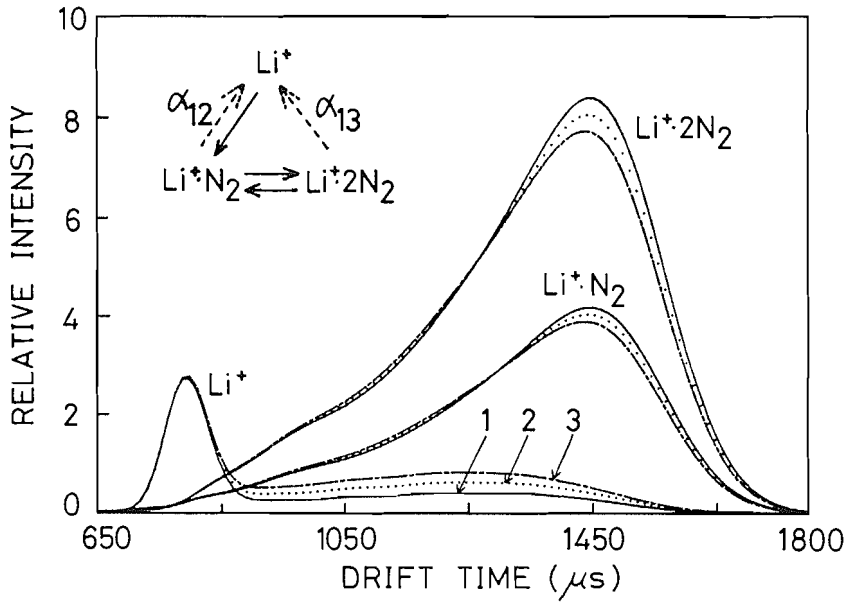


FIG. 8. Arrival time spectra for three different reaction schemes. The solid curves (No. 1) are calculated from the reaction scheme of $\alpha_{12} = 320$ and $\alpha_{13} = 0$/s (same as those of Fig. 6). Dotted curves (No. 2) are those of $\alpha_{12} = \alpha_{13} = 160$/s. Dot–dashed curves (No. 3) are those of $\alpha_{12} = 0$ and $\alpha_{13} = 320$/s. Other kinetic parameters are same as Fig. 6.

"skewness" of the ion swarms, introduced by Skullerud and co-workers in their recent analysis of the Li^+/He system without reactions (26).

Discussion

(a) Initial conditions

In this work, we have adopted two types of initial conditions, the δ function and Gaussian-type function, for the density distributions of initial ion swarms in the axial direction. The former may be useful to obtain the basic information of the dynamic process of multiple ion swarms, specifically to estimate the number of elementary reactions. The latter is recommended for the analysis of more realistic ion swarm phenomena. Basically, however, there is no specific restriction to the mathematical form of the initial condition for the present formulation. Any function can be employed as an initial condition by using a Fourier transform and the orthogonality of Bessel functions.

(b) Radial and axial boundary conditions

To solve the boundary value problem of transport equation, it is essential to choose an appropriate space coordinate suitable for the geometrical structure of experimental apparatus. The cylindrical coordinate is, in this sense, the best choice for the present drift-tube analysis, therefore we can easily introduce the radial boundary effects into [5]. A brief comment on the effects were given by Woo and Whealton (20). However, the treatment of the axial boundary conditions of [5] is not so simple, because [5] is a free boundary solution with respect to the axial coordinate. The method of "negative image swarm" developed by Lowke (27) and applied to analyzing the K^+/N_2 system by Milloy (28). This technique proves to be suitable in the present method. Both boundary conditions were extensively re-examined by Gatland in his review (7).

(c) Neutral gas mixtures

The analysis in gas mixtures is an interesting practical subject in many applied fields. Specifically, in ion chemistry of the earth's atmosphere we have to treat a complex reaction scheme of ion species with a mixture of nitrogen, oxygen, and other neutral species (13). In such a case, each reaction frequency involved in [3] is represented by a summation of several sub-reaction frequencies. If we assume that the mixture is composed of q-neutral gases, [2] is extended to a more general form as

$$[21] \qquad \alpha_{ij} = \sum_{p=1}^{\infty} k_{ij}(p) N_1^{p_1} N_2^{p_2} \cdots N_m^{p_m} \cdots N_q^{p_q}$$

with

$$[22] \qquad p = p_1 + p_2 + \cdots\cdots + p_m + \cdots\cdots + p_q$$

where N_m is the number density of mth neutral gas, p_m is the order of reaction with respect to mth neutral gas, and $k_{ij}(p)$ is the pth order reaction rate from species j to i. While several terms in [21] are absolutely meaningless in the analysis, this formula may be useful for us to classify the above sub-reaction processes into three groups, the direct associative reaction, the associative reaction accompanied by the stabilizing process, and the dissociative reaction. Two-body and three-body reactions are the simplest examples of first and second processes, respectively. The reader can refer to two reviews for details of these processes, the theory of which is mainly based on statistical mechanics (29, 30).

For the diffusion coefficients and drift velocities of ions in gas mixtures, we can resort to several approximate theories and elaborate calculations associated with Blanc's law (31).

(d) Inelastic process

The present formulation can basically cover the inelastic processes of excited ions and molecules in linear swarm phenomena, where the transport coefficients and reaction frequencies are determined phenomenologically as functions of mean translational energies and internal energy states of the species. More precise formulation may be derived from the Wang–Chang – Uhlenbeck – de Boer equation (32).

Can. J. Chem. Downloaded from www.nrcresearchpress.com by 84.41.108.74 on 09/07/12
For personal use only.

(e) Non-linear process

The analysis of non-linear process may be one of the most formidable subjects not only in gas phase ion chemistry, but also in various research fields. In fact, not a few really measureable intermediates and products have been yielded by this process $(O^+(^2P)/O, O^+(^2D)/O, O^-/O_3, O_2^-/O_3, OH^-/O_3, O_3^-/O, CO_3^-/NO$, etc.) in the ionosphere. Moreover, the experimental study on plasma processes involving many charged particles and metastable molecules requires this kind of non-linear analysis. Unfortunately, the two mathematical techniques used to derive the present formulation are not easily extended to treat the non-linear process, because both Fourier transform and matrix algebra are, in essence, tools for analyzing linear phenomena in nature. Thus all contents in this paper may not be applicable to the analysis of non-linear process. However, the only conclusion, which may still hold even in a non-linear process, is that the dynamic equilibrium state is the ultimately attainable phase in the space–time evolution of inter-reacting multiple chemical species.

Summary

A new formulation for the analysis of reactive ion transport of multiple ion swarms in neutral gases has been proposed within the framework of linear process. The dynamic process has been classified into three phases, the initial phase, the non-equilibrium phase, and the dynamic equilibrium phase. A picture of the space–time evolution for four ion swarms has been numerically obtained. Experimental data of kinetic coefficients for $(Li^+, Li^+\cdot N_2, Li^+\cdot 2N_2)/N_2$ system determined by Gatland *et al.* have been examined in a reversible cyclic reaction scheme. Moreover, a procedure for the analysis of experimental arrival time spectra to determine the kinetic coefficients of multiple ion swarms has been obtained in the present formulation.

Acknowledgements

The author wishes to thank Dr. M. Takebe, Dr. S. Sato, and Dr. K. Seto for helpful suggestions.

1. L. B. Loeb. Basic processes of gaseous electronics. 2nd ed. University of California Press, Berkeley, CA. 1960.
2. J. W. T. Spinks and R. J. Woods. Introduction to radiation chemistry, 3rd ed. John Wiley and Sons, New York. 1990.
3. E. A. Mason and E. W. McDaniel. Transport properties of ions in gases. John Wiley and Sons, New York. 1988.
4. H. W. Ellis, R. Y. Pai, E. W. McDaniel, E. A. Mason, and L. A. Viehland. At. Data Nucl. Data Tables, **17**, 177 (1976).
5. H. W. Ellis, E. W. McDaniel, D. L. Albritton, L. A. Viehland, S. L. Lin, and E. A. Mason. At. Data Nucl. Data Tables, **22**, 179 (1978).
6. H. W. Ellis, M. G. Thackston, E. W. McDaniel, and E. A. Mason. At. Data Nucl. Data Tables, **31**, 113 (1984).
7. I. R. Gatland. Case studies in atomic collision physics. Vol. 4. *Edited by* E. W. McDaniel and M. R. C. McDowell. North-Holland, Amsterdam. 1975. p. 369.
8. P. Kebarle. Ion–molecule reactions. Vol. 1. *Edited by* J. L. Franklin. Plenum Press, New York. 1972. p. 315.
9. A. Good, D. A. Durden, and P. Kebarle. J. Chem. Phys. **52**, 212 (1970).
10. D. L. Albritton. At. Data Nucl. Data Tables, **22**, 1 (1978).
11. Y. Ikezoe, S. Matsuoka, M. Takebe, and A. Viggiano. Gas-phase ion–molecule reaction rate constants through 1986. Maruzen, Tokyo. 1987.
12. T. D. Märk. Int. J. Mass Spectrom. Ion Processes, **79**, 1 (1987).
13. M. T. Bowers (*Editor*). Gas-phase ion chemistry. Vols. 1, 2, and 3. Academic Press. 1979, 1979, and 1984.
14. J. M. Farrar and W. H. Saunders, Jr. (*Editors*). Techniques of chemistry. Vol. XX. Techniques for the study of ion–molecule reactions. John Wiley and Sons, New York. 1988.
15. J. H. Seinfeld. Atmospheric chemistry and physics of air pollution. John Wiley and Sons, New York. 1986.
16. J. O. Hirschfelder, C. F. Curtiss, and R. B. Bird. Molecular theory of gases and liquids. John Wiley and Sons, New York. 1964.
17. S. Chapman and T. G. Cowling. The mathematical theory of non-uniform gases. 3rd ed. Cambridge University Press, London. 1970.
18. R. B. Bernstein (*Editor*). Atom–molecule collision theory, a guide for the experimentalist. Plenum Press, New York. 1979.
19. J. H. Whealton and S.-B. Woo. Phys. Rev. Lett. **20**, 1137 (1968).
20. S.-B. Woo and J. H. Whealton. Phys. Rev. **180**, 314 (1969).
21. S. W. Benson. The foundations of chemical kinetics. McGraw-Hill, New York. 1960.
22. B. J. Zwolinski and H. Eyring. J. Am. Chem. Soc. **69**, 2702 (1947).
23. H. Ziereis and F. Arnold. Nature, **321**, 503 (1986).
24. F. L. Eisele. J. Geophys. Res. **93**, 716 (1988).
25. I. R. Gatland, L. M. Colonna Romano, and G. E. Keller. Phys. Rev. A**12**, 1885 (1975).
26. T. H. Løvaas, H. R. Skullerud, O.-H. Kristensen, and D. Linhjell. J. Phys. D: Appl. Phys. **20**, 1465 (1987).
27. J. J. Lowke. Aust. J. Phys. **15**, 39 (1962).
28. H. B. Milloy. Phys. Rev. A**7**, 1182 (1973).
29. D. R. Bates. Fundamental processes in atomic collision physics. *Edited by* H. Kleinpoppen, J. S. Briggs, and H. O. Lutz. Plenum Press, New York. 1985.
30. M. R. Flannery. Recent studies in atomic and molecular processes. *Edited by* A. E. Kingston. Plenum Press, New York. 1987.
31. K. Iinuma, E. A. Mason, and L. A. Viehland. Mol. Phys. **61**, 1131 (1987).
32. C. S. Wang-Chang, G. E. Uhlenbeck, and J. de Boer. Studies in statistical mechanics. Vol. 2. *Edited by* J. de Boer and G. E. Uhlenbeck. North-Holland, Amsterdam. 1964. p. 241.

Appendix

The explicit forms of $g_i(\lambda)$ and $f(\lambda_j)$ in [18] for two, three, and four ion swarms are summarized here, where N_i is a Fourier transformed initial condition for ith ion species. Other notations were already defined in this paper. It is to be noted that the present formulae will become exactly the same as the well-known time-dependent solutions of a set of coupled rate equations for a first-order reaction sequence (9) when we ignore all the transport coefficients and several reaction frequencies of the ion species in them.

(1) Two-ion swarms

[A1] $$g_1(\lambda) = N_1\lambda - N_1T_2 + N_2\alpha_{12}$$

[A2] $$g_2(\lambda) = N_2\lambda - N_2T_1 + N_1\alpha_{21}$$

[A3] $$f(\lambda_1) = \lambda_1 - \lambda_2$$

[A4] $$f(\lambda_2) = \lambda_2 - \lambda_1$$

Can. J. Chem. Downloaded from www.nrcresearchpress.com by 84.41.108.74 on 09/07/12
For personal use only.

(2) Three-ion swarms

[A5] $$g_1(\lambda) = N_1\lambda^2 + \lambda[N_2\alpha_{12} + N_3\alpha_{13} - N_1(T_2 + T_3)] + N_1(T_2T_3 - \alpha_{23}\alpha_{32}) + N_2(\alpha_{13}\alpha_{32} - \alpha_{12}T_3) + N_3(\alpha_{12}\alpha_{23} - \alpha_{13}T_2)$$

[A6] $$g_2(\lambda) = N_2\lambda^2 + \lambda[N_1\alpha_{21} + N_3\alpha_{23} - N_2(T_1 + T_3)] + N_1(\alpha_{23}\alpha_{31} - \alpha_{21}T_3) + N_2(T_1T_3 - \alpha_{13}\alpha_{31}) + N_3(\alpha_{13}\alpha_{21} - \alpha_{23}T_1)$$

[A7] $$g_3(\lambda) = N_3\lambda^2 + \lambda[N_1\alpha_{31} + N_2\alpha_{32} - N_3(T_1 + T_2)] + N_1(\alpha_{21}\alpha_{32} - \alpha_{31}T_2) + N_2(\alpha_{12}\alpha_{31} - \alpha_{32}T_1) + N_3(T_1T_2 - \alpha_{12}\alpha_{21})$$

[A8] $$f(\lambda_1) = (\lambda_1 - \lambda_2)(\lambda_1 - \lambda_3)$$

[A9] $$f(\lambda_2) = (\lambda_2 - \lambda_1)(\lambda_2 - \lambda_3)$$

[A10] $$f(\lambda_3) = (\lambda_3 - \lambda_1)(\lambda_3 - \lambda_2)$$

(3) Four-ion swarms

[A11] $$\begin{aligned} g_1(\lambda) = {} & N_1\lambda^3 + \lambda^2[N_2\alpha_{12} + N_3\alpha_{13} + N_4\alpha_{14} - N_1(T_2 + T_3 + T_4)] \\ & + \lambda\{N_1(T_2T_3 + T_2T_4 + T_3T_4 - \alpha_{23}\alpha_{32} - \alpha_{24}\alpha_{42} - \alpha_{34}\alpha_{43}) + N_2[\alpha_{14}\alpha_{42} + \alpha_{13}\alpha_{32} - \alpha_{12}(T_3 + T_4)] \\ & + N_3[\alpha_{14}\alpha_{43} + \alpha_{12}\alpha_{23} - \alpha_{13}(T_2 + T_4)] + N_4[\alpha_{12}\alpha_{24} + \alpha_{13}\alpha_{34} - \alpha_{14}(T_2 + T_3)]\} \\ & + N_1(\alpha_{34}\alpha_{43}T_2 + \alpha_{24}\alpha_{42}T_3 + \alpha_{23}\alpha_{32}T_4 - \alpha_{23}\alpha_{34}\alpha_{42} - \alpha_{24}\alpha_{32}\alpha_{43} - T_2T_3T_4) \\ & + N_2(\alpha_{12}T_3T_4 + \alpha_{13}\alpha_{34}\alpha_{42} + \alpha_{14}\alpha_{32}\alpha_{43} - \alpha_{14}\alpha_{42}T_3 - \alpha_{13}\alpha_{32}T_4 - \alpha_{12}\alpha_{34}\alpha_{43}) \\ & + N_3(\alpha_{13}T_2T_4 + \alpha_{12}\alpha_{24}\alpha_{43} + \alpha_{14}\alpha_{23}\alpha_{42} - \alpha_{12}\alpha_{23}T_4 - \alpha_{14}\alpha_{43}T_2 - \alpha_{13}\alpha_{24}\alpha_{42}) \\ & + N_4(\alpha_{14}T_2T_3 + \alpha_{12}\alpha_{23}\alpha_{34} + \alpha_{13}\alpha_{24}\alpha_{32} - \alpha_{12}\alpha_{24}T_3 - \alpha_{13}\alpha_{34}T_2 - \alpha_{14}\alpha_{23}\alpha_{32}) \end{aligned}$$

[A12] $$\begin{aligned} g_2(\lambda) = {} & N_2\lambda^3 + \lambda^2[N_1\alpha_{21} + N_3\alpha_{23} + N_4\alpha_{24} - N_2(T_1 + T_3 + T_4)] \\ & + \lambda\{N_1[\alpha_{24}\alpha_{41} + \alpha_{23}\alpha_{31} - \alpha_{21}(T_3 + T_4)] + N_2(T_1T_3 + T_1T_4 + T_3T_4 - \alpha_{34}\alpha_{43} - \alpha_{14}\alpha_{41} - \alpha_{13}\alpha_{31}) \\ & + N_3[\alpha_{24}\alpha_{43} + \alpha_{13}\alpha_{21} - \alpha_{23}(T_1 + T_4)] + N_4[\alpha_{23}\alpha_{34} + \alpha_{14}\alpha_{21} - \alpha_{24}(T_1 + T_3)]\} \\ & + N_1(\alpha_{21}T_3T_4 + \alpha_{23}\alpha_{34}\alpha_{41} + \alpha_{24}\alpha_{31}\alpha_{43} - \alpha_{24}\alpha_{41}T_3 - \alpha_{23}\alpha_{31}T_4 - \alpha_{21}\alpha_{34}\alpha_{43}) \\ & + N_2(\alpha_{34}\alpha_{43}T_1 + \alpha_{14}\alpha_{41}T_3 + \alpha_{13}\alpha_{31}T_4 - \alpha_{13}\alpha_{34}\alpha_{41} - \alpha_{14}\alpha_{31}\alpha_{43} - T_1T_3T_4) \\ & + N_3(\alpha_{23}T_1T_4 + \alpha_{13}\alpha_{24}\alpha_{41} + \alpha_{14}\alpha_{21}\alpha_{43} - \alpha_{24}\alpha_{43}T_1 - \alpha_{13}\alpha_{21}T_4 - \alpha_{14}\alpha_{23}\alpha_{41}) \\ & + N_4(\alpha_{24}T_1T_3 + \alpha_{14}\alpha_{23}\alpha_{31} + \alpha_{13}\alpha_{21}\alpha_{34} - \alpha_{23}\alpha_{34}T_1 - \alpha_{14}\alpha_{21}T_3 - \alpha_{13}\alpha_{24}\alpha_{31}) \end{aligned}$$

[A13] $$\begin{aligned} g_3(\lambda) = {} & N_3\lambda^3 + \lambda^2[N_1\alpha_{31} + N_2\alpha_{32} + N_4\alpha_{34} - N_3(T_1 + T_2 + T_4)] \\ & + \lambda\{N_1[\alpha_{21}\alpha_{32} + \alpha_{34}\alpha_{41} - \alpha_{31}(T_2 + T_4)] + N_2(\alpha_{34}\alpha_{42} + \alpha_{12}\alpha_{31} - \alpha_{32}(T_1 + T_4)] \\ & + N_3(T_1T_2 + T_1T_4 + T_2T_4 - \alpha_{24}\alpha_{42} - \alpha_{14}\alpha_{41} - \alpha_{12}\alpha_{21}) + N_4[\alpha_{24}\alpha_{32} + \alpha_{14}\alpha_{31} - \alpha_{34}(T_1 + T_2)]\} \\ & + N_1(\alpha_{31}T_2T_4 + \alpha_{21}\alpha_{34}\alpha_{42} + \alpha_{24}\alpha_{32}\alpha_{41} - \alpha_{21}\alpha_{32}T_4 - \alpha_{34}\alpha_{41}T_2 - \alpha_{24}\alpha_{31}\alpha_{42}) \\ & + N_2(\alpha_{32}T_1T_4 + \alpha_{12}\alpha_{34}\alpha_{41} + \alpha_{14}\alpha_{31}\alpha_{42} - \alpha_{34}\alpha_{42}T_1 - \alpha_{12}\alpha_{31}T_4 - \alpha_{14}\alpha_{32}\alpha_{41}) \\ & + N_3(\alpha_{24}\alpha_{42}T_1 + \alpha_{14}\alpha_{41}T_2 + \alpha_{12}\alpha_{21}T_4 - \alpha_{12}\alpha_{24}\alpha_{41} - \alpha_{14}\alpha_{21}\alpha_{42} - T_1T_2T_4) \\ & + N_4(\alpha_{34}T_1T_2 + \alpha_{12}\alpha_{24}\alpha_{31} + \alpha_{14}\alpha_{21}\alpha_{32} - \alpha_{24}\alpha_{32}T_1 - \alpha_{14}\alpha_{31}T_2 - \alpha_{12}\alpha_{21}\alpha_{34}) \end{aligned}$$

[A14] $$\begin{aligned} g_4(\lambda) = {} & N_4\lambda^3 + \lambda^2[N_1\alpha_{41} + N_2\alpha_{42} + N_3\alpha_{43} - N_4(T_1 + T_2 + T_3)] \\ & + \lambda\{N_1[\alpha_{21}\alpha_{42} + \alpha_{31}\alpha_{43} - \alpha_{41}(T_2 + T_3)] + N_2[\alpha_{32}\alpha_{43} + \alpha_{12}\alpha_{41} - \alpha_{42}(T_1 + T_3)] \\ & + N_3[\alpha_{23}\alpha_{42} + \alpha_{13}\alpha_{41} - \alpha_{43}(T_1 + T_2)] + N_4(T_1T_2 + T_1T_3 + T_2T_3 - \alpha_{23}\alpha_{32} - \alpha_{13}\alpha_{31} - \alpha_{12}\alpha_{21})\} \\ & + N_1(\alpha_{41}T_2T_3 + \alpha_{21}\alpha_{32}\alpha_{43} + \alpha_{23}\alpha_{31}\alpha_{42} - \alpha_{21}\alpha_{42}T_3 - \alpha_{31}\alpha_{43}T_2 - \alpha_{23}\alpha_{32}\alpha_{41}) \\ & + N_2(\alpha_{42}T_1T_3 + \alpha_{13}\alpha_{32}\alpha_{41} + \alpha_{12}\alpha_{31}\alpha_{43} - \alpha_{32}\alpha_{43}T_1 - \alpha_{12}\alpha_{41}T_3 - \alpha_{13}\alpha_{31}\alpha_{42}) \\ & + N_3(\alpha_{43}T_1T_2 + \alpha_{12}\alpha_{23}\alpha_{41} + \alpha_{13}\alpha_{21}\alpha_{42} - \alpha_{23}\alpha_{42}T_1 - \alpha_{13}\alpha_{41}T_2 - \alpha_{12}\alpha_{21}\alpha_{43}) \\ & + N_4(\alpha_{23}\alpha_{32}T_1 + \alpha_{13}\alpha_{31}T_2 + \alpha_{12}\alpha_{21}T_3 - \alpha_{12}\alpha_{23}\alpha_{31} - \alpha_{13}\alpha_{21}\alpha_{32} - T_1T_2T_3) \end{aligned}$$

[A15] $$f(\lambda_1) = (\lambda_1 - \lambda_2)(\lambda_1 - \lambda_3)(\lambda_1 - \lambda_4)$$

[A16] $$f(\lambda_2) = (\lambda_2 - \lambda_1)(\lambda_2 - \lambda_3)(\lambda_2 - \lambda_4)$$

[A17] $$f(\lambda_3) = (\lambda_3 - \lambda_1)(\lambda_3 - \lambda_2)(\lambda_3 - \lambda_4)$$

[A18] $$f(\lambda_4) = (\lambda_4 - \lambda_1)(\lambda_4 - \lambda_2)(\lambda_4 - \lambda_3)$$

Can. J. Chem. Downloaded from www.nrcresearchpress.com by 84.41.108.74 on 09/07/12
For personal use only.

Stereoselective syntheses of isomers of 3,7-dimethylnonadecane, a sex pheromone of the alfalfa blotch leafminer (*Agromyza frontella* (Rondani))

DAVID MILLER, FRANÇOIS BILODEAU, AND ROBERT H. BURNELL[1]
Département de chimie, Université Laval, Québec (Québec), Canada G1K 7P4

Received July 24, 1990[2]

DAVID MILLER, FRANÇOIS BILODEAU, and ROBERT H. BURNELL. Can. J. Chem. **69**, 1100 (1991).

Two related stereoselective syntheses of 3,7-dimethylnonadecane, a sex pheromone of the alfalfa leafminer, are described to show that pulegone can serve as a useful starting material for the preparation of chiral aliphatic isoprenoid compounds. The schemes are designed to place the stereogenic center of pulegone at C.3 in one synthesis and at C.7 in the other so that the optical properties of the products can be compared with one another and with the values calculated using Brewster's rules.

Key words: chiral hydrocarbons, stereoselective synthesis, pheromone, *Agromyza frontella*.

DAVID MILLER, FRANÇOIS BILODEAU et ROBERT H. BURNELL. Can. J. Chem. **69**, 1100 (1991).

Deux synthèses apparentées de 3,7-diméthylnonadécane, la phéromone sexuelle de la mouche mineuse de la luzerne, sont présentées pour démontrer l'utilité de la pulégone naturelle comme substance initiale pour préparer certains produits aliphatiques isoprépiques. Les approches placent le carbone stéréogénique de la pulégone en C.3 dans un cas et en C.7 dans l'autre donc la comparaison des propriétés chiroptiques des deux échantillons peut fournir des indices de la stéréosélectivité des réactions critiques dans le schéma synthétique.

Mots clés: hydrocarbures chiraux, synthèses stéréosélectives, phéromone, *Agromyza frontella*.

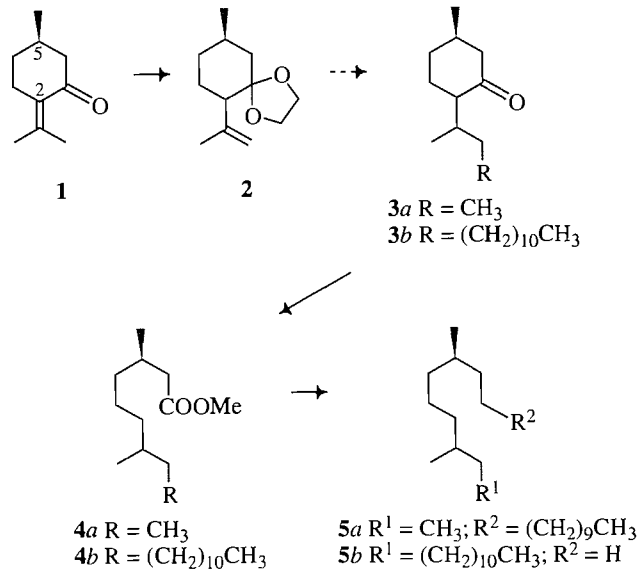
Can. J. Chem. Downloaded from www.nrcresearchpress.com by 198.100.157.202 on 09/07/12
For personal use only.

Introduction

The alfalfa blotch leafminer (*Agromyza frontella* (Rondani)) is a dipteran insect, which spread rapidly in North America after its unintentional introduction from Europe in the late 1960's (1). Studies of mating behavior (2) and subsequent chemical analysis of hexane surface extracts of the male insects identified 3,7-dimethylnonadecane as a female sex pheromone component. Bioassay of the material from a synthetic mixture of racemic hydrocarbons confirmed the general identity of the natural product (3).

The methyl groups on the nonadecane chain are placed with isoprenoid spacing at positions that allow four possible stereoisomers, which probably do not have identical biological activity. It was of interest to design a synthesis that could give selective access to one or more of the stereoisomers. (*R*)-(+)-pulegone **1** was chosen as a chiral starting material due to its availability in a reasonably pure state and because of its fortuitous functionality. Both natural pulegone (4) and isopulegol (5) have been used as chiral starting materials in pheromone synthesis. Usually, however, they only serve as a source of (*R*)-(+)-citronellic acid (yield 50–60%) (6, 7) or its reduction product (*R*)-(+)-citronellol ($LiAlH_4$ reduction of the acid, 90%) (8). In the present syntheses the (*R*)-(+)-pulegone serves directly as the starting product and, should the enantiomeric synthesis be necessary, it can be transformed into (*S*)-(−)-pulegone (9). The commerical product (Aldrich) was fractionally distilled twice under high reflux ratio conditions and then further purified by argentation chromatography. GC analysis showed that the material used in the syntheses was >99% chemically pure and the specific rotation ($[\alpha]_D^{23}$ +21.3 (*c* 6.505, $CHCl_3$)) was unchanged by further purification. Unfortunately several different specific rotations are given in the literature for pulegone but all are similar to the value obtained above.

The first synthesis (Scheme 1) planned the involvement of the cyclic ketal **2** whose terminal double bond would permit, in a few steps, the addition of a methyl group. The ring of the homologous ketone **3***a* could be opened oxidatively (Baeyer–Villiger) and the resulting acyl group in the product **4***a* should allow the facile introduction of the C_{10} chain to complete the 3,7-dimethylnonadecane **5***a*. In this way the chirality at C.5 in pulegone would be located at C.7 in the synthesized pheromone. It was anticipated that there would be considerable induction of a particular stereochemistry at C.3. To a great extent the purpose of the synthesis was to ascertain how important this natural induction would be.



1 **2**

3*a* R = CH_3
3*b* R = $(CH_2)_{10}CH_3$

4*a* R = CH_3
4*b* R = $(CH_2)_{10}CH_3$

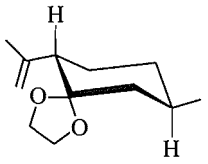
5*a* $R^1 = CH_3$; $R^2 = (CH_2)_9CH_3$
5*b* $R^1 = (CH_2)_{10}CH_3$; $R^2 = H$

SCHEME 1

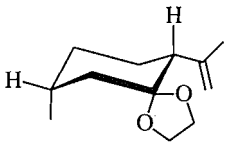
The general method outlined above also afforded another route to the final product (Scheme 1). Using much the same methodology, a C_{11} chain could be added to the terminal double bond in ketal **2**, and the ester moiety in **4***b* arising from ring cleavage of the derived ketone **3***b* could be reduced to afford the hydrocarbon **5***b*. In this case, however, the C.5 chirality of pulegone would reside at the C.3 center of the pheromone. In theory, the two routes would allow us a comparison of the asymmetric induction achieved at the other chiral center.

Strong acid catalysed ketalization of pulegone is normally accompanied by double bond migration (10). In the case of

[1]Author to whom correspondence may be addressed.
[2]Revision received March 4, 1991.



2a



2b

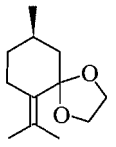
pulegone this introduces a second stereogenic carbon that will eventually lose its chirality, but its importance may be critical while establishing the stereochemistry at the adjacent methyl-bearing carbon, one of the two chiral centers in the final product. The conventional Dean–Stark procedure with benzene provided good yields of the spiroketal in 24–48 h and, with *p*-toluenesulfonic acid as the catalyst, diastereoisomers **2***a* and **2***b* were obtained in the ratio 5.7:1.[3] Since the ketal arises from a long equilibration it is assumed that the major component is **2***a*, in which the two substituents are equatorial to the six-membered ring.

Reexamination of the ketalization brought to light some interesting aspects of the process. Following the progress of the reaction by gas chromatography showed that the product formed more rapidly than all others is neither **2***a* nor **2***b* but rather **6**, in which the double bond has not migrated. After 4.25 h (benzene, *p*-TsOH, reflux Dean–Stark) the concentration of the kinetic product is as high as 16% but **6** disappeared with time to the profit of the normally isolated products. The kinetic product **6** was compared with a sample prepared under conditions where double bond migration is not usually observed (11).

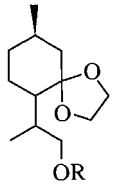
Hydroboration/oxidation of the ketal **2***a* allowed the anti-Markownikow addition to the terminal double bond, affording **7***a*. At this point, the stereochemistry of the final dimethylnonadecane was established and should be preserved to the end of the synthesis.

Primary alcohol **7***a* was converted to the unstable tosylate **7***b*, which was alkylated directly with dimethyllithium cuprate (80%). The resulting ketal **8***a* afforded the ketone **9***a* on hydrolysis (acetone–water, trace HCl: 89%).

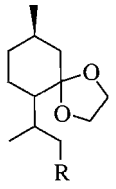
The next three steps were optimized using 2*S*,5*R*-menthone **9***c* as a model. Standard Baeyer–Villiger oxidation of the latter



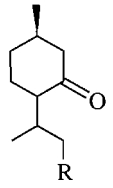
6



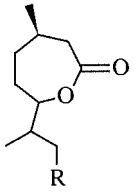
7*a* R = H
7*b* R = Ts



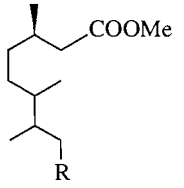
8*a* R = Me
8*b* R = $(CH_2)_{10}CH_3$



9*a* R = Me
9*b* R = $(CH_2)_{10}CH_3$
9*c* R = H



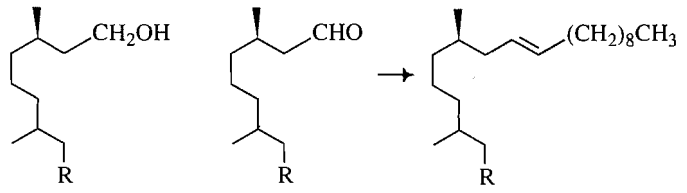
10*a* R = Me
10*b* R = $(CH_2)_{10}CH_3$
10*c* R = H



11*a* R = Me
11*b* R = $(CH_2)_{10}CH_3$
11*c* R = H

[3]More recently it was found that the final equilibrium could be tilted to 12:1 (**2***a* to **2***b*) by using benzene with camphorsulfonic acid. The yield was lower, however (63%).

with *m*-chloroperbenzoic acid led slowly but exclusively to the lactone **10***c* (83%) but, using the Whitesell conditions (12) in which solid sodium bicarbonate is introduced, the reaction had reached an optimal point after only 2.5 h and the isolated yield of lactone **10***c* (90%) was superior to that from the classical procedure. Methanolysis (MeOH, trace H_2SO_4) was virtually quantitative at room temperature and the hydroxy ester **11***c* was tosylated and reduced with lithium aluminium hydride to alcohol **12***c*. The latter gave spectra identical with those of the product obtained by the hydrogenation of geraniol. The model compounds **10***c*, **11***c*, and **12***c* were useful in the assignment of the ^{13}C nmr resonances.



12*a* R = Me
12*b* R = $(CH_2)_{10}CH_3$
12*c* R = H

13

14

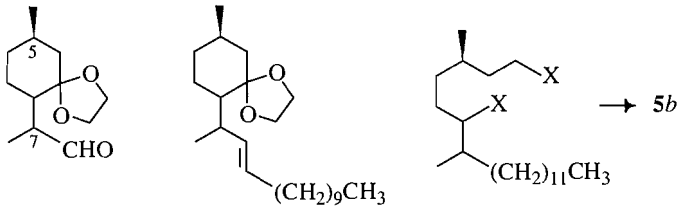
5*a*

In identical fashion homologous ketone **9***a* was oxidized to lactone **10***a* (quantitative), methanolysed to hydroxy ester **11***a* (84%), tosylated, and then reduced ($LiAlH_4$) to 3(*R*),7-dimethylnonanol **12***a* (40%). Oxidation of primary alcohol **12***a* using PCC in methylene chloride gave nonanal **13** (70%). The latter was treated with the ylide prepared from decyltriphenylphosphonium bromide giving 3,7-dimethylnonadec-9-ene **14**, which was hydrogenated over palladium on charcoal to afford the 3,7-dimethylnonadecane **5***a*, $[\alpha]_D$ +2.42.

It was hoped that essentially the same steps could be used in the alternate synthesis. However, the tosylate of **7***a* gave only traces of alkylated product when treated with diundecyllithium cuprate. Consequently, alcohol **7***a* was oxidized to aldehyde **15** (PCC, NaOAc, CH_2Cl_2, room temp.). Wittig reaction with triphenylundecylphosphonium bromide then afforded **16**, which was hydrogenated over Adams' catalyst to give ketal **8***b*. Hydrolysis gave the ketone **9***b*.

Ketone **9***b* was cleaved to lactone **10***b* by Baeyer–Villiger oxidation and methanolysis then afforded ester **11***b*. To remove both oxygen functions at the same time, the latter was reduced with hydride to the diol **17***a* but, despite numerous attempts, no conditions could be found to prepare the ditosyl derivative. Finally, the dibromide **17***b* was prepared using triphenylphosphine and bromine (13) and the halogen substituents removed by hydrogenolysis ($LiAlH_4$) to give the second pheromone **5***b*, $[\alpha]_D$ +3.76. In an alternate route hydroxy ester **11***b* was tosylated and reduced with hydride, affording the primary alcohol **12***b*. The tosylate of the latter was then reduced to **5***b* in the same manner.

Brewster has formulated a series of rules for predicting the



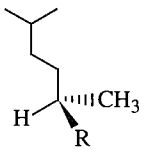
15

16

17*a* X = OH
17*b* X = Br

5*b*

Can. J. Chem. Downloaded from www.nrcresearchpress.com by 198.100.157.202 on 09/07/12
For personal use only.



R	$(M)_D$ calcd.	$(M)_D$ obsd.
Ethyl	13.3	11.9
n-Propyl	3.3	3.5
n-Butyl	1.3	1.5
n-Pentyl	0.0	0.2

FIG. 1

sign and magnitude of the optical properties of hydrocarbons (14). The calculations and examples, such as those in Fig. 1, show that in long-chain hydrocarbons, only chiral centers near the ends of the chains contribute significantly to the molecular rotations. The rules suggest that our synthetic product **5***b*, in which (*R*)-(+)-pulegone's chirality is at C.3, should be dextrorotatory with an $[M]_D$ of 12°. The observed molecular rotation of +11.1° is in acceptable agreement with this calculated value. Comparing this result with that obtained for hydrocarbon **5***a* from the other synthesis allows an assessment of the stereochemistry induced at the other asymmetric carbon because in this case the chirality of pulegone is at C.7 where its effect should be negligible. From the molecular rotation of **5***a* ($[M]_D$ +7.2°) it appears that the first two reactions in the synthesis (ketalization and hydroboration) favor by a factor of 4:1 the configuration that leads to the (*S*)-3 geometry in the final product.

This implies a considerable rotational preference for the isopropenyl group in the ketal. Models suggest no clear preference but, if the major rotamer is that shown in **2***a*, the hydride in the diborane reaction arrives from the remote side of the molecule. Apparently the ketal oxygens do not actively deliver the borane reagent to the appropriate face of the double bond, as the sterically more demanding 9-BBN produced the same alcohol with essentially the same stereochemical preference.

Confirmation of the *S*-configuration at C.3 was obtained from another source. The aldehyde **15** was always treated promptly and with care to avoid epimerization, particularly during the Wittig reaction. It seemed wise to test just how effective the precautions were. At −78°C in the presence of basic catalysts, the aldehyde was virtually unchanged after 3 h but, after the same period at room temperature in methanol containing potassium carbonate, the ^{1}H nmr of the recovered product now showed two doublets for the aldehyde proton, the original at 9.62 and another at 9.26 δ. The latter was considerably more intense (1:3 from the nmr integration), which implies that this is the thermodynamically favoured aldehyde. When the two epimeric structures were examined by the Alchemy II program, the most favoured rotamer of the (*R*)-5,(*S*)-7 isomer of **15** was found to be more stable than the *R,R* compound by about 2 kcal/mol. The aldehyde used to continue the synthesis was the less stable and following this through the sequence (without loss of chirality) would lead to **5***b* with the (*S*)-3,(*S*)-7 configurations.

Experimental

Unless otherwise stated, the conditions and instruments used to characterize the products were as follows: melting points, Electrothermal, uncorrected; ultraviolet spectra, ethanol solutions (ε in parentheses), Hewlett–Packard 8450 A; infrared spectra, carbon tetrachloride solutions, Beckman 4250 and Perkin–Elmer 457; 200-MHz proton and 50-MHz carbon-13 magnetic resonance spectra, deuterochloroform solutions, standard TMS protons and carbon = 0 ppm (where relevant, multiplicity, integrated peak areas, coupling constants, and assignments in parentheses), "dis. D_2O" signifies that the peaks in question disappeared on shaking the solution with a small volume of D_2O, Varian XL-200; mass spectra, Hewlett–Packard 5992; GLC analyses, Varian 3700 and Hewlett–Packard 5792A, flame ionization, DB-1 and SE-30 columns. Elemental analyses were by Galbraith Laboratories, Knoxville, TN. High resolution mass spectra were recorded at the Centre régional de spectrométrie de masse, Université de Montréal. Unless otherwise recorded, dry column chromatography implies the use of Merck Kieselgel 60F (70–230 mesh) and elution with hexane–ether (proportions determined by prior thin-layer chromatography using Baker-flex Silica gel 1B-2F precoated plastic sheets).

First synthesis affording pheromone **5***a*

Ketalization of (R)-(+)*-pulegone*

(*a*) Before use, the *(R)*-(+)-pulegone was fractionally distilled twice and then further purified by argentation chromatography. GC analysis indicated >99% chemical purity and the $[\alpha]_D^{23}$ was +21.3 (*c* 6.505, $CHCl_3$). The pulegone (19.95 g; 131 mmol), ethylene glycol (9.7 g; 161 mmol), and *p*-TsOH (24 mg) were refluxed in benzene (300 mL) with a Dean–Stark separator for 115 h. After concentration, aqueous NaOH (100 mL, 10%) and ether (150 mL) were added. The separated organic phase was washed (water, brine), dried over $MgSO_4$, and concentrated to give a yellow oil. The fraction that distilled at 43°C/0.3 Torr (1 Torr = 133.3 Pa) (Vigreux, 22.7 g; 87%) proved to be a 5.7:1 mixture of the isomers **2***a* and **2***b*; colorless oil, $[\alpha]_D^{23}$ +3.81 (*c* 5.67, $CHCl_3$); ir (neat): 3080, 1645, 1205, and 1145 cm^{-1}; ^{1}H nmr δ: 0.87 (d, *J* = 6.2 Hz, Me-C.5), 1.76 (d, *J* = 1.8 Hz, Me-C.7), 2.16 (dd, *J* = 12.5 and 4.4 Hz, C.2-H), 3.85 (m, 4H, ketal CH_2), and 4.80 (m, 2H, $+CH_2$); ^{13}C nmr: Table 1; ms *m/z*: 196(2, M^+), 181(11), 139(15), 126(12), 114(15), 113(100), and 86(19). Exact Mass calcd. for $C_{12}H_{20}O_2$: 196.1463; found: 196.1435.

(*b*) Using exactly the same procedure, pulegone (8.49 g), ethylene glycol (3.92 g), and *p*-TsOH (11mg) were refluxed in benzene for 4.25 h (Dean–Stark). Gas chromatography showed the presence of unreacted pulegone, ketal **2***a*, and ketal **6** (16%). Distillation of the product gave a fraction that contained 56% of the ketal **6**. The nmr of the major component was δ: 0.84 (s, 3H, *Me*-CH), 1.62 (s, 3H, Me-C=C), and 1.86 (d, 3H, *J* = 1.5 Hz, Me-C=C).

(*c*) To excess trimethylsilyltrifluoromethane sulfonate (3 drops) in CH_2Cl_2 (1 mL) cooled to −78°C was added 1,2-bis(trimethylsiloxy)-ethane (2.08 g) and *(R)*-(+)-pulegone (0.85 g). After stirring at room temperature for 117 h, the reaction was stopped by adding pyridine (0.5 mL) and pouring into saturated aqueous $NaHCO_3$ (15 mL). The crude product obtained by ether extraction was quickly distilled under vacuum to afford a mixture of pulegone (23%) and ketal **6** (67%); ^{1}H nmr δ: 0.88 (d, 3H, *J* = 1.5 Hz, *Me*-CH), 1.66 (s, 3H, Me-C=C), 1.91 (d, 3H, *J* = 1.47 Hz, Me-C=C), 3.70–4.00 (m, 4H, $-OCH_2-CH_2O-$). The respective methyl peaks for pulegone are at 0.98, 1.75, and 1.95 δ. The ^{13}C nmr (Table 1) was obtained from the spectrum of this mixture.

Hydroboration of the ketal **2***a*

(*a*) To the ketal (17.7 g; 83 mmol) in dry THF (40 mL) was added dropwise a 1 M THF solution of B_2H_6 (100 mL). After stirring for 2 h at room temperature, water (15 mL) was slowly added, followed by H_2O_2 (20 mL, 30 vol.) and aqueous NaOH (20 mL, 30%). Ether was added after 30 min at room temperature and the separated organic layer was washed with brine and dried ($MgSO_4$). The oil obtained was fractionated, affording alcohol **7***a* (bp 74–78°C/0.5 Torr: 13.4 g; 82%); colorless oil, $[\alpha]_D^{20}$ −32.6 (*c* 4.05, MeOH); ir (neat): 3425 cm^{-1}; ^{1}H nmr δ: 0.78 (d, 6H, *J* = 7.0 Hz, Me at C.3 and C.7), 3.17 (dd, *J* = 11.0 and 5.1 Hz, CH_2OH), 3.36 (dd, *J* = 11.0 and 9.5 Hz, CH_2OH), 3.78 (m, 4H, ketal CH_2); ^{13}C nmr: Table 1; ms *m/z*: 214(4, M^+), 199(2), 183(28), 127(14), and 113(100).

(*b*) Under argon at 0°C, a solution of 9-BBN (120 mL of 0.5 M in THF) was added to the ketal **2***a* (11.0 g). After 2 h, the temperature was allowed to rise to ambiant and stirring was continued for 12 h. The mixture was cooled in ice, excess 9-BBN was destroyed with a small quantity of H_2O, and then aqueous NaOH (5 mL, 3 N) and H_2O_2 (10 mL, 30 vol.) were added. After stirring for 30 min the product was obtained by hexane extraction and then chromatographed (pet.

Can. J. Chem. Downloaded from www.nrcresearchpress.com by 198.100.157.202 on 09/07/12
For personal use only.

Can. J. Chem. Downloaded from www.nrcresearchpress.com by 198.100.157.202 on 09/07/12
For personal use only.

ether/ether 95:5) to afford some starting material **2***a* (1.12 g) and the alcohol **7***a* (10.36 g; 86%), $[\alpha]_D^{23}$ −35.85 (*c* 4.798, MeOH). Exact Mass calcd. for $C_{12}H_{22}O_3$: 214.1569; found: 214.1582. Other physical properties were identical with those for the product from method (*a*) (above).

Alkylation at C.8 via the tosylate

(*a*) *Preparation of the tosylate* **7**b. Freshly recrystallized *p*-tosyl chloride 10.0 g; 52.5 mmol) was added to the alcohol **7***a* (10.1 g; 47.2 mmol) in pyridine (30 mL) at 0°C. The mixture was stirred for 2.5 h at 0°C and then poured into 5% HCl (200 mL), washed with more HCl, then with saturated $NaHCO_3$, dried, and concentrated to give the crude tosylate **7***b* (17.1 g; 98%). The product was unstable at room temperature and was used without further purification; ir: 3100–3000, 1600, 1452, 1356, and 1175 cm^{-1}; ^1H nmr δ: 0.83 (d, *J* = 6.6 Hz), 0.95 (d, *J* = 7.0 Hz), 2.42 (s, Me-Ar), 3.75 (m, 4H), 4.43 (dd, *J* = 10.0 and 3.7 Hz, CH_2-OTs), 7.29 and 7.75 (2d, *J* = 8.4 Hz, Ar-H).

(*b*) *Reaction with dimethyl lithium cuprate*. A solution of methyl lithium (1.4 M in ether) was added drop by drop to a suspension of cuprous iodide (10.03 g; 54.2 mmol) in dry ether (25 mL) at 0°C until the bright yellow color initially formed had disappeared. Tosylate **7***b* (8.76 g; 23.77 mmol) in ether was added dropwise and the solution was stirred for 1 h at 0°C. Saturated aqueous NH_4Cl was added slowly with stirring and the resulting mixture then poured into water and extracted with ether. The organic phase was washed with brine, dried, concentrated, and purified by chromatography to afford **8***a* as a colorless oil (4.37 g; 82%), *1-ethylenedioxy-2-(1-methylpropyl)-5-methylcyclohexane*; $[\alpha]_D^{23}$ −17.1 (*c* 4.79, $CHCl_3$); ir (neat): 2980–2840 and 1100 cm^{-1}; ^1H nmr δ: 0.84 (m, 9H, Me-C), 1.3–1.8 (m, 10H, ring CH_2 and CH), 3.9 (m, 4H, ketal CH_2); ^{13}C nmr: Table 1; ms *m*/*z*: 212(7, M^+), 183(20), 155(11), 127(11), and 113(100). Exact Mass calcd. for $C_{13}H_{24}O_2$: 212.1776; found: 212.1836.

Hydrolysis of ketal **8**a *to ketone* **9**a

Ketal **8***a* (4014 g; 18.9 mmol) was taken up in acetone (50 mL) and water (7 mL). Three drops of concentrated HCl were added and the mixture refluxed for 15 min. After cooling, saturated aqueous $NaHCO_3$ was added, most of the acetone was evaporated, and the residue was diluted with water and extracted with ether. Concentration of the dried ethereal solution and chromatography of the oil gave the ketone **9***a* (3.01 g; 89%), *2-(1-methylpropyl)-5-methylcyclohexanone*; $[\alpha]_D^{23}$ −31.4 (*c* 0.92 $CHCl_3$); ir: 1707 cm^{-1}; ^{1} H nmr δ: (t, *J* = 6.6 Hz), 0.84 (d, *J* = 6.6 Hz), and 0.96 (d, *J* = 5.9 Hz, three C-Me), 2.29 (ddd, *J* = 11.8, 3.6, and 2.2 Hz, H-C.2); ^{13}C nmr: Table 1; ms *m*/*z*: 168(4, M^+), 139(8), 113(9), 112(100), 97(29), 84(20), 83(19).

Baeyer–Villiger oxidation of ketone **9**a

Ketone **9***a* (127 mg; 0.76 mmol) was added to a stirred solution of *m*-CPBA (180 mg of 80%; 0.76 mmol) in CH_2Cl_2 containing a suspension of $NaHCO_3$ (71 mg; 0.84 mmol) as suggested by Whitesell *et al.* (12). After stirring for 18 h at room temperature, aqueous KI and aqueous $NaHSO_3$ were added to reduce excess reagent. The organic phase was washed with brine, dried, and concentrated to afford the lactone **10***a* (140 mg; quant.), *3-methyl-6-(1-methylpropyl)-caprolactone*, colorless oil; ir: 1735 cm^{-1}; ^1H nmr δ: 0.86 (t, *J* = 5.9 Hz, Me-terminal), 0.88 (d, *J* = 6.6 Hz, Me-CH), 2.38 (dm, *J* = 13.2 Hz, H-C.2), 2.50 (dd, *J* = 13.2 and 12.1 Hz, H-C.2), 4.12 (dd, *J* = 9.2 and 3.3 Hz, H-C.6); ^{13}C nmr: Table 1; ms *m*/*z*: 184(0.9, M^+), 127(65), 126(7), 99(93), 98(41), and 81(100).

In the same manner 2(*S*),5(*R*)-menthone **9***c* was oxidized to the lactone **10***c* in 90% yield after 5.5 h. For comparison the ^{13}C nmr of the 3-methyl-6-isopropylcaprolactone **10***c*, mp 49°C, is given in the table. In the absence of the bicarbonate the yield was 80% after 27 h.

Methanolysis of lactone **10**a *to ester* **11**a

To the lactone **10***a* (2.81 g; 15.3 mmol) in MeOH (20 mL) was added concentrated H_2SO_4 (2 drops) and the mixture was refluxed for 5 min. After cooling, saturated aqueous $NaHCO_3$ was added, most of the MeOH was evaporated, and the residue was taken up in ether. Washing (brine), drying, and concentrating gave the hydroxy ester **11***a* (2.78 g; 84%), *methyl 6-hydroxy-3,7-dimethylnonanoate*, colorless oil; ir: 3450, 1722, 1200, and 1160 cm^{-1}; ^1H nmr δ: 0.81 (d, *J* = 6.0 Hz), 0.85 (t, *J* = 7.0 Hz), and 0.90 (d, *J* = 6.6 Hz, three C-Me), 2.09 (dd, *J* = 14.4 and 7.9 Hz, H-C.2), 2.29 (dd, *J* = 14.4 and 6.2 Hz, H-C.2), 3.43 (m, H-C.6), and 3.60 (s, Me-O); ^{13}C nmr: Table 1; ms *m*/*z*: no M^+, 185(0.6), 159(18), 127(100), 115(25), 87(18), and 81(44).

In the same manner, lactone **10***c* afforded *methyl 6-hydroxy-3,7-dimethyloctanoate* **11***c* in 97% yield, $[\alpha]_D^{20}$ −12.1 (*c* 7.68, $CHCl_3$); ir: 3440, 1737, 1200, and 1160 cm^{-1}; ^1H nmr δ: 0.87 (d, *J* = 6.6 Hz), 0.89 (d, *J* = 6.6 Hz), and 0.93 (d, *J* = 6.6 Hz, three C-Me), 2.10 (dd, *J* = 14.7 and 7.7 Hz, H-*C*2), 2.30 (dd, *J* = 14.7 and 5.9 Hz, H-C.2), 3.30 (m, *H*-C-OH), and 3.64 (s, *Me-O*); ^{13}C nmr: Table 1; ms *m*/*z*: no M^+, 185(0.5), 159(30), 153(11), 127(25), 109(20), 101(37), 87(47), and 81(57).

Conversion of hydroxy ester **11**a *to primary alcohol* **12**a

Tosyl chloride (414 mg; 2.17 mmol) was added to ester **11***a* (443 mg; 2.05 mmol) in dry pyridine (3 mL) and the solution was kept in the dark at 0°C for 6 h. Ether was added (50 mL) and the mixture was washed thoroughly with aqueous HCl, saturated aqueous $NaHCO_3$ and brine, and dried and concentrated to afford the tosylate (683 mg; 90%); ir: 2980, 1735, 1594, 1453, 1170 cm^{-1}; ^1H nmr δ: 0.81 (m, 9H, C-Me), 2.40 (s, Me-arom), 3.61 (s, COOMe), 4.47 (m, 1H, H-C.6), 7.28 (d, *J* = 8.4 Hz), and 7.74 (d, *J* = 8.4 Hz, arom-H).

The tosylate (3.75 g; 10.14 mmol, from above used without further purification) was dissolved in dry ether (100 mL) and reduced with $LiAlH_4$ (500 mg; 133.2 mmol) by stirring at room temperature for 4 h. Excess hydride was destroyed with 5% aqueous H_2SO_4 and, after adding more water, the product obtained by ether extraction was chromatographed (pet. ether/ether 3:2), affording *3,7-dimethylnonanol* **12***a* (690 mg; 40%) as a colorless oil; ir: 3325 cm^{-1}; ^1H nmr δ: 0.8 (d, *J* = 5.5 Hz), 0.84 (t, *J* = 5.9 Hz), and 0.88 (d, *J* = 6.6 Hz, three C-Me), 3.67 (t, *J* = 6.6 Hz), and 3.69 (t, *J* = 6.6 Hz, CH_2OH); ^{13}C nmr: Table 1; ms *m*/*z*: no M^+, 125(9), 97(14), 83(22), 71(23), 70(64), 69(54), and 55(100).

In the same manner ester **11***c* gave the corresponding tosylate (90%), which in turn afforded 3,7-dimethyloctanol **12***c* (70%). The latter was identical (ir, ^1H and ^{13}C nmr; for the latter see Table 1) with the product obtained by hydrogenating geraniol over 10% Pd on C in MeOH.

Oxidation of alcohol **12**a *to aldehyde* **13**

Alcohol **12***a* (170 mg; 1 mmol) in CH_2Cl_2 (1 mL) was added quickly to a suspension of PCC (370 mg; 1.7 mmol) in CH_2Cl_2. After 1 h a 1:1 mixture of ether and pentane was added and the mixture filtered through Celite and then rapidly chromatographed. The *3,7-dimethylnonanal* **13** (118 mg; 70%) was sensitive to air and was used immediately for the following step; ir: 2710, 1721 cm^{-1}; ^1H nmr δ: 0.78 (m, 6H) and 0.89 (d, *J* = 6.6 Hz, C-Me), 2.35 (ddd, *J* = 15.5, 5.9, and 2.2 Hz, H-C.2), 9.69 (t, *J* = 2.2 Hz, CHO); ^{13}C nmr: Table 1; ms *m*/*z*: no M^+, 157(4, M−CHO), 139(2), 112(2), 111(4), 107(6), 97(12), and 87(42).

Wittig reaction of aldehyde **13** *to give alkene* **14**

A 0.168 M solution of decyltriphenylphosphonium bromide in THF (5.4 mL; 0.9 mmol) prepared according to Sonnet (see ref. 14) was cooled to −10°C and *n*-butyllithium (0.79 mL of 1.14 M; 0.9 mmol) was added dropwise. The resulting orange solution of the ylide was cooled to −78°C and a solution of the aldehyde **13** (118 mg; 0.7 mmol) in THF was added dropwise. The mixture was allowed to warm to room temperature (ca. 2 h) and then poured into water and extracted with hexane. The product was chromatographed (silica gel:hexane) affording the *3,7-dimethyl-9-nonadecene* **14** (90 mg; 44%) as a colorless oil; $[\alpha]_D^{20}$ 0.3 (*c* 2.06, $CHCl_3$); ir: 2995 cm^{-1}; ^1H nmr δ: 0.85 (t, 6H, *J* = 5.5 Hz, two CH_3-CH_2), 0.86 (d, 6H, *J* = 6.6 Hz, two CH_3-CH), 5.37 (dm, 2H, *J* = 11.2 Hz, -CH=CH-); ^{13}C nmr: Table 1; ms *m*/*z*: 294(3.1, M^+), 195(3.5), 126(5.6), 125(10), 111(14), 97(28), 85(38), and 71(72). Exact Mass calcd. for $C_{21}H_{42}$: 294.3286; found: 294.3242.

Hydrogenation of alkene **14** *to alkane* **5**a

Alkene **14** (45.7 mg; 0.155 mmol) in hexane (25 mL) was shaken under hydrogen (35 psi; 1 psi = 6.9 kPa) in a Parr apparatus for 6 h. The mixture was filtered through Celite and chromatographed (silica

TABLE 1. ^{13}C nuclear magnetic resonance data[a]

(*a*)

	Compound								
Carbon[b]	**1**	**2***a*	**6**	**7***a*	**8***a*	**8***b*	**9***a*	**9***b*	**9***c*
1	203.71	110.85	110.80	110.42	111.85	111.93	211.92	212.03	211.90
2	131.55	45.24	124.71	48.57	44.89	49.93	55.08	55.39	55.77
3	28.49	29.34	35.56	30.14	30.63	30.67	25.56	28.11	25.85
4	32.67	34.31	29.11	34.31	34.78	34.84	35.29	35.31	35.40
5	31.47	30.61	30.89	32.31	32.27	32.00	33.98	34.07	33.87
6	50.70	51.64	40.63	43.20	49.84	44.88	50.84	50.93	50.77
7	141.47	145.67	130.88	23.45	24.07	24.07	28.09	31.23	27.81
8	22.87	113.18	22.98	64.12	24.98	32.29	32.69	33.13	21.16
9	21.98	23.41	20.43	17.85	19.21	19.87	17.10	17.72	18.15
10	21.65	22.10	21.90	21.76	22.16	22.19	22.27	22.36	22.23
11		(64.85)	(64.43)	(64.47)	13.08	28.60	11.81	27.56	
12		(64.63)	(65.72)	(63.89)	(64.41)	29.80		30.07	
13					(64.60)	29.80		29.76	
14						29.80		29.76	
15						29.80		29.76	
16						29.80		29.76	
17						29.80		29.76	
18						29.80		29.76	
19						32.29		32.00	
20						22.77		22.78	
21						14.19		14.21	
						(64.61)			
						(64.38)			

(*b*)

	Compound							
Carbon[b]	**10***a*	**10***b*	**10***c*	**11***a*	**11***b*	**11***c*	**12***a*	**12***b*
1	174.75	174.86	174.72	173.44	179.48	173.54	61.23	61.12
2	82.84	83.37	84.60	74.87	75.27	76.84	37.47	37.51
3	31.42	30.45	30.91	39.87	33.10	33.07	24.43	24.41
4	37.36	37.60	37.40	33.23	33.40	31.50	36.89	37.20
5	30.29	31.96	33.29	30.47	27.45	30.56	29.56	29.40
6	42.40	42.60	42.51	41.44	41.49	41.46	40.07	40.00
7	40.20	38.77	30.38	31.76	38.16	33.42	34.44	32.80
8	25.32	31.63	18.39	26.01	31.80	17.03	29.56	37.36
9	13.46	27.32	17.08	13.12	15.30	18.94	19.21	20.30
10	23.85	24.05	23.96	19.83	19.90	19.96	19.65	19.70
11	11.63	29.40		11.86	27.45	(51.41)	11.46	27.14
12		29.87)		(51.32)	30.54			30.10
13		29.69			29.80			30.00
14		29.69			29.71			30.50
15		29.69			29.71			30.50
16		29.69			29.71			30.50
17		29.69			29.71			30.50
18		29.69			29.40			30.10
19		32.76			31.94			32.60
20		22.74			22.72			23.20
21		14.03			13.83			14.10
					(51.37)			

Can. J. Chem. Downloaded from www.nrcresearchpress.com by 198.100.157.202 on 09/07/12
For personal use only.

TABLE 1. (*concluded*)

(*c*)

Carbon[b]	Compound							
	12*c*	**13**	**14**	**15**	**16**	**17***a*	**17***b*	**5***b*
1	61.10	202.97	128.37	110.33	111.25	60.88	40.02	27.20
2	39.18	37.24	36.96	43.35	49.37	75.56	66.14	37.47
3	24.61	24.43	24.70	30.40	34.73	33.56	34.85	24.58
4	37.29	36.64	36.96	34.45	30.45	31.87	33.14	37.53
5	29.45	29.45	33.54	25.10	31.96	29.40	31.98	32.85
6	39.87	51.15	37.09	44.95	44.33	39.77	40.15	37.24
7	27.89	34.46	34.56	48.24	25.09	38.24	45.53	34.51
8	22.52	29.54	29.56	204.11	126.81	31.94	32.60	29.47
9	22.61	19.19	19.30	12.04	21.59	14.17	17.30	19.36
10	19.57	20.01	19.70	21.92	22.12	19.83	18.79	19.79
11		11.46	11.53	(64.39)	133.61	27.47	27.38	11.53
12			130.59	(63.83)	27.30	30.00	29.89	30.12
13			27.43		29.71	29.72	29.72	29.80
14			29.67		29.71	29.72	29.72	29.80
15			29.85		29.71	29.72	29.72	29.80
16			29.85		29.71	29.72	29.72	29.80
17			29.85		29.71	29.72	29.72	29.80
18			29.67		29.71	29.72	29.72	29.65
19			32.02		29.71	33.40	31.18	32.02
20			22.92		22.74	22.72	22.78	22.79
21			14.24		14.17	13.59	14.23	14.23
					(64.14)			
					(64.14)			

[a]In ppm from TMS = 0.

[b]For convenience, C.1 to C.10 are always the original carbons from pulegone. From C.11 upwards, the alkyl chains are numbered starting with the shorter (in **14** for example, the double bond carbons are C.1 and C.12). Incidental carbons (ketals, esters, etc.) are reported in parentheses.

Can. J. Chem. Downloaded from www.nrcresearchpress.com by 198.100.157.202 on 09/07/12
For personal use only.

gel:hexane) to give *3,7-(R)-dimethylnonadecane* **5***a* (quant: colorless liquid); $[\alpha]_D^{20}$ 2.42 (*c* 1.60, $CHCl_3$); the spectral data for this sample were identical with those described for alkane **5***b*.

Second synthesis affording pheromone **5**a

Oxidation of alcohol **7**a *to aldehyde* ***15***

Hydroxy ketal **7***a* (4.544 g; 21 mmol) was added to a stirred suspension of PCC (6.9 g; 32 mmol) and sodium acetate (0.7 g; 8.6 mmol) in CH_2Cl_2 (20 mL). After stirring for 80 min at room temperature, ether and pentane were added and the reaction mixture was filtered through Celite and then through a short silica gel column to give the *1-ethylenedioxy-2-(2-formylethyl)-5-methylcyclohexane* **15** (3.50 g; 79%); $[\alpha]_D^{23}$ −58 (*c* 3.2, $CHCl_3$); ir: 1720 cm^{-1}; ^1H nmr δ: 0.87 (d, *J* = 6.6 Hz), 1.02 (d, *J* = 6.3 Hz, two C-methyls), 2.65 (m, 1H, *H*-C-CHO), 4.0 (m, 4H, ketal CH_2), 9.64 (d, *J* = 3.3 Hz, CHO); ^{13}C nmr; Table 1; ms *m/z*: 212(1,M^+), 184(22), 183(20), 127(31), and 113(100).

Wittig reaction of aldehyde ***15*** *to give alkene* ***16***

n-Butyllithium (1.35 mL; 9.2 M) was added dropwise at −10°C under N_2 to a stirred THF solution of undecyltriphenylphosphonium bromide (6.173 g; 12.4 mmol, from refluxing undecyl bromide and triphenylphosphine in toluene for 36 h). The resulting dark red solution was cooled to −78°C, the aldehyde **15** (2.815 g; 13.39 mmol) was added dropwise, and the solution then allowed to warm to room temperature over 5 h. Water was added and the product was obtained by extraction with hexane, washing with aqueous sodium bisulfite, drying, and concentration. Rapid chromatographic purification afforded alkene **16** (2.27 g; 52%), *1-ethylenedioxy-2-(1-methyltridecenyl)-5-methylcyclohexane*, as a viscous oil; $[\alpha]_D^{20}$ −20.2 (*c* 3.825, $CHCl_3$); ir: 3010, 1640, 1103, and 1062 cm^{-1}; ^1H nmr δ: 0.85 (d, *J* = 6.2 Hz), 0.86 (t, *J* = 7.0 Hz), and 0.95 (d, *J* = 7.0 Hz, three C-methyls), 1.71 (m, 2H, H-C.6), 2.01 (m, 1H, H-C.7), 3.88 (m, ketal CH_2), and 5.25 (m, 2H, =CH-); ^{13}C nmr: Table 1; ms *m/z*: 350(2.6, M^+), 335(7), 240(13), 226(9), and 113(100). Exact Mass calcd. for $C_{23}H_{42}O_2$: 350.3284; found: 350.3167.

Hydrogenation of alkene ***16*** *to give ketal* ***8***b

Alkene **16** (2.27 g; 6.49 mmol), Adams' catalyst (175 mg), and hexane (50 mL) were shaken under H_2 in a Parr apparatus at 35 psi for 9.5 h. The mixture was filtered through Celite and concentrated to afford ketal **8***b* (2.122 g; 93%), *1-ethylenedioxy-2-(1-methyltridecyl)-5-methylcyclohexane* colorless liquid; $[\alpha]_D^{20}$ −25.4 (*c* 11.71, acetone); ir: 2980–2840, 1455, 1375, and 1100 cm^{-1}; ^1H nmr δ: 0.87 (m, 9H, methyls), 1.24 (br s, 18H, CH_2), 3.88 (m, 4H, ketal CH_2); ^{13}C nmr: Table 1; ms *m/z*: 352(11, M^+), 337(2), 183(24), 113(100). Exact Mass calcd. for $C_{23}H_{44}O_2$: 352.3190; found: 352.3341.

Hydrolysis of ketal **8**b *to give ketone* ***9***b

Ketal **8***b* (1.67g; 5.42 mmol) was dissolved in acetone (20 mL) and water (3 mL), concentrated HCl (2 drops) was added, and the mixture was refluxed for 2 h. Saturated aqueous $NaHCO_3$ was added, most of the acetone was evaporated, and the residue was taken up in ether, washed, and dried. Concentration gave a colorless liquid, which was chromatographed (silica gel: pet. ether/2% ether) to give ketone **9***b* (1.515 g: quant.), *2-(1-methyltridecyl)-5-methylcyclohexanone*; $[\alpha]_D^{20}$ 16.9 (*c* 1.88, $CHCl_3$); ir: 1707 cm^{-1}; ^1H nmr δ: 0.86 (t, *J* = 6.2 Hz), 0.87 (d, *J* = 6.6 Hz), and 0.98 (d, *J* = 6.2 Hz, three C-methyls), 1.8–2.6 (overlapping multiplets, 4H), 2.33 (m, 1H, H-C.2); ^{13}C nmr: Table 1; ms *m/z*: 308(0.8, M^+), 139(13), 113(10), and 112(100). Exact Mass calcd. for $C_{21}H_{40}O$: 308,3079; found: 308.3042.

Baeyer–Villiger oxidation of ketone **9**b

Following the procedure described for **9***a*, ketone **9***b* (1.364 g) afforded the lactone **10***b* (1.214 g: 85%) after chromatography (pet.

ether/2% ether) as a viscous oil that slowly crystallized, mp 49°C, *6-(1-methyltridecyl-3-methylcaprolactone*; $[\alpha]_D^{20}$ −10.5 (*c* 4.03, $CHCl_3$); ir: 1740 and 1262 cm^{-1}; ^1H nmr δ: 0.86 (t, *J* = 7.0 Hz), 0.93 (d, *J* 6.9 Hz), and 1.02 (d, *J* = 6.6 Hz, three C-methyls), 1.24 (m, 21H), 2.5 (m, 2H, CH_2CO), 4.14 (dd, *J* = 8.8 and 3.3 Hz, H-C.6); ^{13}C nmr: Table 1; ms *m/z*: 324(1, M^+), 240(3), 226(3), 156(22), 127(100), 99(58), and 98(24). Exact Mass calcd. for $C_{21}H_{40}O_2$: 324.3028; found: 324.3156.

Reduction of lactone ***10***b *to diol* ***17***a

To lactone ***10****b* (788 mg) in dry ether (40 mL) was added excess $LiAlH_4$ and the mixture was stirred overnight. After the cautious addition of a few drops of aqueous H_2SO_4, brine was added and the diol obtained by ether extraction. On standing, the *3,7-dimethyl-1,6-nonadecanediol* ***17****a* crystallized as a waxy solid (670 mg; 84%), mp 48°C; $[\alpha]_D^{20}$ −7.57 (*c* 9.345, $CHCl_3$); ir: 3340 cm^{-1}; ^1H nmr δ: 0.87 (m, 9H, C-methyls), 3.45 (m, H-C.6), and 3.67 (m, 2H, CH_2OH); ^{13}C nmr: Table 1; ms *m/z*: M^+, 240(0.6), 227(4), 226(3), 131(100), 113(87), and 95(80).

Dibromo alkane ***17***b *and reduction to alkane* ***5***b

Triphenylphosphine (362 mg; 1.38 mmol) was dissolved in CH_2Cl_2 (10 mL) and bromine was added dropwise until the yellowish color persisted. The diol ***17****a* (226 mg; 0.69 mmol) in CH_2Cl_2 (1 mL) was introduced and, after stirring at room temperature for 8 h, a few drops of MeOH were added and the solvent evaporated. Lixiviation with hexane (three times) afforded a solution that was chromatographed. Petroleum ether eluted the dibromide ***17****b* (231 mg; 74%), *1,6-dibromo-3,7-dimethylnonadecane*; $[\alpha]_D^{20}$ 3.30 (*c* 6.215, $CDCl_3$); ir: 2945, 1457, 1375, 1255, 1235, and 1205 (CH_2-Br) cm^{-1}; ^1H nmr δ: 0.8–1.03 (m, 9H, C-methyls), 3.43 (m, 2H, CH_2Br), and 4.00 (m, 1H, CH-Br); ^{13}C nmr: Table 1; ms *m/z*: no M^+, 375(9) and 373(9.9, M−Br), 163(4.5), 155(4.8), and 141(5.5).

The dibromide ***17****b* (151 mg) was refluxed with an excess of $LiAlH_4$ in dry THF (15 mL) for 2.5 h. After cooling, excess hydride was destroyed with aqueous 5% H_2SO_4. Ether was added and the organic phase washed with brine, dried, and concentrated and the crude product was chromatographed. Elution with hexane afforded the *3,7-dimethylnonadecane* ***5****b* (65.7 mg; 67%); $[\alpha]_D^{20}$ 3.76 (*c* 3.285, hexane); ir: 2880–2840, 1455, and 1372 cm^{-1}; ^1H nmr δ: 0.85 (t and d, 12H, *J* = 5.8 Hz, C-methyls), 1.25 (br s, 32H); ^{13}C nmr: Table 1; ms *m/z*: 296(4.8, M^+), 267(5), 239(4), 197(9), 196(13), and 141(5). Exact Mass calcd. for $C_{21}H_{44}$: 296.3443; found: 296.3337.

Alternate route from lactone ***10***b *to alkane* ***5***b

Methanolysis of lactone **10**b *to ester* **11**b. In the manner described previously, the lactone ***10****b* (623 mg) in MeOH (20 mL) containing H_2SO_4 (1 drop) was stirred at room temperature for 12 h. Neutralization and extraction afforded ester ***11****b* (670 mg; 98%) as a colorless oil; $[\alpha]_D^{23}$ −10.3 (*c* 4.75, $CHCl_3$); ir: 3400(br) and 1740 cm^{-1}; ^1H nmr δ: 0.83 (d, *J* = 6.3 Hz, Me-C.3), 0.85 (t, *J* = 7.7 Hz, Me-terminal), 0.93 (d, *J* = 6.6 Hz, Me-C.7), 2.11 (dd, *J* = 14.5 and 8.1 Hz, H-C.2), 2.31 (dd, *J* = 14.5 and 5.9 Hz, H-C.2), 3.64 (s, Me-O): ^{13}C nmr: Table 1; ms *m/z*: no M^+, 325(1), 159(57), and 127(100). Exact Mass calcd. for $C_{22}H_{44}O_3$: 356.3290; found: 356.3265.

Alcohol ***12***b *via the tosylate*. Hydroxy ester ***11****b* (668 mg) was stirred with tosyl chloride in pyridine (6 mL) at 0°C for 48 h. The crude tosylate (934 mg) obtained by extraction (see above) was taken up in ether (25 mL) and reduced at room temperature with $LiAlH_4$ (150 mg). Extraction and chromatography afforded the primary alcohol ***12****b* (503 mg; 88%); $[\alpha]_D^{20}$ 2.7 (*c* 3.07, $CHCl_3$); ir: 3400 cm^{-1}; ^1H nmr δ: 0.81 (d, 6H, *J* = 6.2 Hz) and 0.88 (d, 3H, *J* = 5.1 Hz, three C-methyls), 3.64 (dt, *J* = 4.2 and 1.8 Hz, CH_2OH); ^{13}C nmr: Table 1; ms *m/z*: no M^+, 294(M−18). Exact Mass calcd. for $C_{21}H_{44}O$: 312.3392; found: 312.3403.

Alkane ***5***b *via tosylate*. Alcohol ***12****b* (117 mg) and tosyl chloride (185 mg) were stirred in the dark in pyridine (7.0 mL) for 48 h. Extraction (as described above) afforded the crude tosylate (145 mg; 83%); ^1H nmr δ: 0.78 −0.89 (m, 9H, three Me-C), 2.44 (s, 3H, Me-Ar), 4.06 (t, *J* = 6.2 Hz, CH_2-OR), 7.33 and 7.79 (2d, *J* = 8.0 Hz, arom-H).

The tosylate (141 mg) was reduced with $LiAlH_4$ (23 mg) in ether (25 mL) at room temperature. To be sure of its purity, the crude product was chromatographed three times over silica gel (pet. ether), affording alkane ***5****b* (56 mg; 63%); colorless oil; $[\alpha]_D^{20}$ 3.76 (*c* 3.28, hexane). The other spectral properties were identical with the product from the route described above.

Acknowledgments

We thank the Natural Sciences and Engineering Research Council of Canada and the Ministère de l'éducation du Québec (F.C.A.R.) for operating grants. We are indebted to Professor Jeremy N. McNeil, Département de biologie, Université Laval, for his continued interest and financial help (graduate bursary, D.M.).

1. D. E. Miller and G. L. Jensen. J. Econ. Entomol. **63**, 1337 (1970).
2. Y. Carriere and J. N. McNeil. J. Insect Behav. **1**, 29 (1988)
3. Y. Carriere, J. Millar, J. N. McNeil, and D. J. Miller. J. Chem. Ecol. **14**, 947 (1988).
4. K. Mori, S. Kuwahara, and H. Ueda. Tetrahedron, **39**, 2439 (1983).
5. K. Mori, S. Masuda, and T. Suguro. Tetrahedron, **37**, 1329 (1981).
6. K. Mori and S. Kuwahara. Tetrahedron, **38**, 521 (1982).
7. C. G. Overberger and H. Kaye. J. Am. Chem. Soc. **89**, 5640 (1967).
8. S. Chattopadhay, V. R. Mamdapur, and M. S. Chadha. Synth. Commun. **20**, 825 (1990).
9. H. E. Ensley and R. V. C. Carr. Tetrahedron Lett. 513 (1977).
10. A. J. Meskens. Synthesis, 501 (1981).
11. T. Tsunoda, M. Suzuki, and R. Noyori. Tetrahedron Lett. **21**, 1357 (1980).
12. J. K. Whitesell, R. S. Matthews, and A. M. Helbing. J. Org. Chem. **43**, 785 (1978).
13. A. G. Anderson, Jr. and F. J. Freenor. J. Org. Chem. **37**, 626 (1972).
14. J. H. Brewster. J. Am. Chem. Soc. **81**, 5475 (1959).

Can. J. Chem. Downloaded from www.nrcresearchpress.com by 198.100.157.202 on 09/07/12
For personal use only.

Synthèse et études structurales de nouveaux complexes polyhydroxamiques du fer(III) potentiellement utilisables en imagerie par résonance magnétique nucléaire. I : Obtention des ligands

FRÉDÉRIC CHAUBET,[1] MARGUERITE NGUYEN VAN DUONG, JACQUES COURTIEU ET ALAIN GAUDEMER[1]

Institue de chimie moléculaire d'Orsay, Unité de recherche associée au Centre national de la recherche scientifique, n° 1384, Université de Paris Sud, 91405 Orsay, France

AURORE GREF

Institut de chimie moléculaire d'Orsay, Unité de recherche associée au Centre national de la recherche scientifique, n° 255, Université de Paris Sud, 91405 Orsay, France

ET

A. L. CRUMBLISS

Paul M. Gross Laboratory, Department of Chemistry, Duke University, Durham, NC 27706, U.S.A.

Reçu le 19 juin 1990[2]

FRÉDÉRIC CHAUBET, NGUYEN VAN DUONG, JACQUES COURTIEU, ALAIN GAUDEMER, AURORE GREF et A. L. CRUMBLISS. Can. J. Chem. **69**, 1107 (1991).

Dans le but d'obtenir des complexes stables du fer(III) utilisables comme agents de contraste en imagerie de résonance magnétique, nous avons synthétisé une série de dihydroxamates analogues d'un sidérophore naturel : l'acide rhodotorulique. Ces nouveaux ligands sont obtenus par condensation du dichlorure de l'acide pyridine-2,6-dicarboxylique avec la *N*-aminopropyl-*N*-acétylhydroxylamine protégée et en introduisant en position 4 différents substituants : O-C_2H_5, O-nC_5H_{11}, O-nC_3H_6CN, O-$nC_4H_8NH_2 \cdot HCl$. Cinq ligands **18***a–e* ont ainsi été préparés.

Mots clés : imagerie médicale, agents de contraste, acide rhodotorulique, synthèse d'analogues.

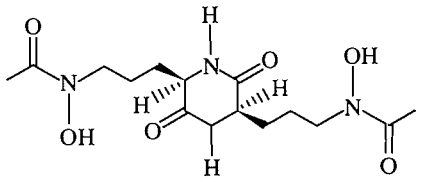
FRÉDÉRIC CHAUBET, NGUYEN VAN DUONG, JACQUES COURTIEU, ALAIN GAUDEMER, AURORE GREF, and A. L. CRUMBLISS. Can. J. Chem. **69**, 1107 (1991).

With a view to preparing stable iron(III) complexes that can be used as contrast agents in magnetic resonance imaging, we have prepared a series of dihydroxamates that are analogs of rhodotorulic acid, a natural siderophore. These new ligands have been synthesized by condensation of 2,6-pyridine dicarboxylic acid chloride with protected *N*-aminopropyl-*N*-acetylhydroxylamine. In addition to the ligand derived from 2,6-pyridine dicarboxylic acid, four other ligands have thus been prepared, having substituents O-C_2H_5, O-nC_5H_{11}, O-nC_3H_6CN, O-$nC_4H_8NH_2 \cdot HCl$. respectively, in the 4 position.

Key words: medical imaging, contrast agents, rhodotorulic acid, synthesis of analogs.

Introduction

Au-delà des progrès technologiques, l'utilisation de l'imagerie par résonance magnétique (IRM) pour le diagnostic médical a rapidement nécessité l'emploi de substances chimiques nouvelles permettant d'augmenter le contraste des images. Parmi celles-ci, les complexes d'ions métalliques paramagnétiques font l'objet à l'heure actuelle des études les plus nombreuses. Le problème principal consistant à protéger l'organisme de la toxicité de ces ions, nous avons porté notre choix sur les ligands spécifiques du fer(III) : les sidérophores. Les sidérophores sont des chélatants spécifiques du fer(III) de faible poids moléculaire et qui forment avec cet ion des complexes extrèmement stables (1). À l'état naturel, ces composés sont le plus souvent isolés de cultures de bactéries pour lesquelles ils assurent la séquestration et le transport du fer essentiel à leur croissance (2). lls appartiennent à deux grandes famille : les acides polyhydroxamiques et les polycatéchols. En plus d'une très grande spécificité, ces composés donnent avec l'ion ferrique des complexes ayant des constantes de stabilité thermodynamique souvent supérieures à 10^{25} M^{-1} (3, 4). La complexation est assurée essentiellement par des groupements hydroxamates ou catécholates. Depuis une quinzaine d'années, les sidérophores, du fait de leur assez faible toxicité, de la puissance et de la spécificité de complexation de l'ion ferrique, ont été employés en médecine pour traiter les empoisonnements par le fer (5, 6). Plus récemment, pour ces mêmes raisons, les complexes formés par ces composés avec le fer(III) ont été envisagés comme agents de contraste potentiels pour l'IRM (7). Dans cette optique, nous nous sommes intéressés aux acides polyhydroxamiques et plus particulièrement à l'acide rhodotorulique **I**, un dihydroxamate naturel produit par *Rhodotorula pilimanae* et formant avec l'ion ferrique un complexe binucléaire de formule générale Fe_2L_3 entre pH 2 et pH 12, domaine où il présente une constante de stabilité thermodynamique de $10^{62,2}$ (8, 9).



I

Notre objectif a été de synthètiser de nouveaux dihydroxamates susceptibles de se comporter vis-à-vis du fer comme l'acide rhodotorulique et pouvant se prêter à des variations structurales susceptibles d'en modifier les propriétés biologiques, en particulier leur biodistribution. Les voies de synthèses décrites pour l'acide rhodotorulique étant longues et ne permettant pas aisément l'introduction de modifications structurales (10–12), nous nous sommes engagés dans la synthèse d'analogues structuraux de ce composé d'accès un peu plus faciles par des voies de synthèse aptes à permettre

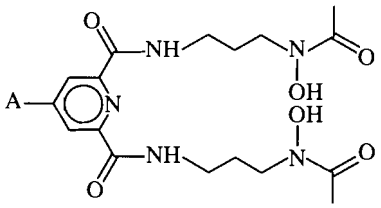
1. Auteurs à qui adresser toute correspondance.
2. Revision recue le 12 février 1991.

Printed in Canada / Imprimé au Canada

Can. J. Chem. Downloaded from www.nrcresearchpress.com by 198.100.157.202 on 09/07/12
For personal use only.

Can. J. Chem. Downloaded from www.nrcresearchpress.com by 198.100.157.202 on 09/07/12
For personal use only.

l'introduction de substituants variés indépendants des sites de complexation et ne perturbant pas cette dernière. À la lumière des travaux de Miller et coll. (13, 14), nous avons entrepris de synthétiser un modèle de sidérophore ayant pour unité centrale le noyau pyridinique et portant, en plus de deux fonctions hydroxamiques en positions α et α′, un substituant en position 4. Nous avons ainsi synthétisé les produits suivants II:



II

avec A = H, O-nC$_5$H$_{11}$, OC$_2$H$_5$, OC$_3$H$_6$CN, O-nC$_4$H$_8$NH$_2$·HCl. Ces composés forment une famille de ligands dihydroxamates tétradentés, aux propriétés chélatantes sans doute identiques mais dont on peut penser que les propriétés physiologiques dépendront de la nature du substituant A. La description de cette synthèse fait l'objet du présent article.

Partie expérimentale

1. Matériels et méthodes

Les spectres de RMN ^{1}H ont été enregistrés à 200 ou 250 MHz sur un appareil Bruker AM 200 ou AM 250. Les spectres de RMN ^{13}C ont été enregistrés à 50 MHz sur un appareil Bruker AM 200. Les déplacements chimiques δ sont exprimés en ppm par rapport au signal de résonance de tétraméthylsilane pris comme référence interne. Les abréviations utilisées sont les suivantes : s = singulet; d = doublet; d×d = doublet dédoublé; t = triplet; q^{dt} = quadruplet; q^{pt} = quintuplet; m = multiplet; J = constante de couplage en Hz. Les spectres infra-rouge ont été mesurés sur un appareil Beckman Acculab 10, en pastille de KBr ou entre deux lames de NaCl (film liquide). Les spectres de masse ont été enregistrés sur un appareils Ribermag R-10-10 par ionisation chimique (I.C.). Les valeurs données entre parenthèses représentent le pourcentage relatif des fragments. Les microanalyses ont été réalisées au Service Central de Microanalyse du CNRS (Gif-sur-Yvette et Vernaison). Les points de fusion ont été mesurés sur un banc Kofler étalonné ou au microscope à platine chauffante Reichert. Les chromatographies sur colonnes ont été effectuées avec de la silice Kieselgel 60 (70–230 mesh, Merck réf. : 7734, et 230–400 mesh, Merck réf. : 9385) et la chromatographie sur couche mince, sur gel de silice Kieselgel 60F254 (Merck réf. : 5735).

*3-(*tert*-Butoxycarbonylamino)-1-propanol* **2**

À une solution de 0,1 mol de 3-amino-1-propanol dans 150 mL d'un mélange dioxanne–eau (2 : 1) refroidie dans un bain de glace, on ajoute en une fois, sous agitation, 0,11 mol (24 g) de ditertiobutyldicarbonate. On complète le mélange réactionnel avec 50 mL de NaOH 1 N et on laisse la solution sous agitation à 5°C une nuit. Le dioxanne est évaporé et le produit de réaction est extrait par l'acétate d'éthyle. La phase organique est lavée successivement avec une solution de citrate 0,5 M, de l'eau, une solution de $NaHCO_3$ 5% et finalement avec une solution de NaCl concentré. Elle est ensuite séchée sur sulfate de sodium et le solvant est évaporé. Le produit **2** est obtenu avec un rendement de 92% et ne nécessite pas de purification ultérieure. IR (NaCl film), ν : 3300 (N-H,O-H); 1670 (C=O) cm^{-1}. RMN ^{1}H ($CDCl_3$) : 1,39 (s, 9H); 1,63 (q^{pt}, J = 6, 2H); 3,02 (d×d, J = 6, J = 7, 2H); 3,05 (s); 3,6 (t, J = 6, 2H); 4,95 (s, 1H). Spectrométrie de masse par I.C. (NH_3), m/z : 281 (M + H$^+$) (100). Anal. calc. pour $C_8H_{17}NO_3$: C 54,84; H 9,78; N 7,99; trouvé : C 54,94; H 9,72; N 8,18.

*3-(*tert*-Butoxycarbonylamino)-1-propanal* **3**

Une solution de 114,6 mmol de chlorure d'oxalyle dans 275 mL de CH_2Cl_2 anhydre est agitée dans un réacteur maintenu à −65°C. À l'aide d'une ampoule à brome on ajoute goutte à goutte une solution de 229 mmol de DMSO dans 55 mL de CH_2Cl_2 anhydre, en surveillant la température du milieu réactionnel afin qu'elle ne dépasse pas −40°C. Quand l'addition est terminée, on laisse agiter 3 min puis on ajoute en 5 min une solution de 104 mmol du produit **2** dans 104 mL de CH_2Cl_2 anhydre. Après 15 min d'agitation supplémentaires, on ajoute 520 mmol de triéthylamine, puis on retire le bain de refroidissement et on laisse revenir le mélange réactionnel à température ambiante. La solution est lavée avec 250 mL d'eau qui sont réextraits par 150 mL de CH_2Cl_2. Les phases organiques sont rassemblées et lavées avec HCl, 1%; Na_2CO_3, 5%; H_2O; puis NaCl. L'extrait est filtré sur papier Whatman, séché, et évaporé à sec. Le rendement brut est de l'ordre de 95% mais l'aldéhyde étant particulièrement instable nous n'avons pas cherché à le purifier et l'avons identifié par le signal RMN ^{1}H du groupement CHO à 9,87 ppm ($CDCl_3$). Il est immédiatement utilisé pour la réaction suivante.

*3-(*tert*-Butoxycarbonylamino)propanol-O-benzyloxime* **4**

Dans un mélange méthanol–eau (2 : 1) sont dissoutes 99,3 mmol de chlorhydrate de *O*-benzylhydroxylamine et cette solution est maintenue à 0°C. À l'aide d'une solution de KOH 6 N, le pH est ajusté à 5. On ajoute alors 90,3 mmol de l'aldéhyde **3** en maintenant le pH à 5. La solution est agitée toute 1 nuit à 5°C puis extraite avec 100 mL d'acétate d'ethyle. La phase organique est lavée successivement avec 50 mL de citrate 0,5 M (2 fois), 100 mL d'eau, et 100 mL de NaCl. L'extrait organique est séché sur sulfate de sodium et, aprés évaporation, on obtient une huile jaune. Le produit de réaction est purifié par chromatographie sur silice « flash » avec un mélange hexane – acétate d'éthyle (50 : 50) comme éluant. Le produit **4** est obtenu avec un rendement de 82% à partir de l'amino alcool protégé **2**. IR (NaCl film); ν : 3385 (N-H); 1690 (C=O); 1510 (C=C aromatiques) cm^{-1}. RMN ^{1}H ($CDCl_3$) : On identifie les deux isomères *syn* et *anti* de l'oxime dans des proportions respectives de 60% et 40%, confirmées par chromatographie en phase gazeuse (colonne Carbowax 120°C à 220°C, 40 min) : 1,42 (s, 9H); 2,33 (d×d, J = 6, 1,2H, isomère *syn*); 2,52 (d×d, J = 6, 0,8H, isomère *anti*); 3,26 (m, 2H); 4,82 (s, 1H); 5,03 (s, 1,2H, isomère *syn*); 5,08 (s, 0,8H, isomère *anti*); 6,72 (t, J = 5,5, 0,4H, isomère *anti*); 7,32 (m, 5H); 7,42 (t, J = 5,5, 0,6H, isomère *syn*). Anal. calc. pour $C_{15}H_{22}N_2O_3$: C 64,73; H 7,97; N 10,06; O 17,24; trouvé : C 64,41; H 8,06; N 10,32; O 17,33.

*1-(*tert*-Butoxycarbonylamino)-3-(benzyloxyamino)propane* **5**

Dans 50 mL d'acide acétique glacial sont dissoutes 29,1 mmol de l'oxime **4** et traitées avec 30,5 mmol de cyanoborohydrure de sodium ajoutées par petites portions, sous agitation à 10°C, et sous argon. Aprés 16 h d'agitation on ajoute 50 mL d'acétate d'éthyle. L'acide acétique est éliminé par évaporation et les traces d'acide sont neutralisées par une solution à 20% de KOH. La phase organique est lavée successivement par H_2O (2 fois), NaCl (1 fois) et séchée sur Na_2SO_4. Le solvant est évaporé et le produit brut est chromatographié sur silice flash avec le mélange hexane – acétate d'éthyle (2 : 1) comme éluant. On obtient une huile incolore avec un rendement de 70%. IR (NaCl film), ν : 3350 (N-H); 1690 (C=O); 1500 (C=C aromatiques) cm^{-1}. RMN ^{1}H ($CDCl_3$) : 1,4 (s, 9H, CH_3 du groupement *tert*-butyl); 1,68 (q^{pt}, J = 6,51, 2H); 2,96 (t, J = 6,5, 2H); 3,16 (d×d, J = 5,7, J = 6,5, 2H); 4,70 (s, 2H, H benzyliques); 4,82 (s, 1H, NH); 5,15 (massif); 7,33 (m, 5H, H aromatiques). Spectrométrie de masse par I.C. (NH_3), m/z : 281 (M+H$^+$)(100). Anal. calc. pour $C_{15}H_{24}N_2O_3$: C 64,26; H 8,63; N 9,99; O 17,12; trouvé : C 64,04; H 8,52; N 9,78; O 17,31.

*1-(*tert*-Butoxycarbonylamino)-3-(acétylbenzyloxyamino)-propane* **6**

Deux millimoles (2 mmol) de l'hydroxylamine *O*-benzylée **5** sont agitées dans un excès d'anhydride acétique à température ambiante pendant 3 h. On ajoute alors 20 mL d'acétate d'éthyle et on lave le mélange réactionnel avec KOH 5% plusieurs fois, puis avec NaCl jusqu'à ce que le pH soit neutre. L'extrait organique est séché sur Na_2SO_4 et évaporé. Le résidu huileux obtenu est chromatographié sur silice flash avec le mélange hexane – acétate d'éthyle (50 : 50) comme éluant. On obtient le produit **6** sous forme d'une huile incolore

Can. J. Chem. Downloaded from www.nrcresearchpress.com by 198.100.157.202 on 09/07/12
For personal use only.

avec un rendement de 73%. IR (NaCl film), ν : 3350 (N-H); 1700 (C=O de CONH); 1650 (C=O acétyl); 1500 (C=C aromatiques) cm^{-1}. RMN ^1H ($CDCl_3$) : 1,41 (s, 9H, CH_3 du groupement *tert*-butyl); 1,75 (q^{pt}, J = 6,5, 2H); 2,09 (s, 3H); 3,07 (d×d, J = 6,5, 2H); 3,68 (t, J = 6,5, 2H); 4,80 (s, 2H, H); 5,05 (massif); 7,36 (m, 5H). Spectrométrie de masse par I.C. (NH_3), m/z : 323 ($M+H^+$)(96), 267 [($M-Me_3C$)+H^+](100). Anal. calc. pour $C_{17}H_{26}N_2O_4$: C 63,33; H 8,19; N 8,69; O 19,85; trouvé : C 63,09; H 8,02; N 8,95; O 20,05.

Trifluoroacétate de 1-amino-3-(acétylbenzyloxyamino)propane **7**a

Dans un ballon, refroidi dans un bain de glace, on place 3 mmol du produit **6**, sous agitation et sous argon et, à l'aide d'une ampoule à brome, on ajoute 20 mmol d'acide trifluoroacétique, en 5 min. L'agitation est poursuivie à température ambiante pendant 1 demi-heure puis on ajoute à cette solution 50 mL d'éther anhydre. Le trifluoroacétate précipite. La suspension est maintenue à 5°C pendant 1 nuit, filtrée sur Büchner, et rincée à l'éther anhydre plusieurs fois pour éliminer le TFA excédentaire. Le produit est séché au dessiccateur chauffant à 60°C. On obtient le produit **7***a* sous forme d'une fine poudre blanche avec un rendement de 88%. *F* : 110–111°C. IR (KBr), ν : 3100 (N-H, O-H); 1710 (C=O de TFA); 1635 (C=O acétohydroxamique); 1450 (C=C aromatiques); 1200 (C-F) cm^{-1}. RMN ^1H (CD_3OD) : 1,88 (m, J = 6,5, 2H); 2(s, 1H); 2,84 (d×d, J = 7,6, 2H); 3,72 (t, J = 6,5, 2H); 4,85 (s, 2H); 7,34 (m, 10H). Spectrométrie de masse par I.C. (NH_3) : On analyse l'ion moléculaire M′ correspondant à M′−CF_3COOH, m/z : 223 (M′+H^+)(100), 117[(M−C_6H_5−OH)+H^+]. Anal. calc. pour $C_{13}H_{19}F_3N_2O_4$: C 50,00; H 5,69; N 8,33; F 16,95; trouvé : C 50,12; H 5,66; N 8,36; F 16,87.

Chlorhydrate de 1-amino-3-(acétylbenzyloxyamino)propane 7b

On dissout 3,24 mmol du produit **6** dans 70 mL d'éther à 0°C. Dans cette solution on fait barboter HCl gazeux (préalablement séché par H_2SO_4 pur) et aprés 1 demi-heure il se forme un précipité blanc floconneux. Le ballon est laissé au froid pendant 1 nuit, puis on filtre les cristaux blancs formés qui sont dissous dans le minimum de méthanol anhydre et précipités à nouveau par l'éther. Le produit est filtré sur Büchner et séché 24 h dans un dessiccateur à KOH pour conduire au chlorhydrate **7***b* pur avec un rendement de 22%. *F* : 69–74°C (litt. (14) *F* : 69–72°C. IR (KBr), ν : 3500 (N-H); 1630 (C=O acétohydroxamique); 1420–1470 (C=C aromatiques) cm^{-1}. RMN ^1H (D_2O) : 1,97 (q^{pt}, J = 6, 2H); 2,08 (s, 3H); 2,97 (t, J = 6, 2H); 3,81 (t, J = 6, 2H); 4,95 (s, 2H); 7,47 (m, 5H). Spectrométrie de masse par I.C. (NH_3) : On analyse l'ion moléculaire M′ =M−HCl, m/z : 223 (M′+H^+)(100). Anal. calc. pour $C_{12}H_{19}N_2O_2Cl{\cdot}1{,}9\ H_2O$: C 49,26; H 7,85; N 9,57; O 21,33; trouvé : C 49,26; H 7,64; N 9,61; O 21,01.

Dichlorhydrate de 1-amino-3-(benzyloxyamino)propane 7c

On évapore le premier filtrat de l'expérience précédente (**7***b*) et le solide jaunâtre obtenu est redissous dans le minimum de méthanol. Par addition d'éther on précipite un produit blanc floconneux. On laisse cette suspension à 5°C pendant 1 nuit. Le produit est filtré sur Büchner et sèché au dessiccateur à KOH. On obtient le dichlorhydrate **7***c* avec un rendement de 47%. *F* : 158°C. IR (KBr), ν : 3400 (N-H); 1410–1460 (C=C aromatiques) cm^{-1}. RMN ^1H (D_2O) : 2,11 (q^{pt}, J = 6, 2H); 3,08 (t, J = 6, 2H); 3,43 (t, J = 6, 2H); 5,11 (s, 2H); 7,48 (m, 5H). Spectrométrie de masse par I.C. (NH_3) : On analyse l'ion moléculaire M′ =M−2HCl, m/z : 181 (M′+H^+)(100), 107(C_6H_5C=OH^+). Anal. calc. pour $C_{10}H_{17}N_2OCl_2$: C 47,44; H 7,17; N 11,06; O 6,32; Cl 28,01; trouvé : C 47,68; H 7,24; N 10,86; O 6,29; Cl 27,82.

Dichlorure de l'acide-4-hydroxy-2,6-pyridinedicarboxylique **10**

Dans un ballon de 125 mL à deux tubulures on place 10,9 mmol d'acide 4-hydroxy-2,6-pyridine dicarboxylique (acide chélidamique). À l'aide d'une ampoule à brome munie d'une garde à potasse, on ajoute 43,6 mmol de dichlorophénylphosphine. Le mélange réactionnel est agité à 130°C pendant 3 h, sous argon. On observe un fort dégagement de HCl. On laisse alors revenir la température à 50°C (le mélange se solidifie) et on procède à une extraction du milieu par l'hexane bouillant (2×50 mL). Les extraits sont rassemblés, refroidis, et laissés 1 nuit à 5°C. Il se forme de minuscules cristaux. Après recristallisation dans l'hexane, ces cristaux sont filtrés, séchés, et sublimés sous vide pour conduire au produit **10** sous forme de paillettes cristallines blanches, avec un rendement de 57%. *F* : 96–98°C (litt. (26) *F* : 94–96°C). IR (KBr), ν : 1720–1750 (C=O); 1560 (C=C et C-N pyridinique) cm^{-1}. RMN ^1H (DMSO-d_6) : 8,3 (s). RMN ^{13}C (DMSO-d_6) (découplage large bande) : 168,5; 147,8; 128,9; 149,9. Spectre de masse par I.C. (NH_3), m/z : 255 ($M+NH_4^+$) (100), 238 ($M+H^+$)(45,8). Anal. calc. pour $C_7H_2Cl_3O_2$: C 35,26; H 0,85; N 5,87; O 13,42; trouvé : C 35,72; H 0,83; N 5,89; O 13,62.

4-Chloro-2,6-pyridinedicarboxylate d'éthyle **11**a

Dans 15 mL de dichlorométhane anhydre sont dissoutes 2 mmol du chlorure d'acide **10**. On ajoute 2 mL d'éthanol anhydre et la solution obtenue est chauffée à reflux sous agitation et sous atmosphère d'argon. Au bout de 2 h le solvant est évaporé et le résidu solide est recristallisé dans l'heptane pour conduire, après filtration sur Büchner, au produit **11***a* avec un rendement de 52%. *F* : 92–94°C. IR (KBr), ν : 2960–3060 (C-H alkyle); 1700 (C=O ester); 1555 (C=C et C-N pyridiniques) cm^{-1}. RMN ^1H ($CDCl_3$) : 1,4 (t, J = 6,9, 6H); 4,44 (q^{dt}, J = 6,9, 4H); 8,22 (s, 2H). Spectrométrie de masse par I.C. (NH_3), m/z : 258 ($M+H^+$)(100), 275 ($M+NH_4^+$)(24). Anal. calc. pour $C_{11}H_{12}ClNO_4$: C 51,27; H 4,69; N 5,44; Cl 13,76; trouvé : C 51,30; H 4,80; N 5,29; Cl 12,99.

4-Éthoxy-2,6-pyridinedicarboxylate d'éthyle **12**

Dans 5 mL de THF anhydre sont dispersées 11,7 mmol de NaH 60%. On y ajoute 1 mL d'éthanol anhydre, et la solution est agitée, sous argon, pendant 1 h à température ambiante. On ajoute alors 7,76 mmol du composé **11***a* dissous dans 10 mL de THF anhydre, et quelques milligrammes d'éther couronne (18-c-6). La solution est chauffée à reflux pendant 1 h, puis les solvants sont évaporés et le résidu final est repris dans 15 mL d'acétate d'éthyle. Après lavage avec NaCl 5% (2×10 mL), et séchage sur sulfate de sodium, l'extrait est évaporé. Une recristallisation du résidu dans l'heptane conduit au produit **12** sous forme de paillettes blanches avec un rendement de 70%. *F* : 87–88°C. IR (KBr), ν : 1700–1730 (C=O); 1580 (C=C et C-N pyridiniques) cm^{-1}. RMN ^1H ($CDCl_3$) : 1,43 (t, J = 6,9, 6H); 1,47 (t, J = 6,9, 3H); 4,19 (q^{dt}, J = 6,9, 2H); 4,45 (q^{dt}, J = 6,9, 4H); 7,73 (s, 2H). Spectrométrie de masse par I.C. (NH_3), m/z : 268 ($M+H^+$)(100), 195 [($M-COOCH_2CH_3$)+H^+](15).

Acide 4-pentoxy-2,6-pyridinedicarboxylique **13***a*

Préparation du pentanolate de sodium : 220 mg de NaH 60% sont dispersés dans 10 mL de pentane à 0°C. À l'aide d'une ampoule à brome on ajoute, goutte à goutte, 0,7 mL de 1-pentanol dans 5 mL de pentane. Après addition on laisse agiter pendant 1 demi-heure à température ambiante, puis le solvant est évaporé. Le résidu blanc obtenu est ensuite repris par 10 mL de benzène anhydre.

Préparation du produit **13***a*: 10 mmol de 1-pentanol sont ajoutées à une solution de 5 mmol du chlorure d'acide **10** dans 15 mL de dichlorométhane anhydre. Le mélange réactionnel est porté à reflux pendant 1 h. Il se produit un dégagement de HCl. Après évaporation du solvant, le résidu repris dans 15 mL de benzène anhydre est additionné à une solution de pentanolate de sodium (1,1 équivalent) dans 10 mL de benzène anhydre. On ajoute quelques milligrammes d'éther couronne (15-c-5) et on laisse la solution sous agitation et sous argon 1 nuit à température ambiante. Le benzène est alors évaporé et on ajoute au résidu huileux 25 mL d'une solution de KOH 0,4 M. La solution est portée à reflux pendant 2 h sous agitation vive. Après refroidissement et neutralisation, une extraction à l'éther (10 mL) permet d'éliminer le 1-pentanol excédentaire. Un solide blanc précipite par addition de HCl concentré à la solution. Le précipité est filtré sur Büchner, rincé avec H_2O glacée plusieurs fois et recristallisé dans l'éthanol. Le reflux au Dean–Stark dans le benzène permet d'éliminer toutes traces d'eau. Le produit **13***a*, lavé à l'éther anhydre et séché au dessiccateur sous vide, est obtenu pur avec un rendement de 75,7% sous forme d'une poudre pulvérulente de couleur crème. *F* : 154–155°C. RMN ^1H (CD_3OD) : 0,85 (t, J = 6,9, 3H); 1,36 (m, 4H); 1,78 (q^{pt}, J = 6,8, 2H); 4,2(t, J = 6,8, 2H); 7,69(s, 2H). Spectrométrie de masse par I.C. (NH_3), m/z : 254 ($M+H^+$)(11),

Can. J. Chem. Downloaded from www.nrcresearchpress.com by 198.100.157.202 on 09/07/12
For personal use only.

210 [(M−CO_2)+H^+](100). Anal. calc. pour $C_{12}H_{15}NO_5$: C 56,90; H 5,97; N 5,53; O 31,59; trouvé : C 56,98; H 5,55; N 5,55; O 31,91.

Acide 4-éthoxy-2,6-pyridinedicarboxylique ***13b***

La synthèse de ce produit est identique à celle du produit **13*a***. L'éthanol est utilisé à la place du pentanol. Le produit **13*b*** est recristallisé dans l'éthanol, sèché par le benzène à reflux pour être obtenu pur sous forme d'une poudre blanche pulvérulente avec un rendement de 72%. *F* : 186–188°C. IR (KBr), ν : 3250 (OH acide); 1730 (C=O acide); 1600 (C=C et C-N pyridiniques) cm^{-1}. RMN ^1H (DMSO-d_6) : 1,33 (t, *J* = 6,7, 3H); 4,25 (q^{pt}, *J* = 6,7, 2H); 7,63(s, 2H); 13(s large, 2H). Spectrométrie de masse par I.C. (NH_3), *m*/*z* : 229 (M+NH_4^+)(10), 212 (M+H^+)(100), 168 [(M−CO_2)+H^+] (14). Anal. calc. pour $C_9H_9NO_5$: C 51,19; H 4,29; N 6,63; O 37,88; trouvé : C 51,03; H 4,55; N 6,44; O 38,08.

Dichlorure de l'acide 4-pentoxy-2,6-pyridinedicarboxylique ***14a***

Dans 10 mL de $SOCl_2$ sont dispersées 4,45 mmol du diacide **13*a*** avec quelques gouttes de DMF comme catalyseur. La solution est portée à reflux pendant 3 h, puis l'excès de $SOCl_2$ est éliminé à l'évaporateur rotatif. Les dernières traces de $SOCl_2$ sont entrainées par plusieurs évaporations successives de benzène anhydre ajouté au résidu. On obtient le produit **14*a*** après recristallisation dans l'heptane, avec un rendement de 80%. IR (KBr), ν : 1750 (C=O); 1590 (C=C et C-N pyridiniques) cm^{-1}. RMN ^1H (CD_2Cl_2) : 0,95 (t, 3H, *J* = 6,9); 1,38 (m, 4H); 1,86 (q^{pt}, *J* = 6,8); 4,18 (t, *J* = 6,6); 7,81 (s, 2H). Anal. calc. pour $C_{12}H_{13}NO_3Cl_2$: C 49,67; H 4,51; N 4,55; trouvé : C 49,59; H 4,71; N 4,83.

Dichlorure de l'acide 4-éthoxy-2,6-pyridinedicarboxylique ***14b***

Dans 10 mL de $SOCl_2$ sont dispersées 3,35 mmol du diacide **13*b*** avec quelques gouttes de DMF comme catalyseur. La solution est portée à reflux pendant 3 h, puis l'excès de $SOCl_2$ est éliminé à l'évaporateur rotatif. Les dernières traces de $SOCl_2$ sont entrainés par plusieurs évaporations successives de benzène anhydre ajouté au résidu. Le résidu est recristallisé dans l'hexane pour conduire au produit **14*b*** avec un rendement de 85%. *F* : 76–77°C (litt. (36) *F* : 76–78°C). IR (KBr), ν : 1750 (C=O); 1590 (C=C et C-N pyridiniques) cm^{-1}. RMN ^1H ($CDCl_3$) : 1,52 (t, *J* = 6,9, 3H); 4,26 (q^{dt}, *J* = 6,9, 2H); 7,79 (s, 2H). Spectrométrie de masse par I.C. (NH_3), *m*/*z* : 249 (M+H^+). Anal. calc. pour $C_9H_7Cl_2NO_3$: C 43,57; H 2,85; N 5,65; trouvé : C 43,78; H 2,96; N 5,52.

Dichlorure de l'acide 4-(3-nitrile-propyloxy)-2,6-pyridinedicarboxylique ***14c***

Dans 30 mL d'une solution 0,3 M de KOH sont dispersées 4,4 mmol de diester **16**. Cette solution est agitée à température ambiante pendant 18 h puis lavée avec 10 mL d'éther. La phase aqueuse est acidifiée avec HCl concentrée jusqu'à précipitation d'un produit blanc. Après 3 h à 5°C, le produit est filtré sur Büchner puis séché pendant 4 h avec un montage de Dean–Stark. Après filtration et plusieurs rinçages faits à l'éther anhydre, le produit est séché sous vide (pour retirer les traces d'éther) et dispersé dans 15 mL de $SOCl_2$ auxquels on ajoute une goutte de DMF. Après 6 h de reflux sous argon le $SOCl_2$ excédentaire est évaporé. Le résidu est repris par le benzène anhydre plusieurs fois et les solutions sont réévaporées afin d'entrainer les dernières traces de $SOCl_2$. La poudre jaune obtenue est recristallisée dans l'heptane pour conduire au chlorure d'acide **14*c***, sous forme de minuscules cristaux blancs, avec un rendement de 55%. *F* : 94°C. IR (KBr), ν : 2220 (C≡N); 1745–1765 (C=O); 1585 (C=C et C-N pyridiniques) cm^{-1}. RMN ^1H ($CDCl_3$) : 2,24 (q^{pt}, 2H, *J* = 6,7); 2,63 (t, 2H, *J* = 6,9); 4,30 (t, 2H, *J* = 5,5); 7,8 (s, 2H). Spectrométrie de masse par I.C. (NH_3), *m*/*z* : 287 (M+H^+)(100), 306 (M+NH_4^+)(16). Anal. calc. pour $C_{11}H_8N_2O_3Cl_2$: C 46,22; H 3,02; N 8,75; trouvé : C 46,02; H 2,81; N 8,76.

4-Hydroxy-2,6-pyridinedicarboxylate ***15***

Dans 180 mL d'éthanol anhydre contenant 2% d'acide sulfurique sont dispersés 100 mmol d'acide chélidamique **9**. La suspension est chauffée à reflux pendant 48 h, puis l'éthanol est évaporé. Le résidu de couleur crème est recristallisé dans 30 mL d'un mélange éthanol–eau (3 : 2). Après 1 nuit à 5°C, le solide blanc obtenu est filtré, dispersé dans le benzène et séché pendant 4 h avec un montage de Dean–Stark. La solution est filtrée à chaud. Le produit **15** cristallise dans la solution placée à 5°C. Après filtration sur Büchner et rinçage à l'hexane puis à l'éther anhydre, le diester **15** est obtenu pur sous forme d'une fine poudre blanche avec un rendement de 45%. *F* : 122–123°C (litt .(23) *F* : 120–121°C). IR (KBr), ν : 3450 (O-H), 1730–1740 (C=O); 1610 (C=C et C-N pyridiniques) cm^{-1}. RMN ^1H ($CDCl_3$) : 1,31 (t, 6H, *J* = 7), 4,33 (q^{dt}, 4H, *J* = 7), 7,56 (s, 2H), 11,5 (s large, 1H). Spectrométrie de masse par I.C. (NH_3), *m*/*z* : 240 (M+H^+)(100), 257 (M+NH_4^+)(3). Anal. calc. pour $C_{11}H_{13}NO_3$: C 55,23 H 5,48; N 5,86; O 33,44; trouvé : C 55,21; H 5,38; N 5,90; O 33,42.

4-(3-Nitrile-propyloxy)-2,6-pyridinedicarboxylate d'éthyle ***16***

Dans 50 mL de toluène anhydre sont ajoutées 26,2 mmol du diester **15** à 1,1 équivalent de NaOH (60%). La suspension est chauffée à 60°C sous argon pendant 3 h. On ajoute alors 28,8 mmol de 4-bromobutyronitrile, 2,5% d'éther couronne (15-C-5) et 130 mL de toluène anhydre. La solution est chauffée à reflux, sous argon, pendant 18 h, refroidie et la suspension obtenue filtrée sur filtre plissé. Le solide résiduel est dispersé dans 50 mL d'eau qui sont extraits par le dichlorométhane (2×50 mL). Les phases organiques sont rassemblées et les solvants évaporées. Le résidu est repris dans 50 mL de dichlorométhane et rincé successivement avec Na_2CO_3 saturée et H_2O. La phase organique est séchée sur papier Whatman. Après évaporation du dichlorométhane, l'huile résiduelle est chromatographiée sur silice flash avec le mélange : dichlorométhane – acétate d'éthyle – méthanol (70 : 30 : 2,5) pour conduire au produit **16** avec un rendement de 60%, sous forme d'une huile incolore qui cristallise lentement. IR (NaCl), ν : 2220 (C≡N; 1710–1740 (C=O); 1590 (C=C et C-N pyridiniques) cm^{-1}. RMN ^1H ($CDCl_3$) : 1,42 (t, *J* = 7,1, 6H); 2,2 (q^{pt}, *J* = 6,3, 2H); 2,6 (t, *J* = 7, 2H); 4,24 (t, *J* = 5,7, 2H); 4,44 (q^{dt}, *J* = 7,1, 4H); 7,75 (s, 2H). Spectrométrie de masse par I.C. (NH_3), *m*/*z* : 307 (M+H)$^+$(100). Anal. calc. pour $C_{15}H_{18}N_2O_5$: C 58,82; H 5,92; N 9,14; O 26,12; trouvé : C 58,71; H 6,14; N 9,27; O 26,13.

Méthode générale de synthèse des acides acétylhydroxamiques protégés ***17a–d*** *à partir des chlorures d'acide*

À une solution du chlorure d'acide dans le dichlorométhane anhydre (0,01–0,015 M) on ajoute 3 équivalents de trifluorocétate de 1-amino-3-(acétylbenzyloxyamino)propane **7*ab*** sous forme solide. La solution agitée est refroidie à 0°C et traitée par 5 équivalents de triéthylamine dans le dichlorométhane anhydre (0, 1–0, 15 M) ajoutés goutte à goutte sous atmosphère d'argon. Quand l'addition est terminée on prolonge l'agitation 1 nuit à 5°C puis 1 h à température ambiante. Le dichlorométhane est partiellement évaporé et la solution résiduelle est lavée successivement avec une solution de citrate 0,5 M, de l'eau, une solution de $NaHCO_3$ 0,5 M et finalement avec une solution concentrée de NaCl. La phase organique est séchée par filtration sur papier Whatman et évaporée. Le résidu est purifié par chromatographie sur silice flash avec un mélange dichlorométhane – acétate d'éthyle – méthanol (70 : 30 : 2,5).

N,N′-*Bis [3-(acétylbenzyloxyamino)propyl]-[4-pentoxy-2,6-pyridine]dicarbamide* ***17a***

Le produit **17*a*** est obtenu pur sous forme d'une huile incolore avec un rendement de 50%. RMN ^1H ($CDCl_3$) : 0,9 (t, *J* = 6,9, 3H); 1,39 (m, 4H); 1,77 (q^{pt}, 4H, *J* = 6,5), 1,92 (q^{pt}, *J* = 6,9, 2H); 2,1 (s, 6H); 3,46 (m, *J* = 6,4, 4H); 3,78 (t, *J* = 6,5); 4,1 (t, *J* = 6,8); 4,81 (s, 4H); 7,34 (m, 10H); 7,75 (s, 2H); 9,17 (t, *J* = 6,4, 2H). Spectrométrie de masse par I.C. (NH_3), *m*/*z* : 663 (M+H^+). Anal. calc. pour $C_{36}H_{47}N_5O_7$: C 65,34; H 7,16; N 10,58; O 16,92; trouvé : C 64,99; H 7,13; N 10,63; O 17,24.

N,N′-*Bis[3-(acétylbenzyloxyamino)propyl]-[4-éthoxy-2,6-pyridine]dicarbamide* ***17b***

Le produit **17*b*** est obtenu pur sous forme d'une huile incolore avec un rendement de 40% à partir du chlorure d'acide **14*b***. IR (NaCl), ν : 3300–3350 (N-H); 1725 (C=O acétohydroxamique); 1690–1710 (C=O amide); 1520 (C-C aromatique); 1035 (N-O) cm^{-1}. RMN ^1H ($CDCl_3$) : 1,46 (t, *J* = 6,8, 3H); 1,76 (q^{pt}, *J* = 6,6, 4H); 2,09 (s, 6H); 3,48(m, *J* = 6,5, 4H); 3,80 (t, *J* = 6,6, 4H); 4.14 (t, *J* = 6,8,

Can. J. Chem. Downloaded from www.nrcresearchpress.com by 198.100.157.202 on 09/07/12
For personal use only.

2H); 4,84 (s, 4H); 7,37 (m, 10H); 7,78 (s, 2H); 9,20 (t, J = 6,5, 2H). Spectrométrie de masse par I.C. (NH_3), m/z : 620 ($M+H^+$). Anal. calc. pour $C_{33}H_{41}N_5O_7$: C 63,96; H 6,67; N 11,30; trouvé : C 63,95; H 6,61; N 10,86.

N,N′-*Bis[3-(acétylbenzyloxyamino)propyl]-[4-(3-(nitrile-propyloxy)-2,6-pyridinedicarbamide* **17**c

Le produit **17***c* est obtenu pur sous forme d'une huile incolore avec un rendement de 30% à partir du chlorure d'acide **14***c*. IR (NaCl), ν : 3300–3330 (N-H); 2220 (C≡N), 1725 (C=O acétohydroxamique); 1640 (C=O amide); 1520 (C-C aromatiques); 1040 (N-O) cm^{-1}. RMN ^1H ($CDCl_3$) : 1,78 (q^{pt}, J = 6,5, 4H); 2,10 (s, 6H); 2,2 (m, J = 6,8, 2H); 2,59 (t, J = 6,9); 3,42 (m, J = 6,5, 4H); 3,75 (t, J = 6,6, 4H); 4,24 (t, J = 6,8, 2H); 4,82 (s, 4H); 7,38 (m, 10H); 7,77 (s, 2H); 9,19 (t, J = 6,5, 2H). Spectrométrie de masse par I.C. (NH_3), m/z : 659 ($M+H^+$). Anal. calc. pour $C_{35}H_{42}N_6O_7$: C 62,82; H 6,43; N 12,76; trouvé : C 62,8; H 6,53; N 12,38.

N,N′-*Bis[3-(acétylbenzyloxyamino)propyl]-2,6-pyridine-dicarbamide* **17**d

Le produit **17***d* est obtenu pur sous forme d'une huile incolore avec un rendement de 42% à partir du dichlorure de l'acide-2, 6-pyridine dicarboxylique commercial. IR (NaCl), ν : 3300–3400 (N-H); 1725 (C=O acétohydroxamique), 1690–1710 (C=O amide); 1515 (C-C aromatiques); 1040 (N-O) cm^{-1}. RMN ^1H ($CDCl_3$) : 1,92 (q^{pt}, J = 6,8, 4H); 2,1 (s, 6H); 3,46 (m, J = 6,4, 4H); 3,78 (t, J = 6,6, 4H); 4,81 (s, 4H); 7,36 (m, 10H); 7,96–8,26 (m, 3H); 9,2 (t, J = 6,5, 2H). Spectrométrie de masse par I.C. (NH_3), m/z : 576 ($M+H^+$). Anal. calc. pour $C_{31}H_{37}N_5O_6$: C 64,68; H 6,48; N 12,16; trouvé : C 64,39; H 6,39; N 11,93.

Méthode générale de synthèse des acides N-*acétylhydroxamiques* **18**a–d

À une solution 0,015 M de ligand protégé, dans le méthanol anhydre, on ajoute 10% en poids de Pd/C 10%. On agite la solution sous 1 atmosphère de H_2(1 atm=101,3 kPa) en suivant la réaction par chromatographie sur couche mince avec le mélange dichlorométhane – acétate d'éthyle – méthanol (70 : 30 : 2,5) comme éluant. Après 4–7 h, on filtre le catalyseur sur tissus de verre et on évapore le solvant. Le résidu est redissous dans le minimum de méthanol et on précipite le produit avec un mélange hexane – acétate d'éthyle (1 : 3). Après 1 nuit à 5°C, le produit est filtré, redissous dans le minimum de méthanol anhydre et précipité avec de l'acétate d'éthyle. Puis il est séché sous vide à température ambiante pendant plusieurs heures.

N,N′-*Bis[3-(acétylhydroxyamino)propyl]-[4-pentoxy-2,6-pyridine]dicarbamide* **18**a

Le produit **18***a* est obtenu pur sous forme d'une poudre jaune pâle avec un rendement de 85%. *F* : 133–135°C. IR (KBr), ν : 3200–3600 (O-H); 2980 (C-H alkyle); 1650–1670 (C-O amide); 1620–1640 (C=O acétohydroxamique); 850 (N-O) cm^{-1}. RMN ^1H (CD_3OD) : 0,84 (t, J = 6,9, 3H); 1,33 (m, 4H); 1,82 (m, 6H); 2,01 (s, 6H), 3,33 (m, J = 6,6, 4H); 3,63 (t, J = 6,6, 4H); 4,08 (t, J = 6,9, 2H); 7,62 (s, 2H). Spectrométrie de masse par I.C. (NH_3), m/z : 482 ($M+H^+$). Anal. calc. pour $C_{22}H_{35}N_5O_7$: C 54,87; H 7,33; N 14,54; trouvé : C 55,46; H 7,37; N 14,44.

N,N′-*Bis[3-(acétylhydroxyamino)propyl]-[4-éthoxy-2,6-pyridine]dicarbamide* **18**b

Le produit **18***b* est obtenu pur sous forme d'une poudre blanche avec un rendement de 75%. *F* : 138–140°C. IR (KBr), ν : 3150–3550 (O-H); 1670 (C=O amide); 1600–1620 (C=O acétohydroxamique); 845 (N-O) cm^{-1}. RMN ^1H (CD_3OD) : 1,35 (t, J = 6,9, 3H); 1,82 (m, 6H); 2,01 (s, 6H); 3,35 (t, J = 6,4, 4H); 3,63 (t J = 6,3, 4H); 4,15 (q^{dl}, J = 7, 2H). Spectrométrie de masse par I.C. (NH_3), m/z : 396 ($M+H^+$)(100). Anal. calc. pour $C_{19}H_{29}N_5O_7$: C 51,75; H 6,50; N 16,25; trouvé : C 51,93; H 6,65; N 15,94.

N,N′-*Bis[3-(acétylhydroxyamino)propyl]-[4-(3-nitrilepropyloxy)-2,6-pyridine]dicarbamide* **18**c

Le produit **18***c* est obtenu pur sous forme d'une poudre blanche avec un rendement de 85%. *F* : 137–139°C. IR (KBr), ν : 3320 (O-H libre); 3080–3160 (O-H lié); 2215 (C≡N); 1650 (C=O amide); 1600-1620 (C=O acétohydroxamique); 870 (N-O) cm^{-1}. RMN ^1H (CD_3OD) : 1,83 (q^{pt}, J = 6,6, 4H); 2,02 (s, 6H); 2,58 (t, J = 7, H_3); 3,36 (t, J = 6,6, 4H); 3,63 (t, J = 6,6, 4H); 4,20 (t, J = 5,8, 2H); 7,67 (s, 2H). Spectrométrie de masse par I.C. (NH_3), m/z : 479 ($M+H^+$). Anal. calc. pour $C_{21}H_{30}N_6O_7$: C 52,71; H 6,32; N 17,56; trouvé : C 53,11; H 6,33; N 17,54.

N,N′-*Bis[3-(acétylhydroxyamino)propyl]-2,6-pyridine-dicarbamide* **18**d

Le produit **18***d* est obtenu pur sous forme d'une poudre jaune pâle avec un rendement de 70%. *F* : 76–80°C. IR (KBr), ν : 3180–3500 (O-H); 2950 (C-H alkyle); 1610 (C=O amide); 1640–1660 (C=O acétohydroxamique); 840 (N-O) cm^{-1}. RMN ^1H (CD_3OD) : 1,82 (q^{pt}, J = 6,6, 4H); 2,00 (s, 6H); 3,36 (t, J = 6,7, 4H); 3,63 (t, J = 6,7, 4H); 7,99–8,15 (m, 3H). Spectrométrie de masse par I.C. (NH_3), m/z : 396 ($M+H^+$). Anal. calc. pour $C_{17}H_{25}N_5O_6$: C 51,64; H 6,37; N 17,71; trouvé : C 51,68; H 6,52; N 17,77.

Préparation du chlorohydrate de N,N′-*Bis[3-(acétylhydroxyamino) propyl]-[4-(4-amino-n-butyloxy)-2,6-pyridine]dicarbamide* **18**e

Dans 150 mL de méthanol anhydre sont dissous 300 mg du ligand protégé **17***c*. On y ajoute 490 mg de Pd/C 10% et 6 mL de HCl 0,1 N. La solution est agitée sous 1 atmosphère de H_2 pendant 16 h. Le catalyseur est filtré sur tissus de verre et le solvant est évaporé. Le résidu est traité de la même manière que pour la synthèse des ligands **18***a–d* pour conduire au ligand **18***e* avec un rendement total de 73% sous forme de cristaux hygroscopiques de couleur mauve. Ces cristaux sont lyophylisés et conservés dans un dessiccateur. *F* : 110–112°C. IR (KBr), ν : 3000–3600 (N-H, O-H); 1600 (C=O amide); 1620–1650 (C=O acétyle); 870 (N-O) cm^{-1}. RMN ^1H (CD_3OD) : 1,96 (m, 8H, H2, H3); 2,09 (s, 6H); 3,00 (t, J = 6,5, 2H); 3,43 (t, J = 6,5, 4H); 3,70 (t, J = 6,5, 4H); 4,22 (t, J = 5, 2H); 7,7 (s, 2H). Spectrométrie de masse par I.C. (NH_3) : on analyse l'ion moléculaire M′ =M−HCl, m/z : 483 ($M+H^+$)(74), 439 ($(M-COCH_3)+H^+$)(18,5), 425 ($(M-C_2H_6NH_2)+H^+$)(100). Anal. calc. pour $C_{21}H_{35}N_6O_7Cl$: C 48,60; H 6,80; N 16,19; Cl 6,83; trouvé : C 48,86; H 6,79; N 16,24; Cl 6,93.

Résultats

Le schéma de synthèse des ligands se divise en 3 séquences :

A. Synthèse des « bras hydroxamiques » à partir du 1-amino-3-propanol **1** (Schéma 1).

B. Synthèse à partir de l'acide chélidamique **9** du motif pyridinique substitué en position 4 par des groupes alcoxy et en α et α′ par 2 fonctions chlorure d'acide (Schémas 2 et 3).

C. Condensation des bras hydroxamiques avec le synthon pyridinique et libération des fonctions chélatantes (Schéma 4).

1. Synthèse des « bras hydroxamiques » (Schéma 1)

En nous inspirant des travaux de Miller et coll. (13, 14), nous avons pu optimiser la synthèse du trifluoroacétate de l'amino-1-(acétyl-aminobenzyloxy)-3-propane **7***a* qui a été obtenu à partir du 1-amino-3-propanol en six étapes avec un rendement de 37,5%. Parmi les méthodes décrites dans la littérature (15, 16) concernant la protection de l'amine primaire, seule la méthode de Moroder *et al.* (15) nous a permis d'obtenir quantitativement le produit **2** sous forme d'une huile ne nécessitant pas de purification. L'oxydation de l'alcool primaire **3** été menée par la méthode de Swern et coll. (17). L'aldéhyde **3**, très instable, n'a pu être purifié mais a été immédiatement traité par la *O*-benzylhydroxylamine (OBHA) dans un mélange méthanol–eau avec contrôle du pH (18). Après chromatographie sur silice flash, les deux isomères *syn* et *anti* de l'oxime **4** ont été obtenu avec un rendement de 82% à partir du produit **2**. Le spectre RMN ^1H du produit **4** réalisé à 250 MHz dans $CDCl_3$ permet d'identifier et de quantifier les isomères *syn* et *anti* dans des proportions respectives 60 : 40.

Le mélange de ces deux isomères, qui ne sont pas séparés,

Can. J. Chem. Downloaded from www.nrcresearchpress.com by 198.100.157.202 on 09/07/12
For personal use only.

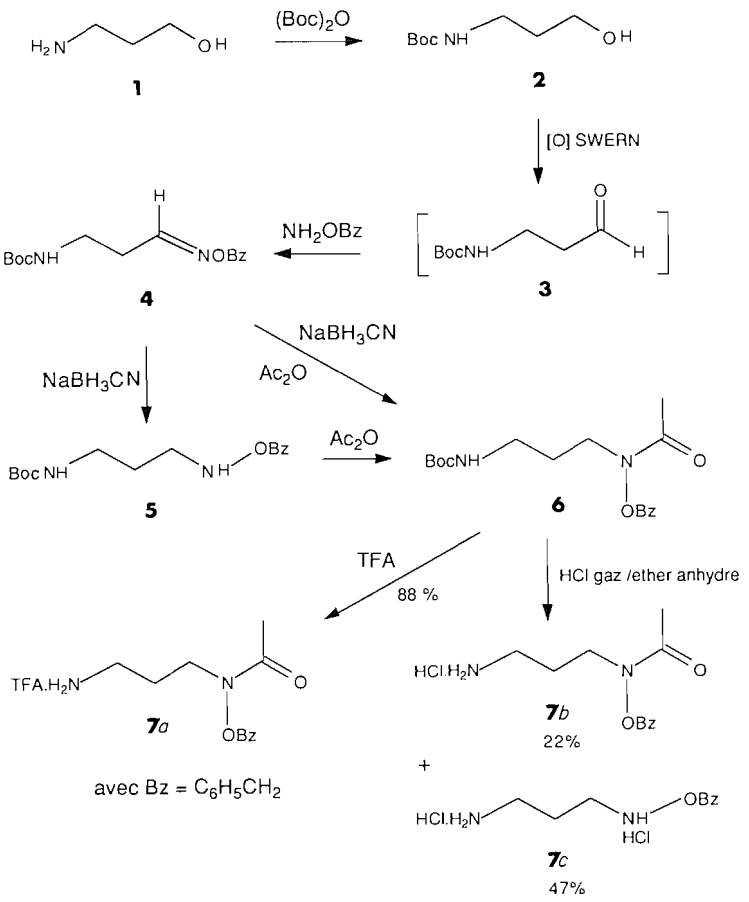


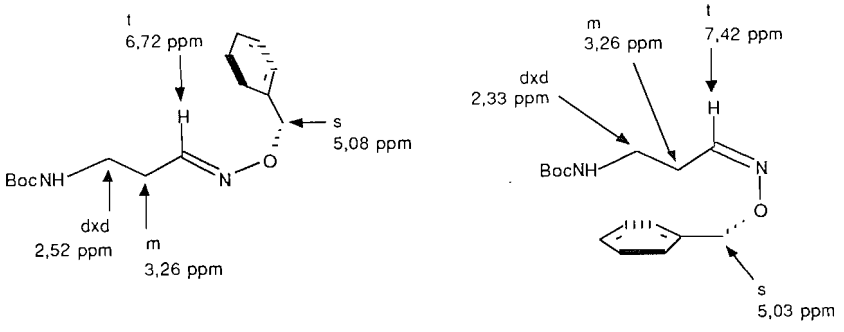
SCHÉMA 1. Synthèse du « bras hydroxamique » **7***a*.

est traité par le cyanoborohydrure de sodium dans l'acide acétique (19) pour conduire à la *O*-benzyl-*N*-(3-(*tert*-butoxycarbonyl-amino)-hydroxylamine **5**. Après chromatographie, le produit pur est obtenu sous forme d'une huile laiteuse incolore avec un rendement de 70%. Son acétylation conduit avec un rendement de 73% au composé **6** caractérisé par l'apparition à 2 ppm du singulet du méthyle du groupement acétohydroxamique protégé. Le rendement de cette séquence réactionnelle a pu être amélioré en réalisant la réduction de la benzyloxime **4** et l'acétylation de l'hydroxylamine **5** sans isolement du produit **4** avec un rendement global de 65%. Par action de HCl gazeux sur le produit **6** dans l'éther éthylique anhydre, le composé **7***b* est obtenu avec un rendement de 22% bien inférieur à celui qui est rapporté dans la littérature (96%) (14). Nous avons pu déterminer que le produit majeur formé au cours de la réaction est en fait le dichlorhydrate **7***c* avec un rendement de 47%. (Nous avons pu séparer et identifier ces deux composés.) L'absence de signal à 2 ppm sur le spectre RMN ^{1}H du produit **7***c* ainsi que le spectre de masse ont permis de le différencier du produit **7***b* sans équivoque. Pour contourner cette difficulté, nous avons procédé à la déprotection du produit **6** par l'acide trifluoroacétique, ce qui conduit au produit **7***a* avec un rendement de 88% (20).

2. Préparation du synthon pyridinique substitué (Schéma 2)

Nous nous sommes basés essentiellement sur les travaux de Markees *et al.* (21–24) et de Bradshaw et coll. (25–27) pour établir notre stratégie de synthèse. Nous avons ainsi développé deux voies synthétiques parallèles à partir de l'acide chélidamique **9**.

La première voie conduit en une étape au dichlorure de l'acide 4-chloro-2,6-pyridine dicarboxylique **10** avec un ren-



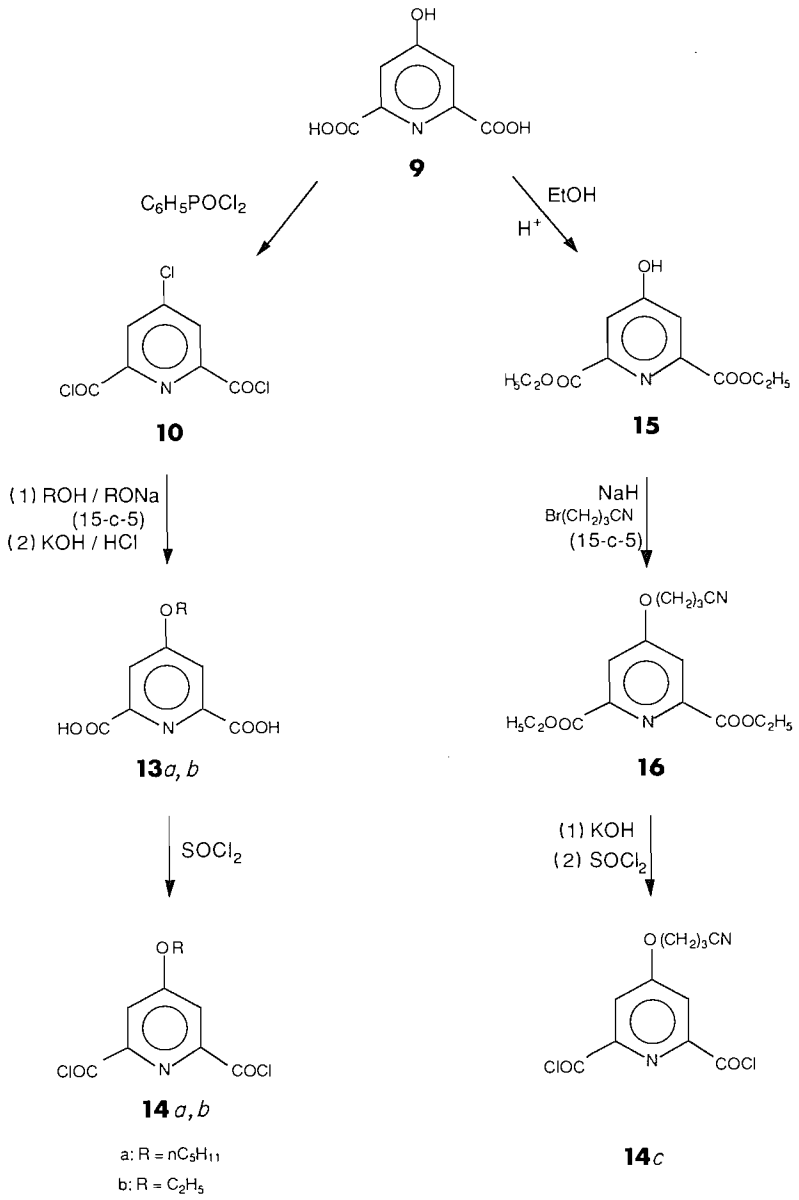


SCHÉMA 2. Synthèse des chlorures d'acide **14***a–c*.

dement de 57% et en 3 étapes aux dichlorures de l'acide 4-pentoxy-2,6-pyridine dicarboxylique **14***a* et de l'acide 4-éthoxy-2,6-pyridine dicarboxylique **14***b* avec des rendement globaux de 34% et de 35% respectivement.

La seconde voie conduit en 3 étapes au dichlorure de l'acide 4-(3-nitrile-*n*-butyloxy)-2,6-pyridine dicarboxylique **14***c* avec un rendement global de 17%.

(a) Synthèse des dichlorures de l'acide 4-pentoxy-2,6-pyridine dicarboxylique ***14***a *et de l'acide 4-éthoxy-2,6-pyridinedicarboxylique* ***14***b

L'acide chélidamique **9** traité par le dichlorure de l'acide phénylphosphonique ($C_6H_5POCl_2$) à 120°C (28) suivi d'une extraction *in situ* par l'hexane bouillant conduit, aprés sublimation, au dichlorure de l'acide 4-chloro-2,6-pyridinedicarboxylique **10**. Ce produit avait été précédemment obtenu par traitement avec le pentachlorure de phosphore (PCl_5) dans le tétrachlorure de carbone ou le chloroforme suivi d'une hydrolyse et d'un reflux dans le chlorure de thionyle ($SOCl_2$) (29) avec un rendement global équivalent ($C_6H_5POCl_2$: 57%; PCl_5 : 59%). Notre méthode présente cependant deux avantages : un gain de temps important et une meilleure reproductibilité des rendements. La substitution du groupement hydroxyle par un atome de chlore est démontrée en RMN ^{13}C par la variation du déplacement chimique de l'atome de carbone en γ (C-OH : δ = 166,7 ppm, C-Cl : δ = 150 ppm). À ce stade deux voies ont été envisagées pour préparer l'acide 4-pentoxy 2,6-pyridinedicarboxylique **13***b*.

Voie 1 (Schéma 3) : Le composé **10** est traité par l'éthanol dans le dichlorométhane afin d'obtenir le diester **11***a* avec un rendement de 52% après recristallisation dans l'heptane. Le produit **11***a* peut également être obtenu avec un rendement de 28% à partir de l'acide chélidamique **9** sans isolement, ni purification du chlorure d'acide intermédiaire **10**. La substitution aromatique de l'atome de chlore en position 4 par l'éthanolate de sodium conduit au produit **12** avec un rendement modeste de 35%. Cependant, l'utilisation d'éther couronne (15-c-5) permet d'augmenter ce rendement jusqu'à 70% (30, 31). En RMN ^1H, on note surtout la variation

Can. J. Chem. Downloaded from www.nrcresearchpress.com by 198.100.157.202 on 09/07/12
For personal use only.

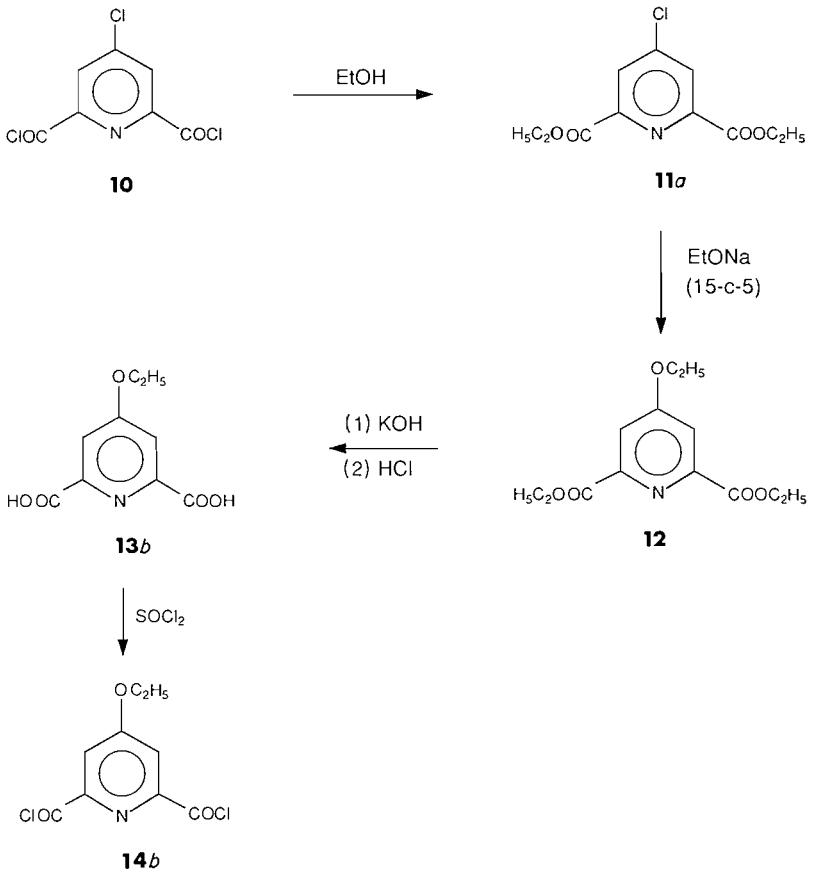


SCHÉMA 3. Synthèse du chlorure d'acide **14***b*.

caractéristique de déplacement chimique des deux atomes d'hydrogène pyridiniques : 8,22 ppm (**11***a*) et 7,72 ppm (**12**). La saponification de l'ester **12** suivie d'une précipitation par HCl, conduit au diacide correspondant avec un rendement de 58%.

Voie 2 (Schéma 2) : Le produit **10** est traité par le *n*-pentanol ou l'éthanol puis saponifié pour conduire aux diacides *para* substitués **13***a* et *b* au cours d'une réaction « one pot » (26), avec un rendement global de 75% et 72% respectivement.

Aprés recristallisation dans l'éthanol, les diacides purs correspondants sont traités par $SOCl_2$ et conduisent aux chlorures d'acide avec des rendements de 80% pour **14***a* et de 85% pour **14***b*.

*(b) Synthèse du dichlorure de l'acide 4-(3-nitrile-*n*-butyloxy)-2,6-pyridinedicarboxylique **14**c*

Nous avons aussi envisagé la substitution du noyau pyridinique par un résidu alkyle portant une fonction nitrile. Cette fonction peut être conservée telle quelle ou être réduite par hydrogénation catalytique en amine primaire qui, sous forme de chlorhydrate, peut avoir une meilleure solubilité dans l'eau. Les travaux de Markees *et al.* (22, 23) nous ont suggéré une stratégie de synthèse du produit **14***c* différente de celle employée pour les chlorures d'acide **14***a* et **14***b*. La fonction hydroxyle de l'acide chélidamique peut être alkylée par un bromure de *n*-alkyle porteur d'une fonction nitrile . L'acide chélidamique **9** estérifié par l'éthanol en présence d'acide sulfuriqe comme catalyseur (32) conduit au produit **15** avec un rendement de 50%. Le traitement de **15** par NaH dans le benzène, suivi de l'addition de 4-bromobutyronitrile et d'une quantité catalytique d'éther couronne (15-c-5) (33), conduit au produit de substitution en position 4 avec un rendement de 60%. Finalement, après saponification, le traitement par $SOCl_2$ du diacide intermédiaire brut conduit au composé **14***c* avec un rendement de 55%.

3. Synthèse des ligands (Schéma 4).

La synthèse des ligands se réduit à deux étapes : (1) condensation des bras hydroxamiques protégés avec les différents chlorures d'acide substitués en position 4 sur le noyau pyridinique (**14***a–c*); (2) hydrogénolyse des groupements benzyliques protecteurs des fonctions acétohydroxamiques. Pour réaliser la condensation, nous avons appliqué la méthode proposée par Lee et Miller pour la synthèse des schizokinen (14) et qui consiste à effectuer la réaction dans le dichlorométhane à 0°C en présence de triéthylamine. Les rendements obtenus, aprés purification par chromotographie sur silice flash, varient de 30 à 50% suivant R. La déprotection des fonctions acétohydroxamiques des produits **14***a–c* s'effectue par hydrogénolyse de la liaison *O*-benzyle dans le méthanol, sous 1 atmosphère de H_2, en présence de Pd/C 10% comme catalyseur (13, 14, 34). Les rendements sont compris entre 70 et 85% suivant R. À ce stade une légère modification des conditions d'hydrogénolyse permet en une seule étape de libérer la fonction acétohydroxamique et de réduire le groupement nitrile du composé **17***c* en amine primaire avec un rendement de 72%. Aux quatre ligands potentiels **18***a–e* nous avons adjoint un cinquième composé dans lequel le noyau pyridinique n'est pas substitué en position 4. Le chlorure de l'acide pyridine-2,6-dicarboxylique, précurseur de ce produit, est disponible commercialement et a été condensé avec les bras hydroxam-

Can. J. Chem. Downloaded from www.nrcresearchpress.com by 198.100.157.202 on 09/07/12
For personal use only.

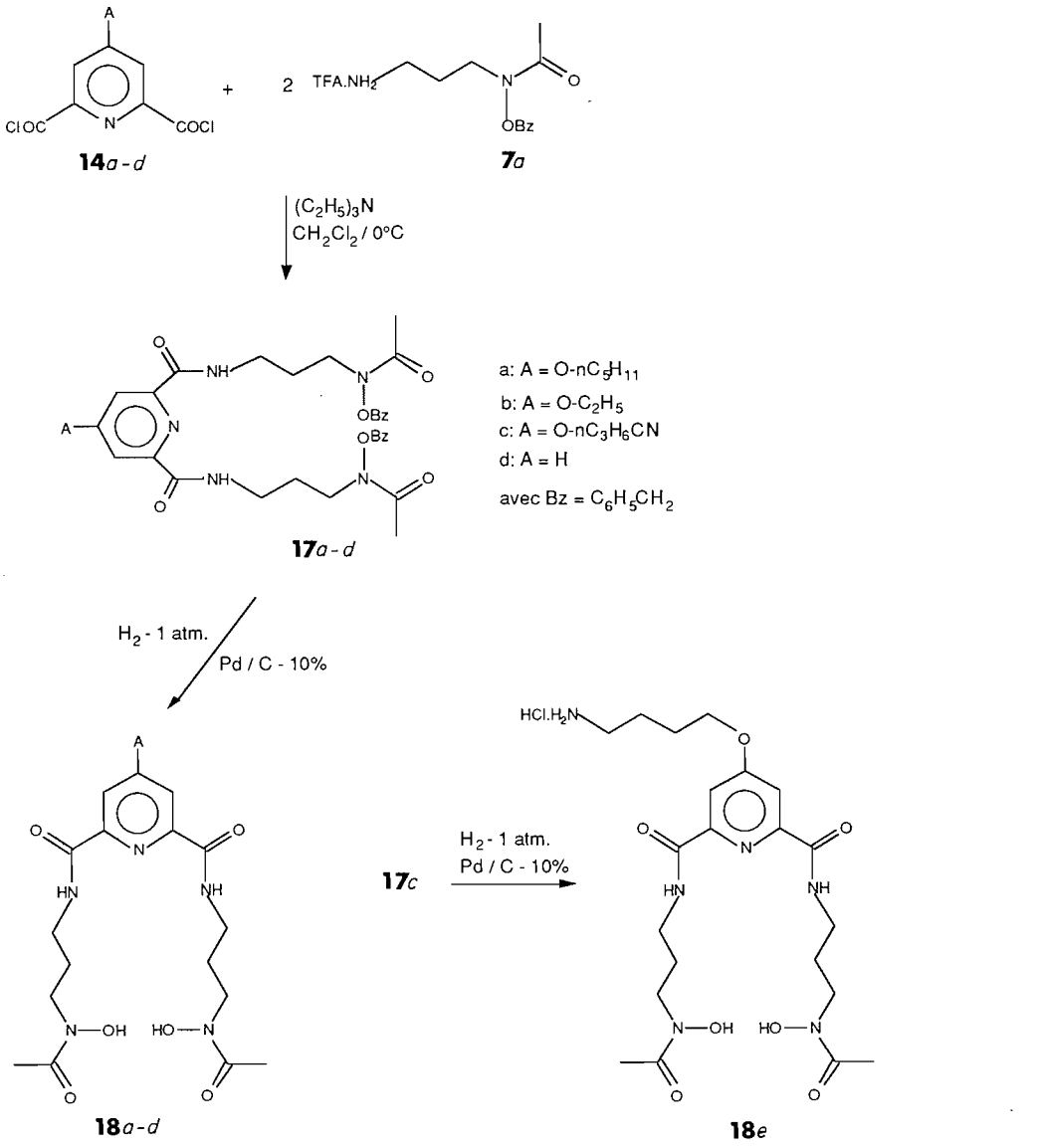


SCHÉMA 4. Synthèse des ligands **18***a–e*.

iques dans les mêmes conditions que pour les composés **17***a–c* pour obtenir le précurseur **17***d*. L'hydrogénolyse catalytique libère, de la même façon, les fonctions acétohydroxamiques pour conduire au produit **18***d* caractérisé en RMN ^1H par les signaux des 3 atomes d'hydrogène pyridiniques entre 7,7 et 8,1 ppm. Nous disposons alors de cinq ligands potentiels de l'ion ferrique, la présence des fonctions chélatantes libres étant confirmée qualitativement par un test avec $FeCl_3$ (35). Le produit **18***d* a été précédemment synthétisé par Miller et coll. (13) par une voie de synthèse faisant intervenir l'acétylation de l'hydroxylamine *O*-benzylée après condensation sur le noyau pyridinique.

Remerciements

L'un d'entre nous (F. Chaubet) remercie la Ligue Nationale Française contre le Cancer pour son soutien financier.

1. B. F. MATZANKE, G. MULLER-MATZANKE et K. N. RAYMOND. Iron carriers and iron proteins. Chap. 21. Phys. Bioinorg. Chem. Ser. **4** (1989).
2. J. B. NEILANDS. Inorganic biochemistry. *Editeur* : G. Eichhorn. Elsevier. New York. 1972.
3. J. B. NEILANDS. Struct. Bonding(Berlin), **1**, 59 (1966).
4. A. E. MARTELL et R. M. SMITH. Critical stability constants. Vol. 1–5. Plenum, New York. 1974–1977.
5. A. E. MARTELL et C. G. PITT. ACS Symp. Ser. **140**, 281 (1980).
6. A. L. CRUMBLISS, R. A. PALMER, K. A. SPRINKLE et D. R. WHITCOMB. *Dans* Development of iron chelators for clinical use. DHEW Publ., U.S. Govt. Printing Office, Bethesda. MD. 1977.
7. R. B. LAUFFER. Chem. Rev. **87**, 901 (1987).
8. C. J. CARRANO, S. R. COOPER et K. N. RAYMOND. J. Am. Chem. Soc. **101**, 599 (1979).
9. C. J. CARRANO et K. N. RAYMOND. J. Am. Chem. Soc. **100**, 5371 (1978).
10. Y. ISOWA, T. TAKASHIMA, M. OHMORI, H. KURITA, M. SATO et K. MORI. Bull. Chem. Soc. Jpn. **45**, 1467 (1972).
11. J. WIDMER et W. KELLER-SCHIERLEIN. Helv. Chim. Acta. **57**, 1904 (1974).
12. B. H. LEE, G. J. GERFEN et M. J. MILLER. J. Org. Chem. **49**, 2418 (1984).
13. B. H. LEE, M. J. MILLER, C. A. PRODY et J. B. NEILANDS. J. Med. Chem. **28**, 323 (1985).

Can. J. Chem. Downloaded from www.nrcresearchpress.com by 198.100.157.202 on 09/07/12
For personal use only.

14. B. H. LEE et M. J. MILLER. J. Org. Chem. **48**, 24 (1983).
15. L. MORODER, A. HALLET, E. WÜNSCH, O. KELLER et G. WERSIN. Hoppe-Seyler's Z. Physiol. Chem. **357**, 1651 (1976).
16. J. W. BLUNT, M. H. G. MUNRO et S. C. YORKE. Tetrahedron Lett. 2793 (1982).
17. A. J. MANCUSO, S. L. HUANG et D. SWERN. J. Org. Chem. **43**, 2480 (1978).
18. R. J. BERGERON et J. J. PEGRAM. J. Org. Chem. **53**, 3131 (1988).
19. G. W. GRIBBLE, R. W. LEIBY et M. N. SHEEHAN. Synthesis, 856 (1977).
20. R. SUNDARAMOORTHI, J. L. FOURREY et B. C. DAS. J. Chem. Soc. Perkin Trans. 1, 2759 (1984).
21. D. G. MARKEES. J. Org. Chem. **29**, 3120 (1964).
22. D. G. MARKEES, V. C. DEWEY et G. W. KIDDER. J. Med. Chem. **13**, 324 (1970).
23. D. G. MARKEES, V. C. DEWEY et G. W. KIDDER. J. Med. Chem. **11**, 126 (1968).
24. D. G. MARKEES et G. W. KIDDER. J. Am. Chem. Soc. **78**, 4130 (1956).
25. J. S. BRADSHAW et coll., F. G. MORIN et D. M. GRANT. J. Org. Chem. **50**, 4865 (1985).
26. J. S. BRADSHAW, N. O. SPENCER, G. R. HANSEN, R. M. IZATT et J. J. CHRISTENSEN. J. Heterocycl. Chem. **20**, 353 (1983).
27. Y. NATATSUJI, J. S. BRADSHAW, P-K TSE, G. ARENA, B. E. WILSON, N. K. DALLEY et R. M. IZATT. J. Chem. Soc. Chem. Commun. 749 (1985).
28. M. M. ROBISON. J. Am. Chem. Soc. **80**, 5481 (1958).
29. J. S. BRADSHAW, G. E. MAAS, J. D. LAMB, R. M. IZATT et J. J. CHRISTENSEN. J. Am. Chem. Soc. **102**, 467 (1980).
30. G. W. GOKEL et H. DUPONT-DURST. Synthesis, 168, (1976).
31. G. W. GOKEL et W. P. WEBER. J. Chem. Educ. **55**, 350 (1978).
32. B. S. GORTON et W. SHIVE. J. Am. Chem. Soc. **79**, 670 (1957).
33. B. FEIBUSH, A. FIGUEROA, R. CHARLES, K. D. ONAN, P. FEIBUSH et B. L. KARGER. J. Am. Chem. Soc. **108**, 3310 (1986).
34. G. STORK et F. H. CLARKE, JR. J. Am. Chem. Soc. **83**, 3121 (1961).
35. J. E. PLOWNAN, T. M. LOEHR, S. J. GOLDMAN et J. SANDERS-LOEHR. J. Inorg. Biochem. **20**, 183 (1984).
36. D. G. MARKEES. J. Am. Chem. Soc. **23**, 1030 (1957).

Can. J. Chem. Downloaded from www.nrcresearchpress.com by 198.100.157.202 on 09/07/12
For personal use only.

Bipyridylacetylenes 1: the synthesis of some bipyridylacetylenes via the palladium-catalyzed coupling of acetylenes with 2,2′-dibromobipyridyl, and the single crystal X-ray structure of 6,6′-bisphenylethynyl-2,2′-bipyridine

IAN R. BUTLER[1] AND CHANTAL SOUCY-BREAU
Chemistry Department, The University of Ottawa, Ottawa, Ont., Canada K1N 6N5

Received January 30, 1990[2]

IAN R. BUTLER and CHANTAL SOUCY-BREAU. Can. J. Chem. **69**, 1117 (1991).

The synthesis of a series of 6,6′-diethynyl-2,2′-bipyridyls from the palladium-catalyzed coupling of 6,6′-dibromo-2,2′-bipyridine with a series of arylacetylenes is reported. The single crystal X-ray structure of 6,6′-phenylethynyl-2,2′-bipyridyl was determined. Crystal data: monoclinic, $A2/a$, with cell constants a = 10.0385(4), b = 9.2166(4), c = 21.4130(8) Å, and β = 102.981(3)°; $D_{calc.}$ = 1.226 g cm^{-3}, Z = 4, R_f = 0.045, S = 1.22, using 886 reflections of the 1443 unique reflections. The packing diagram indicates essentially that the molecules pack in a layered assembly with the nitrogen atoms of the dipyridyl groups on opposite sides and with a dihedral angle of 59.85(16)° between the pyridyl and phenyl groups. The acetylenic bond distances are normal.

Key words: acetylene, palladium, catalysis, coupling, monomers, crystal structure.

IAN R. BUTLER et CHANTAL SOUCY-BREAU. Can. J. Chem. **69**, 1117 (1991).

Faisant appel à un couplage catalysé par le palladium de la 6,6′-dibromo-2,2′-bipyridine avec une série d'arylacétylènes, on a réalisé la synthèse d'une série de 6,6′-diéthynyl-2,2′-bipyridyles. On a déterminé la structure cristalline du 6,6′-phénylélthylnyl-2,2′-bipyridyle par diffraction des rayons-X sur un cristal unique. Les cristaux sont monocliniques, groupe d'espace $A2/a$ avec a = 10,0385(4), b = 9,2166(4) et c = 21,4130(8) Å, β = 102,981(3)°, $D_{calc.}$ = 1,226 g cm^{-3}, Z = 4, R_f = 0,045, S = 1,22 utilisant 886 réflexions de 1443 réflexions uniques. Le diagramme d'entassement indique essentiellement que les molécules s'empilent en couches dans lesquelles les atomes d'azote des groupements dipyridyles se trouvent sur des côtés opposés avec un angle dièdre de 59,85(16)° entre les groupements pyridyle et phényle. La longueur de la liaison acétylénique est normale.

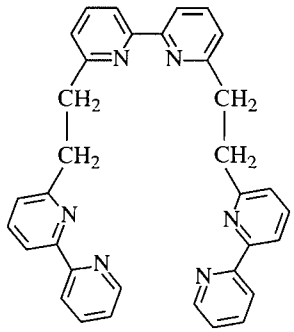
Mots clés : acétylène, palladium, catalyse, coupling, monomère, structure cristalline.

[Traduit par la rédaction]

Introduction

The catalytic coupling reaction of aryl halides with olefins and acetylenes (1–18), mediated by palladium(0), is a reaction that, in the past few years, has been widely used in organic synthesis. We have been interested in this reaction from the standpoint of elucidation of its mechanism; however, during related studies in the synthesis of novel substituted dipyridyl derivatives such as ferrocene-substituted dipyridyls, we developed an interest in the application of the methodology to the synthesis of some acetylene-substituted derivatives.

The palladium-catalyzed reaction of 2-bromopyridine with phenylacetylene was reported initially by Castro and Stephens (19) and later by Ames *et al.* (20) to give excellent yields of 2-pyridylphenylacetylene. In addition, the reaction of 2-bromopyridine with 2-methylbut-3-yne-2-ol (20) and with trimethylsilylacetylene (21, 22), respectively, has been reported, the products of each of these reactions being precursors to 2-ethynylpyridine. In one of our synthetic projects in ligand design and synthesis we were interested in the synthesis of the hexadentate ligand **1**. We envisaged a simple synthesis based on the palladium-catalyzed reaction of 6,6′-dibromo-2,2′-dipyridyl with 6-ethynyl-2,2′-dipyridyl followed by metal-catalyzed reduction. During the course of the synthesis of **1**, we recognized that this work overlapped significantly with another of our current research projects. We are actively engaged in the synthesis of a series of polyacetylene compounds to be used as monomers in the preparation of conducting organic polymers. Thus we decided that some of the acetylene intermediates prepared during the synthesis of **1** may be of a more general interest, and we decided to broaden the scope of the synthesis to include groups other than dipyridyl. The results of these efforts are discussed herein.



1

Experimental section

Solvents used were distilled prior to use, after drying by standard methods, unless otherwise stated. Ferrocenylacetylene (23), 2-pyridylacetylene (20), and 1-naphthylacetylene (24) were prepared following literature procedures. Chromatography was carried out using either neutral alumina (activity grade 1) on a conventional column or using silica gel (Merck 7749-60 PF_{254} plates) on a Harrison Research 7924 chromatatron. Bis(triphenylphosphine)palladium dichloride was prepared from palladium dichloride by adaptation of the literature procedure.[3] The ^{1}H NMR spectra were recorded on Varian XL-300 or Gemini-200 instruments using chloroform-*d*, unless otherwise mentioned (notation used: t = triplet, s = singlet, bd = broad doublet, m = multiplet, ad = asymmetric doublet). Mass spectra were obtained

[1]Author to whom correspondence may be addressed.
[2]Revision received January 29, 1991.

[3]An excess of triphenylphosphine and palladium dichloride was stirred overnight in a biphasic mixture of dichloromethane, methanol, and water containing a small quantity of potassium chloride. This procedure is much simpler than the literature methods.

Can. J. Chem. Downloaded from www.nrcresearchpress.com by 198.100.157.202 on 09/07/12
For personal use only.

Can. J. Chem. Downloaded from www.nrcresearchpress.com by 198.100.157.202 on 09/07/12
For personal use only.

using a VG Analytical 7070E instrument equipped with digital processing, at the University of Ottawa Mass Spectroscopy Centre. All reactions were carried out under an inert (nitrogen or argon) atmosphere.

General product work-up procedure

On completion of the reaction the crude reaction solution was treated with water and dichloromethane (volumes equal to those used as solvent in the reaction). The organic layer was separated and the aqueous layer was further extracted with two portions of dichloromethane. The combined, dried ($MgSO_4$) organic phase was washed through a short neutral alumina column to remove black suspended solids. The volume was reduced under vacuum and the mixture chromatographed using the following procedures.

6,6′-Dibromo-2,2′-bipyridine

The title compound was synthesized using a modest adaptation of the literature procedure (25). The reaction was accomplished by lithiation of 2,6-dibromopyridine (59.5 g, 0.25 mol) with 1.6 M *n*-butyllithium (157 mL) solution in dry diethyl ether (500 mL) cooled to −90°C and stirred for 15 min under a N_2 atmosphere. Anhydrous cupric chloride (16.8 g, 0.13 mol) was then added in portions of 2 g at a time.[4] The reaction mixture was stirred at −70°C for 15 min. Once all the $CuCl_2$ had been added, the brown suspension was stirred for an additional 30 min and kept below −50°C.

Oxidation was carried out with compressed oxygen at −60 to −50°C by bubbling excess O_2 through the mixture for a period of 1 h. The suspension was hydrolyzed with dilute HCl (6 N, 250 mL), and filtered at room temperature. The ether fraction was evaporated to give an additional few grams of product. The solid was dried over Na_2SO_4 and separated on silica gel by column chromatography (eluent: hexane/ethyl acetate 1:1) to give 15 g of a beige solid (40–50% yield), mp 217–218°C (lit. (26) mp 218°C). Further purification by recrystallizing from benzene gave a white solid with mp 220–221°C (lit. (25) mp 221–223°C). ^{1}H NMR, 200 MHz ($CDCl_3$) δ: 8.35 (dd, 2H, $J_{5-3,5'-3'}$ = 0.66, $J_{5-4,5'-4'}$ = 7.66 Hz, *H*-5,5′), 7.75 (t, 2H, $J_{4-3,4'-3'}$ = 7.69, $J_{4-5,4'-5'}$ = 7.55 Hz, *H*-4,4′), 7.48 (dd, 2H, $J_{3-4,3'-4'}$ = 7.85, $J_{3-5,3'-5'}$ = 0.61 Hz, *H*-3,3′). EIMS, *m*/*z* (%): 314 (100), 312 (54), 235 (66), 233 (65), 189 (4.6), 153 (39), 126 (17.5), 116 (7.8), 77 (55), and 50 (31).

Preparation of **2**

Copper(I) iodide (0.16 g, 2 mmol) and bis(triphenylphosphine)palladium dichloride (0.35 g, 4 mmol) were stirred under nitrogen in triethylamine (100 mL) (20). 6,6′-Dibromo-2,2′-dipyridine (22.6 g, 72 mmol), followed by 2-methyl-3-butyn-2-ol (15.15 g, 180 mmol), was added to the mixture, and a precipitate was formed. After 18 h of stirring at room temperature, the solvent was evaporated under vacuum. Dichloromethane (100 mL) was added and the solution was washed with water (3 × 20 mL). The organic phase was dried over anhydrous magnesium sulfate and subsequently evaporated *in vacuo*. The crude product was separated on column chromatographic grade silica gel (eluent: hexane/ethyl acetate 1:1) to afford 21.2 g of nearly pure material. Purification was carried out with a second chromatography (column) to give 6,6′-(2-methylbut-3-yn-2-ol)-2,2′-bipyridine (18 g; 78% yield) with R_f (hexane/EtOAc 1:1) 0.19 and mp 160.5–161.5°C. IR (KBr), ν_{max}: 3380, 3280, 2980, 2940, 2240, 1570, 1450, 1370, 1290, 1200, 1170, 1110, 1080, 990, 970, 920, 810, 750, and 690 cm^{-1}. ^{1}H NMR, 200 MHz ($CDCl_3$) δ: 8.35 (dd, 2H, $J_{3-5,3'-5'}$ = 1.05, $J_{3-4,3'-4'}$ = 7.9 Hz, *H*-3,3′), 7.73 (t, 2H, $J_{4-3,4'-3'}$ = 7.8, $J_{4-5,4'-5'}$ = 7.7 Hz, *H*-4,4′), 7.39 (dd, 2H, $J_{5-3,5'-3'}$ = 1.08, $J_{5-4,5'-4'}$ = 7.7 Hz, *H*-5,5′), 2.29 (5, 2H, Ar-C≡C-C$(CH_3)_2$*O*H), 1.63 (s, 12H, Ar-C≡C-C$(CH_3)_2$OH). EIMS, *m*/*z* (%): 320 (13), 305 (15), 267 (35.8), 259 (12), 247 (25), 219 (70), 204 (15), 139 (28), 118 (99.7), 104 (100), 91 (85), 77 (56.6), and 42 (100). HRMS, calcd. for $C_{20}H_{20}N_2O_2$: 320.3940; found: 320.1513.

[4]We have observed in lithiation reactions of 2,6-dibromopyridine that 6,6′-dibromo-2,2′-bipyridine is produced without the necessity of using the copper salt.

Preparation of **3**a

6,6′-Diethynyl-2,2′-bipyridine was obtained by treatment of **2** (6.9 g, 0.022 mol) with sodium hydroxide (27) (0.8 g, 0.02 mol) in toluene (150 mL). The mixture was heated under reflux for 30 min. Decantation, evaporation under reduced pressure, and separation by silica gel chromatography (eluent: hexane/EtOAc) gave 3.0 g of nearly pure material. Rechromatography on silica gel afforded **3***a* (1.83 g; 42% yield); R_f (hexane/EtOAc 1:1) 0.54; mp 192–193°C; IR (KBr), ν_{max}: 3280, 2360, 1580, 1560, 1440, 1080, 980, 800, and 650 cm^{-1}. ^{1}H NMR, 200 MHz ($CDCl_3$) δ: 8.45 (dd, 2H, $J_{3-5,3'-5'}$ = 1.0, $J_{3-4,3'-4'}$ = 8.0 Hz, *H*-3,3′), 7.76 (t, 2H, $J_{4-5,4'-5'}$ = 7.7, $J_{4-3,4'-3'}$ = 7.9 Hz, *H*-4,4′), 7.48 (dd, 2H, $J_{5-3,5'-3'}$ = 1.06, $J_{5-4,5'-4'}$ = 7.7 Hz, *H*-5,5′), 3.16 (s, 2H, Ar-C≡C-C*H*). EIMS, *m*/*z* (%): 204 (100), 203 (25.7), 179 (97), 76 (3.7), 152 (15.5), 126 (2), 102 (11), 75 (20), and 50 (23.5). HRMS, calcd. for $C_{14}H_8N_2$: 204.2080; found: 204.0690.

Preparation of **3**b, **3**e

In the same manner as **3***a*, 6,6′-dibromo-2,2′-bipyridine (300 mg, 0.95 mmol) was coupled with phenylacetylene (197 mg, 1.9 mmol) in the presence of CuI (0.08 g) and $(PPh_3)_2PdCl_2$ (0.15 g) in triethylamine as solvent (30 mL). After 30 min at room temperature the usual work-up was performed and the crude dark solid was prepurified on a short silica gel column (chromatography) using hexane/CH_2Cl_2 in a 1:1 ratio as eluent. Further separation on silica gel (chromatatron TM, eluent: hexane/CH_2Cl_2 5:1) afforded 6,6′-bis-(phenylethynyl)-2,2′-bipyridine, 153 mg (45%) of a pure white solid of mp 195.8–196.2°C, R_f (hexane/CH_2Cl_2 1:2) 0.13. IR (KBr), ν_{max}: 3060, 2230, 1600, 1568, 1495, 1440, 805, 760, 690, and 640 cm^{-1}. ^{1}H NMR, 200 MHz ($CDCl_3$) δ: 8.46 (dd, 2H, $J_{3-5,3-5}$ = 1.1, $J_{3-4,3'-4'}$ = 7.9 Hz, *H*-3,3′), 7.81 (t, 2H, $J_{4-3,4'-3'}$ = 7.9, $J_{4-5,4'-5'}$ = 7.8 Hz, *H*-4,4′), 7.65–7.59 (m, 10H, Ph), 7.55 (dd, 2H, $J_{5-3,5'-3'}$ = 1.1, $J_{5-4,5'-4'}$ = 7.7 Hz, *H*-5,5′). EIMS, *m*/*z* (%): 356 (100), 355 (24), 279 (15.7), 193 (19), 167 (11), 149 (27), 72 (16), 57 (83), and 41 (41). HRMS, calcd. for $C_{26}H_{16}N_2$: 356.3854; found: 356.1325.

Using an identical procedure coupling 2-pyridylacetylene (1.03 g, 10 mmol) with 6,6′-dibromo-2,2′-dipyridine (1.57 g, 5 mmol) in the presence of CuI (0.08 g) and $(PPh_3)_2PdCl_2$ (0.15 g) gave bis-6,6′-(2-ethynylpyridinyl)-2,2′-dipyridine, **3***e* (89%). ^{1}H NMR, 300 MHz ($CDCl_3$) δ: 7.29 (ddd, 2H, $J_{5'''-4'''}$ = 7.8, $J_{5'''-6'''}$ = 4.8, $J_{5'''-3'''}$ = 1.4 Hz, *H*-5‴, *H*-5⁗), 7.63 (dd, 2H, J_{5-4} = 7.7, J_{5-3} = 1.1 Hz, *H*-5, *H*-5′), 7.67 (ddd, 2H, $J_{3'''-4'''}$ = 7.8, $J_{3'''-6'''}$ = 1.8 Hz, *H*-3‴, *H*-3⁗), 7.71 (td, 2H, $J_{4'''-6'''}$ = 2.7 Hz, *H*‴, *H*-4⁗), 7.84 (t, 2H, J_{4-3} = 8.0 Hz, *H*-4, *H*-4′), 8.50 (dd, 2H, *H*-3, *H*-3′), 8.65 (ddd, 2H, *H*-6‴, *H*-6⁗). Mass spectrum, parent ion *m*/*z* 358 (100%). Anal. calcd. for $C_{24}H_{14}N_4$: C 80.43, H 3.94, N 15.63; found: 80.41, H 3.86, N 15.57.

1-Naphthyl-2-trimethylsilylacetylene

Iodonaphthalene (10 mg, 39 mmol) was coupled with trimethylsilylacetylene (4.0 g, 40 mmol) in diethylamine (40 mL) in the presence of $(PPh_3)_2PdCl_2$ (0.18 g) and CuI (0.05 g) as catalyst. After stirring at room temperature for 18 h, the usual work-up was performed. Separation on a silica column (eluent: hexane) afforded the title compound, 7.0 g (80% yield) as a transparent oil; R_f (hexane) 0.27. IR (film) ν_{max}: 3060, 2960, 2900, 2160, 1590, 1510, 1400, 1250, 1160, 1080, 1050, 1020, 850, 800, 780, and 730 cm^{-1}. ^{1}H NMR, 200 MHz ($CDCl_3$) δ: 8.32 (dd, 1H, Ar), 7.33–7.84 (m, 6H, Ar), 0.32 (s, 9H, Ar-C≡C-Si$(CH_3)_3$). EIMS, *m*/*z* (%): 224 (42), 209 (100), 191 (2.6), 179 (10), 165 (16), 152 (4), 105 (13), 89 (3); HRMS, calcd. for $C_{15}H_{16}Si$: 224.3760; found: 224.1030. Anal. calcd. for $C_{15}H_{16}Si$: C 80.29, H 7.18; found: C 80.19, H 7.05.

1-Ethynylnaphthalene

In a round-bottom flask, under a N_2 atmosphere, were placed 1-naphthyl-2-trimethylsilylacetylene (1.0 g, 4.5 mmol) and a 1 M solution in THF of tetrabutylammonium fluoride (9 mL, 9 mmol) in dry THF (15 mL). The reaction was completed within 10 min at room temperature to give a reddish solution. Hydrolysis was carried out with a water (10 mL) and 2 M HCl (0.5 mL) solution. The solvent (THF) was removed *in vacuo* and the remaining material extracted with diethyl ether (4 × 25 mL) and CH_2Cl_2 (4 × 25 mL). The organic layer

Can. J. Chem. Downloaded from www.nrcresearchpress.com by 198.100.157.202 on 09/07/12
For personal use only.

was washed with a saturated sodium chloride solution (20 mL), then dried over anhydrous $MgSO_4$ to give a crude brown oil (0.99 g). Separation on a short silica column (eluent: pentane) afforded 0.64 g (94% yield) of a pale yellow oil, R_f (pentane) 0.33. IR (film) ν_{max}: 3300, 3070, 2110, 1590, 1510, 1395, 1270, 1020, 800, and 780 cm^{-1}. ^1H NMR, 200 MHz ($CDCl_3$) δ: 8.39 (dd, 1H, Ar), 7.39–7.87 (m, 6H, Ar), 3.48 (s, 1h, Ar-C≡C*H*). EIMS, *m/z* (%): 152 (100), 126 (6.7), 98 (4), 86 (3), 74 (9), 62 (4), and 50 (5). Anal. calcd. for $C_{12}H_8$: C 94.70, H 5.29; found: C 94.46, H 5.51.

Reaction of 6,6′-dibromo-2,2′-bipyridine with 1-ethynylnaphthalene

6,6′-Dibromo-2,2′-bipyridine (200 mg, 0.64 mmol) and 1-ethynylnaphthalene (260 mg, 1.28 mmol), prepared by the palladium-catalyzed coupling of naphthyl iodide with 2-methyl-but-1-yne-2-ol followed by reaction with sodium hydroxide, were reacted in the presence of bis(triphenylphosphine)palladium dichloride (120 mg, 0.17 mmol) and copper(I) iodide (80 mg, 0.42 mmol) in 15 mL of diethylamine. Purification of the crude material on silica gel in the Chromatatron using hexane as eluent afforded 80 mg (30%) of an off-white solid, identified as bis-6,6′-(ethynyl-1-naphthalene)-2,2′-bipyridine, R_f (hexane/CH_2Cl_2 1:2) 0.09, mp 215–216°C. IR (KBr) ν_{max}: 3060, 2140, 1590, 1575, 1505, 1395, 1335, 1270, 1160, 1015, 950, 910, 870, 800, 770, 570, and 440 cm^{-1}. ^1H NMR, 200 MHz ($CDCl_3$) δ: 8.42 (dd, 2H, $J_{3-5,3'-5'}$ = 0.9, $J_{3-4,3'-4'}$ = 8.8 Hz, pyridyl *H*-3,3′), 7.85 (t, 2H, $J_{4-3,4'-3'}$ = 9.9, $J_{4-5,4'-5'}$ = 8.3 Hz, *H*-4,4′), 7.48 (dd, 2H, $J_{5-3,5'-3'}$ = 1.1, $J_{5-4,5'-4'}$ = 7.3 Hz, *H*-5,5′), 7.41–7.66 (m's, 14H, naphthyl). EIMS, *m/z* (%): 456 (12.7), 340 (14), 311 (7), 263 (20), 262 (100), 261 (16), 228 (9), 183 (70), 152 (14), 129 (34), 108 (41), 107 (7), 57 (36), 41 (25), and 28 (19).

NOTE: This reaction can also be achieved by coupling 1-iodonaphthalene (340 mg, 1.3 mmol) with 6,6′-diethynyl-2,2′-bipyridine, **3***a* (130 mg, 0.64 mmol), in DEA (20 mL) in the presence of CuI (0.04 g) and $(PPh_3)_2PdCl_2$ (0.08 g) as catalyst. The reaction gave yields of greater than 30%. A persistent by-product in the former reaction is 1,4-di(1-naphthyl)-1,3-buta-diyne, identified by spectral composition with an authentic sample.

Reaction of 2,6-dibromopyridine with ferrocenylacetylene

1. A mixture of 2,6-dibromopyridine (Aldrich) (300 mg, 1.26 mmol) and ferrocenylacetylene (600 mg, 2.36 mmol) was reacted using the general procedure with bis(triphenylphosphine)palladium dichloride (47 mg, 67 μmol) and copper(I) iodide (40 mg, 209 μmol) in diethylamine (15 mL). The reaction was monitored by TLC (eluent: hexane/diethyl ether 70:30). After 1.5 h a new orange band was observed with a lower R_f than the ferrocenylacetylene. The reaction mixture was worked up using the general method. Column chromatography gave the following bands in order of elution: (i) yellow band of ferrocenylacetylene (25 mg); (ii) an unidentified violet fraction (trace); (iii) a diffuse orange band that gave 6-bromo,2-ethynylferrocenylpyridine (total yield 360 mg, 0.98 mmol, 78%); (iv) red and violet bands (combined weight 100 mg), unidentified; mp 169–170°C. IR (KBr), ν_{max}: 2220, 1575, 1550, 1420, 1200, 1160, 1120, 1110, 1030, 1010, 980, 820, 800, and 680 cm^{-1}. ^1H NMR, δ: 4.24 (s, 5H, η^5-Cp), 4.28 (t, 2H, α-C_5H_4), 4.55 (t, 2H, β-C_5H_3), 7.38 (bad, 2H, *H*-3, *H*-5), 7.45 (at, 1H, *H*-4). Mass spectrum, *m/z* (rel. int. (%)): 368 (20.0), 367 (93.8), 366 (21.3), 365 (100.0), 362 (6.2), 286 (19.1), 285 (52.4), 230 (26.1), 229 (54.6), 228 (57.6), 227 (7.0), 203 (12.0), 202 (15.6), 165 (13.3), 164 (40.5). (High resolution mass spectrum was not possible since the standards used had a reference too close to *m/z* 365/7.)

2. A mixture of 2,6-dibromopyridine (200 mg, 0.84 mmol) and ferrocenylacetylene (400 mg, 1.94 mmol), bis(triphenylphosphine)palladium dichloride (30 mg, 43 μmol), and copper(I) iodide (30 mg, 157 μmol) in diethylamine (15 mL) was stirred for 24 h to give the following products after work-up and column chromatography: ferrocenylacetylene (20 mg); bis-1,4-ferrocenyl-buta-1,3-diyne (36 mg, 8.8%) (28); bis-2,6-(ethynylferrocenyl)pyridine (390 mg, 90.4%); mp: darkens between 240 and 305°C with polymerization. IR (KBr), ν_{max}: 2220, 1565, 1430, 1190, 1110, 800, and 500 cm^{-1}. ^1H NMR, δ: 4.24 (s, 10H, η^5-Cp), 4.26 (t, 4H, α-C_5H_4), 4.55 (t, 4H, β-C_5H_4), 7.36 (d, 2H, *H*-3, *H*-5′), 7.55 (t, 1H, *H*-4). Mass spectrum, *m/z* (rel. int. (%)): 496 (35.6), 495 (100.0, $M^{+\cdot}$), 493 (15.5), 429 (10.0), 374 (6.3), 316 (7.5), 315 (5.2), 309 (5.0), 253 (11.8), 247 (21.2).

Reaction of 6,6′-dibromo-2,2′-bipyridine with ferrocenylacetylene

1. A mixture of 6,6′-dibromo-2,2′-bipyridine (0.75 g, 23.8 mmol) and ferrocenylacetylene (23) (1.0 g, 4.76 mmol) was treated with bis(triphenylphosphine)palladium dichloride (50 mg, 71.3 μmol) and copper(I) iodide (50 mg, 262 μmol) for 24 h. Following work-up and column chromatography bis-1,4-ferrocenyl-buta-1,3-diyne (125 mg, 12.6%) (mp 197–198°C with polymerization. IR (KBr), ν_{max}: 3100, 2160, 1350, 1300, 1110, 1040, 1005, 910, 800 cm^{-1}. HRMS, calcd. for $C_{24}H_{18}Fe_2$: 418.1026; found: 417.9977) and bis-6,6′-(ethynylferrocene)-2,2′-bipyridine (300 mg, 0.524 mmol, 22%) were obtained. Examination of crude intermediate oily fractions of product obtained following column chromatography indicates the presence of 6-bromo-6′-(ethynylferrocene)-2′-bipyridine, parent ion at *m/z* 422/424. ^1H NMR, 300 MHz ($CDCl_3$) δ: 8.32 (d, 1H), 8.30 (d, 1H), 7.65, 7.66 (2t, 2H), 7.47, 7.48 (2d, 2H), 4.49 (t, 2H), 4.26 (s, 5H), 4.23 (t, 2H).

2. A similar reaction using ferrocenylacetylene (240 mg) and 6,6′-dibromo-2,2′-bipyridine (160 mg) with bis(triphenylphosphine)palladium dichloride (50 mg) and copper(I) iodide (30 mg) in diethylamine (20 mL) and THF (20 mL) for 48 h gave bis-6,6′-(ethynylferrocene)-2,2′-dipyridine (260 mg, 89%). Compound **3***d* is obtained as golden yellow microcrystals. It is only sparingly soluble in dichloromethane; mp darkens with polymerization between 240 and 305°C. ^1H NMR, δ: 8.40 (dd, 2H, $J_{5-4,5'-4'}$ = 1.0, $J_{5-3,5'-3'}$ = 7.9 Hz, *H*-5, *H*-5′), 7.78 (t, 2H, $J_{4-5,4-3}$, $J_{4'-5',4'-3'}$ = 7.9 Hz, *H*-4, *H*-4′), 7.49 (dd, 2H, $J_{4-5,4'-5'}$ = 1.0, $J_{3-4,3'-4'}$ = 7.8 Hz, *H*-3, *H*-3′), 4.59 (t, 4H, $J_{H\alpha\text{-}H\beta}$ = 1.8(5), *H*-α-C_5H_4), 4.28 (t, 4H, $J_{H\beta\text{-}H\alpha}$ = 1.8(5) Hz), *H*-β, C_5H_4), 4.27 (s, 10, η^5-C_5H_5). Mass spectrum, *m/e* (rel. int.): 573 (4.3), 572 (100.0, $M^{+\cdot}$), 529 (21.3), 509 (12.8), 508 (70.2), 507 (72.3), 505 (6.4), 454 (8.5), 451 (46.8), 446 (14.9), 444 (17.0), 442 (16.8), 386 (21).

The reaction of 6,6′-dibromo-2,2′-bipyridine with acetylene

The reaction of 6,6′-dibromo-2,2′-bipyridine (1.0 g, 3.2 mmol) with acetylene in the presence of a catalytic mixture of bis(triphenylphosphine)palladium dichloride (50 mg, 71.3 μmol) and copper(I) iodide (40 mg, 0.21 mmol) was carried out using the general procedure. Following the standard work-up, only small quantities of triphenylphosphine oxide and low molecular weight material, *m/z* 665, were observed. The bulk of the product was obtained as a dark brown-black polymeric material (0.64 g).

Structural determination of ***3***b

A suitable crystal of ***3****b* with approximate dimensions 0.15 × 0.15 × 0.10 mm, grown from dichloromethane and diethyl ether by the slow diffusion procedure, was mounted on a glass fibre. The data were collected using CuKα$_1$, λ = 1.54056 Å, radiation using a Picker diffractometer in a room thermostated at 24 ± 1°C. The unit cell parameters and the orientation matrix were obtained from the accurate setting of 32 reflections (100° < 2θ < 120° with CuKα$_1$ radiation). Three standard reflections were measured in every block of 100 measurements and no significant crystal decay was detected. Out of 1589 reflections measured, 1443 were considered unique, of which 886 had $I_{net} \geq 2.5\sigma(I)$. Crystal data: $C_{26}H_{16}N_2$, formula weight = 356.42; space group *A*2/*a* monoclinic[5] (centrosymmetric), *Z* = 4; $D_{calc.}$ = 1.226 g cm^{-3}; μ = 0.52 mm^{-1}; *a* = 10.0385(4), *b* = 9.2166(3), *c* = 21.4130(8) Å; β = 102.981(3)°; *V* = 1930.52(12) Å^3; *F*(000) electrons, 743.87. The polarization coefficient used was taken from ref. 29. The 2θ scan methods using the NRCVAX structure programme package (30, 31), and refined (non-hydrogen atoms anisotropic, hydrogen atom isotropic) using full matrix least squares with minimization of $\Sigma w(|F_o| - |F_c|)^2$ (unit weights). Hydrogen atoms were located in the difference map. The last cycle was calculated with 22 atoms, 160 parameters, and 886 out of the 1443 reflections.

[5]General positions in space group *A*2/*a*: *x*, *y*, *z*; ½ − *x*, *y*, −*z*; *x*, *y* + ½, *z* + ½; ½ − *x*, *y* + ½, ½ − *z*; −*x*, −*y*, −*z*; *x* − ½, −*y*, *z*; −*x*, −*y* − ½, −*z* − ½; *x* − ½, −*y* − ½, *z* − ½.

Can. J. Chem. Downloaded from www.nrcresearchpress.com by 198.100.157.202 on 09/07/12
For personal use only.

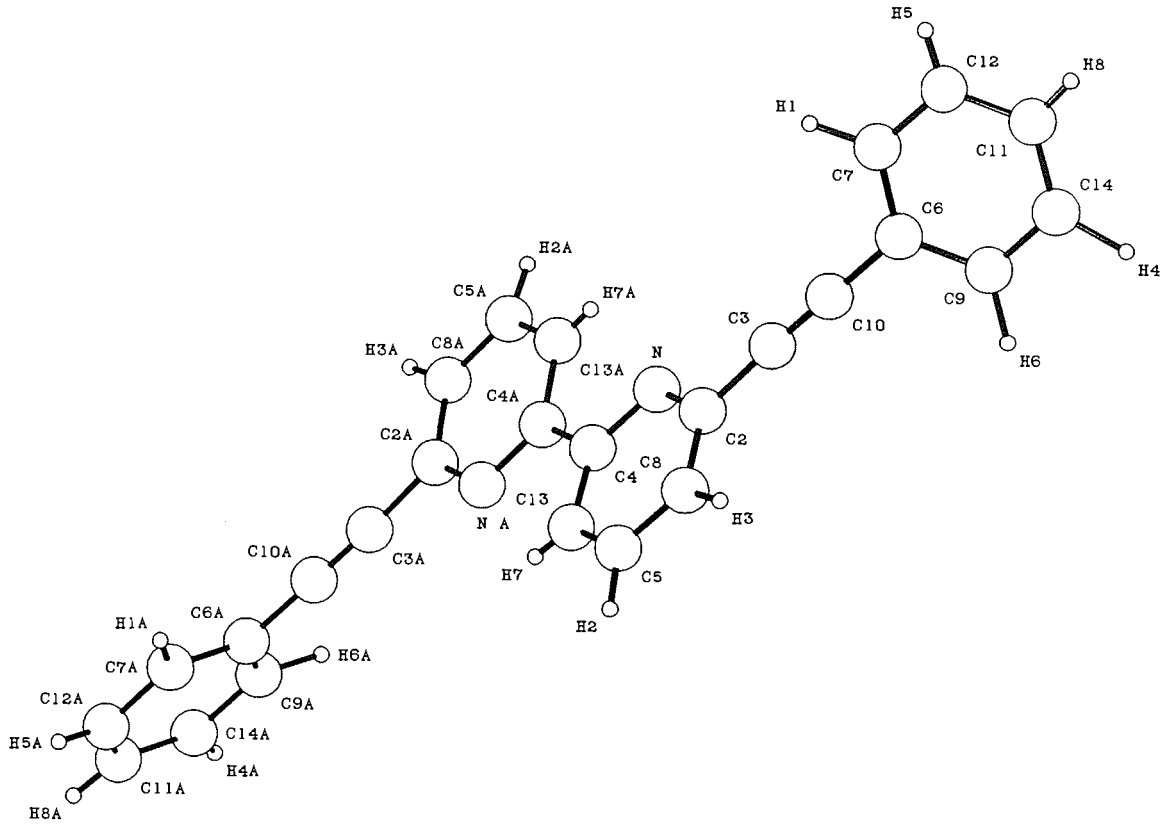


FIG. 1. A PLUTO drawing of **3*b***, indicating the labelling scheme used for atoms.

TABLE 1. Atomic parameters (x, y, z) and B_{iso}

Atom	x	y	z	B_{eq}/B_{iso}
N	0.7483(3)	0.8620(3)	0.91567(11)	3.91
C1	0.6989(3)	0.8583(4)	0.96866(14)	3.86
C2	0.5592(4)	0.8513(4)	0.96690(16)	4.53
C3	0.4681(4)	0.8494(5)	0.90820(17)	5.28
C4	0.5170(4)	0.8550(5)	0.85374(18)	5.18
C5	0.6576(4)	0.8603(4)	0.85857(15)	4.20
C6	0.7129(4)	0.8643(5)	0.80219(16)	4.79
C7	0.7498(4)	0.8659(4)	0.75320(16)	4.45
C8	0.7943(3)	0.8679(4)	0.69384(14)	4.16
C9	0.7536(5)	0.9795(5)	0.65038(18)	5.98
C10	0.7967(6)	0.9801(5)	0.59356(21)	7.38
C11	0.8805(5)	0.8735(5)	0.57976(21)	6.42
C12	0.9212(4)	0.7618(6)	0.62233(18)	5.49
C13	0.8779(4)	0.7598(5)	0.67906(17)	4.80
H2	0.532(3)	0.848(4)	1.0076(16)	5.3(8)
H3	0.366(4)	0.852(4)	0.9059(15)	5.8(9)
H4	0.463(3)	0.853(4)	0.8123(17)	6.2(9)
H9	0.693(4)	1.058(5)	0.6628(19)	7.9(12)
H10	0.767(5)	1.054(5)	0.5681(22)	9.2(14)
H11	0.915(4)	0.873(4)	0.5395(18)	7.4(11)
H12	0.983(4)	0.679(5)	0.6121(18)	7.5(11)
H13	0.900(4)	0.678(4)	0.7075(17)	6.4(10)

The esd's refer to the last digit printed.
B_{eq} is the average of the three principal values of the thermal ellipsoid.

The maximum shift/σ ratio was 0.002. Complex neutral scattering factors were taken from ref. 32. The largest peak in the final difference Fourier synthesis map was located 1.697 Å from H9. No absorption correction was made. The R value ($R = \Sigma||F_o| - |F_c||/\Sigma F_o$) for observed reflections was 0.045; Rw = 0.043 ($Rw = [\Sigma w(|F_o| - |F_c|)^2/\Sigma w F_o^2]^{1/2}$), S = 1.22 ($S = [\Sigma(w(|F_o| - |F_c|)^2/$(no. of reflections − no. of parameters)]$^{1/2}$) and for all reflections R_f was 0.078 and Rw was 0.061. The deepest hole in the final difference Fourier synthesis was −0.102 e Å^{-3} and the highest peak was 0.110 e Å^{-3}. Data for bonds and angles are listed in Table 1 and positional parameters in Table 2. A PLUTO[6] plot of **3*b*** is shown in Fig. 1 and a packing diagram obtained from using NRCVAX PACKER programme is shown in Fig. 2. Anisotropic thermal parameters and final structure factor tables are available as supplementary material.[7]

Results and discussion

There has been much interest in 2,2′-bipyridine and 1,10-phenanthroline based ligands in view of the success in utilization of their complexes in a variety of processes ranging from the reported chemotherapeutic nature of, for example, derivatives of bis-(2,2′-bipyridyl)platinum and -palladium halides (33, 34), through the use of $[Ru(dipy)_3]^{2+}$ as a photosensitizer in the water splitting reaction (35), to the elegant work of Barton's group in the use of ruthenium complexes of modified phenanthrolyl ligands in site-specific DNA cleavage (36–38). Our own interest lies essentially in several areas, namely the preparation of conducting polymers with the ability to coordinate transition metals, and the possible modification of ligands to incorporate an electric field gradient within the molecules, thereby separating reduction and oxidation sites in photo-induced processes.

Our initial work in the dipyridyl system was to synthesize 6,6′-ethynyl-2,2′-bipyridine. This was achieved by the relatively simple modification of the chemistry described for the related pyridyl systems described by Ames *et al.* (20). The route

[6]PLUTO plotting programme developed by W. D. S. Motherwell and W. Clegg, University of Cambridge (1979).

[7]A complete set of data may be purchased from the Depository of Unpublished Data, Document Delivery, CISTI, National Research Council Canada, Ottawa, Canada K1A 0S2.

Can. J. Chem. Downloaded from www.nrcresearchpress.com by 198.100.157.202 on 09/07/12
For personal use only.

TABLE 2

(a) Atomic bond distances (Å) for **3***b*

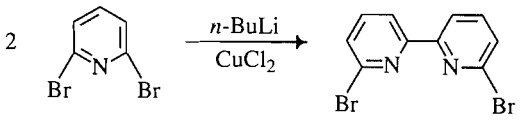
N—C(1)	1.337(4)	C(6)—C(7)	1.189(5)
N—C(5)	1.351(4)[a]	C(7)—C(8)	1.439(5)
C(1)—C(1a)	1.496(6)	C(8)—C(9)	1.385(6)
C(1)—C(2)	1.395(5)	C(8)—C(13)	1.384(6)
C(2)—C(3)	1.379(5)	C(9)—C(10)	1.380(6)
C(3)—C(4)	1.364(5)	C(10)—C(11)	1.368(7)
C(4)—C(5)	1.393(5)	C(11)—C(12)	1.375(7)
C(5)—C(6)	1.438(5)	C(12)—C(13)	1.379(5)

(b) Bond angle data (in deg) for **3***b*

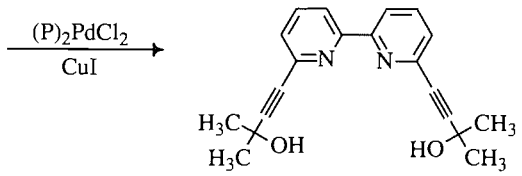
C(1)—N—C(5)	117.6(3)	C(5)—C(6)—C(7)	175.5(4)
N—C(1)—C(1a)	116.8(3)	C(6)—C(7)—C(8)	180.0(4)
N—C(1)—C(2)	122.7(3)	C(7)—C(8)—C(9)	120.4(4)
C(1a)—C(1)—C(2)	120.5(3)	C(7)—C(8)—C(13)	121.1(3)
C(1)—C(2)—C(3)	118.8(3)	C(9)—C(8)—C(13)	118.9(3)
C(2)—C(3)—C(4)	119.1(4)	C(8)—C(9)—C(10)	119.5(4)
C(3)—C(4)—C(5)	119.4(3)	C(9)—C(10)—C(11)	121.1(4)
N—C(5)—C(4)	122.2(3)	C(10)—C(11)—C(12)	120.0(4)
N—C(5)—C(6)	116.8(3)	C(11)—C(12)—C(13)	119.2(4)
C(4)—C(5)—C(6)	121.0(3)	C(8)—C(13)—C(12)	121.3(4)

[a]The second half of the molecule is related by the twofold axis with equation ($\frac{3}{4}$, *y*, 1) through the middle of the C(1)—C(1a) bond. The coordinate transformation to obtain the second half is $\frac{1}{2} - x, y, 2 - z$.

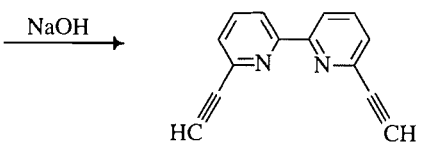
chosen is to couple 2-methylbut-3-yne-2-ol with 6,6′-dibromo-2,2′-bipyridine (25, 39), which in turn is readily available from 2,6-dibromopyridine using a methodology devised by Holm *et al.* (25). The protecting group is removed by treatment of the intermediate diol **2** with sodium hydroxide. In contrast to



1



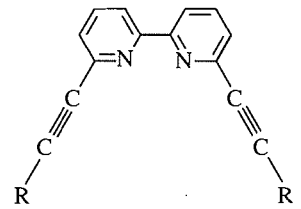
2



3*a*

the liquid 2-ethynylpyridine, which rapidly discolours in air and light in absence of added stabilizers, **3***a* is obtained as a colourless solid, which we have been able to store for periods longer than 2 years without apparent decomposition, although it does polymerize slowly in solution.

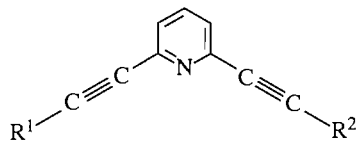
Using a similar strategy, we have been able to prepare a range of related compounds **3***b–e* from **1**. In the case of the ferrocenyl reactions, preliminary test reactions were carried out using 2,6-dibromopyridine. It was found that after 1 h at room



3

3*a*, R = H
3*b*, R = Ph
3*c*, R = 1-naphthyl
3*d*, R = ferrocenyl
3*e*, R = 2-pyridyl

temperature in the presence of approximately 5 mol% (with respect to 2,6-dibromopyridine) of catalyst the monobromo compound **4***d* could be isolated in high yield, while longer reaction times (24 h) gave the disubstituted compound **5***d*. The



4*d*, R^1 = Br, R^2 = -ferrocenyl
5*d*, $R^1 = R^2$ = -ferrocenyl

reactions were carried out at room temperature in diethylamine. In addition to the aforementioned reaction products, a considerable quantity of 1,4-ferrocenyl-but-1,4-diyne (28) is also obtained. Formation of the analogous intermediate monobromo compound is also observed in the reaction of 6,6′-dibromobipyridine, using short reaction times with ferrocenylacetylene, as well as considerable quantities of the diyne. The desired product **3***d* is obtained in high yield, on longer reaction times (24 h). Addition of THF to the amine solvent was found to be useful in increasing the solubility of the dibromo starting material and hence reaction rates. Compound **3***d* is formed as

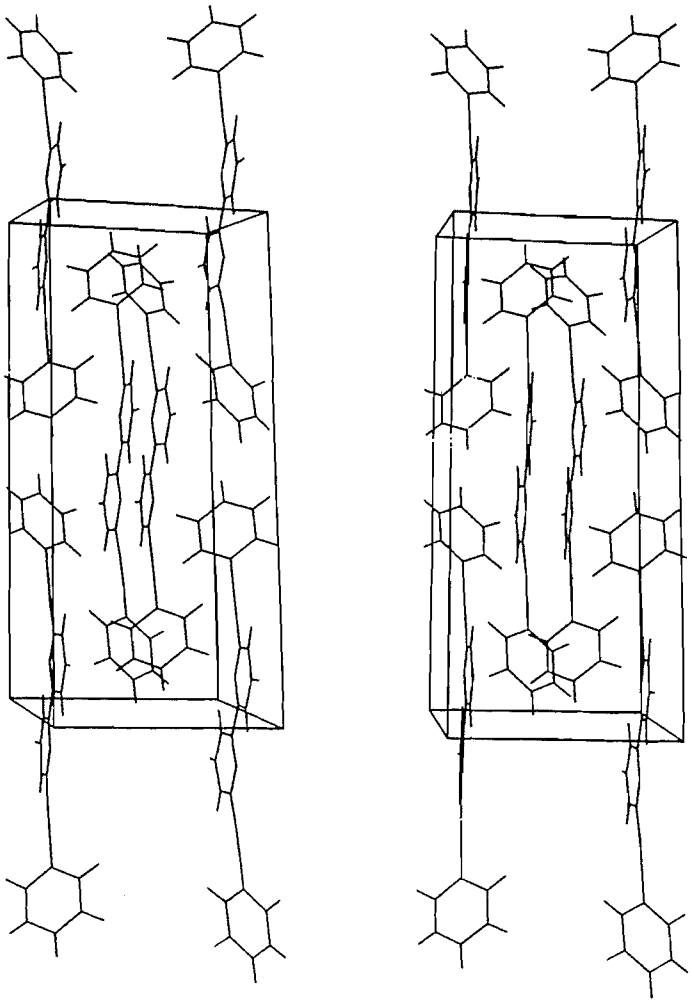


FIG. 2. A stereoscopic view packing diagram, produced using the PACKER programme in the NRCVAX package, showing the molecular packing of compound **3***b* in the unit cell. The *b* axis extends from the left to right and the *c* axis is vertical.

golden orange flakes and is, surprisingly, only sparingly soluble in dichloromethane. Initial attempts to react this compound with (1,5-cyclooctadienyl)palladium dichloride gave a powder from which we were unable to crystallize a single uncontaminated complex.

The ^{1}H NMR spectra for compounds **3***a–e* indicate little influence on the chemical shifts of the bipyridyl protons on changing substituents on the acetylene. The observed chemical shifts of the 3 and 3′ protons adjacent to the acetylene occur at approximately δ 7.5, while the 4 (4′) and 5 (5′) are observed at δ ~7.8 and 8.4 respectively.

The pyridyl rings in compound **3***b* are found with the nitrogen atoms on opposite sides, as expected, to minimize stereoelectronic interactions. The dihedral angle between the phenyl and pyridyl ring planes is 59.85(16)°. In Fig. 2, a packing diagram is shown, to illustrate the parallel packing of the molecules. The C—C triple bond length is 1.189(5) Å and is similar to that of other acetylenes. The closest contact carbon–carbon distance between the layers is approximately 3.6 Å. Compound **3***b*, if it were to serve as a useful ligand in transition metal chemistry, would be significantly hindered to chelated nitrogen coordination due to the pendant acetylenic group. Preliminary investigations indicate that the compound is capable of complex formation; however, there are indications that coordination of large transition metal ions is difficult. Our work in this area is continuing and we have been able to develop methods for the synthesis of novel polymeric compounds based on these monomers. The synthesis of bipyridylacetylene-coupled compounds of 2,2′-bipyridine is more complex and will be published separately.

Acknowledgements

This work was funded in part by a grant from the University of Ottawa faculty development fund, which is gratefully acknowledged. The palladium was supplied on loan from Johnston–Matthey Ltd. This work was made possible by the kind consideration of Professor Peter Morand of the University of Ottawa with whom C.S.-B. has completed her M.Sc. programme. We extend our thanks for the provision of his laboratory facilities to us to complete this work. I.R.B. thanks Dr. Eric Gabe and Yvon LePage of the National Research Council of Canada for their patience and guidance in the crystallographic structural determination and provision of facilities. Finally, we appreciate the extra funding from O.A.P., which was necessary to complete the project.

1. H. A. DIECK and R. F. HECK. J. Organometal. Chem. **93**, 259 (1975).
2. G. H. POSNER. Org. React. **22**, 380 (1975).
3. C. EABORN and D. R. M. WALTON. J. Organometal. Chem. **4**, 217 (1965).
4. E. NEGISHI. *In* Aspects on mechanism and organometallic chemistry. *Edited by* J. H. Brewster. Plenum Press, New York, London. 1978. p. 285.
5. S. G. DAVIES. *In* Organotransition metal chemistry: application to organic synthesis. Vol. 2. *Edited by* J. E. Baldwin. Pergamon Press, Great Britain. 1982. pp. 218–265.
6. P. M. HENRY. Adv. Organomet. Chem. **13**, 363 (1975).
7. K. EDO, H. YAMANAKA, and T. SAKAMOTO. Heterocycles, **9**, 271 (1978).
8. A. OHSAWA, Y. ABE, and H. IGETA. Chem. Lett. 241 (1979).
9. P. M. MAITLIS. *In* The organic chemistry of palladium. Vols. 1 and 2. Academic Press, New York. 1971.
10. J. TSUJI. *In* Organic chemistry with palladium compounds. Springer-Verlag, Berlin. 1980.
11. B. M. TROST. Tetrahedron, **33**, 2615 (1977).
12. J. TSUJI. Adv. Organomet. Chem. **17**, 141 (1979).
13. B. M. TROST and T. R. VEROEVEN. *In* Comprehensive organometallic chemistry. Vol. 8. *Edited by* G. Wilkinson, F. G. A. Stone, and E. W. Abel. Pergamon Press, Great Britain. 1982. p. 913.
14. E. I. BECKER and M. TSUTSUI. Organometallic reactions. Vols. 1–6. Wiley–Interscience, New York. 1970–1977.
15. E. W. STERN. *In* Transition metals in homogeneous catalysis. *Edited by* G. M. Schranzer. Marcel Dekker, New York. 1971. p. 93.
16. W. KITCHING. Organomet. Chem. Rev. **3**, 61 (1968).
17. A. AGUILO. Adv. Organomet. Chem. **5**, 321 (1967).
18. P. M. HENRY. Adv. Organomet. Chem. **13**, 363 (1975).
19. C. E. CASTRO and R. D. STEPHENS. J. Organometal. Chem. **28**, 2163 (1963).
20. D. E. AMES, D. BULL, and C. TAKUNDWA. Synthesis, 364 (1981).
21. W. L. COLLIER and R. S. MACOMBER. J. Org. Chem. **28**, 2163 (1963).
22. N. HAGIHARA, Y. KUROYAMA, and K. SONOGASHIRA. Synthesis, 627 (1980).
23. M. ROSENBLUM, N. BROWN, J. PAPENNMEIER, and M. APPLEBLAUM. J. Organomet. Chem. **6**, 173 (1966).

Can. J. Chem. Downloaded from www.nrcresearchpress.com by 198.100.157.202 on 09/07/12
For personal use only.

24. Y. OKAMOTO, K. L. CHELLAPPA, and S. K. KUNDU. J. Org. Chem. **37**, 3185 (1972).
25. R. H. HOLM, J. E. PARKS, and B. E. WAGNER. J. Organometal. Chem. **56**, 53 (1973).
26. F. H. BURSTALL. J. Chem. Soc. 1662 (1938).
27. YU. A. FIALKOV, A. M. ALEKSANDROV, and L. M. YAGUPOL'SKII. Zh. Obshch. Khim. **38**, 1741 (1968); Chem. Abstr. **70**, 19701 (1969).
28. K. SCHLÖGL and W. STREYRER. **6**, 399 (1966).
29. Y. LE PAGE, E. J. GABE, and L. CALVERT. J. Appl. Crystallogr. **12**, 25 (1979).
30. E. J. GABE, P. S. WHITE, and Y. LE PAGE. American Crystallographic Association Meeting Abstr. **14**, 24 (1986).
31. E. J. GABE, Y. LE PAGE, J.-P. CHARLAND, F. L. LEE, and P. S. WHITE. J. Appl. Crystallogr. **22**, 384 (1989).
32. International tables for X-ray crystallography. Vol. IV. Kynoch Press, Birmingham, England. 1974.
33. G. R. NEWKOME, K. J. THERIOT, F. R. FRONCZEK, and B. VILLAR. Organometallics, **8**, 2513 (1989).
34. G. R. NEWKOME, G. R. PUCKETT, G. E. KIEFER, V. K. GUPTA, F. R. FRONCZEK, D. C. PANTALEO, G. L. MCCLURE, J. B. SIMPSON, and W. A. DEUTSCH. Inorg. Chem. **24**, 811 (1985).
35. T. J. MEYER. Acc. Chem. Res. **22**, 163 (1989), and references therein.
36. A. M. PYLE, J. P. REHMANN, R. MESHOYREV, C. V. KUMAR, N. J. TURRO, and J. K. BARTON. J. Am. Chem. Soc. **111**, 3051 (1989).
37. L. BASILE and J. K. BARTON. J. Am. Chem. Soc. **111**, 1160 (1989).
38. J. K. BARTON. Chem. Eng. News, **66** (39), 30 (1988).
39. G. JUST and R. SINGH. J. Org. Chem. **59**, 4453 (1989).

Can. J. Chem. Downloaded from www.nrcresearchpress.com by 198.100.157.202 on 09/07/12
For personal use only.

Catalysis by β-cyclodextrin in the reaction of *p*-nitrophenyl acetate with α-amino acids

MÓNICA BARRA AND RITA H. DE ROSSI[1]

Instituto de Investigaciones en Físico Química de Córdoba (INFIQC), Departamento de Químicas, Universidad Nacional de Córdoba, Suc. 16, C.C. 61, 5016 Córdoba, Argentina

Received May 4, 1990

MÓNICA BARRA and RITA H. DE ROSSI. Can. J. Chem. **69**, 1124 (1991).

The reactions of *p*-nitrophenyl acetate, **1**, with both enantiomers of the following α-amino acids: alanine (**2***a*), methionine (**2***b*), leucine (**2***c*), and tryptophan (**2***d*), were studied in the presence of β-cyclodextrin (β-CD). All the reactions were catalyzed by β-CD and no chiral discrimination was observed. The reactions of **1** with the D isomers of **2***a* and **2***d* were also studied in the presence of α- and γ-CD. In both cases the catalysis increased in the order α < γ < β-CD. Also, to analyze the influence of the polar nature of the nucleophile, the reactions of **1** with both enantiomers of the methyl esters of **2***a*, **2***c*, and **2***d* were studied in the presence of β-CD. The catalysis observed was significantly smaller than that for the reactions with the amino acids. It is suggested that the catalysis by CDs is due to the formation of a ternary hydrogen-bonding complex that results from the association of the amino acid with the complexed substrate. The effect of the size of the CD cavity on the observed catalysis is attributed to the geometrical requirements for the reaction. The decrease in catalysis in the reactions with the methyl esters is due to a weaker hydrogen-bonding association with these neutral nucleophiles.

Key words: cyclodextrins, catalysis, ester aminolysis.

MÓNICA BARRA et RITA H. DE ROSSI. Can. J. Chem. **69**, 1124 (1991).

On a étudié les réactions de l'acétate de *p*-nitrophényle, **1**, avec les deux énantiomères de acides α-aminés suivants : alanine, **2***a*, méthionine, **2***b*, leucine, **2***c*, et tryptophane, **2***d*, en présence de β-cyclodextrine (β-CD). Toutes les réactions sont catalysées par la β-CD et on n'a observé aucune discrimination chirale. On a aussi étudié les réactions du composé **1** avec les isomères D des produits **2***a* et **2***d*, en présence des α- et des γ-cyclodextrines. De plus, afin d'analyser l'influence de la nature polaire du nucléophile, on a étudié les réactions du composé **1** avec les deux énantiomères des esters méthyliques des composés **2***a*, **2***c* et **2***d*, en présence de β-CD. La catalyse observée est beaucoup plus faible que celle pour les réactions avec les acides aminés. On suggère que la catalyse par les CD est due à la formation d'une liaison hydrogène ternaire complexe résultant de l'association de l'acide aminé avec le substrat complexé. L'effet de la grosseur de la cavité de la CD sur la catalyse observée est attribué à des impératifs géométriques de la réaction. La diminution de la catalyse avec les esters méthyliques est due au fait que la liaison hydrogène avec les nucléophiles neutre est plus faible.

Mots clés : cyclodextrines, catalyse, aminolyse des esters.

[Traduit par la rédaction]

Introduction

Cyclodextrins (CDs) are cyclic oligomers of six to eight glucose units capable of forming inclusion complexes with a great variety of guest compounds (for recent reviews, see ref. 1). As a result, CDs exhibit catalytic properties in various reactions. However, it was recently shown that these catalytic properties may be due not only to the formation of an inclusion complex but also to the formation of a hydrogen-bonding complex (2). The effective formation of the latter results from the large proton-donating ability of the secondary hydroxyl groups located outside the cavity of CDs.

CDs are also capable of chiral recognition, a property that has been shown to have a marked interest in fundamental (3) as well as in applied studies (4). In this regard, we recently reported that the reactions of 1-fluoro-2,4-dinitrobenzene with both enantiomers of natural α-amino acids are selectively catalyzed by β-cyclodextrin (β-CD), the member containing seven glucose units (5). The catalysis and chiral discrimination are ascribed to the formation of a ternary inclusion complex where both reactants are included in the same cavity of β-CD. This study led us to continue analyzing the catalytic properties and potential chiral recognition by β-CD in nucleophilic substitution reactions with α-amino acids as nucleophiles. We wish to report here our results regarding the reaction of *p*-nitrophenyl acetate, **1**, with α-amino acids in the presence of β-CD.

[1]Author to whom correspondence may be addressed.

Results

The reaction of **1** with α-amino acids **2** leads to the formation of *p*-nitrophenol and the corresponding *N*-acetyl-α-amino acids (eq. [1]). Depending on pH, the hydrolysis reaction of **1** competes with eq. [1].[2]

The aminolysis of esters proceeds through a bimolecular mechanism that involves the formation and decomposition of a tetrahedral addition intermediate, **3** (eq. [2]) (7). The decomposition of **3** is characterized by several proton transfers and therefore the aminolysis reaction may be suceptible to acid–base catalysis (8).

To determine the rate-limiting step corresponding to the reaction described in eq. [1], pseudo-first-order rate constants (k_{obs}) for the reaction of **1** with the L isomers of **2** were obtained as a function of amino acid concentration at constant pH (see Table I).[3] In all cases the plots of k_{obs} vs. the total concentration of **2** ($[\mathbf{2}]_T$) were linear, showing that the amino acids did not act as

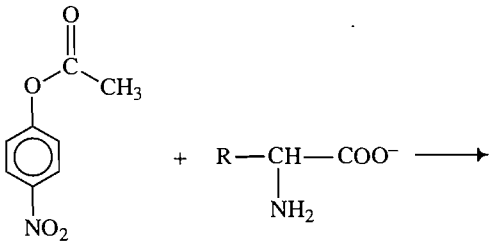
[2]The amino acid is assumed to react only through the nitrogen and not through the carboxylate because it is known that amines are about 10^5 times more reactive than carboxylates, see ref. 6.

[3]Supplementary material: Table I containing the observed pseudo-first-order rate constants for the reaction of **1** with **2** (2 pages), Table II containing rate constants for the reaction of **1** with **4** at varying concentrations of β-CD (2 pages). Copies of these tables may be purchased from: The Depository of Unpublished Data, Document Delivery, CISTI, National Research Council Canada, Ottawa, Canada K1A 0S2.

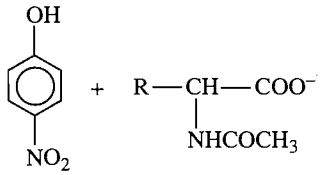
Printed in Canada / Imprimé au Canada

Can. J. Chem. Downloaded from www.nrcresearchpress.com by 198.100.157.202 on 09/07/12
For personal use only.

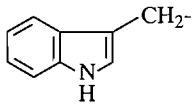
Can. J. Chem. Downloaded from www.nrcresearchpress.com by 198.100.157.202 on 09/07/12
For personal use only.

[1] 

1 **2**

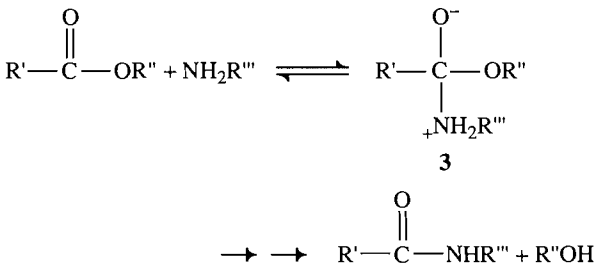


R (amino acid):



CH_3-	$CH_3SCH_2CH_2$-	$(CH_3)_2CHCH_2$-	
Alanine	Methionine	Leucine	Tryptophan
2*a*	**2***b*	**2***c*	**2***d*

catalysts. From the slopes of these plots and the fraction of the anionic form of the corresponding amino acid (nucleophilic species), the second-order rate constant of aminolysis k_A was calculated (Table 1). The values thus obtained decrease as the pK_a value decreases, consistent with the fact that the reactivity of **2** depends mainly on pK_a (9). Besides, the k_A values are independent of pH, indicating that HO^- is not a catalyst. The fact that the second-order rate constant of aminolysis does not depend on either the HO^- or the amino acid concentration indicates that the rate-limiting step for the reaction of **1** and **2** is the addition of the amino acid to generate the tetrahedral intermediate **3** (7).

[2] 

3

Effect of β-cyclodextrin

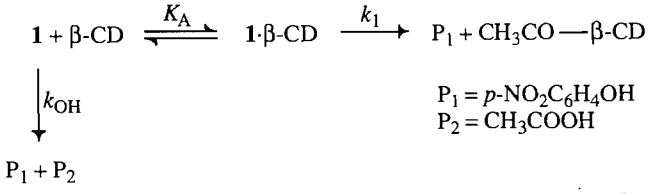
The reaction of **1** with **2** competes, under our experimental conditions (DMSO–water, 2% v/v; pH = 9.878; T = 25°C), with the hydrolysis reaction of **1**. Since it has been shown that the latter reaction is catalyzed by cyclodextrins through a covalent mechanism that involves the nucleophilic attack by one of the HO^- groups of the cyclodextrins on the substrate (10), it was necessary to determine first the kinetic parameters for the hydrolysis of **1** in the presence of β-CD. According to literature data the reaction pathways for this system can be represented as shown in Scheme 1, where **1**·β-CD represents the inclusion complex of **1** with β-CD, K_A represents the association equilibrium constant for this complex, and k_{OH} and k_1 represent the pseudo-first-order rate constants for the hydrolysis of the free substrate and for the release of *p*-nitrophenol by acetylation of β-CD, respectively.

The expression of the pseudo-first-order rate constant (k_{OH}^{CD})

TABLE 1. Second-order rate constants for the reaction of *p*-nitrophenyl acetate with α-amino acids in water solution[a]

Amino acid	pK_a[b]	k_A, $M^{-1}s^{-1}$
Alanine	9.87	0.559 ± 0.004[c]
		0.54 ± 0.07[d]
Leucine	9.74	0.45 ± 0.01[c]
Tryptophan	9.44	0.34 ± 0.01[c]
Methionine	9.27	0.217 ± 0.004[c]

[a]Solvent DMSO–water (2% v/v); μ = 0.2 M (NaCl); T = 25°C.
[b]Reference 20.
[c]pH = 9.878 ± 0.001.
[d]pH = 8.920 ± 0.001.



SCHEME 1

for this scheme is given by eq. [3]:

$$[3]\quad k_{OH}^{CD} = \frac{(k_1 - k_{OH})K_A[\beta\text{-CD}]}{1 + K_A[\beta\text{-CD}]} + k_{OH}$$

Under our experimental conditions, k_{OH} was independently determined in the absence of β-CD whereas k_1 and K_A were calculated by nonlinear adjustment of eq. [3] for k_{OH}^{CD} values obtained at constant pH and varying β-CD concentrations (Table 2). The parameters thus obtained were $k_1 = (1.1 \pm 0.2) \times 10^{-2} s^{-1}$ and $K_A = (67 \pm 22)\ M^{-1}$.

This value of K_A is somewhat lower than that already reported, namely 164 ± 35 M^{-1} (10). To see whether this discrepancy is due to the different reaction conditions, we determined the kinetic parameters under the same conditions as those of the previous work, obtaining $K_A = 79 \pm 12\ M^{-1}$.

To investigate the effect of β-CD on the reaction described in eq. [1], pseudo-first-order rate constants (k_{obs}^{CD}) for the reaction of **1** with the D and L isomers of **2** were determined as a function of β-CD concentration ($[\beta\text{-CD}]_T$), at constant amino acid concentration and at constant pH (Table 3). In all cases, k_{obs}^{CD} increased as $[\beta\text{-CD}]_T$ increased, approaching a maximum saturation value similar to the behavior observed in enzyme kinetics (Fig. 1 is representative). These enzyme-like kinetics are also observed when the pseudo-first-order rate constants for the aminolysis reactions (obtained from the difference between k_{obs}^{CD} and the corresponding k_{OH}^{CD} are plotted vs. $[\beta\text{-CD}]_T$.

We also measured the reaction rate of **1** with the L-alanine **2***a* as a function of soluble starch (a linear analog of cyclodextrins) at constant pH and constant amino acid concentration (Table 3). The observed rate constant in the presence of 2×10^{-3} M starch is about 20% lower than in water at the same pH. These results indicate that the effect of β-CD on eq. [1] involves some specific type of interaction.

The reactions with the L isomers of alanine **2***a* and leucine **2***c* were also studied as a function of amino acid concentration, at

TABLE 2. Effect of β-cyclodextrin on the observed pseudo-first-order rate constants for the hydrolysis of *p*-nitrophenyl acetate[a]

Run	10^3 [β-CD]$_T$, M	10^3 k_{OH}, s^{-1}
1[b]		0.815
2[b]	1.01	1.28
3[b]	4.00	3.14
4[b]	7.01	3.72
5[b]	10.0	5.15
6[b]	15.0	5.83
7[c]		3.97
8[c]	2.01	13.2
9[c]	3.38	18.2
10[c]	4.03	20.2
11[c]	8.06	29.2
12[c]	8.28	30.5
13[c]	10.4	34.2
14[c]	12.0	38.5
15[c]	15.0	39.3

[a]μ = 0.2 M (NaCl); T = 25°C; $[\mathbf{1}]_0 = 4.5 \times 10^{-5}$M.
[b]Solvent DMSO–water (2% v/v); pH = 9.878 ± 0.001.
[c]Solvent acetonitrile–water (0.5% v/v), pH = 10.600, Na_2CO_3 buffer.

constant pH and constant β-CD concentration (Table 3). In both cases the plots of k_{obs}^{CD} vs. $[\mathbf{2}]_T$ are linear, indicating that the presence of β-CD does not induce a change in the rate-limiting step.

To analyze the effect of the size of the cyclodextrin, the reactions of **1** with the D isomers of alanine **2***a* and tryptophan **2***d* were studied as a function of α- (the member with six glucose units) and γ-cyclodextrin (the member with eight glucose units) concentrations (Table 4). In all cases k_{obs} increases linearly as CD concentration increases.

On the other hand, and in order to investigate the influence of the polar nature of the nucleophile on the aminolysis reaction of **1** in the presence of β-CD, we measured the rate of reaction of **1** with the D and L isomers of the methyl esters **4** of alanine, leucine, and tryptophan at pH ≈ 8.3. In the absence of β-CD, the pseudo-first-order rate constant for aminolysis k_A increases linearly with the concentration of ester (Table 5). The reactivity of these nucleophiles (Table 1) is lower than that corresponding to the α-amino acids (Table 2), in agreement with the fact that the proton ionization constants of the methyl esters are smaller than those of the α-amino acids (11). In the presence of β-CD the second-order rate constant of aminolysis shows enzyme-like kinetics as a function of $[\beta\text{-CD}]_T$ (Table II).[3] The catalysis observed is, however, significantly smaller than that for the reaction with **2**. For instance, the rate of aminolysis of **1** is increased by a factor of 7 in the presence of 15 mM β-CD when D-alanine is the nucleophile, and only by a factor of 1.5 when D-alanine methyl ester is the nucleophile.

Discussion

α-Amino acids are capable of forming 1:1 inclusion complexes with cyclodextrins (12) and, therefore, the catalysis observed in the reaction of **1** and **2** in the presence of β-cyclodextrin might involve the complexed amino acids. However, the association equilibrium constants for 1:1 inclusion complexes between β-CD and **2** are smaller than 10 M^{-1} in water (5), and therefore the amount of complexed amino acids will be less than 10% at the highest β-CD concentration used. Under these conditions, the catalytic pathway involving the reaction of **1** with **2**:CD complex would be observed only if it were very efficient.

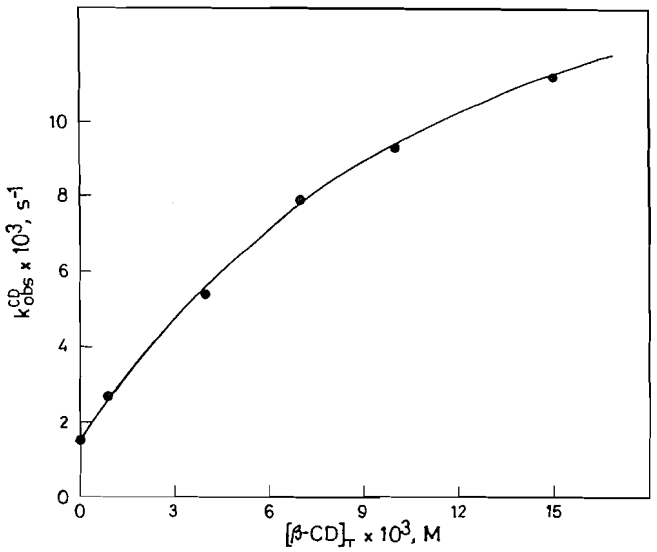


FIG. 1. k_{obs} vs. β-cyclodextrin concentration for the reaction of **1** with L-alanine (data from Table 3).

α-Amino acids are also capable of forming ternary inclusion complexes in which both reactants are included in the same cavity (5), and hence the catalysis might involve a complex of this type. However, since no significant dependence on the size of amino acid or on stereoisomerism has been observed, it is unlikely that the catalytic pathway involves a ternary complex where **1** and **2** are included in the CD cavity.

As we have mentioned previously, it has been shown that the cavity of cyclodextrins is not essential for complex formation and as a consequence, for catalysis (2). The P—O(2′) cleavage of 2′,3′-cyclic monophosphates of ribonucleosides is regioselectively catalyzed by α-cyclodextrin and the catalysis is ascribed to the formation of hydrogen-bonding complexes between α-CD and the ribonucleosides. The effective formation of this type of complex results from the large proton-donating ability of the secondary hydroxyl groups of cyclodextrins (2). Besides, it has also been observed that the hydrogen-bonding association of alcohol molecules with 1:1 inclusion complexes provides additional rigidity to the system, which has been shown to have a marked effect on the properties of the included molecule (13). Thus, the catalysis observed in the reaction of **1** with **2** in the presence of β-CD may be ascribed to the formation of a ternary hydrogen-bonding complex generated by the association between the α-amino acid and the inclusion complex **1**·β-CD as shown in Fig. 2. This association leads to an increase in the residence time of the nucleophile close to the reacting center of the electrophile, which results in a greater effect on rate (14).

We therefore suggest that the overall mechanism for the reaction of **1** with **2** in the presence of β-CD can be described as shown in Scheme 2, where T represents the ternary hydrogen-bonding complex, K_T represents the equilibrium association constant for this complex, and k_2 represents the first-order rate constant for the aminolysis reaction within the ternary complex.

The expression of k_{obs}^{CD} for this scheme is given by eq. [4]:

Can. J. Chem. Downloaded from www.nrcresearchpress.com by 198.100.157.202 on 09/07/12
For personal use only.

TABLE 3. Observed pseudo-first order rate constants for the reaction of *p*-nitrophenyl acetate with α-amino acids in the presence of β-cyclodextrin[a]

Run	10^3 [**2**]$_T$, M	10^3 [β-CD]$_T$, M	$10^3 k_{obs}$, s^{-1}
	D-Alanine		
1	2.02		1.58
2	2.02	1.01	2.77 ± 0.05
3	2.02	4.00	5.02 ± 0.05
4	2.02	7.01	7.40 ± 0.08
5	2.02	10.0	9.60 ± 0.08
6	2.02	15.0	11.2 ± 0.2
	L-Alanine		
7	2.02		1.56
8	2.02	1.01	2.68 ± 0.03
9	2.02	4.00	5.4 ± 0.1
10	2.02	7.01	7.9 ± 0.1
11	2.02	10.0	9.3 ± 0.5
12	2.02	15.0	11.2 ± 0.2
13	2.07	5.01	3.9 ± 0.1
14	4.14	5.01	4.7 ± 0.2
15	6.16	5.01	5.2 ± 0.2
16	8.21	5.01	5.9 ± 0.2
17	10.3	5.01	6.4 ± 0.2
18	2.00	0.67[b]	1.31
19	2.00	1.34[b]	1.43
20	2.00	2.01[b]	1.30
	D-Leucine		
21	2.01		1.33 ± 0.06
22	2.01	1.09	2.59 ± 0.03
23	2.01	4.10	5.19 ± 0.06
24	2.01	7.00	7.05 ± 0.07
25	2.01	10.0	8.78 ± 0.03
26	2.01	15.0	10.5 ± 0.1
	L-Leucine		
27	2.06		1.20 ± 0.02
28	2.06	1.08	2.35 ± 0.01
29	2.06	4.18	5.0 ± 0.1
30	2.06	7.02	6.9 ± 0.1
31	2.06	10.0	8.1 ± 0.2
32	2.06	15.0	9.5 ± 0.4
34	0.509	15.0	10.0 ± 0.3
35	1.02	15.0	10.2 ± 0.3
36	2.04	15.0	10.7 ± 0.2
37	3.06	15.0	11.8 ± 0.2
38	5.09	15.0	12.5 ± 0.2
39	10.2	15.0	15.0 ± 0.1
	D-Tryptophan		
40	2.01		1.56
41	2.01	1.01	2.42 ± 0.02
42	2.01	4.00	5.8 ± 0.1
43	2.01	7.01	7.8 ± 0.3
44	2.01	10.0	9.8 ± 0.3
45	2.01	15.0	12.5 ± 0.2
	L-Tryptophan		
46	2.01		1.63
47	2.01	1.01	2.50 ± 0.09
48	2.01	4.00	5.82 ± 0.03
49	2.01	7.01	8.3 ± 0.2
50	2.01	10.0	9.8 ± 0.5
51	2.01	15.0	12.5 ± 0.2

TABLE 3. (*concluded*)

Run	10^3 [**2**]$_T$, M	10^3 [β-CD]$_T$, M	$10^3 k_{obs}$, s^{-1}
	L-Methionine		
52	2.00		1.04 ± 0.04
53	2.00	1.13	2.33 ± 0.08
54	2.00	3.85	4.8 ± 0.1
55	2.00	7.38	7.2 ± 0.2
56	2.00	15.1	10.5 ± 0.3

[a]Solvent DMSO–water (2% v/v); μ = 0.2 M (NaCl); T = 25°C; $[\mathbf{1}]_0$ = (4–4.5) × 10^{-5} M; pH = 9.878 ± 0.001.

[b]Soluble starch instead of β-cyclodextrin is added; the concentration was calculated assuming FW = 1135.

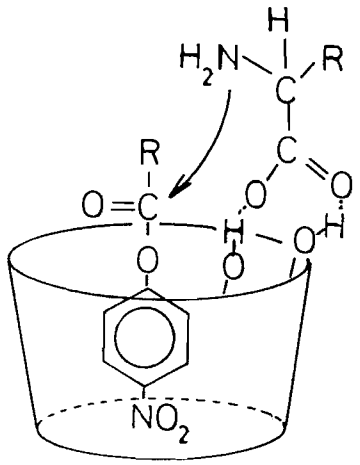
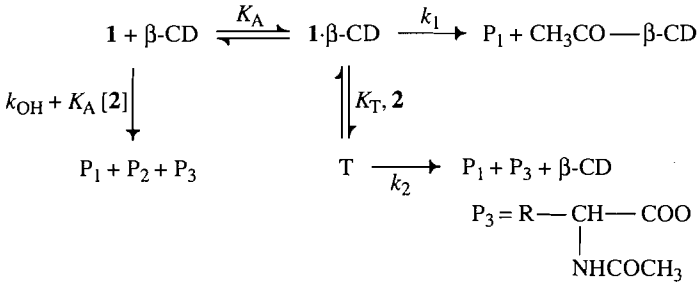


FIG. 2. Schematic representation of the ternary complex of cyclodextrin, *p*-nitrophenyl acetate, and an amino acid.



SCHEME 2

$$[4]\quad k_{obs}^{CD} = k_o + \frac{\{k_1 + k_2 K_T[\mathbf{2}] - k_o(1 + K_T[\mathbf{2}])\} K_A[\beta\text{-CD}]}{1 + K_A(1 + K_T[\mathbf{2}])[\beta\text{-CD}]}$$

$$k_o = k_{OH} + k_A[\mathbf{2}]$$

By nonlinear adjustment of eq. [4] for k_{obs}^{CD} values obtained at constant amino acid concentration and varying concentrations of β-CD, the parameters $P(1) = \{k_1 + k_2 K_T[\mathbf{2}] - k_o(1 + K_T[\mathbf{2}])\}K_A$ and $P(2) = K_A(1 + K_T[\mathbf{2}])$ were calculated (Table 6). The value of $P(2)$ is almost the same for all the amino acids and equal to K_A, indicating that $K_T[\mathbf{2}] << 1$ and therefore $K_T < 100\ M^{-1}$. Also, $P(1)$ does not depend on the stereoisomer.

The expression of k_{obs}^{CD} (eq. [4]) can be simplified to eq. [5]:

Can. J. Chem. Downloaded from www.nrcresearchpress.com by 198.100.157.202 on 09/07/12
For personal use only.

TABLE 4. Observed pseudo-first-order rate constant for the reaction of *p*-nitrophenyl acetate with α-amino acids in the presence of cyclodextrins[a]

Run	$10^3[CD]_T$, M	$10^3 k_{obs}$, s^{-1}	Run	$10^3[CD]_T$, M	$10^3 k_{obs}$, s^{-1}
		D-Alanine			
1[b]		1.18	7[c]		0.675
2[b]	2.18	1.58	8[c]	2.00	1.36
3[b]	4.59	1.51	9[c]	4.46	1.51
4[b]	8.21	1.81	10[c]	7.86	2.35
5[b]	11.8	1.58	11[c]	11.9	3.57
6[b]	17.6	2.31	12[c]	15.1	4.29
		D-Tryptophan			
13[d]		0.946	19[e]		0.708
14[d]	2.83	1.06	20[e]	2.05	1.56
15[d]	4.26	1.25	21[e]	3.98	2.51
16[d]	8.14	1.44	22[e]	8.00	4.25
17[d]	10.2	1.38	23[e]	12.1	6.01
18[d]	15.6	1.64	24[e]	15.0	6.55

[a]Solvent DMSO-water (2% v/v); μ = 0.2 M (NaCl); $[\mathbf{1}]_0 = 4 \times 10^{-5}$ M; T = 25°C.
[b]α-Cyclodextrin; $[\mathbf{2}]_T = 2.03 \times 10^{-3}$ M, pH = 9.78.
[c]γ-Cyclodextrin; $[\mathbf{2}]_T = 2.00 \times 10^{-3}$ M, pH = 9.48.
[d]α-Cyclodextrin; $[\mathbf{2}]_T = 2.09 \times 10^{-3}$ M, pH = 9.66.
[e]γ-Cyclodextrin; $[\mathbf{2}]_T = 2.01 \times 10^{-3}$ M, pH = 9.50.

$$[5] \quad k_{obs}^{CD} = k_o + \frac{(k_1 + k_2 K_T [\mathbf{2}] - k_o) K_A [\beta\text{-CD}]}{1 + K_A [\beta\text{-CD}]}$$

Since k_1 and k_0 are known, it was possible to calculate the product k_2K_T from the $P(1)$ values (Table 6). The values of k_2K_T represent the rate constant for the reaction of the complex **1**·CD with **2**. Comparing these values with the second-order rate constants for **1** and **2** (Table 2), we conclude that the complex is 20–30 times more reactive than the free substrate.

For the reactions of **1** with **2***a* and **2***d* in the presence of α- and γ-cyclodextrins, the plots of k_{obs}^{CD} vs. $[CD]_T$ are linear, indicating that in both cases $K_A[CD] << 1$ and therefore $K_A < 7$ M^{-1}. These results are consistent with the fact that the structure, stability, and reactivity of cyclodextrin complexes depend on the size of the CD cavity (1). The catalytic factor, defined as $C = (k_1 + k_2 K_T [\mathbf{2}] - k_0) K_A$, is shown in Table 7 as a function of the type of cyclodextrin. With both amino acids, C increases in the order α < γ < β and, except with γ-CD, there is no dependence on the type of amino acid. The change in the catalytic factor cannot be attributed to changes either in K_A or in the catalysis for the hydrolysis reaction (k_1), since in such a case a difference of only a factor of three would be expected for α- and β-CD (10). The dependence of the catalytic factor on the size of the CD cavity would reveal a change in the geometry of the complex and hence must be determined by the geometrical requirements to reach the most appropriate distances for reaction. On the other hand, the higher catalysis observed in the reactions with **2***d* in the presence of γ-CD might be due to the contribution of other pathways such as the formation of a tight ternary inclusion complex, which would result in a greater effect on rate.

The effective formation of the hydrogen-bonding ternary complex, and therefore the catalysis, should be reduced if the hydrogen association is prevented. The catalysis observed in the reactions with the methyl esters of alanine, leucine, and tryptophan is significantly smaller than that for the reactions with **2**, and this result is interpreted as a consequence of a weaker association with these neutral nucleophiles. According to Scheme 2, the second-order rate constant for aminolysis (k_A) is given by eq. [6]:

TABLE 5. Observed pseudo-first-order rate constants for the reaction of *p*-nitrophenyl acetate with α-amino acids methyl esters[a]

Run	$10^2[\mathbf{4}]_T$, [b]M	pH	$10^4 k_{obs}$, s^{-1}
	L-Alanine methyl ester		
1	0.553	8.925	1.88
2	0.765	8.682	1.78
3	1.01	9.085	3.65
4	2.18	8.942	6.72
5	3.08	8.690	6.15
6	4.12	8.886	10.4
7	5.10	8.815	12.2
	L-Tryptophan methyl ester		
8	0.539	8.762	1.31
9	1.00	8.540	1.64
10	2.00	8.425	2.64
11	3.01	8.264	3.60
12	4.01	8.265	4.53

[a]Solvent DMSO–water (2% v/v); μ = 0.2 M (NaCl); T = 25°C; $[\mathbf{1}]_0$ = (4–4.5) × 10^{-5} M.
[b]Represents the total concentration of the nucleophile.

TABLE 6. Kinetic parameters for the reactionof *p*-nitrophenyl acetate with α-amino acids in the presence of β-cyclodextrin[a]

Amino acid		$P(1)$, [b]M^{-1} s^{-1}	P (2), [c]M^{-1}	$k_2 K_T$, M^{-1} s^{-1}
Alanine	D	1.3 ± 0.3	61.1 ± 0.3	10.6
	L	1.22 ± 0.09	59.8 ± 0.1	10.9
Leucine	D	1.16 ±0.05	59.7 ± 0.1	8.4
	L	1.1 ± 0.1	59.3 ± 0.2	7.8
Tryptophan	D	1.4 ± 0.2	61.6 ± 0.2	8.5
	L	1.4 ± 0.1	62.2 ± 0.6	8.7
Methionine	L	1.22 ± 0.05	62.2 ± 0.6	6.1

[a]Solvent DMSO–water (2% v/v); μ = 0.2 M (NaCl); T = 25°C; $[\mathbf{1}]_0$ = (4–4.5) × 10^{-5} M.
[b]$P(1) = \{k_1 + k_2 k_T [\mathbf{2}] - k_0 (1 + K_T [\mathbf{2}])\} K_A$.
[c]$P(2) = K_A (1 + K_T [\mathbf{2}])$.

Can. J. Chem. Downloaded from www.nrcresearchpress.com by 198.100.157.202 on 09/07/12
For personal use only.

TABLE 7. Catalytic factor for the reaction of *p*-nitrophenyl acetate with α-amino acids in the presence of cyclodextrins[a]

CD	Alanine	Tryptophan
α	0.050	0.044
γ	0.24	0.44
β	1.3	1.4

[a]Solvent DMSO–water (2% v/v); μ = 0.2 M (NaCl); T = 25°C; $[\mathbf{1}]_o$ = (4–4.5) × 10^{-5} M; catalytic factor = $(k_1 + k_2 K_T [\mathbf{2}] - k_0)K_A$, $M^{-1} s^{-1}$.

TABLE 8. Kinetic parameters for the reaction of *p*-nitrophenyl acetate with α-amino acid methyl esters in the presence of β-cyclodextrin.[a]

		$10^2 k_2 K_T$, $M^{-1} s^{-1}$		
Amino acid	$10^2 k_A$, $M^{-1} s^{-1}$	D	L	f[b]
Alanine	2.3	4.55	4.52	0.5
Leucine	2.2	3.3	3.4	1.8
Tryptophan	1.18	≈1.18	≈1.18	3.4

[a]Solvent DMSO–water (2% v/v); μ = 0.2 M (NaCl); T = 25°C; $[\mathbf{1}]_0$ = (4–4.5) × 10^{-5} M.

[b]Hydrophobicity value (see ref. 15).

$$[6] \quad k_A^{CD} = \frac{(k_2 K_T - k_A) K_A [\beta\text{-CD}]}{1 + K_A [\beta\text{-CD}]} + k_A$$

Since k_A and K_A are known, we could calculate the product $k_2 K_T$ by nonlinear adjustment of eq. [4] for k_A^{CD} values obtained at varying concentrations of β-CD. The resulting data are shown in Table 8 together with the hydrophobicity values (f) for the corresponding α-amino acids (15). Comparing these values, we can see that the catalysis decreases as the pK_a decreases and f increases. The decrease in catalysis as measured by $k_2 K_T$ is higher than that expected from the decrease in the reactivity of the nucleophiles and it is also higher than the decrease observed in $k_2 K_T$ for reactions with **2** (compare the last columns of Tables 6 and 8). This result is ascribed to an increase in the influence of the hydrophobic substituent in the nucleophile on the properties of the ternary hydrogen-bonding complex.

Conclusions

We found that the reactions of *p*-nitrophenyl acetate **1** with α-amino acids **2** are catalyzed by β-CD. The catalysis is attributed to the formation of a hydrogen-bonding complex, which results from the association between the amino acid and the complexed substrate. The effective formation of this type of ternary complex is based on the ability of the nucleophile to form hydrogen bonds with the hydroxyl groups of CDs. This association results in an increase in the rate of reaction of **1** with **2** by about 20–30 times when the substrate is bound to β-CD. The decrease in catalysis observed in the reactions with methyl esters and hence the increase in the influence of the hydrophobic substituent in the nucleophile would be consistent with this mechanism. On the other hand, the dependence of the catalytic factor for the reaction of **1** and **2** upon the size of the CD cavity would be determined by the geometrical requirements for the reaction, this being a characteristic of noncovalent catalysis (1).

Experimental section

Aqueous solutions were made up from water purified in a Millipore apparatus. DMSO was distilled under vacuum and stored over molecular sieves (4 Å).

α-Cyclodextrin (Aldrich), β-cyclodextrin, γ-cyclodextrin, α-amino acids, D- and L-α-tryptophan methyl ester hydrochlorides, and soluble starch (Sigma) were used as received.

p-Nitrophenyl acetate was prepared by the reaction of *p*-nitrophenol (2 mmol) with acetic anhydride (2.5 mmol) in dry pyridine at room temperature. The mixture was stirred for 1 h in the dark, and the product was precipitated by the addition of cold water. The solid was filtered out, washed with aqueous bicarbonate, water, and ethanol, and then dried under vacuum, mp 77–78°C (lit. (16) mp 79–80°C).

Alanine and leucine methyl ester hydrochlorides were prepared by esterification of the corresponding α-amino acid with $SOCl_2$ in dry methanol. The mixture was stirred for 1 h at 0°C and then heated for 2 h at 40°C. After cooling, the solvent was removed under reduced pressure and the product was dried under vacuum. The melting points were in good agreement with the literature data: alanine, mp 110–111°C (lit. (17) mp 109–111°C); leucine, mp 151–152°C (lit. (18) mp 150–151°C).

Kinetic procedures

Reactions with α-amino acids were initiated by adding the substrate dissolved in DMSO to a solution containing all the other constituents, whereas the reactions with α-amino acid methyl esters were initiated by adding 1 N NaOH (in the amount necessary to reach the pH desired) to the solutions containing the substrate and all the other constituents in order to avoid the basic hydrolysis of the nucleophile. The total DMSO concentration was 2%.

All the reactions were run under pseudo-first-order conditions, at 25°C and at constant ionic strength using NaCl as compensating electrolyte. The observed rate constants were determined by following the appearance of *p*-nitrophenoxide ion at 400 nm. The change in absorbance during a kinetic run was recorded on a Beckman 24 spectrophotometer or on a Shimadzu 260 recording spectrophotometer, both with a thermostated cell compartment. The reactions with α-amino acids were followed up to 80–90% conversion, whereas the reactions with methyl esters were followed up to 50% conversion. We did not detect any deviation from the pseudo-first-order behavior in these conditions.

The pH of the solutions containing varying concentrations of cyclodextrin and constant concentrations of α-amino acid was adjusted to the pH of the solution without CD by adding a drop of dilute acid or base. The buffer was the same amino acid. The rate of hydrolysis of **1** at different β-CD concentrations was measured without buffer (Table 2, runs 1–6), with Na_2CO_3 buffer at pH 10.600, and with 0.5% acetonitrile (Table 2, runs 7–16), with latter being the conditions used in a reported work (10). To avoid the basic hydrolysis of α-amino acid methyl esters, the pH of these solutions was measured just at the beginning of each kinetic run and therefore was not adjusted. Thus it was necessary to determine the second-order rate constants for these reactions. Since the rate of acylation of CDs shows a first-order dependence on hydroxide ion below pH 11 (19), we used the observed rate constants for hydrolysis measured at pH 9.878 in the presence of β-CD (k_{OH}^{CD}) to calculate the second-order rate constant of aminolysis (k_A^{CD}) as follows:

$$[7] \quad k_A^{CD} = (k_{obs}^{CD} - k_{OH}^{CD}\, 10^{-9.878}/10^{-pH_{obs}})/[\mathbf{4}]$$

where k_{obs}^{CD} represents the observed pseudo-first-order rate constant, pH_{obs} represents the measured pH, and [**4**] represents the concentration of α-amino acid methyl ester in the neutral form, estimated by using the acid–base dissociation constant in water (11).

Acknowledgments

This research was supported in part by the Consejo Nacional de Investigaciones Científicas y Técnicas, Argentina (CONICET), and the Consejo Provincial de Investigaciones Científicas y Tecnológicas de Córdoba, Argentina (CONI-

Can. J. Chem. Downloaded from www.nrcresearchpress.com by 198.100.157.202 on 09/07/12
For personal use only.

COR). M. Barra is a grateful recipient of a fellowship from CONICET.

1. M. L. BENDER and M. KOMIYAMA. Cyclodextrin chemistry. Springer-Verlag, New York. 1977; W. SAENGER. Angew. Chem. Int. Ed. Engl. **19**, 344 (1980); I. TABUSHI. Acc. Chem. Res. **15**, 66 (1982); C. SIRLIN. Bull. Soc. Chim. Fr. II-5 (1984); I. TABUSHI and Y. KURODA. Adv. Catal. **32**, 417 (1983).
2. M. KOMIYAMA. J. Am. Chem. Soc. **111**, 3046 (1989).
3. R. FORNASIER, F. RENIERO, P. SCRIMIN, and U. TONELLATO. J. Chem. Soc. Perkin Trans. 2, 1121 (1987).
4. D. W. ARMSTRONG. J. Liq. Chromatogr. **7** (S-2), 353 (1984).
5. M. BARRA and R. H. DE ROSSI. J. Org. Chem. **54**, 5020 (1989).
6. W. P. JENCKS and J. CARRIUOLO. J. Am. Chem. Soc. **82**, 1778 (1960).
7. W. P. JENCKS. Catalysis in chemistry and enzymology. McGraw–Hill, New York. 1969. Chap. 10.
8. I. M. KOVACH, M. BELZ, M. LARSON, S. ROUSY, and R. L. SCHOWEN. J. Am. Chem. Soc. **107**, 7360 (1985).
9. W. P. JENCKS and J. CARRIUOLO. J. Am. Chem. Soc. **82**, 675 (1960).
10. R. L. VAN ETTEN, J. F. SEBASTIAN, C. A. CLOWES, and M. L. BENDER. J. Am. Chem. Soc. **89**, 3242 (1967).
11. (*a*) J. W. HAY and L. J. PORTER. J. Chem. Soc. (B), 1261 (1967); (*b*) R. W. HAY and P. J. MORRIS. J. Chem. Soc. (B), 1577 (1970).
12. I. TABUSHI, Y. KURODA, and T. MIZUTANI. J. Am. Chem. Soc. **108**, 4514 (1986).
13. (*a*) G. NELSON, G. PATONAY, and I. M. WARNER. J. Inclusion Phenom. **6**, 277 (1988); (*b*) G. PATONAY, K. FOWLER, G. NELSON, and I. M. WARNER. Anal. Chim. Acta, **207**, 251 (1988).
14. F. M. MENGER. Acc. Chem. Res. **43**, 1273 (1985).
15. Y. NOZAKI and C. TANFORD. J. Biol. Chem. **246**, 2211 (1971).
16. Beilstein. 4th ed. (E III). Band VI. Beilstein-Institut für Literatur der Organischen Chemie. Springer-Verlag, Berlin, 1965. p. 825.
17. M. ZAORAL, J. KOLC, F. KORENCZKI, P. CHERNECKU, and F. SORM. Collect. Czech. Chem. Commun. **32**, 843 (1967); Chem. Abstr. **66**, 86016g (1967).
18. Beilstein. 4th ed. (E III). Band IV. Beilstein-Institut für Literatur der Organischen Chemie. Springer-Verlag, Berlin. 1963. p. 1413.
19. R. L. VAN ETTEN, G. A. CLOWES, J. F. SEBASTIAN, and M. L. BENDER. J. Am. Chem. Soc. **89**, 3252 (1967).
20. R. C. WEAST (*Editor*). Handbook of chemistry and physics. 60th ed. CRC Press, Boca Raton, FL. 1980. p. D-161.

Can. J. Chem. Downloaded from www.nrcresearchpress.com by 198.100.157.202 on 09/07/12
For personal use only.

On the spin trapping of chlorine atoms. Competition from chloride ions

DETLEF REHOREK
Sektion chemie der Karl-Marx-Universität Leipzig, Talstr. 35, Leipzig DDR-7010, Germany
AND
EDWARD G. JANZEN[1] AND YASHIGE KOTAKE[2]
Departments of Clinical Studies and Biomedical Sciences, Ontario Veterinary College, University of Guelph, Guelph, Ont., Canada N1G 2W1

Received October 6, 1990

DETLEF REHOREK, EDWARD G. JANZEN, and YASHIGE KOTAKE. Can. J. Chem. **69**, 1131 (1991).

Chlorine atoms generated by photolysis of hexachloroethane add to *C*-phenyl-*N*-*tert*-butyl nitrone (PBN) to form persistent spin adducts that are readily detectable by EPR spectroscopy. The presence of chloride ions reduces spin adduct formation competitively. Chlorine atoms also react with tetraphenylarsenium ions to liberate phenyl radicals by radical replacement.

Key words: EPR, spin trapping, *C*-phenyl-*N*-*tert*-butyl nitrone, PBN, photolysis, chlorine atoms, tetraphenylarsenium ion, hexachloroethane.

DETLEF REHOREK, EDWARD G. JANZEN et YASHIGE KOTAKE. Can. J. Chem. **69**, 1131 (1991).

Les atomes de chlore générés par photoluse de l'hexachloroéthane s'additionnent à la *C*-phényl-*N*-*tetr*-butyl nitrone (PEN) pour former des adduits de spin persistants que l'on peut facilement détecter par RPE. Par compétition, la présence des ions chlorures réduit la formation d'adduits de spin. Les atomes de chlore réagissent aussi avec les ions tétraphénylarsénium avec libération de radicaux phényles par remplacement de radical.

Mots clés: RPE, piégeage de spin, *C*-phényl-*N*-*tert*-butyl nitrone, PBN, photolyse, atomes de chlore, ion tétraphénylarsénium, hexachloroéthane.

[Traduit par la rédaction]

Introduction

Due to non-zero orbital angular momentum, chlorine atoms are not detectable directly by EPR in liquid solutions. However, it has been shown (1) that chlorine atoms form persistent spin adducts with *C*-phenyl-*N*-*tert*-butyl nitrone (PBN) detectable by EPR spectroscopy even at ambient temperatures. Thus, formation of chlorine atoms by photoinduced cleavage of C—Cl bonds (2–4), photooxidation of a coordinated chloro ligand in metal complexes (5, 6), and electrochemical oxidation of chloride ions (2, 7) has been demonstrated by EPR spin trapping experiments in nonaqueous solutions. It is well known from flash-photolysis experiments in aqueous solutions that chlorine atoms react with chloride ions very rapidly to form $Cl_2^{\cdot-}$ radicals, eq. [1], with $k_1 = 2.1 \times 10^{10}$ L mol^{-1} s^{-1} and $k_{-1} = 1.1 \times 10^5$ s^{-1}, respectively.

$$[1] \qquad {}^{\cdot}Cl + Cl^- \underset{k_{-1}}{\overset{k_1}{\rightleftharpoons}} Cl_2^{\cdot-}$$

A similar behavior has been reported for other halogen atoms and pseudohalide radicals (8). However, so far this reaction has been documented by spin trapping experiments only for thiocyanatyl radicals, $\cdot SCN$ and $(SCN)_2^{\cdot-}$, which both form persistent spin adducts with nitrones (9). Here we wish to report on studies that elucidate the influence of chloride ions on spin trapping of chlorine atoms by PBN in acetonitrile solution.

Experimental

Chlorine atoms were generated by photolysis ($\lambda \geq 310$ nm) of hexachloroethane in acetonitrile. A 75-W Oriel high-pressure mercury lamp mounted on an optical bench and equipped with a Pyrex filter was used as the irradiation source. The samples were photolyzed directly in the cavity of the EPR spectrometer (Bruker model 200 D-SRC) using a quartz flat cell attached to an H-shaped mixing cell (10). A small sample of diphenylpicryl hydrazyl (DPPH) embedded in strips of scotch tape and attached to the back side of the flat cell was used as standard for quantitative measurement. All samples were purged with purified argon for 30 min prior to photolysis. While the concentrations of hexachloroethane (0.1 M) and spin trap (0.01 M) were kept constant, various amounts of either tetraphenylphosphonium chloride ($PPh_4^+Cl^-$) or tetraphenylarsenium chloride ($AsPh_4^+Cl^-$) were added. All chemicals were commercially available (Aldrich, Baker) at high purity. $PPh_4^+Cl^-$ and $AsPh_4^+Cl^-$ were dried by storing at 100°C for at least 2 h prior to use. Acetonitrile was freshly distilled and purified by passing through a column with activated alumina. 2,3,5,6-Tetramethylnitrosobenzene (nitrosodurene) was synthesized according to the literature (11). PBN is commercially available (Aldrich, Sigma). All experiments were carried out at 295 K.

Results and discussion

Homolytic cleavage of the carbon–chlorine bond is accomplished when hexachloroethane is photolyzed with UV light, eq. [2]. Moreover, it is known (12) that haloethyl radicals undergo further decomposition to give ethylene and a second halogen atom.

$$[2] \qquad C_2Cl_6 \xrightarrow{h\nu} \cdot C_2Cl_5 + \cdot Cl$$

$$[3] \qquad \cdot C_2Cl_5 \rightarrow C_2Cl_4 + \cdot Cl$$

Spin adducts of chlorine atoms were the only persistent radicals detected during photolysis of hexachloroethane. The hyperfine splitting constants of this spin adduct ($a_N = 1.233 \pm 0.005$ mT,

$$[4] \qquad C_6H_5CH{=}N(O)C_4H_9 + Cl\cdot \rightarrow C_6H_5CH(Cl)N(O\cdot)C_4H_9$$

$a_H = 0.083 \pm 0.005$ mT, $a_{35\text{-}Cl} = 0.620 \pm 0.005$ mT, $a_{37\text{-}Cl} = 0.512 \pm 0.005$ mT) are in agreement with the data reported in the literature (2–7). Since no spin adducts of $\cdot C_2Cl_5$ radicals were detectable, decomposition according to eq. [3] is assumed

[1]Author to whom correspondance may be addressed.

[2]Present address: Molecular Toxicology Research Program, Oklahoma Medical Research Foundation, Oklahoma City, OK 73104, U.S.A.

Printed in Canada / Imprimé au Canada

Can. J. Chem. Downloaded from www.nrcresearchpress.com by 84.41.108.74 on 09/07/12
For personal use only.

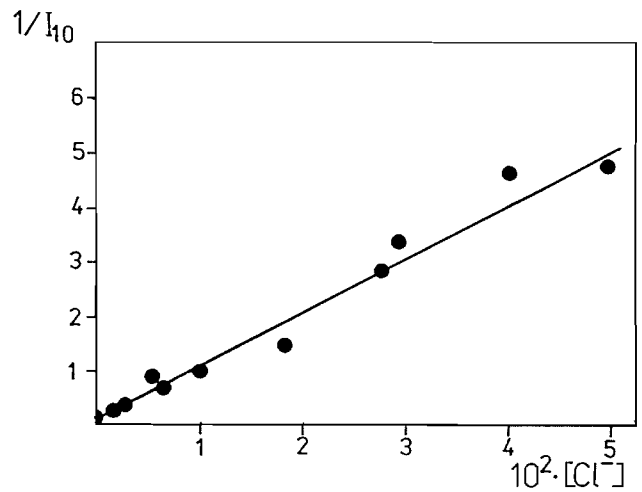


FIG. 1. Reciprocal of EPR intensity of Cl· adduct of PBN after 10 s ($1/I_{10}$) plotted against [$PPh_4^+Cl^-$].

to be fast as compared with additon to the spin trap. After prolonged photolysis, the EPR signal of the benzoyl *tert*-butyl aminoxyl radical (a_N = 0.808 ± 0.005 mT), whch is a known decomposition product of PBN, was also detected.

$C_6H_5C(O)N(O\cdot)C_4H_9$

For a time interval of less than 60 s, the intensity of the EPR signal was linearly dependent on the irradiation time. For given concentrations of spin trap and hexachloroethane and constant irradiation time, the reproductibility of the EPR signal intensity was about ±20%. Deviations are probably due to fluctuations in the intensity of absorbed light mainly caused by slightly different positions of light. Upon addition of $PPh^{4+}Cl^-$, a decrease of chlorine atom spin adduct signal intensity was observed. The plot of $1/I_{10}$ vs. the concentration of chloride ions gave a straight line (Fig. 1). Here, I_{10} is the EPR signal intensity of the chlorine spin adduct after photolyzing the sample for 10 s. This linear relationship is in agreement with the simplified kinetic model given in Scheme 1 and from which the following relationship can be derived by assuming steady state condition for ·Cl and $Cl2_2^{\cdot-}$.

$$[5]\quad 1/I_{10} = \frac{1}{I_a \Phi I_0}\left(1 + \frac{k_1 k_2}{k_t(k_2 + k_{-1})}\frac{[Cl^-]}{[PBN]}\right)$$

Also in this equation I_{10} is assumed to express the average rate of formation of spin adducts. Here, I_a and Φ are the number of light quanta absorbed and the quantum yield of chlorine atom spin adduct, respectively; k_1, k_{-1}, k_2, and k_t are the rate constants defined in Scheme 1.

Using eq. [5], the rate constant $k_t = (1.2 \pm 0.4) \times 10^8$ L mol^{-1} s^{-1} for the trapping reaction can be obtained as a rough estimate from the plot shown in Fig. 1.

If $AsPh_4^+Cl^-$ is used as a source of chloride ions, an additional spin adduct of PBN with a_N = 1.469 ± 0.005 mT and a_H = 0.269 ± 0.005 mT (a_N = 1.465 ± 0.005 mT, a_H = 0.256 ± 0.005 mT in CH_2Cl_2) was detected. By using nitrosodurene as a spin trap, this spin adduct could be assigned to the phenyl radical adduct (a_N = 1.045 ± 0.005 mT, $a_{o,p\text{-}H}$ = 0.287 ± 0.005 mT (3H), $a_{m\text{-}H}$ = 0.100 ± 0.005 mT (2H)). Apparently, an attack of chlorine atoms occurs at the tetraphenylarsenium ion liberating a phenyl radical. Investigations were not undertaken in order to elucidate the fate of the tetraphenylarsenium ion. No chlorine spin adducts were detected for acetonitrile solutions containing water. Instead, the spectrum of

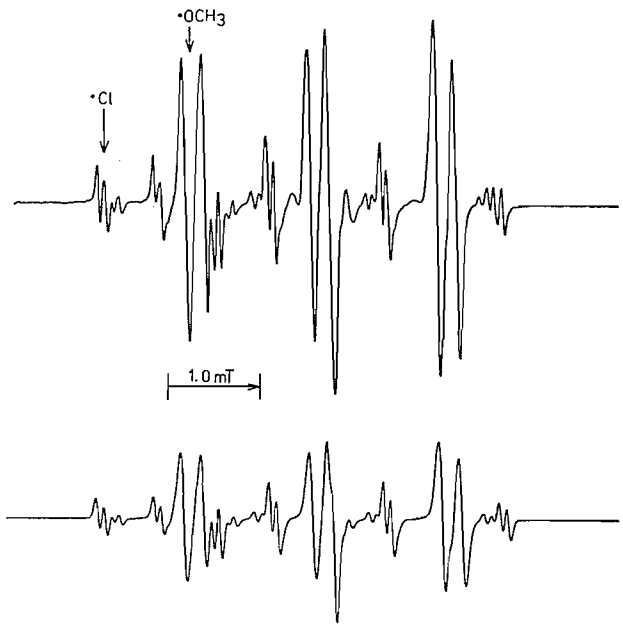
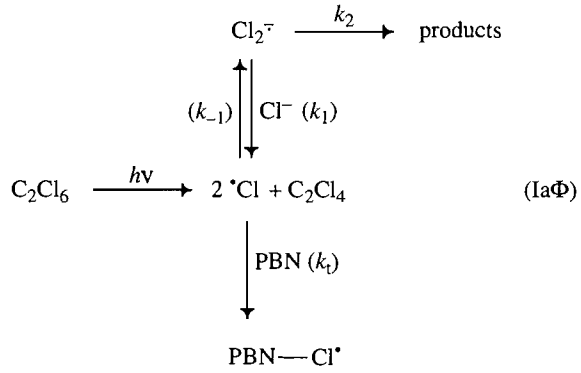


FIG. 2. EPR spectrum of spin adducts obtained during the photolysis of C_2Cl_6 (0.15 M) in benzene solution in the presence of PBN (0.04 M) and methanol (0.04 M). Bottom spectrum is reproduced by spectrum simulation using parameters in the text.



SCHEME 1

the hydroxyl adduct (a_N = 1.34 ± 0.005 mT, a_H = 0.200 ± 0.005 mT) was recorded. However, as previously shown (4), this signal is due to nucleophilic replacement of chloride by water rather than by trapping free ·OH radicals. Interestingly, the reaction between the chlorine spin adduct of PBN and methanol is fairly slow, and both chlorine and methoxy spin adducts could be detected when benzene solutions of C_2Cl_6 were photolyzed in the presence of traces of methanol (a_N = 1.387 ± 0.005 mT, a_H = 0.219 ± 0.005 mT) (Fig. 2).

Gilbert *et al.* (13) have reported formation of radical cations from the reaction of $Cl_2^{\cdot-}$ with alkoxy-substituted olefins. In the current studies, an alternative mechanism leading to hydroxy spin adducts, involving nitrone radical cations (14) rather than intermediate chlorine spin adducts of PBN, cannot be ruled out. However, in the case of methanol, the relatively slow transformation of chlorine spin adducts into methoxy spin adducts provides strong evidence for a nucleophilic replacement reaction route.

Acknowledgments

Financial support from the Natural Sciences and Engineering Research Council of Canada and the Organizing Committee of

Can. J. Chem. Downloaded from www.nrcresearchpress.com by 84.41.108.74 on 09/07/12
For personal use only.

the 2nd International Symposium on Spin Trapping and Aminoxyl Radical Chemistry, which enabled D.R. to travel to the University of Guelph, is gratefully acknowledged.

1. E. G. JANZEN, B. R. KNAUER, L. T. WILLIAMS, and W. B. HARRISON. J. Phys. Chem. **74**, 3025 (1970).
2. E. G. JANZEN, H. J. STRONKS, D. E. NUTTER, E. R. DAVIS, H. N. BLOUNT, J. L. POYER, and P. B. MCCAY. Can. J. Chem. **58**, 1596 (1980).
3. D. REHOREK and E. G. JANZEN. Z. Chem. **24**, 441 (1984).
4. R. KH. FREIDLINA, I. I. KANDROR, and R. G. GASANOV. Usp. Khim. **47**, 508 (1978).
5. P. BERGAMINI, A. MALDOTTI, S. SOSTERO, O. TRAVERSO, and J. SYKORA. Inorg. Chim. Acta, **85**, L15 (1984).
6. D. REHOREK, C. M. DUBOSE, and E. G. JANZEN. Inorg. Chim. Acta, **83**, L7 (1984).
7. T. H. WALTER, E. E. BANCROFT, G. L. MCINTIRE, E. R. DAVIS, L. M. GIERASCH, H. N. BLOUNT, H. J. STRONKS, and E. G. JANZEN. Can. J. Chem. **60**, 1621 (1982).
8. FORNIER DE VIOLET. Rev. Chem. Intermed. **4**, 121 (1981).
9. D. REHOREK and E. G. JANZEN. Inorg. Chim. Acta, **118**, L29 (1986).
10. G. A. RUSSELL, E. G. JANZEN, and E. T. STROM. J. Am. Chem. Soc. **86**, 1807 (1964).
11. L. I. SMITH and F. L. TAYLOR. J. Am. Chem. Soc. **57**, 2460 (1935).
12. M. LAL, J. MONIG, and K.-D. ASMUS. Free Radical Res. Commun. **1**, 235 (1986).
13. B. C. GILBERT, R. O. C. NORMAN, and P. S. WILLIAMS. J. Chem. Soc. Perkin Trans. 2, 647 (1980).
14. H. CHANDRA and M. C. R. SYMONS. J. Chem. Soc. Chem. Commun. 1301 (1986).

Can. J. Chem. Downloaded from www.nrcresearchpress.com by 84.41.108.74 on 09/07/12
For personal use only.

Forbeside D ($C_{62}H_{101}O_{31}SNa$), a new saponin from *Asterias forbesi*. Complete structure by nuclear magnetic resonance (300 MHz) methods

JOHN A. FINDLAY[1] AND ZHENG-QUAN HE
Department of Chemistry, University of New Brunswick, Fredericton, N.B., Canada E3B 6E2
AND
FRANÇOISE SAURIOL
Department of Chemistry, McGill University, 801, Sherbrooke Street West, Montreal, P.Q., Canada H3A 2K6

Received August 16, 1990[2]

JOHN A. FINDLAY, ZHENG-QUAN HE, and FRANÇOISE SAURIOL. Can. J. Chem. **69**, 1134 (1991).

The structure of forbeside D ($C_{62}H_{101}O_{31}SNa$), a saponin from the starfish *Asterias forbesi*, has been deduced entirely by nuclear magnetic resonance methods using a 300 MHz instrument. Based on 2D-COSY, HETCOR, single and multiple RCT, NOESY and HETCORSL experiments, the structure of forebeside D has been shown to be the monosodium salt of 6α-*O*-{β-D-galactopyranosyl-(1→3)-β-D-fucopyranosyl-(1→2)-β-D-fucopyranosyl-(1→4)-[β-D-quinovopyranosyl-(1→2)]-α-L-arabinopyranosyl-(1→3)-β-D-quinovopyranosyl}-20*S*-hydroxy-3β-sulfo-oxy-5α-cholesta-9(11),24-diene. This is the first example of a starfish saponin featuring an arabinopyranosyl unit.

Key words: marine saponin, *Asterias forbesi* saponin, forbeside D structure, structure elucidation by NMR.

JOHN A. FINDLAY, ZHENG-QUAN HE et FRANÇOISE SAURIOL. Can. J. Chem. **69**, 1134 (1991).

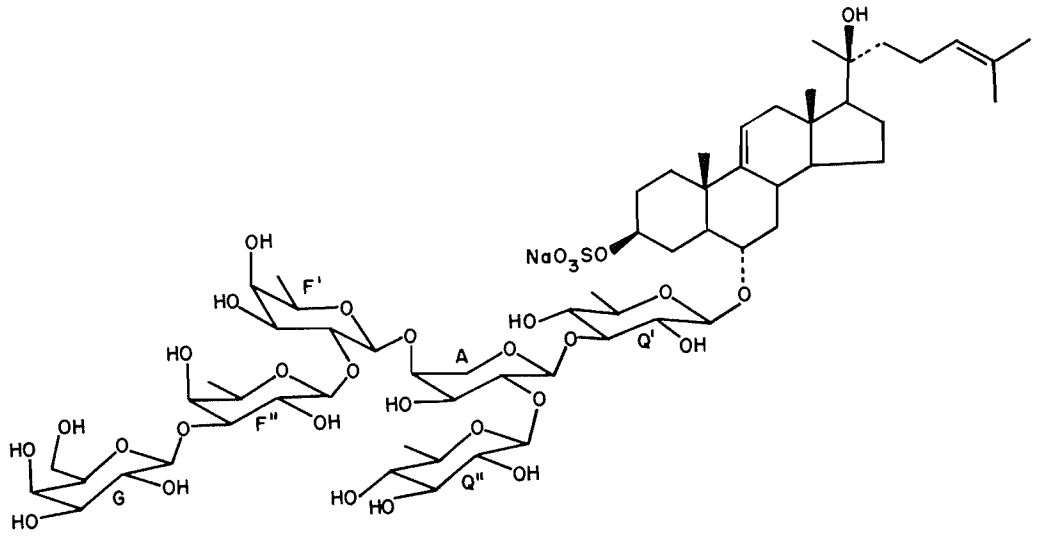
On a déterminé la structure du forbeside D ($C_{62}H_{101}O_{31}SNa$), une saponine isolée de l'étoile de mer *Asterias forbesi*, en faisant appel à des méthodes de résonance magnétique nucléaire à l'aide d'un appareil à 300 MHz. En se basant sur des expériences de 2D-COSY, HETCOR, RCT simple et multiple, NOESY et HETCORSL, on a démontré que le forbeside D est le sel de sodium du 6α-*O*-{β-D-galactopyranosyl-(1→3)-β-D-fucopyranosyl-(1→2)-β-D-fucopyranosyl-(1→4)-[β-D-quinovopyranosyl-(1→2)]-α-L-arabinopyranosyl-(1→3)-β-D-quinovopyranosyl]-20*S*-hydroxy-3β-sulfo-oxy-5α-cholesta-9(11),24-diène. Il s'agit de la première saponine d'étoile de mer à contenir un reste arabinopyranosyle.

Mots clés : saponine marine, saponine de l'*Asterias forbesi*, structure du forbeside D, détermination de structure par RMN.

[Traduit par la rédaction]

In 1987 we reported the structures of forbesides A, B (1), and C (2), the major saponins from the common Atlantic starfish *Asterias forbesi*. Recently we have turned our attention to the minor constituents of the "saponin" fraction and determined the structures of forebesides F, G, and H (3). Forbesides F and G proved to be related to forbeside C, which possesses a thornasterol aglycone connected at C6 to a pentasaccharide side chain. Forbesides F and G feature tetrasaccharide and trisaccharide side chains, respectively, and the nature of the sugars and their connectivity is as in forbeside C. They thus appear to be truncated versions of the prototype forbeside C. Forbeside H was shown to be related to forbeside A, differing only by the lack of the last three sugars of the hexasaccharide side chain. Thus all six saponins from *A. forbesi* so far reported by us feature the thornasterol algycone, and the structures of all were deduced virtually exclusively by NMR methods employing 500 MHz facilities complemented by FAB mass spectral data, and no chemical derivatization or degradation was employed.

We now wish to report the structure **1** for forbeside D, which features a different aglycone and hexasaccharide side chain.



[1]Author to whom correspondence may be addressed.
[2]Revision received March 4, 1991.

Can. J. Chem. Downloaded from www.nrcresearchpress.com by 84.41.108.74 on 09/07/12
For personal use only.

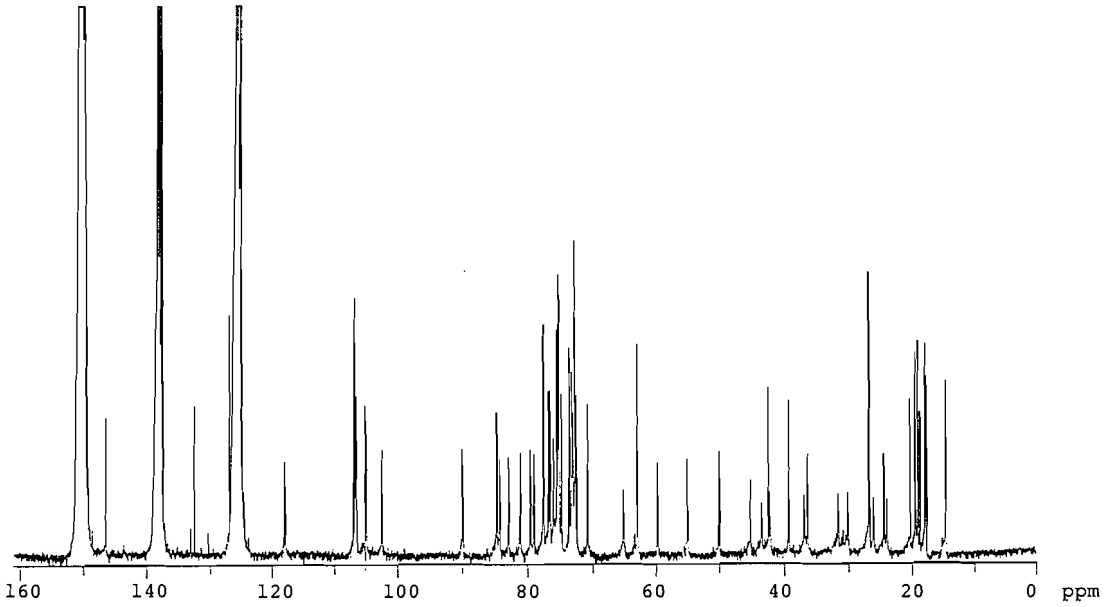


FIG. 1. ^{13}C NMR spectrum of forbeside D.

TABLE 1. NMR data for aglycone of forbeside D in pyridine-d_5/D_2O (5:1)

	^{13}C (δ, ppm)[a]	DEPT	^{1}H (δ, ppm)[b]
1	36.78	CH_2	
2	29.98	CH_2	2.75, 1.83
3	79.39	CH	4.95 m
4	31.41	CH_2	3.31, 1.70
5	49.88	CH	1.50
6	80.93	CH	3.92 m
7	42.08	CH_2	2.69, 1.30
8	36.22	CH	2.06
9	146.31	C	
10	39.17	C	
11	117.77	CH	5.27 br
12	43.40	CH_2	2.26, 2.10
13	42.34	C	
14	54.99	CH	1.29
15	23.94	CH_2	
16	26.02	CH_2	
17	59.55	CH	1.67
18	14.54	CH_3	1.06 s
19	20.19	CH_3	0.97 s
20	75.37	C	
21	26.73	CH_3	1.60 s
22	45.10	CH_2	
23	24.31	CH_2	2.30, 1.75
24	126.44	CH	5.27 br
25	132.25	C	
26	26.72	CH_3	1.78 s
27	18.63	CH_3	1.71 s

[a]Assignments from HCORR and comparison with ref. 4.
[b]Assignments from 2D-COSY.

At the time we isolated and purified forbeside D we did not have access to a 500 MHz NMR facility and the structure was pursued with the aid of a Varian XL300 instrument.

The ^{1}H NMR spectrum of forbeside D at 300 MHz shows, in the downfield region, six anomeric sugar proton doublets at δ 5.23, 5.22, 5.15, 5.02, 4.95, and 4.94. The large coupling constant (J = 7.5 Hz) in each case indicates all anomeric protons have *trans* diaxial coupling partners at their respective C2 positions. The region δ 3.60–4.60 shows the overlapping resonances of the oligosaccharide ring protons. Four methyl doublets at δ 1.88, 1.69, and 1.57 (×2) indicate the presence of four 6-deoxy sugars. The rest of the signals in the upfield region δ 0.90–3.40 are assigned to the aglycone moiety. Five methyl singlets at δ 0.97, 1.06, 1.60, 1.71, and 1.78 are assigned to H19, H18, H21, H27, and H26, respectively. A multiplet at δ 4.85 for H3 and a broad signal at δ 5.27 for two olefinic protons (H11 and H24) are observed. These observations suggested the presence of an aglycone moiety that is identical with that of asterosaponin-4 isolated from *Asterias amurensis* by Okano *et al.* (4).

The ^{13}C NMR spectrum (Fig. 1) and DEPT analysis show six anomeric carbon signals at δ 106.55 (×2), 106.34, 104.91, 104.79, and 102.31. The four methyl signals at δ 19.40, 18.97, 17.81, and 17.66 are consistent with four 6-deoxy sugars in the oligosaccharide moiety. Twenty-one carbon signals assignable to C1–C21 of the aglycone of forbeside D are superimposable with those of forbeside A (1) so that they must share the same steroid ring system but with a different side chain. The ^{1}H and ^{13}C NMR spectra show the presence of a -CH=$C(CH_3)_2$ group and the ^{13}C NMR data of the aglycone of forbeside D (Table 1) are in excellent agreement with those of the free aglycone of asterosaponin-4 (4) except for the downfield shift of C6 (+11 ppm) indicative of a glycosidic linkage. Thus, the preliminary review of NMR data suggested that forbeside D contained a hexasaccharide chain attached to 6α,20*S*-dihydroxy-3β-sulfo-oxy-5α-cholesta-9(11),24-diene at position 6.

Using 2D-COSY-45 (5), single relay, multiple relay COSY (6), *J*-resolved (7), and 2D-NOESY (8) experiments, it is possible to establish the connectivity of all proton resonances in the oligosaccharide moiety as shown in Table 2.

Two quinovose units were identified by 2D-COSY (Fig. 2) and a series of RCT spectra (Fig. 3). Inspection of 2D-COSY-45, single relay, double relay, triple relay, and quadruple relay COSY spectra (Fig. 4) reveals that methyls at δ 1.69 for Q′1 and 1.88 for Q″6 show correlations via each ring proton through

Can. J. Chem. Downloaded from www.nrcresearchpress.com by 84.41.108.74 on 09/07/12
For personal use only.

Can. J. Chem. Downloaded from www.nrcresearchpress.com by 84.41.108.74 on 09/07/12
For personal use only.

TABLE 2. NMR data for oligosaccharide moiety of forbeside D in pyridine-d_5/D_2O (5:1)

	^{13}C (δ, ppm)[a]		^1H (δ, ppm)[b]	
	(30 mg)	(20 mg)	(20 mg)	J (Hz)[c]
Q′1	103.76	104.91	4.94	$J_{1,2}$ = 7.5
2		75.07[d]	4.03	$J_{2,3}$ = 9.6
3	88.76	89.80[d]	4.05	$J_{3,4}$ = 9.6
4		75.07[d]	3.65	$J_{4,5}$ = 9.6
5		72.84	3.85	$J_{5,6}$ = 6.0
6		18.97	1.69	
A 1	105.46	106.55[d]	5.23	$J_{1,2}$ = 7.5
2	82.82	84.08[d]	4.02	$J_{2,3}$ = 9.8
3		75.92[d]	4.31	$J_{3,4}$ = 3.6
4	77.55	78.81	4.29	$J_{4,5\beta}$ = 3.0
5		65.02	4.60	$J_{4,5\alpha}$ = 0.5[e]
			3.95	$J_{5\alpha,5\beta}$ = 11.0
Q″1	105.99	106.55	5.15	$J_{1,2}$ = 7.5
2		76.65	4.08	$J_{2,3}$ = 9.6
3		77.36	4.15	$J_{3,4}$ = 9.6
4		76.40	3.90	$J_{4,5}$ = 9.6
5		74.67	3.80	$J_{5,6}$ = 6.0
6		19.40	1.88	
F′ 1	101.09	102.31[d]	4.95	$J_{1,2}$ = 7.5
2	81.77	82.71[d]	4.38	$J_{2,3}$ = 9.4
3		75.21[d]	4.19	$J_{3,4}$ = 3.8
4		72.49	4.10	$J_{4,5}$ = 0.5[e]
5		72.49	3.95	$J_{5,6}$ = 6.0
6		17.66	1.57	
F″ 1	105.18	106.34	5.02	$J_{1,2}$ = 7.5
2		73.00[d]	4.45	$J_{2,3}$ = 9.5
3	83.35	84.49[d]	4.19	$J_{3,4}$ = 3.5
4		71.49[d]	4.38	$J_{4,5}$ = 0.5[e]
5		72.33	3.80	$J_{5,6}$ = 6.0
6		17.81	1.57	
G 1	103.56	104.79	5.22	$J_{1,2}$ = 7.5
2		73.36	4.50	$J_{2,3}$ = 9.6
3		75.21	4.20	$J_{3,4}$ = 3.5
4		70.55	4.45	$J_{5,6}$ = 0.5[e]
5		77.42	4.15	$J_{5,6A}$ = 6.8
6		62.78	4.30	$J_{5,6B}$ = 5.5
			3.95	$J_{6A,6B}$ = 11.5

[a]From HCORR.
[b]From 2D-COSY, 2D-RCT, 2D-NOESY.
[c]From 2D-J-resolved spectra and 1D ^1H NMR spectrum.
[d]Assignments confirmed by HETCORSL experiment.
[e]Estimate (signal overlap).

to Q′1 and Q″1, respectively. The connectivity and large coupling constants derived from 2D-J-resolved spectra (Fig. 5) are consistent only with β-linked quinovose units.

Methyls at δ 1.57 for F′6 and F″6 show correlation only from F′6 and F″ through F′5 and F″5 to F′4 (δ 4.10) and F″4 (δ 4.40), respectively. The lack of further relayed correlation is due to small coupling constants ($J_{3,4}$ and $J_{4,5}$), which implies the presence of two fucose units. Single relay COSY and multiple relay COSY spectra also show correlation from F′1 (δ 4.95) and F″1 (δ 5.02) to F′4 (δ 4.10) and F″4 (δ 4.40), respectively. Therefore sugars F′ and F″ are assigned to the fucose units. The assignment of chemical shifts of F′5 (δ 3.95) and F″5 (δ 3.80) are obtained from 2D-NOESY experiments, where F′1 (δ 4.95) shows strong *cis* diaxial NOEs with F′3 (δ 4.19) and F′5 (δ 3.95); F″1 (δ 5.02) shows strong *cis* diaxial NOEs with F″3 (δ 4.19) and F″5 (δ 3.80). The NOESY data thus affirm the β anomeric configuration for these sugar units.

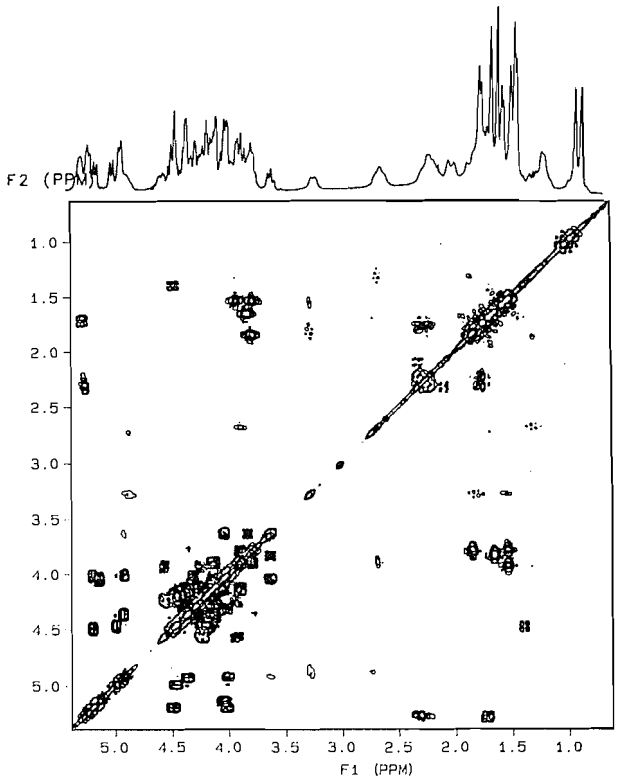


FIG. 2. COSY-45 spectrum of forbeside D.

From the anomeric doublet G1 at δ 5.22, one can locate G2 at δ 4.50 from 2D-COSY-45 spectra (Fig. 2). Single relay COSY spectra show correlation from G1 to G3 (δ 4.20). G3 is further coupled to G4 at δ 4.45, while multiple relay COSY spectra show no cross pattern from G3 to G4, which indicates the presence of a 4β-hydroxy sugar. In the 2D-NOESY spectra (Fig. 6), G1 shows strong *cis* diaxial NOEs with G5 at δ 4.15, which is coupled to G6A at δ 4.30 and G6B at δ 3.95. These findings are consistent only with a β-linked galactose unit. Inspection of the 2D-J-resolved spectrum (Fig. 5) further supported this conclusion due to the observation of double doublets at δ 4.20 for G3 ($J_{2,3}$ = 9.6 Hz, $J_{3,4}$ = 3.5 Hz) and double doublets at δ 4.45 for G4 ($J_{3,4}$ = 3.5 Hz, $J_{4,5}$ = 0.5 Hz).

From 2-D-COSY-45 spectra (Fig. 2) one can trace out the connectivity pathway from A1 at δ 5.23 to A2 at δ 4.02 and A3 at δ 4.31. Single relay COSY spectra also show correlation from A1 to A3 at δ 4.31, while multiple relay COSY spectra show no correlation from A3 to A4 due to a small coupling constant ($J_{3,4}$). In the 2D-COSY spectrum (Fig. 2), a double doublet (1H) is present at δ 4.60, constituting an ABX spin system. The geminal/vicinal coupling pattern is evident from the orientation of the cross peaks and the coupling constants of the proton signal at δ 4.60 ($J_{5,5}$ = 11.0 Hz, $J_{4,5\beta}$ = 3.0 Hz). The assignment of A5α at δ 3.95 was derived from 2D-NOESY spectra (Fig. 6) since A1 shows a strong *cis* diaxial NOE with the A5α proton; thus, A5 at δ 4.60 and A4 at δ 4.29 are assigned. The connectivity and coupling constants from 2D-J-resolved spectra (Fig. 5) are consistent only with an α-arabinose unit. The L configuration of arabinose is preferred because L-arabinose occurs in many starfish saponins while quinovose, fucose, and galactose have only been encountered in the D form in these sources to date.

Can. J. Chem. Downloaded from www.nrcresearchpress.com by 84.41.108.74 on 09/07/12
For personal use only.

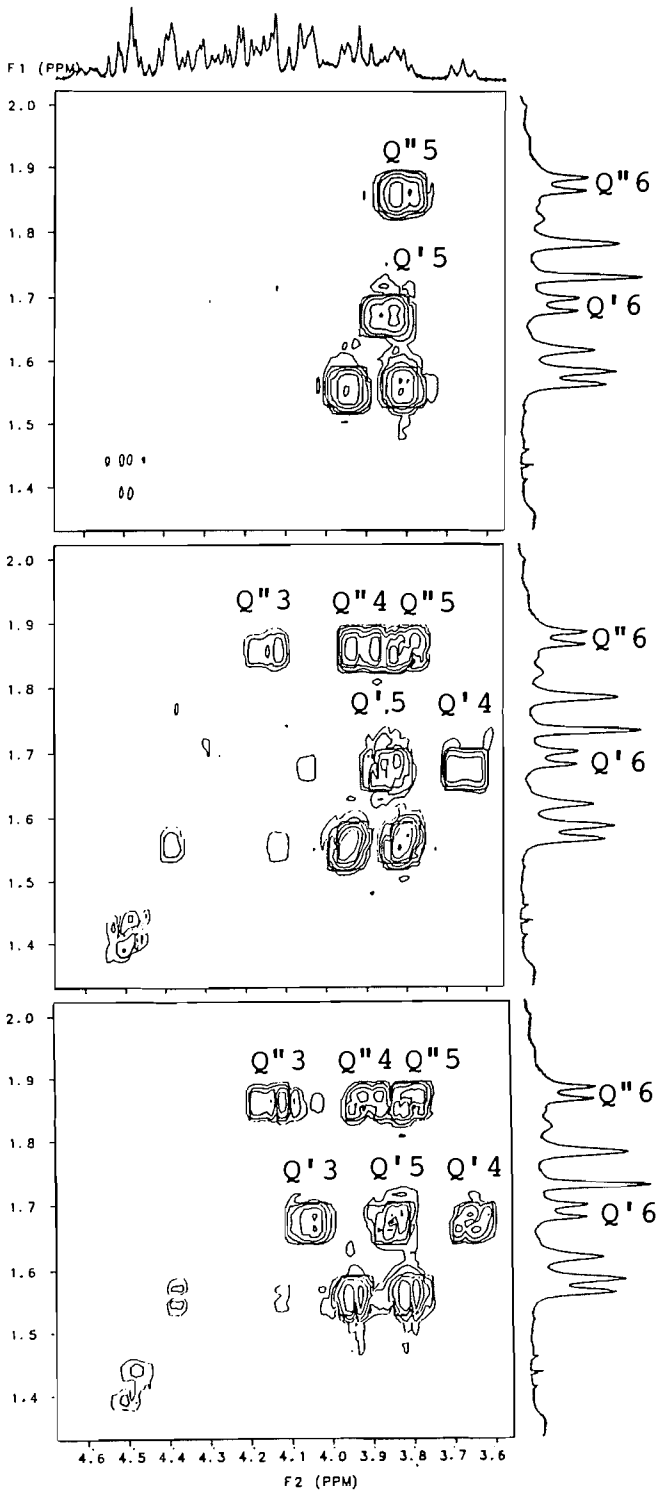


FIG. 3. Portions of COSY-45 spectra of forbeside D; upper, COSY; middle, single relay COSY; lower, double relay COSY.

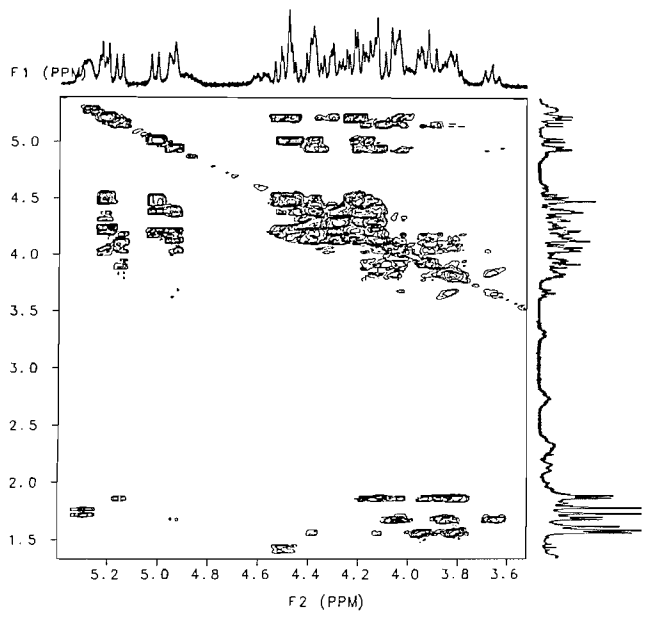


FIG. 4. Portions of quadruple relay COSY spectrum of forbeside D.

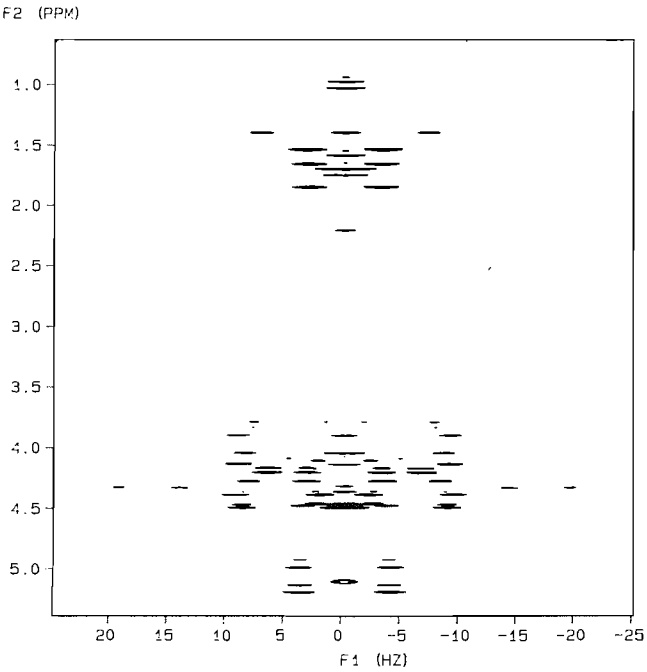


FIG. 5. *J*-Resolved spectrum of forbeside D.

So far, the six sugar units have been identified, solely by ^{1}H NMR experiments, as β-quinovopyranose (×2), β-fucopyranose (×2), β-galactopyranose, and α-arabinopyranose. The sequence of these sugar units in the oligosaccharide chain has been determined by 2D-NOESY and HETCOR (9) and HETCORSL (*vide infra*) experiments.

In the 2D-NOESY spectrum (Fig. 6), Q″1 at δ 5.15 shows strong diaxial NOE interaction with Q″3 at δ 4.15 and Q″5 at δ 3.80, as well as with A2 at δ 4.02 involved in the glycosidic linkage; F″1 at δ 5.02 shows strong diaxial NOE with F″3 at δ 4.19, F″5 at δ 3.80, and F′2 at δ 4.38; A1 at δ 5.23 interacts strongly through space with A3 at δ 4.31, A5α at δ 3.95, and Q′3 at δ 4.05; G1 interacts with G3 at δ 4.20, G5 at δ 4.15, and F″3 (or F′3, *vide infra*) at δ 4.19; Q′1 is correlated to Q′3 at δ 4.05, Q′5 at δ 3.85, and H6 at δ 3.92 of the aglycone; F′1 is correlated to F′3 at δ 4.19, F′5 at δ 3.95, and A4 at δ 4.29.

Inspection of the HETCOR spectrum (Fig. 7) led to the near complete assignment of ^{13}C chemical shifts for the oligosaccharide moiety. The carbon signals Q′3 at δ 89.80 (~ +12 ppm), A2 at δ 84.04 (~ +12 ppm), A4 at δ 78.81 (~ +9 ppm), F′2 at δ 82.71 (~ +10 ppm), F″3 at δ 84.49 (~ +10 ppm) are immediately assigned to glycosidic linkages due to glycosyla-

Can. J. Chem. Downloaded from www.nrcresearchpress.com by 84.41.108.74 on 09/07/12
For personal use only.

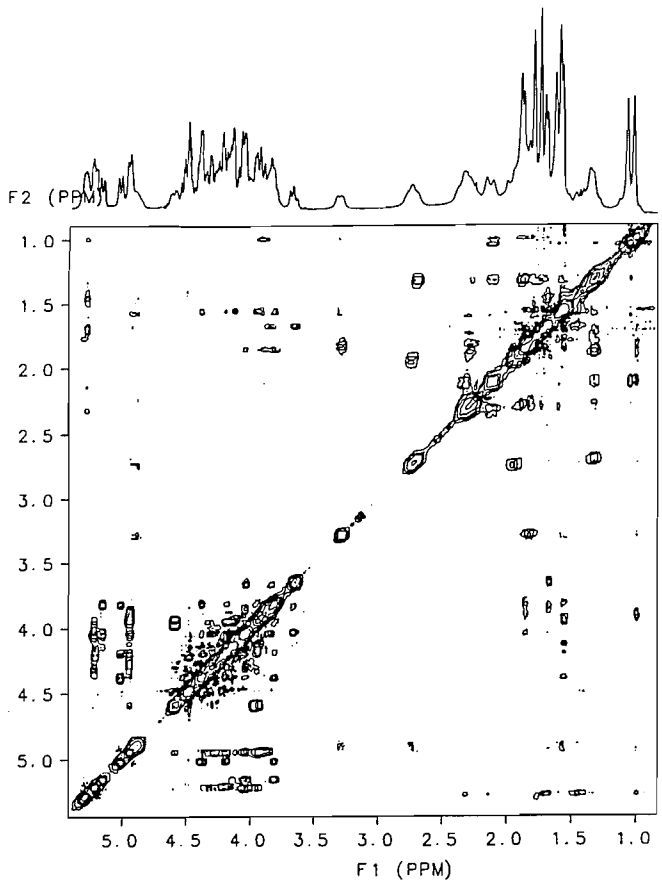


FIG. 6. 2D-NOESY spectrum of forbeside D.

tion shifts by comparison with unsubstituted β-D-quinovopyranosyl, β-D-fucopyranosyl (1, 10), and α-L-arabinopyranosyl units (11). NMR data for the terminal sugars Q″ and G in forbeside D are also in good agreement with those in versicoside A (10) and in forbeside C (2).

In view of the overlap of several proton signals, the analysis of the HETCOR spectrum was not without unambiguity. Thus it was not possible to assign with certainty the Q′2, Q′3, and A2 ^{13}C chemical shifts. Similarly, the F′3 and F″3 carbon assignments could not be decided on the basis of the HETCOR experiments due to coincidence of F′3H and F″3H. Incorrect assignment would of course lead to incorrect location of interglycosidic linkages since these are based, in part, on observation of glycosylation shifts. To overcome this difficulty a heterocorrelation spin lock (HETCORSL) (12) experiment was conducted. This provided unambiguous assignment of the several aforementioned ^{13}C signals. Conventional RELAY-HETCOR experiments (13) are much less sensitive than this more recent HETCOR-RELAY experiment using spin-locking mixing period (12) (HETCORSL). That is why this technique was selected to obtain data complementary to the NOESY experiment. In this HETCOR-RELAY technique, the magnetization transfer between coupled protons is achieved via the homonuclear Hartmann–Hahn cross polarization. The HETCORSL experiment required a more concentrated sample of forbeside D (30 mg) and this showed that some differences existed in ^{13}C and ^{1}H chemical shifts from those of the dilute sample (as per Table 2). Thus it was necessary to repeat COSY and single relay COSY experiments on the concentrated sample prior to interpreting the HETCORSL spectrum. Table 2 compares the ^{13}C chemical shifts for the anomeric and glycosidic carbons of the dilute and concentrated samples.

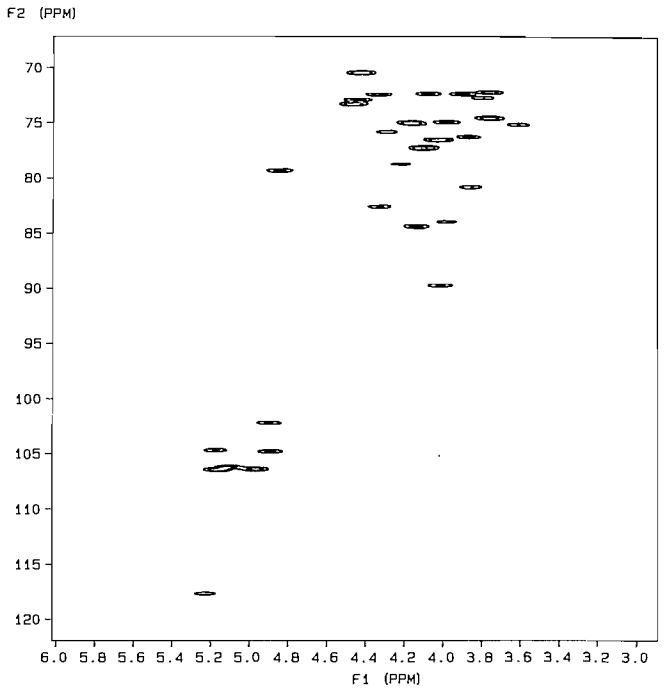


FIG. 7. Portion of HETCOR spectrum of forbeside D.

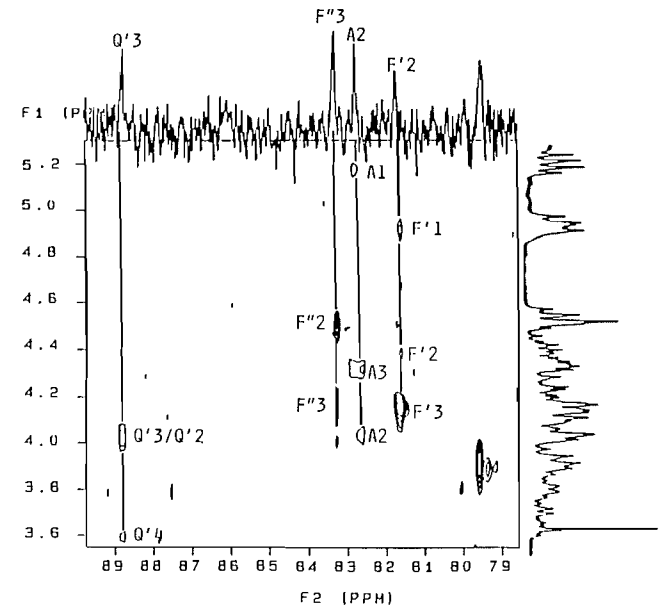


FIG. 8. Portion of HETCORSL spectrum of forbeside D.

The HETCORSL spectrum (see Fig. 8 for a portion) revealed that (a) the ^{13}C signal at δ 88.76 correlates with protons at Q′2, Q′3, and Q′4 and should thus be assigned to Q′3; (b) the signal at δ 83.35 correlates with protons F″2, F″3, and F″4 and must be assigned to F″3; (c) the signal at δ 82.82 correlates with A1, A2, and A3 and must be assigned to A2; (d) the carbon at δ 81.77 correlates with protons F′1 and F′3 and is therefore assigned to F′2. Thus it was possible to complete the ^{13}C chemical shift assignments in an unambiguous fashion and ascertain the sites of interglycosidic linkage via glycosylation shift. This corroborated and complemented the sequencing information derived from NOESY data.

Analysing the 2D-NOESY, HETCOR, and HETCORSL data, the sequence obtained can be summarized as follows:

Can. J. Chem. Downloaded from www.nrcresearchpress.com by 84.41.108.74 on 09/07/12
For personal use only.

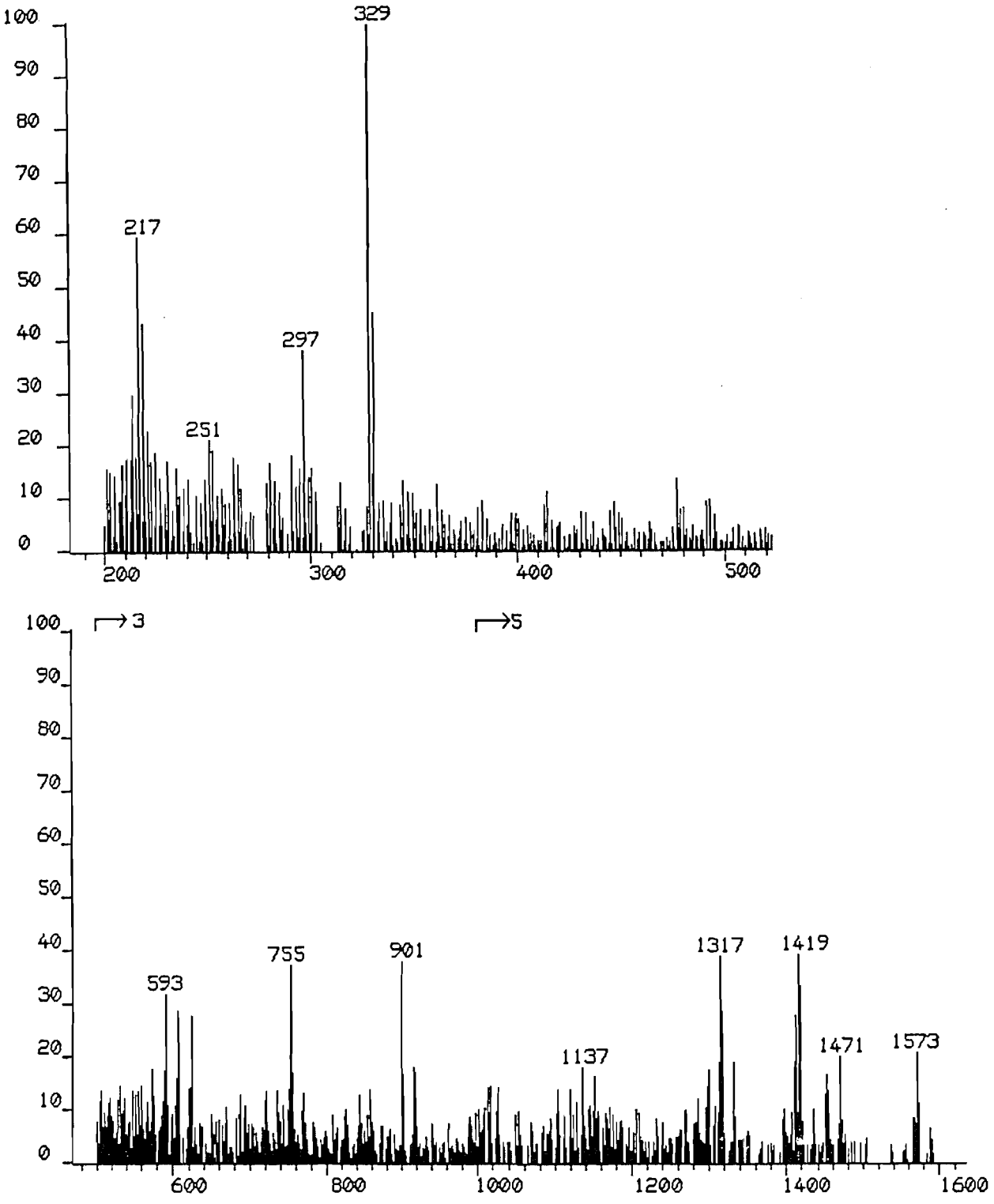
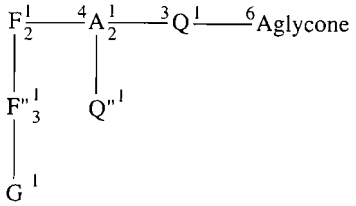


FIG. 91. +FAB mass spectrum of forbeside D.



All sugar units are linked to each other via an *O*-glycosidic bond.

The (+) FAB mass spectrum of fordeside D (Fig. 9) displays pseudomolecular ions at m/z 1419 $[M(C_{62}H_{101}O_{31}SNa) + Na]^+$ and 1397 $[M + H]^+$ indicative of a molecular mass of 1396, which supported the structure determined by NMR methods. It also shows a series of fragment ions readily interpreted on the basis of structure **1** (Table 3).

Hence, forbeside D is the monosodium salt of 6α-O-{β-D-galactopyranosyl-(1→3)-β-D-fucopyranosyl-(1→2)-β-D-fucopyranosyl-(1→4)-[β-D-quinovopyranoslyl-(1→2)]-α-L-arabinopyranosyl-(1→3)-β-D-quinovopyranosyl}-20*S*-hydroxy-3β-sulfo-oxy-5α-cholesta-9(11),24-diene **1**.

TABLE 3. +FAB MS fragmentation of forbeside D

Ion (relative intensity)	Composition
1573(4)	M + Na + matrix
1471(4)	M + Na + matrix − $NaSO_3$ + H
1453(3)	M + Na + matrix − $NaSO_3$ + H − H_2O
1435(2)	M + Na + matrix − $NaSO_3$ + H − $2H_2O$
1419(8)	M + Na
1397(2)	M + H
1317(8)	M + Na − $NaSO_3$ + H
1300(4)	M + Na − $NaSO_4$
1153(3)	M + Na − $NaSO_4$ − 147(Q)
1137(4)	M + Na − $NaSO_4$ − 163(G)
901(13)	M + Na − aglycone − H
755(13)	901 − 146(Q)
609(10)	755 − 146(Q)
593(11)	755 − 162(G)
477(14)	609 − 132(A)
447(9)	609 − 162(G)
331(46)	477 − 146(F)
315(13)	447 − 132(A)
297(38)	315 − H_2O

This new saponin is the first example of a starfish saponin with an arabinopyranosyl unit in the oligosaccharide moiety. It is also the first example of a marine saponin of this complexity whose structure has been deduced entirely on the basis of 300 MHz NMR spectra.

Experimental

Optical rotation was measured with a Perkin–Elmer 241 polarimeter. Mass spectra were recorded with a Kratos MS50 instrument using a magic bullet matrix. Forbeside D (30 mg) was isolated from the crude saponin mixture (4.5 g) obtained from *A. forbesi* as previously described (14). A 20-mg sample was used for all NMR experiments except the HETCORSL, which employed 30 mg of material.

Forbeside D, **1**: colorless powder, mp 213°C (dec.); $[\alpha]_D$ −4.7 (*c* 0.6, H_2O); NMR data, see Tables 1 and 2; (+)FAB-MS (magic bullet), see Fig. 9 and Table 3.

Instrumentation

The NMR spectra were obtained on a Varian XL-300 spectrometer equipped with a proton probe and a 5-mm broadband probe operating at 300 MHz for proton and 75.4 MHz for carbon. The samples were dissolved in a mixture of pyridine-d_5 and D_2O (5:1); the spectra were recorded at 30°C.

2-D-Proton NMR

The COSY-90 and COSY-45 spectra were acquired using 256 increments in the evolution time (t_1) each with four repetitions and a 1 s relaxation delay. The 2D matrix was 1024 × 1024 data points after processing. The data were pseudo echo shaped and symmetrized prior to plotting. The RELAY-COSY experiments were recorded using identical resolution and temperature conditions. The single RELAY experiment required 8 repetitions to complete the phase cycling whereas RELAY-2, RELAY-3, RELAY-4 experiments required 16, 32, and 64 repetitions, respectively.

The phase-sensitive NOESY experiment was recorded under identical conditions (resolution and temperature) as previous 2D experiments, except for the relaxation delay set to 2 s and the number of repetitions set to 16 transients. The mixing time used to perform this experiment was 0.3 s.

C-13 and 2D-heteronuclear experiments

For ^{13}C, a 60° pulse was used with an acquisition time of 0.97 s. Line broadening processing of 1 Hz was used. The DEPT and two-dimensional shift correlation (HETCOR) experiments were performed using 2 and 0.5 s repetition delays, respectively. The 90°C pulse provided by the decoupler was 47 μs. In the DEPT experiment, four spectra were acquired using 45°, 90°, 90°, and 135°; these spectra were edited to provide pure CH, CH_2 and CH_3 sub-spectra. In the 2D-heterocorrelation spectra, 128 free induction decays were acquired in the t_1 domain and 1024 data points were recorded in the t_2 domain. The 2D-heterocorrelation spectra were acquired for 10–15 h at 30°C. The data were pseudo echo shaped and zero filled in the t_1 domain to end up with a 512 × 1024 matrix.

The phase-sensitive relay (HETCORSL) experiment was acquired using 1 s relaxation delay for the 64 increments of the evolution domain. The spectra were recorded at 40°C for 14–15 h. Mild line broadening and zero filling were used to obtain a 512 × 1024 matrix. The spin lock mixing time was selected to be 24 ms, a time sufficient (from previous experiments) to relay magnetization to the next coupled neighboring proton.

Acknowledgements

This study was supported by a grant from the Natural Sciences and Engineering Research Council of Canada. Thanks are due to Daniel Drummond for recording the FAB mass spectra.

1. J. A. FINDLAY, M. JASEJA, D. J. BURNELL, and J.-R. BRISSON. Can J. Chem. **65**, 1384 (1987).
2. J. A. FINDLAY, M. JASEJA, and J.-R. BRISSON. Can. J. Chem. **65**, 2605 (1987).
3. J. A. FINDLAY, Z.-Q. HE, and B. BLACKWELL. Can. J. Chem. **68**, 1215 (1990).
4. K. OKANO, N. OHKAWA, and S. IKEGAMI. Agric. Biol. Chem. **49**, 3823 (1985).
5. A. BAX. Two-dimensional NMR in liquids. Riedel, Boston. 1982; A. BAX and R. FREEMAN. J. Magn. Reson. **44**, 542 (1981): A. BAX, R. FREEMAN, and G. MORRIS. J. Magn. Reson. **42**, 164 (1981).
6. G. EICH, G. BODENHAUSEN, and R. R. ERNST. J. Am. Chem. Soc. **104**, 3731 (1982); A. BAX and G. DROBNY. J. Magn. Reson. **61**, 306 (1985).
7. W. P. AUE, E. BARTHOLDT, and R. R. ERNST. J. Chem. Phys. **64**, 2229 (1976); A. KUMAR, G. WANTER, R. R. ERNST, and K. WUTHRICH. Biochem. Biophys. Res. Commun. **96**, 1156 (1980).
8. S. W. HOMANS, R. A. DWEK, D. L. FERNANDES, and T. W. RADEMACHER. FEBS Lett. **164**, 231 (1983).
9. R. LANZETTA, G. LAONIGRO, and M. PARILLI. Can. J. Chem. **62**, 2874 (1984).
10. Y. ITAKURA, T. KOMORI, and T. KAWASAKI. Liebig's Ann. Chem. 2079 (1983).
11. Y. ASADA, T. YEOKA, and T. FURUYA. Chem. Pharm. Bull. **38**, 142 (1990); I. KITAGAWA, M. SAKAGAMI, F. HASHIUCHI, J. L. ZHOU, M. YOSHIKAWA, and J. L. REN. Chem. Pharm. Bull. **37**, 551 (1989); M. MATSUURA, T. USHIROGUCHI, Y. ITAKURA, and T. FUWA. Chem. Pharm. Bull. **37**, 1390 (1989).
12. A. BAX, D. DAVIS, and S. K. SARKAR. J. Magn. Reson. **63**, 230 (1985).
13. P. H. BOLTON. J. Magn. Reson. **48**, 336 (1982); P. H. BOLTON and G. BODENHAUSEN. Chem. Phys. Lett. **89**, 139 (1982).
14. J. A. FINDLAY, Z.-Q. HE, and M. JASEJA. Can. J. Chem. **67**, 2078 (1989).

Can. J. Chem. Downloaded from www.nrcresearchpress.com by 84.41.108.74 on 09/07/12
For personal use only.

Complexes of the crown thioether ligand 2,5,8-trithia[9]-*o*-benzenophane, (TT[9]OB). Synthesis and molecular structure of [Cu(NCS)(TT[9]OB)]

STEPHEN J. LOEB[1] AND GEORGE K. H. SHIMIZU

Department of Chemistry and Biochemistry, University of Windsor, Windsor, Ont., Canada N9B 3P4

Received January 17, 1991

STEPHEN J. LOEB and GEORGE K. H. SHIMIZU. Can. J. Chem. **69**, 1141 (1991).

The macrocyclic thioether ligand 2,5,8-trithia[9]-*o*-benzenophane (TT[9]OB) reacts with $[Cu(CH_3CN)_4][ClO_4]$ to yield the Cu(I) complex $[Cu(CH_3CN)(TT[9]OB)][ClO_4]$. The coordinated acetonitrile molecule is displaced by the ambidentate, thiocyanate $(NCS)^-$ ion to form the neutral complex [Cu(NCS)(TT[9]OB)] which was characterized by infrared spectroscopy, ^1H NMR spectroscopy, and X-ray crystallography. The title complex crystallized in the orthorhombic space group *Pbca* with $a = 14.447(3)$ Å, $b = 15.034(4)$ Å, $c = 14.851(4)$ Å, $V = 3232.2(14)$ Å^3, and $Z = 8$. The structure refined to $R = 5.15\%$ and $R_w = 5.92\%$ for 1149 reflections with $F_o^2 > 3\sigma(F_o^2)$. The Cu(I) ion has a distorted tetrahedral coordination sphere with TT[9]OB occupying three sites while the fourth site is occupied by the thiocyanate ligand which is N-bound to the metal centre. A comparison is made of the molecular conformations of free TT[9]OB and that found for complexed TT[9]OB in [Cu(NCS)(TT[9]OB)] and $[Cu(Ph_2PMe)(TT[9]OB)][ClO_4]$.

Key words: thioether, macrocyclic metal complex.

STEPHEN J. LOEB et GEORGE K. H. SHIMIZU. Can. J. Chem. **69**, 1141 (1991).

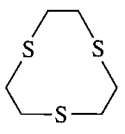
Le ligand thioéther macrocyclique 2,5,8-trithia[9]-*o*-benzénophane, (TT[9]OB) réagit avec le $[Cu(CH_3CN)_4][ClO_4]$ pour conduire au complexe de Cu(I), $[Cu(CH_3CN)(TT[9]OB)][ClO_4]$. La molécule d'acétonitrile coordinée est déplacée par l'ion thiocyanate $(NCS)^-$ ambident pour former le complexe neutre [Cu(NCS)(TT[9]OB)] que l'on a caractérisé par spectroscopies ir et rmn du ^1H et par diffraction des rayons-X. Les cristaux du complexe mentionné dans le titre sont orthorhombiques, ils appartiennent au groupe d'espace *Pbca*, avec $a = 14{,}447(3)$, $b = 15{,}034(4)$ et $c = 14{,}851(4)$ Å, $V = 3232.2(14)$ Å et $Z = 8$. On a affiné la structure jusqu'à des valeurs respectives de $R = 0{,}0515$ et $R_w = 0{,}0592$ pour 1149 réflexions avec $F_o^2 > 3\sigma(F_o^2)$. L'ion Cu(I) est entouré d'une sphère de coordination tétraédrique déformée qui est liée par l'azote au centre métallique. On a réalisé une comparaison des conformations moléculaires du TT[9]OB libre et du TT[9]OB complexé dans le [Cu(NCS)-(TT[9]OB)] et dans le $[Cu(Ph_2PMe)(TT[9]OB)[ClO_4]$.

Mots clés : thioéther; complexe métallique macrocyclique.

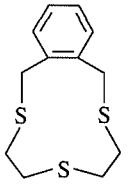
[Traduit par la rédaction]

Introduction

The coordination chemistry of macrocyclic thioether ligands is dominated by the conformational requirements of the free ligand. These cyclic molecules favour the adoption of "inside-out" or exodentate conformations with the S atoms oriented out of the macrocyclic cavity (1–4). It has been shown that this results from the tendency of $SCH_2CH_2SCH_2CH_2S$ chains to adopt a "bracket" structure with *anti* placements for C—C bonds and *gauche* placements for S—C bonds (4). An exception to this observation is the macrocyclic thioether 1,4,7-trithiacyclononane (9S3). For this unique thioether ligand, the exodentate conformation is unfavourable because the conformational constraints of the nine-membered ring force all C—C bonds to adopt *gauche* placements. As a result, the free ligand adopts an endodentate conformation which is essentially the same as the conformation required for *facial* coordination (5). Complexes of 9S3 exhibit remarkable stability and very often unusual coordination geometries and oxidation states that can be attributed to this preorganization of the ligand (1–11).



9S3



TT[9]OB

[1]Author to whom correspondence should be addressed.

The chemistry of 9S3 and recent results on the molecular structures of some acyclic polythioethers (4*c*) suggest that if SCH_2CH_2S linkages are to be used as the structural basis of metal-binding ligands, some perturbation should exist which forces S donor atoms to be preorganized in an endodentate conformation. We have proposed that the incorporation of rigid xylyl units into crown thioethers may limit the conformational flexibilty of the macrocyclic ring or introduce conformational strain into the macrocycle backbone resulting in an endodentate conformation or disposition towards such a conformation. We have recently shown that the reaction of $[Cu(CH_3CN)_4][X]$ with TT[9]OB yields the mononuclear cation $[Cu(CH_3CN)-(TT[9]OB)]^+$ for which the labile acetonitrile ligand can easily be replaced by neutral ancillary ligands such as phosphines and pyridines (12). To complete our studies on the Cu(I) coordination chemistry of TT[9]OB, we have investigated the interaction of the ambidentate anionic ligand $(NCS)^-$ with $[Cu(CH_3CN)(TT[9]OB)]^+$ and this paper describes these results.

Experimental section

General

$[Cu(CH_3CN)_4][ClO_4]$, TT[9]OB, and $[Cu(CH_3CN)(TT[9]OB)]-[ClO_4]$ were prepared using published methods (12, 13). KSCN, CH_3CN, CH_3NO_2, and all deuterated solvents were purchased from Aldrich and used as received. All reactions were conducted under an atmosphere of N_2 using standard Schlenk techniques and all solvents were degassed prior to use. ^1H NMR spectra were recorded at 300.1 MHz, on a Brüker AC300 spectrometer locked to the deuterated solvent. Infrared spectra were recorded on a Nicolet 5DX FTIR spectrometer. Elemental analysis were performed by Microanalytical Services New Westminister, British Columbia, Canada.

Can. J. Chem. Downloaded from www.nrcresearchpress.com by 198.100.157.202 on 09/07/12
For personal use only.

Can. J. Chem. Downloaded from www.nrcresearchpress.com by 198.100.157.202 on 09/07/12
For personal use only.

Preparation of [Cu(NCS)(TT[9]OB)]

To a solution of $[Cu(CH_3CN)(TT[9]OB)][ClO_4]$ (382 mg, 0.83 mmol) in CH_3CN (10 mL), KSCN (166 mg, 0.83 mmol) dissolved in CH_3CN (5 mL) was added dropwise. No visible change occurred as the two colourless solutions were mixed. The mixture was stirred for 3 h at room temperature during which time a white precipitate formed. The solvent was removed and the resulting off-white solid washed with water (3 × 20 mL) and then dried *in vacuo*. The product was then extracted into CH_3NO_2 and recrystallized by vapour diffusion of diethylether into this solution. Yield: 329 mg (64%). ^1H NMR (CD_3CN, 235 K): δ 7.46 (m, 4H, aromatic), 4.10 (d, 2H, benzylic, ^2J = 11.2 Hz), 3.88 (d, 2H, benzylic, ^2J = 11.2 Hz), 3.53 (m, 4H, SCH_2CH_2S), 2.92 (m, 4H, SCH_2CH_2S), IR (KBr): ν(NCS) 2095 cm^{-1}(s). *Anal* calcd, for $C_{13}H_{16}CuNS_4$: C 41.29, H 4.27, S 33.91; found C 41.38, H 4.14, S33.67.

X-ray crystallographic analysis of [Cu(NCS)(TT[9]OB)]

Colourless crystals of [Cu(NCS)(TT[9]OB)] were grown by vapour diffusion of diethylether into a CH_3NO_2 solution of the complex. The diffraction experiment was performed on a four-circle Syntex $P2_1$ diffractometer with graphite-monochromatized MoKα radiation. The initial orientation matrix was obtained from 15 machine-centred reflections selected from a rotation photograph. Partial rotation photographs around each axis were consistent with an orthorhombic crystal system. Utimately, 25 high-angle reflections ($15.2° < 2\theta < 23.4°$) were used to obtain the final lattice parameters and orientation matrix. Machine parameters, crystal data, and data collection parameters are summarized in Table 1. Observed extinctions were consistent with the space group *Pbca* and this was confirmed by a successful solution refinement. Intensity data ($+h,+k,+l$) were collected in two shells ($4.5° < 2\theta < 40°$ and $40° < 2\theta < 45°$). The intensities of three standard reflections (0 0 2, 2 0 0, 3 2 2) were recorded every 197 reflections and showed no statistically significant changes over the duration of the data collection. The absorption coefficient was small and ψ-scans recorded (8 2 2, 4 1 1, 9 2 2, 12 2 3) showed no significant absorption effects. Thus, no absorption correction was applied to the data. The data were processed by using the TEXSAN software package (14) running on a VAX 3520 Workstation. A total of 2469 reflections were collected and 1149 unique reflections with $F_o^2 > 3\sigma(F_o^2)$ were used in the refinement.

The positions of the copper atom and the four sulfur atoms were determined by direct methods from the *E*-map with highest figure of merit. The remaining non-hydrogen atoms were located from a difference Fourier map calculation. In the final cycles of refinement, the copper, sulfur, and nitrogen atoms were assigned anisotropic thermal parameters and the carbon atoms were assigned isotropic thermal parameters. Refinement was carried out by using full-matrix least-squares techniques on *F* minimizing the function $\Sigma w(|F_o| - |F_c|)^2$, where $w = 1/\sigma^2(F_o)$ and F_o and F_c are the observed and calculated structure factors. Atomic scattering factors (15) and anomalous dispersion terms (16, 17) were taken from the usual sources. Fixed H-atom contributions were included with C—H distances of 0.95 Å and thermal parameters 1.2 times the isotropic thermal parameter of the bonded C atoms. No H atoms were refined, but all values were updated as refinement continued. This resulted in $R = \Sigma||F_o| - |F_c|/\Sigma|F_o|| = 0.0515$ and $R_w = (\Sigma w(|F_o| - |F_c|)^2/\Sigma wF_o^2)^{1/2} = 0.0592$ at final convergence.

The Δ/σ value for any parameter in the final cycle was less than 0.001. A final difference Fourier map calculation showed no peaks of chemical significance; the largest was 0.53 electrons/Å^3 and was associated with the Cu atom. Atomic positional parameters are summarized in Table 2 and selected bond distances and angles are summarized in Table 3. Thermal parameters (Table S-1), hydrogen atom parameters (Table S-2), and values of $10|F_o|$ and $10|F_c|$ (Table S-3) are deposited as supplementary material.[2]

[2]Supplementary Tables S-1, S-2, and S-3 may be purchased from the Depository of Unpublished Data, Document Delivery, CISTI, National Research Council of Canada, Ottawa, Ont., Canada K1A 0S2.

TABLE 1. Summary of crystal data, intensity collection, and structure refinement for [Cu(NCS)(TT[9]OB)]

Formula	$C_{13}H_{16}CuNS_4$
Crystal colour, form	Colourless prisms
Formula weight	378.13
a (Å)	14.477(3)
b (Å)	15.034(4)
c (Å)	14.851(4)
Crystal system	Orthorhombic
Space group	*Pbca* (No. 61)
Volume (Å^3)	3232.2(14)
Density (g cm^{-3}), calcd.	1.55
Z	8
Absorption coefficient, μ (cm^{-1})	18.37
Radiation, λ (Å)	0.71069
Temperature (°C)	24
Scan speed (deg min^{-1})	2.0–5.0 (θ/2θ scan)
Scan range (deg)	1.0 below $K\alpha_1$; 1.1 above $K\alpha_2$
Background/scan time ratio	0.5
Data collected	2469
Number of unique data with $F_o^2 > 3\sigma(F_o^2)$	1149
Number of variables	107
Goodness of fit	1.51
$R(F_o)$, %	5.15
$R_w(F_o)$, %	5.92

TABLE 2. Positional parameters and *B* (eq) for [Cu(NCS)(TT[9]OB)]

Atom	*x*	*y*	*z*	*B* (eq)
Cu	0.4438 (1)	0.2893 (1)	0.1914 (1)	3.68 (6)
S1	0.5414 (2)	0.2458 (2)	0.3107 (2)	3.6 (1)
S2	0.5080 (2)	0.3928 (2)	0.0930 (2)	3.8 (1)
S3	0.3766 (2)	0.4015 (2)	0.2802 (2)	3.9 (1)
S4	0.3039 (2)	0.0203 (2)	0.1046 (2)	4.8 (2)
N	0.3850 (6)	0.1830 (6)	0.1428 (6)	4.0 (5)
C1	0.6847 (7)	0.2491 (6)	0.1891 (7)	3.2 (2)
C2	0.7224 (7)	0.1660 (7)	0.1779 (7)	4.1 (2)
C3	0.7488 (8)	0.1359 (8)	0.0918 (8)	5.0 (3)
C4	0.7380 (7)	0.1913 (7)	0.0182 (7)	4.2 (2)
C5	0.7014 (7)	0.2745 (6)	0.0286 (7)	3.3 (2)
C6	0.6732 (6)	0.3059 (6)	0.1124 (6)	2.8 (2)
C7	0.6328 (7)	0.3981 (7)	0.1184 (7)	4.1 (2)
C8	0.4665 (8)	0.4937 (7)	0.1452 (8)	5.0 (3)
C9	0.4565 (7)	0.4899 (7)	0.2474 (8)	4.9 (3)
C10	0.4203 (8)	0.3685 (8)	0.3892 (8)	5.4 (3)
C11	0.5128 (8)	0.3283 (7)	0.3986 (8)	4.9 (3)
C12	0.6620 (8)	0.2800 (7)	0.2826 (7)	4.4 (3)
C13	0.3517 (7)	0.1155 (7)	0.1272 (7)	3.3 (2)

Results

We have previously shown that the Cu(I) complex $[Cu(CH_3CN)(TT[9]OB)][ClO_4]$ can easily be prepared by displacement of three labile acetonitrile ligands from $[Cu(CH_3CN)_4][ClO_4]$ (12). This product is then ideal as a starting material for the incorporation of other ancillary ligands through displacement of the remaining acetonitrile ligand. The addition of one equivalent of potassium thiocyanate to $[Cu(CH_3CN)(TT[9]OB)][ClO_4]$ resulted in the quantitative formation of $KClO_4$ and a single copper containing product formulated as [Cu(NCS)(TT[9]OB)]. Elemental analysis was in agreement with this formulation in which the thiocyanate ion is bonded to the Cu(I) centre rather than $[Cu(CH_3CN)(TT[9]OB)][NCS]$ in

TABLE 3. Selected bond distances and angles for [Cu(NCS)(TT[9]OB)]

Bond	Distance (Å)	Bond	Distance (Å)
Cu1—S1	2.328 (3)	N—C13	1.15 (1)
Cu1—S2	2.353 (3)	C1—C2	1.37 (1)
Cu1—S3	2.359 (3)	C1—C6	1.43 (1)
Cu1—N	1.949 (9)	C1—C12	1.50 (1)
S1—C7	1.85 (1)	C2—C3	1.41 (1)
S1—C8	1.81 (1)	C3—C4	1.38 (1)
S2—C9	1.83 (1)	C4—C5	1.37 (1)
S2—C10	1.81 (1)	C5—C6	1.39 (1)
S3—C11	1.85 (1)	C6—C7	1.51 (1)
S3—C12	1.87 (1)	C8—C9	1.53 (1)
S4—C13	1.62 (1)	C10—C11	1.48 (1)

Atoms	Non-bonding distance (Å)	Atoms	Non-bonding distance (Å)
S1...S2	3.371 (1)	S2...S3	3.374 (4)
S1...S3	3.946 (4)	S1...N1	3.70 (1)
S2...N1	3.869 (9)	S3...N1	3.497 (9)

Bonds	Angle (deg)	Bonds	Angle (deg)
S1—Cu1—S2	92.2 (1)	C2—C3—C4	120 (1)
S1—Cu1—S3	114.7 (1)	C3—C4—C5	120 (1)
S2—Cu1—S3	91.5 (1)	C4—C5—C6	122 (1)
S1—Cu1—N1	119.4 (3)	C1—C6—C5	118.3 (9)
S2—Cu1—N	127.9 (3)	C1—C6—C7	123.1 (9)
S3—Cu1—N	108.2 (3)	C5—C6—C7	118.6 (8)
C7—S1—C8	101.6 (5)	S1—C7—C6	109.2 (7)
C9—S2—C10	102.5 (5)	S1—C8—C9	115.3 (8)
C11—S3—C12	100.5 (5)	S2—C9—C8	110.6 (8)
Cu—N—C13	169.7 (9)	S2—C10—C11	121.0 (9)
C2—C1—C6	120 (1)	S3—C11—C10	114.3 (9)
C2—C1—C12	119 (1)	S3—C12—C1	109.1 (7)
C6—C1—C12	121.7 (9)	S4—C13—N	180 (1)
C1—C2—C3	121 (1)		

Can. J. Chem. Downloaded from www.nrcresearchpress.com by 198.100.157.202 on 09/07/12
For personal use only.

which a simple exchange of non-coordinated anions (NCS^- for ClO_4^-) had occurred.

The room temperature ^1H NMR spectrum (CD_3CN) of [Cu(NCS)(TT[9]OB)] shows three separate sets of broadened resonances assignable to aromatic, benzylic, and methylene SCH_2CH_2S protons. The broadening is likely due to some inversion at the S centres and contributions from ^{63}Cu quadrupole effects. At low temperature (CD_3CN, 235 K), these effects are diminished and the spectrum is well-resolved into discernible patterns. The aromatic region shows a multiplet pattern typical of *ortho* substitution (δ 7.47 (m)) and the benzylic region exhibits a pair of doublets (δ 4.10 (d), 3.88 (d), ^2J = 11.2 Hz) assigned to axial and equatorial protons on the seven-membered chelate ring. The methylene protons of the SCH_2CH_2S chain also resonate as two separate groups (δ 3.53 (m), 2.92 (m)) and are assigned as the protons of C9, C10 and C8, C11 consistent with that observed by ourselves for $[Cu(Ph_2PMe)(TT[9]OB)]^+$ and others for similar compounds containing five-membered chelate ring systems (12, 18). The infrared spectrum clearly shows the ν(NC) stretch of the thiocyanate ion at 2095 cm^{-1} which is indicative of coordinated thiocyanate.

Recrystallization of [Cu(NCS)(TT[9]OB)] by vapour diffusion of diethylether into a relatively dilute solution of the complex produced crystals suitable for X-ray diffraction. The unit cell contains eight molecules of [Cu(NCS)(TT[9]OB)]. A perspective view of [Cu(NCS)(TT[9]OB)], indicating the atom numbering scheme, is shown in Fig. 1. Selected listings of interatomic distances and angles are found in Table 3.

The Cu(I) ion is in a slightly distorted tetrahedral geometry with three coordination sites occupied by coordination to the S atoms of the TT[9]OB ligand and the fourth site occupied by the N atom of the thiocyanate ligand. The Cu—S distances are 2.328(3) Å and 2.359(3) Å for S1 and S3 associated with the *ortho*-xylyl fragment and 2.353 (3) Å for the central S2 atom. The Cu—N distance is 1.949(9) Å. The S—Cu—S angles for the five-membered chelate rings are 92.2(1)° and 91.5(1)° and the S1—Cu—S3 angle of the seven-membered chelate ring involving the *ortho*-xylyl fragment is 114.7(1)°. The parameters associated with the coordination of TT[9]OB to the Cu(I) centre compare well to those found for $[Cu(Ph_2PMe)$-(TT[9]OB)]. The S—Cu—N angles are 119.4(3), 127.9(3), and 108.2(3)° to S1, S2, and S3, respectively. The thiocyanate group is linear with the S4—N—C13 angle measuring 180(1)°. The sulfur–carbon distances in TT[9]OB range from 1.81(1) to 1.87(1) Å and carbon C(sp^2)—C(sp^2) bonds range from 1.37(1) to 1.43(1) Å. The two C(sp^3)—C(sp^3) bonds are 1.48(1) and 1.53 (1) Å and the two C(sp^2)—C(sp^3) bonds are

Can. J. Chem. Downloaded from www.nrcresearchpress.com by 198.100.157.202 on 09/07/12
For personal use only.

TABLE 4. Comparison of torsional angles[a] in TT[9]OB,[b] [Cu(TT[9]OB)(PPh_3)][ClO_4],[c] and [Cu(NCS)(TT[9]OB)]

Bonds	Angle (deg)			
	TT[9]OB	[Cu(TT[9]OB)(PPh_3)]$^+$		[Cu(NCS)(TT[9]OB)]
C1—C6—C7—S1	−100.4	−94.4 (7)	−92.2 (7)	−95 (1)
C6—C7—S1—C8	163.7	164.2 (5)	160.9 (5)	158.4 (7)
C7—S1—C8—C9	−73.9	−68.9 (5)	−70.2 (6)	−77.3 (9)
S1—C8—C9—S2	−62.0	−54.6 (5)	−58.7 (7)	−59 (1)
C8—C9—S2—C10	150.9	133.6 (5)	139.3 (6)	150.1 (8)
C9—S2—C10—C11	−57.0	−133.7 (5)	−129.0 (6)	−64 (1)
S2—C10—C11—S3	−48.6	55.0 (2)	51/3 (9)	−42 (1)
C10—C11—S3—C12	155.0	68.1 (6)	67.4 (8)	135.5 (9)
C11—S3—C12—C1	−152.1	−166.3 (5)	−166.8 (5)	−156.3 (7)
S3—C12—C1—C6	78.6	92.6 (7)	96.3 (7)	94 (1)
C12—C1—C6—C7	0.4	2.2 (9)	1 (1)	−4 (2)

[a]Sign is positive for a clockwise rotation of 1 to 4 viewed down the 2–3 bond.
[b]Data taken from ref. 18. Molecular mechanics calculations for the endodentate conformation.
[c]Data taken from ref. 12. The two sets of values represent two crystallographically independent molecules.

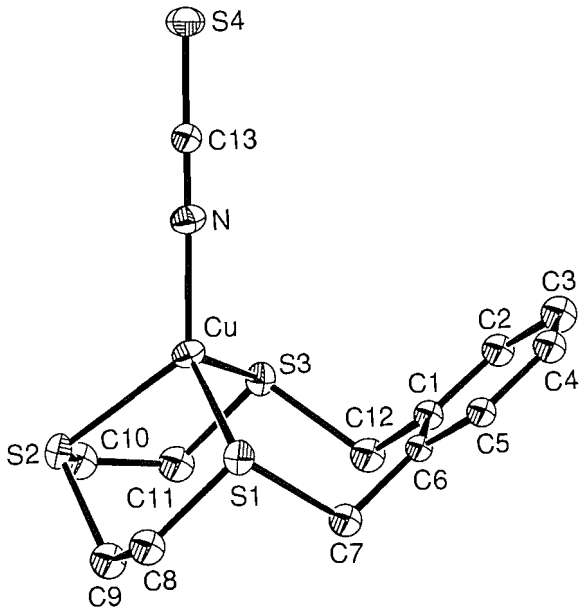


FIG. 1. Perspective ORTEP drawing of [Cu(NCS)(TT[9]OB)] showing the atom-numbering scheme. Thermal ellipsoids of 20% are shown.

1.50(1) and 1.51(1) Å. These parameters are typical for thioether ligands (4) and compare well to those obtained in TT[9]OB (19) and other complexes of TT[9]OB (12, 19, 20).

An interesting structural feature of [Cu(NCS)(TT[9]OB)] is the conformation of the TT[9]OB ligand as described by the torsional angles found in Table 4. The ligand adopts an asymmetric conformation which differs from that found for [Cu(Ph_2PMe)(TT[9]OB)][ClO_4]. The two five-membered chelate rings adopt opposite conformations (δ and λ) in [Cu(Ph_2PMe)-(TT[9]OB)][ClO_4] but adopt the same conformations (δ and δ or λ and λ) in [Cu(NCS)(TT[9]OB)]. Since the thiocyanate ligand offers no steric demands and there is no obvious electronic requirements for NCS^- as a ligand, it could be that the conformation observed for TT[9]OB in [Cu(NCS)(TT[9]OB)] is simply that favoured by the ligand in the absence of any perturbations from the ancillary ligand or anion. Although the energy difference between the two conformations is likely to be small, it should be noted that in our original conformational analysis of TT[9]OB we calculated (Table 4) the low energy endodentate conformation for the free ligand to be the asymmetric version found for TT[9]OB in [Cu(NCS)(TT[9]OB)].

Discussion

The coordination chemistry of 2,5,8-trithia[9]-*o*-benzenophane (TT[9]OB) is different from that found for most macrocyclic thioether ligands. Although the conformation of the free ligand is exodentate (12), there is considerable strain involved in the $SCH_2CH_2SCH_2CH_2S$ bracket and the ligand easily converts to an endodentate conformation (19, 20). This flexibility is in marked contrast to the rigid, preorganized conformation of 9S3.

Studies on the coordination chemistry of 9S3 with Cu(I) have shown that the structure of the complex formed can be very dependent on the ancillary ligands and the counterion used. For example, the product formed in the reaction of [Cu($CH_3CN)_4$][X] with 9S3 depends critically on the nature of X. If X is I^-, PF_6^-, BF_4^-, or ClO_4^-, the products formed are [Cu(I)(9S3)] (21), [Cu(9S3)$_2$][PF_6] (22), [Cu_2(9S3)$_3$][BF_4] (22), and [Cu_3(9S3)$_3$][ClO_4] (21), respectively. Only in the case of the soft anion I^- was a simple mononuclear species of the formula [Cu(9S3)(L)] found. It has recently been shown that if ancillary PPh_3 or $AsPh_3$ ligands are introduced during the reactions involving non-coordinating anions complexes of the type [Cu(PPh_3)(9S3)][X] can also be prepared (11, 23).

In contrast to 9S3, TT[9]OB forms only mononuclear complexes regardless of the nature X or the ancillary ligand. We have shown previously (12) that this is the case for cationic complexes of the formulation [Cu(L)(TT[9]OB)][X] and in this paper we have shown that the same is true for [Cu(NCS)(TT[9]OB)] in which the ancillary ligand is anionic and the complex is neutral. The structural analysis of [Cu(NCS)(TT[9]OB)] demonstrates the subtle conformational differences that can occur for complexes of TT[9]OB and emphasizes the flexible nature of TT[9]OB relative to the conformational rigidity of 9S3.

Acknowledgements

We thank the Natural Sciences and Engineering Research Council of Canada and the Petroleum Research Fund, adminis-

tered by the American Chemical Society for financial support of this research. G.K.S. gratefully acknowledges the award of a NSERC of Canada postgraduate scholarship.

1. S. R. COOPER. Acc. Chem. Res. **21**, 141 (1988).
2. M. SCHRÖDER. Pure Appl. Chem. **60**, 517 (1988).
3. A. J. BLAKE and M. SCHRÖDER. Adv. Inorg. Chem. **35**, 1 (1990).
4. (*a*) R. E. WOLF, J. R. HARTMAN, J. M. E. STOREY, B. M. FOXMAN, and S. R. COOPER. J. Am. Chem. Soc. **109**, 4328 (1987); (*b*) E. JUARISTI. J. Chem. Ed. **56**, 438 (1978) and references therein; (*c*) J. M. DESPER, D. R. POWELL, and S. H. GELLMAN. J. Am. Chem. Soc. **112**, 4321 (1990).
5. R. S. GLASS, G. S. WILSON, and W. N. SETZER. J. Am. Chem. Soc. **102**, 5068 (1980).
6. A. J. BLAKE, R. O. GOULD, A. J. HOLDER, T. I. HYDE, and M. SCHRÖDER. J. Chem. Soc. Chem. Commun. 1861 (1988.)
7. A. J. BLAKE, A. J. HOLDER, T. I. HYDE, H-J. KÜPPERS, M. SCHRÖDER, S. STÖZEL, and K. J. WIEGHARDT. J. Chem. Soc. Chem. Commun. 1600 (1989).
8. A. J. BLAKE, R. O. GOULD, J. A. GREIG, A. J. HOLDER, T. I. HYDE, and M. SCHRÖDER. J. Chem. Soc. Chem. Commun. 876 (1989).
9. A. J. BLAKE, A. J. HOLDER, T. I. HYDE, and M. SCHRÖDER. J. Chem. Soc. Chem. Commun. 1433 (1989).
10. A. J. BLAKE, J. A. GREIG, A. J. HOLDER, T. I. HYDE, A. TAYLOR, and M. SCHRÖDER. Angew. Chem. Int. Ed. Engl. **29**, 197 (1990).
11. A. J. BLAKE, R. O. GOULD, A. J. HOLDER, A. J. LAVERY, and M. SCHRÖDER. Polyhedron, **9**, 2919 (1990).
12. B. DE GROOT, G. R. GIESBRECHT, S. J. LOEB, and G. K. SHIMIZU. Inorg, Chem. **30**, 177 (1991).
13. G. J. KUBAS. Inorg. Synth. **19**, 90 (1979).
14. Texsan-Texray Structure Analysis Package, Molecular Structure Corporation. 1985.
15. D. T. CROMER and J. T. WABER. International tables for X-ray crystallography. Vol. IV, The Kynoch Press, Birmingham, United Kingdom. 1974. Table 2.2A.
16. J. A. IBERS and W. C. HAMILTON. Acta. Crystallogr. **17**, 781 (1974).
17. D. T. CROMER. International tables for X-ray crystallography, Vol. IV, The Kynoch Press, Birmingham, United Kingdom, 1974. Table 2.3.1.
18. C. R. LUCAS, S. LIU, M. J. NEWLANDS, and E. J. GABE. Can. J. Chem. **68**, 1357 (1990).
19. B. DE GROOT and S. J. LOEB. Inorg. Chem. **29**, 4084 (1990).
20. B. DE GROOT and S. J. LOEB. J. Chem. Soc., Chem. Commun. 1755 (1990).
21. H-J. KÜPPERS, K. WEIGHARDT, Y-H. TSAY, C. KRUGER, B. NUBER, and J. WEISS. Angew. Chem. Int. Ed. Engl. **26**, 575 (1987).
22. J. A. CLARKSON, R. Y. YAGBASAN, P. J. BLOWER, and S. R. COOPER. J. Chem. Soc., Chem. Commun. 1244 (1989).
23. A. J. BLAKE and M. SCHRÖDER. Polyhedron, **9**, 2919 (1991).

Can. J. Chem. Downloaded from www.nrcresearchpress.com by 198.100.157.202 on 09/07/12
For personal use only.

Structure and magnetic properties of $[Cp_2M(\mu\text{-}PEt_2)]_2$ (M = Ti, Zr)

DAVID G. DICK AND DOUGLAS W. STEPHAN[1]

Department of Chemistry and Biochemistry, University of Windsor, Windsor, Ont., Canada N9B 3P4

Received January 16, 1991

DAVID G. DICK and DOUGLAS W. STEPHAN. Can. J. Chem. **69**, 1146 (1991).

The complex $[Cp_2Ti(\mu\text{-}PEt_2)]_2$ (**1**) crystallizes in the monoclinic space group $P2_1/n$ with a = 16.591(3) Å, b = 8.662(2) Å, c = 37.407(2) Å, β = 102.40(1)°, Z = 8, and V = 5250(2) Å^3. The Ti_2P_2 core of the dimeric complex is planar and the angles at Ti and P are close to 90°. The Ti...Ti separations were found to be 3.732(1) and 3.706(1) Å in the two independent molecules in the unit cell. Bulk magnetic susceptibility measurements on solid **1** show that the species is diamagnetic over the range 5–340 K. The coupling constant for the antiferromagnetic interaction between the Ti centers of **1** is found to be at least -300 cm^{-1}. Extended Hückel Molecular Orbital calculations suggest that mixing of the frontier $1a_1$ orbitals of the Cp_2Ti fragments with the p orbitals of the phosphide fragments affords a mechanism for super-exchange through the ligands. In THF solution, variable temperature ^1H, and $^{31}P\{^1H\}$ NMR and EPR spectra for **1** are consistent with the generation of the paramagnetic monomeric species Cp_2TiPEt_2, **3**. As well, the data suggest thermal populations of the paramagnetic triplet state of the dimer may occur to a small extent at 340 K. In contrast, the analogous Zr dimer **2** shows no evidence of dissociation or of thermal population of the triplet state at temperatures to 340 K.

Key words: titanium phosphides, structures, magnetic properties.

DAVID G. DICK et DOUGLAS W. STEPHAN. Can. J. Chem. **69**, 1146 (1991).

Le complexe $[Cp_2Ti(\mu\text{-}PEt_2)]_2$ (**1**) cristallise dans le groupe d'espace monoclinique $P2_1/n$, avec a = 16,591(3), b = 8,662(2) et c = 37,407(2) Å, β = 80,07(3)°, Z = 8 et V = 5250(2) Å^3. Le noyau Ti_2P_2 du complexe dimère est plan et les angles au niveau de Ti et de P se rapprochent de 90°. On a trouvé que les distances Ti...Ti sont égale à 3,732(1) et 3,706(1) Å respectivement dans les deux molécules indépendantes de la cellule de base. Des mesures de susceptibilité magnétique globale sur le composé **1** solide montrent que cette espèce est diamagnétique de 5 à 340 K. On a déterminé que la constante de couplage de l'interaction antiferromagnétique entre les centres Ti du composé **1** est égale à au moins -300 cm^{-1}. Des calculs d'OM étendus selon Hückel suggèrent que le mélange des orbitales frontières $1a$, de la portion Cp_2Ti avec les orbitales p des fragments phosphure conduisent à un mécanisme de super-échange à travers les ligands. En solution dans le THF, les spectres rpe et rmn du ^1H et du $^{31}P\{^1H\}$ à température variable du composé **1** sont en accord avec la génération d'espèces paramagnétiques monomères Cp_2TiPE_2, **3**. De plus, les données suggèrent que des populations thermiques de l'état paramagnétique triplet du dimère peuvent être présentes en petites quantités à 340 K. Par opposition, l'analogue dimère **2** du Zr ne présente pas de données suggérant l'existence d'une dissociation ou d'une population thermique de l'état triplet à des températures allant jusqu'à 340 K.

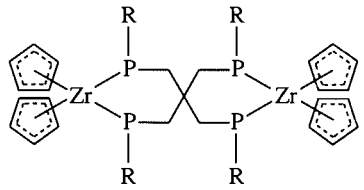
Mots clés : phosphures de titanium, structures, propriétés magnétiques.

[Traduit par la rédaction]

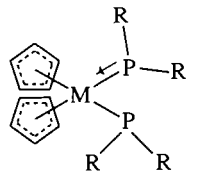
Introduction

As part of a continuing interest in early–late heterobimetallic (ELHB) complexes (1–11) we and others have recently described a route to monophosphido-bridged, ELHB species employing the Ti(III) or Zr(III) phosphido species $[Cp_2M(\mu\text{-}PR_2)]_2$ as precursors. While the chemistry of the derived ELHB complexes is a subject of ongoing investigations, further development in synthetic strategies to such complexes hinges on a thorough understanding of early metal phosphides.

The preparation of the first zironocene(IV) diphosphide species (**a**) was first reported by Ellerman and Poersch in 1967 (12). However, it was not until the report of Baker *et al.* in 1983 (13), that a complete spectroscopic and structural study of metallocene(IV) diphosphides of the form (**b**), was presented.



a (R =Ph)



b (M = Zr, Hf)
(R = Ph, Cy, Et)

The related Ti(III) and Zr(III) phosphide species were first synthesized in 1966 by Issleib and Hackert (14). Subsequent spectroscopic studies suggested several species were formed in the reactions of phosphides with metallocene dihalides (16, 17). The nature of these ill-characterized species was dependent on the mode of preparation, nature of the phosphide substituents, and temperature of reaction. Furthermore, variations in the magnetic properties of the resultant metallocene–phosphide species appear to depend on how the low-valent precursor was generated. This confusion spurred recent structural studies of the complexes $[Cp_2M(\mu\text{-}PMe_2)]_2$ (M = Ti (17), Zr (18)) in which the dimeric structure originally proposed by Issleib and Hackert was confirmed. In this report, we describe the structure and magnetic properties of the dimeric species $[Cp_2M(\mu\text{-}PEt_2)]_2$ (M = Ti, **1**; Zr, **2**). The magneto-structural relationship is discussed in light of Extended Hückel Molecular Orbital considerations.

Experimental section

General data

All preparations were done under an atmosphere of dry, O_2-free N_2 employing a Vacuum Atmospheres inert atmosphere glove box. Solvents were reagent grade, distilled from the appropriate drying agents under N_2, and degassed by the freeze–thaw method at least three times prior to use. ^1H NMR spectra were recorded on Bruker AC-300 spectrometer operating at 300 MHz. Trace amounts of protonated solvents were used as reference and chemical shifts are reported relative to $SiMe_4$. EPR spectra were recorded on a Varian E-12 EPR spectrometer employing DPPH as reference. Variable temperature magnetic susceptibilities were recorded using an S.H.E. Corporation Variable Temperature Superconducting Magnetometer/Susceptometer located at the Michigan State University, East Lansing, MI. Observed magnetic moments were corrected for TIP, the diamagnetism of the

Can. J. Chem. Downloaded from www.nrcresearchpress.com by 84.41.108.74 on 09/07/12
For personal use only.

Can. J. Chem. Downloaded from www.nrcresearchpress.com by 84.41.108.74 on 09/07/12
For personal use only.

bucket, and the diamagnetic contributions using Pascal's constants for C, H, and P. Combustion analyses were performed by Galbraith Laboratories Inc. Knoxville, TN, and Schwarzkopf Laboratories, Woodside, NY. Cp_2TiCl_2 and Cp_2ZrCl_2 were purchased from the Aldrich Chemical Co. $LiPEt_2$ was prepared by the literature method (11) from PEt_2H obtained from the Pressure Chemical Co.

Synthesis of $[Cp_2Ti(\mu\text{-}PEt_2)]_2$, ***1***

The compound $[Cp_2Ti(\mu\text{-}PEt_2)]_2$ **1** was prepared by literature method (14). A solution of $LiPEt_2$ (0.158 g, 1.65 mmol) in 10 mL of THF was added dropwise to a suspension of Cp_2TiCl_2 (0.200 g, 0.804 mmol) in 15 mL of THF. After 1 h of stirring the THF was removed under *vacuo* and 20 mL of benzene was added. The solution was filtered and the fitrate was reduced in volume to about 10 mL. Addition of pentane caused precipitation of the purple, cyrstalline product (0.133 g, 62%). *Anal.* calcd for $C_{28}H_{40}P_2Ti_2$: C 62.93, H 7.54; found: C 62.50, H 7.50. ^1H NMR (C_7D_8, δ, ppm, 295 K): 4.73 (s, Cp), 1.13 (br, s, Et). $^{31}P\{^1H\}$ (C_7H_8, δ, ppm, 185 K) 107.3 (s). EPR (C_7H_8, 323 K) $g = 1.979$.

Synthesis of $[Cp_2Zr(\mu\text{-}PEt_2)]_2$, ***2***

A solution of $LiPEt_2$ (0.145 g, 1.51 mmol) in 10 mL of THF was added dropwise to a solution of Cp_2ZrCl_2 (0.200 g, 0.684 mmol) in 15 mL of THF. After 1 h of stirring the THF was removed under *vacuo* and 20 mL of benzene was added. The solution was filtered and the filtrate was reduced in volume to about 10 mL. Addition of pentane caused precipitation of the red–brown, crystalline product (0.050 g, 24%). *Anal.* calcd for $C_{28}H_{40}P_2Zr_2$: C 54.15, H 6.49; found: C 54.00, H 6.50. ^1H NMR (C_7D_8, δ, ppm, 298 K): 4.65 (t, $|J_{P_H}| = 1.2$ Hz, Cp). 1.34 (s, CH_2), 1.33 (s, CH_3). $^{13}C\{^1H\}$ (C_7D_8, δ, ppm, 298 K): 94.3 (s, Cp), 19.8 (s, CH_2), 13.0 (s, CH_3). $^{31}P\{^1H\}$ (C_7H_8, δ, ppm, 298 K) 88.7 (s).

Extended Hückel molecular orbital calculations

Calculations and plotting were done employing the TRIBBL program package (19) operating on a VAX 11/785. Extended Hückel calculations were performed employing the EHT option of TRIBBL. Cartesian coordinates of the model compound $[Cp_2Ti(\mu\text{-}PH_2)]_2$ were derived from the structural data with the appropriate substitution of hydrogen atoms for the alkyl substituents employing PC-MODEL[1].

X-ray data collection and reduction

X-ray quality crystals of **1** were obtained directly from the preparations as described above. The crystals were manipulated and mounted in capillaries in a glove box, thus maintaining a dry, O_2-free environment for each crystal. Diffraction experiments were performed on a four-circle Syntex $P2_1$ diffractometer with graphite-monochromatized Mo Kα radiation. The initial orientation matrix was obtained from 15 machine-centered reflections selected from rotation photographs. These data were used to determine the crystal system. Partial rotation photographs around each axis were consistent with monoclinic crystal system. Ultimately, 60 reflections ($20° < -\theta < 25°$) were used to obtain the final lattice parameters and the orientation matrices. Machine parameters, crystal data and data collection parameters are summarized in Table 1. The observed extinctions are consistent with the space group $P2_1/n$. The data set was collected in one shell ($4.5° < 2\theta < 45.0°$) and three standard reflections were recorded every 197 reflections. The intensities of the standards showed no statistically significant change over the duration of the data collection. The data were processed using the SHELX-76 program package on the computing facilities at the University of Windsor. The reflections with $F_o^2 > 3\sigma F_o^2$ were used in the refinement.

Structure solution and refinement

Non-hydrogen atomic scattering factors were taken from the literature tabulations (21, 22). The Ti atom positions were determined using direct methods employing SHELX-86. The remaining non-hydrogen atoms were located from successive difference Fourier map calculations. The refinements were carried out by using full-matrix, least squares techniques on F, minimizing the function $w(|F_o| - |F_c|)^2$ where the weight, w, is defined as $4F_o^2/2\sigma(F_o^2)$ and F_o and F_c are the observed and calculated structure factor amplitudes. In the final cycles of refinement all the Ti and P atoms were assigned anisotropic temperature factors. Carbon atoms were described isotropically. Hydrogen atom positions were calculated and allowed to ride on the carbon to which they are bonded assuming a C—H bond length of 0.95 Å. Hydrogen atom temperature factors were fixed at 1.10 times the isotropic temperature factor of the carbon atom to which they are bonded. In all cases the hydrogen atom contributions were calculated, but not refined. The final values of R and R_w are given in Table 1. The maximum Δ/σ on any of the parameters in the final cycles of the refinement and the location of the largest peaks in the final difference Fourier map calculations are also given in Table 1. The residual electron densities were of no chemical significance. The following data are tabulated: positional parameters (Table 2) and selected bond distances and angles (Table 3). Thermal parameters (Table S1), hydrogen atom parameters (Table S2), bond distances and angles associated with the cyclopentadienyl rings (Table S3) and values of 10 F_o and 10 F_c (Table S4) have been deposited as supplementary material.[2]

TABLE 1. Crystallographic parameters for molecule **1**

Formula	$C_{28}H_{40}P_2Ti_2$
Crystal color, form	Purple plates
a (Å)	16.59(3)
b (Å)	8.662(2)
c (Å)	37.402(7)
β (deg)	102.40(1)
Crystal system	Monoclinic
Space group	$P2_1/n$
Vol (Å^3)	5250(2)
Density (g cm^{-3}) calcd.	1.35
Z	8
Crystal dimensions (mm)	0.40 × 0.35 × 0.28
Abs. coeff, μ (cm^{-1})	6.83
Radiation, λ (Å)	Mo Kα (0.71069)
Temp (°C)	24
Scan speed (deg/min)	4.0–10.0 (θ/2θ)
Scan range (deg)	1.0 below Kα1
	1.0 above Kα2
Background/scan time ratio	0.5
Data collected	7478
2θ range (deg)	4.5–45.0
Index range	$\pm h, +k, +l$
Unique data $F_o^2 > 3\sigma(F_o^2)$	4260
Variables	297
R (%)	7.31
R_w (%)	7.94
Largest Δ/σ in final least squares cycle	0.017
Maximum residual (e/Å^3)	0.60
Atom associated	C91

Results and discussion

The known reaction of Cp_2TiCl_2 with $LiPEt_2$ proceeds smoothly, accompanied by the colour changes from red to green to purple (14). The reaction by-product, P_2Et_4 is detected by $^{31}P\{^1H\}$ NMR, and can be removed under *vacuo*. Extraction of the remaining crude products into benzene affords an effective separation of the product **1** from LiCl affording **1** in reasonable yield (62%). The ^1H NMR spectrum of this product at ambient

[1]Commercially available from Serena Software, Bloomington, IN.

[2]Complete set of tables may be purchased from the Depository of Unpublished Data, Document Delivery, CISTI, National Research Council Canada, Ottawa, Canada K1A 0S2.

TABLE 2. Positional parameters for molecule **1**

Atom	x	y	z	Atom	x	y	z
Ti1	23(1)	1348(2)	4118(1)	Ti2	1119(1)	89(2)	3394(0)
Ti3	3589(1)	3691(2)	5874(1)	Ti4	5331(1)	4957(2)	6611(0)
P1	1335(1)	−315(3)	4103(1)	P2	−203(1)	1719(3)	3405(1)
P3	3995(1)	3341(3)	6586(1)	P4	4914(1)	5357(3)	5902(1)
C1	2326(5)	299(10)	4412(2)	C2	3081(6)	−598(12)	4369(3)
C3	1378(6)	−2376(11)	4273(3)	C4	1438(6)	−2484(13)	4686(3)
C5	−265(5)	3706(10)	3211(3)	C6	−1024(6)	4627(12)	3262(3)
C7	−1210(5)	1083(11)	3116(3)	C8	−1282(6)	1183(13)	2705(3)
C9	3236(5)	4003(11)	6855(2)	C10	3513(6)	3881(12)	7272(3)
C11	4106(5)	1335(10)	6785(3)	C12	3302(6)	466(13)	6731(3)
C13	4813(6)	7370(11)	5734(3)	C14	4474(6)	7584(13)	5323(3)
C15	5626(5)	4755(10)	5602(2)	C16	6436(6)	5627(12)	5651(3)
C21	358(5)	4021(11)	4102(3)	C22	1067(5)	3262(10)	4272(3)
C23	945(5)	2652(11)	4600(3)	C24	168(6)	3085(12)	4636(3)
C25	−191(6)	3901(11)	4321(3)	C31	−701(6)	−78(11)	4511(3)
C32	−1239(5)	1032(11)	4317(3)	C33	−1385(5)	626(10)	3949(3)
C34	−931(5)	−686(11)	3913(3)	C35	−510(6)	−1113(12)	4269(3)
C41	1716(6)	2652(12)	3455(3)	C42	2353(6)	1578(11)	3589(3)
C43	2473(7)	637(13)	3314(3)	C44	1901(6)	1113(12)	2982(3)
C45	1464(7)	2308(13)	3081(3)	C51	79(6)	−1681(12)	3086(3)
C52	458(6)	−2357(12)	3408(3)	C53	1294(6)	−2646(13)	3398(3)
C54	1407(7)	−2157(14)	3070(3)	C55	655(8)	−1484(14)	2865(4)
C61	2800(6)	5752(11)	6059(3)	C62	2930(6)	6125(13)	5711(3)
C63	2558(6)	5127(12)	5460(3)	C64	2151(6)	4041(13)	5633(3)
C65	2306(5)	4428(11)	6000(3)	C71	3947(6)	997(12)	5910(3)
C72	4507(6)	1734(11)	5745(3)	C73	4092(6)	2338(12)	5410(3)
C74	3274(6)	1955(13)	5364(3)	C75	3181(6)	1122(12)	5678(3)
C81	4580(6)	6704(12)	6917(3)	C82	4642(6)	7385(11)	6587(3)
C83	5482(6)	7684(13)	6611(3)	C84	5917(8)	7163(14)	6941(3)
C85	5354(7)	6505(14)	7139(4)	C91	5964(6)	2762(13)	6935(3)
C92	5872(6)	2377(12)	6563(3)	C93	6391(5)	3399(11)	6426(3)
C94	6764(7)	4375(14)	6700(3)	C95	6524(7)	4011(14)	7027(4)

Can. J. Chem. Downloaded from www.nrcresearchpress.com by 84.41.108.74 on 09/07/12
For personal use only.

temperature was consistent with the presence of cyclopentadienyl groups and resonances attributable to the ethyl moieties. Although the broadness of the observed resonances suggested the presence of paramagnetic centers, **1** was EPR silent at 298 K. In previous reports in which Cp_2TiCl_2 had been reduced in the presence of phosphide, the product was formulated as a diamagnetic dimer, $[Cp_2Ti(\mu\text{-}PR_2)]_2$ (14–16). Combustion analyses were consistent with the empirical formula Cp_2TiPEt_2 for **1**. The dimeric formulation, that is $[Cp_2Ti(\mu\text{-}PEt_2)]_2$ for **1** was confirmed by a X-ray structural study (*vide infra*).

In a similar fashion, the analogous zirconium reaction was performed. The colorless solution of Cp_2ZrCl_2 gradually became intense red in color with the addition of $LiPEt_2$. Following a work-up procedure similar to that used for **1**, the red–brown product **2** was isolated. The ^1H and $^{13}C\{^1H\}$ NMR spectra of **2** show resonances attributable to cyclopentadienyl groups and the ethyl moieties. The $^{31}P\{^1H\}$ NMR shows a single resonance at 88.7 ppm. Preliminary X-ray experiments[3] showed that crystals of **2** were isomorphous with those of **1**, suggesting that **2** is indeed isostructural to **1**. However, the poor quality of the crystals precluded a full structural study. These data and the results of combustion analyses are consistent with the formulation of **2** as $[Cp_2Zr(\mu\text{-}PEt_2)]_2$.

Structural study of **1**

The crystallographic study of **1** shows that the compound crystallizes in the monoclinic space group $P2_1/n$ with two discrete dimeric molecules per asymmetric unit. The closest approach between the dimers is 2.590 Å (H74...H1A). ORTEP drawings of the two molecules are shown in Fig. 1. Selected bond distances and angles are given in Table 3. The coordination sphere of the Ti atoms are best described as pseudo-tetrahedral, being comprised of two π-bonded cyclopentadienyl groups and two bridging, diethylphosphide moieties. The Ti—C, C—C and P—C bond distances are typical (11, 17, 24–34).

The Ti_2P_2 cores of the crystallographically independent molecules are essentially planar. The Ti—P distances, which range from 2,606(3)–2.631(3) Å, are similar to those reported for $[Cp_2Ti(\mu\text{-}PMe_2)]_2$ (17). The Ti—P distances are slightly shorter than the Zr—P distances found in $[Cp_2Zr(\mu\text{-}PMe_2)]_2$ (18), consistent with smaller covalent radius of Ti. The P—Ti—P angles in **1** were found to be 89.1(1) to 89.8(1)°. This is substantially smaller than the X—Ti—X angles found for related d^0 derivatives. For example, the S—Ti—S angle in $Cp_2Ti(SMe)_2$ is 93.7(1)° (25), while the P—Hf—P angle in $Cp_2Hf(PEt_2)_2$ is 98.64(3)° (13). The smaller angle observed for d^1 metallocene species has been explained in terms of the occupation of the $1a_1$ metal-based molecular orbital (27, 35).

[3]Repeated attempts to obtain crystals of $[Cp_2Zr(\mu\text{-}PEt_2)]_2$ **2** yielded only thin, plate-like crystals which were not of suitable quality for diffraction data collection. In the best case a twinned crystal was examined. The compound was found to crystallize in a monoclinic crystal system with a = 37.58(2) Å, b = 16.776(5) Å, c = 8.813(6) Å, β = 90.67(6)°, V = 5432(4) Å^3. Although this is isomorphorous to **1**, the poor crystal quality precluded further study.

TABLE 3. Selected bond distances and angles for molecule **1**

Bond	Distance (Å)	Bond	Distance (Å)	Bond	Distance (Å)
P1—Ti1	2.622(3)	P2—Ti1	2.631(3)	P1—Ti2	2.619(3)
P2—Ti2	2.616(3)	P3—Ti3	2.620(3)	P4—Ti3	2.613(3)
P3—Ti4	2.606(3)	P4—Ti4	2.618(3)	C21—Ti1	2.385(10)
C22—Ti1	2.377(9)	C23—Ti1	2.384(9)	C24—Ti1	2.425(10)
C25—Ti1	2.390(10)	C31—Ti1	2.428(10)	C32—Ti1	2.385(9)
C33—Ti1	2.369(8)	C34—Ti1	2.382(9)	C35—Ti1	2.421(10)
C41—Ti2	2.422(10)	C42—Ti2	2.396(10)	C43—Ti2	2.379(10)
C44—Ti2	2.390(11)	C45—Ti2	2.384(11)	C51—Ti2	2.409(10)
C52–Ti2	2.392(10)	C53—Ti2	2.387(11)	C54—Ti2	2.395(12)
C55—Ti2	2.390(13)	C61—Ti3	2.402(10)	C62—Ti3	2.394(11)
C63—Ti3	2.394(11)	C64—Ti3	2.382(10)	C65—Ti3	2.365(9)
C71—Ti3	2.404(10)	C72—Ti3	2.396(9)	C73—Ti3	2.387(10)
C74—Ti3	2.397(11)	C75—Ti3	2.394(10)	C81—Ti4	2.401(10)
C82—Ti4	2.387(10)	C83—Ti4	2.375(11)	C84—Ti4	2.368(12)
C85—Ti4	2.381(13)	C91—Ti4	2.375(11)	C92—Ti4	2.429(10)
C93—Ti4	2.431(9)	C94—Ti4	2.382(11)	C95—Ti4	2.383(12)
C1—P1	1.872(8)	C3—P1	1.892(10)	C5—P2	1.861(9)
C7—P2	1.867(9)	C9—P3	1.865(9)	C11—P3	1.885(9)
C13—P4	1.848(10)	C15—P4	1.868(8)	P1—C1	1.872(8)
C1—C2	1.512(12)	P1—C3	1.892(10)	C3—C4	1.531(13)
P2—C5	1.861(9)	C5—C6	1.537(12)	P2—C7	1.867(9)
C7—C8	1.520(14)	P3—C9	1.865(9)	C9—C10	1.531(14)
P3—C11	1.885(9)	C11—C12	1.507(12)	P4—C13	1.848(10)
C14—C13	1.531(13)	C13—C14	1.531(13)	P4—C15	1.868(8)
C15—C16	1.518(12)				

Bonds	Angle (deg)	Bonds	Angle (deg)
P2—Ti1—P1	89.1(1)	P2—Ti2—P1	89.5(1)
P4—Ti3—P3	89.6(1)	P4—Ti4—P3	89.8(1)
Ti2—P1—Ti1	90.8(1)	Ti2—P2—Ti1	90.7(1)
Ti4—P3—Ti3	90.3(1)	Ti4—P4—Ti3	90.2(1)
C1—P1—Ti1	117.0(3)	C1—P1—Ti2	119.9(3)
C3—P1—Ti1	118.8(3)	C3—P1—Ti2	117.0(3)
C3—P1—C1	95.5(4)	C5—P2—Ti1	119.4(3)
C5—P2—Ti2	118.0(3)	C7—P2—Ti1	117.7(3)
C7—P2—Ti2	118.8(3)	C7—P2—C5	94.6(4)
C9—P3—Ti3	117.2(3)	C9—P3—Ti4	118.9(3)
C11—P3—Ti3	119.4(3)	C11—P3—Ti4	118.1(3)
C11—P3—C9	95.1(4)	C13—P4—Ti3	119.6(3)
C13—P4—Ti4	117.0(3)	C15—P4—Ti3	117.2(3)
C15—P4—Ti4	120.5(3)	C15—P4—C13	94.8(4)
C2—C1—P1	115.2(7)	C4—C3—P1	112.8(7)
C6—C5—P2	114.2(6)	C8—C7—P2	115.7(7)
C10—C9—P3	116.0(6)	C12—C11—P3	113.5(7)
C14—C13—P4	116.3(7)	C16—C15—P4	116.5(7)

The Ti—P—Ti′ angles in **1** were found to be between 90.2(1) and 90.8(1)°. In contrast to those found for **1**, the P—Ti—P and Ti—P—Ti′ angles in $[Cp_2Ti(\mu\text{-}PMe_2)]_2$ were found to average 83.3(1) and 96.5(1)°, respectively. In the analogous Zr complex (18) $[Cp_2Zr(\mu\text{-}PMe_2)]_2$, the P—Zr—P angle is 93.8(1)° while the Zr—P—Zr angle is 86.3(1)°. The differences in the angles about the respective M_2P_2 cores give rise to differing metal–metal distances. In **1**, the Ti...Ti average 3.719(1) Å while the corresponding distance in $[Cp_2M(\mu\text{-}PMe_2)]_2$ is 3.918(1) Å for M = Ti (17) and 3.653(1) Å for M = Zr (18). The substantial difference in Ti_2P_2 core geometry and metal–metal separations in **1** and $[Cp_2Ti(\mu\text{-}PMe_2)]_2$ may be attributed to steric interaction between the ethyl substituents on phosphorus and the cyclopentadienyl rings in **1**. This explanation is consistent with the observation of close approaches between the methylene protons of the ethyl moieties and the cyclopentadienyl groups ranging between 2.000 and 2.248 Å in **1**.

Solid state magnetic properties

X-ray quality crystals of **1** were used in all of the magnetic and spectroscopic studies described below. The magnetic susceptibility of a bulk sample of **1** was determined over the temperature range of 5–350 K (Fig. 2) employing a susceptometer. The magnetic data indicate that the sample is essentially diamagnetic with the amount of paramagnetic impurities confined to less than 0.4%. These data imply that antiferromagnetic coupling between the single electrons on the Ti centres in **1** is strong. This is consistent with the slight increase in magnetic moment at 340 K which may forecast the onset of a Curie transition at higher temperatures. However, no evidence for

Can. J. Chem. Downloaded from www.nrcresearchpress.com by 84.41.108.74 on 09/07/12
For personal use only.

Can. J. Chem. Downloaded from www.nrcresearchpress.com by 84.41.108.74 on 09/07/12
For personal use only.

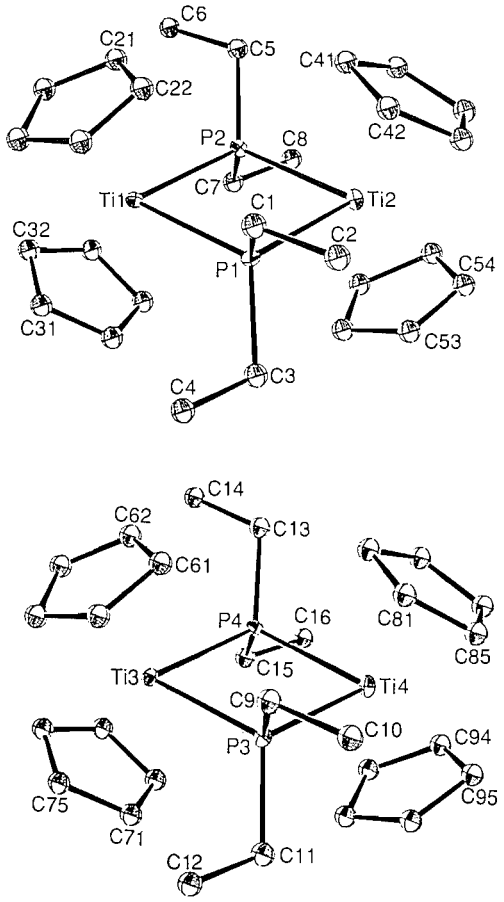


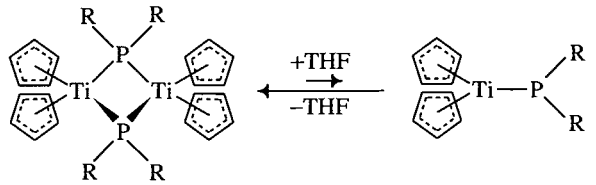
FIG. 1. ORTEP drawing of molecule **1**, 20% thermal ellipsoids are shown. Hydrogen atoms are omitted for clarity but are numbered such that the hydrogen atom numbers correspond to those of the carbon atoms to which they are bonded.

such a transition was obtained as the magnetic fields generated by this instrument are unstable at temperatures above 350° K, although the compound appears thermally stable in the absence of oxygen or moisture to at least 453 K. Based on the present data, an estimate of the coupling constant (J) is, at least, $-300\ cm^{-1}$. These observations are in contrast to those seen for $[Cp_2Ti(\mu\text{-}Cl)]_2$ and $[(MeCp)_2Ti(\mu\text{-}X)]_2$, X = Cl, Br, which exhibit typical antiferromagnetic coupling with Curie temperatures ranging from approximately 140 to 220 K and J values of -111, -160, and $-138\ cm^{-1}$ respectively (36).

A variable temperature, solid state EPR study of **1** showed a resonance at $g = 1.979$ at 350 K. In addition, a weak, half field transition is observed. The intensity of these peaks increases with increasing temperature and the generation of these signals is completely reversible with temperature. The temperature dependence and lack of an EPR signal at 298 K preclude assignment of the observed signals to paramagnetic impurities. Rather, these data suggest the thermal population of the triplet state ($S = 1$) of **1**. However, as mentioned above, the limitations of the apparatus preclude the confirmation of this postulate by high temperature magnetic measurements.

Solution magnetic properties

^1H NMR spectra of the product **1** in THF show resonances at 298 K that are attributable to cyclopentadienyl and ethyl protons, however the signals were observed to be comparatively broad. On cooling to 250 K the spectral lines sharpen and the cyclopentadienyl resonance shifts upfield (Fig. 3). In a similar vien, no $^{31}P\{^1H\}$ NMR signal was observed at 298 K; however, at 223 K a resonance with a linewidth at half height of 1000 Hz was observed at 107.3 ppm. On further cooling to 185 K the line sharpens dramatically to give a linewidth at half height of 110 Hz. These data are consistent with the generation of low concentrations of paramagnetic species with increasing temperature. Variable temperature, EPR studies were also undertaken (Fig. 3). At 298 K in THF, essentially no EPR signal is observed. Two EPR signals are seen on warming. The generation of these signals is reversible with temperature. A doublet at $g = 1.983$ with an $<a,^{31}P>$ value of 33.4 G is observed. This signal is assigned to the mononuclear species Cp_2TiPEt_2, **3**, which is easily generated by dimer dissociation. The formulation of the solvated mononuclear species is further supported by isolation and crystallographic study of the PMe_3 adduct, $Cp_2Ti(PPh_2)(PMe_3)$ (38). The concentration of **3** grows with increasing temperature and is the predominant paramagnetic species in solution at 373 K (eq. [3]). In addition, a singlet resonance at $g = 1.979$ is observed. The g value is identical to that observed in the high temperature solid state EPR spectrum of **1**. Although unconfirmed, this signal is tentatively assigned to the triplet state of **1**. Hyperfine coupling to the phosphorus nuclei is expected but not observed. This may arise as both broader line widths and substantially smaller hyperfine coupling constants are predicted for triplet state dimers (37).



1 **3**

The related Zr species **2** is diamagnetic at 298 K. The sharp lines in the ^1H and $^{31}P\{^1H\}$ NMR spectra show no change in the linewidth of the ^1H NMR resonance attributable to the cyclopentadienyl protons with increasing temperature to 373 K. Thus, unlike the Ti analog, no evidence of either the singlet–triplet or dimer–monomer equilibria is observed.

Bonding considerations

Extended Hückel Molecular Orbital calculations for the model system $[Cp_2Ti(\mu\text{-}PH_2)]_2$ shed some light on the mechanism of the antiferromagnetic coupling between the Ti centers in the dimer **1**. The results of these calculations can be interpreted by considering the frontier orbitals of the phosphide and titanocene fragments. Frontier orbitals for bent metallocenes have been discussed in detail by Hoffman and Lauher (35). Single crystal EPR studies (20), as well as theoretical considerations have shown that for mononuclear paramagnetic metallocene derivatives, the unpaired electron occupies the $1a_1$ metal fragment orbital. Mixing of these $1a_1$ metal fragment orbitals with the p_z orbitals in the bridging phosphorus atoms provides a route for through-ligand coupling of the unpaired electrons on the Ti centres (Fig. 4). This mechanism may explain the observed diamagnetism for **1** and $[Cp_2M(\mu\text{-}PMe_2)]_2$; however, it is surprising that strong antiferromagnetic coupling persists in spite of the substantial differences in the geometries of the M_2P_2 cores. An alternative explanation has been recently offered, in which the notion of a "super-long" bonds has been invoked to explain the diamagnetism of analogous Zr phosphido-bridged dimers (23). Further insight into the subtleties of the magneto-

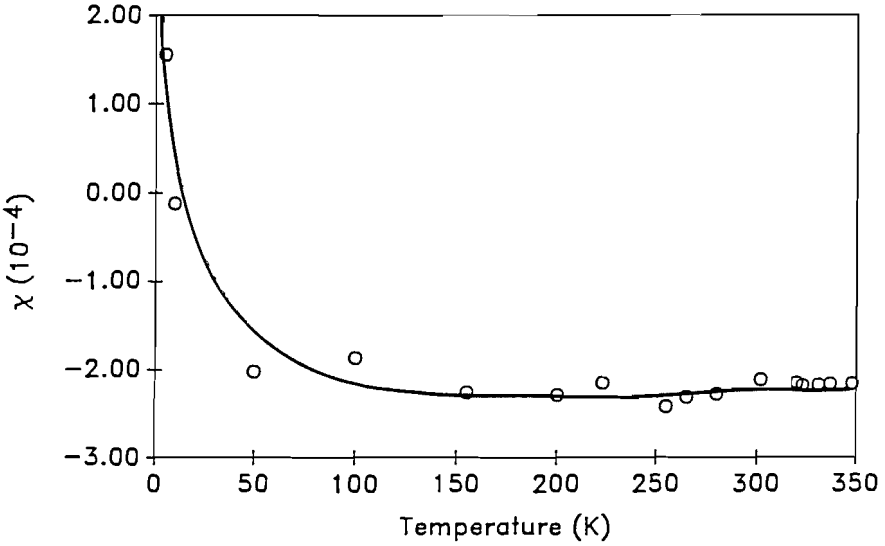


FIG. 2. Plot of χ, molar magnetic susceptibility versus temperature for solid **1**.

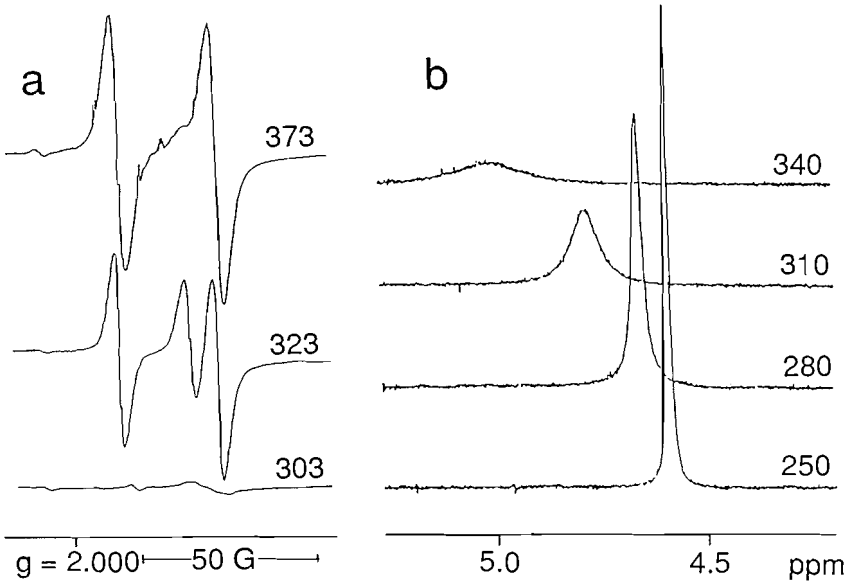


FIG. 3. (*a*) Variable temperature EPR spectra of the THF solution of **1**. (*b*) Variable temperature ^{1}H NMR spectra of a toluene-d^8 solution of **1**, only in resonance due to the cyclopentadienyl protons are shown. In each the temperatures in degrees Kelvin are indicated.

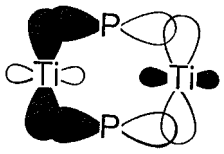


FIG. 4. Possible mechanism for antiferromagnetic coupling in **1**.

structural relationships in these and related d^1 metal dimers awaits the acquisition of additional structural and high temperature, magnetic susceptibility data.

Summary

The dimers $[Cp_2M(\mu\text{-}PR_2)]_2$ (M = Ti, Zr) are diamagnetic at room temperature. The magnetic and structural data for the species $[Cp_2Ti(\mu\text{-}PEt_2)]_2$, **1**, have been examined in detail. Antiferromagnetic coupling is attributed to a through ligand mechanism involving a molecular orbital with both metal $1a_1$ and phosphorus *p* orbital character. The solid state susceptibility, EPR, and NMR data are consistent with dissociation of the dimer **1** to a mononuclear titanocene phosphide species. In addition, the possibility of thermal population of the triplet state of **1** is suggested. In contrast, the Zr dimer shows no evidence of thermal dissociation or population of a triplet state.

Acknowledgements

Financial support from NSERC of Canada is gratefully acknowledged. D.G.D. is grateful for the award of an NSERC Canada postgraduate scholarship. Dr. J. Dye and J. Eglin of Michigan State University are thanked for their assistance in the aquisition of the SQUID magnetic data. Drs. B. R. McGarvey and A. Oszarowski are thanked for helpful discussion.

1. D. W. STEPHAN. Coord. Chem. Rev. **95**, 41 (1989).
2. T. S. TARGOS, R. P. ROSEN, R. R. WHITTLE, and G. L. GEOFFROY. Inorg. Chem. **24**, 1375 (1985).

Can. J. Chem. Downloaded from www.nrcresearchpress.com by 84.41.108.74 on 09/07/12
For personal use only.

3. R. T. BAKER, T. H. TULIP, and S. S. WREFORD. Inorg. Chem. **24**, 1379 (1985).
4. L. GELMINI, L. C. MATASSA, and D. W. STEPHAN. Inorg. Chem. **24**, 2585 (1985).
5. L. GELMINI and D. W. STEPHAN. Inorg. Chim. Acta, **111**, L17 (1986).
6. L. GELMINI and D. W. STEPHAN. Inorg. Chem. **2501**, 1222 (1986).
7. L. GELMINI and D. W. STEPHAN. Organometallics, **7**, 849 (1988).
8. R. T. BAKER and T. H. TULIP. Organometallics, **5**, 839 (1986).
9. P. Y. ZHENG and D. W. STEPHAN. Can. J. Chem. **67**, 1584 (1990).
10. P. Y. ZHENG, T. T. NADASDI, and D. W. STEPHAN. Organometallics, **8**, 1393 (1989).
11. D. G. DICK and D. W. STEPHAN. Organometallics, **9**, 1910 (1990).
12. J. ELLERMAN and P. POERSCH. Agnew. Chem. Int. Ed. Engl. **6**, 355 (1967).
13. R. T. BAKER, J. F. WHITNEY, and S. S. WREFORD. Organometallics, **2**, 1049 (1983).
14. K. ISSLEIB and H. HACKERT. Z. Naturforsch. **21b**, 519 (1966).
15. J. G. KENWORTHY, J. MYATT, and P. F. TODD. J. Chem. Soc. (B) 791 (1970).
16. J. G. KENWORTHY, J. MYATT, and P. F. TODD. J. Chem. Soc. Chem. Commun. 263 (1963).
17. R. PAYNE, J. HACHGENEI, G. FRITZ, and D. FENSKE. Z. Naturforsch. **41b**, 1535 (1986).
18. M. Y. CHIANG, S. GAMBAROTTA, and F. V. BOLHUIS. Organometallics. **7**, 1864 (1988).
19. D. A. PENSAK and J. J. WENDOLOSKI. Quantum Chemistry Program Exchange, Program No. 529.
20. J. L. PETERSEN and L. F. DAHL. J. Am. Chem. Soc. **96**, 2248 (1974).
21. (*a*) D. T. CROMER and J. B. MANN. Acta Crystallogr. Sect. A: Cryst. Phys., Diffr., Theor. Gen. Crystallogr. A**24**, 324 (1968); (*b*) D. T. CROMER and J. B. MANN. Acta Crystallogr. Sect. A.: Cryst. Phys., Diffr., Theor. Gen. Crystallogr. A**24**, 390 (1968).
22. D. T. CROMER and J. T. WABER. International tables for X-ray crystallography. Kynoch Press: Birmingham, England. 1974.
23. M. M. ROHMER and M. BENARD. Organometallics, **10**, 157 (1991).
24. L. B. KOOL, M. D. RAUSCH, H. G. ALT, M. HERBERHOLD, U. THEWALT, and B. WOLF. J. Organomet. Chem. **297**, 159 (1985).
25. T. A. WARK and D. W. STEPHAN. Organometallics, **8**, 2169 (1989).
26. L. B. KOOL, M. D. RAUSCH, H. G. ALT, M. HERBERHOLD, U. THEWALT, and B. WOLF. Angew, Chem. Int. Ed. Engl. **24**, 394 (1985).
27. B. CETINKAYA, P. B. HITCHCOCK, M. F. LAPPERT, S. TORRONI, J. L. ATWOOD, W. E. HUNTER, and M. J. ZAWOROTKO. J. Organomet. Chem. **188**, C31 (1980).
28. L. GELMINI and D. W. STEPHAN. Organometallics, **6**, 1515 (1987).
29. H. ALT, C. E. DENNER, U. THEWALT, and M. D. RAUSCH. J. Organomet. Chem. **356**, C83 (1988).
30. B. H. EDWARDS, R. D. ROGERS, D. J. SIKORA, J. L. ATWOOD, and M. D. RAUSCH. J. Am. Chem. Soc. **105**, 416 (1983).
31. T. A. WARK and D. W. STEPHAN. Inorg. Chem. **29**, 1731 (1990).
32. G. S. WHITE and D. W. STEPHAN. Organometallics, **8**, 903 (1988).
33. G. S. WHITE and D. W. STEPHAN. Organometallics, **6**, 2169 (1987).
34. G. S. WHITE and D. W. STEPHAN. Inorg. Chem. **24**, 1499 (1985).
35. J. W. LAUHER and R. HOFFMAN. J. Am. Chem. Soc. **98**, 1729 (1976).
36. R. JUNGST, D. SEKUTOWSKI, J. DAVIS, M. LULY, and G. STUCKY. Inorg. Chem. **16**, 1645 (1977).
37. R. S. DRAGO. Physical methods in chemistry. W. B. Saunders Co., Philadelphia. 1977.
38. D. G. DICK and D. W. STEPHAN. Organometallics. To be published.

Can. J. Chem. Downloaded from www.nrcresearchpress.com by 84.41.108.74 on 09/07/12
For personal use only.

Synthesis of α-(arylideneamino)alkylamines

ALAN R. KATRITZKY,[1] JINLONG JIANG, AND PHILIP A. HARRIS
Department of Chemistry, University of Florida, Gainesville, FL 32611-2046, U.S.A.

Received November 6, 1990

ALAN R. KATRITZKY, JINLONG JIANG, and PHILIP A. HARRIS. Can. J. Chem. **69**, 1153 (1991).

α-(Arylideneamino)alkylamines **4** are prepared in high yields by the reaction of 1-(benzotriazol-1-yl)-*N*-triphenylphosphorylidenemethylamine (betmip) **2** with lithium amides and treatment of the resulting intermediates **3** with aryl aldehydes.

Key words: benzotriazole, lithium amides, aryl aldehydes.

ALAN R. KATRITZKY, JINLONG JIANG et PHILIP A. HARRIS. Can. J. Chem. **69**, 1153 (1991).

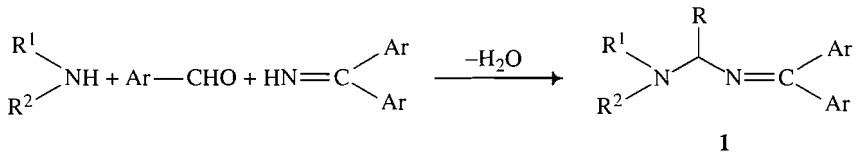
On a préparé des α-(arylidèneamino)alkylamines **4** avec de bons rendements en faisant réagir la 1-(benzotriazol-1-yl)-*N*-triphénylphosphorylidèneméthylamine (betmip) **2** avec des amidures de lithium, puis en traitant les intermédiaires **3** avec des aldéhydes aromatiques.

Mots clés : benzotriazole, amidures de lithium, aldéhydes aromatiques.

[Traduit par la rédaction]

Introduction

Although alkyl diamines (aminals) are well-documented compounds, the corresponding unsaturated α-(diarylideneamino)alkylamines **1** have only been mentioned once in the literature in a report (1) outlining their preparation by a Mannich condensation between diarylketimines, secondary amines, and formaldehyde or aryl aldehydes (see Scheme 1). Diarylketimines require drastic conditions for their preparation, such as the use of sealed tubes at high temperature (2) or the use of molten ketones (3). Other imines with hydrogens on the nitrogen atoms spontaneously polymerize (4).

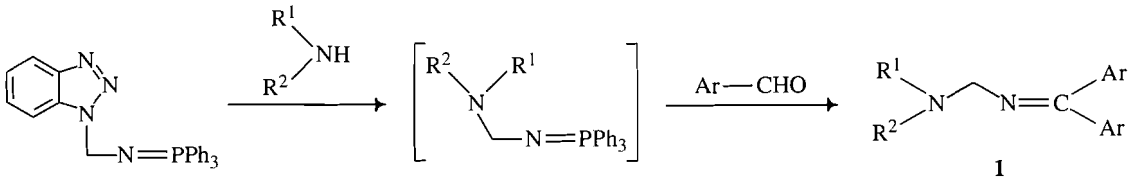


1

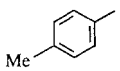
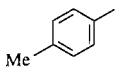
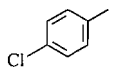
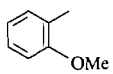
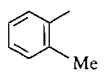
SCHEME 1

Results and discussion

1-(Benzotriazol-1-yl)-*N*-triphenylphosphorylidenemethylamine (betmip) **2** is a new reagent developed in our laboratory. Previously we demonstrated the usefulness of **2** in the novel synthesis of primary amines (5), 1,4,5-trisubstituted imidazoles (6), and in the preparation of carbodimides, imines, isothiocyanates, aziridines, and secondary amines (7). We now report a new route to α-(arylideneamino)alkylamines **4** via nucleophilic displacement of the benzotriazole moiety from **2** with lithium amides, and condensation of the resulting phosphazene intermediates **3** with aryl aldehydes (see Scheme 2).



1

4	R^1	R^2	Ar	**4**	R^1	R^2	Ar
a	Me	Ph		*e*	Pyrrolidine		
b	Me	Ph		*f*	Pyrrolidine		
c	Me	Ph		*g*	Morpholine		
d	Pyrrolidine			*h*	Morpholine		

SCHEME 2

[1]Author to whom correspondence may be addressed.

Can. J. Chem. Downloaded from www.nrcresearchpress.com by 84.41.108.74 on 09/07/12
For personal use only.

TABLE 1. Preparation of α-(arylideneamino)alkylamines **4**

No.	Yield (%)	Boiling point (^{0}C/Torr)[a]	Molecular formula High res. MS (calcd.)	Mass spectra (70 eV)
4*a*	73	162–166/0.9	$C_{15}H_{20}N_2$ 224.1306 (224.1313)	224 (M^+, 7%); 120 (100%); 106 (5%); 91 (26%)
4*b*	70	186–191/0.5	$C_{16}H_{22}N_2$ 238.1478 (238.1475)	238 (M^+, 9%); 132 (11%); 120 (100%); 118 (2%); 106 (14%); 105 (21%)
4*c*	54	170–174/0.5	$C_{16}H_{22}N_2$ 238.1479 (238.1475)	238 (M^+, 7%); 131 (15%); 120 (100%); 118 (5%); 105 (29%)
4*d*	57	145–149/1.2	$C_{13}H_{18}N_2O$ 218.1410 (218.1419)	218 (M^+, 1%); 148 (29%); 134 (14%); 121 (57%); 84 (100%)
4*e*	64	126–130/1.2	$C_{13}H_{18}N_2$ 202.1485 (202.1470)	202 (M^+, 0.4%); 132 (14%); 119 (12%); 105 (14%); 84 (100%)
4*f*	45	119–122/0.3	$C_{12}H_{16}N_2Cl$ 223.0999 (223.1002)	222 (M^+, 0.6%); 152 (5%); 139 (20%) 125 (30%); 84 (100%)
4*g*	43	121–124/0.4	$C_{12}H_{16}N_2O$ 204.1263 (204.1263)	204 (M^+, 2%); 176 (37%); 118 (64%); 91 (100%); 104 (25%)
4*h*	51	138–141/0.5	$C_{13}H_{18}N_2O$ 218.1416 (218.1419)	218 (M^+, 0.5%); 190 (100%); 130 (20%); 105 (65%)

[a]1 Torr = 133.3 Pa.

TABLE 2. ^{1}H NMR data for α-(arylideneamino)alkylamines **4** ($CDCl_3$/TMS)

4	R^1——Amine——R^2	Aryl aldehyde	CH_2 (s, 2H)	CH=N (s, 1H)
a	6.75 (m, 3H), 7.2 (m, 2H) 3.05 (s, 3H)	7.4 (m, 3H), 7.75 (m, 2H)	5.22	8.13
b	6.7 (m, 3H), 7.15 (m, 2H) 3.0 (s, 3H)	2.3 (s, 3H), 7.2 (m, 2H), 7.6 (m, 2H)	5.15	8.15
c	6.7 (m, 3H), 7.2 (m, 2H) 3.05 (s, 3H)	2.35 (s, 3H), 7.2 (m, 3H), 7.85 (m, 1H)	5.20	8.50
d	1.75 (m, 4H), 2.7 (m, 4H)	3.8 (s, 3H), 6.9 (m, 2H), 7.3 (m, 1H), 8.05 (m, 1H)	4.40	8.41
e	1.8 (m, 4H), 2.7 (m, 4H)	2.35 (s, 3H), 7.2 (d, 2H, J = 8), 7.65 (d, 2H, J = 8)	4.4	8.3
f	1.75 (m, 4H), 2.75 (m, 4H)	7.35 (d, 2H, J = 8), 7.7 (d, 2H, J = 8)	4.45	8.3
g	2.65 (m, 4H), 3.75 (m, 4H)	7.4 (m, 3H), 7.75 (m, 2H)	4.27	8.30
h	2.7 (m, 4H), 3.8 (m, 4H)	2.5 (s, 3H), 7.2 (m, 3H), 7.9 (m, 1H)	4.3	8.6

TABLE 3. ^{13}C NMR data for α-(arylideneamino)alkylamines **4** ($CDCl_3$/TMS)

4	R^1——Amine——R^2	Aryl aldehyde	CH_2	CH=N
a	112.4, 117.3, 128.5, 148.7 38.2	128.3, 129.1, 130.7, 135.8	75.4	158.2
b	112.2, 117.1, 128.9, 148.5 37.9	21.2, 128.1, 129.0, 133.1, 140.7	75.2	158.0
c	112.4, 117.3, 129.0, 148.5 38.0	19.1, 126.0, 127.4, 130.1, 130.6, 133.8, 137.6	75.6	157.1
d	23.5, 50.8	55.1, 110.6, 120.3, 127.1, 131.6, 124.0, 128.2	79.3	156.7
	23.1, 52.4	110.5, 120.2, 127.2, 131.6, 124.3	77.2	158.5
e	23.6, 51.0	21.3, 128.2, 129.1, 133.2, 140.8	79.2	160.8
f	23.6, 51.1	128.3, 128.7, 129.4, 130.4	79.0	159.5
g	50.9, 66.6	128.1, 128.3, 130.7, 135.3	82.3	161.2
h	50.9, 66.7	19.3, 125.9, 127.9, 130.3, 130.7, 133.4, 137.7	82.3	160.1

The reaction can be carried out in one pot, without isolation of **3**, and the work-up and isolation procedures are straightforward. After removal of the benzotriazole lithium salt by filtration, the products were separated from the triphenylphosphine oxide side product by distillation. Mass spectrometric analysis (Table 1) of the products showed characteristic peaks resulting from the molecular ion and two fragmentation ions resulting from cleavage of both CH_2—N bonds. The ^{1}H (Table 2) and ^{13}C NMR (Table 3) spectra displayed distinctive signals due to the methylene CH_2 and imino CH=N groups.

In summary, our new method for the preparation of α-(arylideneamino)alkylamines **4** from 1-(benzotriazol-1-yl)-*N*-triphenylphosphorylidenemethylamine **2** offers a new convenient route to this novel class of compounds. Compounds of type

Can. J. Chem. Downloaded from www.nrcresearchpress.com by 84.41.108.74 on 09/07/12
For personal use only.

4 extend the range of aminal functionality, and offer interesting potential substrates for studies of physiological activity, of conformation, and of basicity. The reagent **2** can be readily prepared from benzotriazole in four steps on a large scale and high overall yield (7). It should be noted that attempts at extending this reaction to the use of enolizable aldehydes resulted only in aldol condensation products.

Experimental

^{1}H and ^{13}C NMR spectra were recorded on a Varian VXR 300 MHz spectrometer in $CDCl_3$ using TMS as an internal reference for ^{1}H spectra and $CDCl_3$ for ^{13}C NMR spectra (abbreviations used: s singlet; d doublet; m multiplet). Mass spectra were recorded at 70 eV on an AEI MS-30 mass spectrometer.

Tetrahydrofuran (THF) was dried by distillation from sodium benzophenone ketyl. 1-(Benzotriazol-1-yl)-*N*-triphenylphosphorylidenemethylamine (betmip) **2** (mp 99–101°C) was prepared by the procedure (7) developed in these laboratories.

General procedure for the preparation of α-(arylideneamino)alkylamines ***4***

Butyllithium (5.6 mL, 14 mmol, 2.5 M solution in hexanes) was added to a stirred solution of the secondary amine (14 mmol) in THF (50 mL) at −78°C under argon. A solution of betmip **2** (6.5 g, 16 mmol) in THF (30 mL) was added and stirring continued at room temperature for 20 h during which time a precipitate appeared. The aldehyde (14 mmol) in THF (15 mL) was added and the resulting solution stirred for a further 15 h. After removal of the THF under reduced pressure, the crude product was dissolved in anhydrous ethyl ether and the insoluble by-products filtered off. The solid by-products were washed several times with ether, the ether portions combined, and the ether removed to give the product as an oil. Distillation under vacuum gave the pure α-(arylideneamino)alkylamines **4**.

1. H. BOHME and A. INGENDOH. Liebigs Ann. Chem. 1928 (1978).
2. H. H. STRAIN. J. Am. Chem. Soc. **52**, 820 (1930).
3. G. H. HARRIS, B. R. HARRIMAN, and K. W. WHEELER. J. Am. Chem. Soc. **68**, 846 (1946).
4. S. DAYAGI and Y. DEGANI. *In* The chemistry of the carbon–nitrogen double bond. *Edited by* S. Patai. Interscience, London. 1970. pp. 67–68.
5. A. R. KATRITZKY, JINLONG JIANG, and L. UROGDI. Tetrahedron Lett. 3303 (1989).
6. A. R. KATRITZKY, JINLONG JIANG, and P. A. HARRIS. Heterocycles, **31**, 2187 (1990).
7. A. R. KATRITZKY, JINLONG JIANG, and L. UROGDI. Synthesis, 565 (1990).

Can. J. Chem. Downloaded from www.nrcresearchpress.com by 84.41.108.74 on 09/07/12
For personal use only.

Cycloaddition d'ylures d'azométhine dérivés de la 3,4-dihydro-6,7-diméthoxy-3-méthoxycarbonyl-isoquinoléine

TAHAR LAKHLIFI, AHMED SEDQUI, BERNARD LAUDE,[1] NGUYEN DINH AN ET JOËL VEBREL

Laboratoire de chimie organique, Université de Franche-Comté, La Bouloie, 16 route de Gray, 25030 Besancon CEDEX, France

Reçu le 26 novembre 1990

TAHAR LAKHLIFI, AHMED SEDQUI, BERNARD LAUDE, NGUYEN DINH AN et JOËL VEBREL. Can. J. Chem. **69**, 1156 (1991).

La synthèse de trois précurseurs d'ylures d'azométhine comportant le squelette de la 3,4-dihydro-6,7-diméthoxy-3-isoquinoléine est décrite. Ces produits à caractère dipolaire réagissent avec des dipolarophiles éthyléniques activés pour donner diastéréospécifiquement des dérivés du 4′,5′-diméthoxy-1,2-benzo-4,7-imino-4-méthoxycarbonylcyclohept-1-ène. Les paramètres de résonance magnétique protonique permettent de déterminer la stéréochimie des cycloadduits.

Mots clés : ylures d'azométhine cycliques, composés azabicycliques, stéréochimie.

TAHAR LAKHLIFI, AHMED SEDQUI, BERNARD LAUDE, NGUYEN DINH AN, and JOËL VEBREL. Can. J. Chem. **69**, 1156 (1991).

Three azomethine ylide precursors including the methyl 3,4-dihydro-6,7-dimethoxyisoquinoline-3carboxylate moiety were synthesized. The 1,3-dipolar species formed from these products react with activated dipolarophilic olefines leading diastereospecifically to derivatives of 4′,5′-dimethoxy-1,2-benzo-4,7-imino-4-methoxycarbonyl-1-cycloheptene. Proton magnetic resonance data allowed the determination of the stereochemistry of the cycloadducts.

Key words: cyclic azomethine ylide, azabicyclic compounds, stereochemistry.

Introduction

Les réactions de cycloaddition dipolaire-1,3 des ylures d'azométhine constituent une voie d'accès bien connue aux pyrrolines et pyrrolidines (1). L'espèce ylure d'azométhine peut aussi être insérée dans divers composés cycliques mésoioniques (2). En relation avec ces derniers, il faut signaler l'importante contribution de R. Huisgen et collaborateurs (3) à propos de l'utilisation des Δ-2-oxazolin-5-ones.

Plus récemment, la réactivité dipolaire-1,3 des imines d'α-aminoesters a été mise en évidence simultanément par Joucla et Hamelin (4) et l'équipe de Grigg (5). Cette réactivité a été par la suite largement étudiée par Grigg et collaborateurs (6). À notre connaissance, des imines cycliques dérivés d'α-aminoesters **1** (figure 1) ne sont signalées comme précurseurs d'ylures d'azométhine que dans deux publications des précédents auteurs (7, 8). Les espèces dipolaires dérivées d'imines cycliques alkyloxycarbonylées du type **1** permettent d'accéder à des composés azabicycliques pontés.

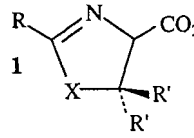
Par ailleurs, Kametani *et al.* (9) ont récemment décrit une synthèse totale de la (−)xylopinine à l'aide de dérivés de la (3*S*)3,4-dihydroisoquinoléine **2** (figure 2) optiquement active, préparés à partir de la L-DOPA selon la méthode de Schrecker et Hartwell (10).

Ces composés **2** sont à l'évidence des précurseurs d'ylures d'azométhine cycliques hexagonaux benzocondensés et nous avons décidé de tester leur réactivité en cycloaddition dipolaire-1,3 vis-à-vis de quelques dipolarophiles éthyléniques. Il n'était pas nécessaire d'utiliser un énantiomère du produit **2** puisque la forme dipolaire en fait disparaître la chiralité et nous avons donc travaillé en série racémique.

Synthèse des précurseurs d'ylures d'azométhine dérivés de la 3,4-dihydro-6,7-diméthoxy-3-méthoxycarbonyl-isoquinoléine *2*

Après avoir exploré diverses voies de synthèse, nous avons retenu et adapté celle décrite par Leonard (11) concernant la préparation de dérivés du 3,4-dihydro-2*H*-pyrrole (figure 2).

Le bromure de 3,4-diméthoxybenzyle est condensé avec un



1*a* R = H, X = S, R' = Me (7)
1*b* R = Ph, X = CH_2, R' = H (8)
1*c* R = Ph, X = $(CH_2)_2$, R' = H (8)

FIG. 1.

acylaminomalonate de diéthyle en présence d'hydrure de sodium dans le DMSO. Les 2-(3,4-diméthoxybenzyl)-2-acylaminomalonates de diéthyle **3** obtenus sont ensuite cyclisés en dérivés du 6,7-diméthoxy-3,4-dihydroisoquinoléine-3,3-dicarboxylate de diéthyle **4** par action de $POCl_3$. La dernière étape s'effectue par transformation du diester diéthylique en monoester méthylique. Dans le cas du produit **4***a* (R = H), on met en oeuvre une hydrolyse acide pour éviter la déshydrogénation du monoacide intermédiaire très rapide en milieu basique. Par contre, la saponification des produits **4***b* et **4***c* (R ≠ H) reste possible et elle est plus rapide que l'hydrolyse acide.

La purification des trois composés **2***a*–*c* doit être faite soigneusement pour éviter leur aromatisation très facile (cf. partie expérimentale). Les énantiomères de configuration absolue (*S*) des imines **2***a* et **2***b* préparés à partir de la L-DOPA par Kametani *et al.* (9) étaient mis en oeuvre à l'état brut (**2***b*(*S*)) ou sous forme de chlorhydrate (**2***a*(*S*), HCl). Seuls les paramètres de résonance magnétique protonique de ce dernier étaient décrits et sans que soient mentionnés ceux du proton H-3 (9).

Réactions de cycloaddition

Elles ont toutes été effectuées en solution dans le toluène et selon le cas soit en tube scellé, soit au reflux du solvant. Dans ces conditions, seuls trois dipolarophiles se sont révélés suffisamment réactifs : les *N*-méthyl et *N*-phénylmaléimide et le fumarate de diméthyle. Les rendements varient de 50 à 70%. D'autres substrats tels que les esters maléique, acrylique et benzylidènemalonique n'ont pas permis d'accéder au cycloadduit : on n'isole que le produit d'aromatisation du précurseur du produit dipolaire. Il se forme également à raison de 20% lors des réactions avec le fumarate de diméthyle et pour plus de 80% lors de l'action du composé **2***b* (R = CH_3) sur le *N*-méthylmaléimide et dans ce cas nous n'avons pas réussi à isoler le cycloadduit correspondant.

1. Auteur à qui adresser toute correspondance.

Printed in Canada / Imprimé au Canada

Can. J. Chem. Downloaded from www.nrcresearchpress.com by 198.100.157.202 on 09/07/12
For personal use only.

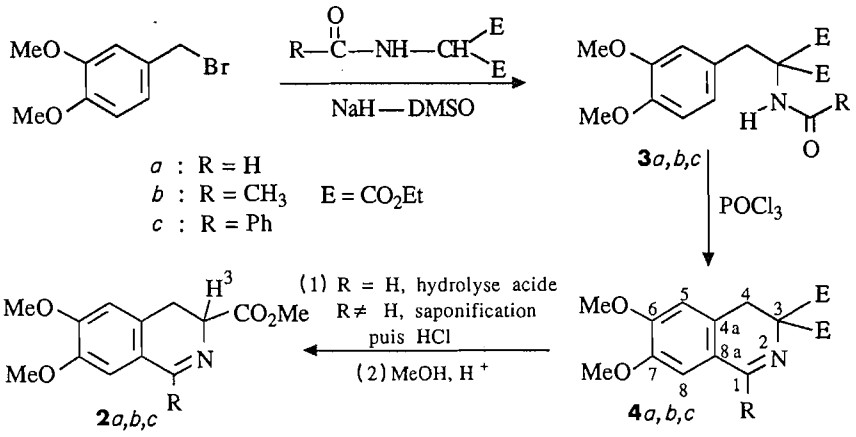


FIG. 2.

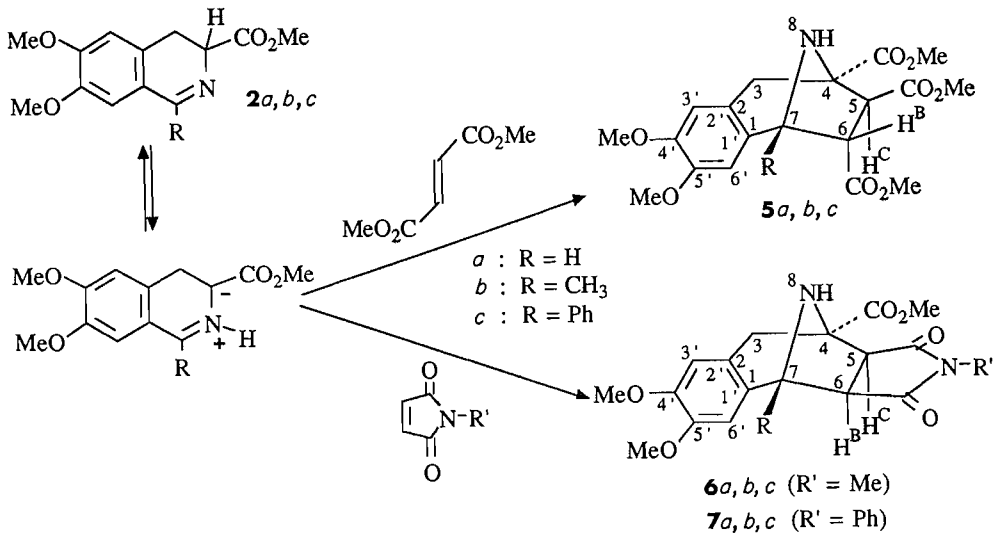


FIG. 3.

Toutes les réactions de cycloaddition sont diastéréospécifiques et les produits obtenus à partir de l'imine **2***a* (R = H) nous ont permis de statuer sans ambiguïté sur la stéréochimie de la réaction avec chaque dipolarophile (figure 3).

L'examen des spectres de résonance magnétique protonique des cycloadduits **5***a*, **6***a* et **7***a* (R = H^A) permet d'observer des signaux en accord avec les structures proposées (12). Ainsi dans le cas du produit **5***a* le proton H^A se manifeste sous forme d'un doublet (δ = 4,61 ppm, $J_{H^A-H^B}$ = 5,90 Hz) ce qui implique que le proton H^B (dd, δ = 3,70 ppm, $J_{H^A-H^B}$ = 5,90 Hz, $J_{H^B-H^C}$ = 7,30 Hz) est en position *exo*. D'autre part, l'inexistence d'un couplage entre H^A et H^B sur les spectres de résonance magnétique protonique des produits **6***a* et **7***a* prouve que l'approche entre les réactifs conduit exclusivement aux cycloadduits comportant le reste maléimido en *exo*. Il est raisonnable de penser que cette stéréochimie peut être valablement étendue aux cas des autres cycloadduits (R ≠ H) qui sont des dérivés du 4′,5′-diméthoxy-1,2-benzo-4,7-imino-4-méthoxycarbonylcyclohept-1-ène.

Il nous a semblé intéressant de comparer le cours stéréochimique de nos réactions avec les maléimides avec celui décrit dans un travail antérieur par Lown et Matsumoto (13). Ces auteurs ont établi, à partir des paramètres de résonance magnétique protonique, la structure du cycloadduit **9** issu de la réaction de l'ylure d'azométhine cyclique benzocondensé **8** avec le *N*-phénylmaléimide (figure 4).

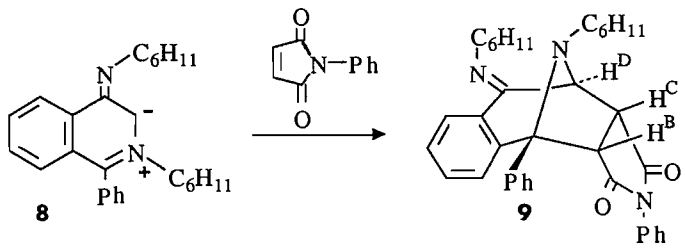


FIG. 4.

Cette stéréochimie *endo* ($J_{H^D-H^C}$ = 9 Hz) pour le reste *N*-phénylmaléimido est contraire à celle que nous avons établie pour les structures **6** et **7**. Mais cette contradiction apparente peut être levée en invoquant l'encombrement stérique dû au reste cyclohexyle fixé sur l'azote ponté de **9**. Ce groupement est suffisamment encombrant pour imposer à la réaction de cycloaddition une stéréochimie conduisant au cycloadduit le moins encombré.

Conclusion

Nous avons donc réussi à mener à bien une synthèse de trois précurseurs d'ylures d'azométhine comportant le squelette de la 3,4-dihydro-6,7-diméthoxyisoquinoléine présent dans de nombreux composés naturels. Ces produits à caractère dipolaire réagissent

Can. J. Chem. Downloaded from www.nrcresearchpress.com by 198.100.157.202 on 09/07/12
For personal use only.

TABLEAU 1. Potentiels d'oxydation (V/ECS) obtenus sur électrode (Pt) tournante ($\omega = 2000\ t\ min^{-1}$) en milieu Et_2Cl_2–CH_3CN (1 : 1) TEAP 0.1 M

Porphyrine	$E^{I}_{1/2}$	$E^{II}_{1/2}$
ZnTPP[a]	0,82	1,13
ZnTPP[b]	0,77	1,16
ZnTPP	0,79	1,14
ZnTPP β-Py^+	0,91	1,23
ZnTPP β-3-Pic^+	0,94	1,26
ZnTPP β-SCN	0,88	1,24
ZnTPP β-$P\phi_3^+$	0,93	1,20

[a]Milieu Et_2Cl_2.
[b]Milieu Et_2Cl_2–CH_3CN–Py.

avec des dipolarophiles éthyléniques très activés pour donner diastéréospécifiquement des dérivés du 4′,5′-diméthoxy-1,2-benzo-4,7-imino-4-méthoxycarbonylcyclohept-1-ène.

Partie expérimentale

Les points de fusion déterminés sur banc Kofler ne sont pas corrigés. Les spectres d'absorption ir ont été obtenus avec un spectrophotomètre Beckman IR 33, les produits étant pastillés dans KBr. Les spectres de rmn protonique ont été obtenus avec un spectromètre Bruker-Spectrospin AC 200, les échantillons étant dissous dans $CDCl_3$ avec le tétraméthylsilane comme référence interne. Les microanalyses ont été assurées par le Service d'Analyses du CNRS à Vernaison.

Le benzamidomalonate de diéthyle est préparé selon la méthode de Leonard (11). Toutes les autres matières premières sont des produits commerciaux.

1. Bromure de 3,4-diméthoxybenzyle

À une solution refroidie à 0°C de 0,1 mol (16,82 g) d'alcool 3,4-diméthoxybenzylique dans 90 mL de benzène anhydre, on additionne goutte à goutte 15 mL de tribromure de phosphore. Après addition, le mélange réactionnel est agité pendant 2 h à température ambiante, versé sur de la glace et décanté. La solution aqueuse est extraite au benzène et les phases organiques sont rassemblées, lavées à l'eau et séchées sur sulfate de sodium. Après filtration et évaporation du benzène, le solide résiduel est recristallisé dans de l'éthanol absolu. On obtient 21,25 g (Rdt. 92%) de bromure de 3,4-diméthoxybenzyle, *F* 52–53°C; rmn ^{1}H, δ : 3,86 (s, 3H, OCH_3), 3,90 (s, 3H, OCH_3), 4,50 (s, 2H, CH_2), 6,24–7,06 (m, 3H).

*2. 2-(3,4-Diméthoxybenzyl)-2-acylaminomalonates de diéthyle (**3**)*

Mode opératoire général : Dans un Erlenmeyer bicol de 250 mL, on introduit sous courant d'azote sec, 1,20 g de NaH (à 80% dans l'huile minérale) et 20 mL de DMSO anhydre. À la suspension agitée magnétiquement, on ajoute goutte à goutte en 1 h une solution de 0,04 mol d'acylaminomalonate de diéthyle dans 60 mL de DMSO anhydre. On additionne ensuite lentement une solution de 0,04 mol (9,25 g) de bromure de 3,4-diméthoxybenzyle dans 40 mL de DMSO anhydre. La solution est maintenue sous agitation pendant 12 h à température ambiante puis versée sur de la glace. On extrait au chloroforme et lave plusieurs fois la phase organique à l'eau salée. Après séchage sur Na_2SO_4 et évaporation du solvant, l'huile résiduelle est reprise par un mélange hexane–propanol (3 : 1). Le solide cristallisé est ensuite filtré et essoré. Chacun des dérivés **3***a–c* est décrit ci-après :

*2-(3,4-Diméthoxybenzyl)-2-formamidomalonate de diéthyle (**3**a)*

On obtient 11,3 g de produit (Rdt. 80%), *F* 92–93°C; ir, ν_{max} : 3360 (NH), 1740 (ester), 1660 (amide); rmn ^{1}H, δ : 1,32 (t, 6H, *J* = 7,00 Hz), 3,65 (s, 2H)), 3,86 (s, 3H, OCH_3), 3,89 (s, 3H, OCH_3), 4,27 (q, 2H, *J* = 7,00 Hz), 4,30 (q, 2H, *J* = 7,00 Hz), 6,89 (sl, 1H, NH), 8,21 (d, 1H, *J* = 1,2 Hz, CHO), 6,50–6,80 (m, 3H). Anal. calc. pour $C_{17}H_{23}NO_7$: C 57,76, H 6,56, N 3,96; tr. : C 57,92, H 6,43, N 3,82.

*2-(3,4-Diméthoxybenzyl)-2-acétamidomalonate de diéthyle (**3**b)*

On obtient 12 g de produit (Rdt. 82%), *F* 81–82°C; ir, ν_{max} : 3280 (NH), 1745 (ester), 1640 (amide); rmn ^{1}H, δ : 1,31 (t, 6H, *J* = 7,00 Hz), 2,00 (s, 3H, R = CH_3), 3,64 (s,2H), 3,81 (s, 3H, OCH_3), 3,84 (s, 3H, OCH_3), 4,25 (q, 2H, *J* = 7,00 Hz), 4,28 (q, 2H, *J* = 7,00 Hz), 6,40 (sl, 1H, NH), 6,45–6,80 (m, 3H). Anal. calc. pour $C_{18}H_{25}NO_7$: C 58,82, H 6,86, N 3,81; tr. : C 58,94, H 6,67, N 3,76.

*2-(3,4-Diméthoxybenzyl)-2-benzamidomalonate de diéthyle (**3**c)*

On obtient 12,2 g de produit (Rdt. 71%), *F* 116–117°C; ir, ν_{max} : 3430 (NH), 1730 et 1750 (ester), 1660 (amide); rmn ^{1}H, δ : 1,32 (t, 6H, *J* = 7,00 Hz), 3,58 (s, 3H, OCH_3), 3,72 (s, 2H), 3,84 (s, 3H, OCH_3), 4,30 (q, 2H *J* = 7,00 Hz), 4,33 (q, 2H, *J* = 7,00 Hz), 7,30 (sl, 1H, NH), 6,50–6,75 (m, 3H), 7,40–7,80 (m, 5H). Anal. calc. pour $C_{23}H_{27}NO_7$: C 64,30, H 6,34, N 3,26; tr. : C 64,12, H 6,42, N 3,37.

*3. Dérivés du 6,7-diméthoxy-3,4-dihydroisoquinoléine-3,3-dicarboxylate de diéthyle (**4**)*

Mode opératoire général : Dans un Erlenmeyer de 100 mL, on place 0,01 mol de composé **3** dans 40 mL d'acétonitrile dans le cas de **3***a* ou **3***b* et dans 40 mL de xylène dans le cas de **3***c*. On ajoute à cette solution 5 mL de $POCl_3$ fraîchement distillé. On maintient ensuite à ébullition et sous agitation magnétique durant un temps variable (5 h pour **4***a* : R = H, 16 h pour **4***b* : R = CH_3 et 72 h pour **4***c* : R = C_6H_5). Après refroidissement, on dilue avec 100 mL de chloroforme (dans le cas de **4***a* et **4***b*) ou de benzène (dans le cas de **4***c*) et 50 mL d'eau puis alcalinise par du carbonate de sodium. Les deux phases sont séparées et la phase organique est lavée à l'eau salée et séchée sur sulfate de sodium anhydre. Après filtration et évaporation des solvants, le residu est repris par un mélange hexane–isopropanol (3 : 1). Le produit cristallisé est filtré et essoré. Chaque dérivé **4***a,b,c* est décrit ci-après :

*6,7-Diméthoxy-3,4-dihydroisoquinoléine-3,3-dicarboxylate de diéthyle (**4**a)*

On obtient 2,7 g de produit (Rdt. 81%), *F* 106–107°C; ir, ν_{max} : 1735 (ester); rmn ^{1}H, δ : 1,25 (t, 6H, *J* = 7,10 Hz), 3,34 (s, 2H, CH_2-4), 3,90 (s, 3H, OCH_3), 3,93 (s, 3H, OCH_3), 4,25 (4H, partie AB d'un système ABX_3, J_{AB} = 14,50 Hz), 6,73 (s, 1H, H–5), 6,90 (s, 1H, H–8), 8,42 (s, 1H, H–1). Anal. calc. pour $C_{17}H_{21}NO_6$: C 60,86, H 6,31, N 4,18; tr. : C 60,72, H 6,52, N 4,25.

*6,7-Diméthoxy-1-méthyl-3,4-dihydroisquinoléine-3,3-dicarboxylate de diéthyle (**4**b)*

On obtient 2,35 g de produit (Rdt. 67%), *F* 109–110°C; ir, ν_{max} : 1740 (ester); rmn ^{1}H, δ : 1,25 (t, 6H, *J* = 7,15 Hz), 2,54 (s, 3H, CH_3), 3,30 (s, 2H, CH_2-4), 3,90 (s, 3H, OCH_3), 3,93 (s, 3H, OCH_3), 4,22 (4H, partie AB d'un système ABX_3, J_{AB} = 13,50 Hz), 6,73 (s, 1H, H–5), 7,07 (s, 1H, H–8). Anal. calc. pour $C_{18}H_{23}NO_6$: C61,86, H 6,63, N 4,01; tr. : C 62,03, H 6,52, N 3,93.

*6,7-Diméthoxy-1-phényl-3,4-dihydroisoquinoléine-3,3-dicarboxylate de diéthyle (**4**c)*

On obtient 2 g de produit (Rdt. 48%), *F* 94–96°C; ir, ν_{max} : 1740 (ester); rmn ^{1}H, δ : 1,21 (t, 6H, *J* = 7,10 Hz), 3,38 (s,2H, CH_2-4), 3,70 (s, 3H, OCH_3), 3,93 (s, 3H, OCH_3), 4,20 (4H, partie AB d'un système ABX_3, J_{AB} = 14,40 Hz), 6,76 (s,1H, H-5), 6,79 (s, 1H, H-8), 7,42–7,51 (m, 5H). Anal. calc. pour $C_{23}H_{25}NO_6$: C 67,12, H 6,13, N 3,40; tr. : C 67,31, H 6,02, N 3,28.

*4. Dérivés du 6,7-diméthoxy-3,4-dihydroisoquinoléine-3-carboxylate de méthyle (**2**)*

(a) Hydrolyse acide par HCl 6 N (R = H) : 0,01 mol de diester **4***a* dans 40 mL de HCl 6 N sont portés à reflux pendant 6 h.

(b) Saponification par KOH 2 N (R = CH_3, Ph) : 0,01 mol de diester **4***b* ou **4***c* sont dissous dans 40 mL d'une solution méthanolique de potasse 2 N. La solution obtenue est portée à reflux pendant 2 h sous agitation magnétique. Le solvant est évaporé et le résidu repris par 50 mL de HCl 2 N.

(c) Traitement commun : La solution acide obtenue est lavée deux fois au chloroforme et décantée. La phase aqueuse est évaporée sous vide de la trompe à eau, le résidu est repris par du benzène et évaporé. On recommence trois fois cette opération puis reprend le résidu par 40 mL de méthanol absolu et 1 mL d'acide sulfurique concentré. Le mélange réactionnel est porté à reflux pendant 2 h puis le méthanol est éliminé par évaporation. L'huile résiduelle est reprise par de l'eau et le mélange

Can. J. Chem. Downloaded from www.nrcresearchpress.com by 198.100.157.202 on 09/07/12
For personal use only.

Can. J. Chem. Downloaded from www.nrcresearchpress.com by 198.100.157.202 on 09/07/12
For personal use only.

neutralisé par addition de petites quantités de carbonate de sodium en veillant à ne pas dépasser la valeur 7 du pH. On extrait alors au chloroforme, lave la phase organique par de l'eau salée et sèche sur Na_2SO_4 anhydre. Le solvant est évaporé sous courant d'azote et le résidu repris sans chauffer par un mélange d'hexane et de propanol (4 : 1). Les produits **2** cristallisés sont essorés et chacun d'entre eux est décrit ci-après :

6,7-Diméthoxy-3,4-dihydroisoquinoléine-3-carboxylate de méthyle (2a)

On obtient 1,67 g de produit (Rdt. 67%), *F* 138–140°C; ir, ν_{max} : 1725 (ester); rmn ^{1}H, δ : 2,96 (d, 2H, $J_{CH_2-H\text{-}3}$ = 10,20 Hz, CH_2-4), 3,85 (s, 3H, OCH_3), 3,91 (s, 3H, OCH_3), 3,95 (s, 3H, OCH_3), 4,32 (dt, 1H, ^3J = 10,20 Hz, $^4J_{H\text{-}3-H\text{-}1}$ = 2,90 Hz, H-3), 6,73 (s, 1H, H-5), 6,88 (s, 1H, H-8), 8,21 (d, 1H, $J_{H\text{-}1-H\text{-}3}$ = 2,90 Hz, H-1). Anal. calc. pour $C_{13}H_{15}NO_4$: C 62,62, H 6,07. N 5,62; tr. : C 62,81, H 5,96, N 5,72.

6,7-Diméthoxy-1-méthyl-3,4-dihydroisoquinoléine-3-carboxylate de méthyle (2b)

On obtient 1,98 g de produit (Rdt. 75%), *F* 110–111°C; ir, ν_{max} : 1730 (ester); rmn ^{1}H, δ : 2,45 (d, 3H, $J_{CH_3-H\text{-}3}$ = 1,90 Hz, CH_3-1), 2,92 (d, 2H, *J* = 9.80 Hz, CH_2-4), 3,83 (s, 3H, OCH_3), 3,91 (s, 3H, OCH_3), 3,93 (s, 3H, OCH_3), 4,20 (tq, $J_{H\text{-}3-CH_2}$ = 9,80 Hz, $J_{H\text{-}3-CH_3}$ = 1,90 Hz, H-3), 6,74 (s, 1H, H-5), 7,02 (s, 1H, H-8). Anal. calc. pour $C_{14}H_{17}NO_4$: C 63,84, H 6,51, N 5,32; tr. : C 63,67, H 6,43, N 5,47.

6,7-Diméthoxy-1-phényl-3,4-dihydroisoquinoléine-3-carboxylate de méthyle (2c)

On obtient 1,05 g de produit (Rdt. 32%), *F* 106–107°C; ir, ν_{max} : 1730 (ester); rmn ^{1}H, δ : 2,95–3,15 (partie AB d'un système ABX avec J_{AB} = 16,40 Hz, J_{AX} = 10,20 Hz, J_{BX} = 5,70 Hz, CH_2-4), 3,72 (s, 3H, OCH_3), 3,81 (s, 3H, OCH_3), 3,95 (s, 3H, OCH_3), 4,35 (partie X d'un système ABX avec J_{AX} = 10,20 Hz, J_{BX} = 5,70 Hz, H-3), 6,79 (s, 1H, H-5), 6,83 (s, 1H, H-8), 7,40–7,65 (m, 5H). Anal. calc. pour $C_{19}H_{19}NO_4$: C 70,12, H 5,89, N 4,31; tr. : C 70,27, H 5,75, N 4,42.

5. Cycloadditions dipolaires

(a) Au reflux du toluène : Un mélange de 1 mmol de dipôle **2** et 1,2 mmol de dipolarophile dissous dans 10 mL de toluène sec est chauffé à reflux sous atmosphère d'azote durant 48 h. Après refroidissement, le toluène est évaporé et le résidu recristallisé dans un solvant précisé dans chaque cas.

4',5'-Diméthoxy-1,2-benzo-4,7-imino-4-méthoxycarbonylcyclohept-1-ène-exo-*5,6-(*N-*méthyldicarboximide) (6a)*

On obtient 0,185 g de produit (Rdt. 52%), *F* 210–211°C de l'éthanol; ir, ν_{max} : 3300 (NH), 1730 (ester), 1700 (imide); rmn ^{1}H, δ : 2,45 (sl, 1H, NH), 3,00 (s, 3H, N-CH_3), 3,16 (d, 1H, *J* = 17,00 Hz) et 3,22 (d, 1H, *J* = 17,00 Hz) : CH_2-3, 3,25 (d, 1H, *J* = 7,10 Hz, H-5 ou H-6), 3,35 (d, 1H, *J* = 7,10 Hz, H-6 ou H-5), 3,84 (s, 3H, OCH_3), 3,87 (s, 3H, OCH_3), 3,90 (s, 3H, OCH_3), 4,65 (s, 1H, H-7), 6,60 (s, 1H), 6.73 (s, 1H). Anal. Calc. pour $C_{18}H_{20}N_2O_6$: C 59,97, H 5,60, N, 7,78; tr. : C 59,95, H, 5,68, N 7,49.

4',5'-Diméthoxy-1,2-benzo-4,7-imino-4-méthoxycarbonyl-7-phénylcyclohept-1-ène-exo-*5,6-(*N-*méthyldicarboximide) (6c)*

On obtient 0,265 g de produit (Rdt. 61%), *F* 250–251°C de l'isopropanol; ir, ν_{max} : 3300 (NH), 1730 (ester), 1700 (imide); rmn ^{1}H, δ : 2,86 (s, 3H, N-CH_3), 3,32 (sl, 1H, NH), 3,34 (d, 1H, *J* = 16,40 Hz) et 3,40 (d, 1H, *J* = 16,40 Hz) : CH_2-3, 3,47 (d, 1H, *J* = 7,10 Hz, H-5 or H-6), 3,94 (d, 1H, *J* = 7,10 Hz), H-6 ou H-5), 3,58 (s, 3H, OCH_3), 3,82 (s, 3H, OCH_3), 3,86 (s, 3H, OCH_3), 6,40 (s, 1H), 6,67 (s, 1H), 7,35–7,85 (m, 5H). Anal. calc. pour $C_{24}H_{24}N_2O_6$: C 66,00, H 5,55, N 6,43; tr. : C 65,87, H 5,58, N 6,37.

4',5'-Diméthoxy-1,2-benzo-4,7-imino-4-méthoxycarbonylcyclohept-1-ène-exo-*5,6-(*N-*phényldicarboximide) (7a)*

On obtient 0,210 g de produit (Rdt. 50%), *F* 150–151°C du *n*-propanol; ir, ν_{max} : 3300 (NH), 1735 (ester), 1700 (imide); rmn ^{1}H, δ : 2,67 (sl, 1H, NH), 3,22 (d, 1H, *J* = 17,20 Hz) et 3,28 (d, 1H, *J* = 17,20 Hz) : CH_2-3, 3,38 (d, 1H, *J* = 7,10 Hz, H-5 ou H-6), 3,53 (d, 1H, *J* = 7,10 Hz, H-6 ou H-5), 3,85 (s, 3H, OCH_3), 3,87 (s, 3H, OCH_3), 3,89 (s, 3H, OCH_3), 4,77 (s, 1H, H-7), 6,63 (s, 1H), 6,75 (s, 1H), 7,20–7,55 (m, 5H). Anal. calc. pour $C_{23}H_{22}N_2O_6$: C 65,37, H 5,25, N 6,63; tr. : C 65,42, H 5,32, N 6,51.

4',5'-Diméthoxy-1,2-benzo-4,7-imino-4-méthoxycarbonyl-7-méthylcyclohept-1-ène-exo-*5,6-(*N-*phényldicarboximide) (7b)*

On obtient 0,262 g de produit (Rdt. 60%), *F* 148–149°C de l'isopropanol; ir, ν_{max} : 3320 (NH), 1730 (ester), 1700 (imide); rmn ^{1}H, δ : 1,90 (s, 3H, CH_3-7), 2,69 (sl, 1H, NH), 3,23 (d, 1H, *J* = 16,80 Hz) et 3,31 (d, 1H, *J* = 16,80 Hz) : CH_2-3, 3,37 (d, 1H, *J* = 7,10 Hz, H-5 ou H-6), 3,47 (d, 1H, *J* = 7,10 Hz, H-6 ou H-5), 3,85 (s, 3H, OCH_3), 3,87 (s, 3H, OCH_3), 3,89 (s, 3H, OCH_3), 6,60 (s, 1H), 6,80 (s, 1H), 7,20–7,55 (m, 5H). Anal. calc. pour $C_{24}H_{24}N_2O_6$: C 66,00, H 5,55, N 6,43; tr. : C 65,78, H 5,62, N 6,35.

(b) En tube scellé : Dans un tube de 10 mL, on introduit 1 mmol de produit dipolaire, 1,2 mmol de dipolarophile et 5 mL de toluène anhydre. Le tube est scellé et placé à 150°C pendant 48 h. Après refroidissement, le mélange réactionnel est repris par du toluène, le solvant est évaporé et le résidu cristallisé dans un solvant (qui sera précisé dans chaque cas) est essoré.

4',5'-Diméthoxy-1,2-benzo-4,7-imino-4-méthoxycarbonyl-7-phénylcyclohept-1-ène-exo-*5,6-(*N-*phényldicarboximide) (7c)*

On obtient 0,350 g de produit (Rdt. 70%), *F* 240–241°C du *n*-propanol; ir, ν_{max} : 3330 (NH), 1735 (ester), 1700 (imide); rmn ^{1}H, δ : 3,35 (sl, 1H, NH), 3,39 (d, 1H, *J* = 16,40 Hz) et 3,47 (d, 1H, *J* = 16,40 Hz) : CH_2-3, 3,56 (d, 1H, *J* = 6,80 Hz, H-5 ou H-6), 4,13 (d, 1H, *J* = 6,80 Hz, H-6 ou H-5), 3,69 (s, 3H, OCH_3), 3,83 (s, 3H, OCH_3), 3,89 (s, 3H, OCH_3), 6,50 (s, 1H), 6,65 (s, 1H), 7,10–7,90 (m, 10H). Anal. calc. pour $C_{29}H_{26}N_2O_6$: C 69.84, H 5,26, N 5,62; tr. : C 70,01, H 5,43, N 5,44.

4',5'-Diméthoxy-1,2-benzo-4,7-imino-4-méthoxycarbonyl-exo-*5-méthoxycarbonyl*-endo-*6-méthoxycarbonylcyclohept-1-ène (5a)*

On obtient 0,192 g de produit (Rdt. 49%), *F* 163–164°C de l'éthanol; ir, ν_{max} : 3300 (NH), 1720 (ester); rmn ^{1}H, δ : 2,84 (sl, 1H, NH), 3,11 (d, 1H, *J* = 16,50 Hz) et 3,26 (d, 1H, *J* = 16,50 Hz) : CH_2-3, 3,62 (d, 1H, *J* = 7,30 Hz, H-5) 3,70 (dd, 1H, *J* = 7,30 Hz, *J* = 5,90 Hz, H-6) 4,61 (d, 1H, *J* = 5,90 Hz, H-7), 3,54 (s, 3H, OCH_3), 3,67 (s, 3H, OCH_3), 3,78 (s, 3H, OCH_3), 3,80 (s, 3H, OCH_3), 3,82 (s, 3H, OCH_3), 6,50 (s, 1H), 6,63 (s, 1H). Anal. calc. pour $C_{19}H_{23}NO_8$: C 57,98, H 5,90, N 3,56; tr. : C 58,12, H 5,95, N 3,46.

4',5'-Diméthoxy-1,2-benzo-4,7-imino-4-méthoxycarbonyl-exo-*5-méthoxycarbonyl*-endo-*6-méthoxycarbonyl-7-méthylcyclohept-1-ène (5b)*

On obtient 0,245 g de produit (Rdt. 60%), *F* 131–132°C de l'isopropanol; ir, ν_{max} : 3320 (NH), 1720 (ester); rmn ^{1}H, δ : 1,90 (s, 3H, CH_3-7), 2,80 (sl, 1H, NH), 3,20 (d, 1H, *J* = 16,40 Hz) et 3,26 (d, 1H, *J* = 16,40 Hz) : CH_2-3, 3,28 (d, 1H, *J* = 7,40 Hz, H-5) 3,74 (d, 1H, *J* = 7,40 Hz, H-6), 3,50 (s, 3H, OCH_3), 3,61 (s, 3H, OCH_3), 3,76 (s, 3H, OCH_3), 3,81 (s, 3H, OCH_3), 3,83 (s, 3H, OCH_3), 6,57 (s, 1H), 6,61 (s, 1H). Anal. calc. pour $C_{20}H_{25}NO_8$: C 58,94, H 6,19, N 3,44; tr. : C 58,65, H 6,22, N 3,40.

4',5'-Diméthoxy-1,2-benzo-4,7-imino-4-méthoxycarbonyl-exo-*5-méthoxycarbonyl*-endo-*6-méthoxycarbonyl-7-phénylcyclohept-1-ène (5c)*

On obtient 0,330 g de produit (Rdt. 70%), *F* 159–160°C de l'isopropanol; ir, ν_{max} : 3300 (NH), 1730 (ester); rmn ^{1}H, δ : 2,30 (sl, 1H, NH), 3,31 (d, 1H, *J* = 16,20 Hz) et 3,39 (d, 1H, *J* = 16,20 Hz) : CH_2-3, 3,45 (s, 3H, OCH_3), 3,51 (s, 3H, OCH_3) 3,68 (s, 3H, OCH_3), 3,77 (s, 3H, OCH_3), 3,85 (s, 3H, OCH_3), 3,93 (d, 1H, *J* = 6,80 Hz, H-5), 4,25 (d, 1H, *J* = 6,80 Hz, H-6), 6,00 (s, 1H), 6,65 (s, 1H), 7,35–7,85 (m, 5H). Anal. calc. pour $C_{25}H_{27}NO_8$: C 63,94, H 5,80, N 2,99; tr. : C 64,08, H 5,92, N 2,77.

1. J. W. Lown. *Dans* 1,3-Dipolar cycloaddition chemistry. Vol. 1. *Éditeur* : A. Padwa. J. Wiley & Sons, New-York. 1984. Chap. 6, et références citées.
2. K. T. Potts. Mesoionic ring systems. *Dans* 1,3-Dipolar cycloaddition chemistry. Vol. 2. *Éditeur* : A. Padwa. J. Wiley & Sons, New-York. 1984. Chap. 1, et références citées.
3. H. Gotthardt, R. Huisgen et H. O. Bayer. J. Am. Chem.

Soc. **92**, 4340 (1970); H. O. BAYER, H. GOTTHARDT et R. HUISGEN. Chem. Ber. **103**, 2356 (1970); **103**, 2368 (1970); H. O. BAYER, R. HUISGEN, R. KNORR et F. C. SCHAEFER. Chem. Ber. **103**, 2581 (1970); R. HUISGEN, H. GOTTHARDT, H. O. BAYER et F. C. SCHAEFER. Chem. Ber. **103**, 2611 (1970); H. GOTTHARDT et R. HUISGEN. Chem. Ber. **103**, 2625 (1970); R. KNORR, R. HUISGEN et G. K. STAUDINGER. Chem. Ber. **103**, 2639 (1970).

4. M. JOUCLA et J. HAMELIN. Tetrahedron Lett. 2885 (1978).
5. R. GRIGG, J. KEMP, G. SHELDRICK et J. TROTTER. J. Chem. Soc. Chem. Commun. 109 (1978).
6. R. GRIGG et J. KEMP. Tetrahedron Lett. 2823 (1978); K. AMORNRAKSA et R. GRIGG. Tetrahedron Lett. 2197 (1980); R. GRIGG et J. KEMP. Tetrahedron Lett. 2461 (1980); R. GRIGG et H. Q. N. GUNARATNE. J. Chem. Soc. Chem. Commun. 384 (1982); Tetrahedron Lett. 1201 (1983); R. GRIGG, H. Q. N. GUNARATNE et J. KEMP. Tetrahedron Lett. 99 (1984); J. Chem. Soc. Perkin Trans. 2, 41 (1984); R. GRIGG, M. JORDAN, A. TANG THONGKUM, F. W. B. EINSTEIN et T. JONES. J. Chem. Soc. Perkin Trans. 1, 47 (1984).
7. R. GRIGG, L. D. BASANAGOUDAR, D. A. KENNEDY, J. F. MALONE et S. THIANPATANAGUL. Tetrahedron Lett. 2803 (1982).
8. A. MKHAIRI et J. HAMELIN. Tetrahedron Lett. 1397 (1987).
9. T. KAMETANI, N. TAGAKI, M. TOYOTA, T. HONDA et K. FUKUMOTO. J. Chem. Soc. Perkin Trans. 1, 2830 (1981).
10. A. W. SCHRECKER et J. L. HARTWELL. J. Am. Chem. Soc. **79**, 3827 (1957).
11. F. LEONARD. U.S. Patents 3,164,597 et 3,185,705 (1965).
12. A. GAUDEMER. *Dans* Stereochemistry: fundamentals and methods. Vol. 1. Spectrometric methods. *Éditeur*: H. Kagan. Georg Thieme, Stuttgart. 1977. p. 109.
13. J. W. LOWN et K. MATSUMOTO. J. Org. Chem. **36**, 1405 (1971).

Can. J. Chem. Downloaded from www.nrcresearchpress.com by 198.100.157.202 on 09/07/12
For personal use only.

β-Substitution de la *méso*-tétraphénylporphyrine de zinc par voie électrochimique

ALAIN GIRAUDEAU[1] ET LANA EL KAHEF

Laboratoire d'électrochimie et de chimie-physique du corps solide, Unité de recherche associée au Centre national de la recherche scientifique, n° 405, Université Louis Pasteur, 4, rue Blaise Pascal, 67000 Strasbourg, France

Reçu le 9 février 1990[2]

ALAIN GIRAUDEAU et LANA EL KAHEF. Can. J. Chem. **69**, 1161 (1991).

L'oxydation par voie électrochimique de la *méso*-tétraphénylporphyrine de zinc dans des solutions mixtes acétonitrile–dichloroéthane et en présence de nucléophiles (Py, 3-Pic, $P\phi_3$, SCN^-) conduit à l'obtention de la métalloporphyrine correspondante monosubstituée. Pour chacun de ces nucléophiles, la substitution a lieu sur un carbone pyrrolique (β-substitution). Les conditions électrochimiques de ces substitutions sont discutées et nous proposons un bilan global pour cette réaction de substitution.

Mots clés : porphyrines, réactions électrochimiques, substitutions nucléophiles.

ALAIN GIRAUDEAU and LANA EL KAHEF. Can. J. Chem. **69**, 1161 (1991).

The electrochemical oxidation of the zinc tetraphenylporphyrin complex in a mixed acetonitrile–dichloroethane solution in the presence of nucleophiles (Py, 3-Pic, $P\phi_3$, SCN^-) leads to the formation of the corresponding monosubstituted metalloporphyrin. For each of these nucleophiles the substitution occurs at a pyrrole carbon atom (β-substitution). The electrochemical conditions of these substitutions are discussed and an overall reaction is proposed.

Key words: porphyrins, electrochemical reactions, nucleophilic substitution.

Introduction

L'oxydation par voie électrochimique d'hydrocarbures aromatiques mono- ou poly-nucléaires permet de réaliser des réactions très diverses telles des réactions d'addition, de dimérisation ou de substitution. Si dans de nombreux cas un même type de réaction peut être réalisé aussi bien par voie chimique qu'électrochimique, cette dernière n'en reste pas moins une méthode originale et très appropriée dès qu'un contrôle de l'étape d'oxydation s'avère être un paramètre important, malgré la multiplicité des paramètres rentrant en jeu dans ces processus d'électrosynthèse (potentiel de réaction, durée d'électrolyse, nature de l'électrode, du solvant ou du sel de fond) et dont le choix peut rendre prépondérantes certaines réactions secondaires.

Dans les métalloporphyrines, le macrocycle porphyrine est un système d'électrons conjugué qui peut être plus ou moins facilement oxydé pour donner les radicaux-cations correspondants (1–3). Cette facilité d'oxydation dépend du macrocycle lui-même, mais est essentiellement fonction de la nature et du degré d'oxydation du cation métallique central de la métalloporphyrine. Les complexes du zinc et du magnésium sont parmi les plus facilement oxydables et ont permis la mise en évidence de la réactivité des radicaux-cations correspondants en réalisant par oxydation chimique des substitutions nucléophiles sur les positions *méso* et (ou) β (4–7). De nombreuses études antérieures ont également traité en détail de la formation des isoporphyrines (8, 9) et se sont attachées à en décrire les mécanismes. Ces travaux ont mis aussi en évidence la possibilité de réaliser des substitutions nucléophiles sur les positions *méso* et (ou) β à partir des dications des porphyrines (9).

Les travaux sur l'oxydation électrochimique des métalloporphyrines en présence de nucléophiles ont été très largement développés, cependant ils se sont focalisés sur l'analyse de la complexation des cations métalliques centraux et très peu sur la réactivité du macrocycle porphyrine (10, 11). Seules à notre connaissance des travaux sur la cyanation de complexes aromatiques par voie électrochimique ont montré que par oxydation à potentiel contrôlé, l'octaéthylporphyrine de zinc formait successivement les complexes mono- à tétra-cyanés correspondants sur les positions *méso* (12, 13).

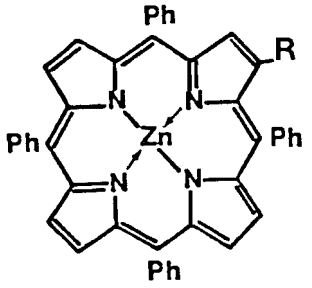


FIG. 1. Structure des porphyrines obtenues. R = Py^+, $3\text{-}Pic^+$, $P\phi_3^+$, SCN.

Récemment, nous avons mis en évidence la possibilité d'effectuer par voie électrochimique des substitutions en position β à partir de la *méso*-tétraphénylporphyrine de zinc, ZnTPP (14). Dans cet article nous décrivons cette réactivité à propos de plusieurs types de nucléophiles et nous donnons le bilan global de la réaction d'obtention de ces porphyrines substituées en position β (fig. 1).

Résultats et discussion

L'oxydation de la *méso*-tétraphénylporphyrine de zinc (ZnTPP) a lieu en deux étapes distinctes (10, 15), avec échanges réversibles successifs d'un électron selon le mécanisme suivant :

[1] $ZnTPP \rightleftarrows ZnTPP^+ + e^-$

[2] $ZnTPP^{+\cdot} \rightleftarrows ZnTPP^{2+} + e^-$

Notre travail et les résultats correspondants concernent uniquement l'étape [1]. Le produit d'oxydation qui est le cation radical $ZnTPP^{+\cdot}$ paramagnétique est aisément identifiable par son spectre d'absorption UV–VIS, sa grande stabilité permet même de l'isoler.

L'allure du signal anodique de la première étape d'oxydation n'est pas affectée par la présence d'un nucléophile; la vague d'oxydation obtenue par voltampérométrie stationnaire (V.S.) conserve la même amplitude et les tracés de voltampérométrie cyclique (V.C.) indiquent une réversibilité inchangée. Le seul

1. Auteur à qui adresser toute correspondence.
2. Révision reçue le 13 décembre 1990.

Printed in Canada / Imprimé au Canada

Can. J. Chem. Downloaded from www.nrcresearchpress.com by 84.41.108.74 on 09/07/12
For personal use only.

Can. J. Chem. Downloaded from www.nrcresearchpress.com by 84.41.108.74 on 09/07/12
For personal use only.

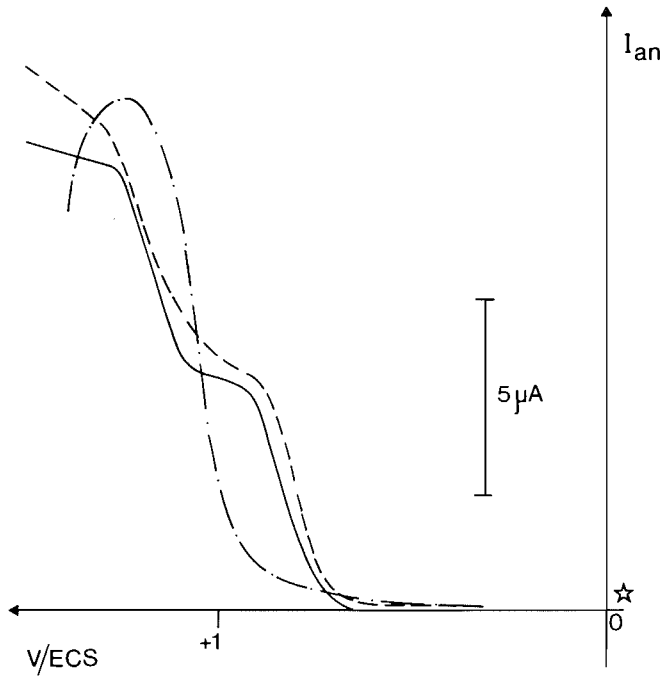


FIG. 2. Voltampérométrie stationnaire de la porphyrine **2**. Electrode, Pt; $\omega = 2000$ t min^{-1}; $v = 10$ mV s^{-1}. Milieu Et_2Cl_2, TBAP 0,1 M : (—). Milieu Et_2Cl_2–CH_3CN–Py, TEAP 0,1 M : avant électrolyse (---); après électrolyse (------).

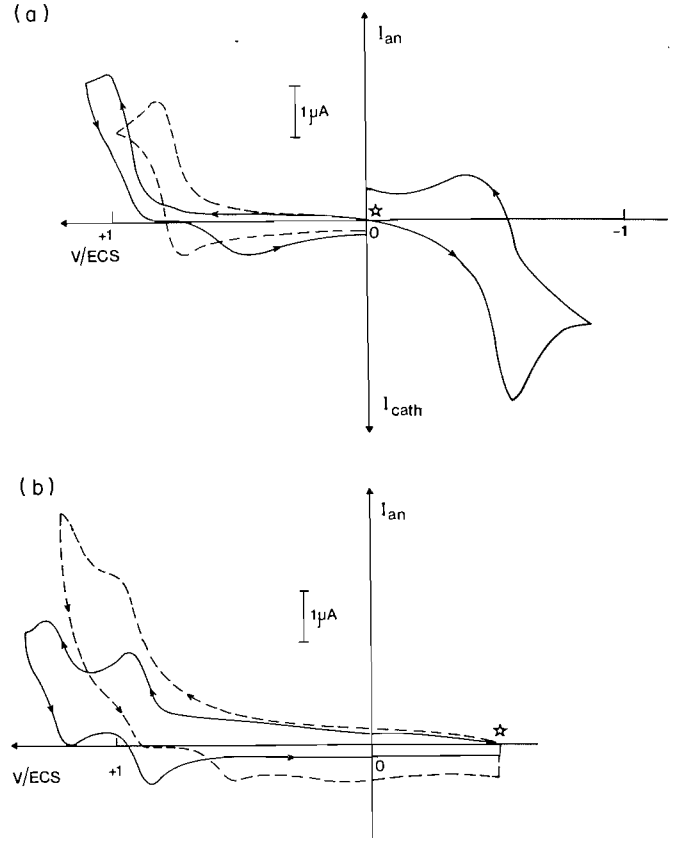


FIG. 3. (a) Voltamétrie cyclique de la porphyrine **2** en milieu Et_2Cl_2–CH_3CN–Py, TEAP 0,1 M. Electrode, Pt; $v = 0,1$ V s^{-1}. Avant électrolyse (---); après électrolyse (—). (b) Voltamétrie cyclique de la porphyrine **3** (5×10^{-4} M) en milieu Et_2Cl_2–CH_3CN, TEAP 0,1 M. Electrode, Pt; $v = 0,1$ V s^{-1}. Absence de pyridine (—); en présence de pyridine 10^{-2} M (---).

effet observé est un déplacement cathodique du potentiel de demi-vague (10) (fig. 2) traduisant la coordination du nucléophile (Nu) sur le métal central selon le mécanisme :

[3] $\quad ZNTPP + Nu \rightleftarrows ZnTPP\,(Nu)$

Lorsqu'on réalise une coulométrie exhaustive de ZnTPP au niveau de la première étape d'oxydation en présence d'un nucléophile, on observe une évolution du spectre optique qui conduit à la fin de l'oxydation à un spectre comprenant toujours une bande Soret intense et deux bandes d'absorption dans le visible (bandes α et β). Par rapport au spectre d'absorption de départ, l'ensemble du nouveau spectre obtenu est décalé vers les plus grandes longueurs d'ondes. En aucun cas on ne retrouve le spectre attendu du radical cation $ZnTPP^{+\cdot}$. Ce résultat suggère la formation d'une nouvelle porphyrine comportant une plus grande délocalisation de la densité électronique sur le cycle porphyrinique.

L'enregistrement des courbes $I = f(t)$ (courant–temps) pendant l'électrolyse montre d'une part que nous n'avons plus une décroissance exponentielle du courant comme observée dans le cas de l'électrolyse de ZnTPP en absence de nucléophile, d'autre part le courant résiduel de fin d'électrolyse n'est plus voisin de zéro. L'analyse de ces courbes $I = f(t)$ indique que nous sommes en présence au moins d'une réaction de type E.C. (Electrochimique–Chimique), ou E.C.E.C., et non plus du mécanisme purement électrochimique [1], de plus la valeur du nombre n d'électrons échangés par mole ZnTPP est comprise dans l'intervalle $2,2 \leq n \leq 2,6$, selon les expériences effectuées. Cette réaction chimique consécutive à l'oxydation de ZnTPP en présence de nucléophile n'est détectable ni par voltampérométrie cyclique (V.C.) ni par voltampérométrie stationnaire (V.S.). En effet le rapport I_{Pa}/P_{Pc} obtenu en V.C. (rapport du courant de pic anodique au courant du pic de réduction associé), pour la première étape d'oxydation, n'est pas modifié par l'addition de nucléophile sur la gamme des vitesses de balayage étudiées (50 mV s^{-1} à 1 V s^{-1}). Les tracés $I = f(c)$ et $1/I = f(\omega^{-1/2})$ (ω vitesse de rotation de l'électrode) obtenus à partir des courbes de V.S. sont linéaires passant par l'origine des coordonnées, analogues à ceux obtenus lors de l'étude de l'oxydation de ZnTPP en l'absence de nucléophile.

Ces résultats sont en accord avec une cinétique d'attaque nucléophile lente sur le produit d'oxydation (radical-cation) de ZnTPP.

En oxydation, l'étude d'une solution après électrolyse montre dans tous les cas l'apparition d'une nouvelle vague vers +1,0 V/ECS (fig. 2). La vague d'oxydation de ZnTPP a disparu. En V.C. ce signal apparaît comme correspondant à une réaction électrochimique irréversible (fig. 3a). Ce signal a été analysé et traduit l'oxydation irréversible du complexe β-substitué formé, en présence d'un excès du nucléophile correspondant. En effet, lorsqu'on réalise en milieu Et_2Cl_2–CH_3CN – TEAP 0,1 M l'oxydation des complexes β-substitués obtenus, on observe qu'ils s'oxydent en deux étapes monoélectroniques et réversibles et qu'en présence du nucléophile correspondant, on n'obtient plus qu'un seul signal dont l'amplitude a doublé (fig. 3b), le transfert électronique étant devenu irréversible.

En réduction, on observe sur la solution après électrolyse un premier signal cathodique vers –0,6 V/ECS auquel est associé un signal retour anodique vers –0,3 V/ECS (fig. 3a). Ces signaux ont été clairement identifiés et sont attribuables à la présence en solution après électrolyse des espèces NuH^+ et correspondent aux

TABLEAU 1. Potentiels d'oxydation (V/ECS) obtenus sur électrode (Pt) tournante ($\omega = 2000\,t\,min^{-1}$) en milieu Et_2Cl_2–CH_3CN (1 : 1) TEAP 0.1 M

Porphyrine	$E^{I}_{1/2}$	$E^{II}_{1/2}$
ZnTPP[a]	0,82	1,13
ZnTPP[b]	0,77	1,16
ZnTPP	0,79	1,14
ZnTPP β-Py^+	0,91	1,23
ZnTPP β-3-Pic^+	0,94	1,26
ZnTPP β-SCN	0,88	1,24
ZnTPP β-$P\phi_3^+$	0,93	1,20

[a]Milieu Et_2Cl_2.
[b]Milieu Et_2Cl_2–CH_3CN–Py.

réactions (16, 17) :

$$NuH^+ + e^- \longrightarrow Nu + 1/2H_2$$

$$1/2H_2 \longrightarrow e^- + H_2$$

Ces résultats permettent de proposer pour la formation de la métalloporphyrine β-substituée le bilan global suivant, en accord avec celui établi par Shine *et al.* (7) :

$$[4]\quad ZnTPP + 2Nu \xrightarrow{+0,82V} 2e^- + ZnTPP\ \beta\text{-}Nu^+ + NuH^+$$

Dans le cas où $Nu = SCN^-$ les observations décrites ci-dessus sont limitées, étant donné qu'à +0,5 V/ECS l'ion thyocianate SCN^- s'oxyde lui-même (18). La formation de ZnTPP (SCN) n'est plus la réaction majeure, de nombreuses réactions secondaires devenant prépondérantes, mais reste néanmoins décrite par le bilan [4] proposé.

La faible différence de potentiel (~120 mV) existant entre les vagues d'oxydation de ZnTPP et de la porphyrine β-substituée formée (tableau 1) montre qu'il est difficile de ne pas oxyder une fraction du produit d'arrivée désiré et permet de comprendre d'une part les valeurs n mesurées supérieures à 2 ainsi que, d'autre part, les valeurs plus élevées qu'attendues du courant résiduel de fin d'électrolyse. Cette faible séparation est également responsable de l'obligation d'électrolyser à des potentiels légèrement voisins du potentiel de demi-vague de l'espèce de départ lorsqu'on veut atteindre un rendement optimum du produit synthétisé.

Cette réactivité de la porphyrine de zinc ZnTPP vis-à-vis de nucléophiles avait déjà été mise en évidence (7) à partir de sels du radical-cation $ZnTPP^{\dot{+}}$ obtenus par voie chimique, cependant des travaux ultérieurs sur l'effet *in situ* de bases de Lewis au cours de l'oxydation électrochimique de ZnTPP n'avaient pas montré d'activité particulière (10) et conclu à la seule formation du radical-cation coordiné $ZnTPP(Nu)^{\dot{+}}$.

Ces observations apparemment contradictoires peuvent s'expliquer raisonnablement en considérant que les études sur la réactivité électrochimique de ZnTPP avaient surtout été conduites par des techniques de spectroélectrochimie en couches minces. Dans ces conditions, les temps d'électrolyse complète sont de l'ordre de la minute. Si on considère que la réaction chimique suivant le transfert électronique est lente, il est tout à fait normal de n'observer dans un premier temps que la formation du radical-cation coordiné. Cette interprétation est confortée par le fait qu'à l'échelle de temps de la voltampérométrie cyclique et même de la voltampérométrie stationnaire, aucun effet n'est observé lors de l'addition d'un nucléophile (si ce n'est sa coordination sur le cation métallique central). Une analyse des courbes de V.S. enregistrées dans nos conditions réactionnelles en appliquant les critères $I = f(c)$ et $1/I = f(\omega^{-1/2})$ ne laisse pas entrevoir de complications cinétiques, ce qui confirme bien que la réaction chimique consécutive au transfert électronique est lente.

Par rapport au spectre RMN de la métalloporphyrine de départ (ZnTPP), l'examen des spectres RMN des produits obtenus montre que la substitution a eu lieu sur une position β du macrocycle porphyrinique, l'aromaticité du cycle étant toujours conservée (7).

Le spectre RMN du complexe ZnTPP–β-SCN est le plus simple. Il montre clairement l'éclatement des signaux dûs aux sept protons β-H du macrocycle porphyrine. Le signal du proton β-H adjacent au substituant (SCN) apparaît, comme attendu, aux champs les plus forts (7) (9,05 ppm). Les six autres protons β-H n'apparaissent pas comme équivalents, l'un d'entre eux donnant un doublet à 8,69 ppm, alors que les cinq autres se confondent en un multiplet (8,87–8,82 ppm). Le doublet peut être raisonnablement attribué au proton β-H situé en *para* du groupe SCN.

Le spectre RMN du complexe ZnTPP–β-Py^+, ClO_4^- est analogue à celui de ZnTPP–β-SCN. Les signaux supplémentaires qui apparaissent, dûs aux protons du substituant (Py^+), se distinguent de ceux des protons β-H par leur intensité plus faible ainsi que leur plus grande largeur de raie. On retrouve les signaux des protons β-H du cycle porphyrinique à des champs voisins de ceux observés précédemment avec éclatement du multiplet 12H des protons *méta* et *para* des phényles en deux multiplets (9H et 3H) correspondants respectivement aux protons des trois phényles les plus lointains du substituant et aux protons du phényle voisin du substituant. Ces résultats sont en plein accord avec ceux décrits antérieurement par Schine *et al.* à propos du même complexe (7).

Lorsque la substitution a lieu avec la 3-picoline, on s'attend à ce que les quatre protons de la 3-picoline ne soient plus équivalents, ce qui est effectivement observé. Le signal du groupe méthyle apparaît aux champs faibles, comme attendu.

Enfin, la substitution avec la triphénylphosphine ($P\phi_3$) conduit à un spectre RMN plus complexe. On observe clairement le multiplet 15H dû aux protons du substituant ($P\phi_3^+$). Le déplacement de l'ensemble du spectre vers les champs plus faibles indique que le pouvoir électroattracteur du substituant est plus faible que celui des précédents; cette observation est également traduite par la valeur des potentiels d'oxydation mesurés pour ces métalloporphyrines (tableau 1).

Pour toutes ces porphyrines, le spectre d'absorption visible enregistré montre, par rapport à celui de la porphyrine de départ ZnTPP, un déplacement des bandes d'absorption vers les plus grandes longueurs d'ondes, caractéristique de la présence de substituants électroattracteurs (21).

Conclusion

L'ensemble de ces résultats montre clairement qu'il est possible de réaliser directement par voie électrochimique des mono-substitutions en positions β sur la porphyrine de zinc ZnTPP avec des nucléophiles bases de Lewis. Les rendements obtenus sont significativement plus élevés que ceux obtenus par la voie chimique. Ils varient de 50 à 63% alors que ceux correspondant à la voie chimique (7) sont plutôt de l'ordre de 35%. Ce résultat s'explique en tenant compte du fait que par voie chimique, une fraction du cation radical retourne à la forme neutre ZnTPP et donc non réactive, la voie électrochimique permettant elle de s'affranchir de cette terminaison puisque la réaction contrôlée est celle de l'oxydation de ZnTPP.

Enfin, la voie électrochimique présente l'avantage de per-

Can. J. Chem. Downloaded from www.nrcresearchpress.com by 84.41.108.74 on 09/07/12
For personal use only.

Can. J. Chem. Downloaded from www.nrcresearchpress.com by 84.41.108.74 on 09/07/12
For personal use only.

mettre la réalisation de substitutions difficiles (ou impossibles) par voie chimique; des travaux sont en cours à ce propos ainsi que pour détailler le bilan global proposé pour ces réactions d'électrosubstitution.

Récemment, nous avons montré également que la base libre H_2TPP pouvait réagir de manière similaire pour conduire à des complexes diversement substitués (22).

Partie expérimentale

La *meso*-tétraphénylporphyrine H_2TPP (**1**) et le complexe de zinc correspondant ZnTPP (**2**) ont été préparés suivant les méthodes habituelles décrites dans la littérature (19, 20). La pyridine (Py), la 3-picoline (3-Pic), le thiocyanate de sodium (NaSCN) et la triphénylphosphine ($P\phi_3$) qui ont conduit respectivement aux porphyrines de zinc β-substituées **3**, **4**, **5** et **6**, étaient des produits commerciaux (Merck) utilisés tels quels.

Appareillage

Les spectres de résonance magnétique nucléaire (RMN) du proton ont été enregistrés en solution dans l'acétone deutériée sur un appareil Brucker SY 200 à 200 MHz.

Les spectres d'absorption UV–VIS ont été effectués en solution CH_2Cl_2 sur un appareil Varian 2200.

Mesures électrochimiques

Voltampérométrie stationnaire et cyclique

L'appareillage était constitué d'un ensemble Bruker E1 30 M, d'un enregistreur Ifélec If 3802 et d'un voltmètre Minisis 2000. La cellule de mesure correspondait à un montage à trois électrodes. L'électrode de travail était un disque de platine (ϕ = 1 mm) et pouvait être utilisée sur une gamme de vitesses de rotation allant de 0 à 5000 t min^{-1}; la contre-électrode était un fil de platine. L'électrode de référence était constituée d'un électrode au calomel saturé (ECS) munie d'un pont de jonction contenant une solution Et_2Cl_2 – TBAP 0,2 M. Les solvants d'étude acétonitrile (CH_3CN) et dichloroéthane (Et_2Cl_2) produits Fluka (qualité puriss) ont été utilisés sans traitements particuliers. Le sel de conductibilité, perchlorate de tétraéthylammonium (TEAP), produit Fluka était purifié selon les méthodes décrites antérieurement (21). Pendant les mesures, la solution d'étude était maintenue sous atmosphère inerte (Argon U).

Electrolyses préparatives

Lors des électrolyses préparatives, les compartiments anodique et cathodique de la cellule de travail étaient séparés par un disque de verre fritté (porosité 4) et seul le compartiment anodique était maintenu sous atmosphère inerte. L'électrode de travail était un fil spirale de platine (ϕ = 0,8 mm) de longueur 30 cm. Le volume de solution dans le compartiment anodique était environ 50 mL.

Le potentiel de travail était contrôlé par un potentiostat Tacussel PRT 100 et sa valeur était fixée à +0,82 ± 0,02 V/ECS. L'évolution du courant d'électrolyse était suivie à l'aide d'un enregistreur Tacussel EPL_2; les durées d'électrolyse étaient en moyenne de 30 min.

Après électrolyse la solution était évaporée sous pression réduite pendant 20 min, puis la phase organique était extraite par lavage dans un mélange H_2O–Et_2Cl_2 (5 : 1).

La solution récupérée était concentrée (10 mL) puis chromatographiée. Après élutions la solution du complexe désiré était séchée (CaH_2), puis après filtration et évaporation du solvant, la porphyrine était recristallisée (Et_2Cl_2, *n*-pentane). Les cristaux obtenus étaient ensuite séchés sous vide à 100°C pendant 24 h.

Adduit **3**[3] : ZnTPP β-Py^+, ClO_4^-

Oxydation de 40 mg de **2** en présence de 0,1 mL Py. La séparation est effectuée sur colonne d'alumine (activité III, Merck) et fournit successivement : eluant $CHCl_3$, 2 mg de **2**; eluant $CHCl_3$–MeOH (25 : 1), 32 mg (63%) de **3**. $F > 350$°C. Spectre visible (CH_2Cl_2), λ_{max} (10^{-4} ε) : 596 (1,21), 557 (1,66) 520 ep. (0,68), 427 (26,9). RMN ^1H ($(CD_3)_2$ C = 0), δ, ppm : 9,51 (d, 2H, J = 5,5 Hz, 3–5 Py^+), 9,43 (s, 1H, β-H adjacent à Py^+), 8,91–8,75 (m, 6H, β-H et 4 Py^+), 8,64 (d, 1H, J = 4,7 Hz, β-H), 8,29–8,13 (m, 8H, *o*-H), 8,05 (d, 2H, J = 5Hz, 2–6 Py^+), 7,88–7,79 (m, 9H, *m*- et *p*-H), 7,53–7,40 (m, 3H, *m*- et *p*-H du phényle voisin de Py^+). Anal. calc. pour $ZnC_{49}H_{32}N_5ClO_4$: C 68,8; H 3,77; N 8,18; Cl 4,14; tr. : C 68,4; H 3,81; N 8,05; Cl 4,17%.

Adduit **4** : ZnTPP β-3-Pic^+, ClO_4^-

Oxydation de 40 mg de **2** en présence de 0,1 mL 3-Pic comme précédemment. Elution avec $CHCl_3$ donne ~5 mg de **2**; eluant $CHCl_3$–MeOH (25 : 1) donne 32 mg (62%) de **4**. F 278–282°C. Spectre visible (CH_2Cl_2), λ_{max} (10^{-4} ε) : 600 (0,92), 560 (1,25), 520 ep. (0,42), 426 (22,0). RMN ^1H ($(CD_3)_2$ C = 0), δ, ppm : 9,39 (d, 1H, J = 5 Hz Pic^+), 9,36 (s, 1H, β-H adjacent à Pic^+), 9,26 (s, 1H, Pic^+), 8,89–8,84 (m, 4H, β-H), 8,80 (d, 1H, J = 4,8 Hz, β-H), 8,63 (d, 1H, J = 4,8 Hz, β-H), 8,57 (d, 1H, = 8 Hz Pic^+), 8,24–8,06 (m, 8 H, *o*-H), 7,97 (d, 1H, J = 7,5 Hz, Pic^+), 7,85–7,80 (m, 9H, *m*- et *p*-H), 7,62–7,48 (m, 2H, *m*-H du phényle voisin de Pic^+), 7,39–7,32 (t, 1H, *p*-H du phényle voisin de Pic^+), 2,60 (q, 3H, CH_3). Anal. calc. pour $ZnC_{50}H_{34}N_5ClO_4$: C 69,0; H 4,05; N 8,04; Cl 4,07; tr. : C 68,1; H 4,16; N 8,06; Cl 4,22%.

Adduit **5** : ZnTPP β-SCN

Oxydation de 40 mg de **2** en présence de 1,2 g NaSCN comme précédemment. L'élution avec $CHCl_2$ donne un mélange **1** plus **2**, 5 mg; eluant $CHCl_3$–$(C_2H_6)_2O$ (10 : 4) donne 24 mg (55%) de **5**. F 340–344°C. Spectre visible (CH_2Cl_2), λ_{max} (10^{-4} ε) : 588 (0,45), 554 (1,91), 510 ep. (0,33), 486 ep. (0,13), 428 (45,25). RMN ^1H ($(CD_3)_2$ C = 0), δ, ppm : 9,05 (s, 1H, β-H adjacent à SCN), 8,87–8,82 (m, 5H, β-H), 8,69 (d, 1H, J = 5 Hz, β-H), 8,25–8,10 (m, 8H, *o*-H), 7,97–7,79 (m, 12H, *m*- et *p*-H). Anal. calc. pour $ZnC_{45}H_{27}N_5S$: C 73,4; H 3,60; N 9,50; Cl 4,03; tr. : C 72,8; H 4,00; N 8,97; Cl 4,02%.

Adduit **6** : ZnTPP β-$P\phi3^+$, ClO_4^-

Oxydation de 40 mg de **2** en présence de 20 mg de $P\phi_3$, colonne de Kieselgel 60 (Merck). Eluant $CHCl_3$ donne ~2 mg de **2**. Eluant éther donne une solution jaune orange (écartée). Eluant $CHCl_3$–$(CH_3)_2CO$ (30 : 20) donne 31 mg (50%) de **6**. F 240–244°C. Spectre visible (CH_2Cl_2), λ_{max} (10^{-4} ε) : 606 (1,05), 566 (1,00), 528 ep. (0,41), 434 (29,3). RMN ^1H ($(CD_3)_2$ C = 0), δ, ppm : 8,94–8,65 (m, 6H, β-H), 8,24–8,04 (m, 7H, β-H et 6 *o*-H), 7,84–7,74 (m, 9H, *m*- et *p*-H), 7,67–7,52 (m, 15H, $P\phi_3$), 7,33–7,17 (m, 3H, *m*- et *p*-H du phényle voisin de $P\phi_3$), 6,87–6,64 (m, 2H, *o*-H du phényle voisin de $P\phi_3^+$). Anal. calc. pour $ZnC_{62}H_{42}N_4PClO_4$: C 71,7; H 4,08; N 5,39; P 2,98; Cl 3,41; tr. : C 71,7; H 4,21; N 5,27; P 2,98; Cl 2,90%.

3. L'attribution des pics des protons de Py^+ (adduit **3**) donnée à la réf. 14 a été modifiée compte tenu des résultats observés à partir des spectres de **4** et **5**.

1. A. STANIENDA. Z. Phys. Chem. **229**, 259 (1964).
2. J. H. FUHRHOPP et D. MAUZERALL. J. Am. Chem. Soc. **91**, 4174 (1969).
3. J. FAJER, D. C. BORG, A. FORMAN, D. DOLPHIN et R. H. FELTON. J. Am. Chem. Soc. **92**, 3451 (1970).
4. G. H. BARNETT et K. M. SMITH. J. Chem. Soc. Chem. Commun. 772 (1974).
5. G. H. BARNETT, B. EVANS et K. M. SMITH. Tetrahedron Lett. 4009 (1976).
6. A. G. PADILLA, S. M. WU et H. J. SHINE. J. Chem. Soc. Chem. Commun. 236 (1976).
7. H. J. SHINE, A. G. PADILLA et S. M. WU. J. Org. Chem. **44**, 4069 (1979).
8. D. DOLPHIN, Z. MULJIANI, K. ROUSSEAU, D. C. BORG, J. FAJER et R. H. FELTON. Ann. N.Y. Acad. Sci. **206**, 349 (1973).
9. D. DOLPHIN, D. J. HALKO, E. C. JOHNSON et K. ROUSSEAU. *Dans* Porphyrin chemistry advances. *Éditeur* : F. R. Longo. Ann Arbor Science, Ann Arbor, MI. 1979. p. 119.
10. K. M. KADISH, L. R. SHINE, R. K. RHODES et L. A. BOTTOMLEY. Inorg. Chem. **20**, 1274 (1981).
11. K. M. KADISH et R. K. RHODES. Inorg. Chem. **20**, 2961 (1981).
12. H. J. CALLOT, A. LOUATI et M. GROSS. Tetrahedron Lett. 3281 (1980).

13. H. J. CALLOT, A. LOUATI et M. GROSS, Bull. Soc. Chim. Fr. 317 (1983).
14. L. EL KAHEF, M. EL MERAY, M. GROSS et A. GIRAUDEAU. J. Chem. Soc. Chem. Commun. 621 (1986).
15. A. GIRAUDEAU, H. J. CALLOT et M. GROSS. Inorg. Chem. **18**, 201 (1979).
16. G. CAUQUIS, J. L. CROS et M. GENIES. Bull. Soc. Chim. Fr. 3765 (1971).
17. G. SCHIAVON, S. ZECCHIN et G. COGONI. J. Electroanal. Chem. Interfacial Electrochem. **48**, 425 (1973).
18. G. CAUQUIS et G. PIERRE. C.R. Acad. Sci. **266**, 883 (1968).
19. A. D. ADLER, F. R. LONGO, J. D. FINARELLI, J. GOLDMACHER, J. ASSOUR et L. KORSAKOFF. J. Org. Chem. **32**, 476 (1967).
20. A. ADLER, F. R. LONGO, F. KAMPAS et K. KIM. J. Inorg. Nucl. Chem. **32**, 2443 (1970).
21. A. GIRAUDEAU, H. J. CALLOT, J. JORDAN, I. EZAHR et M. GROSS. J. Am. Chem. Soc. **101**, 3857 (1979).
22. L. EL KAHEF, M. GROSS et A. GIRAUDEAU. J. Chem. Soc. Chem. Commun. 963 (1989).

Can. J. Chem. Downloaded from www.nrcresearchpress.com by 84.41.108.74 on 09/07/12
For personal use only.

Synthesis and nuclear magnetic resonance spectroscopy of indane structures: indanes mono- and disubstituted in the pentagonal ring

ELBA N. ALESSO, DORA G. TOMBARI, ADRIANA F. IBAÑEZ, AND GRACIELA Y. MOLTRASIO IGLESIAS[1]

Departamento de Química Orgánica, Facultad de Farmacia y Bioquímica, Junin 956 (1113), Universidad de Buenos Aires, Buenos Aires, Argentina

AND

JOSÉ M. AGUIRRE

Departamento de Ciencias Básicas, Universidad Nacional de Luján, Luján, Argentina

Received March 6, 1990[2]

ELBA N. ALESSO, DORA G. TOMBARI, ADRIANA F. IBAÑEZ, GRACIELA Y. MOLTRASIO IGLESIAS, and JOSÉ M. AGUIRRE. Can. J. Chem. **69**, 1166 (1991).

Indanes monosubstituted and 1,2- and 1,3-disubstituted in the pentagonal ring were synthesized, and configurations were assigned to the 1,2-disubstituted compounds by means of nuclear magnetic resonance spectroscopy.

Key words: mono- and disubstituted indanes, conformation, configuration, ^1H and ^{13}C NMR, synthesis.

ELBA N. ALESSO, DORA G. TOMBARI, ADRIANA F. IBAÑEZ, GRACIELA Y. MOLTRASIO IGLESIAS et JOSÉ M. AGUIRRE. Can. J. Chem. **69**, 1166 (1991).

On a synthétisé des indanes mono- ainsi que 1,2- et 1,3-disubstitués sur le cycle pentagonal et on a attribué les configurations des composés 1,2-disubstitués à l'aide de la résonance magnétique nucléaire.

Mots clés : indanes mono- et disubstitués, conformation, configuration, RMN du ^1H et du ^{13}C, synthèse.

[Traduit par la rédaction]

To assign the stereochemistry of indanes obtained by treating 1,2-diarylethylamides and 1-arylethylamides with ethyl polyphosphate (EPP) (1, 2), as a preliminary step in the synthesis of naturally occurring indane structures, we started by preparing the simpler indane models and determining their stereochemistry by means of nmr spectroscopy.

The present work describes the synthesis of indanes monosubstituted and 1,2- and 1,3-disubstituted in the pentagonal ring. Table 1 shows the indanes that were synthesized as well as a summary of the main chemical shifts in ^{13}C and ^1H nmr spectra used to elucidate the stereochemistry of 1,2-disubstituted indanes. Further nmr data are listed in the experimental section.

Given their versatility and ready availability of the starting materials, the approaches presented in Scheme 1 were chosen to synthesize indanes **1**–**9** and **30**. Spectroscopic data for indanes **1**–**4** were assigned according to chemical shifts described for similar compounds in the literature (2, 3).

The *cis* configuration for the indane **5**, which was prepared from chalcone **10**, was assigned on the basis of (a) the stereochemistry of the hydrogenation reaction employed, bearing in mind the steric control exerted by the benzyl group located at C(1) in the indene **22**, and (b) ^1H nmr features of the compound, which agree with those described for *cis*-1-methyl-3-(3,4-dimethoxyphenyl)-5,6-dimethoxyindane in previous work (2).

Starting from indanone **16**, the two stereoisomeric indanes **6** and **7** were obtained. It is recognized that in the *cis* epimer of 1,2-disubstituted indanes the two extreme conformations **I***a* and **I***b* (Fig. 1) would contain an X—C(1)—C(2)—Y array having a smaller torsional angle than the *trans* epimer, which would be represented by the extreme conformations **II***a* and **II***b* (Fig. 1). Therefore it is reasonable to expect, in ^{13}C nmr, a shielding for terminal C atoms (e.g., for X = CH_2Ph) (5) in the *cis* epimer rather than the *trans*, and to a lesser degree this same shielding effect for central C atoms. This is commonly seen in *gauche* butane-type fragments as compared to *anti* fragments in the 1,2-disubstituted cyclopentanes (4).

It was observed that C(1) and C(2) in indane **6** were more shielded then those in **7** (C(1) = 49.60 ppm; C(2) = 50.80 ppm (**6**) and C(1) 55.00 ppm; C(2) = 55.00 ppm (**7**), respectively). As well, the benzyl methylene was more shielded in indane **6** than that in **7** (36.60 ppm and 40.69 ppm, respectively). More specifically, the chemical shift of benzyl methylene in epimer **7** was very similar to that in 1-benzyl-5,6-dimethoxyindane **4** (41.80 ppm). As a result of these observations the *cis* configuration was assigned to compound **6** and the *trans* to **7**. As indane **7** was obtained as a mixture with compound **6**, the comparison of the ^1H nmr spectral data was not suitable for assigning the stereochemistry of compounds **6** and **7**.

To synthesize stereoisomeric indanes **8** and **9**, 2-(3,4-dimethoxyphenyl)-3-phenylindenone **24** was prepared as starting material. A Clemmensen reaction (6) on **24** gave a mixture of stereoisomeric indanes **8** and **9**, in addition to indene **25** (Scheme 1). The *cis* configuration was assigned to the predominant indane **8** and the *trans* configuration to compound **9**. Assignment rationale included: (a) in the ^{13}C nmr spectra, signals for a diastereotopic pair of atoms showed a significant shielding difference (C(1) = 56.80 ppm; C(2) = 51.70 ppm for **8** and C(1) = 59.80 ppm; C(2) = 56.40 ppm for **9**); and (b) the ^1H nmr spectrum of isomer **8** showed lower shielding for H(1) and H(2) than that of isomer **9** (H(1) = 4.61 ppm; H(2) = 3.95 for **8** and H(1) = 4.34 ppm; H(2) = 3.75 ppm for **9**); that is, neither hydrogen atom in isomer **8** was shielded by the *cis* phenyl group bonded to the neighbouring carbon atom (7).

Galton *et al.* in 1970 (6) and Knorr *et al.* in 1980 (8) synthesized *cis*- and *trans*-1,2-diphenylindane by different routes, assigning the *trans* configuration to the isomer having the higher melting point and *cis* to the one with the lower (119–121°C and 83–85°C, respectively). The present authors disagree with such configurational assignment.

We decided to synthesize 1,2-diphenylindanes and compare the data of the ^1H nmr spectra with those obtained by the other

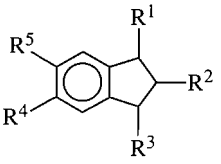
[1]Author to whom correspondence may be addressed.

[2]Revision received March 13, 1991.

Printed in Canada / Imprimé au Canada

Can. J. Chem. Downloaded from www.nrcresearchpress.com by 198.100.157.202 on 09/07/12
For personal use only.

TABLE 1. Substituted indanes and ^{13}C and ^{1}H nmr data



No	R^1	R^2	R^3	R^4	R^5	^{13}C nmr (^{1}H) chemical shifts C-1	C-2	C-3	Other	Carbon
1	4-CH_3-C_6H_4	H	H	CH_3O	CH_3O	51.01	36.90	31.36	20.7	*C*H_3-Ar
2	H	C_6H_5	H	H	H	40.76	45.34	40.76		
3	H	3,4-$(CH_3O)_2$-C_6H_3	H	CH_3O	CH_3O	40.95	45.34	40.95		
4	C_6H_5-CH_2	H	H	CH_3O	CH_3O	46.30	32.20	30.90	41.8	*C*H_2-Ar
5	C_6H_5-CH_2	H	4-CH_3-C_6H_4	CH_3O	CH_3O	45.15	44.86 [a]	49.69	41.8	*C*H_2-Ar
									20.8	*C*H_3-Ar
6	C_6H_5-CH_2	3,4-$(CH_3O)_2$-C_6H_3	H	CH_3O	CH_3O	49.6	50.8	36.1	36.6	*C*H_2-Ar
7	C_6H_5-CH_2	3,4-$(CH_3O)_2$-C_6H_3	H	CH_3O	CH_3O	55.0	55.0	31.86	40.69	*C*H_2-Ar
8	C_6H_5	3,4-$(CH_3O)_2$-C_6H_3	H	H	H	56.8 (4.61)	51.7 (3.95)	37.5		
9	C_6H_5	3,4-$(CH_3O)_2$-C_6H_3	H	H	H	59.8 (4.34)	56.4 (3.75)	39.8		
30	C_6H_5	C_6H_5	H	H	H	56.71	51.70	36.77		

[a]For ^{1}H nmr, δ: 1.70 and 2.75 ppm.

Can. J. Chem. Downloaded from www.nrcresearchpress.com by 198.100.157.202 on 09/07/12
For personal use only.

authors (6, 7) and, in addition, to analyze the ^{13}C nmr chemical shifts of these compounds.

The reduction of 1,2-diphenylindene **26** with Pd(C) 10% as well as the stereospecific hydrogenation of 2,3-diphenylindene **27** with platinum dioxide as catalyst afforded only indane **30** (mp 119–121°C). This indane was also obtained, together with indene **26**, by Clemmensen reduction (9) of 2,3-diphenylindenone **28**. The ^{1}H nmr spectrum for the indane **30** prepared by us agrees with that for the compound obtained by Galton and by Knorr with mp 119–121°C, and displays marked differences in the ^{1}H nmr spectrum from the compound having the lower melting point, as reported by Galton *et al.* (6) and by Knorr *et al.* (8). The comparison of H(1) and H(2) chemical shifts in these isomers shows shielding for hydrogen atoms corresponding to the isomer with the 119–121°C melting point. Furthermore, ^{13}C nmr chemical shifts in indane **30** corresponding to C(1), C(2), and C(3) agree with those for the equivalent carbon atoms in indane **8**, which was assigned the *cis* configuration.

Lastly, ^{1}H nmr spectra for indanes **6** and **8** disclose a highly shielded aromatic proton (a singlet integrating for one hydrogen atom at 6.06 and 6.09 ppm, respectively), and a similar pattern in one of the methoxyl groups (a singlet integrating for three protons at 3.57 and 3.47 ppm, respectively). Such greater shielding would agree with a preferential conformation for these compounds, whereby the 3,4-dimethoxyphenyl group linked to C(2) should be in the axial position, leaving the benzly or phenyl group bonded to C(1) in the *pseudo*-equatorial position (Fig. 1, **I***a*). That conformation would be valid in terms of energy, since it would preclude 1–3 diaxial interaction between the substituents linked to C(1) and H(3). In support, this shielding is not observed in indanes **3** and **9**, which indicates a preferentially equatorial location for the substituent bonded to C(2) in these compounds (Fig.1, **II***a*).

Experimental

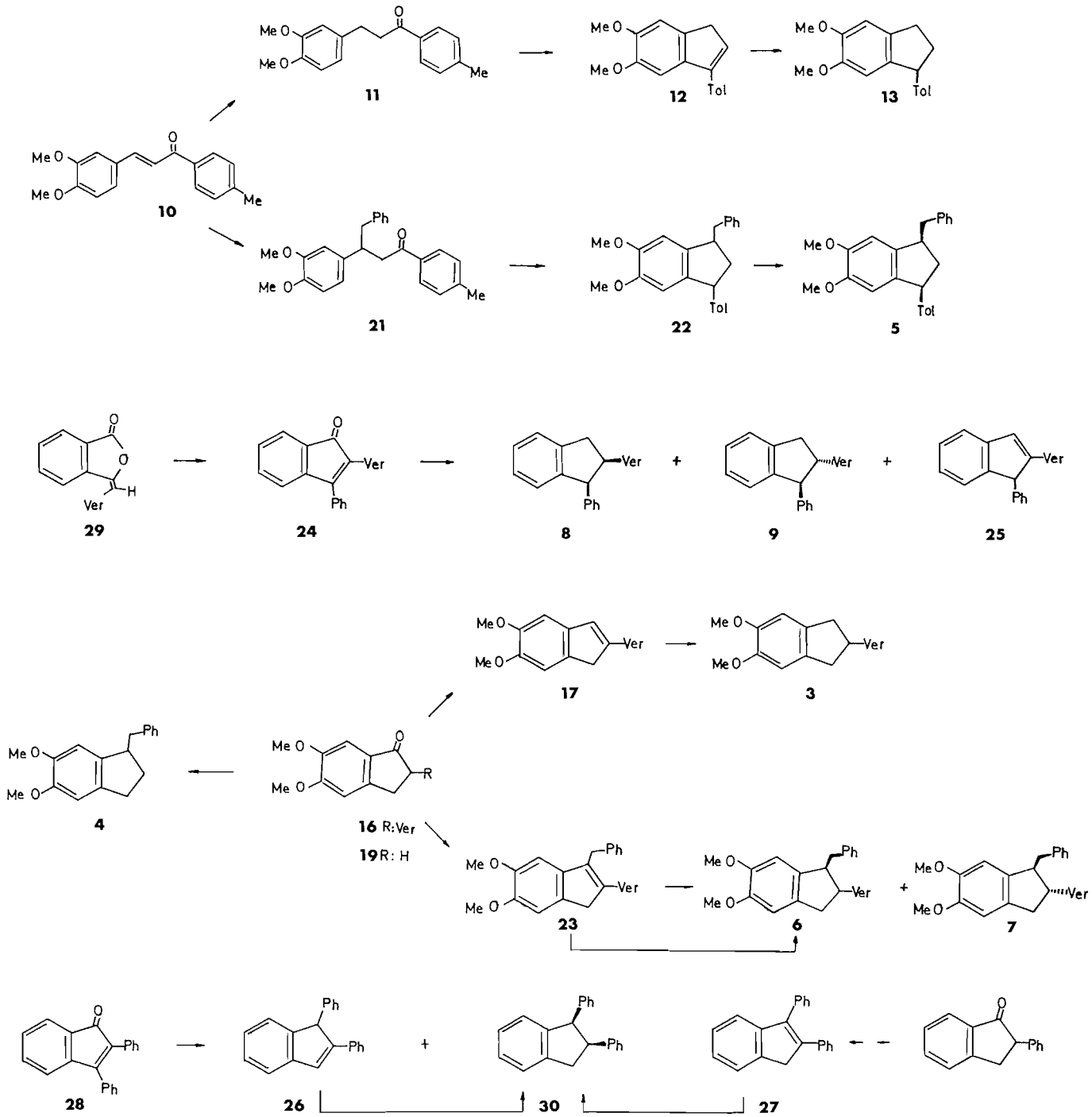
Infrared spectra were obtained on a Shimadzu IR 440 spectrometer. The ^{1}H and ^{13}C nmr spectra were recorded on a Bruker WO 80 SYFT or Varian FT 80A spectrometer using solutions in deuteriochloroform; chemical shifts are reported as values relative to tetramethylsilane as internal standard. Cyclopentene ring carbon and aliphatic carbon shifts were determined by means of model values and APT (Attached Protons Test) experiments. Elemental analyses were carried out in our laboratories using a Coleman analyzer. Melting points (uncorrected) were obtained on a Thomas Hoover apparatus.

1-(4-Methylphenyl)-5,6-dimethoxyindane ***1***

The *1-(4-methylphenyl)-3-(3,4-dimethoxyphenyl)-2-propen-1-one* **10** (11) starting material for the synthesis of **1** was obtained by the general procedure used for the preparation of chalcones (10). Yield 82%; mp 95–96°C (EtOH); ir (mull): 1660 (C=O) cm^{-1}; ^{1}H nmr: 2.4 (s, 3H, CH_3-Ar), 3.9 (s, 6H, OCH_3), 6.70–7.60 (m, 7H, Ar and HC=CH), 7.80 (d, J = 9.0 Hz, 2H, Ar).

A solution of 1.39 g of the propen-1-one **10** in 15 mL of ethyl acetate was hydrogenated with 12 mg of platinum dioxide catalyst at room temperature and 40 psi (1 psi = 6.9 kPa) for 1 h. Removal of catalyst and solvent gave a solid, which crystallized from ethanol to afford colorless needles of *1-(4-methylphenyl)-3-(3,4-dimethoxyphenyl)propan-1-one* ***11***. Yield 73%; mp 46–48°C; ir (mull): 1680 (C=O) cm^{-1}; ^{1}H nmr: 2.4 (s, 3H, CH_3Ar), 2.8–3.5 (m, 4H, H-2 and H-3), 3.85 (s, 6H, OCH_3), 6.8 (s, 3H, Ar), 7.25 (d, J_{ortho} = 8.6 Hz, 2H, Ar), 7.9 (d, J_{ortho} = 8.6 Hz, 2H, Ar). Anal. calcd. for $C_{18}H_{20}O_3$: C 76.12, H 7.10; found: C 76.10, H 7.06.

A solution of 0.56 g of the propan-1-one **11** in 0.45 mL of phosphoric acid (85%) was added slowly with vigorous stirring to a mixture of 0.9 mL of concentrated sulfuric acid and 0.45 mL of phosphoric acid (85%) at 5°C. The reaction mixture was heated at 70–80°C for 30 min and then was poured into 50 mL of ice-water. The white precipitate was collected, washed with cold water, dissolved in chloroform, and the solution washed with sodium bicarbonate (10%) and dried. Evaporation of the solvent afforded a white solid, mp 103–107°C, which was



Ver: 3,4-dimethoxyphenyl; Tol: 4-methylphenyl

SCHEME 1

recrystallized from ethanol to give colourless crystals of *3-(4-methylphenyl)-5,6-dimethoxyindene* **12**. Yield 85%; mp 105–107°C; ^{1}H nmr: 2.4 (s, 3H, CH_3Ar), 3.4 (d, $J_{2,3}$ = 2.1 Hz, 2H, H-3), 3.90, 3.95 (s, 6H, OCH_3), 6.4 (t, $J_{2,3}$ = 2.1 Hz, 1H, H-2), 7.1 (s, 2H, H-4 and H-7), 7.2 (d, J_{ortho} = 8.0 Hz, 2H, Ar), 7.4 (d, J_{ortho} = 8.0 Hz, 2H, Ar). Anal. calcd. for $C_{18}H_{18}O_2$: C 81.27, H 6.82; found: C 81.25, H 6.75.

Hydrogenation of 0.3 g of indene **12** following the above procedure gave *1-(4-methylphenyl)-5,6-dimethoxyindane* **1** as a colorless oil. Yield 90%; ^{1}H nmr: 2.0 (m, 1H, H-2 *cis*), 2.33 (s, 3H, CH_3-Ar), 2.6 (m, 1H, H-2 *trans*), 2.9 (m, 2H, H-3), 3.73, 3.87 (s, 6H, OCH_3), 4.26 (brt, 1H, H-1), 6.49 (s, 1H, H-7), 6.81 (s, 1H, H-4), 7.08 (s, 4H, Ar); ^{13}C nmr: 20.70, 31.36, 36.9, 51.01, 55.6, 107.1, 107.7, 127.5, 128.8, 135.3, 135.6, 138.1, 142.4, 147.8. 147.9. Anal. calcd. for $C_{18}H_{20}O_2$: C 80.66, H 7.52; found: C 80.60, H 7.53.

2-Phenylindane **2**

A solution of 1.0 g of 3-benzylidenephthalide and 0.25 g of sodium in 20 mL of absolute ethanol was heated under reflux for 3 h. Acidification of the cooled reaction mixture gave a yellow solid, which was collected and recrystallized from ethanol to give *2-phenylindan-1,3-dione* **13**. Yield 82%; mp 148–149°C (lit. (6) mp 148–149°C). Clemmensen reduction of the 1,3-indandione following the general

Can. J. Chem. Downloaded from www.nrcresearchpress.com by 198.100.157.202 on 09/07/12
For personal use only.

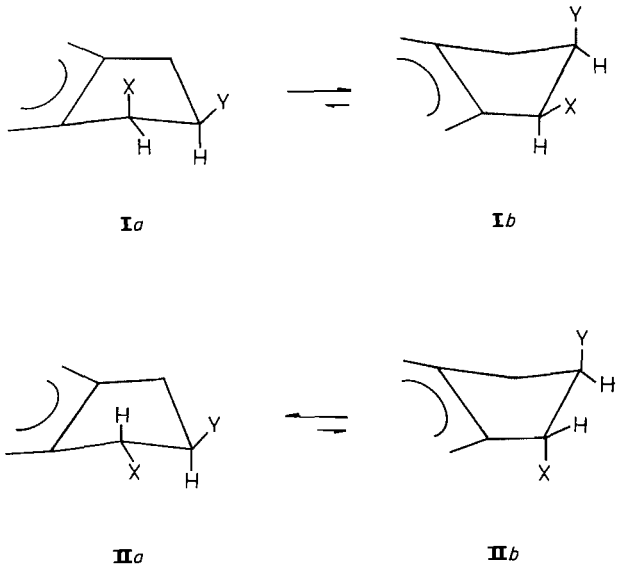


FIG. 1.

conditions of Galton *et al.* (6) afforded 2-phenylindene **14**, which was purified by p-tlc (2 mm thick) on Silica gel G F254. The plates were developed with cyclohexane–benzene 9:1. The *2-phenylindene* **14** was obtained as white crystals. Yield 75%; mp 166–168°C (hexane) (lit. (6) mp 167–168°C); ^{1}H nmr: 3.75 (s, 2H, CH_2), 7.0–7.75 (m, 10H, Ar and H-3).

A solution of 0.5 g of 2-phenylindene **14** in 5 mL of ethanol was hydrogenated with 0.1 g Pd(C) 5% catalyst at room temperature and 35 psi for 2 h. Removal of catalyst and solvent provided a colorless oil. The oil was distilled under reduced pressure to give *2-phenylindane* **2**. Yield 70%; bp 162–165°C/11 Torr) (lit. (6) bp 165°C/11 Torr) (1 Torr = 133.3 Pa); ^{13}C nmr: 40.76, 45.34, 124.16, 126.03, 126.29, 126.88, 128.28. 142.80, 145.29.

2-(3,4-Dimethoxyphenyl)-5,6-dimethoxyindane 3

A solution of 10 g of 3,4-dimethoxyphenylacetic acid, 13.68 g of 3,4-dimethoxybenzaldehyde, 6 mL of triethylamine, and 6 mL of acetic anhydride was refluxed for 35 min. After acidification (hydrochloric acid, 12 mL) the mixture was dissolved in ether, and the solution was washed with water and sodium hydroxide (10%). The combined extracts were acidified (concentrated hydrochloric acid) and filtered. The crude product was hydrogenated in 50 mL of ethanol with 0.9 g of Pd(C) 10% catalyst at room temperature and 35 psi for 2 h; after filtration, the solvent was removed to provide white crystals of *2,3-di-(3,4-dimethoxyphenyl)propanoic acid* **15**, mp 140–141°C. Five grams of the acid **15** were added to 50 g of polyphosphoric acid, and the viscous mass was mixed with an efficient mechanical stirrer and kept at 60–90°C for 2 h. The reaction mixture was then poured into 80 mL of ice-water. The aqueous solution was extracted with ether and the organic extract was washed with cold water, then with sodium bicarbonate solution (10%), and finally dried ($MgSO_4$). Evaporation of the solvent furnished the crude product. Yield 53%; mp 126–130°C. The material was recrystallized from ethanol to give small crystals of *2-(3,4-dimethoxyphenyl)-5,6-dimethoxyindan-1-one* **16**, mp 128–130°C (13); ^{1}H nmr; 3.30 (m, 1H), 3.35–3.90 (m, 2H), 3.80, 3.90, 3.95 (s, 12H, OCH_3), 6.60–6.80 (m, 3H Ar), 6.90 (s, 1H, H-4), 7.20 (s, 1H, H-7).

2-(3,4-Dimethoxyphenyl)-5,6-dimethoxyindene 17

This indene was prepared by the same procedure as described for **14**. Yield 78%; mp 208°C (lit. (12) mp 208°C (benzene)); ^{1}H nmr: 3.65 (s, 2H, CH_2), 3.70, 3.80 (s, 12H, OCH_3), 6.5–7.10 (m, 6H, Ar and H–3).

2-(3,4-Dimethoxphenyl)-5,6-dimethoxyindane 3

This indane was prepared by the same procedure as described for **2**. Yield 80%; mp 152°C (lit. (12) mp 152°C (ethanol); ^{1}H nmr: 2.82–3.67 (m, 5H, H–1 and H–2), 3.85, 3.86 (s, 12H, OCH_3), 6.78 (s, 2H, H–4 and H–7), 6.81 (s, 3H, Ar); ^{13}C nmr: 40.95, 45.34, 55.55, 55.66, 55.79, 107.53, 110.22, 110.96, 118.54, 134.16, 138.11, 147.14, 147.88, 148.61.

1-Benzyl-5,6-dimethoxyindane 4

5,6-Dimethoxyindan-1-one **19** (2) (1.92 g; 10 mmol) dissolved in anhydrous benzene was added to an excess of benzylmagnesium chloride (50 mmol) and the mixture was refluxed for 2 h. The reaction mixture was poured into ice mixed with acetic acid. The organic layer was separated and the aqueous solution was extracted with two portions of methylene chloride. The combined organic extracts were washed with a dilute solution of sodium bicarbonate followed by water, and finally were dried ($MgSO_4$) and the solvent was evaporated. Without further purification the indene **20** was hydrogenated in acetic acid with platinum dioxide at room temperature and 40 psi for 2 h. Removal of catalyst and solvent rendered a yellowish oil that was purified by p-tlc of Silica Gel G F254 and developed with benzene. The upper band afforded 1-benzyl-5,6-dimethoxyindane **4** as a pale yellow oil. Yield 49%; ^{1}H nmr: 2.0 (m, 2H, H–2), 2.75 (m, 4H, H–3 and CH_2-Ar), 3.3 (m, 1H, H–1), 3.75, 3.85 (s, 6H, OCH_3), 6.45 (s, 1H, H–7), 6.70 (s, 1H, H–4), 7.2 (s, 5H, Ar); ^{13}C nmr: 30.9, 32.2, 41.8, 46.3, 55.9, 107.5, 107.7, 125.8, 128.0, 129.0, 135.4, 138.3, 140.7, 147.5, 148.0. Anal. calcd. for $C_{18}H_{20}O_2$: C 80.66, H 7.52; found: C 80.77, H 7.60.

cis-*1-Benzyl-3-(4-methylphenyl)-5,6-dimethoxyindane 5*

The 1-(4-methylphenyl)-4-phenyl-3-(3,4-dimethoxyphenyl)butan-1-one **21**, starting material for the synthesis of indane **5**, was prepared by reaction of **10** with benzylmagnesium bromide and cuprous chloride (2). Yield 65%: mp 96–98°C (ethanol): ir (mull): 1680 (C=O) cm^{-1}; ^{1}H nmr: 2.4 (s, 3H, CH_3-Ar), 2.6–3.6 (m, 5H, H-2, H-3, and H-4), 3.9 (s, 6H, OCH_3), 6.85 (s, 3H, Ar), 7.2 (d, J_{ortho} = 8.0 Hz, 2H, Ar), 7.35 (s, 5H, Ar), 7.8 (d, J_{ortho} = 8.0 Hz, Ar). Anal. calcd. for $C_{25}H_{26}O_3$: C 80.28, H 7.01; found: C 80.34, H 7.07.

The indene **22** was obtained from **21** by the same procedure as described for **12** and without further purification was reduced by the same procedure as described for **1** to give **5** as an oil. Yield 89%; ^{1}H nmr: 1.70 (m, 1H, H-2), 2.3 (s, 3H, CH_3-Ar), 2.75 (m, 1H, H-2), 2.90 (m, 2H, CH_2-Ar), 3.30 (m, 1H, H-1), 3.7, 3.8 (s, 6H, OCH_3), 4.05 (dd, 1H, H-3), 6.4 (s, 1H, H-4), 6.65 (d, 1H, H-7), 7.05 (s, 4H, Ar), 7.20 (s, 5H, Ar); ^{13}C nmr: 20.80, 41.80, 44.86, 45.15, 49.69, 55.83, 55.88, 106.43, 107.84, 125.85, 127.97, 128.16, 128.89, 129.04, 135.68, 138.37, 138.71, 140.52, 142.23, 147.99, 148.23. Anal. calcd. for $C_{25}H_{26}O_2$: C 83.87, H 7.32; found: C 83.60, H 7.26.

cis- *and* trans-*1-Benzyl-2-(3,4-dimethoxyphenyl)-5,6-dimethoxyindane 6* and *7*

2-(3,4-Dimethoxyphenyl)-5,6-dimethoxyindanone (13) **16** (3.23 g; 10 mmol) and benzylmagnesium chloride (50 mmol) were treated in a manner similar to that described for **4**. The crude product was purified by p-tlc of Silica Gel G F254. The plates were developed with benzene. The p-tlc indicated the presence of one major component, which was identified as 3-benzyl-2-(3,4-dimethoxyphenyl)-5,6-dimethoxyindene **23**. It was obtained as an oil. Yield 70%; ^{1}H nmr: 3.60, 3.75, 3.85, 3.90 (s, 12H, OCH_3), 3.70 (s, 2H, H-3), 4.10 (s, 2H, CH_2-Ar), 6.65–7.00 (m, 5H, Ar), 7.20 (s, 5H, Ph). Anal. calcd. for $C_{26}H_{26}O_4$: C 77.68, H 6.52; found: C 77.73, H 6.60.

Hydrogenation of 210 mg of this indene **23** in 50 mL of ethanol with 300 mg of Pd(C) 5% at room temperature and 40 psi afforded 190 mg of the *cis* isomer **6** as an oil. Yield 90.4%; ^{1}H nmr: 2.40 (m, 3H, H-2 and H-3), 3.20 (m, 2H, CH_2-Ar), 3.57 (m, 1H, H-1), 3.75, 3.83, 3.87 (s, 12H, OCH_3), 6.06 (s, 1H, Ar), 6.70–7.20 (m, 9H, Ar); ^{13}C nmr: 36.1, 36.6, 49.6, 50.8, 55.5, 55.6, 55.7, 55.8, 107.6, 108.5, 111.01, 111.9, 119.9, 125.5, 127.7, 129.3, 134.0, 134.4, 137.6, 140.6, 147.0, 147.4, 147.9, 148.5. Anal. calcd. for $C_{26}H_{28}O_4$: C 77.29, H 6.99: found: C 77.36, H 7.07.

The indene **23** was reduced with sodium in boiling pentanol (8). The product, after acidic work-up, was filtered through a short column of basic alumina (Act. 1). Evaporation of the solvent gave an oil. Yield 35%; the ^{13}C nmr data for the oil showed a mixture of *cis* **6** and *trans* **7**.

Can. J. Chem. Downloaded from www.nrcresearchpress.com by 198.100.157.202 on 09/07/12
For personal use only.

trans Isomer **7**: ^{13}C nmr; 31.86, 40.69, 55.00, 55.52, 55.72, 55.95, 103.24, 107.53, 110.78, 110.94, 119.67, 125.68, 127.74, 128.17, 134.8, 134.72, 139.28, 139,37, 146,88, 147.62, 148.00, 148.30.

cis- *and* trans-*1-Phenyl-2-(3,4-dimethoxyphenyl)indane* ***8*** *and* ***9***

The 3-benzylidenephthalide **29** was treated with phenylmagnesium bromide, following the procedure described in the literature (9). The indenone **24** was obtained as a solid. Yield 44%. Recrystallization of **24** from ether – methylene chloride afforded orange needles, mp 134–135°C; ir (KBr): 1770 (C=O) cm^{-1}; ^1H nmr: 3.70, 3.75 (s, 6H, OCH_3), 6.70–7.70 (m, 12H, Ar). Anal. calcd. for $C_{23}H_{18}O_3$; C 80.77, H 5.31; found: C 80.88, H 5.28.

The indene **24** was reduced following Galton's procedure (6). The amalgamated zinc was prepared from 1 g of granulated zinc and 100 mg of mercuric chloride in 1.5 mL of water and 0.05 mL of concentrated hydrochloric acid. To the zinc amalgam was added 0.7 mL of water, a solution of 0.5 g of the indenone **24** in 6 mL of toluene, and 1.75 mL of concentrated hydrochloric acid. This mixture was heated under reflux for 24 h, during which time three 1.5-mL portions of concentrated hydrochloric acid were added. The toluene phase was separated, washed with water, and dried ($MgSO_4$). Evaporation of the solvent afforded a yellow oil (400 mg). A small portion of crystals was separated with the aid of several drops of ethanol. The white needles obtained were crystallized from ethanol. Yield 25%; mp 117–118°C. The structure of this compound was established and assigned to the *cis*-isomer **8**: ^1H nmr: 3.26 (d, J = 8 Hz, 2H, H-3), 3.47, 3.78 (s, 6H, OCH_3), 3.95 (J = 8 Hz, 1H, H-2), 4.61 (d, J = 8 Hz, 1H, H-1), 6.09 (s, 1H, Ar), 6.57 (m, 4H, Ar), 7.18 (m, 7H, Ar); ^{13}C nmr: 37.5, 51.7, 55.4, 55.7, 56.8, 110.4, 111.9, 120.5, 124.16, 125.4, 125.9, 126.8, 126.9, 127.6, 129.1, 133.7, 141.0, 143.8, 145.3, 147.3, 148.0. Anal calcd. for $C_{23}H_{22}O_2$: C 83.71, H 6.72: found: C 83.67, H 6.78.

The filtrate was evaporated and the residue (250 mg) was analyzed by p-tlc of Silica Gel G F254, and developed with benzene. The 1-phenyl-2-(3,4-dimethoxyphenyl) indene **25** was obtained as the upper band. Elution gave white crystals. Yield 23%: mp 127–128°C (ethanol); ^1H nmr: 3.77, 3.82 (s, 6H, OCH_3), 4.91 (brs, 1H, H-1), 6.73 (d, J_{ortho} = 8.8 Hz, 1H, Ar), 7.00–7.40 (m, 12H, Ar and H-3). Anal. calcd. for $C_{23}H_{20}O_2$: C 84.22, H 6.15; found: C 84.30, H 6.23.

The lower band yielded 95 mg of a mixture of *cis* and *trans* indanes **8** and **9**, which was established by ^1H nmr and ^{13}C nmr; ^1H nmr, mixture **8** and **9**: 3.26 (d, J = 8.0 Hz, H-3), 3.36–3.6 (m, H-3), 3.47, 3.73, 3.77, 3.84 (s, OCH_3), 3.75 (m, 1H, H-2), 3.95 (m, H-2), 4.34 (d, J = 8.8 Hz, H-1), 4.61 (d, J = 8.0 Hz, H-1), 6.09 (s, Ar), 6.52–6.76 (m, Ar), 7.0–7.4 (m, Ar); ^{13}C nmr: 37.5, 39.8, 51.7, 55.4, 55.7, 56.3, 56.8, 59.8, 110.4, 110.9, 111.1, 111.9, 119.1, 120.5, 124.1, 124.8, 125.4, 125.9, 126.4, 126.6, 126.8, 127.6, 128.3, 128.5, 129.1, 133.7, 135.6, 141.0, 142.8, 143.3, 143.8, 145.8, 147.2, 147.8, 148.6.

cis-*1,2-Diphenylindane* ***30***

(a) Clemmensen reduction

2,3-Diphenylindenone **28** (1 g) (6) was reduced by the Manning procedure (9). The liquid phase was decanted and extracted with portions of methylene chloride (2 × 10 mL): the organic extracts were washed and dried. Evaporation of the solvent gave 0.85 g of an orange oil, which was analyzed by p-tlc of Silica Gel G F254 and developed with petroleum ether 60–80°C. The upper band gave 0.48 g of 1,2-diphenylindene **26**. Yield 50%; mp 176–178°C (ethanol); ^1H nmr: 4.95 (s, 1H, H-1), 7.00–7.60 (m, 15H, Ar and H-3).

The lower band yielded 0.28 g of *cis*-1,2-diphenylindane **30**. Yield 29%; mp 119–121°C (lit. (6) mp 119–121°C); ^1H nmr: 3.30 (m, 2H, H-3), 4.05 (m, 1H, H-2), 4.70 (d, 1H, J = 8 Hz, H-1), 6.60–7.40 (m, 14H, Ar); ^{13}C nmr: 36.77, 51.70, 56.71, 125.32, 125.81, 126.70, 127.39, 127.94, 128.07, 128.25, 128.61, 128.92, 129.16, 140.87, 141.00, 142.16.

(b) Catalytic hydrogenation of 2,3-diphenylindene ***27***

A solution of 1.0 g of the indene **27** in 15 mL of ethanol was hydrogenated with 10 mg of platinum dioxide catalyst at room temperature and 40 psi for 1 h. Removal of catalyst and solvent gave the indane **10**. Yield 89%.

(c) Catalytic hydrogenation of 1,2-diphenylindene ***26***

The indene **26** was hydrogenated with Pd(C) 5% in ethanol at 50 psi. After 30 min the catalyst was removed and the filtrate was concentrated to give the *cis*-1,2-diphenylindane **30** as white needles, mp 121–122°C. The structure of this compound was established by ^1H nmr and ^{13}C nmr spectroscopy.

Acknowledgments

The authors wish to express their gratitude to the Secretaria de Ciencia y Técnica, Universidad de Buenos Aires, and to CONICET, for support of this study.

1. J. M. Aquirre, E. N. Alesso, D. G. Tombari, C. Somoza, G. Y. Moltrasio, and J. D. Bonafede. An. Asoc. Quim. Argent. **73**, 391 (1985).
2. E. N. Alesso, D. G. Tombari, G. Y. Moltrasio Iglesias, and J. M. Aquirre. Can. J. Chem. **65**, 2568 (1987).
3. M. Miura, M. Yaashida, M. Nojima, and S. Kusabayashi. J. Chem. Soc. Perkin Trans. 1, 79 (1982).
4. H. J. Schneider, N. Nguyen-Ba, and F. Thomas. Tetrahedron, **38**, 2327 (1982).
5. E. Wenker, H. E. Gottlieb, O. R. Gottlieb, M. O. da Pereira, and M. D. Formiga. Phytochemistry, **15**, 1547 (1976).
6. S. A. Galton, M. Kalafer, and F. Marshall Berlinger. J. Org. Chem. **35**, 1 (1970).
7. F. Marcuzzi and G. Melloni. J. Chem. Res. (S), 184 (1979).
8. R. Knorr, E. Lattke, F. Rof, and H. V. Reibig. Chem. Ber. **114**, 1592 (1981).
9. C. Manning, M. R. McClory, and J. J. McCullough. J. Org. Chem. **46**, 919 (1981).
10. A. I. Vogel. Practical organic chemistry. 3rd ed. Longmans, Green and Co., London.
11. K. K. Hau, Y. C. Lin, C. T. Su, and E. J. Lien. T'ai-Wan Yao Hsueh Tsa Chih. **34**, 71 (1982); Chem. Abstr. **99**, 35870e (1983).
12. A. M. Touzin and C. Broquet. Bull. Soc. Chem. Fr. **6**, 2491 (1972).
13. E. V. Kumetsow, D. U. Pruchkin, E. A. Muradyau, and G. N. Dorofunko. Khim. Geterotsikl. Soedin, **1**, 25 (1975); Chem. Abstr. **83**, 9694a (1975).

Can. J. Chem. Downloaded from www.nrcresearchpress.com by 198.100.157.202 on 09/07/12
For personal use only.

Stereochemical studies of the photochemical cycloaddition reaction of alkenes with *N*-benzoylindole and *N*-carboethoxyindole; evidence for biradical intermediacy[1]

DAVID J. HASTINGS AND ALAN C. WEEDON[2]

The Photochemistry Unit, Department of Chemistry, University of Western Ontario, London, Ont., Canada N6A 5B7

Received July 20, 1990[3]

DAVID J. HASTINGS and ALAN C. WEEDON. Can. J. Chem. **69**, 1171 (1991).

The stereochemistries of the 2+2 cycloaddition products obtained from the photochemical addition reaction between *N*-benzoylindole or *N*-carboethoxyindole and the alkenes cyclopentene, cyclohexene, cycloheptene, *cis*- and *trans*-2-butene, and *cis*- and *trans*-4-octene are examined. The structures of the products are shown to be consistent with a photo-cycloaddition mechanism involving the intermediacy of triplet 1,4-biradical species. The quantum yields of adduct formation between *N*-benzoylindole and both *cis*- and *trans*-octene were measured as a function of alkene concentration. The results suggest that *cis*-octene reacts with the indole derivative's triplet excited state with a rate constant of $(1.7 \pm 0.3) \times 10^7\ M^{-1}\ s^{-1}$. The results are also consistent with the immediate products of this reaction being 1,4-biradicals, 98% of which revert to the ground state indole derivative and alkene, and only 2% of which proceed to cycloadduct. In marked contrast, the same treatment suggests that *trans*-octene reacts with the triplet excited state of *N*-benzoylindole with a rate constant estimated to be in the range of 1×10^6 and $6 \times 10^5\ M^{-1}\ s^{-1}$, and it appears that the 1,4-biradicals formed revert much less efficiently to the starting materials; it is estimated that between 67 and 100% of the 1,4-biradicals proceed to cycloadducts. In the reaction with *cis*-octene biradical reversion leads to the formation of *trans*-octene ("Schenk isomerization"); the quantum yield of this process is determined to be 0.074 ± 0.004, which may imply that approximately 75% of the biradicals collapse to *cis*-alkene and 25% collapse to the *trans* isomer.

Key words: indole, photocycloaddition, 1,4-biradicals.

DAVID J. HASTINGS and ALAN C. WEEDON. Can. J. Chem. **69**, 1171 (1991).

On a étudié les stéréochimies des produits de cycloaddition 2+2 obtenus par réaction d'addition photochimique entre le *N*-benzoylindole ou le *N*-carboéthoxyindole et les alcènes suivants : cyclopentène, cyclohexène, cycloheptène, *cis*- et *trans*-but-2-éne et *cis*- et *trans*-oct-4-ène. On démontre que les structures des produits correspondent à celles attendues sur la base d'un mécanisme de photo-cycloaddition impliquant des espèces 1,4-biradicalaires triplets comme intermédiaries. On a déterminé les rendements quantiques pour la formation des adduits entre le *N*-benzoylindole et les *cis*- et *trans*-octènes en fonction de la concentration d'alcène. Les résultats suggèrent que le *cis*-octène réagit avec l'état excité triplet du dérivé de l'indole avec une constante de vitesse de $(1{,}7 \pm 0{,}3) \times 10^7\ M^{-1}\ s^{-1}$. Les résultats sont aussi en accord avec l'existence de 1,4-biradicaux comme produits immédiats de cette réaction dont 98% retourneraient aux états fondamentaux de l'alcène et du dérivé de l'indole alors que seulement 2% conduiraient au produit de cycloadduction. Par ailleurs, un traitement similaire suggère que le *trans*-octène réagit avec l'état excité triplet du *N*-benzoylindole avec une vitesse de réaction qui se situerait entre 1×10^6 et $6 \times 10^5\ M^{-1}\ s^{-1}$ alors que les 1,4-biradicaux qui se forment sont beaucoup moins efficaces pour retourner aux produits de départ; on a évalué que 67–100% des 1,4-biradicaux conduisent aux cycloadduits. Dans la réaction avec le *cis*-octène, le retour des biradicaux vers les produits de départ conduit à la formation du *trans*-octène (« isomérisation de Schenk »); le rendement quantique de ce processus serait de l'ordre de $0{,}074 \pm 0{,}004$ ce qui implique qu'environ 75% des biradicaux conduisent à l'alcène *cis* alors que 25% fournissent l'isomere *trans*.

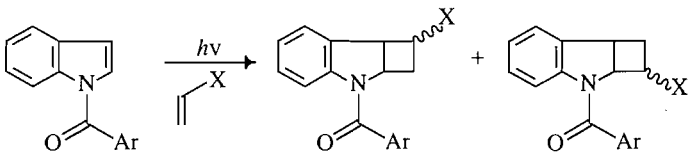
Mots clés : indole, photocycloaddition, biradicaux-1,4.

[Traduit par la rédaction]

Introduction

In 1973 Julian and Foster reported (1) that indoles possessing a benzoyl substituent on the indole nitrogen atom form cyclobutane adducts when irradiated with ultraviolet light in the presence of monosubstituted ethylenes (Scheme 1). The reaction was found to be regioselective, with the isomer **2** favoured over **3**. In a later investigation Ikeda *et al.* confirmed this result (2) and further demonstrated that the reaction is not stereoselective so that in **2** the carbon atom bearing the X-substituent can have both possible configurations.

In principle, this cycloaddition reaction could offer a powerful method for the synthesis of substituted indoles if methods for the selective cleavage or elaboration of the cyclobutane ring of the cycloadducts can be developed. The potential synthetic application of this reaction also requires a knowledge of the mechanism by which the photochemical cycloaddition step



1 Ar = Ph **2** **3**

SCHEME 1

proceeds, so that the effect of further variation of alkene and indole structure upon the reaction efficiency, regiochemistry, and stereochemistry can be predicted.

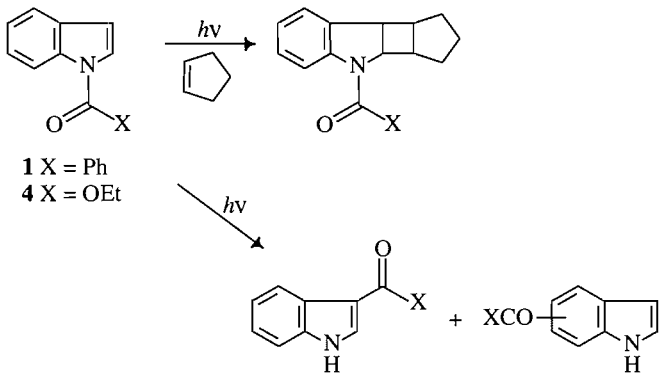
As part of a program of research that, it is hoped, will lead to useful synthetic applications, we have been examining the mechanism of the photochemical cycloaddition reaction between alkenes and *N*-acylindoles (3–5). We have found (3) that *N*-carboethoxyindole, **4** (Scheme 2), also undergoes the photochemical cycloaddition reaction with alkenes and that both *N*-carboethoxyindole and *N*-benzoylindole undergo a photo-Fries rearrangement reaction in competition with cycloaddition. The efficiency of each of these two competing reactions varies

[1]Contribution number 439 from the Photochemistry Unit, University of Western Ontario.

[2]Author to whom correspondence may be addressed.

[3]Revision received March 26, 1991.

Can. J. Chem. Downloaded from www.nrcresearchpress.com by 198.100.157.202 on 09/07/12
For personal use only.



SCHEME 2

differently when either the solvent or the wavelength of the ultraviolet light used for excitation is changed, and this allows selection of one reaction path over the other (3).

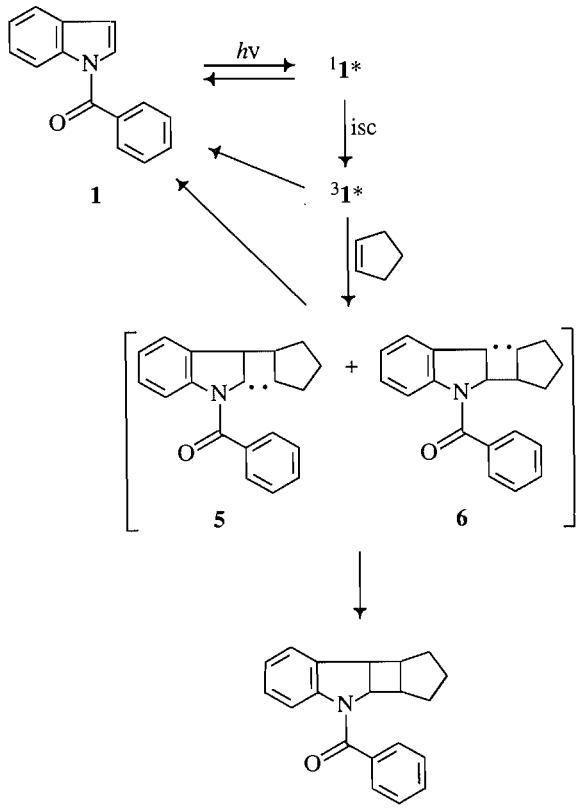
We have also shown (4) for *N*-benzoylindole that the photochemical cycloaddition reaction proceeds by interception of the triplet excited state of the indole derivative by alkene. At high alkene concentrations all of the triplet excited states of *N*-benzoylindole are intercepted, so that the efficiency of the cycloaddition reaction (i.e., the quantum yield of cycloadduct formation, Φ) should approach the efficiency of triplet excited state formation (i.e., the quantum yield of intersystem crossing, Φ_{isc}); however, the value of Φ extrapolated to infinite alkene concentration for the addition of *N*-benzoylindole to cyclopentene was found to be 0.06, which is much smaller than the value of 0.30 determined for Φ_{isc}. To explain this discrepancy we have postulated (4) that an intermediate is formed from the reaction of the triplet excited state of the indole derivative with the alkene and that this intermediate can either proceed to cycloadduct or revert to the ground state starting materials. For the reaction of *N*-benzoylindole with cyclopentene, possible structures for this intermediate could be stereoisomers of the regioisomeric triplet 1,4-biradicals **5** and **6**, as shown in Scheme 3.

If triplet biradicals of the type **5** and **6** are indeed intermediates in this reaction, and if they do revert to the ground state precursors in competition with product formation, then this might be detectable if suitable 1,2-disubstituted alkenes are used as the alkene partner in the photochemical cycloaddition reaction. This possibility is illustrated in Scheme 4. If the putative intermediate biradicals shown in Scheme 4 are sufficiently long-lived, so that any memory of the stereochemistry of the starting alkene is lost, then the stereochemistry of the cyclobutene adducts will be mixed; in addition isomerized alkene will be observed in the reaction mixture. Alternatively, if no biradical intermediates are involved in the reaction, or if they are too short-lived for conformational relaxation, then different products might be expected depending upon which geometrical isomer of the alkene is used, and no isomerized alkene will be seen in the reaction mixture.

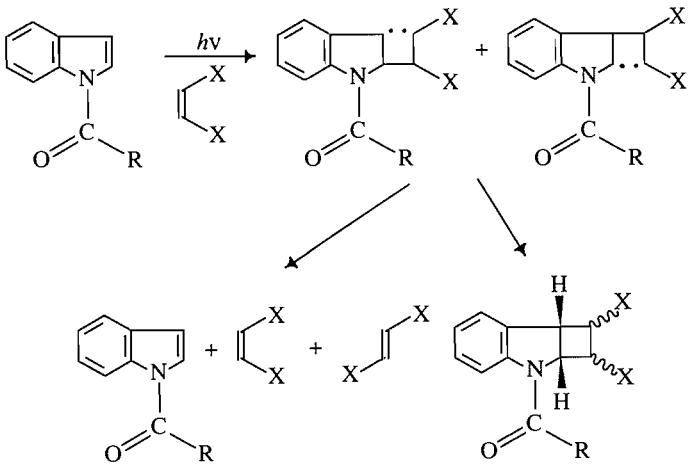
Reported here are the results of an investigation in which *N*-acylindoles have been irradiated in the presence of cyclic and noncyclic 1,2-dialkyl-substituted ethylenes and the stereochemistry of the products examined. These results are then discussed in terms of the possible intermediacy of biradical species.

Results of photochemical cycloaddition and elucidation of the structures of the photoproducts

The addition of a 1,2-disubstituted ethylene to an *N*-acylindole leads to the formation of four chiral centres. The maximum



SCHEME 3



SCHEME 4

number of stereoisomers that can be produced is, however, reduced by the presence of the cyclobutane–cyclopentane ring fusion, which is expected to be *cis* as shown in Scheme 4. Consequently if the two substituents on the ethylene are the same (so that no possibility of regioisomerism exists), then the photoaddition is expected to produce four pairs of enantiomers related as diastereomers. The major analytical problem in this work was to detect, separate, and assign the stereochemistries of these diastereomers.

Several groups have examined the use of nmr spectroscopy for stereochemical assignment of substituted cyclobutane rings (6–16). The use of ^{1}H–^{1}H coupling constants for the hydrogens

Can. J. Chem. Downloaded from www.nrcresearchpress.com by 198.100.157.202 on 09/07/12
For personal use only.

Can. J. Chem. Downloaded from www.nrcresearchpress.com by 198.100.157.202 on 09/07/12
For personal use only.

on the cyclobutane ring has met with some success but ambiguities can be caused by the conformational mobility of the puckered cyclobutane ring (14–16). Recently it was shown that nuclear Overhauser effects between cyclobutane ring hydrogens or substituents can lead to stereochemical assignments (6, 7); however, this has not been demonstrated to be a general method.

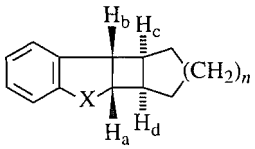
Because of these problems of stereochemical assignment the first alkene examined in this work was cyclopentene. It was anticipated that with this alkene only the two diastereoisomeric pairs of enantiomers represented by structures **7** and **8** would be formed since the sizes of the rings fused to the cyclobutane would preclude the formation of products in which the hydrogens at the cyclopentane–cyclobutane ring fusion positions could be *trans*. It was hoped that the spectroscopic characteristics of the cyclopentene adducts could then be used as models for deduction of the stereochemistry of adducts from other alkenes.

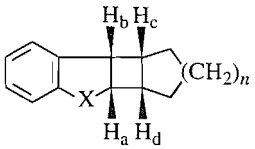
1. Irradiation of N*-benzoylindole and* N*-carboethoxyindole with cyclopentene*

Both gas chromatography (gc) and thin-layer chromatography (tlc) indicated the formation of a single product when a benzene solution of *N*-benzoylindole, **1**, and cyclopentene was irradiated with ultraviolet light under conditions such that only **1** was excited. However, following work-up and removal of unconsumed starting material, the ^{1}H nmr and ^{13}C nmr spectra of the product suggested the presence of two compounds in a 2:1 ratio. The major component was highly crystalline and this allowed its separation from the minor component, which was subsequently isolated from the mother liquors as an oil. The mass spectra of the isolated products indicated them to be adducts of **1** and cyclopentene, and the ^{1}H nmr spectra were consistent with the expected structures **7** and **8**. In particular, the cyclobutane methine protons were clearly visible; for the major isomer they appeared at 3.94, 3.32, 2.84, and 2.66 ppm and these are assigned to protons H_a, H_b, H_c, and H_d, respectively. These assignments are based partly upon the positions calculated using additive chemical shift correlations, and partly on the appearance of the signals and their coupling relationships as deduced from spin–spin decoupling experiments and two-dimensional homonuclear spectra. The signal assigned to H_a appeared as a broad singlet and its splitting by H_b and H_d was unresolved; this is ascribed to slow rotation of the adjacent *N*-benzoyl group. However, the signal assigned to H_b appeared as a double doublet with J = 7.5 and 2.9 Hz. Molecular models of **7** show that the structure is quite rigid and suggest that with the cyclobutane ring in either of its puckered conformations the dihedral angles between H_b and H_a are close to zero, and between H_b and H_c are close to 90°; in this situation the Karplus equations predict the small and large coupling constants observed.

In the minor photoadduct the signal assigned to H_a was also an unresolved broadened singlet and was seen at 4.70 ppm; the signal assigned to H_b was a double doublet at 4.05 ppm with coupling constants of 7.5 and 8.0 Hz. The observation of two large coupling constants between H_b and H_a, and H_b and H_c is consistent with the minor photoadduct having structure **8**, as judged by the inspection of the dihedral angles between the appropriate hydrogens in a molecular model of **8**. The relevant dihedral angles in this case are both close to zero.

To support the above assignments attempts were made to remove the benzoyl group from the photoadducts; it was hoped that in the absence of this group the signal assigned to H_a would be resolved so that the coupling constants to H_b and H_d could be measured independently. The benzoyl group was, however, totally resistant to hydrolysis under both basic and acidic conditions. Eventually it was found that treatment of the photoadducts with lithium aluminum hydride resulted in the formation of a mixture of the *N*-benzyl derivatives **9** and **10** as well as the products of cleavage, **11** and **12**. These compounds were separated by chromatography and their ^{1}H nmr spectra recorded. As anticipated, the signal assigned to H_a in these compounds was resolved as a double doublet and the coupling constants were consistent with the *cis-anti-cis* stereochemistry in **9** and **11**, and the *cis-syn-cis* stereochemistry seen in **10** and **12**. The coupling constant data for the cyclobutane methine hydrogens of these compounds are summarized in Table 1.





7 X = NCOPh, n = 1
9 X = NCH_2Ph, n = 1
11 X = NH, n = 1
13 X = CH_2, n = 1
15 X = NCO_2Et, n = 1
17 X = NCOPh, n = 2
21 X = CH_2, n = 2
25 X = NH, n = 2
29 X = NCOPh, n = 3

8 X = NCOPh, n = 1
10 X = NCH_2Ph, n = 1
12 X = NH, n = 1
14 X = CH_2, n = 1
16 X = NCO_2Et, n = 1
18 X = NCOPh, n = 2
22 X = CH_2, n = 2
26 X = NH, n = 2

The above assignments were further tested by a molecular modelling (MM2) calculation to derive the structures of the most stable conformations of **7**–**12**. The dihedral angles between the cyclobutane methine hydrogens in the most stable conformations were then substituted into the appropriate Karplus equation in order to predict the expected coupling constants. For ease of calculation and because the nitrogen parameters necessary for **7**–**12** were unavailable to us, the indane analogues **13** and **14** were used. The results for **13** and **14** are shown in Table 1 along with the actual coupling constants measured from the ^{1}H nmr spectra of **7**–**12**. The agreement between the calculated values for **13** and **14** and those measured for compounds **7**–**12** is qualitatively very good and quantitatively reasonable, and indicates that for these systems the calculation is reliable for deduction of stereochemistry from coupling constant data, even though indane is being used as a model for indoline, and even though no allowance is made for the effect of an electronegative substituent (the nitrogen atom) on the coupling constants.

The calculated structures of the most stable conformations of **13** and **14** were also used to predict the likely effect of a lanthanide shift reagent complexed to the nitrogen atom of **11** and **12** on the chemical shifts of the cyclobutane methine hydrogens. The calculated relative shifts of the cyclobutane methine hydrogens were then compared with the observed relative shifts when the shift reagent $Eu(fod)_3$ was added to deutero-chloroform solutions of **11** and **12**.

The change in chemical shift of a proton in a rigid molecule induced by a lanthanide shift reagent complexed to a remote Lewis base site in the same molecule is proportional to the magnitude of the pseudocontact interaction, ΔM, between the lanthanide and the proton. The magnitude of ΔM is proportional to $1/r^3$, where r is the distance between the lanthanide and the shifted proton. The magnitude of ΔM is also related to the angle, θ, between the line connecting the lanthanide with the shifted

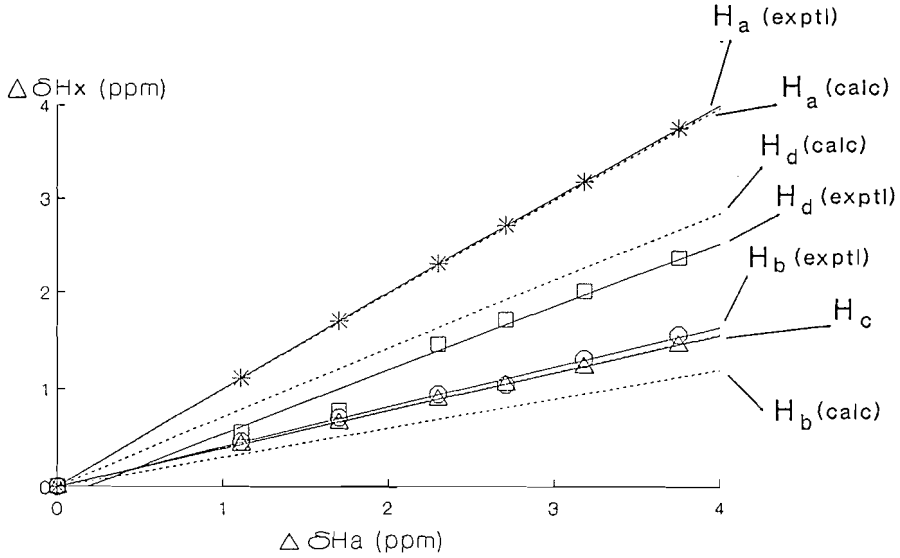


FIG. 1. Calculated (dotted lines) and observed (full lines) changes in chemical shift ($\Delta\delta H_x$) of cyclobutane methine protons in adduct **11** relative to the change in chemical shift of H_a ($\Delta\delta H_a$) consequent upon addition of Eu $(fod)_3$ to $CDCl_3$ solutions of **11**. The calculated and observed lines for H_c are coincident.

TABLE 1. Experimental and calculated $^1H-^1H$ coupling constants (Hz) for cyclobutane methine hydrogens in cyclopentene and cyclohexene adducts of *N*-benzoylindole and *N*-carboethoxyindole

Compound	J_{ab}	J_{ad}	J_{bc}	J_{cd}
7	7.5	2.9	2.9	7.0
8	7.5	7.7	8.0	8.2
9	7.9	2.5	2.7	6.6
10	9.4	9.0	9.0	6.4
11	7.6	2.5	2.7	7.0
12	9.6	9.0	9.2	8.2
13 (calcd.)	7.8	3.6	2.0	8.0
14 (calcd.)	7.8	8.1	7.9	8.0
Isomer I (**18**)	8.5	9.0	9.0	9.5
Isomer II (**17**)	7.0	2.5	2.5	7.0
Isomer I,NBz	8.5	9.3	9.0	9.0
Isomer I,NH (**26**)	8.7	9.3	9.0	9.0
Isomer II,NH (**25**)	8.0	3.0	2.0	8.0
Isomer III,NH (**28**)	6.0	4.0	8.0	7.0
21 (calcd.)	7.8	1.9	3.2	7.3
22 (calcd.)	7.9	8.2	7.9	8.1
23 (calcd.)	7.7	6.8	6.9	6.6
24 (calcd.)	7.3	7.2	7.1	8.5

TABLE 2. Calculated and observed relative lanthanide-induced shifts for cyclobutane methine hydrogens of *N*-acylindole–cycloalkene photochemical adducts and their derivatives[a]

Compound	H_a	H_b	H_c	H_d
11 (calcd.)	1	0.31	0.39	0.71
11 (found)	1	0.40	0.38	0.65
12 (calcd.)	1	0.30	0.25	0.38
12 (found)	1	0.63	0.45	0.45
25 (calcd.)	1	0.33	0.44	0.68
Isomer II,NH (**25**) (found)	1	0.42	0.40	0.90
26 (calcd.)	1	0.27	0.24	0.40
Isomer I,NH (**26**) (found)	1	0.38	0.27	0.40
27 (calcd.)	1	0.29	0.22	0.73
28 (calcd.)	1	0.40	0.61	0.34
Isomer III,NH (**28**) (found)	1	0.47	0.96	0.41

[a]The observed relative lanthanide-induced shift data are obtained from the gradients of the lines in the plot of the change in chemical shift of each proton relative to the change in chemical shift of H_a. Examples are shown in Figs. 1 and 2. The method for derivation of the calculated numbers is described in the text.

proton and the axis of the bond between the lanthanide and the basic site in the molecule, as defined by:

$$\Delta M \alpha \frac{1}{r^3}(3\cos^2\theta - 1)$$

Using this relationship for the most stable conformations of **11** and **12**, with the assumption that the lanthanide complex is attached from the less-hindered face of the molecule to a tetrahedral nitrogen atom, allows the expected relative changes in chemical shifts of the cyclobutane methine hydrogens to be calculated. These can then be compared with the experimental values. The results of such an experiment for compounds **11** and **12** are shown in Figs. 1 and 2 where the experimentally determined lanthanide-induced shifts are expressed relative to the shift observed for H_a, and the calculated values of $1/r^3 \times (3\cos^2\theta - 1)$ for each cyclobutane methine hydrogen are normalized relative to the value for H_a. The gradients of the lines in Figs. 1 and 2 are proportional to ΔM for each hydrogen and these are summarized in Table 2.

The experimental data in Figs. 1 and 2 and Table 2 indicate that for both **11** and **12** the cyclobutane methine closest to the site of lanthanide complexation (i.e., H_a) is the most greatly shifted. In addition, in **11** H_d is more greatly shifted than H_b and H_c, while in **12** H_b, H_c, and H_d are shifted to approximately similar extents. The predicted relative shifts for these hydrogens obtained using the calculated most stable conformations follow the same pattern, with H_a the most greatly shifted in both compounds and H_d more greatly perturbed in **11** only.

For the lanthanide-induced shift experiments it was found

Can. J. Chem. Downloaded from www.nrcresearchpress.com by 198.100.157.202 on 09/07/12
For personal use only.

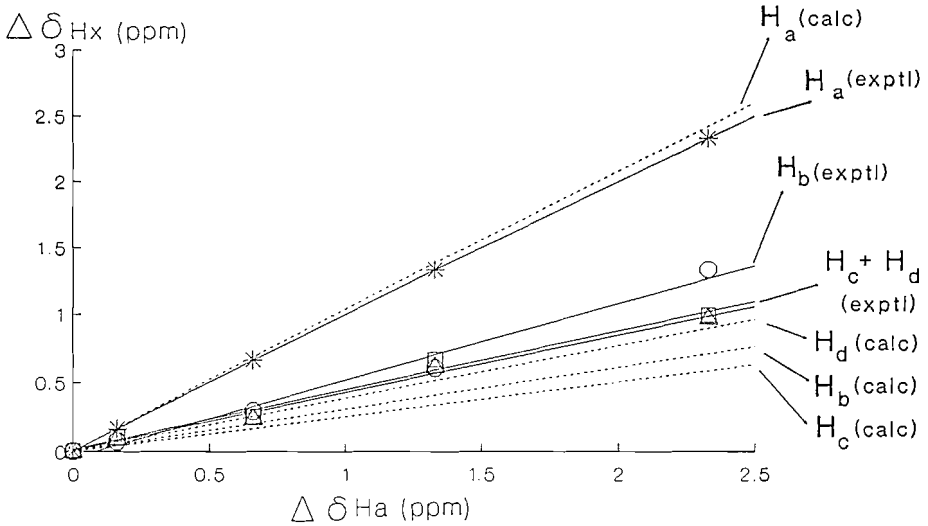
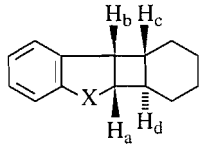


FIG. 2. Calculated (dotted lines) and observed (full lines) changes in chemical shift ($\Delta\delta H_x$) of cyclobutane methine protons in adduct **12** relative to the change in chemical shift of H_a ($\Delta\delta H_a$) consequent upon addition of Eu (fod)$_3$ to $CDCl_3$ solutions of **12**.

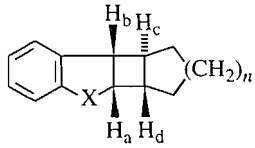
convenient to generate the amine adducts **11** and **12** by photochemical cycloaddition of cyclopentene to *N*-carboethoxyindole, **4**, rather than to *N*-benzoylindole, **1**. The initially formed adducts **15** and **16** were obtained in a 10:1 ratio and were immediately hydrolysed to **11** and **12** by strong base. This gave the amine adducts in good yield and uncontaminated by their benzylated analogues **9** and **10**, which were by-products formed in the removal of the photochemical activating group from the *N*-benzoylindole photoadducts. It was found necessary to use the free amine adducts **11** and **12** for the lanthanide-induced shift study, rather than the *N*-substituted analogues **7**–**10**, since with the latter the lanthanide shift reagent did not form sufficiently strong complexes to give accurately measurable changes in chemical shift.

2. *Irradiation of* N-*benzoylindole and* N-*carboethoxyindole with cyclohexene*

The photochemical cycloaddition of cyclohexene to *N*-benzoylindole could, in principle, yield the four diastereoisomeric pairs of enantiomers represented by **17**–**20**. In fact, when *N*-benzoylindole was irradiated in the presence of cyclohexene only two products were detected. These compounds were not separable by chromatography but one of them was highly crystalline and could be separated in pure form by recrystallization. The second product was isolated as an oil contaminated by small amounts of the crystalline isomer. The mass spectra of these compounds indicated them to be 1:1 adducts between the indole derivative and cyclohexene, and the ^{1}H nmr and ^{13}C nmr spectra were consistent with their being cyclobutane adducts analogous to those formed with cyclopentene. Most importantly, the four cyclobutane methine hydrogens were visible for each compound and their coupling constants could be measured. The coupling constants are shown in Table 1 for the crystalline product ("Isomer I") and its noncrystalline isomer ("Isomer II"). The expected coupling constants for the cyclobutane methine hydrogens in **17**–**20** were estimated from the dihedral angles in the most stable conformations of the indane analogues **21**–**24**. These conformations were derived from molecular modelling calculations in the same way as for the cyclopentane analogues **13** and **14**. The results are shown in Table 1; they suggest that Isomer II is the *cis-anti-cis* stereoisomer **17** because of the small values of J_{ad} and J_{bc} that are predicted for **21** and were seen in



19 X = NCOPh
23 X = CH_2
27 X = NH



20 X = NCOPh, $n = 2$
24 X = CH_2, $n = 2$
28 X = NH, $n = 2$
30 X = NCOPh, $n = 3$

the cyclopentene adduct analogues **7**, **9**, and **11**. However, for Isomer I the estimated and observed coupling constants do not allow determination of stereochemistry. This is because all the coupling constants in **22**, **23**, and **24** are predicted to be of similar magnitude to those in Isomer I.

As with the cyclopentene cycloadducts, the cyclobutane methine H_a was poorly resolved in the ^{1}H nmr spectra of the two cyclohexene adducts and the coupling constants to H_b and H_d could not be seen directly but had to be inferred from the splitting seen in the signals assigned to H_b and H_d. As before, the broadening of the signal for H_a was associated with slow rotation of the *N*-benzoyl group in these compounds. Treatment of the crystalline adduct (Isomer I) with lithium aluminum hydride yielded the *N*-benzyl derivative ("Isomer I,NBz") and the free amine ("Isomer I,NH") in which the signal ascribed to H_a was resolved. The coupling constants of the cyclobutane methine hydrogens seen in the ^{1}H nmr spectra of these two compounds are shown in Table 1 and are similar to those of the parent compound prior to reduction.

Irradiation of *N*-carboethoxyindole, **4**, with cyclohexene also gave two major products, but two minor products were also detected by gc. Examination of these four compounds by gc – mass spectroscopy indicated them to be 1:1 adducts of the indole derivative with the cyclohexene, and the ^{1}H nmr spectrum of the mixture indicated the presence of the characteristic pattern of methine signals associated with the cyclobutane adducts. Gas chromatography indicated that the products were formed in the ratio 1.1:2:142:100. The product mixture was not separated but instead was hydrolysed to the free amines and separated by chromatography. One of the two major isomers present was identical with the product of reduction of Isomer I formed from *N*-benzoylindole (i.e., Isomer I,NH). The ^{1}H nmr spectrum of

Can. J. Chem. Downloaded from www.nrcresearchpress.com by 198.100.157.202 on 09/07/12
For personal use only.

Can. J. Chem. Downloaded from www.nrcresearchpress.com by 198.100.157.202 on 09/07/12
For personal use only.

the other major isomer suggested it to be structure **25**. This was inferred from the values of the coupling constants between the cyclobutane methine hydrogens and these are listed in Table 1.The *cis-anti-cis* relationship of the hydrogens is indicated by the smaller values of J_{ad} and J_{bc}. This assignment was confirmed by lithium aluminum hydride reduction of **17** (i.e., Isomer II), which gave the compound identified as **25** (designated Isomer II,NH).

Of the two minor cyclohexene–*N*-carboethoxyindole cycloadduct isomers present in the original mixture, only one was separated following hydrolysis, the other being inseparable from the major isomers present. This compound is designated "Isomer III,NH" and the coupling constants for the cyclobutane methine hydrogens are shown in Table 1. Comparison of these with the coupling constants predicted for **22**–**24** does not allow unambiguous assignment of any one of the possible structures **26**–**28** to this compound.

To allow a stereochemical assignment of Isomers I and III and to confirm the identification of Isomer II as **17**, the lanthanide-induced shift experiment already described for **11** and **12** was performed using Isomer I,NH and Isomer II,NH (i.e., **25**) and Isomer III,NH. The relative shifts observed for the cyclobutane methine hydrogens of these three isomers are shown in Table 2 and are compared with those estimated for **25**–**28** using conformations calculated (MM2) to be the most stable. For Isomer II,NH the shift reagent perturbs H_a and H_d most highly, and H_b and H_c are much less affected; this mirrors the behaviour of the *cis-anti-cis* cyclopentene cycloadduct **11** and confirms the assignment of structure **25** to Isomer II,NH based upon coupling constant data. Similarly, comparison of the calculated shifts for the methines of **26**–**28** with those found for Isomer I,NH and Isomer III,NH strongly suggests that the former is **2** (H_b, H_c, H_d all similarly shifted) and that the latter is **28** (H_c more shifted than H_b and H_d). It can also be inferred that neither Isomer I,NH nor Isomer III,NH can be **27** since neither shows the predicted selective shift of H_d.

3. *Irradiation of* N-*benzoylindole with cycloheptene*

As with cyclohexene, the photochemical cycloaddition of *N*-benzoylindole to cycloheptene could in principle lead to four pairs of enantiomers related as diastereoisomers. When the irradiation was performed under the same conditions as for cyclopentene and cyclohexene only two products were detected by gc. These were formed in a 20:1 ratio and were shown to be 1:1 adducts between **1** and cycloheptene by gc–ms. The two adducts were separated by chromatography; their ^{1}H nmr spectra exhibited the characteristic signals associated with the cyclobutane methine protons and confirmed them to be the expected cyclobutane adducts. The minor isomer is assigned as structure **29**, which possesses *cis-anti-cis* stereochemistry; this assignment is based upon the observation of coupling constants of 2.5 and 3.0 Hz for J_{ad} and J_{bc}, respectively, which by analogy with the other *cis-anti-cis* stereoisomers in this work is indicative of a *trans* relationship between protons H_a and H_d, and H_b and H_c. Unlike the other *cis-anti-cis* *N*-benzoyl-substituted adducts **7** and **17**, the H_a proton in **29** was not broadened and the coupling constants could be measured without removal of the *N*-benzoyl activating group. This was not the case with the major isomer from the cycloheptene reaction; however, the coupling constants for the H_b methine could be discerned and were 9 and 3 Hz. The former of these can be unambiguosly assigned to the expected larger *cis* coupling between H_a and H_b so that the latter must correspond to J_{bc}. The small value of 3 Hz is strongly suggestive of a *trans* relationship between H_b and H_c and, since the *cis-anti-cis* stereochemistry in **29** has already been assigned to the minor isomer, the major isomer must therefore have the structure **30**, which possesses a *trans* cycloheptane–cyclobutane ring fusion.

4. *Irradiation of* N-*benzoylindole with* cis *and* trans *2-butene and 4-octene*

Irradiation of *N*-benzoylindole with *trans*-2-butene gave all four possible diastereoisomeric 1:1 adducts **31** (Scheme 4) in a ratio 7:21:68:4 as determined by gc and gc–ms. The adducts were separated as a mixture from the other components of the reaction; in the ^{1}H nmr spectrum of the separated mixture the cyclobutane methines of the two major isomers could be discerned, as could high-field doublets corresponding to the methyl substituents on the newly formed cyclobutane rings. The adducts were not further separated. Irradiation of *N*-benzoylindole with the *cis* isomer of 2-butene gave the same four adducts in almost the same ratio (2:21:74:2); the identity of the products of the two reactions was confirmed by gc coinjection and by comparison of the ^{1}H nmr spectra, which were superimposable. Similar results were obtained with *cis* and *trans*-4-octene. In these cases only three of the four possible diastereoisomeric adducts **32** (Scheme 4) were present in detectable quantities; these were formed in the ratio 2:49:49 from the *trans* isomer and 10:47:43 from the *cis* isomer. As with the butene adducts, the cyclobutane methines of the two major octene adducts were clearly visible in the ^{1}H nmr spectrum of the product mixture.

In the reaction with the octenes the reaction mixture was also examined for the presence of isomerized alkene. No *cis*-4-octene was formed in the irradiation of **1** with *trans*-4-octene. However, in the irradiation of **1** with *cis*-4-octene it was found that the *trans* isomer was formed as the irradiation proceeded. In these experiments the concentration of *cis* alkene was kept very high relative to that of **1** so that the *trans* isomer formed would never build up to a high enough concentration to enable it to react with the excited state of **1**; thus the formation of a similar product distribution from both alkenes cannot be attributed to faster reaction of **1** with the *trans* isomer formed during the irradiation.

The formation of *trans*-4-octene during the irradiation of **1** with *cis*-4-octene was quantified at low conversions by measurement of the amount of *trans*-octene produced relative to the amount of light absorbed. The result is shown in Fig. 3 and the gradient of this plot yields a value for the quantum yield of formation of the *trans* isomer of 0.074 ± 0.004.

For reasons that will be discussed below, the quantum yields of formation of the adducts from both the *cis*- and *trans*-octenes were also measured as a function of alkene concentration; the results are given in Table 3.

Discussion

For the reasons outlined in the Introduction, if biradicals are intermediates in the photochemical cycloaddition reactions of *N*-carbonyl-substituted indoles with alkenes, and if their lifetimes are long compared with the time required for conformational relaxation, then it would be expected that *trans*-fused adducts would be obtained from *cis* alkenes and *cis*-fused adducts would be obtained from *trans* alkenes. The conclusion of this work is that this is indeed the case. Thus with cyclohexene three of the four possible diastereoisomeric adducts are formed; these are assigned the structures **17**, **18**, and **20** and of

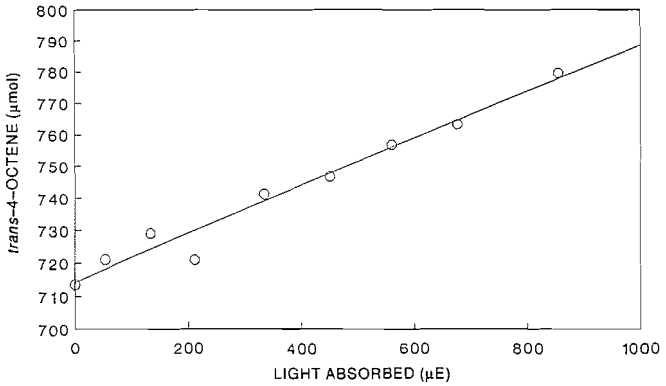


FIG. 3. Plot of amount of *trans*-octene formed during the irradiation (313 nm) of benzene solutions of *N*-benzoylindole, **1** (0.018 M), in the presence of *cis*-octene (5.31 M). The *cis*-octene used contained ca. 4% of the *trans* isomer at the start of the irradiation.

TABLE 3. Quantum yields of photochemical cycloaddition of *N*-benzoylindole, **1**, with *cis* and *trans* 4-octene[a]

[*trans*-Octene]	[*cis*-Octene]	Φ
2.035		0.013
2.379		0.017
2.608		0.018
2.990		0.020
4.060		0.027
5.048		0.033
	4.401	0.0039
	2.797	0.0043
	3.210	0.0046
	3.874	0.0048
	4.350	0.0049
	4.931	0.0052

[a]Excitation wavelength: 313 nm. Solvent: benzene.

these **20** does not preserve the stereochemistry of the alkene. Similarly, with cycloheptene the major product is assigned the structure **30**, which has the same stereochemistry as **20**, the *trans*-fused product formed with cyclohexene, and does not preserve the stereochemistry of the alkene. With the noncyclic alkenes 2-butene and 4-octene, where both the *cis* and *trans* geometrical isomers of the alkene are available, almost the same distribution of products is obtained from each geometrical isomer. This is consistent with the intermediacy of the biradicals shown in Scheme 4 in which all memory of the alkene stereochemistry can be lost. It should be noted that each of the regioisomeric biradicals shown in Scheme 4 has two new chiral centres; it is not necessarily the case that each geometrical isomer of the alkene would produce the same proportions of the regioisomeric and diastereoisomeric biradicals and it is, in fact, quite surprising that the final distribution of the stereoisomeric cyclobutane adducts from each alkene geometrical isomer is so similar.

In our earlier work on the mechanism of photochemical cycloaddition between *N*-benzoylindole and cyclopentene (4), we examined the quantum yield of adduct formation as a function of alkene concentration and were able to show that the quantum yield varied with alkene concentration as predicted by the relationship shown in eq. [1]. This equation was derived assuming the validity of the mechanism shown in Scheme 3.

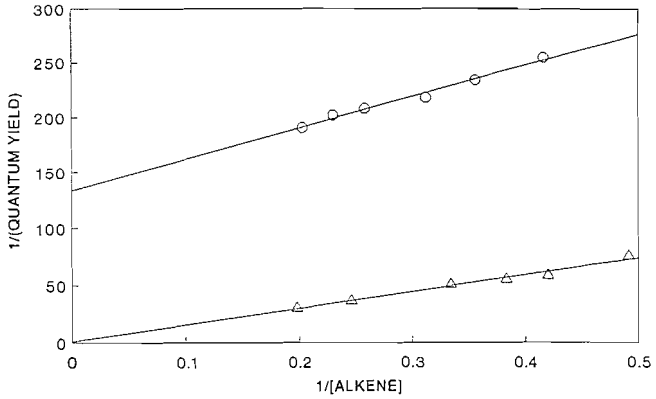


FIG. 4. Plot of reciprocal of quantum yield of formation of photocycloaddition product against reciprocal of alkene concentration for the irradiation (313 nm) of benzene solutions of *N*-benzoylindole, **1** (0.018 M), in the presence of either *cis*- or *trans*-4-octene (5.31 M). Circles: *cis*-4-octene; triangles: *trans*-4-octene.

$$[1] \quad \frac{1}{\Phi} = \frac{1}{\Phi_{isc}}\left\{\frac{k_c}{k_r + k_c}\right\}^{-1}\left\{1 + \frac{k_d}{k_a[A]}\right\}$$

In eq. [1], Φ is the quantum yield of cycloadduct formation, Φ_{isc} is the quantum yield of intersystem crossing, k_d is the rate constant for decay of the triplet excited state of **1**, [A] is alkene concentration, and k_a is the rate constant for reaction of the triplet excited state of **1** with alkene. The rate constants k_c and k_r are those for cyclization of the intermediate biradical to product and reversion to starting materials, respectively. Thus the fraction $k_c/(k_c + k_r)$ is the fraction of the biradicals that proceed to the cycloadducts rather than reverting to the ground state starting materials. This treatment is an approximation since it assumes a single biradical intermediate is involved; because stereoisomeric and regioisomeric biradicals may well be intermediates, the fraction $k_c/(k_c + k_r)$ and k_a are composites for all the intermediate biradicals. The plot of $1/\Phi$ versus $1/[A]$ can be used to yield values of $k_c/(k_c + k_r)$ and k_a if Φ_{isc} and k_d are known. For *N*-benzoylindole, **1**, the values of Φ_{isc} and k_d have been independently determined as 0.39 ± 0.01 and $(3.6 \pm 0.4) \times 10^7\ s^{-1}$, respectively, using the triplet counting procedure; using these values, the quantities $k_c/(k_c + k_r)$ and k_a have been estimated as 0.16 and $(4.0 \pm 0.8) \times 10^6\ M^{-1}\ s^{-1}$, respectively, for the reaction of **1** with cyclopentene (4). This treatment was applied to the photoaddition of both *cis*- and *trans*-4-octene to **1**, and the data shown in Table 3 plotted according to eq. [1] are shown in Fig. 4.

For the addition of *cis*-octene to **1**, the intercept in Fig. 4 yields a value of $k_c/k_c + k_r$ of 0.019 ± 0.001, indicating that only 2% of the intermediate biradicals proceed to cyclobutane adducts and that the remainder revert to ground state **1** and alkene. In addition, the intercept indicates that at very high alkene concentration (i.e., when all of the triplet excited states of **1** are intercepted by alkene) the maximum value of Φ is 0.0075 ± 0.0002. Assuming a value of $3.6 \times 10^7\ s^{-1}$ for k_d, combination of the intercept of the plot for *cis*-octene with the gradient yields a value of k_a, the rate constant for reaction of the triplet excited state of **1** with *cis*-octene, of $(1.7 \pm 0.3) \times 10^7\ M^{-1}\ s^{-1}$, which is slightly faster than that observed for the reaction of **1** with cyclopentene.

The formation of *trans*-4-octene during the irradiation of **1** with *cis*-4-octene is an example of Schenk isomerization, i.e., a photochemical isomerization in which the isomerizing species

Can. J. Chem. Downloaded from www.nrcresearchpress.com by 198.100.157.202 on 09/07/12
For personal use only.

Can. J. Chem. Downloaded from www.nrcresearchpress.com by 198.100.157.202 on 09/07/12
For personal use only.

itself never attains the excited state. The isomerization of *cis*-octene to the *trans* isomer cannot be a result of energy transfer from the triplet excited state of **1** to the alkene since the triplet energy of the latter is higher than that of the indole derivative (4). The quantum yield of Schenk isomerization for *cis*-octene was determined to be 0.074 ± 0.004; the concentration of the alkene in this experiment was 5.31 M. At this concentration >70% of the triplet excited states of **1** are intercepted by the alkene (assuming $k_a = 1.7 \times 10^7$ and $k_d = 3.6 \times 10^7$); since $\Phi_{isc} = 0.39$, the maximum quantum yield of Schenk isomerization possible would be 0.27 if the 98% of the biradicals that do not cyclize to products revert to give only *cis*-octene. The value of 0.074 measured here would appear to indicate that the reverting biradicals prefer to give back *cis*-octene rather than the *trans* isomer. This assumes that no other energy-wasting step leading back to starting materials occurs between interception of the triplet excited state by alkene and the formation of the biradical intermediates; such an energy-wasting step could be exciplex formation and decay.

For the addition of *trans*-octene to **1**, the plot in Fig. 4 yields an intercept of 0.9 ± 3. This is indistinguishable from zero and its reciprocal cannot be used to obtain a reliable value of Φ extrapolated to infinite alkene concentration. However, it does allow limits for this value of Φ to be estimated; the *smallest* value possible, corresponding to the largest value of the intercept, is 0.26, while the largest is 0.39, the value determined for Φ_{isc}. This means that between 67 and 100% of the intermediate biradicals formed from the triplet excited state of **1** and *trans*-octene proceed to the product. Using these extreme values of the intercept, the gradient of the plot in Fig. 4 can be used to estimate limits on the values possible for k_a, the rate constant for reaction between triplet excited **1** and *trans*-octene. The values are 1×10^6 and $6 \times 10^5\ M^{-1}\ s^{-1}$, which are substantially slower than those determined for the photoaddition of **1** to cyclopentene and *cis*-octene.

Conclusions

The products formed from the photochemical addition of alkenes to *N*-benzoylindole and *N*-carboethoxyindole are consistent with the intermediacy of triplet 1,4-biradical intermediates. Quantum yield data suggest *cis*-octene reacts with the triplet excited state of *N*-benzoylindole faster than does the *trans* isomer, but that most of the biradicals revert to starting materials in the case of the former, and proceed to product for the latter.

Experimental

All nmr spectra were recorded in $CDCl_3$ solvent; ^1H nmr spectra were recorded at 200 MHz. The gc–ms analyses were performed using a Finnigan-MAT 8230 mass spectrometer coupled to a gas chromatograph equipped with an SE 54 capillary column.

General irradiation procedures

All preparative irradiations (gram scale) were carried out using a 450-W Hanovia medium pressure mercury lamp housed in a water-cooled Pyrex jacket, which was immersed in the solution to be irradiated. Benzene previously purged with nitrogen was used as the solvent and the solutions of **1** or **4** and the alkenes were briefly purged with nitrogen prior to irradiation. The solutions were stirred under an atmosphere of nitrogen during irradiations. Smaller scale preparative reactions (milligram scale) were performed in benzene solvent in Pyrex tubes sealed under nitrogen; the tubes were placed alongside a 400-W medium pressure mercury lamp housed in a water-cooled Pyrex jacket.

Preparation of N*-benzoylindole,* **1**

To a stirred suspension of indole (5 g, 0.043 mol), powdered NaOH (5 g, 0.125 mol), and $(Bu)_4NBr$ (0.2 g) in dry methylene chloride (150 mL) was added a solution of benzoyl chloride (9.25 g, 0.88 mol) in methylene chloride (25 mL) over 15 min. During addition, the reaction was cooled with ice. After 1.5 h stirring, H_2O (50 mL) was added and the reaction mixture was extracted with CH_2Cl_2. The extracts were dried (K_2CO_3) and solvent removed to give a red oil, which was crystallized from ether/hexanes to yield 8.6 g (91%) of white crystals, mp 63–64°C (lit. (17) mp 57–58°C).

Preparation of N*-carboethoxyindole,* **4**

Indole (12 g, 0.1025 mol), powdered NaOH (10 g), and $(Bu)_4NBr$ (0.5 g) in CH_2Cl_2 (150 mL) were stirred together and ethyl chloroformate (12.5 g, 0.115 mol) was added dropwise with ice cooling. After stirring for 1.5 h the reaction mixture was worked up as for **1** to give a red oil, which was distilled to yield 13.7 g (72%) of a clear pale yellow liquid, bp 133°C at 3 Torr (1 Torr = 133.3 Pa) (lit. (17) bp 142–144°C at 16 Torr); ^1H nmr δ: 8.20 (m, 1H), 7.6–7.0 (m, 4H), 6.55 (d, 1H), 4.43 (q, 2H), 1.38 (t, 3H).

Irradiation of N*-benzoylindole with cyclopentene*

As described in the general procedure, a solution of *N*-benzoylindole (1.626 g, 7.36 mmol) and cyclopentene (7.8 g, 111.5 mmol) in 300 mL of benzene was irradiated for 89 h. Removal of the benzene by distillation under reduced pressure afforded 2.13 g of a brown oil. The oil was purified by column chromatography (silica gel, 30% ether/70% hexanes) to yield unreacted *N*-benzoylindole (0.53 g) and a yellow oil (0.49 g) in which crystals formed. The white crystals were washed with hexanes to yield 0.3 g of *cis-anti-cis* photoadduct **7**, mp 123–126°C; ^1H nmr δ: 8.30 (br s, 1H), 7.44 (m, 5H), 7.4–7.0 (m, 3H), 3.94 (br s, 1H), 3.32 (dd, J = 7.5, 2.9 Hz, 1H), 2.84 (m, 1H), 2.66 (m, 1H), 1.80 (m, 2H), 1.62 (m, 2H), 1.31 (m, 2H); ^{13}C nmr δ: 25.4, 30.9, 32.4 (CH_2), 45.1, 46.2, 47.9, 63.7 (CH), 110.5, 118.3, 124.7, 126.4, 126.8, 127.6, 128.3, 128.4, 130.0, 137.5 (aromatic C), 193.8 (quaternary C=O); *m/e* (%) 289(4.1), 221(46), 105(100), 77(20); M^+ calcd.: 289.14666; found: 289.14654.

The remaining mother liquor was evaporated to yield 0.18 g of yellow oil, determined to be *cis-syn-cis* photoadduct **8**; ^1H nmr δ: 8.30 (br s, 1H), 7.44 (m, 5H), 7.4–7.0 (m, 3H), 4.70 (br s, 1H), 4.05 (br dd, J = 7.5, 8.0 Hz, 1H), 3.08 (br m, 2H), 1.80 (m, 2H), 1.62 (m, 2H), 1.31 (m, 2H); ^{13}C nmr δ: 27.1, 27.9, 28.9 (CH_2), 42.2, 43.4, 45.5, 61.7 (CH), 110.5, 118.3, 125.7, 126.4, 126.8, 127.3, 128.3, 128.4, 130.5, 137.5 (aromatic C), 195.0 (quaternary C=O); M^+ calcd.: 289.14666; found: 289.14656.

Reduction of N*-benzoylindole/cyclopentene adducts* **7** *and* **8**

A sample (570 mg, 1.97 mmol) of the crude products obtained from irradiation of *N*-benzoylindole with cyclopentene, which had been partially purified to remove unreacted *N*-benzoylindole, was dissolved in dry ether (25 mL) and reduced with excess lithium aluminium hydride (121 mg, 318 mmol). After 1 h the reaction was quenched by slow addition of water (50 mL) and the reaction mixture was extracted with ether. The ether extracts were washed with water, dried (K_2CO_3), and solvent removed to yield 534 mg of a green oil. Thin-layer chromatography (silica gel; 30% ether/70% hexanes) revealed the product to be a mixture of three compounds with R_f 0.49, 0.63, and 0.70. The green oil was chromatographed on a column of silica gel (15% ether/85% hexanes) to yield three fractions. The last fraction after removal of eluent yielded 99 mg of light pink crystals of secondary amine **11**, which was recrystallized from $MeOH/H_2O$, mp 95°C; ^1H nmr δ: 7.00 (m, 2H), 6.68 (m, 2H), 3.94 (s, 1H), 3.72 (dd, J = 7.5, 2.5 Hz, 1H), 3.33 (dd, J = 7.6, 2.5 Hz, 1H), 2.68 (m, 2H), 1.78 (m, 4H), 1.48 (m, 2H); ^{13}C nmr δ: 25.6, 31.8, 32.6 (CH_2), 47.2, 47.3, 49.1, 60.8 (CH), 109.9, 118.8, 124.4, 127.3 (aromatic CH), 134.1, 151.5 (quaternary C); *m/e* (%): 185(19), 117(100), 90(33); M^+ calcd.: 185.120449; found: 185.12049.

The second fraction yielded a red oil (50 mg), which crystallized from $MeOH/H_2O$ to afford white crystals of secondary amine **12**, mp 91°C; ^1H nmr δ: 6.93 (m, 2H), 6.62 (m, 2H), 4.81 (s, 1H), 4.42 (dd, J = 9.6, 9.0 Hz, 1H), 4.14 (dd, J = 9.6, 9.2 Hz, 1H), 3.08 (m, 2H), 1.9–1.1 (m, 6H); ^{13}C nmr δ: 26.6, 28.4, 28.8 (CH_2), 42.6, 45.0, 56.4 (CH), 109.1, 117.8, 126.0, 127.2 (aromatic CH), 130.0, 154.0 (quaternary C); *m/e* (%): 185(15), 117(100), 90(30); M^+ calcd.: 185.120449; found: 185.120992.

Can. J. Chem. Downloaded from www.nrcresearchpress.com by 198.100.157.202 on 09/07/12
For personal use only.

The third fraction afforded 254 mg of a brown oil; a sample (60 mg) was chromatographed on preparative tlc plates (silica gel; 100% hexanes) to yield two bands. The first band gave 21 mg of a solid, which was recrystallized from ether/hexanes to afford white crystals of *cis-syn-cis* benzyl adducts **10**, mp 58.5°C; ^{1}H nmr δ: 7.22 (m, 5H), 6.91 (m, 2H), 6.55 (m, 1H), 6.32 (d, J = 4 Hz, 1H), 4.31 (AB, q, J = 16 Hz, 2H), 4.30 (dd, J = 9.4, 9.0 Hz, 1H), 4.11 (dd, J = 9.4, 9.0 Hz, 1H), 3.01 (m, 2H), 1.71 (m, 2H), 1.40 (m, 4H); ^{13}C nmr δ: 27.8, 28.4, 28.7 (CH_2), 42.2, 43.4, 45.5, 62.0 (CH), 51.3 (benzyl CH_2), 105.4, 115.7, 125.8, 116.7, 127.3, 127.4, 128.2 (aromatic CH), 129.5, 138.6, 154.7 (quaternary C); *m/e* (%): 275(3.4), 207(93), 91(100); M^+ calcd.: 275.167399; found: 275.167344.

The second band yielded 14.4 mg of crystals; these were recrystallized from ether/MeOH to afford *cis-anti-cis* benzyl adduct **9**, mp 55°C; ^{1}H nmr δ: 7.17 (m, 5H), 7.00 (m, 2H), 6.58 (m, 5H), 6.36 (d, J = 4 Hz, 1H), 4.33 (AB q, J = 15 Hz, 2H), 3.62 (dd, J = 7.6, 2.5 Hz, 1H), 3.29 (dd, J = 7.6, 2.7 Hz, 1H), 2.80 (d of t, J = 7.0, 2.7 Hz, 1H), 2.68 (d of t, J = 7.0, 2.5 Hz, 1H), 1.9–1.2 (m, 6H); ^{13}C nmr δ: 25.4, 31.5, 32.6 (CH_2), 45.2, 45.3, 46.3, 65.6 (CH), 49.8 (benzyl CH_2), 105.5, 116.5, 124.1, 126.8, 127.44, 127.46, 128.22 (aromatic CH), 133.8, 138.6, 152.3 (quaternary C); *m/e* (%): 275(9.2), 207(100), 91(96); M^+ calcd.: 275.167399; found: 275.167344.

Irradiation of N-*carboethoxyindole*, **4**, with cyclopentene

N-Carboethoxyindole (2.87 g, 15.2 mmol) in 300 mL of benzene containing cyclopentene (16.25 g, 239 mmol) was irradiated for 65 h. The benzene was removed to yield 3.58 g of brown oil. The gc analysis of the oil indicated ca. 30% conversion and the formation of three new products in a ratio of 1:1.24:6.34; gc–ms revealed parent ions for the three products to be *m/e* 189, 257, and 257 respectively. The first of these is isomeric with **4** and the latter two correspond to the adducts **15** and **16** produced from **4** with cyclopentene. A portion (300 mg) of the crude irradiation product was chromatographed on preparative tlc plates (silica gel; 50% ether/50% hexanes) and yielded three bands, which were analyzed by gc–ms. The first band (166 mg) contained a mixture of *N*-carboethoxyindole and the two adducts **15** and **16**, both of which had *m/e* 257(3.0%), 189(100%), 73(32%). The second band was identified as indole by gc–ms and confirmed by gc coinjection. The third band (7.5 mg) was identified as 3-carboethoxyindole, mp 122–124°C (lit. (18) mp 124°C); ^{1}H nmr δ: 8.68 (br s, N-H), 8.18 (m, 1H), 7.93 (d, J = 3 Hz, 1H), 7.30 (m, 3H), 4.40 (q, J = 7 Hz, 2H), 1.40 (t, J = 7 Hz, 3H).

Hydrolysis and decarboxylation of photochemical adducts **15** *and* **16**

A sample (1.66 g) of the crude product obtained from irradiation of *N*-carboethoxyindole with cyclopentene was hydrolyzed by refluxing for 3 h in 25 mL of MeOH/H_2O (2:1) saturated with KOH. The reaction mixture was cooled and acidified with concentrated HCl, and then refluxed for 20 min. The reaction mixture was cooled again and washed with ether. The ether washings were combined and extracted with 10% HCl. The aqueous acid extracts were combined and washed with ether and then CH_2Cl_2 to remove any remaining indole. They were then made basic with saturated NaOH and extracted with CH_2Cl_2. The organic extracts were washed with water, dried (Na_2SO_4), and evaporated to afford 212 mg of white solid. The gc–ms showed two peaks with *m/e* 185 in a ratio of 1:10. Isolation by column chromatography yielded 18 mg of indoline **12** and 190 mg of indoline **11**.

Irradiation of N-*benzoylindole with cyclohexene*

N-Benzoylindole (2.54 g, 0.0115 mol) was irradiated in 300 mL of benzene along with cyclohexene (8.5 g, 0.104 mol) for 48 h. The solution was filtered and solvent removed to yield 3.78 g of brown oil, which was purified on a silica gel column to give unreacted *N*-benzoylindole (1.28 g) and cycloadducts (0.95 g) that appeared as crystals in a yellow oil. Crystallization from CH_2Cl_2/ethyl acetate afforded 0.3 g of white crystals identified as *cis-syn-cis* adduct **18**, mp 170–171°C; ^{1}H nmr δ: 8.28 (br d, J = 4 Hz, 1H), 7.44 (m, 5H), 7.20 (m, 3H), 4.72 (br s, 1H), 4.00 (dd, J = 8.5, 9.0 Hz, 1H), 2.78 (br s, 2H), 1.9–0.9 (m, 8H); ^{13}C nmr δ: 20.9, 21.3, 22.2, 22.4, (CH_2), 32.7, 38.8, 45.3, 61.0 (CH), 118.4, 124.2, 126.1, 127.1, 127.9, 128.3, 130.2 (aromatic CH), 134.6, 137.2, 146.6, 169.0, 205.7 (quaternary C); *m/e* (%): 303(0.55), 221(26), 105(100); M^+ calcd.: 303.162314; found: 303.162570.

The mother liquid (0.7 g) remained as an oil and was identified as *cis-anti-cis* adduct **17**; ^{1}H nmr δ: 8.28 (br d, J = 4 Hz, 1H), 7.44 (m, 5H), 7.20 (m, 3H), 4.63 (br s, 1H), 3.56 (dd, J = 7.7, 2.5 Hz, 1H), 2.60 (m, 1H), 2.11 (m, 1H), 2.00 (m, 2H), 1.9–1.0 (m, 6H); ^{13}C nmr δ: 21.2, 21.6, 22.0, 22.3 (CH_2), 37.6, 39.8, 46.7, 63.7 (CH), 117.8, 126.0, 127.0, 129.3, 139.1, 134.0, 135.4, 136.3, 142.8, 144.7 (aromatic C), 197.2 (quaternary C=O).

Reduction of cis-syn-cis *adduct* **18**

Adduct **18** (106 mg, 0.37 mmol) was treated with lithium aluminium hydride (50 mg) in 15 mL of dry ether for 3 h. After quenching with water the reaction was extracted with ether; the ether extracts were washed with water, dried (K_2CO_3), and solvent removed to yield 81.5 mg of yellow oil, which tlc showed to contain two components that were separated as oils by preparative tlc.

The first of these (40.6 mg) was identified as Isomer I,NBz (see text); ^{1}H nmr δ: 7.61 (m, 1H), 7.15 (m, 5H), 7.00 (m, 1H), 6.59 (m, 1H), 6.38 (d, J = 4 Hz, 1H), 4.38 (AB q, J = 20 Hz, 2H), 4.36 (dd, J = 8.5, 9.2 Hz, 1H), 4.06 (dd, J = 8.5, 9.0 Hz, 1H), 2.78 (m, 1H), 2.66 (m, 1H), 1.50 (m, 4H), 1.24 (m, 4H); ^{13}C nmr δ: 21.1, 21.3, 21.9, 22.6 (CH_2), 34.6, 39.3, 45.4, 63.4 (CH), 51.2 (benzyl CH_2), 105.4, 116.3, 125.6, 126.9, 127.6, 127.2, 128.4, 128.8, 131.2, 138.8 (aromatic C); *m/e* (%): 289(3.5), 207(100), 91(75); M^+ calcd.: 289.183049; found: 289.183068.

The second component (9.2 mg) was identified as secondary amine **26**; ^{1}H nmr δ: 8.14 (br s, 1H), 7.20–7.00 (m, 3H), 4.21 (br s, 1H), 4.12 (s, N-H), 3.80 (ddd, J = 8.7, 9.0, 1.0 Hz, 1H), 2.78 (m, 2H), 2.2–1.6 (m, 8H); ^{13}C nmr δ: 25.2, 26.4, 32.0, 32.7 (CH_2), 34.3, 39.7, 44.6, 52.4 (CH), 111.3, 119.4, 119.7, 121.32, 121.6, 122.2 (aromatic CH); *m/e* (%): 199(2), 117(100), 90(30); M^+ calcd.: 199.136099; found: 199.136103.

Irradiation of N-*carboethoxyindole with cyclohexene*

N-Carboethoxyindole (2.2 g, 0.01 mol) was irradiated in 300 mL of benzene containing cyclohexene (15 g, 0.183 mol) for 48 h. Removal of the benzene afforded 3.55 g of brown oil. The gc analysis revealed five new products in a ratio of 1:1.1:2:142:100. The most minor peak showed *m/e* 189 by gc–ms, and gc coinjection with an authentic sample confirmed this product to be 3-carboethoxyindole. The other four peaks all possessed parent ions of *m/e* 271, indicative of 1:1 photoadducts between **4** and cyclohexene. Characterization of these compounds was not carried any further.

Hydrolysis and decarboxylation of photoadducts from irradiation of N-*carboethoxyindole with cyclohexene*

A sample (6 g) of the crude mixture of products from irradiation of *N*-carboethoxyindole with cyclohexene was hydrolysed by refluxing for 3 h in 75 mL of MeOH/H_2O (2:1) saturated with KOH. The reaction mixture was then acidified (conc. HCl) and refluxed further for 20 min. After cooling, the reaction mixture was washed sequentially with ether and CH_2Cl_2 and made basic by addition of aqueous NaOH. The basified solution was then extracted with CH_2Cl_2. The organic extracts were washed with H_2O, dried (Na_2SO_4), and the solvent removed to yield 4.14 g of brown oil. Gas chromatography revealed three peaks with ratios of 1:17:14. The major portion of the oil (4 g) was then chromatographed (silica gel column; 10% ether/90% hexanes) to yield three fractions. The first fraction (67 mg) afforded yellow crystals identified as secondary amine **28**, mp 69–72°C (ether/hexanes); ^{1}H nmr δ: 6.97 (m, 2H), 6.63 (m, 2H), 4.58 (dd, J = 6, 4 Hz, 1H), 3.98 (br s, N-H), 3.66 (dd, J = 8, 6 Hz, 1H), 2.20–1.90 (m, 2H), 1.90–0.80 (m, 8H); *m/e* (%): 199(7.5), 156(9), 117(100); M^+ calcd.: 199.13601; found: 199.13562.

The second fraction (0.93 g) was isolated as an oil and identified as secondary amine **26**; ^{1}H nmr δ: 7.0 (m, 2H), 6.63 (m, 2H), 4.42 (dd, J = 8, 8 Hz, 1H), 4.04 (dd, J = 8, 8 Hz, 1H), 3.88 (br s, N-H), 2.80 (m, 1H), 2.60 (m, 1H), 2.3–0.8 (m, 8H); *m/e* (%): 199(31), 156(51), 117(100); M^+ calcd.: 199.13601; found: 199.13582.

The third fraction (0.64 g) was isolated as a brown solid. Recrystallization from ether/hexanes afforded crystals of secondary amine **25**, mp 73–75°C; ^{1}H nmr δ: 7.1 (m, 2H), 6.74 (m, 2H), 4.18 (dd, J = 8, 4 Hz,

Can. J. Chem. Downloaded from www.nrcresearchpress.com by 198.100.157.202 on 09/07/12
For personal use only.

1H), 3.65 (br s, N-H), 3.60 (dd, J = 8, 2 Hz, 1H), 2.8–2.25 (m, 2H), 2.25–1.00 (m, 8H); m/e (%): 199(25), 156(48), 117(100); M^+ calcd.: 199.13601; found: 199.13562.

Irradiation of N-*benzoylindole with cycloheptene*

N-Benzoylindole (1.94 g, 8.79 mmol) was irradiated in 300 mL of benzene with cycloheptene (8.7 g, 90.5 mmol) for 22 h. Removal of benzene afforded 2.5 g of a brown oil. The gc analysis showed approximately 40% conversion of the *N*-benzoylindole to three products in a ratio of 1:21:0.05. The oil was hydrolysed to remove unconverted **1** by stirring at room temperature for 3 h in 125 mL of MeOH/H_2O (2:2) saturated with NaOH. The mixture was extracted with ether; drying and removal of solvent yielded 1.1 g of a brown oil. The oil was steam distilled to remove indole and the aqueous stillpot extracted with ether to give 0.7 g of yellow oil. Thin-layer chromatography showed two components, R_f 0.15 and 0.10 (silica gel; 30% ether/70% hexanes). A sample of the oil (122 mg) was chromatographed by preparative tlc (silica gel; 40% ether/60% hexanes) and yielded two bands. The first band (5 mg) afforded an oily film and was assigned structure **29**; ^{1}H nmr δ: 8.25 (m, 1H), 7.80–7.45 (m, 5H), 7.31 (m, 2H), 7.15 (d, J = 4 Hz, 1H), 4.13 (dd, J = 8, 2.5 Hz, 1H), 3.59 (dd, J = 8, 3 Hz, 1H), 2.8–2.35 (m, 2H), 2.2–1.2 (m, 10H); m/e (%): 317(4), 221(100), 105(14); M^+ calcd.: 317.177984; found: 317.178169. The second band (95 mg) yielded an oil assigned structure **30**; ^{1}H nmr δ: 8.28 (br s, 1H), 7.44 (m, 5H), 7.30–6.90 (m, 4H), 4.43 (br s, 1H), 3.46 (dd, J = 9, 3 Hz, 1H), 2.54 (br m, 1H), 2.42 (m, 1H), 2.0–1.0 (m, 10H); m/e (%): 317(0.25), 221(34), 117(100); M^+ calcd.: 317.177984; found: 317.1778534.

Irradiation of N-*benzoylindole with* cis-*2-butene*

A solution of *cis*-2-butene in benzene was prepared by condensing *cis*-2-butene (5 mL) into benzene (5 mL) that had previously been purged with nitrogen. *N*-Benzoylindole (192 mg, 0.87 mmol) was added to the solution, which was then irradiated for 60 h. Gas chromatography revealed four products in the ratio 7:21:68:4. The gc–ms confirmed that the products were 1:1 cycloadducts of **1** with butene (first gc product, m/e (%): 277(1.7), 221(57), 105(100); second gc product, m/e: 277(2.0), 221(59), 105(100), 77(25); third gc product, m/e: 277(1.7), 221(60), 105(100), 77(25); fourth gc product, m/e: 277(2.0), 221(60), 105(100), 77(25)). A sample of the reaction mixture was partially purified by chromatography to give a mixture of the four adducts; in the ^{1}H nmr spectrum of the mixture of adducts a broad singlet at 4.3 ppm was assigned to superimposed signals corresponding to H_a in all the stereoisomers. Similarly, multiplets in the range 2.7–1.9 ppm were assigned to H_c and H_d of all the isomers present. The signal assigned to H_b of the most prevalent isomer was seen as a double doublet at 3.97 ppm, J = 3 and 8 Hz. That corresponding to H_b of the second most prevalent isomer was seen at 3.48 ppm as a triplet, J = 8 Hz. The methyl substituents of both major isomers were seen as overlapping doublets at 1.16 and 0.92 ppm, J = 6 Hz.

Irradiation of N-*benzoylindole with trans-2-butene*

A sample of *trans*-2-butene was prepared by dropwise addition of 2-butanol (100 mL) to 9 M H_2SO_4 (80 mL). The mixture was heated to 90°C (oil bath temperature) and a portion (5 mL) of the *trans*-2-butene, which distilled out, was condensed into benzene (5 mL) that had previously been purged with nitrogen. *N*-Benzoylindole (199 mg, 0.9 mol) was added and the mixture was irradiated for 44 h. Gas chromatography revealed formation of four products in the ratio 2.1:21:74:1.1. The four products were confirmed by gc coinjection to be the same as the products obtained by irradiation of *N*-benzoylindole with *cis*-2-butene (first gc product, m/e (%): 277(1.7), 221(57), 105(100), 77(23); second product, m/e: 277(3), 221(58), 105(100), 77(23); third product, m/e: 277(3), 221(58), 105(100), 77(24); fourth product m/e: 277(3), 221(60), 105(100), 77(24)). The ^{1}H nmr spectrum of the mixture of adducts following their separation by chromatography was identical with that of the mixture of adducts obtained from the irradiation of **1** with the *cis*-alkene.

Preparation of cis-*4-octene*

A sample of 4-octyne (12.2 g, 0.11 mol) was hydrogenated under 1 atm (101.3 kPa) of hydrogen using Lindlar's catalyst (0.8 g) and quinoline (10 mL) in pentane (300 mL) until gc analysis indicated 100% conversion of the octyne. The reaction mixture was filtered, washed with 10% HCl and H_2O, and dried over anhydrous Na_2SO_4. The solvent was removed and the product purified by fractional distillation, which yielded 8.1 g (67%) of *cis*-4-octene (94% pure by ^{1}H nmr analysis); bp 122°C; ^{1}H nmr δ: 5.36 (m, 2H), 2.02 (q, J = 4 Hz, 4H), 1.38 (m, 4H), 0.92 (t, J = 4 Hz, 6H); ^{13}C nmr δ: 129.9, 29.5, 23.1, 13.9.

Irradiation of N-*benzoylindole with* trans-*4-octene*

A solution of *N*-benzoylindole (1 g, 4.5 mmol) in benzene (20 mL) containing *trans*-4-octene (9 g, 80 mmol) was irradiated for 311 h. Removal of benzene yielded 1.18 g of brown oil; gc analysis indicated the presence of three products in the ratio 1:32:32 and 36% conversion of **1**. The oil was chromatographed (5% ether/95% hexanes) to remove *N*-benzoylindole and give 394 mg of yellow oil. The gc–ms of the oil showed three products all with parent ions of m/e 333 indicative of 1:1 photoadducts. First gc product, m/e (%): 333(0.81), 221(78), 105(100); second product, m/e: 333(1.7), 221(80), 105(100); third product, m/e: 333(1.1), 221(82), 105(100). In the ^{1}H nmr spectrum of the mixture a broad singlet at 4.42 ppm was assigned to H_a of both major isomers. Signals between 2.6 and 1.9 ppm were assigned to H_c and H_d of both major isomers also. A signal at 4.03 ppm (triplet, J = 8 Hz) was assigned to H_b of one of the major isomers, and a signal at 3.54 ppm (double doublet, J = 4 and 8 Hz) was assigned to H_b of the second major isomer.

Irradiation of N-*benzoylindole with* cis-*4-octene*

N-Benzoylindole (2.0 g, 0.01 mol) was irradiated in benzene (60 mL) with *cis*-4-octene (11.0 g, 0.09 mol) for 400 h. Removal of benzene afforded 2.14 g of brown oil, which gave three products (7% conversion) by gc analysis in a ratio of 1:5:5 with retention times equivalent to that of the *N*-benzoylindole/*trans*-4-octene irradiation products (confirmed by coinjection). The oil was chromatographed (5% ether/95% hexanes) to yield unreacted *N*-benzoylindole and 0.51 g of yellow oil. The gc–ms of the oil showed three products all with parent ions of m/e 333 indicative of 1:1 photoadducts. First gc product, m/e (%): 333(1.1), 221(78), 105(100); second product, m/e: 333(1.5), 221(75), 105(100); third product, m/e: 333(1.5), 221(79), 105(100). The ^{1}H nmr spectrum of the mixture was identical with that of the products of irradiation of **1** with *trans*-octene.

Schenk isomerization studies

Solutions (5.00 mL) of *N*-benzoylindole (19.6 mg, 0.0886 mmol) in benzene containing either *cis*-4-octene (2.8 g, 0.026 mol) or *trans*-4-octene (2.8 g, 0.026 mol) were prepared and samples (3.00 mL) were irradiated with 313 ± 2 nm light from a 100-W high-pressure mercury lamp. The light intensity was determined by actinometry with azoxybenzene. The amount of isomerized alkene formed was determined by gc with methylcyclohexane as a calibrated internal standard.

Quantum yield of cycloadduct formation in the photoaddition of cis- *and* trans-*4-octene with* ***1***

Solutions (5.00 mL) of *N*-benzoylindole (20.1 mg, 0.0911 mmol) in benzene containing either *cis*-4-octene (2.8 g, 0.026 mol) or *trans*-4-octene (2.8 g, 0.026 mol) were prepared and samples (3.00 mL) were irradiated with 313 ± 2 nm light from a 100-W high-pressure mercury lamp. The light intensity was determined by actinometry with azoxybenzene. The amount of adduct formed was determined by gc with tetracosane as a calibrated internal standard.

Acknowledgements

Financial support from the Natural Sciences and Engineering Research Council of Canada made this work possible. We also wish to express our gratitude to Mr. Doug Hairsine for gc–ms technical support.

1. D. R. JULIAN and R. FOSTER. J. Chem. Soc. Commun. 311 (1973).
2. M. IKEDA, K. OHNO, S. MOHRI, M. TAKAHASHI, and Y. TAMURA. J. Chem. Soc. Perkin Trans. 405 (1984).

3. D. L. OLDROYD and A. C. WEEDON. J. Photochem. Photobiol. **57**, 207 (1991).
4. B. W. DISANAYAKA and A. C. WEEDON. Can. J. Chem. **68**, 1685 (1990).
5. B. W. DISANAYAKA and A. C. WEEDON. Can. J. Chem. **65**, 245 (1987).
6. H. W. ZIFFER, A. BAX, R. J. HIGHET, and B. GREEN. J. Org. Chem. **53**, 895 (1988).
7. M. L. WINZENBURG, E. K. FIELDS, D. P. SINCLAIR, G. J. RAY, M. E. WRIGHT, and H. K. HALL. J. Org. Chem. **53**, 2624 (1988).
8. J. DEKKER, F. J. C. MARTINS, A. M. VILJOEN, and P. L. WESSELS. S. African J. Chem. **34**, 76 (1981).
9. F. J. C. MARTINS, A. M. VILJOEN, and P. L. WESSELS. Tetrahedron, **43**, 225 (1987).
10. N. S. BACCA, L. F. JOHNSTON, L. DUC, and G. W. GRIFFIN. Spectrosc. Lett. **5**, 47 (1972).
11. A. GAMBA and R. MODELLI. Tetrahedron Lett. 2133 (1971).
12. I. FLEMING and D. H. WILLIAMS. Tetrahedron, **23**, 2747 (1967).
13. R. HITTICH. Org. Magn. Reson. **18**, 214 (1982).
14. F. D. LEWIS and S. V. BARANCYK. J. Am. Chem. Soc. **111**, 8653 (1989).
15. E. B. WHIPPLE and G. R. EVANEGA. Org. Magn. Reson. **2**, 1 1970).
16. F. D. LEWIS and R. H. HIRSCH. Tetrahedron Lett. 4947 (1973).
17. V. O. ILLI. Synthesis, 387 (1979).
18. M. SOMEI and M. NATSUME. Tetrahedron Lett. 2451 (1973).

Can. J. Chem. Downloaded from www.nrcresearchpress.com by 198.100.157.202 on 09/07/12
For personal use only.

Azo pigments and their intermediates. A reinvestigation of the tetrazotization of 1,4-diaminoanthraquinone

KOCK-YEE LAW,[1] IHOR W. TARNAWSKYJ, AND SAMUEL KAPLAN
Xerox Webster Research Center, 800 Phillips Road, 0114-39D, Webster, NY 14580, U.S.A.

Received October 10, 1990

KOCK-YEE LAW, IHOR W. TARNAWSKYJ, and SAMUEL KAPLAN. Can. J. Chem. **69**, 1183 (1991).

The azotization of 1,4-diaminoanthraquinone (**1**) by *n*-amyl nitrite in glacial acetic was reinvestigated. The structure of a red-brown precipitate, which was previously identified as anthraquinone-1,4-tetrazonium dichloride (**3**) by Schaarschmidt, was found to be incorrect. In this work, we have identified the red-brown solid as 4-aminoanthraquinone-1-diazonium chloride (**2**), a diazotized product of **1**. The yield of **2** was 80%. The tetrazonium dichloride **3** was actually formed in minute quantity and is soluble in acetic acid. The tetrazonium product of **1** can be isolated as tetrafluoroborate salt **4** in 3.4% yield by adding fluoboric acid into the acetic acid solution. The structure **4** was confirmed by IR and cross-polarization magic angle spinning ^{13}C NMR spectroscopy. Further investigations showed that **1** can be quantitatively tetrazotized by nitrosylsulfuric acid in 78% sulfuric acid. The tetrazonium product was isolated as **4** in 74% yield.

Key words: 1,4-diaminoanthraquinone, diazotization, tetrazotization, azo pigments.

KOCK-YEE LAW, IHOR W. TARNAWSKYJ et SAMUEL KAPLAN. Can. J. Chem. **69**, 1183 (1991).

On a réexaminé la réaction de diazotation de la 1,4-diaminoanthraquinone (**1**) par le nitrite d'amyle dans l'acide acétique glacial. On a déterminé que la structure du précipité brun-rouge, qui avait été identifiée antérieurement par Schaarschmidt comme celle du dichlorure d'anthraquinone-1,4-tétrazonium (**3**), est incorrecte. Il s'agit plutôt du chlorure du 4-aminoanthraquinone-1-diazonium (**2**), un produit de diazotation du produit **1**. Le rendement en produit **2** est d'environ 80%. Le dichlorure de tétrazonium **3** se forme effectivement en très faibles quantités et il est soluble dans l'acide acétique. Le produit tétrazonium de **1** peut être isolé sous la forme d'un tétrafluoroborate (**4**), avec une rendement de 3,4%, par addition d'acide fluoborique à la solution d'acide acétique. On a confirmé la structure du produit **4** par spectroscopie IR et par polarisation croisée de l'angle magique en RMN du ^{13}C. D'autres essais ont permis d'établir que le composé **1** peut être tétrazoté d'un façon quantitative par l'acide nitrosylsulfurique, dans de l'acide sulfurique à 78%. Le produit tétrazonium peut alors être isolé sous forme de produit **4** avec un rendement de 74%.

Mots clés : 1,4-diaminoanthraquinone, diazotation, tétrazotation, colorants azoiques.

[Traduit par la rédaction]

Introduction

Azo dyes and pigments are the most important class of colorant produced in the dye industry, accounting for over 50% of total dyestuff production (1). Depending on the number of azo linkages (-N=N-), these compounds can be further classified into sub-groups, such as monoazo, bisazo, trisazo, and polyazo, etc. Azo compounds are generally prepared by first azotizing an aromatic amine to an azonium salt, followed by coupling the salt with an azoic coupler. The synthesis is simple and is economically attractive. As a result, numerous azo structures for a variety of applications have been synthesized in the industry. In 1975, Champ and Shattuck (2) showed that bisazo pigment Chlorodiane Blue (4,4′-bis(1″-azo-2″-hydroxy-3″-naphthanilide)-3,3′-dichlorobiphenyl) could photogenerate electron-hole pairs in bilayer xerographic devices. This disclosure seemed to inspire a very intensive subsequent effort where thousands of azo pigments with different variations in the amine and the coupler moiety were synthesized and evaluated for xerographic photoreceptor applications (3). Among the amine precursors, isomeric diaminoanthraquinones were studied because of their commerical availability, low cost, and nontoxicity. The uses of 1,5- (4), 2,6- (5), and 2,7-diaminoanthraquinone (6) as precursors have been reported. We were particularly attracted by the prospect of using 1,4-diaminoanthraquinone (**1**) as a presecursor for pigment synthesis, because (a) **1** is commercially available, (b) the azotization procedure for **1** is documented in the literature (7), and (c) **1** absorbs strongly in the red (λ_{max} ~590 nm in DMF). Any success in wavelength extension by 150–200 nm would elevate the utility of the resulting azo pigments, enabling them to be useful in diode laser printers, where photoresponse at 780 nm is needed.

Here we report our reinvestigation of the azotization of **1** by *n*-amyl nitrite. Our results show that the previous structure assignment of the red-brown solid, to anthraquinone-1,4-tetrazonium dichloride (**3**) by Schaarschmidt (7), was incorrect. From the elemental analysis results, and IR and CP MAS ^{13}C NMR spectral data, we reassign the red-brown solid to the diazotized product, 4-aminoanthraquinone-1-diazonium chloride (**2**). Compound **3** was in fact formed, but the yield was very low. A new procedure for the tetrazotization of **1** is reported.

Experimental

Materials

1,4-Diaminoanthraquinone was purchased from Lancaster Synthesis. Nitrosylsulfuric was bought from Aldrich. Fluoboric acid (purified, 48–50%), glacial acetic acid (reagent grade), concentrated hydrochloric acid, and concentrated sulfuric acid were obtained from Fisher. All of these materials were used as received. *n*-Amyl nitrite was prepared from *n*-amyl alcohol (Fisher) and sodium nitrite (Fisher) in the presence of sulfuric acid (8).

General techniques

Elemental analyses were performed by Galbraith Laboratories. IR spectra were taken in KBr pellets on a Perkin–Elmer model 1750 FTIR. Cross-Polarization Magic Angle Spinning (CP MAS) solid state ^{13}C NMR spectra were recorded on a Bruker CXP spectrometer operating at 50.3 MHz in a Cryomagnet Systems, Inc. superconducting magnet system. Proton-enhanced cross polarization used 3–4 ms contact times, high-power (H_1 = 12 G) proton decoupling, and recycle times of 3–6 s. Magic angle spinning (4–4.5 kHz) was performed in a Doty Scientific probe with approximately 100 mg of each sample packed into

[1]Author to whom correspondence may be addressed.

Printed in Canada / Imprimé au Canada

Can. J. Chem. Downloaded from www.nrcresearchpress.com by 84.41.108.74 on 09/07/12
For personal use only.

TABLE 1. Elemental analysis data of 1,4-diaminoanthraquinome and its azotized products

Compound	Formula		C	H	N	Cl
1,4-Diamicoanthraquinone (**1**)	$C_{14}H_{10}N_2O_2$	Calcd.:	70.58	4.23	11.76	—
1·2HCl	$C_{14}H_{12}N_2O_2Cl_2$	Calcd.:	54.04	3.89	9.00	22.79
4-Aminoanthraquinone-1-diazonium chloride (**2**)	$C_{14}H_8N_3O_2Cl$	Calcd.:	58.86	2.82	14.71	12.41
2·HCl	$C_{14}H_9N_3O_2Cl_2$	Calcd.:	52.20	2.82	13.04	22.01
Anthraquinone-1,4-tetrazonium dichloride (**3**)	$C_{14}H_6N_4O_2Cl_2$	Calcd.:	50.48	1.82	16.82	21.28
Red-brown solid		Found:	58.34	2.86	14.37	12.42

6 mm o.d. sapphire rotors. The TOSS technique for sideband suppression was used for all measurements. Typically, 2000–4600 scans were averaged for each spectrum. Spectral assignment is facilitated by distinguishing the protiated and non-protiated carbons using a spin temperature reversal pulse sequence (9, 10). After the cross-polarization mixing periods and prior to carbon observation, proton rf phase is inverted for 100 μs. During this period the carbon spins cross-polarize in the reverse direction, protiated carbons the fastest and non-protiated carbons the slowest. Conveniently, after 100 μs, the protiated carbons are approximately nulled. We find this technique superior in its differentiation of protiated and non-protiated carbons to the commonly used delayed decoupling technique (11).

Azotization of 1,4-diaminoanthraquinone by n*-amyl nitrite*

1,4-Diaminoanthraquinone dihydrogen dichloride, 1.51 g (4 mmol),[2] which was prepared by refluxing 1,4-diaminoanthraquinone in concentrated hydrochloric acid, was suspended in 20 mL of glacial acetic acid. Freshly prepared *n*-amyl nitrite (2.4 mL) was added and the mixture was allowed to react at room temperature for about 2 h. A red-brown precipitate was formed and was isolated by filtration, yield 0.64 g. A second crop of the red-brown solid, 0.27 g, could be obtained by adding diethyl ether (~80 mL) to the filtrate solution. This red-brown solid, compound **2**, was identified as 4-aminoanthraquinone-1-diazonium chloride by elemental analysis data (recrystallized from warm water), and by IR and CP MAS ^{13}C NMR spectroscopy. The combined yield of **2** was ~80%.

To the filtrate solution, 15 mL fluoboric acid was added. After 15 min stirring at room temperature, a bright yellow precipitate, compound **4**, was isolated (0.06 g). Compound **4** was subsequently identified as anthraquinone-1,4-tetrazonium bis(tetrafluoroborate) by IR and CP MAS ^{13}C spectral data, yield 3.4%.

Tetrazotization of 1,4-diaminoanthraquinone

1,4-Diaminoanthraquinone (1.18 g, 5 mmol) was added to a stirred solution containing 2.5 g of nitrosylsulfuric acid in 15 mL 78% sulfuric acid. After stirring at room temperature for 2 h, a clear brown solution was obtained. The tetrazonium product was isolated as tetrafluoroborate salt **4** by adding 25 mL fluoboric acid to the product solution, yield 1.0 g (74%).

Results and discussion

Azotization of 1,4-diaminoanthraquinone by n*-amyl nitrite*

Synthesis and IR spectra

In 1916, Schaarschmidt (7) reported that 1,4-diaminoanthraquinone (**1**) could be tetrazotized in glacial acetic acid by an excess of *n*-amyl nitrite at room temperature, in the presence of hydrochloric acid. A red-brown solid was isolated and was recrystallized from warm (80°C) water. Schaarschmidt identified the red-brown solid as the tetrazotized product, anthraquinone-1,4-tetrazonium dichloride (**3**), on the basis of the nitrogen content of his sample (N calcd.: 16.86%; N found: 16.80%). The chemical yield of **3** was not reported.

We have reinvestigated Schaarschmidt's reaction and obtained identical results, i.e., a red-brown solid was isolated and recrystallized as reported. The C, H, N, Cl elemental analysis data of this solid are given in Table 1. By comparison with the calculated C, H, N, Cl values of the starting compounds and all possible products, we concluded that the red-brown solid is a diazonium product of **1**, 4-aminoanthraquinone-1-diazonium

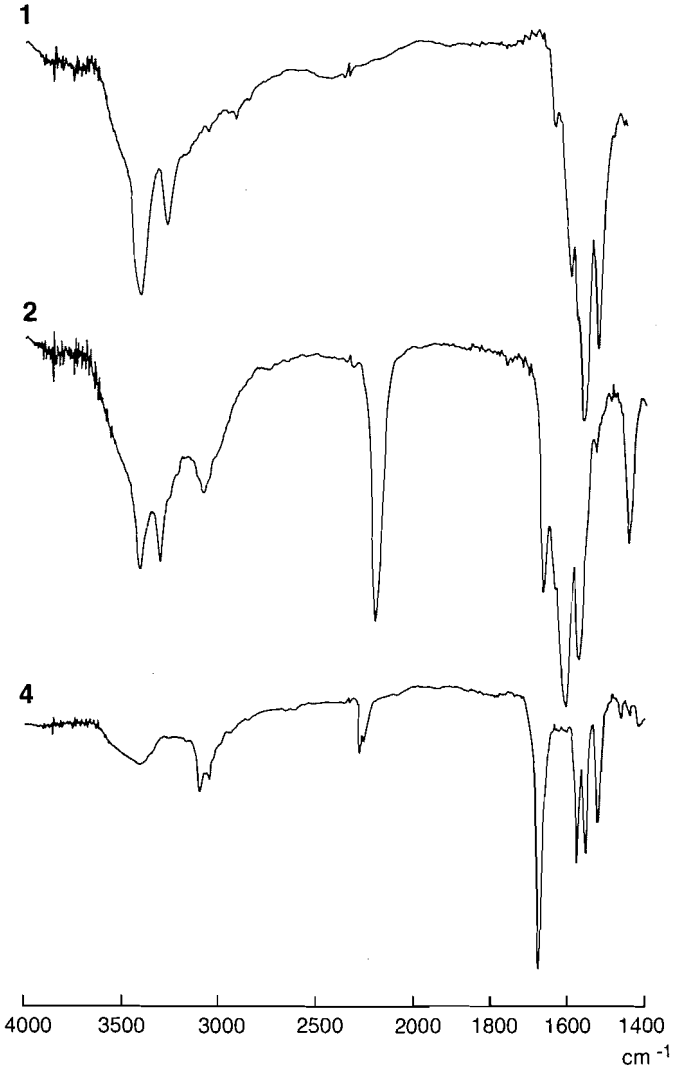


FIG. 1. IR spectra of compounds **1**, **2**, and **4**.

[2]Elemental analysis results show that the hydrogen chloride salt of **1** contains ~15% by weight of water.

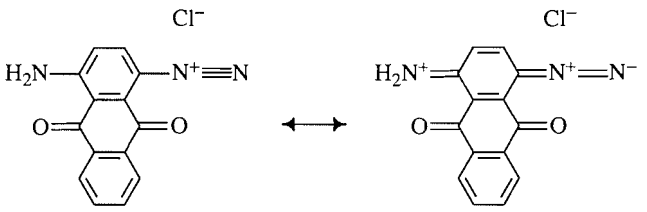
Can. J. Chem. Downloaded from www.nrcresearchpress.com by 84.41.108.74 on 09/07/12
For personal use only.

TABLE 2. IR spectral data of **1**, **2**, and **4**

Compound	Stretching frequency (cm^{-1}) N–H	$-N^+\equiv N$	C=O
1	3400 3200	—	1650 1602
2	3440 3305	2211	1680 1650 (shoulder) 1620
4	—	2271 2292	1690

chloride (**2**).[3] This structure assignment is substantiated by the IR and ^{13}C spectral data reported in this work.

Figure 1 shows the partial IR spectra of **1** and **2** in KBr pellets. The frequency data are listed in Table 2. In the spectrum of **2**, N–H stretchings at 3305 and 3440 cm^{-1} and a strong band at 2211 cm^{-1}, which can be assigned to the $-N^+\equiv N$ stretching (12, 13), are observed. The spectral data suggest that **1** was only partially azotized by *n*-amyl nitrite in acetic acid. The frequency of the $-N^+\equiv N$ stretching in **2** is lower than that of a typical diazonium salt (2283 cm^{-1}) and is comparable to those of 4-aminobenzene-1-diazonium tetrafluoroborate (2183 cm^{-1}) and 4-diethylaminobenzene-1-diazonium tetrafluoroborate (2150 cm^{-1}). The IR spectral data are thus consistent with the structure assignment of **2** because the decrease in $-N^+\equiv N$ stretching frequency can be ascribed to a resonance effect due to the *para* NH_2 group.



Accompanying the appearance of the $-N^+\equiv N$ stretching, a hypsochromic shift is observed in the C=O vibrational stretching, from 1650 cm^{-1} in **1** to 1680 cm^{-1} in **2**. The observed hypsochromic shift is also consistent with the structural assignment of **2**, simply implying that the intramolecular H-bonding between the C=O group and the NH_2 group has been altered due to azotization.

A bright yellow solid, compound **4**, could be isolated from the reaction by introducing fluoboric acid into the filtrate solution. The IR spectral data of this solid are included in Fig. 1 and Table 2. The absence of any N–H stretchings, along with the high-frequency weak bands at 2271 and 2292 cm^{-1} due to the $-N^+\equiv N$ groups (12, 13) and the strong high-frequency C=O stretching at 1690 cm^{-1}, leads us to propose that **4** is anthraquinone-1,4-tetrazonium bis(tetrafluoroborate), a tetrazotized product of **1**. The structure assignment of **4** is confirmed

[3]The carbon content of **2** is off by 0.52 ± 0.03% from the calculated value. We attributed the large difference to the existence of moisture in the sample because extensive high temperature drying of **2** was avoided due to concern of explosion in the drying oven. Moreover, hydrogen chloride salts of amines are known to be hygroscopic. It is likely that a small amount of water may be picked up by **2** during storage.

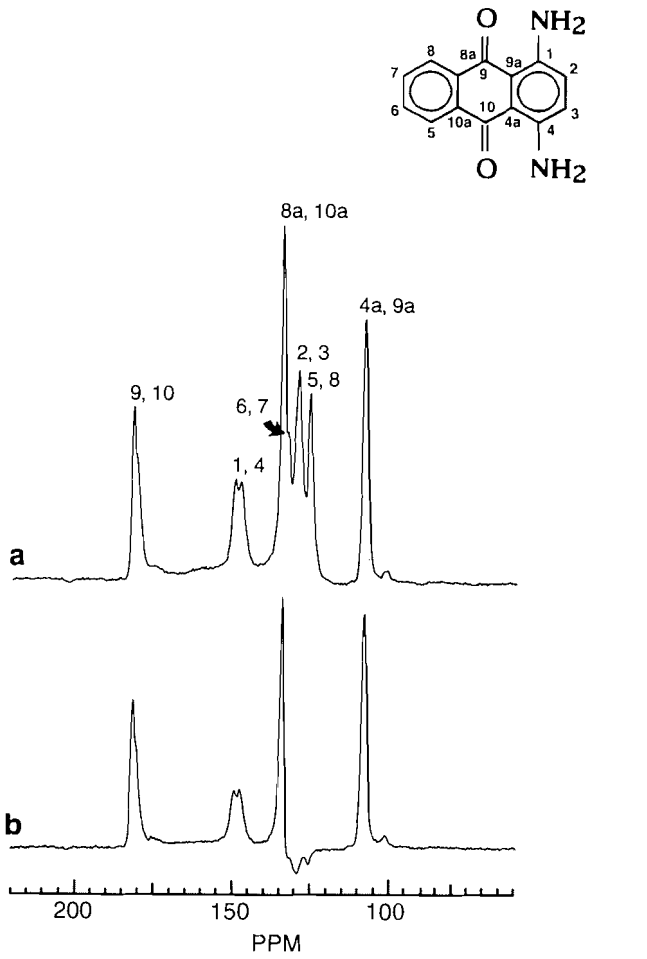


FIG. 2. CP MAS ^{13}C NMR spectra of **1**; (a) cross-polarization time = 3 ms, spinning rate = 4700 Hz, repetition time = 3 s, no. of scans = 3072; (b) same as (a) except with a 100-μs spin temperature reversal time inserted between the cross-polarization and observation periods.

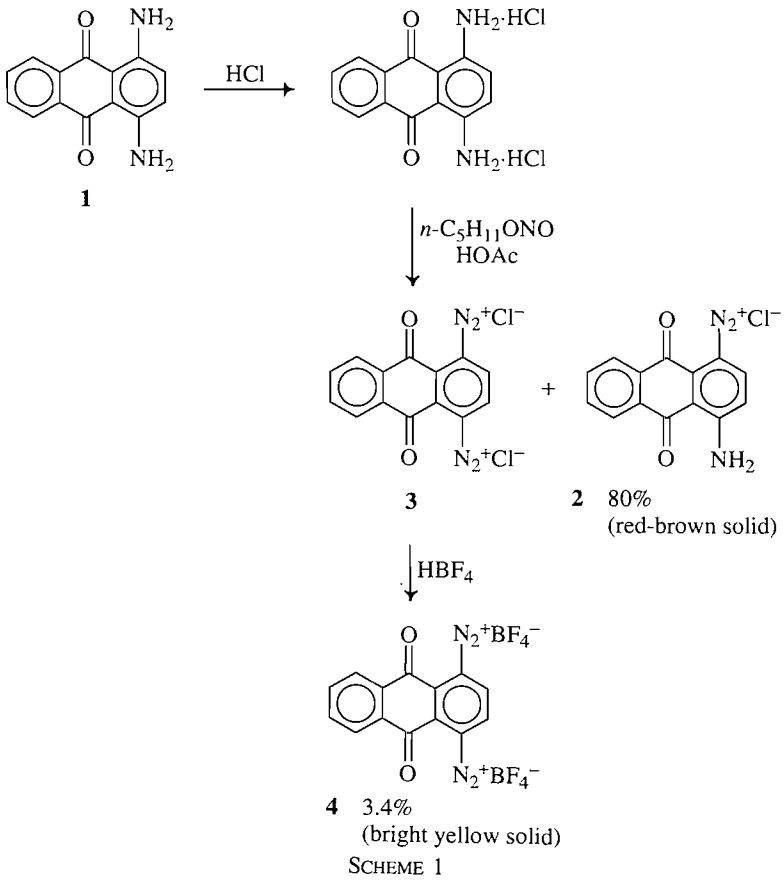
by its CP MAS ^{13}C NMR spectrum. Our results thus reveal that reaction of **1** with *n*-amyl nitrite also yields anthraquinone-1,4-tetrazonium dichloride (**3**) but in a very small quantity (3.4%). Compound **3** is soluble in the acetic acid product solution and the tetrazonium product can be isolated as tetrafluoroborate salt **4**. A schematic summarizing the reaction between 1,4-diaminoanthraquinone and *n*-amyl nitrite is depicted in Scheme 1.

CP MAS ^{13}C NMR studies

Figure 2a shows the CP MAS ^{13}C NMR spectrum of **1** and Fig. 2b shows the corresponding spin temperature reversal experiment with protiated carbons suppressed. Chemical-shift assignments are made by analogy to those observed in DMSO-d_6 (14) and the data are summarized in Table 3. Results show that the chemical shifts observed in the solid state are nearly identical to those observed in solution and that the signals of carbons 1 and 4 are characterized by the doublet splitting resulting from the quadrupolar interactions with neighboring ^{14}N nuclei (15).

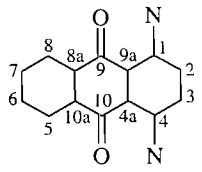
The CP MAS ^{13}C NMR spectrum of **2** is presented in Fig. 3a. Non-protiated carbons of **2** are distinguished by a spin reversal experiment and the ^{13}C spectrum for these carbons is shown in Fig. 3b. The protiated carbons are plotted in Fig. 3c as the

Can. J. Chem. Downloaded from www.nrcresearchpress.com by 84.41.108.74 on 09/07/12
For personal use only.



SCHEME 1

TABLE 3. CP MAS ^{13}C NMR spectra data of **1**, **2**, and **4**



Carbon	Chemical shift (ppm)			
	1 in solution[a]	**1**[b]	**2**[b]	**4**[b]
1 4	146.8	149.5, 147.8[c]	88.6, 91.7[c] 160.5, 159.2[c]	115.5
2 3	128.9	129.4	133–138[d] 122.6	136–139[d,f]
5 8	125.8	125.7	127–130[d]	125–132[d]
6 7	132.2	132.6	133–138[d]	125–132[d,f]
4a 9a	107.7	108.3	119.2, 122.0[e] 139.8, 141.7[e]	131.0
8a 10a	134.2	134.4	134.1[f] 133.0[f]	131.0
9 10	181.2	181.8	180.9[f] 184.5[f]	178.5

[a]In DMSO-d_6, ppm from TMS, data taken from ref. 14.
[b]In solid, reference: methyl carbons of hexamethylbenzene (117.4 ppm).
[c]Doublet from coupling to ^{14}N.
[d]Broad unresolved peak.
[e]Doublet from nonequivalent molecule in crystallographic cell.
[f]Tentatively assigned, may be interchanged.

Can. J. Chem. Downloaded from www.nrcresearchpress.com by 84.41.108.74 on 09/07/12
For personal use only.

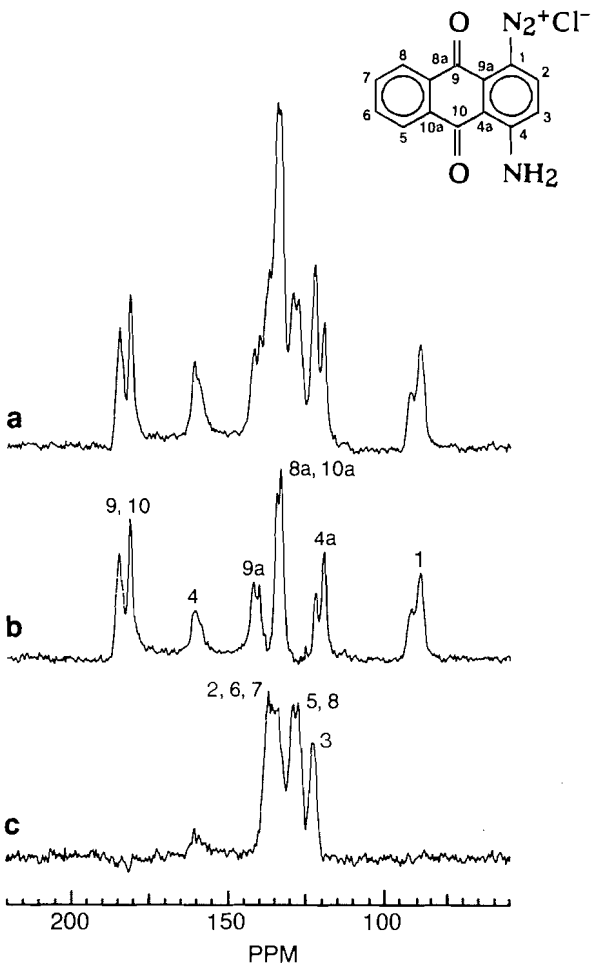


FIG. 3. CP MAS ^{13}C NMR spectra of **2**; (a) cross-polarization time = 4 ms, spinning rate = 4700 Hz, repetition time = 6 s, no. of scans = 4608; (b) same as (a) except with 100-μs spin temperature reversal; (c) spectrum (a) − spectrum (b).

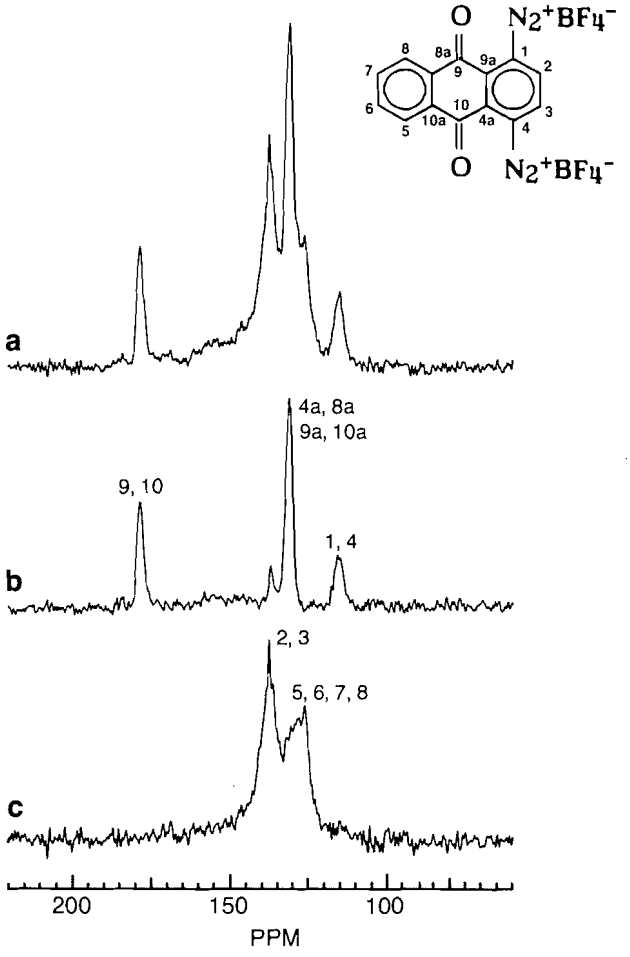
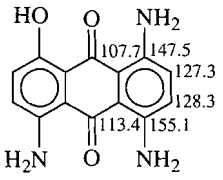
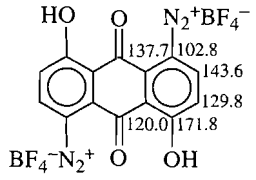


FIG. 4. CP MAS ^{13}C NMR spectra of **4**; (a) cross-polarization time = 4 ms, spinning rate = 4700 Hz, repetition time = 4 s, no. of scans = 2048; (b) same as (a) except with 100-μs spin temperature reversal; (c) spectrum (a) − spectrum (b).

calculated difference of Figs. 3a and b. Chemical-shift assignments are made as follows. The two most downfield peaks at 180.9 and 184.5 ppm are assigned to the two nonequivalent carbonyl carbons. Because of the similarity of the chemical structure between **2** and a previously reported tetrazonium compound **5** (4,8-dihydroxyanthraquinone-1,5-tetrazonium bis(tetrafluoroborate)) (16), we can estimate the chemical-shift changes from **1** to **2** based on the changes from 1,5-diamino-4,8-dihydroxyanthraquinone (**6**) to **5**.



6



5

From the chemical-shift changes of **6** to **5**, the estimated chemical shifts for **2** are C1, 102 ppm; C2, 145 ppm; C3, 130 ppm; C4, 163 ppm; C4a, 114 ppm; and C9a, 138 ppm. By comparsion of these values with the spectral results in Figs. 3a and b, carbons 1, 2, 3, 4, 4a, and 9a are assigned (Table 3). The assignments are consistent with the observed asymmetric broadenings of carbons 1 and 4 due to the quadrupolar interactions with neighboring ^{14}N nuclei.[4] The splitting of peaks of C4a and C9a in **2** may be a consequence of crystal packing. The remaining carbons in **2** (carbons 5, 6, 7, 8, 8a, and 10a) are assigned by comparison with the ^{13}C shifts of **1**, because substituents at carbons 1 and 4 are known to exert very little effect on the chemical shifts of the carbons in the second benzene ring of the anthraquinone system.[5]

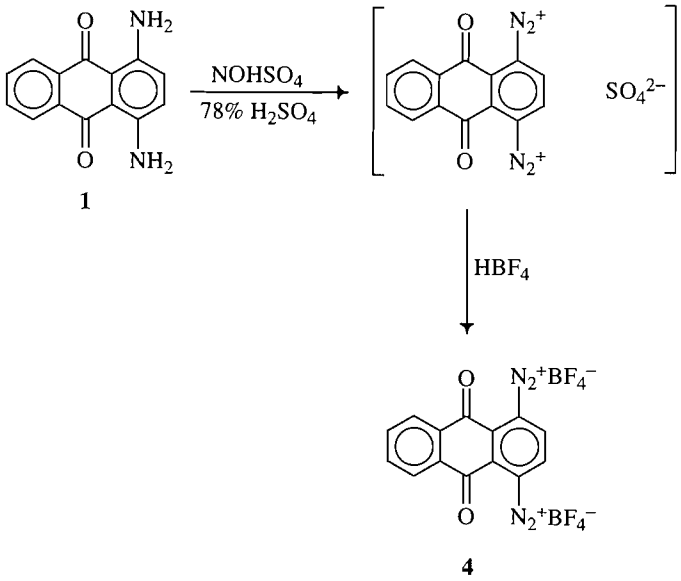
The CP MAS ^{13}C spectrum of **4** is given in Fig. 4a,[4] the non-protiated spectrum in Fig. 4b, and the protiated spectrum in Fig. 4c. The reduction of the number of non-protiated carbons from **2** to **4** suggests that **4** has a twofold symmetry and is the tetrazotized product of **1**.[6] The most downfield peak at 178.5 ppm is assigned to the two equivalent carbonyl carbons 9 and 10 and the most upfield peak at 115.5 ppm is assigned to carbons 1 and 4 because of the strong shielding effect produced

[4]The only useful NMR solvent for **2** and **4** is D_2SO_4. Attempts were made to record the solution ^{13}C NMR spectra of **2** and **4** in D_2SO_4 but failed due to the low thermal stability of these two compounds in sulfuric acid.

[5]Comparison of the ^{13}C data of a large number of monosubstituted anthraquinones (at C-1) and disubstituted anthraquinones (at C-1 and C-4) (14, 17) with those of anthraquinone (18) suggests that substituents at carbons 1 and 4 exert very little influence on the chemical shifts of the carbons in the second benzene ring.

[6]Elemental analysis was not performed for **4** because **4** was found to decompose slowly in the dark at room temperature.

Can. J. Chem. Downloaded from www.nrcresearchpress.com by 84.41.108.74 on 09/07/12
For personal use only.



SCHEME 2

by the diazonium group (19). The peak at 131.0 ppm, which is about twice the intensity of other non-protiated carbons, is attributable to carbons 4a, 8a, 9a, and 10a.

The protiated carbon spectrum of **4**, obtained by the subtraction of Fig. 4b from Fig. 4a, is depicted in Fig. 4c. Since substituents at carbons 1 and 4 are known to exert very small chemical-shift changes on carbons 5, 6, 7, and 8,[5] we assign the unresolved resonance at ~125–132 ppm to carbons 5, 6, 7, and 8 and the broad peak at 136–139 ppm to carbons 2 and 3. The broadening of the carbon peak of 2, 3 may in part be due to the undecoupled dipolar interaction between carbons 2 and 3 with the fluorine atoms of the adjacent tetrafluoroborate anion, analogous to the broadening effect previously observed in 4,8-dihydroxyanthraquinone-1-5-tetrazonium bis(tetrafluoroborate) (16). The ^{13}C NMR spectral data of **4** are consistent with its structure.

Tetrazotization of 1,4-diaminoanthraquinone by nitrosylsulfuric acid

While the yield of the tetrazonium salt of **1** synthesized by the *n*-amyl nitrite method was low, we found that **1** can be quantitatively tetrazotized by nitrosylsulfuric acid in 78% sulfuric acid. The tetrazonium product was isolated as tetrafluoroborate salt **4** in 74% yield (Scheme 2). The sample synthesized by the nitrosylsulfuric method was found to exhibit identical spectroscopic (IR) properties to that prepared by the *n*-amyl nitrite method.

Summary and remarks

The azotization reaction of 1,4-diaminoanthraquinone (**1**) by *n*-amyl nitrite in acetic acid was reinvestigated. The chemical structure of the red-brown solid isolated from the product mixture, which was assigned to anthraquinone-1,4-tetrazonium dichloride (**3**) by Schaarschmidt, was found to be incorrect. On the basis of elemental analysis results, and IR and CP MAS ^{13}C NMR data, we reassigned the red-brown solid to 4-amino-anthraquinone-1-diazonium chloride (**2**). Product analysis showed that **3** was formed in a very low yield in the mixture and that the tetrazonium product can be isolated as tetrafluoroborate salt **4** in 3.4% yield. The structure of **4** was confirmed by IR and CP MAS ^{13}C NMR spectroscopy. Further investigation showed that 1,4-diaminoanthraquinone can be tetrazotized quantitatively by nitrosylsulfuric acid in 78% sulfuric acid. The tetrazonium product, which was isolated as **4**, was obtained in 74% yield.

1. E. N. ABRAHART. Dyes and their intermediates. Chemical Publishing, New York. 1977. Chap. 4.
2. R. B. CHAMP and M. D. SHATTUCK. U.S. Patent 3,898,084 (1975).
3. K. C. NGUYEN and D. S. WEISS. J. Imaging Technol. **15**, 158 (1989).
4. M. HASHIMOTO. Jpn. Patents 59-33455 (1984) and 59-218453 (1984).
5. M. HASHIMOTO. U.S. Patents 4,555,567 (1985) and 4,440,845 (1984).
6. M. HASHIMOTO. U.S. Patent 4,486,522 (1984).
7. A. SCHAARSCHMIDT. Chem. Ber. **49**, 2678 (1916).
8. A. I. VOGEL. Textbook of practical organic chemistry. 4th ed. *Revised by* B. S. Furniss, A. J. Hannaford, V. Rogers, P. W. G. Smith, and A. R. Tatchell. Longman, London and New York. p. 409.
9. M. MELCHIOR. 22nd Experimental NMR Conference, Asilomar, CA. Poster B29. 1981.
10. N. ZUMBULYADIS. J. Chem. Phys. **86**, 1162 (1987).
11. S. J. OPELLA, M. H. FREY, and T. A. CROSS. J. Am. Chem. Soc. **101**, 5854 (1979).
12. K. B. WHETSEL, G. F. HAWKINS, and F. E. JOHNSON. J. Am. Chem. Soc. **78**, 3360 (1956).
13. M. ARONEY, J. W. LEFÉVRE, and R. L. WERNER. J. Chem. Soc. 276 (1955).
14. A. M. BIRCH, A. J. MERCER, A. M. CHIPPENDALE, and C. W. GREENHALGH. J. Chem. Soc. Commun. 745 (1977).
15. A. NAITO, S. GANAPATHY, and C. A. MCDOWELL. J. Magn. Reson. **48**, 367 (1982).
16. K. Y. LAW, S. KAPLAN, and I. W. TARNAWSKYJ. Dyes Pigm. In press.
17. Y. BERGER and A. CASTONGUAY. Org. Magn. Reson. **11**, 375 (1978); F. TOMA, and J. C. BOUHET. Org. Magn. Reson. **7**, 496 (1975); M. L. CASEY, R. C. PAULICK, and H. W. WHITLOCK. J. Org. Chem. **43**, 1627 (1978); Y. BERGER and M. BERGER-DEGUCE. Org. Magn. Reson. **15**, 303 (1981); Y. BERGER, A. COSTANGUAY, and P. BRASSARD. Org. Magn. Reson. **41**, 103 (1980).
18. P. E. HANSEN, O. K. POULSEN, and A. BERG. Org. Magn. Reson. **9**, 649 (1977).
19. D. F. EYRING. Org. Magn. Reson. **12**, 525 (1979).

Can. J. Chem. Downloaded from www.nrcresearchpress.com by 84.41.108.74 on 09/07/12
For personal use only.

Improvements in the quantitation of NMR spectra by the use of statistical methods

ALEX D. BAIN,[1] BRIAN J. FAHIE, TOMASZ KOZLUK, AND WILLIAM J. LEIGH
Department of Chemistry, McMaster University, 1280 Main Street W., Hamilton, Ont., Canada L8S 4M1

Received July 19, 1990[2]

ALEX D. BAIN, BRIAN J. FAHIE, TOMASZ KOZLUK, and WILLIAM J. LEIGH. Can. J. Chem. **69**, 1189 (1991).

In many applications of NMR spectroscopy to chemistry, quantitation plays a key role. This paper argues that peak heights not only *can* be used for quantitative work in NMR but that for careful work they *should* be used. Integrals are accurate, but because they depend on many subjective factors, their precision is suspect. Peak heights are very reproducible on modern spectrometers and so, given this precision, the accuracy can be obtained as well by using calibration methods. An example of the application of these methods is given in the case of a ^{13}C labelling experiment that elucidates a photochemical transformation.

Key words: NMR, labelling, quantitation, peak heights, integrals.

ALEX D. BAIN, BRIAN J. FAHIE, TOMASZ KOZLUK et WILLIAM J. LEIGH. Can. J. Chem. **69**, 1189 (1991).

Dans plusieurs applications chimiques de la RMN, la quantification est importante. Dans ce travail, on fait valoir que non seulement les hauteurs de pics *peuvent* être utilisées dans des travaux quantitatifs de RMN mais que pour des travaux de qualité on *devrait* les utiliser. Les intégrales sont exactes mais, comme elles dépendent de plusieurs facteurs subjectifs, leur précision est suspecte. Les hauteurs des pics sont très reproductibles avec les spectromètres modernes et, tenant compte de cette précision, l'exactitude peut aussi bien être obtenue par des méthodes de calibration. On présente un exemple de l'application de ces méthodes dans le cas d'une expérience de marquage au ^{13}C qui permet d'élucider une transformation photochimique.

Mots clés : RMN, marquage, quantification, hauteurs des pics, intégrals.

[Traduit par la rédaction]

Introduction

NMR is certainly well known as one of the best methods for qualitative analysis: the identification of a molecule. Analysis of ^{13}C and ^{1}H spectra can often solve a structure completely, and the development of two-dimensional NMR methods has dramatically advanced this process (1, 2). These methods are based on spectral analysis, i.e., the positions of the lines in the spectrum, but quantitative analysis has also been an important part of NMR spectroscopy (3, 4). Counting protons using integrals is a very familiar part of proton NMR. Theory says that in the absence of saturation, the integral over a spectral line is directly proportional to the number of spins and the proportionality is the same for all lines in the spectrum. This simple quantitation can be extended and applied so that accurate and precise integration of NMR spectra is important in many fields (5–10). Measurements of enantiomeric and diastereomeric excess are crucial in the design of chiral synthesis. Particularly in isotopic labelling studies, such as the one described in this work, NMR is one of the few methods than can give a detailed picture of the mechanism of the reactions. The important data in this case are relative enrichments at different sites in the molecule (6, 7), so separations are impossible, and mass spectrometry is not selective enough to identify individual sites. However, the validity of these results depends crucially on the precision and accuracy of the quantitation of the NMR data.

Normal methods of quantitation using integration are not without problems (3, 4, 11, 12). In practice, the process involves several subjective decisions on the part of the operator. The choice of integration region, the phasing of the spectrum, and the correction of the baseline are all under the control of the operator, and each may profoundly affect the value of the integral. Careful work with good signal-to-noise ratios and standard conditions can minimize the variation of the results, but there will still be a random component due to the operator's particular choices as well as possible biases between operators (12). Typical estimates of the reliability of an integral are 3–5% (11). Even with relatively poor signal-to-noise, the random errors in an integral are quite small, because of the summation. However, the systematic errors due to the subjective decisions of the operator are much more dangerous and subtle.

This paper aims to avoid many of these problems through the use of peak heights, rather than integrals, in the quantitation of ^{13}C NMR spectra. This is by no means a novel idea (13), but with the improvements in computers and spectrometers, it deserves some further examination. Peak heights require much less operator intervention than integrals, and so are more adaptable to automatic spectral interpretation. Peak heights are precise, as will be shown, but accuracy may be lacking since lines may have different widths. Given the precision, however, the accuracy can be recovered through the use of statistical methods and calibration techniques (14). Generally speaking, an NMR spectrum consists of many repetitions of many data points, but all that is reported is the average. With more powerful computers in spectrometers, and off-line data processing, more care can be given to data analysis. Some very sophisticated methods have been applied to NMR data (15–17), but we suggest that some simple methods can also provide useful information. The application of these statistical methods to NMR spectra will not necessarily improve the data, but it will give a clear and honest estimate of its quality.

Principles

The experiment we propose is conducted as follows. Instead of accumulating many scans on a sample, the scans are broken up into blocks, as in the original block averaging methods, and then not only the average but also the standard deviation of each peak height can be calculated. The sample is also combined with a standard of known concentration, and the peak heights of the standard and the sample are compared. The experiment is then repeated for a series of concentrations of the reference compound. A plot of the peak height of the sample divided by the peak height of the reference against the reciprocal of the reference concentration should then be linear. The slope of this line will then reflect the relative enrichment of each site.

Much work has been published on the experimental para-

[1]Author to whom correspondence may be addressed.
[2]Revision received April 8, 1991.

Can. J. Chem. Downloaded from www.nrcresearchpress.com by 84.41.108.74 on 09/07/12
For personal use only.

meters needed to obtain good quantitative data in NMR (3–12, 18). These include waiting for equilibrium to be re-established between pulses, suppression of the Overhauser effect, and good digital resolution in the spectrum to obtain a faithful representation of the lineshape. Often this research was aimed at finding out when these parameters became important, for instance, how rapidly pulses could be applied, relative to T_1, and still yield useful data. In this paper, we assume that all these precautions have been observed, and we concentrate on the analysis of the data itself.

The main motivation in pursuing peak heights rather than integrals, as a quantitative measure, is the observation that on a modern spectrometer the peak height is very stable. Experiments such as multiple quantum filters (INADEQUATE) and inverse detection methods routinely suppress lines belonging to ^{12}C species relative to their ^{13}C satellites (19–23). For this to happen, the ^{12}C peak must be stable to better than 0.55%. Also, in relaxation measurements it is the usual practice to use peak heights rather than integrals (13, 24). These are ideal conditions, of course, since the sample remains in the magnet all the time, and very little changes from one scan to the next. This performance gives us an estimate of the precision that is attainable.

The parameter, other than electronic stability, that will control the reliability of the peak heights is the stability of the peak widths in the spectrum. In ^{13}C spectroscopy, the linewidths in a proton-decoupled spectrum are mainly determined by two factors: the efficiency of proton decoupling and the apodization function that is applied to the data before Fourier transformation. Of course, the homogeneity of the magnetic field contributes, but it is much less important than in proton spectroscopy. In practice, the proton decoupling usually gives a relatively broad line compared to what can be achieved with careful work (25). Provided the lines are reasonably well separated, a heavy exponential function can be applied to the FID so that the linewidth in the spectrum is dominated by the filter function. Since the intensities in the spectrum are low-frequency information, an exponential filter will cause minimal distortions to the quantitative accuracy. Under these circumstances, the linewidths in the spectrum depend only minimally on the identity of the carbon nucleus or on the concentration of the species.

For accurate integration, the method of choice is to fit the data to a series of theoretical lines (Lorentzian, Gaussian, or some more general form) and then integrate the fitted line (11). The use of peak heights relaxes this assumption, since the only requirement is that the peak shape be stable. Asymmetries and baseline humps, which bedevil lineshape fitting, do not interfere with peak height quantitation.

Small overlaps of lines also affect peak heights less. The wings of a Lorentzian line are notoriously broad, and in the wings the integral only falls off as $1/(\omega - \omega_0)$, where ω_0 is the central frequency of the line. However, the height of the line falls off as $1/(\omega - \omega_0)^2$, so the effects on the peak height are much smaller.

Finally, phase corrections and baseline errors cause fewer problems with peak heights than with integrals. A simple calculation shows that an integral depends on the phase of a Lorentzian line as cos (α) where α is the phase angle relative to pure absorption. The dependence of peak height on α is

$$1/\left[1 + \left(\frac{1 - \cos(\alpha)}{\sin(\alpha)}\right)^2\right]$$

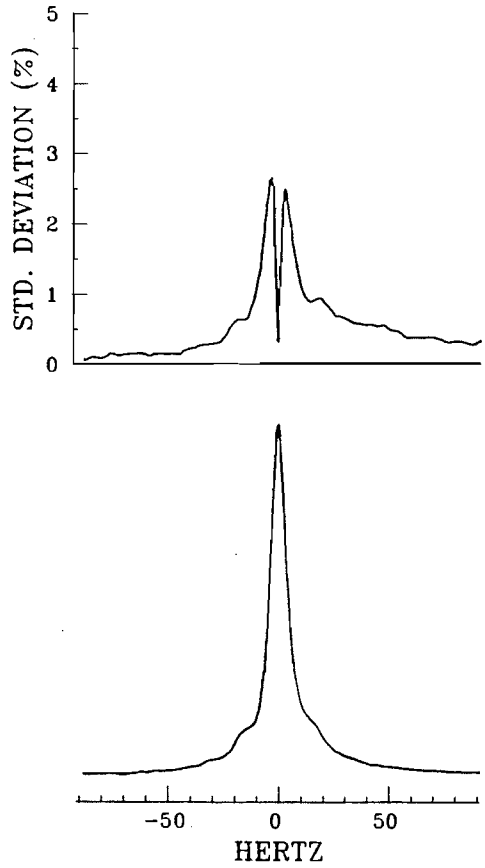


FIG. 1. ^{13}C spectral line (bottom spectrum) and its point-by-point standard deviation on the same horizontal scale (top spectrum). Data wre calculated using the program NMRSTAT.

which is a smaller effect. Small drifts in frequency or phase of the line will affect the wings of the line, but will leave the peak height relatively unaffected. This is illustrated in Fig. 1, where the lower spectrum is a ^{13}C spectral line and the upper spectrum is its standard deviation. In this case the phase drifted accidentally during the course of the experiment, as could be seen from inspection of the individual spectra. This small drift gives the wings of the line a relatively high variation, but the standard deviation of the peak height is similar to that of the baseline. Under ideal conditions, the standard deviation spectrum shows no features near where a spectral line appears in the normal spectrum, but in the presence of small drifts in frequency or in phase, the standard deviation spectrum in Fig. 1 is quite common. This demonstrates that the peak height is stable, even in the presence of small instabilities in the instrument.

In integration, a non-zero baseline will cause slope and curvature of the integral, which mean that the value of the integral will depend strongly on the choice of endpoints. With a peak height, the baseline simply adds or subtracts a constant from the intensity, provided only that the baseline be stable. By plotting the peak height of a sample versus the peak height of a reference of known concentration, as a function of the concentration, we should obtain a straight line. The slope of this line will be proportional to the intensity, and any baseline effects will appear as a non-zero intercept. The intercept can be ignored, since the slope gives us the information we need. This redundancy is built into the experiment. The error bars on the individual peak heights and the linearity of the plot versus

Can. J. Chem. Downloaded from www.nrcresearchpress.com by 84.41.108.74 on 09/07/12
For personal use only.

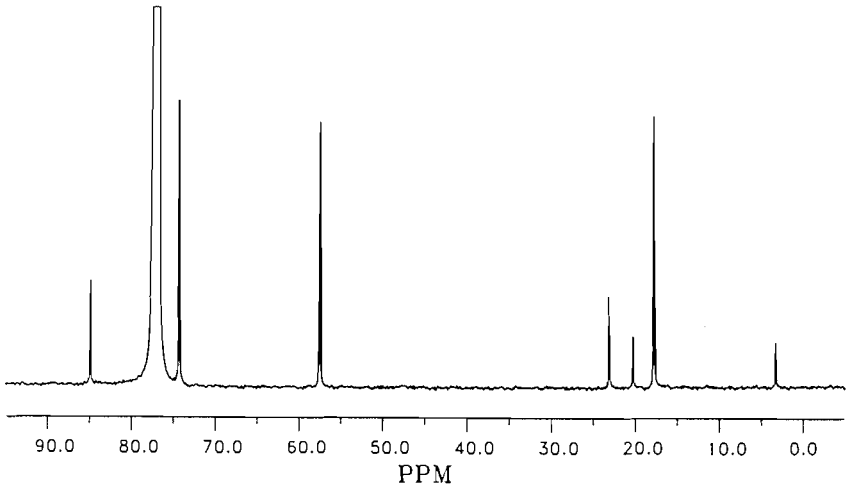


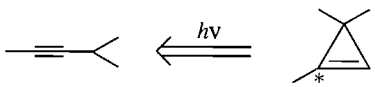
FIG. 2. ^{13}C NMR spectrum (10 000 scans) of compound **1** (labelled) plus the internal standard, ethanol.

reference concentration will then give a clear indication of the quality of the data.

This methodology obviously requires some more work than simply letting the spectrum accumulate for a long period of time, but with modern computer-controlled spectrometers, sample changers, and off-line data processing, much of this work can be automated and these techniques can become routine. We feel that the effort is worthwhile, since the internal consistency of the data will show its reliability.

Results

The compound studied in this paper is 4-methyl-2-pentyne (**1**), which is one of the products of the solution phase photolysis of 1,3,3-trimethylcyclopropene (**2**) (26). To elucidate the mechanism of this reaction,



1 **2**

compound **2** was synthesized with a ^{13}C label at position 1, and the postulated mechanisms lead to this label being at position 2 or position 3 of the alkyne **1** (26). It was therefore crucial to determine the enrichment at the various sites in **1** while working with a restricted amount of material (approximately 3.5 mg).

Compound **1** was dissolved in 0.7 mL of $CDCl_3$ and 4–5 mg of $Cr(acac)_3$ was added to speed up the spin relaxation. Inversion–recovery T_1 experiments indicated that all carbons under these conditions had T_1's of less than 1.1 s. For the quantitative work, a concentric insert (Wilmad WGS-5BL) with a precisely weighed amount of ethanol dissolved in $CDCl_3$ was inserted into the 5-mm NMR tube. Spectra were run on a Bruker AM500 spectrometer operating at 125.7 MHz for ^{13}C, with a $^{13}C/^{1}H$ 5-mm dual probehead. The experimental measurements consisted of 10 blocks of 1000 scans each, with a 7 s delay between scans. The 10 FIDs were processed under identical conditions with an exponential apodization function that added 40 Hz to the line broadening. These spectra were then combined together with a program NMRSTAT, written in Pascal for the ASPECT computer, to form an average spectrum and a standard deviation spectrum. In this way, the standard deviation of each point in the spectrum was calculated. One of the average spectra (i.e., a total of 10 000 scans) is shown in Fig. 2. For all of the present work, the standard deviation of each peak height was less than 4%.

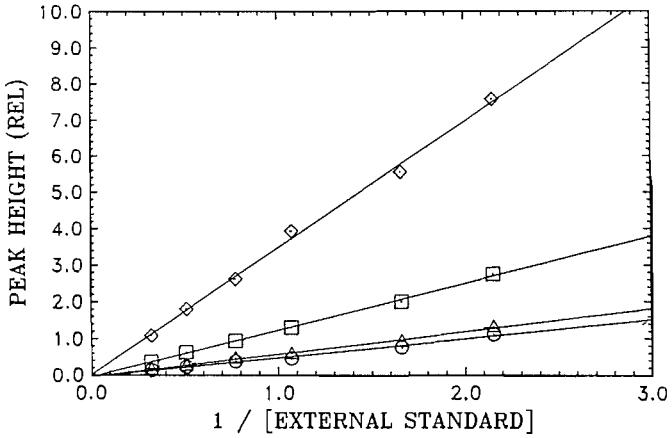


FIG. 3. Plot of normalized height of the peaks of compound **1** in the NMR spectrum versus the reciprocal of the standard concentration. Data are from Table 1. Diamonds represent carbon 2, squares represent carbon 3, circles represent carbon 1, and triangles represent carbon 4. Data from carbons 5 and 6 are not plotted.

The measurements were repeated for a series of ethanol concentrations, and the peak heights of the lines corresponding to compound **1** were divided by the height of the ethanol methylene peak at 57.5 ppm. Figure 3 shows a plot of the peak heights versus the reciprocal of the ethanol concentration for carbons 1, 2, 3, and 4 in compound **1**. Table 1 summarizes the data in Fig. 3, as well as the data for carbons 5 and 6, along with the linear regression slope and its error (two standard deviations) (27). The relative enrichment over natural abundance, defined by eq. [1], is also given in the table, along with its error.

$$[1] \quad \text{Enrichment} = \frac{\text{Slope of carbon}(n) - \text{Slope of carbon}(1)}{\text{Slope of carbon}(1)}$$

An authentic sample of **1** (Farchan Laboratories Inc., Gainesville, Florida) with no labelling was submitted to a similar analysis and the results are presented in the table. The slope of the graph obtained using peak heights corresponding to each peak is given, along with the error (two standard deviations of the slope from the linear regression). Because the signal-to-noise ratio was better for this sample, the integrals for each peak

Can. J. Chem. Downloaded from www.nrcresearchpress.com by 84.41.108.74 on 09/07/12
For personal use only.

TABLE 1. Slopes of the plots of normalized peak heights for the carbons in compound **1** as a function of the inverse of the concentration of the standard (ethanol). Errors quoted are twice the standard deviation of the slope obtained from a linear regression

Carbon no.	1	2	3	4	5, 6
Chemical shift (ppm)	3.29	74.37	84.97	20.61	23.19
Labelled material					
Slope	0.523	3.477	1.282	0.621	1.118
$\pm 2\sigma$	0.054	0.322	0.054	0.044	0.050
Enrichment (eq. [1])	0.0	5.65	1.45	0.19	0.07
$\pm 2\sigma$	—	0.80	0.28	0.15	0.06
Natural abundance material					
Using peak heights					
Slope	0.416	0.414	0.391	0.424	0.834
$\pm 2\sigma$	0.015	0.006	0.055	0.002	0.044
Using integrals					
Slope	0.440	0.446	0.426	0.435	0.875
$\pm 2\sigma$	0.174	0.088	0.130	0.043	0.084

were also calculated by fitting the spectra to Lorentzian curves using a simplex algorithm in the program NMR286 (Softpulse Software, Guelph, Ontario). As shown in the table, the slopes calculated from the integrals agree with those calculated from peak heights, but the integral slopes are considerably less precise.

Discussion

Figure 3 and Table 1 show unequivocally that positions 2 and 3 in compound **1** have been substantially enriched by the ^{13}C label in the starting material. The slopes indicate that these enrichments are about 1.5 times and 5.5 times over natural abundance. The regression and results from carbons 4, 5, and 6 suggest that the error in these measurements is about 15–20% (two standard deviations), assuming that there is no photochemical labelling at these other positions. The errors quoted are the error estimates from the regression, assuming that all the errors are random (27). The data on the natural abundance material indicate that when the signal-to-noise ratio is good, the results can be quite precise, and that the peak height measurement is better than an integration.

For this particular problem, these measurements cast considerable light on the mechanism of this reaction (26). However, these results have much broader application in all of NMR. They show that ^{13}C NMR quantitation on labelled material can be done near the level of natural abundance in a convincing and reliable fashion, and some estimates can be made of the errors. No particular experimental expertise or sophisticated equipment is required to perform these analyses. For careful quantitation, the measurements of peak heights are better, provided they are calibrated as in this work, because they are less susceptible to operator bias, and they give an honest estimate of the errors involved. The novel features of this work are the basic approach, and the computer program to calculate standard deviations of each point in a spectrum. NMR spectroscopists collect a tremendous amount of data in the accumulation of many FIDs for one spectrum. It now is possible to analyze and interpret these data much more fully than simply reporting their sum.

Acknowledgements

We are grateful to the Natural Sciences and Engineering Research Council of Canada, Esso Petroleum Canada, and the McMaster University Science and Engineering Research Board for funding this work, and to IBM Canada for providing computers for data analysis under the McMaster/IBM joint project.

1. J. K. M. SANDERS and B. K. HUNTER. Modern NMR spectroscopy. A guide for chemists. Oxford University Press, Oxford. 1987.
2. A. E. DEROME. Modern NMR techniques for chemistry research. Pergamon Press, Oxford. 1987.
3. J. N. SHOOLERY. Prog. Nucl. Magn. Reson. Spectrosc. **11**, 79 (1977).
4. D. L. RABENSTEIN and T. T. NAKASHIMA. *In* Trace analysis, spectroscopic methods for molecules. *Edited by* G. D. Christian and J. B. Callis. J. Wiley, New York. 1986.
5. M. J. SHAPIRO. *In* NMR spectroscopy techniques. *Edited by* C. Dybowski and R. L. Lichter. Marcel Dekker, New York. p. 203. 1987.
6. J. C. VEDERAS. Nat. Prod. Rep. **4**, 227 (1987).
7. G. J. MARTIN and M. L. MARTIN. Tetrahedron Lett. **22**, 3525 (1981).
8. F. A. L. ANET and M. KOPELEVICH. J. Am. Chem. Soc. **108**, 1355 (1986).
9. Z. RAPPOPORT. Acc. Chem. Res. **21**, 442 (1988).
10. K. ROTH, B. HUBESCH, D. J. MEYERHOFF, S. NARUSE, J. R. GOBER, T. J. LAWRY, M. D. BOSKA, G. B. MATSON, and M. W. WEINER. J. Magn. Reson. **81**, 299 (1989).
11. C. H. SOTAK, C. L. DUMOULIN, and G. C. LEVY. *In* Topics in carbon-13 NMR spectroscopy. Vol. 4. *Edited by* G. C. Levy. J. Wiley, New York. 1984.
12. F. A. L. ANET and D. J. O'LEARY. Tetrahedron Lett. **108**, 1059 (1989).
13. I. A. ARMITAGE, H. HUBER, D. H. LIVE, H. PEARSON, and J. D. ROBERTS. J. Magn. Reson. **15**, 142 (1974).
14. D. L. MASSART, B. G. M. VANDEGINSTE, S. N. DEMING, Y. MICHOTTE, and L. KAUFMAN. Chemometrics: a textbook. Elsevier, Amsterdam. 1988.
15. S. SIBISI, J. SKILLING, R. G. BRERETON, E. D. LAUE, and J. STAUNTON. Nature, **311**, 446 (1984).
16. J. TANG and J. R. NORRIS. J. Magn. Reson. **69**, 180 (1986).
17. H. BARKUIJSEN, R. DEBEER, and D. VAN ORMONDT. J. Magn. Reson. **7**, 553 (1987).
18. C. GIANCASPRO and M. B. COMISAROW. Appl. Spectrosc. **37**, 153 (1983).
19. G. BODENHAUSEN and D. J. RUBEN. Chem. Phys. Lett. **69**, 185 (1980).
20. M. R. BENDALL, D. T. PEGG, D. M. DODDRELL, and J. FIELD. J. Am. Chem. Soc. **103**, 934 (1981).
21. R. BENN and A. RUFINSKA. Magn. Reson. Chem. **26**, 895 (1988).
22. J. CAVANAGH, C. A. HUNTER, D. N. M. JONES, J. KEELER, and J. K. M. SANDERS. Magn. Reson. Chem. **26**, 867 (1988).
23. A. BAX and S. SUBRAMANIAN. J. Magn. Reson. **67**, 565 (1986).
24. R. E. WASYLISHEN. *In* NMR spectroscopy techniques. *Edited by* C. Dybowski and R. L. Lichter. Marcel Dekker, New York. p. 45. 1987.
25. S. R. MAPLE and A. ALLERHAND. J. Magn. Reson. **80**, 394 (1988).
26. B. J. FAHIE and W. J. LEIGH. Can. J. Chem. **67**, 1859 (1989).
27. G. E. P. BOX, W. G. HUNTER, and J. S. HUNTER. Statistics for experimenters. J. Wiley, New York. 1978.

Can. J. Chem. Downloaded from www.nrcresearchpress.com by 84.41.108.74 on 09/07/12
For personal use only.

Photochemistry of the *o*-nitrobenzyl system in solution: effects of O···H distance and geometrical constraint on the hydrogen transfer mechanism in the excited state

D. GRAVEL,[1] R. GIASSON,[1] AND D. BLANCHET
Département de chimie, Université de Montréal, C.P. 6128, Succ. A, Montréal (Québec), Canada H3C 3J7
R. W. YIP[1]
Département de chimie, Université du Québec à Montréal, C.P. 8888, Succ. A, Montréal (Québec), Canada H3C 3P8
AND
D. K. SHARMA
Canadian Centre for Picosecond Spectroscopy, Concordia University, Montréal, P.Q., Canada H3G 1M8

Received October 18, 1990

Can. J. Chem. Downloaded from www.nrcresearchpress.com by 84.41.108.74 on 09/07/12
For personal use only.

D. GRAVEL, R. GIASSON, D. BLANCHET, R. W. YIP, and D. K. SHARMA. Can. J. Chem. **69**, 1193 (1991).

Two rigid nitrobenzene derivatives, 5-nitro-1,2,3,4-tetrahydro-1,4-methanonaphthalene (**6**), and 5-nitro-1,2,3,4-tetrahydro-1,4-ethanonaphthalene (**7**), have been synthesized and studied by picosecond flash absorption spectroscopy, steady-state irradiation, and MMX molecular mechanics calculations. Transients with lifetimes of 770 and 410 ps have been detected and assigned to the excited triplet states of **6** and **7**, respectively. Consistent with prediction, the *o*-quinonoid intermediate is not detected in the time domain between the laser excitation and the end of decay of the triplet state. Intramolecular abstraction of the bridgehead benzylic hydrogen by the cited triplet state proceeds with relative rates of 1:125 for **6** and **7**, respectively. Since structural constraints prohibit the formation of an orthoquinonoid intermediate in these systems, formation of the usual nitroso-alcohol **13** represents the first substantiation of the biradical route to product (**3′** → **4**, Scheme 1). Absorption of the intermediate triplet biradical resulting from hydrogen abstraction by the triplet excited state was not observed, and is therefore believed to be either very weak in the 400–700 nm region, or located outside the detection region. The kinetic results together with structural parameters determined by molecular mechanics show good correlation between structure and reactivity. Hydrogen atom transfer can proceed at up to 53° deviation from linearity of the C—H—O nuclei, with transfer rates decreasing sharply as the O···H distance increases from 1.3 to 1.6 Å. It is suggested that the conditions of the reaction from the excited triplet state meet those required for a hydrogen tunneling mechanism.

Key words: *o*-nitrotoluene photorearrangement, mechanism of; *o*-nitrobenzyl systems, mechanism of photorearrangement; O···H distance, influence of, in hydrogen abstraction mechanism; picosecond flash absorption spectroscopy study of *o*-nitrobenzyl photorearrangement; radical pathway to product in *o*-nitrotoluene photorearrangement.

D. GRAVEL, R. GIASSON, D. BLANCHET, R. W. YIP et D. K. SHARMA. Can. J. Chem. **69**, 1193 (1991).

On a synthétisé deux dérivés rigides du nitrobenzène, les 5-nitro-1,2,3,4-tétrahydro-1,4-méthanonaphtalène (**6**) et 5-nitro-1,2,3,4-tétrahydro-1,4-éthanonaphtalène (**7**) et on les a étudiés par spectroscopie d'absorption éclair (picoseconde), par irradiation à l'état stationnaire et par des calculs de mécanique moléculaire MMX. On a détecté des espèces transitoires de temps de vie de 770 et de 410 ps et on les a attribuées respectivement aux état triplets excités des produits **6** et **7**. En accord avec les prédictions, on n'a pas détecté l'intermédiaire *o*-quinonoïde dans l'espace de temps qui s'écoule entre l'excitation au laser et la fin de la désactivation de l'état triplet. Les vitesses relatives d'arrachement intramoléculaire de l'hydrogène benzylique en tête de pont par les états triplets mentionnés sont respectivement de 1:125 pour les composés **6** et **7**. Puisque des contraintes structurales empêchent la formation d'un intermédiaire *o*-quinonoïde dans ces systèmes, la formation du nitrosoalcool **13** habituel fournit la première preuve de l'existence d'une voie biradicalaire conduisant au produit (**3′** → **4**, schéma 1). On n'a pas observé d'absorption du biradical triplet intermédiaire résultant d'un enlèvement d'hydrogène par l'état triplet excité; on croit donc qu'elle est très faible dans la région de 400–700 nm ou qu'elle est située à l'extérieur de cette région de détection. Les données cinétiques combinées aux paramètres structuraux déterminés par la mécanique moléculaire présentent une bonne corrélation entre la structure et la réactivité. Le transfert de l'atome d'hydrogène peut se produire jusqu'à une déviation de 53° par rapport à la linéarité des noyaux C—H—O; les vitesses de transfert diminuent rapidement lorsque la distance O···H passe de 1,3 à 1,6 Å. On suggère que les conditions de la réaction à partir de l'état triplet excité correspondent à celles requises pour un mécanisme de transfert d'hydrogène par effet tunnel.

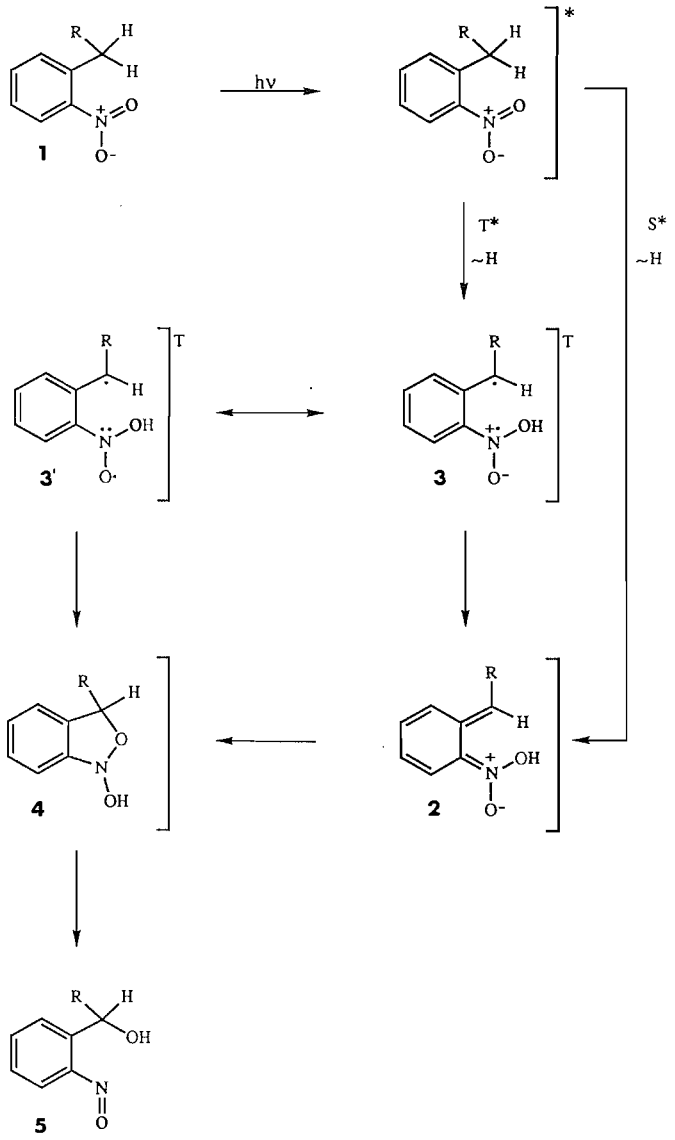
Mots clés: mécanisme de photoréarrangement de l'*o*-nitrotoluène; mécanisme du photoréarrangement de systèmes *o*-nitrobenzyliques; influence de la distance O···H sur le mécanisme d'enlèvement d'hydrogène; étude par spectroscopie d'absorption éclair (picoseconde) du photoréarrangement *o*-nitrobenzylique; voies radicalaires conduisant aux produits dans le photoréarrangement de l'*o*-nitrotoluène.

[Traduit par la rédaction]

Introduction

The well-established general photoreactivity of the *o*-nitrobenzyl system **1** to display intramolecular hydrogen abstraction has been widely exploited in the development of a number of photochromic compounds (1), photolabile protecting groups (2), and, more recently, photoresists (3). According to a general scheme elaborated over the years (4) the primary ground state "product" or intermediate in these reactions is the *o*-quinonoid species, **2**, resulting from intramolecular transfer of the benzylic hydrogen to the nitro group (5) (Scheme 1). The hydrogen atom transfer reaction can, *a priori*, proceed via either (i) an excited $n\pi^*$ triplet state associated with the nitro group to form the triplet biradical **3**, or (ii) an excited singlet state associated with the nitro group to form a short-lived singlet biradical that rapidly collapses to the quinonoid intermediate **2**. Since the geometries of the singlet biradical and the *o*-quinonoid intermediate **2** are

[1]Authors to whom correspondence may be addressed.

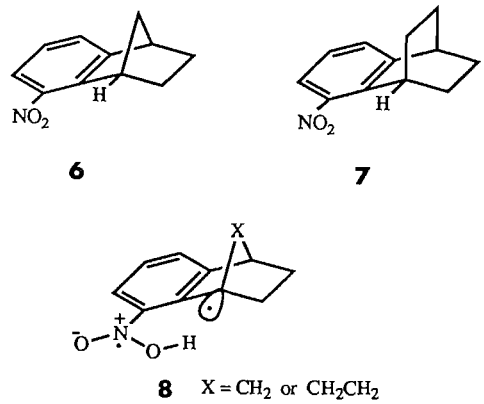


SCHEME 1

not likely to differ significantly, the potential curves of these two species are probably close together. Consequently, the energy barrier separating the singlet biradical and the *o*-quinonoid species **2** is likely to be small and may even be insignificant, so that it may be more appropriate to consider the reaction from the singlet excited state as a concerted [1,5]-sigmatropic shift (6). Our previous demonstration that the singlet state pathway is indeed involved in some of these systems, and that it proceeds extremely rapidly (7), is in accord with these views.

Following the hydrogen transfer step, the primary intermediate(s): *o*-quinonoid **2** and (or) triplet biradical **3**, proceed(s) respectively to the cyclized *N*-hydroxybenzisoxazolidine **4**, the former by a polar cyclization mechanism, and the latter by intersystem crossing to the *o*-quinonoid **2** or, alternatively, by radical cyclization to **4** via the mesomeric form **3′**, following intersystem crossing. (To our knowledge, path **3′** → **4** has never been substantiated in these systems.) Finally, ring chain tautomerism yields the familiar nitrosoalcohol **5**, an internal redox product.

As part of our continuing effort in the study of the reaction mechanism of these systems, we conceived and synthesized two model *o*-nitrobenzyl compounds, **6** and **7**, the rigidity of which provides defined C—H···O—N geometry, distance, and structural constraints. These constraints were expected to simplify the reaction mechanism, and therefore to give us new insight into the H-atom transfer in the excited state. Indeed, fusion of the *o*-nitrobenzyl system to either a bicyclo[2.2.1]-heptane or bicyclo[2.2.2]octane system should, because of Bredt's rule (8), preclude the formation of the *o*-quinonoid intermediate directly from the singlet excited state (7), or following the collapse of a precursor biradical **8**. The choice of



these two rigid models should thus clear up an optical window in the 400–500 nm wavelength region where the *o*-quinonoid intermediate is known to absorb (7). This should facilitate the detection, by time-resolved spectroscopy, of the expected triplet state and corresponding biradical. The triplet excited state of **6** and **7** is not known, but should have similar spectral properties as the triplet excited state of other nitrobenzylic molecules (7, 9), which we have recently studied.

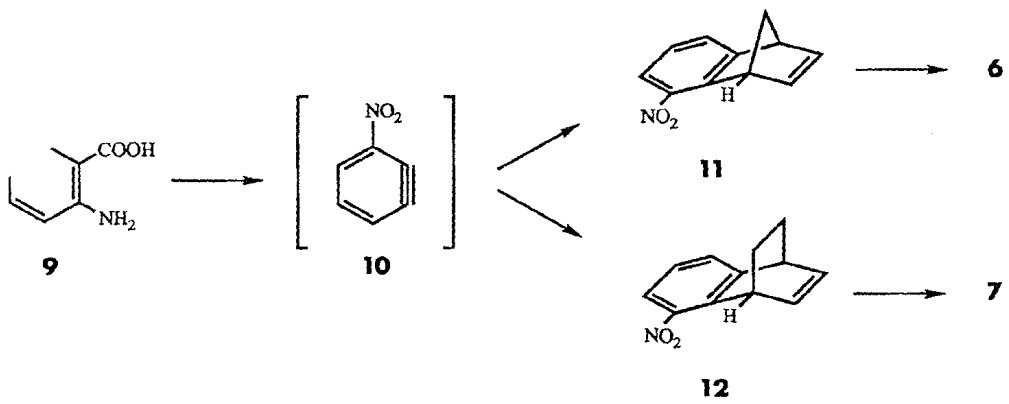
Models **6** and **7** were therefore studied by picosecond absorption spectroscopy and steady-state irradiation to correlate reactivity with the spectroscopic results. The kinetic results and quantum yields, together with the structural parameters of compounds **6** and **7** determined by molecular mechanics, enabled us to obtain *quantitative* data on the effect of geometry, distance, and structural constraints on the efficiency of H-atom transfer and, for the first time, probe the intervention of the radical cyclization path in these systems.

Results and discussion

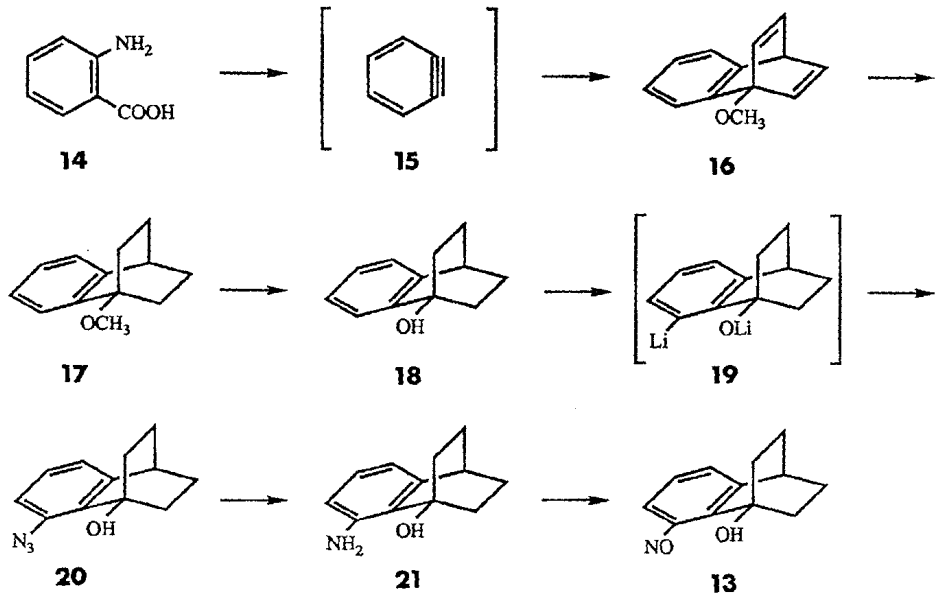
Synthesis of the bicyclic models 6 and 7, and the expected primary photoproduct from 7

As outlined in Scheme 2, synthesis of the bicyclic models **6** and **7** was carried out in a straightforward manner following a procedure reported by Paquette and co-workers (10) for the preparation of bicyclic adduct **11**. Starting from 6-nitroanthranilic acid (**9**), diazotization using isoamyl nitrite leads to 3-nitrobenzyne (**10**), which is trapped *in situ* by [4+2] cycloaddition with either cyclopentadiene or cyclohexadiene, to form respectively the bicyclic adduct **11** or **12**. As reported by Paquette and co-workers (10), adduct **11** is formed in good yield (58–70%) and isolated by simple flash chromatography. The same is not true, however, for the preparation of adduct **12**, which was formed in very low yield and mixed with a number of secondary products resulting mainly from [2+2] and ene reaction (11). In the case of **11**, hydrogenation of the pure material using Wilkinson's catalyst (12), in order to preserve the nitro group, led to 93% of the desired dihydro adduct **6**. In the case of **12**, hydrogenation of the crude reaction product, after

Can. J. Chem. Downloaded from www.nrcresearchpress.com by 84.41.108.74 on 09/07/12
For personal use only.



SCHEME 2



SCHEME 3

elimination of the polar impurities, led to a complex reaction mixture from which 14% of the desired dihydro adduct **7** could be isolated by semi-preparative HPLC.

Scheme 3, on the other hand, depicts a total and unambiguous synthesis of the primary photoproduct **13** expected from the photolysis of model **7**. Essentially, the strategy involves building the bicyclic skeleton with a bridgehead hydroxyl group by a [4+2] cycloaddition analogous to that described above, followed by a β-lithiation reaction of the type reported by Meyer and Seebach (13*a*) for benzyl alcohols to eventually introduce the nitroso group. In a first step, the bicyclic adduct **16** was prepared following a procedure of Tabushi *et al.* (14) that involves diazotization of anthranilic acid (**14**) to yield benzyne (**15**), which is trapped by anisole. The product, isolated with some difficulty in a 25% yield, was then subjected to hydrogenation (10% palladium on carbon) to yield 91% of the tetrahydro adduct **17**, which was demethylated by trimethylsilyliodide (15). The resulting alcohol **18**, which was obtained in 92% yield, was subjected to a β-lithiation reaction (13) and the dilithio compound **19** formed was treated *in situ* with triisopropylbenzenesulfonyl azide (16) to yield 80% of the desired azidoalcohol **20**. The latter was then reduced by sodium borohydride (17) to yield 84% of the corresponding aminoalcohol **21**. Finally, oxidation of **21** to the desired authentic nitrosoalcohol **13** took place in the presence of a sulfuric-acid-free solution of peracetic acid (18); the compound was isolated in the dimeric form (mp 168–170°C) in 72% yield.

Picosecond flash absorption spectroscopy and steady-state photolysis

The transient absorption spectra from picosecond excitation of the bicyclic compounds **6** and **7** at 355 nm (see Fig. 1), using the third harmonic from a YAG laser system, were assigned to the triplet excited state on the basis of the similarity of their spectra and lifetimes with those that we previously reported for other relatively unreactive simple nitrobenzene compounds (5, 9), and by the observed decrease in the transient lifetimes of **6** and **7** on addition of the triplet quencher, 1-hydroxymethyl-1-methyl-2,4-cyclohexadiene[2] ($k_q = (1.2 \pm 0.8) \times 10^9\ M^{-1}\ s^{-1}$ and $(2.6 \pm 0.5) \times 10^9\ M^{-1}\ s^{-1}$ for **6** and **7**, respectively). The two transient absorption bands at 425–450 nm and a weaker band in the 600–650 nm region are almost identical in terms of the peak position, width, and area with those due to the triplet state for the simple nitrobenzene compounds. The transient from the more strained benzobicyclo[2.2.1]heptane derivative **6** decayed with a lifetime, τ, of 710 ps, significantly slower

[2]Synthesis and characterization to be published elsewhere.

Can. J. Chem. Downloaded from www.nrcresearchpress.com by 84.41.108.74 on 09/07/12
For personal use only.

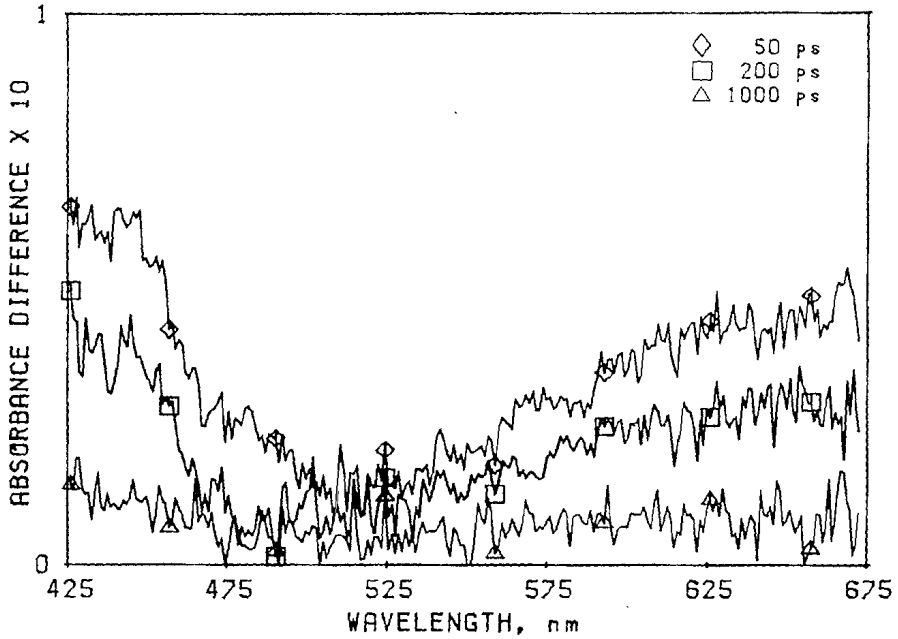


FIG. 1. Picosecond flash photolysis absorption spectra of model compound **7** in acetonitrile: 2-mm path length cell; solute concentration, 0.0079 M; ◇, 50 ps; □, 200 ps; △, 1000 ps.

Can. J. Chem. Downloaded from www.nrcresearchpress.com by 84.41.108.74 on 09/07/12
For personal use only.

than its benzobicyclo[2.2.2]octane homologue **7** (410 ps). On the other hand, the intensities of the absorption of the triplet states of **6** and **7** are similar. Making the reasonable assumption that the extinction coefficients for triplet absorption are similar for the two homologous molecules, the results strongly suggest that the relative triplet yields are similar for **6** and **7**. These results are in sharp contrast with those of more reactive *o*-nitrobenzylic compounds such as the phenyl and *p*-cyanophenyl-*o*-nitrobenzyl ethers (**1**, R = PhO-; *p*-CNC_6H_4O-) that, even at times immediately after the laser pulse, are characterized by a major absorption band in the 425–450 nm region, comprising overlapping *o*-quinonoid and triplet excited states, and a weaker band in the 600–650 nm region due to the triplet excited state alone. We had previously shown that with the ethers **1**, a fast initial singlet excited state contribution to the formation of the *o*-quinonoid intermediate was followed by a slower, most probably triplet, contribution (7). (Schnabel and Wong have also recently shown this duality of contributions for the case of *o*-nitrobenzyl ester groups in polymer matrices (19).) The more reactive phenyl *o*-nitrobenzyl ether was shown to give weaker transient triplet–triplet absorption spectra as a result of more efficient reaction from the singlet.

In an effort to correlate the reactivity of models **6** and **7** with the spectroscopic results, the disappearance rate ratio (relative quantum yields) of both model compounds was measured. Photolysis of 10^{-2} M solutions of compounds **6** and **7** in dioxane at 350 nm using a Rayonet photochemical reactor gave rates of 0.15 and 10, respectively, relative to the disappearance of *o*-nitrotoluene taken as 1 (**1**, R = H). We believe that the enhanced rate of disappearance of **7** is not due to reaction from the singlet excited state. For efficient singlet reaction to occur from **7** and still obtain similar Φ_{IC} for **6** and **7** (*vide supra*), k_{IC} and τ_S would have to change in such a way as to completely compensate for the enhanced k_r from the singlet excited state, which appears highly improbable on the basis of the similarity of the two structures. Furthermore, recent work[3] on a variety of *o*-nitrobenzyl systems suggests that while both the singlet and triplet excited states can contribute to the formation of the *o*-quinonoid reactive intermediate, the singlet excited state seems to contribute significantly for only those more reactive *o*-nitrobenzylic molecules (generally speaking, those with an oxygen substituent at the benzylic carbon are most reactive). Comparing the relative quantum yields of disappearance (relative to *o*-nitrotoluene) of **6** and **7** (0.15 and 10, respectively) with those of methyl *o*-nitrobenzyl ether (**1**, R = CH_3O-) and *p*-cyanophenyl-*o*-nitrobenzyl ether (**1**, R = *p*-CNC_6H_4O-) (31 and 110, respectively), **6** and **7** are clearly in the less reactiv group (11). In the case of the *o*-nitrobenzyl compounds witho structural constraints, the geometries of the singlet biradical ar the *o*-quinonoid intermediate are not likely to differ signi cantly and the potential curves of these two species are probab close together. Consequently, for these compounds, the ener barrier separating the singlet biradical and the *o*-quinon species **2** is likely to be small and may even be insignificant, that it may be more appropriate to consider the reaction from t state as a concerted [1,5]-sigmatropic shift (6), which wc account for the extreme reactivity of the singlet as compare the triplet state. For the geometrically constrained compoun and **7**, however, the low-energy concerted pathway f short-lived excited singlet state to the *o*-quinonoid interme represents a prohibitively high-energy pathway.

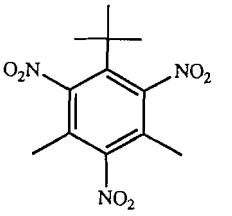
At this point, it remained to be demonstrated that reacti indeed due to benzylic hydrogen abstraction and formatio nitrosoalcohol as primary photoproduct. HPLC analysis lished that four products (see, however, below) are fc during the steady-state photolysis of compound **7** at 350 acetonitrile. To show that one of these peaks corresponds

[3]R. W. Yip, D. K. Sharma, R. Giasson, and D. Gravel. Unpı results.

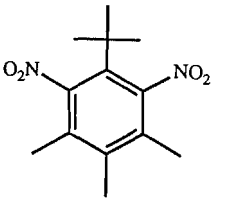
TABLE 1. Geometric parameters of model compounds **6** and **7**, and of **22** and **23**

Compound	C—H···O (degree)	H···O—N (degree)	$r_{H\cdots O}$ (Å)
6	117	105	2.54
7	127	106	2.24
22[a]	136[b]	100[b]	2.57[b]
23[a]	140[b]	99[b]	2.51[b]
Optimal	180[c]	90–120	<2.6[d]

[a]See ref. 21.
[b]Values for the most favored among possible H's.
[c]Assuming linear C—H···O transfer.
[d]2.6 = van der Waals sum for O···H.



22



23

expected photoproduct **13**, small amounts of materials were isolated by semi-preparative HPLC. The small amounts of compounds available and the presence of impurities, however, prevented unambiguous characterization of the products by mass spectrometry and proton NMR. A total synthesis of authentic product **13** was therefore carried out as outlined in Scheme 2 (*vide supra*); the pure compound, isolated as the crystalline nitroso dimer, was characterized by mass spectrometry, proton NMR, and IR. This authentic sample was then used to identify the peak corresponding to the primary photoproduct **13** in the chromatogram of the photolyzed solution of **7**. Furthermore, a solution of synthetic **13** in acetonitrile was also photolyzed at 350 nm. HPLC analysis of the solution showed three peaks due to the formation of photoproducts. These three peaks have retention times identical to those of the three unknown peaks present in the chromatogram of photolyzed solution of **7**. This then demonstrates unambiguously that compound **13** is the only primary photoproduct in the photolysis of **7**, and that the three other photoproducts arise from subsequent photolysis of **13**.

From the set of experiments described above, it follows that intramolecular benzylic hydrogen abstraction does take place in the faster reacting model compound **7** and that it is the only photochemical pathway open to this compound. Indeed, if **7** was to react by intermolecular hydrogen abstraction, other primary photoproducts would be observed. Finally, the formation of **13** also substantiates, for the first time, the intervention of the radical cyclization path $\mathbf{3}' \rightarrow \mathbf{4}$ (Scheme 1) in an *o*-nitrobenzyl system as suggested earlier (2*b*).

From the relative quantum yields of disappearance and triplet lifetimes (τ_6, τ_7), one can calculate the relative rate constants for reaction from the triplet state, k_7/k_6, of **6** and **7**:

$$k_7/k_6 = \Phi_{rel7}/\Phi_{rel6} \times \tau_6/\tau_7 = 125$$

To obtain some explanation why intramolecular H transfer might be more favorable in **7** than in **6**, we carried out molecular mechanics calculations[4] on these two compounds to determine their geometries. The nitro group was rotated around the C—N bond to minimize the distance between the O atom of the nitro group and H atom of the benzylic carbon. The results are recorded in Table 1. Döpp and co-workers (21) have analyzed the geometric requirements for the intramolecular abstraction of the homobenzylic *tert*-butyl hydrogens by the *o*-nitro group of *tert*-butyl-2,6-dinitrobenzylic compounds **22** and **23**, in the solid state. Using X-ray crystallographic structures as models for the excited state, homobenzylic hydrogens in which $r_{H\cdots O} < 2.6$ Å; $136° < \angle$ C—H···O $\leq 180°$; and $90° < \angle$ H···O—N $< 120°$ were identified as those being mainly responsible for the reaction (see Table 1). In the present study, we found compound **7** capable of H-atom abstraction in spite of the fact that its C—H···O angle deviates 53° from linearity. Linearity of the C—H···O angle does not seem to be as critical as H transfer distance (r_{if}),[5] for abstraction to occur. Indeed, we observed that the rate of the reaction decreases by a factor of 125 (*vide supra*) as the transfer distance increases from 1.3 to 1.6 Å, in compounds **7** and **6** respectively. These H transfer distances are sufficiently short for the transfer to occur by hydrogen tunneling across the barrier. In terms of the Golden Rule treatment of Siebrand *et al.* (22), a nonlinear C—H—O reaction would require the inclusion of lower-frequency bending modes resulting in a decreased interaction between the initial and final states, which would be more pronounced for **6** than **7**. The treatment predicts a sensitive dependence on the *transfer distance* and this is most probably the *major factor responsible for the difference in the transfer rates* we have observed for the two model compounds.

Intramolecular hydrogen abstraction by the triplet excited state of compounds **6** and **7** is expected to lead to the corresponding triplet biradical **8**. However, at times of 1–3 ns, corresponding to three times the triplet lifetimes, no signal greater than ca. 0.03 OD units, considered as significant with respect to fluctuations due to noise, baseline reproducibility, and solvent blank signal, etc., was observed. Thus for a signal whose position, band shape, and width are not characterized, the biradical **8** eludes detection because its absorption in the 400–700 nm region is too weak relative to the detectability of the apparatus, or is simply located outside the window accessible by our system. Unlike biradicals whose radical centres are isolated by one (or more) -CH_2- group(s), the location of the absorption of **8** cannot be predicted with certainty. Although to the extent that the biradical spectrum resembles the additive spectrum from the two radical centres because of the minimal orbital overlap between the two centres (on the bridgehead carbon and on the nitrogen and π-system), we expect only a weak absorption band such as that associated with the Ar-NO_2 radical (23), which absorbs at 410–450 (ϵ_{max} = 500 mol^{-1} cm^{-1}).

In conclusion, we have characterized the excited triplet $n\pi^*$ state of the bicyclic compounds **6** and **7** and determined their relative rate constants for H-atom transfer. These results corre-

[4]Calculations using the programs MODEL and MMX. MMX is an enhanced version of Allinger's MMP2 calculations (20).

[5]The H transfer distance (r_{if}) is the distance between the equilibrium position of the hydrogen in the initial state (C—H···O) and the final state (C···H—O): $r_{if} = r_{H\cdots O} - r_{H-O}$. We assumed r_{H-O} to be equal to 0.96 Å, the sum of the covalent radii of the atoms. Probable lengthening and distortion of the N—O bond in the $n\pi^*$ excited state of the nitro group were neglected.

Can. J. Chem. Downloaded from www.nrcresearchpress.com by 84.41.108.74 on 09/07/12
For personal use only.

late well with the structural parameters, and in particular the H···O distance, determined by molecular mechanics. We have shown that the H-atom transfer reaction can proceed at up to 53° deviation from linearity of the C—H—O nuclei, with transfer rates decreasing sharply as the O···H distance increases from 1.3 to 1.6 Å. Further studies on rigid nitrobenzyl systems with different geometries could provide a detailed map of k_r as a function of C—H···O distances, of the angle of the C—H—O nuclei, and of the angle of H—O—N, thus providing an experimental basis for future theoretical calculations. Finally, the formation of nitrosoalcohol **13** in the irradiation of bicyclic model **7** provides unambiguous proof of the biradical pathway to product (**3′** → **4**, Scheme 1) in *o*-nitrobenzyl systems.

Experimental section

General

Melting points were taken on a Büchi apparatus and are uncorrected. ^{1}H NMR spectra were recorded in $CDCl_3$ on Varian VXR300 (300 MHZ), Bruker WH400 (400 MHz), and Bruker WH90 (90 MHz) instruments and chemical shifts are given in ppm relative to TMS. IR spectra were recorded on Perkin–Elmer 710B and Perkin–Elmer 783 spectrophotometers. High and low-resolution mass spectra were determined on AEI MS-902 and V.G. Micromass 12-12 spectrometers, respectively. Photolyses were carried out in Pyrex tubes in a Rayonet RPR-100 photochemical reactor equipped with 16 RPR 3500 Å lamps and a MGR-100 merry-go-round. The HPLC setup used consisted of two Waters 6000A pumps, a Waters 680 gradient controller, a Waters U6K injector, a Waters Lambda-Max 481 variable wavelength UV–visible detector, and a Spectra-Physics SP4270 electronic integrator. The HPLC grade acetonitrile used (BDH Omnisolv or Aldrich Gold Label) was degassed prior to use. Flash chromatographies (24) were carried out using Merck 230–400 mesh silica and glass-distilled solvents (hexanes and ethyl acetate).

1,3-Cyclohexadiene, anthranilic acid, palladium catalyst (10% on carbon), iodotrimethylsilane, sodium borohydride, tetrabutylammonium sulfate, and sodium acetate were purchased from Aldrich and used as received. Anisole (Aldrich) was distilled over sodium, and *N,N,N′,N′*-tetramethylethylenediamine (Aldrich) over calcium hydride. Cyclopentadiene (Aldrich) was distilled prior to use and collected at low temperature (−78°C) to prevent dimerization. Dichloromethane, chloroform, and *n*-heptane were dried by distillation over P_2O_5. Benzene and toluene were dried by distillation over sodium/benzophenone. Acetone was dried by distillation over calcium hydride, and ether by distillation over lithium aluminium hydride.

Flash photolysis experiments

The photophysical experiments used a Nd:YAG laser system consisting of a passively mode-locked (Kodak 9740 dye in chlorobenzene) 7.0 × 90 mm oscillator (ends at Brewster angle), a 7.0 × 115 mm preamplifier, and a 9.35 × 115 mm amplifier, which produced up to ca. 4 mJ frequency-tripled single pulses at 355 nm of ca. 35 ps FWHM pulse duration. Time-resolved spectra were recorded using the pump-probe technique. The 355-nm ultraviolet excitation beam was split off from the colinear second harmonic and fundamental beams by means of a 355-nm reflecting/1.06-μm transmitting beam splitter. The transmitted 1.06-μm pulse was optically delayed by ca. 10 ns and then focussed, by means of a 1-m focal length lens, into a 5-cm cell containing a solution of 30% H_3PO_4 in H_2O to generate the continuum probe pulse, which provided useful coverage from ca. 400 nm to <750 nm. Using a Hamamatsu C979 streak camera equipped with a C1000 type 18 head, the FWHM width of the polychromatic continuum pulse was found to be ca. 35 ps. Variable delays of up to 10 ns between the probe and excitation pulses were obtained by inserting a variable optical delay line in the path of the exciting UV pulse. As both the spectrum and intensity of the probe beam changed from shot to shot, it was necessary to split off a portion of the probe beam (using a prism beam splitter) for use as a "reference" beam. The spectra reference beams (which bypassed the 2-mm pathlength sample cell) were recorded simultaneously along with those of the main "sample" probe beam (which interrogated the excited portion of the sample cell) by focussing both beams at different heights along the slits of a monochromator/spectrograph (Instrument SA (JY) model HR-320) fitted with a SIT vidicon detector (EG&G PAR model 1254) with two-dimensional light-sensing capabilities. Spectroscopic grade acetonitrile was obtained from Caledon Laboratories. The time-resolved spectra were recorded using ca. 1 mJ 355-nm laser pulse energy and ca. 8×10^{-3} M of compounds **6** and **7** in acetonitrile solutions. This excitation energy represents a compromise between the need to minimize the possibility of nonlinear effects (zero laser intensity) and the need for adequate signal (high laser intensities). In flash photolysis studies of *o*-nitrobenzylic compounds with the present system arrangement, we observed that energies up to 3 mJ did not change the shape of the transient spectra nor could we observe any measurable change in the kinetics. We did observe small nonlinearity in the initial concentration of the transients and small baseline changes (ca. equal to or up to twice the noise) at ca. 10 ns due to laser-induced thermal effects above ca. 1.5 mJ; so, for this reason and to more closely approximate the ideal condition for zero nonlinearity at zero excitation intensity, we generally chose to live with slightly noisier signals than with a possible artifact, especially when the frequency of the signal is low (broad band as is the present case) and that of the noise high, and when we are looking for a weak unknown transient. The recoverable triplet excited state signal and the non-appearance of an equally strong *o*-quinonoid signal in terms of the band width, band position, and band area, while not the optimum, are nevertheless adequate for our qualitative interpretation. Typically, nine shots are averaged to obtain better signal-to-noise. With the OMA system used in our experiment there is only a marginal increase in signal-to-noise ratio of the spectrum with further averaging owing to drift within the system. Characterization of the triplet excited states of **6** and **7** is based on the similarity of their spectra and lifetimes to those that we previously reported for other relatively unreactive nitrobenzene compounds (5, 9), and on the observed decrease in the transient lifetimes of **6** and **7** on addition of ca. 1.5 M of the triplet quencher, 1-hydroxymethyl-1-methyl-2,4-cyclohexadiene.[2]

Synthesis of materials

1,4-Dihydro-5-nitro-1,4-methanonaphthalene (11)

Compound **11** was prepared from 6-nitroanthranilic acid (**9**) and cyclopentadiene according to the procedure described by Paquette and co-workers (10). Purification by flash chromatography (hexanes) gave **11** as a yellow solid with a 70% yield (lit. (10) 58%); mp 58.5–59°C (lit. (10) mp 59–60°C).

5-Nitro-1,2,3,4-tetrahydro-1,4-methanonaphthalene (6)

A solution of 1,4-dihydro-5-nitro-1,4-methanonaphthalene (**11**) (0.70 g; 3.7 mmol) and tris(triphenylphosphine)rhodium(I) chloride (12) (0.14 g; 0.15 mmol) in benzene (30 mL) was shaken under hydrogen pressure (50 psi; 1 psi = 6.89 kPa) in a Parr reactor for 17 h. The resulting reaction mixture was filtered over a pad of silica and the solvent evaporated. Distillation of the residue under reduced pressure afforded compound **6** as a yellow oil (0.66 g; 93%); IR ($CHCl_3$) ν:1527 (NO_2), 1360 (NO_2) cm^{-1}; ^{1}H NMR (90 MHz; $CDCl_3$) δ: 7.79 (dd, J = 1.2 and 8.1 Hz, 1H), 7.43 (dd, J = 1.2 and 7.2 Hz, 1H), 7.18 (dd, J = 7.2 and 8.1 Hz, 1H), 4.27 (br s, 1H), 3.45 (br s, 1H), 2.14–1.06 (m, 6H); HRMS m/z calcd.: 189.0790; found: 189.0780.

5-Nitro-1,2,3,4-tetrahydro-1,4-ethanonaphthalene (7)

A solution of 6-nitroanthranilic acid (10) (2.0 g; 11 mmol) and 1,3-cyclohexadiene (13.3 mL; 140 mmol) in acetone (30 mL) was added to a refluxing solution of isoamyl nitrite (25) (1.8 mL; 14 mmol) in CH_2Cl_2 (20 mL). The resulting reaction mixture was stirred under argon for 2 h. After evaporation of the solvent, the residue was dissolved in a 95:5 mixture of hexanes/ethyl acetate and the resulting solution was filtered through a pad of silica in order to remove polar impurities. Evaporation of the solvent gave 1.2 g of a yellow oil containing a mixture of products. The residue was dissolved in benzene (60 mL) and tris(triphenylphosphine)rhodium(I) chloride (12) (0.30 g;

Can. J. Chem. Downloaded from www.nrcresearchpress.com by 84.41.108.74 on 09/07/12
For personal use only.

Can. J. Chem. Downloaded from www.nrcresearchpress.com by 84.41.108.74 on 09/07/12
For personal use only.

0.32 mmol) was added. The solution was shaken under hydrogen pressure (50 psi) for 20 h in a Parr reactor. The reaction mixture was filtered over a pad of silica and the solvent evaporated. The desired compound was isolated from the residue by semi-preparative HPLC (CH_3CN/H_2O 70:30; 9.4 × 250 mm CSC S50DS2 C_{18} column). 5-Nitro-1,2,3,4-tetrahydro-1,4-ethanonaphthalene (**7**) was obtained as a yellow oil (0.32 g; 14%); IR ($CHCl_3$) ν: 1525, 1350 (NO_2) cm^{-1}; ^1H NMR (400 MHz; $CDCl_3$) δ: 7.78 (dd, J = 1.2 and 8.2 Hz, 1H), 7.38 (dd, J = 1.2 and 7.3 Hz, 1H), 7.27 (dd, J = 7.3 and 8.2 Hz, 1H), 3.89 (br s, 1H), 3.11 (br s, 1H), 2.0–1.7 (m, 4H), 1.5–1.3 (m, 4H); HRMS m/z calcd.: 203.0947; found: 203.0912.

*1,4-Dihydro-1-methoxy-1,4-ethenonaphthalene (**16**)*

Compound **16** was prepared from anthranilic acid (**14**) and anisole according to a procedure described by Tabushi *et al.* (14). The desired product, isolated from the reaction mixture by flash chromatography (hexanes/ethyl acetate 95:5), was contaminated with phenyl benzoate. Hydrolysis of phenyl benzoate in refluxing aqueous NaOH (10%), followed by a second flash chromatography (hexanes/ethyl acetate 95:5), gave pure **16** in 25% yield (lit. (14) 25%) as a colorless oil.

*1-Methoxy-1,2,3,4-tetrahydro-1,4-ethanonaphthalene (**17**)*

A catalytic amount of palladium on carbon (10% Pd) was added to a solution of 1,4-dihydro-1-methoxy-1,4-ethenonaphthalene (**16**) (0.48 g; 2.6 mmol) in ethyl acetate (15 mL). The reaction mixture was stirred under hydrogen atmosphere for 3 h. Used catalyst was removed by filtration over a pad of Celite and the solvent was evaporated. Product **17** was purified by flash chromatography (hexanes/ethyl acetate 95:5) and was obtained as a colorless oil (0.45 g, 91%); ^1H NMR (300 MHz; $CDCl_3$) δ: 7.45 (dd, J = 1.4 and 7.2 Hz, 1H), 7.29 (td, J = 1.8 and 7.2 Hz, 1H), 7.23 (td, J = 1.4 and 7.2 Hz, 1H), 7.18 (dd, J = 1.8 and 7.2 Hz, 1H), 3.56 (s, 3H), 2.96 (quintet, J = 2.7 Hz, 1H), 2.05–1.86 (m, 4H), 1.65–1.43 (m, 4H); HRMS m/z calcd.: 188.1201; found: 188.1210.

*1-Hydroxy-1,2,3,4-tetrahydro-1,4-ethanonaphthalene (**18**)*

A solution of 1-methoxy-1,2,3,4-tetrahydro-1,4-ethanonaphthalene (**17**) (0.10 g; 0.53 mmol) and iodotrimethylsilane (0.1 mL; 0.69 mmol) in $CHCl_3$ was stirred for 72 h under argon and at room temperature. Methanol (0.1 mL) was added to the reaction mixture and the solvent was evaporated. The residue was dissolved in ether and the solution washed with saturated aqueous $NaHSO_3$, saturated aqueous $NaHCO_3$, and brine. The solution was dried over $MgSO_4$ and the solvent evaporated. Product **18** was purified by flash chromatography (hexanes/ethyl acetate 80:20) and was obtained as a white solid (85 mg, 92%); mp 131.5–133°C; IR (film) ν: 3500–3100 (OH) cm^{-1}; ^1H NMR (300 MHz; $CDCl_3$) δ: 7.47 (dd, J = 1.4 and 7.3 Hz, 1H), 7.29 (td, J = 1.4 and 7.3 Hz, 1H), 7.22 (td, J = 1.4 and 7.3 Hz, 1H), 7.16 (dd, J = 1.4 and 7.3 Hz, 1H), 2.98 (m, 1H), 1.97–1.83 (m, 4H), 1.62–1.43 (m, 5H); HRMS m/z calcd.: 174.1044; found: 174.1050.

*5-Azido-1-hydroxy-1,2,3,4-tetrahydro-14-ethanonaphthalene (**20**)*

A solution of *n*-BuLi (0.46 mL of a 2.5 M solution in hexane; 1.15 mmol) and *N,N,N',N'*-tetramethylethylenediamine (0.17 mL; 1.15 mmol) in *n*-heptane (0.2 mL) was added slowly to a warm (90°C) solution of 1-hydroxy-1,2,3,4-tetrahydro-1,4-ethanonaphthalene (**18**) (0.10 g; 0.57 mmol) in *n*-heptane (2 mL). The reaction mixture was stirred 2 h at 85°C under argon atmosphere, and then cooled to 0°C (13). A solution of triisopropylbenzenesulfonyl azide (16) (0.40 g; 1.15 mmol) in ether (1 mL) was added, and the resulting reaction mixture was brought to room temperature and stirred for 2 h. The reaction mixture was cooled again to 0°C and quenched by the addition of water (2 mL). The aqueous phase was neutralized with 10% aqueous HCl and extracted twice with ether. The organic extracts were combined, washed with brine, and dried over $MgSO_4$. The solvent was evaporated and the product was isolated by flash chromatography (hexane/ethyl acetate 85:15). Compound **20** was obtained as a yellow solid (0.10 g; 80%); mp 78.5–80.0°C; IR (film) ν: 3600–3200 (OH), 2115 (N_3) cm^{-1}; ^1H NMR (300 MHz; $CDCl_3$) δ: 7.24 (dd, J = 7.3 and 8.2 Hz, 1H), 7.06 (dd, J = 1.1 and 8.2 Hz, 1H), 6.98 (dd, J = 1.1 and 7.3 Hz, 1H), 4.70 (s, 1H), 2.93 (m, 1H), 1.95–1.80 (m, 4H), 1.65–1.40 (m, 4H); HRMS m/z calcd.: 215.1058; found: 215.1050.

*5-Amino-1-hydroxy-1,2,3,4-tetrahydro-1,4-ethanonaphthalene (**21**)*

A solution of $NaBH_4$ (50 mg; 1.32 mmol) in water (0.2 mL) was added to a warm solution (80°C) of 5-azido-1-hydroxy-1,2,3,4-tetrahydro-1,4-ethanonaphthalene (**20**) (95 mg; 0.44 mmol) and tetrabutylammoninum sulfate (15 mg; 0.44 mmol) in toluene (0.5 mL), and the resulting reaction mixture was stirred vigorously at 80°C for 3 h. The reaction mixture was cooled to room temperature and quenched by the addition of 10% HCl. The aqueous phase was made basic with 50% aqueous KOH and was extracted with chloroform. The chloroform extracts were combined, washed with brine, and dried over $MgSO_4$. Compound **21** was obtained as a white solid after recrystallization from $CDCl_3$/petroleum ether (1:2) (70 mg; 84%); mp 165–166°C; IR (film) ν: 3500–3050 (OH), 3435, 3385 (NH_2) cm^{-1}; ^1H NMR (300 MHz; $CDCl_3$) δ: 6.97 (dd, J = 7.3 and 8.0 Hz, 1H), 6.56 (dd, J = 1.1 and 7.3 Hz, 1H), 6.52 (dd, J = 1.1 and 8.0 Hz, 1H), 4.63 (br s, 2H), 3.63 (br s, 1H), 2.85 (m, 1H), 1.98–1.70 (m, 4H), 1.61–1.45 (m, 4H); HRMS m/z calcd.: 189.1153; found: 189.1150.

*1-Hydroxy-5-nitroso-1,2,3,4-tetrahydro-1,4-ethanonaphthalene (**13**)*

A sulfuric-acid-free solution of peracetic acid was prepared by saturating commercial 32% aqueous peracetic acid with sodium acetate, centrifuging the mixture, and collecting the supernatant (18*a*). The resulting solution (0.13 mL; 1.94 mmol) was added to a solution of 5-amino-1-hydroxy-1,2,3,4-tetrahydro-1,4-ethanonaphthalene (**21**) (30 mg; 0.16 mmol) in water (16 mL). The suspension was stirred 3 h at room temperature, followed by 2 h at 40°C. The reaction mixture was made slightly basic by addition of 10% aqueous NaOH and was extracted with CH_2Cl_2. The combined extracts were washed with 10% aqueous HCl and brine, dried over $MgSO_4$, and the solvent was evaporated. Recrystallization of the residue gave the dimeric form of compound **13** as a white solid (23 mg; 72%); mp 168–170°C; IR (film) ν: 3540–3040 (OH), 1262 (NO *trans* dimer) cm^{-1}; ^1H NMR (300 MHz; $CDCl_3$) δ: 7.58 (dd, J = 1.3 and 7.4 Hz, 1H), 7.18 (dd, J = 7.4 and 8.7 Hz, 1H), 7.15 (s, 1H), 6.29 (dd, J = 1.3 and 8.7 Hz, 1H), 3.17 (m, 1H), 2.33–2.21 (m, 2H), 2.14–2.03 (m, 2H), 2.02–1.90 (m, 2H), 1.74–1.61 (m, 2H); LRMS (chemical ionization) m/z: 204 (monomer + H^+), 391 (dimer + H^+ − O).

*Measurement of the relative rates of disappearance of compound **6** upon photolysis*

The relative rate of disappearance of compound **6** was measured using 2-nitrotoluene as reference compound (k_{rd} = 1). Two solutions, one containing 10^{-2} M of compound **6** and one containing 10^{-2} M of 1-nitrotoluene in 1,4-dioxane, were prepared. At this concentration, virtually all of the incident light is absorbed, assuring equal irradiation. The solutions were photolyzed in Pyrex tubes (15 mm × 150 mm) using 16 RPR-3500 Å lamps (emission centered at 350 nm). Samples (1 mL) were taken at regular intervals in both solutions. Samples were analyzed by HPLC using a CH_3CN/H_2O 50:50 mixture as mobile phase, a reversed phase column (3.9 mm × 30 cm; μBondapac C_{18} (5 μm)), and a detection wavelength of 254 nm. A 5% solution of mesitylene in 1,4-dioxane was used as internal standard (1 mL was added to every sample). The natural logarithm of residual concentration as a function of time of photolysis was plotted for both compounds. Rates of disappearance of 2.3×10^{-7} s^{-1} and 1.5×10^{-6} s^{-1} were obtained by least-squares analysis of the resulting plots for compound **6** and 2-nitrotoluene, respectively. Normalization gave a relative rate of disappearance (k_{rd}) of 0.15 for compound **6**.

*Measurement of the relative rate of disappearance of compound **7** upon photolysis*

The procedure used for the determination of the relative rate of disappearance (k_{rd}) of compound **7** is identical to that for compound **6**, with the exception that 1-ethyl-2-nitrobenzene (k_{rd} = 40) (11) was used as reference instead of 2-nitrotoluene (k_{rd} = 1). Rates of disappearance of 9.7×10^{-5} s^{-1} and 3.8×10^{-4} s^{-1} were obtained for compound **7** and 1-ethyl-2-nitrobenzene, respectively. Normalization gave a relative rate of disappearance (k_{rd}) of 10 for compound **7**.

Preparative photolysis of compound 7: Correlation between the expected photoproduct and an authentic synthetic sample of 13

A 10^{-2} M solution of 5-nitro-1,2,3,4-tetrahydro-1,4-ethanonaphthalene (**7**) (20 mg) in acetonitrile (10 mL) was photolyzed in Pyrex tubes for 2 h (70% conversion) at 350 nm. The photolyzed solution was analyzed by HPLC using CH_3CN/H_2O 50:50 (2 mL/min) as mobile phase, a reversed phase column (3.9 mm × 30 cm; μBondapac C_{18} (5 μm)), and a detection wavelength of 320 nm. Chromatograms showed four peaks corresponding to photoproducts at retention times of 2.50, 3.74, 4.44, and 5.08 min. The area under the peak at 4.44 min was increased by the addition of a few drops of a solution of an authentic synthetic sample of **13** in acetonitrile. A small amount of the photoproduct giving rise to the peak at 4.44 min was isolated by semi-preparative HPLC using CH_3CN/H_2O 50:50 (8 mL/min) as mobile phase, a semi-preparative reversed phase column (9.4 mm × 25 cm; CSC S5ODS2 C_{18} (5 μm)), and a detection wavelength of 280 nm. Because only a very small amount of photoproduct was isolated, many of the NMR signals of the photoproduct were obscured by signals generated by the solvent. However, the aromatic region was clear and the following signals were observed: (300 MHz; CH_3CN) δ: 7.67 (dd, J = 1.2 and 7.2 Hz), 7.23 (dd, J = 7.2 and 8.3 Hz), 6.23 (dd, J = 1.2 and 8.3 Hz). These signals are in perfect accord with those of the authentic sample: (300 MHz; CH_3CN) δ: 7.67 (dd, J = 1.3 and 7.5 Hz), 7.22 (dd, J = 7.5 and 8.4 Hz), 6.23 (dd, J = 1.3 and 8.4 Hz). The isolated photoproduct and the authentic synthetic sample were also analyzed by low resolution mass spectrometry using chemical ionization as ion source. Both samples showed peaks at m/z 204, corresponding to the protonated nitroso monomer, and at m/z 391, corresponding to the protonated nitroso dimer after loss of an atom of oxygen.

Photolysis of compound 7 and of its primary photoproduct 13

A solution of 5-nitro-1,2,3,4-tetrahydro-1,4-ethanonaphthalene (**7**) and one of 1-hydroxy-5-nitroso-1,2,3,4-tetrahydro-1,4-ethanonaphthalene (**13**) in acetonitrile were prepared and photolyzed in Pyrex tubes for 20 min at 350 nm. The photolyzed solutions were analyzed by HPLC using CH_3CN/H_2O 50:50 (2 mL/min) as mobile phase, a reversed phase column (3.9 mm × 30 cm; μ Bondapac C_{18} (5 μm)), and a detection wavelength of 254 nm. Chromatograms of the photolyzed solution of model compound **7** showed four peaks growing at retention times of 2.45, 3.85, 4.65, and 5.30 min while the peak corresponding to compound **7** at retention time 11.25 min was decreasing. Chromatograms of the photolyzed solution of synthetic **13**, which is the expected primary product of **7**, showed three peaks growing at retention times of 2.45, 3.85, and 5.30 min while the peak corresponding to compound **13** at a retention time of 4.65 min was decreasing. This experiment shows that **13** is the sole primary photoproduct resulting from photolysis of **7** and that the other products observed result from the subsequent photolysis of the primary product (**13**).

Acknowledgements

The authors are indebted to the Natural Sciences and Engineering Research Council of Canada, le Ministère de l'Éducation du Québec, and Merck Frosst Canada Inc. for financial support. Special thanks are also due to Prof. K. Steliou (Université de Montréal), for kindly providing access to the MODEL and MMX programs, and to W. Siebrand and M. Zgierski (NRC, Ottawa), for discussion.

1. R. Dessauer and J. P. Paris. *In* Advances in photochemistry. Vol. 1. *Edited by* W. A. Noyes, Jr., G. S. Hammond, and J. N. Pitts. Interscience, New York. 1963. p. 275.
2. (*a*) J. Hébert and D. Gravel. Can. J. Chem. **52**, 187 (1987); (*b*) D. Gravel, J. Hébert, and D. Thoraval. Can. J. Chem. **61**, 400 (1983); (*c*) D. Gravel, S. Murray, and G. Ladouceur. Chem. Commun. 1828 (1985); (*d*) B. Amit, U. Zehavi, and A. Patchornik. Isr. J. Chem. **12**, 103 (1974); W. N. R. Pillai. Synthesis, 1 (1981).
3. (*a*) E. Reichmanis, R. Gooden, C. W. Wilkins, Jr., and H. Schonhorn. J. Polym. Sci. Polym. Chem. Ed. **21**, 1075 (1983); (*b*) H. Barzynski and D. Sanger. Angew. Makromol. **93**, 131 (1981).
4. (*a* P. A. Leighton and F. A. Lucy. J. Chem. Phys. **2**, 756 (1934); (*b*) J. A. Berson and E. Brown. J. Am. Chem. Soc. **77**, 447 (1955); (*c*) P. de Mayo and S. T. Reid. Q. Rev. **15**, 393 (1961).
5. (*a*) B. B. Craig and S. J. Atherton. Proc. SPIE—Int. Soc. Opt. Eng. **482**, 96 (1984); (*b*) S. J. Atherton and B. B. Craig. Chem. Phys. Lett. **127**, 7 (1986); (*c*) J. D. Margerum, L. J. Miller, E. Saito, M. S. Brown, and H. S. Mosher. J. Phys. Chem. **66**, 2434 (1962); (*d*) G. Wettermark. J. Phys. Chem. **66**, 2560 (1962); (*e*) G. Wettermark and R. Ricci. J. Chem. Phys. **39**, 1218 (1963); (*f*) M. E. Langmuir, L. Dogliotti, E. D. Black, and G. Wettermark. J. Am. Chem. Soc. **91**, 2204 (1969).
6. R. B. Woodward and R. Hoffmann. The conservation of orbital symmetry. Verlag Chemie, GmbH, Weinheim. 1970. Chap. 7.
7. R. W. Yip, D. K. Sharma, R. Giasson, and D. Gravel. J. Phys. Chem. **89**, 5328 (1985).
8. J. March. Advanced organic chemistry. 3rd ed. Wiley–Interscience, New York. 1985. pp. 138–139.
9. R. W. Yip, D. K. Sharma, R. Giasson, and D. Gravel. J. Phys. Chem. **88**, 5770 (1984).
10. R. A. Snow, D. M. Cottrell, and L. A. Paquette. J. Am. Chem. Soc. **99**, 3734 (1977).
11. R. Giasson. Ph.D. thesis, Université de Montréal, 1988.
12. J. A. Osborn and G. Wilkinson. Inorg. Synth. **10**, 67 (1967).
13. (*a*) N. Meyer and D. Seebach. Chem. Ber. **113**, 1304 (1980); (*b*) C. A. Panetta and A. S. Dixit. Synthesis, 59 (1981).
14. I. Tabushi, H. Yamada, Z. Yoshida, and R. Oda. Bull. Chem. Soc. Jpn. **50**, 285 (1977).
15. (*a*) W. C. Groutas and D. Felker. Synthesis, 861 (1980); (*b*) M. E. Jung and M. A. Lyster. J. Org. Chem. **42**, 3761 (1977).
16. R. E. Harmon, G. Wellman, and S. K. Gupta. J. Org. Chem. **28**, 902 (1963).
17. (*a*) F. Rolla. J. Org. Chem. **47**, 4327 (1982); (*b*) J. N. Reed and V. Snieckus. Tetrahedron Lett. **24**, 3795 (1983).
18. (*a*) K. M. Ibne-Rasa and J. O. Edwards. J. Am. Chem. Soc. **84**, 763 (1962); (*b*) E. J. Corey and A. W. Gross. Tetrahedron Lett. **25**, 491 (1984).
19. W. K. Wong, H. Schupp, and W. Schnabel. Macromolecules, **22**, 2176 (1989).
20. J. T. Spraque, J. C. Tai, Y. Yuh, and N. L. Allinger. J. Comput. Chem. **8**, 581 (1987).
21. K. Padmanabhan, D. Döpp, K. Venkatesan, and V. Ramamurthy. J. Chem. Soc. Perkin Trans. 2, 897 (1986).
22. (*a*) W. Siebrand, T. A. Wildman, and M. Zgierski. Chem. Phys. Lett. **98**, 108 (1983); (*b*) Chem. Phys. Lett. **98**, 108 (1984); (*c*) J. Am. Chem. Soc. **106**, 4083 (1984); **106**, 4089 (1984).
23. (*a*) K. D. Asmus, A. Wigger, and A. Henglein. Ber. Bunsenges. Phys. Chem. **70**, 862 (1966); (*b*) A. Cu and A. C. Testa. J. Am. Chem. Soc. **96**, 1963 (1974).
24. W. C. Still, M. Khan, and A. Mitra. J. Org. Chem. **43**, 2923 (1978).
25. A. I. Vogel. Textbook of practical organic chemistry. Longman, New York. 1978. p. 409.

Can. J. Chem. Downloaded from www.nrcresearchpress.com by 84.41.108.74 on 09/07/12
For personal use only.

Boric acid: a new regiospecific decarboxylating agent. Syntheses of cyclic imines, β-enaminones, and β-enaminodiketones from β-enaminoesters

PHILIPPE DELBECQ, DANIEL BACOS, JEAN PIERRE CELERIER, AND GÉRARD LHOMMET[1]

Laboratoire de chimie des hétérocycles, Unité de recherche associée n°455, Université Pierre et Marie Curie, 4 Place Jussieu, 75252 Paris CEDEX 05, France

Received September 26, 1990

PHILIPPE DELBECQ, DANIEL BACOS, JEAN PIERRE CELERIER, and GÉRARD LHOMMET. Can. J. Chem. **69**, 1201 (1991).

The synthesis of cyclic imines **2**, β-enaminones **6**, and β-enaminodiketones **7** is described. Regio- and stereospecific thermolysis of β-enaminoesters **4** with boric acid permit these preparations in generally good yields.

Key words: boric acid, cyclic β-enaminoesters, decarboxylation, cyclic imines, cyclic β-enaminones.

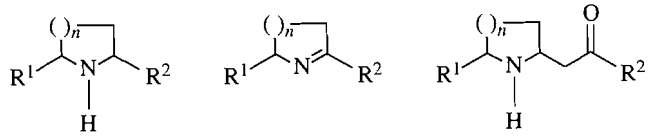
PHILIPPE DELBECQ, DANIEL BACOS, JEAN PIERRE CELERIER et GÉRARD LHOMMET. Can. J. Chem. **69**, 1201 (1991).

La synthèse d'imines **2**, de β-énaminones **6** et de β-énaminodicétones cycliques **7** est décrite. Cette nouvelle voie de synthèse met à profit l'action régio- et stéréo-spécifique de l'acide borique vis-à-vis des β-énaminoesters cycliques **4**.

Mots clés : acid borique, β-énaminoesters cycliques, décarboxylation, imines cycliques, β-énaminones cycliques.

Introduction

The significant bioacid activity of ant venoms has stimulated considerable interest and has led to the isolation of a large number of substances (1). Characteristic components present alkaloid structures with a monocyclic skeleton such as 2,5-dialkyl or dialkenyl pyrrolidines or pyrrolines **1** and **2** ($n = 1$) in the genus *Monomorium* (1) or 2,6-dialkyl piperidines or piperideines **1** and **2** ($n = 2$) in the genus *Solenopsis* (2). Ring substituent configurations are generally *trans* for five- and six-membered rings, but *cis* structures have been found in some species. Functionalized aza-heterocycles such as aminoketones have been isolated in the genus *Cryptolaemus montrouzieri* (3). Aminoketones such as **3** may also be precursors of numerous natural products (4).



1 **2** **3**

R^1, R^2 = alkyl or alkenyl

$( )_n = (CH_2)_n$

Monalkylated derivatives **1**, **2**, and **3** (R^1 = H) are also interesting for their insecticidal activities, and for their synthetic potential (5). Herein we wish to report our studies on the development of a general synthetic methodology for the preparation of monosubstituted cyclic imines and enamines. We describe the decarboxylation of cyclic β-enaminoesters and ketoesters in the presence of boric acid.

The general strategy for synthesis of cyclic imines, enamines, or amines is based on the availability of cyclic β-enaminoesters **4**, which are easily prepared in a few steps from lactams (6). A retrosynthetic study of compounds **1–3** in Scheme 1 shows that β-enaminoesters **4** can serve as key intermediates, which allow versatile preparation of amines or imines. Decarboxylation of **4** can directly lead to imines **2**.

Results and discussion

Compounds **4** are obtained by imidoylation of lactim ethers with Meldrum's acid, followed by monodecarboxylating transesterification (6) and then regiospecific C-alkylation with alkyl or alkenyl halides (*7a*). Results are summarized in Table 1.

TABLE 1. Alkylation of cyclic β-enaminoesters

Compound	n	R	Yield, %	Lit.
4*a*	1	-H	—	6, 7*b*
4*b*	1	$-CH_3$	74	7*a*, 7*b*
4*c*	1	$-C_2H_5$	95	7*a*
4*d*	1	$-CH_2-C_6H_5$	73	7*a*
4*e*	1	$-(CH_2)_3-C_6H_5$	61	—
4*f*	1	$-(CH_2)_2-CH=CH_2$	83	—
4*g*	1	$-(CH_2)_3-CH=CH_2$	55	—
4*h*	1	$-(CH_2)_4-CH=CH_2$	50	—
4*i*	1	$-(CH_2)_6-CH=CH_2$	52	—
4*j*	1	$-(CH_2)_8-CH=CH_2$	50	—
4*k*	1	$-(CH_2)_9-CH_3$	50	—
4*l*	2	-H	—	6, 7*b*
4*m*	2	$-CH_3$	80	7*a*, 7*b*
4*n*	2	$-C_2H_5$	50	7*a*
4*o*	2	$-(CH_2)_2-CH_3$	35	7*a*
4*p*	2	$-CH_2-C_6H_5$	48	7*a*
4*q*	2	$-(CH_2)_3-C_6H_5$	40	—
4*r*	2	$-(CH_2)_9-CH_3$	70	—
4*s*	2	$-(CH_2)_8-CH=CH_2$	50	—
4*t*	3	-H	—	6, 7*b*
4*u*	3	$-CH_3$	70	7*a*
4*v*	3	$-C_2H_5$	64	7*a*
4*w*	3	$-CH_2-C_6H_5$	42	—

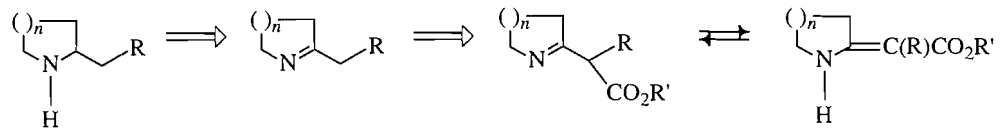
Decarboxylation using boric acid was reported by Wehrli and Chu, who demonstrated that β-ketoesters were transformed into ketones when the initial ester was enolizable (8). Because of the structural analogy existing between β-ketoesters and β-enaminoesters, we find that thermolysis of compounds **4** with boric acid is a good route to cyclic imines **2**. After transesterification by boric acid, a thermal rearrangement takes place. The boric complexes shown in brackets in Scheme 2 are not isolated but are treated with hydrochloric acid to lead to **2**. The yields are generally good, regardless of ring size. Because boric acid catalyzes the interconversion of tautomers **4** and **4'**, our method permits the formation of iminoesters **4'** whose structures are suitable for thermal rearrangement.

This method is particularly useful in preparing not only cyclic

[1]Author to whom correspondence may be addressed.

Printed in Canada / Imprimé au Canada

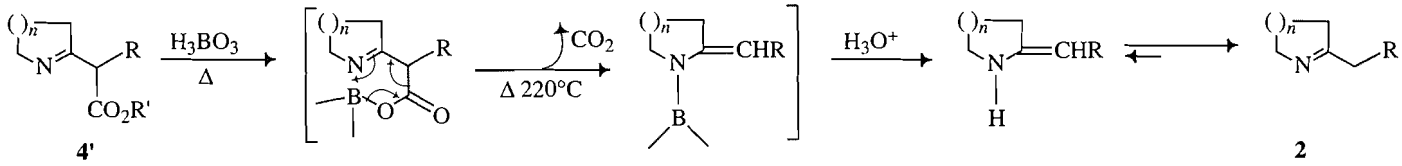
Can. J. Chem. Downloaded from www.nrcresearchpress.com by 84.41.108.74 on 09/07/12
For personal use only.



1 2 4' 4

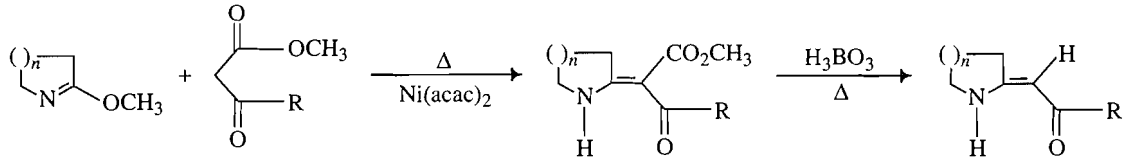
R = alkyl, alkenyl or acyl R' = Et

SCHEME 1



4' 2

SCHEME 2



5 6

SCHEME 3

TABLE 2. Cyclic monoalkylated imines **2**

Compound	*n*	R	Yield, %	Lit.
2*a*	1	-H	80	9, 10
2*b*	1	$-CH_3$	95	9
2*c*	1	$-C_2H_5$	70	9, 10
2*d*	1	$-CH_2-C_6H_5$	80	—
2*e*	1	$-(CH_2)_3-C_6H_5$	40	—
2*f*	1	$-(CH_2)_2-CH=CH_2$	80	—
2*g*	1	$-(CH_2)_3-CH=CH_2$	70	—
2*h*	1	$-(CH_2)_4-CH=CH_2$	80	—
2*i*	1	$-(CH_2)_6-CH=CH_2$	70	—
2*j*	1	$-(CH_2)_8-CH=CH_2$	80	—
2*k*	1	$-(CH_2)_9-CH_3$	90	—
2*l*	2	-H	70	11
2*m*	2	$-CH_3$	65	—
2*n*	2	$-C_2H_5$	65	10, 11
2*o*	2	$-(CH_2)_2-CH_3$	17	11
2*p*	2	$-CH_2-C_6H_5$	70	—
2*q*	2	$-(CH_2)_3-C_6H_5$	30	—
2*r*	2	$-(CH_2)_9-CH_3$	80	12
2*s*	2	$-(CH_2)_8-CH=CH_2$	70	—
2*t*	3	-H	40	10
2*u*	3	$-CH_3$	35	13
2*v*	3	$-C_2H_5$	30	13
2*w*	3	$-CH_2-C_6H_5$	39	—

TABLE 3. Cyclic β-enaminones **6**

Compound	*n*	R	Yield, %	Lit.
6*a*	1	$-CH_3$	50	19
6*b*	1	$-C_3H_7$	46	—
6*c*	1	$-C_6H_5$	60	20, 21
6*d*	2	$-CH_3$	43	7*b*
6*e*	2	$-C_3H_7$	30	—
6*f*	2	$-C_6H_5$	50	21
6*g*	3	$-CH_3$	39	—
6*h*	3	$-C_3H_7$	40	—
6*i*	3	$-C_6H_5$	27	21, 22

TABLE 4. Cyclic β-enaminoketodiesters **5**

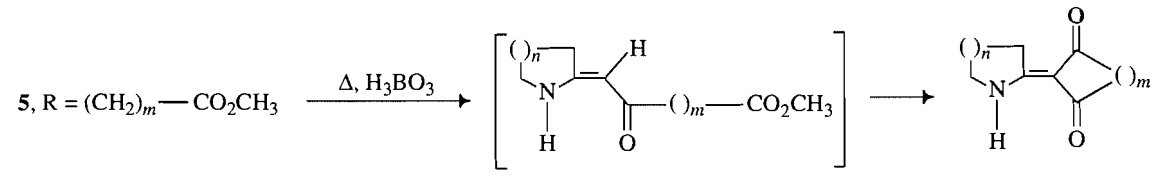
Compound	*n*	*m*	Yield, %
5*a*	1	2	52
5*b*	1	3	47
5*c*	2	2	41
5*d*	2	3	34
5*e*	3	2	21
5*f*	3	3	27

imines **2**, which possess an insecticidal activity comparable with ant venom components, but also other natural products such as *Coniceine* **2** ($n = 2$, R = $-C_3H_7$) (Table 2).

We extended these results by preparing cyclic enaminones **6** in the same way. Such structures are important building blocks for the synthesis of numerous natural products, but only a few enaminones have been isolated due to their unstability. We had previously shown that regiospecificity in the acylation of β-enaminoesters depends on heterocycle size (7), so a direct condensation between lactim ethers and β-ketoesters is the best way to prepare β-enaminoketoesters **5** (14). In any case, this condensation is stereospecific and only *E* compounds **5** are obtained (14) (Scheme 3).

Treatment of **5** with alkoxides has been reported to be regiospecific but leads only to β-enaminoesters **4** via a deacylation reaction (15), and decarboxylations in acidic media (16, 17)

Can. J. Chem. Downloaded from www.nrcresearchpress.com by 84.41.108.74 on 09/07/12
For personal use only.



SCHEME 4

TABLE 5. Cyclic β-enaminoketodiesters **7**

Compound	*n*	*m*	Yield, %	Lit.
7*a*	1	2	12	24
7*b*	1	3	40	—
7*c*	2	2	10	24
7*d*	2	3	36	24
7*e*	3	2	15	24
7*f*	3	3	20	25

are not regiospecific. Under our reaction conditions, however, boric acid can be used to prepare cyclic β-enaminones **6** (18). Once more, the decarboxylation is regio- and stereospecific and *Z* derivatives **6** are obtained (Table 3).

If the R subsituent of the β-ketoester bears another ester function, new β-enaminoketodiesters **5** (R = $-(CH_2)_m-CO_2CH_3$) are prepared (Table 4). Again the thermolysis is regiospecific, only the conjugated ester being decarbalkoxylated with boric acid (Table 5). When R = $-(CH_2)_3-CO_2CH_3$ the five-membered ring compound **6** was isolated, which demonstrates the regiospecificity of the reaction (Scheme 4). However, the enaminone-diester intermediate is generally not isolated and a cyclization by intramolecular C-acylation occurs. Some of these bicyclic β-enaminodiketones **7** have been prepared by direct condensation between lactim ethers and cyclic β-diketones, but our method is more general and permits the syntheses of various compounds **7** regardless of the size of the heterocycle.

Conclusion

In conclusion, this investigation demonstrates that boric acid is a versatile reagent for organic synthesis, especially for the preparation of cyclic imines, β-enaminones, and β-enaminodiketones via stereospecific and regiospecific decarboxylation of substituted cyclic β-enaminoesters.

Experimental

Melting points were determined in open capillaries with a Büchi apparatus and are uncorrected. ^1H NMR spectra were recorded on Varian A60-A and Bruker 80, 200, and 500 MHz spectrometers. Chemical shifts are reported in δ values relative to Me_4Si as internal standard. Abbreviations used are m: multiplet, s: singlet, d: doublet, t: triplet, q: quartet, br s: broad singlet. Infrared spectra were taken on a Philips PU 9700 spectrometer.

Preparation of alkylated cyclic β-enaminoesters 4

General procedure for 5- or 6-membered rings

Cyclic β-enaminoesters (0.02 mol) prepared by imidoylation of lactim ethers as described by Celerier *et al.* (6) were added to a suspension of sodium hydride (0.022 mol) in anhydrous toluene (50 mL). After heating until dissolution of the sodium salt, the mixture was cooled, then halide (0.025 mol) in toluene (50 mL) was added dropwise. After heating 12 h at reflux, water was added and the aqueous phase separated, neutralized with 10% aqueous hydrochloric acid solution, and extracted with chloroform (3 × 30 mL). Organic phases were combined and dried over sodium sulfate. Crude products were purified by distillation or recrystallization.

General procedure for 7-membered rings

Cyclic β-enaminoesters (0.02 mol) (6) were refluxed in 50 mL of alkyl iodide for 12 h. Excess iodide was evaporated; the precipitate was washed three times with diethyl ether, and then poured into 50 mL of saturated aqueous potassium carbonate. The solution was extracted with chloroform (3 × 50 mL), and the organic layers were dried over sodium sulfate, evaporated, and the crude products purified by distillation or recrystallization.

Ethyl 5-phenyl-2-(α-tetrahydropyrrolylidene) pentanoate **4***e*. Yield: 61%; bp (0.01 Torr; 1 Torr = 133.3 Pa): 225°C; IR (neat) ν(cm^{-1}): 3360, 1620, 1570; ^1H NMR ($CDCl_3$) δ(ppm): 1.23 (3H, t, *J* = 7 Hz), 1.50–1.78 (10H, m), 3.20–3.42 (2H, m), 4.15 (2H, q, *J* = 7 Hz), 7.20 (5H, br s), 8.00–8.40 (1H, m). Anal. calcd. for $C_{17}H_{23}NO_2$: C 74.69, H 8.48, N 5.12; found: C 74.48, H 8.37, N 5.29.

Ethyl 2-(α-tetrahydropyrrolyidene)-5-hexenoate **4***f*. Yield: 83%; bp (0.01 Torr): 109°C; IR (neat) ν(cm^{-1}): 3350, 1660, 1590; ^1H NMR ($CDCl_3$) δ (ppm): 1.20 (3H, t, *J* = 7 Hz), 130–2.30 (6H, m), 2.40–2.55 (2H, m), 3.35–3.60 (2H, m), 4.10 (2H, q, *J* = 7 Hz), 4.70–5.20 (2H, m), 5.50–6.15 (1H, m), 8.00–8.30 (1H, m). Anal. calcd. for $C_{12}H_{19}NO_2$: C 68.86, H 9.15, N 6.69; found: C 69.18, H 9.01, N 6.77.

Ethyl 2-(α-tetrahydropyrrolylidene)-6-heptenoate **4***g*. Yield : 55%; bp (1 Torr): 160°C; IR (neat) ν(cm^{-1}): 3350, 1660, 1590; ^1H NMR (CCl_4) δ(ppm): 1.20 (3H, t, *J* = 7 Hz), 1.10–2.35 (8H, m), 2.40–2.60 (2H, m), 3.40–3.55 (2H, m), 4.05 (2H, q, *J* = 7 Hz), 4.60–6.15 (2H, m), 5.70–6.15 (1H, m), 8.00–8.35 (1H, m). Anal. calcd. for $C_{13}H_{21}NO_2$: C 69.92, H 9.48, N 6.27; found: C 70.16, H 9.32, N 6.22.

Ethyl 2-(α-tetrahydropyrrolylidene)-7-octenoate **4***h*. Yield: 50%; bp (0.1 Torr): 170°C; IR (neat) ν(cm^{-1}): 3350, 1660, 1585; ^1H NMR (CCl_4) δ(ppm): 1.25 (3H, t, *J* = 7 Hz), 1.20–2.40 (10H, m), 2.40–2.65 (2H, m), 3.40–3.65 (2H, m), 4.10 (2H, q, *J* = 7 Hz), 4.70–5.20 (2H, m), 5.40–6.10 (1H, m), 8.00–8.35 (1H, m). Anal. calcd. for $C_{14}H_{23}NO_2$: C 70.85, H 9.77, N 5.90; found: C 70.69, H 9.86, N 5.98.

Ethyl 2-(α-tetrahydropyrrolylidene)-9-decenoate **4***i*. Yield: 52%; bp (1 Torr): 190°C; IR (neat) ν(cm^{-1}): 3360, 1660, 1600; ^1H NMR (CCl_4) δ(ppm): 1.24 (3H, t, *J* = 7 Hz), 1.10–2.80 (16H, m), 3.30–3.45 (2H, m), 4.05 (2H, q, *J* = 7 Hz), 4.70–5.20 (2H, m), 5.45–6.15 (1H, m), 8.10–8.45 (1H, m). Anal. calcd. for $C_{16}H_{27}NO_2$: C 72.41, H 10.26, N 5.28; found: C 72.35, H 10.04, N 5.48.

Ethyl 2-(α-tetrahydropyrrolylidene)-11-dodecenoate **4***j*. Yield: 50%; bp (0.01 Torr): 150°C; IR (neat) ν(cm^{-1}): 3340, 1660, 1590; ^1H NMR ($CDCl_3$) δ(ppm): 1.22 (3H, t, *J* = 7 Hz), 1.00–2.30 (18H, m), 2.40–2.65 (2H, m), 3.40–3.60 (2H, m), 4.16 (2H, q, *J* = 7 Hz), 4.75–5.20 (2H, m), 5.50–6.20 (1H, m), 8.20–8.35 (1H, m). Anal. calcd. for $C_{18}H_{31}NO_2$: C 73.67, H 10.65, N 4.77; found: C 73.29, H 10.54, N 4.82.

Ethyl 2-(α-tetrahydropyrrolylidene)-dodecanoate **4***k*. Yield: 55%; bp (0.05 Torr): 140°C; IR (neat) ν(cm^{-1}): 3360, 1650, 1580; ^1H NMR (CCl_4) δ(ppm): 1.24 (3H, t, *J* = 7 Hz), 0.80–2.20 (23H, m), 2.50–2.75 (2H, m), 3.40–3.60 (2H, m), 4.23 (2H, q, *J* = 7 Hz), 8.10–8.35 (1H, m). Anal. calcd. for $C_{18}H_{33}NO_2$: C 73.17, H 11.26, N 4.74; found: C 72.94, H 11.02, N 4.87.

Ethyl 5-phenyl-2-(α-hexahydropyridylidene)-pentanoate **4***q*. Yield:

Can. J. Chem. Downloaded from www.nrcresearchpress.com by 84.41.108.74 on 09/07/12
For personal use only.

Can. J. Chem. Downloaded from www.nrcresearchpress.com by 84.41.108.74 on 09/07/12
For personal use only.

40%; bp (0.01 Torr): 160°C; IR (neat) $\nu(cm^{-1})$: 3350, 1645, 1580; ^1H NMR ($CDCl_3$) δ(ppm): 1.23 (3H, t, J = 7 Hz), 1.40–3.00 (12H, m), 3.10–3.25 (2H, m), 4.15 (2H, q, J = 7 Hz), 7.20 (5H, br s), 8.95–9.20 (1H, m). Anal. calcd. for $C_{18}H_{25}NO_2$: C 75.22, H 8.77, N 4.87; found: C 74.97, H 8.93, N 4.82.

Ethyl 2-(α-hexahydropyridylidene)-dodecanoate **4***r*. Yield: 70%; bp (0.01 Torr): 155°C; IR (neat) $\nu(cm^{-1})$: 3220, 1630, 1590; ^1H NMR ($CDCl_3$) δ(ppm): 0.75–0.95 (3H, m), 1.20–2.25 (25H, m), 2.25–2.55 (2H, m), 3.10–3.45 (2H, m), 4.00–4.20 (2H, m), 9.00–9.25 (1H, m). Anal. calcd. for $C_{19}H_{35}NO_2$: C 73.73, H 11.40, N 4.53; found: C 73.48, H 11.26, N 4.31.

Ethyl 2-(α-hexahydropyridylidene)-dodecenoate **4***s*. Yield: 50%; bp (0.01 Torr): 165°C; IR (neat) $\nu(cm^{-1})$: 3200, 1630, 1580; ^1H NMR ($CDCl_3$) δ(ppm): 1.26 (3H, t, J = 7 Hz), 1.20–2.65 (22H, m), 3.10–3.35 (2H, m), 4.11 (2H, q, J = 7 Hz), 4.80–5.20 (2H, m), 5.50–6.15 (1H, m), 8.80–9.20 (1H, m). Anal. calcd. for $C_{19}H_{33}NO_2$: C 74.22, H 10.81, N 4.56; found: C 74.51, H 10.59, N 4.62.

Ethyl 3-phenyl-2-(α-hexahydroazepinylidene)-propanoate **4***w*. Yield: 42%; bp (0.05 Torr): 155°C; IR (neat) $\nu(cm^{-1})$: 3240, 1630, 1585; ^1H NMR ($CDCl_3$) δ(ppm): 1.16 (3H, t, J = 7 Hz), 1.25–1.75 (6H, m), 2.25–2.60 (2H, m), 3.15–3.30 (2H, m), 3.70 (2H, s), 4.20 (2H, q, J = 7 Hz), 7.10–7.20 (5H, m), 9.05–9.30 (1H, m). Anal. calcd. for $C_{17}H_{23}NO_2$: C 74.69, H 8.48, N 5.12; found: C 74.41, H 8.26, N 5.05.

Cyclic imines **2***: general procedure for preparation*

A mixture of β-enaminoester **4** (0.04 mol) and 2.78 g of solid boric acid (0.045 mol) was heated 1 h at 180°C in an Erlenmeyer equipped with a distillation column to collect water and alcohol. The reaction mixture was then cooled, and water (40 mL) and dichloromethane (10 mL) were added. After the precipitate was dissolved, the aqueous layer was extracted with CH_2Cl_2 (3 × 25 mL), the organic layers combined, dried over sodium sulfate, and solvent removed under reduced pressure. Crude products were then distilled.

2-(1-Phenylethyl)-3,4-dihydro-5H-pyrrole **2***d*. Yield: 80%; bp (0.01 Torr): 110°C; IR (neat) $\nu(cm^{-1})$: 1650, 1610, 1500; ^1H NMR ($CDCl_3$) δ(ppm): 1.70–2.30 (2H, m), 2.45–3.35 (6H, m), 3.85–4.20 (2H, m), 7.35–7.55 (5H, br s); ^{13}C NMR ($CDCl_3$) δ(ppm): 22.6, 32.6, 35.3, 60.9, 126.1, 128.2, 128.4, 141.6, 177.4. Anal. calcd. for $C_{12}H_{15}N$: C 83.19, H 8.73, N 8.09; found: C 83.01, H 8.98, N 7.82.

2-(4-phenylbutyl)-3,4-dihydro-5H-pyrrole **2***e*. Yield: 40%; bp (0.01 Torr): 118°C; IR (neat) $\nu(cm^{-1})$: 1640, 1605, 1495; ^1H NMR ($CDCl_3$) δ(ppm): 1.45–2.05 (6H, m), 2.10–2.75 (6H, m), 3.65–3.90 (2H, m), 7.05–7.25 (5H, br s); ^{13}C NMR ($CDCl_3$) δ(ppm): 22.0, 25.4, 30.7, 33.0, 35.1, 36.6, 125.1, 127.6, 141.7, 177.2. Anal. calcd. for $C_{14}H_{19}N$: C 83.53, H 9.51, N 6.96; found: C 83.16, H 9.73, N 7.15.

2-(1-Pentenyl)-3,4-dihydro-5H-pyrrole **2**f. Yield: 80%; bp (20 Torr): 60°C; IR (neat) $\nu(cm^{-1})$: 3080, 1650; ^1H NMR ($CDCl_3$) δ(ppm): 1.35–2.10 (6H, m), 215–2.50 (4H, m), 3.55–3.85 (2H, m), 4.65–5.00 (2H, m), 5.55–5.90 (1H, m); ^{13}C NMR ($CDCl_3$) δ(ppm): 22.4, 25.4, 32.9, 37.1, 60.6, 114.7, 138.1, 177.9. Anal. calcd. for $C_9H_{15}N$: C 78.77, H 11.02, N 10.21; found: C 79.04, H 11.15, N 9.87.

2-(1-Hexenyl)-3,4-dihydro-5H-pyrrole **2***g*. Yield: 70%; bp (0.5 Torr): 52°C; IR (neat) $\nu(cm^{-1})$: 3080, 1640; ^1H NMR ($CDCl_3$) δ(ppm): 1.35–2.05 (8H, m), 2.10–2.65 (4H, m), 3.60–4.00 (2H, m), 4.80–5.25 (2H, m), 5.35–6.15 (1H, m); ^{13}C NMR ($CDCl_3$) δ(ppm): 22.1, 25.4, 28.3, 33.1, 36.7, 114.0, 138.1, 177.4. Anal. calcd. for $C_{10}H_{17}N$: C 79.40, H 11.34, N 9.26; found: C 79.12, H 11.48, N 9.06.

2-(1-Heptenyl)-3,4-dihydro-5H-pyrrole **2***h*. Yield: 80%; bp (0.05 Torr): 60°C; IR (neat) $\nu(cm^{-1})$: 3080, 1650; ^1H NMR ($CDCl_3$) δ(ppm): 1.20–1.80 (10H, m), 1.85–2.45 (4H, m), 3.45–3.85 (2H, m), 4.75–5.15 (2H, m), 5.35–6.10 (1H, m); ^{13}C NMR ($CDCl_3$) δ(ppm): 22.1, 25.7, 28.2, 28.5, 33.1, 33.3, 36.7, 60.3, 113.8, 138.3, 177.5. Anal. calcd. for $C_{11}H_{19}N$: C 79.94, H 11.59, N 8.48; found: 8.07, H 11.71, N 8.26.

2-(1-Nonenyl)-3,4-dihydro-5H-pyrrole **2***i*. Yield: 70%; bp (3 Torr): 100°C; IR (neat) $\nu(cm^{-1})$: 3080, 1640; ^1H NMR ($CDCl_3$) δ(ppm): 1.10–1.85 (14H, m), 1.90–2.50 (4H, m), 3.50–3.90 (2H, m), 4.75–5.15 (2H, m), 5.30–6.10 (1H, m). ^{13}C NMR ($CDCl_3$) δ(ppm): 22.3, 26.1, 28.6, 28.7, 28.9, 29.1, 33.5, 36.8, 60.5, 113.8, 138.7, 177.8. Anal. calcd. for $C_{13}H_{23}N$: C 80.76, H 11.99, N 7.25; found: C 80.45, H 12.28, N 7.03.

2-(1-Undecenyl)-3,4-dihydro-5H-pyrrole **2***j*. Yield: 80%; bp (0.01 Torr): 105°C; IR (neat) $\nu(cm^{-1})$: 3090, 1645, 1640; ^1H NMR ($CDCl_3$) δ(ppm): 1.10–1.75 (14H, m), 1.80–2.10 (4H, m), 2.15–2.55 (4H, m), 3.60–3.95 (2H, m), 4.75–5.20 (2H, m), 5.55–6.15 (1H, m); ^{13}C NMR ($CDCl_3$) δ(ppm): 22.6, 26.4, 28.9, 29.1, 29.4, 33.8, 37.1, 60.8, 114.1, 139.1, 178.3, Anal. calcd. for $C_{15}H_{27}N$: C 81.38, H 12.29, N 6.33; found: C 81.02, H 12.51, N 6.04.

2-(1-Undecanyl)-3,4-dihydro-5H-pyrrole **2***k*. Yield: 90%; bp (0.01 Torr): 100°C; IR (neat) $\nu(cm^{-1})$: 1635; ^1H NMR ($CDCl_3$) δ(ppm): 0.65–1.00 (3H, m), 1.10–2.20 (20H, m), 2.20–2.60 (4H, m), 3.65–4.00 (2H, m); ^{13}C NMR ($CDCl_3$) δ(ppm): 14.1, 22.6, 26.4, 29.4, 29.5, 29.6, 31.9, 33.9, 37.1, 60.8, 178.3. Anal. calcd. for $C_{15}H_{29}N$: 80.64, H 13.09, N 6.27; found: C 80.37, H 12.83, N 6.52.

2-Methyl-3,4,5,6-tetrahydropyridine **2***m*. Yield: 65%; bp (60 Torr): 70°C; IR (neat) $\nu(cm^{-1})$: 2920, 1660; ^1H NMR ($CDCl_3$) δ(ppm): 1.08 (3H, t, J = 7 Hz), 1.45–1.85 (4H, m), 1.95–2.40 (4H, m), 3.40–3.78 (2H, m); ^{13}C NMR ($CDCl_3$) δ(ppm): 10.6, 19.7, 22.0, 28.8, 33.8, 49.2, 171.8. Anal. calcd. for $C_{17}H_{13}N$: C 75.61, H 11.79, N 12.60; found: C 75.42, H 11.93, N 12.65.

2-(1-Phenylethyl-3,4,5,6-tetrahydropyridine **2***p*. Yield: 70%; bp (0.01 Torr): 85°C; IR (neat) $\nu(cm^{-1})$: 1655, 1590, 1490; ^1H NMR ($CDCl_3$) δ(ppm): 1.30–1.65 (4H, m), 1.70–2.15 (2H, m), 2.20–2.55 (2H, m), 2.60–3.00 (2H, m), 3.35–3.70 (2H, m), 7.05–7.25 (5H, br s); ^{13}C NMR ($CDCl_3$) δ(ppm): 19.6, 21.9, 29.6, 32.6, 42.4, 49.2, 125.8, 128.3, 142.0, 170.1. Anal. calcd. for $C_{13}H_{17}N$: C 83.37, H 9.15, N 7.48; found: C 83.,64, H 9.08, N 7.20.

2-(4-Phenylbutyl)-3,4,5,6-tetrahydropyridine **2***q*. Yield: 30%; bp (0.1 Torr): 1.15°C; IR (neat) $\nu(cm^{-1})$: 1660, 1595, 1500; ^1H NMR ($CDCl_3$) δ(ppm): 1.35–1.80 (8H, m), 1.85–2.30 (4H, m), 2.40–2.75 (2H, m), 3.35–3.70 (2H, m), 7.10–7.30 (5H, br s); ^{13}C NMR ($CDCl_3$) δ(ppm): 19.4, 21.7, 25.8, 28.8, 31.0, 35.6, 40.7, 49.0, 125.4, 128.0, 128.1, 142.3, 170.5. Anal. calcd. for $C_{15}H_{21}N$: C 83.66, H 9.83, N 6.51; found: C 83.51, H 10.05, N 6.44

2-(1-Undecenyl)-3,4,5,6-tetrahydropyridine **2***s*. Yield: 70%; bp (0.01 Torr): 113°C; IR (neat) $\nu(cm^{-1})$: 3075, 1660, 1640, 1640, 1590; ^1H NMR ($CDCl_3$) δ(ppm): 1.15–1.45 (16H, m), 1.50–1.90 (4H, m), 1.95–2.35 (4H, m), 3.25–3.70 (2H, m), 4.80–5.20 (2H, m), 5.45–6.10 (1H, m). Anal. calcd. for $C_{16}H_{29}N$: C 81.63, H 12.42, N 5.95; found: C 81.82, H 12.21, N 5.69.

2-(1-Phenylethyl)-3,4,5,6-tetrahydro-5H-azepine **2***w*. Yield: 39%; bp (0.05 Torr): 105°C; IR (neat) $\nu(cm^{-1})$: 1660, 1580, 1495, 1440; ^1H NMR ($CDCl_3$) δ(ppm): 1.05–1.90 (8H, m), 2.05–3.00 (4H, m), 3.35–3.70 (2H, m), 7.05–7.20 (5H, br s). Anal. calcd. for $C_{14}H_{19}N$: C 84.37, H 8.60, N 7.03; found: 84.17, H 8.85, N 6.91.

β-Enaminones **6***: general procedure for preparation*

A mixture of β-enaminoketoester **5** (0.01 mol) and solid boric acid (0.1 mol for all compounds, except 0.02 mol for acetyl derivatives) was heated 1 h in an oil bath at 225°C. After cooling, the reaction mixture was poured into a beaker containing 30 mL of water, 20 mL of chloroform, and 10 g of potassium carbonate. After agitation (0.5 h) and concentration under reduced pressure to half the original volume, 20 mL of 20% hydrochloric acid and methanol (1:1) was added and the mixture stirred 0.5 h, neutralized with K_2CO_3, extracted with chloroform (3 × 30 mL), dried over sodium sulfate, and the solvents removed under reduced pressure. All crude products were purified by distillation or recrystallization. For thermally sensitive products, purification was achieved by column chromatography.

(α-Tetrahydropyrrolyidene)-propanone **6***a*. Yield: 50%; bp (0.1 Torr): 122°C (19), IR (neat) $\nu(cm^{-1})$: 3300, 2980, 2880, 1610, 1540, 1500, 1430; ^1H NMR ($CDCl_3$) δ(ppm): 1.75–2.20 (2H, m), 2.05 (3H, s), 2.30–2.80 (2H, m), 3.40–3.70 (2H, m), 5.10 (1H, s), 10.50–11.30 (1H, m); ^{13}C NMR ($CDCl_3$) δ(ppm): 21.2, 28.4, 32.1, 47.3, 89.5, 167.2, 194.4.

1-(α-Tetrahydropyrrolylidene)-2-pentanone **6***b*. Yield: 46%; purified by chromatography (silica gel 60, Et_2O, R_f: 0.32); IR ($CHBr_3$) $\nu(cm^{-1})$: 3280, 3020, 2960, 2870, 1610, 1525, 1500, 1460, 1430; ^1H

Can. J. Chem. Downloaded from www.nrcresearchpress.com by 84.41.108.74 on 09/07/12
For personal use only.

NMR ($CDCl_3$) δ(ppm): 0.80–0.95 (3H, m), 1.50–1.70 (2H, m), 1.85–2.10 (2H, m), 2.15–2.30 (2H, m), 2.50–2.65 (2H, m), 3.50–3.60 (2H, m), 5.10 (1H, s), 9.60–10.05 (1H, m); ^{13}C NMR ($CDCl_3$) δ(ppm): 14.1, 19.6, 21.3, 32.3, 43.9, 47.4, 89.3, 167.4, 198.2. Anal. calcd. for $C_9H_{15}NO$: C 70.55, H 9.87, N 9.14; found: C 70.28, H 9.70, N 9.16.

(α-Tetrahydropyrrolylidene)-acetophenone **6***c*. Yield: 60%; mp (ethanol): 109°C (20, 21); IR ($CHBr_3$) ν(cm^{-1}): 3280, 3020, 2880, 1605, 1575, 1510, 1480, 1425; ^1H NMR ($CDCl_3$) δ(ppm): 1.90–2.10 (2H, m), 2.65–2.80 (2H, m), 3.55–3.75 (2H, m), 5.80 (1H, s), 7.30–7.50 (3H, m), 7.80–7.95 (2H, m), 10.10–10.45 (1H, m); ^{13}C NMR ($CDCl_3$) δ(ppm): 21.4, 32.9, 47.7, 86.5, 127.0, 128.1, 130.4, 140.3, 169.2, 188.0.

(α-Hexahydropyridylidene)-propanone **6***d*. Yield: 43%; bp (0.1 Torr): 98°C (7*b*); IR (neat) ν(cm^{-1}): 3400, 2940, 2860, 1605, 1560, 1520, 1445, 1420; ^1H NMR ($CDCl_3$) δ(ppm): 1.50–1.95 (4H, m), 1.85 (3H, s), 2.05–2.45 (2H, m), 3.10–3.50 (2H, m), 4.75 (1H, s), 10.70–11.50 (1H, m); ^{13}C NMR ($CDCl_3$) δ(ppm): 19.2, 22.2, 28.3, 28.4, 40.8, 93.3, 164.1, 193.7.

1-(α-Hexahydropyridylidene)-2-pentanone **6***e*. Yield: 30%; purified by chromatography (silica gel 60, Et_2O, R_f: 0.44); IR ($CHBr_3$) ν(cm^{-1}): 3200, 3020, 2940, 2870, 1600, 1540, 1445, 1420; ^1H NMR ($CDCl_3$) δ(ppm): 0.80–0.95 (3H, m), 1.35–1.85 (6H, m), 2.05–2.20 (2H, m), 2.25–2.35 (2H, m), 3.20–3.35 (2H, m), 4.80 (1H, s), 10.95–11.25 (1H, m); ^{13}C NMR ($CDCl_3$) δ(ppm): 14.0, 19.3, 19.7, 22.3, 28.4, 40.9, 43.9, 92.9, 164.0, 197.1. Anal. calcd. for $C_{10}H_{17}NO$: C 71.81, H 10.25, N 8.38; found: C 72.04, H 10.21, N 8.52.

(α-Hexahydropyridylidene)-acetophenone **6***f*. Yield: 50% (21); purified by chromatography (silica gel 60, Et_2O, R_f: 0.51); IR ($CHBr_3$) ν(cm^{-1}): 3350, 3020, 2940, 2860, 1595, 1580, 1530, 1480, 1440, 1420: ^1H NMR ($CDCl_3$) δ(ppm): 1.60–1.90 (6H, m), 2.40–2.55 (2H, m), 3.30–3.45 (2H, m), 5.00 (1H, s), 7.25–7.50 (3H, m), 7.70–7.90 (2H, m); ^{13}C NMR ($CDCl_3$) δ(ppm): 19.3, 22.2, 28.9. 41.1, 90.1, 126.7, 128.0, 130.2, 140.6, 165.9, 187.1.

(α-Hexahydroazepinylidene)-propanone **6***g*. Yield: 39%; bp (0.05 Torr): 110°C; IR (neat) ν(cm^{-1}): 3400, 2920, 2860, 1600, 1560, 1440; ^1H NMR ($CDCl_3$) δ(ppm): 1.30–1.85 (4H, m), 2.00 (3H, s), 2.10–2.50 (2H, m), 3.10–3.50 (2H, m), 4.75 (1H, s), 10.80–11.70 (1H, m); ^{13}C NMR ($CDCl_3$) δ(ppm): 25.8, 28.7, 29.3, 30.4, 34.6, 44.0, 93.9, 169.4, 194.9. Anal. calcd. for $C_9H_{15}NO$: C 70.55, H 9.87, N 9.14; found: C 70.59, H 9.72, N 8.98.

1-(α-Hexahydroazepinylidene)-2-pentanone **6***h*. Yield: 40%; purified by chromatography (silica gel 60, Et_2O, R_f: 0.64); IR (neat) ν(cm^{-1}): 3350, 3020, 2930, 2870, 1690, 1590, 1460, 1430; ^1H NMR ($CDCl_3$) δ(ppm): 0.75–0.95 (3H, m), 1.40–1.75 (8H, m), 2.05–2.30 (4H, m), 3.15–3.35 (2H, m), 4.90 (1H, s), 10.70–11.20 (1H, m); ^{13}C NMR ($CDCl_3$) δ(ppm): 13.9, 19.5, 25.8, 29.3, 30.4, 34.7, 43.9, 44.0, 93.5, 169.5, 198.3. Anal. calcd. for $C_{11}H_{19}NO$: C 72.88, H 10.57, N 7.73; found: C 72.99, H 10.55, N 7.79.

(α-Hexahydroazepinylidene)-acetophenone **6***i*. Yield: 27% (21, 22); purified by chromatography (silica gel 60, Et_2O, R_f: 0.70); mp: 76°C; IR ($CHBr_3$) ν(cm^{-1}): 3250, 3020, 2920, 2850, 1715, 1590, 1580, 1540, 1460, 1440; ^1H NMR ($CDCl_3$) δ(ppm): 1.50–2.10 (6H, m), 2.40–2.60 (2H, m), 3.40–3.55 (2H, m), 5.40–6.00 (1H, m), 7.10–7.60 (3H, m), 7.70–8.10 (2H, m), 11.50–11.85 (1H, m); ^{13}C NMR ($CDCl_3$) δ(ppm): 25.6, 29.1, 30.6, 35.4, 44.5, 90.7, 126.9, 128.1, 130.4, 140.3, 171.8, 188.2.

Methyl 6-(α-tetrahydropyrrolylidene)-5-oxohexanoate **6** (n = 1, m = 3). Yield: 49% (23); bp (0.1 Torr): 170°C; IR (neat) ν(cm^{-1}): 3280, 3020, 2950, 2880, 1720, 1610, 1530, 1500, 1450, 1430; ^1H NMR ($CDCl_3$) δ(ppm): 1.60–1.95 (4H, m), 1.95–2.30 (4H, m), 2.30–2.55 (2H, m), 3.25–3.50 (2H, m), 3.47 (3H, s), 4.90 (1H, s), 9.50–9.75 (1H, m); ^{13}C NMR ($CDCl_3$) δ(ppm): 21.2, 32.2, 33.4 40.4, 47.4, 51.2, 89.0, 167.5, 173.7, 196.2.

β-Enaminoketodiesters **5***: general procedure for preparation*

Ketodiester (0.05 mol) and 0.055 mol of lactim ether were heated 14 h at 120°C without solvent. Crude products were then purified.

Dimethyl-2-(α-tetrahydropyrrolylidene)-3-oxohexane-1,6-dioate **5***a* (n = 1, m = 2). Yield: 52%; mp (ethanol): 49°C; IR ($CHBr_3$) ν(cm^{-1}): 3200, 3020, 1720, 1670, 1590, 1540, 1470, 1435; ^1H NMR ($CDCl_3$) δ(ppm): 1.85–2.10 (2H, m), 2.45–2.85 (2H, m), 3.05–3.20 (4H, m), 3.50–3.85 (2H, m), 3.65 (3H, s), 3.70 (3H, s), 11.30–11.55 (1H, m); ^{13}C NMR ($CDCl_3$) δ(ppm): 20.9, 29.2, 35.3, 36.7, 47.9, 50.5, 51,5, 98.1, 168.9, 174.3, 174.9, 197.4. Anal. calcd. for $C_{12}H_{17}NO_5$: C 56.46, H 6.71, N 5.49; found: C 56.44, H 6.75, N 5.44.

Dimethyl-2-(α-tetrahydropyrrolylidene)-3-oxoheptane-1,7-dioate **5***b* (n = 1, m = 3). Yield: 47%; mp (ethanol): 61°C; IR ($CHBr_3$) ν(cm^{-1}): 3200, 3020, 2940, 1720, 1670, 1580, 1540, 1435; ^1H NMR ($CDCl_3$) δ(ppm): 1.80–2.10 (4H, m), 2.25–2.40 (2H, m), 2.75–2.85 (2H, m), 3.05–3.15 (2H, m), 3.55–3.70 (2H, m), 3.60 (3H, s), 3.70 (3H, s), 11.25–11.70 (1H, m); ^{13}C NMR ($CDCl_3$) δ(ppm): 21.0, 33.8, 35.2, 40.7, 48.0, 50.6, 51.4, 51.6, 98.4, 169.2, 174.1, 174.7, 199.1. Anal. calcd. for $C_{13}H_{19}NO_5$: C 57.98, H 7.11, N 5.20; found: C 57.86, H 7.05, N 5.10.

Dimethyl-2-(α-hexahydropyridylidene)-3-oxohexane-1,6-dioate **5***c* (n = 2, m = 2). Yield: 41%; purified by chromatography (silica gel 60, Et_2O, R_f: 0.49); IR ($CHBr_3$) ν(cm^{-1}): 3550, 2950, 2870, 1725, 1600, 1460, 1430; ^1H NMR ($CDCl_3$) δ(ppm): 1.55–1.75 (4H, m), 2.40–2.50 (2H, m), 2.55–2.65 (2H, m), 2.75–2.90 (2H, m), 3.20–3.35 (2H, m), 3.55 (3H, s), 3.60 (3H, s), 12.40–12.55 (1H, m); ^{13}C NMR ($CDCl_3$) δ(ppm): 18.9, 21.0, 27.7, 29.3, 35.6, 41.5, 50.9, 51.5, 100.7, 168.9, 169.9, 174.1, 195.1. Anal. calcd. for $C_{13}H_{19}NO_5$; C 57.98, H 7.11, N 5.20; found: C 57.86, H 6.98, N 5.41.

Dimethy-2-(α-hexahydropyridylidene)-3-oxoheptane-1,7-dioate **5***d* (n = 2, m = 3). Yield: 34%; purified by chromatography (silica gel 60, Et_2O, R_f: 0.59); IR ($CHBr_3$) ν(cm^{-1}): 3400, 3020, 2940, 2860, 1720, 1680, 1590, 1470, 1460, 1445, 1430; ^1H NMR ($CDCl_3$) δ(ppm): 1.60–2.00 (6H, m), 2.25–2.35 (2H, m), 2.45–2.55 (2H, m), 2.55–2.65 (2H, m), 3.25–3.40 (2H, m), 3.60 (3H, s), 3.65 (3H, s), 12.65–12.80 (1H, m); ^{13}C NMR ($CDCl_3$) δ(ppm): 19.0, 21.0, 21.1, 27.6, 33.0, 33.6, 39.7, 41.4, 51.0, 101.3, 168.4, 170.2, 173.9. Anal. calcd. for $C_{14}H_{21}NO_5$: C 59.35, H 7.47, N 4.94; found: C 59.47, H 7.57, N 4.89.

Dimethyl-2-(α-hexahydroazepinylidene)-3-oxohexane-1,6-dioate **5***e* (n = 3, m = 2). Yield: 21%; purified by chromatography (silica gel 60, Et_2O, R_f: 0.69); IR ($CHBr_3$) ν(cm^{-1}): 3600, 3000, 2940, 2860, 1730, 1695, 1590, 1575, 1460, 1430; ^1H NMR ($CDCl_3$) δ(ppm): 1.30–1.65 (6H, m), 2.25–2.45 (4H, m), 2.60–2.75 (2H, m), 3.15–3.30 (2H, m), 3.45 (3H, s), 3.55 (3H, s), 11.90–12.25 (1H, m); ^{13}C NMR ($CDCl_3$) δ(ppm): 24.2, 28.2, 28.9, 29.9, 30.9, 35.2, 43.9, 51.0, 51.3, 101.5, 170.3, 173.0, 173.7, 194.7. Anal. calcd. for $C_{14}H_{21}NO_5$: C 59.35, H 7.47, N 4.94; found: C 59.28, H 7.62, N 4.92.

Dimethyl-2-(α-hexahydroazepinylidene)-3-oxoheptane-1,7-dioate **5***f* (n = 3, m = 3). Yield: 27%; purified by chromatography (silica gel 60, Et_2O, R_f: 0.59); IR ($CHBr_3$) ν(cm^{-1}): 3350, 3020, 2940, 2860, 1720, 1690, 1595, 1460, 1430; ^1H NMR ($CDCl_3$) δ(ppm): 1.50–1.80 (6H, m), 1.80–2.00 (2H, m), 2.20–2.40 (2H, m), 2.40–2.70 (4H, m), 3.30–3.50 (2H, m), 3.60 (3H, s), 3.70 (3H, s), 12.05–12.35 (1H, m); ^{13}C NMR ($CDCl_3$) δ(ppm): 20.8, 24.4, 28.4, 30.1, 31.1, 33.6, 39.6, 44.1, 51.4, 102.3, 170.9, 172.8, 173.9, 196.4. Anal. calcd. for $C_{15}H_{23}NO_5$: C 60.59, H 7.80, N 4.71; found: C 60.78, H 7.93, N 4.76.

β-Enaminodiketones **7***: general procedure for preparation*

β-Enaminoketodiester **5** (R = $-(CH_2)_m-CO_2CH_3$) (0.01 mol) and 0.1 mol of solid boric acid were heated 1 h at 230°C. Work-up was similar to the preparation of enaminones.

2-(α-Tetrahydropyrrolylidene)-1,3-cyclopentanedione **7***a* (n = 1, m = 2). Yield: 12% (24); mp (acetone): 210°C; IR ($CHBr_3$) ν(cm^{-1}): 3250, 3020, 1670, 1605, 1570, 1485, 1420; ^1H NMR ($CDCl_3$) δ(ppm): 2.00–2.20 (2H, m), 2.47 (4H, s), 3.15–3.30 (2H, m), 3.65–3.80 (2H, m), 10.30–10.55 (1H, m); ^{13}C NMR ($CDCl_3$) δ(ppm): 20.3, 31.9, 33.8, 48.1, 105.0, 172.8.

2-(α-Tetrahydropyrrolylidene)-1,3-cyclohexanedione **7***b* (n = 1, m = 3). Yield: 40%; mp (ethanol): 158°C; IR ($CHBr_3$) ν(cm^{-1}): 3150, 3020, 2950, 2880, 1630, 1580, 1540, 1470, 1440; ^1H NMR

($CDCl_3$) δ(ppm): 1.60–1.85 (2H, m), 1.85–2.05 (2H, m), 2.20–2.45 (4H, m), 3.15–3.35 (2H, m), 3.45–3.65 (2H, m), 11.70–11.95 (1H, m); ^{13}C NMR ($CDCl_3$) δ(ppm): 19.6, 20.5, 35.5, 38.4, 47.8, 106.7, 176.7, 197.9. Anal. calcd. for $C_{10}H_{13}NO_2$; C 67.02, H 7.31, N 7.82; found: C 66.99, H 7.22, N 7.98.

2-(α-Hexahydropyridylidene)-1,3-cyclopentanedione **7***c* (n = 2, m = 2). Yield: 10% (24); purified by chromatography (silica gel 60, acetone/pentane, 7:3, R_f: 0.38); IR ($CHBr_3$) ν(cm^{-1}): 3300, 3020, 1660, 1600, 1500, 1465, 1400; ^1H NMR ($CDCl_3$) δ(ppm): 1.65–2.00 (4H, m), 2.25–2.60 (4H, m), 3.00–3.25 (2H, m), 3.35–3.55 (2H, m), 11.75–11.95 (1H, m); ^{13}C NMR ($CDCl_3$) δ(ppm): 17.6, 20.9, 26.3, 32.9, 33.9, 41.8, 105.8, 171.1, 202.3, 206.

2-(α-Hexahydropyridylidene)-1,3 cyclohexanedione **7***d* (n = 2, m = 3). Yield: 36% (24); purified by chromatography (silica gel 60, acetone, R_f: 0.73); IR ($CHBr_3$) ν(cm^{-1}): 3400, 3020, 2950, 2870, 1620, 1590, 1560, 1455; ^1H NMR ($CDCl_3$) δ(ppm): 1.60–1.90 (6H, m), 2.30–2.45 (4H, m), 3.00–3.15 (2H, m), 3.30–3.50 (2H, m), 13.10–13.50 (1H, m); ^{13}C NMR ($CDCl_3$) δ(ppm): 18.7, 19.5, 20.4, 29.5, 39.0, 41.9, 107.9, 174.6, 198.1.

2-(α-Hexahydroazepinylidene)-1,3-cyclopentanedione **7***e* (n = 3, m = 2). Yield: 15% (24); purified by chromatography (silica gel 60, acetone/pentane, 3:7, R_f: 0.23); IR ($CHBr_3$) ν(cm^{-1}): 3350, 3020, 2930, 2860, 1660, 1600, 1490, 1460, 1430; ^1H NMR ($CDCl_3$) δ(ppm): 1.45–1.65 (4H, m), 1.65–1.80 (2H, m), 2.35 (4H, br s), 3.20–3.35 (2H, m), 3.35–3.50 (2H, m), 11.95–12.20 (1H, m); ^{13}C NMR ($CDCl_3$) δ(ppm): 23.4, 26.5, 27.5, 30.7, 33.4, 44.7, 105.4, 177.1, 206.6.

2-(α-Hexahydroazepinylidene)-1,3-cyclohexanedione **7***f* (n = 3, m = 3). Yield: 20% (25); purified by chromatography (silica gel 60, acetone, R_f: 0.77); mp: 93°C; IR ($CHBr_3$) ν(cm^{-1}): 3350, 3020, 2930, 2850, 1620, 1565, 1460, 1415; ^1H NMR ($CDCl_3$) δ(ppm): 1.50–1.90 (8H, m), 2.30–2.45 (4H, m), 3.10–3.25 (2H, m), 3.40–3.55 (2H, m), 13.05–13.40 (1H, m); ^{13}C NMR ($CDCl_3$) δ(ppm): 19.5, 23.3, 27.2, 29.6, 30.3, 39.0, 44.2, 108.6, 180.3.

Acknowledgment

We are grateful to E. I. Dupont de Nemours, Wilmington, Deleware, U.S.A., for support of this investigation.

1. T. H. Jones and M. S. Blum. *In* Alkaloids: chemical and biological perspectives. Vol. 1. *Edited by* S. W. Pelletier. J. Wiley & Sons, New York, NY. 1983. pp. 33–84.
2. K. Maruoka, T. Miyazaki, M. Ando, Y. Matsumara, S. Sakane, K. Hattori, and H. Yamamoto. J. Am. Chem. Soc, **105**, 2831 (1983).
3. V. W. Brown and B. P. Moore. Aust. J. Chem. **35**, 1255 (1982).
4. R. B. Herbert. *In* Alkaloids: chemical and biological perspectives. Vol. 3. *Edited by* S. W. Pelletier. J. Wiley & Sons, New York, NY. 1983. pp 241–274.
5. D. Bacos, J. P. Célérier, and G. Lhommet. Tetrahedron Lett. **28**, 2353 (1987); French Patent no. 86/16744 (1987); French Patent no. 86/16745 (1987).
6. J. P. Célérier, E. Deloisy, G. Lhommet, and P. Maitte. J. Org. Chem. **44**, 3089 (1979); Org. Synth. **67**, 170 (1989).
7. (*a*) J. P. Célérier, E. Deloisy-Marchalant, and G. Lhommet. J. Heterocycl. Chem. **21**, 1633 (1984); (*b*) P. H. Lambert, M. Vaultier, and R. Carrié. J. Org. Chem. **50**, 5352 (1985).
8. P. A. Wehrli and V. Chu. J. Org. Chem. **38**, 3436 (1973); Org. Synth. **58**, 79 (1978).
9. A. Etienne and Y. Correia. Bull. Soc. Chim. Fr. 3704 (1969).
10. C. A. Zezza, M. B. Smith, B. A. Ross, A. Arhin, and P. L. E. Cronin. J. Org. Chem. **49**, 4397 (1984).
11. A. Astier and M. M. Plat. Tetrahedron Lett. **19**, 2051 (1978).
12. A. I. Meyers, P. D. Edwards, T. R. Bailey, and G. E. Jagdmann, Jr. J. Org. Chem. **50**, 1019 (1985).
13. V. Dudek and L. Kvan. Collect. Czech. Chem. Commun. **30**, 2472 (1965).
14. P. Brunerie, J. P. Célérier, H. Petit, and G. Lhommet. J. Heterocycl. Chem. **23**, 1183 (1986).
15. T. Yamazaki, K. Matoba, M. Yajima, M. Nagata, and R. Castle. J. Heterocycl. Chem. **12**, 973 (1975).
16. A. E. Wick, P. A. Barlett, and D. Dolphin. Helv. Chim. Acta, **54**, 513 (1971).
17. G. Dannhardt, W. Meindl, S. Gussmann, S. Ajili, and T. Kappe. Eur. J. Med. Chem. **22**, 505 (1987).
18. P. Delbecq, J. P. Célérier, and G. Lhommet. Tetrahedron Lett. **31**, 4873 (1990).
19. M. Natsume, M. Takahashi, K. Kiushi, and H. Sugaya. Chem. Pharm. Bull. **19**, 2648 (1971).
20. W. Führer, V. Rasetti, and G. Rihs. Helv. Chim. Acta, **68**, 1235 (1985).
21. A. Ilvespaa and W. Führer. Ger. Pat. 2 707 658 (1975); Chem. Abstr. **88**, 22609z (1977).
22. Tokyo Stauffer Chem. Co. Ltd. Jap. Pat. 59.164.756 (1986); Chem. Abstr. **102**, 45794e (1984).
23. M. Roth, P. Dubs, E. Götschi, and A. Eschenmoser. Helv. Chim. Acta, **54**, 710 (1971).
24. T. Tsujikawa, Y. Nakagawa, K. Tsukamura, and K. Masuda. Chem. Pharm. Bull. **25**, 2775 (1977).
25. G. Lhommet, M. G. Richaud, and P. Maitte. J. Heterocycl. Chem. **19**, 431 (1982).

Can. J. Chem. Downloaded from www.nrcresearchpress.com by 84.41.108.74 on 09/07/12
For personal use only.

Chemistry of chromotropic acid. ^1H and ^{13}C NMR spectroscopy of chromotropic acid and its derivatives

PARIS E. GEORGHIOU,[1] CHI KEUNG (JIMMY) HO, AND CHESTER R. JABLONSKI
Department of Chemistry, Memorial University of Newfoundland, St. John's, Nfld., Canada A1B 3X7

Received November 9, 1990

This paper is dedicated to Dr. Hugh J. Anderson on the occasion of his 65th birthday

PARIS E. GEORGHIOU, CHI KEUNG (JIMMY) HO, and CHESTER R. JABLONSKI. Can. J. Chem. **69**, 1207 (1991).

The ^1H and ^{13}C NMR spectra of chromotropic acid (CTA) (4,5-dihydroxy-2,7-naphthalenedisulphonic acid) have been unambiguously assigned. Proton NOED spectra were used to show the proximity of both H-3 and H-6 and the hydroxyl groups. Two-dimensional ^1H–^{13}C NMR correlation spectra of CTA, of its corresponding diacetoxy derivative, and of 3-bromo- and 3,6-dibromo-CTA support the assignments. A regioselective deuterium exchange reaction of the C-3 and C-6 protons of CTA with deuterium oxide was observed during the NMR experiments. This latter finding is strongly indicative of the mode of formation, and of the nature of the chromogen formed in the reaction of CTA with formaldehyde in the well-known CTA–formaldehyde analytical reaction.

Key words: chromotropic acid, 3-bromochromotropic acid, 3,6-dibromochromotropic acid.

PARIS E. GEORGHIOU, CHI KEUNG (JIMMY) HO et CHESTER R. JABLONSKI. Can. J. Chem. **69**, 1207 (1991).

On a fait un attribution non-ambiguë des spectres RMN du ^1H et du ^{13}C de l'acide chromotropique (ACT) (acide 4,5-dihydroxy-naphtalène-2,7-disulfonique). On a utilisé les spectres d'EOND du proton pour démontrer que les H-3 et H-6 ainsi que les groupements hydroxyles sont à proximité les uns des autres. Les spectres RMN ^1H–^{13}C de corrélation bidimensionnelle de l'ACT, de son dérivé diacétoxylé et des acides 3-bromo- et 3,6-dibromo-chromotropiques sont en accord avec les attributions. Au cours des expériences de RMN en présence d'oxyde de deutérium, on a observé une réaction d'échange régiosélective du deutérium avec les protons en C-3 et en C-6 de l'ACT. Cette observation est un indice précieux du mode de formation et de la nature du chromogène formé lors de la réaction de l'ACT avec le formaldéhyde au cours de la réaction analytique bien connue de l'ACT–formaldéhyde.

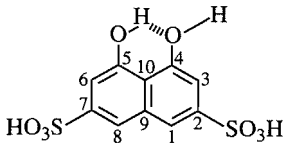
Mots clés : acide chromotropique, acide 3-bromochromotropique, acide 3,6-dibromochromotropique.

[Traduit par la rédaction]

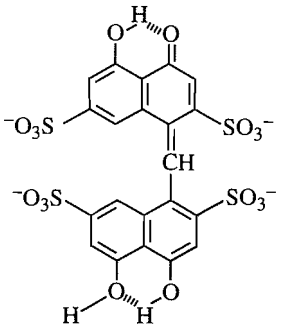
Introduction

Chromotropic acid (CTA) **1** (4,5-dihydroxy-2,7-naphthalenedisulphonic acid) is employed as an analytical reagent and as an intermediate in the syntheses of numerous azo dyes, which are used extensively both in the dye industry and in analytical chemistry (1–3). In North America it has found widespread use as the chromogen-forming reagent in the analysis of formaldehyde using the method recommended by the National Institute for Occupational Safety and Health (NIOSH), Method P&CAM 125 (4, 5). The exact nature of the chromogen and its formation by the reaction of CTA with formaldehyde has, however, not been unambiguously proven. The most often quoted structure (4–8) for the chromogen formed between CTA and formaldehyde has been the *para,para*-quinoidal adduct **2**, but no direct proof of this structure has ever been presented. The structure is based on an analogy to the reaction of formaldehyde with aromatic compounds in the LeRosen test (8).

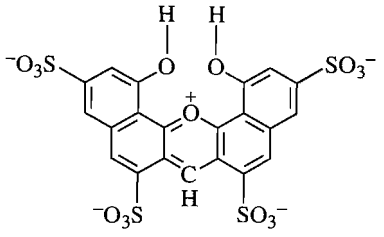
Kamel and Wizinger (9) proposed the mono-cationic dibenzoxanthylium structure **3** as an alternative. This structure is the one that is most consistent with the chemistry of the reaction (10). As part of our ongoing studies of methods for the analysis of formaldehyde we were interested in understanding the chemistry of the formaldehyde–CTA reaction through the use of NMR spectroscopy. Surprisingly, considering its widespread use, there does not appear to be an unambiguous assignment of either its ^1H or ^{13}C NMR spectrum in the literature. Lajunen *et al.* (11) reported a ^{13}C NMR study of CTA, but the ^{13}C NMR spectrum was not definitively assigned. More recently, Freeman *et al.* (12) described the 250-MHz ^1H NMR spectrum of CTA and other naphthalene-based dyestuff intermediates with assignments based on comparisons with mono-substituted naphthalenes. This paper describes our findings using through-bond and through-space NMR correlation techniques, which allowed the unambiguous assignment of the ^1H and ^{13}C NMR spectra of CTA and its mono and dibromo derivatives. These assignments enabled us to propose an hypothesis for the chemistry of the CTA–formaldehyde chromogen-forming reaction (10).



1



2



3

[1]Author to whom correspondence may be addressed.

Can. J. Chem. Downloaded from www.nrcresearchpress.com by 84.41.108.74 on 09/07/12
For personal use only.

Can. J. Chem. Downloaded from www.nrcresearchpress.com by 84.41.108.74 on 09/07/12
For personal use only.

Experimental

^{1}H NMR spectra were recorded with the following instruments at the designated frequencies: Varian Anaspect EM 360 (60 MHz), Bruker WP-80 (80 MHz), or GE GN-300NB (300 MHz) spectrometers. ^{13}C NMR spectra were recorded with the Bruker WP-80 (20.1 MHz) and (or) the GE GN-300NB (75.47 MHz) instrument. The solvent used was either deuterium oxide or water as noted in the experimental details. Proton nuclear Overhauser effect difference (NOED) spectra were determined under steady state conditions (13) on a GE 300-NB instrument using a set of 16K interleaved experiments of 8 transients cycled 12 to 16 times through the list of decoupling frequencies. In each experiment the decoupler was on in continuous wave (CW) mode for 6 s with sufficient attenuation to give an approximate 70–90% reduction in intensity of the irradiated peak. A 24 s delay preceded each frequency change. A set of four "dummy" scans was employed to equilibrate the spins prior to data acquisition. No relaxation delay was applied between successive scans of a given frequency. Difference spectra were obtained on zero-filled 32K data tables that had been digitally filtered with a 1–2 Hz exponential line-broadening function.

Ultraviolet and visible spectra were determined on a Unicam SP.800 ultraviolet spectrophotometer. Infrared spectra were recorded on a Perkin–Elmer 1320 infrared spectrophotometer using KBr disks. Sephadex LH-20 purchased from Pharmacia Fine Chemicals was used in the gel permeation chromatography.

*Purification of 4,5-dihydroxy-2,7-naphthalenedisulphonic acid disodium salt (**1**)*

The material purchased from Sigma Chemical Co. was specified as being only 98% pure. Purified **1** was obtained by dissolving 20 g of the Sigma product in 100 mL of water in a 125-mL Erlenmeyer flask on a hot plate. A solution of 20 g of sodium chloride in 50 mL of hot water was added to the chromotropic acid solution until a precipitate formed. The flask was stoppered and the solution was allowed to first crystallize at room temperature and then at low temperature in a refrigerator. The crystals were filtered with suction and dried in air. The product was almost colourless: UV (H_2O) λ_{max} absorbances: 316, 332, 346 nm. IR (KBr) ν_{max}: 3500 (-SO_2O-H and ArO-H), 1200 (S=O) cm^{-1}. ^{1}H NMR (300 MHz; D_2O, TSP internal standard) δ ppm: 7.20 (d, J = 1.4 Hz, 1H, Ar-H), 7.92 (d, J = 1.4 Hz, 1H, Ar-H). ^{13}C NMR and APT (D_2O) δ ppm: 106.44 (C-3 and C-6), 116.18 (C-10), 118.12 (C-1 and C-8), 134.64 (C-9), 141.36 (C-2 and C-7), 153.76 (C-4 and C-5). 2-D ^{1}H–^{13}C correlation (D_2O): 7.20 ppm correlates with 106.44 (C-3 and C-6), 7.92 ppm correlates with 118.12 (C-1 and C-8).

Deuterium exchange experiments with chromotropic acid

In a typical experiment, an NMR tube was charged with a solution containing 67 mg of purified **1** in 0.30 mL of deuterium oxide. A small amount of DSS as internal standard was added to the solution. The NMR tube was heated in a boiling water bath. ^{1}H NMR spectra were recorded at 10 min intervals until the signal at 7.20 ppm completely disappeared and the signal at 7.92 ppm collapsed to a sharp singlet. The deuterium exchange could be reversed by adding 0.1 mL of water to the NMR tube. The ^{13}C NMR spectra were recorded for a freshly prepared deuterium oxide solution of purified **1**, and following heating of the NMR tube in a boiling water bath for 15 min. Side-by-side comparison of the spectra indicate that the intensity of the 106.44 ppm signal (C-3 and C-6) was reduced by over 90%. All other signals were unchanged.

*4,5-Diacetoxy-2,7-naphthalenedisulphonic acid disodium salt (**4**)*

In a 25-mL Erlenmeyer flask, 1.0 g (2.68 mmol) of chromotropic acid disodium salt was dissolved in 3.0 mL of 3.0 M aqueous sodium hydroxide. To this solution was added approximately 2 g of crushed ice, followed by 0.6 mL of acetic anhydride. The mixture was stirred for 5–10 min with ice-bath cooling. The diacetate separated out as colourless, crystalline needles. It was filtered by suction, washed with portions of absolute ethanol, and dried in air. Recrystallization from water afforded 0.52 g (40%) of crystals having a decomposition point at 320°C. X-ray crystallographic analysis revealed that the compound was a dihydrate: UV (H_2O) λ_{max} absorbances: 315, 329, 339 nm. ^{1}H NMR (D_2O) δ ppm: 2.43 (s, 3H, CH_3-), 7.72 (d, J = 2 Hz, 1H, Ar-H), 8.52 (d, J = 2 Hz, 1H, Ar-H).

*3,6-Dibromo-4,5-dihydroxy-2,7-naphthalenedisulphonic acid disodium salt (**5**a)*

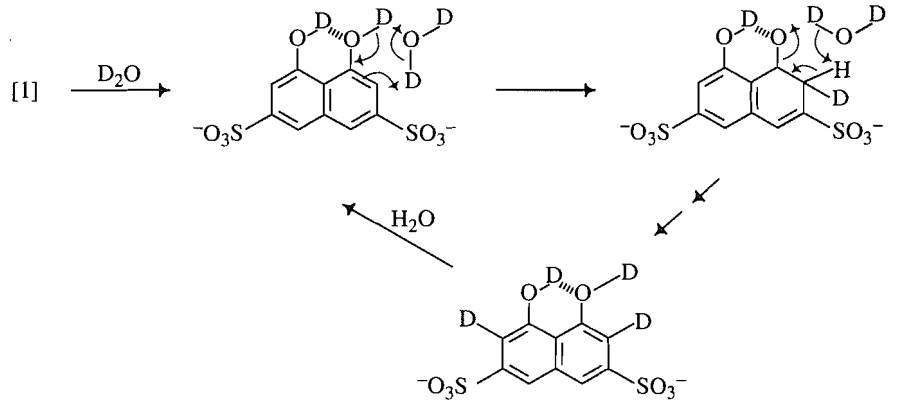
In a 25-mL Erlenmeyer flask, 1.9 g (5.1 mmol) of chromotropic acid disodium salt was mixed with 12 mL of concentrated sulphuric acid (96%, d = 1.84 g/mL). The mixture was heated and stirred at 80°C until all the solid dissolved. The solution was cooled to approximately 15°C and, with continuous cooling and stirring, a solution of 0.8 g (5.0 mmol) of bromine in 3.0 mL of glacial acetic acid was added dropwise over 1 h. After the addition of bromine, the solution was stirred and cooled for an additional 3 h. To this solution, approximately 15 g of ice was added. The white precipitate was filtered off with suction, using a sintered glass funnel. The residue was dissolved in a minimal amount of water at room temperature. To this aqueous solution one half of its volume of concentrated hydrochloric acid solution was added. The grey-white leaflets were suction filtered using a sintered glass funnel, and were press-dried. The residue was further dried under vacuum to afford 1.25 g (46%) of **5***a*, which decomposed above 40°C with liberation of bromine: UV (H_2O) λ_{max} absorbances: 340, 358, 375 nm. ^{1}H NMR (D_2O) δ ppm: 8.10 (s, Ar-H). ^{13}C NMR (D_2O) δ ppm: 102.44 (C-3 and C-6), 116.26 (C-10), 122.04 (C-1 and C-8), 130.74 (C-9), 140.11 (C-2 and C-7), 149.62 (C-4 and C-5). 2-D ^{1}H–^{13}C correlation (D_2O): 8.10 ppm correlates with 122.04 (C-1 and C-8); APT (D_2O): 122.04 ppm (C-1 and C-8, one attached proton).

*3-Bromo-4,5-dihydroxy-2,7-naphthalenedisulphonic acid disodium salt (**6**)*

In a 25-mL Erlenmeyer flask, 1.9 g (5.1 mmol) of chromotropic acid disodium salt was mixed with 12 mL of concentrated sulphuric acid (96%, d = 1.84 g/mL). The mixture was heated and stirred at 80°C until all the solid dissolved. The solution was cooled to approximately 15°C and, with continuous cooling and stirring, a solution of 0.4 g (2.5 mmol) of bromine in 3.0 mL of glacial acetic acid was added dropwise over 3 h. After the addition of bromine, the solution was stirred and cooled for an additional 1 h. To the solution approximately 15 g of ice was added. The white precipitate was suction-filtered using a sintered glass funnel. The residue was dissolved in a minimal amount of water at room temperature. To this aqueous solution one half of its volume of concentrated hydrochloric acid solution was added. The grey-white leaflets were once again filtered off using suction and a sintered glass funnel, and were press-dried. The residue was further dried under vacuum to afford 0.98 g (40%) of **6**, which decomposed at 40°C with liberation of bromine: UV (H_2O) λ_{max} absorbances: 316, 336, 348 nm. ^{1}H NMR (D_2O) δ ppm: 7.17 (d, J = 2 Hz, 1H, Ar-H), 7.80 (d, J = 2 Hz, 1H, Ar-H), 8.10 (s, 1H, Ar-H). ^{13}C NMR (D_2O) δ ppm: 100.51 (C-3), 107.06 (C-6), 115.96 (C-10), 118.62 (C-8), 121.33 (C-1), 132.63 (C-9), 140.17 (C-7), 141.28 (C-2), 151.35 (C-4), 152.23 (C-5).

Results and discussion

The 300-MHz ^{1}H NMR spectrum of CTA shows two AX-type doublets (7.92, 7.20 ppm, J = 1.4 Hz), which is consistent for structure **1** assuming negligible interannular coupling (14). An unambiguous assignment of this spectrum, however, cannot be made on the basis of neighbouring group effects alone. Of the two types of protons on the CTA molecule, one type (on C-3, or C-6) is *ortho* to the sulphonic acid group, and the other type (on C-1, or C-8) is *para* to the hydroxyl but *ortho* to the sulphonic acid group. Since these two types of protons are both *ortho* to the sulphonic acid group, the effect of the electron-withdrawing sulphonic acid group should be the same on both of them. The hydroxyl group on the other hand is *ortho* to the proton on C-3 (or C-6) and *para* to the proton on C-1 (or C-8). It has been shown that the *ortho* and *para* position protons in phenol are equally affected by the hydroxyl group and have similar chemical shifts (15). In naphthalene, however,



SCHEME 1

due to ring current effects (15), the α protons, which are closer to both rings, appear downfield (7.81 ppm) with respect to the β protons (7.46 ppm). By analogy with naphthalene therefore, the signals at 7.92 ppm could be tentatively assigned to the proton on C-1 (and C-8) and the signals at 7.20 ppm can be assigned to the proton on C-3 (and C-6). Nevertheless, the assignment of chemical shifts using only the arguments made above or those made by Freeman *et al.* (12) is clearly not sufficient for a multi-substituted naphthalene derivative such as CTA.

During the ^{1}H NMR experiments on CTA in deuterium oxide it was observed that the signals at 7.20 ppm gradually diminished in intensity. The signals ultimately disappeared completely and the doublet at 7.92 ppm was converted into a sharp singlet. This specific exchange could be reproduced within 0.5 h at 90°C. That a simple hydrogen–deuterium exchange occurred was established by regenerating the original spectrum by the addition of water to the solution contained in the NMR tube. These findings could be accounted for by the pathway shown in Scheme 1.

Even though Scheme 1 shows exchange of the C-3 and C-6 protons, the alternative exchange of the C-1 and C-8 protons could, in principle, be equally likely. This ambiguity is of importance in understanding the reactions of CTA, thus it was necessary to definitively assign the ^{1}H NMR spectrum of CTA.

The corresponding diacetate of CTA, **4**, was synthesized to provide additional evidence for the assignment of the ^{1}H NMR spectrum of CTA. The proximity of the methyl protons of the acetoxy group to the proton on C-3 (or C-6) suggested that a nuclear Overhauser effect (NOE) (16) in the ^{1}H NMR spectrum could be observed. The 300-MHz ^{1}H NMR spectrum of **4** consists of a single signal at 2.19 ppm due to the acetate methyl groups and a pair of sharp AX-type doublets at 8.27 and 7.48 ppm ($J \sim 1.6$ Hz). Assignment of the low-field signals to the C-1, C-8 protons and the C-3, C-6 protons respectively was established by NOED experiments conducted at 300 MHz. Irradiation of the signal at 7.48 ppm enhanced the acetate signals whereas irradiation of the 8.27 ppm signal did not. The assignment of the 7.48 ppm signal to the proton on C-1 (C-8) was confirmed by irradiating the acetate signal, which resulted in a clearly enhanced signal at 7.48 ppm relative to that at 8.27 ppm. Thus, the higher-field signal is due to the protons *ortho* to the acetoxy group. Two-dimensional ^{1}H–^{13}C NMR chemical shift correlation (16) spectra provided additional evidence for these assignments. These results suggest that the higher-field signal that undergoes deuterium exchange in CTA is due to the protons *ortho* to the hydroxyl group, C-3 and C-6.

Proton NOED spectra of CTA itself confirmed the above assignments by unambiguously showing that the higher-field resonance is proximal to the hydroxyl group. The experiments were conducted in DMSO-d_6 solution to slow exchange at the hydroxyl site. To confirm that the assignment of the peaks in DMSO-d_6 is the same as those in D_2O, a dilution study was conducted in DMSO-d_6/D_2O. No change in the relative positions of the two low-field signals was observed. Figure 1 shows a small positive enhancement of the hydroxyl resonance on partial saturation of the higher-field peak. The correlation was confirmed by observation of a selective enhancement of the high-field resonance when the hydroxyl peak was saturated.

Lajunen *et al.* (11) assigned the 25-MHz ^{13}C NMR spectrum of CTA in D_2O, which consisted of six signals (see Table 1), to their respective carbon atoms by analyzing the response of the ^{13}C chemical shifts to varying pH. The largest effect on the chemical shift was observed for the C-4, C-5, and C-10 signals when the pH was changed from 4.5 to 8.0. At basic pH one of the hydroxyl groups is dissociated into the corresponding oxyanion. Dissociation of the second hydroxyl group, however, is not possible in aqueous solution since it is very strongly hydrogen-bonded to the neighbouring oxyanion via an intramolecular six-membered ring. Nevertheless, none of their assignments can be considered to be unambiguous.

We wished to assign the ^{13}C NMR spectrum of CTA using more direct evidence based on through-bond scalar C–H coupling interactions. The 75-MHz broad band decoupled spectrum of CTA in DMSO-d_6 consists of six signals with approximately the same chemical shifts (Table 1) as noted by Lajunen in D_2O. Our experiments confirmed their original assignments. A 2-D HETCOR spectrum optimized for one-bond coupling revealed that the lower-field ^{1}H signal at 7.92 ppm assigned to the proton on C-1 (and C-8) was correlated with the signal at 117.50 ppm. The ^{1}H signal at 7.20 ppm assigned to the proton on C-3 (and C-6) was correlated with the ^{13}C signal at 108.22 ppm.

The proton-coupled ^{13}C NMR spectrum of CTA revealed that the signal due to C-3 (and C-6) was split into a doublet of doublets ($^1J = 162.4$ Hz; $^3J = 6.3$ Hz), the signal due to C-10 was split into an approximate quintet ($^3J = 5.9$ Hz), and that due to C-1 (and C-8) was split into a doublet of triplets ($^1J = 165.1$ Hz; $^3J = 5.0$ Hz). The C-9 signal appeared as an apparent triplet ($^2J = 2.5$ Hz), the signal due to C-2 (and C-7) was an

Can. J. Chem. Downloaded from www.nrcresearchpress.com by 84.41.108.74 on 09/07/12
For personal use only.

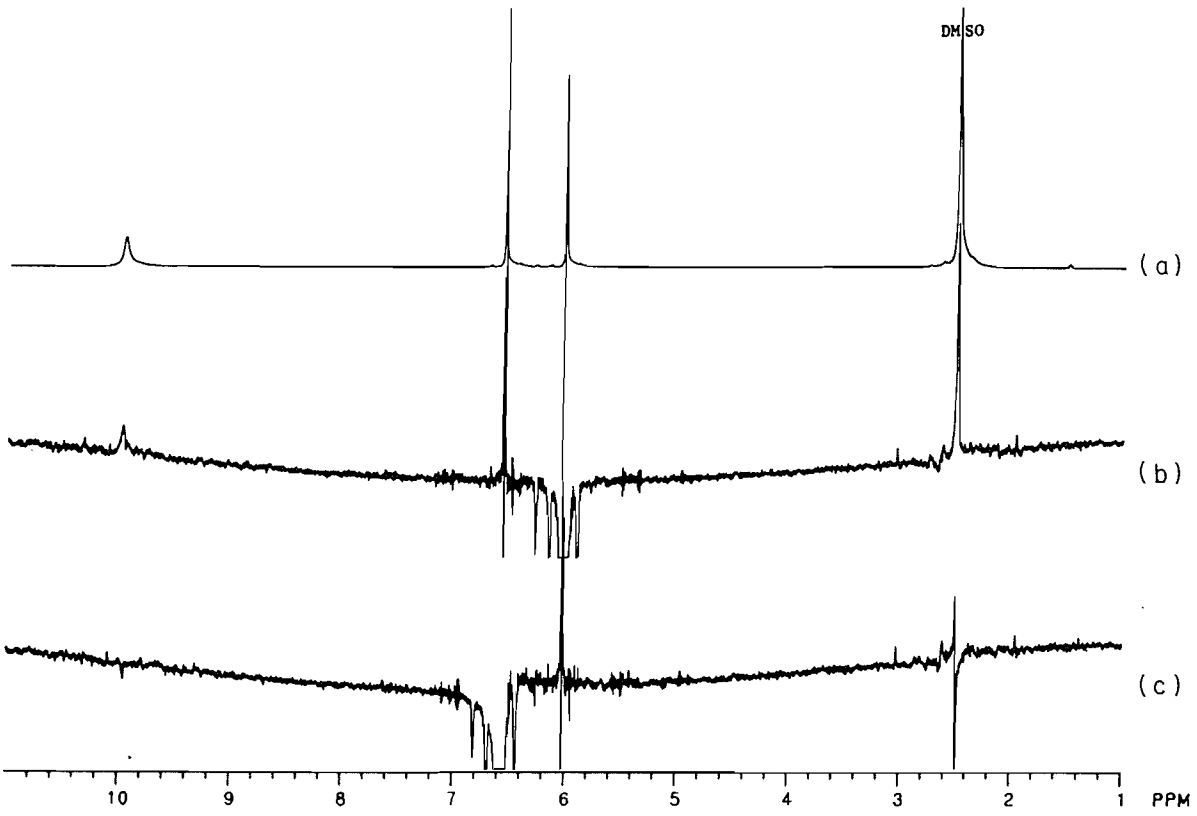


FIG. 1. Proton NOED spectra of chromotropic acid in DMSO-d_6: (a) reference spectrum; (b) saturation (×256) of 6.02 ppm signal showing positive enhancement of 9.98 ppm signal; (c) saturation (×256) of 6.60 ppm signal indicating no enhancement of 9.98 ppm signal.

TABLE 1. ^{13}C NMR chemical shifts for chromotropic acid (**1**) and derivatives (**5***a*, **6**)

Compound (solvent)	C-1	C-2	C-3	C-4	C-5	C-6	C-7	C-8	C-9	C-10	Reference
1 (D_2O)	118.12	141.36	106.44	153.76	153.76	106.44	141.36	118.12	134.64	116.18	This work
1 (DMSO-d_6)	117.50	147.22	108.22	154.98	154.98	108.22	147.22	117.50	135.97	115.65	This work
1 (H_2O)	119.4	142.7	107.8	154.8	154.8	107.8	142.7	119.4	135.9	117.8	11
5*a* (D_2O)	122.04	140.11	102.44	149.62	149.62	102.44	140.11	122.04	130.74	116.26	This work
6 (D_2O)	121.33	141.28	100.51	151.35	152.23	107.06	140.17	118.62	132.63	115.96	This work

unresolved multiplet, and the C-4 (and C-5) signal was split into an apparent doublet (^2J = 1.7 Hz).

Confirmation of the ^{13}C NMR assignments was obtained from two long-range HETCOR experiments (17) optimized for couplings of 10.0 and 7.7 Hz respectively. The ^1H signal of H-3 (and H-6) at 7.20 ppm was correlated ($^2J_{H,C}$) with the ^{13}C signals due to C-4 (and C-5), C-2 (and C-7), as well as ($^3J_{H,C}$) with C-1 (and C-8) and C-10. The ^1H signal of H-1 (and H-8) at 7.92 ppm was correlated ($^2J_{H,C}$) with the ^{13}C signals due to C-9, as well as ($^3J_{H,C}$) with C-1 (and C-8), C-10 and C-3 (and C-6).

The ^{13}C NMR of the deuterium-exchanged CTA in D_2O revealed that the intensity of the signal assigned to C-3 (and C-6) was diminished by over 90%. All other signals were unchanged. Thus it is the C-3 (and C-6) of CTA and not C-1 (and C-8) which are labile.

The 3,6-dibromo, 3,6-dichloro, and 3,6-diiodo derivatives **5***a*,*b*,*c* have been reported in the literature (18) and their NMR spectra were of interest for comparative purposes. Attempts to synthesize these dihalogenated derivatives using the method of Maslowska and Duda (18) were unsuccessful. The procedures reported by Kuznetsov and Basargin (19) for the synthesis of the monobrominated 3-bromo-CTA **6** afforded only the dibrominated product **5***a*. Modification of their procedure, however, afforded **6** in approximately 40% yields. The ^1H NMR spectrum of **5***a* consisted of a single line at 8.10 ppm; that of **6** showed three signals in the aromatic region: one singlet at 8.10 ppm corresponding to the proton on the brominated ring and an AX pattern (7.17 and 7.80 ppm, $J \sim 2$ Hz) for the non-brominated ring. The ^{13}C NMR spectra of **5***a* and **6** consisted of six and 10 signals respectively and their chemical shifts are summarized in Table 1.

The 2-D ^1H–^{13}C HETCOR spectrum of **6** revealed that the singlet at 8.10 ppm in the ^1H NMR spectrum is correlated ($^1J_{H,C}$) with the ^{13}C signal at 121.33 ppm, which is due to C-1 of **6**. The doublet at 7.80 ppm (J = 2 Hz) in the ^1H NMR spectrum is correlated ($^1J_{H,C}$) with the ^{13}C signal at 118.62 ppm, which can be assigned to C-8. The doublet in the proton

Can. J. Chem. Downloaded from www.nrcresearchpress.com by 84.41.108.74 on 09/07/12
For personal use only.

spectrum at 7.17 ppm (J = 2 Hz) is correlated ($^1J_{H,C}$) with the ^{13}C signal at 107.06 ppm, which is due to C-6.

It is interesting that the deuterium exchange reaction at C-3 and C-6 observed with CTA in deuterium oxide is regioselective. This could be due to intermolecular assistance by the proximal hydroxyl groups, or due to steric inaccessibility of the C-1 and C-8 positions. The NMR spectra of **5***a*, **6**, and CTA that follow from the evidence presented here provide essential information for interpreting the spectra observed when the reaction of CTA and formaldehyde was monitored directly by NMR (10). On the basis of these *in situ* experiments and calibration-line studies, it was concluded that the mono-cationic dibenzoxanthylium structure **3** for the chromogen is most consistent with the chemistry of the reaction (10).

1. B. BUDESINSKY. *In* Chelates in analytical chemistry. Vol. 2. *Edited by* H. A. Flaschka and A. J. Barnard. Marcel Dekker, New York. 1969.
2. C. PRAND and T. VENTURINI. J. Chromatogr. Sci. **19**, 308 (1981).
3. P. JANDERA and J. CHURACEK. J. Chromatogr. **197**, 181 (1980).
4. National Institute for Occupational Safety and Health, Manual of analytical methods. 2nd ed. Vol. 1. Washington, DC. 1977. pp. 125–1, 125–9.
5. M. KATZ (*Editor*). Methods of air sampling and analysis. 2nd ed. American Public Health Association Intersociety Committee, American Public Health Association, Washington, DC. 1977. pp. 300–307.
6. F. FEIGL. Spot tests in organic analysis. 7th ed. Elsevier, Amsterdam. 1966. pp. 434–438.
7. E. L. R. KRUG and W. E. HIRT. Anal. Chem. **49**, 1865 (1977).
8. B. A. K. ANDREWS and R. M. REINHARDT. *In* Formaldehyde. Analytical chemistry and toxicology. *Edited by* V. Turoski. Adv. Chem. Ser. 210, p. 88 (1985).
9. M. KAMEL and R. WIZINGER. Helv. Chim. Acta, **79**, 594 (1960).
10. P. E. GEORGHIOU and C. K. HO. Can. J. Chem. **67**, 871 (1989).
11. L. H. J. LAJUNEN, H. RUOTSALAINEN, K. RAISANEN, and S. PARHI. Finn. Chem. Lett. 142 (1980).
12. H. S. FREEMAN, W. N. HSU, J. F. ESANCY, and M. K. ESANCY. Dyes Pigm. **9**, 67 (1988).
13. J. K. SAUNDERS and J. D. MERSH. Prog. Nucl. Magn. Reson. Spectrosc. **15**, 353 (1983).
14. N. JONATHAN, S. GORDON, and B. P. DAILEY. J. Chem. Phys. **36**, 2443 (1962).
15. L. M. JACKMAN and S. STERNHELL. Applications of nuclear magnetic resonance spectroscopy in organic chemistry. 2nd ed. Pergamon Press, Oxford. 1969.
16. J. K. M. SAUNDERS and B. K. HUNTER. Modern NMR spectroscopy. A guide for chemists. Oxford University Press, Oxford. 1987.
17. A. S. ZEKTZER, B. K. JOHN, and G. E. MARTIN. Magn. Reson. Chem. **25**, 752 (1987).
18. J. MASLOWSKA and J. DUDA. Chem. Anal. (Warsaw), **23**, 805 (1978).
19. V. I. KUZNETSOV and N. N. BASARGIN. Zh. Obshch. Khim. **35**, 879 (1965).

Can. J. Chem. Downloaded from www.nrcresearchpress.com by 84.41.108.74 on 09/07/12
For personal use only.

Can. J. Chem. Downloaded from www.nrcresearchpress.com by 84.41.108.74 on 09/07/12
For personal use only.

TABLE 2. Bond lengths (Å) with estimated standard deviations in parentheses

Bond	Length		Bond	Length	
	Uncorr.	Corr.		Uncorr.	Corr.
F(1)—B	1.350(2)	1.370	C(2)—C(8)	1.506(3)	1.520
F(2)—B	1.363(2)	1.386	C(4)—C(5)	1.530(3)	1.534
F(3)—B	1.369(3)	1.391	C(5)—C(6)	1.504(3)	1.516
O(1)—C(1)	1.313(2)	1.323	C(6)—C(7)	1.513(4)	1.525
O(1)—C(2)	1.509(2)	1.524	C(7)—C(8)	1.530(3)	1.535
O(2)—N	1.365(2)	1.371	C(9)—C(10)	1.386(3)	1.393
O(2)—B	1.517(3)	1.530	C(9)—C(14)	1.387(3)	1.395
N —C(1)	1.292(2)	1.317	C(10)—C(11)	1.380(3)	1.383
N —C(3)	1.462(2)	1.474	C(11)—C(12)	1.380(3)	1.388
C(1)—C(9)	1.464(2)	1.468	C(12)—C(13)	1.367(3)	1.374
C(2)—C(3)	1.536(3)	1.554	C(13)—C(14)	1.384(3)	1.387
C(2)—C(4)	1.499(3)	1.512			

TABLE 3. Bond angles (deg) with estimated standard deviations in parentheses

Bonds	Angle (deg)	Bonds	Angle (deg)
C(1)—O(1)—C(2)	109.5(1)	C(5)—C(6)—C(7)	110.6(2)
N —O(2)—B	112.9(1)	C(6)—C(7)—C(8)	111.1(2)
O(2)—N —C(1)	126.0(1)	C(2)—C(8)—C(7)	110.1(2)
O(2)—N —C(3)	120.5(1)	C(1)—C(9)—C(10)	121.1(2)
C(1)—N —C(3)	113.1(2)	C(1)—C(9)—C(14)	118.4(2)
O(1)—C(1)—N	112.6(2)	C(10)—C(9)—C(14)	120.4(2)
O(1)—C(1)—C(9)	119.1(1)	C(9)—C(10)—C(11)	119.5(2)
N —C(1)—C(9)	128.4(2)	C(10)—C(11)—C(12)	120.0(2)
O(1)—C(2)—C(3)	102.7(1)	C(11)—C(12)—C(13)	120.6(2)
O(1)—C(2)—C(4)	107.5(1)	C(12)—C(13)—C(14)	120.3(2)
O(1)—C(2)—C(8)	106.6(1)	C(9)—C(14)—C(13)	119.2(2)
C(3)—C(2)—C(4)	113.1(2)	F(1)—B —F(2)	113.3(2)
C(3)—C(2)—C(8)	113.5(2)	F(1)—B —F(3)	111.3(2)
C(4)—C(2)—C(8)	112.5(2)	F(1)—B —O(2)	103.9(2)
N —C(3)—C(2)	101.5(2)	F(2)—B —F(3)	109.3(2)
C(2)—C(4)—C(5)	110.5(2)	F(2)—B —O(2)	110.0(2)
C(4)—C(5)—C(6)	111.5(2)	F(3)—B —O(2)	108.9(2)

Bond lengths (corrected and uncorrected) and angles are given in Tables 2 and 3 and intra-annular torsion angles in Table 4. Hydrogen atom parameters, anisotropic thermal parameters, bond lengths and angles involving hydrogen, torsion angles, and structure factors have been deposited.[4]

Results and discussion

As already suggested by the spectroscopic data and elemental composition, the crystallographic analysis confirms formula **4**, and thus shows the possibility of cyclocondensation of *N*-(2-hydroxyalkyl)hydroxamic acids in the presence of Lewis acid boron compounds even when chelate-forming reactions such as those observed for the salicylohydroxamate **6** (2) and the hydroxyacetohydroxamate **7** (3) are not involved. The resulting open-chain BF_3-adduct **4** (Fig. 1) is a stable compound and represents a new type of *N*-oxide boron complex with a boron,nitrogen-(1,3)betaine structure (7).

The O(2)BF_3 grouping in **4** has a distorted tetrahedral geometry with bond angles at boron ranging from 103.9(2)° for F(1)—B—O(2) to 113.3(2)° for F(1)—B—F(2). BF_3 itself has a trigonal planar structure both in the gas phase (8) and in the solid state (9, 10). Tetracoordination of the boron atom leads to lengthening of the B—F bonds in **4** (mean 1.382 Å (corr.) and 1.361 Å (uncorr.)) compared to those reported for

TABLE 4. Intra-annular torsion angles (deg) standard deviations in parentheses

Atoms	Torsion angle (deg)
C(2)—O(1)—C(1)—N	1.4(2)
C(3)—N —C(1)—O(1)	−6.4(2)
C(1)—N —C(3)—C(2)	8.1(3)
O(1)—C(2)—C(3)—N	−6.5(2)
C(1)—O(1)—C(2)—C(3)	3.6(2)
C(8)—C(2)—C(4)—C(5)	−55.3(2)
C(2)—C(4)—C(5)—C(6)	55.2(3)
C(4)—C(5)—C(6)—C(7)	−56.3(3)
C(5)—C(6)—C(7)—C(8)	56.8(3)
C(6)—C(7)—C(8)—C(2)	−56.0(3)
C(4)—C(2)—C(8)—C(7)	55.8(2)

[4]Supplementary material mentioned in the text may be purchased from the Depository of Unpublished Data, Document Delivery, CISTI, National Research Council of Canada, Ottawa, K1A 0S2.

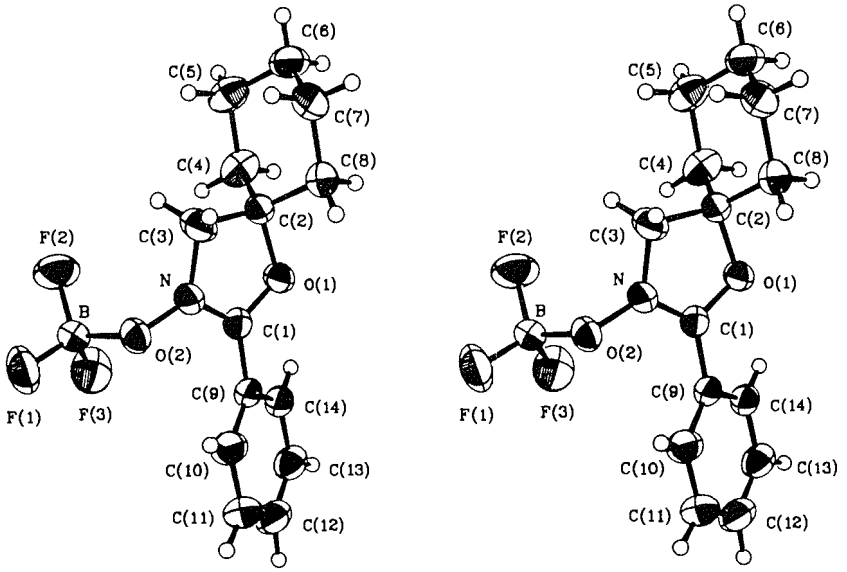


FIG. 1. Stereoview of **4**; 50% probability thermal ellipsoids are shown for the non-hydrogen atoms.

crystalline BF_3: mean values of 1.278 Å (9) and 1.289 Å (10). This is consistent with a weakening of the $pp(\pi)$-interaction between boron and the fluorine ligands upon complex formation. The mean B—F distance in **4** is greater than the corresponding mean B—F bond length (1.345 Å (uncorr.)) reported for pyridine–BF_3 (11). This could result from stronger coordination in the *N*-oxide BF_3-adduct **4** than in pyridine–BF_3. To the best of our knowledge, there are no other structures of heterocyclic *N*-oxide BF_3 complexes in the literature. It is probably safe to assume that the O—B coordinative bond in zwitterionic N—O—B complexes like **4** is generally stronger than the N—B bonds of comparable, but more sterically hindered, N—B adducts.

The libration-corrected O—B bond length in **4** (1.530 Å) is in good agreement with the O—B distance of 1.533 Å derived from semiempirical MNDO calculations on the BF_3 complex of an acetaldehyde adduct of pyridine, **9** (12), which corresponds to an analogous *B,N*-(1,4)betaine structure. An O—B distance of 1.54 Å has been calculated for the BF_3 complex of dimethylsulfoxide (13). While there is a paucity of structural information reported for BF_3 complexes with basic oxides (14), the crystal structure of the related benzaldehyde–BF_3 adduct features an O—B bond length of 1.591 Å (15). The O—B distance in **4** is very similar to the (C)F—B distance of 1.528(8) Å recently reported for an isoelectronic F_3B–FC linkage in a binuclear ferracyclopentadiene derivative (16). The average terminal B—F distance of 1.37(1) Å for the F_3B—FC adduct is similar to that in **4** (see above).

The five-membered 2-oxazoline ring is nearly planar (maximum deviation from the mean plane is 0.070(2) Å for C(3)) and has a flattened C(3)-envelope conformation. The phenyl ring is not coplanar with the oxazoline ring (dihedral angle between normals to the mean planes = 28.8°) in spite of conjugation or possible π-interaction between the imidate moiety and the aromatic ring system. The C(1)—C(9) bond length of 1.468 Å is somewhat longer than the comparable $C(sp^2)$–C(ar) distance of 1.450 Å in compound **6** (2), in which the phenyl ring is held in an approximately coplanar orientation with respect to the oxazoline ring by chelate formation via the *ortho*-phenolic ligand. The cyclohexane ring in **4** has a relatively undistorted chair conformation (see Table 4), with the oxygen atom of the spiro-linked oxazoline ring occupying an equatorial position and the methylene substituent (C(3)) in an axial position.

As observed earlier for compounds **6** (2) and **7** (3), the C(1)—N bond in **4** has distinct double bond character. The bond length of 1.317 Å corresponds to a π-bond order between 0.7 and 0.8 on the basis of a bond length vs. bond order plot (17), and resembles the C=N^+ bond distance in **2** (1) and other boron chelates of hydroxamic acids such as **8** (18) and related hydroxamates (19–23). The double bond character of the iminium C=N^+ bond in the open-chain *B,N*-betaine **4** appears to be somewhat reduced relative to that in the cyclic *B,N*-betaines **6** (1.294 Å) and **7** (1.281 Å). The C(1)—O(1) bond in **4** (1.323 Å) is equal in length to the corresponding bond in the oxazoline moiety of **6** (1.323 Å) and similar to the same bond in the oxazoline ring of **7** (1.310 Å), indicative of greatly reduced double bond character of the imidate C—O bonds in all three compounds. The N—O bond distance in **4** (1.371 Å) is similar to those in **6** (1.369 Å) and **7** (1.367 Å), and can also be compared with that in the difluoroboron chelate **8** (1.374 Å).

In the solid state, the shortest intermolecular contacts may represent three weak C—H···F interactions (H···F = 2.47(3), 2.49(3), and 2.55(2) Å). All other intermolecular distances correspond to normal van der Waals interactions.

Acknowledgements

We thank the Natural Sciences and Engineering Research Council of Canada and the Fonds der Chemischen Industrie, Frankfurt am Main, for financial support.

1. W. KLIEGEL, U. SCHUMACHER, M. TAJERBASHI, S. J. RETTIG, and J. TROTTER. Can. J. Chem. **69,** 545 (1991).
2. W. KLIEGEL, M. TAJERBASHI, S. J. RETTIG, and J. TROTTER. Can. J. Chem. **66,** 2621 (1988).
3. W. KLIEGEL, U. SCHUMACHER, S. J. RETTIG, and J. TROTTER. Can. J. Chem. **69,** 681 (1991).

Can. J. Chem. Downloaded from www.nrcresearchpress.com by 84.41.108.74 on 09/07/12
For personal use only.

4. International tables for X-ray crystallography. Vol. IV. Kynoch Press, Birmingham, U.K. 1974. pp. 99–102, 149 (present distributor Kluwer Academic Publishers: Dordrecht, The Netherlands).
5. V. SCHOMAKER and K. N. TRUEBLOOD. Acta Crystallogr. Sect. B, **24**, 63 (1968).
6. D. W. J. CRUICKSHANK. Acta Crystallogr. **9**, 747 (1956); **9**, 754 (1956); **14**, 896 (1961).
7. W. KLIEGEL. Organomet. Chem. Rev. **A8**, 153 (1972).
8. Gmelin Handbuch der Anorganischen Chemie, Bor, Ergänzungsband. Weinheim. 1954, p. 171; Ergänzungswerk zur 8.Aufl. Bd. 53, Borverbindungen Teil 19. Berlin. 1978. p. 49.
9. D. MOOTZ and M. STEFFEN. Angew. Chem. **92**, 481 (1980).
10. M. YU. ANTIPIN, A. M. ELLERN, V. F. SUKHOVERKHOV, YU. T. STRUCHKOV, and YU. A. BUSALEV. Dokl. Akad. Nauk SSSR, **279**, 892 (1984); Proceed. Acad. Sci. USSR, **279**, 435 (1984).
11. K. TÖPEL, K. HENSEN, and J. W. BATZ. Acta Crystallogr. Sect. C, **40**, 828 (1984).
12. E. ANDERS, F. MARKUS, H. MESKE, J. TROPSCH, and G. MAAS. Chem. Ber. **120,** 735 (1987).
13. G. ROBINET, J. F. LABARRE, and C. LEIBOVICI. Chem Phys. Lett. **22**, 356 (1973).
14. T. D. COYLE and F. G. A. STONE. Progr. Boron Chem. **1**, 83 (1964); Gmelin Handbuch der Anorganischen Chemie, Ergänzungswerk zur 8.Aufl. Bd. 53, Borverbindungen Teil 19. Berlin. 1978. p. 104.
15. M. T. REETZ, M. HÜLLMANN, W. MASSA, S. BERGER, P. RADEMACHER, and P. HEYMANNS. J. Am. Chem. Soc. **108**, 2405 (1986).
16. C. A. MIRKIN, K.-L. LU, G. L. GEOFFROY, and A. L. RHEINGOLD. J. Am. Chem. Soc. **112**, 461 (1990).
17. G. HÄFELINGER. Chem. Ber. **103**, 2941 (1970).
18. W. KLIEGEL, M. TAJERBASHI, S. J. RETTIG, and J. TROTTER. Can. J. Chem. **69,** 673 (1991).
19. S. J. RETTIG, J. TROTTER, W. KLIEGEL, and D. NANNINGA. Can. J. Chem. **55**, 1 (1977).
20. S. J. RETTIG, J. TROTTER, W. KLIEGEL, and D. NANNINGA. Can. J. Chem. **56**, 1676 (1978).
21. W. KLIEGEL, D. NANNINGA, S. J. RETTIG, and J. TROTTER. Can. J. Chem. **61,** 2493 (1983).
22. W. KLIEGEL, M. TAJERBASHI, S. J. RETTIG, and J. TROTTER. Can. J. Chem. **67,** 1644 (1989).
23. W. KLIEGEL, M. TAJERBASHI, S. J. RETTIG, and J. TROTTER. Can. J. Chem. **68,** 69 (1990).

Can. J. Chem. Downloaded from www.nrcresearchpress.com by 84.41.108.74 on 09/07/12
For personal use only.

Structural studies of organoboron compounds. XLVI.[1] 5,5-Pentamethylene-2-phenyl-4,5-dihydrooxazol-*N*-oxide(*N*—*O*—*B*)trifluoroborane

WOLFGANG KLIEGEL AND UTE SCHUMACHER
Institut für Pharmazeutische Chemie der Technischen Universität Braunschweig, Beethovenstrasse 55, 3300 Braunschweig, Bundesrepublik Deutschland

AND

STEVEN J. RETTIG AND JAMES TROTTER
Department of Chemistry, University of British Columbia, 2036 Main Mall, Vancouver, B.C., Canada V6T 1Z1

Received August 31, 1990

WOLFGANG KLIEGEL, UTE SCHUMACHER, STEVEN J. RETTIG, and JAMES TROTTER. Can. J. Chem. **69,** 1212 (1991).

The reaction of *N*-hydroxy-*N*-[(1-hydroxycyclohexyl)methyl]benzamide with dimethylether-boron trifluoride gives 5,5-penta-methylene-2-phenyl-4,5-dihydrooxazol-*N*-oxide(*N*—*O*—*B*)trifluoroborane [3-(2,2,2-trifluoro-1-oxa-2-borataethyl)-5,5-pentamethylene-2-phenyl-1-oxa-3-azonia-2-cyclopentene] in high yield. Crystals of the product are monoclinic, $a = 8.1147(4)$, $b = 15.448(1)$, $c = 11.4144(6)$ Å, $\beta = 95.133(5)°$, $Z = 4$, space group $P2_1/c$. The structure was solved by direct methods and was refined by full-matrix least-squares procedures to $R = 0.043$ and $R_w = 0.058$ for 2178 reflections with $I \geq 3\sigma(I)$. The structure analysis confirms that the title compound has an open-chain boron-nitrogen betaine structure and, as such, is the first isolated and fully characterized open-chain non-chelate boron complex of a cycloimidate *N*-oxide (cyclohydroximate). Bond lengths (corrected for libration) involving the tetrahedrally coordinated boron atom are O—B = 1.530(3) and F—B = 1.370(2)–1.391(2) Å.

Key words: crystal structure, organoboron compound, boron compound.

WOLFGANG KLIEGEL, UTE SCHUMACHER, STEVEN J. RETTIG, et JAMES TROTTER. Can. J. Chem. **69,** 1212 (1991).

La réaction du *N*-hydroxy-*N*-[(1-hydroxycyclohexyl)méthyl]benzamide avec le complexe méthoxyméthane/trifluorure de bore conduit au 5,5-pentaméthylène-2-phényl-4,5-dihydrooxazol-*N*-oxyde(*N*—*O*—*B*)trifluoroborane [3-(2,2,2-trifluoro-1-oxa-2-borataéthyl)-5,5-pentaméthylène-2-phényl-1-oxa-3-azonia-cyclopent-2-ène], avec un rendement élevé. Les cristaux de ce produit sont monocliniques, groupe d'espace $P2_1/c$, avec $a = 8{,}1147(4)$, $b = 15{,}448(1)$ et $c = 11{,}4144(6)$ Å, $\beta = 95.133(5)°$, $Z = 4$. On a résolu la structure par des méthodes directes et on l'a affinée par la méthode des moindres carrés (matrice entière) jusqu'à des valeurs de $R = 0{,}043$ et $R_w = 0.058$ pour 2178 réflexions avec $I \geq 3\sigma(I)$. L'analyse de la structure confirme que le composé mentionné dans le titre existe sous la forme d'une bétaïne bore/azote à chaîne ouverte et qu'il s'agit ainsi du premier complexe d'un cycloimidate *N*-oxyde (cyclohydroximate)/bore, non-chélaté, en chaîne ouverte à être isolé et complètement caractérisé. Les longueurs de liaison (corrigées pour la libration) impliquant l'atome de bore coordiné d'une façon tétraédrique sont O—B = 1,530(3) et F—B = 1.370(2)–1,391(2) Å.

Mots clés: structure cristalline, composé organoborique, composés du bore.

[Traduit par la rédaction]

Introduction

The reaction of the *N*-(2-hydroxyalkyl)-benzohydroxamic acid **1** with oxybis(diphenylborane) yields the diphenylboryl hydroxamate **2** having a five-membered boron chelate structure. Alternative isomeric structures include an open-chain adduct **5** of diphenylborinic acid at a 2-oxazoline *N*-oxide moiety, formed by cyclocondensation during the reaction with the Lewis-acid boron compound. The postulated isomer **5**, however, was ruled out by an X-ray crystallographic analysis (1).

Justification for the inclusion of the cyclocondensate structure **5** in structural considerations is based on earlier observations of similar cyclizations during chelate forming reactions of salicylohydroxamic (2) and hydroxyacetohydroxamic acid derivatives (3), and now, in this work, arises from an experiment designed to result in the formation of the difluoroboron chelate **3** via reaction of **1** with boron trifluoride. The elemental analysis, infrared, and ^{1}H nmr data for the resulting crystalline compound are consistent with the loss of one mole of water and the addition of one mole of BF_3 during the course of the reaction, indicating a non-chelate BF_3 complex with the postulated boron – nitrogen betaine structure **4**. The 2-oxazoline *N*-oxide fragment of **4** resembles the identical moieties within the difluoroboron chelates **6** (2) and **7** (3). In addition, the C=N$^+$ stretching vibration in the infrared spectrum of **4** (at 1650 cm^{-1}) is in good agreement with the corresponding C=N$^+$ bands in the spectra of **6** (1660 cm^{-1}) and **7** (1670 cm^{-1}).

To the best of our knowledge, compound **4** is the first isolated open-chain non-chelate boron complex of a cycloimidate *N*-oxide (cyclohydroximate). Thus an X-ray crystallographic analysis of this compound has been undertaken for proof and structural elucidation.

Experimental

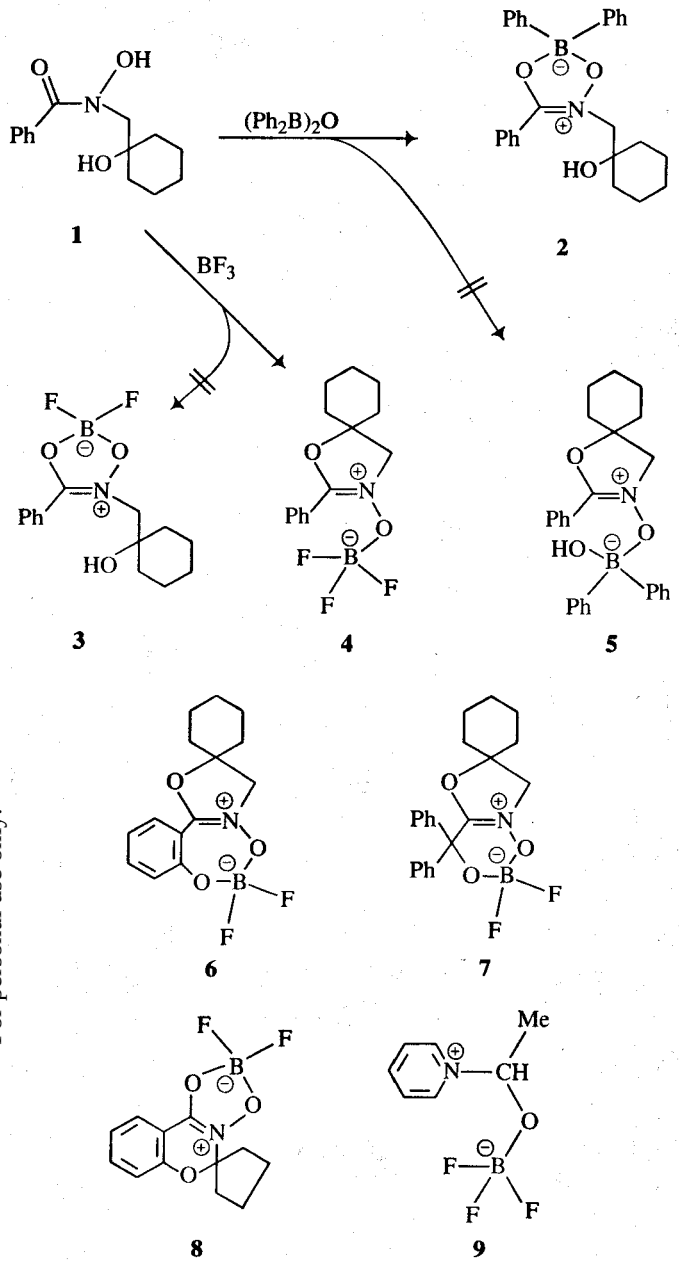
*5,5-Pentamethylene-2-phenyl-4,5-dihydrooxazol-*N*-oxide(*N*—*O*—*B*) trifluoroborane, **4***

N-Hydroxy-*N*-[(1-hydroxycyclohexyl)methyl]benzamide, **1** (2.49 g, 10 mmol),[2] is dissolved in 100–150 mL diethylether. Dimethyl ether-boron trifluoride (1.14 g, 10 mmol) is added and the mixture is left standing at room temperature for 12 h. The solvent is then removed *in vacuo*. Crystallization begins upon cooling and/or upon addition of petroleum ether, giving a colorless material. Yield: 2.74 g (92%). M.p. 146–147°C (from CH_2Cl_2/diethyl ether). *Anal.* calcd. for $C_{14}H_{17}BF_3NO_2$: C 56.22, H 5.73, B 3.61, N 4.68; found: C 56.39, H 5.82, B 3.51, N 4.65. Infrared (KBr): 1650 (shoulder at 1660) cm^{-1} (C=N$^+$). ^{1}H nmr (90 MHz, $CDCl_3$/TMS): δ(ppm) = 1.35–1.88 and 1.88–2.30 (m, 6H, and m, 4H, —$(CH_2)_5$—), 4.29 (s, N—CH_2), 7.35–7.77, and 8.18–8.43 (m, 3H, and m, 2H, C_6H_5). Crystals suitable for X-ray analysis were obtained by recrystallization from absolute ether/CH_2Cl_2.

[1]Previous paper in this series: ref. 3.

[2]Prepared as described in ref. 1.

Can. J. Chem. Downloaded from www.nrcresearchpress.com by 84.41.108.74 on 09/07/12
For personal use only.



X-ray crystallographic analysis of ***4***

A crystal ca. 0.38 × 0.50 × 0.50 mm in size was mounted on a glass fiber. Unit-cell parameters were refined by least-squares on 2 sin θ/λ values for 25 reflections (2θ = 39.8–43.3°) measured on a diffractometer with Mo-K_α radiation ($\lambda_{K\alpha1}$ = 0.70930, $\lambda_{K\alpha2}$ = 0.71359 Å). Crystal data at 21°C are as follows

$C_{14}H_{17}BF_3NO_2$ fw = 299.10

Monoclinic, a = 8.1147(4), b = 15.448(1), c = 11.4144(6) Å, β = 95.133(5)°, V = 1425.1(2) Å^3, Z = 4, ρ_c = 1.394 Mg m^{-3}, $F(000)$ = 624, μ(Mo-K_α) = 1.11 cm^{-1}. Absent reflections: $h0l$, l odd, and $0k0$, k odd, uniquely indicate the space group $P2_1/c$ (No. 14).

Intensities were measured with graphite-monochromated Mo-K_α radiation on an Enraf-Nonius CAD4-F diffractometer. An ω–2θ scan at 1.3–10.0° min^{-1} over a range of (0.80 + 0.35 tan θ)° in ω (scan extended by 25% on each side for background measurement) was employed. Data were measured to 2θ = 55°. The intensities of three check reflections, measured every hour of X-ray exposure time throughout the data collection, showed only small random variations. The data were processed[3] and corrected for Lorentz and polarization effects. Of the 3265 independent reflections measured, 2178 (66.7%) had intensities greater than or equal to 3σ(I) above background where $\sigma^2(I) = [C + 2B + (0.040(C-B))^2]$ with C = scan count, B = normalized total background count.

TABLE 1. Final positional (fractional × 10^5) and isotropic thermal parameters (U × 10^3 Å^2) with estimated standard deviations in parentheses*

Atom	x	y	z	U_{eq}
F(1)	3866(15)	16205(10)	19533(12)	78
F(2)	30910(19)	18605(10)	17142(13)	82
F(3)	23686(19)	7757(8)	28489(13)	77
O(1)	56281(14)	21367(8)	53198(11)	46
O(2)	19578(14)	21982(8)	34928(11)	45
N	34949(17)	23150(10)	40603(13)	43
C(1)	41257(20)	18807(11)	49586(14)	38
C(2)	61123(21)	28823(11)	45688(15)	40
C(3)	45307(27)	30407(15)	37536(23)	59
C(4)	75433(30)	25892(14)	39249(21)	58
C(5)	82577(30)	33477(15)	32733(20)	59
C(6)	87312(28)	40867(17)	40925(22)	64
C(7)	72644(32)	43753(14)	47238(22)	63
C(8)	65595(29)	36234(14)	53946(18)	51
C(9)	33777(21)	11738(11)	55817(14)	39
C(10)	16816(25)	11340(15)	56476(18)	53
C(11)	10265(28)	4773(15)	62812(20)	61
C(12)	20585(29)	−1330(14)	68425(18)	59
C(13)	37316(28)	−928(13)	67808(17)	54
C(14)	44129(24)	5637(11)	61554(16)	43
B	19592(26)	15902(14)	24490(20)	47

*U_{eq} = (1/3) trace (diagonalized U).

The structure was solved by direct methods, the coordinates of all non-hydrogen atoms being determined from an E-map. The non-hydrogen atoms were refined with anisotropic thermal parameters and the hydrogen atoms were refined with isotropic thermal parameters. Scattering factors for all atoms and anomalous dispersion corrections for the non-hydrogen atoms were taken from ref. 4. The weighting scheme $w = 1/\sigma^2(F)$ gave uniform average values of $w(|F_o|-|F_c|)^2$ over ranges of both $|F_o|$ and sin θ/λ and was employed in the final stages of full-matrix least-squares refinement of 258 variables. Reflections with $I < 3\sigma(I)$ were not included in the refinement. Convergence was reached at R = 0.043 and R_w = 0.058 for 2178 reflections with $I \geq 3\sigma(I)$. The function minimized was $\Sigma w(|F_o|-|F_c|)^2$, $R = \Sigma||F_o|-|F_c||/\Sigma|F_o|$, $R_w = (\Sigma w(|F_o|-|F_c|)^2/\Sigma w|F_o|^2)^{1/2}$. On the final cycle of refinement the maximum parameter shift corresponded to 0.03σ. The mean error in an observation of unit weight was 2.08. The final difference map showed maximum fluctuations of −0.21 to +0.29 e Å^{-3}.

The thermal motion has been analyzed in terms of the TLS model (5). The rms error in the temperature factors U_{ij} (derived from the least-squares analysis) is 0.0010 Å^2. Four structural subunits were separately analyzed (rms ΔU_{ij} = 0.0009–0.0024 Å^2). The bond lengths have been corrected for libration (5, 6) using shape parameters q^2 of 0.08 for all atoms. The final positional and (equivalent) isotropic thermal parameters for the non-hydrogen atoms appear in Table 1.

[3]Computer programs used include locally written programs for data processing and locally modified versions of the following: MULTAN80, Multisolution program by P. Main, S. J. Fiske, S. E. Hull, L. Lessinger, G. Germain, J. P. Declercq, and M. M. Woolfson; ORFLS, full-matrix least-squares, and ORFFE, function and errors, by W. R. Busing, K. O. Martin, and H. A. Levy; FORDAP, Patterson and Fourier syntheses, by A. Zalkin; ORTEP II, illustrations, by C. K. Johnson.

Can. J. Chem. Downloaded from www.nrcresearchpress.com by 84.41.108.74 on 09/07/12
For personal use only.

Can. J. Chem. Downloaded from www.nrcresearchpress.com by 84.41.108.74 on 09/07/12
For personal use only.

TABLE 2. Bond lengths (Å) with estimated standard deviations in parentheses

Bond	Length		Bond	Length	
	Uncorr.	Corr.		Uncorr.	Corr.
F(1)—B	1.350(2)	1.370	C(2)—C(8)	1.506(3)	1.520
F(2)—B	1.363(2)	1.386	C(4)—C(5)	1.530(3)	1.534
F(3)—B	1.369(3)	1.391	C(5)—C(6)	1.504(3)	1.516
O(1)—C(1)	1.313(2)	1.323	C(6)—C(7)	1.513(4)	1.525
O(1)—C(2)	1.509(2)	1.524	C(7)—C(8)	1.530(3)	1.535
O(2)—N	1.365(2)	1.371	C(9)—C(10)	1.386(3)	1.393
O(2)—B	1.517(3)	1.530	C(9)—C(14)	1.387(3)	1.395
N —C(1)	1.292(2)	1.317	C(10)—C(11)	1.380(3)	1.383
N —C(3)	1.462(2)	1.474	C(11)—C(12)	1.380(3)	1.388
C(1)—C(9)	1.464(2)	1.468	C(12)—C(13)	1.367(3)	1.374
C(2)—C(3)	1.536(3)	1.554	C(13)—C(14)	1.384(3)	1.387
C(2)—C(4)	1.499(3)	1.512			

TABLE 3. Bond angles (deg) with estimated standard deviations in parentheses

Bonds	Angle (deg)	Bonds	Angle (deg)
C(1)—O(1)—C(2)	109.5(1)	C(5)—C(6)—C(7)	110.6(2)
N —O(2)—B	112.9(1)	C(6)—C(7)—C(8)	111.1(2)
O(2)—N —C(1)	126.0(1)	C(2)—C(8)—C(7)	110.1(2)
O(2)—N —C(3)	120.5(1)	C(1)—C(9)—C(10)	121.1(2)
C(1)—N —C(3)	113.1(2)	C(1)—C(9)—C(14)	118.4(2)
O(1)—C(1)—N	112.6(2)	C(10)—C(9)—C(14)	120.4(2)
O(1)—C(1)—C(9)	119.1(1)	C(9)—C(10)—C(11)	119.5(2)
N —C(1)—C(9)	128.4(2)	C(10)—C(11)—C(12)	120.0(2)
O(1)—C(2)—C(3)	102.7(1)	C(11)—C(12)—C(13)	120.6(2)
O(1)—C(2)—C(4)	107.5(1)	C(12)—C(13)—C(14)	120.3(2)
O(1)—C(2)—C(8)	106.6(1)	C(9)—C(14)—C(13)	119.2(2)
C(3)—C(2)—C(4)	113.1(2)	F(1)—B —F(2)	113.3(2)
C(3)—C(2)—C(8)	113.5(2)	F(1)—B —F(3)	111.3(2)
C(4)—C(2)—C(8)	112.5(2)	F(1)—B —O(2)	103.9(2)
N —C(3)—C(2)	101.5(2)	F(2)—B —F(3)	109.3(2)
C(2)—C(4)—C(5)	110.5(2)	F(2)—B —O(2)	110.0(2)
C(4)—C(5)—C(6)	111.5(2)	F(3)—B —O(2)	108.9(2)

Bond lengths (corrected and uncorrected) and angles are given in Tables 2 and 3 and intra-annular torsion angles in Table 4. Hydrogen atom parameters, anisotropic thermal parameters, bond lengths and angles involving hydrogen, torsion angles, and structure factors have been deposited.[4]

Results and discussion

As already suggested by the spectroscopic data and elemental composition, the crystallographic analysis confirms formula **4**, and thus shows the possibility of cyclocondensation of *N*-(2-hydroxyalkyl)hydroxamic acids in the presence of Lewis acid boron compounds even when chelate-forming reactions such as those observed for the salicylohydroxamate **6** (2) and the hydroxyacetohydroxamate **7** (3) are not involved. The resulting open-chain BF_3-adduct **4** (Fig. 1) is a stable compound and represents a new type of *N*-oxide boron complex with a boron,nitrogen-(1,3)betaine structure (7).

The O(2)BF_3 grouping in **4** has a distorted tetrahedral geometry with bond angles at boron ranging from 103.9(2)° for F(1)—B—O(2) to 113.3(2)° for F(1)—B—F(2). BF_3 itself has a trigonal planar structure both in the gas phase (8) and in the solid state (9, 10). Tetracoordination of the boron atom leads to lengthening of the B—F bonds in **4** (mean 1.382 Å (corr.) and 1.361 Å (uncorr.)) compared to those reported for

TABLE 4. Intra-annular torsion angles (deg) standard deviations in parentheses

Atoms	Torsion angle (deg)
C(2)—O(1)—C(1)—N	1.4(2)
C(3)—N —C(1)—O(1)	−6.4(2)
C(1)—N —C(3)—C(2)	8.1(3)
O(1)—C(2)—C(3)—N	−6.5(2)
C(1)—O(1)—C(2)—C(3)	3.6(2)
C(8)—C(2)—C(4)—C(5)	−55.3(2)
C(2)—C(4)—C(5)—C(6)	55.2(3)
C(4)—C(5)—C(6)—C(7)	−56.3(3)
C(5)—C(6)—C(7)—C(8)	56.8(3)
C(6)—C(7)—C(8)—C(2)	−56.0(3)
C(4)—C(2)—C(8)—C(7)	55.8(2)

[4]Supplementary material mentioned in the text may be purchased from the Depository of Unpublished Data, Document Delivery, CISTI, National Research Council of Canada, Ottawa, K1A 0S2.

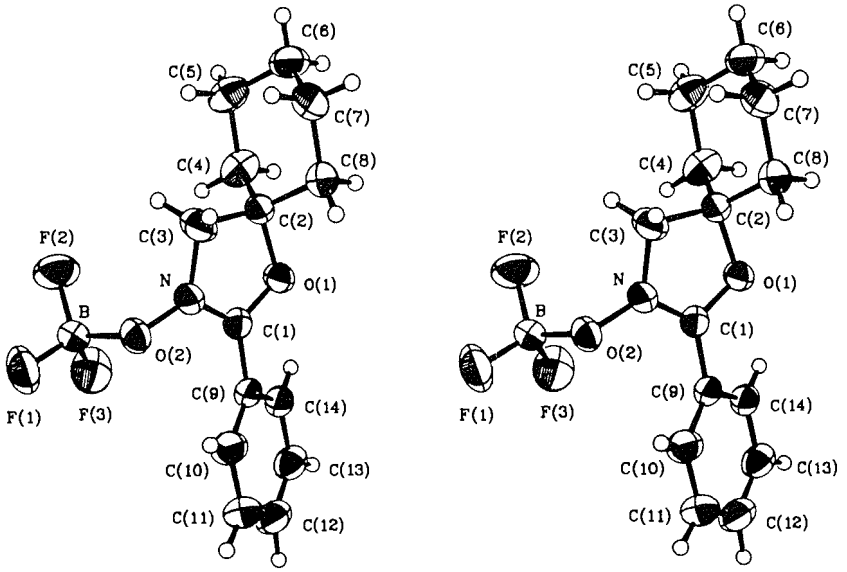


FIG. 1. Stereoview of **4**; 50% probability thermal ellipsoids are shown for the non-hydrogen atoms.

crystalline BF_3: mean values of 1.278 Å (9) and 1.289 Å (10). This is consistent with a weakening of the $pp(\pi)$-interaction between boron and the fluorine ligands upon complex formation. The mean B—F distance in **4** is greater than the corresponding mean B—F bond length (1.345 Å (uncorr.)) reported for pyridine–BF_3 (11). This could result from stronger coordination in the *N*-oxide BF_3-adduct **4** than in pyridine–BF_3. To the best of our knowledge, there are no other structures of heterocyclic *N*-oxide BF_3 complexes in the literature. It is probably safe to assume that the O—B coordinative bond in zwitterionic N—O—B complexes like **4** is generally stronger than the N—B bonds of comparable, but more sterically hindered, N—B adducts.

The libration-corrected O—B bond length in **4** (1.530 Å) is in good agreement with the O—B distance of 1.533 Å derived from semiempirical MNDO calculations on the BF_3 complex of an acetaldehyde adduct of pyridine, **9** (12), which corresponds to an analogous *B,N*-(1,4)betaine structure. An O—B distance of 1.54 Å has been calculated for the BF_3 complex of dimethylsulfoxide (13). While there is a paucity of structural information reported for BF_3 complexes with basic oxides (14), the crystal structure of the related benzaldehyde–BF_3 adduct features an O—B bond length of 1.591 Å (15). The O—B distance in **4** is very similar to the (C)F—B distance of 1.528(8) Å recently reported for an isoelectronic F_3B–FC linkage in a binuclear ferracyclopentadiene derivative (16). The average terminal B—F distance of 1.37(1) Å for the F_3B—FC adduct is similar to that in **4** (see above).

The five-membered 2-oxazoline ring is nearly planar (maximum deviation from the mean plane is 0.070(2) Å for C(3)) and has a flattened C(3)-envelope conformation. The phenyl ring is not coplanar with the oxazoline ring (dihedral angle between normals to the mean planes = 28.8°) in spite of conjugation or possible π-interaction between the imidate moiety and the aromatic ring system. The C(1)—C(9) bond length of 1.468 Å is somewhat longer than the comparable $C(sp^2)$–C(ar) distance of 1.450 Å in compound **6** (2), in which the phenyl ring is held in an approximately coplanar orientation with respect to the oxazoline ring by chelate formation via the *ortho*-phenolic ligand. The cyclohexane ring in **4** has a relatively undistorted chair conformation (see Table 4), with the oxygen atom of the spiro-linked oxazoline ring occupying an equatorial position and the methylene substituent (C(3)) in an axial position.

As observed earlier for compounds **6** (2) and **7** (3), the C(1)—N bond in **4** has distinct double bond character. The bond length of 1.317 Å corresponds to a π-bond order between 0.7 and 0.8 on the basis of a bond length vs. bond order plot (17), and resembles the C=N^+ bond distance in **2** (1) and other boron chelates of hydroxamic acids such as **8** (18) and related hydroxamates (19–23). The double bond character of the iminium C=N^+ bond in the open-chain *B,N*-betaine **4** appears to be somewhat reduced relative to that in the cyclic *B,N*-betaines **6** (1.294 Å) and **7** (1.281 Å). The C(1)—O(1) bond in **4** (1.323 Å) is equal in length to the corresponding bond in the oxazoline moiety of **6** (1.323 Å) and similar to the same bond in the oxazoline ring of **7** (1.310 Å), indicative of greatly reduced double bond character of the imidate C—O bonds in all three compounds. The N—O bond distance in **4** (1.371 Å) is similar to those in **6** (1.369 Å) and **7** (1.367 Å), and can also be compared with that in the difluoroboron chelate **8** (1.374 Å).

In the solid state, the shortest intermolecular contacts may represent three weak C—H···F interactions (H···F = 2.47(3), 2.49(3), and 2.55(2) Å). All other intermolecular distances correspond to normal van der Waals interactions.

Acknowledgements

We thank the Natural Sciences and Engineering Research Council of Canada and the Fonds der Chemischen Industrie, Frankfurt am Main, for financial support.

1. W. KLIEGEL, U. SCHUMACHER, M. TAJERBASHI, S. J. RETTIG, and J. TROTTER. Can. J. Chem. **69,** 545 (1991).
2. W. KLIEGEL, M. TAJERBASHI, S. J. RETTIG, and J. TROTTER. Can. J. Chem. **66,** 2621 (1988).
3. W. KLIEGEL, U. SCHUMACHER, S. J. RETTIG, and J. TROTTER. Can. J. Chem. **69,** 681 (1991).

Can. J. Chem. Downloaded from www.nrcresearchpress.com by 84.41.108.74 on 09/07/12
For personal use only.

4. International tables for X-ray crystallography. Vol. IV. Kynoch Press, Birmingham, U.K. 1974. pp. 99–102, 149 (present distributor Kluwer Academic Publishers: Dordrecht, The Netherlands).
5. V. SCHOMAKER and K. N. TRUEBLOOD. Acta Crystallogr. Sect. B, **24**, 63 (1968).
6. D. W. J. CRUICKSHANK. Acta Crystallogr. **9**, 747 (1956); **9**, 754 (1956); **14**, 896 (1961).
7. W. KLIEGEL. Organomet. Chem. Rev. **A8**, 153 (1972).
8. Gmelin Handbuch der Anorganischen Chemie, Bor, Ergänzungsband. Weinheim. 1954, p. 171; Ergänzungswerk zur 8.Aufl. Bd. 53, Borverbindungen Teil 19. Berlin. 1978. p. 49.
9. D. MOOTZ and M. STEFFEN. Angew. Chem. **92**, 481 (1980).
10. M. YU. ANTIPIN, A. M. ELLERN, V. F. SUKHOVERKHOV, YU. T. STRUCHKOV, and YU. A. BUSALEV. Dokl. Akad. Nauk SSSR, **279**, 892 (1984); Proceed. Acad. Sci. USSR, **279**, 435 (1984).
11. K. TÖPEL, K. HENSEN, and J. W. BATZ. Acta Crystallogr. Sect. C, **40**, 828 (1984).
12. E. ANDERS, F. MARKUS, H. MESKE, J. TROPSCH, and G. MAAS. Chem. Ber. **120,** 735 (1987).
13. G. ROBINET, J. F. LABARRE, and C. LEIBOVICI. Chem Phys. Lett. **22**, 356 (1973).
14. T. D. COYLE and F. G. A. STONE. Progr. Boron Chem. **1**, 83 (1964); Gmelin Handbuch der Anorganischen Chemie, Ergänzungswerk zur 8.Aufl. Bd. 53, Borverbindungen Teil 19. Berlin. 1978. p. 104.
15. M. T. REETZ, M. HÜLLMANN, W. MASSA, S. BERGER, P. RADEMACHER, and P. HEYMANNS. J. Am. Chem. Soc. **108**, 2405 (1986).
16. C. A. MIRKIN, K.-L. LU, G. L. GEOFFROY, and A. L. RHEINGOLD. J. Am. Chem. Soc. **112**, 461 (1990).
17. G. HÄFELINGER. Chem. Ber. **103**, 2941 (1970).
18. W. KLIEGEL, M. TAJERBASHI, S. J. RETTIG, and J. TROTTER. Can. J. Chem. **69,** 673 (1991).
19. S. J. RETTIG, J. TROTTER, W. KLIEGEL, and D. NANNINGA. Can. J. Chem. **55**, 1 (1977).
20. S. J. RETTIG, J. TROTTER, W. KLIEGEL, and D. NANNINGA. Can. J. Chem. **56**, 1676 (1978).
21. W. KLIEGEL, D. NANNINGA, S. J. RETTIG, and J. TROTTER. Can. J. Chem. **61,** 2493 (1983).
22. W. KLIEGEL, M. TAJERBASHI, S. J. RETTIG, and J. TROTTER. Can. J. Chem. **67,** 1644 (1989).
23. W. KLIEGEL, M. TAJERBASHI, S. J. RETTIG, and J. TROTTER. Can. J. Chem. **68,** 69 (1990).

Can. J. Chem. Downloaded from www.nrcresearchpress.com by 84.41.108.74 on 09/07/12
For personal use only.

Structural studies of organoboron compounds. XLVII.[1] 6,8-Bis(1-cyano-1-methylethyl)-2,4-diphenyl-1,3,5-trioxa-6,8-diaza-2,4-diboracyclooctane

WOLFGANG KLIEGEL AND GOTTFRIED LUBKOWITZ

Institut für Pharmazeutische Chemie der Technischen Universität Braunschweig, Beethovenstrasse 55, 3300 Braunschweig, Bundesrepublik Deutschland

AND

STEVEN J. RETTIG AND JAMES TROTTER

Department of Chemistry, University of British Columbia, 2036 Main Mall, Vancouver, B.C., Canada V6T IZI

Received September 24, 1990

WOLFGANG KLIEGEL, GOTTFRIED LUBKOWITZ, STEVEN J. RETTIG, and JAMES TROTTER. Can. J. Chem. **69**, 1217 (1991).

The reaction of *N,N'*-bis(1-cyano-1-methylethyl)-*N,N'*-dihydroxymethanediamine with phenylboronic acid gives 6,8-bis(1-cyano-1-methylethyl)-2,4-diphenyl-1,3,5-trioxa-6,8-diaza-2,4-diboracyclooctane in good yield. Crystals of the product are monoclinic, $a = 9.2681(9)$, $b = 15.946(1)$, $c = 15.491(1)$ Å, $\beta = 95.946(8)°$, $Z = 4$, space group $P2_1/n$. The structure was solved by direct methods and was refined by full-matrix least-squares procedures to $R = 0.047$ and $R_w = 0.064$ for 2936 reflections with $I \geq 3\sigma(I)$. The central eight-membered $O(BON)_2C$ ring has a boat–boat ("saddle") conformation and features cross-ring non-bonding N···B distances of 2.475 and 2.755 Å, which are significantly shorter than the sum of van der Waals radii (~3.15 Å). Features of the molecular geometry are consistent with weak dative N → B interactions, particularly in the case of the shorter transannular contact. The formally trigonal boron atom involved in the short interaction is displaced 0.098 Å from the plane of its three substituents towards the nitrogen atom while the corresponding displacement for the other boron atom is 0.017 Å. The C(phenyl)—B distances are equal within experimental error at the two B atoms (1.545(3) and 1.547(3) Å), but the (B)O—B and (to a lesser extent) the (N)O—B bonds to the boron atom involved in the shorter transannular interaction are longer than the others (1.371(3) and 1.392(3) vs. 1.354(3) and 1.388(3) Å). The structure may be thought of as an intermediate in the transition from an eight-membered monocylic system to a bridged ring system.

Key words: crystal structure, organoboron compound, boron compound.

WOLFGANG KLIEGEL, GOTTFRIED LUBKOWITZ, STEVEN J. RETTIG et JAMES TROTTER. Can. J. Chem. **69**, 1217 (1991).

La réaction de la *N,N'*-bis(1-cyano-1-méthyléthyl)-*N,N'*-dihydroxyméthanediamine avec l'acide phénylboronique conduit au 6,8-bis(1-cyano-1-méthyléthyl)-2,4-diphényl-1,3,5-trioxa-6,8-diaza-2,4-diboracyclooctane, avec un bon rendement. Les cristaux de ce produit sont monocliniques, groupe d'espace $P2_1/n$, avec $a = 9,2681(9)$, $b = 15,946(1)$ et $c = 15,491(1)$ Å, $\beta = 95,946(8)°$ et $Z = 4$. On a résolu la structure par des méthodes directes et on l'a affinée par la méthode des moindres carrés (matrice complète) jusqu'à des valeurs de $R = 0,047$ et $R_w = 0,064$ pour 2936 réflexions avec $I \geq 3\sigma(I)$. Le cycle central à huit chaînons, $O(BON)_2C$ existe dans une conformation bateau–bateau («selle»); les interactions non-liantes N···B à travers le cycle sont caractérisées par des distances de 2,475 et 2,755 Å qui sont beaucoup plus courtes que la somme des rayons de van der Waals (~3,15 Å). Les caractéristiques de la géométrie moléculaire sont en accord avec des interactions datives faibles N → B, en particulier dans le cas du contact transannulaire le plus court. Par rapport au plan de ses trois substituants, l'atome de bore formellement plan trigonal impliqué dans l'interaction la plus courte est déplacé de 0,098 Å vers l'atome d'azote; par comparaison, le déplacement correspondant de l'autre atome de bore est de 0,017 Å. Aux erreurs expérimentales près, les distances C(phényl)—B (1,545(3) et 1,547(3)) sont les mêmes pour les deux atomes de bore; toutefois, les longueurs des liaisons (B)O—B et (à un degré moindre) (N)O—B des atomes de bores impliqués dans l'interaction transannulaire sont plus longues que les autres (1,371(3) et 1,392(3) vs. 1,354(3) et 1,388(3) Å). On peut imaginer que la structure est un intermédiaire dans la transition allant d'un système monocyclique à huit chaînons à un système cyclique ponté.

Mots clés : structure cristalline, composé organoboré, composé boré.

[Traduit par la rédaction]

Introduction

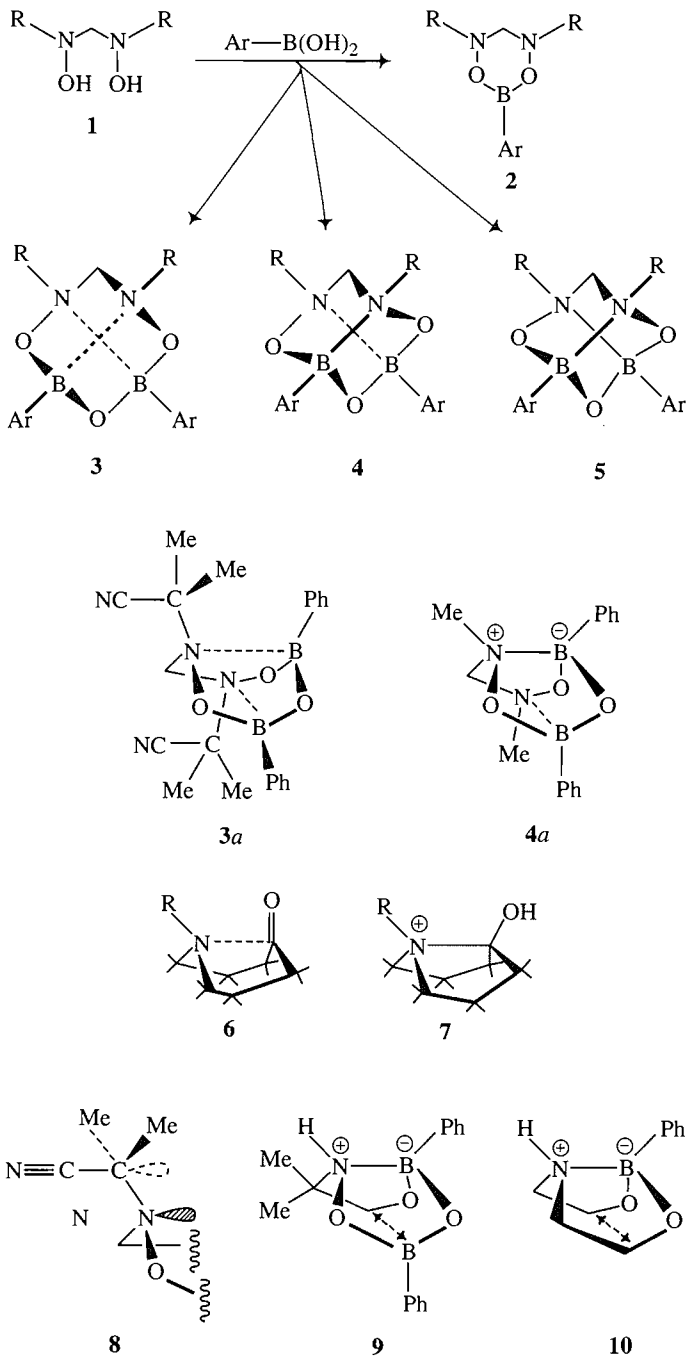
The *N,N'*-dihydroxy-*N,N'*-dialkylaminal **1** reacts with arylboronic acid to give the six-membered cyclocondensate, **2**, provided that the basicity of the aminal nitrogen atom is reduced (e.g. by α-cyanoalkyl substitution) and the boronic acid is sterically hindered (e.g. by *ortho*-substitution of the aryl residue). The structure of the cycloboronate **2***a*, substituted in such a manner (R = $C(CH_3)_2CN$, Ar = 2,4,6-$(CH_3)_3C_6H_2$), has been elucidated by an X-ray crystallographic study (1). In cases of simple *N*-alkyl substitution (R = alkyl) and an unsubstituted phenylboronic acid (Ar = phenyl) the products are bicyclic 1:2 condensates **4** with transannular N → B coordination (2). This was established by an X-ray crystallographic analysis of compound **4***a* (R = CH_3, Ar = C_6H_5) (3).

In this work we describe the reaction of the weakly basic *N,N'*-dihydroxyaminal **1** (R = $C(CH_3)_2CN$) with sterically unhindered phenylboronic acid. Surprisingly this condensation also results in a 1:2 reaction product between the "diol" **1** and the boronic acid, as shown by elemental analysis, nmr and mass spectral data. In the ^{13}C and ^{11}B nmr spectra the "magnetic equivalence" of the carbon nuclei directly attached to N and N' of the aminal function and also of the two boron nuclei suggest an essentially symmetric cyclooctane ring system **3** or, less likely, a highly strained tricyclooctane (dinoradamantane) skeleton **5**. The bicyclo[3.3.0]octane structure **4**, however, cannot be excluded because of possible fluxional behavior in solution leading to nmr signal coalescence during fast topomerization via alternating N→B coordination (2). The presence of an N—B bond, as realized in the bicyclic structure of type **4** in the solid state reported recently (3), would be somewhat contradictory to the assumption of reduced nitrogen donor

[1]Previous paper in this series: ref. 11.

Can. J. Chem. Downloaded from www.nrcresearchpress.com by 84.41.108.74 on 09/07/12
For personal use only.

Can. J. Chem. Downloaded from www.nrcresearchpress.com by 84.41.108.74 on 09/07/12
For personal use only.



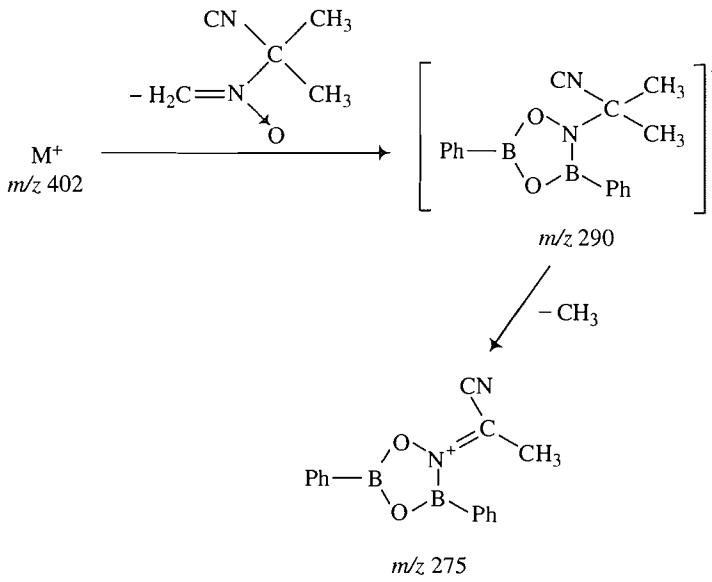


FIG. 1. Mass spectral fragmentation of **3***a* (main fragments).

capacity as a result of the presence of α-cyano groups in the compound under consideration here. An X-ray crystallographic analysis was undertaken in order to provide detailed information on the structure in the solid state.

Experimental

6,8-Bis(1-cyano-1-methylethyl)-2,4-diphenyl-1,3,5-trioxa-6,8-diaza-2,4-diboracyclooctane, **3**a *(R = $C(CH_3)_2CN$, Ar = C_6H_5)*

N,N'-Bis(1-cyano-1-methylethyl)-*N,N'*-dihydroxymethanediamine **1** (R = $C(CH_3)_2CN$) (4) (1.06 g, 5 mmol) and phenylboronic acid (1.22 g, 10 mmol) are suspended in 20 mL of benzene and refluxed for 1 h with continuous removal of water using a Dean Stark trap. Nearly all of the solvent is distilled off *in vacuo*, and petroleum ether (bp 30–70°C) is added. Upon cooling, colorless crystals are formed. Yield: 1.71 g (85%). Mp 149–150°C (from toluene). *Anal.* calcd. for $C_{21}H_{24}B_2N_4O_3$: C 62.73, H 6.02, B 5.38, N 13.94; found: C 62.73, H 6.05, B 5.41, N 13.91. Infrared (KBr): 2240 (very weak, C≡N), 1600 cm^{-1} (aryl C=C). ^1H nmr (90 MHz, $CDCl_3$/TMS): δ (ppm) = 1.47 (s, 2 CH_3), 1.53 (s, 2 CH_3), 3.90 (s, N—CH_2—N), 7.27–7.60 (m, 6 aromatic H, *m*- and *p*-), 7.77–8.00 (m, 4 aromatic H, *o*-). ^{13}C nmr (100 MHz, $CDCl_3$/TMS): δ (ppm) = 24.57 (2 CH_3), 25.97 (2 CH_3), 57.48 (2 *C*—CN), 72.08 (N—CH_2—N), 119.17 (2 *C*N), 127.94, 131.77, and 134.81 (12 aromatic C). ^{11}B nmr (64 MHz, $CDCl_3/Et_2OBF_3$): δ (ppm) = 28.7 (broad). Mass spectrum (70 eV, 60°C): *m/z* = 402 (40%, M^+), 290 (55%, M − H_2C=N(O)—C(CN)$(CH_3)_2$), 275 (100%, M − H_2C=N(O)—C(CN)$(CH_3)_2$—CH_3), 236 (8%), 181 (12%, $C_6H_5BOC_6H_5$), 105 (13%, C_6H_5BOH), 77 (12%, C_6H_5), 68 (6%, $(CH_3)_2C(CN)$). The main fragmentation scheme is shown in Fig. 1.

Crystals suitable for X-ray analysis were obtained by recrystallization from toluene.

X-ray crystallographic analysis of **3**a

A crystal ca. 0.30 × 0.32 × 0.45 mm in size was mounted on a glass fiber. Unit-cell parameters were refined by least squares on setting angles for 25 reflections (2θ = 82.2–102.3°) measured on a diffractometer with Cu-K_α radiation (λ = 1.54178 Å). Crystal data at 21°C are as follows

$C_{21}H_{24}B_2N_4O_3$ f.w. = 402.07

Monoclinic, *a* = 9.2681(9), *b* = 15.946(1), *c* = 15.491(1) Å, β = 95.946(8)°, *V* = 2277.0(3) $Å^3$, *Z* = 4, ρ_c = 1.173 Mg m^{-3}, *F*(000) = 848, μ(Cu-K_α) = 5.98 cm^{-1}. Absent reflections: 0*k*0, *k* odd, and *h*0*l*, *h* + *l* odd, uniquely indicate the space group $P2_1/n$ (No. 14).

Intensities were measured with graphite-monochromated Cu-K_α radiation on a Rigaku AFC6S diffractometer. An ω–2θ scan at 32° min^{-1} over a range of (1.15 + 0.20 tan θ)° in ω (with up to eight rescans, background/scan time ratio = 0.5) was employed. Data were measured to 2θ = 155°. The intensities of three check reflections, measured every 200 reflections throughout the data collection, showed only small random variations. After data reduction,[2] an empirical

[2]TEXSAN/TEXRAY structure analysis package which includes versions of the following: MITHRIL, integrated direct methods, by C. J. Gilmore; DIRDIF, direct methods for difference structures, by P. T. Beurskens; ORFLS, full-matrix least-squares, and ORFFE, function and errors, by W. R. Busing, K. O. Martin, and H. A. Levy; ORTEP II, illustrations, by C. K. Johnson.

TABLE 1. Final atomic coordinates (fractional) and B_{eq} (Å^2)*

Atom	x	y	z	B_{eq}
O(1)	0.1294(1)	0.66946(9)	0.1553(1)	5.11(6)
O(2)	0.3789(2)	0.62997(9)	0.1472(1)	5.49(7)
O(3)	0.3986(1)	0.60100(8)	0.29883(9)	4.97(6)
N(1)	0.1266(2)	0.5996(1)	0.2153(1)	4.94(8)
N(2)	0.3042(2)	0.6731(1)	0.3002(1)	5.08(8)
N(3)	−0.2286(3)	0.6625(2)	0.2180(2)	11.0(2)
N(4)	0.3276(3)	0.6327(2)	0.5164(2)	9.1(2)
C(1)	0.1580(2)	0.6379(1)	0.3003(1)	4.89(9)
C(2)	−0.0165(2)	0.5592(1)	0.1986(2)	5.5(1)
C(3)	−0.1354(3)	0.6184(2)	0.2097(2)	6.9(1)
C(4)	−0.0327(3)	0.5264(2)	0.1063(2)	7.7(1)
C(5)	−0.0233(3)	0.4872(2)	0.2623(2)	7.8(1)
C(6)	0.3557(2)	0.7231(1)	0.3779(2)	6.1(1)
C(7)	0.3428(2)	0.6730(2)	0.4571(2)	6.5(1)
C(8)	0.5142(3)	0.7472(2)	0.3715(2)	7.8(1)
C(9)	0.2614(3)	0.8017(2)	0.3787(3)	10.3(2)
C(10)	0.2939(2)	0.7744(1)	0.0964(1)	4.88(9)
C(11)	0.1853(2)	0.8345(1)	0.0858(2)	6.0(1)
C(12)	0.2042(3)	0.9087(2)	0.0438(2)	7.2(1)
C(13)	0.3330(3)	0.9250(2)	0.0106(2)	7.4(1)
C(14)	0.4435(3)	0.8676(2)	0.0216(2)	7.9(1)
C(15)	0.4244(2)	0.7934(1)	0.0642(2)	6.4(1)
C(16)	0.5023(2)	0.4955(1)	0.2013(1)	4.87(9)
C(17)	0.5251(3)	0.4705(2)	0.1185(2)	6.3(1)
C(18)	0.5923(3)	0.3956(2)	0.1022(2)	6.8(1)
C(19)	0.6393(3)	0.3442(1)	0.1703(2)	6.4(1)
C(20)	0.6198(3)	0.3677(1)	0.2532(2)	6.3(1)
C(21)	0.5528(2)	0.4427(1)	0.2687(2)	5.6(1)
B(1)	0.2711(3)	0.6892(1)	0.1405(2)	4.7(1)
B(2)	0.4215(2)	0.5787(2)	0.2147(2)	4.9(1)

*$B_{eq} = (8/3)\pi^2\Sigma\Sigma U_{ij}a_i^*a_j^*(\mathbf{a}_i\cdot\mathbf{a}_j)$.

absorption correction, based on azimuthal scans for three reflections, was applied. Transmission factors range from 0.86 to 1.00. Of the 4964 reflections measured, 4690 were unique (R_{int} = 0.016) and 2936 (62.6%) had intensities greater than or equal to $3\sigma(F^2)$ above background where $\sigma^2(F^2) = [S^2(C + 4B) + 0.035F^2)^2]/Lp^2$ with S = scan speed, C = scan count, B = total background count, and Lp = Lorentz-polarization factor.

The structure was solved by direct methods, the coordinates of all non-hydrogen atoms being determined from an E-map. The non-hydrogen atoms were refined with anisotropic thermal parameters and the hydrogen atoms were fixed in idealized positions (C—H = 0.98 Å, $B_H = 1.2B_{bonded\ atom}$). A correction for secondary extinction was applied, the final value of the extinction coefficient being 4.95×10^{-6}. Scattering factors for all atoms and anomalous dispersion corrections for the non-hydrogen atoms were taken from ref. 5. The weighting scheme $w = 4F_o^2/\sigma^2(F_o^2)$ gave uniform average values of $w(|F_o| - |F_c|)^2$ over ranges of both $|F_o|$ and $\sin\theta/\lambda$ and was employed in the final stages of full-matrix least-squares refinement of 272 variables. Reflections with $I < 3\sigma(I)$ were not included in the refinement. Convergence was reached at R = 0.047 and R_w = 0.064 for 2936 reflections with $I \geq 3\sigma(I)$. The function minimized was $\Sigma w(|F_o| - |F_c|)^2$, $R = \Sigma||F_o| - |F_c||/\Sigma|F_o|$, $R_w = (\Sigma w(|F_o| - |F_c|)^2/\Sigma w|F_o|^2)^{1/2}$.

On the final cycle of refinement the maximum parameter shift corresponded to 0.08σ. The mean error in an observation of unit weight was 2.24. The final difference map showed maximum fluctuations of ±0.16 e Å^{-3}. The final positional and (equivalent) isotropic thermal parameters for the non-hydrogen atoms appear in Table 1. Bond lengths and angles are given in Tables 2 and 3 and intra-annular torsion angles in Table 4. Hydrogen atom parameters, anisotropic thermal parameters, torsion angles, intermolecular contacts, least-squares planes, bond lengths and angles involving hydrogen, and structure factors have been deposited.[3]

TABLE 2. Bond lengths (Å) with estimated standard deviations

Atom	Atom	Distance	Atom	Atom	Distance
O(1)	N(1)	1.452(2)	C(6)	C(8)	1.532(3)
O(1)	B(1)	1.392(3)	C(6)	C(9)	1.529(3)
O(2)	B(1)	1.371(3)	C(10)	C(11)	1.387(3)
O(2)	B(2)	1.354(3)	C(10)	C(15)	1.389(3)
O(3)	N(2)	1.446(2)	C(10)	B(1)	1.545(3)
O(3)	B(2)	1.388(3)	C(11)	C(12)	1.371(3)
N(1)	C(1)	1.454(3)	C(12)	C(13)	1.372(3)
N(1)	C(2)	1.472(3)	C(13)	C(14)	1.371(4)
N(2)	C(1)	1.467(2)	C(14)	C(15)	1.375(3)
N(2)	C(6)	1.480(3)	C(16)	C(17)	1.381(3)
N(3)	C(3)	1.131(3)	C(16)	C(21)	1.385(3)
N(4)	C(7)	1.142(3)	C(16)	B(2)	1.547(3)
C(2)	C(3)	1.474(4)	C(17)	C(18)	1.383(3)
C(2)	C(4)	1.515(3)	C(18)	C(19)	1.371(4)
C(2)	C(5)	1.520(3)	C(19)	C(20)	1.368(4)
C(6)	C(7)	1.479(4)	C(20)	C(21)	1.380(3)

Results and discussion

The X-ray analysis confirms an eight-membered cyclic pyroboronate structure of the type **3** for compound **3***a* (see Fig. 2). The eight-membered ring has a distorted boat–boat ("saddle") conformation (see Table 4) which is generally only adopted when attractive transannular interactions occur. Analogous conformations for other medium-size heterocyclic rings are also known to be stabilized by such interactions (6). Transannular interactions in **3***a* are possible between the suitably placed donor–acceptor pairs N(1)···B(2) and N(2)···B(1). The intramolecular non-bonded distances of 2.755(3) and 2.475(3) Å, respectively, are suggestive of possible weak dative interactions, particularly in the latter case. Both of these N···B contacts are considerably shorter than the sum of van der Waals radii (~3.15 Å), and they are also shorter than the non-bonding intramolecular N···B contact of 3.082 Å in **4***a* (3) which lies at the upper end of the range between the transannular N—B bond in **4***a* (1.742 Å) and a van der Waals contact. If both of the weak transannular N···B contacts in **3***a* are looked upon as weak dative bonds the ring skeleton of **3** corresponds roughly to a widened form of the tricyclic ("dinoradamantane") skeleton of **5**, which is "half-realized" in the bicyclooctane framework of **4**.

Further support for the significance of the transannular interactions in **3***a* comes from comparison with non-bonded distances in molecules having ring systems geometrically similar to that in **4***a*: C···B = 3.416 Å in **9** (7) and C···C = 3.812 Å in **10** (8). The C···B distance in **9** is expected to be longer than the corresponding N···B distance in **4***a* because of the methylene group in the place of the amine function. The corresponding C···C contact in **10** is strictly non-bonding. Steric strain, particularly that imposed by ring fusion resulting from the formation of the relatively short transannular N—B bond, is most likely responsible for the longer non-bonding

[3]Supplementary material mentioned in the text may be purchased from the Depository of Unpublished Data, Document Delivery, CISTI, National Research Council of Canada, Ottawa, Ont., Canada K1A 0S2.

Can. J. Chem. Downloaded from www.nrcresearchpress.com by 84.41.108.74 on 09/07/12
For personal use only.

TABLE 3. Bond angles (deg) with estimated standard deviations

Atom	Atom	Atom	Angle	Atom	Atom	Atom	Angle
N(1)	O(1)	B(1)	111.0(1)	N(4)	C(7)	C(6)	176.9(3)
B(1)	O(2)	B(2)	128.8(2)	C(11)	C(10)	C(15)	117.1(2)
N(2)	O(3)	B(2)	111.7(2)	C(11)	C(10)	B(1)	121.9(2)
O(1)	N(1)	C(1)	104.0(1)	C(15)	C(10)	B(1)	121.0(2)
O(1)	N(1)	C(2)	107.4(2)	C(10)	C(11)	C(12)	121.7(2)
C(1)	N(1)	C(2)	115.7(2)	C(11)	C(12)	C(13)	120.0(2)
O(3)	N(2)	C(1)	104.9(1)	C(12)	C(13)	C(14)	119.7(2)
O(3)	N(2)	C(6)	107.2(2)	C(13)	C(14)	C(15)	120.2(2)
C(1)	N(2)	C(6)	115.2(2)	C(10)	C(15)	C(14)	121.3(2)
N(1)	C(1)	N(2)	104.9(1)	C(17)	C(16)	C(21)	116.9(2)
N(1)	C(2)	C(3)	111.7(2)	C(17)	C(16)	B(2)	119.6(2)
N(1)	C(2)	C(4)	108.4(2)	C(21)	C(16)	B(2)	123.5(2)
N(1)	C(2)	C(5)	108.3(2)	C(16)	C(17)	C(18)	122.3(2)
C(3)	C(2)	C(4)	109.2(2)	C(17)	C(18)	C(19)	119.3(2)
C(3)	C(2)	C(5)	109.1(2)	C(18)	C(19)	C(20)	119.8(2)
C(4)	C(2)	C(5)	110.2(2)	C(19)	C(20)	C(21)	120.4(2)
N(3)	C(3)	C(2)	178.5(3)	C(16)	C(21)	C(20)	121.3(2)
N(2)	C(6)	C(7)	109.7(2)	O(1)	B(1)	O(2)	121.6(2)
N(2)	C(6)	C(8)	108.3(2)	O(1)	B(1)	C(10)	116.5(2)
N(2)	C(6)	C(9)	108.2(2)	O(2)	B(1)	C(10)	120.5(2)
C(7)	C(6)	C(8)	110.4(2)	O(2)	B(2)	O(3)	120.6(2)
C(7)	C(6)	C(9)	109.9(3)	O(2)	B(2)	C(16)	121.4(2)
C(8)	C(6)	C(9)	110.3(2)	O(3)	B(2)	C(16)	117.9(2)

TABLE 4. Intra-annular torsion angles (deg) with estimated standard deviations in parentheses

Atoms	Value (deg)
B(1)—O(1)—N(1)—C(1)	81.4(2)
O(1)—N(1)—C(1)—N(2)	−64.2(4)
N(1)—C(1)—N(2)—O(3)	−68.1(2)
C(1)—N(2)—O(3)—B(2)	92.5(2)
N(2)—O(3)—B(2)—O(2)	10.9(3)
O(3)—B(2)—O(2)—B(1)	−25.4(3)
B(2)—O(2)—B(1)—O(1)	−54.2(3)
O(2)—B(1)—O(1)—N(1)	27.7(3)

N···B distance in **4***a* compared with that in **3***a*. The better donor qualitifes of the aminal nitrogen atoms in **4***a*, which are responsible for the formation of the "normal" transannular N—B bond, should otherwise lead to shorter N···B distances than in **3***a* with its weakly basic aminal nitrogen atoms.

Considering the difference between the two N···B distances in **3***a* (the N(2)···B(1) contact is 0.28 Å shorter) and the even larger difference between the N—B bond and the N···B contact in **4***a*, along with the general geometry of both molecules, the structure of **3***a* may be thought of as an intermediate in the transition from an eight-membered monocyclic system to the bridged-ring system of **4***a*. Similar relationships have been discussed for cyclic aminoketones **6** (with incipient nucleophilic addition of the amino group to the carbonyl function) and their transannular reaction products **7** (9). X-ray structure analyses of several eight-membered aminoketones **6** revealed transannular N···C(O) non-bonding distances between 2.46 and 2.76 Å (10) while the reaction products **7** show an N^+—C bond length of 1.64 Å (ref. 6, p. 126). These distances are very similar to the analogous N···B/N—B distances in **3***a* and **4***a*. The displacements (towards the cross-ring nitrogen) of the two boron atoms in **3***a* from the planes defined by their substituent atoms are 0.098(2) Å for B(1) and 0.017(2) Å for B(2). The value for B(2), while statistically significant, is not really consistent with any appreciable pyramidalization; values similar to this might easily arise from inter- and/or intramolecular steric forces. The value for B(1) (involved in the shorter of the transannular N···B interactions), however, is substantially larger and since there are no unusually short inter- or intramolecular contacts involving the relevant phenyl and —CMe_2(CN) substituents, indicates partial pyramidalization. If the weak interaction with N(2) is considered, the overall geometry at B(1), an axially elongated trigonal pyramid, is consistent with a system not far along the pathway between trigonal planar and tetrahedral.

The detailed geometry about the boron and nitrogen atoms in **3***a* is also consistent with a weak but significant interaction between B(1) and N(2). The partial pyramidalization of B(1) can also be inferred from the sum of the bond angles at B(1) involving the O and C atoms, 358.6(3)°. The corresponding value for B(2) is 359.9(3)°. The B—C(aryl) distances (1.545(3) and 1.547(3) Å) are nearly the same as that involving the sp^2-boron atom in **4***a* (1.548 Å). The B—O(N) distances do not differ significantly, but that involving B(1) is marginally longer (1.392(3) vs. 1.388(3) Å). Within the anhydridic B(1)—O(2)—B(2) portion of the ring the B—O distance of 1.371(3) Å involving B(1) is significantly longer than that of 1.354(3) Å for B(2) indicative of reduced O—B $pp(\pi)$ interaction, and hence reduced double bond character of the O—B bonds at B(1) relative to B(2). The difference between the two transannular N···B contacts in **3***a* is also reflected by the C—N bonds of the aminal function: C(1)—N(2) (1.467(2) Å) is longer than C(1)—N(1) (1.454(3) Å) in accordance with the increased positive charge at N(2). In compound **4***a* this difference is more pronounced as a result of the greater charge

Can. J. Chem. Downloaded from www.nrcresearchpress.com by 84.41.108.74 on 09/07/12
For personal use only.

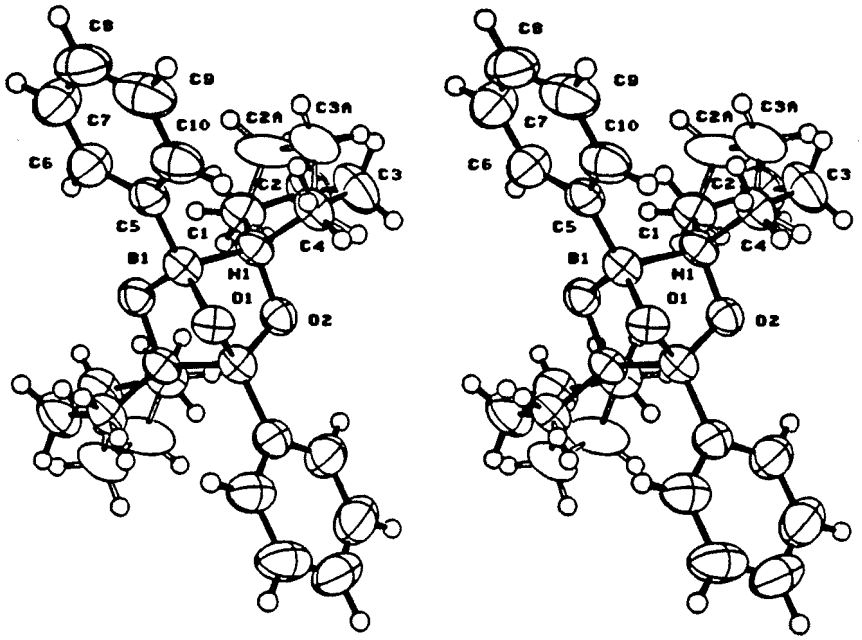


FIG. 2. Stereoview of **3***a*; 33% probability thermal ellipsoids are shown for the non-hydrogen atoms.

difference between the two ring nitrogen atoms: N^+—CH_2 = 1.479, N—CH_2 = 1.452 Å (3). As in **4***a* (3) the N—O bonds of **3***a* show a similar small difference in length, that at the nitrogen atom having the higher positive charge (N(2)—O(3) = 1.446(2) Å) being shorter than that at the other nitrogen atom (N(1)—O(1) = 1.452(2) Å). Once again this difference is less pronounced than in **4***a* where N^+—O = 1.447 and N—O = 1.462 Å. In the six-membered monocyclic arylboronate **2***a* there are no such differences in aminal N—C and N—O bond lengths between the chemically equivalent nitrogen atoms (1).

Similar to **2***a* (1) the α-cyanoalkyl moieties of **3***a* show evidence of stereoelectronic (anomeric) effects. An antiperiplanar orientation of both nitrogen electron pairs with respect to the α-positioned cyano groups, **8**, enables some overlap between the nitrogen *n*-orbitals and the σ* orbitals of the adjacent C—C(cyano) bond, resulting in relatively short C—N(amine) and long C—C(cyano) bonds (the C(2)—N(1) = 1.472(3) and C(6)—N(2) = 1.480(3) Å bond lengths are not significantly different from the usual value of 1.472(5) Å for three-coordinate nitrogen N—C bonds, but the C(2)—C(3) = 1.474(4) and C(6)—C(7) = 1.479(4) Å bonds are significantly longer than the normal C—C(cyano) bond length of 1.44(1) Å). This effect is not as marked as that observed for **2***a*, probably a consequence of the competition for the nitrogen lone pair by the transannular interaction with the unoccupied boron p_z orbitals in **3***a*.

Unlike the monocyclic arylboronate **2***a* (1) which has opposite configurations (*R*,*S*) at the two amine centres, **3***a* has the same configuration at both nitrogen atoms. The molecule shown in Fig. 2 is the (6*R*,8*R*)-enantiomer, the centrosymmetric crystals containing equal numbers of the (6*R*,8*R*)- and (6*S*,8*S*)-enantiomers. If the boron atoms in **3***a* are also considered tetracoordinate the relative configuration is (2*SR*,4*SR*,6*RS*,8*RS*),[4] comparable to that observed for the bicyclic compound **4***a* (3).

As is typical for sterically unhindered arylboronate derivatives, the phenyl rings are approximately coplanar with the O_2BC mean planes. The dihedral angles between normals to the phenyl and O_2C planes are 7.8° for B(1) and 2.1° for B(2). The shortest intermolecular contact involving non-hydrogen atoms, N(4)···C(11) = 3.418(3) Å, corresponds to a normal van der Waals interaction.

Acknowledgements

We thank the Natural Sciences and Engineering Research Council of Canada and the Fonds der Chemischen Industrie, Frankfurt am Main, for financial support.

1. W. KLIEGEL, G. LUBKOWITZ, S. J. RETTIG, and J. TROTTER. Can. J. Chem. **69**, 234 (1991).
2. W. KLIEGEL. J. Organomet. Chem. **253**, 9 (1983).
3. W. KLIEGEL, S. J. RETTIG, and J. TROTTER. Can. J. Chem. **62**, 515 (1984).
4. M. MASUI and C. YIJIMA. Yakugaku Zasshi **89**, 135 (1969).
5. International tables for X-ray crystallography. Vol. IV. Kynoch Press: Birmingham, U.K. (present distributor Kluwer Academic Publishers: Dordrecht, The Netherlands). 1974. pp. 99–102, 149.
6. R. S. GLASS (*Editor*). Conformational analysis of medium-size heterocycles. VCH Publishers, Weinheim. 1988.
7. S. J. RETTIG, J. TROTTER, W. KLIEGEL, and H. BECKER. Can. J. Chem. **54**, 3142 (1976).
8. S. J. RETTIG and J. TROTTER. Can. J. Chem. **53**, 1393 (1975).
9. (*a*) N. J. LEONARD. Rec. Chem. Prog. **17**, 243 (1956); (*b*) J. D. DUNITZ. X-ray analysis and the structure of organic molecules. Cornell University Press, Ithaca, NY. 1979. Chap. 7, p. 301; (*c*) H. B. BÜRGI and J. D. DUNITZ. Acc. Chem. Res. **16**, 153 (1983).
10. M. KAFTORY and J. D. DUNITZ. Acta Crystallogr. Sect. B, **31**, 2912 (1975); Sect. B, **31**, 2914 (1975); Sect. B, **32**, 1 (1976); E. BYE and J. D. DUNITZ. Acta Crystallogr. Sect. B, **34**, 3245 (1978).
11. W. KLIEGEL, U. SCHUMACHER, S. J. RETTIG, and J. TROTTER. Can. J. Chem. **69**, 1212 (1991).

[4]The 2, 4, 6, and 8 positions of the heterocyclic ring correspond to atoms B(1), B(2), N(1), and N(2), respectively.

Can. J. Chem. Downloaded from www.nrcresearchpress.com by 84.41.108.74 on 09/07/12
For personal use only.

Structural studies of organoboron compounds XLVIII.[1] 1,4-Diphenyl-3,3:6,6-bis(tetramethylene)-2,5,7-trioxa-3,6-diazonia-1,4-diboratabicyclo[2.2.1]heptane

WOLFGANG KLIEGEL AND ULF RIEBE

Institut für Pharmazeutische Chemie der Technischen Universität Braunschweig, Beethovenstrasse 55, 3300 Braunschweig, Bundesrepublik Deutschland

AND

STEVEN J. RETTIG AND JAMES TROTTER

Department of Chemistry, University of British Columbia, 2036 Main Mall, Vancouver, B.C., Canada V6T 1Z1

Received September 24, 1990

WOLFGANG KLIEGEL, ULF RIEBE, STEVEN J. RETTIG, and JAMES TROTTER. Can. J. Chem. **69**, 1222 (1991).

The reaction of *N*-hydroxypyrrolidine with either oxybis(diphenylborane) or phenylboronic acid gives 1,4-diphenyl-3,3:6,6-bis(tetramethylene)-2,5,7-trioxa-3,6-diazonia-1,4-diboratabicyclo[2.2.1]heptane in moderate yield. Crystals of the product are orthorhombic, $a = 10.984(2)$, $b = 14.619(2)$, $c = 12.311(2)$ Å, $Z = 4$, space group *Pccn*. The structure was solved by direct methods and was refined by full-matrix least-squares procedures to $R = 0.039$ and $R_w = 0.043$ for 908 reflections with $I \geq 3\sigma(I)$. This is the first heterocyclic [2.2.1]heptane system containing a six-membered BONBON ring and a B—O—B bridge to be structurally characterized. The molecule has exact C_2 symmetry with the twofold axis passing through the bridging oxygen atom. Bond lengths involving the tetrahedrally coordinated boron atom are B—O(B) = 1.423(3), B—O(N) = 1.497(3), B—N = 1.703(3), and B—C(phenyl) = 1.577(4) Å.

Key words: 2,5,7-trioxa-3,6-diazonia-1,4-diboratabicyclo[2.2.1]heptane ring system, crystal structure, organoboron compound.

WOLFGANG KLIEGEL, ULF RIEBE, STEVEN J. RETTIG et JAMES TROTTER. Can. J. Chem. **69**, 1222 (1991).

La réaction de la *N*-hydroxypyrrolidine avec soit l'oxybis(diphénylborane) ou l'acide phénylboronique conduit au 1,4-diphényl-3,3:6,6-bis(tétraméthylène)-2,5,7-trioxa-3,6-diazonia-1,4-diboratabicyclo[2.2.1]hepatane, avec un rendement raisonnable. Les cristaux de ce produit sont orthorhombiques, groupe d'espace *Pccn*, avec $a = 10{,}984(2)$, $b = 14{,}619(2)$ et $c = 12{,}311(2)$ Å et $Z = 4$. On a résolu la structure par des méthodes directes et on l'a affinée par la méthode des moindres carrés jusqu'à des valeurs de $R = 0{,}039$ et $R_w = 0{,}043$ pour 908 réflexions avec $I \geq 3\sigma(I)$. Il s'agit du premier système hétérobicyclo[2.2.1]heptane comportant un cycle à six chaînons BONBON et un pont B—O—B à être caractérisé d'un point de vue structural. La molécule possède une symétrie C_2 exacte, avec un axe binaire passant par l'atome d'oxygène qui crée le pont. Les longueurs des liaisons impliquant l'atome de bore coordiné d'une façon tétraédrique sont : B—O(B) = 1,423(3), B—O(N) = 1,497(3), B—N = 1,703(3) et B—C(phényl) = 1,577(4) Å.

Mots clés : système cyclique 2,5,7-trioxa-3,6-diazonia-1,4-diboratabicyclo[2.2.1]heptane, structure cristalline, composé organoboré.

[Traduit par la rédaction]

Introduction

The reaction of *N*-hydroxypyrrolidine, **1**, and oxybis(diphenylborane) in boiling ethanol did not lead to the diphenylboryloxyamine **2** or its dimer, but resulted instead in the formation of a crystalline product with analytical data consistent with an oxybis(B-pyrrolidinoxy-phenylborane) structure **3**. Compound **3** was identified by elemental analysis, ^{1}H nmr spectroscopy, reaction with diphenylcarbazone,[2] and also by synthesis via condensation of **1** with phenylboronic acid. Three possible structures for the product **3** were considered. The open-chain pyroboronate **3***A*, similar to the ethylboronate **4** proposed as an intermediate in the oxidation of O-(diethylboryl)-acetone oxime (2), can be ruled out on the basis of the ^{11}B nmr chemical shift for **3** ($\delta(Et_2OBF_3) = 9.0$ ppm) which is consistent with a tetrahedral boron species. A trigonal planar phenylboronate with ester and anhydride functions would be expected to display an ^{11}B δ value of approximately 30 ppm (3). Compound **4** has an ^{11}B resonance at 19 ppm (2), intermediate between the above-mentioned values.

The five-membered chelate structure **3***B*, derived from **3***A* by intramolecular N → B coordination, possesses the BOBON ring system present in diphenylboron chelate **5**, the structure of which has been determined by an X-ray crystallographic analysis (4). The ^{11}B nmr spectrum of **5**, however, displays two separate signals at δ = 10.5 and 30.3 ppm (5) as was expected from the presence of two different types of boron atoms (sp^2 and sp^3). Compound **3** displays only one signal in its ^{11}B nmr spectrum, suggesting either fluxional behavior of **3***B* with both boron and both nitrogen atoms involved, a symmetrical bicyclic structure **3***C* with a reasonably strained norbornane ring skeleton, or (less likely) intermolecular N → B adducts of **3***A*. Structure **3***C* represents, formally, an intramolecular N → B adduct of **3***B* or the twofold intramolecular adduct of **3***A*. A somewhat similar strained bicyclic ring system has recently been characterized for compound **6** (6). For unambiguous proof of the bicyclo[2.2.1]heptane structure **3***C* at least in the solid state, an X-ray crystallographic analysis of **3** was performed.

Experimental

1,4-Diphenyl-3,3:6,6-bis(tetramethylene)-2,5,7-trioxa-3,6-diazonia-1,4-diboratabicyclo[2.2.1]heptane, **3**C

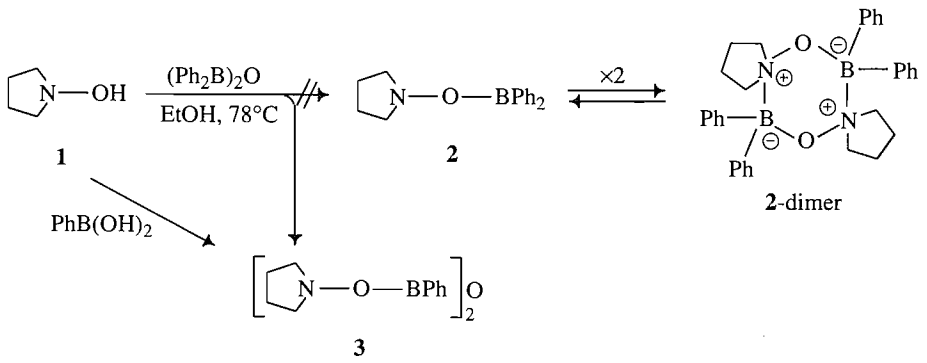
Method (*a*): *N*-hydroxypyrrolidine (0.88 g, 5 mmol) and oxybis(diphenylborane) (0.87 g, 2.5 mmol) are dissolved in 20 mL of ethanol and the mixture is refluxed for 30 min. The solvent is distilled off *in*

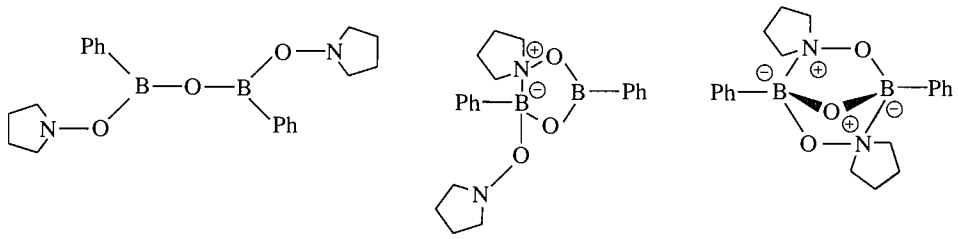
[1]Previous paper in this series: ref. 29.

[2]The blue color reaction indicating the presence of an intact diphenylboron moiety (1) did not occur with compound **3**.

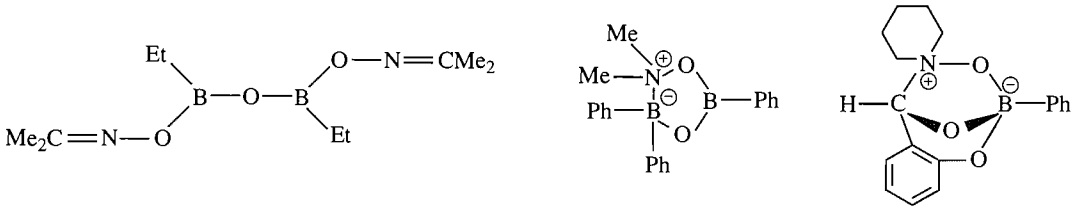
Can. J. Chem. Downloaded from www.nrcresearchpress.com by 84.41.108.74 on 09/07/12
For personal use only.

Can. J. Chem. Downloaded from www.nrcresearchpress.com by 84.41.108.74 on 09/07/12
For personal use only.

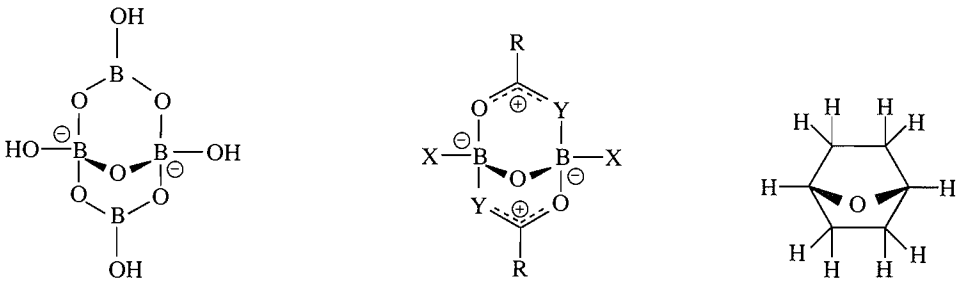




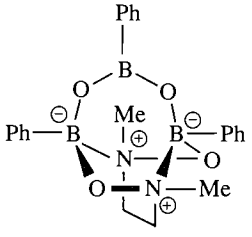
3A 3B 3C



4 5 6



7 8 9



10

vacuo and upon the remaining oil, after cooling down, 20 mL of petroleum ether (bp 30–75°C) are layered. During slow volatilization of the petroleum ether at room temperature (over a period of 3 days) long needle-like crystals grow into the upper layer. Mp (without recrystallization) 170–174°C (decomp.). Yield: 0.66 g (72%).

Method (*b*): *N*-hydroxypyrrolidine (0.88 g, 5 mmol) and phenylboronic acid (0.61 g, 5 mmol) are dissolved in 20 mL of ethanol and the mixture is refluxed for 30 min. After evaporation of solvent *in vacuo* the remaining colorless oil crystallizes slowly at room temperature. Recrystallization from dichloromethane/petroleum ether (1:1) yields

Can. J. Chem. Downloaded from www.nrcresearchpress.com by 84.41.108.74 on 09/07/12
For personal use only.

0.45 g (48%) of colorless crystals which are identical by mp, and infrared spectrum to the material obtained using method (*a*). Mp, 170–171°C (from CH_2Cl_2/petroleum ether).

Infrared (KBr): 1600 cm^{-1} (weak, arom. C=C). ^1H nmr (90 MHz, $CDCl_3$/TMS): δ (ppm) = 1.0–2.3 (m, 2 C—CH_2CH_2—C), 3.05 (m, 2 N—CH_2), 3.35 (t, 2 N—CH_2), 7.2 (m, 6 phenyl—H, *m* and *p*), 7.6 (m, 4 phenyl—H, *o*). ^{11}B nmr ($CDCl_3/Et_2OBF_3$): δ (ppm) = 9.0. Mass spectrum (70 eV): *m/z* (relative intensity): 364 (2.5, M^+), 278 (100, M − C_4H_8NO), 174 (16, M − C_4H_8NO − C_6H_5BO), 105 (11, C_6H_5BOH), 86 (8, C_4H_8NO), 70 (16, C_4H_8N). *Anal.* calcd. for $C_{20}H_{26}B_2N_2O_3$: C 65.98, H 7.20, B 5.95, N 7.69; found: C 65.99, H 7.27, B 6.35, N 7.77. The substance gives a red color reaction with diphenylcarbazone (1%) in methanolic soluton. Crystals of **3***C* suitable for X-ray analysis were obtained by method (*a*) without recrystallization.

X-ray crystallographic analysis of **3**C

A crystal ca. 0.35 × 0.43 × 0.50 mm in size was mounted on a glass fiber. Unit-cell parameters were refined by least-squares on setting angles for 25 reflections (2θ = 20.1–34.0°) measured on a diffractometer with Mo-K_α radiation (λ = 0.71069 Å). Crystal data at 21°C are as follows

$C_{20}H_{26}B_2N_2O_3$ f.w. = 364.06

Orthorhombic, a = 10.984(2), b = 14.619(2), c = 12.311(2) Å, V = 1976.8(5) $Å^3$, Z = 4, ρ_c = 1.223 Mg m^{-3}, $F(000)$ = 776, μ(Mo-K_α) = 0.75 cm^{-1}. Absent reflections: 0*kl*, *l* odd, *h*0*l*, *l* odd, and *hk*0, *h* + *k* odd, uniquely indicate the space group *Pccn* (No. 56).

Intensities were measured with graphite-monochromated Mo-K_α radiation on a Rigaku AFC6S diffractometer. An ω–2θ scan at 16° min^{-1} over a range of (1.20 + 0.35 tan θ)° in ω (with up to eight rescans, background/scan time ratio = 0.5) was employed. Data were measured to 2θ = 55°. The intensities of three check reflections, measured every 150 reflections throughout the data collection, showed only small random variations. After data reduction,[3] an empirical absorption correction, based on azimuthal scans for three reflections, was applied. Transmission factors range from 0.95 to 1.00. Of the 2269 independent reflections measured, 908 (40.0%) had intensities greater than or equal to 3σ(F^2) above background where $\sigma^2(F^2) = [S^2(C + 4B) + (0.035F^2)^2]/Lp^2$ with S = scan speed, C = scan count, B = total background count, and Lp = Lorentz-polarization factor. The relatively small fraction of data having significant intensity is due to the inclusion of reflections with 2θ between 45 and 55°, of which only about 10% were "observed."

The structure was solved by direct methods. The molecule is situated on a crystallographic C_2 axis which passes through the bridging oxygen atom O(1). The pyrrolidine ring was found to be twofold conformationally disordered (78:22), the peripheral atoms C(2) and C(3) were refined using a split-atom twofold disordered model. The site occupancy factors were initially estimated from Fourier map peak heights and were subsequently adjusted (but not refined) to result in approximately equal equivalent isotropic thermal parameters for the two well-resolved components. The non-hydrogen atoms were refined with anisotropic thermal parameters and the hydrogen atoms were fixed in idealized positions (C—H = 0.98 Å, B_H = 1.2 $B_{bonded\ atom}$). A correction for secondary extinction was applied, the final value of the extinction coefficient being 1.23 × 10^{-6}. Scattering factors for all atoms and anomalous dispersion corrections for the non-hydrogen atoms were taken from ref. 7. The weighting scheme $w = 4F_o^2/\sigma^2(F_o^2)$ gave uniform average values of $w(|F_o| - |F_c|)^2$ over ranges of both $|F_o|$ and sin θ/λ and was employed in the final stages of full-matrix least-squares refinement of 142 variables. Reflections with $I < 3\sigma(I)$ were not included in the refinement. Convergence was reached at R = 0.039 and R_w = 0.043 for 908 reflections with $I \geq 3\sigma(I)$. The function minimized was $\Sigma w(|F_o| - |F_c|)^2$, $R = \Sigma||F_o| - |F_c||/\Sigma|F_o|$, $R_w = (\Sigma w(|F_o| - |F_c|)^2/\Sigma w|F_o|^2)^{1/2}$.

On the final cycle of refinement the maximum parameter shift corresponded to 0.01σ. The mean error in an observation of unit weight was 1.89. The final difference map showed maximum fluctuations of ±0.12 e $Å^{-3}$. The final positional and (equivalent) isotropic thermal parameters for the non-hydrogen atoms appear in Table 1. Bond lengths and angles are given in Tables 2 and 3 and intra-annular torsion angles in Table 4. Hydrogen atom parameters, anisotropic thermal parameters, torsion angles, intermolecular contacts, least-squares planes, bond lengths and angles involving hydrogen, and structure factors have been deposited.[4]

TABLE 1. Final atomic coordinates (fractional) and B_{eq} ($Å^2$)*

Atom	*x*	*y*	*z*	B_{eq}
O(1)	1/4	1/4	0.3068(2)	3.9(1)
O(2)	0.3620(1)	0.2961(1)	0.4610(1)	4.3(1)
N(1)	0.3638(2)	0.1971(1)	0.4571(2)	4.0(1)
C(1)	0.3697(3)	0.1608(2)	0.5693(2)	5.1(1)
C(2)′	0.4995(4)	0.1677(4)	0.6029(3)	6.5(3)
C(2A)″	0.450(2)	0.093(1)	0.568(2)	8(1)
C(3)′	0.5732(4)	0.1757(4)	0.4990(4)	7.1(3)
C(3A)″	0.528(2)	0.097(1)	0.474(1)	7(1)
C(4)	0.4830(2)	0.1703(2)	0.4086(2)	5.0(1)
C(5)	0.2246(2)	0.0742(2)	0.3464(2)	4.3(1)
C(6)	0.1473(3)	0.0141(2)	0.4010(3)	6.0(2)
C(7)	0.1357(3)	−0.0757(2)	0.3703(4)	7.9(2)
C(8)	0.2013(4)	−0.1098(2)	0.2845(4)	8.0(2)
C(9)	0.2784(3)	−0.0527(2)	0.2281(3)	7.1(2)
C(10)	0.2897(3)	0.0384(2)	0.2583(2)	5.4(2)
B(1)	0.2359(3)	0.1773(2)	0.3826(2)	4.0(1)

*$B_{eq} = (8/3)\pi^2\Sigma\Sigma U_{ij}\boldsymbol{a}_i^*\boldsymbol{a}_j^*(\boldsymbol{a}_i\cdot\boldsymbol{a}_j)$. The symbols ′ and ″ refer to site occupancy factors of 0.78 and 0.22, respectively.

TABLE 2. Bond lengths (Å) with estimated standard deviations

Atom	Atom	Distance	Atom	Atom	Distance
O(1)	B(1)	1.423(3)	C(3)	C(4)	1.492(5)
O(2)	N(1)	1.447(2)	C(3A)	C(4)	1.43(2)
O(2)	B(1)*	1.497(3)	C(5)	C(6)	1.394(4)
N(1)	C(1)	1.482(3)	C(5)	C(10)	1.400(4)
N(1)	C(4)	1.491(3)	C(5)	B(1)	1.577(4)
N(1)	B(1)	1.703(3)	C(6)	C(7)	1.372(4)
C(1)	C(2)	1.488(5)	C(7)	C(8)	1.373(5)
C(1)	C(2A)	1.33(2)	C(8)	C(9)	1.377(5)
C(2)	C(3)	1.517(6)	C(9)	C(10)	1.388(4)
C(2A)	C(3A)	1.44(2)			

*Symmetry operation: 1/2 − *x*, 1/2 − *y*, *z* (here and elsewhere in this report).

Results and discussion

The X-ray analysis shows that compound **3** indeed forms the bicyclic twofold N—B adduct **3***C* in the solid state (see Fig. 1). The ^{11}B nmr spectrum, which is consistent with the presence of tetracoordinated boron, suggests that the structure **3***C* is stable in solution as well as in the solid state. To the best of our knowledge this is the first example of a full heterocyclic "norbornane" ring system of the BONBON type with a B—O—B

[3]TEXSAN/TEXRAY structure analysis package which includes versions of the following: MITHRIL, integrated direct methods, by C. J. Gilmore; DIRDIF, direct methods for difference structures, by P. T. Beurskens; ORFLS, full-matrix least-squares, and ORFFE, function and errors, by W. R. Busing, K. O. Martin, and H. A. Levy; ORTEP II, illustrations, by C. K. Johnson.

[4]Supplementary material mentioned in the text may be purchased from the Depository of Unpublished Data, Document Delivery, CISTI, National Research Council of Canada, Ottawa, Ont., Canada K1A 0S2.

TABLE 3. Bond angles (deg) with estimated standard deviations

Atom	Atom	Atom	Angle	Atom	Atom	Atom	Angle
B(1)	O(1)	B(1)*	98.0(3)	N(1)	C(4)	C(3A)	105.9(7)
N(1)	O(2)	B(1)*	104.4(2)	C(6)	C(5)	C(10)	116.7(3)
O(2)	N(1)	C(1)	109.1(2)	C(6)	C(5)	B(1)	120.9(2)
O(2)	N(1)	C(4)	106.8(2)	C(10)	C(5)	B(1)	122.4(2)
O(2)	N(1)	B(1)	100.2(2)	C(5)	C(6)	C(7)	121.8(3)
C(1)	N(1)	C(4)	103.9(2)	C(6)	C(7)	C(8)	120.6(4)
C(1)	N(1)	B(1)	118.5(2)	C(7)	C(8)	C(9)	119.4(3)
C(4)	N(1)	B(1)	117.6(2)	C(8)	C(9)	C(10)	120.1(3)
N(1)	C(1)	C(2)	106.0(3)	C(5)	C(10)	C(9)	121.4(3)
N(1)	C(1)	C(2A)	106.5(8)	O(1)	B(1)	O(2)*	107.9(2)
C(1)	C(2)	C(3)	106.4(3)	O(1)	B(1)	N(1)	97.8(2)
C(1)	C(2A)	C(3A)	112(1)	O(1)	B(1)	C(5)	122.5(2)
C(2)	C(3)	C(4)	105.7(3)	O(2)*	B(1)	N(1)	101.6(2)
C(2A)	C(3A)	C(4)	106(1)	O(2)*	B(1)	C(5)	112.0(2)
N(1)	C(4)	C(3)	105.7(3)	N(1)	B(1)	C(5)	112.3(2)

TABLE 4. Intra-annular torsion angles

Atoms	Value
O(2)*—B(1)—N(1)—O(2)	−70.2(2)
B(1)—N(1)—O(2)—B(1)*	−9.6(2)
N(1)—O(2)—B(1)*—N(1)*	78.4(2)
B(1)*—O(1)—B(1)—N(1)	−53.1(1)
O(1)—B(1)—N(1)—O(2)	40.0(2)
B(1)—N(1)—O(2)—B(1)*	−9.6(2)
N(1)—O(2)—B(1)*—O(1)	−23.8(2)
O(2)—B(1)*—O(1)—B(1)	51.8(1)
N(1)—C(1)—C(2)—C(3)	−19.7(5)
C(1)—C(2)—C(3)—C(4)	−1.7(5)
C(2)—C(3)—C(4)—N(1)	22.3(5)
C(3)—C(4)—N(1)—C(1)	−34.5(4)
C(4)—N(1)—C(1)—C(2)	33.4(3)
N(1)—C(1)—C(2A)—C(3A)	18(2)
C(1)—C(2A)—C(3A)—C(4)	−6(2)
C(2A)—C(3A)—C(4)—N(1)	−10(2)
C(3A)—C(4)—N(1)—C(1)	19.8(9)
C(4)—N(1)—C(1)—C(2A)	−23(1)

bridge. Similar B—O—B bridges have previously been found in the less strained bicyclo[3.3.1]nonane skeletons of various boron heterocycles such as **7** (8) and, similarly, in acyloxy- or acylamino-derivatives of boric or boronic acids of the type **8** (9–11).

The molecule **3***C* has exact C_2 symmetry in the solid state, the ring skeleton being similar to that of 7-oxabicyclo[2.2.1]heptane, **9**, which has been shown to possess C_{2v} symmetry in the gas phase by microwave spectroscopy (12). The angle at the B—O—B bridge in **3***C* (98.0(3)°) is somewhat larger than the corresponding angle of 95.3° in **9** (12) and similar to values of 97.4° and 96.6° reported for other derivatives of 7-oxabicyclo-[2.2.1]heptane (13) and 7-oxabicyclo[2.2.1]hept-2-ene (14), respectively. All of these oxygen-bridged species show angles at the bridging oxygen atom larger than the 93.1 angle at the bridging methylene group in norbornane itself (15). The bond angles at the bridging oxygen atoms of the less strained bicyclo[3.3.1]nonane derivatives **7** and **8** are substantially larger: 110.1–111.9° in **7** (16), 109.9° in **8***a* (R = CH_3, X = CH_3COO, Y = O) (9), 108.6° in **8***b* (R = CH_3, X = F, Y = O) (10), and 110.9° in **8***c* (R = CF_3, X = Cl, Y = 2,6-$(CH_3)_2C_6H_3N$) (11).

The N—B bond in **3***C* (1.703(3) Å) is shorter than that in the monocyclic compound **5** (1.728 Å) (4) which contains a similar BOBON ring system. The N—B bond in **5**, however, is subject to more steric hindrance and one of the boron atoms in **5** is sp^2 hybridized and involved in a pp(π) interaction with the hydroxylamine oxygen atom. This is reflected by the considerable difference between the (sp^3)B—O(N) distance of 1.497(3) Å in **3***C* and the (sp^2)B—O(N) distance of 1.422 Å in **5** (4). The (sp^3)B—C(phenyl) bond in **3***C* (1.577(4) Å) is about 0.02 Å longer than the (sp^2)B—C(phenyl) bond in **5** (1.553 Å) (4) and other phenylboronates containing similar BOBON rings (1.548–1.559, mean 1.554 Å) (17–21). The (sp^3)B—C(phenyl) bond in the present structure is the shortest yet observed for a "$PhBO_2N$" compound and is comparable to the recently reported (sp^3)B—C(phenyl) distance of 1.579 Å (21) in a bicyclic pyroboronate with relatively weak transannular N—B bonding. The steric constraints imposed by the formation of the bicyclo[2.2.1]heptane system are at least partly responsible for the shortness of the (sp^3)B—C(phenyl) bond in **3***C*. With the boron atoms in the bridgehead positions, ring constraints result in larger than tetrahedral bond angles about the boron atom involving the phenyl carbon atom (average C—B—O/N = 115.6°). This leads to increased *s*-character in the hybrid orbital at boron involved in the B—C bond and hence a shorter bond distance. As discussed in an earlier paper (22), the sum of all four bonds to boron in tetrahedral "$PhBO_2N$" compounds remains essentially constant. In the present case the short B—C bond is balanced by a relatively long N—B bond. The (sp^3)B—C(phenyl) bond length in the phenylboronate complex **6** (6) of 1.591 Å lies within the range of 1.582 to 1.633 Å reported for (sp^3)B—C(phenyl) distances in other phenylboronate complexes (17–19, 22–28).

The (sp^3)B—O—B(sp^3) bridge in **3***C* (sum of bond lengths 2.846 Å) is, as expected, longer than the (sp^3)B—O—B(sp^2) bridge in **5** (2.816 Å) which contains a characteristic very short anhydridic (sp^2)B—O bond (1.329 Å) and an (sp^3)B—O bond of 1.487 Å (4). The difference of about 0.07 Å between the two types of B—O bonds in **3***C* is roughly the same as the mean difference of 0.05 Å between the (sp^3)B—O(B) and (sp^3)-B—O(N) bonds in the tricyclic compound **10** (22) which incorporates a twisted BONBON boat with a B—OBO—B

Can. J. Chem. Downloaded from www.nrcresearchpress.com by 84.41.108.74 on 09/07/12
For personal use only.

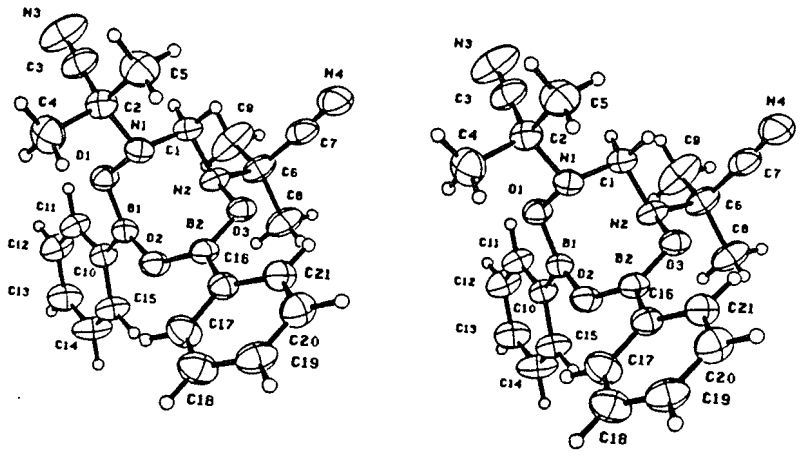


FIG. 1. Stereoview of **3***C*; 50% probability thermal ellipsoids are shown for the non-hydrogen atoms.

bridge, the shorter bond always being the anhydridic "pyroboronate" B—O bond. The bond lengths within the B—O—N sequence in **3***C* (1.497(3) and 1.447(2) Å, respectively) are not significantly different from those in **10** (1.497 and 1.443, 1.492 and 1.452 Å). The main differences between the BONBON moieties in the two compounds are in the N—B bonds (**3***C*: 1.703(3) Å, **10**: 1.649 and 1.658 Å) and in the degree of distortion of the BONBON heterocycle.

Both possible conformations of the pyrrolidine ring (resulting from the disordering of atoms C(2) and C(3)) correspond to slightly distorted *N*-envelopes with the nitrogen atom displaced 0.512(2) Å from the C(1)C(2)C(3)C(4) mean plane and 0.338(2) Å from the C(1)C(2A)C(3A)C(4) mean plane. There are some very short intermolecular distances across the centre of symmetry at (1/2, 0, 1/2) involving the 22% occupied disordered sites (C(2A) ... C(3A) = 2.84(2), C(3A) ... C(3A) = 2.98(4), H(4A) ... H(6A) = 1.33 Å, and three C ... H contacts in the range 1.96–2.37 Å). Adjacent molecules can therefore not both have the minor sites occupied. These short intermolecular contacts are also most likely responsible for the unbalanced occupancies of these otherwise equivalent sites. The phenyl ring is planar within experimental error with the boron atom lying in the phenyl mean plane (displacement 0.001(3) Å).

Acknowledgements

We thank the Natural Sciences and Engineering Research Council of Canada and the Fonds der Chemischen Industrie, Frankfurt am Main, for financial support.

1. R. NEU. Z. Anal. Chem. **176**, 334 (1960); B. FRIESE and F. UMLAND. Anal. Chim. Acta **96**, 303 (1978).
2. O. P. SHITOV, S. L. IOFFE, L. M. LEON'TEVA, and V. A. TARTAKOVSKII. Zh. Obshch. Khim. **43**, 1266 (1973); J. Gen. Chem. USSR **43**, 1257 (1973).
3. H. NOTH and B. WRACKMEYER. Nuclear magnetic resonance spectroscopy of boron compounds. Berlin. 1978; B. WRACKMEYER. Ann. Rep. NMR Spectrosc. **20**, 61 (1988); A. R. SIEDLE. Ann. Rep. NMR Spectrosc. **20**, 205 (1988).
4. W. KLIEGEL, H.-W. MOTZKUS, S. J. RETTIG, and J. TROTTER. Can. J. Chem. **62**, 838 (1984).
5. W. KLIEGEL and B. WRACKMEYER. Unpublished data.
6. W. KLIEGEL, H.-W. MOTZKUS, K. DRÜCKLER, S. J. RETTIG, and J. TROTTER. Can. J. Chem. **68**, 64 (1990).
7. International tables for X-ray crystallography. Vol. IV. Kynoch Press: Birmingham, U.K. (present distributor Kluwer Academic Publishers: Dordrecht, The Netherlands), 1974. pp. 99–102, 149.
8. G. HELLER. Top. Curr. Chem. **131**, 39 (1986).
9. A. DAL NEGRO, L. UNGARETTI and A. PEROTTI. J. Chem. Soc. Dalton Trans. 1639 (1972).
10. H. BINDER, W. MATHEIS, H.-J. DEISEROTH, and F.-S. HAN. Z. Naturforsch. Sect. B, **39**, 1717 (1984).
11. W. CLEGG, M. NOLTEMEYER, G. M. SHELDRICK, W. MARINGGELE, and A. MELLER. Z. Naturforsch. Sect. B, **35**, 1499 (1980).
12. R. A. CRESWELL. J. Mol. Spectrosc. **56**, 133 (1975).
13. M. VAN MEERSSCHE, J. P. DECLERQ, L. A. VAN ROYAN, and P. J. DE CLERQ. Bull. Soc. Chim. Belg. **92**, 115 (1983).
14. M. COSSU, R. VIANI, J. LAPASSET, J. P. AYCARD, C. MARFISI, and H. BODOT. Cryst. Struct. Commun. **11**, 1189 (1982).
15. A. YOKOZEKI and K. KUCHITSU. Bull. Chem. Soc. Jpn. **44**, 3356 (1971).
16. X. SOLANS, M. FONT-ALTABA, J. SOLANS, and M. V. DOMENECH. Acta Crystallogr. Sect. B, **38**, 2438 (1982).
17. S. J. RETTIG, J. TROTTER, W. KLIEGEL, and H. BECKER. Can. J. Chem. **54**, 3142 (1976).
18. W. KLIEGEL, S. J. RETTIG, and J. TROTTER. Can. J. Chem. **62**, 515 (1984).
19. W. KLIEGEL, D. NANNINGA, S. J. RETTIG, and J. TROTTER. Can. J. Chem. **62**, 845 (1984).
20. W. KLIEGEL, D. NANNINGA, S. J. RETTIG, and J. TROTTER. Can. J. Chem. **61**, 2329 (1983).
21. H. AMT, W. KLIEGEL, S. J. RETTIG, and J. TROTTER. Can. J. Chem. **68**, 1797 (1990).
22. H. AMT, W. KLIEGEL, S. J. RETTIG, and J. TROTTER. Can. J. Chem. **66**, 1117 (1988).
23. S. J. RETTIG and J. TROTTER. Can. J. Chem. **53**, 1393 (1975).
24. S. J. RETTIG and J. TROTTER. Can. J. Chem. **61**, 206 (1983).
25. E. EBELING, W. KLIEGEL, S. J. RETTIG, and J. TROTTER. Can. J. Chem. **67**, 933 (1989).
26. N. FARFAN, T. MANCILLA, D. CASTILLO, G. URIBE, L. CARRILLO, P. JOSEPH-NATHAN, and R. CONTRERAS. J. Organomet. Chem. **381**, 1 (1990).
27. W. KLIEGEL, L. PREU, S. J. RETTIG, and J. TROTTER. Can. J. Chem. **63**, 509 (1985).
28. M. YALPANI and R. BOESE. Chem. Ber. **116**, 3347 (1983).
29. W. KLIEGEL, G. LUBKOWITZ, S. J. RETTIG, and J. TROTTER. Can. J. Chem. **69**, 1217 (1991).

Can. J. Chem. Downloaded from www.nrcresearchpress.com by 84.41.108.74 on 09/07/12
For personal use only.

Structural studies of organoboron compounds. XLIX.[1] 4,6-Bis(1-phenyl-2-nitroethyl)-2-(4-methoxyphenyl)-1,3-dioxa-4,6-diaza-2-boracyclohexane

WOLFGANG KLIEGEL AND GOTTFRIED LUBKOWITZ

Institut für Pharmazeutische Chemie der Technischen Universität Braunschweig, Beethovenstrasse 55, 3300 Braunschweig, Bundesrepublik Deutschland

AND

STEVEN J. RETTIG AND JAMES TROTTER

Department of Chemistry, University of British Columbia, 2036 Main Mall, Vancouver, B.C., Canada V6T 1Z1

Received November 2, 1990

WOLFGANG KLIEGEL, GOTTFRIED LUBKOWITZ, STEVEN J. RETTIG, and JAMES TROTTER. Can. J. Chem. **69**, 1227 (1991).

The preparation of *N,N'*-bis(1-phenyl-2-nitroethyl)-*N,N'*-dihydroxymethanediamine and its subsequent reaction with 4-methoxyphenylboronic acid to yield 4,6-bis(1-phenyl-2-nitroethyl)-2-(4-methoxyphenyl)-1,3-dioxa-4,6-diaza-2-boracyclohexane are described. Crystals of the latter compound are monoclinic, a = 8.4790(8), b = 16.2100(9), c = 9.4367(6) Å, β = 109.342(5)°, Z = 2, space group $P2_1$. The structure was solved by direct methods and was refined by full-matrix least-squares procedures to R = 0.032 and R_w = 0.039 for 1749 reflections with $I \geq 3\sigma(I)$. The molecule has a six-membered BONCNO cycloboronate structure. Bond lengths involving the trigonal planar boron atom are (N)O—B = 1.362(4) and 1.364(5), (aryl)C—B = 1.548(4) Å.

Key words: organoboron compound, crystal structure, cycloboronate, methanediamine.

WOLFGANG KLIEGEL, GOTTFRIED LUBKOWITZ, STEVEN J. RETTIG et JAMES TROTTER. Can. J. Chem. **69**, 1227 (1991).

On décrit la préparation de la *N,N'*-bis(1-phényl-2-nitroéthyl)-*N,N'*-dihydroxyméthanediamine et sa réaction subséquente avec l'acide 4-méthoxyphénylboronique qui conduit au 4,6-bis(1-phényl-2-nitroethyl)-2-(4-méthoxyphényl)-1,3-dioxa-4,6-diaza-2-boracyclohexane. Les cristaux de ce dernier composé sont monocliniques, avec a = 8,4790(8), b = 16,2100(9) et c = 9,4367(6) Å, β = 109,342(5)°, Z = 2 et groupe d'espace $P2_1$. On a résolu la structure par des méthodes directes et on l'a affinée par la méthode directes et on l'affinée par la méthode des moindres carrés jusqu'à des valeurs respectives de R = 0,032 et R_w = 0,039 pour 1749 réflexions avec $I \geq 3\sigma(I)$. La molécule contient une structure cycloboronate BONCNO à six chaînons. Les longeurs des liaisons impliquant l'atome de bore plan trigonal sont (N)O—B = 1,362(4) et 1,364(5), (aryl)C—B = 1,548(4) Å.

Mots clés : composé organoboré, structure cristalline, cycloboronate, méthanediamine.

[Traduit par la rédaction]

Introduction

The condensation of a newly synthesized *N*-(β-nitroalkyl) substituted dihydroxyaminal **2***a* (R = $CHPhCH_2NO_2$) with *p*-methoxyphenylboronic acid (Ar = 4-$MeOC_6H_4$) did not lead to the 1:2 reaction product with the general structure **1** which is the usual product of the reaction of simple *N*-alkyl derivatives **2** with arylboronic acids (1, 2). The elemental analysis and spectral data for the isolated crystalline substance was consistent with a 1:1 condensation product of **2***a* and the boronic acid, having a probable structure **3**. As we have recently reported (3), a six-membered cyclic arylboronate **3***b* has been obtained by condensation of a weakly basic aminal **2***b* (R = CMe_2CN) with a sterically hindered arylboronic acid (Ar = 2,4,6-$Me_3C_6H_2$). On the basis of this result, the formation of a cyclic condensate **3***a* would be plausible on the grounds of an attenuation of the basicity at the aminal nitrogen centres by the electron-withdrawing β-nitroalkyl residues. The arylboronic acid moiety in **3***a*, however, is not hindered sterically, but its Lewis acidity may perhaps be reduced by the inductive and mesomeric effects of the *p*-methoxy group (4).

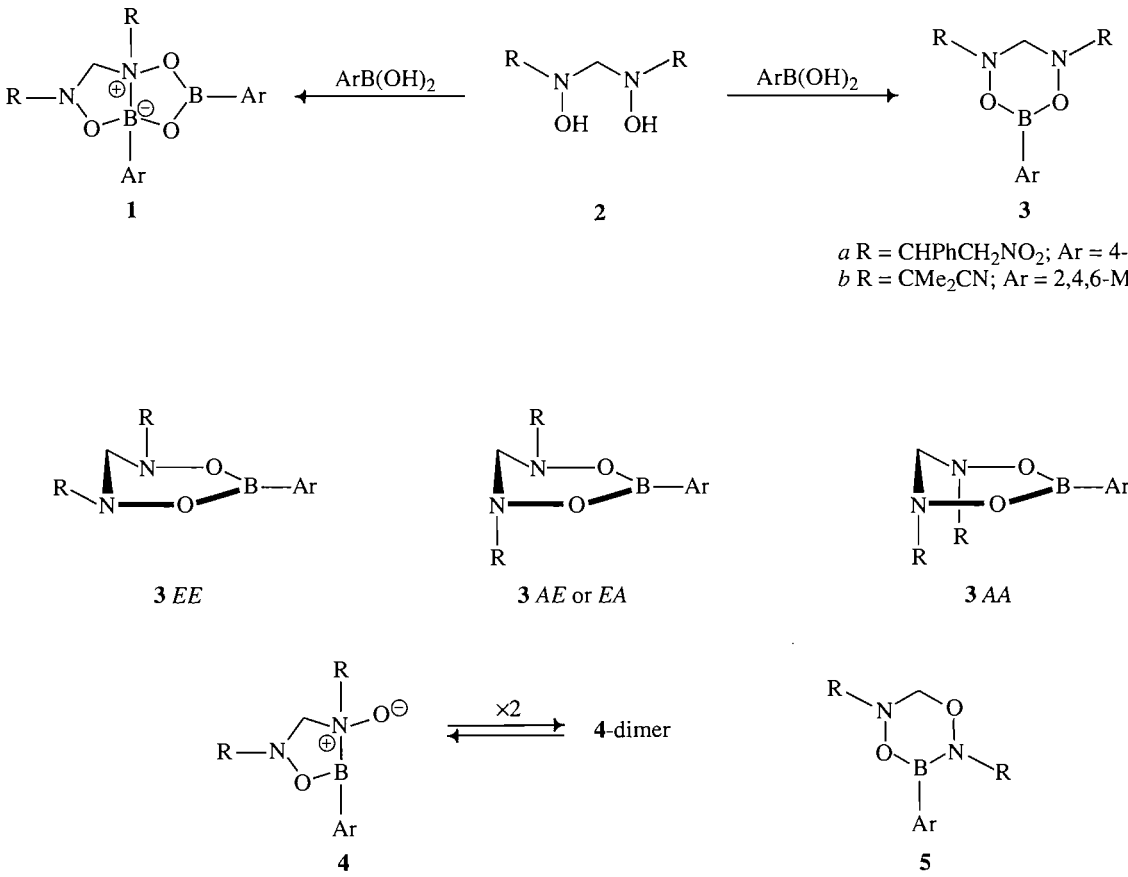
In compound **3***b* both of the bulky *N*-cyanoalkyl substituents were found to occupy equatorial positions of a semiplanar ring ("sofa" conformation) **3 EE**, most likely stabilized by the minimization of steric interactions (3). For compound **3***a*, having less bulky *N*-alkyl substituents, the axial-equatorial isomer (**3 AE or EA**) must be considered. Axial-equatorial isomers are known to be the predominant form present in solutions of 3,5-dimethyl-1-oxa-3,5-diazacyclohexane (5), the only form present in solutions of a related seven-membered cyclic aminal (6), and in equilibrium with other isomers in solutions of simple 1,3-diazacyclohexanes (7). The axial-axial conformer **3 AA** is thought to be highly unfavorable due to 1,3-*syn*-diaxial steric interaction, inducing the inversion at nitrogen leading to **3 AE/EA** or the ring inversion converting **3 AA** directly to **3 EE**. Other possible structures for the condensation product include the five-membered ring system **4** or its dimer, and the six-membered cycloboronate **5**, which could be considered as a rearrangement product of **4** resulting from an aminal-*N*-oxide rearrangement to an *N,O*-acetal (8).

Infrared and nmr spectroscopic data do not allow for an unambiguous assignment of one of the alternative structures **3–5**. In the ^1H nmr spectrum, two different signals were found for the CH_2 protons of the aminal methylene group, one predominant signal at 3.68 ppm (65–80% of the total peak area for CH_2) and another signal at 3.58 ppm (20–35%). It is not yet clear whether this phenomenon results from an equilibrium between two forms in solution, or from partial decomposition in the chosen solvent.[2] An X-ray crystallographic study has been

[1]Previous paper in this series: ref. 18.

[2]*N*-(β-Nitroalkyl)aminals of the type **2***a* seem to be quite unstable compounds (see Experimental section). Preliminary variable-temperature nmr studies of the cycloboronate **3***a* show broadening and splitting of the dominant methylene signal into an AB pattern at lower temperatures, the minor signal remaining unaffected.

Can. J. Chem. Downloaded from www.nrcresearchpress.com by 84.41.108.74 on 09/07/12
For personal use only.



undertaken in order to determine the structure and conformation of this material in the solid state.

Experimental

N,N′-Bis(1-phenyl-2-nitroethyl)-N,N′-dihydroxymethanediamine, 2a

N-(1-Phenyl-2-nitroethyl)-hydroxylamine (9) (5.46 g, 30 mmol) is dissolved, with slight heating, in 30 mL ethanol (96%). The solution is cooled down to room temperature and mixed with aqueous formaldehyde (15 mmol of a 40% solution). Stirring is continued until crystallization commences. The solution is then cooled down to −18°C and, after 6 h, filtered. The crystalline precipitate is washed with ethanol.[3] Yield: 3.27 g (58%). Melting point 116–117°C (from ethanol/petroleum ether). *Anal.* calcd. for $C_{17}H_{20}N_4O_6$: C 54.25, H 5.36, N 14.89; found: C 54.21, H 5.39, N 14.82. Infrared (KBr): 3180 (O—H), 1600 (C⋯C, weak), 1550 cm^{-1} (NO_2). ^1H nmr (90 MHz, $CDCl_3$/TMS): δ (ppm) = 3.50 (s, N—CH_2—N), 4.22–5.02 (ABX pattern, 2 CH_2CH), 7.08–7.52 (m, 2 C_6H_5), 9.35 (s, 2 OH, exchangeable). Mass spectrum (70 eV, 60°C): *m/z* = 150 (25%, $C_6H_5CHCH_2NO_2$), 104 (100%, $C_6H_5CHCH_2$), 91 (12%, C_7H_7), 77 (19%, C_6H_5).

4,6-Bis(1-phenyl-2-nitroethyl)-2-(4-methoxyphenyl)-1,3-dioxa-4,6-diaza-2-boracyclohexane, 3a

2*a* (0.75 g, 2 mmol) and 4-methoxyphenylboronic acid (0.30 g, 2 mmol) are suspended in 20 mL of benzene and refluxed for 1 h with continuous removal of water using a Dean Stark trap. After partial evaporation of the solvent *in vacuo*, petroleum ether (bp 30–75°C) is added. Colorless crystals form upon slow cooling. Yield: 0.85 g (86%). Melting point (decomp.) 148–149°C (from benzene). *Anal.* calcd. for $C_{24}H_{25}BN_4O_7$: C 58.56, H 5.12, B 2.20, N 11.38; found: C 58.53, H 5.17, B 2.48, N 11.38. Infrared (KBr): 1600 (C⋯C), 1555 cm^{-1} (NO_2). ^1H nmr (90 MHz, $CDCl_3$/TMS): δ (ppm) = 3.58 and 3.68 (s and s, 20–35% and 65–80%,[4] N—CH_2—N), 3.78 (s, OCH_3), 4.35–5.33 (overlapping ABX systems, 2 CH_2CH), 6.85 and 7.50 (dd, *J* = 9 Hz, B—C_6H_4), 7.00–7.35 (m, 2 C_2H_5). Mass spectrum (70 eV, 150°C): *m/z* = 492 (9%, M^+), 432 (4%, M − CH_2NO_2), 372 (6%, M − 2(CH_2NO_2)), 328 (11%, M − N = $CH(C_6H_5)CH_2NO_2$), 281 (6%), 268 (13%, $(CH_3OC_6H_4BO)_2$), 197 (6%), 150 (13%, $C_6H_5CHCH_2NO_2$), 134 (16%, $CH_3OC_6H_4BO$), 121 (20%), 104 (100%, $C_6H_5CHCH_2$), 91 (39%, C_7H_7), 77 (36%, C_6H_5), 65 (15%).

X-ray crystallographic analysis of 3a

A crystal ca. 0.10 × 0.20 × 0.25 mm in size was mounted on a glass fiber. Unit-cell parameters were refined by least-squares on setting angles for 25 reflections (2θ = 69.6–94.0°) measured on a diffractometer with Cu-K_α radiation (λ = 1.54178 Å). Crystal data at 21°C are as follows

$C_{24}H_{25}BN_4O_7$ fw = 492.29

Monoclinic, *a* = 8.4790(8), *b* = 16.2100(9), *c* = 9.4367(6) Å, β = 109.342(5)°, *V* = 1223.8(1) $Å^3$, *Z* = 2, ρ_c = 1.336 Mg m^{-3}, *F*(000) = 516, μ(Cu-K_α) = 7.83 cm^{-1}. Absent reflections: 0*k*0, *k* odd, space group $P2_1$ (No. 4) from structure analysis.

Intensities were measured with graphite-monochromated Cu-K_α radiation on a Rigaku AFC6S diffractometer. An ω–2θ scan at 16° min^{-1} over a range of (1.00 + 0.20 tan θ)° in ω (with up to eight rescans, background/scan time ratio = 0.5) was employed. Data were measured to 2θ = 155°. The intensities of three check reflections, measured every 200 reflections throughout the data collection, showed

[3]The product thus obtained is analytically pure. During recrystallization from ethanol, decomposition to *N,N*-bis(1-phenyl-2-nitroethyl)-hydroxylamine, mp 103–105°C, occurs (10). The thermal instability of **2***a* can also be seen in the EI mass spectrum which does not display a molecular ion peak.

[4]Variable for successive experiments at room temperature over a period of several hours.

Can. J. Chem. Downloaded from www.nrcresearchpress.com by 84.41.108.74 on 09/07/12
For personal use only.

Can. J. Chem. Downloaded from www.nrcresearchpress.com by 84.41.108.74 on 09/07/12
For personal use only.

TABLE 1. Final atomic coordinates (fractional) and B_{eq} (Å^2)*

Atom	x	y	z	B_{eq}
O(1)	0.4746(2)	0.2559	0.4705(2)	4.4
O(2)	0.5390(2)	0.3764(2)	0.3521(2)	4.5
O(3)	−0.2435(3)	0.3347(2)	−0.0299(3)	6.5
O(4)	0.5572(3)	0.1560(3)	0.2337(3)	6.0
O(5)	0.4038(3)	0.0741(3)	0.3084(3)	7.1
O(6)	0.5191(4)	0.5598(3)	0.2630(3)	7.3
O(7)	0.5444(4)	0.4905(3)	0.0809(3)	8.7
N(1)	0.6418(3)	0.2567(2)	0.5824(3)	4.1
N(2)	0.7125(3)	0.3707(2)	0.4518(3)	3.8
N(3)	0.5276(4)	0.1166(3)	0.3314(3)	4.9
N(4)	0.5942(4)	0.5137(3)	0.2094(3)	5.2
C(1)	0.7039(3)	0.3403(3)	0.5953(3)	3.8
C(2)	0.7439(4)	0.1976(3)	0.5304(4)	4.1
C(3)	0.6544(4)	0.1170(3)	0.4864(4)	4.7
C(4)	0.9061(4)	0.1848(3)	0.6599(4)	4.3
C(5)	0.9083(5)	0.1496(3)	0.7933(4)	5.9
C(6)	1.0583(6)	0.1398(4)	0.9088(4)	7.2
C(7)	1.2043(6)	0.1666(3)	0.8929(5)	7.5
C(8)	1.2043(5)	0.2004(3)	0.7612(6)	7.5
C(9)	1.0550(4)	0.2094(3)	0.6444(5)	5.8
C(10)	0.7723(4)	0.4568(3)	0.4601(3)	3.8
C(11)	0.7641(4)	0.4859(3)	0.3051(4)	4.3
C(12)	0.9527(4)	0.4589(2)	0.5633(3)	3.7
C(13)	0.9989(4)	0.5071(3)	0.6920(4)	4.5
C(14)	1.1642(4)	0.5069(3)	0.7873(4)	5.3
C(15)	1.2815(4)	0.4596(3)	0.7555(4)	5.2
C(16)	1.2363(4)	0.4128(3)	0.6275(4)	5.2
C(17)	1.0726(4)	0.4127(3)	0.5316(4)	4.7
C(18)	0.2499(4)	0.3181(3)	0.2539(3)	4.1
C(19)	0.1325(4)	0.2610(3)	0.2638(3)	4.1
C(20)	−0.0342(4)	0.2639(3)	0.1729(3)	4.2
C(21)	−0.0849(4)	0.3249(3)	0.0671(4)	4.6
C(22)	0.0286(5)	0.3819(3)	0.0523(4)	6.5
C(23)	0.1917(4)	0.3783(3)	0.1444(4)	6.0
C(24)	−0.3703(4)	0.2828(4)	−0.0121(5)	7.5
B(1)	0.4321(4)	0.3160(3)	0.3633(4)	4.0

*$B_{eq} = (8\pi^2/3)\Sigma\Sigma U_{ij} a_i^* a_j^* (\mathbf{a}_i \cdot \mathbf{a}_j)$.

only small random variations. After data reduction,[5] an empirical absorption correction, based on azimuthal scans for three reflections, was applied. Transmission factors range from 0.89 to 1.00. Of the 2785 reflections measured, 2606 were unique (R_{int} = 0.021) and 1749 (67.1%) had intensities greater than or equal to $3\sigma(F^2)$ above background where $\sigma^2(F^2) = [S^2(C + 4B) + (0.025F^2)^2]/Lp^2$ with S = scan speed, C = scan count, B = total background count, and Lp = Lorentz-polarization factor.

The structure analysis was initiated in the noncentrosymmetric space group on the basis of the E-statistics, this choice being confirmed by the subsequent successful solution and refinement of the structure. The structure was solved by direct methods, the coordinates of all non-hydrogen atoms being determined from an E-map. The non-hydrogen atoms were refined with anisotropic thermal parameters and the hydrogen atoms were fixed in idealized positions (C—H = 0.98 Å, $B_H = 1.2B_{bonded\ atom}$). A correction for secondary extinction was applied, the final value of the extinction coefficient being 5.46×10^{-4}. Scattering factors for all atoms and anomalous dispersion corrections for the non-hydrogen atoms were taken from ref. 11. The weighting scheme $w = 4F_o^2/\sigma^2(F_o^2)$ gave uniform average values of $w(|F_o| - |F_c|)^2$ over ranges of both $|F_o|$ and $\sin\theta/\lambda$ and was employed in the final stages of full-matrix least-squares refinement of 325 variables. Reflections with $I < 3\sigma(I)$ were not included in the refinement. Convergence was reached at R = 0.032 and R_w = 0.039 for 1749 reflections with $I \geq 3\sigma(I)$. The function minimized was $\Sigma w(|F_o| - |F_c|)^2$, $R = \Sigma||F_o| - |F_c||/\Sigma|F_o|$, $R_w = (\Sigma w(|F_o| - |F_c|)^2/\Sigma w|F_o|^2)^{1/2}$. A parallel refinement of the mirror-image structure resulted in marginally higher residuals, the R and R_w factor ratios being 1.003 and 1.002, respectively.

On the final cycle of refinement the maximum parameter shift corresponded to 0.06σ. The mean error in an observation of unit weight was 1.45. The final difference map showed maximum fluctuations of ±0.12 e Å^{-3}. The final positional and (equivalent) isotropic thermal parameters for the non-hydrogen atoms appear in Table 1. Bond lengths and angles are given in Tables 2 and 3 and intra-annular torsion angles in Table 4. Hydrogen atom parameters, anisotropic thermal

[5]TEXSAN/TEXRAY structure analysis package which includes versions of the following: MITHRIL, integrated direct methods, by C. J. Gilmore; DIRDIF, direct methods for difference structures, by P. T. Beurskens; ORFLS, full-matrix least-squares, and ORFFE, function and errors, by W. R. Busing, K. O. Martin, and H. A. Levy; ORTEP II, illustrations, by C. K. Johnson.

TABLE 2. Bond lengths (Å) with estimated standards deviations

Atom	Atom	Distance	Atom	Atom	Distance
O(1)	N(1)	1.460(3)	C(5)	C(6)	1.384(5)
O(1)	B(1)	1.364(5)	C(6)	C(7)	1.367(7)
O(2)	N(2)	1.463(3)	C(7)	C(8)	1.358(7)
O(2)	B(1)	1.362(4)	C(8)	C(9)	1.384(5)
O(3)	C(21)	1.362(4)	C(10)	C(11)	1.517(4)
O(3)	C(24)	1.418(5)	C(10)	C(12)	1.517(4)
O(4)	N(3)	1.214(4)	C(12)	C(13)	1.387(4)
O(5)	N(3)	1.213(4)	C(12)	C(17)	1.374(4)
O(6)	N(4)	1.198(4)	C(13)	C(14)	1.392(5)
O(7)	N(4)	1.205(4)	C(14)	C(15)	1.366(6)
N(1)	C(1)	1.443(4)	C(15)	C(16)	1.370(5)
N(1)	C(2)	1.480(4)	C(16)	C(17)	1.383(4)
N(2)	C(1)	1.465(4)	C(18)	C(19)	1.384(4)
N(2)	C(10)	1.478(4)	C(18)	C(23)	1.389(5)
N(3)	C(3)	1.501(4)	C(18)	B(1)	1.548(4)
N(4)	C(11)	1.494(4)	C(19)	C(20)	1.390(4)
C(2)	C(3)	1.500(5)	C(20)	C(21)	1.370(5)
C(2)	C(4)	1.521(4)	C(21)	C(22)	1.374(5)
C(4)	C(5)	1.377(5)	C(22)	C(23)	1.369(5)
C(4)	C(9)	1.377(5)			

TABLE 3. Bond angles (deg) with estimated standard deviations

Atom	Atom	Atom	Angle	Atom	Atom	Atom	Angle
N(1)	O(1)	B(1)	119.0(2)	C(7)	C(8)	C(9)	119.6(4)
N(2)	O(2)	B(1)	117.3(3)	C(4)	C(9)	C(8)	121.0(4)
C(21)	O(3)	C(24)	118.1(3)	N(2)	C(10)	C(11)	109.7(3)
O(1)	N(1)	C(1)	108.0(2)	N(2)	C(10)	C(12)	108.1(3)
O(1)	N(1)	C(2)	106.8(2)	C(11)	C(10)	C(12)	109.0(3)
C(1)	N(1)	C(2)	113.5(2)	N(4)	C(11)	C(10)	113.8(3)
O(2)	N(2)	C(1)	105.6(2)	C(10)	C(12)	C(13)	120.5(3)
O(2)	N(2)	C(10)	103.2(2)	C(10)	C(12)	C(17)	120.6(3)
C(1)	N(2)	C(10)	113.0(2)	C(13)	C(12)	C(17)	118.9(3)
O(4)	N(3)	O(5)	123.2(3)	C(12)	C(13)	C(14)	119.8(3)
O(4)	N(3)	C(3)	118.5(3)	C(13)	C(14)	C(15)	120.7(3)
O(5)	N(3)	C(3)	118.3(3)	C(14)	C(15)	C(16)	119.5(3)
O(6)	N(4)	O(7)	124.2(4)	C(15)	C(16)	C(17)	120.3(4)
O(6)	N(4)	C(11)	118.3(3)	C(12)	C(17)	C(16)	120.8(3)
O(7)	N(4)	C(11)	117.4(4)	C(19)	C(18)	C(23)	115.7(3)
N(1)	C(1)	N(2)	111.5(2)	C(19)	C(18)	B(1)	121.5(3)
N(1)	C(2)	C(3)	111.0(3)	C(23)	C(18)	B(1)	122.8(3)
N(1)	C(2)	C(4)	107.1(2)	C(18)	C(19)	C(20)	122.9(3)
C(3)	C(2)	C(4)	110.1(3)	C(19)	C(20)	C(21)	118.9(3)
N(3)	C(3)	C(2)	114.0(3)	O(3)	C(21)	C(20)	125.1(3)
C(2)	C(4)	C(5)	121.7(3)	O(3)	C(21)	C(22)	115.0(3)
C(2)	C(4)	C(9)	119.5(3)	C(20)	C(21)	C(22)	119.9(3)
C(5)	C(4)	C(9)	118.8(3)	C(21)	C(22)	C(23)	120.1(4)
C(4)	C(5)	C(6)	119.9(4)	C(18)	C(23)	C(22)	122.5(3)
C(5)	C(6)	C(7)	120.4(4)	O(1)	B(1)	O(2)	123.5(3)
C(6)	C(7)	C(8)	120.2(4)	O(1)	B(1)	C(18)	118.1(3)
				O(2)	B(1)	C(18)	118.4(3)

TABLE 4. Intra-annular torsion angles (deg) with estimated standard deviations in parentheses

Atoms	Torsion angle
B(1)—O(1)—N(1)—C(1)	24.3(4)
O(1)—N(1)—C(1)—N(2)	−59.8(3)
N(1)—C(1)—N(2)—O(2)	66.7(3)
C(1)—N(2)—O(2)—B(1)	−38.0(3)
N(2)—O(2)—B(1)—O(1)	6.1(5)
O(2)—B(1)—O(1)—N(1)	1.7(5)

parameters, torsion angles, intermolecular contacts, least-squares planes, bond lengths and angles involving hydrogen, and structure factors have been deposited.[6]

Results and discussion

The X-ray analysis establishes the cycloboronate structure **3***a* for the condensation product of **2***a* with *p*-methoxyphenylboronic acid (Ar = 4-$CH_3OC_6H_4$). This is the second reported example of the new BONCNO heterocycle **3**, the only other fully characterized member of this class being **3***b* (3). In striking contrast to the *N*-(α-cyanoalkyl) substituted **3***b*, which has both of the *N*-substituents in equatorial positions of the semiplanar C(1)-envelope ring (form **3 EE**), the *N*-(β-nitroalkyl) derivative **3***a* exists in the **3 AE** form in the solid state (Fig. 1). This difference could result from a less sterically hindered axial *N*-alkyl substituent in **3***a*, as well as from dipolar and stereoelectronic effects would could favor the axial position of one of the *N*-substituents. In such an arrangement the antiperiplanar orientation of the non-bonding electron pair at N(1) with respect to the C(1)—N(2) bond could contribute to the stabilization of the molecular geometry by a generalized anomeric effect via n–σ* overlap (12) and/or minimization of the destablilizaing, through space, n–n interaction between the two nitrogen lone pairs (13). The presence of an n–σ*(π) effect is suggested by the relatively short N(1)—C(1) bond (1.443(4) Å) compared to the adjacent C(1)—N(2) bond (1.465(4) Å). In addition, the axially positioned substituent at N(1) does not interfere with the substituent at B(1) because of the essentially planar arrangement at the sp^2 boron, the nearly coplanar orientation of the *B*-aryl ring (dihedral angle between normals to the mean planes is 17.3°), and the near planarity of the N—O—B—O—N moiety of **3***a* (planar to within 0.066(3) Å).

Although the nitro group of the axial N(1) substituent neighbors the boronate function, the O(4)···B(1) non-bonding distance (3.196 Å) approaching the normal van der Waals distance of 3.07 Å (14), it is unlikely to contribute to the stabilization of the conformation **3 AE**. Any significant O···B interaction should result in some degree of pyramidalization above the O(1)—O(2)—C(18) plane at the B(1) atom due to partial rehybridization of the sp^2 boron atom. The boron atom is actually displaced from the plane of its substituents by a considerable 0.109(4) Å, but in the opposite direction from O(4), probably a result of packing forces (see Fig. 2) in view of the otherwise normal geometry for a trigonal planar boron atom at B(1). An example of true partial pyramidalization, with a similar displacement of the boron atom, has recently been reported for an eight-membered heterocycle containing a weak transannular N···B interaction (15).

[6]Supplementary material mentioned in the text may be purchased from the Depository of Unpublished Data, Document Delivery, CISTI, National Research Council of Canada, Ottawa, Canada K1A 0S2.

Can. J. Chem. Downloaded from www.nrcresearchpress.com by 84.41.108.74 on 09/07/12
For personal use only.

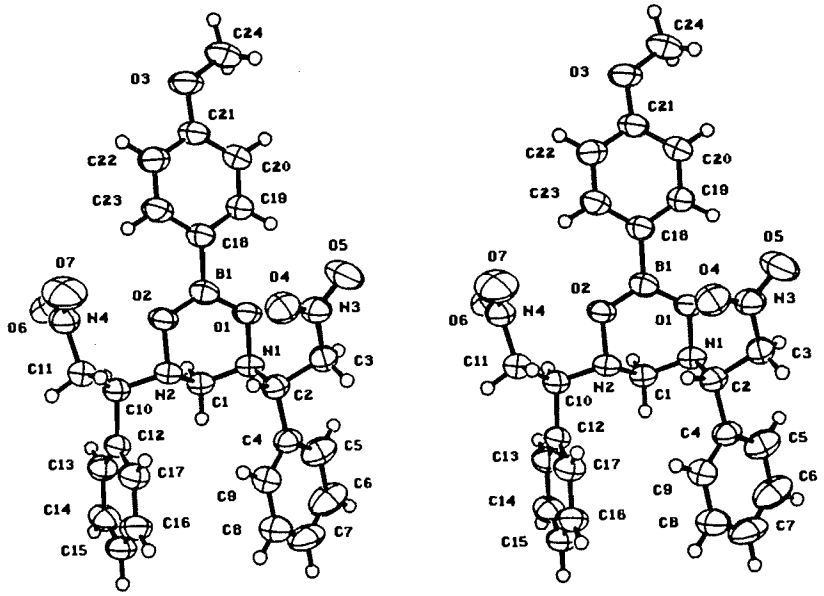


FIG. 1. Stereoview of the 4,6-bis(1-phenyl-2-nitroethyl)-2-(4-methoxyphenyl)-1,3-dioxa-4,6-diaza-2-boracyclohexane molecule; 50% probability thermal ellipsoids are shown for the non-hydrogen atoms.

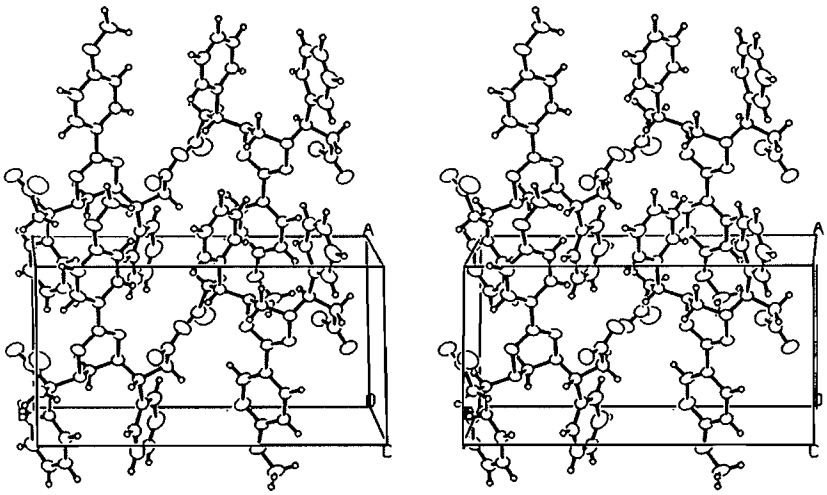


FIG. 2. Stereoview of the packing arrangement of 4,6-bis(1-phenyl-2-nitroethyl)-2-(4-methoxyphenyl)-1,3-dioxa-4,6-diaza-2-boracyclohexane; 32% probability thermal ellipsoids are shown for the non-hydrogen atoms.

The size of the *N*-(β-nitroalkyl) substituents might account for the fact that bisaxial conformer **3 AA** is not observed in the solid state. The **3 AA** conformer would undergo severe 1,3-*syn*-diaxial steric interactions, thus **3 AE** represents the preferred (and perhaps exclusive) form of compound **3***a*. Similar experimental findings for 3,5-dimethyl-1-oxa-3,5-diazacyclohexane in solution explained the most stable axial-equatorial form in terms of the anomeric effect and reduced 1,3-diaxial interactions (5). *Ab initio* studies of the basic 1-oxa-3,5-diazacyclohexane system, however, revealed the diaxial form as the most stable geometry of this cyclic aminal, interpreted as a consequence of anomeric interactions (16). Another indication of an anomeric effect involving one of the nitrogen lone pairs might be the widening of the N(1)—C(1)—N(2) angle in the **3 AE** form of **3***a* (111.5(2)°) relative to the corresponding angle of 106.4° in the **3 EE** form of **3***b* (3). Similar tendencies have been calculated for the **AE** and **EE** forms of *N,N'*-dimethyl-1-oxa-3,5-diazacyclohexane: 109.09 and 107.25°, respectively (16); the N—C—N angle for the **AA** form is larger still: 113.05° (16).

The N—O bond lengths in **3***a* (mean 1.462 Å) are very similar to those observed in **3***b* (mean 1.461 Å) (3) and in the simple aminal **2** (R = CH_3) (1.458 Å) (17). As in **3***b* (3), the partial double bond character (corresponding to a π-bond order of ~0.5) of the O—B bonds in the approximately planar N—O—B—O—N ring fragment is reflected by short O—B distances (mean 1.363 Å) resulting from *pp*(π) back donation. The B(1)—C(1) distance of 1.548(4) Å is slightly shorter than the corresponding B—C(aryl) bond of 1.560 Å in **3***b*, the latter value being typical for six-membered phenylboronates (ref. 3 and references therein). Inductive effects resulting from the presence of the *p*-methoxy group in **3***a* probably contribute to the slight shortening of the B—C(aryl) bond. The orientation of

Can. J. Chem. Downloaded from www.nrcresearchpress.com by 84.41.108.74 on 09/07/12
For personal use only.

the *B*-aryl substituent with respect to the boron coordination plane (see above) is similar to that reported for most arylboronates except the mesityl derivative **3***b* which has a nearly perpendicular orientation of these groups.

Because of the axial and equatorial positioning of the *N*-alkyl groups in **3***a* (**AE** form) the compound displays the same configuration at both amine centres (S,S), in contrast to the opposite configurations (R,S) observed at the amine nitrogen atoms in the **EE** form of **3***b* (3). The chiral centres at C(2) and C(10) also both have S configurations, thus the stereoisomer shown in Fig. 1 is the S,S,S,S isomer. Since the material crystallizes in a chiral space group ($P2_1$), each crystal consists of only one stereoisomer. Presumably the bulk sample contains equal numbers of crystals composed of S,S,S,S and R,R,R,R isomers (assuming that the aminal **2***a*, synthesized from racemic starting materials, is a racemate as well). It has not yet been determined whether other stereoisomers such as that derived by inversion at both nitrogen atoms (R,R,S,S, diastereoisomer — results from ring inversion) are also formed.

Acknowledgements

We thank the Natural Sciences and Engineering Research Council of Canada and the Fonds der Chemischen Industrie, Frankfurt am Main, for financial support.

1. W. KLIEGEL. J. Organomet. Chem. **253**, 9 (1983).
2. W. KLIEGEL, S. J. RETTIG, and J. TROTTER. Can. J. Chem. **62**, 515 (1984).
3. W. KLIEGEL, G. LUBKOWITZ, S. J. RETTIG, and J. TROTTER. Can. J. Chem. **69**, 234 (1991).
4. K. TORSSELL. Progr. Boron Chem. **1**, 369 (1964); H. C. BEACHELL and D. W. BEISTEL. Inorg. Chem. **3**, 1028 (1964); A. R. SIEDLE and G. M. BODNER. Inorg. Chem. **11**, 3108 (1972).
5. V. J. BAKER, I. J. FERGUSON, A. R. KATRITZKY, R. PATEL, and S. RAHIMI-RASTGOO. J. Chem. Soc. Perkin Trans. II, 377 (1978).
6. F. G. RIDDELL. The conformational analysis of heterocyclic compounds. London. 1980; T. A. CRABB and A. R. KATRITZKY. Adv. Heterocycl. Chem. **36**, 1 (1984).
7. R. ST. AMOUR and M. ST. JACQUES. Tetrahedron Lett. **26**, 13 (1985).
8. W. KLIEGEL and G.-H. FRANCKENSTEIN. Liebigs Ann. Chem. 2294 (1976); 956 (1977) and references therein.
9. C. D. HURD and J. PATTERSON. J. Am. Chem. Soc. **75**, 285 (1953).
10. W. KLIEGEL and G. LUBKOWITZ. Unpublished results.
11. International tables for X-ray crystallography. Vol. IV. Kynoch Press, Birmingham, U.K. (present distributor Kluwer Academic Publishers: Dordrecht, The Netherlands), 1974. pp. 99–102 and 149.
12. A. J. KIRBY. The anomeric effect and related stereoelectronic effects at oxygen. Berlin. 1983; P. DESLONGCHAMPS. Stereoelectronic effects in organic chemistry. Oxford. 1983.
13. V. G. S. BOX. Heterocycles, **31**, 1157 (1990).
14. A. BONDI. J. Phys. Chem. **68**, 441 (1964).
15. W. KLIEGEL, G. LUBKOWITZ, S. J. RETTIG, and J. TROTTER. Can. J. Chem. **69**, 1217 (1991).
16. L. CARBALLEIRA, B. FERNANDEZ, and M. A. RIOS. J. Mol. Struct. (Theochem) **206**, 29 (1990).
17. W. KLIEGEL, S. J. RETTIG, and J. TROTTER. Can. J. Chem. **67**, 1959 (1989).
18. W. KLIEGEL, U. RIEBE, S. J. RETTIG, and J. TROTTER. Can. J. Chem. **69**, 1222 (1991).

Can. J. Chem. Downloaded from www.nrcresearchpress.com by 84.41.108.74 on 09/07/12
For personal use only.

Photoelectrochemical transduction between ionic and electronic conduction mediated by bis(maleonitriledithiolato)nickelate(II) in a polyviologen film

MARK C. LEFEBVRE, DAVID A. BIRO, AND COOPER H. LANGFORD[1]

Laboratories for Inorganic Materials, Department of Chemistry and Biochemistry, Concordia University, 1455 de Maisonneuve W., Montreal (Que.), Canada H3G 1M8

Received

MARK C. LEFEBVRE, DAVID A. BIRO, and COOPER H. LANGFORD. Can. J. Chem. **69**, 1233 (1991).

The photoelectrochemistry of a polymer coated electrode exploiting the chromophore bis(maleonitriledithiolato)nickelate(II) to link the redox self-exchange conductor poly(xylylviologen) to the solution couple $Fe(CN)_6^{3-/4-}$ is described. The diffusion coefficient for the $Fe(CN)_6^{3-/4-}$ redox couple in the film is 4.2×10^{-9} cm^2/s. The system was developed in an attempt to improve on a system where a quaternary ammonium substituted polystyrene/polyvinylpyridine blend films functioned as a good ionic conductor but poor electronic conductor in consequence of the trap states. The expected improvement in electronic conductivity is seen but at the expense of lower ionic mobility.

Key words: polyviologen, bis(maleonitriledithiolato)nickelate(II), polymer conduction, photoelectrode.

MARK C. LEFEBVRE, DAVID A. BIRO et COOPER H. LANGFORD. Can. J. Chem. **69**, 1233 (1991).

Nous avons etudié la photoélectrochimie du chromophore bis(maleonitriledithiolato)nickelate(II) dispersé dans le polymère redox poly(xylylviologène) qui est utilisé comme mediateur pour le transfert d'électron entre le polymère et le couple redox $Fe(CN)_6^{3-/4-}$. Le coefficient de diffusion pour le $Fe(CN)_6^{3-/4-}$ dans ces filmes est de $4{,}2 \times 10^{-9}$ cm^2/s. Le système a été developpé pour améliorer un autre système ou des films d'un mélange de polystyrène et polyvinylpyridine contenant des groupements ammonium quaternaires fonctionnait comme un bon conducteur ionique, mais un mauvais conducteur électronique. La conductivité électronique du nouveau polymère est augmenté tel qu'attendu, mais sa mobilité ionique est plus faible.

Mots clés : polyviologène, bis(maleonitriledithiolato)nickelate(II), conduction dans polymers, photoélectrode.

Can. J. Chem. Downloaded from www.nrcresearchpress.com by 84.41.108.74 on 09/07/12
For personal use only.

Introduction

In a series of publications (1–3) we have described ion-exchange polymer coatings based on quaternary ammonium derivatized polystyrene blended with polyvinylpyridine for use on transparent electrodes. The polymer mediates the transduction of ionic to electronic currents via the excited states of dyes located at the interface between hydrophobic domains (where ions migrate readily) and hydrophilic domains (where current is carried by electron hopping). The physics of these systems is now becoming well characterized. The principal limit on their performance is imposed by the characteristics of the hydrophobic domain. In the hydrophilic domain, ion mobilities are near those for aqueous solution.

As the slow response to switching first indicated (1–3), electronic conduction involves a broad distribution of deep and shallow trap sites in these complex amorphous materials. This report describes an attempt to overcome the main limitation by exploiting a polyviologen polymer known to have favourable redox hopping characteristics and acceptor states well matched to the low-lying excited state of the chromophore (4, 5). In this work the chromophore is bis(maleonitriledithiolato)nickelate(II).

The maleonitriledithiolate (mnt) ligand forms a square planar complex with nickel which is strongly coloured. Its spectral characteristics are retained with different counterions. The complex is also known to be electrochemically and photoelectrochemically active in solution and in polymer films (6). The solution electrochemistry of the complex displays a reversible one electron transfer between 2− and 1− ion charges. Reduction from 2− to 3− or oxidation from 1− to 0 is less reversible (6). The photoelectrochemical activity of the complex is not easily exploited in solution since the states excited with visible light have been shown to have a very short lifetime (7).

Poly(xylyl)viologen (PXV), a cationic redox polymer can be used as an electrode modifier. Viologens have been used as electron acceptors in previous photoelectrochemical schemes (4, 5). They have several useful characteristics: reversible one electron reduction to a monocation radical, ion exchange capacity, and a distinct change in colour between the two oxidation states. Facile redox processes are considered to be the primary mode of charge transport in this conducting polymer (8).

Any given system can have a combination of three channels of charge migration, metal-like electronic conduction, redox (self exchange) hopping, and ion diffusion. In wet junction cells one mode must be ion migration and this is usually coupled to a second. The channels may often be considered to correspond to *hydrophylic* domains where the solvent soluble ions readily move and *hydrophobic* domains where the spacing and orientation of molecules necessary for intermolecular electron jumping (electronic and redox self-exchange) is attained (2).

Polymers, which are amorphous or semicrystalline, may have very many localized energy states over a wide band of energies arising from chain ends, interphase regions between amorphous and crystalline zones, interphase regions between hydrophylic and hydrophobic zones, and the effects of local or bulk dipoles induced by the material's structure. This can give rise to broad distributions of acceptor and donor states for the polymer. All these localized states are capable of trapping (partially stabilizing) a charge carrier. Trap-controlled migration is charge diffusion which is highly dependent upon the depths of the intrinsic traps of the conducting medium.

The $Ni(mnt)_2^{2-}$ chromophore has been ion exchanged into polymeric films to extend the excited state lifetimes and to improve charge separation efficiency (3, 6). The support polymer showed the ability to segregate into hydrophobic and hydrophylic domains. The charge transport mechanism is believed to occur via the combination of localized trap states in the hydrophobic domains with ionic charge transport in the hydrophylic domains (similar behaviour was noted for films containing porphyrin and phthalocyanine complexes (2)). Ionic conduction appeared good, but overall response was poor due to trap-

[1]To whom correspondence should be addressed.

controlled migration. The system was probably limited by poor overlap of the complex's excited state with the accepting states of the polymer as well as the deep trap nature of the polymer. PXV-Ni(mnt)$_2$ is studied here in an effort to match the accepting levels of the polymer with the excited state of the mnt more closely, and to exploit a polymer with better carrier transport characteristics (4, 5).

Experimental

Materials

All materials were reagent grade unless otherwise specified. $[(C_2H_5)_4N]_2[Ni(S_4C_6N_4)_2)_2]$ (Ni(mnt)$_2$) was prepared according to the method outlined by Persaud and Langford (9).

Poly(xylyl)viologen bromide (PXV-Br$_2$) was prepared by reacting equimolar amounts of 4,4′-bipyridyl (Fluka) with α,α′-dibromo-(*p*)-xylene (Aldrich) in acetonitrile (Caledon HPLC grade) in a sealed vessel for 24 h (10). This condensation polymerization gave yields over 85%. The average polymer so produced is know to contain eight or nine repeat units giving an average molecular weight of roughly 3500 g/mol (10, 11). A polymer blend of PXV-Br$_2$ with polyethylene oxide (PEO) was prepared with 1% (w/v) aqueous PXV-Br$_2$ and 1% (w/v) aqueous PEO (Aldrich 100 000 g/mol).

Methods

Electrodes, roughly 1 × 5 cm, were cut from sheets of SnO_2-coated Pyrex glass (Swift Glass Co., Connecticut). They were cleaned in chromic acid, rinsed, and stored in ethanol. Aliquots of 0.2 mL of aqueous solutions of the preformed polymer were drop cast upon levelled dry electrodes and allowed to dry slowly for uniform film formation. The electrodes were bordered with a clear inert insulating lacquer (that gave no background electrochemical signal) leaving an area of 1 cm^2 exposed. Contact to the electrodes was established with nickel alligator clip contacts. Film thicknesses were measured with a micrometer. The Ni(mnt)$_2^{2-}$ ion was incorporated into the prepared films by ion exchange from acetonitrile solutions of the Ni(mnt)$_2^{2-}$ tetraethylammonium salt. The electrodes were left in the solutions for 15 h.

Solutions for electrochemical measurements were 0.10 M KCl and 2.00 mM of $K_3Fe(CN)_6 \cdot 3H_2O$ and $K_4Fe(CN)_6$ in 0.10 M KCl. Measurements were carried out in an electrochemical cell equipped with a platinum counter electrode and an Ag/AgCl (saturated KCl) reference electrode. The volume of solutions was typically 25 mL. Cyclic voltammetry was done using a Metrohm E506 potentiostat coupled with a Metrohm E612 scanner. Voltammetric experiments were done at scan rates from 10 to 100 mV/s. Potentials and peak separation data tabulated here are those evaluated at 100 mV/s scan rate. All solutions were deoxygenated with prepurified nitrogen for 10 min prior to experiments.

A tungsten halogen lamp (EKN 300W Sylvania) coupled with a locally made power supply was used as an adjustable light source to obtain short-circuit photocurrents. A 5 cm water filter was used in conjunction with an ultraviolet filter to remove IR and UV radiation. Dark currents for all experiments were allowed to stabilize (10–15 min). Short-circuit current measurements were taken using a multimeter (Kiethley model 177) coupled to a strip chart recorder. Irradiation intensities were evaluated using a Coherent 210 power meter and were adjusted to 100 mW/cm^2. All solutions were deoxygenated for 10 min with prepurified nitrogen while the systems attained a steady current. Solutions were also stirred at a constant rate.

Ultraviolet–visible spectra were obtained on an Hewlett Packard 8452A diode array spectrophotometer interfaced to an IBM/PC. Near infrared spectra were measured on a Shimadzu UV-160. Some spectra of solid films in SnO_2-coated electrodes, blanked accordingly when scatter from the opaque films was not too great, were recorded. In most cases, however, films were dissolved into known quantities of either water or dimethylformamide (Aldrich, Spec grade) and solution spectra obtained. Fluorescence of solid films was measured using a Perkin Elmer MPF-44. Fourier transform infrared spectra were obtained from films on an IRTRAN2 disc on a Bomem Michelson 102 FTIR.

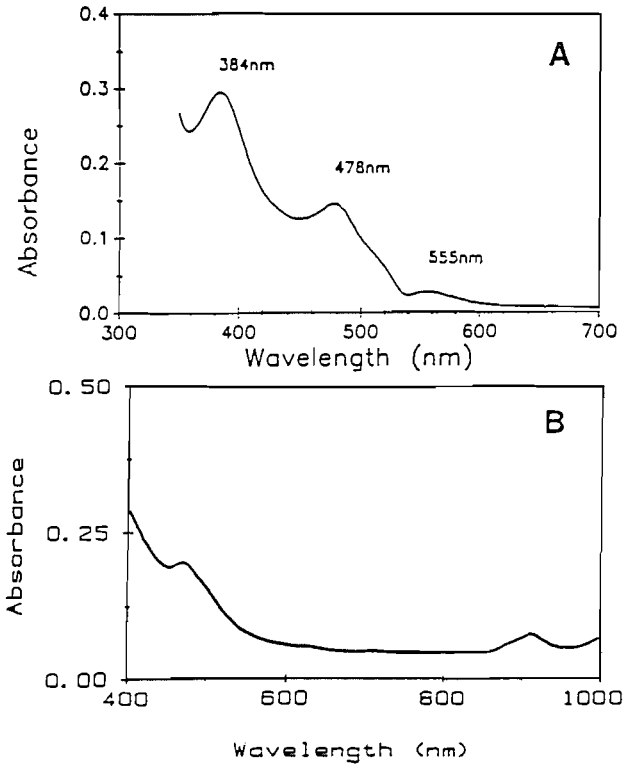


FIG. 1. (*a*) Absorption spectrum of PXV-Ni(mnt)$_2$ 0.045 mM in DMF. (*b*) Near infrared spectrum of same solution.

Results

Physical characterization

Solutions of PXV-Br$_2$ (1% (w/v)) as well as the 1:1 blend with PEO were cast upon clean SnO_2 electrodes. These were light yellow coloured films. PXV-Br$_2$ is water soluble, but upon ion-exchange with Ni(mnt)$_2^{2-}$ the films become water insoluble, thus allowing aqueous electrochemistry. With Ni(mnt)$_2^{2-}$ present, the films were brown in colour. PXV-Ni(mnt)$_2$/PEO films appeared darker than the PXV-Ni(mnt)$_2$ films.

Spectroscopy

PXV-Br$_2$ exhibited strong absorbance at 260 nm in good agreement with a published spectrum (10). A broad peak at 540 nm due to the reduced viologen moiety was obtained by the addition of a small amount of sodium hydrogen sulfite to aqueous PXV-Br$_2$. Re-oxidation of the viologen by ambient oxygen was complete in about 10 min. Ni(mnt)$_2^{2-}$ was ion exchanged into the PXV-Br$_2$ film to investigate possible interactions between the polymer and the Ni(mnt)$_2^{2-}$ counterion. A spectrum is shown in Fig. 1*a*. Discernible peaks for the PXV-Ni(mnt)$_2$ film were observed at 478, 388 nm (intensities: 3800, 6600 M^{-1} cm^{-1}, respectively) which compare very closely in wavelength and intensity to reported spectra of Ni(mnt)$_2$ complexes (9, 12). Also noted was a small peak near 555 nm which may reflect absorption by the reduced form of viologen (11) indicating some ground state oxidation of the dye by PXV.

Figure 1*b* shows the spectrum from 400 nm to the near infrared for PXV-Ni(mnt)$_2$. The principle visible region absorption is observed at 478 nm. A broad low intensity peak is noted for PXV-Ni(nmt)$_2$ near 890 nm which is not observed in either the Ni(mnt)$_2^{2-}$ or the PXV^{2+} salts. This absorbance is assigned to PXV-Ni(mnt)$_2$ charge transfer.

The vibrational spectrum of the PXV-Br$_2$ (Fig. 2*a*) corres-

Can. J. Chem. Downloaded from www.nrcresearchpress.com by 84.41.108.74 on 09/07/12
For personal use only.

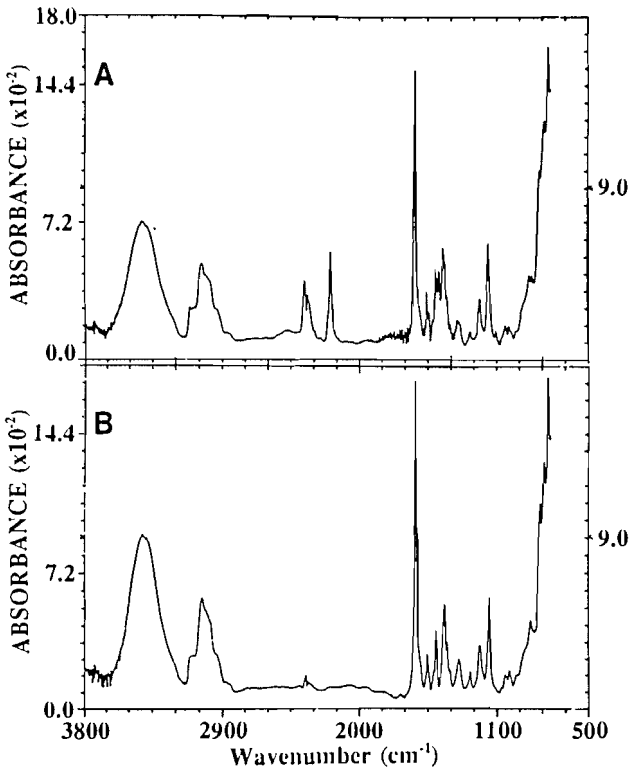


FIG. 2. (*a*) FTIR spectrum of PXV-Ni(mnt)$_2$ on AgCl and (*b*) PXV-Br$_2$ on AgCl.

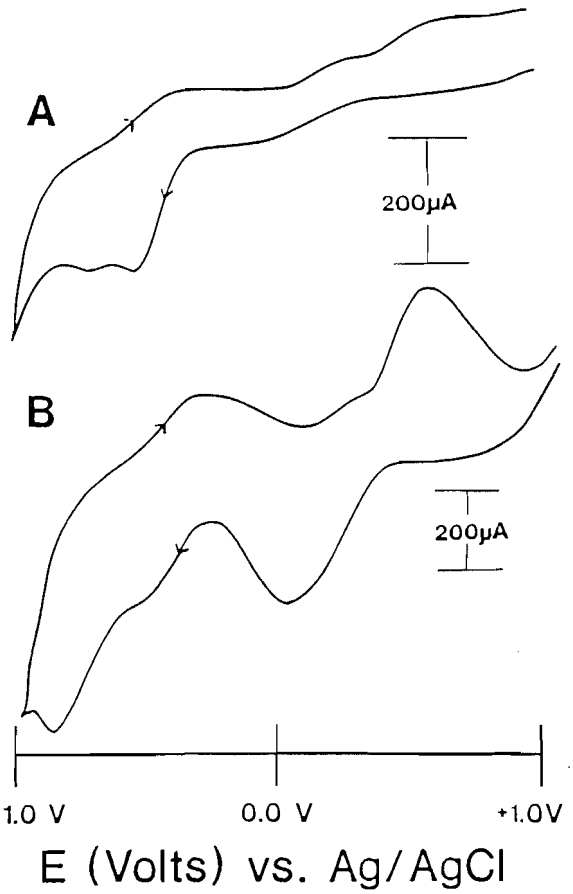


FIG. 3. Cyclic voltammograms of a SnO$_2$/PXV-Ni(mnt)$_2$ modified electrodes (*a*) in contact with 0.10 M KCl and (*b*) in contact with 2.00 mM Fe(CN)$_6^{3-/4-}$ and 0.10 M KCl. Scan rate was 100 mV/s for both starting at an initial potential of +0.8 V. Anodic currents are upwards and anodic potentials are to the right. Voltammograms were qualitatively similar at KCl = 1.00 M.

ponds very closely to a published spectrum for a similar polyviologen (13). Pronounced viologen peaks were at 1631 cm^{-1} (attributed to ν(C=N)), 1445 cm^{-1} (ν(C—N)) and 1155 cm^{-1} (ν(C—C)). Upon incorporation of Ni(mnt)$_2^{2-}$ new peaks observed in the PXV-Ni(mnt)$_2$ spectrum (Fig. 2*b*) corresponded closely to published IR data for Ni(mnt)$_2^{2-}$ salts (14). Prominent mnt peaks at 2191 cm^{-1} (ν(C≡N)), 1489 cm^{-1} (ν(C=C)), and weaker ones at 1105 cm^{-1} (π(C—CN) and 865 cm^{-1} (ν(C—S)) were observed. PXV peaks at 3400, 3000, 1630 cm^{-1} (the 1630 cm^{-1} peak being tentatively assigned to ν(C—N$^+$)) (13) exhibited a decrease in intensity. Distinct PXV peaks shifts were also noted at 1156 and 1216 cm^{-1}. Strong electrostatic interactions between the ion pair is a proposed explanation for the changes in the PXV related peaks.

Fluorescence emission was undetectable in steady-state room temperature measurements of Ni(mnt)$_2^{2-}$. Upon incorporation into the polymer film irradiation at 478 nm (the main visible absorption of the chromophore) results in emission at 555 nm.

Electrochemistry

In the absence of a redox couple cyclic voltammograms show small peaks for the Ni(mnt)$_2^{2-}$ one-electron oxidation (Fig. 3*a*). The waves were often very broad and appeared irreversible with ΔE_p = 0.30 V at 10 mV/s. The observed Ni(mnt)$_2^{2-}$ potentials are consistent with literature values (12). Upon continuous cycling these peaks decrease in intensity. This decrease is not due to leaching of the chromophore from the film since none was subsequently observed in the supporting electrolyte, but is attributed to crosslinking of the polymer and expulsion of counterions from the film. On the cathodic scan, films turn from their brown colour to a deep violet–blue at potentials less than −0.6 V (versus Ag/AgCl), indicating the presence of the viologen radical cation, but this colour develops only slowly. The films also return to their initial colour slowly at a potential more anodic than +0.4 V, thus reflecting the electrochromic nature of the viologen.

The viologen (4,4′-bipyridyl) peaks on the negative sweep of the voltammogram are weak and are not well defined since they occur near the cathodic limit of the solvent. In some cases the second reduction peak of the viologen was not observed. It has been suggested that the lack of the second reduction peak in viologens may be due to a conproportionation reaction [1] of the viologen (15, 16).

[1] $(PXV)^0 + (PXV)^{2+} = 2(PXV)^{1+}$

The viologen dication to radical monocation reduction potential, observed at −0.45 V agrees with the literature (10). The PXV-Ni(mnt)$_2$/PEO blend showed a slightly more negative value of −0.49 V. Cyclic voltammograms for the blend did not show any significant advantage over films of the neat viologen polymer.

The second reduction of viologen is known to be irreversible (16). When the system was cycled more cathodic than this second reduction potential a decrease in all voltammetric peaks was observed due to loss of electro-activity of the polymer. This loss of electro-activity is attributed to crosslinking and contraction of the polymer film (17). Also, when the viologen is reduced counterions are forced from the film into solution (18).

An equimolar solution of the ferri/ferrocyanide redox couple greatly improved the conduction of the films (Fig. 3*b*). The Fe(CN)$_6^{3-/4-}$ couple showed a voltammetric wave at 0.27 V

Can. J. Chem. Downloaded from www.nrcresearchpress.com by 84.41.108.74 on 09/07/12
For personal use only.

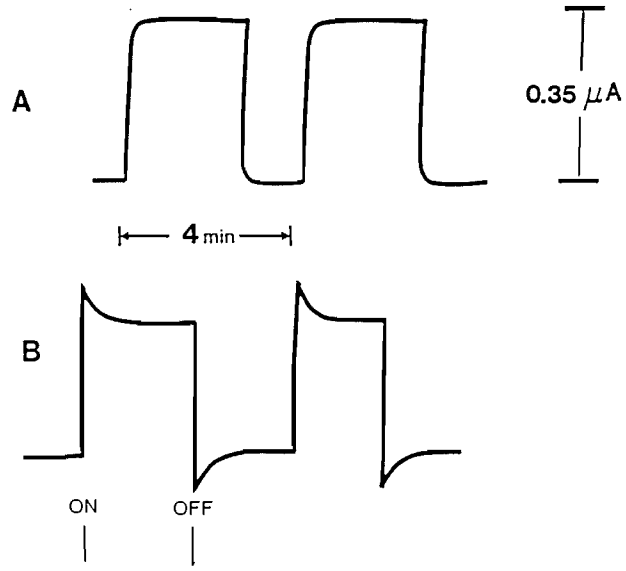


FIG. 4. Short-circuit photocurrents as a function of illumination time for PXV-Ni(mnt)$_2$ modified SnO_2 electrodes in contact with 2.00 mM $Fe(CN)_6^{3-/4-}$ and 0.10 M KCl. (*a*) A profile showing fast temporal response and (*b*) a profile showing capacitive response. Both were illuminated with light greater than 400 nm with an intensity of 100 mW/cm^2.

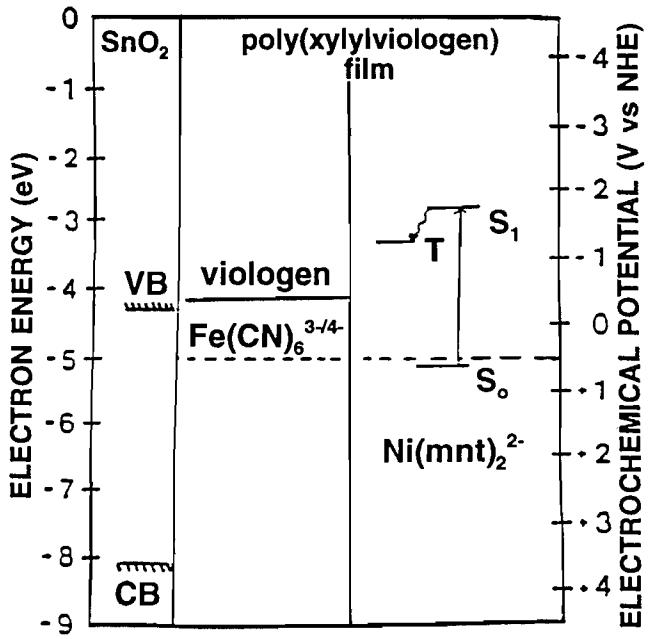


FIG. 5. Energy level diagram. The acceptor level of the polymer film is shown here relative to the energy levels of the SnO_2 electrode, the solution redox couple, and the Ni(mnt)$_2$ dye.

with ΔE_p = 200 to 400 mV for scan rates from 10 to 100 mV/s. The redox couple readily penetrates the film, but loaded films subsequently placed into supporting electrolyte alone showed leaching of 75% of the $Fe(CN)_6^{3-/4-}$ into solution within 30 min as evidenced by the decrease in $Fe(CN)_6^{3-/4-}$ currents. The $Fe(CN)_6^{3-/4-}$ signal largely masked the $Ni(mnt)_2^{2-}$ reduction signal as the redox couple penetrated the film. Solutions showed no evidence of leaching of the chromophore upon incorporation of the redox couple. The concentration of the redox couple in one film evaluated by integration of the area underneath the voltammetric waves was determined to be 1.2×10^{-4} mol/cm^3 while the concentration of $Ni(mnt)_2^{2-}$ was 2.8×10^{-5} mol/cm^3.

The rate of charge transport through a polymer film can be described by effective diffusion coefficients which include electron hopping, ion migration, and other aspects of carrier mobilities (19). The coefficient from three films containing the $Fe(CN)_6^{3-/4-}$ couple evaluated using a potential step from 0 to +1.0 V was $4.2 \pm 0.8 \times 10^{-9}$ cm^2/s, this being two orders of magnitude below that found for the redox couple in another ion-exchange polymer studied in this laboratory (3).

Photoelectrochemistry

The photoelectrochemical behaviour of polymer films was studied in background electrolyte in the presence and absence of $Fe(CN)_6^{3-/4-}$ redox couple. The background current for all electrodes studied was non-zero (−20 to +20 nA) and all photocurrents were anodic. Short-circuit photocurrents in only background electrolyte were all very small (≈30 nA) for intensities of 100 mW/cm^{-2} and the temporal response of the films was typical of a trap-controlled process (3). The magnitude of the photocurrents was 365 ± 25 nA/cm^2 for a series of three PXV-Ni(mnt)$_2$ electrodes at 100 mW/cm^2 in 2.00 mM $Fe(CN)_6^{3-/4-}$ in 0.10 M KCl. The PEO containing polymer blend fabricated in an effort to increase the hydrophilicity and hence the ionic conductivity of the films resulted in even smaller photocurrents. The photocurrents of PXV-Ni(mnt)$_2$/PEO films which had higher $Ni(mnt)_2^{2-}$ concentrations were 2/3 those of PXV-Ni(mnt)$_2$ films. These blends reflected an effort to create hydrophylic domains within the films to improve ionic diffusion. The perchlorate electro-inactive anion was incorporated into the PXV film to render the PXV film insoluble to allow examination of aqueous photoelectrochemistry of the polymer without the dye. Short-circuit photocurrents reached 50 ± 5 nA/cm^2 for electrodes not containing the dye most likely due to light absorption by the $Fe(CN)_6^{3-/4-}$ redox couple.

Photocurrent profiles for the polymer films studied are illustrated in Fig. 4. New PXV-Ni(mnt)$_2$ films demonstrated prompt response to light on/light off switching reaching a steady state current in about 10 seconds (Fig. 4*a*). After 1 h of use, however (shorter in some cases), the films would start to show slight capacitive response to switching (Fig. 4*b*). Cross-linking within the polymer and loss of ions from the film are probable causes.

Discussion

Exchange of $Ni(mnt)_2^{2-}$ anions into a catonic film has proven to be an effective method to exploit the short-lived metal to ligand charge transfer states excited by irradiation with visible light (3). In the earlier study photocurrent increased linearly with film thickness up to >6 μm, allowing construction of films harvesting a high fraction of the light. Overall conversion efficiency, however, remained low. Time dependence of the photocurrents revealed the probable limit. Charge migration across the film required trap-controlled electron migration via the acceptor states of an amorphous polymer film with many deep trap sites. The present study was designed to ameliorate this problem by exploiting a polymer known for facile electron exchange conduction. Unfortunately, the present study highlights the major *advantage* of the previously studied film, the ionic mobility across the film is similar to that in water.

A proposed energy level diagram for the photovoltaic system is illustrated in Fig. 5. The acceptor level of the PXV^{2+} would lie close to the potential for the viologen dication to radical

Can. J. Chem. Downloaded from www.nrcresearchpress.com by 84.41.108.74 on 09/07/12
For personal use only.

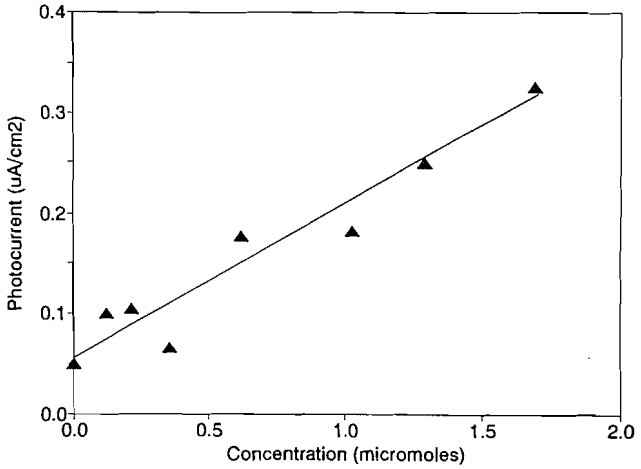


FIG. 6. Short-circuit photocurrent as a function of $Ni(mnt)_2^{2-}$ concentration within polymer film modified electrodes in contact with 2.00 mM $Fe(CN)_6^{3-/4-}$ and 0.10 M KCl. Electrodes were irradiated with light greater than 400 nm with an intensity of 100 mW/cm^2.

cation reduction. The excited states of the dye are assigned on the basis of absorption bands (9) of the mnt complexes.

A proposed reaction sequence for the system is as follows. The $Ni(mnt)_2^{2-}$ absorbs in the visible region populating its excited states. The proximity of the dye to the polymer cations leads to oxidation of the dye's excited state by the polymer's viologen moiety. Redox self-exchange of the viologen along with migration of compensating counterions shuttles the electron to the electrode surface and ultimately into the conduction band of the semiconductor giving an anodic photocurrent. $Fe(CN)_6^{4-}$ in the film reduces the oxidized $Ni(mnt)_2^{1-}$ species and excess $Fe(CN)_6^{3-}$ diffuses out to be reduced itself at the Pt cathode, thus completing the circuit.

It is known that if redox sites are bound to polymer chains electron-hopping can be significant (20), but there is the possibility that the redox carrier could be the $Ni(nmt)_2^{2-}$ dye itself. Figure 6 shows the $Ni(nmt)_2^{2-}$ concentration dependence of the observed short-circuit photocurrents. This result is roughly linear which, when extrapolated to zero concentration, corresponds to the observed short-circuit photocurrents in the absence of $Ni(nmt)_2^{2-}$. Should $Ni(mnt)_2^{2-}$ have been the primary redox carrier in this system Fig. 6 would have appeared parabolic (redox self-exchange being bimolecular). The observed increase in short-circuit photocurrents is simply due to the increase in light absorption, implying that primary redox exchange conduction is via the polymer backbone.

The temporal photocurrent profile for the PXV-$Ni(mnt)_2$ system illustrates improved conduction within the film over the trap-controlled migration observed for the ion-containing polymer blend studied previously (3). Fewer deep traps and more efficient charge separation are responsible for the fast response to light on/light off switchings.

Electro-activity of redox centres in most redox polymer films depends on ionic conductivity. The migration of charge compensating ions in the opposite direction to charge migration is necessary to preserve electroneutrality in local regions of the film. Ionic diffusion coefficients within the PXV^{2+} film were two orders of magnitude smaller than in the previously studied ion containing polymer blend (3), whereas photocurrents were one order of magnitude smaller. Thus spatial charge separation appears more efficient, but the loss of ionic mobility within the film gives an overall loss of performance. A maximally efficient device needs a combination of the electronic conductivity afforded by an efficient redox self-exchange polymer and the ionic mobility afforded the very hydrophylic films of Biro and Langford (3). In this case, improvement of one parameter was accomplished at the more than compensating expense of the other.

Acknowledgements

We thank the Natural Science and Engineering Research Council of Canada for the Strategic and Operating grants. The Laboratory for Inorganic Materials is funded by the MESS du Québec.

1. A. M. CROUCH and C. H. LANGFORD. J. Electroanal. Chem. **83**, 221 (1987).
2. A. M. CROUCH, I. ORDONEZ, C. H. LANGFORD, and M. F. J. LAWRENE. J. Phys. Chem. **92**, 6058 (1988).
3. D. A. BIRO and C. H. LANGFORD. Inorg. Chem. **27**, 3601 (1988).
4. D. C. BOOKBINDER and M. S. J. WRIGHTON. J. Am. Chem. Soc. **102**, 5123 (1980).
5. H. D. ABRUNA and A. J. BARD. J. Am. Chem. Soc. **103**, 6898 (1981).
6. L. PERSAUD and C. H. LANGFORD. Inorg. Chem. **25**, 3438 (1986).
7. L. PERSAUD. D. K. SHARMA, and C. H. LANGFORD. Inorg. Chim. Acta, **114**, L5 (1986).
8. N. OYAMA, T. OHSAKA, H. YAMAMOTO, and M. KANEKO. J. Phys. Chem. **90**, 3850 (1986).
9. L. PERSAUD and C. H. LANGFORD. Inorg. Chem. **24**, 3562 (1985).
10. A. FACTOR and G. E. HEINSOHN. Polym. Lett. **9**, 289 (1971).
11. S. E. CREAGER and M. A. FOX. J. Electroanal. Chem. **258**, 431 (1989).
12. J. A. MCCLEVERTY. *In* Progress in inorganic chemistry. Vol. 12. *Edited by* F. A. Cotton. Interscience Publishers, New York. 1968. p. 49.
13. H. SATO and T. TAMAMURA. J. Appl. Polym. Sci. **24**, 2075 (1979).
14. C. W. SCHLAPFER and K. NAKAMOTO. Inorg. Chem. **14**, 1338 (1975).
15. E. M. KOSOWER and J. L. COTTER. J. Am. Chem. Soc. **86**, 5524 (1964).
16. C. L. BIRD and A. T. KUHN. Chem. Soc. Rev. **10**, 49 (1981).
17. Y. M. TSOU, H. Y. HUI, and A. J. BARD. J. Electrochem. Soc. **135**, 1669 (1988).
18. D. A. SEANOR. *In* Electrical properties of polymers. Academic Press, New York. 1982. p. 304.
19. K. SUMI and F. C. ANSON. J. Phys. Chem. **90**, 3845 (1986).
20. D. A. BUTTRY and F. C. ANSON. J. Electroanal. Chem. **150**, 333 (1981).

Can. J. Chem. Downloaded from www.nrcresearchpress.com by 84.41.108.74 on 09/07/12
For personal use only.

Study of the properties of pyridine-2-azo-*p*-phenyltetramethylguanidine as a metal ion complexing agent[1]

KENNETH T. LEFFEK AND ARNOLD JARCZEWSKI[2]
Department of Chemistry, Dalhousie University, Halifax, N.S., Canada B3H 4J3

Received January 2, 1991

KENNETH T. LEFFEK and ARNOLD JARCZEWSKI. Can. J. Chem. **69**, 1238 (1991).

Pyridine-2-azo-*p*-phenyltetramethylguanidine (PAPT) was synthesized and the properties of this compound examined. The dissociation constants of the conjugate acids in H_2O are pK'_a H_2O = 10.41 ± 0.06, and pK''_a H_2O = 2.62 ± 0.02 at 25°C at I = 0.1, and in acetonitrile are pK'_a = 18.0 ± 0.2 and pK''_a = 10.4 ± 0.2. The properties of metal–ligand chelates in acetonitrile have been examined and the stability constants for Ni^{2+}, Co^{2+}, and Zn^{2+} complexes measured. The rates of reaction of PAPT with Ni^{2+}, Co^{2+}, and Zn^{2+} in acetonitrile have been determined and the activation parameters measured for the complex formation of LNi^{2+}. The stability constants for both complexing centres of PAPT have been calculated. The ^{13}C NMR spectra for PAPT and LNi^{2+} are quoted. The expected enhancement of the metal ion complexing ability of PAPT due to the strongly electron-releasing nature of the tetramethylguanidinyl group was not found.

Key words: metal ion complexes, pyridine-2-azo-*p*-phenyltetramethylguanidine, stability constants, pK_a.

KENNETH T. LEFFEK et ARNOLD JARCZEWSKI. Can. J. Chem. **69**, 1238 (1991).

On a synthétisé la pyridine-2-azo-*p*-phényltétraméthylguanidine (PAPT) et on a examiné ses propriétés. Dans l'eau, les constantes de acides conjugués sont pK'_a H_2O = 10,41 ± 0,06 et pK''_a H_2O = 2,62 ± 0,02, à 25°C, avec I = 0,1 alors que, dans l'acétonitrile, pK'_a = 18,0 ± 0,2 et pK''_a = 10,4 ± 0,2. On a déterminé les propriétés des chélates métal–ligand dans l'acétonitrile et on a déterminé les constantes de stabilité des complexes avec Ni^{2+}, Co^{2+} et Zn^{2+}. On a déterminé les vitesses de réaction du PAPT avec Ni^{2+}, Co^{2+} et Zn^{2+} dans l'acétonitrile et on a mesuré les paramètres d'activation pour la formation du complexe LNi^{2+}. On a calculé les constantes de stabilité des deux centres de complexation du PAPT. On rapporte les spectres RMN du ^{13}C NMR PAPT et du LNi^{2+}. Bien que le groupe tétraméthylguanidinyle soit fortement électrodonneur, on n'a pas observé l'augmentation attendue de la capacité du PAPT à former des complexes avec les ions métalliques.

Mots clés : complexes d'ions métalliques, pyridine-2-azo-*p*-phényltétraméthylguanidine, constantes de stabilité, pK_a.

[Traduit par la rédaction]

Introduction

Pyridine-2-azo-*p*-dimethylaniline (PADA), originally synthesized by Faessinger and Brown (1), has been thoroughly examined with respect to its ability to chelate several metal ions with the *d*-orbitals (2–6). Of the bivalent metal ions, nickel(II) has received considerably more attention than the others (2, 3, 7, 8–12). The usefulness of PADA lies, in part, in the magnitude of the stability constants of the appropriate metal complexes in water (2, 7) as well as in various nonaqueous solvents (9, 11, 12). The kinetics of metal ion binding to PADA have been measured using a variety of methods (3, 6, 7, 8–11, 13–15), and the activation parameters and mechanism of reactions have been discussed (7–11, 13, 14, 16, 17). The Eigen–Wilkins formulation (18) of the mechanism for metal complex formation is valid for water (7, 9, 10), nonaqueous solvents (9, 11), and mixed solvents (8).

PADA–metal complex formation was used as a model system to examine and discuss the mechanism of biologically important reactions of enzymes containing either Co^{2+} or Zn^{2+} (16). Also, PADA appears to be a useful ligand for the study of the kinetics and mechanism of fast metal–ligand substitution processes taking place in aqueous and micellar solutions (10).

This work seeks to develop a new complexing agent with a stronger electron-releasing group than the dimethylamino group in PADA.

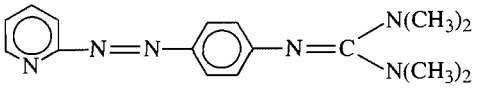
A series of 2-phenyl-1,1,3,3-tetramethylguanidine first synthesized by Kesler and Liebfritz (19), and extended by Pruszynski (20) and Leffek *et al.* (21), offers an opportunity to introduce such a group. The ^{35}Cl nuclear quadrupole resonance spectra for a series of five chloro-substituted 2-phenyltetramethylguanidines (22) indicated a very strong electron-releasing effect for the TMG group with a Hammett σ_p value of −0.88. This was confirmed (21) by a correlation of the pK of the conjugate acids and σ for 12 *meta*- and *para*-substituted 2-phenyl-1,1,3,3-tetramethylguanidines, from which it was calculated that σ_p for the TMG group was −0.80.

Taking into account the usefulness of PADA as a metal ion complexing agent and the strongly electron-releasing effect of the TMG group (21), we decided to synthesize the PADA analogue with the TMG group substituted for *p*-dimethylaniline, a weaker electron-releasing group, in the hope that the new compound would have a stronger ability to bond the metal ions than PADA itself. Therefore the purpose of the present work is to synthesize and study the properties of pyridine-2-azo-*p*-phenyltetramethylguanidine (PAPT) as a complexing ligand.

Results and discussion

The ^{13}C NMR spectra of pyridine-2-azo-*p*-phenyltetramethylguanidine (PAPT) synthesized according to a modified Faessinger–Brown method (1) were run in acetonitrile, dimethyl sulfoxide, and dimethyl sulfoxide/D_2O mixture (3:1). The ^{13}C NMR data for these spectra are collected in Table 1.

The spectra show no evidence of impurities. The peaks were assigned by analogy with those observed by Holloway and Hubbard (12) for pyridine-2-azo-*p*-dimethylaniline (PADA), which are also shown in Table 1. The spectra of these two compounds are very similar except for the signals arising from



PAPT

[1]Presented, in part, at the 10th IUPAC Conference on Physical Organic Chemistry, Haifa, Israel, August 1990.

[2]Visiting scientist from A. Mickiewicz University, Poznań, Poland.

Can. J. Chem. Downloaded from www.nrcresearchpress.com by 84.41.108.74 on 09/07/12
For personal use only.

TABLE 1. ^{13}C NMR data for pyridine-2-azo-*p*-phenyltetramethylguanidine (PAPT) in DMSO, DMSO/D_2O (3:1), and CH_3CN solvents

		PADA[a]		PAPT			
Ring	Carbon	Calcd.	Assign. DMSO/D_2O	Calcd.	Assign. DMSO	Assign. DMSO/D_2O	Assign. CD_3CN
Pyridine	2	173.8	163.8	164.1	163.4	164.4	164.4
	3	117.8	114.5	115.6	112.6	117.4	113.6
	4	136.0	139.9	140.9	138.5	146.7	139.1
	5	125.8	125.2	126.4	124.5	127.0	125.1
	6	150.1	149.7	150.0	149.1	150.2	150.1
Phenyl	1	153.1	154.3	154.3	157.7	158.6	159.1
	2,6	113.1	112.5	121.0	121.5	123.1	122.6
	3,5	123.5	126.7	122.2	124.8	127.0	125.7
	4	140.7	143.0	142.8	144.9	141.4	146.5
$N(CH_3)_2$			40.2	39.4	40.2	40.7	40.0
Guanidinyl				159.3	160.1	163.5	161.6

[a]From ref. 12.

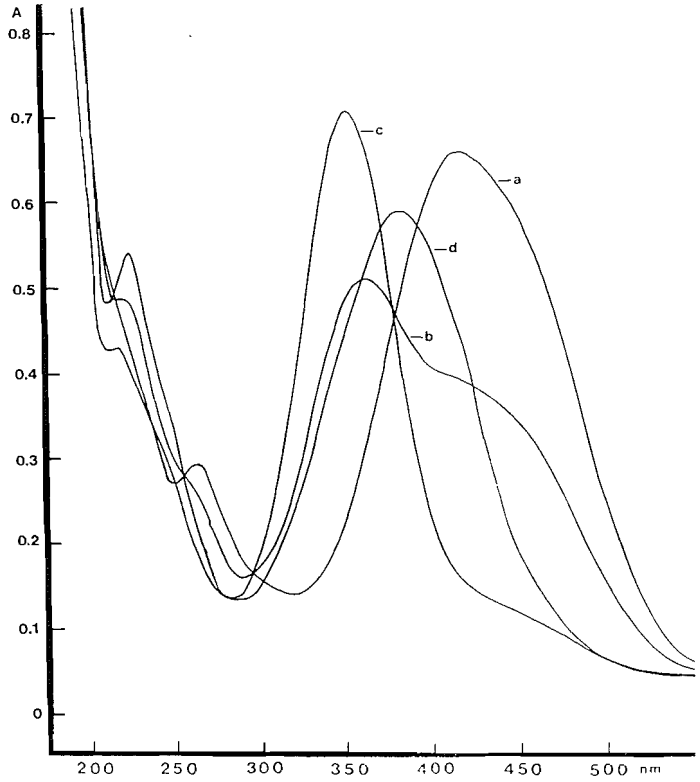


FIG. 1. Spectra of pyridine-2-azo-*p*-phenyltetramethylguanidine (PAPT) (5×10^{-5} M) in water: (a) pH 11.5; (b) pH 10.3; (c) pH 9.0; (d) pH 1.0.

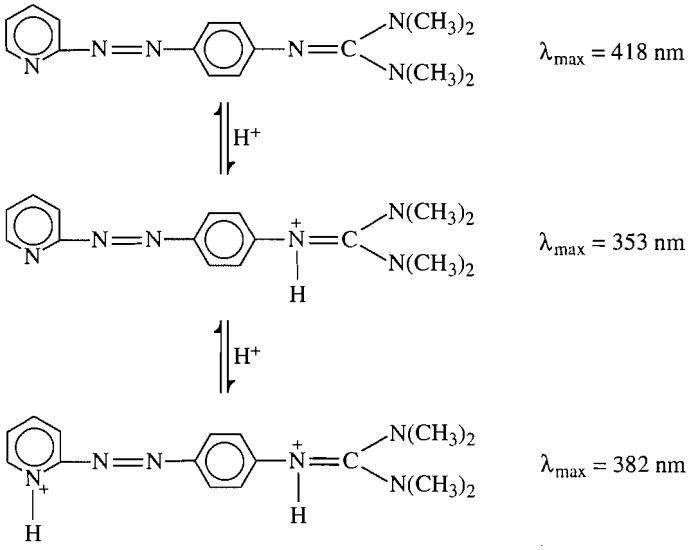
the 2 and 6 carbon atoms of the phenyl ring, where the PAPT molecule shows a marked downfield shift relative to PADA. The spectra of nine ring-substituted phenyltetramethylguanidines recently published (21) show similar peaks for the 2 and 6 carbon atoms, but phenyltetramethylguanidine itself does not (23). Its *ortho* carbon atoms appear at 114.4 ppm. The calculated values for the pyridine ring were obtained (24) using eq. [1] in which $\delta C_{(k)}$ is the chemical shift of carbon atom k in the pyridine ring and A_{ik} is the shift increment predicted for carbon k upon the introduction of a substituent R at carbon i. The A_{ik} values for the azo group were taken from Holloway and Hubbard (12). The calculated values for the phenyl ring were obtained (24) using eq. [2] in which $A_i(R_i)$ is the chemical shift for a substituent in the ith position. A_i values for the azo group were taken from the literature (25, 26) and A_i values for the TMG group were average values from the nine published spectra of ring-substituted phenyltetramethylguanidines (21), i.e., A_{Cl}, +23.6; A_{ortho}, −7.8; A_{meta}, −0.5; A_{para}, −9.7. The calculated values for the dimethylamino carbons and the guanidinyl carbon are averages from the nine published spectra (21).

$$[1] \quad \delta C_{(k)} = C_{(k)} + \sum_i A_{ik}(R)$$

$$[2] \quad \delta C_{(k)} = 128.5 + \sum_i A_i(R_i)$$

As was concluded for PADA (12), the ^{13}C NMR spectra are consistent with a single isomer of PAPT, with a *trans* arrangement across the azo double bond.

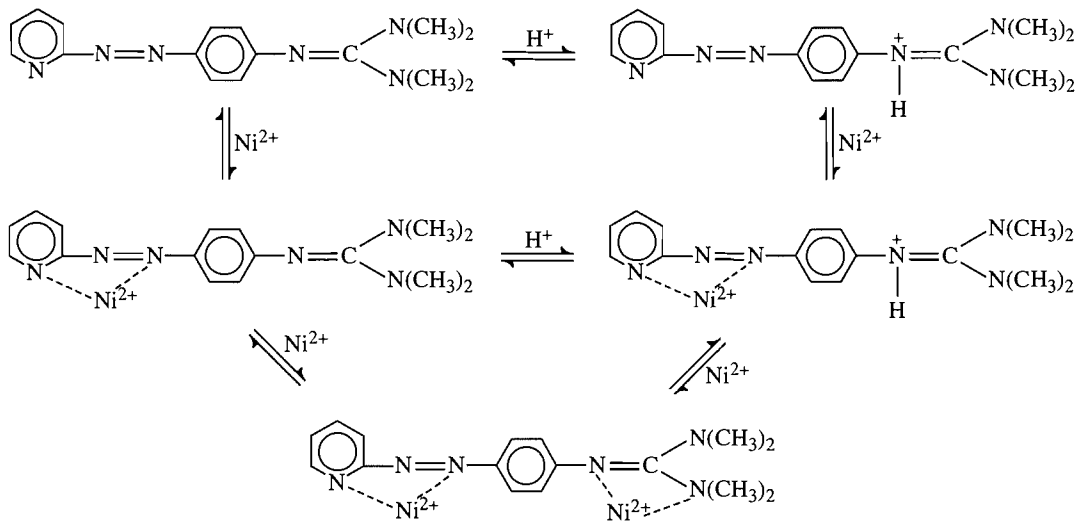
The UV–visible spectra of pyridine-azo-*p*-phenyltetramethylguanidine (PAPT) in water give three absorption maxima at λ 418, 353, and 382 nm, indicating the following equilibria:



An isosbestic point between PAPT and protonated PAPT is observed at 374 nm, as illustrated in Fig. 1.

It is noted that the unprotonated form exists only under

Can. J. Chem. Downloaded from www.nrcresearchpress.com by 84.41.108.74 on 09/07/12
For personal use only.



SCHEME 1

strongly alkaline conditions, and already at pH 10 two forms exist, the unprotonated form and the monoprotonated form (Fig. 1). At pH 9 almost all the compound exists in the monoprotonated form. Strongly acid conditions, from pH 2.5 to 1.0, shift the equilibrium to the diprotonated form.

The dissociation constant values pK'_a and pK''_a at 25°C, at constant ionic strength $I = 0.1$, maintained with KCl, were measured as: $pK'_a = 10.41 \pm 0.06$, $pK''_a = 2.62 \pm 0.02$.

In acetonitrile solvent the three forms L, LH^+, and LH_2^{2+} have λ_{max} at 411, 343, and 402 nm respectively, with an isosbestic point at 371 nm as shown in Fig. 2. The curves were obtained by gradual acidification with perchloric acid in acetonitrile, which is a strong acid in this solvent (27).

The appropriate values of pK_a in acetonitrile solvent were measured with dipicrate–monopicrate and monopicrate-free base buffers (28, 29) using a method already described (21). The pK'_a and pK''_a at 25°C were 18.0 ± 0.2 and 10.4 ± 0.2 respectively.

Since the nitrogen electrons of the guanidinyl substituent are delocalized in the direction of the pyridine-2-azo group, then, compared to PADA, we can expect three effects concerning the complexing abilities of PAPT towards metal cations with *d* electrons:

1. Only the free, unprotonated ligand can show a strong complexing ability.
2. The monoprotonated form will have a strongly reduced complexing power, since the protonated guanidinyl group will not be a powerful electron-donating group.
3. Both complexing centres can bond M^{2+} cations, giving LM^{2+} and $L(M^{2+})_2$ complexes.

In acetonitrile solvent we can distinguish the species shown in Scheme 1. These equilibria are demonstrated in Figs. 2–4.

It is obvious that protonation of PAPT will reduce its complexing power due to the decreased value of the pK''_a (2.62), which is even smaller than the corresponding value for 2-aminopyridine ($pK_a = 6.71$). When PAPT is protonated, the electron-releasing properties of the guanidinyl substituent will not only be suppressed but the positive charge of its NH group will cause a reverse effect, pulling the π electrons out of the phenyl ring and decreasing the equilibrium constant for the formation of LH^+M^{2+} complexes (Scheme 1).

The existence of the $LNi^{2+}H^+$ complex was deduced from the

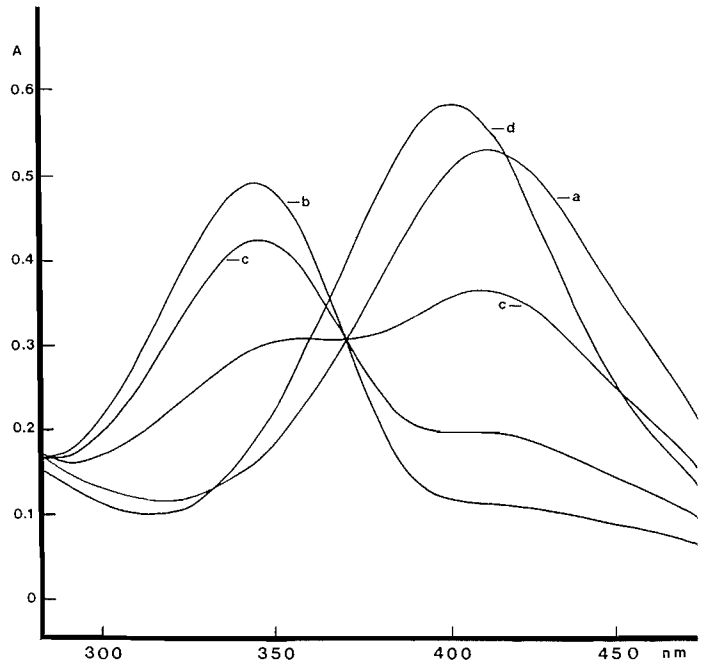


FIG. 2. Spectra of pyridine-2-azo-*p*-phenyltetramethylguanidine (PAPT) (4×10^{-5} M) in acetonitrile solvent: (a) unprotonated; (b) monoprotonated; (c) equilibrium between L and LH^+; (d) diprotonated.

^{13}C NMR spectra. The ^{13}C NMR spectrum of the free ligand in DMSO/D_2O (3:1) mixture is summarized in Table 1, together with the resonance peaks in DMSO and CD_3CN. The addition of the anhydrous $Ni(ClO_4)_2$ to the solutions of PAPT in these solvents caused a progressive relaxation of the resonance with increasing Ni^{2+} concentration by the paramagnetic nature of the system. The solution of the free ligand was systematically dosed with Ni^{2+} up to a 1:1 molar ratio of the metal to ligand. The spectrum showed a decrease in the intensity of the NMR peaks with each addition of Ni^{2+}, but no broadening of the peaks was observed.

The spectrum in the DMSO/D_2O mixture showed the same relaxed resonances in the presence of Ni^{2+} as observed in DMSO solvent, indicating that the presence of water, which strongly protonates the basic centre in the guanidinyl group

Can. J. Chem. Downloaded from www.nrcresearchpress.com by 84.41.108.74 on 09/07/12
For personal use only.

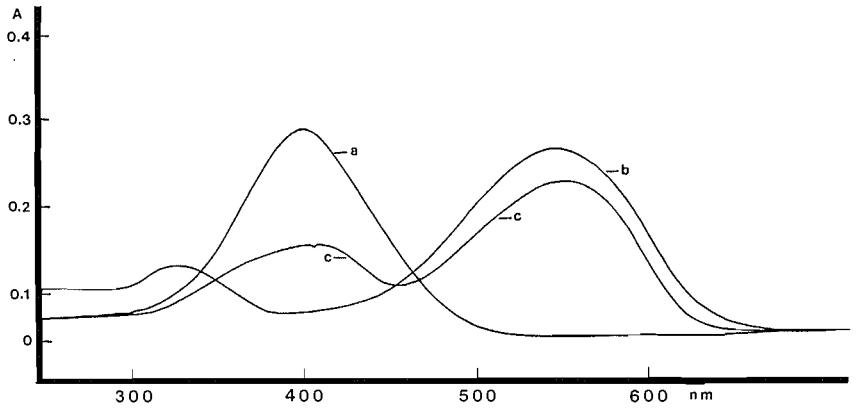


FIG. 3. Spectra of pyridine-2-azo-*p*-phenyltetramethylguanidine (2×10^{-5} M) with $Ni(ClO_4)_2$ (2×10^{-3} M) in acetonitrile solvent: (a) free ligand; (b) L:Ni^{2+}, 1:1; (c) large excess of Ni^{2+} over ligand, 1:400.

(Scheme 1), does not prevent the complexing by the pyridine azo group. The same conclusion can be reached from the relaxed spectrum of LNi^{2+} in CD_3CN. The addition of D_2O did not change the paramagnetic character of the system, indicating the presence of protonated LNi^{2+} complex (Scheme 1).

Reaction of PAPT with Ni(II) in acetonitrile solvent

PAPT in acetonitrile solvent, absorbing at $\lambda_{max} = 411$ nm, appears to be in the unprotonated form (Fig. 3(a)). The addition of anhydrous $Ni(ClO_4)_2$ (1:1) gives a blue-coloured species absorbing at $\lambda_{max} = 556$ nm (Fig. 3(b)). A large excess of Ni^{2+} over PAPT produces a shift from 556 nm to $\lambda_{max} = 565$ and 414.5 nm. These two maxima are assigned to LNi^{2+} (λ_{max} 556 nm) and $L(Ni^{+2})_2$ (λ_{max} 415 nm) (Fig. 3(c); Scheme 1).

The $LNi^{2+}H^+$ complex is not seen in the visible spectrum since its absorption is masked by the absorption peak of the LH^+ moiety. The protonation of LNi^{2+} shifts the absorption maximum from 556 to 345 nm, which is much closer to the LH^+ absorption than to that of LNi^{2+}, as shown by spectra (a) and (c) in Fig. 4.

The reaction of PAPT with Ni^{2+} to produce LNi^{2+} is much faster than the reaction with the second complexing centre (Fig. 5). In the first moment only the blue colour of the LNi^{2+} complex is observed at $\lambda_{max} = 565$ nm (Scheme 1), but in time an equilibrium with $L(Ni^{2+})_2$ (λ_{max} 415 nm) is reached. There was no indication of $L(Ni^{2+})_2$ when the ligand was in excess over Ni^{2+}.

Stability constants for LNi^{2+} and $L(Ni^{2+})_2$ formation have been measured spectrophotometrically using both stopped-flow and conventional spectrophotometry.

The following equilibria were considered:

$$L + Ni^{2+} \leftrightharpoons LN^{2+}$$

$$LNi^{2+} + Ni^{2+} \leftrightharpoons L(Ni^{2+})_2$$

Then

$$K_1 = \frac{[LNi^{2+}]}{[Ni^{2+}]\,[L]} \qquad \lambda_{max} = 565\ \text{nm}$$

$$K_2 = \frac{[L(Ni^{2+})_2]}{[LNi^{2+}]\,[Ni^{2+}]} \qquad \lambda_{max} = 415\ \text{nm}$$

$$\beta = K_1K_2 = \frac{[L(Ni^{2+})_2]}{[Ni^{2+}]^2\,[L]}$$

The stability constants were determined by standard methods

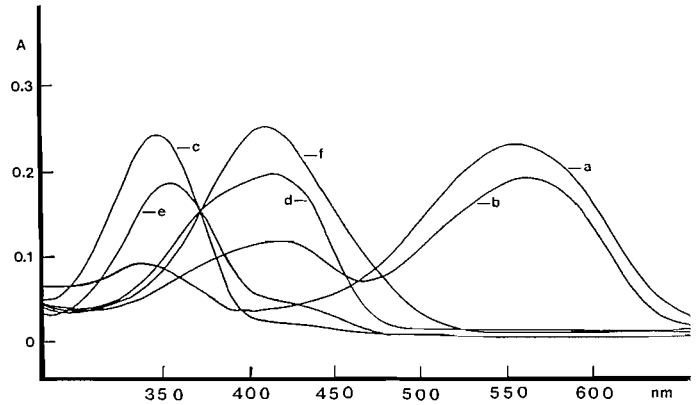


FIG. 4. The influence of water on the complex of pyridine-2-azo-*p*-phenyltetramethylguanidine (L) with Ni^{2+}: (a) L:Ni^{2+}, 1:1 (2×10^{-5} M); (b) L:Ni^{2+}, 1:400 ($L = 2 \times 10^{-5}$ M); (c) L:Ni^{2+}, 1:1 (2×10^{-5}) with H_2O added to 1 M; (d) as (b) with 1 M H_2O; (e) as (b) with 4 M H_2O; (f) free ligand (2×10^{-5} M).

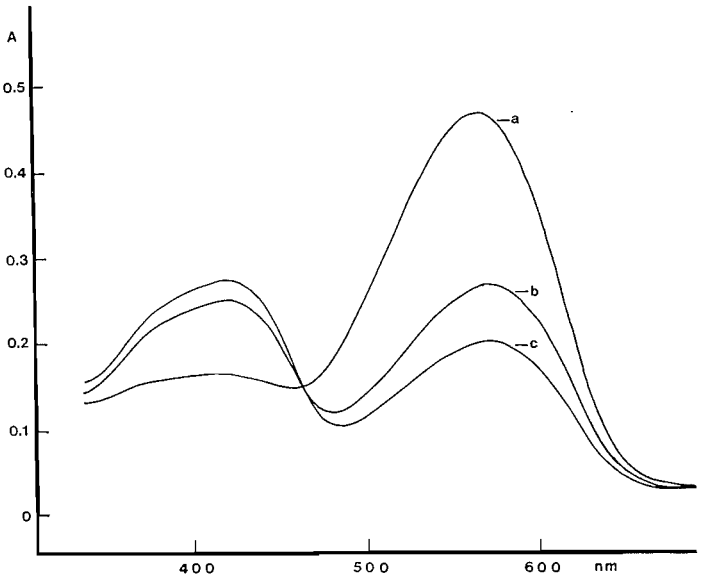


FIG. 5. Spectra of pyridine-2-azo-*p*-phenyltetramethylguanidine (2×10^{-5} M) with $NiClO_4)_2$ (2×10^{-4} M) in acetonitrile: (a) about 20 s after mixing; (b) 300 s after mixing; (c) 1200 s after mixing.

Can. J. Chem. Downloaded from www.nrcresearchpress.com by 84.41.108.74 on 09/07/12
For personal use only.

TABLE 2. Observed rate constants k_{obs} and derived rate constants k_f and k_b for the reaction of nickel(II) ion with pyridine-2-azo-*p*-phenyltetramethylguanidine[a] (PAPT) in acetonitrile solvent

T (°C)	$10^4[Ni^{2+}]$ (M)	k_{obs} (s^{-1})	$10^{-3}k_f$ ($dm^3\,mol^{-1}\,s^{-1}$)	k_b (s^{-1})
10.0	0.8	0.41		
	1.6	0.57		
	2.4	0.78		
	3.9	1.14		
	6.0	1.66	2.43±0.05	0.20±0.01
15.0	0.8	0.30		
	1.6	0.58		
	2.4	0.83		
	3.9	1.25		
	6.0	1.84	2.93±0.07	0.10±0.02
20.0	0.8	0.39		
	1.6	0.74		
	2.4	1.02		
	3.9	1.49		
	6.0	2.16	3.35±0.11	0.18±0.04
25.0	0.8	0.65		
	1.6	0.97		
	2.4	1.26		
	3.9	1.89		
	6.0	2.64	3.85±0.7	0.35±0.02
35.0	0.8	0.74		
	1.6	1.38		
	2.4	1.695		
	3.9	2.41	5.2±0.5	0.4±0.1

[a]Initial concentration, 2×10^{-5} M.

(2, 16) using a constant initial concentration of the ligand and a varying excess of Ni^{2+}. Since the equilibrium constants are large, the optical density of the complexed solutions did not change very much with varying Ni^{2+} concentration. Reasonable agreement was obtained between the method of Klotz and Loh Ming (2) and that of Cayley and Hague (16), but the reported values cannot be considered to be precisely determined. Since the method of Cayley and Hague is the simpler of the two, it was used for all of these reported stability constant values. In this procedure d, the optical density of the complexed solution, is plotted against $d - d_0/[M]$ in which d_0 is the optical density of the ligand alone and [M] is the total metal ion concentration. The slope of this graph is $-1/K$. A least-squares fit to measurements carried out at 565 and 415 nm for the first and second equilibria at 25°C gave $K_1 = (6.1 \pm 0.9) \times 10^5\,L\,mol^{-1}$; $K_2 = (8.4 \pm 1.8) \times 10^3\,L\,mol^{-1}$, so that $\beta = (5.1 \pm 1.3) \times 10^9\,L^2\,mol^{-2}$.

The first equilibrium is fairly well separated from the second one (Scheme 1), allowing kinetic measurements for this reaction to be made.

The addition of water destroys the blue-coloured LN^{2+}, producing the complex $LNi^{2+}H^+$, absorbing at 345 nm (Fig. 4). Only the ^{13}C NMR study indicates that this is $LNi^{2+}\,H^+$, and not LH^+, which absorbs at 343 nm (Fig. 2). Therefore the kinetic measurements for the first, fast, reaction (Scheme 1) of PAPT with Ni^{2+} to yield the product LNi^{2+} can be performed in a dry system and in a limited range of excess of Ni^{2+} concentration.

The concentration of PAPT was 2×10^{-5} M and the concentration of Ni^{2+} was set in a moderate range, always in excess to fit the pseudo-first-order conditions, low enough to minimize the influence of the second step of reaction to produce the $L(Ni^{2+})_2$ complex (Scheme 1). The kinetic measurements were performed for five different concentrations of $Ni(ClO_4)_2$ in the range of 8×10^{-5} to 6×10^{-4} M, at five temperatures between 10° and 35°C.

Each k_{obs} value at a particular Ni^{2+} concentration was obtained from five separate kinetic runs, which were averaged electrically by a data collector coupled to a stopped-flow spectrophotometer.

The plots of k_{obs} against Ni^{2+} concentration are linear, yielding the second-order rate constant, k_f, from the slope. The intercept, k_b, would be the first-order rate constant for the dissociation of the LNi^{2+} complex to the starting materials, if the second complexation equilibrium had no interfering effect. The rate constants k_f and k_b, with their standard deviations, were computed from the plots of k_{obs} against the Ni^{2+} concentration using a least-squares fit. The results are presented in Table 2. The k_f^{25} value of $3.85 \times 10^3\,dm^3\,mol^{-1}\,s^{-1}$ is about four times smaller than the corresponding rate constant for the reaction of PADA in acetonitrile solvent ($1.7 \times 10^3\,cm^4\,mol^{-1}\,s^{-1}$ (9)). This result is surprising if the tetramethylguanidinyl group is more strongly electron releasing than the dimethylamino group in PADA.

In Table 2 the rate constants, k_b, have significant values. Bennetto and Imani (9) found for the reaction of PADA with Ni^{2+} in CH_3CN that the plots of the first-order rate constants against Ni^{2+} concentration passed through the origin, indicating $k_b \sim 0$ and a very large equilibrium constant for the metal ion – ligand reaction.

The equilibrium constant (K_1), measured as the ratio $k_f/k_b = 1 \times 10^4$ at 25°C, is very much smaller than that measured at equilibrium. This discrepancy is attributed to interferences of the second complexation reaction with another Ni^{2+} ion. Since the equilibrium constant of the first complexation is so large, the

Can. J. Chem. Downloaded from www.nrcresearchpress.com by 84.41.108.74 on 09/07/12
For personal use only.

Can. J. Chem. Downloaded from www.nrcresearchpress.com by 84.41.108.74 on 09/07/12
For personal use only.

second reaction would not introduce any error in the determination of k_f, but would give rise to a spurious k_b.

The values of the activation parameters for the reaction were calculated as $\Delta H^{\neq} = 4.6 \pm 0.1$ kcal mol^{-1} and $\Delta S^{\neq} = -26.6 \pm 0.4$ cal mol^{-1} deg^{-1}. The enthalpy of activation $\Delta H^{\neq}$ is smaller by 1.5 kcal mol^{-1} and the entropy of activation $\Delta S^{\neq}$ is more negative by 7.3 cal mol^{-1} deg^{-1} than the same reaction for PADA (9). The free energy value is smaller by 0.8 kcal mol^{-1} for the reaction of PADA in the same conditions (9).

The second complex $L(Ni^{2+})_2$ formed by the reaction of LNi^{2+} with Ni^{2+} at the guanidinyl centre, absorbing at $\lambda_{max} =$ 415 nm, has a smaller stability constant, $K_2 = (8.41 \pm 1.6) \times 10^3$, and this equilibrium was reached in a slower step, as is shown in Fig. 5.

To compare the complexing abilities of the pyridine azo centre and the guanidinyl centre, the equilibrium constant for the reaction of phenyltetramethylguanidine with $Ni(ClO_4)_2$ in acetonitrile was also measured, at 236 nm, the maximum of the absorption peak of an equimolar mixture of these two compounds. The value of K^{25} for a phenyltetramethylguanidine concentration equal to 2×10^{-5} M and a varying concentration of Ni^{2+}, at $\lambda_{max} = 236$ nm, was $(1.8 \pm 0.9) \times 10^4$ L mol^{-1}. This confirms that Ni^{2+} complexes with both the pyridine and TMG parts of the PAPT molecule and that the pyridine azo centre forms the more stable complex.

The second-order rate constant, k_f, was also determined for the reaction of Ni^{2+} with phenyltetramethylguanidine at 236 nm and was found to be 46.8 ± 0.7 dm^3 mol^{-1} s^{-1} at 25°C. This is about 80 times smaller than the corresponding value of PADA with Ni^{2+} (9), confirming the qualitative results shown in Fig. 5.

In conclusion, the new complexing agent pyridine-2-azo-*p*-phenyltetramethylguanidine (PAPT) reacts with Ni^{2+} ion in CH_3CN, giving two complexes, LNi^{2+} and $L(Ni^{2+})_2$. The first complex, LNi^{2+}, is formed in a faster reaction, which is, however, slower than the analogous reaction with PADA, and the second, $L(Ni^{2+})_2$, is formed in a slower reaction. The $\beta = (K_1K_2 = 5 \times 10^9)$ for both steps is very large. However, the TMG substituent group does not manifest itself as a more powerful electron-releasing group than the dimethylamino group.

Reaction of PAPT with Co(II) in acetonitrile solvent

A $Co(ClO_4)_2$ solution was used as the complexing agent. The reaction of an equimolar (2×10^{-5} M) concentration of PAPT and Co^{2+} gave two absorption peaks at 568 and 411 nm assigned to LCo^{2+} and $L(Co^{2+})_2$ respectively. The second step of the reaction to give the $L(Co^{2+})_2$ complex is relatively faster than the corresponding reaction of Ni^{2+}.

The estimated value of the stability constant $K_1^{25} = (1.2 \pm 0.4) \times 10^5$ L mol^{-1} for LCo^{2+} was in the same order of magnitude as that for LNi^{2+}. The estimated value of the rate constant of the reaction was $K_f^{25} = (4.2 \pm 0.6) \times 10^4$ dm^3 mol^{-1} s^{-1}. Both the stability and the rate constants were measured using a stopped-flow spectrophotometer. The LCo^{2+} complex was less stable than LNi^{2+}, making a precise kinetic study very difficult.

Reaction of PAPT with Zn(II) in acetonitrile solvent

Anhydrous $ZnCl_2$ was used to examine the reaction of PAPT with Zn^{2+}. The reaction shows two absorption peaks at 557 and 585 nm after the solutions of PAPT and $ZnCl_2$ were mixed. These were assigned to two different LZn^{2+} complexes, one in which the Zn^{2+} is complexed at the pyridine azo site and the other in which the Zn^{2+} is complexed at the guanidinyl site. In time, both peaks decreased while a third one at 409 nm, assigned to $L(Zn^{2+})_2$, grew. The addition of water causes a slow decomposition of the coloured species, giving λ_{max} at 340 nm, assigned to the protonated $LZn^{2+}H^+$ complex.

Using moisture-free conditions and the stopped-flow technique, the stability constant at 557 nm was determined as $K^{25} = (6.9 \pm 0.6) \times 10^4$ dm^3 mol^{-1}.

These values for the reaction of PAPT with Co^{2+} and Zn^{2+} are considered as preliminary results.

Experimental

Materials

The synthesis of pyridine-2-azo-*p*-phenyltetramethylguanidine (PAPT) was carried out starting with 2-(4-nitrophenyl)tetramethylguanidine (20). This compound (0.05 mol, 11.8 g) was dissolved in dry toluene (75 mL) and clean sodium (0.1 mol, 2.4 g) was added with stirring under a positive pressure of dry nitrogen. The mixture was carefully warmed until the reaction started, after which cooling was necessary to keep the reaction under control. After the vigorous reaction had stopped, the reaction mixture was refluxed until the sodium had disappeared. To this suspension of the disodium derivative, 2-aminopyridine (0.05 mol, 4.7 g) was added all at once and the reaction mixture was refluxed for another hour. When the reaction was complete, the solvent was removed under reduced pressure. After work-up (1), the crude oily product was extracted with benzene and the extract applied to a column filled with Kieselgel 100, 70–230 mesh, suspended in benzene. The subsequent elution with benzene and acetone gave the product, which after crystallization from heptane gave red crystals, mp 89°C; *m/z* (rel.int.%) 296(25.7), 268(12.6), 224(15.4), 197(12.9), 190(21.0), 146(20.3).

There were two other by-products, mp 175°C and 212°C. The product with mp 175°C is pyridine-2-azo-aniline; *m/z* (rel.int.%) 198(1.9), 170(27.5), 120(5.9), 92(39.8), 56(15.1). The product with mp 212°C gave a mass spectrum *m/z* (rel.int.%) 431(7.7), 413(23.0), 312(8.2), 397(6.2). This high molecular weight product, which must be formed by another coupling reaction, was not identified.

The anhydrous salts of $Ni(ClO_4)_2$ and $Co(ClO_4)_2$ were prepared from their hexahydrates by heating small samples of them over P_2O_5 in a vacuum oven at 120°C (9). Analysis of these anhydrous salts showed no evidence of decomposition. The samples were weighed in a dry-box and the solutions were prepared by dissolving the salt in dry (less than 0.01% water) acetonitrile.

Determination of dissociation constants

The determination of the dissociation constants pK_a of PAPT in water was accomplished spectrophotometrically using the method described by Albert and Serjeant (30), at 25°C at constant ionic strength $I = 0.1$ maintained by KCl, by means of a Cary 219 spectrophotometer and an Orion Research model 601 meter. To remove CO_2, doubly distilled water was boiled and during subsequent cooling saturated with nitrogen.

The dissociation constants of PAPT in acetonitrile solvent were measured using the Coetzee and Padmanabham method (28), according to the procedure already described (21).

Determination of stability constants

The stability constants of the complex of PAPT with Ni^{2+}, Co^{2+}, and Zn^{2+} in CH_3CN were measured spectrophotometrically at the λ_{max} characteristic of the appropriate complex, using a stopped-flow (Durrum–Gibson) or a UV–vis (Cary 219) spectrophotometer, depending on the type of reaction. The measurements for LNi^{2+}, LCo^{2+}, and LZn^{2+} were followed by the stopped-flow method and those for LNi^{2+} and $L(Ni^{2+})_2$ by conventional spectrophotometry using a Cary 219. The concentrations of the solutions for measurement of LNi^{2+}, LCo^{2+}, and LZn^{2+} were $[L] = 2 \times 10^{-5}$ M, with the concentration of M^{2+} reaching 200-fold excess.

The stability constants K were determined by measuring the optical

densities of the solutions of a fixed total ligand concentration with a varying excess of total metal ion concentration (2, 16). If d is the optical density of the solution of the complex and d_0 that of the ligand alone, a plot of d against $(d - d_0)/[M^{2+}]$ gives a straight line of slope $-1/K$. The measurements for LNi^{2+} were also performed according to the procedure described by Klotz and Loh Ming (2). There was no difference in the results obtained by these very similar methods.

Kinetic measurements

The kinetic measurements were performed using a stopped-flow Durrum–Gibson spectrophotometer with the metal ion concentration in an excess to assure pseudo-first order conditions. In both the equilibrium and kinetic measurements the reaction cells were thermostated to keep the temperature constant within ±0.1°C.

The solutions were always freshly prepared before the measurements and they were kept under a positive pressure of dry nitrogen to prevent atmospheric moisture.

Acknowledgment

The authors are grateful for financial support from the Natural Sciences and Engineering Research Council of Canada.

1. R. W. Faessinger and E. V. Brown. J. Am. Chem. Soc. **73**, 4606 (1951).
2. I. M. Klotz and W. C. Loh Ming. J. Am. Chem. Soc. **75**, 4159 (1953).
3. R. G. Wilkins. Inorg. Chem. **3**, 520 (1964).
4. D. N. Hague and M. Eigen. Trans. Faraday Soc. **62**, 1236 (1966).
5. D. N. Hague, S. R. Martin, and M. S. Zetter. J. Chem. Soc. Faraday Trans. 1, **68**, 37 (1972).
6. D. N. Hague and M. S. Zetter. Trans. Faraday Soc. **66**, 1176 (1970).
7. M. A. Cobb and D. N. Hague. J. Chem. Soc. Faraday Trans. 1, **68**, 932 (1972).
8. E. F. Caldin and P. Godfrey. J. Chem. Soc. Faraday Trans. 1, **70**, 2260 (1974).
9. H. P. Bennetto and Z. S. Imani. J. Chem. Soc. Faraday Trans. 1, **71**, 1143 (1975).
10. B. H. Robinson and N. C. White. J. Chem. Soc. Faraday Trans. 1. **74**, 2625 (1978).
11. E. F. Caldin and R. C. Greenwood. J. Chem. Soc. Faraday Trans. 1, **77**, 773 (1981).
12. C. E. Holloway and C. D. Hubbard. Inorg. Chim. Acta, **98**, 131 (1985).
13. M. A. Cobb and D. N. Hague. Trans. Faraday Soc. **67**, 3069 (1971).
14. E. F. Caldin, M. W. Grant, and B. B. Hasinoff. J. Chem. Soc. D, 1351 (1971).
15. M. W. Grant and C. J. Wilson. J. Chem. Soc. Faraday Trans 1, **72**, 1362 (1976).
16. G. R. Cayley and D. N. Hague. Trans. Faraday Soc. **67**, 786 (1971).
17. E. F. Caldin, M. W. Grant, and B. B. Hasinoff. J. Chem. Soc. Faraday Trans. 1, **68**, 2247 (1972).
18. M. Eigen and R. G. Wilkins. *In* Mechanism of inorganic reactions. *Edited by* R. F. Gould. Adv. Chem. Ser. No. 49, p. 55 (1965).
19. H. Kessler and D. Liebfritz. Tetrahedron, **26**, 1805 (1970).
20. P. Pruszynski. Can. J. Chem. **65**, 626 (1987).
21. K. T. Leffek, P. Pruszynski, and K. Thanapaalasingham. Can. J. Chem, **67**, 590 (1989).
22. B. Nogaj and P. Pruszynski. Magn. Reson. Chem. **25**, 301 (1987).
23. H.-O. Kalinowski and H. Kessler. Org. Magn. Reson. **6**, 305 (1974).
24. F. W. Wehrli, A. P. Marchand, and S. Wehrli. Interpretation of carbon-13 NMR spectra. 2nd ed. John Wiley, Chichester. 1988. Chap. 2.
25. L. F. Johnson and W. C. Jankowski. Carbon-13 NMR spectra. John Wiley, New York. 1972.
26. H.-O. Kalinowski, S. Berger, and S. Braun. Carbon-13 NMR spectroscopy. John Wiley, New York. 1988, p. 315.
27. I. M. Kolthoff, S. Bruckenstein, and M. K. Chantooni, Jr. J. Am. Chem. Soc. **83**, 3927 (1961).
28. J. F. Coetzee and G. R. Padmanabhan. J. Am. Chem. Soc. **87**, 5005 (1965).
29. I. M. Kolthoff, M. K. Chantooni, Jr., and S. Bhowmik. J. Am. Chem. Soc. **90**, 23 (1968).
30. A. Albert and E. P. Serjeant. *In* The determination of ionization constants. 3rd ed. Chapman and Hall, New York. 1984.

Can. J. Chem. Downloaded from www.nrcresearchpress.com by 84.41.108.74 on 09/07/12
For personal use only.

La photochimie du *cis*-penta-1,3-diène, en phase gazeuse à 184,9 et 147,0 nm

GUY J. COLLIN[1] ET HÉLÈNE DESLAURIERS

Département des sciences fondamentales, Université du Québec à Chicoutimi, Chicoutimi (Québec), Canada G7H 2B1

ET

GEORGE R. DE MARÉ

Laboratoire de chimie physique moléculaire, Faculté des sciences, C.P. 160, Université Libre de Bruxelles, 50, avenue F.-D. Roosevelt, B-1050 Bruxelles, Belgique

Reçu le 4 mars 1991

GUY J. COLLIN, HÉLÈNE DESLAURIERS et GEORGE R. DE MARÉ. Can. J. Chem. **69**, 1245 (1991).

La photochimie du *cis*-penta-1,3-diène a été étudiée à 184,9 et à 147,0 nm en phase gazeuse. Les produits majeurs observés à 184,9 nm, outre le *trans*-penta-1,3-diène, sont le cyclopenta-1,3-diène, et divers radicaux révélés par l'addition d'iodure d'hydrogène. Le cyclopentadiène est formé très probablement via l'élimination successive de deux atomes d'hydrogène avec isomérisation concurrente du radical pentadiènyle vers la structure cyclopentènyle : Φ_0(cyclo-C_5H_6) ≈ 0,25. L'élimination du radical méthyle (Φ_0 = 0,50) est également importante. Il y a formation concomitante des radicaux CH_2=CHCH=$\dot{C}$H*, et dans une moindre mesure des radicaux CH_2=C=CH$\dot{C}H_2$*. On n'a cependant pas pu établir si ce dernier radical provient de l'isomérisation du précédent, ou s'il provient d'une molécule de penta-1,2-diène** résultant de l'isomérisation de la molécule photoexcitée. On a pu enfin observer une isomérisation conduisant vers la formation de penta-1,4-diène ($\Phi_0 \approx 0{,}03_5 \pm 0{,}01_5$). À 147,0 nm, on retrouve les mêmes caractéristiques, avec une fragmentation plus poussée des intermédiaires. L'énergie supérieure disponible à cette longueur d'onde explique cette observation. Globalement, la photofragmentation du *cis*-penta-1,3-diène s'apparente beaucoup plus à la photochimie des alcènes acycliques et assez peu à celle du buta-1,3-diène qui passe surtout pas l'isomérisation vers la structure buta-1,2-diène.

Mots clés : penta-1,3-diène, photolyse, UV lointain, réactions monomoléculaires, fragmentation, stabilisation.

GUY J. COLLIN, HÉLÈNE DESLAURIERS, and GEORGE R. DE MARÉ. Can. J. Chem. **69**, 1245 (1991).

We have studied the 184.9 and 147.0 nm photochemistry of gaseous *cis*-1,3-pentadiene: the main products observed at 184.9 nm are *trans*-1,3-pentadiene and 1,3-cyclopentadiene. The formation of radicals also occurs as shown through the use of DI as a radical scavenger. Cyclopentadiene is the likely product of successive eliminations of two hydrogen atoms from the photoexcited molecule after rearrangement of the pentadienyl radical to the cyclopentenyl structure: Φ_0(cyclo-C_5H_6) ≈ 0.25. Elimination of a methyl radical ($\Phi_0 \approx 0.50$) also occurs, with formation of CH_2=CHCH=$\dot{C}$H* and, in a lower yield, CH_2=C=CH$\dot{C}H_2$*. However, it is not possible to identify properly the mechanism of the formation of the latter radical. It may be the result of the isomerization of either the first photoexcited molecule or the excited 1,3-butadienyl radicals. A small amount of 1,4-pentadiene formation is also observed ($\Phi_0 \approx 0.03_5 \pm 0.01_5$). At 147.0 nm, the same characteristics are observed, together with higher fragmentation due to the higher energy content of the photoexcited molecules. It appears that the photofragmentation at both wavelengths is more in line with that of acyclic alkenes than with that of 1,3-butadiene, which tends to undergo isomerization of the photoexcited molecules to the 1,2-butadiene structure.

Key words: 1,3-pentadiene, far UV, vacuum UV, photolysis, monomolecular, fragmentation, stabilization.

Introduction

La photochimie des diène-1,3 a été relativement bien étudiée, tout particulièrement à 253,7 nm, donc par voie photosensibilisée. Elle a fait l'objet de rapport dans plusieurs manuels de référence (1, 2). Plus spécifiquement, la photoisomérisation *cis–trans* en solution, de même que la formation de cyclopropènes et de cyclobutènes substitués a été observée (3–5). À plus courtes longueurs d'onde, les travaux sont plus rares. Il est cependant pertinent de mentionner un travail réalisé à 228,8 nm. On y rapporte la mise en évidence d'un excimère (6). Aucun travail ne semble avoir spécifiquement porté sur la fragmentation de la molécule excitée et à plus courtes longueur d'onde.

La photofragmentation du buta-1,3-diène est mieux connue (7, 8). Nous avons, en particulier, montré que la molécule photoexcitée (buta-1,3-diène)** s'isomérise vers la forme (buta-1,2-diène)** avant rupture de la liaison C—CH_3.

[1] CH_2=CH—CH=CH_2 + $h\nu$ → (CH_2=CH—CH=CH_2)**

[2] (CH_2=CH—CH=CH_2)** → (CH_2=C=CH—CH_3)**

[3] (CH_2=C=CH—CH_3)** → CH_2=C=$\dot{C}$H + ·CH_3

1. Auteur à qui adresser toute correspondance.

Le présent travail se propose de vérifier la validité du mécanisme précédent dans le cas du *cis*-penta-1,3-diène (cPd13). Si ce mécanisme est acceptable, il se propose également d'étudier la chimie du radical CH_2=C=CH—$\dot{C}H_2$ qui pourrait être éventuellement formé par décomposition de la molécule (CH_2=C=CH—CH_2—CH_3)** excitée.

Partie expérimentale

Photoirradiation

Les techniques expérimentales sont bien connues. La lampe à mercure, basse pression (Philipps), émet principalement à 184,9 nm et surtout à 253,7 nm (9). La lampe de résonance à xénon émet presqu'exclusivement à 147,0 nm entre 120 et 250 nm (10). Ces émissions, ainsi que les coefficients d'absorption du penta-1,3-diène, sont vérifiées à l'aide d'un monochromateur McPherson d'un demi-mètre. La formation du butane normal dans la photolyse de l'éthylène sert d'actinomètre. Toutes les irradiations sont réalisées à la température de la pièce : $T = 20 \pm 2$°C.

Quelques irradiations ont été réalisées avec un filtre en Vycor. Ce filtre éliminait complètement la raie située à 184,9 nm et atténuait de quelque 30% la raie située à 253,7 nm.

Produits chimiques

Le *cis*-penta-1,3-diène est un produit A.P.I. (99,91 ± 0,02%). La principale impureté observée est le *trans*-penta-1,3-diène dont la

Can. J. Chem. Downloaded from www.nrcresearchpress.com by 84.41.108.74 on 09/07/12
For personal use only.

TABLEAU 1. Photolyse du *cis*-penta-1,3-diène en présence d'intercepteur à 184,9 nm. Rendements quantiques de composés linéaires en C_5

cPd13[a]	O_2[a]	DI[a]	D_2S[a]	SF_6[a]	Φ(penta-1,4-diène)	trPd13	cP2	trP2
0,94	—	—	—	—	0,013	0,44	—	—
1,70	—	—	—	—	0,019	0,80	—	—
0,96	0,1	—	—	—	0,015	1,2	—	—
1,90	0,2	—	—	—	0,031	0,95	—	—
1,90	0,2	—	—	100	0,057	0,93	—	—
0,96	—	0,2	—	—	0,03	30–65	4	7
0,95	—	—	0,15	—	0,02	≈50	0,0	0,0
0,95	—	0,2	—	51	0,043	300	11	6
5,1	0,85	0,50	—	—	n.m.[b]	2200	1,3	0,55

[a]En Torr (1 Torr = 133 Pa).
[b]n.m. ≡ non mesuré.

TABLEAU 2. Photolyse du *cis*-penta-1,3-diène à 184,9 nm en présence d'oxygène

cPd13[a]	O_2[a]	Φ(CH_4)	Φ(C_2H_2)	Φ(C_2H_4)	Φ(C_3H_6)	Φ(cyclo-C_5H_6)
0,50	0,05	0,013	0,05	0,035	(0,047)[b]	0,24
0,96	0,10	0,017	0,06	0,04	(0,035)	0,23
2,38	0,24	0,016	0,06	0,031	(0,040)	0,19
5,04	0,50	0,009	0,045	0,020	(0,043)	0,11
9,98	1,0	0,010	0,045	0,020	n.m.	0,03
1,92	0,19	0,03	0,066	0,056	0,055	0,282
1,92	0,8	n.m.	0,058	0,031	0,049	0,23
1,92	5,0	0,006	0,055	0,028	0,048	0,18
1,92	9,2	0,015	0,056	0,031	0,050	0,24
1,92	19,3	n.m.	0,043	0,019	0,037	0,09
1,92	45	n.m.	0,046	0,037	0,091	0,09
1,92	73	n.m.	0,045	0,032	0,038	0,03

[a]En Torr.
[b]Valeurs obtenues en l'absence d'oxygène.

concentration variait entre 0,06 et 0,12% dépendamment de l'échantillon utilisé. Ces échantillons contenaient des traces de C_2H_4 + C_2H_6 (4–26 ppm), d'acétylène (3–15 ppm), de cyclopenta-1,3-diène (8 ppm). L'oxygène (99,99%) et l'hexafluorure de soufre (99,99%) proviennent de chez Matheson et l'iodure de deutérium de chez Merck Sharp and Dohme du Canada. Tous ces produits sont utilisés tels que reçus, après dégasage à la température de l'azote liquide lorsque leur pression de vapeur saturante le permet.

Analyses

Toutes les analyses sont effectuées par chromatographie en phase gazeuse avec détecteur à flammes ionisantes. On a utilisé de façon séparée, deux colonnes remplies en acier inoxydable. La première (6 m, ϕ : 6 mm) en est une de squalane (20%) déposée sur «firebrick» (11). La seconde en est de Ucon LB 550X (7,50 m, ϕ : 6 mm) maintenue à 50°C (12).

Résultats

(a) À 184,9 nm

La photolyse du cPd13, en l'absence d'additif montre la formation importante du *trans*-penta-1,3-diène (trPd13). Le rendement quantique de ce produit varie entre 0,4 et 1,7 avec une incertitude relative au moins égale à ±25% étant donné le niveau d'impuretés (tableau 1). Ce rendement quantique semble augmenter légèrement avec l'augmentation de pression. Le penta-1,4-diène est aussi formé avec un rendement beaucoup plus faible que ce soit en l'absence ou en présence d'intercepteurs (tableau 1) : $\Phi(\text{penta-1,4-diène}) \approx 0{,}03_5 \pm 0{,}01_5$ quelle que soit la pression au sein du réacteur. D'autres produits, tels que le méthane (Φ <0,01), l'éthylène, l'acétylène, le propylène, buta-1,3-diène sont aussi observables avec des rendements quantiques inférieurs à 0,05. En présence de 10% d'oxygène, la photolyse montre la formation des mêmes produits (tableau 2). Le produit majeur observable est le cyclopenta-1,3-diène dont le rendement décroît rapidement avec l'augmentation de la pression. L'ajout de SF_6 a un effet similaire sur la plupart des rendements (figure 1).

L'irradiation réalisée à travers le filtre en Vycor ne produit qu'une faible isomérisation *cis–trans* à peine discernable du niveau d'impureté.

En présence de DI ou de D_2S, le méthane est un produit majeur (Φ ≈ 0,5 sous une pression de 1 Torr), de même que les *cis*- et *trans*-pentène-2 et surtout le trPd13 (tableau 3). On retrouve également des quantités importantes d'éthylène, de propène, de buta-1,3-diène, et dans de moindres quantités, d'acétylène, de buta-1,2-diène et un peu de cyclopentène.

(b) À 147,0 nm

Les caractéristiques principales relevées à 184,9 nm se retrouvent à 147,0 nm. Les produits majeurs sont encore le *trans*-penta-1,3-diène, le cyclopentadiène, l'acétylène et le vinylacétylène. On ne retrouve cependant pas de penta-1,4-diène et la formation de produits légers semble quantitativement plus importante. Les rendements de ces produits diminuent avec l'augmentation de la pression (tableau 4, figure 2).

L'effet combiné de l'oxygène et de l'iodure de deutérium a

Can. J. Chem. Downloaded from www.nrcresearchpress.com by 84.41.108.74 on 09/07/12
For personal use only.

TABLEAU 3. Photolyse du *cis*-penta-1,3-diène à 184,9 nm. Effet d'intercepteurs radicalaires sur les rendements quantiques

cPd13[a]	DI[a]	Autres[a]	CH_4	C_2H_2	C_2H_6	C_2H_6	C_3H_6	C_4H_6-1,3	C_4H_6-1,2	cyclo-C_5H_8
0,96	0,2	—	0,50	0,06	0,21	0,04	0,19	0,26	0,025	Traces
0,96	0,2	SF_6:51	0,10	0,03	0,11		0,06	0,065	—	n.m.
0,96	0,2	SF_6:100	n.m.	0,007	0,043	0,012	0,04	0,047	0,00	0,02
2,86	0,6	—	0,6±0,1	0,05	0,22	0,04	0,19	0,42	0,02	0,03
5,1	1,0	—	0,26	0,06	0,13	n.m.	0,11	0,22	Traces	n.m.
0,95	—	D_2S:0,15	0,24	0,08	0,20	0,03	0,08	0,11	0,00	0,00
2,85	—	D_2S:0,40	0,30	0,08	0,22	0,04	0,08	0,11	0,00	0,00

[a]En Torr.

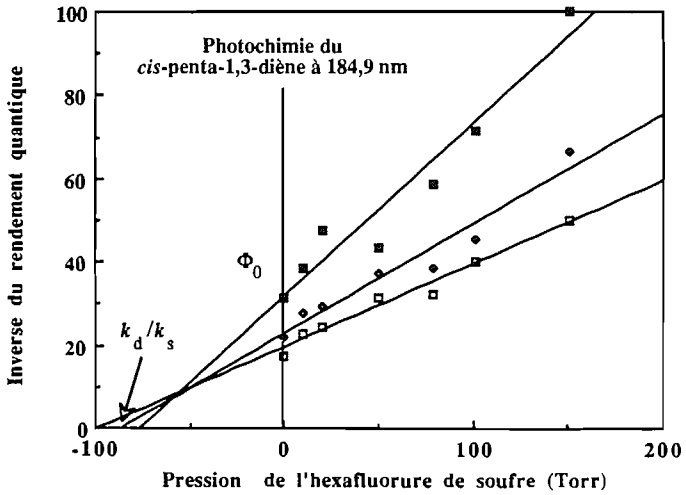


FIG. 1. Photochimie du mélange *cis*-penta-1,3-diène : oxygène (1,0 : 0,12 Torr) à 184,9 nm. Effet du SF_6 sur l'inverse des rendements quantiques de l'acétylène : (□) $y = 19,5 + 0,20x$; $r^2 = 0,98$; du propène : (◇) $y = 22,6 + 0,26x$; $r^2 = 0,95$; et de l'éthylène : (■) $y = 31,5 + 0,42x$; $r^2 = 0,94$.

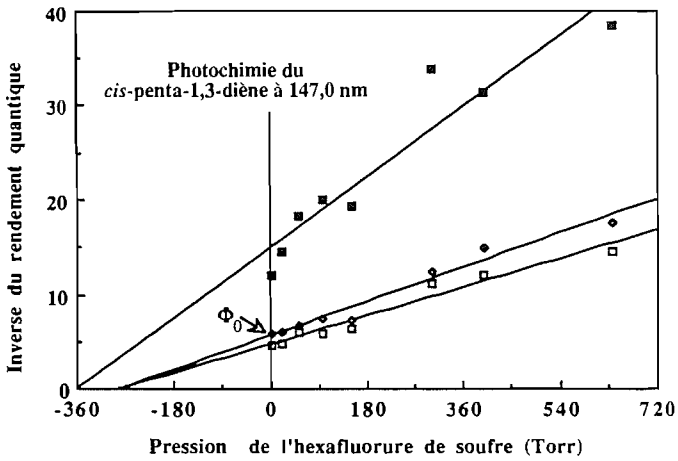


FIG. 2. Photochimie du mélange *cis*-penta-1,3-diène : oxygène (1,0 : 0,12 Torr) à 147,0 nm. Effet du SF_6 sur l'inverse des rendements quantiques de l'acétylène : (□) $y = 4,68 + 0,017x$; $r^2 = 0,96$; du vinylacétylène : (◇) $y = 5,60 + 0,020x$; $r^2 = 0,97$; et de l'éthylène : (■) $y = 14,9 + 0,041x$; $r^2 = 0,90$.

été exploré. L'oxygène diminue la formation des *cis*- et *trans*-pentène-2 générés par le DI sans toutefois vraiment interférer avec l'isomérisation *cis–trans* du monomère (tableau 5).

Discussion

1. À 184,9 nm

(a) Isomérisation de la molécule photoexcitée

Le principal produit observé à 184,9 nm est le *trans*-penta-1,3-diène. L'isomérisation *cis–trans* du penta-1,3-diène a été maintes et maintes fois observée et discutée, que ce soit en photosensibilisation (2, 3, 6), en radiolyse (13), dans des systèmes catalysés (14) ou par voie thermique (15). La photoisomérisation à 366 nm catalysée par le Pyrex a aussi été observée (16), de même que la photochimie directe à 253,7 nm (17). Les possibilités sont donc nombreuses. La quantité d'informations recueillies ici est insuffisante pour permettre une discussion éclairée. Rappelons seulement que la formation d'une molécule éthylénique électroniquement excitée dans l'état V (π,π^*) permet un retour vers l'état fondamental soit vers la structure *cis*, soit vers la structure *trans* (réf. 2, p. 475). La présence de radicaux et d'atomes d'hydrogène ou d'iode permet aussi d'obtenir cette isomérisation *cis–trans* à travers leur addition réversible sur cette double liaison (14). Le rendement quantique voisin de l'unité, mesuré en présence ou en l'absence d'oxygène (tableau 1), compte tenu des réactions de fragmentations observées, laisse entrevoir la possibilité d'un mécanisme en chaîne.

Un autre isomère linéaire observé est le penta-1,4-diène. Son rendement est relativement peu affecté par la présence d'intercepteurs : $\Phi([5] = 0,03_5 \pm 0,01_5$. L'observation de ce produit a aussi été faite en photochimie directe à 253,7 nm et il a permis de calculer un temps de vie de la molécule excitée de 2×10^{-8} s (18). On peut donc suggérer une réaction d'isomérisation directe de la molécule photoexcitée à travers un déplacement sigmatropique [1,3] d'un atome d'hydrogène. Ce processus a été observé dans divers alcènes cycliques (19) et acycliques (20). Dans ce dernier cas, les rendements sont d'autant plus importants que la liaison éthylénique déplacée est d'autant plus substituée (21). Cette isomérisation semble impliquer la molécule photoexcitée après sont retour à l'état fondamental, donc à partir de la molécule vibrationnellement très chaude (22).[2]

[4] $cPd13 + h\nu \rightarrow (cPd13)^{**}$, I

[5] $(cPd13)^{**} \rightarrow CH_2{=}CHCH{=}CHCH_3{\ddagger}$

[6] $CH_2{=}CHCH{=}CHCH_3{\ddagger} \rightarrow CH_2{=}CHCH_2CH{=}CH_2$

2. Un arbitre a très justement remarqué que le rendement en penta-1,4-diène présente une tendance nette (bien que faible) à l'augmentation en présence de SF_6. Cette augmentation est tout à fait en accord avec la présence de molécules vibrationnellement chaudes.

Can. J. Chem. Downloaded from www.nrcresearchpress.com by 84.41.108.74 on 09/07/12
For personal use only.

TABLEAU 4. Photolyse du *cis*-penta-1,3-diène à 147,0 nm. Rendements quantiques

cPad13 (Torr)	0,45	4,50	10,0	0,45	9,0	1,05	1,05	1,05[a]	3,07[b]
O_2 (Torr)	—	—	—	0,10	1,0	0,1	0,1	—	—
DI (Torr)	—	—	—	—	—	—	—	0,2	0,6
SF_6 (Torr)	—	—	—	—	—	150	640	—	—
Méthane	0,032	0,04	0,03	n.m.	n.m.	0,02	n.m.	0,21	0,21
Acétylène	0,22	0,27	0,24	0,22	0,22	0,15	0,02	0,07	0,04
Éthylène	0,07	0,08	0,07	$0,09_5$	0,07	0,06	0,02	0,12	0,012
Éthane	0,05	0,03	0,02	0,00	0,00	0,00	0,00	0,05	0,00
Propène	0,05	0,06	0,05	0,05	0,05	0,045	0,025	0,017	$0,01_6$
Propyne	0,02	0,03	$0,03_5$	0,12	0,04	$0,02_4$	0,011	0,018	0,02
Allène	0,04	0,04	$0,02_5$	0,035	$0,02_4$	0,014	0,005	n.m.	n.m.
Buta-1,3-diène	0,09	0,04	$0,02_5$	0,09	0,03	0,01	0,008	0,10	0,06
Vinylacétylène	0,20	0,22	0,19	0,17	0,19	0,14	$0,05_6$	0,087	0,07
trans-Penta-1,3-diène	0,3	0,9	0,9	0,59	n.m.	0,08	0,06	129	744
Cyclopenta-1,3-diène	0,25	0,19	$0,2_3$	0,26	0,25	$0,16_6$	$0,02_5$	n.m.	n.m.
Me-4-P-2	0,13	0,10	0,06	0,00	0,00	n.m.	n.m.	n.m.	n.m.

[a]Φ(pentène-2) = 8,60.
[b]Φ(pentène-2) = 24,4 avec rapport *trans*/*cis* ≈ 2.

TABLEAU 5. Photochimie du *cis*-penta-1,3-diène à 147,0 nm. Effet combiné de l'oxygène et de l'iodure d'hydrogène. Rendements quantiques

cPd13 (Torr)	4,95	4,95	4,95	4,95
O_2 (Torr)	—	0,5	1,0	2,0
DI (Torr)	0,5	0,5	0,5	0,5
Méthane	$0,17_7$	0,26	0,27	0,24
Éthylène	0,07	0,13	0,13	$0,10_5$
Buta-1,3-diène	0,025	0,05	0,05	0,07
trans-Pentène-2	10,7	3,0	0,30	0,18
cis-Pentène-2	5,9	2,2	0,26	0,12
tPd13	1080	1200	2470	620

(b) L'élimination d'un atome d'hydrogène

La décroissance observée du rendement en cyclopentadiène-1,3, que ce soit à 184,9 ou à 147,0 nm, est importante. Dans un premier temps, on peut supposer que un ou plusieurs intermédiaires sont impliqués dans le processus de formation, selon le mécanisme suivant :

[7] $(cPd13)^{**} \rightarrow \overline{CH_2CHCHCHCH_2}^* + H$

[8] $(cPd13)^{**} \rightarrow$ autres produits

[9] $(cPd13)^{**} + M \rightarrow cPd13 + M$

[10] $\overline{CH_2CHCHCHCH_2}^* \rightarrow$ cyclo-C_5H_7*

[11] $\overline{CH_2CHCHCHCH_2}^* + M \rightarrow \overline{CH_2CHCHCHCH_2} + M$

[12] cyclo-C_5H_7* → cyclo-C_5H_6 + H

[13] cyclo-C_5H_7* + M → cyclo-C_5H_7 + M

L'application du principe de quasi-stationarité des concentrations des espèces réactives à ce mécanisme conduit à l'expression suivante, où $[M]$ est la pression :

$$[14] \quad [\Phi(\text{cyclo-}C_5H_6)] = \frac{k_7 k_{10} k_{12}}{(k_{10} + k_{11}[M])(k_{12} + k_{13}[M])(k_5 + k_7 + k_8 + k_9[M])}$$

L'inverse du rendement quantique du cyclopenta-1,3-diène est donc une fonction cubique de la pression. La régression d'ordre 3, appliquée à la courbe :

$$[15] \quad [\Phi(\text{cyclo-}C_5H_6)]^{-1} = a + b[M] + c[M]^2 + d[M]^3$$

montre un coefficient de corrélation excellent ($r^2 = 0,971$) (figure 3). Un calcul similaire obtenu avec une régression d'ordre 2 conduit à un coefficient de corrélation au moins aussi bon, avec cependant une constante b, du produit $b[M]$, négatif. Ces résultats indiquent clairement l'effet de stabilisation dû à l'effet de pression sans pouvoir vraiment choisir entre un mécanisme faisant intervenir deux (23) ou trois étapes de stabilisation (trois intermédiaires susceptibles de stabilisation).

Afin d'améliorer la sensibilité du traitement statistique, les mêmes résultats ont été traités en traçant la fonction :

$$[16] \quad \frac{\left(\frac{1}{\Phi} - a\right)}{P} = b' + c'[M] + d'[M]^2$$

où a, b', c' et d' sont des constantes positives composées des coefficients k_7 à k_{13}. On obtient ainsi (figure 4) une courbe quadratique ayant trois coefficients positifs, avec un coefficient de corrélation convenable, légèrement meilleur que celui obtenu à partir d'une relation linéaire. On peut donc raisonnablement préférer un mécanisme impliquant trois intermédiaires susceptibles de stabilisation.

Nous avons, par ailleurs, montré récemment que les radicaux pentadiényles excités, formés dans la photochimie à 184,9 nm du méthyl-3 penta-1,4-diène, conduisent facilement à la formation de cyclopenta-1,3-diène (24). Cependant, la nature exacte de ce processus (cyclisation 1–5 du radical pentadiényle ou passage via un intermédiaire vinylcyclopropyle) n'a pu être précisée (25).

Il faut enfin relever que, par extrapolation à pression nulle, donc en l'absence de réaction de stabilisation, le rendement en cyclopenta-1,3-diène est voisin de 0,25, permettant d'afficher une valeur minimum du rendement de la réaction [7] : $\phi([7]) \geq 0,25$.

(c) L'élimination d'un radical méthyle

La mesure des radicaux méthyles s'effectue relativement bien en présence de DI ou de D_2S : réaction suivante (26, 29) :

[17] $\cdot CH_3 + DI \text{ ou } D_2S \rightarrow CH_3D + \cdot I \text{ ou } \cdot SD$

Sous une pression de 1 Torr, $\Phi_{DI}(\text{méthane}) \approx \Phi_{D_2S}(\text{méthane})$

Can. J. Chem. Downloaded from www.nrcresearchpress.com by 84.41.108.74 on 09/07/12
For personal use only.

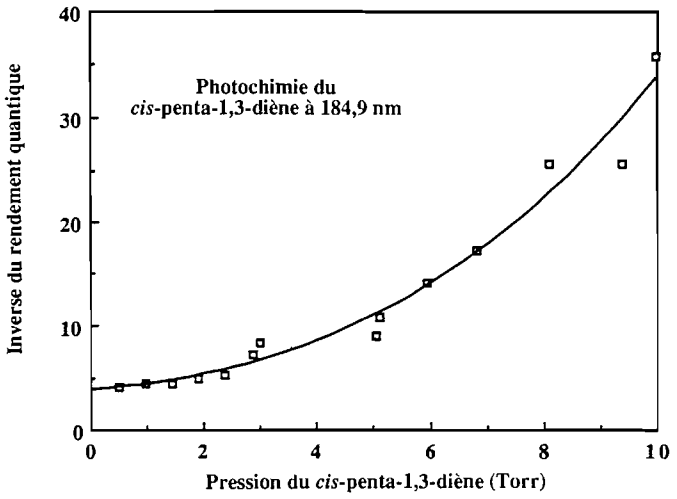


FIG. 3. Photochimie du mélange *cis*-penta-1,3-diène : oxygène (100 : 10) à 184,9 nm. Effet de la pression totale sur l'inverse du rendement quantique du cyclopenta-1,3-diène : $y_2 = 4{,}20 - 0{,}039x + 0{,}29x^2$; $r^2 = 0{,}973$; ou $y_3 = 3{,}82 + 0{,}42x + 0{,}14x^2 + 0{,}0115x^3$; $r^2 = 0{,}971$.

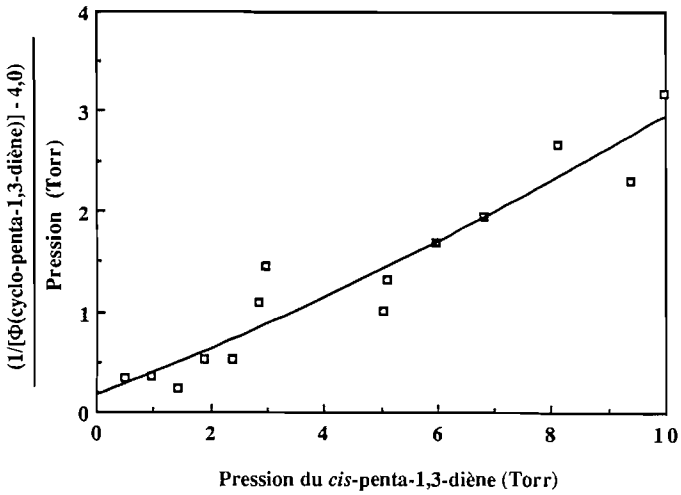


FIG. 4. Photochimie du mélange *cis*-penta-1,3-diène : oxygène (100 : 10) à 184,9 nm. Effet de la pression totale sur la fonction

$$\left(\frac{1}{\Phi(\text{cyclo-}C_5H_6)} - 4{,}0\right) \Big/ P = f([M]):$$

$y = 0{,}166 + 0{,}22M + 0{,}006M^2$; $r^2 = 0{,}97$.

$\approx 0{,}50 \pm 0{,}03$, alors qu'en l'absence d'interception ou en présence d'oxygène, le rendement en méthane ne dépasse pas 0,02. On peut donc estimer un rendement en radicaux méthyles voisin de $0{,}48 \pm 0{,}04$.

[18] $(cPd13)^{**} \rightarrow CH_2{=}CH{-}CH{=}CH^* + \cdot CH_3$

[19] $(cPd13)^{**} \rightarrow CH_2{=}C{=}CH{-}CH_2{-}CH_3{**}$

[20] $CH_2{=}C{=}CH{-}CH_2{-}CH_3{**} \rightarrow CH_2{=}C{=}CH{-}\dot{C}H_2{*} + \cdot CH_3$

La réaction [18] prévoit la rupture directe de la liaison C—CH_3 de la molécule *cis*-penta-1,3-diène photoexcitée. Les réactions [19] et [20], à l'exemple du buta-1,3-diène cité plus haut, proposent l'isomérisation de la molécule photoexcitée, via un transfert interne, 1,3, d'un atome d'hydrogène avant rupture d'une liaison C—CH_3 située en position β par rapport à une double liaison. Cette liaison est, en générale, la plus fragile dans les hydrocarbures insaturés acycliques. Elle entraîne une décomposition relativement facile des molécules vibrationnellement excitées (30).

La présence des radicaux C_4H_5 est confirmée à travers la formation observée en présence de DI des buta-1,3- et -1,2-diène (réactions d'interception similaire à la réaction [17]). Cela n'implique pas nécessairement la concurrence des deux mécanismes, puisque l'interconversion (isomérisation) des deux radicaux C_4H_5* excités ne peut pas être complètement éliminée (il s'agit aussi d'un transfert interne 1,3 d'un atome d'hydrogène) :

[21] $CH_2{=}CH{-}CH{=}\dot{C}H^* \Leftrightarrow CH_2{=}C{=}CH{-}\dot{C}H_2{*}$

(d) La rupture d'une liaison carbone–carbone (autre que C—CH_3)

La formation d'un certain nombre de produits légers en C_2 et C_3 réclame la rupture d'une liaison C—C située à l'intérieur de la molécule photoexcitée. C'est le cas de la formation de l'acétylène, de l'éthylène, du propène, ... Les rendements quantiques de ces produits suivent une loi de type Stern–Volmer (23) :

[22] $[\Phi(x)]^{-1} = [\Phi_0(x)]^{-1}(1 + k_s/k_d[M])$

où k_d est la constante de vitesse d'ordre 1 et k_s la constante de vitesse d'ordre 2, respectivement des réactions de décomposition et de stabilisation de l'intermédiaire excité.

[23] $(cPd13)^{**} \rightarrow CH_2{=}\dot{C}H^* + \cdot CH{=}CHCH_3$

[24] $CH_2{=}\dot{C}H^* \rightarrow CH{\equiv}CH + H$

[25] $CH_2{=}\dot{C}H^* + M \rightarrow CH_2{=}\dot{C}H + M$

L'équation [22] devient :

[26] $[\Phi(C_2H_2)]^{-1} = \Phi_0(C_2H_2)^{-1}(1 + k_{25}/k_{24}[M])$

où Φ_0 est le rendement mesuré par extrapolation à pression nulle. Au moins deux autres propositions de mécanismes sont disponibles :

[27] $(cPd13)^{**} \rightarrow CH_2{=}\dot{C}H + \cdot CH{=}CHCH_3{*}$

[28] $\cdot CH{=}CHCH_3{*} \rightarrow CH{\equiv}CH + \cdot CH_3$

[29] $(cPd13)^{**} \rightarrow \cdot CH_3 + CH_2{=}CHCH{=}CH^*$

[30] $CH_2{=}CHCH{=}CH^* \rightarrow CH_2{=}\dot{C}H + CH{\equiv}CH$

réactions auxquelles il faut ajouter les réactions de stabilisation des radicaux excités. Ces deux derniers mécanismes montrent que l'on ne peut pas indiquer l'ordre chronologique des fragmentations, réactions [23]–[24], [27]–[28] ou [29]–[30]. Ajoutons seulement que, compte tenu de l'énergie disponible à 184,9 nm, il est peu probable que deux radicaux excités issus de la même molécule puissent aussi se fragmenter. Les radicaux vinyles et propèn-1-yles apparaissant simultanément dans les réactions [23] et [27], ne sont pas susceptibles de fragmentation conjointe.

Si l'on ne peut connaître avec certitude l'identité du précurseur, la droite Stern–Volmer permet cependant d'obtenir une idée assez juste du temps de vie de l'intermédiaire. Ainsi, le rapport de sa pente divisée par son ordonnée à l'origine permet de connaître le rapport k_d/k_s mesuré, en terme d'unité de pression. En utilisant la pression comme horloge interne, ou plus scientifiquement, en identifiant k_s à la constante de vitesse

Can. J. Chem. Downloaded from www.nrcresearchpress.com by 84.41.108.74 on 09/07/12
For personal use only.

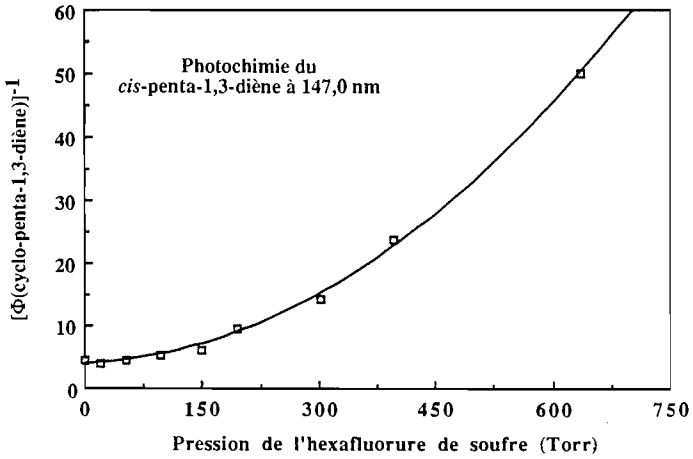


FIG. 5. Photochimie du mélange *cis*-penta-1,3-diène : oxygène (1,0 : 0,12 Torr) à 147 nm. Effet du SF_6 sur l'inverse du rendement quantique du cyclopenta-1,3-diène : $y_2 = 4{,}00 + 0{,}0043x + (1{,}07 \times 10^{-4})x^2$; $r^2 = 0{,}998$ ou $y_3 = 4{,}46 + 0{,}0097x + (1{,}71 \times 10^{-4})x^2 - (6{,}87 \times 10^{-8})x^3$; $r^2 = 0{,}999$.

de collision physique, on peut évaluer k_d et donc le temps de vie de l'intermédiaire.

Les rapports k_d/k_s ainsi calculé pour l'acétylène, l'éthylène et le propène sont, respectivement, égaux à 97,5, 76 et 86 Torr. Avec une fréquence de collision sous une pression de 1 Torr telle que $\omega = 1{,}45 \times 10^7\ s^{-1}$, le temps de vie de l'intermédiaire responsable de la formation du propène est de 0,80 ns. Ce temps de vie est relativement long comparativement au temps de vie calculé pour la molécule pentène-1 photoexcitée à 184,9 nm (31). On peut donc raisonnablement proposer que la stabilisation porte plutôt sur l'intermédiaire radicalaire que sur la molécule (cPd13)** elle-même.

2. À 147,0 nm

(a) La fragmentation par rupture de liaison

La photodécomposition de la molécule photoexcitée à 147,0 nm conduit à une variété importante de produits (tableau 4), donc de chemins réactionnels. L'énergie disponible (811 kJ E^{-1}) est énorme relativement aux énergies nécessaires à la rupture d'une liaison C—H ou C—CH_3. Compte tenu du mécanisme proposé à 184,9 nm et de ce que l'on connaît, par ailleurs, de la photochimie des alcènes acycliques à la même longueur d'onde (29), on peut proposer le mécanisme de type suivant :

[31] $(cPd13)^{**} \rightarrow \cdot R_1^* + \cdot R_2$

[32] $\cdot R_1^* \rightarrow \cdot R_3 + M$

où $\cdot R_1^*$ est un radical suffisamment excité pour donner lieu à une réaction de fragmentation subséquente, $\cdot R_2$ et $\cdot R_3$ sont, soit un atome d'hydrogène, soit un radical et M une molécule stable. En ne comptant pas le méthane, l'éthane, et le méthyl-4 pentène-2 qui sont probablement produits par réactions radicalaires, et le *trans*-penta-1,3-diène dont on ne sait pas très bien comment il est formé (voir plus haut), la somme des produits moléculaires légers apparaissant à 0,45 Torr (tableau 4) est de 0,94 ($\pm$0,15). Cette identité entre le nombre de molécules photoexcitées et le nombre de molécules qui se décomposent est peut-être fortuite. En effet, bien que les cas soient relativement rares et de peu d'importance quantitative, la photofragmentation pourrait produire en une seule étape deux molécules stables (32). Ce type de réaction commande une réorganisation (isomérisation) et une énergie relativement exigeante de la molécule photoexcitée pour atteindre une géométrie convenable :

[33] $CH_3CH{=}CHCH{=}CH_2^{**} \rightarrow (M)^{**} \rightarrow CH_3CH{:} + C_3H_4$

[34] $CH_3CH{:} \rightarrow C_2H_4$

En retournant au mécanisme type mentionné plus haut, la formation du cyclopenta-1,3-diène rapportée à 184,9 nm (réactions [7]–[13] sont de ce type) : $\Phi_0(\text{cyclo-}C_5H_6) \approx 0{,}25$ (figure 5). La courbure positive de la droite Stern–Volmer est ici, aussi, évidente. Malgré une coefficient de corrélation exemplaire ($r^2 = 0{,}999$), on doit remarquer que la régression du 3^e degré introduit des coefficients négatifs alors qu'ils devraient être tous positifs. Un traitement similaire à celui réalisé à 184,9 nm (figure 4) montre que les résultats ne peuvent définitivement pas être traités à l'aide d'une régression d'ordre trois, ne laissant que la possibilité d'un ordre deux, donc d'un mécanisme ne faisant intervenir que deux étapes de stabilisation.

Il en est de même de la formation de l'acétylène, réactions [23]–[30], du vinylacétylène, réaction [18] suivie de

[35] $CH_2{=}CH{-}CH{=}\dot{C}H^* \rightarrow CH_2{=}CHC{\equiv}CH + \cdot H$

Les formations de l'éthylène et du propène peuvent aussi se rattacher à ce type de mécanisme pourvu, cependant, qu'il soit précédé par un réarrangement de la molécule photoexcitée. L'efficacité du SF_6, pour stabiliser les intermédiaires, est ici plus faible que ce qui a été observé à 184,9 nm. L'énergie plus importante disponible à 147,0 nm est sans doute responsable d'une durée de vie plus courte des intermédiaires excités. Les temps de vie, calculés à travers les droites Stern–Volmer pour les intermédiaires présidant à la formation de l'acétylène et du vinylacétylène sont voisins : 0,25 ns.

L'identification et la mesure des rendements quantiques des radicaux ne sont pas nécessairement simples. Il faut tenir compte des réactions radical–radical, de l'addition des atomes d'hydrogène sur le penta-1,3-diène, ... Les formations de l'éthane et du méthyl-4 pentène-2, en l'absence d'intercepteurs radicalaires, sont à mettre au compte de ces réactions :

[36] $\cdot CH_3 + \cdot CH_3 \rightarrow C_2H_6$

[37] $\cdot H + cPd13 \rightarrow CH_3CH{=}CHCHCH_3$

[38] $CH_3CH{=}CHCHCH_3 + CH_3 \rightarrow CH_3CH{=}CHCH(CH_3)_2$

Ces réactions permettent d'établir une valeur minimum des rendements en radicaux méthyles et en atomes d'hydrogène : $\Phi(\cdot CH_3) > 2\Phi(C_2H_6) + \Phi(C_6H_{12}) \approx 0{,}23$ et $\Phi(\cdot H) > \Phi(C_6H_{12})$.

L'augmentation des rendements en méthane et en éthylène en présence d'iodure d'hydrogène confirme la présence des radicaux méthyles et vinyles. La quantification est cependant plus problématique. En effet, l'iodure de deutérium initie la formation d'une quantité importante de *cis*- et de *trans*-pentène-2. Il en ressort qu'en fin d'irradiation, la majeure partie de l'additif est consommé. Il n'agit donc plus avec toute l'efficacité requise. L'addition simultanée d'oxygène et d'iodure d'hydrogène augmente de façon importante le rendement en méthane, tout en réduisant la formation de ces deux pentène-2. Les rendements en méthane alors obtenus $\Phi_{DI+O_2}(\text{méthane}) \approx$ 0,24–0,27 sont probablement plus réalistes. Il ne faut pas oublier que l'oxygène est lui-même capable d'intercepter les radicaux méthyles. Les valeurs $\Phi(\cdot CH_3)$ doivent donc être supérieures aux valeurs $\Phi_{DI+O_2}(\text{méthane})$, mesurées.

Can. J. Chem. Downloaded from www.nrcresearchpress.com by 84.41.108.74 on 09/07/12
For personal use only.

Remerciements

Nous voulons exprimer notre gratitude au Conseil de recherche en sciences naturelles et en génie du Canada ainsi que le Department of Scientific Affairs de l'OTAN (RG n° 85/0484) pour l'aide apportée à la réalisation de cette étude. Les auteurs veulent aussi témoigner leur gratitude à M. L. Arteaga, Univ. de Cochabamba, Bolivia, pour les conseils apportés pendant la préparation de ce travail.

1. J. G. CALVERT et J. N. PITTS, JR. *Dans* Photochemistry. John Wiley & Sons, New York. 1967. pp. 508–509.
2. N. J. JURRO. *Dans* Modern molecular photochemistry. Benjamin/Cummings, Menlo Park. 1978. pp. 476–480.
3. S. BOUÉ et R. SRINIVASAN. J. Am. Chem. Soc. **92**, 3226 (1970).
4. R. SRINIVASAN et S. BOUÉ. J. Am. Chem. Soc. **93**, 5606 (1971).
5. S. BOUÉ et R. SRINIVASAN. Mol. Photochem. **4**, 93 (1972).
6. P. VANDERLINDEN et S. BOUÉ. Bull. Soc. Chim. Belg. **86**, 785 (1977).
7. R. DOEPKER. J. Phys. Chem. **72**, 4037 (1968).
8. G. J. COLLIN, H. DESLAURIERS, G. R. DE MARÉ et R. POIRIER. J. Phys. Chem. **94**, 134 (1990).
9. H. DESLAURIERS et G. J. COLLIN. J. Chim. Phys. **82**, 1033 (1985).
10. H. DESLAURIERS et G. J. COLLIN. Can. J. Chem. **63**, 3168 (1985).
11. R. A. HIVELY et R. E. HINTON. J. Gas Chromatogr. **6**, 203 (1968).
12. J. GAWLOWSKI, J. NIEDZIELSKI et A. BIERYNSKI. Chem. Anal. **15**, 721 (1970).
13. G. J. COLLIN, P. M. PERRIN et F.-X. GARNEAU. Can. J. Chem. **52**, 2337 (1974).
14. K. W. EGGER et S. W. BENSON. J. Am. Chem. Soc. **87**, 3311 (1965); **87**, 3314 (1965).
15. W. M. MARLEY et P. M. JEFFERS. J. Phys. Chem. **79**, 2085 (1975).
16. R. L. DAUBENDIEK et G. R. MCMILLAN. J. Am. Chem. Soc. **95**, 1374 (1973).
17. M. BIGWOOD et S. BOUÉ. Tetrahedron Lett. **44**, 4311 (1973).
18. A. DELABY et S. BOUÉ. J. Chem. Soc. Chem. Commun. 818 (1973).
19. P. J. KROPP, H. G. FRAVEL, JR. et T. RANDALL FIELDS. J. Am. Chem. Soc. **98**, 841 (1976).
20. T. D. R. MANNING et P. J. KROPP. J. Am. Chem. Soc. **103**, 889 (1981).
21. G. J. COLLIN et H. DESLAURIERS. Can. J. Chem. **63**, 1424 (1985).
22. R. A. BACK et G. J. COLLIN. J. Phys. Chem. **90**, 5684 (1986).
23. J. A. BARLTROP et J. D. COYLE. *Dans* Principles of photochemistry. J. Wiley & Sons, New York. 1978. pp. 148–155.
24. G. R. DE MARÉ, H. DESLAURIERS et G. J. COLLIN. Res. Chem. Intermed. **14**, 133 (1990).
25. G. R. DE MARÉ et G. J. COLLIN. J. Mol. Structure, Theochem. Sous presse.
26. P. AUSLOOS et S. G. LIAS. J. Chem. Phys. **90**, 5684 (1986).
27. P. AUSLOOS, R. E. REBBERT et S. G. LIAS. J. Photochem. **2**, 267 (1973–1974).
28. G. J. COLLIN et K. BUKKA. J. Photochem. **6**, 381 (1976–1977).
29. Z. DIAZ et R. D. DOEPKER. J. Phys. Chem. **81**, 1442 (1977).
30. W. TSANG. Int. J. Chem. Kinet. **1**, 245 (1969).
31. J. GAWLOWSKI et G. J. COLLIN. J. Photochem. **23**, 241 (1983).
32. G. J. COLLIN. Adv. Photochem. **14**, 135 (1988).

Can. J. Chem. Downloaded from www.nrcresearchpress.com by 84.41.108.74 on 09/07/12
For personal use only.

Reactions of Muonium with simple biochemical solutes in water and micelles

MARY V. BARNABAS[1] AND DAVID C. WALKER
Department of Chemistry and TRIUMF, University of British Columbia, Vancouver, B.C., Canada V6T 1Y6
Received February 15, 1991

MARY V. BARNABAS and DAVID C. WALKER. Can. J. Chem. **69**, 1252 (1991).

Rate constants are reported for the reaction of muonium atoms in water with some 36 organic compounds, many of interest in biology. These k_M values range from $<10^5$ to 7×10^{10} M^{-1} s^{-1}, according to the *type* of reaction involved, with the sugar–phosphate backbones of nucleic acids being at the low end and their bases at the high end. They are compared with corresponding published H-atom data (k_H), where possible, and show kinetic-isotope-effects ranging over five orders of magnitude. Since all k_H data were obtained at pH = 1, while k_M values refer to pH ~ 7 of the natural state, the pH-dependence of k_M was examined in representative cases. The changes found result from protonation of the solute rather than a changed reactivity of Mu on being converted to MuH^+. On localizing the solutes in the hydrophobic phase of dilute micelles, the reactivity of Mu was again measured ($k_{M(mic)}$). The resulting "enhancement" factor was considered in terms of: the reaction mechanism, its dependence on microenvironment (solvation), and the concentrating effect of mutual confinement to small sections of a biphasal system.

Key words: kinetic isotope effects, muonium, biochemicals, micelles.

MARY V. BARNABAS et DAVID C. WALKER. Can. J. Chem. **69**, 1252 (1991).

On a déterminé les constantes de vitesse, dans l'eau, d'atomes de muonium avec 36 composés organiques, dont plusieurs ont un intérêt biologique. Ces valeurs de k_M varient de $< 10^5$ à 7×10^{10} M^{-1} s^{-1} suivant le *type* de réaction impliqué; les composés comportant les phosphates de sucre des acides nucléiques réiques réagissent généralement les moins rapidement alors que leurs bases se trouvent à l'autre bout du spectre de réactivité. Lorsque c'est possible, on a comparé ces valeurs avec les données correspondantes publiées pour les atomes d'hydorgène (k_H); on a observé des effets isotopiques cinétiques s'étiques s'étalant sur cinq ordres de grandeur. Puisque toutes les données relatives aux k_H ont été déterminées à un pH = 1, alors que les valeurs de k_M se réfèrent au des pH = 7 de l'état naturel, on a examiné la relation entre le pH et les valeurs des k_M, pour des cas représentatifs. Les changements qui ont été observés sont plutôt dus à la protonation du soluté qu'à un changement de réactivité du Mu lorsqu'il se transforme en MuH^+. On a de nouveau mesuré la réactivité des Mu ($k_{M(mic)}$) aprés leur localisation dans les phases hydrophobes de micelles diluées. On a évalué le facteur d'« augmentation » de la réactivité en fonction: du mécanisme de la réaction, de sa dépendance sur le microenvironnement (solvatation) et sur l'effet d'augmentation de la concentration par un confinement mutuel dans des faibles sections d'un système à deux phases.

Mots clés : effets isotopiques cinétiques, muonium, biochimiques, micelles.

[Traduit par le rédaction]

Introduction

Simple organic compounds which are basic constituents of biological systems were selected for this study. The principal functional groups targeted were carbonyls, amides, thiocarbonyls, carboxylic acids, amino acids, as well as representative DNA and RNA bases, their sugars, nucleosides and nucleotides.

These compounds were subjected to reaction with free muonium atoms in aqueous solution as produced by muon bombardment of water. Muonium (Mu) is the hydrogen-like atom with a positive muon of 2.2 μs lifetime as its nucleus (1). Mu has one-ninth the mass of ^1H, and is produced at the end of ~38% of the high energy muon tracks in water. Given a suitable muon beam, one can directly observe rates of reaction of Mu and expect to see subtle kinetic isotope effects compared to ^1H because of the unusually large isotopic–mass ratio. Muonium reaction rates are observed by the nuclear physics counting technique of muon spin rotation (μSR) (1, 2). In this technique the species of interest (Mu) is both produced and detected, one atom at a time. A summation is then made over a large number of such events to determine the relaxation of the spin precession — from which the chemical rate constant is determined.

Experimental

In the μSR technique (1, 2) each muon is timed as it arrives at the sample and its decay-positron is timed when the muon decays. A lifetime histogram is then composed from the accumulation of ~10^7 such events. With the sample placed in an external transverse magnetic field the direction of emission of positrons fluctuates as the muon's spin precesses, because the positron is ejected predominantly along the muon's spin vector at the moment it decays. This means that a positron detector in the plane of precession sees a typical lifetime histogram with the Mu precession frequency superposed on it. The amplitude of this oscillation is proportional to the yield and the rate of damping is proportional to Mu's rate of reaction. In pure water the oscillation has a half-life of about 4 μs, but as Mu reacts with solutes this is reduced by a factor proportional to k_M.

An eight parameter MINUIT χ^2-minimization fitting procedure is applied to each histogram and gives the muonium relaxation, λ in eq. (1), as one of these parameters.

$$[1] \qquad N_t = N_0 \exp(-t/\tau)[1 + A_M \exp(-\lambda t)\cos(\omega_M t + \phi_M) + A_D \cos(\omega_D t + \phi_D)] + Bg$$

where N_t is the number of counts in the histogram corresponding to time t; N_0 a normalization factor; τ the mean muon lifetime; A_M and A_D, ω_M and ω_D, and ϕ_M and ϕ_D are the asymmetries, angular speed, and initial phases of the "muonium atoms" and "diamagnetic muon components", respectively; and Bg is the time-independent background signal. λ is the relaxation in the presence of solute, λ_0 the value with [solute] = 0, so that $\Delta\lambda = \lambda - \lambda_0 = k_M[S]$.

μSR equipment was used on beamlines M20 and M13 at the TRIUMF cyclotron in Vancouver. Aqueous solutions were made from triply distilled water and thoroughly deoxygenated by bubbling with pure N_2. The micelles used were cetyltrimethylammonium bromide (CTAB), sodium dodecylsulphate (SDDS), and sodium octylsulphate (SOS). A typical micelle consists of 50–80 surfactants so the inherent impurities of the surfactant molecules contribute to the "background" relaxation λ_0. The solutes were invariably Reagent Grade or better.

[1]Present address: Chemistry Division, Argonne National Laboratory, Argonne, IL 60439, U.S.A.

Can. J. Chem. Downloaded from www.nrcresearchpress.com by 84.41.108.74 on 09/07/12
For personal use only.

TABLE 1. Rate constants for the reaction of muonium: and comparison with H, and effect of added micelles

Solute	$k_M/M^{-1}\,s^{-1}$	k_M/k_H[a]	$k_{M(mic)}/k_M$[c]	Reaction
Formamide[b]	$<10^5$	—	≤70†	Abstraction
Acetamide[b]	$<10^5$	<1	≤10000*	Abstraction
N-Methylacetamide[b]	$<10^5$	—	≤10000*	Abstraction
Dimethylacetamide[b]	$<10^5$	—	≤200†	Abstraction
Urea*	$<10^5$	<3	≤10000*	Abstraction
Tetramethylurea[b]	$\leq 4 \times 10^5$	—	<5000*	Abstraction
Guanidine[b]	$\leq 3 \times 10^5$	≤0.2	≤3000*	Abstraction
Thiourea[b]	4×10^7	0.007	≤20*, 1.4†	?
Tetramethylthiourea	4×10^{10}	—	0.5*	Addition
Thioacetamide[b]	3×10^{10}	5	1*	Addition
Dimethylthioformamide	7×10^{10}	—	—	Addition
Thiouracil	2×10^{10}	—	—	Addition
Acetone	8.7×10^7	33	290*	Addition
2-Propanol	1.3×10^6	0.01	20000*	Abstraction
Acrylamide	2×10^{10}	0.6	~1*	Addition
Methylcyanoacetate	1×10^8	—	<10*	Addition
Benzophenone	2×10^{10}	3	—	Addition
Benzoquinone[b]	2.5×10^{10}	3	~1*	Addition
Acetic acid	$<10^5$	≤1	—	?
Pyruvic acid	1×10^9	0.4	—	Addition
Oxalic acid (pH = 1)	2×10^8	750	—	(Addition?)
Valine	5×10^6	0.5	≤20*, 10†	Abstraction
Histidine	2.5×10^9	10	~1*	Addition
Methionine	1.4×10^7	0.04	1‡	Abstraction
Penicillamine	4×10^9	2	1*	Abstraction
Cysteine	6×10^9	5	—	Abstraction
Uracil[b]	6×10^9	15	1*	Addition
Cytosine	3×10^9	35	—	Addition
Thymine[b]	3×10^9	5	1*	Addition
Adenine[b]	2×10^9	20	1*	Addition
Ribose	2×10^6	0.03	50‡	Abstraction
2-Deoxyribose	2×10^6	0.015	10†	Abstraction
Adenosine	2×10^9	12	1*	Addition
Ribose-5-phosphate	1×10^7	—	—	Abstraction
Na_2HPO_4	$<10^5$	—	—	?
AMP	2×10^9	10	1*	Addition

[a] k_H data from ref 12(*b*).
[b] k_M reported in ref 4 and now includes $k_{M(mic)}$ modified.
[c] Micelles used: *, CTAB; †, SOS; ‡, SDDS.

Impurities could be a problem for the weakly reacting solutes but not for efficient ones.

An experiment was usually repeated at a few solute concentrations, so that a plot of relaxation against solute concentration yielded a mean value of k_M. However, only a small range of concentrations can be used for an given solute due to a restriction imposed by μSR. This technique requires one to adjust the solute concentration until the muonium *chemical* lifetime falls into the narrow observational time-window around the 2 μs lifetime when its muon decays. For solutes with $k_M \sim 10^{10}$ this requires only $\sim 10^{-4}$ M, but for solutes with $k_M < 10^6$ one needs concentrations of 1 M or more. In the latter cases impurities could be responsible for the observed reaction and only upper limits on k_M are reliable. With the micelle experiments there were additional limitations: first the impurities in the surfactants pushed λ_0 up and restricted the highest usable concentrations, so that only lower limits of $k_{M(mic)}$ were measureable; and second, the lowest concentrations usable were at about two times the crictical-micelle-concentrations, which put an upper limit on rate measurements.

Results

Table 1 records values of k_M for 36 compounds and $k_{M(mic)}$ values (many just limits) for 26 of them. For 17 of these compounds k_M has been reported previously (3, 4) and only the $k_{M(mic)}$ values are new. They are grouped according to functionality. Included among them are simple aliphatic amides and diamides, ring amides, thio-amides, carboxylic acids, purine and pyrimidine bases, constituents of nucleic acids' sugar–phosphate backbones, and a few common compounds added for comparison purposes. The structures are given in Fig. 1. All these data refer to solutions at natural pH (usually close to 7). Table 2 presents k_M data at two different pH values for a range of reaction types, including three inorganic compounds.

These data are subject to a number of experimental errors. Each μSR measurement carries a statistical uncertainty, usually taken as one standard deviation. In any one run there

Can. J. Chem. Downloaded from www.nrcresearchpress.com by 84.41.108.74 on 09/07/12
For personal use only.

TABLE 2. Rate constants for the reaction of Mu with selected compounds at natural pH and at pH = 1

Solute	Reaction[b]	$k_M/M^{-1}s^{-1}$ pH = 7	$k_M/M^{-1}s^{-1}$ pH = 1	Qualitative pH effect
$NaNO_3$	?	1.5×9	1.9×10^9	None
$K_3Fe(CN)_6$	Reduction	2×10^{10}	3.2×10^{10}	(Small) acid ↑
$KMnO_4$	Reduction	2.5×10^{10}	1.7×10^{10}	None
HCOONa	Abstraction	8×10^6	9.2×10^5	Acid ↓
$(CH_3)_2CHOH$	Abstraction	1.3×10^6	5.9×10^5	Acid ↓
$(CH_3)_2CO$	Addition	1.1×10^8	8.7×10^7	None
Urea	Abstraction	$<10^5$	$<10^6$	—
Thiourea	?	5×10^7	2×10^9	Acid ↑
TMTU	Addition	4×10^{10}	3×10^9	Acid ↓
Uracil	Addition	6×10^9	4.3×10^9	None
Oxalic acid	(Addition ?)	9×10^7	2.5×10^8	Acid ↓

[a]?, reaction type not known.

are three or four separate counters involved, each producing its own histogram, fit independently and yielding a separate value for λ. These counters have different efficiencies and intrinsic asymmetries and the spread of their separate results tend, surprisingly, not to be covered by the statistical error bars. Nevertheless one has obtained three or four independent values of Δλ and hence k for a given solution. These can be averaged, and another solution made up and run, thus reducing the probability of errors from impurities, weighings, dilutions, deoxygenations, etc. Overall, however, even when Δλ is in the accurate range around 1×10^6 s^{-1}, the rate constants probably have at least a ±25% error associated with them. In the k regions where [S] > 0.1 M there is also the considerable uncertainty stemming from the possibility of impurities.

Discussion

The major objectives of this research were (*i*) to measure k_M for molecules of biological significance in the hope of drawing general inferences about basic reaction mechanisms; (*ii*) to compare Mu with ^1H as a measure of general kinetic isotope effects; and (*iii*) to study these reactions in micelles to explore the role of membrane isolated processes, and to compare reactions in water with those in hydrophobic microenvironments. All three aspects can have implications for radiobiology (5).

(*i*) k_M *values – effect of structure on reactivity*

Figure 2 displays the k_M data of Table 1 in a form which groups the compounds into four categories. The ordinate is logarithmic so a considerable range of reactivities is involved. k_M depends on the type of reaction and its detailed mechanism and therefore on the nature of each functional group present. Muonium atoms are usually regarded as strong reducing agents like e^-_{aq}; but they also undergo a variety of completely different *types* of reactions, like H. For instance, Mu is seen to "add" across a double or triple bond, "abstract" an H or halogen, "substitute" in place of a bonded H or halogen, undergo an acid-base reaction by exchanging a proton (in this case a muon) to yield e^-_{aq}, or, when interacting with a paramagnetic chemical entity, Mu may either "combine" with it to form a diamagnetic molecule or merely change its multiplicity in an electron-exchange interaction (6). Of all these possible Mu reactions, the *products* can be detected or identified only in the case of addition — and then only because level-crossing-resonance spectroscopy (LCR) allows muonated free radicals to be seen (7). In general one must rely on chemical inferences to deduce mechanisms. In Mu's reactions with the organic compounds of this study addition and abstraction seem to dominate.

To exemplify the diversity of Mu reactivity, compare acetamide, acetone and thioacetamide, with k_M values of $<10^5$, 1.1×10^8 and 3×10^{10} $M^{-1}s^{-1}$ respectively. Changing the —NH_2 group to —CH_3 increases the rate by at least 2 orders of magnitude, and the change of carbonyl to thiocarbonyl increases the rate by >5 orders of magnitude. This tendency can be explained qualitatively in the following terms: The —$CONH_2$ linkage of acetamide is rigid and planar with maximum conjugation of πe^-s in the C=O bond with the non–bonding pair of N. This makes it less reactive to addition by Mu than a free carbonyl, so only abstraction occurs (from —CH_3 or —NH_2). In the case of acetone, the carbonyl π system is available for attack and Mu is known to add to the O (8). This directional preference in attaching to the O may be partly because Mu is weakly nucleophilic (9) and put off the C by its two electron–releasing methyls, and partly because the C-centered >Ċ—OMu radical formed is stabilized by hyperconjugation. In thioacetamide, however, the Mu–addition is known to be different and to occur at C, giving rise to a thiyl radical (RṠ) (10, 11). The dipole moments of thioamides are larger than those of corresponding amides, and the C=S group is inherently more polarizable than the C=O group on account of the larger kernal of electrons in the S atom, with the result that the double bond is weakened so that Mu adds rapidly at C.

Unfortunately, thioacetone was not available for comparison with the above, but thiourea was. It shows a reaction even less efficient than acetone, and shows by far the slowest reaction of all the C=S-containing molecules. Also, in an LCR study (11), thiourea showed no RṠ resonance where the other thiocompounds did. All these suggests Mu adds at the S rather than the C for the specific case of thiourea. In contrast to thiourea, tetramethylthiourea reacts with Mu at $k_M = 4 \times 10^{10}$, while thioacetamide and dimethylthioformamide are also highly reactive toward Mu and have been seen to give thiyl LCRs (11): so it looks as if the double keto–enol exchange stabilization of thiourea must play a unique role in eliminating reaction of Mu at the C of its C=S.

Almost every system has a different message and the following are worth drawing attention to: (*a*) Mu abstracts

Can. J. Chem. Downloaded from www.nrcresearchpress.com by 84.41.108.74 on 09/07/12
For personal use only.

Can. J. Chem. Downloaded from www.nrcresearchpress.com by 84.41.108.74 on 09/07/12
For personal use only.

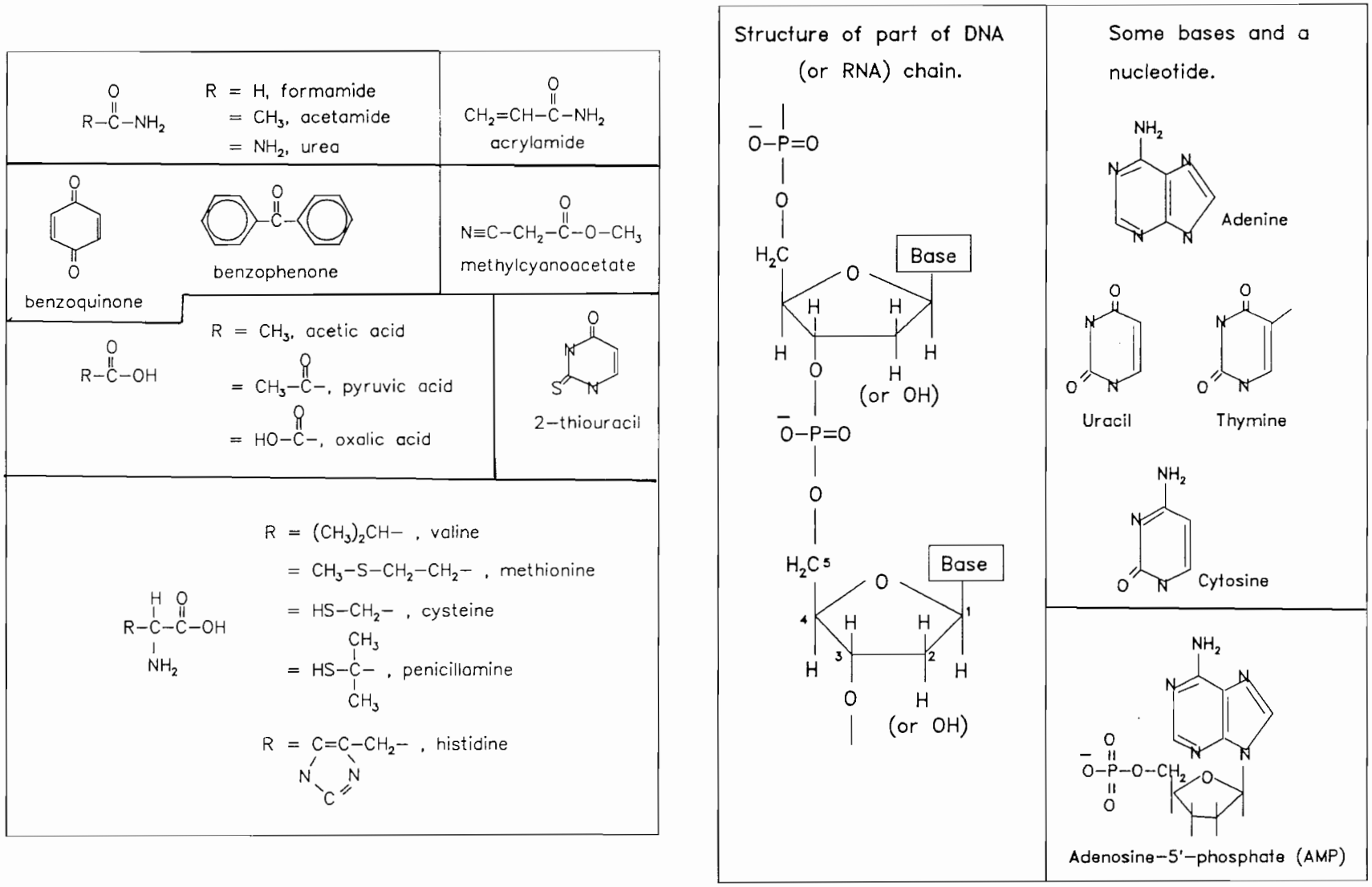


FIG 1. Structures of most of the chemicals used here.

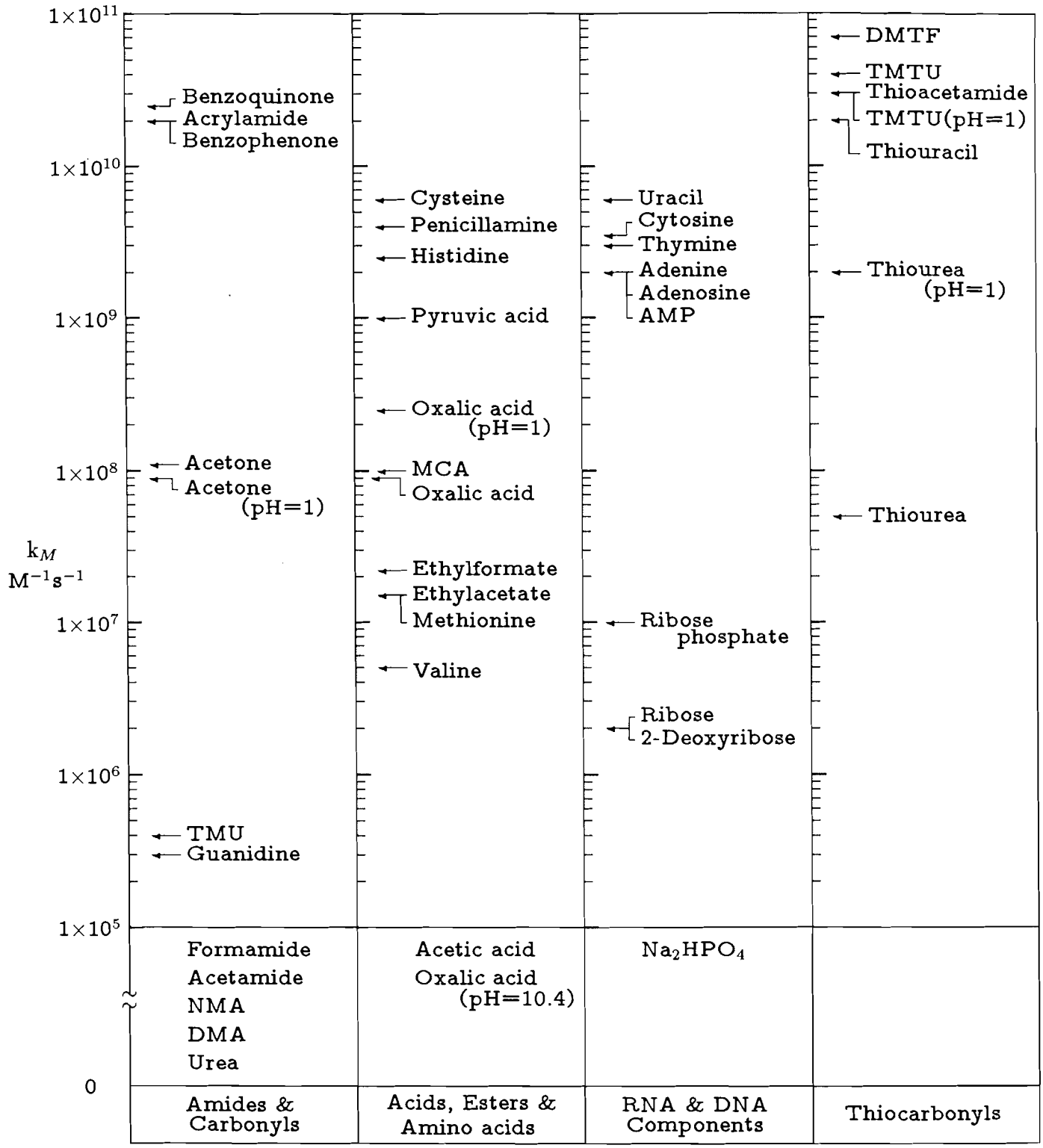


FIG 2. A sketch showing the variation of k_M, separated into compounds of different functional groups.

an H from the —SH of penicillamine with $k_M = 4 \times 10^9$, which is orders of magnitude faster than Mu abstractions from C—H, and faster than H-atoms abstract (12). (*b*) Mu adds to the —C≡N bond of methylcyanoacetate faster than to the >C=N of guanidine. (*c*) Mu adds across an unsubstituted cyclic C=C, as in uracil, faster than across a methyl- or methylene- substituted one, as in thymine or histidine — *i.e.* Mu is significantly sterically hindered by CH_3 in C=C addition. (*d*) Both benzoquinone and benzophenone react with Mu much faster than benzene or acetone. (*e*) Carboxylic groups are unreactive towards Mu, whether as esters, anions or undissociated —COOH, so the reaction with oxalic acid is probably an addition reaction, like H (13). (*f*) The DNA and RNA sugar–phosphate backbones, either as separate units or as ribose-5-phosphate, are essentially unreactive (not above the level where impurities dominate) whereas the purine or

Can. J. Chem. Downloaded from www.nrcresearchpress.com by 84.41.108.74 on 09/07/12
For personal use only.

pyrimidine bases are quite reactive, whether as separate chemicals (*eg* adenine) or nucleosides (adenosine) or nucleotides (adenosine-5-phosphate, AMP). One can therefore expect the radiobiology of nucleic acids to arise by attack of radiolysis species at the inner bases rather than at the helical backbone.

(*ii*) *Kinetic isotope effects* – k_M/k_H

Use is made of muonium as an isotope of H primarily because Mu is easier to detect (given a source of muons!) due to its radioactive nature, spin characteristics and magnetic moment. In comparing k_M with the corresponding k_H, note must be taken of the fact that most H-atom data obtained by pulse radiolysis involve converting e^-_{aq} to H by having the water at pH $\sim$ 1; whereas the data of Fig. 2 were obtained for Mu reactions at pH $\sim$ 7, as in nature. For several solutes (Table 2 and others (14)) the analogous pH = 1 solutions were studied. For most solutes unaffected by acid, k_M didn't change, implying, as expected, that the reactivity of muonium atoms themselves are not altered significantly by protonation to MuH^+. Furthermore Mu's pK_a (to give e^-_{aq} by muon transfer to OH^-) is known to be about 10 (15). However, some solutes are protonated at pH 1 but not at pH 7, so their reactivity towards Mu could be altered for that reason. Oxalic acid seems to fall into that category, possibly aided towards an addition reaction when both carboxylic groups are protonated. Another change arises for thiourea (already seen to be at odds with general concepts) and tetramethylthiourea. The former increases at low pH while the latter decreases, and they happen to finish with almost the same k_M at pH 1. But for molecules like acetone there is no change with pH and even an alcohol such as 2-propanol shows only a two-fold change in k_M.

Bearing in mind these possible differences from protonation, the comparison of Mu with ^1H is shown in the central column of Table 1. This kinetic isotope effect is seen to range from 750 (oxalic acid) and 33 (acetone — known to be an addition reaction (8)) to $\sim$0.01 for abstraction reactions (2-deoxyribose or 2-propanol).

At least three factors have to be considered when analysing kinetic isotope effects. First is the pre-exponential encounter-frequency term given by the ratio of mean velocities or diffusion constants, where the ratio k_M/k_H should be $\sim$3; second is the activation barrier favouring H because of the higher vibrational energy of the Mu-transition state; and third is the quantum tunneling effect, where Mu should be favoured if the effect of reduced mass wins out over the larger barrier height and width (6). Fast addition reactions seem to comply with the first, slow abstractions with the second, and odd ones such as carbonyls with the third.

(iii) *Effect of added micelles*

Micelles are the simplest artificial systems to be used to mimic biological membranes. In fact they are far from uniformly spherical and show considerable water penetration (16). Organic solutes localize at micelles according to Poisson statistics, so, for three times as many solutes as micelles in solution — as in these experiments — there should be <6% unoccupied micelles and <8% with more than six solutes. The presence of micelles creates three microenvironments in which reaction may occur: an inner hydrocarbon core, an external aqueous medium containing lose ion atmospheres, and the boundary region (Stern layer). The latter may be the most important for all polar solutes forced by bulk water out of its interstices. It may be the region where Mu reacts and where large phenomenological reaction-rate enhancements occur (17).

A few general comments about muonium-micelle reactions are in order. Muonium is not itself significantly "localized" at micelles — that is, its mean residence time was found to be no longer than the time it would take to diffuse through that volume of an equally viscous liquid (18). This lack of *mutual* localization by Mu (in addition to the organic solute) means that the "concentration" to be used in evaluating k_M is **not** the local intra-micellar concentration, but merely the mean value based on total volume of solution (19). Therefore, there is no automatic concentrating-effect arising from the fact that the organic solute is confined to the small volume of a micelle. In fact, for a highly efficient reaction, the effective rate constant can be diminished by the bunching of solute molecules at micelles. $k_{M(mic)}$ values can be expected to depend on the type of reaction, its rate constant in water, the region of micelle in which the solute is localized, and on the number of solute molecules per micelle. Some solutes do not preferentially localize due to their much greater solubility in water than in hydrocarbons: one such example here, thiourea, supports the proposition that Mu is not strongly localized at micelles (18), in not showing $k_M \gg k_{M(mic)}$. Finally, H-atoms cannot be similarly studied in micelles (20) because H reacts $\sim 10^2$ times faster than Mu with the surfactants themselves.

Of the $k_{M(mic)}$ data which are not just showing an upper limit, there are enhancement factors up to 20 000 (2-propanol — a very slow abstraction), 290 (acetone — conversion from addition to abstraction (21)), values of 10–50 (for aminoacids and sugars), to no-change (for a range of rates from diffusion-limited additions, such as acrylamide, to moderately fast abstactions, as with methionine). It was hoped that the enhancement factor would be useful in deciding what reaction mechanism was involved, but there is not yet a simple enough pattern present to do that.

Conclusions

The rate constants of Mu reactions present a range of almost six orders of magnitude, while kinetic isotope effects (relative to H) differ for different types of reactions from 0.007 to 750. The change in apparent reactivity on adding micelles varies in a variety of ways for different functional groups. The reactions of Mu with the many components of DNA and RNA show that the addition reaction with the bases is much more favourable than the abstraction of a H from a sugar unit. There are no significant micelle–induced enhancement effects for the major components of nucleic acids.

Acknowledgements

Gratitude is extended to our colleagues Dr. K. Venkateswaran, Dr. J. M. Stadlbauer, Dr. B. W. Ng and Mr. Z. Wu who helped perform these experiments, and to Curtis Ballard and Keith Hoyle for their technical wizardry. NSERC of Canada provided some of the funding needed.

1. S. F. J. Cox. J. Phys. C, **20**, 3187 (1987).
2. J. H. Brewer and K. M. Crowe. Ann. Rev. Nucl. Part. Sci. **28**, 239 (1978).
3. P. W. Percival, E. Roduner, H. Fischer, M. Camani, F. N. Gygax, and A. Schenck. Chem. Phys. Lett. **17**, 11 (1977).
4. M. V. Barnabas, K. Venkateswaran and D. C. Walker. Can. J. Chem. **67**, 120 (1989).
5. C. von Sonntag. The chemical basis of radiation biology. Taylor and Francis, London. 1987.
6. D. C. Walker. Muon and Muonium chemistry. Cambridge University Press, Cambridge. 1983.

Can. J. Chem. Downloaded from www.nrcresearchpress.com by 84.41.108.74 on 09/07/12
For personal use only.

7. R. F. KIEFL. Hyperfine Interactions, **32**, 707 (1986).
8. E. RODUNER, P. W. PERCIVAL, D. G. FLEMING, J. HOCHMANN, and H. FISCHER. Chem. Phys. Lett. 57, 37 (1978).
9. J. M. STADLBAUER, B. W. NG, R. GANTI, and D. C. WALKER. J. Am. Chem. Soc. **106**, 3151 (1984).
10. C. J. RHODES, M. C. R. SYMONS, and E. RODUNER. J. Chem. Soc. Chem. Commun. 3 (1988).
11. M. V. BARNABAS and D. C. WALKER. Chem. Phys. Lett. **168**, 9 (1990).
12. (*a*) P. NETA, Chem. Rev. **73**, 533 (1972); (*b*) G. V. BUXTON, C. L. GREENSTOCK, W. P. HELMAN, and A. B. ROSS. Phys. Chem. Ref. Data, **17**, 513 (1988).
13. R. A. WITTER and P. NETA. J. Org. Chem. **38**, 484 (1973).
14. M. V. BARNABAS. Ph.D. Thesis. University of British Columbia, Vancouver, B.C. 1989.
15. B. W. NG, J. M. STADLBAUER, and D. C. WALKER. J. Phys. Chem. **88**, 857 (1984).
16. (*a*) F. M. MENGER and B. J. BOYER, J. Am. Chem. Soc. 102, 5936 (1980); (*b*) J. H. FENDLER, Membrane mimetic chemistry. Wiley-Interscience, New York, 1982.
17. K. VENKATESWARAN, M. V. BARNABAS, Z. WU, J. M. STADLBAUER, B. W. NG, and D. C. WALKER. Chem. Phys. Lett. **143**, 313 (1988).
18. K. VENKATESWARAN, M. V. BARNABAS, B. W. NG and D. C. WALKER. Can. J. Chem. **66**, 1979 (1988).
19. K. VENKATESWARAN, M. V. BARNABAS, J. M. STADLBAUER, and D. C. WALKER. Can. J. Phys. **68**, 952 (1990).
20. M. GRATZEL, J. K. THOMAS, and L. K. PATTERSON. Chem. Phys. Lett. **29**, 393 (1974).
21. D. C. WALKER. Can. J. Chem. **68**, 1719 (1990).

Can. J. Chem. Downloaded from www.nrcresearchpress.com by 84.41.108.74 on 09/07/12
For personal use only.

Excess molar volumes of (a cycloalkane + an alkanol) at 298.15 K

T. M. LETCHER AND J. MERCER-CHALMERS
Department of Chemistry, Rhodes University, Grahamstown, South Africa

Received December 7, 1990

T. M. LETCHER and J. MERCER-CHALMERS. Can. J. Chem. **69**, 1259 (1991).

In this work we report the excess molar volumes, V_m^E for the miscible mixtures $\{xc\text{-}C_5H_{10} + (1 - x)CH_3OH\}$ and $\{xc\text{-}C_kH_{2k} + (1 - x)C_lH_{2l+1}OH\}$ where $k = 5, 6, 7, 8$, or 10 and $l = 2$ or 3. The V_m^E results are discussed in terms of the size of the cycloalkane ring and the type of alcohol.

Key words: Excess volumes, cycloalkane + alkanol.

T. M. LETCHER et J. MERCER-CHALMERS. Can. J. Chem. **69**, 1259 (1991).

On a déterminé les volumes molaires en excès, V_m^E, pour des mélanges miscibles de $\{xc\text{-}C_5H_{10} + (1 - x)CH_3OH\}$ et de $\{xc\text{-}C_kH_{2k} + (1 - x)C_lH_{2l+1}OH\}$ dans lesquels $k = 5, 6, 7, 8$ ou 10 et $l = 2$ ou 3. On discute des valeurs de V_m^E obtenues en fonction de la grandeur du cycloalcane et du type d'alcool.

Mots clés : volumes en excès; cycloalcane + alcool.

Can. J. Chem. Downloaded from www.nrcresearchpress.com by 84.41.108.74 on 09/07/12
For personal use only.

Introduction

The excess molar volume, V_m^E was measured as a function of mole fraction x at 298.15 K and one atmospheric pressure for the mixtures $\{xc\text{-}C_5H_{10} + (1 - x)CH_3OH\}$ and $\{xc\text{-}C_kH_{2k} + (1 - x)C_lH_{2l+1}OH\}$ where $k = 5, 6, 7, 8$, or 10 and $l = 2$ or 3. The mixtures defined by $k = 6, 7, 8$, or 10 with $l = 1$ are not included as they are not miscible over the whole composition range. Of the sixteen data sets presented in this work four have been reported (1–4).

Experimental

The cycloalkanes were purified as previously described (5). The alkanols were dried as before (6, 7) and in all cases the water impurity (by Karl Fischer titration) was found to be less than 2×10^{-3} mole fraction. The cycloalkanes and the alkanols were analysed by g.l.c. and in all cases the purity was found to be better than 99.8 mol%.

The V_m^E values were calculated from molar masses and densities of pure liquids and mixtures using an Anton-Paar DMA 601 vibrating-tube density meter, thermostated at 298.15 ± 0.002 K. The method has been described (8).

Results

The V_m^E results have been deposited with the National Research Council of Canada[1] and the Redlish Kister equation:

$$[1] \quad V_m^E = x(1 - x)\Sigma_{r=0}A_r(1 - 2x)^r$$

has been fitted to the results. The coefficients A_r are given in Table 1, together with the standard deviation σ calculated from

$$\sigma = \sqrt{\Sigma(V_{m,exp} - V_{m,calc})^2/(n - n_p)}$$

where n is the number of observations and n_p the number of parameters.

Discussion

Our V_m^E results for (cyclopentane + ethanol) and (cyclohexane + ethanol) are within 0.005 $cm^3\ mol^{-1}$ of the results

TABLE 1. Coefficients A_r for eq. [1] for $xC_kH_{2k} + (1 - x)C_mH_{2m+1}$ at 298.15 K together with the standard deviation σ

Mixture	A_0	A_1	A_2	A_3	$10^3\sigma$ / $cm^3\ mol^{-1}$
$xC_5H_{10} + (1 - x)CH_3OH$	1.9514	0.4342	0.9656	−0.1687	4.1
$xC_5H_{10} + (1 - x)C_2H_5OH$	1.6064	−0.0402	0.5416	−0.5086	2.2
$xC_5H_{10} + (1 - x)C_3H_7OH$	0.8450	−0.5754	0.0151	−0.2571	4.1
$xC_5H_{10} + (1 - x)CH_3CH(OH)CH_3$	1.5852	−0.8136	0.3208	−0.1953	4.1
$xC_6H_{12} + (1 - x)C_2H_5OH$	2.2415	0.0929	0.5840		2.3
$xC_6H_{12} + (1 - x)C_3H_7OH$	1.6630	0.4139	0.5662	0.2748	2.3
$xC_6H_{12} + (1 - x)CH_3CH(OH)CH_3$	2.2612	−0.5714	0.7348	−0.4252	3.1
$xC_7H_{14} + (1 - x)C_2H_5OH$	2.1221	−0.1844	1.0334		2.2
$xC_7H_{14} + (1 - x)C_3H_7OH$	1.4371	−0.3566	0.5649	−0.1863	2.0
$xC_7H_{14} + (1 - x)CH_3CH(OH)CH_3$	1.8969	−0.6406	0.6743		1.8
$xC_8H_{16} + (1 - x)C_2H_5OH$	1.6103	−0.0137	0.8618	−0.2123	3.1
$xC_8H_{16} + (1 - x)C_3H_7OH$	1.1572	−0.4122	0.5879	−0.1477	3.0
$xC_8H_{16} + (1 - x)CH_3CH(OH)CH_3$	1.4506	−0.6456	0.4786		2.7
$xC_{10}H_{20} + (1 - x)C_2H_5OH$	0.9207	−0.2672	0.4438		2.6
$xC_{10}H_{20} + (1 - x)C_3H_7OH$	0.6797	−0.6150	0.2116	−0.2023	2.9
$xC_{10}H_{20} + (1 - x)CH_3CH(OH)CH_3$	0.5563	−0.6250	−0.1743		2.0

[1]Copies of the results may be purchased from the Depository of Unpublished Data, Document Delivery, CISTI, National Research Council of Canada, Ottawa, Ont., Canada K1A 0S2.

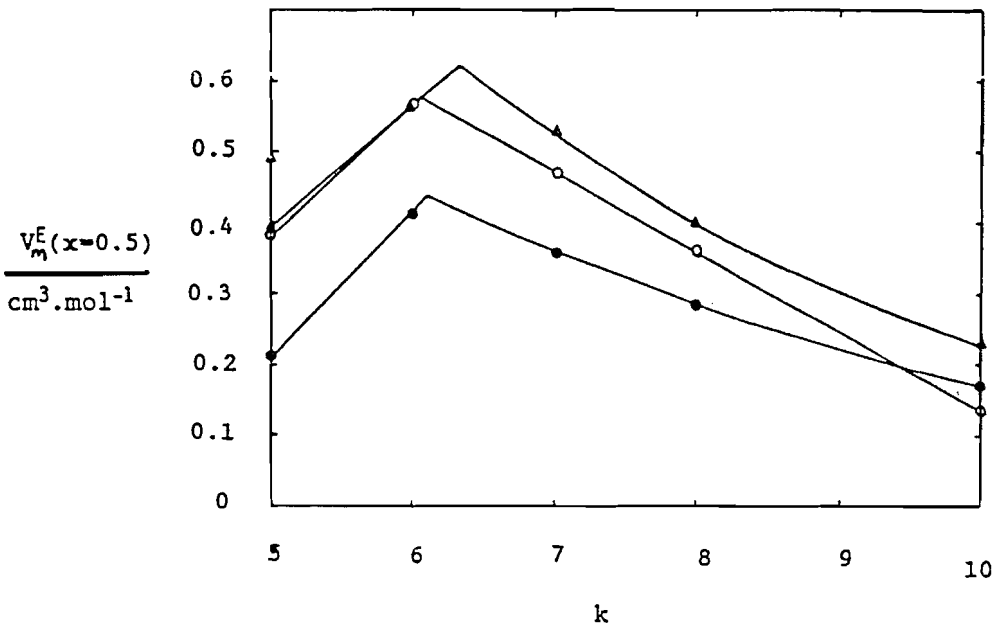


FIG. 1. $V_m^E(x = 0.5)$ for $\{x\text{c-}C_kH_{2k} + (1 - x)C_lH_{2l+1}OH\}$ against k. △, CH_3OH; ▲, C_2H_5CH; ●, C_3H_7OH; ○, $CH_3CH(OH)CH_3$.

reported by Marsh and Burfitt (1). The V_m^E values reported here for (cyclohexane + ethanol) and those of ref. 1 compare well to those reported by Pardo and van Ness (2) but differ by as much as 0.03 $cm^3\ mol^{-1}$, in the worst case, when compared to the published results of Scatchard and Satkiewicz (3). Our results for (cyclohexane + 1-propanol) compare reasonably well with those published by Janssens and Ruel (4) and differ by only 0.012 $cm^3\ mol^{-1}$ from their smoothing curve.

The V_m^E values for all the mixtures, except for (cyclodecane + 2-propanol) at low cyclodecane concentrations, are positive over the whole composition range. This is most likely a result of the breakdown of the hydrogen bonding between the alcohol molecules on addition of the cycloalkane. The $V_{m,maximum}^E$ for all the systems presented here lie between +0.16 and +0.57 $cm^3\ mol^{-1}$.

The $V_m^E(x = 0.5)$ results for all sixteen systems has been plotted as a function of cycloalkane carbon number, k, in Fig. 1. The values for the cyclopentane systems are very much lower than the values predicted by the pattern generated by the other cycloalkanes. This is reminiscent of the $V_m^E(x = 0.5)$ values obtained for cycloalkane + n-alkane mixtures (9). For these mixtures the $V_m^E(x = 0.5)$ values for the cyclopentane systems are all less positive than the $V_m^E(x = 0.5)$ predicted by the pattern generated by the cyclohexane, cycloheptane, cyclooctane, and cyclodecane systems. It is possible that the small size of the cyclopentane molecule results in a compact packing structure within the hydrogen bonded network of alcohol molecules, resulting in a small overall volume of mixing.

The magnitude of $V_m^E(x = 0.5)$, for mixtures of a cycloalkane + a 1-alkanol is also dependant on the 1-alkanol chain length. From Fig. 1, for any given cycloalkane, $V_m^E(x = 0.5)$ decreases with increasing alkanol chain length. This could be a direct result of the fact that hydrogen bonding decreases in alcohols with increasing chain length. The breakdown of this hydrogen bonding on mixing results in methanol producing a more positive V_m^E than ethanol, and ethanol in turn producing a more positive effect than 1-propanol. The effect of the branched alkane chain in 2-propanol produces an effect which lies between that of ethanol and 1-propanol.

Acknowledgement

The authors thank the F.R.D. (South Africa) for financial assistance.

1. K. N. MARSH and C. BURFITT. J. Chem. Thermodyn. **7**, 955 (1975).
2. F. PARDO and H. C. VAN NESS. J. Chem. Eng. Data, **10**, 163 (1965).
3. G. SCATCHARD and F. G. SATKIEWICZ. J. Am. Chem. Soc. **86**, 130 (1964).
4. J.-M. JANSSENS and M. RUEZ. Can. J. Chem. Eng. **50**, 591 (1972).
5. T. M. LETCHER. J. Chem. Thermodyn. **16**, 805 (1984).
6. T. M. LETCHER, C. HEYWARD, S. WOOTEN, and B. SHUTTLEWORTH. Fuel, **65**, 891 (1986).
7. T. M. LETCHER, S. WOOTEN, B. SHUTTLEWORTH, and C. HEYWARD. J. Chem. Thermodyn. **18**, 1037 (1986).
8. T. M. LETCHER and B. W. SCOONES. J. Chem. Thermodyn. **14**, 185 (1982).
9. T. M. LETCHER and C. HEYWARD. Thermochim. Acta, **65**, 61 (1983).

Can. J. Chem. Downloaded from www.nrcresearchpress.com by 84.41.108.74 on 09/07/12
For personal use only.

The photocycloaddition of naphthoates with acetylacetone; dramatic acid promotions of product quantum yields

YUAN L. CHOW[1] AND XIAO-YUN LIU

Department of Chemistry, Simon Fraser University, Burnaby, B.C., Canada V5A 1S6

Received December 20, 1990

YUAN L. CHOW and XIAO-YUN LIU. Can. J. Chem. **69**, 1261 (1991).

In acetonitrile and methanol, methyl 1- and methyl 2-naphthoate (1- and 2-$NpCO_2CH_3$) underwent [2+2] photocycloaddition with acetylacetone (acacH) from a reactive species derived from the lowest spectroscopic singlet excited state to give cyclobutane derivatives such as **9** that ring-opened to afford addition products of acetyl and acetonyl moieties at the 7,8-position for 1-$NpCO_2CH_3$ (**2** and **3**) and the 1,2-position for 2-$NpCO_2CH_3$ (**7**). Further irradiation of **3** and **7** caused a deep-seated rearrangement of **3** to give **4** and an intramolecular addition of **7** to give the caged product **8**. The photocycloaddition quantum yields were increased remarkably in the presence of a trace amount (<0.001 M) of protic acids. For example, the limiting quantum yield of **2** and **3** with $\Phi_{adducts} = 0.033$ (in the absence) increased to $\Phi_{adducts} > 0.5$ under comparable conditions in the presence of $[H_2SO_4] = 0.001$ M, approaching the maximum asymptotically at about this concentration; the increases of the quantum yield could not be correlated with H_2SO_4 concentrations. The acid promotion of the product formation elevated the photocycloaddition to a significantly useful preparative reaction. The photocycloaddition of 2-$NpCO_2CH_3$ was quenched by tributylamine, dimethylaniline, and methyl iodide, and could not be initiated by typical triplet sensitization. Strong fluorescence of 2-$NpCO_2CH_3$ at 358 nm in CH_3CN was quenched by acetylacetone, tributylamine, dimethylaniline, and methyl iodide, the last of which concurrently enhanced the phosphorescence intensity of 2-$NpCO_2CH_3$. In the presence of $[H_2SO_4] > 0.005$ M the fluorescence intensity at 358 nm was quenched and a new fluorescence at 470 nm corresponding to protonated ^{1}2-$NpCO_2CH_3$ appeared. However, in the $[H_2SO_4] < 0.002$ M region, the new fluorescence was not observed, indicating that the protonation scarcely occurred. The Stern–Volmer constant, obtained by the quantum yield monitor, of the 2-$NpCO_2CH_3$ photocycloaddition with acacH was more than an order of magnitude smaller than that obtained by the quenching of 2-$NpCO_2CH_3$ fluorescence by acacH. The discrepancies outlined above clearly demonstrate that the reactive intermediate of the photocycloaddition is not the exciplex of the spectroscopic singlet excited species of ^{1}2-$NpCO_2CH_3$ and acacH, but one that is derived from the exciplex. It is speculated that this unknown reactive intermediate interacts with a proton to promote the photocycloaddition.

Key words: photocycloaddition of naphthoates, photorearrangement of styryl ketones, acid catalysis of quantum yields, fluorescence of protonated naphthoates, acid enhancement of singlet quenching.

YUAN L. CHOW et XIAO-YUN LIU. Can. J. Chem. **69**, 1261 (1991).

Dans l'acétonitrile et le méthanol, les 1- (et 2-) naphtoates de méthyle (1- et 2-$NpCO_2CH_3$) subissent une photocycloaddition [2+2] avec l'acétylacétone (acacH), par le biais d'une espèce réactive obtenue à partir de l'état excité singulet spectroscopique le plus bas, conduisant à des dérivés du cyclobutane du type **9** qui donnent lieu à une ouverture de cycle et à la formation de produits d'addition des portions acétyle et acétonyle sur les positions 7 et 8 du 1-$NpCO_2CH_3$ (**2** et **3**) et sur les positions 1 et 2 du 2-$NpCO_2CH_3$ (**7**). Une irradiation prolongée des composés **3** et **7** provoque des transpositions profondes de **3** en **4** et une addition intramoléculaire de **7** en **8**, un composé en forme de cage. Les rendements quantiques de photocycloaddition augmentent d'une façon remarquable en présence d'une trace (<0,001 M) d'acide protique. Par exemple, le rendement quantique limite des produits **2** et **3** passe de $\Phi_{(produits)} = 0{,}033$ (absence d'acide) à plus de 0,5 (pour $[H_2SO_4] = 0{,}001$ M) avec une croissance asymptotique qui atteint son maximum autour de cette valeur; on n'a pas pu établir de corrélation entre le rendement quantique et la concentration en H_2SO_4. La catalyse acide de la formation des produits a transformé la photocycloaddition en une réaction préparative d'une grande utilité. La photocyloaddition du 2-$NpCO_2CH_3$ est désactivée par la tributylamine, la diméthylaniline et l'iodure de méthyle et elle ne peut pas être initiée par des sensibilisateurs typiques de triplets. La fluorescence importante du 2-$NpCO_2CH_3$ à 358 nm est désactivée par l'acétylacétone, la tributylamine, la diméthylaniline et l'iodure de méthyle; ce dernier produit provoque en même temps une augmentation de l'intensité de la phosphorescence du 2-$NpCO_2CH_3$. En présence d'une $[H_2SO_4] > 0{,}005$ M, l'intense fluorescence à 358 nm est désactivée et il y a apparition d'une nouvelle fluorescence à 470 nm, correspondant au ^{1}2-$NpCO_2CH_3$. Toutefois, lorsque la $[H_2SO_4] < 0{,}002$ M, on n'observe pas la nouvelle fluorescence ce qui indiquerait que la protonation se produit à peine. La constante de Stern–Volmer de la photocycloaddition du 2-$NpCO_2CH_3$ avec l'acacH, obtenue en observant le rendement quantique, est au moins 10 fois plus faible que celle obtenue par la désactivation de la fluorescence du 2-$NpCO_2CH_3$ par l'acacH. Les différences mentionnées plus haut démontrent clairement que l'intermédiaire réactif de la photocycloaddition n'est pas l'exciplexe des espèces excitées singulets spectroscopiques du ^{1}2-$NpCO_2CH_3$ et de l'acacH, mais plutôt un autre qui est dérivé de cet exciplexe. On suppose que cet intermédiaire réactif inconnu interagit avec un proton pour promouvoir la photocycloaddition.

Mots clés : photocycloaddition des naphtoates, photoéarrangement de styrylcétones, rendements quantiques acido-catalysés, fluorescence de naphtoates protonés, désactivation acido-catalysée de singulets.

[Traduit par la rédaction]

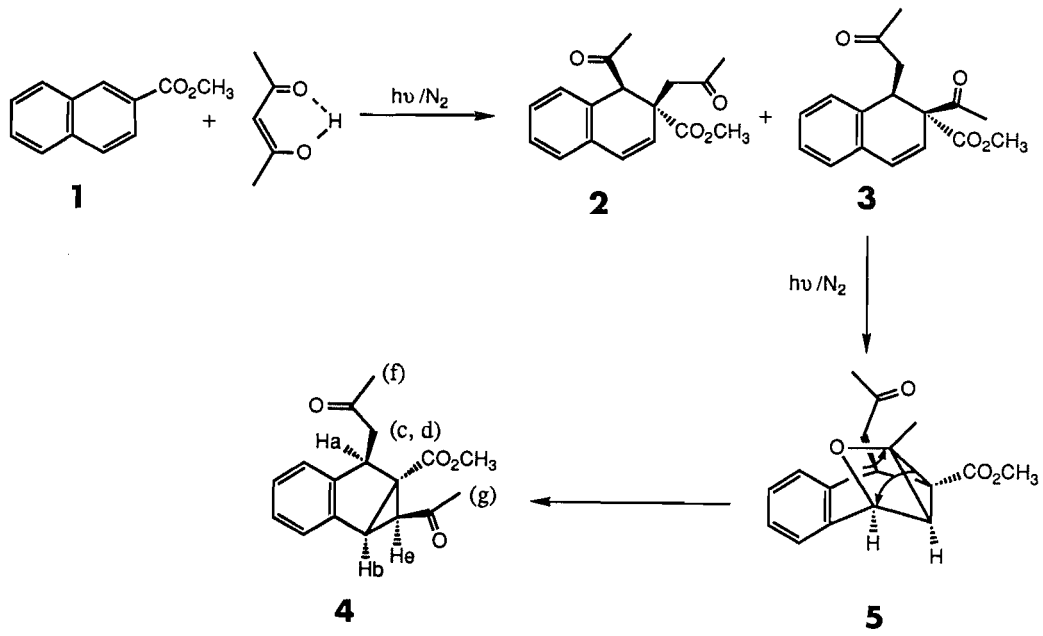
Introduction

Whereas photocycloaddition of naphthalene derivatives with olefins has been well established (1), there is an obscure area in photochemistry where the reaction involves naphthalene derivatives and enones (2–7). As the excited state of both classes of compounds can initiate photochemical reactions (1–7), their mutual photoreactions appear to have escaped the attention of investigators. This was the reason that we undertook a mechanistic investigation after finding the photocycloaddtion of acetylacetone (acacH) and methyl naphthoates.

Cyano group substituted naphthalenes have been shown to undergo singlet excited state photocycloaddition with electron-

[1]Author to whom correspondence may be addressed.

Can. J. Chem. Downloaded from www.nrcresearchpress.com by 84.41.108.74 on 09/07/12
For personal use only.



rich olefins to give cyclobutane and azetine products (1, 8). The published investigations reveal important aspects of the mechanisms, in which the intermediacy of an exciplex has been implied (8–11). Other types of naphthalene derivatives have also been investigated but not as extensively as the photocycloaddition of naphthonitriles (1, 12). On the other hand, [2+] photocycloaddition of acacH to simple olefins is a well-established reaction, known as the de Mayo reaction (2–7, 13), in which the net result involves the addition of acetyl and acetonyl groups across a C=C double bond. This reaction has been claimed to occur from the triplet excited acacH (14); though its quantum yields are generally low, it has been used in many synthetic applications, providing excellent to satisfactory results (2, 3, 7). As far as we are aware, the photocycloaddition of acacH to aromatic compounds has not been reported except for our preliminary communications (15–17).

Results

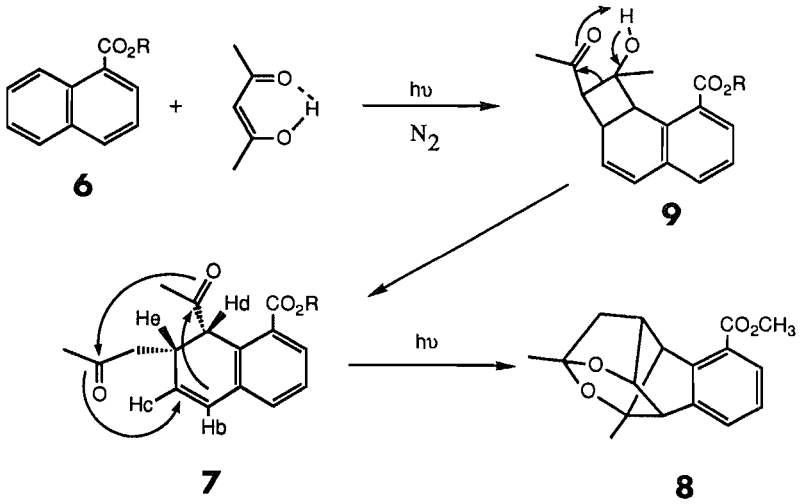
Photocycloaddition

Photolysis of methyl 2-naphthoate (2-$NpCO_2CH_3$, **1**) and acetylacetone in acetonitrile for 15 h resulted in slow formation of the addition product **2** in 33% yield, in addition to a trace amount (<2%) of another isomer **3**: this isomer became the major product in the presence of a trace amount of H_2SO_4 (0.0005 M) in which **2** was also isolated as the minor product. Unreacted 2-$NpCO_2CH_3$ was recovered to fill the balance of the percentage yields. The formation of **2** and **3** was extraordinarily accelerated in the presence of H_2SO_4 up to 0.001 M concentration. The structure of **2** was readily decided on the basis of, firstly, ^{13}C NMR signals at 207.5, 205.8 (for two unconjugated CO), and 173.7 ppm (for a CO_2R carbonyl) and, secondly, a broad IR absorption at 1730 cm^{-1} and, finally, two AB quartets and a singlet at 4.47 ppm (18). One AB quartet at 5.81 and 6.51 ppm (J = 9.5 Hz) arises from the neighboring protons of the conjugated olefinic bond, and the other at 3.19 and 3.03 ppm (J = 18.5 Hz) from the diastereotopic geminal methylene protons. For **3** the ^{13}C NMR signals and IR absorptions were comparable; in addition the similar olefinic protons were present, showing an AB quartet at 6.41 and 6.50 ppm (J = 10 Hz). The ^1H NMR spectrum also showed an ABX pattern at 4.71, 2.28, and 2.56 ppm (J = 18, 7.5, and 5.5 Hz). The ^1H NMR coupling patterns and their chemical shifts clearly indicated that both **2** and **3** were the isomeric products in the addition of acetyl and acetonyl groups on the 1,2-position of **1**, with alternate regiochemistry. A 2+2 photocycloaddition followed by the cyclobutane ring opening was assumed, in analogy to the de Mayo reaction (2, 13); that led us to assign the stereochemistry as shown, which was also consistent with the subsequent reaction. The NOE results of **2** also supported the assignment by showing that the methine proton (4.47 ppm) and the methoxy methyl are close to each other (19). Similar photolysis of solutions of 2-$NpCO_2CH_3$ and acacH in various solvents in a merry-go-round gave **2** in 0% (in cyclohexane), 10% (in benzene), 9.3% (in THF), 19.5% (in acetonitrile), and 19% (in CH_3OH) yields. This trend was shown to be opposite to that observed in the de Mayo reaction (2).

Photolysis of **3** led to the formation of diketo-ester **4**, in 60% yield, which was also formed as a by-product in prolonged irradiation of the photocycloaddition of **1**. For **4**, the ^{13}C NMR and IR spectra showed the necessary signals for the carbonyl groups, and an ABX system at 4.63, 3.19, and 3.15 ppm (J = 18, 8, and 4.5 Hz) was still present in the ^1H NMR spectra. However, the two olefinic protons in **3** were converted to what appeared to be two cyclopropyl protons that were oriented *cis* to each other, as shown by an AB quartet of H_b (d, 3.17 ppm, J = 9 Hz) and H_e (d, 3.06 ppm, J = 9 Hz). The NOE experiments (19) demonstrated that irradiation of H_f (s, 2.28 ppm) or H_a (dd) caused the enhancement of H_c and H_d, and that irradiation of H_b and H_a (s, 1.99 ppm) caused the enhancement of H_e. An excited state of **3** should be able to undergo an oxa-di-π-methane rearrangement or a similar path by the formation of a strained oxetane intermediate **5** and a subsequent ring opening as shown (20, 21) to give **4**. This mechanistic consideration led to the assigned stereochemistry.

Similar photolysis of methyl-1-naphthoate **6** (1-$NpCO_2CH_3$) and acacH in CH_3CN under similar conditions for 8 h gave diketone **7**, in 30% yield, which was most likely formed by a similar pathway as described above via the intermediate **9**. In the presence of a trace amount of H_2SO_4 (0.0001–0.001 M), while no new product appeared, the formation of **7** was accelerated enormously. Prolonged photolysis of a neutral photolysate gave a caged product **8**, which was also obtained in a 40% yield by

Can. J. Chem. Downloaded from www.nrcresearchpress.com by 84.41.108.74 on 09/07/12
For personal use only.



irradiation of diketone **7** with a 200-W Hanovia lamp through a Pyrex filter. In the latter photolysis of **7**, a small amount of a product short of the CH_3CO − H moiety was also detected by GC–MS analysis. This compound was assumed to be methyl 7-acetonyl-1-naphthoate. The structure of **7** was easily decided from ^1H and ^{13}C NMR and IR spectra, which showed the expected carbonyl signals (see Experimental). Decoupling experiments showed that H_c (dd, 5.78 ppm, J = 9.5 and 25 Hz) was coupled with H_b (6.51 ppm) and H_e (m, 3.33 ppm), and that the latter (H_e) was coupled with H_d (d, 4.32 ppm, J = 7 Hz) and H_c. However, a combined effort of spectroscopic investigations could not solve the structure of **8** except to show that both ketone groups and the olefinic moiety had disappeared as the consequence of irradiation. Multiplicity sorting in ^{13}C NMR indicated the presence of six quaternary carbons, which require a caged structure. The presence of proton singlets at 3.13 and 3.72 ppm was useless in illuminating the structural features. Eventually the structure was determined to be **8**, as shown by single crystal X-ray crystallography (15). The formation of **8** from an excited state diketone **7** can be visualized as an intramolecular cycloaddition involving three π-bonds (two C=O groups and one C=C group) as shown. It is probably initiated from the lowest triplet state of the styrene moiety in **7** by a radical mechanism. Though we failed to find a precedent for such a photocyloaddition, cycloadditions involving three olefinic π-bonds are known (21, 22). From this reaction, it required that the H_d and H_e protons in **7** must be *cis*-oriented, which was also indicated by their coupling constant of 7 Hz.

Photocycloaddition of ethyl 2-naphthoate and ethyl 1-naphthoate with acacH also gave the corresponding ethyl analogues of 1,5-diketones **2** and **7**. These products were described in the thesis submitted by one of the authors (17).

Mechanistic studies

The photocycloaddition of 2-$NpCO_2CH_3$ with acacH in acetonitrile was used as a model to carry out mechanistic studies. Owing to the overlap of absorption in the 300–330 nm area (Fig. 1) and the closeness of excited state energies for 2-$NpCO_2CH_3$ (E_s = 84.5, E_T = 59 kcal/mol) and acacH ($E_s \leq$ 90, E_T = 69–74 kcal/mol), the first question concerning this photocycloaddition was the excited state responsible for the cycloaddition. The quantum yields of 2-$NpCO_2CH_3$ disappearance (Φ_{Np}) in the photocycloaddition with acacH were determined in acetonitrile using RPR 3000 A as the light source under two sets of conditions; first was constant [2-$NpCO_2Me$] =

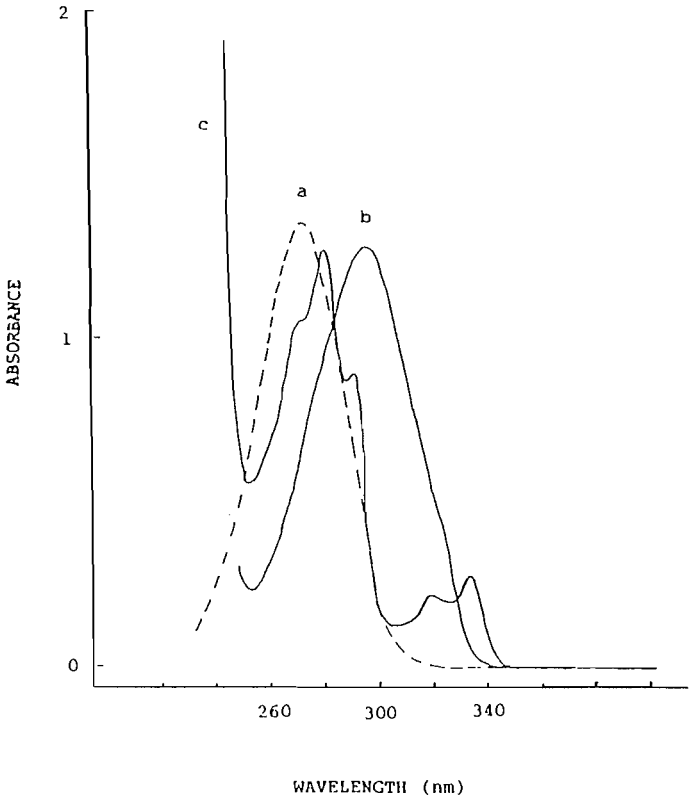


FIG. 1. The absorption spectra of (a) acacH (0.002 M), (b) 1-$NpCO_2CH_3$ (0.0002 M), and (c) 2-$NpCO_2CH_3$ (0.0002 M) in acetonitrile.

0.05 M with varying [acacH], 0.05–0.1 M, and the second was constant [acacH] = 0.05 M, with varying [2-$NpCO_2CH_3$], 0.05–0.1 M. The light intensity absorbed by 2-$NpCO_2CH_3$ (the first case) or by acacH (the second case) was estimated from the concentration and molar extinction coefficient at 300 nm as shown in the Experimental; the fraction of the intensity absorbed by 2-$NpCO_2CH_3$ or by acacH was used for the calculation of Φ_{Np} in two cases, respectively. While in the second case Φ_{Np} remained constant with increasing [2-$NpCO_2CH_3$], Φ_{Np} in the first case increased with increasing [acacH] (Fig. 2). For 1-$NpCO_2CH_3$, the results were similar within experimental errors (17). These clearly indicated that light absorption by naphthoates produced the primary excited species, initiating the train of events pertaining to the photocycloaddition. In our

Can. J. Chem. Downloaded from www.nrcresearchpress.com by 84.41.108.74 on 09/07/12
For personal use only.

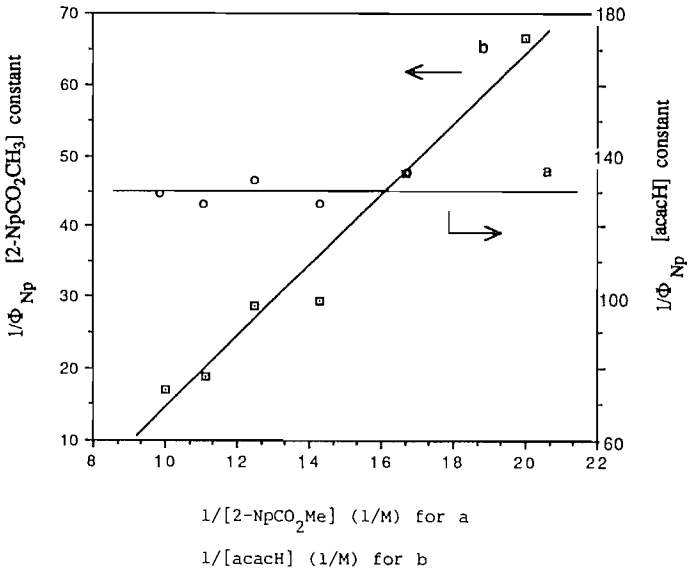


FIG. 2. The dependence of the quantum yields of the 2-$NpCO_2CH_3$ (Φ_{Np}) disappearance in the photocycloaddition (a) under the constant concentration of acacH (0.05 M), and (b) under the constant concentration of 2-$NpCO_2Me$ (0.05 M) in acetonitrile with 300 nm irradiation.

communication (15), we wrongly stated that the excitation of acacH caused the photocycloaddition; the erroneous experiment was caused by wrong absorbancy correction processes.

The quantum yield of **2** (Φ_p) for the photocycloaddition of 2-$NpCO_2CH_3$ in acetonitirile was determined as a function of [acacH] = [A], 0.08–0.3 M, in which appropriate corrections on light absorbed by 2-$NpCO_2CH_3$ were made. The plots of $1/\Phi_p$ vs. 1/[A] yielded a straight line with slope = 14.2 and intercept = 30; calculated $k_q\tau_0$ and the limiting Φ_p are 2.1 ± 0.3 M^{-1} and 0.033 ± 0.004, respectively, average values from repeated experiments. The plot was done according to eq. [1] assuming that an unspecified reactive state of 2-$NpCO_2CH_3$ reacted with a substrate at a rate ratio of $k_q\tau_0$ and the limiting quantum yield of β (21); in the present case the reaction rate constant with acetylacetone is k_{ca} (Table 1). It will be shown later, in the Discussion, that this reactive state is not the spectroscopic singlet excited state but an unknown species derived therefrom.

$$[1]\quad 1/\Phi_p = 1/\beta + 1/\beta k_q\tau_0[A])$$

The photocycloaddition of 2-$NpCO_2CH_3$ could not be sensitized by typical triplet sensitizers such as xanthone (E_T 74.1 kcal/mol) and benzophenone (E_T 69.2 kcal/mol) under conditions such that either the 2-$NpCO_2CH_3$ or acacH concentration was overwhelmingly higher than the other and the sensitizer absorbed the incident light. Also this photocycloaddition was efficiently quenched by tributylamine or dimethylaniline; at the 0.01 M level the quantum yield of **2** was reduced to about 1/6 and 1/3 respectively. This photocycloaddition in the presence of [acacH] = 0.08 M was quenched by tributylamine, giving $k_{TBA}\tau' = 233 \pm 30\,M^{-1}$ (Table 1) from two series of experiments and standard Stern–Volmer plots according to eq. [2],

$$[2]\quad \frac{\Phi^0}{\Phi} = 1 + k_{TBA}\tau'[TBA]$$

where $\tau' = 1/(1/\tau_0 + k_{CA}[acacH])$. Φ^0 and Φ are the quantum yields of **2** in the absence and presence of TBA, which is shown to interact with the spectroscopic singlet excited state 2-

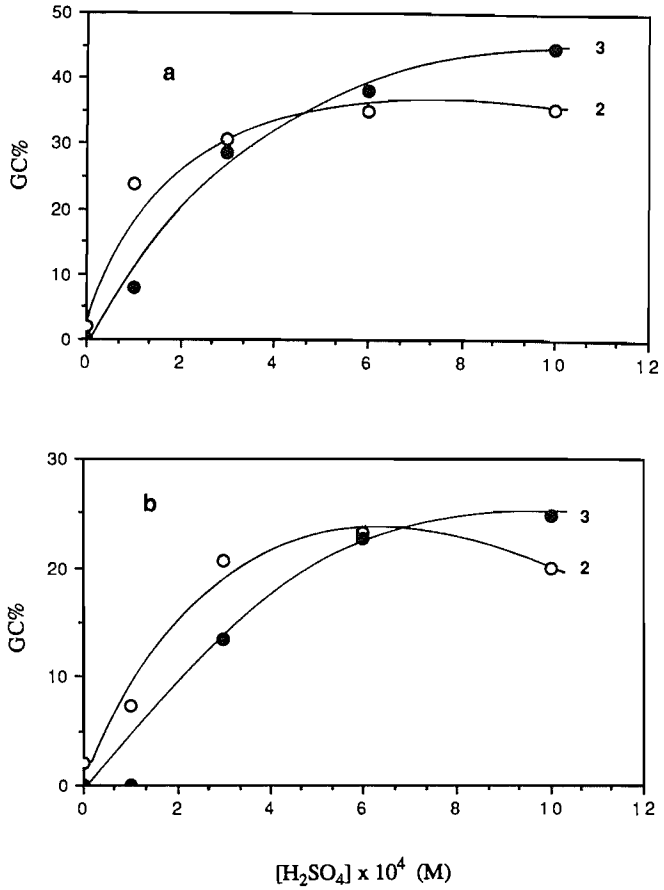


FIG. 3. The effects of sulfuric acid on percentage yields of photocycloaddition of 2-$NpCO_2CH_3$ (0.02 M) and acacH (0.05 M) in (a) acetonitrile and (b) methanol; nitrogen-purged samples were irradiated with 300-nm light in a merry-go-round under the same conditions.

$NpCO_2CH_3$ having a lifetime τ_0 = 8.5 ns measured by fluorescence quenching (*vide infra*). Likewise, oxygen (air-saturated solution) and biacetyl quenched the photocycloaddition efficiently. In contrast, the photocycloaddition of acacH with cyclohexene (a de Mayo reaction) was not quenched by tributylamine and dimethylaniline. This observation supported the conclusion that excited acacH is not the reactive species in the present photocycloaddition of naphthoates and acacH. In the presence of small amounts of iodomethane (<0.002 M), the quantum yield of **2** was drastically reduced, but in the [CH_3I] >0.005 M region, the yields of **3** increased significantly and that of **2** also started to increase. These photolysates were shown to contain an acid (probably HI), which was detectd by wet litmus paper. It was certain the photolytically generated HI in the higher [CH_3I] region acted as acid catalyst to promote the photocycloaddition.

Under a set of photolysis conditions, photocycloaddition of 2-$NpCO_2CH_3$ (0.02 M) with acacH (0.08 M) in acetonitrile was carried out in the presence of a trace amount of acid. As shown in Table 1, the formations of **2** and **3** were dramatically increased in the presence of less than 10^{-3} M acid. The acid catalysis was the largest with sulfuric acid, and the percent increases of **2** and **3** were shown to be asymptotically approaching maximum values at about 0.001 M H_2SO_4 (Fig. 3); the combined quantum yield of **2** and **3** was estimated to be 0.16 in the presence of [H_2SO_4] = 0.001 M as compared to 0.0045 in the absence of

Can. J. Chem. Downloaded from www.nrcresearchpress.com by 84.41.108.74 on 09/07/12
For personal use only.

TABLE 1. The quenching of 2-$NpCO_2CH_3$ fluorescence intensities and photocycloaddition in acetonitrile[a]

	$k_q\tau(m^{-1})$	τ(ns)	$k_q(m^{-1}\,s^{-1})$
Biacetyl (k_{BA})	95±2	3.5[d]	(k_{diff} = 2.7 × 10^{10})[c]
acacH (k_{AA})	28.7±1.5	8.5[e,f]	3.4 (±0.2) × 10^9
Tributylamine (k_{TBA})	127±2	3.5[d]	3.6 (±0.1) × 10^{10}
Iodomethane (k_{1M})	40±1	8.5[e]	4.7 (±0.1) × 10^9
H_2SO_4 (k_{H^+})	35.3±1.1	3.5[d]	1.01 (±0.03) × 10^{10}
H_2SO_4 (k_{H^+}) ([acacH] = 0.08 M)	13.2±0.4	1.8[d,g]	7.3 (±0.2) × 10^9
acacH (k_{AA}) ([H_2SO_4] = 0.001 M)	28.4±0.6	7.8[e,h]	3.6 (±0.1) × 10^9
acacH (k_{CA})[b]	2.1	(8.5)[e]	(2.5 × 10^8
Tributylamine (k_{TBA})[b] [acacH] = 0.08 M)	233±30	7.25[e,i]	3.2 (±0.4) × 10^{10}

[a]All experiments were run in acetonitrile either under nitrogen or under air, except the last two; relative intensities of 2-$NpCO_2CH_3$ fluorescence at 358 nm were monitored with the excitation at 330 nm.

[b]In these two experiments, the quantum yield of **2** in the photocycloaddition of 2-$NpCO_2CH_3$ with acacH was monitored: irradiation used Rayonet RPR 3000 lamps under nitrogen.

[c]The diffusion-controlled rate constant at 25°C in acetonitrile is assumed as the bimolecular quenching rate constant in order to calculate τ values in the presence of oxygen quenching from the air. In methanol, $k_q\tau$ = 71 and k_{diff} = 1.8 × 10^{10} M^{-1} s^{-1}, which gives τ = 3.9 ns.

[d]These reactions were run without N_2 purging, and τ = 3.5 ns was used for calculation.

[e]This reaction was run udner N_2 and τ_0 = 8.5 ns was used; τ_0 was obtained from biacetyl quenching under nitrogen assuming k_q = 2.7 × 10^{10} M^{-1} s^{-1}.

[f]In methanol $k_q\tau_0$ and k_q are 24.4 ± 0.9 M^{-1} and 2.6 (±0.1) × 10^9 M^{-1} s^{-1}.

[g]The lifetime was modified from the contribution of k_{AA} [acacH] to 1.8 ns.

[h]The lifetime was modified from the contribution of k_{H^+} [H_2SO_4] to 7.8 ns.

[i]The lifetime was modified from the contribution of k_{CA} [acacH] to 7.25 ns.

H_2SO_4. In the presence of [H_2SO_4] = 0.001 M and [acacH] = 0.9–1.2 M the combined quantum yields were ≥0.5. Similarly, the yields of **7** were increased in the same pattern as Fig. 3, by more than 10-fold at [H_2SO_4] = 0.001 M. Attempts to correlate the quantum yields with the concentrations of H_2SO_4 did not yield reproducible results and failed to give a recognizable plot.

Naphthoate fluorescence studies

Taking advantage of the strong fluorescence shown by naphthoates, we studied quenching patterns of singlet excited naphthoates with various substrates. The fluorescence intensity of 2-$NpCO_2CH_3$ was quenched rapidly in unpurged solution by biacetyl to give the Stern–Volmer rate of $k_{BA}\tau$ = 95 M^{-1} in acetonitrile and 71 M^{-1} in methanol. Adapting k_{BA} as being equal to the diffusion-controlled rate constant, 2.7 × 10^{10} M^{-1} s^{-1} in acetonitrile and 1.8 × 10^{10} M^{-1} s^{-1} in methanol (23), τ was calculated to be 3.5 and 3.9 ns in these solvents, respectively. Similar quenching experiments with a nitrogen-purged solution of 2-$NpCO_2CH_3$ and the same calculation procedure gave a lifetime τ_0 of 8.5 ns in acetonitrile and 9.4 ns in methanol; τ_0 was longer than τ since oxygen quenching was eliminated, and was regarded as the inherent lifetime of lowest singlet excited 2-$NpCO_2CH_3$ without bimolecular processes (24, 25).

The fluorescence intensities of 2-$NpCO_2CH_3$ (10^{-4}–10^{-3} M in acetonitrile) in the absence (I^0) and presence (I) of a substrate were measured to obtain a Stern–Volmer plot and to calculate the slope ($k_q\tau$ value); unless specified, experiments were carried out in acetonitrile (Table 1) (21). The rate constant of the interaction of singlet excited state 2-$NpCO_2CH_3$ with a substrate (k_q) can be calculated on the basis of lifetimes (τ or τ_0) estimated above and is shown in Table 1. Owing to the overlaps of absorption curves between acacH and 2-$NpCO_2CH_3$ in the 300-nm region, the fluorescence intensities have to be corrected for the amount absorbed by acacH. The plots were examined at three different excitation wavelengths to give very similar $k_q\tau$ values. Such interference did not exist with other substrates. While tributylamine most likely interacted with singlet excited 2-$NpCO_2CH_3$ by electron transfer (26), methyl iodide did so by promoting its intersystem crossing (27). The latter was confirmed by the observation of proportionately enhanced phosphorescence spectra at 77 K for a solution containing increasing concentrations of methyl iodide (see Fig. 5, later). The quenching of 2-$NpCO_2CH_3$ fluorescence intensities by acacH was examined at 7, 22, and 50°C; the Stern–Volmer plots gave slopes ($k_q\tau_0$ values) of 31 ± 1, 24 ± 1, and 8.5 ± 1.0 M^{-1} respectively, tending to decrease with increasing temperature. Assuming that the unimolecular reactions of singlet excited 2-$NpCO_2CH_3$ involving electron demotion were not affected significantly in this temperature range, τ_0 could be taken as approximately constant. Therefore the rate constant of the acacH interaction with singlet excited 2-$NpCO_2CH_3$ decreases with increasing temperature; such a negative temperature effect in fluorescence quenching suggests the presence of an exciplex (27, 28), i.e., *(2-$NpCO_2CH_3$ ... acacH).

The fluorescence pattern of 2-$NpCO_2CH_3$ was not affected in the presence of [H_2SO_4] 0.0002–0.002 M, but in the region of [H_2SO_4] > 0.005 M, the fluorescence intensity at 359 nm started to be reduced and a new fluorescence peak emerged at 470 nm with the isosbestic point at 414 nm (Fig. 4). A similar fluorescence change in the presence of sulfuric acid was published recently when this work was completed (29). In the presence of [acacH] = 0.08 M, the 2-$NpCO_2CH_3$ fluorescence spectra also varied on addition of H_2SO_4 with a pattern similar to that shown in Fig. 4. In both cases the Stern–Volmer plots monitored at 359 nm gave good straight-line correlations, and

Can. J. Chem. Downloaded from www.nrcresearchpress.com by 84.41.108.74 on 09/07/12
For personal use only.

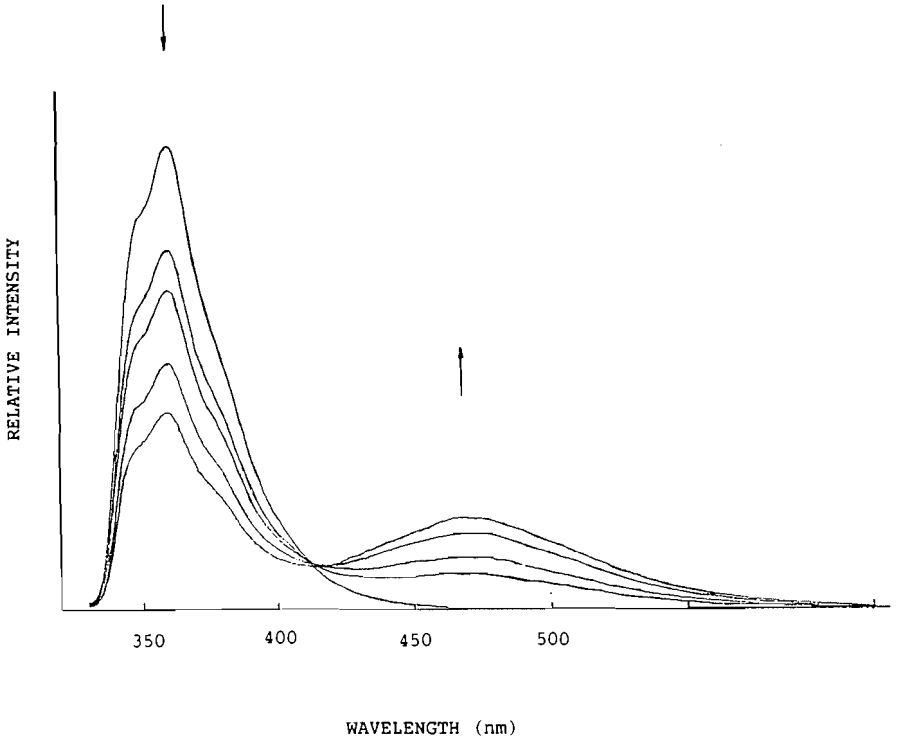


FIG. 4. The effects of H_2SO_4 (0, 0.0063, 0.0125, 0.0250, 0.375 M) on 2-$NpCO_2CH_3$ fluorescence in acetonitrile, under air at room temperature with the excitation wavelength at 300 nm; the fluorescence peak of ^{1}2-$NpCO_2CH_3$ at 359 nm and that of protonated ^{1}2-$NpCO_2CH_3$ at 470 nm.

TABLE 2. Acid promotion on the photocycloaddition of methyl 2-naphthoate and acacH in acetonitrile[a]

Acids (M)	% Conversion **1**	% Formation **3**	% Formation **2**
None (control)	2.06	0	2.06
H_2SO_4 (0.0003)	66.6	20.8	24.4
H_3PO_4 (0.0003)	12.6	4.4	8.2
HCl (0.0003)	22.0	7.2	10.6
BF_3OEt_2 (0.0003)	37.4	9.2	20.2
CF_3COOH (0.0005)	13.7	2.9	10.5

[a]The solutions containing 2-$NpCO_2Me$ (0.02 M), acacH (0.05 M), and one of above acids were irradiated under nitrogen for 3 h (6 h for CF_3COOH) in a merry-go-round; the photolysates were analysed with GC with error margin ±5%.

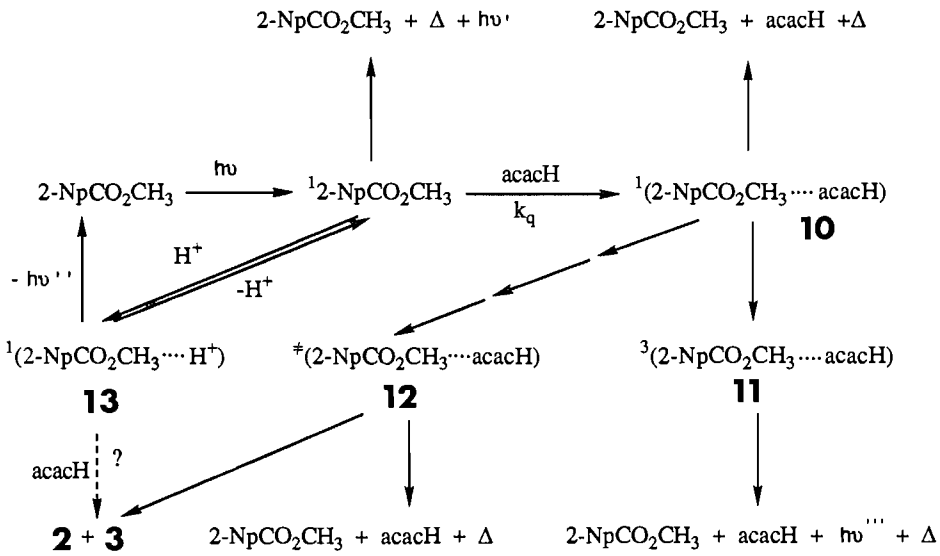
calculated rate constants of the acid association of singlet excited 2-$NpCO_2CH_3$ are comparable whether in the presence or absence of acacH (Table 1). The quenching of 2-$NpCO_2CH_3$ fluorescence by acacH in the presence of a low concentration of H_2SO_4 (0.001 M) showed that the $k_q\tau$ value monitored at 359 nm was 28.4 (±0.6) M^{-1} and was indistinguishable from that in the absence of H_2SO_4. This lack of effect was a significant contrast to the acid effects on quantum yields displayed in Fig. 3 and Table 2. Thus we failed to find experimental confirmation of the dramatic acid effects with 2-$NpCO_2CH_3$ fluorescence. In acetonitrile, 1-$NpCO_2CH_3$ exhibited a fluorescence peak at 362 nm, which was quenched by the increasing concentrations of $[H_2SO_4]$ = 0.005–0.06 M (but not in the <0.005 M region), giving a relatively weak new fluorescence peak at 470 nm with the isosbestic point at 423 nm. The new peak was assumed to arise from the acid complex species of the lowest singlet excited 1-$NpCO_2CH_3$.

Finally, the absorption spectra of neither naphthoates nor acacH in acetonitrile and methanol were modified in the presence of the other in the concentration range of 0.01–0.5 M for either component. Likewise, these absorption spectra were not changed in the presence of sulfuric acid up to 0.01 M. These experiments indicated that there were no ground state complex formations under the photolysis conditions.

Discussion

The photocycloaddition of 2-$NpCO_2CH_3$ to acacH exhibits low quantum efficiency (e.g., a limiting Φ of 0.033) but gives acceptable yields of the final products in a prolonged photolysis. As the photoreaction simultaneously introduces acetyl and acetonyl groups across a naphthalene double bond, it is a synthetically effective reaction to construct carbon skeletons. While the product resembles the de Mayo reaction, the present photocycloaddition originates from a reactive state of naphthoates, as clearly indicated by the agreement in the rate constants, k_{TBA} (see Table 1), of tributylamine quenching of the product

Can. J. Chem. Downloaded from www.nrcresearchpress.com by 84.41.108.74 on 09/07/12
For personal use only.



SCHEME 1

quantum yields (see estimation below) and the fluorescence intensity. The fact that tributylamine does not quench the photocycloaddition of acacH with cyclohexene demonstrates fundamental mechanistic differences between the present photocycloaddition and the de Mayo reaction. However, the most significant observation in this photocycloaddition is the dramatic promotion of product quantum yields by trace amounts of various protic acids (Table 2 and Fig. 3), which elevates this photocycloaddition to a synthetically significant reaction.

Owing to the fact that the primary cyclobutane adducts are destroyed in the secondary reaction, the stereochemistry of the photocycloaddition is reduced to the orientation of the acetyl and acetonyl groups on the ring; their orientation is shown to be the *cis* mode, from ^{1}H NMR data and subsequent reactions. While the primary photoreaction can be explained by a common reaction pathway of the addition and ring opening, with a cyclobutane such as **9** as the intermediate, the secondary photoreactions of **7** to **8** and **3** to **4** are extraordinary and only possible because of the particular disposition of the participating functional groups. From a structural point of view, the photoreaction of **7** to **8** should involve a coordinated addition of three π-bonds (two carbonyl and one carbon–carbon double bond) to give the caged product by electron shifts as indicated by arrows. The photorearrangement of **7** should occur from the lowest excited state, which is most likely to be the triplet excited state localized at the styrene moiety (21, 23). Regardless of stepwise reaction or otherwise, the *cis* orientation of the two ketone groups can allow the coordinated cyclization by 1,5-bond formations as shown in **8**, owing to stereochemical constraints. The excitation of **3** causes a net 1,2-migration of the acetyl group with the concomitant bond shift to form a cyclopropane ring that can be visualized as an oxa-di-π-methane rearrangement (20, 21). In theory, the strained structure **5** can be formed from excited intramolecular oxetane formation from **3**; the strain energy in **5** may promote electron reorganization to give **4**. Whether the intermediate is **5** or the corresponding 1,4-diradical cannot be easily resolved; the intermediate **5** provides better visualization of the stereochemical consequence in **4**.

Extensive efforts to unravel the mechanism of the photocycloaddition using fluorescence quenching of 2-$NpCO_2CH_3$ as the model have not been fruitful at this stage. There are a number of indications that the reactive species originates from the lowest spectroscopic singlet excited state, which emits at about 359 nm (^{1}2-$NpCO_2CH_3$ in Scheme 1). Firstly, iodomethane imparts heavy atom effects by promoting intersystem crossing (21) of singlet excited 2-$NpCO_2CH_3$ as shown by k_{IM} in fluorescence quenching and phosphorescence enhancement; Fig. 5b demonstrates such enhancement through the interaction within "a quenching sphere" of ^{1}2-$NpCO_2CH_3$ with iodomethane in a solid solution to generate the triplet state. The quantum yield of product **2** is indeed reduced in the low concentration region of $[CH_3I] \sim 0.001$ M. Secondly, quenchers of 2-$NpCO_2CH_3$ fluorescence such as biacetyl and *tertiary* amines Table 1) also quench the quantum yield of product **2** in the photoaddition. Because the reactive state of the photocycloaddition is uncertain, a quantitative correlation is possible only if we assume that $k_{CA}\tau_0 = 2.1\,M^{-1}$ represents the portion of successful photocycloaddition in the total quenching of singlet excited 2-$NpCO_2CH_3$ (τ_0 = 8.5 ns, Table 1); k_{CA} is estimated to be $2.5 \times 10^8\,M^{-1}\,s^{-1}$. This allows us to estimate $\tau' = 7.25$ ns in eq. [2] and, therefore, $k_{TBA} = 3.2 \times 10^{10}\,M^{-1}\,s^{-1}$. The agreement with that obtained from fluorescence quenching of $k_{TBA} = 3.6 \times 10^{10}\,M^{-1}\,s^{-1}$, in spite of entirely different conditions and nature of monitors, indicates convincingly the involvement of singlet state 2-$NpCO_2CH_3$.

Thirdly, while 2-$NpCO_2CH_3$ fluorescence intensities are systematically quenched by acacH in a frozen state at a low range of <0.02 M, 2-$NpCO_2CH_3$ phosphorescence intensities are not reduced even by high concentrations of acacH except for small decreases at the peaks that may arise from low quantum yields of the photocycloaddition of 2-$NpCO_2CH_3$ to form **2** and **3** (Fig. 5a). Such fluorescence quenching in solid solution is controlled by the probability of quencher being present in the vicinity (i.e., within a quenching sphere) as formulated by Perrin (in ref. 21). In view of the fact that the generation of neither 2-$NpCO_2CH_3$ nor acacH triplet states by sensitization initiates the photocycloaddition, and that the excitation of 2-$NpCO_2CH_3$ is responsible for the photocycloaddition with acacH, the photocycloaddition must originate from a singlet state, and, most likely, from that of 2-$NpCO_2CH_3$. Singlet excited acacH is not likely the originator owing to a short lifetime; if it is, tributylamine should not be able to quench the photocycloaddition. The pattern of emission with a near total conservation of the original triplet population of 2-$NpCO_2CH_3$

Can. J. Chem. Downloaded from www.nrcresearchpress.com by 84.41.108.74 on 09/07/12
For personal use only.

Can. J. Chem. Downloaded from www.nrcresearchpress.com by 84.41.108.74 on 09/07/12
For personal use only.

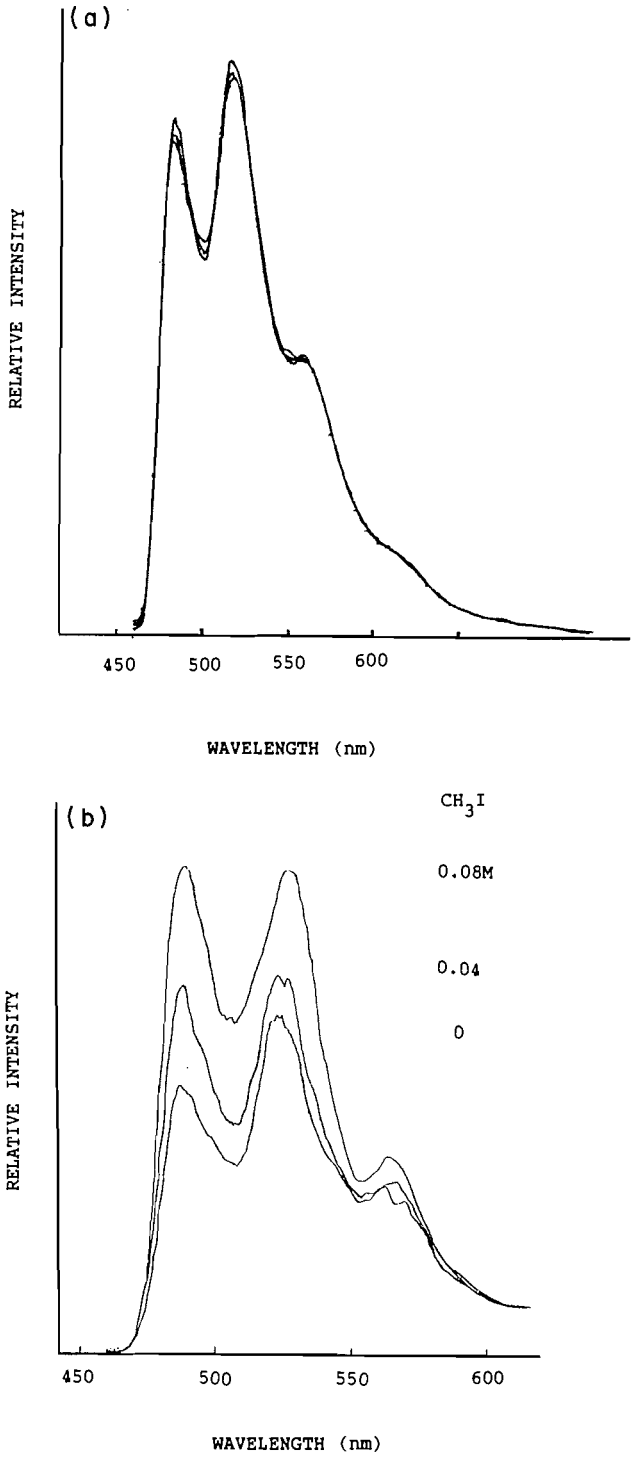


FIG. 5. (a) The phosphorescence spectra of 2-$NpCO_2CH_3$ (0.02 M) in a mixture of isopropanol and ether (1:3 ratio by volume) at 77 K under nitrogen in the presence of acacH (0.0–0.5 M); λ excitation 350 nm. (b) The enhancement of the 2-$NpCO_2CH_3$ phosphorescence spectrum in the presence of methyl iodide.

demonstrates interesting energy transfer, most likely occurring within excited state complexes such as those proposed as singlet and triplet exciplexes **10** and **11** in Scheme 1. Within these exciplexes one can envisage rapid migration along the energy ladder scheme without other energy wasting radiationless decays; ^{1}2-$NpCO_2CH_3$ + acacH → **10** → (2-$NpCO_2CH_3$... ^{1}acacH) → (2-$NpCO_2CH_3$...^{3}acacH) → (^{3}2-$NpCO_2CH_3$... acacH) (**11**) → 2-$NpCO_2CH_3$ + phosphorescence.

While evidence listed above supports the 2-$NpCO_2CH_3$ reaction arising from the singlet excited manifold, there is other critical evidence indicating that *the spectroscopic singlet state (Scheme 1, ^{1}2-$NpCO_2CH_3$) is not directly involved in the photocycloaddition*. The primary reason is the mismatch of the Stern–Volmer constant ($k_q\tau_0$) obtained from fluorescence quenching as compared to that from the quantum yield monitor of **2** (k_{AA} vs. k_{CA}, Table 1); the former is more than an order of magnitude larger than the latter. Secondly, whereas H_2SO_4 promotes the quantum yields of **2** and **3** very significantly in the [H_2SO_4] <0.001 M range, the protonation of spectroscopic singlet excited 2-$NpCO_2CH_3$ cannot be detected in this range by fluorescence emission either at 359 nm or 470 nm. We propose complex **12** derived from the singlet exciplex **10** as the immediate reactive state to give **2** and **3**, as shown in Scheme 1. While 2-$NpCO_2CH_3$ in **10** has the well-defined lowest spectroscopic singlet state, that in **12** possesses an unknown electronic state and its quantitative relation with respect to **10** has not been defined. Certain types of photochemical reactions originating from excited states of olefins and enones are susceptible to acid catalysis (30–32) for which the protonation of an intermediate, suggested to be a twisted state (32–35), has been proposed as the reactive intermediate. It is tempting to suggest a twisted state of 2-$NpCO_2CH_3$ to complex **12** without specifying the structures and electronic states. The kinetic relations among **10**, **11**, and **12** must be resolved to illuminate the reactive state.

The quenching by TBA and methyl iodide is definitely demonstrated to occur at the spectroscopic singlet excited state of 2-$NpCO_2CH_3$ according to fluorescence quenching studies; these quenching effects should be transmitted proportionally along the subsequent steps leading to complexes **11** and **12** to affect the quantum yields. The proportionality is supported by the agreement in k_{TBA} obtained by two types of quenching in the presence and absence of acacH as shown in Table 1. However, the crucial question is how a low concentration of H_2SO_4 manages to promote the photocycloaddition. The protonation of ^{1}2-$NpCO_2CH_3$ would be insignificant under the experimental conditions of Fig. 3 at [acacH] = 0.08 and [H_2SO_4] $<10^{-3}$ M, as can be judged from rate constants k_{AA} and k_{H^+} in Table 1. It is proposed that sulfuric acid at <0.001 M in acetonitrile can interact with complex **12** to render the observed promotional effects. While the exact pathway remains obscure at this stage, this proposal implies that the reactive complex **12**, †(2-$NpCO_2CH_3$...acacH), probably carries higher electron polarization than ^{1}2-$NpCO_2CH_3$, which would allow **12** to localize higher electron density in one site, where it would be protonated more easily. The possibility of an interaction of complex **10** with an acid is deemed less likely because the 2-$NpCO_2CH_3$ portion in **10** possesses a reasonably similar electronic configuration and chemical reactivity to that of the spectroscopic singlet state. Further, if this protonation occurs, the effects should be reflected in a Stern–Volmer analysis of the quantum yields of **2**. The failure to correlate the quantum yield of products **2** and **3** with [H_2SO_4] indicates the complexity of the reactions involving acid participation. It is clear that such reactions do not involve protonated ^{1}2-$NpCO_2CH_3$, **13**, which fluoresces with a broad band at 420 nm, as the reactive intermediate in acid promotion processes, as shown by previous calculations and in Figs. 3 and 4. In view of the indistinguishable $k_q\tau$ values for ^{1}2-$NpCO_2CH_3$ fluorescence quenching by acacH, either in the absence or presence of [H_2SO_4] = 0.001 (28.7 and 28.4 M^{-1}, see Table 1), it is the formation pathways beyond **10** that must be involved in acid promotions.

Inability to resolve kinetics of the photocycloaddition pre-

TABLE 3. ^{1}H NMR data of the products

Compound	Data (ppm in $CDCl_3$)	
1	4.0 (s, 3H); 7.58 (m, 2H)	7.89 (d, 2H)
2	3.03 (d, 1H, J=18.5 Hz)	2.12 (s, 6H)
	3.19 (d, 1H, J=18.5 Hz)	3.59 (s, 3H)
	5.81 (d, 1H, J=9.5 Hz)	4.47 (s, 1H)
	6.51 (d, 1H, J=9.5 Hz)	7.07–7.24 (m, 4H)
3	1.94 (s, 3H)	2.23 (s, 3H)
	2.56 (d, 2H, J=6 Hz)	3.63 (s, 3H)
	6.17 (dd, 1H, J=9.5 Hz, J=1 Hz)	4.34 (m, 1H)
	6.59 (d, 1H, J=9.5 Hz)	7.05 (m, 1H)
	7.16 (m, 3H)	
(in C_6D_6)	1.46 (s, 3H)	2.11 (s, 3H)
	2.28 (dd, 1H, J=18 Hz, J=7.5 Hz)	3.05 (s, 3H)
	2.56 (dd, 1H, J=5.5 Hz, J=7.5 Hz)	6.95 (M, 2H)
	6.5 (dd, 1H, J=10 Hz, J=1.5 Hz)	
	6.83 (dd, 1H, J=7 Hz, J=2 Hz)	
	7.32 (dd, 1H, J=7 Hz, J=1.5 Hz)	
4	3.06 (d, 1H, J=9 Hz)	1.99 (s, 6H)
	3.15 (dd, 1H, J=18 Hz, J=4.5 Hz)	2.28 (s, 3H)
	3.19 (dd, 1H, J=18 Hz, J=8 Hz)	3.75 (s, 3H)
	3.17 (d, 1H, J=9 Hz)	7.0 (d, 1H, J=7 Hz)
	4.63 (dd, 1H, J=8 Hz, J=4.5 Hz)	7.12–7.24 (m, 3H)
6	4.0 (s, 1H); 7.52 (m, 2H)	7.62 (dd, 1H)
	7.88 (d, 1H); 8.03 (d, 1H)	8.19 (dd, 1H)
	8.91 (d, 1H)	
7	1.87 (s, 3H)	2.23 (s, 3H)
	2.70 (dd, 1H, J=18 Hz, J=7.5 Hz)	3.33 (m, 1H)
	2.98 (dd, 1H, J=18 Hz, J=7.5 Hz)	3.88 (s, 3H)
	4.33 (d, 1H, J=7 Hz)	7.3–7.78 (m, 3H)
	5.78 (dd, 1H, J=9 Hz, J=2.5 Hz)	
	6.52 (dd, 1H, J=9 Hz, J=3 Hz)	
8	1.87 (dd, 1H, J=7 Hz, J=11 Hz)	1.02 (s, 3H)
	2.05 (d, 1H, J=11 Hz)	1.58 (s, 3H)
	2.55 (dd, 1H, J=5.5 Hz, J=7 Hz)	3.13 (s, 1H)
	4.48 (dd, 1H, J=5.5 Hz, J=8 Hz)	3.95 (s, 3H)
	7.4 (d, 1H, J=7 Hz)	7.78 (dd, 1H, J=8 Hz)

Can. J. Chem. Downloaded from www.nrcresearchpress.com by 84.41.108.74 on 09/07/12
For personal use only.

vents us from going beyond this point. Naphthalenes and other aromatic derivatives are known to be polarized on excitation, generating extraordinary excited state acidic or basic properties (36, 37), which last as long as their lifetimes. Napththoates (pK^0 = −8 to −9) and naphthoic acid (pK^0 = −7 to −8) obviously become much more basic with pK^* = 1–2 in their singlet excited state (38, 39), and can be protonated under ordinary reaction conditions, as shown in the literature and here. A pertinent question in this regard is whether complex **13** is also reacting with acacH to give products **2** and **3** in a high H_2SO_4 concentration region.

Interim conclusion

In acetonitrile and methanol, 1- and 2-$NpCO_2CH_3$ photolytically undergo photocycloaddition with acacH to give products **2**, **3**, and **7** with the addition of acetyl and acetonyl groups in low quantum yields. This useful synthetic method is significantly improved when run in the presence of H_2SO_4 at about 0.001 M, in which the quantum yield of the product is increased by more than an order of magnitude to ≥0.5. Mechanistic studies show that the photocycloaddition of 2-$NpCO_2CH_3$ occurs from an unknown species originating from its spectroscopic singlet excited state. Whereas this singlet-state 2-$NpCO_2CH_3$ exhibited an interesting fluorescence pattern in the reaction with H_2SO_4, the protonated singlet excited 2-$NpCO_2CH_3$ is not the key species in the acid-promoted reaction. Thus while the acid-promoted photocycloaddition is synthetically useful, its mechanism remains unknown.

Experimental

General conditions

Unless otherwise specified, the following experimental conditions were used. Melting points (mp) were determined on a Fisher–Johns apparatus, and were uncorrected. Infrared spectra (IR) were recorded with a Perkin–Elmer 559B spectrophotometer using neat liquid film, Nujol mull, or KBr pellet. Ultraviolet and visible spectra (UV) were taken with a Varian Cary 210 spectrophotometer. Mass spectra (MS) and gas chromatography – mass spectra (GC–MS) were obtained on a Hewlett–Packard 5985 GC–MS system either by electron ionization or by chemical ionization. Proton nuclear magnetic resonance (^{1}H NMR) spectra were recorded with a Bruker WM-400 spectrometer in $CDCl_3$ solution using tetramethylsilane (TMS) as an internal standard. Chemical shifts are reported in δ values in ppm and coupling constants (J) in Hz. The coupling patterns are presented as s (singlet), d (doublet), t (triplet), q (quartet), and m (multiplet). The chemical shifts of ^{13}C NMR spectra are also reported in ppm relative to TMS. Elemental analyses were carried out by Mr. M. K. Yang using a Carlo Erba model 1106 elemental analyzer. Gas chromatography (GC) analyses were performed on a Hewlett–Packard 5790A chromatograph (FID), equipped with an OV-1 capillary column and a Hewlett–Packard 3390A chart integrator. Retention times (R_t) are reported in minutes (min). Phosphorescence and fluorescence spectra were taken with a Perkin–Elmer MPF 44B spectrophotometer and were uncorrected. Percentage yields in preparative experiments were calculated

TABLE 4. ^{13}C NMR data of products

Compound	Data (ppm in $CDCl_3$)				
2	207.5	206.8	173.7	132.2	131.8
	129.3	128.6	128.4	128.3	128.1
	127.3	56.4	52.4	47.6	47.3
	29.99	29.96			
3	206.4	203.6	170.2	137.0	130.8
	129.4	128.7	127.97	127.4	127.1
	124.6	65.0	52.7	44.4	37.8
	30.6	26.8			
4	207.9	202.1	172.1	145.5	136.6
	127.8	126.9	124.2	123.9	52.5
	45.8	40.5	39.7	39.4	38.6
	31.4	30.1			
6	167.9	133.8	133.3	131.3	130.1
	128.5	127.7	127.1	126.1	125.8
	124.4	52.0			
7	208.27	206.97	167.77	135.43	135.10
	132.78	130.59	129.99	129.44	127.57
	127.53	52.14	50.62	44.90	32.57
	30.44	29.95			
8	167.15(s)		147.17(s)		141.87(s)
	127.97(d)		127.56(d)		
	126.09(d)		124.70(s)		104.86(s)
94.04(s)	82.22(d)				
	54.87(d)	54.60(d)	51.80(q)	4.28(d)	41.50(t)
	21.83(q)	18.24(q)			

based on the amount of the naphthalene derivatives present at the start of the reaction.

Chemicals and apparatus

For the preparative photochemical reactions, reagent grade solvents were distilled prior to use. Acetonitrile was distilled over P_2O_5. For spectroscopy, commercial spectroscopic grade solvents were used as supplied. Methyl 1-naphthoate (1-$NpCO_2Me$), and methyl 2-naphthoate (2-$NpCO_2Me$) were prepared from the corresponding naphthoic acids by H_2SO_4-catalyzed esterfication. The spectral data are listed in Tables 3–6. Acetylacetone (BDH) was distilled.

Photolysis apparatus and quantum yield determination

The first apparatus was a Hanovia-type reaction vessel (180 mL, Pyrex glass) fitted with a 200-W Hanovia medium-pressure mercury lamp (654A 36). The second apparatus consisted of eight quartz tubes (to accommodate 5 mL of solution) placed in a Rayonet photochemical reactor equipped with RPR 3000 Å lamps (16 × 21 W) or RPR 3500 Å lamps (16 × 24 W); a fan to circulate the air provided a constant temperature of 31 ± 1°C. Sometimes, a long cylindrical reaction vessel (3 × 20 cm, quartz) was inserted into a quartz water-cooled lamp housing; this set-up was used instead of test tubes.

The actinometer solution was prepared as follows. Benzophenone (456 mg, 2.50 mmol) and benzhydrol (921 mg, 5.0 mmol) were dissolved in benzene (25 mL). An aliquot (3 mL) from each of the above stock solutions was pipetted into a test tube. The actinometer solution (5 mL) containing 0.050 M benzophenone and 0.10 M benzhydrol was transferred into a quartz tube and purged with nitrogen for 10 min. The actinometer known to have the quantum yield of 0.74 (40) was irradiated, together with sample solutions, for 5 min. The absorbance (A) at 342 nm of benzophenone was measured with 0.10-cm optical path cells before and after irradiation, respectively. The light intensity was calculated by absorbance changes.

Quantum yields were determined using the second type of apparatus equipped with 350-nm or 300-nm light sources. Photolysates were analyzed by GC with octadecane ($C_{18}H_{38}$, added into the sample solution before irradiation) or xanthone (added after irradiation) as an internal standard (IS). The amount of a product formed or a starting material reacted was calculated from predetermined calibration curves

TABLE 5. IR data of the products

Compound	Absorptions (cm^{-1})				
1	3040(w)	1700(s)	1715(s)		
2	3028(w)	2959(w)	1738(s)	1439(w)	1362(m)
	1194(s)	1084(m)	789(w)		
3	3072(w)	2959(w)	1728(s)	1437(w)	1364(m)
	1223	791	748		
4	2940(m)	1703(s)	1430(m)	1350(m)	12400(m)
	1150(m)	755(m)			
6	3070(w)	2970(m)	1720(s)	1600(m)	1582(m)
	1517(m)	1440(m)	1290(s)	1255(s)	1210(s)
	1143(s)	1080(m)	1045(m)	1025(m)	955(w)
	825(m)	793(s)			
7	3044(w)	2961(w)	1736(s)	1439(m)	1362(m)
	1281(s)	1194(m)	1142(s)	756(m)	
8	3040(w)	1717(s)	1300(s)	1250(w)	1200(w)
	1150(s)	990(m)	960(m)	870(w)	840(m)
	765(m)	725(m)			

and the corresponding quantum yield Φ was calculated using the benzophenone–benzhydrol actinometry.

Since both naphthoates and acacH absorb light in the 300-nm region, the fraction of the incident light absorbed by naphthoates was determined according to the following equation:

$$A = A^0 [(\epsilon_{Np} C_{Np})/(\epsilon_{Np} C_{Np} + \epsilon_{acacH} C_{acacH})]$$

where A^0 is the light absorbed, ϵ_{Np} and ϵ_{acacH} are the extinction coefficients of NpR and acacH at 300 nm, respectively, and C_{Np} and C_{acacH} are the concentrations of NpR and acacH, respectively. Similarly, the fraction of the incident light absorbed by acacH could be calculated by replacing the numerator of $\epsilon_{Np}C_{Np}$ with $\epsilon_{acacH}C_{acacH}$.

The photocycloaddition of naphthoates with acetylacetone

An acetonitrile solution of acetylacetone and a naphthoate was placed in eight quartz tubes. After the solution was sealed and purged

Can. J. Chem. Downloaded from www.nrcresearchpress.com by 84.41.108.74 on 09/07/12
For personal use only.

TABLE 6. Mass spectral data of the products

Compound	Mode	m/e (%)			
1	EI	186(M^+, 80)	155(100)	127(62)	
2	EI	286(M^+, 3.4)	227(1.5)	211(18.8)	
186(100)					
		167(20)	155(74)	141(62)	115(17)
	CI	287(M+1, 38)	269(29)	241(100)	227(9)
		186(26)			
3	EI	268(2)	186(100)	155(80)	141(23)
		127(32)	43(25)		
	CI	287(M+1, 100)	269(38)	186(36)	
4	EI	286(M^+, 2)	254(20)	243(2)	229(1)
		211(25)	186(50)	165(20)	155(70)
		141(65)	127(50)	115(55)	43(100)
	CI	287(M+1, 100)	269(30)	255(40)	227(80)
		186(37)			
6	EI	186(M^+, 90)	155(100)	127(90)	115(7)
7	EI	286(M^+, 0.5)	268(3)	244(2)	229(25)
		211(100)	186(45)	168(20)	155(50)
		141(28)	127(25)	115(20)	43(45)
8	CI	287(M+1, 100)	269(30)	255(40)	227(80)
		186(37)			

with oxygen-free nitrogen for 10 min, the tubes were irradiated with a light source of 300 or 350 nm. Reactions were monitored by GC. A zero-hour sample was kept in the dark and analyzed by GC as a control. To avoid secondary photoreactions, the irradiation was stopped when the conversion of naphthalene derivative was around 50–60% as determined by GC. The residue was flash-chromatographed to give product. The spectral data are listed in Tables 3–6.

Methyl 2-naphthoate

A solution of 2-$NpCO_2Me$ (300 mg, 1.6 mmol) and acacH (1.6 g, 16 mmol) in acetonitrile (50 mL) was irradiated with 300-nm lamps. After irradiation for 15 h, the light yellow photolysate gave two GC (200°C) peaks at R_t 2.73 min for 2-$NpCO_2Me$ and at R_t 5.02 min for **2** in the ratio of 1:1. A trace amount of a second product (R_t 4.83 min) was also detected. The yellow residue was chromatographed using 30% ethyl acetate in hexanes as the eluant to give 2-$NpCO_2Me$ (112.8 mg) and a yellow oily compound (152 mg, 33%) of 1-acetyl-2-acetonyl-2-carbomethoxy-1,2-dihydronaphthalene (**2**), which was distilled bulb-to-bulb. Anal. calcd. for $C_{17}H_{18}O_4$: C 71.33, H 6.29; found: C 71.29, H 6.42%.

A solution of 2-$NpCO_2Me$ (300 mg, 1.6 mmol), acacH (500 mg, 5 mmol), and a trace amount of sulfuric acid (about 0.0005 M) in acetonitrile (50 mL) was irradiated with 300-nm lamps for 9 h. The light brown photolysate showed three GC peaks (200°C) at R_t 4.83 min (**3**, 45%), 5.02 min (**2**, 23%), and 2.73 min (2-$NpCO_2Me$, 15%). The residue was flash-chromatographed using 30% ethyl acetate in hexanes as the eluant to give a yellow oily compound of **2** (36 mg, 8%) and a light yellow powder (**3**, 72 mg, 16%) of 1-acetonyl-2-acetyl-2-carbomethoxy-1,2-dihydronaphthalene. The latter was further purified by recrystallization from cyclohexane to afford white crystals (70 mg, mp 81–82°C). Anal. calcd. for $C_{17}H_{18}O_4$: C 71.33, H 6.29; found: C 71.51, H 6.08%.

When a similar solution was over-irradiated for 24 h under similar conditions, the photolysate afforded two major product peaks at R_t 6.07 min (**4**, 31%) and 5.02 min (**2**, 15%). The crude product was chromatographed as above, followed by preparative TLC separation (using 50% ethyl acetate in hexanes) to give **4** (51 mg) as a yellow oil.

A solution of **3** (2.3 mg, 0.008 mmol) in acetonitrile (0.4 mL) in a quartz tube was irradiated similarily for 1 h. GC analysis of the photolysate showed 3.5% of **3** and 61% of **4**.

Methyl 1-naphthoate

A solution of 1-$NpCO_2Me$ (300 mg, 1.6 mmol) and acacH (1.6 g, 16 mmol) in acetonitrile (50 mL) was irradiated with 300-nm lamps. After irradiation for 8 h, the GC analysis (200°C) of the photolysate showed that 52% of 1-$NpCO_2Me$ survived (R_t 2.62 min) and 34% of **7** (R_t 6.91 min) was formed. The yellow oily residue was flash-chromatographed twice using 30% ethyl acetate in hexanes as eluant to give a pale yellow powder (139 mg, 30.4%) and 1-$NpCO_2Me$ (120 mg). The former was further recrystallized from acetonitrile to afford white crystals of 1-carbomethoxy-7-acetonyl-8-acetyl-7,8-dihydronaphthalene (**7**, mp 107–107.5°C).

A solution of 1-$NpCO_2Me$ (1 g, 5.6 mmol) and acacH (430 mg, 4.3 mmol) in methylene chloride (180 mL) was irradiated in the Hanovia apparatus. After irradiation for 187 h, GC analysis (column at 150–230°C at 10°C/min) of the photolysate showed that 62% of 1-$NpCO_2Me$ (R_t 3.57 min) survived and two products were formed with R_t 6.31 min (**8**, 30%) and 7.99 min (**7**, 7%). The residue was flash-chromatographed using 20% ethyl acetate in hexanes as eluant to give a crude product (66.5 mg, R_t 6.31 min), which was recrystallized from acetonitrile to give white crystals of 1,8-dimethyl-2,9-dioxa-5,6-(3′-carbomethoxybenzo)tetracyclo[5, 2, $0^{3,11}$ $0^{4,8}$]undecane (**8**, 31 mg): mp 117–117.5°C. Anal. calcd. for $C_{17}H_{18}O_4$: C 71.33%, H 6.29%; found: C 71.42% and 71.23%, H 6.47% and 6.34%. The structure of **8** was determined by X-ray crystallography (15).

A solution of **7** (4.2 mg, 0.015 mmol) in methylene chloride (1 mL) in a quartz tube was irradiated at 300 nm. A sample solution was withdrawn at 1-h intervals and analyzed by GC. After 6 h of irradiation, the GC analysis (150–230°C at 10°C/min) showed three peaks at R_t 7.99 min for **7** (24%), R_t 6.31 min for **8** (16%), and an unknown product (R_t 7.33 min, 39%). The unknown product showed GC–MS (CI) peaks at m/e 243 (M+1, 47%), 211 (100%). No further study of this unknown compound was done.

A solution of **7** (4.7 mg, 0.016 mmol) in methylene chloride (1 mL) was irradiated through a Pyrex filter with a 200-W Hanovia lamp. After 6 h of irradiation, GC (150–230°C at 10°C/min) analysis of the photolysate showed three peaks at R_t 7.99 for **7** (22%), R_t 6.31 min for **8** (46%), and R_t 7.33 min for the unknown compound (14%).

Triplet sensitization

A stock soslution of 2-$NpCO_2CH_3$ (0.02 M), acacH (0.08 M), and octadecane (IS) was prepared. Three sample solutions were prepared in quartz tubes in which No. 1 contained the stock solution (5 mL) without a sensitizer, No. 2 the solution (5 mL) and xanthone (0.05 M), and

Can. J. Chem. Downloaded from www.nrcresearchpress.com by 84.41.108.74 on 09/07/12
For personal use only.

No. 3 the solution (5 mL) with benzophenone (0.05 M). The above three solutions were irradiated for 6 h at 350 nm. While **2** was obtained (22%) from No. 1 solution, this product could not be detected by GC for No. 2 and No. 3 solutions.

Quenching

Five acetonitrile solutions (1 mL) containing 2-$NpCO_2Me$ (0.02 M), acacH (0.08 M), octadecane (as IS, 0.005 M), and TBA (0, 0.0015, 0.003, 0.0045, and 0.006 M) were irradiated at 350 nm for 2 h. The quantum yields were determined and analysed by the Stern–Volmer relation (eq. [1]) to afford slopes ($k_q\tau$) of 237 ± 29 and 230 ± 31 in two series of experiments. Two solutions (5 mL) were prepared in quartz tubes, in which No. 1 contained no DMA, and No. 2 contained DMA (0.01 M). The solutions were irradiated for 4 h to afford quantum yields of **2** of 0.0043 for No. 1 and 0.0008 for No. 2.

Quenching of the de Mayo reaction

Three solutions (5 mL) in hexanes were prepared in quartz tubes, each of them containing acacH (0.05 M, 0.25 mmol), cyclohexene (0.5 M, 2.5 mmol), and decahydronaphthalene (as IS, 0.004 M, 0.02 mmol); No. 2 tube also contained *N*,*N*-dimethylaniline (0.01 M, 0.05 mmol) and No. 3 tube tributylamine (0.01 M, 0.05 mmol), while No. 1 tube was used as a control. The solutions were irradiated in the second apparatus at 300 nm for 4 h. The relative yields of the addition product (identified by coinjection with an authentic compound) were 11.8% for No. 1, 9.4% for No. 2, and 10.7% for No. 3 solution.

Acknowledgement

The authors are grateful to the Natural Sciences and Engineering Research Council of Canada for generous support of this research project.

1. J. J. McCULLOUGH. Chem. Rev. **87**, 811 (1987).
2. A. C. WEEDON. *In* Synthetic organic photochemistry. *Edited by* W. Horspool. Plenum, New York. 1984. pp. 61–143.
3. W. A. WENDER. *In* Photochemistry in organic synthesis. *Edited by* J. D. Coyle. Royal Society of Chemistry, London, England. 1986. Chap. 9.
4. W. OPPOLZER. Acc. Chem. Res. **15**, 135 (1982).
5. P. DE MAYO. Acc. Chem. Res. **4**, 41 (1971).
6. P. E. EATON. Acc. Chem. Res. **1**, 50 (1968).
7. P. G. BOUSLAUGH. Synthesis, 287 (1970).
8. J. J. McCULLOUGH, W. K. MACINNIS, C. J. L. LOCK, and R. FAGGIANI. J. Am. Chem. Soc. **104**, 4644 (1982), and the papers cited herein.
9. J. MICHL. Photochem. Photobiol. **25**, 141 (1977).
10. W. R. WARE, D. WATT, and J. D. HOLMES. J. Am. Chem. Soc. **96**, 7853 (1974).
11. J. B. BIRK. Photophysics of aromatic molecules. Wiley–Interscience, London. 1970. Chap. 7.
12. (*a*) T. TEITEL, D. WELLS, T. H. SPURLING, and W. H. F. SASSE. Aust. J. Chem. **31**, 85 (1978); (*b*) A. ALBANI and L. GIANNANTONIA. J. Org. Chem. **49**, 8863 (1983).
13. P. DE MAYO and H. TAKESHITA. Can. J. Chem. **41**, 440 (1963).
14. H. NOZAKI, M. KURITA, T. MORI, and R. NOYORI. Tetrahedron, **24**, 1821 (1968).
15. YUAN L. CHOW, X.-Y. LIU, and S. Z. HU. J. Chem. Soc. Chem. Commun. 1047 (1988).
16. Y. L. CHOW, G. E. BUONO-CORE, X. Y. LIU, K. ITOH, and P. QIAN. J. Chem. Soc. Chem. Commun. 913 (1987).
17. X. Y. LIU. Ph.D. Thesis, Simon Fraser University, 1990.
18. R. M. SILVERSTEIN, G. C. BASSLER, and T. C. MORRILL. Spectrometric identification of organic compounds, Wiley, New York. 1981.
19. J. K. SAUNDERS and J. W. EASTON. *In* Determination of organic structures by physical methods. Vol. 8. *Edited by* F. S. Nachod, J. J. Zucherman, and E. W. Randall. Wiley, New York. 1976, p. 271.
20. K. N. HOUK. Chem. Rev. **76**, 1 (1976).
21. N. J. TURRO. Modern molecular photochemistry. Benjamin Cummings, Menlo Park. 1978. p. 487.
22. R. B. WOODWARD and R. HOFFMAN. Angew. Chem. Int. Ed. **8**, 781 (1969).
23. S. L. MUROV. Handbook of photochemistry. Marcel Dekker, New York. 1973.
24. D. CREED, R. A. CALDWELL, and M. ULRICH. J. Am. Chem. Soc. **100**, 5831 (1978).
25. J. L. CHARLTON, D. E. TOWNSEND, B. D. WATSON, P. SHANON, J. KOWALEWSKA, and J. SALTIEL. J. Am. Chem. Soc. **99**, 5992 (1977).
26. S. G. COHEN, A. PAROLA, and G. H. PARSON. Chem. Rev. **73**, 141 (1973).
27. T. OKADA, H. MATSUI, H. OOHARI, H. MATSUMOTO, and N. MATAGA. J. Chem. Phys. **49**, 4717 (1968).
28. H. KNIBBE, D. REHM, and A. WELLER. Ber. Bunsen-ges. Phys. Chem. **73**, 839 (1969).
29. S. CHEN, C. GUO, and H. XU. J. Photochem. Photobiol. Chem. **49**, 187 (1989).
30. J. C. McEWEN and K. YATES. J. Am. Chem. Soc. **109**, 5800 (1987), and other papers from this group.
31. G. G. WUBBELS. Acc. Chem. Res. **16**, 285 (1983).
32. A. RUDOLPH and A. C. WEEDON. J. Am. Chem. Soc. **111**, 8756 (1989).
33. D. I. SCHUSTER, P. B. BROWN, L. J. CAPPONI, C. A. RHODES, J. C. SCAIANO, P. C. TUCKER, and D. WEIR. J. Am. Chem. Soc. **109**, 2533 (1987).
34. W. G. DAUBEN, H .C. H. A. VAN RIEL, J. D. ROBINS, and G. J. WAGNER. J. Am. Chem. Soc. **101**, 6383 (1979).
35. R. BONNEAU, J. JOUSSOT-DUBIEN, L. SALEM, and A. J. YARWOOD. J. Am. Chem. Soc. **98**, 4329 (1976).
36. H. SHIZUKA. Acc. Chem. Res. **18**, 141 (1985), and papers cited therein.
37. J. F. IRELAND and P. A. H. WYATT. Adv. Phys. Org. Chem. **12**, 131 (1976).
38. P. J. KOVI and S. G. SCHULMAN. Spectrosc. Lett. **5**, 443 (1972).
39. A. R. WATKINS. J. Chem. Soc. Faraday Trans., **68**, 28 (1972).
40. W. M. MOORE and M. KETCHUM. J. Am. Chem. Soc. **84**, 1388 (1962).

Can. J. Chem. Downloaded from www.nrcresearchpress.com by 84.41.108.74 on 09/07/12
For personal use only.

Structural studies on the polysaccharide portion of "A-band" lipopolysaccharide from a mutant (AK1401) of *Pseudomonas aeruginosa* strain PAO1[1]

TODD L. ARSENAULT, DONALD W. HUGHES, AND DAVID B. MACLEAN[2]
Department of Chemistry, McMaster University, Hamilton, Ont., Canada L8S 4M1

WALTER A. SZAREK[2]
Department of Chemistry, Queen's University, Kingston, Ont., Canada K7L 3N6

ANDREW M. B. KROPINSKI
Department of Microbiology and Immunology, Queen's University, Kingston, Ont., Canada K7L 3N6

AND

JOSEPH S. LAM
Department of Microbiology, University of Guelph, Guelph, Ont., Canada N1G 2W1

Received September 11, 1990

TODD L. ARSENAULT, DONALD W. HUGHES, DAVID B. MACLEAN, WALTER A. SZAREK, ANDREW M. B. KROPINSKI, and JOSEPH S. LAM. Can. J. Chem. **69**, 1273 (1991).

AK1401 is a mutant of *Pseudomonas aeruginosa* strain PAO1 (serotype O5) that does not express O-antigen, but does express "A-band" lipopolysaccharide (LPS). The polysaccharide portion of the A-band LPS (A-PS) from AK1401 was found to consist mainly of D-rhamnose, with smaller amounts of 3-*O*-methylrhamnose, ribose, mannose, glucose, and a 3-*O*-methylhexose. ^{1}H nuclear magnetic resonance spectra of the intact A-PS indicated that the main structural feature was a repeating trisaccharide of α-D-rhamnose having the following structure:

$$[\rightarrow 2\text{-}\alpha\text{-D-Rha}p\text{-}(1\rightarrow 3)\text{-}\alpha\text{-D-Rha}p\text{-}(1\rightarrow 3)\text{-}\alpha\text{-D-Rha}p\text{-}(1\rightarrow]_n$$

The ^{1}H NMR spectrum of the repeating unit was completely assigned through the use of 2D shift-correlated and relayed coherence transfer NMR spectroscopy. The linkage positions and sequence of residues were found by nuclear Overhauser enhancement difference spectroscopy.

Key words: *Pseudomonas aeruginosa*, lipopolysaccharide, ^{1}H NMR.

TODD L. ARSENAULT, DONALD W. HUGHES, DAVID B. MACLEAN, WALTER A. SZAREK, ANDREW M. B. KROPINSKI et JOSEPH S. LAM. Can. J. Chem. **69**, 1273 (1991).

Le AK1401 est une espèce mutante du *Pseudomonas aeruginosa* de la lignée PAO1 (sérotype O5) qui n'exprime pas de O-antigène, mais qui exprime un lipopolysaccharide (LPS) de «bande-A». On a trouvé que la portion polysaccharide du LPS de bande-A du AK1401 est principalement formée de D-rhamnose, avec des quantités plus faibles de 3-*O*-méthylrhamnose, de ribose, de mannose, de glucose et d'un 3-*O*-méthylhexose. Les spectres de résonance magnétique nucléaire du ^{1}H du PS-A indiquent que la caractéristique structurale principale est un motif trisaccharide de α-D-rhamnose, de structure :

$$[\rightarrow 2\text{-}\alpha\text{-D-Rha}p\text{-}(1\rightarrow 3)\text{-}\alpha\text{-D-Rha}p\text{-}(1\rightarrow 3)\text{-}\alpha\text{-D-Rha}p\text{-}(1\rightarrow]_n$$

Faisant appel à la RMN en 2D avec corrélation des déplacements et transfert de cohérence par relais, on a fait une attribution complète du spectre RMN du ^{1}H du motif. On a déterminé les positions de liaison et la séquence des résidus par l'effet Overhauser nucléaire différentiel.

Mots clés : *Pseudomonas aeruginosa*, lipopolysaccharide, RMN du ^{1}H.

[Traduit par la rédaction]

Introduction

Pseudomonas aeruginosa is an opportunistic pathogen that infects persons having compromised immune systems, such as burn victims, organ transplant recipients taking anti-rejection drugs, and cystic fibrosis (CF) patients. CF patients commonly suffer respiratory tract infections of *P. aeruginosa* that are potentially fatal (1). *Pseudomonas aeruginosa* infections in general are very difficult to eradicate because of resistance to a wide variety of antibiotics (1), but the mucoid colonies present in CF lungs are even more persistent because the cell-surface lipopolysaccharide (LPS) antigens change upon colony formation (1, 2). This latter phenomenon can make vaccination ineffective, since the bacteria no longer express the LPS antigens to which antibodies were raised.

Lipopolysaccharides are cell-surface molecules common to all Gram-negative bacteria. They consist of a carbohydrate/lipid portion ("Lipid A", which anchors the LPS in the outer membrane) and a carbohydrate portion, consisting of a short "core oligosaccharide" and a high molecular weight "side-chain polysaccharide" (3). The carbohydrate portion is linked to the Lipid A by a very acid-labile linkage involving 2-keto-3-deoxyoctulosonic acid (KDO), and thus may be liberated by mild acid-catalyzed hydrolysis, which results in precipitation of the insoluble Lipid A. Within a species, there is little variation in the structures of the core and lipid A, but the side-chain polysaccharides are highly variable; in the case of *P. aeruginosa*, they consist of repeating units composed of 2–5 monosaccharides, and commonly contain uronic acids, amino sugars, and some unusual sugars (see ref. 4). These side-chain structures are often called "O-antigens", and their variation is used in immunological typing schemes to define serotypes within a particular species. Vaccines currently used against pathogenic

[1]Presented in part at the First Congress of the International Endotoxin Society, San Diego, CA, May 10–12, 1990; Abstract I-P-14.

[2]Authors to whom correspondence may be addressed.

Can. J. Chem. Downloaded from www.nrcresearchpress.com by 84.41.108.74 on 09/07/12
For personal use only.

Can. J. Chem. Downloaded from www.nrcresearchpress.com by 84.41.108.74 on 09/07/12
For personal use only.

Gram-negative bacteria commonly consist of a mixture of O-antigens from several serotypes of the same species.

Rivera *et al.* (5) have described a minor type of LPS, designated "A-band" LPS, from *P. aeruginosa* strain PAO1 (serotype O5), which differed from the classical LPS ("B-band" LPS) described above in its mobility on polyacrylamide gel electrophoresis. It was shown that this new type of LPS did not react with monoclonal antibodies to the O-antigen; also, the side-chain polysaccharide contained only neutral sugars, and was shorter than the O-antigen. Rivera and McGroarty (6) later postulated that the A-band LPS is present along with B-band LPS in cultures, but that the B-band expression stops under certain conditions (such as prolonged antibiotic therapy) leaving the A-band LPS as the principal cell-surface antigen.

Upon establishment of colonies in a CF lung, *P. aeruginosa* becomes non-typable, a result which implies that the O-antigens are no longer present. However, Lam *et al.* (2) have shown, through the use of monoclonal antibodies, that expression of A-band LPS is conserved in a high percentage of clinical isolates from CF patients. Furthermore, this antigen was found to be present in 11 of the 17 IATS[3,4] serotypes (2), thus indicating that it is a "common antigen". Since the A-band LPS is conserved upon infection, and since it is a common antigen, vaccines based on this type of LPS might be more successful in preventing pulmonary infections of *P. aeruginosa* than the current vaccines based on O-antigens.

AK1401 is a rough mutant of strain PAO1 (7) that, in spite of being defective in the synthesis of O-antigen, produces a high molecular weight LPS that reacts with A-band specific monoclonal antibodies (2). Thus, AK1401 is a potentially attractive source of A-band LPS because the LPS can be obtained free from contaminating O-antigen. Rough B-band LPS is still produced; however, this is easily removed by size-exclusion chromatography. Because of the lack of O-antigens, AK1401 can be used also to screen serum samples for the presence of antibodies to A-band LPS. Accordingly, we undertook a structural study of the A-band LPS from AK1401 with the intention of preparing synthetic vaccines based upon subunits of the structure that could be used for protection against *Pseudomonas* infections.

In the present work the structure of the polysaccharide portion of A-band LPS (A-PS) from AK1401 was examined by a combination of spectroscopic and degradative techniques. The monosaccharide composition was found by gas chromatography (GC) and gas chromatography – mass spectrometry (GC–MS) (8) of the alditol acetates derived from a hydrolysate of the A-PS. The absolute configuration of the rhamnose component was found by GC and GC–MS of (−)-2-octyl glycoside peracetates (9). The anomeric configurations were found by determination of the C-1–H-1 coupling constants (10). The ^{1}H NMR spectrum was assigned for the principal monosaccharides with the aid of ^{1}H–^{1}H shift-correlated (COSY) and relayed coherence transfer (RELAY) experiments, and this assignment was used to infer the linkage positions and sequence of residues in the polysaccharide by observation of inter-residue nuclear Overhauser enhancements (nOe's). The similarity of this structure with those of other neutral LPS's from *P. aeruginosa* (11–13) is discussed.

Experimental

Sample preparation

AK1401 cells were grown overnight at 37°C in 500 mL of tryptic soy broth (Difco) and then used to inoculate 4.5 L of tryptic soy broth in an SLS fermentor (Labline). The temperature was maintained at 37°C, the rotation rate was 200 rpm, and the aeration rate was 10 L min^{-1}. The cells were harvested, at late logarithmic or early stationary phase, by centrifugation. LPS was isolated by the method of Darveau and Hancock (14), and hydrolyzed in 1% acetic acid at 100°C for 90 min. The lipid A was removed by centrifugation, and the supernatant was lyophilized to dryness. The residue was dissolved in 0.05 M pyridinium acetate buffer (pH 5.3) and chromatographed on Bio-Gel P-4 (minus 400 mesh). The component of highest molecular weight was used in this study.

Prior to analysis, the A-PS sample was chromatographed on Sephadex G-50 in 0.05 M pyridinium acetate buffer. The void-volume fraction was collected and lyophilized. For ^{1}H and ^{13}C NMR analysis, an A-PS sample (7 mg) was exchanged three times with 99.9% D_2O (MSD Isotopes), the sample being lyophilized after each exchange. Finally, the sample was dissolved in 0.8 mL of 99.996% D_2O ("D_2O PLUS", MSD Isotopes).

Compositional analysis

A sample of A-PS (<1 mg) was dissolved in 1 mL of 2 M HCl in a thick-walled Teflon screw-cap vial (capacity ≈ 8 mL), and the solution was kept for 3 min in a Panasonic 700-W microwave oven at medium-high power;[5] the sample was cooled at least 15 min before opening the reaction vial. The sample was evaporated to near dryness under reduced pressure, and residual water and acid were removed by evaporating with 3 portions of 1-propanol. Alternatively, hydrolysis was performed at 120°C in 1 mL of 2 M trifluoroacetic acid in a sealed glass tube for 1.5 h; the water and acid then were removed under reduced pressure.

The dry residue was dissolved in 1 mL of water, and the solution was treated with 5 mg of sodium borohydride at ambient temperature for 4 h (or overnight). The reaction mixture was quenched by the addition of 5% acetic acid in methanol, and evaporated. Further portions of 5% acetic acid in methanol were added, and the solution was distilled until the presence of boron could no longer be detected (flame test). The residue was dried under vacuum and treated with 1 mL of acetic anhydride at 110°C for 2 h. The reaction mixture was cooled, poured into water, and extracted with chloroform. The combined chloroform extracts were washed extensively with 5% aqueous sodium hydrogen carbonate, dried over anhydrous sodium sulfate, and concentrated.

A series of alditol acetate standards (arabinitol, xylitol, 2-deoxyglucitol, 6-deoxygalactitol, and 3-*O*-methylrhamnitol peracetates) was prepared from the corresponding aldoses as described above. Rhamnitol, ribitol, glucitol, galactitol, and mannitol peracetates were prepared on a larger scale as follows. The sugar (0.5 g) was reduced with 0.5 g of sodium borohydride in 10 mL of water as described above. The alditols were acetylated using 10 mL of acetic anhydride; in the cases of glucitol, mannitol, and galactitol peracetates, the products were obtained by pouring the reaction mixture into methanol and collecting the crystalline materials. Overall yields were ≈50%. The identity of all products was confirmed by GC and CI-MS using ammonia as the reagent gas.

Gas chromatography was performed on a 30 m × 0.5 mm DB1701 wide-bore capillary column (J&W Scientific) using a Hewlett–Packard 5890 instrument equipped with an on-column injector and a HP3390A integrator. The oven temperature was 200°C, and the flame-ionization

[3]IATS refers to "International Antigenic Typing System"; for definition, see P. V. Liu, H. Matsumoto, H. Kusama, and T. Bergan. Int. J. System. Bacteriol. **33**, 256 (1983).

[4]It has been found recently that the antigen is present in 12 of the 17 serotypes (M. Y. C. Lam. Ph.D. Thesis, University of Guelph, Guelph, Ont. 1990).

[5]This experiment was similar to that described for the rapid total hydrolysis of proteins (S.-T. Chen, S.-H. Chiou, Y.-H. Chu, and K.-T. Wang. Int. J. Peptide Protein Res. **30**, 572 (1987)). The reaction vessel was fabricated from a 1 in. diameter Teflon rod; the minimum wall thickness was 6 mm, and the thread depth was 1 cm.

detector was kept at 280°C. The carrier gas was helium at a pressure of 8 psig (1 psi = 6.89 kPa).

GC–MS was performed on a VG Micromass 7070F mass spectrometer equipped with a Varian model 3700 GC having a J&W Scientific on-column injector. The column described above was used, except that the oven temperature was reduced to 180°C and the helium backing pressure was only 2 psig. The interface temperature was kept at 250°C, the ion source at 200°C, the electron energy at 70 eV, and the accelerating potential at 4 kV. The mass spectrometer was scanned from either 350 or 300 to 40 amu at 2 s per decade, with a 1-s interscan delay. The data were acquired and processed on a Digital Electronics Corporation PDP 11/24 computer using VG 11/250 software.

Absolute configuration

A sample of A-PS hydrolysate was treated with 0.5 mL of (−)-2-octanol and 1 drop of trifluoroacetic acid in a sealed tube at 140°C for 20 h. The mixture was evaporated under reduced pressure, and the residue was treated with 10 mg of fused sodium acetate and 1 mL of acetic anhydride at 110°C for 1 h. The reaction mixture was poured into water and extracted with chloroform. The extracts were washed extensively with 5% aqueous sodium hydrogen carbonate, dried, and concentrated. Standard samples for retention-time comparison were prepared similarly, using L-rhamnose with either (−)-2-octanol or (±)-2-octanol. GC analysis was performed as above.

Nuclear magnetic resonance spectroscopy

All of the NMR spectra were recorded on a Bruker AM-500 spectrometer. The ^1H spectra were acquired at 500.137 MHz using a 5-mm dual frequency $^1H/^{13}C$ probe. Spectra were acquired over 2.45 kHz in 8K data points (1.671 s acquisition time). Sample temperature was maintained at 30°C by a Bruker BVT-1000 variable temperature unit. The residual HDO signal was suppressed by saturation for 1.0 s prior to acquisition. The free induction decays (FID's) were processed using Gaussian multiplication for resolution enhancement, and before Fourier transformation were zero-filled to 16K.

Nuclear Overhauser enhancement (nOe) difference spectra were obtained by subtraction of the off-resonance control free induction decay (FID) from the on-resonance FID. The proton of interest was selectively irradiated for 0.2 s, and the decoupler was gated off during acquisition. A 2.0-s relaxation delay was used. For each irradiation 8 scans were acquired with the cycle of irradiations repeated 20 times. FID's were processed using exponential multiplication (line-broadening 4.0 Hz) and were zero-filled to 32K before Fourier transformation. The sample was not degassed, so the enhancements were not quantitated. All of the observed nOe's were negative.

COSY and RELAY 2D NMR spectra were acquired in the absolute-value mode using the standard pulse sequences $90°–t_1–90°–$ACQ and $90°–t_1–90°–\tau–180°–\tau–90°–$ACQ, respectively. Spectra in $F2$ were acquired over a 2.45-kHz spectral width in 1K data points. The COSY data were acquired in 96 scans for each of the 256 FID's, whereas the RELAY data were acquired in 128 scans. The 90° ^1H pulse width was 19.2 μs. A 1.0-s relaxation delay was used, during which the HDO signal was suppressed by presaturation. The RELAY experiments used the phase cycling scheme given in ref. 15, and used a fixed delay τ of 0.040 s. Zero-filling in $F1$ produced a 512 × 512 data matrix with a digital resolution of 4.787 Hz/point in both dimensions. During 2D Fourier transformation a sine-bell squared window function was applied to both dimensions. The transformed data were then symmetrized.

The ^{13}C spectra were recorded at 125.759 MHz using the 5-mm dual frequency probe. The spectra were acquired in 105 000 scans over 29.4-kHz spectral width in 32K data points. A 30° pulse width of 2.0 μs was used. The data were processed using exponential multiplication (line broadening 4.0 Hz). The values of the $^1H–^{13}C$ one-bond coupling constants were obtained using the gated decoupling technique. A 0.5-s relaxation delay was used. The FID was processed using exponential multiplication (line broadening 3.0 Hz) and was zero-filled to 64K before Fourier transformation.

Chemical shifts for the ^1H NMR spectra are reported in ppm relative to TMS using the HDO signal at 4.60 ppm as internal reference. The ^{13}C chemical shifts were referenced relative to 1,4-dioxane in D_2O at 67.4 ppm as an external reference.

Results and discussion

Examination of the ^1H and ^{13}C NMR spectra of the A-PS (see Fig. 1) shows that the main structural feature is a trisaccharide repeating unit of 6-deoxyhexoses. The H-1 signal for each monosaccharide appeared as a broad singlet (linewidth ≈ 3 Hz), indicating that the value of the H-1–H-2 coupling constant is of this magnitude; this result is consistent with all of the three monosaccharides having the *manno* configuration. Analysis of the alditol acetates showed rhamnose to be the principal monosaccharide (see Table 1). Thus, the bulk of the A-PS is a polymer of rhamnose (a "rhamnan") with three distinct rhamnose units.

Rhamnans have been previously reported to be present in lipopolysaccharide preparations from *Pseudomonas aeruginosa* (11, 12), as well as *P. syringae* (16, 17) and *P. cepacia* (18). Those from *P. aeruginosa* occur as minor components of the LPS, and their presence is seen only after the major O-antigens are selectively hydrolyzed with acid or base; the rhamnans found in the other species are in fact the side chains of the principal LPS's. The two known rhamnans from *P. aeruginosa* (and that from *P. syringae*) have the same repeating unit, comprised of two α-(1→3)-linked rhamnoses and one α-(1→2)-linked rhamnose. A polymer of this repeating unit was synthesized by Tsvetkov *et al.* (13), and its ^{13}C NMR spectrum was reported to be identical with that of the natural rhamnan identified in ref. 12. The reported values of the ^{13}C NMR chemical shifts are ≈0.1 ppm higher than those found for the A-PS (see Table 2), suggesting that the polysaccharide portion of A-band LPS from AK1401 has the same repeating unit. Since the differences in chemical-shift values are consistent, they may be attributable to slight differences in standardization of the two instruments. The similarity between the A-band LPS described by McGroarty and co-workers (5, 6) and the "common antigen" described by Yokota *et al.* (11) had been established by the use of a monoclonal antibody (MAb E87, see ref. 6). The present data confirm this observation, since they show that the repeating unit of the polysaccharide portion of A-band LPS from AK1401 is the same as the repeating unit of the common antigen.

Some differences do exist in the structure of the A-PS from AK1401 compared to the polysaccharides reported previously, notably in the types of monosaccharides that are present as minor components. The monosaccharide composition of A-PS from AK1401 was found by GC and GC–MS analysis of the alditol acetates, and the results obtained under two sets of hydrolytic conditions are shown in Table 1; the difference in the results obtained under the two sets of conditions is noteworthy. Identities were confirmed by coinjection of standard samples, except for the 3-*O*-methylhexose, which was identified from its mass spectrum alone, and which was distinguished from a 4-*O*-methylhexose by GC–MS analysis of the alditol-d_1 acetates.[6]

The minor monosaccharides found for the A-PS derived from AK1401 are slightly different from those found in other rhamnan-based polysaccharides of *Pseudomonas*. For example, Yokota *et al.* (11) found that the polysaccharide from *P. aeruginosa* ATCC 27584 contained rhamnose, a 6-deoxy-3-*O*-methylhex-

[6]The sample of alditol-d_1 acetates was prepared by Dr. A. Sen (Queen's University); the GC–MS data were acquired by J. Peltier (McMaster University).

Can. J. Chem. Downloaded from www.nrcresearchpress.com by 84.41.108.74 on 09/07/12
For personal use only.

Can. J. Chem. Downloaded from www.nrcresearchpress.com by 84.41.108.74 on 09/07/12
For personal use only.

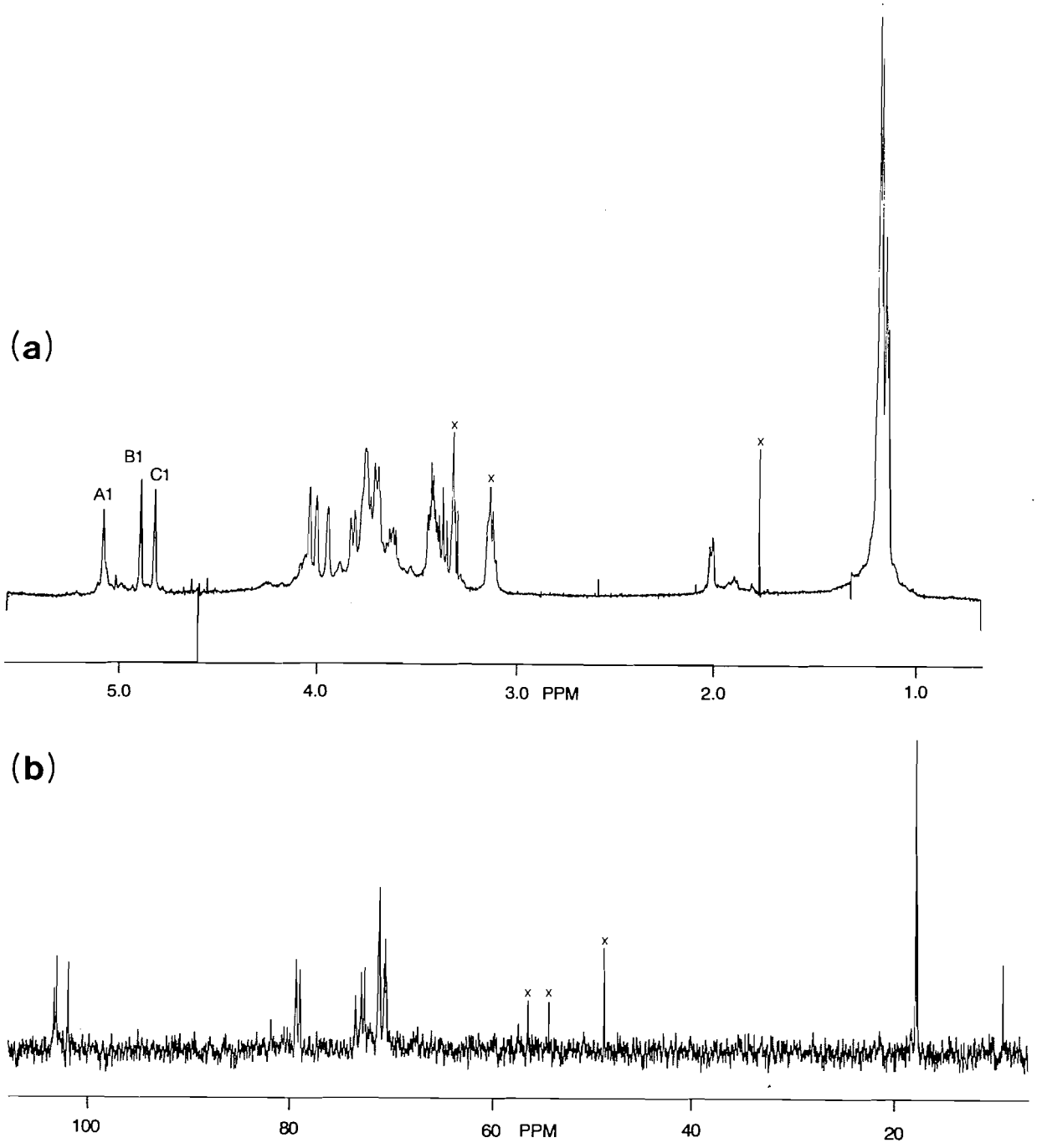


FIG. 1. (a) The 500-MHz ^{1}H NMR spectrum of A-PS from AK1401 in D_2O. The signals for the anomeric protons of residues A, B, and C are indicated. Peaks marked "X" are unassigned. (b) The 125-MHz ^{13}C NMR spectrum.

ose, xylose, glucose, and galactosamine. In the polysaccharide from *P. aeruginosa* serotype O7, Kocharova *et al.* (12) found rhamnose, mannose, glucose, and an unidentified sugar, which was first thought to be ribose; however, no ribitol pentaacetate was found by GC analysis of the alditol acetates derived from the polysaccharide. In contrast, our results clearly show the presence of ribitol pentaacetate in the same type of analysis performed on the A-PS from AK1401. Smith *et al.* (16, 17) studied a polysaccharide from the plant pathogenic species *P. syringae*, and found it to be composed almost entirely of rhamnose, with several minor sugars occurring in much lower amounts than those found in *P. aeruginosa*.

The rhamnose in the A-PS was found to be the unusual D-enantiomer. The same result was reported for the rhamnan from *P. aeruginosa* ATCC 27584 by Yokota *et al.* (11), based on the sign of the optical rotation of the methyl rhamnoside derived from a hydrolysate. Kocharova *et al.* (12) concluded that the rhamnan from *P. aeruginosa* serotype O7 also had only D-rhamnose, based on the sign of the optical rotation of the intact polysaccharide, and by analogy to the results of Smith *et al.* (17), who found only D-rhamnose in a rhamnan, having the same repeating unit, from *P. syringae*. The latter result was obtained using the same method as in the present work, which is better than methods based on optical rotations, since it shows directly that no L-rhamnose is present.

The anomeric configuration of each of the three principal

TABLE 1. Composition of the A-PS from *P. aeruginosa* AK1401

Retention time (min)	Component[a]	Relative intensity[b] A[c]	Relative intensity[b] B[d]
7.9	3-*O*-Methylrhamnitol tetraacetate	26 (1)	9 (0.5)
8.5	Rhamnitol pentaacetate	100	100
9.2	Ribitol pentaacetate	11 (0.5)	13 (0.8)
19.1	3-*O*-Methylhexitol pentaacetate	3	—
20.6	Mannitol hexaacetate	9 (0.5)	13 (3)
22.9	Glucitol hexaacetate	8 (0.6)	20 (4)

[a]Identities are based on electron-impact mass spectra and coelution on GC with authentic standards.
[b]Relative intensities were determined by normalizing the integrated areas from the chromatogram obtained by GC with a flame-ionization detector (referenced to rhamnitol pentaacetate = 100) and averaging several runs. The values in parentheses are the standard deviations for each average intensity.
[c]Values obtained using 2 M HCl in a Teflon vial. In this determination ethyl stearate and ethyl palmitate were detected also; ethyl palmitate coelutes with 3-*O*-methylrhamnitol tetraacetate under the GC conditions used, an aspect that accounts for the elevated relative intensity of this component.
[d]Values obtained using 2 M trifluoroacetic acid in a sealed glass tube.

TABLE 2. Comparison of ^{13}C chemical-shift data for A-PS from AK1401 and a synthetic rhamnan

This work	Ref. 13
103.43	103.5
103.19	103.3
102.01	102.1
79.29	79.4 (2C)
78.96	79.1
73.35	73.5
72.79	72.9
72.46	72.6
71.03	71.2 (3C)
70.54	70.6
70.35	70.5 (2C)
17.81	17.9 (3C)

TABLE 3. Chemical-shift data for signals of anomeric protons and carbons in *Pseudomonas* rhamnans

Source	^1H NMR	^{13}C NMR
Yokota *et al.* (11)	4.96, 5.04, 5.20	—
Kocharova *et al.* (12)	5.02, 5.09, 5.26	102.0, 103.1(2C)
Smith *et al.* (16, 17)	5.05, 5.13, 5.25	101.04, 102.17(2C)
This work	4.82, 4.89, 5.08	102.01, 103.19, 103.43

rhamnose units seen in the NMR spectra was found to be α. The values of J_{C1-H1} were 176, 173, and 173 Hz, and the chemical shifts of the ^{13}C resonances (see Table 3) were 102.0, 103.2, and 103.4 ppm, respectively; Table 3 also shows the chemical shifts of the anomeric ^{13}C and ^1H resonances reported by others. This assignment is in agreement with those of Yokota *et al.* (11) and Kocharova *et al.* (12), which were based on comparisons of chemical shifts using reference compounds. It should be noted that the assignment of the anomeric configuration by determination of the J_{H1-H2} could not be made in this case, because the signals for the anomeric protons were not sufficiently resolved in the spectrum of the A-PS.[7] In contrast, the values of J_{C1-H1} are markedly different between α- and β-rhamnopyranosides (18, 19).

The assignment of the pyranoid ring to the rhamnose units was based on the similarity of the NMR spectral data to those reported by Tsvetkov *et al.* (13) and Smith *et al.* (17); the assignments by these groups were confirmed by synthesis and by methylation analysis, respectively.

The signals for each of the three principal monosaccharides in the 500-MHz ^1H NMR spectrum of the intact A-PS could be assigned, in spite of several overlapping signals, through the use of 2D shift-correlated (COSY) and relayed coherence transfer (RELAY) experiments. The signals of the three anomeric protons were labelled A1, B1, and C1 (where A1 refers to the signal of H-1 of residue A, and so on) starting with the resonance at lowest field (see Fig. 1). COSY spectra were interpreted by starting from the signal of the anomeric proton of each residue, and locating the signal of H-2 of that residue by finding the coupled resonance (by observation of an off-diagonal peak in the COSY spectrum). Thus, proton A1 at 5.079 ppm is coupled to the proton at 3.946 ppm, since there is an off-diagonal peak in the COSY spectrum that correlates them; therefore, the signal at 3.946 ppm is assigned to proton A2, and its neighbor (A3) may be found in a similar fashion. In this way, all of the resonances of a given monosaccharide may be found by analysis of the nearest-neighbor connectivities shown in the COSY spectrum.

In the case of residue B, there are two potential B3-B4 crosspeaks, one of which correlates B3 to the multiplet at 3.442 ppm, and the other correlates B3 with the resonance at 3.13 ppm. This feature may be the result of overlapping resonances at the position of the signal assigned to proton B3, or alternatively B3 has two neighbors in addition to B2. The use of the RELAY experiment in resolving the ambiguity caused by overlapping resonances is illustrated in Fig. 2. Since this experiment shows next-nearest-neighbor connectivities in addition to nearest-neighbor connectivities (the information

[7]It has been reported (A. de Bruyn, M. Anteunis, R. de Gussem, and G. G. S. Dutton. Carbohydr. Res. **47**, 158 (1976)) that J_{H1-H2} = 1.8 Hz for α-rhamnopyranose, 1.1 Hz for β-rhamnopyranose, and 1.7 Hz for methyl α-rhamnopyranoside.

Can. J. Chem. Downloaded from www.nrcresearchpress.com by 84.41.108.74 on 09/07/12
For personal use only.

Can. J. Chem. Downloaded from www.nrcresearchpress.com by 84.41.108.74 on 09/07/12
For personal use only.

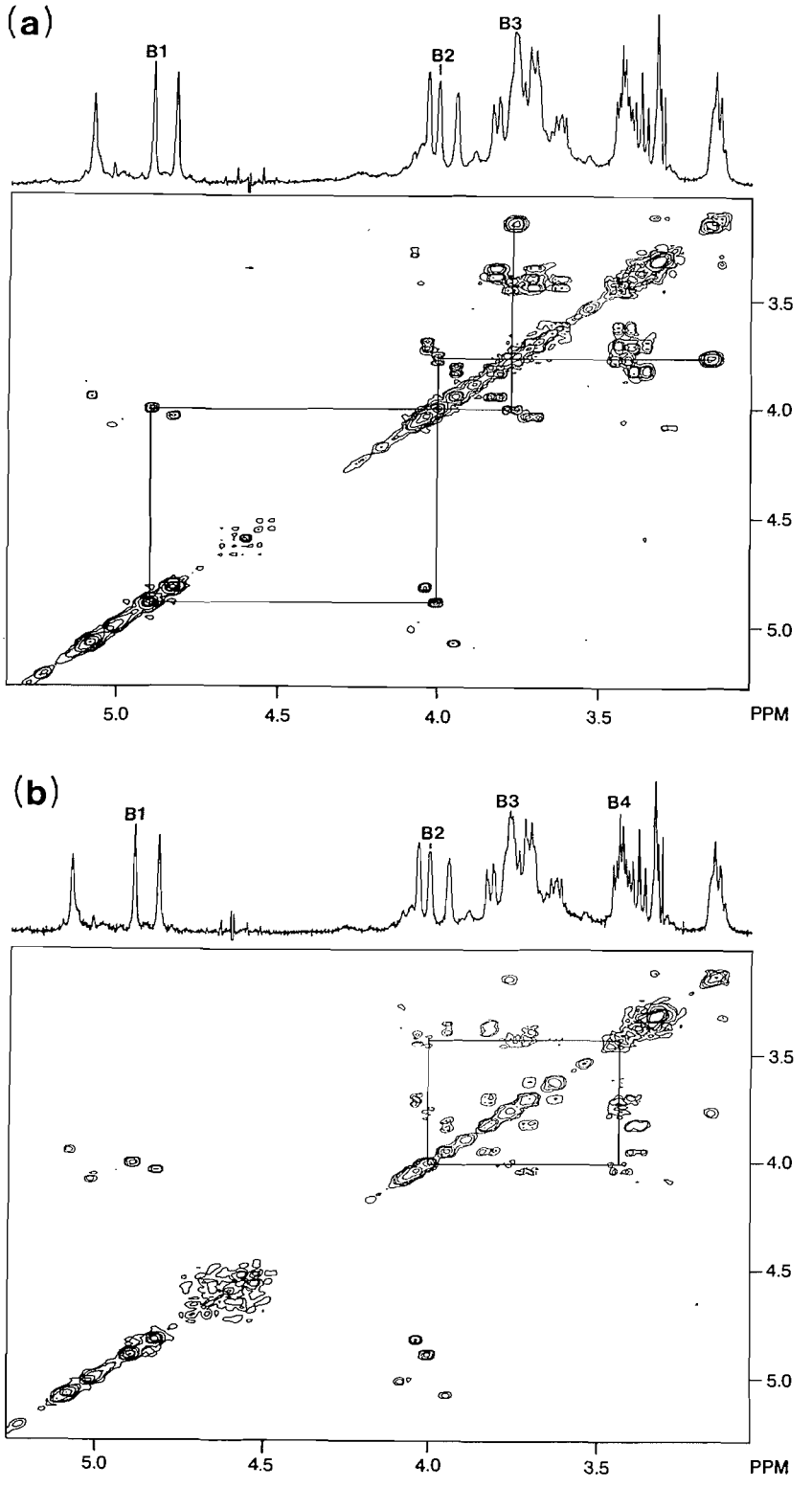


FIG. 2. Portions of the COSY and RELAY spectra of the A-PS from AK1401 in D_2O. In the COSY experiment (a), the signals for protons B1, B2, and B3 may be assigned, since crosspeaks are evident for B1–B2 and B2–B3; however, the assignment of B4 is ambiguous because there are two possible B3–B4 crosspeaks (due to overlapping signals on the diagonal). In the RELAY experiment (b), an additional crosspeak for B2-B4 was observed, thus allowing the assignment of B4; only the B2-B4 correlation is indicated for clarity.

contained in a COSY spectrum), the assignment of the signal for proton B4 is clarified by the presence of an additional crosspeak which correlates B2 to B4. Thus, the RELAY experiment shows a correlation between the known B2 resonance at 4.002 ppm and the B3 resonance at ≈3.77 ppm (as in COSY), and also a correlation between the B2 resonance and the resonance at 3.442 ppm. Therefore, the signal at 3.442 ppm is assigned to proton B4, and the additional crosspeak seen in the COSY spectrum that correlated the B3 resonance to the resonance at 3.13 ppm must be the result of another resonance overlapped

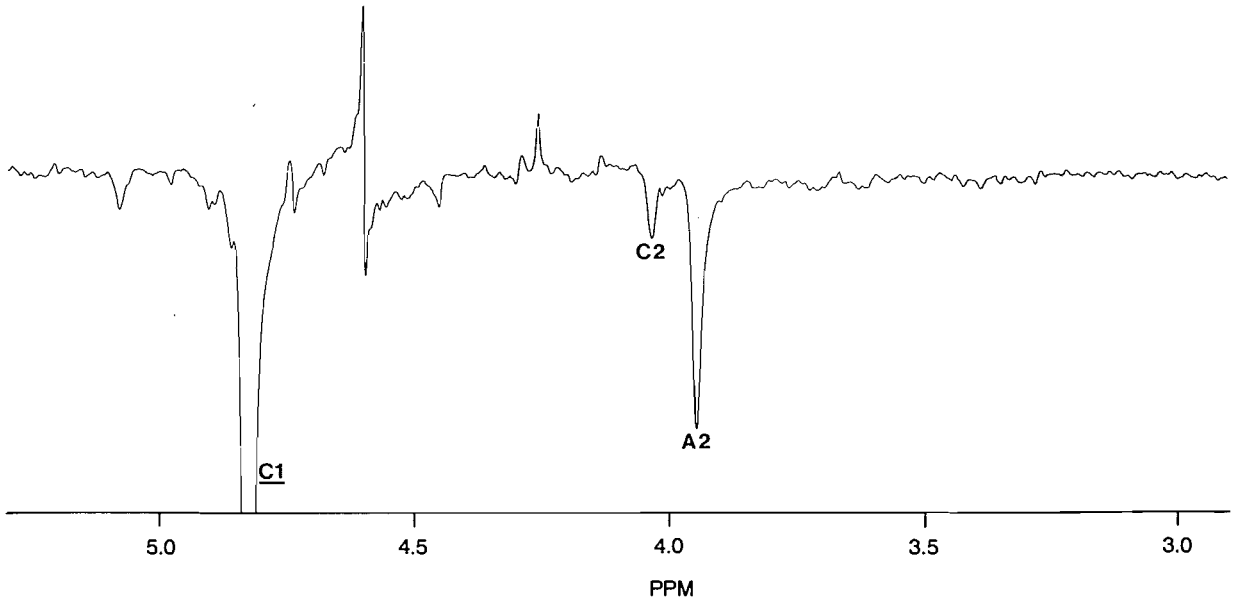


FIG. 3. A representative nOe difference experiment. Upon irradiation of proton C1, negative enhancements of A2 and C2 were observed. The inter-residue enhancement allowed the assignment of the sequence of residues (C → A) and the linkage position {C-(1→2)-A}.

TABLE 4. ^{1}H NMR data for A-PS from AK1401 in D_2O

Proton	Chemical shift	Multiplicity	Coupling constant(s)
Residue A			
H-1	5.079	br s	$J_{1,2}$ = 1.7 Hz[a]
H-2	3.946	br s	$J_{2,3}$ = 3.3 Hz[a]
H-3	3.825	dd	$J_{3,4} \approx 10$ Hz
H-4	3.374	apparent t	$J_{4,5} \approx 10$ Hz
H-5	3.71	m[b]	—
H-6,6′,6″	1.175	d	$J_{5,6}$ = 5.5 Hz
Residue B			
H-1	4.894	br s	$J_{1,2} < 2$ Hz
H-2	4.002	br s	$J_{2,3} \approx 3$ Hz
H-3	3.77	br m[c]	$J_{3,4} \approx 10$ Hz
H-4	3.442	sextet[d]	$J_{4,5} \approx 10$ Hz
H-5	3.76	br m[c]	—
H-6,6′,6″	1.175	d	$J_{5,6}$ = 5.5 Hz
Residue C			
H-1	4.823	br s	$J_{1,2} < 2$ Hz
H-2	4.037	br s	$J_{2,3} \approx 3$ Hz
H-3	3.71	m[b]	$J_{3,4} \approx 10$ Hz
H-4	3.432	sextet[d]	$J_{4,5} \approx 10$ Hz
H-5	3.62	dq	—
H-6,6′,6″	1.140	d	$J_{5,6} \approx 6$ Hz

[a] $J_{1,2}$ and $J_{2,3}$ for residue A were determined from the spectrum at 80°C.
[b] The signals of H-5 of residue A and H-3 of residue C were overlapped.
[c] H-3 and H-5 of residue B are part of the same multiplet, together with an unknown resonance.
[d] The H-4 signals of residues B and C were overlapped.

TABLE 5. Observed nuclear Overhauser enhancements

Irradiated proton	Enhanced signals[a]
A1	B3 (strong), C5, A2, H-6's
B1	B2, C3-A5 multiplet
C1	A2 (strong), C2
A2	C1 (strong), A3, A1
B2	B1, C3-A5 multiplet
C2	C1, B5, C3-A5 multiplet
A3	A2 (weak)
B3–B5	A1, C2, H-6's, B2
C3–A5	B1, H-6's, C2, B2, B4-C4 multiplet, A4
C5	H-6's, A1, B4-C4 multiplet
C6	C4-B4 (weak), C5
A6–B6	C3-A5, B5, A4, B4-C4 multiplet

[a] Enhanced signals are listed in order of decreasing intensity.

with that of B3. The nature of this additional resonance was not clarified by the RELAY spectrum, so that it and the resonance at 3.13 ppm remain unassigned. It is interesting to note that the signal at 3.13 ppm is absent when the A-band LPS from AK1401 was obtained by extraction using a different procedure (phenol–chloroform – petroleum ether). A summary of the signal assignments is given in Table 4. Some of the coupling constants were obtained by observation of the ^{1}H NMR spectrum at 80°C; however, the chemical shifts reported are those from the room-temperature spectrum.

The sequence of and linkage positions between residues A, B, and C were determined by observation of inter-residue nOe's. The result of a representative nOe experiment is shown in Fig. 3, and the data are in Table 5. If one considers the linkage α-D-Rha*p*-(1→2)-D-Rha*p*, it is apparent from a Dreiding model that the anomeric proton cannot approach within a distance of 3 Å to the H-3 of the next residue. Thus, an α-(1→2) linkage would not show a significant nOe of the signal of H-3 upon irradiation of the anomeric proton of the neighboring unit (see also ref. 18). Since irradiation of protons A1 and B1 resulted in nOe's of the signals of protons B3 and C3, respectively, neither of the linkages, A → B and B → C, can be α-(1→2). Since irradiation of C1 gave a strong nOe of the signal of A2, but not of any H-3 signal, only C → A can be a 1 → 2 linkage, whereas A → B and B → C are α-(1→3) linkages. Furthermore, the results of the nOe difference experiments involving intra-residue connectivities provide confirmatory evidence for the α configuration, as indicated, for example, by the absence of an nOe of H-3 or H-5 upon irradiation of H-1. Thus, the repeating-unit structure of the A-PS from AK1401 is as follows.

Can. J. Chem. Downloaded from www.nrcresearchpress.com by 84.41.108.74 on 09/07/12
For personal use only.

$$[\rightarrow 2\text{-}\alpha\text{-D-Rha}p\text{-}(1\rightarrow 3)\text{-}\alpha\text{-D-Rha}p\text{-}(1\rightarrow 3)\text{-}\alpha\text{-D-Rha}p\text{-}(1\rightarrow]_n$$

A **B** **C**

This complete assignment of the ^{1}H NMR spectrum complements the assignment of the ^{13}C NMR spectrum of this repeating unit reported by Tsvetkov *et al.* (13).

Although this repeating unit is the same as that found by other workers (11, 12, 16), our work represents the first complete assignment of the ^{1}H NMR spectrum of the polysaccharide. Work is in progress to determine the role of the minor sugar constituents in the structure of the A-PS.

Conclusions

The polysaccharide portion of A-band LPS from *Pseudomonas aeruginosa* mutant AK1401 (derived from strain PAO1, serotype O5) was found to have the same repeating-unit structure as other rhamnans from *P. aeruginosa* (11, 12), and from *P. syringae* (16, 17). The A-PS consists principally of rhamnose, but also has lesser amounts of 3-*O*-methylrhamnose, ribose, glucose, mannose, and a 3-*O*-methylhexose; these minor sugars differ from those found in other rhamnans from *Pseudomonas*. The rhamnose was shown to be the unusual D-enantiomer. The ^{1}H NMR spectrum of the intact A-PS was assigned for the three rhamnose units of the repeating structure, and this assignment allowed the determination of the linkage positions and sequence of residues by nOe difference spectroscopy.

Acknowledgements

This work was supported by grants from the Canadian Cystic Fibrosis Foundation (CCFF) and the Natural Sciences and Engineering Research Council of Canada. One of us (T.L.A.) gratefully acknowledges the receipt of Ontario Graduate Scholarships (1986–1987 and 1988–1989) and a CCFF Studentship (1989–1990). The authors would like to thank Dr. J. C. Richards (National Research Council, Ottawa) for helpful discussion regarding the nOe experiments, Dr. G. O. Aspinall (York University) for kindly providing a sample of 3-*O*-methylrhamnose, Dr. A. Sen (Queen's University) for preparing A-band LPS isolated by phenol–chloroform – petroleum ether extraction, and for preparing the sample of alditol-d_1 acetates, and J. Peltier for some of the GC–MS data.

1. J. R. W. Govan and S. Glass. Rev. Med. Microbiol. **1**, 19 (1990).
2. M. Y. C. Lam, E. J. McGroarty, A. M. Kropinski, L. A. MacDonald, S. S. Pedersen, N. Hoiby, and J. S. Lam. J. Clin. Microbiol. **27**, 962 (1989).
3. L. Kenne and B. Lindberg. *In* The polysaccharides. Vol. 2. *Edited by* G. O. Aspinall. Academic Press, New York, NY. 1983. pp. 287–363.
4. Y. A. Knirel, E. V. Vinogradov, N. A. Kocharova, N. A. Paramonov, N. K. Kochetkov, B. A. Dmitriev, E. S. Stanislavsky, and B. Lanyi. Acta Microbiol. Hung. **35**, 3 (1988).
5. M. Rivera, L. E. Bryan, R. E. W. Hancock, and E. J. McGroarty. J. Bacteriol. **170**, 512 (1988).
6. M. Rivera and E. J. McGroarty. J. Bacteriol. **171**, 2244 (1989); E. J. McGroarty and M. Rivera. Infect. Immun. **58**, 1030 (1990).
7. D. Berry and A. M. Kropinski. Can. J. Microbiol. **32**, 436 (1986).
8. A. Fox, S. L. Morgan, and J. Gilbart. *In* Analysis of carbohydrates by glc and ms. *Edited by* C. J. Biermann and G. D. McGinnis. CRC Press, Boca Raton, FL. 1989. pp. 87–117.
9. K. Leontein, B. Lindberg, and J. Lönngren. Carbohydr. Res. **62**, 359 (1978).
10. K. Bock and C. Pedersen. J. Chem. Soc. Perkin Trans. 2, 293 (1974).
11. S.-I. Yokota, S. Kaya, S. Sawada, T. Kawamura, Y. Araki, and E. Ito. Eur. J. Biochem. **167**, 203 (1987).
12. N. A. Kocharova, Y. A. Knirel, N. K. Kochetkov, and E. S. Stanislavskii. Bioorg. Khim. **14**, 701 (1988).
13. Y. E. Tsvetkov, L. V. Backinowsky, and N. K. Kochetkov. Carbohydr. Res. **193**, 75 (1989).
14. R. P. Darveau and R. E. W. Hancock. J. Bacteriol. **155**, 831 (1983).
15. D. W. Hughes, R. A. Bell, T. Neilson, and A. D. Bain. Can. J. Chem. **63**, 3133 (1985).
16. A. R. W. Smith, S. E. Zamze, and R. C. Hignett. J. Gen. Microbiol. **131**, 963 (1985).
17. A. R. W. Smith, S. E. Zamze, S. M. Munro, K. J. Carter, and R. C. Hignett. Eur. J. Biochem. **149**, 73 (1985).
18. A. S. Shashkov, Y. A. Knirel, N. V. Tanatar, and N. K. Kochetkov. Carbohydr. Res. **146**, 346 (1986).
19. L. D. Hall and G. A. Morris. Carbohydr. Res. **82**, 175 (1980).

Can. J. Chem. Downloaded from www.nrcresearchpress.com by 84.41.108.74 on 09/07/12
For personal use only.

Effets des sels de terres rares sur quelques phosphates dérivés des métabolites de la glycolyse

CLAUDE RABILLER,[1] PHILIPPE EYMARD ET MAHMOUD MESBAHI
Laboratoire de RMN et réactivité chimique, Unité associée 472 du Centre national de la recherche scientifique, Faculté des sciences et techniques, 2 rue de la Houssinière, 44072 Nantes CEDEX 03, France

Reçu le 13 décembre 1990

CLAUDE RABILLER, PHILIPPE EYMARD et MAHMOUD MESBAHI. Can. J. Chem. **69**, 1281 (1991).

Les dérivés phosphatés du glucose et du fructose sont des intermédiaires importants dans la fermentation des sucres. L'étude du devenir de leurs protons (ou deutérons) par spectroscopie RMN doit fournir des informations sur les transferts de protons (ou deuterons) susceptibles d'intervenir au cours de cette bio-transformation. Dans cette note, nous décrivons l'influence de la complexation de ces métabolites avec le chlorure de praséodyme ainsi que celle du pH sur leurs déplacements chimiques protoniques. On décrit par ailleurs les conditions dans lesquelles tous les protons des formes α et β de ces sucres cycliques sont individualisés. On a trouvé que le glucose-1-phosphate présente les meilleures aptitudes pour ce type d'étude. De plus, la comparaison du comportement de ces composés avec celui de l'acide 2-phosphoglycérique permet de préciser la conformation de ce dernier.

Mots clés : dérivés phosphatés des sucres, RMN, effets des terres rares.

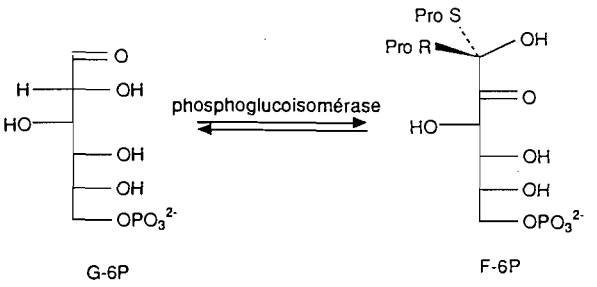
CLAUDE RABILLER, PHILIPPE EYMARD, and MAHMOUD MESBAHI. Can. J. Chem. **69**, 1281 (1991).

Phosphate derivatives of glucose and fructose are well-known intermediates in sugar fermentation. Proton and deuterium NMR spectroscopy studies of the fermentation process provide information about proton (deuteron) transfers that are likely to occur in such biotransformations. In this paper we describe the influence of complexation of those metabolites with praseodymium trichloride and of pH on their proton NMR chemical shifts. We determine the conditions under which all the protons of both the α and β forms of these cyclic sugars are separated. Glucose-1 phosphate was found to be the most suitable derivative for this type of study. Furthermore, comparing the behaviour of these compounds with 2-phosphoglyceric acid allows us to specify the exact conformation of the latter.

Key words: phosphate sugar derivatives, NMR, LIS effects.

Introduction

La bioconversion du glucose en alcool, en glycérol ou en acide lactique fait intervenir un certain nombre de métabolites bien connus tels que les dérivés phosphatés du glucose, du fructose et des sucres à trois atomes de carbone. Les transferts de protons accompagnant les différentes étapes de cette bio-transformation suscitent encore de nombreux travaux (1–4). Il en est ainsi par exemple de l'isomérisation du glucose-6-phosphate (G-6P) en fructose-6-phosphate (F-6P) :



G-6P F-6P

Le proton introduit en position pro-*R* provient à la fois du milieu et d'un transfert intramoléculaire (3, 4). On ignore cependant avec certitude dans quelle proportion et quels sont les facteurs susceptibles de la modifier. Pour ce type d'étude, la RMN du proton ou du deutérium en abondance naturelle (5–8) est susceptible d'apporter des renseignements complémentaires dans la mesure où les différents sites « protons » ou « deutérons » d'une molécule donnée sont bien séparés.

Cependant, qu'il s'agisse du glucose, du fructose, de leurs dérivés monophosphatés, bis-phosphatés ou de l'acide gluconique, la quasi-isochronie des déplacements chimiques rend cette approche très délicate. Ainsi, par exemple, les sept protons du fructose-1,6 bis-phosphate résonnent sur une plage de 0,5 ppm !

Lorsque l'on veut étudier ces métabolites, on a en général recours à leurs dérivés dont certains présentent des spectres mieux résolus. Des renseignements intéressants, bien qu'incomplets, ont pu être obtenus sur le glucose (9) à partir de son pentaacétate par RMN du deutérium. Il faut cependant souligner que les techniques de dérivatisation utilisées dans la chimie des sucres sont souvent délicates à manier et nécessitent de plus la mise en oeuvre de laborieuses techniques de séparation.

Une autre approche consiste à utiliser les effets de sels de terres rares en milieu aqueux (Lanthanide Induced Shift : LIS). La littérature recèle de très nombreux travaux relatifs aux effets LIS en milieu organique. Assez curieusement, peu d'études ont été consacrées aux solutions aqueuses et moins encore aux sucres dans ce milieu. Le comportement des déplacements chimiques des acides glycérique, gluconique et lactobionique a cependant fait l'objet d'un travail détaillé (10). Une très grande dépendance des déplacements chimiques en fonction de la concentration en sel de terre rare et du pH y est observée. Les nitrates d'europium et de praséodyme déplacent les protons à champ faible alors qu'une augmentation du pH provoque l'effet inverse.

On imagine alors le parti que l'on peut tirer de ces deux effets contradictoires en vue d'individualiser les différents protons ou deutérons des métabolites que nous nous proposons d'étudier. L'objet de ce travail est donc de déterminer si les phosphates dérivés du glucose présentent le même type de comportement que les acides de l'étude précédente et, dans l'affirmative, d'optimiser les conditions de concentration et de pH pour obtenir la meilleure séparation des massifs. Seront ainsi étudiés les glucose-6- et -1-phosphates (G-6P et G-1P), le fructose-6-phosphate (F-6P), le fructose-1,6 bis-phosphate (F-1,6P), l'acide gluconique et à titre de comparaison, l'acide 2-phospho-

1. Auteur à qui adresser toute correspondance.

Can. J. Chem. Downloaded from www.nrcresearchpress.com by 84.41.108.74 on 09/07/12
For personal use only.

Can. J. Chem. Downloaded from www.nrcresearchpress.com by 84.41.108.74 on 09/07/12
For personal use only.

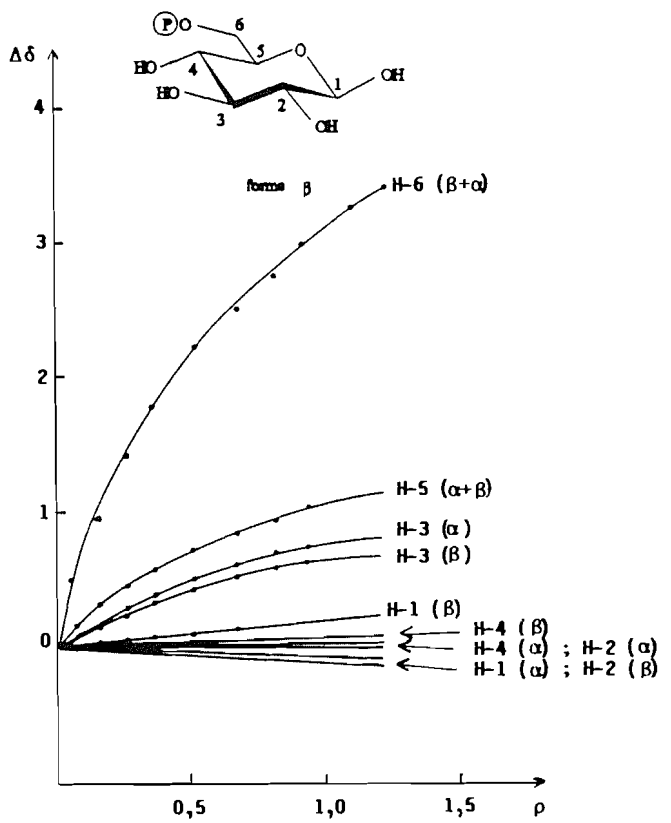


FIG. 1. Variation des déplacements chimiques des protons du glucose-6-phosphate **1** en fonction de la concentration en sel de praséodyme; $\Delta\delta$ (ppm) = δ_H (ρ = 0) − δ_H (ρ = x); ρ = [$PrCl_3 \cdot 6H_2O$] [Glucose-6-phosphate]; C = 0,1 mol/L dans D_2O.

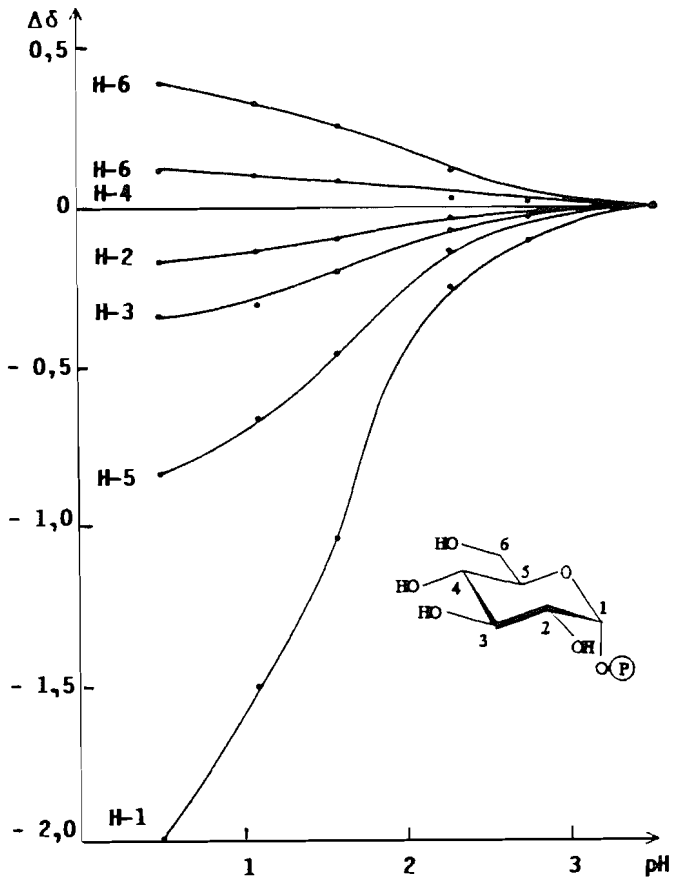


FIG. 2. Variation des déplacements chimiques des protons du glucose-1-phosphate **2** complexé à $PrCl_3 \cdot 6H_2O$ (ρ = 0,25), en fonction du pH; $\Delta\delta$ (ppm) = δ_H (pH = 3,5) − δ_H (pH = x); ρ = 0,25 = constante; C = 0,1 mol/L dans D_2O.

glycérique (2-PG) ainsi que l'acide phosphoénolpyruvique (PEP). Le sel de terre rare utilisé est le chlorure de praséodyme $PrCl_3 \cdot 6H_2O$.

Partie experimentale

Les différents composés phosphorés étudiés au cours de ce travail proviennent de chez Sigma. Ils ont été utilisés sans autre purification. Le chlorure de praséodyme $PrCl_3 \cdot 6H_2O$ a été fourni par Ventron (Karlsruhe). Nous l'avons transformé en $PrCl_3 \cdot 6D_2O$ par dissolution dans D_2O (fournie par le service des Molécules Marquées, CEA Saclay) suivie d'un séchage sous pression réduite.

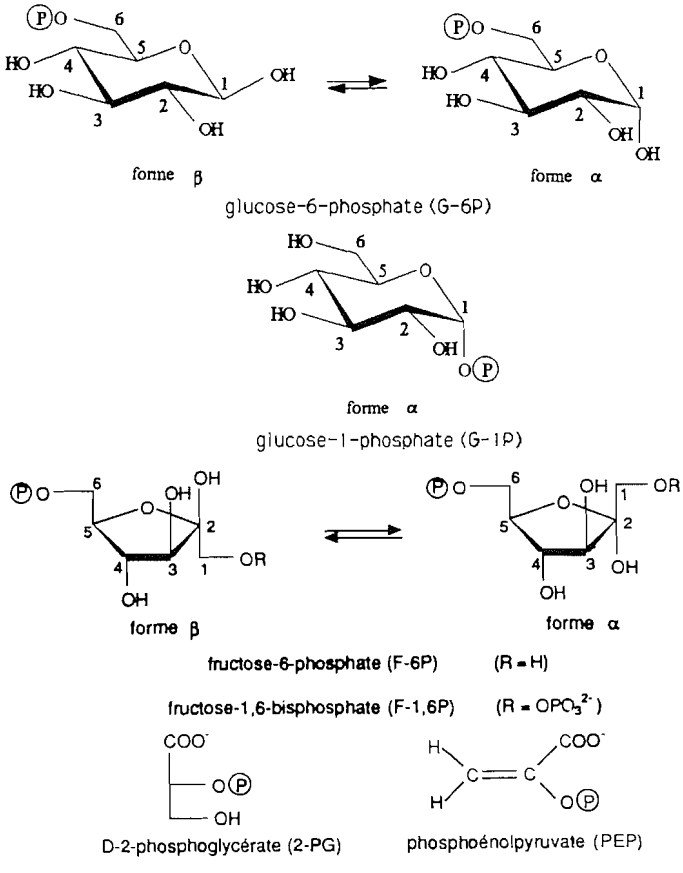
Les spectres de RMN ont été enregistrés sur un appareil Bruker WM opérant à la fréquence de 250 MHz pour le proton. Les expériences COSY-HH ont été menées sur un spectromètre Bruker AM 500 MHz à l'aide d'un train de séquences multiimpulsionnelles pré-programmées sur l'appareil (programme COSY-H-H-DQC) avec l'élimination du pic de l'eau.

Les déplacements chimiques (en ppm) sont mesurés à partir du sel de sodium de l'acide 4,4-diméthyl-4-silapentanesulfonique (DSS) (Merck).

Les solutions sont préparées par introduction de 0,5 mmol de produit et d'une petite quantité de DSS dans 5 mL d'eau lourde. On introduit progressivement des quantités connues de sel de praséodyme $PrCl_3 \cdot 6D_2O$, détermine à chaque fois la valeur de ρ et mesure le pH correspondant. Si nécessaire, on acidifie le milieu à l'aide d'une solution 6,2 N DCl, pour solubiliser le complexe formé. Avant chacune des mesures de RMN, ces solutions sont filtrées.

Résultats et discussion

Les structures des différents hydrates de carbone phosphatés étudiés sont les suivantes :[2]



2. Dans la suite du texte, le groupement phosphate sera schématisé par O Ⓟ.

Can. J. Chem. Downloaded from www.nrcresearchpress.com by 84.41.108.74 on 09/07/12
For personal use only.

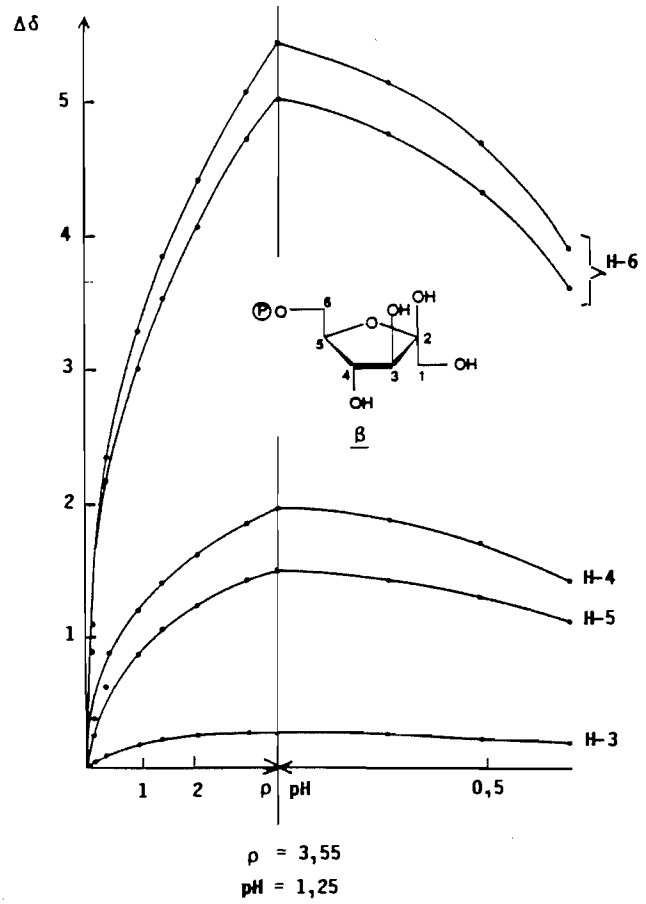


FIG. 3. Variation des déplacements chimiques des protons du fructose-6-phosphate **3** en fonction de la concentration en sel de praséodyme [$PrCl_3 \cdot 6H_2O$] et du pH (seuls les protons de la forme β sont représentés).

$$\Delta\delta\ (\text{ppm}) = \delta_H\ (\rho = 0) - \delta_H\ (\rho = x) \qquad 0 \leq \rho \leq 3{,}55$$
puis $$\Delta\delta\ (\text{ppm}) = \delta_H\ (\text{pH} = 1{,}25 - \delta_H\ (\text{pH} = x) \quad 1{,}25 \leq \text{pH} \leq 0{,}17$$

avec ρ = constante = 3,55; C = 0,1 mol/L dans D_2O.

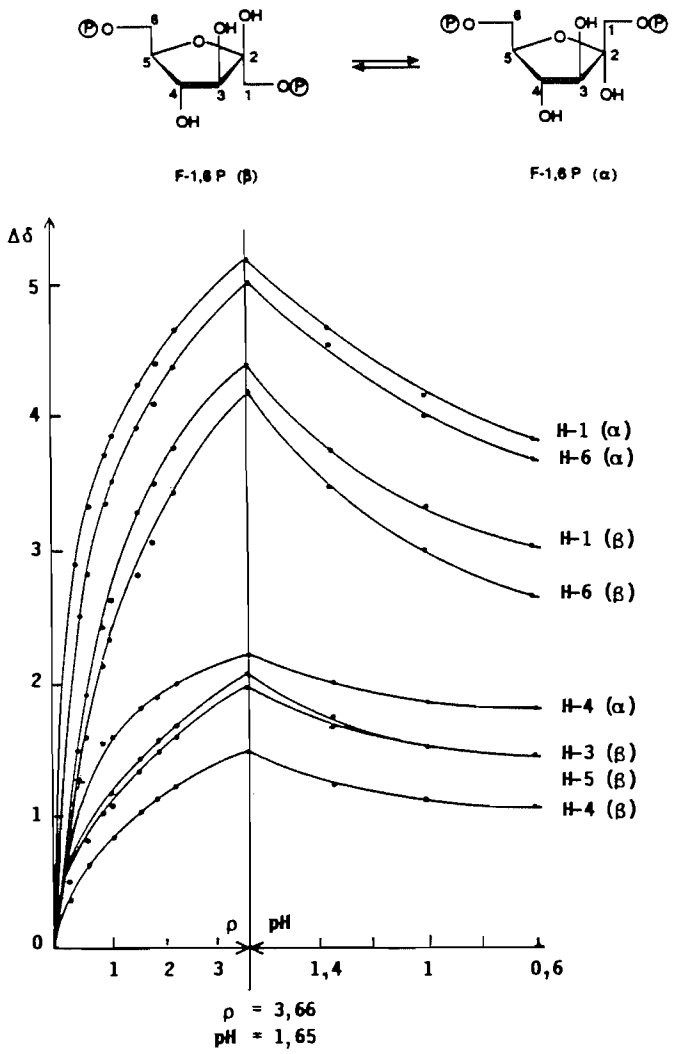


FIG. 4. Variation des déplacements chimiques des protons du fructose-1,6 bis phosphate **4** en fonction de la concentration en $PrCl_3 \cdot 6H_2O$ et du pH.

$$\Delta\delta\ (\text{ppm}) = \delta_H\ (\rho = 0) - \delta_H\ (\rho = x) \qquad 0 \leq \rho \leq 3{,}66$$
puis $$\Delta\delta\ (\text{ppm}) = \delta_H\ (\text{pH} = 1{,}65) - \delta_H\ (\text{pH} = x) \quad 1{,}65 \leq \text{pH} \leq 0{,}6$$

Les courbes de variation des déplacements chimiques protoniques avec la concentration en sel de praséodyme et en fonction du pH sont représentées sur les figures 1 (glucose-6-phosphate), 2 (glucose-1-phosphate), 3 (fructose-6-phosphate), 4 (fructose-1,6 bis-phosphate), 5 (acide D-phospho-2 glycérique) et 6 (acide phosphoénolpyruvique). Il faut noter que l'addition de $PrCl_3 \cdot 6H_2O$ aux solutions des sucres étudiés se traduit non seulement par de fortes variations de déplacement chimique mais également par un élargissement des raies d'autant plus important que la valeur de ρ est grande. Il peut être ainsi délicat d'attribuer les protons du fait de l'impossibilité d'analyser la multiplicité des massifs et de mesurer les constantes de couplage. L'attribution a alors été réalisée à l'aide de la séquence RMN bi-dimensionnelle COSY-HH. La figure 7 représente ainsi le spectre 2D COSY-HH du F-1,6P. Les variations de déplacement sont calculées à partir de la récente attribution du spectre ^1H de ce composé (11). L'analyse des raies du glucose-1-phosphate a été réalisée sur la base de travaux antérieurs (12). Par ailleurs, le complexe substrat–$PrCl_3 \cdot 6H_2O$ est totalement insoluble à pH = 6–7. Il est nécessaire d'acidifier le milieu dans tous les cas jusqu'à une valeur de pH ~ 2–3 pour obtenir une dissolution totale. L'examen des figures 1–6 indique que tous les protons sont déplacés à champs faibles sous l'influence du chlorure de praséodyme. Un effet inverse intervient pour les protons éloignés du phosphore : c'est le cas par exemple des protons H-4 et H-2 du G-6P ou H-6 du G-1P.

De plus, compte tenu des valeurs Δδ observées, il est clair que le centre de complexation se situe essentiellement sur la fonction phosphate. Les protons localisés à proximité du phosphore sont très fortement déplacés. C'est le cas des protons H-6, H-5 du G-6P, H-1, H-5 du G-1P, H-6, H-5, H-4 du F-6P ou H-1, H-6 du F-1,6P. La comparaison des formes structurales α et β de ce dernier illustre également ce propos. La forme α qui possède les deux groupes phosphates en *cis* présente des variations de déplacement $\Delta\delta_{H\text{-}1\alpha}$ et $\Delta\delta_{H\text{-}6\alpha}$ plus intenses que les correspondantes de la forme β. Le proton H-4 du F-1,6P (α) qui se trouve en *cis* des deux fonctions phosphate subit également des écarts de déplacement plus importants que ceux observés pour H-4β (voir figure 4).

Au contraire, pour une valeur de ρ donnée, une diminution du pH entraîne un abaissement des déplacements chimiques des protons proches du phosphore et une augmentation des déplacements protons éloignés (cas des H-6 du G-1P, voir figures 2 et 8). Ces tendances sont également confirmées en comparant le comportement des formes α et β du G-6P.

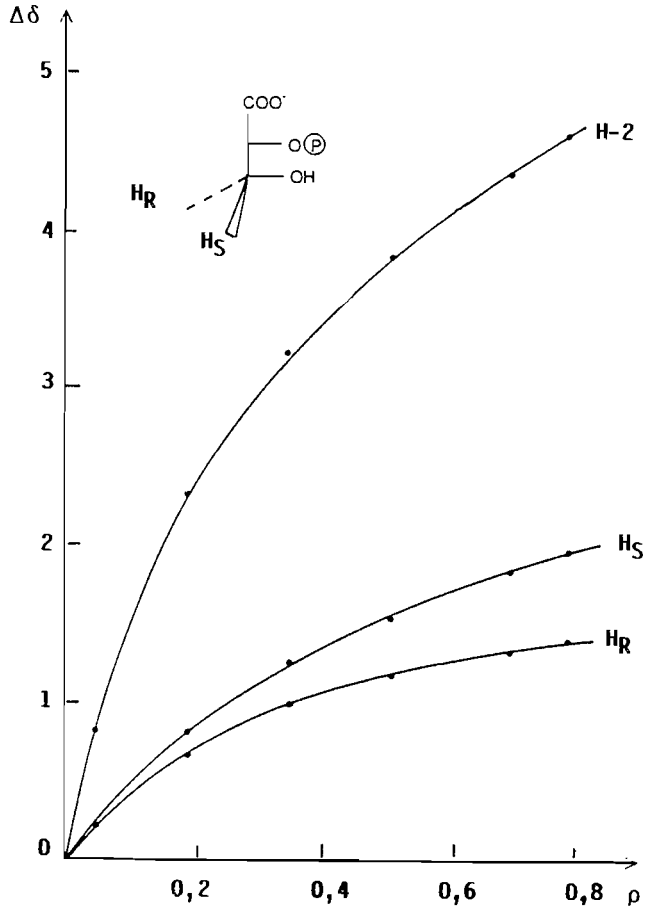
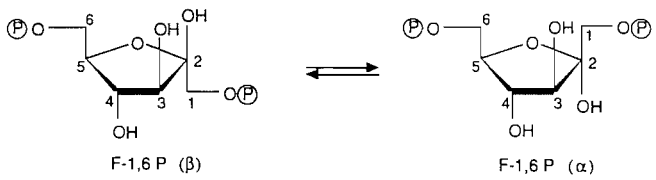
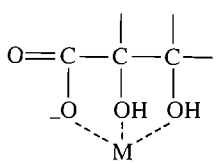


FIG. 5. Variation des déplacements chimiques des protons de l'acide D-2-phosphoglycérique **5** avec la concentration en $PrCl_3 \cdot 6H_2O$; $\Delta\delta$ (ppm) = δ_H (ρ = 0) − δ_H (ρ = x); C = 0,1 mol/L; pH = 1,8 (à ρ = 0).



Il faut noter de plus que l'allure des courbes $\Delta\delta$ en fonction de ρ est manifestement le résultat de deux phénomènes puisque l'addition du $PrCl_3 \cdot 6H_2O$ se traduit non seulement par la complexation du substrat, mais également par une modification non négligeable du pH. Nous donnons à titre indicatif cette variation dans le cas de l'étude $\Delta\delta = f(\rho)$ pour le F-1,6P (voir tableau 1). L'écart de 0,7 unité de pH, en passant de ρ = 0 à ρ = 3,66, est susceptible d'infléchir grandement la courbe de variation $\Delta\delta = f(\rho)$. En effet à ρ = constante (3,55), on note sur la figure 3 un abaissement des déplacements chimiques d'environ 1,5 ppm par unité de pH pour les protons H-6 du F-6P. Ces observations vont tout à fait dans le sens de celles effectuées antérieurement sur des composés analogues possédant une fonction acide carboxylique (10). De plus, les auteurs de ce travail postulent l'existence d'une complexation à trois centres du type :



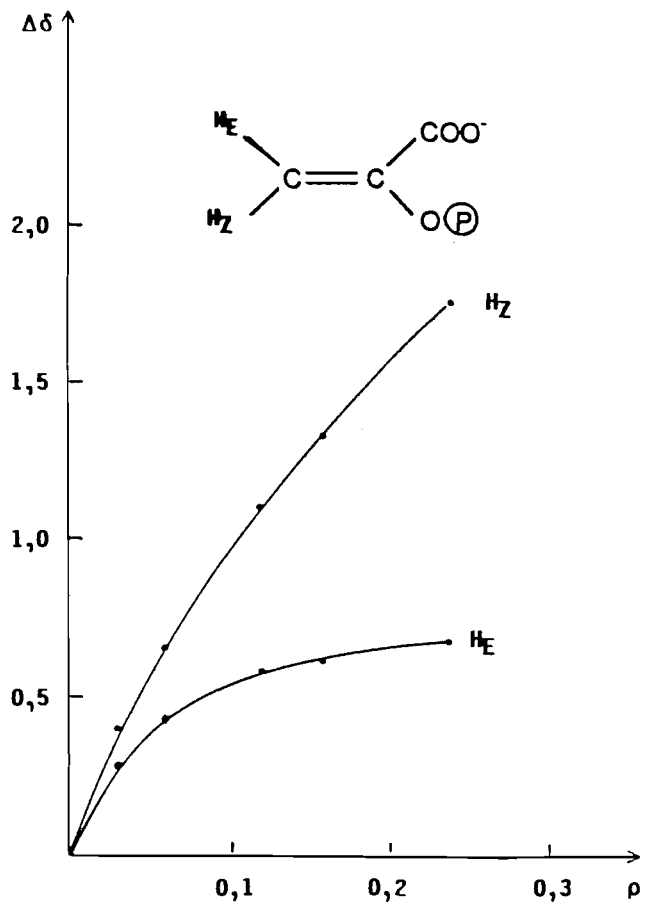


FIG. 6. Variation des déplacements chimiques des protons de l'acide phosphoénolpyruvique **6** en fonction de la concentration en $PrCl_3 \cdot 6H_2O$; $\Delta\delta$ (ppm) = δ_H (ρ = 0) − δ_H (ρ = x); C = 0,1 mol/L.

TABLEAU 1. Variation du pH avec la concentration en $PrCl_3 \cdot 6\ H_2O$ d'une solution de fructose-1,6 bis phosphate (0,1 mol/L dans D_2O; pH ajusté à 2,35 avec une solution 6,2 N de DCl)

ρ^a	0	0,29	0,48	0,61	1,09	1,88	2,33	3,6
pH	2,35	2,25	2,15	2,05	2,00	1,85	1,80	1,65

[a] ρ = [$PrCl_3 \cdot 6\ H_2O$] [Substrat]

Cela ne semble pas être le cas en ce qui concerne les formes α ou β du G-1P ou G-6P et du F-6P ou du F-1,6P, dont les structures se prêtent mal à l'établissement d'une telle association. On trouvera dans le tableau 2, les meilleures conditions de séparation pour les divers métabolites étudiés.

De plus, le PEP, qui ne possède que deux centres de complexation, voit cependant ses protons fortement déplacés (voir figure 6). La fonction phosphate apparaît donc comme un puissant agent de complexation pour le praséodyme. Cette tendance est également fortement confirmée par l'amplitude relative des variations de déplacements des protons éthyléniques H(Z) et H(E). L'attribution des protons du PEP a été réalisée sur la base d'expériences de deutération stéréosélective enzymatique (13) et chimiques (14). En solution aqueuse, on mesure $\delta_{H(Z)}$ = 5,51 ppm et $\delta_{H(E)}$ = 5,87 ppm (référence DSS). Lors des additions successives de $PrCl_3 \cdot 6H_2O$, on constate que H(Z) se déplace beaucoup plus rapidement que H(E) (H(Z) « double » H(E)). Pour une valeur de ρ = 0,24, on a $\Delta\delta_{H(Z)}$ = 1,75 ppm et $\Delta\delta_{H(E)}$ = 0,68 ppm. Ces mesures montrent sans ambiguité une nette préférence pour le groupe OPO_3H_2 par

Can. J. Chem. Downloaded from www.nrcresearchpress.com by 84.41.108.74 on 09/07/12
For personal use only.

Can. J. Chem. Downloaded from www.nrcresearchpress.com by 84.41.108.74 on 09/07/12
For personal use only.

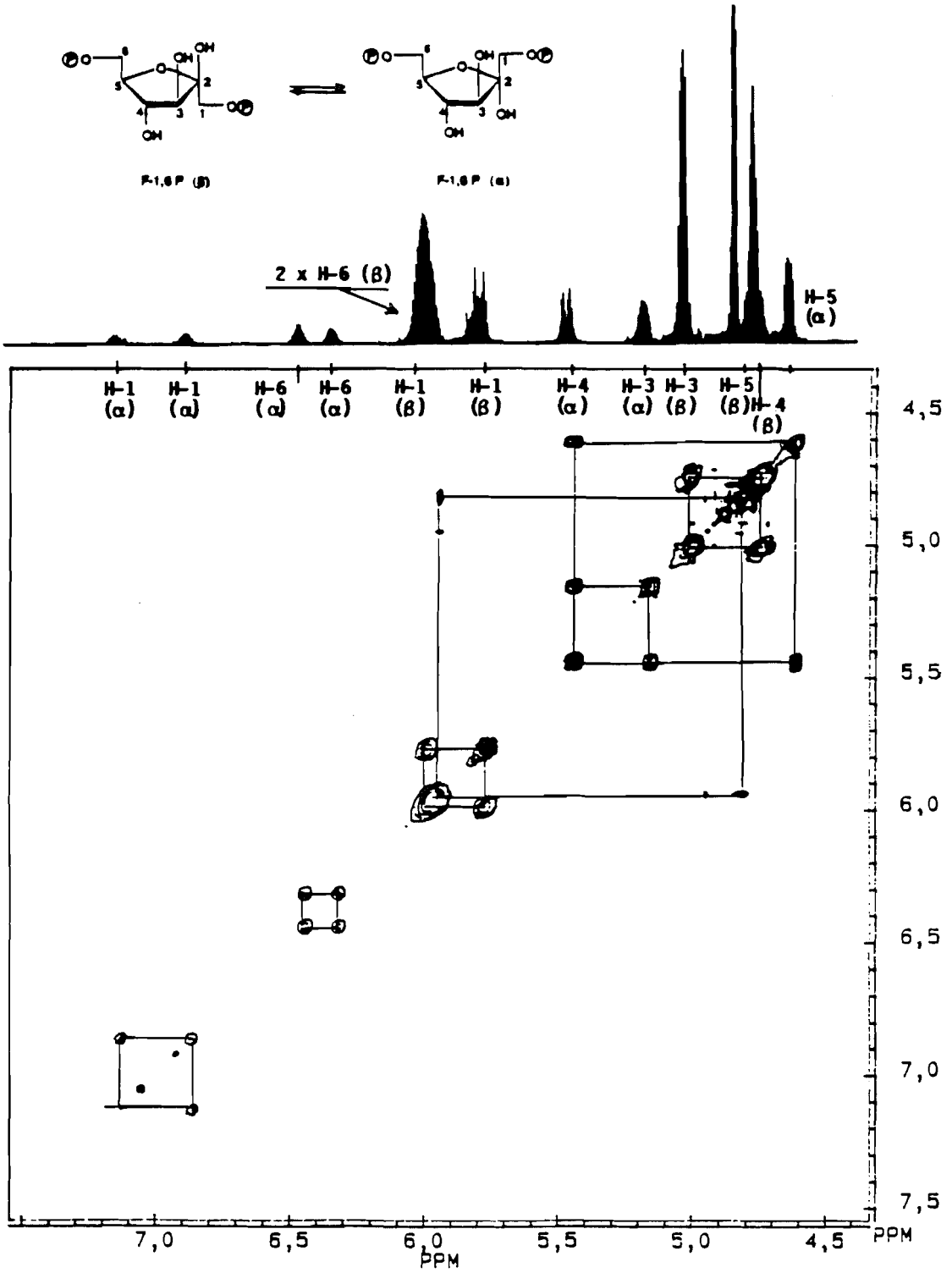


FIG. 7. Spectre COSY H–H du fructose-1,6 phosphate en présence de $PrCl_3 \cdot 6H_2O$ (ρ = 1,09, pH = pH = 1,2), C = 0,1 mol/L dans D_2O [SW = 1600 Hz, NE = 128, SI = 1K, NS = 400, D_1 = 2,0 s, D_4 = 2 × 10^{-3} s, P_1 = 14,5 μs, D_0 = 5 μs, P_2 = 7,3 μs). La transformation du signal est effectuée sur une matrice de 512K. La corrélation entre H-5 et H-6 n'est pas observée pour la forme α, ce qui n'est pas étonnant compte tenu de la faible intensité présentée par cette même corrélation pour la forme β largement majoritaire.

rapport au groupe COOH. On peut appliquer cette remarque à l'étude conformationnelle de l'acide 2-phosphoglycérique (2-PG). La figure 5 montre l'évolution des déplacements de chacun des trois protons de cette molécule. Le proton H-2 se déplace très rapidement à champ faible ($\Delta\delta_{H\text{-}2}$ = 4,3 ppm pour ρ = 0,79). Quant aux protons H-1*R* et H1-*S*, ils présentent une différence notable de comportement ($\Delta\Delta\delta_{H\text{-}1}$ = ($\Delta\delta_{H\text{-}1R}$ − $\Delta\delta_{H\text{-}1S}$) ≅ 0,5 ppm pour une valuer de ρ = 0,79). L'attribution de ces deux protons a été réalisée par la synthèse du 3 *S*-[3-^{2}H]-2-phosphoglycérate.[3] La méthode utilisée met en oeuvre la préparation du *Z*-[3-^{2}H]-PEP (14), suivie de l'action réversible de l'énolase (17). On peut écrire, pour cette molé-

3. C. Rabiller. Résultats non publiés.

Can. J. Chem. Downloaded from www.nrcresearchpress.com by 84.41.108.74 on 09/07/12
For personal use only.

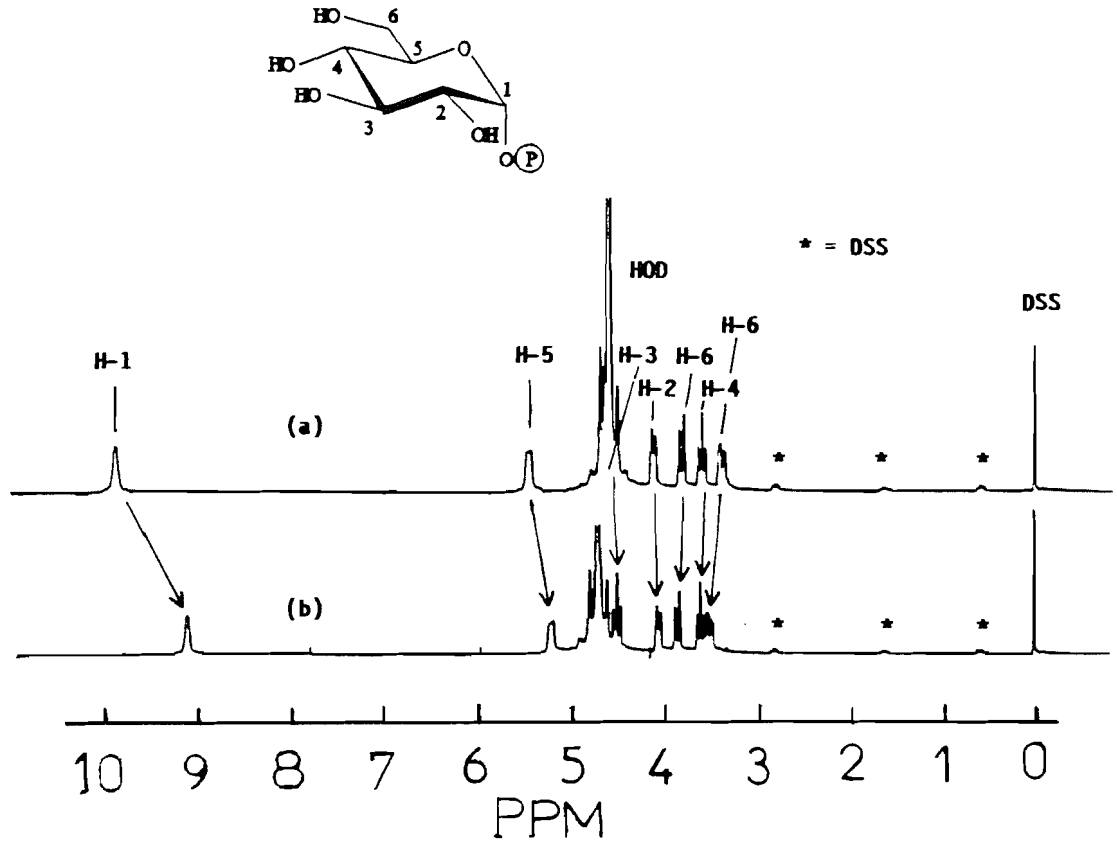


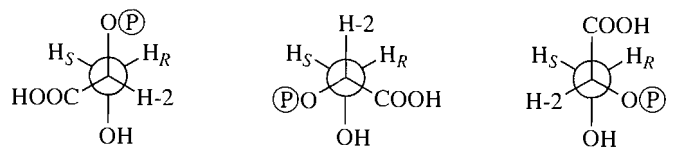
FIG. 8. Spectre protonique du glucose-1-phosphate à 250 MHz en solution aqueuse (solution 0,1 M dans D_2O); (a) ρ = 0,25; pH = 2,3; (b) ρ = 0,25; pH = 1,6.

TABLEAU 2. Déplacements chimiques δ_H mesurés par rapport au DSS dans les meilleures conditions de séparation en présence de $PrCl_3 \cdot 6\ H_2O$

	ρ	pD	δ_{H_2O}	H-1[a] *	H-1′ *	H-2	H-3	H-4	H-5	H-6 *	H-6′ *
G-1P											
α	0,25	2,3	4,60	9,90		4,12	4,64	3,60	5,46	3,38	3,82
G-6P											
α	0,35	2,1	4,76	5,15		3,5	3,96	3,73	4,60	6,56	6,56
β				4,68		3,2	3,92	3,54	4,16	6.49	6,49
F-6P[b]											
β	3,55	1,25	4,75	3,19	3,34		4,32	5,84	5,65	8,85	9,40
F-1,6P											
α	1,09	2,0	4,73	7,68	8,06		5,39	5,79		6,92	7,12
β				6,41	6,71		5,24	4,88	4,98	6,62	6,62
2-PG	0,85	1,8				9,30	5,82 (*S*) 5,20 (*R*)				

[a]Protons (*) prochiraux non attribués.
[b]Les protons de la forme α n'ont pas été assignés du fait de la faible abondance de cette structure.

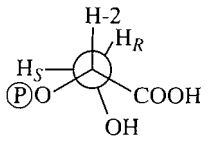
cule, les trois conformères *gauches* autour de la liaison C2—C3 :



1 2 3

Peu de choses sont connues actuellement sur la conformation privilégiée de cette molécule en solution. L'analyse conformationnelle sur la base des constantes de couplage est en effet difficile à mener du fait de la décevante simplicité du spectre de RMN des protons H(*R*) et H(*S*) à pH acide (15). L'induction de grandes variations de déplacement en présence de chlorure de praséodyme permet une analyse au premier ordre du spectre des protons H-2, H(*R*) et H(*S*). H-2 présente ainsi deux couplages de valeurs respectives 2,5 et 5,0 Hz. Ces valeurs sont en accord

avec une structure *gauche* du type **2**, pour laquelle H(*S*) se trouve à proximité du phosphore avec un angle dièdre $\phi_{H\text{-}2,H(S)}$ proche de 90°. L'existence d'une telle conformation serait justifiée par l'établissement d'une liaison hydrogène entre les fonctions alcool et acide carboxylique, la fonction OPO_3H_2 étant déjà complexée au praséodyme :



Conclusion

Au cours de ce travail, nous avons montré que la fonction phosphate constituait un excellent agent de complexation pour le praséodyme. Les grandes variations de déplacement chimique observées en fonction de la concentration en sel de terre rare et du pH autorisent l'étude séparée de presque tous les protons des dérivés phosphatés des sucres (G-1P, G-6P, F-6P ou -F,6P). Il est même possible de séparer les formes α et β. Nous avons rassemblé, dans le tableau 2, les déplacements chimiques de chacune de ces substances dans les meilleures conditions expérimentales de séparation. Le G-1P existant uniquement sous forme α, est très certainement le composé qui se prêtera le mieux à des études mécanistiques par RMN du proton ou du deutérium. Les déplacements chimiques sont en effet bien individualisés pour des valeurs de ρ assez faibles (ρ ~ 0,25) et la résolution dans ces conditions est encore satisfaisante, ainsi que l'indiquent les deux spectres réalisés à pH = 2,3 et 2,6 représentés sur la figure 8. Une contribution concernant l'analyse conformationnelle de l'acide 2-phosphoglycérique a pu également être apportée.

Remerciements

Les auteurs remercient vivement Monsieur Michel Bonneau pour son assistance technique dans la réalisation des figures ainsi que la Société Eurofins (Nantes) pour la réalisation des spectres COSY à 500 MHz.

1. Y. J. Topper. J. Biol. Chem. **225**, 419 (1957).
2. I. A. Rose et E. L. O'Connell. J. Biol. Chem. **236**, 3086 (1961).
3. V. Liemans, F. Malaisse-Lagae, R. Willem et W. J. Malaisse. Biochim. Biophys. Acta, **998**, 11 (1989).
4. W. J. Malaisse, F. Malaisse-Lagae, V. Liemans, R. Ottinger and R. Willem. Mol. Cell. Biochem. **93**, 153 (1990).
5. M. L. Martin, B. L. Zhang et G. J. Martin. FEBS Lett. **158**, 131 (1983).
6. G. J. Martin, B. L. Zhang et M. L. Martin. Biochem. Biophys. Res. Commun. **111**, 890 (1983).
7. G. J. Martin, B. L. Zhang, N. Naulet et M. L. Martin. J. Am. Chem. Soc. **108**, 5116 (1986).
8. C. Rabiller, M. Mesbahi et M. L. Martin. Chirality, **2**, 85 (1990).
9. G. J. Martin, B. L. Zhang, N. Naulet et M. L. Martin. J. Am. Chem. Soc. **108**, 5116 (1986).
10. T. Taga, Y. Kuroda et M. Ohashi. Bull. Chem. Soc. Jpn. **51**, 2278 (1978).
11. R. J. Voll, S. Ramaprasad, D. Vargas, E. S. Younathan, L. Laban et T. A. W. Koerner. Carbohydr. Res. **203**, 173 (1990).
12. L. D. Field et B. A. Messerle. J. Magn. Reson. **62**, 453 (1985).
13. I. A. Rose and D. J. Kuo. Biochemistry, **28**, 9579 (1989).
14. M. P. Gore, P. Nanjappan, G. C. Hoops et R. W. Woodward. J. Org. Chem. **55**, 758 (1990).
15. E. H. Curzon, G. E. Hawkes et E. W. Randall. J. Chem. Soc. Perkin Trans. 2, 495 (1981).
16. M. Cohn, J. E. Person, E. L. O'Connell and I. A. Rose. J. Am. Chem. Soc. **92**, 4095 (1970).

Can. J. Chem. Downloaded from www.nrcresearchpress.com by 84.41.108.74 on 09/07/12
For personal use only.

Inhibition of papain by peptide nitriles: conversion of the nitrile group into other functionalities via the papain:nitrile thioimidate ester adduct[1]

BARBARA J. GOUR-SALIN,[2] PAULE LACHANCE, AND ANDREW C. STORER
Biotechnology Research Institute, 6100 Royalmount Ave., Montreal, P.Q., Canada H4P 2R2

Received December 21, 1990

BARBARA J. GOUR-SALIN, PAULE LACHANCE, and ANDREW C. STORER. Can. J. Chem. **69**, 1288 (1991).

Peptide nitriles are reversible inhibitors of papain that form thioimidates with the cysteine thiol in the enzyme's active site. These thioimidates undergo reactions with thiols and amines to form acids and amidines, respectively. These reactions were also found to be stereospecific. Only a thioimidate derived from an L-amino acid nitrile will react with exogenous nucleophiles. These reactions were followed by ^{13}C and ^{15}N NMR techniques.

Key words: papain, nitrile, ^{13}C NMR, ^{15}N NMR, thioimidate.

BARBARA J. GOUR-SALIN, PAULE LACHANCE et ANDREW C. STORER. Can. J. Chem. **69**, 1288 (1991).

Les nitriles de peptides sont des inhibiteurs réversibles de la papaïne qui forment des thioimidates avec le thiol de la cystéine du site actif de l'enzyme. Ces thioimidates réagissent avec les thiols et les amines pour former respectivement des acides et des amidines. On a aussi observé que ces réactions sont stéréospécifiques. Seul un thioimidate obtenu à partir d'un nitrile d'un acide L-aminé pourra réagir avec des nucléophiles exogènes. On a observé ces réactions à l'aide de techniques RMN du ^{13}C et du ^{15}N.

Mots clés : papaïne, nitrile, RMN du ^{13}C, RMN du ^{15}N, thioimidate.

[Traduit par la rédaction]

Can. J. Chem. Downloaded from www.nrcresearchpress.com by 84.41.108.74 on 09/07/12
For personal use only.

Enzymes are now widely recognized as practical catalysts for synthesis (1). Esterases and lipases are used for the cleavage of racemic esters to yield optically active acids and for the removal of acyl groups from racemic acylates to produce optically active alcohols. Alcohol dehydrogenases are increasingly used to catalyze the oxidation and reduction of hydroxyl and carbonyl compounds.

In 1937 Weiss (2) suggested that papain acts as a catalyst in the hydrolysis of peptide bonds by virtue of the sulfhydryl group, which can accept the acyl group of a substrate RCO-NHR′ to form an intermediate acyl-enzyme, which then can undergo hydrolysis or aminolysis. Although this hypothesis was long disregarded, the evidence for its validity is now substantial (3); the reactive sulfhydryl group of Cys-25 can readily donate its proton ot His-159 (4), thus making it a strong nucleophile in the thiolysis of amides.

More recently, papain has also been exploited in the field of preparative peptide synthesis where it is used for the formation rather than the cleavage of peptide bonds (5). This methodology has been used in the synthesis of such biologically important compounds as the enkephalins (5*a*) and dynorphin (5*e*). In these cases, the reaction mechanism is the microscopic reverse of that describing the pathway of proteolysis. This paper focuses on the exploration of the possibility of using papain for the catalysis of different reactions.

Peptide nitriles such as *N*-(*N*-acetyl-L-phenylalanyl)glycinenitrile (*N*-Ac-L-PheGlyCN) (**1***a*) and benzoylamidoacetonitrile (hippurylnitrile) (**1***b*) are strong competitive inhibitors of papain (6). The nitrile functionality forms a covalent adduct with the thiol group of cysteine 25 in the active site of papain yielding a thiomidate ester (**2**) linkage (Scheme 1) (7). Thioimidates are the precursors of a large number of heterocyclic compounds. For example, thioimidates readily undergo nucleophilic attack by a wide range of amino compounds. The most usual pathway involves loss of the thiol with formation of an amidine system (8) but the alternative, loss of ammonia and its replacement with the nucleophile, can also take place (9). Subsequent reaction of the amidine with β-keto-esters, β-diketones, or malonic acid derivatives results in the production of pyrimidines. Bifunctional amines such as the *o*-phenylenediamines condense with thioimidates to yield benzimidazoles (9) whereas condensation with *o*-aminophenols yields benzoxazoles (9) and with hydrazines gives 1,2,4-triazoles (9). Unlike non-enzyme bound thioimidates, which hydrolyze very quickly at neutral pH's (10), the papain:nitrile thioimidate complex is very slow to hydrolyze at pH 6.0 (11). The hydrolysis of the non-enzyme bound thioimidate proceeds via addition of H_2O to the protonated thioimidate, presumably to form a tetrahedral intermediate that then collapses to either the amide and thiol, or thiol acid and free amine. In this case the pK_a of the enzyme-bound thioimidate must be much lower than the unbound one and at pH 6.0 most of the thioimidate adduct is in its non-protonated state, a fact accounting for its slow hydrolysis. Because of this it seemed feasible that the enzyme-bound thioimidate might be able to undergo reactions with nucleophiles. This was shown to be the case in a preliminary communication (11) in which the thioimidate **2***a* formed from the reaction of papain and *N*-(*N*-acetyl-L-phenylalanyl)glycinenitrile (**1***a*) does indeed react with external thiols. We now report further examples of the addition of external nucleophiles to a variety of nitrile:papain thiomidate adducts.

Experimental

Papain was prepared by the method of Storer and Carey (12). Enzyme prepared in this manner was found to contain >0.8 mol of active cysteine per mol of protein.

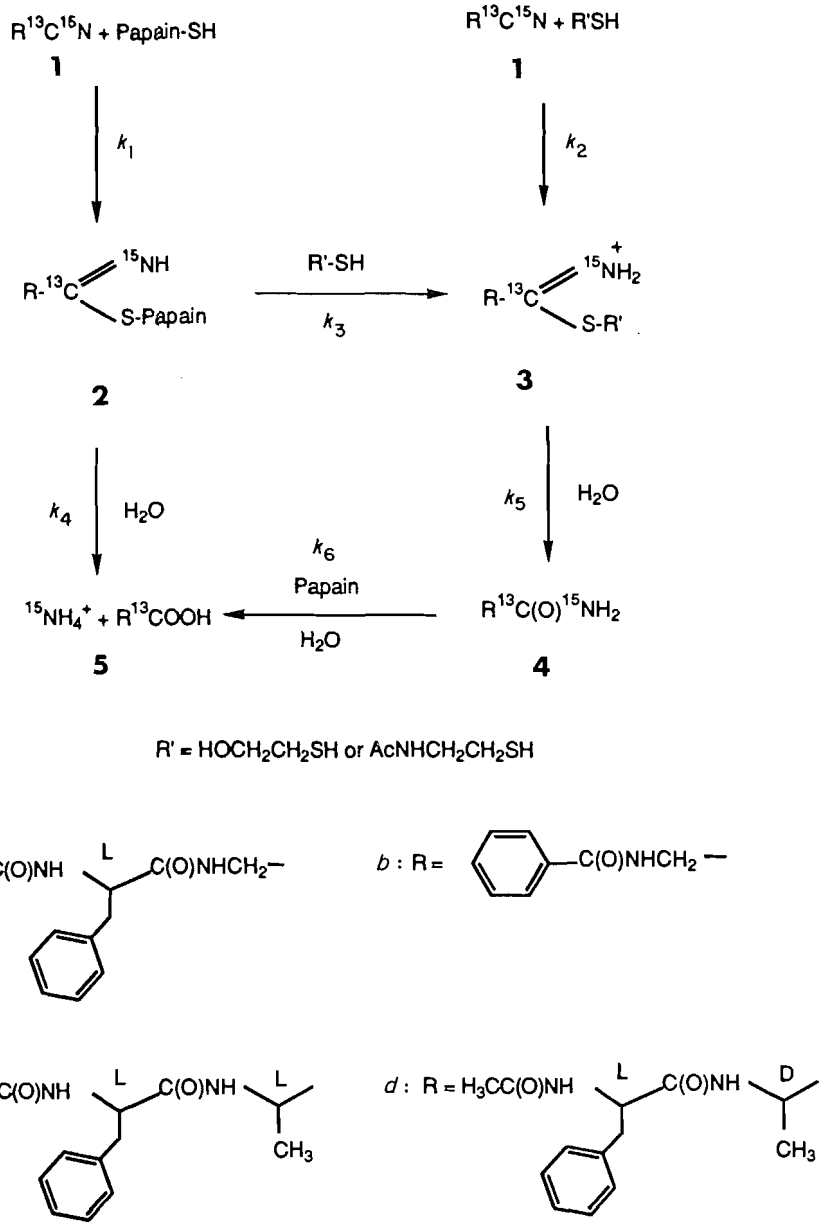
All compounds were checked for purity either by HPLC or TLC and all new compounds were then subjected to high resolution Exact Mass analysis to confirm their identities.

NMR measurements

^{13}C and ^{15}N NMR samples were prepared in 10-mm NMR tubes in 25 mM phosphate buffer (0.5 mM EDTA), pH 6.0 containing 10% D_2O and 10% acetone. The pH of all samples was checked before and after data acquisition and did not change appreciably. All spectra were recorded at 298 K by using a Bruker AM 500 spectrometer operating at 125 MHz. The carbon-13 spectra were collected with 32K data points over a range of 30 kHz using a 30° pulse width of 8 μs and a relaxation delay of 1 s. The internal reference was the methyl carbon resonance of acetone assigned to 30.7 ppm, as had previously been determined from a blank sample containing TSP (sodium 3-trimethylsilylpropionate-

[1]NRCC No. 32423.

[2]Author to whom correspondence may be addressed.



SCHEME 1

2,2,3,3-d_4) and acetone. The ^{15}N NMR spectra were collected at 298 K at 50 MHz. For these spectra, a neat sample of nitromethane was used as an external reference. The spectra were acquired using 32K data points over a range of 20 kHz with a 30° pulse width of 8 μs and no relaxation delay. The ^1H NMR spectra were collected at 298 K at 500 MHz. Tetramethylsilane was used as an internal reference.

Kinetic measurements

Papain was assayed with the substrate carbobenzoxy-L-phenylalanyl-L-arginine-4-methyl-coumarinyl-7-amide (Cbz-L-Phe-Arg-MCA). Hydrolysis of the substrate was monitored on a Perkin–Elmer LS-5B fluorimeter by excitation at 380 nm and measuring fluorescence emission at 440 nm upon release of the 7-amino-4-methylcoumarin (MCA) product. Assay solutions contained 2 nM papain, 12.5 mM phosphate, 0.2 mM EDTA, and 15% acetone. All kinetic experiments were carried out at pH 6.20 and 25.0°C. Inhibitor and substrate concentrations were kept in excess of the enzyme and the inhibitor concentration covered a range of at least $0.3–10\,K_i$ to optimize the precision of the K_i determination. The inhibition constant K_i was obtained from initial rate measurements by plotting the reciprocal of initial rate versus inhibitor concentration (Dixon plot) for various substrate concentrations. At least eight inhibitor concentrations were used for each substrate concentration. With the *N*-Ac-L-Phe-D-AlaCN derivative, the kinetic analysis showed evidence that a slow binding step occurs after formation of the initial enzyme-inhibitor complex.

Molecular modelling

A search of conformational space was carried out to locate low-energy structures for the *N*-Ac-L-Phe-D,L-Ala thioimidate intermediates. These calculations, which were done using SYBYL 5.32 (Tripos Assoc. Inc.) on a Silicon Graphics 4D/280 computer, indicate that the favored (ϕ,φ) angles for *N*-Ac-L-Phe-L-Ala thioimidate are in the (−90, 150) region of ϕ–φ space. This corresponds to the so-called "A-conformer" (13). For *N*-Ac-L-Phe-D-Ala thioimidate, the favored (ϕ,φ) angles are reversed, (150, −90). In these calculated structures the alanine methyl group hinders attack on the thioimidate carbon in the D-Ala but not in the L-Ala isomer.

Mass spectrometric measurements

All FAB and EI (70 eV) mass spectrometric measurements were conducted using a VG Analytical ZAB-EQ tandem hybrid mass spectrometer equipped with a VG 11-250J data system. Chemical

Can. J. Chem. Downloaded from www.nrcresearchpress.com by 84.41.108.74 on 09/07/12
For personal use only.

Can. J. Chem. Downloaded from www.nrcresearchpress.com by 84.41.108.74 on 09/07/12
For personal use only.

ionization (Cl) analyses using isobutane reagent gas were performed on a Finnigan 4500 quadrupole mass spectrometer equipped with an INCOS data system. Sample sizes in the range of 100–300 nmol were dissolved in 1–2 μL of glycerol or 2-hydroxyethyl sulfide (Sigma Chemicals) and deposited on a gold probe tip prior to their FAB analyses. An 8-keV Xe^0 beam (Ion Tech FAB gun 1 mA discharge current) was used. Conventional FAB mass spectra were obtained at a resolving power (10% valley definition) of 1000, scanning the range m/z 50–1000 Da with a cycle time of approximately 10 s. Mass assignments were reliable to within 0.1 Da. In Cl analyses approximately 0.1 mg of material was deposited in a glass capillary prior to its thermal desorption. The probe was heated for 25–300°C at a rate of 20°C/min and the quadrupole mass analysor was scanned from 50–700 with a cycle time of 3 s.

Accurate mass measurements of ions formed in FAB ionization were performed by peak matching using a matrix cluster (m/z: 185, 277, 369, 461) as reference ion. The resolving power was typically 8000 in all mass measurements.

N-*(N-Acetyl-L-phenylalanyl)-[1-^{13}C]glycinenitrile (^{13}C-**1**a)*

This compound was prepared by the procedure outlined by Liang and Abeles (7*a*). Doubly labelled K^{13}C^{15}N was used to obtain ^{13}C^{15}N-**1***a*: mp 188–189°C (lit. (7*a*) mp 189°C). ^{1}H NMR (acetone-d_6, **1***a*), δ: 1.85 (s, 3H, $CH_3C(O)$), 2.91 (d of d, J = 8.65, 13.9 Hz, 1H, ArCH), 3.16 (d of d, J = 5.61, 13.9 Hz, 1H, ArCH), 4.18 (d, 2H, J = 7 Hz, CH_2CN), 4.64 (d of d, J = 5.61, 8.65 Hz, 1H, α-CH), 7.2–7.27 (m, 5H, ArH). ^{13}C NMR (80% H_2O, 10% D_2O, 10% acetone, ^{13}C-**1***a*, partial), δ: 117.1 (^{13}CN), 127.6, 129.2, 129.6, 136.5 (ArC), 174.1 (C(O)NH), 174.3 (C(O)NH). ^{15}N NMR (80% H_2O, 10% D_2O, 10% acetone, ^{13}C^{15}N-**1***a*), δ: −142.3 (d, J = 17.6 Hz, ^{13}C^{15}N), −257.8 (d, J = 20.4 Hz, C(O)NH), −278 (d, J = 33.1 Hz, C(O)NH). MS (El), calcd.: 245.1164; found: 245.1163.

N-*(N-Acetyl-L-phenylalanyl)-[1-^{13}C]glycinamide (^{13}C-**4**a)*

The amide was prepared by the method of Thompson, Andrews, and Hanzlik (14). The ^{13}C label was introduced by using ^{13}C-labelled glycine in the synthesis of methyl glycinate: mp 184°C (lit. (14) mp 184°C). ^{1}H NMR ($CDCl_3$, *N*-(*N*-acetyl-L-phenylalanyl)glycine-[1-^{13}C]methyl ester), δ: 1.98 (s, 3H, $CH_3C(O)$), 3.08 (m, 2H, CH_2), 3.7 (d, J = 3.9 Hz, 3H, $^{13}C(O)OCH_3$), 3.9 (m, 1H, CHAr), 4.0 (m, 1H, CHAr), 4.7 (m, 1H, α-CH), 7.2–7.3 (m, 5H, ArH). ^{1}H NMR (CD_3OD, *N*-(*N*-acetyl-L-phenylalalanyl)-[1-^{13}C]glycinamide), δ: 1.95 (s, 3H, CH_3), 2.92 (d of d, J = 8.67, 13.7 Hz, 1H, CHAr), 3.12 (d of d, J = 6.47, 13.7 Hz, 1H, CHAr), 3.65 (d of d, J = 5.2, 17.1 Hz, 1H, $CH^{13}C(O)$), 3.84 (d of d, J = 5.2, 17.1 Hz, 1H, $CH^{13}C(O)$), 4.49 (d of d, J = 6.5, 8.6 Hz, 1H, α-CH), 7.12–7.22 (m, 5H, ArH). ^{13}C NMR (80% H_2O, 10% D_2O, 10% acetone, *N*-(*N*-acetyl-L-phenylalanyl)-[1^{13}C]glycinamide, partial), δ: 174.7 ($C(O)NH_2$) ppm. ^{15}N NMR (80% H_2O, 10% acetone, *N*-(*N*-acetyl-L-phenylalanyl)-[1-^{13}C]glycinamide), δ: −257.1 (d, J = 18.0 Hz, C(O)NH), −271 (d, J = 30.2 Hz, C(O)NH), −277 (d, J = 16.7 Hz, $C(O)NH_2$) ppm.

N-*(N-Acetyl-L-phenylalanyl)-[1-^{13}C]glycine (^{13}C-**5**a)*

The ^{13}C labelled *N*-(*N*-acetyl-L-phenylalanyl)glycine methyl ester was hydrolyzed by the method of Knowles *et al.* (15) to give the ^{13}C-carboxylic acid, but in very low yields. Consequently, the methyl ester was cleaved enzymatically using the methodology of Sabbioni and Jones (16). *N*-(*N*-Acetyl-L-phenylalanyl)glycine methyl ester (1.0 g, 3.59 mmol) was dissolved in an aqueous solution of KH_2PO_4 (20 mL) adjusted to pH 7.0 using 1 M NaOH at room temperature. Pig liver esterase (800 units) was added and the pH was maintained at 7.0 by pH-stat controlled addition of 1 M aqueous NaOH. The hydrolysis was continued until 1 equivalent of base had been taken up. The reaction mixture was washed with Et_2O (6 × 50 mL) and the emulsion that formed was broken by vacuum filtration. The aqueous phase was acidified to pH 2 using 2 M HCl and extracted with ethyl acetate (3 × 50 mL). The organic layer was dried and the solvent removed *in vacuo* to yield 480 mg (1.82 mmol, 51% yield) of the acid: mp 158.5–159°C (lit. (15) mp 164.5–165.5°C). ^{1}H NMR (DMSO-d_6), δ: 1.8 (s, 3H, $CH_3C(O)$), 2.71 (d of d, J = 10.6, 13.8 Hz, 1H, ArCH), 3.0 (d of d, J = 4.4, 10.6 Hz, 1H, ArCH), 3.76 (d, J = 5.7 Hz, 2H, CH_2), 4.53 (m, 1H, α-CH), 7.1–7.3 (m, 5H, ArH), 8.1 (d, J = 8.6 Hz, 1H, NH), 8.3 (t, J = 6.0 Hz, 1H, NH), 12.6 (br s, 1H, COOH). ^{13}C NMR (80% H_2O, 10% D_2O, 10% acetone, partial), δ: 176.2 (COOH).

N-*(N-Acetyl-L-phenylalanyl)-[1-^{13}C^{15}N]glycine anilide (^{13}C^{15}N-**6**a)*

The synthesis of this compound was based on the method Lowe and Yuthavong (17) used for the preparation of *N*-(*N*-acetyl-L-phenylalanyl)glycine *p*-nitroanilide. To a suspension of *N*-(*N*-acetyl-L-phenylalanyl)-[1-^{13}C]glycine (**5***a*) (21.9 mg, 8.29 × 10^{-2} mmol) in CH_2Cl_2 (10 mL) was added triethylamine (0.006 mL, 8.29 × 10^{-5} mol). A clear solution formed, which was cooled to −10°C under N_2. A solution of ethyl chloroformate (0.008 mL, 8.29 × 10^{-2} mmol) in methylene chloride was added dropwise. After 15 min a solution of ^{15}N-aniline (0.007 mL, 8.29 × 10^{-2} mmol) in CH_2Cl_2 (2 mL) was added to the stirred solution. Stirring was continued for 1 h after which the white precipitate was filtered off, washed with saturated $NaHCO_3$, and recrystallized from EtOAc/hexane to give 9.7 mg (2.86 × 10^{-2} mmol, 34.5% yield) of the desired amide (**6***a*). ^{1}H NMR (acetone-d_6), δ: 1.93 (s, 3H, CH_3), 2.99 (d of d, J = 8.8, 13.6 Hz, 1H, CHAr), 3.19 (d of d, J = 5.8, 13.6 Hz, 1H, CHAr), 3.79 (d of t, J = 5.35, 16.9 Hz, 1H, $CH^{13}C(O)^{15}N$),4.02 (d of t, J = 5.8, 16.9 Hz, 1H, $CH^{13}C(O)^{15}N$), 4.53 (m, 1H, α-CH), 7.0–8.0 (m, ArH, NH). ^{13}C NMR (80% H_2O, 10% D_2O, 10% acetone, partial), δ: 169.18 (d, J = 15.8 Hz, $^{13}C(O)^{15}NH$). ^{15}N NMR (80% H_2O, 10% D_2O, 10% acetone, partial), δ: −253.3 (d, J = 15.8 Hz, ^{15}NHAr).

*[1-^{13}C^{15}N]Benzoylamidoacetonitrile (^{13}C^{15}N-**1**b)*

Benzoylamidoacetonitrile ($BzNHCH_2CN$) (**1***b*) was prepared by the method of Storer and co-workers (7*b*). Doubly labelled K^{13}C^{15}N was used to obtain ^{13}C^{15}N-**1***b* and K^{13}CN was used to obtain ^{13}C-**1***b*, mp 133–136°C (lit. (18) mp 144°C). ^{1}H NMR (DMSO-d_6, **1***b*), δ: 4.45 (d, J = 5.6 Hz, 2H, CH_2), 7.6–8.1 (m, 5H, ArH), 9.34 (br s, 1H, NH). ^{13}C NMR (DMSO-d_6, ^{13}CN-**1***b*), δ: 172.5 (C(O)NH), 137.8, 134.4, 133.2 (ArC), 123.5 (d, ^{13}C^{15}N), 33.6 (CH_2). ^{13}C NMR (80% H_2O, 10% D_2O, 10% acetone, ^{13}C^{15}N-**1***b*), δ: 170.8 (C(O)NH), 117.6 (d, J = 17.9 Hz, ^{13}C^{15}N). ^{15}N NMR (80% H_2O, 10% D_2O, 10% acetone, ^{13}C^{15}N-**1***b*), δ: −142.5 (d, J = 17.9 Hz, ^{13}C^{15}N). MS (El), calcd.: 160.0636; found:160.0641.

*[1-^{13}C]Benzoylamidoacetamide (^{13}C-**4**b)*

This compound was synthesized using the method of Thompson *et al.* (14). The sodium salt of hippuric acid (2 g, 10.0 mmol) was dissolved in MeOH (25 mL) and cooled to 0°C. Hydrogen chloride was bubbled through the stirred solution for 1 h. The reaction mixture was stirred overnight and the NaCl filtered off. The methanol was removed *in vacuo* to yield a yellow oil, which was recrystallized from ethyl acetate/hexane to give methyl hippurate (1.9 g, 9.8 mmol, 98% yield). ^{1}H NMR (D_2O, TSP), δ: 3.7 (s, 3H, OCH_3), 4.1 (s, 2H, CH_2), 7.45–7.77 (m, 5H, ArH). This was redissolved in methanol, cooled to 0°C, and NH_3 was bubbled through the solution for 8 h. The methanol was removed and the product recrystallized from MeOH to give 1.4 g (7.7 mmol, 78% yield, mp 167–170°C (dec.)) of [1-^{13}C]benzoylamidoacetamide (^{13}C-**4***b*). ^{1}H NMR (DMSO-d_6), δ: 3.8 (d, J = 5.85 Hz, 2H, CH_2), 7.47–7.9 (m, 5H, ArH), 8.7 (br s, 1H, NH). ^{13}C NMR (80% H_2O, 10% D_2O, 10% acetone, partial NMR), δ: 170.5 (ArC(O)NH), 174.5 ($C(O)NH_2$). ^{15}N NMR (80% H_2O, 10% D_2O, 10% acetone), δ: −276.4 ($C(O)NH_2$). MS (El), calcd.: 178.0743; found: 178.0748.

N-*(N-Acetyl-L-phenylalanyl)-D,L-[^{13}C^{15}N]alaninenitrile (^{13}C^{15}N-**1**c,d)*

α-Aminopropionitrile was prepared by modifying the procedure for the synthesis of alanine (19). A solution of acetaldehyde (112 μL, 2.2 mmol) in diethyl ether (70 μL) was cooled to 0°C and NH_4Cl (117 mg, 2.2 mmol) in water (390 μL) was added. Potassium cyanide (K^{13}C^{15}N) (130 mg, 2.2 mmol) in water (300 μL) was added slowly and after stirring for 30 min the reaction was allowed to warm to room temperature and stirred for an additional 4 h to yield a solution of α-aminopropionitrile.

To a solution of *N*-acetyl-L-phenylalanine (310 mg, 1.5 mmol) in

Can. J. Chem. Downloaded from www.nrcresearchpress.com by 84.41.108.74 on 09/07/12
For personal use only.

methylene chloride (5 mL) at −15°C was added *N*-methylmorpholine (164 μL, 1.5 mmol) and a solution of isobutylchloroformate (193 μL, 1.5 mmol) in CH_2Cl_2 (20). The solution was stirred for 15 min. At this time *N*-methylmorpholine (217 μL, 2.2 mmol) was added to the α-aminopropionitrile solution and the whole was slowly added to the solution containing the mixed anhydride of *N*-acetyl-L-phenylalanine. The reaction mixture was stirred at −15°C for 1.5 h and overnight at room temperature. Water (15 mL) was added and the aqueous layer was extracted with CH_2Cl_2 (2 × 15 mL), washed with saturated $NaHCO_3$, 2 N HCl, and saturated NaCl. The organic layer was dried and the solvent removed *in vacuo* to give the desired nitrile, which was recrystallized from ethyl acetate (30% yield). ^{1}H NMR (DMSO-d_6, both diastereomers), δ: 1.29 (d, J = 7.2 Hz, CH_3), 1.4 (d, J = 6.7 Hz, CH_3), 1.75 (s, $CH_3C(O)$), 1.78 (s, $CH_3C(O)$), 2.7–2.8 (m, CHAr), 2.89–2.97 (m, CHAr), 4.45 (m, α-CH), 4.72 (m, α-CH), 7.15–7.32 (m, ArH), 8.2 (m, NH), 8.75 (m, NH). ^{13}C NMR (80% H_2O, 10% D_2O, 10% acetone, partial, both diastereomers), δ: 174.3, 174.3 (C(O)NH), 173.4, 173.3 (C(O)NH), 119.8 (d, J = 11.4, $^{13}C^{15}N$), 119.9 (d, J = 115 Hz, $^{13}C^{15}N$). ^{15}N NMR (80% H_2O, 10% D_2O, 10% acetone, partial, both diastereomers), δ: −144.5 (d, J = 11.4 Hz, $^{13}C^{15}N$), −144.7 (d. J = 11.5 Hz, $^{13}C^{15}N$). MS (El), calcd.: 259.1322; found; 259.1325.

N-(N-*Acetyl-L-phenylalanyl)-L-[1-^{13}C]alanine methyl ester (^{13}C-**8**)*

N-Acetyl-L-phenylalanine (5 g, 24.1 mmol) and the hydrochloride salt of L-alanine methyl ester (21) (3.37 g, 24.1 mmol) were suspended in methylene chloride (75 mL) and cooled to 0°C. Triethylamine (3.36 mL, 24.1 mmol) was added dropwise and the mixture stirred 20 min at which time HOBt (3.26 g, 24.1 mmol) was added. After a further 20 min stirring, DCC (4.98 g, 24.1 mmol) was added and the solution stirred at 0°C overnight. The solvent was removed *in vacuo* and the residue suspended in EtOAc. The DCU was removed by filtration and the organic layer washed with 5% citric acid, saturated $NaHCO_3$ solution, and brine. The organic layer was dried, the solvent removed, and the residue recrystallized from ethyl acetate to give 7.05 g (90% yield) of the desired product: mp 188–189°C. IR (KBr disk): 3280, 1750, 1635, 1540, 1380 cm^{-1}. ^{1}H NMR (DMSO-d_6), δ: 1.3 (d of d, J = 4.6, 7.2 Hz, 3H, CH_3), 1.73 (s, 3H, CH_3), 2.7 (d of d, J = 10.1, 13.8 Hz, 1H, CHAr), 3.0 (d of d, J = 4.3, 13.8 Hz, 1H, CHAr), 3.6 (s, 3H, OCH_3), 4.3 (m, 1H, α-CH), 4.55 (m, 1H, α-CH), 7.2–7.3 (m, 5H, ArH), 8.05 (d, J = 8.5 Hz, 1H, NH), 8.47 (d, J = 7.0 Hz, 1H, NH). MS (El), calcd.: 292.1423; found: 292.1416.

N-(N-*Acetyl-L-phenylalanyl)-L-[1-^{13}C]alaninamide (^{13}C-**4**c)*

The amide was prepared using the methodology of Thompson, Andrews, and Hanzlik (14). *N*-(*N*-Acetyl-L-phenylalanyl)-L-[1-^{13}C]-alanine methyl ester (**8**) (1.33 g, 4.81 mmol) was dissolved in methanol and cooled to 0°C in an ice bath. NH_3 was bubbled through the solution for 3 h. The solution was allowed to warm to room temperature and stirred for an additional 8 h. The solvent was removed *in vacuo* and the white precipitate was recrystallized from MeOH/ EtOAc/Et_2O to give 0.76 g (2.89 mmol, 60% yield) of the desired amide (mp > 230°C). IR (KBr disk): 3300, 1620, 1545 cm^{-1}. ^{1}H NMR (DMSO-d_6), δ: 1.2 (d of d, J = 4.1, 7.1 Hz, 3H, CH_3), 1.75 (s, 3H, CH_3), 2.72 (d of d, J = 9.9, 13.8 Hz, 1H, CHAr), 3.05 (d of d, J = 4.5, 13.8 Hz, 1H, CHAr), 4.2 (m, 1H, α-CH), 4.5 (m, 1H, α-C), 6.9 (s, 1H, NH), 7.13 (s, 1H, NH), 7.2–7.3 (m, 5H, ArH), 8.02 (d, J = 7.5 Hz, 1H, NH), 8.08 (d, J = 8.3 Hz, 1H, NH). ^{13}C NMR (80% H_2O, 10% D_2O, 10% acetone, partial), δ: 177.6 ($C(O)NH_2$), 174.4 (C(O)NH), 173.4 (C(O)NH), 136.7, 129.6, 129.2, 127.7 (ArC). ^{15}N NMR (80% H_2O, 10% D_2O, 10% acetone), δ: −256.4 (C(O)(NH), −257.8 (C(O)NH), −277.8 ($C(O)NH_2$). MS(El), calcd.: 277.1426; found: 277.1433.

N-(N-*Acetyl-L-phenylalanyl)-L-[1-^{13}C]alaninenitrile (^{13}C-**1**c)*

The amide was dehydrated to the nitrile using the method of Stephens *et al.* (22). The amide (0.75 g, 2.71 mmol) was dissolved in 5 mL of pyridine and cooled to 0°C. A solution of *p*-toluenesulfonyl-chloride (0.71 g, 3.72 mmol) in anhydrous pyridine (5 mL) was added drop by drop over a period of 30 min. The solution was allowed to warm to room temperature and stirred overnight. Water (5 mL) was added and the solution stirred for an additional 1 h. The solvent was removed *in vacuo* and the residue dissolved in EtOAc, washed with saturated Na_2CO_3 solution, decolourized with carbon, filtered, and the solvent removed *in vacuo*. The solid was recrystallized from EtOAc to yield 21.0 mg (30% yield) of the desired product: mp 207–210°C. IR (KBr disk): 3220, 3030, 1630, 1540 cm^{-1}. ^{1}H NMR ($CDCl_3$), δ: 1.4 (d of d, J = 5.8, 7.3 Hz, 3H, CH_3), 2.0 (s, 3H, CH_3), 3.0 (d of d, J = 8.2, 13.8 Hz, 1H, CHAr), 3.1 (d of d, J = 6.5, 13.8 Hz, 1H, CHAr), 4.6 (m, 1H, α-CH), 4.7 (m, 1H, α-CH), 6.1 (br s, 1H, NH), 6.2 (br s, 1H, NH), 7.2–7.4 (m, 5H, ArH). ^{13}C NMR (80% H_2O, 10% D_2O, 10% acetone, partial), δ: 174.3 (C(O)NH), 173.3 (C(O)NH), 136.4, 129.7, 129.2, 127.6 (ArC), 119.8 (^{13}CN). ^{15}N NMR (80% H_2O, 10% D_2O, 10% acetone, partial), δ: −144.5 (d, J = 11.4 Hz, $^{13}C^{15}N$). MS (El),calcd.: 259.1321; found: 259.1327.

N-(N-*Acetyl-L-phenylalanyl)-D-[1-^{13}C]alaninenitrile (^{13}C-**1**d)*

This diastereomer was synthesized in the same manner as *N*-(*N*-acetyl-L-phenylalanyl)-L-[1-^{13}C]alaninenitrile except that in this case D-alanine-1-^{13}C was used as starting material; mp 194–195°C. ^{1}H NMR (DMSO-d_6, *N*-(*N*-acetyl-L-phenylalanyl)D-[1-^{13}C]alanine methyl ester), δ: 1.2 (d of d, J = 4.85, 7.1 Hz, 3H, CH_3), 1.76 (s, 3H, CH_3), 2.7 (d of d, J = 9.4, 13.6 Hz, 1H, CHAr), 2.9 (d of d, J = 5.25, 13.6 Hz, 1H, CHAr), 3.65 (s, 3H, OCH_3), 4.25 (m, 1H, α-CH), 4.55 (m, 1H, α-CH), 7.2–7.3 (m, 5H, ArH), 8.05 (d, J = 8.4 Hz, 1H, NH), 8.4 (d, J = 7.3 Hz, 1H, NH). ^{1}H NMR (DMSO-d_6, *N*-(*N*-acetyl-L-phenylalanyl)-D-[1-^{13}C]alaninamide) (^{13}C-**4***d*), δ: 1.1 (d of d, J =4.1, 7.1 Hz, 3H, CH_3), 1.77 (s, 3H, CH_3), 2.78 (d of d, J = 9.0, 13.6 Hz, 1H, CHAr), 2.92 (d of d, J = 6.0, 13.6 Hz, 1H, CHAr), 4.12 (m, 1H, α-CH), 4.42 (m, 1H, α-CH), 7.0 (br s, NH), 7.2–7.3 (m, 5H, ArH), 8.1 (d, J = 7.9 Hz, 1H, NH), 8.15 (d, J = 7.4 Hz, 1H, NH). ^{13}C NMR (80% H_2O, 10% D_2O, 10% acetone, partial), δ: 178.1 ((CO)NH), 136.5, 129.6, 127.7 (ArC). ^{15}N NMR (80% H_2O, 10% D_2O, 10% acetone, partial), δ: −277.6 ($C(O)NH_2$). ^{1}H NMR (DMSO-d_6, *N*-(*N*-acetyl-L-phenylalanyl)-D-[1-^{13}C]alaninenitrile) (^{13}C-**1***d*), δ: 1.28 (t, J = 6.0 Hz, 3H, CH_3), 2.0 (s, 3H, CH_3), 2.77 (d of d, J = 9.1, 13.6 Hz, 1H, CHAr), 2.9 (d of d, J = 5.7, 13.6 Hz, 1H, CHAr), 4.45 (m, 1H, α-CH), 4.70 (m, 1H, α-CH, 7.1–7.4 (m, 5H, AH), 8.2 (d, J = 8.2 Hz, 1H, NH), 8.77 (d, J = 7.3 Hz, 1H, NH). ^{13}C NMR (80% H_2O, 10% D_2O, 10% acetone, partial), δ: 174.3 ((CO)NH), 173.3 ((CO)NH), 136.3, 129.6, 127.6 (ArC), 119.9 (CN). ^{15}N NMR (80% H_2O, 10% D_2O, 10% acetone, partial), δ: −144.8 (d, J = 11.5 Hz, CN). MS (El), calcd.: 259.1322; found: 259.1238.

Results and discussion

As reported (11), *N*-(*N*-acetyl-L-phenylalanyl)glycinenitrile (*N*-Ac-L-PheGlyCN) **1***a* reacts with mercaptans in the absence of enzyme to form *N*-(*N*-acetyl-L-phenylalanyl)glycinamide (*N*-Ac-L-PheGlyNH_2) **4***a*, probably via the thioimidate **3***a* (Scheme 1). In the presence of papain, in a parallel reaction, the formation of this amide is catalyzed. This additional parallel conversion to amide **4***a* probably results from the attack of the thiol on the enzyme-bound thioimidate **2***a* to yield a free non-enzymic thioimidate **3***a* that, relative to the enzyme-bound thioimidate adduct **2***a*, is known to hydrolyze rapidly to give **4***a* (10). The amide **4***a* is subsequently hydrolyzed via papain's well-characterized amidase activity to the carboxylic acid (23) (*N*-Ac-L-PheGlyCOOH) **5***a*. (Scheme 1). Here we wish to report the interaction of a variety of enzyme-bound thioimidates **2** with different nucleophiles.

First, the reaction of aniline with the thioimidate formed from papain and *N*-(*N*-acetyl-L-phenylalanine)glycinenitrile will be discussed. Control experiments were conducted. It has been already established (11) that, in the absence of any added nucleophile, the reaction of $^{13}C^{15}N$-**1***a* with papain slowly leads to the corresponding carboxylic acid ^{13}C-**5***a* and ammonium ion. A second control experiment involved reacting *N*-Ac-L-PheGlyCN with an excess of aniline. No enzyme was present.

Can. J. Chem. Downloaded from www.nrcresearchpress.com by 84.41.108.74 on 09/07/12
For personal use only.

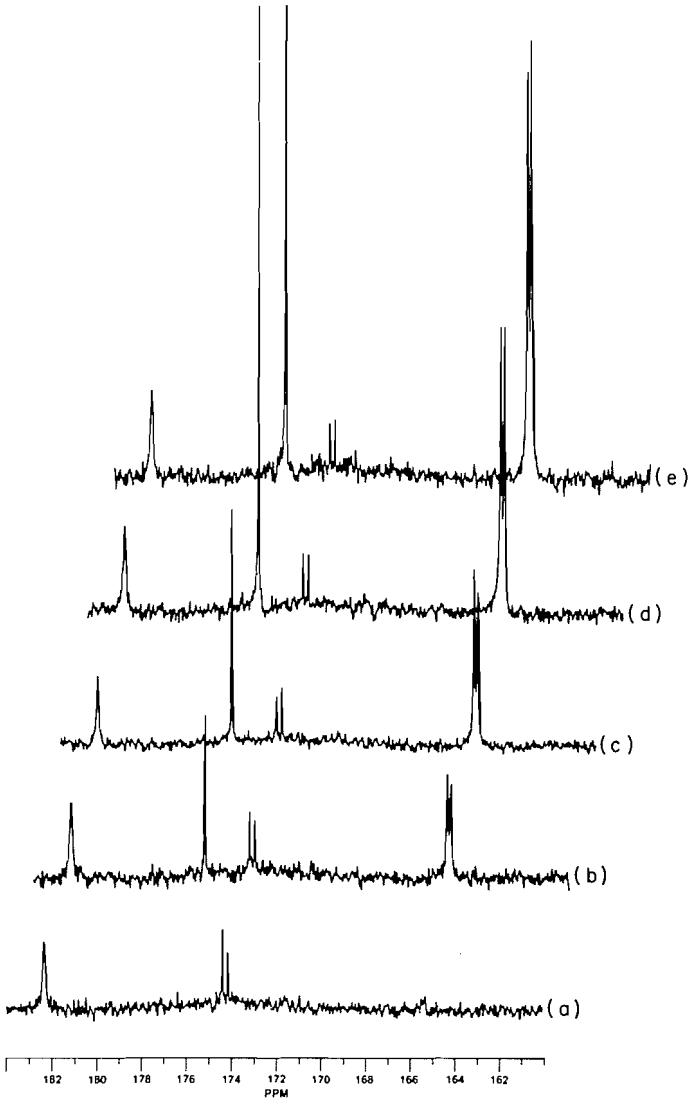
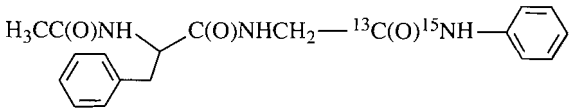


FIG. 1. Partial ^{13}C NMR spectra of 10 mM *N*-Ac-L-PheGly-$^{13}C^{15}N$ ($^{13}C^{15}N$-**1***a*) + 0.18 mM papain + 30 mM aniline (a) after 1 day; (b) after 8 days; (c) after 15 days; (d) after 22 days; (e) after 42 days.

After a period of 22 days there had been no reaction between aniline and *N*-Ac-L-PheGlyCN. Additionally, after a period of 26 days there was no reaction between aniline and the enzyme alone.

In Fig. 1 the partial ^{13}C NMR spectra of the reaction $^{13}C^{15}N$-**1***a* and papain in the presence of aniline are shown as a function of time. Spectrum (a) was taken one day after mixing and indicates only the presence of starting materials as indicated by the two resonances at 174.0 and 174.2 ppm, which represent the two carbonyl carbons of the amide functionalities in the starting material. The resonance at 182.4 ppm corresponds to the papain thioimidate adduct $^{13}C^{15}N$-**2***a*. After 7 days (spectrum (b)) the resonance at 176.8 ppm indicates that the acid ^{13}C-**5***a* is present. Ammonium ion can also be detected simultaneously in the ^{15}N NMR spectrum. A doublet at 165.4 ppm ($J_{^{13}C^{15}N}$ = 20.0 Hz) also appears. Concomitantly, a doublet centred at −277.9 ($J_{^{13}C^{15}N}$ = 20.0 Hz) appears in the ^{15}N NMR spectrum (Table 1). These peaks are not observed in the control experiments and result from the interaction of aniline with the papain:nitrile thioimidate adduct. When ^{13}C-**1***a* is used instead of $^{13}C^{15}N$-**1***a*, the resonance at 165.4 appears as a singlet. If ^{13}C-**1***a* is used in conjunction with aniline-^{15}N, the adduct appears as a doublet centred at 165.4 ($J_{^{13}C^{15}N}$ = 20.0 Hz) in the ^{13}C NMR spectrum and a new doublet at −255.8 ppm ($J_{^{13}C^{15}N}$ = 20.0 Hz) appears in the ^{15}N NMR spectrum. If $^{13}C^{15}N$-**1***a* is used in conjunction with aniline-^{15}N, the adduct appears as a triplet centred at 165.4 ($J_{^{13}C^{15}N}$ = 20.0 Hz). In the ^{15}N NMR spectrum, a doublet at −255.8 ($J_{^{13}C^{15}N}$ = 20.0 Hz) and a multiplet centred at −277.9 appear (Table 1).

The coupling indicates that neither of the amides, *N*-(*N*-acetyl-L-phenylalanyl)glycinamide **4***a* nor *N*-(*N*-acetyl-L-phenylalanyl)glycine anilide **6***a* can be the product in this case.



6*a*

This information was confirmed by synthesizing both amides (14, 17). The ^{13}C NMR spectrum for [1-^{13}C]*N*-Ac-L-PheGlyNH$_2$ indicates that the amide carbonyl of the terminal amide functionality absorbs at 174.7 ppm. The three amide resonances of this compound appear at −257.4, −271.2, and −276.7 ppm in the ^{15}N NMR spectrum. For [1-$^{13}C^{15}N$]*N*-(*N*-acetyl-L-phenylalanyl)glycine anilide $^{13}C^{15}N$-**6***a* the terminal carbonyl resonance appears as a doublet at 169.2 ppm ($J_{^{13}C^{15}N}$ = 15.8 Hz) and the anilide resonance in the ^{15}N NMR spectrum appears at −253.3 ppm ($J_{^{13}C^{15}N}$ = 15.5 Hz) (Table 1).

This would indicate that the product is an amidine. The amidine group is the nitrogen analog of carboxylic acids. It combines the properties of an azomethine-like C=N double bond (24) with an amide-like C—N single bond (25). The two nitrogens in an amidine group are nonequivalent. However, monosubstituted amidines may exhibit tautomerism. For example ^{15}N NMR data are reported for *N*-phenylbenzamidine and *N*-methylbenzamidine (25) in DMSO. For *N*-phenylbenzamidine there is a preference for the amino form over the imino form, δ ^{15}N (−151, −275 ppm). However, for *N*-methylbenzamidine there appears to be no clear preference for one form over the other, δ ^{15}N (−234, −238 ppm).

If the amidine is protonated to give the amidinium cation there is complete charge delocalization and the two nitrogens become equivalent. This is reflected in the ^{15}N NMR data for the amidinium cations of *N*-phenylbenzamidine (δ −270, −280 ppm) and *N*-methylbenzamidine (δ −269, −270 ppm). The difference in resonances is dependent only on the difference in the substitution of the nitrogens. Unsubstituted amidines are stronger bases than aliphatic amines. Benzamidine (26) has a pK_a of 11.2. In our pH 6.0 reaction mixture we would expect to have the benzamidinium cation and for it to exhibit one ^{15}N resonance as the two nitrogens become equivalent in the cationic form. And indeed for benzamidine we find only one ^{15}N resonance at −278.0 ppm. This evidence would suggest that in our case the amidinium cation **7***a* is being formed from the reaction of *N*-Ac-L-PheGlyCN and aniline via the intermediacy of the thioimidate:papain adduct (Scheme 2). Unlike the amide formed from the reaction of *N*-Ac-L-PheGlyCN with papain in the presence of thiols, the amidine is not hydrolyzed to *N*-Ac-L-PheGlyCOOH. The peak representing ^{13}C-**5***a* appears at the same rate with or without aniline in the reaction mixture.

To summarize, there is no reaction between aniline and the nitrile without papain. With papain an amidine that does not hydrolyze to a carboxylic acid is formed. This represents a

TABLE 1. ^{13}C and ^{15}N NMR resonances (25 mM phosphate buffer (0.5 mM EDTA) pH 6.0 containing 10% D_2O, 10% acetone)

Compound	^{13}C NMR (peak identity) ppm[a]	^{15}N NMR (peak identity) ppm[b]
1. *N*-Ac-L-PheGlyCN (**1***a*)	174.0 (C(O)NH)	−142.3 (CN)
	174.2 (C(O)NH)	
	117.1 (CN)	
2. *N*-Ac-L-PheGly-C(NH)-*S*-papain (**2***a*)	182.4 (C(NH-*S*-papain)	−124.8 (C(NH)-*S*-papain)
3. *N*-Ac-L-PheGly-NH_2 (**4***a*)	174.7 (C(O)NH_2)	−276.7 (NH_2)
		−271.2 (NH)
		−257.4 (NH)
4. *N*-Ac-L-PheGly (**5***a*)	176.8 (COOH)	
5. NH_4^+		−362.6 (NH_4^+)
6. Aniline	146.3 (CNH_2)	−328.2 (NH_2)
7. *N*-Ac-L-PheGly-C(NHPh)NH_3^+ (**7***a*)	165.4 (C(NHPh)NH_3^+)	−277.9 (NH_2)
		−255.8 (NHPh)
8. *N*-Ac-L-PheGly-NHPh (**6***a*)	169.2 (C(O)NH_2)	−253.3 (NHPh)
9. Benzamidinium cation	167.5 (C(NH)NH_3^+)	−278.0 $(NH_2)_2$
10. BzC(O)$NHCH_2CN$ (**1***b*)	117.6 (CN)	−142.5 (CN)
	170.8 (C(O)NH)	
11. BzC(O)$NHCH_2$C(NH)-*S*-papain (**2***b*)	182.9 (C(NH)-*S*-papain)	−125.3 (C(NH)-*S*-papain)
12. BzC(O)$NHCH_2$C(O)NH_2 (**4***b*)	170.5 (C(O)NH)	−275.3 (NH)
	174.8 (C(O)NH_2)	−276.4 (NH_2)
13. BzC(O)$NHCH_2COOH$ (**5***b*)	176.8 (COOH)	
14. BzC(O)$NHCH_2$C(NHPh)NH_3^+ (**7***b*)	166.1 (C(NHPh)NH_3^+)	
15. *N*-Acetylcysteamine	174.6 (C(O)NH)	−259.2 (NH)
16. *N*-Ac-L-Phe-L-AlaCN (**1***c*)	119.8 (CN)	−144.5 (CN)
	173.3 (C(O)NH)	
	174.3 (C(O)NH)	
17. *N*-Ac-L-Phe-L-Ala-C(NH)-*S*-papain (**2***c*)	186.4 (C(NH)-*S*-papain)	
18. *N*-Ac-L-Phe-L-Ala-NH_2 (**4***c*)	177.7 (C(O)NH_2)	−277.8 (NH_2)
19. *N*-Ac-L-Phe-L-Ala (**5***c*)		
20. *N*-Ac-L-Phe-L-Ala-C(NHPh)NH_3^+ (**7***c*)	169.1 (C(NHPh)NH_3^+)	
21. *N*-Ac-L-Phe-D-AlaCN (**1***d*)	173.3 (C(O)NH)	−144.8 (CN)
	174.3 (C(O)NH)	
	119.9 (CN)	
22. *N*-Ac-L-Phe-D-Ala-C(NH)-*S*-papain (**2***d*)	186.8 (C(NH)-*S*-papain)	
23. *N*-Ac-L-Phe-D-Ala-NH_2 (**4***d*)	178.8 (C(O)NH_2)	−277.6 (NH_2)

[a]Internal reference was the methyl carbon resonance of acetone assigned to 30.7 ppm.
[b]Nitromethane was used as an external reference.

reaction that is very difficult to do synthetically but can be accomplished, at least on small scale, at neutral pH's and ambient temperatures with papain. In fact all attempts to synthesize the authentic amidine **7***a* by the method of Bailey *et al.* (27) failed. Other amino nucleophiles were also used. The reaction of benzylamine with *N*-Ac-L-PheGly$^{13}C^{15}N$ also resulted in the formation of an amidine, as evidenced by a doublet at 164.0 ppm (J = 19.6 Hz). However, for aliphatic amines such as ethylamine and ethylenediamine no reaction took place.

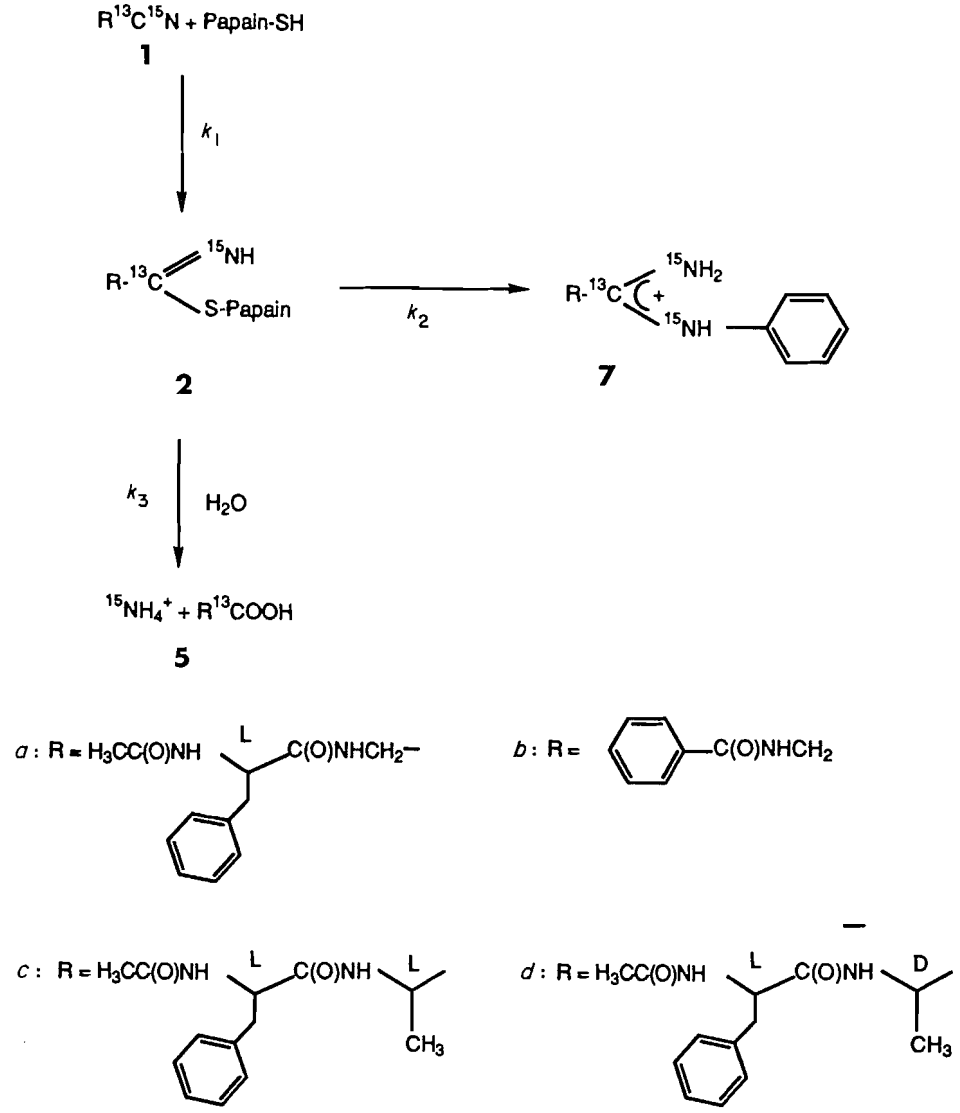
Now that it has been established that the thioimidate adduct resulting from the reaction of *N*-(*N*-acetyl-L-phenylalanyl)-glycinenitrile and papain reacts with a variety of nucleophiles to yield a variety of products, it was decided that other nitrile inhibitors should be investigated. The same reactions were carried out using benzoylamidoacetonitrile (BzNHCH$_2$CN) **1***b*, another known inhibitor of papain. Incubation of ^{13}C-**1***b* with papain resulted in the immediate formation of the thioimidate represented by a peak at 182.9 ppm (Fig. 2c). The peak at 170.8 ppm represents the amide carbonyl of $^{13}C^{15}N$-**1***b*. After a period of 1 day we see a small peak from the hydrolysis of the thioimidate to the corresponding carboxylic acid **5***b* at 176.8 ppm. Concomitantly the NH_4^+ is released and appears in the ^{15}N NMR spectrum (Table 1). The identification of the acid was further verified by acquisition of the ^{13}C NMR spectrum of a known sample of benzoylamidoacetic acid (BzNHCH$_2$COOH) **5***b*. The carbon of the carboxylic acid functionality appears at the same position as that found in the reaction mixture.

When $^{13}C^{15}N$-**1***b* is treated with an excess of thiol (β-mercaptoethanol, *N*-acetylcysteamine), a doublet centred at 174.8 ppm ($J_{^{13}C^{15}N}$ = 17.0 Hz) appears in the ^{13}C NMR spectrum (Fig. 2a) and concomitantly a doublet appears in the ^{15}N NMR spectrum (−276.4 ppm, $J_{^{13}C^{15}N}$ = 17.0 Hz). A corresponding signal appears as a singlet when ^{13}C-**1***b* is used as starting material (Fig. 2b). The ^{13}C chemical shift is identical to the carbonyl absorption of authentic benzoylamidoacetamide-1-^{13}C (BzNHCH$_2$C(O)NH_2) ^{13}C-**4***b* synthesized by the method of Thompson *et al.* (14).

Two days after mixing β-mercaptoethanol and benzoylamidoacetonitrile in the presence of papain (Fig. 3a), a large doublet representing the amide $^{13}C^{15}N$-**4***b* appears in the ^{13}C NMR spectrum, as does a singlet indicating the presence of the corresponding acid ^{13}C-**5***b*. The amide **4***b* is being formed and converted to the acid **5***b* at approximately twice the rate (by

Can. J. Chem. Downloaded from www.nrcresearchpress.com by 84.41.108.74 on 09/07/12
For personal use only.

Can. J. Chem. Downloaded from www.nrcresearchpress.com by 84.41.108.74 on 09/07/12
For personal use only.



SCHEME 2

NMR integration) as amide is formed from the reaction of the nitrile **1***b* with β-mercaptoethanol alone. As the reaction proceeds, the carboxylic acid **5***b* resonance enlarges at the expense of the nitrile **1***b* and the amide **4***b* resonances. When cysteamine is used in place of β-mercaptoethanol, the reaction proceeds in a similar manner. As in the case with *N*-(*N*-acetyl-L-phenylalanyl)glycinenitrile, it seems clear that the conversion to amide **4***b* results from the attack of the thiol on the enzyme-bound thioimidate to yield a non-enzymic thioimidate that hydrolyzes rapidly (10) to yield the amide **4***b*, which in the presence of papain is further hydrolyzed to the carboxylic acid **5***b* (Scheme 1).

The reaction of benzoylamidoacetonitrile ($BzNHCH_2CN$) with aniline was also investigated. Control experiments indicated that there is no reaction between [1-$^{13}C^{15}N$]benzoylamidoacetonitrile $^{13}C^{15}N$-**1***b* and aniline (no papain) over a period of months. Similarly, there is no reaction between aniline and papain. As before, benzoylamidoacetonitrile and papain will react slowly to form the carboxylic acid **5***b*. As with the reaction of *N*-(*N*-acetyl-L-phenylalanyl)glycinenitrile and aniline in the presence of papain, benzoylamidoacetonitrile and aniline react to form the amidinium ion **7***b*, as evidenced by the growth of a doublet at 166.1 ppm in the ^{13}C NMR spectrum (Scheme 2).

Enzymes are recognized as practical catalysts for asymmetric syntheses, with their abilities to undergo stereospecific transformations (28). Therefore, the stereoselectivity of the reaction of exogenous nucleophiles with the thioimidate adduct resulting from the interaction of two diastereomers *N*-(*N*-acetyl-L-phenylalanyl)-L-alaninenitrile (*N*-Ac-L-Phe-L-AlaCN) **1***c* and *N*-(*N*-acetyl-L-phenylalanyl)-D-alaninenitrile (*N*-Ac-L-Phe-D-AlaCN) **1***d* was investigated. Firstly we had to ensure that *N*-AcPheAlaCN was also a covalent inhibitor of papain and underwent the same types of reactions as *N*-AcPheGlyCN. A diastereomeric mixture of *N*-Ac-L-Phe-L-Ala$^{13}C^{15}N$ and *N*-Ac-L-Phe-D-Ala$^{13}C^{15}N$ was synthesized based on the method of Storer and co-workers (29). When the diastereomeric mixture was incubated with papain, two thioimidate resonances appeared in the ^{13}C NMR spectrum (186.3, 186.8 ppm). It appeared that only one of these was hydrolyzed to form the *N*-(*N*-acetyl-L-phenylalanyl)alanine (*N*-Ac-L-PheAla^{13}COOH) (179.6 ppm) and $^{15}NH_4^+$. Both diastereomers yielded amides *N*-(*N*-acetyl-L-phenylalanyl)-[1-

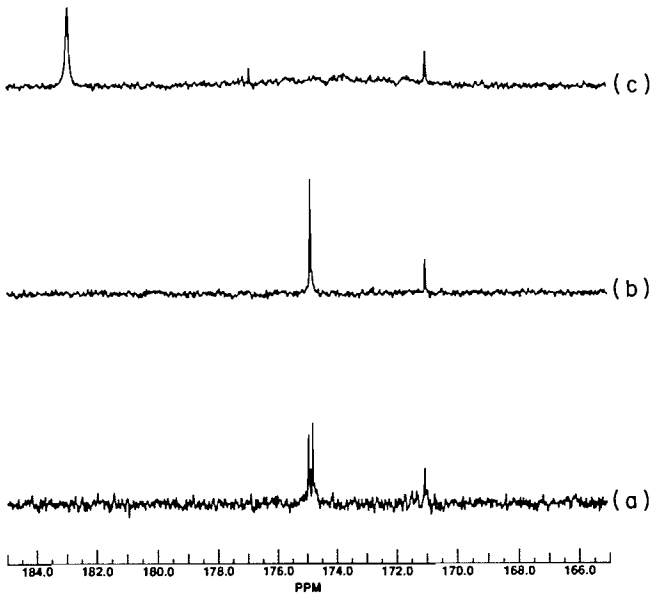


FIG. 2. Partial ^{13}C NMR spectra (a) 10 mM $BzNHCH_2{}^{13}C^{15}N$-**1***b*) + 30 mM β-mercaptoethanol (after 1 day); (b) 10 mM $BzNHCH_2{}^{13}CN$ (^{13}C-**1***b*) + 30 mM β-mercaptoethanol (after 1 day); (c) 10 mM $BzNHCH_2{}^{13}CN$ (^{13}C-**1***b*) + 0.19 mM papain (after 1 day).

^{13}C]alaninamide (*N*-AcPhe-[1-^{13}C]Ala$^{15}NH_2$) **4***c*, **4***d* when incubated with an excess of β-mercaptoethanol at pH 6 (178.8, 177.7 ppm) (Table 1).

To clarify the role of each diastereomer, they were synthesized separately. L-Alanine-[1-^{13}C]methyl ester was synthesized from [1-^{13}C]L-alanine by the method of Brenner and Huber (21). L-Alanine methyl ester was coupled to *N*-acetyl-L-phenylalanine. The resulting ester (^{13}C-**8**) was then converted to an amide (^{13}C-**4***c*), which in turn was dehydrated to yield the desired nitrile ^{13}C-**1***c*. The D analog was synthesized in a similar manner starting from [1-^{13}C]D-alanine. *N*-Ac-L-Phe-L-Ala^{13}CN reacts with papain (Fig. 4b) to form the thioimidate ^{13}C-**2***c* whose resonance is centred at 186.4 ppm. The thioimidate is slowly hydrolyzed to give *N*-Ac-L-Phe-L-Ala$^{13}COOH$ (^{13}C-**5***c*) (179.6 ppm) (Fig. 4b). *N*-Ac-L-Phe-L-Ala^{13}CN reacts with an excess of β-mercaptoethanol to give *N*-Ac-L-Phe-L-[1-^{13}C]-AlaNH_2 (^{13}C-**4***c*) (177.7 ppm) whose terminal amide carbonyl carbon resonance was verified by comparison with the resonance for authentic *N*-Ac-L-Phe-L-[1-^{13}C]AlaNH_2 (^{13}C-**4***c*). When the time course of the reaction of ^{13}C-**1***c* and papain in the presence of β-mercaptoethanol was undertaken, the results were similar to those found for the reaction of *N*-Ac-L-PheGly^{13}CN + β-mercaptoethanol. At the concentration of enzyme used in this reaction (0.324 mM), build-up of amide ^{13}C-**4***c* is not observed. Only the production of acid (^{13}C-**5***c*) at the expense of the nitrile (^{13}C-**1***c*) (119.8 ppm) is observed. Analysis of the peak integrations indicate that acid is formed at approximately 1.5 times the sum of the rate for amide formation in the blank and the rate of hydrolysis of the thioimidate to form acid. If a lower concentration of papain is employed (0.18 mM), an amide resonance is observed. When doubly labelled starting material is used one also sees an absorption at −277.8 ppm in the ^{15}N NMR spectrum, which is consistent with the authentic amide $^{13}C^{15}N$-**4***c*. Therefore, the mechanism appears to be the same as that outlined in Scheme 1 (Table 1).

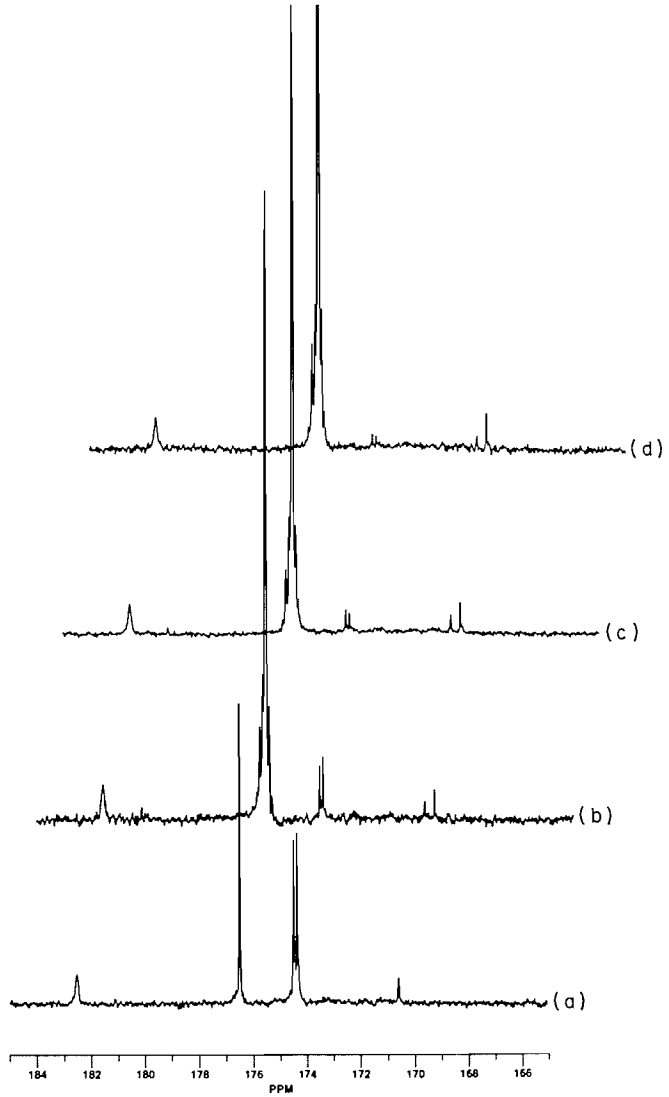


FIG. 3. Partial ^{13}C NMR specrtra of 10 mM $BzNHCH_2{}^{13}C^{15}N$ ($^{13}C^{15}N$-**1***b*) + 0.19 mM papain + 30 mM β-mercaptoethanol (a) after 2 days; (b) after 6 days; (c) after 10 days; (d) after 13 days.

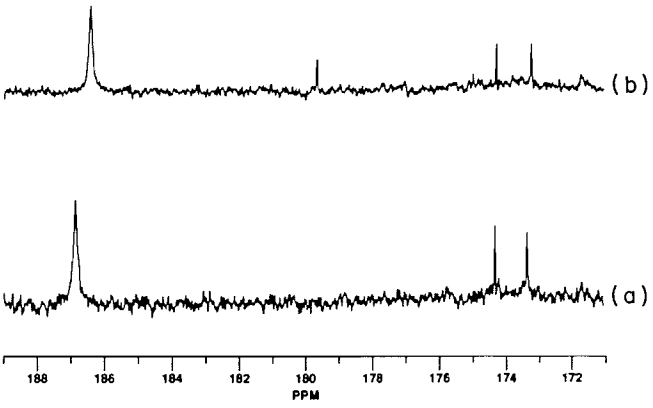


FIG. 4. Partial ^{13}C NMR spectra (a) 10 mM *N*-Ac-L-Phe-D-Ala^{13}CN (^{13}C-**1***c*) + 0.30 mM papain (after 21 days); (b) 10 mM *N*-Ac-L-Phe-L-Ala^{13}CN (^{13}C-**1***c*) + 0.29 mM papain (after 1 day).

Can. J. Chem. Downloaded from www.nrcresearchpress.com by 84.41.108.74 on 09/07/12
For personal use only.

Can. J. Chem. Downloaded from www.nrcresearchpress.com by 84.41.108.74 on 09/07/12
For personal use only.

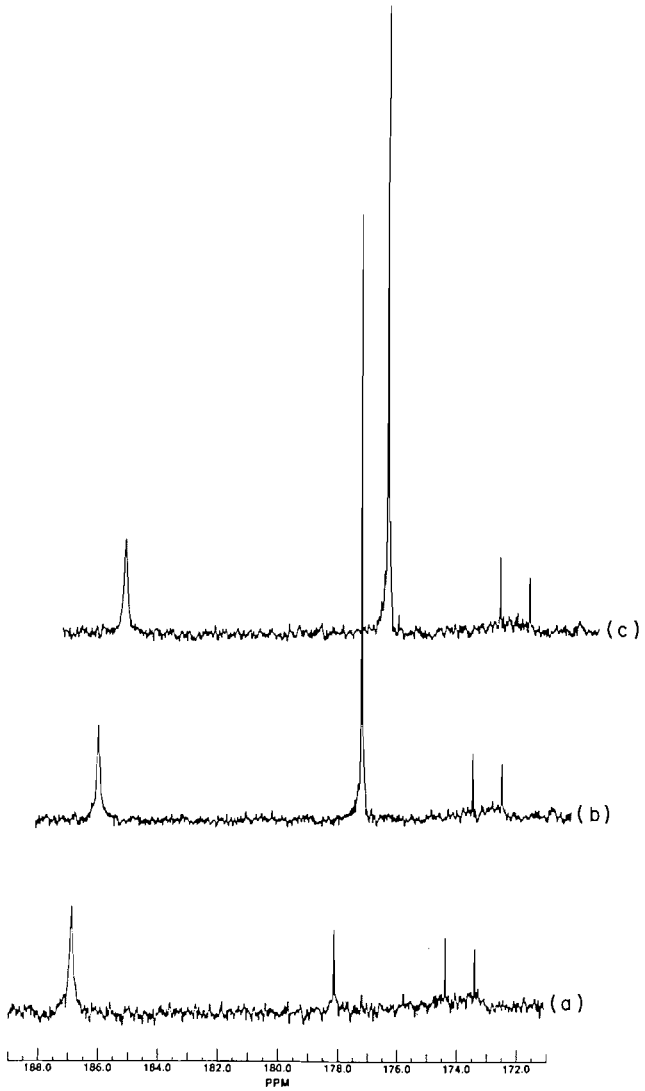


FIG. 5. Partial ^{13}C NMR spectra of 10 mM *N*-Ac-L-Phe-D-Ala^{13}CN (^{13}C-**1***d*) + 0.30 mM papain + 30 mM β-mercaptoethanol (a) after 1 day; (b) after 6 days; (c) after 27 days.

The same series of reactions was carried out with *N*-Ac-L-Phe-D-Ala^{13}CN. This diastereomer reacts with papain to form the thioimidate ^{13}C-**2***d*, which absorbs at 186.8 ppm. This thioimidate ^{13}C-**2***d* does not hydrolyze to the acid ^{13}C-**5***d* even after a period of 4 weeks (Fig. 4a). The nitrile reacts with β-mercaptoethanol to yield the corresponding amide ^{13}C-**4***d* (178.8 ppm) (Table 1). This reaction is not catalyzed in a parallel reaction by papain as is the L,L diastereomer. When the time course of the reaction of *N*-Ac-L-Phe-D-Ala^{13}CN (^{13}C-**1***d*), papain, and β-mercaptoethanol was run, there was no conversion of the amide (^{13}C-**4***d*) to the acid (^{13}C-**5***d*) (Fig. 5). One sees only build-up of the amide at the same rate as that formed from the reaction of nitrile and β-mercaptoethanol alone. In this case, in Scheme 1, k_3, k_4, and $k_6 = 0$.

With aniline as a nucleophile, the following results were obtained. Aniline and *N*-Ac-L-Phe-L,D-AlaCN in the absence of papain do not react even after a period of 6 weeks. A time course of the reaction of the L,L diastereomer, papain, and aniline indicates the formation of the amidine **7***c* (169.4 ppm). The thioimidate ^{13}C-**1***c* formed from the reaction of papain and *N*-Ac-L-Phe-L-Ala^{13}CN (^{13}C-**1***c*) is slowly hydrolyzed to the acid ^{13}C-**5***c*. However, with the L,D diastereomer there is formation of the thioimidate ^{13}C-**2***d* (186.8 ppm) but no hydrolysis to acid (^{13}C-**5***d*) nor reaction with aniline to form the amidine (Table 1). For *N*-Ac-L-Phe-D-AlaCN, $k_2 = k_3 = 0$ in the reactions depicted in Scheme 2.

The inhibition constants for the deactivation of papain with *N*-Ac-L-Phe-L-AlaCN and *N*-Ac-L-Phe-D-AlaCN were measured and the values of 6 and 18 μM, respectively, were obtained. This would indicate that while both diastereomers are good inhibitors, something must be blocking the attack of external nucleophiles in the case of the L,D diastereomer. Molecular modelling and energy minimization experiments indicate that the A-conformer thioimidate (13) is the lowest energy form for both diastereomers, but nucleophilic attack on this thioimidate intermediate is blocked in the case of the L,D diastereomer by the methyl side chain of the alanine residue, the backbone of Trp 26, and the backbone of Ser 24.

The viability of using papain as a nitrile hydrolyzing enzyme has been established, as well as its ability to do stereospecific transformations. Using the above reactions, papain can be used as an enantioselective nitrilase. This leads to the possibility of the production of optically pure amino acids, which can be produced by an enzymatic Strecker synthesis.

Acknowledgements

We would like to acknowledge the contribution of Dr. P. Thibault and Mr. D. Embree, Atlantic Research Laboratory, National Research Council, Halifax, Nova Scotia, by their mass determinations, Dr. R. Menard and Ms. C. Plouffe by their inhibition constant measurements, and Dr. E. Purisima by his molecular modelling work.

1. H. G. DAVIES, R. H. GREEN, D. R. KELLY, and S. M. ROBERTS (*Editors*). Biotransformations in preparative organic chemistry: the use of isolated enzymes and whole cell systems in synthesis. Academic Press, New York. 1989.
2. J. WEISS. Chem. Ind. 685 (1937).
3. (*a*) G. LOWE. Philos. Trans. R. Soc. London B: **257**, 237 (1970); (*b*) Tetrahedron, **32**, 291 (1976).
4. (*a*) L. POLGAR. Int. J. Biochem. **8**, 171 (1977); (*b*) A. R. FERSHT. J. Am. Chem. Soc. **93**, 3504 (1971).
5. (*a*) W. KULLMAN. Biochem. J. **220**, 405 (1984); (*b*) Y. ISOWA, M. OHMORI, T. ICHIKAWA, H. KURITA, M. SATO, and K. MORI. Bull. Chem. Soc. Jpn. **50**, 2762 (1977); (*c*) C. F. BARBAS and C-H. WONG. J. Chem. Soc. Chem. Commun. 533 (1987); (*d*) Y. V. MITIN, N. P. ZAPEVALOVA, and E. Y. GORBUNOVA. Int. J. Peptide Protein Res. **23**, 528 (1984); (*e*) W. KULLMAN. J. Org. Chem. **47**, 5300 (1982).
6. E. C. LUCAS and A. WILLIAMS. Biochemistry, **8**, 5125 (1969).
7. (*a*) T-C. LIANG and R. H. ABELES. Arch. Biochem. Biophys. **252**, 626 (1987); (*b*) J. R. BRISSON, P. R. CAREY and A. C. STORER. J. Biol. Chem. **261**, 9087 (1986); (*c*) J. B. MOON, R. S. COLEMAN, and R. P. HANZLIK. J. Am. Chem. Soc. **108**, 1350 (1986).
8. P. REYNAUD, R. C. MOREAU, and N. H. THU. C. R. Hebd. Seances Acad. Sci. **253**, 2540 (1961).
9. S. PATAI (*Editor*). The chemistry of amidines and imidates. Interscience, London. 1975.
10. (*a*) R. K. CHATURVEDI, A. E. MACMAHON, and G. L. SCHMIR. J. Am. Chem. Soc. **89**, 698 (1967); (*b*) R. K. CHATURVEDI and G. L. SCHMIR. J. Am. Chem. Soc. **91**, 737 (1969).
11. B. J. GOUR-SALIN, A. C. STORER, A. KRANTZ, V. ROBINSON, and A. CASTELHANO. Enzyme Microb. Technol. **13**, 408 (1991).
12. A. C. STORER, H. LEE, and P. R. CAREY. Biochemistry, **22**, 4789 (1983).
13. (*a*) H. LEE, R. H. ANGUS, A. C. STORER, K. I. VARUGHES, and

P. R. CAREY. Biochemistry, **27**, 250 (1988); (*b*) H. LEE, R. H. ANGUS, A. C. STORER and P. R. CAREY. Biochemistry, **27**, 258 (1988); (*c*) R. H. ANGUS, A. C. STORER, and P. R. CAREY. Biochemistry, **27**, 264 (1988).
14. S. A. THOMPSON, P. R. ANDREWS, and R. R. HANZLIK. J. Med. Chem. **29**, 104 (1986).
15. J. R. KNOWLES, H. SHARP, and P. GREENWALL. Biochem. J. **13**, 343 (1969).
16. G. SABBIONI and J. B. JONES. J. Org. Chem. **52**, 4565 (1987).
17. G. LOWE and Y. YUTHAVONG. Biochem. J. **124**, 107 (1971).
18. A. KLAGES and O. HAACK. Ber. Dtsch. Chem. Ges. **36**, 1646 (1903).
19. E. C. KENDALL and B. F. MCKENZIE. Org. Synth. Coll. Vol. 1, 21 (1964).
20. K. A. VARUGHESE, R. H. ANGUS, P. R. CAREY, H. LEE, and A. C. STORER. Can. J. Chem. **64**, 1668 (1986).
21. M. BRENNER and W. HUBER. Helv. Chim. Acta, **36**, 1109 (1953).
22. R. STEPHENS, E. J. BIANCO, and F. J. PILGRIM. J. Am. Chem. Soc. **77**, 1710 (1955).
23. (*a*) B. ASBOTH and L. POLGAR. Acta Biochim. Biophys. Acad. Sci. Hung. **12**, 223 (1977); (*b*) A. STOCKWELL and E. SMITH. J. Biol. Chem. **227**, 1 (1957).
24. S. PATAI (*Editor*). The chemistry of the carbon–nitrogen double bond. Interscience, London. 1970.
25. J. ZABICKY (*Editor*). The chemistry of amides. Interscience, London. 1972.
26. B. CLEMENT and T. KAMPCHEN. Chem. Ber. **119**, 1101 (1986).
27. D. BAILEY, C. J. DEGRAZIA, D. WOOD, and J. SIGGINS. J. Med. Chem. **17**, 702 (1974).
28. (*a*) G. M. WHITESIDES, J. DAHMER, and H. K. CHENAULT. J. Am. Chem. Soc. **111**, 6354 (1989); (*b*) M. A. LUYTEN, D. BUR, H. WYNN, W. PARRIS, M. GOLD, J. D. FRIESEN, and J. B. JONES. J. Am. Chem. Soc. **111**, 6800 (1989); (*c*) J. B. JONES, L. K. P. LAM, C. M. BROWN, B. DEJESO, L. LYM, and E. J. TOONE. J. Am. Chem. Soc. **110**, 4409 (1988); (*d*) C. H. WONG and G. M. WHITESIDES. Angew. Chem. Int. Ed. Engl. **24**, 617 (1985); (*e*) J. B. JONES. Tetrahedron, **42**, 3351 (1986).
29. R. H. ANGUS, P. R. CAREY, H. LEE, A. C. STORER, and K. I. VARUGHESE. Can. J. Chem. **63**, 2169 (1985).

Can. J. Chem. Downloaded from www.nrcresearchpress.com by 84.41.108.74 on 09/07/12
For personal use only.

X-ray crystal structure determination and NMR solution studies of 3′,3″,5′,5″-tetrabromophenolphthalein ethyl ester

ANTONY C. CHIVERTON AND SUZANNE FORTIER[1]
Department of Chemistry, Queen's University, Kingston, Ont., Canada K7L 3N6
JOHN W. BOVENKAMP[1] AND D. THORAVAL
Defence Research Establishment Ottawa, Ottawa, Ont., Canada K1A 0Z4
G. W. BUCHANAN[1]
Ottawa–Carleton Institute for Research and Graduate Studies in Chemistry, Carleton University, Ottawa, Ont., Canada K1S 5B6
AND
B. A. DAWSON
Health and Welfare Canada, Ottawa, Ont., Canada K1A 0L2

Received November 20, 1990[2]

ANTONY C. CHIVERTON, SUZANNE FORTIER, JOHN W. BOVENKAMP, D. THORAVAL, G. W. BUCHANAN, and B. A. DAWSON. Can. J. Chem. **69**, 1298 (1991).

The crystal structure of 3′,3″,5′,5″-tetrabromophenolphthalein ethyl ester (TBPE) has been determined by X-ray diffraction at room temperature. This compound crystallizes in space group $P\bar{1}$, with a = 12.361(4), b = 12.533(4), c = 9.986(2) Å, α = 99.57(3), β = 112.76(2), γ = 100.73(3) °, and Z = 2. The structure was solved by direct methods and refined by full-matrix least-squares calculations to a residual of 0.034 for 1862 observed reflections. TBPE is propeller shaped about the central carbon and crstallizes with one molecule of benzene solvent per asymmetric unit. In 1:1 CD_2Cl_2:$CDCl_3$ solution complete ^1H and ^{13}C NMR signal assignments have been made via $^1H^1H$ COSY and $^1H^{13}C$ HETCOR experiments. The quinoidal and phenolic integrities are retained on the NMR timescale. By contrast for an acetone-d_6 solution only 14 ^{13}C resonances are found and the colour of the solution changed from green to dark blue. These changes in acetone solution are attributed to the presence of a trace of base which induces the loss of the phenolic proton of TBPE and the existence of resonance forms which render the phenolic and quinoidal rings equivalent.

Key words: crystal structure, NMR, 3′3″5′5″-tetrabromophenolphthalein ethyl ester.

ANTONY C. CHIVERTON, SUZANNE FORTIER, JOHN W. BOVENKAMP, D. THORAVAL, G. W. BUCHANAN et B. A. DAWSON. Can. J. Chem. **69**, 1298 (1991).

On a déterminé la structure cristalline de l'ester éthylique de la 3′,3″,5′,5″-tétrabromophénolphthaléïne (ETBP) par diffraction des rayons-X, à la température ambiante. Ce composé cristallise dans le groupe d'espace $P\bar{1}$, avec a = 12,361(4), b = 12,533(4), c = 9,986(2) Å, α = 99,57(3), β = 112,76(2), γ = 100,73(3)° et Z = 2. On a résolu la structure par des méthodes directes et on l'a affinée par des calculs de moindres carrés (matrice entière) jusqu'à une valeur de R = 0,034 pour 1862 réflexions observées. L'ETBP a la forme d'une hélice avec un atome de carbone au centre et il cristallise avec une molécule de benzène par unité asymétrique. En solution dans un mélange $CD_2Cl_2/CDCl_3$ 1:1, on a fait une attribution complète des raies des spectres rmn du ^1H et du ^{13}C en faisant appel à des expériences de $^1H^1H$ COSY et $^1H^{13}C$ HETCOR. À l'échelle de temps de la rmn, les intégrités quinonoïdales et phénoliques sont maintenues. Par ailleurs, avec les spectres détermines dans l'acétone-d_6, on n'observe que 14 résonances ^{13}C et la couleur de la solution change du vert à bleu foncé. On attribue les changements observés dans l'acétone à la présence d'une trace de base qui induit la perte du proton phénolique de l'ETBP et à l'existence de formes de résonance qui rendent les cycles phénoliques et quinonoïdales équivalentes.

Mots clés : structure cristalline, rmn, ester ethylique de la 3′,3″,5′,5″-tétrabromophénolphthaléïne.

[Traduit par la rédaction]

Introduction

Indicator dyes have been found useful for the detection of droplets of toxic liquids containing a basic nitrogen. Consequently they have been incorporated into adhesive backed detector papers. In 1981, the commonly used indicator dye ethyl-bis(2,4-dinitrophenyl) acetate was found to be mutagenic (1). TBPE has been suggested as a replacement (2) and it has been found to be non-mutagenic by the Ontario Research Foundation (3).

TBPE is an acid/base indicator dye which, unlike most phenolphthaleins, exists in an open ester form rather than the usual lactone form. The phenolic proton is removed in the pH range 3.6–4.2 (4). The resulting charge is delocalized between the phenol and quinoid rings producing a change in colour from yellow, at pH below the 3.6–4.2 range, to dark blue above this pH range. TBPE was first synthesized by Davis and Schuhmann (5), using a five-step procedure starting with phenolphthalein. Other synthetic studies were reported by Sun *et al.* (6). The synthetic route which was used to produce the samples for this work is described in ref. 2. Patents have been submitted for the use of TBPE for the detection of toxic liquids (7). The present paper reports single crystal X-ray diffraction and soluton NMR studies on TBPE.

Experimental

X-ray crystal structure determination

The title compound was synthesized by procedures presented previously (2, 5). Pertinent data about the crystal used and the measurement of diffraction intensities are summarized in Table 1. The crystal was mounted at the end of a glass fibre. The intensity data were collected on an Enraf-Nonius CAD-4 diffractometer using graphite

[1]To whom correspondence should be addressed.
[2]Revision received April 4, 1991.

Can. J. Chem. Downloaded from www.nrcresearchpress.com by 84.41.108.74 on 09/07/12
For personal use only.

TABLE 1. Crystal data

Parameter	Crystal data
Molecular formula	$C_{22}Br_4O_4H_{14}$, C_6H_6
Molecular weight,	740.08 (661.98 + 78.11)
Space group, Z	$P\bar{1}$, 2
a, Å	12.361(4)
b, Å	12.533(4)
c, Å	9.987(2)
α, deg	99.57(3)
β, deg	112.76(2)
γ, deg	100.73(3)
V, Å^3	1352.4
T, K	292
F(000)	720
No. refl'ns used for determination of unit cell parameters, 2θ range, deg	24, 20–32
Density (calcd), g/cm^3	1.817
Number of measured reflections	2358
Number of observed reflections, $I \geq 3\sigma(I)$	1862
Total loss of intensity, %	5.2
2θ range scanned, deg	1.0 → 40.0
sin θ_γ max.	0.4807
h,k,l range scanned	0 → 11, −12 → 12, −9 → 9
λ(MoKα), Å	0.71073
μ, cm^{-1}	59.162
Crystal dimensions, mm	0.25 × 0.20 × 0.15
Final R, R_w	0.034. 0.041
Largest shift/error in final least-squares cycle, δ/σ	0.09
Maximum and minimum residual electron density in final difference fourier map, $\bar{e}$/Å^3	0.349, −0.315
Standard deviation of an observation of unit weight, σ	1.658

monochromated radiation, Mo Kα (λ = 0.71073 Å). The intensities were collected using the θ–2θ scanning procedure and three reflections were measured after every 7200 s of exposure time to check on the stability of the crystal. A 5.2% loss in intensity was observed and a linear decay correction was applied; the maximum and average corrections were 1.0270 and 1.0136, respectively. The data were corrected for Lorentz and polarization effects. The structure was solved by direct methods using the program MULTAN80 (8). All of the hydrogen positions, except for five, were found in different Fourier maps. The positions of H21A, H21B, H22B, H22C, and H24 were calculated. The structure was refined by full-matrix least-squares. The function minimized was $\Sigma w||F_0| - |F_c||^2$, where $w = 4F^2[\sigma^2(F^2) + (0.04F^2)^2]$. All reflections with $I \geq 3\sigma(I)$ were used. Anisotropic temperature factors were used for the non-hydrogen atoms. Isotropic temperature factors equal in magnitude to the equivalent isotropic values of their parent atoms were assigned to the hydrogens. The hydrogen atoms were included in the calculations, but neither their positions nor their temperature factors were refined. The scattering factors were taken from Cromer and Waber (9). Anomalous dispersion coefficients were taken from Cromer (10). All calculations were done on a PDP 11/23 computer using the Enraf-Nonius SDP program package (11). The program ORTEP (12) was used for the preparation of the illustration.[3]

Nuclear magnetic resonance studies

All spectra were recorded at 298 K on a Bruker AM-400 spectrometer equipped with an Aspect 3000 computer and process controller using DISNMR version 87. Standard microprograms from the Bruker Software Library were employed.

The $^1H^1H$ COSY experiment used N-type phase cycling with a 45° mixing pulse. Typically, the free induction decays were acquired over 1024 data points for each of the 256 values of the evolution time, with a digital resolution of *ca.* 5 Hz/point. The raw data were zero filled in F1 prior to Fourier transformation using the sine-bell window function for both F1 and F2. The matrix was symmetrized about the diagonal.

The $^1H^{13}C$ COSY spectra were obtained using a low decoupler power in the CW mode (composite phase decoupling) with polarization transfer from ^1H to ^{13}C. Typically, the FID's were acquired over 4096 data points for each of the 128 or 256 values of the evolution time, with digital resolution of 7 Hz/point F2 and 5–10 Hz/point in F1. The raw data were zero filled in F1 prior to Fourier transformation using the sine bell window function. Proton relaxation delays of 3–5 s were utilized. For the long range correlations, the delays were chosen normally to emphasize couplings of *ca.* 7.5 Hz.

Discussion

X-ray crystal structure determination of TBPE

The atomic parameters are given in Table 2 and an ORTEP (12) illustration of the molecule with the atomic numbering and ring labelling schemes used throughout is shown in Fig. 1. Hydrogen atoms are omitted to simplify the picture. The labelling of the hydrogen atoms refers to the number of their parent atom. Bond lengths and angles are listed in Table 3.

All bond lengths were found to be within the expected ranges given by Allen *et al.* (13). There is no evidence of any hydrogen bonding effects as there are no oxygen–oxygen distances less than 4.448(9) Å. The three rings of TBPE are planar. The maximum perpendicular distance between any atom in one of the rings, the phenolic (A), quinoid (B), or ethyl ester (C) and the calculated least-squares plane of that ring is 0.04(1), 0.02(1), and 0.02(1) Å, respectively. The three-ring structure of

[3]Tables of positional parameters, temperature factors, F values, and bond distances may be purchased from the Depository of Unpublished Data, CISTI, Document Delivery, National Research Council of Canada, Ottawa, Ont., Canada K1A 0S2.

Can. J. Chem. Downloaded from www.nrcresearchpress.com by 84.41.108.74 on 09/07/12
For personal use only.

TABLE 2. Fractional coordinates and equivalent isotropic thermal parameters for all non-H atoms with esd's in parentheses

Atom	x/a	y/b	z/c	U
Br(1)	0.0083(1)	0.5035(1)	0.2626(1)	* 0.0522(6)
Br(2)	−0.3559(1)	0.6471(1)	0.3911(1)	* 0.0558(6)
Br(3)	−0.0866(1)	0.7571(1)	1.0940(1)	* 0.0655(7)
Br(4)	0.2972(1)	1.1484(1)	1.2502(1)	* 0.0541(6)
C(1)	0.1193(9)	0.8440(8)	0.734(1)	* 0.036(5)
C(2)	0.0223(9)	0.7550(8)	0.599(1)	* 0.036(5)
C(3)	0.055(1)	0.6840(9)	0.509(1)	* 0.039(6)
C(4)	−0.035(1)	0.5996(9)	0.388(1)	* 0.039(6)
C(5)	−0.159(1)	0.5858(9)	0.353(1)	* 0.042(6)
O(5)	−0.2508(7)	0.5044(6)	0.2347(9)	* 0.059(4)
O(11)	0.0879(7)	0.9879(6)	1.2635(8)	* 0.054(4)
O(20a)	0.4810(8)	0.8173(7)	0.947(1)	* 0.069(5)
O(20b)	0.2842(8)	0.7267(7)	0.8557(9)	* 0.060(5)
C(6)	−0.1884(9)	0.6604(9)	0.438(1)	* 0.036(5)
C(7)	−0.101(1)	0.7468(9)	0.565(1)	* 0.043(6)
C(8)	0.1124(9)	0.8763(9)	0.867(1)	* 0.037(5)
C(9)	0.0249(9)	0.8106(9)	0.907(1)	* 0.039(6)
C(10)	0.0201(9)	0.8454(9)	1.039(1)	* 0.040(6)
C(11)	0.098(1)	0.9528(9)	1.149(1)	* 0.038(6)
C(12)	0.1893(9)	1.0131(9)	1.109(1)	* 0.038(5)
C(13)	0.1968(9)	0.9777(9)	0.980(1)	* 0.040(5)
C(14)	0.224(1)	0.9028(9)	0.709(1)	* 0.035(5)
C(15)	0.343(1)	0.8908(8)	0.783(1)	* 0.036(5)
C(16)	0.438(1)	0.956(1)	0.766(1)	* 0.050(6)
C(17)	0.415(1)	1.027(1)	0.674(2)	* 0.061(7)
C(18)	0.299(1)	1.037(1)	0.596(1)	* 0.058(7)
C(19)	0.205(1)	0.973(1)	0.616(1)	* 0.048(6)
C(20)	0.363(1)	0.805(1)	0.865(1)	* 0.043(6)
C(21)	0.515(1)	0.734(1)	1.027(2)	* 0.082(8)
C(22)	0.554(2)	0.656(2)	0.952(2)	* 0.11(1)
C(23)	0.273(1)	0.573(2)	0.172(2)	* 0.09(1)
C(24)	0.257(2)	0.674(2)	0.183(3)	* 0.10(1)
C(25)	0.297(2)	0.744(1)	0.311(4)	* 0.11(1)
C(26)	0.354(2)	0.713(3)	0.442(2)	* 0.12(1)
C(27)	0.367(1)	0.605(2)	0.428(3)	* 0.09(1)
C(28)	0.327(2)	0.537(1)	0.295(3)	* 0.09(1)

TBPE exhibits a propeller geometry with A, B, and C rings making angles of 12.6(5), 39.9(5), and 69.9(5)° with the plane defined by the central carbon and the three connecting ring carbons (the central plane). In the so-defined central plane, the maximum perpendicular distance of any atom to the least-squares plane is 0.02(1) Å. The open ester form is observed in the title compound.

A search for molecules containing a central carbon with only three six-membered aromatic rings attached was performed using the Cambridge Structural Database (14). The search found 12 structures (15–22) that satisfied these criteria. As expected all of these structures exhibit a propeller shape. Indeed, Brooks and Stucky (15) state that due to steric requirements three phenyl rings attached to a single central carbon cannot be coplanar. The rings, therefore, are twisted out of the central plane and form a propeller shape. All of the structures found were charged species, either cations, anions, or radicals, in contrast to TBPE, which is a neutral molecule. Typical values for the twist angles of the rings out of the central plane cluster around 30° as shown in Pararosaniline (17). In this case the three aniline rings are twisted out of the central plane by 34.1, 34.1, and 27.4°. The structure of triphenylmethyllithium tetramethylethylenediamine (15) exhibits a larger range of twist angles, with values of 19.7, 30.6, and 44.8°. A set of five

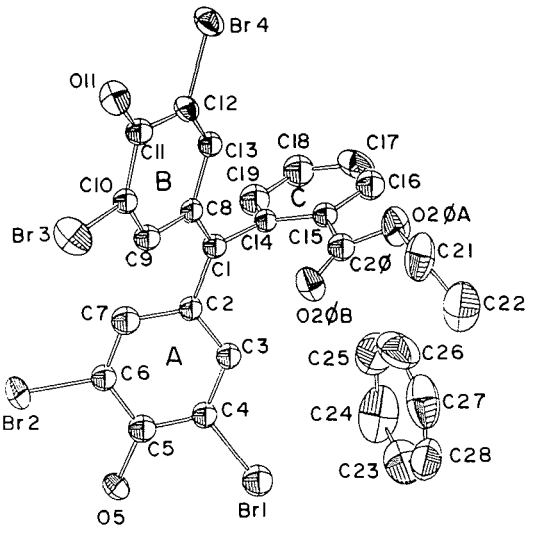


FIG. 1. Ortep illustration of TBPE.

triphenylmethyl radical structures with varying degrees of chlorine substitution at the *ortho*-position of the phenyl rings was determined by Veciano *et al.* (22). Depending on the extent of substitution, the rings were twisted out of the central plane by angles ranging from 37.7 to 65.3°. The average twist angle was 49.9°. TBPE can also be compared to structures in which one of the phenyl rings is replaced by a five-membered ring. For example, ferrocenyldiphenylcarbenium tetrafluoroborate (23) is also a propeller-shaped molecule. In this structure the three rings make angles of 18.3, 38.2, and 56.8° with the central plane. The ferrocenyl cyclopentadiene ring makes the smallest twist angle with the central plane.

TBPE is seen to have a considerably larger range of twist angles, from 12.6 to 69.90°, than all of the structures mentioned above. The quinoid ring (B) has a twist angle of 12.6(5)°. This relatively small angle is due to the presence of the double bond which, indeed, would suggest that this ring should be coplanar with the central plane. Steric requirements, however, force the quinoid ring to deviate from this ideal coplanarity and twist into a propeller shape. The phenolic ring (A) is twisted out of the plane by 39.9(3)°. This value is the closest to the magnitudes previously reported. The phenolic ring is also the ring which most closely resembles the rings present in the previous studies. The ethyl ester ring (C) exhibits the largest twist angle of 69.9(5)°. Veciana *et al.* (22) and McKechnie and Paul (18) have suggested that the magnitude of the twist angle is determined largely by the extent of substitution at the *ortho*-positions of the phenyl rings. If this hypothesis is extended to include the effects of the size of the substituent, then the structure of TBPE supports this suggestion. The large ethyl ester group at the *ortho*-position of ring C appears to force this ring to deviate from coplanarity with the central plane to a greater degree than the single atom substituents used in the previously cited studies. In addition, the larger range for twist angles found in TBPE can be explained by the fact that TBPE is a neutral molecule in contrast to all of the twelve structures in the comparison group.

Nuclear magnetic resonance studies

(i) ^1H NMR spectrum

The chemical shifts for the fourteen protons of TBPE are presented in Table 4. The numbering scheme is the same as in the X-ray study with the hydrogen atoms labelled according to their parent atom.

The absence of correlations in the $^1H^1H$ COSY (24) experi-

Can. J. Chem. Downloaded from www.nrcresearchpress.com by 84.41.108.74 on 09/07/12
For personal use only.

TABLE 3. Selected bond lengths and angles with esd's in parentheses

Bond	Distance (Å)	Bond	Distance (Å)
C1—C2	1.50(1)	C17—C18	1.39(2)
C1—C8	1.36(2)	C18—C19	1.38(2)
C1—C14	1.49(2)	C21—C22	1.40(3)
C2—C3	1.38(2)	C23—C24	1.30(4)
C2—C7	1.41(2)	C23—C28	1.35(3)
C3—C4	1.38(1)	C24—C25	1.28(4)
C4—C5	1.40(2)	C25—C26	1.38(4)
C5—C6	1.36(2)	C26—C27	1.38(4)
C6—C7	1.41(1)	C27—C28	1.30(3)
C8—C9	1.46(2)		
C8—C13	1.45(1)	C5—O5	1.36(1)
C9—C10	1.34(2)	C11—O11	1.22(2)
C10—C11	1.47(1)	C20—O20a	1.33(1)
C11—C12	1.46(2)	C20—O20b	1.21(2)
C12—C13	1.34(2)	O20a—C21	1.44(2)
C14—C15	1.42(2)		
C14—C19	1.37(2)	C4—Br1	1.89(1)
C15—C16	1.39(2)	C6—Br2	1.90(1)
C15—C20	1.46(2)	C10—Br3	1.87(1)
C16—C17	1.37(2)	C12—Br4	1.885(8)

Bonds	Angles (deg)	Bonds	Angles (deg)
C2—C1—C8	125(1)	O11—C11—C12	123.2(9)
C2—C1—C14	114(1)	C11—C12—C13	123.5(8)
C8—C1—C14	121.0(8)	C11—C12—Br4	115.8(8)
C1—C2—C3	120(1)	C13—C12—Br4	120.7(9)
C1—C2—C7	119(1)	C8—C13—C12	122(1)
C3—C2—C7	121.2(8)	C1—C14—C15	122(1)
C2—C3—C4	119(1)	C1—C14—C19	119(1)
C3—C4—C5	122(1)	C15—C14—C19	119(1)
C3—C4—Br1	119(1)	C14—C15—C16	119(1)
C5—C4—Br1	118.9(7)	C14—C15—C20	121(1)
C4—C5—O5	124(1)	C16—C15—C20	120(1)
C4—C5—C6	117.9(8)	C15—C16—C17	120(1)
O5—C5—C6	118(1)	C16—C17—C18	122(1)
C5—C6—C7	124(1)	C17—C18—C19	118(1)
C5—C6—Br2	119.2(6)	C14—C19—C18	123(1)
C7—C6—Br2	117.2(9)	C15—C20—O20a	112(1)
C2—C7—C6	116(1)	C15—C20—O20b	126(1)
C1—C8—C9	123.0(8)	O20a—C20—O20b	122(1)
C1—C8—C13	121(1)	C20—O20a—C21	118(1)
C9—C8—C13	116(1)	P20a—C21—C22	112(2)
C8—C9—C10	121.5(8)	C24—C23—C28	122(2)
C9—C10—C11	123(1)	C23—C24—C25	122(3)
C9—C10—Br3	121.3(7)	C24—C25—C26	120(2)
C11—C10—Br3	116(1)	C25—C26—C27	118(2)
C10—C11—O11	123(1)	C26—C27—C28	120(2)
C10—C11—C12	114(1)	C23—C28—C27	119(2)

Can. J. Chem. Downloaded from www.nrcresearchpress.com by 84.41.108.74 on 09/07/12
For personal use only.

ment identified the OH proton at 6.40 ppm. The most deshielded proton resonance is the doublet of doublets at 8.05 ppm, which is due to H16. This assignment follows from the observation of a long range (^3J) correlation to the ester carbonyl carbon at 165.48 ppm and is consistent with the known deshielding influence of an ester function on *ortho* aromatic protons (25). With this assignment in hand the $^1H^1H$ COSY experiment leads to ready identification of resonances for H17, H18, and H19. From the spin coupling pattern, chemical shifts, and integrated intensities the CH_2 and CH_3 groups are readily identified.

The remaining resonances in the ^1H spectrum consist of a three-proton singlet at 7.40 ppm and a one-proton singlet at 7.90 ppm. Due to rapid rotation about the C1—C2 bond, the protons on C3 and C7 will have identical chemical shifts and thus two of the three protons at 7.40 can be assigned to H3 and H7. The remaining two singlets of one proton intensity must therefore arise from the non-equivalent H9 and H13 sites of the quinoid ring. The proton having the chemical shift of 7.90 ppm must lie in the deshielding "outer" region of one of the adjacent aromatic moieties.

From the X-ray data one can obtain information regarding the preferred conformation of TBPE in the solid. Assuming similar solution geometry, a distinction between H9 and H13 resonances can be made.

The X-ray data show that the interplanar angle between rings A and B is 45.8(4) while that between rings B and C is 102.1(4)

Can. J. Chem. Downloaded from www.nrcresearchpress.com by 84.41.108.74 on 09/07/12
For personal use only.

TABLE 4. ^{1}H NMR chemical shifts (δ_H from TMS ± 0.01) for TBPE*

Position	δ_H
OH	6.40
H3, 7	7.40
H9	7.90
H13	7.40
H16	8.05
H17	7.63
H18	7.68
H19	7.27
H21	4.15
H22	1.20

*For 0.1 M solution in 1:1 $CD_2Cl_2CDCl_3$.

TABLE 5. ^{13}C chemical shifts for TBPE (δ_C from TMS ± 0.01)*

δ_C	Relative intensity	Type	Assignment
13.75	1	CH_3	C22
61.63	1	CH_2	C21
109.83	2	Quaternary	C4, 6
124.02	1	Quaternary	C12
124.69	1	Quaternary	C10
129.71	1	Quaternary	C8
130.26	1	CH	C17
130.90	1	CH	C16
131.56	1	CH	C19
131.53	1	Quaternary	C15
131.92	1	CH	C18
132.62	1	Quaternary	C1
134.94	2	CH	C3, 7
139.36	1	CH	C9
139.49	1	Quaternary	C14
139.59	1	CH	C13
151.53	1	Quaternary	C2
158.98	1	Quaternary	C5
165.47	1	Quaternary	C20
172.96	1	Quaternary	C11

*0.1 M solution in 1:1 CD_2Cl_2:$CDCl_3$.

and between A and C is 92.2(4)°. From molecular models it is clear that H9 lies in the "outer" *i.e.* deshielding region of ring B while H13 is situated almost directly above the C14 site of ring C. On the basis of the known anisotropic effect of aromatic rings on ^{1}H resonances (26), one can assign H9 as giving rise to the deshielded resonance at 7.90 ppm.

(ii) ^{13}C NMR spectrum

The ^{1}H decoupled ^{13}C NMR spectrum of TBPE in 1:1 CD_2Cl_2:$CDCl_3$ solution at 298 K shows 20 resonances, whose chemical shifts are presented in Table 5.

Initially, the APT (27) experiment was used to distinguish between protonated and nonprotonated aromatic carbons. Secondly, the relative intensities of the resonances as determined from a suppressed nuclear Overhauser experiment furnished information regarding sites which are averaged by bond rotation, since only 20 lines are observed for TBPE which possesses 22 carbons.

Since the ^{1}H spectrum has been completely assigned, the ^{13}C chemical shifts for the ten carbons bearing hydrogen follow directly from the 1-bond ^{1}H–^{13}C correlation experiment (24). A typical spectrum illustrating these correlations is shown in Fig. 2. The double intensity ^{13}C resonance at 134.94 ppm for the C3,C7 pair, which are rendered equivalent by rapid rotation about the C1—C2 bond, is readily apparent.

TABLE 6. ^{13}C chemical shifts for TBPE in acetone-d_6 (δ_C from TMS ± 0.01)*

δ_C	Relative intensity	Assignment
14.28	1	CH_3(C22)
62.75	1	CH_2(C21)
117.96	4	C4,6,10,12
131.35	1	C17
131.55	1	C16
132.04	1	C15
132.87	1	C19
133.02	1	C18
133.16	1	C1
138.60	4	C3,7,9,13
138.89	1	C14
140.24	2	C2,8
160.72	2	C5,11
166.62	1	C20

*0.05 M solution.

For assignment of the non-protonated (quaternary) aromatic carbon resonances, the long range (*i.e.* ^2J or ^3J) correlation experiments are valuable along with consideration of chemical shifts for related molecules. The brominated quinoid carbons C10 and C12 are distinguished by the fact that C12 exhibits a ^2J correlation to the proton at 7.40 ppm (H13) while C10 correlates to the proton resonance at 7.90 ppm (H9). The quinoid carbonyl (C11) at 172.69 ppm correlates to both H9 and H13 as expected, and its chemical shift is in close accord with data for related 1,3-dibromo-2 quinoid molecules (28).

In the phenolic ring, the well-documented effects of substituents on aromatic ^{13}C shifts (29) lead to the prediction that the brominated carbons C4,C6 should resonate near 110 ppm. The intensity of the quaternary resonance at 109.83 ppm shows the expected single long range (^2J) correlation to the H3,H7 protons. For C5 the expected chemical shift is near 160 ppm based on model phenolic compounds (29). Accordingly, the resonance at 158.98 can be assigned to C5 and it shows the expected correlation (^3J) to the H3,H7 protons. The remaining quaternary carbon which correlates to H3,H7 only, appears at 151.26 ppm and must, by elimination, be attributed to C2.

At this point, four resonances remain to be assigned which arise from the quaternay carbons C1, C8, C14, and C15. The resonance at 139.49 ppm shows "long range" correlation to H16 and H18, while the 131.53 resonance correlates with H17 and H19. Initially, the delays in the long range C—H correlation experiment were set to emphasize C—H couplings of 7.5 Hz so that the strongest correlations will be observed for couplings of this magnitude. It is known from early work (30) that $^3J_{CCCH}$ in benzene is 7.4 Hz, while the $^2J_{CCH}$ value is 1.0 Hz. Hence the correlations which are observed under these conditions will arise via ^3J networks. Accordingly, we assign the 139.49 resonance to C14 and the 131.53 line to C15. Finally, the ^{13}C resonance at 132.62 ppm shows a correlation with a proton resonance at 7.40 ppm while the carbon at 129.71 shows no correlations under these conditions. The remaining unassigned carbons are C1 and C8. In the case of C8, there are no vicinal hydrogens and hence the lack of observed correlations would not be surprising in view of the lower magnitudes for ^2J

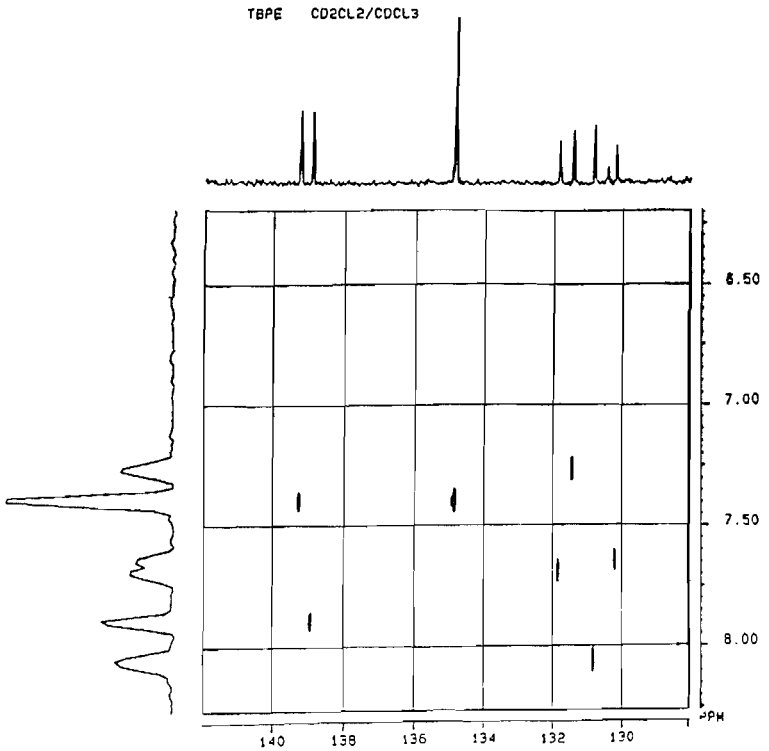


FIG. 2. ^{1}H ^{13}C correlation experiment spectrum for TBPE in CD_2Cl_2:$CDCl_3$.

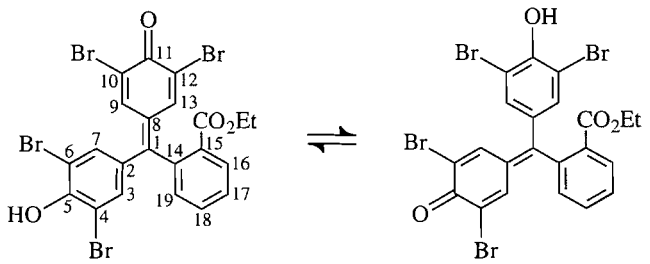
couplings mentioned above. For C1, however, there are five vicinal hydrogens. Failure to observe correlations to more than one site here must be due to dihedral angle effects arising from the non-planarity of the three aromatic rings with respect to the plane occupied by C1, C2, C8, and C14. From the X-ray data, the dihedral angle between C1 and H19 is 110.1°. Assuming a similar geometry in solution, the $^{3}J_{CCCH}$ value is expected to be less than 2 Hz (31). Again on the basis of the X-ray data, the expected dihedral angles between C1 and the H3,H7 pair will be *ca.* 40° different from the planar situations which lead to maximal coupling. In the solid state, however, the H9 and H13 sites are within 12.6° of being coplanar with C1. Thus it is reasonable to expect a correlation with one or both of these sites. Experimentally, the correlation to the 7.40 proton resonance indicates that this arises from the vicinal C1—H13 interaction.

With the delays set to emphasize 3.75 Hz ^{13}C—^{1}H coupling, the ^{13}C resonance at 129.71 correlates to the ^{1}H line at 7.90 ppm. This confirms the identity of C8 and the correlation arises from a ^{2}J pathway to H9.

(iii) ^{13}C NMR spectrum in acetone-d_6

The initial point to note here is that the colour of the acetone-d_6 solution of TBPE is dark blue in contrast to the green solution in the 1:1 CD_2Cl_2–$CDCl_3$ solvent mixture. A further difference is that the ^{13}C NMR spectrum in acetone-d_6 shows a total of 14 resonances in contrast to the 20 observed in the CD_2Cl_2–$CDCl_3$ medium. Methods of resonance assignment were similar for the two solvent media and results are presented in Table 6 for the acetone-d_6 case. Clearly there is, in acetone-d_6, a situation in which the environments of C4,6,10,12 are averaged to one as are the environments of C3,7,9,13 as well as the C2,8 and C5,11 pairs, respectively.

We believe that the explanation for the colour change between the two media and the differing number of ^{13}C resonances lies with the normal trace of acid present in $CDCl_3$. This gives the solution in CD_2Cl_2–$CDCl_3$ a lower pH, consistent with its green colour. In this medium there is a keto–enol type tautomerism as shown below. These equilibria are usually slow on the NMR timescale and hence separate ^{13}C resonances are seen for the phenolic vs. the quinoidal ring carbons of TBPE.



As stated in the Introduction, TBPE loses its phenolic proton above pH 4.2 and changes colour to dark blue. The ^{13}C NMR behaviour of TBPE in acetone-d_6 is consistent with such an occurrence, since the groups of carbons C4,6,10,12; C3,7,9,13; C5,11 and C2,8 are rendered degenerate due to the existence of resonance between rings **A** and **B** as depicted below.

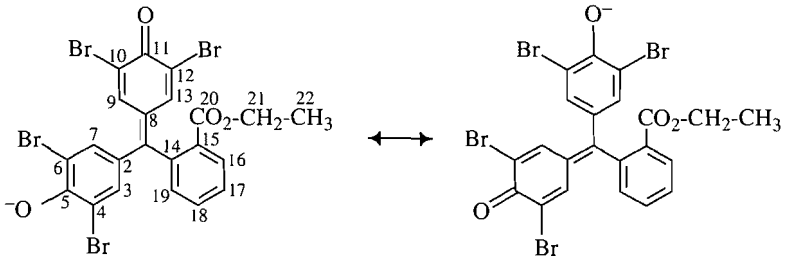
Assuming minimal influence of solvent on ^{13}C chemical shifts, one can check for the existence of averaging of the assigned ^{13}C shifts in the two media using additivity and weighted chemical shift averaging. Such data are presented in Table 7. It is evident that the agreement between predicted and observed shifts on the basis of averaging is excellent for the C4,6,10,12 positions as well as for the C3,7,9,13 and C2,8 sites.

There is poor agreement between predicted and observed ^{13}C data for the C5,11 pair, with the observed shift in acetone-d_6 being *ca.* 5 ppm more shielded than predicted. This is, however, entirely *consistent* with the suggested deprotonation of the phenolic site in acetone-d_6. Such a deprotonation will lead

Can. J. Chem. Downloaded from www.nrcresearchpress.com by 84.41.108.74 on 09/07/12
For personal use only.

TABLE 7. Comparison of observed ^{13}C shifts for TBPE in acetone-d_6 and values predicted on the basis of averaging of shifts in CD_2Cl_2–$CDCl_3$

Site	δ_C in CD_2Cl_2–$CDCl_3$	Average	δ_C in acetone-d_6
C4,6; C10; C12	109.83; 124.69; 124.02	117.09	117.96
C3,7; C9; C13	134.94; 139.36; 139.59	137.21	138.60
C2; C8	151.53; 129.71	140.62	140.28
C5; C11	158.98; 172.96	165.97	160.72



A B

to an increase in electron density at the C5,11 site and thus a more shielded ^{13}C resonance.

The question arises at this point as to why TBPE, with a pK_a of *ca.* 4 should behave as a strong acid in acetone, since the pK_a of protonated acetone is *ca.* −7 (32). A possible explanation for this observation is that the acetone-d_6 contains traces of base, since the commercial material (MSD isotopes) is prepared from the protio precurser via base-catalyzed exchange in D_2O. To check this possibility, the pH of a 50:50 (by volume) mixture of commercial acetone-d_6 and ultrapure water was compared to that of ultrapure water alone, using a Fisher Accumet 925 pH meter. The pH of the acetone-d_6 mixture was 0.7 units higher than that of ultrapure water, suggesting that there is indeed a trace of base present. In a 0.05 M solution of TBPE in acetone, the acetone is present at a concentration of *ca.* 15 M, so that the effect of any trace impurity on the solute properties will be greatly enhanced.

Additional support for the proposed existence of the monoanionic form of TBPE in acetone-d_6 comes from the ^{13}C NMR spectrum of the pure K^+ salt of TBPE (5) in acetone-d_6. Again the solution is dark blue in colour and 14 ^{13}C resonances are observed, whose chemical shifts are generally within 2 ppm of those for TBPE itself in the same solvent medium.

1. E. R. NESTMANN, D. J. KOWBEL, and J. A. WHEAT. Carcinogenisis, **2**, 879 (1981).
2. D. THORAVEL, J. W. BOVENKAMP, R. W. BETS, and B. V. LACROIX. Defence Research Establishment Ottawa, Report No. 963. June 1988.
3. A. J. HORTON. Ontario Research Foundation, Report No. 48-30082. 1984.
4. E. A. FEHNEL and E. D. AMSTURZ. Ind. Eng. Chem. Anal. **16**, 53 (1944).
5. M. M. DAVIS and P. J. SCHUHMANN. J. Res. Natl. Bur. Stand. **39**, 221 (1947).
6. C.-L. SUN, Y.-T. SHEN, and I. C. SHEN. Hua Hsueh Shih Chieh, **13**, 570 (1958); C.A. **54**, 22486*c* (1960).
7. D. THORAVAL and J. W. BOVENKAMP. Canadian Patent Application, 562, 507 (25 March 1988); US Patent Application 263, 186 (27 October 1988); European Patent Application 89302952 0 (23 March 1988).
8. P. MAIN, S. J. FRISKE, S. E. HULL, L. LESSINGER, G. GERMAIN, J.-P. DECLERCQ, and M. M. WOOLFSON. MULTAN80. A system of computer programs for the automatic solution of crystal structures from X-ray diffraction data. Univs. of York, England, and Louvain, Belgium. 1980.
9. D. T. CROMER and J. T. WABER. International tables for X-ray crystallography. Vol. IV. Birmingham, Kynoch Press. (Present distributor Kluwer Academic Publishers, Dordrecht) 1974.
10. D. T. CROMER. International tables for X-ray crystallography. Vol. IV. Birmingham, Kynoch Press. (Present distributor Kluwer Academic Publishers, Dordrecht). 1974.
11. B. A. FRENZ. Enraf-Nonius structure determination package. Enraf-Nonius, Delft, The Netherlands. 1979.
12. C. K. JOHNSON. ORTEP. Report ORNL-3794. Oak Ridge National Laboratory, TN, USA. 1965.
13. F. H. ALLEN, O. KENNARD, D. G. WATSON, L. BRAMMER, A. J. ORPEN, and R. TAYLOR. J. Chem. Soc. Perkin Trans. II S1 (1987).
14. F. H. ALLEN, S. A. BELLARD, M. D. BRICE, B. A. CARTWRIGHT, A. DOUBLEDAY, H. HIGGS, T. HUMMELINK, B. G. HUMMELINK-PETERS, O. KENNARD, W. D. S. MOTHERWELL, J. R. RODGERS, and D. G. WATSON. Acta Crystallogr. B**35**, 2331 (1975).
15. J. J. BROOKS and G. D. STUCKY. J. Am. Chem. Soc. **94**, 7333 (1972).
16. A. H. GOMES DE MESQUITE, C. H. MACGILLAVRY, and K. ERIKS. Acta Crystallogr. **18**, 437 (1965).
17. L. L. KOH and K. ERIKS. Acta Crystallogr. C**27**, 1405 (1977).
18. J. S. MCKECHNIE and I. C. PAUL. J. Chem. Soc. B. 918 (1971).
19. M. M. OLMSTEAD and P. P. POWER. J. Am. Chem. Soc. **107**, 2174 (1985).
20. K. KOSTER and E. WEISS. J. Organomet. Chem. **168**, 273 (1979).
21. P. ANDERSON and B. KLEWE. Acta Chem. Scand. **21**, 2599 (1967).
22. J. VECIANO, O. ARMET, C. ROVIRA, J. RIERA, J. CASTANER, E. MOLINS, J. RIUS, C. MIRAVITLLES, S. OLIVELLA, and J. BRICHFEUS. J. Phys. Chem. **91**, 5608 (1987).
23. D. BEHRENS. J. Organomet. Chem. **182**, 89 (1979).

Can. J. Chem. Downloaded from www.nrcresearchpress.com by 84.41.108.74 on 09/07/12
For personal use only.

24. A. BAX. Two-dimensional nuclear magnetic resonance in liquids. Reidel Bonston (1982) and references cited therein.
25. L. M. JACKMAN. Applications of nuclear magnetic resonance in organic chemistry. Pergamon Press, New York, NY. 1959.
26. N. JONATHAN, S. GORDON, and B. P. DAILEY. J. Chem. Phys. **36**, 2443 (1962).
27. S. L. PATT and J. N. SHOOLERY. J. Mag. Res. **46**, 535 (1982).
28. S. BERGER and A. RIEKER. Tetrahedron, **28**, 3123 (1972).
29. J. B . STOTHERS. Carbon-13 NMR spectroscopy. Academic Press, New York, NY. 1972. p. 197.
30. F. J. WEIGERT and J. D. ROBERTS. J. Am. Chem. Soc. **89**, 2967 (1967).
31. F. W. WEHRLI and T. WIRTHLIN. Interpretation of carbon-13 NMR spectra. Heyden, New York, NY (1976) and references cited therein.
32. N. C. DENO and M. J. WISOTSKY. J. Am. Chem. Soc. **85**, 1735 (1963).

Can. J. Chem. Downloaded from www.nrcresearchpress.com by 84.41.108.74 on 09/07/12
For personal use only.

Crystal and molecular structures of two polymorphs of 2,2-di(*p*-nitrophenyl)-1-picrylhydrazine dichloromethane, $C_{18}H_{11}N_7O_{10}\cdot CH_2Cl_2$

HONG WANG, RICHARD J. BARTON, AND BEVERLY E. ROBERTSON[1]
Department of Chemistry, University of Regina, Regina, Sask., Canada S4S 0A2

AND

JOHN A. WEIL AND KEITH C. BROWN
Department of Chemistry, University of Saskatchewan, Saskatoon, Sask., Canada S7N 0W0

Received July 5, 1990[2]

HONG WANG, RICHARD J. BARTON, BEVERLY E. ROBERTSON, JOHN A. WEIL, and KEITH C. BROWN. Can. J. Chem. **69**, 1306 (1991).

Two polymorphic crystal forms (yellow and orange) of 2,2-di(*p*-nitrophenyl)-1-picrylhydrazine were crystallized from the same dichloromethane solution, and their crystal structures determined. The yellow form is triclinic, $P\bar{1}$, a = 9.055(3), b = 10.396(4), c = 13.3187(3) Å, α = 89.83(2), β = 79.89(3), γ = 70.83(3)° at 228 K; R = 0.060, and R_w = 0.057 for 3511 reflections with $I > 2\sigma_I$. The orange form is monoclinic, $P2_1/c$, a = 8.999(3), b = 25.041(11), c = 12.207(5) Å, β = 121.66(2)° at 223 K; R = 0.053, and R_w = 0.058 for 3651 reflections with $I > 2\sigma_I$. The molecular structures in the two crystal forms are very similar. Both forms contain one solvent molecule per molecule of 2,2-di(*p*-nitrophenyl)-1-picrylhydrazine. In each, the two hydrazine nitrogen atoms have strong resonance interactions with the vicinal aromatic groups and both are sp^2 hybridized. The molecular structure around the N—N linkage shows a staggered conformation. Thus the resonance interaction between the picryl group and the other two *p*-nitrophenyl groups is negligible. The difference in color between the two crystal forms is attributed to a difference in molecular packing.

Key words: crystal structure, polymorphism, picrylhydrazine, conformation.

HONG WANG, RICHARD J. BARTON, BEVERLY E. ROBERTSON, JOHN A. WEIL et KEITH C. BROWN. Can. J. Chem. **69**, 1306 (1991).

À partir d'une même solution de dichlorométhane, les deux formes polymorphes (jaune et orange) de la 2,2-di(*p*-nitrophényl)-1-picrylhydrazine ont pu être obtenues à l'état cristallin et on a déterminé leur structure cristalline. La forme jaune est triclinique, $P\bar{1}$, a = 9,055(3), b = 10,396(4) et c = 13,3187(3) Å, α = 89,83(2), β = 79,89(3) et γ = 70,83(3)°, à 228 K; R = 0,060 et R_w = 0,057 pour 3511 réflexions avec $I > 2\sigma_I$. La forme orange est monoclinique, $P2_1/c$, a = 8,999(3), b = 25,041(11) et c = 12,207(5) Å, β = 121,66(2)°, à 223 K; R = 0,053 et R_w = 0,058 pour 3651 réflexions avec $I > 2\sigma_I$. Les structures moléculaires des deux formes cristallines sont très semblables. Les deux formes contiennent une molécule de solvant par molécule de 2,2-di(*p*-nitrophényl)-1-picrylhydrazine. Dans chacune, il existe de fortes interactions de résonance entre les deux atomes d'azote de l'hydrazine et les groupements aromatiques vicinaux et les deux ont une hybridation du type sp^2. Dans la structure moléculaire, la liaison N—N présente une conformation décalée. L'interaction de résonance entre le groupe picryle et les deux autres groupes *p*-nitrophényles est donc négligeable. On attribue les différences dans la couleur des deux formes cristallines à une différence dans l'empilement moléculaire.

Mots clés : structure cristalline, polymorphisme, picrylhydrazine, conformation.

[Traduit par la rédaction]

Introduction

The results presented here are part of ongoing structural studies of a series of diaryl picrylhydrazine derivatives. These show a variety of interesting structural effects. For example, the structure determination of 2,2-diphenyl-1-picrylhydrazine has shown that it forms a clathrate-type host–guest inclusion compound with some organic solvents (1). If the two phenyl rings are constrained to be approximately coplanar, as in 9-(2,4,6-trinitroanilino)-carbazole (2), the electron affinity of the picryl group and the electron-donation property of the planar carbazole moiety promote a π-molecular charge-transfer interaction between adjacent molecules. This leads to a structure based on infinite stacks, similar to those in many π-molecular donor–acceptor compounds, but here containing only one molecular species.

In 2,2-diphenyl-1-picrylhydrazine and in the carbazole, the conformation of each molecule, and other properties dependent on the conformation, are strongly influenced by the existence of an intramolecular hydrogen bond between one hydrazine nitrogen atom, N(1), and an oxygen atom of an *ortho*-nitro substituent on the picryl group (3, 4).

In nitroaromatic compounds, the electron-withdrawing property of the nitro groups tends to make such molecules strongly dipolar, at least locally. As a consequence, such molecules tend to co-crystallize with solvent molecules, and exhibit polymorphism. The clathration and π-molecular properties of the picrylhydrazines too are related to the tendency of these groups to form strong electric dipoles.

The related diphenylpicrylhydrazyl free radicals also exhibit polymorphism and a tendency to include solvent molecules in their crystal structures (5, 6). The crystal structure of the potassium salt of the 1-(*N,N*-diphenylhydrazono)-2,4,6-trinitrobenzenide anion has also been reported (7).

Because the 2,2-di(*p*-nitrophenyl)-1-picrylhydrazine molecule contains nitro substituents on the phenyl rings on both sides of the hydrazine linkage, it is less polar as a unit than any of the species discussed above. The 2,2-di(*p*-nitrophenyl)-1-picrylhydrazine molecule was first reported by Weil, Sane, and Kinkade (8), and its potassium salt was reported by Weil

[1]To whom correspondence should be addressed.
[2]Revision received April 15, 1991.

Can. J. Chem. Downloaded from www.nrcresearchpress.com by 84.41.108.74 on 09/07/12
For personal use only.

TABLE 1. Crystal data and experimental parameters and refinement data for D2N(y) and D2N(o)

Parameter	Value	
	D2N(y)	D2N(o)
Formula	$C_{18}H_{11}N_7O_{10}\cdot CH_2Cl_2$	$C_{18}H_{11}N_7O_{10}\cdot CH_2Cl_2$
Molar mass (g/mol)	570.259	570.259
Color	Yellow	Orange
Crystal system	Triclinic	Monoclinic
Space group	$P1$	$P2_1/c$
a (Å)	9.055(3)	8.999(3)
b (Å)	10.396(4)	25.041(11)
c (Å)	13.3187(3)	12.207(5)
α (°)	89.83(2)	90.00
β (°)	79.89(3)	121.66(2)
γ (°)	70.83(3)	90.00
V (Å^3)	1163.7(7)	2341(2)
Z	2	4
F(000)	580	1160
D_{calcd} (g/cm^3)	1.627	1.618
Reflections used in refinement of cell constants	40	34
2θ range (°)	38.0–45.0	40.0–46.0
Temperature (K)	228(4)	223(4)
Linear absorption coefficient, μ (cm^{-1})	3.56	3.03
Melting temperature (°C)	124.8	119.5
Crystal dimensions (mm)	0.20 × 0.32 × 0.80	0.50 × 0.60 × 1.40
Octants	$\pm h, k, \pm l$	$\pm h, k, l$
2θ max (deg)	45	46
R^a	0.060	0.053
$R_w{}^a$	0.057	0.058
S^a	1.482	1.181
Least-squares variables	395	395
Independent reflections	4106	4129
Reflections used in refinements	3511	3651
2θ range (deg)	3.0–45.0	3.0–45.0
ρ_{max} e Å^{-3}	0.182	0.217

$^aR = \frac{\Sigma||F_o| - |F_c||}{\Sigma|F_o|}$, $R_w = \left\{\frac{\Sigma w(|F_o| - |F_c|)^2}{\Sigma wF_o{}^2}\right\}^{1/2}$, $S = \left\{\frac{\Sigma w(|F_o| - |F_c|)^2}{n - m}\right\}^{1/2}$.

and Janusonis (9).[3] When this compound is crystallized from dichloromethane, two distinctly different crystal forms are simultaneously obtained from the same solution: one is yellow, D2N(y), and the other orange, D2N(o).

Experimental

The compound 2,2-di(*p*-nitrophenyl)-1-picrylhydrazine was synthesized following the method described by Weil, Sane, and Kinkade (8), and was crystallized from dichloromethane.

The space groups and approximate unit-cell parameters for the yellow and orange forms were determined by X-ray diffraction, using precession photographs, at room temperature. The intensity data collection and the accurate unit-cell parameter determination for both forms was carried out on a modified four-cricle diffractometer using a θ–2θ scan mode, graphite-monochromated Mo$K\alpha$ radiation and reduced temperature. Reduced temperatures were maintained using an Enraf-Nonius low temperature nitrogen flow system modified to accommodate a computerized control mechanism (λ(Mo$K\alpha$) = 0.71069 Å for data collection; λ(Mo$K\alpha_1$) = 0.70926 Å for unit-cell parameter determination).

The crystal data and experimental parameters for both forms are listed in Table 1. Three reference reflections were measured after every 47 reflections. The intensities of the standard reflections fell by 0% and 5% for D2N(y) and D2N(o), respectively. The variances σ_I of intensities were estimated both from counting statistics and from machine instability.

The intensities were corrected for the Lorentz and polarization effects and reduced to structure amplitudes. No dispersion or absorption corrections were made. The structure amplitudes, and their variances, of reflections for which the intensities were less than $3\sigma_I$ were calculated from the intensities and σ_I by the Baysian statistical method (10).

The structures of both crystal forms were solved by direct methods and Fourier syntheses. After the positions of all the non-hydrogen atoms were located and refined, the positions of the hydrogen atoms were found by difference Fourier synthesis. For both forms, solvent molecules (in a 1:1 ratio) were included in the crystals. The final structures were refined by full-matrix least squares with anisotropic temperature factors for non-hydrogen atoms and isotropic temperature factors for hydrogen atoms. Only those reflections with $I > 2\sigma_I$ were used.

The least-squares weights w for the refinements were calculated from the expression $w = (\sigma_c{}^2 + \sigma_m{}^2)^{-1}$. The $\sigma_c{}^2$ are the aforementioned variances calculated from σ_I; the $\sigma_m{}^2$ were calculated in order to remove systematic trends with respect to F and sin θ/λ from the weighted deviates of the structure factors, $w(|F_o| - |F_c|)^2$ (11, 12). The refinement data for the crystal structures are also listed in Table 1. All the calculations were performed using the XTAL system

[3]In ref. 9, p. 1250, "with triethyl-*n*-butyl ammonium hydroxide" should read "with trichloroacetic acid".

Can. J. Chem. Downloaded from www.nrcresearchpress.com by 84.41.108.74 on 09/07/12
For personal use only.

Can. J. Chem. Downloaded from www.nrcresearchpress.com by 84.41.108.74 on 09/07/12
For personal use only.

TABLE 2. Atom coordinates and temperature factors for 2,2-di(*p*-nitrophenyl)-1-picrylhydrazine (yellow form), D2N(y)

Atom	*x*	*y*	*z*	U_{eq}[a] (×10² Å²)
H(7)	0.040(5)	0.793(3)	0.417(3)	2.6(6)
C(1)	0.2376(2)	0.7715(1)	0.4260(2)	2.5
C(2)	0.2653(2)	0.8423(2)	0.5206(2)	2.8
C(3)	0.4061(3)	0.8604(2)	0.5491(2)	3.0
C(4)	0.5239(2)	0.8089(2)	0.4826(2)	2.9
C(5)	0.5041(2)	0.7356(2)	0.3930(2)	2.9
C(6)	0.3613(2)	0.7158(1)	0.3705(2)	2.7
N(2)	0.1481(3)	0.9037(2)	0.5927(2)	3.8
O(21)	0.1814(3)	0.9639(2)	0.6715(3)	6.5
O(22)	0.0213(2)	0.8911(2)	0.5740(2)	5.3
N(4)	0.6740(2)	0.8308(2)	0.5103(2)	3.9
O(41)	0.7836(2)	0.7929(2)	0.4376(2)	4.6
O(42)	0.6806(3)	0.8841(3)	0.6030(3)	8.0
N(6)	0.3366(2)	0.6241(1)	0.2951(2)	3.3
O(61)	0.2182(2)	0.5597(1)	0.3507(2)	4.3
O(62)	0.4406(3)	0.6153(2)	0.1885(2)	5.3
N(7)	0.1060(2)	0.7586(1)	0.3891(2)	2.7
N(8)	0.1171(2)	0.7254(1)	0.2589(2)	2.7
C(11)	−0.0117(2)	0.6501(1)	0.2539(2)	2.7
C(12)	−0.0344(3)	0.6317(2)	0.1294(2)	3.8
C(13)	−0.1597(3)	0.5579(2)	0.1223(3)	3.9
C(14)	−0.2613(3)	0.5047(2)	0.2402(3)	3.4
C(15)	−0.2403(3)	0.5213(2)	0.3650(3)	3.6
C(16)	−0.1132(3)	0.5931(2)	0.3707(2)	3.2
N(14)	−0.3948(3)	0.4277(2)	0.2342(3)	4.3
O(43)	−0.3997(3)	0.4037(2)	0.1224(3)	6.5
O(44)	−0.4986(3)	0.3938(2)	0.3432(3)	6.7
C(21)	0.1795(2)	0.8081(2)	0.1543(2)	2.7
C(22)	0.3155(3)	0.8019(2)	0.0460(2)	3.3
C(23)	0.3779(3)	0.8805(2)	−0.0541(3)	3.7
C(24)	0.3015(3)	0.9627(2)	−0.0428(2)	3.2
C(25)	0.1667(3)	0.9698(2)	0.0649(3)	4.3
C(26)	0.1048(3)	0.8918(2)	0.1639(3)	4.2
N(24)	0.3677(3)	1.0458(2)	−0.1496(2)	3.8
O(45)	0.4953(3)	1.0429(2)	−0.2369(2)	5.1
O(46)	0.2902(3)	1.1126(2)	−0.1462(2)	5.8
C(51)[b]	0.2066(4)	0.3282(3)	0.2179(4)	7.7
Cl(1)[b]	0.0119(1)	0.3502(1)	0.2556(1)	5.56
Cl(2)[b]	0.2545(1)	0.2477(1)	0.0859(1)	6.47

[a] $U_{eq} = (1/3)\Sigma_{ij}U_{ij}a_i^*a_j^*\mathbf{a}_i\cdot\mathbf{a}_j$.
[b] Solvent molecule.

TABLE 3. Atom coordinates and temperature factors for 2,2-di(*p*-nitrophenyl)-1-picrylhydrazine (orange form), D2N(o)

Atom	*x*	*y*	*z*	U_{eq}[a] (×10² Å²)
H(7)	1.000(4)	0.397(1)	0.579(3)	2.4(7)
C(1)	0.7946(3)	0.38650(9)	0.5864(2)	2.7
C(2)	0.6759(3)	0.42040(9)	0.4841(2)	2.7
C(3)	0.5139(3)	0.4332(1)	0.4629(2)	3.0
C(4)	0.4635(3)	0.4119(1)	0.5416(2)	3.0
C(5)	0.5633(3)	0.3741(1)	0.6341(2)	3.1
C(6)	0.7217(3)	0.3606(1)	0.6514(2)	3.0
N(2)	0.7198(3)	0.44422(9)	0.3958(2)	3.4
O(21)	0.6096(3)	0.4708(1)	0.3063(2)	5.4
O(22)	0.8655(2)	0.43695(9)	0.4140(2)	4.7
N(4)	0.2959(3)	0.42767(9)	0.5227(2)	3.5
O(41)	0.2554(2)	0.40869(9)	0.5959(2)	4.6
O(42)	0.2069(2)	0.45935(9)	0.4372(2)	4.9
N(6)	0.8053(3)	0.31301(9)	0.7303(2)	3.8
O(61)	0.8461(3)	0.27784(8)	0.6819(2)	5.2
O(62)	0.8164(3)	0.3097(1)	0.8338(2)	6.1
N(7)	0.9625(3)	0.38038(9)	0.6209(2)	3.0
N(8)	1.0864(3)	0.36337(8)	0.7459(2)	3.1
C(11)	1.2036(3)	0.3241(1)	0.7526(2)	3.1
C(12)	1.3665(3)	0.3175(1)	0.8656(3)	3.7
C(13)	1.4786(3)	0.2780(1)	0.8728(3)	3.8
C(14)	1.4296(3)	0.2463(1)	0.7674(3)	3.6
C(15)	1.2702(4)	0.2529(1)	0.6538(3)	4.1
C(16)	1.1567(3)	0.2913(1)	0.6473(2)	3.5
N(14)	1.5469(3)	0.2040(1)	0.7752(2)	4.6
O(43)	1.6797(3)	0.1953(1)	0.8780(2)	5.7
O(44)	1.5087(5)	0.1788(2)	0.6804(3)	11.5
C(21)	1.1416(3)	0.4045(1)	0.8421(2)	3.1
C(22)	1.1401(4)	0.3936(1)	0.9524(3)	4.5
C(23)	1.1872(4)	0.4324(1)	1.0455(3)	4.8
C(24)	1.2350(3)	0.4816(1)	1.0262(3)	4.1
C(25)	1.2384(5)	0.4934(1)	0.9177(3)	5.7
C(26)	1.1893(5)	0.4545(1)	0.8238(3)	5.1
N(24)	1.2825(3)	0.5230(1)	1.1243(2)	5.0
O(45)	1.2432(3)	0.5160(1)	1.2057(2)	6.2
O(46)	1.3622(4)	0.5623(1)	1.1212(3)	7.8
C(51)[b]	0.9534(5)	0.3488(2)	0.2667(4)	6.6
Cl(1)[b]	1.1646(1)	0.31922(5)	0.3492(1)	8.09
Cl(2)[b]	0.8738(2)	0.35391(6)	0.1035(1)	10.34

[a] $U_{eq} = (1/3)\Sigma_{ij}U_{ij}a_i^*a_j^*\mathbf{a}_i\cdot\mathbf{a}_j$.
[b] Solvent molecule.

of crystallographic programs (12) and the scattering factors used were those contained in the XTAL system. The function minimized was $\Sigma w(|F_o| - |F_c|)^2$.

Results and discussion

Molecular structure

The coordinates and temperature factors of the non-hydrogen atoms of the D2N(y) and D2N(o) molecules are listed in Tables 2 and 3, respectively.[4] The bond lengths, bond angles, and selected dihedral angles are listed in Tables 4 and 5. Figure 1 is a stereoscopic view of the D2N(y) molecule. The atom-numbering scheme is given in Fig. 2.[5] Labels for the planes of the molecule are defined in Fig. 3. The estimated standard deviations of all functions of the atom parameters were calculated using both the variances and the covariances of the atom parameters (12).

Both crystal forms contain one solvent molecule (CH_2Cl_2) per asymmetric unit. The 2,2-di(*p*-nitro-phenyl)-1-picrylhydrazine molecules adopt similar conformations in the two polymorphic forms. However, significant differences exist, such as in the extent of rotation of the *p*-nitro groups (of the mono-nitrophenyl groups) out of the planes of their phenyl rings. The influence of the dihedral angles between each of the two mono-nitrophenyl planes and the picryl plane is also significant, as shown in Table 5.

[4] Lists of structure amplitudes, anisotropic temperature factors, H-atom coordinates, least-squares planes, and bond distances and angles and figures showing the correlations of the dihedral angles of the nitro groups with endocyclic angles and C—NO_2 bond lengths for picrylhydrazine derivatives, diphenylhydrazyl, diphenylpicryl hydrazinate and trinitroanaline, the correlation between the endocyclic angles and all C—NO_2 bond lengths for D2N(y) and D2N(o), and packing diagrams for D2N(y) and D2N(o), may be purchased from the Depository for Unpublished Data, Document Delivery, CISTI, National Research Council of Canada, Ottawa, Ont., Canada K1A 0S2.

[5] Note that the crystallographic numbering convention is such that the mono- and di-substituted hydrazine atoms are N(7) and N(8), respectively.

TABLE 4. Bond lengths (Å) and bond angles (deg) in 2,2-di(*p*-nitrophenyl)-1-picrylhydrazine

Bond	Length (Å)	
	Yellow form	Orange form
C(1)—C(2)	1.411(3)	1.421(3)
C(1)—C(6)	1.416(3)	1.424(4)
C(2)—C(3)	1.382(3)	1.378(3)
C(3)—C(4)	1.362(3)	1.368(4)
C(4)—C(5)	1.376(3)	1.383(4)
C(5)—C(6)	1.369(3)	1.368(4)
C(11)—C(12)	1.390(3)	1.398(4)
C(11)—C(16)	1.387(3)	1.391(4)
C(12)—C(13)	1.386(4)	1.382(4)
C(13)—C(14)	1.373(4)	1.374(4)
C(14)—C(15)	1.384(4)	1.385(4)
C(15)—C(16)	1.379(4)	1.374(4)
C(21)—C(22)	1.384(3)	1.380(4)
C(21)—C(26)	1.388(4)	1.381(4)
C(22)—C(23)	1.384(4)	1.382(4)
C(23)—C(24)	1.379(4)	1.365(5)
C(24)—C(25)	1.376(4)	1.372(5)
C(25)—C(26)	1.370(4)	1.388(5)
C(1)—N(7)	1.351(3)	1.347(3)
C(11)—N(8)	1.414(3)	1.413(3)
C(21)—N(8)	1.450(3)	1.440(3)
C(2)—N(2)	1.461(3)	1.457(3)
C(4)—N(4)	1.460(3)	1.455(3)
C(6)—N(6)	1.473(3)	1.468(3)
C(14)—N(14)	1.459(3)	1.462(4)
C(24)—N(24)	1.467(3)	1.468(4)
C(51)—Cl(1)	1.753(3)	1.740(4)
C(51)—Cl(2)	1.728(4)	1.743(5)
N(7)—N(8)	1.400(3)	1.402(3)
N(2)—O(21)	1.217(3)	1.218(3)
N(2)—O(22)	1.209(3)	1.223(3)
N(4)—O(41)	1.221(3)	1.224(3)
N(4)—O(42)	1.206(4)	1.218(3)
N(6)—O(61)	1.221(3)	1.219(3)
N(6)—O(62)	1.217(3)	1.217(3)
N(14)—O(43)	1.217(4)	1.215(3)
N(14)—O(44)	1.236(4)	1.199(4)
N(24)—O(45)	1.220(4)	1.230(4)
N(24)—O(46)	1.221(4)	1.229(4)
N(7)—H(7)	0.80(4)	0.85(4)
C(51)—Cl(1)	1.753(4)	1.744(4)
C(51)—Cl(2)	1.728(4)	1.751(4)

Bonds	Angle (deg)	
	Yellow form	Orange form
C(2)—C(1)—C(6)	114.3(2)	114.0(2)
C(1)—C(2)—C(3)	122.6(2)	122.5(2)
C(2)—C(3)—C(4)	119.0(2)	119.0(2)
C(3)—C(4)—C(5)	122.0(2)	121.8(2)
C(4)—C(5)—C(6)	118.0(2)	118.2(2)
C(1)—C(6)—C(5)	123.7(2)	123.3(2)
C(12)—C(11)—C(16)	119.8(2)	119.6(2)
C(11)—C(12)—C(13)	120.2(2)	119.9(2)
C(12)—C(13)—C(14)	118.9(2)	119.4(2)
C(13)—C(14)—C(15)	121.9(2)	121.5(2)
C(14)—C(15)—C(16)	118.8(2)	119.3(2)
C(11)—C(16)—C(15)	120.4(2)	120.2(2)
C(22)—C(21)—C(26)	121.2(2)	120.0(2)
C(21)—C(22)—C(23)	119.3(2)	120.5(3)

TABLE 4 (*concluded*)

Bonds	Angle (deg)	
	Yellow form	Orange form
C(22)—C(23)—C(24)	118.6(2)	118.7(3)
C(23)—C(24)—C(25)	122.5(2)	122.0(3)
C(24)—C(25)—C(26)	118.9(2)	119.2(3)
C(21)—C(26)—C(25)	119.6(2)	119.6(3)
C(2)—C(1)—N(7)	123.4(2)	123.0(2)
C(6)—C(1)—N(7)	122.4(2)	122.9(2)
C(1)—C(2)—N(2)	122.1(2)	121.6(2)
C(3)—C(2)—N(2)	115.3(2)	115.9(2)
C(3)—C(4)—N(4)	118.6(2)	118.8(2)
C(5)—C(4)—N(4)	119.3(2)	119.4(2)
C(1)—C(6)—N(6)	120.8(2)	120.5(2)
C(5)—C(6)—N(6)	115.1(2)	115.8(2)
C(12)—C(11)—N(8)	119.3(2)	120.2(2)
C(16)—C(11)—N(8)	120.9(2)	120.2(2)
C(13)—C(14)—N(14)	119.4(2)	119.5(2)
C(15)—C(14)—N(14)	118.7(2)	119.0(2)
C(22)—C(21)—N(8)	118.4(2)	118.6(2)
C(26)—C(21)—N(8)	120.5(2)	121.4(2)
C(23)—C(24)—N(24)	118.4(2)	118.7(3)
C(25)—C(24)—N(24)	119.1(2)	119.4(3)
Cl(1)—C(51)—Cl(2)	111.6(2)	112.2(2)
C(11)—N(8)—C(21)	118.5(2)	121.5(2)
C(1)—N(7)—N(8)	118.4(2)	119.7(2)
C(11)—N(8)—N(7)	115.0(2)	114.6(2)
C(21)—N(8)—N(7)	112.6(2)	114.0(2)
C(2)—N(2)—O(21)	118.2(2)	118.6(2)
C(2)—N(2)—O(22)	118.9(2)	119.1(2)
C(4)—N(4)—O(41)	117.1(2)	117.4(2)
C(4)—N(4)—O(42)	118.0(2)	118.3(2)
C(6)—N(6)—O(61)	116.6(2)	116.7(2)
C(6)—N(6)—O(62)	117.7(2)	118.0(2)
C(14)—N(14)—O(43)	118.1(2)	118.9(2)
C(14)—N(14)—O(44)	117.6(2)	119.1(2)
C(24)—N(24)—O(45)	118.0(2)	118.3(3)
C(24)—N(24)—O(46)	117.7(2)	117.7(3)
O(21)—N(2)—O(22)	122.8(2)	122.3(2)
O(41)—N(4)—O(42)	124.9(2)	124.3(2)
O(61)—N(6)—O(62)	125.5(2)	124.9(2)
O(43)—N(14)—O(44)	124.2(2)	121.9(2)
O(45)—N(24)—O(46)	124.2(2)	124.0(3)
N(8)—N(7)—H(7)	113(2)	118(2)
C(1)—N(7)—H(7)	122(2)	119(2)
Cl(1)—C(51)—Cl(2)	108.7(4)	111.7(3)

The hydrazine hydrogen atom forms an intramolecular bond with one oxygen atom, O(22), of one of the nitro groups on the picryl group *ortho* to the N—N linkage, as in the related picrylhydrazine derivatives (1, 2, 13) and nitroaniline derivatives (14, 15). Because of this, the hydrogen-bonded nitro group is forced to be nearly coplanar with the picryl plane. The interatomic distances and angles associated with the hydrogen bond, for several picrylhydrazine derivatives and for the trinitroaniline molecule, are given in Table 6. The distances N(7)···O(22) (Table 6) are considerably shorter than the normal value 2.90 Å (16) for N—H···O bonds, because the angle N—H···O is far from 180°.

The bond lengths and the torsional angles of the central fragment of the picrylhydrazine derivatives and of other related molecules are summarized in Tables 7 and 8. In the picrylhydrazine derivatives, all the C(1)—N(7) bonds have similar

Can. J. Chem. Downloaded from www.nrcresearchpress.com by 84.41.108.74 on 09/07/12
For personal use only.

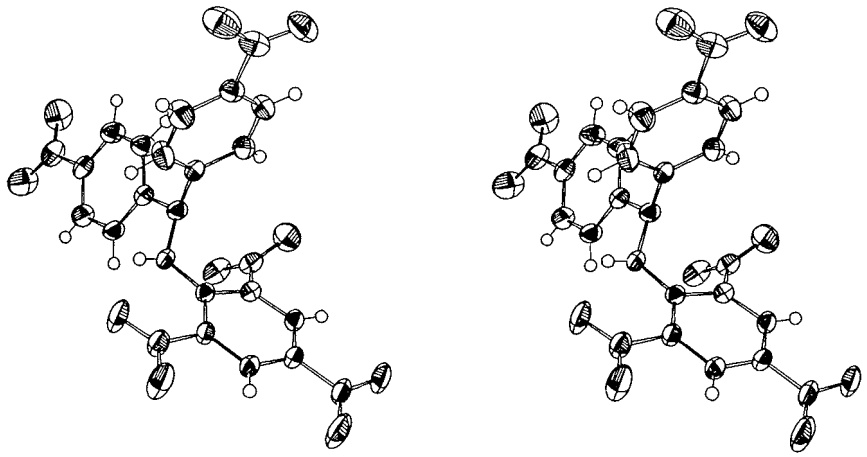


FIG. 1. Stereoscopic view of the molecule of 2,2-di(*p*-nitrophenyl)-1-picrylhydrazine (yellow form), D2N(y).

TABLE 5. Dihedral angles (deg) between planes least-squares fitted to positions of atoms, as defined in Fig. 3 for 2,2-di(*p*-nitrophenyl)-1-picrylhydrazine

		Dihedral angle	
Plane 1	Plane 2	Yellow form	Orange form
A	B	1.4(3)	6.7(2)
A	C	10.2(1)	4.7(3)
A	D	52.9(1)	51.1(2)
A	F	71.0(1)	71.4(1)
A	G	87.4(1)	82.6(1)
A	E	61.4(1)	52.9(1)
E[a]	F	13.2(1)	21.6(1)
E	G	77.5(1)	66.5(1)
F	G	86.6(1)	77.1(1)
F	I	11.7(1)	6.3(1)
G	J	7.3(1)	16.1(2)

Plane least-squares fitted to the position of atoms N(7), N(8), C(11), C(21).

lengths. All of them are significantly shorter than the average C—N single bond (1.456 Å) (17) and some of them are close in length to the C—N partial double bond in the related hydrazyl (6) (1.352 Å) and in trinitroaniline (18) (1.340 Å).

The sum of the three bond angles around the N(7) atom are 356.4(4) and 353.0(4)° for D2N(y) and D2N(o), respectively, suggesting that the N(7) atom is close to being sp^2 hybridized. The sums of the three bond angles around N(8) in D2N(y) and D2N(o) are 346.1 and 350.1°, respectively. The deviations of the nitrogen-atom position from the plane of the N(8) σ-bond system[6] are 0.226(2) and 0.249(1) Å. These parameters indicate that N(8) also is close to having sp^2 hybridization, but with a more appreciable amount of sp^3 character.

Table 7 lists the angles between the phenyl planes and the plane of the N(8) σ-bond system. In all cases except trinitroanilinocarbazole, the phenyl rings adopt the configuration of two propellers of a three-propeller system. In D2N and in diphenylpicrylhydrazine, the two propellers are turned by substantially different amounts from coplanarity with the N(8) σ-bond system, the difference being largest for D2N.

[6]The plane of the σ-bond system is the plane fitted (by least squares) to the central atom and the three atoms connected to it by bonds.

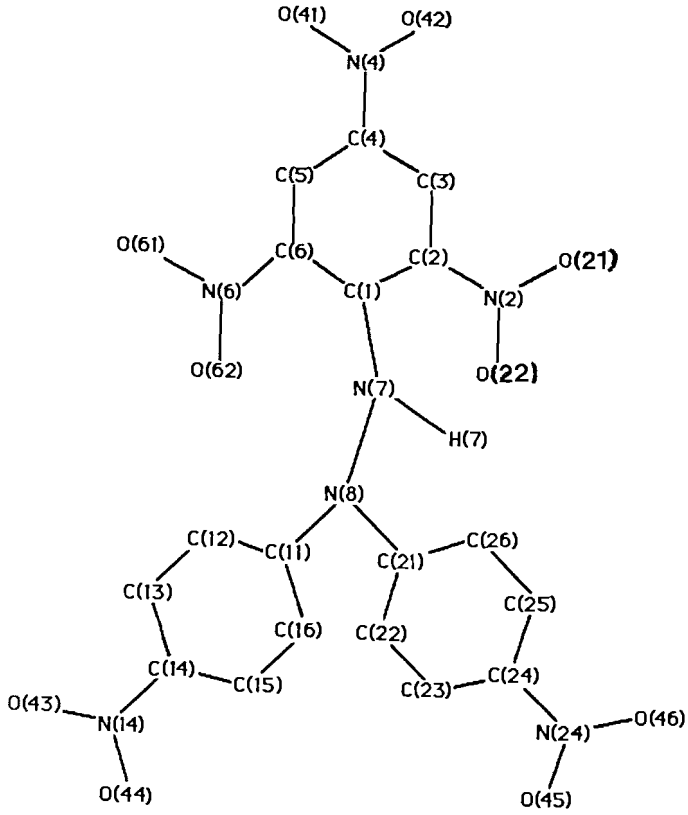


FIG. 2. Atom numbering scheme of 2,2-di(*p*-nitrophenyl)-1-picrylhydrazine.

The dihedral angles between the plane fitted to the phenyl ring of the picryl group and the plane formed by atoms C(1), N(7), and N(8) are 28.1(3) and 23.7(2)° in D2N(y) and D2N(o), respectively. The angles between the plane of the N(8) σ-bond system and the plane fitted to the phenyl ring formed by atoms C(11) to C(16) are 13.2(1) and 21.6(1)°, respectively. The nitrogen lone-pair *p* orbitals are able to interact with the π-electrons of the picryl group in the former case and those of the phenyl ring in the latter.

The angles between the plane of the N(8) σ-bond system and the plane fitted to the phenyl ring formed by atoms C(21) to C(26) are 77.5(1) and 66.5(1)° for D2N(y) and D2N(o), respectively. It follows that here less π-interaction occurs.

Can. J. Chem. Downloaded from www.nrcresearchpress.com by 84.41.108.74 on 09/07/12
For personal use only.

TABLE 6. Interatomic distances (Å) and angles (deg) associated with the intramolecular hydrogen bond for 2,2-di(*p*-nitrophenyl)-1-picrylhydrazine and related compounds

Compound	N(7)—H(7)	O(22)—H(7)	N(7)—O(22)	N(7)—H(7)—O(22)
D2N(y)	0.80(4)	2.06(3)	2.623(3)	127(4)
D2N(o)	0.85(4)	1.99(2)	2.614(3)	129(2)
TNAC(I)[a]	0.82(3)	1.97(3)	2.596(4)	132(2)
TNAC(II)[a]	0.87(3)	1.95(3)	2.608(4)	131(2)
D(t)[b]	0.85(5)	2.02(4)	2.600(6)	125(3)
D(c)[b]	0.84(7)	2.08(5)	2.596(6)	119(5)
Trinitroaniline[c]	0.92(5)	1.87(5)	2.616(5)	136(4)
Normal value[d]	1.00	2.00	2.90	—

[a]TNAC: 2,4,6-Trinitroanilinocarbazole. Reference 2.
[b]2,2-Diphenyl-1-picrylhydrazine crystallized from tetrahydrofuran, D(t) and chloroform, D(c). Reference 1.
[c]Reference 18.
[d]Reference 16.

TABLE 7. Bond lengths (Å) and dihedral angles (deg) of the central moiety of 2,2-di(*p*-nitrophenyl)-1-picrylhydrazine and related molecules

Compound	N(7)—N(8)	C(1)—N(7)	C(11)—N(8)	C(21)—N(8)	Φ[a]EF	Φ[a]EG
D2N(y)	1.400(3)	1.351(3)	1.414(3)	1.450(3)	13.2(1)	77.5(1)
D2N(o)	1.402(3)	1.347(3)	1.413(3)	1.440(3)	21.6(1)	66.5(1)
TNAC(I)[b]	1.381(3)	1.355(4)	1.408(4)	1.392(3)	0.4(1)[g]	3.3(1)
TNAC(II)[b]	1.380(4)	1.361(4)	1.384(4)	1.396(4)	3.3(1)	2.2(1)
D(t)[c]	1.381(5)	1.355(9)	1.444(6)	1.437(6)	14.8(2)	47.9(2)
D(c)[c]	1.400(5)	1.348(7)	1.429(7)	1.428(6)	18.1(2)	46.2(2)
DPPH(I)[d]	1.334	1.369	1.429	1.430	31.1	36.9
DPPH(II)[d]	1.349	1.358	1.422	1.419	27.1	42.4
DPPHK[e]	1.412(3)	1.303(4)	1.423(4)	1.425(4)	37.3	42.6
Carbazole[f]	—	—	1.388(4)	1.388(4)	—	—

[a]Angles between planes E and F and planes E and G, as defined in Fig. 3, and equivalent planes in other molecules.
[b,c]See Table 6.
[d]DPPH: 2,2-diphenyl-1-picrylhydrazyl. Reference 6.
[e]DPPHK: potassium 1-(*N*,*N*-diphenylhydrazono)-2,4,6-trinitrobenzenide. Reference 7.
[f]Reference 30.
[g]The plane equivalent to plane E in D2N is defined differently in TNAC.

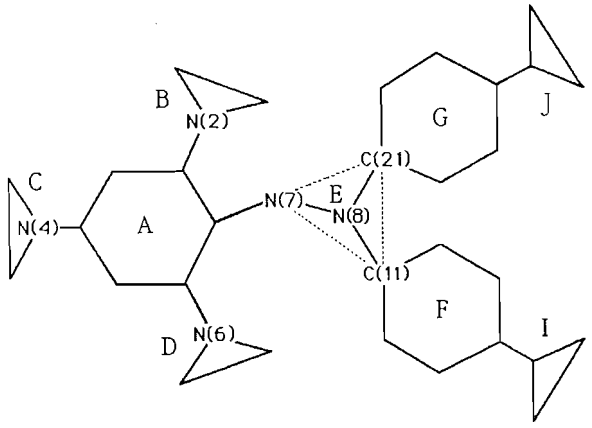


FIG. 3. Designation of planes in 2,2-di(*p*-nitrophenyl)-1-picrylhydrazine.

TABLE 8. Torsional angles (deg) around the N—N linkage[a]

Compound	α_1	α_2	α_3	α_4
D2N(y)	136.3(2)	77.1(3)	81(2)	66(2)
D2N(o)	137.4(2)	82.7(2)	72(2)	68(2)
TNAC(I)[b]	121.1(3)	74.8(4)	74(2)	90(2)
TNAC(II)[b]	120.3(3)	75.7(4)	77(3)	86(3)
D(t)[c]	125.2(5)	82.8(5)	86(4)	65(4)
D(c)[c]	125.0(5)	82.6(6)	80(4)	73(4)
DPPH(I)[d]	145.9	28.1	—	—
DPPH(II)[d]	145.9	28.1	—	—
DPPHK[e]	118.5	26.9	—	—

[a]See Fig. 4.
[b]Reference 2.
[c]Reference 1.
[d]Reference 6.
[e]Reference 7.

Consistent with this, the N(8)—C(11) bond lengths are significantly shorter than the N(8)—C(21) bond lengths. A similar correlation between the dihedral angles and the C—N bond length was observed in the 2,2-diphenyl-1-picrylhydrazyl free radical (5, 6, 19).

For 2,2-diphenyl-1-picrylhydrazine, the dihedral angles between the N(8) σ-bond system and one of the phenyl planes (formed by atoms C(11)—C(21)) are 14.8 and 18.1° for the crystals obtained from tetrahydrofuran and chloroform, respectively (1). The bond lengths equivalent to the N(8)—C(11) bond lengths are 1.437(6) and 1.428(6), respectively, for 2,2-diphenyl-1-picrylhydrazine, which are larger than the

Can. J. Chem. Downloaded from www.nrcresearchpress.com by 84.41.108.74 on 09/07/12
For personal use only.

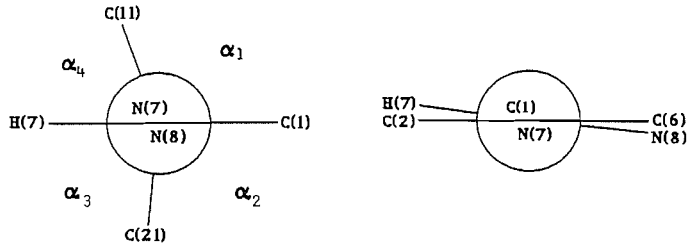


FIG. 4. Newman projections of the central fragment of picrylhydrazine derivatives (*a*) the N—N linkage, (*b*) the C(1)—N(7) bond. Values of α_1, α_2, α_3, and α_4 are given in Table 8.

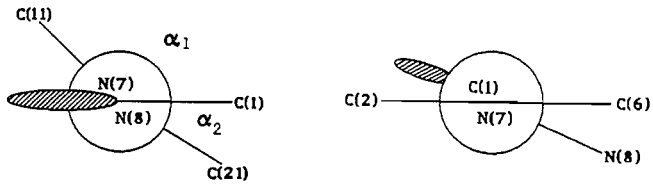


FIG. 5. Newman projections of the central fragment of the diphenylpicrylhydrazyl free radical (*a*) the N—N linkage, (*b*) the C(1)—N(7) bond. Values of α_1, α_2, are given in Table 8. The shaded area represents the assumed location of the lone-pair orbitals of N(7).

values found here (*i.e.*, 1.414(3) and 1.413(3) Å for D2N(y) and D2N(o), respectively). This illustrates the role of the *p*-nitro substitutes in enhancing resonance interaction with the hydrazine nitrogen atoms when the interplanar angles between the phenyl ring and nitrogen plane permit such interaction.

The *p*-nitro substituents may also be assumed to play a role in enhancing resonance interaction between the picryl group and the hydrazine atom N(7). However, the N(7)—C(1) distances are much shorter than the bonds to N(8), suggesting that the *o*-nitro groups of the picryl ring further enhance the resonance interaction.

The dihedral angles between the planes fitted to the picryl ring and to atoms C(1), N(7), and N(8) are larger than those (17.1(5)°) found for 2,2-diphenyl-1-picrylhydrazine (1) and those (14.8(3) and 12.8(2)°) for the two independent molecules in 2,4,6-trinitroanalinocarbazole (2). However, they are smaller than the values (31.6 and 34.5°) found for the related hydrazyl, where the conformational flexibility is not restricted by an intramolecular hydrogen bond (6).

Views of the Newman projections (20) along the N(7)—N(8) bond and along the C(1)—N(7) are given in Fig. 4 for the D2N molecule, and Fig. 5 for the picrylhydrazyl. The atom arrangement around the N—N linkage shows a staggered conformation, which minimizes the steric repulsions between the picryl group at one end of the N—N linkage and the aromatic groups at the other.

The large torsional angles (α_3 and α_4 in Table 8) between the N(7) σ-bond plane and the N(8) σ-bond plane indicate suppression of resonance interaction between the picryl group and the aromatic groups, through the N—N linkage, consistent with the observation that the influence of the *para*-substituents of the phenyl groups on the chemical shift of the hydrazine proton and carbon atoms of the picryl groups is insignificant (21).

The hydrazine nitrogen atoms in the picrylhydrazine molecules are sp^2 hybridized and the N—N bond lengths are essentially those of a single bond. However, they are shorter than the N—N bond lengths of 1.449(4) Å in the hydrazine (H_2N—NH_2) molecule (22) and 1.451(3) Å in dimethyldi(di-

TABLE 9. Puckering coefficients[a] of the aromatic rings in D2N

Plane	*q*2	*q*3	*f*2	*q*2	*Q*
D2N(y)					
C(1)...C(6)	0.056	−0.017	149.91	107.30	0.059
C(11)...C(16)	0.022	−0.006	132.86	105.48	0.023
C(21)...C(26)	0.004	−0.004	20.64	134.07	0.005
D2N(o)					
C(1)...C(6)	0.099	−0.026	168.21	104.47	0.102
C(11)...C(16)	0.016	−0.001	70.09	94.89	0.016
C(21)...C(26)	0.007	0.006	278.39	45.80	0.009

[a]See ref. 25 for definitions.

phenylphosphino)hydrazine (23), but are much longer than the N—N double bond (1.24 Å) in the 2,2′,4,4′,6,6′-hexanitroazobenzene molecule (24).

The shortening of the N(8)—C(11) bond through resonance interaction with the *p*-nitro group on the phenyl group C(11)—C(16) leads to an increase in the N(7)—N(8) bond lengths to 1.414(3) and 1.413(3) Å, from the values of 1.381(5) and 1.400(5) Å found in the structures of crystals of 2,2-diphenyl-1-picrylhydrazine crystallized from tetrahydrofuran and chloroform (1), and 1.381(3) and 1.380(4) Å found for the two independent molecules in the structure of 2,4,6-trinitroaniline (2).

The *o*-nitro substituent on the picryl group not involved in the intramolecular hydrogen bond forms a large dihedral angle (angle between planes A and D in Table 5) with the plane of the picryl group, because of steric repulsion from the aromatic groups at the other end of the N—N linkage. The *p*-nitro substituent of the picryl group forms a non-zero rotation angle (angles between planes A and C in Table 5) with respect to the picryl plane, caused by the steric hindrance effect of neighboring molecules in the crystals. In 2,2-diphenyl-1-picrylhydrazyl (6) and in potassium 1-(*N*,*N*-diphenylhydrazono)-2,4,6-trinitrobenzenide (7) there is no intramolecular hydrogen bonding, and both *o*-nitro groups are rotated significantly from coplanarity with the picryl ring.

The deviations of the angles of the picryl ring from 120° are related to the properties of the substituents (25). The larger endocyclic angles at atoms C(2), C(4), and C(6) are induced by the electron-withdrawing properties of the nitro groups attached there. As a consequence of these enlarged angles, the endocyclic angles at C(1), C(3), and C(5) are decreased to maintain closure of the phenyl ring. The relatively larger decrease of the angle at C(1) arises from the electron-donating property of the hydrazine group attached there.

The endocyclic angles at atoms C(2), C(4), and C(6), the dihedral angles formed by the nitro groups with the phenyl plane, and the C—NO_2 bond lengths are all mutually correlated, as expected.

The puckering of the six-member ring of the trinitroanilino groups was analyzed using the method of Cremer and Pople (26–28). The configuration is described by the amplitude of the puckering with respect to the mean plane of the molecule and by phase angles which define the character of the puckering. The results indicate that the picryl rings have half-boat[7] conforma-

[7]The half-boat conformation of the six-membered ring is analogous to the envelope conformation which applies to five-membered rings, except that five (rather than four), atoms are near a common plane in the case of the six-membered ring.

Can. J. Chem. Downloaded from www.nrcresearchpress.com by 84.41.108.74 on 09/07/12
For personal use only.

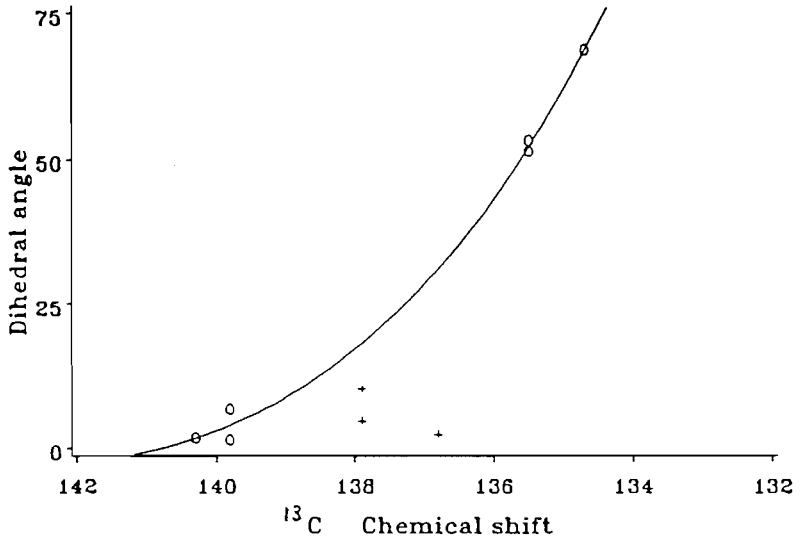


FIG. 6. Correlation of the out-of-plane rotation angles (deg) of the nitro groups and the ^{13}C chemical shifts (ppm) of the carbon atom on which the nitro group is substituted for the picryl rings in D2N(o) and D2N(y) and 2,2-diphenyl-1-picrylhydrazine. The values of the chemical shifts are given with respect to the internal TMS peaks. (○, *o*-nitro groups; +, *p*-nitro groups).

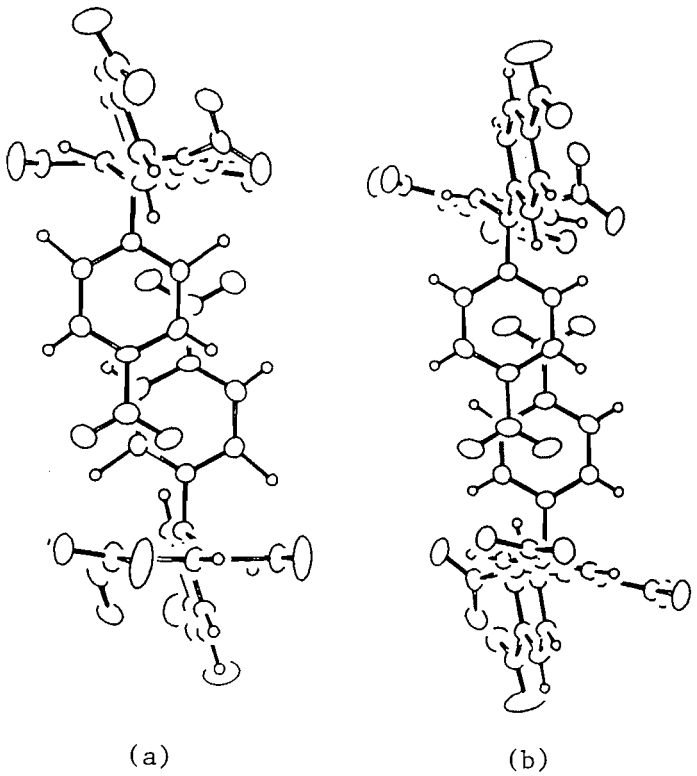


FIG. 7. Overlap of adjacent molecules of (*a*) D2N(y), (*b*) D2N(o).

tions. The puckering amplitudes Q of the picryl rings in the hydrazines (0.059 and 0.102 in D2N(y) and D2N(o)) are larger than that in the hydrazyl free radical (6) but smaller than that in the hydrazinate (0.23). The puckering coefficients of all three substituted phenyl rings in the hydrazines D2N(y) and D2N(o) are listed in Table 9.

Since the NMR chemical shift is directly related to the electron density at the nucleus, its magnitude for the carbon (^{13}C) atom on which a nitro group is substituted will be affected by the rotation angle of the nitro group with respect to the picryl plane. Unfortunately, the available chemical shifts were measured in liquid solution, whereas the rotation angles of the nitro groups were obtained in the crystal. The molecular structure in the crystal is not necessarily identical to that in solution. However, the steric hindrance between the diarylamino group and the picryl group, as well as the intramolecular hydrogen bond, restrict the *o*-nitro groups from rotating about their C—N bonds, and the rotation angles of the two *o*-nitro groups in the solid state are expected to be similar to those in solution.

A plot of the dihedral angle between the plane of the nitro groups on the picryl rings and the plane of the ring to which they are bonded (as determined from the X-ray diffraction results) versus the ^{13}C chemical shift of the nitro-bonded carbon atoms for D2N and 2,2-diphenyl-1-picrylhydrazine, is given in Fig. 6. The ^{13}C NMR spectra of D2N and 2,2-diphenyl-1-picrylhydrazine were obtained at 250 K in acetone-d_6 by Currie *et al.* (21). All *p*-nitro groups, including those on the picryl rings, have greater freedom to assume a variety of angular positions about their N—C bonds than do the *o*-nitro group, in response to the variations in their environments in the liquid. The rotational freedom of the *p*-nitro groups is manifested by their large temperature factors. Therefore, the curve through the points in Fig. 6 was fitted only to those points representing the *o*-nitro groups. The large deviations of those points representing the *p*-nitro groups from the curve indicates either that their N—C rotation angles in the solid state are substantially smaller than the time-averaged values in solution, or that carbon atoms with *para* substituents have considerably different chemical shifts than those with *ortho* substituents (24).

Molecular packing

In many cases, for a given molecule, crystal forms with different molecular packing may be obtained under different crystallization conditions, particularly from different solutions. In our case, however, the yellow form and the orange form of D2N were crystallized virtually simultaneously, from a common dichloromethane solution.

The two crystal forms were examined by EPR to investigate the possibility that one or the other might have been nucleated

Can. J. Chem. Downloaded from www.nrcresearchpress.com by 84.41.108.74 on 09/07/12
For personal use only.

by picrylhydrazyl free radicals, possibly present as an impurity in the original solution. However, the EPR spectral traces showed no evidence for the presence of free radicals in either crystal form.

The two forms of D2N have similar melting points, 124.8°C for the yellow form and 119.5°C for the orange form. They presumably have similar enthalpies of crystallization and similar probabilities of nucleating in dichloromethane solution. The difference in color between the two crystal forms must be a consequence of the difference in molecular packing. For example, a recent study of a series of perylene derivatives by Klebe *et al.* (29) showed such an effect. The absorption characteristics of these derivatives were assumed to be influenced by the electronic interaction between two adjacent perylene moieties which packed with their planes roughly coplanar, and which were separated by 3.34–3.65 Å. In both D2N(y) and D2N(o), the plane of the *p*-nitrophenyl group containing C(21) is coplanar with the plane of the same group of an adjacent molecule related by a center of symmetry. The overlapping area of the two planes for molecules in the D2N(y) crystal is only slightly different than that in the D2N(o) crystal, as illustrated in Fig. 7. Nevertheless, the small difference in overlap may account for the difference in color.

D2N crystals do not form chains, as is the case in 9-(2,4,6-trinitroanilino)carbazole (2). This may be related to the presence of the *p*-nitro substituents on the phenyl group, which decreases the overall polarity of the molecule, and to the absence of a bond forcing the two phenyl groups to be nearly coplanar.

Acknowledgements

The authors thank the Canadian International Development Agency for the support of H.W., and the Natural Sciences and Engineering Research Council of Canada for operating grants to R.J.B. and B.E.R. and to J.A.W.

1. H. Wang, R. J. Barton, B. E. Robertson, J. A. Weil, and K. C. Brown. J. Inclusion Phenom. Mol. Recogn. Chem. **10**, 203 (1991).
2. H. Wang, R. J. Barton, B. E. Robertson, J. A. Weil, and K. C. Brown. Can. J. Chem. **65**, 1322 (1987).
3. J. Heidberg, J. A. Weil, G. A. Janusonis, and J. K. Anderson. J. Chem. Phys. **41**, 1033 (1964).
4. R. L. Tyson and J. A. Weil. J. Phys. Chem. **94**, 3951 (1990).
5. D. E. Williams. J. Am. Chem. Soc. **89**, 4280 (1967).
6. C. Th. Kiers, J. L. DeBoer, R. Olthof, and A. L. Spek. Acta Crystallogr. **B32**, 2297 (1976).
7. R. Gopal, B. E. Robertson, and J. A. Weil. Can. J. Chem. **61**, 2735 (1983).
8. J. A. Weil, K. V. Sane, and J. M. Kinkade, Jr. J. Phys. Chem. **65**, 710 (1961).
9. J. A. Weil and G. A. Janusonis. J. Org. Chem. **27**, 1248 (1962).
10. S. French and K. Wilson. Acta Crystallogr. **A34**, 517 (1978).
11. H. Wang and B. E. Robertson. Struct. Stat. Crystallogr., Proc. Symp. 1984. *Edited by* A. J. C. Wilson. Adenine Press, Guiderland, NY. 1985. pp. 125–136.
12. S. R. Hall and J. M. Stewart. XTAL crystallographic system of programs. Universities of Western Australia and Maryland. 1988.
13. J. L. Flippen-Anderson and D. S. Dudis. Acta Crystallogr. **C45**, 1107 (1989).
14. G. Ploug-Soerensen and E. K. Andersen. Acta Crystallogr. **C39**, 112 (1983).
15. L. Parkanyi and A. Kalman. J. Mol. Struct. **125**, 315 (1984).
16. W. C. Hamilton and J. A. Ibers. Hydrogen bonding in solids; methods of molecular structure determination. W. A. Benjamin, New York, NY. 1968.
17. International tables for X-ray crystallography. Vol. II. Kynoch Press, Birmingham, England. 1974. pp. 17–19.
18. J. R. Holden, C. W. Dickinson, and C. M. Bock. J. Phys. Chem. **76**, 3597 (1972).
19. M. Sternberg. Compt. Rend. **240**, 990 (1955).
20. A. Streitwieser Jr. and C. H. Heathcock. Introduction to organic chemistry. Macmillan, New York, NY. 1976.
21. P. F. Currie, J. W. Quail, A. C. M. Rusk, and J. A. Weil. Can. J. Chem. **61**, 1760 (1983).
22. Y. Morino, T. Iijima, and Y. Murata. Bull. Chem. Soc. Jpn. **33**, 46 (1960).
23. J. B. Faught. Can. J. Chem. **54**, 738 (1976).
24. E. J. Graeber and B. Morosin. Acta Crystallogr. **B30**, 310 (1974).
25. A. Domenicano, A. Vaciago, and C. A. Coulson. Acta Crystallogr. **B31**, 221 (1975).
26. D. Cremer and J. A. Pople. J. Am. Chem. Soc. **97**, 1354 (1975).
27. D. Cremer. Fortran Program RING, Quantum Chemical Program Exchange, Program No. 288. University of Indiana, Bloomington, IN. 1975.
28. D. Cremer. Isr. J. Chem. **20**, 12 (1980).
29. G. Klebe, F. Graser, E. Haedicke, and J. Berndt. Acta Crystallogr. **B45**, 69 (1989).
30. V. K. Bel'skii. Sov. Phys. Crystallogr. **30**, 112 (1985).

Can. J. Chem. Downloaded from www.nrcresearchpress.com by 84.41.108.74 on 09/07/12
For personal use only.

An unexpected acyloin rearrangement and oxidation of a camphor derivative

JOHN M. MCINTOSH[1] AND KENNETH C. CASSIDY[2]

Department of Chemistry and Biochemistry, University of Windsor, Windsor, Ont. Canada N9B 3P4

Received February 15, 1991

JOHN M. MCINTOSH and KENNETH C. CASSIDY. Can. J. Chem. **69**, 1315 (1991).

The trimethylsiyl ether **7** derived in two steps from camphor underwent ring expansion via an acylion rearrangement to afford two products (**8** and **9**) when desilylation was attempted. Compound **9** was stable but **8** was oxidized in air to homocamphoric acid anhydride **11**.

Key words: camphor, acyloin rearrangement.

JOHN M. MCINTOSH et KENNETH C. CASSIDY. Can. J. Chem. **69**, 1315 (1991).

Lorsqu'on essaie d'effecteur une désilylation de l'éther triméthylsilylé **7**, obtenu en deux étapes à partir du camphre, celui-ci subit une extension de cycle par le biais d'une transposition aux acyloïnes qui conduit à deux produits (**8** et **9**). Le composé **9** est stable, mais le produit **8** est oxydé par l'air en anhydride de l'acide homocamphorique **11**.

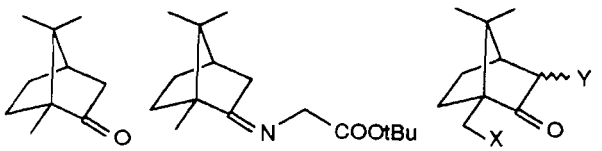
Mots clés : camphor, transposition aux acyloïnes.

[Traduit par la rédaction]

Introduction

The literature on the chemistry of camphor (**1**) is enormous. This extraordinarily compact structure has been exposed to almost every conceivable reaction condition and a great diversity of products has been isolated (1). Recently the chemistry of camphor has enjoyed a renaissance due to its use in asymmetric synthesis. It has served as both a direct source of chiral centres of known configuration (2) and as a chiral directing agent (3).[3] The factors that make camphor attractive in this area are its ready availability in both enantiomeric forms, its rigid structure, which limits the influence of conformational change on reaction pathways, and the number and diversity of known transformations that allow access to other chiral molecules of known configuration, which frequently are not obviously related to **1**.

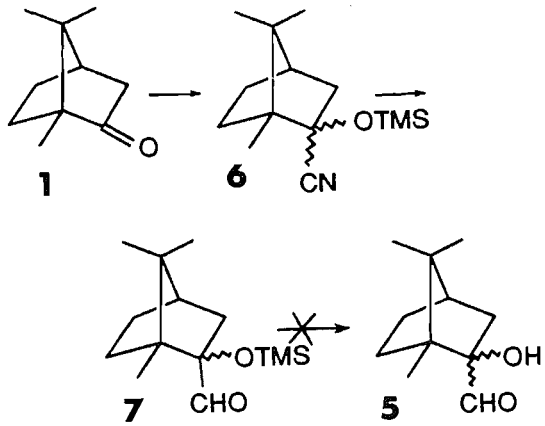
For a number of years, we have been engaged in a study of the stereochemistry of the alkylation of chiral imines of glycinate esters. Much of the work has centred on the use of the camphor imine **2**. Our results in this area have been documented (4), as has our inability to perform aldol condensations on the enolate of **2**. A number of reports (5) suggested to us that the incorporation of a second centre, hydroxylic in nature, into the skeleton of **1** might facilitate such aldol condensations. We have already reported (6) the approaches we took to the preparation of **3** and **4**, and the unexpected product obtained when **4** was



1 **2** **3** X=H, Y=OH **4** X=OH, Y=H

condensed with *tert*-butyl glycinate. We now report the unexpected transformation found when the preparation of the camphor derivative **5** was attempted.

The proposed synthesis of **5** is shown in Scheme 1. The mixture of cyanohydrin ether stereoisomers **6** was prepared in 95% yield as previously described (7). Reduction of **6** with



1 **6** **7** **5**

SCHEME 1

DIBAL-H proceeded uneventfully to give the silyl ether (**7**) of the desired hydroxyaldehyde **5**. NMR analysis of both **6** and **7** indicated an approximately 6:1 ratio of stereoisomers. The accepted mechanism (7) for the formation of cyanohydrin TMS ethers with TMSiCN involves attack of cyanide ion on a ketone–trimethylsilyl complex. Assuming that this is a kinetically controlled process, it suggests that the isomer of **6** with an *endo*-oriented cyano group should be preferred.

The desilylation of **7** proved to be anything but routine. Exposure to either Bu_4NF or $BF_3 \cdot OEt_2$ in CH_2Cl_2 afforded two products (**8** and **9**) that were isomeric with both product **5** and each other. However, neither of these exhibited the expected aldehyde proton in the ^1H NMR. The ratio of these was found to be approximately the same as the ratio of the stereoisomers **6** and **7**.

Both **8** and **9** had the molecular weight (mass spectra) of 182 ($C_{11}H_{18}O_2$). The ^1H and ^{13}C NMR spectra for **8** and **9** are given in Tables 1 and 2. The infrared of both compounds indicated the presence of both a carbonyl and an alcohol group. The ^{13}C NMR (both proton decoupled and DEPT-135 edited) of the major product showed three quaternary methyl groups, a ketonic carbon, a secondary carbinol carbon, three methylene groups, and one other methine carbon. The ^1H NMR confirmed the presence of three methyl groups (singlets) and a one-proton triplet. Decoupling experiments revealed that the signal at δ = 4.21 was coupled with protons resonating at δ = 2.32 and 2.15

[1]Author to whom correspondence may be addressed.

[2]Holder, NSERC predoctoral fellowship, 1988–1991.

[3]For a recent review (3*a*) and for some recent references (3*b*).

Can. J. Chem. Downloaded from www.nrcresearchpress.com by 84.41.108.74 on 09/07/12
For personal use only.

TABLE 1. ^{1}H NMR data for compounds **8** and **9**

Compound **8**				Compound **9**			
δ (ppm)	No. of H (mult.)	*J* (Hz)	Assignment	δ (ppm)	No. of H (mult.)	*J* (Hz)	Assignment
4.21	1(t)	9.0	3-en	4.00	1(bs)		2-ex
3.50	1(d)	18	O*H* (D_2O)	3.65	1(d)	2.3	O*H* (D_2O) ex
2.32	1(m)		4-ex	2.75	1(d)	15.6	4-ex
2.15	1(m)		4-en	2.3	1(dd)	15.6,3.1	4-en
1.95	1(m)		5	1.9	1(m)		
1.8–1.5	4(m)	6,7		1.8	1(m)		
1.00	3(s)		[11]	1.7	1(m)		
0.90	3(s)		[10]	1.4–1.25	2(m)		
0.70	3(s)	[9]		1.25	3(s)		9
				0.95	3(s)		11
				0.92	3(s)		10

TABLE 2. ^{13}C NMR data for **8**, **9**, and **10**

Compound **8**			Compound **9**			Compound **10**[a]	
δ (ppm)	Mult.	Assignment	δ (ppm)	Mult.	Assignment	δ (ppm)	Assignment
215.0	s	C2	211.8	s	C3	212.6	C3
70.17	d	C3	78.9	d	C2	53.94	C2
56.8	s	C1	51.5	s	C1	44.46	C1
48.0	s	C8	46.3	d	C5	45.75	C5
44.4	d	C5	44.6	t	C4	47.04	C4
38.0	t	C7	44.4	s	C8	43.12	C8
34.1	t	C4	28.6	t	C6	27.44	C6
27.3	t	C6	26.8	t	C7	36.15	C7
23.3	q	[C10]	24.1	q	C10	23.58	C10
19.8	q	[C9]	18.4	q	C9	20.77	C9
13.4	q	[C11]	16.4	q	C11	18.84	C11

[a]See ref. 9.

On the basis of these data, the assignments given in Table 1 were made and the structure **8** assigned to this compound. The stereochemistry is inferred from the coupling constants calculated for the energy-minimized conformation of **8**. The dihedral angles bewteen protons A and B (151°) and A and C (35°) respectively predict (8) coupling constants of similar magnitude (ca. 8 Hz) and this agrees with the observed triplet. The lack of extraneous signals in the ^{13}C NMR of **8** and in the ^{1}H and ^{19}F NMR of its Mosher ester indicates that only one of the possible diastereomers was present. The dihedral angles calculated for the epimer (30° and 85°) lead to coupling constants that vary widely in magnitude and do not agree well with those observed.

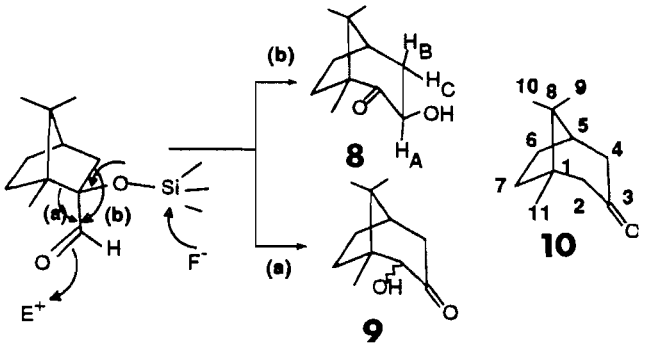
The minor isomer had many of the same characteristics but the Mosher ester could not be formed. The NMR data ensure that only one steroisomer is present and the most obvious differences with **8** were the presence of an AB quartet with signals at δ = 2.75 and 2.3 and that the secondary carbinol proton appeared as a slightly broadened *singlet* (δ = 4.00). Decoupling experiments showed that this signal was coupled only to the OH proton. Further, the signals at 2.75 and 2.3 were coupled to each other and the latter was also coupled to a signal at 2.0. These data and other decoupling experiments led to the assignments shown in Table 2. On the basis of the NMR evidence and a proposed mechanism, the structure **9** was suggested for this compound. The proton and carbon NMR data for the related compound **10** have been reported by Lightner and co-workers (9). The resonance assignments were made without comment and the values we obtained for **9** were consistent with those reported. In an effort to assign the stereochemistry of **9**, the NOE difference spectrum was obtained. The secondary carbinol proton showed a strong positive correlation with the methyl group at 1.25 ppm and a much weaker interaction with the methyl group resonating at 0.95 ppm in the ^{1}H spectrum. The 1.25 ppm methyl singlet also showed close proximity to the proton resonating at 2.75 ppm. These data appear to require the *endo* configuration of the C-2 hydroxy group in **9**. If structure **9** is correct, the methyl resonance at 1.25 would necessarily be due to C(9) and that at 0.95 would be C(11), assignments that do not correspond to those reported for compound **10**. That our assignments for **9** are correct was shown by the proton–carbon correlated 2-D spectra, which indicated the positive correlations shown in Table 3.

It is possible that **8** and **9** are formed independently as shown in Scheme 2 or that they represent a mixture that can be formed from, and equilibrate via, a common ene-diol intermediate. Such an equilibrium was observed in reactions of **3** (6). The latter case seems unlikely since the same ratio of **8** and **9** was

Can. J. Chem. Downloaded from www.nrcresearchpress.com by 84.41.108.74 on 09/07/12
For personal use only.

TABLE 3. Proton–carbon correlations for compound **9**

δC (ppm)	δH (ppm)
78.9 (CH)	4.00 (s)
46.3 (CH)	1.9 (m)
44.6 (CH_2)	2.3 (dd), 2.7 (d)
28.6 (CH_2)	1.4 (m)
26.6 (CH_2)	1.3 (m)
24.1 (Me)	0.92 (s)
18.4 (Me)	1.25 (s)
16.4 (Me)	0.95 (s)



SCHEME 2

obtained using Bu_4NF and $BF_3 \cdot OEt_2$ and the former would be unlikely to cause enolization of either **8** or **9**. In the former case, the stereoisomer of **8** and **9** that is produced will, of course, depend on which of the two diastereotopic faces of the aldehyde carbonyl group is attacked by the migrating bond.

At this point, the 2-D spectra of **8** were desired to compare with those of **9**. In preparation for these experiments, the normal spectra were re-recorded and it was clear that the original material had been essentially completely converted into another product **11**. This process had occurred while crystals of **8** had been allowed to stand in air at ambient temperature. This material showed a doubling of the carbonyl band in a region suggestive of a six-membered ring anhydride, but *no* hydroxyl absorptions in the infrared spectrum. Both the mass spectrum (molecular weight = 198, $C_{11}H_{16}O_3$) and the DEPT-135 edited ^{13}C NMR indicated the presence of only 16 protons, suggesting an oxidation had occurred. In addition, the ^{13}C NMR (Table 4) showed two carbonyl carbons at 173 and 170 ppm and no sp^3 carbon attached to oxygen. These data seemed best accommodated by homocamphoric anhydride **11** (Fig. 1).

Hydrolysis of **11** provided the known (10) diacid **12** (homocamphoric acid). The NMR spectra of homocamphoric acid have apparently not been described. However, the similarity of the ^1H and ^{13}C spectra with those of the well-known camphoric acid (11*a,c*) and camphoric anhydride (11*b*; ^1H NMR) and the coincidence of the melting point of **12** obtained in this work to that reported (10) in the literature ensure the structural assignment.

The facile rearrangement of **5** to **8** and **9** is an example of an acyloin rearrangement (12). The stereospecific acid-catalyzed reaction has been most thoroughly studied in the context of the expansion of the D-ring of steroids, but alkaloid and terpene

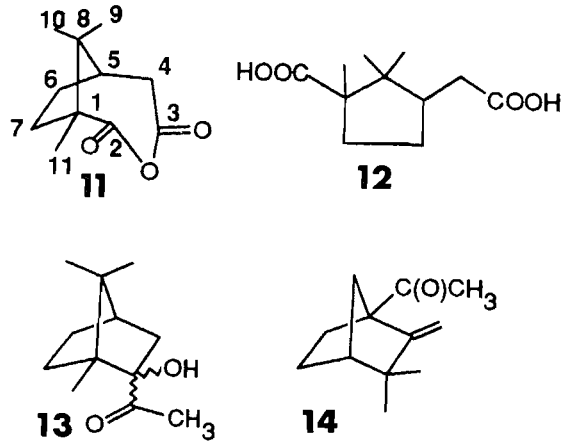


FIG. 1.

examples are also well known (see, for example, ref. 13). However, to our knowledge, it does not seem to have been reported in the literature on camphor. Relief of ring strain would seem to be the likely driving force for the rearrangement, but the corresponding methyl ketone **13** ("2-acetylborneol") has been prepared (14) and rearranged under vigorously acidic conditions ($KHSO_4$, 180°C) to give **14** ("2-acetylcamphene"). A variety of other ring-opened and rearranged bicyclo[2.2.1]heptyl products, but no ring-expanded products, were described. The rearrangement outlined here must be considered to be yet another chapter in the story of the molecular gymnastics of camphor derivatives.

It is not clear why **8** should be so sensitive to aerial oxidation. The isomer **9** does not exhibit this reactivity, nor do more highly strained molecules such as 3-hydroxycamphor (6). The failure of **9** to undergo the same oxidation also argues against the interconversion of **8** and **9** as noted previously. At this time we cannot comment meaningfully on this reaction.

Experimental

Infrared spectra were run as neat liquids or KBr mulls; NMR spectra were run at 300 MHz for ^1H and 75 MHz for ^{13}C in $CDCl_3$ solution. Assignments shown in brackets ([ ]) may be interchanged. DEPT editing refers to the DEPT-135 pulse sequence. Where this was performed, the multiplicities that would have been seen in the proton-coupled spectra are indicated. Column chromatography utilized silica gel 60 (Merck), solvents were removed under reduced pressure, and the drying agent used was anhydrous magnesium sulfate. Mosher esters were prepared from commercially available (*R*)-(+)-α-(trifluoromethyl)phenylacetic acid using the literature procedure (15). Elemental analyses were performed by Galbraith Laboratories, Knoxville, Tenn.

Preparation of 2-hydroxy-1,7,7-trimethylbicyclo[2.2.1]heptane-2-carboxaldehyde TMS ether (7)

To a cooled solution of 62 g (0.25 mol) of crude **6** (7) in 100 mL of dry toluene was added 190 mL of a solution of DIBAL (1.5 M in toluene) dropwise with stirring. After the addition was complete, the solution was allowed to warm to ambient temperature. TLC (4% pet. ether/ether) analysis showed starting material was still present so the solution was refluxed gently for 3 h. The cooled solution was poured slowly over a mixture of 75 mL of H_2SO_4 and stirred overnight. The solution was filtered, the organic layer separated, and the aqueous layer extracted with toluene. The combined organic layers were dried and evaporated to afford an oil (60 g), which was distilled to give **7** as a 6:1 mixture of epimers (48 g, 75%), bp 75–80°C (0.1 Torr; 1 Torr = 133.3 Pa); IR (neat): 2957, 1731, 1252, 1124 cm^{-1}; ^1H NMR: 9.52 [9.41] (s, 1H), 2.15 (m, 1H), 1.82–1.5 (m, 3H), 1.45–1.00 (m, 3H), 0.95 [0.97] (s, 3H), 0.91 [0.90] (s, 3H), 0.82 (s, 3H), 0.09 (s, 9H).

Can. J. Chem. Downloaded from www.nrcresearchpress.com by 84.41.108.74 on 09/07/12
For personal use only.

TABLE 4. ^1H and ^{13}C NMR data for compound **11**

^1H NMR				^{13}C NMR		
δ (ppm)	No. of H (mult.)	*J* (Hz)	Assignment	δ (ppm)	Mult.	Assignment
2.92	1 (1/2 ABq)	14.4	4-ex	172.2	s	[C2]
2.72	1 (1/2 ABq)	14.4, 6.7		167.5	s	[C3]
			4-en	56.23	s	C1
2.5–2.0	3 (m)			46.88	d	C5
1.9–1.7	2 (m)			46.09	s	C8
1.27	3 (s)		[11]	38.61	t	C4
1.14	3 (s)		[9]	33.10	t	C6
1.03	3 (s)		[10]	26.92	t	C7
				26.01	q	C11
				20.72	q	[C9]
				20.50	q	[C10]

Anal. calcd. for $C_{14}H_{26}O_2$: C 65.88, H 10.27; found: C 65.74, H 10.32.

Chromatography failed to separate the epimers.

Attempted preparation of 2-hydroxy-1,7,7-trimethylbicyclo[2.2.1]-heptane-2-carboxaldehyde (5)

To 10 mL of CH_2Cl_2 was added 3.5 g (0.014 mol) of **7**. The solution was cooled to 0°C in ice and 1.8 mL (0.015 mol) of $BF_3O \cdot OEt_2$ was added slowly. After 15 min, GC (column A) showed no starting material. The solution was allowed to warm to room temperature and then quenched by the slow addition of saturated aqueous $NaHCO_3$. The organic layer was separated, the aqueous layer was extracted with ether, and the combined organic layers dried and evaporated to afford a white solid that showed two components on TLC analysis (R_f 0.37 and 0.52, 2:1 pet. ether:ether). The mixture was chromatographed to afford 0.4 g of **9** (MS: m/z = 182; mp 154–156°C; IR: 3481, 2922, 1716, 1059 cm^{-1}) and 1.04 g of **8** (MS: m/z = 182; mp 175–184°C (dec); IR: 3475 (br), 2966, 1707, 1024 cm^{-1}). The ^1H and ^{13}C NMR data for **8** and **9** can be found in Tables 1 and 2. Anal. calcd. for **9** ($C_{11}H_{18}O_2$): C 72.49, H 9.95; found: C 72.05, H 9.94.

The same result was obtained when **7** was treated with $Bu_4N^+F^-$ in THF.

Only unsatisfactory analytical data could be obtained for **8**, presumably due to oxidation to **11**.

The Mosher ester of **8** was prepared as follows. To 1 mL of dry pyridine was added 100 mg of **8**. The solution was cooled to 0°C and 0.15 g of MPTA-Cl (14) was added. A precipitate formed instantly. The mixture was stirred overnight while warming to ambient temperature, then poured into 5 mL of 10% HCl and extracted with ether. The ether was dried and evaporated to give 0.27 g of a yellow oil, which was purified by column chromatography. The yield of purified ester was 71%; IR: 2972, 1750, 1721, 1258, 1169 cm^{-1}; ^1H NMR: 7.72 (m, 2H), 7.45 (m, 3H), 5.62 (t, 1H, J = 9.6 Hz), 3.71 (s, 3H), 2.30–1.05 (m, 7H), 1.02 (s, 3H), 0.95 (s, 3H), 0.82 (s, 3H); ^{13}C NMR: 207.11, 166.03, 132.41, 129.52, 128.31, 127.50, 73.83, 57.78, 55.78, 47.40, 44.29, 34.19, 33.66, 27.15, 23.15, 19.81, 13.61; ^{19}F NMR: 5.55 (TFA = 0).

After standing at room temperature in air for several days, compound **8** had been transformed into **11**. This was separated from residual **8** by chromatography and obtained as a white solid, mp 138–140°C; IR: 2972, 1782, 1745, 1118, 1041 cm^{-1}. The ^1H and ^{13}C NMR data are given in Table 4.

Homocamphoric acid (12)

Anhydride **11** (50 mg, 0.25 mmol) was added to 1 mL of H_2O containing 50 mg of NaOH. The mixture was refluxed 1 h, cooled, and stirred at room temperature overnight. Acidification with concentrated HCl gave a white precipitate, which was dissolved in ether, washed with brine, dried, and evaporated to afford **12** (81%) as a white powder, mp 237–238°C (dec.) (lit. (10) mp 238°C); IR: 3266–2800, 2945, 1696, 1313, 1303 cm^{-1}; ^1H NMR: 11.05 (s, 2H), 2.4–2.04 (m, 3H), 2.02–1.75 (m, 2H), 1.40–1.15 (m, 2H), 1.10 (s, 3HO, 0.98 (s, 3H), 0.65 (s, 3H); ^{13}C NMR: 177.36 (s), 174.40 (s), 54.87 (s), 44.29 (s), 43.20 (d), 35.26 (t), 31.92 (t), 26.61 (t), 21.81 (q), 21.39 (q), 19.32 (q).

Acknowledgements

We acknowledge the financial support of the Natural Sciences and Engineering Research Council of Canada in the form of a scholarship (to K.C.C.) and operating grants (to J.M.M.). The able technical assistance of M. Fuerth in obtaining the 2-D spectra used contributed signifcantly to the completion of this work.

1. (*a*) T. MONEY. Nat. Prod. Rep. **2**, 253 (1985); (*b*) T. MONEY. *In* Studies in natural products chemistry. Vol. 4. *Edited by* A. Rahman. Elsevier, New York. 1989. p. 625; (*c*) J. L. SIMONSEN. The terpenes. Vol. 2. Cambridge University Press, London. 1948. pp. 272ff; (*d*) P. DE MAYO. Mono- and sesquiterpenoids. Interscience, New York. 1959.
2. R. V. STEVENS, F. C. A. GAETA, and D. S. LAWRENCE. J. Am. Chem. Soc. **105**, 7713 (1983); R. V. STEVENS, J. H. CHANG, R. LAPALME, S. SCHOW, M. G. SCHLAGATER, R. SHAPIRO, and H. N. WELLER. J. Am. Chem. Soc. **105**, 7719 (1983).
3. (*a*) W. OPPOLZER. Tetrahedron, **43**, 1969 (1987); (*b*) T. ISHIZUKA, S. ISHIBUCHI, and T. KUNIEDA. Tetrahedron Lett. **30**, 3449 (1989); W. OPPOLZER and A. J. KINGMA. Helv. Chim. Acta, **72**, 1337 (1989).
4. (*a*) J. M. MCINTOSH and P. M. MISHRA. Can. J. Chem. **64**, 726 (1985); (*b*) J. M. MCINTOSH and R. K. LEAVITT. Tetrahedron Lett. **27**, 3839 (1986); (*c*) J. M. MCINTOSH, R. K. LEAVITT, P. M. MISHRA, K. C. CASSIDY, J. E. DRAKE, and R. CHADHA. J. Org. Chem. **53**, 1947 (1988).
5. (*a*) L. CASELLA, G. JOMMI, S. MONTANARI, and M. SISTI. Tetrahedron Lett. **29**, 2067 (1988); (*b*) A. EL ACHQAR, M.-L. ROUMESTANT, and P. VIALLEFONT. Tetrahedron Lett. **29**, 2441 (1988); (*c*) J. BAJGROWICZ, A. EL ACHQAR, M.-L. ROUMESTANT, C. PIGIÉRE, and P. VIALLEFONT. Heterocycles, **24**, 2165 (1986), and references therein.
6. J. M. MCINTOSH, K. C. CASSIDY, and L. C. MATASSA. Tetrahedron, **45**, 5449 (1989).
7. D. A. EVANS, G. L. CARROLL, and L. K. TRUESDALE. J. Org. Chem. **39**, 914 (1974).
8. L. M. JACKMAN and S. STERNHELL. Applications of nuclear magnetic resonance in organic chemistry. Pergamon Press, New York. 1969.

Can. J. Chem. Downloaded from www.nrcresearchpress.com by 84.41.108.74 on 09/07/12
For personal use only.

9. B. V. CRIST, S. L. RODGERS, and D. A. LIGHTNER. J. Am. Chem. Soc. **104**, 6040 (1982).
10. W. S. JOHNSON and W. E. SCHELBERG. J. Am. Chem. Soc. **67**, 1754 (1945).
11. (*a*) C. J. POUCHERT and J. R. CAMPBELL. The Aldrich library of NMR spectra. Aldrich Chemical Co. Milwaukee, WI. 1974. Vol. 2. p. 185; (*b*) Vol. 3, p. 86; (*c*) W. H. PIRKLE and P. L. RINALDI. J. Org. Chem. **42**, 2080 (1977).
12. N. L. WENDER. *In* Molecular rearrangements. *Edited by* P. de Mayo. Interscience, New York. 1964. pp. 1114ff.
13. (*a*) J. F. KING and P. DE MAYO. *In* Molecular rearrangements. *Edited by* P. de Mayo. Interscience, New York. 1964. p. 801ff. (*b*) E. WARNOFF. *In* Molecular rearrangements. *Edited by* P. de Mayo. Interscience, New York. 1964. p. 917.
14. M. KAGAWA. Chem. Pharm. Bull. **7**, 306 (1959).
15. J. A. DALE, D. L. DULL, and H. S. MOSHER. J. Org. Chem. **34**, 2543 (1969).

Can. J. Chem. Downloaded from www.nrcresearchpress.com by 84.41.108.74 on 09/07/12
For personal use only.

Déplacements homolytiques intramoléculaires. 19. Stéréochimie de la décomposition induite de peroxydes insaturés conduisant à la formation d'hétérocycles à trois et quatre chaînons

X. LUBEIGT, F. FLIES, M. J. BOURGEOIS ET E. MONTAUDON[1]
Laboratoire de chimie appliquée, Université Bordeaux I, F-33405, Talence CEDEX, France

ET

B. MAILLARD[1]
Laboratoire de chimie organique et organométallique, associé au Centre national de la recherche scientifique (Unite de recherche associée n° 35), Université Bordeaux I, F-33405, Talence CEDEX, France

Reçu le 6 décembre 1990

X. LUBEIGT, F. FLIES, M. J. BOURGEOIS, E. MONTAUDON et B. MAILLARD. Can. J. Chem. **69**, 1320 (1991).

La décomposition induite dans le chlorure de méthylène de peroxydes β- et γ-insaturés comportant un substituant sur la chaîne liant la fonction peroxydique et la double liaison est étudiée. La stéréochimie des oxiranes et oxétanes disubstitués obtenus est déterminée par RMN ^{13}C. La stéréosélectivité de la réaction est discutée.

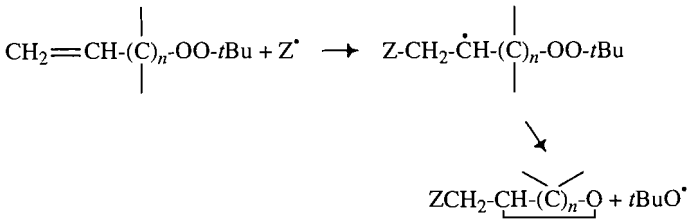
Mots clés : peroxydes insaturés, substitution homolytique intramoléculaire, addition radicalaire, hétérocycles oxygénés.

X. LUBEIGT, F. FLIES, M. J. BOURGEOIS, E. MONTAUDON, and B. MAILLARD. Can. J. Chem. **69**, 1320 (1991).

Homolytic decomposition induced by addition of dichloromethyl radicals to β- and γ-unsaturated peroxides having a substituent on the chain linking the unsaturation and the peroxide function was studied. The stereochemistry of the heterocycles produced was determined by ^{13}C NMR and the stereoselectivity of intramolecular homolytic substitution on the peroxidic bond discussed.

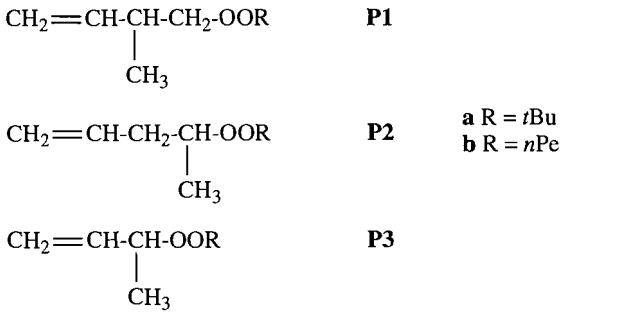
Key words: unsaturated peroxides, homolytic intramolecular substitutions, radical additions, oxygenated heterocycles.

Depuis plusieurs années nous avons abordé l'étude de la décomposition induite de composés peroxydiques insaturés et montré l'intérêt synthétique de cette réaction pour l'obtention d'hétérocycles oxygénés :



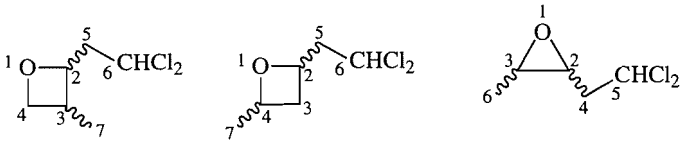
Nous avons, au cours de travaux précédents (1), déterminé les limites d'application de cette réaction. Nous venons d'aborder l'étude de la stéréochimie des substitutions homolytiques intramoléculaires de radicaux alkyle sur des liaisons peroxydiques. Cette analyse a été réalisée à partir des additions radicalaires du chlorure de méthylène à des composés peroxydiques insaturés comportant un substituant sur la chaîne liant les deux fonctions réactives que sont la double liaison et la liaison O—O. Nous avons ainsi mis en évidence l'existence d'une certaine stéréosélectivité dans la formation d'hétérocycles à cinq chaînons (2). La prédominance de l'isomère *cis* ou *trans* dépend tout d'abord de la position relative des substituants et est influencée notamment par leur taille et celle du radical oxyle partant; par contre le volume du radical Z attaquant la double liaison et la température à laquelle est effectuée la réaction n'ont que peu d'influence sur la stéréosélectivité.

Ayant vu précédemment (3, 4) que les peroxydes β- et γ-insaturés subissent une décomposition homolytique induite pour conduire à des oxiranes et des oxétanes, nous avons voulu compléter le travail précédent par l'étude de la stéréochimie des hétérocycles susceptibles de se former par addition radicalaire du chlorure de méthylène aux peroxydes modèles suivants :



Identification des éthers cycliques

Les hétérocycles attendus sont les suivants :



1 **2** **3**

La technique généralement utilisée pour identifier les hétérocycles diastéréoisomères X et Y repose sur l'analyse des spectres RMN ^{13}C des mélanges : (1) les signaux correspondant à X et à Y sont repérés : ceci ne présente de difficultés que si X et Y sont en proportions relatives peu différentes; (2) la corrélation signal–carbone basée sur des déplacements chimiques est facilitée par la technique du DEPT et, éventuellement, par analogie avec les spectres de composés voisins décrits dans la littérature; (3) l'attribution *cis–trans* est réalisée par comparaison des différences de déplacements chimiques ($\Delta\delta$) de chaque carbone des deux isomères avec les valeurs correspondantes des modèles de la littérature, lorsque ceux-ci sont connus. Dans les cas où cette analyse n'est pas possible ou ne permet pas de tirer des conclusions, d'autres méthodes d'identification sont utilisées.

1. Auteurs à qui adresser toute correspondance.

Printed in Canada / Imprimé au Canada

Can. J. Chem. Downloaded from www.nrcresearchpress.com by 84.41.108.74 on 09/07/12
For personal use only.

TABLEAU 1. RMN $^{13}C^a$ des oxétanes disubstitués en 2,3

Oxétane		Carbone 2	3	4	5	6	7	Attribution
	trans	85,0	37,4	73,5	22,8		17,5	
R1	*cis*	79,6	31,8	74,5	16,9		13,0	
	$\Delta\delta^b$	+5,4	+5,6	−1	+5,9		+4,5	
	X	86,5	36,4	78,0	51,3	70,2	18,4	*trans*
1	Y	81,8	32,5	79,4	46,7	70,8	14,6	*cis*
	$\Delta\delta^b$	+4,7	+3,9	−1,4	+4,6		+3,8	

[a] δ en ppm par rapport au TMS.
[b] Pour la référence, $\Delta\delta = \delta(trans) - \delta(cis)$; pour **1**, $\Delta\delta = \delta(X) - \delta(Y)$.

2-(2,2-Dichloroéthyl)-3-méthyloxétane, 1

Le composé modèle le plus proche est le 2,3-diméthyloxétane, **R1** (5). Le repérage des signaux correspondant à X et à Y d'une part, la corrélation signal–carbone d'autre part, ne présentent pas de difficultés. Les variations de déplacement chimique des différents carbones montrent que les composés X et Y ont respectivement les configurations *trans* et *cis* (tableau 1).

2-(2,2-Dichloroéthyl)-4-méthyloxétane, 2

Cette étude s'avérait difficile en raison de la faible différence de proportions des diastéréoisomères d'une part, et de l'absence de données de la littérature d'autre part. L'obtention d'une fraction enrichie en l'un des isomères, par HPLC, a permis d'éliminer la première difficulté. Afin de pallier la seconde, nous avons calculé, par une technique d'incrémentation, les déplacements chimiques des carbones du 2,4-diméthyloxétane, **R2**, à partir de ceux du 1,3-diméthylcyclobutane, du 2-méthyloxétane et du méthylcyclobutane (5, 6).

La comparaison des déplacements chimiques des carbones des méthylcyclobutane et 2-méthyloxétane permet de déterminer l'influence de l'oxygène sur les carbones vicinaux (figure 1). Les déplacements chimiques des carbones des isomères *trans* et *cis* de **R2** peuvent alors être estimés empiriquement, à partir des spectres des 1,3-diméthylcyclobutanes *trans* et *cis* et des incréments calculés. Les valeurs théoriques ainsi estimées sont rapportées dans le tableau 2.

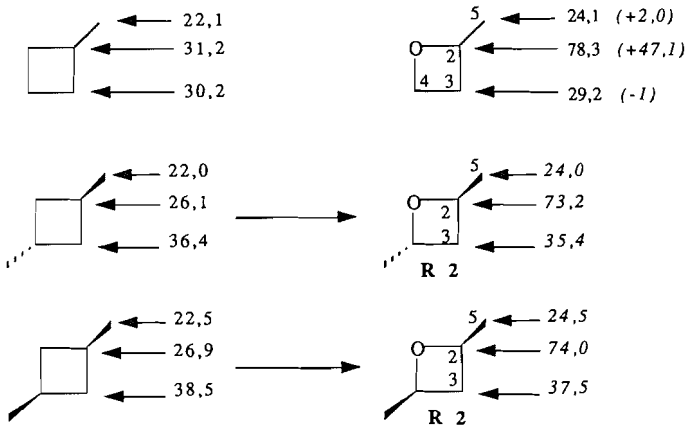
Les quantités relatives voisines des composés X et Y dans le mélange rendent difficiles le repérage des isomères et la corrélation signal–carbone : il reste d'ailleurs une indétermination au niveau des carbones 2 et 4. La comparaison des spectres des oxétanes chlorés avec ceux calculés pour les 2,4-diméthyloxétanes suggère l'attribution indiquée dans le tableau 2.

1,1-Dichloro-3,4-époxypentane

Les modèles de la littérature (7, 8) apportent peu d'éléments de comparaison; le 2,3-époxypentane, **R3**, est décrit dans le tableau 3 à titre d'exemple. L'attribution *cis–trans* ne peut donc se faire comme précédemment.

Les diastéréoisomères X et Y constituant l'époxyde **3** ont pu être séparés par HPLC, ce qui a facilité l'analyse. Si le repérage des carbones 4, 5 et 6 est aisé, grâce aux techniques habituelles (tableau 3), il n'en est pas de même pour les carbones 2 et 3 qui ne peuvent être différenciés a priori; une proposition sera formulée.

L'identification de X et Y (respectivement *trans* et *cis*) est rendue possible grâce aux carbones 4 et 6 (tableau 4). Il est en effet connu, et cela peut être observé dans les dérivés des oxétanes et des tétrahydrofuranes (2), que dans les composés



expérimental ; *calculé*

FIG. 1.

comportant deux substituants vicinaux (ici CH_3 et CH_2CHCl_2), les carbones correspondants sont plus blindés par effet γ dans l'isomère *cis* que dans l'isomère *trans*.

Proposition d'attribution des carbones 2 et 3

Une proposition peut être faite pour lever l'indétermination relative au repérage des carbones 2 et 3 de chacun des diastéréoisomères X et Y de l'époxyde **3**. Il s'agit d'un calcul empirique, basé sur des observations effectuées sur le 2-éthyl-3-méthyltétrahydrofurane et son homologue dichloré (figure 2) : on remarque en effet que la présence de deux chlores sur le substituant éthyle entraîne un fort blindage du carbone γ (carbone 2) et un déblindage du carbone δ (carbone 3).

Si cette remarque est également valable dans le cas des époxydes, on peut alors essayer de différencier les carbones 2 et 3 pour chaque isomère, à partir des données de la littérature (7) et de ces incréments. Les valeurs indiquées dans la figure 2 ne constituent qu'une proposition et non une affirmation, compte tenu du mode de détermination des incréments (issus d'un hétérocycle différent) d'une part, et des faibles différences des déplacements chimiques observés d'autre part.

Résultats

L'addition radicalaire du dichlorométhane aux différents peroxydes insaturés a été réalisée en présence de peracétate de *tert*-butyle, à 110°C, durant 12 h (rapport molaire 50 : 1 : 0,5). L'influence de la température sur la stéréosélectivité de la substitution homolytique intramoléculaire a été étudiée en

Can. J. Chem. Downloaded from www.nrcresearchpress.com by 84.41.108.74 on 09/07/12
For personal use only.

TABLEAU 2. RMN $^{13}C^{a}$ des oxétanes disubstitués en 2,4

Oxétane		Carbone 2	3	4	5	6	7	Attribution
	trans	73,2	35,4	73,2	24,0		24,0	
R2[c]	*cis*	74,0	37,5	74,0	24,5		24,5	
	$\Delta\delta^{b}$	−0,8	−2,1	−0,8	−0,5		−0,5	
	X	74,4 ou 76,1	33,7	76,1 ou 74,4	51,1	69,7	23,8	*trans*
2	Y	73,5 ou 75,5	35,0	75,5 ou 73,5	52,4	69,4	24,8	*cis*
	$\Delta\delta^{b}$		−1,3		−1,3		−1,0	

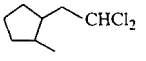
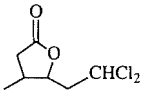
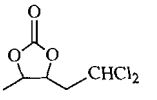
[a]δ en ppm par rapport au TMS.
[b]Pour la référence, $\Delta\delta = \delta(trans) - \delta(cis)$; pour **2**, $\Delta\delta = \delta(X) - \delta(Y)$.
[c]Calculé par incrémentation (voir figure 1).

TABLEAU 3. RMN $^{13}C^{a}$ des oxiranes disubstitués en 1,2

Epoxyde		Carbone 2	3	4	5	6	Attribution
R3	*trans*	60,7	54,1				
	cis	58,1	52,4				
3	X	56,0[b]	55,3[b]	46,6	70,9	17,8	*trans*
	Y	52,9[b]	53,6[b]	42,4	71,2	13,9	*cis*

[a]δ en ppm par rapport au TMS.
[b]Déterminé par comparaison avec les valeurs obtenues par incrémentation (voir figure 2).

TABLEAU 4. Déplacements chimiques[a] de CH_3 et CH_2CHCl_2 observés dans les hétérocycles à 4 et 5 chaînons

Hétérocycle	CH_2CHCl_2	CH_3	Isomère
	48,9	16,5	*trans*
	45,7	14,4	*cis*
	48,1	16,8	*trans*
	44,6	14,3	*cis*
	47,0	19,0	*trans*
	43,2	14,9	*cis*
1	51,3	18,4	*trans*
	46,7	14,6	*cis*

[a]δ en ppm par rapport au TMS.

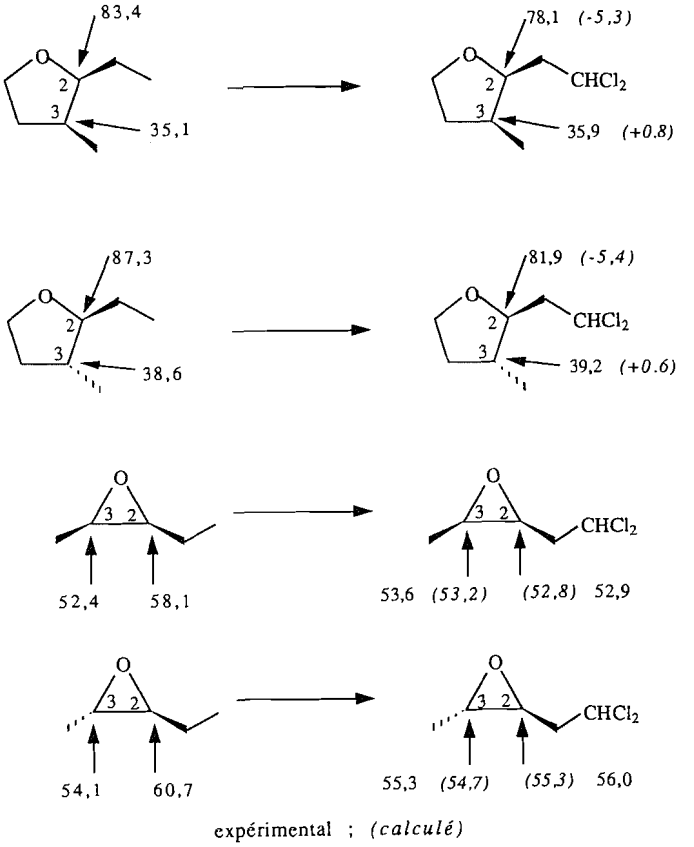


FIG. 2.

opérant à 80°C et à 40°C en présence de peroxyde de benzoyle et de perdicarbonate de diéthyle respectivement. Les résultats sont rassemblés dans le tableau 5.

Discussion

Comme dans le cas de la formation des hétérocycles oxygénés à cinq chaînons, nous voyons que la position relative des substituants est un facteur important sur la distribution des oxiranes et oxétanes diastéréoisomères. Par contre, que les substituants se trouvent portés par des carbones en α (essais 1, 2, 5 et 6) ou en β (essais 3 et 4) dans l'éther obtenu, c'est le composé *trans* qui est majoritaire.

L'explication de la formation préférentielle du dérivé *trans* dans le cas des dérivés α-disubstitués est la même que celle avancée pour la création des cycles à cinq chaînons : le radical attaquant adopte préférentiellement la conformation B (figure 3) dans laquelle les substituants vicinaux sont les plus éloignés. Il importe à ce niveau de remarquer que la distribution des isomères varie peu avec la taille du cycle (essais 1 et 5, et 2 et 6), la nature du radical partant, *tert*-butoxyle ou *n*-pentyloxyle (essais 1 et 2, et 5 et 6), ou la température de réaction (essais 7, 8, 1 et 11, 12, 5).

Dans le cas des cycles β-disubstitués, on observe que la taille du cycle a une influence non négligeable sur la répartition des diastéréoisomères puisque l'oxétane *trans* prédomine légère-

Can. J. Chem. Downloaded from www.nrcresearchpress.com by 84.41.108.74 on 09/07/12
For personal use only.

TABLEAU 5. Addition radicalaire[a] de chlorure de méthylène aux peroxydes γ- et β-insaturés

Essai	Peroxyde	Hétérocycle	Rdt (%)[b]	*cis*/*trans*[c]
1[d]	**P1a**	**1**	24	25 : 75
2[d]	**P1b**	**1**	29	25 : 75
3[d]	**P2a**	**2**	10	44 : 56
4[d]	**P2b**	**2**	11[c]	47 : 53
5[d]	**P3a**	**3**	58	23 : 77
6[d]	**P3b**	**3**	50	20 : 80
7[e]	**P1a**	**1**	20[c]	25 : 75
8[f]	**P1a**	**1**	20[c]	24 : 76
9[e]	**P2a**	**2**	12[c]	43 : 57
10[f]	**P2a**	**2**	13[c]	43 : 57
11[e]	**P3a**	**3**	60[c]	25 : 75
12[f]	**P3a**	**3**	66[c]	25 : 75

[a]Rapports molaires chlorure de méthylène/peroxyde/peracétate de *tert*-butyle : 50 : 1 : 0,5.
[b]En produit distillé, sauf indication contraire.
[c]Déterminé par CPG.
[d]110°C; 12 h; peracétate de *tert*-butyle.
[e]40°C; 8 jours; perdicarbonate de diéthyle.
[f]80°C; 24 h; peroxyde de benzoyle.

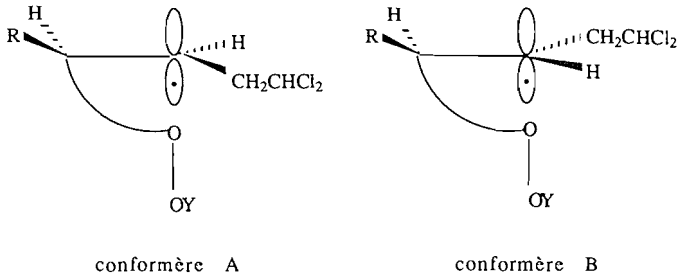


FIG. 3.

ment, alors que c'est l'inverse en série tétrahydrofurane (*cis*/*trans* : 53 : 47) (2). Ceci peut s'expliquer si l'on admet que la structure de l'éther est préétablie par la conformation qu'adopte le radical adduit dans l'état de transition. En effet, dans le tétrahydrofurane, la forme C (précurseur du composé *cis*) a une énergie plus basse que la forme D (précurseur du *trans*); dans l'oxétane, la situation est inversée (figure 4). En ce qui concerne la nature du groupe partant (essais 3 et 4) et la température de la réaction (essais 9, 10 et 3), elles n'ont pratiquement pas d'influence sur le cours de la réaction.

Une remarque importante est relative aux rendements d'obtention des oxétanes : ils sont modestes (24 et 10%, essais 1 et 3) comparativement à ceux des hétérocycles à trois (58%, essai 5) et cinq chaînons (43–58%) (2) formés à partir des peroxydes de *tert*-butyle par exemple. À côté de ces oxétanes, des peroxydes adduits **PA1** et **PA2** sont obtenus respectivement à partir des peroxydes **P1** (rendement 21%) et **P2** (rendement 20%) (figure 5) : ceci confirme que la vitesse de la substitution homolytique intramoléculaire est dans ce cas-là plus faible que celle du transfert d'hydrogène du solvant (4).

Conclusion

Les substitutions homolytiques intramoléculaires de radicaux alkyle sur les liaisons peroxydiques conduisant à la formation d'éthers cycliques à trois et quatre chaînons donnent préférentiellement l'isomère *trans*. Toutefois, on n'observe une certaine stéréosélectivité de la réaction que pour l'obtention des dérivés 2,3-disubstitués.

Partie expérimentale

Techniques analytiques

L'analyse des produits de réaction par chromatographie en phase gazeuse a été effectuée sur les appareils suivants : Intersmat IGC 112 F (ionisation de flamme, gaz vecteur : azote), équipé de colonnes en acier inox de 2 mm de diamètre intérieur : OV 17 (10% sur Chromosorb W HP, 80–100 mesh, longueur 1,5 m), FFAP (10% sur Chromosorb W AW, 80–100 mesh, longueur 2 m) et Carbowax 20 M (5% sur Chromosorb W DMCS, 80–10 mesh, longueur 3 m); et Delsi DI 200 (ionisation de flamme, gaz vecteur : azote), équipé de colonnes capillaires en silice fondue : CP Sil 5 CB (longueur 25 m, diamètre intérieur 0,32 mm) et BP 20 (longueur 25 m, diamètre intérieur 0,22 mm). Ces appareils sont associés à un intégrateur Intersmat ICR-1B donnant les temps de rétention et les surfaces des pics. Les dosages ont été effectués par la méthode de l'étalon interne.

Les spectres RMN ^1H ont été enregistrés sur des appareils Perkin–Elmer R 24B fonctionnant à 60 MHz et Bruker AC 250 fonctionnant à 250 MHz. Tous les composés étudiés sont en solution dans le tétrachlorure de carbone, en présence de TMS ou de benzène comme référence interne. Les spectres RMN ^{13}C ont été enregistrés dans des solutions de chloroforme deutéré sur des appareils Bruker WP 90 fonctionnant à 23,6 MHz et AC 250 fonctionnant à 62,9 MHz.

Les spectres de masse ont été réalisés sur un spectromètre à simple focalisation VG Micromass 16F, couplé avec un chromatographe en phase gazeuse Intersmat IGC 121M.

Techniques réactionnelles

Les réactions sont effectuées sur des mélanges constitués par le chlorure de méthylène, le peroxyde et l'amorceur dans les rapports molaires 50 : 1 : 0,5.

La durée et la température des réactions dépendent de la nature de l'amorceur : perdicarbonate de diéthyle (PDCE) : 40°C; 8 jours; peroxyde de benzoyle (PB) : 80°C; 24 h; peracétate de *tert*-butyle (PA) : 110°C; 12 h. Les conditions propres à chaque expérience sont rappelées dans les tableaux de la partie théorique.

(i) Études analytiques

La solution (2 cm^3) est introduite dans une ampoule de 10 cm^3. Celle-ci, fermée hermétiquement, est placée dans un bain d'huile thermostaté.

Les rendements sont déterminés par CPG directement sur le mélange réactionnel selon la méthode de l'étalon interne. Les proportions relatives des différents diastéréoisomères sont déduites des surfaces relatives des pics correspondants, ceux-ci étant supposés avoir le même coefficient de réponse.

(ii) Études préparatives

La solution (90 cm^3) est introduite dans un autoclave en acier de 125 cm^3 que l'on place dans une étuve préalablement chauffée à 110, 80 ou 40°C.

Après élimination du solvant, l'hétérocycle est isolé par distillation. La structure de chaque isomère est déterminée à l'aide de la RMN ^1H et ^{13}C, par comparaison avec des molécules modèles voisines de la littérature. Les pourcentages relatifs *cis*/*trans* sont obtenus par CPG.

Matières premières

(i) Amorceurs

Le *peroxyde de benzoyle*, produit commercial, est purifié par extraction au chloroforme. Le *peracétate de* tert-*butyle et le perdicarbonate de diéthyle* sont respectivement synthétisés selon les références 9 et 10.

(ii) Précurseurs des peroxydes

À l'exception de l'*hydroperoxyde de* tert-*butyle* (produit commercial séparé du peroxyde de di-*tert*-butyle, avec lequel il est en mélange, par distillation de ce dernier), du *but-3-ène-2-ol* et du *1-bromopentane*, tous les précurseurs doivent être préparés.

L'*hydroperoxyde de pentyle* est préparé selon la référence 11 par

Can. J. Chem. Downloaded from www.nrcresearchpress.com by 84.41.108.74 on 09/07/12
For personal use only.

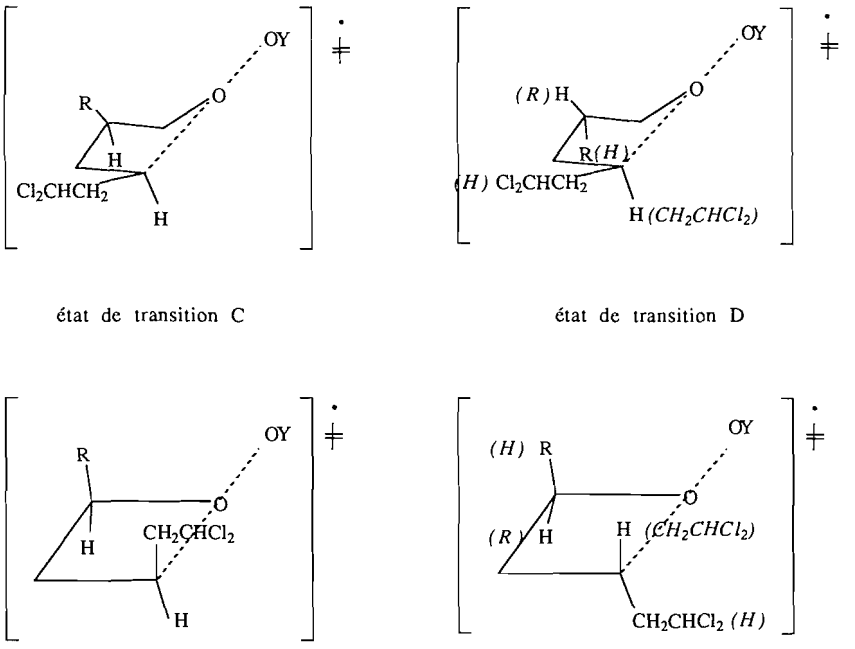
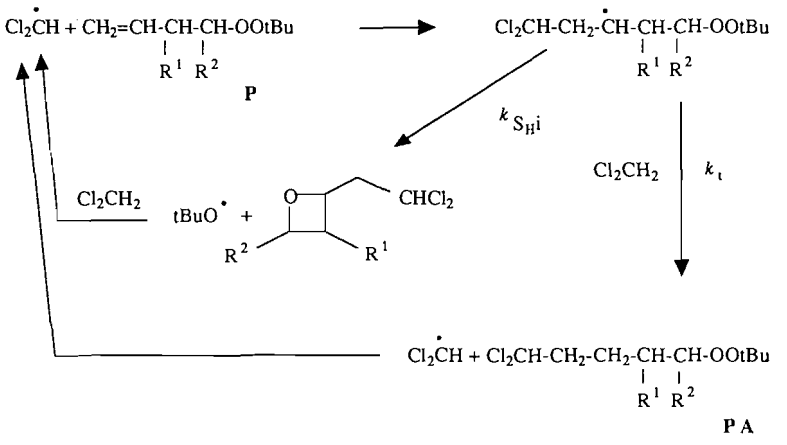


FIG. 4.



P1, PA1 : $R^1 = CH_3$, $R^2 = H$
P2, PA2 : $R^1 = H$, $R^2 = CH_3$

FIG. 5.

action de l'eau oxygénée en milieu basique sur le mésylate de 1-pentyle; Rdt 56%; n_D^{20} 1,4127; Eb_{10} 54°C (litt. (11) : Eb_4 41–42°C).

L'*hydroperoxyde de 1-méthylprop-2-ényle* est synthétisé par photo-oxygénation du but-2-ène, selon un protocole dérivé de la référence 12. Dans 100 cm^3 de CCl_4 refroidi à −20°C, on introduit lentement 40 g de but-2-ène et des traces de tétraphénylporphyrine. Un courant d'oxygène traverse la solution irradiée par une lampe de sodium de 400 W et maintenue à −20°C. Au bout de 5 h, l'hydroperoxyde est transformé en son sel de sodium à l'aide de 200 cm^3 d'une solution de NaOH 1 N. La phase aqueuse séparée est acidifiée. L'hydroperoxyde ainsi régénéré est alors extrait à l'éther. Cette solution éthérée est lavée à l'eau, puis séchée sur sulfate de sodium anhydre. Après évaporation du solvant, la pureté de l'hydroperoxyde est vérifiée par dosage; Rdt 22%.

Le *2-méthylbut-3-ène-1-ol* provient de la réduction de l'acide 2-méthylbut-3-énoïque lui-même issu de la carbonatation du bromure de but-3-ène-2-ylemagnésium.

Le *pent-4-ène-2-ol* est obtenu par condensation organomagnésienne du bromure d'allylemagnésium sur l'éthanal.

(iii) Peroxydes

Ils sont synthétisés par action de l'hydroperoxyde correspondant, en milieu basique, sur le mésylate de l'alcool convenable (préparé selon la référence 13) ou sur le 1-bromopentane (pour **P3b**), selon des méthodes mises au point au laboratoire (14–16). Leurs caractéristiques physiques et spectroscopiques sont rassemblées dans le tableau 6.

Produits de réaction

*2-(2,2-Dichloroéthyl)-3-méthyloxétane, **I*** : n_D^{20} 1,4677; $Eb_{0,6}$ 38°C; RMN ^1H (δ) : 5,9–5,6 (m, 1H, H-6), 4,7–4,3 (*trans*) et 4,3–3,9 (*cis*) (2m, 3H, H-2 et H-4), 3,2–2,3 (m, 3H, H-3 et H-5), 1,2 (*trans*) et 1,1 (*cis*) (2d, J = 7 Hz, 3H, H-7); SM (pics principaux) M^+ *trans* : 55 (32), 42 (100), 41 (26), 28 (41); *cis* : 55 (33), 42 (100), 41 (23), 28 (29). Anal. calc. pour $C_6H_{10}OCl_2$: C 42,63; H 5,96; Cl 41,94; tr. : C 42,35; H 5,99; Cl 41,85.

Can. J. Chem. Downloaded from www.nrcresearchpress.com by 84.41.108.74 on 09/07/12
For personal use only.

TABLEAU 6. Caractéristiques physiques et spectroscopiques des peroxydes

Peroxyde	Rdt (%)	n_D^{20}	RMN ^{1}H (δ)
P1a	10	1,4144	6,1–4,7 (m, 3H, CH_2=CH), 3,9–3,6 (m, 2H, CH_2O), 2,8–2,1 (m, 1H, CH), 1,1 (s, 9H, $(CH_3)_3C$), 1 (d, J = 7 Hz, 3H, CH_3CH)
P1b	21	1,4280	6,1–4,7 (m, 3H, CH_2=CH), 4,1–3,5 (m, 4H, CH_2OOCH_2), 2,8–2,2 (m, 1H, CH), 1,9–0,9 (m, 12H, autres H)
P2a	8	1,4116	6,1–4,7 (m, 3H, CH_2=CH), 4,3–3,7 (m, 1H, CHO), 2,7–1,9 (m, 2H, CH_2), 1,2 (s, 9H, $(CH_3)_3C$), 1,15 (d, J = 7 Hz, 3H, CH_3CH)
P2b	10	1,4265	6,2–4,8 (m, 3H, CH_2=CH), 4,3–3,6 (m, 3H, CH_2OOCH), 2,7–0,9 (m, 8H, autres H), 1,2 (d, J = 7 Hz, 3H, CH_3CH), 0,9 (t, J = 7 Hz, 3H, CH_3CH_2)
P3a	17	1,4044 (Eb_{45} 47°C)	6,2–4,9 (m, 3H, CH_2=CH), 4,6–4,1 (m, 1H, CH), 1,25 (d, J = 8 Hz, 3H, CH_3CH), 1,2 (s, 9H, $(CH_3)_3C$), 1,15 (s, 3H, CH_3)
P3b	17	1,4150	6,2–4,7 (m, 3H, CH_2=CH), 4,7–4,2 (m, 1H, CHO), 4–3,6 (m, 2H, CH_2O), 1,9–0,8 (m, 9H, autres H)

2-(2,2-Dichloroéthyl)-4-méthyloxétane, 2 : n_D^{20} 1,4602; $Eb_{0,3}$ 36°C; RMN ^{1}H (δ) : 6,0–5,6 (m, 1H, H-6), 5,1–4,5 (m, 2H, H-2 et H-4), 3–2,1 (m, 4H, H-3 et H-5), 1,4 (d, J = 6 Hz, 3H, H-7); SM (pics principaux) M^+ *trans* : 88 (38), 71 (33), 42 (100), 41 (66), 27 (32); *cis* : 88 (47), 71 (20), 43 (51), 42 (100), 41 (75), 27 (37). Anal. calc. pour $C_6H_{10}OCl_2$: C 42,63; H 5,96; Cl 41,94; tr. : C 42,21; H 5,85; Cl 42,48.

1,1-Dichloro-3,4-époxypentane, 3 : n_D^{20} 1,4589; Eb_3 48°C; RMN ^{1}H (δ) : 5,9–5,6 (m, 1H, H-5), 2,95–2,6 (*trans*) et 3,2–2,8 (*cis*) (m, 2H, H-2 et H-3), 2,5–2,1 (m, 2H, H-4), 1,25 (*trans*) et 1,2 (*cis*) (d, J = 7 Hz, 3H, H-6); SM (pics principaux) M^+ *trans* : 71 (100), 45 (39), 43 (21), 28 (59); *cis* : 71 (100), 45 (64), 43 (45), 28 (83). Anal. calc. pour $C_5H_8OCl_2$: C 38,74, H 5,20; Cl 45,74; tr. : C 38,48, H 5,11; Cl 45,82.

Peroxyde de tert*-butyle et de 5,5-dichloro-2-méthylpentyle, PA1* : n_D^{20} 1,4579; $Eb_{0,1}$ 46°C; RMN ^{1}H (δ) : 5,7 (t, 1H, $CHCl_2$), 3,7 (d, 2H, CH_2OO), 2,5–1,4 (m, 5H, autres H), 1,2 (s, 9H, $(CH_3)_3C$), 1 (d, 3H, CH_3).

Peroxyde de tert*-butyle et de 5,5-dichloro-1-méthylpentyle, PA2* : $Eb_{0,1}$ 50°C; RMN ^{1}H (δ) : 5,7 (t, 1H, $CHCl_2$), 4,2–3,7 (m, 1H, CHOO), 2,6–1,4 (m, 6H, autres H), 1,2–1,1 (s et d, 12H, $(CH_3)_3C$ et CH_3).

1. E. MONTAUDON, M. CAMPAGNOLE, F. FLIES et B. MAILLARD. J. Heterocycl. Chem. **28**, 459 (1991), et mémoires antérieurs.
2. E. MONTAUDON, X. LUBEIGT et B. MAILLARD. J. Chem. Soc. Sous presse.
3. E. MONTAUDON, F. RAKOTOMANANA et B. MAILLARD. Bull. Soc. Chim. Fr. 198 (1985).
4. M. AGORRODY, M. CAMPAGNOLE, E. MONTAUDON et B. MAILLARD. Tetrahedron, **43**, 3429 (1987).
5. D. F. EWING, K. A. HOLBROOK et R. A. SCOTT. Org. Magn. Reson. **7**, 554 (1975).
6. E. ELIEL et K. M. PETRUSIEWICZ. Org. Magn. Reson. **13**, 193 (1980).
7. D. R. PAULSON, F. Y. N. TANG, G. F. MORAN, A. S. MURRAY, B. P. PELKA et E. M. VASQUEZ. J. Org. Chem. **40**, 184 (1975).
8. S. G. DAVIES et G. H. WHITHAM. J. Chem. Soc. Perkin Trans. 2, 861 (1975).
9. P. D. BARTLETT et R. R. HIATT. J. Am. Chem. Soc. **80**, 1398 (1958).
10. F. STRAIN, W. E. BISSINGER, W. R. DIAL, H. RUDOFF, B. J. DEWITT, H. C. STEVENS et J. H. LANGSTON. J. Am. Chem. Soc. **72**, 1254 (1950).
11. H. R. WILLIAMS et H. S. MOSHER. J. Am. Chem. Soc. **76**, 2984 (1954).
12. W. ADAM et A. GRIESBECK. Synthesis, 1050 (1986).
13. A. SEKERA et C. S. MARVEL. J. Am. Chem. Soc. **55**, 345 (1933).
14. M. J. BOURGEOIS, E. MONTAUDON et B. MAILLARD. Synthesis, 700 (1989).
15. J. MOULINES, M. J. BOURGEOIS, M. CAMPAGNOLE, A. M. LAMIDEY, B. MAILLARD et E. MONTAUDON. Synth. Commun. **20**, 349 (1990).
16. M. CHIRON-CHARRIER, M. CAMPAGNOLE, M. J. BOURGEOIS et E. MONTAUDON. Bull. Soc. Chim. Belg. **100**, 93 (1991).

Can. J. Chem. Downloaded from www.nrcresearchpress.com by 84.41.108.74 on 09/07/12
For personal use only.

A facile preparation of 4-aryl-3-[(*tert*-butyldimethylsilyl)oxymethyl]furans

BRIAN A. KEAY[1]
Department of Chemistry, University of Calgary, Calgary, Alta., Canada T2N 1N4

AND

JEAN-LOUIS J. BONTRONT
Department of Chemistry and Biochemistry, University of Windsor, Windsor, Ont., Canada N9B 3P4

Received September 10, 1990[2]

BRIAN A. KEAY and JEAN-LOUIS J. BONTRONT. Can. J. Chem. **69**, 1326 (1991).

A series of aryl bromides undergo a palladium-catalyzed coupling reaction with 3-[(*tert*-butyldimethylsilyl)oxymethyl]-4-(tri-*n*-butylstannyl)furan to provide 4-aryl-3-[(*tert*-butyldimethylsilyl)oxymethyl]furans in moderate to good yields.

Key words: palladium, cross-couplings, stannanes, 3,4-disubstituted furans.

BRIAN A. KEAY et JEAN-LOUIS J. BONTRONT. Can. J. Chem. **69**, 1326 (1991).

Des réactions de couplage, catalysées par le palladium, entre divers bromures d'aryle et le [(*tert*-butyldiméthylsilyl)oxyméthyl]-3-(triméthylstannyl)-4-furanne conduisent avec des rendements relativement faibles aux aryl-4-[(*tert*-butyldiméthylsilyl)oxyméthyl]-3-furannes.

Mots clés : palladium, couplage croisé, stannanes, furannes disubstitués en positions 3 et 4.

[Traduit par la rédaction]

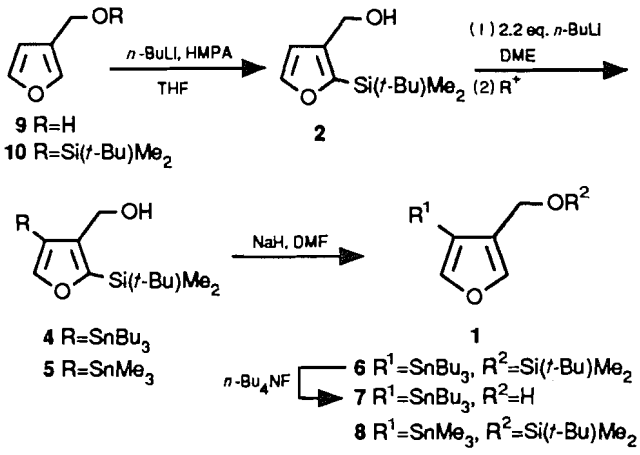
Can. J. Chem. Downloaded from www.nrcresearchpress.com by 84.41.108.74 on 09/07/12
For personal use only.

The preparation of 3,4-disubstituted furans is a formidable task since furan derivatives tend to lithiate (1) and add electrophiles (2) in the C-2 and C-5 positions. Elaborate methods for the preparation of 3,4-disubstituted furans have therefore been developed to overcome these tendencies. Some of these include inter- (3) and intra-molecular (4) Diels–Alder–retro-Diels–Alder sequences, synthesis of the furan ring from acyclic (5) and cyclic (6) precursors, and chemical modifications of commercially available 3,4-furandicarboxylic acid (7). We have recently described a simple preparation of 3,4-disubstituted furans **1** (8) via a regiospecific C-4 lithiation of 2-(*tert*-butyldimethylsilyl)-3-(hydroxymethyl)furan **2** (Scheme 1). Quenching the dianion with electrophiles followed by a carbon to oxygen silyl migration afforded 3,4-disubstituted furans **1** in good yields.

The scope of these procedures does not include the preparation of 4-aryl-3-substituted furans. Since furan rings can be converted to a variety of other ring systems (Scheme 2), we sought a general method for the preparation of 4-aryl-3-substituted furans for further elaboration into natural products such as Heritol **3**, the ichthyotoxic constituent of the mangrove plant *Heritiera littoralis* (9).

A suitable method for the introduction of aryl groups at the C-4 position of furan rings could involve the palladium-catalyzed coupling reaction between aryl halides and organostannanes developed by Stille and co-workers (10). Recent reports of successful arylhalide–arylstannyl couplings (11) and the lack of examples reported utilizing stannylfurans (12)[3] led us to study the palladium-catalyzed coupling reaction between various arylbromides and stannylfurans **4**–**7** (Scheme 1). We herein report our findings.

Stannylfurans **4**–**8** were prepared as outlined in Scheme 1. Thus, 3-(hydroxymethyl)furan **9** was silylated to provide the silyl alcohol **10** (95%) (15). Treatment of **10** with 1.7 equivalents



SCHEME 1

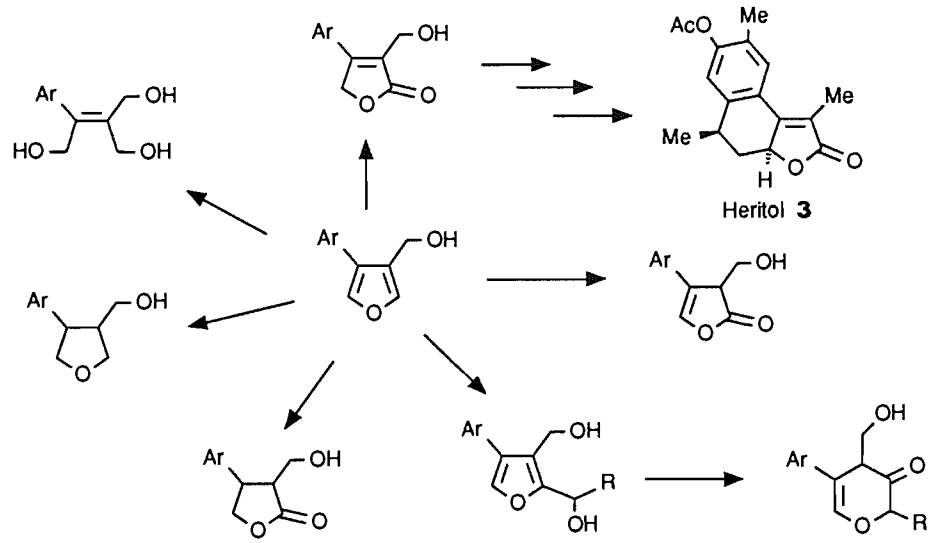
of *n*-butyllithium (THF, HMPA) provided furan **2** (87%) via a 1,4 O→C silyl migration (8*a*). Regiospecific lithiation of furan **2** at C-4 with 2.2 equivalents of *n*-butyllithium (DME, 0°C), followed by trapping of the dianion with either tri-*n*-butyl- or trimethyl-stannyl chloride (1.1 equivalents), provided stannylfurans **4** (89%) and **5** respectively (8*b*). A 1,4 C→O silyl migration of compounds **4** and **5** (NaH, DMF) provided stannylfurans **6** and **8** respectively (>95%) (8*c*). Desilylation of furan **6** with tetra-*n*-butylammonium fluoride (THF, room temperature) afforded alcohol **7** (88%).

Stannylfuran **4** was initially employed in the coupling reaction with bromobenzene (1.1 equiv.) and tetrakis(triphenylphosphine)palladium(0) (TTPP, 2 mol%) in refluxing toluene. Analysis of the reaction mixture after 5 h indicated that only 50% of the bromobenzene had reacted. The addition of another 2 mol% of palladium catalyst and refluxing for another 6 h were required to provide coupled furan **11** (51%) and 10% of destannylated furan **2** (Scheme 3). The long reaction time, poor yield of furan **11**, and the presence of destannylated furan **2** are in contrast to results reported from typical coupling reactions using bromobenzene (10, 11*g*). No improvement in the yield

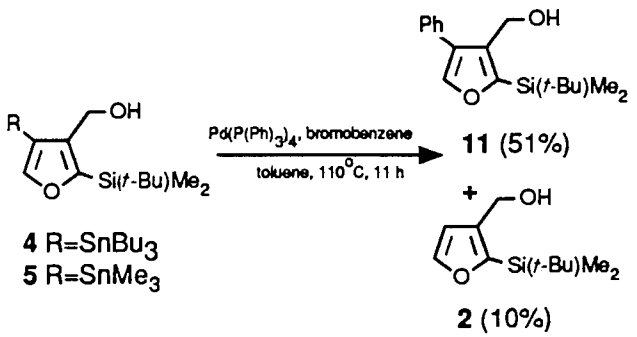
[1]Author to whom correspondence may be addressed.

[2]Revision received April 16, 1991.

[3]Furylzinc and furylboronic acids have been used in palladium-catalyzed coupling reactions, see refs. 13 and 14 respectively.



SCHEME 2



SCHEME 3

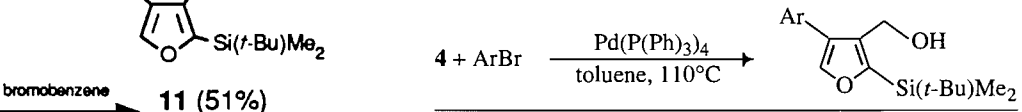
of furan **11** was observed when the trimethylstannylfuran **5** was employed with bromobenzene under identical conditions; destannylated furan **2** was also isolated (11%). These observations were not limited to bromobenzene, as both 3-bromotoluene and 2-bromonaphthalene coupled with furan **4** to provide furans **12** and **13** respectively in poor yields (Table 1).

The disappointing results obtained for the coupling reactions of furans **4** and **5** were overcome by the use of furan **6** as the starting material. Compound **6** coupled smoothly with bromobenzene to provide coupled furan **14** in 90% yield within 1 h (Table 2). Destannylated furan **10** (Scheme 1) was neither detected (by ^{1}H NMR) nor isolated.

The coupling reaction was extended to a number of aromatic bromides (Table 2). In general, yields were high, and reaction times were short (1–6 h, entries 1, 2, 5, and 7). Exceptions were noted when sterically hindered aryl bromides were employed (entries 3, 4, and 6). Longer reaction times and, in the case of bromomesitylene, additional palladium catalyst were required for the reaction to proceed to completion. The absence of any coupled product from the reaction with 2-bromopyridine was surprising since it has been used successfully in other palladium-catalyzed couplings (16). The reaction also failed for 1-bromo-2-methoxybenzene despite the addition of more catalyst after 6 and 12 h.[4] This result may be due to both steric interactions and electronic factors (6).

[4]It is well documented that couplings with methoxy-substituted aryl bromides proceed slowly, and usually require additional catalyst, see ref. 10.

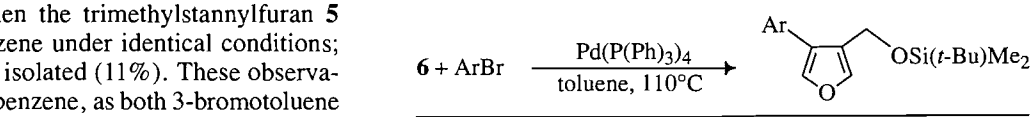
TABLE 1. Palladium-catalyzed coupling reactions of furan **4**



	ArBr	Time (h)	Yield (%)
1.	Bromobenzene	18	**11** (51)[a]
2.	3-Bromotoluene	18	**12** (55)[a]
3.	2-Bromonaphthalene	18	**13** (46)[a]

[a](10–12%) Destannylated furan **2** was also isolated.

TABLE 2. Palladium-catalyzed coupling reactions of furan **6**



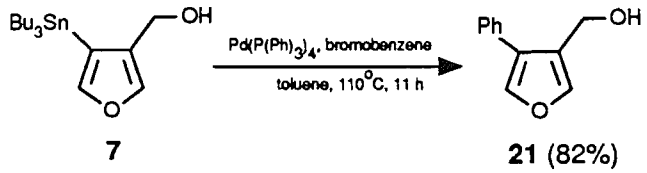
	ArBr	Time (h)	Yield (%)
1.	Bromobenzene	1	**14** (90)
2.	2-Bromobenzaldehyde	1	**15** (85)
3.	2-Bromomesitylene	6[a]	**16** (55)
4.	1-Bromo-2-methylbenzene	4	**17** (80)
5.	4-Bromobiphenyl	3	**18** (70)
6.	1-Bromo-2-methylnaphthalene	3	**19** (82)
7.	1-Bromo-4-chlorobenzene	1	**20** (88)
8.	2-Bromopyridine	18[b]	n.r.[c]
9.	1-Bromo-2-methoxybenzene	18[b]	n.r.[d]

[a]Added more catalyst after 3 h.
[b]Added more catalyst after 6 and 12 h.
[c]Recovered 80% of furan **6**.
[d]Recovered 20% of furan **6**.

The poor results observed for stannyl furans **4** and **5** are in contrast to results reported from typical coupling reactions with bromobenzene. These observations could be due to the presence of the unprotected hydroxymethyl group at C-3 and (or) the bulky *tert*-butyldimethylsilyl moiety at C-2 of furans **4** and **5** (Scheme 1). Further experiments were performed to elucidate the reason for our observation.

To determine if the free hydroxyl group in our systems was responsible, we coupled stannyl furan **7** with bromobenzene

Can. J. Chem. Downloaded from www.nrcresearchpress.com by 84.41.108.74 on 09/07/12
For personal use only.



SCHEME 4

(Scheme 4) under the same conditions used for furans **4** and **5**. Coupled product **21** was obtained in 82% yield after 3 h (110°C); no destannylated furan **9** (Scheme 1) was observed (by ^{1}H NMR). This result clearly indicates that the hydroxyl group was not interfering with the reaction. Echavarren and Stille reported similar results with palladium-catalyzed cross-couplings between aryl triflates and vinyl stannanes containing free hydroxyl groups (17).

The presence of the *tert*-butyldimethyl silyl group at C-2 of furans **4** and **5** was shown to be responsible for the destannylation of furans **4** and **5**. Refluxing either furan **4** or **5** in toluene for 12 h in the absence of both the palladium catalyst and bromobenzene provided destannylated furan **2** in 13% yield. Stannylated furans **6** and **7**, and **8** (with no C-2 silyl group), did not provide destannylated furans **10** and **9** respectively under identical conditions. Furans **4** and **5** were also found to undergo facile protiodestannylation (18) when treated with 0.1% aqueous HCl (THF, 10 min) while furans **6–8** showed no signs of protiodestannylation after 1 h under identical conditions.

Examination of molecular models indicated that the trisubstituted compound **4** is sterically congested. These unfavourable steric interactions are not observed in stannyl furans **6–8** since the furan rings are only disubstituted (at C-3 and C-4). In the absence of a substituent at C-2, the C-3 moiety can rotate away from the stannyl group, thereby reducing the steric interactions in furans **6–8** when compared to furans **4** and **5**. Thus protiodestannylation occurs to relieve the strong steric interaction among the substituents in furans **4** and **5**. In addition, the hindered nature of furan **4** may be the reason for the longer reaction times (18 h vs. 1 h for furan **6**) required for the cross-coupling with bromobenzene (Table 1).

We have therefore shown that 4-aryl-3-substituted furans can be prepared via a palladium-catalyzed coupling reaction. The reactions are simple to perform and the products are easily purified. In addition, the silyl-protected hydroxymethyl group on the furan ring can be modified to convert the products from the coupling reaction into other 3,4-disubstituted furans. Synthetic applications of this methodology towards Hertiol **3** are currently in progress.

Experimental

Nuclear magnetic resonance spectra were obtained with a Bruker AC300 spectrometer using deuterochloroform as solvent (and internal standard). All ^{1}H NMR and ^{13}C NMR spectra were obtained at 300 and 75 MHz respectively. Infrared spectra were obtained with a Nicolet 5DK-FTIR spectrometer. Low and high resolution mass spectra were obtained with either a Varian CH5 or VG 7070F and a Kratos MS80RFA spectrometer respectively. Elemental analyses were performed by either Guelph Chemical Laboratories, Guelph, Ontario, or at the University of Calgary.

Flash column chromatography was performed using E. Merck silica gel (230–400 mesh A.S.T.M.) by the method developed by Still *et al.* (19). All solvents were dried and distilled prior to use.

*3-[(*tert*-Butyldimethylsilyl)oxymethyl]furan (**10**)*

To a solution of *tert*-butyldimethylsilyl chloride (6.1 g, 40 mmol) in DMF (20 mL) at 0°C under an atmosphere of argon was added imidazole (5.7 g, 84 mmol) and 3-hydroxymethylfuran **9** (3.6 g, 37 mmol). After 12 h at 25°C, diethyl ether and aqueous sodium chloride were added. The organic layer was washed six times with saturated aqueous sodium chloride, dried (Na_2SO_4), and the solvent removed *in vacuo* to afford, after distillation, a clear colourless oil **10** (95%), bp 106–109°C/20 Torr (1 Torr = 133.3 Pa); IR (neat): 1063 cm^{-1}; ^{1}H NMR δ: −0.04 (s, 6H), 0.81 (s, 9H), 4.54 (s, 2H), 6.42 (m, 1H), 7.51 (m, 2H); ^{13}C NMR δ: −2.85, 18.21, 25.80, 57.52, 109.66, 125.85, 139.38, 143.14; mass spectrum, *m/e*: 212 ($M^{\cdot+}$). Anal. calcd. for $C_{11}H_{20}O_2Si$: C 62.21, H 9.49; found: C 62.34, H 9.43.

*2-(*tert*-Butyldimethylsilyl)-3-(hydroxymethyl)furan (**2**)*

To a mixture of furan **10** (0.69 g, 3.3 mmol) and HMPA (0.62 mL, 3.6 mmol) dissolved in THF (10 mL) under an atmosphere of argon at −78°C was added *n*-butyllithium (1.43 mL, 2.5 M in hexane, 3.6 mmol). The solution was allowed to come to room temperature over 6 h and stirred at room temperature overnight. Saturated ammonium chloride was added and the solution extracted with diethyl ether. The organic layer was washed three times with saturated copper sulfate, dried (Na_2SO_4), and the solvent removed *in vacuo* to afford, after distillation, a white crystalline solid **2** (87%), bp 75–78°C/0.02 Torr; IR (KBr): 3319, 1070 cm^{-1}; ^{1}H NMR δ: 0.01 (s, 6H), 0.89 (s, 9H), 1.5 (bs, 1H), 4.57 (s, 2H), 6.46 (d, 1H, J = 1.8 Hz), 7.57 (d, 1H, J = 1.8 Hz); ^{13}C NMR δ: −5.73, 18.12, 25.69, 57.10, 110.52, 135.87, 146.69, 154.96; mass spectrum, *m/e*: 212 ($M^{\cdot+}$). Anal. calcd. for $C_{11}H_{20}O_2Si$: C 62.21, H 9.49; found: C 62.27, H 9.47.

*2-(*tert*-Butyldimethylsilyl)-3-(hydroxymethyl)-4-(tri-*n*-butylstannyl)furan (**4**)*

To a solution of furan **2** (1.5 g, 6.9 mmol) in dry DME (20 mL) at −78°C under an atmosphere of argon was added *n*-butyllithium (7.6 mL, 2.0 M in hexane, 15.2 mmol). After 15 min at 0°C, tri-*n*-butylstannyl chloride (1.9 mL, 6.9 mmol) was added and the solution stirred for 1 h. Saturated ammonium chloride was added, the solution extracted with ethyl acetate, and the solvent removed *in vacuo* to afford, after silica gel column (petroleum ether/ethyl acetate 20:1) and distillation, stannylated furan **4** (89%) as a clear colourless oil, bp 148–150°C/0.12 Torr; IR (neat): 3425, 1464, 1251 cm^{-1}; ^{1}H NMR δ: 0.28 (s, 6H), 0.87 (t, 9H, J = 4.1 Hz), 0.88 (s, 9H), 0.94 (t, 6H, J = 3.7 Hz), 1.2–1.4 (m, 6H), 1.44–1.55 (m, 6H), 2.05 (s, 1H), 4.50 (s, 2H), 7.35 (s, 1H); ^{13}C NMR δ: −5.52, 9.95, 13.65, 17.33, 26.37, 27.29, 29.18, 58.30, 115.75, 141.02, 151.53, 154.78(s); mass spectrum, *m/e*: 444 ($M^{\cdot+}$ − *t*-Bu); HRMS (EI) calcd. for $C_{19}H_{37}O_2Si^{120}Sn$ ($M^{\cdot+}$ − *t*-Bu): 445.1585; found ($M^{\cdot+}$ − *t*-Bu): 445.1578.

*2-(*tert*-Butyldimethylsilyl)-3-(hydroxymethyl)-4-(trimethylstannyl)furan (**5**)*

The above procedure was used, followed by quenching the dianion with trimethylstannyl chloride. Work-up provided furan **5** (88%) as a clear colourless oil, bp 88–92°C/0.04 Torr; IR (neat): 3450, 1471, 972 cm^{-1}; ^{1}H NMR δ: 0.30 (s, 9H, $J_{H,Sn}$ = 54.6 and 57.1 Hz), 0.30 (s, 6H), 0.92 (s, 9H), 4.57 (s, 2H), 7.40 (s, 1H); ^{13}C NMR δ: −8.77, −5.48, 17.32, 26.40, 58.12, 116.50, 140.89, 151.59, 154.54; mass spectrum, *m/e*: 361 ($M^{\cdot+}$ − Me); HRMS (EI) calcd. for $C_{13}H_{25}O_2Si^{120}Sn$ ($M^{\cdot+}$ − Me): 361.0653; found: 361.0625.

*3-[(*tert*-Butyldimethylsilyl)oxymethyl]-4-(tri-*n*-butylstannyl)furan (**6**)*

To a solution of stannylfuran **4** (0.32 g, 0.63 mmol) in dry DMF (1 mL) was added sodium hydride (0.8 mg, 0.04 mmol) under an atmosphere of argon. After 5 min at 25°C, diethyl ether and saturated sodium chloride were added. The diethyl ether was washed six times with saturated sodium chloride, dried (Na_2SO_4), and the solvent removed *in vacuo* to afford, after distillation, compound **6** (98%) as a clear colourless oil, bp 138°C/0.21 Torr; IR (neat): 1464, 1254, 1106, 1073, 1040, 842 cm^{-1}; ^{1}H NMR δ: 0.08 (s, 6H), 0.89 (t, 9H, J = 7.0 Hz), 0.92 (s, 9H), 1.05 (t, 6H, J = 5.1 Hz), 1.43 (m, 6H), 1.51 (m, 6H), 4.55 (s, 2H), 7.14 (s, 1H), 7.44 (s, 1H); ^{13}C NMR δ: −5.25, 9.71, 13.65, 18.48, 25.98, 27.32, 29.14, 59.11, 114.14, 130.77,

Can. J. Chem. Downloaded from www.nrcresearchpress.com by 84.41.108.74 on 09/07/12
For personal use only.

Can. J. Chem. Downloaded from www.nrcresearchpress.com by 84.41.108.74 on 09/07/12
For personal use only.

139.63, 147.82; mass spectrum, *m/e*: 444 ($M^{\cdot+}$ − *t*-Bu); HRMS (EI) calcd. for $C_{19}H_{37}O_2Si^{120}Sn$ ($M^{\cdot+}$ − *t*-Bu): 445.1585; found ($M^{\cdot+}$ − *t*-Bu): 445.1594.

*3-[(*tert*-Butyldimethylsilyl)oxymethyl]-4-(trimethylstannyl)furan (**8**)*

The above procedure was followed using furan **5** to afford furan **8** (88%) after work-up and distillation, bp 78–82°C/0.04 Torr; IR (neat): 1257, 1074, 839 cm^{-1}; ^1H NMR δ: 0.08 (s, 6H), 0.28 (s, 9H, $J_{H,Sn}$ = 55.0 and 57.3 Hz), 4.56 (s, 2H), 7.17 (s, 1H), 7.44 (s, 1H); ^{13}C NMR δ: −9.03, −5.15, 18.51, 26.03, 58.53, 115.59, 130.50, 139.67, 147.92; mass spectrum, *m/e*: 361 ($M^{\cdot+}$ − Me); HRMS (EI) calcd. for $C_{13}H_{25}O_2Si^{120}Sn$ ($M^{\cdot+}$ − Me): 361.0653; found: 361.0638.

*3-(Hydroxymethyl)-4-(tri-*n*-butylstannyl)furan (**7**)*

To a solution of furan **6** (100 mg) in THF (5 mL) at 0°C was added 1.1 equivalents of tetra-*n*-butylammonium fluoride. After 5 h at 0°C, diethyl ether and saturated ammonium chloride were added. The organic layer was separated, dried, and removed *in vacuo* to leave an oil. Flash chromatography (silica gel, EtOAc/pet. ether 1:5) followed by distillation provided furan **7** (92%) as a colourless oil, bp 80–84°C/0.04 Torr; IR (neat): 3423, 1496, 1040 cm^{-1}; ^1H NMR δ: 1.92 (t, 9H), 1.08 (m, 6H), 1.38 (m, 6H), 1.51 (m, 6H), 4.51 (s, 2H), 7.18 (s, 1H), 7.52 (s, 1H); ^{13}C NMR δ: 9.58, 13.59, 27.24, 29.11, 58.05, 114.97, 130.31, 140.02, 148.17; mass spectrum, *m/e*: 331 ($M^{\cdot+}$ − *n*-Bu); HRMS (EI) calcd. for $C_{13}H_{23}O_2{}^{120}Sn$ ($M^{\cdot+}$ − *n*-Bu): 331.0724; found: 331.0755.

General tin coupling procedure

To a solution of a stannylated furan (82 mg, 0.16 mmol) in dry toluene (2 mL) were added an aryl bromide (0.18 mmol) and tetrakis(triphenylphosphine)palladium(0) (2 mol%). The mixture was refluxed. After the appropriate time (Table 1 or 2) either the solution was worked up or more catalyst was added. The work-up was as follows: the solution was cooled to room temperature, water (1 mL) added, and the mixture filtered through Celite. The mixture was extracted with diethyl ether, dried (Na_2SO_4), and the solvent removed *in vacuo*. Silica gel chromatography (petroleum ether/ethyl acetate 50:1), followed by either a distillation or recrystallization, afforded coupled products.

*2-(*tert*-Butyldimethylsilyl)-3-(hydroxymethyl)-4-phenyl furan (**11**)*

Yield 51%; bp 105°C/0.3 Torr; IR (neat): 3450, 1488, 1254, 1099, 999, 829, 782 cm^{-1}; ^1H NMR δ: 0.35 (s, 6H), 0.94 (s, 9H), 1.6 (bs, 1H), 4.60 (s, 2H), 7.27–7.31 (m, 1H), 7.36–7.41 (m, 2H), 7.52–7.55 (m, 2H), 7.70 (s, 1H); ^{13}C NMR δ: −5.55, 17.51, 26.41, 55.13, 127.11, 127.25, 128.27, 128.72, 132.29, 133.93, 144.00, 158.09; mass spectrum, *m/e*: 231 ($M^{\cdot+}$ − *t*-Bu): HRMS (EI) calcd. for $C_{13}H_{15}O_2Si$ ($M^{\cdot+}$ − *t*-Bu): 231.0842; found ($M^{\cdot+}$ − *t*-Bu): 231.0836.

*2-(*tert*-Butyldimethylsilyl)-3-(hydroxymethyl)-4-(3-methylphenyl)-furan (**12**)*

Yield 55%; bp 120–125°C/0.05 Torr; IR (neat): 3431, 1608, 1471, 1251 cm^{-1}; ^1H NMR δ: 0.38 (s, 6H), 0.97 (s, 9H), 2.40 (s, 3H), 4.63 (s, 2H), 7.27 (m, 1H), 7.3–7.5 (m, 2H), 7.35 (s, 1H), 7.71 (m, 1H); ^{13}C NMR δ: −5.53, 17.27, 21.45, 26.44, 55.20, 125.37, 127.16, 127.69, 128.81, 129.03, 132.21, 134.06, 136.25, 143.96, 157.92; mass spectrum, *m/e*: 245 ($M^{\cdot+}$ − *t*-Bu). Anal. calcd. for $C_{18}H_{26}O_2Si$: C 71.47, H 8.67; found: C 71.37, H 8.79.

*2-(*tert*-Butyldimethylsilyl)-3-(hydroxymethyl)-4-(2-naphthyl)furan (**13**)*

Yield 46%; bp 155–160°C/0.05 Torr; IR (neat): 3456, 1601, 1392 cm^{-1}; ^1H NMR δ: 0.41 (s, 6H), 1.01 (s, 9H), 4.42 (s, 1H), 7.40–7.55 (m, 4H), 7.71 (s, 1H), 7.8–8.0 (m, 3H); ^{13}C NMR δ: −5.55, 17.37, 26.54, 55.51, 124.52, 125.36, 125.73, 125.94, 126.26, 128.07, 128.11, 128.35, 129.63, 132.70, 133.60, 136.10, 145.09, 157.10; mass spectrum, *m/e*: 281 ($M^{\cdot+}$ − *t*-Bu); HRMS (EI) calcd. for $C_{17}H_{17}O_2Si$ ($M^{\cdot+}$ − *t*-Bu): 281.0998; found: 281.0980.

*3-[(*tert*-Butyldimethylsilyl)oxymethyl]-4-phenylfuran (**14**)*

Yield 90%; bp 89°C/0.03 Torr; IR (neat): 1468, 1255, 1095, 1074, 857, 776 cm^{-1}; ^1H NMR δ: 0.08 (s, 6H), 0.93 (s, 9H), 4.68 (s, 2H), 7.27–7.31 (m, 1H), 7.35–7.41 (m, 2H), 7.45–7.55 (m, 4H); ^{13}C NMR δ: −5.29, 19.23, 25.86, 56.53, 124.42, 126.23, 127.01, 127.89, 128.59, 132.38, 139.95, 141.73; mass spectrum, *m/e*: 288 ($M^{\cdot+}$), 231 ($M^{\cdot+}$ − *t*-Bu); HRMS (EI) calcd. for $C_{13}H_{15}O_2Si$ ($M^{\cdot+}$ − *t*-Bu): 231.0842; found ($M^{\cdot+}$ − *t*-Bu): 231.0859.

*3-[(*tert*-Butyldimethylsilyl)oxymethyl]-4-(2-formylphenyl)furan (**15**)*

Yield 85%; bp 82–85°C/0.02 Torr; IR (neat): 1694, 1468, 1256, 1075, 839, 774 cm^{-1}; ^1H NMR δ: −0.05 (s, 6H), 0.82 (s, 9H), 0.47 (s, 2H), 7.40–7.71 (m, 5H), 8.01 (dd, 1H, *J* = 8.1 and 2.3 Hz), 10.05 (s, 1H); ^{13}C NMR δ: −5.58, 16.21, 25.77, 58.09, 121.66, 125.79, 127.43, 128.1, 131.8, 133.51, 134.86, 135.7, 141.23, 141.98, 192.12; mass spectrum, *m/e*: 259 ($M^{\cdot+}$ − *t*-Bu); HRMS (EI) calcd. for $C_{14}H_{15}O_3Si$ ($M^{\cdot+}$ − *t*-Bu): 259.0791; found ($M^{\cdot+}$ − *t*-Bu): 259.0795.

*3-[(*tert*-Butyldimethylsilyl)oxymethyl]-4-(2,4,6-trimethylphenyl)-furan (**16**)*

Yield 55%; bp 90°C/0.07 Torr; IR (neat): 1471, 1256, 1078, 849 cm^{-1}; ^1H NMR δ: −0.1 (s, 6H), 0.83 (s, 9H), 2.05 (s, 6H), 2.29 (s, 3H), 4.29 (s, 2H), 6.89 (s, 2H), 7.17 (d, *J* = 1.6 Hz, 1H), 7.48 (d, *J* = 1.6 Hz, 1H); ^{13}C NMR δ: −5.74, 19.4, 20.58, 21.01, 25.84, 56.94, 123.00, 125.64, 127.85, 128.08, 137.07, 137.76, 139.79, 140.66; mass spectrum, *m/e*: 330 ($M^{\cdot+}$), 273 ($M^{\cdot+}$ − *t*-Bu); HRMS (EI) calcd. for $C_{16}H_{21}O_2Si$ ($M^{\cdot+}$ − *t*-Bu): 273.1311; found ($M^{\cdot+}$ − *t*-Bu): 273.1324.

*3-[(*tert*-Butyldimethylsilyl)oxymethyl]-4-(2-methylphenyl)furan (**17**)*

Yield 80%; bp 85°C/0.1 Torr; IR (neat): 1550, 1082, 841, 780 cm^{-1}; ^1H NMR δ: −0.06 (s, 6H), 0.84 (s, 9H), 2.23 (s, 3H), 4.42 (s, 2H), 7.12–7.25 (m, 4H), 7.30 (d, 1H, *J* = 1.3 Hz), 7.45 (d, 1H, *J* = 1.3 Hz); ^{13}C NMR δ: −5.59, 18.28, 20.33, 25.83, 56.65, 124.59, 125.46, 125.69, 127.56, 129.98, 130.60, 131.60, 137.01, 140.38, 140.57; mass spectrum, *m/e*: 245 ($M^{\cdot+}$ − *t*-Bu); HRMS (EI) calcd. for $C_{14}H_{17}O_2Si$ ($M^{\cdot+}$ − *t*-Bu): 245.0998; found ($M^{\cdot+}$ − *t*-Bu): 245.0991.

*3-[(*tert*-Butyldimethylsilyl)oxymethyl]-4-[4-(phenyl)phenyl]furan (**18**)*

Yield 70%; bp 95°C/0.13 Torr; IR (neat): 1470, 1256, 1075, 838, 765 cm^{-1}; ^1H NMR δ: 0.11 (s, 6H), 0.92 (s, 9H), 4.71 (s, 2H), 7.31–7.63 (m, 11H); ^{13}C NMR δ: −5.30, 18.25, 25.83, 56.49, 124.40, 125.91, 126.99, 127.27, 128.21, 128.55, 128.76, 139.83. 140.02, 140.76, 141.18, 141.83; mass spectrum, *m/e*: 364 ($M^{\cdot+}$), 307 ($M^{\cdot+}$ − *t*-Bu); HRMS (EI) calcd. for $C_{19}H_{19}O_2Si$ ($M^{\cdot+}$ − *t*-Bu): 307.1155; found ($M^{\cdot+}$ − *t*-Bu): 307.1152.

*3-[(*tert*-Butyldimethylsilyl)oxymethyl]-4-(2-methylnaphthyl)furan (**19**)*

Yield 82%; bp 103°C/0.09 Torr; IR (neat): 1470, 1256, 1084, 838, 793, 743 cm^{-1}; ^1H NMR δ: −0.28 (s, 3H), −0.25 (s, 3H), 0.74 (s, 9H), 2.32 (s, 3H), 4.25 (s, 2H), 7.35–7.45 (m, 5H), 7.60 (s, 1H), 7.75–7.82 (m, 2H); ^{13}C NMR δ: −5.90, 18.22, 20.78, 25.76, 56.87, 121.87, 124.81, 125.79, 126.00, 126.59, 127.71, 128.40, 131.89, 133.65, 135.20, 140.74, 140.99; mass spectrum, *m/e*: 352 ($M^{\cdot+}$), 295 ($M^{\cdot+}$ − *t*-Bu); HRMS (EI) calcd. for $C_{18}H_{19}O_2Si$ ($M^{\cdot+}$ − *t*-Bu): 295.1155; found ($M^{\cdot+}$ − *t*-Bu): 295.1164.

*3-[(*tert*-Butyldimethylsilyl)oxymethyl]-4-(4-chlorophenyl)furan (**20**)*

Yield 88%; bp 95°C/0.1 Torr; IR (neat): 1515, 1092, 837 cm^{-1}; ^1H NMR δ: 0.07 (s, 6H), 0.89 (s, 9H), 4.60 (s, 2H), 7.33 (d, 2H, *J* = 4.8 Hz), 7.43 (d, 2H, *J* = 1.3 Hz), 7.48 d, 2H, *J* = 4.8 Hz), 7.53 (d, 1H, *J* = 1.3 Hz); ^{13}C NMR δ: −5.30, 18.25, 25.82, 56.16, 124.14, 125.43, 128.73, 129.16, 130.83, 132.90, 140.06, 141.98; mass spectrum, *m/e*: 265 ($M^{\cdot+}$ − *t*-Bu), 230 ($M^{\cdot+}$ − *t*-Bu − Cl); HRMS (EI) calcd. for $C_{13}H_{14}O_2SiCl$ ($M^{\cdot+}$ − *t*-Bu): 265.5293; found ($M^{\cdot+}$ − *t*-Bu): 265.5281.

*3-(Hydroxymethyl)-4-(phenyl)furan (**21**)*

Yield 82%; bp 70–72°C/0.04 Torr; IR (KBr): 3338, 1601, 1051 cm^{-1}; ^1H NMR δ: 4.65 (s, 2H), 7.3–7.6 (m, 7H); ^{13}C NMR δ: 55.20, 123.68, 126.81, 127.4, 128.34, 129.15, 131.61, 139.85, 141.62; mass spectrum, *m/e*: 174 ($M^{\cdot+}$); HRMS (EI) calcd. for $C_{11}H_{10}O_2$: 174.0680; found: 174.0672.

Acknowledgements

We thank the Natural Sciences and Engineering Research Council of Canada for (a) financial support and (b) a post-graduate scholarship to J.-L. J. B. The Lithium Corporation of America (Lithco, Gastonia, N.C.) is thanked for a generous gift of *tert*-butyldimethylsilyl chloride.

1. H. W. GSCHWEND and H. R. RODRIGUEZ. Org. React. **26**, 1 (1979).
2. (*a*) F. M. DEAN. Adv. Heterocycl. Chem. **30**, 167 (1982); (*b*) F. M. DEAN. Adv. Heterocycl. Chem. **31**, 238 (1982).
3. (*a*) C. D. WEIS. J. Org. Chem. **27**, 3520 (1962); (*b*) M. F. ANSELL, M. P. L. CANTON, and P. C. NORTH. Tetrahedron Lett. **22**, 1727 (1981), and references therein.
4. Y. YASUCHIKA, N. TATSUTA, S. SOEJIMA, K. HAYAKAWA, and K. KANEMATSU. Heterocycles, **30**, 223 (1990).
5. (*a*) H. J. REICH and R. E. OLSON. J. Org. Chem. **52**, 2315 (1987); (*b*) F. R. KINDER and A. PADWA. Tetrahedron Lett. **31**, 6835 (1990).
6. (*a*) T. SUZUKI, K. KUBOMURA, H. FUCHII, and H. TAKAYAMA. J. Chem. Soc. Chem. Commun. 1687 (1990); (*b*) W. TOCHTERMANN, G. OLSSON, E. PETERS, K. PETERS, and H. G. VON SCHNERING. Tetrahedron, **44**, 4797 (1988); (*c*) J. HUNGER, C. WOLFF, W. TOCHTERMANN, E. PETERS, K. PETERS, and H. G. VON SCHNERING. Chem. Ber. **119**, 2698 (1986).
7. (*a*) A. G. SCHULTZ and L. A. MOTYKA. J. Am. Chem. Soc. **104**, 5800 (1982); (*b*) A. G. SCHULTZ, L. A. MOTYKA, and M. PLUMMER. J. Am. Chem. Soc. **108**, 1056 (1986); (*c*) E. J. COREY, D. N. CROUSE, and J. E. ANDERSON. J. Org. Chem. **40**, 2140 (1975).
8. (*a*) E. J. BURES and B. A. KEAY. Tetrahedron Lett. **28**, 5965 (1987); (*b*) Tetrahedron Lett. **29**, 1247 (1988); (*c*) P. G. SPINAZZE and B. A. KEAY. Tetrahedron Lett. **30**, 1765 (1989).
9. D. H. MILES, D. L. HO, A. A. DE LA CRUZ, E. D. GOMEZ, J. A. WEEKS, and J. L. ATWOOD. J. Org. Chem. **52**, 2930 (1987).
10. D. R. MCKEAN, G. PARRINELLO, A. F. RENALDO, and J. K. STILLE. J. Org. Chem. **52**, 422 (1987).
11. (*a*) V. FARINA and S. I. HAUCK. Synlett, 157 (1991); (*b*) A. J. MAJEED, O. ANTONSEN, T. BENNECHE, and K. UNDHEIM. Tetrahedron, **45**, 993 (1989); (*c*) Y. YAMAMOTO, S. TOSHMA, and H. NEMOTO. J. Org. Chem. **54**, 4734 (1989); (*d*) M. E. KROLSKI, A. F. RENALDO, D. E. RUDISILL, and J. K. STILLE. J. Org. Chem. **53**, 1170 (1988); (*e*) J. M. CLOUGH, I. S. MANN, and D. A. WIDDOWSON. Tetrahedron Lett. **28**, 2645 (1987); (*f*); A. DONDONI, M. FOGAGNOLO, G. FANTIN, A. MEDICI, and P. PEDRINI. Tetrahedron Lett. **27**, 5269 (1986); (*g*) J. K. STILLE. Angew. Chem. Int. Ed. Engl. **25**, 508 (1986).
12. (*a*) F. K. SHEFFY, J. P. GODSCHALX, and J. K. STILLE. J. Am. Chem. Soc. **106**, 4833 (1984); (*b*) I. PATERSON and M. GARDNER. Tetrahedron, **45**, 5283 (1989).
13. (*a*) A. ARCADI, A. BURINI, S. CACCHI, M. DELMASTRO, F. MARINELLI, and B. PIETRONI. Synlett, 47 (1990); (*b*) D. S. ENNIS and T. L. GILCHRIST. Tetrahedron, **46**, 2623 (1990); (*c*) E. NEGISHI, T. TAKAHASHI, and A. O. KING. Org. Synth. **66**, 67 (1988); (*d*) E. NEGISHI, F.-T. LUO, R. TRISBEE, and H. MATSUSHITA. Heterocycles, **18**, 117 (1982).
14. Y. YANG. Synth. Commun. **19**, 1001 (1989).
15. E. J. COREY and A. VENKATESWARLU. J. Am. Chem. Soc. **94**, 6190 (1972).
16. (*a*) J. E. PLEVIJAK and R. F. HECK. J. Org. Chem. **43**, 2454 (1978); (*b*) A. TAMMURA, Y. YAMMADA, and Z. YOSHIDA. Tetrahedron, **35**, 329 (1979); (*c*) N. MUJAWA and A. J. SUZUKI. J. Chem. Soc. Chem. Commun. 866 (1979); (*d*) D. MILSTEIN. Organometallics, **1**, 888 (1982).
17. A. M. ECHAVARREN and J. K. STILLE. J. Am. Chem. Soc. **109**, 5478 (1987).
18. N. MOUFID and Y. CHAPLEUR. Tetrahedron Lett. **32**, 1799 (1991); J. ARDISSON, J. P. FEREZOU, M. JULIA, and A. PANCRAZI. Tetrahedron Lett. **28**, 2001 (1987).
19. W. C. STILL, M. KAHN, and A. MITRA. J. Org. Chem. **43**, 2923 (1978).

Can. J. Chem. Downloaded from www.nrcresearchpress.com by 84.41.108.74 on 09/07/12
For personal use only.

1,3-Diketonatoboron difluoride sensitized cation radical reactions

Y. L. CHOW[1] AND XIANEN CHENG
Department of Chemistry, Simon Fraser University, Burnaby, B.C., Canada V5A 1S6

Received October 6, 1990[2]

Y. L. CHOW and XIANEN CHENG. Can. J. Chem. **69**, 1331 (1991).

Dibenzoylmethanatoboron difluoride ($DBMBF_2$) and allied BF_2 complexes interact from their singlet excited state with *trans*-anethole (*t*-A), quadricyclene (QC), and norbornadiene (NBD) by electron transfer to generate the corresponding cation radicals, which undergo the reported reactions. By sensitization, *t*-A undergoes dimerization to form the *anti* head-to-head and *syn* head-to-head dimers with retention of stereochemistry. The formation is reversible under sensitization conditions, leading to accumulation of the more stable *anti* isomer. However, irradiation of the absorption band of the $DBMBF_2$ – *t*-A ground state complex did not lead to dimerization of *t*-A. By $DBMBF_2$ sensitization, QC is cleanly converted to NBD while NBD is not affected. The calculation shows $QC^{+\cdot}$ possesses higher energy than $NBD^{+\cdot}$ by 7.5 kcal/mol, hence an irreversible rearrangement. Other sensitizers (e.g., cyanoaromatics and tetrachlorobenzoquinone) also promote these cation radical reactions but not as cleanly as $DBMBF_2$.

Key words: photosensitization by boron complexes, cation radical rearrangement, cation radical cycloaddition, electron transfer sensitization, photoreaction of ground state complexes.

Y. L. CHOW et XIANEN CHENG. Can. J. Chem. **69**, 1331 (1991).

Le difluorure de dibenzoylméthanatobore ($DBMBF_2$) et ses complexes apparentés réagissent dans leur état excité singulet avec l'anéthole-*trans* (*t*-A), le quadricyclène (QC) et le norbornadiène (NBD) par transfert d'électron pour générer les cations radicalaires correspondants qui subissent les réactions mentionnées. Le *t*-A sensibilisé donne les dimères tête–tête *anti* et tête–tête *syn* avec rétention de la stéréochimie. Cette réaction sensibilisée est réversible et conduit majoritairement à l'isomère *anti* le plus stable. Cependant l'irradiation de la bande d'absorption du complexe $DBMBF_2$–*t*-A dans l'état fondamental ne conduit pas à une dimérisation du *t*-A. Le QC sensibilisé par le $DBMBF_2$ se transforme proprement en NBD tandis que le NBD n'est pas affecté dans les mêmes conditions. Les calculs montrent que l'énergie du cation radicalaire $QC^{+\cdot}$ est de 7,5 kcal/mol supérieure à celle du cation radicalaire $NB^{+\cdot}$ et que le réarrangement est par conséquent irréversible. D'autres sensibilisateurs (par exemple les cyanoaromatiques et la tétrachlorobenzoquinone) favorisant également ces réactions mais pas aussi proprement que le $DBMBF_2$.

Mots clés : photosensibilisation par des complexes de bore, réarrangement des cations radicalaires, cycloaddition des cations radicalaires, sensibilisation par transfert d'électrons, réaction photochimique des complexes à l'état fondamental.

[Traduit par la rédaction]

Introduction

We have reported that dibenzoylmethanatoboron difluoride ($DBMBF_2$) reacts from its singlet excited state with simple olefins to form cycloaddition products (1, 2), and that 2-acetylcyclohexanonatoboron difluoride ($ACHBF_2$) and acetylacetonatoboron difluoride ($AABF_2$) similarly undergo photocycloaddition with a number of benzene derivatives (3). These primary photocycloadducts generally undergo hydrolysis at a certain stage to eliminate the BF_2 moiety and rearrange by acid catalysis to give final products under the photolysis conditions. In $DBMBF_2$ photocycloadditions to cyclic olefins, it has been established that the excimer reacts with cyclic olefins while the monomer of excited state $DBMBF_2$ contributes very little in the addition (2, 4). Strangely, a similar photocycloaddition to acyclic olefins exhibits the opposite pattern.

In a preliminary publication, evidence showed that the singlet excited $DBMBF_2$ interacts with many types of olefins to form exciplexes that are assumed to be the precursors of the subsequent chemical events, such as cycloadditions, cation radical reactions, and reverse electron transfer (1). The correlation of the $DBMBF_2$ fluorescence quenching rate constants (log k_q) by olefins against the ionization potential of donor olefins shows a departure from the Rehm–Weller full electron transfer model (1) involving an excited state electron acceptor (*A), such as $*DBMBF_2$, and a donor (D), as shown in eq. [1]. The near flat correlation region (Fig. 1 of ref. 1) involving electron-rich olefins coincides with specific types of chemical reactions that can be characterized as cation radical initiated reactions. We wish to describe such cation radical reactions promoted by singlet excited $DBMBF_2$ and to provide evidence for electron transfer processes.

Two model reactions chosen here are well established to involve cation radicals as the reactive intermediate. Bauld and co-workers (5, 6) demonstrated that the aminium radical initiated dimerization of *trans*-anethole (**1**) in CH_2Cl_2 ($E_{\frac{1}{2}}^{ox}$ = 1.11 V) follows formally concerted [$\pi^2 s + \pi^1 s$] cycloadditions with retention of configuration to give the head-to-head *trans*, *anti*,*trans*-cyclobutane **2** and the head-to-head *trans*,*syn*,*trans*-cyclobutane **3** in about 1:1 ratio at −35°C; at room temperature only the *anti* isomer **2**, the more stable of the two, is obtained (eqs. [2] and [3]). The reaction is nicely demonstrated to be a reversible cation radical chain reaction of $\mathbf{1}^{+\cdot}$ arising from thermal electron transfer to tris(*p*-bromophenyl)aminium hexachloroantimonate, and its activation parameters are determined through kinetic studies (6). Recently Lewis and Kojima (7, 8) used photoinitiated electron transfer sensitization (9,10-dicyanoanthracene and other cyano aromatics) of *trans*-anethole to induce its dimerization, leading to qualitatively similar results to those obtained by Bauld's group (5, 6). The less stable *syn* isomer **3** is the only product in direct photolysis of *tert*-anethole (7, 9). Applications of the addition of $\mathbf{1}^{+\cdot}$ to other olefins have also been reported (10).

The sensitized interconversion of quadricyclene (QC or **4**) and norbornadiene (NBD or **5**) is well characterized, as shown in eq. [4] (11–14). Triplet sensitization by aromatic ketones exclusively converts **5** to **4** (13, 14). This remarkable photoisomerization was beautifully demonstrated to involve different

[1]Author to whom correspondence may be addressed.
[2]Revision received April 30, 1991.

Can. J. Chem. Downloaded from www.nrcresearchpress.com by 84.41.108.74 on 09/07/12
For personal use only.

TABLE 1. Thermodynamic parameters and quantum efficiencies (Φ) of the valence isomerization of QC and NBD[a]

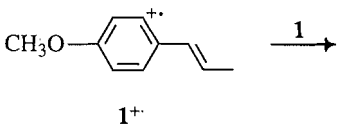
Sensitizer E_S or E_T	$E_{\frac{1}{2}}^{red}$ (V)	Solvent	Starting isomer	ΔG^b (kcal/mol)	Φ	Reference
$AABF_2$	−1.78	CD_2Cl_2	QC		0.06	This work
($E_S < 86$)		CD_3CN	QC	−24.0	0.02	This work
		CD_2Cl_2	NBD		0.000	This work
		CD_3CN	NBD	−9.5	0.000	This work
$DBMBF_2$	−1.30	CD_2Cl_2	QC		0.07	This work
($E_S = 73$)		CD_3CN	QC	−22.2	0.02	This work
($E_T = 62$)		CD_2Cl_2	NBD		0.000	This work
		CD_3CN	NBD	−7.6	0.000	This work
1-CN-Np	−1.8	CD_3CN	QC	−22.8	~0.01	19
($E_S = 87$)		CD_3CN	NBD	−8.3	~0.01	17
TCB	0.02	CD_3CN	QC	−41.7	~0.6	16
($E_T = 62$)		CD_3CN	NBD	−27.2	0.000	16

[a]The oxidation potentials of QC (0.91 V) and NBD (1.54 V) are cited from refs. 16 and 17.
[b]The thermodynamic free energy was approximately calculated according to $\Delta G = E_{(D/D^+)} - E_{(A^-/A)} - E_{00} - E_{coulombic}$ (20).

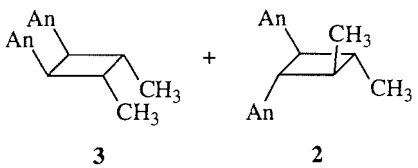
energy surfaces and a schematic representation of preferential transitions has been given (12). However, Solomon, Steel, and Weller pointed out earlier that the singlet state sensitized **4** → **5** isomerization is most likely to involve electron transfer (15), i.e., the isomerization occurs through cation radicals $\mathbf{4}^{+\cdot} \rightarrow \mathbf{5}^{+\cdot}$ in a radical ion pair. The involvement of these two distinct cation radicals is elegantly demonstrated by CIDNP results in electron transfer (e.g., 1-cyanonaphthalene and chloranil) sensitized reactions (16–18); the potential energy of $\mathbf{4}^{+\cdot}$ is estimated to be higher by 9–14 kcal/mol than that of $\mathbf{5}^{+\cdot}$, which drives the one-way isomerization. Extensive studies on similar sensitized interconversions have been published (19).

[1] $*A + D \longrightarrow A^{-\cdot} + D^{+\cdot}$

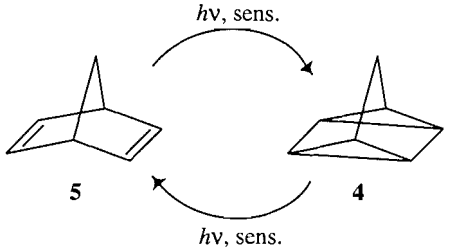
[2] $D + Ar_3N^{+\cdot} \longrightarrow D^{+\cdot} + Ar_3N$

[3] 

$\mathbf{1}^{+\cdot}$



3 **2**

[4] 

Results

The valence isomerization of quadricyclene (**4**) and norbornadiene (**5**) could be sensitized with acetylacetone or $AABF_2$ using a 300-nm light source or with $DBMBF_2$ using a 350-nm light source at about 30°C under concentrations in which the sensitizers absorbed all incident light. The photolysis was carried out either in CD_2Cl_2 or in CD_3CN solution using NMR spectroscopy to monitor progress. Taking advantage of the fact that NBD showed distinct low-field signals 3.6 and 6.8 ppm for the allylic and olefinic protons, and that these protons would shift to higher fields at ca. 1.4 ppm on isomerization to QC, the conversions either way could be monitored readily and unambiguously. In CD_2Cl_2, acetylacetone sensitized the conversion of NBD to QC smoothly, but did not affect the reverse isomerization, QC → NBD, in 12 h of irradiation. In contrast, $AABF_2$ and $DBMBF_2$ sensitized the conversion of QC to NBD but not that of NBD to QC in CD_2Cl_2 solution. The quantum yields of the conversion were determined and are listed in Table 1 together with reported sensitization data. Table 1 also contains the singlet and triplet energy levels, and redox potentials of compounds participating in the photoinduced electron transfer reaction, the free energy of which (ΔG) is calculated according to Weller's equation (20).

In CH_3CN, both $AABF_2$ and $DBMBF_2$ showed a similar sensitization pattern but with a lower quantum efficiency than that observed in CD_2Cl_2. Both sensitizers showed a quantum yield of 0.02 for conversion of QC to NBD. Taking advantage of the strong fluorescence of monomeric $DBMBF_2$ at 397 and 416 nm (4), the quenching of fluorescence intensities was studied in acetonitrile at $[DBMBF_2] = 5 \times 10^{-6}$ M using a Stern–Volmer type analysis to correlate the efficiency. Interestingly, both valence isomers quenched the fluorescence strongly with slopes ($k_q\tau_0$) of 14.1 M^{-1} for QC (**4**) and 6.8 M^{-1} for NBD (**5**). Using τ_0 of $DBMBF_2$ as 2.7 ns (4), the quenching rate constants (k_q) were 5.2×10^9 and $2.5 \times 10^9\ M^{-1}\ s^{-1}$, respectively (Table 2). $AABF_2$ showed fluorescence only at a concentration of 0.05 M (21); as its origin was uncertain, quenching experiments were not carried out. In all these irradiations the BF_2 complexes were not consumed and no other product(s) was detected by GC analysis.

Irradiation of an acetonitrile solution of **1** (0.5 M) containing a sensitizer gave a mixture of *syn* isomer **3** and *anti* isomer **2**, the ratio of which favored the latter increasingly with the duration of irradiation. With $DBMBF_2$ as the sensitizer, 4 h of irradiation yielded *anti*-**2** and *syn*-**3** in a 6:1 ratio. This ratio was very close

Can. J. Chem. Downloaded from www.nrcresearchpress.com by 84.41.108.74 on 09/07/12
For personal use only.

TABLE 2. Parameters of fluorescence intensity quenching

Sensitizer E_S (eV); τ_0 (ns)	Quencher	Solvent	$k_q\tau_0$ (M^{-1})	$10^{-9}k_q$ (M^{-1} s^{-1})	Reference
9-Cyanoanthracene 2.96;17.2	**1**	CH_3CN	248	14	8
$DBMBF_2$ 3.17;2.7	**1**	CH_3CN	13.1	4.8	This work
1-Cyanonaphthalene 3.75;8.9	**4**	CH_3CN	18.7	2.1	19
$DBMBF_2$	**4**	CH_3CN	14.1	5.2	This work
$DBMBF_2$	**5**	CH_3CN	6.8	2.5	This work

Can. J. Chem. Downloaded from www.nrcresearchpress.com by 84.41.108.74 on 09/07/12
For personal use only.

to that sensitized by 9,10-dicyanoanthracene in CH_3CN, reported recently (8). The GC analysis of the photolysate did not show a peak corresponding to *cis*-anethole, but no effort was made to confirm its absence. When this investigation was nearly complete, detailed investigations of the dimerization and isomerization of **1** by sensitization and direct excitation were published (7, 8). We will report the aspects not covered by these two most recent publications.

In view of the proven efficiency as electron acceptors in their excited state (16, 17), 9-cyanoanthracene (CA) and tetrachloro-1,4-benzoquinone (TCB) were also used as sensitizers in addition to the BF_2 complexes. The formations of *syn* isomer **3** and *anti* isomer **2** were plotted against irradiation times elapsed in the presence of $DBMBF_2$ as shown in Fig. 1. The formation profiles showed that both **2** and **3** were formed at about the same rate in the beginning, but the production of the less stable *syn* isomer **3** rapidly leveled off at about 30–60 min irradiation time while that of more stable *anti* isomer **2** increased steadily. TCB sensitized dimerization of *trans*-anethole (**1**) was also included for comparison (Fig. 2B). It exhibited a different profile from that of $DBMBF_2$ sensitization (Fig. 2A); both **2** and **3** were formed at about the same rate, though the *syn* isomer **3** started to increase more rapidly beyond 4 h of irradiation. The difference arises from the fact that TCB sensitizes the dimerization from its lowest triplet state with a lower energy (E_T 62 kcal/mol) participating electron transfer. CA and benzoylacetonatoboron difluoride ($BABF_2$) sensitized cases showed reaction profiles similar to that shown by $DBMBF_2$; these plots are described in the Ph.D. thesis presented by one of us (21).

$DBMBF_2$ also sensitized the cycloreversion of dimers **2** and **3** under comparable photolysis conditions to those used above to give *trans*-anethole **1** without the formation of *cis*-anethole. As shown in the profile of cycloreversions in Fig. 2, under comparable conditions the *syn* isomer **3** was sensitized to give **1** faster and in better yields than the *anti* isomer **2**. The poor yields of the monomer **1** in these cycloreversions (i.e., 18% from **2** and 71% from **3** based on reacted dimers) appeared to arise from polymerization as found in the aminium radical initiated cycloreversion reaction (5). No effort was made to identify polymers of **1**. The rapid cycloreversion of **3** was followed by the much slower formation of **2** as shown in Fig. 2A. It should be mentioned that in these sensitized reactions, whether dimerizations or cycloreversions, $DBMBF_2$ and $BABF_2$ remained unreacted during photolysis. During the reaction CA decreased slightly, showing some side reactions.

A colourless solution of $DBMBF_2$ turned bright yellow on addition of one of these and other electron-rich donors (20). Inspection of the UV spectra of these mixture solutions showed that the end absorption was red-shifted to various extents,

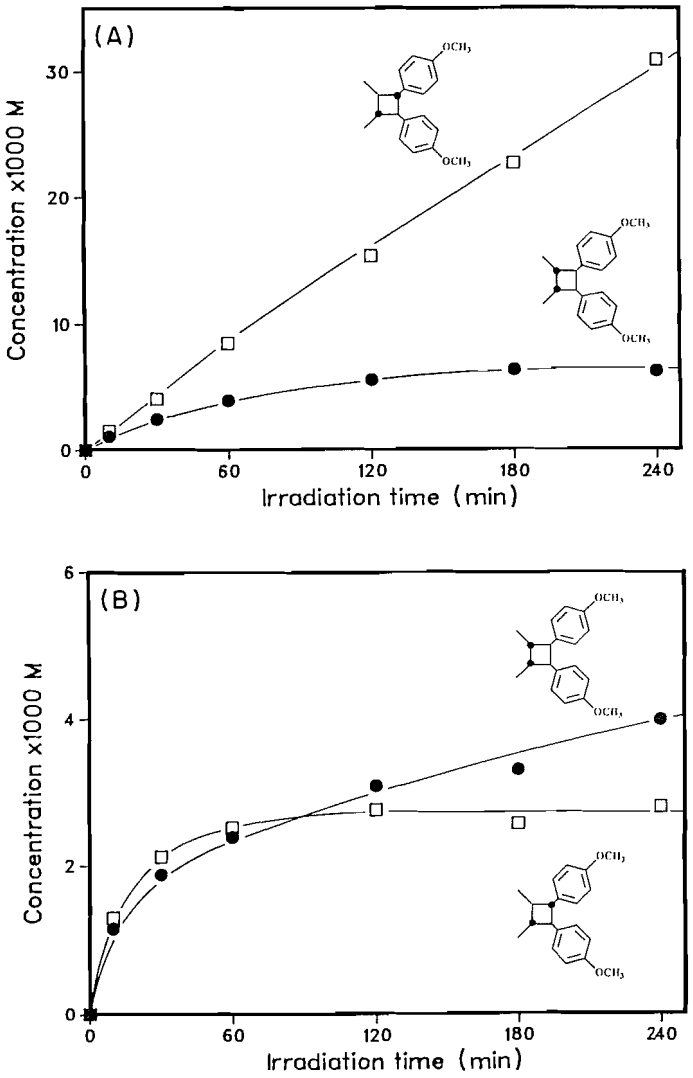


FIG. 1. The formation profile of the *syn*-**3** and *anti*-**2** dimers in the $DBMBF_2$ (A, 0.02 M) and tetrachlorobenzoquinone (B, 0.02 M) sensitized photolysis of **1** (0.5 M) in CH_3CN.

indicating the formation of charge transfer (CT) complexes. Among these, the red shift induced by **1** was most extensive (up to 500 nm) and the association constant was determined to be 0.44 M^{-1} by the Benesi–Hildebrand relation (4). The shifts induced by **4** and **5** were smaller. A solution containing $DBMBF_2$ (0.02 M) and *trans*-anethole **1** in CH_3CN was irradiated with monochromatic light at 312.8 nm for $DBMBF_2$ and at 437.0 nm for the $DBMBF_2$–**1** ground state complex, and

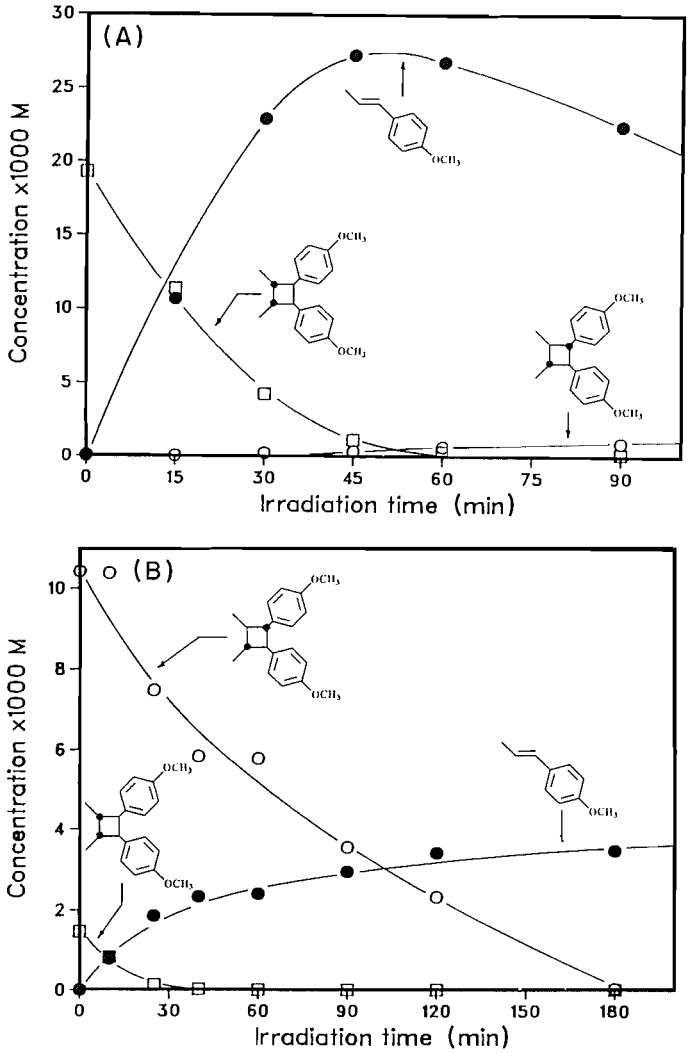


FIG. 2. $DBMBF_2$ (0.02 M) sensitized cycloreversion of the *anti*-**2** dimer (B, 0.02 M) and the *syn*-**3** dimer (A, 0.0192 M) in CH_3CN solution. In the upper figure A, the starting sample contains *syn*-**3** (12%).

the photolysates were analysed by GC. By taking into account the light intensities at these slit openings and the absorbancy, we could estimate the relative quantum yields of *anti*-**2** at 437 nm irradiation to be, at the maximum, 1% of that at 312.8 nm irradiation (see Experimental). It should be noted that at λ_{ex} = 312.8 nm, the incident light was absorbed by $DBMBF_2$ and **1** as well as by the CT complex of $DBMBF_2$–**1**. The fraction of light absorbed by the complex is relatively small owing to the small formation constant. As $DBMBF_2$ singlet excited state energy (E_s 73 kcal/mol) (4) is much lower than that of *trans*-anethole (81 kcal/mol estimated from the longest wavelength of the absorption curve at 355 nm), the excitation at 312.8 nm should be mainly localized in $DBMBF_2$. The results led to the surprising conclusion that excitation of the $DBMBF_2$–**1** ground state complex did not afford the dimerization initiated by $\mathbf{1}^{+\cdot}$. It must be mentioned that the excitation of the $DBMBF^2$–**1** absorption band did not show emission at all. Also $DBMBF_2$ fluoresence was quenched by **1** without showing new emission. The quenching efficiency was determined in the usual manner and the result from a Stern–Volmer analysis is listed in Table 2.

Discussion

Without detailed estimations of thermodynamic parameters (energetics), the results clearly indicated that the BF_2 complex

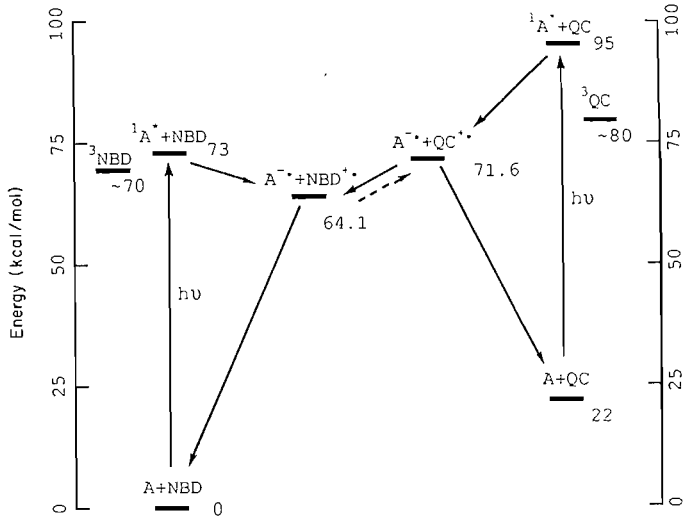


FIG. 3. Energy levels of relevant species in $DBMBF_2$ sensitized isomerization of QC and NDB.

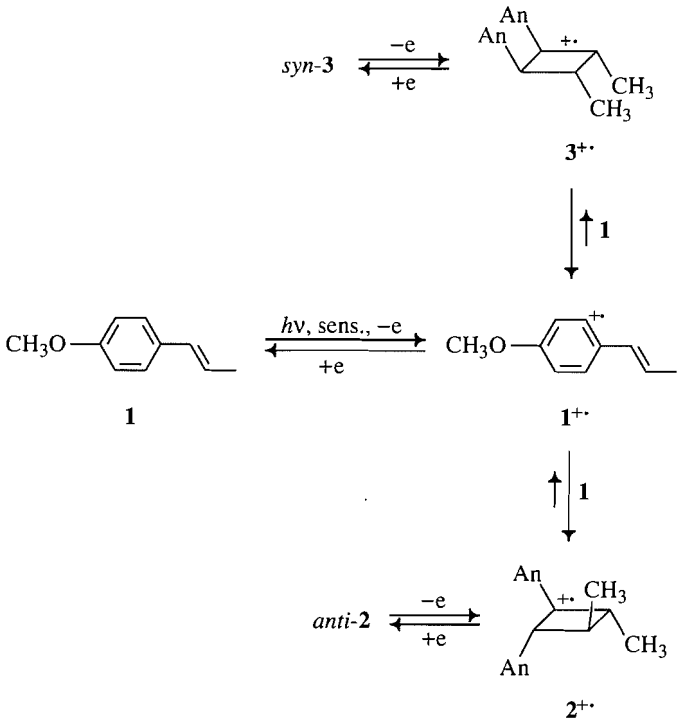
sensitized isomerization of QC to NBD (**4**→**5**) and those of the dimerization of *trans*-anethole (**1**) are initiated by the primary intermediates, the corresponding cation radicals. This means that the primary photoreaction in these cases is a *bona fide* electron transfer process, in which the singlet excited states of BF_2 complexes are the electron acceptors, to give the anion radicals (e.g., $DBMBF_2^{-\cdot}$ and $AABF_2^{-\cdot}$) to counterbalance the cation radicals. As the correlation of the k_q values of these processes with ionization potential indicates (1), the solvent-separated ion pair could have been formed either in the encounter stage or from the solvent penetration of an exciplex radical ion pair (22, 23). With the help of reported data we wish to discuss the thermodynamics and mechanism of the overall reactions.

The acetylacetone (E_T = 69–74 kcal/mol) sensitized conversion of NBD to QC is analogous to acetophenone sensitization (13, 14), namely, by triplet energy transfer to NBD but not to QC, to induce one-way conversion (see Fig. 3 for the E_T levels). While both TCB (16, 17) and BF_2 complexes sensitize a clear conversion of QC to NBD, the former reacts from its triplet excited state as opposed to the singlet state of the latter. The interaction of singlet excited state $DBMBF_2$ with QC and NBD has been demonstrated by the fluorescence quenching to be nearly diffusion controlled (Table 2). Though no exciplex emission is observed, the energy level of the excitation is estimated as shown in Fig. 3 (where $DBMBF_2$ = A) by adapting the ground state of QC lying 22 kcal/mol above that of NBD (16, 17), which is arbitrarily taken as the base line. The potential energy of ion radical pairs (E_{IRP}) can be calculated from the reduction potential of the acceptor ($E_{A^-/A}$) and the oxidation potential of donor E_{D/D^+} according to eq. [1], where the Coulombic factor E_C is about −0.06 eV in CH_3CN (20).

$$E_{IRP} = E_{D/D^+} - E_{A^-/A} + E_C$$

The calculated energy levels of the ion radical pairs (Fig. 3) indicate that $QC^{+\cdot}$ must be at least 7.5 kcal/mol higher than $NBD^{+\cdot}$ in these pairs. This energy difference deters the $NBD^{+\cdot} \rightarrow QC^{+\cdot}$ conversion and accounts for the one-way valence isomerization QC → NBD. However, the ion radical pair generated from $AABF_2$ ($E_{A^-/A}$ = 1.78 V) with NBD should have the energy level high enough (by >5.2 kcal/mol) to cause triplet recombination, and is possible to generate triplet state NBD (E_T 68–70 kcal/mol). This is an analogous argument to

Can. J. Chem. Downloaded from www.nrcresearchpress.com by 84.41.108.74 on 09/07/12
For personal use only.



SCHEME 1

the case of 1-cyanonaphthalene sensitization (16, 17), though such a process is inefficient as shown by the low quantum yield of 0.01 (Table 1). The failure of $AABF_2$ sensitization to convert NBD to QC may arise from the slow intersystem crossing of $^1(AABF_2^-–NBD^+) \rightarrow {}^3(AABF_2^-–NBD^+)$, which can effectively retard the generation of triplet state NBD.

The formation of *syn*-**3** and *anti*-**2** in the sensitized dimerization of *trans*-anethole exhibits a pattern similar to those recently published by Lewis and Kojima (8) and to the early observations by Bauld's group (5, 6). The GC traces in Fig. 1 clearly show that in the early stage of the sensitized dimerization, *syn*-**3** and *anti*-**2** are formed in nearly equal probability. Owing to the more facile cycloreversion of *syn*-**3** than that of *anti*-**2**, the former reaches a stationary state rapidly while the latter increases nearly linearly. This suggests that the stereochemical approach of $\mathbf{1}^{+\cdot}$ and **1** is regiospecific in the head-to-head mode but in either *syn* or *anti* orientation. Subsequent cyclization has been proposed to be a stereospecific $[\pi^2 s + \pi^1 s]$ cycloaddition with retention of *trans* configuration (5). The lack of *cis* isomerization and the formation of other stereoisomeric dimers clearly indicate that the intermediacy of acyclic 1,4-cation radicals is not compatible in $\mathbf{1}^{+\cdot}$ initiated reactions and the cycloreversions. Such 1,4-cation radicals have been proposed to be viable intermediates in certain dimerizations (24, 25). Our conclusion agrees with those obtained in the thermally initiated and 9,10-dicyanoanthracene sensitized dimerization of **1** (5, 8).

We propose Scheme 1 to account for the sensitized reversible photodimerization of **1** (E_{D/D^+} = 1.11 V in CH_2Cl_2) to give **2** and **3**; the key step is the fast reversion of $\mathbf{3}^{+\cdot}$ in comparison to that of $\mathbf{2}^{+\cdot}$, probably owing to steric compressions. We believe that this step is responsible for accumulating *anti*-**2** and causing fast cycloreversion of *syn*-**3**. The step of electron transfer and reversal (i.e., **2** or **3** $\rightarrow \mathbf{2}^{+\cdot}$) is not responsible because of the fact that the oxidation potentials for *syn*-**2** (E_{D/D^+} 1.75 V) and *anti*-**3** (E_{D/D^+} 1.85 V) are very close to each other (8); such electron transfer reactions to either dimer should occur with comparable rates.

During the excitation of the charge transfer band of the $DBMBF_2$–**1** complex the failure to give dimerization of **1** is very surprising in view of the fact that the contact radical ion pair CIP must have been formed. It is assumed that the $DBMBF_2$–**1** complex in its excited state may possess a geometry prone to reverse electron transfer, which destroys cation radical $\mathbf{1}^{+\cdot}$ rapidly within the ion CIP so that $\mathbf{1}^{+\cdot}$ has no chance to diffuse away for reactions even in polar solvent. The significance of this negative result and proposal resides in the fact that the dynamic interaction of singlet excited $DBMBF_2$ with **1** can even initiate dimerization. The extension of the assumption made above leads us to propose that a solvent separated radical ion pair (SSIP) is derived from dynamic processes and undergoes slower reverse electron transfer because of geometrical factors. Therefore $\mathbf{1}^{+\cdot}$ can diffuse away to initiate dimerization. Such a SSIP may be formed from an encounter complex or generated by solvent penetration of exciplex ion pairs in polar solvent (22, 23). We have observed a similar example where excitation of a ground state complex failed to undergo a reaction, contrary to expectations (26). Such phenomena must be related to the exciplex reactivity and geometry, which increasingly attract the attention of photochemists.

Experimental

Materials and conditions

The instrumentation and conditions were the same as those described in refs. 2 and 4. NBD, 9-cyanoanthracene, *trans*-anethole (**1**), and tetrachlorobenzoquinone were recrystallized or redistilled from commercial products. QC was prepared by acetophenone sensitized isomerization of NBD (13). $DBMBF_2$ and $AABF_2$ were prepared in the previous work (2, 3). The authentic sample of the *syn*-**3** dimer was prepared by direct photolysis of **1** through a Pyrex filter (9), that of the *anti*-**2** by TCB sensitized dimerization in which *syn*-**3** was also formed. The latter was chromatographed to give a sample of *anti*-**2** contaminated with 12% of *syn*-**3**.

Sensitized dimerization of 1

A CH_3CN solution containing **1** (5.0×10^{-1} M), a sensitizer (2×10^{-2} M), and octadecane (9.0×10^{-3} M) as the internal standard was irradiated with a 350-nm light source. When TCB was used as the sensitizer, the solution was purged with nitrogen. At intervals, samples were withdrawn for GC analysis. The calibration curves of dimers **2** and **3** with respect to the internal standard were used to read percentage yields directly. At the end of a 4-h irradiation, $DBMBF_2$ and $BABF_2$ remained unchanged in concentration. When 9-cyanoanthracene was used as the sensitizer, its amount decreased by about 40% in 4 h of irradiation. TCB in CH_3CN developed a dark purple colour on addition of **1**; this colour disappeared on irradiation. But the amount of TCB could not be accurately analyzed by GC with a FID detector.

Sensitized cycloreversion of dimers

A CH_3CN solution containing $DBMBF_2$ (2.0×10^{-2} M), a dimer ($\sim 1 \times 10^{-2}$ M), and octadecane (2.0×10^{-3} M) was irradiated and analysed as above.

The monochromatic photolysis

A CH_3CN solution (2 mL) of $DBMBF_2$ (2.0×10^{-2} M), *trans*-anethole **1** (5.0×10^{-1} M), and octadecane (as the internal standard, 2.0×10^{-3} M) was placed in a 1-cm UV cell and was irradiated for 120 min at 312.8 nm. Separately, the same solution and conditions were used to irradiate at 437 nm. The light source used was a Kratos GM252 grating monochrometer, LH150 lamp housing, and LPS251HR power supply mounted on a light bench. The UV cell holder was placed 15 cm before the tip of the GM252. The settings for operating conditions were as follows: the current of the power supply at 8.20 A, the band width at 5 nm, and slit width at entry and exit at 15 nm. The

Can. J. Chem. Downloaded from www.nrcresearchpress.com by 84.41.108.74 on 09/07/12
For personal use only.

200-W Xenon–mercury lamp (Oriel) had an output of 43 $\mu W/cm^2$ at 312.8 nm, and 27 $\mu W/cm^2$ at 437 nm. The relative yields of dimers **2** and **3** were calculated from the GC peaks with respect to the internal standard; these were 0.025 at 437 nm and 0.34 at 312.8 nm.

At 312.8 nm, the molal absorbance of **1** (ϵ_1) was 1833, and that of $DBMBF_2$ (ϵ_A) was 4100; taking the concentrations into consideration, only 8.2% of incident light was absorbed by $DBMBF_2$. The quantum yields at 437 nm (Φ(437 nm)) are estimated by the following equation to be 0.01 × Φ(312.7 nm).

$$\Phi(437\text{ nm}) = (\text{yield of dimers at 437 nm})/(\text{yield of dimers at 312.8 nm}) \times (\text{output ratio of the lamp}) \times (\text{fraction of light absorbed by } DBMBF_2 \text{ at 312.8 nm}) \times 1/(\text{fraction of light absorbed by the complex at 437 nm}) \times \Phi(312.7\text{ nm}) = 0.01\,\Phi(312.7\text{ nm})$$

Sensitized valence isomerization of QC and NBD

A solution containing a sensitizer and QC (or NBD) in CD_2Cl_2 (or CH_3CN) was placed in an NMR tube (5 mm i.d.), which was irradiated with a Rayonet reactor equipped either with RPR-3000 Å or RPR-3500 Å lamps. The progress of the reaction was followed with ^1H NMR spectroscopy with a Bruker 100SY equipped with Aspect 2000 software. The solvent peak $CHDCl_2$ (or CHD_2CN) was used as the internal standard. The peak ratios of NBD (4 olefinic protons) and QC (6 tertiary protons) at various concentrations with respect to the solvent peak were established before these experiments. The concentrations of QC or NBD were calculated on the basis of the integral ratios to the standard and the quantum yields were calculated based on benzophenone–benzhydrol actinometry. The error by this method is estimated to be ±10%, mainly arising from uncertainties in integrations. The details of the method are given in ref. 21.

Acknowledgement

The authors wish to thank the Natural Sciences and Engineering Research Council of Canada for generous financial support of this project.

1. Y. L. CHOW and X. E. CHENG. J. Chem. Soc. Chem. Commun. 1043 (1990).
2. Y. L. CHOW and X. E. CHENG. Can. J. Chem. In press.
3. Y. L. CHOW and X. X. OUYANG. CAN. J. CHEM. **69**, 423 (1991).
4. Y. L. CHOW, X. E. CHENG, and C. I. JOHANSSON. J. Photochem. Photobiol. A: **57**, 247 (1991).
5. N. L. BAULD and R. RABON. J. Am. Chem. Soc. **105**, 633 (1983).
6. K. T. LORENZ and N. L. BAULD. J. Am. Chem. Soc. **109**, 1157 (1987).
7. F. D. LEWIS and M. KOJIMA. J. Am. Chem. Soc. **110**, 8660 (1988).
8. F. D. LEWIS and M. KOJIMA. J. Am. Chem. Soc. **110**, 8664 (1988).
9. H. NOZAKI, R. NOYORI, and M. KAWANISI. Tetrahedron, **24**, 3183 (1968).
10. D. W. REYNOLDS and N. L. BAULD. Tetrahedron, **42**, 6189 (1986).
11. W. G. DAUBEN and R. L. CARGILL. Tetrahedron, **16**, 197 (1961).
12. N. J. TURRO, W. R. CHERRY, M. F. MIRBACH, and M. J. MIRBACH. J. Am. Chem. Soc. **99**, 7388 (1977).
13. G. S. HAMMON, C. D. DEBOER, and N. J. TURRO. J. Am. Chem. Soc. **86**, 2532 (1964).
14. S. MUROV and G. S. HAMMOND. J. Phys. Chem. **72**, 3797 (1968).
15. B. S. SOLOMON, C. STEEL, and A. WELLER. Chem. Commun. 927 (1969).
16. H. D. ROTH, M. L. M. SCHILLING, and G. JONES II. J. Am. Chem. Soc. **102**, 4303 (1980).
17. H. D. ROTH, M. L. M. SCHILLING, and G. JONES II. J. Am. Chem. Soc. **103**, 1246 (1981).
18. H. D. ROTH and M. L. M. SCHILLING. J. Am. Chem. Soc. **103**, 7210 (1981).
19. G. JONES II, S.-H. CHIANG, W. G. BECKER, and J. A. WELCH. J. Phys. Chem. **86**, 2805 (1982) and references cited.
20. H. KNIBBE, D. REHM, and A. WELLER. Ber. Bunsen-ges. Phys. Chem. **72**, 257 (1968).
21. X. E. CHENG. Ph.D. thesis. Simon Fraser University, 1990.
22. (*a*) I. R. GOULD, R. MOODY, and S. FARID. J. Am. Chem. Soc. **110**, 7242 (1988). (*b*) E. R. GOULD, J. E. MOSER, D. EGE, and S. FARID. J. Am. Chem. Soc. **110**, 1991 (1988).
23. D. REHM and A. WELLER. Z. Phys. Chem. NF, **69**, 183 (1970).
24. S. L. MATTES, H. R. LUSS, and S. FARID. J. Phys. Chem. **87**, 4779 (1983).
25. S. L. MATTES and S. FARID. Org. Photochem. **6**, 233 (1983).
26. Y. L. CHOW, X. M. ZHOU, T. J. GAITAN, and Z. Z. WU. J. Am. Chem. Soc. **111**, 3813 (1989).

Can. J. Chem. Downloaded from www.nrcresearchpress.com by 84.41.108.74 on 09/07/12
For personal use only.

072240019

π-Facial stereoselectivity in the Diels–Alder reactions of benzene oxides

JAMES R. GILLARD, MICHAEL J. NEWLANDS, JOHN N. BRIDSON, AND D. JEAN BURNELL[1]
Department of Chemistry, Memorial University of Newfoundland, St. John's, Nfld., Canada A1B 3X7

Received April 8, 1991

This paper is dedicated to Professor Hugh J. Anderson on the occasion of his 65th birthday

JAMES R. GILLARD, MICHAEL J. NEWLANDS, JOHN N. BRIDSON, and D. JEAN BURNELL. Can. J. Chem. **69**, 1337 (1991).

The Diels–Alder reactions of *N*-phenylmaleimide and dimethyl acetylenedicarboxylate with benzene oxide (1,3,5-cyclohexatriene 1,2-oxide, **3**) and its more substituted derivatives 1,2-dimethyl-1,3,5-cyclohexatriene 1,2-oxide (**7**) and 10-oxatricyclo[4.3.1.0]deca-2,4-diene (**11**) in a kinetic manner gave exclusively products of addition *anti* to the plane-nonsymmetrical oxygen. The structures of the adducts were determined unequivocally by nuclear Overhauser enhancements in their ^{1}H nuclear magnetic resonance spectra and by X-ray crystallographic methods. The π-facial stereoselectivity was rationalized in terms of unfavorable orbital interactions, steric hindrance between the dienophile and the *syn* face of benzene oxide, and σ-donation by the oxygen.

Key words: cycloaddition, Diels–Alder, *syn–anti*, π-facial stereoselectivity, benzene oxide.

JAMES R. GILLARD, MICHAEL J. NEWLANDS, JOHN N. BRIDSON et D. JEAN BURNELL. Can. J. Chem. **69**, 1337 (1991).

Les réactions de Diels–Alder de la *N*-phénylmaléimide et de l'acétylène dicarboxylate de méthyle avec l'oxyde de benzène (cyclohexatriène-1,3,5-oxyde-1,2, **3**) et avec ses dérivés plus substitués : le diméthyl-1,2-cyclohéxatriène-1,3,5-oxyde-1,2 (**7**) et le oxa-10-tricyclo[4.3.1.0]décadiène-2,4 (**11**) donnent uniquement et de façon cinétique les produits d'addition en position *anti* par rapport à l'oxygène plan-non symétrique. On a déterminé sans ambiguïté la structure des adduits en faisant appel à l'exaltation Overhauser nucléaire de leurs spectres de résonance magnétique nucléaire du ^{1}H et à la cristallographie de rayons X. On interprète la stéréosélectivité π-faciale en fonction des interactions défavorables des orbitales, de l'encombrement stérique entre le diénophile et la face *syn* de l'oxyde de benzène, et du comportement de l'oxygène comme donneur σ.

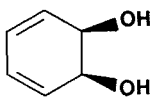
Mots clés : cycloaddition, Diels–Alder, *syn–anti*, stéréosélectivité π-faciale, oxyde de benzène.

[Traduit par la rédaction]

Introduction

Diels–Alder reactions involving some 5-heterosubstituted cyclopentadienes lead predominantly to products that arise by addition to the face of the diene *syn* to the heteroatom, i.e., to the more substituted face (1, 2). Other heteroatoms in a similar position force the cycloaddition to take place mainly *anti* to the heteroatom (2, 3), as do simple hydrocarbon substituents (4).[2] Other cyclic and acyclic systems with allylic heteroatom substituents have been examined: some add *syn* while others add *anti* (6).

There has been much less work on the π-facial (*syn–anti*) stereoselectivity of 1,3-cyclohexadiene derivatives with allylic heteroatom substitution (7). *cis*-Cyclohexa-3,5-diene-1,2-diol (**1**) and many of its derivatives add to ethylenic dienophiles



1

mainly *syn* to the oxygens (8).[3] On the other hand, *anti* addition is predominant with a 1,2,4-triazoline-3,5-dione dienophile (10), and singlet oxygen also adds mainly *anti* to the oxygen of **1** (11). The stereochemistry of the products of each of these processes has been determined in an unequivocal manner.

The benzene oxides are obvious structural relatives of the diols of type **1**, but the stereochemistry of their cycloaddition reactions has not, in most instances, been rigorously proven (12). Excellent pioneering work from the laboratory of Vogel focused on the valence tautomerism that exists between benzene oxides and oxepins (13). The oxide forms were trapped with dienophiles such as maleic anhydride, but the stereochemistry of the adducts was not determined. Reports of more recent work in which benzene oxides have been trapped with carbon dienophiles show each adduct as the result of addition to the face of the benzene oxide that is *anti* to the oxygen, but no evidence was provided for this stereochemical assignment (14). Similarly, adducts derived from 1,2,4-triazoline-3,5-dione dienophiles have been reported as the products of *anti* addition (15), but this assignment of stereochemistry was based on one structure that was determined by X-ray crystallography (16). In contrast, on acetone-sensitized excitation, diazomethane added to the face of a benzene oxide *syn* to the oxygen (17).

We report here the Diels–Alder cycloadditions of three benzene oxides with carbon dienophiles, and the first irrefutable proof for the stereochemistry of the products.

Results

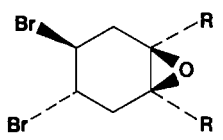
Benzene oxide was prepared by a procedure very similar to that of Vogel *et al.* (18). Briefly, 1,4-cyclohexadiene was monobrominated in the cold, and epoxidation with *meta*-chloroperoxybenzoic acid gave **2**. Double dehydrobromination was effected with DBU. The ^{1}H nmr of the product displayed a single set of signals, but Vogel and Günther (13) demonstrated that this is really an average of the signals of benzene oxide (**3**) and its valence tautomer, oxepin (**4**). The addition of *N*-phenylmaleimide to an ether solution of the tautomeric mixture resulted in smooth conversion to a *single* adduct. The nmr data indicated a symmetrical molecule, i.e., the adduct was not formed from **4**. Nuclear Overhauser enhancement (nOe) measurements led to the structure **5** for the adduct, which was the result of an *endo* addition, *anti* to the oxygen. This *anti* addition was in marked contrast to the many known examples of an allylic oxygen atom directing addition *syn* to itself (1, 2, 8), so it

[1]Author to whom correspondence may be addressed.

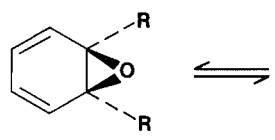
[2]One example with 5-methyl-1,3-cyclopentadiene was reported to have no selectivity (5).

[3]Some older studies (9) incorrectly assumed these added *anti*.

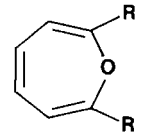
Can. J. Chem. Downloaded from www.nrcresearchpress.com by 84.41.108.74 on 09/07/12
For personal use only.



2 R = H
6 R = CH_3
10 R = $-CH_2CH_2CH_2-$



3 R = H
7 R = CH_3
11 R = $-CH_2CH_2CH_2-$



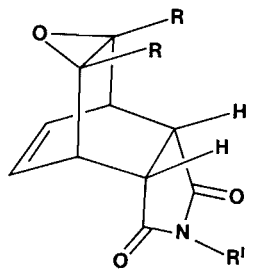
4 R = H
8 R = CH_3
12 R = $-CH_2CH_2CH_2-$

seemed prudent to corroborate the structure by X-ray crystallography (Fig. 1).

The reactions of two more substituted, and seemingly more sterically hindered, benzene oxides were also examined. The order of the reactions in their preparation was different. The Birch reduction product of *ortho*-xylene was first epoxidized and then brominated to afford **6**. Double dehydrobromination with potassium *tert*-butoxide gave the dimethyl benzene oxide **7** along with its valence tautomer **8** (19). Reaction with *N*-phenylmaleimide was very much slower than with the unsubstituted diene. This observation was consistent with Vogel's work, which showed that the **7** ⇄ **8** equilibrium is very much in favor of the oxepin **8** form, due to eclipsing of the two methyls in the benzene oxide tautomer **7** (13). Nevertheless, the Diels–Alder reaction did take place and, as before, only one adduct was formed. The nmr data led to an unequivocal assignment of structure. The adduct was symmetrical, i.e., it was derived from **7** and not from **8**.[4] Irradiation of the methyl singlet in the ^1H nmr resulted in a significant nOe of the signal due to the protons α to the carbonyls, and vice versa. Thus, the structure of the adduct could only have been **9**, the product of *endo* addition, *anti* to the oxygen. Therefore, in spite of the much larger size of two methyl groups compared to two hydrogens, the cycloaddition still demonstrated complete π-facial stereoselectivity.

The same sequence of reactions as above, but starting with indan, led via **10** to the valence tautomers **11** and **12**. In this case Vogel (13) had reported that the equilibrium lies very much in favor of the benzene oxide form because in **12** there would be a very considerable amount of angle strain. The cycloaddition with *N*-phenylmaleimide was rapid. A single symmetrical adduct was obtained, and nOe measurements showed conclusively that the adduct possessed structure **13**.

The benzene oxide **11** reacted with *N*-methylmaleimide to give **14** in a manner very similar to the reaction of the *N*-phenyl dienophile. Then **13** was heated in $CHCl_3$ with *N*-methylmaleimide, and **14** was heated with *N*-phenylmaleimide. In neither



5 R = H, R' = Ph
9 R = CH_3, R' = Ph
13 R = $-CH_2CH_2CH_2-$, R' = Ph
14 R = $-CH_2CH_2CH_2-$, R' = CH_3

case was any exchange detected. These experiments demonstrated that the adducts of **11** and, presumably, the adducts of the other two benzene oxides were formed under kinetic rather that thermodynamic control.

The Diels–Alder reaction of **11** with dimethyl acetylenedicarboxylate, a sterically less demanding dienophile, still gave only one adduct. Attempts to determine its stereochemistry unequivocally by means of nOe measurements failed. Therefore, the structure was determined by X-ray crystallography, and, as is evident from Fig. 2, the adduct was once again the result of addition to the face of **11** *anti* to the oxygen. In the crystal the molecule appears somewhat twisted, with the two carbomethoxy groups in slightly different conformations.

Discussion

These benzene oxides added exclusively *anti*, while similar cyclopentadienyl and cyclohexadienyl dienes with allylic oxygen functions all add *syn*. While there have been many theories forwarded to explain these *syn* additions, the *anti* additions that have been observed with other substituents have usually been rationalized by invoking steric hindrance. It is instructive to examine why the factors that might otherwise direct addition *syn* to an oxygen function fail completely to do so with **3**, **7**, and **11**.

Fukui and co-workers (21) postulated that in cyclopentadienyl systems mixing of diene π-orbitals with lone-pair orbitals associated with a plane-nonsymmetrical heteroatom leads to a perturbation of the π-system such that the electron density of the HOMO is significantly larger on the *syn* face. More recently, Inagaki *et al.* (22) used orbital mixing (π-system with *s*-orbitals on the sp^2 carbons of the diene) to explain differences in selectivity between different heteroatoms. An idea forwarded by Kahn and Hehre (23) was that for electrostatic reasons dienophiles should add to the more nucleophilic (i.e., *syn*) face. Anh (24) suggested a direct, favorable interaction between the heteroatom lone pair and the LUMO of the incoming dienophile.

Ab initio calculations[5] show that in the HOMO of benzene oxide (**3**) (Fig. 3) the *s*-orbital coefficients on the diene carbons are tiny, so the π-system could be only very slightly biased on the side of the oxygen due to "orbital mixing" of the type described by Fukui and Inagaki. Therefore, it is unlikely that the complete facial stereospecificity observed in this study can arise by this phenomenon. Also, it is obvious from Fig. 3 that a node must exist between the component of the HOMO residing on the oxygen and the LUMO of the incoming dienophile. The four next-highest occupied molecular orbitals are either symmetrical or have very small coefficients on oxygen. Therefore, the oxygen of the benzene oxides cannot be directly facilitating *syn* addition by any of the mechanisms mentioned above.

The geometry of the benzene oxides is such that the oxygen is almost perpendicular to the plane of the diene moiety whereas

[4]In contrast, adducts derived from this type of disubstituted benzene oxide ⇄ oxepin react with nitrogen dienophiles via the oxepin forms to give unsymmetrical adducts (15, 20).

[5]A communication that summarizes our parallel computational work with plane-nonsymmetrical diene systems is in preparation.

Can. J. Chem. Downloaded from www.nrcresearchpress.com by 84.41.108.74 on 09/07/12
For personal use only.

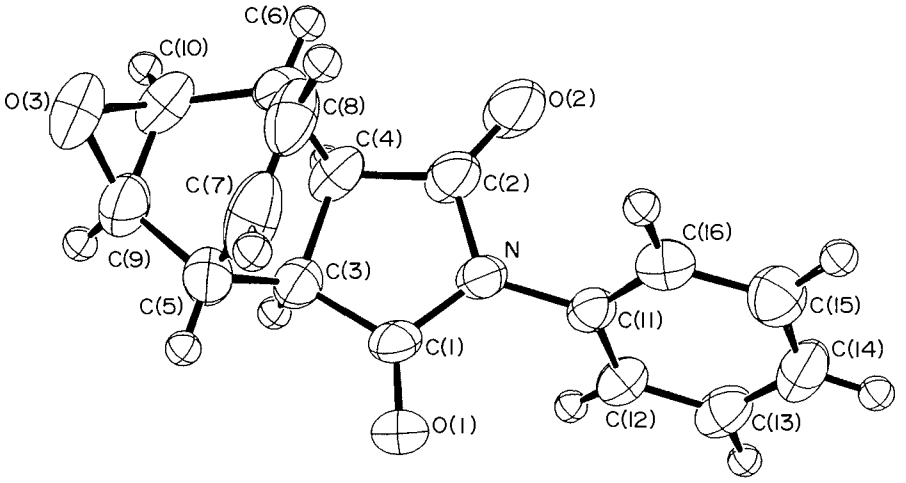


FIG. 1. Perspective view of **5** with ellipsoids scaled to 50% probability. Hydrogen atoms have been added to clarify the relative stereochemistry. (Numbering of the atoms conforms with the data in Table 2.)

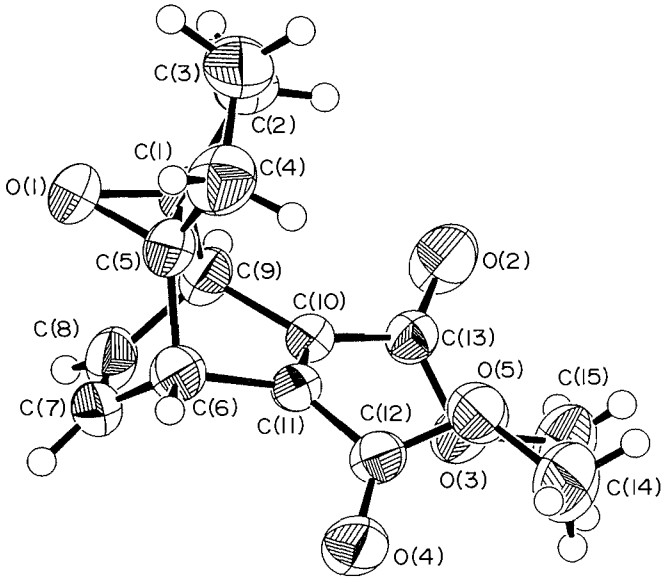


FIG. 2. Perspective view of **15** with ellipsoids scaled to 50% probability. (Numbering of the atoms conforms with the data in Table 4.)

the "oxirane substituents" (two hydrogens for **3**, two methyls for **7**, and $CH_2CH_2CH_2$ for **11**) are roughly coplanar with the diene moiety. There must be a significant steric interaction between the oxygen and an incoming dienophile on the *syn* face. Therefore, in marked contrast to other oxygen-bearing dienes (e.g., **1**), the unfavorable steric interactions in a *syn* transition state of a benzene oxide are not overwhelmed by an opposing attractive force. In fact, the molecular geometry leaves addition to the *anti* face unencumbered, and *anti* addition eventuates with both ethylenic and acetylinic dienophiles.

A model, based on work by Cieplak (25), that considers the σ-donor ability of an *anti* substituent has been espoused recently by le Noble and co-workers and by Macaulay and Fallis (2). Hydrogen and carbon have much greater σ-donor abilities than has oxygen (26). However, the Cieplak model specifies that facial selectivity can be modulated only by a σ bond *antiperiplanar* to the face of attack. The relative positions of the oxygen

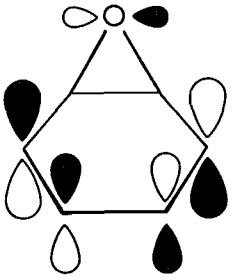


FIG. 3. Representation of the atomic orbital components of the highest occupied molecular orbital (HOMO) of **3**.

and the oxirane substituents vis-à-vis the plane of the diene moiety suggest that only σ-donation by the weaker σ-donor, the oxygen, can be considered to be operative. Thus, the facially specific addition of dienophiles *anti* to the oxygen of a benzene oxide is not inconsistent with the proposals of le Noble and Fallis (2).

Experimental

Melting points (mp) were determined on a Fisher–Johns apparatus and are uncorrected. Infrared spectra were recorded on a Mattson FT instrument. Mass spectral data were from a V.G. Micromass 7070HS instrument. Nuclear magnetic resonance (nmr) spectra were obtained on a General Electric GE 300-NB instrument or a Varian 360 instrument: ^1H shifts are relative to internal tetramethylsilane in $CDCl_3$; ^{13}C shifts are relative to the solvent resonance ($CDCl_3$ = δ 77.0). Nuclear Overhauser enhancement (nOe) data were obtained from sets of interleaved ^1H experiments (16K) of 8 transients cycled 12–16 times through the list of irradiated frequencies. The decoupler was gated on in CW mode for 6 s with sufficient attenuation to give a 70–90% reduction in intensity of the irradiated peak. Frequency changes were preceded by a 60-s delay. Four scans were used to equilibrate spins before data acquisition, but a relaxation delay was not applied between scans at the same frequency. The nOe difference spectra were obtained from zero-filled 32K data tables to which a 1–2 Hz exponential line-broadening function had been applied. Reactions were run under an atmosphere of dry nitrogen. Solvents were distilled, and aqueous solutions are implied for saturated NaCl, etc.

trans-*4,5-Dibromocyclohexene oxide (2)*

trans-4,5-Dibromo-1-cyclohexene (27) (10.0 g, 41.7 mmol) and 10.0 g of 85% *meta*-chloroperoxybenzoic acid in $CHCl_3$ (150 mL) were heated at reflux for 16 h. The mixture was cooled in ice and

Can. J. Chem. Downloaded from www.nrcresearchpress.com by 84.41.108.74 on 09/07/12
For personal use only.

TABLE 1. Crystallographic data

Parameter	Value	
	Adduct **5**	Adduct **15**
Molecular formula	$C_{16}H_{13}NO_3$	$C_{15}H_{16}O_5$
Formula weight	267.27	276.28
Crystal system	Monoclinic	Monoclinic
Space group	$P2_1/n$	$P2_1/c$ (no. 14)
Cell dimensions a (Å)	10.8686 (11)[a]	12.137 (2)
b (Å)	6.6307 (7)	9.022 (2)
c (Å)	17.499 (3)	13.482 (2)
β (deg)	92.973 (10)	108.56 (4)
Cell volume (Å^3)	1259.4 (3)	1399.3 (4)
Z	4	4
d_{calc} (g cm^{-3})	1.410	1.311
$F(000)$	680	584
μ (mm^{-1})	0.09	0.092
Crystal dimensions (mm)	0.20 × 0.20 × 0.20	0.40 × 0.30 × 0.20
T (K)	295	296
Index	$-11 \leq h \leq 11; 0 \leq k \leq 6; 0 \leq l \leq 18$	$0 \leq h \leq 14; 0 \leq k \leq 14; -16 \leq l \leq 14$
$2\theta_{max}$ (deg)	44.8	50.0
Independent reflections	1628	2643
Acceptance ($I_{net}/\sigma I_{net} \geq$)	2.5	3.0
Observed reflections	1115	1399

[a]Estimated standard deviations in parentheses refer to the last digits.

Can. J. Chem. Downloaded from www.nrcresearchpress.com by 84.41.108.74 on 09/07/12
For personal use only.

filtered, and the solid was discarded. The solution was washed with 20% $NaHSO_3$ (100 mL), saturated $NaHCO_3$ (2 × 100 mL), and saturated NaCl (200 mL), then dried ($MgSO_4$) and concentrated *in vacuo* to provide a yellow oil. Crystallization from cold hexane gave colorless **2** (6.97 g, 65%): mp 68–69°C; ir (KBr pellet) ν_{max}: 1415, 1009, 889 cm^{-1}; ^{1}H nmr δ: 4.30 (1H, ddd, J = 4.6, 6.7, 7.7 Hz), 4.20 (1H, ddd, J = 6.3, 6.3, 7.7 Hz), 3.24 (2H, m), 2.99 (1H, br dd, J = 4.5, 16.0 Hz), 2.90 (1H, ddd, J = 3.5, 6.3, 16.5 Hz), 2.65 (1H, dd, J = 6.3, 16.5 Hz), and 2.46 (1H, ddd, J = 3.2, 6.7, 16.0 Hz); ^{13}C nmr δ: 50.7 and 50.2 (oxirane carbons), 48.7 and 47.3 (2 × CHBr), 33.3 and 32.3 (2 × CH_2); ms m/z (%): 256 (M^+, 0.1), 177 (3), 176 (2), 175 (3), 174 (2), 95 (21), and 67 (100). Exact mass calcd. for $C_6H_8{}^{81}BrO$ (M^+ − Br): 176.9738; found: 176.9742; calcd. for $C_6H_8{}^{79}BrO$ (M^+ − Br): 174.9759; found: 174.9752.

*1,3,5-Cyclohexatriene 1,2-oxide/oxepin (**3** ⇄ **4**)*

A solution of **2** (1.07 g, 4.17 mmol) and DBU (2.50 g, 16.4 mmol) in anhydrous ether (20 mL) was stirred at room temperature for 24 h (19*a*), then poured into saturated $NaHCO_3$. Approximately 50 mL of ether was added, and the organic layer was washed with saturated $NaHCO_3$ (2 × 100 mL) and saturated NaCl (100 mL), and dried over anhydrous K_2CO_3. Evaporation of the solvent yielded **3** ⇄ **4** as a yellow liquid (0.270 g, 67%): ir (film) ν_{max}: 3028, 1609, 1431, and 1072 cm^{-1}; ^{1}H nmr δ: 6.26 (2H, complex m), 5.88 (2H, m), and 5.12 (2H, d, J = 4.5 Hz); ^{13}C nmr δ: 130.7, 128.6, 122.3, 120.2, 110.0, and 107.5; ms *ms*/*z* (%): 94 (M^+, 61), 78 (7), 68 (35), 66 (100), and 65 (68). Exact mass calcd. for C_6H_6O: 94.0418; found: 94.0420.

*Diels–Alder reaction of **3** with N-phenylmaleimide*

To the ether solution obtained after work-up of a reaction of 0.837 g (3.27 mmol) of **2** and 2.00 g of DBU was added 0.584 g (3.37 mmol) of *N*-phenylmaleimide in $CHCl_3$ (25 mL). After stirring at room temperature for 16 h, the solvents were evaporated. The ^{1}H nmr of the residue showed signals for only one adduct, which was rigorously purified by flash chromatography, then recrystallized from $CHCl_3$–C_6H_6 to yield 0.274 g (31% from **2**) of very pure **5**: mp 218–219°C; ir (KBr pellet) ν_{max}: 1709, 1388, 1195, and 726 cm^{-1}; ^{1}H nmr δ: 7.46–7.13 (5H), 5.91 (2H, apparent dd, J = 3.6, 4.6 Hz, vinyl H's), 3.65 (2H, m, bridgehead H's), 3.37 (2H, m, oxirane H's), and 3.05 (2H, apparent t, J = 1.8 Hz, H's α to C=O's); nOe data: irradiate 5.91: nOe at 3.65 (6%); irradiate 3.65: nOe's at 5.91 (6%), 3.37 (6%), and 3.05 (5%); irradiate 3.37: nOe's at 3.65 (7%) and 3.05 (5%); irradiate 3.05: nOe's at 3.65 (6%) and 3.37 (6%); ^{13}C nmr δ: 176.0, 131.4, 128.9, 128.6, 126.5, 126.2, 47.1 (oxirane carbons), 41.9 (α to C=O's), and 35.6 (bridgeheads); ms m/z (%): 267 (M^+, 35), 173 (22), 119 (32), and 91 (100). Exact mass calcd. for $C_{16}H_{13}NO_3$: 267.0895; found: 267.0892.

*X-ray structure determination of **5***

Data collection was on an Enraf–Nonius CAD-4 diffractometer with a graphite-crystal monochromator with MoKα_1 radiation (λ = 0.70930 Å). Crystallographic data are summarized in Table 1. Cell dimensions were determined by least squares from 25 reflections ($35.0 < 2\theta < 38.0°$). Integrated intensities were obtained by the $\theta/2\theta$ scan mode. Reference reflections measured during data collection showed no decrease in intensity. Corrections were applied for Lorentz and polarization effects, but not for absorption. The structure was solved by direct and Fourier methods. Least-squares refinements on F with anisotropic factors given to non-H atoms converged to R = 0.037, R_w = 0.035, S = 0.31. Weights were based on counting statistics, $w = 1/\sigma^2$ (F_o); Δ/s (max.) = 1.482. The largest peaks in the final difference map were +0.153 and −0.160 e/Å^3. All calculations were made with the NRC VAX Crystal Structure System (28), and atomic scattering factors were from International tables for X-ray crystallography (20). Figure 1 was prepared from the output of ORTEPII (30). Bond lengths and angles are given in Table 2, and positional and thermal parameters for refined atoms appear in Table 3.[6]

trans*-4,5-Dibromo-1,2-dimethylcyclohexene oxide (**6**)*

1,2-Dimethyl-1,4-cyclohexadiene (11.09 g, 102.7 mmol) was added to a solution of 31.8 g of the magnesium salt of monoperoxyphthalic acid (80%) hexahydrate (MMPP) (31) in 95% ethanol (500 mL). After stirring at room temperature for 3 h, H_2O (1 L) was added, and this was extracted with CH_2Cl_2 (300 mL). The organic extract was washed with H_2O (200 mL) and saturated NaCl (200 mL), dried ($MgSO_4$), and concentrated. Flash chromatography (4% acetone in pentane) of the residue yielded 5.4 g (42%) of the mono-epoxide: ^{1}H

[6]Complete sets of crystallographic data may be purchased from the Depository of Unpublished Data, Document Delivery, CISTI, National Research Council Canada, Ottawa, Canada K1A 0S2.

Can. J. Chem. Downloaded from www.nrcresearchpress.com by 84.41.108.74 on 09/07/12
For personal use only.

TABLE 2. Selected bond distances, angles, and torsional angles for **5**[a]

Bond	Distance (Å)	Bonds	Angle (deg)
O(1)—C(1)	1.205 (4)	O(1)—C(1)—N	124.3 (3)
O(3)—C(9)	1.428 (5)	O(1)—C(1)—C(3)	127.1 (3)
N—C(1)	1.382 (5)	O(3)—C(9)—C(5)	119.0 (4)
N—C(11)	1.440 (4)	O(3)—C(9)—C(10)	60.1 (3)
C(1)—C(3)	1.508 (5)	N—C(11)—C(12)	119.1 (3)
C(3)—C(4)	1.519 (5)	C(1)—N—C(2)	112.4 (3)
C(3)—C(5)	1.534 (5)	C(1)—C(3)—C(4)	105.0 (3)
C(5)—C(7)	1.466 (7)	C(1)—C(3)—C(5)	113.1 (3)
C(5)—C(9)	1.520 (6)	C(3)—C(4)—C(6)	109.2 (3)
C(6)—C(8)	1.491 (7)	C(3)—C(5)—C(7)	106.8 (3)
C(7)—C(8)	1.295 (9)	C(3)—C(5)—C(9)	103.9 (3)
C(9)—C(10)	1.419 (7)	C(5)—C(7)—C(8)	115.5 (4)
C(11)—C(12)	1.383 (4)	C(5)—C(9)—C(10)	112.3 (4)
C(12)—C(13)	1.379 (5)	C(7)—C(5)—C(9)	109.2 (4)
C(13)—C(14)	1.379 (6)	C(9)—O(3)—C(10)	59.7 (3)

Bonds	Angle (deg)
O(3)—C(9)—C(10)—C(6)	110.9 (4)
C(1)—N—C(11)—C(12)	63.8 (3)
C(1)—C(3)—C(5)—C(7)	59.8 (3)
C(1)—C(3)—C(5)—C(9)	175.2 (5)
C(2)—N—C(11)—C(16)	66.3 (3)

[a]See Fig. 1 for atom numbering. Estimated standard deviations in parentheses refer to the last digits.

TABLE 3. Positional parameters and equivalent isotropic temperature factors for **5**

Atom	x	y	z	B_{iso}[a]
O(1)	0.70278(22)	0.3201(4)	0.04379(15)	4.83(12)
O(2)	0.67636(24)	−0.1271(5)	0.23828(16)	7.41(17)
O(3)	0.24010(21)	0.3032(4)	0.16757(15)	5.47(13)
N	0.71647(22)	0.0788(4)	0.13735(14)	3.20(12)
C(1)	0.6677 (3)	0.2499(5)	0.10235(20)	3.32(14)
C(2)	0.6533 (3)	0.0227(7)	0.20095(19)	4.26(18)
C(3)	0.5657 (3)	0.3288(6)	0.14938(22)	3.84(17)
C(4)	0.5535 (3)	0.1743(6)	0.21264(20)	3.87(17)
C(5)	0.4425 (4)	0.3504(7)	0.10326(25)	4.98(20)
C(6)	0.4225 (3)	0.0817(7)	0.20626(25)	4.71(19)
C(7)	0.4094 (3)	0.1490(9)	0.0743 (3)	5.7 (3)
C(8)	0.3995 (3)	0.0108(8)	0.1259 (3)	5.28(24)
C(9)	0.3525 (4)	0.4128(7)	0.1626 (3)	5.46(22)
C(10)	0.3415 (3)	0.2648(7)	0.22046(23)	4.60(20)
C(11)	0.8246 (3)	−0.0249(5)	0.11400(16)	2.99(15)
C(12)	0.9369 (3)	0.0737(6)	0.11917(19)	3.49(16)
C(13)	1.0410 (3)	−0.0265(7)	0.09807(20)	4.10(20)
C(14)	1.0329 (4)	−0.2236(7)	0.07323(21)	4.50(19)
C(15)	0.9204 (4)	−0.3209(7)	0.06821(20)	4.38(19)
C(16)	0.8155 (3)	−0.2208(6)	0.08840(19)	3.71(17)

[a]B_{iso} is the mean of the principal axes of the thermal ellipsoid.

nmr (60 MHz) δ: 5.3 (2H, apparent s), 2.3 (4H, apparent s), and 1.3 (6H, s). This was dissolved in $CHCl_3$ (100 mL) and cooled to −50°C. Bromine (5.64 g, 35.2 mmol = 0.81 mol-equiv.) (19*b*) was added dropwise at a rate that ensured that the solution not become orange. After warming to room temperature the solvent was evaporated in *in vacuo*. Recrystallization of the residue from hexane gave 7.59 g (76%) of **6** as colorless needles: mp 82–83°C; ir (KBr pellet) ν_{max}: 1466, 1384, 1322, 1167, 842, and 670 cm^{-1}, ^1H nmr δ: 4.26 (1H, ddd, J = 4.5, 8.3, 9.1 Hz), 4.15 (1H, ddd, J = 6.8, 7.7, 9.1 Hz), 2.90 (1H, dd, J = 4.5, 15.4 Hz), 2.69 (1H, dd, J = 6.8, 16.1 Hz), 2.61 (1H, dd, J = 7.7, 16.1 Hz), 2.29 (1H, dd, J = 8.3, 15.4 Hz), 1.34 (3H, s), and 1.32 (3H, s); ^{13}C nmr δ: 61.9 and 61.0 (oxirane carbons), 50.5 and 49.6 (2 × CHBr), 40.8 and 39.9 (2 × CH_2), 19.9 and 19.5 (2 × CH_3); ms m/z (%): 205 (11), 203 (12), 165 (1), 163 (1), 123 (20), 95 (7), 81 (17), 79 (11), and 43 (100).

*1,2-Dimethyl-1,3,5-cyclohexatriene 1,2-oxide/2,7-dimethyloxepin (**7** ⇄ **8**)*

Following the procedure of Paquette and Barrett (19*b*): **6** (2.1355 g, 7.52 mmol) in dry ether (50 mL) was cooled to 0°C before addition of 2.00 g of potassium *tert*-butoxide in four portions over 1 h. After stirring for 1 h the reaction was poured into H_2O (75 mL). After addition of more ether, the organic solution was washed with H_2O (75 mL), saturated $NaHCO_3$ (75 mL), and saturated NaCl (75 mL), then dried ($MgSO_4$) and concentrated to provide 0.7535 g (82%) of dimethylbenzene oxide/oxepin as a yellow liquid: ir (film) ν_{max}: 1658, 1160, and 743 cm^{-1}; ^1H nmr δ: 5.99 (2H, distorted t, $J \approx 3$ Hz), 5.44 (2H, complex m), and 1.91 (6H, s); ^{13}C nmr δ: 149.9, 127.5, 112.2, and 21.1; ms m/z (%): 122 (M^+, 43), 107 (8), 91 (14), 79 (90), 77 (56), and 43 (100). Exact mass calcd. for $C_8H_{10}O$: 122.0731; found: 122.0725.

*Diels–Alder reaction of **7** with N-phenylmaleimide*

A solution of 0.1286 g (1.05 mmol) of dimethylbenzene oxide/oxepin (**7**/**8**) and *N*-phenylmaleimide (0.1660 g, 0.958 mmol) in $CHCl_3$ (50 mL) was heated at reflux for 10 h. The ^1H nmr of the crude mixture showed signals for only one adduct (**9**), which was isolated by flash chromatography as colorless crystals: mp 261–262°C; ir (KBr pellet) ν_{max}: 1709, 1388, 1195, and 726 cm^{-1}; ^1H nmr δ: 7.47–7.13 (5H), 5.97 (2H, dd, J = 3.6, 4.5 Hz), 3.38 (2H, m), 3.13 (2H, apparent t, J = 1.6 Hz), and 1.44 (6H, s); nOe data: irradiate 5.97: nOe at 3.38 (7.5%); irradiate 3.38: nOe's at 5.97 (8.5%), 3.13 (5%), and 1.44 (1%); irradiate 3.13: nOe's at 3.38 (9.5%) and 1.44 (2.5%); irradiate 1.44: nOe's at 3.38 (12%) and 3.13 (10.5%); ^{13}C nmr δ: 176.5, 131.5, 129.0, 128.7, 127.5, 126.3, 57.6 (oxirane carbons), 42.2 (α to C=O's), 41.7 (bridgeheads), and 13.8 (2 × CH_3); ms m/z (%): 295 (M^+, 7), 253 (29), 175 (10), 161 (9), 148 (8), 133 (8), 119 (11), 106 (77), 105 (76), 93 (19), 91 (23), 77 (28), and 43 (100). Exact mass calcd. for $C_{18}H_{17}NO_3$: 295.1207; found: 295.1209.

trans-*3,4-Dibromo-10-oxatricyclo[4.3.1.0^{1,6}]decane (**10**)*

To a stirred, room temperature solution of 5,8-dihydroindan (28.47 g, 0.237 mol) in $CHCl_3$ (350 mL) was added 1.0 g of Aliquat 336 (Aldrich) and, over a period of 2 h, a solution of 88 g of 80% MMPP in H_2O (450 mL). This was stirred vigorously for a further 2 h. A white solid that formed at the interface was dissolved by addition of 1 M NaOH (100 mL). The organic layer was washed with H_2O (200 mL), saturated $NaHCO_3$, and saturated NaCl (400 mL), then dried ($MgSO_4$) and concentrated. Flash chromatography (4% acetone in hexane) gave 23.89 g (74%) of the mono-epoxide: ^1H nmr (60 MHz) δ: 5.3 (2H, br s) and 2.8–1.3 (10H as complex m) including a large narrow m at δ 2.4 (approx. 4H). This was brominated as for **6**, to provide **10** as a crystalline solid (87%): mp 87–88°C; ir (KBr pellet) ν_{max}: 1415, 1069, and 933 cm^{-1}; ^1H nmr δ: 4.41 (1H, ddd, J = 4.3, 5.4, 6.6 Hz), 4.30 (1H, ddd, J = 4.9, 6.2, 6.6 Hz), 3.01 (1H, dd, J = 4.3, 15.8 Hz), 2.82 (1H, dd, J = 6.2, 16.4 Hz), 2.67 (1H, dd, J = 4.9, 16.4 Hz), 2.42 (1H, dd, J = 5.4, 15.8 Hz), 2.04 (2H, distorted quintet), 1.59 (3H, distorted septet), and 1.42 (1H, m); ^{13}C nmr δ: 65.5 and 64.6 (oxirane carbons), 49.9 and 47.0 (2 × CHBr), 34.6, 33.5, 31.8, 31.2, and 19.6; ms m/z (%): 298 (0.3), 296 (0.7) and 294 (0.4) all M^+, 217 (0.7), 215 (0.7), 135 (100), 117 (13), 107 (24), 93 (44), 91 (25), 79 (62), 77 (24), and 55 (32).

*10-Oxatricyclo[4.3.1.0]deca-2,4-diene (**11**)*

The dibromide **10** (1.1975 g, 4.05 mmol) was dehydrobrominated in the same manner as **6** to give **11** (0.4940 g, 91%) as a pale yellow liquid: ir (film) ν_{max}: 1437, 1271, 1187, 1055, 911, 868, and 773 cm^{-1}; ^1H nmr (60 MHz) δ: 6.3 (4H, symmetrical m) and 2.9–1.1 (6H as a complex m); ^{13}C nmr δ: 128.3, 126.9, 70.7, 29.4, and 18.1; ms m/z

Can. J. Chem. Downloaded from www.nrcresearchpress.com by 84.41.108.74 on 09/07/12
For personal use only.

(%): 134 (M^+, 67), 133 (21), 117 (17), 115 (18), 106 (21), 105 (38), 91 (86), 79 (43), 78 (100), 77 (39), and 51 (48). Exact mass calcd. for $C_9H_{10}O$: 134.0731; found: 134.0737.

Diels–Alder reaction of ***11*** *with* N*-phenylmaleimide*

A solution of **11** (95.3 mg, 0.710 mmol) and *N*-phenylmaleimide (120.3 mg) in $CDCl_3$ (1.0 mL) was stirred at room temperature for 16 h. The ^1H nmr of the crude mixture showed signals for only one adduct (**13**), which was isolated as colorless crystals (0.1565 g, 72%) following flash chromatography (30% ethyl acetate in hexane): mp 261–262°C; ir (KBr pellet) ν_{max}: 1713, 1597, 1385, and1185 cm^{-1}; ^1H nmr δ: 7.48–7.14 (5H), 6.03 (2H, dd, J = 3.3, 4.7 Hz), 3.65 (2H, m), 3.26 (2H, apparent t, J = 1.7 Hz), 2.03 (2H, m), and 1.89–1.74 (4H, multiplets); nOe data: irradiate 6.03: nOe at 3.65 (10.5%); irradiate 3.65: nOe's at 6.03 (11%) and 3.26 (5.5%); irradiate 3.26: nOe's at 3.65 (12%) and a multiplet at approx. 1.75 (4%); irradiate 2.03: nOe's at 3.65 (3%) and 1.75 (10.5%); irradiate 1.75: nOe's at 3.26 (13.5%) and 2.03 (30%); ^{13}C nmr δ: 176.4, 131.4, 129.0, 128.6, 127.9, 126.3, 64.2 (oxirane carbons), 42.2 (α to C=O's), 37.4 (bridgeheads), 25.3 (2 × CH_2), and 25.0 (CH_2); ms m/z (%): 307 (M^+, 74), 173 (33), 160 (17), 159 (14), 134 (100), 133 (30), 132 (29), 131 (32), 117 (31), 104 (42), 93 (34), 91 (47), 78 (42), and 77 (32). Exact mass calcd. for $C_{19}H_{17}NO_3$: 307.1207; found: 307.1193.

Diels–Alder reaction of ***11*** *with* N*-methylmaleimide*

A solution of **11** (0.231 g, 1.72 mmol) and *N*-methylmaleimide (0.192 g, 1.72 mmol) in $CDCl_3$ (2 mL) was stirred at room temperature for 16 h, after which time ^1H nmr indicated that most of the diene had been consumed, and signals for only one adduct were evident. The adduct was purified by flash chromatography (50% ethyl acetate in hexane) to give colorless crystals of **14** (0.327 g, 77%): mp 151–153°C; ir (KBr pellet) ν_{max}: 1772 (w) and 1702 cm^{-1}; ^1H nmr δ: 5.88 (2H, dd, J = 3.3, 4.6 Hz), 3.52 (2H, m, bridgeheads), 3.06 (2H, narrow m, α to C=O's), 2.89 (3H, s, *N*-CH_3), and 2.05–1.62 (6H, multiplets); nOe data: irradiate 3.06: nOe's at 3.52 (8%) and ca. 2.75 (3%); irradiate ca. 2.75: nOe's at 3.52 (3%), 3.06 (15%), and ca. 2.00 (35%); ^{13}C nmr δ: 177.2, 127.6, 64.0, 42.0, 36.9, 25.2, 24.8, and 24.4 (CH_3); ms m/z (%): 245 (M^+, 16), 244 (6), 217 (29), 186 (32), 160 (21), 159 (18), 134 (100), 133 (44), 132 (47), 131 (57), 104 (86), 91 (66), 78 (88), and 77 (45). Exact mass calcd. for $C_{14}H_{15}NO_3$: 245.1051; found: 245.1056.

Diels–Alder reaction of ***11*** *with dimethyl acetylenedicarboxylate*

A solution of **11** (0.166 g, 1.24 mmol) and dimethyl acetylenedicarboxylate (150 μL, 1.24 mmol) in $CHCl_3$ (5 mL) was stirred at room temperature for 16 h, after which time ^1H nmr indicated the presence of only one adduct. Flash chromatography (20% acetone in hexane) yielded **15** as a pale yellow oil (0.344 g, 84%) that crystallized slowly on standing: mp 72–75°C; ir (film) ν_{max}: 2954, 1717, 1635, and 1270 cm^{-1}; ^1H nmr δ: 6.32 (2H, dd, J = 3.5, 4.2 Hz), 4.16 (2H, apparent br t, J = 3.7 Hz), 3.80 (6H, s), and 1.60–1.98 (6H, m); irradiation of the signal at δ 3.80 resulted in no significant nOe's; ^{13}C nmr δ: 166.2, 147.2, 131.3, 70.9, 52.3 (2 × OCH_3), 44.9 (bridgeheads), 27.2 (2 × CH_2), and 25.9 (CH_2); ms m/z (%): 276 (M^+,15), 244 (93), 220 (34), 217 (50), 205 (53), 189 (77), 188 (60), 185 (76), 157 (50), and 129 (100).

X-ray structure determination of ***15***

Data collection was on a Rigaku AFC6S diffractometer with a graphite monochromator with MoKα radiation (λ = 0.71069 Å). Crystallographic data are summarized in Table 1. Cell constants and an orientation matrix for data collection were obtained by least squares using the setting angles of 25 reflections ($38.3 < 2\theta < 43.4°$). Data collection used the ω–2θ scan technique. Omega (ω) scans of several intense reflections, made before data collection, had an average width at half-height of 0.03° with a take-off angle of 6.0°. Scans of (1.05 + 0.30 tan θ)° were made at a speed of 32.0°/min (in ω). The weak reflections ($I < 10.0\sigma(I)$) were rescanned (maximum of 2 rescans), and the counts were accumulated to assure good counting statistics. Stationary background counts were recorded on each side of the reflection. The ratio of peak counting time to background counting time was 2:1. Three reference reflections, measured every 150 reflections, remained constant. Intensities were corrected for Lorentz and polarization effects; a correction for secondary extinction was applied. The structure was solved by direct methods. Full-matrix least-squares refinement with anisotropic factors given to all non-H atoms converged

TABLE 4. Selected bond distances, angles, and torsional angles for **15**[a]

Bond	Distance (Å)	Bonds	Angle (deg)
O(1)—C(1)	1.452 (3)	O(1)—C(1)—C(2)	112.8 (3)
O(2)—C(13)	1.192 (3)	O(1)—C(1)—C(5)	60.5 (2)
O(3)—C(13)	1.318 (3)	O(1)—C(1)—C(9)	118.3 (3)
O(3)—C(15)	1.445 (4)	O(1)—C(5)—C(1)	59.9 (2)
C(1)—C(2)	1.505 (4)	O(2)—C(13)—O(3)	124.5 (3)
C(1)—C(5)	1.447 (4)	O(2)—C(13)—C(10)	123.8 (3)
C(1)—C(9)	1.530 (4)	C(1)—O(1)—C(5)	59.5 (2)
C(2)—C(3)	1.533 (6)	C(1)—C(2)—C(3)	103.8 (3)
C(6)—C(7)	1.513 (5)	C(1)—C(9)—C(8)	107.4 (3)
C(6)—C(11)	1.537 (4)	C(1)—C(9)—C(10)	103.0 (3)
C(7)—C(8)	1.300 (5)	C(2)—C(1)—C(9)	125.2 (3)
C(10)—C(11)	1.332 (4)	C(2)—C(3)—C(4)	116.0 (3)
C(10)—C(13)	1.482 (4)	C(6)—C(7)—C(8)	114.2 (3)
		C(6)—C(11)—C(10)	113.3 (3)
		C(6)—C(11)—C(12)	119.6 (3)
		C(7)—C(6)—C(11)	106.8 (3)
		C(8)—C(9)—C(10)	106.0 (3)
		C(10)—C(11)—C(12)	126.9 (3)

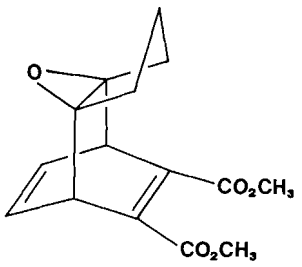
Bonds	Angle (deg)
O(1)—C(1)—C(2)—C(3)	49.7 (4)
O(1)—C(5)—C(4)—C(3)	−48.9 (4)
O(2)—C(13)—C(10)—C(9)	40.0 (5)
O(4)—C(12)—C(11)—C(6)	43.9 (4)
C(1)—C(9)—C(10)—C(13)	−121.6 (3)
C(5)—C(6)—C(11)—C(12)	123.2 (3)

[a]See Fig. 2 for atom numbering. Estimated standard deviations in parentheses refer to the last digits.

TABLE 5. Positional parameters and equivalent isotropic temperature factors for **15**

Atom	x	y	z	B_{iso}[a]
O(1)	0.1754(2)	0.5031(2)	0.2595(2)	5.1(1)
O(2)	0.2850(2)	−0.0053(3)	0.4541(2)	6.4(1)
O(3)	0.3903(2)	−0.0844(2)	0.3567(2)	5.4(1)
O(4)	0.3334(2)	0.0282(3)	0.0809(2)	5.8(1)
O(5)	0.2181(2)	−0.0855(3)	0.1563(2)	6.1(1)
C(1)	0.1834(3)	0.3600(3)	0.3105(3)	4.0(1)
C(2)	0.0733(4)	0.3175(5)	0.3320(4)	5.5(2)
C(3)	−0.0219(4)	0.3424(6)	0.2269(4)	6.8(2)
C(4)	0.0380(4)	0.3284(5)	0.1429(3)	5.8(2)
C(5)	0.1621(3)	0.3665(3)	0.1988(3)	4.2(1)
C(6)	0.2688(3)	0.3115(4)	0.1710(3)	4.2(2)
C(7)	0.3737(3)	0.3977(4)	0.2363(4)	5.1(2)
C(8)	0.3915(3)	0.3906(4)	0.3365(4)	4.9(2)
C(9)	0.3043(3)	0.2981(3)	0.3682(3)	4.0(1)
C(10)	0.3027(2)	0.1461(3)	0.3170(2)	3.2(1)
C(11)	0.2826(2)	0.1524(3)	0.2141(2)	3.3(1)
C(12)	0.2815(3)	0.0265(4)	0.1433(2)	3.7(1)
C(13)	0.3233(3)	0.0119(3)	0.3838(2)	3.6(1)
C(14)	0.2235(4)	−0.2198(4)	0.0982(3)	8.2(2)
C(15)	0.4093(3)	−0.2244(4)	0.4116(3)	7.3(2)

[a]B_{iso} is the mean of the principal axes of the thermal ellipsoid.



15

to $R = 0.045$, $R_w = 0.040$, $S = 1.83$. The weighting scheme was based on counting statistics. The maximum shift/error in the final cycle was 0.12. The largest peaks in the final difference map were +0.22 and −0.15 e/Å^3. Atomic scattering factors were from International tables for X-ray crystallography (29); anomalous dispersion effects were included in F (32). All calculations were made with the TEXSAN crystallographic software package (33). Figure 2 was prepared from the output of ORTEPII (30). Bond lengths and angles are given in Table 4, and positional and thermal parameters for refined atoms appear in Table 5.[6]

Acknowledgements

We thank Dr. B. Gregory and Miss M. Baggs for mass spectra, and Dr. C. R. Jablonski and Ms. N. Brunet for nmr spectra. We are grateful to Dr. E. J. Gabe, Division of Chemistry, National Research Council of Canada, for his assistance in the X-ray structure determination of **5**. The Natural Sciences and Engineering Research Council of Canada provided financial support.

1. S. WINSTEIN, M. SHATAVSKY, C. NORTON, and R. B. WOODWARD. J. Am. Chem. Soc. **77**, 4183 (1955); K. L. WILLIAMSON, Y.-F. L. HSU, R. LACKO, and C. H. YOUN. J. Am. Chem. Soc. **91**, 6129 (1969); K. L. WILLIAMSON and Y.-F. L. HSU. J. Am. Chem. Soc. **92**, 7385 (1970); V. A. MIRONOV, M. E. DOLGAYA, V. T. LUKYANOV, and S. A. YANKOVSKII. Zh. Organich. Khim. **12**, 1436 (1976); D. W. JONES. J. Chem. Soc. Chem. Commun. 739 (1980).
2. W.-S. CHUNG, N. J. TURRO, S. SRIVASTAVA, H. LI, and W. J. LE NOBLE. J. Am. Chem. Soc. **110**, 7882 (1988); J. B. MACAULAY and A. G. FALLIS. J. Am. Chem. Soc. **112**, 1136 (1990).
3. R. BRESLOW, J. M. HOFFMAN, JR., and C. PERCHONOCK. Tetrahedron Lett. 3723 (1973); M. ISHIDA, T. AOYAMA, and S. KATO. Chem. Lett. 663 (1989); A. M. NAPERSTKOW, J. B. MACAULAY, M. J. NEWLANDS, and A. G. FALLIS. Tetrahedron Lett. **30**, 5077 (1989).
4. V. A. MIRONOV, T. M. FADEEVA, and A. A. AKHREM. Dokl. Akad. Nauk SSSR, **174**, 852 (1967); E. J. COREY, N. M. WEINSHENKER, T. K. SCHAAF, and W. HUBER. J. Am. Chem. Soc. **91**, 5675 (1969); D. J. BURNELL and Z. VALENTA. J. Chem. Soc. Chem. Commun. 1242 (1985).
5. S. MCLEAN and P. HAYNES. Tetrahedron, **21**, 2313 (1965).
6. P. G. MCDOUGAL, J. G. RICO, and D. VAN DERVEER. J. Org. Chem. **51**, 4492 (1986); T. KOIZUMI, Y. ARAI, H. TAKAYAMA, K. KURIYAMA, and M. SHIRO. Tetrahedron Lett. **28**, 3689 (1987); M. J. FISHER and L. E. OVERMAN. J. Org. Chem. **53**, 2630 (1988); R. TRIPATHY, R. W. FRANCK, and K. D. ONAN. J. Am. Chem. Soc. **110**, 3257 (1988); M. J. FISHER, W. J. HEHRE, S. D. KAHN, and L. E. OVERMAN. J. Am. Chem. Soc. **110**, 4625 (1988).
7. H. AUKSI and P. YATES. Can. J. Chem. **59**, 2510 (1981).
8. J. R. GILLARD and D. J. BURNELL. J. Chem. Soc. Chem. Commun. 1439 (1989).
9. D. T. GIBSON, M. HENSLEY, H. YOSHIOKA, and T. J. MABRY. Biochemistry, **9**, 1626 (1970); D. T. GIBSON, G. E. CARDINI, F. C. MASELES, and R. E. KALIO. Biochemistry, **9**, 1631 (1970); D. T. GIBSON, B. GSCHWENDT, W. K. YEH, and V. M. KOBAL. Biochemistry, **12**, 1520 (1973); D. G. H. BALLARD, A. COURTIS, I. M. SHIRLEY, and S. C. TAYLOR. J. Chem. Soc. Chem. Commun. 954 (1983).
10. V. M. KOBAL, D. T. GIBSON, R. E. DAVIS, and A. GARZA. J. Am. Chem. Soc. **95**, 4420 (1973).
11. T. HUDLICKY, H. LUNA, G. BARBIERI, and L. D. KWART. J. Am. Chem. Soc. **110**, 4735 (1988); H. A. J. CARLESS and O. Z. OAK. Tetrahedron Lett. **30**, 1719 (1989); H. A. J. CARLESS, J. R. BILLINGE, and O. Z. OAK. Tetrahedron Lett. **23**, 3113 (1989); T. HUDLICKY, J. D. PRICE, H. LUNA, and C. M. ANDERSEN. Synlett, 309 (1990); H. A. J. CARLESS and K. BUSIA. Tetrahedron Lett. **31**, 1617 (1990).
12. *Review*: T. MUKAI, T. KUMAGAI, and Y. YAMASHITA. Heterocycles, **15**, 1569 (1981).
13. E. VOGEL and H. GÜNTHER. Angew. Chem. Int. Ed. Engl. **6**, 385 (1967).
14. R. M. DEMARINIS, C. N. FILER, S. M. WARASZKIEWICZ, and G. A. BERCHTOLD. J. Am. Chem. Soc. **96**, 1193 (1974); G. W. HOLBERT, L. B. WEISS, and B. GANEM. Tetrahedron Lett. 4435 (1976); H. PRINZBACH, H. BINGMANN, J. MARKERT, G. FISCHER, L. KNOTHE, W. EBERBACH, and J. BROKATZKY-GEIGER. Chem. Ber. **119**, 589 (1986).
15. D. R. BOYD and G. A. BERCHTOLD. J. Org. Chem. **44**, 468 (1979).
16. K.-L. HOFFMANN, G. MAAS, and M. REGITZ. J. Org. Chem. **52**, 3851 (1987).
17. H. PRINZBACH, D. STUSCHE, M. BREUNINGER, and J. MARKERT. Chem. Ber. **109**, 2823 (1976).
18. E. VOGEL, W. A. BÖLL, and H. GÜNTHER. Tetrahedron Lett. 609 (1965).
19. (*a*) E. VOGEL, R. SCHUBART, and W. A. BÖLL. Angew. Chem. **76**, 535 (1964); (*b*) L. A. PAQUETTE and J. H. BARRETT. Org. Synth. Coll. Vol. **5**, 467 (1973).
20. W. H. RASTETTER and T. J. RICHARD. Tetrahedron Lett. 2999 (1978).
21. S. INAGAKI, H. FUJIMOTO, and K. FUKUI. J. Am. Chem. Soc. **98**, 4054 (1976).
22. M. ISHIDA, Y. BENIYA, S. INAGAKI, and S. KATO. J. Am. Chem. Soc. **112**, 8980 (1990).
23. S. D. KAHN and W. J. HEHRE. J. Am. Chem. Soc. **109**, 663 (1987).
24. N. T. ANH. Tetrahedron, **29**, 3227 (1973).
25. A. S. CIEPLAK. J. Am. Chem. Soc. **103**, 4540 (1981); A. S. CIEPLAK, B. D. TAIT, and C. R. JOHNSON. J. Am. Chem. Soc. **111**, 8447 (1989).
26. N. D. EPIOTIS, W. R. CHERRY, S. SHAIK, R. L. YATES, and F. BERNARDI. Top. Curr. Chem. **70**, 1 (1977).
27. J. P. WIBAUT and F. A. HAAK. Recl. Trav. Chim. Pays-Bas, **67**, 85 (1948).
28. E. J. GABE, F. L. LEE, and Y. LE PAGE. *In* Crystallographic computing III. *Edited by* G. M. Sheldrick, C. Kluger, and R. Goddard. Clarendon Press, Oxford. 1985. pp. 167–174.
29. International tables for X-ray crystallography. Vol. IV. Kynoch Press, Birmingham. 1974. (Present distributor D. Reidel, Dordrecht.)
30. C. K. JOHNSON. ORTEPII. Report ORNL-5138, Oak Ridge National Laboratory, Oak Ridge, Tennessee. 1976.
31. P. BROUGHAM, M. S. COOPER, D. A. CUMMERSON, H. HEANEY, and N. THOMPSON. Synthesis, 1015 (1987).
32. J. A. IBERS and W. C. HAMILTON. Acta Crystallogr. **17**, 781 (1964).
33. TEXSAN–TEXRAY structure analysis package. Molecular Structure Corporation, The Woodlands, Texas. 1985.

Can. J. Chem. Downloaded from www.nrcresearchpress.com by 84.41.108.74 on 09/07/12
For personal use only.

Complexes binaires du nickel(II) et du zinc(II) avec la 1-canavanine et la 1-arginine, études potentiométriques et spectroscopiques

ABDALLAH ALBOURINE, MICHELLE PETIT-RAMEL[1] ET GERMAINE THOMAS-DAVID
Laboratoire de chimie analytique II, Université Claude Bernard, Lyon I, 43 Boulevard du 11 Novembre 1918, 69622 Villeurbanne, CEDEX, France

ET

JEAN JACQUES VALLON
Laboratoire de chimie analytique III, Université Claud Bernard, Faculté de pharmacie, 8 Avenue Rockefeller, 69373 Lyon CEDEX 2, France

Reçu le 1er août 1990

ABDALLAH ALBOURINE, MICHELLE PETIT-RAMEL, GERMAINE THOMAS-DAVID et JEAN JACQUES VALLON. Can. J. Chem. **69**, 1344 (1991).

Les constantes de stabilité des complexes binaires de la 1-canavanine (Can) et la 1-arginine (Arg) avec Ni^{2+} et Zn^{2+} ont été déterminées à 25°C et à force ionique $\mu = 0{,}1$ ($NaNO_3$). Cette technique est complétée par des mesures spectrophotométriques et de dichroïsme circulaire dans les domaines ultraviolet et visible. Ainsi nous avons calculé les absorbances molaires et les dichroïsmes circulaires molaires de la 1-canavanine et la 1-arginine ligands et de leurs complexes avec Ni^{2+} et Zn^{2+}. Pour le nickel(II), ces différentes mesures mettent en évidence trois complexes, NiL, NiL_2 et NiL_3. La 1-canavanine, ligand tridenté, prend un caractère bidenté lors de la formation du complexe $Ni(Can)_3$. En ce qui concerne le zinc(II), cette étude conduit à deux espèces complexées : ZnL et ZnL_2.

Mots clés : 1-arganine, 1-canavanine, coordination binaire du nickel, coordination binaire du zinc, dichroïsme circulaire.

ABDALLAH ALBOURINE, MICHELLE PETIT-RAMEL, GERMAINE THOMAS-DAVID, and JEAN JACQUES VALLON. Can. J. Chem. **69**, 1344 (1991).

The stability constants of binary complexes of 1-canavanine (Can) and 1-arginine (Arg) with Ni^{2+} and Zn^{2+} have been calculated at 25°C and at ionic strength $\mu = 0.1$ ($NaNO_3$). This technique is completed with spectrophotometry and circular dichroïsm measurements in the ultraviolet and visible ranges. Thus we determined the molar absorbances and the molar circular dichroïsm of ligands and complexes with Ni^{2+} and Zn^{2+}. Concerning the nickel(II), these measurements display three complexes, NiL, NiL_2, and NiL_3. 1-Canavanine, which generally has a tridentate ligand behaviour, becomes a bidentate ligand in the $Ni(Can)_3$ complex. With regard to zinc(II), this study only displays the ZnL and ZnL_2 species.

Key words: 1-arginine, 1-canavanine, circular dichroïsm, nickel binary coordination, zinc binary coordination.

Introduction

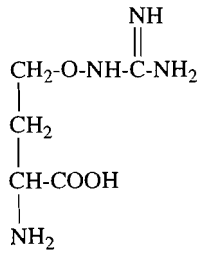
Ce mémoire se situe dans le prolongement d'un examen comparé des propriétés complexantes de la 1-canavanine et de la 1-arginine avec le cuivre(II) (1).

La 1-canavanine ou acide amino-2 (guanidinoxy)-4 butyrique, analogue structural de la 1-arganine, entre dans la composition des germes de certaines légumineuses (2). Fischer et Belitz l'utilisent comme indicateur de protéines de soja dans les produits alimentaires carnés (3). En outre, elle se révèle très utile pour l'étude des mécanismes bactériens de la dégradation des protéines anormales et le contrôle génétique des réactions métaboliques (2).

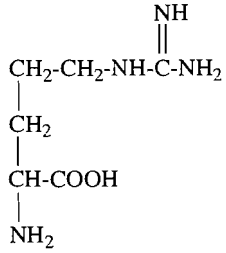
Nous avions signalé que la 1-canavanine possède, cependant, des propriétés antimétaboliques car elle provoque des altérations structurales et fonctionnelles fatales pour la protéine (2). Cette toxicité provient de sa ressemblance structurale avec la 1-arginine qui lui permet de réagir avec les enzymes spécifiques de celle-ci (4).

Bien que les composés minéraux ne constituent qu'une fraction très faible des tissus cellulaires, ils restent cependant essentiels au maintien de la vie. Parmi ces éléments, les métaux alcalins et alcalino-terreux ont toujours eu une place prépondérante vis-à-vis des protéines et acides aminés.

En ce qui concerne les métaux de transition, nous retiendrons le caractère essentiel du nickel chez les animaux supérieurs (5–8) dont la carence entraîne certains syndromes chez plusieurs animaux tel que le rat (9). Le nickel est également essentiel pour les plantes : l'uréase du Jack bean (canavalia ensiformis) et du soja (glycine max) contenant de la 1-canavanine, sont en effet des métalloenzymes à nickel (10–13). De même, il induit l'hydrolyse de l'arginine par l'uréase du soja.



1-Canavanine



1-Arginine

Quant au zinc, élément indispensable au métabolisme humain, il entre de même dans la composition de nombreuses enzymes. Il faut noter que la dose quotidienne de zinc nécessaire à l'homme adulte (0,3 mg/kg) est facilement obtenue par des conditions normales d'alimentation (14). Le zinc(II), notamment considéré comme un catalyseur acide, favorise la coupure des chaînes péptidiques dans la mesure où il est susceptible de former des complexes stables avec les acides aminés constituant l'enchaînement (15).

La démarche suivie pour la mise en évidence des espèces complexées $M_pH_qL_rL'_s$ ainsi que le calcul de leurs constantes de stabilité β_{pqrs} et de leurs facteurs intensifs émane directement du protocole développé dans le précédent mémoire (1).

1. Auteur à qui adresser toute correspondance.

Printed in Canada / Imprimé au Canada

Can. J. Chem. Downloaded from www.nrcresearchpress.com by 84.41.108.74 on 09/07/12
For personal use only.

Can. J. Chem. Downloaded from www.nrcresearchpress.com by 84.41.108.74 on 09/07/12
For personal use only.

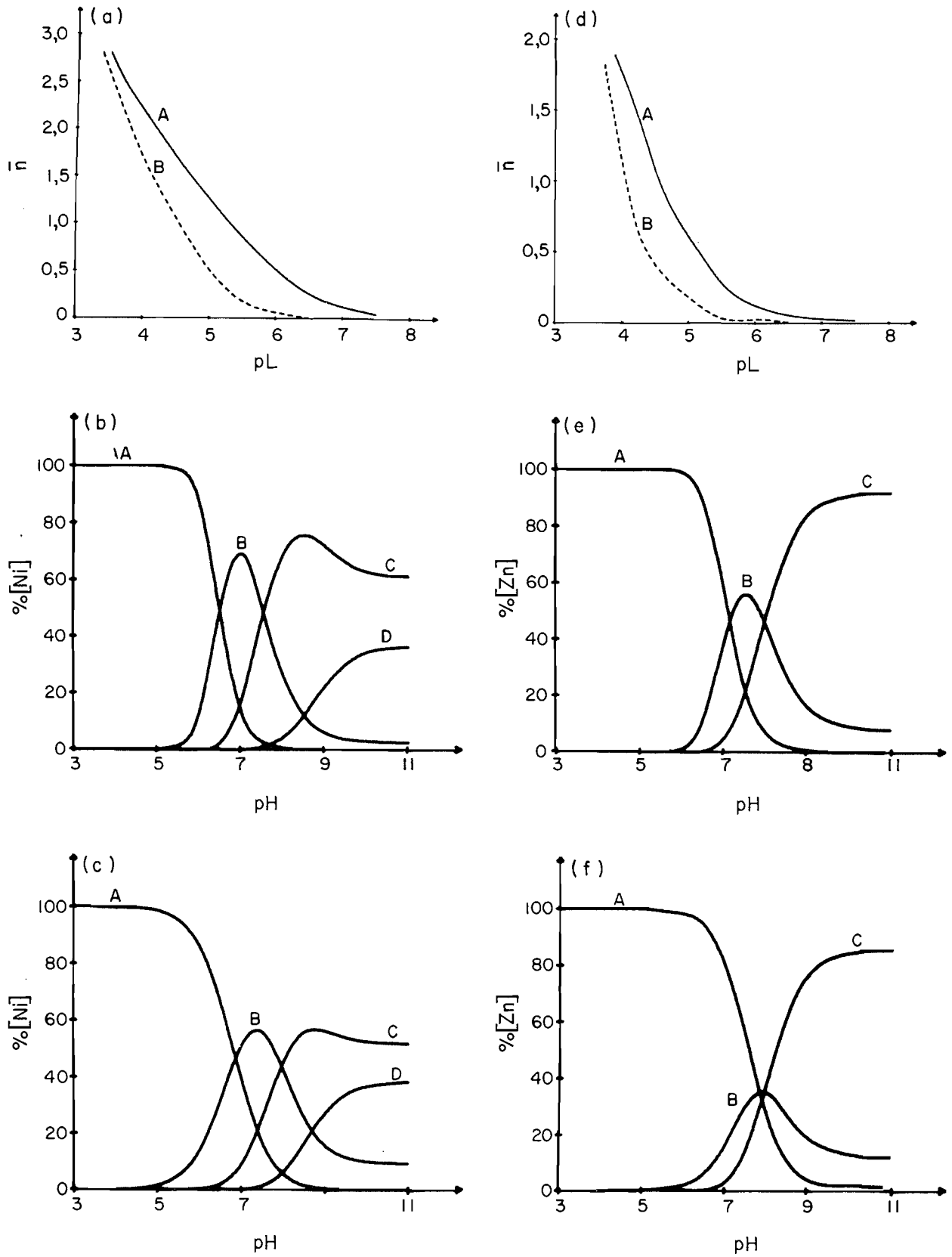


FIG. 1. (a) Nombre moyen de ligand fixé par atome de nickel(II) en fonction de pL; A : système 1-canavanine–nickel(II); B : système 1-arginine–nickel(II). (b) Répartition des complexes de la 1-canavanine avec le nickel(II) rapport 3 : 1; A : Ni^{2+}; B : NiCan; C : $Ni(Can)_2$; D : $Ni(Can)_3$. (c) Répartition des complexes de la 1-arginine avec le nickel(II) rapport 3 : 1; A : Ni^{2+}; B : NiArg; C : $Ni(Arg)_2$; D : $Ni(Arg)_3$. (d) Nombre moyen de ligand fixé par atome de zinc(II) en fonction de pL; A : système 1-canavanine–zinc(II); B : système 1-arginine–zinc(II). (e) Répartition des complexes de la 1-canavanine avec le zinc(II) rapport 3 : 1; A : Zn^{2+}; B : ZnCan; C : $Zn(Can)_2$. (f) Répartition des complexes de la 1-arginine avec le zinc(II) rapport 3 : 1; A : Zn^{2+}; B : ZnArg; C : $Zn(Arg)_2$.

TABLEAU 1. Constantes des stabilités des complexes binaires de Ni^{2+} et Zn^{2+} avec la 1-canavanine et la 1-arginine; $t = 25°C$ et $\mu = 0,1$ ($NaNO_3$)

	pqrs	log β_{pqrs}	log *K*	Domaine de formation	Références 16	Références 21
NiCan	1001	6,00	6,00	pH 5,5–11		
$Ni(Can)_2$	1002	10,69	4,69	pH 6,25–11		
$Ni(Can)_3$	1003	13,77	3,08	pH 7,25–11		
NiArg	1010	4,88	4,88	pH 4,75–11	4,98	5,18
$Ni(Arg)_2$	1020	8,89	4,01	pH 6,25–11	4,32	4,31
$Ni(Arg)_3$	1030	12,04	3,15	pH 7,50–11	3,21	
ZnCan	1001	5,00	5,00	pH 5,50–11		
$Zn(Can)_2$	1002	9,20	4,20	pH 6,75–11		
ZnArg	1010	4,00	4,00	pH 5,50–11	4,19	4,11
$Zn(Arg)_2$	1020	7,95	3,95	pH 6,75–11	3,91	3,96

Résultats

Rappelons que la déprotonation du groupement guanidyle (log $K = 11,58$) de la 1-arganine n'intervient pas dans le domaine de pH correspondant à la complexation des métaux de transition (pH <10). Seuls le groupement aminé (log $K = 8,98$) d'une part et le groupement carboxylate (log $K = 2,22$) d'autre part sont concernés (1).

Dans le cas de la 1-canavanine, au contraire, les trois groupements : aminé (log $K = 9,16$), guanidyle (log $K = 6,98$) et carboxylate (log $K = 2,15$) participent à la chélation (1).

Il faut noter que, si les travaux concernant la 1-arginine complexée ou non sont nombreux (16, 19), nous ne disposons d'aucune donnée bibliographique concernant la complexation du nickel et du zinc par la 1-canavanine.

1. Ni(II)–1-canavanine et Ni(II)–1-arginine

1. A. Mesures potentiométiques

Les rapports métal : ligand (1 : 3 et 1 : 5) étudiés conduisent aux classiques courbes de formation $\bar{n} = f(pL)$ (fig. 1a). Pour les deux systèmes, elles tendent vers $\bar{n} = 3$, ce qui implique la formation des espèces successives ML, ML_2 et ML_3 dont on peut apprécier graphiquement les constantes de stabilité. Les valeurs définitives des constantes affinées par la méthode de pit-mapping, ainsi que les données bibliographiques, sont rassemblées dans le tableau 1. Les courbes de répartition sont représentées sur les figures 1b et 1c. Quel que soit le ligand, 1-canavanine ou 1-arginine, le complexe ML_2 reste toujours majoritaire.

1. b. Mesures spectroscopiques

Les solutions utilisées pour les mesures spectrophotométriques sont 0,010 M en Ni^{2+} et 0,025 M en 1-canavanine d'une part; 0,020 M en Ni^{2+} et 0,050 M en 1-arginine d'autre part. Le domaine de longueur d'onde envisagé est compris entre 300 et 800 nm.

Pour des pH inférieurs à 5, comme le montrent les deux faisceaux de spectres (fig. 2a et fig. 2b), nous sommes en présence de deux bandes attendues, correspondant au nitrate de nickel(II) : l'une étroite dont le maximum très aigu est à 370 nm, l'autre beaucorp plus large possède deux maxima (640 et 650 nm). Ces observations ont conformes aux travaux de Nicholls (18).

Pour les pH supérieurs à 5, ces transitions de très faible absorbance se trouvent amplifiées et décalées vers les plus faibles longueurs d'onde grâce à l'effet hypsochrome normal du

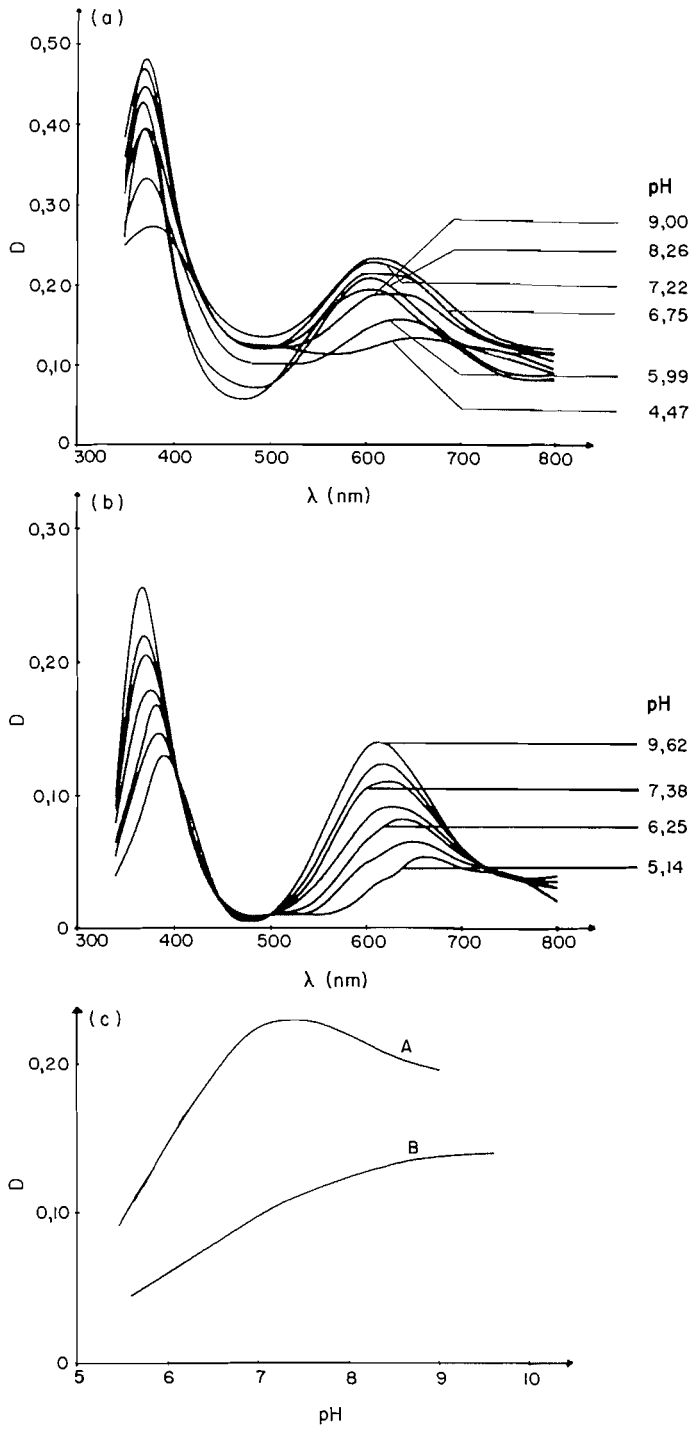


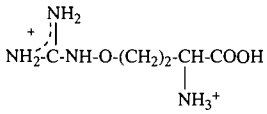
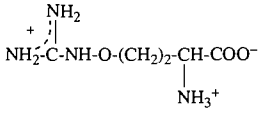
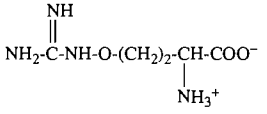
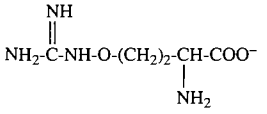
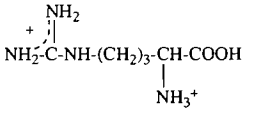
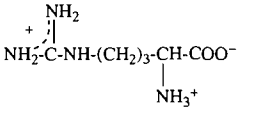
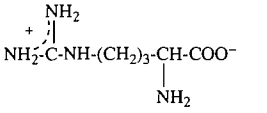
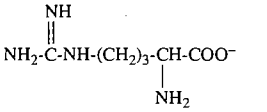
FIG. 2. (a) Faisceau des spectres d'absorption du système 1-canavanine (0,025 M)–nickel(II) (0,01 M). (b) Faisceau des spectres d'absorption du système 1-arginine (0,05 M)–nickel(II) (0,02 M). (c) Variation du maximum d'absorption (610 nm) en fonction du pH pour les systèmes 1-canavanine–nickel(II) (A) et 1-arginine–nickel(II) (B).

champ de ligand de chaque coordinat. En outre, les deux maxima de la bande située vers 640 nm tendent à s'aplatir et à se confondre en un seul vers 610 nm.

L'absorbance molaire du système Ni(II)–1'arginine (fig. 2c) augmente progressivement au delà de pH 5 de manière analogue à celle du système Cu(II)–l'arginine (1). Ceci se justifie par la formation graduelle des complexes NiArg, $Ni(Arg)_2$ et $Ni(Arg)_3$ de plus en plus stables. L'absorbance molaire de chaque

Can. J. Chem. Downloaded from www.nrcresearchpress.com by 84.41.108.74 on 09/07/12
For personal use only.

TABLEAU 2. Facteurs intensifs spectrophotométriques et dichroïques de la l-canavanine et de la l-arginine

	Spectrophotométrie		Dichroïsme circulaire	
	λ(nm)	ε	λ(nm)	Δε
l-Canavanine				
	213	324	213	+1,06
	213	375	213	+0,62
	213	3717	213	+0,66
	213	3392	213	+1,67
l-Arginine				
	200	2000	210	+1,59
	200	2000	210	+0,94
	200	2000	210	+0,07
	200	2000	210	+4,64

complexe est calculée puis affinée à 610 nm (tableau 2). Elle croit normalement avec l'augmentation du nombre de cycles de chélation.

Dans le cas du système Ni(II)–l-canavanine, il faut distinguer deux étapes (fig. 2c): (*i*) $5 < pH < 7.5$: l'absorbance augmente avec le pH, les courbes de répartition indiquant la formation successive des complexes NiCan et $Ni(Can)_2$. (*ii*) $7.5 < pH < 9$: l'absorbance diminue lorsqu'apparait le complexe $Ni(Can)_3$.

Cette dernière observation, après calcul des absorbances molaires à 610 nm (tableau 3), tend à montrer que le nombre de cycles de chélation est plus faible pour l'espèce $Ni(Can)_3$ que pour l'espèce $Ni(Can)_2$.

Les mêmes solutions sont ensuite examinées par dichroïsme circulaire entre 300 et 750 nm (fig. 3a et fig. 3b). L'examen des spectres dichroïques montre que pour chacun des deux ligands, les complexes obtenus présentent un comportement dichroïque différent : Le système nickel–l-canavanine fait apparaître cinq bandes bien différenciées (357, 410, 553, 620 et 695 nm) alors que le système nickel–l-arginine ne comporte que trois bandes (355, 568 et 667 nm). Les amplitudes dichroïques des complexes évoluent de la même manière que leur densité optique.

TABLEAU 3. Facteurs intensifs spectrophotométriques et dichroïques des complexes de la l-canavanine et de la l-arginine avec Ni^{2+} et Zn^{2+}

	Spectrophotométrie		Dichroïsme circulaire	
	λ (nm)	ε	λ (nm)	Δε
NiCan	610	9,67	620	−0,0019
$Ni(Can)_2$	610	12,31	620	−0,0203
$Ni(Can)_3$	610	6,10	620	−0,0126
NiArg	610	4,67	568	−0,0009
$Ni(Arg)_2$	610	5,74	568	−0,0080
$Ni(Arg)_3$	610	9,59	568	−0,0091
ZnCan	—	—	213	+0,22
$Zn(Can)_2$	—	—	213	−9,00
ZnArg	—	—	210	−1,75
$Zn(Arg)_2$	—	—	210	−0,02

Les figures 3a et 3b permettent de calculer le dichroïsme circulaire molaire en fonction du pH à 620 nm pour la l-canavanine et à 586 nm pour la l-arginine et d'estimer, pour ces longueurs d'onde, les facteurs intensifs dichroïques respec-

Can. J. Chem. Downloaded from www.nrcresearchpress.com by 84.41.108.74 on 09/07/12
For personal use only.

Can. J. Chem. Downloaded from www.nrcresearchpress.com by 84.41.108.74 on 09/07/12
For personal use only.

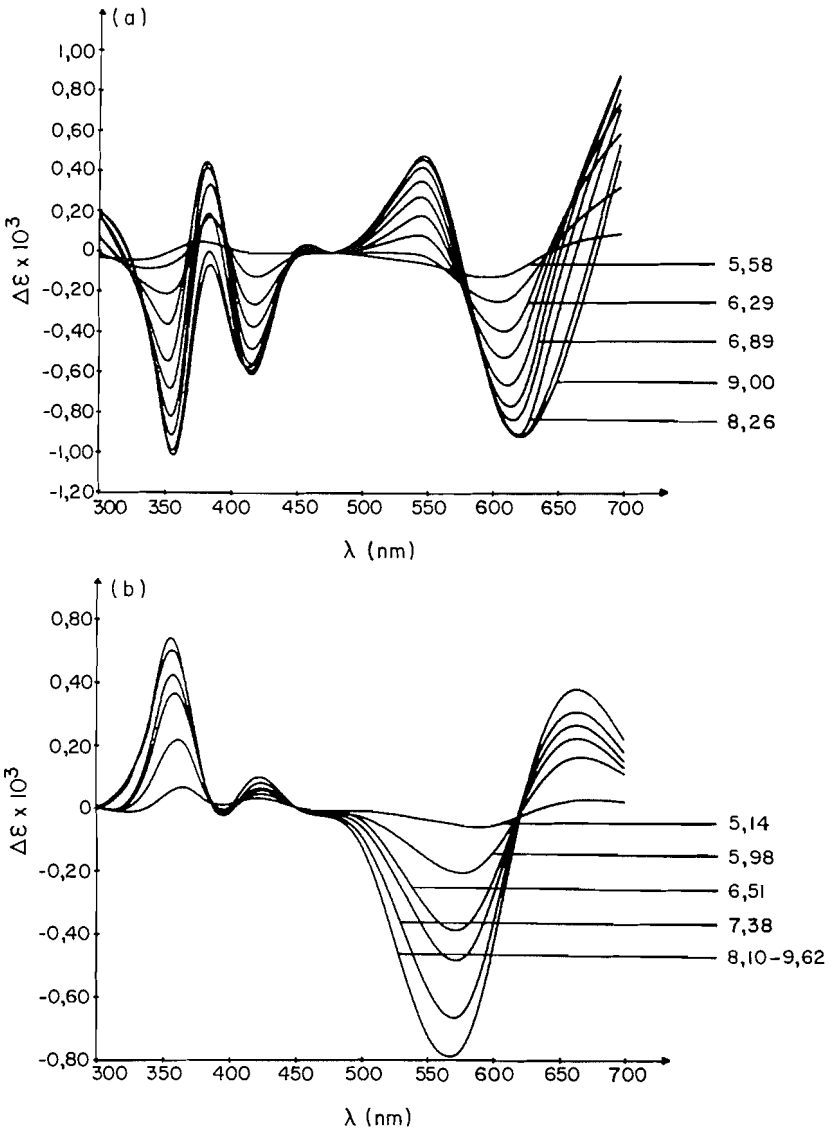


FIG. 3. (a) Faisceau des spectres d'absorption dichroïque du système 1-canavanine (0,025 M)–nickel(II) (0,01 M). (b) Faisceau des spectres d'absorption dichroïque du système 1-arginine (0,05 M)–nickel(II) (0,02 M).

tifs de chaque complexe. Ces paramètres sont ensuite affinés et consignés dans le tableau 3.

2. Zn(II)–1-canavanine et Zn(II)–1-arginine

2. A. Mesures potentiométriques

Les deux rapports métal : ligand (1 : 3 et 1 : 5) conduisent aux courbes de formation $\bar{n} = f(\mathrm{pL})$ de la figure 1d.

Dans ce cas, seuls se forment les complexes ML et ML_2. Leurs constantes de stabilité sont réunies dans le tableau 1 et les courbes de répartition représentées sur les figures 1e et 1f.

2. B. Mesures spectroscopiques

Les mesures spectrophotometriques et dichroïques sont réalisées dans le domaine de l'ultraviolet (190–250 nm) où absorbent également chacun des ligands. Outre les espèces complexées, nous devons, alors, tenir compte de la contribution de leurs formes protonées.

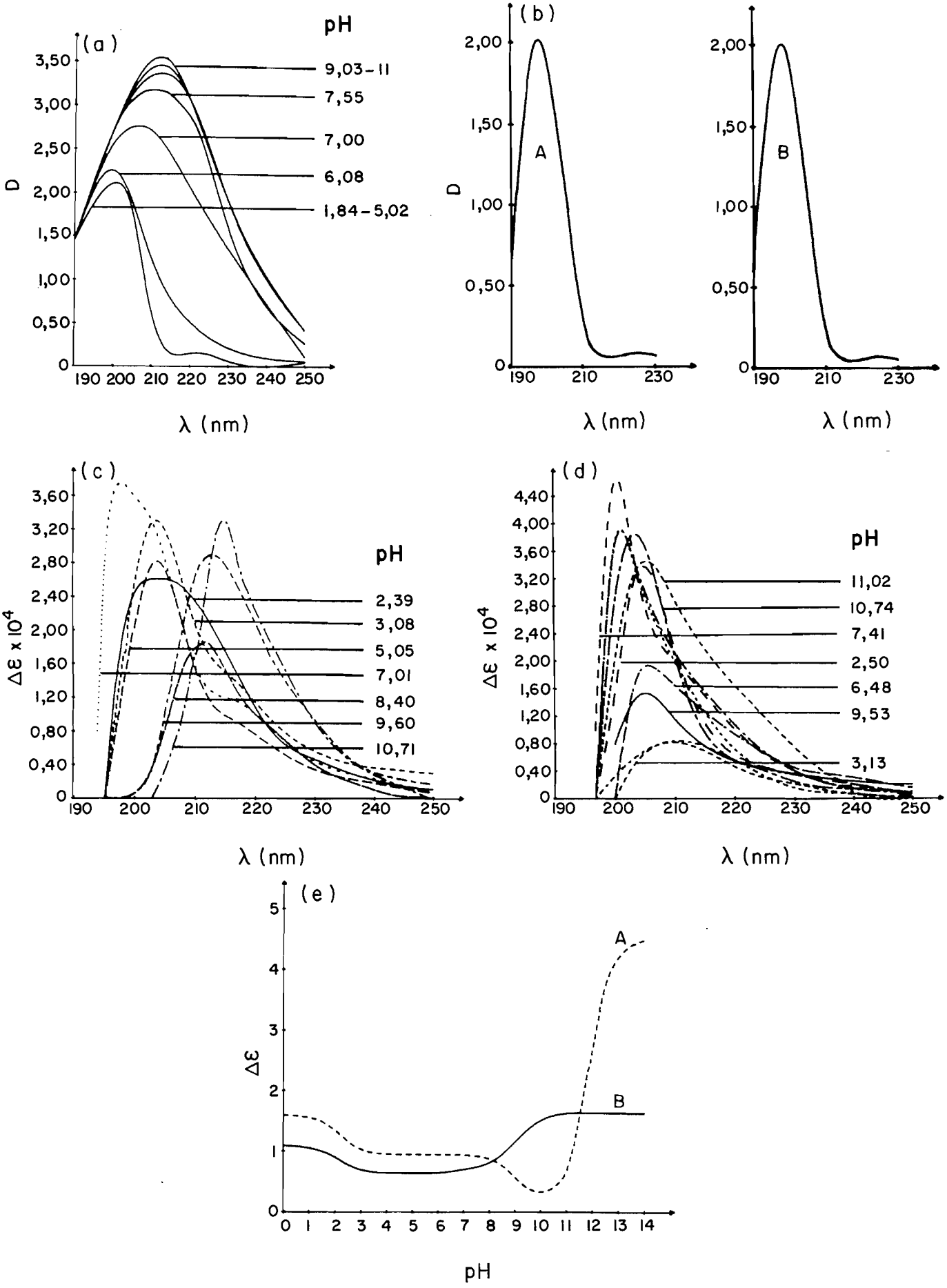
(a) Ligands: Nous avons contrôlé les variations d'absorbance et de dichroïsme circulaire avec le pH de manière à mettre en évidence les facteurs intensifs de chaque forme protonée.

Les solutions de 1-canavanine et de 1-arginine étudiées sont 0,01 M en acide aminé. Les spectres d'absorption lumineuse et de dichroïsme circulaire ont été enregistrés entre 190 et 250 nm.

En ce qui concerne les mesures spectrophotométriques, dans le cas de la 1-canavanine (fig. 4a), nous observons une évolution de la longueur d'onde du maximum d'absorption ainsi que de l'amplitude d'absorption au fur et à mesure que le pH augmente. Les valeurs des facteurs intensifs des formes protonées sont estimées et affinées à 213 nm (tableau 2).

Pour la 1-arginine (fig. 4b), quel que soit le pH, la position et l'amplitude de la bande d'absorption restent invariables. Le maximum d'absorption est situé à 200 nm pour toutes les formes protonées; leur absorbance molaire est la même (tableau 2).

FIG. 4. (a) Faisceau des spectres d'absorption de la 1-canavanine (0,01 M). (b) Spectres d'absorption de la 1-arginine (0,01 M); A : pH = 5; B : pH = 10. (c) Spectres d'absorption dichroïque de la 1-canavanine (0,01 M). (d) Spectres d'absorption dichroïque de la 1-arginine (0,01 M). (e) Dichroïsme circulaire molaire de la 1-canavanine (213 nm) (B) et de la 1-arginine (210 nm) (A) en fonction du pH.



Can. J. Chem. Downloaded from www.nrcresearchpress.com by 84.41.108.74 on 09/07/12
For personal use only.

Can. J. Chem. Downloaded from www.nrcresearchpress.com by 84.41.108.74 on 09/07/12
For personal use only.

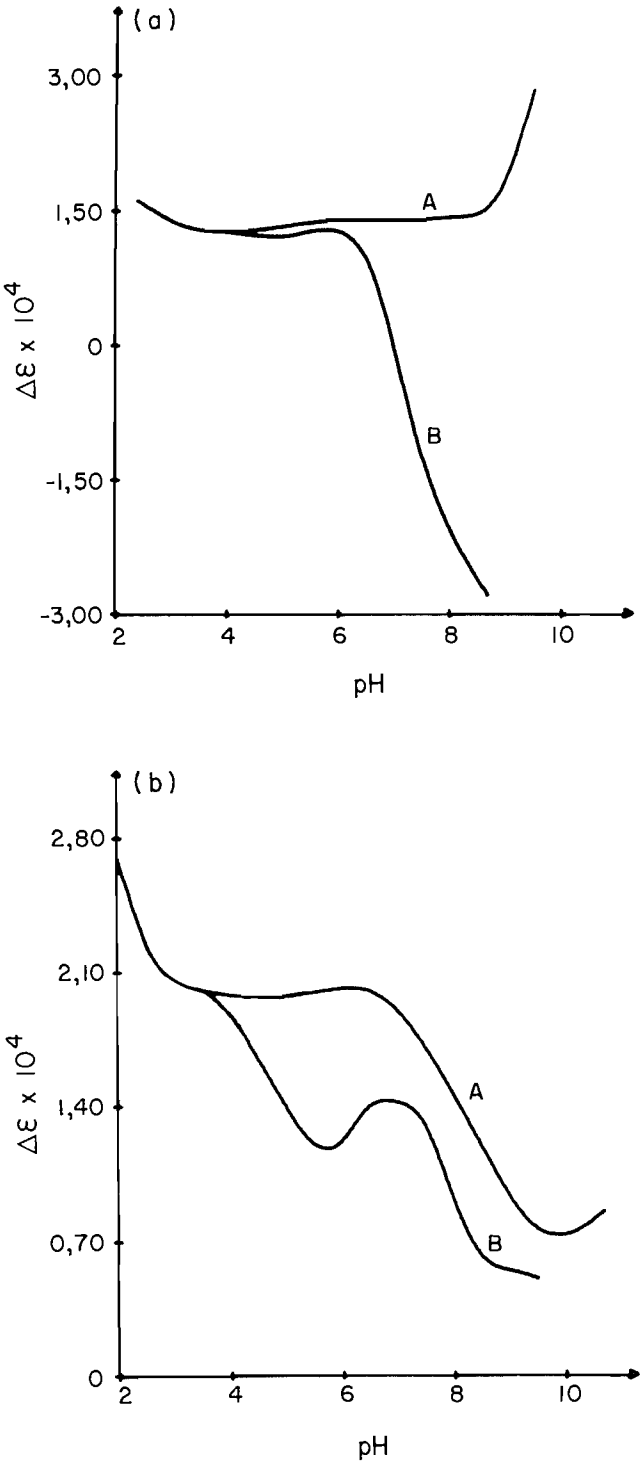


FIG. 5. (a) Absorption dichroïque de la 1-canavanine seule (0,01 M) (A) et du système 1-canavanine (0,01 M)–zinc(II) (0,002 M) (B) en fonction du pH à 213 nm. (b) Absorption dichroïque de la 1-arginine seule (0,01 M) (A) et du système 1-arginine (0,01 M)–zinc(II) (0,002 M) (B) en fonction du pH à 210 nm.

Quant au dichroïsme circulaire, que ce soit pour la 1-canavanine (fig. 4c) ou la 1-arginine (fig. 4d), la dépronation des molécules se traduit par un déplacement bathochrome des maxima d'absorption dichroïque.

Nous calculons de façon approchée les facteurs intensifs relatifs à chaque forme protonée pour une longueur d'onde donnée (213 nm pour la 1-canavanine et 210 nm pour la 1-arginine) qui sont ensuite affinés (tableau 2).

La figure 4e représente les dichroïsmes circulaires molaires en fonction du pH recalculés à l'aide des facteurs intensifs dichroïques pour les deux ligands. Ces deux courbes mettent parfaitement en évidence les différentes formes protonées.

(b) Zn(II)–1-canavanine : Les concentrations utilisées, pour les mesures spectrophotométriques et dichroïques, sont 0,01 M en ligand et 0,002 M en métal; soit un rapport ligand : métal égal à 5 de manière à éviter la formation d'espèces hydroxylées.

Nous n'avons pas observé de variation appréciable de longueur d'onde ou de densité optique par spectrophotométrie. Cette méthode ne permet donc pas de mettre en évidence les complexes formés entre la 1-canavanine et le zinc(II).

Par contre, les spectres dichroïques permettent de tracer la variation du dichroïsme circulaire du système en fonction du pH à 213 nm (fig. 5a, courbe B).

$2 < pH < 5$: les courbes A et B sont confondues, la réponse dichroïque correspond au ligand libre non complexé.

$pH > 5,5$: le dichroïsme circulaire de la 1-canavanine subit une profonde modification : formation des complexes ZnCan et surtout $Zn(Can)_2$ en bon accord avec les mesures potentiométriques (fig. 1e). Les dichroïsmes circulaires molaires des complexes ZnCan et $Zn(Can)_2$ sont notés dans le tableau 3.

(c) Zn(II)-1-arginine : Les concentrations de travail restent les mêmes et, comme précédemment, la spectrophotométrie ne permet pas d'identifier les différents complexes.

La figure 5b montre au contraire une variation appréciable de l'amplitude dichroïque avec le pH lors de la formation des complexes, notamment de l'espèce ZnArg. Les valeurs des dichroïsmes molaires des deux complexes affinées à 210 nm sont données dans le tableau 3.

Discussion

1. Complexation avec le nickel(II)

La 1-canavanine et la 1-arginine génèrent trois espèces successives complexes NiL, NiL_2 et NiL_3 mises en évidence par potentiométrie, spectrophotométrie et dichroïsme circulaire.

Les courbes de répartitions (fig. 1b et fig. 1c) montrent dans chaque cas un complexe ML_2 majoritaire.

Les mesures spectrophotométriques et surtout dichroïques du système nickel(II)–1-arginine confirment ces résultats dans la mesure où les absorbances molaires comme les dichroïsmes circulaires molaires des complexes NiArg, $Ni(Arg)_2$ et $Ni(Arg)_3$ augmentent avec le degré de coordination, donc avec le nombre de cycles de chélation (19, 20).

Ceci nous conduit à souligner un point intéressant concernant le nombre de positions chélatantes de la 1-canavanine. Nous avons montré, en effet, que la 1-canavanine, contrairement à la 1-arginine, présente un caractère tridenté vis-à-vis du cuivre(II) dans un état de coordinence 6 (1). Or, le nickel(II) favorise la formation d'une espèce $Ni(Can)_3$ dans laquelle la 1-canavanine ne peut être qu'un coordinat bidenté.

Les mesures spectrophotométriques présentent une augmentation de l'absorbance molaire du complexe $Ni(Can)_2$ par rapport à NiCan ensuite une diminution de l'absorbance du complexe $Ni(Can)_3$. Les complexes NiArg, $Ni(Arg)_2$ et $Ni(Arg)_3$ présentent au contraire une absorbance molaire régulièrement croissante.

Les mesures dichroïques dépendant étroitement du nombre de cycles de chélation (20) recoupent aisément cette hypothèse dans la mesure où le dichroïsme circulaire molaire de NiCan (deux cycles de chélation, ligand tridenté) est inférieur à celui

du complexe $Ni(Can)_3$ (trois cycles de chélation, ligand bidenté) lui-même inférieur à celui du complexe $Ni(Can)_2$ (quatre cycles de chélation, ligand tridenté).

Si l'examen comparé des spectres dichroïques des complexes du cuivre (1) ne permet pas une différenciation nette entre la 1-arginine et la 1-canavanine, les spectres de chaque complexe du nickel(II), très différents (fig. 3a et fig. 3b), devraient pouvoir être considérés comme des facteurs intéressants de contrôle de qualité.

2. Complexation avec le zinc(II)

Les complexes de zinc(II) formés avec la 1-canavanine et la 1-arginine identifiés par potentiométrie sont au nombre de deux : ZnL et ZnL_2.

L'étude spectroscopique de ces complexes nécessite un examen préalable des propriétés optiques des deux coordinats.

La spectrophotométrie ultraviolet montre que la 1-canavanine et la 1-arginine, comme la plupart des acides aminés (17), absorbent dans le domaine de longueurs d'onde 200–220 nm. Cette technique confirme la différence existant entre la 1-canavanine et la 1-arginine (fig. 4a et fig. 4b) malgré leur ressemblance structurale : les spectres d'absorption de la 1-arginine ne subissent aucune modification en fonction du pH; les spectres d'absorption de la 1-canavanine présentent en fonction du pH un effet bathochrome appréciable.

En outre, les mesures de dichroïsme circulaire à 213 nm pour la 1-canavanine et 210 nm pour la 1-arginine permettent de tracer les courbes de dichroïsme circulaire en fonction du pH. Ces courbes mettent parfaitement en évidence les différentes formes protonées ainsi que leur domaine d'existence. Ces résultats sont conformes à l'étude potentiométrique de ces deux ligands (1).

Si la spectrophotométrie ultraviolet ne permet pas l'identification des chélates de la 1-canavanine et la 1-arginine, les spectres dichroïques des espèces compléxées traduisent beaucoup mieux l'influence de la coordination sur la variation du dichroïsme circulaire des formes protonés des ligands. Nous avons, en outre, mis en évidence la différence nette de comportement dichroïque des formes $Zn(Arg)_2$ et $Zn(Can)_2$.

Nous avons signalé dans l'introduction une certaine toxicité de la 1-canavanine ainsi que le rôle du nickel et du zinc dans les enzymes. Cette toxicité peut être liée à la stabilité des complexes métalliques formés avec ces oligo-éléments enzymatiques plus importante pour la 1-canavanine que pour la 1-arginine. Il existe en effet une corrélation entre la stabilité et l'effet chélate important dû au caractère tridenté de la 1-canavanine.

Partie expérimentale

Matériel

Nous disposons d'une chaîne de mesures étalonnée avec précision : électrode de verre|solution thermostatée|KCl saturé|électrode calomel.

Le jeu d'électrodes est relié à un potentiomètre Isis 2000 Tacussel et les mesures sont effectuées sur des solutions aqueuses thermostatées à 25°C ± 0,1°C et sous atmosphère d'azote. La force ionique de chaque solution est maintenue constante à l'aide d'une solution de $NaNO_3$ 0,1 M.

Les spectres d'absorption sont tracés à l'aide d'un spectrophotomètre Varian 634 et les spectres dichroïques à l'aide d'un dichrographe Jobin–Yvon Mark IV. Les cuves Hellma sont en quartz et ont des trajets optiques différents : 1 cm pous les mesures d'absorption dans le visible; 1 mm pour les mesures d'absorption dans l'ultraviolet; 5 cm pour les mesures dichroïques dans le visible; 0,2 mm pour les mesures dichroïques dans l'ultraviolet.

Réactifs

La 1-canavanine est sous forme sulfate de canavanine ou sous forme « free base » (Sigma) et la 1-arginine sous forme free base (Sigma). Ces acides aminés sont conservés à basse température.

Les sels métalliques sont introduits d'une part sous forme de nitrate de nickel(II) : $Ni(NO_3)_2 \cdot 6H_2O$ (Prolabo) et d'autre part sous forme de sulfate de zinc(II) : $ZnSO_4 \cdot 7H_2O$ (Prolabo). Ils sont dissous dans l'eau distillée et leurs titres sont déterminés par un dosage complexométrique à l'EDTA.

1. A. Albourine, M. Petit-Ramel, G. Thomas-David et J. J. Vallon. Can. J. Chem. **67**, 959 (1989).
2. G. A. Rosenthal. Anal. Biochem. **77**, 147 (1977).
2. K. H. Fischer et H. D. Belitz. Z. Lebensm.-Unters.-Forsch. **162**, 227 (1976).
4. S. Natelson. J. Agric. Food Chem. **33**, 413 (1985).
5. F. H. Nielsen. Studies on the essentiality of nickel. *Dans* : Newer trace elements in nutrition. *Éditeurs* : W. Nertz et W. E. Cornatzer. Marcel Dekker, New York. 1971.
6. M. Kirchgessner, J. Perth et A. Schnegg. Arch. Tierernähr. **30**, 10 (1980).
7. M. Anke, M. Partschefeld, M. Grun et B. Groppel. Arch Tierernähr. **28**, 83 (1978).
8. F. W. Sunderman, Jr. Disorders of mineral metabolism. Vol. 1. *Éditeurs* : F. Bronner et J. W. Coburn. Academic Press, New York. 1981.
9. M. Kirchgessener. Trace element metabolism in man and animals. Proc. 3rd Symp. Arbeitskreis f. Tierernähr. Weihenstephan. Tech. Univ. München. Freising–Weihenstephan. 1978.
10. N. E. Dixon, R. L. Blakley et B. Zerner. Can J. Biochem. **58**, 481 (1980).
11. J. C. Polacco. Plant. Physiol. **58**, 350 (1976).
12. J. C. Polacco. Plant. Physiol. **59**, 827 (1977).
13. N. E. Dixon, C. Gazzola, C. J. Asher, D. S. W. Lee, R. L. Blakley et B. Zerner. Can. J. Biochem. **58**, 474 (1980).
14. L. Levesque. Les micropoluants minéraux dans les eaux superficielles, revue. Association française pour l'étude des eaux. rapport n° 4. 1978.
15. D. R. Williams. The metal of life. Van Nostrand Reinhold Company, London. 1971.
16. S. Pelletier. These Doctorat d'État Paris. 1960.
17. M. Legrand et R. Viennet. Acad. Sci. **258**, 676 (1964).
18. D. Nicholls. Comprehensive inorganic chemistry. Oxford Univ. Press, Oxford. 1973.
19. J. E. Crooks. The spectrum in chemistry. Academic Press, London. 1978.
20. G. Snatzke (*Éditeur*). Optical rotary disperssion and circular dichoïsm in organic chemistry. Heyden and Son, Ltd., London. 1967.
21. E. R. Clare et A. E. Martell. J. Inorg. Nucl. Chem. **32**, 911 (1970).

Can. J. Chem. Downloaded from www.nrcresearchpress.com by 84.41.108.74 on 09/07/12
For personal use only.

Triterpenoid glycosides from the Northeastern Pacific marine sponge *Xestospongia vanilla*

SANDRA A. MORRIS, PETER T. NORTHCOTE, AND RAYMOND J. ANDERSEN[1]

Departments of Chemistry and Oceanography, University of British Columbia, Vancouver, B.C., Canada V6T 1Z4

Received March 18, 1991

SANDRA A. MORRIS, PETER T. NORTHCOTE, and RAYMOND J. ANDERSEN. Can. J. Chem. **69**, 1352 (1991).

Isoxestovanin A (**6**), xestovanin B (**7**), xestovanin C (**8**), dehydroxestovanin A (**9**), epidehydroxestovanin A (**10**), dehydroxestovanin C (**11**), and secodehydroxestovanin A (**12**), seven new triterpenoid glycosides, have been isolated from the Northeastern Pacific sponge *Xestospongia vanilla*. The structures of the metabolites were determined by a combination of spectroscopic analysis and chemical degradation. The aglycone of **6** has the new isoxestovanane triterpenoid carbon skeleton. Compounds **7**, **8**, and **11** are the first *X. vanilla* triterpenoid glycosides known to contain three monosaccharide subunits.

Key words: triterpenoid, glycoside, sponge, Xestospongia.

SANDRA A. MORRIS, PETER T. NORTHCOTE et RAYMOND J. ANDERSEN. Can. J. Chem. **69**, 1352 (1991).

On a isolé des extraits de sept nouveaux glycosides triterpéniques : la isoxestovanine A (**6**), la xestovanine B (**7**), la xestovanine C (**8**), la déhydroxestovanine A (**9**), la épidéhydroxestovanine A (**10**), la déhydroxestovanine C (**11**) et la secodéhydroxestovanine A (**12**), á partir de la *Xestospongia vanilla*, l'éponge du Pacifique Nord-est. On a déterminé la structure des métabolites par analyse spectrale et par dégradation chimique. L'aglycone du composé **6** a le sequelette carboné du nouveau triterpène isoxestovanane. Les composés **7**, **8** et **11** sont les premiers glycosides triterpéniques *X. vanilla* connus qui contiennent trois sous-unités monosaccharides.

Mots clés : triterpène, glycoside, éponge, Xestopongia.

[Traduit par la rédaction]

Can. J. Chem. Downloaded from www.nrcresearchpress.com by 84.41.108.74 on 09/07/12
For personal use only.

The Northeastern Pacific sponge *Xestospongia vanilla* is an extremely rich source of terpenoid metabolites. We have previously reported the isolation of xestodiol (1), xestovanin A (**1**) (2), secoxestovanin A (**2**) (2), xestenone (**3**) (3), secoxestenone (**4**) (4), and xestolide (**5**) (4) from *X. vanilla*. Xestodiol is an 18-carbon apocarotenoid, xestovanin A (**1**) and secoxestovanin A (**2**) are triterpenoid glycosides with the new xestovanane and secoxestovanane carbon skeletons, and xestenone (**3**), secoxestenone (**4**), and xestolide (**5**) are degraded triterpenoids (4) that represent three additional unprecedented terpenoid skeletons. The discovery of triterpenoid glycosides in *X. vanilla* is of particular interest because only one other marine sponge, *Asteropus sarsinosum*, has been found to contain this type of metabolite (5). Prior to their discovery in the sponges *X. vanilla* and *A. sarsinosum*, the only known marine sources of triterpenoid glycosides were echinoderms (6).

A continuing investigation of the terpenoid metabolism of *X. vanilla* has led to the isolation of seven new metabolites, isoxestovanin A (**6**), xestovanin B (**7**), xestovanin C (**8**), dehydroxestovanin A (**9**), epidehydroxestovanin A (**10**), dehydroxestovanin C (**11**), and secodehydroxestovanin A (**12**), whose structures are reported herein. One of the metabolites, isoxetovanin A (**6**), has the new isoxestovanane triterpenoid carbon skeleton, five (compounds **7**, **8**, **9**, **10**, and **11**) have the xestovanane carbon skeleton, and one (compound **12**) has the secoxestovanane skeleton. As part of this investigation, an interesting geographic variation in the metabolite content of *X. vanilla* has been observed.

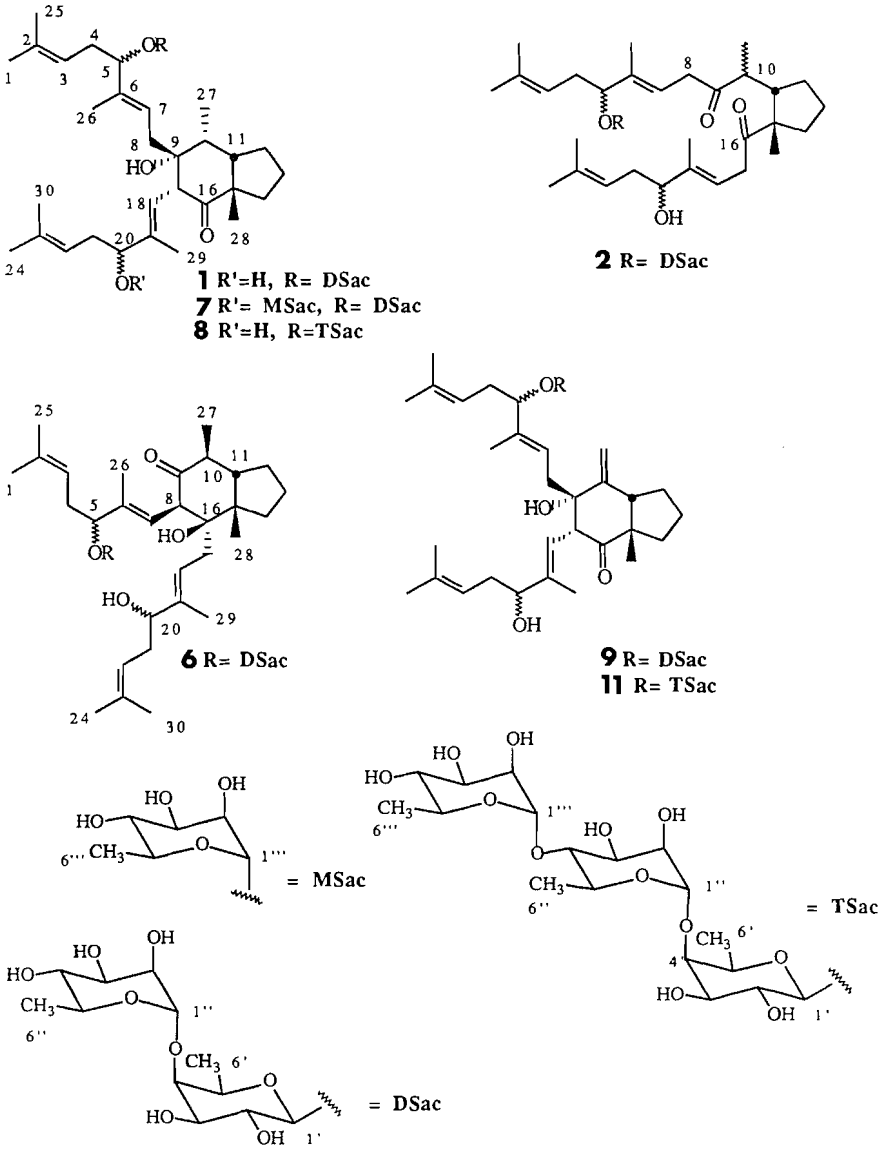
Specimens of *X. vanilla* were collected by hand using SCUBA in exposed surge channels along the shoreline of the Deer group of islands in Barkley Sound and along the northern tip of Anthony Island in the Queen Charlotte Islands group, British Columbia. The Bamfield specimens of *X. vanilla* (1000 g, dry weight) yielded the previously described metabolites xestovanin A (**1**) (50 mg) and secoxestovanin A (**2**) (5 mg) along with the new metabolites isoxestovanin A (**6**) (11 mg), xestovanin B (**7**) (12 mg), xestovanin C (**8**) (10 mg), dehydroxestovanin A (**9**) (12 mg), and secodehydroxestovanin A (**12**) (20 mg), whereas the Anthony Island specimens yielded dehydroxestovanin A (**9**) (15 mg), epidehydroxestovanin A (**10**) (14 mg), dehydroxestovanin C (**11**) (10 mg), and secodehydroxestovanin A (**12**) (20 mg).

New metabolites from the Bamfield specimens

Isoxestovanin A (**6**) was isolated as an optically active ($[\alpha]_D$ −4.4 (*c* 0.16, MeOH)) colorless glass that gave an intense pseudomolecular ion at m/z 787 Da ($C_{42}H_{68}O_{12}$ + Na) in the FABMS. A comparison of the ^1H and ^{13}C NMR data obtained for isoxestovanin A (**6**) (Tables 1 and 2) with the NMR data previously obtained for xestovanin A (**1**) showed that the two molecules were closely related triterpenoid glycosides. Therefore, the highest mass ion observed in the EIHRMS of **6** at m/z 436.3336 Da ($C_{30}H_{44}O_2$, ΔM −0.5 mmu) could be attributed to the loss of a disaccharide substituent and one molecule of water from the parent ion to give a fragment containing the carbon skeleton of the triterpenoid aglycone. The presence of an intense peak at m/z 311 Da in the FABMS of isoxestovanin A (**6**), which could be assigned to a disaccharide fragment ($C_{12}H_{22}O_9$ + H), provided further evidence for a general structure consisting of a triterpenoid aglycone attached to a disaccharide.

A total of 42 resonances were observed in the ^{13}C NMR spectrum of isoxestovanin A (**6**) (Table 2), an APT experiment (7) identified 61 protons attached to carbon atoms (10 × CH_3, 6 × CH_2, 19 × CH), and the ^1H NMR spectrum (Table 1) contained resonances that could be assigned to six secondary hydroxyl protons and one tertiary alcohol proton. The combined NMR data provided carbon and hydrogen counts that were in agreement with the molecular formula ($C_{42}H_{68}O_{12}$) inferred for **6** from the FABMS and EIHRMS data. A detailed analysis of the ^{13}C NMR, ^1H NMR, NOE, and COSY data

[1]Author to whom correspondence may be addressed.



for **6** (Tables 1, 2, and 4[2]) led to the identification of two acyclic aglycone fragments (Fragment A: C1–C8 plus Me25 and Me26; Fragment B: C17–C24 plus Me29 and Me30) and the attached disaccharide and alcohol substituents that were nearly identical to the corresponding fragments of xestovanin A (**1**). Additional support for the nature of the C5 disaccharide substituent came from a standard GC analysis (8) (see Experimental) of the monosaccharides present in **6**. Only L-rhamnose and D-fucose were detected as expected from the NMR data. The magnitudes of the $^1J_{C,H}$ for the anomeric carbons and their attached protons in **6** were determined from a gated decoupled ^{13}C NMR experiment (fucose $^1J_{C,H}$ 156.8 Hz; rhamnose $^1J_{C,H}$ 171.0 Hz). They were consistent with a fucose β glycosidic linkage and a rhamnose α glycosidic linkage (9), as in xestovanin A (**1**).

The remaining portion of the aglycone in **6** had to contain 10 carbon atoms, it had to incorporate ketone (IR, 1710 cm^{-1}; ^{13}C NMR, acetone-d_6, δ 210.5), tertiary alcohol (^{13}C NMR, δ 83.6,s; ^1H NMR, Me_2SO-d_6, δ 4.42,s), secondary methyl (^1H NMR, δ 0.88,d), and tertiary methyl (^1H NMR, δ 0.96,s) functionalities, and it had to be bicyclic. Consideration of all of the spectral data for isoxestovanin A (**6**), in conjunction with the assumption that the aglycone had an unrearranged triterpenoid carbon skeleton, led to the conclusion that the 10-carbon bicyclic portion of its aglycone had a constitution corresponding to the expected product of intramolecular aldol condensation between the C8 methylene carbon and the C16 ketone functionality in secoxestovanin A (**2**). The resulting bicyclic fragment (see Fig. 1) contained a cyclohexanone functionality as required by the IR and ^{13}C NMR data for **6** (IR, 1710 cm^{-1}; ^{13}C NMR, acetone-d_6, δ 210.5). Correlations observed between the Me28 (δ 1.09) protons and C16 (δ 83.6) and between the Me27 protons (δ 0.95) and C9 (δ 210.5) in the HMBC spectrum (10) (acetone-d_6) of **6** provided strong support for the proposed structure. Additional HMBC correlations between both the Me27 (δ 0.95) and Me28 (δ 1.09) protons and the C11 resonance (δ 55.5) provided direct evidence for the C11—C15 bond. Further support for the proposed structure

[2]Supplemental material (24 pages): Table 4 (NOE results); selected ^1H and ^{13}C NMR spectra for compounds **6–12**; ^1H NMR data (acetone-d_6) for compounds **6**, **8**, **9**, **10**, and **11**; and spectral data for the peracetates of **6** and **9** has been deposited. A complete set of data may be purchased from The Depository of Unpublished Data, Document Delivery, CISTI, National Research Council Canada, Ottawa, Canada K1A 0S2.

Can. J. Chem. Downloaded from www.nrcresearchpress.com by 84.41.108.74 on 09/07/12
For personal use only.

TABLE 1. ^{1}H NMR data. Recorded at 400 MHz in Me_2SO-d_6.

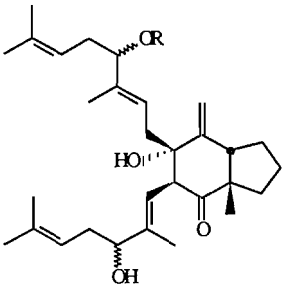
Carbon no.	Xestovanin A (**1**)	Isoxestovanin A (**6**)	
	^{1}Hδ	^{1}Hδ	COSY
1	1.55, s	1.55, s	H3
3	4.93, t(7.0)	4.86, t(6.5)	H1, H4, H4′, H25
4	2.20, m	2.14, m	H3, H4′, H5
4′	2.25, m	2.29, ddd(13.6, 6.5, 5.7)	H3, H4, H5
5	4.04, dd(8.7, 5.9)	4.08, dd(5.7, 9.5)	H4, H4′
7	5.22, bd(8.1)	5.58, bd(10.6)	H8, H26
8	1.97, m	3.79, d(10.6)	H7, 16OH
8′	2.24, m		
9OH	4.40, s		
10	2.07, dq(6.2, 5.5)	2.10, dq(10.9, 6.3)	H11, H27
11	1.86, m	1.69, m	H10, H12, H12′
12		1.47, m	H11, H12′, H13
12′		1.81, m	H11, H12, H13
13	1.32, m	1.52, m	H12, H12′, H13, H14
13′		1.60, m	H13
14	1.10, m	1.42, m	H13, H14′
14′	2.43, ddd(13.0, 8.0, 5.5)	2.04, m	H14
16OH	—	4.42, s	H8
17	3.59, d(9.9)	1.92, m	H17′, H18
17′	—	2.42, dd(10.2, 14.2)	H17, H18
18	5.46, bd(9.9)	5.12, bd(10.2)	H17, H17′, H29
20	3.90, dt(7.5, 4.1)	3.72, dt(7.0, 4.6)	H21, 20OH
20OH	4.67, d(4.1)	4.48, d(4.6)	H20
21	2.05, m	2.09, m	H20, H22
21′	2.17, m	2.09, m	H20, H22
22	4.96, t(9.1)	5.05, t(6.6)	H21, H24, H30
24	1.58, s	1.61, s	H22
25	1.55, s	1.52, s	H3
26	1.53, s	1.49, s	H7
27	0.95, d(6.2)	0.88, d(6.3)	H10
28	1.30, s	0.96, s	
29	1.41, s	1.50, s	H18
30	1.53, s	1.53, s	H22
1′	3.97, d(7.3)	4.10, d(7.7)	H2′
2′	3.28, ddd(9.6, 7.3, 4.3)	3.22, m	H1′, H3′, 2′OH
2′OH	4.92, d(4.3)	4.73, d(4.4)	H2′
3′	3.31, ddd(9.6, 4.0, 1.8)	3.30, m	H2′, H4′, 3′OH
3′OH	5.03, d(4.0)	4.90, d(4.4)	H3′
4′	3.61, bd(1.8)	3.60, m	H3′, H5′
5′	3.39, brq(6.3)	3.32, m	H4′, H6′
6′	1.15, d(6.3)	1.15, d(6.4)	H5′
1″	5.10, d(2.0)	5.08, d(1.8)	H2″
2″	3.76, ddd(4.2, 3.1, 2.0)	3.77, m	H1″, H3″, 2″OH
2″OH	4.57, d(4.2)	4.54, d(4.3)	H2″
3″	3.46, ddd(9.3, 5.7, 3.1)	3.48, ddd(9.5, 5.5, 3.3)	H2″, H4″, 3″OH
3″OH	4.48, d(5.7)	4.46, d(5.5)	H3″
4″	3.18, dt(9.3, 5.8)	3.19, ddd(9.5, 9.3, 5.7)	H3″, H5″, 4″OH
4″OH	4.64, d(5.8)	4.60, d(5.7)	H4″
5″	3.56, dq(9.2, 6.2)	3.57, m	H4″, H6″
6″	1.10, d(6.2)	1.12, d(6.2)	H5″
1‴			
2‴			
2‴OH			
3‴			
3‴OH			
4‴			
4‴OH			
5‴			
6‴			

Can. J. Chem. Downloaded from www.nrcresearchpress.com by 84.41.108.74 on 09/07/12
For personal use only.

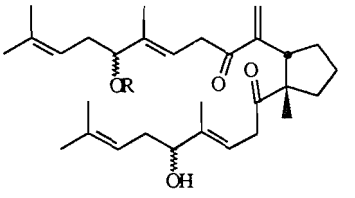
Chemical shifts are in ppm from internal TMS

Xestovanin B (**7**)		Xestovanin C (**8**)	
^{1}Hδ	COSY	^{1}Hδ	COSY
1.59, s	H3	1.59, s	H3
4.94, t(6.9)	H1, H4, H4′, H25	4.93, bt(6.9)	H1, H4, H4′, H25
2.20, m	H3, H4′, H5	2.23, m	H3, H4′, H5
2.25, m	H3, H4, H5	2.29, m	H3, H4, H5
4.05, m	H4, H4′	4.03, dd(6.0, 8.7)	H4, H4′
5.22, bd(8.0)	H8, H8′, H26	5.20, bd(7.4)	H8, H8′, H26
1.95, m	H7, H8′	2.01, m	H7, H8′
2.26, m	H7, H8	2.25, m	H7, H8
4.50, s	H17[a]	4.37, s	H17[a]
2.14, m	H11, H27	2.11, dq(6.9, 5.6)	H11, H27
1.95, m	H10	1.86, m	H10, H12, H12′
		1.55, m	H11, H12′, H13, H13′
		1.60, m	H11, H12, H13, H13′
1.33, m		1.34, m	H12, H12′, H13′, H14, H14′
1.53, m		1.40, m	H12, H12′, H13, H14, H14′
1.12, m	H13, H13′, H14′	1.14, m	H13, H13′, H14′
2.42, m	H13, H13′, H14	2.43, ddd(13.0, 7.5, 5.4)	H13, H13′, H14
		—	
3.57, d(9.3)	9OH[a], H18	3.57, d(9.9)	9OH[a], H18
		—	
5.51, d(9.3)	H17, H29	5.45, bd(9.9)	H17, H29
3.95, m	H21, H21′	3.88, dt(7.4, 4.1)	20OH, H21, H21′
—		4.64, d(4.1)	H20
2.06, m	H20, H21′, H22	2.08, m	H20, H21′, H22
2.23, m	H20, H21, H22	2.18, m	H20, H21, H22
4.98, t(7.5)	H21, H21′, H24, H30	4.96, bt(9.2)	H21, H21′, H24, H30
1.55, s	H22	1.57, s	H22
1.59, s	H3	1.54, s	H3
1.53, s	H7	1.52, s	H7
0.95, d(6.8)	H10	0.92, d(6.8)	H10
1.27, s		1.26, s	
1.35, s	H18	1.40, s	H18
1.55, s	H22	1.52, s	H22
3.96, d(7.4)	H2′	3.94, d(7.3)	H2′
3.26, m	H1′, 2′OH	3.25, m	H1′, 2′OH, H3′
4.98, d(4.3)	H2′	4.90, d(4.3)	H2′
3.31, m	3′OH, H4′	3.30, m	H2′, 3′OH, H4′
5.00, d(4.1)	H3′	5.03, d(4.0)	H3′
3.60, m	H3′	3.60, bs	H3′, H5′
3.39, m	H6′	3.39, m	H4′, H6′
1.15, d(5.8)	H5′	1.13, d(6.1)	H5′
5.09, d(1.6)	H2″	5.06, bs	H2″
3.76, m	H1″, 2″OH, H3″	3.75, m	H1″, 2″OH, H3″
4.55, d(4.3)	H2″	4.76, d(4.5)	H2″
3.48, m	H2″, 3″OH, H4″	3.61, m	H2″, 3″OH, H4″
4.46, d(5.7)	H3″	4.68, d(6.8)	H3″
3.19, m	H3″, 4″OH, H5″	3.39, m	H3″, H5″
4.63, d(5.7)	H4″	—	—
3.58, m	H4″, H6″	3.64, m	H4″, H6″
1.11, d(6.1)	H5″	1.14, d(6.1)	H5″
4.61, bs		5.06, bs	H2‴
3.44, m	2‴OH	3.71, m	H1‴, 2‴OH, 3‴
4.44, d(5.7)	H2‴	4.55, d(4.2)	H2‴
3.49, m	3‴OH	3.37, m	H2‴, 3‴OH, H4‴
4.59, d(4.5)	H3‴	4.42, d(5.8)	H3‴
3.18, m	H5‴, 4‴OH	3.19, ddd(9.4, 9.2, 5.6)	H3‴, H5‴
4.67, d(5.3)	H4‴	4.62, d(5.6)	H4‴
3.44, m	H4‴, H6‴	3.49, dq(9.2, 6.2)	H4‴, H6‴
1.13, d(5.8)	H5‴	1.11, d(6.2)	H5‴

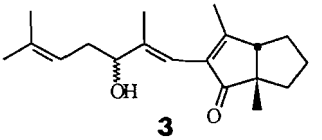
Can. J. Chem. Downloaded from www.nrcresearchpress.com by 84.41.108.74 on 09/07/12
For personal use only.



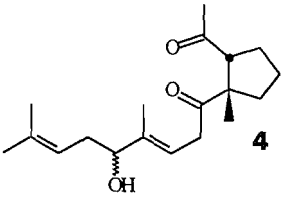
10 R= DSac



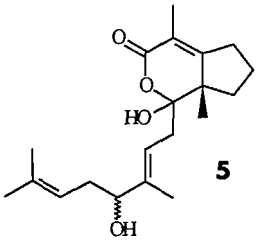
12 R= DSac



3



4



5

came from the COSY data for **6**, which contained correlations that could be assigned to the continuous spin system extending from the Me27 protons, through the H11 methine, and around the cyclopentane ring to H14 and H14′ (Table 1).

A series of NOE difference experiments helped establish the relative stereochemistry around the bicyclic ring system in isoxestovanin A (**6**) and also supported the proposed constitution. Irradiation of Me28 (δ 1.09: acetone-d_6) induced NOEs in H11 (δ 1.81), H14 (δ 1.65), and in the C16 hydroxyl proton (δ 3.49), and irradiation of H11 (δ 1.81) induced NOEs in Me27 (δ 0.95) and Me28 (δ 1.09). This series of NOEs were consistent with a *cis* ring fusion. Congestion in the ^{1}H NMR

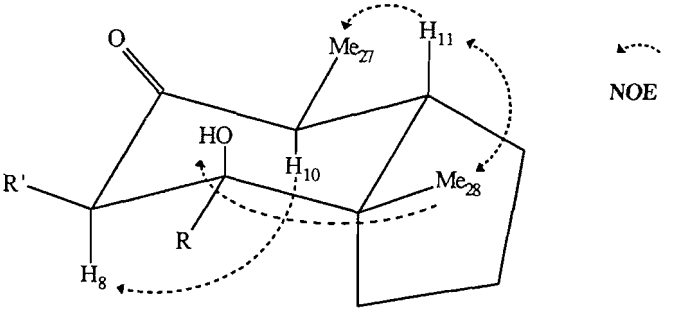
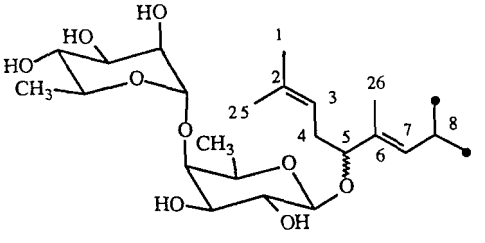
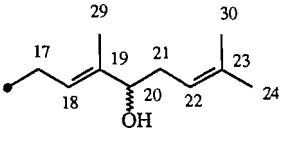


FIG. 1.



Fragment A



Fragment B

spectrum of isoxestovanin A (**6**) recorded in Me_2SO-d_6 (Table 1) or acetone-d_6[2] precluded the use of NOE experiments to establish the relative stereochemistries at C8 and C10. However, in the ^{1}H NMR spectrum of isoxestovanin A (**6**), recorded in 10:1 acetone-d_6/benzene-d_6, the H8 and H10 resonances were well resolved and irradiation of H10 (δ 2.17) induced an NOE (8%) in H8 (δ 3.95), demonstrating that the two protons were 1,3 diaxial to each other as shown in Fig. 1. The 1,3-diaxial NOE between H8 and H10 also supported the proposed placement of the 10-carbon side chain containing the disaccharide substituent (Fragment A), which terminates in C8, adjacent to the C9 ketone functionality (i.e., 1,3 to C10). A COSY correlation (Table 1) between H8 (δ 3.79) and the 16OH proton (δ 4.42) was assigned to W coupling, indicating that H8 and the 16OH group were attached to adjacent carbons and that the 16OH was axial. Additional information about the conformation and relative stereochemistry of the bicyclic ring system came from a measurement of the H10/H11 vicinal coupling

Can. J. Chem. Downloaded from www.nrcresearchpress.com by 84.41.108.74 on 09/07/12
For personal use only.

TABLE 2. ^{13}C NMR data for xestovanin A (**1**), isoxestovanin A (**2**), xestovanin B (**3**), and xestovanin C (**4**). Recorded at 75 MHz in acetone-d_6

Carbon no.	Xestovanin A (**1**)	Isoxestovanin A (**6**)	Xestovanin B (**7**)	Xestovanin C (**8**)	Dehydroxestovanin A (**9**)	Epidehydroxestovanin A (**10**)	Dehydroxestovanin C (**11**)
1	26.0[a]	25.8	26.0	26.0[a]	26.0	26.0	26.0
2	133.1[b]	133.1[a]	133.1[i]	133.1[b]	132.9	133.0	132.9
3	121.1	121.2	121.1[g]	121.2	121.2	121.3	121.3
4	34.9[c]	35.2	32.9[c]	34.9[c]	34.8[a]	34.7[a]	34.8[a]
5	83.0	82.9	82.9[f]	83.1	83.1	83.1	83.1
6	135.4	135.7	135.9[j]	135.4	136.1	136.5	136.1
7	127.0	128.0	126.4[h]	127.0	126.1	125.3	126.1
8	37.7	53.2	37.9	37.8	38.8	38.7	38.9
9	83.3	210.5	83.0	83.4	79.4	79.4	79.4
10	34.9	46.9	34.8	35.0	150.4	150.3	150.5
11	56.2	55.5	56.1	56.3	52.5	52.8	52.5
12	27.9	33.7	28.0	28.0	29.0	32.6	29.0
13	22.3	21.6	22.4	22.4	22.9	23.4	22.9
14	35.7	37.1	35.5	35.4	36.4	34.7[a]	36.4
15	55.8	52.6	55.8	55.9	56.2	55.5	56.2
16	213.3	83.6	212.5	213.0	212.7	212.6	212.7
17	52.0	32.3	52.4	52.0	57.6	59.0	57.6
18	122.1	122.5	126.2[h]	122.2	120.3	119.7	120.4
19	141.1	138.4	136.8[j]	141.1	142.7	143.9	142.7
20	78.3	77.9	81.4[f]	78.4	77.5	77.5	77.5
21	32.5[c]	35.2	32.7[c]	32.6[c]	32.7[a]	32.9[a]	32.7[a]
22	122.1	122.2	121.7[g]	122.1	122.1	121.9	122.1
23	132.7[b]	133.0[a]	133.6[i]	132.7[b]	132.9	133.0	132.9
24	25.9[a]	26.0	26.0	25.9[a]	26.0	26.0	26.0
25	18.0[d]	18.0	18.0[b]	18.0	18.0	18.1	18.0[b]
26	11.0	12.2	11.2[a]	11.0	11.1	11.1	11.1
27	13.7	13.5	13.7	13.7	111.0	110.3	111.0
28	25.9[a]	21.6	25.9	26.0	25.9	26.6	25.9
29	11.5	11.1	11.3[a]	11.6	12.7	13.0	12.7
30	18.1[d]	18.0	18.2[b]	18.0	18.0	18.1	18.1[b]
1′	99.7	99.4	99.9	99.8	99.9	110.1	99.9
2′	71.9	72.0	71.9[d]	71.8	71.9	71.0	71.9
3′	76.0	76.2	76.1	76.1[d]	76.0	75.9	75.9
4′	78.1	78.3	78.0	78.6	78.1	78.2	78.6
5′	71.2	70.8	71.2	72.4	70.9	70.8	72.4
6′	17.8	17.8	17.8[b]	17.8	17.7	17.7	17.7
1″	102.5	102.5	102.5	102.5	102.5	102.5	102.4
2″	71.7	72.0	71.8[d]	72.5	71.9	71.0	72.5
3″	72.4	72.5	72.5[d]	73.0	72.5	72.5	73.0
4″	73.5	73.7	73.6[e]	79.7[d]	73.6	73.6	79.6
5″	69.7	69.7	69.7	68.3	69.7	69.7	68.2
6″	18.1	18.1	18.0[b]	18.7	18.0	18.0	18.7
1‴			96.9	102.2			102.2
2‴			72.2[d]	72.0			72.0
3‴			72.6[d]	71.2			70.8
4‴			73.9[e]	73.7			73.6
5‴			69.1	69.8			69.7
6‴			17.9[b]	18.0			18.0

[a–j]May be interchanged within a column. Hydrogen attachments were determined via APT. Assignments are partially based on HETCOR data. The di- and trisaccharide assignments are tentative.

constant in **6** (10:1 acetone-d_6/benzene-d_6). Irradiation of the Me27 resonance (δ 1.05) caused the H10 resonance (δ 2.17) to collapse to a doublet with $J = 11.1$ Hz, indicative of a *trans* diaxial coupling. The H10/H11 coupling constant in xestovanin A (**1**), where H10 is axial and H11 is equatorial, was found to be 5.9 Hz. Taken together, the above results completely defined the relative stereochemistry and conformation of the bicyclic portion of **6** to be that shown in Fig. 1.

Isoxestovanin A (**6**) has the new isoxestovanane triterpenoid carbon skeleton. As with the previously reported xestovanins (2), the absolute configurations of the sugar carbons are correct as shown in the structure for **6**, the relative stereochemistries at C8, C10, C11, C15, and C16 are correct as drawn but their configurations relative to the sugars is arbitrary, and no information is available about the configurations at C5 and C20. Repeated attempts to determine the complete stereochemistry of the xestovanins, either by X-ray of a suitable crystalline derivative or by chemical degradation, have been unsuccessful. It is interesting to note that isoxestovanin A (**6**) and xestovanin A (**1**) have the opposite relative configurations at C10. The relative stereochemistry at C10 of secoxestovanin A (**2**) had originally been assigned to be the same as that of xesto-

Can. J. Chem. Downloaded from www.nrcresearchpress.com by 84.41.108.74 on 09/07/12
For personal use only.

Can. J. Chem. Downloaded from www.nrcresearchpress.com by 84.41.108.74 on 09/07/12
For personal use only.

vanin A (**1**), assuming a biogenetic relationship between them (2). It is now clear that the original assumption about the C10 configuration in **2** is unjustified and it must be considered undetermined as shown.

Xestovanin B (**7**) was isolated as an optically active ($[\alpha]_D$ −45.5 (*c* 0.3, MeOH)) colorless oil that gave a pseudomolecular ion at *m/z* 933 Da (M^+ + Na) in the FABMS consistent with a molecular formula of $C_{48}H_{78}O_{16}$. The ^{13}C NMR (48 resolved resonances: Table 2), APT (69 hydrogen atoms attached to carbon: 11 × CH_3, 6 × CH_2, 24 × CH), and ^1H NMR data (eight secondary and one tertiary alcohol protons: Table 1) substantiated the carbon and hydrogen counts in the molecular formula of **7**.

The ^1H NMR spectra of xestovanin B (**7**) recorded in either acetone-d_6 or Me_2SO-d_6 showed a strong resemblance to the ^1H NMR spectra of xestovanin A (**1**) recorded in the same solvents[2] (Table 1), and COSY and NOE experiments conducted on **7** established a series of connectivities and stereochemical relationships that demonstrated the presence of the same aglycone found in xestovanin A (**1**). The chemical shifts of the resonances assigned to H18, H20, H21, and H21′ in **7** showed slight downfield shifts relative to the corresponding resonances in xestovanin A (**1**) (Table 1). In the COSY spectrum of xestovanin B(**7**) (Table 1), the resonances assigned to the H5 and H20 methine protons (δ 4.05 and 3.95) failed to show correlations into hydroxyl protons, indicating that in **7** there were ether linkages at both C5 and C20.

Acetal resonances at δ 95.8(s), 98.7(s), and 101.2(s) and 12 deshielded methine resonances in the region δ 71.2–78.0 in the ^{13}C NMR spectrum (Table 2), and three methyl doublet resonances in the ^1H NMR spectrum (δ 1.11, 1.13, and 1.15) of xestovanin B (**7**) that could not be accounted for by the aglycone were assigned to three 6-deoxyhexose residues. A standard GC analysis (8) (see Experimental) of the monosaccharides liberated from **7** identified only L-rhamnose and D-fucose. Correlations in the COSY spectrum of **7** (Table 1) identified two independent spin systems with chemical shifts that were virtually identical to the chemical shifts observed for the protons in the fucose and rhamnose components of the C5 disaccharide substituent in xestovanin A (**1**) (Table 1). In addition, scalar couplings were observed in the COSY spectrum of **7** between alcohol protons and the methine protons at H2′ and H3′ of the fucose and at H2″, H3″, and H4″ of the rhamnose, and an NOE was observed between the anomeric proton (H1″) of the rhamnose and H4′ of the fucose (Table 4[2]). Two of the acetal resonances in the ^{13}C NMR spectrum of **7** (δ 98.7 and 101.2) had chemical shifts identical to the resonances assigned to the rhamnose and fucose anomeric carbons (δ 98.6 and 101.2) in xestovanin A (**1**) and a gated decoupled ^{13}C NMR spectrum revealed that the one-bond C–H coupling constants for these two anomeric carbons in **7** were in agreement with the α and β anomeric configurations at rhamnose and fucose, respectively (9). Therefore, it was apparent that xestovanin B (**7**) had a disaccharide substructure that was identical to the disaccharide substituent at C5 of xestovanin A (**1**) and it had to be attached at either C5 or C20 of the aglycone. Congestion in the ^1H NMR spectrum of **7** made it impossible to locate the position of attachment of the disaccharide substituent by NOE experiments.

A methyl resonance at δ 1.13(d) and a deshielded methine resonance at δ 4.61 in the ^1H NMR spectrum of xestovanin B (**7**) were assigned to the protons on C6 and C1 of the remaining monosaccharide. Starting with these two resonances, it was possible to assign resonances to the remainder of the protons in the monosaccharide on the basis of correlations observed in the COSY spectrum (Table 1). The resonances assigned to H2, H3, and H4 in this 6-deoxyhexose unit each showed further COSY correlations to alcohol protons, indicating that the monosaccharide was linked to the rest of the molecule only through the anomeric carbon. Irradiation of the anomeric proton (δ 4.61) induced a strong NOE in the H20 resonance (δ 3.95) of the aglycone, consistent with the connection of the sugar through a glycosidic linkage to C20. Attachment of a monosaccharide substituent to C20 implied that by default the disaccharide substituent had to be attached to the aglycone at C5 in xestovanin B (**7**), just as it is in xestovanin A (**1**).

The results of the sugar analysis carried out on xestovanin B (**7**) required that the 6-deoxyhexose attached to C20 had to be either D-fucose or L-rhamnose. The resonance assigned to H4 (δ 3.38: acetone-d_6) of this monosaccharide appeared as a triplet with a coupling constant of 8.5 Hz, indicating that the proton was axial and that the sugar was L-rhamnose. The C–H coupling constant between the remaining anomeric carbon (δ 95.8) resonance and its attached proton was found to be 171.9 Hz, indicating that the L-rhamnose was attached to C20 through an α-glycosidic linkage (9) as shown in the representation **7** of the complete structure of xestovanin B.

Xestovanin C (**8**) was isolated as an optically active ($[\alpha]_D$ −25 (*c* 0.2, MeOH)) colorless glass that also gave a pseudomolecular ion in the FABMS at *m/z* 933 Da (M^+ + Na) appropriate for a molecular formula of $C_{48}H_{78}O_{16}$, suggesting that it was an isomer of xestovanin B (**6**). The electron impact mass spectrum of xestovanin C (**8**) failed to show a parent ion. A fragment ion observed at *m/z* 436.3342 Da ($C_{30}H_{44}O_2$) was the highest mass observed in the HREIMS and it was attributed to the loss of a trisaccharide substituent plus one molecule of water from the parent molecule to give a fragment containing the carbon skeleton of a triterpenoid aglycone. The presence of an intense fragment ion at *m/z* 455 Da in the FABMS of **8**, which could be assigned to a trisaccharide fragment ($C_{18}H_{32}O_{13}$), supported this analysis. The ^{13}C NMR (48 resolved resonances: Table 2), APT (69 protons attached to carbon: 11 × CH_3, 6 × CH_2, 24 × CH), and ^1H NMR data (nine OH protons: Table 1) for **8** confirmed the carbon and hydrogen counts in the molecular formula.

A careful comparison of the ^1H NMR, ^{13}C NMR, COSY, and NOE data (Tables 1, 2, and 4[2]) recorded for xestovanin C (**8**) with the data recorded for xestovanin A (**1**) indicated that the two molecules contained identical triterpenoid aglycones. Further analysis of the ^1H and ^{13}C NMR data recorded for xestovanin C (**8**) suggested that there were three 6-deoxyhexose moieties in the molecule. Resonances at δ 99.8(d), 102.2(d), and 102.5(d) in the ^{13}C NMR spectrum were assigned to the anomeric carbons and resonances at δ 1.11(d), 1.13(d), and 1.14(d) in the ^1H NMR spectrum were assigned to the C6 protons of the three monosaccharides. A standard GC analysis (8) (see Experimental) of the sugars liberated from xestovanin C (**8**) identified only L-rhamnose and D-fucose. Comparison of the chemical shifts of the anomeric proton and carbon resonances (acetone-d_6) assigned to the monosaccharides in xestovanin C (**8**) (δ, ^1H: 4.19, 5.25, and 5.29; ^{13}C: 99.8, 102.2, and 102.5) with the chemical shifts of the anomeric protons and carbons in the fucose (δ, ^1H: 4.17; ^{13}C: 99.7) and rhamnose (δ, ^1H: 5.27; ^{13}C: 102.5) units in xestovanin A (**1**) showed that one fucose and two rhamnose units were present in **8**. The H20 methine resonance in **8**

showed coupling into an alcohol proton and it also underwent an acetylation shift upon conversion of **8** to the octaacetate **13**, whereas the H5 methine proton did not couple to an alcohol proton and it did not undergo an acetylation shift. Therefore, it was apparent that xestovanin C (**8**) had a trisaccharide substituent at C5 of the aglycone.

Irradiation of the fucose anomeric proton (H1′) in xestovanin C octaacetate (**13**) (δ 4.30) induced NOEs in H5 of the aglycone (δ 4.10) and in H3′ (δ 4.93) and H5′ (δ 3.55) of the fucose itself, demonstrating that the fucose was attached to C5 of the aglycone through a β glycosidic linkage. The magnitude of the scalar couplings observed between H1′ and H2′ (J = 7.2 Hz) and between C1′ and H1′ (J = 156.3 Hz) (9) of the fucose residue in **8** confirmed the β-anomeric configuration. Analysis of the sugar methine to alcohol proton correlations observed in the COSY data obtained for xestovanin C (**8**) revealed that H2′ and H3′ of the fucose, H2″ and H3″ of one rhamnose, and H2‴, H3‴, and H4‴ of the second rhamnose were vicinal to alcohol protons (Table 1). All of the resonances assigned to these same protons underwent acetylation shifts as a result of the conversion of xestovanin C (**8**) to its octaacetate **13** (see Experimental). The COSY and acetylation shift data showed that the fucose was linked to the anomeric carbon of one rhamnose through C4′ and that the two rhamnose units were also joined through a 1,4 linkage. One-bond scalar couplings of 170.0 and 171.0 Hz were observed between the anomeric protons (δ H1″ and H1‴) and the anomeric carbons (δ C1″ and C1‴) of the two rhamnose residues, indicating that both had α glycosidic linkages in xestovanin C (**8**) as shown (9).

Dehydroxestovanin A (**9**) was isolated as an optically active ($[\alpha]_D$ −45 (c 0.8, MeOH)) pale yellow glass. ^{1}H and ^{13}C NMR spectra recorded on **9** (Tables 2 and 3) showed strong similarities to those of xestovanin A (**1**) (Tables 1 and 2), suggesting that **9** was a triterpenoid glycoside closely related to **1**. The molecular formula of dehydroxestovanin A (**9**) was determined by considering a number of pieces of MS and NMR evidence. An intense pseudomolecular ion (M^+ + Na), appropriate for a molecular formula of $C_{42}H_{66}O_{12}$, was observed at m/z 785 Da in the FABMS spectrum of **9**. Clearly resolved resonances for 42 carbon atoms were observed in the ^{13}C NMR spectrum, an APT experiment showed that there were 59 hydrogen atoms bonded to carbon (9 × CH_3, 7 × CH_2, 18 × CH) (Table 2), and the ^{1}H NMR and COSY spectra revealed that the seven remaining hydrogen atoms were associated with one tertiary and six secondary alcohol functionalities (Table 3). The highest mass peak that was observed in the EIHRMS of **9** appeared at m/z 434.3191 Da ($C_{30}H_{42}O_2$, ΔM +0.6 mmu) and it was attributed to the loss of a disaccharide substituent and one equivalent of water from the parent molecule to give a fragment containing the carbon skeleton of the triterpenoid aglycone. Both the pseudomolecular ion in the FABMS and the aglycone fragment ion in the HREIMS of **9** were found at two mass units less than the corresponding ions in the mass spectra of xestovanin A (**1**), indicating that the aglycone of **9** was a dehydro derivative of the aglycone of **1**.

The characteristic resonances assigned to the Me27 and H10 protons in the ^{1}H NMR spectra of xestovanin A (**1**) (Table 1) were missing in the ^{1}H NMR spectrum of dehydroxestovanin A (**9**) (Table 3) and the ^{13}C NMR spectrum of **9** contained one less aliphatic methine resonance, one less aliphatic methyl resonance, and two more olefinic resonances than the ^{13}C NMR spectrum of xestovanin A (**1**) (Table 2). Analysis of the COSY spectrum (Table 3) showed that a pair of olefinic resonances at δ 5.04 and 5.17 were coupled to each other and that they were both coupled to a methine resonance assigned to H11 (δ 2.67), indicating that dehydroxestovanin A (**9**) possessed an olefinic bond between C10 and C27. Irradiation of H27*E* (δ 5.17) induced an NOE in H11 (δ 2.67) in agreement with the presence of a $\Delta^{10,27}$ olefinic functionality (Table 4[2]). Resonances at δ 150.4 and 111.0 in the ^{13}C NMR spectrum of **9** were assigned to C10 and C27, respectively.

Comparison of the ^{1}H NMR, COSY, NOE, and ^{13}C NMR data obtained for dehydroxestovanin A (**9**) (Tables 2 and 3) with the same data obtained for xestovanin A (**1**) (Tables 1 and 2) showed that, except for the oxidation level of the C10/C27 bond, the remaining portions of the aglycones in the two molecules were identical. Standard sugar analysis (8) (see Experimental) identified D-fucose and L-rhamnose residues and inspection of the NMR data (Tables 2 and 3) assigned to the sugars showed that dehydroxestovanin A (**9**) contained the same disaccharide substituent found in xestovanin A (**1**). COSY (Table 3) evidence demonstrated that the disaccharide was attached to C5 in dehydroxestovanin A (**9**) just as in xestovanin A (**1**).

Secodehydroxestovanin A (**12**) was isolated as a colorless oil that gave a pseudomolecular peak (M^+ + Na) in the FABMS consistent with a molecular formula of $C_{42}H_{66}O_{12}$. The ^{13}C NMR, APT, and ^{1}H NMR data agreed with the assigned molecular formula. A detailed analysis of the ^{13}C NMR (Experimental), ^{1}H NMR (Table 3), and COSY data (Table 3) showed that **12** was the $\Delta^{10,27}$ analogue of secoxestovanin A (**2**). Thus, COSY and NOE experiments (Tables 3 and 4[2]) identified two 10-carbon aglycone fragments (C1–C8 plus Me25 and Me26: C17–C24 plus Me29 and Me30) and their attached alcohol and disaccharide substituents, which were identical to the corresponding fragments in secoxestovanin A (**2**). The chemical shifts of two carbonyl resonances in the ^{13}C NMR spectrum of **12** indicated the presence of one saturated (δ 211.5: C16) and one unsaturated (δ 199.6: C9) ketone, and two deshielded singlets in the ^{1}H NMR spectrum (δ 5.68 and 6.15: acetone-d_6) were assigned to the methylene protons on the $\Delta^{10,27}$ olefin that was conjugated to the unsaturated ketone. A COSY experiment optimized for long-range couplings showed a correlation between H27*Z* (δ 5.68) and a methine assigned to H11 (δ 3.17: acetone-d_6), and in the normal COSY spectrum it was possible to find correlations starting with the H11 methine and continuing around the cyclopentane ring to the C14 methylene protons (Table 3). An NOE between the H11 methine resonance (δ 3.17) and a methyl singlet resonance at δ 1.33, which was assigned to Me28, confirmed their *cis* relationship on the cyclopentane ring. Irradiation of the H27*Z* resonance at δ 6.15 induced an NOE in a resonance at δ 3.40 that was assigned to one of the H8 methylene protons on the basis of COSY correlations. The observation of an NOE between H27*Z* and H8 demonstrated that the 10-carbon fragment (C1–C8 plus Me25 and Me26) containing the disaccharide substituent was attached to the enone system at C9 as shown in **12**.

New metabolites from the Anthony Island specimens

Epidehydroxestovanin A (**10**) was isolated as an optically active ($[\alpha]_D$ −3.8 (c 3.8, MeOH)) pale yellow glass. An intense pseudomolecular ion at m/z 785 Da ($C_{42}H_{66}O_{12}$ + Na) was observed in the FABMS of **10** even though the highest mass ion observed in the EIHRMS was at m/z 434.3189 Da,

Can. J. Chem. Downloaded from www.nrcresearchpress.com by 84.41.108.74 on 09/07/12
For personal use only.

TABLE 3. ^{1}H NMR data. All spectra were recorded in Me_2SO-d_6 at 400 MHz.

Carbon No.	Dehydroxestovanin A (**9**)		Epidehydroxestovanin A (**10**)	
	^{1}H δ	COSY	^{1}H δ	COSY
1	1.60, s	H3	1.63, s	H3, H4*, H4′*
3	4.90, bt(7.0)	Me1, H4, H4′, Me25	4.89, bt(7.1)	Me1, H4, H4′, Me25
4	2.18, m	H3, H4′, H5	2.16, m	H1*, H3, H4′, H5, Me25*
4′	2.21, m	H3, H4, H5	2.22, m	Me1*, H3, H4, H5, Me25*
5	3.95, dd(8.8, 5.7)	H4, H4′	3.93, m	H4, H4′
7	5.26, bt(5.9)	H8, H8′, Me26*	5.32, t(6.6)	H8, H8′, Me26
8	2.20, m	H7, H8′, Me26*	2.26, m	H7, Me26*
8′	2.34, dd(14.5, 5.6)	H7, H8, Me26	2.26, m	H7, Me26*
9OH	4.64, s		4.57, s	
11	2.57, bt (6.1)	H12, H12′, H27*E**	2.45, bt(6.8)	H12, H12′, H27*E**
12	1.89, m	H11, H12′, H13*, H13′*	1.90, m	H11, H12′, H13, H13′
12′	2.01, m	H11, H12, H13, H13′	2.03, m	H11, H12, H13, H13′
13	1.53, m	H12*, H12′, H13′, H14, H14′	1.50, m	H12, H12′, H13′, H14, H14′
13′	1.59, m	H12, H12′, H13, H14, H14′	1.61, m	H12, H12′, H13, H14, H14′
14	1.24, m	H13, H13′H14′	1.37, ddd(12.2, 7.5, 4.5)	H13, H13′, H14′
14′	1.93, m	H13, H13′, H14	2.04, m	H13, H13′, H14
17	3.56, d(8.8)	H18	3.38, d(9.5)	H18
17′	—		—	
18	5.44, d(8.8)	H19, Me29	5.27, d(9.5)	H17, H29
20	3.84, bdt(6.6, 4.1)	H21, H21′, 20OH	3.81,bdt(6.2, 4.0)	H21, H21′, 20OH
20OH	4.64, d(4.6)	H20	4.56, d(4.0)	H20
21	2.09, m	H20, H22, Me24*, Me30*	2.09, m	H20, H22, Me24*, Me30*
21′	2.09, m	H20, H22, Me24*, Me30*	2.09, m	H20, H22, Me24*, Me30*
22	5.02, bt(5.7)	H21, H21′, Me24, Me30	5.01, bt(7.0)	H21, H21′, Me24, Me30
24	1.60, s	H22	1.59, s	H21*, H21′*, H22
25	1.54, s	H3	1.54, s	H3, H4*, H4′*
26	1.49, s	H7, H8, H8′	1.46, s	H7, H8*, H8′*
27*E*	5.04, s	H11, H27*Z*	5.07, s	H11*, H27*Z*
27*Z*	5.17, s	H11*, H27*E*	5.14, s	H27*E*
28	1.12, s		1.05, s	—
29	1.48, s	H17*, H18	1.52, s	H17*, H18
30	1.53, s	H22	1.52, s	H21*, H21′*, H22
1′	3.92, d(7.7)	H2′	3.94, d(7.6)	H2′
2′	3.21, ddd(9.6, 7.7, 4.7)	H1′, H3′, 2′OH	3.23, ddd(9.6, 7.6, 4.6)	H1′, H3′, 2′OH
2′OH	4.81, d(4.7)	H2′	4.76, d(4.7)	H2′
3′	3.33, m	H2′, H4′, 3′OH	3.35, m	H2′, H4′, 3′OH
3′OH	4.97, d(4.3)	H3′	4.94, d(4.2)	H3′
4′	3.56, m	H3′, H5′	3.55, m	H3′, H5′
5′	3.44, bq(6.2)	H4′, H6′	3.43, bq(6.2)	H4′, H6′
6′	1.12, d(6.2)	H5′	1.09, d(6.2)	H5′
1″	5.07, d(1.4)	H2″	5.07, bs	H2″
2″	3.75, m	H1″, H3″, 2″OH	3.75, m	H1″, H3″, 2″OH
2″OH	4.55, d(4.2)	H2″	4.53, d(4.2)	H2″
3″	3.45, m	H2″, H4″, 3″OH	3.45, m	H2″, H4″, 3″OH
3″OH	4.47, d(5.8)	H3″	4.46, d	H3″
4″	3.17, dt(9.5, 5.9)	H3″, H5″, 4″OH	3.17, ddd(9.5, 9.3, 5.7)	H3″, H5″, 4″OH
4″OH	4.63, d(5.9)	H4″	4.61, d(5.7)	H4″
5″	3.58, m	H4″, H6″	3.57, m	H4″, H6″
6″	1.09, d(6.2)	H5″	1.09, d(6.2)	H5″
1‴				
2‴				
2‴OH				
3‴				
3‴OH				
4‴				
4‴OH				
5‴				
6‴				

[a]May be interchanged within a column.
*Observed in a long-range COSY only.

Can. J. Chem. Downloaded from www.nrcresearchpress.com by 84.41.108.74 on 09/07/12
For personal use only.

Chemical shifts are reported in ppm from internal TMS

Dehydroxestovanin C (**11**)		Secodehydroxestovanin A (**12**)	
^{1}H δ	COSY	^{1}H δ	COSY
1.61, s	H3, H4*, H4′*	1.63, s	H3
4.90, bt(6.6)	Me1, H4, H4′, Me25	4.95, t(7.2)	H1, H4, H4′, Me25
2.16, m	H1*, H3, H4′, H5	2.25, m	H3, H4′, H5
2.19, m	Me1*, H3, H4, H5	2.17, m	H3, H4, H5
3.95, dd(8.7, 6.1)	H4, H4′	4.02, dd(8.8, 6.0)	H4, H4′
5.26, bt(6.8)	H8, H8′, Me26	5.35, t(6.3)	H8, H8′, Me26
2.20, m	H7, H8′, Me26*	3.57, m	H7, H8′
2.34, dd(15.0, 6.8)	H7, H8, Me26*	3.31, m	H7, H8
4.64, s		—	
2.62, m	H12, H12′	3.07, t(7.6)	H12, H12′
1.86, m	H11, H12′, H13, H13′	1.87, m	H11, H12′
2.01, m	H11, H12, H13, H13′	1.58, m	H11, H12
1.57, m	H12, H12′, H14, H14′	1.75, m	H13′, H14, H14′
1.57, m	H12, H12′, H14, H14′	1.68, m	H13, H14
1.24, m	H13, H13′, H14′	2.25, m	H13, H13′, H14′
1.94, m	H13, H13′, H14	1.41, m	H13, H14
3.56, d(8.9)	H18	3.05, dd(17.4, 7.0)	H17′, H18
—		2.93, dd(17.4, 7.2)	H17, H18
5.44, d(8.8)	H17, H29	5.31, bt(6.5)	H17, H17′, Me29
3.84, dt(7.1, 4.9)	H21, H21′, 20OH	3.79, m	H21, H21′, 20OH
4.63, d(5.0)	H20	4.60, d(4.2)	H20
2.09, m	H20, H22, Me24*, Me30*	2.07, m	H20, H22
2.09, m	H20, H22, Me24*, Me30*	2.07, m	H20, H22
5.02, m	H21, H21′, Me24, Me30	5.03, bt(7.0)	H21, H21′, Me24, Me30
1.60, s	H21*, H21′*, H22	1.63, s	H3
1.54, s	H3	1.55, s	H22
1.47, s	H7, H8*, H8′*	1.54, s	H7
5.04, bs	H27*Z*	6.12, s[a]	
5.17, bs	H27*E*	5.66, s[a]	
1.10, s	—	1.24, s	
1.48, s	H18	1.46, s	H18
1.53, s	H21*, H21′*, H22	1.54, s	H22
3.92, d(7.6)	H2′	3.97, d(7.7)	H2′
3.22, m	H1′, H3′, 2′OH	3.24, m	H1′, 2′OH
4.80, d(4.7)	H2′	4.79, d(4.7)	H2′
3.30, m	H2′, H4′, 3′OH	3.33, m	H4′, 3′OH
4.99, d(4.3)	H3′	4.95, d(4.2)	H3′
3.57, m	H3′, H4′	3.50, m	H3′
3.39, m	H4′, H6′	3.47, m	H6′
1.09, d(6.1)	H5′	1.12, d(5.2)	H5′
5.06, bs	H2″	5.08, d(1.3)	H2″
3.74, bs	H1″, H3″, 2″OH	3.77, m	H1″, H3″, 2″OH
4.76, d(4.5)	H2″	4.55, d(4.2)	H2″
3.60, m	H2″, H4″, 3″OH	3.47, m	H2″, H4″, 3″OH
4.69, d(6.8)	H3″	4.47, d(5.6)	H3″
3.39, t(9.3)	H3″, H5″	3.19, m	H3″, H5″, 4″OH
—		4.63, d(5.6)	H4″
3.62, m	H4″, H6″	3.59, m	H4″, H6″
1.13, d(6.1)	H5″	1.11, d(6.1)	H5″
5.06, bs	H2‴		
3.71, bs	H1‴, 2‴OH, H3‴		
4.56, d(4.3)	H2‴		
3.38, m	H2‴, 3‴OH, H4‴		
4.43, d(5.8)	H3‴		
3.18, m	H3‴, H5‴		
4.62, d(5.9)	H4‴		
3.49, dq(9.3, 6.2)	H4‴, H6‴		
1.10, d(6.2)	H5‴		

Can. J. Chem. Downloaded from www.nrcresearchpress.com by 84.41.108.74 on 09/07/12
For personal use only.

corresponding to an elemental composition of $C_{30}H_{42}O_2$ (ΔM +0.5 mmu). The pseudomolecular ion in the FABMS of **10** had the same mass as the pseudomolecular ion in the FABMS of dehydroxestovanin A(**9**), and the highest mass ion observed in the EIHRMS of **10**, attributed to the aglycone portion of the molecule, had the same mass and elemental composition as the highest mass ion in the EIHRMS of **9**. Furthermore, a comparison of the ^{13}C and ^{1}H NMR data for epidehydroxestovanin A (**10**) with the NMR data for dehydroxestovanin A (**9**) (Tables 2 and 3) revealed that the two molecules had nearly identical triterpenoid glycoside structures.

A detailed analysis of the COSY data for epidehydroxestovanin A (**10**) showed that the triterpenoid aglycone portion of the molecule possessed the same scalar coupled spin systems as the aglycone in dehydroxestovanin A (**9**) (Table 3). The only notable differences in the ^{1}H NMR data for the two molecules were slight changes in the chemical shifts of several resonances assigned to protons in the region of the bicyclic ring system. In particular, the resonances assigned to H11, H17, H18, and Me28 were slightly more shielded in epidehydroxestovanin A (**10**) (acetone-d_6: δ 2.54(H11), 3.58(H17), 5.52(H18), 1.13(Me28)) than the resonances assigned to the same protons in dehydroxestovanin A (**9**) (acetone-d_6: δ 2.67(H11), 3.67(H17), 5.60(H18), 1.21(Me28)). Since all of the MS and NMR data indicated that compounds **9** and **10** had identical constitutions, it was apparent that they were stereoisomers. Inspection of the ^{1}H and ^{13}C NMR data for **10**, along with the results of a standard GC analysis of the monosaccharides released upon hydrolysis (D-fucose and L-rhamnose), confirmed that the acyclic fragments C1–C8 and C18–C24, including the C5 disaccharide substituent, had identical stereochemical configurations in dehydroxestovanin A (**9**) and epidehydroxestovanin A (**10**) (Tables 2 and 3). Therefore, the stereochemical difference had to be in the bicyclic region of the aglycone.

The nearly identical ^{13}C NMR chemical shifts of the resonances assigned to C8, C9, C10, and C11 in epidehydroxestovanin A (**10**) (δ 38.7(C8), 79.4(C9), 150.3(C10), 52.8(C11)) and in dehydroxestovanin A (**9**) (δ 38.8(C8), 79.4(C9), 150.4(C10), 52.5(C11)) indicated that the relative configurations at C9 and C11 were identical in the two molecules. However, a series of NOE experiments carried out on **10** showed that the one point of stereochemical difference between **9** and **10** was the configuration at C17. Thus, irradiation of H11 (δ 2.54) induced NOEs in H27*E* (δ 5.15), H12 (δ 1.99), and Me28 (δ 1.13) confirming the usual *cis* relationship between H11 and Me28. Irradiation of Me28 (δ 1.13) induced NOEs in H11 (δ 2.54), H14 (δ 1.42), and H18 (δ 5.52). The observation of an NOE between Me28 and H18 in **10** was in contrast to the NOE results observed for dehydroxestovanin A (**9**), where irradiation of Me28 induced an NOE in H17, and this Me28/H18 NOE in **10** required that the side chain containing C18 be *cis* to Me28 as shown in Fig. 2.

Dehydroxestovanin C (**11**) was isolated as an optically active ($[\alpha]_D$ −24.6 (*c* 0.08, MeOH)) colorless glass that gave an intense pseudomolecular ion in the FABMS at *m/z* 931 Da ($C_{48}H_{76}O_{16}$ + Na) and a highest mass peak in the EIHRMS at *m/z* 434.3191 Da ($C_{30}H_{42}O_2$: ΔM +0.6 mmu). The structure of dehydroxestovanin C (**11**) was readily assigned by comparing its ^{1}H and ^{13}C NMR data (Tables 2 and 3) with the corresponding NMR data for xestovanin C (**8**) and dehydroxestovanin A (**9**) (Tables 1–3). This comparison showed that **11** contained an aglycone portion that was identical to the aglycone of dehydroxestovanin A (**9**) and a trisaccharide portion that was identical to the trisaccharide portion of xestovanin C (**7**). COSY, NOE, and HETCOR data obtained for **11** supported the assigned structure, and GC analysis (8) (see Experimental) of the sugars released from **11** identified only L-rhamnose and D-fucose as expected.

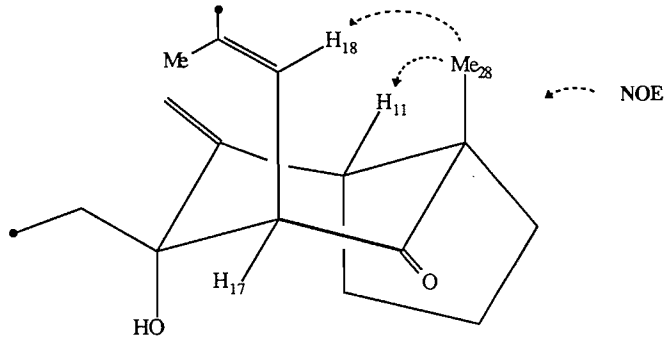


FIG. 2.

Discussion

The new *X. vanilla* triterpenoid glycosides reported here include the first example of the isoxestovanane carbon skeleton (i.e., **6**) and the first example of a xestovanin containing a trisaccharide substituent (i.e., **8**). Scheme 1 shows a proposed biogenetic pathway to the *X. vanilla* triterpenoid aglycones starting from squalene. The secoxestovanane skeleton can readily arise from a single proton initiated cyclization and the xestovanane and isoxestovanane skeletons represent alternate intramolecular aldol cylization pathways on a 9,16-diketosecoxestovanane precursor. It is interesting to note that all of the triterpenoids from the Anthony Island specimens (i.e., **9**, **10**, **11**, and **12**) have a $\Delta^{10,27}$ olefinic functionality, while the major triterpenoids from the Bamfield specimens (i.e., **1**, **2**, **6**, **7**, and **8**) have the $\Delta^{10,27}$ olefin reduced. Detailed examination of repeated collections of *X. vanilla* from Bamfield failed to show any major seasonal variation in metabolite content. Therefore, one possible explanation for the observed geographic variation would be an absence in the Anthony Island population of *X. vanilla* of the enzyme that reduces the $\Delta^{10,27}$ olefin. Some members of the *X. vanilla* family of triterpenoid glycosides exhibit moderate antifungal and antibacterial activities (see Experimental).

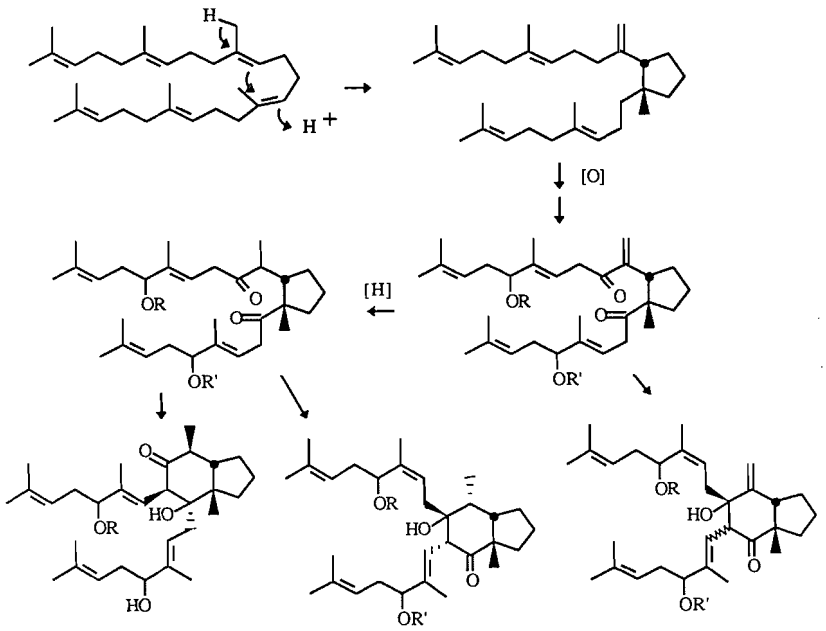
Experimental

Freshly collected sponge (1000 g) was homogenized with methanol in a Waring blender. Concentration of the methanol extract *in vacuo* gave an aqueous suspension that was exhaustively extracted first with hexane and then with dichloromethane. Purification of the dichloromethane soluble material by Sephadex LH20 chromatography (9:1 MeOH/CH_2Cl_2) gave a series of early eluting fractions containing crude mixtures of triterpenoid glycosides. The mixtures of glycosides were further purified by sequential application of open column reversed-phase chromatography (multi-step gradient: 2:3 acetone/H_2O to 7:3 acetone/H_2O) and reversed-phase HPLC (eluents: either 55:45 acetone/H_2O (compounds **1**, **2**, **6**, **7**, **8**, **11**, **12**) or 3:1 MeOH/H_2O (compounds **9**, **10**)) to give pure metabolites.

Determination of the absolute configurations of the sugars

A small sample (5–10 mg) of triterpenoid glycoside was hydrolyzed with 3 M aqueous trifluoroacetic acid at 60°C for 4 h. (Note: The C5 disaccharide could also be obtained by treating the xestovanins with 1 mL of MeOH and 1 mL of 0.5 M $KOH_{(aq)}$ followed by heating to 90°C for 2 h.) Removal of the water and trifluoroacetic acid under reduced pressure gave a clear gum that was reacted with

Can. J. Chem. Downloaded from www.nrcresearchpress.com by 84.41.108.74 on 09/07/12
For personal use only.



SCHEME 1

250 μL of (+)-2-octanol and 1 drop of trifluoroacetic acid in a sealed vial at 130°C for 12 h (8). Removal of the reagents *in vacuo* gave a mixture of 2-octylglycosides that were reacted with acetic anhydride and pyridine (0.5 mL of each) at 100°C for 30 min. Excess reagents were removed *in vacuo* to yield a mixture of peracetylated (+)-2-octylglycosides. Standards were prepared in an identical fashion from D- and L-fucose and L-rhamnose. A sample of D-rhamnose was not available; therefore, L-rhamnose was derivatized with (−)-2-octanol to provide the enantiomer of (+)-2-octyl-D-rhamnoside. The product mixture and standards were analysed by capillary GC (HP SE54 column; temperature programme: 120°C for 2 min followed by an increase in temperature of 20°C/min to a final temperature of 250°C). The observed retention times for the standards were as follows: peracetylated (+)-2-octyl-D-fucoside (5.24, 5.33, 5.40 min); peracetylated (+)-2-octyl-L-fucoside (5.31, 5.45, 5.63 min); peracetylated (+)-2-octyl-L-rhamnoside (5.00, 5.07, 5.21, 5.36 min); peracetylated (−)-2-octyl-L-rhamnoside (5.14, 5.28, 5.52 min). The observed retention times (in minutes) for the peracetylated (+)-2-octylglycosides obtained from the isoxestovan A (**6**) hydrolysate were 5.02, 5.08, 5.23, 5.34, and 5.40. These retention times corresponded to the expected values for a mixture of D-fucose and L-rhamnose. Similar values were obtained for all of the other new *X. vanilla* triterpenoid glycosides.

Xestovanin A (***1***): The data obtained for this compound were the same as those found previously. Additional data are the following: $[\alpha]_D$ −42.0 (*c* 0.30, MeOH); ^{13}C NMR (acetone-d_6, 75 MHz), see Table 2.

Isoxestovanin A (***6***): Colorless glass; $[\alpha]_D$ −4.4 (*c* 0.16, MeOH); IR (film), ν_{max}: 3406, 1710, 1512, 1448, 1070, 1030 cm^{-1}; ^{1}H NMR (acetone-d_6, 400 MHz), see supplemental material; ^{1}H NMR (DMSO-d_6, 400 MHz), see Table 1; ^{13}C NMR (acetone-d_6, 75 MHz), see Table 2; LRFABMS, pseudomolecular ion, *m/z*: 787 ($M^+(C_{42}H_{68}O_{12})$ + 23 (Na)), 437 ($C_{30}H_{45}O_2$), 418 ($C_{30}H_{42}O$), 367 ($C_{25}H_{35}O_2$), 311 ($C_{12}H_{23}O_9$); LREIMS, *m/z* (formula, relative intensity): 436 ($C_{30}H_{44}O_2$, 29), 418 ($C_{30}H_{42}O$, 4), 367 ($C_{25}H_{35}O_2$, 88), 349 ($C_{25}H_{33}O$, 10), 163 ($C_{11}H_{15}O$, 40); HREIMS *m/z*: 436.3336 ($C_{30}H_{44}O_2$, Δ*M* −0.5 mmu: $M^+ - C_{12}H_{22}O_9 - H_2O$).

Xestovanin B (***7***): Colorless oil; $[\alpha]_D$ −45.5 (*c* 0.29, MeOH); ^{1}H NMR (Me_2SO-d_6), see Table 1; ^{13}C NMR (acetone-d_6, 75 MHz), see Table 2; LRFABMS, pseudomolecular ion, *m/z*: 933 ($C_{48}H_{78}O_{16}$ + Na).

Xestovanin C (***8***): Colorless glass; $[\alpha]_D$ −25.0 (*c* 0.12, MeOH); IR (film), ν_{max}: 3423, 2933, 1708, 1366, 1225, 1045, 838, 801, 766 cm^{-1}; ^{1}H NMR (acetone-d_6, 400 MHz), see supplemental material; ^{1}H NMR (DMSO-d_6, 400 MHz), see Table 1; ^{13}C NMR (acetone-d_6, 75 MHz), see Table 2; LRFABMS, pseudomolecular ion, *m/z*: 933 (M^+ ($C_{48}H_{78}O_{16}$) + 23 (Na)), 455 ($C_{18}H_{31}O_{13}$), 436 ($C_{30}H_{44}O_2$); LREIMS, *m/z* (formula, relative intensity): 436 ($C_{30}H_{44}O_2$, 34), 418 ($C_{30}H_{42}O$, 7), 385 ($C_{25}H_{37}O_3$, 9), 367 ($C_{25}H_{35}O_2$, 33), 349 ($C_{25}H_{33}O$, 18), 301 ($C_{20}H_{29}O_2$, 14), 229 ($C_{16}H_{21}O$, 14), 203 ($C_{14}H_{19}O$, 26), 163 ($C_{11}H_{15}O$, 15), 147 ($C_{11}H_{15}$, 14), 139 ($C_9H_{15}O$, 10); HREIMS, *m/z*: 436.3342 ($C_{30}H_{44}O_2$, Δ*M* 0.0 mmu: $M^+ - C_{18}H_{32}O_{13} - H_2O$).

Xestovanin C octaacetate (***13***): A 5-mg sample of xestovanin C was acetylated at room temperature with acetic anhydride and pyridine. The pure compound was isolated as a pale yellow glass; IR (film), ν_{max}: 3385, 3000, 2929, 1751, 1716, 1371, 1242, 1227, 1072, 1041 cm^{-1}, ^{1}H NMR ($CDCl_3$, 400 MHz), δ: 1.08 (d, *J* = 7.0 Hz, 3H, H27), 1.20 (m, 1H, H14), 1.21 (d, *J* = 6.3 Hz, 3H, H6‴), 1.33 (d, *J* = 6.4 Hz, 3H, H6″), 1.34 (d, *J* = 6.4 Hz, 3H, H6′), 1.35 (s, 3H, H28), 1.42 (m, 1H, H13), 1.50 (m, 1H, H13), 1.50 (br s, 3H, H26), 1.52 (br s, 3H, H29), 1.60 (br s, 3H, H25), 1.61 (br s, 3H, H30), 1.64 (br s, 3H, H1), 1.67 (br s, 3H, H24), 1.70 (m, 1H, H12), 1.81 (m, 1H, H12), 1.99 (m, 1H, H11), 1.99 (s, 3H, −OCO*CH*$_3$), 2.01 (s, 3H, −OCO*CH*$_3$), 2.03 (s, 3H, −OCO*CH*$_3$), 2.05 (s, 3H, −OCO*CH*$_3$), 2.06 (s, 3H, −OCO*CH*$_3$), 2.10 (s, 3H, −OCO*CH*$_3$), 2.14 (s, 3H, OCO*CH*$_3$), 2.15 (m, 1H, H8), 2.17 (s, 3H, −OCO*CH*$_3$), 2.22 (m, 1H, H4), 2.27 (dq, *J* = 7.0, 5.9 Hz, 1H, H10), 2.28 (m, 1H, H8), 2.30 (m, 1H, H21), 2.42 (m, 1H, H21), 2.43 (m, 1H, H4), 3.55 (dq, *J* = 6.4, <1 Hz, 1H, H5′), 3.60 (d, *J* = 9.6 Hz, 1H, H17), 3.70 (t, *J* = 9.4 Hz, 1H, H4″), 3.81 (dd, *J* = 3.0, <1 Hz, 1H, H4′), 3.98 (dq, *J* = 9.8, 6.3 Hz, 1H, H5‴), 4.00 (dq, *J* = 9.5, 6.4 Hz, 1H, H5″), 4.20 (dd, *J* = 9.3, 5.6 Hz, 1H, H5), 4.30 (d, *J* = 7.9 Hz, 1H, H1′), 4.82 (d, *J* = 2.0 Hz, 1H, H1″), 4.90 (br t, *J* = 7.9 Hz, 1H, H3), 4.93 (dd, *J* = 10.4, 3.1 Hz, 1H, H3′), 5.00 (d, *J* = 1.8 Hz, 1H, H1‴), 5.01 (br t, *J* = 7.3 Hz, 1H, H22), 5.07 (t, *J* = 9.8 Hz, 1H, H4‴), 5.16 (dd, *J* = 3.3, 2.0 Hz, 1H, H2‴), 5.17 (br t, *J* = 6.9 Hz, 1H, H20), 5.20 (dd, *J* = 10.4, 7.9 Hz, 1H, H2′), 5.26 (br d, *J* = 9.4 Hz, 1H, H7), 5.26 (dd, *J* = 9.8, 3.3 Hz, 1H, H3‴), 5.30 (dd, *J* = 9.4, 3.2 Hz, 1H, H3″), 5.42 (dd, *J* = 3.2, 2.0 Hz, 1H, H2″), 5.65 (br d, *J* = 9.8 Hz, 1H, H18) ppm; LRFABMS, pseudomolecular ion, *m/z*: 1269 ($M^+(C_{64}H_{94}O_{24})$ + 23 (Na)).

Dehydroxestovanin A (***9***): Pale yellow glass; $[\alpha]_D$ −45.0 (*c* 0.78, MeOH); IR (film), ν_{max}: 3406, 2979, 2938, 2896 (sh), 1701, 1660 (sh), 1464, 1381, 1253, 1129, 1072, 1046, 1031, 981 cm^{-1}; ^{1}H NMR (acetone-d_6, 400 MHz), see supplemental material; ^{1}H NMR (DMSO-d_6, 400 MHz), see Table 3; ^{13}C NMR (acetone-d_6, 75 MHz), see Table 2; LRFABMS, pseudomolecular ion, *m/z*: 785 ($M^+(C_{42}H_{66}O_{12})$ + 23(Na)), 435 ($M^+ - C_{12}H_{21}O_9 - H_2O$), 309 ($C_{12}H_{21}O_9$); LREIMS,

Can. J. Chem. Downloaded from www.nrcresearchpress.com by 84.41.108.74 on 09/07/12
For personal use only.

m/z (formula, relative intensity): 434 ($C_{30}H_{42}O_2$, 41), 416 ($C_{30}H_{40}O$, 14), 365 ($C_{25}H_{33}O_2$, 69), 349 ($C_{25}H_{33}O$, 10), 265 ($C_{19}H_{21}O$, 13); HREIMS, m/z: 434.3191 ($C_{30}H_{42}O_2$, ΔM +0.6 mmu: $M^+ - C_{12}H_{22}O_9 - H_2O$)

*Epidehydroxestovanin A (**10**)*: Pale yellow glass; $[\alpha]_D$ −3.8 (*c* 3.8, MeOH); IR (film), ν_{max}: 3493, 2919, 1703, 1509, 1376, 1229, 1070, 991, 909, 838, 808 cm^{-1}; ^1H NMR (acetone-d_6, 400 MHz), see supplemental material; ^1H NMR (DMSO-d_6, 400 MHz), see Table 3; ^{13}C NMR (acetone-d_6, 75 MHz), see Table 2; LRFABMS, pseudomolecular ion, m/z: 785 ($M^+(C_{42}H_{66}O_{12})$ + 23(Na)), 435 ($M^+ - C_{12}H_{21}O_9 - H_2O$), 309 ($C_{12}H_{21}O_9$); LREIMS, m/z (formula, relative intensity): 434 ($C_{30}H_{42}O_2$, 10), 365 ($C_{25}H_{33}O_2$, 24), 349 ($C_{25}H_{33}O$, 4); HREIMS, m/z: 434.3189 ($C_{30}H_{42}O_2$, ΔM +0.5 mmu: $M^+ - C_{12}H_{22}O_9 - H_2O$)

*Dehydroxestovanin C (**11**)*: Colorless glass; $[\alpha]_D$ −24.6 (*c* 0.08, MeOH); IR (film), ν_{max}: 3385, 3036, 2933, 2329, 1698, 1538, 1376, 1192, 1044, 856 cm^{-1}; ^1H NMR (acetone-d_6, 400 MHz), see supplemental material: ^1H NMR (DMSO-d_6, 400 MHz), see Table 3; ^{13}C NMR (acetone-d_6, 75 MHz), see Table 2; LRFABMS, pseudomolecular ion, m/z: 931 ($M^+(C_{48}H_{76}O_{16})$ + 23(Na)), 453 ($C_{18}H_{29}O_{13}$), 435 ($M^+ - C_{18}H_{31}O_{13} - H_2O$), 309 ($C_{12}H_{21}O_9$); LREIMS, m/z (formula, relative intensity): 434 ($C_{30}H_{42}O_2$, 11), 383 ($C_{25}H_{35}O_3$, 16), 365 ($C_{25}H_{33}O_2$, 41); HREIMS, m/z: 434.3191 ($C_{30}H_{42}O_2$, ΔM +0.6 mmu: $M^+ - C_{12}H_{22}O_9 - H_2O$).

*Secodehydroxestovanin A (**12**)*: Colorless oil; IR (film), ν_{max}: 3401, 2969, 2930, 1700, 1447, 1376, 1229, 1067 cm^{-1}; ^1H NMR (Me_2SO-d_6), see Table 3; ^{13}C NMR (75 MHz, Me_2SO-d_6), δ: 211.5(C), 199.6(C), 148.9(C), 139.7(C), 135.9(C), 132.0(C), 131.3(C), 124.9(CH_2), 122.2(CH), 121.4(CH), 120.2(CH), 117.2(CH), 101.2(CH), 99.0(CH), 81.4(CH), 76.8(CH), 75.7(CH), 74.4(CH), 71.9(CH), 70.8(CH), 70.6(CH), 70.0(CH), 69.4(CH), 68.9(CH), 58.9(C), 48.0(CH), 38.4(CH_2), 37.0(CH_2), 35.6(CH_2), 34.1(CH_2), 31.7(CH_2), 31.6(CH_2), 25.6(CH_3), 25.6(CH_3), 25.4(CH_3), 22.6(CH_2), 17.8(CH_3), 17.8(CH_3), 17.8(CH_3), 17.5(CH_3), 11.8(CH_3), 10.5(CH_3); LRFABMS, pseudomolecular ion, m/z: 785 ($M^+(C_{42}H_{66}O_{12})$ + Na(23)), LREIMS, m/z: 452, 434, 383, 365 (100%).

Antifungal and antibacterial activities

Inhibition of test microorganisms was measured in a standard disc assay. Xestovanin A (**1**), dehydroxestovanin A (**9**), and epidehydroxestovanin A (**10**) inhibited the fungus *Pythium ultimum* (200 μg/disc). Dehydroestovanin C (**11**) inhibited *Staphylococcus aureus*, *Bacillus subtilis*, and *Candida albicans* (150 μg/disc).

Acknowledgements

Financial support was provided by an NSERC grant to R.J.A. S.M. and P.T.N. were supported by NSERC Postgraduate Fellowships and P.T.N. also received a Polysar Fellowship. The authors wish to thank M. LeBlanc, the staff of the Bamfield Marine Station, and the crew of the J.P. Tully for assisting the collection of *X. vanilla*.

1. P. T. NORTHCOTE and R. J. ANDERSEN. J. Nat. Prod. **50**, 1174 (1987).
2. P. T. NORTHCOTE and R. J. ANDERSEN. J. Am. Chem. Soc. **111**, 6276 (1989).
3. P. T. NORTHCOTE and R. J. ANDERSEN. Tetrahedron Lett. **29**, 4357 (1988).
4. P. T. NORTHCOTE and R. J. ANDERSEN. Can. J. Chem. **67**, 1359 (1989).
5. (*a*) I. KITIGAWA, M. KOBAYASHI, Y. OKAMOTO, M. YOSHIKAWA, and Y. HAMAMOTO. Chem. Pharm. Bull. **35**, 5036 (1987); (*b*) F. J. SCHMITZ, M. B. KSEBATI, S. P. GUNASEKERA, and S. J. AGARWAL. J. Org. Chem. **53**, 5941 (1988); (*c*) M. B. KSEBATI, F. J. SCHMITZ, and S. P. GUNASEKERA. J. Org. Chem. **53**, 3917 (1988).
6. D. J. BURNELL and J. W. APSIMON. *In* Marine natural products: chemical and biological perspectives, Vol. 5. Edited by P. J. Schueuer. Academic Press, New York. 1983. Chap. 6.
7. S. PATT and J. N. SHOOLERY. J. Magn. Reson. **46**, 535 (1982).
8. K. LEONTEIN, B. LINDBERG, and J. LONNGREN. Carbohydr. Res. **62**, 359 (1978).
9. A. LIPTAK, P. NANASI, A. NESZMELYI, and H. WAGNER. Tetrahedron, **36**, 1261 (1980).
10. (*a*) M. F. SUMMERS, L. G. MARZILLI, and A. BAX. J. Am. Chem. Soc. **108**, 4285 (1986); (*b*) A. BAX and M. F. SUMMERS. J. Am. Chem. Soc. **108**, 2093 (1986).

Can. J. Chem. Downloaded from www.nrcresearchpress.com by 84.41.108.74 on 09/07/12
For personal use only.

Cleavage of the radical cations of alkenes; 1-butene and 4,4-dimethyl-1-pentene. *Ab initio* calculations on the interaction between the allyl and alkyl radical and carbocation moieties[1]

XINYAO DU, DONALD R. ARNOLD,[2] RUSSELL J. BOYD, AND ZHENG SHI
Department of Chemistry, Dalhousie University, Halifax, N.S., Canada B3H 4J3
Received March 15, 1991

XINYAO DU, DONALD R. ARNOLD, RUSSELL J. BOYD, and ZHENG SHI. Can. J. Chem. **69**, 1365 (1991).

Carbon–carbon bond cleavage of the radical cations of 1-butene ($C_4H_8^{\dagger}$) and 4,4-dimethyl-1-pentene ($C_7H_{14}^{\dagger}$) will generate the allyl and alkyl radical and carbocation fragments. Alternative bonding arrangements between the allyl and methyl moieties in $C_4H_8^{\dagger}$ and between the allyl and *tert*-butyl moieties in $C_7H_{14}^{\dagger}$, possible metastable intermediates or transition states preceding complete separation of the fragments, have been investigated by *ab initio* molecular orbital calculations. Structures were fully optimized at the UHF/6-31G* or UHF/STO-3G levels, and some of the calculations on $C_4H_8^{\dagger}$ were expanded with single point MP2/6-31G*//UHF/6-31G* computations. The $C_4H_8^{\dagger}$ radical cation, having a structure similar to that of 1-butene, is more stable than the separated fragments: 183 kJ mol^{-1} lower in energy than the sum of the energies of the allyl cation and the methyl radical, and 385 kJ mol^{-1} lower than the sum of the energies of an allyl radical and a methyl cation, at the MP2/6-31G* level. The corresponding values at the UHF/STO-3G level are 276 and 415 kJ mol^{-1}, respectively. There is less bonding interaction between the allyl and *tert*-butyl moieties in $C_7H_{14}^{\dagger}$. The summation of the energies of the allyl radical and *tert*-butyl cation is 123 kJ mol^{-1} lower than the summation of the energies of the allyl cation and *tert*-butyl radical, and 115 kJ mol^{-1} higher in energy than the bonded radical cation $C_7H_{14}^{\dagger}$, at the UHF/STO-3G level. These calculated values are compared with thermochemical data and with experimental results on the cleavage of these, and related, radical cations.

Key words: radical cation, cleavage, *ab initio* calculations, electron transfer, photochemistry.

XINYAO DU, DONALD R. ARNOLD, RUSSELL J. BOYD et ZHENG SHI. Can. J. Chem. **69**, 1365 (1991).

La rupture de la liaison carbone–carbone des cations radicalaires du butène-1 ($C_4H_8^{\dagger}$) et du diméthyl-4,4-pentène ($C_7H_{14}^{\dagger}$) génèrent des fragments de radicaux alkyles et de carbocations. Faisant appel aux calculs *ab initio* d'orbitales moléculaires, on a étudié des dispositions alternatives de la liaison entre les unités alkyle et méthyle du $C_4H_8^{\dagger}$ et entre les unités allyle et *tert*-butyle du $C_7H_{14}^{\dagger}$ qui sont des intermédiaires métastables possibles ou des états de transition précédants la séparation complète des fragments. On a optimisé ces structures aux niveaux UHF/6-31G* ou UHF/STO-3G et on a développé certains calculs relatifs au cation radicalaire $C_4H_8^{\dagger}$ avec des calculs du point unique MP2/6-31G*//UHF/6-31G. Le cation radicalaire $C_4H_8^{\dagger}$, ayant une structure similaire à celle du butène-1, est plus stable que les fragments séparés : l'énergie est de 183 kJ mol^{-1} inférieure à la somme des énergies du cation allyle et du radical méthyle et de 385 kJ mol^{-1} inférieure à la somme des énergies du radical allyle et du cation méthyle au niveau MP2/6-31G*. Les valeurs correspondantes au niveau UHF/STO-3G sont respectivement de 276 et de 415 kJ mol^{-1}. Il y a moins d'interaction de liaison entre les unités allyle et *tert*-butyle du $C_7H_{14}^{\dagger}$. La sommation des énergies du radical allyle et du cation *tert*-butyle est de 123 kJ mol^{-1} inférieure à la sommation des énergies du cation allyle et du radical *tert*-butyle, et de 115 kJ mol^{-1} supérieure à l'énergie du cation radicalaire lié $C_7H_{14}^{\dagger}$, au niveau UHF/STO-3G. On a comparé ces valeurs calculées aux données thermochimiques et aux résultats expérimentaux obtenus lors de la rupture de ces cations radicalaires et des cations radicalaires apparentés.

Mots clés : cation radicalaire, rupture, calculs *ab initio*, transfert d'électrons, photochimie.

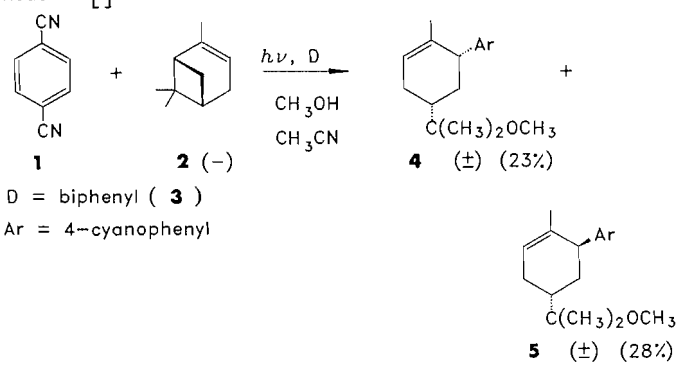
[Traduit par la rédaction]

Introduction

When a solution of 1,4-dicyanobenzene (**1**), (−) α-pinene (**2**), and biphenyl (**3**) in acetonitrile–methanol (3:1) was irradiated, the 1:1:1 adducts (±) **4** and (±) **5** were obtained in good yield (reaction [1]) (2). The key step in the mechanism proposed to explain this result, following the photoinduced single electron transfer, involves cleavage of the initially formed α-pinene radical cation $\mathbf{2}^{\dagger}$ to the distonic radical cation $\mathbf{6}^{\dagger}$ (Scheme 1). Reaction of the resulting tertiary cationic centre with methanol and coupling of the ambident allylic radical, at either end (symmetric) and from both sides, with the radical anion $\mathbf{1}^{\cdot-}$, followed by rearomatization by loss of cyanide ion, completes the sequence. There was no evidence for any reaction of the initially formed alkene radical cation ($\mathbf{2}^{\dagger}$) other than cleavage to $\mathbf{6}^{\dagger}$. Unreacted α-pinene recovered from the reaction mixture was not racemized; formation of $\mathbf{6}^{\dagger}$ was not reversible. Furthermore, **4** and **5** are formed in almost equal amounts; there was no evidence for an interaction between the allylic radical and the cationic centre of the distonic radical cation $\mathbf{6}^{\dagger}$ that might sterically hinder formation of the *cis* product (**4**).

A strong bonding interaction between the cationic centre and the central carbon of the allylic radical in $\mathbf{6}^{\dagger}$ would lead to the same radical cation as that which would be formed initially from tricyclene (1,7,7-trimethyltricyclo[2.2.1.$0^{2,6}$]heptane) (**7**).

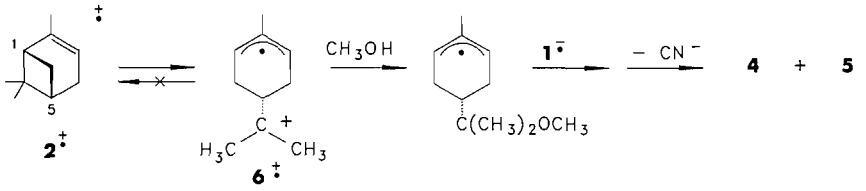
Reaction [1]



[1]This is Part 28 of the series "Radical ions in photochemistry." The preceding publication in this series is ref. 1*a*.

[2]Author to whom correspondence may be addressed.

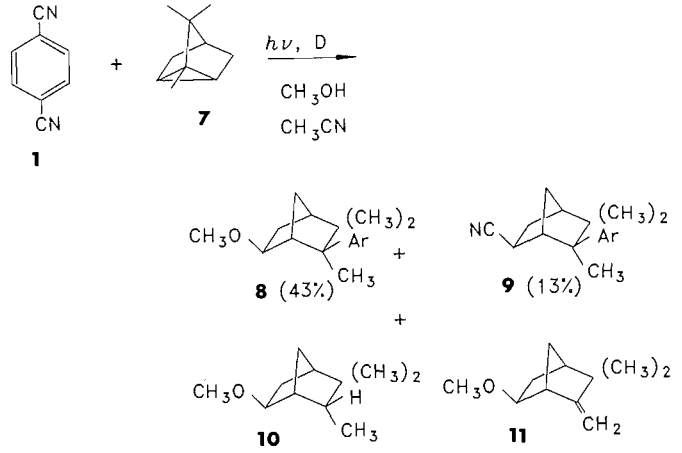
Can. J. Chem. Downloaded from www.nrcresearchpress.com by 84.41.108.74 on 09/07/12
For personal use only.



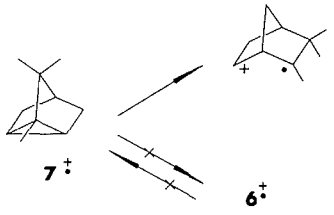
SCHEME 1

However, when **7** was subjected to these reaction conditions (reaction [2]), different products (**8–11**) were obtained.[3] These products were not detected in the reaction mixture starting with α-pinene (**2**) (reaction [1]); thus there is good evidence that the radical cations **2**·+, **6**·+, and **7**·+ do not interconvert under these conditions (Scheme 2). Cleavage of the radical cation of **7** occurs at the more heavily substituted C1—C2 bond. However, the stereochemistry and the regiochemistry of the products (**8–11**), and the fact that the nitrile **9** is a major product, are all indicative of nucleophilic assistance during the cleavage of **7**·+.[4]

Reaction [2]



Similar reactions, carbon–carbon bond cleavages (3) and rearrangements (4), of radical cations are known; however, little is known about the detailed course of these reactions. As in the examples just described, direct observation of these processes is made difficult by the fact that radical cations of this type are generally unstable transient species. Furthermore, when the radical cation is generated by photoinduced single electron transfer, deactivation by back electron transfer is usually rapid. Back electron transfer from the radical anion to the radical cation within the radical ion pair has a rate constant of ca. 10^8 s^{-1} (5), so that cleavage and rearrangement must be even more rapid in order to compete.



SCHEME 2

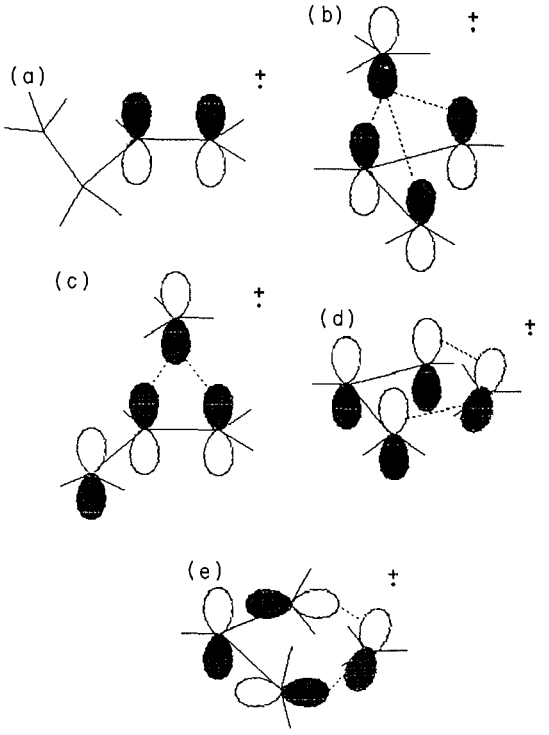


FIG. 1. Possible metastable intermediates/transition states preceding the complete separation of the allyl and alkyl fragments from the radical cation of alkenes.

One of the main objectives of this programme is to gain insight into the detailed nature of these cleavage and rearrangement processes. We have applied *ab initio* molecular orbital calculations to the problem. α-Pinene (**2**) and tricyclene (**7**) are relatively large molecules, currently beyond the scope of all but the simplest *ab initio* molecular orbital calculation methods. Therefore we began our study by choosing the radical cations of 1-butene (**12**) and 4,4-dimethyl-1-pentene (**13**) as archetypical examples of alkene radical cations that are small enough to treat by reliable methods (MP2/6-31G*, UHF/6-31G*, and UHF/STO-3G).

There is experimental evidence that illustrates the complexity of the problem even with these relatively simple alkenes. The normal electron impact ionization mass spectra of the C_4H_8 isomers, 1-butene (**12**), *cis*- and *trans*-2-butene (**14**), and the cyclic isomers methylcyclopropane (**15**) and cyclobutane (**16**), are all very similar (6). The molecular ions equilibrate to a common structure(s) before or during fragmentation. The behaviour of the initially formed radical cations has been studied by neutralization–reionization mass spectrometry.

[3]D. R. Arnold and X. Du. Unpublished results.

[4]The solvent acetonitrile–methanol (3:1) is ca. 6 M methanol. The cyanide ion is present in relatively low concentration, generated upon rearomatization of the intermediate 4-cyanocyclohexadienyl anion (Scheme 1). Nucleophilic assistance during the cleavage of cyclopropane radical cations has been reported (3*a*).

Can. J. Chem. Downloaded from www.nrcresearchpress.com by 84.41.108.74 on 09/07/12
For personal use only.

Can. J. Chem. Downloaded from www.nrcresearchpress.com by 84.41.108.74 on 09/07/12
For personal use only.

Using this technique it was possible to show that even though the initially formed radical cations readily undergo carbon–carbon bond cleavage, carbon–hydrogen bond cleavage, and rearrangement, five distinct radical cations ($C_4H_8^{+\cdot}$) could still be characterized (6*a*).

Additional evidence for the structure and reactivity of the C_4H_8 radical cations comes from electron spin resonance (ESR) studies carried out in Freon matrices at low temperatures under conditions where the radical cations are relatively stable (7). Butene-1 (**12**), *cis*- and *trans*-2-butene (**14**), and 2-methylpropene (**17**) all give distinct ESR spectra attributed to their respective radical cations (7*a*). Analysis of the ESR proton hyperfine splitting of the radical cations of **12** and *cis*- and *trans*-**14** indicates that these radical cations maintain a structure similar to that of the original alkene; they are essentially planar (7, 8).

Computational

Molecular orbital calculations are particularly valuable for revealing the structure and relative energy of local minima, possible metastable intermediate(s), preceding the complete separation of the allyl and alkyl fragments from the radical cation formed initially.

In addition to the structure closely resembling the alkene (Fig. 1a), a possible bridged structure for the radical cation would have the alkyl moiety interact with the allyl moiety, approaching in two nearly parallel planes (Fig. 1b). This is a structure that might also result from cleavage of the radical cation of an alkylcyclopropane or as an intermediate/transition state in the suprafacial 1,3-sigmatropic rearrangement of an alkene radical cation (9).[5] In the case of $C_4H_8^{+\cdot}$ this structure has C_s symmetry.

Another possible structure would have the alkyl moiety interact with adjacent carbons of the allyl moiety (Fig. 1c). A similar "nonclassical" structure has been proposed to explain the ESR spectrum of the radical cation of methylenecyclobutane (**17**$^{+\cdot}$) (10).

Other possible structures for the radical cation were not given detailed consideration because of obvious unfavourable energetics or symmetry. Alternative arrangements having the allyl and alkyl moieties approach along two perpendicular planes (Figs. 1d and 1e) are unlikely; either the orbital overlap is unsymmetric (Fig. 1d) or overlap throughout the allyl system is lost (Fig. 1e).

The *ab initio* molecular orbital calculations were carried out with the GAUSSIAN 86 series of programs (11). The charge and spin distributions were calculated by Mulliken population analysis (12). Structures were fully optimized at the UHF/6-31G* and UHF/STO-3G levels. The energies for some optimized structures were corrected for electron correlation using single point MP2/6-31G*//UHF/6-31G* computations. Limitations of these methods have been discussed (13). The calculated energies for the neutral alkenes, for several alternative structures of the alkene radical cations, and for the fragment alkyl and allyl radicals and cations are listed in Table 1.

TABLE 1. The calculated (*ab initio*) total energies for the neutral alkenes **12** and **13**, for several alternative structures of the alkene radical cations, and for the fragment alkyl and allyl radicals and cations

	STO-3G	6-31G*	MP2/6-31G*
$C_4H_8^{+\cdot}$			
12$^{+\cdot}$**b** (Fig. 3)	−153.92624	−155.75745	−156.22480
12$^{+\cdot}$ *anti*		−155.81037	
12$^{+\cdot}$ *eclipsed*	−153.99062	−155.81122	
12$^{+\cdot}$ *skew* (Fig. 2)	−153.99177	−155.81173	−156.28136
$C_7H_{14}^{+\cdot}$			
13$^{+\cdot}$**b** (Fig. 5)	−269.68224		
13$^{+\cdot}$ *eclipsed*	−269.72788		
13$^{+\cdot}$ *anti*	−269.73289		
13$^{+\cdot}$ *skew* (Fig. 4)	−269.73564		
12 *gauche*		−156.10162[a]	
12 *anti*		−156.10238[a]	
12 *eclipsed*		−156.10471[a]	
12 *skew*		−156.10608[b]	−156.62021
		−156.10586[a]	
13 *anti*	−269.96601		
13 *skew*	−269.97122[c]		
Allyl radical	−115.05429[d]	−116.46810[d]	−116.80964
Allyl cation	−114.80953[d]	−116.19321[d]	−116.54301
Methyl radical	−39.07701[d]	−39.55899[d]	−39.66867
Methyl cation	−38.77948[d]	−39.23064[d]	−39.32514
tert-Butyl radical	−154.83549		
tert-Butyl cation	−154.63766	−156.44241[e]	

[a]Optimized using RHF 6-31G*/3-21G (ref. 14*a*).
[b]IP obtained from the energy of the HOMO is 9.7 eV (935.9 kJ mol^{-1}).
[c]IP obtained from the energy of the HOMO is 8.45 eV (815.3 kJ mol^{-1}).
[d]Reference 14*b*.
[e]Reference 14*c*.

Calculations on the 1-butene (12) system

The geometry optimization of the radical cation of 1-butene (**12**$^{+\cdot}$), having a structure similar to that of the alkene (Fig. 1a), was carried out at both the UHF/STO-3G and UHF/6-31G* levels. Minima were found for three of the four possible conformers around the C2—C3 carbon–carbon single bond.[6] The conformer with the methyl group *skew* and a hydrogen on C3 *eclipsed* with the vinyl group is the global minimum (**12**$^{+\cdot}$**a**, Fig. 2). The related conformation, that having the methyl group *gauche* and a hydrogen on C3 *anti* to the vinyl group, is not a minimum; calculations starting with this initial structure collapsed to the global minimum. The conformer next in energy above the minimum has C1, C2, C3, and C4 all in a plane, with the methyl group *eclipsed* with the vinyl group. The least stable conformer has the alternative planar structure with the methyl group *anti* to the vinyl group. Calculations on the neutral molecule 1-butene (**12**) find the same relative order of stability for the conformers (14).

The bridged structure analogous to Fig. 1b was also fully optimized at both the UHF/STO-3G and at the UHF/6-31G* levels. The initial search for a minimum imposed a C_s symmetry constraint and confined the allyl moiety to a plane. Having identified a stationary point, a similar structure (**12**$^{+\cdot}$**b**, Fig. 3)

[5]An *ab initio* (UHF/6-31G*) study of the 1,3-hydrogen migration of the radical cation of 1-propene has identified a similar structure as a transition state (9*a*). An earlier calculation using semi-empirical methods (MINDO/3) indicated the same structure was an intermediate; however, no energy minimum was found for the 1,3-methyl migration of the radical cation of 1-butene (**12**$^{+\cdot}$) (9*b*).

[6]The four possible conformers of 1-butene resulting from rotation around the C2—C3 carbon–carbon single bond are as follows: with the methyl group and the vinyl group at an angle of ca. 0° (*eclipsed*), 60° (*gauche*), 120° (*skew*), and 180° (*anti*).

Can. J. Chem. Downloaded from www.nrcresearchpress.com by 84.41.108.74 on 09/07/12
For personal use only.

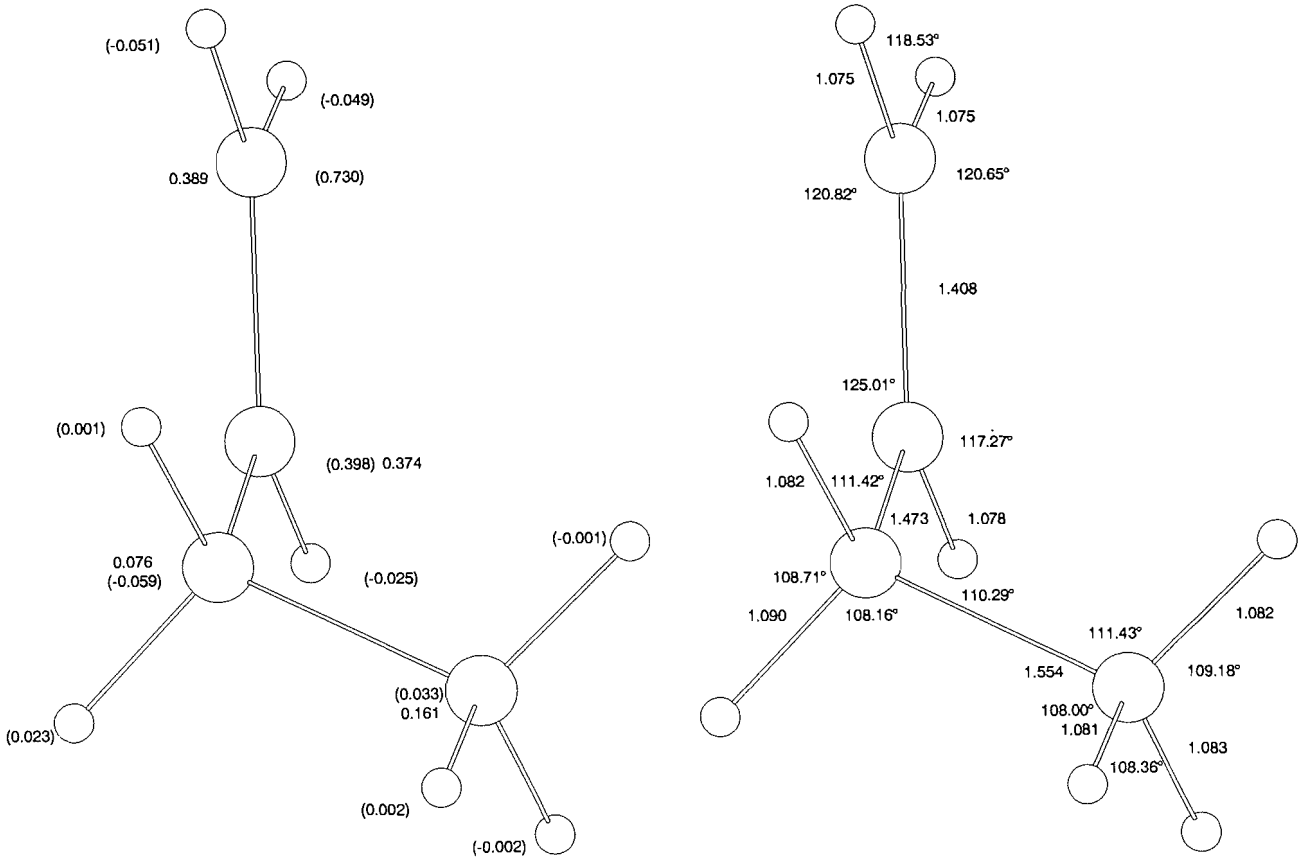


FIG. 2. The global minimum structure for the radical cation of 1-butene (**12**†**a**); left: the spin and charge densities on the radical cation **12**†**a**; right: the optimized (UHF/6-31G*) structure of the radical cation **12**†**a**.

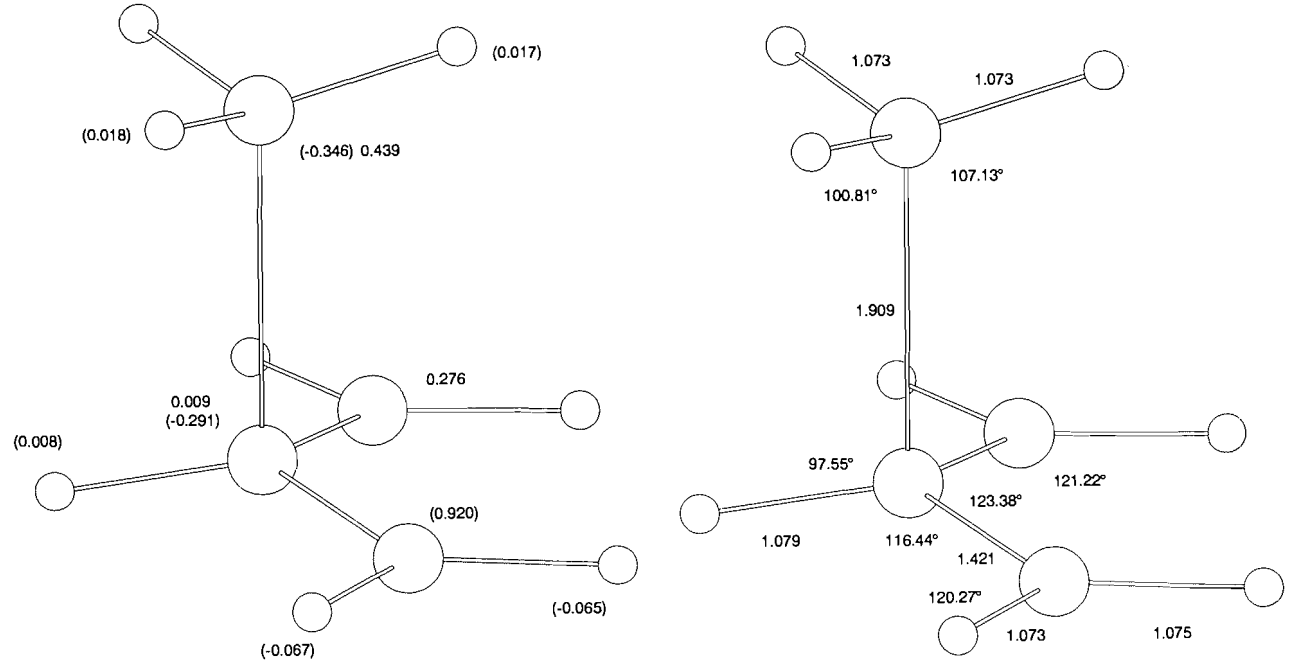


FIG. 3. A stationary point (transition state) for the radical cation of 1-butene (**12**†**b**); left: the spin and charge densities on the radical cation **12**†**b**; right: the optimized (UHF/6-31G*) structure of the radical cation **12**†**b**.

Can. J. Chem. Downloaded from www.nrcresearchpress.com by 84.41.108.74 on 09/07/12
For personal use only.

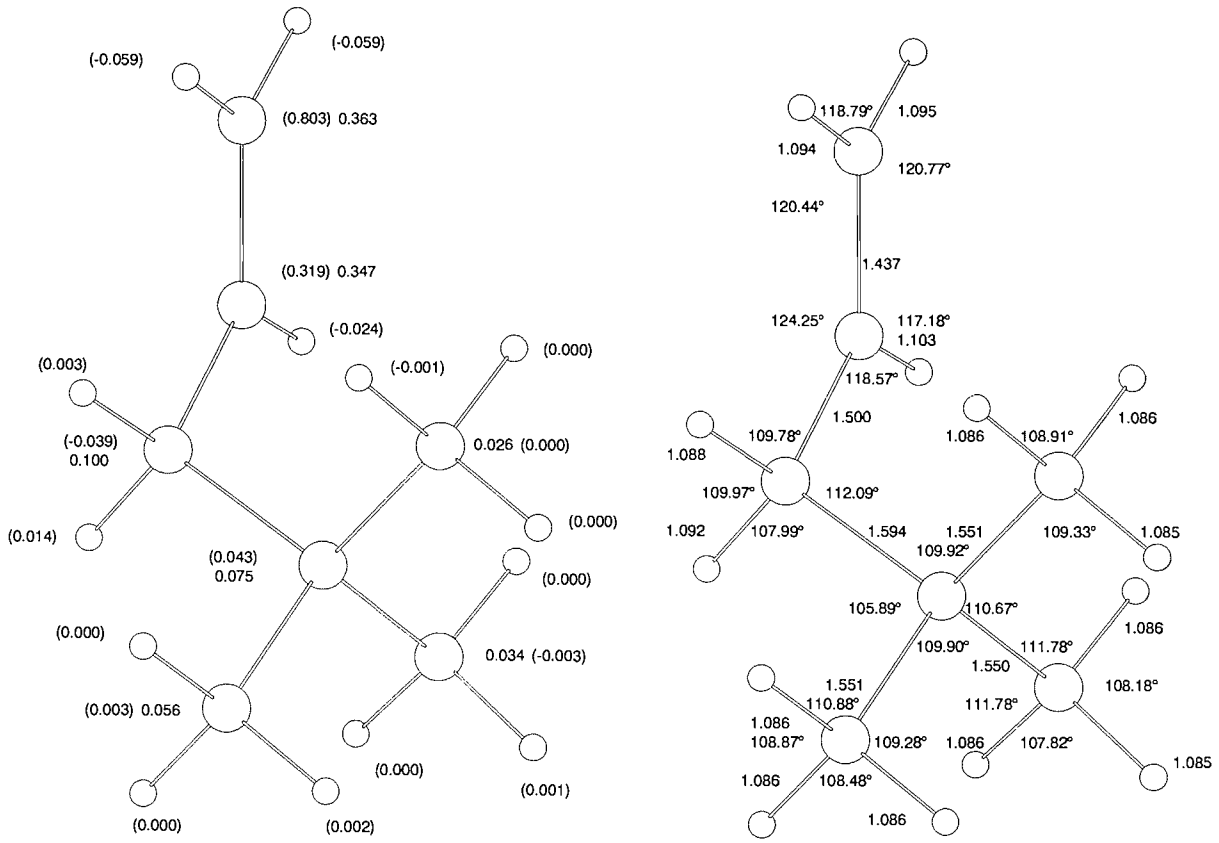


FIG. 4. The global minimum structure for the radical cation of 4,4-dimethyl-1-pentene (**13⁺a**); left: the spin and charge densities on the radical cation **13⁺a**; right: the optimized (UHF/STO-3G) structure of the radical cation **13⁺a**.

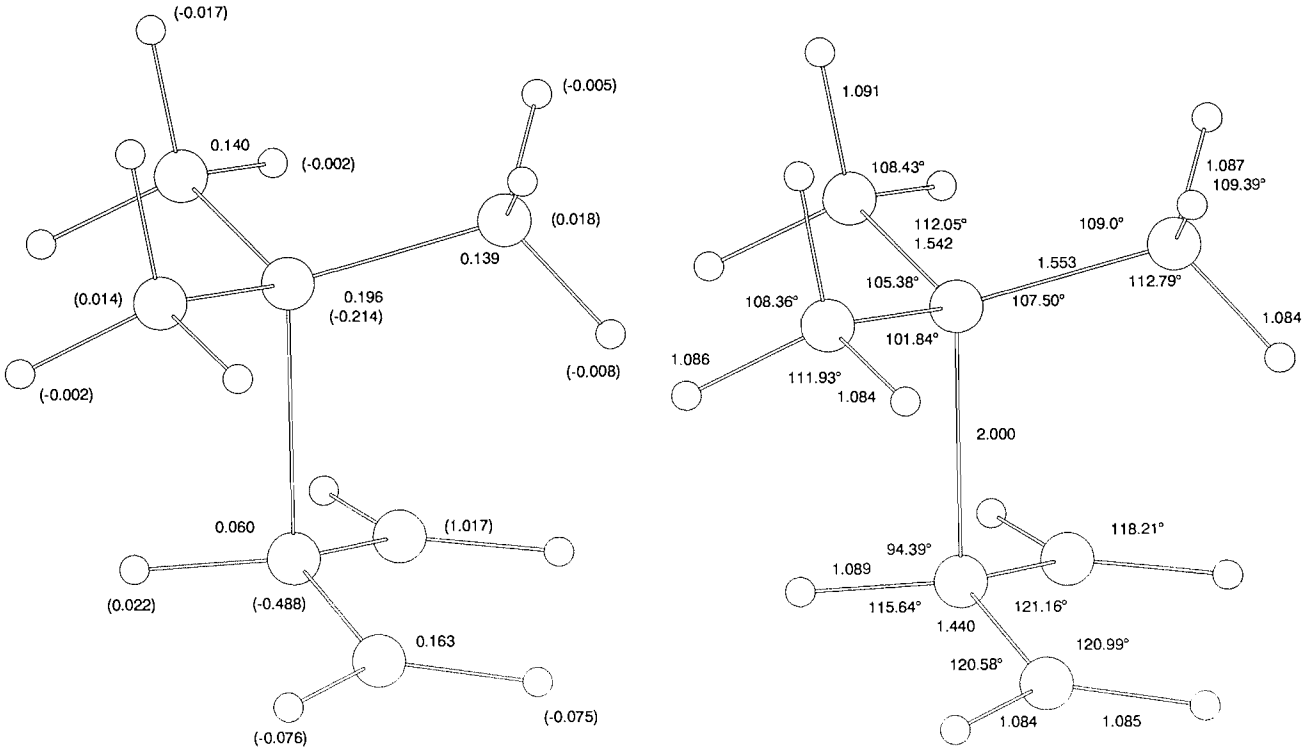


FIG. 5. A stationary point (transition state) for the radical cation of 4,4-dimethyl-1-pentene (**13⁺b**); left: the spin and charge densities on the radical cation **13⁺b**; right: the optimized (UHF/STO-3G) structure for the radical cation **13⁺b**.

Can. J. Chem. Downloaded from www.nrcresearchpress.com by 84.41.108.74 on 09/07/12
For personal use only.

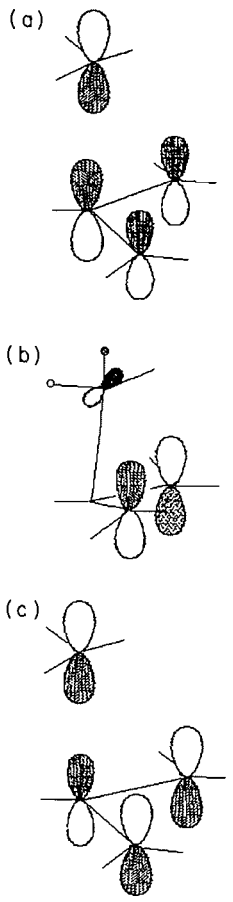


FIG. 6. (a) The highest filled molecular orbital (HOMO) of the radical cation **12**‡**b**. (b) The singly occupied molecular orbital (SOMO) of the radical cation **12**‡**b**. (c) The lowest unoccupied molecular orbital (LUMO) of the radical cation **12**‡**b**.

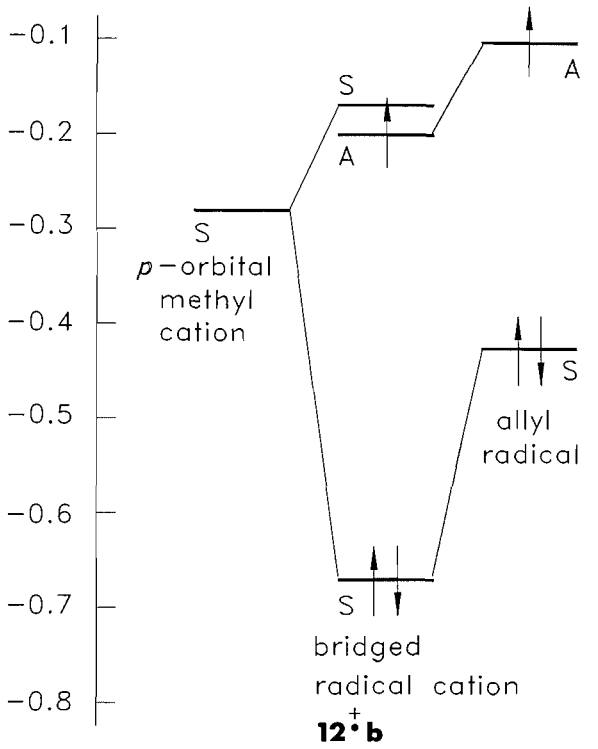


FIG. 7. Orbital correlation diagram for the cleavage of the radical cation **12**‡**b**. Cleavage of the radical cation to the allyl radical and methyl cation is orbital symmetry allowed.

was obtained without imposing these constraints. Further characterization of the stationary point showed one imaginary frequency on diagonalization of the force constant matrix; therefore, while the UHF/6-31G* calculations identify **12**‡**b** as a stationary point, more stable than the separated fragments, it is a transition state, not an intermediate (15).

Calculations on the structure analogous to Fig. 1c were attempted only at the UHF/STO-3G level and were initially subject to constraint; the C4 carbon of the methyl moiety was confined to a plane perpendicular to the C1—C2 bond lying between the C1 and C2 atoms. Even with this constraint the calculation did not converge. When the constraints were removed the calculation converged to the global minimum structure **12**‡**a** shown in Fig. 2. Therefore, calculations at the UHF/STO-3G level do not find a stable structure analogous to Fig. 1c for $C_4H_8^{\ddagger}$ and this structure was not considered further.

Single point calculations (MP2/6-31G*//UHF/6-31G*) were carried out on the neutral molecule (**12**) and on the radical cation in structures **12**‡**a** and **12**‡**b**; the results are summarized in Table 1.

Calculations on the 4,4-dimethyl-1-pentene (13) system

The geometry optimization of the radical cation of 4,4-dimethyl-1-pentene (**13**‡), in a structure similar to that of the alkene, was carried out only at the UHF/STO-3G level. All four possible conformers were considered and three minima were identified. As in the case of the 1-butene radical cation (**12**‡), the global minimum for **13**‡ has the *tert*-butyl group *skew* (ca. 120°) to the plane of the vinyl group (**13**‡**a**, Fig. 4). The conformers having the *tert*-butyl group *eclipsed* and *anti* to the vinyl group were energy minima but were considerably higher in energy. Calculations initiated with the radical cation in the conformation having the *tert*-butyl group *gauche* (ca. 60°) with the plane of the vinyl group converged to the global minimum. This order of stability for the conformers of the radical cation of **13** is the same as that observed for the parent molecule (16).

Calculations on the bridged structure analogous to Fig. 1b were also performed at the UHF/STO-3G level. Initially the structure was confined to C_s symmetry with the central carbon of the *tert*-butyl moiety in a plane perpendicular to the allyl moiety and through C2. The resulting stationary point was then fully optimized without these constraints; C_s symmetry was maintained (**13**‡**b**, Fig. 5). This structure is less stable than the separated *tert*-butyl cation and allyl radical fragments, one imaginary frequency was found on diagonalization of the force constant matrix; therefore, **13**‡**b** is not an intermediate.

Results and discussion

The most stable of the structures considered for the radical of 1-butene (**12**‡) is very similar to that of the alkene (**12**‡**a**, Fig. 2). The hydrogen on C3 and the three carbons, C1, C2, and C3, are all in the same plane. The allyl moiety is nearly planar, the terminal methylene group is only slightly (<1°) twisted out of the C1—C2—C3 plane. The methyl group is *skew* (119.8°) to the plane of the vinyl group and the C3—C4 bond length (1.554 Å) is normal. The singly occupied molecular orbital (SOMO) is largely associated with the π bond between C1 and C2. There is little positive change (0.161)

Can. J. Chem. Downloaded from www.nrcresearchpress.com by 84.41.108.74 on 09/07/12
For personal use only.

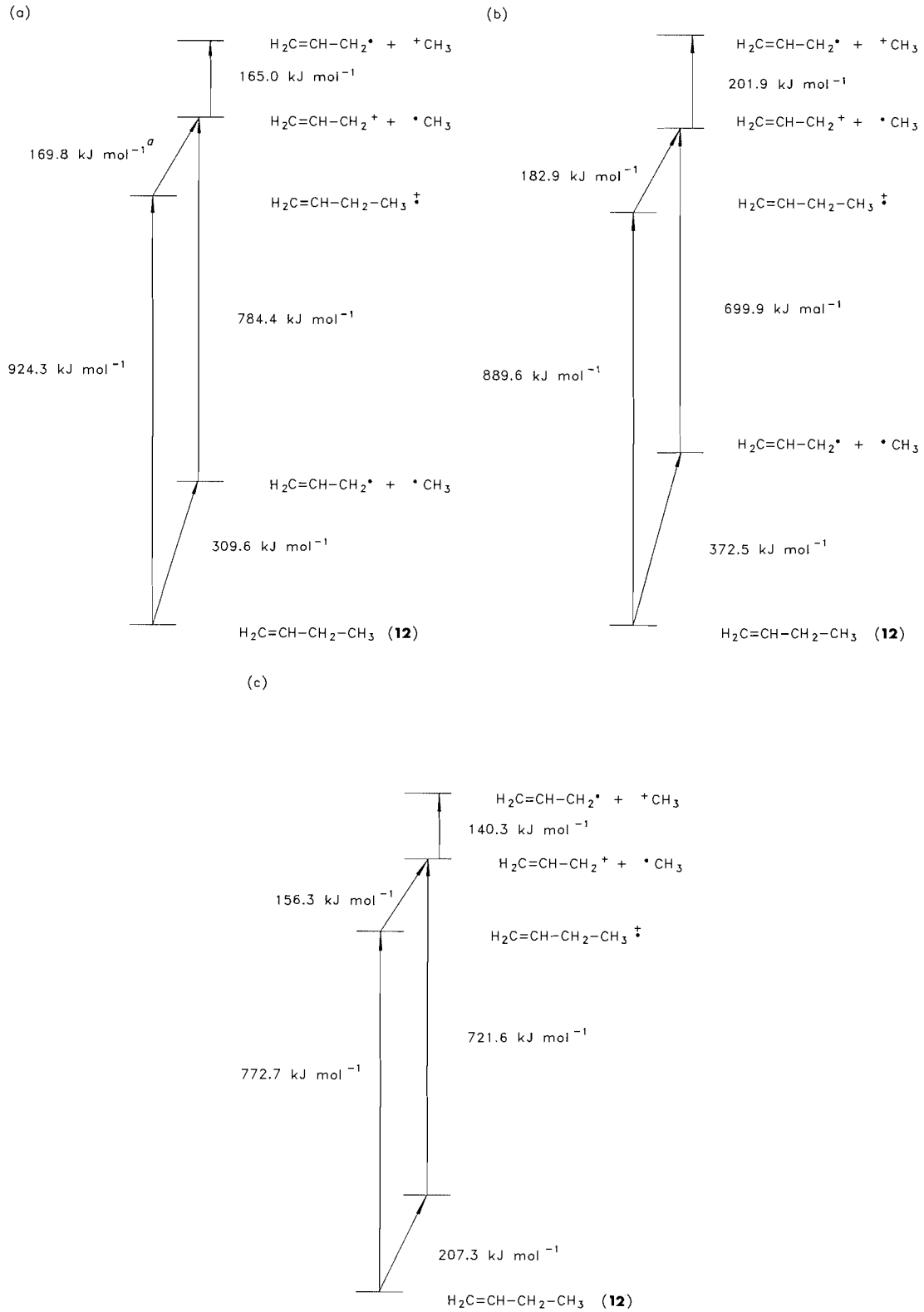


FIG. 8. Thermochemical cycles for the cleavage of the radical cations **12‡a**. (a) Experimental results (17). (b) Differences in calculated (MP2/6-31G*//UHF/6-31G*) total energies. (c) Differences in calculated (UHF/6-31G*) total energies.
[a]Value calculated by completing the cycle.

or spin (0.033) density on the methyl moiety. This conformer is only 1.3 kJ mol^{-1} more stable than the conformer having C1, C2, C3, and C4 all essentially in the same plane, with the methyl group *eclipsed* with the vinyl group. The alternative planar arrangement, that with the methyl group *anti* to the vinyl group, is 3.5 kJ mol^{-1} above the global minimum.

Analysis of the ESR spectrum of the radical cation of 1-butene (**12‡**) in a Freon matrix at low temperature shows

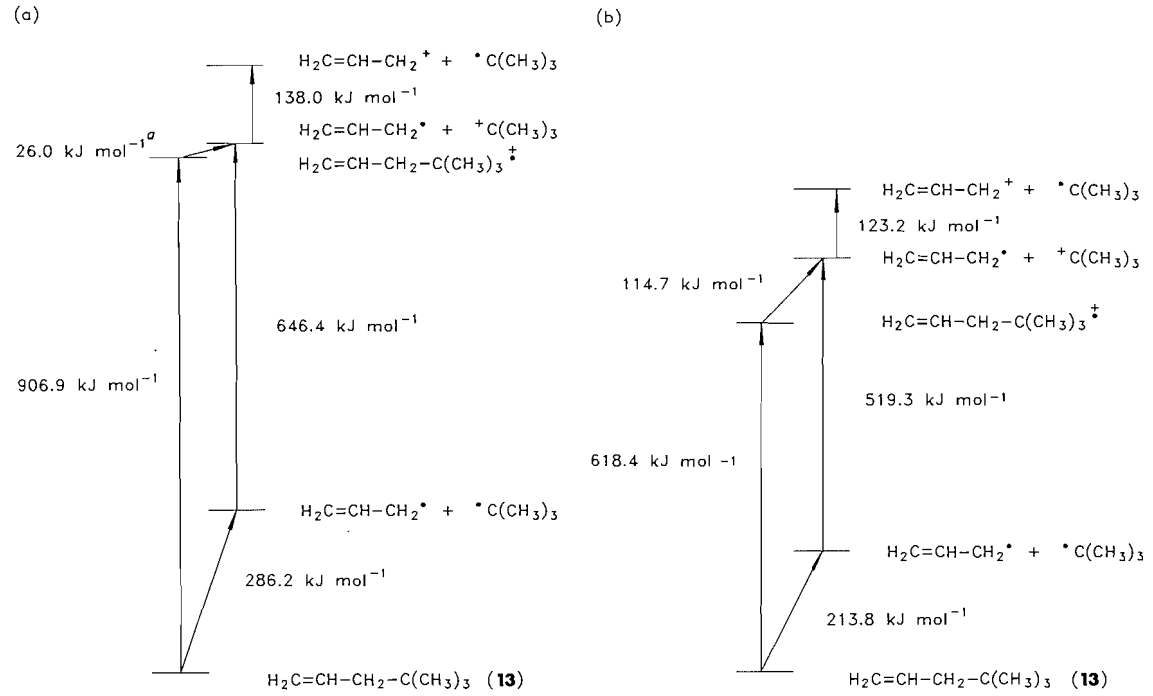


FIG. 9. Thermochemical cycles for the cleavage of the radical cation **13‡a**. (a) Experimental results (17). (b) Differences in calculated (UHF/STO-3G) total energies.
[a]Value calculated by completing the cycle.

equivalent hyperfine coupling due to the hydrogens on C3. This has led to the assignment of the planar structure, that having the methyl group *eclipsed* with the vinyl group, for the radical cation (*7b*). The results of these calculations lead us to suggest that the *skew* conformer is in fact favoured; however, the two hydrogens on C3 appear equivalent in the ESR spectrum because the rotational barrier, which equilibrates the two hydrogens, through the planar conformer is small.

The bridged structure **12‡b** (Fig. 3) is an energy maximum, a possible transition state in the suprafacial 1,3-sigmatropic methyl migration of **12‡**. This structure is 148.5 kJ mol^{-1} less stable than the global minimum **12‡a** (Fig. 2) and is only 34.4 kJ mol^{-1} more stable than the sum of the energy of the allyl cation and the methyl radical (MP2/6-31G*). The structure is similar to that found for the transition state for the 1,3-hydrogen migration in the propene homolog (*9a,b*). The allyl moiety is almost planar, H3 is only 21° out of the plane of C1, C2, and C3, and the C2—C4 bond length is relatively long (1.909 Å). The angle between H3—C2—C4 is 97.6°. Significant positive charge (0.439) and spin (−0.292) density are on the methyl moiety. This structure is related to the radical cation that could form upon cleavage of methylcyclopropane. However, when the radical cation of methylcyclopropane cleaves, fragmentation to give the alternative radical cation, that having the more heavily substituted (i.e., the more stable secondary) cationic centre, would be preferred.

An accurate description of the bonding involved in **12‡b** is provided by an analysis of the individual molecular orbitals (Fig. 6). In the highest filled molecular orbital (Fig. 6a) the orbital coefficients for the p_x orbitals on C1 and C3 are small; bonding involves both σ and π bonds. The major contributors to the singly occupied molecular orbital (SOMO) are the p_y atomic orbitals on C1 and C3 (Fig. 6b). This species (**12‡b**) is best described as having the methyl moiety partially bonded to all of the carbons of the allyl moiety. The positive charge density is largely associated with the methyl moiety while the unpaired electron is largely distributed between the terminal carbons of the allyl moiety. These bonding orbitals correlate with the orbitals of the methyl cation and the allylic radical. Correlation with the methyl radical and allylic cation is symmetry forbidden (Fig. 7).

Calculations on the radical cation of 4,4-dimethyl-1-pentene (**13‡**) were carried out only at the UHF/STO-3G level. Comparison of the results from the two basis sets calculations on **12‡** indicates that the minimum structures for the radical cation are relatively more stable, compared to the energy of the separated fragments, with the lower level basis set (UHF/STO-3G). In the case of **13‡** the minimum having the structure close to that of the alkene (**13‡a**, Fig. 4) is closer in energy (114.7 kJ mol^{-1}) to the separated fragments and, while the calculation of the radical cation having the bridged structure **13‡b** (Fig. 5) does converge, the calculated energy at the stationary point is higher (25 kJ mol^{-1}) than the sum of the energy of the separated fragments. The C2—C4 bond length (2.00 Å), in this transition state, is relatively long. Bonding between the *tert*-butyl and allyl moieties in **13‡** is weaker than bonding between the methyl and allyl moieties in **12‡**. The calculated stability of these bonded radical cation structures (**13‡a** and **13‡b**) would be even less if the larger basis set (UHF/6-31G*) was used.

The cleavage process

These radical cations can undergo carbon–carbon bond cleavage in two modes: formation of the allyl radical and alkyl cation, or formation of the allyl cation and alkyl radical. The energy requirements for these alternatives can be estimated both from experimental thermochemical data (Figs. 8a and 9a (17)) and from the calculated values listed in Table 1 (Figs. 8b,

Can. J. Chem. Downloaded from www.nrcresearchpress.com by 84.41.108.74 on 09/07/12
For personal use only.

Can. J. Chem. Downloaded from www.nrcresearchpress.com by 84.41.108.74 on 09/07/12
For personal use only.

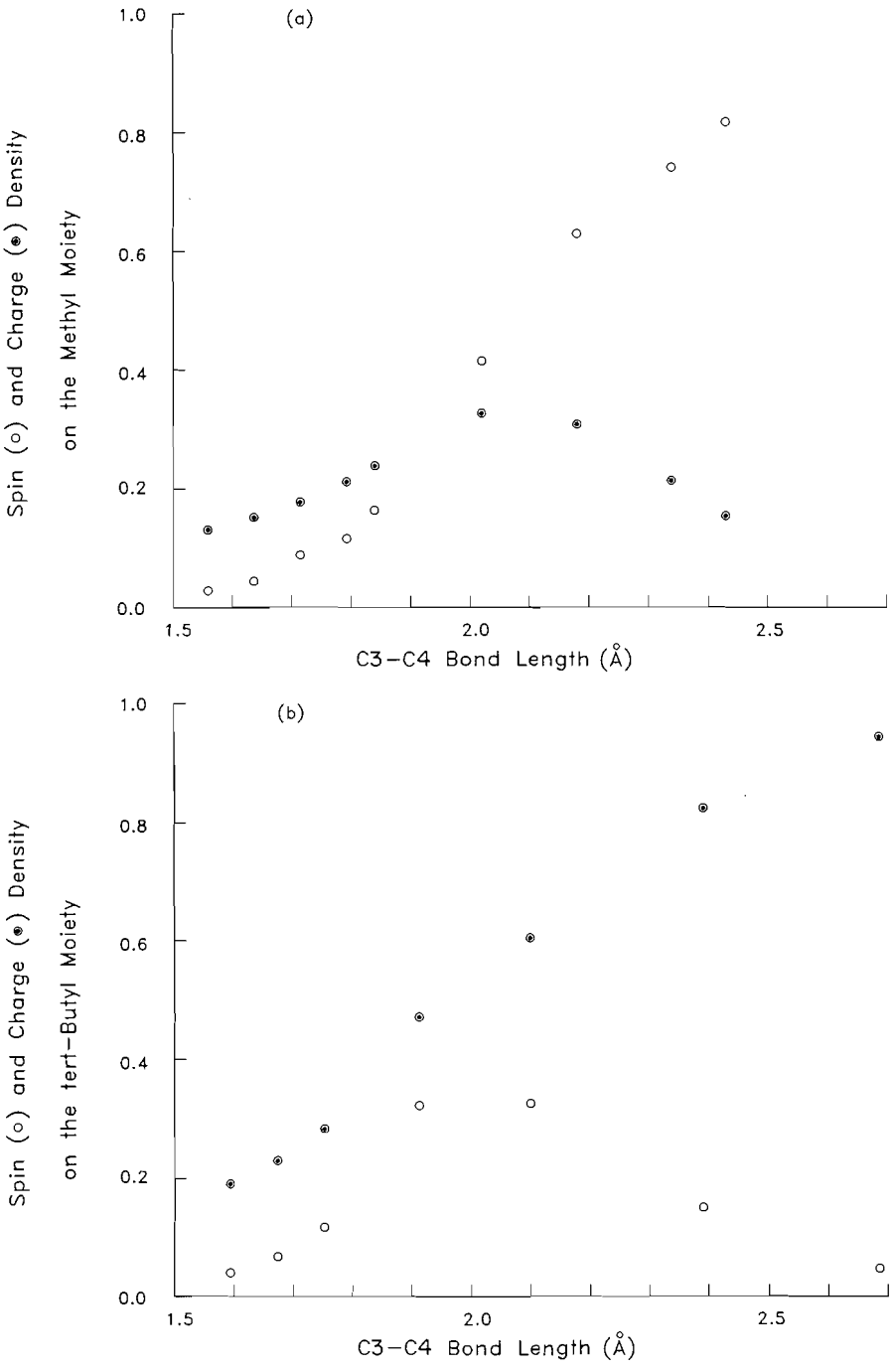


FIG. 10. The calculated (UHF/STO-3G) spin and charge densities on the alkyl fragment of the radical cation (a) **12**‡**a** and (b) **13**‡**a** as a function of allylic bond length.

8c, and 9b). For the cleavage of the radical cation of 1-butene (**12**‡), there is good agreement between the experimental results and the calculated energy values when the larger basis set is used and when electron correlation is considered (MP2/6-31G*) (Fig. 8b). The largest discrepancy caused by neglect of electron correlation involves the calculated homolytic C3—C4 bond dissociation energy. Bond dissociation energies calculated using Hartree–Fock theory are generally low (13). While formation of the alkyl radical and allylic cation is favoured in the case of **12**‡, cleavage to the alkyl cation and allyl radical is favoured in the case of **13**‡.

When the radical cations **12**‡**a** and **13**‡**a** cleave, there is no intrinsic barrier that favours cleavage in either mode. The singly occupied orbital of the product, alkyl or allyl radical, is determined on the basis of energetics. Figures 10a and b show the calculated (UHF/STO-3G) spin and charge densities on the methyl and *tert*-butyl fragments as the allylic C3—C4 bond is progressively lengthened; the rest of the structure was optimized. The initial stages of bond lengthening increase both charge and spin densities on both the methyl moiety and the *tert*-butyl moiety. However, as the bond lengthening increases beyond ca. 2 Å, spin density increases on the methyl moiety while charge density increases on the *tert*-butyl group.

There is experimental evidence indicative of these alterna-

tive modes of cleavage of 12^+ and 13^+. The mass spectrum of 1-butene (**12**) shows the base peak at $m/z = 41$, the allyl cation, and the peak at $m/z = 15$ for the methyl cation has a relative abundance of only 6%; there is a significant (40%) peak due to the molecular ion ($m/z = 56$). The base peak in the mass spectrum of 4,4-dimethyl-1-pentene (**13**) is due to the *tert*-butyl cation ($m/z = 57$) and the peaks due to the allylic cation ($m/z = 41, 53\%$) and the molecular ion ($C_7H_{14}^+$, $m/z = 98$, <1%) are both relatively minor (18).

The interaction of an alkenyl radical cation with an alkene results in formation of an excited complex that fragments to yield new cations, radicals, and alkenes. This process has been studied by triple quadrupole mass spectrometry and the principal reaction between the ethenyl radical cation and ethylene yields a $C_4H_8^+$ complex that fragments exclusively to the allyl cation and the methyl radical. In marked contrast, reaction of the radical cation of 2-methylpropene with 2-methylpropene gives a $C_7H_{14}^+$ complex that yields the 2-methylallyl radical and the *tert*-butyl cation as the only products (19).

Conclusions

Removal of a single electron from 1-butene yields a relatively stable radical cation 12^+**a** with a structure closely resembling the original alkene. This intact radical cation is significantly more stable than the separated allyl and alkyl fragments. Fragmentation to the allyl cation and the methyl radical is energetically favoured over formation of the allyl cation and methyl radical. The alternative bridged structure for the radical cation, 12^+**b**, formed by interaction of allyl and methyl fragments in which the unpaired electron resides mainly on the terminal carbons of the allyl moiety and nearly half the positive charge is distributed on the methyl moiety, is not an energy minimum.

Substitution of a *tert*-butyl group in place of the methyl group has a profound effect on the nature of the radical cation. Removal of a single electron from 4,4-dimethyl-1-pentene yields a radical cation, 13^+**a**, which is only slightly more stable than the separated fragments. Cleavage of the $C_7H_{14}^+$ radical cation to the allyl radical and *tert*-butyl cation is favoured over the alternative formation of the allyl cation and *tert*-butyl radical. These differences between 12^+ and 13^+ can be attributed to variation in the difference in the ionization potential of the two alternative fragments and to the variation in the stability of the alkyl cation: (1) Fragmentation of the radical cation occurs in the direction that gives the carbocation of that fragment having the lower ionization potential. (2) If the carbocation is stable, cleavage of the radical cation is favoured and bonding interaction between the fragments is minimized. These correlations have been recognized previously for cleavage of radical cations in solutions of polar solvents (3*b*, 20). Cleavage of radical cations in acetonitrile–methanol (3:1) solution occurs in the direction that gives the carbocation of that fragment having the lower oxidation potential.

The results of these calculations are in good agreement with the observed behaviour of the radical cations of α-pinene (reaction [1]) and tricyclene (reaction [2]). The initial single electron transfer step in reaction [1] should give a weakly bonded radical cation (2^+). Cleavage of 2^+ to 6^+ will be assisted by relief of strain associated with the four-membered ring (9*c*). Formation of the allylic radical and *tert*-carbocation is consistent with these calculations. Furthermore, the absence of a minimum for structure 13^+**b** makes it unlikely that there is significant bonding interaction between the allyl radical and carbocation centres in 6^+. This is consistent with the observed stereochemistry; there is little preference for formation of the *trans* products **5**, and no rearrangement to the radical cation obtained from **7**. Nucleophilic assistance in the cleavage of the radical cation of tricyclene (**7**) is also consistent with theory. The radical cation of cyclopropane maintains the three-membered ring; cleavage to the trimethylene radical cation is endothermic (21).

Acknowledgements

This work was supported by grants from the Natural Sciences and Engineering Research Council of Canada. We also thank Dalhousie University Computing and Information Services for generous allocation of computer time.

1. (*a*) D. R. ARNOLD, L. J. LAMONT, and A. L. PERROTT. Can. J. Chem. **69**, 225 (1991); (*b*) D. R. ARNOLD, X. DU, and K. M. HENSELEIT. Can. J. Chem. **69**, 839 (1991).
2. D. R. ARNOLD and X. DU. J. Am. Chem. Soc. **111**, 7666 (1989).
3. (*a*) J. P. DINNOCENZO, W. P. TODD, T. R. SIMPSON, and I. R. GOULD. J. Am. Chem. Soc. **112**, 2462 (1990); (*b*) R. POPIELARZ and D. R. ARNOLD. J. Am. Chem. Soc. **112**, 3068 (1990); (*c*) X. CI and D. G. WHITTEN. J. Am. Chem. Soc. **111**, 3459 (1989); (*d*) P. MASLAK and J. N. NARVAEZ. Angew. Chem. Int. Ed. Engl. **29**, 283 (1990).
4. (*a*) H. D. ROTH. Acc. Chem. Res. **20**, 343 (1987); (*b*) F. W. MCLAFFERTY, M. P. BARBALAS, and F. TURECEK. J. Am. Chem. Soc. **105**, 1 (1983); (*c*) N. L. BAULD. Tetrahedron, **45**, 5307 (1989); (*d*) J. P. DINNOCENZO and D. A. CONLON. J. Am. Chem. Soc. **110**, 2324 (1988); (*e*) A. PADWA, C. S. CHOU, and W. F. RIEKER. J. Org. Chem. **45**, 4555 (1980).
5. I. R. GOULD, D. EGE, S. L. MATTES, and S. FARID. J. Am. Chem. Soc. **109**, 3794 (1987).
6. (*a*) R. FENG, C. WESDEMIOTIS, M.-Y. ZHANG, M. MARCHETTI, and F. W. MCLAFFERTY. J. Am. Chem. Soc. **111**, 1986 (1989); (*b*) T. HSIEH, J. P. GILMAN, M. J. WEISS, and G. G. MEISELS. J. Phys. Chem. **85**, 2722 (1981).
7. (*a*) T. SHIDA, Y. EGAWA, and H. KUBODERA. J. Chem. Phys. **73**, 5963 (1980); (*b*) J. FUJISAWA, S. SATO, K. SHIMOKOSHI, and T. SHIDA. J. Phys. Chem. **89**, 5481 (1985); (*c*) K. USHIDA, T. SHIDA, M. IWASAKI, K. TORIYAMA, and K. NUNOME. J. Am. Chem. Soc. **105**, 5496 (1983); (*d*) M. IWASAKI, K. TORIYAMA, and K. NUNOME. Faraday Disc. Chem. Soc. **78**, 19 (1984); (*e*) K. TORIYAMA, K. NUNOME, M. IWASAKI, T. SHIDA, and K. USHIDA. Chem. Phys. Lett. **122**, 118 (1985); (*f*) J. FUJISAWA, S. SATO, K. SHIMOKOSHI. Chem. Phys. Lett. **124**, 391 (1986).
8. T. CLARK and S. F. NELSON. J. Am. Chem. Soc. **110**, 868 (1988).
9. (*a*) T. CLARK. J. Am. Chem. Soc. **109**, 6838 (1987); (*b*) Y. HOPPILLIARD and G. BOUCHOUX. Org. Mass Spectrom. **17**, 534 (1982); (*c*) N. L. BAULD. J. Comput. Chem. **11**, 896 (1990).
10. K. USHIDA, T. SHIDA, and J. C. WALTON. J. Am. Chem. Soc. **108**, 2805 (1986).
11. M. J. FRISCH, J. S. BINKLEY, H. B. SCHLEGEL, K. RAGHAVACHARI, C. F. MELIUS, R. L. MARTIN, J. J. P. STEWART, F. W. BOBROWICZ, C. M. ROHLFING, L. R. KAHN, D. J. DEFREES, R. SEEGER, R. A. WHITESIDE, D. J. FOX, E. M. FLEUDER, and J. A. POPLE. GAUSSIAN 86. Release H; Carnegie–Mellon University, Pittsburgh, PA. 1984.
12. R. S. MULLIKEN. J. Chem. Phys. **23**, 1833 (1955); **23**, 1841 (1955); **23**, 2338 (1955); **23**, 2343 (1955).
13. (*a*) W. J. HEHRE, L. RADOM, P. V. R. SCHLEYER, and J. A. POPLE. Ab initio molecular orbital theory. Wiley, New York. 1986; (*b*) J. B. COLLINS and A. STREITWIESER. J. Comput. Chem. **1**, 81 (1980); (*c*) H. P. LUTHI, J. H. AMMETER, J. ALMLOF, and K. FAEGRI. J. Chem. Phys. **77**, 2002 (1982); (*d*) A. E. REED, R. B. WEINSTOCK, and F. WEINHOLD. J. Chem. Phys. **83**, 735 (1985).
14. (*a*) K. B. WIBERG and E. MARTIN. J. Am. Chem. Soc. **107**, 5035 (1985); (*b*) R. A. WHITESIDE, M. J. FRISCH, and J. A. POPLE. The Carnegie–Mellon Quantum Chemistry Archive, 3rd

Can. J. Chem. Downloaded from www.nrcresearchpress.com by 84.41.108.74 on 09/07/12
For personal use only.

ed. Carnegie–Mellon University, Pittsburgh, PA. 1983; (*c*) W. L. JORGENSEN and J. K. BUCKNER. J. Am. Chem. Soc. **109**, 1891 (1987).
15. (*a*) H. B. SCHLEGEL. New theoretical concepts for understanding organic reactions. *Edited by* J. Bertran and I. G. Csizmadia. Kluwer Academic Publishers, Dordrecht. 1989. p. 33; (*b*) H. B. SCHLEGEL. Adv. Chem. Phys. **67**, 249 (1987).
16. A. A. BOTHNER-BY, C. NAAR-COLIN, and H. GUNTHER. J. Am. Chem. Soc. **84**, 2748 (1962).
17. (*a*) H. M. ROSENSTOCK, K. DRAXL, B. W. STEINER, and J. T. HERRON. J. Phys. Chem. Ref. Data, **6**, Suppl. 1 (1977); (*b*) F. P. LOSSING. Can. J. Chem. **50**, 3973 (1972); (*c*) D. P. WANG, L. C. LEE, S. K. SRIVASTAVA. Chem. Phys. Lett. **152**, 513 (1988); (*d*) J. L. HOLMES and F. P. LOSSING. Int. J. Mass Spectrom. Ion Processes, **58**, 113 (1984); (*e*) D. GRILLER, J. M. KANOBUS-KAMINSKA, and A. MACCOLL. Theochem. **40**, 125 (1988); (*f*) P. MASCLET, D. GROSJEAN, and G. MOUVIER. J. Electron Spectrosc. Relat. Phenom. **2**, 225 (1973); (*g*) W. TSANG. J. Am. Chem. Soc. **107**, 2872 (1985).
18. E. STENHAGEN, S. ABRAHAMSSON, and F. W. MCLAFFERTY (*Editors*). Registry of mass spectral data. John Wiley and Sons, Toronto. 1974. pp. 9 and 76.
19. A. L. MITCHELL and J. M. TEDDER. J. Chem. Soc. Perkin Trans. 2, 1197 (1986).
20. A. OKAMOTO and D. R. ARNOLD. Can. J. Chem. **63**, 2340 (1985).
21. (*a*) D. D. M. WAYNER, R. J. BOYD, and D. R. ARNOLD. Can. J. Chem. **63**, 3283 (1985); (*b*) D. A. HROVAT, P. DU, and W. T. BORDEN. Chem. Phys. Lett. **123**, 337 (1986).

Can. J. Chem. Downloaded from www.nrcresearchpress.com by 84.41.108.74 on 09/07/12
For personal use only.

A theoretical approach to the acid-catalyzed hydration of the carbonyl group: the case of formaldehyde

DANIEL PEETERS AND GEORGES LEROY

Laboratoire de chimie quantique, Université Catholique de Louvain, Pl. Louis Pasteur n° 1, B 1348, Louvain-la-Neuve, Belgium

Received November 13, 1990[1]

DANIEL PEETERS and GEORGES LEROY. Can. J. Chem. **69**, 1376 (1991).

The analysis of the hydration of formaldehyde in the presence of a hydrated proton was performed. Molecular quantum chemistry methods were used to explore the potential energy hypersurface. Calculations were performed at RHF-4-31G level. The structures were obtained through the use of first and second derivatives of the potential energy hypersurface thereby guaranteeing the nature of the extremum. The incidence of one or two water molecules on the reaction is discussed. It has been found that a low energy reaction path exists when the hydration process is catalyzed by a proton and two water molecules. The reaction mechanism rests on successive addition/elimination processes and reveals the respective roles of the oxygen lone pairs and of the C=O double bond upon the mechanism.

Key words: ab initio calculations, carbonyl reactivity, acid catalysis, hydration, reaction mechanism.

DANIEL PEETERS et GEORGES LEROY. Can. J. Chem. **69**, 1376 (1991).

L'hydration du formaldéhyde en présence d'un proton hydraté a été analysée. Les méthodes de la chimie quantique moléculaire sont utilisées dans l'analyse de l'hypersurface d'énergie potentielle. Les structures d'équilibre ont été obtenues à partir de méthodes utilisant les dérivées première et seconde de l'énergie potentielle, garantissant par là la nature de l'extrémum local. L'influence d'une et deux molécules d'eau supplémentaires est discutée. Cette étude montre l'existence d'un chemin de réaction à basse énergie dans l'hydratation catalysée par un proton en présence de deux molécules d'eau. Le méchanisme repose sur une succession d'étapes d'addition/elimination et montre les rôles respectifs des paires libres de l'atome d'oxygène et de la double liaison C=O dans ce mécanisme.

Mots clés : calcul ab initio, reactivité du carbonyl, catalyse acide, hydratation, mécanisme de réaction.

I. Introduction

The reactivity of the carbonyl group within a given molecule is known to be an important feature in both organic chemistry and biochemistry. Among many other reactions of this functional group reversible hydration is also important. Some of the hydrates are known to be stable solids, others which do not give solid hydrates can nevertheless be observed in an aqueous solution reaction:

$$R_1R_2CO + H_2O \rightleftarrows R_1R_2C(OH)_2$$

Even when this process is not clearly identified in a reaction mechanism, it is often suggested that it takes place with a small equilibrium constant. The hydrate may be difficult to detect, but it will be subsequently introduced as an intermediate in a sequence of elementary processes leading to an overall mechanism. In the gas phase, this reaction usually does not take place, although in some cases a small, but meaningful, equilibrium constant exists in the vapor mixture. These reactions are further subject to acid and base catalysis. Some reaction mechanisms involving several water molecules have been proposed. A review of the experimental approach to these considerations may be found in the comprehensive review of Bell (1) and the mechanism of general acid and base catalysis of the reactions of water and alcohols with formaldehyde has been described by Jencks and co-workers (2). These authors have arrived at the conclusion that the general acid catalysis of the addition of water to the carbonyl group occurs through a class "e" mechanism.

In the case of formaldehyde, various experimental approaches attest to the ease of such a reaction with an equilibrium constant close to 2×10^3. The reaction itself takes place in two steps, the first step leads to a molecular complex with a release of the heat of solution (1.63 to 1.96 kcal mol^{-1} for acetaldehyde (3)) followed by a hydration process corresponding to a reaction enthalpy ranging from 5.7 to 14.6 kcal mol^{-1}, with a suggested value of 8.0 kcal mol^{-1} (to be compared to a value of circa 5.0 kcal mol^{-1} for acetaldehyde (1)). It is further well established that the solution polymerizes to paraformaldehyde upon evaporation. If the formaldehyde is subjected to sulfuric acid catalysis, it forms a trimer (trioxane), if it is distilled it forms a linear polymer (Delrin).

This reaction is of particular theoretical interest. It is the simplest reaction of the carbonyl group and can be taken as a model for more complex situations. It also constitutes a challenge for theoreticians due to the fact that it does not take place in the gas phase, but requires the introduction of water into the computation in order to be followed realistically by quantum mechanics. The interaction between a single water molecule and formaldehyde has been analyzed by various authors. Quite recently, an extensive analysis of the many complexes appearing on the energy hypersurface has been performed by Kumpf and Danewood (4). The properties of these complexes, namely the behavior of the electronic spectrum of formaldehyde perturbed by the presence of water, has been studied by Blair and co-workers (5). The hydration process itself has been studied for neutral species by Williams *et al.* in several papers (6). Since an extensive analysis of the literature has been performed by these authors, we shall refer our readers to these reviews. These authors studied in a first approach the catalyzed addition mechanism (6*a*) and completed the examination by studying the influence of solvation on this mechanism (6*b*).

In this work we intend to study, from a theoretical point of view, the behavior of the carbonyl group of formaldehyde in the presence of water molecules, one of these bearing a proton. This will be accomplished by the analysis of various extrema appearing on the potential energy hypersurface. In the "supermolecule" approach, some well-defined situations of $H_2CO \cdot H^+ \cdot (H_2O)_n$ and $H_2C(OH)_2 \cdot H^+ \cdot (H_2O)_{n-1}$ clusters (where n equals

[1]Revision received April 18, 1991.

Printed in Canada / Imprimé au Canada

Can. J. Chem. Downloaded from www.nrcresearchpress.com by 84.41.108.74 on 09/07/12
For personal use only.

TABLE 1. Neutral and protonated methanediol and water formaldehyde complex (total energy in atomic units, relative energies in kcal mol^{-1}, and entropy in cal mol^{-1} K^{-1})

System	Reference to Fig. 1	E (SCF/4-31G)	ΔE	ZPE	E (0-298.15)	S^0
$H_2CO \cdot H_2O^{\neq}$	A'	−189.60864	12.09	33.71	3.66	74.19
$H_2CO \cdot H_2O$	A	−189.61248	9.68	34.45	3.80	76.04
$H_2C(OH_2)$	B'	−189.62073	4.50	37.57	2.69	64.96
$H_2C(OH)_2$	B	−189.62791	0.00	38.38	2.31	60.63
$H_2O \cdot H_2CO \cdot H^+$	D'	−189.93216	13.02	45.22	2.61	65.24
$H_2O \cdot H_2CO \cdot H^+$	D	−189.94098	7.49	45.35	2.89	66.10
$H_2CO \cdot H^+ \cdot H_2O$	C	−189.95292	0.00	42.10	3.54	72.17

1, 2, and 3) are examined. This paper may be considered a continuation of our previous work (7) on the behavior of water molecules sharing a proton. Some $H^+ \cdot (H_2O)_n$ clusters were studied with a special interest on the proton exchange between the various acceptor sites. In this case, a formaldehyde molecule will replace a water molecule. The clusters obtained will be allowed to rearrange on that part of the reaction hypersurface which describes diol formation. This analysis may also be considered a prerequisite to other reactions involving the carbonyl group.

II. Method

Our approach consists of first, the determination of the fully optimized geometry of the various structures. These structures are further solvated to small clusters and are treated as supermolecular systems. Any symmetry constraint has *a priori* been removed. As the most important entities concerned in this work are composed of three water molecules, we limited our choice of the basis set to the valence split 4-31G basis of Pople and coworkers using the GAUSSIAN series of programs (8, 9). Nevertheless this allows an analytical computation of the first and second derivatives of the energy hypersurface of any system studied, guaranteeing the nature of the local extremum.

The current reproaches to such a supermolecule approach invoke the basis set limitations leading to a well-known basis set superposition error and the lack of electron correlation. It is known that currently all these requirements can not be satisfied for the systems under consideration. As the second derivatives are the only guarantee of the nature of the extremum, we have chosen a methodological approach allowing this constraint to be fulfilled. Indeed, on our own experience, algorithms resting solely on first derivatives very often lead to improper points on the hypersurface giving one or even more negative eigenvalues when treated properly. Along the same lines, the natural tendency to start the optimization with symmetrical structures also presents many drawbacks. Thus the strategy we have employed throughout this paper starts from broken symmetry, followed by a full optimization of the structure guaranteed by the local analysis of the hypersurface up to the second order. To avoid basis set superposition error, which exists but is crudely corrected for by counterpoise calculations, we have decided to rest our discussion on structures belonging to the same hypersurface as fas as possible (i.e. presenting the same number of variables and parameters). In this case, the error is minimized for an error of the same magnitude should be observed for all partners. In addition, the intermolecular correlation energy of these systems remains almost constant on the hypersurface. This conclusion rests on arguments deduced from a preceding paper (6).

The results obtained in this way may be used in the computation of some thermodynamical properties. Indeed, as soon as the geometry of the system is known, one may calculate its moment of inertia and obtain the related rotational data. Furthermore, the knowledge of the normal modes of vibrations and their frequencies allows the introduction of zero point energy (ZPE) corrections. Consideration of the translational, rotational, and vibrational motions allows the computation of the internal energy under standard conditions. In addition, the entropy may be estimated from the use of statistical thermodynamics. Some care must be taken in using this datum, as it is only meaningful under the assumption of "perfect" behavior of the system. This means that we admit that the counter ion plays no explicit role for ionized system; that the neighborhood does not interact further with the structure under consideration and that the internal motions remain conventional vibrational modes at the temperature considered.

III. Results

The results are grouped by the number of water molecules added to formaldehyde. Thus Table 1 presents the data obtained following the procedure described in the preceding paragraph for $H_2CO \cdot 1H_2O$ and its rearranged counter parts such as $CH_2(OH)_2$. Figure 1 presents the corresponding structures accompanied by the most relevant bond lengths. To clarify the presentation, the position index of the structure in the figure is added as the second entry in the table, the first being the most appropriate chemical formula. In this case neutral, as well as protonated species, are shown explicitly. The tables report the fully optimized total energy and the energy increase relative to the most stable structure on the surface. The zero point energies, thermal corrections from 0 to 298.15 K and the entropies obtained within the harmonic approximation are also given. These data are not corrected for the possible free internal rotations. In this context, Tables 2 and 3, complemented by Figs. 2 and 3, present the data and structures obtained by adding one or two additional water molecules to the previous systems. This addition is made in the presence of an extra proton to simulate an acidified medium. Finally, for the purpose of completing our discussion, Table 4 and Fig. 4 present some structures obtained by replacing a water molecule with methanol.

One must keep in mind that such systems contain many degrees of freedom (36 for those with 14 atoms) and present a number of stable structures which may be important. In addition, the presence of labile parameters in clusters and complexes makes the determination of a true extremum quite difficult. Thus we do not pretend the list of structures reported here is exhaustive. However, all of these structures are true extrema presenting no negative eigenvalue for the second

Can. J. Chem. Downloaded from www.nrcresearchpress.com by 84.41.108.74 on 09/07/12
For personal use only.

TABLE 2. Protonated complexes of methanediol and formaldehyde with two water molecules (total energy in atomic units, relative energies in kcal mol^{-1}, and entropy in cal mol^{-1} K^{-1})

System	Reference to Fig. 2	E (SCF/4-31G)	ΔE	ZPE	E (0-298.15)	S^0
$H_2O \cdot H_2CO \cdot H^+ \cdot H_2O$	*D*	−265.88018	20.99	61.17	4.98	83.21
$H_2O \cdot H_2CO \cdot H^+ \cdot H_2O^{\neq}$	*F*	−265.88210	19.79	61.61	4.11	77.49
$H_2O \cdot H_2CO \cdot H^+ \cdot H_2O^{\neq}$	*E*	−265.89427	12.15	60.48	4.48	81.00
$H_2O \cdot H_2CO \cdot H^+ \cdot H_2O$	*B*	−265.89516	11.59	60.79	4.92	84.28
$H_3O^+ \cdot H_2C(OH_2)$TS	*H*	−265.90028	8.38	62.31	3.77	75.52
$H_2O \cdot H_2O \cdot H_2CO \cdot H^{+\neq}$	*G*	−265.90030	8.37	61.40	3.74	75.02
$H_3O^+ \cdot H_2C(OH_2)$	*C'*	−265.90066	8.14	61.93	4.17	78.07
$H_2O \cdot H_2O \cdot H_2CO \cdot H^+$	*C*	−265.90227	7.13	62.27	4.23	80.14
$H_2CO \cdot H_5O_2^+$	*A*	−265.91364	0.00	59.60	5.18	88.45

TABLE 3. Protonated complexes of methanediol and formaldehyde with three water molecules (total energy in atomic units, relative energies in kcal mol^{-1}, and entropy in cal mol^{-1} K^{-1})

System	Reference to Fig. 3	E (SCF/4-31G)	ΔE	ZPE	E (0-298.15)	S^0
$H_2O \cdot H_2CO \cdot H_5O_2^+$	*B*	−341.84138	14.40	75.79	7.04	106.49
$H_2O \cdot H_2C(OH_2) \cdot H_3O^{+\neq}$	*C'*	−341.84216	13.90	77.51	5.53	90.55
$H_2O \cdot H_2O \cdot H_2CO \cdot H^+ \cdot H_2O$	*C*	−341.84536	11.90	78.83	6.10	95.61
$(H_2O)_2H_2C(OH_2) \cdot H^+$	*D'*	−341.85420	6.35	79.28	6.08	96.97
$(H_2O)_3 \cdot H_2CO \cdot H^+$	*D*	−341.85637	4.99	79.51	5.94	95.48
$H_2CO \cdot H_7O_3^+$	*A'*	−341.85896	3.37	75.64	6.90	105.83
$H_2C(OH_2) \cdot H_5O_2^+$	*B'*	−341.85969	2.91	79.67	5.18	86.91
$H_2CO \cdot H_7O_3^+$	*A*	−341.86433	0.00	76.61	7.17	107.55

Can. J. Chem. Downloaded from www.nrcresearchpress.com by 84.41.108.74 on 09/07/12
For personal use only.

derivatives matrix, or at most one for transition states. In the case of transition states, the eigenvector corresponding to this negative curvature has been analyzed to ensure its correct behavior along the reaction path, avoiding undesirable transition states such as those related to rotations or flip-flop motions. In conclusion, other stable structures which could be determined are believed to bring no further insight to the problem.

IV. Discussion

(a) Methyleneglycol

A crude examination of the equilibrium structures obtained for the complex "water–formaldehyde" and the methanediol molecule provides information for the reaction

$$H_2CO \cdot H_2O \rightleftarrows H_2C(OH)_2$$

The reaction energy found at 0 K equals -9.68 kcal mol^{-1}, which is slightly decreased by ZPE and thermal corrections to a value of -7.24 kcal mol^{-1}. This difference is essentially due to the ZPE corrections as low frequency modes are present in the complex but not in the reactant molecules. The same kind of considerations lead to an overall entropy change of some -15.41 eu bringing the Gibbs free energy to -2.64 kcal mol^{-1} for the described process. This results compares favorably to the experimental values of -4.0 to -4.5 kcal mol^{-1} for the global reaction in solution.[2] The transition state shown in Fig. 1 corresponds to the rotation of the formaldehyde molecule in the complex and may not, in any case, be considered an addition transition state. Indeed, the corresponding reaction coordinate contains no contribution from the bonds in formation. Such a transition state presents a high energy and, as shown by Williams, the introduction of more water molecules is required to maintain the reaction in an acceptable energy range.

It should be mentioned that a second conformer is obtained for methyleneglycol. In this conformer, an OH bond bisects the CH_2 group, while in the most stable conformer a hydrogen bridge is established with the opposite oxygen center. The anomeric effect (10) predicts that this species is slightly less stable (45 kcal mol^{-1}) than the first. However, since it presents nearly the same vibrators and entropy, the Gibbs free energy between this species and the complex falls to a small value (-0.13 kcal mol^{-1}) which justifies a nearly one-to-one equilibrium for this species even though globally the overall constant is much smaller.

Finally the association step described by the reaction:

$$H_2CO + H_2O \rightleftarrows H_2CO \cdot H_2O$$

is highly exothermic from a theoretical point of view (-7.04 kcal mol^{-1}) but may not be considered so exothermic when compared to the experimental value (-1.6, -2.0 kcal mol^{-1}) as it does not describe the global solvation process (i.e. the reorganization of all the associated solvent molecules).

Since it is well known that the reactions of carbonyls respond to acid catalysis (2), we examined the various species obtained by protonation of the preceding systems. The addition of a bare proton either on the complex or on the diol leads in both cases to a molecule–ion complex. In the former the proton is captured by the water molecule yielding a $H_2CO \cdot H_3O^+$ complex (Fig. 1*C*). In the latter, the proton is trapped by an hydroxyl group giving

[2]These values are obtained from the association constants given in Table 1 of ref. 1. The K_2 values range from 10^{-3} to 4.5×10^{-4}, giving Gibb's free energies between 4.09 and 4.56 kcal mol^{-1}.

Can. J. Chem. Downloaded from www.nrcresearchpress.com by 84.41.108.74 on 09/07/12
For personal use only.

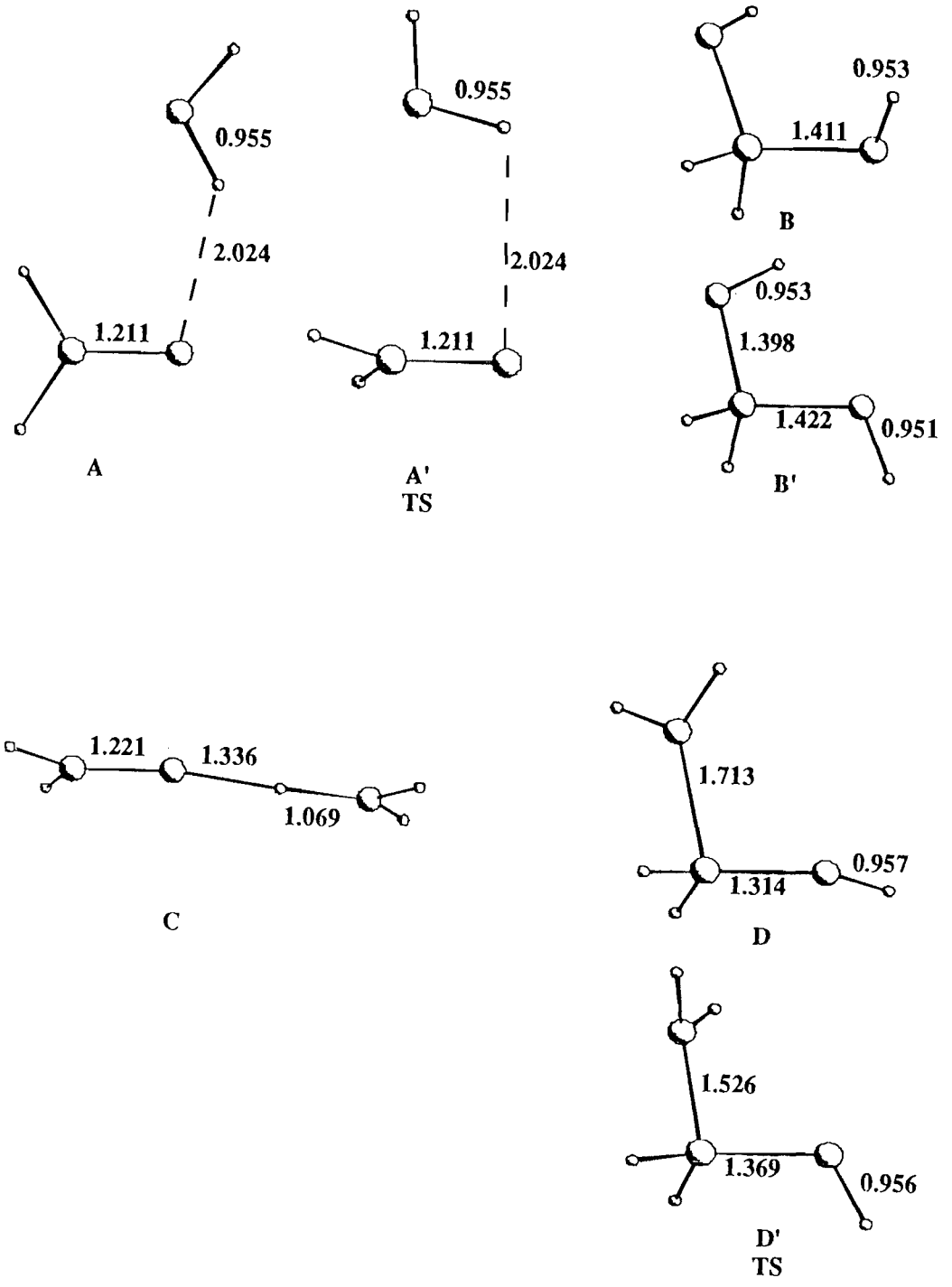


FIG. 1. Structures of neutral and protonated methanediol and the complexes between water and formaldehyde (distances in Å).

another complex symbolized by $H_2COH^+ \cdot H_2O$ (Fig. 1*D*) which is some 7.49 kcal mol^{-1} less stable. Entropy as well as thermal corrections increase this tendency towards instability. All the other conformations obtained by rotating the OH bonds about the CO bond have led to rotational transition states rather than stable conformers. It may be surprising to find a transition structure (Fig. 1*D'*) resembling a protonated diol with no corresponding minimum, but we have explored the hypersurface and followed carefully the corresponding eigenvector in both directions. No minimum could be found and the structure smoothly rearranges upon rotation to the stable complex (Fig. 1*D*). During this rotation, the CO bond shortens while the water molecule moves off. Finally, a direct proton transfer transition structure can be obtained; however, it passes through an impressive activation barrier of some 29.6 kcal mol^{-1}. Summarizing these first observations, we may conclude that an anlaysis of the protonated energy hypersurface corresponding to the protonated diol molecule does not lead to such minimum, as only molecular cationic complexes are found.

(b) Systems with a second water molecule

Further hydration of the previously protonated systems will

Can. J. Chem. Downloaded from www.nrcresearchpress.com by 84.41.108.74 on 09/07/12
For personal use only.

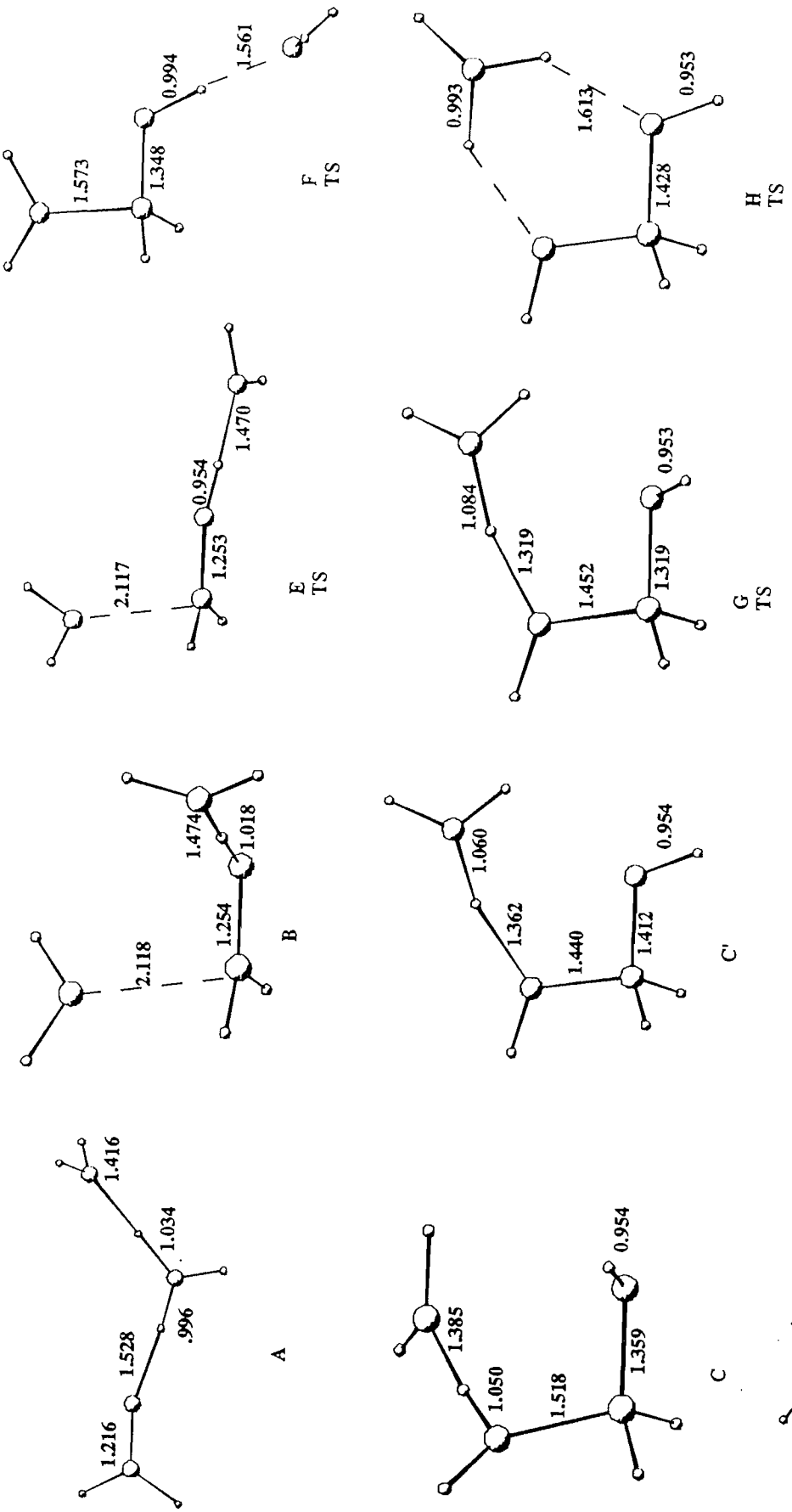


FIG. 2. Structures of solvated methanediol and the related complexes of formaldehyde in the presence of a proton (distances in Å).

produce many chemically distinct species as shown in Fig. 2. Starting from the $H_2CO \cdot H_3O^+$ complex (Fig. 1*C*), one may add an extra water molecule either on the hydronium part, or on the carbon center (Fig. 2*A*, *B*). Both lead to stable minima, even though the former is energetically more stable. Starting from the $H_2COH^+ \cdot H_2O$ complex (Fig. 1*D*), a molecule may be added on the water site or undeneath the complex on the carbon center (Fig. 2*C*, *D*). Both situations lead to stable structures. Looking at the former situation, a second stable minimum is obtained by a 90° rotation of the OH bond about the CO bond (Fig. 2*C'*).

The most stable system obtained from an energetic point of view, corresponds to the $H_2CO \cdot H_5O_2^+$ complex (Fig. 2*A*) while the less stable structure corresponds to the double hydration of the H_2COH^+ ion (Fig. 2*D*). On examination of their geometry, one notices that in the latter structure the addition of a second water molecule appreciably repels both molecules from the carbon centre. In the first complex, the identification of the formula relies on the OH distances reported from the structure. It has been established previously that in the $H_7O_3^+$ species the OH bonds shared by two oxygen atoms are equivalent and close to the standard bond length of H_3O^+. In this case, the bond pointing toward the carbonyl group is close to the conventional bond length of a water molecule while the other bond is much longer, even though the proton is not symmetrically located between the two water molecules.

The three remaining structures appear between these two extremes and are those related to our problem. The system described by Fig. 2*B* reveals that the two water molecules also exert an important mutual interaction in this case. The presence of a molecule near the protonated carbonyl group repels the other molecule connected to the carbon center. However, the proton initially attached to the water molecule (Fig. 1*C*) moves to the carbonyl center no matter what the orientation taken by the water molecule. In some sense, the presence of these two water molecules extensively reorganizes the structure of the carbonyl group. Nevertheless, this molecule–ion complex does not evolve to a diol-like system.

Finally, two more stable structures can be proposed (Fig. 2*C*, *C'*). The first one corresponds to a sensibly stabilized complex between the protonated formaldehyde and a water dimer. The distance between the carbon center and the water molecule decreases significantly (0.2 Å) if one compares this situation to the one water molecule complex (Fig. 1*B*) and prepares the formation of the CO bond. This bond formation is completed in the other conformer which lies 1 kcal mol^{-1} higher in terms of total energy and 1.23 kcal mol^{-1} higher in Gibbs free energy. Such a difference allows for a good thermodynamical equilibrium between these structures.

Some transition states connecting the previously described systems can be found. For example, rotation transition states can be observed. When the water molecule located close to the carbonyl oxygen rotates (Fig. 2*E* one finds a transition state lying some 0.56 kcal mol^{-1} higher in energy. This difference is totally resorbed by the ZPE, thermal corrections and, at the free energy level, by the entropy. This allows globally for a free rotation of the system.

Since the conformer described by Fig. 2*C'* is a stable one, one may ask what happens when the second water molecule is added on the second hydroxyl group (Fig. 2*F*). In this case the structure becomes a rotation transition state leading to Fig. 2*B*. Its internal coordinates are quite close to the latter, and after a careful analysis of the hyperstructure, no stable structure could be found in this region of the potential hypersurface. Upon rotation of the OH function, the CO bond shortens and the water molecule moves off as described before (Fig. 1*D* and *D'*).

Finally, two more transition structures merit our attention. The first one (Fig. 2*G*) connects the two stable structures of diol type (Fig. 2*C*, *C'*) at less than 1 kcal mol^{-1} of free activation energy, ensuring by the way a good transformation rate. This corresponds to a rotation of the $(H_2O)_2$ moiety coupled to a synchronous rotation of the OH group. The second transition structure (Fig. 2*H*) describes the proton exchange between the two hydroxyl groups through a H_3O^+ relay in energetic conditions close to the preceding example.

At this stage, one may thus conclude that even though the most stable situation does not correspond to a diol structure, as soon as this level is attained on the potential hypersurface, an important reorganization of the structures is made possible at low energy constrain and at high rate due to the presence of a second water molecule in the system,

(c) Systems with a third water molecule

Having noticed the influence of a second water molecule on the reorganization of the system, we thought it would be appropriate to investigate the behavior of a third water molecule. We find that the structures corresponding to the complex $H_2CO \cdot H_7O_3^+$ are the most stable (Fig. 3*A*, *A'*), with an energetic preference of some 3.37 kcal mol^{-1} in favour of the complexation of the hydrated H_3O^+ part rather than the H_2O terminal group. Similarly, the situation corresponding to the addition of a water molecule onto the carbon center of $H_2CO \cdot H_5O_2^+$ (Fig. 3*B*) is again unfavorable when compared to $H_2CO \cdot H_3O^+$. The distance between the incoming oxygen atom and the carbon center is the largest described so far (2.495 Å). This intermediate may be taken as the limiting structure describing the reaction between water and the $H_2CO \cdot H_5O_2^+$ structure, even though the corresponding reaction energy equals 11.98 kcal mol^{-1}.

The addition of the water molecule either on the carbonyl proton (Fig. 2*C*) or on the water site (Fig. 2*B*) leads to a new structure (Fig. 3*C*) which is a compromise between the two intermediates previously reported. Indeed the CO distance of the entering water molecule approaches a bond length close to a diol-like system as it increases slightly when we compare it to the diol-like situation (Fig. 2*C*). This is due to the repulsion of the water molecule close to the protonated carbonyl. On the other hand, the OH distance between the carbonyl group and the proton shortens when compared to the carbonyl-like situation (Fig. 2*B*). The situation corresponding to a hydration of the diol (Fig. 3*C'*) is again a rotation transition state related to the preceding complex. No definite diol-like compounds appear with this arrangement.

The addition of the extra water molecule may also lead to a complex between a water trimer and the protonated formaldehyde molecule. In this case two stable conformers may be found (Fig. 3*D*, *D'*) whose structures resemble more closely the diol molecule as the number of water molecules increases. Indeed, in this case both CO distances are modified towards the diol CO equilibrium distance. Upon successive hydration the carbonyl elongates (Figs. 1*D*, 2*C*, 3*D*) by some 0.004 Å, while the other conformer, initially a transition state (Fig. 1*D'*) is stabilized to a diol resembling complex (Figs. 2*C'*, 3*D'*). This situation has an energy of about 5 kcal mol^{-1} higher than the most stable structure and may plausibly lie along the reaction path.

Finally, another very stable diol structure exists. It corresponds to a complex between $CH_2(OH)_2$ and $H_5O_2^+$ shown in

Can. J. Chem. Downloaded from www.nrcresearchpress.com by 84.41.108.74 on 09/07/12
For personal use only.

Can. J. Chem. Downloaded from www.nrcresearchpress.com by 84.41.108.74 on 09/07/12
For personal use only.

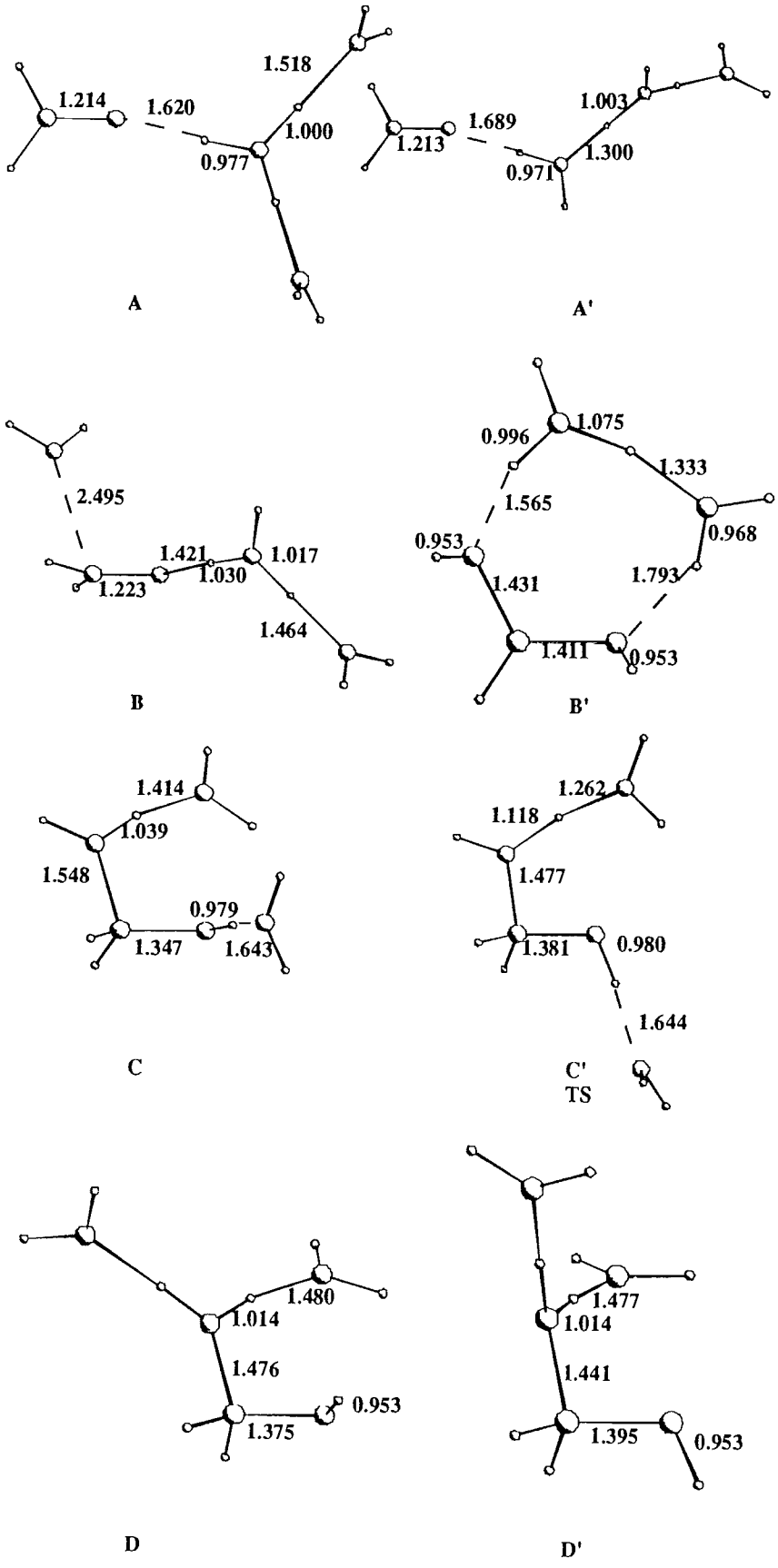


FIG. 3. Structures of methanediol solvated by two water molecules and the related complexes of formaldehyde (distances in Å).

TABLE 4. Protonated complexes of formaldehyde with methanol and water (total energy in atomic units, relative energies in kcal mol^{-1}, and entropy in cal mol^{-1} K^{-1})

System	Reference to Fig. 4	E (SCF/4-31G)	ΔE	ZPE	E (0-298.15)	S^0
$CH_3OH \cdot H_2CO \cdot H^+$	*A*	−228.92002	0.00	65.09	3.67	74.99
$CH_3OH \cdot H_2CO \cdot H^{+\neq}$	*A'*	−228.91653	2.19	64.37	3.52	75.02
$CH_3OH \cdot H_2CO \cdot H_3O^+$	*C*	−304.86602	7.19	81.52	5.57	92.05
$CH_3OCH_2OH \cdot H_3O^+$	*D*	−304.86999	4.70	80.82	5.07	86.97
$H_2CO \cdot H^+ \cdot CH_3OH \cdot H_2O^{\neq}$	*B'*	−304.87510	1.49	80.70	4.91	86.48
$H_2CO \cdot H^+ \cdot CH_3OH \cdot H_2O$	B	−304.87748	0.00	81.70	5.18	88.30

Fig. 3*B'*. This structure is the second structure examined with respect to the energy of the various species. It lies only 2.80 kcal mol^{-1} higher than the most stable structure. In this case, therefore, we have two energetically low-lying species which belong explicitly to either the protonated formaldehyde class, or to the diol system.

(d) A brief summary

At this stage it is worthwhile summarizing the most important points from this discussion. (*i*) The protonated form of methanediol rearranges to either a complex between a water molecule and a protonated formol; or a complex between formaldehyde and a hydronium ion. No diol-like structure has been found for such a system. (*ii*) The additon of a single water molecule leads to a stable $H_2CO \cdot H_5O_2^+$ complex. A complex between methanediol and a hydronium ion is found some 8.14 kcal mol^{-1} higher. This complex is itself 1 kcal mol^{-1} higher than a diol-like structure obtained by the complexation of a water dimer and protonated formaldehyde. (*iii*) The addition of a second water molecule confirms the stability of the $H_2CO \cdot H^+(H_2O)_n$ complexes, but in this case a $H_2C(OH)_2 \cdot H_5O_2^+$ appears at only 2.80 kcal mol^{-1} from the most stable previous complex. This hypersurface is thus the only one containing a diol molecule.

From this point of view, one may propose a global reaction correspondong to

$$R_1R_2CO \cdot H_5O_2^+ + H_2O \rightleftarrows R_1R_2C(OH)_2 \cdot H_5O_2^+$$

Before considering the reaction mechanism itself, it is worthwhile to have a look at the effect of the substitution of a water molecule by some other solvating species such as methanol.

(e) Incidence of the co-reactant

In the presence of a methanol molecule, the product will be a hemiacetal. To achieve this analysis, we have optimized the most important structures lying along the reaction pathway, substituting a hydrogen atom by a methyl group. The corresponding results are reported in Fig. 4 and Table 4 and will be discussed below. If one considers a neutral methanol molecule added to a protonated formaldehyde, two almost isoenergetic structures appear (ΔE = 0.61 kcal mol^{-1}). Only the most pertinent to our discussion is shown. This structure resembles a protonated hemiacetal more than a complex between methanol and formaldehyde. Indeed the bond lengths are not far from the conventional valence bond length (1.40 and 1.42 Å for C—O in the neutral hemiacetal). The other structure is obtained by rotation of the methanol moiety by some 140° about the C-O axis. Rotation of the proton about the CO bond generates a rotation transition structure lying at 2.19 kcal mol^{-1}. This is the same for both conformers. Starting from this first structure, a water molecule has been added to the various sites of interest yielding the structures presented in the figure. These structures can be compared to the two water molecule case.

Some tendencies previously presented remain: (*i*) The addition of a water molecule on the methanol site produces a significant shortening of the C—O bond in formation and a lengthening of the other CO bond. (*ii*) The addition of a water molecule on the protonated carbonyl site repels the methanol and shortens the CO bond.

These results confirm that, qualitatively, methanol acts comparable to water, in which case this second water molecule may be considered as a model for a second methanol molecule.

On the other hand, the main differences are: (*i*) The complexes or molecules in the methanol case show much shorter bond lengths than in the water case. It is surprising to notice that these bond lengths are close to the isoelectronic system with two or three water molecules (Fig. 4*A*, *A'* and Fig. 2*C*, *C'*; Fig. 4*B*, *B'* and Fig. 3*D*, *D'*). This suggests that the structure is determined by the number of electrons rather than by the number and nature of the molecules involved in the complex. (*ii*) A rotation transition state rather than a stable structure is obtained upon rotation of the OH bond (Fig. 4*B'*). (*iii*) Even though the structures seem to be more like molecules than complexes, the interconversion energies are about twice those obtained between water and formaldehyde.

Finally, the exchange of a proton from the methoxy to the alcohol site through a hydronium ion relay is very easy, requiring only 2.19 kcal mol^{-1}. The corresponding transition state is close to the product, in structure as well as in energy.

These observations allow us to conclude that the deductions stated for the hydration process of formaldehyde can be generalized to the hemiacetal formation process.

V. A possible reaction mechanism

At this stage, it is interesting to look at a reaction mechanism relating the formol reactant to the diol product in the presence of an acid catalyst such as a hydrated proton. Taking into account the global reaction proposed in the previous section:

$$R_1R_2CO \cdot H_5O_2^+ + H_2O \rightleftarrows R_1R_2C(OH)_2 \cdot H_5O_2^+$$

this reaction mechanism must be viewed from three complementary viewpoints: the energy of the system, the geometry of the various intermediates, and the electronic structure of the various partners.

(a) From an energy viewpoint

The reactant can be described by Fig. 2*A* which leads upon

Can. J. Chem. Downloaded from www.nrcresearchpress.com by 84.41.108.74 on 09/07/12
For personal use only.

Can. J. Chem. Downloaded from www.nrcresearchpress.com by 84.41.108.74 on 09/07/12
For personal use only.

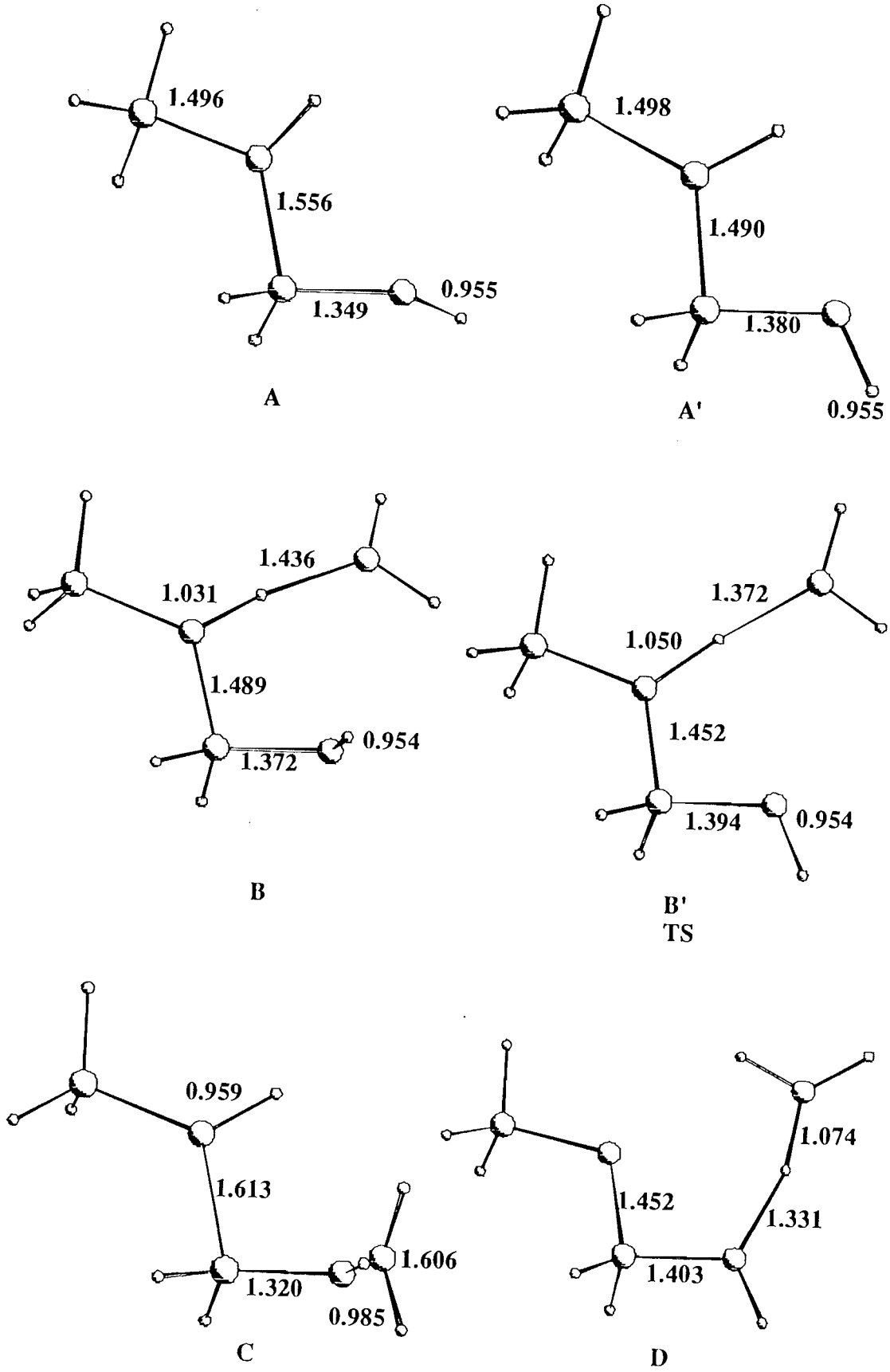


FIG. 4. Structures of protonated metoxy methanol and the related complexes of formaldehyde in the presence of methanol and a proton (distances in Å).

Can. J. Chem. Downloaded from www.nrcresearchpress.com by 84.41.108.74 on 09/07/12
For personal use only.

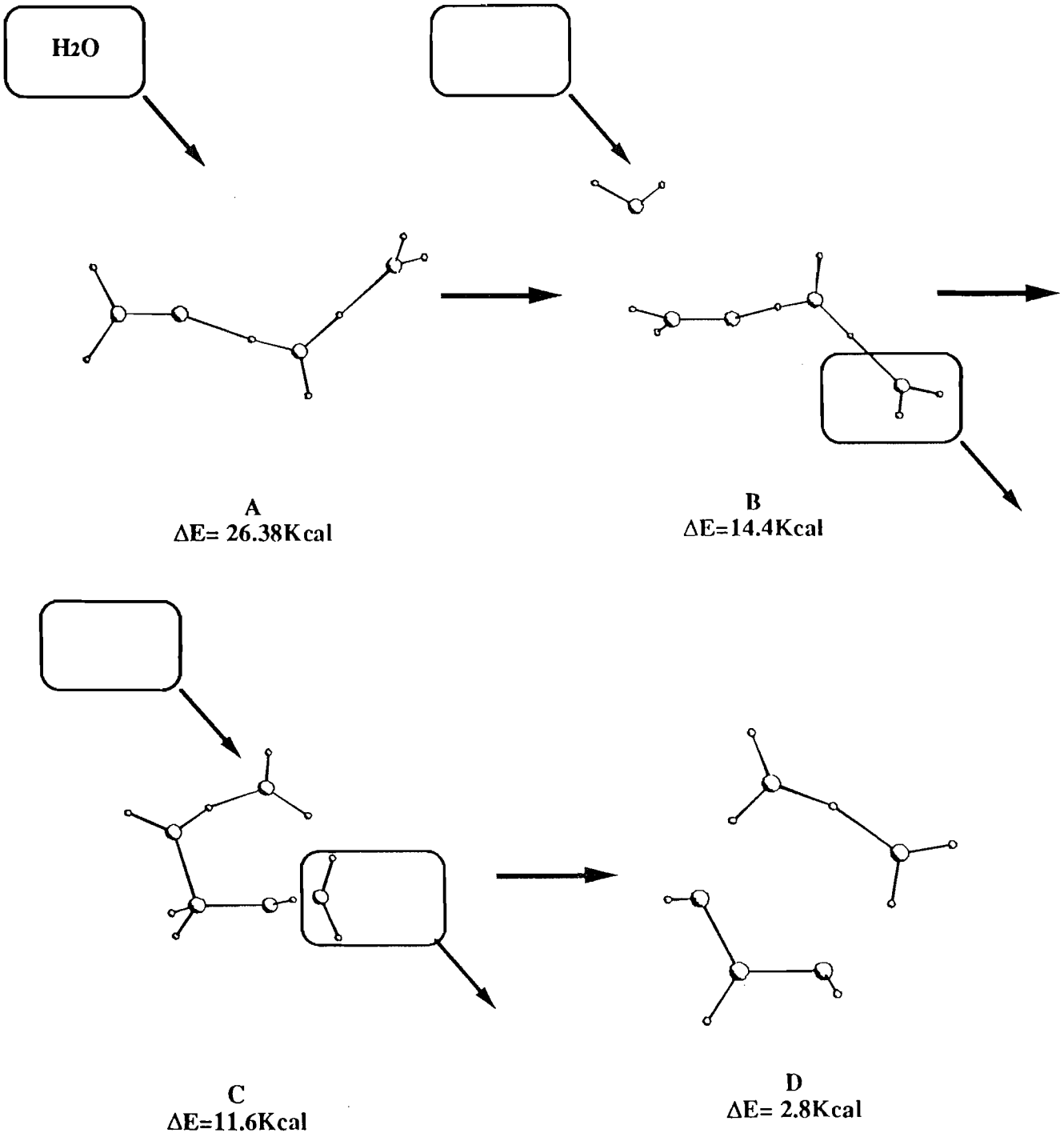


FIG. 5. Reaction energies of the hydration of formaldehyde in the presence of a proton and water molecules (the energies are given relative to the most stable structure of the potential energy hypersurface $H_2CO \cdot H^+ \cdot (H_2O)_3$).

addition of a water molecule to the reactant complex (Fig. 3*B*). The successive rearrangements of water molecules, one leaving one site while presumably another adding to another site, produce a logical sequence of low energy lying elimination/addition situations presented in Fig. 5. The relative energies are given with reference to the most stable structure belonging to the surface (Fig. 3*A*). The complete sequence refers to the acid catalysts in presence of two water molecules, i.e., $H_5O_2^+$ with a low reaction energy of 2.8 kcal. Considering the structural complementarity of $H_5O_2^+$ and methanediol, one may admit that the addition of any supplementary water molecule will not change the reaction energy nor the mechanism. It will probably change the relative energies of the intermediate species by stabilizing structures such as B through a complementary solvation process, and reduce the overall "activation" energy.

(b) From a structural viewpoint

As the water molecule enters the system, a complex is formed

Can. J. Chem. Downloaded from www.nrcresearchpress.com by 84.41.108.74 on 09/07/12
For personal use only.

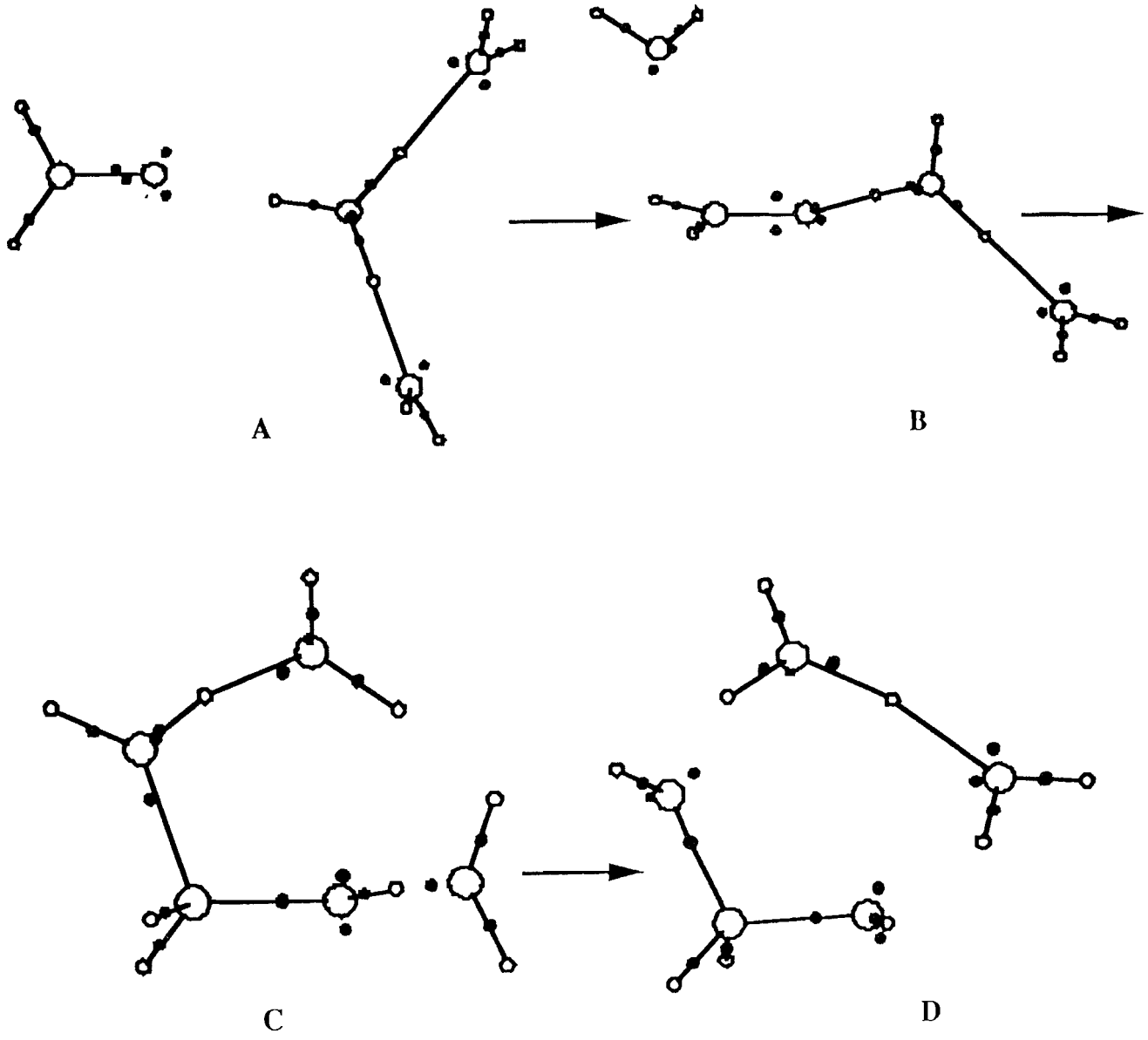
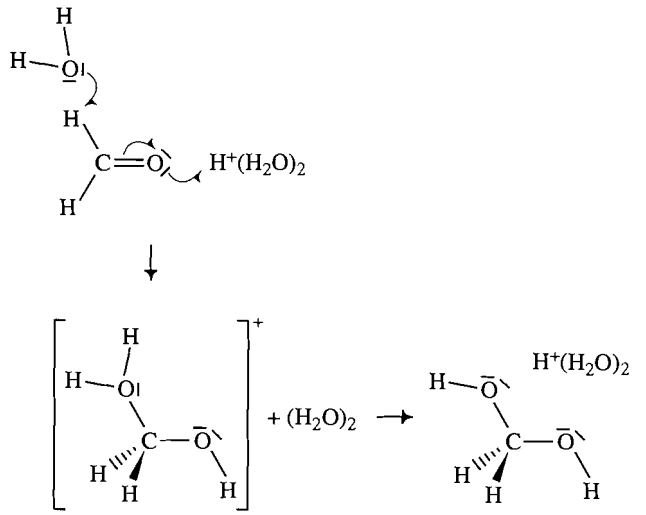


FIG. 6. Centroids of localized orbitals associated with the various structures along the reaction path of the hydration of formaldehyde in the presence of a proton.

with the initial $H_2CO \cdot H_5O_2^+$ species (Fig. 5*B*). Three steps have been determined to induce this reaction. First, the proton shifts from the $H_5O_2^+$ water entity to the carbonyl group. Meanwhile, one water molecule leaves $H_5O_2^+$ and another enters, forming a water dimer (Fig. $5B \rightarrow D$). This reaction mechanism is totally compatible with the suggestions of Eigen (11) and Bell (1, 12) who stated that the transition state for the addition of water to formaldehyde would contain one or two water molecules. In the proposed mechanism, these water molecules appear in intermediate complexes, related to the reactants and products by energetically low lying transition states.

(c) From an electronic viewpoint

The chemist is generally interested in the electronic description of a reaction mechanism. To this end, we have localized the molecular orbitals (13) obtained for the most pertinent structures lying on the hypersurface. The results of this procedure are presented in Fig. 6. The dots represent the centroids of charges giving the mean position of the electron pair associated with a localized orbital. The formation of the diol appears to follow a clear and simple electronic mechanism. Indeed, the exchanged proton coming from the water complex, lies in the formaldehyde molecular plane (Fig. 6*A*, *B*). It is captured by a lone pair of formaldehyde during the approach of a water molecule perpendicular to this molecular plane. Meanwhile, a σ C—O bond is formed and the C=O double bond rearranges. In the latter case, the π electron pair moves to the lone pair domain of the oxygen atom. Finally, a proton from the added water molecule moves into the lone pair domain of an ancillary water molecule, which then rearranges its electronic structure to a $H_5O_2^+$ complex. This mechanism may be shown schematically in the following way:



Let us point out here that this theoretical description of the mechanism is in full agreement with the conclusions obtained by Jencks and co-workers (2) from their experimental approach. Nevertheless, our method provides a better insight of the molecular elementary processes successively taking place during the reaction.

VI. Conclusions

In this paper we have analyzed the addition of water molecules to formaldehyde. This reaction mechanism was studied under the influence of a proton to model the effect of an acid catalyst. The main conclusions of this work are that: (*i*) In the presence of a single proton, no methanediol molecule is obtained. The molecule evolves to a molecule-ion complex. (*ii*) The same reaction, in the presence of a water molecule, leads to various situations, among which the complex $H_2CO \cdot H_5O_2^+$ is the most stable. Nevertheless, stable structures corresponding to the chemical formula of methanediol appear on the potential energy hypersurface. They are situated at some 8 kcal mol^{-1} higher than the most stable structure but they define a region on the hyperstructure where their interconversion can be fulfilled easily and at a fairly good rate. (*iii*) A second water molecule acts on the system in a similar way, i.e. the $H_2CO \cdot H_7O_3^+$ complex is the most stable structure but the number of diol-like situations increases. These compounds are more stable than those obtained previously, as they lie at only 2.8 kcal mol^{-1} higher than the most stable structure and inside the range of accessible conformers of $H_2CO \cdot H_7O_3^+$. In this sense, reactants and products coexist in chemical equilibrium on the hypersurface. (*iv*) This analysis leads us to propose a reaction mechanism for the acid catalyzed hydration of formaldehyde. In the first step of this mechanism, the hydrated proton aligns with a lone pair of formaldehyde. This proton is captured by the lone pair forming a covalent C—O bond, while the π electron pair shifts to become a lone pair. This rearrangement allows the concomitant addition of a water molecule on the carbon site by the formation of a second C—O covalent bond. Finally, the proton located on this oxygen moves back to the surrounding water molecules. (*v*) The preceding conclusions can be generalized to other reactions, namely those in which an alcohol molecule replaces a water molecule, leading to the formation of a hemiacetal.

Acknowledgments

This work has been made possible thanks to continuous support to our laboratory by the National Fund for Scientific Research (Belgium). The authors would like to thank Dr. Steven J. Berthel for reading and improving the English of their manuscript.

1. R. P. Bell. Adv. Phys. Org. Chem. **4**, 1 (1966).
2. L. H. Funderburk, L. Aldwin, and W. P. Jencks. J. Am. Chem. Soc. **100**, 5444 (1978).
3. R. P. Bell and J. C. Clunie. Trans. Faraday Soc. **48**, 439 (1952).
4. R. A. Kumpf and J. R. Damewood, Jr. J. Phys. Chem. **93**, 4478 (1989).
5. J. T. Blair, J. D. Westbrook, R. M. Levy, and K. Krogh-Jespersen. Chem. Phys. Lett. **154**, 531 (1989).
6. (*a*) I. H. Williams, G. M. Maggiora, and R. L. Schowen. J. Am. Chem. Soc. **102**, 7832, (1980); (*b*) I. H. Williams, D. Spangler, D. A. Femec, G. M. Maggiora, and R. L. Schowen. J. Am. Chem. Soc. **105**, 31 (1983); (*c*) I. H. Williams, D. Spangler, G. M. Maggiora, and R. L. Schowen. J. Am. Chem. Soc. **107**, 7717 (1985).
7. (*a*) D. Peeters and G. Leroy. Bull. Soc. Chim. Belg. **97**, 931 (1988); (*b*) D. Peeters and G. Leroy. J. Mol. Struct. (Theochem). **209**, 263 (1990).
8. (*a*) M. J. Frisch, J. S. Binkley, H. B. Schlegel, K. Raghavachari, C. F. Melius, R. L. Martin, J. J. P. Stewart, F. W. Bobrowicz, C. M. Rohlfing, L. R. Kahn, D. J. Defrees, R. Seeger, R. A. Whiteside, D. J. Fox, E. M. Fleuderand, and J. A. Pople. GAUSSIAN 86, Carnegie Mellon Chemistry Publishing Unit, Pittsburgh, PA. 1984.
9. W. J. Hehre, R. Ditchfield, and J. A. Pople. J. Chem. Phys. **56**, 2257 (1972).
10. G. A. Jeffrey, J. A. Pople, and L. Random. Carbohyd. Res. **25**, 117 (1972).
11. M. Eigen. Discuss. Faraday Soc. **39**, 7 (1965).
12. R. P. Bell and P. G. Evans. Proc. R. Soc. London Ser. A, **291**, 297 (1966).
13. (*a*) S. F. Boys. Rev. Mod. Phys. **323**, 296 (1960); (*b*) S. F. Boys. *In* Quantum theory of atoms, molecules and the solid state. *Edited by* P. O. Löwdin. Academic Press, New York. 1966. (*c*) A localization program has been written for the Gaussian Package by one of the authors (D.P.).

Can. J. Chem. Downloaded from www.nrcresearchpress.com by 84.41.108.74 on 09/07/12
For personal use only.

Thermodynamical detection of hydrophobic hydration of tris(2,4-pentanedionato)-cobalt(III) and tris(3,5-heptanedionato)cobalt(III) in water

YASUKI YOSHIMURA

Laboratory of Chemistry, College of Humanities and Social Sciences, Iwate University, Ueda, Morioka, 020 Japan

Received December 20, 1990

YASUKI YOSHIMURA. Can. J. Chem. **69**, 1388 (1991).

The solubilities of tris(2,4-pentanedionato)cobalt(III) and tris(3,5-heptanedionato)cobalt(III) in water, heptane, and 1,2-ethanediol were determined over the temperature range 5–50°C and from these data the thermodynamic quantities of solution at 25°C were estimated. The free energy (ΔG_t^0), enthalpy (ΔH_t^0), and entropy (ΔS_t^0) of transfer of these chelates from heptane to some solvents were calculated from the corresponding thermodynamic quantities of solution. When ΔH_t^0 and ΔS_t^0 were separately plotted against ΔG_t^0, the data of transfer from heptane to water deviated markedly from a correlation obtained for the data of transfer to the solvents other than water. This finding indicates that these chelates are subject to hydrophobic hydration in their aqueous solutions. The solubility of tris(glycinato)cobalt(III) in water was also determined over the temperature range 5–60°C and its temperature dependence of the solubility is compared with that for the cobalt(III) chelates of the β-diketones.

Key words: tris cobalt(III) chelates of β-diketones and glycine, temperature dependence of solubility, thermodynamic parameters of solution, thermodynamic parameters of transfer, hydrophobic hydration.

YASUKI YOSHIMURA. Can. J. Chem. **69**, 1388 (1991).

On a déterminé les solubilités du tris-(pentadionato-2,4)cobalt(III) et du tris(heptadionato-3,5)cobalt(III) dans l'eau, dans l'heptane et dans l'éthanediol dans un intervalle de température allant de 5 à 50°C. À partir de ces données on a évalué les paramètres thermodynamiques de solution à 25°C. On a calculé, l'énergie libre (ΔG_t^0), l'enthalpie (ΔH_t^0) et l'entropie (ΔS_t^0) de transfert de ces chélates à partir de l'heptane vers d'autres solvants, en se basant sur les paramètres thermodynamiques de solution. Les courbes de ΔH_t^0 et de ΔS_t^0 en fonction de ΔG_t^0 dévient beaucoup d'une corrélation obtenue pour les données de transfert vers des solvants autres que l'eau. Ces observations indiquent que ces chélates sont sujets à une hydratation hydrophobe dans leurs solutions aqueuses. On a également déterminé la solubilité du tris(glycinato)cobalt(III) dans l'eau dans l'intervalle de température allant de 5 à 60°C et on a comparé l'influence de la température sur la solubilité avec celle des chélates de cobalt(III) de β-dicétones.

Mots clés : chélates de tris cobalt(III) de β-dicétones, influence de la température sur la solubilité, paramètres thermodynamiques de solution, paramètres thermodynamiques de transfert, hydratation hydrophobe.

[Traduit par la rédaction]

The author has investigated through solubility measurements a dissolution behavior of tris(2,4-pentanedionato)cobalt(III) ($Co(acac)_3$) in the aqueous mixed solvents of dimethyl sulfoxide (DMSO) (1), 1,4-dioxane (D) (2), 2-methyl-2-propanol (TBA) (2), 2-butoxyethanol (BE) (3), and 2-ethoxyethanol (EE) (3). The enthalpy (ΔH_s^0) and entropy of solution (ΔS_s^0) for $Co(acac)_3$ in water estimated from temperature dependence of the solubility are negative (1) and its heat capacity of solution ($\Delta C_{p,s}^0$) is positive (2).

It has been extensively found that nonpolar nonelectrolytes dissolve in water with negative ΔH_s^0 and ΔS_s^0, and with positive $\Delta C_{p,s}^0$ (see, for example, ref. 4). This finding is explained in terms of hydrophobic hydration. Thus $Co(acac)_3$ seems to behave as a hydrophobic solute in water. For alkanes which are typically hydrophobic nonelectrolytes their hydrophobic properties increase with an increase in number of carbon atoms (5). From an analogy, the substitution of alkyl groups for two terminal methyl groups of 2,4-pentanedione (acac) in $Co(acac)_3$ is expected to increase the hydrophobic property.

The hydrophobic hydration is brought about by an effect of hydrophobic solutes on the hydrogen-bonded network structure of water and is phenomenon characteristic of aqueous solution (6–8). To make sure that metal chelates such as $Co(acac)_3$ are subject to the hydrophobic hydration, their thermodynamic quantities of solution in water need to be compared with those in some solvents other than water. This confirmation seems to provide useful information in a field such as solvent ex trac tion of metal chelates.

In this study, some alkyl-substituted β-diketones and their cobalt(III) chelates are synthesized and the solubilities of these chelates in water (W), heptane (Ht), and 1,2-ethanediol (ethylene glycol, EG) are determined over the temperature range 5–50°C. From these data the thermodynamic quantities of solution at 25°C are estimated and these quantities in W are compared with those in Ht and EG. Furthermore, in order to establish an unique feature for temperature dependence of the solubilities of these chelates in W, the solubility of tris(glycinato)cobalt(III) ($Co(gly)_3$) in W is also determined over the temperature range 5–60°C.

Experimental

Preparation of cobalt(III) chelates

3,5-Heptanedione (dipropionylmethane, DPrM), 2,6-dimethyl-3,5-heptanedione (diisopropionylmethane, DIPrM), and 2,2,6,6-tetramethyl-3,5-heptanedione (dipivaloylmethane, DPM) were synthesized according to the procedure of Adams and Hanser (9). Cobalt(III) chelates of these β-diketones were synthesized by the same method as $Co(acac)_3$ (10). The crude chelates were recrystallized from acetone solutions. *Anal.* calcd. for $Co(DPrM)_3$ ($Co(C_7H_{11}O_2)_3$): C 57.27, H 7.55; found: C 56.96, H 7.59. *Anal.* calcd. for $Co(DPM)_3$ ($Co(C_{11}H_{19}O_2)_3$): C 65.11, H 9.44; found: C 64.89, H 9.61. The melting point of the purified $Co(DPrM)_3$ was 55.7–56.1°C. As crystalline $Co(DIPrM)_3$ decomposed on standing in a silica gel desiccator, the solubility measurement of this chelate was not carried out. The purification of commercial $Co(acac)_3$ was described previously (1).

fac-Isomer of $Co(gly)_3$ was synthesized by methods reported in literatures (11, 12), recrystallized from aqueous sulphuric acid solution

Can. J. Chem. Downloaded from www.nrcresearchpress.com by 84.41.108.74 on 09/07/12
For personal use only.

TABLE 1. Solubilities (S_m) of $Co(acac)_3$ in Ht, EG, and E*

	Ht	EG	E
T/°C	$S_m \times 10^4$/(mol kg^{-1})	$S_m \times 10^3$/(mol kg^{-1})	$S_m \times 10^2$/(mol kg^{-1})
5			1.84 ± 0.02
10	1.83 ± 0.01		2.17 ± 0.01
15	2.46 ± 0.03	2.32 ± 0.03	2.57 ± 0.01
20	3.21 ± 0.01	2.72 ± 0.03	3.06 ± 0.01
25	4.19 ± 0.03	3.15 ± 0.05	3.64 ± 0.03
30	5.38 ± 0.06	3.73 ± 0.04	4.32 ± 0.03
35	6.79 ± 0.02	4.32 ± 0.07	5.17 ± 0.05
40	8.67 ± 0.05	4.97 ± 0.04	6.17 ± 0.06
45		5.71 ± 0.04	7.35 ± 0.12
50	14.2 ± 0.1	6.54 ± 0.01	
55		7.53 ± 0.05	
25†	4.19 ± 0.04	3.25 ± 0.06	3.66 ± 0.01

*Errors denote 95% confidence levels.

†Solubility values obtained by the experiment that the solutions equilibrated at the highest temperatures are allowed to attain equilibrium at 25°C are listed.

(about 50% by volume), and then dried for 3 h at 160°C. *Anal.* calcd. for $Co(gly)_3$ ($Co(C_2H_4O_2N)_3$): C 25.64, H 4.30, N 14.95; found: C 25.28, H 4.45, N 15.01.

Solvent

Commercial Ht (reagent grade, Wako Chemical Industries Ltd.) was stirred with concentrated sulphuric acid for 24 h with a magnetic stirrer, washed with dilute sodium hydroxide solution and water, refluxed over calcium hydride for 2 h, and then finally distilled. EG (reagent grade, Wako Chemical Industries Ltd.) was dried over molecular sieves (type 4A) for a week and distilled three times under reduced pressure. Commercial 99.5% ethanol (E) (Wako Chemical Industries Ltd.) was dried over molecular sieves (type 4A) for a week and distilled. The water contents in the purified Ht, EG, and E, measured by Karl Fischer titration, were less than 0.01, 0.05, and 0.02% by weight, respectively.

Solubility measurement

The solubility measurement was carried out by using the same apparatus and procedure as described previously (1–3). In the procedure, an aliquot of solution saturated with each chelate was withdrawn in 5 or 10 cm^3 volumetric flask by weight and diluted to the mark with water (for the systems other than Ht) or Ht (for Ht system). The concentration (in mol dm^{-3}) of the chelate in this solution was analyzed spectrophotometrically and the solubility in mol kg^{-1} (S_m) was obtained by calculating the mole numbers of the chelate in the aliquot of the saturated solution from the concentration. In the spectrophotometric determination, the absorbance was measured at the following wavelengths in the respective systems: for $Co(acac)_3$, 323 nm (W, EG, and E systems), 322 nm (Ht system); for $Co(DPrM)_3$, 323.5 nm (W and EG systems), 594 nm (Ht system); for $Co(DPM)_3$, 588 nm (Ht system); for *fac*-$Co(gly)_3$, 217 nm (W system). For all chelates, calibration curves in both aqueous and Ht solutions were straight in the concentration regions tested and the Beer's law equations were obtained by using the least-squares method. Since the absorbance in aqueous solutions was not affected by adding small amount of EG or E, the calibration curves in aqueous solutions were used for the solubility measurement in the EG and E systems.

In the preparation of the calibration curve for *fac*-$Co(gly)_3$, stock solution of the chelate was prepared by dissolving weighed crystal in 1 cm^3 of about 20% solution (by volume) of perchloric acid because of low solubility in W. Since the resulting calibration curve referred to the solutions containing 0.5 cm^3 of 20% perchloric acid per 5 cm^3, in the procedure of solubility measurement also the working solution to determine spectrophotometrically the concentration of the chelate was made up by adding 0.5 cm^3 of 20% perchloric acid solution to the aliquot of the saturated solution withdrawn in 5 cm^3 volumetric flask.

Determination of partition coefficient

The partition coefficient (P) of $Co(DPrM)_3$ between W and Ht was determined by the same procedure as used for the determination of P for $Co(acac)_3$ between W and dodecane (3). The equilibrium concentrations of $Co(DPrM)_3$ in both the phases were determined spectrophotometrically. The value of P was calculated as the ratio of the equilibrium concentration in aqueous phase to that in Ht phase.

Results

Solubilities of cobalt(III) chelates

The S_m values of $Co(acac)_3$ in Ht, EG, and E, of $Co(DPrM)_3$ in W, Ht, and EG, and of $Co(DPM)_3$ in Ht are tabulated in Tables 1, 2, and 3, respectively. The solubility measurement was repeated at least three times at each temperature. The errors given in these tables denote deviations at a 95% confidence level and are less than 2% in most cases.

In the previous work (1), it has been found that the solubility values of $Co(acac)_3$ in W obtained from absorbances at two different wavelengths agree with each other, and that $Co(acac)_3$ is not decomposed in W under the condition adopted in the solubility measurement. In the present systems also, the solubility data at 25°C were reproducible within the experimental errors when the solutions at the end of experiment at the highest temperature were allowed to attain equilibrium at 25°C. This result shows that these chelates are not decomposed in the course of the equilibration as well.

The solubility of $Co(DPM)_3$ in W was examined by extracting the chelate in saturated aqueous solution with dodecane. But the reproducibility of this method was poor because of its extremely low solubility (S_m was roughly $\sim 10^{-7}$ mol kg^{-1} at 25°C). When EG was stirred with $Co(DPM)_3$ for 72 h at 50°C, no absorption due to $Co(DPM)_3$ was detected in the EG phase. Accordingly, the solubility of $Co(DPM)_3$ in EG seems to be lower than that in W.

The solubilities of $Co(acac)_3$ and $Co(DPrM)_3$ in W decreased with an increase in temperature. This temperature dependence of solubility markedly differs from that in solvents such as Ht, EG, E, DMSO, D, TBA, BE, and EE. It is interesting to examine whether the above temperature dependence

Can. J. Chem. Downloaded from www.nrcresearchpress.com by 84.41.108.74 on 09/07/12
For personal use only.

TABLE 2. Solubilities (S_m) of $Co(DPrM)_3$ in W, Ht, and EG*

	W	Ht	EG
T/°C	$S_m \times 10^4$/(mol kg^{-1})	S_m/(mol kg^{-1})	$S_m \times 10^2$/(mol kg^{-1})
5	7.43 ± 0.04	0.277 ± 0.002	0.490 ± 0.001
10	5.68 ± 0.06	0.432 ± 0.005	0.586 ± 0.007
15	4.58 ± 0.05	0.703 ± 0.009	0.712 ± 0.007
20	3.68 ± 0.05	1.20 ± 0.03	0.864 ± 0.006
25	3.13 ± 0.02	2.29 ± 0.05	1.04 ± 0.01
27.5			1.14 ± 0.01
30	2.74 ± 0.04	5.25 ± 0.13	1.25 ± 0.01
32.5			1.38 ± 0.01
35	2.55 ± 0.03		1.49 ± 0.01
37.5			1.66 ± 0.01
40	2.40 ± 0.01		1.82 ± 0.01
42.5	2.31 ± 0.04		
45	2.28 ± 0.01		2.18 ± 0.01
47.5	2.23 ± 0.03		2.43 ± 0.01
25†	3.17 ± 0.04	2.29 ± 0.04	1.03 ± 0.01

*,†See footnotes in Table 1.

TABLE 3. Solubility (S_m) of $Co(DPM)_3$ in Ht*

T/°C	$S_m \times 10$/(mol kg^{-1})
5	1.24 ± 0.01
10	1.50 ± 0.02
15	1.76 ± 0.02
20	2.09 ± 0.03
25	2.42 ± 0.01
30	2.88 ± 0.05
35	3.32 ± 0.03
40	3.89 ± 0.05
45	4.50 ± 0.07
50	5.26 ± 0.08
25†	2.41 ± 0.02

*,†See footnotes in Table 1.

TABLE 4. Solubility (S_m) of *fac*-$Co(gly)_3$ in W*

	$S_m \times 10^4$/(mol kg^{-1})	
T/°C	From 217 nm†	From 520 nm‡
5	3.09 ± 0.03	
10	3.78 ± 0.03	
15	4.59 ± 0.04	
20	5.57 ± 0.07	
25	6.56 ± 0.09	
30	7.67 ± 0.14	
35	8.90 ± 0.07	
40	10.3 ± 0.1	10.6 ± 0.2
45	11.8 ± 0.1	12.1 ± 0.2
50	13.5 ± 0.1	13.8 ± 0.2
55	15.5 ± 0.1	15.8 ± 0.2
60	17.6 ± 0.1	18.1 ± 0.3
25§	6.47 ± 0.05	

*Errors denote 95% confidence levels.

†,‡Solubility values obtained from the absorbances at 217 and 520 nm, respectively.

§Solubility value obtained by reequilibrating at 25°C the solution saturated at 60°C.

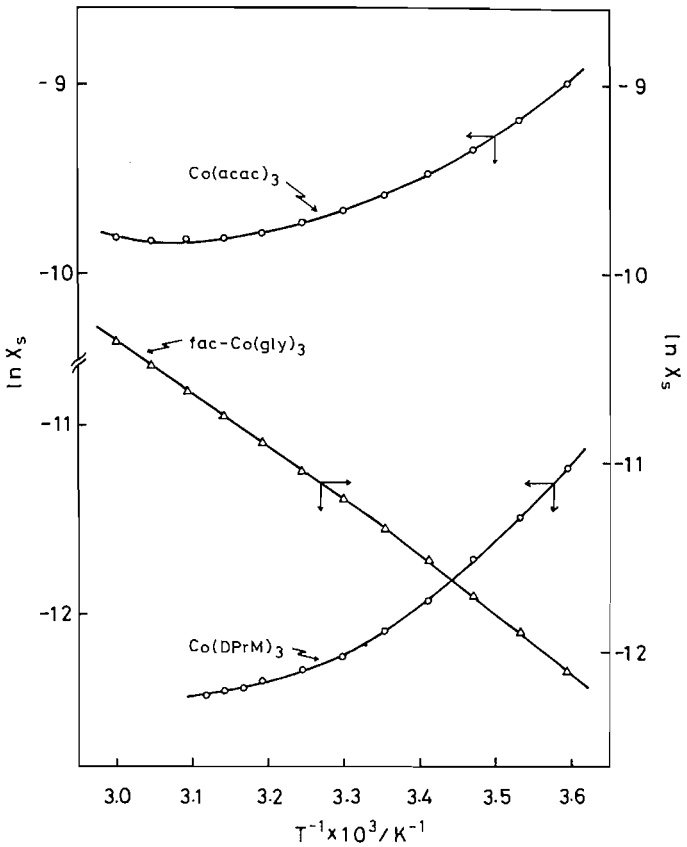


FIG. 1. Solubility curves of $Co(acac)_3$, $Co(DPrM)_3$, and *fac*-$Co(gly)_3$ in W depicted by plotting ln X_s against $1/T$.

of solubility observed in W is characteristic of $Co(acac)_3$ and $Co(DPrM)_3$ or not. Thus, the solubility of *fac*-$Co(gly)_3$ in W was also determined.[1]

The solubility of *fac*-$Co(gly)_3$ in W is listed in Table 4. At the temperatures above 40°C, the solubility values were obtained from absorbances not only at 217 nm but at 520 nm. These solubility values agreed with each other within the experimental errors. Furthermore, when the solution saturated at 60°C was re-equilibrated at 25°C, the solubility data at 25°C was reproducible (see Table 4). These results confirm that *fac*-$Co(gly)_3$ is not decomposed under the experimental condition.

The S_m values were converted to solubility in mole fraction (X_s) and ln X_s was plotted against $1/T$. These solubility curves for $Co(acac)_3$, $Co(DPrM)_3$, and *fac*-$Co(gly)_3$ in W are shown in Fig. 1. Figure 1 suggests that the temperature dependence of solubility found for $Co(acac)_3$ and $Co(DPrM)_3$ in W results from a peculiar interaction of these chelates with water.

Activity coefficient of cobalt(III) chelates in saturated solutions

Since infinite dilution is selected as the standard state for solute, it is required to examine whether the saturated solutions examined in this work may be regarded as ideal dilute solutions or not. In the previous work (3), it has been demonstrated that the P values of $Co(acac)_3$ between W or

[1]The solubility of *mer*-$Co(gly)_3$ in W was also determined and it was found that when the values for ln S_m were plotted against $1/T$, the solubility curve broke suddenly at around 35–45°C. An explanation of this anomalous behavior is investigated and will be reported elsewhere.

Can. J. Chem. Downloaded from www.nrcresearchpress.com by 84.41.108.74 on 09/07/12
For personal use only.

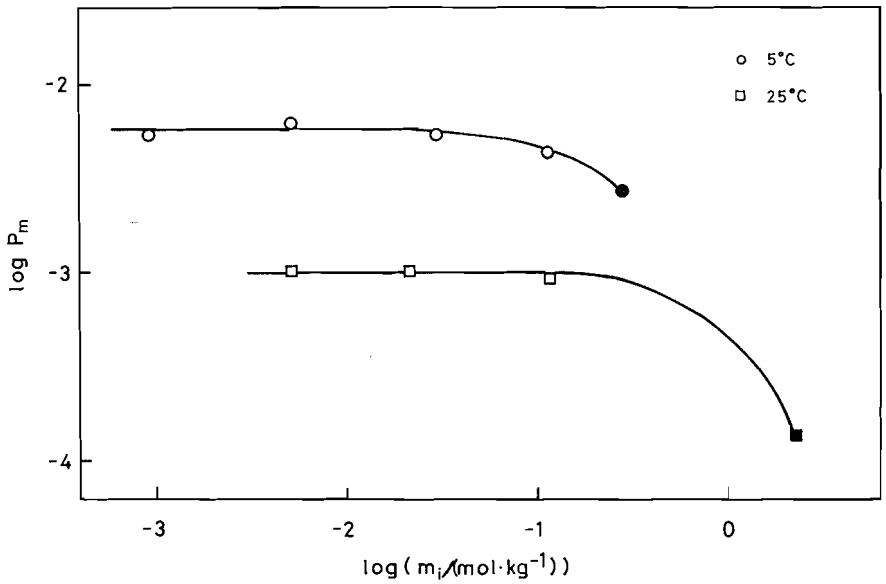


FIG. 2. Dependence of the partition coefficient based on molality (P_m) of $Co(DPrM)_3$ between W and Ht on the initial concentration of $Co(DPrM)_3$ in Ht phase (m_i). Full symbols denote the ratio of the solubility in molality of $Co(DPrM)_3$ in W to that in Ht.

DMSO and dodecane are in accord with the ratios of solubilities in the respective solvents and that the activity coefficients of $Co(acac)_3$ in these saturated solutions may be regarded as unity. The solubilities of $Co(acac)_3$ in EG or Ht, of $Co(DPrM)_3$ in W, and of *fac*-$Co(gly)_3$ in W are similar in magnitude to the solubility of $Co(acac)_3$ in W (1). The solubilities of $Co(acac)_3$ in E and of $Co(DPrM)_3$ in EG are similar in magnitude to the solubility of $Co(acac)_3$ in DMSO (1). Since it has been demonstrated that the activity coefficient of $Co(acac)_3$ in its saturated aqueous or DMSO solution is unity, it seems to be reasonable that the activity coefficients of $Co(acac)_3$ in EG, Ht, or E, of $Co(DPrM)_3$ in W or EG, and of *fac*-$Co(gly)_3$ in W may be regarded as unity.

Figure 2 shows a dependence of the partition coefficient based on mol kg^{-1} (P_m) for $Co(DPrM)_3$ between W and Ht on its initial concentration in Ht phase (m_i). The P_m values were nearly independent of m_i over the values of 9.2×10^{-4} to 0.115 mol kg^{-1} at both 5 and 25°C. But the ratio of the solubility in W to that in Ht was lower than P_m at both temperatures. This result indicates that the activity coefficient must be taken into account for the saturated solution of $Co(DPrM)_3$ in Ht because the activity coefficient of $Co(DPrM)_3$ in the saturated aqueous solution is regarded as unity.

In order to estimate the activity coefficient of $Co(DPrM)_3$ in Ht (γ(Ht)), P_m was determined four times at each temperature where the solubility in Ht was measured (m_i was 9.0×10^{-3} mol kg^{-1}) and converted to the partition coefficient based on mole fraction (P_x). The γ(Ht) value was calculated by

$$[1] \quad \gamma(\mathrm{Ht}) = X_s(\mathrm{W})/(P_x X_s(\mathrm{Ht}))$$

where X_s(W) and X_s(Ht) denote the solubility in W and Ht, respectively. In Table 5, the values for P_x, $X_s(W)/X_s(Ht)$, and γ(Ht) of $Co(DPrM)_3$ are listed.

The solubility of $Co(DPM)_3$ in Ht is also fairly high and from an analogy to the result shown in Fig. 2 it may be inferred that in this case also the activity correction is required. Unfortunately, the above procedure to estimate γ(Ht) could not be applied because of extremely low solubility of $Co(DPM)_3$ in W.

TABLE 5. Partition coefficient (P_x) of $Co(DPrM)_3$ between W and Ht and activity coefficient (γ(Ht)) of $Co(DPrM)_3$ in saturated Ht solution

T/°C	$P_x \times 10^4$*	$(X_s(W)/X_s(Ht)) \times 10^4$†	γ(Ht)‡
5	9.64 ± 0.17	4.95	0.513
10	6.08 ± 0.19	2.47	0.406
15	4.10 ± 0.11	1.25	0.305
20	2.69 ± 0.11	0.617	0.229
25	1.85 ± 0.05	0.302	0.163
30	1.32 ± 0.04	0.143	0.108

*P_x is defined as the ratio of equilibrium concentration of $Co(DPrM)_3$ (on mole fraction scale) in aqueous phase to one in Ht phase and mean of the values measured four times at the $Co(DPrM)_3$ concentration of 9.0×10^{-3} mol kg^{-1} is listed. Errors denote 95% confidence levels.

†Ratio of solubility in mole fraction in W to that in Ht of $Co(DPrM)_3$.

‡Calculated from [1].

Thermodynamic quantities of solution for cobalt(III) chelates

The values for ΔH_s^0, ΔS_s^0, $\Delta C_{p,s}^0$, and the free energy of solution (ΔG_s^0) were estimated by using Clarke and Glew procedure (13, 14). In the estimation, the values of $R \ln X_s$ (R = 8.3144 J K^{-1} mol^{-1}) were fitted, except for the dissolution of $Co(DPrM)_3$ in Ht where the $R \ln (\gamma X_s)$ values were fitted. Other details of the estimation have been reported elsewhere (3). The thermodynamic parameters thus estimated are listed in Table 6, where the values for the same process of $Co(acac)_3$ estimated from the solubility data in W, DMSO, D, BE, EE, and TBA reported previously (1–3) are also contained.

Discussion

The solubilities of the β-diketone cobalt(III) chelates studied in this work increase in the following sequence: $Co(DPM)_3 \ll Co(DPrM)_3 < Co(acac)_3$ in W; $Co(acac)_3 < Co(DPM)_3 < Co(DPrM)_3$ in Ht; $Co(DPM)_3 \ll Co(acac)_3 < Co(DPrM)_3$ in

Can. J. Chem. Downloaded from www.nrcresearchpress.com by 84.41.108.74 on 09/07/12
For personal use only.

TABLE 6. Thermodynamic quantities of solution for cobalt(III) chelates at 25°C*

Thermodynamic quantities	$Co(acac)_3$ in following solvents								
	Ht	W†	EG	DMSO†	D‡	BE§	EE§	TBA‡	E
ΔG_s^0	25.0	23.8	21.1	13.9	10.6	14.9	14.3	19.4	15.8
ΔH_s^0	38.5	−14.3	23.1	16.1	15.6	15.8	15.0	26.2	25.7
ΔS_s^0	45.3	−127.8	6.7	7.4	16.8	3.0	2.3	22.8	33.2
$\Delta C_{p,s}^0$	0	572	0	114	55	386	179	0	214

Thermodynamic quantities	$Co(DPrM)_3$ in following solvents			$Co(DPM)_3$	*fac*-$Co(gly)_3$
	Ht¶	W	EG	Ht	W
ΔG_s^0	8.7	29.9	18.2	9.2	28.1
ΔH_s^0	30.5	−21.1	27.8	23.2	24.1
ΔS_s^0	73.1	−171.0	32.2	46.9	−13.2
$\Delta C_{p,s}^0$	360	836	188	0	−127

*The units for ΔG_s^0 and ΔH_s^0 are kJ mol^{-1} and for ΔS_s^0 and $\Delta C_{p,s}^0$ are J K^{-1} mol^{-1}.
†Recalculated from the data given in ref. 1.
‡Recalculated from the data given in ref. 2.
§Reference 3.
¶Calculated from the solubility values corrected by using the γ(Ht) values listed in Table 5.

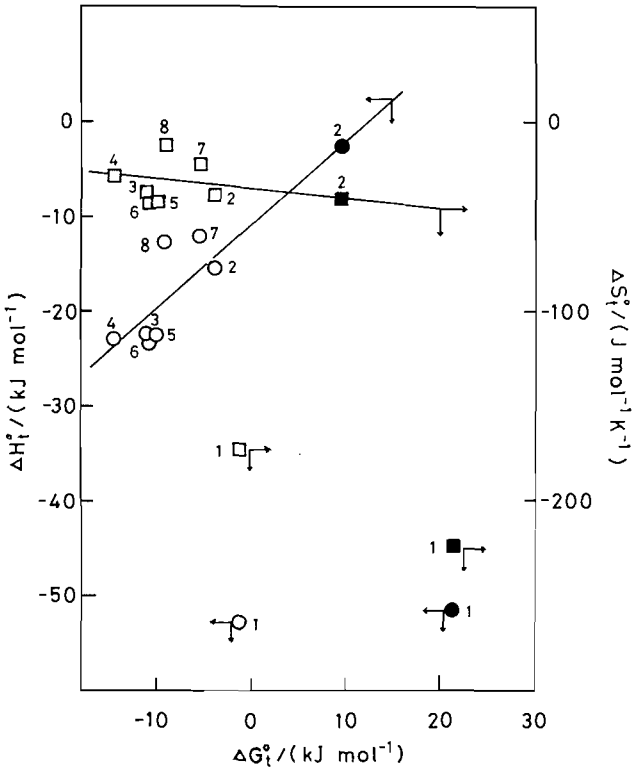


FIG. 3. Correlation between the enthalpy (ΔH_t^0) or entropy of transfer (ΔS_t^0) and the free energy of transfer (ΔG_t^0) for the transfer process of $Co(acac)_3$ and $Co(DPrM)_3$ from Ht to the following solvents: 1, W; 2, EG; 3, DMSO; 4, D; 5, BE; 6, EE; 7, TBA; 8, E. Circles are the plot of ΔH_t^0 vs. ΔG_t^0 and squares are the plot of ΔS_t^0 vs. ΔG_t^0. Full symbols denote the data for $Co(DPrM)_3$ and open symbols denote the data for $Co(acac)_3$.

EG. The solubilities of the corresponding copper(II) chelates in W also increase in the same order as the cobalt(III) chelates, whereas the solubilities in Ht increase in order $Cu(acac)_2 < Cu(DPrM)_2 < Cu(DPM)_2$ (15). On the basis of the theoretical prediction that in a homologous series, a solid having higher melting point is less soluble in nonpolar solvent such as Ht than one having lower melting point at a given temperature (16), the solubility sequence for $Co(DPM)_3$ and $Co(DPrM)_3$ in Ht can be explained by the low melting point of $Co(DPrM)_3$. The solubility sequence of the copper(II) chelates in Ht is also consistent with the above prediction (15).

The thermodynamic parameters of solution for $Co(acac)_3$ and $Co(DPrM)_3$ in W are peculiar compared to those in the other solvents in the following aspects: (*i*) ΔH_s^0 and ΔS_s^0 in W are negative, while those in the other solvents are positive; (*ii*) $\Delta C_{p,s}^0$ in W is large positive value, while that in the other solvents is near to 0. In order to make clear a difference in solvation of these chelates, a comparison of the thermodynamic parameters of transfer of the chelates from a solvent to the other solvents is more favorable.

Thus, the free energy (ΔG_t^0), enthalpy (ΔH_t^0), and entropy of transfer (ΔS_t^0) of $Co(acac)_3$ and $Co(DPrM)_3$ from Ht to the other solvents at 25°C were calculated by substracting the corresponding parameters of solution in Ht from those in the other solvents. For the transfer of $Co(DPrM)_3$ from Ht to W, the values thus obtained (ΔG_t^0; ΔH_t^0, 21.2; −51.6 kJ mol^{-1}; ΔS_t^0, −244 J K^{-1} mol^{-1}) agreed nearly with the values obtained from the plot of ln P_x vs. $1/T$ (ΔG_t^0; ΔH_t^0, 21.2; −55.7 kJ mol^{-1}; ΔS_t^0, −258 J K^{-1} mol^{-1}).

In Fig. 3, the values for both ΔH_t^0 and ΔS_t^0 are plotted against ΔG_t^0. Both ΔH_t^0 and ΔS_t^0 are negative in all cases. This result implies that the solvation of $Co(acac)_3$ or $Co(DPrM)_3$ in W, EG, DMSO, D, BE, EE, TBA, and E is stronger than the solvation in Ht. This conclusion is reasonable. For the transfer process to the solvents other than W, a rough linear correlation was found between ΔH_t^0 or ΔS_t^0 and ΔG_t^0. While ΔG_t^0 decreases with a decrease in ΔH_t^0 and with an increase in ΔS_t^0, the decrease in ΔG_t^0 is governed by decreasing ΔH_t^0 rather than by increasing ΔS_t^0 except for TBA and E. The data for the transfer to W deviate markedly from the correlation lines. This result shows definitely that some solvation characteristic of W, that is, hydrophobic hydration occurs.

If the above deviation for the transfer process from Ht to W may be attributed to the hydrophobic hydration, larger devia-

Can. J. Chem. Downloaded from www.nrcresearchpress.com by 84.41.108.74 on 09/07/12
For personal use only.

tion for $Co(DPrM)_3$ indicates that the hydrophobic hydration of $Co(DPrM)_3$ is stronger than that of $Co(acac)_3$. This conclusion is reasonable because hydrophobic parts of $Co(DPrM)_3$ are larger than those of $Co(acac)_3$.

$Co(acac)_3$ in W gives the solubility curve with a minimum at 50–55°C (see Fig. 1). $Cr(acac)_3$ also yields similar solubility curve in W (17). The solubility curve of $Co(DPrM)_3$ in W is also essentially identical. On the other hand, the solubility curve of *fac*-$Co(gly)_3$ in W is practically straight.

fac-$Co(gly)_3$ seems to be essentially hydrophilic. It has been found that the crystal of *fac*-$Cr(gly)_3 \cdot H_2O$ has a three-dimensional network of intermolecular hydrogen bonds between the chelate molecules, and that the water molecule in the crystal also serves to link two molecules of the chelate (18). These facts suggest that the dissolution of *fac*-$Co(gly)_3$ in W results from hydrophilic hydration composed of the hydrogen bond between the carboxylic and/or amino groups of the chelate and water molecules. Yamamoto and Nishi have also investigated a behavior of the hydration for a series of alkyl carboxylic acids in aqueous solutions and suggested that formic acid, which has no methyl group, undergoes the hydrophilic hydration through the hydrogen bond between the carboxylic group and water molecules (19).

The thermodynamic parameters of solution in W for *fac*-$Co(gly)_3$ listed in Table 6 also do not show the pronounced trend for the hydrophobic hydration, that is, large negative ΔH_s^0 and ΔS_s^0, and large positive $\Delta C_{p,s}^0$. The negative ΔS_s^0 found for *fac*-$Co(gly)_3$ is interesting in connection with the three-dimensional network of crystalline *fac*-$Cr(gly)_3 \cdot H_2O$. But an interpretation of this finding requires further examination.

The hydrophobic hydration has been interpreted as the phenomenon that a hydrophobic solute brings about a lowering of both enthalpy and entropy by increasing order of the network structure of water around the solute (4). Since the order of the water structure decreases with an increase in temperature (see, for example, ref. 20), the effect of the hydrophobic hydration may also be expected to diminish with increasing temperature (21). Thus, the hydrophobic effect seems to disappear at sufficiently high temperatures. Shinoda has pointed out that the disappearance of the hydrophobic hydration brings about a straightening of solubility curve at sufficiently high temperatures (22). The substitution of alkyl group for a hydrogen atom of the methylene group in glycine is expected to increase the hydrophobic property. In view of the finding that *fac*-$Co(gly)_3$ in W gives the straight solubility curve, an examination of the solubility in W for cobalt(III) chelates of the alkyl substituted α-amino acids is of interest in connection with the above Shinoda's viewpoint. Such examination is carried out and will be reported elsewhere.

1. Y. YOSHIMURA, N. SATO, and M. KIKUCHI. Bull. Chem. Soc. Jpn. **59**, 2135 (1986).
2. Y. YOSHIMURA. Can. J. Chem. **65**, 1218 (1987).
3. Y. YOSHIMURA. Can. J. Chem. **67**, 2108 (1989).
4. T. S. SARMA and J. C. AHLUWALIA. Chem. Soc. Rev. **2**, 203 (1973).
5. F. M. MENGER and U. V. VENKATARAM. J. Am. Chem. Soc. **108**, 2980 (1986).
6. R. LUMRY, E. BATTISTEL, and C. JOLICOEUR. Faraday Symp. Chem. Soc. **17**, 93 (1982).
7. E. GRUNWALD. J. Am. Chem. Soc. **108**, 5719 (1986).
8. N. MULLER. J. Solution Chem. **17**, 661 (1988).
9. J. T. ADAMS and C. R. HANSER. J. Am. Chem. Soc. **66**, 1220 (1944).
10. Inorg. Synth. Vol. V. p 188.
11. H. LEY and H. WINKLER. Ber. (*a*) **42**, 3900 (1909). (*b*) **45**, 375 (1912).
12. R. G. NEVILLE and G. GORIN. J. Am. Chem. Soc. **78**, 4893 (1956).
13. E. C. W. CLARKE and D. N. GLEW. Trans. Faraday Soc. **62**, 539 (1966).
14. S. F. DEC and S. J. GILL. J. Chem Educ. **62**, 879 (1985).
15. H. KOSHIMURA. J. Inorg. Nucl. Chem. **38**, 1705 (1976).
16. J. H. HILDEBRAND and R. L. SCOTT. The solubility of nonelectrolytes. Dover, New York. 1950. pp. 26–28.
17. M. YAMAMOTO. J. Phys. Chem. **88**, 3356 (1984).
18. R. F. BRYAN, P. T. GREENE, P. F. STOKELY, and E. W. WILSON, Jr. Inorg. Chem. **10**, 1468 (1971).
19. K. YAMAMOTO and N. NISHI. J. Am. Chem. Soc. **112**, 549 (1990).
20. A. INOUE, K. KOJIMA, Y. TANIGUCHI, and K. SUZUKI. J. Solution Chem. **16**, 727 (1987).
21. (*a*) M. SH. RAMADAN, D. F. EVANS, and R. LUMRY. J. Phys. Chem. **87**, 4538 (1983); (*b*) M. SH. RAMADAN, D. F. EVANS, R. LUMRY, and S. PHILSON. J. Phys. Chem. **89**, 3405 (1985).
22. K. SHINODA. J. Phys. Chem. **81**, 1300 (1977).

Can. J. Chem. Downloaded from www.nrcresearchpress.com by 84.41.108.74 on 09/07/12
For personal use only.

The thermodynamics of the vaporization of liquid indium(I) bromide by modified entrainment

PETER J. GARDNER AND STEVE R. PRESTON

Department of Chemistry, Royal Holloway and Bedford New College, University of London, Egham Hill, Egham, Surrey, TW20 0EX United Kingdom

Received January 28, 1991

PETER J. GARDNER and STEVE R. PRESTON. Can. J. Chem. **69**, 1394 (1991).

The transport of gaseous In(I)Br in an argon carrier gas was studied in the temperature range 680 to 935 K by the modified entrainment method. Combination of the entrainment results with a literature equation for the total vapour pressure above the liquid gave the following expressions for the temperature dependence of the vapour pressures of the monomer (InBr) and dimer (In_2Br_2) respectively: $\ln (p_1^0/p^0) = -(13457 \pm 59)/T + (24.240 \pm 0.077) - (1.306 \pm 0.014) \ln T - (0.001164 \pm 0.000021)T$, (680–950 K) and $\ln (p_2^0/p^0) = -(6490 \pm 1650)/T + (2.9 \pm 2.2)$, (680–810 K); $p^0 = 10^5$ Pa. The dimer concentration is *ca.* 14% at 680 K and decreases to *ca.* 4% at 810 K.

Key words: high temperature thermodynamics, indium(I) bromide, vaporization thermodynamics.

PETER J. GARDNER et STEVE R. PRESTON. Can. J. Chem. **69**, 1394 (1991).

On a étudié le transport du bromure d'indium gazeux In(I) Br par l'argon, à des températures allant de 680 à 935 K en utilisant la méthode d'entrainement modifié. En combinant les résultats obtenus par entrainement avec une équation relative à la pression de vapeur totale au-dessus du liquide répertoriée dans la littérature, on peut représenter l'effet de la température sur les pressions de vapeur du monomère (InBr) et du dimère (In_2Br_2) respectivement par les expressions suivantes : $\ln (p^0/p^0) = -(13457 \pm 59)/T + (24{,}240 \pm 0{,}077) - (1{,}306 \pm 0{,}014) \ln T - (0{,}001164 \pm 0{,}000021)T$, (680–950 K) et $\ln (p_2^0/p^0) = -(6490 \pm 1650)/T + (2{,}9 \pm 2{,}2)$, (680–810 K); $p^0 = 10^5$ Pa. La concentration du dimère est approximativement de 14% à 680 K et elle diminue à 4% environ à 810 K.

Mots clés : thermodynamique des hautes températures, bromure d'indium(I), thermodynamique des vaporisations.

[Traduit par la rédaction]

Can. J. Chem. Downloaded from www.nrcresearchpress.com by 84.41.108.74 on 09/07/12
For personal use only.

Introduction

Metal halides, for example, indium(I) bromide, have been used since the early 1960s in the development of the current generation of "metal halide" mercury discharge lamps (1). The effect of the inclusion of the metal halide within the lamp envelope is to improve significantly the spectral distribution and the colour rendition of the lamp. To simulate the spectral distribution it is necessary to know the thermodynamic and transport properties of the included halides over a wide range of temperature. A recent examination (2) of the vaporization of indium(I) bromide gave an equation for the total vapour pressure above the liquid between 570 and 950 K.

This paper describes a study of indium(I) bromide vaporization by a complementary technique, the modified entrainment method, and in combination with the results above, yields separate vapour pressure equations for the monomer and dimer species.

Experimental

Materials

Indium(I) bromide, a bright orange crystalline material, was prepared by reaction of high purity samples of indium metal and bromine; it was part of the same batch used in the quasi-static vapour pressure manometry study (2) and its synthesis has been described (2) in detail. Indium analyses by EDTA titration were 58.98 and 58.52 mass% and bromine analysis by potentiometric titration of the hydrolysate using a reversible silver: silver bromide electrode gave 41.0 mass percent (for InBr, In = 58.96%; Br = 41.04%).

Argon was purified by passage through a commercial rare gas purifer (model RGP-4, B.O.C. Ltd.) which removes O_2 and N_2 (titanium getter at 700°C), H_2, hydrocarbons, and CO (CuO at 450°C), CO_2 and H_2O (molecular sieves).

Apparatus

The modified entrainment apparatus and recent improvements to it have been described elsewhere (3–6). Briefly, the sample is contained in a spherical silica capsule suspended from one arm of a recording microbalance (Cahn R100). The opening of the capsule is in the form of a vertical capillary (*ca.* 20 mm long × 1 mm i.d.) that is inset into the capsule by approximately 5 mm. Argon gas flows downwards (90 cm^3 (stp) min^{-1}) over the end of the capillary, flushing away emergent gasses; the argon flow rate was controlled by a mass flow controller. The capsule was suspended in a silica furnace tube at the centre of a temperature plateau of a vertically mounted tube furnace (Trans Temp Inc.). Temperature measurement (±1 K) was via a calibrated chromel: alumel thermocouple mounted axially just below the capsule. The experimental parameter is the rate of mass loss ($\dot{w}$) at a preset temperature and which varied in this work from $\approx 5.1 \times 10^{-11}$ kg s^{-1} (680 K) to $\approx 1.1 \times 10^{-8}$ kg s^{-1} (935 K). The capillary length was determined by a travelling microscope and the mean capillary radius was obtained by filling the capillary with mercury and weighing; length (l) = 1.8815 ± 0.0019 cm, radius (r) = 0.05301 ± 0.00062 cm giving a diffusive resistance ($l/\pi r^2$) of 213.1 ± 2.5 cm^{-1}.

Results and discussion

A mass spectrometric study (2, 7) of the vapour above liquid In(I)Br at 500 K indicates the presence of both monomer and dimer species with the monomer predominant. No higher states of aggregation were detected. Consequently, our results were interpreted assuming the following equilibria

[1] $\mathrm{InBr(l)} \rightleftharpoons \mathrm{InBr(g)} \qquad \Delta H_1, \Delta S_1$

[2] $\mathrm{2InBr(g)} \rightleftharpoons \mathrm{In_2Br_2(g)} \qquad \Delta H_2, \Delta S_2$

If the ratio of the dimer to monomer flux in the capillary is β, then the partial pressures of the monomer (p_1^0) and the dimer (p_2^0) may be written as

$$[3] \quad p_1^0 = \frac{P}{(1+\beta)}\left(1 - \exp\left(\frac{-\dot{w}RTl(1+\beta)}{D_1AM_1P(1+2\beta)}\right)\right)$$

$$[4] \quad p_2^0 = \frac{P\beta}{(1+\beta)}\left(1 - \exp\left(\frac{-\dot{w}RTl(1+\beta)}{D_2AM_1P(1+2\beta)}\right)\right)$$

In these equations, P is the operating pressure (≈9 mm Hg

Can. J. Chem. Downloaded from www.nrcresearchpress.com by 84.41.108.74 on 09/07/12
For personal use only.

TABLE 1. Some typical values from the simultaneous soluton of eqs. [3] to [5]

T/K	p_1^0/Pa	p_2^0/Pa	β
703	1400	175	0.091
769	5730	557	0.073
790	8980	426	0.036

above atmospheric pressure), $\dot{w}$ is the rate of mass loss at temperature (T), l/A is the diffusive resistance, and M_1 is the monomer molecular mass. Transport occurs in a three component system (InBr, In_2Br_2, Ar) so D_i are multicomponent diffusion coefficients of i into the mixture. An outline of the derivation of eqs. [3] and [4] and the estimation of D_i are described in an Appendix. Using results from the quasi-static vapour pressure manometry study (2), an equation for the total pressure (p_T) of dimer and monomer may be written

$$[5] \quad p_T = p_1^0 + p_2^0$$

Given reliable estimates of D_i (see Appendix), eqs. [3]–[5] contain three unknowns, β, p_1^0, and p_2^0; an analytic solution is not feasible so the expressions were solved numerically with an initial guess of $0 < \beta < 10$. The analytical form of the minimized function was explored at different temperatures to establish that only one root existed in this range. Some typical values are collected in Table 1.

The algorithm failed for input data above ≈830 K in that negative roots for β (and hence p_2^0) were obtained. If the diffusion coefficients were exact and the experimental input was free from random error then β should tend asymptotically to zero at high temperatures. Given small errors in D_i and scatter in $\dot{w}$, catstrophic failure occurs for $T > 830$ K. To extract some information from the high temperature data points we note that eqs. [3]–[5] reduce to [6] as $\beta \rightarrow 0$ and $p_1^0 \rightarrow p_T$.

$$[6] \quad p_T = P\left(1 - \exp\left(\frac{-\dot{w}RTl}{\mathfrak{D}_1 A M_1 P}\right)\right)$$

Transport now occurs in a two component system (Ar, InBr) and $\mathfrak{D}_1$ is the binary diffusion coefficient of InBr in Ar. This diffusion coefficient was extracted by inversion of eq. [6] and checked against the estimated values given in the Appendix; agreement to within ≈5% was noted.

Of the 70 data points ($\dot{w}$, T) recorded only 30 gave a positive root for β and realistic values for p_1^0 and p_2^0. The results for p_2^0 were linearly regressed to the form ln (p_2^0/p^0) vs. $1/T$ to yield the following vapour pressure equation ($p^0 = 10^5$ Pa)

$$[7] \quad \ln\left(\frac{p_2^0}{p^0}\right) = \frac{-(6490 \pm 1650)}{T} + (2.9 \pm 2.2)$$

The equilibrium to which this equation applies is

$$[8] \quad 2InBr(l) \rightleftharpoons In_2Br_2(g) \qquad \Delta H_8, \Delta S_8$$

and the valid temperature range for eq. [7] is 680–810 K. The uncertainty intervals (± standard deviation) are large because p_2^0 is obtained as a difference between two large pressures of similar magnitude, p_T and p_1^0.

The treatment of the results for p_1^0 was different in that an expression for $\Delta C_p(l \rightarrow g)$ was included in the regression. The heat capacity for lnBr(l) has been reported (8) in the form $C_p = a + bT$ over the range 580–700 K. It was assumed valid over our experimental temperature range and combined with a corresponding expression for C_p(g) obtained by the usual statistical thermodynamic procedures using molecular parameters from Huber and Herzberg (9). From 650 to 950 K,

TABLE 2. Enthalpy and entropy changes at 815 K for reactions [1], [2], and [8]

Reaction	ΔH kJ mol^{-1}	ΔS J K^{-1} mol^{-1}
[1] InBr(l) ⇌ In Br(g)	96.8±0.2	102.2±0.3
[2] 2InBr(g) ⇌ In_2Br_2(g)	−140±14	−180±18
[8] 2InBr(l) ⇌ In_2Br_2(g)	54±14	24±18

$$[9] \quad C_p\,(InBr,l)/J\,K^{-1}\,mol^{-1} = (47.93 \pm 0.12) + (0.01964 \pm 0.00018)T$$

$$[10] \quad C_p\,(InBr,g)/J\,K^{-1}\,mol^{-1} = (37.07 \pm 0.02) + (0.00028 \pm 0.00002)T$$

$$[11] \quad \Delta C_p/\,J\,K^{-1}\,mol^{-1} = (-10.86 \pm 0.12) - (0.01936 \pm 0.00018)T$$

With ΔC_p in the form $A + BT$ (as in eq. [11]), regression of $[R \ln (p_1^0/p^0) + A \ln T + 0.5BT]$ vs. $1/T$ gave

$$[12] \quad \ln\left(\frac{p_1^0}{p^0}\right) = \frac{-(13457 \pm 59)}{T} - (1.306 \pm 0.014)\ln T - (0.001164 \pm 0.000021)T + (24.240 \pm 0.077)$$

Included in this regression are 11 high temperature points from ref. 2 from 839 to 950; this is the temperature range where the dimer concentration is vanishingly small so $p_1 \approx p_T$. The valid temperature range for eq. [12] is now 680–950 K. A simpler two-parameter equivalent of equation [12] is

$$[13] \quad \ln\left(\frac{p_1^0}{p^0}\right) = \frac{-(11641 \pm 31)}{T} + (12.29 \pm 0.04)$$

Uncertainty intervals are ±one standard deviation of the regression coefficients for eqs. [7] to [13]. The principal uncertainty in p_2^0 arises from the random error given by the standard deviations of the regression coefficients in eq. [7]. Other contributing errors, from the uncertainty in diffusive resistance (2%) and from the estimation of diffusion coefficients (5%) are trivial. For p_1^0, however, these minor uncertainties contribute significantly to the overall error. The error in the partial pressures arising from random error in the regression coefficients A and B in an equation of the form $\ln p = A - BT$ was evaluated from eq. [14] (10).

$$[14] \quad \sigma_p = [(p'_B)^2\sigma^2_B + (p'_A)^2\sigma^2_A + 2p'_Bp'_A\sigma_A\sigma_B\rho(A,B)]^{1/2}$$

In eq. [14], p'_x are first derivatives of p with respect to X, σ_x are standard deviations of the regression coefficients and $\rho(A,B)$ is the cross correlation coefficient for A and B, which is effectively $\rho(\Delta S_v, \Delta H_v)$. This was estimated as 0.88 from the correlation between ΔS_v and ΔH_v of the twelve group I halides (MX; M = Na, K, Rb, Cs; X = Cl, Br, I) obtained from Topor's results (11). The variation of p_1^0 and p_2^0 with temperature and with appropriate uncertainty intervals is shown in Fig. 1.

The thermodynamic constants for eqs. [1], [2], and [8] are connected via $\Delta H_2 = \Delta H_8 - 2\Delta H_1$ and values are collected in Table 2. The value for the dimerization enthalpy (ΔH_2) fits satisfactorily with the trend in ΔH_2 vs. molecular mass for other (12, 13) monovalent bromide dimers, M_2Br_2 (−228 (M = Li),

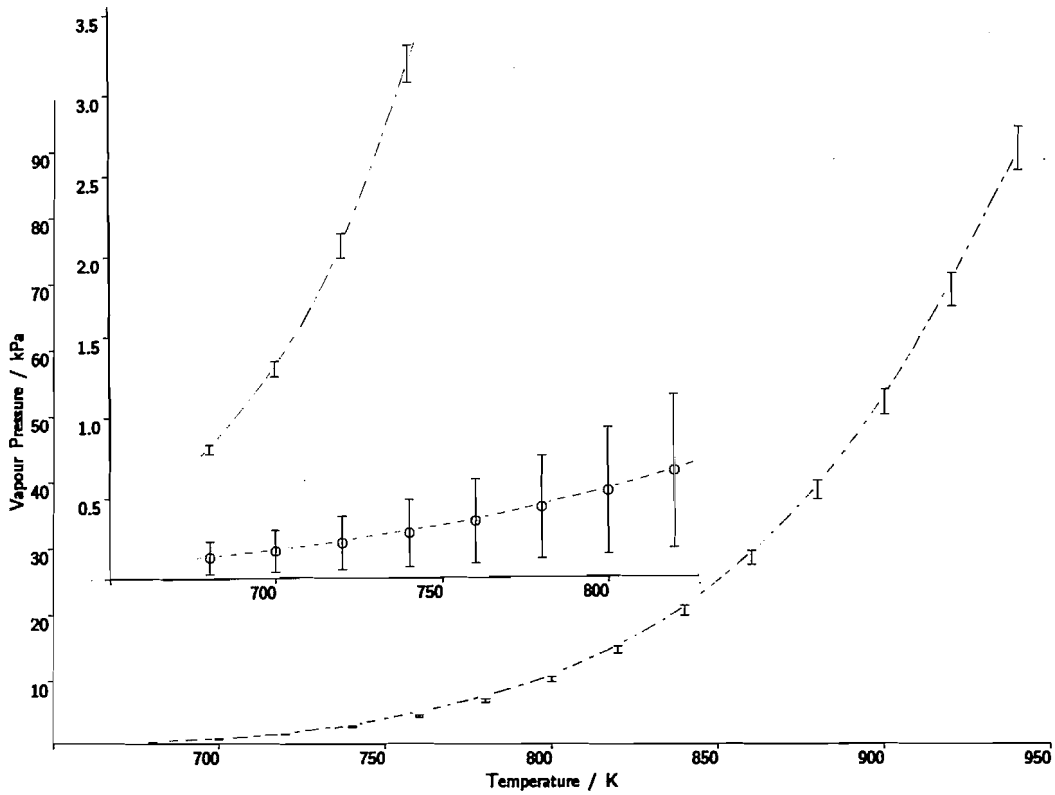


FIG. 1. The variation of the partial pressure of the indium bromide monomer (----) and dimer (○, – – – –) with temperature. Uncertainty bars indicate the probable error (50% c.i., from eq. [14]).

−200 (M = Na), −182 (M = K), and −127 (M = Cs) kJ mol^{-1}).

Acknowledgement

The authors gratefully acknowledge Dr. S. A. Mucklejohn and Mr. N. W. O'Brien (GE Thorn Lamps Ltd.) for helpful discussion and the gift of materials and Mr. J. Turner for skilful silica work.

1. M. A. CAYLESS and A. M. MARSDEN. Lamps and lighting. 3rd ed., Edward Arnold. 1983.
2. T. R. BRUMLEVE, S. A. MUCKLEJOHN, and N. W. O'BRIEN. J. Chem. Thermodyn. **21**, 1193 (1989).
3. D. BATTAT, M. M. FAKTOR, I. GARRETT, and R. H. MOSS. J. Chem. Soc. Faraday I, **70**, 2267 (1974).
4. A. FINCH, P. J. GARDNER, E. TARBOX, and S. YARDLEY. J. Chem. Soc. Faraday I, **75**, 545 (1979).
5. B. DE LARGY, A. FINCH, P. J. GARDNER, and N. KELL. J. Chem. Soc. Faraday I, **79**, 383 (1983).
6. P. J. GARDNER and P. PANG. Can. J. Chem. **66**, 566 (1988).
7. T. M. BRUMLEVE, S. A. MUCKLEJOHN, and N. W. O'BRIEN. Proc. Symp. High Temp. Lamp Chem. *Edited by* E. G. Zubler. The Electrochemical Society. 1988.
8. P. J. GARDNER and S. R. PRESTON. Thermochim. Acta, **180**, 281 (1991).
9. K. P. HUBER and G. HERZBERG. Molecular spectra and molecular structure. IV. Constants of diatomic molecules. Van Nostrand. 1979.
10. A. A. CLIFFORD. Multivariate error analysis. Applied Science Publishers 1973. p. 34.
11. L. TOPOR. J. Chem. Thermodyn. **4**, 759 (1972).
12. S. TRUGMAN and R. G. GORDON. J. Chem. Phys. **64**, 4625 (1976).
13. D. D. WAGMAN, W. H. EVANS, V. B. PARKER, R. H. SCHUMM, I. HALOW, S. M. BAILEY, K. L. CHURNEY, and R. M. NUTTALL. J. Phys. Chem. Ref. Data, Supplement no. 2, 1982.
14. D. BATTAT, M. M. FAKTOR, I. GARRETT, and R. H. MOSS. J. Chem. Faraday I, **70**, 2302 (1974).
15. P. J. GARDNER and P. PANG. Can. J. Chem. **66**, 2137 (1988).
16. D. E. SANDS. J. Chem. Ed. **51**, 473 (1974).
17. R. C. REID, J. M. PRAUSNITZ, and T. K. SHERWOOD. The properties of gases and liquids. McGraw-Hill. 1977.
18. J. G. HARTLEY and M. FINK. J. Chem. Phys. **87**, 5477 (1987).
19. R. A. SVEHLA. NASA Tech. Rept. R-132, Lewis Research Centre, Cleveland, OH, U.S.A. 1962.
20. M. RIGBY, E. B. SMITH, W. A. WAKEHAM, and G. C. MAITLAND. The forces between molecules. Clarendon Press, Oxford. 1986.
21. P. D. NEUFELD, A. R. JANZEN, and P. A. AZIZ. J. Chem. Phys. **51**, 1100 (1972).
22. S. CHAPMAN and T. G. COWLING. The mathematical theory of non-uniform gases. Cambridge Univ. Press. 1960.
23. D. BATTAT, M. M. FAKTOR, I. GARRETT, and R. H. MOSS. J. Chem. Soc. Faraday I, **70**, 2293 (1974).

Appendix

Flux equations and partial pressures

The partial pressure of the ith species at the bottom of the capillary (p_i^0) is related to the pressure at the open end of the capillary (p_i^l), the total pressure (P), the flux of the ith species (j_i) and the total flux (J) by eqs. [A1] and [A2] (14)

$$[A1] \quad \frac{p_i^0}{P} = \frac{j_i}{J} - \left[\frac{j_i}{J} - \frac{p_i^l}{P}\right] e^{-\xi_i}$$

$$[A2] \quad \xi_i = \frac{JRTl}{D_i P}$$

Quantities in eq. [A2] have been defined in the main text under eqs. [3] and [4]. The downward flow of carrier gas flushes away emergent gas from the top of the capillary so $p_i^l = 0$. If a coupling parameter (β), defined as $j(In_2Br_2)/j(InBr)$, is used to

Can. J. Chem. Downloaded from www.nrcresearchpress.com by 84.41.108.74 on 09/07/12
For personal use only.

connect the two contributing equilibria [1] and [2], then

$$[A3] \quad \frac{j_1}{J} = \frac{1}{(1+\beta)}, \quad \frac{j_2}{J} = \frac{\beta}{(1+\beta)}$$

where 1 = InBr and 2 = In_2Br_2. Substitution of [A3] into [A1] with $p_i^l = 0$ gives the partial pressure eqs. [3] and [4] directly. The central assumption of modified entrainment is that the *equilibrium* partial pressure obtains in the capsule and this assumption has been discussed (15).

An expression for p_T, the total pressure, is used in eq. [5] and was obtained by a weighted 3-parameter regresson of the raw results for p_T (2)

$$[A4] \quad \ln(p_T/\text{Pa}) = 41.550 - 2.368 \ln T - \frac{13120.7}{T}$$

This is not identical to the corresponding equation from ref. 2 as these workers regressed their data with an estimated constant value of $\Delta C_p(l \rightarrow g, 650\text{–}950\ K) = -33.5\ J\ K^{-1}\ mol^{-1}$. From eq. [11] it is clear that this estimate is in error; at the mid-temperature, eq. [11] gives $\Delta C_p(l \rightarrow g, 800\ K) = -26.3\ J\ K^{-1}\ mol^{-1}$. Secondly, Mucklejohn *et al.* (2) did not weight their results during regression; the importance of appropriate weighting in the regression of logarithmic functions has been stressed (16). Equation [A4] includes the weighting factor, $w_i = p_T^2$.

Diffusion coefficients

There are no literature data for diffusion coefficients for the indium bromide/argon system. However, reliable estimation procedures are well-established; Reid *et al.* (17) tabulate estimated diffusion coefficients for over 100 binary systems with an overall absolute deviation of 7%. In this work we estimate the Lennard–Jones collision diameter (σ) from an empirical correlation between σ and moment of inertia (6).

$$[A5] \quad \sigma/\text{Å} = (3.411 \pm 0.087) + (0.549 \pm 0.047) \times 10^{19} \, (I/\text{g cm}^2)^{1/2}$$

With molecular dimensions for InBr from Huber *et al.* (9) and estimated (see below) constants for In_2Br_2, σ(InBr) = 4.65 Å and $\sigma(In_2Br_2)$ = 5.54 Å. The symmetry for In_2Br_2 was assumed D_{2h} and structural constants were estimated by analogy with the alkali metal bromide dimers which have been studied by electron diffraction (18). For those bromides, plots of θ_{dimer}(Br—M—Br) vs. $r_{monomer}$(M—Br) and r_{dimer}(M—Br) vs. $r_{monomer}$(M—Br) are approximately linear and interpolation at r(In—Br) = 2.54 Å gave estimated constants for In_2Br_2; r(In—Br) = 2.78 Å, θ(In—Br—In) = 78°, θ(Br—In—Br) = 102° and $I_xI_yI_z = 3.48 \times 10^{-111}$ g^3 cm^6. Diffusion coefficients are relatively insensitive to choice of well-depth (ϵ_i) and these were estimated using Svehla's (19) linear correlation between ϵ_i and T_B, the normal boiling temperature. Hence (ϵ/k_B)InBr = 1109 K and $(\epsilon/k_B)In_2Br_2$ = 1723 K. With the Lorentz–Berthelot combining rules (20) for σ_{12} and ϵ_{12}/k_B and Neufeld's formula (21) for the diffusion collision integral, diffusion coefficients were calculated from the standard kinetic theory of gases equation (22) and regressed to a power law in T over the experimental temperature range (680–940 K).

TABLE A1. Representative ternary diffusion coefficient correction factors (γ_i in eq. [A8])

T/K	γ_i	γ_2
680	0.996	0.992
747	0.980	0.963
790	0.954	0.915
810	0.933	0.878

$$[A6] \quad \mathfrak{D}(\text{InBr, Ar})/\text{m}^2\,\text{s}^{-1} = 6.26 \times 10^{-6}\left(\frac{T}{273}\right)^{1.802}$$

$$[A7] \quad \mathfrak{D}(In_2Br_2, \text{Ar})/\text{m}^2\,\text{s}^{-1} = 4.32 \times 10^{-6}\left(\frac{T}{273}\right)^{1.848}$$

In these equations $\mathfrak{D}_i$ are the binary gaseous diffusion coefficients. A second order treatment (23) was used to quantify ternary (Ar, InBr, In_2Br_2) diffusion coefficients. This treatment permits the ternary diffusion coefficient ($D_{i,\text{mixture}}$) to be written in terms of $\mathfrak{D}_{ij}$, where j is the majority component (Ar).

$$[A8] \quad D_{i,\text{mixture}} = \frac{\mathfrak{D}_{i,\text{Ar}}}{\gamma_i}$$

$$[A9] \quad \gamma_i = 1 + B_i\,\bar{\xi}_i$$

$$[A10] \quad B_1 = 0.5\left(\frac{D(3,2)D(1,2)\beta}{(1+\beta)} - 1\right)$$

$$[A11] \quad B_2 = 0.5\left(\frac{D(3,1)D(2,1)}{(1+\beta)} - 1\right)$$

$$[A12] \quad \bar{\xi}_i = \frac{\dot{w}RTl(1+\beta)}{D_{i,\text{mix}}AM_1P(1+2\beta)}$$

$$[A13] \quad D(k,l) = \left(\frac{M_l}{M_k}\right)^{1/2} - 1$$

Notice in this sequence of equations that γ_i in [A9] is itself a function [A12] of the ternary coefficient [A8] that is being estimated; hence a reiterative procedure is employed initially setting $\gamma_i = 1$ and terminating when successive estimates of γ_i are within 1 in 10^4. Less than six iterations were sufficient in all cases. Some typical values of γ_i are collected in Table A1.

Can. J. Chem. Downloaded from www.nrcresearchpress.com by 84.41.108.74 on 09/07/12
For personal use only.

Thermolysis of α-hydroperoxyalkyl diazenes. Spin trapping of radical intermediates and spin trapping kinetics

LUKOSE MATHEW, EMMANUEL Y. OSEI-TWUM,[1] AND JOHN WARKENTIN[2]
Department of Chemistry, McMaster University, Hamilton, Ont., Canada L8S 4M1
Received February 8, 1991

LUKOSE MATHEW, EMMANUEL Y. OSEI-TWUM, and JOHN WARKENTIN. Can. J. Chem. **69**, 1398 (1991).

α-Hydroperoxyalkyl diazenes ($Me_2C(OOH)N{=}NR$, **1**, R = CH_2CF_3, CH_2CH_2OMe, $CH(Me)_2$, CMe_3, CH_2Ph, Ph, CH_2CH_2OPh, and *c*-$C_3H_5CD_2$) decompose in benzene, at 50°C or less, by a mechanism involving free radical (R•) intermediates. The radicals were trapped with 1-methyl-4-nitroso-3,5-diphenylpyrazole, **2**, to afford spin adducts (nitroxyls) that were observed by ESR spectroscopy. When the solvent was ethyl vinyl ether, radicals from **1** (R = CH_2CH_2OPh) were trapped by the solvent and the adduct radicals so formed were spin trapped by **2**. These observations support free radical mechanisms for thermolysis of **1** and for the hydroxyalkylations that occur when **1** are decomposed in solutions containing enol ethers or other unsaturated substrates. The ring-opening of cyclopropylmethyl radicals (cpm) to 3-butenyl radicals was used to estimate the rate constant for radical trapping by **2**. For cpm the rate constant is given by $\log k_{cpm} = (10.7 \pm 0.4) - (3.9 \pm 0.5)/\theta$ where $\theta = 2.3\,RT$ kcal mol^{-1}. At 25°C, the spin trapping rate constant has the value 6.9×10^7 M^{-1} s^{-1}.

Key words: hydroperoxyalkyl diazenes; radicals, spin trapping; spin trapping, rate constant.

LUKOSE MATHEW, EMMANUEL Y. OSEI-TWUM et JOHN WARKENTIN. Can. J. Chem. **69**, 1398 (1991).

Les α-hydropéroxyalkyldiazènes ($Me_2C(OOH)N{=}NR$, **1**, R = CH_2CF_3, CH_2CH_2OMe, $CH(Me)_2$, CMe_3, CH_2Ph, Ph, CH_2CH_2OPh et *c*-$C_3H_5CD_2$) se décomposent dans le benzène à une température égale ou inférieure á 50°C selon un mécanisme impliquant des radicaux libres (R•) intermédiaires. On a piégé les radicaux libres avec le méthyl-1-nitroso-4-diphényl-3,5-pyrazole, **2**, pour obtenir des adduits de spin (nitroxyles) que l'on a observés par spectroscopie de ESR. L'éther ethylvinylique utilisé comme solvant piège les radicaux provenant du composé **1** (R = CH_2CH_2OPh) et les adduits radicalaires ainsi formés sont captés par le composé **2**. Ces observations tendent à prouver que la thermolyse du composé **1** et l'hydroxyalkylation, qui se produit lorsque le composé **1** se décompose dans des solutions contenant des éthers énoliques ou d'autres substrats insaturés, impliquent un mécanisme radicalaire. On s'est basé sur l'ouverture du cycle des radicaux cyclopropylméthyles (cpm) qui conduit aux radicaux buténynl-3 pour évaluer la constante de vitesse de la capture des radicaux par le composé **2**. Pour le cpm, la constante de vitesse est donnée par la rélation : $\log k_{cpm} = (10{,}7 \pm 0{,}4) - (3{,}9 \pm 0{,}5)/\theta$ où $\theta = 2{,}3\,RT$ kcal mol^{-1}. On évalue la constante de capture de spin à $6{,}9 \times 10^7$ M^{-1} s^{-1} à 25°C.

Mots clés : hydropéroxyalkyldiazènes; radicaux, capture de spin; capture de spin, constante de vitesse.

[Traduit par la rédaction]

Introduction

Spin trapping is a well-known technique (1–4) for the indirect detection of a short-lived free radical (R•). The method involves an addition reaction of such a radical to an efficient scavenger (spin trap) to afford a long-lived radical (spin adduct). The latter is easily detected and its ESR spectrum contains information about the radical of interest (R•).

Nitroso compounds are important spin traps because they are readily available and because they react rapidly and irreversibly with many radicals, eq. [1]. Moreover, hyperfine in-

[1] $$R'NO + R^{\bullet} \longrightarrow R'RNO^{\bullet}$$

teractions between the unpaired electron and magnetic nuclei in R of the adduct can be large because R is attached directly to N, which carries much of the spin density of a nitroxyl radical. Disadvantages of nitroso compounds as spin traps include the tendency of some (e.g., Me_3CNO) toward photolysis and subsequent self-generated ESR spectra and the tendency of others to form nitroso dimers that are in equilibrium with the monomers (4). Although the monomer/dimer equilibrium does not present a problem in studies where identification of radicals is the objective, there are difficulties with kinetic studies. First, the highest concentration of monomeric nitroso compound is severely limited by dimer formation. Second, the actual concentration of nitroso spin trap is subject to greater uncertainty if dimerization is important.

In 1982, Kaur and Perkins (5) reported the use of 1-methyl-4-nitroso-3,5-diphenylpyrazole (**2**) for spin trapping of alkyl and aryl radicals. The advantages of **2** over some other nitroso spin traps are that it is monomeric in solution to at least 0.03 M (5), and that it is stable to visible light and is, therefore, not by itself a source of nitroxyl radicals.

α-Hydroperoxyalkyl diazenes ($R^1R^2C(OOH)N{=}NR^3$) and some cyclic analogues have been known for some time as sources of free radicals (6–8) including the hydroxyl radical (9). However, some of them afford diazonium ion intermediates instead (10) and others cause oxygen atom transfers that convert olefins to epoxides (11) and thioethers to sulfoxides (12) by non-radical mechanisms under neutral conditions.

In this paper we report spin trapping, with **2**, to demonstrate the formation of free radicals during thermal decomposition of a family of hydroperoxyalkyl diazenes ($Me_2C(OOH)N{=}NR$, **1**). The Arrhenius equation for spin trapping of cyclopropylmethyl with **2** is reported also.

Methods, results, and discussion

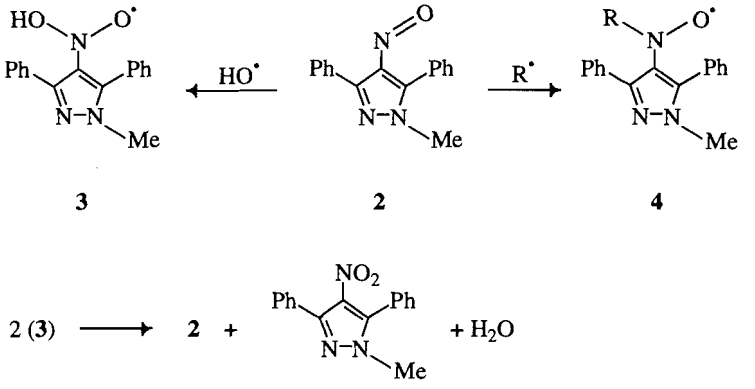
α-Hydroperoxyalkyl diazenes (**1**) decompose slowly at ambient temperature in solution (eq. [2]):

[2] $$Me_2C(OOH){=}NR \longrightarrow HO^{\bullet} + Me_2CO + N_2 + R^{\bullet}$$

a: R = CH_2CF_3; *b*: R = CH_2CH_2OMe; *c*: R = $CHMe_2$; *d*: R = CMe_3; *e*: R = CH_2Ph; *f*: R = Ph; *g*: R = $CD_2C_3H_5$ (C_3H_5 = cyclopropyl); *h*: R = CH_2CH_2OPh

[1]Present address: Research Institute Division V, King Fahd University of Petroleum and Minerals, KFUPM, Box 1472, Dhahran 31261, Saudi Arabia.
[2]Author to whom correspondence may be addressed.

Can. J. Chem. Downloaded from www.nrcresearchpress.com by 84.41.108.74 on 09/07/12
For personal use only.



SCHEME 1

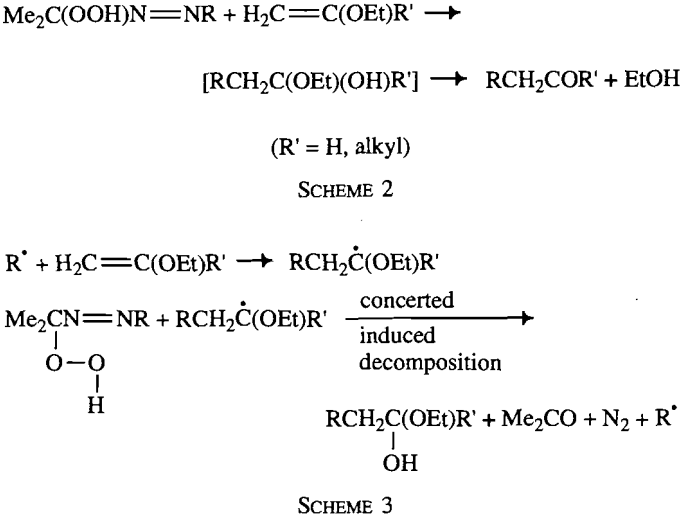
Consequently ESR spectra of spin adducts between R·(from **1**) and spin trap **2** could be recorded within minutes of warming a cold benzene solution of the reactants to room temperature in the ESR cavity. The initial ESR spectrum was complicated, however, probably because of the presence of hydroxyl radical spin adduct **3** together with spin adduct **4**, Scheme 1. Spin adducts of hydroxyl radicals and nitroso compounds are unstable (13), affording nitro compound, nitroso precursor, and water as illustrated in Scheme 1. That process could explain why the ESR spectra became clean and simple as time progressed, the concentration of **4** increasing steadily until its spectrum dominated after about 10 min.

The ESR spectra of **4***c*–**4***f* were reported by Kaur and Perkins (5). Our ESR spectra for those adducts are in good to fair agreement with published (5) spectra (lit. values in parentheses); **4***c*: g = 2.0061, a_N = 13.1 (13.2) G, a_H (1H) = 5.8(5.9) G; **4***d*: a_N = 14.4(13.4) G; **4***e*: g = 2.0068, a_N = 13.0(13.0) G, a_H (2H) = 7.5(7.7) G; **4***f*: g = 2.0056, a_N = 9.8(9.8) G, a_H (3H) = 2.63(2.65) G, a_H (2H) = 0.85 (0.8) G.

The ESR spectra of the new members of the family **4** appear to be normal; **4***a*: a_N = 11.5 G, a_H (2H) = 6.3 G, a_F (3F) = 1.13 G (Fig. 1); **4***b*: a_N = 12.6 G, a_H (2H) = 8.8 G, splitting to the more remote CH_2 group not resolved: **4***g*: g = 2.0057, a_N = 12.8 G, a_D (2D) = 1.5 G; **4***h*: a_N = 12.6 G, a_H (2H) = 8.6 G. Observation of all of the ESR spectra, **4***a*–**4***h*, from prescursors **1***a*–**1***h*, serves to support a free radical mechanism for thermolysis of α-hydroperoxyalkyldiazenes (**1**) as a class.

In a previous report (8) the use of compounds of type **1** for hydroxyalkylation of olefinic substrates was described. Best yields were obtained in the hydroxyalkylation of enol ethers (Scheme 2) to afford aldehydes or ketones (8). Those products, and the fact that rapid decomposition of hydroperoxy diazenes of type **1** is strongly inhibitied by 2,2,6,6-tetramethylpiperidine-*N*-oxyl radical (TMPO) led to the suggestion of a radical chain mechanism for hydroxyalkylation, with chain-carrying steps illustrated in Scheme 3 (8).

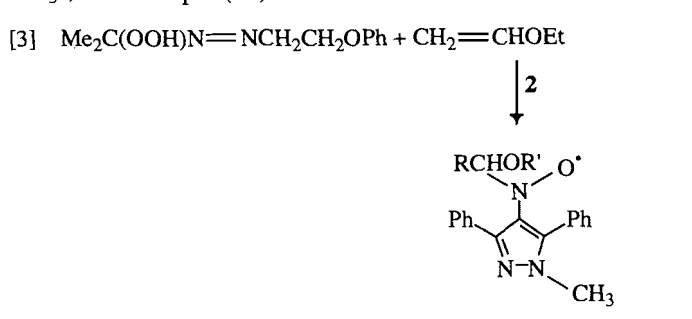
It was possible to provide support for that mechanism by intercepting the α-ethoxyalkyl radical intermediate of Scheme 3. A solution of **1***h* in ethyl vinyl ether containing **2** (1.0×10^{-3} M) gave rise, at ambient temperature, to the ESR spectrum of a radical to which structure **5***a* could be assigned, eq. [3]. The ESR spectrum, with g = 2.0063, a_N = 12.0 G, a_H (1H) = 4.25 G resembles that of **5***b* (3), with a_N = 13.5 G, a_H = 4.6 G (in ethanol), and that of $PhCH(OCHMe_2)N(O^{\cdot})CMe_3$, with g = 2.0063, a_N = 13.7 G, a_H = 1.17 G (14).



SCHEME 2

SCHEME 3

Although additional weak signals were superimposed on the spectrum of **5***a*, it is clear that addition of $PhOCH_2CH_2^{\cdot}$ to ethyl vinyl ether (ca. 10 M) competes effectively with spin trapping of $PhOCH_2CH_2^{\cdot}$ by **2** (1.0×10^{-3} M). If the latter trapping has a rate constant near 1.1×10^8 M^{-1} s^{-1} at 50°C (see below) then the rate constant for addition to ethyl vinyl ether must have a value greater than 4.5×10^4 M^{-1} s^{-1}. This calculation includes the estimate that at least 80% of the radicals detected were **5***a* and that the other 20% were spin adducts from $PhOCH_2CH_2^{\cdot}$ and **2**. We were unable to find rate constants in the literature for addition of any radicals to any enol ethers. However, the rate constants for addition of alkyl radicals to vinyl acetate (a reasonable model) are about one order of magnitude smaller; 2×10^3 M^{-1} s^{-1} at 50°C for $CCl_3^{\cdot}$, for example (15).



5*a* R = $PhO(CH_2)_3$, R' = Et
5*b* R = Me, R' = H

Can. J. Chem. Downloaded from www.nrcresearchpress.com by 84.41.108.74 on 09/07/12
For personal use only.

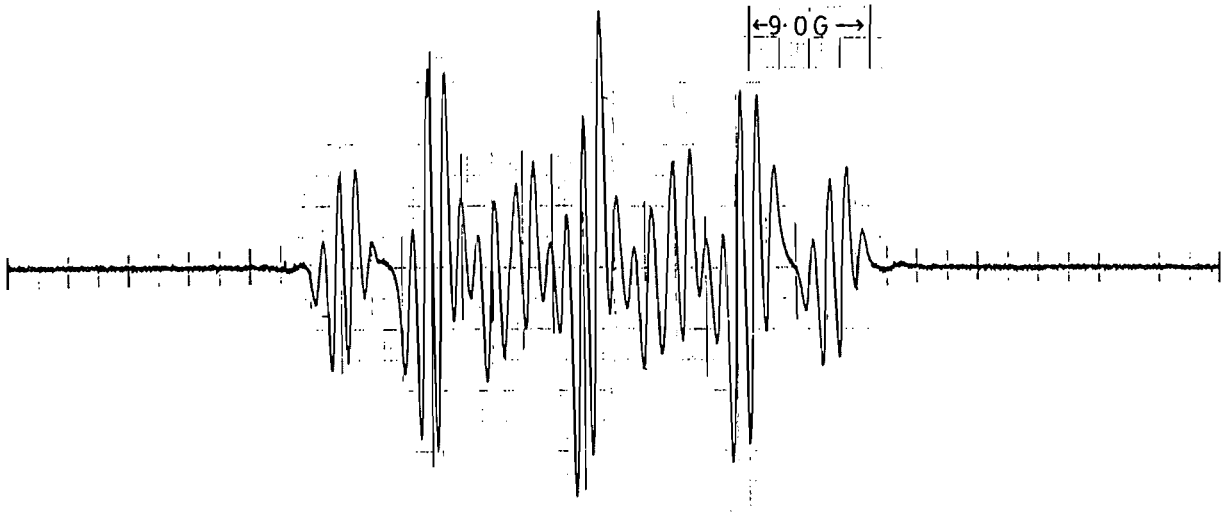


FIG. 1. ESR spectrum of nitroxyl radical from addition of $CF_3CH_2^{\cdot}$ to **2** in benzene.

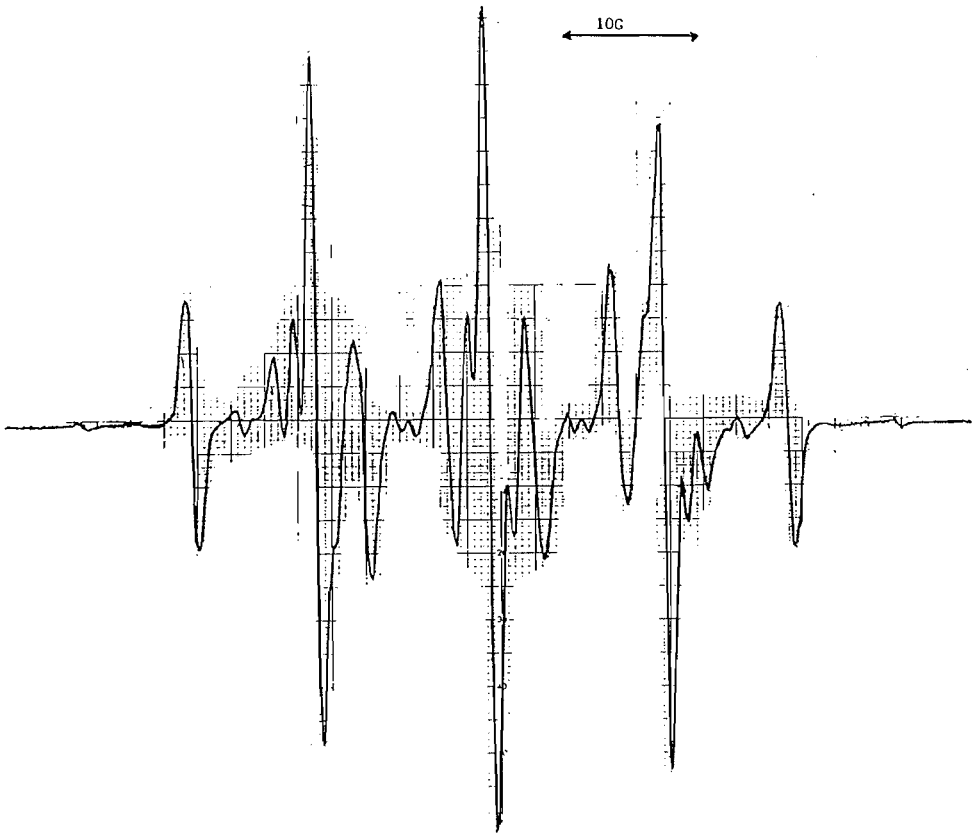
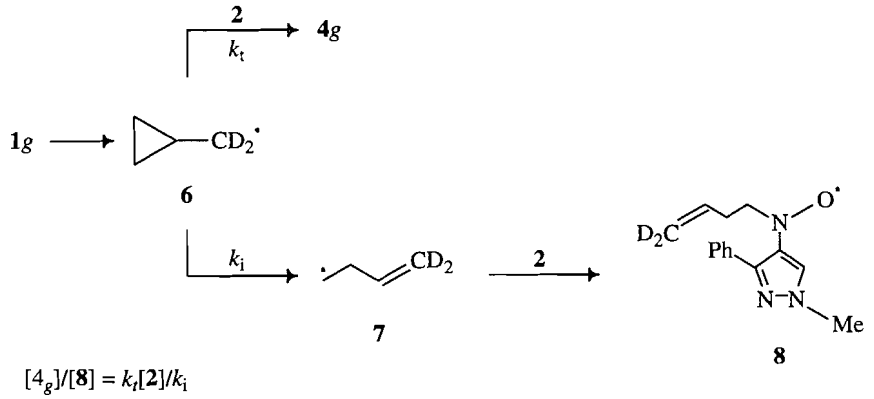


FIG. 2. Superimposed ESR spectra of **4***g* and **8**. See text and Scheme 4.

In addition to the spectra of radical adducts of **2**, Kaur and Perkins (5) estimated the rate constant, at 40°C, for spin trapping of undecyl radical (U$^{\cdot}$) with **2**. That rate constant was obtained from an experiment in which phenyl-*N*-*tert*-butylnitrone (PBN) was allowed to compete with **2** for U$^{\cdot}$ and the rate constant for reaction of U$^{\cdot}$ with PBN was taken to be 1.3×10^5 M^{-1} s^{-1}, the value reported for trapping of 5-hexenyl radicals (16) by PBN. It is very important, because of the interdependence of rate constants for free radical reactions, to obtain derived numbers from as many sources as possible, to provide for a consistent set of data (17). For that reason, we decided to estimate the rate constant for spin trapping of a primary radical by **2** against a different clock, the well-calibrated (18–22) and frequently used cyclopropylmethyl (cpm) free radical clock.

To distinguish between the spin adducts from cpm and 3-buten-1-yl radicals by ESR spectroscopy, the deuterated precursor **1***g* was prepared. Thermolysis of **1***g* afforded **6**, which in the presence of **2** underwent competitive spin trapping and ring-opening to afford **4***g* and **7** (Scheme 4). The latter was spin trapped also to form **8** and the ratio **4***g*/**8** was determined by double integration of the ESR spectra (Fig. 2), which are significantly different because of the different splitting constants to protium and deuterium; for **8**, $g = 2.0039$, $a_N = 12.8$ G, a_H (2H) = 9.27 G. That ratio was related to the rate

Can. J. Chem. Downloaded from www.nrcresearchpress.com by 84.41.108.74 on 09/07/12
For personal use only.



$[4_g]/[\mathbf{8}] = k_t[\mathbf{2}]/k_i$

SCHEME 4

TABLE 1. Extinction coefficients at λ = 738 nm for benzene solutions of **2**

T(°C)	[**2**] (M)[a]	A[b]	l[c] (cm)	ϵ
40	0.192	1.81	0.1	94
40	0.0779	0.744	0.1	96
40	0.0312	0.292	0.1	94
40	0.0124	1.19	1.0	96
40	0.00499	0.481	1.0	97
40	0.00199	0.185	1.0	93
23	0.196	1.87	0.1	95
23	0.0795	0.720	0.1	91
23	0.0318	0.295	0.1	93
23	0.0127	0.112	0.1	88

[a]Thermal expansion of benzene was included in calculating concentrations at 40°C from concentrations at 23°C.
[b]Absorbance.
[c]Cell path length.

TABLE 2. Product ratios and derived rate constants, k_t

Temperature (K)	[**4g**]/[**8**][a]	[**2**][b]	$10^{-7}\,k_i^c$ (s^{-1})	$10^{-7}\,k_t^d$ ($M^{-1}\,s^{-1}$)
283	0.82	0.963	5.63	4.79
293	0.55	0.950	8.50	4.92
295	0.63	0.948	9.20	6.11
295	0.59	0.948	9.20	5.73
298	0.50	0.944	10.3	5.46
300	0.54	0.942	11.2	6.42
313	0.46	0.927	17.9	8.88
333	0.33	0.905	34.6	12.6

[a]Ratio of spin adducts (Scheme 4), from the ESR spectra.
[b]Corrected for temperature effects on volume, through use of the coefficient of cubical expansion of the solvent benzene.
[c]Calculated (19) from $\log(k_i/s^{-1}) = 13.31 - 7.26/\theta$.
[d]Calculated from the relationship in Scheme 4.

constants for spin trapping of cpm and for rearrangement of cpm in the usual (23) way, Scheme 4, and the spin trapping rate constant (k_t) was calculated by substituting for k_i its numerical value from the Arrhenius equation (19), $\log (k_i/s^{-1}) = 13.31 - 7.26/\theta$. The hydrogen/deuterium kinetic isotope effect on k_i was assumed to be negligible and trapping by **2** was treated as pseudo first order.

To attain ratios (**4g/8**) near the ideal value of unity, relatively large concentrations of **2** were required and it was necessary to establish that **2** remains monomeric in solution at high concentrations. Measurements of the extinction coefficient of **2** at λ = 738 nm in benzene were made at both 23 and 40°C over the concentration range (2.0–196) × 10^{-3} M (Table 1). Within experimental error, the extinction coefficient was independent of concentration and temperature (ϵ = 95 ± 2 at 40°C; 92 ± 3 at 23°C) in complete agreement with the findings of Kaur and Perkins (5) for concentrations up to 0.03 M. The reasonable assumption was then made that **2** remains monomeric at concentrations (0.91–0.96 M) nearly fivefold higher than the maximum concentration at which ϵ could be measured (0.20 M).

Data for competitive spin trapping and isomerization of **6**, for the temperature range 283–333 K are in Table 2. A least-squares treatment of the data gives eq. [4] as the Arrhenius expression for the spin trapping rate constant, k_t, with correlation coefficient 0.97. At 40°C, eq. [4] gives $k_t = 9.4 \times 10^7$ M^{-1} s^{-1}, which is in satisfactory agreement (roughly three-fold larger) with the value reported (5) for spin trapping of undecyl radicals with **2**.[3] At 25°C, $k_t = 6.9 \times 10^7$ M^{-1} s^{-1}. These numbers are minimum values, presumably, that would rise if **2** actually is partly dimeric at concentrations near 0.96 M (Table 2).[3]

[4] $\log (k_t/M^{-1}\,s^{-1}) = (10.7 \pm 0.4) - (3.9 \pm 0.5)/\theta$

where $\theta = 2.3\,RT$ kcal mol^{-1}

Both the pre-exponential factor and the activation energy are larger than those for trapping of 5-hexenyl radicals with 2-methyl-2-nitrosopropane, for which $\log A = 8.4$ and $E_a = 2$ kcal mol^{-1} were reported (25).[4] Qualitatively, the difference can be rationalized. In 2-methyl-2-nitrosopropane the nitroso nitrogen is very hindered (neopentylic) but not conjugated, whereas in **2** the nitroso group presumably has less steric protection but some conjugative interaction with the pyrazole ring. The larger frequency factor and activation barrier for **2** are therefore in accord with expectation. The 25°C rate constant (6.9×10^7 M^{-1} s^{-1}) is, within experimental error, the same as that (3.9×10^7 M^{-1} s^{-1}) for trapping a primary alkyl radical with nitrosodurene (16).

Experimental

Electron spin resonance (ESR) spectra were recorded at ambient temperature with a Bruker ER 100 D spectrometer operating at 9.6 GHz and equipped with a Te-102 rectangular cavity. Proton NMR

[3]The new data imply that rate constants based on spin trapping with **2**, and referred to the Kaur and Perkins number, can probably be increased by a factor of two (24).

[4]These numbers become $\log A = 8.6$ and $E_a = 1.8$ kcal mol^{-1} if the most recent value (26) of the rate constant for cyclization of 5-hexenyl to cyclopentylmethyl is used.

Can. J. Chem. Downloaded from www.nrcresearchpress.com by 84.41.108.74 on 09/07/12
For personal use only.

spectra were obtained with a Varian EM-390, a Bruker WP-80, or a Bruker WM-250 spectrometer, while ^{13}C and ^{19}F spectra were run on Bruker WP-80 and WM-250 spectrometers, respectively. Tetramethylsilane and $CDCl_3$ were used as internal references for ^1H and ^{13}C spectra, respectively. External trichlorofluoromethane was used to calibrate ^{19}F spectra. Solvents from Caledon Chemical Co. Ltd., Georgetown, were distilled in glass and stored over molecular sieves.

Synthesis of 1-methyl-4-nitroso-3,5-diphenylpyrazole, 2

The nitrosopyrazole was prepared[5] by the procedure of Boyd and Norris (27). Recrystallized material melted at 92–94°C. ^1H NMR (200 MHz, $CDCl_3$) δ: 3.83 (s, 3H), 7.46–7.56 (m, 8H), 7.99–8.10 (m, 2H). ^{13}C NMR (50 MHz, $CDCl_3$) δ: 37.3 (CH_3), 127.1 (C-4, tent.), 129.7 (C-4 of Ph); 128.5, 128.8, 129.1, 130.1 (4 × C-2, C-3 of Ph), 130.4 (C-4 of Ph), 131.0 (C-1 of Ph), 158.0 (C-3, tent.), two quaternary carbon signals are apparently coincident with ArH signals.

Synthesis of α-hydroperoxyalkyldiazenes, 1

Caution: 1 are probably explosive! The procedure for preparation of **1** by autoxidation of substituted hydrazones of acetone has been described and some NMR spectra (^1H and ^{13}C) and mass spectra of the precursors and products have been reported (8). Those NMR spectra are included here, together with additional spectra (^{13}C NMR, IR, and UV) to provide all the spectroscopic data in one place. The UV extinction coefficients for all except **1***g* are ca. 20.

$Me_2C(OOH)N{=}NCH_2CF_3$, **1***a*: IR (CCl_4) cm^{-1}: 3520 (br, OH), UV(λ_{max}, hexane) nm: 372. ^1H NMR (90 MHz, $CDCl_3$) δ: 1.40 (s, 6H), 4.27 (q, J_{HF} = 9 Hz, 2H), 8.80 (s, br, 1H). ^{19}F NMR (235.4 MHz), δ: −66.8 (t, J_{HF} = 9 Hz). ^{13}C NMR (22.6 MHz) δ: 21.30 (Me), 68.58 (q, J_{CF} = 29.1 Hz, CH_2), 104.22 (Me_2C), 123.69 (q, J_{CF} = 251.0 Hz, CF_3).

$Me_2C(OOH)N{=}NCH_2CH_2OMe$, **1***b*: UV ($\lambda_{max}$, hexane) nm: 365. ^1H NMR (90 MHz, $CDCl_3$) δ: 1.32 (s, 6H), 3.30 (s, 3H), 3.80 (t, J = 5.9 Hz, 2H), 4.01 (t, J = 5.9 Hz, 2H), 9.35 (s, br, 1H). ^{13}C NMR (22.6 MHz) δ: 21.43 (Me_2), 58.64 (OMe), 68.09 (NCH_2), 69.40 (CH_2O), 104.76 (Me_2C).

$Me_2C(OOH)N{=}NCHMe_2$, **1***c*: UV (λ_{max}, hexane) nm: 362. ^1H NMR (90 MHz, $CDCl_3$) δ: 1.27 (d, J = 6.0 Hz, 6H), 1.42 (s, 6H), 3.70 (sept, J = 6.0 Hz, 1H), 9.50 (s, br, 1H). ^{13}C NMR (22.6 MHz,) δ: 20.27 (Me_2CH), 21.62 (Me_2C), 67.92 (NCH), 102.45 (Me_2C).

$Me_2C(OOH)N{=}NCMe_3$, **1***d*: IR (CCl_4 cm^{-1}: 3538. UV (λ_{max}, hexane) nm: 363. ^1H NMR (90 MHz, $CDCl_3$) δ: 1.20 (s, 9H), 1.33 (s, 6H), 9.21 (s, br, 1H). ^{13}C NMR (22.6 MHz) δ: 21.58 (Me_2), 26.68 (Me_3), 67.97 (Me_3C), 102.75 (Me_2C).

$Me_2C(OOH)N{=}NCH_2Ph$ **1***e*: ^1H NMR (90 MHz, CCl_4) δ: 1.35 (s, 6H), 4.88 (s, 2H), 7.27 (s, 5H), 9.11 (s, br, 1H). ^{13}C NMR (22.6 MHz, $CDCl_3$) δ: 21.52 (Me_2), 73.24 (NCH_2), 103.03 (Me_2C), 127.73, 128.70, 128.83, 134.76 (C-3, C-4, C-2, C-1, respectively, of Ph).

$Me_2C(OOH)N{=}NPh$ **1***f*: IR (CCl_4 cm^{-1}: 3640, 3450. UV (λ_{max}, hexane) nm: 260, 372. ^1H NMR (90 MHz, $CDCl_3$) δ: 1.50 (s, 6H), 7.55 (m, 5H), 9.10 (s, br, 1H). ^{13}C NMR (22.6 MHz, $CDCl_3$) δ: 21.98 (Me_2), 103.99 (Me_2C), 122.68, 127.25, 131.45, 151.21 (C-2, C-3, C-4, C-1, respectively, of Ph).

$Me_2C(OOH)N{=}NCH_2C_3H_5$ (C_3H_5 = cyclopropyl), **1***g*: IR (neat) cm^{-1}: 3320 (br). UV (λ_{max}, hexane) nm: 292, 358. ^1H NMR (90 MHz, $CDCl_3$) δ: 0.17–0.77 (m, 4H), 1.03–1.40 (m, 1H), 1.47 (s, 6H), 3.67 (d, 2H), 9.47 (s, br, 1H). ^{13}C NMR (22.6 MHz, $CDCl_3$) δ: 3.51 (cp-CH_2) 9.20 (CH), 21.84 (Me_2), 73.60 (CH_2), 102.89 (Me_2C).

$Me_2C(OOH)N{=}NCH_2CH_2OPh$, **1***h*: IR ($CCl_4$ cm^{-1}: 3520 (br). UV (λ_{max}, hexane) nm: 280, 365. ^1H NMR (90 MHz, $CDCl_3$) δ: 1.32 (s, 6H), 4.19 (t, J = 6.0 Hz, 2H), 4.48 (t, J = 6.0 Hz, 2H), 6.94 (m, 3H), 7.28 (m, 2H), 9.30 (s, br, 1H). ^{13}C NMR (22.6 MHz). δ: 21.71 (Me_2C), 64.91 (NCH_2), 67.70 (CH_2O), 103.32 (Me_2C), 114.91, 121.32, 129.63, 158.66 (C-2, C-4, C-3, C-1, respectively, of Ph).

Acknowledgements

This work was financed from a grant provided by the Natural Sciences and Engineering Research Council of Canada. We thank Dr. P. A. Risbood for a sample of **2** and Messrs. B. G. Sayer and J. I. A. Thompson for assistance with the spectroscopy.

[5]Synthesis by Dr. P. A. Risbood.

1. G. R. CHALFONT, M. J. PERKINS, and A. HORSFIELD. J. Am. Chem. Soc. **90**, 7141 (1968).
2. E. G. JANZEN and B. J. BLACKBURN. J. Am. Chem. Soc. **91**, 4481 (1969).
3. S. FORSHULT, C. LAGERCRANTZ, and K. TORSSELL. Acta Chem. Scand. **23**, 522 (1969).
4. E. G. JANZEN. Acc. Chem. Res. **4**, 31 (1971).
5. H. KAUR and M. J. PERKINS. Can. J. Chem. **60**, 1587 (1982).
6. F. MINISCI. Gazz. Chim. Ital. **89**, 626 (1959); Gazz. Chim. Ital. **90**, 1307 (1960); F. MINISCI and U. PALLINI. Gazz. Chim. Ital. **90**, 1318 (1960).
7. R. E. MACLEAY and C. S. SHEPPARD. U. S. Patent No. 4010152 (1977).
8. E. Y. OSEI-TWUM, D. MCCALLION, A. S. NAZRAN, R. PANICUCCI, P. A. RISBOOD, and J. WARKENTIN. J. Org. Chem. **49**, 336 (1984); E. Y. OSEI-TWUM and J. WARKENTIN. J. Org. Chem. **50**, 4725 (1985); C. LAKHANI, L. MATHEW, and J. WARKENTIN. Can. J. Chem. **65**, 1748 (1987).
9. R. D. GRANT, E. RIZZARDO, and D. H. SOLOMON. J. Chem. Soc. Perkin Trans. 2, 379 (1985); N. NARITA and T. TEZUKA. J. Am. Chem. Soc. **104**, 7316 (1982); T. TEZUKA, H. MARUSAWA, and K. ICHIKAWA. Chem. Lett. 2145 (1984).
10. G. E. LEWIS and G. L. SPENCER. Aust. J. Chem. **28**, 1733 (1974); T. TEZUKA and S. ANDO. Chem. Lett. 1621 (1985); J. GRIFFITHS and C. HAWKINS. J. Chem. Soc. Perkin Trans. **2**, 747 (1977).
11. A. L. BAUMSTARK. Bioorg. Chem. **14**, 326 (1986); A. L. BAUMSTARK and P. C. VASQUEZ. Tetrahedron Lett. **24**, 123 (1983); J. Org. Chem. **50**, 3657 (1985).
12. A. L. BAUMSTARK and P. C. VASQUEZ. J. Org. Chem. **48**, 65 (1983); A. L. BAUMSTARK and D. R. CHRISOPE. Tetrahedron Lett. **22**, 4591 (1981).
13. R. KONAKA and S. SAKATA. Chem. Lett. 411 (1982).
14. M. V. MERRITT and R. A. JOHNSON. J. Am. Chem. Soc. **99**, 3713 (1977).
15. J. P. LORAND. *In* Landolt-Bornstein (New Series), Radical reactions in liquids. Vol. 13. subvolume a. *Edited by* H. Fischer. Springer Verlag, Berlin. 1984. p. 135.
16. P. SCHMIDT and K. U. INGOLD. J. Am. Chem. Soc. **100**, 2493 (1978).
17. L. J. JOHNSTON, J. LUSZTYK, D. D. M. WAYNER, A. N. ABEYWICKREYMA, A. L. J. BECKWITH, J. C. SCAIANO, and K. U. INGOLD. J. Am. Chem. Soc. **107**, 4594 (1985); D. A. LINDSAY, J. LUSZTYK, and K. U. INGOLD. J. Am. Chem. Soc. **106**, 7087 (1984).
18. M. NEWCOMB and A. G. GLENN. J. Am. Chem. Soc. **111**, 275 (1989).
19. A. L. J. BECKWITH and V. W. BOWRY. J. Org. Chem. **54**, 2681 (1989).
20. A. L. J. BECKWITH, V. W. BOWRY, and G. MOAD. J. Org. Chem. **53**, 1632 (1988).
21. L. MATHEW and J. WARKENTIN. J. Am. Chem. Soc. **108**, 7981 (1986).
22. B. MAILLARD, D. FORREST, and K. U. INGOLD. J. Am. Chem. Soc. **98**, 7024 (1976).
23. D. GRILLER and K. U. INGOLD. Acc. Chem. Res. **13**, 317 (1980).
24. C. CHATGILIALOGLU, K. U. INGOLD, I. TSE-SHEEPY, and J. WARKENTIN. Can. J. Chem. **61**, 1077 (1983).
25. Y. MAEDA and K. U. INGOLD. J. Am. Chem. Soc. **101**, 4975 (1975).
26. C. CHATGILIALOGLU, K. U. INGOLD, and J. C. SCAIANO. J. Am. Chem. Soc. **103**, 7739 (1981).
27. G. V. BOYD and T. NORRIS. J. Chem. Soc. Perkin Trans. 1, 1028 (1974).

Can. J. Chem. Downloaded from www.nrcresearchpress.com by 84.41.108.74 on 09/07/12
For personal use only.

Kadsulignan C and D, two novel lignans from *Kadsura longipedunculata*

JIA-SEN LIU,[1] MEI-FEN HUANG, AND HONG-XING ZHOU
Shanghai Institute of Materia Medica, Academia Sinica, 319 Yueyang Rd., Shanghai 200031, China

Received February 7, 1991

JIA-SEN LIU, MEI-FEN HUANG, and HONG-XING ZHOU. Can. J. Chem. **69**, 1403 (1991).

Two novel lignans, kadsulignan C (**4**) and D (**5**), were isolated from the root bark of *Kadsura longipedunculata*. Their structures, including absolute configurations, were elucidated by 2D $^1H-^{13}C$ long-range COSY experiments and chemical transformation to the known compound **10**.

Key words: isolation and structure, absolute configuration, kadsulignan C, kadsulignan D, lignans, *Kadsura longipedunculata*.

JIA-SEN LIU, MEI-FEN HUANG et HONG-XING ZHOU. Can. J. Chem. **69**, 1403 (1991).

On a isolé de l'écorce de la racine du *Kadsura longipedunculata* deux nouveaux lignanes, les kadsuligane C (**4**) et D (**5**). On a élucidé leur structure et établi leur configuration absolue à l'aide d'expériences COSY à longue distance en résonance magnetique nucléaire du ^1H et du ^{13}C, et en les transformant chimiquement pour aboutir au composé **10** connu.

Mots clés : isolation et structure, configuration absolue, kadsulignane C, kadsulignane D, lignanes, *Kadsura longipedunculata*.
[Traduit par la rédaction]

Can. J. Chem. Downloaded from www.nrcresearchpress.com by 84.41.108.74 on 09/07/12
For personal use only.

Introduction

The bark of the root *Kadsura longipedunculata* Finet. et Gapnep. is used as a traditional Chinese drug (1) to improve circulation of the blood, invigorate vital energy, and to treat rheumatoid arthritis as well as gastric or duodenal ulcer. In our previous papers we reported the isolation and structure elucidation of three new compounds, (+)-anwulignan (**1**) (2), schisanlactone E (**2**), and changnanic acid (**3**) (3) from plant material collected in the Zhejiang province of China. The pharmacological screening of compounds **1–3** indicated that each exhibits activity against leukemia P388 cell *in vitro* (IC_{50}, 1.5, 1.0, and 10 μg/mL respectively for **1**, **2**, and **3**). In addition, compound **1** shows an inhibitory effect to HBsAg of human serum of chronic hepatitis B carriers *in vitro* (2). A recent bioassay indicated that **2** and **3** show antagonistic activity to leukotriene D_4 *in vitro*.[2] Each of these findings support traditional medical usage of the root bark.

In our continuing studies on the chemistry of *K. longipedunculata* two new lignan compounds, which we have named kadsulignan C (**4**) and D (**5**), were isolated from the root bark extract. Both compounds **4** and **5** show moderate cytotoxicity against leukemia P388 cell *in vitro* (IC_{50} 50 and 10 μg/mL, respectively).[2] In the present paper we report the isolation, structure elucidation, and absolute configuration of kadsulignan C (**4**) and D (**5**). A discussion of the absolute configuration of benzoyl oxokadsurane (**12**), an analogous compound recently reported in the literature (8), is also presented.

Results and discussion

Kadsulignan C (**4**), $C_{31}H_{30}O_{11}$, is a pale yellow crystalline compound, the spectra of which display partial features similar to the dibenzocyclooctadiene lignans commonly found in this family of plants. Its infrared (ir), ^1H and ^{13}C nmr, and high resolution mass spectra (hrms) indicate the presence of the cyclooctadiene ring substituted with hydroxyl, acetoxyl, benzoxyl, and two methyl groups. However, its ultraviolet (uv) spectrum (λ_{max} 220, 276, 335 nm) shows that kadsulignan C (**4**) possesses a spiroenone ring different from the spirodienone

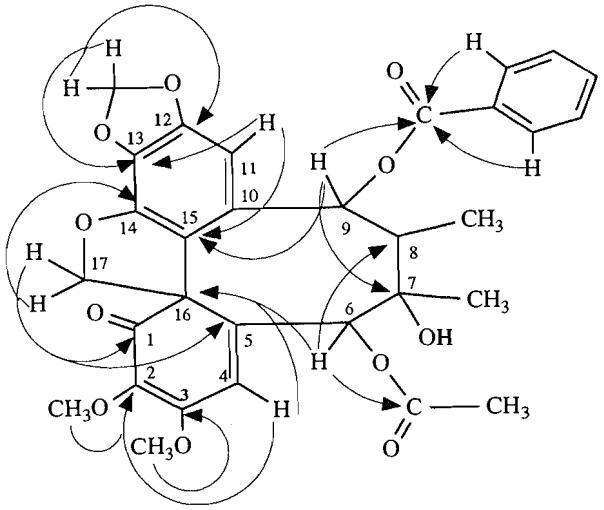


FIG. 1. 2D $^1H-^{13}C$ long-range shift correlation via $^3J_{CH}$ in kadsulignan C (**4**).

lignans kadsulignan A (**6**) and B (**7**) recently reported in our previous paper (4). A comparison of the ^{13}C nmr data of **4** with those of the spirodienone lignan **6** (4) reveals that the spiro carbon (C-16, δ 62.8, s) in compound **4** shifts upfield about 25 ppm while the carbonyl carbon (C-1, δ 194.9, s) of the enone ring shifts downfield over 10 ppm relative to the same carbons in compound **6**. These facts show that the spiro carbon (C-16) is not connected to oxygen and that the enone ring **4** is not an α,β,α′,β′-dienone. Furthermore, the ^1H nmr (δ 4.68, 4.04, d each, J = 9.1, H-17) and ^{13}C nmr spectra (δ 79.3, t, C-17) suggest the presence of a methylene group adjacent to an oxygen atom in the molecule of **4**. Analysis of 2D $^1H-^{13}C$ COSY and 2D $^1H-^{13}C$ long-range COSY spectra allowed us to establish the connectivity between carbon–hydrogen nuclei via $^1J_{CH}$ and between carbon–carbon nuclei via $^3J_{CH}$. In the 2D long-range COSY spectrum, the oxymethylene protons (H-17) correlate to the carbonyl carbon (C-1), C-5, and C-14 while H-4 and H-6 correlate to the spiro carbon (C-16) via $^3J_{CH}$. Thus, a spiro ring skeleton is established for kadsulignan C as shown in Fig. 1. A further analysis of the 2D $^1H-^{13}C$ long-range COSY spectrum illustrated each substituent position, benzoxyl at C-9, acetoxyl at C-6, methylenedioxyl at C-12 and C-13, and two methoxyls at C-2 and C-3 (Fig. 1). Nuclear Overhauser experiments (nOe,

[1]Author to whom correspondence may be addressed. The present address is SynPhar Laboratory Inc., 4290-91A Street, Edmonton, Alta., Canada T6E 5V2.

[2]Department of Pharmacology, Shanghai Institute of Materia Medica, personal communications.

Printed in Canada / Imprimé au Canada

TABLE 1. The ^1H nmr data[a] of kadsulignan C (**4**) and D (**5**)

Proton		Compound 4	Compound 5
4		6.45,d(1.3)	6.50,s
6		5.69,d(1.3)	5.69,s
8		2.19,q(7.2)	2.13,q(7.2)
9		5.82,s	5.60,s
11		6.49,s	6.40,s
17		4.68,4.04,d each(9.1)	4.64,4.03,d each(8.9)
CH_3-7		1.30,s	1.25,s
CH_3-8		1.36,d(7.2)	1.32,d(7.2)
OCH_2O		6.02,5.95,d each(1.4)	5.95,5.91,d each(1.3)
CH_3O-3		3.87,s	4.02,s
CH_3O-2		3.15,s	3.70,s
OH		2.84,s	2.87,s
Ac		1.78,s	
Bz	2′,6′	7.69,dd(8.3/1.2)	
	3′,5′	7.37,dd(8.3/7.5)	
	4′	7.54,dddd(7.5/7.5/1.2/1.2)	
Ang-9	3′		6.00,brq(7.1)
	CH_3-2′		1.71,brs
	CH_3-3′		1.84,brd(7.1)
Ang-6	3′		6.08,brq(7.1)
	CH_3-2′		1.33,brs
	CH_3-3′		1.89,brd(7.1)

[a]δ, ppm, in $CDCl_3$ (400 MHz); *J*, Hz, in parentheses; the assignments are based on selective decoupling and nOe experiments.

Table 3) provided further evidence for the structure and elucidated the relative stereochemistry of kadsulignan C as shown in structure **4**.

Kadsulignan D (**5**), $C_{32}H_{36}O_{11}$, is also a pale yellow crystalline compound with a similar uv to that of **4**. Comparison of the ^1H and ^{13}C nmr spectra of **4** and **5** (Tables 1 and 2) indicates that the structural difference between **4** and **5** is in the acid moiety: two angeloyl groups in compound **5** replace the benzoyl and acetyl groups in compound **4**. Further support of the presence of two angeloxyls is provided by the hrms fragmentation pattern, which displays fragment peaks of $[M - C_5H_8O_2]^+$ and $[M - C_{10}H_{16}O_4]^+$. The 2D ^1H–^{13}C COSY and 2D ^1H–^{13}C long-range COSY spectra of kadsulignan D (**5**) show similar correlations to those shown in Fig. 1 except that H-6 and H-9 correlate respectively to a carbonyl carbon of each angeloxyl group. Furthermore, nOe enhancements are observed between the olefinic hydrogen (H-3′) and both methyls (H-5′ and H-4′) of the acid moiety (Table 3). This experiment distinguishes the angeloxyl from tigloxyl, a geometric isomer of angeloxyl, since in the case of tigloxyl, only the nOe enhancement between the olefinic hydrogen H-3′ and the methyl H-4′ would be observed. In addition, these nOe experiments also indicate that kadsulignan D (**5**) has the same relative stereochemistry as compound **4**.

An attempt to apply the exciton chirality method of circular dichroic spectroscopy (cd) (5) to assign the absolute configurations of **4** and **5** was unsuccessful because multiple chromophores complicated the Cotton curves. However, chemical conversion of **4** and **5** into a known dibenzocyclooctadiene lignan enabled us to assign their absolute configurations. Thus, treatment of **4** with chlorotrimethylsilane/sodium iodide in anhydrous acetonitrile (6) cleaved the spirooxy ring with concomitant aromatization and demethylenation to afford compound **8**. Compound **8** was methylated and hydrolyzed, affording deacetyl deangeloyl kadsurarin (**10**) (7). Since the absolute configuration of **10** is known, the absolute configuration of **4** may be unambiguously assigned as 6*S*,7*S*,8*S*,9*R*,16*S*. Similarly kadsulignan D (**5**) also gave compound **10** upon chemical conversion. Therefore, its configurations are the same as those of **4**. It is interesting to note that the cd spectra of **4** and **5** are considerably different (see Table 4) and this fact is attributed to differences in perturbance of multiple chromophores.

Recently, the isolation and structure of an analogous lignan, benzoyl oxokadsurane (**12**), from *K. coccinea* was reported (8). Comparison of the cd data of compounds **4** and **12** (see Table 4) reveals that the cd curves of **12** are similar to those of compound **4**, indicating the same absolute configurations of C-16 and C-9 in both compounds **4** and **12**. Based on the absolute configuration assignment of **4**, benzoyl oxokadsurane (**12**) may have a 7*R*,8*R*,9*R*,16*S* configuration. This conclusion is the same as that in the literature (8). However, the absolute configuration reported was assigned by the cd exciton chirality method (5) using a negative Cotton effect at 230–270 nm to predict an *R* configuration for the benzoate (C-9). Since there are three negative Cotton effects and no positive diagnostic Cotton effect in the region 230–270 nm (Table 4), the cd spectrum of compound **12** has no feature of exciton coupling in that region (5). Therefore, the cd exciton chirality method is not applicable to the prediction of absolute configuration of the benzoate in compound **12**.

Can. J. Chem. Downloaded from www.nrcresearchpress.com by 84.41.108.74 on 09/07/12
For personal use only.

Can. J. Chem. Downloaded from www.nrcresearchpress.com by 84.41.108.74 on 09/07/12
For personal use only.

TABLE 2. The ^{13}C nmr data[a] of kadsulignan C (**4**) and D (**5**)

Carbon (multiplicity)		Compound 4	Compound 5
1 (s)		194.86	194.85
2 (s)		132.12	132.63
3 (s)		154.65	154.94
4 (d)		123.82	123.57
5 (s)		140.69	141.33
6 (d)		82.19	82.55
7 (s)		75.24	75.30
8 (d)		44.08	44.30
9 (d)		83.52	82.55
10 (s)		129.39	129.83
11 (d)		101.18	101.09
12 (s)		150.16	150.31
13 (s)		130.00	130.15
14 (s)		143.28	143.80
15 (s)		119.91	119.86
16 (s)		62.79	63.24
17 (t)		79.30	78.98
CH_3-7 (q)		28.52	28.42
CH_3-8 (q)		17.76	17.90
CH_3O (q) × 2		58.54	58.59
OCH_2O (t)		101.95	101.78
Bz	CO (s)	165.47	
	1′ (s)	128.91	
	2′, 6′ (d)	129.39	
	3′, 5′ (d)	128.31	
	4′ (d)	133.10	
Ac	CO (s)	169.72	
	CH_3 (q)	20.27	
Ang-6	1′ (s)		166.34
	2′ (s)		126.42
	3′ (d)		141.01
	4′ (q)		15.42
	5′ (q)		19.10
Ang-9	1′ (s)		165.85
	2′ (s)		125.37
	3′ (d)		140.57
	4′ (q)		15.70
	5′ (q)		20.28

[a]δ, ppm, in $CDCl_2$ (25.18 MHz); the assignments are based on DEPT spectra, 2D ^1H–^{13}C COSY, and 2D ^1H–^{13}C long-range COSY experiments.

TABLE 3. The nOe enhancements of kadsulignan C (**4**) and D (**5**)

Irradiation	Observation	nOe enhancement (%) 4	nOe enhancement (%) 5
CH_3O-3	H-4	18	20
H-4	H-6	15	18
	OH	5	6
H-6	H-4	18	19
CH_3-7	H-6	18	17
	H-8	16	11
CH_3-8	OH	6	5
	H-9	12	12
H-9	H-11	22	20
H-11	H-9	13	15
Ang-9 H-5′	H-3′		19
	OH		16
H-4′	H-3′		15
Ang-6 H-5′	H-3′		20
	OH		0
H-4′	H-3′		19

Experimental

Melting points were determined on a Kofler hot stage apparatus and are uncorrected. The following instruments were used to record spectra: uv, Shimadzu uv-3000; ir, Perkin Elmer 599B; ^1H nmr and *n*Oe experiments, Bruker AM400 (400 MHz); ^{13}C nmr, 2D ^1H–^{13}C COSY, and 2D ^1H–^{13}C long-range COSY experiments, Bruker AC100 (25.19 MHz for ^{13}C nmr, 100 MHz for ^1H nmr); hrms, Varian MAT-711; cd, Jasco J500A; optical rotations, Jasco DIP181. Silica gel for column chromatography was manufactured at the Quingdao Haiyang Chemical Factory. The hptlc plates were manufactured at the Yantai Institute of Chemical Technology.

*Isolation of kadsulignan C (**4**) and D (**5**)*

The crude alcoholic extract of the root bark (3.5 kg) of *K. longipedunculata* collected in the Lin-An district of Zhejiang province, China, was suspended in water and extracted with ether. The ether was chromatographed on a silica gel eluting, in turn, with petroleum ether, benzene, benzene – ethyl acetate (10:1 and 4:1). The mid-fractions eluted with benzene – ethyl acetate (4:1) gave a crystalline mixture containing mainly two compounds. The crystalline mixture was rechromatographed over silica gel using benzene – ethyl acetate (6:1) as eluent. Concentration of the early fractions led to the isolation of kadsulignan C (**4**), 310 mg, which was crystallized from chloroform – petroleum ether. The mother liquor of the crystalline mixture was chromatographed repeatedly over silica gel eluting with petroleum ether – diethyl ether (1:1). Collection of the later fractions from the separations led to the isolation of kadsulignan D (**5**), 250 mg, which was crystallized from diethyl ether – petroleum ether.

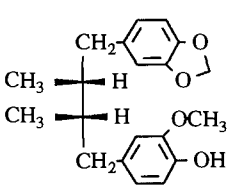
*Kadsulignan C (**4**)*: mp 244–246°C, $[\alpha]_D^{17}$ −86.3 (*c* 0.4516, $CHCl_3$); uv (CH_3OH) λ_{max} (log ε): 220 (4.73), 276 (3.57), 335 (3.71) nm; ir (KBr) ν_{max}: 3560, 1735, 1725 (sh), 1660, 1640, 1580 cm^{-1}; ^1H nmr and ^{13}C nmr: see Tables 1 and 2; hrms *m/z*: 578.1786 (M^+, 2% calcd. for $C_{31}H_{30}O_{11}$, 578.1788), 518.1579 (M^+ − CH_3COOH, 1%), 456.1422 (M^+ − PhCOOH, 7%), 414.1334 (M^+ − PhCOO − CH_3CO, 40%), 396.1207 (M^+ − PhCOOH − CH_3COOH, 13%), 385.0926 (M^+ − $C_{11}H_{13}O_3$, 66%), 353.1026 (M^+ − $C_{11}H_{13}O_5$, 18%), 341.1014 (M^+ − $C_{12}H_{13}O_5$, 44%), 325.0741 (M^+ − $C_{13}H_{17}O_5$, 35%), 105.0343 (PhCO, 100%); cd (CH_3OH): see Table 4.

*Kadsulignan D (**5**)*: mp 160–161°C, $[\alpha]_D^{10}$ −1.2 (*c* 2.238, $CHCl_3$); uv (CH_3OH) λ_{max} (log ε): 220 (4.83), 335 (3.64) nm; ir (KBr) ν_{max}: 3540, 3480, 1720, 1660, 1645, 1580 cm^{-1}; ^1H nmr and ^{13}C nmr: see Tables 1 and 2; hrms *m/z*: 596.2265 (M^+, 7% calcd. for $C_{32}H_{36}O_{11}$, 596.2273), 496.1775, (M^+ − $CH_3CH{=}C(CH_3)COOH$, 9%), 396.1212 (M^+ − $CH_3CH{=}C(CH_3)COOH$ ×2, 24%), 353.0968 ($C_{20}H_{17}O_6$, 22%), 344.1209 ($C_{19}H_{20}O_6$, 25%), 343.1173 ($C_{19}H_{19}O_6$, 100%), 325.0700 ($C_{18}H_{13}O_6$, 48%), 313.0668 ($C_{17}H_{13}O_6$, 46%); cd (CH_3OH): see Table 4.

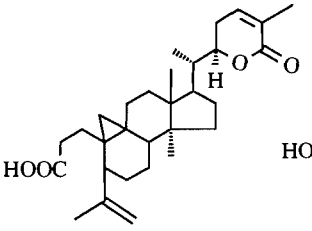
*Compound **8***

Kadsulignan C (**4**, 50 mg) and sodium iodide (200 mg) were dissolved in anhydrous acetonitrile (6 mL) at room temperature under a nitrogen atmosphere, then cooled to −17°C. Chlorotrimethylsilane (0.2 mL) was added to the solution and the reaction mixture was stirred at −17°C for 1 h. The reaction was quenched with 20% aqueous sodium thiosulfate and extracted with ether. The ether extract was separated by hptlc using diethyl ether – petroleum ether (3:1) containing 1% acetonitrile. The component with the lowest R_f was

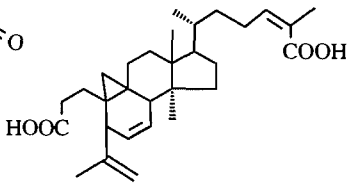
Can. J. Chem. Downloaded from www.nrcresearchpress.com by 84.41.108.74 on 09/07/12
For personal use only.



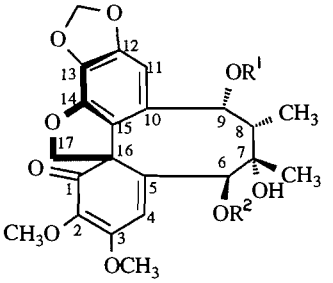
1

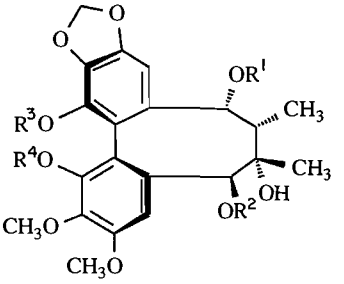


2



3



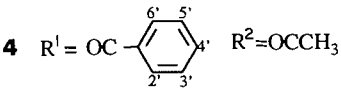


8 R^1=OCPh R^2=$OCCH_3$ R^3=R^4=H

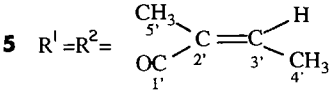
9 R^1=OCPh R^2=$OCCH_3$ R^3=R^4=CH_3

10 R^1=R^2=H R^3=R^4=CH_3

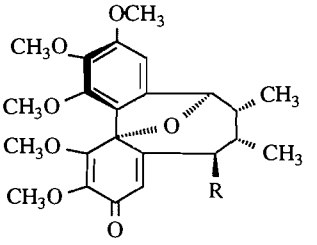
11 R^1=R^2=(Z)$OC(CH_3)C$=$CHCH_3$ R^3=R^4=H



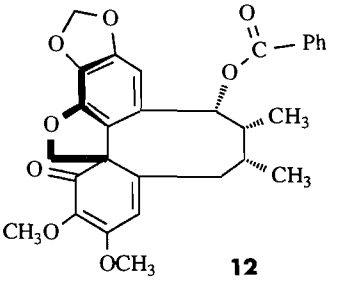
4 R^1= OC R^2=$OCCH_3$



5 R^1=R^2=



6 R =H 7 R=$OOCCH_3$



12

TABLE 4. Comparison on cd data of kadsulignan C (**4**), D (**5**), and benzoyl oxokadsurane (**12**) in methanol

	4	**5**[a]	**12**[b]
Δε (nm)	−12.10(120)	−14.26(219)	−2.30(230)
	−11.96(245)		−8.90(245)
	−8.49(285)		−4.08(270)
	−18.20(318)	−0.62(331)	−13.09(317)
	0 (346)		0 (345)
	+11.90(372)		+8.38(364)

[a]The Cotton effect at long wavelength is too weak to be observed.
[b]In ethanol, cited from ref. 8.

collected and purified by hptlc using chloroform–methanol (100:2) to give compound **8**, 5.0 mg; uv (CH_3OH) λ_{max} (log ε): 224 (4.46), 250 (sh), 284 (3.35) nm; ^{1}H nmr ($CDCl_3$) δ: 1.32 (3H, d, J = 7.1 Hz, Me-8), 1.38 (3H, s, Me-7), 2.29 (1H, s, D_2O exchangeable, OH-7), 2.29 (1H, q, J = 7.1 Hz, H-8), 3.38, 3.94 (3H each, s, OCH_3 ×2), 5.09, 5.71 (1H each, brs, D_2O exchangeable, OH-1, OH-14), 5.64, 5.88 (1H each, s, H-9, H-6), 5.98, 5.99 (1H each, d, J = 1.4 Hz, OCH_2O), 6.53, 6.74 (1H each, s, H-11, H-4), 1.62 (3H, s, CH_3CO), 7.28 (2H, td, J = 1.5, 6.6 Hz, H-2′, H-6′), 7.45 (1H, td, J = 1.5, 6.2 Hz, H-4′), 7.25 (2H, overlapping solvent peak, H-3′, H-5′); hrms m/z: 566.1818 (M^+, 11% calcd. for $C_{30}H_{30}O_{11}$, 566.1788), 444.1481 (M^+ − PhCOOH, 73%), 384.1247 (M^+ − PhCOOH − CH_3COOH, 48%), 341.1045 (M^+ − $C_{11}H_{13}O_5$, 100%); cd (CH_3OH) Δε (nm): +8.8 (221), 0 (229), −20.2 (240), −3.7 (280).

Methyl ether (9) of compound 8

Compound **8** (5.0 mg) was methylated with an ethereal solution of CH_2N_2 for 7 days. The reaction mixture was worked up in the usual way, then purified by hptlc using petroleum ether – diethyl ether (1:1) to provide compound **9**, 4.2 mg, ^{1}H nmr ($CDCl_3$) δ: 1.28 (3H, d, J = 7.1 Hz, Me-8), 1.34 (3H, s, Me-7), 2.22 (1H, q, J = 7.1 Hz, H-8), 2.27 (1H, brs, D_2O exchangeable, OH-7), 3.13, 3.45, 3.82, 3.97 (3H each, s, OCH_3 ×4), 5.74, 6.03 (1H each, s, H-9, H-6), 5.94, 5.95 (1H each, d, J = 1.4 Hz, OCH_2O), 6.55, 6.86 (1H each, s, H-11, H-4), 7.46 (1H, brt, J = 7.0 Hz, H-4′), 7.19–7.30 (4H, m, overlapping solvent peak, Ph-H ×4); ms m/z: 594 (M^+), 472 (M^+ − PhCOOH), 412 (M^+ − PhCOOH − CH_3COOH), 369, 359, 122, 105.

Deacetyl deangeloyl kadsurarin (10)

Compound **9** (4.2 mg) dissolved in 10% methanolic potassium hydroxide (3 mL) was refluxed for 7.5 h. The reaction mixture was treated with a)ter (2 mL) and extracted with ether. The ether extract was purified by hptlc using petroleum ether – ethyl acetate (1:1) to give **10**, 2.4 mg. The ^{1}H nmr, ms, ir, and cd of the reaction product are identical with an authentic sample of compound **10** derived from kadsurarin (7).

Compound **11** treated with CH_2N_2 for 12 days and worked up in the usual way; it was hydrolyzed with 10% methanolic potassium hydrox-

ide as described above. The product obtained from this reaction is identical with compound **10**.

Compound 11

Kadsulignan D (**5**) (100 mg) was treated for 20 min with chlorotrimethylsilane (0.3 mL) and sodium iodide (300 mg) in anhydrous acetonitrile (9 mL) in the manner described for the preparation of compound **8**. Compound **11**, 20.4 mg, was isolated from the reaction mixture; ^{1}H nmr ($CDCl_3$) δ: 1.29 (3H, s, Me-7), 1.30 (3H, d, J = 7.1 Hz, Me-8), 1.39, 1.42 (3H each, s, Me-2′ ×2), 1.82, 1.86 (3H each, dd, J = 7.9, 1.4 Hz, Me-3′ ×2), 2.22 (1H, q, J = 7.1 Hz, H-8), 2.29 (1H, brs, D_2O exchangeable, OH-7), 3.88, 3.92 (3H each, s, OCH_3 ×2), 4.94, 5.81 (1H each, brs, D_2O exchangeable, OH-1, OH-14), 5.52, 5.60 (1H each, s, H-9, H-6), 5.93, 5.95 (1H each, brs, OCH_2O), 5.91–6.00 (2H, m, covered, H-3′, ×2), 6.43, 6.69 (1H each, s, H-11, H-4); ms m/z: 584 (M^+), 484 ($M^+ - CH_3CH{=}C(CH_3)COOH$), 412 ($M^+ - CH_3CH{=}C(CH_3)COOH - C_4H_8O$), 384 ($M^+ - CH_3CH{=}C(CH_3)COOH$ ×2).

Acknowledgements

Financial support was provided by the National Natural Science Foundation of China. The authors are grateful to Professor Yu-Hu Liu, Huanan Institute of Botany, Academia Sinica, China, for the botanical identification of materials investigated; the Department of Analytical Chemistry, Shanghai Institute of Materia Medica, Academia Sinica, China, for uv, ir, nmr, ms, and cd measurements; and to Dr. Lois M. Browne and Prof. William A. Ayer, Department of Chemistry, University of Alberta, Canada, for reviewing the manuscript of this paper and helpful discussion.

1. Pharmacopoeia of People's Republic of China. Vol. 1. 1977. p. 396.
2. Jia-Sen Liu and Mei-Fen Huang. Youji Huaxue, **8**, 227 (1988).
3. Jia-Sen Liu and Mei-Fen Huang. Huaxue Xuebao, **49**, 502 (1991).
4. Jia-Sen Liu, Liang Li, and Han-Gang YuMei-Fen. Can. J. Chem. **67**, 682 (1989).
5. N. Harada and K. Nakanishi. Circular dichroic spectroscopy — Exciton coupling in organic stereochemistry. Oxford University Press, Oxford. 1983.
6. G. A. Olah, S. C. Narang, B. G. B. Gupta, and R. Malhotra. J. Org. Chem. **44**, 1247 (1979).
7. Jia-Sen Liu and Yu-Ting Ma. Huaxue Xuebao, **46**, 465 (1988).
8. Lian-Niang Li and Hong Xue. Phytochemistry, **29**, 2730 (1990).

Can. J. Chem. Downloaded from www.nrcresearchpress.com by 84.41.108.74 on 09/07/12
For personal use only.

A theoretical study of conformational deuterium isotope effects and bond dissociation energies of diastereotopic hydrogens

SAUL WOLFE[1,2] AND CHAN-KYUNG KIM[1]

Department of Chemistry, Queen's University, Kingston, Ont., Canada K7L 3N6
and the Department of Chemistry and Biochemistry, Simon Fraser University, Burnaby, B.C., Canada V5A 1S6

Received July 23, 1990[3]

SAUL WOLFE and CHAN-KYUNG KIM. Can. J. Chem. **69**, 1408 (1991).

In the conformations that correspond to the C6-X1-C2-X3-C4 moieties of 1,3-dioxane, 1,3-dithiane, and cyclohexane in their chair conformations, the model systems $CH_2(OH)_2$, $CH_2(SH)_2$, and *gauche*-butane contain "axial" and "equatorial" hydrogens. The vibrational frequencies of the diastereomeric monodeuterated CHD derivatives of these model compounds have been computed *ab initio* at the 6-31G*//6-31G* level of theory, scaled by 0.9, and used to calculate the conformational deuterium isotope effects in these systems, as well as the stretching and bending components of these isotope effects. The results are in very good agreement with the experimental observations and with some of the interpretations given by Anet for the six-membered rings. Using an equation suggested by McKean, the scaled isolated stretching frequencies have been used to predict the bond dissociation energies of the diastereotopic hydrogens of these molecules. The results suggest that the preference for radical abstraction of the axial C2 hydrogen in a 1,3-dioxane will be diminished in cyclohexane, and reversed in a 1,3-dithiane.

Key words: stereochemistry, isotope effects, bond dissociation energies.

SAUL WOLFE et CHAN-KYUNG KIM. Can. J. Chem. **69**, 1408 (1991).

Les systèmes modèles, $CH_2(OH)_2$, $CH_2(SH)_2$ et le butane *gauche* contiennent des hydrogènes « axial » et « équatorial», dans les conformations qui correspondent aux unités C6-X1-C2-X3-C4 du 1,3-dioxane, du 1,3-dithiane et du cyclohexane dans leur conformation chaise. On a calculé les fréquences de vibration des dérivés diastéréoisomères monodeutériés CHD de ces composés modèles à l'aide de calculs *ab initio* au niveau théorique 6-31G*//6-31G* gradué à 0,9 et on les a utilisés pour calculer l'effet isotopique du deutérium dans ces systèmes, aussi bien que les composantes de la déformation et de l'élongation de ces effets isotopiques. Les résultats s'accordent parfaitement avec les résultats expérimentaux et avec certaines interprétations de Anet relatives aux cycles à six chaînons. On a utilisé les fréquences isolées d'élongation graduées pour prédire les énergies de dissociation des liaisons des hydrogènes diastéréoisomères de ces molécules en utilisant une équation suggérée par McKean. Les résultats suggèrent que la préférence pour une abstraction radicalaire de l'hydrogène axial en C9 dans le 1,3-dioxane sera moins marquée dans le cyclohexane et sera inversée dans le 1,3-dithiane.

Mots clés : stéréochimie, effets isotopiques du deutérium, énergies de dissociation des liaisons.

[Traduit par la rédaction]

Can. J. Chem. Downloaded from www.nrcresearchpress.com by 84.41.108.74 on 09/07/12
For personal use only.

Introduction

Linear correlations exist between C—H bond lengths and isolated C–H stretching frequencies (1), between isolated C–H stretching frequencies and C—H bond dissociation energies (1, 2), and between one-bond C–H coupling constants and the inverse of C—H bond lengths (3). Since diastereotopic hydrogens in organic compounds have different bond lengths (3), their different stretching frequencies, bond dissociation energies, and C–H coupling constants lead to a multiplicity of stereoelectronic "effects", including the Bohlmann bands (infrared), Perlin effect (nmr) (3), relative rates of radical abstraction (4), and conformational deuterium isotope effects (5).

In the course of a recent study of the Perlin effect (3), we calculated the 6-31G* (6) optimized geometries of a number of molecules $CH_2(XH)_2$ in conformations that simulate the chair conformations of six-membered rings containing the X-C-X moiety. In every case the trends in C—H bond lengths of the model structures were found to reproduce those observed for the cyclic structures. Three of the molecules of the earlier study, namely, X = S (**1**), X = O (**2**), and *gauche*-butane (**3**) are shown in Fig. 1; in each case the diastereotopic "axial" and "equatorial" hydrogens are readily identified. Using a modification of LINK 716 of GAUSSIAN 86 (7, 8*a*),[4] we have now calculated the vibrational frequencies of the diastereomeric monodeuterated analogs of **1**–**3** and, by use of the computer programme provided as Supplementary Data,[5] have employed these frequencies to obtain the "equatorial" ⇄ "axial" equilibrium constants.

Conformational deuterium isotope effects

In the cases of **1** and **2**, analysis of individual frequencies allowed the total equilibrium constant to be partitioned into its stretching and bending components. It is generally observed that frequencies computed at the 6-31G* level are systematically too high by 10% (2, 9); a uniform scaling factor of 0.9 was, therefore, employed throughout. It has recently been shown (10) that this practice amounts to an empirical simulation of the effect of electron correlation.

The results are summarized in Table 1, together with the experimental results of Anet and Kopelevich for cyclohexane and the 5,5-dimethyl-1,3-dioxanes and 1,3-dithianes (5*a*–*c*),

[1]Present address: Department of Chemistry and Biochemistry, Simon Fraser University, Burnaby, B.C., Canada V5A 1S6.

[2]Canada Council Killam Research Fellow, 1990–1992.

[3]Revision received May 13, 1991.

[4]GAUSSIAN 90 now allows computation of the frequencies of isotopically labelled molecules. See ref. 8*b*. Frequencies calculated using GAUSSIAN 86 with the protocol of ref. 8*a* are identical to those calculated using GAUSSIAN 90.

[5]This programme may be purchased from the Depository of Unpublished Data, Document Delivery, CISTI, National Research Council Canada, Ottawa, Canada K1A 0S2.

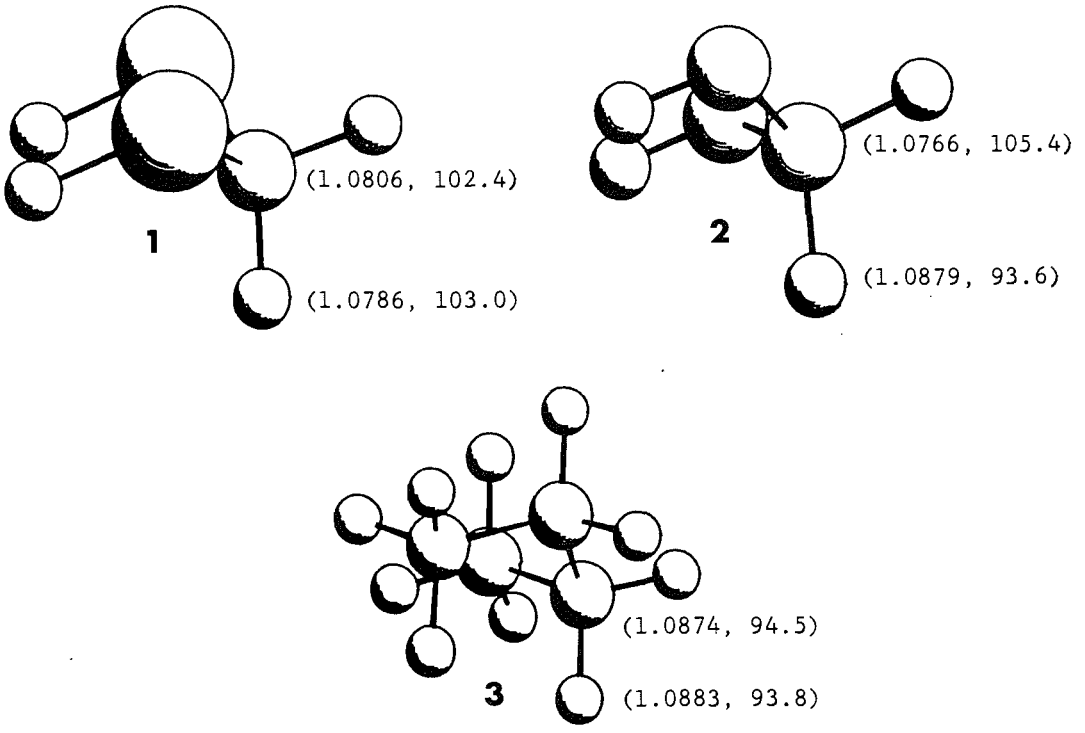


FIG. 1. Structures **1**–**3**, showing the "equatorial" and "axial" hydrogens in each case. The numbers in parentheses are (bond length in Å, bond dissociation energy in kcal/mol).

TABLE 1. Bond lengths, isolated stretching frequencies, equilibrium isotope effects, and their stretching and bending components

					ΔG^b		
Molecule	C—H bond	r(C—H)[a]	ν^{is}_{C-H}[c,d]	ν^{is}_{C-D}[c,e]	Total	Stretch	Bend
$CH_2(SH)_2$	eq	1.0806	2977	2192	−7.1	19.4	−26.4
1	ax	1.0786	2985	2185	0±1.2[f]		
$CH_2(OH)_2$	eq	1.0766	3012	2115	56.6	39.6	17.0
2	ax	1.0879	2879	2220	49.0±3.6[g]		
Butane	eq	1.0874	2890	2118	7.3		
3	ax	1.0883	2882	2124	6.3±1.5[h]		
					≅50[i]		
					14.1[j]		

[a]In angstrom.
[b]Refers to the equilibrium eq(C–D) ⇄ ax(C–D), in cal/mol at 23°C.
[c]In cm^{-1}, after scaling by 0.9.
[d]All hydrogens other than the unique hydrogen have been replaced by deuterium in the calculations.
[e]The unique hydrogen has been replaced by deuterium in the calculations.
[f]Experimental value for 5,5-dimethyl-1,3-dithiane at 23°C (5*c*).
[g]Experimental value for 5,5-dimethyl-1,3-dioxane at 23°C (5*b*).
[h]Experimental value for cyclohexane at 23°C (5*a*).
[i]Experimental value for cyclohexane at −75°C (5*d*).
[j]Theoretical value for cyclohexane at −88°C using the 3-21G basis set (5*e*).

Aydin and Günther for cyclohexane (5*d*), and the theoretical calculations of Williams on cyclohexane (5*e*).

In **2** and **3**, the "axial" hydrogen (deuterium) has the longer bond, and the lower stretching frequency. This trend is reversed in **1**. Considing only the zero-point energy differences that might be expected to result from the differences in the C–H (C–D) stretching frequencies, the "axial" deuterated isomer should be preferred in the case of **1**, and the "equatorial" deuterated isomer shoud be preferred in the cases of **2** and **3** (5*a*–*c*).

As can be seen, the sign of ΔG is in each case consistent with an analysis based only on the presumed zero-point energy differences. Moreover, the ΔG calculated for the model systems seem to agree with experiment, especially in the comparison of **2** with a 1,3-dioxane, and the comparison of *gauche*-butane with cyclohexane. However, when the primary and secondary

Can. J. Chem. Downloaded from www.nrcresearchpress.com by 84.41.108.74 on 09/07/12
For personal use only.

TABLE 2. Analysis of the stretching frequencies[a] of the diasteromeric monodeuterated derivatives of **1** and **2**

Molecule	Location of deuterium	Frequency ν_1	ν_2	ν_3	ν_4	ν_5	ν_6
1	Equatorial	277	699	2185	2618	2619	2985
	Axial	279	729	2977	2618	2619	2192
	ν(ax) − ν(eq)	2	30	792	0	0	−793
2	Equatorial	1062	1097	2220	2879	3687	3688
	Axial	1037	1120	3012	2115	3688	3688
	ν(ax) − ν(eq)	−25	23	792	−764	1	0

[a]In cm^{-1}, after scaling by 0.9.

TABLE 3. Analysis of the bending frequencies[a] of **1** and **2**, and their diasteromeric monodeuterated derivatives

Molecule	Location of deuterium	Frequency[b] ν_1	ν_2	ν_3	ν_4	ν_5	ν_6	ν_7	ν_8	ν_9
1	None	148	228	621	723	851	1052	1215	1272	1438
	Equatorial	148	227	572	686	813	1012	1017	1225	1281
	Axial	148	225	613	633	829	1027	933	1258	1280
	ν(ax) − ν(eq)	0	−2	41	−53	16	15	−84	33	−1
2	None	113	375	530	1000	1132	1394	1348	1443	1519
	Equatorial	113	373	524	889	941	1284	1230	1385	1423
	Axial	113	370	529	886	955	1343	1166	1414	1402
	ν(ax) − ν(eq)	0	−3	5	−3	14	59	−64	29	−21

[a]In cm^{-1}, after scaling by 0.9.
[b]ν_1, ν_2: XH torsion; ν_3: XCX bend; ν_4: CH_2 rock; ν_5: CXH bend + CH_2 twist; ν_6: CXH bend + CH_2 rock; ν_7: CH_2 twist; ν_8: CH_2 wag; ν_9: CH_2 scissor.

Can. J. Chem. Downloaded from www.nrcresearchpress.com by 84.41.108.74 on 09/07/12
For personal use only.

isotope effects associated with all of the other stretching and bending vibrations are examined, a more subtle discussion of **1** becomes necessary. The stretching contribution to ΔG has the *same* sign in **1** and **2**, but the stretching and bending contributions to the free energy difference in **1** have *opposite* signs, and the *bending* contributions dominate. Thus an analysis of **1** that emphasizes C–H (C–D) stretching would not account for the sign of ΔG.

Table 2 examines all of the stretching frequencies of the diastereomeric monodeuterated derivatives of **1** and **2**. In **2**, ν_1 and ν_2 refer to O–C–O stretching, ν_5 and ν_6 refer to O–H stretching, and ν_3 and ν_4 are the C–H (C–D) stretching frequencies. The O–C–O and O–H effects cancel so that, as expected, differences in C–H (C–D) vibrations are the dominant factor that determines the stretching contribution to the conformational preference. Examination of ν_3 and ν_4 reveals that the C–D (2220 → 2115 cm^{-1}) and C–H (3012 → 2879 cm^{-1}) stretching frequencies are lower when the D (H) are "axial". Since the decrease in the C–H frequency is larger, the final result is that the isomer in which hydrogen is "axial" (and deuterium is "equatorial") has the lower zero-point energy. The result of this analysis is consistent with the idea (3) that in the oxygen compound **2** the (n_p,σ^*_{CH}) orbital interaction controls the geometry of the CH_2 moiety.

In **1**, ν_1 and ν_2 are the symmetric and antisymmetric S–C–S stretching frequencies, ν_4 and ν_5 are the symmetric and antisymmetric S–H stretching frequencies, and ν_3 and ν_6 are the

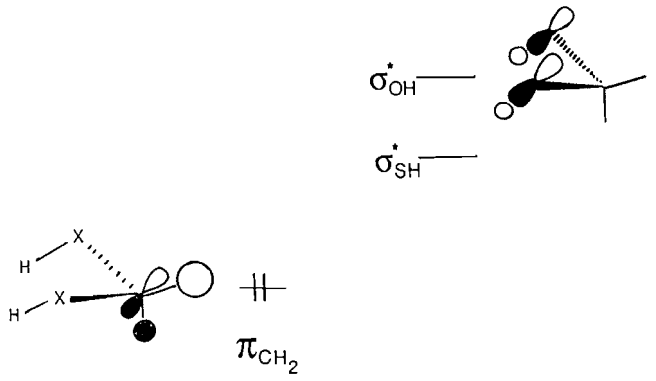


FIG. 2. Orbital interaction diagram for $CH_2(XH)_2$, showing charge transfer from π_{CH_2} to $\sigma^*_{(XH)_2}$.

C–H (C–D) stretching frequencies. Here we observe that the C–H (C–D) and S–H differences between the isomers cancel, but both of the S–C–S stretching freqencies are lower in the isomer having "equatorial" deuterium. This means that in **1** the "equatorial" preference of the stretching contribution to the equilibrium isotope effect is not caused by C–D (C–H) directly, but through an effect transmitted from C–D (C–H) to the C—S bonds. The picture suggested by this finding can be conveyed in two ways: (i) in terms of hyperconjugation, the description (H—S—C— $H_{eq} \Leftrightarrow H^+$ S=C H^-_{eq}) predicts concomitant C–H_{eq} weakening and S–C strengthening; (ii) in terms of

TABLE 4. Calculated bond dissociation energies of diastereotopic hydrogens

Molecule	C—H hydrogen	$\nu^{is}_{C—H}$[a]	C—H bond dissociation energy[b]
Methanol	Antiperiplanar[c]	2968 (2979)[d]	101.5
	gauche[c]	2893 (2921)[d]	94.8 (95.5)[d]
1	Equatorial	2977	102.4
	Axial	2985	103.0
2	Equatorial	3012	105.4
	Axial	2879	93.6
3	Equatorial	2890	94.5
	Axial	2882	93.8

[a]In cm^{-1}, after scaling by 0.9.
[b]In kcal/mol.
[c]With respect to the O—H bond.
[d]Experimental value (1*b*).

orbital interactions (11), the low-lying σ^*_{SH} acceptor orbitals control the geometry of the CH_2 moiety via charge transfer from π_{CH_2} (see Fig. 2). This charge transfer is strengthened by a strengthening of the S–C bond, accompanied by a preferential weakening of the C—H_{eq} bond, because H_{eq} has the larger coefficient in π_{CH_2} (3).

The charge transfer argument leads to the prediction that the H—C—H angle in **1** will be smaller than tetrahedral (12). Because the coefficients of the two hydrogen atomic orbitals are out-of-phase in the donor orbital, π_{CH_2}, depopulation of this orbital will be facilitated by a decrease in the H—C—H angle (11). Indeed, the H—C—H angles of **1** and **2** are 108.0° and 110.2°, respectively.

Table 3 summarizes the bending frequencies of the undeuterated and the "equatorial" and "axial" deuterated derivatives of **1** and **2**. For the undeuterated compounds, all C–H bending frequencies are lower in **1**. The largest effect of monodeuteration of this compound is seen in ν_4 and ν_7. In each case the frequency of the bending vibration is lower when deuterium is "axial"; this is the origin of the large negative ΔG_{bend} seen in Table 1. Interestingly, in **2**, the conformational effect of isotopic substitution on ν_4 is negligible, so that when all bending vibrations are taken into account, deuterium prefers the "equatorial" site (positive ΔG_{bend}).

Bond dissociation energies

McKean (1) has advocated the use of eq. [1] to estimate C—H bond dissociation energies from "isolated" C–H stretching frequencies. Since the appropriate degree of deuteration of **1**–**3** allows the isolated C–H stretching frequencies of these compounds to be computed, and the equilibrium isotope effects described above seem to be reasonable, we have used eq. [1] to calculate the "axial" and "equatorial" C—H bond dissociation energies (D.E.). Table 4, which includes the diastereotopic deuterium isolated (2) methyl hydrogens of methanol as a benchmark, summarizes the results.

$$[1] \quad \text{D.E. (kcal/mol)} = 0.08963\nu(\text{C–H})_{is} - 164.5$$

The value for the weaker *gauche* hydrogen of methanol is in excellent agreement with experiment, and both calculated frequencies are within 1% of the experimental values (13). Since the *gauche* hydrogen of methanol is topologically equivalent to the "axial" C2 hydrogen in a pyranose ring, it follows that this hydrogen will react preferentially in radical abstraction (4). The same trend is seen in **2**: the "axial" C2 hydrogen will be more reactive in radical abstraction (4). The difference in bond dissociation energies favoring "axial" abstraction is greatly diminished in **3**, and reversed in **1**. We expect that radical attack upon C—H bonds of a cyclohexane ring will exhibit little axial–equatorial selectivity, but radical abstraction from C2 of a 1,3-dithiane should exhibit a preference opposite to that of a 1,3-dioxane.

Acknowledgments

The authors thank the Natural Sciences and Engineering Research Council of Canada for financial support, and Computing Services of Queen's University and Simon Fraser University for generous allocation of resources.

1. (*a*) D. C. McKean. Chem. Soc. Rev. **7**, 399 (1978); (*b*) Int. J. Chem. Kinet. **21**, 445 (1989).
2. A. L. Aljibury, R. G. Snyder, H. L. Strauss, and K. Raghavachari. J. Chem. Phys. **84**, 6872 (1986).
3. S. Wolfe, B. M. Pinto, V. Varma, and R. Y. N. Leung. Can. J. Chem. **68**, 1051 (1990).
4. V. Malatesta and K. U. Ingold. J. Am. Chem. Soc. **103**, 609 (1981); A. J. L. Beckwith and C. J. Easton. J. Am. Chem. Soc. **103**, 615 (1981); D. Griller, J. Howard, P. R. Marriott, and J. C. Scaiano. J. Am. Chem. Soc. **103**, 619 (1981).
5. (*a*) F. A. L. Anet and M. Kopelevich. J. Am. Chem. Soc. **108**, 1355 (1986); (*b*) J. Am. Chem. Soc. **108**, 2109 (1986); (*c*) J. Chem. Soc. Chem. Commun. 595 (1987); (*d*) R. Aydin and H. Günther. Angew. Chem. Int. Ed. Engl. **20**, 985 (1981); (*e*) I. H. Williams. J. Chem. Soc. Chem. Commun. 627 (1986).
6. P. C. Hariharan and J. A. Pople. Theor. Chim. Acta, **28**, 213 (1973).
7. M. J. Frisch, J. S. Binkley, H. B. Schlegel, K. Raghavachari, C. F. Melius, R. L. Martin, J. J. P. Stewart, F. W. Bobrowicz, C. M. Rohlfing, L. R. Kahn, D. J. DeFrees, R. Seeger, R. A. Whiteside, D. J. Fox, E. M. Fluder, and J. A. Pople. GAUSSIAN 86, Gaussian Inc., Pittsburgh, PA. 15213.
8. (*a*) S. Wolfe, S. Hoz, C.-K. Kim, and K. Yang. J. Am. Chem. Soc. **112**, 4186 (1990); (*b*) M. J. Frisch, M. Head-Gordon, G. W. Trucks, J. B. Foresman, H. B. Schegel, K. Raghavachari, M. A. Robb, J. S. Binkley, C. Gonzalez, D. J. DeFrees, D. J. Fox, R. A. Whiteside, R. Seeger, C. F. Melius, J. Baker, R. L. Martin, L. R. Kahn, J. J. P. Stewart, S. Topiol, and J. A. Pople. GAUSSIAN 90. Gaussian, Inc., Pittsburgh PA. 1990.

Can. J. Chem. Downloaded from www.nrcresearchpress.com by 84.41.108.74 on 09/07/12
For personal use only.

9. J. A. POPLE, R. KRISHNAN, H. B. SCHLEGEL, and J. S. BINKLEY. Int. J. Quant. Chem. Symp. **13**, 225 (1979); J. A. POPLE, H. B. SCHLEGEL, R. KRISHNAN, D. J. DEFREES, J. S. BINKLEY, M. J. FRISCH, R. A. WHITESIDE, R. A. HOUT, and W. J. HEHRE. Int. J. Quant. Chem. Symp. **15**, 269 (1981).
10. V. I. PUPYSHEV, Y. N. PANCHENKO, C. W. BOCK, and G. PONGOR. J. Chem. Phys. **94**, 1247 (1991).
11. T. A. ALBRIGHT, J. K. BURDETT, and M. H. WHANGBO. Orbital interactions in chemistry. John Wiley, New York. 1985.
12. B. M. PINTO, H. B. SCHLEGEL, and S. WOLFE. Can. J. Chem. **65**, 1658 (1987).
13. W. J. HEHRE, L. RADOM, P. V. R. SCHLEYER, and J. A. POPLE. Ab initio molecular orbital theory. Wiley–Interscience, New York. 1986. p. 250.

Can. J. Chem. Downloaded from www.nrcresearchpress.com by 84.41.108.74 on 09/07/12
For personal use only.

Origin of the dual-band laser emission from 7-diethylamino-4-methylcoumarin (C1) in solution: effect of hydrogen-bonding interaction by hydroxylic molecules[1,2]

R. W. YIP[3] AND Y. X. WEN

Département de chimie, Université du Québec à Montréal, C.P. 8888, Succ. A, Montréal, Qué, Canada H3C 3P8

Received August 20, 1990[4]

R. W. YIP and Y. X. WEN. Can. J. Chem. **69**, 1413 (1991).

Ultraviolet absorption measurements on 7-diethylamino-4-methylcoumarin (C1) and its rigid analogue C102 in which the 7-amino group is structurally prevented from twisting in *n*-butyl acetate (*n*BuOAc) solutions containing submolar concentrations of *n*-butyl alcohol showed weak 2:1 alcohol:dye complexation. These results contrast with those from fluorescence measurements which revealed a 1:1 alcohol:dye excited state complex for the C1 dye. These results together with N_2 laser excited amplified spontaneous emission (ASE), and laser gain measurements on C1 and C102 in *n*BuOAc with alcohol or acetonitrile co-solvent show that dual ASE from C1 originates from a quasi-equilibrium concentration of hydrogen-bonded or acetonitrile-solvated excited state complex. The results are inconsistent with a TICT–*n*BuOAc exciplex for C1 in *n*BuOAc. The laser gain of the twin ASE peaks at 420 nm and 455 nm from C1 can be tuned by adding a small quantity of hydroxylic co-solvent to dried *n*BuOAc. ASE was found to be a selective probe for a H-bonded C1 complex whose fluorescence is normally obscured by that from the "free" dye.

Key words: aminocoumarins, dual amplified spontaneous emission, excited state hydrogen-bonding complex, laser gain.

R. W. YIP et Y. X. WEN. Can. J. Chem. **69**, 1413 (1991).

Les spectres d'absorption UV de la 7-diéthylamino-4-méthylcoumarine (C1) et de son analogue rigide C102, dans lequel on bloque la rotation du groups 7-amino, on été déterminé en solution dans l'acétate de *n*-butyle contenant des concentrations submolaires d'alcool *n*-butylique; ils montrent une faible complexation alcool–colorant dans un rapport de 2:1. Ces résultats contrastent avec ceux obtenus à partir des mesures de fluorescence qui révèlent la présence d'un complexe de l'état excité alcool–colorant 1:1 pour le colorant C1. Ces résultats combinés à une émission spontanée amplifiée provoquée par un laser au N_2 (ASE) et à des mesures d'amplification par un laser sur les composés C1 et C102 dans le *n*-BuOAc avec l'alcool ou l'acétonitrile comme co-solvant montrent que l'émission spontanée double obtenue à partir du composé C1 provient d'une concentration à l'état de quasi-équilibre de liaisons hydrogènes ou de complexes à l'état excité solvatés par l'acétonitrile. Les résultats sont imcompatibles avec l'existence d'un exciplexe TICT–*n*BuoAc dans le nBuOAc. On peut synthoniser l'amplification par un laser des deux pics à 420 et à 455 nm du composé C1, en ajoutant des petites quantités de co-solvant hydroxylé au nBuOAc sec. On a trouvé que l'émission spontanée induite par un laser au N_2 (ASE) est une sonde sélective pour les complexes liés par des liaisons hydrogènes dont la fluorescence est normalement cachée par celle du colorant "libre".

Mots clés: Aminocoumarines, émission spontanée doublement amplifiée, complexe lié par des liaisons hydrogènes dans l'état excité, amplification au laser.

[Traduit par la rédaction]

Introduction

Unlike the model *p*-*N*,*N*-dimethylaminobenzonitrile system, which exhibits *dual* internal charge transfer (ICT) emissions from the planar and the perpendicularly twisted ICT (TICT) R_2N—Ph conformations (1, 2), the important bichromophoric fluorescent 7-diethylamino-4-methylcoumarin (C1) laser dye exhibits only a *single* fluorescence band with near-TICT solvatochromic properties (3, 4). Since the cross section $\sigma_E(\lambda)$ for amplified spontaneous emission (ASE) is related to the fluorescence profile $F(\lambda)$ (5), a *single* ASE band is expected. Surprisingly, *dual* ASE ascribed to a planar and a TICT form has been reported for C1 in moderately polar solvents such as *n*-butyl acetate (*n*BuOAc), ethers, and chloroalkanes (6). The TICT form is believed to exist as a TICT–solvent exciplex (stabilized by specific interaction with the solvent O or Cl heteroatom) at laser-excited transitory concentrations that relaxes back to the planar form (6). However, recent excited state absorption (ESA) studies on C1 and the rigidized analogue, C102 (2,3,5,6-1*H*, 4*H*-tetrahydro-8-methylquinolazino[9,9*a*,1-*gh*]coumarin) failed to reveal a unique ESA absorption due to the TICT form (7). In view of the fundamental importance of the TICT state in the photophysics of bichromofluorophores (1, 2), the unexpected implication of a large σ_E for the TICT exciplex, and the possible modification of the laser gain profile of the aminocoumarins, we now report uv absorption, fluorescence, and ASE results on C1 and C102 as part of our study of conformationally sensitive excited states.

Experimental section

ASE studies used a 50 μJ PRA LN100 N_2 laser for transverse excitation (7*d*, 8) (2″ focal length quartz cylindrical lens) of a dye solution contained in an upright 1 cm rectangular 4-window fluorescence quartz cell, and a JY HR 320 monochromator and a silicon diode array/OMA (EG&G 1412F/1461) system for detection of the emission. The transverse excitation geometry has been previously described (8). Briefly it consisted of a laser excitation beam which is at right angle to the axis passing through the cell and the centre of the monochromator slits. The line image formed by focussing the N_2 laser excitation beam with a cyclindrical lens defines the ASE gain region which is coaxial with the axis passing through the cell and the centre of the monochromator slits. The length of the line image was controlled by a pair of slits placed near the cell in the excitation beam. The cell

[1]Presented in part at the 17th Annual Ontario–Quebec Physical Organic Minisymposium, Quebec City, Quebec, Nov. 10–12, 1989.

[2]Dedicated to Professor Paul de Mayo, a notable and incisive contributor to Canadian chemistry, on the occasion of his 65th birthday, for pedagogically encouraging his students to extend their critical faculties.

[3]To whom correspondence should be addressed.

[4]Revision received May 3, 1991.

Can. J. Chem. Downloaded from www.nrcresearchpress.com by 84.41.108.74 on 09/07/12
For personal use only.

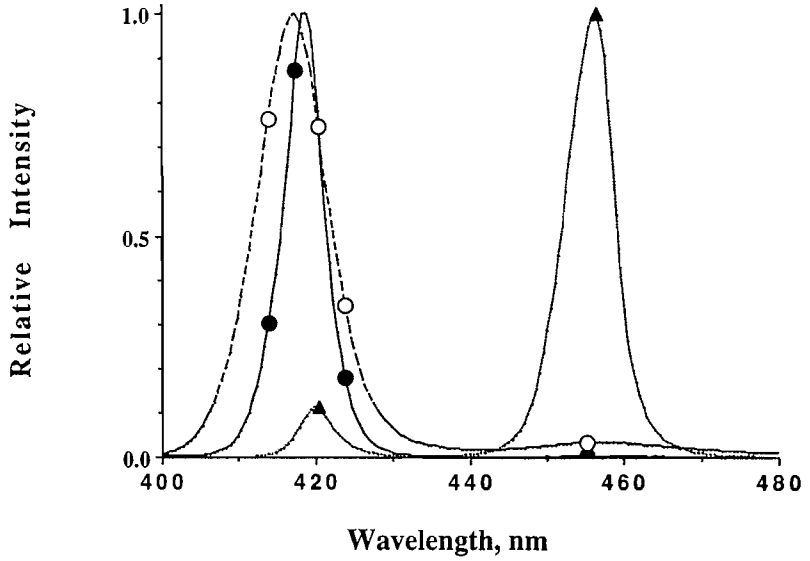


FIG. 1. ASE of C1 O, unpurified *n*BuOAc; OO, dried *n*BuOAc; V, water-saturated *n*BuOAc.

was canted several degrees to avoid feedback from reflection at the parallel cell walls. Digital data from the 1461 detector interface was collected and analyzed using an IBM AT clone connected to the 1461 interface unit via serial interfacing. Typically, the emission from 10 excitation pulses were integrated over 3 min. Appropriate glass neutral density filters were used to keep the signal counts below the maximum limit of ca. 15 000 counts. At a detector temperature of −15°C, the background over this period was < 10 counts and was subtracted from the signal. The wavelength of the monochromator-OMA system was calibrated with an Ultra-Violet Products Inc. Hg and Kr Pen-Ray lamp. Solvents (Caledon distilled in glass) and nBuOAc (Fisher reagent) were refluxed over CaH_2 for 1 h and distilled. The C1 and C102 (Exciton Corp.) were recrystallized from methanol–water and sublimed. Absorption and fluorescence spectra were measured with a Cary-2200 uv/vis spectrophotometer and a Perkin-Elmer MPF-44 spectrofluorimeter, respectively.

Results and discussion

The ASE spectrum of C1 but not the rigidized C102 in unpurified *n*BuOAc showed two bands at 420 and 455 nm, consistent with previous observations (6). However, further investigations of C1 in dried *n*BuOAc (or THF) revealed a single ASE band at 420 nm, with only a trace of the 455 nm band; and conversely in water-saturated *n*BuOAc solution. These results (Fig. 1) show conclusively that the dual ASE 455 nm band from C1 in *n*BuOAc originates from traces of water probably *H*-bonded (6*d*, 9) to the excited C1 dye and not from a TICT–solvent exciplex (6*a-c*).

The role of hydrogen bonding in the dual ASE of C1 in *n*BuOAc was investigated by adding submolar concentrations of methanol or *n*-butyl alcohol (*n*BuOH). Figure 2*a* shows that the *proportion* of the long to short wavelength bands was altered by the addition of methanol. In contrast, the ASE spectra from C102 showed the normally observed continuous shift in the wavelength *position* of the single peak with increasing alcohol concentration. Though less dramatic, dual ASE was also observed for C1 in *n*BuOAc + dried acetonitrile (AN) as co-solvent (Fig. 2*b*). This unanticipated result seem to suggest that high dielectric constant solvents like AN can also participate in complexing with the highly dipolar excited state of C1. At high or neat concentrations of methanol (or *n*BuOH), structure, due possibly to specific alcohol self-associated complexes

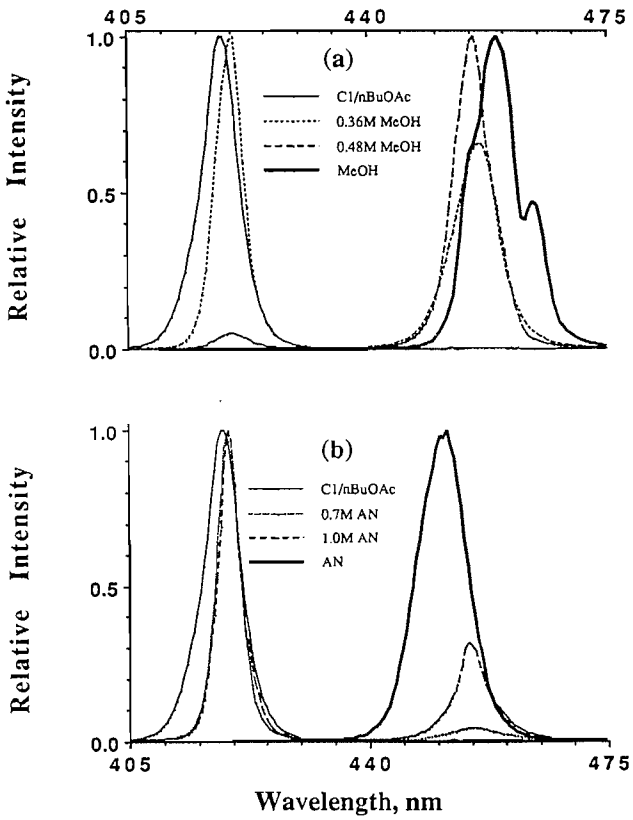


FIG. 2. ASE of C1 in (*a*) *n*BuOAc + methanol; (*b*) *n*BuOAc + acetonitrile.

with C1, can be observed reproducibly in the long-wavelength C1 ASE band. Should this suggestion be substantiated by future experiments, ASE would then be a powerful technique to study alcohol self-association (10) in solution, since, as far as we are aware, there is no method of direct measurement in solution at ambient temperature of specific signals due to particular associated species of alcohol, although important indirect information can be gained from thermodynamic (10*a*, *b*) and other methods (10*c*, *d*).

Can. J. Chem. Downloaded from www.nrcresearchpress.com by 84.41.108.74 on 09/07/12
For personal use only.

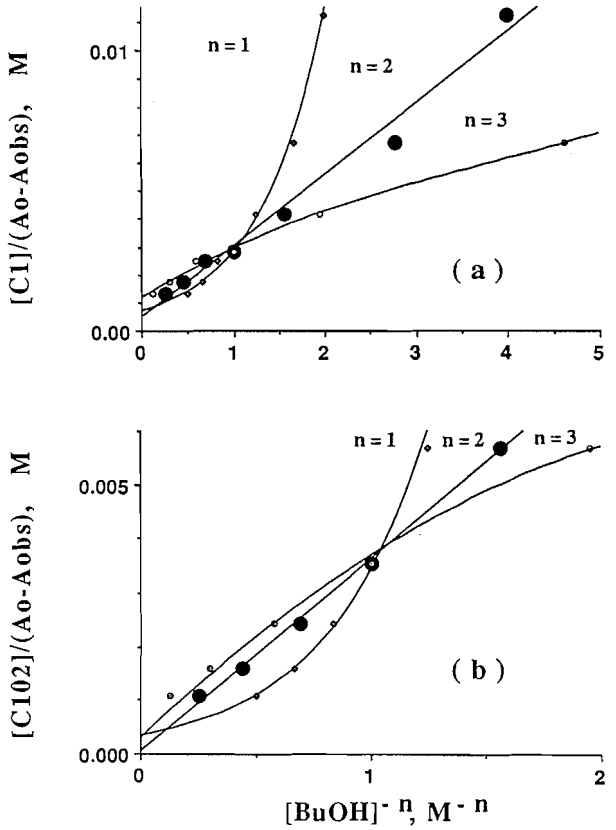


FIG. 3. Plot of $[dye]/(A_0 - A_{obs})$ vs. $[BuOH]^{-n}$ for (*a*) C1 and (*b*) C102 coumarin dyes. Solid points represent the experimental data for $n = 2$. $[Dye] = 3.98 \times 10^{-5}$ M; $[BuOH] \approx 0 - 2$ M.

The uv absorption of C1 (and C102) in *n*BuOAc + *n*BuOH was studied to determine whether, as was in the case of 1-methylindole and *n*BuOH (11), ground state complexation was solely responsible for the fluorescence properties. The uv absorption spectra of C1 and C102 in *n*BuOAc with different concentrations of *n*BuOH showed isosbestic wavelengths λ_{iso}^{ab} at 369 and 378 nm, respectively, which show that the dyes form complexes with alcohol. For the equilibrium:

$$D + n\text{ROH} = D..n\text{ROH}$$

the corresponding absorbance A_{obs}, from both the free and complexed dye as a function of [ROH], is

$$[1] \quad [D]_0/(A_0 - A_{obs}) = [(\epsilon - \epsilon_{cx})L]^{-1}(1 + K_{gs}^{-1}[ROH]^{-n})$$

where ϵ and ϵ_{cx} are the extinction coefficients of the "free" and complexed dye D, and A_0 is the absorbance and $[D]_0$ is the dye concentration at [ROH] = 0. This equation follows from the definition of the equilibrium for formation of a dye–alcohol complex, in which the free dye concentration is expressed as a difference in concentration between the initial dye concentration and the concentration of complexed dye, *i.e.*., $[D]_0 - [D_{cx}]$; and replacing the free and complexed dye concentrations by their optical absorbances. Figure 3*a* shows the fit to the data for C1 and Fig. 3*b* for C102 to eq. [1] for different values of *n*, the number of alcohol molecules complexed with each dye molecule. The data clearly show a best fit for $n = 2$ (D..2(*n*BuOH), D = C1 or C102) for both coumarin dyes. From the above plot we obtained $K_{gs} = 0.19 \pm 0.03$ (C1) and 0.016 ± 0.003 M^{-2} (C102), which shows that C102 is only weakly complexed to alcohol in the ground state. C1 shows small non-negligible extent of complexation with alcohol in the ground state.

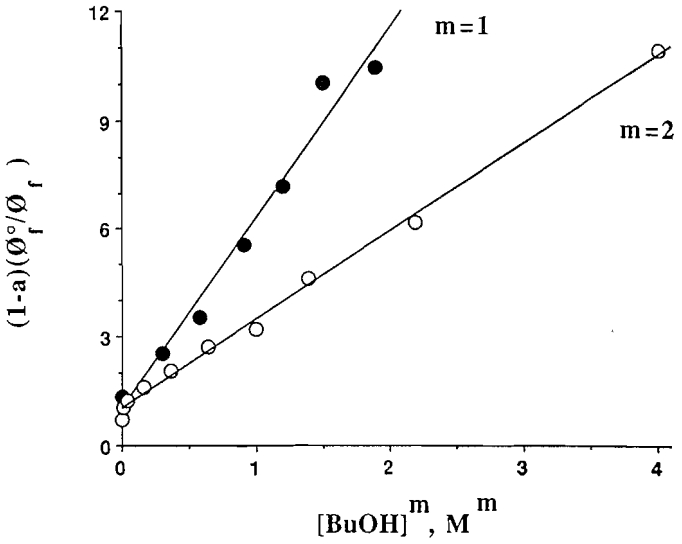


FIG. 4. Plot of $(1 - a)(\Phi_f^0/\Phi_f)$ vs. $[BuOH]^m$. Solid circles are data for C1 with $m = 1$ and open circles are data for C102 with $m = 2$. $[Dye] = 3.98 \times 10^{-5}$ M; [BuOH] = 0–2 M.

The fluorescence spectra of C1 and C102 in *n*BuOAc with different amounts of added *n*BuOH showed a distinct isosbestic wavelength for C1 (λ_{iso}^{fl} at 425 nm) but not for C102. The results suggest that with C1 but not C102, an equilibrium exists between the excited state dye and its alcohol complex. This would explain the presence of only one ASE band for C102. To assess the relative contribution of ground and excited state dye interaction in the alcohol to the fluorescence quenching by alcohol, the Stern–Volmer constant for fluorescence quenching of the "free" excited state dye by alcohol was determined by calculating the fraction of the total *absorbed light* and *fluorescence intensity* due to the free dye. The analysis was facilitated by exciting the dyes at their *absorption* λ_{iso}^{ab} and keeping the dye concentration constant. Under these conditions, the intensity of light absorbed by the system is independent of the alcohol concentration and remains constant. Knowing the ground state equilibrium constant, the fraction of the total light absorbed by the free dye can be calculated from the equation

$$[2] \quad a = (K_{gs}[ROH]^n)/(1 + K_{gs}[ROH]^n)$$

The fluorescence quantum yield ratio for the *uncomplexed* excited state dye, Φ_f/Φ_f^0, where $\Phi_f = \Phi_f^0$ at [ROH] = 0, can be obtained from the measured total fluorescence intensity ratios I/I^0, where I and I^0 are the intensities in the presence and absence of [ROH]:

$$[3] \quad I/I^0 = \Phi_f/\Phi_f^0 + \beta(\lambda)\Phi_{cx}/\Phi_{cx}^0$$

where $\beta(\lambda) = I_{cx}^{\infty}/I_f^0$ and I_{cx}^{∞} = intensity when the solvent has been completely replaced by the ROH, and I_f^0 = intensity for [ROH] = 0. From Φ_f/Φ_f^0 as a function of [ROH], K_{sv} can be obtained from

$$[4] \quad \Phi_f/\Phi_f^0 = (1 - a)/(1 + K_{sv}[ROH]^m)$$

The data from C1 and *n*BuOH (Fig. 4) displayed a good fit

Can. J. Chem. Downloaded from www.nrcresearchpress.com by 84.41.108.74 on 09/07/12
For personal use only.

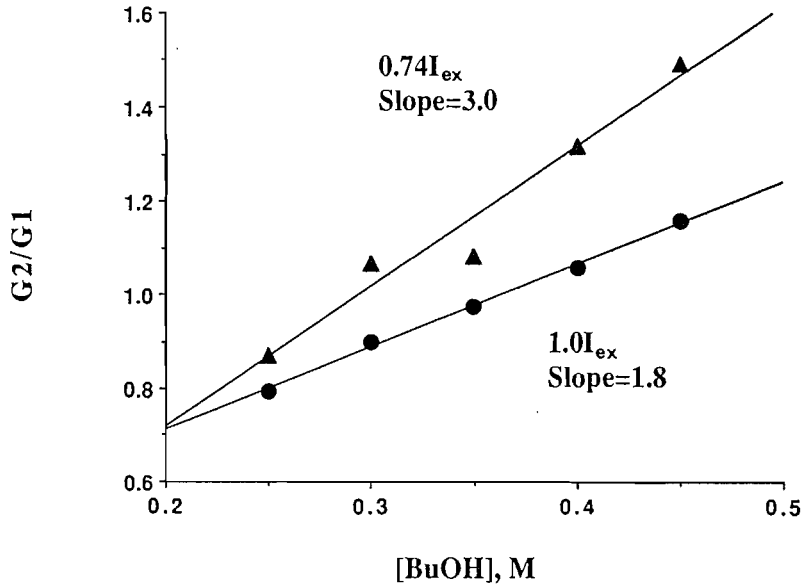


FIG. 5. Ratio of gains at 455 and 420 nm, G(455 nm)/G(420 nm) vs. [BuOH] for C1 in *n*BuOAc at two relative intensities.

to equation [4] with $m = 1$ and $K_{sv} = 5.3 \pm 0.8$ M^{-1}, which implies detachment of one alcohol molecules upon excitation of the complex, consistent with a large dipole change (*i.e.*, a highly dipolar C1*) and rupture of a H...N bond in C1*. The fluorescence results taken together with those from absorption show that *the principal quenching process by alcohol is dynamic quenching of the excited state dye* and not that due to ground state complexation.

The data presented thus far suggest that in the presence of a hydroxylic component such as alcohol, excited C1 and its hydrogen-bonded complex are in equilibrium:

$$C1^* + HOR = [C1..HOR]^*$$

and that the two ASE bands (at 420 and 455 nm) are due to free and complexed dye molecules. If this is correct, then the ratio of the gain factors for the two ASE bands, G(455 nm)/G(420 nm) should be linearly dependent on the alcohol concentration, and an excited equilibrium constant extracted from the data should be considerably larger than that associated with the ground state equilibrium. Neglecting absorption losses (7), the laser gain G is given by

$$[5] \quad G(\lambda) = \sigma_E(\lambda)N(\lambda)$$

where σ_E is the stimulated emission cross section (6), and N is the population of the fluorescing state. Thus the quantity σ(455 nm)N(455 nm)/σ(420 nm)N(420 nm) for the two ASE bands can be determined by measuring their laser gains (8).

The ASE gain of the C1 dye was determined by changing the gain length of a transversely excited of dye solution cell according to a method previously described (8). Using the same experimental arrangement as that used in determining the ASE spectra, the focussed line excitation image on the cell was masked so that the excitation length (the gain region) can be altered between L and $2L/3$ to give ASE intensities I_L and $I_{2L/3}$. The gain $G(\lambda)$ in this case is given by:

$$[6] \quad G(\lambda) = (3/L \ln \{\tfrac{1}{2}((R-1) + [(R-1)^2 + 4(R-1)]^{1/2})\}$$

where $R = I_L(\lambda)/I_{2L/3}(\lambda)$. By measuring R, and knowing L, the gain G can be calculated. A concentration of 7.4 mM of C1 dye in *n*BuOAc was used in the measurements.

The results (Fig. 5) for the two threshold- and maximum-limited relative excitation intensities (I_{ex}) show linear G(455 nm)/G(420 nm) — (*n*BuOH] plots and a smaller slope at the *higher laser intensity, i.e.*, a *lower* gain for the 455 nm ASE band. These results are in harmony with our model in which we expect (*a*) a linear dependance of G(455 nm)/G(420 nm) on [*n*BuOH]; and (*b*) a decreased population of the complexed species at the higher intensity, since it is well known that at high laser intensities incomplete equilibration occurs because of a decrease in lifetime of the initially formed species (12). The previous explanation for the long-wavelength ASE band (455 nm in *n*BuOAC) — that due to an enhanced transitory TICT-exciplex populations (6*a*) — implies a higher population at high I_{ex}, contrary to our results. We can also crudely estimate[5] the extrapolated zero-excitation intensity slope and hence K_{es} from

$$[7] \quad G(455 \text{ nm})/G(420 \text{ nm}) \approx N(455 \text{ nm})/N(420 \text{ nm}) = K_{es}[ROH]$$

The value of K_{es} (6.4 M^{-1}) from eq. [7] is considerably greater than that corresponding to the ground state equilibrium.

In conclusion, dual ASE from C1 in a polar environment originates from a quasi-excited state equilibrium concentration of H-bonded or acetonitrile-solvated complex. The results are inconsistent with a planar ICT and an evanescent laser-excited population of TICT–*n*BuOAc exciplex as an explanation for the previously reported dual ASE from C1 in *n*BuOAc. The present results and those from parallel ESA studies (7) of C1 in *n*BuOAc indicate a single non-90° conformational (with respect to the ring C—N bond) excited state species which is significantly more polar than that of C102. Of significance in the use of coumarin dyes in laser applications is the sensitive dependence of the ASE profile from C1 in dried *n*BuOAc on

[5]Assuming similar σ_E for the 422 and 455 nm bands. Difference in the σ_E (ref. 5) due to the factors λ^4, τ_f, and Φ_f is estimated to be <10%.

Can. J. Chem. Downloaded from www.nrcresearchpress.com by 84.41.108.74 on 09/07/12
For personal use only.

the concentration of hydroxylic co-solvent. This suggests that the lasing profile can be tuned by adding a small quantity of alcohol. In addition, this sensitive ASE dependence on hydroxylic co-solvents can be used to selectively probe for H-bonded excited-state dye molecules whose normal fluorescence is usually obscured by that from the free C1 dye. The results for the coumarin C1 dye illustrate that the strongly overlapping normal fluorescence bands can be experimentally "deconvolved" into two characteristic ASE bands due to distinct species of a fluorophore. The origin of the structures observed in the ASE of C1 in *n*BOAc at high to neat alcohol concentrations are not known but may be due to solvent structure.

Acknowledgements

We thank NSERC for funding this research, and PAFACC (UQAM) for the nitrogen laser.

1. Z. R. GRABOWSKI, K. ROTKIEWICZ, A. SIEMIARCZUK, D. J. COWLEY, and W. BAUMANN. Nouv. J. Chim. **3**, 443 (1979) and references therein.
2. W. RETTIG. Angew. Chem. Int. Ed. Engl. **25**, 971 (1986).
3. W. RETTIG and A. KLOCK. Can. J. Chem. **63**, 1649 (1985).
4. (*a*) G. J. JONES II, W. R. JACKSON, C-Y CHOI, and W. R. BERGMARK. J. Phys. Chem. **89**, 294 (1985); (*b*) G. J. JONES II, W. R. JACKSON, S. KANOKTANAPORN, and A. M. HALPERN. Opt. Commun. **33**, 315 (1980).
5. O. G. PETERSON, J. P. WEBB, W. C. MCCOLGIN, and J. H. EBERLY. J. Appl. Phys. **42**, 1917 (1971).
6. (*a*) V. MASILAMANI *et al.* Opt. Commun. **59**, 203 (1986); (*b*) V. MASILAMANI *et al.* **62**, 389 (1987); (*c*) A. RAMALINGAM, P. K. PALANISAMY, V. MASILAMANI, and B. M. SIVARAM. J. Photochem. Photobiol. A, **49**, 89 (1989); (*d*) V. MASILAMANI and B. M. SIVARAM. J. Lumin. **27**, 137 (1982).
7. R. W. YIP and Y-X WEN. J. Photochem. Photobiol. A, **54**, 263 (1990).
8. W. T. SILFVAST and J. S. DEECH. Appl. Phys. Lett. **11**, 97 (1967); C. V. SHANK, A. DIENES, and W. T. SILFVAST. Appl. Phys. Lett. **17**, 307 (1970).
9. A. DECLEMY, C. RULLIÈRE, and PH. KOTTIS. Chem. Phys. Lett. **101**, 401 (1983).
10. (*a*) B. D. ANDERSON, J. H. RYTTING, S. LINDENBAUM, and T. HIGUCHI, J. Phys. Chem. **79**, 2340 (1975); (*b*) L. ANDREOLI-BALL, M. COSTAS, P. PAQUET, D. PATTERSON, and M. S. VICTOR. Pure Appl. Chem. **61**, 1075 (1989); (*c*) J. KORPPI-TOMMOLA and R. W. YIP. Can. J. Chem. **59**, 191 (1981); (*d*) J. KORPPI-TOMMOLA, J. Mol. Struct. **40**, 13 (1977).
11. B. SKALSKI, D. M. RAYNER, and A. G. SZABO. Chem. Phys. Lett. **70**, 587 (1980).
12. E. LIPPERT. *In* Organic molecular photophysics. Vol. 2. *Edited by* J. B. Birks. J. Wiley, New York. NY. 1975. p. 7.

Can. J. Chem. Downloaded from www.nrcresearchpress.com by 84.41.108.74 on 09/07/12
For personal use only.

Voltammetric determination of Al(III) with adsorptive preconcentration of the pyrocatechol violet complex

DRAGIC V. VUKOMANOVIC, JOHN A. PAGE,[1] AND GARY W. VANLOON
Department of Chemistry, Queen's University, Kingston, Ont., Canada K7L 3N6
Received January 11, 1991

DRAGIC V. VUKOMANOVIC, JOHN A. PAGE, and GARY W. VANLOON. Can. J. Chem. **69**, 1418 (1991).

A method is described for the determination of aluminium in aqueous samples by linear scan voltammetry after adsorptive accumulation of the pyrocatechol violet (PCV) complex. A pH 6.5 triethanolamine/perchloric acid electrolyte is used for the determination with adsorption onto a mercury drop electrode at −0.50 V (vs a Ag/AgCl/satd KCl reference). Scanning cathodically after adsorption gave a current peak at −0.70 V for reduction of adsorbed PCV and a peak at −0.90 V for reduction of the adsorbed Al–PCV complex. The peaks were well resolved. Using 1.0 μM PCV and a 60 s adsorption period gave linear calibration curves for Al in the range 1 to 25 ng mL^{-1} Al. The detection limit was 0.1 ng mL^{-1} Al. For analysis, calibration by the method of standard additions is required. Most other metal species do not interfere, but vanadium (V(IV) and V(V)) forms a complex with PCV that is adsorbed and reduced at the same potential as Al–PCV. The interference may be eliminated by complexation of the V with citrate. Al and V present together may be determined by analysis in the absence of citrate (total: Al + V) and in the presence of citrate (Al); V is determined as the difference in the two values.

The analysis of a range of samples with Al concentrations from 6 ng mL^{-1} to 3 μg mL^{-1} gave results which were in good agreement with those obtained by other methods.

Key words: aluminium, pyrocatechol violet, adsorption, voltammetry, environmental.

DRAGIC V. VUKOMANOVIC, JOHN A. PAGE et GARY W. VANLOON. Can. J. Chem. **69**, 1418 (1991).

On décrit une méthod de détermination de l'aluminium en solutions aqueuses par voltamétrie à balayage linéaire après une accumulation de l'adsorption du complexe violet de pyrocathécol (PCV). On utilise un électrolyte de type triéthanolamine/acide perchlorique à un pH de 6,5 pour effectuer cette détermination avec adsorption sur une électrode à goutte de mercure à −0,50 V (par rapport à une électrode de réference de type Ag/AgCl/KCl saturé). Le balayage de la cathode après l'adsorption donne un pio de courant à −0,70 V pour la réduction du PCV adsorbé et un pio à −0,90 V pour la réduction du complexe Al–PCV adsorbé. Les pice sont bien résolus En utilisant 1,0 μM de PCV avec une période d'adsotion de 60 s on obtient des courbes d'étalonnage linéaires pour le Al avec des concentrations de Al allant de 1 à 25 ng mL^{-1}. La limite de détection est de 0,1 ng mL^{-1}. Il faut utiliser la méthode des additions standards pour l'étalonnage en vue de l'analyse. Cette détermination ne subit pas l'influence de la plupart des autres métaux mais le vanadium V(IV) et le vanadium V(V) forment un complexe avec le PCV qui est adsorbé et réduit au même potentiel qui le complexe Al–PCV. On peut éliminer cette interférence en complexant le vanadium avec le citrate. On peut déterminer par analyse en l'absence de citrate l'aluminium et le vanadium présents (Al + V total) et en présence du citrate on déterminer l'aluminium uniquement. La différence entre ces deux valeurs donne alors le vanadium seul. L'analyse d'un certain nombre d'échantillons contenant des concentrations en aluminium allant de 6 ng mL^{-1} à 3 μg mL^{-1} donne des résultats qui s'accordent très bien avec ceux obtenus par d'autres méthodes.

Mots clés : aluminium, pyrocathécol violet, adsorption, voltamétrie, environmental.

[Traduit par la rédaction]

Introduction

Aluminium analysis at the trace level is of importance because of the possible human and environmental toxic properties of the element. However, direct voltammetric methods for the element are limited by the difficulty of reduction of the Al(III) species and a concurrent reduction of hydrogen ion from aqueous acid solution at a Hg electrode.

While there are no anodic stripping methods (ASV) for Al, adsorptive accumulation followed by a voltammetric measurement of the adsorbed species (AdV) can be used in cases where the metal species itself is not readily determined by ASV. In the usual form of AdV, an excess of a ligand is used to convert the analyte species to a complex that can be adsorbed on the surface of a microelectrode. The adsorption is carried out in such a way that the rate of accumulation on the electrode is proportional to the concentration of the analyte species in the solution. The adsorbed species is then measured, usually by linear scan voltammetry (LSV), with a current peak for oxidation or reduction of the coordinate ligand. Some of the excess free ligand may also be adsorbed and undergo reaction in the LSV step and this must not interfere with the analyte measurement. The method must be calibrated under conditions of use, usually by standard additions of the analyte species. The method was first used for the determination of Ni(II) as the dimethylglyoxime complex (1) and AdV procedures have now been published for some 20 elements with detection limits in the range 0.001 to 1 ng mL^{-1} of the element (2). The method has also been used for the determination of adsorbable organic species (3).

Two AdV methods have been described for Al(III). In one (4), Solochrome Violet RS (SVRS), a di-*o*-hydroxy phenyl azo reagent is used to complex the Al(III). Adsorption on a Hg drop electrode at −0.45 V (vs. Ag/AgCl/satd. KCl) and subsequent LSV gives a current peak at −0.61 V for reduction of the metal complex. Using a pH 4.5 acetate electrolyte and 120 s adsorption from stirred solution, analysis was carried out in the range 0.27 to 11 ng mL^{-1} Al. The estimated detection limit, based on 10 min adsorption, was 0.15 ng mL^{-1}. It was necessary to heat the sample solution to 90°C to ensure quantitative formation of the metal complex. If significant concentrations of Cu(II) and Fe(III) were present in the sample, these interfered in the analysis.

[1]To whom correspondence should be addressed.

Can. J. Chem. Downloaded from www.nrcresearchpress.com by 84.41.108.74 on 09/07/12
For personal use only.

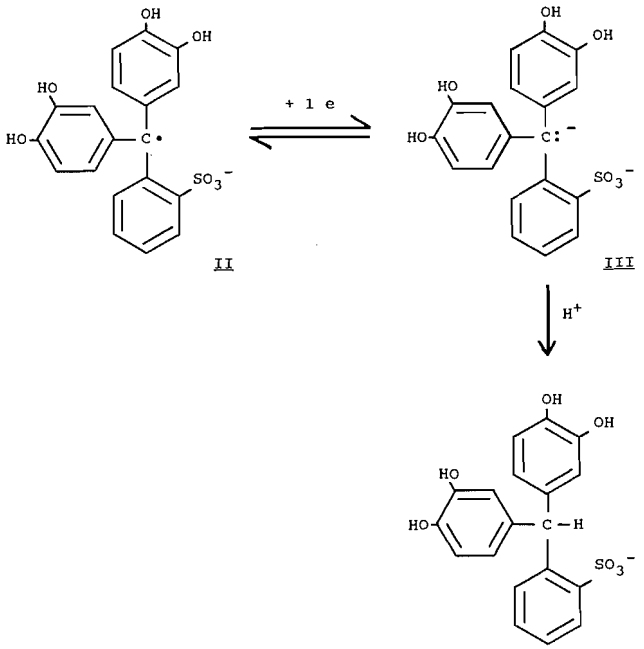


FIG. 1. Structure and ionization of pyrocatechol violet (PCV) — H_4L and H_3L^- forms only.

In the second method (5), 1,2-dihydroxy anthraquinone-3-sulfonic acid (DASA) is used as the ligand. The metal complex adsorbs on a Hg drop electrode at −0.90 V (vs. Ag/AgCl/satd. KCl) and gives a current peak for reduction of the complex near −1.1 V, depending on the electrolyte. The measurement was carried out at pH 7.1 in a buffered electrolyte. The detection limit, based on 45 s adsorption from stirred solution, was 0.03 ng mL^{-1} Al, while the sensitivity was 7 na (ng $mL^{-1})^{-1}$. A serious interference was identified in Zn(II) but this element could be masked by the addition of ethylenediaminetetracetate (EDTA). The method was employed for the analysis of aquatic samples, but surface active organic species were found to interfere.

This paper reports on the use of pyrocatechol violet (PCV: 3,3′,4′-trihydroxyfuchsone-2″-sulfonic acid, H_4L) for the determination of Al(III). The reagent is a member of a class of sulfonephthalein compounds and the structure can be written either as a quinone or as a zwitterion (6, 7) as shown in Fig. 1. The PCV is a strong acid with respect to the ionization of the H_4L, but a weak acid with respect to further ionization. The pK_a values for ionization of the —OH protons in aqueous solution at 25°C are $H_3L^- = 7.8$, $H_2L^{2-} = 9.8$, and $HL^{3-} = 11.7$, respectively (8). The reagent forms complexes with metal ions by coordination through the —OH groups. Complexes with metal ions coordinated to both catechol rings of the PCV have been reported as well as complexes with a single metal ion coordinated to one, two, and three PCV groups. Reported values (8) for the stepwise coordination of Al(III) to the L^{4-} form of PCV are log $K_1 = 25.1$, log $K_2 = 22.3$, log $K_3 = 20.7$ and an Al_2L_1 complex with log $K_{21} = 24.1$ has also been reported. PCV has been used for the spectrophotometric determination of a number of metal ions (9) and is recommended for the spectrophotometric determination of Al(III) (10–12). A pH of 6.1 to 6.2 is optimal for the determination. The complex is readily formed at room temperature and is stable in neutral solutions. Voltammetric studies of PCV and its metal complexes do not appear to have been reported.

Experimental

A Princeton Applied Research Corporation Model 174A Polarographic Analyzer was employed with a Model 303 Static Mercury Drop Electrode. The voltammograms were recorded using a Hewlett–Packard Model 7004A X–Y recorder. The three electrode system consisted of a 15 mL quartz glass cell with a static Hg electrode, a Pt auxiliary electrode and a Ag/AgCl/satd. aq KCl reference electrode separated from the analytical solution by a Vycor frit bridge. For polarography, a 2 s drop life was employed. The electrolyte was stirred as required using a 0.9 cm Teflon "Spin Fin" driven at a rotation rate of 500 Hz. All potentials reported are relative to the Ag/AgCl reference electrode. The usual AdV experiment involved adsorption for 60 s from stirred solution on a Hg drop (size "M", $A = 0.018$ cm^2) at −0.50 V. The stirring was turned off and after a 10 s pause, the voltammetric measurement was made by scanning the electrode potential from −0.50 to −1.00 V at 0.05 V s^{-1}.

The electrolytes were deaerated with N_2 gas and blanketed with the gas throughout the experiment. The N_2 gas was CANOX "oxygen free" grade purified by passage over hot BASF catalyst (30% by wt. Cu on support material). The sample and cell manipulations were carried out in a laminar flow clean hood with a high efficiency air filter. The glassware was cleaned by soaking in 3 M aq. HNO_3, rinsed with good quality distilled water and conditioned with pure electrolyte before use. Losses of Al(III) were found to be significant with freshly cleaned "active" vessels.

The PCV was a reagent grade chemical supplied by BDH Chemicals. The ^1H NMR spectrum indicated a pure material. For AdV, a stock 0.10 mM PCV solution was prepared by dissolving a weighed amount of the reagent (pure material assumed) in distilled water. The solution was stable for periods exceeding 6 weeks.

The stock Al(III) solution was prepared by dissolution of 2.006 g of Al turnings (99.8%) in 50 mL of 12 M hydrochloric acid and dilution to exactly 2 L with distilled water. A 1.003 μg mL^{-1} Al standard for analytical work was prepared by dilution of the stock solution with a pH 2.0 HCl electrolyte.

The supporting electrolyte solutions were prepared from reagent grade chemicals. The triethanolamine (TEA) was a 97% by wt. reagent. The stock 0.5 M triethanolamine perchlorate electrolyte ((TEAH)(ClO_4) = THX) was made up by addition of 1.0 M aq. TEA to 1.0 M aq. $HClO_4$ to give a pH of 6.5 (near equal volumes). The stock 0.5 M HOAc/0.5 M NaOAc buffer solution was prepared by addition of aq. NaOH to aq. HOAc to give a pH of 4.7. Other buffer systems including BES (*N*,*N*-bis(2-hydroxyethl)-2-aminoethane sulfonic acid), $NH_2OH.HCl$ and HEPES, MES, PIPES, TRIS and BIS-TRIS (13) were also investigated. These systems were prepared from reagent grade chemicals as needed.

Results and discussion

I. Pyrocatechol violet (PCV)

Polarography of a 0.10 mM PCV solution in a 0.020 M THX electrolyte at pH 6.5 gave two reduction steps with $E_{1/2}$ values of −0.70 V and −1.05 V. The limiting current of the first (principal) wave was about 6/7 that of the total limiting current of the two waves. Polarography of Cd(II) in a 0.10 M KCl electrolyte gave a limiting current value ~5% greater than the total limiting current observed for the same molar concentration of PCV, indicating that the overall reduction of the PCV was a two-electron process.

The behaviour is consistent with that observed in an electrochemical study of some closely related species (7, 14). The reduction mechanism proposed in these definitive studies is shown in Fig. 2. In neutral or slightly acidic solutions the PCV will be largely present as a H_3L^- species. This species undergoes protonation to species I which then undergoes a one-electron reduction to a radical species II. The radical can undergo a further one-electron reduction to species III or it

Can. J. Chem. Downloaded from www.nrcresearchpress.com by 84.41.108.74 on 09/07/12
For personal use only.

Can. J. Chem. Downloaded from www.nrcresearchpress.com by 84.41.108.74 on 09/07/12
For personal use only.

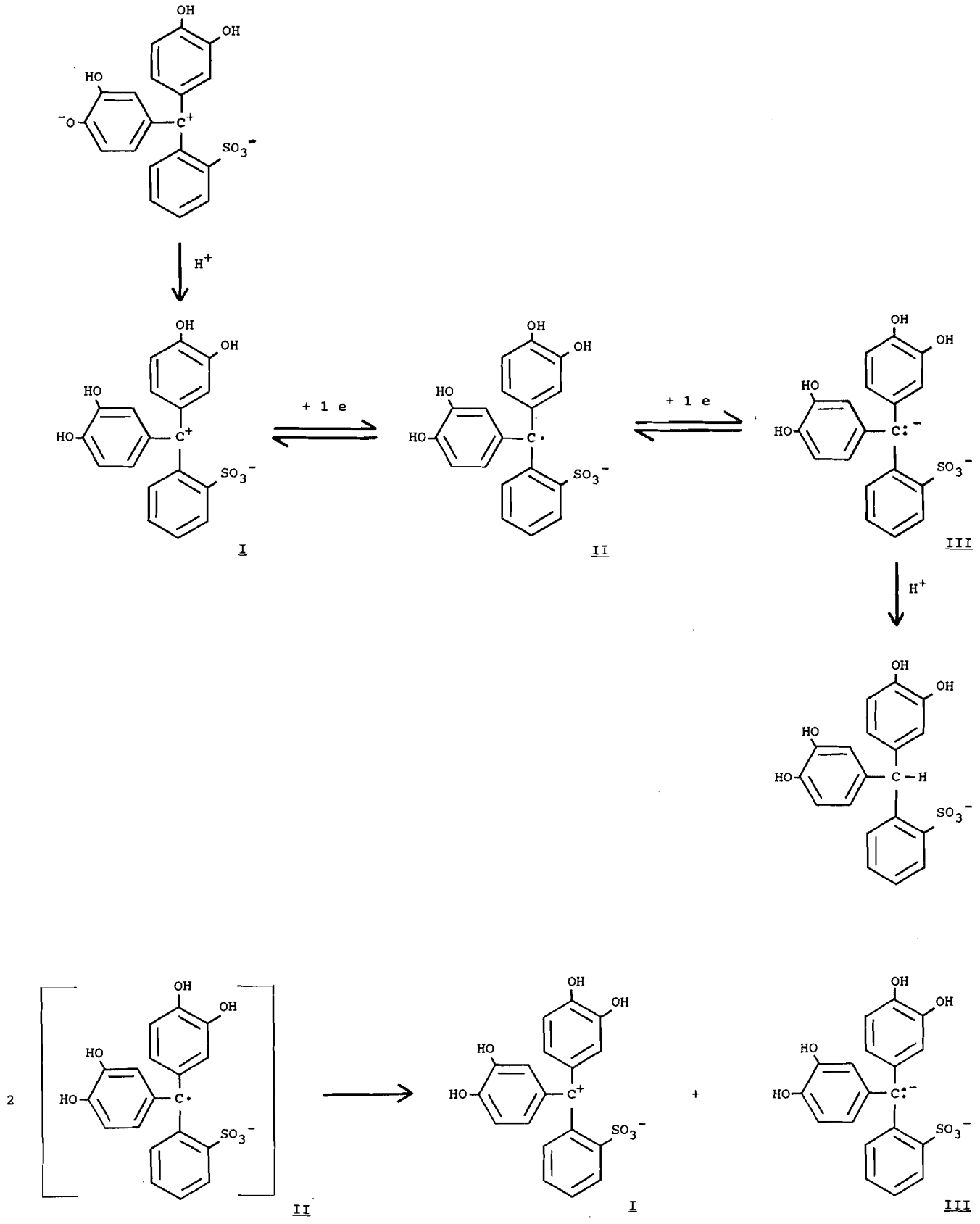


FIG. 2. Reduction mechanism for pyrocatechol violet (PCV) — adapted from that for phenol red (7, 14).

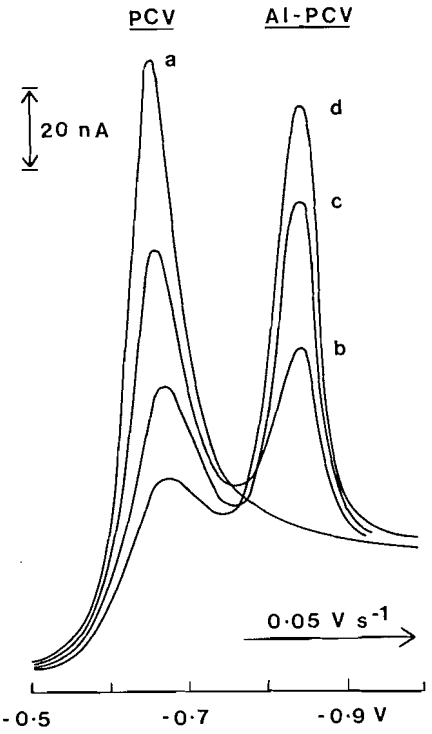


FIG. 3. Reduction of adsorbed PCV and Al–PCV: I vs E; 0.020 M THX electrolyte, pH 6.5, 60 s ads 0.5 μM PCV; *a*: 0, *b*: 5, *c*: 10, *d*: 15 ng mL^{-1} Al(III).

can disproportionate to give III and regenerate I. The stability with respect to disproportionation is dependent upon the substituents present and differs from member to member in a series of sulfonephthaleins. In the final step, species III is protonated to give a stable reduced H_5L^- species. The first polarographic wave observed with PCV represents the formation of III via a one-electron reduction and disproportionation of the intermediate while the second wave represents the formation of III by direct reduction of the intermediate formed in the first step. Controlled potential reduction at potentials on the plateau of either step leads to a two-electron reduction of the PCV.

The behaviour of adsorbed PCV is shown in Fig. 3*a*. The sharply defined cathodic peak is expected for the reduction of a surface layer of adsorbed PCV (15). At pH 6.5, the peak was independent of the adsorption potential over the range 0.00 to −0.50 V and independent of the ionic strength of the THX electrolyte over the range 0.010 to 0.10 M. With increasing electrolyte pH, the peak potential shifted to more negative values as shown in Fig. 4*a* indicating consumption of hydrogen ion in the reduction process. There was a slight increase in the peak current and little change in peak shape with increasing pH. The peak width at half-maximum was ~0.08 V.

The AdV behaviour was dependent on adsorption time as shown in Fig. 5. Initially, the current peak increased as expected for adsorption at a rate dependent upon the PCV concentration, but the peak grew only to a maximum then decreased with time. The maximum was dependent upon the concentration of PCV in the solution. There was no change in peak potential or shape over the range of adsorption times. In other experiments, the PCV was adsorbed from stirred solution for various times, then the electrode was held at the adsorption potential for up to 300 s in an unstirred electrolyte before reduction of the adsorbed material. A negligible additional adsorption of PCV would be expected in the waiting period. The additional residence time of the PCV on the electrode did not affect the PCV peak, indicating that the adsorbed PCV was stable. Extrapolation of the response at low adsorption times indicates that at the higher surface concentrations some of the adsorbed PCV becomes electroinactive. Given the quinoid nature of the PCV, the deactivation may result from a polymerization of the adsorbed species initiated by a radical intermediate in the reduction process.

II. Aluminium(III)/pyrocatechol violet (Al–PCV)

The combining ratio of Al with PCV in the THX electrolyte at pH 6.5 was determined spectrophotometrically. The total PCV concentration was maintained at 0.05 mM and Al(III) was added to excess. The PCV absorption (λ_{max} 444 nm) decreased while that of the Al–PCV (λ_{max} 596 nm) grew with a well-defined isosbestic point at 515 nm. Under these conditions, the mole ratio of Al and PCV in the complex was 1:1 as determined from the changes in the peak absorbance of either the PCV or the Al–PCV.

Direct current polarography of 0.10 mM PCV/0.056 mM Al(III) in a 0.050 M THX electrolyte at pH 6.5 gave two reduction waves with $E_{1/2}$ values of −0.64 and −1.02 V. The steps were near equal while the total limiting current was equal to that for the same concentration of free PCV. Increasing the Al(III) concentration resulted in a decrease in the first step and a growth in the second step, with the total limiting current constant. The first wave results from the reduction of free PCV, while the second represents the reduction of complexed PCV, both presumably by an overall two-electron process.

The AdV behaviour of Al–PCV is shown in Fig. 3*b*, *c*, *d*. The adsorbed Al–PCV was more difficult to reduce than adsorbed PCV but both current peaks were well defined. Addition of Al(III) to the PCV solution resulted in a decrease in the AdV peak for PCV and an increase in the Al–PCV peak. The reaction between the PCV and Al(III) was rapid. The peak height data shown in Fig. 6 indicates a 1:1 mole combining ratio and similar adsorption and reduction processes for free and complexed PCV.

The AdV peak current for Al–PCV increased linearly with scan rate over the range 0.02 to 0.5 V s^{-1}. Triangular wave voltammetry gave no evidence of anodic processes corresponding to oxidation of the products of reduction. The peak potential for reduction of the absorbed complex shifted to more negative values with increasing pH as shown in Fig. 4*b*. The separation of the peak potentials for PCV and Al–PCV was a maximum near pH 6.5 The Al–PCV peak from a given concentration of added Al(III) was a maximum at pH 6.5 as shown in Fig. 7. The decrease at high pH may result from partial hydrolysis of the added Al(III) while that at low pH may be due to an incomplete reaction of the Al(III) with PCV. At pH 6.5, increasing the concentration of the THX electrolyte resulted in a slight decrease in the Al–PCV peak current.

The AdV peaks for PCV and Al–PCV were dependent upon the adsorption time as shown in Fig. 8. With a fixed PCV concentration, the Al–PCV peak grew with time to a limiting value dependent upon the Al(III) concentration. At short times there was a peak for reduction of adsorbed PCV but this peak grew to a maximum and then decreased with adsorption time.

The AdV peak corresponding to surface saturation with Al–

Can. J. Chem. Downloaded from www.nrcresearchpress.com by 84.41.108.74 on 09/07/12
For personal use only.

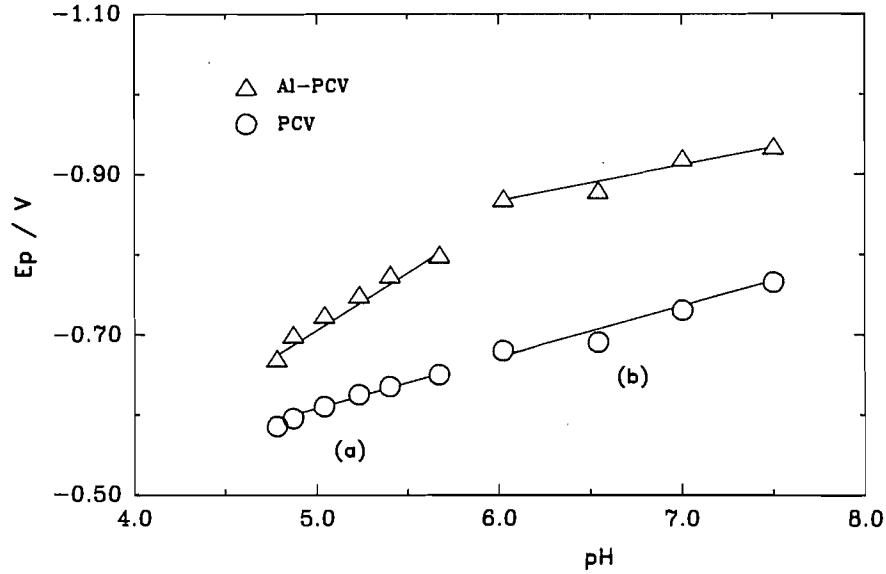


FIG. 4. Reduction of adsorbed PCV and Al–PCV: E_p vs pH; (*a*) acetate and (*b*) THX electrolytes, 60 s ads, v = 0.05 V s^{-1} 0.5 μM PCV/10 ng mL^{-1} Al(III).

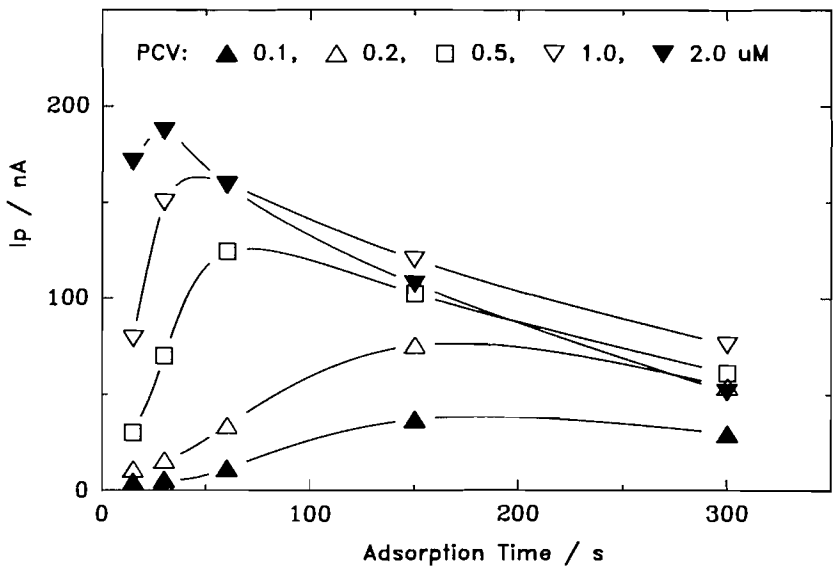


FIG. 5. Reduction of adsorbed PCV: I_p vs adsorption time; 0.020 M THX electrolyte, pH 6.5, 60 s ads, v = 0.05 V s^{-1}.

PCV was a function of the electrolyte composition. In the case of a 4.0 μM PCV/3.0 μM Al(III) solution, the peak for the Al–PCV reduction limited at 295 nA and 0.56 μC with a scan rate of 0.05 V s^{-1}. Assuming a two-electron reduction, this gives 1.8×10^{12} molecules of Al–PCV on the 0.018 cm^2 Hg drop (1.04 nm^2 per Al–PCV). The area is near that calculated for surface saturation with other metal complexes in AdV (1).

III. pH

While pH 6.5 is optimal with good resolution of the PCV and Al–PCV peaks and good sensitivity with respect to added Al(III), the buffer capacity of the THX is minimal at this pH (pK_a $TEAH^+$ = 7.8). Experiments using other buffered electrolytes were carried out to investigate the effect of buffer capacity. At pH 6.5, PIPES (pK_a = 6.8), MES (pK_a = 6.2), TRIS (pK_a = 8.1), and $NH_2OH.HCl$ (pK_a = 6.0) electrolytes gave peak resolution and sensitivity approaching that of the THX, while BES (pK_a = 7.2), BIS-TRIS (pK_a = 6.8), and HEPES (pK_a = 7.6) electrolytes gave poor resolution of the PCV and Al–PCV reduction peaks. In no case did the increased buffer capacity of the solution produce better defined or separated peaks for the reduction of the adsorbed species.

Aluminium analysis

For analysis of aqueous samples in the range 3 to 10 ng mL^{-1} Al, a pH 6.5 electrolyte, 0.020 M in THX with 1.0 μM added PCV is recommended. The pH adjustment should be made by dropwise addition of 0.05 and 0.01 M aq. $HClO_4$ or TEA solutions to the sample as required. Samples with high Al(III) concentrations should be diluted before pH adjustment to bring them within the recommended concentration range. Care should be taken to avoid local excesses of base that might produce irreversible hydrolysis of the Al(III). The pH adjustment is followed by the addition of 400 μL of 0.5

Can. J. Chem. Downloaded from www.nrcresearchpress.com by 84.41.108.74 on 09/07/12
For personal use only.

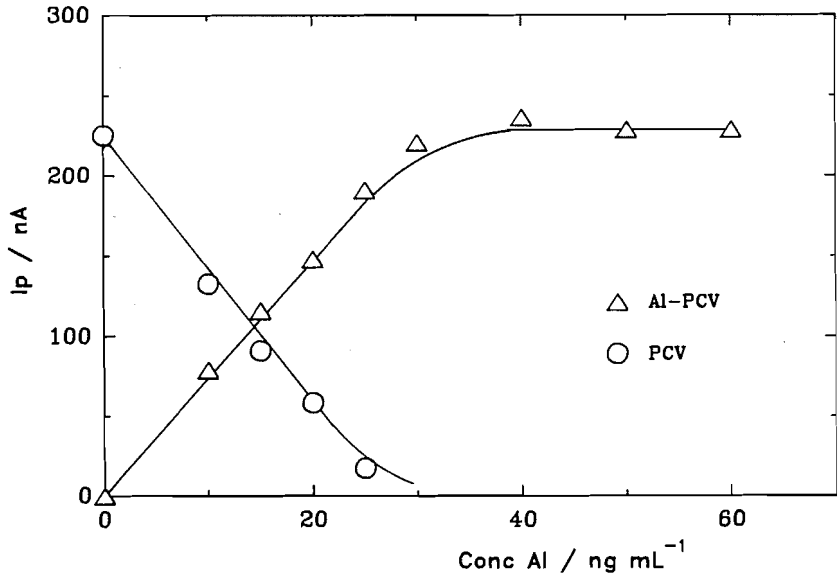


FIG. 6. Reduction of adsorbed PCV and Al–PCV: I_p vs. conc. Al(III); 0.020 M THX electrolyte, pH 6.5, 60 s ads, $\nu = 0.05$ V s^{-1}, 1.0 μM PCV with added Al(III).

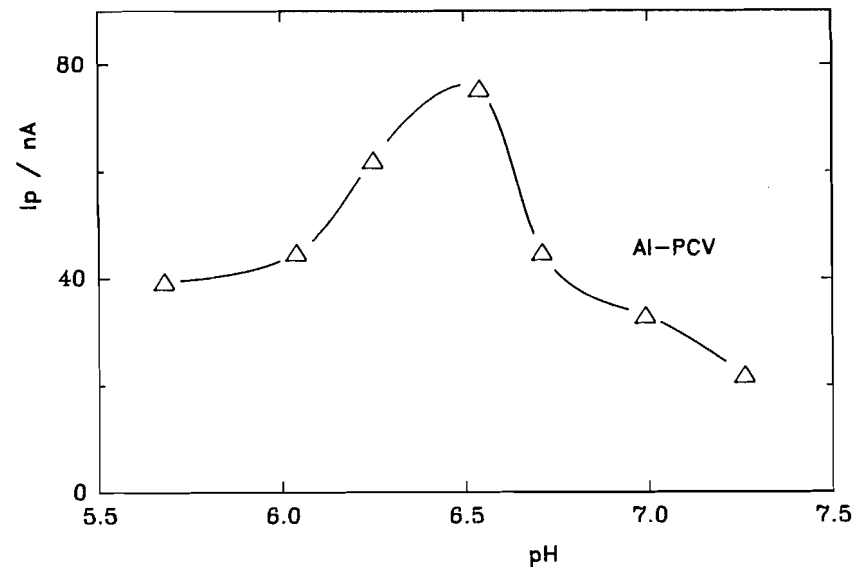


FIG. 7. Reduction of adsorbed Al–PCV: I_p vs. pH; 0.020 M THX electrolyte, 60 s ads, $\nu = 0.05$ V s^{-1}, 0.5 μM PCV/10 ng mL^{-1} Al(III).

M THX (pH = 6.5) and 100 μL of 100 μM PCV solution per 10 mL of electrolyte. The final pH should be in the range 6.0–7.0.

The AdV should be carried out as described in the Experimental section with the Al–PCV peak measured from an estimated baseline. Calibration of the method should be by standard additions of Al(III). Three standard additions with a single AdV measurement after each addition are recommended. The total concentration of Al(III) after the additions should not exceed 20 ng mL^{-1}.

In the absence of interferences, the conditions give an amount of PCV in the sample in excess of the Al(III). If species such as Cu(II) and Pb(II) that coordinate with the ligand are present, the amount of added PCV must be increased. A peak for PCV must persist through the analysis and standard additions of Al(III). The 60 s adsorption gives a low fractional surface coverage of the electrode with adsorbed species. The recommended pH gives a good separation of the peaks for PCV and Al–PCV.

Using standards prepared from the standard Al(III) solution, the method gave a linear calibration curve over the range 1 to 20 ng mL^{-1} Al. The slope of the calibration line (sensitivity) was 10 nA (ng mL^{-1})$^{-1}$. The detection limit (DL) was estimated by analyses of a 3 ng mL^{-1} Al standard. The standard deviation of the signal for 10 replicate analyses was ±0.30 nA, giving a detection limit of 0.10 ng mL^{-1} based on a protection factor of 3 (16). For samples with low Al(III) concentrations (<1 ng mL^{-1}), the PCV concentration may be reduced and the adsorption time increased to enhance the Al–PCV signal.

Interferences

A number of metal ions were tested for interference in the

Can. J. Chem. Downloaded from www.nrcresearchpress.com by 84.41.108.74 on 09/07/12
For personal use only.

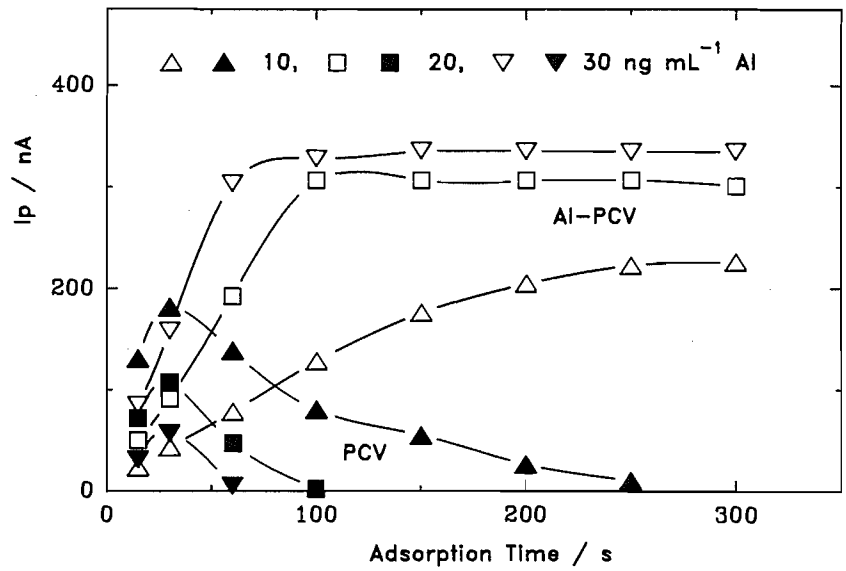


FIG. 8. Reduction of adsorbed PCV and Al–PCV: I_p vs. adsorption time; 0.020 M THX electrolyte, pH 6.5, 60 s ads, v = 0.05 V s^{-1}, 4.0 μM PCV with added Al(III).

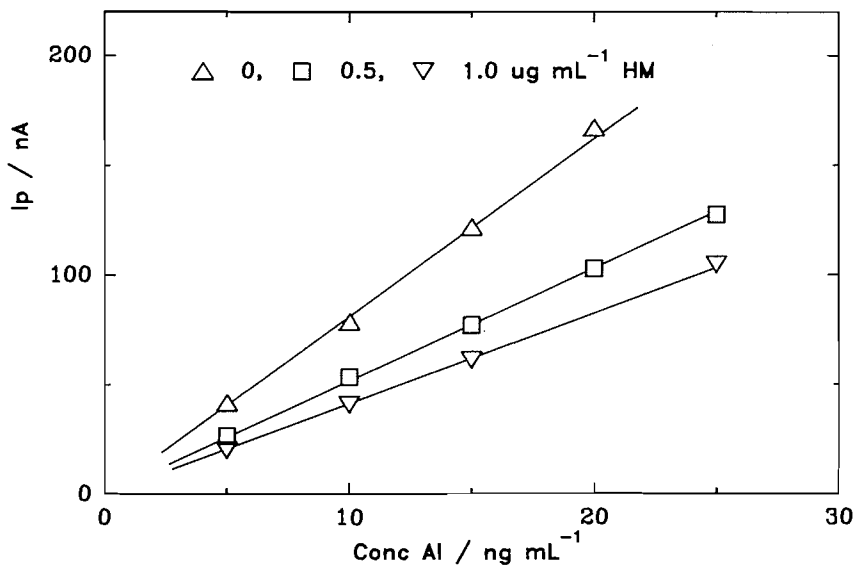


FIG. 9. Adsorption and reduction of Al–PCV: I_p vs. conc. Al(III), 0.020 M THX electrolyte, pH 6.5, 60 s ads, v = 0.05 V s^{-1}, 1.0 μM PCV with added humic material.

determination using a 1.0 μM PCV electrolyte with 10 ng mL^{-1} added Al(III), with addition of various metal ions.

Of the species tested, Ag(I), Cd(II), Co(II), Fe(III), Hg(II), Mn(II), Mo(VI), Ni(II), Pb(II), Sn(II), and Zn(II) did not interfere at concentrations up to 0.2 μg mL^{-1}. The addition of Cr(III), Th(IV), and Ti(III) produced small shifts in the baseline but did not otherwise interfere at concentrations up to 0.2 μg mL^{-1}. The addition of Ga(III), In(III), Sn(II), and U(VI) gave peaks overlapping those for PCV and Al–PCV but the sensitivity was low and interference significant only when their concentrations were greater than 0.01, 0.13, 0.2, and 0.02 μg mL^{-1}, respectively, representing unusually high levels for aqueous environmental samples. The addition of Cr(VI) produced an interfering peak at −0.90 V, but Cr(III) did not interfere at concentrations up to 0.2 μg mL^{-1}. Reduction of the Cr(VI) by the addition of $NH_2OH.HCl$ (200 μg mL^{-1} sample) removed the interference.

Added Cu(II) and Pb(II) were found to form metal complexes that could be adsorbed and reduced. Adsorption at −0.05 V gave peaks for reduction of adsorbed Cu–PCV at −0.21 V, Pb–PCV at −0.47 V, PCV at −0.70 V and Al–PCV at −0.90 V, suggesting simultaneous analysis. The Cu–PCV and Pb–PCV were more readily reduced than PCV itself indicating reduction of the metal centre of the absorbed complex. With 60 s adsorption, the sensitivity for Cu, Pb, and Al was 10, 3, and 10 nA (ng mL^{-1})$^{-1}$, respectively. In the determination of Al(III) with adsorption at −0.50 V, Cu–PCV and Pb–PCV species would be adsorbed and simultaneously reduced and would not interfere in the determination, provided the PCV was sufficient for complexation of all species.

Can. J. Chem. Downloaded from www.nrcresearchpress.com by 84.41.108.74 on 09/07/12
For personal use only.

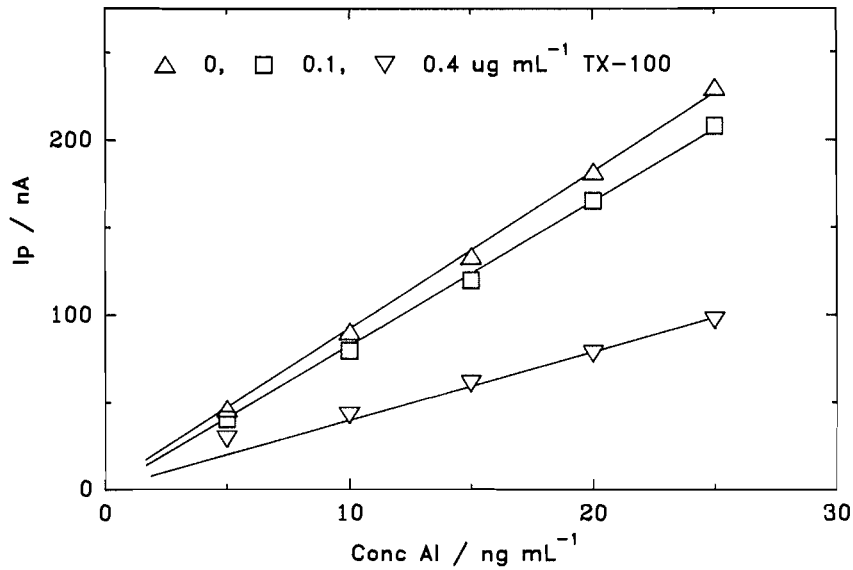


FIG. 10. Adsorption and reduction of Al–PCV: I_p vs. conc. Al(III), 0.020 M THX electrolyte, pH 6.5, 60 s ads, v = 0.05 V s^{-1} 1.0 μM PCV with added Triton X-100.

Both V(IV) and V(V) were found to give a well-defined peak with PCV at the same peak potential as that for reduction of adsorbed Al–PCV. In the absence of Al(III), the peak was suitable for V analysis. Using a 60 s adsorption, the sensitivity for V was 4 nA (ng mL^{-1})$^{-1}$.

The method was also tested for interference from various anionic species. The testing was performed using a 1.0 μM PCV solution with 10 ng mL^{-1} added Al(III), with the anions added as solutions of their Na salts.

The addition of Cl^-, SO_4^{2-}, and PO_4^{3-} at concentrations up to 2 μg mL^{-1} did not alter the response with respect to Al. The addition of F^-, oxalate, and tartrate decreased the sensitivity without shifting the potential of the PCV and Al–PCV reduction peaks. Additions of Al(III) in the presence of up to 2 μg mL^{-1} of each of these (six) species gave linear calibration curves indicating analysis was possible by the method of standard additions. With citrate, there was no peak for Al–PCV in the presence of 1 μg mL^{-1} of the anion and it appeared that complexation of the Al(III) prevented the formation of the PCV complex. The AdV peak for V–PCV was not affected by citrate. It is possible to determine V(IV) and V(V) without interference from Al(III) in the presence of citrate and stepwise analysis for both elements is also possible. The combined Al–PCV and V–PCV peak is first recorded and standard additions of Al(III) are made. Sodium citrate is then added to the sample (1 mg L^{-1}) to complex the Al(III) and the V-PCV peak recorded. The V-PCV peak is then used to provide the reference value for extrapolation of the standard addition data to give the Al(III) concentration. The concentration of the V species can then be determined using standard additions of a V species in the presence of citrate.

Surface active materials present in the electrolyte are also a potential interference. Figures 9 and 10 show that while a linear calibration can be obtained for Al in the presence of surface active materials, the sensitivity is reduced. On a weight scale the suppressive effect of Triton X-100, a nonionic alkylphenylethoxylate surfactant was greater than that of a natural humic material. Analysis by standard addition calibration would appear to be valid in the presence of the surface active agents.

TABLE 1. Analysis of natural water samples

Source	Al(III)/(ng mL^{-1})	Note
1. Lake Ontario water	6.2 ± 1.6	
2. Tap water (Kingston)	95.7 ± 13	100.3[a]
3. SLRS-1	18.5 ± 0.8; 18.2 ± 2.1	23.5[b]
Source	**Al(III)/(μg mL^{-1})**	
4. Soil pore water #1 (pH 7)	1.45 ± 0.12; 1.51 ± 0.19; 1.51 ± 0.61	
	2.69 ± 0.06[c]	3.3[a]
5. Soil pore water #2 (pH 4)	1.34 ± 0.23; 1.36 ± 0.38	1.2[a]
6. Soil pore water #3 (pH 4)	3.37 ± 0.49; 3.16 ± 1.3	3.4[a]

[a]Comparative value by ICP-MS.
[b]Certificate value for St. Lawrence River Water Standard Material.
[c]Acidification of neutral pore water to pH 2 followed by analysis at pH 6.5.

Analysis

Using the standard procedure, a number of water samples representing a range of electrolytes were analyzed for Al(III) with the results tabulated in Table 1. The tap waters were drawn from the local water supplies while the pore waters were obtained in a soil chemistry study (17). One sample was a St. Lawrence River Water Sample (SLRS-1) certified by the Marine Analytical Chemistry Standards Program of the National Research Council of Canada. The samples were diluted with distilled water before analysis to bring them within the recommended concentration range for analysis.

In each case the analyses were carried out at pH 6.5 with measurements on the sample and on the sample after each of three standard additions. Each measurement was repeated 4 times (4 × 4 = 16 data points per analysis). The confidence interval reported represents the uncertainty in the result derived from extrapolation of the calibration data. Compara-

Can. J. Chem. Downloaded from www.nrcresearchpress.com by 84.41.108.74 on 09/07/12
For personal use only.

tive ICP-MS data obtained on the samples was generally in good agreement with the AdV results. In the case of Sample #4, a soil pore water of neutral pH, analysis at pH 6.5 after a 200-fold dilution of the sample gave a result which was significantly less than that obtained by the ICP-MS method. When the sample was acidified to pH 2 with HNO_3 before dilution and then analyzed at pH 6.5, the Al(III) concentration value was comparable to that found by ICP-MS. It is known (17) that a substantial portion of the Al(III) in a neutral soil pore water is present in the form of organic complexes and it is possible that the method does not measure Al(III) in these forms. Acidification appears to release the bound Al(III) and it is not taken up on readjustment of the sample pH to 6.5. Advantage could be taken of this irreversible release of Al(III) to measure bound Al(III) in solution. The other pore water samples analyzed were acidic in nature and the results after adjustment to pH 6.5 compared well with the total Al(III) value obtained by ICP-MS.

Acknowledgements

Support from the Natural Sciences and Engineering Research Council of Canada in the way of an operating grant and scholarship support from Queen's University for D. V. Vukomanovic is gratefully acknowledged. We are indebted to Professor D. Beauchemin for the ICP-MS results reported in this study.

1. H. W. NURNBERG. Pure Appl. Chem. **54**, 853 (1982).
2. J. WANG. *In* Electroanalytical chemistry. Vol. 16. *Edited by* Allen J. Bard. Marcel Dekker, Inc. 1989. pp. 1–89.
3. J. WANG. Am. Lab. **17**, 41 (May 1985).
4. J. WANG, P. A. M. FARIAS, and J. S. MAHMOUD. Anal. Chim. Acta. **172**, 57 (1985).
5. C. M. G. VAN DEN BERG, K. MURPHY, and J. P. RILEY. Anal. Chim. Acta. **188**, 177 (1986).
6. R. G. BATES. *In* Determination of pH. 2nd ed. John Wiley and Sons. 1972, pp. 134–138.
7. J. K. SENNE and L. W. MARPLE. Anal Chem. **42**, 1147 (1970).
8. D. D. PERRIN (*Editor*). Stability constants of metal ion complexes. Part B. Organic ligands. IUPAC Chemical Data Series, No. 22. Pergamon Press Ltd. 1979.
9. E. B. SANDELL and H. ONISHI. *In* Photometric determination of trace metals. Vol. 3. Part I. 4th ed. John Wiley and Sons. 1978. pp. 320–321.
10. W. K. DOUGAN and A. L. WILSON. Analyst, **99**, 413 (1974).
11. O. ROYSET. Anal. Chim. Acta. **178**, 223 (1985).
12. O. ROYSET. Anal. Chim. Acta. **185**, 75 (1986).
13. D. C. HARRIS. *In* Quantitative chemical analysis. 2nd ed. W. H. Freeman and Company. 1987. pp. 198–199.
14. P. J. KUDIRKA and R. S. NICHOLSON. Anal. Chem. **44**, 1786 (1972).
15. E. LAVIRON. J. Electroanal. Chem. **52**, 355 (1974).
16. J. D. WINEFORDNER. *In* Trace analysis. Wiley-Interscience. 1976. Chap. 1.
17. S. J. DUFFY, G. W. HAY, R. K. MICKLETHWAITE, and G. W. VANLOON. Sci. Total Environ. **76**, 203 (1988).

Can. J. Chem. Downloaded from www.nrcresearchpress.com by 84.41.108.74 on 09/07/12
For personal use only.

A novel type of active site at the surface of crystalline SiO_2 (*a*-quartz) and its possible impact on pathogenicity

DOMINIQUE COSTA,[1] BICE FUBINI,[2] ELIO GIAMELLO, AND MARCO VOLANTE
Dipartimento di Chimica Inorganica, Chimica Fisica e Chimica dei Materiali, via Pietro Giuria 9, 10125 Torino, Italy
Received May 31, 1990[3]

DOMINIQUE COSTA, BICE FUBINI, ELIO GIAMELLO, and MARCO VOLANTE. Can. J. Chem. **69**, 1427 (1991).

A new type of surface site, different from those previously described, which gives rise to a paramagnetic oxygen species upon adsorption of O_2 at low temperature, has been found at the surface of crystalline quartz. This site is abundant on freshly cleaved surfaces or on chemically etched ones but absent on crystal growth faces or on samples annealed at high temperature. The abundance of this site is not related to the other surface radicals characteristic of the quartz surface originated by mechanical grinding in air. The EPR spectral features of the signal suggest an ozonide type radical O_3^-. The adsorption of oxygen onto quartz dusts variously treated in order to modulate their fibrogenic potential *in vivo* indicates that a relationship may exist between the presence of this site and quartz pathogenicity.

Key words: quartz, oxygen radical species, ozonide, silicosis, EPR.

DOMINIQUE COSTA, BICE FUBINI, ELIO GIAMELLO et MARCO VOLANTE. Can. J. Chem. **69**, 1427 (1991).

On a trouvé à la surface du quartz cristallin un nouveau site de surface, différent de ceux décrits antérieurement, qui conduit à une espèce d'oxygène paramagnétique lors de l'adsorption de l'oxygène à basse température. Ce site se trouve en abondance sur les surfaces fraichement coupées ou sur celles qui sont décapées alors qu'il est absent sur les faces des cristaux en croissance ou sur des échantillons condensés à haute température. L'abondance de ce site n'est pas relié aux radicaux de surface caractéristiques de la surface du quartz travaillée par broyage mécanique dans l'air. Les caractéristiques spectrales du signal en RPE suggèrent un radical du type ozonide O_3^-. L'adsorption de l'oxygène sur de la poussière de quartz, traitée de différentes façons dans le but de moduler leur potentiel fibrogénique *in vivo*, indique qu'il peut exister une relation entre la présence de ce site et la pathonégicité du quartz.

Mots clés : quartz, espèce d'oxygène radicalaire, ozonide, silicose, RPE.

[Traduit par la rédaction]

Introduction

Most crystalline silica polymorphs are toxic to humans when inhaled in particulate forms, as they cause silicosis, the well-known pulmonary fibrosis, that afflicts people exposed to silica dusts for long periods of time (1, 2). In recent years the possible carcinogenicity of quartz has also been under debate (3, 4). The mechanism of action of the silica particle at the molecular level is still unknown, particularly as far as the specific role of the quartz surface is concerned. While the surface chemistry of amorphous silica (non-toxic) has been widely investigated because of its industrial use as high surface area material, few papers (5, 6) have been devoted to the characterisation of the surface of quartz dusts. Among the various surface functionalities which may be regarded as possible initiators of the chain of events ending up in formation of the pneumonoconiotic lesions typical of silicosis, surface radicals should be taken into account. Indeed, such a hypothesis has been recently put forward by some of us and other authors (7–15). Various radical centres are in fact present at the surface of freshly ground and of aged dusts, originated by rupture of the silicon–oxygen bond and subsequent reaction of dangling bonds with atmospheric components. Active oxygen forms, such as silylperoxide, $SiO_2\cdot$ and superoxide O_2^- anions, whose potential toxicity is widely accepted, have been suggested to exist on samples ground in air (8–12). The assignments have been made on the basis of literature data both on bulk (16, 17) and on powdered samples (18–22). It must, however, be pointed out that these paramagnetic species are rather stable with time and mild thermal treatments (9). Moreover, the modifications detected in the EPR spectrum after long standing in aqueous solutions mimicking the biological environment do not seem to indicate that these particular radical species are the only initiators of the pathogenic process (10, 11). It is in fact unlikely that one of these forms alone would trigger the biochemical reactions originating macrophage activation and release of fibroblast stimulating factors. Most probably the action of the quartz surface is due to a complex interplay, during phagocytosis, between different kinds of surface functionalities. Animal experiments have shown (23, 24) that freshly ground dusts are more fibrogenic, or at least provoke lesions in much shorter time, than aged dusts (13). The latter, however, are still fibrogenic even years after standing in air, *e.g.*, DQ 12 or Min-U-Sil, largely used in medical research (F. Pott, private communication, 1990). The primary cause of the overall toxicity, if due to radical species, has thus to be sought in a complex interplay between biological entities (cell membranes, macrophage metabolites) and the various active sites at the dust surface or others originated in a biological medium.

The present paper reports new data on an additional site which is EPR silent but can be evidenced by the formation of a paramagnetic form upon adsorption of molecular oxygen at 77 K. This radical, already reported in a previous paper by some of us (25), occurs similarly to the one reported years ago and assigned to $SiO_3\cdot$ by Radtsig and co-workers on vacuum-ground fused silica (19), but its origin appears unrelated to the formation of the other known radical sites. Several quartz samples, known to exhibit distinct fibrogenic effects, have been examined in the present paper: freshly ground and aged dusts, samples heated *in vacuo*, chemically etched dusts, and micro-

[1]On leave from Laboratoire de Reactivite de Surface et Structure, UA1106, CNRS, Universite P. et M. Curie, 4 pl. Jussieu, 75252 Paris, Cedex 05, France.

[2]To whom correspondence should be addressed.

[3]Revision received May 8, 1991.

Printed in Canada / Imprimé au Canada

Can. J. Chem. Downloaded from www.nrcresearchpress.com by 84.41.108.74 on 09/07/12
For personal use only.

crystals grown in hydrothermal conditions. The effect on the active site of substances capable of inhibiting silicosis (*e.g.*, Al salts, polyvinylpyridine-*N*-oxide ≡ PVPNO) has also been investigated.

Experimental

Materials

(1) Freshly ground pure crystals were obtained from extremely pure *a*-quartz chips (purified by subsequent melting and recrystallization, 99.999%, Atomergic) (9) and from natural Madagascar quartz crystals (a relatively pure natural *a*-quartz). Grinding was performed in an agate ball mill either in a water-free atmosphere or in presence of a substantial water vapour pressure (20 Torr). A dry atmosphere favors the formation of surface radicals, whereas a moist one depresses it (10, 12, 14). The product is not uniform in size, being made up of submicron particles in contact with larger ones (25).

(2) Microcrystals grown in hydrothermal conditions have been prepared at CRSOCI-CNRS Orleans, with the help of Dr. Erre, following a procedure previously described (26).

(3) The typical *SiO_2 aged dust, i.e.* kept standing in air long periods of time (years), was Min-U-Sil 5 *a*-quartz (Pennsylvania Glass Sand Co) with particle size below 5 μm and BET surface area of about 2 m^2 g^{-1}.

Thermal and chemical treatments

(1) Thermally heated samples were prepared either by heating pure quartz dusts in vacuum at 1073 K for 12 h or by heating this material in nitrogen atmosphere at 1573 K for the same period of time. This procedure provides samples with virtually no surface radicals left. The former still bears a substantial amount of silanols and is thus hydrophilic, whereas the latter one is hydrophobic (results to be published).

(2) HF-etched and NaOH-etched quartz samples were obtained by keeping samples ground in moist atmosphere respectively in aqueous solutions of HF (0.1 and 1 M) (from a commercial 40% solution in water, Merck) or of NaOH (0.1 M) for 2 h at 313 K. The samples were then washed several times and dried *in vacuo* at room temperature. In the case of the HF 1 M etching, 35% in weight was lost because of solubilization of SiO_2.

(3) Catechol (1,2-dihydroxybenzene)-etched quartz was obtained by contacting some 80 mg of Madagascar quartz ground in moist atmosphere with 10 mL of a 5×10^{-2} M aqueous solution of catechol (Janssen Chimica) at 313 K then washing it and vacuum-drying at room temperature.

(4) The *PVPNO* treatment was realized by contacting some 80 mg of the quartz powder with a PVPNO solution (50 mg PVPNO in 10 mL water) for 1/2 h and subsequently drying without washing.

(5) The *aluminum* treatment was carried out contacting some 80 mg of Madagascar quartz ground in moist atmosphere with 10 mL of a saturated solution of $NaAlO_2$ in water. The sample was then washed several times in water and dried *in vacuo* at room temperature.

To evaluate separately the effect of modifications due to the basicity of the solution from those induced by the AlO_2^- ion itself, a treatment was also made in a pure NaOH aqueous solution having the same pH (11.4) as the $NaAlO_2$ one.

Electron spin resonance

Electron spin resonance spectra were taken on a Varian E 109 spectrometer operating at X band. The spectra were recorded *in vacuo* at 77 K. These are appropriate conditions for detection of most of the surface paramagnetic species (9).

For the oxygen adsorption experiments, an appropriate EPR cell was employed which allowed the sample to be kept *in vacuo* for long periods of time and also to submit it to treatments with gases. Oxygen adsorption was performed by admitting oxygen onto the sample and then cooling the sample to 77 K. Spectra were recorded either in the presence of the gas or after evacuation at 77 K, in order to leave only the layer irreversibly adsorbed at this temperature.

To enable comparison between spectra arising from different samples, the same sample weight was always employed (some 60 mg); because of different particle size, quantitative comparisons between different kind of samples have to be made on the basis of the respective surface areas. Varian pitch ($g = 2.0029$) was used as reference standard for g value calibration.

Results

Evidence for a weakly bound oxygen paramagnetic form on quartz dusts

Upon contact of quartz dusts with oxygen at 77 K, a paramagnetic adsorbed species is formed, which is detectable by EPR. Figure 1 reports the typical spectrum of a pure quartz dust ground in dry air (*a*), after contact with oxygen and subsequent evacuation at 77 K (*b*), under 25 Torr of oxygen (*c*) and of the standard aged dust (Min-U-Sil), both in vacuum (*d*), and under 25 Torr of oxygen (*e*). The spectra under vacuum have been largely discussed in previous papers (7, 9); they are produced by the cleavage of Si—O—Si bonds during grinding and subsequent reaction with atmospheric components. The final product is mainly $SiO_2\cdot$ (silylperoxide $g_{zz} = 2.064$, $g_{yy} = 2.007$, $g_{xx} = 2.002$) and O_2^- (superoxide anion, $g_{zz} = 2.044$, $g_{yy} = 2.010$, $g_{xx} = 2.002$). A few unreacted Si· radicals (usually called E′ centres) are detectable having the $g_\perp$ component at $g = 2.000$. On Min-U-Sil at 77 K, there are also some sets of lines superimposed onto the major spectrum which are very likely sextets of hyperfine components due to isolated aluminum atoms as impurities in the quartz matrix (27).

Upon contact with O_2 at 77 K, on both solids (spectra *b*, *c*, *e* in Fig. 1) a new sharp line appears at $g = 2.0000 \pm 0.0005$ (indicated hereafter as O_2(ads)) superimposed on the spectrum of Si· in the original spectrum. The intensity of this line is greater on the freshly ground sample than on the aged dust. In spite of the coincidence of the g values, this line arises from a paramagnetic form different from the E′ center. Inspection of the saturation curves (intensity vs. microwave power) of the E′ signal and of the one obtained for O_2(ads) in Fig. 2 in fact reveals two different behaviors. Upon evacuation of the sample at room temperature, the initial spectra (Fig. 1, *a* and *d*) are restored. If the evacuation is carried out at 77 K, a part of the paramagnetic adsorbed species remains at the surface as the signal does not disappear even after prolonged outgassing at 77 K. This is clearly visible with the freshly ground sample, Fig. 1*b*. At 77 K this form is thus stable, even in the absence of oxygen in the gas phase. Figure 3 reports the spectra obtained by subsequently contacting a freshly ground dust with oxygen at increasing pressure. The intensity I of the $g = 2.000$ signal, measured by the peak-to-peak height of the line, increases with the oxygen pressure; the linewidth is unaffected by the presence of oxygen in the gas phase. In the inset a sort of adsorption isotherm is reported, where the relative intensity of the O_2(ads) signal in arbitrary units is reported as a function of the equilibrium pressure. This has been obtained by subtraction, from the overall signal at $g = 2.000$, of the contribution of the E′ center measured before contact with oxygen. Such a behavior of the isotherm (Langmuirian type) is typical of a reversible adsorption process.

It is noteworthy that, upon regrinding of Min-U-Sil and of other aged dusts, the intensity of the adsorbed oxygen signal increases. The centers capable of forming O_2(ads), which hereafter we will call O_2(ads) "precursor sites", are thus mainly located at the freshly created surfaces.

Can. J. Chem. Downloaded from www.nrcresearchpress.com by 84.41.108.74 on 09/07/12
For personal use only.

Can. J. Chem. Downloaded from www.nrcresearchpress.com by 84.41.108.74 on 09/07/12
For personal use only.

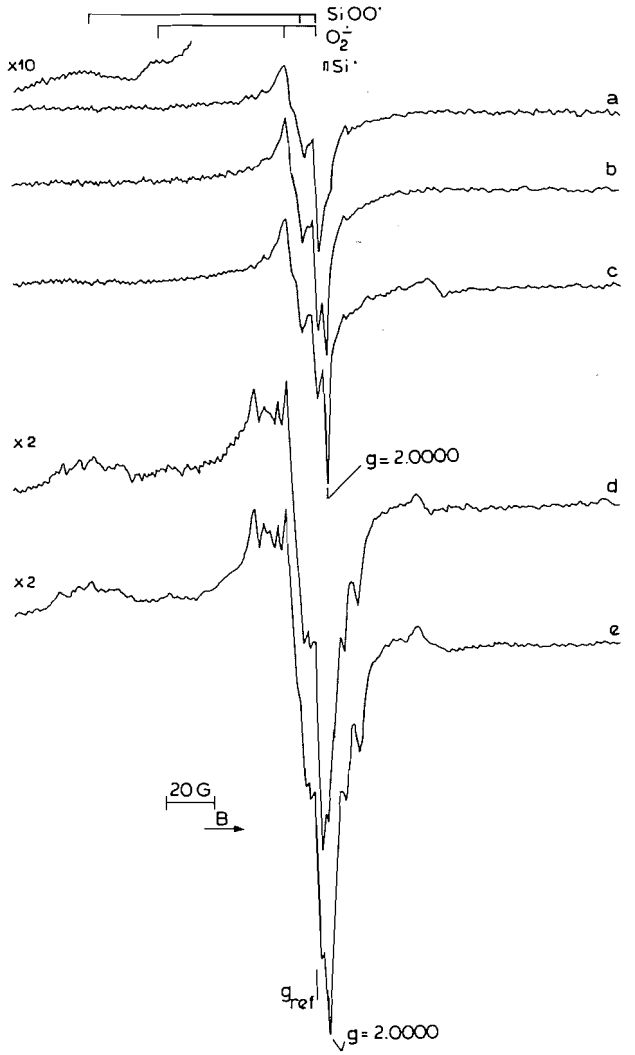


FIG. 1. Electron paramagnetic resonance spectra of freshly ground pure quartz dust: (*a*) in vacuum, (*b*) after contact with oxygen followed by evacuation of oxygen at 77 K, (*c*) and under 25 torr O_2; Min-U-Sil 5 dust (*d*) in vacuum and (*e*) under 25 Torr O_2. Spectra recorded at 77 K.

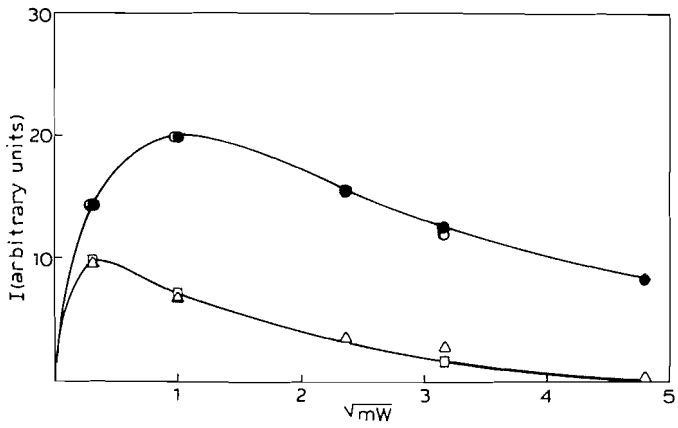


FIG. 2. Freshly ground pure quartz dusts: saturation curves (intensity of the line, measured as peak-to-peak height of the $g = 2.000$ component, versus the square root of microwave power) of (*a*) the E′ signal before contact with oxygen and (*b*) after evacuation at room temperature (Fig. 1*a*) (□, △) and of the O_2(ads) signal under 20 Torr oxygen (○) and 30 Torr oxygen (●).

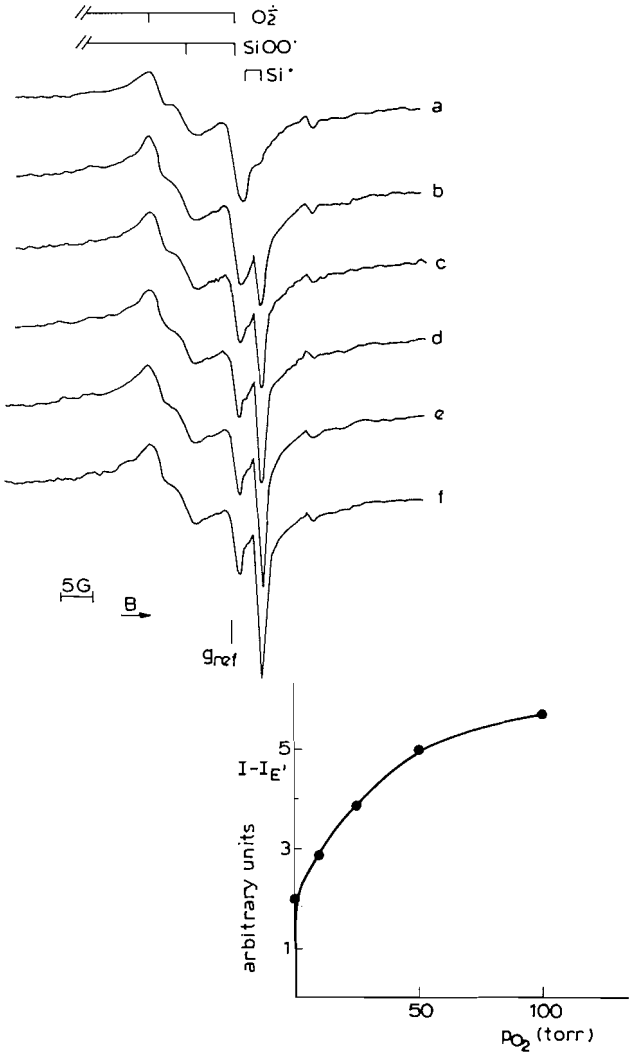


FIG. 3. Electron paramagnetic resonance spectra (at 77 K) of freshly ground pure quartz dust, (*a*) before and (*b*) after adsorption of O_2 followed by evacuation at 77 K and under increasing oxygen pressure: (*c*) 10, (*d*) 25, (*e*) 50, and (*f*) 100 Torr. Inset: intensity of the O_2(ads) signal (arbitrary units) obtained by subtraction from total intensity of the signal at $g = 2.0000$ (superimposition of O_2(ads) and E′ signals) of the intensity of the E′ signal alone, observed when recording under vacuum (spectrum *a*).

Relationship between the center for O_2 adsorption and the other paramagnetic forms: effect of chemical treatments

To investigate if the O_2(ads) precursor site is related to the presence of the other paramagnetic forms, the same experiment was carried out on samples where the other radicals were progressively eliminated. This can be done either *chemically*, *e.g.*, by immersion in solutions reacting with the SiO_2 framework itself (such as HF, NaOH, catechol) or *thermally*, *e.g.*, by heating the dusts *in vacuo* or nitrogen atmosphere. Details on this procedure will be reported in a future paper. Figure 4*a* reports the spectrum obtained before (upper trace) and after (lower trace) contact with O_2 ($p = 25$ Torr) of a sample previously left standing 2 h in an 0.1 M HF solution. The chemical treatment affects the radical population by destroying the outermost layers of the particle. In contrast, the O_2(ads) precursor site is still present and in this case the O_2(ads) signal dominates the spectrum. The same thing happens on treatment of

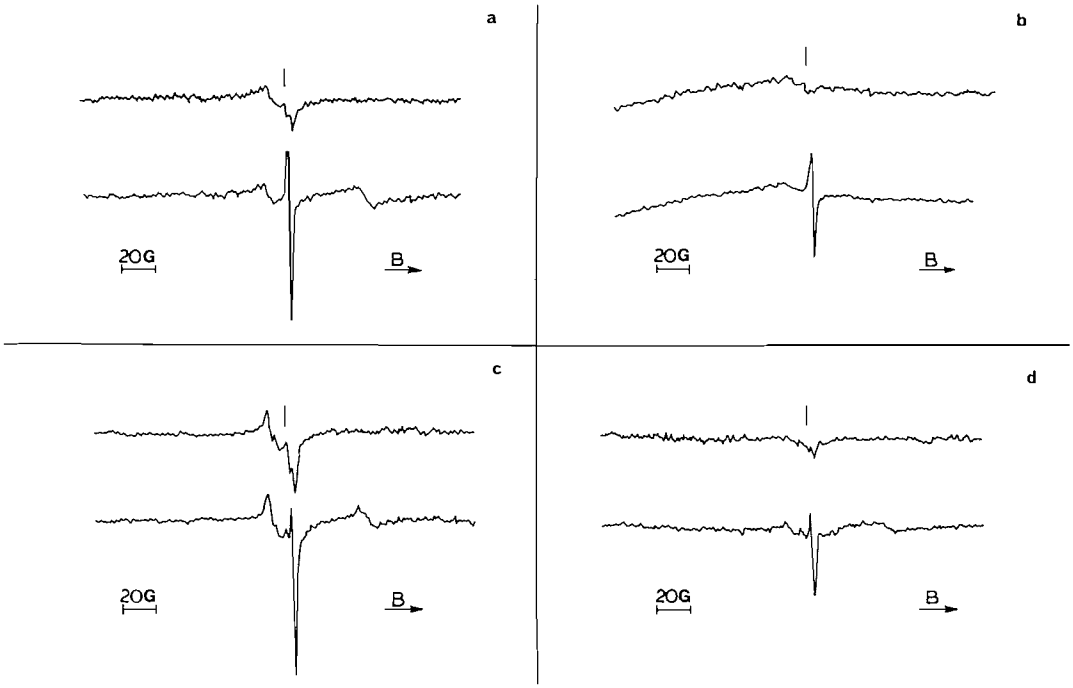


FIG. 4. Influence of etching on the O_2(ads) signal. Electron paramagnetic resonance spectra (at 77 K), recorded before (upper trace) and after (lower trace) adsorption of oxygen (25 Torr) on: (*a*) freshly ground pure quartz crystals after HF etching, 0.1 M, 2 h; (*b*) Madagascar quartz ground in moist air after HF etching, 1 M, 2 h; (*c*) freshly ground pure quartz crystals after NaOH etching, 0.1 M, 2 h; (*d*) Madagascar quartz ground in moist air after catechol etching, 5×10^{-2} M, 30 min.

the same sample with aqueous NaOH (Fig. 4*c*). The chemical treatment erodes some of the paramagnetic sites, modifying the EPR spectrum (by a different mechanism and to a different extent than HF) but either leaves unaffected or recreates the sites capable of interaction with O_2. A more severe treatment (HF 1 M, 2 h, elimination of 35% of weight of the material) on a sample with initially few radicals (Madagascar quartz ground in moist air) completely erodes the radical signals (Fig. 4*b*, upper trace). Even in such a case the paramagnetic adsorbed oxygen is formed (Fig. 4*b*, lower trace). The spectrum consists only of the O_2(ads) signal, which is apparently axial (expanded spectrum in Fig. 5) with $g_\perp = 2.0000 \pm 0.0005$ and $g_\parallel \sim 2.0015 \pm 0.0005$.

Figure 5 reports a spectrum obtained by subtraction of the two spectra in Fig. 4*a* for the evaluation of the modifications produced by the contact with oxygen; it is noteworthy that the spectrum obtained in this way is very similar to the one obtained on a radical-free surface. This clearly indicates that the reaction with oxygen occurs independently of other radical species. To check whether some modifications in the signal features might be observed at increasing oxygen pressure, the saturation of the signal was tested in two well-defined conditions: (*1*) after contact with oxygen and evacuation at 77 K (spectra *b* in Figs. 1 and 3) thus leaving at the surface only the fraction of adsorbate irreversibly held at 77 K, and (*2*) under an equilibrium pressure of 200 Torr. The curves are reported in Fig. 5. Despite the different position of the maximum, likely due to the influence of the large amount of O_2 present in the cell on the relaxation of the centres, the two curves behave similarly to the upper curve in Fig. 2, suggesting that the same species O_2(ads) is present on the two kinds of samples (freshly ground and chemically etched samples). It is also noteworthy that the lower curve in Fig. 5 (O_2(ads) in the absence of any residual oxygen pressure) is definitely different from the lower curve in Fig. 2 (E' centres) being both recorded in the absence of residual oxygen in the gas phase.

Figure 4 also presents the spectra obtained on Madagascar quartz ground in moist air treated with catechol and subsequently contacted with oxygen (Fig. 4*d*, upper trace and lower trace, respectively). Catechol is known to be one of the most powerful organic chemicals able to react with the silica framework (28). In fact, most of the radicals present in the original sample are eroded after the chemical treatment. Upon contact with oxygen, however, the same EPR signal appears.

All data in Fig. 4 thus confirm two main facts: *(i) Most of the original radicals are located at the surface or in the subsurface layer*, microcracks, etc..., as already hypothesized in previous papers (7, 9). Chemical treatments with HF, NaOH, and catechol, all capable of reacting with the silica framework, erode the original radicals. The loss in weight, which is around 10% for 0.1 M treatments, indicates how the reaction has not proceeded in depth. Details on the differences in reactivity of the three reagents will be reported elsewhere. In the present paper, we only stress that all these treatments modify the state of the surface. *(ii) The chemical treatments leave mainly unaffected or else recreate the site responsible for oxygen adsorption* and formation of the labile oxygen radical.

Effect of thermal treatments

Upon thermal treatment the original surface radicals on quartz dusts are modified and progressively eliminated (9). In some cases, mainly on samples with complex spectra, such as Min-U-Sil (9), even after treatment *in vacuo* at 1073 K a broad signal remains. Conversely, on pure quartz or cristobalite (unpublished results) all radicals are annealed between 873 and 1073 K, and thus no EPR signals are detected. Under

Can. J. Chem. Downloaded from www.nrcresearchpress.com by 84.41.108.74 on 09/07/12
For personal use only.

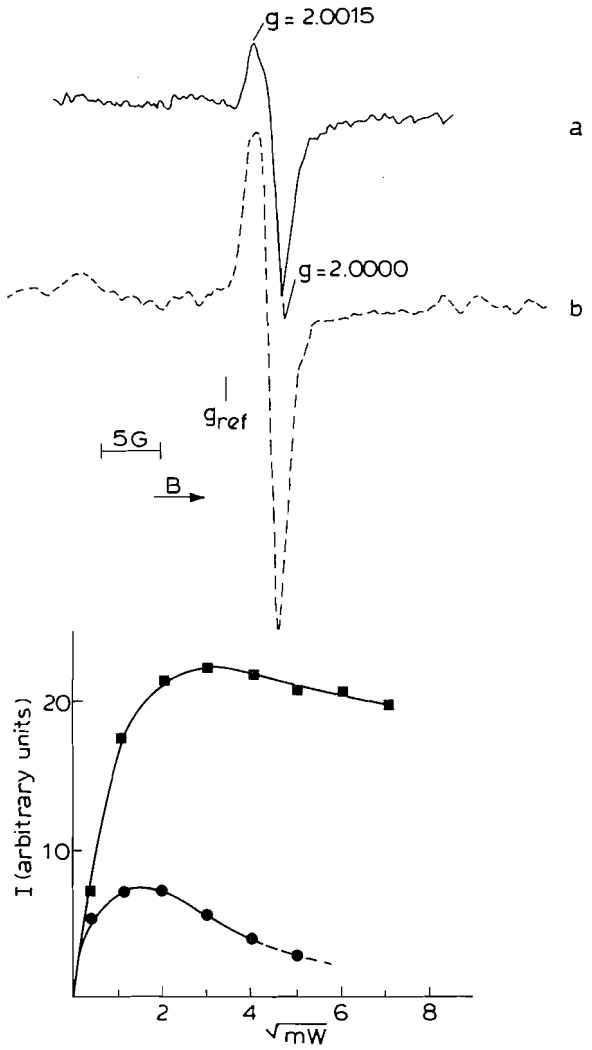


FIG. 5. O_2(ads) adsorbed oxygen signal on HF-etched samples: (*a*) as in Fig. 4*b*, recorded on an expanded scale; (*b*) EPR spectrum of the O_2(ads) signal, obtained by computer subtraction of the first of the two spectra in figure 4a from the second one. Inset: saturation curves of the O_2(ads) signal (Signal intensity, arbitrary units, versus square root of microwave power), for the fraction of O_2(ads) left at the surface after outgassing at 77 K (●) and O_2(ads) in equilibrium with pO_2 = 200 Torr (■).

these conditions the quartz samples, in contrast to amorphous silicas, are still largely hydrophilic (29), whereas after treatment at 1573 K they are mainly hydrophobic (unpublished results).

The interaction with O_2 at 77 K was tested on two samples of Madagascar quartz treated respectively at 873 and 1573 K, in order to have two samples deprived of their radicals, one largely hydrophilic, *i.e.*, bearing patches of vicinal silanols, and the other one, hydrophobic, thus exhibiting at the surface only siloxane bridges and isolated silanols (29). In both cases no signals were observed upon contact with oxygen even at high pressure. These results indicate that thermal treatments, unlike chemical treatments, destroy the sites reacting with oxygen at 77 K.

Origin of the samples

All the samples examined so far were either fresh or aged crystalline quartz dusts obtained by mechanical grinding. To investigate the role of crystallinity and of the grinding process, two other samples have been considered: Aerosil 50, a pyrogenic amorphous silica with a relatively low surface area (already employed by some of us in adsorption work (30) and as standard in studies on the toxicity of mineral dusts (31)), and a powder made up of microcrystals obtained by hydrothermal growth, *i.e.*, only exposing growth faces (26). In both cases, no signal was observed upon contact with O_2. It can therefore be concluded that the formation of the paramagnetic form upon adsorption of oxygen at 77 K only occurs when the exposed surface is *created by grinding* and is not inhibited by chemical etching of the ground surface.

Stability of the sites reacting with O_2

The sites responsible for the formation of the paramagnetic oxygen species at 77 K are more abundant on freshly ground than on aged dusts (Fig. 1). It has already been mentioned that grinding aged dusts enhances the formation of this species, by creating new sites. As to the stability of these sites, it has been seen (by contacting the sample periodically with O_2 and then running EPR spectra) that their number slowly decays with time, particularly if the sample is kept in moist atmosphere.

Effect of treatments with substances used to prevent quartz pathogenicity: Al^{3+} ions and PVPNO

Polyvinylpyridine-*N*-oxide (PVPNO) is a polymer used to prevent silicosis (32). Its mechanism of action is not known; it may simply cover the surface by hydrogen bonding to silanols (33), or it may react via its —N═O group with active sites (34). Figure 6 reports the spectra of Madagascar quartz ground in moist air before and after contact with O_2 (Fig. 6*a*) and the same treated with PVPNO and subsequently contacted with O_2 (Fig. 6*b*). The treatment with PVPNO clearly inhibits the formation of O_2(ads). This inhibition may be caused by simple adsorption of the polymer on the quartz surface, thus screening the active sites. Alternatively a reaction may occur between the polymer and the surface involving modification or elimination of the site itself.

Administration of aluminum salts is another method used to prevent silicosis. The effect of Al^{3+} in blunting SiO_2 toxicity has been largely confirmed by *in vivo* experiments by Le Bouffant *et al.* (35). One quartz sample (the same batch of Madagascar quartz ground in moist air used for the PVPNO experiment) was contacted with a $NaAlO_2$ solution for 1 h. The final spectrum (in Fig. 6*c*, upper trace) shows that the original paramagnetic signals are decreased, indicating that $NaAlO_2$ also affects the active sites population. This effect, which differs from what happens after a treatment with NaOH solution with the same pH of the $NaAlO_2$ solution, will be extensively discussed in a future paper. Only a very small signal appears after contact with O_2 (Fig. 6*c*, lower trace), indicating that treatment with the aluminum ions interferes with the relevant sites and inhibits the formation of the oxygen radical form. In conclusion, via different chemical of physico-chemical paths, both of the above substances inhibit the formation of the oxygenic paramagnetic form.

Discussion

There is clear evidence that in some cases a particular site is present at the quartz surface, which reacts with dioxygen at 77 K to give a weakly bound paramagnetic adduct. To understand the chemical nature of the site and of the paramagnetic form to which it gives rise, both the physico-chemical condi-

Can. J. Chem. Downloaded from www.nrcresearchpress.com by 84.41.108.74 on 09/07/12
For personal use only.

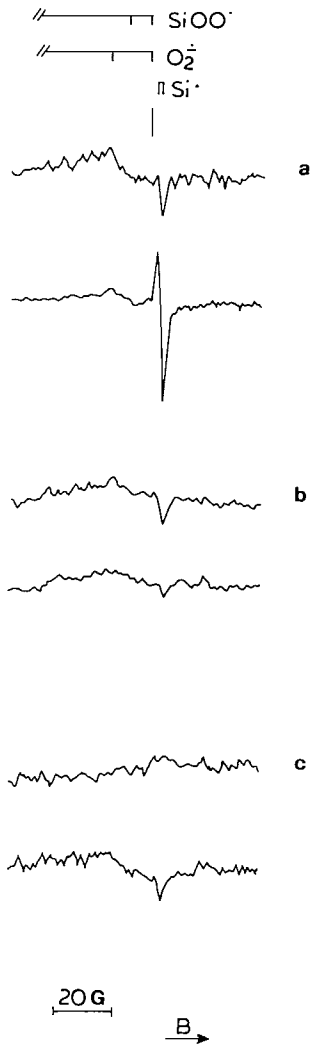


FIG. 6. Electron paramagnetic resonance spectra (77 K) of Madagascar quartz ground in moist air, under vacuum (upper trace) and under 25 Torr of oxygen (lower trace), after different chemical treatments: (*a*) before any treatment; (*b*) after treatment with aqueous PVPNO; (*c*) after treatment with aqueous $NaAlO_2$.

tions in which the site appears and the EPR spectral features must be considered.

(1) State of the ground surface and origin of the site

The site appears to be present only on surfaces of crystalline material which are powdered by mechanical grinding. The maximum abundance is found on freshly ground samples and the number of sites decays with time, particularly in moist atmosphere. Regrinding again increases the number of the sites.

It is known since the work of Antonini and Hochstrasser on quartz (18) that mechanical treatments such as grinding originate homolytic rupture of the Si—O bond, as demonstrated by the appearance of an EPR spectrum due to Si· dangling bonds (also called E′ centres). The same conclusions were derived by Radtsig and co-workers who extensively investigated the grinding of vitreous silica under vacuum and the reactivity of the ground materials with several molecules (19, 20). These authors claim that SiO· centres, formed in parallel with Si· during grinding, are also present on the solid, even though (having a degenerate ground level) they are not visible by EPR (16, 19).

The effect of mechanical treatments on various crystalline polymorphs of SiO_2 in air and in controlled atmospheres has been reported by some of us (7, 9, 12). It has been shown that radical centres are formed by the simultaneous action of grinding and reaction of oxygen with the newly created surface. The most abundant centres so formed are the silylperoxide radical (SiOO·) and the superoxide ($O_2^{\cdot-}$) radical ion. The former is created by reaction between Si· and molecular oxygen. The superoxide species are very likely formed during grinding by electron transfer from the solid to molecular oxygen. The electrons released by the solid are probably those of defects, generated upon mechanical treatment, analogous to those observed on several oxides submitted to other kind of activation such as γ- or neutron irradiation.

In conclusion, the surface of quartz ground in air exhibits, beside the typical silica functionalities (silanols and siloxanes), radical centres such as SiOO·, $O_2^{\cdot-}$, and unreacted residual Si· (all observed by EPR) and SiO· which is EPR silent. The above-mentioned species are fairly stable with time, but a decrease with time in the intensity of the spectra was found both by Vallyathan *et al.* (13) and by some of us (8), the decrease being more pronounced in moist than in dry atmosphere. The newly discovered site too seems to be affected by moist atmosphere, confirming its relationship with the other radicals. However, its abundance seems unrelated to the others, particularly when chemical treatments have caused the original radical population to be partially or completely eroded (Fig. 5). On the basis of these findings we can assume that the site is produced, like the others, by mechanical grinding. In contrast to the others, this site either is located in a surface region which is not affected by chemical treatments (e.g. microcracks) or is progressively eliminated and restored by the chemical treatment. In contrast, thermal treatments, whereby most surface radicals are annealed, also eliminate this site. In such a case, even after prolonged exposure to various substances which does in fact create some radicals (unpublished results), this form is still absent.

(2) Assignments

The perpendicular component of the EPR signal of O_2(ads) falls at $g = 2.0000$, corresponding exactly to that of the well known E′ center (Si·) in polycrystalline SiO_2. The presence of two superimposed signals is proved by the fact that the two lines have a different saturation curve (Figs. 2 and 5). The dependence on the oxygen pressure indicates that the spectrum arises from reaction of O_2 with a suitable surface site, so as to produce a paramagnetic form.

Several lines arising from the O_2 spectrum, if large doses of O_2 are admitted on the sample at 77 K ($p_{O_2} > 10$ Torr), can be seen in various parts of the spectrum. These lines, however, are distinguishable from the signal under discussion because, unlike the $g = 2.0000$ component, they are broadened with increasing O_2 pressure, and they disappear by simple evacuation at 77 K.

The new signal is therefore produced by reaction of an EPR-silent surface species with dioxygen.

The assignment of a detailed structure to the observed species is not straightforward. Some observations reported in the literature were particularly interesting due to the clear analogies with our case. The first one is reported by Radtsig and co-workers (19, 20) on the surface chemistry of ground

Can. J. Chem. Downloaded from www.nrcresearchpress.com by 84.41.108.74 on 09/07/12
For personal use only.

fused SiO_2. A surface species is formed upon oxygen adsorption which has the same adsorptive behavior (appearance–disappearance as a function of the oxygen pressure) found in the present work. In that case too the observation of the whole spectrum of the oxygen adduct was seriously limited by overlap with other signals. The authors only report a component at $g = 2.008$, *i.e.*, a value quite different from that observed for O_2(ads). The species was assigned by Radtsig to $SiO_3\cdot$ arising from the reaction of O_2 with the EPR-silent $SiO\cdot$ site. No discussion about the chemical bonding in the species (ionicity–covalency) or about its geometry is done in Radtsig's papers, where the $SiO_3\cdot$ representation is merely indicative of the chemical composition of the species.

The second case is that of the ionic triatomic oxygen species observed on several oxides (36, 37). These are two species: the ozonide O_3^- ion which shows stability and g values very different from those of O_2(ads) and the T-shaped "so-called" ozonide. The latter species on V_2O_5 (38) exhibits $g_\perp = 2.0001$ (very close to the O_2(ads) component observed in the present case), $g_\parallel = 2.0017$ and is destroyed by evacuation at 150 K. The structure of the species (an oxygen molecule coordinated "side on" onto an O^- site) has been demonstrated by employing ^{17}O-enriched oxygen (39). The same experimental approach is, unfortunately, impossible in our case due to the low intensity of the observed signal. It is therefore not possible to assign a detailed structure to O_2(ads) even though the two above-mentioned species, $SiO_3\cdot$ (19, 20) and the T-shaped side-on O_3^-, show a behavior very close to that observed for O_2(ads). It is clear, however, that a weakly bound polynuclear oxygen radical is formed upon selective reaction of dioxygen with an EPR-silent site on the surface of quartz.

(3) Possible relationship with quartz pathogenicity

The site reacting with oxygen may be related somehow to the molecular event occurring during macrophage activation, ending up with the formation of fibroblast-stimulating growth factors (1, 40). In contrast to the other oxygen paramagnetic species which are strongly bound at the surface, oxygen is bound very weakly to the O_2(ads) site. Such a site could thus interact in a biological medium with various molecules, and perhaps act as a catalytic site where the biochemical cascade reactions are triggered.

Some facts would be in agreement with such a hypothesis: (*i*) It is well known that freshly ground dusts are more pathogenic and yield the fibrotic response in a shorter time than aged dusts (23, 26). The O_2(ads) precursor site is by far more abundant on freshly cleaved surfaces than on aged ones. (*ii*) The well-known inhibitors of quartz toxicity, the polymer PVPNO and aluminum ions, also blunt the specific O_2(ads) sites. In the case of PVPNO the action may be just a screening of the site by the polymer. As to the effect of $NaAlO_2$, it is noteworthy that a sample kept at the same pH as the $NaAlO_2$ solution but in NaOH does not lose its capability of reacting with O_2. In such a case there is thus a direct chemical action of the aluminum ion on the active site. (*iii*) Etching in HF increases fibrogenicity (41, 42) and on HF-etched quartz, unlike other radicals, the ozonide is still present. (*iv*) Thermal treatments which decrease fibrogenicity (43) also decrease or eliminate the active site.

One datum, namely the absence of the ozonide on the hydrothermally grown microcrystals, does not fit this correlation. In fact a similar specimen was found to be relatively fibrogenic (24, 26) although the fibrogenic response was delayed by comparison with ground material of the same size. In such a case it is possible that the active sites are created after prolonged immersion in a biological environment where several molecules may slowly react with the SiO_2 framework. The biochemical process of macrophage activation during quartz phagocytosis is somehow complex as many growth factors are released in the medium. It is therefore not easy to identify which are the surface-active sites responsible for the pathogenic biological response. It is likely, moreover, that several chemical functionalities will play some role in the overall toxicity, acting at different stages of particle inhalation and retention (25). This renders even more difficult the possibility of drawing clear-cut conclusions from the comparison of surface states and fibrogenicity *in vivo*. Nevertheless, the above-mentioned facts indicate that this site, reacting with O_2, should be considered as one of the possible agents of quartz pathogenicity.

Conclusions

A polynuclear paramagnetic species, probably of the ozonide type, is formed, when O_2 is contacted with crystalline silica dusts at 77 K, on a specific site at the surface which is EPR silent. The purity of the quartz employed samples ensures that the site arises from the silica framework and cannot be originated by any sort of impurity. Possible candidates are the $SiO\cdot$ or O^- species originated during grinding. This active form is also detectable in the absence of the other well-known surface radicals, if the latter ones have been eliminated by chemical treatments, whereas thermal treatments also eliminate the sites capable of O_2(ads) formation. A correspondence has been found between the presence of the site, giving rise to the ozonide form on variously treated quartz dusts and their fibrogenicity, which suggest a relationship between this site and silica pathogenicity.

Acknowledgements

Financial help from CECA, convention No 7280/03/006, is acknowledged. One of us, D. Costa, is indebted to the Groupe d'Etudes et Recherches sur les Pneumopathies Professionnelles (GERP) for a grant. The authors are also indebted to Dr. Pezerat (Université Pierre et Marie Curie, Paris) for helpful discussions and to Dr. Erre (CNRS-CRSOCI, Orleans) for helping in the preparation and characterization of the hydrothermally grown quartz sample.

1. G. S. DAVIS. Lung, **164**, 139 (1986).
2. Silicosis and Silicate Disease Committee. Diseases associated with exposure to silica and non-fibrous silicate minerals. Arch. Pathol. Lab. Med. **112**, 673 (1988).
3. D. F. GOLDSMITH, D. M. WINN, and C. M. SHY. Silica, silicosis and cancer. Controversy in occupational medicine. Praeger Publisher, New York, NY. 1986.
4. Silica and some silicates. IARC Monographs on the Evaluation of the Carcinogenic Risk of Chemicals to Humans. Vol. 42. Lyon, France. 1987.
5. K. ROBOCK. Beitr. Silikose Forsch. **92**, 1 (1967).
6. A. M. LANGER. Q. Rev. Biophys. **11**, 534 (1978).
7. B. FUBINI, V. BOLIS, and E. GIAMELLO. Inorg. Chim. Acta, Bioinorg. Chem. **138**, 193 (1987).
8. B. FUBINI, V. BOLIS, E. GIAMELLO, L. PUGLIESE, and M. VOLANTE. Effects of mineral dusts on cells. NATO ASI Ser. Vol. H. 30. *Edited by* B. T. Mossman and R. O. Begin. Springer-Verlag, Berlin Heidelberg, Germany. 1989. p. 205.
9. B. FUBINI, E. GIAMELLO, L. PUGLIESE, and M. VOLANTE. Solid State Ionics, **32–33**, 334 (1989).

Can. J. Chem. Downloaded from www.nrcresearchpress.com by 84.41.108.74 on 09/07/12
For personal use only.

10. B. FUBINI, E. GIAMELLO, and M. VOLANTE. Inorg. Chem. Acta, **163**, 187 (1989).
11. B. FUBINI, V. BOLIS, E. GIAMELLO, M. VOLANTE, and D. COSTA. *In* Les pneumopathies professionnelles. *Edited by* P. Sebastien. INSERM, Paris, France. 1991. p. 317.
12. E. GIAMELLO, B. FUBINI, M. VOLANTE, and D. COSTA. Colloids Surf. **45**, 155 (1990).
13. V. VALLYATHAN, X. SHI, N. S. DALAL, W. IRR, and V. CASTRANOVA. Am. Rev. Respir. Dis. **138**, 1213 (1988).
14. X. SHI, N. S. DALAL, X. HU, and V. VALLYATHAN. J. Env. Health, **27**, 435 (1989) and references therein.
15. H. PEZERAT. *In* Les pneumoconioses professionnelles. *Edited by* P. Sebastien. INSERM, Paris, France. 1991. p. 71.
16. D. L. GRISCOM. Phys. Rev. B, **22**, 4192 (1980).
17. J. A. WEIL. Phys. Chem. Miner. **10**, 149 (1984) and references therein.
18. F. ANTONINI and G. HOCHSTRASSER. Surf. Sci. **32**, 644 (1972).
19. V. A. RADTSIG and A. V. BYSTRIKOV. Kinet. Katal. **19**, 713 (1978).
20. V. A. RADTSIG. Kinet. Katal. **121**, 1019 (1980).
21. U. STEINICKE, U. KRETZSCHMAR, I. EBERT, and H. P. HENNING. React. Solids, **4**, 1 (1987) and references therein.
22. Y. KUBOKAWA, M. ANPO, and C. YUN. Proc. 7th Int. Congr. Catal. B, 1170 (1981).
23. C. GOTHE, L. LIDSTROM, and A. SWENSSON. Med. Lav. **63**, 357 (1971).
24. M. CZERNICHOWSKI, H. VAN DAMME, and R. ERRE. *In* Les pneumopathies professionnelles. *Edited by* P. Sebastien. INSERM, Paris, France. 1991. p. 271.
25. B. FUBINI, E. GIAMELLO, M. VOLANTE, and V. BOLIS. J. Toxicol. Indust. Health, **6**, 571 (1991).
26. M. CZERNICHOWSKI. Doctoral Thesis, Universite d'Orleans, France. 1989.
27. D. L. GRISCOM. *In* The physics of SiO_2 and its interfaces. *Edited by* S. T. Pantelides. Pergamon Press, New York, NY. 1979. p. 232.
28. R. K. ILER. The chemistry of silica. Wiley, New York, NY. 1979. p. 59.
29. B. FUBINI. Thermochim. Acta, **135**, 19 (1988); V. BOLIS, B. FUBINI, L. MARCHESE, G. MARTRA, and D. COSTA. J. Chem. Soc. Faraday Trans. **87**, 497 (1991).
30. V. BOLIS, S. COLUCCIA, L. MARCHESE, and B. FUBINI. Ads. Sci. Tech. **5**, 239 (1988).
31. J. FOURNIER, B. FUBINI, V. BOLIS, and H. PEZERAT. Can. J. Chem. **67**, 289 (1989).
32. H. W. SCHLIPKOTER, W. HILSCHER, F. POTT, and E. G. BECK. *In* Inhaled particles and vapour. Vol. I. *Edited by* W. A. Walton. Pergamon Press, U.K. 1970. p. 379.
33. P. F. HOLT and E. T. NASRALLAH. J. Chem. Soc. B, **3**, 233 (1968).
34. M. GULUMIAN and A. VAN WIK. Med. Lav. **78** (2), 124 (1987).
35. L. LE BOUFFANT, H. DANIEL, and J. C. MARTIN. *In* Inhaled particles and vapours. Vol. IV. *Edited by* W. A. Walton. Pergamon Press, London, U.K. 1976. p. 389.
36. M. CHE and A. J. TENCH. Adv. Catal. **31**, 77 (1982).
37. M. CHE and A. J. TENCH. Adv. Catal. **32**, 1 (1982).
38. V. V. NIKISHA, B. N. SHELIMOV, V. A. SHVETS, A. P. GRIVA, and V. B. KAZANSKY. J. Catal. **28**, 230 (1972).
39. B. N. SHELIMOV, C. NACCACHE, and M. CHE. J. Catal. **37**, 279 (1975).
40. A. G. HEPPLESTON. Environ. Health Perspect. **55**, 111 (1984).
41. F. M. ENGLEBRECHT, M. YOGANATHAN, E. J. KING, and G. NAGELSCHMIDT. A.M.A. Archives of Industrial Health, **17**, 287 (1958).
42. U. SAFFIOTTI. *In* Silica, silicosis and cancer. *Edited by* D. F. Goldsmith, D. M. Winn, and C. M. Shy. Praeger Publisher, New York, NY. 1986. p. 287.
43. K. ROBOCK and W. KLOSTERKOTTER. Staub Reinh. Luft, **33**, 60 (1973).

Can. J. Chem. Downloaded from www.nrcresearchpress.com by 84.41.108.74 on 09/07/12
For personal use only.

Photochemical probes of conformational mobility in liquid crystals. The photochemistry of β-phenyl-4-methoxypropiophenone in the nematic and smectic B phases of CCH-*n* and OS-*nm* liquid crystals

MARK S. WORKENTIN, BRIAN J. FAHIE,[1] AND WILLIAM J. LEIGH[2]
Department of Chemistry, McMaster University, Hamilton, Ontario, Canada L8S 4M1
Received May 14, 1991

MARK S. WORKENTIN, BRIAN J. FAHIE, and WILLIAM J. LEIGH. Can. J. Chem. **69**, 1435 (1991).

The photochemistry of β-phenyl-4-methoxypropiophenone (**1**) in the isotropic and liquid crystalline (nematic and smectic B) phases of *trans,trans*-4′-alkyl-(1,1′-bicyclohexyl)-4-carbonitrile (CCH-*n*) and *trans*-4-alkylcyclohexyl-*trans*-4′-alkylcyclohexylcarboxylate (OS-*nm*) mesogens has been investigated using nanosecond laser flash photolysis techniques. Solubility limits of **1** as a function of temperature in the smectic phases have been rigorously determined by ^{2}H NMR spectroscopy, using α-, methoxy-, and β-phenyl-deuterated analogs of the ketone. Triplet decay of **1** in the smectic (Crystal B) phase of CCH-4 is multiexponential, suggesting that the ketone is solubilized in a distribution of conformations in the highly-ordered liquid crystalline lattice. The average triplet lifetime of **1** at various temperatures throughout the smectic phase is about a factor of three longer than that in homologous nematic and isotropic phases at the same temperature. The differences in the Arrhenius parameters for triplet decay in the smectic and nematic/isotropic phases are very small, however. The present results for **1** in the smectic phase of the CCH-*n* mesogens correct the interpretation of previously reported data obtained with higher concentration mixtures, and afford an accurate indication of the true effects of smectic B liquid crystalline order on the conformation-dependent triplet state behavior of this molecule. In OS-*nm* liquid crystals, triplet decay follows clean first order kinetics in all phases, but the variations in Arrhenius dependence with solvent phase are similar to those observed in the CCH-*n* liquid crystals.

Key words: smectic, liquid crystals, ^{2}H NMR, nanosecond laser flash photolysis, intramolecular triplet quenching, photochemistry.

MARK S. WORKENTIN, BRIAN J. FAHIE et WILLIAM J. LEIGH. Can. J. Chem. **69**, 1435 (1991).

On a étudié la photochimie de la β-phényl-4-méthoxypropiophénone (**1**) dans les phases isotropes et cristalline liquide (nématique et smectique) des mésogènes *trans,trans*-4′-alkyl-(1,1-bicyclohexyl)-4-carbonitrile (CCH-*n*) et *trans*-4-alkylcyclohexyl-*trans*-4′-alkyl-cyclohexanecarboxylate (OS-*nm*) en utilisant la technique de photolyse éclair avec un laser à nanoseconde. On a déterminé rigoureusement par la rmn du ^{2}H, la limite de solubilité du composé **1** en fonction de la température dans la phase smectique, en utilisant les analogues α-méthoxy et β-phényl deutériés de la cétone. La décroissance du triplet du composé **1** dans la phase smectique (cristal B) du CCH-4 est multiexponentielle, suggérant ainsi que la cétone est solubilisée avec une distribution de conformations dans le réseau cristallin liquide fortement ordonné. La durée de vie moyenne du triplet du composé **1** à différentes températures à travers la phase smectique est environ trois fois plus longue que celle du triplet dans les phases homologues nématique et isotrope à la même température. Cependant la différence dans les paramètres d'Arrhénius pour la décroissance du triplet dans les phases smectique et nématique/isotrope, est très faible. Les résultats actuels relatifs au composé **1** dans la phase smectique du mésogène CCH-*n* corrigent l'interprétation des résultats obtenus antérieurement avec des mélanges dont la concentration était plus élevée, et fournissent une indication précise sur les effets réels de l'ordre cristallin du liquide smectique B sur la conformation de cette molécule qui dépend du comportement du triplet. Dans les cristaux liquides du OS-*nm*, la décroissance du triplet suit parfaitement une cinétique d'ordre un dans toutes les phases mais les variations d'Arrhénius en fonction du solvant sont semblables à celles observées dans les cristaux liquides du CCH-*n*.

Mots clés : smectique, cristaux liquides, rmn du ^{2}H, photolyse éclair au laser à nanoseconde, blocage du triplet intramoléculaire, photochimie.

[Traduit par la rédaction]

Introduction

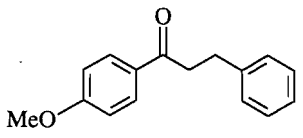
There is considerable interest in the potential effects of liquid crystalline order on the molecular and conformational mobility of dissolved solutes, as well as on various aspects of chemical reactivity that depend on these factors (1). Photochemical and photophysical techniques have been most useful in providing information on the effects of liquid crystals on the rates of conformational and diffusive motions of solutes. These techniques have included static and time-resolved spectroscopic techniques, as well as more qualitative product analysis methods.

We have reported the results of nanosecond laser flash photolysis studies on the triplet state behavior of β-phenyl-4-methoxypropiophenone (**1**) and several derivatives in the smectic (crystal-B) and nematic liquid crystalline phases of *trans,trans*-4′-butylbicyclohexyl-4-carbonitrile (CCH-4) and the 4′-ethyl homolog (CCH-2) (2, 3). β-Phenyl ketones such as **1** possess characteristically short triplet lifetimes in fluid isotropic solvents owing to efficient intramolecular quenching of the carbonyl triplet state by through-space interactions with the β-phenyl ring (4, 5). These interactions involve the n,π* state (6) (which must be either the lowest state or within 2–3 kcal/mol of the lowest state) and require prior formation of a gauche conformation of the molecule (5–8); see eq. [1]. Re-

[1]Present address: Department of Chemistry, University of British Columbia, Vancouver, B.C., Canada V6T 1W5.

[2]Natural Sciences and Engineering Research Council (Canada) University Research Fellow (1983–1993). Author to whom correspondence may be addressed.

Can. J. Chem. Downloaded from www.nrcresearchpress.com by 84.41.108.74 on 09/07/12
For personal use only.

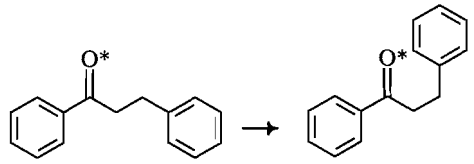


1



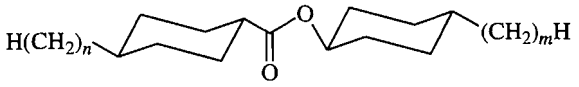
CCH-4: $n = 4$
CCH-2: $n = 2$
CCH-3: $n = 3$

stricting the conformational mobility of the molecule results in an increase in the triplet lifetime. This has been demonstrated for **1** and its parent molecule (β-phenylpropiophenone) using various organized media such as zeolites (7), polymers (6), and cyclodextrin inclusion complexes (8), as well as thermotropic liquid crystals (2, 3). Under these conditions, the triplet lifetime may provide a direct measure of the rates of those conformational motions that allow the molecule to assume the gauche quenching geometry.

[1] 

Our original studies of **1** in the isotropic and liquid crystalline phases of CCH-4 and CCH-2 employed 1.0 mol% samples, a composition that was chosen because it provided adequate optical densities for laser flash photolysis experiments with a nitrogen laser (337 nm) and using 0.7 mm thick cells (2). Under these conditions, triplet decay appears to follow reasonably clean first order kinetics. For the mixtures of **1** with CCH-4, Arrhenius plots of the triplet decay rate showed a distinct change in slope at a temperature close to the smectic–nematic (S–N) transition temperature of the pure mesogen. They indicated increases of ca. 12 kcal/mol and ca. 35 eu in the energy and entropy of activation for triplet decay of **1** in the bulk smectic phase relative to the corresponding values for the nematic and isotropic phases (2). These results were touted as being among the largest reported effects on the conformational mobility and chemical reactivity of solutes dissolved in liquid crystalline media. On the other hand, phase-independent triplet Arrhenius behavior was observed for similar (1.0 mol%) mixtures of **1** in CCH-2 (2). This result is surprising since the smectic phase of this mesogen is known to be more highly ordered than that of CCH-4 (9).

Recently, we have published ^{2}H NMR evidence which indicates that the physical nature of the 1.0 mol% mixture of **1** and CCH-4 that was studied previously is in fact much more complicated than we originally supposed (10). It was shown that the solubility limit of **1** in the smectic phase is temperature dependent and much lower than 1 mol%. It was further shown that the portion of solute in excess of the solubility limit is localized in a solute-enriched nematic phase throughout the 35–53°C temperature range (10), and in a highly concentrated isotropic liquid below 35°C (10–12). We suggested that the triplet lifetimes reported for **1** over the 28–53°C temperature range are actually average values of those due to the ketone in the coexisting smectic and nematic (above 35°C) or isotropic (below 35°C) solutions. Since the proportions of the two co-existing phases — and the concentration of solute in them — varies with temperature, the reported Arrhenius behavior affords an inaccurate indication of the true effects of the smectic phase on the conformational mobility of **1**. We have subsequently suggested (11, 12) that similar problems are likely to have plagued many of the reported studies of solute reactivity or spectroscopy in highly-ordered smectic phases, particularly those using CCH-*n* mesogens (2, 3, 13–16).



OS-53: $n = 5$; $m = 3$
OS-35: $n = 3$; $m = 5$

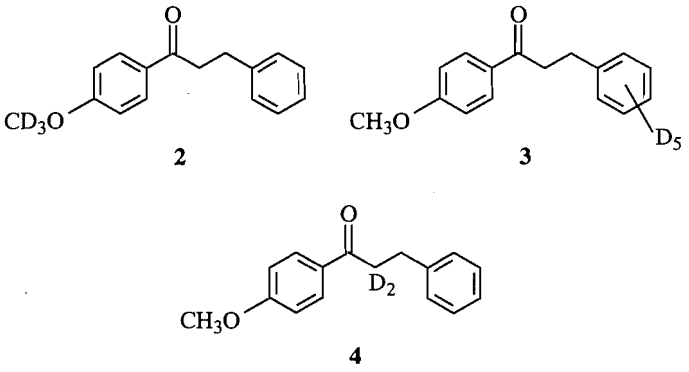
We now report the results of laser flash photolysis and further ^{2}H NMR studies of **1** in the liquid crystalline and isotropic phases of several CCH-*n* mesogens. This work features a careful determination of the solubility limits of the probe in the smectic phases and triplet lifetime data obtained from homogeneous samples of composition well below the solubility limit. By employing various selectively deuterated analogs of **1**, we have now successfully observed distinct ^{2}H NMR spectra of the solute as homogeneous solutions in both the smectic and nematic phases of CCH-4. These allow a more accurate determination of the solubility limits of **1** in the smectic phase than was possible with the α-deuterated analog, which does not exhibit an observable ^{2}H NMR spectrum in this liquid crystalline phase (10). For comparison, we have also carried out similar experiments with mixtures of **1** in the isotropic and liquid crystalline phases of two *trans*-4-alkylcyclohexyl-*trans*-4′-alkylcyclohexylcarboxylate (OS-*nm*) liquid crystals. The smectic phases of these materials have been previously characterized by X-ray diffraction methods (17). The present results afford a true, generalizable indication of the effects of highly ordered smectic liquid crystals on the conformation-dependent triplet state behavior of this molecule.

Results

The selectively deuterated derivatives of **1** that have been employed in this work for ^{2}H NMR experiments (**2–4**) were synthesized using modifications of the reported procedure for the synthesis of **1** (*6a*) (see Experimental section).

Deuterium NMR spectra of **2–4** as 0.1–0.6 mol% mixtures with CCH-4, CCH-2, and the two OS-*nm* liquid crystals were recorded on a 500 MHz spectrometer (operating at 76.8 MHz) at various temperatures throughout the 0–84°C temperature range using the quadrupolar echo pulse sequence (18). Spectra were recorded at 3–5°C intervals starting at the upper end of the temperature range, to ensure that those recorded in the bulk smectic phases are those of uniformly aligned samples. The solvents are all aligned spontaneously by the spectrometer magnetic field when in the nematic phase, and the alignment persists as the temperature is lowered into the corresponding smectic phase (10–12). Sample concentrations were adjusted by trial and error to establish the solubility limits of **1** at representative temperatures throughout the smectic phase ranges

Can. J. Chem. Downloaded from www.nrcresearchpress.com by 84.41.108.74 on 09/07/12
For personal use only.



of CCH-4 (K-28°-S-53°-N-80°-I) (9), OS-53 (K-25°-S-39°-N-53°-I) (17), and OS-35 (K-24°-S-52°-N-54°-I) (17), following the procedure reported previously (10–12). Figure 1 shows representative 76.8 MHz ^2H NMR spectra of 0.21–0.25 mol% samples of **2** and **3** in the nematic and smectic phases of CCH-4 and OS-35. The 0.25 mol% sample of **2**/CCH-4 is homogeneous from 12–45°C, as revealed by the presence of only a single quadrupolar doublet in the NMR spectrum (*e.g.* Fig. 1*a*; 38°C). Similarly, 0.1 mol% samples of **4** in OS-53 and **2** in OS-35 were found to be homogeneous from 4–34°C and 10–46°C, respectively (the smectic–solid transitions (K–S) of all three materials supercool substantially). Compound **4** shows no detectable spectral features in homogeneous smectic solutions of OS-35 or CCH-4, but does so in OS–53. Depending on the temperature, spectra of biphasic mixtures (*i.e.*, of composition above the smectic phase solubility limit) showed smectic + nematic or smectic + isotropic phase components in all cases. A few examples of spectra of this type are included in Fig. 1.

We are unable to observe spectra of **2** and **4** in the smectic phase of CCH-2. Even with 0.1 mol% samples, spectra in the 20–44°C range exhibit only an isotropic singlet, indicating that the solubility of **1** in this smectic phase is substantially lower than 0.1 mol%.

Table 1 lists quadrupolar splittings obtained from the spectra of **2–4** in each of the nematic and smectic phases studied. Those listed for nematic phases were recorded within 1–2°C of the smectic–nematic (S–N) transition temperature, while those listed for the smectic phases were generally recorded at 30 ± 2°C.

Spectra of **2** and **3** as 0.25 mol% solutions in CCH-4 were also recorded at 37°C with a 400 MHz solid state spectrometer (at 61.4 MHz) employing a home-built deuterium probe. The sample was oriented in the spectrometer magnet by cooling from the nematic phase, with the sample tube arranged so that its long axis was parallel to the field direction. Spectra recorded for **2** under these conditions were similar to those recorded with the 500 MHz spectrometer (*e.g.*, Fig. 1*a,b*). Those for **3** were somewhat better resolved, because of a shorter 90° pulse and higher accumulated S/N on the 400 MHz spectrometer. The spectrum of **3** on this spectrometer shows two doublets: a strong inner doublet of splitting 10.5 kHz and a weaker outer doublet of splitting 84.0 kHz (at 37°C). Spectra were then recorded with the sample tube oriented perpendicular to the field direction. In both cases, the appearance of the spectrum changes dramatically with sample orientation, indicating the solute to be well oriented in the liquid crystal (19).

Nanosecond laser flash photolysis experiments employed the pulses from an excimer laser filled with N_2/He (337 nm;

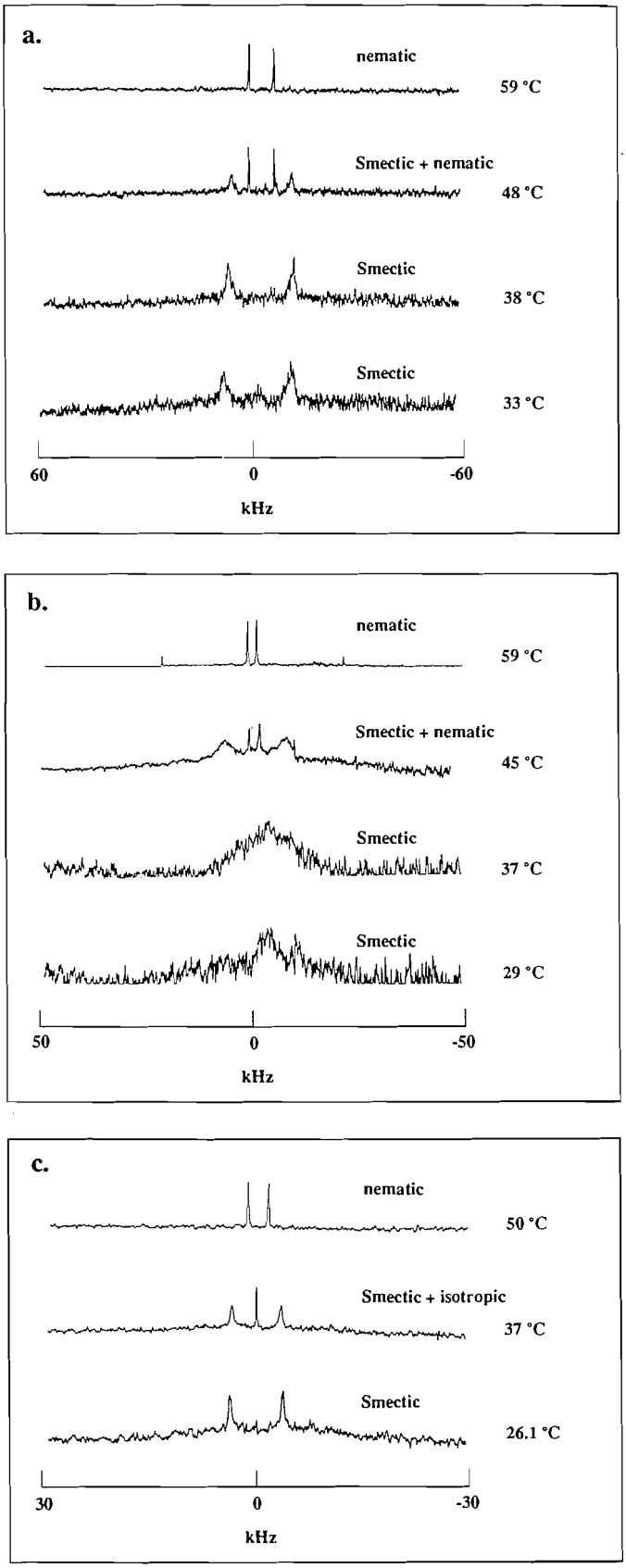


FIG. 1. ^2H NMR spectra of mixtures of (*a*) **2** (0.25 mol%) and (*b*) **3** (0.21 mol%) with CCH-4 and (*c*) **2** (0.25 mol%) with OS-35, recorded at various temperatures between 24 and 84°C using the quadrupolar echo pulse sequence.

Can. J. Chem. Downloaded from www.nrcresearchpress.com by 84.41.108.74 on 09/07/12
For personal use only.

TABLE 1. Quadrupolar splittings from ^2H NMR spectra of **2**–**4** in the nematic and smectic B phases of CCH-*n* and OS-*nm* liquid crystals[a]

Liquid crystal	Phase	**2**	**3**		**4**
			ortho/meta	*para*	
CCH-4	N[b]	7.7	2.1	43.5	25.2
	S[c]	19.4	10.5[d]	84.0[d]	[e]
CCH-2	N[b]	5.1	[f]	[f]	18.8
OS-53	N[b]	4.4	0.2	28.7	22.2
	S[c]	6.5	1.6	[e]	33.0
OS-35	N[b]	2.9	0.4	19.1	14.3
	S[c]	7.3	3.9	[e]	[e]

[a]Recorded at 76.8 MHz, using the quadrupolar echo pulse sequence. Errors in splittings are ca. ±0.1 kHz.
[b]N = nematic; spectra were recorded 1–2° above the S–N transition temperature.
[c]S = smectic; spectra were recorded at 30°C.
[d]Recorded at 61.4 MHz, 37°C.
[e]No signals observable.
[f]Not recorded.

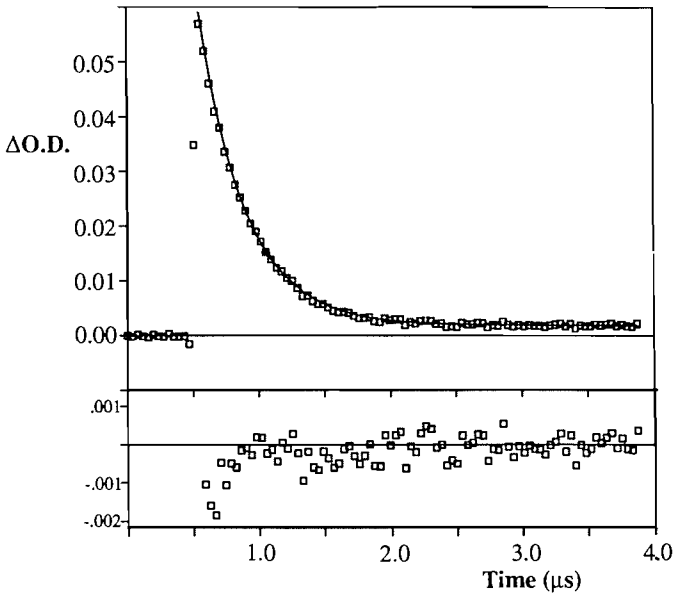


FIG. 2. Representative decay trace from nanosecond laser flash photolysis of a degassed 0.1 mol% solution of **1** in OS-53 at 9.5°C. A plot of the residuals from single-exponential least squares analysis of the data is included.

<6 ns) or Xe/HCl/H_2/He (308 nm; ≤12 ns) mixtures and a microcomputer-controlled detection system (20). Low concentration samples of **1** in CCH-4 and the OS-*nm* liquid crystals were sealed in 3 × 7 mm Suprasil quartz cells after degassing with several freeze–pump–thaw cycles. Sample compositions were 0.25 mol% for CCH-4 and 0.1 mol% for the OS-*nm* liquid crystals. In general, the samples were allowed to anneal for several days at a temperature roughly midway through the smectic phase range, and then slowly cooled to the lower temperature limit. Handling the samples in this way insures that they are homeotropically aligned (*i.e.* glassy). Samples that were cooled quickly from the nematic phase or allowed to sit at room temperature for extended periods of time crystallized and were unsuitable for laser flash photolysis experiments. Static UV absorption spectra of **1** in the various phases of each of the liquid crystals studied showed no discernible differences as a function of solvent phase.

Experiments were also carried out with 1.0 mol% mixtures of **1** with CCH-2 (K-29°-S-44°-N-48°-I) (9), a 2:1 mixture of CCH-2 and CCH-4 (CCH-2/4; K-10°-S-25°-N-57°-I) (9), and CCH-3 (S_2-39°-S_1-53°-N-80°-I) (9). Flash photolysis experiments with solutions of **1** in the nematic phases were carried out using 1.0 mol% samples in 0.7 × 7 mm Pyrex cells, because the turbidity of the unoriented nematic phases rendered the 3 × 7 mm nematic samples opaque, resulting in low light transmission and poor quality results. Experiments were also carried out with deoxygenated 1×10^{-3} M solutions of **1** in acetonitrile over the 5–60°C range.

Laser flash photolysis of all these samples yields intense transient absorptions (λ_{max} = 385 nm) assignable to the triplet state of **1** (2, 3, 6–8). Triplet decays for the nematic and isotropic phase samples followed clean first order kinetics in every case. Decays also followed clean first order kinetics for the smectic solutions of **1** in OS-53 and OS-35; a representative example is shown in Fig. 2. In the case of the 0.25 mol% **1**/CCH-4 sample however, triplet decay is multiexponential at all temperatures throughout the 30–50°C range. Figure 3 shows representative decay traces for this sample at 30.4 and 45.8°C. With each trace is included a plot of the residuals obtained from curve-fitting of the data to two exponential decays. In general, the fit of the data to two exponentials improves at higher temperatures in the smectic phase range. However, the relative contributions of the two components and their lifetimes vary erratically, probably owing to the quality of the data. For this reason, least squares fitting of the data to a single exponential decay was employed to extract average triplet lifetimes for **1** in the smectic phase of CCH-4, using a minimum of 100 data points in each case. These analyses gave linear correlation coefficients of 0.99 or better in every case. Small amounts of residual absorption were frequently evident in the decay traces for the smectic phase samples, but these were not reproducible and never amounted to more than 5–10% of the maximum transient O.D. The fit to two exponentials does not improve at lower laser power, ruling out possible contributions to transient decay from bimolecular triplet processes.

The Arrhenius plot for the 0.25 mol% **1**/CCH-4 mixture is shown in Fig. 4*a*. The (upper) nematic phase line was constructed by combining data from the 1.0 mol% samples with the less extensive data from the 0.25 mol% samples in this range. Also included in this plot are the data obtained from the 1.0 mol% sample of **1** in CCH-2/4, which is nematic over the 25–54°C range (9). Figure 4*b* shows the Arrhenius plot obtained from the lifetime data obtained in OS-53; that obtained with OS-35 is similar to the OS-53 plot and is not shown. Nematic and isotropic phase data for these solvents were obtained from samples of two concentrations (0.1 and 0.6 mol%). Sample opaqueness is a particular problem at temperatures within the S–N transition, making it difficult to obtain data over these ranges. Activation parameters obtained from least-squares analysis of the data according to the Arrhenius and Eyring equations are summarised in Table 2. Table 2 also includes triplet lifetimes for **1** at 30°C in each of the

Can. J. Chem. Downloaded from www.nrcresearchpress.com by 84.41.108.74 on 09/07/12
For personal use only.

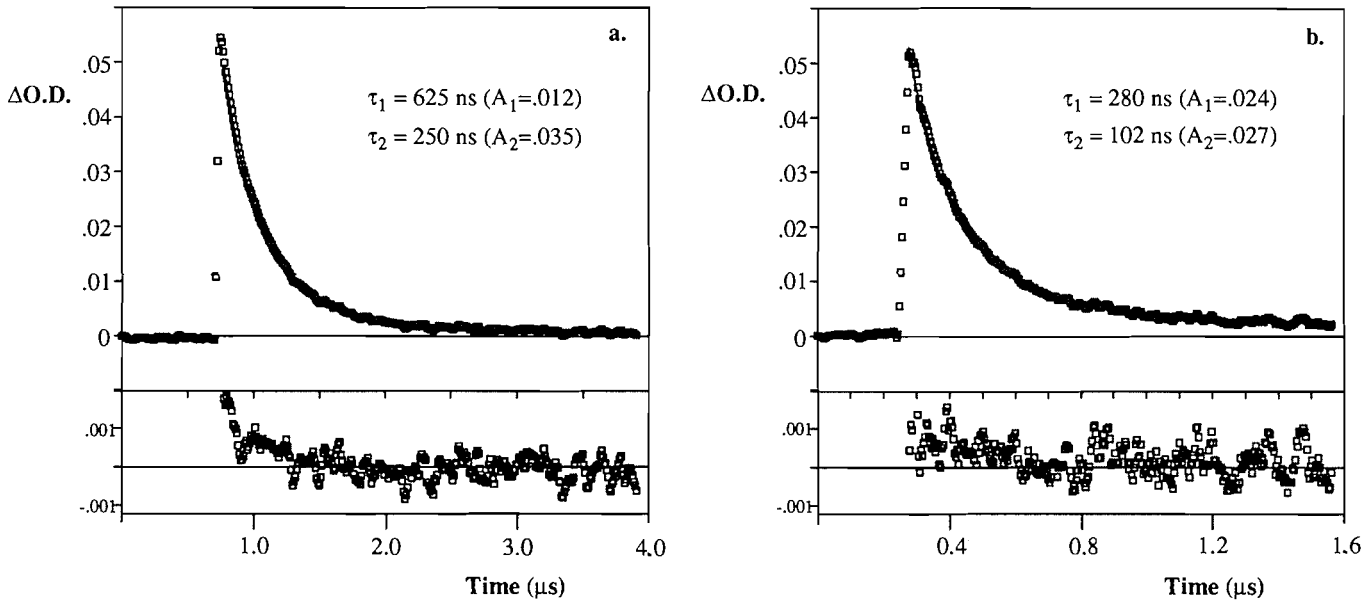


FIG. 3. Representative decay traces from nanosecond laser flash photolysis of a degassed 0.25 mol% smectic solution of **1** in CCH-4 at (*a*) 30.4°C and (*b*) 45.8°C. A plot of the residuals from two-exponential curve-fitting of the data is included for each trace.

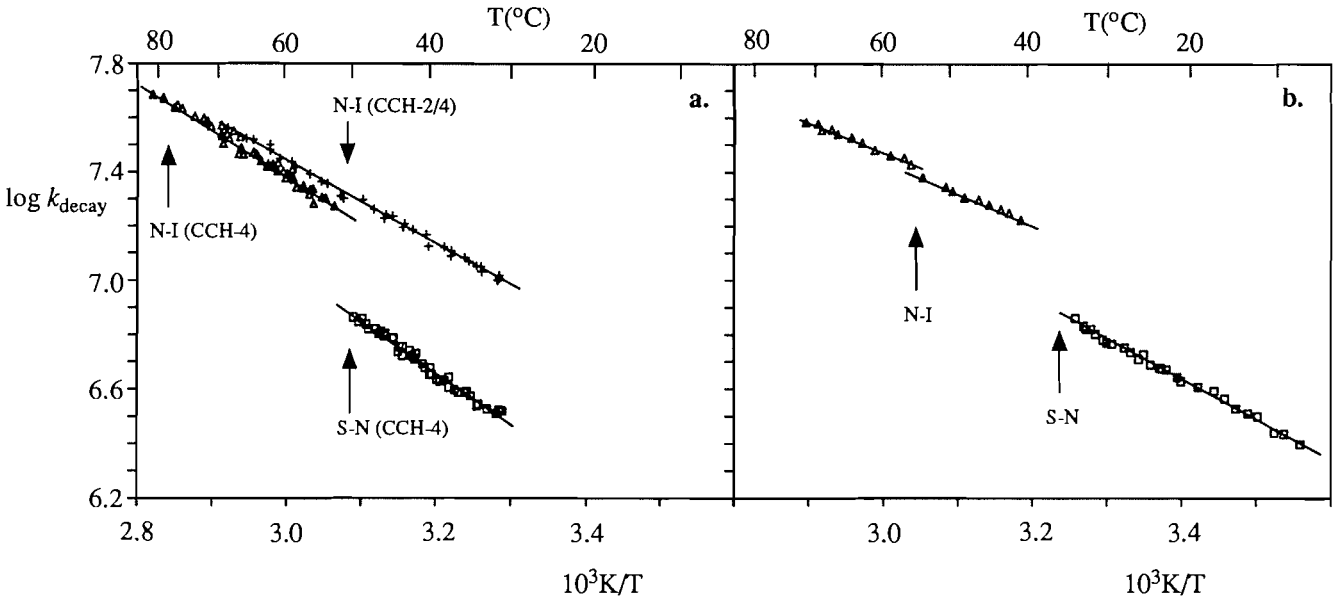


FIG. 4. Arrhenius plots for triplet decay of **1** in (*a*) CCH-*n* and (*b*) OS-53 liquid crystals. (*a*) □, 0.25 mol% **1** in CCH-4; △, 1.0 mol% **1** in CCH-4; +, 1.0 mol% **1** in CCH-2/4; (*b*) 0.1 mol% **1** in OS-53; □, smectic phase data; △, nematic and isotropic phase data.

phases studied; in some cases, these were estimated by extrapolation of the Arrhenius plots defined by data determined at higher temperatures.

Laser flash photolysis experiments were also carried out for 0.01 and 0.1 mol% samples of **1** in purified CCH-2 from 30–70°C (3 × 7 mm cells; 308 nm laser). Decay traces from the 0.1 mol% sample analysed for clean first order kinetics and the lifetimes were superimposable on the Arrhenius plot reported previously for a 1.0 mol% sample (2). The 0.01 mol% sample afforded poor quality traces that appear to be at least two-component in nature. The poor quality of these traces is due to light scattering, which is more pronounced with samples of this mesogen than with those of CCH-4, combined with weak transient signals. The long-lived component of these traces analysed for a lifetime in excess of 1 μs, with a fairly large (±60%) associated error.

Discussion

The morphologies of the smectic phases of the materials employed in the present work have all been established by X-ray diffraction methods (17, 21). That of CCH-4 is classified as a bilayer crystal-B phase (21–23); the constituent molecules are arranged in correlated bilayers of thickness just slightly less than twice the molecular length. Within the

Can. J. Chem. Downloaded from www.nrcresearchpress.com by 84.41.108.74 on 09/07/12
For personal use only.

TABLE 2. Activation parameters and triplet lifetimes for solutions of **1** in liquid crystalline and isotropic solvents[a]

Solvent	Phase	E_a (kcal/mol)	log A (s^{-1})	$\Delta S^{\ddagger}$ (eu)	$\tau_{30°}$ (ns)
CCH-4	S[b]	8.8±0.4	12.8±0.2	−2.1±0.1	346
	N[c]	8.0±0.4	12.6±0.3	−3.0±0.1	150
CCH-2/4	N/I[c]	7.0±0.1	12.0±0.1	−5.8±0.1	112
CCH-2	I[c]	6.0±0.1	11.4±0.1	−8.6±0.1	78[g]
CCH-3	N/I[c]	6.8±0.3	11.9±0.1	−6.2±0.2	105[g]
OS-53	S[d]	6.7±0.2	11.6±0.1	−7.4±0.1	165
	N/I[f]	5.8±0.3	11.3±0.2	−9.2±0.2	73[g]
OS-35	S[d]	7.9±0.4	12.3±0.3	−4.3±0.3	259
	N/I[f]	6.8±0.2	11.9±0.2	−6.6±0.1	96[g]
ACN	I[e]	4.7±0.1	10.8±0.1	−11.5±0.1	40

[a]Errors in Arrhenius parameters are quoted as $\pm 2\sigma$. Errors in lifetimes are ca. 10%. S = smectic; N = nematic; I = isotropic.
[b]Sample composition = 0.25 mol%.
[c]Sample composition = 1.0 mol%.
[d]Sample composition = 0.1 mol%.
[e]Sample concentration = 0.001 M.
[f]Sample composition = 0.5 mol%.
[g]Extrapolated from Arrhenius plot.

bilayers, the molecules are hexagonally close-packed and oriented parallel to one another and perpendicular to the layer plane (21–23). Crystal-B phases possess some degree of three-dimensional positional order (22). The 4′-butyl derivative (CCH-4) forms an enantiotropic smectic phase, and is hence more useful as a reaction solvent than the 4′-propyl derivative (CCH-3), which forms monotropic smectic phases (24*a*). The enantiotropic smectic phase of CCH-2 is characterized by rhombohedral packing and threefold symmetry (21). Miscibility studies have shown that it is a more highly-ordered smectic phase than those of CCH-4 and CCH-3 (9). As a photochemical reaction solvent, it has found considerably less extensive use than CCH-4 (2, 3, 14).

On the basis of X-ray diffraction data, De Maria and coworkers have assigned the smectic phases of OS-53 and OS-35 as smectic B (hexagonal packing of molecules in single layers, with the long axes perpendicular to the layer planes). To the extent that these phases show long-range positional order (17), they should probably also be classified as crystal B. On a qualitative level, they can thus be viewed as similar in order and rigidity to the crystal B phase of CCH-4. However, on a more quantitative level, their relationship to each other and to CCH-4 and CCH-2 are unknown.

The ^2H NMR spectra of the 0.21–0.25 mol% samples of **2**–**4** in CCH-4 which are shown in Fig. 1*a*,*b* define the distinctive spectral patterns characteristic of homogeneous solubilization of these probes in the nematic (53–78°C) and smectic (<48°C) phases of this mesogen. Solubilization in the isotropic phase (>80°C) is characterized by a narrow-line singlet. The nematic phase spectra are characterized by one or more quadrupolar doublets depending on the number of non-equivalent deuteria in the solute. The magnitude of the quadrupolar splitting is a function of the time-averaged angle subtended by the applied magnetic field and the individual C—D bond direction, which is dictated by the overall time-averaged orientation of the solute (25). The maximum splittings observed for each derivative thus vary according to the deuteration site. In the nematic phase, these are 7.7 kHz for **2** and 25.2 kHz for **4** and occur at the lower end of the nematic phase temperature range (*i.e.*, at the *bulk* S–N transition temperature, where ordering in the nematic phase is at a maximum). The nematic phase spectra for **3** are similar to those reported previously for ring-deuterated alkylphenones in CCH-4 (12). They exhibit two sets of doublets: a relatively strong inner doublet with a maximum splitting of 2.1 kHz due to the *ortho*- and *meta*-deuterons, and a weak outer doublet of 43.5 kHz maximum splitting due to the *para*-deuteron. The large difference between the quadrupolar splittings of the *para*- and *ortho*-/*meta*-deuterons is due to differences in their time-averaged orientation with respect to the applied field. The larger value observed for the former indicates that the solute is preferentially oriented with the *para*-C—D bond axis of the β-phenyl ring near perpendicular to the applied magnetic field, parallel to the preferred orientation of the host matrix (because CCH-4 has negative diamagnetic anisotropy (26)). The quadrupolar splitting is at a maximum for deuteria in this orientation.

The smectic phase spectra of **2** and **3** consist of considerably broader absorptions and much larger quadrupolar splittings compared to the nematic phase spectra. In the case of **2**, the doublet splitting is *ca.* 2.5 times larger than in the nematic phase and does not vary appreciably with temperature throughout the 25–50°C range. In the case of **3**, the spectrum consists of broad absorptions flanked by a weaker doublet. The weak outer doublet, which is presumably due to the *para*-deuterons, is unobservable with the spectrometer used to record the spectra shown in Fig. 1*b*. The appearance of the broad inner absorptions changes dramatically as the temperature is lowered below 40°C. Using the 400 MHz solid state NMR spectrometer, both components of the spectrum of **3** can be resolved; at 37°C, the inner doublet splitting is ca. five times larger than in the nematic phase, while the splitting of the weaker outer doublet is *ca.* two times larger. No spectral features are observable at any temperature for homogeneous solutions of **4** in the smectic phase of CCH-4, as noted previously (10). This

Can. J. Chem. Downloaded from www.nrcresearchpress.com by 84.41.108.74 on 09/07/12
For personal use only.

Can. J. Chem. Downloaded from www.nrcresearchpress.com by 84.41.108.74 on 09/07/12
For personal use only.

may indicate that the reorientation rate of the α-CD bonds in the solute is similar in magnitude to the quadrupolar coupling constant, *ca.* 185 kHz (12, 27). The consistently larger splittings observed for **2** and **3** in the smectic compared to the nematic phase indicates that as expected, the solute experiences a greater degree of order (at both ends of the molecule) in the former type of phase. The fact that the appearance of the spectrum changes with sample orientation indicates that the solute is also well-aligned in the smectic phase (19).

The ^{2}H NMR spectra of **2–4** in the liquid crystalline phases of OS-53 and OS-35 are qualitatively similar to those in CCH-4, as expected since OS-*nm* liquid crystals also possess negative diamagnetic anisotropy (24*b*). The splittings are comparatively smaller, however. This presumably indicates that the solute is somewhat less ordered in the nematic and smectic phases of the OS-*nm* liquid crystals than it is in the corresponding phases of CCH-4. As well, a discernible doublet is observed for smectic solutions of **4** in OS-53, in contrast to the behavior of this analogue in smectic solutions of CCH-4 and OS-35.

Spectra recorded at temperatures within phase transitions show signals due to the solute in both the upper- and lower-temperature phases. As we have noted previously, these characteristics can be employed to determine the solubility limits of a solute in the smectic phase as a function of temperature, as well as the type of phases that are present in biphasic liquid crystalline samples. The spectra shown in Fig. 1*a*,*c* demonstrate that the solubility limit of **1** in the crystal B phase of CCH-4 is 0.21 mol% at some temperature higher than 38°C but lower than 48°C (43–44°C, in fact). The solubility limit increases with decreasing temperature throughout the smectic phase range (for example, in a 0.34 mol% **2**/CCH-4 mixture, the nematic phase signals persist to 38°C). At temperatures corresponding to *ca.* 5°C below the S–N transition temperatures of the pure mesogens, the solubility limit of **1** in the OS-*nm* smectic phases is roughly half that in the crystal B phase of CCH-4.

Spectra of a 1.0 mol% mixture of **2** and CCH-4 verify our previous conclusion (10) that a 1.0 mol% **1**/CCH-4 mixture is biphasic throughout the complete 30–52°C range: smectic + nematic between 35 and 52°C, and smectic + isotropic below 35°C.

The Arrhenius plots in Fig. 4 show that the average triplet decay rate of **1** undergoes a significant decrease (by a factor of 2–3) as the samples transform from nematic to smectic solutions. The difference can be ascribed to a sudden change in the conformational mobility of the solute at the S–N transition, consistent with the considerable difference in the degree of order present in the two phases. Sudden "jumps" of this type are observed in many of the properties associated with liquid crystals at transitions between weakly-ordered and highly-ordered phases (28). For a single liquid crystal, the effect is not due to changes in the local polarity experienced by the solute in the two phase types, since there is no change in the static UV absorption spectra of the samples at the phase transitions. The similarities in the Arrhenius plots for homogeneous solutions of **1** in CCH-4, OS-53, and OS-35 indicate that the effect is quite general.

The Arrhenius behavior observed for **1** in CCH-4 in the present work represents the true effects of this liquid crystal on the conformational mobility of the molecule. It confirms our suggestion (10) that the reported behavior of **1** in this liquid crystal (2), which was obtained using a 1 mol% sample, is distorted due to the biphasic nature of a sample of that concentration. The reported triplet lifetimes obtained with that sample represent average values of the lifetime of the ketone in the mobile (nematic or isotropic) phase and the smectic phase, weighted according to the distribution of ketone in the two phases. Since this distribution varies with temperature (mostly nematic at 50°C and mostly smectic at 30°C) (10), the resulting Arrhenius line would be expected to span from the nematic phase line at its low temperature extreme to the true smectic phase line at its low temperature extreme, as was observed (2).

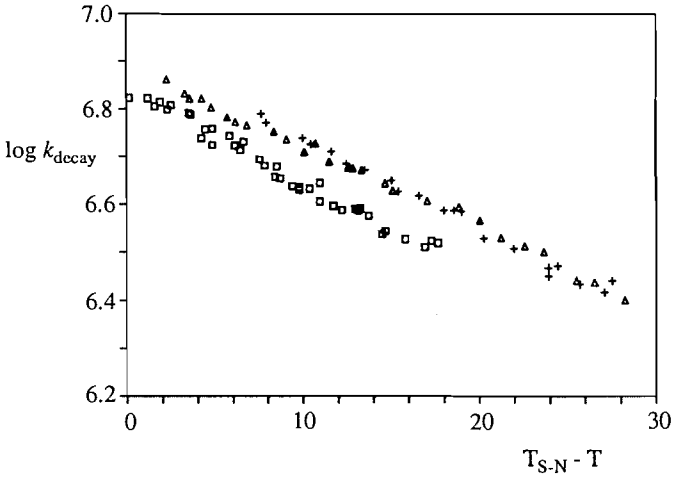


FIG. 5. Plot of log k_{decay} vs. reduced temperature ($T_{S-N} - T$) for triplet decay of **1** in the smectic B phases of CCH-4 and OS-*nm* liquid crystals: □, 0.25 mol% **1** in CCH-4; △, 0.1 mol% **1** in OS-53; +, 0.1 mol% **1** in OS-35. T_{S-N} is the lower temperature onset of the bulk smectic–nematic transition, taken to be 48.5°C for CCH-4, 36°C for OS-53, and 48°C for OS-35.

Figure 5 shows a plot of log k_{decay} versus reduced temperature ($T_{S-N} - T$), constructed by combining the data for *all three* of the smectic phases studied. The T_{S-N} values used to calculate the reduced temperatures were defined as 1°C below the midpoint of the S–N transition range for the mixtures as determined by ^{2}H NMR. The data for the two OS-*nm* smectic phases fall on the same line and appear to be displaced (by 4–5°C) from that defined by the CCH-4 data. We interpret the coincidence of the data for the OS-*nm* liquid crystals as indicating that the factors responsible for determining the triplet lifetime of **1** — local solvent polarity (8b) and rigidity — are similar in the two liquid crystals. The observed displacement of the data for smectic CCH-4 from the line defined by the OS-*nm* data could result from the solute experiencing higher local polarity (6) or greater rigidity in CCH-4. The fact that the nematic/isotropic phase data for the **1**/OS-*nm* mixtures are similarly displaced from those of the **1**/CCH-4 mixtures suggests that the difference in the behavior of **1** in the two classes of smectic phases is largely due to differences in local solvent polarity.

Triplet decay of **1** in CCH-2 was previously reported to be phase-independent, and this was taken to indicate that the solute experiences very little restraint to its conformational mobility in the smectic phase of this mesogen (2). In fact, the present NMR studies of **2** and **4** in CCH-2 indicate that the solubility limit of **1** in smectic CCH-2 is well below 0.1 mol% throughout its complete temperature range, and the bulk of the solute is solubilized in an isotropic liquid phase that coexists with a smectic phase of composition >99.9 mol%

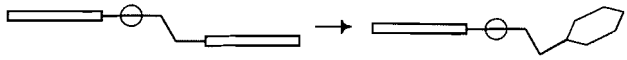
Can. J. Chem. Downloaded from www.nrcresearchpress.com by 84.41.108.74 on 09/07/12
For personal use only.

CCH-2. Thus, the phase-independent triplet state behavior of **1** in CCH-2 is due to the fact that the solute resides largely in an isotropic (and briefly, a nematic) phase throughout the complete temperature range investigated. Below the bulk S–N transition, it is solubilized in a highly concentrated isotropic liquid, but experiences similar effects on mobility as at lower concentrations in the bulk isotropic phase. The much longer lifetimes observed for **1** in a 0.01 mol% sample of smectic CCH-2 suggest that this phase does indeed reduce the mobility of the ketone compared to the isotropic phase.

Triplet decay of **1** in the crystal B phase of CCH-4, even for homogeneous solutions, follows multi-exponential kinetics. This indicates that the ketone is solubilized in a distribution of sites in the liquid crystalline lattice (with varying effects on the conformational mobility of the probe), or in a distribution of conformations. Since triplet decay in these cases can be fairly successfully modelled with a simple first order treatment, the distribution of lifetimes spans only a factor of two or three. The lifetime distribution is comparatively narrower in the OS-*nm* smectic phases, since triplet decay is more accurately represented by simple first order kinetics.

Interestingly, the noticeable changes that occur in the triplet decay rate of **1** in CCH-4 and OS-*nm* at the S–N transitions are the result of barely perceptible alterations in the Arrhenius parameters for triplet decay in the two phase types. For CCH-4, the activation energy and entropy for triplet decay in the crystal-B phase are less than 1.0 kcal/mol and 2 eu higher, respectively, than the corresponding values for the nematic phase. Similar small differences are observed for the OS-*nm* liquid crystals. These barely perceptible changes in the energetics associated with intramolecular quenching at the S–N phase transition may indicate that the solute is in fact rather poorly restrained in the smectic B phases, in spite of the high degree of liquid crystalline order that is known to be associated with this type of phase (21, 22). An alternate possibility is that the solute is well-restrained in the smectic phase, but need undergo only small-amplitude conformational motions to achieve the quenching geometry. This could be the case if the preferred conformation (or distribution of similar conformations) is one in which the β-phenyl ring is already close to that required for intramolecular triplet quenching to occur, or if the spatial requirements for β-phenyl quenching are not as stringent as is implied in eq. [1]. While β-phenyl quenching is known to require overlap of the β-phenyl π-system with the carbonyl *n*-orbital (and hence a *gauche* or eclipsed conformation), the precise geometry or range of geometries required for quenching is unknown.

It is well-known that solutes are incorporated in liquid crystals in a manner dictated by best-packing considerations (28). In liquid crystals of rod-like molecules, rod-like solutes tend to assume the same average orientation as that defined by the solvent matrix (29). However, it does not follow that flexible solutes will necessarily adopt all-*trans* conformations; rather, they will prefer whatever conformations are stabilized the most by the liquid crystalline matrix. Semi-empirical dihedral driver calculations (AM1(30)) for **1** indicate that there exists a *gauche* conformation which is only 2 kcal/mol less stable than the lowest energy all-*trans* conformation; space-filling models indicate that the overall shape of this rod-like conformer is only slightly bulkier than that of the *trans* conformer. Even with reasonably tight packing of the solute in the crystal-B phase, intramolecular quenching in these conformers could occur with relatively slight changes in the overall shape of the

[2] 

excited solute (see reaction [2]), and thus with only slight restriction due to the ordered solvent matrix.

The two solubilization models that are consistent with the flash photolysis data — loose packing with little restriction on large-amplitude conformational motions versus tight packing with little restriction on small-amplitude conformational motions — could presumably be distinguished by further ^{2}H NMR studies that afford quantitative information on the motional rates of the β-phenyl ring deuteria. The first model requires that the β-phenyl ring reorient at rates similar to or faster than the triplet decay rate of **1**, while the second allows for reorientation rates much slower than the triplet decay rate. Studies of this type are in progress.

The Arrhenius parameters for triplet decay of **1** in the various nematic and isotropic phases vary slightly throughout the series (see Table 2). While this may be due to variations in solvent microviscosity, it is difficult to rule out the possibility that minor quenching impurities account for the slight variations in lifetime throughout the series of mesogenic solvents. For CCH-2/4 and the OS-*nm* liquid crystals, for which data have been collected throughout substantial temperature ranges in both the nematic and isotropic phases, there is little or no detectable change in triplet Arrhenius behavior at the N–I transition temperatures. This generalizes our previous conclusion that intramolecular quenching in **1** is unaffected by nematic solvent order in CCH-*n* liquid crystals (2, 3).

Summary and conclusions

The triplet decay rate of β-phenyl-4-methoxypropiophenone (**1**) is a factor of *ca.* 2.5 slower in the smectic B liquid crystalline phases of CCH-*n* and OS-*nm* mesogens than in the corresponding nematic and isotropic phases. Triplet decay is multiexponential in the smectic phase of CCH-4, indicating that the ketone is solubilized in a distribution of conformations or in a distribution of sites in the liquid crystal lattice. The substantial difference in the triplet lifetimes of **1** in the smectic and nematic/isotropic phases is the result of barely perceptible differences in Arrhenius parameters for decay in the highly-ordered and mobile phases, however. The results indicate that, in spite of the high degree of order associated with this type of liquid crystal, the solute experiences fairly small restrictions to the conformational motions required for β-phenyl quenching. This could be the case if the solute's preferred conformation (or distribution of similar conformations) in the liquid crystal is one in which the β-phenyl ring is already close to that required for intramolecular triplet quenching to occur, or if the spatial requirements for β-phenyl quenching are not as stringent as is commonly thought.

Experimental

^{1}H NMR spectra were recorded on Varian EM390 (90 MHz) or Bruker AC200 (200 MHz) spectrometers in deuteriochloroform solution, and are reported in parts per million downfield from tetramethylsilane. Ultraviolet absorption spectra were recorded on a Hewlett-Packard HP8451 UV spectrometer. Mass spectra and exact masses were recorded on a VGH ZABE mass spectrometer; the latter employed a mass of 12.000000 for carbon. Melting points were determined on a hot stage microscope with a Cole-Parmer Model 8110-10 Type K thermocouple.

Acetonitrile (Caledon HPLC) was refluxed over calcium hydride and distilled under nitrogen. Acetone (BDH Reagent) used in the

Can. J. Chem. Downloaded from www.nrcresearchpress.com by 84.41.108.74 on 09/07/12
For personal use only.

preparation of **1** was refluxed over anhydrous potassium carbonate and distilled.

β-Phenyl-4-methoxypropiophenone (**1**) (3), β-phenyl-4-methoxypropiophenone-α,α-d_2 (**4**) (10), and β-phenyl-4-hydroxypropiophenone (4) were prepared in earlier studies. Bromobenzene-d_5, 4-methoxyacetophenone, 4-hydroxyacetophenone, iodomethane-d_3 (all from Aldrich Chemical Co.), dichloromethane (Baker, HPLC grade), CCH-4, CCH-3, CCH-2, OS-35, and OS-53 (E. Merck) were used as received from the suppliers. For some of the flash photolysis experiments, CCH-2 was recrystallised three times from pentane (Baker Photrex).

β-Phenyl-4-(methoxy-d_3)propiophenone (**2**) was prepared from β-phenyl-4-hydroxypropiophenone, iodomethane-d_3, and potassium carbonate in refluxing acetone (4), and was recrystallized twice from aqueous ethanol (mp = 94–95°C). It exhibited the following ^{1}H NMR spectrum: δ(ppm) = 3.1 (m, 2H), 3.2 (m, 2H), 6.9 (d, 2H), 7.2 (s, 5H), 7.9 (d, 2H). Exact mass: calcd. for $C_{16}H_{13}O_2D_3$: 243.1350; found: 243.1346.

β-(Phenyl-d_5)-4-methoxypropiophenone (**3**) was prepared by condensing 4-methoxyacetophenone with benzaldehyde-d_5 (prepared from phenyl-d_5 magnesium bromide and *N*-formylmorpholine (31)) and hydrogenation of the resulting chalcone derivative over Raney nickel in deoxygenated ethyl acetate (4). Compound **3** was recrystallised twice from 95% ethanol (mp 95–97°C) and exhibited the following ^{1}H NMR spectrum: δ(ppm) = 3.04 (m, 2H), 3.24 (m, 2H), 3.85 (s, 3H), 6.90 (d, 2H), 7.92 (d, 2H). Exact mass: calcd. for $C_{16}H_{11}O_2D_5$: 245.1464; found: 245.1465.

Deuterium NMR spectroscopy

^{2}H NMR experiments were carried out at 76.78 MHz on a Bruker AM500 NMR spectrometer equipped with an Aspect 3000 computer, a Bruker BVT-100 Variable Temperature Unit, and a 10 mm VSP broadband probe. Temperatures were controlled to within 0.2°C and were calibrated with a copper–constantan thermocouple. Samples were prepared by combining the appropriate amounts of solute and liquid crystal and heating to the isotropic phase to ensure complete sample mixing. They were then placed in 5 mm NMR tubes. The sample and probe were allowed to equilibrate at each temperature for 10–20 min prior to recording the spectrum. Spectra were recorded on stationary samples using the quadrupolar echo pulse sequence (18), collecting 16K data points per scan over a 40–170 kHz sweep width. Depending on the bulk concentration and temperature, 96–12000 scans were collected with a 0.2–0.4 s delay between scans, and averaged. A few experiments were carried out at 61.4 MHz on a Bruker MSL400 NMR spectrometer equipped with an Aspect 3000 computer, Bruker BVT-100 Variable Temperature Unit, and a home-built deuterium probe. The π/2 pulse width was determined to be 14–16 μs for the AM500 and 4 μs for the MSL400 spectrometers by trial and error using $CDCl_3$(10%)/$CHCl_3$ solutions. The data were processed using exponential multiplication and 80–100 Hz line-broadening prior to obtaining the Fourier transform.

Laser flash photolysis

Nanosecond laser flash photolysis experiments employed the pulses from a Lumonics TE-861M excimer laser filled with Xe/HCl/H_2/He (308 nm, 15 ns, *ca.* 40 mJ) or N_2/He (337 nm, 6 ns, *ca.* 4 mJ) mixtures and the microcomputer-controlled detection system which has been described elsewhere (20). The sample compartment was surrounded by an insulated quartz sleeve, through which heated nitrogen was passed in order to heat the sample. Sample temperatures were measured using a copper-constantan thermocouple or a Cole-Parmer Type K digital thermocouple thermometer and are accurate to ±0.1°C. The samples were allowed to equilibrate at each temperature for at least 20 min prior to recording the decay trace.

Samples were contained in 3 × 7 mm or 0.7 × 7 mm cells constructed from rectangular Suprasil quartz or Pyrex tubing, respectively (Vitro Dynamics). Except for the low concentration samples in CCH-2, they were prepared by weighing out the appropriate amount of solute and liquid crystal and heating to the isotropic phase to ensure complete sample mixing. Samples of composition <0.1 mol% were prepared by adding an aliquot of a standard solution of **1** in dichloromethane to the appropriate amount of liquid crystal. The mixture was dissolved completely in dichloromethane and the solvent was removed on a rotary evaporator and then pumped under high vacuum (*ca.* 10^{-4} Torr) for several hours. Samples of 1 mol% or greater **1** were contained in the 0.7 mm cells, while all others were contained in the 3 mm cells. They were degassed with five freeze–pump–thaw cycles and sealed on a vacuum line. Except where noted, samples were annealed for several days at 38°C, which produced homeotropically aligned samples.

Acknowledgments

We wish to thank E. Merck (Darmstadt) for generous gifts of the CCH-*n* and OS-*nm* liquid crystals, and Dr. C. Fyfe (University of British Columbia) for the use of his solid state NMR spectrometer. The financial support of the Natural Sciences and Engineering Research Council of Canada is gratefully acknowledged.

1. For reviews see (*a*) V. RAMAMURTHY. Tetrahedron, **42**, 5753 (1986); (*b*) W. J. LEIGH. *In* Photochemistry on solid surfaces. *Edited by* T. Matsuura and M. Anpo. Elsevier, Amsterdam. 1989. Chapt. 9.2; (*c*) M. F. SONNENSCHEIN and R. G. WEISS. *In* Photochemistry on solid surfaces. *Edited by* T. Matsuura and M. Anpo. Elsevier, Amsterdam. 1989. Chapt. 9.4; (*d*) R. G. WEISS. Tetrahedron, **44**, 3413 (1988); (*e*) W. J. LEIGH. *In* Liquid crystals – applications and uses. Vol. II. *Edited by* B. Bahadur. World Interscience, Bangalore. 1991. Chapt. 27.
2. W. J. LEIGH. J. Am. Chem. Soc. **107**, 6114 (1985).
3. W. J. LEIGH. Can. J. Chem. **64**, 1130 (1986).
4. (*a*) D. G. WHITTEN and W. E. PUNCH. Mol. Photochem. **2**, 77 (1980); (*b*) P. J. WAGNER, P. A. KELSO, A. E. KEMPPAINEN, A. HAUG, and D. R. GRABER. Mol. Photochem. **2**, 81 (1980); (*c*) D. E. STERMITZ, V. P. MURALIDHARAN, and C. M. O'DONNEL. Mol. Photochem. **2**, 87 (1980).
5. J. C. SCAIANO, M. J. PERKINS, J. W. SHEPPARD, M. S. PLATZ, and R. L. BARCUS. J. Photochem. **21**, 137 (1983).
6. (*a*) J. C. NETTO-FERREIRA, W. J. LEIGH, and J. C. SCAIANO. J. Am. Chem. Soc. **107**, 2617 (1985); (*b*) W. J. LEIGH, J. C. SCAIANO, C. I. PARASKEVOPOULOS, G. M. CHARETTE, and S. E. SUGAMORI. Macromolecules, **18**, 2148 (1985).
7. H. C. CASAL and J. C. SCAIANO. Can. J. Chem. **62**, 628 (1984).
8. (*a*) H. C. CASAL, J. C. NETTO-FERREIRA, and J. C. SCAIANO. J. Incl. Phenom. **3**, 395 (1985); (*b*) J. C. NETTO-FERREIRA and J. C. SCAIANO. J. Photochem. Photobiol. A, **45**, 109 (1988).
9. D. S. MITCHELL and W. J. LEIGH. Liq. Cryst. **4**, 39 (1989).
10. B. J. FAHIE, D. S. MITCHELL, and W. J. LEIGH. Can. J. Chem. **67**, 148 (1989).
11. B. J. FAHIE, D. S. MITCHELL, M. S. WORKENTIN, and W. J. LEIGH. J. Am. Chem. Soc. **111**, 2916 (1989).
12. M. S. WORKENTIN, W. J. LEIGH, and K. R. JEFFREY. J. Am. Chem. Soc. **112**, 7329 (1990).
13. (*a*) V. C. ANDERSON and R. G. WEISS. J. Am. Chem. Soc. **106**, 6628 (1984); (*b*) D. A. HROVAT, J. H. LIU, N. J. TURRO, and R. G. WEISS. J. Am. Chem. Soc. **106**, 7033 (1984); (*c*) R. G. ZIMMERMAN, J. H. LIU, and R. G. WEISS. J. Am. Chem. Soc. **108**, 5264 (1986); (*d*) R. L. TREANOR and R. G. WEISS. J. Phys. Chem. **91**, 5552 (1987).
14. W. J. LEIGH and S. K. JAKOBS. Tetrahedron, **43**, 1393 (1987).
15. (*a*) B. M. FUNG and M. GANGODA. J. Am. Chem. Soc. **107**, 3395 (1985); (*b*) M. GANGODA and B. M. FUNG. Chem. Phys. Lett. **120**, 527 (1985).
16. H. FUJIWARA, J. HIRAI, Y. SASAKI, and K. TAKAHASHI. Mol. Cryst. Liq. Cryst. **150B**, 387 (1987).
17. P. DE MARIA, P. MARIANI, F. RUSTICHELLI, and B. SAMORI. Mol. Cryst. Liq. Cryst. **116**, 115 (1984).
18. (*a*) J. H. DAVIS, K. R. JEFFREY, M. BLOOM, M. I. VALIC, and

T. P. HIGGS. Chem. Phys. Lett. **42**, 390 (1976); (*b*) M. BLOOM, J. H. DAVIS, and M. I. VALIC. Can. J. Phys. **58**, 1510 (1980).
19. R. HENTSCHEL, H. SILLESCU, and H. W. SPIESS. Polymer, **22**, 1516 (1981).
20. W. J. LEIGH, M. S. WORKENTIN, and D. J. ANDREW. J. Photochem. Photobiol. A: Chem. **57**, 97 (1991).
21. E. RAHIMZADEH, T. TSANG, and L. YIN. Mol. Cryst. Liq. Cryst. **139**, 291 (1986).
22. (*a*) G. J. BROWNSEY and A. J. LEADBETTER. J. Phys. (Les Ulis, Fr.) **42**, L135 (1981); (*b*) A. J. LEADBETTER, J. C. FROST, and M. A. MAZID. J. Phys. (Les Ulis, Fr.) **40**, L325 (1979).
23. G. W. GRAY and J. W. G. GOODBY. Smectic liquid crystals — textures and structures. Leonard Hill: London, 1984.
24. (*a*) Licristal Liquid Crystals, EM Chemicals, Hawthorne, NY. 1985; (*b*) DR. V. BECKER (E. Merck, Co., Darmstadt, FRG). Private communication.
25. (*a*) A. G. AVANT, J. M. EMSLEY, S. NG, and S. M. VENABLES. J. Chem. Soc. Perkin Trans. II, 1855 (1984); (*b*) J. W. EMSLEY, R. HASHIM, G. R. LUCKHURST, and G. N. SHILSTONE. Liq. Cryst. **1**, 437 (1986).
26. (*a*) L. POHL, R. EIDENSCHINK, J. KRAUSE, and G. WEBER. Phys. Lett. A, **65**, 169 (1978); (*b*) L. POHL and R. EIDENSCHINK. Anal. Chem. **50**, 1934 (1978).
27. H. W. SPIESS and H. SILLESCU. J. Magn. Reson. **42**, 381 (1981).
28. H. KELKER and R. HATZ. Handbook of liquid crystals. Verlag Chemie, Weinheim. 1980.
29. E. SACKMANN, P. KREBS, H. U. REGA, J. VOSS, and H. MÖHWALD. Mol. Cryst. Liq. Cryst. **24**, 283 (1973).
30. AM1 calculations were carried out with Version 2.1 of the general purpose molecular orbital computational package AMPAC: Austin Method 1 Package, 1.0 QCPE 506. Dewar Research Group and J. P. Stewart, QCPE Bull. **6**, 24a,b (1986).
31. G. A. OLAH, L. OHANNESIAN, and M. ARVANAGHI. J. Org. Chem. **49**, 3856 (1984).

Can. J. Chem. Downloaded from www.nrcresearchpress.com by 84.41.108.74 on 09/07/12
For personal use only.

Stereochemistry and kinetics of amines addition to acetylenic esters

SABER M. SHARAF, SAMIR K. EL-SADANY, EZZAT A. HAMED, AND ABDEL-HAMID A. YOUSSEF[1]
Department of Chemistry, Faculty of Science, Alexandria University, Alexandria, Egypt

Received October 19, 1990

SABER M. SHARAF, SAMIR K. EL-SADANY, EZZAT A. HAMED, and ABDEL-HAMID A. YOUSSEF. Can. J. Chem. **69**, 1445 (1991).

The reactions of a series of methyl *para*-substituted phenylpropiolates **1***a–e* with piperidine, morpholine, and diethylamine in methanol and dimethylformamide (DMF) have been studied and their rates measured. The products were methyl β-(*N*,*N*-dialkylamino)-*p*-substituted cinnamates **2–4***a–e*. ^{1}H NMR spectra were used to determine the configuration of the products. The ρ values in methanol ranged between 0.34 and 1.24 whereas in DMF they were between 0.85 and 1.88. The values of $\Delta S^{\neq}$ favor a bimolecular rate-limiting step mechanism.

Key words: nucleophilic addition to acetylenic esters.

SABER M. SHARAF, SAMIR K. EL-SADANY, EZZAT A. HAMED et ABDEL-HAMID A. YOUSSEF. Can. J. Chem. **69**, 1445 (1991).

On a étudié les réactions d'une série de phenylpropiolates de méthyle substitués en position *para*, **1***a–e* avec la pipéridine, la morpholine et la diéthylamine dans le méthanol et dans le diméthylformamide (DMF) et on a également mesuré les vitesses de réaction. On a obtenu des β-(*N*,*N*-dialkylamino)cinnamates de méthyle substitués en position *para* **2–4***a–e* et on a déterminé leur configuration à partir des spectres RMN du ^{1}H. La valeur de ρ se situent entre 0,34 et 1,24 dans le méthanol et entre 0,85 et 1,88 dans le DMF. Les valeurs de $\Delta S^{\neq}$ suggèrent qu'une réaction bimoléculaire constitue l'étape déterminante.

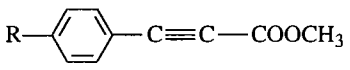
Mots clés : addition nucléophile aux esters acétyléniques.

[Traduit par la rédaction]

Introduction

Nucleophilic additions to activated alkynes have been studied from synthetic and stereochemical points of view (1, 2). Previously, it was suggested (3, 4) that the reaction of amines with acetylenic compounds may involve *cisoid* additions, whereas others (2, 5) have found *transoid* products. Both types of additions depend upon many factors. These include the basicity, steric requirements of the amines, substituents in the aromatic ring conjugated with the acetylenic bond, and the nature of the solvent as well as the temperature (5–10).

In continuation of our studies on the reactions of acetylenic compounds (9), this work involves the study of the stereochemistry and kinetics of the addition of piperidine, morpholine, and diethylamine to methyl *p*-substituted phenylpropiolates **1***a–e* in methanol and dimethylformamide (DMF).



1 *a–e*

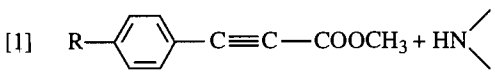
a, R = H; *b*, R = CH_3; *c*, R = Br; *d*, R = Cl; *e*, R = NO_2

Results and discussion

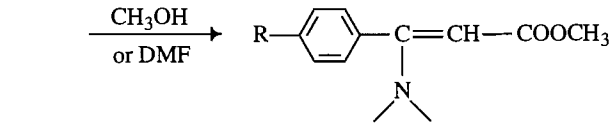
The products obtained from the reaction of amines and the acetylenic esters **1***a–e* in methanol and DMF have been isolated and identified as methyl β-(*N*,*N*-dialkylamino) *p*-substituted cinnamates, eq. [1]. ^{1}H NMR data indicate the presence of only one piperidino, morpholino, or *N*,*N*-diethylamino group. The IR bands at 1495–1560 cm^{-1} indicate a double bond stretching, which is a typical conjugated β-enamino-ester structure (11). The strong band at 1690–1700 cm^{-1} was assigned to the >C=O of the conjugated ester group (12).

Configuration of the products

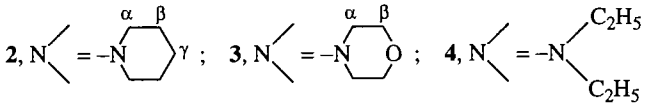
The elucidation of the configuration of the products was, however, difficult due to the fact that only one geometrical isomer (except **2–4***e* in DMF) is accessible. The ^{1}H NMR data of the products obtained from the reaction of **1***a–e* with piperidine, morpholine, and diethylamine in methanol showed a

[1] 

1 *a–e*

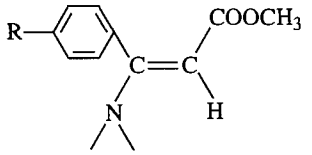


2–4*a–e*

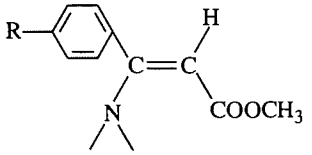


singlet for a vinylic proton at δ 4.72–5.00. The *E* configuration of these products was established by comparing the chemical shifts of the vinylic protons in their ^{1}H NMR spectra to the related derivatives (9, 13, 14). Furthermore, the calculated chemical shift values of the vinylic protons, obtained by applying the NMR rules of additivity (15, 16), for *E*- and *Z*-β-(*N*,*N*-dialkylamino) cinnamate esters ($\delta_{calc.}$ = 4.72 and 5.20 ppm, respectively) indicated the *E* configuration for the isolated products **2–4***a–e* (δ_{obs} = 4.72–5.00 ppm).

The products obtained from these reactions in DMF also gave a singlet vinylic proton for *E* adducts **2***a–d*, **3***a–d*, and **4***a–d*, whereas **2***e*, **3***e*, and **4***e* showed two vinylic protons at δ 4.72–5.00 and 5.23–5.63 ppm indicating the presence of a mixture of *E* and *Z* isomers, respectively. Similarly, two singlets at δ 3.47–3.50 and 3.62–3.65 ppm were observed for the OCH_3 group of the *p*-nitro esters with a ratio *E*:*Z* of 73:27%; 67:33%; 63:37%, respectively, depending on the amine used.



E-**2***e*, **3***e*, **4***e*



Z-**2***a–e*, **3***a–e*, **4***a–e*

[1]Author to whom correspondence may be addressed.

Printed in Canada / Imprimé au Canada

Can. J. Chem. Downloaded from www.nrcresearchpress.com by 84.41.108.74 on 09/07/12
For personal use only.

TABLE 1. Rate constants and activation parameters for the reaction of compounds **1***a–e* with amines

Compound no.	Amine	$k_2^a \times 10^5$ (L mol^{-1} s^{-1}) 30°C	40°C	50°C	$\Delta H^{\neq}$ (kcal mol^{-1})	$\Delta S^{\neq}$ (eu)	$k_3^b \times 10^3$ (L mol^{-2} s^{-1}) 30°C	40°C	50°C	$\Delta H^{\neq}$ (kcal mol^{-1})	$\Delta S^{\neq}$ (eu)
1*a*	Piperidine	151.0	263.0	267.0	12.2	−31.3	72.2	79.9	133.3	5.3	−46.2
1*b*		63.7	226.0	469.0	18.8	−11.1	49.3	73.3	10.3	6.6	−42.9
1*c*		156.0	333.0	600.0	12.5	−30.3	105.2	156.7	212.3	6.2	−42.6
1*d*		177.0	400.0	750.0	13.4	−26.9	112.5	166.7	222.5	6.1	−42.8
1*e*		667.0	950.0	1330.0	5.1	−51.5	213.4	253.6	305.3	3.0	−51.7
1*a*	Diethylamine	42.0	111.1	294.4	18.2	−13.9	12.4	20.3	32.8	8.8	−38.2
1*b*		25.6	64.8	277.6	22.4	−9.7	4.5	10.7	21.7	14.6	−21.0
1*c*		75.9	194.4	395.9	15.4	−21.9	29.2	36.5	46.1	3.8	−52.9
1*d*		77.8	203.7	422.2	14.3	−25.5	30.3	36.8	46.5	3.5	−53.8
1*e*		284.4	406.7	568.8	6.1	−50.2	233.3	313.9	406.3	4.7	−45.8
1*a*	Morpholine	6.9	22.8	70.4	21.9	−5.4	4.2	10.4	26.4	17.1	−12.9
1*b*		4.3	17.4	47.2	22.7	−3.7	1.9	6.4	15.3	19.3	−7.1
1*c*		19.1	43.2	102.0	15.5	−23.9	10.6	22.69	34.4	10.8	−29.7
1*d*		18.1	43.2	106.0	16.5	−21.1	10.8	23.1	38.2	11.6	−29.2
1*e*		63.8	146.0	276.0	13.6	−28.3	211.1	255.0	308.3	3.0	−51.7

[a]Methanol.
[b]DMF.

Kinetics of the reactions

The kinetics of the formation of methyl β-(*N*,*N*-dialkylamino) *p*-substituted cinnamates in methanol and DMF were studied by following the gradual decrease of amine concentration as a function of time. The reactions in methanol showed second-order kinetics, those in DMF followed third-order kinetics, first order in the substrate and second order in the amine (Table 1).

The rates of amine addition to **1***a–e* in both solvents depend on the type of amine and the *p*-substituent. The order of reactivity of amines is piperidine > morpholine > diethylamine, suggesting that these reactions are controlled not only by the basicity of the amines but also by their steric requirements (17).

Hammett plots gave good straight lines for these reactions with a slight deviation from linearity for the reactions of **1***e* in DMF. The ρ values ranged between +0.34:1.24 and +0.85:1.88 in methanol and DMF respectively, depending on the temperature and the amine used. These values of ρ, as shown before (9), point to the formation of a transition state with some anionic character developed at the carbon atom adjacent to the carbomethoxy group.

The thermodynamic parameters $\Delta S^{\neq}$ and $\Delta H^{\neq}$ were calculated using the least-squares method, Table 1. The observed negative entropies of activation $\Delta S^{\neq}$ are expected for adduct formation from neutral species, and the magnitudes of $\Delta S^{\neq}$ values point to the formation of highly ordered transition states. This suggests that the mechanism of these addition reactions is a bimolecular one (17, 18).

Mechanism of the reaction

The reaction in methanol involves an initial rate-limiting addition step of the amine to the appropriate acetylenic ester **1***a–e*. The function of the methanol molecule can be regarded as a proton donor through a six-membered transition state **6** leading to the formation of the *E* isomer, predominantly independent of the substrate/amine molar ratio.

The reaction in DMF, however, showed a second-order dependence of the amine used, since the amine molecule exists as a hydrogen-bonded dimer (17). The participation of the amine dimer can be interpreted as a synchronous proton transfer in which one molecule of the acetylenic ester shares with it to form a cyclic transition state **6**, Scheme 1. A similar mechanism was suggested earlier for the reaction of 1,3-diphenyl-2-propyn-1-one with morpholine in dioxane (18) and *trans*-chalcone with pyrrolidine in heptane (19).

The reactions of **1***e* with amines in DMF yielded a mixture of *E* and *Z* isomers (Scheme 1). This could occur by either a two-step process in which addition of the amine led to **5**, which underwent protonation to the *E*/*Z* mixture, or by the competing formation of **5** and **6**.

The reaction of **1***e* with morpholine in methanol and DMF was followed by ^{1}H NMR spectroscopy. In methanol only the *E* product was identified throughout the whole reaction. However, in DMF two vinylic protons were observed and their ratio did not change with time. This indicates that the mechanism proceeds via *syn*-addition with absence of isomerization of the product under the reaction conditions.

In conclusion, *syn*-additon via **6** is favored for the reaction of **1***a–e* with different amines in methanol and **1***a–d* in DMF, since it leads to the formation of only the *E* isomer, as observed. In the case of the reaction of **1***e* with amines in DMF there is a competing *anti*-protonation, giving a mixture of *E* and *Z* isomers.

Experimental

Infrared and ultraviolet spectra were measured on Pye Unicam SP 1025 and SP 800 spectrometers, respectively.

The ^{1}H NMR spectra were measured on a Varian EM 390 90-MHz spectrometer. Microanalyses were done at the microanalytical laboratories, Alexandria University; melting points and boiling points are uncorrected.

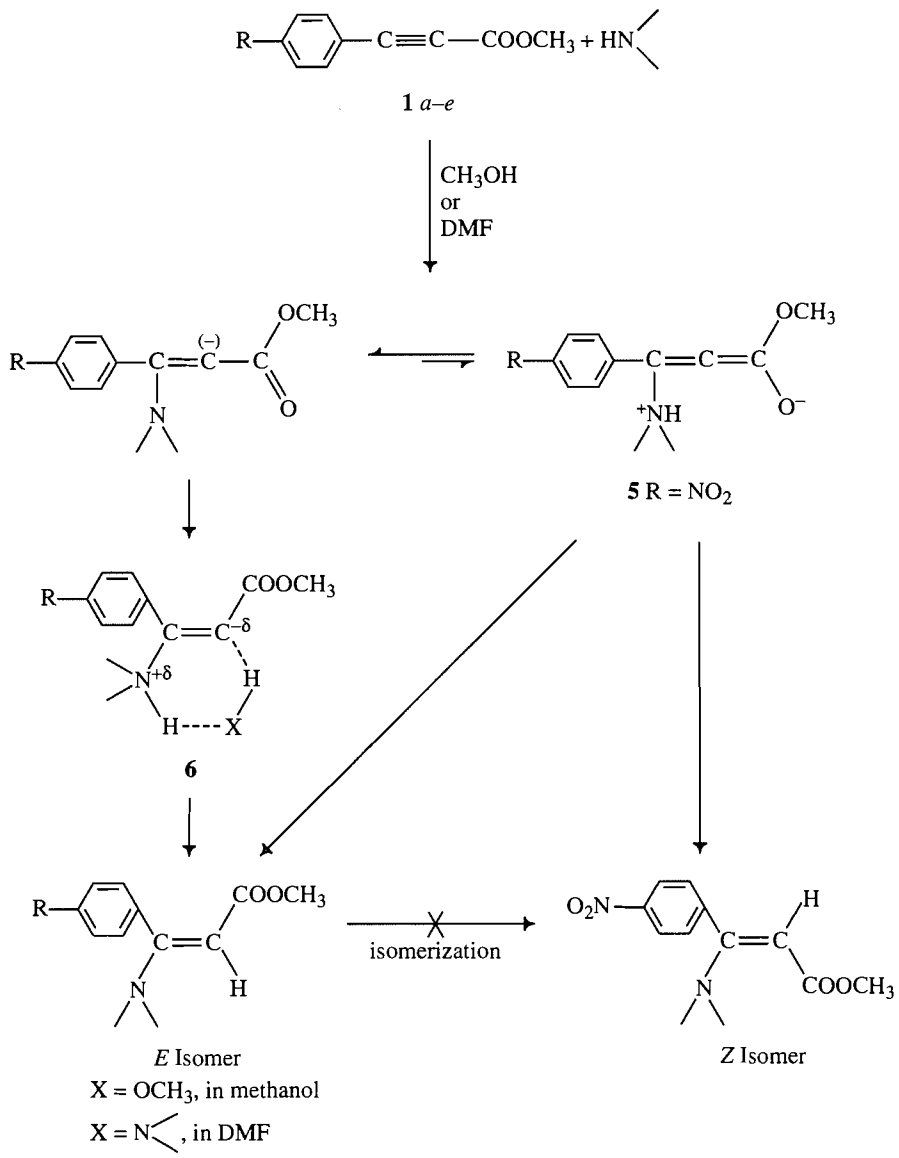
Preparation of starting materials

para-Substituted phenylpropiolic acids were prepared by heating methyl 2,3-dibromo-3-(*p*-substituted phenyl)-propanoates (20) with 25% methanolic potassium hydroxide on a steam bath. The methyl esters **1***a–e* were, however, obtained by treatment of the acids with dry hydrogen chloride gas in methanol.

Methyl phenylpropiolate ***1****a*

Pale yellow oil; bp 110°C/20 Torr (1 Torr = 133.3 Pa); IR (Nujol): 1610, 1720, and 2225 cm^{-1}; UV (methanol): λ = 260 nm (ε = 10 000);

Can. J. Chem. Downloaded from www.nrcresearchpress.com by 84.41.108.74 on 09/07/12
For personal use only.



SCHEME 1

^{1}H NMR ($CDCl_3$) δ: 7.23–7.80 (m, 5H, Ph), 3.83 (s, 3H, -OCH_3) ppm.

Methyl p-*methylphenylpropiolate* **1**b

Colourless plates from methanol, mp 62°C; IR(KBr): 1605, 1710, and 2230 cm^{-1}; UV (methanol): λ = 267 nm (ε = 17 600); ^{1}H NMR ($CDCl_3$) δ: 7.37, 7.03 (dd, 4H, aryl), 3.73 (s, 3H, OCH_3), and 2.31 (s, 3H, *p*-CH_3) ppm. Anal. calcd. for $C_{11}H_{10}O_2$: C 75.86, H 5.75; found: C 75.55, H 5.77.

Methyl p-*bromophenylpropiolate* **1**c

Colourless plates from methanol, mp 105°C; IR(KBr): 1585, 1730, and 2240 cm^{-1}; UV (methanol): λ = 247 nm (ε = 16 000); ^{1}H NMR ($CDCl_3$) δ: 7.60–7.10 (m, 4H, aryl), 3.70 (s, 3H, OCH_3) ppm. Anal. calcd. for $C_{10}H_7BrO_2$: C 50.20, H 2.93; found: C 50.36, H 3.10.

Methyl p-*chlorophenylpropiolate* **1**d

Colourless plates from methanol, mp 88°C; IR(KBr): 1590 and 2240 cm^{-1}; UV (methanol): λ = 265 nm (ε = 24 000); ^{1}H NMR ($CDCl_3$) δ: 7.65–7.10 (m, 4H, aryl), 3.74 (s, 3H, OCH_3) ppm. Anal. calcd. for $C_{10}H_7ClO_2$: C 61.71, H 3.63; found: C 61.99, H 3.65.

Methyl p-*nitrophenylpropiolate* **1**e

Pale yellow plates from methanol, mp 110°C; IR(KBr): 1595, 1715, and 2240 cm^{-1}; UV (methanol): λ = 285 nm (ε = 19 800); ^{1}H NMR ($CDCl_3$) δ: 8.13, 7.63 (dd, 4H, aryl), 3.80 (s, 3H, OCH_3) ppm. Anal. calcd. for $C_{10}H_7NO_4$: C 58.54, H 3.44, N 6.83; found: C 59.00, H 3.60, N 6.94.

Reaction products

The desired acetylenic ester (0.001 mol) was dissolved in the appropriate solvent (10 mL) and threefold molarity of the amine was added. The mixture was thermostated at 40°C for 10 half-lives. The reaction mixture was poured into ice-cold water and the solid formed was filtered and recrystallized from methanol–water. The samples used for ^{1}H NMR studies were those isolated from the reaction before recrystallization.

Reaction in methanol

E-*Methyl* β-*piperidino-cinnamate* **2**a

Colurless needles, yield 91%; mp 56°C; IR(KBr): 1720 and 2840 cm^{-1}; UV (methanol): λ = 294 nm (ε = 19 200); ^{1}H NMR ($CDCl_3$) δ: 7.60–7.00 (m, 5H, Ph), 4.85 (s, 1H, *E*-olefinic), 3.40 (s, 3H, -OCH_3), 3.20–2.80 (m, 4H, α-$2CH_2$), and 1.80–1.10 (m, 6H, β- and γ-$3CH_2$) ppm. Anal. calcd. for $C_{15}H_{19}O_2$: C 73.43, H 7.81, N 5.71; found: C 72.99, H 7.70, N 5.78.

E-*Methyl* β-*piperidino*-p-*methylcinnamate* **2**b

Colourless needles, yield 88%; mp 54°C; IR(KBr): 1685, 2860, and 2940 cm^{-1}; UV (methanol): λ = 274 nm (ε = 18 600); ^{1}H NMR ($CDCl_3$) δ: 7.50–7.00 (m, 4H, aryl), 4.93 (s, 1H, *E*-olefinic), 3.37 (s, 3H, -OCH_3), 3.32–2.70 (m, 4H, α-$2CH_2$), 2.37 (s, 3H, *p*-CH_3), and 1.73–1.10 (m, 6H, β- and γ-$3CH_2$) ppm. Anal. calcd. for $C_{16}H_{21}NO_2$: C 74.09, H 8.16, N 5.40; found: C 74.23, H 8.03, N 5.14.

Can. J. Chem. Downloaded from www.nrcresearchpress.com by 84.41.108.74 on 09/07/12
For personal use only.

Can. J. Chem. Downloaded from www.nrcresearchpress.com by 84.41.108.74 on 09/07/12
For personal use only.

E-*Methyl* β-*piperidino*-p-*bromocinnamate* **2**c

Colourless plates, yield 95%, mp 105°C; IR(KBr): 1700, 2860, and 3000 cm^{-1}; UV (methanol): λ = 294 nm (ε = 15 200); ^1H NMR ($CDCl_3$) δ: 7.45–7.00 (m, 4H, aryl), 4.93 (s, 1H, *E*-olefinic), 3.50 (s, 3H, $-OCH_3$), 3.25–2.90 (m, 4H, α-$2CH_2$), and 1.86–1.24 (m, 6H, β- and γ-$3CH_2$) ppm. Anal. calcd. for $C_{15}H_{18}BrNO_2$: C 55.58, H 5.59, N 4.32; found: C 55.33, H 5.39, N 4.40.

E-*Methyl* β-*piperidino*-p-*chlorocinnamate* **2**d

Colourless plates, yield 91%; mp 102°C; IR(KBr): 1690, 2800, and 3000 cm^{-1}; UV (methanol): λ = 295 nm (ε = 29 000); ^1H NMR ($CDCl_3$) δ: 7.50–6.95 (m, 4H, aryl), 4.90 (s, 1H, *E*-olefinic), 3.47 (s, 3H, $-OCH_3$), 3.25–2.85 (m, 4H, α-$2CH_2$), and 1.90–1.22 (m, 6H, β- and γ-$3CH_2$) ppm. Anal. calcd. for $C_{15}H_{18}ClNO_2$: C 64.39, H 6.48, N 5.00; found: C 64.55, H 6.57, N 5.19.

E-*Methyl* β-*piperidino*-p-*nitrocinnamate* **2**e

Yellow plates, yield 93%; mp 125°C; IR(KBr): 1690, 2860, and 2980 cm^{-1}; UV (methanol): λ = 278 nm (ε = 22 600); ^1H NMR ($CDCl_3$) δ: 8.20, 7.37 (dd, 4H, aryl); 4.94 (s, 1H, *E*-olefinic), 3.47 (s, 3H, $-OCH_3$), 3.25–2.90 (m, 4H, α-$2CH_2$), and 1.85–1.26 (m, 6H, β- and γ-$3CH_2$) ppm. Anal. calcd. for $C_{15}H_{18}N_2O_2$: C 62.06, H 6.25, N 9.65; found: C 62.44, H 6.21, N 9.83.

E-*Methyl* β-*morpholino-cinnamate* **3**a

Colourless needles, yield 90%; mp 74°C; IR(KBr): 1710, 2860, and 2960 cm^{-1}; UV (methanol): λ = 288 nm (ε = 17 000); ^1H NMR ($CDCl_3$) δ: 7.64–7.10 (m, 5H, Ph), 5.00 (s, 1H, *E*-olefinic), 3.85–3.55 (m, 4H, β-$2CH_2$), 3.50 (s, 3H, $-OCH_3$), and 3.28–2.92 (m, 4H, α-$2CH_2$) ppm. Anal. calcd. for $C_{14}H_{17}NO_3$: C 67.99, H 6.93, N 5.66; found: C 67.80, H 7.00, N 5.66.

E-*Methyl* β-*morpholino*-p-*methylcinnamate* **3**b

Colourless plates, yield 93%; mp 54°C; IR(KBr): 1710 and 2980 cm^{-1}; UV (methanol): λ = 288 (ε = 19 000); ^1H NMR ($CDCl_3$) δ: 7.34–6.85 (m, 4H, aryl), 4.93 (s, 1H, *E*-olefinic), 3.80–3.55 (m, 4H, β-$2CH_2$), 3.50 (s, 3H, $-OCH_3$), 3.28–2.85 (m, 4H, α-$2CH_2$), and 2.40 (s, 3H, *p*-CH_3) ppm. Anal. calcd. for $C_{15}H_{19}NO_3$: C 74.09, H 8.16, N 5.40; found: C 74.23, H 8.03, N 5.14.

E-*Methyl* β-*morpholino*-p-*bromocinnamate* **3**c

Colourless needles, yield 95%; mp 98°C; IR(KBr): 1710, 2800, and 3000 cm^{-1}; UV (methanol): λ = 288 nm (ε = 14 400); ^1H NMR ($CDCl_3$) δ: 7.47, 7.15 (dd, 4H, aryl), 4.93 (s, 1H, *E*-olefinic), 3.76–3.54 (m, 4H, β-$2CH_2$), 3.47 (s, 3H, $-OCH_3$), and 3.18–2.85 (m, 4H, α-$2CH_2$) ppm. Anal. calcd. for $C_{14}H_{16}BrNO_3$: C 51.55, H 4.94, N 4.29; found: C 51.43, H 5.00, N 4.19.

E-*Methyl* β-*morpholino*-p-*chlorocinnamate* **3**d

Colourless needles, yield 96%; mp 85°C; IR(KBr): 1700, 2840, and 2980 cm^{-1}; UV (methanol): λ = 288 nm (ε = 14 000); ^1H NMR ($CDCl_3$) δ: 7.44, 7.00 (m, 4H, aryl), 4.93 (s, 1H, *E*-olefinic), 3.78–3.56 (m, 4H, β-$2CH_2$), 3.47 (s, 3H, $-OCH_3$), and 3.20–2.90 (m, 4H, α-$2CH_2$) ppm. Anal. calcd. for $C_{14}H_{16}ClNO_3$: C 59.68, H 5.72, N 4.97; found: 59.94, H 5.67, N 5.05.

E-*Methyl* β-*morpholino*-p-*nitrocinnamate* **3**e

Yellow crystals, yield 98%; mp 123°C; IR(KBr): 1690 and 2900 cm^{-1}; UV (methanol): λ = 274 nm (ε = 30 000); ^1H NMR ($CDCl_3$) δ: 8.30, 7.50 (dd, 4H, aryl), 5.00 (s, 1H, *E*-olefinic), 3.73–3.60 (m, 4H, β-$2CH_2$), 3.46 (s, 3H, $-OCH_3$), and 3.13–2.96 (m, 4H, α-$2CH_2$) ppm. Anal. calcd. for $C_{14}H_{16}N_2O_5$: C 57.43, H 5.52, N 9.58; found: C 57.43, H 5.53, N 9.40.

E-*Methyl* β-*(*N,N-*diethylamino)-cinnamate* **4**a

Colourless crystals, yield 96%; mp 35°C; IR(KBr): 1700 and 2990 cm^{-1}; UV (methanol): λ = 290 nm (ε = 21 160); ^1H NMR ($CDCl_3$) δ: 7.85–7.25 (m, 5H, Ph), 4.83 (s, 1H, *E*-olefinic), 3.60 (s, 3H, $-OCH_3$), 3.50–3.10 (q, 4H, $2CH_2$), and 1.40–1.05 (t, 6H, $2CH_3$) ppm. Anal. calcd. for $C_{14}H_{19}NO_2$: C 72.05, H 8.21, N 6.00; found: C 71.90, H 8.16, N 5.90.

E-*Methyl* β-*(*N,N-*diethylamino)*-p-*methylcinnamate* **4**b

Colourless crystals, yield 96%; mp 47°C; IR(KBr): 1690 and 2990 cm^{-1}; UV (methanol): λ = 288 nm (ε = 21 120); ^1H NMR ($CDCl_3$) δ: 7.32–6.96 (m, 4H, aryl), 4.77 (s, 1H, *E*-olefinic), 3.43 (s, 3H, $-OCH_3$), 3.33–2.88 (q, 4H, $2CH_2$), 2.67 (s, 3H, *p*-OCH_3), and 1.24–0.92 (t, 6H, $2CH_3$) ppm. Anal. calcd. for $C_{15}H_{21}NO_2$: C 72.84, H 8.53, N 5.66; found: C 72.81, H 8.70, N 5.68.

E-*Methyl* β-*(*N,N-*diethylamino)*-p-*bromocinnamate* **4**c

Colourless needles, yield 95%; mp 96°C; IR(KBr): 1690, 2980, and 3000 cm^{-1}; UV (methanol): λ = 296 nm (ε = 21 600); ^1H NMR ($CDCl_3$) δ: 7.50–7.15 (dd, 4H, aryl), 4.80 (s, 1H, *E*-olefinic), 3.47 (s, 3H, $-OCH_3$), 3.28–2.98 (q, 4H, $2CH_2$), and 1.28–1.00 (t, 6H, $2CH_3$) ppm. Anal. calcd. for $C_{14}H_{18}BrNO_2$: C 53.87, H 5.81, N 4.48; found: C 53.76, H 5.65, N 4.30.

E-*Methyl* β-*(*N,N-*diethylamino)*-p-*chlorocinnamate* **4**d

Colourless needles, yield 96%; mp 85°C; IR(KBr): 1690 and 2990 cm^{-1}; UV (methanol): λ = 290 nm (ε = 25 000); ^1H NMR ($CDCl_3$) δ: 7.35–7.20 (dd, 4H, aryl), 4.83 (s, 1H, *E*-olefinic), 3.50 (s, 3H, $-OCH_3$), 3.28–2.92 (q, 4H, $2CH_2$), and 1.28–0.95 (t, 6H, $2CH_3$) ppm. Anal. calcd. for $C_{14}H_{18}ClNO_2$: C 62.29, H 6.78, N 5.89; found: C 62.59, H 6.86, N 5.60.

E-*Methyl* β-*(*N,N-*diethylamino)*-p-*nitrocinnamate* **4**e

Yellow crystals, yield 96%; mp 123°C; IR(KBr): 1700 and 3000 cm^{-1}; UV (methanol): λ = 280 nm (ε = 54 666); ^1H NMR ($CDCl_3$) δ: 8.18, 7.40 (dd, 4H, aryl), 4.72 (s, 1H, *E*-olefinic), 3.50 (s, 3H, $-OCH_3$), 3.28–2.94 (q, 4H, $2CH_2$), and 1.18–0.95 (t, 6H, $2CH_3$) ppm. Anal. calcd. for $C_{14}H_{18}N_2O_4$: C 60.43, H 6.47, N 10.07; found: C 59.99, H 6.34, N 10.04.

Reaction in DMF

The same products were isolated as in methanol with all amines, except that **1***e* gave two isomers.

E- *and* Z-*Methyl* β-*piperidino*-p-*nitrocinnamate*

This compound showed the same IR, UV, and elemental analyses as the *Z* isomer **2***e*. ^1H NMR ($CDCl_3$) δ: 8.40–7.94, 7.44–7.00 (2m, 4H, aryl), 5.23 (s, 1H, *Z*-olefinic, 27%), 4.97 (s, 1H, *E*-olefinic, 73%), 3.65 (s, 3H, *Z*-OCH_3, 27%), 3.47 (s, 3H, *E*-OCH_3, 73%), 3.20–2.85 (m, 4H, α-$2CH_2$), and 1.85–1.10 (m, 6H, β- and γ-$2CH_2$) ppm.

E- *and* Z-*Methyl* β-*morpholino*-p-*nitrocinnamate*

This compound showed the same IR, UV, and elemental analyses as that isolated from the reaction in methanol. ^1H NMR ($CDCl_3$) δ: 8.34–7.86, 7.50–6.98 (2m, 4H, aryl), 5.63 (s, 1H, *Z*-olefinic, 33%), 5.00 (s, 1H, *E*-olefinic, 67%), 3.85–3.63 (m, 4H, β-$2CH_2$), 3.62 (s, 3H, *Z*-OCH_3, 33%), 3.47 (s, 3H, *E*-OCH_3, 67%); and 3.18–2.80 (m, 4H, α-$2CH_2$) ppm.

E- *and* Z-*Methyl* β-*(*N,N-*diethylamino)*-p-*nitrocinnamate*

This compound showed the same IR, UV, and elemental analyses as the product isolated from methanol. ^1H NMR ($CDCl_3$) δ: 8.40–7.86, 7.60–6.85 (2m, 4H, aryl), 5.37 (s, 1H, *Z*-olefinic, 37%), 4.72 (s, 1H, *E*-olefinic, 63%), 3.65 (s, 3H, *Z*-OCH_3, 37%), 3.50 (s, 3H, *E*-OCH_3), 3.34–2.90 (q, 4H, $2CH_2$), and 1.40–0.85 (t, 6H, $2CH_3$) ppm.

Kinetic measurements

The rate of reaction was determined by following the decrease in amine concentration by titration against hydrochloric acid using methyl red as indicator (21).

The reactions of **1***a–e* (0.1–0.025 M) with amines (0.1–0.025) in methanol were measured under second-order kinetics (1:1). Plots of log $-dc/dt$ vs. log C_{mean} showed that these reactions are second order. The observed rate constants k_2 were calculated from the special second-order rate constant equation:

$$k_2 = 1/t \cdot 1/a \cdot x/a-x$$

where t, a, and x are time, initial concentration of the amine, and concentration of amine consumed in the reaction, respectively.

The reactions of **1***a–e* (0.025 M) with amines (0.05 M) in DMF were carried out using a 1:2 molar ratio respectively. Mathematical calculation indicates that the reaction is third order. The third-order rate constants k_3 were calculated from the equation:

$$k_3 = 1/t\,(1/C_t^2 - 1/C_0^2)$$

where t, C_0, and C_t are time, initial concentration of the amine, and concentration of the amine consumed during the reaction.

1. J. I. DICKSTEIN and S. I. MILLER. Chemistry of the carbon–carbon triple bond. Part 2. *Edited by* S. Patai. Wiley, New York. 1978.
2. W. E. TRUCE, H. G. KLEIN, and R. B. KRUSE. J. Am. Chem. Soc. **83**, 4636 (1961).
3. E. R. JONES and M. C. WHITING. J. Chem. Soc. 1423 (1949).
4. W. E. TRUCE and B. F. HEINE. J. Am. Chem. Soc. **79**, 5311 (1957).
5. W. E. TRUCE and D. W. ONKEN. J. Org. Chem. **40**, 3200 (1975).
6. J. B. HENDRICKSON, R. REES, and J. F. TEMPLETON. J. Am. Chem. Soc. **86**, 107 (1964).
7. W. E. TRUCE and D. G. BRADY. J. Am. Chem. Soc. **88**, 3543 (1966).
8. W. E. TRUCE and L. D. MARKLEY. J. Org. Chem. **35**, 3275 (1970).
9. E. A. HAMED, S. M. SHARAF, S. A. ABDEL-BAKY, M. F. IBRAHIM, and A. A. YOUSSEF. J. Phys. Org. Chem. **3**, 627 (1990).
10. J. E. DOLFINI. J. Org. Chem. **30**, 1298 (1965).
11. S. I. YAKIMOVICH, V. N. NIKALAEV, and N. V. KOSHMINA. Zh. Org. Khim. **18** (6), 1173 (1982).
12. L. J. BELLAMY. Infrared spectra of complex molecules. John Wiley and Son, New York. 1959.
13. A. A. YOUSSEF, S. M. SHARAF, S. K. EL-SADANY, and E. A. HAMED. J. Org. Chem. **46**, 3813 (1981).
14. A. A. YOUSSEF and H. M. ABDEL-MAKSOUD. J. Org. Chem. **40**, 3227 (1975).
15. S. W. TOBEY. J. Org. Chem. **34**, 1281 (1969).
16. U. E. MATTER, C. PASCUAL, E. PRETCH, A. PROSS, W. SIMON, and S. STERNHELL. Tetrahedron, **25**, 691 (1969).
17. S. T. MCDOWELL and C. M. STIRLING. J. Chem. Soc. B, 343 (1967).
18. C. B. KORSHUNOV and H. A. KOPRIAVESSA. Zh. Org. Khim. **8**, 1913 (1970).
19. F. MENGER and I. H. SMITH. J. Am. Chem. Soc. **91**, 4211 (1969).
20. M. A. WILSON and P. D. WOODGATE. J. Chem. Soc. Perkin Trans. 2, 141 (1976).

Can. J. Chem. Downloaded from www.nrcresearchpress.com by 84.41.108.74 on 09/07/12
For personal use only.

Cadmium chloride mediated regiocontrol of dienolates and ketene thioacetals: γ condensation with aldehydes

BO LEI AND ALEX G. FALLIS

The Ottawa–Carleton Chemistry Institute, Department of Chemistry, University of Ottawa, Ottawa, Ont., Canada K1N 6N5

Received February 7, 1991

BO LEI and ALEX G. FALLIS. Can. J. Chem. **69**, 1450 (1991).

The use of cadmium chloride to control the regioselectivity of vinylogous anions upon condensation with aldehydes is described. Addition occurred preferentially at the γ position with substituted crotonates and 2-ethylidene-1,3-dithiane (**6**). Experiments demonstrated that this selectivity arose as a consequence of isomerization of the initially formed kinetic α product to the thermodynamic γ product (e.g., **2** to **4**). The optimum results were achieved with 2 equivalents of cadmium chloride and quenching at 0°C.

Key words: vinylogous anions, cadmium, condensation, dithiane.

BO LEI et ALEX G. FALLIS. Can. J. Chem. **69**, 1450 (1991).

On décrit l'utilisation du chlorure de cadmium pour contrôler la régiosélectivité de la réaction de condensation entre les anions vinylogues et les aldéhydes. Les crotonates substitués et l'éthylidène-2-dithiane-1,3 (**6**) conduisent à une addition préférentielle en position γ. Les expériences démontrent que cette sélectivité résulte de l'isomérisation du produit cinétique α formé initialement en produit thermodynamique γ (e.g., **2** à **4**). On obtient les meilleurs résultats lorsqu'on utilise deux équivalents de chlorure de cadmium avec refroidissement à 0°C.

Mots clés : anions vinylogues, cadmium, condensation, dithiane.

[Traduit par la rédaction]

Can. J. Chem. Downloaded from www.nrcresearchpress.com by 84.41.108.74 on 09/07/12
For personal use only.

Introduction

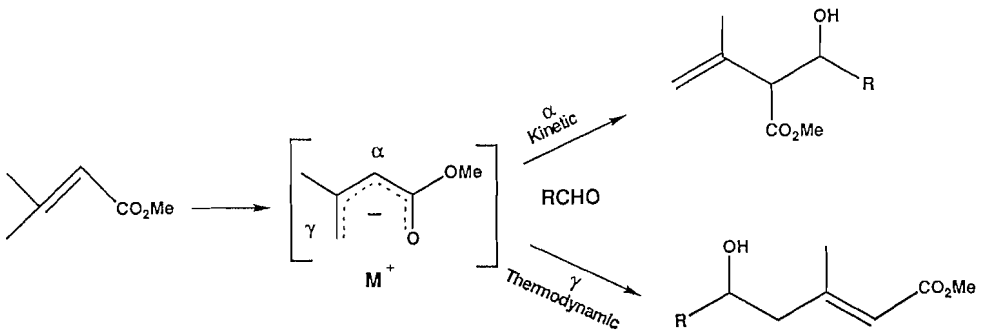
Synthetic applications of allylic carbanions, such as those employed in allyl transfer (1–3), the vinylogous Reformatsky reaction (4–7), and related species derived from ketene dithioacetals (8-10) are of widespread current interest. In spite of considerable study, the effective control of the new carbon–carbon bond at either the α or the γ position is still a significant challenge. The regioselective condensation of heteroatom-stabilized allylic anions and resonance-stabilized enolates depends upon the complex interplay of several different factors. These include the nature of the heteroatom(s), the extent of charge delocalization, steric effects, solvation, the type of electrophile, and the characteristics of the counterion. Synthetic difficulties are compounded by the observation that halides and carbonyl systems often exhibit the opposite regiochemistry (9). In addition, as illustrated in Scheme 1, the kinetic and thermodynamic products frequently differ. Nevertheless, this circumstance can be utilized to facilitate the desired control.

Selective carbon–carbon bond formation at the γ position is important for the synthesis of terpenoid natural products and consequently a variety of methods have been developed to control the reactive site (11–15). A number of different metals and counterions have been examined, including lithium, magnesium, zinc, tin, silicon, palladium, etc. We wish to report that organocadmium reagents generated *in situ* from the corresponding alkyl lithium derivatives condense preferentially, under thermodynamic conditions, with aldehydes at the γ position of the allylic anion (preliminary communication: ref. 16). This is in contrast to the reported behaviour of the "crotylcadmium" reagent prepared from crotyl magnesium bromide, which afforded exclusively the methallyl adducts (17, 18).

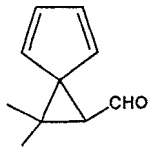
Results and discussion

We required a reliable procedure for the direct introduction of a conjugated allyl unit for our total synthesis of (+)-longifolene (19). In spite of the previous studies in this area (referenced above) this transformation is often not as straightforward as it appears. The spiro-cyclopropyl aldehyde **1** was prepared in 84% yield by oxidation (active MnO_2) of the corresponding alcohol, itself available in two steps from cyclopentadiene (20). Treatment of methyl 3-methylcrotonate (methyl 3,3-dimethylacrylate) with lithium diisopropylamide (LDA) at −78°C in tetrahydrofuran (THF), to generate the anion, followed by condensation with aldehyde **1** afforded the α product **2** exclusively (Table 1, Entry 1). This is in accord with the normal regiochemical behaviour encountered with lithium enolates. Dugger and Heathcock (11) established that upon condensation with benzaldehyde the product mixture was influenced by the length of the reaction time and the quenching temperature. For example, after a reaction time of 10 s followed by quenching at −70°C the hydroxy-ester **5** was formed, while if the initial reaction mixture was allowed to warm to 10–15°C before quenching the γ isomer **3** and the corresponding lactone were isolated. Similar results were reported by Johnson and White (12) who examined the behaviour of the lithium dianion from the corresponding acid. They noted that the kinetic α products were formed at −78°C while at higher temperatures (22 and 65°C) the reaction was reversible and the more stable γ products dominated. Hudlicky and co-workers (4) found that the regioselectivity in the Reformatsky reaction of ethyl 4-bromocrotonate with carbonyl substrates was dependent on the polarity of the solvent and the hardness of the metal. Under their modified conditions (dry Zn, THF) we found that methyl 3-bromomethyl-2-butenoate (Table 1, Entry 2) reacted with benzaldehyde to give only **3**. In contrast, when the spiro-cyclopropyl aldehyde **1** was used we obtained a 40:60 α/γ mixture of **2** and **4**; this ratio became 60:40 when methyl 4-bromocrotonate was employed (Table 1, Entry 4). This change in regiochemistry may partly be a consequence of the hindered carbonyl group in **1**, since the dianion studies (12) indicated that steric effects could exert a prominent influence. Modification of the conditions using an ultrasonic bath and (or) dimethoxyethane (DME) as the solvent provided no significant improvement in the α/γ ratio.

In a parallel series of experiments various lithium anion–



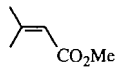
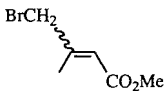
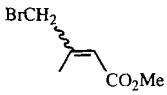
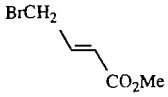
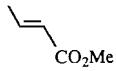
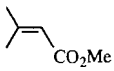
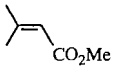
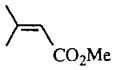
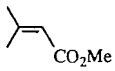
RCHO = PhCHO or



1

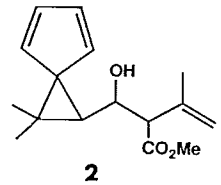
SCHEME 1

TABLE 1. Crotonate condensations

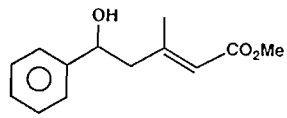
Entry	Aldehyde	Substrate	Metal/salt	α:γ	Isolated yield (%)
1.	**1**		LDA[a]	100:0	79
2.	PhCHO		Zn(THF)	0:100	85
3.	**1**		Zn(THF)	40:60	63
4.	**1**		Zn(THF)	60:40	60
5.	PhCHO		$LiNCy_2/CdCl_2$ HMPA	50:50	90
6.	PhCHO		$LDA/CdCl_2$	15:85	75
7.	PhCHO		LDA/CdI_2	10:90	65
8.	**1**		$LDA/CdCl_2$	15.85	90
9.	**1**		$LDA/CdCl_2$	20:80	73

[a]Reaction temperature, −78°C; quenched, −78°C; other entries quenched at 0°C.

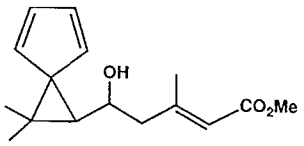
Can. J. Chem. Downloaded from www.nrcresearchpress.com by 84.41.108.74 on 09/07/12
For personal use only.



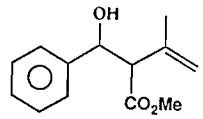
2



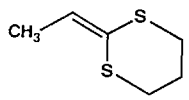
3



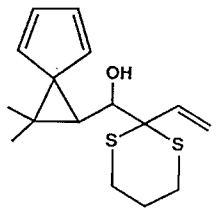
4



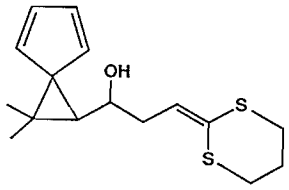
5



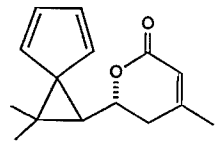
6



7



8



9

salt combinations derived from 2-ethylidene-1,3-dithiane (**6**) were examined (Table 2). Previously Ziegler and Tam (8) had established that alkylation of the lithium anion derived from **6** afforded the α product preferentially. A similar result was encountered with **1**, in which **7** was the dominant product (Table 2, Entry 1). The corresponding copper derivative, derived from **6**, gave the γ allylation product exclusively when they employed a variety of allylic halides as the electrophiles. However, with the spiro-cyclopropyl aldehyde **1**, even the copper derivative afforded a significant quantity of the undesired α product **7** in addition to the γ isomer **8** (Table 2, Entry 3), and **7** became the dominant product in the presence of zinc chloride (Table 2, Entry 2).

Except for the reaction of organocadmium reagents with acyl halides, organocadmium species have received relatively little attention (21). Pure, salt-free alkyl cadmiums do not react with carbonyl compounds but this reactivity may be altered significantly by the addition of magnesium or lithium salts (22). Thus, various combinations of cadmium salts and organometallics would be expected to alter the reactivity and possibly also the selectivity in our systems. This was found to be the case.

The addition of anhydrous cadmium chloride powder to the preformed lithium anion at −78°C, followed by warming and quenching at 0°C with saturated aqueous ammonium chloride, markedly increased the quantity of the γ product **8**. The α/γ ratio was changed to 10:90 for both benzaldehyde and the spiro-aldehyde **1** (Table 2, Entries 4 and 5). This effect appears to be general and added cadmium salts also worked well with

TABLE 2. Dithioketene acetal condensations[a]

Entry	Aldehyde	Metal/salt	α:γ	Isolated yield (%)
1.	**1**	LDA	90:10	96
2.	**1**	LDA/$ZnCl_2$	60:40	70
3.	**1**	LDA/CuI·$P(OMe)_3$	35:65	61
4.	**1**	LDA/$CdCl_2$	10:90	90
5.	PhCHO	LDA/$CdCl_2$	10:90	95

[a]Substrate: 

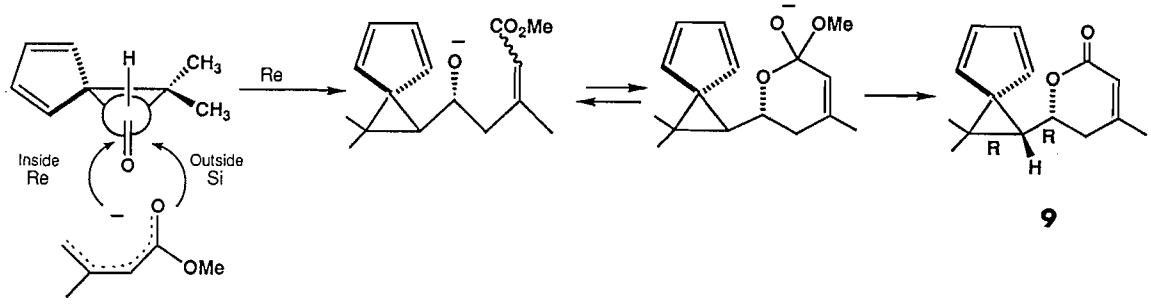
substituted crotonates so that the γ product **4** predominated as summarized in Table 1 (Entries 6–9). Thus cadmium halides reverse the normal regiochemical behaviour encountered with simple lithium enolates and do not require heating the reaction mixture above 0°C. Lithium dialkylamides undergo 1,4-addition to methyl crotonate unless hexamethylphosphoramide (HMPA) is added, in which case deprotonation occurs (23). To encourage deprotonation the bulkier base lithium dicyclohexylamide was employed with added HMPA. Unfortunately the presence of the polar solvent HMPA reduced the influence of the cadmium chloride (Table 1, Entry 5).

Relatively few investigations into the composition and structure of organocadmium reagents have been conducted. "Purified" organocadmiums, isolated by distillation, such as di-*n*-butylcadmium (24) have a dialkyl structure. It is assumed that the *in situ* reagents were similar, although clearly they must be part of a complex equilibrium, since yields were less if the ratio of the lithium to cadmium species was not 2:1. Solvation effects are also important, as the γ selectivity diminished in the presence of polar additives such as HMPA while more soluble salts such as cadmium iodide only altered the ratio slightly and the yields tended to be lower.

Quenching studies established that the γ condensation product **4** arose from isomerization of the alkoxide of the initial kinetic product **2**. The standard reaction with lithium diisopropylamide and cadmium chloride was quenched at −78°C with acetic acid in THF. Work-up established that only the α product **2** was present. This material was redissolved in THF and treated separately with lithium diisopropylamide and cadmium chloride, initially at −78°C and then at 0°C for 1 h. The products consisted of **2** and **4** in a similar α/γ ratio (15:85) to the one observed previously. In addition a small quantity of the unsaturated lactone **9** was formed. This lactone **9** was the only γ product (Table 1, Entry 9) when the (+)-*R*-spiro-aldehyde **1** was employed. The reaction was conducted in the standard manner with the cadmium chloride mediated anion and quenched at 0°C after stirring for 2 h. This result is similar to earlier studies (11) in which dihydro-α-pyrones were the major products upon quenching at 15°C in related reactions with LDA as the base. Spectral data established the lactone structure **9**. These included the vinyl methyl singlet at δ 1.87, the cyclopropyl hydrogen as a doublet (δ 2.31, J = 4.4 Hz), and the methine proton on the carbon bearing oxygen as doublet of doublet of doublets at δ 4.48 (J = 4.4, 10.1, 11.1 Hz) in the ^{1}H nmr spectrum. A COSY spectrum confirmed that the cyclopropyl hydrogen was adjacent to this methine hydrogen, which was itself adjacent to the ring methylene protons.

In principle this condensation with methyl 3,3-dimethylacrylate anion in the presence of cadmium chloride could generate two diastereomers, depending upon the approach of the

Can. J. Chem. Downloaded from www.nrcresearchpress.com by 84.41.108.74 on 09/07/12
For personal use only.



SCHEME 2

reagent from either the "inside" Re face or the "outside" Si direction. A combination of beneficial electronic and steric interactions contributes to the selectivity of this reaction. Inside attack is favoured sterically as nonbonded interactions with the adjacent methyl groups are avoided, particularly when the carbonyl lies in approximately the same plane as the cyclopentadiene. In addition, this may allow the delocalized π system of the organocadmium reagent to interact favourably with the π system of the diene. The net result would be predominant attack from the inside Re face to generate the C5-(*R*)-lactone **9** (73%). The stereochemical assignment of the major lactone was confirmed by additional chemical transformations (19). A small amount (12%) of the C5-(*S*) diastereomer was also isolated. Only the *Z*-olefin can form the six-membered ring lactone and the *E*-olefin hydroxy-ester was not detected amoung the products. Thus, as illustrated in Scheme 2, the alkoxide that resulted from the initial condensation must have added to the ester carbonyl, when the geometry was favourable, to generate **9** after loss of methoxide. Isomerization to the observed product continued until the reaction was complete, and was consistent with the thermodynamic features of this reaction elucidated above.

In conclusion, cadmium chloride exerts a beneficial influence on vinylogous anions to alter their normal regiochemical behaviour. This process involves an equilibrium that facilitates the preparation of the γ condensation product and may be conducted at 0°C. This feature makes it useful for sensitive substrates where higher temperatures are deleterious. These procedures to influence the regioselectivity of carbonyl condensations will also be useful in other synthetic applications.

Experimental

Melting points were determined in capillary tubes with a Thomas–Hoover Uni-Melt apparatus, or with a Fisher–Johns melting point apparatus, and are uncorrected. Infrared (ir) spectra were recorded on a Perkin–Elmer 783 or 983G infrared spectrophotometer, and were calibrated with the 1601 cm^{-1} band of polystyrene film. Proton magnetic resonance spectra (^1H nmr) were measured at 80 MHz with a Bruker WP80 spectrometer or at 200 MHz with a Varian Gemini spectrometer or at 300 MHz with a General Electric GN 300 or a Varian XL-300 spectrometer in deuterochloroform. Carbon magnetic resonance spectra (^{13}C nmr) were measured at 50 MHz with a Varian Gemini spectrometer or at 75 MHz with a General Electric GN 300 spectrometer or a Varian XL-300 spectrometer. The residual solvent signal ($CDCl_3$) was used as an internal lock; $CDCl_3/^1H$: δ 7.262, ^{13}C: δ 77.00; and chemical shifts are reported in ppm downfield from tetramethylsilane (δ scale) as an internal standard. The number of protons, multiplicity, coupling constants, and proton assignments are indicated in parentheses. Mass spectra were determined on a V.G. Micromass 7070 HS instrument using an ionization energy of 70 eV, or on a Hewlett–Packard 5890A gas chromatograph – 5970B mass selective detector equipped with a 12.5 m capillary column (0.2 mm i.d.) coated with cross-linked dimethyl silicone (0.33 μm). Optical rotations were measured using a Perkin–Elmer 241 polarimeter (sodium light, cell length = 10 cm, c = g/100 mL).

Gas–liquid chromatographic analyses were conducted on a Hewlett–Packard 402B gas chromatograph equipped with a column (3 m × 6 mm i.d.) containing 1.5% OV-17 supported on Gas Chrome Q using helium as the carrier gas. Analytical thin-layer chromatography (tlc) employed commercial aluminum sheets precoated (0.2 mm layer) with silica gel 60 F_{254} (E. Merck). Flash column chromatography using E. Merck silica gel 60 (230–400 mesh) was employed for all column chromatography. The purity of all title compounds was judged to be ≥95% as determined by a combination of gc–ms, ^1H nmr, and ^{13}C nmr analysis.

Petroleum ether refers to a fraction with boiling range 30–60°C. Anhydrous diethyl ether (ether), tetrahydrofuran (THF), dimethoxyethane (DME), and dioxane were obtained by distillation from $LiAlH_4$ or potassium/benzophenone. Methanol and absolute ethanol were dried by distillation from magnesium. Dry hexamethylphosphoramide (HMPA), dimethylformamide (DMF), dimethyl sulfoxide (DMSO), and diisopropylamine were prepared by distillation from calcium hydride. Solutions in organic solvents were dried over anhydrous magnesium sulfate and stripped of solvent with a Büchi rotary evaporator connected to a water aspirator. Unless otherwise indicated, all reactions were conducted under an atmosphere of dry nitrogen.

2,2-Dimethylspiro[2,4]hepta-4,6-diene-1-ylcarboxaldehyde (1)

2,2-Dimethyl-1-hydroxymethylspiro[2,4]hepta-4,6-diene (3.0 g, 0.02 mmol) (20) in dichloromethane (25 mL) was added dropwise to a stirred, refluxing suspension of active MnO_2 (20) (30 g, 40 g if mixed with charcoal) in dichloromethane (250 mL). The mixture was stirred under reflux for 12 h, cooled to room temperature, and filtered through Celite and anhydrous $MgSO_4$. The solid residue was washed thoroughly with dichloromethane (200 mL) and the combined filtrates concentrated. The crude product was purified by flash chromatography (5% ethyl acetate/petroleum ether) to afford the spiro-aldehyde **1** (2.5 g, 84%) as a pale yellow liquid; ir (film): 2825 (H-CO), 2720 (H-CO), 1704 (C=O) cm^{-1}; ^1H nmr (300 MHz) δ: 1.42 (s, 3H, CH_3), 1.56 (s, 3H, CH_3), 2.78 (d, 1H, J = 6 Hz, cyclopropyl H), 6.17 (m, 1H, cyclopentadienyl H), 6.53 (m, 2H, cyclopentadienyl H), 6.60 (m, 1H, cyclopentadienyl H), 9.56 (d, 1H, J = 6 Hz, H-C=O); ^{13}C nmr δ: 198.0, 135.5, 132.4, 131.6, 131.4, 56.8, 49.4, 37.1, 26.8, 20.7. Exact Mass calcd. for $C_{10}H_{12}O$: 148.0888; found: 148. 0888.

Methyl 4-bromo-3-methyl-2-butenonate (lit. (25))

Methyl 3,3-dimethylacrylate (5.4 g, 47 mmol) was dissolved in carbon tetrachloride (50 mL) containing *N*-bromosuccinimide (NBS) (8.7 g, 49 mmol, Aldrich) and azobisisobutryonitrile (AIBN) (0.078 g). The mixture was stirred under reflux for 8 h, cooled, and filtered to remove the precipitate. The filtrate was concentrated and purified by distillation under reduced pressure (bp 45–70°C/0.6 Torr; 1 Torr = 133.3 Pa) (lit. (25) bp 112–130°C/35 Torr) to afford the bromoester (6.9 g, 68%) as a 1:1 *Z*,*E* mixture: ^1H nmr (80 MHz) *Z*, δ: 1.99 (d, 2H, J = 2 Hz, CH_3-C=C), 3.65 (s, 3H, OCH_3), 4.47 (m, 2H, CH_2Br), 5.68 (d, 1H, J = 2 Hz, H-C=C); *E*, δ: 2.21 (d, 3H, J = 2 Hz, CH_3-C=C), 3.65 (s, 3H, OCH_3), 3.86 (d, 2H, J = 1 Hz, CH_2Br), 5,87 (m, 1H, H-C=C).

Can. J. Chem. Downloaded from www.nrcresearchpress.com by 84.41.108.74 on 09/07/12
For personal use only.

Can. J. Chem. Downloaded from www.nrcresearchpress.com by 84.41.108.74 on 09/07/12
For personal use only.

General procedure for Reformatsky reaction

Active zinc powder (5 molar equivalents, zinc dust (Aldrich) was quickly washed with 50% acetic acid, filtered, rinsed thoroughly with water and DME, and dried under vacuum at 110°C for 12 h) suspended in anhydrous THF (2 mL) was placed in a three-necked flask equipped with a condenser and a dropping funnel (4). The aldehyde (benzaldehyde or **1**, ca. 2 mmol) and the bromoester in anhydrous THF (10 mL) were placed in the dropping funnel. A few drops of the THF solution containing the starting materials were added to the stirred suspension, followed by a small crystal of iodine, and the reaction heated. Once reflux commenced and the iodine color discharged, the remainder of the THF solution was added dropwise to the reaction while stirring under reflux. After the addition was complete, reflux was continued for another hour, the reaction cooled to room temperature, quenched with saturated aqueous ammonium chloride, and filtered. The filtrate was extracted with ether (2 × 10 mL) and the combined extracts washed with brine, dried, filtered, and concentrated. The product was purified by chromatography (20% ethyl acetate/petroleum ether) (see Table 1 for α : γ ratios and yields).

Methyl 2-isopropylidenyl-3-hydroxy-3-(2',2'-dimethylspiro[2.4]-hepta-4',6'-dien-1'-yl)propanoate (**2**): ir ($CHCl_3$): 3660 (OH), 1730 (C═O), 1650 (C═C) cm^{-1}; ^1H nmr (300 MHz) δ: 1.41 (s, 3H, CH_3), 1.48 (s, 3H, CH_3), 1.68 (s, 3H, CH_3-C═C), 2.28 (d, 1H, J = 10.5 Hz, cyclopropyl H), 2.82 (br s, 1H, OH), 3.47 (d, 1H, J = 7.5 Hz, CH-CO_2Me), 3.69 (s, 3H, OCH_3), 4.02 (m, 1H, CH-O), 4.76 (s, 1H, H-C═C),4.83 (s, 1H, H-C═C), 6.18 (m, 2H, cyclopentadienyl H), 6.41 (m, 1H, cyclopentadienyl H), 6.50 (m, 1H, cyclopentadienyl H); ^{13}C nmr δ: 172.9, 139.1, 137.9, 132.5, 132.2, 129.0, 115.6, 71.0, 59.8, 51.9, 51.5, 46.8, 35.7, 26.4, 22.0, 21.0, ms m/z: 262 (M^+), 244 ($M^+ - H_2O$).

Methyl 5-hydroxy-3-methyl-5-(2',2'-dimethylspiro[2.4]hepta-4',6'-dien-1'-yl)-2-pentenoate (**4**): ir (film): 3480 (OH), 3060 (H-C═C), 1720 (C═O), 1635 (C═C) cm^{-1}; ^1H nmr (300 MHz) δ: 1.38 (s, 3H, CH_3), 1.43 (s, 3H, CH_3), 1.71 (s, 3H, CH_3), 1.95 (d, 2H, J = 6.5 Hz, CH_2-C═C), 2.15 (d, 1H, J = 10.6 Hz, cyclopropyl H), 3.35 (br s, 1H, OH), 3.62 (s, 3H, OCH_3), 4.22 (m, 1H, CH-O), 5.15 (s, 1H, H-C═C), 6.15 (m, 2H, cyclopentadienyl H), 6.38 (m, 2H, cyclopentadienyl H), 6.50 (m, 2H, cyclopentadienyl H); ^{13}C nmr ($CDCl_3$) δ: 164.4, 138.7, 137.8, 132.5, 131.3, 128.9, 127.7, 70.5, 56.3, 52.1, 51.2, 42.9, 34.5, 27.1, 22.5, 19.9; ms m/z: 262 (M^+), 244 ($M^+ - H_2O$).

Methyl 5-hydroxy-3-methyl-5-phenyl-2-pentenoate (**3**) (lit. (11)): ir (film): 3450 (OH), 1725 (C═O), 1640, 1600 (C═C) cm^{-1}; ^1H nmr (80 MHz) δ: 1.57 (s, 3H, CH_3), 3.02 (d, 1H, J = 4.4 Hz, CH_2), 3.40 (d, 1H, J = 8.8 Hz, CH_2), 3.74 (s, 3H, OCH_3), 4.83 (s, 1H, H-C═C), 4.85 (s, 1H, OH), 5.05 (dd, 1H, J = 4.4, 8.8 Hz, *H*-C-OH), 7.33 (s, 5H, phenyl H); ms m/z: 220 (M^+).

Methyl 5-hydroxy-5-(2',2'-dimethylspiro[2.4]hepta-4',6'-dien-1'-yl)-2-pentenoate: ir (film): 3450 (OH), 1720 (C═O), 1650 (C═C) cm^{-1}; ^1H nmr (80 MHz) δ: 2.05 (d, 1H, J = 3.5 Hz, cyclopropyl H), 2.25 (br s, 1H, OH), 2.30–2.60 (m, 2H, CH_2), 3.72 (s, 3H, OCH_3), 4.55 (m, 1H, *H*-C-OH), 5.76 (d, 1H, J = 6 Hz, C═C*H*-CO_2Me), 6.18 (m, 2H, cyclopentadienyl H), 6.43 (m, 2H, cyclopentadienyl H), 6.88 (m, 1H, H-C═C-CO_2Me); ms m/z: 248 (M^+).

Methyl 2-vinyl-3-hydroxy-3-(2',2'-dimethylspiro[2.4]hepta-4',6'-dien-1'-yl)propanoate: ir (film): 3490 (OH), 1730 (C═O), 1640 (C═C) cm^{-1}; ^1H nmr (80 MHz) δ: 2.80 (d, 1H, J = 3 Hz, OH), 3.25 (dd, 1H, J = 6, 12 Hz H-C-CO_2Me), 3.65 (s, 3H, OCH_3), 4.52 (m, 1H, *H*-C-OH), 5.25 (m, 2H, CH_2═C), 5.60–5.90 (m, 1H, *H*C═CH_2), 6.22 (m, 1H, cyclopentadienyl H), 6.45 (m, 1H, cyclopentadienyl H); ms m/z: 248 (M^+).

Condensations of aldehydes with 2-ethylidene-1,3-dithiane (**6**)

The 2-ethylidene-1,3-dithiane was prepared by Grignard addition to carbon disulfide and alkylation (8, 26, 27) and distilled to yield 3.81 g (52%) of dithiane **6** as a foul smelling, pale yellow, liquid: bp 61–62°C/0.3 Torr (lit. (8) bp 43–44°C/0.1 Torr); ^1H nmr (80 MHz) δ: 1.76 (d, 3H, J = 7 Hz, CH_3), 2.18 (m, 2H, CH_2), 2.87 (m, 4H, SCH_2), 6.00 (q, 1H, J = 7 Hz, H-C═C); ms m/z: 146 (M^+).

A: LDA only

An LDA solution was prepared from diisopropylamine (0.232 g, 2.3 mmol, Aldrich) and *n*-butyllithium (2.5 M in hexane, 0.9 mL, 2.2 mmol, Aldrich) in anhydrous THF (5 mL) at −25°C. Dithiane **6** (0.321 g, 2.2 mmol) in anhydrous THF (2 mL) was added, forming a yellow solution. After stirring at −25°C for 30 min, the solution was cooled to −78°C, and a THF solution (10 mL) of the spiro-aldehyde **1** (0.220 g, 1.5 mmol) added dropwise. The resulting solution was stirred at −78°C for a further 30 min, warmed to 0°C, and quenched with saturated aqueous ammonium chloride. The mixture was extracted with ether (2 × 20 mL) and the combined ether extracts were washed with brine, dried, filtered, and concentrated. The product was purified by chromatography (20% ethyl acetate/petroleum ether) to give 0.349 g (86%) of the α dithiane **7** and 0.051 g (10%) of γ dithiane **8**; α : γ = 90:10, total yield 96%.

2-Vinyl-2-[1-hydroxy-1-(2',2'-dimethylspirol[2.4]hepta-4',6'-dien-1'-yl)]-1,3-dithiane (**7**): ^1H nmr (80 MHz) δ: 1.39 (s, 3H, CH_3), 1.45 (s, 3H, CH_3), 1.89 (m, 2H, -SCH_2-C*H*$_2$-SCH_2-), 2.35 (d, 1H, J = 9.9 Hz, OH), 2.53 (d, 1H, J = 4.5 Hz, cyclopropyl H), 2.83 (m, 4H, SH_2), 3.89 (dd, 1H, J = 4.5, 9.9 Hz, *H*-C-OH), 5.11–5.59 (m, 3H, H-C═C), 6.15–6.50 (m, 4H, cyclopentadienyl H). Exact Mass calcd. for $C_{16}H_{22}OS_2$: 294.1111; found: 294.1115.

2-[3-Hydroxy-3-(2',2'-dimethylspiro[2.4]hepta-4',6'-dien-1'-yl)propylidene]-1,3-dithiane (**8**): ir (film): 3410 (OH), 1600 (C═C) cm^{-1}; ^1H nmr (300 MHz) δ: 1.39 (s, 3H, CH_3), 1.41 (s, 3H, CH_3), 2.03 (d, 1H, J = 9.6 Hz, cyclopropyl H), 2.18 (m, 2H, -SCH_2-C*H*$_2$-SCH_2-), 2.58 (dd, 2H, J = 5.7, 7.5 Hz, CH_2-C═C), 2.88 (t, 4H, J = 6.0 Hz, SCH_2), 2.97 (s, 1H, OH), 3.41 (m, 1H, *H*-C-OH), 6.07 (t, 1H, J = 7.5 Hz, H-C═C), 6.37 (m, 1H, cyclopentadienyl H), 6.44 (m, 1H, cyclopentadienyl H), 6.49 (m, 2H, cyclopentadienyl H). Exact Mass calcd. for $C_{16}H_{22}OS_2$: 294.1111; found: 294.1119.

B: LDA/$ZnCl_2$

2-Ethylidene-1,3-dithiane (**6**) (0.204 g, 1.4 mmol) in anhydrous THF (2 mL) was added dropwise to an LDA solution prepared from diisopropylamine (0.152 g, 1.5 mmol) and *n*-butyllithium (2.5 M in hexane, 0.6 mL, 1.5 mmol, Aldrich) in anhydrous THF (5 mL) at −40°C. The yellow solution was stirred at −40°C for 40 min and zinc chloride (0.2031 g, 1.5 mmol, Aldrich) added. After stirring at −40°C for an additional 30 min, the reaction was cooled to −78°C, and the spiro-aldehyde **1** (0.192 g, 1.3 mmol) in anhydrous THF (10 mL) was added dropwise. The reaction was continued for a further hour at −78°C, warmed to 0°C, and quenched with saturated aqueous NH_4Cl. The mixture was extracted with ether (2 × 20 mL) and the combined ether extracts were washed with brine, dried, filtered, concentrated, and purified by chromatography (15% ethyl acetate/petroleum ether) to give 0.163 g (43%) of triene **7** (α product) and 0.104 g (27%) of triene **8** (γ product); α : γ = 60:40, total yield 70%.

C: LDA/CuI·P(MeO)$_3$

An LDA solution was prepared from diisopropylamine (0.36 mL, 2.6 mmol) and *n*-butyllithium (2.7 M in hexane, 0.96 mL, 2.6 mmol, Aldrich) in anhydrous THF at −25°C. Dithiane **6** (0.365 g, 2.5 mmol) in anhydrous THF (1 mL) was added to the solution. The reaction solution was stirred at −25°C for 30 min, and cooled to −78°C, followed by addition of trimethylphosphite cuprous iodide complex (0.906 g, 2.8 mmol) in anhydrous THF (2 mL) (based on ref. (8). A yellow precipitate gradually formed during 1 h of stirring. The spiro-aldehyde **1** (0.370 g, 2.5 mmol) in anhydrous THF (10 mL) was added dropwise to the yellow suspension over a period of 30 min, resulting in a greenish solution. The solution was stirred at −78°C for 1 h, warmed to 0°C, stirred at 0°C for 30 min, and quenched with saturated aqueous NH_4Cl. A minimum amount of water was added to just dissolve the white precipitate and the mixture was stirred at 0°C for 10 min and extracted with ether (3 × 15 mL). The combined ether extracts were washed with brine, dried, filtered, and concentrated. Chromatography (20% ethyl acetate/petroleum ether) gave 0.159 g (22%) of **8** (α product) and 0.289 g (39%) of **7** (γ product); α : γ = 35:65, total yield 61%.

Can. J. Chem. Downloaded from www.nrcresearchpress.com by 84.41.108.74 on 09/07/12
For personal use only.

D: LDA/$CdCl_2$

The dithiane **6** (2.2 mmol) in anhydrous THF (5 mL) was added dropwise to an LDA solution prepared from diisopropylamine (2.3 mmol) and *n*-butyllithium (2.5 M in hexane, 2.3 mmol) in anhydrous THF (10 mL) at −40°. After stirring at −40°C for 30 min, the reaction was cooled to −78°C and cadmium chloride powder (1.5 mmol, Aldrich, Gold label, previously ground in a mortar and dried in vacuum at 110°C) was added in one portion. The resulting white suspension was stirred at −78°C for 30 min and an anhydrous THF solution (10 mL) containing aldehyde (benzaldehyde or spiro-aldehyde **1**, 1.0 mmol) was added over a period of 30 min. After the addition was complete, the reaction was conducted at −78°C for a further hour, warmed to 0°C, stirred at 0°C for 0.5 h, and quenched with saturated aqueous NH_4Cl. The mixture was filtered through Celite and the filtrate extracted with ether (2 × 15 mL). The combined ether extracts were washed with brine, dried, filtered, and concentrated. The oily residue was purified by chromatography (15% ethyl acetate/petroleum ether) to give the α product and the γ product in total yield of 90–95%; 10:90 ratio (Table 2).

2-[3-Hydroxy-3-phenylpropylidene)-1,3-dithiane: ir (film): 3410 (br, OH), 1605, 1585 (C=C), 705 (s, C-S) cm^{-1}; ^1H nmr (80 MHz) δ: 2.01–2.27 (m, 3H), 2.60–2.93 (m, 6H), 4.74 (t, 1H, J = 6.4 Hz, HC-O), 5.97 (t, 1H, J = 7.4 Hz, H-C=C), 7.37 (m, 5H, phenyl H). Exact Mass calcd. for $C_{13}H_{16}OS_2$: 252.0642; found: 252.0647.

2-Vinyl-2-(1-hydroxy-1-phenyl)-1,3-dithiane: ir (film): 3450 (br, O-H), 3080, 3060, 3025 (phenyl H), 1625 (C=C) cm^{-1}; ^1H nmr (80 MHz) δ: 1.94 (m, 2H, CH_2), 2.80 (m, 4H, SCH_2), 2.94 (d, 1H, J = 3.2 Hz, OH), 4.90 (d, 1H, J = 3.2 Hz, H-C-O), 5.35–6.00 (m, 3H, H-C=C), 7.26–7.48 (m, 5H, phenyl H). Exact Mass calcd. for $C_{13}H_{16}OS_2$: 252.0642; found: 252.0657.

E: LDA/$CdCl_2$ reaction with methyl 3,3-dimethylacrylate

An LDA solution (2.1 equiv.) was prepared from diisopropylamine and *n*-butyllithium in anhydrous THF at −78°C. A THF solution of the methyl acrylate (2.0 equiv.) was added dropwise to the solution, to form a pale yellow solution. After stirring for 30 min at −78°C, cadmium chloride powder (1 equiv., Aldrich, Gold label, ground in a mortar and dried under vacuum at 110°C overnight) was added in one portion and the resulting suspension stirred for 30 min further, followed by addition of aldehyde (benzaldehyde or spiro-aldehyde **1**) in THF with a syringe pump (0.1 mL/min). After the addition was complete, the reaction was continued for an additional hour, then allowed to warm to 0°C, stirred for 30 min at 0°C, and quenched with saturated aqueous NH_4Cl. The mixture was filtered through Celite and the filtrate extracted with ether (2 × 20 mL). The combined ether extracts were washed with brine, dried, filtered, and concentrated. Chromatography (20% ethyl acetate/petroleum ether) afforded the hydroxy-ester **4** or **3** (γ product) and the hydroxy-ester **2** or **5** (α product); (see Table 1 for α : γ ratios and yields).

F: Thermodynamic study of LDA/$CdCl_2$ reaction

Methyl 3,3-dimethylacrylate (0.114 g, 1.0 mmol, THF, 5 mL) was treated with LDA, as described above, at −78°C and, after stirring for 30 min, cadmium chloride powder (0.0916 g, 0.5 mmol, Aldrich, Gold label, previously ground in a mortar and dried under vacuum at 110°C overnight) was added in one portion. The suspension was stirred for 30 min at −78°C and an anhydrous THF solution (10 mL) containing the spiro-aldehyde **1** (0.074 g, 0.5 mmol) was added dropwise over a period of 45 min. The reaction was stirred for 1 h at −78°C and then quenched by slowly adding acetic acid (1 mL) in anhydrous THF (2 mL). The mixture was filtered through Celite and the filtrate extracted with ether (2 × 20 mL). The combined ether layers were washed with brine, dried, filtered, and concentrated. Chromatography (20% ethyl acetate/petroleum ether) yielded hydroxy-ester **2** (0.103 g, 79%).

An LDA solution (0.8 mmol) in THF (5 mL) was treated with cadmium chloride powder (0.046 g, 0.4 mmol) at −78°C as described above. A solution of the hydroxy-ester **2** (0.103 g, 0.39 mmol) in anhydrous THF (10 mL) was added and the resulting suspension stirred for 1 h at −78°C. The reaction was warmed to 0°C, stirred for 1 h, and then quenched with saturated aqueous NH_4Cl. Ether extraction and work-up as above followed by chromatography (15% ethyl acetate/petroleum ether) gave hydroxy-ester **4** (0.076 g, 73%) and recovered starting material **2** (0.014 g, 13%), α : γ = 15:85.

G: LDA/CdI_2 reaction of benzaldehyde with methyl 3,3-dimethylacrylate

The lithium anion of methyl 3,3-dimethylacrylate (1.03 g, 9 mmol, THF, 5 mL) was generated at −78°C with LDA as described above. The solutions was stirred for an additional 30 min, followed by addition of cadmium iodide (1.65 g, 4.5 mmol, Aldrich, Gold label, dried under vacuum for 2 h at 110°C) in one portion. The cadmium iodide slowly dissolved and formed a light yellow solution. Benzaldehyde (0.424 g, 4 mmol, Aldrich, redistilled) in anyhdrous THF (5 mL) was added dropwise. The resulting solution was stirred for 1 h at −78°C, for 30 min at 0°C, and quenched with saturated aqueous NH_4Cl. The mixture was worked up as above by extraction with ether (2 × 20 mL) and flash chromatography (20% ethyl acetate/petroleum ether) to give hydroxy-ester **3** (γ product, 0.519 g, 59%) and hydroxy-ester **5** (α product, 0.051 g, 6%), α : γ = 10:90, 65% total yield.

H: $LiNCy_2$/$CdCl_2$ reaction of benzaldehyde with methyl crotonate

A THF solution (2 mL) containing hexamethylphosphoramide (HMPA) (1.79 g, 10 mmol, Aldrich) was added to a lithium dicyclohexylamide ($LiNCy_2$) solution prepared from dicyclohexylamine (1.63 g, 9 mmol) and *n*-butyllithium (2.6 M in hexane, 3.5 mL, 9 mmol) in anhydrous THF (20 mL) at 0°C. The solution was stirred for 30 min at 0°C, then cooled to −78°C, followed by the addition of methyl crotonate (0.905 g, 9 mmol, Aldrich) in anhydrous THF (5 mL). After stirring for 30 min at −78°C, cadmium chloride powder (0.825 g, 4.5 mmol, Aldrich, Gold label, previously ground in a mortar and dried under vacuum at 110°C overnight) was added in one portion. The resulting suspension was stirred for 30 min at −78°C and a solution of benzaldehyde (0.424 g, 4 mmol, Aldrich, redistilled) in anhydrous THF (5 mL) was added dropwise to the suspension. The reaction was continued at −78°C for 1 h, at 0°C for 30 min, and quenched with saturated aqueous NH_4Cl. The mixture was filtered through Celite, and the filtrate was extracted with ether (2 × 20 mL). The combined organic extracts were washed with brine, dried, filtered, concentrated, and purified by chromatography (20% ethyl acetate/petroleum ether) to give methyl 5-hydroxy-5-phenyl-2-pentenoate (γ product, 0.338 g, 41%) and methyl 2-vinyl-3-hydroxy-3-phenylpropanoate (α product, 0.328 g, 40%), α : γ = 50:50, 81% total yield.

Methyl 5-hydroxy-5-phenyl-2-pentenoate (lit. (12)): ir (film): 3490 (OH), 3080, 3060, 3030 (phenyl C-H), 1715 (C=O), 1600 (C=C) cm^{-1}; ^1H nmr (80 MHz) δ: 2.13 (m, 2H, CH_2), 2.80–3.15 (m, 2H, H-C-O, OH), 3.69 (s, 1H, OCH_3), 5.81 (m, 1H, C=CH-CO_2Me), 6.85 (m, 1H, H-C=C-CO_2Me), 7.25 (m, 5H, phenyl H).

Methyl 2-vinyl-3-hydroxy-3-phenylpropanoate (lit. (12)): ir (film): 3490 (OH), 1725 (C=O), 1460 (C=C) cm^{-1}; ^1H nmr (80 MHz) δ: 2.89 (d, 1H, J = 2.6 Hz, OH), 3.35 (dd, 1H, J = 2.6, 5.8 Hz, H-C-CO_2Me), 3.61 (s, 3H, OCH_3), 5.05 (m, 1H, *H*-C-OH), 5.32 (m, 2H, C=CH_2), 5.96 (m, 1H, -C=CH_2), 7.32 (m, 5H, phenyl H). Exact Mass calcd. for $C_{12}H_{14}O_3$: 206.0942; found: 206.0968.

*(+)-(5R,1′R)-3-Methyl-5-(2′,2′-dimethylspiro[2.4]hepta-4′,6′-dien-1′-yl)-6-oxa-2-cyclohexenone (**9**)*

An LDA solution was prepared from diisopropylamine (0.32 mL, 2.3 mmol) and *n*-butyllithium (2.5 M, 0.9 mL, 2.3 mmol, Aldrich) in anhydrous THF (5 mL) at −40°C, and a solution of methyl 3,3-dimethylacrylate (0.2510 g, 2.2 mmol) in anhydrous THF (2 mL) was added dropwise. After stirring for 20 min, cadmium chloride powder (0.366 g, 2.0 mmol, Aldrich, Gold label, previously ground in a mortar and dried overnight under vacuum at 110°C) was added in one portion. The suspension was stirred for 30 min at −40°C, and a solution of (+)-spiro-aldehyde **1** (0.159 g, 1.1 mmol) (15) in anhydrous THF (5 mL) was added by syringe pump (0.1 mL/min). After the addition was complete, stirring was continued for a further 30 min at −40°C. The reaction was allowed to warm to 0°C, stirred for 2 h at

0°C, and then quenched with saturated aqueous NH_4Cl. The mixture was filtered through Celite and the filtrate was extracted with ether (2 × 15 mL). The combined organic layers were dried, filtered, and concentrated. Chromatography (15% ethyl acetate/petroleum ether) afforded (+)-triene lactone **9** (0.185 g, 73%), as a colourless liquid, and α product **4** (0.038 g, 15%). (+)-Triene-lactone **9**; $[\alpha]^{22}$ +17.7° (*c* 3.4, $CHCl_3$); ir (film): 1710 (C=O), 1650 (C=C) cm^{-1}; ^1H nmr (200 MHz) δ: 1.39 (s, 3H, CH_3), 1.43 (s, 3H, CH_3), 1.87 (s, 3H, CH_3-C=C), 1.93 (m, 1H, axial HC-C=C), 2.09 (m, 1H, eq. CH-C=C), 2.31 (d, 1H, J = 4.4 Hz, cyclopropyl H), 4.48 (ddd, 1H, J = 4.4, 10.1, 11.1 Hz, H-C-O), 5.76 (s, 1H, H-C=C), 6.17 (m, 1H, cyclopentadienyl H), 6.28 (m, 1H, cyclopentadienyl H), 6.49 (m, 1H, cyclopentadienyl H), 6.58 (m, 1H, cyclopentadienyl H); ^{13}C nmr and DEPT δ: 164.6 (C=O), 156.0 (C=C), 136.4 (C=CH), 132.3 (C=CH), 131.6 (C=CH), 129.7 (C=CH), 116.8 (C=CH), 76.6 (CH), 51.1 (quaternary C), 42.1 (CH), 35.6 (CH_2), 31.9 (quaternary C), 27.2 (CH_3), 23.0 (CH_3), 20.4 (CH_3). Exact Mass calcd. for $C_{15}H_{18}O_2$: 230.1302; found: 230.1303. Anal. calcd. for $C_{15}H_{18}O_2$: C 78.21, H 7.88; found: C 78.02, H 7.69.

Acknowledgments

We are grateful to the University of Ottawa, Memorial University of Newfoundland (where this work was initiated and represents part of the Ph.D. research of B. L.), and the Natural Sciences and Engineering Research Council of Canada for financial support of this research.

1. Y. YAMAMOTO. Acc. Chem. Res. **20**, 243 (1987).
2. E. J. COREY, C-M. YU, and S. KIM. J. Am. Chem. Soc. **111**, 5495 (1989).
3. W. R. ROUSH, L. K. HOONG, M. A. J. PALMER, and J. C. PARK. J. Org. Chem. **55**, 4109 (1990).
4. T. HUDLICKY, M. G. NATCHUS, L. D. KWART, and B. L. CALWELL. J. Org. Chem. **50**, 4300 (1985); L. E. RICE, M. C. BOSTON, H. O. FINKLEA, B. J. SUDER, J. O. FRAZIR, and T. HUDLICKY. J. Org. Chem. **49**, 1845 (1984).
5. R. L. FAN and T. HUDLICKY. Tetrahedron Lett. **30**, 5533 (1989).
6. Y. YAMAMOTO, S. HATSUYA, and J. YAMADA, Chem. Commun. 86 (1988).
7. M. BELLASSOUED, F. DARDOIZE, Y. FRANGIN, and M. GAUDEMAR. J. Organomet. Chem. **219**, C1 (1981); M. BELLASSOUED, M. GAUDEMAR, A. EL BORGI, and B. BACCAR. J. Organomet. Chem. **280**, 165 (1985).
8. F. E. ZIEGLER and C. C. TAM. J. Org. Chem. **44**, 3428 (1979); F. E. ZIEGLER and C. M. CHAN. J. Org. Chem. **43**, 3065 (1978).
9. J. BIELLMANN and J. DUCEP. Org. React. **27**, 1 (1982).
10. J.-M. FANG, L.-F. LIAO, and B.-C. HONG. J. Org. Chem. **51**, 2828 (1986); J.-M. FANG, B.-C. HONG, and L.-F. LIAO. J. Org. Chem. **52**, 855 (1987).
11. R. W. DUGGER and C. H. HEATHCOCK. J. Org. Chem. **45**, 1181 (1980).
12. P. R. JOHNSON and J. D. WHITE. J. Org. Chem. **49**, 4424 (1984).
13. P. ALBAUGH-ROBERTSON and J. A. KATZENELLENBOGEN. J. Org. Chem. **48**, 5288 (1983).
14. M. MAJEWSKI, G. B. MPANGO, M. T. THOMAS. A. WU, and V. SNIECKUS. J. Org. Chem. **46**, 2029 (1981).
15. A. S. KENDE and J. CHEN. J. Am. Chem. Soc. **107**, 7184 (1985).
16. B. LEI and A. G. FALLIS. Tetrahedron Lett. **27**, 5193 (1986).
17. D. ABENHAIM and E. HENRY-BASCH. C. R. SEANCES Acad. Sci. Ser. C: **267**, 87 (1968).
18. D. ABENHAIM, E. HENRY-BASCH, and P. FREON. Bull. Soc. Chim. Fr. 4043 (1969).
19. B. LEI and A. G. FALLIS. J. Am. Chem. Soc. **112**, 4609 (1990).
20. K. ANTCZAK, J. F. KINGSTON, and A. G. FALLIS. Can. J. Chem. **62**, 2451 (1984).
21. P. R. JONES and R. J. DESIO. Chem. Rev. **78**, 491 (1978).
22. J. KOLLONITSCH. J. Chem. Soc. A: 453 (1966); 456 (1966).
23. J. L. HERRMANN, G. R. KIECZYKOWSKI, and R. H. SCHLESSINGER. Tetrahedron Lett. 2433 (1973).
24. J. R. SANDERS and E. C. ASHBY. J. Organomet. Chem. **25**, 277 (1970).
25. A. LOFFLER, F. NORRIS, W. TAUB, K. L. SWANHOLT, and A. S. DREIDING. Helv. Chem. Acta, **53**, 403 (1970).
26. A. J. FATIADI, Synthesis, **65**, 133 (1976); L. A. Carpino. J. Org. Chem. **35**, 3971 (1970).
27. J. MEIJER, P. VERMEER, and L. BRANSMA. Recl. Trav. Chim. Pays-Bas, **92**, 601 (1972).

Can. J. Chem. Downloaded from www.nrcresearchpress.com by 84.41.108.74 on 09/07/12
For personal use only.

Synthesis and electrochemistry of linear and cofacial conjugated binuclear phthalocyanines covalently linked by alkyne and alkene bridges

STEVEN VIGH, HERMAN LAM, PAVEL JANDA, A. B. P. LEVER,[1] AND CLIFFORD C. LEZNOFF[1]
Department of Chemistry, York University, North York (Toronto), Ont., Canada M3J 1P3

AND

RONALD L. CERNY
Midwest Center for Mass Spectrometry, University of Nebraska–Lincoln, Lincoln, NE 68558, U.S.A.

Received October 31, 1990[2]

STEVEN VIGH, HERMAN LAM, PAVEL JANDA, A. B. P. LEVER, CLIFFORD C. LEZNOFF, and RONALD L. CERNY. Can. J. Chem. **69**, 1457 (1991).

Semihydrogenation of 1,2-bis(3,4-dicyanophenyl)ethyne gave *cis*-1,2-bis(3,4-dicyanophenyl)ethene. From these precursors, binuclear phthalocyanines were produced containing linear binuclear phthalocyanines having an ethyne bridge and a mixture of *cis* and *trans* isomers of binuclear phthalocyanines linked by an ethene bridge. The *cis* and *trans* isomers could be separated and differentiated by gel permeation chromatography as the very extended *trans* isomer elutes faster than the cofacial globular *cis* isomer. Strong coupling between the conjugated binuclear phthalocyanine was not observed when examined by cyclic voltammetry.

Key words: phthalocyanines, cofacial, binuclear, cyclic voltammetry.

STEVEN VIGH, HERMAN LAM, PAVEL JANDA, A. B. P. LEVER, CLIFFORD C. LEZNOFF et RONALD L. CERNY. Can. J. Chem. **69**, 1457 (1991).

La semi-hydrogénation du 1,2-bis(3,4-dicyanophényl)éthyne conduit au *cis*-1,2-bis(3,4-dicyanophényl)éthène. À l'aide de ces précurseurs, on a préparé des phthalocyanines binucléaires contenant des phthalocyanines binucléaires linéaires possédant un pont éthyne et un mélange des isomères *cis* et *trans* des phtalocyanines binculéaires liées par un pont éthène. On a pu séparé et différencié les isomères *cis* et *trans* grâce à la chromatographie à perméation de gel; en effet l'isomère *trans*, plus étendu, s'élue plus rapidement que l'isomère *cis* globulaire cofacial. Lorsqu'on les a soumis à de la voltampérométrie cyclique, on n'a pas observé de couplage important entre la phtalocyanine binucléaire conjuguée.

Mots clés : phtalocyanines, cofacial, binucléaire, voltampérométrie cyclique.

[Traduit par la rédaction]

Introduction

It has been shown (1–4) that binuclear porphyrins, constrained to lie in cofacial configurations, are effective in catalyzing the 4e reduction of O_2 to H_2O. The long-term instability of these porphyrin catalysts, however, has led us to prepare the more stable cofacial binuclear and multinuclear (5–7) phthalocyanines (8–10), having bridges of five (5, 8), four (6), three (7), two (6), one (9), zero (7), and even "(−1)" bridges (10). The electrochemistry of some of these cofacial (7, 11) and conjugated planar (10) metallophthalocyanines exhibted interesting mixed valence species, but only the 2e reduction of O_2 was observed, albeit with greater efficiency than mononuclear species. We had never attempted to prepare a binuclear phthalocyanine that is both conjugated and cofacial but we have now succeeded in this quest and report its synthesis, and its spectroscopic and electrochemical properties.

Results and discussion

Synthetic aspects

Semihydrogenation of 1,2-bis(3,4-dicyanophenyl)ethyne (**1**) (6) in acetonitrile with Lindar's catalyst (12) gave *cis*-1,2-bis(3,4-dicyanophenyl)ethene (**2**) in 94% yield. Treatment of **1** and **2** with gaseous ammonia in a solution of sodium methoxide in methanol (5, 13) gave their respective diiminoisoindolines **3** and **4**. Mixed condensation (5, 13) of **3** with the diiminoisoindoline (**5**) (5) derived from 4-neopentoxyphthalonitrile (5, 14) gave, upon chromatographic purification using flash (15) and gel permeation chromatography (8, 16), 2,9,16,23-tetraneopentoxyphthalocyanine (**6**) in 49% yield and the desired binuclear phthalocyanine (**7**), linked by an ethyne group in 7.4% yield (Scheme 1). Binuclear phthalocyanine **7** was readily converted into its diCo(II) derivative (**8**) by treatment with anhydrous $CoCl_2$ in 77% yield. Similarly, condensation of **4** and **5** gave mononuclear **6** in 53% yield and a mixture of the *cis* and *trans* binuclear phthalocyanines **9** and **10**, linked by ethene groups (Scheme 1). Gel permeation chromatography, using tetrahydrofuran as eluant, succeeded in separating the linear fast-moving *trans*-binuclear bisphthalocyaninylethene (**10**) from the slower cofacial *cis*-binuclear bisphthalocyaninylethene (**9**). The infrared spectra of **9** and **10** were not characteristically different for these *cis* and *trans* isomers and their mass spectral data were identical. Unfortunately, the NMR spectra of **8–10** were uninformative due to their insolubility in appropriate solvents and the fact that these compounds consist of a mixture of 36 regioisomers, with the result that most NMR signals are broad and featureless. Both isomers gave good elemental analysis. These isomers exhibted similar spectral and analytical data but did show mobility differences on gel permeation chromatography. In addition, the major product is the *cis*-**9**, the predicted product, while the formation of *trans*-**10** by known facile *cis–trans* isomerization is understandable. Metallation of **9** with $CoCl_2$ or $Zn(OAc)_2$ gave the diCo(II) and diZn(II) derivatives **11** and **12** respectively.

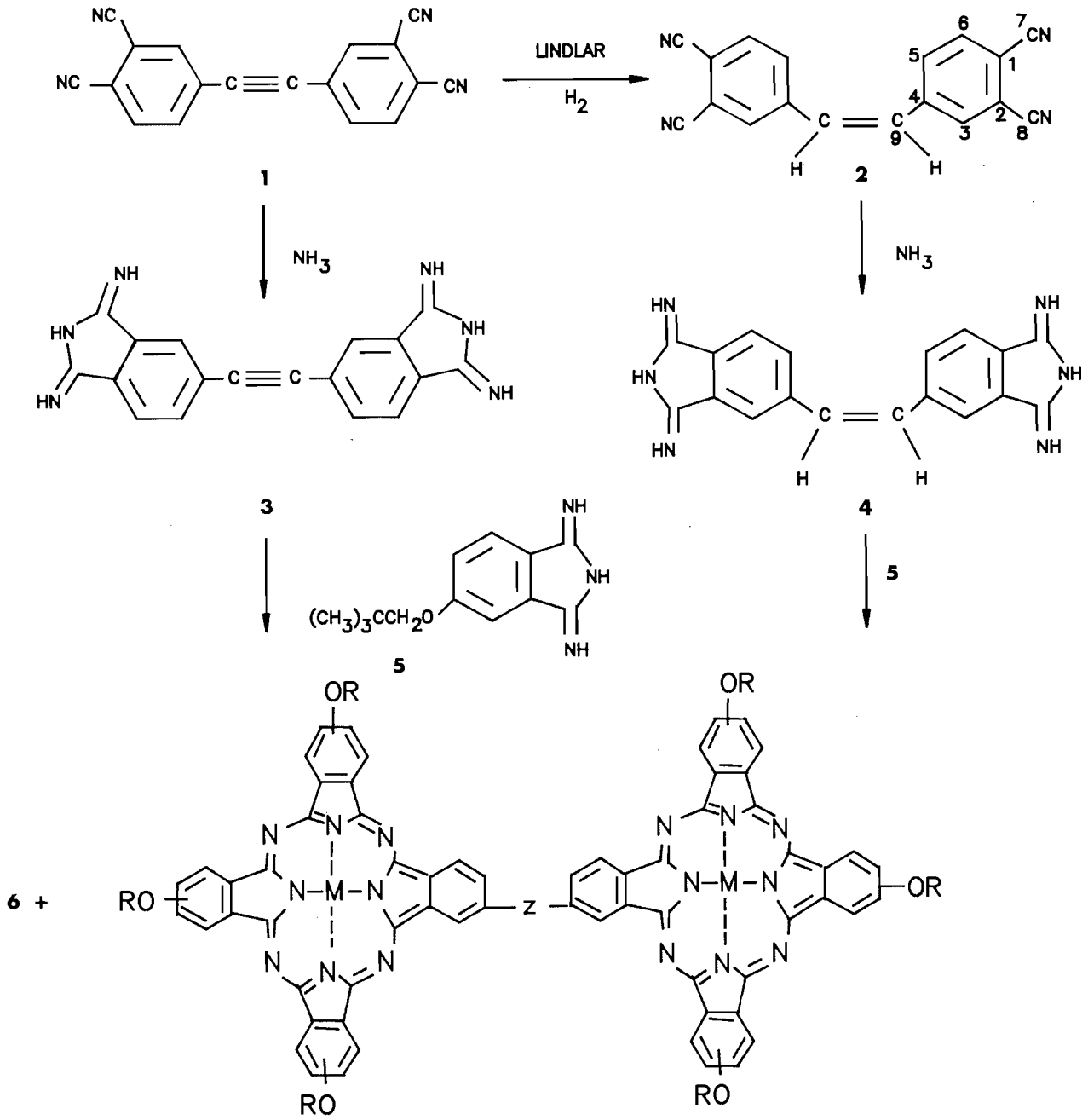
Electronic spectra

The *trans* metal-free species **10** has an electronic spectrum typical of a largely uncoupled mononuclear metal-free phthalocyanine (5, 18) while the *cis* isomer **9** has a blue-shifted *Q*-band spectrum consistent with extensive intramolecular coupling

[1]Authors to whom correspondence may be addressed.
[2]Revision received May 27, 1991.

Printed in Canada / Imprimé au Canada

Can. J. Chem. Downloaded from www.nrcresearchpress.com by 84.41.108.74 on 09/07/12
For personal use only.



SCHEME 1

(18–20). Similar extensive intramolecular coupling is observed in the spectra of the *cis* dimetallated species **11** and **12**, which exhibit typical broad, blue-shifted *Q*-band absorption (8, 11, 18, 19, 21, 22) (Fig. 1). They likely therefore adopt a basically cofacial conformation required by the *cis*-ethene linkage.

Electrochemistry

Differential pulse voltammetry (DPV) data for the cobalt complexes **8** and **11** are reported in Table 1. These complexes are not nearly so well behaved electrochemically as most previously described cobalt phthalocyanine derivatives (8, 11,18). Although DPV peaks were obtained as listed, the cyclic voltammograms were generally broad and ill-defined, showing a series of overlapping and apparently irreversible waves.

Comparison with the control, CoTNPc (18) species leads to fairly obvious assignments. The ethyne derivative, **8**, has redox processes, as assigned, at potentials almost identical with those of the corresponding mononuclear CoTNPc. No splitting of these waves is noted. The first oxidation is then assigned to the simultaneous oxidation of both rings to the *bis*-$Co^{II}Pc(-1)$

Can. J. Chem. Downloaded from www.nrcresearchpress.com by 84.41.108.74 on 09/07/12
For personal use only.

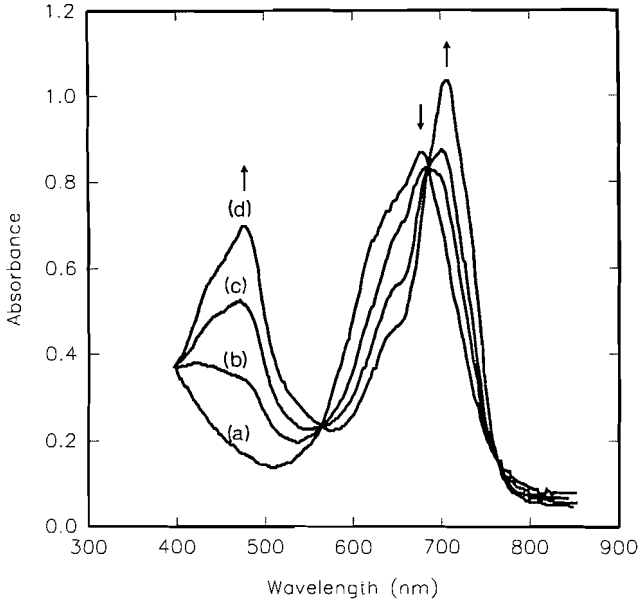


FIG. 1. Spectroelectrochemistry of CoPc=PcCo in DCB solution with 0.1 M TBAP, deoxygenated by Ar. Bulk electrolysis at −1 V vs. SCE reference electrode. Spectra taken using the Guided Wave fiber optic probe: (a) starting oxidized form $Co^{II}Pc = PcCo^{II}$; (d) final reduced form $Co^{I}Pc{=}PcCo^{I}$. Spectra changed during the bulk electrolysis from (a) to (d) according to arrows.

TABLE 1. Electrochemical data[a]

	Process			
Complex	I	II	?	III
CoTNPc[b]	0.03	−0.91	−2.07	
Ethyne **8**	0.14	−0.87	−2.09	
cis-Ethene **11**	0.13	−0.91	−1.52	−1.80

[a]Differential pulse voltammetry data, $E_{\frac{1}{2}}$ values approximated as the means of the forward and reverse peak positions, in DCB, in volts vs. ferricenium/ferrocene. This couple is observed in these studies at 0.495 V vs. AgCl/Ag on a platinum electrode surface.

[b]Data from ref. 18.

radical phthalocyanine species, and reduction involves the simultaneous reduction to the *bis*-$Co^{I}Pc(-2)$ species, and then subsequently, at −2.09 V (vs. ferrocene), reduction to the *bis*-$Co^{I}Pc(-3)$ species.

The *cis* cobalt ethene complex **11** also shows potentials at roughly those exhibited by CoTNPc but the apparent $[Co^{I}Pc(-2)]_2^{2-}/[Co^{I}Pc(-3)]_2^{4-}$ process is about 0.2 V more positive than expected. This last observation is reminiscent of the behaviour of recently described napthalene (11, 21) and anthracene (11) bridged cobalt phthalocyanines, which show splitting of their Co^{II}/Co^{I} couples and the formation of mixed valence $Co^{II}Pc \cdot Co^{I}Pc$ species. Spectroelectrochemical studies (Fig. 1) polarized just negative of this wave (at −1.0/ V vs. ferrocene) give a spectrum λ_{max} 475 nm (MLCT), 708 nm (*Q* band) typical of a fully reduced cobalt(I) phthalocyanine species (5, 8, 10, 11, 18, 21, 22), and unlike a mixed valence $Co^{II}Pc \cdot Co^{I}Pc$ binuclear species. The reduction is fully reversible (Fig. 2) since spectroelectrochemical reoxidation regenerated the original spectrum. There is no spectroscopic evidence for a mixed valence intermediate.

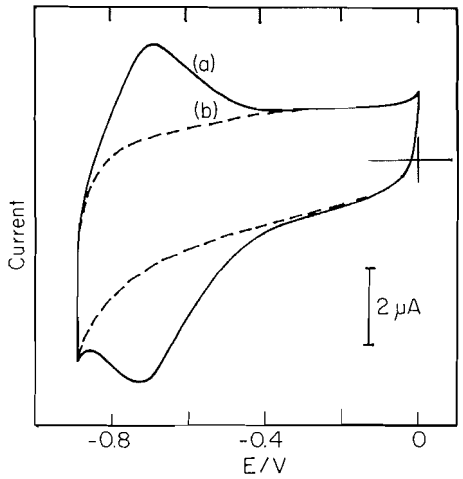


FIG. 2. Cyclic voltammetry of HOPG/CoPc=PcCo electrode in aqueous solution of 0.1 M phosphate buffer, pH = 7, Ar, scan rate v = 100 V/s, potential vs. SCE. (a) HOPG/CoPc=PcCo; (b) HOPG (residual current).

We conclude therefore that the interaction between the rings in the ethene derivative **11** is too small to stablize the mixed valence $Co^{II}Pc \cdot Co^{I}Pc$ species. Moreover, there appears to be an additional redox process at −1.52 V (vs. ferrocene). The origin of the −1.52 V couple is obscure; it may indeed be due to an impurity process.

Oxygen reduction

Complexes **8** and **11** were also deposited as monolayer films on highly pyrolytic graphite rotating disk electrodes following methods described earlier (23). These modified electrodes electrocatalyse the reduction of molecular oxygen in a two-electron process to hydrogen peroxide. No four-electron reduction to oxygen was observed. Since we have extensively discussed the two-electron reduction of oxygen by cobalt phthalocyanines in the past (11, 23) no further discussion is presented here.

Experimental

Matheson high purity argon was used to maintain inert atmosphere conditions. Infrared (ir) spectra were recorded on a Pye Unicam SP1000 infrared spectrophotometer using KBr discs. Nuclear magnetic resonance (nmr) spectra for protons and carbons were recorded on a Bruker AM300 nmr spectrometer. The position of signals is reported in δ units. (The splitting of the signals is described as singlets (s), doublets (d), triplets (t), quartets (q), doublets of doublets (dd), or multiplets (m)). The ^1H nmr spectra of 10^{-4} M solutions of the phthalocyanines were obtained by averaging 500–3000 scans over the absorption range. The ultraviolet–visible spectra (uv) were recorded on a Hewlett Packard HP8451A diode array spectrophotometer. Mass spectra (ms) were recorded at 70 eV on a VG Micromass 16F mass spectrometer in the EI mode. The FAB spectra were obtained with a Kratos MS-50 triple analyzer mass spectrometer equipped with a FAB ion source of standard Kratos design and Ion Tech atom gun. The sample was dissolved in chloroform and a microlitre of the resulting solution added to a microlitre of *m*-nitrobenzyl alcohol on the probe tip. The spectra of the molecular ions of the binuclear phthalocyanines were obtained by signal averaging up to 256 scans over the approximate mass range. The number in parentheses after the indaicated ion shows the percentage of the base peak represented by that ion. Melting points (mp) were determined using a Kofler hot stage melting point apparatus and are uncorrected. Flash chromatography was performed using silica gel of particle size 20–45 μm. All reactions were stirred with a magnetic stirrer. All solvents were freshly distilled before use. Thin-layer

Can. J. Chem. Downloaded from www.nrcresearchpress.com by 84.41.108.74 on 09/07/12
For personal use only.

Can. J. Chem. Downloaded from www.nrcresearchpress.com by 84.41.108.74 on 09/07/12
For personal use only.

chromatography (tlc) was performed using silica gel G as the absorbant. Microanalyses were performed by Guelph Chemical Laboratories Ltd., Guelph, Ontario.

Electrochemical data were obtained with a Princeton Applied Research (PARC) model 173 potentiostat, or a PARC model 174A polarographic analyzer coupled to a PARC model 175 universal programmer. Cyclic voltammetry and differential pulse voltammetry (DPV) were carried out under an atmosphere of argon, or nitrogen, using a conventional three-electrode cell. The working electrode was described by the cross-sectional area of a 27-gauge platinum wire (area 10^{-3} cm^2), and sealed in glass. A platinum wire also served as the counter electrode. The reference electrode was a silver wire quasireference electrode, referenced internally to the ferricenium/ferrocene (Fc^+/Fc) couple.

Spectroelectrochemical measurements were made with a 0.45-mm path-length optically transparent thin-layer electrode (OTTLE) cell, utilizing a gold minigrid (500 lines/in., 60% transmittance) (17), in conjunction with the Hitachi Perkin–Elmer model 340 spectrometer.

Preparation of 1,2-bis(3,4-dicyanophenyl)ethylene (1)

Compound **1** was prepared as reported by Marcuccio *et al.* (6); yield 85%, mp 285–287°C (lit. (6) mp 286–288°C); ^{1}H nmr (DMSO-d_6, 300 MHz) δ: 8.42 (d, J = 1.6 Hz, 2H, Ar*H*-3), 8.22 (d, J = 8 Hz, 2H, Ar*H*-6), 8.11 (d, J = 8 Hz, 2H, Ar*H*-5).

Preparation of 1,2-bis(3,4-dicyanophentl)ethene (2)

A solution of 1.0 g (3.6 mmol) of pure **1** in 300 mL of acetonitrile was stirred under hydrogen (1 atm (101.3 kPa), 25°C) in the presence of Lindlar's catalyst (12) (250 mg) until absorption of hydrogen (88 mL) had ceased. The catalyst was filtered and the filtrate was evaporated to give 0.950 g (94% yield) of a yellow powder **2**. Recrystallization in methanol yielded white, needle-like crystals, mp 196–197°C; ir (cm^{-1}): 3090–2920, 2210 (CN), 1590, 1550, 1490, 1380, 1230, 920, 870, 850, 810, 770, 720; uv (CH_3CN) λ_{max} (log ε): 308 (4.09), 276 (4.07), 224 (4.38); ^{1}H nmr (DMSO-d_6, 300 MHz) δ: 8.00 (s, 2H, Ar*H*-3), 7.98 (d, J = 8 Hz, 4H, Ar*H*-6), 7.61 (d, J = 8 Hz, 2H, Ar*H*-5), 6.95 (s, 2H, C*H*=CH); ^{13}C nmr δ: 141.2 (C-4), 134.1 + 134.0 (C-5 + C-9), 133.6 (C-3), 131.0 (C-6), 115.8 + 115.6 (C-7 + C-8), 115.1 (C-2), 113.3 (C-1); ms m/z: 280(M^+), 254. Anal. calcd. for $C_{18}H_8N_4$: C 77.13, H 2.87, N 19.98; found: C 77.10, H 3.21, N 20.17.

Preparation of the bis-1,3-diiminoisoindoline of 1,2-bis(3,4-dicyanophenyl)ethyne (3)

The bisphthalonitrile **1**, 0.30 g (1.08 mmol), was added to a solution of 30 mg of sodium in 30 mL of dry methanol. Since the bisphthalonitrile **1** did not dissolve, the mixture was heated to 60°C. The mixture was stirred at 60°C for 0.75 h under reflux conditions, while ammonia gas was bubbed into the solution. The reaction mixture gradually turned green during which time a green precipitate was observed. The reaction was cooled to room temperature and the addition of ammonia gas was discontinued. Evaporation of the solvent gave crude **3**, which was used directly in condensation reactions without further purification. Compound **3** did not exhibit a nitrile absorption in its ir spectrum.

Preparation of the bis-1,3-diiminoisoindole of 1,2-bis(3,4-dicyanophenyl)ethene (4)

The bisphthalonitrile **2**, 0.300 g (1.07 mmol), was added to a solution of 30 mg of sodium in 30 mL of dry methanol. The mixture was stirred at room temperature for 0.75 h while ammonia gas was bubbled into the solution. The reaction mixture gradually became green, during which time a green precipitate was observed. The addition of ammonia gas was discontinued. Evaporation of the solvent gave crude **4**, which was used directly in condensation reactions without further purification. Compound **4** did not exhibit a nitrile absorption in its ir spectrum.

Preparation of the 1,2-bis-2'-(9',16',23'-trineopentoxyphthalocyaninyl)ethyne (7)

The two crude diiminoisoindolines **5** and **3**, obtained from 6.0 g (28 mmol) of 4-neopentoxyphthalonitrile (5) (**5**), and 300 mg (1.08 mmol) of **1**, were heated to 150°C (oil bath) in 30 mL of 2-*N*,*N*-dimethylaminoethanol for 72 h under an argon atmosphere. The mixture was cooled to room temperature, diluted with water, filtered, and washed thoroughly with water followed by methanol until the filtrate was almost clear. The crude product was extracted with methanol in a Soxhlet apparatus until the extract was clear of brown and yellow impurities. The crude product was purified by flash chromatography using a 5 cm diameter column packed with flash silica gel 12 cm high. The crude product was preabsorbed on a small amount of flash silica gel and eluted with toluene to give 300 g of the monomeric 2,9,16,23-tetraneopentoxyphthalocyanine (**6**) in 49% yield. Further elution with 2-methoxyethanol/toluene (2:98) gave a fraction consisting largely of dimer **7**, containing traces of monomer and some green material. Finally, elution with 2-methoxyethanol/toluene (1:4) gave a green fraction consisting largely of trimer and impurities. The dimer fraction was further purified by gel permeation chromatography (8, 16). Elution wih tetrahydrofuran removed all traces of monomer and green material from the major dimer band. Evaporation of the solvent gave a dark blue product. This product was washed with acetonitrile/acetone to remove traces of fluorescent impurities, detectable by tlc using toluene/2-methoxyethanol (98:2) as eluant to give, in 7.4% yield, 125 mg of **7** as a dark blue, shiny solid; ir (cm^{-1}): 3300 (N-H), 1610, 1480, 1400, 1240, 1100, 1020 (N-H), 750; uv (*o*-dichlorobenzene (DCB)) λ_{max} (log ε): 678 (4.36), 660 (4.39), 648 (4.45); ms m/z: 1569.8 (23), 1568.8 (58), 1567.8 (M^+ + 1, 100), 1566.8 (M^+, 86). Anal. calcd. for $C_{96}H_{94}N_{16}O_6$: C 73.54, H 6.04, N 14.29; found: C 73.30, H 5.95, N 13.94.

Preparation of 1,2-bis-2'-(9',16',23'-trineopentoxyphthalocyaninyl)-ethyne dicobalt(II) (8)

A mixture of 50 mg (0.032 mmol) of metal-free dimer **7** and 100 mg (0.77 mmol) of anhydrous cobalt(II) dichloride in 10 mL of a 1:1 mixture of 2-methoxyethanol/dichlorobenzene was heated at 16°C for 20 h under an argon atmosphere. The crude reaction mixture, after cooling, was evaporated under high vacuum to remove the 2-methoxyethanol/dichlorobenzene. The remaining residue was precipitated with a water/methanol (1:1) mixture. After filtering, the dark blue, shiny solid obtained was extracted with methanol in a Soxhlet apparatus until the extract was clear. The dark blue solid was dried to give 41 mg (76% yield) of **8**; ir (cm^{-1}): 1620, 1530, 1480, 1410, 1380, 1240, 1100, 760; uv (DCB) λ_{max} (log ε): 686 (4.21), 658 (4.23), 650 (4.19), 638 (4.18), 630 (4.19), 302 (4.33), 262 (4.04); ms m/z: 1683.6 (23), 1682.6 (58), 1681.6 (M^+ + 1, 100), 1680.6 (M^+, 86). Anal. calcd. for $C_{96}H_{90}N_{16}O_6Co_2$: C 68.56, H 5.39, N 13.39, Co 7.01; found: C 67.82, H 5.68, N 12.99, Co 6.80.

Preparation of cis *and* trans *1,2-bis-2'-(9',16',23'-trineopentoxyphthalocyaninyl)ethene (9 and 10)*

The two crude diiminoisoindolines, **5** and **4**, obtained from 6.0 g (28 mmol) of 4-neopentoxyphthalonitrile (5) and 300 mg (1.07 mmol) of **2**, were heated to 150°C (oil bath) in 30 mL of 2-*N*,*N*-dimethylaminoethanol for 72 h under an argon atmosphere. The mixture was cooled to room temperature, diluted with water, filtered, and washed thoroughly with water followed by methanol until the filtrate was almost clear. The crude product was extracted with methanol in a Soxhlet apparatus until the extract was clear of brown and yellow impurities. The crude product was purified by flash chromatography using a 5 cm diameter column packed with flash silica gel 12 cm high. The crude product was preabsorbed on a small amount of flash silica gel and eluted with toluene/hexane (1:1) to give 3.2 g of the monomeric **6** in 53% yield. Further elution with toluene gave a fraction consisting largely of dimer and monomer. Finally, elution with 2-methoxyethanol/toluene (2:98) gave a green fraction consisting largely of trimer and impurities. The dimer fraction was further purified by flash chromatography (3 cm diameter column). Elution with toluene/hexane (25:75) up to 100% toluene gave an even purer fraction of dimer with a small trace of monomer. This dimer fraction was further purified by gel permeation chromatography (8, 16) applying no more than 50 mg of dimer per chromatographic run. Elution with tetrahydrofuran removed all traces of monomer. The main dimer band of **9** was observed but a front-running blue band consisting of **10** was also noticed. These two

fractions were collected separately. Evaporation of the solvent gave 470.3 mg of **9** and **10** (28% yield, 378 mg of **9** and 92.3 mg of **10**) as dark blue solids, having identical ir and ms spectroscopic properties; ir (cm^{-1}): 3300 (N-H), 1620, 1480, 1400, 1240, 1100, 10.20 (N-H), 750; uv for **9** (DCB) λ_{max} (log ε): 704 (5.06), 650 (5.00), 344 (5.08); uv for **10** λ_{max} (log ε): 704 (4.76), 678 (4.77), 658 (4.78), 650 (4.77), 340 (4.86); ms *m/z*: 1571.7 (23), 1570.7 (58), 1569.7 (M^+ + 1, 100), 1568.7 (M^+, 86). Anal. calcd. for $C_{96}H_{90}N_{16}O_6Co_6$ for **9**: C 73.44, H 6.16, N 14.27; found: C 73.51, H 6.52, N 14.24. Anal. calcd. $C_{96}H_{96}N_{16}O_6$ for **10**: C 73.44, H 6.16, N 14.27; found: C 73.85, H 6.39, N 14.55.

*Preparation of the 1,2-bis-2'-(9',16',23'-trineopentoxyphthalocyaninyl)ethyne dicobalt(II) (**11**)*

A mixture of 50 mg (0.032 mmol) of metal-free dimer (**9**) and 100 mg (0.77 mmol) of anhydrous cobalt(II) dichloride in 13 mL of a 5:3:5 mixture of 2-methoxyethanol/dichlorobenzene/toluene was heated at 160°C for 20 h under an argon atmosphere. Flash chromatography of the crude reaction mixture on a 3 cm diameter column of flash silica gel and elution with dimethylformamide (DMF) gave, in 78.5% yield, 42.2 mg of **11** as a dark blue solid; ir (cm^{-1}): 1615, 1480, 1400, 1240, 1100, 1015, 755; uv (DCB) λ_{max} (log ε): 682 (4.82), 650 (4.76), 300 (4.91); ms *m/z*: 1685.6 (23), 1684.6 (58), 1683.6 (M^+ + 1, 100), 1682.6 (M^+, 86). Anal. calcd. for $C_{96}H_{92}N_{16}O_6Co_2$: C 68.48, H 5.50, N 13.31, Co 7.00; found: C 68.71, H 5.85, N 13.54, Co 6.50.

*Preparation of 1,2-bis-2'-(9',16',23'-trineopentoxyphthalocyaninyl)-ethene dizinc(II) (**12**)*

A mixture of 60 mg (0.038 mmol) of metal-free dimer **9** and 100 mg (0.54 mmol) of anhydrous zinc acetate in 13 mL of a 5:3:5 mixture of 2-methoxyethanol/dichlorobenzene/toluene was heated at 160°C for 20 h under an argon atmosphere. Flash chromatography of the crude reaction mixture on a 3 cm diameter column of flash silica gel and elution with 2-methoxyethanol/toluene (1:3) gave, in 89% yield, 57.7 mg of **12** as a dark blue solid; ir (cm^{-1}): 1610, 1490, 1395, 1340, 1235, 1100, 1060, 1015, 750; uv (DCB) λ_{max} (log ε): 688 (4.99), 658 (4.91), 650 (4.88), 342 (4.99), 300 (4.85); ms *m/z*: 1701.6 (18), 1700.6 (31), 1699.6 (46), 1698.6 (68), 1697.6 (84), 1696.6 (100), 1695.6 (82), 1694.6 (85), 1693.6 (M^+ + 1, 54), 1692.6 (M^+, 47). Anal. calcd. for $C_{96}H_{92}N_{16}O_6Zn_2$: C 67.96, H 5.46, N 13.20, Zn 7.70; found: C 67.53, H 5.40, N 13.03, Zn 7.22.

Acknowledgements

Financial support by the Natural Sciences and Engineering Research Council of Canada and by The Office of Naval Research (Washington) is gratefully acknowledged. The work was also funded by the Midwest Center for Mass Spectrometry, a National Science Foundation Regional Instrumentation Facility (Grant No. CHE8620177).

1. J. P. Collman, P. Denisevich, Y. Konai, M. Marrocco, C. Koval, and F. C. Anson. J. Am. Chem. Soc. **102**, 6027 (1980); J. P. Collman, F. C. Anson, S. Bencosme, A. Chong, T. Collins, P. Denisevich, E. Evitt, T. Geiger, J. A. Ibers, G. Jameson, Y. Konai, C. Koval, K. Meier, P. Oakley, R. B. Pettman, E. Schmittou, and J. Sessler. *In* Organic synthesis today and tomorrow. *Edited by* B. M. Trost and C. R. Hutchinson. Pergamon, Oxford. 1981.
2. R. R. Durand, C. S. Benscome, J. P. Collman, and F. C. Anson. J. Am. Chem. Soc. **105**, 2710 (1983); J. P. Collman, F. C. Anson, C. E. Barnes, C. S. Benscome, T. Geiger, E. R. Evitt, R. P. Kreh, K. Meier, and R. B. Pettman. J. Am. Chem. Soc. **105**, 2694 (1983).
3. C. K. Chang and I. Abdalmuhdi. J. Org. Chem. **48**, 5388 (1983); C. K. Chang, H. Y. Liu, and I. Abdalmuhdi. J. Am. Chem. Soc. **106**, 2725 (1984); C. K. Chang and I. Abdalmuhdi. Angew. Chem. **23**, 164 (1984); H. Y. Liu, I. Abdalmuhdi, C. K. Chang, and F. C. Anson. J. Phys. Chem. **89**, 665 (1985).
4. J. P. Fillers, K. G. Ravichandran, I. Abdalmuhdi, A. Tulinsky, and C. K. Chang. J. Am. Chem. Soc. **108**, 417 (1986).
5. C. C. Leznoff, S. M. Marcuccio, S. Greenberg, A. B. P. Lever, and K. B. Tomer. Can. J. Chem. **63**, 623 (1985).
6. S. M. Marcuccio, P. I. Svirskaya, S. Greenberg, A. B. P. Lever, C. C. Leznoff, and K. B. Tomer. Can. J. Chem. **63**, 3057 (1985).
7. H. Lam, S. M. Marcuccio, P. I. Svirskaya, S. Greenberg, A. B. P. Lever, C. C. Leznoff, and R. L. Cerny. Can. J. Chem. **67**, 1087 (1989); C. C. Leznoff, H. Lam, W. A. Nevin, N. Kobayashi, P. Janda, and A. B. P. Lever. Angew. Chem. Int. Ed. Engl. **26**, 1021 (1987).
8. W. A. Nevin, W. Liu, S. Greenberg, M. R. Hempstead, S. M. Marcuccio, M. Melnik, C. C. Leznoff, and A. B. P. Lever. Inorg. Chem. **26**, 891 (1987).
9. S. Greenberg, S. M. Marcuccio, C. C. Leznoff, and K. B. Tomer. Synthesis, 406 (1986).
10. C. C. Leznoff, H. Lam, S. M. Marcuccio, W. A. Nevin, P. Janda, N. Kobayashi, and A. B. P. Lever. J. Chem. Soc. Chem. Commun. 699 (1987).
11. N. Kobayashi, H. Lam, W. A. Nevin, P. Janda, C. C. Leznoff, and A. B. P. Lever. Inorg. Chem. **29**, 3415 (1990).
12. H. Lindlar. Helv. Chim. Acta, **35**, 446 (1952); E. N. Marvell and T. Li. Syntheses, 457 (1973).
13. P. J. Brach, S. J. Grammatica, O. A. Ossanna, and L. Weinberger. J. Heterocycl. Chem. **7**, 1403 (1970).
14. W. R. Barger, A. W. Snow, H. Wohltjen, and N. J. Thomas. Thin Solid Films, **132**, 113 (1985).
15. W. C. Still, M. Khan, and A. Mitra. J. Org. Chem. **43**, 2923 (1978).
16. J. A. Anton, J. Kwong, and P. A. Loach. J. Heterocycl. Chem. **13**, 717 (1976).
17. W. A. Nevin and A. B. P. Lever. Anal. Chem. **60**, 727 (1988).
18. W. A. Nevin, M. R. Hempstead, W Liu, C. C. Leznoff, and A. B. P. Lever. Inorg. Chem. **26**, 570 (1987).
19. W. A. Nevin, W. Liu, and A. B. P. Lever. Can. J. Chem. **65**, 855 (1986).
20. E. S. Dodsworth, A. B. P. Lever, P. Seymour, and C. C. Leznoff. J. Phys. Chem. **89**, 339 (1985).
21. W. Liu, M. R. Hempstead, W. A. Nevin, M. Melnik, A. B. P. Lever, and C. C. Leznoff. J. Chem. Soc. Dalton Trans. 2511 (1987).
22. C. C. Leznoff, H. Lam, W. A. Nevin, N. Kobayashi, P. Janda, and A. B. P. Lever. Angew. Chem. Int. Ed. Engl. **26**, 1021 (1987).
23. M. R. Hempstead, A. B. P. Lever, and C. C. Leznoff. Can. J. Chem. **65**, 2677 (1987); P. Janda, N. Kobayashi, P. Ashburn, H. Lam, C. C. Leznoff, and A. B. P. Lever. Can. J. Chem. **67**, 1109 (1989).

Can. J. Chem. Downloaded from www.nrcresearchpress.com by 84.41.108.74 on 09/07/12
For personal use only.

Syntheses of glycosyl phosphates by phase transfer catalysis

RENÉ ROY,[1] FRANÇOIS D. TROPPER, AND CHANTAL GRAND-MAÎTRE
Department of Chemistry, University of Ottawa, Ottawa, Ont., Canada K1N 6N5

Received February 13, 1991

RENÉ ROY, FRANÇOIS D. TROPPER, and CHANTAL GRAND-MAÎTRE. Can. J. Chem. **69**, 1462 (1991).

The peracetylated glycosyl bromides of D-glucose (**1**), D-galactose (**2**), and D-lactose (**5**) were treated with dibenzyl phosphate in a catalytic two-phase system using tetrabutylammonium hydrogen sulfate as catalyst. The reactions proceeded by complete inversion at the anomeric centers and afforded a new stereospecific entry into 1,2-*trans*-β-D-glycosyl phosphates of peracetylated D-glucose (**3**), D-galactose (**4**), and the disaccharide D-lactose (**6**) in 83, 73, and 83% yields respectively. Interestingly, the glycosyl chloride **7** furnished the oxazoline **9** rather than the expected glycosyl phosphate **8**.

Key words: phase transfer catalysis, glycosyl phosphates, phosphotriesters.

RENÉ ROY, FRANÇOIS D. TROPPER et CHANTAL GRAND-MAÎTRE. Can. J. Chem. **69**, 1462 (1991).

Les bromures de glycosyles peracétylés du D-glucose (**1**), du D-galactose (**2**) et du D-lactose (**5**) ont été traités en présence de phosphate de dibenzyle dans des conditions de catalyse par transfert de phase utilisant le bisulfate de tétrabutylammonium comme catalyseur. Les réactions ont conduit à une inversion complète des centres anomériques et fournissent une nouvelle entrée stéréospécifique aux phosphates peracétylés des 1,2-*trans*-β-D-glycosyles du D-glucose (**3**), du D-galactose (**4**) et du disaccharide D-lactose (**6**) avec des rendements de 83, 73, and 83% respectivement. Il est intéressant de noter que le chlorure de glycosyle **7** a conduit à la formation de l'oxazoline **9** au lieu du phosphate de glycosyle attendu **8**.

Mots clés: catalyse par transfert de phase, phosphate de glycosyles, phosphotriesters.

Can. J. Chem. Downloaded from www.nrcresearchpress.com by 84.41.108.74 on 09/07/12
For personal use only.

Introduction

Carbohydrate phosphates are important intermediates in a wide variety of biosynthetic processes (1). They constitute integral components of the core and lipid A region of lipopolysaccharides, sugar nucleotides, teichoic acids, bacterial polysaccharides, glycophospholipids, and phosphoinositides.

Previous methods for the synthesis of glycosyl 1-phosphates are essentially based on two fundamental concepts. In the first one, phosphoric acid, their salts, or dialkyl phosphates were used as nucleophiles on glycose peracetates (2), 1,2-orthoesters (3), halogenoses (4), 1,2-oxazolines (5), Brigl anhydrides (6), or on trichloroacetimidates (7). In the second approach, the anomeric hydroxyl groups were activated as lithium (8) or thallium (9) salts and reacted with electrophilic dialkyl phosphorochloridates. More recently, the phosphoramidite and H-phosphonate methods have also attracted interest (10). These methods and the occurrence of carbohydrate phosphates have been reviewed (11).

The widespread utilization of phase transfer catalysis (PTC) in carbohydrate chemistry (12) coupled with our own interests (13, 14) stimulated the application of this methodology to the synthesis of anomeric glycosyl phosphates from halogenoses. It was anticipated that dibenzylphosphate would be a potent nucleophile under a catalytic two-phase system. This procedure would give access to carbohydrate phosphotriesters from readily available reagents. We describe herein the successful practical syntheses of 1,2-*trans*-β-D-anomeric phosphates of peractylated D-glucose (**3**), D-galactose (**4**), and D-lactose (**6**). The reactions proceded by inversion at the anomeric centers and occurred with complete stereocontrol.

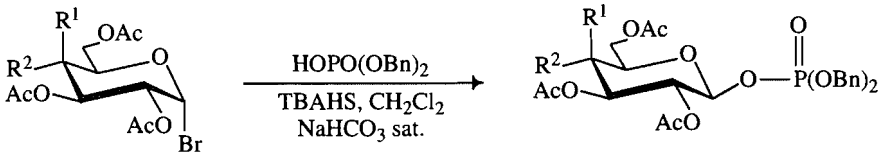
Results and discussion

Although there have been a number of recent applications of phase transfer catalysis (PTC) in carbohydrate chemistry (12–14), none of these dealt with the preparation of anomeric glycosyl phosphates. Because of the widespread occurrence of these important derivatives, it was decided to utilize PTC as a simple, practical entry into this class of carbohydrates. Our previous experience in PTC with a number of nucleophiles (phenoxides, thiophenoxides, azides, and carboxylates) (13, 14) prompted us to test the validity of using dibenzyl phosphate as nucleophile under the previously described conditions (13, 14). Thus, treatment of the α-bromides **1**, **2**, and **5** in methylene chloride and saturated sodium hydrogen carbonate with dibenzyl phosphate (2 equiv.) and tetrabutylammonium hydrogen sulfate (1 equiv.) at room temperature (1.5–3 days) afforded the corresponding β-D-glycosyl phosphates **3**, **4**, and **6** in 73–83% yields. Obviously, the reactions were much slower than those using phenoxides and thiophenoxides as nucleophiles (<45 min). The reactions occurred with complete inversion at the anomeric centers. Only traces of hydrolysis and dehydrobromination by-products were formed as side reactions. Changing the solvent, the catalyst, or the base (14) resulted in slower reactions and in lower yields.

The case of the 2-acetamido-3,4,6-tri-*O*-acetyl-2-deoxy-α-D-glucopyranosyl chloride (**7**) is worthy of comment. We previously determined the usefulness of **7** as electrophile under PTC conditions with a wide variety of nucleophiles (13, 14). In these studies, it was also shown that the 2-methyl-(3,4,6-tri-*O*-acetyl-1,2-dideoxy-α-D-glucopyrano)-[2,1-*d*]-oxazoline (**9**) was the major product isolated under PTC conditions in the absence of extraneous nucleophiles (>6 h). This was attributed to the slow formation of the β-chloride analogue of **7** with concomitant anchimeric participation of the 2-acetamido group, thus providing the oxazoline **9**. In the actual case, however, even with added dibenzyl phosphate, the oxazoline **9** was the major product formed (TLC; ^{1}H NMR) within the first hour of reaction instead of the expected glycosyl phosphate **8**. Therefore, it is believed that the nucleophilic displacement of the α-chloride by dibenzyl phosphate might have occurred, followed by rapid intramolecular displacement of the phosphate by the amide function to provide the oxazoline **9**. This could be rationalized by a favored anchimeric participation from the acetamido group over the acetyl groups in **3**, **4**, and **6**.

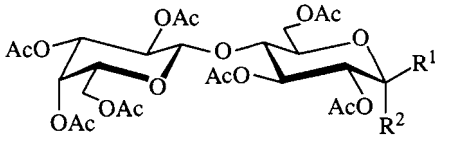
The anomeric configurations of the above glycosyl phosphates were unambiguously established by ^{1}H and ^{13}C NMR spectroscopy (Tables 1 and 2). The complete assignments of all the protons and carbons were confirmed by COSY and

[1]Author to whom correspondence may be addressed.

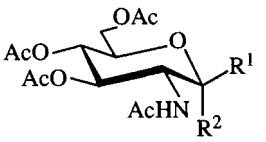


1 R^1 = H, R^2 = OAc
2 R^1 = OAc, R^2 = H

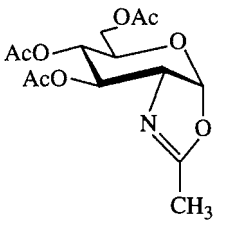
3 R^1 = H, R^2 = OAc
4 R^1 = OAc, R^2 = H



5 R^1 = H, R^2 = Br
6 R^1 = OPO(OBn)$_2$, R^2 = H



7 R^1 = H, R^2 = Cl
8 R^1 = OPO(OBn)$_2$, R^2 = H



9

SCHEME 1

TABLE 1. ^{13}C NMR chemical shifts (ppm) and C–P coupling constants (Hz) of the glycosyl phosphate derivatives (300 MHz, $CDCl_3$, 25°C)

Compound no.	C-1 ($^2J_{C,P}$)	C-2 ($^3J_{C,P}$)	C-3 ($^4J_{C,P}$)	C-4	C-5	C-6	CH_2Ph ($^2J_{C,P}$)
3	96.2 (4.7)	71.1 (9.2)	72.3 (1.5)	67.4	72.6	61.4	69.62, 69.57 (5.8), (5.5)
4	96.7[a] (4.8)	68.6 (8.8)	70.4 —	66.4	71.7	61.0	69.60, 69.55 (5.9, (6.1)
6 Glc	96.1 (4.9)	71.5 (9.0)	72.3 —	75.6	73.4	61.5	69.6, 69.5 (6.2, (6.3)
Gal	101.0	69.0	70.9	66.5	70.7	60.8	

[a] $^1J_{C\text{-}1,H\text{-}1}$ = 167 Hz.

HETCOR experiments. The anomeric carbons of **3**, **4**, and **6** appeared at 96.2 ($^2J_{C,P}$ 4.7 Hz), 96.7 ($^2J_{C,P}$ 4.8 Hz), and 96.1 ($^2J_{C,P}$ 4.9 Hz) ppm respectively (Table 1). The anomeric proton of the glucosyl phosphate **3** appeared as a doublet of doublets centered at 5.33 ppm with $J_{1,2}$ and $^3J_{1,P}$ couplings of 7.5 Hz. The same coupling constants were obtained for the anomeric proton (5.30 ppm) of the glucosyl residue of the lactosyl phosphate **6** (Fig. 1). The case of the galactosyl phosphate **4** was, however, somewhat ambiguous (in $CDCl_3$) since the H-1 and H-2 protons appeared as an ABX system (300 MHz). Although the C-1 chemical shift and the $^2J_{C,P}$ coupling constant were similar to those observed for the β-phosphates **3** and **6** and thus indicative of the β-D configuration, it was decided to further confirm this assumption. A one-bond $^{13}C-^1H$ coupling constant, which showed a $^1J_{H1,C1}$ of 167 ± <1 Hz for **4**, was obtained by a heteronuclear gated decoupling experiment (300 MHz). This value indicated that the H-1 proton should have been equatorially disposed (α-anomer) since 160 Hz is assumed to be typical of β-anomers while 170 Hz is typical of the α-anomers (15). Since the literature cited (15) has not been applied or demonstrated on anomeric glycosyl phosphates, the ambiguity still remained. The anomeric region of the ^{1}H NMR spectra of **4** was then simulated (Fig. 2) based on the estimated chemical shifts of H-1, H-2, and H-3 obtained from the $^1H-^1H$ homonuclear shift correlated experiment. The data obtained (Table 2) showed a $J_{1,2}$ coupling constant of 8.1 Hz ($CDCl_3$),

Can. J. Chem. Downloaded from www.nrcresearchpress.com by 84.41.108.74 on 09/07/12
For personal use only.

Can. J. Chem. Downloaded from www.nrcresearchpress.com by 84.41.108.74 on 09/07/12
For personal use only.

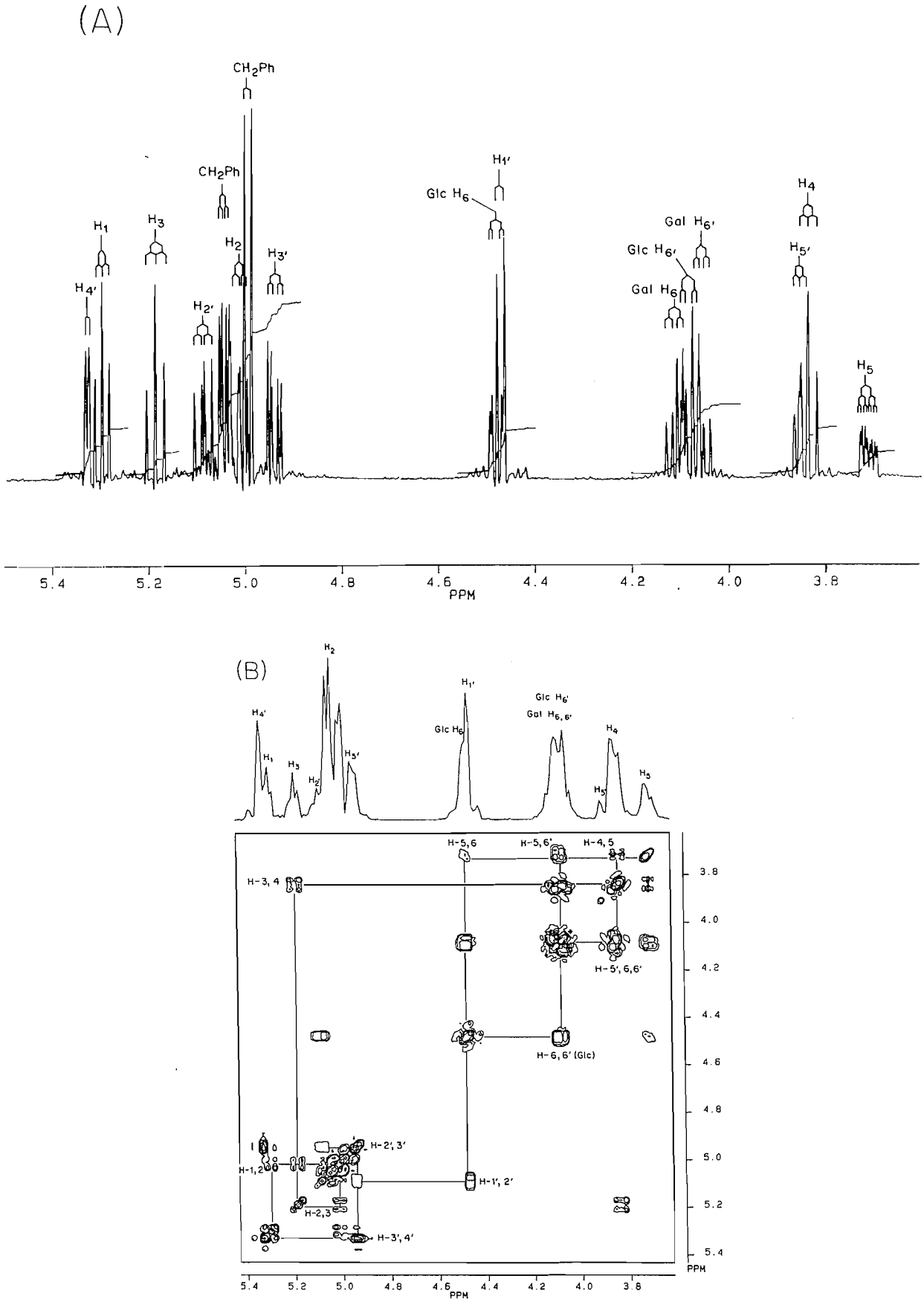


FIG. 1. (A) Resolution-enhanced 500 MHz ^{1}H NMR spectrum of dibenzyl (per-*O*-acetylated β-D-lactosyl) phosphates **6**. (B) Expanded COSY contour plot of the ring proton region (3.60–5.40 ppm) of **6**.

TABLE 2. Selected ^1H NMR chemical shifts and coupling constants (Hz) of the glycosyl phosphate derivatives

Compound no.	H-1 ($^3J_{1,P}$, $J_{1,2}$)	H-2 ($J_{2,3}$)	H-3 ($J_{3,4}$)	H-4 ($J_{4,5}$)	H-5 ($J_{5,6}$, $J_{5,6'}$)	H-6 ($J_{6,6'}$)	H-6′
3[a]	5.33 (7.5, 7.5)	5.11 (9.2)	5.20 (9.2)	5.09 (9.9)	3.79 (2.2, 4.8)	4.09 (12.3)	4.22
4[a]	5.30[c] (7.4, 8.1)	5.31[c] (9.8)	5.01[c] (3.5)	5.40 (1.2)	4.00 (6.0, 6.8)	4.08 (11.0)	4.14
	5.50[d] (7.8, 8.0)	5.79 (10.5)	5.14 (3.5)	5.40 (1.1)	3.27 (6.5, 6.5)	4.99–5.09[e] (–)	
6[b] Glc	5.30 (7.5, 7.5)	5.01 (9.3)	5.19 (9.2)	3.84 (10.0)	3.71 (2.1, 5.1)	4.48 (12.2)	4.02
Gal	4.47 (7.8)	5.09 (10.4)	4.94 (3.5)	5.33 (<1 Hz)	3.85 (6.9, 6.3)	4.11 (11.2)	4.06

[a]At 300 MHz in $CDCl_3$.
[b]At 500 MHz in $CDCl_3$.
[c]From the simulated spectra, Fig. 2. Other data are observed values.
[d]At 300 MHz in C_6D_6.
[e]Unresolved ABX system.

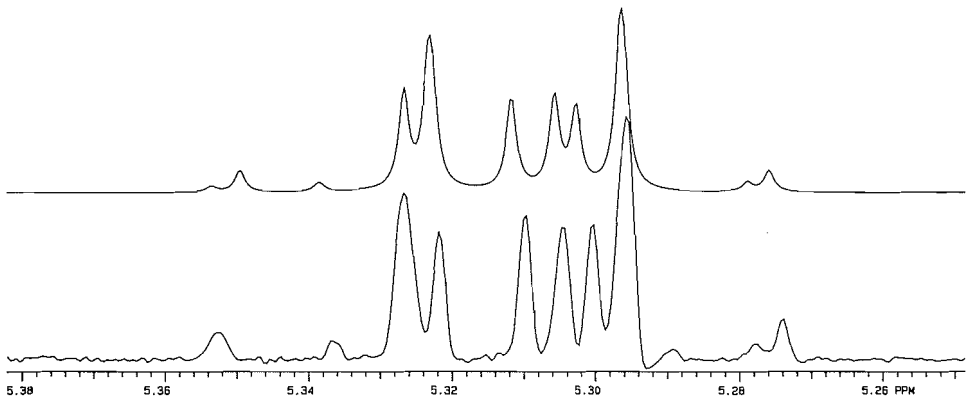


FIG. 2. Partial ^1H NMR spectra (300 MHz) of **4** in $CDCl_3$ showing H-1 and H-2 as a second-order pattern. Simulated (top); observed spectrum (bottom).

typical of β-D-glycosides (axial proton). The apparent ambiguity was finally completely eliminated by running the ^1H NMR spectra of **4** in C_6D_6. The chemical shifts and coupling constants are included in Table 2. The H-1–H-3 system no longer appeared as an ABX pattern and was completely resolved.

In conclusion, treatment of halogenoses with dibenzyl phosphate under a catalytic two-phase system afforded 1,2-*trans*-β-D-glycosyl phophotriesters in good yields with complete stereocontrol. The method presents clear advantages over the previous ones because all the reagents are stable, nontoxic, and readily available. Moreover, β-glycosyl phosphates can give access to α-glycosyl phosphates by Lewis acid catalyzed anomerization (7) and were shown to act as useful glycosyl donors (16–18).

Experimental

General methods

The description of the general methods used is essentially the same as that recently published (14). The ^1H and ^{13}C NMR spectra at 300 and 75.4 MHz respectively were recorded on a Varian XL-300 spectrometer. The ^1H NMR spectra of **6** were recorded on a Bruker AM-500 MHz spectrometer. We acknowledge the assistance of NRC (Ottawa) for providing this instrument. The analyses were done as a first-order approximation. The carbon and proton chemical shifts are given relative to internal (deutero)chloroform at 77.0 and 7.24 ppm respectively. The homonuclear ^1H–^1H 45° COSY experiments on **6** were obtained on the Bruker instrument operating at 500.132 MHz. The spectra were collected as 512 × 256 blocks of data, which were processed using sinusoidal multiplication in each dimension before zero-filling to 1024 words in both dimensions followed by double Fourier transformation. The final data matrix was symmetrized. ^1H NMR simulations were performed using the standard NMR simulation package of the Varian XL-300 software (version 6.2, revision E). An initial spectrum was obtained using estimates of the chemical shifts (2D-COSY) and typical values for $J_{1,2}$ (7.5 Hz), $J_{2,3}$ (9 Hz), $J_{2,P}$, and $J_{3,P}$ (0 Hz) and a set value of $J_{1,P}$ (6.8 Hz) as measured from the ^{31}P NMR spectrum. This allowed initial assignment of the appropriate transitions. The measured experimental transition frequencies with their appropriate assignments were fixed in the simulation. Iteration on this data set gave the simulation shown in Fig. 2 and the final data are shown in Table 2. The peracetylated glycosyl bromides **1**, **2**, and **5** were prepared by the usual HBr/HOAc treatment of the peracetates (19).

Can. J. Chem. Downloaded from www.nrcresearchpress.com by 84.41.108.74 on 09/07/12
For personal use only.

Can. J. Chem. Downloaded from www.nrcresearchpress.com by 84.41.108.74 on 09/07/12
For personal use only.

*Dibenzyl(2,3,4,6-tetra-*O*-acetyl-β-*D*-glucopyranosyl) phosphate 3*

A solution of dibenzyl phosphate (135 mg, 0.49 mmol) and tetrabutylammonium hydrogen sulfate (82.5 mg, 0.24 mmol) in saturated sodium hydrogen carbonate (2 mL) was added to acetobromoglucose **1** (100 mg, 0.24 mmol) in methylene chloride (2 mL). The two-phase reaction mixture was stirred at room temperature for 72 h. Care was taken to maintain the pH of the aqueous phase at pH 8–9 by addition of a few drops of the saturated $NaHCO_3$ solution as required. Ethyl acetate was added (20 mL) and the resulting organic phase was successively washed with saturated $NaHCO_3$, water, and saturated NaCl. The organic phase was then dried with magnesium sulfate, filtered, and evaporated under reduced pressure. The residue was purified by radial silica gel chromatography using 2% *tert*-butanol in methylene chloride as eluant (with a few drops of triethylamine) to afford the pure glycosyl phosphate **3** (123 mg, 83%). Crystallization from diisopropyl ether gave needles of analytically pure **3**; mp 74.6–75.6°C; $[\alpha]_D$ −7.6 (*c* 1.0, $CHCl_3$) (lit. (7*b*) mp 76°C; $[\alpha]_D$ −6.5 (*c* 1.0, $CHCl_3$); lit. (3*a*) mp 76.5–78°C, $[\alpha]_D$ −8.4 (*c* 3, $CHCl_3$)). ^1H NMR (300 MHz) ($CDCl_3$) δ: 7.28 (m, 10H, Ph), 5.33 (dd, 1H, $J_{1,2}$ = 7.5, $^3J_{1,P}$ = 7.5 Hz, H1), 5.20 (dd, 1H, $J_{2,3}$ = 9.2, $J_{3,4}$ = 9.2 Hz, H3), 5.11 (dd, 1H, H2), 5.09 (dd, 1H, $J_{4,5}$ = 9.9 Hz, H4), 5.07 (d, 2H, $^3J_{H,P}$ = 7.4 Hz, CH_2Ph), 5.00 (d, 2H, $^3J_{H,P}$ = 7.1 Hz, CH_2Ph), 4.22 (dd, 1H, $J_{5,6'}$ = 4.8, $J_{6,6'}$ = 12.3 Hz, H6′), 4.09 (dd, 1H, $J_{5,6}$ = 2.2, H6), 3.79 (ddd, 1H, H5), 2.02, 1.99, 1.88 (4s, 12H, OAc). ^{13}C NMR ($CDCl_3$) δ: 170.4, 169.9, 169.3, 169.2 (OAc), 135.4, 135.2, 128.6, 128.5, 127.8, 127.7 (Ph), 96.2 (d, $^2J_{C,P}$ = 4.7 Hz, Cl), 72.6 (C5), 72.3 (d, $^4J_{C,P}$ = 1.5 Hz, C3), 71.1 (d, $^3J_{C,P}$ = 9.2 Hz, C2), 69.62 (d, $^2J_{C,P}$ = 5.8 Hz, CH_2Ph), 69.57 (d, $^2J_{C,P}$ = 5.5 Hz, CH_2Ph), 67.8 (C4), 61.4 (C6), 20.5, 20.45 (2×), 20.36 (OAc). CI (ether) *m/z*: 609 (21%, M + H^+). Anal. calcd. for $C_{28}H_{33}O_{13}P$: C 55.25, H 5.47, P 5.09; found: C 55.07, H 5.52, P 4.93.

*Dibenzyl (2,3,4,6-tetra-*O*-acetyl-β-*D*-galactopyranosyl) phosphate 4*

When the above procedure was applied on acetobromogalactose **2**, the title galactosyl phosphate **4** was obtained as an oil in 73% yield; $[\alpha]_D$ +3.3 (*c* 1.0, $CHCl_3$). ^1H NMR (300 MHz) ($CDCl_3$) δ: 7.33 (m, 10H, Ph), 5.40 (dd, 1H, $J_{3,4}$ = 3.5, $J_{4,5}$ = 1.2 Hz, H4), 5.31 (dd, 1H, $J_{1,2}$ = 8.1, $J_{2,3}$ = 9.8 Hz, H2), 5.30 (dd, 1H, $^3J_{1,P}$ = 7.4 Hz, H1), 5.07 (d, 2H, $^3J_{H,P}$ = 7.3 Hz, CH_2Ph), 5.03 (dd, 1H, $J_{3,4}$ = 3.5 Hz, H3), 5.00 (dd, 2H, $^3J_{H,P}$ = 7.0 Hz, CH_2Ph), 4.14 (dd, 1H, $J_{5,6'}$ = 6.8, $J_{6,6'}$ = 11.0 Hz, H6′), 4.08 (dd, 1H, $J_{5,6}$ = 6.0, H6), 4.00 (ddd, 1H, H5), 2.15, 1.97, 1.95, 1.90 (4s, 12H, OAc). ^1H NMR (300 MHz) (C_6D_6) δ: 7.12 (m, 10H, Ph), 5.79 (dd, 1H, $J_{1,2}$ = 8.0, $J_{2,3}$ = 10.5 Hz, H2), 5.51 (dd, 1H, $^3J_{1,P}$ = 7.8 Hz, H1), 5.40 (dd, 1H, $J_{3,4}$ = 3.5, $J_{4,5}$ = 1.1 Hz, H4), 4.97 (d, 2H, $^3J_{H,P}$ = 7.1 Hz, CH_2Ph), 5.14 (dd, 1H, H3), 4.99–5.09 (2H, ABX, H6,6′), 3.90 (d, 2H, $^3J_{H,P}$ = 7.1 Hz, CH_2Ph), 3.27 (ddd, 1H, $J_{5,6}$ = $J_{5,6'}$ = 6.5 Hz, H5), 1.71, 1.70, 1.56, 1.55 (4s, OAc). ^{13}C NMR ($CDCl_3$) δ: 170.2, 170.0, 169.8, 169.4 (OAc), 135.3, 135.2, 128.6, 128.55, 128.52, 127.8, 127.7 (Ph), 96.7 (d, $^2J_{C,P}$ = 4.8 Hz, C1), 71.7 (C5), 70.4 (C3), 69.6 (d, $^2J_{C,P}$ = 5.9 Hz, CH_2Ph), 69.55 (d, $^2J_{C,P}$ = 6.1 Hz, CH_2Ph), 68.6 (d, $^3J_{C,P}$ = 8.8 Hz, C2), 66.6 (C4), 61.0 (C6), 20.6, 20.5 (4 × OAc). CI (ether) *m/z*: 609 (1.1%, M + H^+). Anal. calcd. for $C_{28}H_{33}O_{13}P$: C 55.25, H 5.47, P 5.09; found: C 55.44, H 5.57, P 4.88.

*Dibenzyl (hepta-*O*-acetyl-β-*D*-lactosyl) phosphate 6*

Acetobromolactose **5** (250 mg, 0.36 mmol), dibenzyl phosphate (149 mg, 0.54 mmol, 1.5 equiv.), and tetrabutylammonium hydrogen sulfate (120 mg, 0.35 mmol, 1 equiv.) were dissolved in methylene chloride (2 mL). Saturated sodium hydrogen carbonate (2 mL) containing sodium carbonate (70 mg, pH 9.0) was then added to the organic solution. The two-phase reaction mixture was vigorously stirred at room temperature for 34 h until TLC (0.1% Et_3N in hexane:ethyl acetate, 1:1 v/w) indicated complete conversion of **5** (R_f 0.38) into the glycosyl phosphate **6** (R_f 0.27). Addition of ethyl acetate (20 mL) and washings of the organic phase as above, followed by drying (Na_2SO_4), filtration, and evaporation of the organic phase, furnished a glassy solid. Purification on silica gel column chromatography using chloroform:isopropanol as eluant (40:1, v/v) afforded 12 mg of the 2-acetoxylactal resulting from a dehydrobromination side-reaction, followed by **6** (266 mg, 83%) as a glassy solid; $[\alpha]_D$ −7.5 (*c* 0.97, $CHCl_3$). ^1H NMR (500 MHz) ($CDCl_3$) δ: 7.20–7.36 (m, 10H, Ph), 5.33 (dd, 1H, $J_{3,4}$ = 3.5, $J_{4,5}$ < 1 Hz, H4′), 5.30 (dd, 1H, $J_{1,2}$ = 7.5, $^3J_{1,P}$ = 7.5 Hz, H1), 5.19 (dd, 1H, $J_{3,4}$ = 9.2, $J_{2,3}$ = 9.3 Hz, H3), 5.09 (dd, 1H, $J_{1,2}$ = 7.8, $J_{2,3}$ = 10.4 Hz, H2′), 5.01 (dd, 1H, H2), 4.99 (app. d, 2H, $^2J_{C,P}$ = 7.3 Hz, J_{gem} < 1 Hz, CH_2Ph), 4.94 (dd, 1H, H3′), 5.03 (dd, 2H, $^2J_{C,P}$ = 7.3, J_{gem} = 2.8 Hz, CH_2Ph), 4.48 (dd, 1H, $J_{5,6}$ = 2.1, $J_{6,6'}$ = 12.2 Hz, H6 Glc), 4.47 (d, 1H, $J_{1,2}$ = 7.8 Hz, H1′), 4.11 (dd, 1H, $J_{5,6}$ = 6.9, $J_{6,6'}$ = 11.2 Hz, H6 Gal), 4.06 (dd, 1H, H6′ Gal), 4.02 (dd, 1H, $J_{5,6'}$ = 5.1 Hz, H6′ Glc), 3.85 (app. dd, 1H, $J_{5,6'}$ = 6.3 Hz, H5′), 3.84 (dd, 1H, $J_{4,5}$ = 10.0 Hz, H4), 3.71 (ddd, 1H, H5), 2.13, 2.04, 2.02 (2×), 2.00, 1.94, 1.88 (7s, 21H, OAc). ^{13}C NMR (300 MHz) ($CDCl_3$) δ: 170.3, 170.1 (2×), 170.0, 169.5, 169.0 (OAc), 135.3 (d, $^3J_{C,P}$ = 23.3 Hz, C-*ipso* Ph), 128.6 (C-*para*), 128.58, 128.54 (C-*meta*), 127.8, 127.7 (C-*ortho*), 101.0 (Cl′), 96.1 (d, $^2J_{C,P}$ = 4.9 Hz, Cl), 75.6 (C4), 73.4 (C5), 72.3 (C3), 71.5 (d, $^3J_{C,P}$ = 9.0 Hz, C2), 70.9 (C3′), 70.7 (C5′), 69.6 (d, $^2J_{C,P}$ = 6.2 Hz, CH_2Ph), 69.5 (d, $^2J_{C,P}$ = 6.3 Hz, CH_2Ph), 69.0 (C2′), 66.5 (C4′), 61.5 (C6), 60.8 (C6′), 20.7 (2×), 20.6 (3×), 20.5, 20.4 (OAc). Negative FAB MS *m/z*: 809 (M^- − benzyl). Anal. calcd. for $C_{40}H_{49}O_{21}P$: C 53.57, H 5.51, P 3.45; found: C 53.45, H 5.62, P 3.71.

Acknowledgements

We acknowledge the financial support of this work by NSERC. Mr. F. D. Tropper is grateful to NSERC and Mrs. C. Grand-Maître to FCAR for graduate scholarships. We also thank Dr. C. Kazakoff for running mass spectra and Mr. R. Capoor and Dr. A. J. Williams for some of the NMR experiments. Utilization of the Bruker AM-500 MHz spectrometer from NRC (Ottawa) is also acknowledged.

1. H. Nikaido and W. Z. Hassid. Adv. Carbohydr. Chem. Biochem. **26**, 351 (1971).
2. (*a*) D. L. MacDonald. Methods Enzymol. **8**, 121 (1966); (*b*) Carbohydr. Res. **3**, 117 (1966), and references therein.
3. (*a*) L. V. Volkova, L. L. Danilov, and R. P. Evstigneeva. Carbohydr. Res. **32**, 165 (1974); (*b*) M. A. Salam and E. J. Behrman. Carbohydr. Res. **90**, 83 (1981).
4. (*a*) E. W. Putman. Methods Carbohydr. Chem. **2**, 261 (1963); (*b*) T. Posternak, J. Am. Chem. Soc. **72**, 4824 (1950); (*c*) F. J. Reithel, J. Am. Chem. Soc. **67**, 1056 (1945); (*d*) D. L. MacDonald and H. G. Fletcher, Jr. J. Am. Chem. Soc. **82**, 1832 (1960).
5. T. Yamasaki, C. D. Warren, A. Herscovies, and R. W. Jeanloz. Can. J. Chem. **59**, 2247 (1981).
6. C. L. Stevens and R. E. Harman. Carbohydr. Res. **11**, 99 (1969).
7. (*a*) R. R. Schmidt, M. Stumpp, and J. Michel. Tetrahedron Lett. **23**, 405 (1982); (*b*) R. R. Schmidt and M. Stumpp. Liebigs Ann. Chem. 680 (1984).
8. M. Inage, H. Chaki, S. Kusumoto, and T. Shiba. Chem. Lett. 1281 (1982).
9. A. Granata and A. S. Perlin. Carbohydr. Res. **94**, 165 (1981).
10. P. Westerduin, G. H. Veeneman, G. A. van der Marel, and J. H. van Boom. Tetrahedron Lett. **27**, 6271 (1986).
11. J. Theim and M. Franzkowiak. J. Carbohydr. Chem. **8**, 1 (1989).
12. (*a*) K. Brewster, J. M. Harrison, and T. D. Inch. Tetrahedron Lett. 5051 (1979); (*b*) D. Dess, H. P. Kleine, D. V. Weinberg, R. J. Kaufman, and R. S. Sidhu. Synthesis, 883 (1981); (*c*) J. Bogusiak and W. Szeja. Pol. J. Chem. **59**, 293 (1985); (*d*) W. Szeja. Synthesis, 223 (1988); (*e*) H. Kunz and H. Waldman. Angew. Chem. Int. Ed. Engl. **24**, 883 (1985); (*f*) F. Chrétien, P. Di Cesare, and B. Gross. J. Chem. Soc. Perkin Trans. 1, 3297 (1988), and references cited therein.
13. (*a*) R. Roy and F. D. Tropper. Synth. Commun. **20**, 2097 (1990); (*b*) R. Roy, F. D. Tropper, A. Romanowska, M. Letellier,

L. COUSINEAU, S. MEUNIER, and J. BORATYNSKI. Glycoconjugate J. **8**, 75 (1991); (*c*) F. D. TROPPER, F. O. ANDERSON, C. GRAND-MAÎTRE, and R. ROY. Synthesis, 734 (1991) (*d*) R. ROY, F. D. TROPPER, T. MORRISON, and J. BORATYNSKI, J. Chem. Soc. Chem. Commun. 536 (1991).
14. R. ROY and F. D. TROPPER. Can. J. Chem. **69**, 817 (1991).
15. K. BLOCK and V. PEDERSEN. J. Chem. Soc. Perkin Trans. 2, 293 (1974).
16. S.-I. HASHIMOTO, T. HONDA, and S. IKEGAME. J. Chem. Soc. Chem. Commun. 685 (1989).
17. M. MICHALSKA and J. MICHALSKI. Heterocycles, **28**, 1249 (1989).
18. (*a*) R. R. SCHMIDT, H. GADEN, and H. JATZKE. Tetrahedron Lett. **31**, 327 (1990); (*b*) R. R. SCHMIDT, M. BEHRENDT, and A. TOEPFER. Synlett. 694 (1990).
19. R. W. JEANLOZ and P. J. STOFFYN. Methods Carbohydr. Chem. **1**, 221 (1962).

Can. J. Chem. Downloaded from www.nrcresearchpress.com by 84.41.108.74 on 09/07/12
For personal use only.

Nucleic acid related compounds. 66. Improved syntheses of 5′-chloro-5′-deoxy- and 5′-*S*-aryl(or alkyl)-5′-thionucleosides[1]

MORRIS J. ROBINS,[2] FRITZ HANSSKE, STANISLAW F. WNUK, AND TADASHI KANAI

Departments of Chemistry, University of Alberta, Edmonton, Alta., Canada T6G 2G2 and Brigham Young University, Provo, UT 84602, U.S.A.

Received March 27, 1991

MORRIS J. ROBINS, FRITZ HANSSKE, STANISLAW F. WNUK, and TADASHI KANAI. Can. J. Chem. **69**, 1468 (1991).

Treatment of ribonucleosides with thionyl chloride/pyridine/acetonitrile (0°C to ambient temperature) resulted in essentially quantitative formation of 5′-chloro-5′-deoxy-2′,3′-*O*-sulfinylnucleoside derivatives. These diastereomeric sulfite esters underwent deprotection readily with aqueous methanolic ammonia. This gave 5′-chloro-5′-deoxynucleosides without use of the suspected carcinogen, hexamethylphosphoramide (HMPA). Nucleophilic displacement with sodium thiolates in dimethylformamide (−30°C to ambient temperature) gave 5′-*S*-aryl(or alkyl)-5′-thionucleosides in high yields. Treatment of ribonucleosides with thionyl chloride/acetonitrile without pyridine followed by aqueous work-up gave diastereomeric 2′,3′-*O*-sulfinylnucleosides with an unmodified 5′-hydroxyl group. Diagnostic NMR shifts for cyclic sulfite ester stereochemistry are noted.

Key words: adenosine, 5′-*S*-aryl(or alkyl)-5′-thionucleosides, 5′-chloro-5′-deoxynucleosides, uridine, nucleosides.

MORRIS J. ROBINS, FRITZ HANSSKE, STANISLAW F. WNUK et TADASHI KANAI. Can. J. Chem. **69**, 1468 (1991).

Les ribonucléosides traités par un mélange de chlorure de thionyle/pyridine/acétonitrile donnent essentiellement et quantitativement des dérivés du chloro-5′-déoxy-5′-*O*-sulfinyl-2′,3′-nucléoside. Ces sulfites d'esters diastéréoisomères sont déprotégés facilement par l'ammoniac dans du méthanol aqueux pour donner les chloro-5′-déoxy-5′-nucléosides sans l'utilisation de l'hexaméthylphosphoramide (HMPA) soupçonné d'être cancérigène. Le déplacement nucléophile avec les thiolates de sodium dans le diméthylformamide (−30°C jusqu'à la température ambiante) donne les *S*-aryl(ou alkyl)-5′-thio-5′-nucléosides avec des rendements élevés. Le traitement des nucléosides par le mélange de chlorure de thionyle/acétonitrile sans la pyridine et le traitement aqueux subséquent donnent les *O*-sulfinyl-2′,3′-nucléosides avec le groupe hydroxyl-5′ non modifié. On a enregistré les déplacements chimiques en RMN relatifs à la stéréochimie de ces sulfites d'esters cycliques.

Mots clés : adénosine, *S*-aryl(ou alkyl)-5′-thio-5′-nucléosides, chloro-5′-déoxy-5′-nucléosides, uridine, nucléosides.

[Traduit par la rédaction]

Introduction

Procedures for modification at C5′ of ribonucleosides classically used 2′,3′-*O*-isopropylidene protection and activation of the 5′-hydroxyl group by *p*-toluenesulfonylation (1). Direct conversions of 2′,3′-*O*-isopropylidene nucleosides to 5′-chloro derivatives were reported with neat thionyl chloride (2) or thionyl chloride/dimethylformamide (DMF) (Vilsmeier–Haack reagent) (3). Dods and Roth also noted that treatment of unprotected uridine with thionyl chloride/DMF gave 5′-chloro-5′-deoxyuridine (3). Kikugawa and Ichino (4) reported that treatment of cytidine with thionyl chloride/DMF gave the 2,2′-anhydroarabinonucleoside (4*a*), but treatment of cytidine or adenosine with thionyl chloride/hexamethylphosphoramide (HMPA) followed by aqueous work-up gave the unprotected 5′-chloro-5′-deoxynucleosides (4*b*). Hogenkamp invoked HMPA-mediated oxyphosphonium activation at C5′ and pentavalent cyclic phosphorus bonding at O2′ and O3′ to rationalize this selective C5′ chlorination (5). However, Normant and Deshayes had reported the *absence* of Vilsmeier–Haack type phosphonium activation in conversions of alcohols to alkyl chlorides by thionyl chloride/HMPA and had noted acid–base complexation of hydrogen chloride by HMPA (6). Successful substitution of trimethyl phosphate for HMPA in this reaction was reported by Gibbs and Verkade (7), and Hřebabecký and Beránek (8) identified the formation of 2′,3′-cyclic sulfite ester intermediates in HMPA as well as other solvents. Thus, the formation of 2′,3′-*O*-sulfinyl intermediates (8, 9) that undergo displacement of the 5′-halosulfite group by halide in the polar solvating HMPA medium (6) is indicated, whereas the formerly considered chemical participation (1*c*, 5) of HMPA is unlikely. A number of 5′-chloro-5′-deoxynucleosides have been prepared by this thionyl chloride/HMPA procedure (4*b*), and earlier studies have been summarized (1, 10–12).

Sowa and Tsunoda reported that treatment of pyrimidine (13) or purine (14) nucleosides with thionyl chloride/acetonitrile followed by water resulted in formation of 2′,3′-*O*-sulfinyl esters with an unmodified 5′-hydroxyl group. We have confirmed these results and found that the addition of 2 equivalents of pyridine to suspensions of ribonucleosides and excess thionyl chloride in acetonitrile resulted in essentially quantitative conversions to the 5′-chloro-5′-deoxy-2′,3′-*O*-sulfinylnucleoside intermediates. Pyridine was not required for the conversion of 5′-substituted nucleosides to their 2′,3′-cyclic sulfite esters, and adenosine-1-oxide was converted to its 5′-chloro-5′-deoxy-2′,3′-*O*-sulfinyl derivatives without modification of the *N*-oxide function. The diastereomeric cyclic sulfite esters underwent hydrolysis readily in aqueous methanolic ammonia to provide an economical overall route to the synthetically useful 5′-chloro-5′-deoxynucleosides without use of the suspected carcinogen, and sometimes difficultly removable, HMPA.

Results and discussion

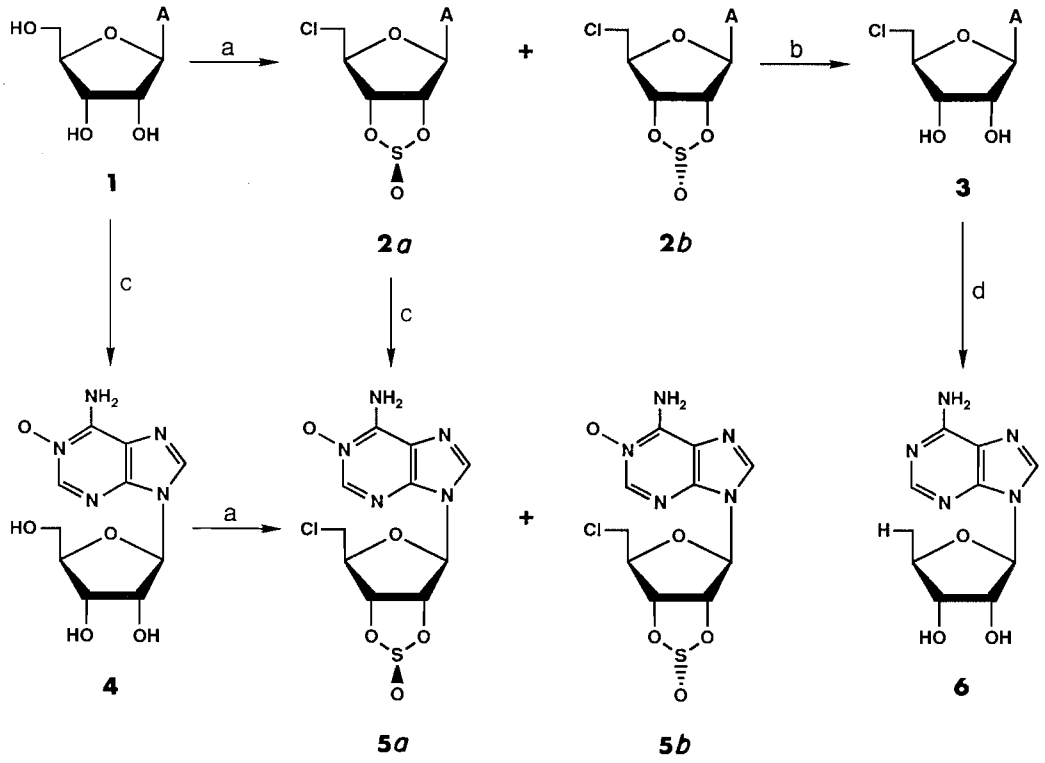
Treatment of a stirred suspension of adenosine (**1**, Scheme 1) with 3 equivalents of thionyl chloride and 2 equivalents of pyridine in acetonitrile at ~0°C followed by warming to ambient temperature resulted in quantitative (TLC, NMR) formation of a mixture of 5′-chloro-5′-deoxy-2′,3′-*O*-sulfinyladenosines (**2***a*/**2***b*). Fractional crystallization of the cyclic sulfite ester diastereomers occurred to give highly enriched *exo* isomer (**2***a*)

[1]For the previous paper in this series see ref. 30.

[2]Author to whom correspondence may be addressed at Brigham Young University.

Printed in Canada / Imprimé au Canada

Can. J. Chem. Downloaded from www.nrcresearchpress.com by 84.41.108.74 on 09/07/12
For personal use only.



(a) $SOCl_2/C_6H_5N/MeCN$. (b) $NH_3/H_2O/MeOH$. (c) $3\text{-}ClC_6H_4CO_3H$/solvent. (d) $LiEt_3BH/THF/Me_2SO$

SCHEME 1

and an enriched sample of the *endo* isomer (**2***b*). It has been established that the ^1H NMR frequencies of geminal protons on 5-membered cyclic sulfite ester rings (1,3,2-dioxathiolan-2-oxides) are shifted downfield when proximal to the exocyclic oxygen atom and upfield when distal (9, 15–17). Known correlations for cyclic sulfite ^{13}C NMR shifts (9, 16) also were in harmony with our observed ^1H and ^{13}C NMR spectra (Tables 1 and 2). The isolation of several forms of these cyclic sulfite esters is noted in the experimental section. Treatment of **2***a*/**2***b* with aqueous methanolic ammonia at ambient temperature resulted in smooth deprotection to give 5′-chloro-5′-deoxyadenosine (**3**, 94%). Direct processing of crude **2***a*/**2***b* gave **3** with overall yields of >90%.

Treatment of **3** with lithium triethylborohydride/THF/DMSO at ambient temperature resulted in reductive dechlorination (18) to give 5′-deoxyadenosine (**6**, 93%) (19). This chlorination/deprotection/reduction sequence provides a concise and efficient route to **6** that offers an ambient temperature alternative to the radical-mediated dechlorination with tributylstannane (8, 11).

A modified oxidation of **1** to adenosine-1-oxide (**4**, 96%) (20) is noted in the experimental section. Treatment of **4** with $SOCl_2$/pyridine/acetonitrile gave the diastereomeric 5′-chloro-5′-deoxy-2′,3′-*O*-sulfinyladenosine-1-oxides (**5***a*/**5***b*, 94%) with no effect on the purine *N*-oxide functionality. Alternatively, oxidation of **2***a* with 3-chloroperoxybenzoic acid gave the *exo* isomer **5***a* (90%) without observed oxidation of the sulfite ester (21).

Treatment of 5′-azido-5′-deoxyadenosine (**7***a*, Scheme 2) or 5′-*O*-benzoyladenosine (**7***b*) with $SOCl_2$/acetonitrile resulted in formation of the respective 2′,3′-*O*-sulfinyl derivatives (**8***a*/**9***a* (96%) or **8***b*/**9***b* (95%)). Cytidine (**7***c*) and uridine (**7***d*) were converted to their 2′,3′-*O*-sulfinyl derivatives (**8***c*/**9***c* (84%) and **8***d*/**9***d* (82%)) analogously, as described (13). Inclusion of 2 equivalents of pyridine in the mixture with uridine resulted in formation of the 5′-chloro-5′-deoxy-2′,3′-*O*-sulfinyluridine diastereomers (**8***e*/**9***e*), which were deprotected to give 5′-chloro-5′-deoxyuridine (**10**, 82%).

Several methods have been employed for the nucleophilic displacement of leaving groups with thiols at C5′ of nucleoside derivatives (1, 22–26). However, the procedure of Borchardt *et al.* requires the condensation of liquid ammonia (25) and variable yields have been noted. The disulfide/phosphine procedure of Hata and co-workers (26) is conceptually elegant and gives high yields, but the use of tributylphosphine and purification from phosphine oxide by-products is required.

Treatment of the readily accessible adenine and uracil 5′-chloro-5′-deoxynucleosides (**3** and **10**, Scheme 3) with sodium thiolates (derived by treatment of thiols in dimethylformamide with sodium hydride at low temperature) resulted in rapid and quantitative conversion to the corresponding 5′-*S*-aryl(or alkyl)-5′-thionucleoside derivatives (**11***a–e*, 86–94% analytically pure). Other 5′-thioether derivatives have been prepared with equivalently high yields (unpublished results).

In summary, treatment of adequately soluble ribonucleosides and their 5′-substituted derivatives with thionyl chloride in acetonitrile resulted in essentially quantitative formation of the diastereomeric 2′,3′-*O*-sulfinyl derivatives. Presumably, the 5′-*O*-chlorosulfinyl group was hydrolyzed from unsubstituted nucleosides during work-up. Inclusion of 2 equivalents of pyridine in the reaction mixture with ribonucleosides resulted in near quantitative conversion to 5′-chloro-5′-deoxy-2′,3′-*O*-

Can. J. Chem. Downloaded from www.nrcresearchpress.com by 84.41.108.74 on 09/07/12
For personal use only.

TABLE 1. ^{1}H NMR spectral data[a,b]

Compound	H1′[c] ($J_{1'-2'}$)	H2′[d] ($J_{2'-3'}$)	H3′[d] ($J_{3'-4'}$)	H4′[e] ($J_{4'-5'}$)	H5′[d] ($J_{5'-5''}$)	H5″[d,f] ($J_{5''-4'}$)	H2[g] or H5[c] (J_{5-6})	H8[g] or H6[c]	NH_2[h] or NH[h]	Aromatic (J_{A-B}) and (or) others
1	5.91 (6.1)	4.64[e] (5.5)	4.16[e] (2.8)	3.99 (3.3)	3.69[e] (12.2)	3.57[e] (3.5)	8.16	8.37	7.39	5.48[c] (5.8,[i] OH2′) 5.44[j] (5.0,[k] OH5′) 5.22[c] (5.0,[i] OH3′)
2*a*	6.42 (3.0)	6.34 (6.0)	5.90 (4.0)	4.52 (6.4)	3.94 (12.0)	3.89 (6.4)	8.21	8.37	7.40	
2*b*	6.68 (3.0)	6.25 (7.5)	5.83 (4.0)	4.75 (6.5)	4.01 (11.5)	3.90 (6.5)	8.20	8.44	7.40	
3	5.94 (5.5)	4.75[e] (4.5)	4.24[e] (4.0)	4.10 (6.5)	3.85[l,m]		8.17	8.34	7.27	5.57[c] (6.0,[i] OH2′) 5.43[c] (5.0,[i] OH3′)
4	5.88 (5.5)	4.54[l]	4.14[l]	3.94[l]	3.60[h,m]		8.62[n]	8.55[n]	7.8–9.2	5.58[h] (OH2′) 5.22[h] (OH3′) 5.06[h] (OH5′)
5*a*	6.43 (3.0)	6.30 (6.5)	5.85 (4.0)	4.54 (6.0)	3.88[d,m] (6.0)[o]		8.70	8.52	8.0–9.0	
5*a*[p,q]	6.50 (3.0)	6.28 (6.0)	5.84 (4.0)	4.58 (6.0)	3.94[c,m] (6.0)[o]		8.91	8.80		9.49,[h] 10.10[h] (=NH_2) 8.5–10.5[h] (N-OH)
5*b*[p,q]	6.68 (3.0)	6.18 (6.0)	5.74 (4.0)	4.78 (6.0)	3.94[c,m] (6.0)[o]		8.91	8.82		9.49,[h] 10.10[h] (=NH_2) 8.5–10.5[h] (N-OH)
6	5.85 (5.0)	4.66[l]	3.98[l]	3.98[l]			8.16	8.32	7.26	5.42[h] (OH2′) 5.15[h] (OH3′) 1.30[c] (6.0,[r] CH_3)
8*a*	6.40 (3.0)	6.37 (6.0)	5.89 (3.7)	4.48 (5.0)	3.70[d,m] (5.5)[o]		8.22	8.39	7.45	
9*a*[q]	6.64 (3.3)	6.29 (7.5)	5.76 (4.0)	4.70 (6.0)	3.71[d,m] (5.5)[o]		8.20	8.45	7.45	
8*b*	6.43[l]	6.43[l] (5.5)	6.11 (4.0)	4.66 (6.0)	4.54[l,m] (6.0)[o]		8.13	8.33	7.42	7.53–7.96[l]
9*b*[q]	6.64 (3.0)	6.33 (7.5)	5.97 (4.3)	4.93 (6.0)	4.54[l,m] (6.0)[o]		8.12	8.40	7.42	7.53–7.96[l]
8*c*[p,q]	5.92 (2.5)	5.82 (7.0)	5.57 (4.0)	4.37[l] (5.0)	3.67[l,m]		6.20 (8.0)	8.12	10.05, 8.80	s
9*c*[p,q]	6.16 (2.5)	5.74 (7.0)	5.46 (4.0)	4.62[l] (5.0)	3.67[l,m]		6.20 (8.0)	8.16	10.05, 8.80	s
8*d*[q]	5.92 (3.0)	5.81 (6.5)	5.57 (4.0)	4.19[l] (5.0)	3.63[c,m] (5.0)[o]		5.67 (8.0)	7.83	11.42	s
9*d*[q]	6.28 (2.5)	5.73 (6.5)	5.48 (4.0)	4.48[l] (5.0)	3.63[c,m] (5.0)[o]		5.67 (8.0)	7.86	11.42	s
8*e*[t]	5.99[l]	5.99[l] (5.5)	5.61 (4.5)	4.33 (6.0)	3.92 (11.4)	3.84 (6.3)	5.69 (8.0)	7.75	11.40	
9*e*[t]	6.16 (2.2)	5.88 (7.5)	5.56 (4.2)	4.62 (6.6)	3.93 (11.2)	3.83 (6.5)	5.69 (8.0)	7.85	11.40	

sulfinylnucleoside diastereomers. Treatment of these mixtures with aqueous methanolic ammonia effected deprotection to give the 5′-chloro-5′-deoxynucleosides in high yields. Nucleophilic displacement with sodium thiolates in DMF gave quantitative conversion to the 5′-*S*-aryl(or alkyl)-5′-thionucleoside derivatives, which were isolated in high yields. All of these conversions were effected at or below ambient temperature with readily available and inexpensive reagents under common bench-top conditions.

Experimental

Uncorrected melting points were determined with a microstage block. UV spectra were recorded with a Hewlett Packard 8451A diode array spectrophotometer. ^{1}H and ^{13}C NMR spectra were recorded with Bruker WH-200, WH-400, or Varian Gemini-200 spectrometers. Electron impact (MS) and chemical ionization (CI, NH_3) mass spectra were determined with AEI MS-50 and MS-12 instruments, respectively. Reagents and solvents were of commercial reagent quality. Thionyl chloride and all solvents were distilled before use. Pyridine was dried by reflux over, and distillation from, calcium hydride.

*5′-Chloro-5′-deoxy-2′,3′-*O*-sulfinyladenosines* **2a/2b**

Method A

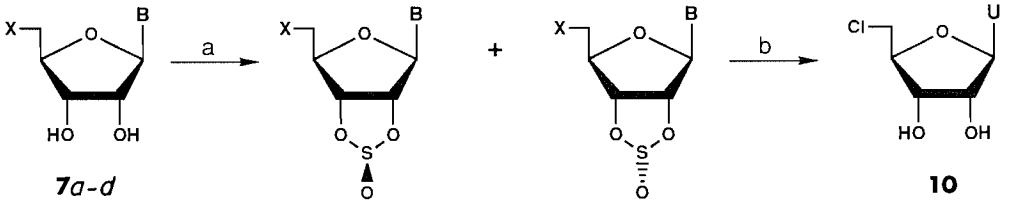
A stirred suspension of adenosine (**1**, 13.35 g, 50 mmol) in CH_3CN (50 mL) was cooled in an ice/H_2O bath for 5 min. Addition of $SOCl_2$ (11 mL, 17.9 g, 150 mmol) was followed by cooling to 0°C. Pyridine (8.1 mL, 7.9 g, 100 mmol) was added and the resulting light yellow solution was stirred for 3–4 h at 0°C and allowed to warm to ambient temperature overnight. The mixture was cooled in ice/H_2O and H_2O (150 mL) was added to dissolve the colorless precipitate. The solution was carefully neutralized to pH 5–6 (solid $NaHCO_3$) and a colorless precipitate separated. The mixture was extracted with EtOAc (400 mL followed by 2 × 200 mL) and the combined organic phase was washed with saturated $NaHCO_3$/H_2O (200 mL) and H_2O, dried (Na_2SO_4), and filtered. Toluene (100 mL) was added and the solution concentrated (<30°C) *in vacuo* to ~300 mL. Toluene (100 mL) was added and evaporation was continued to ~100 mL. This mixture was cooled (4°C) for 4 h and filtered to give 12.6 g (67%) of the major *exo* diastereomer (**2***a*) as a colorless crystalline hemisolvate (verified by ^{1}H NMR): mp 178–181°C (softening transition), 232–233°C (dark brown "crystals" melting to dark fluid). Anal. calcd. for $C_{10}H_{10}ClN_5O_4S{\cdot}0.5C_4H_8O_2$ (375.8): C 38.35, H 3.76, N 18.64; found: C 38.44, H 3.77, N 18.40.

Can. J. Chem. Downloaded from www.nrcresearchpress.com by 84.41.108.74 on 09/07/12
For personal use only.

TABLE 1 (*concluded*)

Compound	H1′[c] ($J_{1'-2'}$)	H2′[d] ($J_{2'-3'}$)	H3′[d] ($J_{3'-4'}$)	H4′[e] ($J_{4'-5'}$)	H5′[d] ($J_{5'-5''}$)	H5″[d,f] ($J_{5''-4'}$)	H2[g] or H5[c] (J_{5-6})	H8[g] or H6[c]	NH_2[h] or NH[h]	Aromatic (J_{A-B}) and (or) others
10	5.81 (6.0)	4.14 (5.0)	3.96 (4.4)	4.00 (4.3)	3.91 (11.5)	3.82 (5.8)	5.69 (8.0)	7.67	11.40	5.52[h] (OH2′) 5.37[h] (OH3′)
11*a*	5.93 (6.0)	4.80[e] (5.0)	4.19[e] (4.0)	4.07 (5.7)	2.94 (14.0)	2.83 (6.5)	8.16	8.37	7.33	5.55[c] (6.0,[i] OH2′) 5.38[c] (4.7,[i] OH3′) 2.1[g] (SCH_3)
11*b*	5.93 (6.0)	4.95[e] (5.0)	4.22[e] (4.0)	4.04 (5.0)	3.48 (14.0)	3.36 (7.0)	8.18	8.38	7.32	7.2–7.4[l] 5.58[c] (6.0,[i] OH2′) 5.43[c] (5.0,[i] OH3′)
11*c*	5.91 (6.0)	4.84[e] (5.0)	4.19[e] (3.5)	3.98 (6.0)	3.29 (13.0)	3.17 (7.0)	8.18	8.38	7.34	6.90,[c] 7.39[c] (8.5) 5.55[c] (6.0,[i] OH2′) 5.25[c] (5.0,[i] OH3′) 3.78[g] (OCH_3)
11*d*	5.75 (6.0)	4.14[e] (5.5)	3.85[e] (4.0)	3.79 (5.9)	3.20 (14.0)	3.08 (6.5)	5.63 (8.0)	7.62	11.35	6.89,[c] 7.35[c] (8.5) 5.41[c] (5.5,[i] OH2′) 5.25[c] (5.0,[i] OH3′) 3.72[g] (OCH_3)
11*e*	5.78 (6.0)	4.15[h] (5.0)[u]	3.89[l] (4.0)[u]	3.82 (6.0)	3.18 (14.0)	3.06 (6.5)	5.65 (8.0)	7.64	11.28	6.75,[c] 7.28[c] (8.5) 9.62[h] (C_6H_4OH) 5.42[h] (OH2′) 5.25[h] (OH3′)

[a]Chemical shifts (δ) at 400 MHz in Me_2SO-d_6/Me_4Si unless otherwise noted.
[b]"Apparent" first-order coupling constants (in parentheses).
[c]Doublet unless otherwise noted.
[d]Doublet of doublets (unless otherwise noted).
[e]Doublet of doublets of doublets (unless otherwise noted).
[f]Upfield resonance assigned to 5″(pro-*R*)-H.
[g]Singlet.
[h]Broad singlet.
[i]$^3J_{HO-CH}$.
[j]Triplet.
[k]$^3J_{HO-CH_2}$.
[l]Multiplet.
[m]"Collapsed" signals for H5′,5″.
[n]After heating a solution of **4** in D_2O at 100°C for 5.5 h in a sealed ampoule, its spectrum lacked the "exchangeable" proton peaks and the signal at δ 8.55.
[o]$J_{5''-4'}$.
[p]Hydrochloride salt.
[q]Signals were assigned from a spectrum of the diastereomeric mixture (correlated with integrated intensities).
[r]$^3J_{CH_3-4'}$.
[s]No signal was observed for OH5′.
[t]Determined at 200 MHz.
[u]Coupling constant obtained from a D_2O-exchanged spectrum.



Series	B	X
a	adenin-9-yl	N_3
b	adenin-9-yl	OBz
c	cytosin-1-yl	OH
d	uracil-1-yl	OH
e	uracil-1-yl	Cl

(a) $SOCl_2$/MeCN for *a*-*d*, $SOCl_2$/C_6H_5N/MeCN for *e*. (b) NH_3/H_2O/MeOH

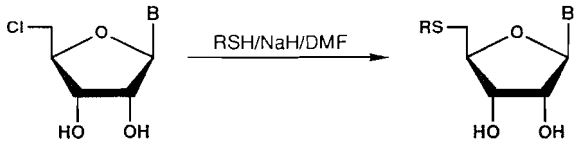
SCHEME 2

Can. J. Chem. Downloaded from www.nrcresearchpress.com by 84.41.108.74 on 09/07/12
For personal use only.

TABLE 2. ^{13}C NMR spectral data[a,b]

Compound	C2	C4	C5	C6	C8	C1′	C2′	C3′	C4′	C5′
1	152.29	149.00	119.33	156.09	139.87	87.93	73.44	70.61	85.86	61.62
2*a*	152.85	148.68	118.14	156.26	139.85	87.31	85.86	85.37	83.67	43.39
2*b*	152.85	148.75	119.14	156.26	139.85	89.31	89.22	88.13	86.08	43.62
3	153.20	149.80	119.47	156.38	140.30	88.10	73.27	71.60	83.98	45.00
4	143.22	142.31	118.73	148.19	141.78	87.39	70.08	73.74	85.44	61.11
5*a*	143.44	142.53	118.84	148.46	141.07	87.33	85.83	85.13	83.71	43.37
5*a*[c,d]	145.47	144.93	119.35	148.99	143.27	87.71	86.23	85.08	84.05	43.93
5*b*[c,d]	145.47	144.93	119.35	148.99	143.27	89.65	89.16	87.71	86.49	43.58
6	152.60	149.40	119.20	156.04	139.85	87.83	74.56	73.12	79.73	18.90
8*a*	152.86	148.84	119.05	156.17	139.87	87.22	85.59	84.74	82.72	50.95
9*a*[d]	152.86	148.69	119.05	156.17	139.87	89.02[e]	89.02[e]	87.45	84.99	51.20
8*b*[f]	152.73	148.69	119.09	156.09	139.72	87.40	85.71	84.25	81.65	63.35
9*b*[d,f]	152.73	148.69	119.09	156.09	139.72	89.29	89.02	86.93	83.92	63.76
8*c*[c,d]	159.89	147.00	93.83	145.22		91.60	86.97	86.11	84.30	60.37
9*c*[c,d]	159.89	147.00	95.68	145.43		93.39	89.71	88.39	87.54	60.76
8*d*[d]	150.24	163.07	101.90	141.87		90.14	86.32	84.81	84.27	60.53
9*d*[d]	150.26	163.07	101.65	142.08		92.10	89.56	87.34[e]	87.34[e]	60.95
8*e*	150.76	163.59	102.43	143.33		91.56	86.83	85.32	84.53	43.48
9*e*	150.76	163.62	102.38	143.91		94.15	90.15	87.95	87.25	43.65
10	151.15	163.50	102.15	141.25		88.15	72.20	70.80	83.10	44.90
11*a*[g]	153.03	149.83	119.39	156.42	140.18	87.50	72.74[e]	72.74[e]	83.85	36.07
11*b*[h,i]	153.70	150.11	119.67	156.44	141.14	88.40	73.65[j]	73.26[j]	83.92	36.16
11*c*[k]	152.62	149.47	119.20	156.06	139.94	87.33	72.57[j]	72.52[j]	82.96	37.41
11*d*[l]	151.02	163.27	102.34	141.24		88.28	72.48[j]	72.36[j]	82.63	37.49
11*e*[m]	150.73	162.97	102.03	141.04		87.89	72.20[j]	72.03[j]	82.04	37.71

[a]Chemical shifts (δ) at 75.5 MHz.
[b]All proton-decoupled peaks appeared as singlets.
[c]Hydrochloride salt.
[d]Assignments were made from a spectrum of the diastereomeric mixture.
[e]Peaks were not resolved.
[f]Peaks also at δ 128.63, 129.05, 129.25, 133.47 (Ar); 165.29 (CO).
[g]A peak also at δ 15.52 (SCH_3).
[h]Data parallel literature values (29).
[i]Peaks also at δ 127.14, 129.35, 130.11, 136.32 (Ar).
[j]Assignments might be reversed.
[k]Peaks also at δ 55.71 (OCH_3); 114.71, 125.50, 132.99, 158.46 (Ar).
[l]Peaks also at δ 55.48 (OCH_3); 115.06, 125.79, 132.55, 158.76 (Ar).
[m]Peaks also at δ 116.40, 123.17, 132.94, 156.83 (Ar).



3, B = adenin-9-yl
10, B = uracil-1-yl

11*a*, B = adenin-9-yl, R = CH_3
11*b*, B = adenin-9-yl, R = C_6H_5
11*c*, B = adenin-9-yl, R = 4-$CH_3OC_6H_4$
11*d*, B = uracil-1-yl, R = 4-$CH_3OC_6H_4$
11*e*, B = uracil-1-yl, R = 4-HOC_6H_4

SCHEME 3

This product was dried at 60°C *in vacuo* for 2 days to give **2***a*: mp 176–178°C (transition), 236–237°C (dec.); MS (CI, NH_3) *m/z*: 332 (100, M + 1, ^{35}Cl), 334 (40, M + 1, ^{37}Cl (and ^{35}Cl, ^{34}S)). Anal. calcd. for $C_{10}H_{10}ClN_5O_4S$ (331.7): C 36.21, H 3.04, Cl 10.69, N 21.11, S 9.67; found: C 36.20, H 3.05, Cl 10.55, N 21.03, S 9.88. Beautifully crystalline **2***a* was obtained by rapid crystallization from dry CH_3CN.

Three successive additions of toluene and concentrations of the mother liquor resulted in deposition of 5.4 g (29%) of an ~1:1 mixture of **2***a*/**2***b* hemisolvate. Slow concentration of this filtrate resulted in separation of 1.4 g (7%) of an ~1:4 mixture of this material. A portion of the latter solid was purified by preparative TLC (EtOAc/hexane, 20:1) to give colorless material with MS (CI, NH_3) *m/z*: 332 (100, M + 1, ^{35}Cl), 334 (40, M + 1, ^{37}Cl (and ^{35}Cl, ^{34}S)); and NMR spectral data (see Tables 1 and 2) for **2***b*.

Method B

Filtration and washing of the colorless precipitate obtained after neutralization to pH 5–6 in Method A and drying *in vacuo* gave 8.7 g (52%) of analytically pure **2***a* (found: C 36.10, H 3.11, Cl 10.63, N 21.02).

Method C (hydrochloride)

To a stirred suspension of **1** (1.34 g, 5 mmol) in pyridine (0.81 mL, 0.79 g, 10 mmol) and CH_3CN (15 mL) cooled in an ice/H_2O bath was slowly added $SOCl_2$ (1.84 mL, 3.0 g, 25 mmol). Stirring was continued at ~5°C for 3–4 h with warming to ambient temperature overnight. The resulting precipitate was filtered under a stream of dry N_2 and dried *in vacuo* over KOH and P_4O_{10} to give 1.69 g (92%) of colorless hygroscopic crystals of (**2***a*/**2***b*)·HCl: mp 165–175°C (transition), ~228°C (dec.); MS (CI, NH_3) *m/z*: 332 (26, M + 1, ^{35}Cl), 136 (100, B + 2). Anal. calcd. for $C_{10}H_{10}ClN_5O_4S$·HCl (368.2): C 32.62, H 3.01, Cl 19.26, N 19.02; found: C 32.64, H 2.93, Cl 19.11, N 18.98.

5′-Chloro-5′-deoxyadenosine **3**

To a stirred suspension of (**2***a*/**2***b*)·HCl (3.5 g, 9.5 mmol) MeOH (50 mL) was added H_2O (10 mL) and concentrated NH_3/H_2O

Can. J. Chem. Downloaded from www.nrcresearchpress.com by 84.41.108.74 on 09/07/12
For personal use only.

Can. J. Chem. Downloaded from www.nrcresearchpress.com by 84.41.108.74 on 09/07/12
For personal use only.

(5 mL). Stirring was continued for 30 min at ambient temperature and the clear, TLC-homogeneous solution was evaporated. The resulting colorless solid was crystallized from H_2O and dried *in vacuo* over P_4O_{10} to give 2.55 g (94%) of **3**: mp ~108–110°C (softening), ~188–190°C (dec.) (lit. (4*b*) mp 190°C (dec.), (7) mp 185–187°C (dec.)); MS *m/z*: 285.0627 (5.4, M^+(285.0629, ^{35}Cl)), 287.0599 (1.5, M^+(287.0599, ^{37}Cl)), 136.0616 (100, B + 2). Anal. calcd. for $C_{10}H_{12}ClN_5O_3$ (285.7): C 42.04, H 4.23, Cl 12.41, N 24.51; found: C 41.84, H 4.20, Cl 12.08, N 24.24.

5′-Deoxyadenosine ***6***

To a solution of **3** (286 mg, 1 mmol) in Me_2SO (15 mL) was added 1 M $LiEt_3BH$/THF (15 mL) and the solution stirred overnight at ambient temperature. **Cautious** addition of 5% HOAc/H_2O (40 mL) was followed by purging the **pyrophoric** Et_3B from the solution with N_2. The slightly yellow mixture was evaporated *in vacuo* at 50°C (bath temperature) and the residual syrup was dissolved in H_2O (30 mL) and applied to a column of Dowex 1 × 2 (OH^-) resin (2 × 20 cm). The column was washed with H_2O and the product eluted with MeOH/H_2O (3:2). Evaporation of the eluate and recrystallization of the product from H_2O gave 234 mg (93%) of **6**: mp ~134°C, with resolidification and remelting at 210–212°C (lit. (19*b*) mp 212–213°C (softens 135–140°C)); MS *m/z*: 251.1016 (M^+: 251.1018). Anal. calcd. for $C_{10}H_{13}N_5O_3$ (251.2): C 47.81, H 5.22, N 27.88; found: C 47.67, H 5.32, N 27.69.

Adenosine-1-oxide ***4***

A mixture of **1** (2.67 g, 10 mmol) and 3-chloroperoxybenzoic acid (6.09 g, 30 mmol as 85% reagent) in HOAc (40 mL) was stirred for 18 h at ambient temperature. To the white suspension was added Et_2O (50 mL). The crystalline product was filtered, washed thoroughly with Et_2O, and dried over KOH and P_4O_{10} to give 3.88 g (96%) of **4**·2HOAc (verified by ^1H NMR). Recrystallization of this material (95% EtOH) and drying gave **4**: mp 223–224°C (lit. (20) mp 155°C; 160°C (dec.)). Anal. calcd. for $C_{10}H_{13}N_5O_5$ (283.2): C 42.41, H 4.63, N 24.73; found: C 42.02, H 4.73, N 24.42.

*5′-Chloro-5′-deoxy-2′,3′-O-sulfinyladenosine-1-oxide hydrochlorides (***5***a/***5***b)·HCl*

A stirred suspension of **4** (1.42 g, 5 mmol) in CH_3CN (20 mL) was cooled in an ice/H_2O bath and $SOCl_2$ (1.1 mL, 1.8 g, 15 mmol) was added. The mixture was cooled to 0°C and pyridine (0.81 mL, 0.79 g, 10 mmol) was added. Stirring was continued and the mixture allowed to warm to ambient temperature overnight. The colorless precipitate was filtered (under dry N_2), washed with dry CH_3CN, and dried *in vacuo* over KOH and P_4O_{10} to yield 1.80 g (94%) of (**5***a*/**5***b*)·HCl (~6:1 by ^1H NMR). Anal. calcd. for $C_{10}H_{10}ClN_5O_5S$·HCl (384.2): C 31.26, H 2.89, N 18.23; found: C 31.84, H 2.90, N 18.20.

5′-Chloro-5′-deoxy-2′,3′-O-exo-sulfinyladenosine-1-oxide **5**a

A suspension of 3-chloroperoxybenzoic acid (3.05 g, 15 mmol as 85% reagent) and **2***a*·0.5EtOAc (1.88 g, 5 mmol) in 1,4-dioxane (15 mL) and EtOAc (50 mL) was stirred at ambient temperature overnight. The mixture was evaporated *in vacuo* to ~15 mL, stirred with Et_2O (100 mL), filtered, and the crystals washed thoroughly with Et_2O. This material was recrystallized (EtOAc/MeOH) and dried to yield 1.57 g (90%) of **5***a*: mp >195°C (dec.). Anal. calcd. for $C_{10}H_{10}ClN_5O_5S$ (347.7): C 34.54, H 2.90, Cl 10.20, N 20.14; found: C 34.34, H 2.88, Cl 10.23, N 20.22.

5′-Azido-5′-deoxy-2′,3′-O-sulfinyladenosines **8**a/**9**a

A stirred suspension of 5′-azido-5′-deoxyadenosine (27) (**7***a*, 1.17 g, 4 mmol) in CH_3CN (12 mL) was cooled in an ice/H_2O bath and $SOCl_2$ (0.88 mL, 1.43 g, 12 mmol) was added. Stirring at ambient temperature was continued for 6 h, H_2O (20 mL) added, and the resulting solution carefully neutralized to pH 5–6 (solid $NaHCO_3$) and extracted with EtOAc (3 × 30 mL). The combined organic phase was washed with saturated $NaHCO_3$/H_2O (20 mL) and H_2O (20 mL), dried (Na_2SO_4), and evaporated to give 1.3 g (96%) of **8***a*/**9***a* (~1.7:1 by ^1H NMR). Recrystallizations (EtOAc) gave the major *exo* isomer (**8***a*): mp 172–173°C; MS (CI, NH_3) *m/z*: 339 (100, M + 1). Anal. calcd. for $C_{10}H_{10}N_8O_4S$ (338.3): C 35.50, H 2.98, N 33.12, S 9.48; found: C 35.61, H 2.86, N 33.06, S 9.40.

5′-O-Benzoyl-2′,3′-O-sulfinyladenosines **8**b/**9**b

A cooled suspension of 5′-*O*-benzoyladenosine (28) (**7***b*, 1.48 g, 4 mmol) in CH_3CN (20 mL) was treated with $SOCl_2$ (1.28 mL, 2.1 g, 17.6 mmol) and worked up as described for the conversion of **7***a* → **8***a*/**9***a* to give 1.58 g (95%) of **8***b*/**9***b* (~1.5:1 by ^1H NMR). Recrystallizations (EtOAc) gave **8***b*: mp 186–187°C; MS (CI, NH_3) *m/z*: 418 (68, M + 1), 136 (100, B + 2). Anal. calcd. for $C_{17}H_{15}N_5O_6S$ (417.4): C 48.92, H 3.62, N 16.78, S 7.68; found: C 49.09, H 3.40, N 16.56, S 7.61.

*2′,3′-O-Sulfinylcytidine hydrochlorides (***8***c/***9***c)·HCl*

This mixture was prepared as described (13) (84% yield after drying *in vacuo* at 60°C over P_4O_{10}). **8***c*/**9***c*·HCl (~1.2:1 by ^1H NMR) had mp ~155–170°C (transition), 252–253°C (dec.) (lit. (13) mp 253–254°C). Anal. calcd. for $C_9H_{11}N_3O_6S$·HCl (325.7): C 33.19, H 3.71, Cl 10.88, N 12.90, S 9.84; found: C 33.18, H 3.60, Cl 10.90, N 12.95, S 9.84.

2′,3′-O-Sulfinyluridines **8**d/**9**d

This mixture was prepared as described (13) except the precipitated product was washed with MeOH/Et_2O (1:2). Drying *in vacuo* at ambient temperature over P_4O_{10} gave 82% of **8***d*/**9***d* (~2.3:1 by ^1H NMR) with mp 104–107°C (lit. (13) mp 104–105°C). Anal. calcd. for $C_9H_{10}N_2O_7S$ (290.3): C 37.24, H 3.47, N 9.65, S 11.05; found: C 36.94, H 3.39, N 9.64, S 10.78.

5′-Chloro-5′-deoxyuridine ***10***

A stirred suspension of uridine (**7***d*, 12.2 g, 50 mmol) in pyridine (8.1 mL, 7.9 g, 100 mmol) and CH_3CN (100 mL) was cooled in an ice/H_2O bath and $SOCl_2$ (18.2 mL, 29.7 g, 250 mmol) was slowly added. Stirring was continued at ambient temperature overnight and the mixture was evaporated *in vacuo* to give a slightly yellow solid foam. (When EtOAc and $NaHCO_3$/H_2O were added, the organic phase worked up, and the product mixture chromatographed on a silica column (C_6H_6/EtOAc, 1:1) as described (8), diastereomers **8***e* and **9***e* were obtained. See Tables 1 and 2 for NMR data.) The crude solid foam was dissolved in H_2O/MeOH (50:215 mL), concentrated NH_3/H_2O (30 mL) added, and the mixture stirred at ambient temperature for 1 h. The precipitated solids were filtered, and the filtrate concentrated to a small volume and then applied to a column of Dowex 1 × 2 (OH^-) resin. The column was washed with H_2O, the product eluted with 0.2 M $Et_3NH_2CO_3$/H_2O, and the eluate evaporated followed by additions and evaporations of H_2O *in vacuo*. The residue was recrystallized (MeOH/H_2O, 1:9) and dried over P_4O_{10} to give 10.7 g (82%) of colorless needles of **10**: mp 176–177°C (lit. (8) mp 176–178°C); MS *m/z*: 262.0354 (6.1, M^+(262.0357, ^{35}Cl)), 264.0326 (2.1, M^+(264.0327, ^{37}Cl)). Anal. calcd. for $C_9H_{11}ClN_2O_5$ (262.6): C 41.16, H 4.22, Cl 13.50, N 10.67; found: C 41.17, H 4.23, Cl 13.40, N 11.03.

General procedure for 5′-S-aryl(or alkyl)-5′-thionucleosides (details with ***11***a*)*

5′-S-Methyl-5′-thioadenosine ***11***a

Sodium hydride (0.29 g of 50% NaH/mineral oil, 6 mmol) was washed with Et_2O (2 × 10 mL) and suspended in anhydrous DMF (30 mL) at −30°C. Methanethiol (0.31 mL, 0.27 g, 5.5 mmol) was added slowly with magnetic stirring. When evolution of H_2 had ceased, a solution of **3** (1.43 g, 5 mmol) in anhydrous DMF (40 mL) was added dropwise. The mixture was allowed to warm to ambient temperature, stirred overnight, and evaporated *in vacuo*. The residue was treated with H_2O (50 mL), neutralized to pH 7 with dilute HCl/H_2O, and cooled. The crude product that separated was recrystallized from MeOH/H_2O (1:1, 150 mL) to give 1.28 g (86%) of colorless needles of **11***a*: mp 212°C (lit. (22) mp 207°C, (23) mp 213–214°C); UV (MeOH) max: 259 nm (ε 15 400); min: 226 nm (ε 2900); MS *m/z*: 297.0896 (8.5, M^+(297.0896)). Anal. calcd. for $C_{11}H_{15}N_5O_3S$ (297.3): C 44.43, H 5.09, N 23.55, S 10.78; found: C 44.25, H 5.07, N 23.52, S 10.99.

5′-S-Phenyl-5′-thioadenosine ***11****b*

Treatment of **3** with benzenethiol by the *general procedure* gave **11***b* (92%): mp 136–137°C (lit. (23) mp 136–138°C, (24) 139°C); UV (MeOH) max: 254 nm (ε 21 300); min 228 nm (ε 6000); MS *m/z*: 359.1055 (5.2, M^+(359.1052)), 136.0624 (100, B + 2H). Anal. calcd. for $C_{16}H_{17}N_5O_3S$ (359.4): C 53.47, H 4.77, N 19.49, S 8.92; found: C 53.53, H 4.69, N 19.27, S 8.90.

5′-S-(4-Methoxyphenyl)-5′-thioadenosine ***11****c*

Treatment of **3** with 4-methoxybenzenethiol by the *general procedure* gave **11***c* (87%): mp 123–124°C; UV (MeOH) max: 257, 229 nm (ε 22 700, 10 900); min: 235, 223 nm (ε 10 600, 10 200); MS *m/z*: 389.1155 (8.1, M^+(389.1158)), 136.0626 (100, B + 2H). Anal. calcd. for $C_{17}H_{19}N_5O_4S$ (389.4): C 52.43, H 4.92, N 17.98, S 8.23; found: C 52.14, H 4.81, N 17.66, S 8.31.

5′-S-(4-Methoxyphenyl)-5′-thiouridine ***11****d*

Treatment of **10** with 4-methoxybenzenethiol by the *general procedure* gave **11***d* (94%): mp 203–204°C; UV (MeOH) max: 256, 227 nm (ε 17 500, 10 700); min: 237, 221 nm (ε 9600, 10 300); MS *m/z*: 366.0891 (31, M^+(366.0886)), 195.0482 (100). Anal. calcd. for $C_{16}H_{18}N_2O_6S$ (366.4): C 52.45, H 4.95, N 7.65, S 8.75; found: C 52.07, H 4.85, N 7.56, S 8.96.

5′-S-(4-Hydroxyphenyl)-5′-thiouridine ***11****e*

Treatment of **10** with 4-hydroxybenzenethiol by the *general procedure* and recrystallization of the crude product (MeOH/$CHCl_3$, 1:2) gave **11***e* (92%): mp 169–170°C; UV (MeOH) max: 256 nm (ε 16 600); min: 236 nm (ε 9000); MS *m/z*: 352.0728 (2.9, M^+(352.0729)), 112.0276 (32, B + H), 69.0006 (100). Anal. calcd. for $C_{15}H_{16}N_2O_6S$ (352.4): C 51.13, H 4.58, N 7.95, S 9.10; found: C 50.96, H 4.45, N 7.71, S 8.86.

Acknowledgements

We thank the Natural Sciences and Engineering Research Council of Canada, the National Cancer Institute of Canada, and the American Cancer Society (Grant No. CH-405) for generous support. We thank Mrs. Kathryn M. Rollins for assistance with the manuscript.

1. (*a*) J. G. MOFFATT. *In* Nucleoside analogues: chemistry, biology, and medical applications. *Edited by* R. T. Walker, E. De Clercq, and F. Eckstein. Plenum Press, New York. 1979. pp. 71–164; (*b*) T. UEDA. *In* Chemistry of nucleosides and nucleotides. *Edited by* L. B. Townsend. Plenum Press, New York. 1988. pp. 1–112; (*c*) P. C. SRIVASTAVA, R. K. ROBINS, and R. B. MEYER, JR. *In* Chemistry of nucleosides and nucleotides. *Edited by* L. B. Townsend. Plenum Press, New York. 1988. pp. 113–281.
2. (*a*) P. C. SRIVASTAVA, K. L. NAGPAL, and M. M. DHAR. Experientia, **25**, 356 (1969); (*b*) P. C. SRIVASTAVA and R. J. ROUSSEAU. Carbohydr. Res. **27**, 455 (1973).
3. R. F. DODS and J. S. ROTH. Tetrahedron Lett. 165 (1969).
4. (*a*) K. KIKUGAWA and M. ICHINO. Tetrahedron Lett. 867 (1970); (*b*) Tetrahedron Lett. 87 (1971); (*c*) J. Org. Chem. **37**, 284 (1972).
5. H. P. C. HOGENKAMP. Biochemistry, **13**, 2736 (1974).
6. J. F. NORMANT and H. DESHAYES. Bull. Soc. Chim. Fr. 2854 (1972).
7. D. E. GIBBS and J. G. VERKADE. Synth. Commun. **6**, 563 (1976).
8. H. HŘEBABECKÝ and J. BERÁNEK. Nucleic Acids Res. **5**, 1029 (1978).
9. Y. WANG and H. P. C. HOGENKAMP. Carbohydr. Res. **76**, 131 (1979).
10. M. J. ROBINS, P. SPORNS, and W. H. MUHS. Can. J. Chem. **57**, 274 (1979).
11. Y. WANG, H. P. C. HOGENKAMP, R. A. LONG, G. R. REVANKAR, and R. K. ROBINS. Carbohydr. Res. **59**, 449 (1977).
12. P. DRAŠAR and J. BERÁNEK. Collect. Czech. Chem. Commun. **54**, 1358 (1989).
13. T. SOWA and K. TSUNODA. Bull. Chem. Soc. Jpn. **48**, 505 (1975).
14. T. SOWA and K. TSUNODA. Bull. Chem. Soc. Jpn. **48**, 3243 (1975).
15. J. G. PRITCHARD and P. C. LAUTERBUR. J. Am. Chem. Soc. **83**, 2105 (1961).
16. Z. HAVLAS, M. SYNÁČKOVÁ, H. HŘEBABECKÝ, J. FARKAŠ, and J. BERÁNEK. Collect. Czech. Chem. Commun. **46**, 400 (1981).
17. C. H. GAGNIEU, A. GUILLER, and H. PACHECO. Carbohydr. Res. **180**, 223 (1988).
18. H. C. BROWN and S. KRISHNAMURTHY. J. Am. Chem. Soc. **95**, 1669 (1973).
19. (*a*) H. M. KISSMAN and B. R. BAKER. J. Am. Chem. Soc. **79**, 5534 (1957); (*b*) J. R. MCCARTHY, JR., R. K. ROBINS, and M. J. ROBINS. J. Am. Chem. Soc. **90**, 4993 (1968).
20. M. A. STEVENS, D. I. MAGRATH, H. W. SMITH, and G. B. BROWN. J. Am. Chem. Soc. **80**, 2755 (1958).
21. Y. GAO and K. B. SHARPLESS. J. Am. Chem. Soc. **110**, 7538 (1988).
22. J. BADDILEY and G. A. JAMIESON. J. Chem. Soc. 4280 (1954).
23. R. KUHN and W. JAHN. Chem. Ber. **98**, 1699 (1965).
24. D. SHIRE, P. BLANCHARD, A. RAIES, F. LAWRENCE, M. ROBERT-GERO, and E. LEDERER. Nucleosides Nucleotides, **2**, 21 (1983).
25. R. T. BORCHARDT, J. A. HUBER, and Y. S. WU. J. Org. Chem. **41**, 565 (1976).
26. I. NAKAGAWA, K. AKI, and T. HATA. J. Chem. Soc. Perkin Trans. 1, 1315 (1983).
27. W. JAHN. Chem. Ber. **98**, 1705 (1965).
28. R. MENGEL and M. BARTKE. Angew. Chem. Int. Ed. Engl. **17**, 679 (1978).
29. Y. LOOZE, L. GILLET, M. DECONINCK, J. LÉONIS, and M. GELBOKE. Anal. Lett. **13**, 871 (1980).
30. M. J. ROBINS, S. MANFREDINI, S. G. WOOD, R. J. WANKLIN, B. A. RENNIE, and S. L. SACKS. J. Med. Chem. In press.

Can. J. Chem. Downloaded from www.nrcresearchpress.com by 84.41.108.74 on 09/07/12
For personal use only.

Monolayer properties of mixed chlorophyll *a*-digalactosyldiacylglycerol at the nitrogen–water interface

DANIEL DUCHARME,[1] OSAMU SHIBATA,[2] GAÉTAN MUNGER, AND ROGER M. LEBLANC
Centre de recherche en photobiophysique, Université du Québec à Trois-Rivières, Trois-Rivières, Qué., Canada G9A 5H7

Received July 4, 1990[3]

DANIEL DUCHARME, OSAMU SHIBATA, GAÉTAN MUNGER, and ROGER M. LEBLANC. Can. J. Chem. **69**, 1475 (1991).

Surface pressure, surface potential, and ellipsometric–area isotherms have been measured to investigate the properties of chlorophyll *a* – digalactosyldiacylglycerol monolayers at the nitrogen – water interface. The surface pressure – area isotherms of the mixed film show a pronounced negative deviation with respect to ideality, whereas the surface potential isotherms follow the additivity law for mixed films. As the mole fraction of Chl *a* increases from 0.1 to 0.5, each of the corresponding ellipsometric isotherm is shifted towards more negative values in the liquid expanded region. As the mole fraction is increased above 0.5, the ellipsometric $\delta\Delta$ values become more positive, with this trend continuing throughout the 0.5 to 0.9 mole fraction range. The combined effects of anisotropy in both the refractive indices and the absorption coefficient can explain the turnover observed in the ellipsometric $\delta\Delta$ isotherms as the mole fraction of Chl *a* becomes larger than 0.5.

Hydrophilic interactions have been ruled out on the basis of the agreement with the additivity law, which is observed for surface potentials of the mixed monolayers. The observed deviation exhibited in the π–*A* isotherms is interpreted in terms of the intermolecular cavity effect.

Key words: chlorophyll *a*, digalactosyldiacylglycerol, mixed monolayer, ellipsometry.

DANIEL DUCHARME, OSAMU SHIBATA, GAÉTAN MUNGER et ROGER M. LEBLANC. Can. J. Chem. **69**, 1475 (1991).

On a mesuré les isothermes de pression superficielle, de potentiel de surface et ellipsométrique pour étudier les propriétés des monocouches pures et en milange de la chlorophylle *a* et du digalactosyldiacylglycérol à l'interface azote-eau. Les isothermes de surface pression superficielle des films mixtes montrent une déviation négative prononcée par rapport au cas idéal, tandis que les isothermes de potentiel de surface suivent la loi d'additivité des films mixtes. Lorsque la fraction molaire de la chlorophylle *a* augmente à partir de 0,1 jusqu'à 0,5 chacun des isothermes ellipsométriques correspondants se déplace vers des valeurs plus négatives dans la région expansée de liquide. Lorsque la fraction molaire dépasse 0,5 jusqu'a atteindre 0.9 la valeur ellipsométrique $\delta\Delta$ devient plus positive. Les effets combinés de l'anisotopie à la fois dans les indices de réfraction et dans le coefficient d'adsorption peuvent expliquer le changement observé dans les isothermes $\delta\Delta$ ellipsométriques lorsque la fraction molaire de la chl *a* devient supérieure à 0,5.

On a écarté les interactions hydrophiles en raison de l'accord existant avec les lois d'additivité que l'on observe pour les potentiels de surface des monocouches mixtes. On attribue à l'effet de cavité intermoléculaire la déviation observée dans les isothermes π–*A*.

Mots clès : chlorophylle *a*, digalactosyldiacylglycérol, monocouche mixte, ellipométrie.

[Traduit par la rédaction]

1. Introduction[4]

The thylakoid membrane system of chloroplasts, the site of light-harvesting reactions of photosynthesis, contains, in addition to chlorophylls, a large proportion of glycolipids. The major lipid components are the uncharged MGDG and DGDG, which combined amount to about 60 to 70 mol% of the total lipids present in the membrane (1). Charged SQDG and PG are also present as minor glycolipid components. Considering the importance of Chl *a* in photosynthesis, it is necessary to have a good knowledge of the way this pigment interacts with its environment.

The results reported here, with monolayers as a model system, differ from those reported elsewhere using different models. With the introduction of Chl *a* into phospholipid bilayer membranes, evidence has been obtained for compound formation between Chl *a* and lipids involving interaction of the lipid phosphate with the magnesium ion in chlorophyll (2). Interactions of Chl *a* with the lipids of the thylakoid membrane have also been reported (3). From lifetime measurements of Chl *a* in lipid liposomes, as well as in vesicles of MGDG, DGDG, and SQDG, reports have also suggested that association of Chl *a* occurs with these lipids (4, 5).

However, information about Chl *a* – galactolipid interactions in monolayers at the gas–water interface is scarce (6). The results reported in the present work for Chl *a* – DGDG show a larger negative deviation from the additivity law than those reported for the Chl *a* – MGDG system (6).

This negative deviation, typically indicating condensation of mixed monolayers (7), has been interpreted in several ways. Explanations have included van der Waals interactions, configuration entropy effects, alterations of water molecules near the monolayer, and an intermolecular cavity effect (8, 9). Ellipsometric and surface potential isotherms of the system under study in this work reveal features which help in the understanding of the condensing effect observed in surface pressure isotherms.

Applying the additivity law to surface potential values of the mixture, it is shown that agreement between calculated and experimental values suggests the absence of any particular interactions between the monolayer components.

The ellipsometric angle $\delta\Delta$ is sensitive to changes of

[1]Département de Chimie, Cegep de Shawinigan, Shawinigan, Qué., Canada G9N 6V8.

[2]College of General Education, Kyushu University–01, Roppon-matsu, Fukuoka 810, Japan.

[3]Revision received April 26, 1991.

[4]Abbreviations: Chl, chlorophyll; MGDG, monogalactosyldiacylglycerol; DGDG, digalactosyldiacylglycerol; SQDG, sulfoquinovosyldiacylglycerol; PG, phosphatidylglycerol; TLC, thin-layer chromatography; HPLC, high performance liquid chromatography; GC, gas chromatography.

Can. J. Chem. Downloaded from www.nrcresearchpress.com by 84.41.108.74 on 09/07/12
For personal use only.

TABLE 1. Fatty acid composition of the galactolipid*

Acid		DGDG†	
		Present work	Reference 11
Palmitic	16:0	3.2	10.0
Palmitoleic	16:1	0.3	
Palmitolenic	16:3	0.5	
Stearic	18:0	0.5	0.9
Oleic	18:1	4.8	3.5
Linoleic	18:2	2.5	3.0
Linolenic	18:3	88.2	82.6

*Results are expressed as percentages.
†Extracted from barley leaves and purified by HPLC.

refractive indices, to changes in the sign of the difference between refractive indices of an anisotropic film (birefringence), to the extent of absorption of the film, to the anisotropic character of the absorption coefficient, and to film thickness. Thus, ellipsometric isotherms can provide valuable information on interactions between mixed film components.

Analysis of the results based on both the surface potential, which is in agreement with the additivity law for mixed films, and ellipsometric behavior of the mixed films, does not provide evidence of any specific interactions between monolayer components within the 5 to 25 mN/m surface pressure range. The negative deviation observed in the π–A isotherms in this surface pressure range may be explained by the intermolecular cavity effect in the monolayer.

2. Methodology

(A) Pure components

Chl *a* was extracted from barley leaves and purified according to the method described in ref 10. TLC (G plate, Mandel Sci. Co., ON, Canada) was used to test the purity of the pigment, which resulted in a single spot of a R_f value of 0.40, using as the elution solvent a mixture of *n*-hexane/acetone (7:3, v/v). DGDG was extracted from barley leaves and purified by HPLC, using as the elution solvent a mixture of hexane/isopropanol/water (70:30:3, v/v/v). Fatty acid composition of the galactolipid, shown in Table 1, was determined by GC and found to be in good agreement with published values (11). The molar weights of Chl *a* and DGDG are 894 and 936 g mol^{-1}, respectively. These compounds were stored under argon at −134°C. Prior to use, they were dissolved in a mixture of *n*-hexane/ethanol (9:1, v/v). All solvents were distilled before use. Chl *a* was studied with two different spreading solvents: benzene and *n*-hexane/ethanol (9:1, v/v). Measurements were carried out on a phosphate buffer subphase (10^{-3} mol L^{-1}, pH = 8.0). The phosphate salts (Na_2HPO_4 and NaH_2PO_4, 99.5 mol%, J. T. Baker Chemical Co., Phillipsburg, NJ) employed for the buffer were used as received.

Deionized and prepurified water (Nanopure filter system, Barnsted, Boston, MA) was twice distilled in a quartz still (Model Bi-18, Amerisil Inc., Sayreville, NJ). Specific resistivity of water was 18 MΩ cm, with a surface tension ≥71 mN/m. Surface potential was measured by using an ^{241}Am electrode (Nuclear Radiation Development, Grand Island, NY) placed 1–2 mm above the subphase and located at approximately 12 cm from the float. The reference electrode was dipped in the subphase behind the float; reference surface potential was −350 mV with a standard deviation of ±30 mV. These variations in the reference potential are attributed to the variations, from run to run, of the water content in the gas phase surrounding the electrodes (7). These changes in the water content could have been related to fluctuations in the nitrogen flow close to the nitrogen–water interface.

The buffer subphase was allowed to stand 15 min in the trough and then compressed. The movable barrier was brought to approximately 1 cm from the float, and impurities were removed by vacuum aspiration with a pipette. Impurities were removed from the buffer by repeated compression and decompression cycles and vacuum aspirations, until no surface pressure could be detected. After zeroing the surface pressure transducer, the subphase was allowed to rest an additional 15 min and compressed again to check for the presence of any remaining impurities. Only after this procedure was carried out was the solution spread over the subphase. Experiments have shown that the baseline of the surface pressure does not drift by more than 1 mN/m within a 2-hour period for a clean subphase.

Surface pressure, surface potential, and ellipsometric isotherms were obtained according to the methods and instrumentation described previously (12). The film was compressed at a speed of 5 $Å^2$ $molecule^{-1}$ min^{-1}. Each of the three types of isotherms were measured at least 10 times for each of the compounds and averaged. The area per molecule was measured to ±3 and ±1.5 $Å^2$ $molecule^{-1}$ for Chl *a* and DGDG, respectively; the surface potential to an accuracy of ±15 mV; the ellipsometric $\delta\Delta$ to ±0.05° for Chl *a* as compared to ±0.02° for DGDG, and the ellipsometric $\delta\psi$ to ± 0.02°.

All measurements were carried out under dim green light and in a nitrogen environment. To ensure that Chl *a* does not bleach under illumination of the laser beam used for ellipsometric measurements, surface pressure was recorded during a 2-h irradiation of a compressed monolayer of Chl *a*. The observed decrease in surface pressure was comparable to that obtained with the laser turned off. Relative humidity within the Plexiglass enclosure was measured with a needle-type hygrometer (Cole Parmer, ON, Canada) and remained approximately constant at 50 ± 5% during the experiments. The temperature of the aqueous subphase was controlled at 20 ± 1°C.

(B) Mixed component films

Measurements of surface pressure, surface potential, and ellipsometric isotherms for mixed films were each repeated at least three times. Maximum deviations between extremes for each type of isotherm were in the same range as those reported above for the pure galactolipid. The uncertainties in the ellipsometric angles become higher the higher the mole fraction of Chl *a*.

3. Results

Surface pressure, surface potential, and ellipsometric isotherms

(A) Pure component films

Figure 1 shows the surface pressure (π), surface potential (ΔV), and ellipsometric ($\delta\Delta$ and $\delta\psi$) – area (A) isotherms of pure Chl *a*, DGDG and mixed component monolayers. For sake of clarity, some of the isotherms of the mixtures are not included.

The surface pressure – area isotherms have been measured by both a continuous and a step-wise compression method. The "step-wise" compression technique is necessary since, in obtaining experimental ellipsometer readings, approximately 5 to 10 min are required to measure the angles at one specific molecular area. The collapse pressure of Chl *a* was observed to be dependent on the method used. As shown in Fig. 1, from the liftoff at 138 $Å^2$ $molecule^{-1}$ to approximately 85 $Å^2$ $molecule^{-1}$ (π = 25 mN/m), no difference is observed between the two methods. However, from a molecular area of 85 $Å^2$ $molecule^{-1}$, the surface pressure isotherm measured by the step-wise method (solid line) deviates from that obtained by continuous compression (dashed line). The collapse pressure obtained by continuous compression is in close agreement with published values (6, 13).

For pure DGDG monolayer films, the liftoff was observed at approximately 145 $Å^2$ $molecule^{-1}$, with the collapse pressure measured at 42 mN/m. At a surface pressure of 10 mN/m, the

Can. J. Chem. Downloaded from www.nrcresearchpress.com by 84.41.108.74 on 09/07/12
For personal use only.

Can. J. Chem. Downloaded from www.nrcresearchpress.com by 84.41.108.74 on 09/07/12
For personal use only.

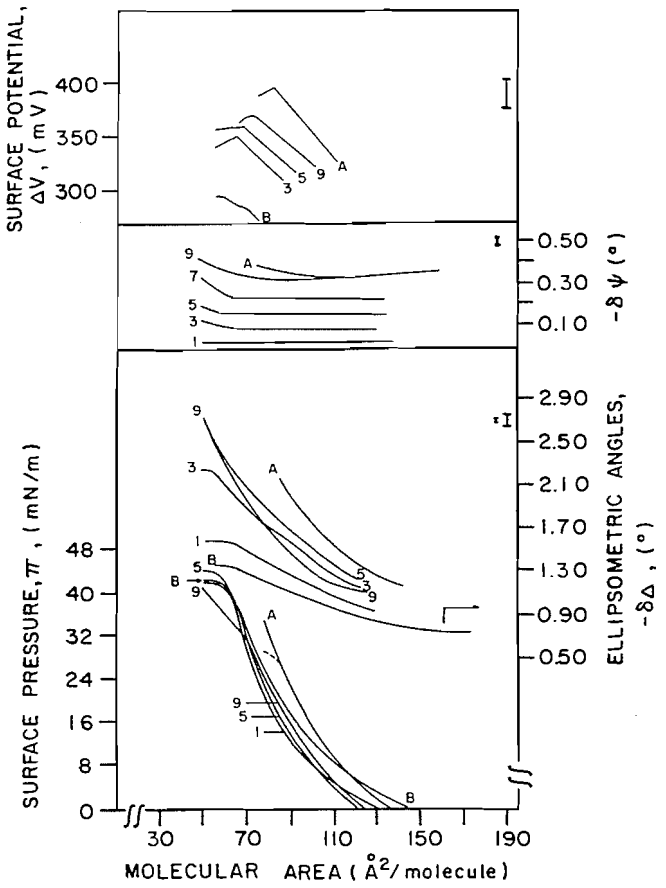


FIG. 1 Surface pressure (π), surface potential (ΔV) and ellipsometric ($\delta\Delta$ and $\delta\psi$) — area (A) isotherms of pure and mixed Chl *a* — DGDG at the nitrogen–water interface. The subphase was buffered at pH 8.0 using phosphate, 10^{-3} mol L^{-1}. Temperature was maintained at 20 ± 1°C for all experiments. Isotherms A and B are for pure Chl *a* and DGDG, respectively. Isotherm A measured by continuous (···) and, step-wise (—) compression, respectively. Values (1, 3, 5, 7, 9) represent mole fractions (0.1, 0.3, 0.5, 0.7, 0.9) of Chl *a* in the mixed film, measured by step-wise compression. Ellipsometric parameters: ϕ = 60.00 ± 0.05°; λ = 6328 Å. Bars at the upper right of each frame represent the maximum experimental error on each type of measurement. The two bars in the lowest frame are experimental errors on mixed films (shorter bar) and Chl *a*.

π–*A* isotherm of the galactolipid is more expanded than galactolipid extracted from Beta vulgaris (ref. 11) by approximately 10 to 15 Å^2 molecule^{-1}. The discrepancy in molecular area decreases as surface pressure increases. This could be due in part to the different subphase and spreading solvent which were used in the work with Beta vulgaris, in which case pure water and chloroform were employed. In this work, a phosphate buffer was used as a subphase and hexane: ethanol (9:1, v/v) as spreading solvent. Collapse pressures cannot be compared since the authors did not report this value.

As shown in Fig. 1, DGDG exhibits an ellipsometric "jump angle" of −0.72° at a molecular area of approximately 170 Å^2 molecule^{-1}. This jump angle corresponds to the onset of a photometric signal which allows reliable azimuth readings to be taken. From that molecular area and onward with further compression, $\delta\Delta$ decreases slowly as a function of the reduction of molecular area, and plateaus at approximately −1.34°. The onset of this plateau occurs at approximately 65 Å^2 molecule^{-1}. The shape and values of this ellipsometric isotherm resemble those of previously published isotherms for unsaturated phospholipids (14).

The ellipsometric behavior of Chl *a* is substantially different from that of the galactolipid. From the observed jump angle of −1.10° for Chl *a* and onward, $\delta\Delta$ decreases almost exponentially as a function of the reduction of the molecular area, reaching a value of approximately −2.1° in the collapse pressure region, as observed in the π–*A* isotherm (Fig. 1). Moreover, in contrast to DGDG, the change in the relative amplitude for the reflected to the incident light beam components, which is a measure of absorption, shows, as expected, a non-null $\delta\psi$ value for Chl *a*. The ellipsometric values obtained in this work differ from published data (15), in which these researchers report both $\delta\Delta$ and $\delta\psi$ first becoming positive, and then changing signs at about 150 Å^2 molecule^{-1}. From this area to approximately 80 Å^2 molecule^{-1}, the reported $\delta\Delta$ value changes from −1.30 to −1.90°, as compared to −1.10 to −2.1° in the present work. Concurrently, $\delta\psi$ is reported to vary from −0.14 to −0.19°, as compared to an essentially constant value of −0.35° in the present study.

Due to large photometric signal fluctuations at high molecular area, reliable measurements could not be taken prior to a molecular area of approximately 150 Å^2 molecule^{-1}. Therefore it is impossible to compare changes in sign of the ellipsometric angles in this work to those reported previously (15). In addition, it was necessary to reduce the sensitivity of the lock-in amplifier to the 25 mV scale, as compared to a 10 mV scale used with the galactolipid and the mixed films. Large fluctuations in the photometric signal have been reported for pentadecanoic acid in the G–LE (gaseous–liquid expanded) phase (16). These fluctuations have been attributed to the condensation of a liquid from the gas phase, characterized by the appearance of high density phase domains coexisting with the low density phase. As a function of the average density, the domains grow at the expense of the low density phase until a full condensation has taken place. As these domains are being moved in and out of the probe area by the convective motion of the water, fluctuations in the photometric signal arise. However, another explanation can be given for this phenomenon. For DPPC dye-labeled monolayers in the G–LE region, Lösche and Möhwald (17) have noted the appearance of holes. These holes are surrounded by molecules. At large molecular area, their instability, *i.e.* variation in size due to a low molecular density environment, can also give rise to the observed fluctuations in the photometric signal as the holes are moved in and out of the light beam by the convective motion of the water. A similar phenomenon could be responsible for the fluctuations observed in this study.

Benzene and *n*-hexane:ethanol (9:1, v/v) were used as spreading solvents for Chl *a*. Ellipsometric $\delta\Delta$ isotherms of Chl *a* measured with *n*-hexane:ethanol as the spreading solvent exhibit much better reproducibility (±0.05°) than those measured with benzene (±0.1°). From these observations, it has been decided that in further experiments, *n*-hexane:ethanol is the solvent of choice. With this solvent system, the π–*A* and the ΔV–*A* isotherms do not show significant spreading solvent-related differences.

The ΔV–*A* isotherms of both pure components exhibit the following features: (*i*) the onset of stable surface potential occurs at a slightly larger molecular area than the onset of surface pressure; (*ii*) a steady increase in surface potential is observed as molecular area decreases; (*iii*) in the collapse region, DGDG exhibits a plateau at 300 ± 15 mV, whereas

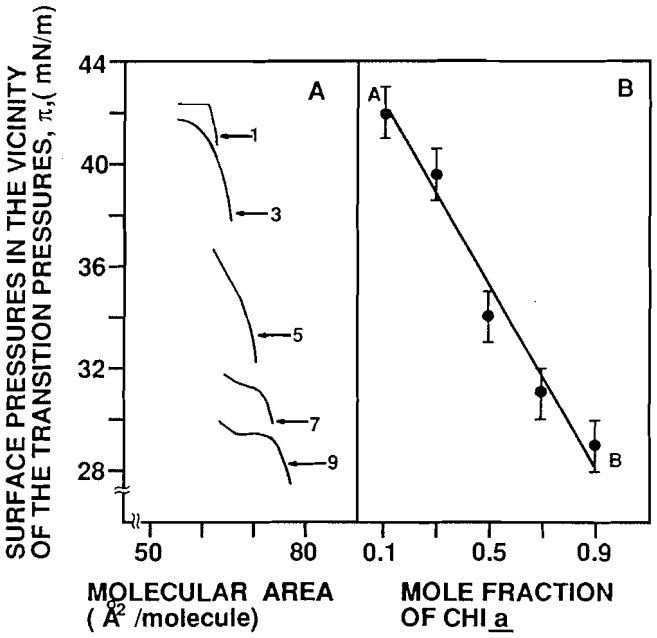


FIG. 2. (*A*) Surface pressures in the vicinity of the transition pressures as a function of molecular area measured by continuous compression. Labels and experimental conditions are identical to those of Fig. 1. (*B*) Surface pressures at the transition pressures as a function of mole fraction of Chl *a*. Area below line AB is the one phase region.

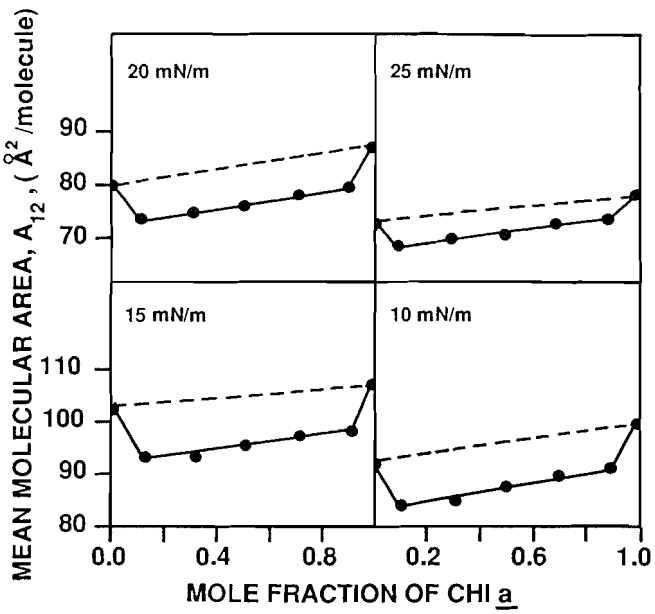


FIG. 3. Mean molecular areas (A_{12}) of mixed Chl *a* – DGDG monolayers as a function of mole fraction of Chl *a* at four different surface pressures (10, 15, 20, and 25 mN/m). Dashed curves are calculated results assuming the additivity rule. Solid circles are the experimental values.

Chl *a* shows a sudden decrease in surface potential at a molecular area that corresponds closely to the onset of collapse surface pressure observed in the π–*A* isotherm. Because of the scale of Fig. 1, it may not be apparent that the surface potential of DGDG has plateaued. The maximum value for surface potential values of Chl *a* is approximately 400 mV, which is in close agreement with published values (6).

(B) Mixed component films

Monolayer films of five mixtures of Chl *a* – DGDG have been measured, shown in Fig. 1 as mole fraction of Chl *a* (0.1, 0.3, 0.5, 0.7, 0.9). For π–*A* isotherms measured either by step-wise or continuous compression, none of the isotherms of the mixed films fall between those of the pure components as expected by the additivity rule for ideal mixtures. Step-wise compression of the 0.5, 0.7, and 0.9 mixtures did not show transition points in pressure (the transition points correspond to the surface pressure where a sudden change in slope in the π–*A* isotherms takes place) as well defined as those obtained by continuous compression. For mixtures with a higher content in Chl *a* (0.5, 0.7, and 0.9), the transition points measured by continuous compression were lower than those obtained by the step-wise technique. However, up to the transition points, no differences could be observed between the two methods. The mixed films, with the exception of the 0.9 mole fraction Chl *a*, measured by both techniques showed nearly a constant collapse pressure, with a transition point varying according to the mixture composition. Results obtained for continuous compression are presented in Fig. 2*A*. Application of the surface phase rule to this system shows that below the line AB (Fig. 2B), the two-components would be completely miscible.

The deviation from ideality is illustrated in Fig. 3, where mean molecular area (A_{12}) is plotted as a function of mole fraction of Chl *a*, for surface pressures of 10, 15, 20, and 25 mN/m. It is seen that the deviation from the additivity law tends to increase as the mole fraction of Chl *a* decreases, with the average gap between experimental and calculated values becoming smaller the higher the surface pressure. It is to be noted that an increased instability in the surface pressure arises after the onset of transition point pressures.

In contrast to the behavior of the π–*A* isotherms, those of the ellipsometric $\delta\Delta$–A isotherms for the mixtures fall between those of the pure components. In the 5 to 25 mN/m range, from approximately 125 to 80 Å^2 molecule^{-1}, with an increasing mole fraction of Chl *a* (0.1 to 0.5), each of the corresponding ellipsometric isotherms is shifted towards more negative $\delta\Delta$ values. The higher the mole fraction of Chl *a*, the lower the $\delta\Delta$ values (Fig. 1). However, a significant change in this trend is observed as the mole fraction of Chl *a* is increased above 0.5. The corresponding ellipsometric isotherms for the 0.7 (not shown) and 0.9 mole fractions are more positive than those of 0.5 and 0.3 mole fraction, with the 0.9 fraction of Chl *a* being the most positive. Although small, these observed differences in ellipsometric angles are larger than the uncertainties of the measurements. Furthermore, only the 0.1 and 0.3 mixtures show the same ellipsometric behavior as the pure galactolipid, with an ellipsometric plateau occurring at lower molecular areas (65 Å^2 molecule^{-1} for the 0.1 as compared to approximately 55 Å^2 molecule^{-1} for the 0.3 mole fraction). Concurrently, regardless of surface pressure, measured from 5 to 25 mN/m, the $\delta\psi$ angle decreases almost linearly as a function of increasing mole fraction of Chl *a* (see Fig. 4). At low molecular areas, below approximately 65 Å^2/molecule, in contrast to what is mentioned above, no differences in the $\delta\Delta$–A isotherms could be observed for the mixtures of the 0.5, 0.7, and 0.9 mole fraction of Chl *a*. Furthermore, in this molecular area region, with the exception of the 0.1 mole fraction, a significant decrease in $\delta\psi$ sets-in for all mixtures (see Fig. 1).

From the π–*A* isotherms (Fig. 1), the ellipsometric $\delta\Delta$ angle has been plotted as a function of the mole fraction of Chl *a* in Fig. 5 A, at five different surface pressures (5, 10, 15, 20, and 25 mN/m). This has been accomplished by selecting the molecular area, at the appropriate surface pressure of interest,

Can. J. Chem. Downloaded from www.nrcresearchpress.com by 84.41.108.74 on 09/07/12
For personal use only.

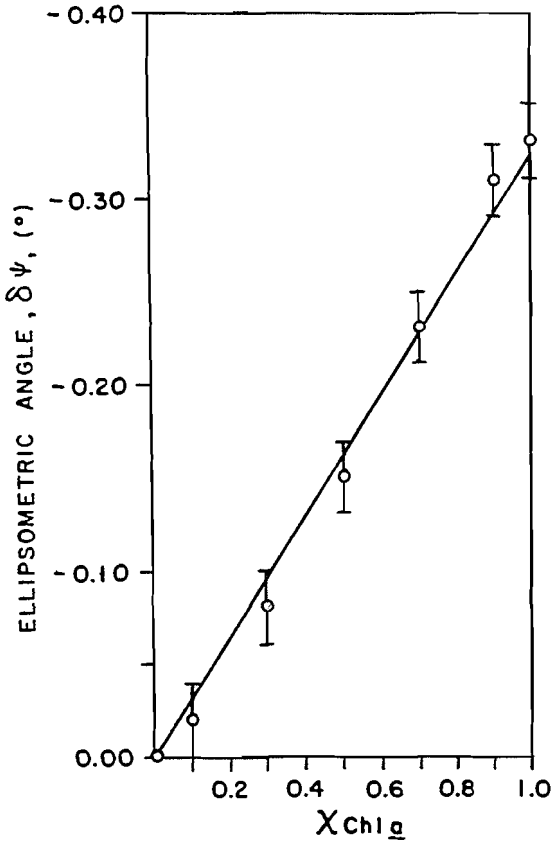


FIG. 4. Ellipsometric angle δψ as a function of mole fraction (χ) of Chl *a* for the Chl *a* – DGDG system for surface pressures between 5 and 25 mN/m. The ellipsometric parameters are identical to those of Fig. 1.

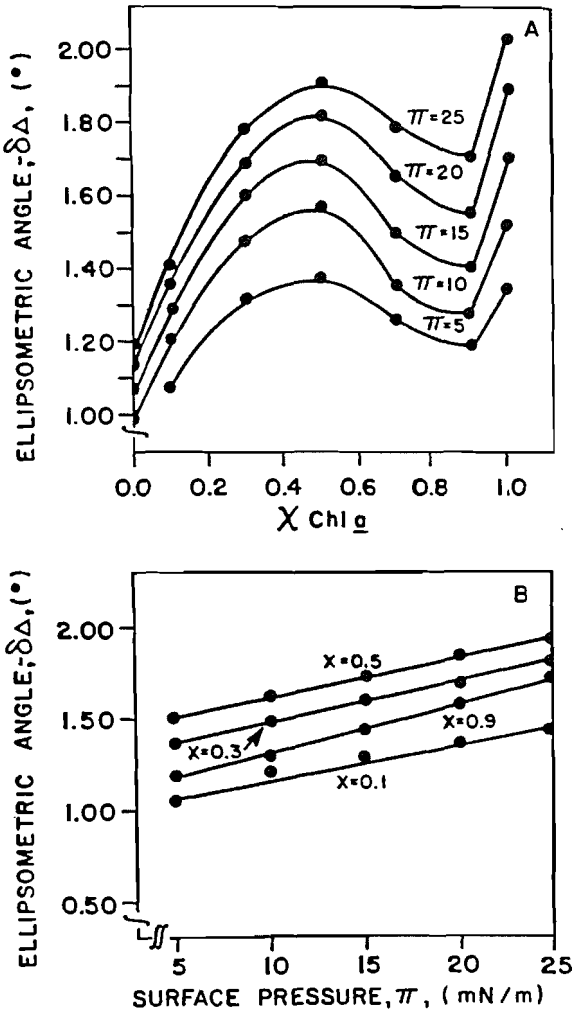


FIG. 5. (*A*) Ellipsometric angle δΔ as a function of mole fraction (χ) of Chl *a* for the Chl *a* – DGDG system at different surface pressures (5, 10, 15, 20, and 25 mN/m). (*B*) Ellipsometric angle δΔ as a function of surface pressure for the Chl *a* – DGDG system at different mole fractions of Chl *a*.

for pure compounds and each mole fraction of Chl *a*. The five curves in Fig. 5A exhibit a salient feature: each of them shows a minimum at $X_{\text{Chl }a}$ of 0.5. Furthermore, if the variation of δΔ is plotted as a function of the increasing surface pressure, a linear relationship, at constant mole fraction, is obtained for each of the mole fractions. These results are presented in Fig. 5*B*.

The Δ*V*–*A* isotherms, presented in Fig. 1, for the Chl *a* – DGDG mixtures have essentially the same features as the pure Chl *a*. We may point out the following significant features: (*i*) the Δ*V* isotherms are shifted towards higher values as the mole fraction of Chl *a* increases; (*ii*) each mixture shows a sudden decrease in surface potential at a molecular area which varies with the composition of the mixture; (*iii*) the change of slope in the Δ*V*–*A* isotherms corresponds approximately to the onset of the transition point, as shown in the π–*A* isotherms.

From surface potential values for the mixtures, the surface dipole moment has been calculated at several surface pressures (10, 15, 20, and 25 mN/m). The results for surface potential and surface dipole moment are plotted in Fig. 6 as a function of mole fraction of Chl *a*, from which it can be seen that the additivity rule is closely followed. The difference between these results and those shown in ref. 18 is due to a transcription error in the latter reference.

4. Discussion

This work was undertaken to determine the nature of interactions in mixed monolayers of Chl *a* – DGDG. The surface pressure – area isotherms for the mixed monolayers have shown a pronounced negative deviation from ideality for mixed films.

Figure 5*A* illustrates that over the surface pressure of interest, from 5 to 25 mN/m, and independent of surface pressure, the δΔ values show a minimum at a $X_{\text{Chl }a}$ value of 0.5. The ellipsometric values were observed to become more positive as the mole fraction of Chl *a* increases from 0.5 to 0.9, after which point, as seen in Fig. 5*A*, δΔ decreases again. At first glance, this is rather surprising since the ellipsometric δΔ is known to be more sensitive to refractive index than to film thickness (19). Since the length of the hydrophobic moieties of both components Chl *a* and DGDG are comparable, it can be assumed that the film thickness is constant at a given surface pressure, and independent of the species in excess. The refractive index of Chl *a* has been reported to be approximately 1.58 (15), a value that is likely to be higher than that of the galactolipid. The shape and values of the ellipsometric isotherm of the galactolipid resemble those of unsaturated phospholipids, for which the refractive index has been evaluated at approximately 1.46 (14, 20, 21). As a consequence, one would expect that, as the mole fraction of Chl *a* increases, the δΔ values would continuously decrease. The work in this report has shown that this ellipsometric

Can. J. Chem. Downloaded from www.nrcresearchpress.com by 84.41.108.74 on 09/07/12
For personal use only.

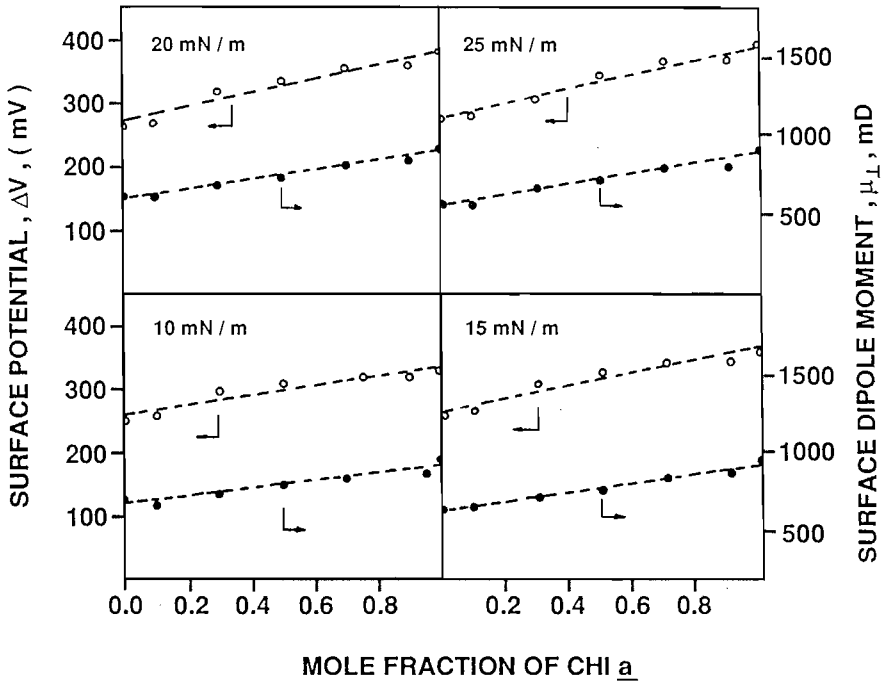


FIG. 6. Surface potential (● ←) and calculated surface dipole moment (● →) of Chl *a* – DGDG as a function of mole fraction of Chl *a* at different surface pressures (10, 15, 20, and 25 mN/m).

behavior is not a characteristic of the Chl *a* – DGDG mixed monolayers (see Fig. 5*A*). The reader is referred to ref. 15 for the pertinent ellipsometric equations.

Some investigators (22, 23) have argued that the Chl *a* molecule anchors to the aqueous substrate by the carbonyl group and neighbouring carboxymethyl group in ring V of the porphyrin ring. Based on this assumption, and from the onset of the ellipsometric jump angle, the experimental results imply that Chl *a* is oriented, becoming more vertically oriented upon monolayer compression. Since polarizability parallel to the porphyrin ring is higher than polarizability perpendicular to the ring (15), then as *d* increases, n_z increases at the expense of n_x. As compression proceeds, $\delta\Delta$ becomes more and more negative. Concurrently, as the porphyrin ring becomes more vertically oriented, k_z, associated with the optical *Z*-axis perpendicular to the water surface, is expected to increase at the expense of k_x. However, our results suggest that the *k* values are mainly a function of the concentration of Chl *a* (see Fig. 1, $\delta\psi$–*A* isotherms), and not as sensitive to orientation as reported elsewhere (15).

The lower or more negative $\delta\Delta$ values obtained for the Chl *a* isotherm, as compared to those for DGDG, can be attributed mainly to the higher refractive indices of the pigment. However, for a given film thickness (*d*), the permutation of the refractive indices makes $\delta\Delta$ more negative, for n_x larger than n_z. Similarly, for n_z greater than n_x and with the same film thickness, the $\delta\Delta$ values become more positive. The birefringence corresponds to this difference between refractive indices of the film. In addition to this effect, the extent of absorption, as indicated by the magnitude of the *k* values with $k_z > k_x$, contributes to making $\delta\Delta$ more positive.

The ellipsometric behavior of the mixed film may be explained applying the following assumptions: (*i*) the mixed film is governed by the same ellipsometric equations as the pure anisotropic homogeneous monolayer; (*ii*) refractive indices are additive; (*iii*) in the liquid expanded state, the polyunsaturated galactolipid aliphatic chains result in kinks which contribute to negative anisotropy (n_x larger than n_z) (24); (*iv*) at constant surface pressure, film thickness remains constant, independent of the species in excess; (*v*) the *k* values increase as the mole fraction of Chl *a* increases. Moreover, because of the high degree of hydration of the polar head groups, it is assumed that only the hydrophobic moiety is detected by ellipsometry. In consideration of these assumptions, the results presented in Fig. 5*A* may be explained on the basis of the difference in sign of the birefringence and the increase in absorption as Chl *a* increases in the mixed film. For $X_{\text{Chl } a}$ values of 0.1 to 0.5, where the galactolipid is in excess, the overall ellipsometric effect in the film is as if n_x were greater than n_z. This results in more negative $\delta\Delta$ values.

As the mole fraction of Chl *a* becomes larger than 0.5, the pigment is in excess. Since the rigid porphyrin ring in the Chl *a* molecule is more or less vertically oriented, as evidenced by the occurrence of the ellipsometric jump angle, and since the main contribution to refractive indices of the pigment is mainly from the extended π-electron system of the ring, it is expected that a change of sign ($n_z > n_x$) in birefringence combined with higher *k* values ($k_z > k_x$) would lead to more positive $\delta\Delta$ values. This change in birefringence, coupled with increased absorption (see Fig. 4), can explain, in the 5 to 25 mN/m range, why $\delta\Delta$ values of the 0.9 Chl *a* mole fraction are more positive than those for the 0.3 mole fraction (Fig. 5*A*), despite the fact that the refractive index of Chl *a* is greater than that of the galactolipid.

As seen in Fig. 5*B*, for each of the given mole fraction mixtures, $\delta\Delta$ decreases linearly as π increases up to 25 mN/m. At these surface pressures, the films are in the liquid expanded state. Since at a given mole fraction absorption does not vary (see Fig. 1 $\delta\psi$–*A* isotherms) and refractive indices remain nearly constant (24), $\delta\Delta$ decreases linearly as film thickness (*d*) increases as predicted by the ellipsometric equation.

For the pure galactolipid, an ellipsometric plateau ($\delta\Delta$–*A*) is observed in the final stage of compression. It is shown in Fig. 1 that for the mixed monolayers with the lower content in

Can. J. Chem. Downloaded from www.nrcresearchpress.com by 84.41.108.74 on 09/07/12
For personal use only.

Chl *a*, the 0.1 and 0.3 Chl *a* – DGDG mixtures, this plateau in the ellipsometric isotherm is also observed. These plateaus occur in the same molecular area range as for the pure carbohydrate-containing lipid monolayer. This is not the case for mixed monolayers with a higher concentration of Chl *a*. When Chl *a* is in excess with respect to the lipid, the ellipsometric plateau is no longer observed, even if the film is compressed to lower molecular areas. These observations suggest that the optical properties of the mixed film are controlled by the species in excess in the film.

As observed in Fig. 4, $\delta\psi$ decreases linearly as a function of the increasing mole fraction of Chl *a*. This relationship, analogous to Beer's law for dilute solutions, does not provide evidence of interactions between monolayer components in Chl *a* – DGDG monolayers.

Under the experimental subphase conditions used in this work, *i.e.*, constant pH and ionic concentration, the negative deviations with respect to the ideality law in the π–*A* isotherm, cannot be attributed to the interactions of the polar head group components. This is shown from surface potential isotherms of the Chl *a* – DGDG monolayer mixtures. In any case, if interactions of this type occur, they are not evidenced in the surface potential isotherms. As shown in Fig. 6, the additivity rule is closely followed, strongly suggesting that for mixed monolayers the negative deviation in the π–*A* isotherms cannot be attributed to any specific interactions between the monolayer components. The surface dipole moment, which is proportional to the average surface potential per molecule, has been calculated and plotted as a function of the mole fraction of Chl *a* (Fig. 6). The conclusion concerning interactions of the polar head groups is the same as for surface potentials.

In the 0.1 to 0.5 mole fraction range of Chl *a*, DGDG is in excess with respect to the pigment. In the liquid-expanded state, the kinked aliphatic chains of DGDG may produce cavities which can be partially occupied by the hydrophobic moiety of the Chl *a*, leading to a reduction in the average area per molecule. The porphyrin ring is bulky and has about the same dimensions as the galactolipid chains (based on a CPK atomic model). Since the deviation from the additivity law seen in the π–*A* isotherms is negative, the porphyrin ring would occupy the cavity produced by the aliphatic DGDG chains in a plane perpendicular to this cavity. As the mole fraction of Chl *a* exceeds 0.5, the negative deviation observed may be explained by intermolecular cavities in the following manner. In L-B films of Chl *a*, for films deposited at 20 mN/m, the distance between the two adjacent porphyrin planes has been determined by infrared spectroscopy to be 7.1 Å (23). This distance would be sufficient to allow the aliphatic chains of DGDG to find room between adjacent porphyrin rings, thus reducing the molecular area of the mixed film.

A significant and interesting characteristic in the $\delta\psi$ and ΔV isotherms is the upturn in $\delta\psi$ and the downturn in ΔV at lower molecular areas (see Fig. 1). These features both vary with composition, and occur at approximately the same molecular area as that of the onset of the transition point pressure. The rapid decrease in $\delta\psi$ in this range is not attributed to an increase in optical absorption, but rather to increasing film thickness (25), and is in agreement with the model for partial or total rejection of the more easily collapsible component, Chl *a*, out of the monolayer (26, 27). A change in slope in the $\delta\Delta$–*A* isotherms is also observed in this molecular area range. However, the onset of the change in slope, in the surface potential and ellipsometric $\delta\psi$ isotherms, is close, but does not exactly coincide in molecular area values with the corresponding change in slope observed for the ellipsometric $\delta\Delta$ isotherms. It is tempting to correlate these observed changes to the phenomenon occurring at the onset of transition point pressures. These pressures are associated with the rejection of Chl *a* from the film.

Acknowledgments

This work was supported by the Natural Sciences and Engineering Research Council of Canada and Fonds pour la Formation de Chercheurs et l'Aide à la Recherche (FCAR). One author (D.D.) gratefully acknowledges le Cegep de Shawinigan et le Fonds FCAR for their support. We also gratefully acknowledge Ms. Cynthia Palmer and Dr. C. Salesse for a careful and critical reading of the manuscript.

1. M. NISHIHARA, K. YOKOTA, and M. KITO. Biochim. Biophys. Acta, **617**, 12 (1980).
2. P. DEA and S. I. CHAN. Biochim. Biophys. Acta, **854**, 1 (1986).
3. K. E. EIGENBERG, W. R. CROASMUN, and S. I. CHAN. Biochim. Biophys. Acta, **642**, 438 (1981).
4. G. S. BEDDARD, S. E. CARLIN, and G. PORTER. Chem. Phys. Lett. **43**, 27 (1976).
5. M. VAN GRUP, G. VAN GINKEL, and Y. K. LEVINE. Biochim. Biophys. Acta, **938**, 71 (1988).
6. P. TANCRÈDE, G. MUNGER, and R. M. LEBLANC. Biochim. Biophys. Acta, **689**, 45 (1982).
7. G. L. GAINES, JR. Insoluble monolayers at liquid–gas interfaces. John Wiley and Sons, 1966. Chap. 6.
8. R. A. DEMEL, L. L. M. VAN DEENEN, and B. A. PETHICA. Biochim. Biophys. Acta, **135**, 11 (1967).
9. D. O. SHAH. Progr. Surface Sci. **3**, 221 (1972).
10. T. OMATA and N. MURATA. Plant Cell Physiol. **24**, 1093 (1983).
11. D. G. BISHOP, J. R. HENRICK, J. H. BAYSTON, A. S. MACPHERSON, and S. R. JOHNS. Biochim. Biophys. Acta, **602**, 248 (1980).
12. D. DUCHARME, A. TESSIER, and R. M. LEBLANC. Rev. Sci. Instrum. **58**, 571 (1987).
13. R. E. HIRSCH and S. S. BRODY. Photochem. Photobiol. **29**, 589 (1979).
14. D. DUCHARME, C. SALESSE, and R. M. LEBLANC. Thin Solid Films, **132**, 83 (1985).
15. D. DEN ENGELSEN and B. DE KONING. J. Chem. Soc. Faraday Trans. 1, **70**, 2100 (1974).
16. TH. RASING, H. HSIUNG, Y. R. SHEN, and M. W. KIM. Phys. Rev. A, **37**, 2732 (1988).
17. M. LÖSCHE and H. MÖHWALD. Colloids Surf. **10**, 217 (1984).
18. D. DUCHARME, O. SHIBATA, G. MUNGER, and R. M. LEBLANC. Thin Solid Films, **180**, 135 (1989).
19. A. F. ANTIPPA, R. M. LEBLANC, and D. DUCHARME. J. Opt. Soc. Am. A, **3**, 1794 (1986).
20. C. LUSSAN, A. HOU, and P. BOTHOREL. C.R. Acad. Sci. Ser. D. 639 (1969).
21. R. J. CHERRY and D. CHAPMAN. J. Mol. Biol. **30**, 551 (1967).
22. W. D. BELLAMY, G. L. GAINES JR., and A. G. TWEET. J. Chem. Phys. **39**, 2528 (1963).
23. C. CHAPADOS and R. M. LEBLANC. Biophys. Chem. **17**, 211 (1983).
24. D. DUCHARME, J. J. MAX, C. SALESSE, and R. M. LEBLANC. J. Phys. Chem. **94**, 1925 (1990).
25. A. N. SAXENA, J. Opt. Soc. Am. **55**, 1061 (1965).
26. P. TANCRÈDE, L. PARENT, P. PAQUIN, and R. M. LEBLANC. J. Colloid Interface Sci. **83**, 606 (1981).
27. A. I. FEHER, F. D. COLLINS, and T. W. HEALY. Aust. J. Chem. **30**, 511 (1977).

Can. J. Chem. Downloaded from www.nrcresearchpress.com by 84.41.108.74 on 09/07/12
For personal use only.

The synthesis of some novel *N*-chloro-Δ^1-4-azasteroids by efficient *N*-chlorination of azasteroid lactams with trichloroisocyanuric acid

THOMAS G. BACK,[1] JOSEPH H.-L. CHAU, BRIAN P. DYCK, AND PATRICIA L. GLADSTONE
Department of Chemistry, University of Calgary, Calgary, Alta., Canada T2N 1N4

Received March 4, 1991

THOMAS G. BACK, JOSEPH H.-L. CHAU, BRIAN P. DYCK, and PATRICIA L. GLADSTONE. Can. J. Chem. **69**, 1482 (1991).

The preparation of *N*-chloro-Δ^1-4-azasteroids **2***a*–**2***c* from lactams **1***a*–**1***c* was achieved conveniently and in high yield with trichloroisocyanuric acid. The treatment of 20β-hydroxy-4-aza-5α-pregn-1-en-3-one (**1***d*) with this reagent produced the less stable *N*-chloro compound **2***d*, which reacted further to afford 4-aza-5α-pregn-1-en-3,20-dione (**4**) as the principal product. The similar chlorination of 4-azacholest-5-en-3-one (**5**) occurred at C-6, giving 6-chloro-4-azacholest-5-en-3-one (**6**). Photolysis of *N*-chloro-4-aza-5α-cholest-1-en-3-one (**2***a*) in methanol produced the transient *N*-acyl imine **7**, which was trapped by the solvent to afford 5-methoxy-4-azacholest-1-en-3-one (**8**), along with 4-azacholesta-1,5-dien-3-one (**9**) and its 6-chloro derivative **10**.

Key words: *N*-chloroazasteroid, Δ^1-4-azasteroid, *N*-chloro-Δ^1-4-azasteroid, trichloroisocyanuric acid, *N*-chlorination.

THOMAS G. BACK, JOSEPH H.-L. CHAU, BRIAN P. DYCK et PATRICIA L. GLADSTONE. Can. J. Chem. **69**, 1482 (1991).

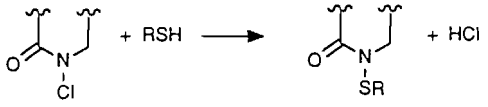
Utilisant les lactames **1***a*–**1***c* et l'acide trichloroisocyanurique, on a préparé les *N*-chloro-Δ^1-4-azastéroïdes (**2***a*–**2***c*) avec aisance et d'excellents rendements. Lorsqu'on traite la 20β-hydroxy-4-aza-5α-pregn-1-èn-3-one (**1***d*) avec ce réactif, on obtient le composé *N*-chloro **2***d* qui est plus réactif et qui, par réaction subséquente, fournit la 4-aza-5α-pregn-1-èn-3,20-dione (**4**) comme produit principal. La chloration semblable de la 4-azacholest-5-èn-3-one (**5**) se produit en C-6 et fournit la 6-chloro-4-azacholest-5-èn-3-one (**6**). La photolyse de la *N*-chloro-4-aza-5α-cholest-1-èn-3-one (**2***a*) dans le méthanol fournit la *N*-acyl imine (**7**) transitoire qui est piégée par le solvant pour conduire à la 5-méthoxy-4-azacholest-1-èn-3-one (**8**) aux côtés de la 4-azacholesta-1,5-dièn-3-one (**9**) et de son dérivé 6-chloro (**10**).

Mots clés : *N*-chloroazastéroïde; Δ^1-4-azastéroïde; *N*-chloro-Δ^1-4-azastéroïde; acide trichloroisocyanurique; *N*-chloration.

[Traduit par la rédaction]

Many types of azasteroids are known (1) and some display interesting biological activity (for example, see ref. 2). The Δ^1-4-azasteroids **1** are of special current interest because certain such derivatives function as potent inhibitors of the enzyme 5α-reductase, as recently demonstrated by Rasmusson and co-workers (3). This enzyme is responsible for the conversion of testosterone to dihydrotestosterone, which has been implicated as the principal trophic hormone of the prostate gland (4). Thus, 5α-reductase inhibitors offer a possible nonsurgical alternative for the treatment of benign prostatic hypertrophy, a common affliction of elderly men. The Δ^1-4-azasteroids and related compounds are believed to function as competitive transition state inhibitors of this enzyme. However, new compounds that could bind to its active site through covalent bond formation are also of interest as potential affinity labels and irreversible inhibitors (5).

We recently reported (6) that certain *N*-chloroazasteroids react with model thiols to produce sulfenamides through the formation of new S—N bonds (eq. [1]). These *N*-chloro

[1] 

compounds are therefore envisaged to behave as chemoselective affinity labels for thiol (sulfhydryl) groups within active sites (7). We now report the preparation of a series of novel *N*-chloro-Δ^1-4-azasteroids **2** by chlorination of the corresponding lactams **1**. These compounds may be of value in future labelling and inhibition studies of 5α-reductase.

To date, our syntheses of other *N*-chloroazasteroids employed *N*-chlorosuccinimide (NCS) as the chlorinating agent (6). Other reagents such as sodium or *tert*-butyl hypochlorite were also investigated, but proved inferior. Although NCS gives generally satisfactory results, it suffers from several disadvantages. It can be used in stoichiometric amounts at room temperature in the presence of 1 equivalent of potassium *tert*-butoxide, or in excess amounts in refluxing chloroform without the added base. The former method can result in competing chlorination of the α-position of the lactam carbonyl group, as well as its epimerization if it is a chiral center. The latter method requires prolonged reaction times and the occasionally troublesome chromatographic removal of excess unreacted NCS. We now report that trichloroisocyanuric acid (TCIA) is an exceptionally efficient and convenient reagent for this purpose that avoids these problems.

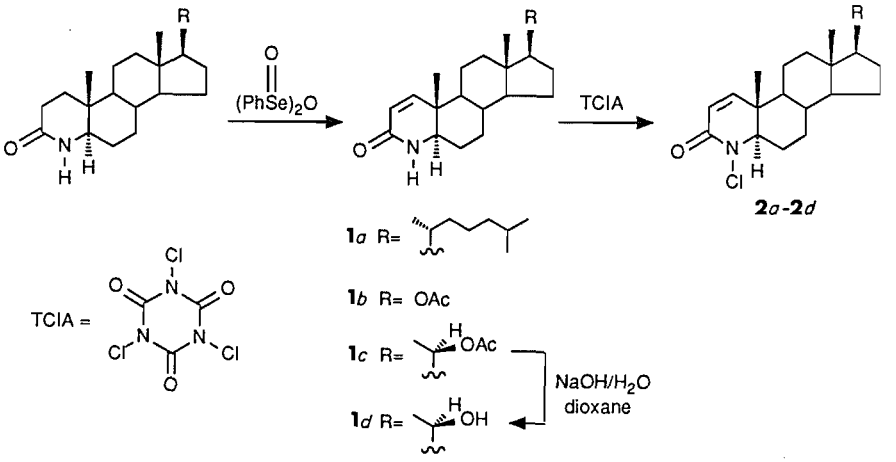
Results and discussion

The required Δ^1-4-azasteroids **1***a*–**1**c were prepared by the dehydrogenation of the corresponding saturated lactams with benzeneseleninic anhydride (Scheme 1) by a procedure reported earlier (8). An alternative method employing 2,3-dichloro-5,6-dicyano-1,4-benzoquinone (DDQ) has also been reported for this purpose (9). Compound **1***d* was obtained by saponification of the acetate moiety of **1***c*.

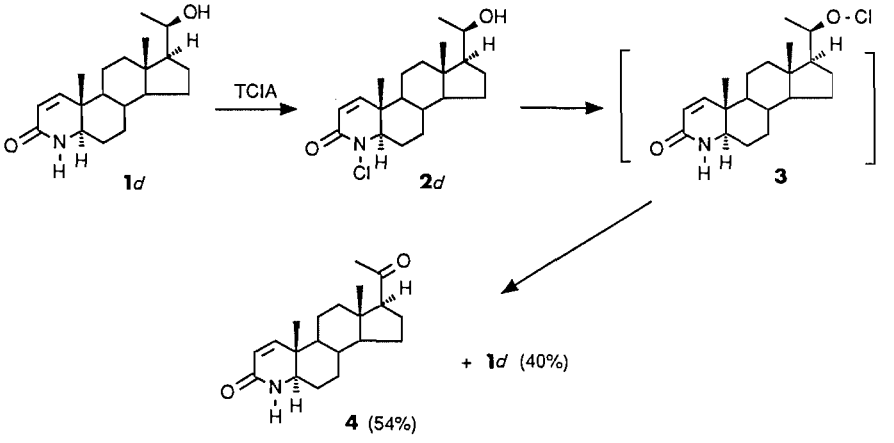
The *N*-chlorination of azasteroids **1***a*–**1***c* with TCIA in chloroform solution afforded the *N*-chloro derivatives **2***a*–**2***c* in excellent isolated yields. The reaction is illustrated in Scheme 1 and the results are summarized in Table 1. Results obtained with NCS as the chlorinating reagent are also included in Table 1 for comparison. TCIA is an inexpensive, commercially available reagent that has previously been employed in other chlorination processes (10). It decomposes rapidly in basic aqueous media to form water-soluble products. This permits the use of excess reagent to ensure completion of the reaction and requires only a simple work-up with aqueous sodium bicarbonate to obtain essentially quantitative yields of the desired *N*-chloro compounds in high states of purity. The reactions in Table 1 were performed with 0.50–0.74 molar equivalents (i.e., 1.5–2.2 equivalents of chlorine) of TCIA and the mixtures were briefly

[1]Author to whom correspondence may be addressed.

Can. J. Chem. Downloaded from www.nrcresearchpress.com by 84.41.108.74 on 09/07/12
For personal use only.



SCHEME 1



SCHEME 2

TABLE 1. Preparation of *N*-chloroazasteroids

Entry	Lactam	Reagent (molar equiv.)	Time[a]	Product	Yield (%)[b,c]
1	**1***a*	NCS (5.2)	12 h	**2***a*	85
2	**1***a*	TCIA (0.50)	2 h	**2***a*	99
3	**1***b*	NCS (5.5)	18 h	**2***b*	80
4	**1***b*	TCIA (0.74)	30 min	**2***b*	100
5	**1***c*	NCS (6.1)	16 h	**2***c*	78
6	**1***c*	TCIA (0.50)	45 min	**2***c*	97

[a]All reactions were performed in refluxing chloroform.

[b]Isolated yields are reported on products that were homogeneous on TLC with ^{1}H NMR and IR spectra identical to those of analytical samples.

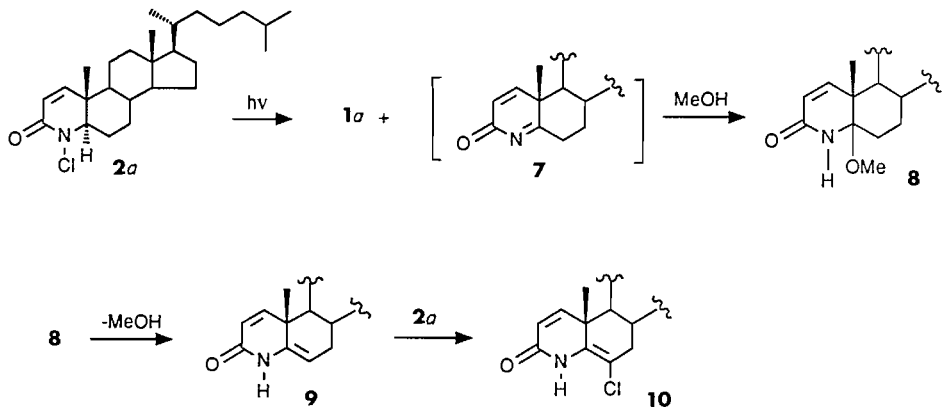
[c]Products in entries 1, 3, 5, and 6 were isolated by preparative TLC; those in entries 2 and 4 did not require chromatographic purification.

refluxed to ensure the complete consumption of the starting materials. However, these reactions proceed rapidly even at room temperature, as evidenced by TLC analysis. Their rapid progress in the absence of pyrolytic initiation suggests that electrophilic, rather than free-radical mechanisms, are involved. Furthermore, adventitious photoinitiation was ruled out in a control experiment in which **1***a* and TCIA reacted rapidly (1 h) at room temperature in the dark. No significant side reactions were noted in any of the examples employing TCIA. The products are stable, crystalline solids that can be subjected to routine manipulation such as chromatography and stored for extended periods in the dark at or below 0°C. It is clear from these experiments that TCIA is superior to NCS for this purpose, both from the point of view of efficiency and convenience.

The *N*-chloro-20β-hydroxy derivative **2***d* proved to be less stable than **2***a*–**2***c*. Lactam **1***d* was chlorinated with TCIA in deuteriochloroform solution at room temperature, and the reaction was monitored by TLC and NMR. The formation of **2***d* was complete after 2 h, as evident from the appearance of a less polar product, along with the disappearance of the ^{1}H NMR signal at δ 5.68 (NH of **1***d*), and the shift to lower field of signals from δ 3.33 (C-5) and δ 0.98 (C-19) to δ 3.59 and δ 1.07, respectively. However, longer reaction times under these conditions, or attempts to isolate the product by the usual work-up, resulted in the decomposition of **2***d* to afford the 20-ketone **4** and the original lactam **1***d*, isolated in yields of 54 and 40%, respectively. This is consistent with the rearrangement of **2***d* to the isomeric hypochlorite **3**, followed by elimination of HCl, or hydrolysis to the free alcohol, as shown in Scheme 2. Related oxidations of secondary alcohols to ketones with various other *N*-halo reagents have been previously reported (11).

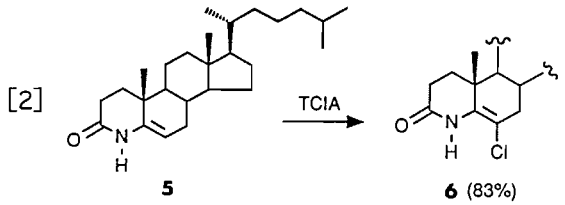
We also investigated the chlorination of azasteroid **5**, the Δ^5-isomer of **1***a*, with TCIA under similar conditions. Enamide **5** is an ambident nucleophile, where both the nitrogen atom and

Can. J. Chem. Downloaded from www.nrcresearchpress.com by 84.41.108.74 on 09/07/12
For personal use only.



SCHEME 3

C-6 are potential sites for electrophilic attack. In this case, none of the *N*-chloro compound was observed, and the 6-chloro derivative **6** (eq. [2]) was produced in 83% yield. Thus, *C*-chlorination is favoured over *N*-chlorination in this example, although we cannot rule out the possibility of initial kinetically controlled *N*-chlorination, followed by rapid isomerization to **6**.



We previously reported (6) that some *N*-chloroazasteroids undergo photochemical dehydrochlorination to generate reactive *N*-acyl imines (12). Some of these intermediates were trapped by solvent addition when the photolyses were performed in methanol. These results suggested that *N*-chloroazasteroids could function as photoaffinity labels (13), and we therefore attempted to determine whether the Δ^1-analogues would behave similarly. Thus, photolysis of **2***a* in methanol produced the enamide **9** and its 6-chloro derivative **10**, along with the parent lactam **1***a*, as shown in Scheme 3. These products are analogous to the ones previously obtained from the corresponding 1,2-saturated *N*-chloroazasteroid, and are presumably formed by a similar pathway, described earlier (6). However, in contrast to the saturated analogue, careful chromatography of the reaction mixture in the present example permitted the isolation of a small amount of the relatively unstable carbinolamide methyl ether **8**, which was characterized by IR and ^{1}H NMR spectroscopy. This confirms the generation of the *N*-acyl imine intermediate **7** under these conditions.

In conclusion, we have demonstrated that TCIA is a remarkably effective *N*-chlorinating reagent that permitted the facile preparation of several novel *N*-chloro-Δ^1-4-azasteroids with potentially interesting biological properties.

Experimental

Azasteriods **1***a*–**1***c* were prepared as described previously (8). Compound **1***c* was assumed to have the 20β configuration (14) as it was obtained by the sodium borohydride reduction of the 20-keto group of 4-aza-5α-pregnan-3,20-dione, prior to acetylation and dehydrogenation with benzeneseleninic anhydride. Enamide **5** was prepared according to a literature procedure (15). NCS and TCIA were obtained from the Aldrich Co. and were used without further purification. Melting points were determined on an A. H. Thomas hot-stage apparatus and are uncorrected. The IR spectra were recorded on a Nicolet 5DX spectrometer and NMR spectra were obtained on a Bruker ACE 200 instrument at 200 MHz in deuteriochloroform solvent with either chloroform or tetramethylsilane as the internal standard. Mass spectra were recorded on a Kratos MS 80 or a VG 7070 spectrometer by Drs. R. Yamdagni and Q. Wu. Elemental analyses were performed on an SCP Science model 440 elemental analyzer by Ms. D. Fox. Preparative TLC was carried out with Analtech 20 × 20 cm glass plates coated with 1 mm of silica gel GF.

Preparation of N*-chloro-4-aza-5α-cholest-1-en-3-one (***2***a) with NCS; typical procedure*

4-Azacholest-1-en-3-one (**1***a*) (98 mg, 0.255 mmol) and NCS (176 mg, 1.32 mmol) were refluxed for 12 h in 15 mL of chloroform. The solvent was then removed *in vacuo* and the residue was separated by preparative TLC (30% ethyl acetate – hexanes) to afford 91 mg (85%) of **2***a*, with R_f 0.62; mp 109–110°C (from hexanes); IR (Nujol); 1694, 1278, 805 cm^{-1}; ^{1}H NMR δ: 6.83 (d, J = 9.8 Hz, 1H), 5.94 (d, J = 9.8 Hz, 1H), 3.58 (dd, J = 12.5, 3.9 Hz, 1H), 2.32 (m, 1H), 2.06 (m, 1H), 1.06 (s, 3H), 0.92 (d, J = 6.4 Hz, 3H), 0.874 (d, J = 6.6 Hz, 3H), 0.871 (d, J = 6.6 Hz, 3H), and 0.69 (s, 3H); mass spectrum, *m/z* (relative intensity, %): 419 (M^+, 2), 385 (M^+ of **1***a*, presumably formed by thermal decomposition of **2***a* in the sample inlet, 75), 384 (36), 370 (23), 110 (100). Anal. calcd. for $C_{26}H_{42}ClNO$: C 74.34, H 10.08, N 3.33; found: C 74.43, H 10.29, N 3.47.

Preparation of N*-chloro-4-aza-5α-cholest-1-en-3-one (***2***a) with TCIA; typical procedure*

4-Azacholest-1-en-3-one (**1***a*) (109 mg, 0.283 mmol) and TCIA (33 mg, 0.14 mmol) were refluxed for 2 h in 5 mL of chloroform. The reaction mixture was extracted three times with aqueous $NaHCO_3$ solution, the combined aqueous layers were extracted once with chloroform, and the combined chloroform layers were dried ($MgSO_4$) and evaporated to constant weight *in vacuo* to afford 118 mg (99%) of **2***a*, which solidified upon standing, mp 103–108°C. It was homogeneous on TLC and gave IR and ^{1}H NMR spectra identical to those of the analytical sample produced in the preceding procedure.

The following compounds were prepared similarly (See Table 1 for yields and conditions).

*N-Chloro-17β-acetoxy-4-aza-5α-androst-1-en-3-one (***2***b)*: mp 136–137°C (from dichloromethane–hexanes); IR (film): 1733, 1690, 1248, 1038 cm^{-1}; ^{1}H NMR δ: 6.82 (d, J = 9.8 Hz, 1H), 5.94 (d, J = 9.8 Hz, 1H), 4.62 (dd, J = 9.0, 7.5 Hz, 1H), 3.59 (dd, J = 12.5, 3.9 Hz, 1H), 2.05 (s, 3H), 1.07 (s, 3H), 0.82 (s, 3H); mass spectrum, *m/z* (relative intensity, %): 365 (M^+, 5), 330 (96), 313 (26), 288 (22), 110 (75), 43 (100). Anal. calcd. for $C_{20}H_{28}ClNO_3$: C 65.64, H 7.71, N 3.82; found: C 65.67, H 7.98, N 3.72.

*N-Chloro-20β-acetoxy-4-aza-5α-pregn-1-en-3-one (***2***c)*: mp 112–113°C (from dichloromethane–hexanes); IR (Nujol): 1723, 1683, 1244, 1122, 810 cm^{-1}; ^{1}H NMR δ: 6.82 (d, J = 9.8 Hz, 1H), 5.94 (d, J = 9.8 Hz, 1H), 4.85 (dq, J = 10.2, 6.1 Hz, 1H), 3.59 (dd, J = 12.6,

Can. J. Chem. Downloaded from www.nrcresearchpress.com by 84.41.108.74 on 09/07/12
For personal use only.

Can. J. Chem. Downloaded from www.nrcresearchpress.com by 84.41.108.74 on 09/07/12
For personal use only.

3.9 Hz, 1H), 2.31 (m, 1H), 2.03 (s, 3H), 1.16 (d, J = 6.1 Hz, 3H), 1.06 (s, 3H), 0.67 (s, 3H); mass spectrum, m/z (relative intensity, %): 393 (M^+, 2), 391 (8), 359 (32, M^+ of **1***c*, presumably formed by thermal decomposition of **2***c* in the sample inlet), 284 (32), 110 (69), 43 (100). Anal. calcd. for $C_{22}H_{32}ClNO_3$: C 67.07, H 8.19, N 3.56; found: C 67.01, H 8.31, N 3.58.

*20β-Hydroxy-4-aza-5α-pregn-1-en-3-one (1*d)

20β-Acetoxy-4-aza-5α-pregn-1-en-3-one (**1***c*) (183 mg, 0.510 mmol) was stirred for 20 h in 8 mL of 1,4-dioxane and 5 mL of 1 M aqueous NaOH solution at 60°C. The solvent was evaporated *in vacuo*, the residue was taken up in water, acidified with 10% HCl solution, and extracted three times with chloroform. The chloroform layers were washed three times with aqueous $NaHCO_3$ solution, once with aqueous NaCl, dried ($MgSO_4$), and evaporated *in vacuo*. The residue crystallized from methanol–water to afford 122.5 mg (76%) of the title compound, mp 287–290°C; IR (Nujol): 3451, 3204, 1669, 1597, 1292, 1117, 816 cm^{-1}; ^1H NMR δ: 6.82 (d, J = 9.9 Hz, 1H), 5.81 (d, J = 9.9 Hz, 1H), 5.68 (br s, 1H), 3.74 (m, 1H), 3.33 (m, 1H), 2.15 (m, 1H), 1.15 (d, J = 6.1 Hz, 3H), 0.98 (s, 3H), 0.78 (s, 3H); mass spectrum, m/z (relative intensity, %): 317 (M^+, 73), 316 (11), 299 (16), 283 (18), 232 (19), 110 (100). Exact Mass calcd. for $C_{20}H_{31}NO_2$: 317.2355; found: 317.2344.

*Chlorination of 20β-hydroxy-4-aza-5α-pregn-1-en-3-one (1*d*) with TCIA*

The lactam (**1***d*) (18.6 mg, 0.059 mmol) and TCIA (4.6 mg, 0.020 mmol) were stirred in 2 mL of deuteriochloroform at room temperature for 90 min. TLC analysis (10% methanol–benzene) revealed the presence of a new component at R_f 0.37, as well as a trace of unreacted **1***d*. Additional TCIA (2.2 mg, 0.010 mmol) was added and stirring continued for 30 min to effect the complete disappearance of the starting material. An NMR spectrum then indicated the nearly quantitative formation of the *N*-chloro derivative **2***d* with signals at δ 6.84 (d, J = 9.8 Hz, 1H), 5.94 (d, J = 9.8 Hz, 1H), 3.74 (dq, J = 10.2, 6.2 Hz, 1H), 3.59 (dd, J = 12.6, 3.9 Hz, 1H), 2.30 (m, 1H), 2.16 (m, 1H), 1.15 (d, J = 6.1 Hz, 3H), 1.07 (s, 3H), 0.78 (s, 3H). New signals attributed to the ketone **4** (*vide infra*) were apparent after an additional 5 h.

The reaction was repeated with lactam **1***d* (43 mg, 0.13 mmol) and TCIA (16 mg, 0.068 mmol) in 3 mL of chloroform. After 75 min, the reaction mixture was washed three times with aqueous $NaHCO_3$ solution and the $NaHCO_3$ washings were extracted twice with chloroform. The combined chloroform layers were dried ($MgSO_4$) and evaporated *in vacuo*. The residue was separated by preparative TLC in 10% methanol–benzene to afford 17 mg (40%) of lactam **1***d*, R_f 0.21, identical to an authentic sample (TLC, IR, NMR), and 23 mg (54%) of 4-aza-5α-pregn-1-ene-3,20-dione (**4**), R_f 0.33; mp: sublimes from 300°C (recrystallized from dichloromethane–hexanes); IR (film): 3194, 1697, 1680, 1605, 829 cm^{-1}; ^1H NMR δ: 6.81 (d, J = 9.9 Hz, 1H), 5.82 (dd, J = 9.9, 1.5 Hz, 1H), 5.34 (br s, 1H), 3.34 (m, 1H), 2.55 (crude t, 1H), 2.14 (s, 3H), 0.98 (s, 3H), 0.65 (s, 3H), 0.65 (s, 3H); mass spectrum, m/z (relative intensity, %): 315 (M^+, 33), 300 (7), 272 (8), 244 (11), 110 (95), 43 (100). Exact Mass calcd. for $C_{20}H_{31}NO_2$: 315.2198; found: 315.2235. Further verification of the structure of **4** was obtained by its reduction with sodium borohydride in ethanol to produce **1***d* in 73% yield, identical to an authentic sample (TLC, IR, ^1H NMR).

When lactam **1***d* (53 mg, 0.17 mmol) was refluxed with NCS (63 mg, 0.47 mmol) in 10 mL of chloroform for 18 h, TLC and NMR analyses revealed the presence of starting material, ketone **4**, and several unidentified components.

Chlorination of 4-azacholest-5-en-3-one (5) with TCIA

The enamide **5** (121 mg, 0.314 mmol) and TCIA (24 mg, 0.103 mmol) were stirred for 1 h at room temperature in 5 mL of chloroform. The solution was then concentrated *in vacuo* and separated by preparative TLC (ethyl acetate) to afford 110 mg (83%) of 6-chloro-4-azacholest-5-en-3-one (**6**), R_f 0.75, identified by comparison of its IR and ^1H NMR spectra with those of an authentic sample (6).

Photolysis of N*-chloro-4-aza-5α-cholest-1-en-3-one (2*a*)*

A solution of compound **2***a* (132 mg, 0.314 mmol) in 15 mL of methanol was irradiated for 20 min in a Pyrex vessel with a Rayonet UV apparatus equipped with four 300-nm lamps. The reaction mixture was concentrated *in vacuo* and separated by preparative TLC (70% ethyl acetate – hexanes) to afford 17 mg (13%) of 6-chloro-4-azacholesta-1,5-dien-3-one (**10**) as an amorphous solid, R_f 0.79; IR (film): 3393, 1690, 1618, 1300, 1119, 1109 cm^{-1}; ^1H NMR δ: 7.27 (br s, 1H), 6.73 (d, J = 10.0 Hz, 1H), 5.87 (dd, J = 10.0, 1.9 Hz, 1H), 2.37 (dd, J = 17.1, 6.2 Hz, 1H), 1.26 (s, 3H), 0.92 (d, J = 6.4 Hz, 3H), 0.87 (d, J = 6.5 Hz, 6H), 0.71 (s, 3H); mass spectrum, m/z (relative intenstiy, %): 417 (M^+, 41), 402 (13), 41 (100). Exact Mass calcd. for $C_{26}H_{40}ClNO$: 417.2798; found: 417.2858. A more polar band afforded 29 mg (24%) of 4-azacholesta-1,5-dien-3-one (**9**), R_f 0.55; mp 214–216°C (from chloroform – ethyl acetate); IR (Nujol): 3190, 1693, 1618, 1223, 1178 cm^{-1}; ^1H NMR δ: 7.61 (br s, 1H), 6.73 (d, J = 10.0 Hz, 1H), 5.82 (dd, J = 10.0, 1.8 Hz, 1H), 5.00 (m, 1H), 2.08 (m, 2H), 1.23 (s, 3H), 0.92 (d, J = 6.4 Hz, 3H), 0.87 (d, J = 6.5 Hz, 6H), 0.71 (s, 3H): mass spectrum, m/z (relative intensity, %): 383 (M^+, 90), 369 (19), 135 (53), 40 (100). Anal. calcd. for $C_{26}H_{41}NO$: C 81.40, H 10.77, N 3.65; found: C 81.31, H 10.46, N 3.50. A polar component near the baseline afforded 46 mg (38%) of lactam **1***a*, identical to an authentic sample (TLC, ^1H NMR). Several overlapping bands between R_f 0.6 and 0.7 contained the carbinolamide methyl ether **8** (NMR), *vide infra*, which decomposed upon further attempts at purification.

In a separate experiment, **2***a* (65 mg, 0.16 mmol) was similarly irradiated and separated as quickly as possible by preparative TLC in a less polar solvent (30% ethyl acetate – hexanes). The band with R_f 0.44 afforded 8 mg (12%) of **8**; IR (film): 3250, 1686, 1623, 1068, 756 cm^{-1}; ^1H NMR δ: 6.46 (d, J = 10.0 Hz, 1H), 6.25 (br s, 1H), 5.84 (dd, J = 10.0, 2.0 Hz, 1H), 3.24 (s, 3H), 1.45 (s, 3H), 0.90 (d, J = 6.0 Hz) overlapping with 0.87 (d, J = 6.5 Hz, total 9H), 0.74 (s, 3H); ^{13}C NMR δ: 166.3 (C=O, C-3), 156.3 (CH, C-1), 119.7 (CH, C-2), 88.0 (quaternary C, C-5), 47.8 (MeO).

Acknowledgement

We gratefully acknowledge the financial support of the Natural Sciences and Engineering Research Council of Canada and Merck Frosst Canada Inc. P.L.G. and B.P.D. were summer research assistants sponsored by a Studentship from the Natural Sciences and Engineering Research Council of Canada and a University of Calgary Faculty of Science Special Award, respectively. We thank Dr. Leo Milward of Agriculture Canada for providing several high resolution mass spectra.

1. (*a*) H. O. Huisman. Angew. Chem. Int. Ed. Engl. **10**, 450 (1971); (*b*) *In* Steroids. *Edited by* W. F. Johns. International Review of Science, Organic Chemistry Series 1. Vol. 8. Butterworths, London. 1973. Chap. 9; (*c*) H. O. Huisman and W. N. Speckamp. *In* Steroids. *Edited by* W. F. Johns. International Review of Science, Organic Chemistry Series 2. Vol. 8. Butterworths, London. 1976. Chap. 8.
2. (*a*) R. E. Dolle, H. S. Allaudeen, and L. I. Kruse. J. Med. Chem. **33**, 877 (1990); (*b*) M. Brandt and M. A. Levy. Biochemistry, **28**, 140 (1989); (*c*) H. Singh, T. R. Bhardwaj, N. K. Ahuja, and D. Paul. J. Chem. Soc. Perkin Trans. 1, 305 (1979); (*d*) A. Gandiha, I. G. Marshall, D. Paul, and H. Singh. J. Pharm. Pharmacol. **26**, 871 (1974); (*e*) R. W. Chesnut, N. N. Durham, R. A. Brown, E. A. Mawdsley, and K. D. Berlin. Steroids, **27**, 525 (1976); (*f*) W. E. Solomons and N. J. Doorenbos. J. Pharm. Sci. **63**, 19 (1974); (*g*) N. J. Doorenbos and W. E. Solomons. J. Pharm. Sci. **62**, 638 (1973).
3. (*a*) G. H. Rasmusson, G. F. Reynolds, N. G. Steinberg, E. Walton, G. F. Patel, T. Liang, M. A. Cascieri, A. H. Cheung, J. R. Brooks, and C. Berman. J. Med. Chem. **29**, 2298 (1986); (*b*) G. H. Rasmusson, G. F. Reynolds, T. Utne, R. B. Jobson, R. L. Primka, C. Berman, and J. R. Brooks. J.

Med. Chem. **27**, 1690 (1984); (*c*) J. R. CARLIN, G. H. RASMUSSON, and W. J. A. VANDENHEUVEL. European Patent Appl. EP 271,220, June 15, 1988; U. S. Patent Appl. 932,550, Nov. 20, 1986; Chem. Abstr. **109**, 129456b (1988).

4. (*a*) M. G. LOUGHLIN and N. BRUCHOVSKY. *In* Benign prostatic hypertrophy. *Edited by* F. Hinman, Jr. Springer-Verlag, New York. 1983. Chap. 12. (*b*) J. P. KARR and G. P. MURPHY. *In* Benign prostatic hypertrophy. *Edited by* F. Hinman, Jr. Springer-Verlag, New York. 1983. Chap. 18.
5. For existing examples of irreversible inhibitors of 5α-reductase, see: (*a*) B. ROBAIRE, D. F. COVEY, C. H. ROBINSON, and L. L. EWING. J. Steroid Biochem. **8**, 307 (1977); (*b*) V. PETROW, Y. WANG, L. LACK, and A. SANDBERG. Steroids, **38**, 121 (1981); (*c*) T. R. BLOHM, B. W. METCALF, M. E. LAUGHLIN, A. SJOERDSMA, and G. L. SCHATZMAN. Biochem. Biophys. Res. Commun. **95**, 273 (1980). For examples of other types of steroidal 5α-reductase inhibitors, see: (*d*) D. A. HOLT, M. A. LEVY, D. L. LADD, H.-J. OH, J. M. ERB, J. I. HEASLIP, M. BRANDT, and B. W. METCALF. J. Med. Chem. **33**, 937 (1990); (*e*) D. A. HOLT, M. A. LEVY, H.-J. OH, J. M. ERB, J. I. HEASLIP, M. BRANDT, H.-Y. LAN-HARGEST, and B. W. METCALF. J. Med. Chem. **33**, 943 (1990); (*f*) D. A. HOLT, H.-J. OH, M. A. LEVY, and B. W. METCALF. Steroids, **56**, 4 (1991); (*g*) P. M. WEINTRAUB, T. R. BLOHM, and M. LAUGHLIN. J. Med. Chem. **28**, 831 (1985).
6. T. G. BACK and K. BRUNNER. J. Org. Chem. **54**, 1904 (1989).
7. For examples of other reactive, thiophilic steroids, see (*a*) S. S. SIMONS, JR., M. PONS, and D. F. JOHNSON. J. Org. Chem. **45**, 3084 (1980); (*b*) C.-C. CHIN and J. C. WARREN. J. Biol. Chem. **243**, 5056 (1968).
8. T. G. BACK. J. Org. Chem. **46**, 1442 (1981).
9. A. BHATTACHARYA, L. M. DIMICHELE, U.-H. DOLLING, A. W. DOUGLAS, and E. J. J. GRABOWSKI. J. Am. Chem. Soc. **110**, 3318 (1988).
10. M. FIESER and L. F. FIESER. *In* Reagents for organic synthesis. Vol. 2. J. Wiley, New York. 1969. pp. 426–427; Vol. 3. 1972. p. 297; Vol. 5. 1975. p. 687; Vol. 6. 1977. pp. 605–606; M. FIESER and J. G. SMITH. *In* Reagents for organic synthesis. Vol. 13. J. Wiley, New York. 1988. p. 322.
11. R. FILLER. Chem. Rev. **63**, 21 (1963).
12. For related photochemical dehydrochlorination of *N*-chloroamides, see: (*a*) R. S. NEALE, N. L. MARCUS, and R. G. SCHEPERS. J. Am. Chem. Soc. **88**, 3051 (1966); (*b*) X. T. PHAN and P. J. SHANNON. J. Org. Chem. **48**, 5164 (1983). For silver-mediated dehydrochlorinations of *N*-chloramines, see: (*c*) O. E. EDWARDS, D. VOCELLE, and J. W. APSIMON. Can. J. Chem. **50**, 1167 (1972); (*d*) O. E. EDWARDS, D. H. PASKOVICH, and A. H. REDDOCH. Can. J. Chem. **51**, 978 (1973). For other examples of *N*-acyl imines formed by dehydrohalogenation, see: (*e*) J. E. BALDWIN, F. L. URBAN, R. D. G. COOPER, and F. L. JOSE. J. Am. Chem. Soc. **95**, 2401 (1973); (*f*) R. A. FIRESTONE and B. G. CHRISTENSEN. J. Org. Chem. **38**, 1436 (1973); (*g*) U. SCHMIDT, A. LIEBERKNECHT, and J. WILD. Synthesis, 159 (1988); (*h*) H. POISEL and U. SCHMIDT. Chem. Ber. **108**, 2547 (1975); (*i*) H. POISEL. Chem. Ber. **110**, 942 (1977); (*j*) Chem. Ber. **110**, 948 (1977); (*k*) Chem. Ber. **111**, 3136 (1978); (*l*) J. KÖPPEN, D. MATTHIES, and H. SCHWEIM. Liebigs Ann. Chem. 2283 (1985); (*m*) M. SEKI, T. MORIYA, and K. MATSUMOTO. Agric. Biol. Chem. **48**, 1251 (1984); (*n*) D. D. KEITH, R. YANG, J. A. TORTORA, and M. WEIGELE. J. Org. Chem. **43**, 3713 (1978); (*o*) M. D. GRIM, V. CHAUHAN, Y. SHIMOHIGASHI, A. J. KOLAR, and C. H. STAMMER. J. Org. Chem. **46**, 2671 (1981); (*p*) Y. SHIMOHIAGASHI and C. H. STAMMER. J. Chem. Soc. Perkin Trans. 1, 803 (1983); (*q*) G. STOLL, J. FRANK, H. MUSSO, H. HENKE, and W. HERRENDORF. Liebigs Ann. Chem. 1968 (1986). For examples of other steroidal *N*-acyl imines, see: (*r*) W. A. COURT, O. E. EDWARDS, C. GRIECO, W. RANK, and T. SANO. Can. J. Chem. **53**, 463 (1975); (*s*) T. G. BACK, N. IBRAHIM, and D. J. MCPHEE. J. Org. Chem. **47**, 3283 (1982); (*t*) T. G. BACK, K. BRUNNER, P. W. CODDING, and A. W. ROSZAK. Heterocycles, **28**, 219 (1989); (*u*) K. TSUDA and R. HAYATSU. J. Am. Chem. Soc. **78**, 4107 (1956).
13. (*a*) J. A. KATZENELLENBOGEN, H. N. MYERS, and H. J. JOHNSON, JR. J. Org. Chem. **38**, 3525 (1973); (*b*) J. A. KATZENELLENBOGEN, H. J. JOHNSON, JR., and H. N. MYERS. Biochemistry, **12**, 4085 (1973).
14. L. F. FIESER and M. FIESER. *In* Steroids. Reinhold, New York. 1959. pp. 337–340 and pp. 567–568.
15. N. J. DOORENBOS, C. L. HUANG, C. R. TAMORRIA, and M. T. WU. J. Org. Chem. **26**, 2546 (1961).

Can. J. Chem. Downloaded from www.nrcresearchpress.com by 84.41.108.74 on 09/07/12
For personal use only.

Diels–Alder reactions of activated 2*H*-thiopyrans

DALE E. WARD,[1] YUANZHU GAI, AND WAJDI M. ZOGHAIB
Department of Chemistry, University of Saskatchewan, Saskatoon, Sask., Canada S7N 0W0
Received March 19, 1991

DALE E. WARD, YUANZHU GAI, and WAJDI M. ZOGHAIB. Can. J. Chem. **69**, 1487 (1991).

The Diels–Alder reactivity of various 2*H*-thiopyrans bearing electron-donating substituents has been investigated. The approximate order of reactivity among the 2*H*-thiopyrans studied was 4,6-disubstituted >> 5-substituted > 4-substituted, 3,5-disubstituted >> 3-substituted. Good yields of predominantly *endo* adducts are obtained with reactive dienophiles. With less reactive dienophiles, reactions are much slower and yields are attenuated due to the competing thermal decomposition of the dienes under the reaction conditions. The adducts obtained are equivalent (via desulfurization) to those from unreactive *cis*-substituted dienes.

Key words: Diels–Alder, 2*H*-thiopyran.

DALE E. WARD, YUANZHU GAI et WAJDI M. ZOGHAIB. Can. J. Chem. **69**, 1487 (1991).

On a examiné la réactivité dans les réactions de Diels–Alder de divers 2*H*-thiopyranes portant divers groupes électrodonneurs. L'ordre approximatif de réactivité des divers 2*H*-thiopyranes étudiés est disubstitués en 4,6 >> substitués en 5 > substitués en 4, disubstitués en 3,5 >> substitués en 3. Avec des diénophiles réactifs, on a obtenu de bons rendements des adduits principalement *endo*. Avec des diénophiles moins réactifs, les réactions sont beaucoup plus lentes et les rendements sont atténués à cause de la réaction compétitive de décomposition thermique des dienes dans ces conditions réactionnelles. Les adduits obtenus sont équivalents (via la désulfurisation) à ceux obtenus à partir des dienes non-réactifs *cis*-substitués.

Mots clés : Diels–Alder, 2*H*-thiopyrane.

[Traduit par la rédaction]

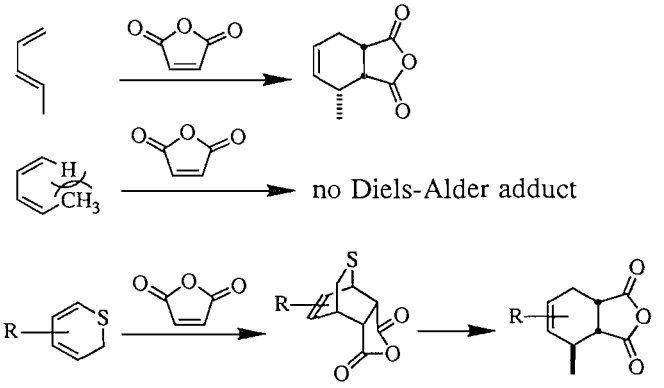
Introduction

The Diels–Alder reaction is of fundamental importance to both the theory and the practice of organic chemistry (1). The formation of two carbon–carbon bonds and up to four stereogenic centers with predictable stereoselectivity and wide applicability are among the more notable attributes of this reaction. Recent advances include intramolecular applications (2), applications in asymmetric synthesis (i.e., the preparation of chiral scalemic adducts) (3), and the use of hetero dienes and dienophiles (4). The scope of the Diels–Alder reaction has broadened significantly with the use of Lewis acids (3, 5) or high pressure (6) or both (7) to enhance reactivity and (or) selectivity.

A major limitation of the Diels–Alder reaction is the lack of reactivity associated with *cis*-substituted dienes (8). For example, the reaction of *cis*-1,3-pentadiene with maleic anhydride (9) or with tetracyanoethylene (10) does not give an adduct under conditions where the *trans* isomer reacts quantitatively. Similarly, *trans*-1,3-pentadiene is 10^3 times more reactive than 4-methyl-1,3-pentadiene towards tetracyanoethylene (10). The low reactivity of *cis*-dienes towards [4+2] cycloaddition is attributed to the steric destabilization that occurs in the necessary *s-cis* conformation.

A potential strategy to overcome the low reactivity of *cis*-dienes involves the use of 2*H*-thiopyrans. Diels–Alder reactions of 2*H*-thiopyrans with dienophiles should provide adducts that, after desulfurization, would be synthetically equivalent to an adduct derived from a *cis*-diene (see Scheme 1). If 2*H*-thiopyrans could act as functional equivalents to the unreactive *cis*-dienes the scope of the Diels–Alder reaction might be significantly expanded.

The Diels–Alder reactions of 2*H*-thiopyrans have not been extensively investigated. Flemming and Murray studied (11) the reaction of the parent compound with three dienophiles and found that predominantly *endo* adducts were produced



SCHEME 1

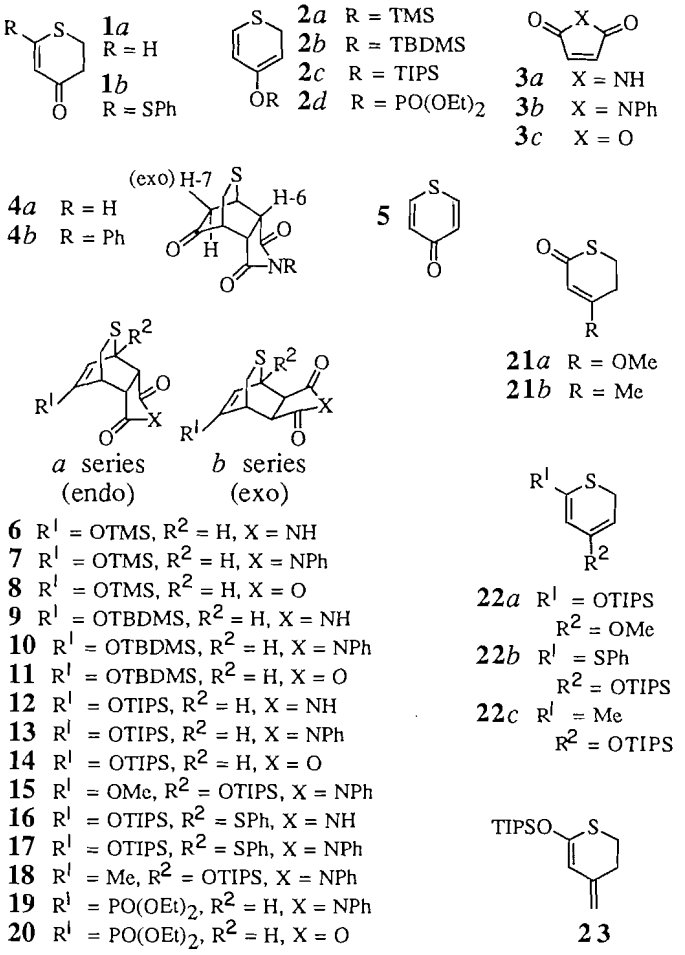
in low yield. Harayama and Otsuyama reported (12) that reaction of the 4-trimethylsilyloxy derivative with dienophiles produced both Diels–Alder and Michael adducts in low yield. In an effort to find suitably reactive analogues, we investigated (13) Diels–Alder reactions of 2*H*-thiopyrans that were activated by electron-donating substituents. In contrast to Harayama and Otsuyama, we found that 4-trialkylsilyloxy-2*H*-thiopyrans react with typical dienophiles to give fair to excellent yields of Diels–Alder adducts with *endo* stereoselectivity. Desulfurization of these adducts provided compounds equivalent to an *endo* Diels–Alder adduct from the unreactive (*E*)-3-trimethylsilyloxy-1,3-pentadiene in good overall yield. To further define the scope of this use of 2*H*-thiopyrans as functional equivalents of *cis*-dienes we have examined the Diels–Alder reactivity of a variety of substituted derivatives and herein report the full results of this study.

Results and discussion

Our initial efforts focussed on the preparation of 2*H*-thiopyrans bearing an oxygen substituent at C-4. Treatment of the readily available 2*H*-thiopyran-4(3*H*)-one (**1***a*) (14) with chlorotrimethylsilane (TMSCl) under Danishefsky's con-

[1]Author to whom correspondence may be addressed.

Can. J. Chem. Downloaded from www.nrcresearchpress.com by 84.41.108.74 on 09/07/12
For personal use only.



ditions (15) provided the diene **2***a*. Reaction with maleimide (**3***a*, 1 equiv.) in refluxing xylene for 16 h gave the adduct **4***a* (35%) along with **1***a* (20%) and 4*H*-thiopyranone (14*b*) (**5**, 25%).

The ^{1}H NMR spectrum of the crude reaction mixture indicated the presence of a 10:1 mixture of the stereoisomeric adducts **6***a*,*b* along with **1***a* and **5**. After chromatography over silica gel, only a single isomer of the hydrolyzed adduct (**4***a*) was isolated, which was assigned the *endo* stereochemistry on the basis of ^{1}H NMR. Specifically, in the spectrum of **4***a*, H-7$_{exo}$ exhibited a long-range W-coupling to H-6 with ^4J = 2 Hz; by contrast H-3$_{anti}$ was not spin coupled to H-5 (cf. Fig. 1). Although not isolated, we believe[2] that the *exo* isomer **6***b* is the minor component in the crude adduct **6***a*,*b*.

Monitoring the reaction of **2***a* with **3***a* by ^{1}H NMR revealed that both **1***a* and **5** were formed during reaction. The addition of a small amount of 2,6-di-*tert*-butyl-4-methylphenol (BHT) was effective in reducing the formation of **5**. However, despite pretreating the glassware with base and (or) with TMSCl and using carefully dried solvent, we were unable to completely suppress the formation of **1***a*. Under optimal conditions (**3***a*,

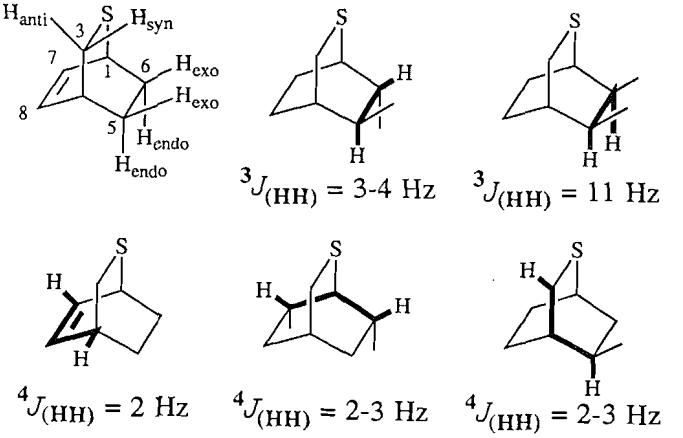


FIG. 1. Numbering system, labelling system, and typical H–H coupling constants for 2-thiabicyclo[2.2.2]oct-7-enes and 2-thiabicyclo[2.2.2]octanes.

2 equiv.; BHT, 0.2 equiv.; xylene, 110°C, 16 h) we obtained the adduct **4***a* (62%) along with **1***a* (28%) and **5** (9%).

Analogous results were obtained using *N*-phenylmaleimide (**3***b*) as the dienophile (Table 1). Attempted reaction of **2***a* with maleic anhydride (**3***c*) resulted in the rapid formation of **1***a*; in some experiments various amounts of the Diels–Alder adduct **5** (as a 3:1 mixture of *endo* and *exo* isomers[2]) could be detected but not isolated.

In an effort to obtain dienes that would be more stable, we prepared **2***b* and **2***c* by treatment of **1***a* with *tert*-butyldimethylsilyl trifluoromethanesulfonate (TBDMSOTf) and triisopropylsilyl trifluoromethanesulfonate (TIPSOTf), respectively, in the presence of Et_3N. Reaction of **2***b* with **3***a* (2 equiv.; BHT, 0.1 equiv.; xylene, 110°C, 16 h) gave the adduct **9***a* (53%) along with **1***a* (30%) and **5** (10%). Although the ^{1}H NMR spectrum of the crude reaction mixture indicated[2] the presence of a 10:1 mixture[3] of the stereoisomeric adducts **9***a*,*b*, only a single isomer was isolated. The *endo* stereochemistry was assigned to **9***a* based on the absence of W-coupling between H-3$_{anti}$ and H-5 in the ^{1}H NMR spectrum (cf. Fig. 1). The stereochemistry was confirmed by conversion of **9***a* into **4***a* ($HF_{(aq)}$, CH_3CN). Similar results were obtained in the reaction of **2***b* with **3***b* (Table 1). The reaction of **2***b* with **3***c* produced a 3:1 mixture of *endo*:*exo*[2] adducts **11** (54%) along with **1***a* (38%) and **5** (8%) as determined by ^{1}H NMR of the crude reaction mixture using an internal standard. The adducts could not be purified without extensive decomposition.

In contrast with **2***a* and **2***b*, reaction of **2***c* with dienophiles proceeded without significant production of **1***a* or **5** and addition of BHT to the reaction mixture was not necessary. Good yields of predominantly *endo* adducts were obtained in reactions of **2***c* with **3**. The *endo* stereochemistry was readily assigned to the major adduct on the basis of the lack of coupling between H-3$_{anti}$ and H-5 in the ^{1}H NMR spectrum[4] (cf. Fig. 1).

Reactions of **2***c* with **24** were much slower than those with

[2]The spectral characteristics (^{1}H and (or) ^{13}C NMR) of the major and minor adducts in the spectrum of the crude adduct closely resemble those of the homogeneous *endo* (e.g., **13***a*, **14***a*, **36***a*, and **39***a*) and *exo* (e.g., **19***b*, **36***b*, and **39***b*) adducts, respectively. Stereochemistry was readily assigned based on the consistent presence of coupling between H-3$_{anti}$ and H-5 only in the *exo* isomer (^4J = 2–3 Hz, cf. Fig. 1).

[3]This is presumably a kinetic mixture since control experiments show that individual solutions (toluene-d_8 or $CDCl_3$) of **13***a*, **19***a*, **19***b*, **26***a*, **26***b*, **36***a*, and **36***b* are unchanged after heating at 120°C for at least 48 h.

[4]The minor isomer shows coupling between H-3$_{anti}$ and H-5, J = 2–3 Hz.

Can. J. Chem. Downloaded from www.nrcresearchpress.com by 84.41.108.74 on 09/07/12
For personal use only.

TABLE 1. Diels–Alder reactions of activated 2*H*-thiopyrans

Entry	Diene	Dienophile	Temperature (°C)	Time (h)	*endo*:*exo*[a]	Products[b]
1	**2***a*	**3***a*	110	16	10:1	**4***a*, 62% (86%)
2	**2***a*	**3***b*	110	16	10:1	**4***b*, 56% (84%)
3	**2***b*	**3***a*	110	24	10:1	**9***a*,*b*, 53% (76%)
4	**2***b*	**3***b*	110	16	10:1	**10***a*, 60% (81%)
5	**2***b*	**3***c*	110	16	3:1	(**11***a*,*b* (3:1), 54% (87%))[c]
6	**2***c*	**3***a*	120	72	10:1	**12***a*,*b* (10:1), 72%
7	**2***c*	**3***b*	120	48	10:1	**13***a*, 77%
8	**2***c*	**3***c*	110	36	4:1	(**14***a*,*b* (4:1), 89%)[c] **14***a*, 6%
9	**2***c*	**24***a*	120	168	2.3:1	**25***a*,*b* (2.3:1), 41%
10	**2***c*	**24***b*	120	144	1.7:1	**25***a*,*b* (1.7:1), 56%
11	**2***c*	**24***c*	120	144	1:1	**25***a*,*b* (1:1), 43%
12	**2***c*	Fumarate	120	168	2.5:1	**28**, **29** (2.5:1), 12%
13	**2***c*	Maleate	120	168	1.2:1	**28**, **29** (1.2:1), 29%
14	**2***d*	**3***b*	110	70	10:1	**19***a*, 59%; **19***b*, 8%
15	**2***d*	**3***c*	110	70	6:1	(**19***a*,*b* (6:1), 80%)[c] **19***a*, 12%
16	**22***a*	**3***b*	80	4	4:1	**15***a*,*b* (4:1), 20% (40%)
17	**22***b*	**3***a*	110	17	1.2:1	**16***a*,*b* (2:1), 53% (71%)
18	**22***b*	**3***b*	110	17	2:1	**17***a*, 57%
19	**30**	**3***a*	110	127	3:1	**35***a*,*b* (3:1), 50%
20	**30**	**3***b*	110	78	2:1	**36***a*,*b* (2:1), 69%
21	**30**	**24***a*	110	240	2.5:1	**41**, **42** (8:1), 14% **44**, 5.6%
22	**33***a*	**3***b*	110	120	?[d]	**38***a*, 14%
23	**33***b*	**3***b*	110	270	>10:1	**40***a*, 50%; **40***b*, 5%
24	**34***a*	**3***b*	110	24	?[d]	**37***a*, 57%
25	**34***b*	**3***b*	110	51	10:1	**39***a*, 77%; **39***b*, 6%

[a]Ratio determined by ^{1}H NMR before purification.
[b]Isolated products and yields; yields in parentheses are based on recovered hydrolysed diene.
[c]Yields determined by ^{1}H NMR using an internal standard.
[d]*exo* Isomer not detected.

Can. J. Chem. Downloaded from www.nrcresearchpress.com by 84.41.108.74 on 09/07/12
For personal use only.

3, and both the yields obtained and the stereoselectivity were attenuated (Table 1). The stereochemistry of the adducts (**25**–**27**) was determined by analysis of the coupling constants observed in the ^{1}H NMR spectra. The resonance for H-5$_{endo}$ was readily assigned on the basis of its W-coupling to H-3$_{anti}$ (ca. 2–3 Hz, cf. Fig. 1). The magnitude of the coupling constant between H-5$_{endo}$ and H-6 provides the basis for the assignment of stereochemistry at C-6 (see Fig. 1). The lower yields obtained in these cases are attributable to the thermal instability of the diene. A toluene-d_8 solution of **2***c* at 120°C decomposes to unidentified products (polymerization?) with $t_{1/2}$ = 6 days (^{1}H NMR). At higher temperatures the lifetime of the diene is substantially shortened.

The reaction of **2***c* with dimethyl fumarate or dimethyl maleate was also slow at 120°C and gave, in each case, a mixture of only the *trans* adducts **28** and **29**.[5] The stereochemistry of the adducts was assigned based on the coupling constants observed in the ^{1}H NMR spectra. The *trans* relationship between the carbomethoxy groups in both **28** and **29** was evident from the coupling constants between H-5 and H-6 (5.5 and 5 Hz, respectively) while the stereochemistry at C-5 was assigned based on the presence (1.5 Hz for **28**) or absence (0 Hz for **27**) of coupling between H-3$_{anti}$ and H-5 (cf. Fig. 1).

Thus far, we have been unable to isolate Diels–Alder adducts in reactions of **2***c* with acetylenic dienophiles. For example, reaction of **2***c* with dimethyl acetylenedicarboxylate (C_6D_6, 80°C) gave a complex mixture of products from which dimethyl 4-triisopropylsilyloxy-1,2-benzenedicarboxylate could be isolated in low yield. Similarly, reaction of **2***c* with methyl propiolate gave methyl 4-triisopropylsilyloxybenzoate along with several unidentified products.[6] The production of these aromatic esters is presumably the result of a facile retro Diels–Alder elimination of thioformaldehyde from the initially formed adduct (16). Attempted Diels–Alder reaction of **2***c* with benzoquinone resulted in the formation of **5**.

To further enhance Diels–Alder reactivity, we sought to prepare 2*H*-thiopyrans with two activating substituents. The *in situ* trapping of photochemically generated thioformaldehyde with Brassard's diene (17) according to the procedure of Vedejs *et al.* (14*a*) provided the thiopyranone **21***a* (50%). Treatment of the lithium diisopropylamide (LDA) derived enolate of **21***a* with TIPSOTf gave the unstable diene **22***a*. The reaction of **22***a* with **3***b* proceeded at 80°C within 4 h to give a 4:1 mixture[2] of **15***a*,*b* (20%) together with **21***a* (49%). The

[5]Dimethyl maleate is isomerized into dimethyl fumarate (^{1}H NMR) under the reaction conditions.

[6]Some products were tentatively identified by ^{1}H NMR (13).

Can. J. Chem. Downloaded from www.nrcresearchpress.com by 84.41.108.74 on 09/07/12
For personal use only.

more stable diene **22***b* was available by treating thiopyranone **1***b* with TIPSOTf in the usual way. Diels–Alder reaction of **22***b* with **3***a* at 110°C for 17 h provided the adducts **16***a,b* as a 1.2:1 mixture[3] of *endo*:*exo* diastereomers.[2] The reaction of **22***b* with **3***b* gave similar results (Table 1).

As expected, the dienes **22***a* and **22***b* are more reactive than **2***c*. Comparing reactions with similar dienophiles, the reactions of **22***a* and **22***b* proceed faster and at lower temperature than those of **2***c* (Table 1). However, the increased reactivity of **22***a* and **22***b* is offset by increased thermal instability and Diels–Alder adducts could not be obtained with the less reactive dienophiles **24**.

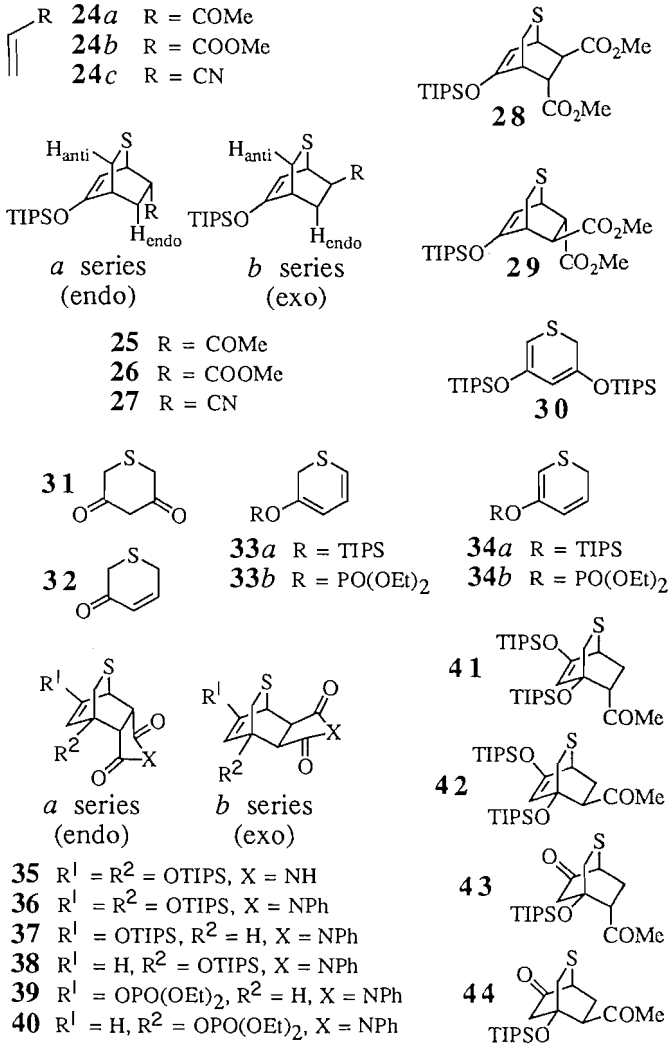
Alternatively, the 3,5-disubstituted 2*H*-thiopyran **30** was prepared from readily available **31** (18) by treatment with TIPSOTf (2.2 equiv.). The diene **30** reacted sluggishly with **3***a* and **3***b* to give adducts in fair yield with modest *endo*[2] selectivity (Table 1). Reactions with **24**[7] were much slower and resulted in low yields of adducts with poor stereoselectivity. The 3,5-disubstituted 2*H*-thiopyran **30** is similar to **2***c* in terms of stability and reactivity. However, **30** is considerably more stable and less reactive than the 4,6-disubstituted 2*H*-thiopyrans **22***a* and **22***b*.

Treatment of **21***b* (14*a*) with TIPSOTf gave an inseparable 3.6:1 mixture of **23** and the 6-substituted 2*H*-thiopyran **22***c*, respectively. Diels–Alder reaction of this mixture of dienes with **3***b* in $CDCl_3$ at 100°C gave a low yield of the *endo* adduct **18***a*. However, heating the 3.6:1 mixture of dienes **23** and **22***c* at 100°C in $CDCl_3$ in the presence of a catalytic amount of dichloromaleic anhydride (19) resulted in a 1:3 mixture of **23** and **22***c* (ca. 60%) together with **21***b* (ca. 40%) after 24 h (^{1}H NMR). Reaction of the 3.6:1 mixture of **23** and **22***c* with **3***b* in the presence of dichloromaleic anhydride ($CDCl_3$, 100°C, 24 h) gave the adduct **18***a* (30%) along with **21***b* (36%). These results imply that **22***c* is more reactive than **2***c*.

The 3- and 5-substituted 2*H*-thiopyrans **33***a* and **34***a* were available from **32** (20). Treatment of **32** with TIPSOTf and Et_3N gave a 1:4 mixture of **34***a* and **33***a* while treatment of the LDA derived enolate of **32** with TIPSOTf gave up to a 4:1 mixture of **34***a* and **33***a*. Heating a 4:1 mixture of **34***a* and **33***a* in toluene-d_8 at 100°C for 48 h resulted in a 1:4 mixture of **34***a* and **33***a* (^{1}H NMR). Conversely, after heating a toluene-d_8 solution of **33***a* at 100°C for 48 h, **34***a* could not be detected in the mixture. Prolonged heating (8 days) led to decomposition into unidentified products. The reaction of a 2:3 mixture of **34***a* and **33***a* with **3***b* (toluene-d_8, 100°C) for 24 h resulted in the complete disappearance of **34***a*, and the adduct **37***a* along with **33***a* were obtained after chromatography. Heating a toluene-d_8 solution of **33***a* and **3***b* at 100°C for 5 days gave the adduct **38***a* in 14% yield. The much lower reactivity of **33***a* compared to **34***a* is presumably the result of increased steric hindrance by the TIPS group at the bonding carbon (21).[8]

The use of dienol phosphates as stable analogues of dienol silyl ethers in Diels–Alder reactions has recently been reported (22). We examined the reactivity of the diethylphosphoryloxy-2*H*-thiopyrans **2***d*, **33***b*, and **34***b* and the results are presented in Table 1. In general, the phosphate dienes were more stable and less reactive than their silyl ether counterparts and little if any improvement in yields of Diels–Alder adducts was obtained.

Attempted reaction of **2***d* with **24***a* or **24***b* gave no adduct (^{1}H NMR) after 100 h at 140°C in toluene-d_8; increasing the reaction temperature to 160°C resulted in the decomposition of the diene to unidentified products within 24 h. In analogy with **34***a*, the diene **34***b* isomerizes to **33***b*. Heating a toluene-d_8 solution of **34***b* at 140°C for 72 h results in a 1:3 mixture of **34***b* and **33***b* (^{1}H NMR). By contrast, we did not detect evidence for the formation of **34***b* after prolonged heating of a solution of **33***b*. As with the silyl ether analogues, **33***b* is considerably less reactive than **34***b*.



Conclusion

2*H*-Thiopyrans bearing electron-donating substituents show enhanced Diels–Alder reactivity. By comparing the time and temperature of reactions of various dienes with similar dienophiles, the approximate order of reactivity among the 2*H*-thiopyrans is 4,6-disubstituted >> 5-substituted > 4-substituted, 3,5-disubstituted >> 3-substituted. Good yields of predominantly *endo* adducts are obtained with reactive dienophiles. With less reactive dienophiles, reactions are much slower and yields are attenuated due to the competing thermal decomposition of the dienes under the reaction conditions. The thermal

[7]Although adducts were detected in reactions of **30** with **24***a*, **24***b*, and **24***c*, only those from **24***a* were isolated and fully characterized.

[8]*trans*-Pentadiene is 1.5 times more reactive than 2-methylbutadiene towards maleic anhydride. Similarly, *trans*-1-methoxybutadiene is 3 times more reactive than 2-methoxybutadiene. By contrast, 2-*tert*-butylbutadiene is greater than 500 times more reactive than 1-*tert*-butylbutadiene (21).

instability of the silyloxydienes precludes the use of reaction temperatures above 120°C. This limitation is likely to be surmountable by the use of high pressure (6).

Desulfurization of the adducts derived from 2*H*-thiopyrans can provide products that are synthetically equivalent to Diels–Alder adducts of unreactive *cis*-substituted dienes (13). The coupling of an efficient Diels–Alder reaction of a 2*H*-thiopyran with desulfurization should provide a viable strategy to prepare compounds previously unavailable by Diels–Alder methods. Studies on the application of this strategy will be reported in due course.

Experimental

All solvents were distilled prior to use. Pyridine, *i*-Pr_2NH, and Et_3N were distilled from CaH_2 and stored over KOH pellets. Diethyl ether and THF were distilled from benzophenone potassium ketyl. Benzene, toluene, xylene, and CH_2Cl_2 were distilled from P_2O_5 under argon and stored over 3 Å molecular sieves. Toluene-d_8 was passed through neutral alumina immediately before use. $ZnCl_2$ was dried by melting several times under vacuum. Maleic anhydride was recrystallized from CCl_4. Unless otherwise noted, other commercially available reagents were used as received. Unless otherwise noted, reactions were carried out under an atmosphere of argon and reaction temperatures refer to the bath. Unless otherwise noted, all reported compounds were homogeneous by thin-layer chromatography (TLC) and by NMR.

Preparative thin-layer chromatography (PTLC) was carried out on glass plates (20 × 20 cm) precoated (0.25 mm) with silica gel 60 F_{254}. Materials were detected by visualization under an ultraviolet lamp (254 nm) and (or) by treating a 1-cm vertical strip removed from the plate with a solution of phosphomolybdic acid (5%) containing a trace of ceric sulfate in aqueous sulfuric acid (5% v/v), followed by charring on a hot plate. Flash column chromatography (FCC) was performed according to Still *et al.* (23) with Merck Silica Gel 60 (40–63 μm).

Mass spectra (MS) were recorded on a VG analytical retrofit of a single-sectored, magnetic scanning MS-12 linked to a Zenith computer. Electron impact (EI) ionization was accomplished at 70 eV and chemical ionization (CI) at 50 eV with ammonia as the carrier gas. Only partial data are reported. Infrared (IR) spectra were recorded on a Biorad FTS-40 Fourier transform interferometer using a diffuse reflectance cell. Only diagnostic peaks are reported. ^1H nuclear magnetic resonance (^1H NMR) spectra and ^{13}C nuclear magnetic resonance (^{13}C NMR) spectra were measured at 300 MHz and 75 MHz, respectively, on a Bruker AM-300 spectrometer. Unless otherwise noted, NMR spectra were obtained in $CDCl_3$ solution. For ^1H NMR, residual $CHCl_3$ in $CDCl_3$ was employed as the internal standard and assigned as 7.26 ppm downfield (δ) from tetramethylsilane (TMS). For ^{13}C NMR, $CDCl_3$ was employed as the internal standard and assigned as 77.0 δ relative to TMS. The ^1H NMR assignments are made on the basis of chemical shift, multiplicity, and, where necessary, confirmed by homonuclear decoupling and (or) NOE experiments. Chemical shifts and coupling constants were determined assuming first-order behavior. Multiplicity is indicated by one or more of: s (singlet), d (doublet), t (triplet), q (quartet), m (multiplet), br (broad); the list of coupling constants (*J*) corresponds to the order of the multiplicity assignment. ^1H NMR spectra were obtained with a digital resolution of 0.244 Hz/pt (sweep width = 4000 Hz, FID = 32 K data points) and coupling constants are reported to the nearest 0.5 Hz. The ^{13}C NMR assignments are made on the basis of chemical shift, multiplicity, and consistency within a series of similar structures. The multiplicity of ^{13}C NMR signals refers to the number of attached H's (i.e., s = C, d = CH, t = CH_2, q = CH_3) and was determined by *J*-modulation (24). Melting points were determined on a Gallenkamp melting point apparatus and are uncorrected.

6-Phenylthio-2H-thiopyran-4(3H)-one (1b)

NCS (71 mg, 0.52 mmol) was added portionwise to a solution of 2-phenylthiotetrahydro-4*H*-thiopyran-4-one (25) (112 mg, 0.5 mmol) in CCl_4 (6 mL) at 0°C. After stirring for 4 h at 0°C, the reaction mixture was filtered, and the combined filtrate and washings were concentrated and fractionated by PTLC (70% ether in hexane) to give **1***b* as an oil (45 mg, 41%); IR: 3276, 1661, 1647, 1519 cm^{-1}; ^1H NMR δ: 7.46 (5H, m, SC_6H_5), 5.92 (1H, s, H-5), 3.15 (2H, m, H-2), 2.65 (2H, m, H-3); ^{13}C NMR δ: 191.9 (s, C-4), 165.0 (s, C-6), [137.1 (s), 135.5 (d ×2), 130.5 (d), 129.8 (d ×2), SC_6H_5], 119.1 (d, C-5), 37.4 (t, C-3), 28.7 (t, C-2); MS (EI), *m/z* (relative intensity): 222 (M^+, 100), 189 (73).

4-Trimethylsilyloxy-2H-thiopyran (2a)

A solution of $ZnCl_2$ (1 mL, 1.5 M in ether) was added to a solution of **1***a* (114 mg, 1 mmol) in CH_2Cl_2 (10 mL), and Et_3N (0.85 mL, 6 mmol) and TMSCl (0.38 mL, 3 mmol) were added with stirring at room temperature. After 5 min the reaction mixture was concentrated and triturated with hexane. The combined hexane washings were concentrated and distilled to give **2***a* as a clear liquid (138 mg, 74%); bp 64–66°C, 2 Torr (1 Torr = 133.3 Pa); IR: 3045, 1627 cm^{-1}; ^1H NMR δ: 6.32 (1H, dd, *J* = 0.5, 10 Hz, H-6), 5.86 (1H, dd, *J* = 1.5, 10 Hz, H-5), 4.68 (1H, ddt, *J* = 0.5, 1.5, 5.5 Hz, H-3), 3.37 (2H, d, *J* = 5.5 Hz, H-2), 0.22 (9H, s, $Si(CH_3)_3$); ^{13}C NMR δ: 149.7 (s, C-4), 125.8 (d, C-6), 122.7 (d, C-5), 93.3 (d, C-3), 25.6 (t, C-2), 0.2 (q, $Si(CH_3)_3$); MS (CI), *m/z* (relative intensity): 187 ($[M + 1]^+$, 100), 186 (M^+, 23), 90 (26), 73 (15).

General procedure for preparation of silyloxy-2H-thiopyrans

To a solution of thiopyranone and Et_3N (3 equiv.) in CH_2Cl_2 (ca. 10 mL/mmol of thiopyranone) was added TBDMSOTf or TIPSOTf (1.05–1.2 equiv.) with stirring at room temperature. After 5 min the reaction mixture was concentrated and fractionated by FCC (hexane or pentane) using a column prepared from a slurry of silica gel in 3% v/v Et_3N in hexane or pentane. The yields obtained are essentially quantitative. The 2*H*-thiopyrans could not be distilled without extensive decomposition.

4-tert-Butyldimethylsilyloxy-2H-thiopyran (2b): IR: 3056, 1622 cm^{-1}; ^1H NMR δ: 6.32 (1H, dd, *J* = 0.5, 10 Hz, H-6), 5.88 (1H, dd, *J* = 1.5, 10 Hz, H-5), 4.67 (1H, ddt, *J* = 0.5, 1.5, 5.5 Hz, H-3), 3.37 (2H, d, *J* = 5.5 Hz, H-2), 0.22 (9H, s, $SiC(CH_3)_3$), 0.14 (6H, s, $Si(CH_3)_2$); ^{13}C NMR δ: 150.0 (s, C-4), 125.8 (d, C-6), 122.8 (d, C-5), 93.3 (d, C-3), 25.6 (t and q, C-2 and $SiC(CH_3)_3$), 18.1 (s, $SiC(CH_3)_3$), −4.5 (q, $Si(CH_3)_2$); MS (EI), *m/z* (relative intensity): 228 (M^+, 40), 187 (68), 75 (100).

4-Triisopropylsilyloxy-2H-thiopyran (2c): IR: 3043, 1614 cm^{-1}; ^1H NMR δ: 6.32 (1H, dd, *J* = 0.5, 10 Hz, H-6), 5.93 (1H, dd, *J* = 1.5, 10 Hz, H-5), 4.70 (1H, ddt, *J* = 0.5, 1.5, 5.5 Hz, H-3), 3.35 (2H, d, *J* = 5.5 Hz, H-2), 1.10 (21H, m, $Si(CH(CH_3)_2)_3$); ^{13}C NMR δ: 150.3 (s, C-4), 125.8 (d, C-6), 122.9 (d, C-5), 92.6 (d, C-3), 25.8 (t, C-2), 17.9 (q, $Si(CH(CH_3)_2)_3$), 12.6 (d, $Si(CH(CH_3)_2)_3$); MS (EI), *m/z* (relative intensity): 270 (M^+, 45), 227 (65), 97 (100), 59 (61).

4-Diethylphosphoryloxy-2H-thiopyran (2d)

Methyllithium (0.17 mL, 1.27 M in hexanes, 0.22 mmol) was added dropwise to a solution of diisopropylamine (0.031 mL, 0.22 mmol) in THF (2 mL) at −78°C. After stirring for 10 min, a solution of **1***a* (20 mg, 0.18 mmol) in THF (1 mL) was added dropwise via syringe. After stirring for 1 h, diethyl chlorophosphate (0.064 mL, 0.44 mmol) was added and the reaction mixture was allowed to warm to room temperature and stirred for an additional 2.5 h. The reaction mixture was diluted with ether, washed with saturated NH_4Cl, saturated $NaHCO_3$, brine, dried over $MgSO_4$, concentrated, and fractionated by FCC (50% EtOAc in hexanes) to give **2***d* as an oil (23 mg, 54%); IR: 3052, 1640, 1552, 1274, 1029 cm^{-1}; ^1H NMR δ: 6.39 (1H, dt, *J* = 10, 1 Hz, H-6), 6.01 (1H, ddd, *J* = 0.5, 1.5, 10 Hz, H-5), 5.25 (1H, m, H-3), 4.15 (4H, dq, *J* = 8, 7 Hz, OCH_2), 3.44 (2H, ddd, *J* = 0.5, 2, 5.5 Hz, H-2), 1.32 (6H, dt, *J* = 1, 7 Hz, CH_3); ^{13}C NMR δ: 146.6 (s, C-4), 127.6 (d, C-6), 119.4 (d, C-5), 98.0 (d, C-3), 64.6 (t, OCH_2), 25.0 (t, C-2), 16.1 (q, CH_3), [C-3, 4, 5, and OCH_2CH_3

Can. J. Chem. Downloaded from www.nrcresearchpress.com by 84.41.108.74 on 09/07/12
For personal use only.

show coupling to ^{31}P, J = 4–8 Hz]; MS (CI), *m/z* (relative intensity): 268 ([M + 18]$^+$, 36), 251 ([M + 1]$^+$, 100).

(1R,4R*,5R*,6S*)-2-Thiabicyclo[2.2.2]octan-8-one-5,6-dicarboxylic acid imide (**4**a)*

A solution of **2***a* (240 mg, 1.3 mmol), **3***a* (252 mg, 2.6 mmol), and BHT (57 mg, 0.26 mmol) in xylene (3 mL) was heated at 110°C for 16 h. The ^1H NMR spectrum of the crude product indicated[2] the presence of a 10:1 mixture[3] of the adducts **6**. Fractionation by FCC (gradient elution: 25–50% EtOAc in hexane) gave **1***a* (41 mg, 28%) and **4***a* (170 mg, 62%); mp 215–217°C (MeOH); IR: 3381, 3176, 1778, 1720, 1708 cm^{-1}; ^1H NMR δ: 3.67 (1H, ddd, J = 2, 3.5, 9.5 Hz, H-6), 3.61 (1H, dt, J = 3.5, 3 Hz, H-1), 3.33 (1H, dd, J = 3, 9.5 Hz, H-5), 3.27 (1H, q, J = 3 Hz, H-4), 3.21 (1H, dd, J = 3, 11.5 Hz, H-3$_{syn}$), 3.13 (1H, dd, J = 3, 11.5 Hz, H-3$_{anti}$), 2.88 (1H, ddd, J = 2, 3, 20 Hz, H-7$_{exo}$), 2.63 (1H, dd, J = 3, 20 Hz, H-7$_{endo}$); ^{13}C NMR δ: ($(CD_3)_2CO$) δ: 208.0 (s, C-8), 178.1 and 177.5 (s, imide C=O), 48.7 (d, C-6), 45.8 (t, C-7), 44.6 and 44.0 (d, C-4, 5), 35.5 (d, C-1), 27.1 (t, C-3); MS (EI), *m/z* (relative intensity): 211 (M$^+$, 100), 183 (68), 112 (42), 97 (65).

Eluting the column with 20% MeOH in CH_2Cl_2 gave the polar **5** (13 mg, 9%).

(1R,4R*,5R*,6S*)-N-Phenyl-2-thiabicyclo[2.2.2]octan-8-one-5,6-dicarboxylic acid imide (**4**b)*

A solution of **2***a* (95 mg, 0.51 mmol), **3***b* (88 mg, 0.51 mmol), and BHT (22 mg, 0.1 mmol) in xylene (1 mL) was heated at 110°C for 16 h. The ^1H NMR spectrum of the crude product indicated[2] the presence of a 10:1 mixture[3] of the adducts **7**. Fractionation by FCC (gradient elution: 25–50% EtOAc in hexane) gave **1***a* (19 mg, 33%) and **4***b* (82 mg, 56%); mp 223–225°C (EtOAc); IR: 3064, 1772, 1708 cm^{-1}; ^1H NMR δ: 7.15–7.50 (5H, m, C_6H_5), 3.78 (1H, ddd, J = 2, 3.5, 9.5 Hz, H-6), 3.72 (1H, dt, J = 3.5, 3 Hz, H-1), 3.47 (1H, dd, J = 3, 9.5 Hz, H-5), 3.37 (1H, q, J = 3 Hz, H-4), 3.22 (2H, m, H-3$_{syn}$ and H-3$_{anti}$), and 2.92 (1H, ddd, J = 2, 3, 20 Hz, H-7$_{exo}$), 2.65 (1H, dd, J = 3, 20 Hz, H-7$_{endo}$); ^{13}C NMR δ: 206.7 (s, C-8), 175.2 and 174.8 (s, imide C=O), [131.0 (s), 129.4 (d ×2), 129.2 (d), 126.2 (d ×2), N-C_6H_5], 46.6 (d, C-6), 45.2 (t, C-7), 43.9 and 42.3 (d, C-4, 5), 34.9 (d, C-1), 26.6 (t, C-3); MS (EI), *m/z* (relative intensity): 287 (M$^+$, 60), 86 (52), 84 (75), 57 (100).

Eluting the column with 20% MeOH in CH_2Cl_2 gave the polar **5** (5 mg, 9%).

(1R,4R*,5R*,6S*)-8-*tert*-Butyldimethylsilyloxy-2-thiabicyclo[2.2.2]-oct-7-ene-5,6-dicarboxylic acid imide (**9**a) and (1R*,4R*,5S*,6R*)-8-*tert*-butyldimethylsilyloxy-2-thiabicyclo-[2.2.2]oct-7-ene-5,6-dicarboxylic acid imide (**9**b)*

A solution of **2***b* (20 mg, 0.088 mmol) and **3***a* (25 mg, 0.26 mmol) in xylene (1 mL) was heated at 110°C for 24 h. The ^1H NMR spectrum of the crude product indicated[2] the presence of a 10:1 mixture[3] of the adducts **9**. Fractionation by FCC (40% EtOAc in hexane) gave **1***a* (3 mg, 30%) and **9***a,b* (10:1, 15 mg, 53%) as an oil; IR: 3144, 3042, 1774, 1717, 1633 cm^{-1}; ^1H NMR δ for **9***a*: 8.70 (1H, brs, NH), 5.26 (1H, dd, J = 2, 7.5 Hz, H-7), 3.97 (1H, dd, J = 3.5, 7.5 Hz, H-1), 3.39 (1H, dd, J = 3.5, 8.5 Hz, H-6), 3.39 (1H, m, H-4), 3.04 (1H, dd, J = 3, 10.5 Hz, H-3$_{syn}$), 2.98 (1H, dd, J = 2.5, 8.5 Hz, H-5), 2.84 (1H, dd, J = 3, 10.5 Hz, H-3$_{anti}$), 0.87 (9H, s, $SiC(CH_3)_3$), 0.13 (3H, s, $SiCH_3$), 0.08 (3H, s, $SiCH_3$); partial data for **9***b*: 8.90 (1H, brs, NH), 5.46 (1H, dd, J = 2, 7.5 Hz, H-7), 3.89 (1H, dd, J = 3.5, 7.5 Hz, H-1), 2.64 (1H, ddd, J = 1.5, 2.5, 11 Hz, H-3$_{anti}$); ^{13}C NMR δ for **9***a*: 176.6 and 175.5 (s, imide C=O), 153.7 (s, C-8), 103.3 (d, C-7), 49.6 (d, C-6), 43.3 (d, C-5), 39.1 (d, C-4), 36.3 (d, C-1), 31.8 (d, C-3), 25.5 (q, $SiC(CH_3)_3$), 17.9 (s, $SiC(CH_3)_3$), −4.3 (q, $SiCH_3$), −5.0 (q, $SiCH_3$); MS (CI), *m/z* (relative intensity): 326 ([M + 1]$^+$, 100), 268 (30), 132 (29).

Eluting the column with 20% MeOH in CH_2Cl_2 gave the polar **5** (1 mg, 10%).

(1R,4R*,5R*,6S*)-N-Phenyl-8-*tert*-butyldimethylsilyloxy-2-thiabicyclo[2.2.2]oct-7-ene-5,6-dicarboxylic acid imide (**10**a)*

A solution of **2***b* (15 mg, 0.066 mmol) and **3***b* (30 mg, 0.17 mmol) in xylene (1 mL) was heated at 110°C for 16 h. The ^1H NMR spectrum of the crude product indicated[2] the presence of a 10:1 mixture[3] of *endo* and *exo* adducts **10**. Fractionation by FCC (25% EtOAc in hexane) gave **1***a* (2 mg, 26%) and **10***a* (16 mg, 60%) as an oil; IR: 3056, 1776, 1702, 1634 cm^{-1}; ^1H NMR δ: 7.15–7.50 (5H, m, C_6H_5), 5.32 (1H, dd, J = 1.5, 7.5 Hz, H-7), 4.11 (1H, dd, J = 3.5, 7.5 Hz, H-1), 3.54 (1H, dd, J = 3.5, 8.5 Hz, H-6), 3.52 (1H, m, H-4), 3.14 (1H, dd, J = 3, 10.5 Hz, H-3$_{syn}$), 3.13 (1H, dd, J = 3, 8.5 Hz, H-5), 2.89 (1H, dd, J = 3, 10.5 Hz, H-3$_{anti}$), 0.89 (9H, s, $SiC(CH_3)_3$), 0.15 (3H, s, $SiCH_3$), 0.10 (3H, s, $SiCH_3$); ^{13}C NMR δ: 176.6 and 175.5 (s, imide C=O), 153.7 (s, C-8), [131.7 (s), 129.1 (d ×2), 128.6 (d), 126.2 (d ×2), N-C_6H_5], 103.3 (d, C-7), 49.6 (d, C-6), 43.3 (d, C-5), 39.1 (d, C-4), 36.3 (d, C-1), 31.8 (d, C-3), 25.5 (q, $SiC(CH_3)_3$), 17.9 (s, $SiC(CH_3)_3$), −4.6 (q, $SiCH_3$); MS (CI), *m/z* (relative intensity): 402 ([M + 1]$^+$, 72), 344 (100), 171 (20).

Eluting the column with 20% MeOH in CH_2Cl_2 gave the polar **5** (0.9 mg, 12%).

(1R,4R*,5R*,6S*)-8-Triisopropylsilyloxy-2-thiabicyclo[2.2.2]oct-7-ene-5,6-dicarboxylic acid imide (**12**a) and (1R*,4R*,5S*,6R*)-8-triisopropylsilyloxy-2-thiabicyclo[2.2.2]-oct-7-ene-5,6-dicarboxylic acid imide (**12**b)*

A solution of **2***c* (185 mg, 0.69 mmol) and **3***a* (100 mg, 1 mmol) in xylene (2.5 mL) was heated at 120°C for 72 h. The ^1H NMR spectrum of the crude product indicated[2] the presence of a 10:1 mixture[3] of the adducts **12**. Fractionation by FCC (25% EtOAc in hexane) gave **12***a,b* (10:1, 184 mg, 72%) as an oil; IR: 3154, 3059, 1780, 1718, 1630 cm^{-1}; ^1H NMR δ for **12***a*: 5.24 (1H, dd, J = 2, 7.5 Hz, H-7), 3.96 (1H, dd, J = 3.5, 7.5 Hz, H-1), 3.43 (1H, m, H-4), 3.39 (1H, dd, J = 3.5, 8.5 Hz, H-6), 3.06 (1H, dd, J = 3, 10.5 Hz, H-3$_{syn}$), 2.98 (1H, dd, J = 2.5, 8.5 Hz, H-5), 2.83 (1H, dd, J = 3, 10.5 Hz, H-3$_{anti}$), 1.10 (21H, m, $Si(CH(CH_3)_2)_3$); partial data for **12***b*: 5.45 (1H, dd, J = 2, 8 Hz, H-7), 3.88 (1H, dd, J = 4, 8 Hz, H-4), 2.66 (1H, m, H-3$_{anti}$); ^{13}C NMR δ for **12***a*: 177.5 and 176.5 (s, imide C=O), 153.6 (s, C-8), 102.4 (d, C-7), 50.6 (d, C-6), 44.6 (d, C-5), 38.9 (d, C-4), 35.9 (d, C-1), 31.7 (d, C-3), 17.8 (q, $Si(CH(CH_3)_2)_3$), 12.4 (d, $Si(CH(CH_3)_2)_3$); MS (CI), *m/z* (relative intensity): 368 ([M + 1]$^+$, 100), 324 (62).

(1R,4R*,5R*,6S*)-N-Phenyl-8-triisopropylsilyloxy-2-thiabicyclo-[2.2.2]oct-7-ene-5,6-dicarboxylic acid imide (**13**a)*

A solution of **2***c* (95 mg, 0.35 mmol) and **3***b* (100 mg, 0.57 mmol) in xylene (2 mL) was heated at 120°C for 48 h. The ^1H NMR spectrum of the crude product indicated[2] the presence of a 10:1 mixture[3] of *endo* and *exo* adducts **13**. Fractionation by FCC (20% EtOAc in hexane) gave **13***a* (120 mg, 77%) as an oil; IR: 3066, 1778, 1713, 1633 cm^{-1}; ^1H NMR δ: 7.15–7.50 (5H, m, C_6H_5), 5.33 (1H, dd, J = 2, 7.5 Hz, H-7), 4.11 (1H, dd, J = 3.5, 7.5 Hz, H-1), 3.58 (1H, m, H-4), 3.55 (1H, dd, J = 3.5, 8.5 Hz, H-6), 3.17 (1H, dd, J = 3, 10.5 Hz, H-3$_{syn}$), 3.13 (1H, dd, J = 2.5, 8.5 Hz, H-5), 2.89 (1H, dd, J = 3, 10.5 Hz, H-3$_{anti}$), 1.10 (21H, m, $Si(CH(CH_3)_2)_3$); ^{13}C NMR δ: 176.6 and 175.5 (s, imide C=O), 153.7 (s, C-8), [131.7 (s), 129.0 (d ×2), 128.5 (d), 126.2 (d ×2), N-C_6H_5], 102.3 (d, C-7), 49.6 (d, C-6), 46.3 (d, C-5), 39.3 (d, C-4), 36.5 (d, C-1), 31.9 (d, C-3), 17.9 (q, $Si(CH(CH_3)_2)_3$), 12.5 (d, $Si(CH(CH_3)_2)_3$); MS (CI), *m/z* (relative intensity): 444 ([M + 1]$^+$, 100), 400 (53), 227 (17).

Reactions of 2b *and* 2c *with* 3c

Solutions of **3***c* (20 mg, 0.2 mmol) in toluene-d_8 (0.5 mL) containing **2***b* (23 mg, 0.1 mmol) and **2***c* (27 mg, 0.1 mmol), respectively, were sealed in NMR tubes and heated at 110°C for 16 h and 36 h, respectively. Using the residual protons in toluene-d_8 as an internal standard, ^1H NMR spectra of the solutions revealed the presence of **11***a* (41%), **11***b* (13%), **1***a* (38%), and **5** (8%) from **2***b*, and **14***a* (71%) and **14***b* (18%) from **2***c*. We were unable to purify the adducts without extensive decomposition. In one case, a reaction from **2***c* (42 mg, 1.5 mmol) gave, after FCC (75% ether in hexane), a small sample of pure **14***a* (6 mg, 11%).

(1R,4R*,5R*,6S*)-8-Triisopropylsilyloxy-2-thiabicyclo[2.2.2]oct-7-ene-5,6-dicarboxylic acid anhydride (**14**a)*: IR: 3056, 1866, 1779, 1723, 1633 cm^{-1}; ^1H NMR δ: 5.32 (1H, dd, J = 2, 7.5 Hz, H-7), 4.06 (1H, dd, J = 3.5, 7.5 Hz, H-1), 3.66 (1H, dd, J = 3.5, 9 Hz, H-6),

Can. J. Chem. Downloaded from www.nrcresearchpress.com by 84.41.108.74 on 09/07/12
For personal use only.

Can. J. Chem. Downloaded from www.nrcresearchpress.com by 84.41.108.74 on 09/07/12
For personal use only.

3.53 (1H, m, H-4), 3.25 (1H, dd, J = 2.5, 9 Hz, H-5), 3.09 (1H, dd, J = 3, 10.5 Hz, H-3$_{syn}$), 2.87 (1H, dd, J = 3, 10.5 Hz, H-3$_{anti}$), 1.10 (21H, m, Si(CH(CH$_3$)$_2$)$_3$); ^{13}C NMR δ: 171.4 and 170.0 (s, anhydride C=O), 154.0 (s, C-8), 102.8 (d, C-7), 50.1 (d, C-6), 43.9 (d, C-5), 39.0 (d, C-4), 35.8 (d, C-1), 31.1 (d, C-3), 17.8 (q, Si(CH(*C*H$_3$)$_2$)$_3$), 12.4 (d, Si(*C*H(CH$_3$)$_2$)$_3$); MS (CI), *m/z* (relative intensity): 369 ([M + 1]$^+$, 100), 325 (22), 148 (25).

(1R,4R*,5R*,6S*)-8-Methoxy-*N*-phenyl-1-triisopropylsilyloxy-2-thiabicyclo[2.2.2]oct-7-ene-5,6-dicarboxylic acid imide (**15**a) and (1R*,4R*,5S*,6R*)-8-methoxy-*N*-phenyl-1-triisopropylsilyloxy-2-thiabicyclo[2.2.2]oct-7-ene-5,6-dicarboxylic acid imide (**15**b)*

A solution of **22***a* (40 mg, ca. 80% pure by ^{1}H NMR, prepared from 14.4 mg of **21***a*) and **3***b* (17.3 mg, 0.1 mmol) in toluene-d_8 (0.4 mL) was sealed in an NMR tube under vacuum and heated at 80°C. After 4 h, ^{1}H NMR revealed the absence of **22***a*. The solution was concentrated and fractionated by PTLC (75% ether in hexane) to give **21***a* (7 mg, 49% from **21***a*) and a 4:1 mixture[2] of the adducts **15** (9.5 mg, 20% from **21***a*); IR: 3066, 1778, 1716, 1637 cm^{-1}; ^{1}H NMR δ for **15***a*: 7.15–7.50 (5H, m, NC$_6$H$_5$), 5.25 (1H, d, J = 1.5 Hz, H-7), 3.73 (1H, d, J = 8 Hz, H-6), 3.56 (1H, m, H-4), 3.54 (3H, s, OCH$_3$), 3.26 (1H, dd, J = 2.5, 10.5 Hz, H-3$_{syn}$), 3.20 (1H, dd, J = 2.5, 8.5 Hz, H-5), 3.04 (1H, dd, J = 2.5, 10.5 Hz, H-3$_{anti}$), 1.15 (21H, m, Si(CH(CH$_3$)$_2$)$_3$); partial data for **15***b*: 5.37 (1H, d, H-7), 3.60 (3H, s, OCH$_3$), 2.79 (1H, ddd, J = 2, 2, 10 Hz, H-3$_{anti}$); ^{13}C NMR δ for **15***a*: 176.2 and 172.2 (s, imide C=O), 156.4 (s, C-8), [131.4 (s), 129.2 (d ×2), 128.6 (d), 126.6 (d ×2), NC$_6$H$_5$], 103.2 (d, C-7), 83.7 (s, C-1), 56.6 (q, OCH$_3$), 55.3 (d, C-6), 43.7 (d, C-5), 37.4 (d, C-4), 35.0 (t, C-3), 18.4 (q, Si(CH(*C*H$_3$)$_2$)$_3$), 13.5 (d, Si(*C*H(CH$_3$)$_2$)$_3$); partial data for **15***b*: 159.1 (s, C-8), 105.6 (d, C-7), 31.8 (t, C-3); MS (EI), *m/z* (relative intensity): 473 (M$^+$, 4), 440 (100).

(1S,4R*,5R*,6S*)-1-Phenylthio-8-triisopropylsilyloxy-2-thiabicyclo-[2.2.2]oct-4-ene-5,6-dicarboxylic acid imide (**16**a) and (1S*,4R*,5S*,6R*)-1-phenylthio-8-triisopropylsilyloxy-2-thiabicyclo[2.2.2]oct-4-ene-5,6-dicarboxylic acid imide (**16**b)*

A solution of **22***b* (100 mg, 0.26 mmol), **3***a* (38 mg, 0.38 mmol), and BHT (4 mg, 0.02 mmol) in CDCl$_3$ (0.5 mL) was sealed in an NMR tube and heated at 110°C. After 17 h, ^{1}H NMR revealed the absence of **22***b* and the presence of a 1.2:1 mixture[2] of *endo*:*exo* adducts **16**. The solution was concentrated and fractionated by PTLC (75% ether in hexane) to give **1***b* (15 mg, 26%) and a 2:1 mixture of **16***a*,*b* (65 mg, 53%); IR: 3217, 3066, 1777, 1715, 1625 cm^{-1}; ^{1}H NMR δ for **16***a*: 8.45 (1H, brs, NH), [7.89 (2H, m), 7.36 (3H, m), SC$_6$H$_5$], 5.20 (1H, d, J = 2 Hz, H-7), 3.47 (1H, d, J = 8.5 Hz, H-6), 3.45 (1H, m, H-4), 3.14 (1H, dd, J = 3, 10 Hz, H-3$_{syn}$), 3.05 (1H, dd, J = 2, 8.5 Hz, H-5), 2.99 (1H, dd, J = 2.5, 10 Hz, H-3$_{anti}$), 1.10 (21H, m, Si(CH(CH$_3$)$_2$)$_3$); for **16***b*: 8.68 (1H, brs, NH), [7.67 (2H, m), 7.36 (3H, m), SC$_6$H$_5$], 5.19 (1H, d, J = 2 Hz, H-7), 3.28 (4H, m, H-3$_{syn}$, 4, 5, 6), 2.78 (1H, ddd, J = 2, 2, 10 Hz, H-3$_{anti}$), 1.10 (21H, m, Si(CH(CH$_3$)$_2$)$_3$); ^{13}C NMR δ for **16***a*: 176.7 and 173.8 (s, imide C=O), 154.0 (s, C-8), [137.3 (d ×2), 129.6 (s and d), 128.7 (d ×2), SC$_6$H$_5$], 105.6 (d, C-7), 56.4 (s, C-1), 54.2 (d, C-6), 46.2 (d, C-5), 40.0 (d, C-4), 36.8 (t, C-3), 17.8 (q, Si(CH(*C*H$_3$)$_2$)$_3$), 12.4 (d, Si(*C*H(CH$_3$)$_2$)$_3$); for **16***b*: 177.0 and 174.6 (s, imide C=O), 155.5 (s, C-8), [136.4 (d ×2), 131.0, 129.1 (d), 128.9 (d ×2), SC$_6$H$_5$], 108.3 (d, C-7), 56.3 (s, C-1), 55.7 (d, C-6), 47.3 (d, C-5), 37.6 (d, C-4), 33.5 (t, C-3), 17.7 (q, Si(CH(*C*H$_3$)$_2$)$_3$), 12.2 (d, Si(*C*H(CH$_3$)$_2$)$_3$); MS (CI), *m/z* (relative intensity): 475 ([M + 1]$^+$, 12), 442 (100), 367 (43), 324 (88), 97 (89).

(1S,4R*,5R*,6S*)-*N*-Phenyl-1-phenylthio-8- triisopropylsilyloxy-2-thiabicyclo[2.2.2]oct-7-ene-5,6-dicarboxylic acid imide (**17**a)*

A solution of **22***b* (45 mg, 0.12 mmol), **3***b* (27 mg, 0.16 mmol), and BHT (2 mg, 0.01 mmol) in CDCl$_3$ (0.5 mL) was sealed in an NMR tube and heated at 110°C. After 17 h, ^{1}H NMR revealed the absence of **22***b* and the presence of a 2:1 mixture[2] of *endo*:*exo* adducts **17**. The solution was concentrated and fractionated by PTLC (75% ether in hexane) to give **1***b* (2 mg, 7.5%) and **17***a* (38 mg, 57%; contaminated by a small amount (ca. 5%) of a structurally related, inseparable impurity); IR: 3059, 1777, 1717, 1623 cm^{-1}; ^{1}H NMR δ: [7.89 (2H, m), 7.15–7.50 (8H, m), SC$_6$H$_5$ and NC$_6$H$_5$], 5.26 (1H, d, J = 2 Hz, H-7), 3.57 (1H, m, H-4), 3.56 (1H, d, J = 8.5 Hz, H-6), 3.22 (1H, dd, J = 3.5, 10 Hz, H-3$_{syn}$), 3.15 (1H, dd, J = 2, 8.5 Hz, H-5), 3.04 (1H, dd, J = 3, 10 Hz, H-3$_{anti}$), 1.10 (21H, m, Si(CH(CH$_3$)$_2$)$_3$); ^{13}C NMR δ: 175.8 and 172.5 (s, imide C=O), 154.0 (s, C-8), [137.4 (d ×2), 129.7 (s), 129.6 (d), 128.6 (d ×2), SC$_6$H$_5$], [131.5 (s), 128.9 (d ×2), 128.6 (d), 126.2 (d ×2), N-C$_6$H$_5$], 106.0 (d, C-7), 57.0 (s, C-1), 52.9 (d, C-6), 45.0 (d, C-5), 40.3 (d, C-4), 36.9 (t, C-3), 17.8 (q, Si(CH(*C*H$_3$)$_2$)$_3$), 12.5 (d, Si(*C*H(CH$_3$)$_2$)$_3$); MS (CI), *m/z* (relative intensity): 552 ([M + 1]$^+$, 4), 444 (32), 400 (10), 121 (100).

(1R,4R*,5R*,6S*)-8-Methyl-*N*-phenyl-1-triisopropylsilyloxy-2-thiabicyclo[2.2.2]oct-7-ene-5,6-dicarboxylic acid imide (**18**a)*

A solution of **23** and **22***c* (3.6:1, 28 mg, 0.098 mmol), **3***b* (17.3 mg, 0.1 mmol), and dichloromaleic anhydride (2 mg) in CDCl$_3$ (0.4 mL) was sealed in an NMR tube and heated at 100°C for 22 h. The reaction mixture was concentrated and fractionated by PTLC (75% ether in hexane) to give **21***b* (4.5 mg, 36%) and **18***a* (13.7 mg, 30% from the diene mixture); IR: 1777, 1715 cm^{-1}; ^{1}H NMR δ: [7.40 (3H, m) and 7.13 (2H, m), NC$_6$H$_5$], 6.17 (1H, brs, H-7), 3.69 (1H, d, J = 8.5 Hz, H-6), 3.46 (1H, m, H-4), 3.28 (1H, dd, J = 3.5, 10.5 Hz, H-3$_{syn}$), 3.21 (1H, dd, J = 2.5, 8.5 Hz, H-5), 2.90 (1H, dd, J = 2.5, 10.5 Hz, H-3$_{anti}$), 1.90 (3H, d, J = 1.5 Hz, CH$_3$), 1.15 (21H, m, Si(CH(CH$_3$)$_2$)$_3$); ^{13}C NMR δ: 176.8 and 172.4 (s, imide C=O), 137.7 (s, C-8), 131.8 (d, C-7), [131.8 (s), 129.2 (d ×2), 128.6 (d), 126.6 (d ×2), NC$_6$H$_5$], 81.8 (s, C-1), 55.7 (d, C-6), 44.3 (d, C-5), 38.2 (d, C-4), 35.0 (t, C-3), 20.9 (q, CH$_3$), 18.3 (q, Si(CH(*C*H$_3$)$_2$)$_3$), 13.5 (d, Si(*C*H(CH$_3$)$_2$)$_3$); MS (CI), *m/z* (relative intensity): 458 ([M + 1]$^+$, 100), 414 (86), 366 (30).

(1R,4R*,5R*,6S*)-8-Diethylphosphoryloxy-*N*-phenyl-2-thiabicyclo-[2.2.2]oct-7-ene-5,6-dicarboxylic acid imide (**19**a) and (1R*,4R*,5S*,6R*)-8-diethylphosphoryloxy-*N*-phenyl-2-thiabicyclo[2.2.2]oct-7-ene-5,6-dicarboxylic acid imide (**19**b)*

A solution of **2***d* (15 mg, 0.06 mmol), **3***b* (14 mg, 0.08 mmol), and BHT (2 mg, 0.01 mmol) in CDCl$_3$ (0.4 mL) was sealed in an NMR tube and heated at 110°C. After 70 h, ^{1}H NMR revealed the absence of **2***d* and the presence[2] of a 10:1 mixture[3] of *endo*:*exo* adducts **19**. The solution was concentrated and fractionated by PTLC (75% EtOAc in hexane) to give **19***a* (15 mg, 59%); IR: 3066, 1777, 1710, 1643, 1279, 1027 cm^{-1}; ^{1}H NMR δ: 7.15–7.50 (5H, m, NC$_6$H$_5$), 6.08 (1H, brd, J = 7.5 Hz, H-7), 4.18 (1H, dd, J = 3.5, 7.5 Hz, H-1), 4.09 (4H, m, OCH$_2$), 3.75 (1H, m, H-4), 3.58 (1H, dd, J = 3.5, 8.5 Hz, H-6), 3.16 (1H, dd, J = 2.5, 8.5 Hz, H-5), 3.15 (1H, dd, J = 3, 10.5 Hz, H-3$_{syn}$), 3.01 (1H, dd, J = 3, 10.5 Hz, H- 3$_{anti}$), 1.29 (3H, t, J = 7 Hz, CH$_3$), 1.27 (3H, t, J = 7 Hz, CH$_3$); ^{13}C NMR δ: 176.0 and 175.0 (s, imide C=O), 148.4 (s, C-8), [131.6 (s), 129.1 (d ×2), 128.6 (d), 126.6 (d ×2), NC$_6$H$_5$], 111.8 (d, C-7), 64.9 (t, OCH$_2$), 48.9 (d, C-6), 43.4 (d, C-5), 37.2 (d, C-4), 35.6 (d, C-1), 32.0 (t, C-3), 16.0 (q, CH$_3$), [C-4, 7, 8, and OCH$_2$CH$_3$ show coupling to ^{31}P, J = 4–8 Hz]; MS (CI), *m/z* (relative intensity): 441 ([M + 18]$^+$, 55), 424 ([M + 1]$^+$, 100), 249 (70), 172 (32), 155 (48); and **19***b* (ca. 2 mg, 8%); IR: 3066, 1778, 1712, 1648, 1272, 1029 cm^{-1}; ^{1}H NMR δ: 7.15–7.50 (5H, m, NC$_6$H$_5$), 6.24 (1H, brd, J = 7.5 Hz, H-7), 4.23 (4H, m, OCH$_2$), 4.12 (1H, m, H-1), 3.64 (1H, m, H-4), 3.30 (2H, m, H-5, 6), 3.20 (1H, dd, J = 3, 11 Hz, H-3$_{syn}$), 2.80 (1H, brd, J = 11 Hz, H-3$_{anti}$), 1.39 (6H, brt, J = 7 Hz, CH$_3$); MS (EI), *m/z* (relative intensity): 423 (M$^+$, 10), 249 (100), 155 (67), 127 (58).

(1R,4R*,5R*,6S*)-8-Diethylphosphoryloxy-2-thiabicyclo[2.2.2]oct-7-ene-5,6-dicarboxylic acid anhydride (**20**a)*

A solution of **2***d* (25 mg, 0.1 mmol), **3***c* (15 mg, 0.15 mmol), and BHT (3 mg, 0.015 mmol) in CDCl$_3$ (0.4 mL) was sealed in an NMR tube and heated at 110°C. After 56 h, ^{1}H NMR revealed the absence of **2***d* and the presence[2] of **1***a* (ca. 10%) and a 6:1 mixture[3] of *endo*:*exo* adducts **20** (ca. 80%). The solution was concentrated and fractionated by PTLC (75% EtOAc in hexane) to give **20***a* (4.4 mg, 12%); IR: 3066, 1866, 1778, 1642, 1278, 1030 cm^{-1}; ^{1}H NMR δ: 6.10 (1H, ddd, J = 1.5, 1.5, 7.5 Hz, H-7), 4.16 (5H, m, OCH$_2$, and

Can. J. Chem. Downloaded from www.nrcresearchpress.com by 84.41.108.74 on 09/07/12
For personal use only.

H-1), 3.75 (1H, m, H-4), 3.71 (1H, dd, J = 3.5, 9 Hz, H-6), 3.27 (1H, dd, J = 2.5, 9 Hz, H-5), 3.10 (1H, dd, J = 3, 10.5 Hz, H-3_{syn}), 3.00 (1H, dd, J = 3, 10.5 Hz, H-3_{anti}), 1.36 (3H, dt, J = 1, 7 Hz, CH_3), 1.35 (3H, dt, J = 1, 7 Hz, CH_3); ^{13}C NMR δ: 170.8 and 169.5 (s, anhydride C=O), 148.5 (s, C-8), 112.4 (d, C-7), 65.1 (t, OCH_2), 49.4 (d, C-6), 44.0 (d, C-5), 36.9 (d, C-4), 34.9 (d, C-1), 31.3 (t, C-3), 16.0 (q, CH_3), [C-4, 7, 8, and OCH_2CH_3 show coupling to ^{31}P, J = 4–8 Hz]; MS (CI), *m/z* (relative intensity): 366 ([M + 18]$^+$, 100), 349 ([M + 1]$^+$, 56), 249 (24), 172 (16), 155 (45).

*4-Methoxy-*2H*-thiopyran-6(*3H,6H*)-one (**21***a*)*

A solution of methyl phenacyl sulfide (26) (166 mg, 1 mmol) in benzene (14 mL) was deaerated by bubbling argon through for 10 min. 1,3-Dimethoxy-1-trimethylsilyloxy-1,3-butadiene (17) (505 mg, 2.5 mmol) was added and the solution was irradiated in a Rayonette reactor (305 nm) through a 5% $CuSO_4$ filter at ca. 10–15°C for 4 h (14*a*). Concentration and fractionation by FCC (75% ether in hexane) gave **21***a* as an oil (72 mg, 50%); IR: 3032, 1737, 1627, 1611 cm^{-1}; ^{1}H NMR δ: 5.42 (1H, s, H-5), 3.68 (3H, s, OCH_3), 3.12 (2H, m, H-2), 2.66 (2H, m, H-3); ^{13}C NMR δ: 190.4 (s, C-6), 175.6 (s, C-4), 101.6 (d, C-5), 55.7 (q, OCH_3), 29.1 (t, C-3), 26.3 (t, C-2); MS (EI), *m/z* (relative intensity): 144 (M$^+$, 10), 86 (60), 84 (100).

*4-Methoxy-6-triisopropylsilyloxy-*2H*-thiopyran (**22**a)*

Butyllithium (0.092 mL, 2.18 M in hexanes, 0.2 mmol) was added dropwise to a solution of diisopropylamine (0.034 mL, 0.25 mmol) in THF (1 mL) at 0°C. After stirring at 0°C for 10 min, the solution was cooled to −78°C and a solution of **21***a* (14.4 mg, 0.1 mmol) in THF (1 mL) was added dropwise via syringe. After stirring for 1 h, TIPSOTf (0.06 mL, 0.22 mmol) was added and the reaction mixture was stirred for 0.5 h at −78°C and for an additional 4 h with the cooling bath removed. The reaction mixture was diluted with ether, washed with 5% Na_2CO_3, dried over $MgSO_4$, and concentrated to give the unstable **22***a* as an oil (40 mg, ca. 80% pure by ^{1}H NMR, main contaminant is **21***a*); ^{1}H NMR δ: 5.36 (1H, d, J = 1.5 Hz, H-5), 4.33 (1H, dt, J = 1.5, 5.5 Hz, H-3), 3.54 (3H, s, OCH_3), 3.49 (2H, d, J = 5.5 Hz, H-2), 1.15 (21H, m, $Si(CH(CH_3)_2)_3$).

*6-Phenylthio-4-triisopropylsilyloxy-*2H*-thiopyran (**22**b)*

Prepared from **1***b* according to the general procedure for the preparation of silyloxy dienes outlined above. The neat diene decomposes rapidly and is thus used immediately in the next step. ^{1}H NMR δ: 7.41 (5H, m, SC_6H_5), 6.09 (1H, d, J = 1.5 Hz, H-5), 4.78 (1H, dt, J = 1.5, 5.5 Hz, H-3), 3.36 (2H, d, J = 5.5 Hz, H-2), 1.10 (21H, m, $Si(CH(CH_3)_2)_3$).

*4-Methyl-6-triisopropylsilyloxy-*2H*-thiopyran (**22**c) and 3,4-dihydro-4-methylene-6-triisopropylsilyloxy-*2H*-thiopyran (**23**)*

Treatment of **21***b* (prepared in 65% yield by the method of Vedejs *et al.* (14*a*)) according to the general procedure for the preparation of silyloxy dienes outlined above gave a 3.6:1 mixture of **23** and **22***c*; ^{1}H NMR δ for **23**: 5.75 (1H, s, H-5), [4.63 (1H, m) and 4.57 (1H, m), C=CH_2], 2.92 (2H, m, H-2), 2.58 (2H, m, H-3), 1.15 (21H, m, $Si(CH(CH_3)_2)_3$); for **22***c*: 5.42 (1H, s, H-5), 5.03 (1H, tq, J = 4, 1.5 Hz, H-3), 3.36 (2H, dq, J = 4, 1.5 Hz, H-2), 1.75 (3H, dt, J = 1.5, 1.5 Hz, CH_3), 1.15 (21H, m, $Si(CH(CH_3)_2)_3$).

General procedure for reactions of 2c *with* **24**

The distilled dienophile (0.67 mmol) was added to a solution of **2***c* (68 mg, 0.25 mmol) in toluene-d_8 (0.5 mL, filtered through neutral alumina) in a 5-mm NMR tube. The tube was evacuated, sealed, and heated at 120°C. Reaction was monitored by ^{1}H NMR and when the diene was consumed the tube was opened and the reaction mixture fractionated by FCC (25% EtOAc in hexane). The ratio of *endo*:*exo* adducts[2] did not change significantly over the course of the reaction.

Reaction with **24**a

A mixture[3] of **25***a,b* (2.3:1, 35 mg, 41%) was obtained after 168 h. Pure samples of **25***a* and **25***b* were obtained by PTLC (30% CH_2Cl_2 in hexane, five elutions).

*(1*R*,4R*,6S*)-6-Acetyl-8-triisopropylsilyloxy-2-thiabicyclo[2.2.2]-oct-7-ene (**25**a)*: IR: 3054, 1712, 1636 cm^{-1}; ^{1}H NMR δ: 5.24 (1H, dd, J = 2, 7.5 Hz, H-7), 3.89 (1H, dd, J = 2.5, 7.5 Hz, H-1), 3.15 (1H, ddd, J = 2.5, 4, 10 Hz, H-6), 3.01 (1H, dd, J = 3, 9.5 Hz, H-3_{syn}), 2.97 (1H, m, H-4), 2.78 (1H, dt, J = 9.5, 2 Hz, H-3_{anti}), 2.14 (1H, m, H-5_{endo}) [coupled with H-3_{anti}, J = 2 Hz], 2.13 (3H, s, $COCH_3$), 1.79 (1H, ddd, J = 1.5, 10, 13.5 Hz, H-5_{exo}), 1.10 (21H, m, $Si(CH(CH_3)_2)_3$); ^{13}C NMR δ: 206.4 (s, $COCH_3$), 156.1 (s, C-8), 103.1 (d, C-7), 56.7 (d, C-6), 36.9 and 36.8 (d, C-1, 4), 33.3 (t, C-3), 27.8 (q, $COCH_3$), 26.7 (t, C-5), 17.9 (q, $Si(CH(CH_3)_2)_3$), 12.5 (d, $Si(CH(CH_3)_2)_3$); MS (EI), *m/z* (relative intensity): 340 (M$^+$, 35), 293 (79), 227 (26), 157 (30), 115 (54), 59 (100).

*(1*R*,4R*,6R*)-6-Acetyl-8-triisopropylsilyloxy-2-thiabicyclo[2.2.2]-oct-7-ene (**25**b)*: IR: 3064, 1712, 1639 cm^{-1}; ^{1}H NMR δ: 5.46 (1H, dd, J = 2, 8 Hz, H-7), 3.89 (1H, dd, J = 3, 8 Hz, H-1), 2.98 (1H, dd, J = 3.5, 10 Hz, H-3_{syn}), 2.87 (1H, m, H-4), 2.75 (1H, ddd, J = 3, 5.5, 11 Hz, H-6), 2.73 (1H, dt, J = 10, 2.5 Hz, H-3_{anti}), 2.24 (1H, ddd, J = 1.5, 5.5, 13.5 Hz, H-5_{exo}), 2.13 (3H, s, $COCH_3$), 1.67 (1H, dddd, J = 2.5, 4.5, 11, 13.5 Hz, H-5_{endo}), 1.10 (21H, m, $Si(CH(CH_3)_2)_3$); ^{13}C NMR δ: 206.7 (s, $COCH_3$), 157.0 (s, C-8), 105.4 (d, C-7), 55.2 (d, C-6), 37.5 and 36.5 (d, C-1, 4), 33.7 (t, C-3), 28.5 (q, $COCH_3$), 25.1 (t, C-5), 17.9 (q, $Si(CH(CH_3)_2)_3$), 12.5 (d, $Si(CH(CH_3)_2)_3$); MS (EI), *m/z* (relative intensity): 340 (M$^+$, 99), 297 (69), 293 (44), 227 (68), 157 (46), 115 (79), 59 (100).

Reaction with **24**b

A mixture[3] of **26***a,b* (1.7:1, 49 mg, 56%) was obtained after 144 h. Pure samples of the **26***a* and **26***b* were obtained by PTLC (30% CH_2Cl_2 in hexane, four elutions).

*(1*R*,4R*,6S*)-8-Triisopropylsilyloxy-2-thiabicyclo[2.2.2]oct-7-ene-6-carboxylic acid, methyl ester (**26**a)*: IR: 3022, 1739, 1638 cm^{-1}; ^{1}H NMR δ: 5.27 (1H, dd, J = 2, 7.5 Hz, H-7), 3.95 (1H, dd, J = 3, 7.5 Hz, H-1), 3.63 (3H, s, OCH_3), 3.16 (1H, ddd, J = 3.5, 3.5, 10 Hz, H-6), 2.96 (2H, m, H-3_{syn}, 4), 2.74 (1H, m, H-3_{anti}) [coupled to H-5_{endo}, J = 2 Hz], 2.19 (1H, m, H-5_{endo}) [coupled with H-3_{anti}, J = 2 Hz], 1.87 (1H, ddd, J = 1.5, 10, 13.5 Hz, H-5_{exo}), 1.10 (21H, m, $Si(CH(CH_3)_2)_3$); ^{13}C NMR δ: 173.3 (s, $COOCH_3$), 156.0 (s, C-8), 103.5 (d, C-7), 51.9 (q, OCH_3), 48.2 (d, C-6), 37.1 and 36.6 (d, C-1, 4), 33.3 (t, C-3), 27.7 (t, C-5), 17.9 (q, $Si(CH(CH_3)_2)_3$), 12.5 (d, $Si(CH(CH_3)_2)_3$); MS (EI), *m/z* (relative intensity): 356 (M$^+$, 51), 309 (36), 227 (34), 115 (50), 59 (100).

*(1*R*,4R*,6R*)-8-Triisopropylsilyloxy-2-thiabicyclo[2.2.2]oct-7-ene-6-carboxylic acid, methyl ester (**26**b)*: IR: 3063, 1740, 1639 cm^{-1}; ^{1}H NMR δ: 5.43 (1H, dd, J = 2, 8 Hz, H-7), 3.88 (1H, dd, J = 3, 8 Hz, H-1), 3.72 (3H, s, OCH_3), 3.02 (1H, dd, J = 3.5, 10 Hz, H-3_{syn}), 2.87 (1H, m, H-4), 2.82 (1H, ddd, J = 3, 5.5, 11.5 Hz, H-6), 2.75 (1H, dt, J = 10, 2.5 Hz, H-3_{anti}), 2.19 (1H, ddd, J = 1.5, 5.5, 13.5 Hz, H-5_{exo}), 1.83 (1H, dddd, J = 2.5, 4.5, 11.5, 13.5, H-5_{endo}), 1.10 (21H, m, $Si(CH(CH_3)_2)_3$); ^{13}C NMR δ: 173.3 (s, $COOCH_3$), 156.6 (s, C-8), 105.2 (d, C-7), 52.2 (q, OCH_3), 47.6 (d, C-6), 38.1 and 36.3 (d, C-1, 4), 33.8 (t, C-3), 26.3 (t, C-5), 17.9 (q, $Si(CH(CH_3)_2)_3$), 12.5 (d, $Si(CH(CH_3)_2)_3$); MS (EI), *m/z* (relative intensity): 356 (M$^+$, 39), 323 (31), 270 (21), 227 (26), 115 (34), 59 (100).

Reaction with **24**c

A mixture[3] of **27***a,b* (1:1, 35 mg, 43%) was obtained after 144 h. Pure samples of the **27***a* and **27***b* were obtained by PTLC (30% CH_2Cl_2 in hexane, three elutions).

*(1*S*,4R*,6S*)-8-Triisopropylsilyloxy-2-thiabicyclo[2.2.2]oct-7-ene-6-carbonitrile (**27**a)*: IR: 3050, 2234, 1637 cm^{-1}; ^{1}H NMR δ: 5.42 (1H, dd, J = 2, 7.5 Hz, H-7), 3.76 (1H, dd, J = 3, 7.5 Hz, H-1), 3.29 (1H, ddd, J = 3, 3.5, 10 Hz, H-6), 2.96 (2H, m, H-3_{syn}, 4), 2.77 (1H, m, H-3_{anti}) [coupled to H-5_{endo}, J = 2 Hz], 2.13 (1H, ddd, J = 1.5, 10, 13.5 Hz, H-5_{exo}), 1.90 (1H, m, H-5_{endo}) [coupled with H-3_{anti}, J = 2 Hz], 1.10 (21H, m, $Si(CH_3)_2)_3$); ^{13}C NMR δ: 156.4 (s, C-8), 121.5 (s, CN), 102.7 (d, C-7), 37.0 and 35.7 (d, C-1, 4), 33.4 (d, C-6), 32.9 (t, C-3), 29.9 (t, C-5), 17.9 (q, $Si(CH(CH_3)_2)_3$), 12.5 (d, $Si(CH(CH_3)_2)_3$); MS (EI), *m/z* (relative intensity): 323 (M$^+$, 55), 227 (100), 115 (41), 97 (48), 59 (68).

Can. J. Chem. Downloaded from www.nrcresearchpress.com by 84.41.108.74 on 09/07/12
For personal use only.

(1S,4R*,6R*)-8-Triisopropylsilyloxy-2-thiabicyclo[2.2.2]oct-7-ene-6-carbonitrile (27b)*: IR: 3060, 2238, 1638 cm^{-1}; ^1H NMR δ: 5.37 (1H, dd, J = 2, 8 Hz, H-7), 3.70 (1H, dd, J = 2.5, 8 Hz, H-1), 3.12 (1H, dd, J = 3.5, 10 Hz, H-3_{syn}), 2.93 (1H, m, H-4), 2.89 (1H, ddd, J = 2.5, 6, 11.5 Hz, H-6), 2.81 (1H, dt, J = 10, 2.5 Hz, H-3_{anti}), 2.08 (1H, dddd, J = 2.5, 4.5, 11.5, 13.5 Hz, H-5_{endo}), 1.89 (1H, ddd, J = 1.5, 6, 13.5 Hz, H-5_{exo}), 1.10 (21H, m, $Si(CH(CH_3)_2)_3$); ^{13}C NMR δ: 155.8 (s, C-8), 121.8 (s, CN), 104.3 (d, C-7), 37.9 and 35.8 (d, C-1, 4), 34.0 (t, C-3), 33.9 (d, C-6), 28.7 (t, C-5), 17.9 (q, $Si(CH(CH_3)_2)_3$), 12.5 (d, $Si(CH(CH_3)_2)_3$); MS (EI), *m/z* (relative intensity): 323 (M^+, 67), 323 (31), 227 (43), 147 (71), 59 (100).

(1R,4R*,5R*,6R*)-8-Triisopropylsilyloxy-2-thiabicyclo[2.2.2]oct-7-ene-5,6-dicarboxylic acid, dimethyl esther (28) and (1R*,4R*,5S*,6S*)-8-triisopropylsilyloxy-2-thiabicyclo[2.2.2]-oct-7-ene-5,6-dicarboxylic acid, dimethyl ester (29)*

A solution of **2***c* (68 mg, 0.25 mmol) and dimethyl fumarate (144 mg, 1 mmol) in toluene-d_8 (0.5 mL) was sealed in an NMR tube and heated at 120°C for 168 h. Fractionation by FCC (25% EtOAc in hexane) gave a 2.5:1 mixture of the adducts **28** and **29** (13 mg, 12%) as an oil; IR: 3060, 1738, 1639 cm^{-1}; ^1H NMR (C_6D_6) δ for **28**: 5.28 (1H, dd, J = 2, 7.5 Hz, H-7), 3.98 (1H, dd, J = 3, 8 Hz, H-1), 3.62 (1H, dd, J = 3, 5.5 Hz, H-6), 3.58 (1H, dd, J = 1.5, 5.5 Hz, H-5), 3.42 (3H, s, OCH_3), 3.36 (3H, s, OCH_3), 3.31 (1H, m, H-4), 2.79 (1H, dd, J = 3, 10.5 Hz, H-3_{syn}), 2.61 (1H, dd, J = 3, 10.5 Hz, H-3_{anti}), 1.10 (21H, m, $Si(CH(CH_3)_2)_3$); for **29**: 5.27 (1H, dd, J = 2, 7.5 Hz, H-7), 4.08 (1H, dd, J = 2.5, 5 Hz, H-6), 4.00 (1H, dd, J = 2.5, 7.5 Hz, H-1), 3.67 (1H, ddd, J = 1.5, 4.5, 5 Hz, H-5), 3.52 (1H, m, H-4), 3.30 (3H, s, OCH_3), 3.28 (3H, s, OCH_3), 3.08 (1H, dd, J = 3, 11 Hz, H-3_{syn}), 2.64 (1H, ddd, J = 1.5, 2.5, 11 Hz, H-3_{anti}), 1.10 (21H, m, $Si(CH(CH_3)_2)_3$); ^{13}C NMR δ for **28**: 173.5 and 172.1 (s, $COOCH_3$), 154.4 (s, C-8), 104.6 (d, C-7), 52.3 (q ×2, OCH_3), 51.0 (d, C-6), 43.9 (d, C-5), 39.4 and 38.0 (d, C-1, 4), 33.1 (t, C-3), 17.9 (q, $Si(CH(CH_3)_2)_3$), 12.5 (d, $Si(CH(CH_3)_2)_3$); for **29**: 172.6 and 173.3 (s, $COOCH_3$), 156.0 (s, C-8), 103.5 (d, C-7), 52.2 (q ×2, OCH_3), 50.7 (d, C-6), 44.1 (d, C-5), 39.2 and 37.1 (d, C-1, 4), 28.3 (t, C-3), 17.9 (q, $Si(CH(CH_3)_2)_3$), 12.5 (d, $Si(CH(CH_3)_2)_3$); MS (EI), *m/z* (relative intensity): 414 (M^+, 58), 371 (58), 309 (41), 227 (64), 59 (100).

An identical experiment carried out with dimethyl maleate for 226 h gave a 1.2:1 mixture of the *trans* adducts **28** and **29** (30 mg, 29%). Dimethyl maleate isomerizes to dimethyl fumarate under the reaction conditions (^1H NMR).

3,5-Bis(triisopropylsilyloxy)-2H-thiopyran (30)

Prepared from 2*H*-thiopyran-3,5(4*H*,6*H*)-dione (**31**) (18) according to the general procedure for the preparation of silyloxy dienes outlined above using twice the amount of reagents; IR: 3061, 1631 cm^{-1}; ^1H NMR δ: 5.13 (1H, d, J = 0.5 Hz, H-4), 4.97 (1H, d, J = 0.5 Hz, H-6), 3.21 (2H, s, H-2), 1.10 (42H, m, $Si(CH(CH_3)_2)_3$); ^{13}C NMR δ: 149.5 and 148.2 (s, C-3, 5), 104.5 (d, C-4), 88.7 (d, C-6), 29.2 (t, C-2), 17.8 (q, $Si(CH(CH_3)_2)_3$), 12.5 (d, $Si(CH(CH_3)_2)_3$); MS (EI), *m/z* (relative intensity): 442 (M^+, 100), 399 (16), 286 (20), 243 (24), 115 (37), 87 (38), 73 (53), 59 (95).

3-Triisopropylsilyloxy-2H-thiopyran (33a) and 5-triisopropylsilyloxy-2H-thiopyran (34a)

Butyllithium (0.082 mL, 2.18 M in hexanes, 0.18 mmol) was added dropwise to a solution of diisopropylamine (0.030 mL, 0.22 mmol) in THF (18 mL) at 0°C. After stirring at 0°C for 10 min, the solution was cooled to −78°C and a solution of **32** (20) (15.2 mg, 0.13 mmol) in THF (1 mL) was added dropwise via syringe. After stirring for 1 h, TIPSOTf (0.038 mL, 0.14 mmol) was added and the reaction mixture was stirred for 0.5 h at −78°C and saturated $NaHCO_3$ (ca. 1 mL) was added. The reaction mixture was diluted with CH_2Cl_2, washed with saturated $NaHCO_3$, dried over Na_2SO_4, concentrated, and fractionated by FCC (hexane, SiO_2 was pretreated with Et_3N) to give a 2:1–4:1 mixture of **34***a* and **33***a* as an oil (31 mg, 85%). Alternatively, treatment of **32** with TIPSOTf according to the general procedure for the preparation of silyloxy dienes outlined above gave a 1:4 mixture of **34***a* and **33***a*. The above mixtures were used in Diels–Alder reactions without further purification. Pure samples of the individual dienes were obtained by PTLC (hexane, two elutions).

For **33***a*: IR: 3059, 3026, 1631, 1555 cm^{-1}; ^1H NMR δ: 5.99 (1H, dd, J = 6.5, 9 Hz, H-5), 5.78 (1H, d, J = 9 Hz, H-6), 5.26 (1H, d, J = 6.5 Hz, H-4), 3.32 (2H, s, H-2), 1.10 (21H, m, $Si(CH(CH_3)_2)_3$); ^{13}C NMR δ: 144.7 (s, C-3), 122.4 (d, C-5), 111.5 (d, C-6), 103.1 (d, C-4), 28.7 (t, C-2), 17.9 (q, $Si(CH(CH_3)_2)_3$), 12.6 (d, $Si(CH(CH_3)_2)_3$); MS (EI), *m/z* (relative intensity): 270 (M^+, 84), 227 (83), 115 (71), 87 (61), 59 (100).

For **34***a*: IR: 3036, 1626, 1547 cm^{-1}; ^1H NMR δ: 5.84 (1H, dm, H-4), 5.73 (1H, ddt, J = 0.5, 10, 5 Hz, H-3), 5.36 (1H, brs, H-6), 3.13 (2H, dm, J = 5 Hz, H-2), 1.10 (21H, m, $Si(CH(CH_3)_2)_3$); ^{13}C NMR δ: 147.4 (s, C-5), 127.3 (d, C-4), 119.0 (d, C-3), 98.3 (d, C-6), 23.9 (t, C-2), 17.9 (q, $Si(CH(CH_3)_2)_3$), 12.5 (d, $Si(CH(CH_3)_2)_3$); MS (EI), *m/z* (relative intensity): 270 (M^+, 93), 227 (100), 97 (72), 59 (53).

3-Diethylphosphoryloxy-2H-thiopyran (33b) and 5-diethylphosphoryloxy-2H-thiopyran (34b)

Using the procedure described for the preparation of **2***d*, **32** (75 mg, 0.65 mmol) gave after fractionation by FCC (17% EtOAc in ether) **33***b* (14.2 mg, 9%); IR: 3052, 1647, 1278, 1029 cm^{-1}; ^1H NMR δ: 6.02 (2H, m, H-5, 6), 5.86 (1H, m, H-4), 4.21 (4H, dq, J = 8, 7 Hz, OCH_2), 3.49 (2H, brs, H-2), 1.38 (6H, dt, J = 1, 7 Hz, CH_3); MS (CI), *m/z* (relative intensity): 268 ($[M + 18]^+$, 52), 251 ($[M + 1]^+$, 100), 96 (64); and **34***b* (66.8 mg, 40%); IR: 3049, 1626, 1273, 1030 cm^{-1}; ^1H NMR δ: 5.98 (1H, brs, H-6), 5.91 (1H, d, J = 10 Hz, H-4), 5.68 (1H, dt, J = 10, 5.5 Hz, H-3), 4.12 (4H, dq, J = 8, 7 Hz, OCH_2), 3.20 (2H, dd, J = 1, 5.5 Hz, H-2), 1.35 (6H, t, J = 7 Hz, CH_3); ^{13}C NMR δ: 142.3 (s, C-5), 124.2 (d, C-4), 118.6 (d, C-3), 107.0 (d, C-6), 64.5 (t, OCH_2), 23.8 (t, C-2), 16.1 (q, CH_3), [C-4, 5, 6, and OCH_2CH_3 show coupling to ^{31}P, J = 4–8 Hz]; MS (CI), *m/z* (relative intensity): 268 ($[M + 18]^+$, 66), 251 ($[M + 1]^+$, 100), 155 (22), 96 (25).

(1S,4R*,5S*,6S*)-4,7-Bis(triisopropylsilyloxy)-2-thiabicyclo[2.2.2]-oct-7-ene-5,6-dicarboxylic acid imide (35a) and (1S*,4R*,5R*,6R*)-4,7-bis(triisopropylsilyloxy)-2-thiabicyclo-[2.2.2]oct-7-ene-5,6-dicarboxylic acid imide (35b)*

A solution of **30** (446 mg, 1 mmol) and **3***a* (97 mg, 1.3 mmol) in toluene (6 mL) was heated under reflux under Ar for 127 h. The reaction mixture was concentrated and fractionated by FCC (20% EtOAc in hexane) to give a mixture[3] of **35***a,b* (3:1, 270 mg, 50%); IR: 3209, 3078, 1782, 1718, 1631 cm^{-1}; ^1H NMR δ for **35***a*: 8.02 (1H, brs, NH), 4.93 (1H, d, J = 2 Hz, H-8), 3.68 (1H, dd, J = 2, 3.5 Hz, H-1), 3.46 (1H, dd, J = 3.5, 8.5 Hz, H-6), 2.96 (1H, d, J = 9.5 Hz, H-3_{syn}), 2.92 (1H, d, J = 8.5 Hz, H-5), 2.77 (1H, d, J = 9.5 Hz, H-3_{anti}), 1.10 (21H, m, $Si(CH(CH_3)_2)_3$); for **35***b*: 8.18 (1H, brs, NH), 5.12 (1H, d, J = 2 Hz, H-8), 3.58 (1H, dd, J = 2, 4 Hz, H-1), 3.39 (1H, dd, J = 4, 10 Hz, H-6), 3.16 (1H, d, J = 10 Hz, H-3_{syn}), 2.97 (1H, dd, J = 2, 10 Hz, H-5), 2.65 (1H, dd, J = 2, 10 Hz, H-3_{anti}), 1.10 (21H, m, $Si(CH(CH_3)_2)_3$); ^{13}C NMR δ for **35***a*: 175.5 and 174.5 (s, imide C=O), 152.5 (s, C-7), 104.5 (d, C-8), 77.1 (s, C-4), 51.0 and 50.8 (d, C-5, 6), 39.5 (t, C-3), 37.8 (d, C-1), 18.3 and 17.8 (q, $Si(CH(CH_3)_2)_3$), 13.4 and 12.5 (d, $Si(CH(CH_3)_2)_3$); for **35***b*: 176.2 and 175.4 (s, imide C=O), 153.8 (s, C-7), 108.3 (d, C-8), 76.2 (s, C-4), 52.2 and 50.7 (d, C-5, 6), 38.4 (d, C-1), 36.4 (t, C-3), 18.2 and 17.8 (q, $Si(CH(CH_3)_2)_3$), 13.4 and 12.5 (d, $Si(CH(CH_3)_2)_3$); MS (CI), *m/z* (relative intensity): 540 ($[M + 1]^+$, 100), 496 (61), 384 (22), 340 (43), 148 (49).

(1S,4R*,5S*,6S*)-N-Phenyl-4,7-bis(triisopropylsilyloxy)-2-thiabicyclo[2.2.2]oct-7-ene-5,6-dicarboxylic acid imide (36a) and (1S*,4R*,5R*,6R*)-N-phenyl-4,7-bis(triisopropylsilyloxy)-2-thiabicyclo[2.2.2]oct-7-ene-5,6-dicarboxylic acid imide (36b)*

A solution of **30** (380 mg, 0.86 mmol) and **3***b* (175 mg, 1 mmol) in toluene (6 mL) was heated under reflux under Ar for 78 h. The reaction mixture was concentrated and fractionated by FCC (10% EtOAc in hexane) to give a mixture[3] of **36***a,b* (2:1, 365 mg, 69%). Pure samples of **36***a* and **36***b* were obtained by PTLC (10% ether in hexane, three elutions).

Can. J. Chem. Downloaded from www.nrcresearchpress.com by 84.41.108.74 on 09/07/12
For personal use only.

For **36***a*: IR: 3045, 1779, 1719, 1631 cm^{-1}; ^1H NMR δ: 7.15–7.50 (5H, m, C_6H_5), 4.99 (1H, d, J = 2 Hz, H-8), 3.81 (1H, dd, J = 2, 3.5 Hz, H-1), 3.58 (1H, dd, J = 3.5, 8.5 Hz, H-6), 3.05 (1H, d, J = 8.5 Hz, H-5), 3.05 (1H, d, J = 9 Hz, H-3_{syn}), 2.82 (1H, d, J = 9 Hz, H-3_{anti}), 1.10 (42H, m, $Si(CH(CH_3)_2)_3$); ^{13}C NMR δ: 174.4 and 173.4 (s, imide C═O), 152.7 (s, C-7), [131.9 (s), 129.0 (d ×2), 128.4 (d), 126.4 (d ×2), N-C_6H_5], 104.6 (d, C-8), 77.4 (s, C-4), 49.8 and 49.7 (d, C-5, 6), 39.9 (t, C-3), 38.1 (d, C-1), 18.3 and 17.9 (q, $Si(CH(CH_3)_2)_3$), 13.5 and 12.5 (d, $Si(CH(CH_3)_2)_3$); MS (CI), *m/z* (relative intensity): 616 ($[M + 1]^+$, 100), 572 (93), 442 (31), 148 (87).

For **36***b*: IR: 3062, 1780, 1719, 1633 cm^{-1}; ^1H NMR δ: 7.15–7.50 (5H, m, C_6H_5), 5.18 (1H, d, J = 2 Hz, H-8), 3.73 (1H, dd, J = 2, 3.5 Hz, H-1), 3.49 (1H, dd, J = 3.5, 10 Hz, H-6), 3.19 (1H, d, J = 10 Hz, H-3_{syn}), 3.12 (1H, dd, J = 2, 10 Hz, H-5), 2.68 (1H, dd, J = 2, 10 Hz, H-3_{anti}), 1.10 (42H, m, $Si(CH(CH_3)_2)_3$); ^{13}C NMR δ: 175.3 and 174.4 (s, imide C═O), 154.0 (s, C-7), [131.7 (s), 129.2 (d ×2), 128.7 (d), 126.7 (d ×2), N-C_6H_5], 108.6 (d, C-8), 76.5 (s, C-4), 51.1 and 49.4 (d, C-5, 6), 39.3 (d, C-1), 36.6 (t, C-3), 18.3 and 17.7 (q, $Si(CH(CH_3)_2)_3$), 13.4 and 12.6 (d, $Si(CH(CH_3)_2)_3$); MS (CI), *m/z* (relative intensity): 616 ($[M + 1]^+$, 100), 572 (61), 442 (26), 148 (33).

(1S,4S*,5R*,6S*)-*N*-Phenyl-7-triisopropylsilyloxy-2-thiabicyclo-[2.2.2]oct-7-ene-5,6-dicarboxylic acid imide (**37**a) and (1R*,4R*,5S*,6S*)-*N*-phenyl-4-triisopropylsilyloxy-2-thiabicyclo[2.2.2]oct-7-ene-5,6-dicarboxylic acid imide (**38**a)*

A solution of **34***a* and **33***a* (2:3, 49 mg, 0.18 mmol) and **3***b* (29 mg, 0.17 mmol) in toluene-d_8 (0.5 mL) was sealed in an NMR tube and heated at 110°C. After 24 h the ^1H NMR spectrum of the reaction mixture revealed the absence of **34***a*. The reaction mixture was concentrated and fractionated by FCC (20% EtOAc in hexane) to give **33***a* (21 mg, 42%), **32** (2 mg, 4%), and **37***a* (19 mg, 57% from **34***a*); IR: 3060, 3030, 1780, 1710, 1637 cm^{-1}; ^1H NMR δ: 7.15–7.50 (5H, m, C_6H_5), 4.98 (1H, dd, J = 2, 7.5 Hz, H-8), 3.87 (1H, dd, J = 2, 3.5 Hz, H-1), 3.67 (1H, dq, J = 7.5, 2.5 Hz, H-4), 3.55 (1H, dd, J = 3.5, 8.5 Hz, H-6), 3.11 (1H, dd, J = 2.5, 10 Hz, H-3_{syn}), 3.01 (1H, dd, J = 2.5, 8.5 Hz, H-5), 2.70 (1H, dd, J = 3, 10 Hz, H-3_{anti}), 1.10 (21H, m, $Si(CH(CH_3)_2)_3$); ^{13}C NMR δ: 177.4 and 175.0 (s, imide C═O), 154.5 (s, C-7), [131.7 (s), 129.0 (d ×2), 128.6 (d), 126.3 (d ×2), N-C_6H_5], 98.9 (d, C-8), 48.9 (d, C-6), 43.6 (d, C-5), 38.7 (d, C-1), 34.1 (d, C-4), 33.8 (t, C-3), 17.9 (q, $Si(CH(CH_3)_2)_3$), 12.5 (d, $Si(CH(CH_3)_2)_3$); MS (EI), *m/z* (relative intensity): 443 (M^+, 6), 400 (100), 227 (42).

A solution of **33***a* (21 mg, 0.078 mmol) and **3***b* (14 mg, 0.08 mmol) in toluene-d_8 (0.5 mL) was sealed in an NMR tube and heated at 110°C. After 120 h the ^1H NMR spectrum revealed the absence of **33***a*. The reaction mixture was concentrated and fractionated by FCC (20% EtOAc in hexane) to give **38***a* (5 mg, 14%, contaminated (ca. 5%) with a structurally related inseparable impurity); IR: 3055, 1779, 1716 cm^{-1}; ^1H NMR δ: 7.15–7.50 (5H, m, C_6H_5), 6.47 (1H, dd, J = 6.5, 9 Hz, H-7), 6.25 (1H, dd, J = 9 Hz, H-8), 3.99 (1H, dd, J = 3, 6.5 Hz, H-1), 3.66 (1H, dd, J = 3, 8.5 Hz, H-6), 3.12 (1H, d, J = 8.5 Hz, H-5), 3.08 (1H, d, J = 9.5 Hz, H-3_{syn}), 2.77 (1H, d, J = 9.5 Hz, H-3_{anti}), 1.10 (21H, m, $Si(CH(CH_3)_2)_3$); ^{13}C NMR δ: 175.1 and 173.1 (s, imide C═O), 135.4 and 130.6 (d, C-7, 8), [131.8 (s), 129.2 (d ×2), 128.7 (d), 126.5 (d ×2), N-C_6H_5], 75.7 (s, C-4), 50.3 and 48.8 (d, C-5, 6), 38.5 (t, C-3), 32.7 (d, C-1), 18.3 (q, $Si(CH(CH_3)_2)_3$), 13.5 (d, $Si(CH(CH_3)_2)_3$); MS (CI), *m/z* (relative intensity): 444 ($[M + 1]^+$, 100), 400 (59).

(1S,4S*,5R*,6S*)-7-Diethylphosphoryloxy-*N*-phenyl-2-thiabicyclo-[2.2.2]oct-7-ene-5,6-dicarboxylic acid imide (**39**a) and (1S*,4S*,5S*,6R*)-7-diethylphosphoryloxy-*N*-phenyl-2-thiabicyclo[2.2.2]oct-7-ene-5,6-dicarboxylic acid imide (**39**b)*

A solution of **34***b* (19 mg, 0.076 mmol) and **3***b* (26 mg, 0.15 mmol) in $CDCl_3$ (0.4 mL) was sealed in an NMR tube and heated at 110°C. After 51 h, ^1H NMR revealed the absence of **34***b* and the presence[2] of a 10:1 mixture[3] of *endo*:*exo* adducts **39**. The solution was concentrated and fractionated by PTLC (75% EtOAc in ether) to give **39***a* (25 mg, 77%); IR: 3066, 1777, 1710, 1642, 1282, 1027 cm^{-1}; ^1H NMR δ: 7.15–7.50 (5H, m, NC_6H_5), 5.78 (1H, brd, J = 7.5 Hz, H-8), 4.13 (4H, m, OCH_2), 4.02 (1H, m, H-1), 3.80 (1H, dddd, J = 2.5, 3, 3, 7.5 Hz, H-4), 3.58 (1H, dd, J = 3.5, 8.5 Hz, H-6), 3.13 (1H, dd, J = 3, 10.5 Hz, H-3_{syn}), 3.05 (1H, dd, J = 3, 8.5 Hz, H-5), 2.77 (1H, dd, J = 3, 10.5 Hz, H-3_{anti}), 1.31 (3H, t, J = 7 Hz, CH_3), 1.21 (3H, t, J = 7 Hz, CH_3); ^{13}C NMR δ: 176.6 and 174.6 (s, imide C═O), 149.2 (s, C-7), [131.6 (s), 129.2 (d ×2), 128.9 (d), 126.6 (d ×2), NC_6H_5], 107.1 (d, C-8), 64.8 (t, OCH_2), 49.0 (d, C-6), 43.1 (d, C-5), 36.7 (d, C-1), 34.0 (d, C-4), 32.8 (t, C-3), 16.0 (q, CH_3), [C-1, 7, 8 and OCH_2CH_3 show coupling to ^{31}P, J = 4–8 Hz]; MS (EI), *m/z* (relative intensity): 423 (M^+, 35), 377 (20), 250 (91), 230 (83), 104 (100); and **39***b* (ca. 2 mg, 6%); IR: 1778, 1712, 1648, 1278, 1029 cm^{-1}; ^1H NMR δ: 7.15–7.50 (5H, m, NC_6H_5), 6.00 (1H, ddd, J = 1.5, 2, 8 Hz, H-8), 4.23 (4H, m, OCH_2), 4.00 (1H, dd, J = 2, 4 Hz, H-1), 3.71 (1H, dddd, J = 2.5, 3, 5, 8 Hz, H-4), 3.49 (1H, dd, J = 4, 10 Hz, H-6), 3.18 (1H, dd, J = 3, 11 Hz, H-3_{syn}), 3.06 (1H, ddd, J = 1.5, 5, 10 Hz, H-5), 2.77 (1H, ddd, J = 1.5, 2.5, 11 Hz, H-3_{anti}), 1.40 (3H, t, J = 7 Hz, CH_3), 1.39 (3H, t, J = 7 Hz, CH_3); MS (EI), *m/z* (relative intensity): 423 (M^+, 14), 377 (6), 250 (36), 249 (39), 29 (100).

(1R,4S*,5S*,6S*)-4-Diethylphosphoryloxy-*N*-phenyl-2-thiabicyclo-[2.2.2]oct-7-ene-5,6-dicarboxylic acid imide (**40**a) and (1R*,4S*,5R*,6R*)-4-diethylphosphoryloxy-*N*-phenyl-2-thiabicyclo[2.2.2]oct-7-ene-5,6-dicarboxylic acid imide (**40**b)*

A solution of **33***b* (18 mg, 0.072 mmol) and **3***b* (20.8 mg, 0.12 mmol) in $CDCl_3$ (0.4 mL) was sealed in an NMR tube and heated at 110°C. After 270 h, ^1H NMR revealed the presence[2] of a >10:1 mixture of *endo*:*exo* adducts **40**. The solution was concentrated and fractionated by PTLC (33% EtOAc in ether) to give **33***b* (4 mg, 22%), the *endo* adduct **40***a* (15 mg, 50%); IR: 3065, 1778, 1714, 1597, 1279, 1033 cm^{-1}; ^1H NMR δ: 7.15–7.50 (5H, m, NC_6H_5), 6.52 (1H, dd, J = 7, 9 Hz, H-7), 6.41 (1H, d, J = 9 Hz, H-8), 4.10–4.40 (4H, m, OCH_2), 4.01 (1H, dd, J = 3, 7 Hz, H-1), 3.87 (1H, d, J = 8 Hz, H-5), 3.68 (1H, dd, J = 3, 8 Hz, H-6), 3.60 (1H, d, J = 10 Hz, H-3_{syn}), 3.00 (1H, d, J = 10 Hz, H-3_{anti}), 1.36 (3H, t, J = 7 Hz, CH_3), 1.35 (3H, t, J = 7 Hz, CH_3); ^{13}C NMR δ: 174.5 and 173.0 (s, imide C═O), 132.0 (s, C-8), [131.6 (s), 129.2 (d ×2), 128.9 (d), 126.5 (d ×2), NC_6H_5], 131.1 (d, C-7), 80.7 (s, C-4), 64.7 and 64.2 (t, OCH_2), 49.6 (d, C-6), 45.8 (d, C-5), 34.0 (t, C-3), 33.1 (d, C-1), 16.1 (q, CH_3), [C-4, 5, 8 and OCH_2CH_3 show coupling to ^{31}P, J = 4–8 Hz]; MS (CI), *m/z* (relative intensity): 424 ($[M + 1]^+$, 100), 250 (29), 155 (30); and **40***b* (ca. 1.5 mg, 5%); IR: 1778, 1713, 1499, 1272, 1030 cm^{-1}; ^1H NMR δ: 7.15–7.50 (5H, m, NC_6H_5), 6.74 (1H, d, J = 9 Hz, H-8), 6.64 (1H, dd, J = 7, 9 Hz, H-7), 4.05–4.40 (4H, m, OCH_2), 4.00 (1H, dd, J = 3.5, 7 Hz, H-1), 3.89 (1H, dd, J = 2, 10 Hz, H-5), 3.39 (1H, dd, J = 3.5, 10 Hz, H-6), 3.35 (1H, d, J = 10 Hz, H-3_{syn}), 2.81 (1H, dd, J = 2, 10 Hz, H-3_{anti}), 1.37 (6H, m, CH_3); MS (EI), *m/z* (relative intensity): 424 ($[M + 1]^+$, 100), 250 (52), 155 (89).

(1S,4R*,5S*)-5-Acetyl-4-triisopropylsilyloxy-2-thiabicyclo[2.2.2]-octan-7-one (**43**) and (1S*,4R*,5R*)-5-acetyl-4-triisopropylsilyloxy-2-thiabicyclo[2.2.2]octan-7-one (**44**)*

A solution of **30** (110 mg, 0.25 mmol) and **24***a* (70 mg, 1 mmol) in toluene-d_8 (0.5 mL) was sealed in an NMR tube and heated at 110°C for 240 h. The reaction mixture was concentrated and fractionated by FCC (20% EtOAc in hexane) to give a mixture[2] of **41** and **42** (8:1, 18 mg, 14%) and **44** (5 mg, 5.6%). Attempted separation of **41** and **42** (PTLC, 10% EtOAc in hexane, three elutions) resulted in the isolation of **43**.

For **41** and **42** (8:1); ^1H NMR δ for **41**: 4.96 (1H, d, J = 1 Hz, H-8), 3.23 (1H, m, H-1), 3.05 (1H, dd, J = 6, 10 Hz, H-5), 2.96 (1H, d, J = 9 Hz, H-3_{syn}), 2.74 (1H, d, J = 9 Hz, H-3_{anti}), 2.26 (1H, ddd, J = 3, 10, 13 Hz, H-6_{exo}), 2.18 (3H, s, $COCH_3$), 2.01 (1H, ddd, J = 3, 6, 13 Hz, H-6_{endo}), 1.15 (42H, m, $Si(CH(CH_3)_2)_3$); partial data for **42**: 5.19 (1H, br, H-8), 2.31 (3H, s, $COCH_3$).

For **43**; IR: 1729, 1716 cm^{-1}; ^1H NMR δ: 3.30 (1H, ddd, J = 2, 6.5, 10.5 Hz, H-5), 3.14 (1H, dd, J = 2, 18 Hz, H-8_{endo}), 3.00 (1H, dd, J = 3, 3.5 Hz, H-1), 2.93 (1H, d, J = 9.5 Hz, H-3_{anti}), 2.88 (1H, dd, J = 2, 9.5 Hz, H-3_{syn}), 2.57 (1H, dd, J = 2, 18 Hz, H-8_{exo}), 2.46

(1H, ddd, J = 3, 6.5, 14 Hz, H-6$_{endo}$), 2.39 (1H, ddd, J = 3.5, 10.5, 14 Hz, H-6$_{exo}$), 2.30 (3H, s, $COCH_3$), 1.10 (21H, m, $Si(CH(CH_3)_2)_3$); ^{13}C NMR δ: 210.8 (s, C-7), 201.2 (s, $COCH_3$), 75.6 (s, C-4), 52.1 (d, C-5), 46.5 (t, C-8), 40.5 (d, C-1), 36.0 (t, C-3), 34.3 (q, $COCH_3$), 30.4 (t, C-5), 18.2 (q, $Si(CH(CH_3)_2)_3$), 13.4 (d, $Si(CH(CH_3)_2)_3$); MS (CI), *m/z* (relative intensity): 374 ($[M + 18]^+$, 100), 357 ($[M + 1]^+$, 46), 313 (63).

For **44**; IR: 1719 cm^{-1}; ^1H NMR δ: 3.39 (1H, dd, J = 2, 10 Hz, H-3$_{syn}$), 3.10 (1H, ddd, J = 2, 7.5, 11 Hz, H-5), 3.01 (1H, d, J = 18 Hz, H-8$_{exo}$), 2.98 (1H, dd, J = 2, 4.5 Hz, H-1), 2.67 (1H, dd, J = 2, 10 Hz, H-3$_{anti}$), 2.60 (1H, ddd, J = 2, 7.5, 14.5 Hz, H-6$_{exo}$), 2.54 (1H, dd, J = 2, 18 Hz, H-8$_{endo}$), 2.31 (3H, s, $COCH_3$), 2.30 (1H, ddd, J = 4.5, 11, 14.5 Hz, H-6$_{endo}$), 1.10 (21H, m, $Si(CH(CH_3)_2)_3$); ^{13}C NMR δ: 210.8 (s, C-7), 201.5 (s, $COCH_3$), 74.8 (s, C-4), 53.2 (d, C-5), 52.0 (t, C-8), 40.4 (d, C-1), 34.1 (q, $COCH_3$), 28.8 and 28.4 (t, C-3, 5), 18.3 (q, $Si(CH(CH_3)_2)_3$), 13.4 (d, $Si(CH(CH_3)_2)_3$); MS (CI), *m/z* (relative intensity): 357 ($[M + 1]^+$, 100), 313 (61).

Acknowledgement

Financial support from the Natural Sciences and Engineering Research Council of Canada and the University of Saskatchewan is gratefully acknowledged.

1. (*a*) J. SAUER. Angew. Chem. Int. Ed. Engl. **5**, 211 (1966); (*b*) A. WASSERMAN. *In* Diels–Alder reactions. American Elsevier, New York. 1965; (*c*) A. S. ONISHENKO. *In* Diene synthesis. Daniel Davey, New York. 1964; (*d*) J. SAUER and R. SUSTMANN. Angew. Chem. Int. Ed. Engl. **19**, 779 (1980).
2. (*a*) E. CIGANEK. Org. React. **32**, 1 (1984); (*b*) A. FALLIS. Can. J. Chem. **62**, 183 (1984); (*c*) D. F. TABER. *In* Intramolecular Diels–Alder and ene reactions. Springer-Verlag, Berlin. 1984; (*d*) D. CRAIG. Chem. Soc. Rev. **16**, 187 (1987).
3. (*a*) L. A. PAQUETTE. *In* Asymmetric synthesis. Vol. 3. *Edited by* J. D. Morrison. Academic Press, New York. 1984. Chap. 7; (*b*) M. J. TASHNER. *In* Organic synthesis—theory and applications. Vol. 1. *Edited by* T. Hudlicky. JAI Press, Greenwich, CT. 1989. pp. 1–102.
4. (*a*) D. L. BOGER and S. M. WEINREB. *In* Hetero Diels–Alder methodology in organic synthesis. Academic Press, New York. 1987; (*b*) T. KAMETANI and S. HIBINO. Adv. Heterocycl. Chem. **42**, 242 (1987); (*c*) L. F. TIETZE. Heterocycl. Chem. **27**, 47 (1990).
5. R. DICKENSON, R. KUBELA, G. MACALPINE, Z. STOJANIC, and Z. VALENTA. Can. J. Chem. **50**, 2377 (1972).
6. (*a*) W. J. LE NOBLE (*Editor*). Organic high pressure chemistry. Elsevier Science Publishers B.V., Amsterdam. 1988; (*b*) J. JURZAK and B. BARANOWSKI (*Editors*). High pressure chemical synthesis. Elsevier, Amsterdam. 1989.
7. T. A. ENGLER, U. SAMPATH, S. NAGANATHAN, D. VANDER VELDE, and F. TAKUSAGAWA. J. Org. Chem. **54**, 2712 (1989).
8. J. G. MARTIN and R. K. HILL. Chem. Rev. **61**, 537 (1961).
9. D. CRAIG. J. Am. Chem. Soc. **65**, 1006 (1943).
10. C. A. STEWART. J. Org. Chem. **28**, 3320 (1963).
11. R. H. FLEMMING and B. H. MURRAY. J. Org. Chem. **44**, 2280 (1979).
12. T. HARAYAMA and M. OTSUYAMA. Yagugaku Zasshi, **103**, 1096 (1983).
13. D. E. WARD, W. M. ZOGHAIB, C. K. RHEE, and Y. GAI. Tetrahedron Lett. **31**, 845 (1990).
14. (*a*) E. VEDEJS, T. H. EBERLEIN, D. J. MAZUR, C. K. MCCLURE, D. A. PERRY, R. RUGGERI, E. SCHWARTZ, J. S. STULTS, D. L. VARIE, R. G. WILDE, and S. WITTENBERGER. J. Org. Chem. **51**, 1556 (1986); (*b*) C. H. CHEN, G. A. REYNOLDS, and J. A. VAN ALLEN. J. Org. Chem. **42**, 2777 (1977).
15. S. DANISHEFSKY, T. KITAHARA, and P. SCHUDA. Org. Synth. **61**, 147 (1983).
16. E. VEDEJS, J. S. STULTS, and R. G. WILDE. J. Am. Chem. Soc. **110**, 5452 (1988).
17. J. SAVARD and P. BRASSARD. Tetrahedron, **40**, 3455 (1984).
18. E. A. FEHNEL and A. P. PAUL. J. Am. Chem. Soc. **77**, 4241 (1955).
19. A. J. BIRCH and K. P. DASTUR. J. Chem. Soc. Perkin Trans. 1, 1650 (1973).
20. K. SKINNEMOEN and K. UNDHEIM. Acta. Chem. Scand. B, **33**, 767 (1977).
21. D. CRAIG, J. J. SHIPMAN, and R. B. FOWLER. J. Am. Chem. Soc. **83**, 2885 (1961).
22. (*a*) C. KOULKLOVSKY, A. POUILHÉS, and Y. LANGOIS. J. Am. Chem. Soc. **112**, 6672 (1990); (*b*) T. CALOGEROPOULOU and D. F. WEIMER. J. Org. Chem. **53**, 2295 (1988); (*c*) H.-J. LIU and T. K. NGOOI. Can. J. Chem. **62**, 2676 (1984).
23. W. C. STILL, M. KAHN, and A. MITRA. J. Org. Chem. **43**, 2923 (1978).
24. D. W. BROWN, T. T. NAKASHIMA, and D. L. RABENSTEIN. J. Magn. Reson. **45**, 302 (1981).
25. V. K. KANSAL and R. J. K. TAYLOR. J. Chem. Soc. Perkin Trans. 1, 703 (1984).
26. A. J. H. LABUSCHAGNE, J. S. MALHERBE, C. J. MEYER, and D. F. SCHEIDER. J. Chem. Soc. Perkin Trans. 1, 955 (1978).

Can. J. Chem. Downloaded from www.nrcresearchpress.com by 84.41.108.74 on 09/07/12
For personal use only.

Hétéropolyanions de type Dawson. 2. Synthèses de polyoxotungstoarsénates lacunaires dérivant de l'octadécatungstodiarsénate. Étude structurale par RMN du tungstène-183 des octadéca(molybdotungstovanado)diarsénates apparentés[1]

ROLAND CONTANT[2] ET RENÉ THOUVENOT

Laboratoire de physicochimie inorganique, Unité de recherche associée au Centre national de la recherche scientifique, n° 419, Université Pierre et Marie Curie, 4, Pl. Jussieu, 75252 Paris Cedex 05, France

Reçu le 18 avril 1991

ROLAND CONTANT et RENÉ THOUVENOT. Can. J. Chem. **69**, 1498 (1991).

Les tungstoarsénates lacunaires di-, tri- et hexavacants α-$[HAs_2W_{16}O_{59}]^{11-}$, α-$[As_2W_{15}O_{56}]^{12-}$ et α-$[H_2As_2W_{12}O_{48}]^{12-}$ ont été préparés par dégradation alcaline ménagée de l'anion de type Dawson α-$[As_2W_{18}O_{62}]^{6-}$. Les relations entre tous ces anions et les deux isomères α-$[As_2W_{17}O_{61}]^{10-}$ ont été établies. Les dérivés mixtes saturés α-$[As_2V_xW_{18-x}O_{62}]^{(6+x)-}$ (x = 1,2,3) et α-$[As_2Mo_xW_{18-x}O_{62}]^{6-}$ (x = 1,3) ont été obtenus en comblant les lacunes avec le vanadium et le molybdène respectivement. L'anion mixte monovacant α_2-$[As_2Mo_2W_{15}O_{61}]^{10-}$ a aussi été obtenu et a été utilisé concurremment avec α-$[HAs_2W_{16}O_{59}]^{11-}$ pour synthétiser α-$[As_2Mo_2W_{16}O_{62}]^{6-}$; dans les deux cas il se forme simultanément les anions α-$[As_2Mo_xW_{18-x}O_{62}]^{6-}$ (x = 1 et 3). Toutes les espèces ont été caractérisées par polarographie et par spectrométrie IR. En s'appuyant sur la ressemblance des propriétés oxydo-réductrices et des processus de synthèse avec ceux des tungstophosphates lacunaires et mixtes correspondants, des structures ont été proposées pour toutes ces espèces. Dans le cas des tungstovanado- et molybdotungstoarsénates saturés les structures postulées ont été confirmées par RMN du tungstène-183 en solution. En outre, les spectres RMN de ces mêmes espèces ont été discutés en relation avec ceux des dérivés phosphoriques analogues. Finalement, les principales différences avec les anions tungstophosphoriques résident (i) dans l'existence d'un anion $[HAs_2W_{16}O_{59}]^{11-}$, dont la protonation permet de satisfaire la règle de Lipscomb, (ii) dans l'absence d'un oligomère analogue à $[P_8W_{48}0_{184}]^{40-}$, et (iii) dans la plus faible stablité des octadéca(molybdotungsto)diarsénates.

Mots clés : hétéropolyanions, tungstoarsénate, molybdotungstoarsénate, tungstovanadoarsénate, RMN ^{183}W.

ROLAND CONTANT and RENÉ THOUVENOT. Can. J. Chem. **69**, 1498 (1991).

The di-, tri-, and hexavacant lacunary tungstoarsenates α-$[HAs_2W_{16}O_{59}]^{11-}$, α-$[As_2W_{15}O_{56}]^{12-}$, and α-$[H_2As_2W_{12}O_{48}]^{12-}$ were prepared by controlled alkaline degradation of the Dawson-type anion α-$[As_2W_{18}O_{62}]^{6-}$. The relationships between all these anions and the two α-$[As_2W_{17}O_{61}]^{10-}$ isomers were established. The mixed saturated derivatives α-$[As_2V_xW_{18-x}O_{62}]^{(6+x)-}$ (x = 1,2,3) and α-$[As_2Mo_xW_{18-x}O_{62}]^{6-}$ (x = 1, 3) were obtained by refilling the lacunas with vanadium and molybdenum respectively. The new mixed anion α_2-$[As_2Mo_2W_{15}O_{61}]^{10-}$ was used concurrently with α-$[HAs_2W_{16}O_{59}]^{11-}$ to obtain α-$[As_2Mo_2W_{16}O_{62}]^{6-}$; in both cases minor parts of α-$[As_2Mo_xW_{18-x}O_{62}]^{6-}$ (x = 1 and 3) were obtained simultaneously. All species have been characterized by polarography and by IR spectrometry. Proposed structures, based on the similarity of the redox properties and syntheses processes to those of the corresponding Dawson-type lacunary and mixed tungstophosphates, were given for all these species. The structures of the "saturated" tungstovanado- and molybdotungstoarsenates were confirmed by ^{183}W solution NMR. In addition the ^{183}W solution NMR spectra of all these latter species are discussed in relation to those of the analogous phosphoric derivatives. Finally, the main differences with the corresponding tungstophosphoric anions lie in (i) the existence of $[HAs_2W_{16}O_{59}]^{11-}$, whose protonation satisfies Lipscomb's rule, (ii) the lack of a stable oligomer like $[P_8W_{48}O_{184}]^{40-}$, and (iii) the lower stability of the octadeca(molybdotungsto)diarsenates.

Key words : heteropolyanions, tungstoarsenate, molybdotungstoarsenate, tungstovanadoarsenate, ^{183}W NMR.

Introduction

Alors que les tungstophosphates ont fait l'objet ces dernières années de nombreuses publications (1–3), les tungstoarsénates(V) ont été très peu étudiés. Nous nous sommes intéressés ici à l'hydrolyse alcaline de l'anion α-octadécatungstodiarsénate α-$[As_2W_{18}O_{62}]^{6-}$ à structure de Dawson (4)[3] (en abrégé α-As_2W_{18}) (figure 1) dans le but d'isoler de nouveaux composés lacunaires (6) permettant la synthèse d'hétéropolyanions mixtes. En effet, en remplaçant dans ce type de complexe le phosphore(V) par l'arsenic(V), on peut espérer obtenir des espèces analogues mais avec des stabilités modifiées. Ces modifications, même de faible ampleur, peuvent être intéressantes pour la compréhension des mécanismes de formation ou pour les applications notamment catalytiques (7). L'étude, de l'hydrolyse alcaline entraînant le départ progressif d'atomes de tungstène, et de la réaction inverse d'acidification des espèces lacunaires d'une part, la comparaison des propriétés des tungstoarsénates ainsi obtenus avec celles des tungstophosphates correspondants d'autre part, permettent de déterminer la position probable de la lacune. Cette étude a été complétée par des mesures de RMN du tungstène-183 sur les composés mixtes saturés contenant du molybdène ou du vanadium.

Partie expérimentale

Préparations

α-$K_6As_2W_{18}O_{62} \cdot 14H_2O$

Un échantillon de 220 g de $Na_2WO_4 \cdot 2H_2O$ (0,67 mol) est dissous dans 300 mL d'eau, puis acidifié peu à peu par 100 mL d'acide HCl 4 M (0,4 mol). Dès que la solution est limpide, 150 mL d'acide arsénique concentré (1,65 mol) sont ajoutés rapidement et la solution est portée 4 h à reflux. À la solution refroidie sont ajoutés 140 g de NH_4Cl. Le précipité jaune est filtré et essoré puis redissous dans 250 mL d'eau. La solution est alors abandonnée 24 h vers 7°C. Les cristaux qui apparaissent en très faible quantité sont ceux d'un isomère récemment identifié (8–10). Le filtrat est alors traité par 40 g de KCl. Le précipité est filtré, essoré et recristallisé dans environ 150 mL d'eau. Anal. calc.

1. Partie 1, voir la référence 1.

2. Auteur à qui adresser toute correspondance.

3. Les atomes de tungstène et les atomes substituants sont numérotés conformément aux recommandations de l'Union internationale de chimie pure et appliquée (5). Cependant, pour faciliter les comparaisons, la numérotation des atomes de vanadium est analogue à celle des atomes de molybdène.

Printed in Canada / Imprimé au Canada

Can. J. Chem. Downloaded from www.nrcresearchpress.com by 84.41.108.74 on 09/07/12
For personal use only.

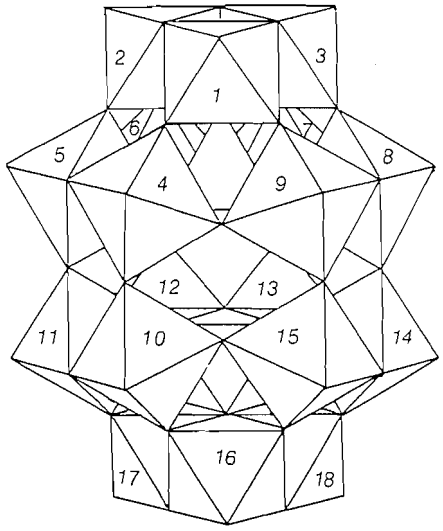


FIG. 1. Représentation en polyèdre de coordination de l'anion α-$[As_2W_{18}O_{62}]^{6-}$ et de ses dérivés de substitution (4, 5).

pour $K_6As_2W_{18}O_{62} \cdot 14H_2O$: K 4,75; W 67,01; As 3,04; H_2O 5,10; trouvé : K 4,71; W 66,67; As 3,07; H_2O 5,07.

α_2-$K_{10}As_2W_{17}O_{61} \cdot 21H_2O$

Un échantillon de 118,5 g (24 mmol) de $K_6As_2W_{18}O_{62} \cdot 14H_2O$ est dissous dans 360 mL d'eau puis traité par 360 mL (0,36 mol) d'une solution molaire de $KHCO_3$. Au bout de 40 min, le précipité est filtré, essoré puis redissous dans 500 mL d'eau chaude. Il apparaît au refroidissement un précipité blanc qui est filtré, essoré et séché à l'air. Anal. calc. pour $K_{10}As_2W_{17}O_{61} \cdot 21H_2O$: K 7,79; W 62,25; As 2,99; H_2O 7,53; trouvé : K 7,62; W 62,19; As 3,00; H_2O 7,52.

α-$K_{11}HAs_2W_{16}O_{59} \cdot xH_2O$

À une solution de 39,5 g (8 mmol) de $K_6As_2W_{18}O_{62} \cdot 14H_2O$ dans 150 mL d'eau sont ajoutés rapidement 100 mL (0,2 mol) d'une solution de tris(hydroxyméthyl)aminométhane 2 M puis au bout de 5 min 150 mL d'une solution de chlorure de potassium demi-saturée. Le précipité est filtré, essoré, lavé deux fois avec 50 mL d'éthanol puis séché à l'air. Anal. calc. pour $K_{11}HAs_2W_{16}O_{59} \cdot 28H_2O$: K 8,65; W 59,2; As 3,02; (H_2O + As_2O_5) 14,96; trouvé : K 8,43; W 59,0; As 3,05; (H_2O + As_2O_5) 15,01. Cette espèce est thermiquement peu stable. Sur le diagramme d'analyse thermique, il n'apparaît aucun palier avant la sublimation totale de As_2O_3.

α-$Na_{12}As_2W_{15}O_{56} \cdot 21H_2O$

À une solution de 99 g (20 mmol) de $K_6As_2W_{18}O_{62} \cdot 14H_2O$ dans 350 mL d'eau est ajouté 89 g (0,57 mol) de $NaClO_4 \cdot H_2O$. Le mélange est agité énergiquement, refroidi vers 10°C et le $KClO_4$ solide est filtré. On ajoute au filtrat 270 mL (0,27 mol) d'une solution molaire de carbonate de sodium. Le précipité est décanté puis filtré, essoré, lavé à l'éthanol et séché à l'air. Anal. calc. pour $Na_{12}As_2W_{15}O_{56} \cdot 21H_2O$: Na 6,19; W 61,9; As 3,36; H_2O 8,48; trouvé : Na 6,23; W 62,1; As 3,35; H_2O 8,54.

α-$K_{12}H_2As_2W_{12}O_{48} \cdot 23H_2O$

À une solution de 74 g (15 mmol) de $K_6As_2W_{18}O_{62} \cdot 14H_2O$ dans 250 mL d'eau sont ajoutés 250 mL (0,5 mol) d'une solution de tris(hydroxyméthyl)aminométhane 2 M. Au bout de 2,5 h d'évolution à température ambiante, on ajoute 75 g de KCl solide. S'il apparaît un précipité, il est filtré et au filtrat est ajouté 200 mL d'une solution de carbonate de potassium 2 M. Le précipité qui apparaît immédiatement est filtré, essoré et lavé deux fois à l'éthanol puis séché à l'air. Anal. calc. pour $K_{12}H_2As_2W_{12}O_{48} \cdot 23H_2O$: K 11,70; W 55,0; As 3,74; H_2O 10,77; trouvé : K 11,90; W 55,05; As 3,88; H_2O 10,87.

α-$(K_8LiH_3As_2W_{12}O_{47} \cdot 16,5H_2O)_n$

Un échantillon de 8 g (2 mmol) de α-$K_{12}H_2As_2W_{12}O_{48} \cdot 23H_2O$ est dissous dans une solution de 250 mL de chlorure de lithium molaire acidifiée par 6 mL d'acide chlorhydrique molaire. Après 3 h d'évolution à la température ambiante, 50 mL de chlorure de potassium saturé sont ajoutés. Le précipité est filtré, essoré, lavé à l'éthanol et séché à l'air. Anal. calc. pour $K_8LiH_3As_2W_{12}O_{47} \cdot 16,5H_2O$: K 8,39; Li 0,17; W 59,2; As 4,02; H_2O 8,69; trouvé : K 8,40; Li 0,22; W 58,7; As 4,20; H_2O 8,62.

1,2-$K_{10}As_2Mo_2W_{15}O_{61} \cdot 21H_2O$

À une solution de 150 mL de chlorure de lithium molaire acidifiée par 3 mL d'acide chlorhydrique molaire sont ajoutés 13,5 g (3 mmol) de $Na_{12}As_2W_{15}O_{56} \cdot 21H_2O$ puis 6 mL (6 mmol) d'une solution molaire de molybdate et peu à peu 15 mL d'acide chlorhydrique molaire. Le pH doit alors se fixer vers 4,5. On ajoute 60 mL d'une solution de chlorure de potassium saturée. Le précipité est filtré, essoré, lavé à l'alcool et séché à l'air. Anal. calc. pour $K_{10}As_2Mo_2W_{15}O_{61} \cdot 21H_2O$: K 8,07; W 56,92; Mo 3,96; As 3,10; H_2O 7,80; trouvé : K 8,21; W 57,12; Mo 3,97; As 3,06; H_2O 7,96.

1,2,3-$K_6As_2Mo_3W_{15}O_{62} \cdot 14H_2O$

À un mélange de 125 mL d'acide chlorhydrique molaire et 15 mL (15 mmol) de molybdate de sodium molaire on ajoute en agitant 20 g (4,4 mmol) de $Na_{12}As_2W_{15}O_{56} \cdot 21H_2O$. Après dissolution, on ajoute 25 g de chlorure de potassium. Le précipité est filtré, essoré puis recristallisé dans le minimum d'eau acidulée (pH = 2). Anal. calc. pour $K_{10}As_2Mo_3W_{15}O_{62} \cdot 14H_2O$: K 5,02, W 59,0; Mo 6,16; As 3,21; H_2O 5,39; trouvé : K 4,84; W 58,7; Mo 6,14; As 3,20; H_2O 5,21.

1,2-$K_6As_2Mo_2W_{16}O_{62}$

Cette espéce n'a pas été isolée à l'état pur mais a été identifiée comme la composante principale d'un mélange obtenu comme suit. À un mélange de 50 mL d'acide chlorhydrique molaire et de 4 mL (4 mmol) de molybdate de sodium molaire sont ajoutés 10 g (2 mmol) de $K_{11}HAs_2W_{16}O_{59}$,aq. Après agitation énergique, la solution, éventuellement filtrée, est additionnée de 8 g de chlorure de potassium. Le précipité jaune est filtré puis recristallisé dans le minimum d'eau acidulée (pH = 2). Anal. calc. pour $K_6As_2Mo_2W_{16}O_{62} \cdot 15H_2O$: K 4,91; W 61,5; Mo 4,02; As 3,14; H_2O 5,65; trouvé : K 4,62; W 61,9; Mo 3,98; As 3,09; H_2O 5,71.

Les mesures polarographiques et de RMN du tungstène-183 montrent que ce produit contient toujours une certaine proportion de $As_2Mo_3W_{15}$, de 1-As_2MoW_{17} et même de As_2W_{18}. Le résultat est analogue si la synthèse est effectuée en ajoutant du tungstate à $As_2Mo_2W_{15}$.

1-$K_6As_2MoW_{17}O_{62} \cdot 14H_2O(\alpha_2)$

À un mélange de 100 mL d'acide chlorhydrique molaire et 5 mL (5 mmol) de molybdate de sodium 1 M sont ajoutés 25 g (5 mmol) de α_2-$K_{10}As_2W_{17}O_{61} \cdot 21H_2O$. Après dissolution, 20 g de chlorure de potassium sont ajoutés. Le précipité jaune est filtré et recristallisé dans le minimum d'eau acidulée (pH = 2). Anal. calc. pour $K_6As_2MoW_{17}O_{62} \cdot 14H_2O$: K 4,84; W 64,4; Mo 1,98; As 3,09; H_2O 5,20; trouvé : K 4,72; W 65,2; Mo 1,91; As 3,09; H_2O 5,07.

4-$K_6As_2MoW_{17}O_{62} \cdot 15H_2O(\alpha_1)$

À un mélange de 40 mL d'acide chlorhydrique molaire et de 2 mL (2 mmol) de molybdate de lithium sont ajoutés 10 g (2 mmol) de α_1-$K_9LiAsw_{17}O_{61} \cdot 20H_2O$ (11). Quand la dissolution est totale, le sel de potassium est précipité par 10 g de KCl solide. Le précipité est filtré et essoré puis recristallisé dans 20 mL d'eau acidulée (pH = 2). Anal. calc. pour $K_6As_2MoW_{17}O_{62} \cdot 15H_2O$: K 4,82; W 64,2; Mo 1,97; As 3,08; H_2O 5,55; trouvé : K 4,97; W 63,7; Mo 1,97; As 3,07; H_2O 5,53.

1,2,3-$K_9As_2V_3W_{15}O_{62} \cdot 21H_2O$

À un mélange de 75 mL d'acide chlorhydrique molaire et de 19 mL (9,5 mmol) de $NaVO_3$ 0,5 M sont ajoutés 13,5 g de $Na_{12}As_2W_{15}O_{56} \cdot 21H_2O$ (3 mmol). Après dissolution, on ajoute 12 g de chlorure de potassium. Le précipité est filtré, essoré et recristallisé dans le minimum d'eau. Anal. calc. pour $K_9As_2V_3W_{15}O_{62} \cdot 21H_2O$: K 7,35; W 57,6; V 3,19; H_2O 7,90; trouvé : K 7,17; W 57,6; V 3,05; H_2O 7,77.

1,2-$K_8As_2V_2W_{16}O_{62} \cdot 19H_2O$

À une solution de 22 mL (11 mmol) de $NaVO_3$ 0,5 M additionnée de 45 mL de HCl molaire et 35 mL d'eau sont ajoutés 28 g de $K_{11}HAs_2W_{16}O_{59} \cdot 28H_2O$ (5,6 mmol). Après 15 min d'agitation énergique, la partie insoluble est filtrée. Au filtrat sont ajoutés 25 g de KCl solide. Le précipité jaune orangé est filtré, essoré et redissous dans 65 mL d'eau. Le louche qui apparaît est filtré sur papier et on laisse

Can. J. Chem. Downloaded from www.nrcresearchpress.com by 84.41.108.74 on 09/07/12
For personal use only.

cristalliser. Anal. calc. pour $K_8As_2V_2W_{16}O_{62} \cdot 19H_2O$: K 6,46; W 60,8; V 2,11; H_2O 7,06; trouvé : K 6,67; W 60,1; V 2,05; H_2O 7,15.

1-$K_7As_7VW_{17}O_{62} \cdot 16\ H_2O(\alpha_2)$

À une solution de 6 mL (3 mmol) de $NaVO_3$ 0,5 M additionée de 18 mL de HCl molaire et 75 mL d'eau sont ajoutés 15 g de α_2-$K_{10}As_2W_{17}O_{61} \cdot 21H_2O$ (3 mmol). Après dissolution, on ajoute 20 g de KCl solide. Le précipité jaune est filtré, essoré puis recristallisé dans le minimum d'eau. Anal. calc. pour $K_7As_2VW_{17}O_{62} \cdot 16\ H_2O$: K 5,61; W 64,04; V 1,04; H_2O 5,90; trouvé : K 6,04; W 62,9; V 1,03; H_2O 5,96.

Analyses

Les méthodes d'analyse du tungstène, du molybdène et du vanadium ont été décrites dans un article précédent (1). L'arsenic a été dosé par colorimètrie du complexe α-$[AsMo_{12}O_{40}]^{3-}$ en milieu eau–dioxanne (12), après séparation sous forme de Li_3AsO_4. Cette méthode n'est pas utilisable en présence de vanadium. Les métaux alcalins ont été dosés par spectrophotométrie de flamme et dans certains cas le potassium a été dosé par gravimétrie du tétraphénylborate (13). L'état d'hydratation, qui a été déterminé par analyse thermogravimétrique, est donné à titre indicatif, car il dépend des conditions de stockage.

Mesures physiques

Les spectres RMN du tungstène-183 ont été enregistrés sur des appareils à transformée de Fourier Bruker WM 250 ou AM 500 à 10,4 MHz et 20,8 MHz respectivement. Les déplacements chimiques du tungstène-183 ont été mesurés par rapport à une référence externe de Na_2WO_4 2 M dans D_2O alcalinisé, en utilisant comme référence secondaire une solution aqueuse saturée d'acide dodécatungstosilicique α-$[SiW_{12}O_{40}]^{4-}$ ($\delta = -103,8$ ppm). Les déplacements chimiques, sans correction de susceptibilité magnétique, sont donnés conformément aux recommandations de l'Union internationale de Chimie pure et appliquée, à savoir δ négatif correspond à une fréquence de résonance inférieure à celle de la référence (écran nucléaire plus élevé). Les solutions concentrées ont été obtenues en dissolvant environ 6 g du sel de potassium de l'hétéropolyanion dans 2 mL de $LiClO_4$ saturé; aprés la filtration, opérée directement dans le tube de RMN (Wilmad diamètre externe 10 mm), on ajoute 0,22 mL de D_2O.

Résultats

Polarographie

Toutes les espèces décrites sont suffisamment stables en solutions diluées pour pouvoir être caractérisées par polarographie (tableau 1). Il est bien connu (2) que pour les hétéropolyanions les processus de réduction dépendent de la structure plutôt que de la nature de l'hétéroatome. Il est donc possible de comparer les tungstoarsénates dérivant de As_2W_{18} aux tungstophosphates de type Dawson dont les structures peuvent être considérées comme établies (13). Ainsi ont pu être identifiés α_1- et α_2-As_2W_{17} dont les polarogrammes comme ceux des tungstophosphates correspondants se différencient essentiellement par le $E_{1/2}$ de la troisème vague (tableau 1). De même, les polarogrammes de As_2W_{15}, As_2W_{12} et des dérivés mixtes saturés molybdiques et vanadiques sont pratiquement identiques à ceux des tungstophosphates lacunaires et mixtes analogues. Par contre, P_2W_{16} n'a pas été isolé et le polarogramme de As_2W_{16} n'est pas suffisamment différent de ceux de α_2-As_2W_{17} et α-As_2W_{15} pour permettre de le caractériser sans ambiguïté.

Spectroscopies

Le spectre UV de α-$[As_2W_{18}O_{62}]^{6-}$ présente deux épaulements vers 240 et 300 nm respectivement sur une bande très intense dont le maximum est inférieur à 200 nm. Avec les espèces lacunaires, le pied de cette bande d'absorption se déplace vers l'ultraviolet au fur et à mesure de l'agrandissement de la lacune (6). Par contre, pour les composés mixtes saturés, dans lesquels un ou plusieurs atomes de vanadium ou de molybdène sont substitués aux atomes de tungstène, l'extrémité de la bande située dans le proche UV est déplacée vers le visible et les solutions sont rouges ou jaunes, mais il n'apparaît jamais de maximum permettant d'indentifier ces composés.

TABLEAU 1. Potentiels de demi-vague (volts/ECS) de quelques tungstoarsénates, molybdotungstoarsénates et tungstovanadoarsénates de type Dawson

Espèce	$E_{1/2}$ (nombre d'électrons)			
α-As_2W_{18}[a]	+0,08(1)	−0,10(1)	−0,39(1)	
α_1-As_2W_{17}[b]	−0,47(2)	−0,57(2)	−0,95(2)	
α_2-As_2W_{17}[b]	−0,44(2)	−0,55(2)	−0,79(2)	
α-As_2W_{16}[b]	−0,45(2)	−0,56(2)	−0,78(2)	
α-As_2W_{15}[b]	−0,52(4)	−0,74(2)		
α-As_2W_{12}[b]	−0,60(2)	−0,70(2)		
1,2-$As_2Mo_2W_{15}$[b]	−0,42(2)	−0,53(2)	−0,69(6)	−0,81(2)
1-As_2MoW_{17}[a](α_2)	+0,28(1)	−0,11(1)	−0,29(2)	
4-As_2MoW_{17}[a](α_1)	+0,45(1)	0,00(1)	−0,36(2)	
1,2-$As_2Mo_2W_{16}$[a]	+0,29(1)	+0,11(1)	−0,30(2)	
1,2,3-$As_2Mo_3W_{15}$[a]	+0,31(1)	+0,18(1)	−0,09(1)	−0,30(1)
1-As_2VW_{17}[c]	+0,46(1)			
1,2-$As_2V_2W_{16}$[c]	+0,42(2)			
1,2,3-$As_2V_3W_{15}$[c]	+0,32(3)			

[a]Electrode de carbone tournante : pH 1,0; HCl 0,1 M/NaCl 0,9 M.
[b]Electrode à goutte de mercure : pH 4,6 acide acétique/acétate de lithium 1 M.
[c]Electrode de platine tournante : pH 1,0; HCl 0,1 M/NaCl 0,9 M.

Les bandes d'absorption IR dans la région 700–1000 cm^{-1} sont indiquées dans le tableau 2. Comme toujours dans le cas des polyanions fortement hydratés, les bandes sont larges et plus ou moins bien différenciées. Par rapport à l'anion As_2W_{18} (D_{3h}), les modes d'élongation ν(M—O—M) des ponts μ_{oxo} (14) apparaissent à des fréquences inférieures et généralement sous la form de bandes à plusieurs maxima et épaulements.

Le premier effet, déplacement de fréquences vers les faibles nombres d'ondes, est plus important pour les espèces polyvacantes et les espèces polysubstituées, ce qui est en accord avec une diminution de la stabilité de l'édifice polyanionique (diminution des constantes de force) (15).

Le second effet, éclatement des bandes de vibration, est relié à l'abaissement de la symétrie du polyanion dans les composés lacunaires et substitués : du fait de cet abaissement de symétrie, les tétraèdres AsO_4, non équivalents, devraient donner plusieurs bandes d'élongation. Cependant, contrairement à ceux du tétraèdre PO_4 ($\bar{\nu} > 1000\ cm^{-1}$) (16), les modes du tétraèdre AsO_4 apparaissent dans le domaine de vibration des liaisons M—O ($\bar{\nu} \approx 900\ cm^{-1}$) (14) et l'on n'observe au mieux, qu'une seule bande faible ou un épaulement; pour les autres espèces, les bandes du tétraèdre AsO_4 sont vraisemblablement masquées sous les bandes larges et intenses ν_{as}(M—O).

La technique spectroscopique la plus performante pour caractériser les différentes espèces est la RMN du tungstène-183. Elle a été utilisée pour les composés « saturés » contenant du molybdène et (ou) du vanadium. Les résultats qui apportent aussi des informations structurales sont discutés plus loin.

Hydrolyse partielle de l'anion α-$[As_2W_{18}O_{62}]^{6-}$: formation de composés lacunaires

La première étape de l'hydrolyse conduit toujours à α_2-As_2W_{17}. La réaction, qui est catalysée par les bases, est du premier ordre par rapport au polyanion (13). La vitesse dépend également de la nature du contre-ion : avec les alcalins par

Can. J. Chem. Downloaded from www.nrcresearchpress.com by 84.41.108.74 on 09/07/12
For personal use only.

TABLEAU 2. Bandes d'absorption infra-rouge (700–1000 cm^{-1}) des tungstoarsénates et tungstoarsénates mixtes de type Dawson

Composé	ν (cm^{-1})[a]		
	ν_{as}(M—O_{ter})[b]	ν(As—O)[b]	ν_{as}(M—O—M)[b]
α-$K_6As_2W_{18}O_{62}$	978F	930f.	896f, 870f, 840f, 768F
α_1-$K_9LiAs_2W_{17}O_{61}$	952F		875ép, 862m, 830ép, 780ép, 735F
α_2-$K_{10}As_2W_{17}O_{61}$	948F		865F, 822f, 795ép, 740F
α-$K_{11}HAs_2W_{16}O_{59}$	942F		890ép, 870f, 815f, 785f, 720F
α-$Na_{12}As_2W_{15}O_{56}$	940F	910ép	890ép, 870m, 820f 790f, 770m, 715F
α-$K_{12}H_2As_2W_{12}O_{48}$	968m	935ép, 920f	840F, 795f, 750m
α-$(K_8LiH_3As_2W_{12}O_{47})_n$	972f	950ép, 935f	853F, 765ép, 700f
1,2-$K_{10}As_2Mo_2W_{15}O_{61}$	948F		867F, 825f, 793f, 730F
1-$K_6As_2MoW_{17}O_{62}$	972F	925ép	8,90f, 865f, 840f, 772F
4-$K_6As_2MoW_{17}O_{62}$	972F	925ép	892f, 863f, 830f, 770F
1,2-$K_6As_2Mo_2W_{16}O_{62}$	970F	922f	888f, 860ép, 828m, 765F
1,2,3-$K_6As_2Mo_3W_{15}O_{62}$	973F	928f	892f, 860ép, 832m, 770F
1-$K_7As_2VW_{17}O_{62}$	968F		892ép, 865f, 830ép, 775F
1,2-$K_8As_2V_2W_{16}O_{62}$	956F		880F, 820ép, 764F
1,2,3-$K_9As_2V_3W_{15}O_{62}$	952F		876F, 835f, 755F

[a]F: fort; m: moyen; f: faible; ép: épaulement.
[b]Attribution d'après ref. 14.
[c]Mélange de molybdotungstoarsénates, voir texte.

Can. J. Chem. Downloaded from www.nrcresearchpress.com by 84.41.108.74 on 09/07/12
For personal use only.

exemple, elle varie dans l'ordre $K^+ > Na^+ > Li^+$. L'influence de la nature du contre-ion ou de la base devient plus importante au cours des étapes suivantes. Cette propriété est utilisée pour orienter l'hydrolyse vers la formation ou la séparation d'une espèce déterminée. Ainsi l'addition, à une solution de α_2-As_2W_{17}, de carbonate ou d'hydroxyde de sodium ou de potassium conduit à la formation simultanée de As_2W_{16} et As_2W_{15}. Les sels de ce dernier étant beaucoup moins solubles, ils précipitent même en solution diluée, permettant ainsi la séparation. L'utilisation d'une base aminée comme le tris(hydroxyméthyl)-aminométhane entraîne des modifications importantes: il se forme rapidement As_2W_{16}, puis, lentement, As_2W_{12}. Ce processus peut encore être perturbé par la présence, même en faible proportion, de Li^+, qui stabilise As_2W_{16}, ou de Na^+ qui favorise la formation et la stabilisation de As_2W_{15}.

Equilibre As_2W_{17}/As_2W_{16}

Ainsi, en présence des ions Li^+ ($c > 0,1$ M), la vitesse de formation de As_2W_{12} devient pratiquement nulle et il est alors possible d'étudier entre pH 7,5 et pH 8 l'équilibre qui s'établit entre les espèces As_2W_{17} et As_2W_{16}. Après addition du tampon tris(hydroxyméthyl)aminométhane dans la cellule polarographique (20°C), il faut environ 20 min pour que l'équilibre s'établisse, par conséquent les mesures sont effectuées au bout de 30 et 45 min.

La proportion de As_2W_{17} a été déterminée à partir de la hauteur de la première vague polarographique qui est nettement moins négative que la vague correspondante de As_2W_{16} (−0,66 et −0,77 volts/ECS respectivement à pH 7,85). En faisant varier la concentration en tungstate et en traçant log ($[As_2W_{17}]/[As_2W_{16}]$) en fonction de log $[WO_4^{2-}]$ à différents pH on obtient une série de droites de pente 1 (figure 2). À partir des valeurs de pK_{app} (tableau 3) obtenues à différents pH, il est facile de montrer que $\Delta pK_{app}/\Delta pH$ est voisin de moins 3 et que par conséquent les résultats sont en accord avec l'équilibre

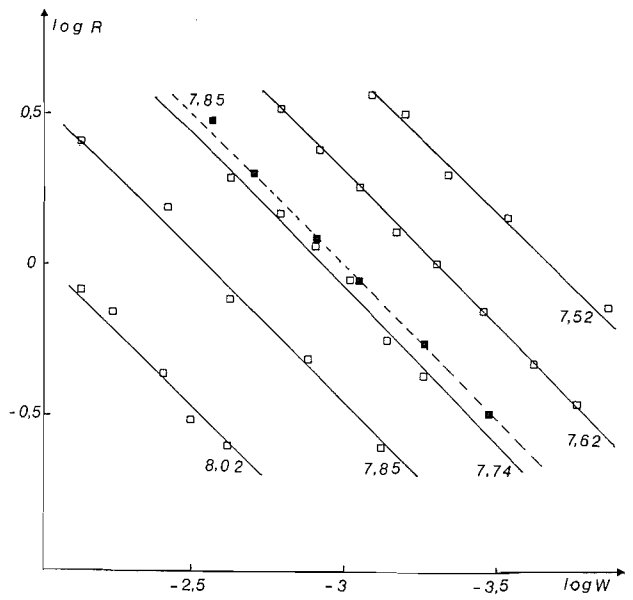


FIG. 2. Droites log $R = f(log\ W)$ ($R = [As_2W_{17}]/[As_2W_{16}]$; $W = [WO_4^{2-}]$) à différents pH : les conditions de force ionique ($I = 1,0$ M) et de concentration en Li^+ ($c = 0,80$ M) restent inchangées sauf pour la droite en pointillé ($I = 0,6$ M; $c = 0,40$ M).

suivant :

[1] $[As_2W_{17}O_{61}]^{10-} + 3H_2O \rightleftharpoons [HAs_2W_{16}O_{59}]^{11-} + WO_4^{2-} + 3H_3O^+$ (constante K)

Cette constante est fonction de la concentration de Li^+, celui-ci favorisant la formation de As_2W_{16} aux dépens de α_2-As_2W_{17}. Comme ce dernier donne un complexe 1–1 avec l'ion Li^+ (11), As_2W_{16} doit donner un complexe plus riche en Li^+. Compte tenu de la différence de force ionique, les résultats

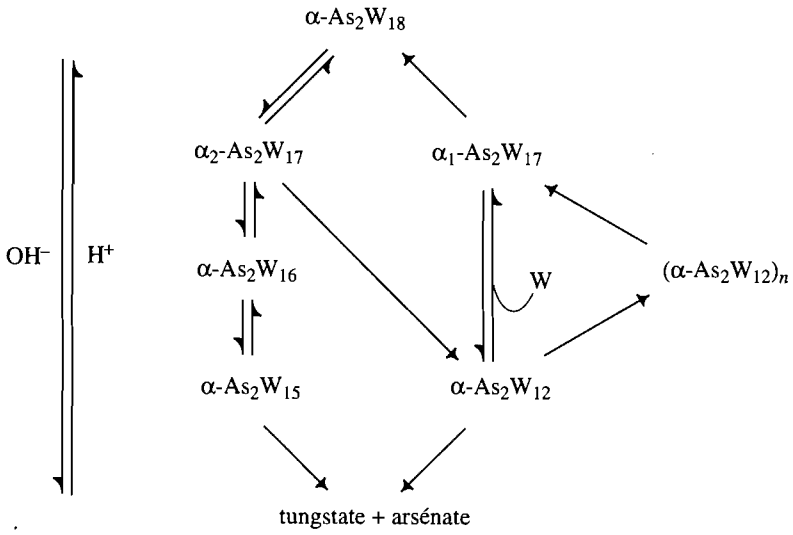


SCHÉMA 1

TABLEAU 3. Constantes de l'équilibre $[HAs_2W_{16}O_{59}]^{11-}/[As_2W_{17}O_{61}]^{10-}$ dans différentes conditions

$[Li^+]$ (M)	$[Cl^-]$ (M)	pH[a]	pK_{app}[b]	K_{app}	pK^b
0,80	1,00	7,52	3,66	$2,19\cdot10^{-4}$	26,22
0,80	1,00	7,62	3,30	$5,01\cdot10^{-4}$	26,16
0,80	1,00	7,74	2,94	$1,15\cdot10^{-3}$	26,16
0,80	1,00	7,85	2,56	$2,75\cdot10^{-3}$	26,11
0,80	1,00	8,02	2,04	$9,12\cdot10^{-3}$	26,10
0,40	0,60	7,85	2,99	$1,02\cdot10^{-3}$	26,54

[a]Le pH est fixé par le tampon tris(hydroxyméthyl)aminométhane, la concentration de $[(CH_2OH)_3\cdot CNH_3]^+$ étant maintenue égale à 0,2 M.
[b]Voir texte.

du tableau 3 ne sont pas en désaccord avec un complexe 2–1, ce qui correspondrait à l'équilibre :

$$[2] \quad [LiAs_2W_{17}O_{61}]^{9-} + Li^+ + 3H_2O \rightleftharpoons [Li_2HAs_2W_{16}O_{59}]^{9-} + WO_4^{2-} + 3H_3O^+$$

Ceci explique que les ions Li^+ stabilisent à la fois As_2W_{17} et As_2W_{16} et que le passage à As_2W_{12} et l'hydrolyse totale se trouvent fortement ralentis.

Stabilité des espèces lacunaires

L'ensemble des relations existant entre les différentes espèces dérivant de α-As_2W_{18} est représenté sur le schéma 1.

Parmi les espèces lacunaires décrites, α_2-As_2W_{17} est la seule qui soit stable en solution aqueuse; sa zone de stabilité est comprise entre pH 1 et pH 7. As_2W_{15} est plus stable que le composé phosphorique analogue, mais se transforme cependant en α_2-As_2W_{17}. Cette évolution est accélérée en milieu acide, mais ralentie par la présence de Li^+. As_2W_{16} est l'espèce qui, acidifiée, se transforme le plus rapidement même en présence de Li^+, le terme final étant aussi α_2-As_2W_{17}.

En solution aqueuse, As_2W_{12} n'est pas stable et, en milieu non tamponné, le stade ultime de l'évolution est un mélange contenant α_2-As_2W_{17} et les espèces provenant de l'hydrolyse basique (voir Schéma 1). En milieu acide, il se forme en outre As_2W_{18}. La présence de Li^+ ne modifie certainement pas le processus, mais elle modifie les vitesses, ce qui permet la séparation des composés intermédiaires. L'addition de tungstate à As_2W_{12} en présence de Li^+ et d'une quantité convenable d'acide, conduit quantitativement à α_1-As_2W_{17}. Dans les mêmes conditions, sans ajout de tungstate, il se forme un mélange d'espèces plus condensées $(As_2W_{12})_n$. Ces espèces se transforment en α_1-As_2W_{17} d'autant plus rapidement que la solution est plus diluée. Il ne se forme donc vraisemblablement pas d'oligomère cyclique analogue à P_8W_{48} (3*a*). Par contre, le comportement de α_1-As_2W_{17} est analogue à celui de α_1-P_2W_{17} : le solide doit être isolé en présence de Li^+ qui ralentit l'isomérisation $\alpha_1 \rightarrow \alpha_2$. Cette dernière est aussi ralentie par la protonation. Dans les mêmes conditions, l'isomérisation de α_1-As_2W_{17} est environ cinq fois plus rapide que celle de α_1-P_2W_{17}.

Action des ions métalliques sur les espèces lacunaires

Les hétéropolytungstates lacunaires monovacants sont connus pour donner des complexes 1–1 avec presque tous les métaux. Les complexes des deux isomères α_1- et α_2-As_2W_{17} avec les ions métalliques divalents et alcalins ont déjà été étudiés (11).

As_2W_{15} a un comportement analogue à celui de P_2W_{15} (17, 18): avec la plupart des ions divalents, il se forme les complexes $M_2(As_2W_{15})_2$ et $M_4(As_2W_{15})_2$; avec les métaux à haut degré d'oxydation comme Mo(VI) et V(V), il se forme $As_2M_3W_{15}$; avec les métaux de degré d'oxydation III ou IV, le comportement est intermédiaire et il peut se former soit l'un, soit l'autre type de complexes, soit éventuellement les deux.

As_2W_{16}, qui est un polyanion divacant, réagit avec de nombreux métaux en jouant probablement le rôle d'un ligand polydenté, mais seul $As_2V_2W_{16}$ a pu être isolé à l'état pur.

À partir de As_2W_{12}, il ne nous a pas été possible d'obtenir des composés mixtes purs : par exemple, contrairement à ce qui est observé avec P_2W_{12}, qui permet de préparer $P_2Mo_6W_{12}$ (6), l'action sur As_2W_{12} du molybdate en milieu acide ne conduit pas à $As_2Mo_6W_{12}$, mais à un mélange d'espèces saturées moins riches en molybdène.

Discussion

Considérations structurales

α-$[As_2W_{18}O_{62}]^{6-}$ possède la structure de Dawson établie sur

Can. J. Chem. Downloaded from www.nrcresearchpress.com by 84.41.108.74 on 09/07/12
For personal use only.

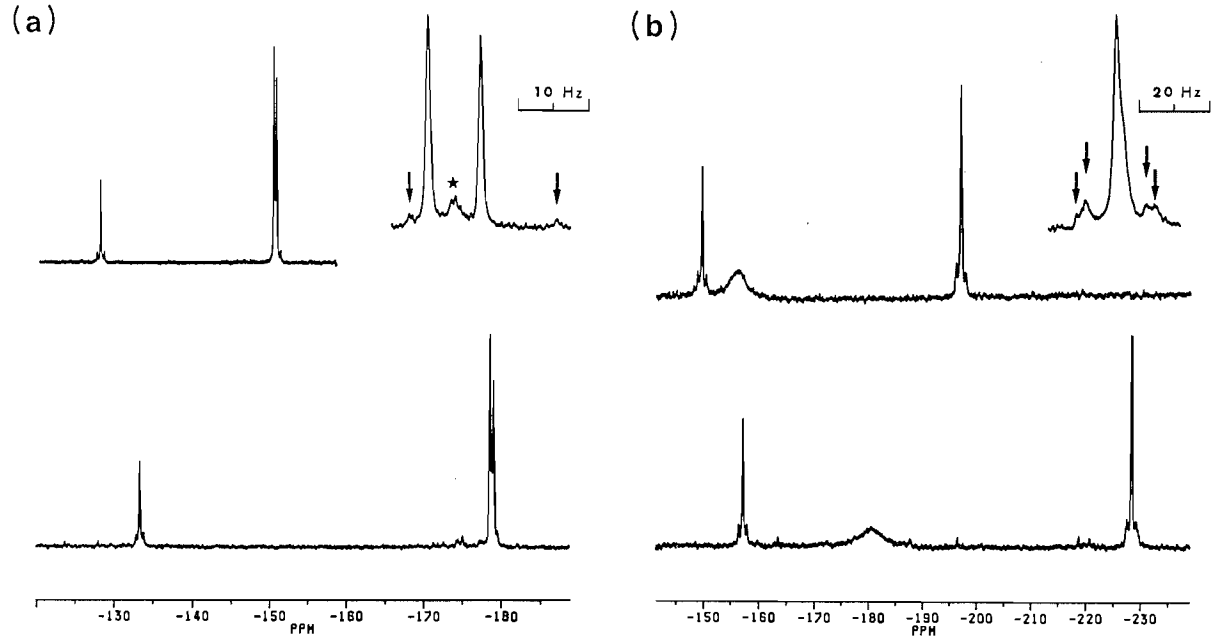


FIG. 3. Comparaison des spectres RMN du tungstène-183 (a) des ions $[As_2Mo_3W_{15}O_{62}]^{6-}$ (haut) et $[P_2Mo_3W_{15}O_{62}]^{6-}$ (bas) et (b) des ions $[As_2V_3W_{15}O_{62}]^{9-}$ (haut) et $[P_2V_3W_{15}O_{62}]^{9-}$ (bas). Conditions expérimentales : solutions aqueuses saturées des sels de lithium; concentration environ 0,5 M.

$[As_2Mo_3W_{15}O_{62}]^{6-}$: 20,8 MHz; 1546 acquisitions; facteur d'élargissement 1 Hz; la partie expansée, obtenue avec un facteur de rétrécissement de 0,4 Hz représente les deux signaux de résonance des tungstène équatoriaux; l'étoile indique les deux composantes internes (confondues) du système AB résultant de leur couplage mutuel ($\Delta\nu$ = 7,5 Hz, $^2J_{W-W} \approx 30$ Hz); les deux flèches localisent la paire de satellites autour du pic basse fréquence ($^2J_{W-W}$ = 20,5 Hz) correspondant au couplage polaire–équatorial dans la sous-unité AsW_9O_{34}. $[P_2Mo_3W_{15}O_{62}]^{6-}$: 20,8 MHz; 1802 acquisitions; facteur d'élargissement 1 Hz.

$[As_2V_3W_{15}O_{62}]^{9-}$: 10,4 MHz; 12 183 acquisitions; facteur d'élargissement 1 Hz; la partie expansée, obtenue avec un facteur d'élargissement de 0,3 Hz représente le signal de résonance du tungstène équatorial de la sous-unité AsW_9O_{34}; les flèches localisent les deux paires de satellites correspondant aux couplages équatorial–équatorial ($^2J_{W-W}$ = 21,5 Hz) et polaire–équatorial ($^2J_{W-W}$ = 17,4 Hz) respectivement. $[P_2V_3W_{15}O_{62}]^{9-}$: 10,4 MHz; 24 208 acquisitions; facteur d'élargissement 1 Hz.

le composé phosphorique (4) (figure 1). Pour les dérivés lacunaires dont les homologues phosphoriques existent, on peut considérer que, dans la mesure où les processus de synthèse et les propriétés oxydo-réductrices sont voisins, les structures sont identiques. Ainsi les lacunes se situent vraisemblablement (figure 1) (i) en position équatoriale (octaèdre 4) pour α_1-As_2W_{17}, (ii) en position polaire (octaèdre 1) pour $\alpha_2As_2W_{17}$, (iii) à la place d'un groupe W_3O_{13} polaire (octaèdres 1, 2 et 3) pour As_2W_{15}, (iv) à la place des six tungstènes qui forment le tiers longitudinal du polyanion saturé (octaèdres 1, 4, 9, 10, 15 et 16) pour As_2W_{12}. De la même manière, $As_2Mo_2W_{15}$ qui résulte du remplissage partiel de la lacune de As_2W_{15} conserve une lacune dans le même groupe polaire que les deux atomes de molybdène.

As_2W_{16} est la seule espèce pour laquelle in n'existe pas d'équivalent phosphorique stable. Étant donné que ce composé se met en équilibre avec α_2-As_2W_{17} et α-As_2W_{15}, il est probable que sa structure soit intermédiaire, c'est-à-dire que la lacune divacante serait située dans un groupement polaire (octaèdres 1 et 2). Cette hypothèse est parfaitement en accord avec le fait que l'addition d'un atome de tungstène sur $As_2Mo_2W_{15}$ et l'addition de deux atomes de molybdène sur As_2W_{16} conduisent instantanément au même $As_2Mo_2W_{16}$, caractérisé par polarographie et par RMN du tungstène-183.

If faut noter que la structure attribuée à As_2W_{16} entraînerait l'existence sur l'anion déprotoné « $[As_2W_{16}O_{59}]^{12-}$ » d'un octaèdre WO_6 possédant trois atomes d'oxygène non partagés et par conséquent violant la règle de Lipscomb (19) qui affirme

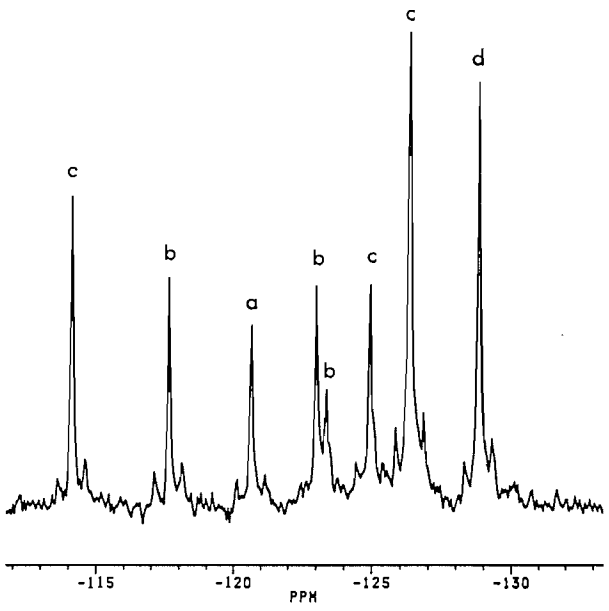


FIG. 4. Partie haute fréquence (résonance des tungstènes polaires) du spectre RMN du tungstène-183 d'une solution contenant $[As_2W_{18}O_{62}]^{6-}$ (pic a; 5%), $[As_2MoW_{17}O_{62}]^{6-}$ (pics b; 20%), $[As_2Mo_2W_{16}O_{62}]^{6-}$ (pics c; 50%) et $[As_2Mo_3W_{15}O_{62}]^{6-}$ (pic d; 25%). Conditions expérimentales : solution aqueuse saturée du sel de lithium; concentration globale environ 0,5 M; 20,8 MHz; 8762 acquisitions; facteur d'élargissement 1,2 Hz.

Can. J. Chem. Downloaded from www.nrcresearchpress.com by 84.41.108.74 on 09/07/12
For personal use only.

TABLEAU 4. Données RMN du tungstène-183 des molybdotungstoarsénates $As_2Mo_xW_{18-x}$; déplacements chimiques en ppm par rapport à Na_2WO_4 2 M dans D_2O alcalinisé; constantes de couplage $^2J_{W-W}$ entre parenthèses

	α-As_2W_{18}[a]	As_2MoW_{17}	$As_2Mo_2W_{16}$	$As_2Mo_3W_{15}$
^{183}W polaires de la sous-unité $AsMo_xW_{9-x}$	−120,8 [6W] (J = 21,4 Hz)[b]	−117,8 [2W] (J = 20 Hz)	−114,1 [1W] (J = 20 Hz)	
^{183}W polaires de la sous-unité AsW_9		−123,1 [2W] (J = 20 Hz)	−124,9 [1W] (J = 20 Hz)	
		−123,6 [1W]	−126,6 [2W] (J = 20 Hz)	−128,8 [3W] (J = 20,7 Hz)[b]
Amplitude Δδ		5,8	12,5	
^{183}W équatoriaux	−144,1 [12W] (J = 21,4 Hz)[b]	−141,9 [2W] −144,7 [2W] −147,4 [2W] −148,0 [2W] −148,2 [2W] −149,8 [2W]	−145,3 [2W] −146,6 [2W] −147,6 [2W] −147,8 [2W] −151,4 [2W] −155,0 [2W]	−151,3 [6W] −151,7 [6W] (J = 20,5 Hz)[b]
δ moyen		−146,7	−148,9	−151,5
Amplitude Δδ		7,9	9,7	0,4

[a]δ reporté à −121,9 et −145,3 ppm par Acerete *et al.* (9).
[b]Système AB léger à 10,4 MHz.

qu'une telle structure est instable. C'est sans doute pourquoi l'espèce obtenue, aussi bien à l'état solide qu'en solution, est l'espèce protonée $[HAs_2W_{16}O_{59}]^{11-}$, dans laquelle le proton doit se situer sur l'un des trois atomes d'oxygène externes de l'octaèdre WO_6. Ainsi la règle de Lipscomb est respectée, mais ceci explique la faible stabilitié, notamment thermique, de cette espèce.

RMN du tungstène-183 sur les espèces saturées

Les spectres sont comparables à ceux des composés phosphoriques analogues (1) (figure 3); cependant, contrairement à ^{31}P, ^{75}As (I = 3/2; 100%) ne donne lieu à aucun couplage observable et toutes les raies du tungstène-183 sont des singulets. Le spectre de α-As_2W_{18} a déjà été décrit (8, 9). Il présente deux pics d'intensité 2 (−144,1 ppm) et 1 (−120,8 ppm) correspondant respectivement aux 12 atomes de tungstène équatoriaux et aux 6 atomes polaires. On peut remarquer que le faible écart entre les deux signaux (23,4 ppm soit 243 Hz à 10,4 MHz) permet d'observer un léger effet de second ordre (système AB) pour les satellites tungstène–tungstène autour de chacun de ces pics ($^2J_{W—O—W}$ = 21,4 Hz). Pour les composés $As_2M_3W_{15}$, la symétrie est abaissée de D_{3h} à C_{3v} et si les trois atomes de tungstène polaires restent équivalents, il existe deux types de tungstènes équatoriaux et on doit s'attendre à trois pics d'intensité 2 : 2 : 1. Pour les composés $As_2M_2W_{16}$ et As_2MW_{17}, la symétrie est C_s puisqu'il ne reste qu'un plan miroir et les atomes de tungstènes équatoriaux se répartissent en six groupes de deux, tandis que les tungstènes polaires doivent donner trois pics dans les rapports 2 : 1 : 1 pour $As_2M_2W_{16}$ et 2 : 2 : 1 pour As_2MW_{17}.

Dérivés molybdotungstiques

Pour les composés molybdotungstiques, le nombre et les intensités relatives des raies correspondent effectivement à ces prévisions. Cependant, comme $P_2Mo_2W_{16}$, l'espèce $As_2Mo_2W_{16}$ n'a pas pu être obtenue pure et dans le spectre de ^{183}W de sa solution sont aisément identifiés As_2W_{18} (5%), As_2MoW_{17} (20%) et $As_2Mo_3W_{15}$ (25%) (figure 4). Par ailleurs, l'anion $As_2Mo_3W_{15}$, dont la solution ne présente initialement que les trois raies attendues, évolue progressivement vers un mélange de ces différentes espèces. Il semble donc que chacun de ces espèces conduise à un mélange dont la composition dépend, entre autres, du rapport molybdène tungstène initial.

Les régions de résonance des tungstènes polaires (amplitude maximale 12 ppm) et équatoriaux (amplitude maximale 10 ppm) sont toujours nettement séparées, cependant l'intervalle entre ces deux zones est notablement plus faible que dans les composés phosphoriques, de l'ordre de 20–25 ppm et 40–

Can. J. Chem. Downloaded from www.nrcresearchpress.com by 84.41.108.74 on 09/07/12
For personal use only.

TABLEAU 5. Données RMN du tungstène-183 des tungstovanadoarsénates $As_2V_xW_{18-x}$; déplacements chimiques en ppm par rapport à Na_2WO_4 2 M dans D_2O alcalinisé; constantes de couplage $^2J_{W-W}$ (ou largeur de raie) entre parenthèses

	α-As_2W_{18}[a]	As_2VW_{17}	$As_2V_2W_{16}$	$As_2V_3W_{15}$
^{183}W polaires de la sous-unité AsV_xW_{9-x}	−120,8 [6W] (J = 21,4 Hz)[b]	−99,3 [2W] ($\Delta\nu_{1/2}$ 50 Hz)	−78 [1W] ($\Delta\nu_{1/2}$ 40 Hz)	
^{183}W polaires de la sous-unité AsW_9		−119,8 [2W] (J = 21,4 Hz) −164,5 [1W] (J = 17,1 Hz)	−111,8 [1W] (J = 19,8 Hz) −159,9 ou −160,3 [2W]	−149,3 [3W] (J = 16,4 Hz)
δ moyen(AsW_9)		134,7	144,1	
Amplitude Δδ		44,7	48	
^{183}W équatoriaux	−144,1 [12W] (J = 21,4 Hz)[b]	~ −140 [2W] ($\Delta\nu_{1/2}$ 170 Hz −149,9 [2W] −157,0 [2W] −157,4 [2W] −158,5 [2W] −182,2 [2W]	~ −150 [4W] (très large) −160,3 ou −159,9 [2W] −168,4 [2W] −190 [2W] −193,3 [2W]	−156 [6W] ($\Delta\nu_{1/2}$ 30 Hz) −196,6 [6W] (J = 17,4 et 21,5 Hz)
δ moyen		−157,5	−168,6	−176,3
Amplitude Δδ		42	43	40,6

[a]δ reporté à −121,9 et −145,3 ppm par Acerete *et al.* (9).
[b]Système AB léger à 10,4 MHz.

45 ppm respectivement (tableau 4). À cette remarque près, le spectre ^{183}W de chacun des molybdotungstoarsénates est très semblable à celui du molybdotungstophosphate analogue (1) : en particulier, chaque région de résonance (tungstènes polaires d'une part, tungstènes équatoriaux d'autre part) de la solution de $As_2Mo_2W_{16}$ est pratiquement superposable à la région de résonance correspondante de la solution de $P_2Mo_2W_{16}$. Ainsi les atomes de tungstène subissent des incréments structuraux identiques dans les deux familles, à savoir un déblindage d'environ 3 ppm par atome de molybdène pour les atomes W dans le même groupement polaire que Mo, et un blindage de, en moyenne, 2,5 ppm par atome de molybdène pour les atomes de W du groupement polaire opposé confondus en projection avec le (ou les) atome(s) de molybdène.

Dérivés tungstovanadiques

Dans le cas des tungstovanadoarsénates, l'amplitude importante des déplacements chimiques pour chaque région de résonance entraîne un chevauchement de ces zones pour As_2VW_{17} et $As_2V_2W_{16}$. Les attributions respectives sont faites par comparaison avec les composés phosphoriques analogues (1) (tableau 5).

La proximité d'un atome de vanadium se traduit par une raie large (octuplet plus ou moins coalescé) pour les atomes W polaires et très large pour les atomes W équatoriaux (20). Le nombre de raies fines attendues est donc 2 pour $As_2V_3W_{15}(C_{3v})$, 6 pour $As_2V_2W_{16}(C_s)$ et 7 pour $As_2VW_{17}(C_s)$, ce qui est effectivement observé (figure 5). Relativement à As_2W_{18}, les variations de déplacements chimiques sont beaucoup plus importantes qu'en présence du molybdène, mais ces variations sont comparables à celles observées avec les composés phosphoriques : par exemple, pour As_2VW_{17} et $As_2V_2W_{16}$, les deux raies de résonance des tungstènes dans le groupement polaire ne contenant pas de vanadium sont séparées par plus de 40 ppm, le signal blindé correspondant au(x) tungstène(s) se confondant en projection avec le(s) atome(s) de vanadium. La raie de plus haute fréquence est attribuée aux atomes W adjacents au vanadium dans le groupement polaire, son déplacement chimique augmente d'environ 20 ppm par atome de vanadium. De même, les atomes de W équatoriaux adjacents au vanadium sont

Can. J. Chem. Downloaded from www.nrcresearchpress.com by 84.41.108.74 on 09/07/12
For personal use only.

Can. J. Chem. Downloaded from www.nrcresearchpress.com by 84.41.108.74 on 09/07/12
For personal use only.

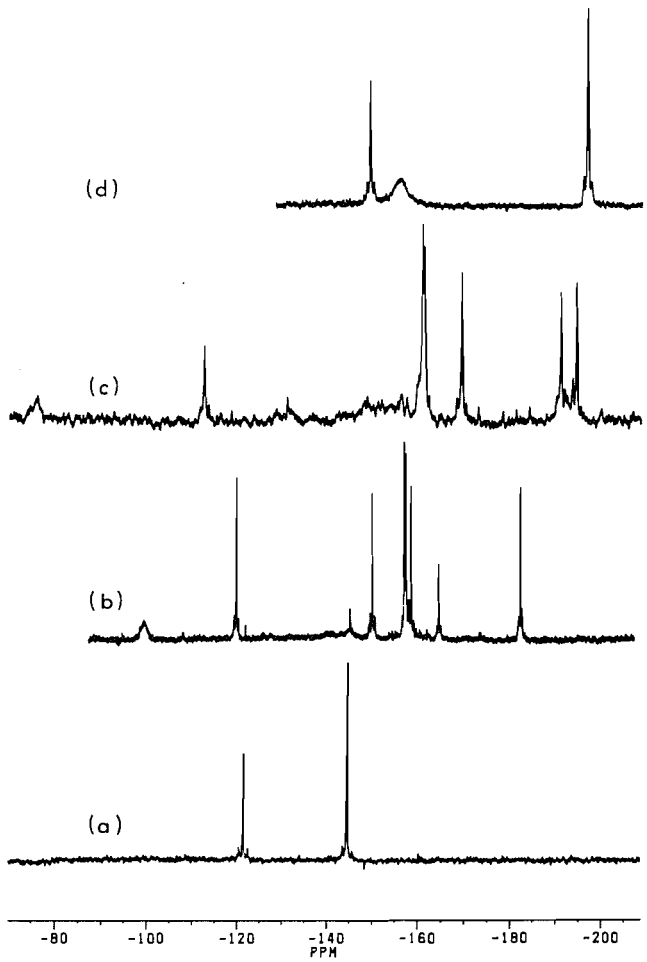


FIG. 5. Spectres RMN du tungstène-183 des anions $[As_2W_{18}O_{62}]^{6-}$ (a), $[As_2VW_{17}O_{62}]^{7-}$ (b), $[As_2V_2W_{16}O_{62}]^{8-}$ (c) et $[As_2V_3W_{15}O_{62}]^{9-}$ (d). Conditions expérimentales : solutions aqueuses saturées des sels de lithium; concentration environ 0,5 M. (a) $[As_2W_{18}O_{62}]^{6-}$: 10,4 MHz; 1000 acquisitions; facteur d'élargissement 1Hz; (b) $[As_2VW_{17}O_{62}]^{7-}$: 20,8 MHz; 17 221 acquisitions; facteur d'élargissement 1 Hz; (c) $[As_2V_2W_{16}O_{62}]^{8-}$: 10,4 MHz; 105 432 acquisitions; facteur d'élargissement 2 Hz; (d) $[As_2V_3W_{15}O_{62}]^{9-}$: 10,4 MHz; 12 183 acquisitions; facteur d'élargissement 1 Hz.

responsables des signaux larges vers -140 à -150 ppm, résonances de plus haute fréquence des raies équatoriales. Il est à remarquer que, pour l'espèce $As_2V_3W_{15}$, le signal est relativement fin (30 Hz au lieu de 150 à 200 Hz) (figures 3 et 5) du fait de la relaxation très rapide du noyau vanadium.

Tous ces résultats sont analogues à ceux observés sur les composés phosphoriques (1).

Les constantes de couplage de $As_2V_3W_{15}$ méritent quelques commentaires : les deux valeurs observées, soit, d'une part, entre tungstène polaire et tungstène équatorial d'un demi-anion AsW_9, environ 17 Hz et, d'autre part, entre tungstènes équatoriaux des demi-anions AsW_9 et AsV_3W_6, 21,5 Hz, sont nettement inférieures aux constantes de couplage analogues dans les anions tungstiques et molybdotungstiques qui sont de l'ordre de 20–21 Hz pour la première dans α-As_2W_{18} et $As_2Mo_3W_{15}$ (tableau 4) et 30,3 Hz pour la seconde dans le polytungstate dissymétrique β-As_2W_{18} (8). Cet affaiblissement des constantes de couplage homonucléaire tungstène–tungstène, attribué à un effet *trans* induit par les atomes de vanadium, est discuté en détail dans un autre article traitant de molybdotungstovanadosilicates à structure de Keggin.[4]

Remerciements

Les auteurs remercient Martine Richet pour sa collaboration technique.

1. M. ABBESSI, R. CONTANT, R. THOUVENOT et G. HERVÉ. Inorg. Chem. **30**, 1695 (1991).
2. M. T. POPE. Heteropoly and isopoly oxometalates. Inorganic Chemistry Concepts 8. Springer-Verlag, Berlin. 1983.
3. (*a*) R. CONTANT et A. TÉZÉ. Inorg. Chem. **24**, 4610 (1985); (*b*) W. H. KNOTH, P. J. DOMAILLE et R. D. FARLEE. Organometallics, **4**, 62 (1985); (*c*) W. H. KNOTH, P. J. DOMAILLE et R. L. HARLOW. Inorg. Chem. **25**, 1577 (1986); (*d*) R. THOUVENOT, A. TÉZÉ, R. CONTANT et G. HERVÉ. Inorg. Chem. **27**, 524 (1988).
4. B. DAWSON. Acta Crystallogr. **6**, 113 (1953).
5. Y. JEANNIN et M. FOURNIER. Pure Appl. Chem. **59**, 1529 (1987).
6. R. CONTANT et J. P. CIABRINI. J. Chem. Res. Synop. 222 (1977); Miniprint, 2601 (1977).
7. M. MISONO. Catal. Rev. **29**, 269, (1987).
8. (*a*) R. CONTANT et R. THOUVENOT. 29ème congrès de l'UICPA, Cologne. juin 1983. Communication p. 24 du recueil des abstracts; (*b*) R. CONTANT, G. HERVÉ et R. THOUVENOT. Atelier des polyoxométallates, St-Lambert des Bois, France. juillet 1983.
9. R. ACERETE, C. F. HAMMER et L. C. W. BAKER. Inorg. Chem. **23**, 1478 (1984).
10. H. NEUBERT et J. FUCHS. Z. Naturforsch., B: Chem. Sci., **42**, 951 (1987).
11. R. CONTANT. J. Chem. Res. Synop. 120 (1984); Miniprint, 1063 (1984).
12. R. CONTANT. Thèse, Paris. 1972.
13. R. CONTANT et J. P. CIABRINI. J. Inorg. Nucl. Chem. **43**, 1525 (1981).
14. C. ROCCHICCIOLI-DELTCHEFF, R. THOUVENOT et R. FRANCK. Spectrochimi. Acta, Part A, **52A**, 587 (1976).
15. (*a*) C. ROCCHICCIOLI-DELTCHEFF et R. THOUVENOT. C. R. Seances Acad. Sci. Ser. C: **278**, 857 (1974); (*b*) J. Chem. Res. Synop. 46 (1977); Miniprint, 0549 (1977); (*c*) R. THOUVENOT. Thèse d'État, Paris. 1978.
16. C. ROCCHICCIOLI-DELTCHEFF et R. THOUVENOT. Spectrosc. Lett. **12**, 127 (1979).
17. R. G. FINKE, M. W. DROEGE et P. J. DOMAILLE. Inorg. Chem. **26**, 3886 (1987).
18. J. P. CIABRINI. Thèse d'État, Paris. 1982.
19. W. N. LIPSCOMB. Inorg. Chem. **4**, 132 (1965).
20. P. J. DOMAILLE. J. Am. Chem. Soc. **106**, 7677 (1984)

4. E. Cadot, R. Thouvenot, A. Tézé et G. Hervé, manuscrit en preparation.

Reaction of carbonyl ylides with chloroform

MICHEL BÉKHAZI, WITOLD LAWRYNOWICZ, AND JOHN WARKENTIN[1]
Department of Chemistry, McMaster University, Hamilton, Ont., Canada L8S 4M1
Received April 17, 1991

MICHEL BÉKHAZI, WITOLD LAWRYNOWICZ, and JOHN WARKENTIN. Can. J. Chem. **69**, 1507 (1991).

Carbonyl ylides **2**, generated by thermolysis of alkoxyoxadiazolines **1** in chloroform, react with chloroform to form ketals (**3**) of 1,1,1-trichloropropanone. The isotope effect at 80°C, determined by analysis of products from thermolysis of **1** in mixed solvent ($CHCl_3/CDCl_3$, both in large excess) was estimated to be $k_H/k_D = 5$. A mechanism involving concerted C—Cl and C—H bond formation between the ylide C atoms and the Cl and H atoms of chloroform is proposed. The ketals of 1,1,1-trichloropropanone are the first to be reported.

Key words: carbonyl ylide, reaction with chloroform; chloroform, reaction with carbonyl ylides; ketals, of 1,1,1-trichloropropanone; 1,1,1-trichloropropanone, ketals of.

MICHEL BÉKHAZI, WITOLD LAWRYNOWICZ et JOHN WARKENTIN. Can. J. Chem. **69**, 1507 (1991).

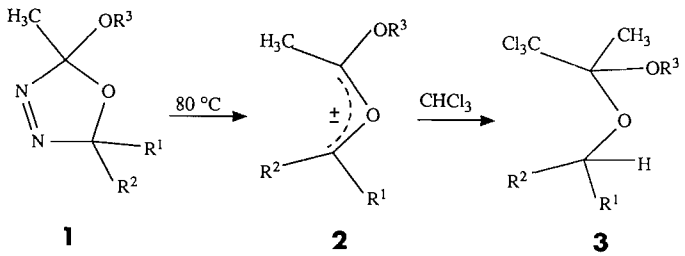
Les ylures de carbonyle **2**, obtenus par thermolyse d'alkoxyoxadiazolines **1** dans le chloroforme, réagissent avec le chloroforme pour former des cétals (**3**) de la 1,1,1-trichloropropanone. En se basant sur une analyse des produits de la thermolyse du composé **1** dans un mélange de solvants ($CHCl_3/CDCl_3$, les deux en très grand excès), on a évalué que, à 80°C, l'effet isotopique (k_H/k_D) est égal à 5. On propose un mécanisme impliquant une formation concertée de liaisons C—Cl et C—H à partir des atomes de C de l'ylure et les atomes de Cl et de H du chloroforme. Les cétals de la 1,1,1-trichloropropanone sont les premiers à être préparés.

Mots clés : ylure de carbonyle, réaction avec le chloroforme; chloroforme, réaction avec les ylures de carbonyle; cétals de la 1,1,1-trichloropropanone; 1,1,1-trichloropropanone, cétals de.

[Traduit par la rédaction]

Introduction

Well-known thermal reactions of carbonyl ylides[2] include electrocyclic ring closures to oxiranes (1, 2), cycloadditions to dipolarophiles (3–6), 1,4-sigmatropic hydrogen shifts to form enol ethers (7–9), fragmentations to carbonyl compounds and carbenes (9–11), and reactions with alcohols to form ketals (10, 12, 13).[3] The latter reactions involve (formally) the protonation of one ylide carbon and alkoxylation of the other. To the best of our knowledge analogous reactions of carbonyl ylides with acids weaker than alcohols or water have not been reported nor are there any examples of such reactions of ylides with carbon acids of any pK_a. We now report the first examples of the trapping of carbonyl ylides by chloroform, a carbon acid of pK_a 24.1 (14).



1 **2** **3**

(*a*: $R^1 = R^2 = R^3 = CH_3$; *b*: $R^1 = R^2 = CH_3$, $R^3 = CH_2CH_3$; *c*: $R^1 = R^2 = CH_3$, $R^3 = CH(CH_3)_2$; *d*: $R^1 = R^2 = CH_3$, $R^3 = C(CH_3)_3$; *e*: $R^1 = R^2 = CH_3$, $R^3 = CH_2CH_2OCH_3$; *f*: $R^1 = R^2 = (CH_2)_4$, $R^3 = CH_3$; *g*: $R^1 = R^2 = (CH_2)_5$, $R^3 = CH_3$)

SCHEME 1

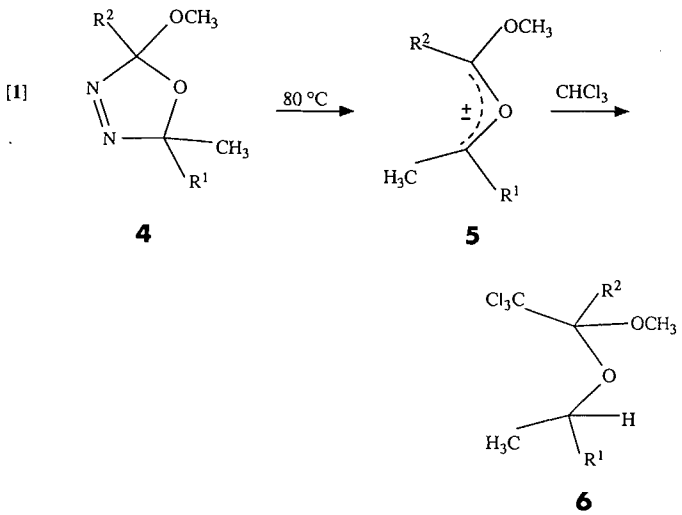
[1]Author to whom correspondence may be addressed.

[2]The literature concerning reactions of carbonyl ylides is extensive and only a few references to each type are given.

[3]In general, rate constants for the reactions listed are strongly substituent dependent and it is not possible to observe them all for a given ylide by judicious choice of the reaction conditions.

Methods, results, and discussion

Oxadiazolines, **1**, prepared by oxidation of *N*-acetylhydrazones of ketones with $Pb(OAc)_4$ (15), were thermolyzed at 80°C in degassed chloroform solutions (0.6–0.9 M) in sealed tubes (Scheme 1). Ketals (**3***a*–**3***g*) of 1,1,1-trichloropropanone (yields ranging from 18 to 55%) were separated by preparative gc and identified by ^1H nmr spectroscopy and by mass spectrometry. Oxadiazolines **4**, prepared by analogous approaches, afforded ketals **6** on thermolysis at 80°C in chloroform (eq. [1]).

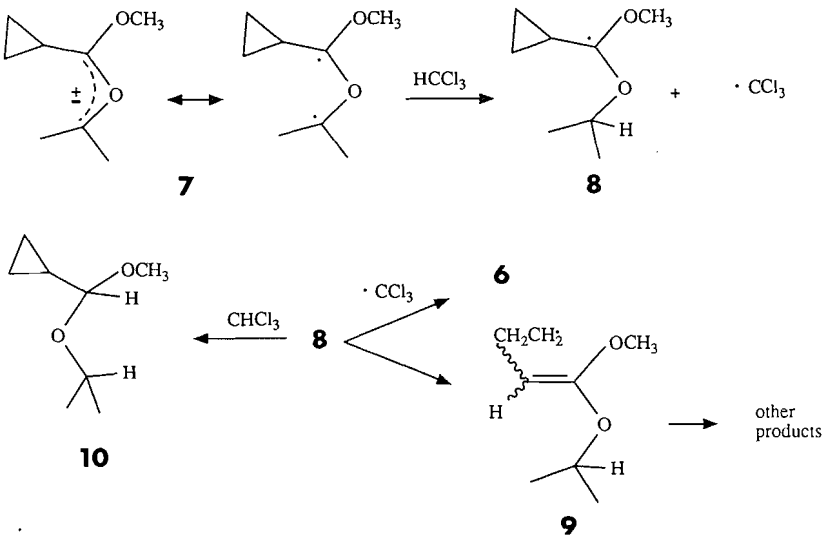


4 **5** **6**

(*a*: $R^1 = CH_3$, $R^2 = CH_2CH_3$; *b*: $R^1 = CH_3$, $R^2 = c\text{-}C_3H_5$)

Major by-products ($(CH_3)_2CO$, $CH_3CO_2CH_3$, $CH_3CH{=}CH_2$, and $CH_3CH(OCH_3)OC(CH_3){=}CH_2$, from **1***a*) were those expected from carbonyl ylide and carbene intermediates (16). Thermolysis of **1***a* in neat $HSnBu_3$ afforded those same products without any materials containing isopropoxy groups. Formation of **3** from a free-radical intermediate, which abstracts H from $CHCl_3$, is therefore unlikely. Support for that

Can. J. Chem. Downloaded from www.nrcresearchpress.com by 84.41.108.74 on 09/07/12
For personal use only.

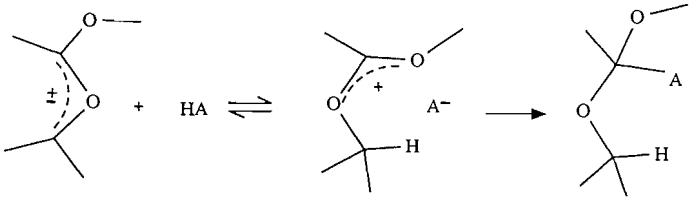


SCHEME 2

conclusion came from the finding that the 2-cyclopropyl analogue (**4***b*), prepared by oxidation of $(CH_3)_2C{=}NNHCO{-}\triangleleft$ with $Pb(OAc)_4$ in methanol (15) afforded **6***b* in a yield (25%) comparable to the yields from **1***a*–**1***c* (reaction [1]). If the process occurred by a free-radical pathway (e.g., Scheme 2) then significant ring opening to radical **9**, in competition with coupling to form **6***b*, could be expected because the rate constant for ring opening of cyclopropylmethyl to the 3-buten-1-yl radical is very large.[4] Moreover, radical **8** (and particularly its analogues from the other oxadiazolines) should be capable of H abstraction from $CHCl_3$ to form the appropriate acetal (**10**). Compounds of that type, which are very easily recognized by ^1H nmr spectroscopy ($\delta \simeq 5.1$) (11) were not obtained.

Finally, there is no precedent for radical chemistry of carbonyl ylides, nor is there any reason to expect ylides **2**, if they have singlet diradical character as expressed with **7** (Scheme 2), to be much more reactive towards $CHCl_3$ than toward $HSnBu_3$. In fact, data from the literature indicate that the reverse is probably true. Alkyl radicals (1°, 2°, and 3°) abstract from $HSnBu_3$ with rate constants in the range (1–2) $\times$ 10^6 M^{-1} s^{-1} at 300 K (18) whereas *n*-hexyl and *tert*-butyl radicals abstract H from $CHCl_3$ with rate constants 4.8 $\times$ 10^3 M^{-1} s^{-1} at 263 K (18) and 2.5 $\times$ 10^2 M^{-1} s^{-1} at 310 K (19), respectively. Thus $HSnBu_3$ is more reactive than $CHCl_3$, toward alkyl radicals, by a factor between about 10^2 and 10^4. Although the effects of oxy substituents on those rate constants are not known, it would be surprising if such substituents reversed the reactivity order.

A polar mechanism (Scheme 3) can be ruled out on the basis of the finding that carbon acids comparable to or stronger than $CHCl_3$ (pK_a = 24.1) (14), such as diethyl malonate (pK_a = 13) (20), nitromethane (pK_a = 11) (20, 21), and acetonitrile (pK_a = 25) (20) failed to form isopropoxy groups[5] from **2***a*.



SCHEME 3

It is therefore unlikely that the initial process in chloroform is the proton transfer depicted in general form in Scheme 3. Dichloromethane likewise failed to intercept ylides **2** to form a product or products containing isopropoxy groups.

In light of the evidence against radical and simple acid–base chemistry in the first step, and in view of the fact that the regioisomers of **3** were not formed,[6] we propose the novel polar mechanism of Scheme 4 for the reaction of **2** and **5** with $CHCl_3$.

The mechanism of Scheme 4, involving concerted formation of ylide **12** and its subsequent conversion, either by a concerted 1,2-rearrangement or to **3** by way of ion pair **13**, can account for all of the observations. First, by involving both electrophilic attack at Cl and nucleophilic attack at H of $CHCl_3$, with a six-membered transition state, that mechanism differentiates $CHCl_3$ from carbon acids such as carbonyl and nitro compounds. For them, the analogous transition state would be 7-membered. The alternative mechanism, proton transfer as in Scheme 3, would involve separation of charges. That is largely avoided in the first step of Scheme 4 by having one ylide give way to another. For CH_2Cl_2, the analogous step would require the breaking of a stronger C—H bond or, from the point of view of product stability, the formation of an ylide less stabilized than **12**. Moreover, attack on $CHCl_3$ with the regiochemistry opposite to that depicted would involve a transition state analogue of **11** with partial charges less favourably disposed. Ion pair **13**, derived from **12** by a heterolytic dissociation, would be expected to collapse to **3** without much of a barrier.

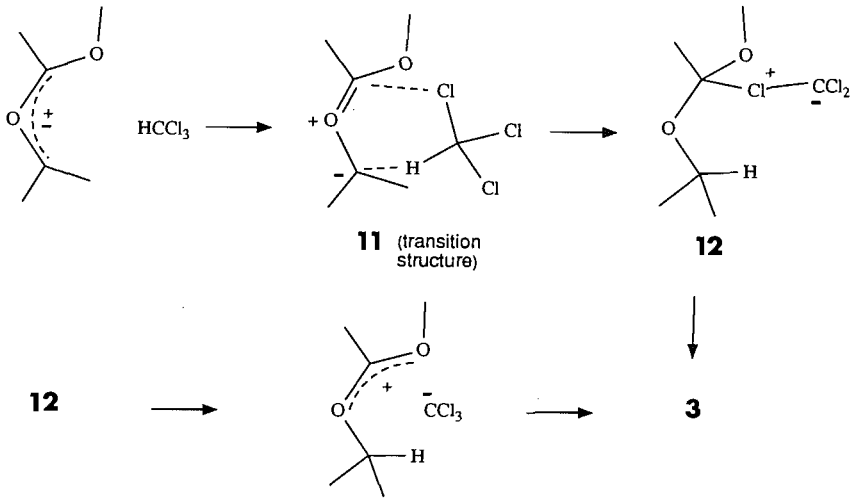
The proposed mechanism (Scheme 4) is novel and there are relatively few obvious ways of testing it. One consequence of

[4]About 6.2 $\times$ 10^8 s^{-1} at 80°C (17). The two alkoxy substituents of **7** would be expected to retard its ring opening relative to that of the parent radical, but the rate constant is unlikely to be smaller than 10^6 s^{-1}.

[5]Some of the products formed in those solvents were not identified. Major products from **1***a* were acetone, methyl acetate, and $CH_3CH(OCH_3)OC(CH_3){=}CH_2$, which arise from fragmentations and from a 1,4-sigmatropic hydrogen shift in the carbonyl ylide intermediate. The minor products, although unidentified, did not have the easily recognized isopropoxy multiplets of **3** ($R^1 = R^2 = CH_3$).

[6]We estimate that we would have detected less than 5% of such products.

Can. J. Chem. Downloaded from www.nrcresearchpress.com by 84.41.108.74 on 09/07/12
For personal use only.



SCHEME 4

that mechanism is that there should be a hydrogen/deuterium kinetic isotope effect for reaction in a solvent consisting of $CHCl_3$ and $CDCl_3$, because C—H bond rupture is part of the rate-determining step. Such an isotope effect has been demonstrated, with oxadiazoline **1***b* as starting material and with a 1:1 solution of $CDCl_3$ in $CHCl_3$. Separation of the ketal **3***b* together with its labelled analogue, and integration of the ^1H nmr spectrum ($((CH_3)_2C(H)O$ vs. CH_3CH_2O) gave $k_H/k_D = 5$. That is a substantial kinetic isotope effect, in keeping with expectation for the concerted mechanism.

The products, like the mechanism by which they are formed, are of interest. A search of the literature revealed that the most congested ketals of acetone that have been prepared are the diisopropyl and the dicyclohexyl ketals (22), formed by treatment of the ketone with the alcohol and *p*-toluenesulfonic acid in the presence of molecular sieves. Ketals of 1,1,1-trichloro-2-propanone, including the most simple ones (the dimethyl and ethylene ketals) appear to be unknown, neither are its hemiketals nor the hydrate described. Apparently there is not a single method for the preparation of ketals of 1,1,1-trichloro-2-propanone, probably because of the steric hindrance caused by the trichloromethyl group. Models of the diisopropyl ketal (**3***c*) indicate that nonbonded interactions are substantial and that there are four distinct methyl group environments. Only two were evident from the ^1H nmr spectrum, which has the characteristics of compounds of the type $XYC[CH(CH_3)_2]$ with a molecular plane of symmetry but without such a plane through the isopropyl groups.

Experimental

The ^1H nmr spectra were recorded with an EM 390 spectrometer, on solutions made with $CDCl_3$ and reference TMS. Mass spectra were obtained with a VG 70-70F double focusing spectrometer or with a ZAB-E triple focusing instrument. Samples were introduced with the direct insertion probe and ionization was achieved by electron impact (70 eV) or by chemical means, with NH_3.

Ketals **3** were purified, in general, by centrifugal chromatography with a Chromatotron no. 7924 instrument fitted with a glass plate coated with silica (Merck Kieselgel 60 PF 254). The coating was 2 mm thick and 12 cm wide. Solvents for elution were distilled in glass before use. In most instances preparative glpc was required to remove remaining impurities from a ketal isolated by centrifugal chromatography. Preparative glpc was carried out with a steel column (0.25 in. × 8 ft) packed with OV-17 (10%) in a Varian Aerograph A90-P3 machine.

Chloroform from Caledon Laboratories, Ltd., and chloroform-*d* from Merck, Sharpe, and Dohme were used as received. Shaking the chloroform with aqueous bicarbonate, drying, and distillation did not affect the results (tested with **1***a* only), and most of the reactions were therefore done with ordinary chloroform.

The acetyl hydrazine and the ketones required to synthesize acetyl hydrazone precursors of **1** were from Aldrich Chemical Co., Inc.

Ketone acetylhydrazones

The general procedure involved stirring of 0.07 mol of acetylhydrazine with excess ketone and 0.02 mole of anhydrous sodium sulfate at room temperature for 4 h. Absolute ethanol was added, a little at a time, to dissolve the solid organic product and the solution was filtered to remove sodium sulfate hydrates. Evaporation of the ethanol and excess ketone under vacuum afforded crude acetyl hydrazone in quantitative yield. The hydrazones were recrystallized from absolute ethanol/petroleum ether.

2-Alkoxy-2,5,5-trialkyl-Δ^3-1,3,4-oxadiazolines, 1

Compounds **1** were prepared by oxidative cyclization of acyl hydrazones of ketones with lead tetraacetate in alcohol R^3OH or in a solution of that alcohol in methylene chloride (9, 10). They were purified, first by methanolysis (MeO^-, MeOH) of the 2-acetoxy oxadiazoline that is formed as a by-product, and then by bulb-to-bulb distillation at ca. 0.05 Torr (1 Torr = 133.3 Pa) (9, 10).

The ^1H nmr spectra of new oxadiazolines are listed below. All were run at 90 MHz in solvent $CDCl_3$ containing TMS.

Oxadiazoline **1***b*, δ: 1.20 (t, J = 7 Hz, 3H), 1.47 (s, 3H), 1.58 (s, 3H), 1.63 (s, 3H), 3.30 (m, diastereotopic, 2H). **1***c*, δ: 1.17 (d, J = 7 Hz, 6H), 1.45 (s, 3H), 1.58 (s, 3H), 1.62 (s, 3H), 3.53 (sept, J = 7 Hz, 1H). **1***d*, δ: 1.35 (s, 9H), 1.50 (s, 3H), 1.58 (s, 3H), 1.75 (s, 3H). **1***e*, δ: 1.43 (s, 3H), 1.57 (s, 3H), 1.63 (s, 3H), 3.37 (s) superimposed upon 3.16–3.66 (m), total 7H. **1***f*, δ: 1.60 (s, 3H), 1.65–2.40 (m, 8H), 3.07 (s, 3H). **1***g*, δ: 1.17–2.10 (m) with 1.55 (s) superimposed (13H), 3.06 (s, 3H); **4***a*, δ: 1.02 (t, J = 7.5 Hz, 3H), 1.48 (s, 3H), 1.60 (s, 3H), 1.87 (q, J = 7.5 Hz, 2H), 3.13 (s, 3H); **4***b*, δ: 0.10–0.37 (m, 4H), 0.97–1.37 (m, 1H), 1.33 (s, 3H), 1.40 (s, 3H), 3.09 (s, 3H).

Thermolysis of oxadiazolines

The general procedure involved sealing a solution of the oxadiazoline (0.8–1.0 M) in chloroform into an nmr tube after several cycles of freeze–pump–thaw degassing. The ^1H nmr spectrum was recorded and the tube was immersed in an oil bath and heated at 80°C for 5 days. An ^1H nmr spectrum, taken with the tube still sealed, was used for estimates of the yields. The sample was then analyzed by

Can. J. Chem. Downloaded from www.nrcresearchpress.com by 84.41.108.74 on 09/07/12
For personal use only.

gc and gc/ms and the product of greatest interest (**3**) was separated and purified by preparative gc, on OV-17 packing at 180°C. Yields reported above in the text are averages of at least two runs except for the case of **1***b*, which was a single experiment. Yields from duplicate or triplicate runs were reproducible. For example, the yields of **3***c* from **1***c* were 32, 33, and 29% in three separate experiments.

Spectroscopic data for ketals 3 and 6

All ^{1}H nmr spectra of ketal products are 90 MHz spectra unless otherwise indicated. The solvent and reference were $CDCl_3$ and TMS throughout. Diastereotopism was observed in all cases where it was expected. The mass spectra confirmed the presence of three chlorine atoms, with M, M + 2, and M + 4 signals in the intensity ratio 1:1:0.3, where M is the signal corresponding to 3 × ^{35}Cl for the parent less OR, where OR is the smallest alkoxy group. M + 6 signals, expected at relative intensity 0.03, were not above noise in most cases.

Data for **3**a: ^{1}H nmr, δ: 1.26 (d, J = 6.1 Hz, 3H), 1.29 (d, J = 6.1 Hz, 3H), 1.78 (s, 3H), 3.53 (s, 3H), 4.26 (sept, J = 6.1 Hz, 1H), ms (EI), m/z (%): 203 (25), 205 (26), 207 (9), P − OCH_3; 175 (100), 177 (98), 179 (32), P − $OCH(CH_3)_2$. **3***b*, ^{1}H nmr δ: 1.23 (d, J = 6.0 Hz, 3H), 1.24 (t, J = 7.0 Hz, 3H), 1.28 (d, J = 6.0 Hz, 3H), 1.77 (s, 3H), 3.83 (q, J = 7.0 Hz, 2H), 4.26 (sept, J = 6.0 Hz, 1H); ms (m/z, %): 203 (6), 205 (6), 207 (2), P − OCH_2CH_3; 189 (19), 191 (19), 193 (7), P − $OCH(CH_3)_2$; ms (CI, NH_3), m/z: 266, 268, 270, M + NH_4^+. **3***c*, ^{1}H nmr, δ: 1.24 (d, J = 6.1 Hz, 6H), 1.28 (d, J = 6.1 Hz, 6H), 1.81 (s, 3H), 4.33 (sept, J = 6.1 Hz, 2H); ms (EI), m/z (%): 203 (28), 205 (30), 207 (12), P − $OCH(CH_3)_2$; 161 (100), 163 (96), 165 (33), $C_3H_4Cl_3O$; 103 (93), $C_5H_{11}O_2$. **3***d*, ^{1}H nmr, δ: 1.20 (d, J = 6.4 Hz, 3H), 1.23 (d, J = 6.4 Hz, 3H), 1.35 (s, 9H), 1.84 (s, 3H), 4.38 (sept, J = 6.4 Hz, 1H); ms (EI), m/z (%): 203 (11), 205 (11), 207 (3), P − $OC(CH_3)_3$; 161 (25), 163 (25), 165 (7), $C_3H_4Cl_3O$; 103 (100), $C_5H_{11}O_2$. **3***e*, ^{1}H nmr, δ: 1.25 (d, J = 6.2 Hz, 3H), 1.29 (d, J = 6.2 Hz, 3H), 1.80 (s, 3H), 3.41 (s, 3H), 3.58 (t, J = 5.4 Hz, 2H), 3.93 (t, J = 5.4 Hz, 2H), 4.28 (sept, J = 6.2 Hz, 1H); ms (EI), m/z (%): 219 (8), 221 (9), 223 (3), P − $OCH(CH_3)_2$; 203 (8), 205 (8), 207 (3), P − OCH_2CH_2OMe; 61 (100), $C_2H_5O_2$. **3***f*, ^{1}H nmr, δ: 1.4–1.9 (m, 8H), 1.66 (s, 3H), 3.40 (s, 3H), 4.40 (m, 1H); ms (EI), m/z (%): 229 (0.7), 231 (0.7), P − OCH_3; 175 (100), 177 (99), 179 (31), 181 (3.4), P − $OCH(CH_2)_4$; 161 (2.5), 163 (2.3), 165 (1.0), $C_3H_4Cl_3O$; 97 (26), 99 (17), 101 (3), $C_2H_3Cl_2$. **3***g*, ^{1}H nmr, δ: 1.1–1.4 (m) with 1.81 (s) superimposed, total 13H, 3.56 (s, 3H), 3.93 (m, 1H); ms (EI), m/z (%): 243 (2), 245 (2), P − OCH_3; 175 (100), 177 (100), 179 (32), 181 (3), P − $OCH(CH_2)_5$; 161 (4), 163 (4), 165 (1). **3***b*, (D-analogue, from $CDCl_3$), ^{1}H nmr, δ: 1.20 (t, J = 7.0 Hz), with D-coupled multiplets, ca. δ 1.2 superimposed, total 9H, 1.78 (s, 3H), 3.87 (q, J = 7.0 Hz, 2H); ms (EI), m/z (%): 204 (4), 206 (4), 208 (1), P − OCH_2CH_3; 189 (14), 191 (15), 193 (6), P − $OCD(CH_3)_2$; 161 (32), 163 (32), 165 (13), $C_2Cl_3O_2$; 125 (24), 127 (17), 129 (8), $C_2H_3Cl_2O$; 89 (96), $C_4H_9O_2$; 61 (100), $C_2H_5O_2$. **6***a*, ^{1}H nmr, δ: 0.23–1.00 (m, 5H), 1.08 (d, J = 6.2 Hz, 3H), 1.10 (d, J = 6.2 Hz, 3H), 3.47 (s, 3H), 4.47 (sept, J = 6.2 Hz, 1H).

Isotope effect

The H/D kinetic isotope effect was determined by the method of competition and product analysis. To **1***b* (0.155 g, 0.89 mmol) was added chloroform (0.72 g, 6.0 mmol) and deuteriochloroform (0.71 g, 5.9 mmol). The resulting solution, in an nmr tube, was degassed by means of three freeze–pump–thaw cycles. The tube was sealed and placed in a constant temperature bath at 80 ± 1°C for 5 days. The tube was cut, the volatiles were evaporated, and the residue was analyzed by nmr spectroscopy (500 MHz) using a 10-s delay time between pulses. The ratio of protio to deuterio adducts (**6***f*) was determined by integrating the methine septet against the methylene quartet several times and averaging. An isotope effect of 5 ± 1 was estimated from the average of two runs.

Acknowledgements

This project was supported by the Natural Sciences and Engineering Research Council of Canada. We are grateful to Professor M. J. McGlinchy for helpful discussions, to Dr. R. W. Smith and Mr. F. A. Ramelan for the mass spectra, and to Mr. B. G. Sayer for some of the nmr spectra.

1. R. Huisgen. Angew. Chem. Int. Ed. Engl. **16**, 572 (1977).
2. L. E. Manring and K. S. Peters. J. Am. Chem. Soc. **106**, 8077 (1984).
3. G. A. Lee. J. Org. Chem. **41**, 2656 (1976).
4. (*a*) J. P. K. Wong, A. A. Fahmi, G. W. Griffin, and N. S. Bhacca. Tetrahedron, **37**, 3345 (1981); (*b*) P. K. Das and G. W. Griffin. J. Org. Chem. **49**, 3452 (1984).
5. P. C. Wong, D. Griller, and J. C. Scaiano. J. Am. Chem. Soc. **104**, 6631 (1982).
6. A. Padwa, S. P. Carter, H. Nimmesgern, and P. D. Stull. J. Am. Chem. Soc. **110**, 2894 (1988).
7. (*a*) A. C. Lottes, J. A. Landgrebe, and K. Larsen. Tetrahedron Lett. **30**, 4089 (1989); (*b*) Tetrahedron Lett. **30**, 4093 (1989).
8. (*a*) A. P. Hitchcock, S. Zweep, T. Steel, M. Békhazi, and J. Warkentin. Can. J. Chem. **60**, 2914 (1982); (*b*) M. W. Majchrzak and J. Warkentin. Can. J. Chem. **67**, 1753 (1989).
9. M. Békhazi and J. Warkentin. J. Am. Chem. Soc. **61**, 619 (1983).
10. M. Békhazi and J. Warkentin. J. Am. Chem. Soc. **103**, 2473 (1981).
11. M. Békhazi and J. Warkentin. J. Am. Chem. Soc. **105**, 1289 (1983).
12. C. V. Kumar, P. K. Das, W. I. O'Sullivan, S. N. Ege, and G. W. Griffin. J. Chem. Soc. Perkin Trans. 2, 1745 (1984).
13. N. Shimizu and P. D. Bartlett. J. Am. Chem. Soc. **100**, 4260 (1978).
14. A. C. Lin, Y. Chiang, D. B. Dahlberg, and A. J. Kresge. J. Am. Chem. Soc. **105**, 5380 (1983).
15. J. Warkentin. Synthesis, 279 (1970).
16. M. Békhazi and J. Warkentin. Can. J. Chem. **61**, 619 (1983).
17. A. L. J. Beckwith, V. W. Bowry, M. O'Leary, G. Moad, E. Rizzardo, and D. H. Solomon. J. Chem. Soc. Chem. Commun. 1003 (1986); (*b*) L. Mathew and J. Warkentin. J. Am. Chem. Soc. **108**, 7981 (1986); (*c*) M. Newcomb and A. G. Glenn. J. Am. Chem. Soc. **111**, 275 (1989).
18. N. Q. Tuan and T. Gäumann. Radiat. Phys. Chem. **10**, 263 (1977).
19. P. G. Frith and K. A. McLauchlan. J. Chem. Soc. Faraday Trans. 2, **72**, 87 (1976).
20. F. G. Bordwell and J. E. Bartmess. J. Org. Chem. **43**, 3101 (1978).
21. R. G. Pearson and R. L. Dillon. J. Am. Chem. Soc. **75**, 2439 (1953).
22. D. P. Roelofson and H. Van Bekkum. Synthesis, 419 (1972).

Can. J. Chem. Downloaded from www.nrcresearchpress.com by 84.41.108.74 on 09/07/12
For personal use only.

Structural and surface aspects of thermally treated copper aluminium mixed hydroxides

AWAD I. AHMED, S. E. SAMRA, AND S. A. EL-HAKAM
Chemistry Department, Faculty of Science, Mansoura University, Mansoura, A.R. Egypt
Received February 16, 1990[1]

AWAD I. AHMED, S. E. SAMRA, and S. A. EL-HAKAM. Can. J. Chem. **69**, 1511 (1991).

$CuO–Al_2O_3$ catalysts containing various amounts of copper oxide have been prepared by precipitation. The phase changes were studied by X-ray diffraction. The results obtained revealed that the thermal treatment of solid $CuO–Al_2O_3$ at 700°C produced only crystalline CuO. Heating to 900°C led to the formation of copper alumina spinel together with unreacted CuO and γ-Al_2O_3. The spinel content was found to increase with increasing copper content. Nitrogen adsorption–desorption isotherms on the calcined samples have been measured. Surface areas have been calculated and the pore structure analysed. The textural properties of the system were found to depend on both the copper content and the calcination temperature.

Key words: CuO, Al_2O_3 catalysts, structure, surface area, pore structure.

AWAD I. AHMED, S. E. SAMRA et S. A. EL-HAKAM. Can. J. Chem. **69**, 1511 (1991).

On a préparé, par précipitation, des catalyseurs de type $CuO–Al_2O_3$ contenant différentes quantités d'oxyde de cuivre. On a étudié les changements de phase par diffraction de rayons X. Les résultats obtenus révèlent que le traitement thermique du $CuO–Al_2O_3$ solide à 700°C produit uniquement du CuO cristallin. Le chauffage jusqu'à 900°C conduit à la formation de spinelle de cuivre alumine avec du CuO et du γ-Al_2O_3 qui n'ont pas réagi. On a trouvé que la spinelle augmente avec la teneur en cuivre. On a mesuré les isothermes d'adsorption–désorption de l'azote des échantillons calcinés. On a calculé les aires de surface et on a analysé la structure des pores. On a trouvé que les propriétés texturales du système dépendent à la fois de la teneur en cuivre et de la température de calcination.

Mots clés : CuO, Al_2O_3, catalyseurs, structure, aires de surface, structure des pores.

[Traduit par la rédaction]

1. Introduction

Metal oxides have long attracted attention since they are widely used and find many applications in several fields of investigation related to catalysis. It is found that better catalysts (1–6), refractories, and adsorbents are frequently produced by mixing two or more metal oxides. It is well known that for a better understanding of the function of catalysts their physical structure must be elucidated since structure may be greatly affected by their method of preparation and treatment (7). Attention is also currently directed towards certain aspects of the physical structure of active solids which characterize their "texture". These include surface area, pore geometry, and pore size distribution.

The catalytic activity and selectivity of catalysts may be greatly influenced by the geometrical characteristics of their surface. According to Schwab and Block (8) the dehydrogenation reaction takes place on flat surfaces whereas dehydration occurs in narrow pores.

The $CuO–Al_2O_3$ system may be considered as one of the most interesting binary system. The co-existence of CuO and Al_2O_3 in a binary system increases the range application of the mixed oxide solid.

In recent years copper oxide alumina systems have attracted considerable interest because of their selective properties in reactions involving hydrogen (9–13), selective hydrogenation of carbonyl groups in unsaturated aldehydes and ketones (14) and hydrogen transfer to ketones over hydroxyapatites (15). However, some aspects of the textural and catalytic behaviour of copper-containing catalysts are not completely understood.

The present investigation reports a study on the effect of thermal treatment on the structural and textural properties of copper aluminium mixed hydroxides.

2. Experimental

2.1 Materials

Different copper aluminium mixed hydroxide samples of various compositions were prepared from solutions of copper and aluminium chloride using 1 M NH_4OH at 70°C (BDH grade). Depending on the desired composition of mixed hydroxide, appropriate, calculated volumes of chloride solution were taken, and the NH_4OH solution was added dropwise with continuous stirring to give a pH of about 7.5. The precipitate was washed several times with distilled water till free from chloride and ammonium ions and dried at 100°C for 48 h.

The mixed oxide samples were obtained by heating the corresponding mixed hydroxide in air to temperatures between 300 and 900°C for 24 h. The compositions of the prepared mixed oxides were 0.10 CuO 1 Al_2O_3, (AC10), 0.25 CuO 1 Al_2O_3 (AC25), 0.50 Cu 1 Al_2O_3 (AC50), and 1 CuO 1 Al_2O_3 (AC1:1). The thermal products of the mixed oxides are designated AC10-*T*, AC25-*T*, AC50-*T*, and AC1:1-*T*, where *T* is the calcination temperature.

2.2 Techniques

The adsorption by nitrogen was measured at −196°C on the calcination products of the mixed oxides using a conventional volumetric apparatus. The adsorption was followed until near saturation and then the desorption was followed down to relative pressures at which the desorption branches of the isotherm join the adsorption ones. The samples were outgassed at 4 h under a reduced pressure of 10^{-5} Torr prior to any adsorption measurement.

An X-ray investigation of the thermal products of mixed hydroxide samples was carried out using a Geiger Flex D/MAX-IA X-ray diffractometer system. The patterns were obtained using nickel-filtered copper radiation (λ = 1.5405 Å) at 36 kV and 16 mA; the diffraction angle 2° was scanned at a rate of 2° min^{-1}.

3. Results and discussion

The X-ray investigation of the products of thermal treatment of AC50 at temperatures between 300 and 500°C (Fig. 1*a* and *b*) revealed the amorphous nature of the solids. On increasing the calcination temperature to 700°C (Fig. 1*c*) only

[1]Revision received May 16, 1991.

Printed in Canada / Imprimé au Canada

Can. J. Chem. Downloaded from www.nrcresearchpress.com by 84.41.108.74 on 09/07/12
For personal use only.

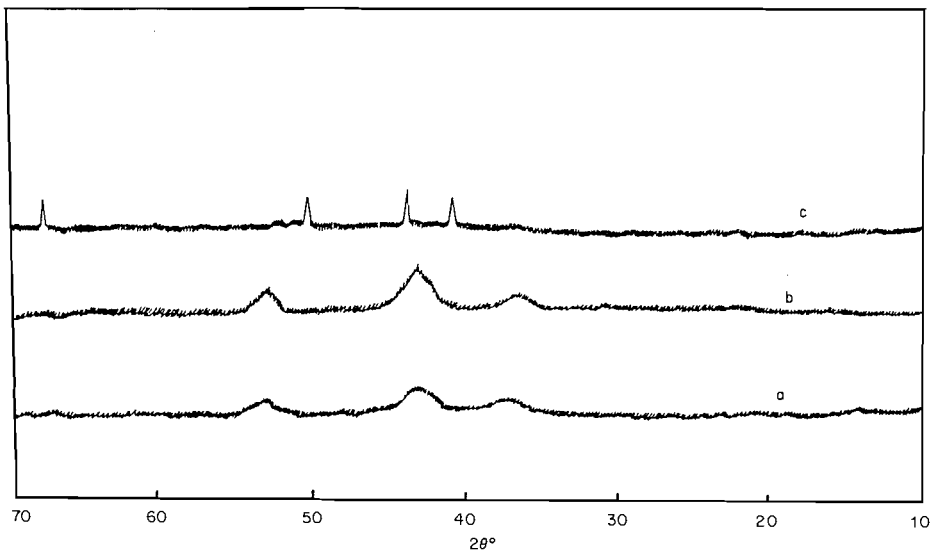


FIG. 1. X-ray diffraction patterns of (*a*) AC50-300, (*b*) AC50-500, and (*c*) AC50-700.

the crystalline CuO phase was obtained at *d* values of 1.174, 1.084, 0.918, and 0.832 Å. At temperatures lower than 500°C a mutual interaction between the two oxyhydroxides and the substitution of the cationic sites are common in the transition metal hydroxide gels as well as oxides, e.g. the $Co(OH)_2$–$Mg(OH)_2$ systems observed by Matyshak *et al.* (16). These observations were also observed by Mani and Rao (17) for the $Fe(OH)_3$–$Al(OH)_3$ system. They found that the samples calcined at 420°C were amorphous to X-rays, they also found from electron microscopic and diffraction studies the presence of clusters in these samples.

Figure 2 represents the X-ray diffraction patterns of the different mixed oxides calcined at 900°C. All the characteristic lines of both CuO and γ-Al_2O_3 and copper(II) aluminate ($CuAl_2O_4$) spinel were detected. The peaks, at 1.522 and 0.874 Å, are characteristic of γ-alumina, while the bands at *d* = 1.288, 1.130, and 0.996 Å are characteristic of $CuAl_2O_4$. The intensity of the diffraction lines of the $CuAl_2O_4$ spinel formed increases with increased copper content. A maximum intensity for the $CuAl_2O_4$ lines was attained at solid composition AC1:1-900. It is also seen from Fig. 2 that the increase in copper content was accompanied by the appearance of some copper(I) metal aluminate ($CuAlO_2$) phase besides $CuAl_2O_4$. This process may be represented as follows:

$$CuO + Al_2O_3 \rightarrow CuAl_2O_4$$

$$2CuAl_2O_4 \rightarrow 2CuAlO_2 + Al_2O_3 + \tfrac{1}{2}O_2$$

The presence of unreacted CuO and γ-Al_2O_3, together with the spinel phases, in all specimens heated to 900°C revealed that the solid-state reaction between copper and aluminium oxides yielding $CuAl_2O_4$ is a slow diffusion reaction (18). According to this mechanism CuO reacts with Al_2O_3 by diffusion of CuO to the $CuAl_2O_4$ interface. Since the O—Cu bond in CuO and O—Al bonds in Al_2O_3 are respectively ionic and covalent, the mobility of Cu^{2+} ions may be considerably higher than that of Al^{3+}.

Adsorption–desorption isotherms of nitrogen at −196°C were measured on the calcination products of AC10, AC25, AC50, and AC1:1 thermally treated at 300–900°C. Figure 3 shows a set of representative adsorption–desorption isotherms of nitrogen on the calcination products of AC10. The adsorption of nitrogen on all the thermal products of CuO–Al_2O_3 samples exhibits hysteresis. It is also shown that the area and shape of the hysteresis loops change with calcination temperature. The isotherms of all samples investigated are situated between types II and IV of the EDDT classification (19).

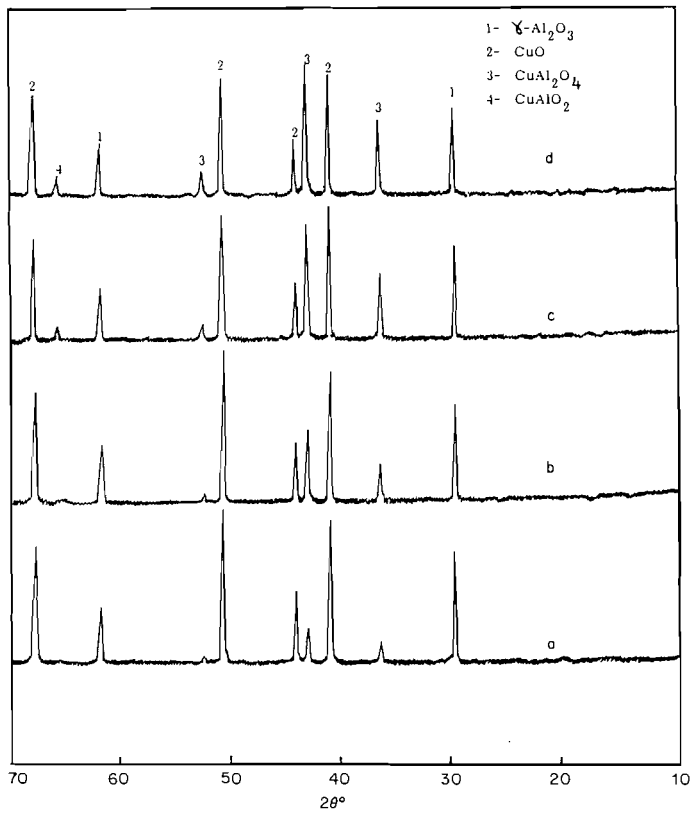


FIG. 2. X-ray diffraction patterns of (*a*) AC10-900, (*b*) AC25-900, (*c*) AC50-900, and (*d*) AC1:1-900.

From an analysis of the adsorption isotherms by the BET equation (20), the specific surface area values S_{BET} ($m^2\ g^{-1}$) were calculated, adopting a cross-sectional area for the nitrogen molecule of 16.2 Å (21). The specific surface areas and BET-*C* constants of the above samples are given in Table 1.

Can. J. Chem. Downloaded from www.nrcresearchpress.com by 84.41.108.74 on 09/07/12
For personal use only.

TABLE 1. Surface characteristics of $CuO-Al_2O_3$

Sample	S_{BET} $m^2\ g^{-1}$	S_t $m^2\ g^{-1}$	S_{cum} $m^2\ g^{-1}$	V_{cum} $mL\ g^{-1}$	V_T $mL\ g^{-1}$	BET C	r_H nm
AC10-300	303.8	312.5	318.6	0.3728	0.3454	26	1.1
AC10-500	276.6	279.2	271.6	0.4321	0.4075	20	1.5
AC10-700	190.7	187.6	213.8	0.3891	0.3500	19	1.8
AC10-900	94.4	95.2	95.2	0.1671	0.1364	9	1.5
AC25-300	298.9	285.4	311.8	0.3634	0.3651	51	1.2
AC25-500	261.7	258.3	281.5	0.4067	0.3924	12	1.5
AC25-700	175.3	178.1	161.5	0.3763	0.3901	11	2.2
AC25-900	78.3	84.4	89.3	0.1985	0.1563	12	2.0
AC50-300	287.4	289.6	298.3	0.3969	0.3666	38	1.3
AC50-500	166.7	168.8	178.1	0.5121	0.5136	17	3.1
AC50-700	147.6	148.8	154.9	0.4102	0.3984	16	2.7
AC50-900	54.3	59.4	73.3	0.1021	0.0970	21	1.8
AC1:1-300	234.2	229.2	245.9	0.3056	0.2985	23	1.3
AC1:1-500	109.6	100.6	119.4	0.3521	0.3287	14	3.0
AC1:1-700	78.6	77.1	70.8	0.2106	0.2101	17	2.7
AC1:1-900	67.1	65.6	81.9	0.1417	0.1545	19	2.3

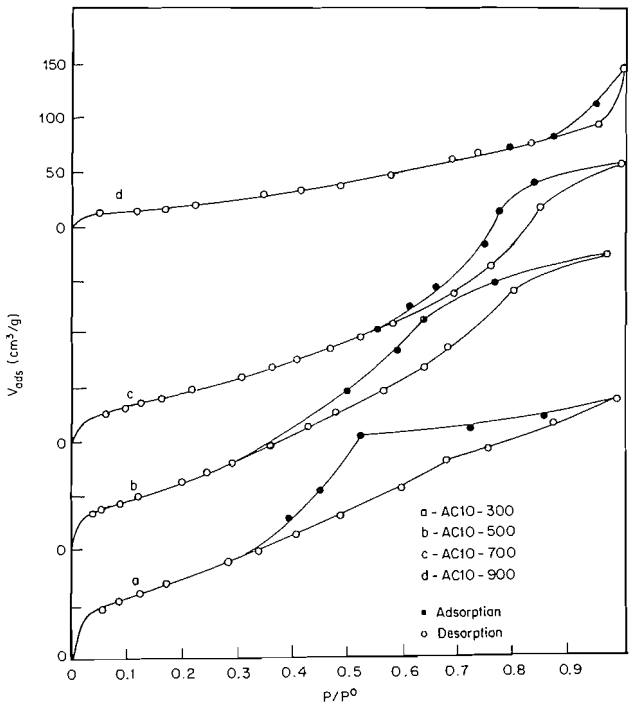


FIG. 3. Adsorption–desorption isotherms of nitrogen at −196°C on the calcination products of AC10.

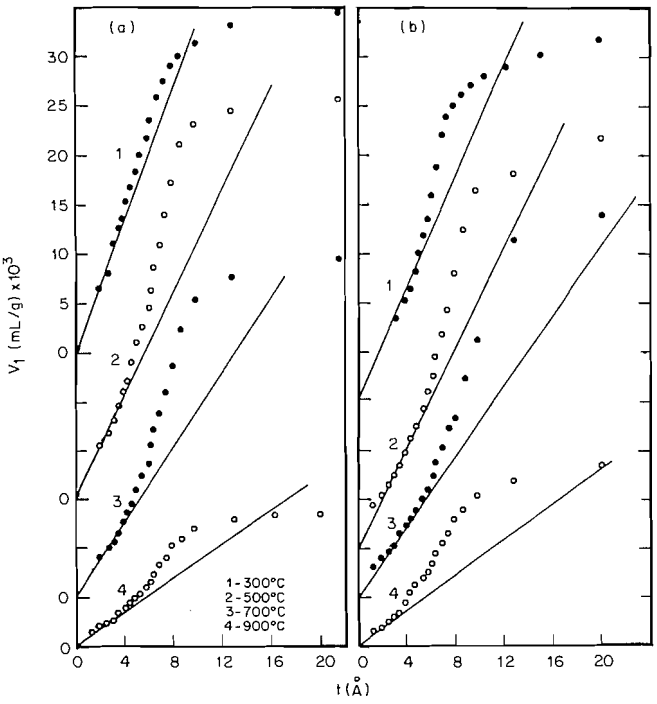


FIG. 4. V_1–t plots of nitrogen adsorbed on the calcination products of (*a*) AC10 and (*b*) AC25.

The surface areas of $CuO-Al_2O_3$ calcined in the temperature range 300–900°C reveal clearly that the increase of copper content in the precipitated alumina is associated with a marked decrease in the surface area. The effects were more pronounced at higher calcination temperatures. This may be interpreted by the diffusion of divalent copper ions in the matrix of alumina which appears to be associated with a more effective elimination of a good fraction of smaller pore, leading to a marked decrease in surface area. Within the temperature range investigated, the BET C constant changes with temperature and metal content.

The t plot of De Boer and co-workers (22, 23) has attracted a good deal of attention as a simple and direct means of interpreting nitrogen adsorption isotherms and characterising the porosity of solid adsorbents. The method consists of plotting the volume of nitrogen adsorbed on the solid under investigation against the corresponding statistical thickness, t, of the adsorbed layer of nitrogen on a nonporous reference solid. Lippens *et al.* (22) calculated the mean monolayer thickness as 3.541 Å and used this to calculate t ($t = 0.354V/V_m$) at the corresponding P/P^0 (where V is the volume of nitrogen adsorbed and V_m is the monolayer capacity). The slope of the linear t plot provides a measure of the surface area S_t ($m^2\ g^{-1}$) of the solid, according to the relation

$$S_t = \frac{V_1}{t} \times 10^4$$

Can. J. Chem. Downloaded from www.nrcresearchpress.com by 84.41.108.74 on 09/07/12
For personal use only.

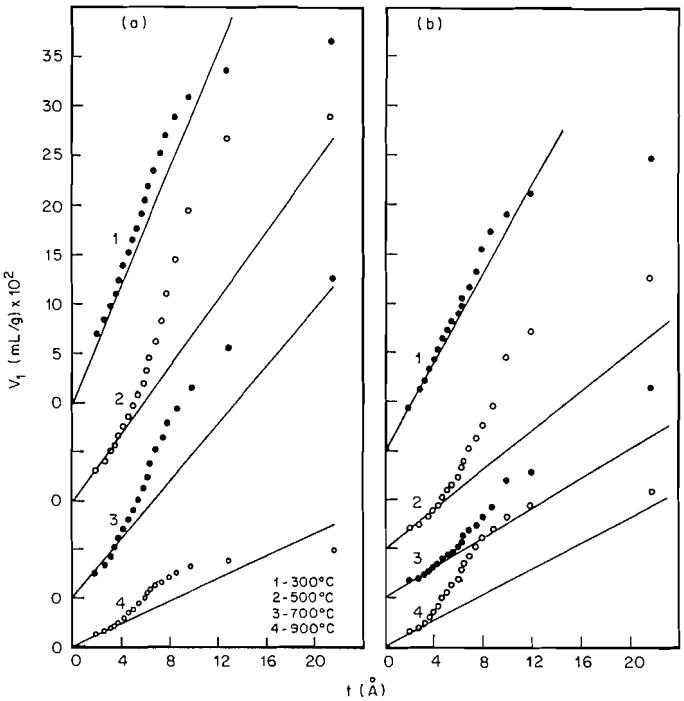


FIG. 5. V_l–t plots of nitrogen adsorbed on the calcination products of (*a*) AC50 and (*b*) AC1:1.

De Boer and co-workers have demonstrated that a deviation from the straight line is associated with the existence of pores in the solid. A downward deviation from the straight line (negative deviation) indicates the presence of micropores; their filling by the adsorbate molecules cuts down their surface from further adsorption, while an upward deviation from the straight line (positive deviation) indicates the presence of mesopores in which capillary condensation can take place, causing the amount adsorbed to increase beyond the straight line in the V_l–t plot. In these plots, the t curves of De Boer and co-workers (22, 23) and Mikhail *et al.* (24) were used.

Surface-area values calculated by the V_l–t method (S_t) are given in Table 1. Satisfactory agreement is observed between the corresponding S_{BET} and S_t values, indicating the correctness in the choice of the t curve used in the analysis. The V_l–t plots constructed for samples AC10, AC25, AC50, and AC1:1 heated at different temperatures are shown in Figs. 4 and 5. From these plots, an upward deviation is found to commence at lower t value for samples heated to 300°C. This positive deviation does not continue and reverts back at relatively higher t value ($\simeq$10 Å) indicating that the samples form a mixed pore system. When the temperature is raised above 300°C, most of the micropores are changed to mesopores. These changes are also reflected in the total pore volume (V_T), determined by the volume adsorbed at $P/P^0 = 0.95$ and the average pore radii.

Thermal treatment of CuO–Al_2O_3 samples up to 900°C is accompanied by a continuous decrease in surface area. The average pore radius indicates some widening up to 500°C for AC50 and AC1:1 and continuous to 700°C for AC10 and AC25. At this temperature it may be postulated (25) that, during calcination, the cryptocrystalline material moves from the surface of wider pores to fill the smaller capillaries or pores, so that the average pore radius increases. The increase in the total pore volume (V_T) observed at 500°C may be attributed to the removal of water molecules held in the intercrystalline pores, leading to an increase of the accessibility to the nitrogen molecules. Increasing the calcination temperature is accompanied by a decrease in pore radius and the appearance of microporosity as clearly shown in V_l–t plots (Figs. 4 and 5), indicating the commencement of a process of shrinkage.

There is another way to evaluate the total surface area, which might be used under favourable conditions as a substitute for the BET method. This comes from pore size analysis and the surface associated with the different groups of pores present. The pore size analysis carried out using nitrogen adsorption was made by using the corrected model-free method (26) for mesopore analysis, and the micropore method (27) for micropore analysis. Computation was carried out starting from $P/P^0 = 0.95$ down to $P/P^0 = 0.3$, so as to completely cover the hysteresis region of adsorption. It was decided that the parallel plate model can reasonably describe the shape of the pores. The results shown in Table 1 fulfill all criteria for correct pore structure analysis, namely agreement between the cumulative surface area (S_{cum}) and S_{BET}, as well as agreement between cumulative pore volume (V_{cum}) and total pore volume (V_T).

Pore volume distribution curves could be constructed and they are shown in Figs. 6 and 7, for the samples calcined at 500°C and AC25 calcined in the temperature range (300–

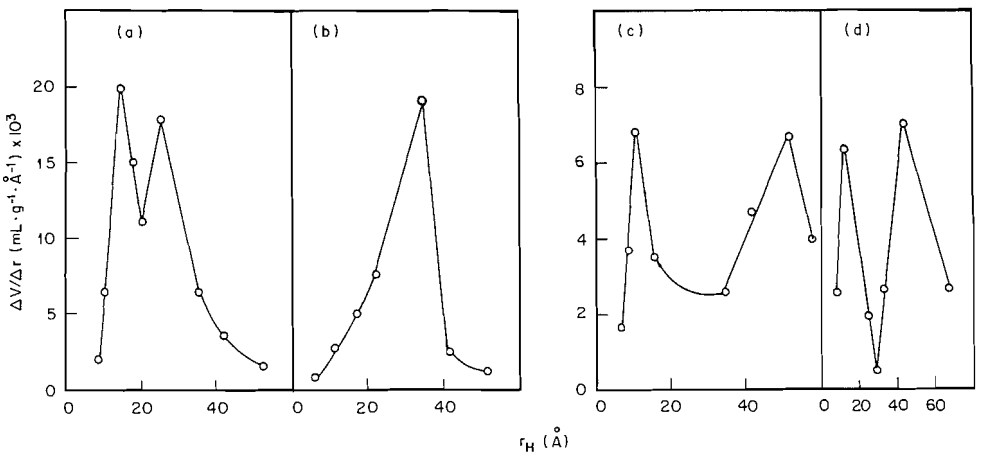


FIG. 6. Pore-volume distribution curves of (*a*) AC10-500, (*b*) AC25-500, (*c*) AC50-500, and (*d*) AC1:1-500.

Can. J. Chem. Downloaded from www.nrcresearchpress.com by 84.41.108.74 on 09/07/12
For personal use only.

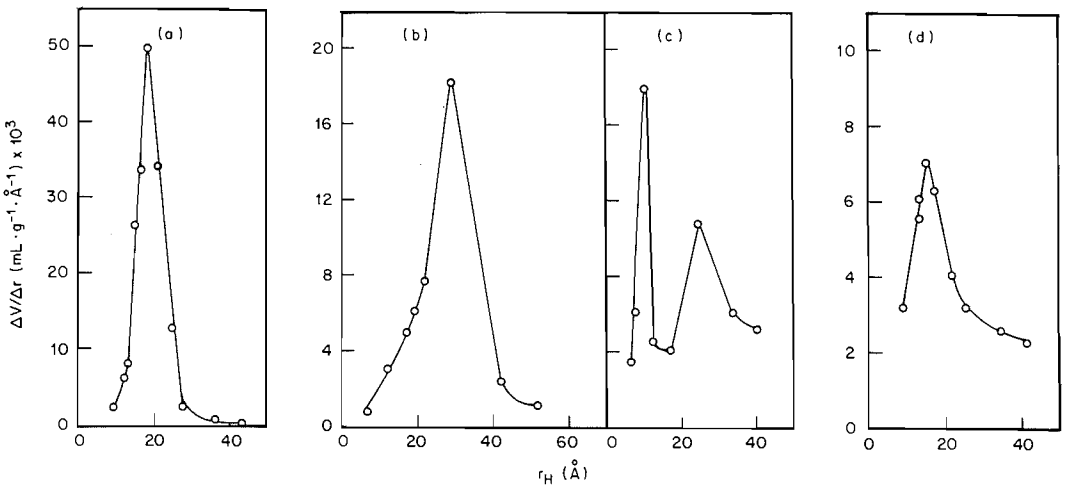


FIG. 7. Pore–volume distribution curves of (*a*) AC25-300; (*b*) AC25-500; (*c*) AC25-700, and (*d*) AC25-900.

900°C). The pore volume distribution curves reveal several interesting points: (*1*) The number of pores, as shown by the height of the distribution curve, is substantially reduced on increasing both the copper content and the calcination temperature. This decrease parallels the decrease in surface area. (*2*) Solids with high copper oxide content have a noticeable effect on both the meso- and micropores in both number and size. A more significant effect was noticed for AC50 and AC1:1 where microporous (X-ray) amorphous solids are formed. (*3*) The effect of calcination temperature on the pore volume curves is mainly reflected in a decrease of their number. Small shifts to higher pore radii were observed specially at 500°C. On increasing the calcination temperature to 700°C a group of narrow pores was formed, owing to the formation of small crystallites of CuO. The presence of both micropores and mesopores in the samples points to inhomogeneity of the samples. At 900°C copper alumina spinels were formed which were characterised by a low degree of heterogeneity due to their crystallinity, and this is indicated by the drastic decrease in surface area and the disappearance of the sample mesoporosity. This is in accordance with the X-ray findings.

1. M. SAMAANE and S. J. TEICHNER. Bull. Soc. Chim. Fr. **1927**, 1934 (1968).
2. M. E. DRY and F. S. STONE. Discuss. Faraday Soc. **28**, 192 (1955).
3. P. KOSTAD. Non-stoichiometry, diffusion and electrical conductivity in binary metal oxides. Wiley-Interscience, New York. 1972.
4. D. DOLLIMORE and T. E. JONES. J. Appl. Chem. Biotechnol. **23**, 29 (1973).
5. K. C. KHULBE, R. S. MANN, D. SHOPOV, A. ANDREE, and L. PETROV (*Editors*). Proc. 3rd Int. Symp. Heterogen. Catal. Varna, 1975, Bulgarian Academy of Sciences, Sofia. 1978. p. 468.
6. R. F. COOLEY and J. S. REED. J. Am. Ceram. Soc. **55**, 395 (1972).
7. W. B. IMNES. Anal. Chem. **29**, 1069 (1957).
8. G. M. SCHWAB and J. BLOCK. J. Chim. Phys. **51**, 664 (1954).
9. K. KLIER. Adv. Catal. **31**, 243 (1982).
10. H. H. KUNG. Catal. Rev. Sci. **22**, 235 (1980).
11. T. VAN HERWIJNEN and W. A. DE JONG. J. Catal. **63**, 83 (1980).
12. A. HIROMIOHI, S. YASUKAGU, and Y. YUKIO. J. Catal. **9**, 146 (1967); **10**, 128 (1968).
13. A. P. RUDENKO and E. M. EZZO. Kinet. Katal. **11**, 1064 (1970).
14. J. JENK and J. E. GERMAIN. **65**, 141 (1980); **65**, 133 (1980).
15. C. L. KIBBY and W. K. HALL. J. Catal. **31**, 65 (1973).
16. V. A. MATYSHAK, M. YA. KUSHNEV, M. P. SHIBANOV, A. A. KADUSHIN, and O. V. KRYLOV. Kinet. Catal. **17**, 457 (1976).
17. B. MANI and V. SITAKARA RAO. Thermochim. Acta, **53**, 183 (1982).
18. R. E. CARTER. J. Am. Ceram. Soc. **44**, 116 (1961).
19. S. BRUNAUER, L. S. DEMING, W. S. DEMING, and E. TELLER. J. Am. Chem. Soc. **62**, 1723 (1940).
20. S. BRUNAUER, P. H. EMMETT, and E. TELLER. J. Am. Chem. Soc. **60**, 309 (1938).
21. D. M. YOUNG and A. D. CROWELL. Physical adsorption of gases. Butterworths, London. 1962. p. 108.
22. B. C. LIPPENS, B. G. LINSEN, and J. H. DE BOER. J. Catal. **3**, 32 (1964).
23. B. C. LIPPENS and J. H. DE BOER. J. Catal. **4**, 319 (1965).
24. R. SH. MIKHAIL, S. A. SELIM, and F. I. ZEIDAN. J. Appl. Chem. Biotechnol. **26**, 191 (1976).
25. H. E. RIES. Adv. Catal. **4**, 87 (1952).
26. S. BRUNAUER, R. SH. MIKHAIL, and E. E. BODOR. J. Colloid Interface Sci. **24**, 451 (1967).
27. R. SH. MIKHAIL, S. BRUNAUER, and E. E. BODOR. J. Colloid Interface Sci. **26**, 45 (1968).

Can. J. Chem. Downloaded from www.nrcresearchpress.com by 84.41.108.74 on 09/07/12.
For personal use only.

A tensammetric study of the adsorption of cationic polymers and copolymers

TRUIS SMITH-PALMER[1] AND CHERYL ROBERTS
Chemistry Department, Saint Francis Xavier University, Antigonish, Nova Scotia B2G 1C0

Received December 10, 1990[2]

TRUIS SMITH-PALMER and CHERYL ROBERTS. Can. J. Chem. **69**, 1516 (1991).

The tensammograms of several sets of cationic polyacrylamide copolymers are discussed and compared. Tensammograms are not affected by molecular weight, but plots of capacitive current at a chosen potential versus charge density give regular curves.

Key words: tensammetry, cationic, polyacrylamide, charge density.

TRUIS SMITH-PALMER and CHERYL ROBERTS. Can. J. Chem. **69**, 1516 (1991).

On a comparé et on discute des tensammogrammes de plusieurs ensembles de copolymères cationiques du polyacrylamide. Les tensammogrammes ne sont pas affectés par la masse moléculaire, mais des courbes du courant capacitif à un potentiel donné en fonction de la densité de charge fournissent des droites régulières.

Mots clés : tensammétrie, cationique, polyacrylamide, densité de charge.

[Traduit par la rédaction]

Can. J. Chem. Downloaded from www.nrcresearchpress.com by 84.41.108.74 on 09/07/12
For personal use only.

Introduction

Cationic polyacrylamide copolymers come with a wide variety of functional groups and in a wide variety of molecular weights, although for the most part their weights tend to be smaller than those of their anionic counterparts, which are often 1–20 million. These cationic polymers are used in a variety of industries, often to help flocculate systems of negatively charged particles. There has been much discussion in the literature on their mechanism of action — whether it is due to charge neutralization (1), bridging, or a combination thereof (2) which depends on molecular weight and charge density. Whichever the mechanism, adsorption of the polymers must be considered as a first step. Many colloids of industrial interest such as clays, coal, and silica have negatively charged surfaces. However, the surfaces can become positively charged in the presence of certain modifiers, and there are other particles, e.g. goethite, which have positively charged surfaces. The nature of the surface charge would naturally be expected to affect the adsorption process.

Tensammograms are effectively plots of capacitive current versus applied potential (3). As the potential is scanned from 0 to −2 V, the surface of a static mercury drop is at first positively charged, with the charge gradually decreasing to zero then becoming increasingly negative. The capacitive current depends on the nature of the ions and/or molecules which are adsorbed onto the surface of the mercury drop at the potential in question. For surface-active molecules and some small polymers such as polyethylene glycol, there is usually a distinct potential range where surface adsorption occurs, and at the limits of this range, adsorption/desorption peaks are often seen (e.g. refs. 4, 5). Polyelectrolytes are also surface active, but are very much larger than detergents and are made up of alternating hydrophyllic and hydrophobic regions rather than the distinct "heads" and "tails" of detergents. The tensammograms of large polyelectrolytes do not always exhibit absorption or desorption peaks, as their size makes them absorb so strongly that such peaks would be outside the useful 0–2 V potential range. However, their tensammograms are distinctly different from the tensammogram for KCl alone and the general shape of the tensammograms of anionic and nonionic polyelectrolytes are distinctly different from those of cationic polyelectrolytes (6). Ions such as chloride which can adsorb onto the Hg surface can be replaced by the much larger polyelectrolytes, which can then undergo various rearrangements on the surface (7), or undergo partial desorption where just some of the segments desorb. Although the adsorption of different kinds of species effects the capacitive current differently (3), for a series of related compounds the effects on the current should be of the same sign but of varying magnitude. The surface of the mercury is featureless (structurally homogeneous), and should not itself influence the binding of the polymer. Thus by measuring the capacitive current at various potentials, one can gain insight into how the adsorption changes with surface charge.

We have previously shown that we can determine the concentration of polyacrylamides and cationic and anionic acrylamide copolymers using both polarographic maximum suppression (8) and tensammetry (6), and that we can use tensammetry to determine the mol% anionicity of anionic acrylamide/acrylate copolymers after complexation with tetraethylammonium chloride (9). In this paper we compare the tensammetric behaviour of various cationic polymers and copolymers in order to study parameters which affect their adsorption at various potentials. We have also examined the use of tensammetry in determining the charge densities (mol%) of the cationic acrylamide copolymers themselves. Various titrations (conductimetric, colorimetric) are currently used by most labs to determine the charge densities of cationic copolymers. These titrations rely on knowledge of the exact amount of polymer present, and for some the change of colour of the indicator is not sharp.

Experimental

Tensammograms were recorded, as described previously (6, 9), using a Princeton Applied Research (PAR) Model 174A Polarographic Analyzer and a Model 303 static mercury drop electrode (SMDE) in conjunction with a PAR Model 174A/50 AC Polarographic Analyzer Interface and a PAR Model 122 Lock-in Amplifier. The analog output of the polarograph was digitized using an Apple IIe microcomputer with Interactive Microware software (Lab Data Manager, Scientific Plotter) and hardware (ADALAB Interface card, ADA-AMP Instrumentation Amplifier). A modulation amplitude of 10 mV (p-p) at 200 Hz was used. The phase was adjusted to be 135 degrees away from the phase of the reference modulation to minimize faradaic currents. The hanging mercury drop electrode (small) and a scan rate of 5 mV/s were used. All potentials reported are relative to a silver-silver chloride reference electrode containing KCl (saturated).

The Magnifloc polymers were obtained from the American Cyanamid Corp. The Praestol polymers were obtained from Energy, Mines

[1]Author to whom correspondence should be addressed.
[2]Revision received May 15, 1991.

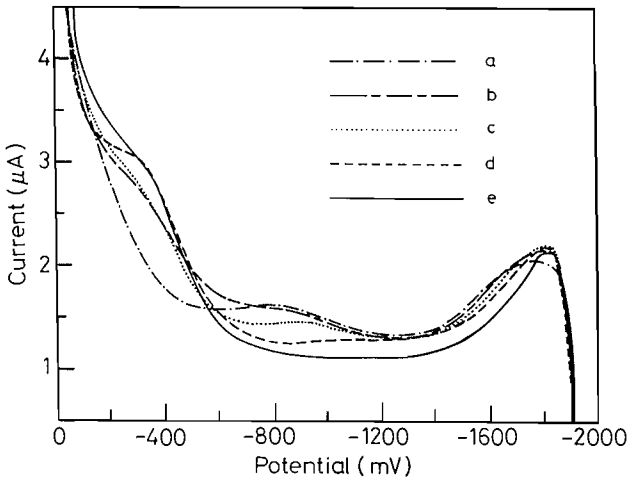


FIG. 1. Tensammograms of 50 ppm solutions of Magnifloc 905N (*a*), 491C (*b*), 492C (*c*), 494C (*d*), and 496C (*e*) in 0.25 M KCl.

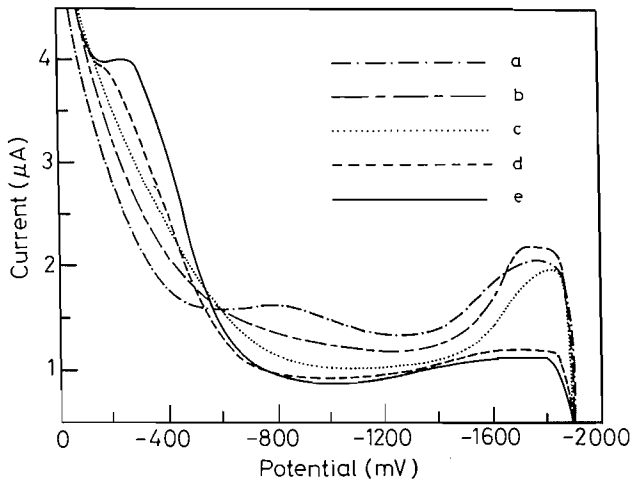


FIG. 2. Tensammograms of 50 ppm solutions of Magnifloc 905N (*a*), Praestol 411k (*b*), Praestol 421k (*c*), Praestol 534K (*d*), and Praestol 444k (*e*) in 0.25 M KCl.

and Resources (Edmonton) and Stockhausen, Germany. Standard deviations were determined using 12 measurements.

Results and discussion

At low concentration, capacitive current is a function of the concentration of surface active material in solution, as well as a function of the structure of that material. However, at concentrations upward of ~20 ppm, depending on the polymer in question, the adsorbed monolayer is saturated and tensammograms are not affected by concentration. Solutions of KCl give a tensammogram which has a characteristic hump at ~−300 mV where specific adsorption of Cl^- occurs (6), and another hump at ~−1800 mV which we attribute to the potassium ions (10). The tensammograms of a non-ionic polyacrylamide, Magnifloc 905N, and a set of standard cationic polyacrylamide copolymers, Magnifloc 491, 492, 494, and 496 (50 ppm) are shown in Fig. 1. These so-called "cationic polyacrylamides" are co-polymers of acrylamide and the methyl chloride quaternary of dimethyl aminoethyl acrylate [CH_2=$CHCO_2CH_2CH_2N(CH_3)_3Cl$]. The tensammograms of the cationic copolymers cross each other, and that of the non-ionic polyacrylamide, just before −600 mV.

At this potential only non-specific attraction of polymers to the electrode surface must occur, i.e., there will be no electrostatic attraction or repulsion between the surface and the polymers at this potential. However, as the water molecules near the surface will be oriented at random in the absence of a charge on the surface, polymers are able to readily approach the surface and are then held there by dispersion forces. The curve for the non-ionic polymer shows no Cl^- hump in the ~−300 mV region and the capacitive current there is depressed with respect to that of KCl alone (6). At this potential the surface of the mercury drop is positively charged and the cationics would be expected to adsorb to a lesser extent than does the polyacrylamide. The capacitive currents of the cationic copolymers become progressively higher as their charge densities increase, indicating that their effectiveness in replacing chloride ions from the surface decreases. Adsorption of positively charged polymers onto a positively charged surface has been reported previously (1). There the adsorption is not electrostsatic, but is the non-specific (dispersion forces) kind of bonding shown by non-ionic polymers. However, this attraction would be expected to be increasingly countered by electrostatic repulsion as the positive charge increased, thence the increase in capacitive current with % charge. At potentials more negative than the

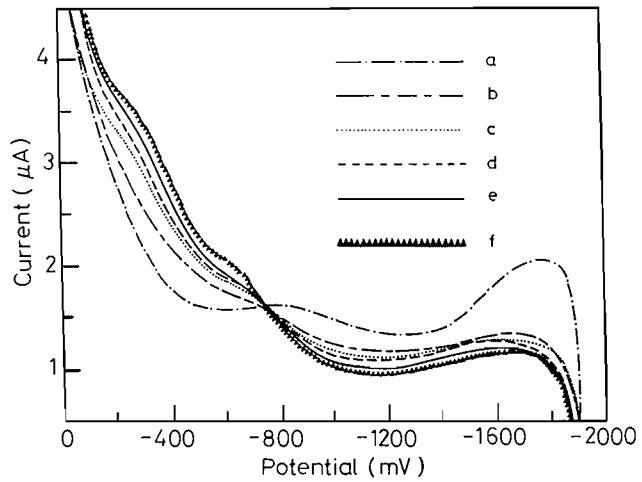


FIG. 3. Tensammograms of 50 ppm solutions of Magnifloc 905N (*a*), Praestol 611BC (*b*), Praestol 650BC (*c*), Praestol 644BC (*d*), Praestol 655BC (*e*), and Praestol 666 BC (*f*) in 0.25 M KCl.

crossover point, the cationic polymers would be expected to be increasingly attracted to the mecury surface as compared to the non-ionic polymer, as their % charge increases. This is manifested in the tensammograms by a decrease in the capacitive current. At potentials around −1600 mV the capacitive currents of all these polymers and of KCl show a similar rise. At this point the adsorption of potassium ions presumably predominates (10). The tensammograms of another series of copolymers where the cationic monomer is the methacrylate, [$CH_2C(Me)CO_2$-$CH_2N(CH_3)_3Cl$] are shown in Fig. 2. The presence of the extra methyl group is seen to have little effect on the overall shape of the tensammograms, or the crossover point. The most significant difference is that the tensammograms of the two copolymers of highest charge do not show a hump in the −1800 mV region, showing that they can effectively compete with the potassium ions. The tensammograms of a further series where the copolymer is the methyl chloride quaternary of dimethylaminopropylacrylamide (Fig. 3) are all fairly flat in the −1800 mV region and we must assume that the change in the copolymer makes it much better able to compete with K^+, even at low charge densities. The crossover point on these tensam-

Can. J. Chem. Downloaded from www.nrcresearchpress.com by 84.41.108.74 on 09/07/12
For personal use only.

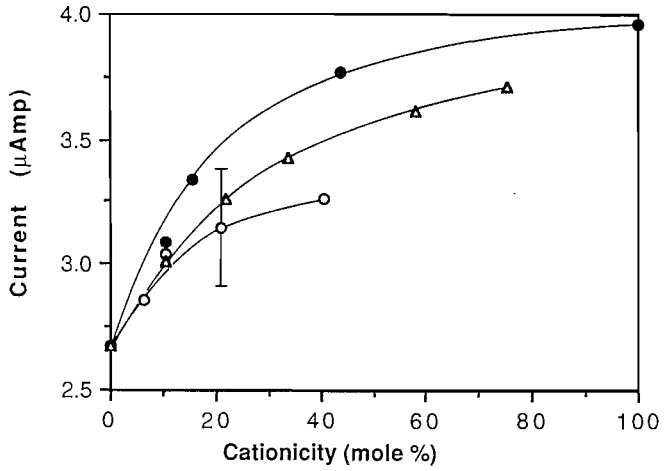


FIG. 4. Plot of current at −220 mV versue cationicity for 50 ppm solutions of: copolymers of acrylamide and the methyl chloride quaternary of dimethylaminoethylacrylate (○, acrylamide and the methyl chloride quaternary of dimethylaminoethylmethacrylate (●), and acrylamide and the methyl chloride quaternary of dimethylaminopropylacrylamide (△) in 0.25 M KCl.

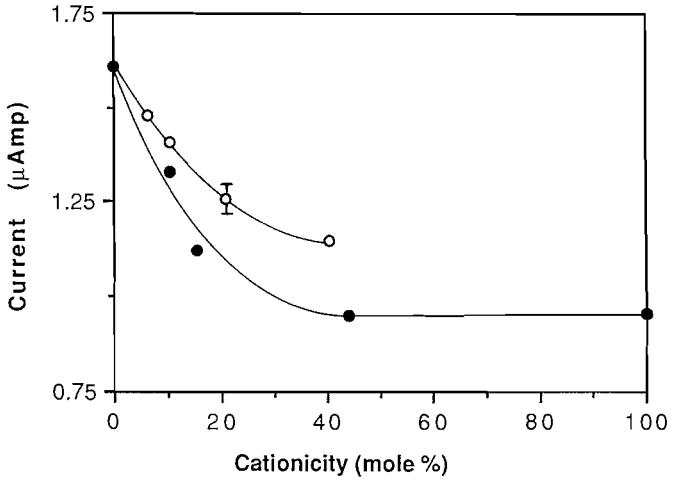


FIG. 5. Plot of current at −800 mV versus cationicity for 50 ppm solutions of dimethylaminoethylacrylate (○), and acrylamide and the methyl chloride quaternary of dimethylaminoethylmethacrylate (●) in 0.25 M KCL.

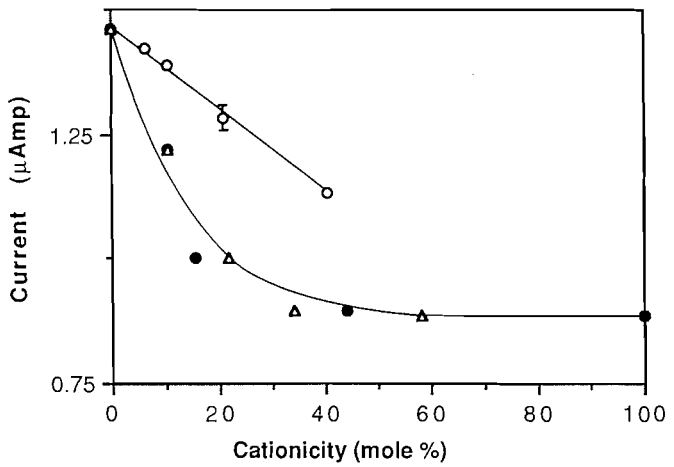


FIG. 6. Plot of current at −1100 mV versus cationicity for 50 ppm solutions of: copolymers of acrylamide and the methyl chloride quaternary of dimethyl aminoethylacrylate (○), acrylamide and the methyl chloride quaternary of dimethylaminoethylmethacrylate (●), and dimethylaminopropylacrylamide (△) in 0.25 M KCl.

mograms is at −760 mV, significantly more negative than for the acrylate copolymers.

By inspection of the tensammograms, potentials of −220 mV, −800 mV, and −1000 mV, were identified as points where the biggest changes in current occurred as a function of the copolymers' charge densities. Plots of capacitive current versus mol% cationicity are shown in Figs. 4, 5, and 6 for each of the potentials respectively. The plots show that the changes with charge density are fairly regular for each set, but that changing the cationic polymer does affect the capacitive current.

If the identity of the cationic monomer was known, the appropriate standard curves could be used to determine the mol% cationicity of a polymer. This method has the advantage of not being concentration dependent once a critical concentration is present, which is useful for polymers whose purity is questionable. The graphs at −800 mV and −1000 mV are the most useful because the tensammetric curves tend to be much more reproducible in this region. The actual currents measured in the tensammograms depend on the particular capillary being used. The electrodes were cleaned in HF and siliconized before use, but these cationic copolymers strongly adsorb onto glass and capillaries have to be changed fairly frequently. The tensammograms shown comparing the different cationic copolymers were all run on the same day using the same electrode, and using polymer solutions which were all prepared together 5 days prior to use. We have found that solutions of cationic polymers show aging effects — when freshly prepared they produce very fast settling rates of kaolin slurries, whereas much older solutions bring about drastically slower settling rates which depend more on the charge density (unpublished result). This may be due to the hydrolysis of the polymers, although aging effects have previously been reported for solutions of polyacrylamides (12).

When using tensammetry to determine the charge density of anionic acrylamide/acrylic acid copolymers, we found that the complexes formed with tetraethylammonium chloride gave distinct desorption peaks which were related to the charge density. For the cationic polymers above, the presence of ethanesulphonic, or pentanesulphonic acid changed the shapes of the tensammograms somewhat, but lead to no new distinct peaks, nor to improved 'standard' curves.

We next examined the tensammograms of a series of cationic polyelectrolytes (Magnifloc 567, 572, 573, 577 and 581) based on the reaction of dimethylamine and epichlorohydrin, giving [CH_2—$CH(OH)CH_2$—$N(CH_3)_2Cl$], with a range of average molecular weights varying from 5 000 to 250 000 respectively. Their tensammograms are almost identical to each other, with some slight differences occurring at their beginning. These polymers have high charge densities, and this is particularly shown by the lack of any hump at −1800 mV, similar to the tensammograms for the most highly charged Praestols. The tensammograms of three polydiallylydimethyl ammonium chlorides of different molecular weights, Magnifloc 585, 587, and 591, were also found to be independent of molecular weight, and to show a greatly decreased capacitive current with respect to KCl at −1800 mV.

Thus in general the molecular weight of a cationic polymer has little effect on its tensammogram. A similar result has been

Can. J. Chem. Downloaded from www.nrcresearchpress.com by 84.41.108.74 on 09/07/12
For personal use only.

reported previously for polyacrylamide (9). Thus we can say that the adsorption of these polymers onto a neutral or a negatively or positively charged mercury surface is independent of molecular weight. If this result can be extrapolated to smaller particles of various other identities where molecular weight is known to be an important parameter in controlling settling rates, it suggests that it is only the flocculation step and not the initial adsorption step that is molecular weight dependent. Adsorption isotherms determined on a system which is undergoing flocculation do not reveal this. If flocculation is occurring very fast with polymers of high molecular weight, particles are quickly bound together and removed from solution before the adsorption process is completed.

Conclusions

Positively charged polymers can adsorb onto a positively charged surface, but the extent of adsorption decreases with charge density. The adsorption onto the negatively charged mercury surface increases with charge density. However, as the surface becomes very negatively charged there is greater competition with cations and only the polyectrolytes of highest potential and charge effectively compete with K^+. The dependence of adsorption (as manifested by the capacitive current) on charge density can be used to estimate the charge density of unknown polymers to within ±5%.

Acknowledgements

We thank NSERC for an Operating Grant and UCR, St. F.X.U. for a summer stipend for C.R.

1. F. MABIRE, R. AUDEBERT, and C. QUIVORON. J. Colloid Interface Sci. **97**, 120 (1984).
2. R. I. S. Gill and T. M. HERRINGTON. Colloids Surfaces, **25**, 297 (1987).
3. B. BREYER and H. H. BAUER. Chemical analysis. Vol. 13. Alternating current polarography and tensammetry. Interscience, Wiley & Sons, New York, NY. 1963.
4. K. S. SHARMA. Kolloid–Zeitschrift und Zeitsch rift für Polymere, Band 233. Heft 1-2, 962. 1969.
5. D. R. CANTERFORD. Anal. Chim. Acta, **94**, 377 (1977).
6. T. SMITH-PALMER, B. R. WENTZELL, J. C. DONINI, and R. J. JERRARD. Can. J. Chem. **66**, 2658 (1988).
7. B. B. DAMASKIN and V. E. KAZARINIV. *In* Comprehensive treatise of electrochemistry. Vol. 1. The double layer. *Edited by* J. O. M. Bockris, B. E. Conway, and E. Yeager. Plenum Press, New York, NY. 1980. p. 356.
8. B. R. WENTZELL, T. SMITH-PALMER, and J. C. DONINI. Can. J. Chem. **65**, 557 (1987).
9. T. SMITH-PALMER and B. R. WENTZELL. Can. J. Chem. **68**, 26 (1990).
10. A. K. SHALLAL and H. H. BAUER. Anal. Lett. **4**(4), 205 (1971).
11. J. R. MILLER and D. C. GRAHAME. J. Coll. Sci. **16**, 23 (1961).
12. W. P. SHYLUK and F. S. STOW, JR. J. Appl. Polym. Sci. **13**, 1023 (1969).

Can. J. Chem. Downloaded from www.nrcresearchpress.com by 84.41.108.74 on 09/07/12
For personal use only.

Hydrogen-bonded complexes of perfluoro-*t*-butanol with acetone and nitromethane in low temperature solutions and matrices[1]

LOUISE SCHRIVER[2] AND ANDRÉ SCHRIVER
Laboratoire de Physique Moléculaire et Atmosphérique, CNRS UPR 136, 4 place Jussieu, F-75252 Paris Cedex 05, France[3]
STEFAN PEIL
Fachbereich Physikalische Chemie, Philipps-Universität, Hans-Meerwein Straße, D-3550 Marburg, Germany
AND
OTTO SCHREMS
Alfred Wegener Institute for Polar and Marine Research, Columbus Straße, D-2850 Bremerhaven, Germany[4]
Received December 7, 1990

LOUISE SCHRIVER, ANDRÉ SCHRIVER, STEFAN PEIL, and OTTO SCHREMS. Can. J. Chem. **69**, 1520 (1991).

Infrared spectra are reported for binary complexes between perfluoro-*tert*-butanol as proton donor and nitromethane and acetone as bases. The complexes have been investigated in low temperature solutions and in cryogenic matrices. The spectra have been evaluated in terms of frequency shifts ($\Delta\nu_{OH}$), half widths (FWHH) and anharmonicities (κ) caused by the hydrogen bonding of these complexes. The influence of the environment (solvents and solid matrices) as well as temperature on the spectra of the complexes has also been studied and is discussed in detail.

Key words: hydrogen bonding, temperature effects, solutions, matrix.

LOUISE SCHRIVER, ANDRÉ SCHRIVER, STEFAN PEIL et OTTO SCHREMS. Can. J. Chem. **69**, 1520 (1991).

On rapporte les spectres infrarouges des complexes binaires entre le perfluoro-*tert*-butanol, en tant que donneur de protons et le nitrométhane et l'acétone en tant que bases. On a étudié les complexes en solutions à basse température et dans des matrices cryogéniques. On a évalué les spectres en fonction des déplacements des fréquences ($\Delta\nu_{OH}$), des largeurs à mi-hauteur (FWHH) et des harmonicités (κ) provoquées par les liaisons hydrogènes dans ces complexes. On a également étudié l'influence de l'environnement (solvants et matrices solides) aussi bien que de la température sur les spectres des complexes, et on en discute largement.

Mots clés : liaisons, hydrogènes, effet de temperature, solutions, matrix.

[Traduit par la rédaction]

Introduction

Because of its strong acidic properties (pK_a = 5.4 at 298 K) (1) and weak tendency for self-association, perfluoro-*tert*-butanol (PFTB) is an excellent candidate as proton donor in the experimental studies of hydrogen bonded systems (2, 3). Schrems *et al.* (4) examined the PFTB – dimethyl ether complex in the gas phase, CCl_4 solution and solid argon as part of their studies on proton donor abilities of fluoroalcohols. Iskanderov *et al.* (5, 6) investigated hydrogen-bonded complexes between PFTB and various bases in cryosolvents like Kr, Xe, and Freons by means of IR spectroscopy. They also studied the low frequency spectra of some of these complexes (7). Recently, Luck *et al.* (8) examined in detail the IR spectra of the complexes between PFTB and acetonitrile-D_3 (AN-d_3) in dilute solutions of a large variety of solvents and isolated in solid Ne, Ar, Kr, Xe, and N_2 matrices. The near-infrared studies performed by Burneau (9) of the same system provided complementary information. The present report consequently extends the last two studies with two further proton acceptor molecules. In detail, we have investigated the IR and NIR spectra of two complexes involving PFTB as proton donor interacting with nitromethane (NM) and acetone (AC) for which only scarce information has been available so far (3). NM with a proton donor affinity (PA) of 180 kcal/mol is a weaker base than AN (PA = 187 kcal/mol) while AC (PA = 195 kcal/mol) is somewhat stronger. The aim of these studies is to manifest the correlation between base strength and spectral properties (frequency shifts $\Delta\nu_{OH}$, $\Delta 2\nu_{OH}$, band profiles, intensities and multiplicities, isotope shifts) obtained from the different phases and temperatures.

Experimental

The experiments were performed under similar conditions as previously described (8). PFTB was obtained from SCM Chemicals (Gainesville, FL, USA) and the rare gases were supplied by Messer Griesheim (Düsseldorf, FRG). Deuterated PFTB was prepared by successive exchanges with D_2O and vacuum distillation to an isotopic enrichment of 95%. Acetone, acetone-d_6, and nitromethane-d_3 (NM-d_3) were UVASOL® grade and obtained from Merck (Darmstadt, FRG). The Freons (from Dupont Nemours, France) were distilled and kept over P_2O_5 at 273 K. The spectra were resolved with an accuracy of 1 cm^{-1}. Careful attention was paid to the spectral backgrounds. The solvent absorptions have been subtracted. In matrix studies the experimental details have been found to be identical to those described in ref. 8.

Results

1. Complexes between PFTB and NM-d_3

Measurements in solution

Typical spectra of the fundamental and overtone OH stretching region of dilute solutions of PFTB and NM-d_3 in cryosolvent solutions (1:1 volume mixture of Freon 11 and Freon 114B2) at various temperatures (range 295–113 K) are pre-

[1]This paper is dedicated to Professor Werner A. P. Luck, University of Marburg, on the occasion of his reaching Emeritus status.

[2]To whom correspondence should be adressed.

[3]A part of this work was also taken account to Laboratoire de Spectrochimie Moléculaire, CNRS UA 508.

[4]Contribution number 418 of the Alfred Wigener Institut for Polar and Marine Research, Bremerhaven, Germany.

Printed in Canada / Imprimé au Canada

Can. J. Chem. Downloaded from www.nrcresearchpress.com by 84.41.108.74 on 09/07/12
For personal use only.

Can. J. Chem. Downloaded from www.nrcresearchpress.com by 84.41.108.74 on 09/07/12
For personal use only.

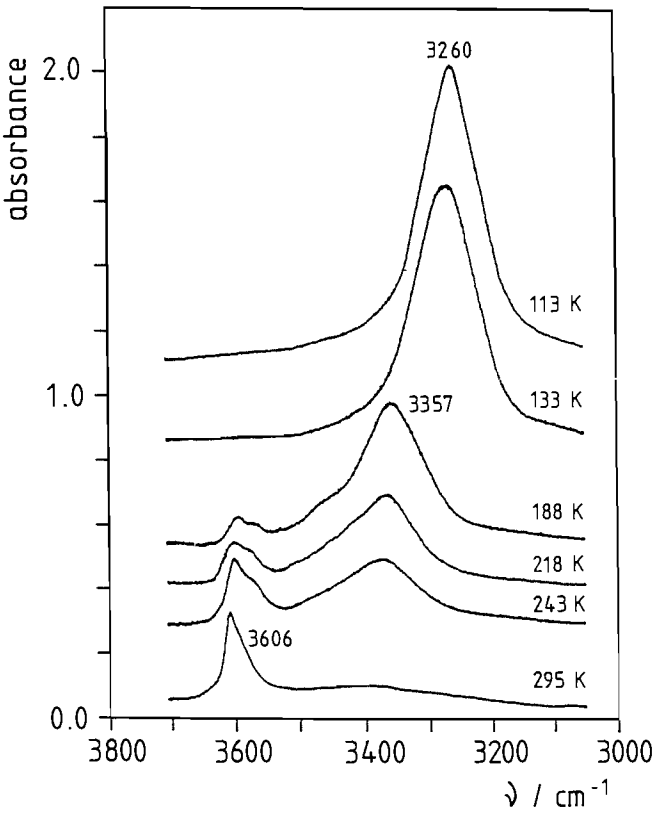


FIG. 1. Temperature effect on the fundamental ν_{OH} absorption of the PFTB···NM-d_3 complex diluted in a mixture of Freon 11 and Freon 114B2 (volume ratio 1:1). Concentrations (c) at room temperature were c[PFTB] = 0.015 mol, c(NM-d_3] = 0.03 mol. Pathlength (d) = 2 mm.

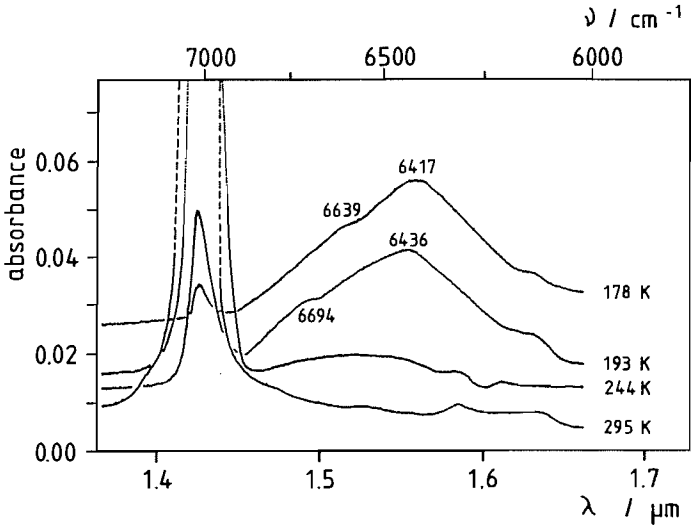


FIG. 2. Temperature effect on the first overtone of the OH stretching vibration of the PFTB···NM-d_3 complex diluted in Freon 11 and Freon 114B2 (volume ratio 1:1). Concentrations (c) at room temperature were c[PFTB] = 0.03 mol, c(NM-d_3] = 0.04 mol. Pathlength (d) = 44 mm.

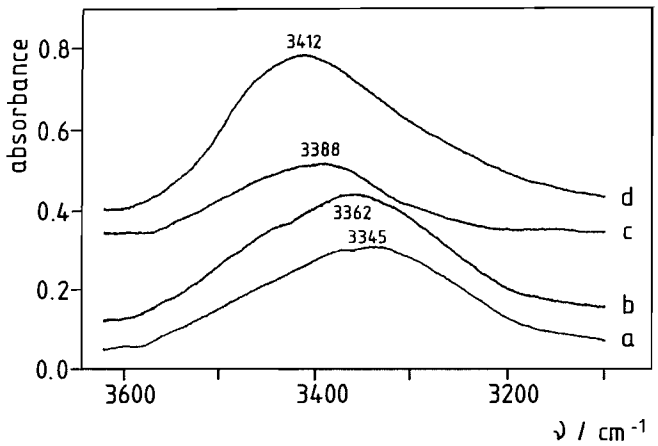


FIG. 3. Absorption spectra of PFTB/NM-d_3 mixtures at two molar fractions in the 3600–2900 cm^{-1} region:

(a) 0.5 mol PFTB in NM-d_3, pathlength (d) = 54 μm;
(b) Solution (a) diluted (1:2) in Freon mixture, d = 103 μm;
(c) Solution (a) diluted (1:10) in Freon mixture, d = 383 μm;
(d) 0.5 mol NM-d_3 in PFTB, pathlength (d) = 54 μm.

sented in Figs. 1 and 2. This 1:1 mixture of the Freons remains a liquid down to 130 K and becomes vitreous on passing to even lower temperatures (10). At room temperature we observe mainly the free OH absorption band ($\nu_{OH,f}$) at 3606 cm^{-1} in the ν_{OH} fundamental region. However, there is also a weak and broad OH absorption band ($\nu_{OH,b}$) with a maximum at about 3395 cm^{-1}.

The tendency for hydrogen bond formation increases with decreasing temperature. This can be illustrated by the decrease of the free OH band at 3606 cm^{-1} and the increase of the absorption band associated with bonded OH groups ($\nu_{OH,b}$). At 133 K, $\nu_{OH,f}$ has even disappeared completely, whereas $\nu_{OH,b}$ shows an intense symmetric band which is finally shifted to 3260 cm^{-1} at 113 K. Simultaneously, the half width of the band (FWHH) has been strongly reduced on passing from 295 to 243 K. At 133 K, the lowest temperature measured, FWHH reaches about 100 cm^{-1}. The shift of $\nu_{OH,b}$ from 3395 to 3260 cm^{-1} at 113 K clearly indicates that the hydrogen bond strength increases with decreasing temperature. From Fig. 1 it can be demonstrated that low temperatures do not only strengthen the hydrogen bond but also reduce the half width of $\nu_{OH,b}$.

In the 6000 to 7100 cm^{-1} region (see Fig. 2), a broad but weak band at about 6500 cm^{-1} appears with decreasing temperature while the $2\nu_{OH,f}$ of monomeric PFTB at 7033 cm^{-1} decreases simultaneously. The first overtone of the stretching mode of OH interacting with NM-d_3 increases in intensity with decreasing temperature as the associated $\nu_{OH,b}$ fundamental mode does. The maximum of the band is shifting from about 6490 cm^{-1} at 244 K to 6417 cm^{-1} at 178 K. It should be noted that at 193 K a submaximum is observed at about 6700 cm^{-1} which could be a combination tone of $2\nu_{OH,b}$ with a low frequency mode. At the same temperature, two further bands occur at 4303 and 3968 cm^{-1}. The first one is assigned to the combination mode of $\nu_{OH,b} + \nu_{6(CF_3)}$. By comparison with the PFTB–AN complex (9, 11) the second band is most likely a combination of $\nu_{OH,b}$ with the *out-of-plane bending mode* (τ_{OH}) assuming that τ_{OH} has its maximum absorption at 611 cm^{-1}.

For comparison spectra of two different binary mixtures recorded at room temperature are shown in Fig. 3. The spectra demonstrate the effect of changes in concentration as well as the influence of the nature of the solvent. Increasing concentration of either acceptor or proton donor favours complex formation. In solutions of PFTB in NM-d_3 the band maximum

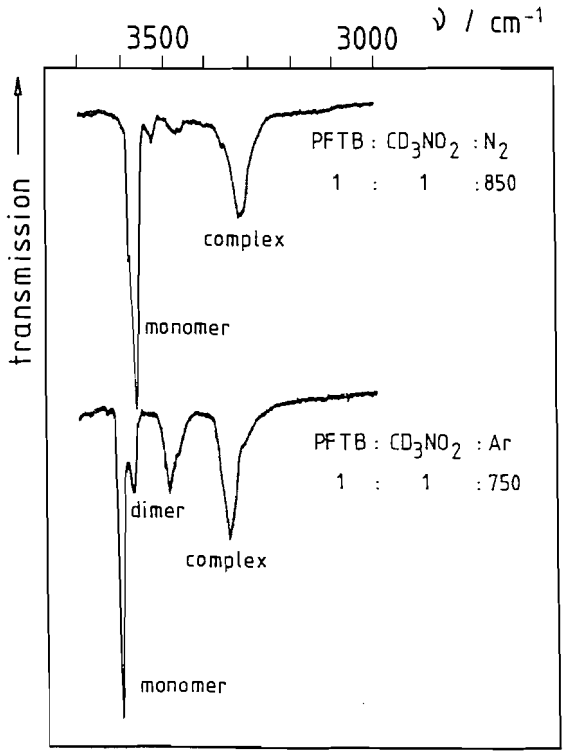


FIG. 4. OH stretching absorptions of PFTB/NM-d_3 in argon and nitrogen matrices at 10 K.

shifts to 3345 cm^{-1} with a half width (FWHH) of about 270 cm^{-1}. On the other hand, NM-d_3 dissolved in PFTB provides spectra with band maxima at higher frequencies than in dilute Freon solutions as demonstrated in Fig. 3. The interaction of the complexes with NM-d_3 as solvent is obviously stronger than with Freons. PFTB as solvent provides an environment which seems to be slightly more inert than the Freons.

Formation of 2:1 complexes has also to be kept in mind. However, we found no indication for the existence of a $(PFTB)_2\cdots$NM-d_3 complex in the binary solution of 0.5 mol NM-d_3 in PFTB while such a 2:1 complex was detected in a binary solution with AN-d_3 (8). The weaker hydrogen bonding with NM-d_3 obviously does not enhance a cooperative effect by increasing the oxygen basicity when the hydrogen bond is formed in the 1:1 complex.

Measurements in matrices

PFTB$\cdots$NM-d_3 complexes have also been studied in low temperature matrices. Typical spectra of PFTB$\cdots$NM-d_3 1:1 mixtures in Ar (PFTB:NM-d_3: Ar = 1:1:750) and N_2 (PFTB:NM-d_3:N_2 = 1:1:850) matrices are shown in Fig. 4. Infrared matrix spectra have been reported in the literature for PFTB (12–14) as well as for NM (15). In the matrices with PFTB:AN-d_3 1:1 mixtures the strongest new bands appear at 3358 cm^{-1} in Ar and at 3324 cm^{-1} in N_2. They can clearly be assigned to $\nu_{OH,b}$ of the 1:1 complex. In comparison with spectra obtained from solutions a substantial narrowing of the $\nu_{OH,b}$ absorption is observed. However, the bands are asymmetric on the low frequency side even at very high dilution.

Annealing of the matrices caused the appearance of a second component at about 3342 cm^{-1} in Ar and 3315 cm^{-1} in N_2. This shoulder could have several origins: (*i*) the existence of two conformations, (*ii*) contributions from 1:2 complexes of the type PFTB$\cdots$(AN-d_3)$_2$, (*iii*) other types of intermolecular interactions (16).

In both Ar and N_2 matrices the OH *bending mode* was observed at 1418 cm^{-1} with a blue shift of 36 cm^{-1} compared to the absorption of non-hydrogen bonded OH groups.

Deuterated PFTB was also investigated in Ar matrices. The ν_{OD} band is observed at 2498 cm^{-1}, providing an isotopic ratio $\nu_{OH}/\nu_{OD} = 1.34$. The halfwidth (FWHH) of the stretching band decreased by a factor of $\sqrt{2}$ on deuteration.

2. Complexes between PFTB and AC-d_6

Measurements in mixed Freon solutions

The experiments with PFTB/AC-d_6 mixtures have been performed in analogy to those with NM-d_3. From Fig. 5 it can be seen that remarkable changes occur in the band contours of $\nu_{OH,b}$ of PFTB (0.1 mol) complexed with AC-d_6 (0.15 mol) when the temperature is lowered from 295 to 98 K. At room temperature the band centered at about 3240 cm^{-1} is very broad (FWHH $\approx$ 340 cm^{-1}) with ill-defined submaxima. With decreasing temperature the intensity of this band increases gradually, showing considerably narrowing and frequency shifts. At 98 K this band becomes fairly symmetric and shows a well-defined maximum at 3030 cm^{-1}. Simultaneously, however, other bands appear at about 2830, 2715, and 2610 cm^{-1}. The absorption at 2827 cm^{-1} grows strongly with decreasing temperature. These band structures are similar to those observed for the PFTB$\cdots$AN-d_3 complex (8). They have been interpreted in terms of resonances between the ν_{OH} and either $2\nu_2$ (2827 cm^{-1} absorption) or combinations involving ν_2 to ν_6 modes (2708, 2610 cm^{-1} bands). The shift of the ν_{OH} absorption towards lower frequencies permits Fermi resonance with decreasing temperature and providing an enhancement of its intensity.

In the region of the first overtone a broad and weak absorption is observed at 298 K (Fig. 6). Its center is located at about 5640 cm^{-1} and shifts to lower frequencies with decreasing temperature. At 129 K its maximum is at 5258 cm^{-1} and a shoulder at 6037 cm^{-1}. Submaxima could be indications of contributions of resonances between the $2\nu_{OH}$ and various combination levels. Assignments of overtone and combination modes beyond all doubt are difficult to make, as for example for the two further absorptions in the spectra at about 4600 and 3930 cm^{-1}. With decreasing temperature their intensity diminishes slightly showing that they cannot belong to associated species. At 298 K the first one consists of two overlapped bands with maxima at 4722 and 4621.5 cm^{-1}. The 4722 cm^{-1} component disappears at low temperatures while the other one shifts its maximum to 4594 cm^{-1}. This could be due to a combination involving the ν_{OH} mode. The band at 3930 cm^{-1} is tentatively assigned to a combination of ν_{OH} with the *out-of-plane bending mode* τ_{OH}.

Measurements in matrices

Argon matrices

A typical spectrum of a mixture of PFTB and AC-d_6 isolated in solid argon at 6 K (PFTB:AC-d_6:Ar = 1:1:150) is shown in Fig. 7. The spectrum is characterized by absorption structures involving Fermi resonance similar to those observed in solutions at 88 K. Band maxima are located at 3071, 2837, 2708, and 2625 cm^{-1}. Annealing of the matrices generally leads to additional complex formation within the matrix but also to narrowing of the complex bands. As previously reported (17) a more favourable orientation of the complex and/or

Can. J. Chem. Downloaded from www.nrcresearchpress.com by 84.41.108.74 on 09/07/12
For personal use only.

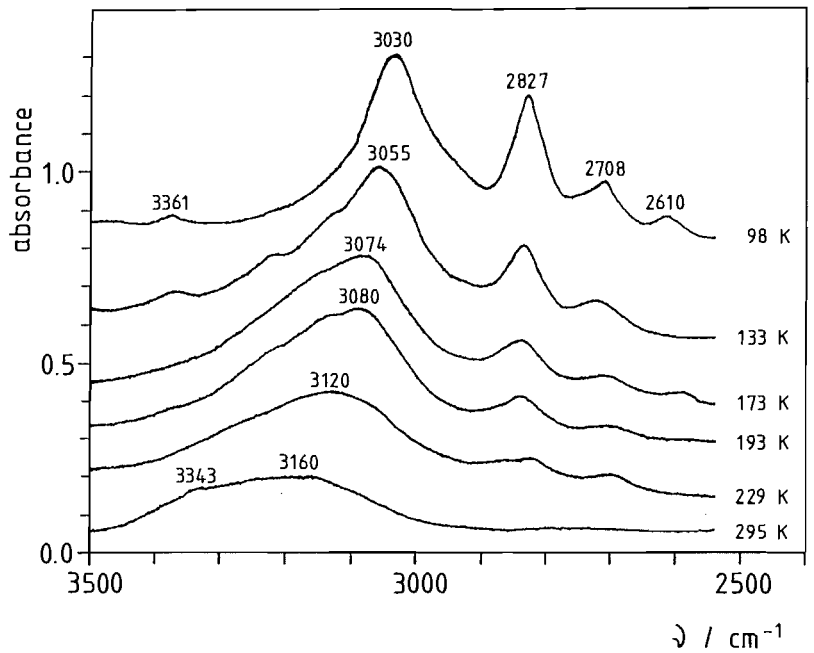


FIG. 5. Temperature effect on the ν_{OH} absorption of the PFTB···AC-d_6 complex diluted in a mixture of Freon 11 and Freon 114B2 (volume ratio 1:1). Concentrations (c) at room temperature were c[PFTB] = 0.1 mol, c(AC-d_6] = 0.15 mol. Pathlength (d) = 200 μm.

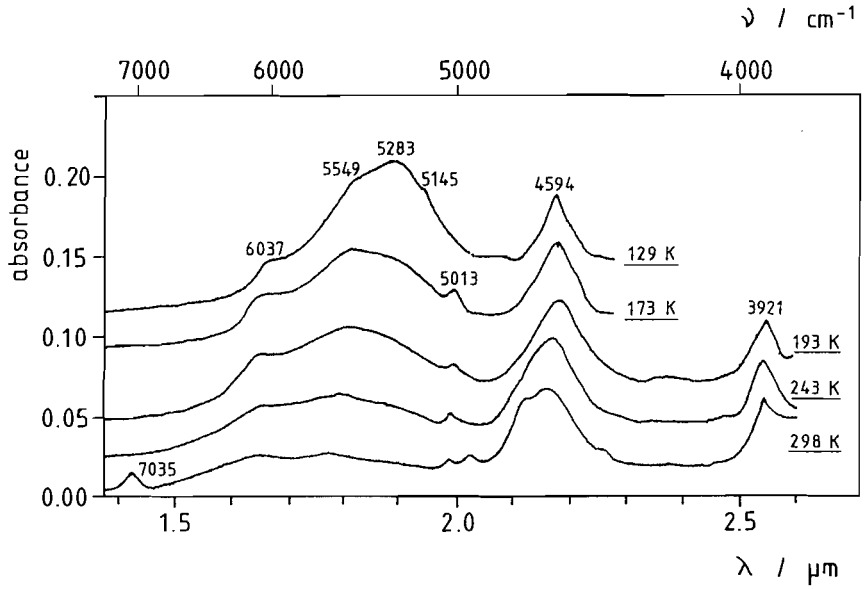


FIG. 6. Temperature effect on the first overtone of the OH stretching vibration in the PFTB···AC-d_6 complex diluted in a mixture of Freon 11 and Freon 114B2 (volume ratio 1:1). Concentrations (c) at room temperature were c[PFTB] = 0.1 mol, c(AC-d_6] = 0.15 mol. Pathlength (d) = 10 μm.

closer packing in the matrix after the annealing process might be responsible for this observation.

After deposition at 6 K the strong absorption at 3071 cm^{-1} also shows a shoulder at ≈3150 cm^{-1}. This shoulder disappears when AC-d_6 is replaced by AC. Consequently, it could be assigned to the combination $\nu_{s(CD_3)} + \delta_{s(CD_3)}$ previously observed in the IR spectra of AC-d_6 in solution (18). The OH bending mode of the complex appears at 1437.5 cm^{-1} with a blue shift of 55.5 cm^{-1} (Fig. 7). With increasing concentration of PFTB and after annealing to 35 K a shoulder on the low frequency side of the 3085 cm^{-1} band is observed at 3023 cm^{-1}. This is probably caused by 2:1 complexes of the type ROH···ROH···AC-d_6 (Fig. 8).

We have also performed some experiments with deuterated PFTB. The main absorption of the complex $\nu_{OD,b}$ was identified at 2298 cm^{-1}.

Nitrogen matrices

In nitrogen matrices the ν_{OH} absorption has maxima at 3054 cm^{-1} (FWHH ≈ 100 cm^{-1}) for the strongest band, and at 2840 cm^{-1} ($2\nu_2$ in resonance) and 2705 cm^{-1}. The OH *bending mode* has its maximum at 1436 cm^{-1}. The ν_{CO} absorption at

Can. J. Chem. Downloaded from www.nrcresearchpress.com by 84.41.108.74 on 09/07/12
For personal use only.

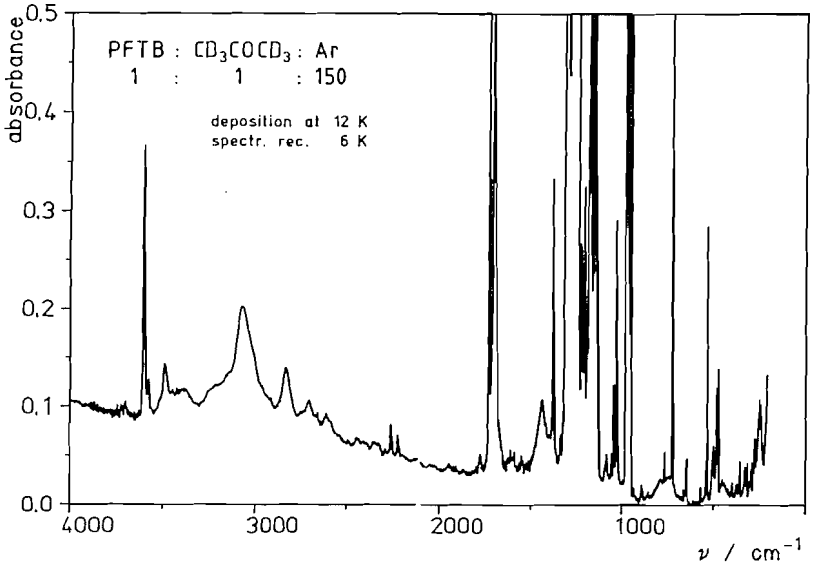


FIG. 7. Infrared spectrum of a PFTB/AC-d_6 mixture in argon matrix at 6 K.

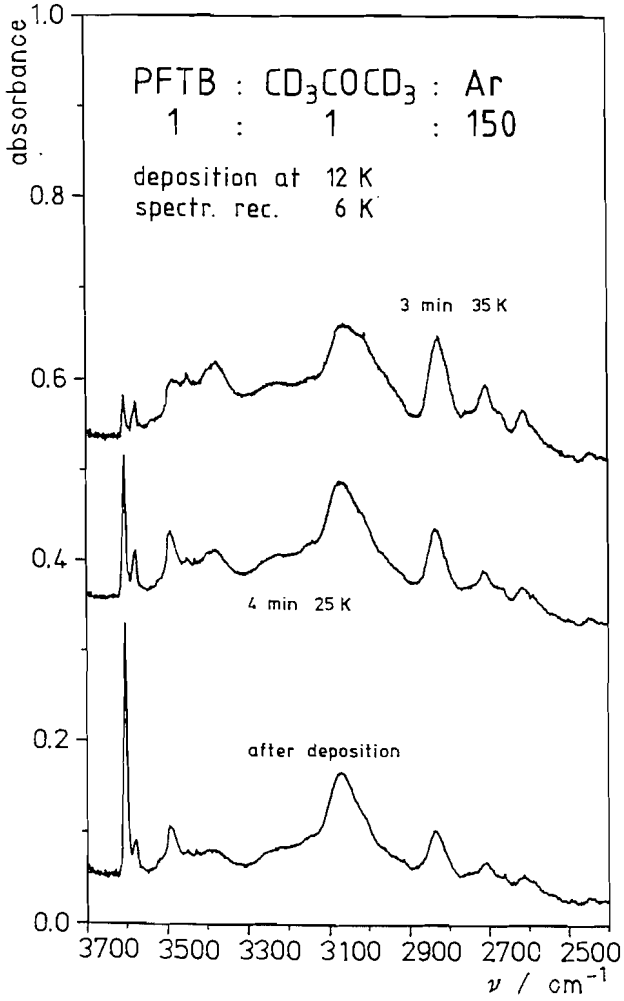


FIG. 8. Spectra of a PFTB/AC-d_6 mixture in argon matrix after deposition at 6 K (bottom) and after annealing experiments (middle and top).

1696 cm^{-1} shows a red shift comparable to the one observed for AC:HI (19).

Discussion

The influence of the strength of the hydrogen bond on OH stretching frequencies, frequency shifts, bandwidths, and anhrmonicities is discussed on the basis of the experimental results described above.

(i) Frequency shifts

In Table 1 the maxima of the fundamental ν_{OH} absorptions are given for the two systems studied in solutions and matrices. For comparison, the results for the PFTB···AN-d_3 complex obtained from previous studies (8) are also included. As expected, $\Delta\nu_{OH}$ ($\Delta\nu_{OH} = \nu_{OH,gas} - \nu_{OH,b}$) increases with the strength of the base. However, in solutions at room temperature this observation is not so evident because of the broad $\nu_{OH,b}$ absorption. At low temperatures the band maxima are much better defined. Figure 9 shows the correlation between the observed frequency ν_{OH} and the temperature. A linear relation is obtained for the PFTB···AC-d_6 complex for the whole temperature range measured with the coefficient $d\nu/dT = 0.40$ cm^{-1} K^{-1}. In the case of the PFTB···NM-d_3 complex the relation is linear only at temperatures above 150 K with $d\nu/dT = 0.70$ cm^{-1} K^{-1}. For comparison $d\nu/dT = 0.55$ cm^{-1} K^{-1} for the PFTB···AN-d_3 complex (8). Obviously, there is a correlation of $d\nu/dT$ with the strength of the proton acceptor: the higher the $d\nu/dT$ value the stronger is the proton affinity of the acceptor. The fracture in the curve of the PFTB···NM-d_6 system at about 150 K indicates the phase transition from the liquid to the viterous phase.

The $\Delta\nu$ values observed at 185 K in solution are lower than those in matrices at 6 K, demonstrating the importance of the solvent effect.

Recently, a linear dependence between the observed frequencies ν_{OH} of alcohols on $T_c^{1/2}$ (T_c = critical temperature) of the solvent and matrix materials has been found (20). Differences in band shifts ($\Delta\nu_{OH}$) between different solvents can

Can. J. Chem. Downloaded from www.nrcresearchpress.com by 84.41.108.74 on 09/07/12
For personal use only.

TABLE 1. Frequencies $\nu_{OH,b}$, frequency shifts $\Delta\nu_{OH}$ and bandwidths FWHH of PFTB··· acceptor complexes in a Freon mixture at 298 and 113 K and in Ar and N_2 matrices at 6 K (values are given in cm^{-1})

Solution	T = 298 K			T = 113 K		
	$\nu_{OH,b}$	$\Delta\nu_{OH}$	FWHH	$\Delta\nu_{OH,b}$	$\Delta\nu_{OH}$	FWHH
			Solutions in Freon 11 + Freon 114B2			
PFTB/CD_3NO_2	3395	235	200	3260	370	109
PFTB/CD_3CN	3266	364	127	3136	494	
				3104	526	122
PFTB/$(CD_3)_2CO$	~3240	390	340	3030	600	130
			Matrices (6 K)			
		Argon			Nitrogen	
PFTB/CD_3NO_2	3359	271	25	3324	306	25
PFTB/CD_3CN	3245	385	25	3196	434	26
PFTB/$(CD_3)_2CO$	3071	559	60	3054	576	100

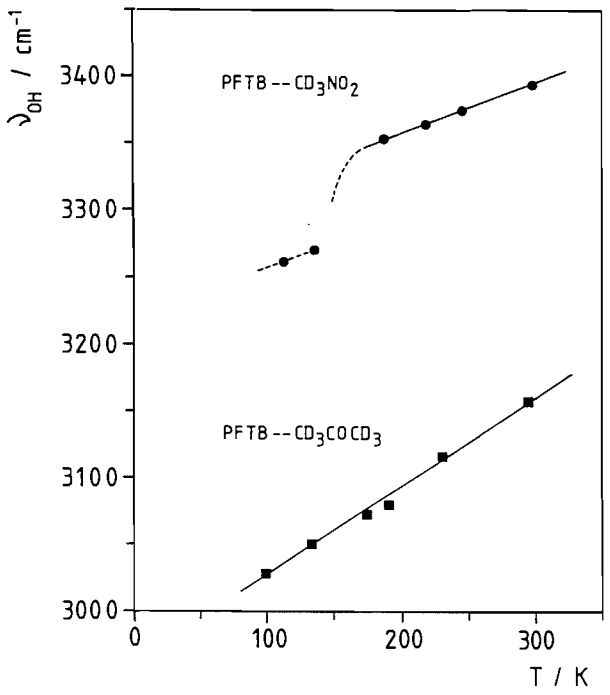


FIG. 9. OH stretching frequencies $\nu_{OH,b}$ for PFTB···AC-d_6 and PFTB···NM-d_3 complexes plotted as a function of temperature.

in a first approximation be considered as a measure of the intermolecular potential. Taking into account that the Lennard–Jones parameter ϵ_0 can be estimated at the critical temperature T_c as

$$\epsilon_0 = 0.74\, kT_c$$

and the pair potential U_{12} of dispersion forces between two different molecules 1 and 2 is given by

$$U_{12} = (U_{11} \cdot U_{22})^{1/2} \approx (T_{c1} \cdot T_{c2})^{1/2}$$

linear relationships between ν_{OH} of alcohols and $T_c^{1/2}$ of the solvent or matrix material have been obtained (20).

For ν_{OH} (Freon), extrapolated to temperatures where the matrix spectra are recorded (≈10 K) and the following proportionality holds:

$$\frac{\Delta\nu_{OH(Freon)}}{\Delta\nu_{OH(matrix)}} \sim \frac{T_{c(Freon)}^{1/2}}{T_{c(matrix)}^{1/2}}$$

with $\Delta\nu_{OH(Freon)} = \nu_{OH(gas)} - \nu_{OH,b(Freon)}$.

We have applied this relation for the two systems investigated. $\nu_{OH,b}$ in Freons, extrapolated to 10 K, are at 3282 ($\Delta\nu_{OH}$ = 348 cm^{-1}) and 2963 cm^{-1} ($\Delta\nu_{OH}$ = 667 cm^{-1}) for NM-d_3 and AC-d_6, respectively. $\nu_{OH,b}$ values for argon matrices are given in Table 2, $T_{c(Argon)}$ is 170.7 K. The good agreement between the two calculated Freon values for T_c (≈260 K) supports the approach described above.

In Fig. 10 we have plotted the ratio $(\nu_{gas} - \nu_{OH,b})/\nu_{gas}$ ($\nu_{OH,b}$ are values from argon matrices) against the proton affinity (PA). Results obtained with other bases like dimethyl ether (DME) (4), NH_3 (20), C_5D_5N (21) have also been included, as well as the results obtained with the proton donors HCl and HI (23, 24).

For weak and medium strong hydrogen-bonded complexes between hydrogen halides and various bases (15–25), the electrostatic interaction is the dominant term in the intermolecular potential. The observed $\Delta\nu/\nu_0$ ratio decreases from HF towards HI (22), correlating with the dipole moment of the HX bond. Figure 10 shows that for PFTB $\Delta\nu/\nu_0$ values are lower than for HCl but higher than for HI in cases of weak and medium strong hydrogen bonds. With very strong bases (PA > 200 kcal/mol) proton transfer has to be considered. How ever, proton sharing and proton transfer are only observed with HX molecules whose valence electrons are easily polarizable. Despite the strong acidity of PFTB no proton transfer reactions or proton sharing are observed, probably due to the weak polarizability of the OH oscillator.

(ii) Halfwidths (FWHH) of the complex bands

In the case of the PFTB···NM-d_3 complex the $\nu_{OH,b}$ absorption is much broader than that observed for the PFTB···AN-d_3 complex, thus indicating the existence of different conformations of the complex. For the PFTB···AC-d_6 complex, the ν_{OH} absorption obviously overlaps with combination tones. With decreasing temperature, strong narrowing is observed. The

Can. J. Chem. Downloaded from www.nrcresearchpress.com by 84.41.108.74 on 09/07/12
For personal use only.

TABLE 2. ν_{OD} and ν_{OH} frequencies of PFTB and PFTB···complexes in low temperature matrices and deduced values κ_{11}*; comparison with κ_{11}** values, calculated from $\nu_{0\to1}$ and $\nu_{0\to2}$, of PFTB and the same complexes in solution (values are given in cm^{-1})[a]

Solution	Matrices (6 K)				Solutions (298 K)			
		ν_{OH}	ν_{OD}	κ_{11}*		ν_{OH}	$2\nu_{OH}$	κ_{11}**
PFTB	N_2	3567	2634	100.4	C_6F_{14}	3620	7074	83
	Ar	3606	2662	99.5	Freon	3595	7039	76
PFTE/CD_3CN	Ar	3245	2418.5	146.0				
PFTB/CD_3NO_2	Ar	3359	2498	137.0	Freon	3344	6417	135
PFTB/$(CD_3)_2CO$	Ar	3071	2298	162.0	(200 K)			

[a]The formula for the calculations of κ_{11}* and κ_{11}** are given in text.

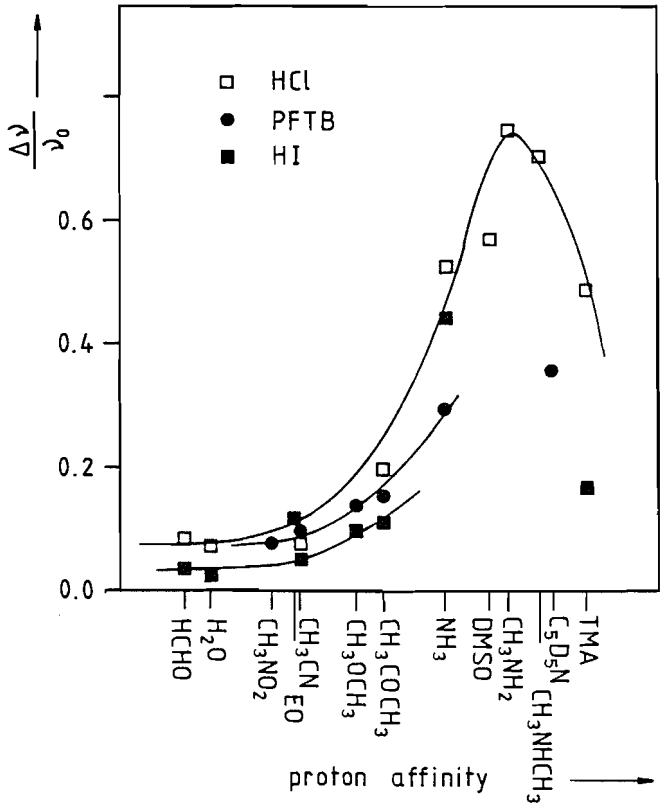


FIG. 10. Frequency ratio $\Delta\nu/\nu_0$ of the OH stretching band of PFTB complexes with different acceptors as function of the proton affinity PA of the base. For comparison, values for HCl and HI are also included.

slope d(FWHH)/dT is about 1.1 cm^{-1} K^{-1} for the first band of the AC-d_6 complex and 0.49 cm^{-1} K^{-1} for the NM-d_3 complex in the temperature interval 193 to 250 K. These values are considerably higher than those reported for the PFTB···AN-d_3 complex (0.15 cm^{-1} K^{-1} to 0.2 cm^{-1} K^{-1} depending on the nature of the solvent) (8). At the lowest temperature reached in solution (83 K) the observed bandwidth of $\nu_{OH,b}$ for the different complexes within the same solvent shows only weak dependence on base strength:

FWHH	Complex
109cm^{-1}	PFTB···NM-d_3
122cm^{-1}	PFTB···AN-d_3
131cm^{-1}	PFTB···AC-d_6

In the theories of hydrogen bonding, it is generally assumed that main band shaping factors are the mechanical and electrical coupling of the internal and external modes of the hydrogen bonds (26, 27). Broadening of the ν_s bands have been explained by stochastic effects in liquids (28–30) and rovibrational structure in the gas phase (31). However, in matrices usually a substantial narrowing of the absorption bands is observed due to the extreme low temperatures. This has been found for weak hydrogen bonding ($\Delta\nu/\nu_0 < 0.1$), where the ν_s band is very narrow (FWHH < 10 cm^{-1}). In the case of medium strong hydrogen bonding ($\Delta\nu/\nu_0$ between 0.1 and 0.2) two situations were encountered: (*i*) either narrow bands as for HF···NH_3 (32) and HCl···$S(CH_3)_2$ (33) systems, or (*ii*) broad bands with a strong narrowing on deuterium substitution as for HCl···DME (34) and HCl···ethylene oxide (35) complexes. The PFTB···NM-d_3 complex is weakly hydrogen bonded; the observed ν_{OH} bandwidth (25 cm^{-1}) is broader than expected. The band shows an asymmetrical profile with a shoulder after annealing.

The PFTB···AC-d_6 complex (medium strong hydrogen bonding) shows an OH band as broad as in solutions at 113 K. As suggested for HCl···DME or HCl···ethylene oxide complexes by Bernadet and Limonzi (36), the bandwidth could be an intrinsic property of the hydrogen bond.

(iii) Anharmonicity

From the IR and NIR absorptions the anharmonicity coefficient κ_{11} of the $\nu_{0\to1}$ OH vibration can be calculated according to the following relation (in Table 2 this coefficient ist marked as κ_{11}^{**}):

$$\kappa_{11} = \nu_{0\to1} - (\nu_{0\to2})/2$$

However, as previously demonstrated (37) the $2\nu_{OH}$ profiles are unlike and very broad at room temperature.

Another method described in references 9, 38 is to evaluate κ_{11} from ν_{OH} and ν_{OD} frequencies. The following relation is used with the assumption that the OH oscillator is isolated and the potential energy limited to the quartic term (in Table 2 this coefficient is market as κ_{11}^{*}):

$$\kappa_{11}^{*} = \frac{\varphi(\varphi\nu_{OD} - \nu_{OH})}{2(\varphi - 1)} \varphi = \left(\frac{\mu_{OD}}{\mu_{OH}}\right)^{1/2}$$

where μ = reduced mass.

Table 2 summarizes the results obtained for κ_{11} calculated by both methods for the PFTB···NM-d_3 complex. Only the second method was used for the PFTB···AC-d_6 complex. We observe that the anharmonicity coefficients are similar for the

Can. J. Chem. Downloaded from www.nrcresearchpress.com by 84.41.108.74 on 09/07/12
For personal use only.

three systems reported here, indicating that the role played by the base strength is of minor importance. For the PFTB$\cdots$NM-d_3 complex κ_{11} values have been obtained at different temperatures. The results suggest that the anharmonicity coefficient is temperature independent as previously reported by Perchard and Perchard (38) for some associated alcohols.

Finally, from the spectra of the PFTB$\cdots$AC-d_6 complexes in matrices the anharmonicity coefficient of the deformation mode (κ_{22}) can be calculated according to the relation:

$$\kappa_{22} = \delta_{0\to1} - (\delta_{0\to2})/2$$

The obtained value $\kappa_{22} = 18.7\ cm^{-1}$ indicates a considerable increase of the anharmonicity due to hydrogen bonding as previously reported by Asselin and Sandorfy (39).

Acknowledgements

We thank the Ministere des Affaires Etrangeres, Paris, and the Deutsche Akademische Austauschdienst, Bonn, for financial assistance in the frame of the French–German Procope cooperation (project No. 1988/118, 1989/086) and the Deutsche Forschungsgemeinschaft, Bonn, for funds.

The authors would also like to thank Danièle Carrère for technical assistance, and one of the anonymous referees for valuable comments.

1. A. D. SHERRY and K. F. PURCELL. J. Am. Chem. Soc. **94**, 1853 (1972).
2. L. SCHRIVER and A. BURNEAU. J. Chim. Phys. Paris, **78**, 723 (1976).
3. A. BURNEAU, A. LOUTELLIER, and L. SCHRIVER. J. Mol. Struct. **61**, 397 (1980).
4. O. SCHREMS, H. M. OBERHOFFER, and W. A. P. LUCK. J. Phys. Chem. **88**, 4335 (1984).
5. T. A. ISKANDEROV, Y. A. KIMEL'FEL'D, E. M. SMIRNOVA, H. V. JOGANSEN, and M. SH. ROZENBERG. Opt. Spectrosc. (USSR), **61**, 618 (1987).
6. T. A. ISKANDEROV, Y. A. KIMEL'FEL'D, and E. M. SMIRNOVA. Chem. Phys. **112**, 379 (1987).
7. T. A. ISKANDEROV, Y. A. KIMEL'FEL'D, and E. M. SMIRNOVA. J. Mol. Struct. **177**, 221 (1987).
8. W. A. P. LUCK, S. PEIL, L. SCHRIVER, and A. SCHRIVER. J. Mol. Struct. **224**, 185 (1990).
9. A. BURNEAU. Spectrochim. Acta, **45A**, 1305 (1989).
10. C. SANDORFY. Can. J. Spectrosc. **10**, 85 (1965).
11. P. V. HUONG, M. COUZI, and J. LASCOMBE. J. Chim. Phys. Paris. **64**, 1056 (1967).
12. J. MURTO, A. KIVINEN, J. KORPPI-TOMMOLA, R. VIITALA, and J. HYÖMÄKI. Acta Chem. Scand. **27**, 107 (1973).
13. L. SCHRIVER and A. BURNEAU. J. Chem. Soc. Faraday Trans. 2, **81**, 503 (1985).
14. W. A. P. LUCK and S. PEIL. J. Mol. Struct. **224**, 175 (1990).
15. F. D. VERDERAME, J. A. LANNON, L. E. MARRIS, W. I. G. THOMAS, and E. A. LUCIA. J. Chem. Phys. **56**, 2638 (1971).
16. L. SCHRIVER, A. SCHRIVER, and J. P. PERCHARD. J. Chem. Soc. Faraday Trans. 2, **81**, 1407 (1985).
17. W. A. P. LUCK and O. SCHREMS. Spectrosc. Lett. **13**, 719 (1980).
18. G. DELLEPIANE and J. OVEREND. Spectrochim. Acta. **22**, 593 (1966).
19. L. SCHRIVER. Trans. Faraday. Soc. **85(6)**, 607 (1989).
20. A. BEHRENS-GRIESENBACH, W. A. P. LUCK, and O. SCHREMS. J. Chem. Soc. Faraday. Trans. 2, **80**, 579 (1984).
21. L. SCHRIVER. To be published.
22. A. J. BARNES. J. Mol. Struct. **100**, 259 (1983).
23. A. J. BARNES. Personal communication. 1987.
24. L. SCHRIVER, A. SCHRIVER, and J. P. PERCHARD. J. Mol. Struct. **222**, 141 (1990).
25. E. E. TRUSCOTT and B. S. AULT. J. Phys. Chem. **88**, 2323 (1984).
26. G. N. ROBERTSON. Phil. Trans. R. Soc. London, A**286**, 25 (1977).
27. Y. BOUTEILLER and Y. GUISSANI. Mol. Phys. **38**, 617 (1979).
28. S. BRATOS. J. Chem. Phys. **63**, 3499 (1975).
29. V. P. SAKUN. Chem. Phys. **99**, 457 (1985).
30. W. G. JOHNSON and D. W. OXTOBY. J. Chem. Phys. **87**, 781 (1987).
31. J. LASCOMBE and J. C. LASSÈGUES. Mol. Phys. **40**, 969 (1980).
32. L. ANDREWS. J. Mol. Struct. **100**, 281 (1983).
33. G. MAES and M. GRAINDOURZE. J. Mol. Spectrosc. **113**, 410 (1985).
34. L. SCHRIVER, A. LOUTELLIER, A. BURNEAU, and J. P. PERCHARD. J. Mol. Struct. **95**, 37 (1982).
35. P. BERNADET and L. SCHRIVER. J. Mol. Struct. **130**, 193 (1985).
36. P. BERNADET and F. FILLAUX. Chem. Phys. **106**, 447 (1986).
37. A. BURNEAU and J. LIMOUZI. Mol. Phys. **33**, 399 (1971).
38. C. PERCHARD and J. P. PERCHARD. J. Raman Spectrosc. **3**, 277 (1975).
39. M. ASSELIN and C. SANDORFY. Can. J. Chem. **49**, 1540 (1971).

Can. J. Chem. Downloaded from www.nrcresearchpress.com by 84.41.108.74 on 09/07/12
For personal use only.

Hydroxyproline adsorption on a mercury electrode in neutral solution

M. M. GÓMEZ

Departamento de Química Física Aplicada, Facultad de Ciencias, Universidad Autónoma, 28049-Madrid, Spain

Received December 24, 1990

M. M. GÓMEZ. Can. J. Chem. **69**, 1528 (1991).

The adsorption of hydroxyproline (HPRO) on mercury in aqueous solutions of 10^{-2} M $KClO_4$ has been determined from electrocapillary and capacity measurements. Comparison of the results obtained for HPRO with those reported for proline (PRO) shows that the presence of a hydroxyl group in the molecule has a small effect on the adsorption process. The respective values for adsorption parameters are -7 and -5 μC cm^{-2} for the charges of maximum adsorption, -13.0 and -10.4 kJ mol^{-1} for the standard Gibbs energies of adsorption at zero charge, and -1.28 and $+0.6$ for the α parameter in the Frumkin isotherms. According to the analysis carried out for the normal component of the dipole moment of HPRO, -0.8 D, the more probable orientation of this aminoacid adsorbed on mercury is with the pyrrolidine ring parallel to the electrode surface resting the OH group away from the surface.

Key words: adsorption, double layer, aminoacids, hydroxyproline.

M. M. GÓMEZ. Can. J. Chem. **69**, 1528 (1991).

On a mesuré l'adsorption de l'hydroxyproline (HPRO) sur le mercure dans des solutions aqueuses de 10^{-2} M $KClO_4$ en utilisant les mesures de capacité et d'électrocapillarité. Les résultats obtenus, comparés à ceux répertoriés dans la littérature pour la proline (PRO), révèlent que la présence du groupe hydroxyle dans la molécule a très peu d'influence sur le processus d'adsorption. Les paramètres d'adsorption sont respectivement sont de -7 et de -5 μC cm^{-2} pour les charges d'adsorption maximum et $-13,0$ et $-10,4$ kJ mol^{-1} pour les énergies d'adsorption standard de Gibbs pour une charge nulle. La valeur de α est de $-1,28$ et 0,6 dans les isothermes de Frumkin. L'analyse de la composante normale du moment dipolaire de la HPRO, $-0,8$ D révèle que l'orientation la plus probable de cet acide aminé adsorbé sur le mercure est celle où le cycle de la pyrrolidine est parallèle à la surface de l'électrode avec le groupe hydroxyle éloigné de la surface.

Mots clés : adsorption, couche double, acides aminés, hydroxyproline.

[Traduit par la rédaction]

Introduction

The elucidation of properties of biological molecules in solution is an essential step in the understanding of their physiological functions. The several studies carried out about the surface activity of primary aminoacids allowed one to establish relationships between molecular properties and the adsorption behaviour of these compounds. However, information about the surface properties of secondary aminoacids is not very extensive.

The secondary protein aminoacids comprise those whose structures are stable to acid hydrolysis. Of this group *N*-methyl and *C*-hydroxy derivatives are the most numerous. Hydroxyproline is the most abundant hydroxylated aminoacid, occurring in considerable amounts in hydrolysates of collagen and elastin (the principal proteins of connective tissue). Most of the hydroxyproline is hydroxylated in the γ-position (Fig. 1), but some forms of connective tissue also contain amounts of β-hydroxyproline (1).

Proline and hydroxyproline are very different from the other aminoacids in that they contain the pyrrolidine five-membered ring. In a previous paper, the adsorption of proline on a mercury electrode has been studied (2). The aim of the present study was to determine the structure of the mercury/solution interface for γ-hydroxyproline and to analyze how the presence of a hydroxyl group affects the adsorption process by comparing the results with those obtained for proline. Consequently, the same methods and procedures used for proline (PRO) have been applied to hydroxyproline (HPRO) and they will not be described in detail further. Potassium perchlorate was used as support electrolyte and the pH of the solution was kept equal to 5.8 in order to study the zwitterion form of HPRO.

Molecular structure of hydroxyproline

In addition to the normal conformational descriptors the conformation of PRO and derivatives is described by the mode of puckering of the pyrrolidine ring. The conformational analysis of five-membered rings is greatly facilitated by the concept of pseudorotation. The endocyclic torsion angles τ_j (Fig. 1*a*) are interrelated via the well-known pseudorotation equation. The puckering of the ring may be specified by the pseudorotational parameters P (phase angle of pseudorotation) and τ_m (puckering amplitude) computed from the τ_j angles (2).

It was stated that the atoms C_δ—N—C_α—C_β are nearly

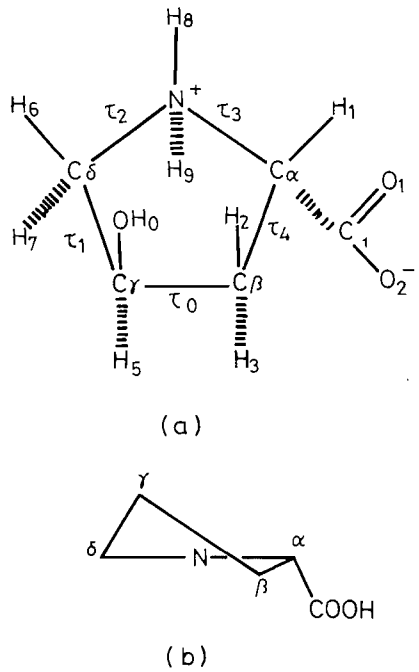


FIG. 1. (*a*) Labeling of the carbon atoms and protons of hydroxyproline in zwitterion form and τ notation of endocyclic angles; (*b*) perspective views of the N-type hydroxyproline ring conformation (3).

Can. J. Chem. Downloaded from www.nrcresearchpress.com by 84.41.108.74 on 09/07/12
For personal use only.

TABLE 1. Bond distances, bond angles, and torsion angles used for zwitterion of hydroxyproline (see text). Atom numbering is given in Fig. 1

Bond	Distances (Å)	Bond	Angles (deg)	Bonds	Torsion angles (deg)
C_α—C_β	1.533	C_α—C_β—C_γ	100.9	C_α—C_β—C_γ—C_δ	39.2
C_β—C_γ	1.532	C_β—C_γ—C_δ	101.7	C_β—C_γ—C_δ—N	−29.9
C_γ—C_δ	1.535	C_γ—C_δ—N	107.1	C_γ—C_δ—N—C_α	7.6
C_δ—N	1.463	C_δ—N—C_α	107.5	C_δ—N—C_α—C_β	18.2
C_α—N	1.462	C_β—C_α—C_1	112.8	N—C_α—C_β—C_γ	−36.3
C_α—C_1	1.530	C_α—C_1—O_1	117.8	N—C_α—C_1—O_1	−3.2
C_1—O_1	1.247	C_α—C_1—O_2	116.6	N—C_α—C_1—O_2	178.7
C_1—O_2	1.245	N—C_α—H_1	107.8	N—C_α—C_β—H_2	−157.3
C_α—H_1	1.095	C_α—C_β—H_2	113.2	N—C_α—C_β—H_3	80.2
C_β—H_2	1.116	C_α—C_β—H_3	110.2	C_α—C_β—C_γ—O	−78.1
C_β—H_3	1.117	C_β—C_γ—O	107.1	C_α—C_β—C_γ—H_5	157.7
C_γ—O	1.403	C_β—C_γ—H_5	114.2	C_β—C_γ—C_δ—H_6	−152.3
C_γ—H_5	1.107	C_γ—C_δ—H_6	112.3	C_β—C_γ—C_δ—H_7	87.3
C_δ—H_6	1.116	C_γ—C_δ—H_7	109.7	C_γ—C_δ—N—H_8	−113.9
C_δ—H_7	1.117	C_δ—N—H_8	111.4	C_γ—C_δ—N—H_9	127.8
N—H_8	1.016	C_δ—N—H_9	109.8	C_δ—N—C_α—H_1	−99.7
N—H_9	1.016	C_γ—O—H_0	107.3	C_δ—N—C_α—C_1	141.1
O—H_0	0.972				

coplanar and C_γ displaced from this plane. All conformations that are characterized by a positive value of torsion angle τ_0 (Fig. 1*a*) are denoted by N-type forms (Fig. 1*b*) and all conformations having a negative angle τ_0 by S-type forms.

The HPRO ring system in neutral or acidic medium displays a pure N-type state (3). The pseudorotational parameters calculated from the coupling constants of HPRO measured at pD = 6.5 are $P_N = 12.8°$ and $\tau_N = 43.6°C$ (Table IX in ref. 3).

From a neutron diffraction study (4) a value of −3.2° was estimated for the torsion angle O_1—C_1—C_α—N. The existence of an intramolecular hydrogen bond is not clear. The H_9....O_1 distance, 2.082 Å, is more than 0.3 Å smaller than 2.4 Å, the appropriate sum of van der Waals radii. Therefore, Donohue and Trueblood (5) have preferred not call to this short intramolecular contact a hydrogen bond.

In order to discuss the results of the present work, optimized geometries of HPRO have been estimated for the more favored conformation in neutral solution. First, the geometry of HPRO in molecular form was optimized by using the MM2 force field (6, 7). Then, the geometry in zwitterion form was built up from the MM2 geometry for the ring and from the neutron diffraction geometry for the $^+NH_2$—CH—COO^- fragment (4), see Table 1.

There are a lot of possible orientations of the HPRO molecule resting onto three different atoms over the electrode surface (XY plane). Those orientations with one oxygen atom resting onto the surface were rejected because the value of the perpendicular component μ_i of the dipole moment is positive, contrary to the results of the present work (see below). For all the remaining orientations, three different hydrogen atoms were placed in the XY plane and the corresponding molecular areas projected onto the electrode surface and the molecular heights were calculated from the optimized geometry given in Table 1. The molecular heights were calculated by adding the corresponding van der Waals radii to the higher and lower atoms. Likewise, the components μ_i of the dipole moment were obtained using the INDO method (8). The obtained results for the individual orientation, defined by the three hydrogen atoms contacting the electrode surface, are given in Table 2. Values of A_i correspond to the average molecular area obtained for orientations of the OH group of 30, 180, and 300°. The orientations of HPRO are grouped in two types. For the A-type the molecule is adsorbed with the ring perpendicular to the electrode surface. For the B-type orientation, the HPRO ring is adsorbed flat with the COO^- group away from the electrode surface. The total dipolar moment, calculated using the INDO method, was 12.6 D.

TABLE 2. Area, A_i, height, X_i, and perpendicular dipole moments, μ_i, for the individual orientations of N-type conformations of the zwitterion of hydroxyproline; three different hydrogen atoms contact the electrode surface for each individual orientation (see text)

Type of orientation	Contacting atoms	A_i/nm²	X_i/nm	μ_i/D
A	H_2—H_3—H_5	0.47	0.67	1.9
	H_6—H_7—H_9	0.43	0.68	−5.8
	H_8—H_9—H_6	0.42	0.69	−5.5
	H_6—H_7—H_5	0.44	0.81	−11.0
	Average	0.44	0.71	
B	H_3—H_7—H_9	0.47	0.63	3.6
	H_3—H_5—H_7	0.53	0.60	−1.2
	H_8—H_6—O_0	0.48	0.64	−7.4
	H_1—H_8—O_0	0.44	0.60	−2.6
	Average	0.48	0.62	

Results and analysis

Electrocapillary and capacity measurements were carried out in aqueous solutions of 10^{-2} M $KClO_4$ at seven concentrations of HPRO in the same range used for PRO (2). The double-layer capacity was determined with an impedance bridge using a SCE as reference electrode and the cell which was described in a previous paper (9). The pzc was measured by means of a streaming electrode. The maximum interfacial tension was obtained by using a classical electrometer (10).

The dependence of the differential capacity of the mercury

Can. J. Chem. Downloaded from www.nrcresearchpress.com by 84.41.108.74 on 09/07/12
For personal use only.

TABLE 3. Zero-charge coordinates for mercury/aqueous solution of proline and hydroxyproline interfaces in 10^{-2} M $KClO_4$ solution at 25°C (pH = 5.8)

	$E_{\sigma=0}$/V vs. SCE		$C_{\sigma=0}/\mu F\ cm^{-2}$		$\gamma_{\sigma=0}/mN\ m^{-1}$	
Conc./mol L^{-1}	PRO[a]	HPRO	PRO[a]	HPRO	PRO[a]	HPRO
0	−0.451	−0.451	16.83	16.83	427.3	427.3
10^{-3}	−0.450	−0.450	16.85	16.78	427.1	427.2
10^{-2}	−0.446	−0.448	16.92	16.75	426.7	427.1
5×10^{-2}	−0.440	−0.447	17.03	16.24	425.5	426.6
10^{-1}	−0.438	−0.446	17.10	16.24	424.6	426.1
1.5×10^{-1}	−0.437	−0.445	17.15	16.20	424.0	425.5
2.25×10^{-1}	−0.435	−0.443	17.21	16.30	423.2	424.9
3×10^{-1}	−0.434	−0.441	17.35	16.61	422.5	424.1

[a]Data from ref. 2.

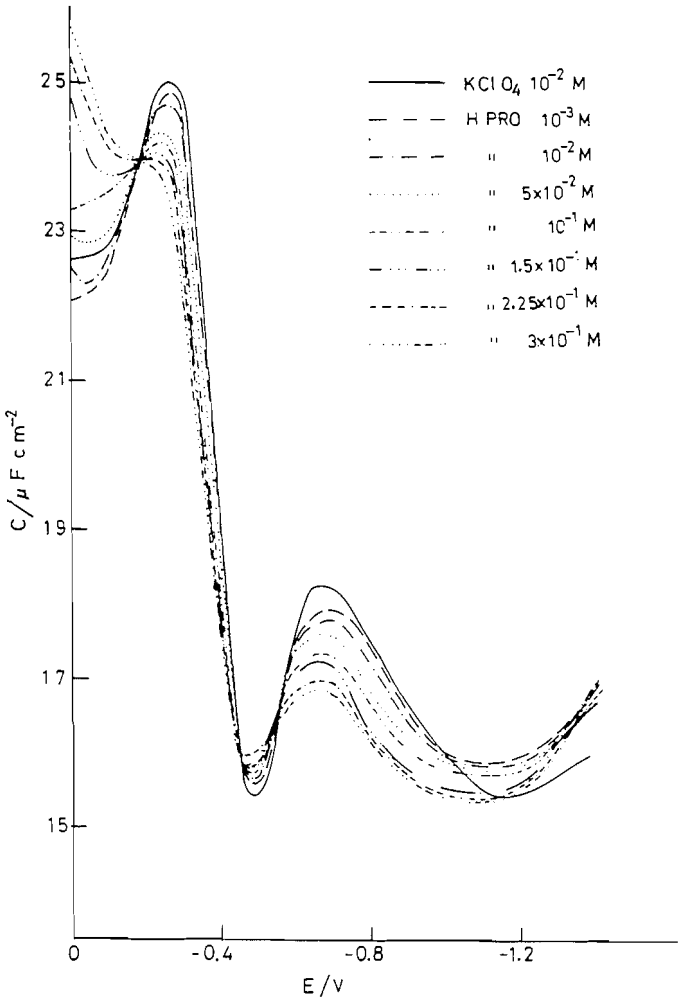


FIG. 2. (*a*) Capacity–potential (against saturated calomel electrode) curves for aqueous 10^{-2} M $KClO_4$ solutions containing different concentrations of hydroxyproline.

electrode on potential is close to that found for PRO (Fig. 2). Integration of the capacity curves provides the corresponding curves for electrode charge, σ^M, against the potential. The electrocapillary curves were obtained by integration of these curves. Results at zero charge for the potential, E, the capacity, C, and the interfacial tension, γ, given in Table 3, show small differences from the corresponding values found for PRO.

The relative surface excess, Γ, was determined at constant charge by numerical differentiation of the Parsons function, $\xi = \gamma + \sigma^M E$, with respect to the logarithm of the HPRO concentration, log c_{org}. The liquid junction potential in all solutions was assumed to remain constant. Activity coefficients for HPRO in water have been measured (11). These are very close to unity, being 1.001 at 0.3 mol dm^{-3}. However, there is no information about the activity coefficients in the present system which would allow the correct analysis to be done. The calculations were therefore carried out assuming a constant activity coefficient equal to unity. The error involved in this approximation would be small, probably comparable with experimental error. The variation of Γ with σ^M is shown in Fig. 3, where a maximum is observed for a charge about -5 μC cm^{-2}.

The saturation values of Γ, Γ_s, determined by extrapolation of $1/\Gamma$ vs. $1/c_{org}$ curves at different charges to $1/c_{org} = 0$ (12) do not seem to be reliable because no saturation is approached. The calculated values for the individual orientations of HPRO (Table 2) are spread between 0.42 and 0.53 nm^2, corresponding to 4.0 and 3.1×10^{-10} mol cm^{-2}, respectively. An average value of 0.46 nm^2 was taken as the actual value of the molecular area ($\Gamma_s = 3.6 \times 10^{-10}$ mol cm^{-2}).

The maximum coverage reached experimentally does not exceed 0.4. Therefore, the following analysis could not be entirely reliable.

The adsorption isotherm was analysed from the surface excess values. The coverage, θ, was calculated from $\theta = \Gamma/\Gamma_s$ with $\Gamma_s = 3.6 \times 10^{-10}$ cm^{-2}. A linear dependence of $\log \theta/(1-\theta)c$ upon θ was obtained in the range of studied charges. The fact that these straight lines show the same positive slope indicates that the adsorption follows a Frumkin isotherm (eq. [1]) which is apparently congruent to charge. The obtained value of +0.6 for the interaction parameter, α, indicates that an attractive force acts among the adsorbed molecules,

$$[1] \quad \beta c = \theta(1-\theta)^{-1} \exp(-2\alpha\theta)$$

where β is the adsorption coefficient.

The adsorption isotherm was also analysed by plotting the surface pressure as a function of the logarithm of HPRO concentration at constant charge within the range +3 to −9 μC cm^{-2}.

The surface pressure at constant charge (Φ) was determined from the expression $\Phi = \xi^b - \xi$, where ξ^b is the value for 10^{-2} M $KClO_4$ solution in the absence of HPRO at a given value of σ^M.

Can. J. Chem. Downloaded from www.nrcresearchpress.com by 84.41.108.74 on 09/07/12
For personal use only.

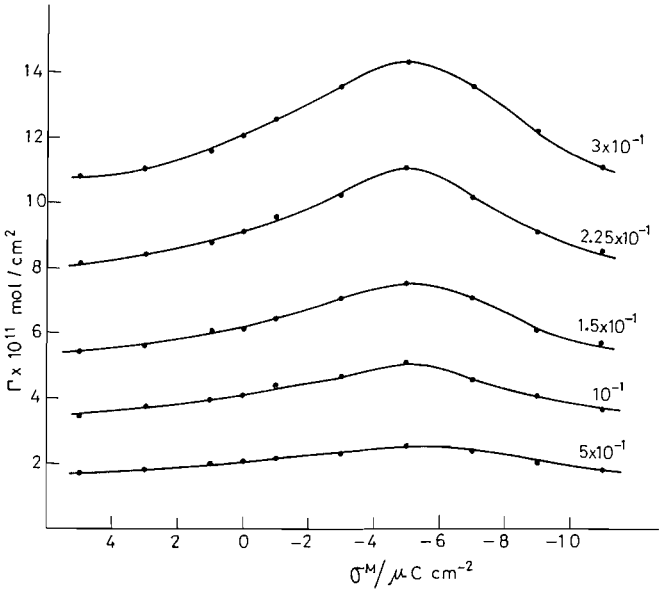


FIG. 3. Surface excess of hydroxyproline as a function of the surface charge density on a mercury electrode at 25°C. The hydroxyproline concentration, in mol L^{-1}, is indicated for each curve.

According to the Frumkin isotherm, the pressure-coverage relation is represented by eq. [2]:

$$[2] \quad \Phi = \Gamma_s RT[\ln(1-\theta) + \alpha\theta^2]$$

where R is the gas constant and T is the temperature in K.

The surface pressure vs. log HPRO concentration was plotted for eight values of σ^M. When the resulting curves are shifted along the x axis, it is observed that there is good superimposition and the curves coincide, within the experimental error, with the solid line corresponding to a Frumkin isotherm with $\alpha = 0.6$ and $\Gamma_s = 3.6 \times 10^{-10}$ mol cm^{-2} (Fig. 4). On the contrary, the composite surface pressure curve at constant potential shows points more scattered.

The standard Gibbs energy of adsorption, ΔG^0, of HPRO on the mercury electrode was calculated by the Parsons' method (13) and by the test of the Frumkin isotherm (eq. [1]). The results in both cases was very close. The value of ΔG^0 obtained at the charge of maximum adsorption, $\sigma^M_{max} = -5$ μC cm^{-2}, was −10.8 kJ mol^{-1}, the standard states being "ideally" pure substance both in solution and the interface (14). It was found that the standard Gibbs energy displays a parabolic variation with a maximum at charges around −5 μC cm^{-2}. Figure 5 shows a quadratic dependence of $(\Delta G^0 - \Delta G^0_{max})$ on $(\sigma^M - \sigma^M_{max})$ within the charge range of +5 to −11 μC cm^{-2}. The adsorption of the support electrolyte could be detectable by a breakdown of the quadratic dependence of the standard Gibbs energy with charge at positives charges (15, 16). Such a deviation has not been observed in the present system. Therefore, it is reasonable to assume that the adsorption of ClO_4^- in presence of HPRO was weak.

The change in the rational potential drop across the inner layer, $\Delta\phi^{M-2}$, at constant charge, shows a linear dependence on the relative surface excess, Γ (Fig. 6). Values of $\Delta\phi^{M-2}$ were calculated from:

$$[3] \quad \Delta\phi^{M-2} = E^N_\sigma - E^{base}_{\sigma=0} - \phi^{2-s}_\sigma$$

where E^N_σ is the measured potential in the presence of HPRO, $E^{base}_{\sigma=0}$ is the pzc of the base electrolyte and ϕ^{2-s}_σ is the diffuse-layer potential drop given by the Gouy–Chapman theory. The zero gradient at $\sigma^M \simeq -5$ μC cm^{-2} corresponds to the charge of maximum adsorption.

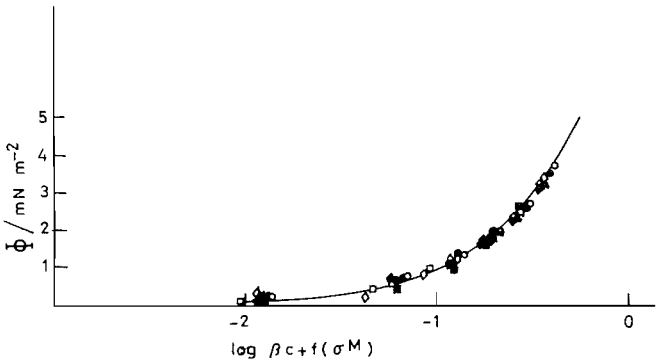


FIG. 4. Composite pressure curve for hydroxyproline adsorption on mercury electrode. The line was calculated from the Frumkin isotherm with $\alpha = 0.6$ and $\Gamma_s = 3.6 \times 10^{-10}$ mol cm^{-2}. Charges on mercury (μC cm^{-2}): (◇) +3; (◆) +1; (▲) 0; (△) −1; (●) −3; (○) −5; (■) −7; (□) −9.

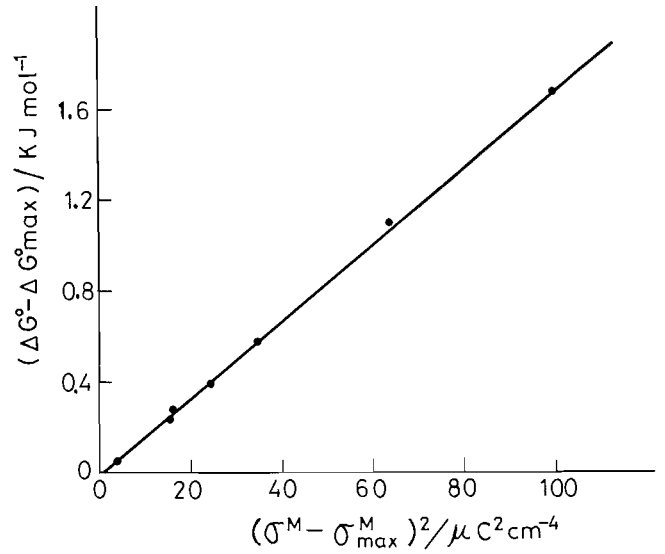


FIG. 5. Variation of the standard Gibbs energy of adsorption of hydroxyproline with the electrode charge. Charges ranging between +5 to −11 μC cm^{-2}.

The linear dependence of the gradient $(\partial\Delta\phi^{M-2}/\partial\theta)_{\sigma^M}$ on the electrode charge σ^M, which corresponds to a quadratic dependence for the standard Gibbs energy (17), is observed in all the charge range studied (Fig. 7).

The inner layer capacity at constant amount adsorbed, C_i, which is defined by eq. [4], was calculated from Fig. 6 by plotting potential-charge curves at selected coverage values and differentiating at constant charge.

$$[4] \quad C_i = (\partial\sigma^M/\partial\phi^{M-2})_\Gamma$$

Figure 8 shows that $1/C_i$ is a linear function of coverage, which is in accord with the model of two series capacitors:

$$[5] \quad \frac{1}{C_i} = \frac{1-\theta}{C_0} + \frac{\theta}{C_1}$$

where C_1 and C_0 are the inner layer capacities at saturation in the presence and in the absence of adsorbate, respectively (12). The C_0 capacity was calculated by using the Gouy–Chapman

Can. J. Chem. Downloaded from www.nrcresearchpress.com by 84.41.108.74 on 09/07/12
For personal use only.

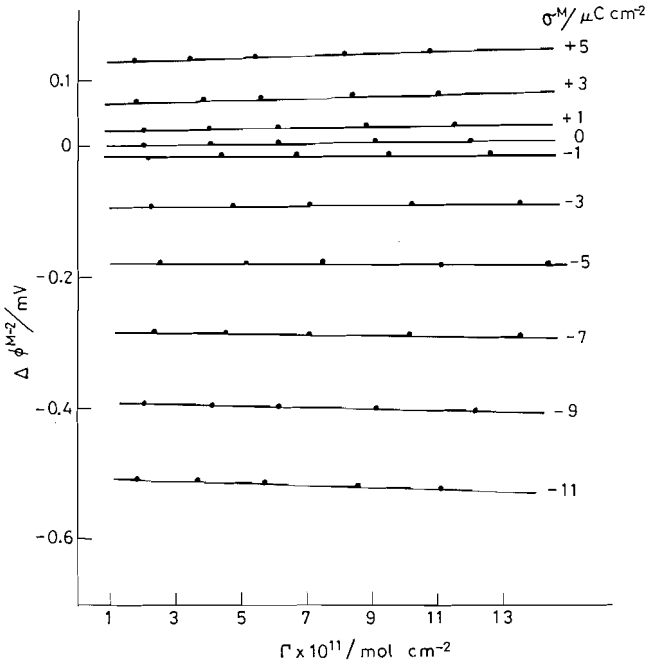


FIG. 6. Change in the potential drop across the inner layer upon adsorption of hydroxyproline at constant charge. The charge values are indicated for each curve.

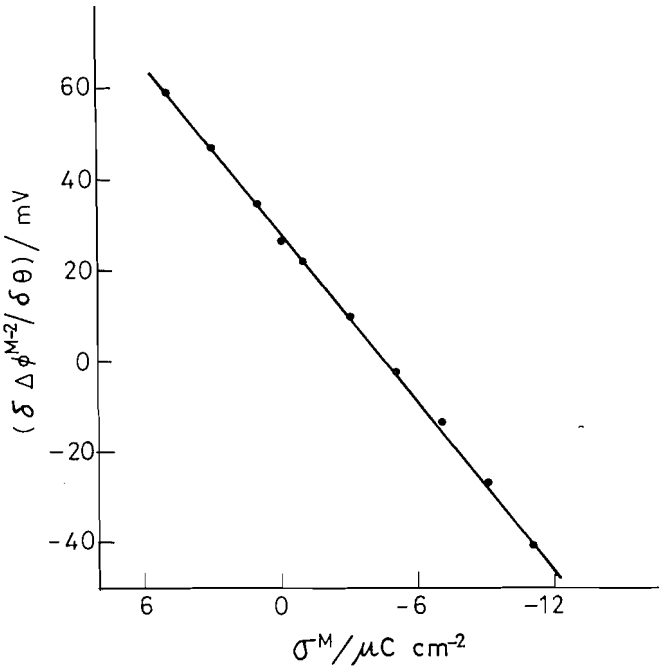


FIG. 7. Plot of the function $(\partial\Delta\phi^{M-2}/\partial\Gamma)_{\sigma^M}$ vs. the electrode charge for adsorption of hydroxyproline.

theory for the supporting electrolyte with values for $\partial\sigma^i/\partial\sigma^M$ estimated from the data of Payne (18). The C_1 capacity at different charges was obtained extrapolating values of $1/C_i$ in Fig. 8 to $\theta = 1$. The inner layer capacities are dependent on the electrode charge. The C_1 values increase as the charge is made less negative.

The capacity of the inner layer, regarded as a parallel plate condenser, is

$$[6] \quad C_i = \frac{\epsilon_i}{4\pi X_i}$$

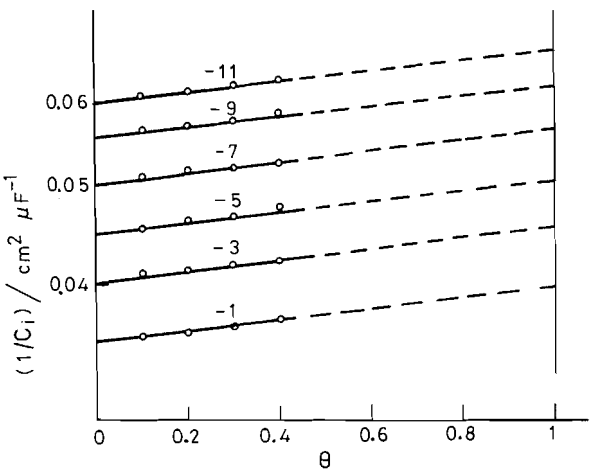


FIG. 8. Reciprocal of the inner layer capacity at constant amount adsorbed as a function of the coverage of hydroxyproline at constant charge as indicated by figures in the lines (in $\mu C\ cm^{-2}$).

TABLE 4. Inner layer parameters at saturation with hydroxyproline and water

$\sigma^M/\mu C\ cm^{-2}$	−1	−3	−5	−7	−9	−11
$C_1/\mu F\ cm^{-2}$	25.0	21.5	19.3	17.5	16.1	15.2
$C_0/\mu F\ cm^{-2}$	28.8	25.0	22.0	19.5	17.8	16.6
ϵ_a	18.7	16.1	14.5	13.1	12.1	11.4
ϵ_ω	10.0	8.7	7.6	6.8	6.2	5.8

TABLE 5. Adsorption parameters of proline (2) and hydroxyproline from aqueous solutions of 10^{-2} M $KClO_4$ on a mercury electrode at 25°C

Parameter	Proline[a]	Hydroxyproline
Isotherm	Frumkin	Frumkin
$\alpha_{\sigma_{max}}$	−1.28	+0.6
$\sigma^M_{max}/\mu C\ cm^{-2}$	−7	−5
$\Delta G^0_{\sigma=0}/kJ\ mol^{-1}$	−13.0	−10.4
$\Delta G^0_{max}/kJ\ mol^{-1}$	−14.4	−10.8
$\Delta E_{\sigma=0}/mV$	58	29

[a]Data from ref. 2.

where ϵ_i is the dielectric constant and X_i is the separation between the plates which can be considered equal to the height of the adsorbed molecules (12, 19). The dielectric constants of the inner layer at saturation (ϵ_a) and in the absence of HPRO (ϵ_ω) and the C_0 and C_1 values are given in Table 4 as a function of the surface charge. The ϵ_a and ϵ_ω values were calculated from eq. [6] assuming $X_a = 0.67$ nm and $X_\omega = 0.31$ nm for HPRO and water, respectively.

Discussion

The adsorption of HPRO on mercury shows small differences with the adsorption of PRO, as can be deduced by comparing the values of the corresponding parameters given in Table 5. Both compounds are weakly adsorbed obeying a Frumkin isotherm. However, there are some definite differences in the values determined for the shift of the potential of zero charge from $\theta = 0$ to $\theta = 1$, $\Delta E_{\sigma=0}$, the charge of the maximum adsorption, σ^M, the interaction parameter, α, and the standard Gibbs energy ΔG^0_σ.

Can. J. Chem. Downloaded from www.nrcresearchpress.com by 84.41.108.74 on 09/07/12
For personal use only.

Can. J. Chem. Downloaded from www.nrcresearchpress.com by 84.41.108.74 on 09/07/12
For personal use only.

The shift of the zero-charge potential upon a transition from $\theta = 0$ to $\theta = 1$ can be considered to be the difference between the potential drops due to the oriented adsorption of the organic substance dipoles and water, respectively, at $\sigma^M = 0$. The shift of pzc of HPRO was estimated by extrapolating the plot at $\sigma^M = 0$ in Fig. 6 to $\Gamma = \Gamma_s$. A value of 29 mV was obtained for $\Delta E_{\sigma=0}$ by assuming a linear relationship of ϕ^{M-2} with θ. The more negative value of σ^M_{max} and larger $\Delta E_{\sigma=0}$ for PRO suggest a larger normal component of the dipole moment (20).

At a given charge, σ^M = constant $\neq 0$, the potential shift, ΔE_σ, could be due to three factors: the replacement of the water dipoles already oriented at the electrode, the orientation of the adsorbate molecule, and a change in the inner layer thickness due to the adsorption of the adsorbate molecules. In general, ΔE_σ can be represented by (12, 21):

$$[7] \quad \Delta E_\sigma/\theta = \Gamma_s N \left(\frac{\mu_a}{\epsilon_a} - \frac{n\mu_\omega}{\epsilon_\omega}\right) - \sigma\left(\frac{X_a}{\epsilon_a} - \frac{X_\omega}{\epsilon_\omega}\right)$$

where n is the number of water molecules displaced by adsorption of one adsorbate molecule, N is the Avogadro's number and μ_a and μ_ω are the effective dipole moments of the adsorbate and water on the electrode, respectively. Although all the terms on the right-side in eq. [7] have the possibility to change with charge, Γ_s and X_a can be assumed constant for the adsorption of HPRO whose orientation on the mercury electrode does not change. It should be noted that the dipole moment and dielectric constant are influenced not only by the orientation of permanent dipoles, but also by induced dipoles formed in the electric field. Therefore, μ_a cannot be constant when the adsorbate shows a high polarizability although the orientation is constant (12).

The component of the dipole moment of HPRO perpendicular to the mercury surface was calculated at maximum adsorption, where there is no potential change (Fig. 6). The replacement of possible ClO_4^- ions present in the interface has not been considered. The term $n\mu_\omega$ was calculated from the potential drop due to the water dipoles adsorbed on the electrode, Δg^ω_{dipole}. Using the data of Bockris and Habib (22), Δg^ω_{dipole} was estimated to be -0.012 V at a charge of -5 μC cm^{-2}. By substituting values in eq. [7], a value of -0.8 D (1 D $\equiv 3.336 \times 10^{-30}$ Cm) was obtained for μ_a with the positive pole towards the electrode.

In the case of the adsorption of PRO (2), the component of the dipole moment and the dielectric constant at maximum charge was calculated by taking average values for the molecular height ($X_a = 0.65$ nm) and for the saturation surface concentration ($\Gamma_s = 3.7 \times 10^{-10}$ mol cm^{-2}) (see ref. 2). The obtained values were $\mu_a = -1.9$ D and $\epsilon_a = 10.6$. However, these values must be taken as rough estimates because the zwitterion of PRO could be adsorbed in a conformational equilibrium between N- and S-type forms.

The interaction parameter in the Frumkin isotherm is negative for PRO ($\alpha = -1.28$ at σ^M_{max}) and positive for HPRO ($\alpha = +0.6$). The difference between these values can be expressed in terms of adsorbate–adsorbate and adsorbate–solvent interaction differences (23):

$$[8] \quad RT(\alpha_P - \alpha_H) = (\Delta G^0_{s-P} - \Delta G^0_{s-H}) - (1/2)(\Delta G^0_{P-P} - \Delta G^0_{H-H})$$

where P, H, and s stand for PRO, HPRO, and solvent respectively. The empirical difference of -4.6 kJ mol^{-1} for $RT(\alpha_P - \alpha_H)$ could then be due to greater interfacial solubility and/or adsorbate-adsorbate repulsion for PRO than for HPRO. A more favourable interaction adsorbate/solvent at the interface for PRO is according with a greater bulk solubility (24). The estimation of the last term in eq. [8], due to the difference between the normal component of the dipole moment is only 0.34 kJ mol^{-1}. This figure was calculated by using the expression:

$$[9] \quad (\Delta G^0_{AA}) = 9.24\theta\mu_a^2/\epsilon_a R^3$$

which gives the free energy for dipole–dipole interaction by assuming localized adsorption for parallel hexagonal arrays (25). Taking values of $R = 0.79$ nm and $R = 0.81$ nm for the distance at full coverage and $\epsilon_a = 10.6$ and $\epsilon_a = 14.5$ for the dielectric constants of PRO and HPRO respectively, the calculated values of (ΔG^0_{AA}) for PRO and HPRO are 0.38 and 0.04 kJ mol^{-1}, respectively. On the other hand, differences in the α parameter could also be due to different specific interactions between pairs of adsorbed molecules of aminoacid i.e. hydrogen bonds. It was found that a short intermolecular hydrogen bond may contribute to the stability of the crystal structure of HPRO (4).

The standard Gibbs energy of adsorption is determined by two factors: the free transfer energy of the organic compound from the bulk solution to the surface, and the free energy of interaction between the electrode and the substance.

The surface activity of PRO and HPRO in aqueous solutions of 10^{-2} $KClO_4$ has been determined from surface tension measurements (26). The difference between the transfer free energies of HPRO and PRO at the air/solution interface was found to be 1.2 kJ mol^{-1}. This value is appreciably smaller than 3.4 kJ mol^{-1} estimated by Nozaki and Tanford (27) as a contribution of a hydroxyl group to the transfer energy. At the interface, the OH group of HPRO is probably only partially dehydrated because a part of the adsorbed molecule should be exposed to the aqueous phase, whereas on transfer of the molecule from water to nonaqueous solvent the hydroxyl group must completely be dehydrated and surrounded by nonaqueous medium.

At the mercury/solution interface, the standard Gibbs energy at $\sigma^M = 0$ for HPRO is 2.6 kJ mol^{-1} smaller than that obtained for PRO (see Table 5). By assuming that the transfer energy of an organic compound from the bulk to the uncharged mercury/solution interface is close to that for air/solution interface, the difference in the interaction energies of PRO and HPRO with the electrode would be *ca.* 1.4 kJ mol^{-1}. Therefore, it seems that the OH group addition to PRO affects very slightly the specific interaction electrode/adsorbate. Such a small contribution must be expected if one takes into account the fact that both molecules interact almost flat on the electrode surface and the OH group rest away from the surface.

The comparison of the empirical value of -0.8 D for the effective dipole moment derived from interfacial parameters with the calculated ones is not very reliable because the interfacial data provide macroscopic parameters. However, some information about the orientation of HPRO can be obtained from the results given in Table 2. The smaller values of μ_i are calculated for B-type orientations. When the molecule rests onto the H_3—H_5—H_7 atoms a value of -1.2 D was calculated for μ_i. Therefore, the zwitterion of HPRO could be adsorbed with the ring parallel to the electrode and the carboxyl and hydroxyl groups towards the bulk solution.

Acknowledgement

This study has been supported by the Dirección General de Investigación Científica y Técnica of Spain (Project PS88-0014).

1. P. BORNSTEIN. Ann. Rev. Biochem. **43**, 567 (1974).
2. M. M. GÓMEZ, R. MOTILLA, and E. DIEZ. Electrochim. Acta, **34**(6), 831 (1989).
3. C. A. G. HAASNOOT, F. A. A. M. DE LEEUW, H. P. M. DE LEEUW, and C. ALTONA. Biopolymers, **20**, 1211 (1981).
4. T. F. KOETZLE, M. S. LEHMANN, and W. C. HAMILTON. Acta Crystallogr. B**29**, 231 (1973).
5. J. DONOHUE and K. N. TRUEBLOOD. Acta Crystallogr. **5**, 414 (1952).
6. N. L. ALLINGER. J. Am. Chem. Soc. **99**, 8127 (1977).
7. N. L. ALLINGER and Y. H. YUH. QCPE, **12**, 395 (1980).
8. J. A. POPLE, D. L. BEVERIDGE, and P. A. DOBOSH. J. Chem. Phys. **47**, 2026 (1967).
9. M. M. GÓMEZ, A. MANZANO, A. ALDAZ, and J. M. VARA. An Quim. **76**A, 35 (1980).
10. M. M. GÓMEZ, E. DIEZ, E. ALDA, and A. ALDAZ. J. Electroanal. Chem. **165**, 207 (1984).
11. P. K. SMITH and E. R. B. SMITH. J. Biol. Chem. **132**, 57 (1940).
12. O. IKEDA, K. KOGO, and H. TAMURA. J. Electroanal. Chem. **95**, 177 (1979).
13. R. PARSONS. Proc. R. Soc. A, **261**, 79 (1961).
14. J. JASTRZEBSKA, M. JURKIEWICZ-HERBICH, and S. TRASATTI. J. Electroanal. Chem. **216**, 21 (1987).
15. R. PARSONS and R. PEAT. J. Electroanal. Chem. **122**, 299 (1981).
16. M. M. GÓMEZ, E. DIEZ, E. ALDA, and A. ALDAZ. J. Electroanal. Chem. **193**, 265 (1985).
17. R. PARSONS. Trans. Faraday Soc. **55**, 999 (1959).
18. R. PAYNE. J. Phys. Chem. **70**, 204 (1966).
19. R. PARSONS, R. PEAT, and R. M. REEVES. J. Electroanal. Chem. **62**, 151 (1975).
20. G. BORGHESANI. Electrochim. Acta, **28**, 483 (1983).
21. B. DAMASKIN and A. N. FRUMKIN. J. Electroanal. Chem. **34**, 291 (1972).
22. J. O'M. BOCKRIS and M. A. HABIB. Electrochim. Acta, **22**, 41 (1977).
23. F. PULIDIRI, G. BORGHESANI, R. PERIALI, A. DE BATTISTI, and S. TRASATTI. J. Chem. Soc. Faraday Trans. I, **74**, 79 (1978).
24. R. C. WEAST (*Editor*). Handbook of chemistry and physics. CRC Press, Cleveland. 1969. p. C703.
25. F. O'M. BOCKRIS and D. A. J. SWINKELS. J. Electrochem. Soc. **111**, 736 (1964).
26. M. M. GÓMEZ. An. Quim. In press.
27. Y. NOZAKI and C. TANFORD. J. Biol. Chem. **246**, 2211 (1971).

Can. J. Chem. Downloaded from www.nrcresearchpress.com by 84.41.108.74 on 09/07/12
For personal use only.

The photochemistry of RDX in solid argon at 10 K

JEFF ALIX AND SUSAN COLLINS
Department of Chemistry, California State University, Northridge, CA 91330, U.S.A.

Received September 4, 1990[1]

JEFF ALIX and SUSAN COLLINS. Can. J. Chem. **69**, 1535 (1991).

The photochemistry of RDX was studied in argon matrices at 10 K and examined by FTIR spectroscopy. The spectra and kinetics of product growth indicate that there are two decomposition pathways:

[I] $RDX \rightarrow 4NO + 2CH_2O + N_2 + CH_2 \rightarrow 4NO + 2CO + N_2 + CH_4 + H_2$

[II] $RDX \rightarrow N_2O + [O_3 + N_2]$ or $[N_2O_3] + CO_2 + C_2H_2 + N_2 + 2H_2$

The mechanism II nitrogen products can easily be rationalized for the chair configuration of RDX with axial NO_2 groups adjacent (C_s symmetry). When considering the carbon products of II, it may be necessary to postulate intermolecular reactions. Our studies gave no evidence for the symmetric triple fission path, which leads to N_2O and CH_2O, nor for the NO_2 stripping mechanism reported for the gas-phase thermal reactions, which leads to the formation of NO_2 and HCN. Rather, our findings were more consistent with the known condensed phase products. The production of CH_4, C_2H_2, N_2O_3, and O_3 are unique to the matrix study.

Key words: RDX, photochemistry, argon matrices.

JEFF ALIX et SUSAN COLLINS. Can. J. Chem. **69**, 1535 (1991).

Opérant à 10 K, dans des matrices d'argon et utilisant la spectroscopie FTIR, on a étudié la photochimie du RDX. Les spectres et la cinétique de la croissance des produits indiquent qu'il existe deux voies de décomposition :

[I] $RDX \rightarrow 4NO + 2CH_2O + N_2 + CH_2 \rightarrow 4NO + 2C0 + N_2 + CH_4 + H_2$

[II] $RDX \rightarrow N_2O + [O_3 + N_2]$ ou $[N_2O_3] + CO_2 + C_2H_2 + N_2 + 2H_2$

La formation des produits azotés par le méchanisme II peut facilement être rationalisée à partir de la configuration chaise du RDX et du NO_2 adjacent axial (syméthrie C_s). Lorsqu'on considère les produits carbonés obtenus par le mécanisme II, il peut être nécessaire de postuler des réactions intramoléculaires. Nos études n'ont pas permis de déceler des données permettant de suggérer l'existence du mécanisme impliquant une voie de fission triple syméthrique qui conduirait à du N_2O et à du CH_2O ou du mécanisme d'élimination de NO_2 rapporté pour les réaction thermiques en phase gazeuse et qui conduit à la formation de NO_2 et de HCN. Les résultats obtenus sont plutôt en accord avec les produits connus de la phase condensée. La formation de CH_4, de C_2H_2, de N_2O_2 et de O_3 ne se produit que dans les matrices.

Mots clés : RDX, photochimie, matrices d'argon.

[Traduit par la rédaction]

Introduction

The technique of matrix isolation has proven to be extremely valuable for isolation of intermediates which are crucial in establishing chemical and photochemical mechanisms. 1,3,5-Trinitrohexahydro-*s*-triazine, RDX, is known to decompose by several pathways. The products obtained depend on the phase and temperature of the starting material. The condensed-phase decomposition occurs just above the melting point giving NO, N_2O, H_2, CO, CH_2O, and CO_2 (3). Another study showed that a primary deuterium kinetic isotope effect ($k_H/k_D = 1.5$) is associated with C—H breakage during the rate determining step under these conditions (4). When decomposition is studied at higher temperatures producing gas phase molecules, two other mechanisms predominate (3, 5). The first involves the NO_2 stripping mechanism in which all three NO_2 groups are removed before the triazine fragment decomposes to form HCN and presumably H_2. The second pathway, which clearly has been seen in molecular beam studies, is the symmetric triple fission to form CH_2NNO_2 fragments which then further decompose to form CH_2O and N_2O (6). Our study was motivated by the possibility of trapping the CH_2NNO_2 fragment and obtaining its infrared spectrum, and to determine whether the mechanisms in the matrix is similar to the gas or to the condensed phase mechanisms. We report here the matrix FTIR spectra of RDX and its photoproducts and their kinetic behavior at 10 K.

Experimental

The apparatus used for these experiments has been described recently (1). FTIR spectra were recorded on a Nicolet 20 DXB instrument with 1.0 cm^{-1} resolution. The RDX was deposited by heating it to approximately 200°C in a stainless steel vacuum line positioned in front of the CsI substrate window. Argon was passed over it at 1–2 mmol per h for 1 h. The argon stream entrained the RDX vapors and mixing occurred before deposition. The photolysis light source was an Oriel medium pressure xenon lamp. Broad band irradiation was used for all experiments.

An independent study involving the photolysis of a 1/1/200 matrix of $N_2O/CH_2O/Ar$ was necessary to elucidate some mechanistic features. The N_2O and CH_2O were deposited by separate jets and combined at the CsI substrate window. A lower limit of approximately five percent reactive pairs is expected at this concentration.

RDX was kindly supplied to us by Dr. Steve Rodgers at the Edwards Air Force Base. Argon (Matheson, 99.995%) and occasionally nitrogen (Airco, 99.995%) were used as matrix gases, and they were used without further purification. No significant experimental differences were found when the reaction was carried out in argon or nitrogen matrices. N_2O (Aldrich, 95%) was used without further purification. Formaldehyde was prepared from paraformaldehyde according to ref. 2.

Results

The present section will describe the infrared absorptions of the photochemical products and intermediates in Ar at 10 K.

The infrared spectra of RDX in argon at 10 K are shown in Fig. 1*A*. Photolysis of RDX is 80% complete in 40 min resulting

[1]Revision received May 22, 1991.

Printed in Canada / Imprimé au Canada

Can. J. Chem. Downloaded from www.nrcresearchpress.com by 84.41.108.74 on 09/07/12
For personal use only.

TABLE 1. Kinetic behavior of product bands

Frequency (cm^{-1})	Photolysis 2 min	Photolysis 40 min	Photolysis 11 h	Curve in Fig. 2	Kinetics type	Assignment
3291.2	0	100	70	—	B	C_2H_2
2227.5	2	20	100	—	B	N_2O
2218.9	2	25	100	*f*	B	N_2O
2140.0	0	18	100	*i*	C	CO
2085.0	0	31	100	*k*	C	CHO
1851.0	0	100	46	*c*	A	NO
1777.5	0	100	53	*d*	A	$(NO)_2$
1740.0	20	42	0	*a*	A	CH_2O
1693.2	10	50	100	*h*	B	N_2O_3
1498.1	20	45	0	*b*	A	CH_2O
1300.0	0	23	100	*j*	C	CH_4
1283.0	2	20	100	—	B	N_2O
1045.3	4	96	90	*e*	B	O_3
733.3	4	20	100	—	B	N_2O
586.3	4	20	100	—	B	N_2O

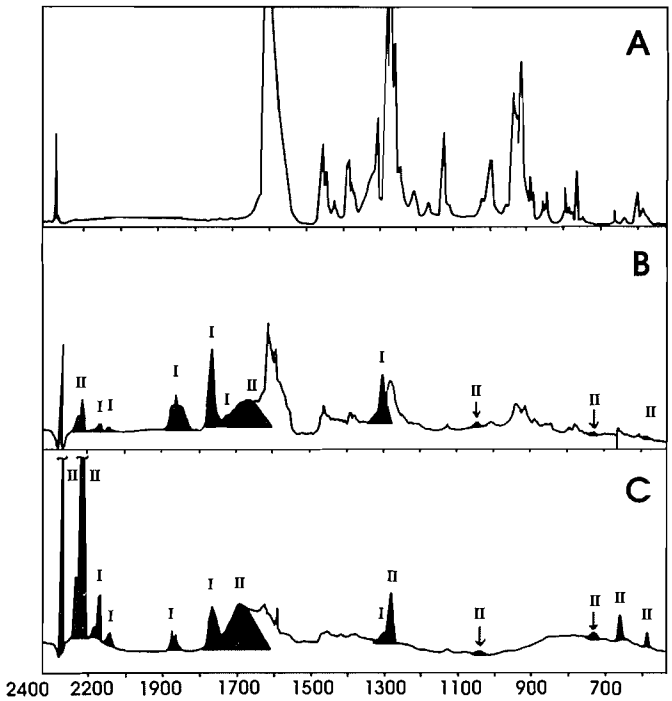


FIG. 1. FTIR absorption bands (*A*) of RDX is Ar at 10 K, (*B*) after 40 min photolysis, and (*C*) after 11 h photolysis. Bands with dark shading are product bands. Bands marked I and II are associated with mechanisms I and II, respectively.

in the product spectrum shown in Fig. 1*B*. After continued irradiation for 11 h, there is complete disappearance of the RDX bands and evidence of secondary photochemical reactions. Figure 1*C* shows the photolysis bands after eleven hours. Of the three spectra, only the 40 min spectrum contains RDX and products together as positive bands. The product bands in 1*B* and 1*C* are indicated by dark shading. Table 1 gives the frequencies and relative intensities of the product bands, normalized to the most intense band of its kind, at three different photolysis times. The molecule assignments associated with the listed bands will be discussed in the next section.

Figure 2 illustrates the kinetics of the product bands. Three distinct behavior patterns, types *A*, *B*, and *C*, are illustrated in 2*A*, 2*B*, and 2*C*. Type A behavior is characterized by simple first-order kinetics and by a fast rise at early photolysis times. Type B behavior also is first order, but these bands rise more slowly. At long photolysis times, some bands from types A and B disappear with a concomitant rise of type C bands. Thus at least two examples of consecutive reaction kinetics are seen.

In a separate argon matrix experiment, N_2O and CH_2O were deposited together and photolysed. After 1 h photolysis there was evidence of CH_2O decomposition to form CO, and annealing of the N_2O was evidenced by the sharpening of the N_2O FTIR bands. There was no evidence of any photoreaction between N_2O and CH_2O.

Discussion

We will discuss the assignment of the product bands and develop a mechanism for the reactions in terms of the kinetic behavior. All of the product molecules are known molecules, and in all cases, literature matrix spectra are available.

Mechanism I

NO. The bands at 1851.0 and 1777.5 cm^{-1} are assigned as NO and the $(NO)_2$ dimer. They follow type A kinetics. These bands appear in a unique portion of the IR spectrum and they compare very well with the literature argon matrix spectra of NO and $(NO)_2$ (7). After 11 h of photolysis, there appears to be some degradation of both the monomer and dimer.

CO. The band at 2140.0 cm^{-1} follows type C kinetics and is assigned to CO. This band also is very well known and appears in many photochemical studies (e.g., ref. 2).

CH_2O, CH_4, HCO, CH_2. The bands at 1740.0 and 1498.1 cm^{-1} appear at early photolysis times with type A kinetics. Consistent with these band frequencies is the molecule formaldehyde (8). The kinetics support the assignment since formaldehyde is known to photolyse in the matrix (9). CO is expected to be a photoproduct, and indeed, the band at 2140.0 cm^{-1} assigned to CO exhibits type C kinetics. Other

Can. J. Chem. Downloaded from www.nrcresearchpress.com by 84.41.108.74 on 09/07/12
For personal use only.

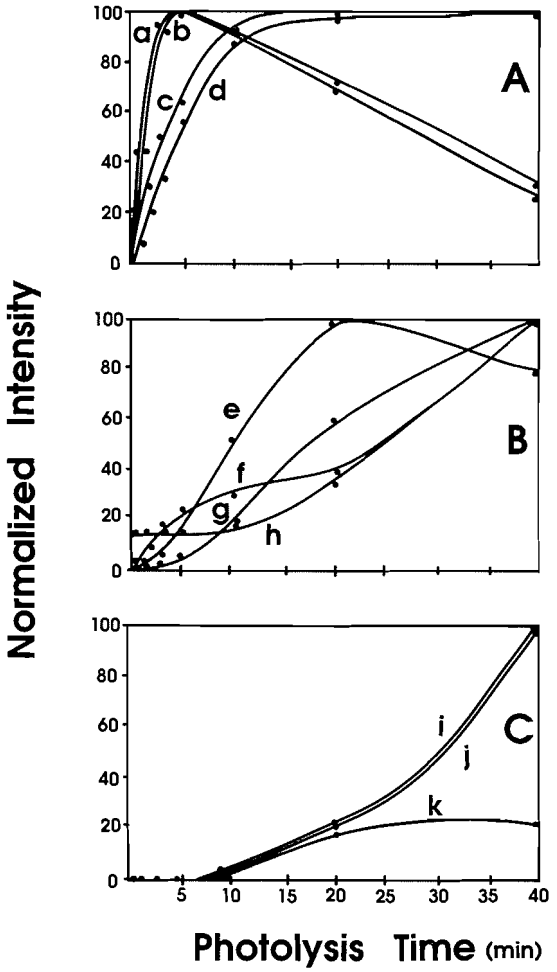


FIG. 2. Normalized FTIR product band intensities versus time. Curves marked *a*–*k* are from bands with the following frequencies; *a*, 1740.0; *b*, 1498.1; *c*, 1851.0; *d*, 1777.5; *e*, 1045.3; *f*, 2218.9; *g*, 733.3; *h*, 1693.2; *i*, 2140.0; *j*, 1300.0; *k*, 2085.0

bands appearing with type C kinetics due to the decomposition of formaldehyde appear at 1300.0 and 2085.0 cm^{-1}. We assign these bands as CH_4 and HCO (10, 11). The methane would account for the uptake of hydrogen from the formaldehyde photolysis, conceivably by the reaction of CH_2 with excited CH_2O. For this, the formation of methylene also must be postulated as a product. To date, there are no literature reports of a matrix spectrum of CH_2. All attempts to stablize methylene under matrix conditions have failed due to its extreme reactivity (12). The band at 2085.0 cm^{-1} is assigned to formyl. This is tentative at best and at least consistent with the photochemical breakdown of formladehyde. Another possibility is HCN, but this is ruled out since the known band for the CH bend at 717 cm^{-1} is not seen in our experiments. Thus we postulate that one of the decomposition mechanisms of RDX results in NO, CH_2O, and CH_2 which later react to form NO, CO, and CH_4. In order to balance the reaction, the production of N_2 and H_2 must be postulated to give the overall balanced reaction as:

$$[I] \quad RDX \rightarrow 4NO + 2CH_2O + N_2 + CH_2 \rightarrow 4NO + 2CO + N_2 + CH_4 + H_2$$

The CH_4 band at 1300.0 cm^{-1} is intense relative to the CO band at 2140.0 cm^{-1} in Fig. 1*B*, possibly due to some absorption of the parent RDX overlapping in that region. Alternatively, it may be necessary to postulate extra hydrogen from other sources, i.e., impurities, to react with methylene to give excess methane. Also one should note that a weak absorbance at 1740.0 cm^{-1} due to formaldehyde still remains in Fig. 1*B*.

Mechanism II

N_2O. The second decomposition reaction is characterized by type B, slower rise, kinetics. The bands at 2227.5, 2218.9, 1283.0, and 586.3 cm^{-1} are due to N_2O (13). These bands all follow type B kinetics. As an independent check, an authentic matrix sample of N_2O in argon (M/R = 1/100) was prepared and it gave an identical spectrum.

N_2O_3. The very broad band at 1693.2 cm^{-1} has type B growth behavior. This band is assigned as symmetric N_2O_3 which has an absorption band at 1690.6 cm^{-1} in the literature (14). It is known to be a product of the reaction of NO + O_2 or NO + O_3 in argon matrices. It is not necessary to postulate these reactions, however, since it can form directly from RDX. One could easily envision its formation from RDX in the chair conformation with the axial NO_2 groups adjacent to each other (C_s symmetry).

O_3. A type B band which exhibits consecutive reaction kinetics is at 1045.3 cm^{-1}. The assignment of O_3 is consistent with the IR spectrum (15). Such an intermediate certainly would be trapped at 10 K. Further support for this assignment comes from the similarity between the type B kinetics and the known tendency for decomposition under matrix photolysis conditions (16). Again, considering the C_s-symmetry chair configuration known for solid phase RDX, the two NO_2 groups are adjacent and they easily could react to form N_2O, O_3, and N_2 (17).

C_2H_2. The next set of type B bands are at 733.3 and 3291.2 cm^{-1}. These bands also are well known and are easily assigned to acetylene (18). The reaction of two adjacent methylene groups produced from the chair configuration of RDX would give acetylene. The reaction of two methylene groups in the matrix is known to produce highly vibrationally excited ethylene which immediately decomposes to form acetylene and hydrogen (19). As in mechanism I, the presence of another methylene group could conceivably result in the rapid formation of methane.

CO_2, H_2O. Comparison of the band at 2340.8 cm^{-1} in Figs. 1*A*, 1*B*, and 1*C* shows that CO_2 is present in the deposition spectrum as a consequence of our deposition method. There is only a slight increase during the initial 40 min of irradiation, but there is a dramatic increase during the 11 h photolysis. This is much more than we normally see in this period of time when the background pressure is 10^{-6} Torr. Thus, CO_2 certainly is a product associated with mechanism II. Matrix water at 1625.0 and 1597.6 cm^{-1} are seen in our experiments and are very well known to other researchers (e.g., ref. 14). We see normal amounts in the eleven hour spectrum compared to CO_2 absorbances in the 40 min spectrum, therefore we conclude that water is not a photoproduct of RDX.

If we consider one RDX molecule leading to products, then N_2 and H_2 must be postulated to balance the reaction:

$$[II] \quad RDX \rightarrow N_2O + [N_2O_3] \text{ or } [N_2 + O_3] + C_2H_2 + CO_2 + 2H_2 + N_2$$

This reaction would involve considerable movement of the atoms in forming the carbon products from one RDX molecule.

Can. J. Chem. Downloaded from www.nrcresearchpress.com by 84.41.108.74 on 09/07/12
For personal use only.

Alternatively, more than one RDX molecule may participate in the formation of the carbon products.

While mechanisms I and II are consistent with the observed products and kinetic behavior, it might be considered that the two decomposition pathways are not necessarily primary processes, i.e., that the initial fragmentation involves the triple fission or NO_2 stripping mechanisms, and that these intermediates are not stabilized at 10 K. This can be ruled out in any event, since neither NO_2 nor HCN are observed products in our studies. The NO_2 photoproduct NO is seen in mechanism I, but it is not accompanied by HCN. The symmetric triple fission products, N_2O and CH_2O, also can be ruled out since our matrix deposition and photolysis of N_2O and CH_2O do not give our final mechanisms I or II products. Rather, no reaction occurs between them.

Conclusions

Reactions [I] and [II] are consistent with the condensed phase thermal chemistry and inconsistent with the gas phase thermal chemistry. The formation of methylene, ethylene, methane, N_2O_3, and ozone in our studies seems at first to be different from the known condensed phase chemistry. These differences may be unique to the matrix environment, the cryogenic temperature, the absence of true isolation, and possibly the photochemical process. In the limit that internal conversion is faster than chemical decomposition where thermal and photochemical studies are comparable, the matrix study shows that there must be two pathways leading to the higher temperature condensed phase results. The NO_2 stripping mechanism and the symmetric triple fission mechanism are results of high temperature gas phase studies only.

The conformation of the RDX in the solid phase is known to be the chair configuration with C_s symmetry. A consequence of the C_s symmetry is that the NO_2 groups are axial and adjacent. This structure could easily explain mechanisms I and II since no geometric rearrangement of RDX is necessary for product formation except perhaps the carbon products in mechanism II. Furthermore the C_{3v} averaged configuration, expected at higher temperatures, has the nitro groups pointing away from each other in the equatorial positions. This structure could more easily explain the stripping NO_2 mechanism and the symmetric triple fission processes seen in the gas-phase studies. Thus perhaps the barrier to the formation of the C_{3v} averaged configuration provides the cutoff, above which the NO_2 stripping and symmetric triple fission mechanisms occur and below which our mechanisms I and II give rise to the condensed phase products. The barrier may be thermal or viscous in nature.

Acknowledgements

The authors would like to thank Dr. Steve Rodgers from Edward Air Force Base for suggesting this project and supplying us with the RDX. We would like to thank Mary McMannamon for the formaldehyde and N_2O experiments. We also would like to acknowledge partial support from the Universal Energy Systems (grant # 210-S-9MG-115) and partial support from the Petroleum Research Foundation (grant # 19114-GB4) for this project.

1. W. Moran and S. Collins. J. Mol. Struct. **222**, 235 (1990).
2. T. Miyazawa and K. S. Pitzer. J. Chem. Phys. **30**, 1076 (1959).
2. M. Farber and R. Srivastava. Chem. Phys. Lett. **64**, 307 (1979).
4. S. Bulusu, D. Weinstein, J. Autura, and R. Veliky. J. Phys. Chem. **90**, 4121 (1986).
5. C. Capellos, S. Lee, S. Bulusu, and L. Gamss. Advances in chemical reaction dynamics. D. Reidel Publishers. 1986. pp. 398–404.
6. X. Zhao, E. Hintsa, and Y. T. Lee. J. Chem. Phys. **88**, 801 (1988).
7. W. Guillory and C. Hunter. J. Chem. Phys. **50**, 3516 (1969).
8. H. Khoshkhoo and E. Nixon. Spectrochim. Acta, **29**A, 603 (1973).
9. J. Sodeau and E. Lee. Chem. Phys. Lett. **57**, 71 (1978).
10. S. Collins, J. Phys. Chem. **94**, 5240 (1990).
11. G. Ewing, A. Thompson, and G. C. Pimentel. J. Chem. Phys. **32**, 927 (1960).
12. C. B. Moore, T. D. Goldfarb, and G. C. Pimentel. J. Chem. Phys. **43**, 63 (1965).
13. W. B. Demore and N. Davidson. J. Am. Chem. Soc. **81**, 5869 (1959).
14. S. Bhatia and J. Hall. J. Phys. Chem. **84**, 3255 (1980).
15. L. Andrews and R. Spiker Jr. J. Phys. Chem. **76**, 3208 (1972).
16. D. Lucas and G. Pimentel. J. Phys. Chem. **31**, 204 (1939).
17. R. Karpowicz and T. Brill. J. Phys. Chem. **88**, 348 (1984).
18. A. Engdahl and B. Nelander. Chem. Phys. Lett. **100**, 129 (1983).
19. Y. P. Lee and G. C. Pimentel. J. Chem. Phys. **75**, 4241 (1981).

Can. J. Chem. Downloaded from www.nrcresearchpress.com by 84.41.108.74 on 09/07/12
For personal use only.

Electronic absorption and fluorescence spectra of 2-phenyl-substituted benzothiazoles: study of excited-state proton transfer reactions

JOYKRISHNA DEY AND SNEH K. DOGRA[1]

Department of Chemistry, Indian Institute of Technology, Kanpur – 208016, India

Received January 7, 1991

JOYKRISHNA DEY and SNEH K. DOGRA. Can. J. Chem. **69**, 1539 (1991).

The absorption and fluorescence spectral properties of 2-(3′-hydroxyphenyl)-, 2-(4′-hydroxyphenyl)-, and 2-(3′,4′-dihydroxyphenyl)-, and 2-(4′-hydroxy-3′-methoxyphenyl), 2-(3′-hydroxy-4′-methoxyphenyl)-, and 2-(3′-methoxyphenyl)benzothiazoles have been studied in a number of solvents of varying polarity. The ionization constants (pK_a) for various prototropic reactions of these molecules in both S_0 and S_1 states are determined. The effect of substitution on the spectral properties and on the pK_a values are discussed. The molecules have been found to undergo biprotonic phototautomerism in dilute acid solutions. On the basis of the fluorimetric titration behaviour of the molecules (except 2-(3′-methoxyphenyl)benzothiazole), the existence of monocation–zwitterion equilibrium in the S_1 state is proposed. PPP-SCF-MO-CI method has been used to calculate charge densities on the heteroatoms.

Key words: spectra, proton transfer.

JOYKRISHNA DEY et SNEH K. DOGRA. Can. J. Chem. **69**, 1539 (1991).

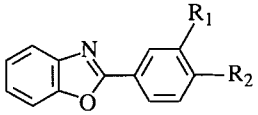
On a étudié, dans un certain nombre de solvants de polarité différente, les propriétés spectrales d'absorption et de fluo rescence des composés suivants : 2-(hydroxy-3′-phényl), 2-(hydroxy-4′-phényl), 2-(3′,4′-dihydroxyphényl)-, 2-(4′-hydroxy-3′-méthoxyphényl), 2-(3′-hydroxy-4′-méthoxyphényl)-, et 2-(3′-méthoxyphényl)benzothiazole. On a déterminé les constantes d'ionisation (pK_a) de plusieurs réactions prototropiques de ces molécules dans les états S_0 et S_1. On discute de l'effet des substitutions sur les propriétés spectrales et sur les valeurs du pK_a. On a trouvé que les molécules subissent un phototautomérisme biprotonique en solution diluée acide. On propose l'existence d'un équilibre monocation-zwittérion dans l'état S_1 en se basant sur le comportement du titrage fluorométrique des molécules (à l'exception du 2-(3′-méthoxyphényl)-benzothiazole). On a utilisé la méthode PPP-SCF-MO-CI pour calculer la densité de charge des hétéroatomes.

Mots clés : spectres, transfert de proton.

[Traduit par la rédaction]

1. Introduction

The excited state proton-transfer (ESPT) reactions in organic molecules capable of emitting fluorescence has been a subject of great interest among researchers. It has been observed that the basicity or acidity of aromatic amines and alcohols changes by several orders of magnitude upon electronic excitation. The proton dissociation constants (pK_a^*) in the lowest excited singlet state (S_1) of a large number of organic acids and bases have been reported (1–5). The ESPT reactions of naphthols (6, 7) in aqueous and micellar media are well studied. Recently, the excited-state intramolecular proton-transfer reaction of 2-(2′-hydroxyphenyl)benzothiazole (8) and similar molecules (9, 10), because of their uses as potential proton-transfer lasers (11), have been studied extensively. However, no attention has been paid for such studies to 2-(3′-hydroxyphenyl)- and 2-(4′-hydroxyphenyl)benzothiazoles. In a continuation of our studies on the proton-transfer reactions of 2-[phenyl-substituted]benzazoles (benzimidazoles (10, 12), benzoxazoles (9*a*, 13), and benzothiazoles (14)) we have undertaken this investigation to study the absorption and fluorescence spectral properties of **I** and **II** in organic solvents of different polarity and in aqueous solutions of various acid/base concentrations. To study the effect of substituent on the spectral properties and proton-transfer reactions of **I** and **II** we have also included **III**, **IV**, **V**, and **IM**.



I: $R_1 = OH$, $R_2 = H$ — **IV**: $R_1 = OCH_3$, $R_2 = OH$
II: $R_1 = H$, $R_2 = OH$ — **V**: $R_1 = OH$, $R_2 = OCH_3$
III: R_1, $R_2 = OH$ — **IM**: $R_1 = OCH_3$, $R_2 = H$

To support our experimental results semiempirical PPP-SCF-MO-CI calculations have been performed to calculate charge densities on the basic centers of **I**, **II**, and **III**.

2. Experimental

Materials

All compounds were prepared as described in the literature (15) and purified by repeated recrystallization from aqueous ethanol. The purity of the compounds was established by TLC, melting points, and fluorescence excitation spectra in methanol. H_2SO_4 (98%), KOH (B.D.H.), and ortho-H_3PO_4 (B.D.H.) were all reagent grade. Analytical grade cyclohexane (SRL), 1,4-dioxane (E. Merck), acetonitrile (E. Merck), and methanol (B.D.H.) were purified by usual methods (16). Spectrograde ethylacetate (B.D.H.) and analytical grade ethanediol and glycerol (SRL) were used directly. Triply distilled water was used for studies in aqueous solution. The solvents thus obtained showed no detectable fluorescence in the region 250 to 500 nm. pH values of the solutions made by mixing appropriate amount of dilute KOH and H_3PO_4 solutions were measured in a Toshniwal digital 46 CL pH-meter fitted with a combined glass electrode. Aqueous solutions of higher acidity/basicity were prepared following the Hammett's acidity (H_0) (17*a*) and Yagil's basicity (H_-) (17*b*) scales. The fluorescence quantum yields were measured in solutions having absorbances less than 0.1, by comparison with a quinine bisulfate (0.1 N H_2SO_4) solution ($\phi_f = 0.55$) (18). The fluorophore concentration of the solutions (containing not more than 1% (v/v) methanol) was $\sim 5 \times 10^{-5}$ M. All solutions were prepared just before measurements. No attempt was made to remove oxygen from the solutions for fluorescence measurements. All experiments were carried out at ~298 K.

Absorption and fluorescence spectra

The absorption spectra were measured on Shimadzu UV-190 spectrophotometer. All fluorescence measurements were performed in the spectrofluorimeter fabricated in our laboratory which has been described earlier (19). Fluorescence spectra reported here are all corrected.

[1]Author to whom correspondence may be sent.

Printed in Canada / Imprimé au Canada

Can. J. Chem. Downloaded from www.nrcresearchpress.com by 84.41.108.74 on 09/07/12
For personal use only.

TABLE 1. Absorption maxima (λ_a nm) and molar extinction coefficient (log ϵ) of molecules **I** to **V** in different solvents

	I		II		III		IV		V	
Solvent	λ_a	log ϵ	λ_a	log ϵ	λ_a	log ϵ	λ_a	log ϵ	λ_a	log ϵ
Cyclohexane	301		316	(sh)			332	(sh)	332	(sh)
	255		303				323	—	320	—
	247		257				310	(sh)	310	(sh)
			249				297	(sh)	295	(sh)
Dioxane	303	4.32	318	4.41	335	(sh)	335	(sh)	332	(sh)
	256	3.92	307	4.41	326	4.43	326	4.47	324	4.45
			258	3.85	313	(sh)	313	(sh)	313	(sh)
			250	3.87	300	(sh)	297	(sh)	300	(sh)
Acetonitrile	300	4.30	316	4.42	335	(sh)	332	(sh)	332	(sh)
	255	3.91	306	4.42	323	4.41	324	4.45	322	4.43
			257	3.85	310	(sh)	313	(sh)	300	(sh)
			249	3.86	300	(sh)	300	(sh)		
Ethylacetate	294	4.29	317	4.47	333	(sh)	332	(sh)	330	(sh)
			307	4.47	324	4.43	324	4.47	322	4.41
					313	(sh)	313	(sh)	313	(sh)
					300	(sh)	300	(sh)	300	(sh)
Methanol	298	4.28	318	4.42	328	4.42	335	(sh)	324	4.40
					313	(sh)	327	4.46	300	(sh)
					300	(sh)	300	(sh)		
Dichloromethane	308	(sh)	316	(sh)	330	(sh)	332	(sh)	332	(sh)
	300	4.22	306.5	4.33	321	4.48	324	4.43	322.5	4.33
					313	(sh)	313	(sh)	312	(sh)
					300	(sh)	300	(sh)	295	(sh)
Water (pH 6.7)	302	4.24	316	4.34	323	4.38	324	4.38	321	4.33

Method of calculation

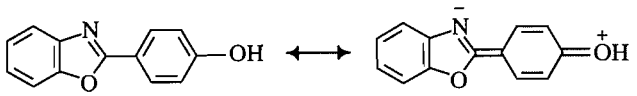
The molecular orbital calculations have been performed by using the semi-empirical PPP-SCF-MO method combined with a singly excited CI calculation (20–22). The one center repulsion integrals ($\gamma_{\mu\mu}$) were calculated from the corresponding valence-state ionization potentials (I_μ) and electron affinities (A_μ) by using the Pariser–Parr approximation. The two-centre repulsion integrals ($\gamma_{\mu\nu}$) were determined by using the Nishimoto–Mataga (22*b*) approximation. The two-centre core resonance integrals ($\beta_{\mu\nu}$) were calculated by the Nishimato–Forster (22*c*) approximation. The empirical parameters used for the calculations were the same as given in ref. 13. The C—C and C—O bond lengths were assumed to be 1.395 and 1.35 Å, respectively. The bond angles were taken to be equal to those of regular hexagon (120°) and pentagon (108°).

The calculations have been carried out on our institute's Dec-1090 computer. The program (23) for the calculations was obtained from QCPE, Indiana University, Bloomington, USA.

3. Results and discussion

3.1. Solvent dependence of absorption and fluorescence spectra

The absorption and fluorescence spectral data of the molecules studied in different solvents are compiled in Tables 1 and 2, respectively. The absorption spectra of the molecules in methanol agree with those reported in the literature (24). The long wavelength absorption band of **II** is red-shifted relative to that of **I** and can be explained by the resonance effect of the —OH group. This increases the magnitude of transition moment vector, which is reflected by the high intensity (log ϵ, Table 1) of the lowest energy absorption band and by the higher fluorescence quantum yield. The absorption spectrum



II **II'**

of **I** closely resembles that of 2-phenylbenzothiazole (PBT) (24) and is consistent with the fact that the charge migration from the —OH group at 3′ position will be localized on the phenyl ring rather than delocalized over the whole molecule and therefore, it has very little effect on the absorption spectrum of (PBT).

The absorption spectra of **III**, **IV**, and **V** are structured and are not very different from each other. The longest wavelength absorption bands of these molecules are red-shifted compared to that of **II**. This can be explained by the resonance effect as described earlier for **II**. The structured absorption spectra may be caused by the formation of hydrogen bond between the hydroxyl proton and the oxygen atom of adjacent —OH or —OCH_3 group. This intramolecular hydrogen bond (IHB), which makes the molecule more rigid, may also be one of the reasons for the red shift of the longest wavelength absorption band of the molecules.

The absorption spectra of the molecules almost remain unaffected by the solvents employed, except for the loss of the vibrational structure and a small blue shift in water. This is consistent with the fact that the resonance effect of hydroxyl group is smaller than that of amino group and thereby the absorption spectra will not be affected much by the solvents. Water, being a very strong hydrogen-bonding solvent, will

Can. J. Chem. Downloaded from www.nrcresearchpress.com by 84.41.108.74 on 09/07/12
For personal use only.

TABLE 2. Fluorescence maxima (λ_f nm) and quantum yields (ϕ_f) of molecules **I** to **V** in different solvents

	I		II		III		IV		V	
Solvent	λ_f	ϕ_f	λ_f	ϕ_f	λ_f	ϕ_f	λ_f	ϕ_f	λ_f	ϕ_f
Cyclohexane	370	0.03	370	0.05			380 360 350	0.11	377 360 350	0.09
Dioxane	365	0.04	380	0.11	375	0.32	374	0.25	375	0.23
Acetonitrile	370	0.06	370	0.13	380	0.38	380	0.35	380	0.35
Ethylacetate	365	0.06	370	0.17	380	0.35	380	0.27	380	0.25
Methanol	380	0.05	380	0.28	400	0.60	390	0.73	395	0.41
Dichloromethane	360	0.03	370	0.09	373	0.17	373 360	0.19	370	0.17
Water (pH 6.7)	390	<0.001	380	0.36	410	0.02	400	0.02	400	<0.001

break the IHB in **III**, **IV**, and **V**, resulting in a blue-shifted broad absorption band. Like absorption spectra, the fluorescence spectra of **III**, **IV**, and **V** in cyclohexane are also structured and the emission maxima are red-shifted relative to that of **I** or **II**. This can be explained on the same lines as described above for the absorption spectra. In contrast to the absorption spectra, the fluorescence spectra of the molecules are red-shifted in hydrogen-bonding solvents. It is well known that —OH group becomes more acidic in the S_1 state. As a result the hydrogen bond between the positively polarized hydrogen of the —OH group and the acceptor atom of the proton acceptor solvent becomes stronger in S_1 state and thus the fluorescence maximum shifts to longer wavelength.

The results in Table 2 indicate that the fluorescence quantum yields of the molecules increase with the increase of polarity and hydrogen-bonding capacity of solvents. The higher quantum yield of **II** in polar solvents can be attributed to the stabilization of the rigid structure **II′**. The same is also true for **III**, **IV**, and **V**. Moreover, it is now firmly established that the presence of IHB enhances the rates of radiationless transitions in a molecule (25). This explains the low fluorescence quantum yields for **III**, **IV**, and **V** in cyclohexane. In polar and protic solvents, IHB is partially broken in competition with the intermolecular hydrogen bond resulting in an increase of quantum yield. The very low fluorescence quantum yield of all the neutral molecules in dichloromethane is due to fluorescence quenching by the solvent molecules, as it is well established (26) that dichloromethane quenches the fluorescence of the fluorophores although not too efficiently. Similar behaviour in water is explained below.

I exhibits a dual fluorescence (λ_f = 390 nm, 510 nm) in methanol and water. The longest wavelength emission band is relatively weak and is only observed at higher solute concentration ($\sim 10^{-4}$ M). When water is added to methanol the intensity of 510 nm band increases and reaches a maximum in solution containing 35% (v/v) water, whereas the intensity of 390 nm band decreases and reaches a minimum at this composition of methanol–water. With further increase in the percentage of water, intensity of the long wavelength band decreases. Similar behaviour has also been observed in acetonitrile–water and dioxane–water mixtures, indicating that the dual fluorescence in methanol, acetonitrile, and dioxane is due to the presence of a trace amount of water. We attribute the appearance of the 510 nm band to the formation of anion, a result of deprotonation from the —OH group. The very low ϕ_f value of the neutral molecule in water is thus due to monoanion formation, whereas similar behaviour is not observed in **II** and thus its fluorescence quantum yield increases as compared to other solvents. This assignment is based on the following facts.

(*i*) The fluorescence excitation spectra (pH ~ 7) recorded for both emission bands are similar and resemble the absorption spectra of neutral species. This indicates that both species have the same ground state precursor, *i.e.* neutral molecule.

(*ii*) The addition of KOH to the solution in 35% water – methanol mixture increases the intenstiy of the 510 nm band and decreases that of the other fluorescence band (390 nm). Furthermore, on acidification (3 < pH < 7) the opposite behaviour is observed. This proves that the species in the S_1 state are in reversible equilibrium.

(*iii*) Under similar conditions the methoxy derivative (**IM**) of the molecule **I** exhibits only the normal Stokes-shifted band characteristic of the neutral molecule. Therefore, the excited state process in **I** must involve deprotonation from the —OH group.

(*iv*) The fluorescence excitation spectrum (in the basified water–methanol mixture) recorded at the 510 nm emission band is similar to the absorption spectrum of anion in the same solution.

Assignment of 510 nm fluorescence band to the formation of excimer or exciplex is neglected on the ground that the ratio of fluorescence intensities at the band maxima (I_{510}/I_{390}) does not change with the increase of solute concentration.

Thus water molecules in methanol, acetonitrile, or dioxane act as proton acceptors leading to the following reaction.

$$[1] \quad ROH^* + H_2O \rightleftharpoons RO^- + H_3O^+$$

The decrease of fluorescence intensities of neutral and monoanion species with the increase of percentage of water (>35%) may be due to quenching by water molecules.

Effect of acid concentrations

The absorption and fluorescence spectra of all the molecules have been studied in the H_-/pH/H_0 range of 16 to −10.4. The spectral properties of the prototropic species of all molecules, compiled in Table 3, are discussed under the following headings.

*2-(3′-Methoxyphenyl)benzothiazole (**IM**)*

IM is present as a neutral in the H_-/pH range of 16 to 3.0. In solutions of pH less than 3.0 both absorption and fluorescence spectra shift to longer wavelengths. Based on earlier results (14) (*i.e.* protonation at tertiary nitrogen atom leads to

Can. J. Chem. Downloaded from www.nrcresearchpress.com by 84.41.108.74 on 09/07/12
For personal use only.

TABLE 3. Absorption (λ_a nm) and fluorescence maxima (λ_f nm), molar extinction coefficient (log ϵ), and fluorescence quantum yields of different prototropic species of molecules **I** to **V** and **IM** in aqueous solution

	Prototropic species									
	Neutral		Monocation		Dication		Monoanion		Dianion	
Molecule	λ_a (log ϵ)	λ_f (ϕ_f)	λ_a (log ϵ)	λ_f (ϕ_f)	λ_a (log ϵ)	λ_f (ϕ_f)	λ_a (log ϵ)	λ_f (ϕ_f)	λ_a (log ϵ)	λ_f (ϕ_f)
I	302 (4.24)	390 (<0.001)	320 (4.31)	440 (0.05)			345 298 (4.26)	510 (<0.001)		
II	316 (4.34)	380 (0.36)	349 (4.5)	410 (0.68)	343 (4.42)		348 (4.55)	420 (0.11)		
III	323 (4.38)	410 (0.02)	363 (4.43) 248 (3.97)	440 (0.12)	348 (4.38) 240 (3.63)	415	358 (4.42)	443 (0.02)	394 (4.34) 322 (4.01) 277 (4.17)	
IV	324 (4.38)	400 (0.02)	364 (4.46) 248 (4.02)	440 (0.16)	360 (4.40) 246 (3.95)	420	362 (4.54)	443 (0.04)		
V	321 (4.33)	400 (<0.001)	361 (4.38) 249 (3.9)	440 (0.22)	356 (4.41) 248	420	353 (4.1) 313 (4.12) 268 (4.16)	510 (<0.001)		
IM	301 (4.3)	380 (0.1)	319 256	445 (0.11)	—	—	—	—	—	—

a red shift in the absorption and fluorescence spectra if $\pi \rightarrow \pi$ is the lowest energy transition) the red-shifted absorption and fluorescence bands can be assigned to the monocation formed by protonation of the ring nitrogen atom. The value of the acidity constant for the monocation–neutral equilibrium (Table 4) as well as the similarity of the spectral characteristics of monocation of **IM** with those of PBT (27) (λ_f = 390 nm) also confirm this assignment. The fluorescence intensity of the neutral band (λ_a = 380 nm) decreases with the concomitant rise of the monocation band (λ_f = 445 nm) as the pH is lowered. No further change in the spectral properties is observed when acid concentration is increased below H_0 = 0.0. The spectral characteristics of neutral and monocation forms of **IM** are depicted in Fig. 1 and the relative intensity change of the monocation and neutral molecule are plotted as a function of pH/H_0 in Fig. 2.

Compounds II, III, IV, and V

The absorption of fluorescence spectra of these molecules are red-shifted in solutions of pH > 7.0. This can be ascribed to the formation of the monoanion. The absorption spectra of **III** exhibit a further red shift in solutions of pH > 10.0. Since **III** has two dissociable —OH groups, the latter shift is due to the dianion formation. The red shifts in the absorption and fluorescence maxima of the monoanions relative to those of the corresponding neutral molecules (**II**, **III**, and **IV**) are almost similar, indicating thereby that monoanions are formed by the deprotonation of the 4′-OH groups. Consequently the dianion of **III** is formed from dissociation of 3′-OH group. This is further manifested by the fact that pK_a for neutral–monoanion equilibrium is nearly similar for **II**, **III**, and **IV** (Table 4). The fluorescence spectrum (λ_f = 510 nm) of the monoanion of **V** is very significantly red-shifted, as compared to those of **II**, **III**, and **IV**, although there is not much difference in the absorption band maxima of this species in these molecules. This is due to the large solvent relaxation in the excited state as observed in **I** as discussed below. In all cases, as the pH is raised, the fluorescence intensity of the monoanion increases simultaneously with the decrease of the neutral band. Since **III** decomposes at higher pH, it was not possible to record fluorescence spectra in solutions of pH above 11.0.

In the pH region of 7 to 3, the molecules are neutral in both the S_0 and S_1 states. Like **IM**, the absorption and fluorescence spectra shift to longer wavelengths (except for **II**) at $H_0 < 0$ and red-shifted bands can be assigned to monocation formed by protonating tertiary nitrogen atom. The fluorescence intensity of the monocation species of the compounds, especially for **III** and **IV**, increases slowly up to H_0 −3 and then sharply with further increase of acidity. Although nice isosbestic points are observed in the absorption spectra of these conjugate acid–base pair in the pH/H_0 range of 3 to −1.0, no correspondence is noticed between the decrease in the fluorescence intensity of the neutral species and increase in the fluorescence intensity of monocation (see Fig. 3). This indicates that either the fluorescence intensity of the neutral molecule is quenched by the protons (because the fluorescence intensity of neutral species is not quenched by the equivalent amount of SO_4^{2-} ions, obtained by the addition of K_2SO_4) or

Can. J. Chem. Downloaded from www.nrcresearchpress.com by 84.41.108.74 on 09/07/12
For personal use only.

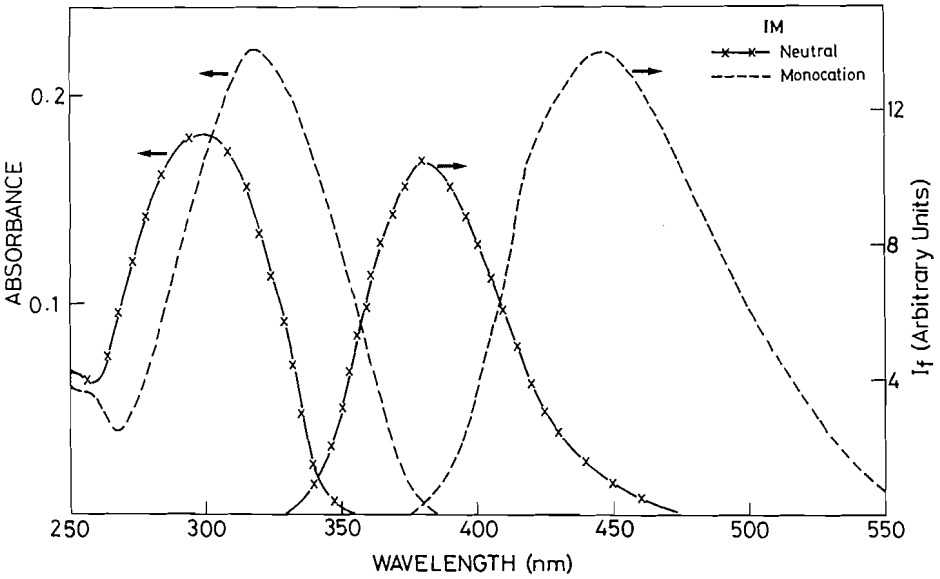


FIG. 1. Absorption (left) and fluorescence (right) spectra of the prototropic species of 2-(3′-methoxyphenyl)benzothiazole (**IM**).

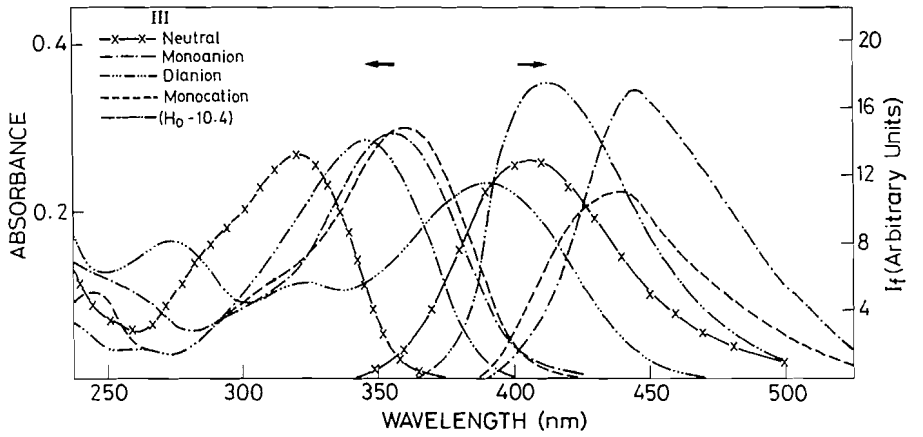


FIG. 2. Absorption (left) and fluorescence (right) spectra of the prototropic species of 2-(3′,4′-dihydroxyphenyl)benzothiazole (**III**).

there exists a non-fluorescent species in between neutral and monocation. The existence as well as nature of this species will be established in the subsequent section. In concentrated H_2SO_4 acid (H_0 −10.4), the absorption and fluorescence spectra of the monocations of all these molecules shift to shorter wavelengths which can be ascribed to the protonation on the —OH or —OCH_3 group at the 4′ position (since the protonation of —OH or —OCH_3 group at the 3′ position in **I** or **IM** does not bring about any spectral change) forming dications. The spectral profiles of the various prototropic species of **III** are depicted in Fig. 3.

2-(3′-Hydroxyphenyl)benzothiazole (I)

The absorption properties of I in aqueous solutions of pH/H_0 ranging from 13 to −10.4 are similar to those of the **II**, **III**, **IV**, and **V**. Thus the red-shifted absorption spectra of **I** (Fig. 4) at pH 13.0 and H_0 −1.0 can be assigned to the monoanion and monocation, respectively. The fluorescence characteristics of I in solutions pH/H_0 <2 are also similar to those observed for molecules discussed in the last section.

The fluorescence spectral characteristics in the pH range 0.0 to 13 are different from the ground state reactions and also different from those of the other molecules. The molecule exhibits dual fluorescence (λ_f = 390, 510 nm) in this pH region. As already mentioned the short and long wavelength bands are due to the neutral molecule and monoanion, respectively. The intensities of the bands remain unchanged in the pH range 3.0 to 8.0. When the pH increases to above 8.0 the intensity of the 510 nm band increases and that of 390 nm band decreases. On the other hand, when the pH is decreased to below 3.0, the intensities of both bands decrease. The relative intensity change of the 510 nm band as a function of pH/H_0 is shown in Fig. 3. The plot thus obtained is a stretched sigmoid curve with two inflection points, one corresponds to the ground state pK_a value (9.8) and the other to the excited state pK_a value (1.8). The intensity change of the 390 nm band could not be plotted because of its very low intensity in aqueous solutions. Similar features have also been observed in 1-, 2-naphthols (6) and 9-phenanthrol (28). This indicates that the rate of proton transfer in the S_1 state of **I** is comparable to the rate of its fluorescence decay.

The appearance of the monoanion fluorescence band in the region of pH 3 to 8 must be due to the excited state prototropic reaction because anionic species is completely absent in solu-

Can. J. Chem. Downloaded from www.nrcresearchpress.com by 84.41.108.74 on 09/07/12
For personal use only.

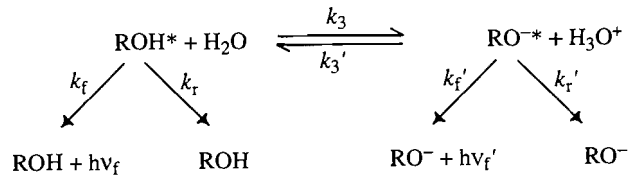
Can. J. Chem. Downloaded from www.nrcresearchpress.com by 84.41.108.74 on 09/07/12
For personal use only.

TABLE 4. pK_a and pK_a^* values of the prototropic equilibria of molecules **I**, **II**, **III**, **IV**, **V**, and **IM**

Molecules/equilibrium 1			pK_a 2	pK_a^* FT 3	pK_a^* FC[a] 4	pK_a^* FC[f] 5
I	Dication	⇌ monocation	<−10.4	—	—	—
	Monocation	⇌ zwitterion		−6.6	—	—
	Neutral	⇌ zwitterion			—	—
	Monocation	⇌ neutral	0.7	—	4.6	—
	Neutral	⇌ monoanion	9.5	1.5	0.8	−3.1
II	Dication	⇌ monocation	<−10.4	—	—	—
	Monocation	⇌ zwitterion		−2.7	—	—
	Neutral	⇌ zwitterion		1.6	—	—
	Monocation	⇌ neutral	1.5	—	7.8	—
	Neutral	⇌ monoanion	8.8	9.0	2.5	3.5
III	Dication	⇌ monocation	<−10.4	—	—	—
	Monocation	⇌ zwitterion		−7.0	—	—
	Neutral	⇌ zwitterion		1.5	—	—
	Monocation	⇌ neutral	1.5	—	8.7	—
	Neutral	⇌ monoanion	8.5	8.3	2.1	4.7
	Monoanion	⇌ dianion	12.5	—	7.1	—
IV	Dication	⇌ monocation	<−10.4	—	—	—
	Monocation	⇌ zwitterion		−6.3	—	—
	Neutral	⇌ zwitterion		1.4	—	—
	Monocation	⇌ neutral	1.4	—	8.5	—
	Neutral	⇌ monoanion	9.1	9.2	2.3	4.0
V	Dication	⇌ monocation	<−10.4	—	—	—
	Monocation	⇌ zwitterion		−7.0	—	—
	Neutral	⇌ zwitterion		1.4	—	—
	Monocation	⇌ neutral	1.4	—	8.6	—
	Neutral	⇌ monoanion	9.3	9.6	3.4	−2.0
IM	Monocation	⇌ neutral	0.7	1.2	4.6	8.8

[a,f]Calculated using absorption and fluorescence maxima of the species, respectively.

tions of pH < 7 in the ground state. Therefore, the fluorescence properties in the region corresponding to the complete titration curve can be explained by the kinetics of the excited state reaction. The pathways of decay available to the excited-state prototropic species can be represented by the scheme



SCHEME 1

where k_3 and k_3' are the pseudo first order rate constants for the deprotonation and second order protonation reactions, k_f and k_r are the radiative and non-radiative decay constants for ROH* and k_f' and k_r' are the corresponding quantities for RO^{-}*. If the equations derived by Weller (2), using the steady-state principle, are applied, then the relative fluorescence intensities of the neutral and monoanion species can be given by the equations

$$[5] \quad I/I_0 = \frac{1 + k_3'\tau_0'[H_3O^+]}{1 + k_3\tau_0 + k_3'\tau_0'[H_3O^+]}$$

$$[6] \quad I'/I_0' = \frac{k_3\tau_0}{1 + k_3\tau_0 + k_3'\tau_0'[H_3O^+]}$$

where I_0 or I_0' is the fluorescence intensity of only one species, and I or I' is the same for the species at any pH in which both the conjugate acid and base are present; τ_0 and τ_0' are the radiative life times of the neutral and monoanion species, respectively. Since in the pH region 8.0 to 3.0, the concentration of H_3O^+ is very small, the rate (k_3') of the backward reaction will be very small compared to the radiative decay rate ($1/\tau_0'$) of the monoanion. Under such condition the eqs. [5] and [6] reduce to equations

$$[7] \quad I/I_0 = \frac{1}{1 + k_3\tau_0}$$

and

$$[8] \quad I'/I_0' = \frac{k_3\tau_0}{1 + k_3\tau_0}$$

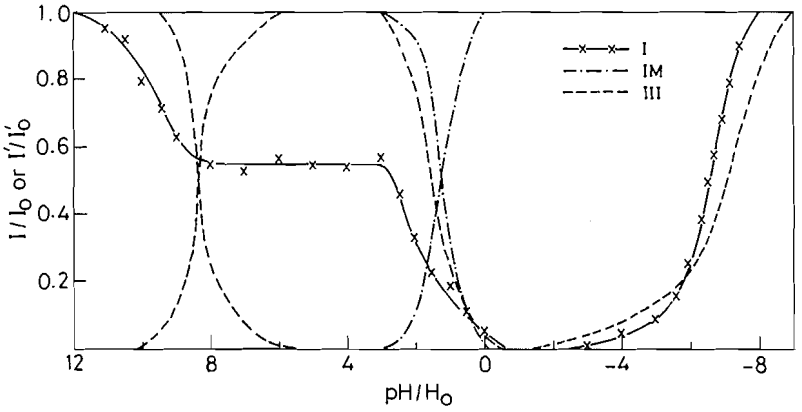


FIG. 3. Fluorimetric titration curves for compounds **I**, **IM**, and **III**.

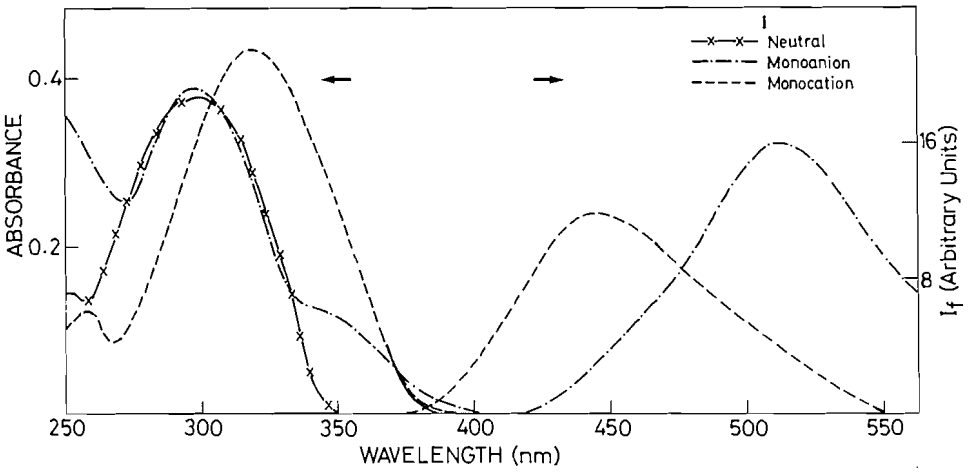


FIG. 4. Absorption (left) and fluorescence (right) spectra of the prototropic species of 2-(3′-hydroxyphenyl)benzothiazole (**I**).

respectively, which clearly show that the relative intensities of the neutral and anion forms are independent of $[H_3O^+]$ in the above pH region. Substituting the value of $I'/I_0' = 0.55$ in eq. [8] we get $k_3\tau_0 = 1.22$. Thus knowing τ_0 one can calculate k_3.

Acidity constants

The acidity constants of the various prototropic reactions, as mentioned below, in the S_0 state are determined using absorption spectral data and the pK_a values so obtained are tabulated in Table 4.

[1] Dication $\rightleftharpoons$ monocation + H^+

[2] Monocation $\rightleftharpoons$ neutral + H^+

[3] Neutral $\rightleftharpoons$ monoanion + H^+

[4] Monoanion $\rightleftharpoons$ dianion + H^+

Equilibrium [4] is possible only for **III**. The pK_a value for equilibrium [1] could not be determined as the formation of dication was not complete even at H_0 −10.4. From the data of Table 4, it is clear that for **II**, the pK_a[3] value of reaction [3] is much smaller and that of reaction [2] is higher than that for **I**. This is consistent with the fact, as discussed earlier, that **II** is resonance-stabilized, as a result of which the hydroxyl proton becomes more acidic and the pyridinic nitrogen atom becomes more basic. MO calculations show that the π-electron density (Table 5) at the oxygen atom of —OH group in **II** is smaller than that in **I**. This is more pronounced in the S_1 state thus providing that —OH group becomes more acidic upon excitation. On the other hand, charge density at the tertiary nitrogen atom of **II** is more than that in **I** and thus making it more basic. Based on this discussion, pK_a[3] value for **III** indicates that the first deprotonation will occur from the hydroxyl group at position 4′, followed by from position 3′. Little higher values of pK_a[3] for **IV** and **V** could be because of the presence of electron donating methoxy group at the ortho-position to the hydroxyl group. Similarity of pK_a[2] values for compounds **I** and **IM** and higher value for **II** can be explained on the same lines as has been done before for pK_a[3].

The pK_a* values for the various prototropic reactions have been determined using fluorimetric titrations and Forster cycle method employing absorption and fluorescence data wherever applicable and are compiled in Table 4. The Forster cycle method cannot be used to calculate (*a*) pK_a*[1], because ground state pK_a value is not known, (*b*) pK_a*[2], because the prototropic reaction involved in the ground state is different from that occurring in the S_1 state (see below), (*c*) pK_a*[4] cannot be determined using fluorescence data as the dianion of **III** is non-fluorescent. As expected, pK_a*[3] values indicate that hydroxyl group become stronger acid on excitation. On the other hand, ground state pK_a[3] values have been obtained

Can. J. Chem. Downloaded from www.nrcresearchpress.com by 84.41.108.74 on 09/07/12
For personal use only.

TABLE 5. π-Electron densities on the hetero atoms of 3′-HPBT, 4′-HPBT, and 3′,4′-DHPBT

Molecule	Atom	π-Electron density S_0	π-Electron density S_1
3′-HPBT	S	1.422	1.457
	N	1.382	1.443
	O	1.917	1.915
4′-HPBT	S	1.427	1.438
	N	1.385	1.457
	O	1.907	1.887
3′,4′-DHPBT	S	1.426	1.471
	N	1.385	1.436
	O[a]	1.933	1.901
	O[b]	1.936	1.932

[a,b]Oxygen atom of the —OH group at 4′ and 3′ position, respectively.

from the fluorimetric titrations curves (Fig. 3) for **II**, **III**, **IV**, and **V**, indicating that prototropic equilibrium [3] is not established in the S_1 state during the lifetimes of these molecules. Stretched sigmoid fluorimetric titration curves have been noticed for **I** in the pH range to 11, giving two pK_a[3] values, one agreeing with the ground state pK_a[3] value and the other the excited state pK_a[3] value. This indicates that the lifetimes of the respective conjugate acid–base pair of **I** are comparable with the reciprocal rate constants of these prototropic reactions.

As mentioned earlier, no correspondence is observed between the decrease in the fluorescence intensity of neutral species and the increase in the fluorescence intensity of monocation. On the basis of the following discussion, we conclude that the decrease in the fluorescence intensity of neutral species is due to the formation of non-fluorescent zwitterion rather than due to proton-induced fluorescence quenching. (*i*) Prototropic equilibrium for the monocation–neutral reaction of **IM** has clearly established that formation of non-fluorescent species is because of the presence of —OH group, which is absent in **IM**. Further the structures of **I** and **IM** are not very different from each other. If **I** undergoes proton-induced fluorescence quenching it should also be observed for **IM**. On the other hand, the proton-induced fluorescence quenching has been observed for both 2-naphthol and 2-methoxy naphthalene (29). (*ii*) pK_a* values are generally determined from the formation curve of that species. The pK_a*[2] values thus obtained for the monocations of these molecules indicate that the tertiary nitrogen atom become weaker base upon excitation, which is contrary to the established results. (*iii*) Our PPP calculations have also indicated that charge density increases at the basic nitrogen atom, suggesting that the tertiary nitrogen atom becomes a stronger base in the S_1 state. (*iv*) Since the formation of zwitterion in the S_1 state involves biprotonic mechanism, its formation will depend on the environments. That is why it is only formed in the pH/H_0 range 3 to −2. (*v*) When similar titration is performed in cyclohexane with trifluoroacetic acid the formation of monocation is complete at much lower acid concentration and the increase in the intensity of monocation is comparable with the decrease of the neutral species. This is because the formation of zwitterion will be less favourable in non-polar than in polar media.

It has also been noticed that the shape of the fluorimetric titration (Fig. 3) curves for the formation of monocation do not conform to the trend observed in the titration curves for neutral molecules, *i.e.* it rises very slowly in the beginning and then sharply, as if there are two breaks. Since no changes have been noticed in the absorption spectra at $H_0 < -2$, we attribute this to an excited state phenomenon. In our opinion, the first break is due to the formation of monocation from non-fluorescent zwitterion and the increase of intensity in the second step is due to the decrease in the rates of radiationless processes in monocation. This could be due either to an increase in viscosity of the medium or a decrease in the number of free water molecules to solvate the monocations with the increase of acid concentration. Because of this, only the approximate values of pK_a* for the monocation–zwitterion equilibria are reported.

Conclusions

The higher values of molar extinction coefficient of the lowest energy transition and fluorescent quantum yield and low value of pK_a[3] of **II** compared to the corresponding values of **I** indicate the resonance effect of the —OH group leading to structure **II′**. The structured absorption and fluorescence spectra exhibited by **III**, **IV**, and **V** are indicative of the presence of intramolecular hydrogen bond between the —OH proton and the oxygen atom of the adjacent —OH or —OCH_3 group. The rate of deprotonation reaction in molecules **II**, **III**, **IV**, and **V** is slower than the rates of radiative decays whereas in **I** the proton-transfer rate is comparable to the rate of radiative decay. The prototropic reactions of the molecules, except for **IM**, in the acidity region of $H_0 = 0.0$ to $H_0 = -9.0$ in the S_1 state are different from those in the S_0 state. The fluorimetric titration curves in this region of acidity have led to a prediction of the monocation–zwitterion equilibrium. The zwitterions are formed from neutral molecules as a result of biprotonic photoautomerism.

Acknowledgements

The authors thank the Department of Science and Technology, New Delhi, for financial support of the project entitled "Proton transfer reactions in the excited states in micelles".

1. (*a*) TH. FORSTER. Z. Elektrochem. Angew. Phys. Chem. **54**, 42 (1950); **54**, 531 (1950); (*b*) A. WELLER. Ber. Bunsenges. Phys. Chem. **56**, 662 (1952); **66**, 1144 (1956).
2. A. WELLER. Z. Phys. Chem. N.F. Bd. **3**, 238 (1955); **60**, 1144 (1950); **61**, 956 (1957); A. WELLER. Discuss. Faraday Soc. **27**, 28 (1959); G. JACKSON and G. PORTER. Proc. R. Soc. (London), **260**A, 13 (1961); A. WELLER. Progress in reaction kinetics. Vol. 1. *Edited by* G. Porter. Pergamon Press, Oxford. 1961. p. 189.
3. E. VANDER DONCKT. Progress in reaction kinetics. Vol. 5. *Edited by* G. Porter. Pergamon Press, Oxford. 1970. p. 273; J. F. IRELAND and P. A. H. WYATT. Adv. Phys. Org. Chem. **12**, 131 (1976).
4. E. L. WEHRY and L. B. ROGERS. Fluorescence and phosphorescence analyses. *Edited by* D. M. Hercules. Wiley Interscience, New York. 1966. p. 125.
5. W. BARTOCK, R. B. HARTMAN, and P. J. LUCCHESI. Photochem. Photobiol. **4**, 499 (1965); I. AVIGAL, J. FEITELSON, and M. OBOLENGHI. J. Chem. Phys. **50**, 2614 (1969); W. KLOPFFER. Advances in photochemistry. Vol. 10. *Edited by* J. N. Pitts Jr., G. S. Hammond, and K. Gollnick. Wiley Interscience, New York. 1977. p. 311.

Can. J. Chem. Downloaded from www.nrcresearchpress.com by 84.41.108.74 on 09/07/12
For personal use only.

6. A. WELLER. Z. Phys. Chem. N.F. **17**, 224 (1958); E. L. WEHRY and L. B. ROGERS. J. Am. Chem. Soc. **88**, 357 (1966); J. L. ROSENBERG and I. BRINN. J. Phys. Chem. **76**, 3558 (1972); K. TSUTSUMI and H. SHIZUKA. Chem. Phys. Lett. **52**, 485 (1977); Z. Phys. Chem. N.F. **111**, 129 (1978); H. SHIZUKA and S. TABITA. J. Am. Chem. Soc. **104**, 6919 (1982); C. M. HARRIS and B. K. SELLINGER. J. Phys. Chem. **84**, 891 (1980).
7. C. M. HARRIS and B. K. SELLINGER. Z. Phys. Chem. (N.F.) **134**, 65 (1983).
8. M. D. COHEN and S. FLAVIAN. J. Chem. Soc. B, 317 (1967); 321 (1967); 329 (1967); 334 (1967); D. L. WILLIAMS and A. HELLER. J. Phys. Chem. **74**, 4473 (1970); R. NAKAGAKI, T. KOBAYASHI, S. NAKAMURA, and S. NAGAKURA. Bull. Chem. Soc. Jpn. **50**, 1909 (1977); P. F. BARBARA, L. E. BRUS, and P. M. RENTZEPIS. J. Am. Chem. Soc. **103**, 2156 (1981); R. S. BECKER, C. LENOBLE, and A. ZEIN. J. Phys. Chem. **91**, 3509 (1987); W. E. BREWER, M. L. MARLINEZ, and P. T. CHOU. J. Phys. Chem. **94**, 1915 (1990).
9. M. KRISHNAMURTHY and S. K. DOGRA. J. Photochem. **32**, 235 (1986); M. ITOH and Y. FUJIWARA. J. Am. Chem. Soc. **107**, 1562 (1985) and references therein.
10. H. K. SINHA and S. K. DOGRA. Chem. Phys. **102**, 337 (1986) and references therein.
11. A. U. KHAN and M. KASHA. Proc. Natl. Acad. Sci. U.S.A. **80**, 1767 (1983); P. CHON, D. MCMORROW, T. J. AARTSMA, and M. KASHA. J. Phys. Chem. **88**, 4596 (1984).
12. H. K. SINHA and S. K. DOGRA. J. Photochem. **36**, 149 (1987); A. K. MISHRA and S. K. DOGRA. Indian J. Chem. **24A**, 285 (1985); **24A**, 815 (1985); Indian J. Phys. **58B**, 480 (1984); Bull. Chem. Soc. Jpn. **58**, 3587 (1985); J. Photochem. **31**, 333 (1985).
13. J. K. DEY and S. K. DOGRA. Chem. Phys. **143**, 97 (1990); Indian J. Chem. **29A**, 1153 (1990) and references therein.
14. J. K. DEY and S. K. DOGRA. Unpublished results.
15. HOFFMANN. Ber. **13**, 1236 (1880); M. T. BOGERT and A. STULL. J. Am. Chem. Soc. **47**, 3078 (1925).
16. J. A. RIDDICK and W. B. BUNGER. Organic solvents. Wiley Interscience, New York. 1970. pp. 592–594, 798–805.
17. (*a*) M. L. JORGENSON and R. D. HARTER. J. Am. Chem. Soc. **85**, 878 (1983); (*b*) G. YAGIL. J. Phys. Chem. **71**, 1034 (1967).
18. W. H. MELLWISH. J. Phys. Chem. **65**, 229 (1961).
19. M. SWAMINATHAN and S. K. DOGRA. Indian J. Chem. A, **22**, 853 (1983).
20. R. PARISER and R. G. PARR. J. Chem. Phys. **21**, 466 (1953).
21. J. A. POPLE. Trans. Faraday Soc. **49**, 1315 (1953).
22. (*a*) J. DELBENE and H. H. JAFFE. J. Chem. Phys. **48**, 1807 (1968); (*b*) N. MATAGA and K. NISHIMOTO. Z. Phys. Chem. (Frankfurt), **12**, 335 (1957); **13**, 140 (1957); (*c*) K. NISHIMOTO and L. S. FORSTER. Theoret. Chim. Acta, **3**, 407 (1965).
23. QCPE Program No. QCMP007, Indiana University, Chemistry Department, Bloomington, USA.
24. R. PASSARINI. J. Chem. Soc. 2261 (1954).
25. J. R. MERRILL and R. BENNETT. J. Chem. Phys. **43**, 1401 (1965); J. A. OTTERSTEDT. J. Chem. Phys. **58**, 5716 (1973); H. SHIZUKA, K. MATSUI, T. OKAMURA, and I. TANAKA. J. Phys. Chem. **79**, 2731 (1975); W. F. RICHY and R. S. BECKER. J. Phys. Chem. **49**, 2092 (1968); M. D. COHEN, G. M. J. SCHIMIDT, and (in part) (MRS.) S. FLAVIAN. J. Chem. Soc. 2041 (1964); M. D. COHEN and (MRS.) S. FLAVIAN. J. Chem. Soc. B, 317 (1967).
26. (*a*) D. GOSWAMI, R. S. SARPAL, and S. K. DOGRA. Bull. Chem. Soc. Jpn. In press; (*b*) R. O. LOUTFY and A. C. SOMERSALT. Can. J. Chem. **54**, 76 (1976).
27. C. A. S. POTTER and R. G. BROWN. Chem. Phys. Lett. **153**, 7 (1988).
28. M. SWAMINATHAN and S. K. DOGRA. J. Chem. Soc. Perkin Trans. 2, 947 (1984).
29. R. E. BURTON and W. J. DEVIS. J. Chem. Soc. 1766 (1964); S. SCHULMAN and Q. FERNANDO. J. Phys. Chem. **71**, 2668 (1967); K. TSUTSUMI and H. SHIZUKA. Z. Phys. Chem. N.F. Bd. **122**, 129 (1980); H. SHIZUKA and S. TOBITA. J. Am. Chem. Soc. **104**, 6919 (1982).

Can. J. Chem. Downloaded from www.nrcresearchpress.com by 84.41.108.74 on 09/07/12
For personal use only.

Ternary mutual diffusion coefficients of $MgCl_2$ + $MgSO_4$ + H_2O and Na_2SO_4 + $MgSO_4$ + H_2O from Taylor dispersion profiles

ZHIPENG DENG AND DEREK G. LEAIST[1]
Department of Chemistry, University of Western Ontario, London, Ont., Canada N6A 5B7
Received December 5, 1990[2]

ZHIPENG DENG and DEREK G. LEAIST. Can. J. Chem. **69**, 1548 (1991).

The Taylor dispersion (peak-broadening) technique is used to measure the ternary mutual diffusion coefficients of the mixed salt solutions $MgCl_2$ + $MgSO_4$ + H_2O and Na_2SO_4 + $MgSO_4$ + H_2O at 25°C. The dispersion of the solutes is followed by differential refractometry. A simple least-squares procedure is developed to calculate the ternary diffusion coefficients from the refractive index profiles. The coefficients are measured at 0.04, 0.20, or 0.40 mol dm^{-3} total salt for the molar salt ratios 1:3, 1:1, or 3:1. The measured diffusion coefficients are compared with the limiting values for the completely dissociated salts.

Key words: mixed salt solutions, multicomponent diffusion, Taylor dispersion, ternary diffusion coefficients.

ZHIPENG DENG et DEREK G. LEAIST. Can. J. Chem. **69**, 1548 (1991).

On a utilisé la technique de dispersion de Taylor (élargissement des bandes) pour mesurer les coefficients de diffusion mutuels ternaires de solutions mixtes de sels $MgCl_2$ + $MgSO_4$ + H_2O et Na_2SO_4 + $MgSO_4$ + H_2O, à 25°C. On a suivi la dispersion des solutés par réfractométrie différentielle. On a développé une méthode simple des moindres carrés pour calculer les coefficients de diffusions ternaires à partir des profils des indices de réfraction. On a mesuré les coefficients à des concentrations totales de sel de 0,04, 0,20 et 0,40 mol dm^{-3}, pour des rapports molaires de sel de 1:3, 1:1 et 3:1. On a comparé les coefficients de diffusion mesurés avec les valeurs limites obtenues pour les sels complètement dissociés.

Mots clés : solutions de sels mixtes, diffusion à plusieurs composantes, dispersion de Taylor, coefficients de diffusion ternaire.

[Traduit par la rédaction]

1. Introduction

Relatively few diffusion studies have dealt with mixed salt solutions despite the practical importance of these systems and their interesting properties. Most of the reported data (1–8) have been obtained for 1–1, 1–2, or 2–1 salts. The present study was undertaken to measure the ternary mutual diffusion coefficients of the higher-valent systems $MgCl_2$ + $MgSO_4$ + H_2O and N_2SO_4 + $MgSO_4$ + H_2O. The information available for mixtures of 1–2 or 2–1 salts might not be a reliable guide to the behavior of 1–2 + 2–2 or 2–1 + 2–2 systems owing to the strong association of 2–2 salts (9–12).

Diffusion data for mixtures of 1–1 + 2–2 salts (such as NaCl + $MgSO_4$ + H_2O) would also be useful. Unfortunately, the diffusion of two salts lacking a common ion (13) is a more complicated quaternary process (three independent solute fluxes) which is beyond the scope of the present study.

Multicomponent diffusion is usually studied by optical (3–6), conductimetric (14, 15) or diaphragm-cell (13) techniques. These techniques are reliable, but they have not gained wide popularity, largely because the experimental procedures are so laborious. Recently, the more convenient Taylor dispersion (peak-broadening) technique (1, 16–19) for measuring binary diffusion was extended to three- and four-component systems (20–23). In a Taylor experiment, a narrow band of solution is injected into a laminar carrier stream of different composition which flows in a long capillary tube. The injected solutes spread out as they flow along the tube. A liquid-chromatography detector (usually a differential refractometer) monitors the broadened distribution of dispersed solutes as they flow out of the tube. Ternary diffusion coefficients can be calculated by moments analysis (21) or, more accurately, by fitting the dispersion equations to the eluted solute peaks (22, 23).

The dispersion technique has significant advantages over other diffusion experiments. Most important of all, it is immune to errors from convection, even if the injected solution is less dense than the carrier stream. A wide range of dilute or concentrated solutions can be studied if differential refractometry is used to detect the eluted solutes. By connecting the detector to a microcomputer, the collection of the data is easily automated. The run times are conveniently short, and calibration of the dispersion tube is not required.

In this paper an improved least-squares procedure is developed to calculate ternary diffusion coefficients from dispersion profiles.

2. Experimental

Reagent grade $MgSO_4$ (Baker), $MgCl_2 \cdot 6H_2O$ (BDH) and Na_2SO_4 (BDH) were used as received. The water content of each salt was checked by drying samples to constant weight in a vacuum oven at 350°C. Solutions were prepared with distilled deionized water in calibrated volumetric flasks. Solutions of $MgCl_2$, Na_2SO_4, and $MgSO_4$ (0.10 mol dm^{-3}) had the respective pH values 5.7, 5.9, and 7.3.

The dispersion equipment consisted of a metering pump, an injection valve fitted with a 20×10^{-6} dm^{-3} sample loop, a Teflon capillary tube (length 25.90 m, inner radius 4.339×10^{-4} m), and a differential refractometer detector (Waters Model 401, 10^{-5} dm^{-3} flow cells) at the tube outlet. The refractometer output voltage was measured at accurately-timed 20–30 s intervals with a digital voltmeter (Hewlett-Packard Model 3478A). The dispersion tube was coiled in a 0.7 m-diameter helix and held at 25.00 ± 0.03°C during the experiments. Sample retention times were typically 5000–6000 s.

3. Theory

Diffusion in a three-component solution composed of solute 1 + solute 2 + solvent 0 obeys the ternary Fick equations (1)

[1]To whom correspondence should be addressed.
[2]Revision received May 15, 1991.

Can. J. Chem. Downloaded from www.nrcresearchpress.com by 84.41.108.74 on 09/07/12
For personal use only.

Can. J. Chem. Downloaded from www.nrcresearchpress.com by 84.41.108.74 on 09/07/12
For personal use only.

[1] $j_1 = -D_{11}\nabla c_1 - D_{12}\nabla c_2$

[2] $j_2 = -D_{21}\nabla c_1 - D_{22}\nabla c_2$

where j_1 and j_2 are the molar flux densities of the solutes in the volume-fixed frame; c_1 and c_2 are the solute concentrations in moles per unit volume. The ternary diffusion coefficient D_{ik} gives the flux of solute i produced by the gradient ∇c_k in the concentration of solute k. The cross-terms $-D_{12}\nabla c_2$ and $-D_{21}\nabla c_1$ allow for coupled diffusion: the transport of each solute produced by gradient in the other solute. Fluxes of dissolved salts, for example, tend to be strongly coupled by electrostatic forces. Association reactions can also lead to large cross-terms.

The flux of solvent (component 0), which does not appear explicitly in the diffusion equations, can be evaluated by solving eqs. [1] and [2] together with the condition of zero volume flow: $j_1V_{1m} + j_2V_{2m} + j_0V_{0m} = 0$. V_{im} is the partial molar volume of component i.

Consider a ternary dispersion experiment in which a laminar carrier stream of composition $\bar{c}_1$, $\bar{c}_2$ flows at mean speed U in a long capillary tube of inner radius r. Diffusion is initiated at time $t = 0$ by injecting a small volume of ΔV of solution of composition $\bar{c}_1 + \Delta c_1$, $\bar{c}_2 + \Delta c_2$ into the carrier stream. The solution near the center of the tube flows more rapidly than the solution near the tube wall. Consequently, the injected solutes spread out as they flow along the tube. The broadened distribution of the solutes is monitored at the tube outlet, a distance L downstream from the point of injection.

Price (20) has shown that the radially-averaged concentrations of the eluted solutes are given by

[3] $$c_i(t) = \bar{c}_i + (2/r^3U)(3/\pi^3t)^{1/2} \times \sum_{k=1}^{2} A_{ik}D_k^{1/2} \exp\left[-12D_k(t - t_R)^2/r^2t\right] \qquad (i = 1,2)$$

t_R is the mean retention time, L/U. D_1 and D_2 are the eigenvalues of the 2 by 2 matrix $\mathbf{D}$ of the ternary diffusion coefficients.

[4] $$D_1 = \{D_{11} + D_{22} + (D_{11} - D_{22})[1 + 4D_{12}D_{21}/(D_{11} - D_{22})^2]^{1/2}\}/2$$

[5] $$D_2 = \{D_{11} + D_{22} - (D_{11} - D_{22})[1 + 4D_{12}D_{21}/(D_{11} - D_{22})^2]^{1/2}\}/2$$

The A_{ik} coefficients are abbreviations for

[6] $A_{11} = \Delta V[(D_{22} - D_1)\Delta c_1 - D_{12}\Delta c_2]/(D_2 - D_1)$

[7] $A_{12} = \Delta V[(D_{22} - D_2)\Delta c_1 - D_{12}\Delta c_2]/(D_1 - D_2)$

[8] $A_{21} = \Delta V[(D_{11} - D_1)\Delta c_2 - D_{21}\Delta c_1]/(D_2 - D_1)$

[9] $A_{22} = \Delta V[(D_{11} - D_2)\Delta c_2 - D_{21}\Delta c_1]/(D_1 - D_2)$

Equations [3] are valid provided the flow is laminar and (17, 24) $0.8r^2/D_i < t_R < Lr/50D_i$.

It is difficult in practice to measure the concentration of each eluted solute. Instead, the broadened distribution of the solutes is followed indirectly by measuring the refractive index profile $n(t)$ across the eluted sample.

[10] $n(t) = \bar{n} + R_1[c_1(t) - \bar{c}_1] + R_2[c_2(t) - \bar{c}_2]$

where $\bar{n}$ is the baseline refractive index of the bulk of the carrier solution; $R_1 = dn/dc_1$ and $R_2 = dn/dc_2$ are the molar refractivities of the solutes, evaluated at the carrier stream composition, $\bar{c}_1$, $\bar{c}_2$.

Highly sensitive flow-through differential refractometers are available commercially. These instruments give a linear response — the voltage $v(t)$ — to the changes in the refractive index $n(t)$ of the eluted solution relative to the background refractive index $\bar{n}$ of the carrier stream. The detector signal is represented by the expression

[11] $v(t) = k[n(t) - \bar{n}] + B_0 + B_1t$

where k is the detector sensitivity, dv/dn, and B_0 is the baseline detector voltage. The term B_1t is often included to allow for small linear drifts in the baseline signal.

Equations [3] and [6]–[11] may be combined to give the working equations

[12a] $$v(t) = v_{max}\left(\frac{t_R}{t}\right)^{1/2}\left[W_1 \exp\left(-\frac{12D_1(t - t_R)^2}{r^2t}\right) + (1 - W_1)\exp\left(-\frac{12D_2(t - t_R)^2}{r^2t}\right)\right] + B_0 + B_1t$$

[12b] $$W_1 = (a + b\alpha_1)D_1^{1/2}/[(a + b\alpha_1)D_1^{1/2} + (1 - a - b\alpha_1)D_2^{1/2}]$$

for the detector signal. v_{max} represents the height of the eluted solute peak relative to the baseline. α_1 stands for the fraction of the initial refractive index contributed by solute 1:

[13] $\alpha_1 = R_1\Delta c_1/(R_1\Delta c_1 + R_2\Delta c_2)$

W_1 and $1 - W_1$ give the normalized weights of the exponential terms. The parameters a and b are constants for a given system and carrier stream composition.

D_1, D_2, v_{max}, B_0, and B_1 are most easily evaluated by using least squares to fit eq. [12] to the measured detector voltages. a and b can also be evaluated provided the data set includes two or more peaks with different values of α_1. (For better accuracy the values of α_1 should be widely separated, such as 0.0 and 1.0 rather than 0.4 and 0.6.) The retention time t_R can also be treated as a least-squares parameter, in which case flow-rate calibrations are unnecessary. Conveniently, detector calibration is not required because the refractometer sensitivity k is not used in the calculations.

The solute peaks obtained for ternary diffusion closely resemble two overlapping Gaussians, centered on time t_R, with variances $r^2L/24D_1U$ and $r^2L/24D_2U$. Notice, however, that for the special initial conditions satisfying $a + b\alpha_1^{(1)} = 1$, the exponential term in D_2 vanishes, leaving the eigenfunction in D_1. The concentration vector

[14] $$\begin{pmatrix} \alpha_1^{(1)}/R_1 \\ (1-\alpha_1^{(1)})/R_2 \end{pmatrix} = b^{-1}\begin{pmatrix} (1-a)/R_1 \\ (a+b-1)/R_2 \end{pmatrix}$$

is therefore an eigenvector of **D**, with eigenvalue D_1. Similarly, the exponential term in D_1 vanishes for initial conditions satifying $a + b\alpha_1^{(2)} = 0$. The vector

[15] $$\begin{pmatrix} \alpha_1^{(2)}/R_1 \\ (1-\alpha_1^{(2)})/R_2 \end{pmatrix} = b^{-1}\begin{pmatrix} -a/R_1 \\ (a+b)/R_2 \end{pmatrix}$$

is therefore an eigenvector of **D**, with eigenvalue D_2.

Once the eigenvalues and the eigenvectors of **D** have been evaluated, **D** itself can be recovered by the similarity transform (21, 25)

[16] $$\mathbf{D} = \begin{pmatrix} (1-a)R_1 & -a/R_1 \\ (a+b-1)/R_2 & (a+b)/R_2 \end{pmatrix}\begin{pmatrix} D_1 & 0 \\ 0 & D_2 \end{pmatrix}\begin{pmatrix} (1-a)R_1 & -a/R_1 \\ (a+b-1)/R_2 & (a+b)/R_2 \end{pmatrix}^{-1}$$

and hence

[17] $$D_{11} = D_1 + [a(1-a-b)/b](D_1 - D_2)$$

[18] $$D_{12} = (R_2/R_1)(a/b)(1-a)(D_1 - D_2)$$

[19] $$D_{21} = (R_1/R_2)[(a+b)(1-a-b)/b](D_2 - D_1)$$

[20] $$D_{22} = D_2 + [a(1-a-b)/b](D_2 - D_1)$$

The initial concentration differences Δc_1, Δc_2 should be small enough to ensure that the diffusion coefficients do not vary appreciably across the eluted solute peaks. If this condition is met, the calculated D_{ik} coefficients represent differential values at the composition $\bar{c}_1$, $\bar{c}_2$ of the carrier stream.

4. Results

The ternary diffusion coefficients of $MgCl_2(1) + MgSO_4(2) + H_2O$ and $Na_2SO_4(1) + MgSO_4(2) + H_2O$ were measured at total salt concentrations of 0.04, 0.20, or 0.40 mol dm^{-3} and molar salt ratios of 1:3, 1:1, or 3:1.

Solute peaks for the system $MgCl_2(1) + MgSO_4(2) + H_2O$ are illustrated in Fig. 1. Peak number 1 was generated by injecting excess $MgCl_2$ ($\Delta c_1 = 0.05$, $\Delta c_2 = 0.00$ mol dm^{-3}; $\alpha_1 = 1.00$) into the carrier stream. Peak number 2 was generated by injecting excess $MgSO_4$ ($\Delta c_1 = 0.00$, $\Delta c_2 = 0.050$ mol dm^{-3}; $\alpha_1 = 0.00$). The composition of the carrier stream in this example is: $\bar{c}_1 = 0.10$, $\bar{c}_2 = 0.10$ mol dm^{-3}.

A least-squares procedure (22, 25, 26) based on Newton's method was used to fit eq. [12] to the measured solute peaks. The object was to minimize the sum S of the squared deviations between the measured detector voltages and those calculated from eq. [12].

[21] $$S = \sum_i [v(t_i)_{meas} - v(t_i)_{calc}]^2$$

The minimization was accomplished by adjusting the values of the fitting parameters a, b, D_1, D_2 and, for each peak, v_{max}, t_R, B_0, and B_1.

Given initial estimates of the various fitting parameters, represented by p_1^0, p_2^0, ..., the calculated detector voltages can be approximated by the first-order Taylor series (a different Taylor!) in the parameters

[22] $$v(t_i)_{calc} = v^0(t_i)_{calc} + \sum_m [\partial v^0(t_i)_{calc}/\partial p_m]\Delta p_m$$

The least-squares conditions $\partial S/\partial \Delta p_m = 0$ provide the set of linear equations

[23] $$\sum_m \sum_i \frac{\partial v^0(t_i)_{calc}}{\partial \Delta p_l}\frac{\partial v^0(t_i)_{calc}}{\partial \Delta p_m}\Delta p_m = \sum_i \frac{\partial v^0(t_i)_{calc}}{\partial \Delta p_l}[v(t_i)_{meas} - v^0(t_i)_{calc}]$$

which are easily solved (with a microcomputer) for the parameter increments Δp_m which reduce S. The calculations are repeated using the improved parameter estimates $p_1^0 + \Delta p_1$, $p_2^0 + \Delta p_2$, ..., and so on, until the minimum in S is located, as indicated by negligible parameter changes.

Two to four peaks with different values of α_1 were fitted simultaneously. In most cases convergence was achieved after 3–5 iterations. The standard deviations between the measured and the calculated voltages was typically 0.3% of the peak voltage. The values of α_1 were in the range 0.0–1.0.

Once a, b, D_1, and D_2 had been evaluated, eqs. [17]–[20] were used to calculate the D_{ik} coefficients. The standard deviation of the D_{ik} values, $\pm 0.01 \times 10^{-9}$ m^2 s^{-1}, was estimated by repeating the fitting procedure for 3–4 sets of replicate peaks. The average values of the D_{ik} coefficients obtained at each composition are given in Tables 1 and 2. The ratio R_2/R_1 of the salt refractivities required to calculate the cross-coefficients D_{12} and D_{21} was calculated by taking the ratio of the peak areas generated per mole of excess injected salt (22, 23).

The initial concentration differences (Δc_1, Δc_2) were typically 0.05 mol dm^{-3}. A few runs were made with concentration differences one-half as large. Since the results did not differ significantly, the measured diffusion coefficients can be interpreted as differential values at the composition of the carrier stream ($\bar{c}_1$, $\bar{c}_2$).

As the solute fraction of salt 1

[24] $$f_1 = \bar{c}_1/(\bar{c}_1 + \bar{c}_2)$$

drops to zero, D_{12} vanishes by definition because the gradient in salt 2 cannot produce a coupled flow of salt 1 if the solution is free of salt 1. In this limit D_{22} approaches the value of the binary diffusion coefficient for salt 2. Similarly, as $f_1 \rightarrow 1$, D_{21} vanishes and D_{11} approaches the binary value for salt 1.

These ideas are illustrated in Fig. 2 where the diffusion coefficients of $MgCl_2(1) + MgSO_4(2) + H_2O$ for 0.40 mol dm^{-3} total salt are plotted against the solute fraction of $MgCl_2$. Figure 3 shows the diffusion coefficients of the $Na_2SO_4(1) + MgSO_4(2) + H_2O$ system plotted against the solute fraction of Na_2SO_4. The values of D_{12} and D_{21} appear to extrapolate

Can. J. Chem. Downloaded from www.nrcresearchpress.com by 84.41.108.74 on 09/07/12
For personal use only.

Can. J. Chem. Downloaded from www.nrcresearchpress.com by 84.41.108.74 on 09/07/12
For personal use only.

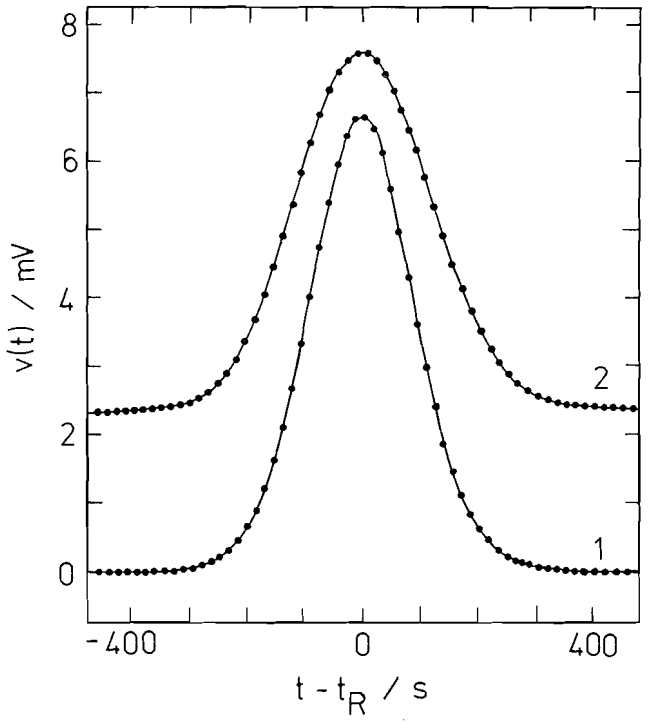


FIG. 1. Refractometer output voltage plotted against time for $MgCl_2$ ($\bar{c}_1$ = 0.100 mol dm^{-3}) + $MgSO_4$ ($\bar{c}_2$ = 0.100 mol dm^{-3}) + H_2O. Peak 1, initial gradient in $MgCl_2$ (Δc_1 = 0.050, Δc_2 = 0.000 mol dm^{-3}; α_1 = 1.00). Peak 2, initial gradient in $MgSO_4$ (Δc_1 = 0.000, Δc_1 = 0.050 mol dm^{-3}; α_1 = 0.00). ●, measured voltages. —, calculated voltages (eq. [12]). The baseline of peak 2 has been offset for clarity.

TABLE 1. Mutual diffusion coefficients of $MgCl_2$(1) + $MgSO_4$(2) + H_2O at 25°C

$\bar{c}_1$	$\bar{c}_2$	D_{11}	D_{12}	D_{21}	D_{22}	R_2/R_1
0.00	0.04	—	0.00	—	0.614[b]	—
0.01	0.03	1.58	−0.03	−0.53	0.67	1.04
0.02	0.02	1.37	−0.09	−0.32	0.74	1.01
0.03	0.01	1.20	−0.11	−0.16	0.80	1.01
0.04	0.00	1.057[c]	—	0.00	—	—
0.00	0.20	—	0.00	—	0.525[b]	—
0.05	0.15	1.51	−0.04	−0.53	0.61	1.01
0.10	0.10	1.32	−0.08	−0.32	0.67	0.98
0.15	0.05	1.16	−0.10	−0.13	0.72	0.99
0.20	0.00	1.038[c]	—	0.00	—	—
0.00	0.40	—	0.00	—	0.473[b]	—
0.10	0.30	1.39	0.00	−0.46	0.54	0.98
0.20	0.20	1.25	−0.03	−0.24	0.60	0.98
0.30	0.10	1.14	−0.08	−0.07	0.65	0.98
0.40	0.00	1.050[c]	—	0.00	—	—

[a]Units: $\bar{c}_i$ in mol dm^{-3}; D_{ik} in 10^{-9} m^2 s^{-1}.
[b]Reference 27.
[c]Reference 28.

correctly to zero for both systems. (A precise extrapolation is not possible because the functional form of D_{ik} versus f_1 is not known.) In addition, the extrapolated values of D_{11} and D_{22} appear to be consistent with the previously reported (27, 28) binary diffusion coefficients of $MgCl_2$, Na_2SO_4, and $MgSO_4$ at 0.40 mol dm^{-3}. Similar agreement is obtained at 0.04 and 0.20 mol dm^{-3} total salt.

TABLE 2. Mutual diffusion coefficients of $NaSO_4$(1) + $MgSO_4$(2) + H_2O at 25°C

$\bar{c}_1$	$\bar{c}_2$	D_{11}	D_{12}	D_{21}	D_{22}	R_2/R_1
0.00	0.04	—	0.00	—	0.614[b]	—
0.01	0.03	1.14	−0.01	−0.12	0.61	1.16
0.02	0.02	1.12	−0.01	−0.08	0.64	1.13
0.03	0.01	1.07	−0.03	−0.04	0.66	1.12
0.04	0.00	1.034[b]	—	0.00	—	—
0.00	0.20	—	0.00	—	0.525[b]	—
0.05	0.15	1.10	−0.01	−0.14	0.56	1.13
0.10	0.10	1.03	−0.03	−0.07	0.58	1.14
0.15	0.05	0.99	−0.05	−0.03	0.61	1.12
0.20	0.00	0.922[b]	—	0.00	—	—
0.00	0.40	—	0.00	—	0.473[b]	—
0.10	0.30	0.99	−0.01	−0.12	0.52	1.15
0.20	0.20	0.93	−0.02	−0.07	0.53	1.14
0.30	0.10	0.89	−0.05	−0.03	0.56	1.16
0.40	0.00	0.831[b]	—	0.00	—	—

[a]Units: $\bar{c}_i$ in mol dm^{-3}; D_{ik} in 10^{-9} m^2 s^{-1}.
[b]Reference 27.

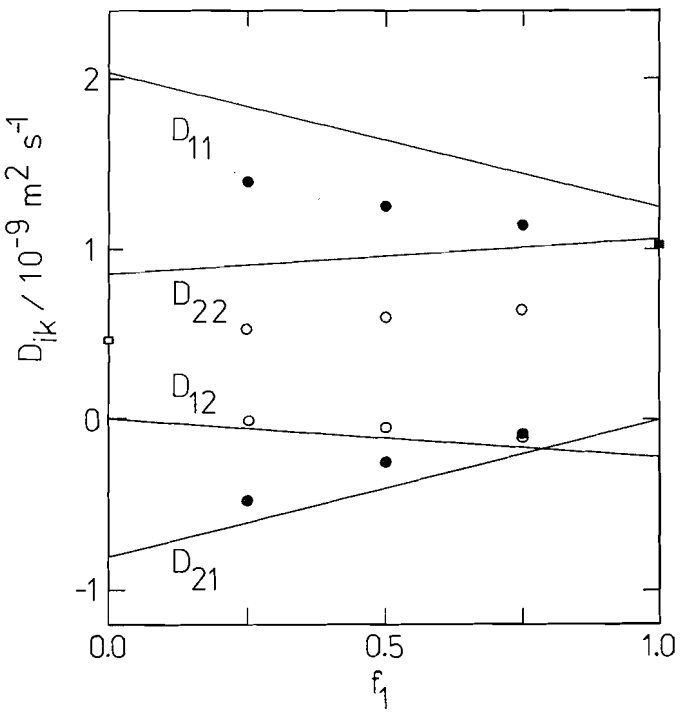


FIG. 2. Measured diffusion coefficients of $MgCl_2$(1) + $MgSO_4$(2) + H_2O at 0.40 mol dm^{-3} total salt: ●,○, ternary values (this work); ■,□, binary values (27, 28). The solid lines give limiting ternary diffusion coefficients calculated from eqs. [25]–[28].

5. Discussion

In an earlier least-squares analysis of Taylor profiles (22), D_{11}, D_{12}, D_{21}, and D_{22} were treated as fitting parameters, rather than the a, b, D_1, and D_2 parameters used here. However, the expressions for the derivatives $\partial v^0/\partial D_{ik}$ are so complicated that it was necessary to resort to numerical differentiation. By contrast, the derivatives with respect to a, b, D_1, and D_2 are easy to evaluate analytically, which simplifies the equations and speeds up the convergence. For these reasons the present least-squares procedure represents an improvement. Check cal-

Can. J. Chem. Downloaded from www.nrcresearchpress.com by 84.41.108.74 on 09/07/12
For personal use only.

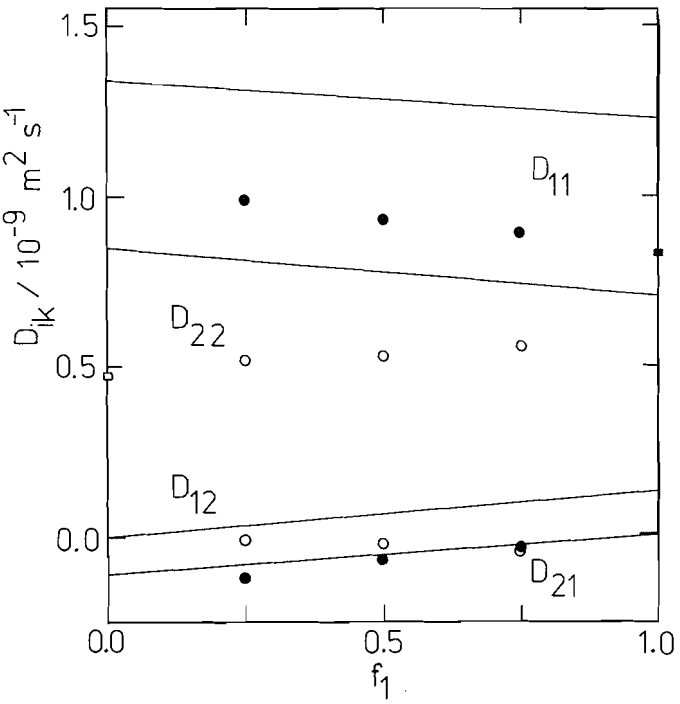


FIG. 3. Measured diffusion coefficients of $Na_2Cl_4(1)$ + $MgSO_4(2)$ + H_2O at 0.40 mol dm^{-3} total salt; ●,○, ternary values (this work); ■,□, binary values (27, 28). The solid lines give limiting ternary diffusion coefficients calculated from eqs. [25]–[28].

culations showed that the two procedures gave identical D_{ik} values within the experimental precision.

The accuracy of the ternary dispersion technique was checked by measuring the diffusion coefficients of sucrose + KCl + H_2O and $MgCl_2$ + NaCl + H_2O at 25°C. The measured diffusion coefficients agreed closely (standard deviation 0.03 × 10^{-9} m^2 s^{-1}) with accurate values obtained previously by optical interferometry (29, 30). Details of the comparison are given in ref. 22.

The D_{ik} coefficients can also be calculated from the temporal moments of the eluted solute peaks (21). Unfortunately, small drifts in the baseline detector signal magnify the errors in the higher moments. Consequently, least-squares procedures are more reliable (22).

Accurate limiting ternary diffusion coefficients of infinitely dilute, completely dissociated salts can be calculated from the limiting ionic conductivities by using the extended Nernst equations:

$$[25]\quad D^0_{11} = \hat{D}_1 + t_1(\hat{D}_3 - \hat{D}_2)$$

$$[26]\quad D^0_{12} = t_1(\hat{D}_3 - \hat{D}_1)$$

$$[27]\quad D^0_{21} = t_2(\hat{D}_3 - \hat{D}_2)$$

$$[28]\quad D^0_{22} = \hat{D}_2 + t_2(\hat{D}_3 - \hat{D}_1)$$

$$[29]\quad \hat{D}_i = RT\Lambda_i/(z_iF)^2$$

$$[30]\quad t_i = \hat{c}_i z_i^2 \hat{D}_i \Big/ \sum_k \hat{c}_k z_k^2 \hat{D}_k$$

where $\hat{c}_i$, z_i, Λ_i, $\hat{D}_i$, and t_i are, respectively, the concentration, charge, limiting molar conductivity, diffusion coefficient and transference number of ion 1.

For the $MgCl_2$ + $MgSO_4$ + H_2O system, the ions are numbered as follows: $Cl^-(1)$, $SO_4^{2-}(2)$, $Mg^{2+}(3)$. For the Na_2SO_4 + $MgSO_4$ + H_2O system they are numbered: $Na^+(1)$, $Mg^{2+}(2)$, $SO_4^{2-}(3)$. In both cases ion 3 is the common ion. At 25°C, the limiting conductivities of aqueous Na^+, Cl^-, Mg^{2+}, and SO_4^{2-} ions are respectively (12) 0.005010, 0.007635, 0.01060, and 0.01600 S m^2 mol^{-1}. The corresponding limiting ionic diffusion coefficients are 1.334 × 10^{-9}, 2.033 × 10^{-9}, 0.706 × 10^{-9}, and 1.065 × 10^{-9} m^2 s^{-1}.

In Fig. 2 the limiting ternary diffusion coefficients of $MgCl_2(1)$ + $MgSO_4(2)$ + H_2O (solid lines) are plotted against the solute fraction of $MgCl_2$. The diffusion coefficient of the weakly-hydrated Cl^- ions is almost three times larger than the diffusion coefficient of the Mg^{2+} ions. Consequently, a relatively large electric field is generated by the gradient in $MgCl_2$. The field slows down the Cl^- ions and speeds up the Mg^{2+} ions to maintain electroneutrality. If dissolved $MgSO_4$ is present, the electric field will also drive a substantial coupled flow of SO_4^{2-} ions, countercurrent to the flow of $MgCl_2$, which explains why the cross-coefficient D^0_{21} takes larger, negative values.

In the limit $f_1 \rightarrow 0$, the diffusion coefficient D^0_{11} for the $MgCl_2(1)$ salt corresponds to the tracer diffusion coefficient of Cl^- ions in supporting $MgSO_4$ solutions. D^0_{11} therefore rises as f_1 decreases. The composition-dependence of D^0_{12} and D^0_{22} is much weaker because the Mg^{2+} and SO_4^{2-} ions have similar diffusivities.

Similar considerations apply to the limiting ternary diffusion coefficients of $Na_2SO_4(1)$ + $MgSO_4(2)$ + H_2O plotted in Fig. 3. The composition-dependence of D^0_{11} and D^0_{21} is less pronounced for this system because Na^+ is less mobile than Cl^-.

The ternary diffusion coefficients calculated from limiting ionic conductivities are of course accurate only at infinite dilution. Nevertheless, experience has shown that D^0_{ik} values can provide a qualitative guide to the diffusion behavior of dilute or even moderately-concentrated univalent mixed-salt solutions.

Figures 2 and 3 show that the diffusion coefficients at 0.40 mol dm^{-3} total salt, after allowance is made for the 20–30% higher viscosity of the solutions relative to pure water, agree qualitatively with the limiting D^0_{ik} values calculated for the completely dissociated salts. Similar agreement is found at 0.20 and 0.40 mol dm^{-3} total salt. This result is surprising. Except in very dilute solutions, an appreciable fraction of the dissolved $MgSO_4$ diffuses as neutral ion pairs, unaffected by the electric field induced by gradients in $MgCl_2$ or Na_2SO_4. One might therefore expect only weak interactions between the diffusing salts. Yet Fig. 2 shows that the magnitude of D_{21} can exceed D_{22} (at high $MgSO_4$ salt fractions), which indicates that the concentration gradient in $MgCl_2$ can produce a larger flow of $MgSO_4$ than the gradient in $MgSO_4$. The reasonable agreement between the measured diffusion coefficients and the limiting values must be fortuitous.

Acknowledgement

The authors thank the Natural Sciences and Engineering Research Council for financial support.

1. H. J. V. TYRRELL and K. R. HARRIS. Diffusion in liquids. Butterworths, London. 1984.

2. E. L. CUSSLER. Multicomponent diffusion. Elsevier, Amsterdam. 1976.
3. J. A. RARD and D. G. MILLER. J. Phys. Chem. **91**, 4614 (1987).
4. V. VITAGLIANO, R. LAURENTINO, and L. COSTANTINO. J. Phys. Chem. **73**, 2456 (1969).
5. V. VITAGLIANO, R. SARTORIO, P. PADULANO, R. LAURENTINO, and O. ORTONA. Gazz. Chim. Ital. **109**, 427 (1979).
6. R. SARTORIO, V. VITAGLIANO, G. GUARINO, and O. ORTONA. J. Solution Chem. **16**, 935 (1987).
7. R. A. NOULTY and D. G. LEAIST. J. Solution Chem. **16**, 813 (1987).
8. O. W. EDWARDS, R. L. DUNN, J. D. HATFIELD, E. O. HUFFMAN, and K. L. ELMORE. J. Phys. Chem. **70**, 217 (1966).
9. E. C. RIGHELLATO and C. W. DAVIES. Trans. Faraday Soc. **26**, 592 (1930).
10. C. W. DAVIES. J. Chem. Soc. 2410 (1930).
11. H. W. JONES and C. B. MONK. Trans. Faraday Soc. **48**, 929 (1952).
12. R. A. ROBINSON and R. H. STOKES. Electrolyte solutions. 2nd ed. Academic Press, New York. 1959.
13. D. G. LEAIST. J. Chem. Soc. Faraday Trans. 1, **83**, 829 (1987).
14. D. G. LEAIST and R. A. NOULTY. Can. J. Chem. **63**, 476 (1985).
15. D. G. LEAIST. Can. J. Chem. **63**, 2933 (1985).
16. G. I. TAYLOR. Proc. R. Soc. London, A**219**, 186 (1953).
17. K. C. PRATT and W. A. WAKEHAM. Proc. R. Soc. London, A**342**, 401 (1975).
18. A. ALIZADEH, C. A. NIETO DE CASTRO, and W. A. WAKEHAM. Int. J. Thermophys. **1**, 243 (1980).
19. S. CHEN, H. T. DAVIS, and D. F. EVANS. J. Chem. Phys. **77**, 2540 (1982).
20. W. E. PRICE. J. Chem. Soc. Faraday Trans. 1, **84**, 2431 (1988).
21. D. G. LEAIST. J. Phys. Chem. **94**, 5180 (1990).
22. D. G. LEAIST. J. Chem. Soc. Faraday Trans. **87**, 597 (1991).
23. D. G. LEAIST. Ber. Bunsenges. Phys. Chem. **95**, 117 (1991).
24. W. N. GILL and R. SANKARASUBRAMANIAN. Proc. R. Soc. London, A**316**, 341 (1970).
25. H. MARGENAU and G. M. MURPHY. The mathematics of physics and chemistry. 2nd ed. Van Nostrand, Princeton. 1956.
26. P. R. BEVINGTON. Data reduction and error analysis for the physical sciences. McGraw-Hill, New York. 1969.
27. J. A. RARD and D. G. MILLER. J. Solution Chem. **8**, 755 (1979).
28. D. G. MILLER, J. A. RARD, L. B. EPSTEIN, and J. G. ALBRIGHT. J. Phys. Chem. **82**, 5739 (1984).
29. E. L. CUSSLER and P. J. DUNLOP. J. Phys. Chem. **70**, 1880 (1960).
30. J. G. ALBRIGHT, R. MATHEW, D. G. MILLER, and J. A. RARD. J. Phys. Chem. **93**, 2176 (1989).
31. D. G. LEAIST and P. A. LYONS. J. Phys. Chem. **86**, 564 (1982).

Can. J. Chem. Downloaded from www.nrcresearchpress.com by 84.41.108.74 on 09/07/12
For personal use only.

Novel, intramolecular hydrogen-transfer and cyclo-addition photochemistry of cyclic 1,3-dienes

FRANCISCUS W. A. M. MIESEN,[1] HANS C. M. BAETEN, HARM A. LANGERMANS, AND LEO H. KOOLE
Laboratory of Organic Chemistry, Eindhoven University of Technology, P. O. Box 513, 5600 MB Eindhoven, The Netherlands

AND

HENK A. CLAESSENS
Laboratory of Instrumental Analysis, Eindhoven University of Technology, P. O. Box 513, 5600 MB Eindhoven, The Netherlands

Received March 18, 1991

FRANCISCUS W. A. M. MIESEN, HANS C. M. BAETEN, HARM A. LANGERMANS, LEO H. KOOLE, and HENK A. CLAESSENS. Can. J. Chem. **69**, 1554 (1991).

With use of one- and two-dimensional NMR spectroscopy and deuterium labelling, the photochemistry of 9-*endo*-hydroxy-9-*exo*-vinyl-bicyclo[4.2.1]nonadiene (**1**) and the 9-*exo*-(11-dimethylvinyl)- (**2**) and 9-*exo*-ethyl- (**3**) analogues has been studied. Irradiation of **1–3** gave novel 8-membered ring systems **4–6** by a light-induced rearrangement process, in which the hydroxyl proton is transferred on one side of the molecule toward one of the termini of the endocyclic diene. This rearrangement process thus involves a formal hydrogen transfer, during which either H^+ or $H^\bullet$ may be transferred to a reactive diene intermediate. Replacement of the hydroxyl proton by deuterium in **1–3**, and ^2H NMR of the corresponding photoproducts, confirmed that the hydrogen translocation occurs intramolecularly. Prolonged irradiation of **4** and **5** results in the formation of pyran products **10** and **11** by an intramolecular photocycloaddition of the triplet excited state of the α,β-unsaturated ketone to 1,3-*cis,cis*-cyclooctadiene, via a stabilized bisallylic biradical intermediate. Conformational studies of the structurally more rigid system **10**, which is derived from **4**, revealed that the hydroxyl proton was transferred on the *endo* side of the molecule.

Key words: intramolecular hydrogen transfer, photochemistry of hydroxy-alkyl-bicyclononadienes, intramolecular photocycloaddition, conformational studies.

FRANCISCUS W. A. M. MIESEN, HANS C. M. BAETEN, HARM A. LANGERMANS, LEO H. KOOLE et HENK A. CLAESSENS. Can. J. Chem. **69**, 1554 (1991).

Faisant appel à la spectroscopie RMN en une ou en deux dimensions et au marquage par le deutérium, on a étudié la photochimie du 9-*endo*-hydroxy-9-*exo*-vinyl-bicyclo[4.2.1]nonadiène (**1**) et de ses analogues 9-*exo*-(11-diméthylvinyl)- (**2**) et 9-*exo*-éthyl- (**3**). L'irradiation des composés **1–3** conduit à de nouveaux systèmes cycliques à 8 chaînons (**4–6**) par un processus de transposition induit par la lumière dans lequel le proton hydroxylique est transféré d'un côte de la molécule vers l'une des extrémités du diène endocyclique. Ce réarrangement implique donc un transfert formel d'hydrogène au cours duquel soit un H^+ ou un $H^\bullet$ est transféré vers un intermédiaire diénique réactif. Le remplacement du proton hydroxylique des composés **1–3** par du deutérium et la RMN du ^2H des photoproduits correspondants a permis de confirmer que la translocation de l'hydrogène se produit d'une façon intramoléculaire. Une irradiation prolongée des composés **4** et **5** conduit à la formation des pyranes **10** et **11** qui résultent d'une photocycloaddition intramoléculaire de l'état triplet de la cétone α,β-insaturée sur le 1,3-*cis,cis*-cyclooctadiène, par le biais d'un intermédiaire biradicalaire bisallylique stabilisé. Des études conformationnelles du système plus rigide du composé **10** dérivé du produit **4** révèlent que le proton hydroxylique est transféré vers la face *endo* de la molécule.

Mots clés: transfert d'hydrogène intramoléculaire, photochimie d'hydroxy-alkyl-bicyclononadiènes, photocycloaddition intramoléculaire, études conformationnelles.

[Traduit par la rédaction]

Introduction

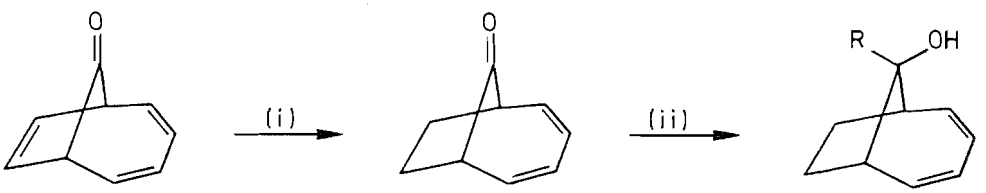
Photo-excitation of cycloalkenes may result in a substantial apparent increase of molecular basicity, leading in protic media to light-induced protonation of the olefin. On direct and sensitized irradiation in methanol, cyclohexenes, cycloheptenes, and cyclooctenes show initial *cis/trans* isomerization followed by protonation of the resulting highly strained isomers (1–5). This process is facilitated by the concomitant relief of strain in this intermediate (6). In striking constrast, cyclopentenes do not undergo photoprotonation on direct irradiation in methanol (7), but afford a mixture of products as a result of trapping a radical-cation intermediate. Such a radical cation may be the result of an electron ejection from a Rydberg excited state, rather than a ($\pi\pi^*$) state (8–10). On sensitized irradiation, cyclopentenes and other highly constrained cyclic olefins exhibit reactions involving radical intermediates, which probably originate from intermolecular reactions by the ($\pi\pi^*$) excited state itself (5, 11). This behaviour is thought to be associated with the inability of these olefins to undergo *cis/trans* isomerization. Although photoprotonation of cycloalkenes in protic media is thus well documented, the photochemistry of compounds combining such chromophores and suitably positioned hydroxyl groups enjoyed only limited study (12, 13). Under UV irradiation alcohols add to olefins in two modes: (a) the addition takes place at the hydroxyl group or (b) the addition takes place at the carbon atom to which the hydroxyl group is attached.

In the present paper we describe a photochemical study of 9-*endo*-hydroxy-9-*exo*-vinyl-bicylo[4.2.1]nona-2,4-diene (**1**), and the 9-*exo*-(2′-methylpropenyl)- (**2**) and 9-*exo*-ethyl- (**3**) analogues. We have studied the photochemistry of these compounds partly on the basis of deuterium labelling experiments. The structural and conformational properties of the isolated photoproducts were investigated with one- and two-dimensional NMR techniques, low temperature ^{13}C NMR, and semi-empirical AM1 quantum-chemical calculations.

[1]Author to whom correspondence may be addressed.

Printed in Canada / Imprimé au Canada

Can. J. Chem. Downloaded from www.nrcresearchpress.com by 84.41.108.74 on 09/07/12
For personal use only.



1 R = $-CH=CH_2$

2 R = $-CH=C(CH_3)_2$

3 R = $-CH_2CH_3$

SCHEME 1. (i) H_2/Ni_2B, see refs. 15–17; (ii) (a) RMgBr in THF, (b) H^+.

Can. J. Chem. Downloaded from www.nrcresearchpress.com by 84.41.108.74 on 09/07/12
For personal use only.

Results and discussion

Synthesis, purification, and identification

Compounds **1–3** were prepared in two steps from bicyclo-[4.2.1]nona-2,4,7-triene-9-one (Scheme 1) (14). The first step involves selective hydrogenation of the C(7)—C(8) bond, using Ni_2B as a catalyst (15–17). The product, bicyclo[4.2.1]nona-2,4-diene-9-one, was obtained in pure form after silica gel column chromatography. The second step in the synthesis of **1–3** is a Grignard reaction with vinyl-, 2,2-dimethylvinyl-, or ethylmagnesium bromide, respectively. It should be noted that this reaction affords the 9-*endo*-hydroxy epimers exclusively (18, 19). Compounds **1–3** were purified by silica gel column chromatography; their identity and purity were assessed by one- and two-dimensional ^1H NMR (COSY), ^{13}C NMR (including INEPTP), and two-dimensional $^1H/^{13}C$ correlation (for a survey of these techniques see ref. 20), and mass spectrometry. All photoproducts were isolated via preparative HPLC separation of the crude reaction mixtures. Molecular structures could be unequivocally established by the above-mentioned methods.

Photochemistry

UV irradiation of compounds **1–3** in *n*-hexane led to the formation of the novel 8-membered ring systems **4–6**, resulting from a new intramolecular formal hydrogen-transfer reaction (Scheme 2). Simultaneously, the expected products of a disrotatory electrocyclic ring closure reaction **7–9** were formed. Prolonged irradiation of photoproducts **4** and **5** led to the strained pyran structures **10** and **11** (Scheme 3).

In studying the photochemistry of **1–3**, we monitored the kinetics of formation and disappearance of materials at different photolysis time intervals (GC analysis). The results for the irradiation of **1** are presented in Fig. 1. Our data clearly show that **1** is initially converted to **4** and **7**; compound **10** is formed from **4** in a secondary photoreaction.

Analogously, irradiation of compound **2** initially produces **5** and **8**, and compound **5** is converted to **11** upon prolonged irradiation. The experiments with compound **3** merely showed formation of **6** and **9**, i.e., compound **6** does not show the secondary photoreaction.

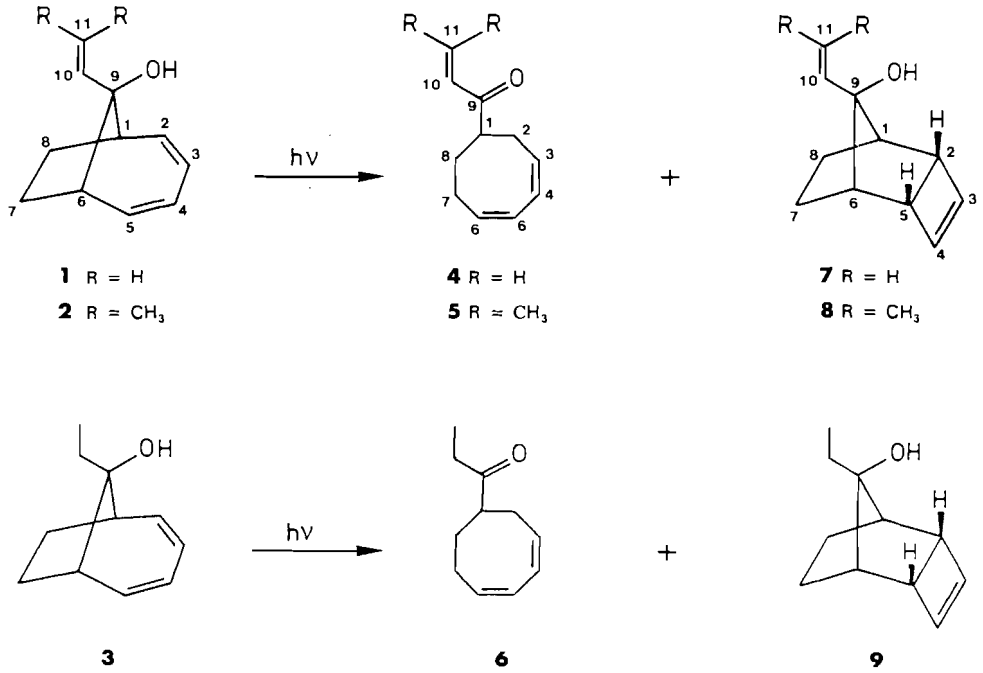
Verification of the stereochemistry of these reactions could be obtained with compound **1***a* (Scheme 4). Transfer of deuterium toward C(2) was evident from the ^1H and ^{13}C NMR spectra of **4***a*. The ^2H NMR spectrum of **4***a*, recorded at 77 MHz, showed a singlet signal at δ 2.3 ppm, exactly at the position of one of the H(2) protons in compound **4** (compare Figs. 2a and 2b). This demonstrates that the transfer of deuterium occurs at one face of the molecule exclusively.

The light-induced conversions **1** → **4**, **2** → **5**, and **3** → **6** may be formulated as proceeding via an initial photoprotonation process followed by a collapse of the resulting carbocation intermediate (cf. the photofragmentation of homoallylic alcohols (7, 21, 22)). Such a photoprotonation process, concomitant with the breaking of one of the bridgehead bonds, would be in line with the involvement of an olefinic intermediate exhibiting enhanced reactivity (6, 7). However, at present the exact nature of this intermediate cannot be defined and transfer of the hydroxylic hydrogen in the form of $H^\bullet$ or even H^- cannot be excluded. Even the cyclic reorganization of electrons (as shown in Fig. 3) involved in the overall reaction may be formulated as an 8-electron analogue of an oxy-retro-ene reaction (23).[2]

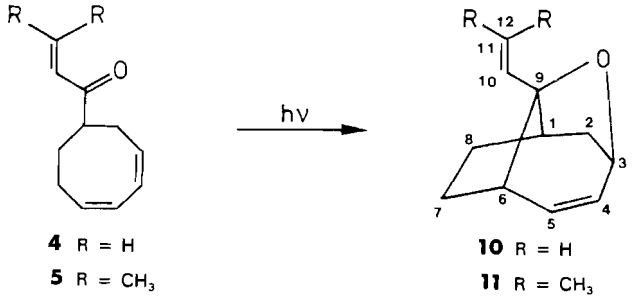
Concerning the stereochemistry, we could not establish *exo* or *endo* orientation of deuterium in **4***a*, since the conformational flexibility of the 8-membered ring precludes the application of Karplus-type equations to translate the vicinal proton–proton *J*-coupling constants into proton–proton dihedral angles (24). However, for the structurally more rigid system **10***a*, which is derived from **4***a* (Scheme 4), it could be unequivocally established that deuterium is located on the *endo* face of **10***a* and hence also on the *endo* face of **4***a* (see section of conformational studies). Additional evidence for the presence of deuterium on C(2) was obtained from a comparison of the ^{13}C NMR spectra of **4** and **4***a*. In **4***a*, the C(2) signal is split into three lines of equal intensity and $J = 19.4$ Hz due to one-band *J*-coupling with deuterium ($I = 1$). Interestingly, a small signal is also visible at δ 1.6 ppm in the ^2H NMR spectrum of **4***a*. The small peak is found exactly at the position of one of the H(8) protons in compound **4** (compare Figs. 3a and 3b). The explanation for the appearance of the small peak in Fig. 3b may lie in the occurrence of a thermal suprafacial [1,5]-H sigmatropic shift, occurring during the thermal isomerization of *cis,trans*-cyclooctadiene (COD) to *cis,cis*-COD, according to Scheme 5 (25, 26). Evidently this [1,5]-H shift would place deuterium in an isochronous position in the ^2H NMR spectrum, when compared with the *endo*-located H(8) in compound **4**.

Of course, the occurrence of this [1,5]-H shift is not detectable from the ^1H and ^{13}C NMR spectra of compound **4**. It may be noted that the UV irradiation of **1** and **2** does not induce a sigmatropic [1,3]-OH shift in the head group. In fact, we anticipated that this reaction could occur, in analogy with the previous work of our group on the photochemistry of 8-hydroxygermacrene B (12) and 4-methyl, 4-ethyl disubstituted 3-alkylidene 2-naphthalenol compounds (13, 27). For these

[2]We wish to thank one of the reviewers for suggesting this possible explanation.



SCHEME 2



SCHEME 3

systems, the occurrence of a planar photochemical [1,3]-OH shift was firmly established on the basis of experimental and theoretical data (27–29).

The 8-membered ring systems **4** and **5** are converted into the strained pyrans **10** and **11** in a secondary photoreaction (in ≈16 and 6% yields respectively). To the best of our knowledge, this reaction represents a novel photocycloaddition, which is reminiscent of the Paterno–Buchi reaction of ketones with alkenes, leading to the formation of oxetanes (30, 31). These reactions generally proceed from an attack of an (n,π^*) state of the carbonyl compound on an unsaturated substrate. In general, photocycloadditions of (n,π^*) states are expected to proceed via diradical intermediates (32, 33). These intermediates are produced either directly or indirectly from $S_1(n,\pi^*)$ or $T_1(n,\pi^*)$ states in the oxetane formation.

In our system the α,β-unsaturated ketone would have a singlet (n,π^*) state of lower energy than the singlet state of the conjugated *cis,cis*-COD system, while the triplet (n,π^*) state is almost equal to the triplet of the *cis,cis*-COD system. For the saturated ketone, however, the photocycloaddition is absent, and its triplet state is considerably higher than the triplet of the *cis,cis*-COD system. Consequently the triplet of the saturated ketone would be quenched by energy transfer many times faster than the α,β-unsaturated ketones, because of the large exothermicity of the process. For approximate energy levels see Table 1.

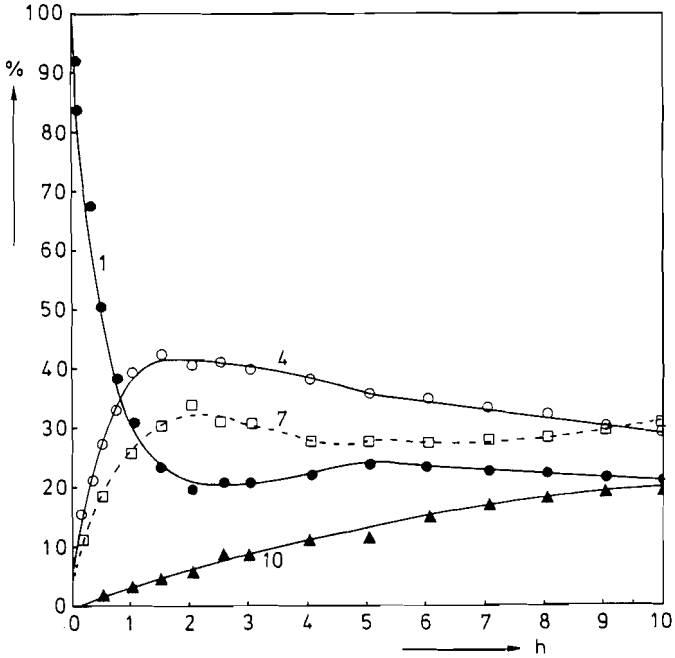


FIG. 1. Plot for conversion (%) of compound **1** to photoproducts **4**, **7**, and **10** as function of time (h).

Energy transfer to the *cis,cis*- or *cis,trans*-COD system results in a photostationary state composition of *cis,cis*- and *cis,trans*-cyclooctadienes (35, 36). It should be noted that the *cis,trans* isomer may isomerize to *cis,cis* either by a *cis/trans* isomerization about the *trans* double bond or by a [1,5]-H shift for the thermal isomerization (25, 26).

Since intersystem crossing (ISC) is very fast in α,β-unsaturated ketones, and singlet processes are normally too slow to compete, a mechanism involving a triplet excited state is

Can. J. Chem. Downloaded from www.nrcresearchpress.com by 84.41.108.74 on 09/07/12
For personal use only.

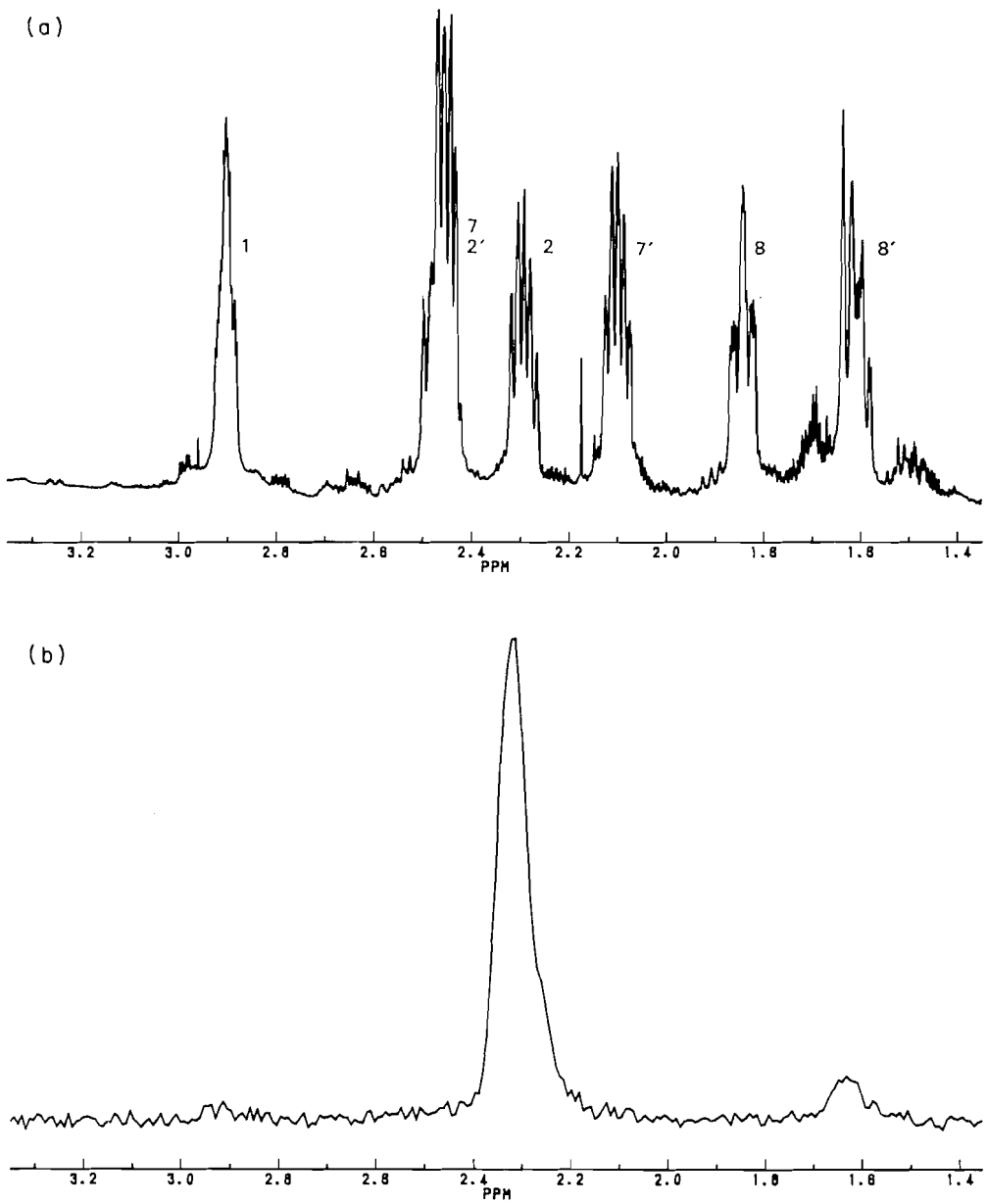
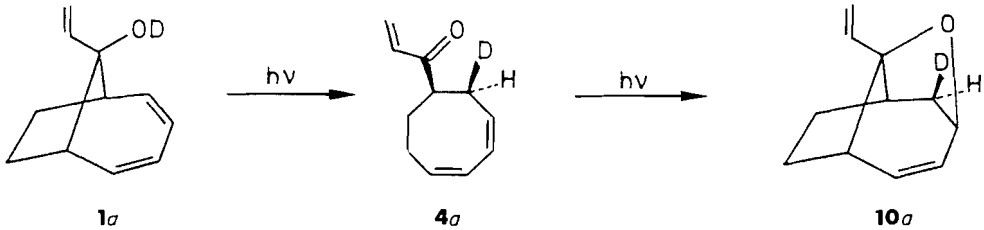


FIG. 2(a). The ^1H NMR (400 MHz) and (b) the ^2H NMR (77 MHz) spectrum of **4***a* in $CDCl_3$. The assignments of protons were obtained from two-dimensional homonuclear NMR spectra (COSY).



1*a* **4***a* **10***a*

SCHEME 4

preferred over a singlet excited process. A mechanism involving the formation of a charge-transfer, stabilized exciplex, leading to a biradical that can collapse to the strained pyrans or undergo radiationless decay to the ground-state molecules, is rather remote for the *cis,cis*-COD system (37, 38). In the oxetane formation of acetone and COD (ISC is slower in this case) the total rate of fluorescence quenching of the ketone is significantly slower than the rate of ISC (38). Therefore we consider the pyran formation to occur predominantly from the triplet state of the α,β-unsaturated ketone, and a chemical reaction can indeed compete with the triplet energy transfer to the COD, because of the decrease in diene character of the 8-membered ring. Based on an alkoxy model (39), the intramolecular pyran formation, like intramolecular cycloaddition, is

Can. J. Chem. Downloaded from www.nrcresearchpress.com by 84.41.108.74 on 09/07/12
For personal use only.

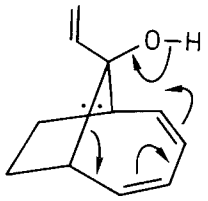
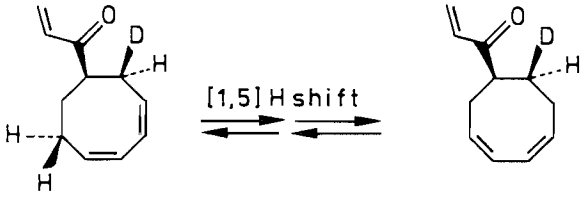


FIG. 3. Schematic representation for the formal hydrogen-transfer reaction.



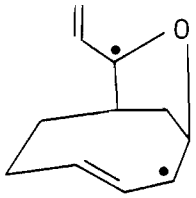
SCHEME 5

TABLE 1. Approximate singlet and triplet energy levels

Compound	S_1 (kcal/mol)	T_1 (kcal/mol)
α,β-Unsaturated ketone[a]	74	70
Saturated ketone[a]	84	78
cis,cis-Cyclooctadiene[b]	>80	70–73
cis,trans-Cyclooctadiene[b]	—	<70

[a]Data obtained from N. J. Turro (34).
[b]Data obtained from R. S. H. Liu (in ref. 36).

expected to obey a "rule of five" (40), involving the stabilized diradicaloid intermediate:



The formation of photoproducts **7–9** involves a ring closure of the endocylic dienes in **1–3**. As can be seen in Fig. 1, the photoprotonation reaction and the ring closure occur with approximately equal probability during the irradiation of **1**. Similar results were obtained for **2** and **3**. The photochemical ring closure of **1–3** follows a disrotatory route, as predicted by the Woodward and Hoffmann rules (41). The *endo* orientation of the protons H(2) and H(5) was established on the basis of the NMR spin–spin coupling constant $J_{H(1)-H(2)}$, and comparison with literature data (42).

Conformational studies

The ^{1}H NMR spectrum of the compounds **1–3** in the ground state showed a long-range spin–spin coupling between H(10) and the hydroxyl proton ($^4J_{HCCOH} \approx 1.5$ Hz). This reveals that the coupling path is in all-*trans* ("W") conformation, i.e., the OH group resides in the plane of C(9), C(10), and C(11). The C(10)—C(11) double bond in **1** and **2** is therefore approximately orthogonal with respect to the endocyclic diene system. The conformational properties of **1–3** were investigated further on the basis of semi-empirical MO calculations. Dreiding models of **1–3** provided initial starting conformations. The geometries of **1–3** were optimized using the AM1 Hamiltonian of the AMPAC program (43, 44). The optimized conformations of **1–3** showed *trans* conformation of the coupling path H-O-C(9)-C(10)-H(10) in the head group (Fig. 4a).

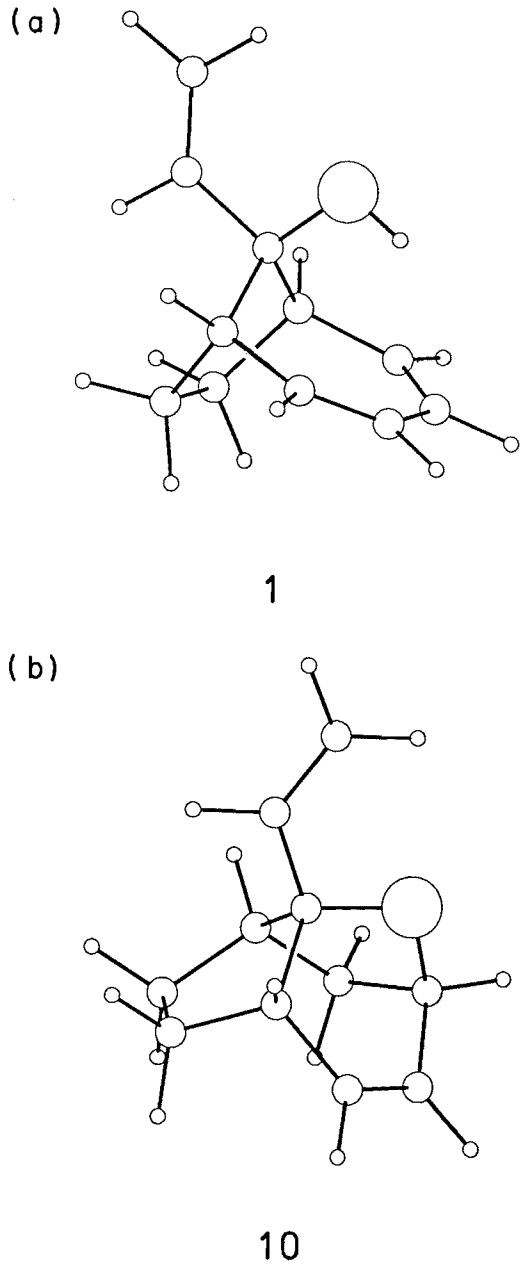


FIG. 4(a). Optimized conformation of **1** studied with AM1 calculation method showing *trans* conformation of the coupling path in the head group ($\Delta H_f = -2.78$ kcal/mol). (b) Optimized conformation of **10** from which proton–proton torsion angles for the Karplus relations have been extracted ($\Delta H_f = -8.03$ kcal/mol).

Inspection of the AM1-optimized conformation of **1** confirms that the hydroxyl proton is proximate to C(2) ($r_{OH-proton-C(2)} = 2.52$ Å). Essentially the same conformation was found in the AM1 calculation on structures **2** and **3**. (The AM1 calculations on **1–3**, **10**, and **11** resulted in the following enthalpies of formation (ΔH_f): ΔH_f(**1**) = −2.78 kcal/mol, ΔH_f(**2**) = −17.80 kcal/mol, ΔH_f(**3**) = −34.67 kcal/mol, ΔH_f(**10**) = −8.03 kcal/mol, ΔH_f(**11**) = −23.47 kcal/mol.)

Can. J. Chem. Downloaded from www.nrcresearchpress.com by 84.41.108.74 on 09/07/12
For personal use only.

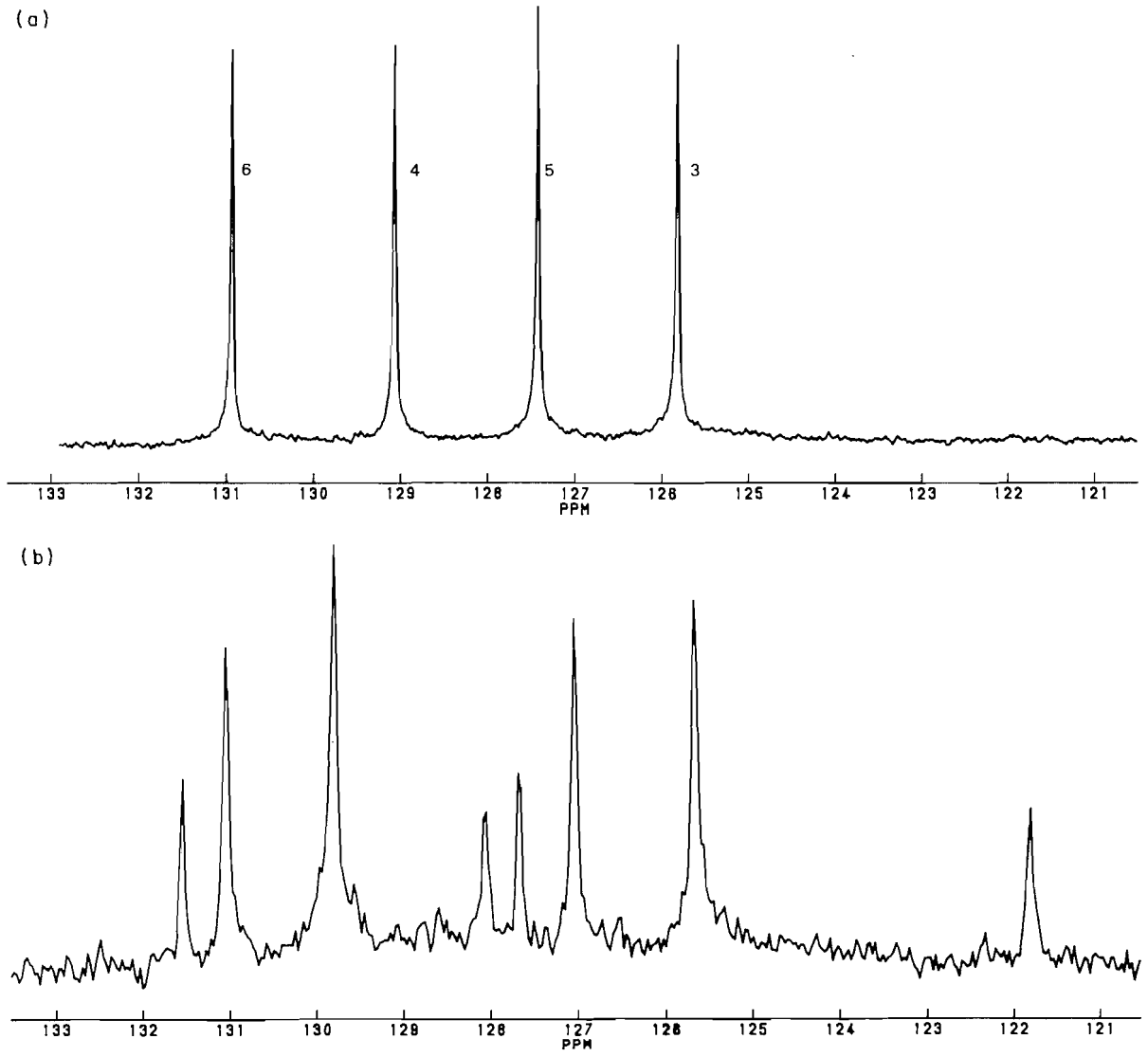


FIG. 5.(a). Olefinic region of the ^{13}C NMR spectrum in of **6** at 20°C (100 MHz, solvent CD_2Cl_2). The assignments are based on a ^{13}C–^{1}H correlation experiment. (b) Decoalescence in the olefinic region of ^{13}C NMR spectrum of **6** at −90°C (100 MHz, solvent CD_2Cl_2). Clearly, two distinct molecular conformations are present in a ratio of approximately 1:2 at this temperature. These observations closely resemble the data of Anet *et al.* on *cis,cis*-cyclooctadiene, and *cis,cis*-cyclooctadiene mono-epoxide (refs. 45–47).

The conformational properties of the 8-membered ring compounds **4**–**6** are more difficult to characterize, since there is no obvious starting geometry for the AM1 calculations. Rather it must be expected from the work of Anet and Yavari on *cis,cis*-1,3-cyclooctadiene and *cis,cis*-cyclooctadiene mono-epoxide (45–47) that compounds **4**–**6** are involved in a complex conformational equilibrium. We obtained convincing evidence for the flexible nature of compounds **4**–**6** from variable-temperature ^{13}C NMR measurements. Upon lowering the sample temperature from 20 to −90°C in CD_2Cl_2 we observed decoalescence phenomena for **4**–**6**. As a typical example, Figs. 5a and 5b show the olefinic regions in the ^{13}C NMR spectra of compound **6**, as measured at 20°C and −90°C.

The observation of two sets of ^{13}C NMR peaks at −90°C clearly shows that at least two distinct conformations coexist at this temperature. It should be noted that our ^{13}C NMR spectral data on compounds **4**–**6** closely resemble the data of Anet and Yavari on *cis,cis*-1,3-cyclooctadiene and *cis,cis*-cyclooctadiene mono-epoxide (45–47). The conformational properties of the strained pyrans **10** and **11** were again studied with the AM1 calculation method. Starting geometries were obtained from Dreiding molecular models. In the optimized conformation of **10** (Fig. 4b) we especially focused on the proton–proton torsion angles Φ_1 (H(1)-C(1)—C(2)-H(2)) = −2.2°; Φ_2 (H(1)-C(1)—C(2)-H(2′)) = 119.2°; Φ_3 (H(3)-C(3)—C(2)-H(2)) = −23.6°; Φ_4 (H(3)-C(3)—C(2)-H(2′)) = 96.4°. Thus, from a simple Karplus dependency of $^{3}J_{HH}$ on the proton–proton torsion angle (24), one expects that $^{3}J_{H(1)-H(2,endo)}$ and $^{3}J_{H(3)-H(2,endo)}$ are substantially larger than $^{3}J_{H(1)-H(2',exo)}$ and $^{3}J_{H(3)-H(2',exo)}$. Interestingly, these tentative conclusions are in line with the experimental ^{1}H NMR data on compound **10**, which show that the downfield H(2) proton (δ 2.24 ppm) has relatively large coupling constants with its vicinal neighbours H(1) and H(3) (i.e., 10.1 and 6.2 Hz, respectively, see experimental section), while the upfield H(2) proton (δ 1.63 ppm) shows much smaller $^{3}J_{HH}$ couplings with H(1) and H(3) (i.e., <1 Hz in both cases). Therefore, we tentatively assign the downfield H(2) proton as H(2,*endo*), and the upfield H(2′) proton as H(2′,*exo*). Having

Can. J. Chem. Downloaded from www.nrcresearchpress.com by 84.41.108.74 on 09/07/12
For personal use only.

this assignment, it is worthwhile to reexamine the ^{1}H NMR spectrum of the C(2)-deuterated compound **10***a*. Now it seems likely that it is H(2,*endo*) and not H(2′,*exo*) that is replaced by deuterium in **10***a*. Thus the photochemical formal proton transfer reaction **1** → **4** proceeded *exclusively* on the *endo* face of the molecule. We anticipate that this holds also for the analogous photochemical reactions **2** → **5** and **3** → **6**.

Concluding remarks

UV irradiation of compounds **1**–**3** leads to a new photochemical rearrangement process, in which the hydroxyl hydrogen is transferred on the *endo* side of the molecule toward one of the terminals of the endocyclic diene. This reaction is probably driven by the enhanced reactivity of the diene moiety after photo-excitation, leading to a protonation of the olefin. However, the reaction can also be considered as an oxy-retro-ene type reaction. The 8-membered ring structures **4** and **5** are converted relatively slowly to the strained pyrans **10** and **11** in a secondary photoreaction. This reaction is not observed for the ethyl counterpart **6**. Most likely, the reaction of **4** and **5** is a photo-cycloaddition, resembling the Paterno–Buchi reaction. We believe that the reaction develops from the T_1 excited state of the α,β-unsaturated ketone, leading to the strained pyran products, which may arise from a bisallylic radical intermediate.

Experimental

General procedures

All solvents and commercial reagents were reagent grade and dried with the appropriate drying agents. Argon was dried over Drierite pellets. Column chromatography was performed using Silica-60 as the stationary phase. Proton, deuterium, and carbon-13 NMR spectra were recorded on a Bruker AM400[3] or a Bruker AM600[4] spectrometer in $CDCl_3$ solution. Chemical shifts are reported in ppm (δ), relative to tetramethylsilane as an internal standard. Coupling constants (*J*) are given in Hz. GC analyses were performed on a Kipp Analytica 8200 instrument with FID detection (25 m × 0.22 mm i.d.; column type: WCOT fused silica; stationary phase CP WAX 51). All HPLC separations were run on a system that consists of a Waters 6000A pump, a 4 × 100 mm Lichrosorb 60 (5 μm) column, and a Philips Unicam PU4020 UV detector (254 nm). Mass spectral data were obtained on a Hewlett Packard 5970A system by electron ionization at 70 eV.

Synthesis

Bicyclo[4.2.1]nona-2,4-diene-9-one

This compound was prepared via selective hydrogenation of the C(7)—C(8) bond in bicyclo[4.2.1]nona-2,4,7-triene-9-one (14) (Scheme 3). This reaction is not straightforward, as is evident from the work of Brown (15), Gilissen *et al.* (16,17), and Schuster and Kim (18). We used Ni_2B as hydrogenation catalyst, which was prepared as follows: $Ni(Ac)_2 \cdot 4\,H_2O$ (230 mg, 0.92 mmol) was dissolved under an argon atmosphere with magnetic stirring in 20 mL of ethanol in a 500-mL Erlenmeyer flask. A solution of 33 mg $NaBH_4$ in 20 mL of ethanol was transferred dropwise into the reaction vessel, yielding a black suspension of Ni_2B. Subsequently, bicylo[4.2.1]nona-2,4,7-triene-9-one (1 g, 7.4 mmol) was added, and hydrogen gas was allowed into the flask (atmospheric pressure). Stirring was continued until 170 mL (6.9 mmol) hydrogen gas was absorbed. Ethanol was evaporated, and the residue was dissolved in 100 mL of dry ether. Standard work-up (addition of 50 mL saturated aqueous $NaHCO_3$, filtration, and repeated washing of the aqueous phase with ether) yielded a mixture of the desired diene, and the starting compound (ratio ≈ 5:1), which was chromatographed on a silica gel column using CH_2Cl_2 as eluent (R_f diene = 0.43; R_f triene = 0.49). This afforded 460 mg of the desired product (yield 45%). ^{1}H NMR ($CDCl_3$) δ: 5.58–5.96 (4H, m, H(2–5)), 2.69–2.87 (2H, m, H(1,6)), 2.10–2.46 (4H, m, H(7,8)). ^{13}C NMR ($CDCl_3$) δ: 216.44 (s, C(9)), 129.55 (d, C(2,5)), 126.12 (d, C(3,4)), 50.35 (d, C(1,6)). 34.55 (t, C(7,8)). EI-MS; 134 (m^+), 106, 91, 78 (base peak), 51, 39, 27.

9-endo-Hydroxy-9-exo-vinyl-bicyclo[4.2.1]nona-2,4-diene (1)

Magnesium turnings (1.27 g, 52.7 mmol) and 15 mL of dry THF were transferred into a 250-mL reaction flask equipped with a reflux cooler (connected with a methanol cryostat (−60°C)), a dropping funnel, and a mechanical stirrer. During the experiment, dry argon was slowly passed through the reaction vessel. Vinyl bromide (0.5 g, 4.7 mmol) and a small iodine crystal were added. After start-up of the reaction, 15 mL of dry THF was added immediately, followed by the main portion of vinyl bromide (6.25 g, 58.3 mmol) in 10 mL of dry THF, over a period of 1 h. After completion of the addition, the mixture was stirred for 1 h, and cooled to 0°C with an ice bath. Bicyclo[4.2.1]-nona-2,4-diene-9-one (1.68 g, 12.5 mmol), dissolved in 15 mL of dry THF, was added dropwise over a period of 1 h. The reaction was allowed to proceed for 6 h at 0°C, and for 14 h at ambient temperature. Then, the reaction was finished through addition of 35 mL of 3 N HCl at 0°C. THF was removed and the residue was mixed with 100 mL of diethyl ether. The organic layer was washed with $NaHCO_3$, dried over $MgSO_4$, and concentrated. Column chromatography using CH_2Cl_2 as eluent afforded 5.19 g of pure **1** (R_f 0.35, yield 91%). ^{1}H NMR ($CDCl_3$) δ: 6.18–6.34 (1H, dd, H(10)), 5.75–6.01 (4H, m, H(2–5)), 5.38–5.49 (1H, dd, H(11, *trans*)), 5.12–5.22 (1H, dd, H(11, *cis*)), 3.07 (1H, d, OH), 2.48–2.58 (2H, m, H(1,6)), 2.02–2.08 (4H, m, H(7,8)). ^{13}C NMR ($CDCl_3$) δ: 142.81 (d, C(10)), 136.13 (d, C(2,5)), 126,14 (d, C(3,4)), 113.88 (t, C(11)), 77.49 (s, C(9)), 49.44 (t, C(1,6)), 38.17 (t, C(7,8)). EI-MS: 147, 115, 107, 95, 91, 79 (base peak), 65, 55, 39, 27.

9-endo-Hydroxy-9-exo-(2′-methylpropenyl)-bicyclo[4.2.1]nona-2,4-diene (2)

The Grignard reagent was prepared from 1-bromo-2-methylpropene (2.35 g, 17.4 mmol) and magnesium turnings (0.37 g, 15.2 mmol) in 30 mL of dry THF. The reaction was allowed to proceed for 6 h at 40°C. Bicyclo[4.2.1]nona-2,4-diene-9-one (1 g, 7.45 mmol) in 10 mL of dry THF was slowly added in 30 min. The reaction mixture was stirred for 48 h, poured onto crushed ice, and 100 mL 1 N NH_4Cl solution was added. Subsequently, the pH of the solution was lowered to 5, via addition of 1 N HCl solution. Usual work-up procedure and repeated column chromatography, using hexane–dichloromethane (30:70) as eluent, afforded pure **3** (R_f 0.20, yield 0.44 g, 31%). ^{1}H NMR ($CDCl_3$) δ: 5.70–6.11 (4H, m, H(2–5)), 5.45–5.55 (1H, m, H(10)), 2.87–2.88 (1H, d, OH), 2.55–2.72 (2H, m, H(1,6)), 1.95–2.04 (4H, m, H(7,8)), 1.91–1.92 (3H, d, CH_3), 1.77–1.78 (3H, d, CH_3). ^{13}C NMR ($CDCl_3$) δ: 138.21 (s, C(11)), 136.37 (d, C(2,5)), 130.59 (d, C(10)), 125.76 (d, C(3,4)), 76.57 (s, C(9)), 48.58 (d, C(1,6)), 37.92 (t, C(7,8)), 27.83 and 20.60 (q, CH_3). EI-MS: 190 (m^+), 175, 147, 105, 83 (base peak), 55, 41, 39, 29, 27.

9-endo-Hydroxy-9-exo-ethyl-bicyclo[4.2.1]nona-2,4-diene (3)

The Grignard reagent was prepared from ethyl bromide (1.21 g, 11.1 mmol) and magnesium turnings (0.27 g, 11.1 mmol) in 30 mL of dry diethyl ether. Bicyclo[4.2.1]nona-2,4-diene-9-one (1.36 g, 10.1 mmol), dissolved in 15 mL of dry diethyl ether, was added dropwise in 30 min at 0°C. After completion of the reaction (30 min at 0°C and 90 min at ambient temperature), the suspension was poured onto 30 g of crushed ice. Hydrochloric acid (25 mL of a 1 N solution) was slowly added. Standard work-up and column chromatography with CH_2Cl_2 as eluent yielded 0.92 g (54%) of pure **2** (R_f 0.33). ^{1}H NMR ($CDCl_3$) δ: 5.80–6.05 (4H, m, H(2–5)), 2.84 (1H, s, OH), 2.40–2.55 (2H, m, H(1,6)), 1.95–2.05 (4H, m, H(7,8)), 1.69–1.86 (2H, q, H(10)), 0.92–1.11 (3H, t, H(11)). ^{13}C NMR ($CDCl_3$) δ: 136.45 (d, C(2,5)), 125.71 (d, C(3,4)), 77.44 (s, C(9)), 48.17 (d, C(1,6)), 37.83 (t, C(10)), 32.05 (t, C(7,8)), 9.34 (q, C(11)). EI-MS: 164 (m^+), 135, 117, 107, 91, 79, 65, 57 (base peak), 41, 39, 29.

[3]NMR facility of the Eindhoven University of Technology.

[4]The 600-MHz ^{1}H NMR spectra were recorded on the Bruker AM600 NMR spectrometer of the Dutch National hf NMR facility at Nijmegen, The Netherlands.

Can. J. Chem. Downloaded from www.nrcresearchpress.com by 84.41.108.74 on 09/07/12
For personal use only.

TABLE 2. Irradiation of bicyclononadienes[a]

Olefin	Amount (mg)	Time (h)	Yield (%)[b] 1–3	4–6	7–9	10,11
1	460	1.5	22	41	30	4
		10	21	30	30	16
2	440	1.5	23	18	56	—
		8	1	15	73	6
3	460	1.5	16	34	50	0
		10	1	34	65	0

[a]Irradiations were conducted as described in this section using ≈500 mL of *n*-hexane containing ≈3 mmol of olefin.

[b]Yields were determined by gas-chromatographic analysis of aliquots removed periodically from the irradiation mixture.

Irradiation procedure

All photochemical experiments (as shown in Table 2) on **1–3** were performed in ≈500 mL of *n*-hexane (concentration ≈6 mM), which was dried over sodium prior to use.

Irradiations were performed using a 500-W medium Hg lamp (Hanau TQ78) through quartz. Cooling of the lamp and the reaction mixture was accomplished by means of a closed circuit filled with methanol. In this way, the temperature in the reaction vessel was maintained around 0°C. Before and during irradiation, the reaction mixture was purged by a stream of dry argon, to remove all traces of oxygen. All photoreactions were monitored by means of gas chromatography. After irradiation, the solvent was removed on a rotatory evaporator. The reaction mixture was separated by HPLC using CH_2Cl_2/hexane (10:90 or 15:85) as eluent. Isolation of products was continued until sufficient material was obtained for NMR characterization.

Spectral and analytical data of photoproducts

The nomenclature of compounds is according to the IUPAC convention. However, to obtain as much consistency as possible, the numbers in the NMR data were assigned as in Schemes 2 and 3, and may differ from IUPAC convention.

6-(1'-Oxo-propenyl)-1,3-cis,cis-*cyclooctadiene (**4**)*

^{1}H NMR ($CDCl_3$) δ: 6.46 (1H, dd, H(10)), 6.26 (1H, dd, H(11, *trans*)), 5.95–5.84 (2H, m, H(4,5), $^3J_{H(4)-H(3)}$ = 11.3 Hz, $^3J_{H(4)-H(5)}$ = 4.28 Hz, $^3J_{H(5)-H(6)}$ = 11.3 Hz), 5.76 (1H, dd, H(11, *cis*)), 5.65 (2H, m, H(3,6), $^3J_{H(3)-H(2)}$ = 7.12 Hz, $^3J_{H(3)-H(2')}$ = 2.5 Hz, $^3J_{H(6)-H(7)}$ = 7.04 Hz, $^3J_{H(6)-H(7')}$ = 2.50 Hz), 2.93 (1H, m, H(1), $^3J_{H(1)-H(2)}$ = 9.13 Hz, $^3J_{H(1)-H(2')}$ = 2.27 Hz, $^3J_{H(1)-H(8)}$ = 4.36 Hz, $^3J_{H(1)-H(8')}$ = 8.86 Hz), 2.48 (1H, m, H(2')), 2.48 (1H, m, H(7) or H(7')), 2.30 (1H, m, H(2), $^2J_{H(2)-H(2')}$ = 15.29 Hz), 2.12 (1H, m, H(7') or H(7)), 1.85 (1H, m, H(8) or H(8')), 1.63 (1H, m, H(8') or H(8)). ^{13}C NMR ($CDCl_3$) δ: 204.50 (s, C(9)), 136.11 (d, C(10)), 132.06 (d, C(3) or C(6)), 130.17 (d, C(6) or C(3)), 129.03 (t, C(11)), 128.64 (d, C(4) or C(5)), 127.15 (d, C(5) or C(4)), 45.48 (d, C(1)), 30.60 (t, C(2)), 27.67 (t, C(7)), 26.75 (t, C(8)). EI-MS: 162 (m^+), 147, 145, 107, 91, 79 (base peak), 55, 41, 39, 27.

(2-Deutero)-6-(1'-oxo-propenyl)-1,3-cis,cis-*cyclooctadiene (**4**a)*

^{1}H NMR ($CDCl_3$): identical to **4** except for the H(2) signal at δ = 2.30, which is lacking. ^{2}H NMR ($CDCl_3$) δ: 2.32 (1D, s, D(2)), 1.64 (1D, s, D(2)[5]). ^{13}C NMR ($CDCl_3$); identical to **4** except for the C(2) signal: δ = 30.66 (m, C(2)). EI-MS: 163 (m_D^+), 162 (m_H^+), 148, 147, 107, 91, 79 (base peak), 55, 39, 27.

6-(3'-Methyl-1'-oxo-but-2'-enyl)-1,3-cis,cis-*cyclooctadiene (**5**)*

^{1}H NMR ($CDCl_3$) δ: 6.12 (1H, m, H(10)), 5.93–5.80 (2H, m, H(4,5)), 5.64 (2H, m, H(3,6)), 2.58 (1H, m, H(1)), 2.45 (1H, m, H(2')), 2.45 (1H, m, H(7) or H(7')), 2.24 (1H, m, H(2)), 2.14 (3H, d, H(12) or H(13)), 2.07 (1H, m, H(7') or H(7)), 1.90 (3H, d, H(13) or H(12)), 1.83 (1H, m, H(8) or H(8')), 1.57 (1H, m, H(8') or H(8)). ^{13}C NMR ($CDCl_3$) δ: 205.30 (s, C(9)), 156.77 (s, C(11)), 132.18 (d, C(10)), 130.64, 128.35 (d, C(3,6)), 126.99, 124.15 (d, C(4,5)), 48.73 (d, C(1)), 30.66 (t, C(2)), 28.86, 21.85 (q, C(12,13)), 27.80 (t, C(7)), 26.59 (t, C(8)). EI-MS: 190 (m^+), 175, 147, 83 (base peak), 55, 39.

6-(1'-Oxo-propyl)-1,3-cis,cis-*cyclooctadiene (**6**)*

^{1}H NMR ($CDCl_3$) δ: 5.94–5.80 (2H, m, H(4,5)), 5.60 (2H, m, H(3,6)), 2.63 (1H, m, H(1), $^3J_{H(1)-H(2)}$ = 3.87 Hz), 2.49 (2H, q, H(10)), 2.42 (1H, m, H(2')), 2.42 (1H, m, H(7) or H(7')), 2.27 (1H, m, H(2)), 2.08 (1H, m, H(7') or H(7)), 1.85 (1H, m, H(8) or H(8')), 1.60 (1H, m, H(8') or H(8)), 1.06 (3H, t, H(11)). ^{13}C NMR ($CDCl_3$) δ: 215.77 (s, C(9)), 132.08 (d, C(3) or C(6)), 130.21 (d, C(6) or C(3)), 128.62 (d, C(4) or C(5)), 127.01 (d, C(5) or C(4)), 47.91 (d, C(1)), 35.21 (t, C(10)), 30.56 (t, C(2)), 27.87 (t, C(7)), 26.69 (t, C(8)), 9.06 (q, C(11)). EI-MS: 165, 164 (m^+), 146, 135, 107, 91, 79 (base peak), 57, 41, 39, 29.

*9-endo-Hydroxy-9-exo-vinyl-tricyclo[4.2.1.0^{2,5}]nona-3-ene (**7**)*

^{1}H NMR ($CDCl_3$) δ: 6.23 (1H, dd, H(10)), 6.23 (2H, m, H(3,4)), 5.40 (1H, dd, H(11, *trans*)), 5.15 (1H, dd, H(11, *cis*)), 3.33 (2H, m, H(2,5)), 1.95 (2H, m, H(1,6)), 1.55 (2H, m, H(7,8) or H(7',8')), 1.42 (2H, m, H(7',8') or H(7,8)). ^{13}C NMR ($CDCl_3$) δ: 142.42 (d, C(10)), 140.70 (d, C(3,4)), 115.66 (t, C(11)), 93.61 (s, C(9)), 50.72 (d, C(2,5)), 47.84 (d, C(1,6)), 24.63 (t, C(7,8)). EI-MS: 161, 147, 134, 107, 96, 91, 79 (base peak), 55, 39, 27.

*9-endo-Hydroxy-9-exo-(2'-methyl-propenyl)-tricyclo[4.2.1.0^{2,5}]-nona-3-ene (**8**)*

^{1}H NMR ($CDCl_3$) δ: 6.27 (2H, m, H(3,4)), 5.50 (1H, dd, H(10)), 3.29 (2H, dd, H(2,5)), 2.03 (2H, m, H(1,6)), 1.85 (3H, d, H(12) or H(13)), 1.85 (2H, m, H(7,8) or H(7',8')), 1.74 (3H, d, H(13) or H(12)), 1.45 (2H, m, H(7',8') or H(7,8)). ^{13}C NMR ($CDCl_3$) δ: 140.72 (d, C(3,4)), 129.65 (d, C(10)), 50.72 (d, C(2,5)), 47.70 (d, C(1,6)), 27.74 (q, C(12) or C(13)), 24.39 (t, C(7,8)), 20.63 (q, C(13) or C(12)). EI-MS: 190 (m^+), 175, 147, 109, 91, 83 (base peak), 55, 39.

*9-endo-Hydroxy-9-exo-propyl-tricyclo[4.2.1.0^{2,5}]nona-3-ene (**9**)*

^{1}H NMR ($CDCl_3$) δ: 6.28 (2H, m, H(3,4)), 3.28 (2H, dd, H(2,5)), 1.85 (2H, m, H(1,6)), 1.69 (2H, q, H(10)), 1.51 (2H, m, H(7,8) or H(7',8')), 1.37 (2H, m, H(7',8') or H(7,8)), 1.01 (3H, t, H(11)). ^{13}C NMR ($CDCl_3$) δ: 141.06 (d, C(3,4)), 95.43 (s, C(9)), 50.60 (d, C(2,5)), 45.52 (d, C(1,6)), 30.80 (t, C(10)), 24.73 (t, C(7,8)), 9.47 (q, C(11)). EI-MS: 164 (m^+), 163, 149, 135, 107, 91, 79 (base peak), 57, 41, 39, 29.

*9-Oxa-8-vinyl-tricyclo[5.2.1.0^{4,8}]dec-2-ene (**10**)*

^{1}H NMR ($CDCl_3$) δ: 6.13 (1H, dd, H(10)), 6.13 (1H, dd, H(4), $^3J_{H(4)-H(5)}$ = 4.8 Hz, $^3J_{H(4)-H(3)}$ = 9.6 Hz, $^3J_{H(4)-H(6)}$ = 1.0 Hz), 5.53 (1H, dd, H(5), $^3J_{H(5)-(6)}$ = 3.5 Hz), 5.27 (1H, dd, H(11, *trans*)), 5.12 (1H, dd, H(11, *cis*), 4.44 (1H, m, H(3), $^3J_{H(3)-H(2)}$ = 6.2 Hz, $^3J_{H(3)-H(2')}$ = <0.1 Hz), 2.70 (1H, m, H(6)), 2.34 (1H, m, H(1), $^3J_{H(1)-H(2)}$ = 10.1 Hz, $^3J_{H(1)-H(2')}$ = <0.1 Hz), 2.24 (1H, m, H(2), $^2J_{H(2)-H(2')}$ = 11.7 Hz), 2.10 (1H, m, H(7) or H(8) or H(7') or H(8')), 1.63 (1H, m, H(8) or H(7) or H(7') or H(8')), 1.80 (1H, m, H(7') or H(8) or H(7) or H(8')), 1.51 (1H, m, H(8') or H(8) or H(7') or H(7)). ^{13}C NMR ($CDCl_3$) δ: 140.80 (d, C(10)), 113.92 (t, C(11)), 134.39 (d, C(4)), 129.50 (d, C(5)), 93.51 (s, C(9)), 73.95 (d, C(3)), 45.92 (d, C(6)), 45.63 (t, C(1)), 44.86 (t, C(2)), 32.03 (t, C(7) or C(8)), 29.42 (t, C(8) or C(7)). EI-MS: 163, 162 (m^+), 147, 134, 133, 120, 107, 91, 79 (base peak), 55, 41, 39, 27.

*(10-Deutero)-9-oxa-8-vinyl-tricyclo[5.2.1.0^{4,8}]dec-2-ene (**10**a)*

^{1}H NMR ($CDCl_3$): identical to **10** except for the H(10) signal at δ = 2.24, which is lacking. ^{2}H NMR ($CDCl_3$) δ: 2.21 (1D, s, D(2)). ^{13}C NMR ($CDCl_3$) δ: 141.03 (d, C(10)), 134.20 (d, C(4)), 129.59 (d, C(5)), 113.89 (t, C(11)), 93.53 (s, C(9)), 73.88 (d, C(3)), 46.08 (d, C(6)), 45.78 (t, C(1)), 44.61 (m, C(2)), 32.02, 29.52 (t, C(7,8)). EI-MS: 163 (m_D^+), 162 (m_H^+), 148, 147, 129, 108, 107 (base peak), 92, 91, 79, 55, 39.

*9-Oxa-8-(2'-methyl-propen-1'-yl)-tricyclo[5.2.1.0^{4,8}]dec-2-ene (**11**)*

Could not be isolated as pure (11). Its existence was verified by GC analyses (6.5% after 8 h).

[5]Signal due to [1,5]-H shift.

Can. J. Chem. Downloaded from www.nrcresearchpress.com by 84.41.108.74 on 09/07/12
For personal use only.

Acknowledgements

This investigation has been supported by the Netherlands Foundation for Chemical Research (SON), with financial aid from the Netherlands Organization for Scientific Research (NWO). We wish to thank Mr. J. van Dongen for the skillful HPLC separations. Finally we express our gratitude to Professor J. W. Verhoeven, for his interest in this project and for several valuable discussions concerning the mechanisms of these reactions.

1. J. A. MARSHALL. Acc. Chem. Res. **2**, 33 (1973).
2. P. J. KROPP and H. J. KRAUS. J. Am. Chem. Soc. **89**, 5199 (1967).
3. P. J. KROPP. Pure Appl. Chem. **24**, 585 (1970).
4. P. J. KROPP and H. FAUBLE. J. Am. Chem. Soc. **92**, 948 (1970).
5. P. J. KROPP. J. Am. Chem. Soc. **91**, 5783 (1969).
6. J. A. MARSHALL and H. FAUBL. J. Am. Chem. Soc. **92**, 948 (1970).
7. P. J. KROPP, E. J. REARDON, JR., Z. L. F. GAIBEL, K. F. WILLIARD, and J. H. HATTAWAY, JR. J. Am. Chem. Soc. **95**, 7059 (1973).
8. A. J. MERER and R. S. MULLIKEN. Chem. Rev. **69**, 639 (1969).
9. P. BORRELL and F. C. JAMES. Trans. Faraday Soc. **62**, 2452 (1966).
10. P. BORRELL and P. CASHMORE. Trans. Faraday Soc. **65**, 2412 (1969).
11. R. R. SAUERS, W. SHIMSKY, and M. M. MASON. Tetrahedron Lett. 4763 (1972).
12. H. R. FRANSEN and H. M. BUCK. J. Chem. Soc. Chem. Commun. 786 (1982).
13. W. J. G. M. PEIJNENBURG and H. M. BUCK. Tetrahedron, **44**, 4821 (1988); **44**, 4927 (1988).
14. T. A. ANTKOWIAK, D. C. SANDERS, G. B. TRIMITSIS, J. B. PRESS, and H. SHECHTER. J. Am. Chem. Soc. **94**, 5366 (1972).
15. C. A. BROWN, J. Chem. Soc. Chem. Commun. 600 (1969).
16. H. M. J. GILISSEN, P. SCHIPPER, P. J. J. M. VAN OOL, and H. M. BUCK. J. Org. Chem. **45**, 319 (1980).
17. H. M. J. GILLISSEN. PhD Thesis, Eindhoven University of Technology (1982).
18. D. SCHUSTER and C. W. KIM. J. Org. Chem. **40**, 505 (1975).
19. A. DIAZ, J. FULCHER, R. CETINA, M. RUBIO, and R. REYMOSO. J. Org. Chem. **40**, 2459 (1975).
20. A. E. DEROME. *In* Modern NMR techniques for chemistry research. 2nd ed. Pergamon, Oxford. 1987.
21. P. J. KROPP and H. J. KRAUSS. J. Am. Chem. Soc. **91**, 7466 (1969).
22. R. T. ARNOLD and J. F. DOWDALL. J. Am. Chem. Soc. **70**, 2590 (1948).
23. J. MARCH. *In* Advanced organic chemistry. 3rd ed. John Wiley & Sons, New York. 1985. p. 711, and references therein.
24. C. A. G. HAASNOOT, F. A. A. M. DE LEEUW, and C. ALTONA. Tetrahedron, **36**, 2783 (1988).
25. S. L. MUROV, L. YU, and L. P. GIERING. J. Am. Chem. Soc. **95**, 4329 (1973).
26. J. J. BLOOMFIELD and J. S. MCCONAGHY. Tetrahedron Lett. 3723 (1969).
27. G. J. M. DORMANS, H. R. FRANSEN, and H. M. BUCK. J. Am. Chem. Soc. **106**, 1213 (1984).
28. G. J. M. DORMANS, G. C. GROENENBOOM, and H. M. BUCK. J. Chem. Phys. **86**, 4895 (1987).
29. G. J. M. DORMANS, W. J. G. M. PEIJNENBURG, and H. M. BUCK. J. Mol. Struct. (Theochem), **119**, 367 (1985).
30. J. MARCH. *In* Advanced organic chemistry. 3rd ed. John Wiley & Sons, New York. 1985. p. 868.
31. D. R. ARNOLD. Adv. Photochem. **6**, 301 (1968).
32. W. HERNDON. Tetrahedron Lett. 125 (1971).
33. N. J. TURRO. Pure Appl. Chem. **27**, 697 (1972).
34. N. J. TURRO. *In* Modern molecular photochemistry. The Benjamin/Cummings Publishing Co., Menlo Park, Cal. 1978. p. 292.
35. W. J. NEBE and G. J. FONKEN. J. Am. Chem. Soc. **91**, 1249 (1969).
36. R. S. H. LIU. J. Am. Chem. Soc. **89**, 112 (1967).
37. K. SHIMA, Y. SAKAI, and H. SAKURAI. Bull. Chem. Soc. Jpn. **44**, 215 (1917).
38. R. R. HAUTALA and N. J. TURRO. J. Am. Chem. Soc. **93**, 5595 (1971).
39. J. M. SURZUR and M. P. BERTRAND. Bull. Soc. Chim. Fr. 5b, 1861 (1973).
40. R. SRINIVASAN and K. J. CARLOUGH. J. Am. Chem. Soc. **89**, 4933 (1967).
41. R. B. WOODWARD and R. HOFFMANN. *In* The conservation of orbital symmetry. Academic Press, New York. 1970.
42. D. I. SCHUSTER and C. W. KIM. J. Am. Chem. Soc. **96**, 7437 (1974).
43. M. J. S. DEWAR, E. G. ZOEBISCH, E. P. HEALY, and J. J. P. STEWART. J. Am. Chem. Soc. **107**, 3902 (1985).
44. M. J. S. DEWAR and J. J. P. STEWART. QCPE Bull. **6**, 24 (1986); QCPE Program No. 506 (version 2.10).
45. F. A. L. ANET and I. YAVARI. Tetrahedron Lett. **43**, 1567 (1975).
46. F. A. L. ANET and I. YAVARI. J. Am. Chem. Soc. **100**, 7814 (1978).
47. N. L. ALLINGER, J. F. VISKOCIL, U. BURKERT, and Y. YUH. Tetrahedron, **32**, 33 (1976).

Can. J. Chem. Downloaded from www.nrcresearchpress.com by 84.41.108.74 on 09/07/12
For personal use only.

Enantiospecific syntheses of (+)-hyosamine and (−)-hyosamine

HANS H. BAER,[1] TONG CHEN, AND JERZY B. GIZIEWICZ

The Ottawa–Carleton Chemistry Institute, Department of Chemistry, University of Ottawa, Ottawa, Ont., Canada K1N 6N5

Received April 15, 1991

HANS H. BAER, TONG CHEN, and JERZY B. GIZIEWICZ. Can. J. Chem. **69**, 1563 (1991).

Two constituent components of the stereoisomeric aminocyclitol antibiotics hygromycin B and destomycin A, namely, (+)-hyosamine and (−)-hyosamine (1L- and 1D-(1,3/2,4,6)-4-amino-6-methylamino-1,2,3-cyclohexanetriol **1** and **2**, respectively) were synthesized independently in enantiospecific fashion from the common preparative precursor **3**, 1L-(1,3/2,4,6)-6-azido-1,2-*O*-isopropylidene-4-nitro-1,2,3-cyclohexanetriol, which is conveniently accessible from D-mannose. The key strategy involved selective and sequential reduction of the nitrogenous functions in **3** to the amino stage and installation of an *N*-methyl group in appropriately blocked derivatives. Several variations based on this principle were examined, and one approach to **1** as well as two approaches to **2** were successfully completed. The target amines were characterized as their crystalline penta-*N*,*O*-acetyl derivatives **12** and **22**.

Key words: aminocyclitol antibiotics, enantiospecific syntheses of hyosamines, nitrogen-substituted 1,2,3-cyclohexanetriols.

HANS H. BAER, TONG CHEN et JERZY B. GIZIEWICZ. Can. J. Chem. **69**, 1563 (1991).

Le 1L-(1,3/2,4,6)-6-azido-1,2-*O*-isopropylidène-4-nitro-cyclohexane-1,2,3-triol (**3**), facilement accessible à partir du D-mannose, a été utilisé comme produit de départ commun pour la synthèse énantiospécifique indépendante de deux aminocyclitols stéréo-isomères présents dans les antibiotiques hygromycine B et destomycine A, soit les (+)-hyosamine et (−)-hyosamine (1L- et 1D-(1,3/2,4,6)-4-amino-6-méthylamino-cyclohexane-1,2,3-triols, respectivement **1** et **2**). La stratégie clé implique la réduction sélective et séquentielle des fonctions azotées du composé **3** en fonctions aminées et l'incorporation d'un groupe *N*-méthyle dans les dérivés adéquatement bloqués. On a examiné plusieurs variations basées sur ce principe; une approche conduisant au composé **1** et deux approches conduisant au produit **2** ont été complétées avec succès. Les amines recherchées ont été caractérisées par leurs dérivés cristallins penta-*N*,*O*-acétylés, **12** et **22**.

Mots clés: antibiotiques dérivés de l'aminocyclitol, synthèses énantiospécifiques d'hyosamines, cyclohexane-1,2,3-triols substitués par de l'azote.

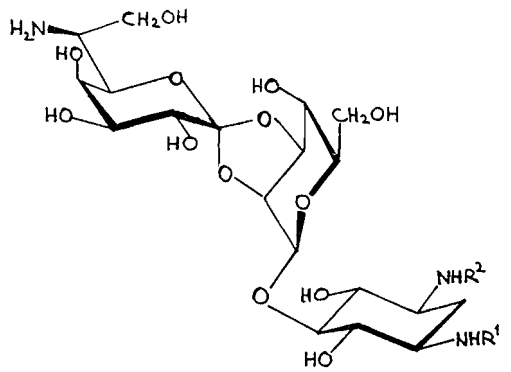
[Traduit par la rédaction]

Introduction

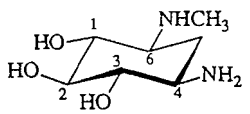
The aminocyclitol antibiotics hygromycin B and destomycin A produced by *Streptomyces hygroscopicus* and *Streptomyces rimofaciens*, respectively, are diastereomers. Each consists of an amino-methylamino-cyclohexanetriol unit (an *N*-methyl-2-deoxystreptamine) to which is glycosidically linked the rare sugar D-talose, which, in turn, bears on its O-2,O-3 positions a 6-amino-6-deoxyheptono-1,5-lactone, attached in orthoester fashion. The sole structural difference between the two antibiotics is the enantiotopic position of the *N*-methyl substituent in the diaminocyclitol (1). Thus, hygromycin B yields on hydrolysis the dextrorotatory fragment **1**, termed (+)-hysamine (1L-(1,3/2,4,6)-4-amino-6-methylamino-1,2,3-cyclohexanetriol), whereas destomycin A gives the 1D enantiomer, levorotatory (−)-hyosamine (**2**).

Although racemic hyosamine was synthesized in the laboratories of Nakajima (2) and Suami (3), no enantiospecific synthesis of **1** appears to have been recorded. Two chiral syntheses of **2** have been described by the same groups of workers. The first synthesis (4) started from achiral 1,2,4,5/3-cyclohexanepentol and used an enantiospecific biochemical oxidation as the key step of generating chirality, and after numerous further steps the optically active target compound was obtained in low overall yield. The second approach (5) was carbohydrate based, commencing with *N*-acetyl-D-glucosamine and employing nitroalkane cyclization strategy. Again, the overall yield over many steps was very poor.

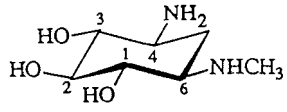
The present paper presents new, enantiospecific approaches to **1** and **2** that start from a common chiral precursor. We recently developed (6) a new synthesis of 2-deoxystreptamine (i.e., **1** or **2** without the *N*-methyl group) that starts from



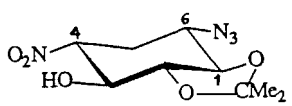
hygromycin B: $R^1 = H$, $R^2 = CH_3$
destomycin A: $R^1 = CH_3$, $R^2 = H$



1
(+)-hyosamine



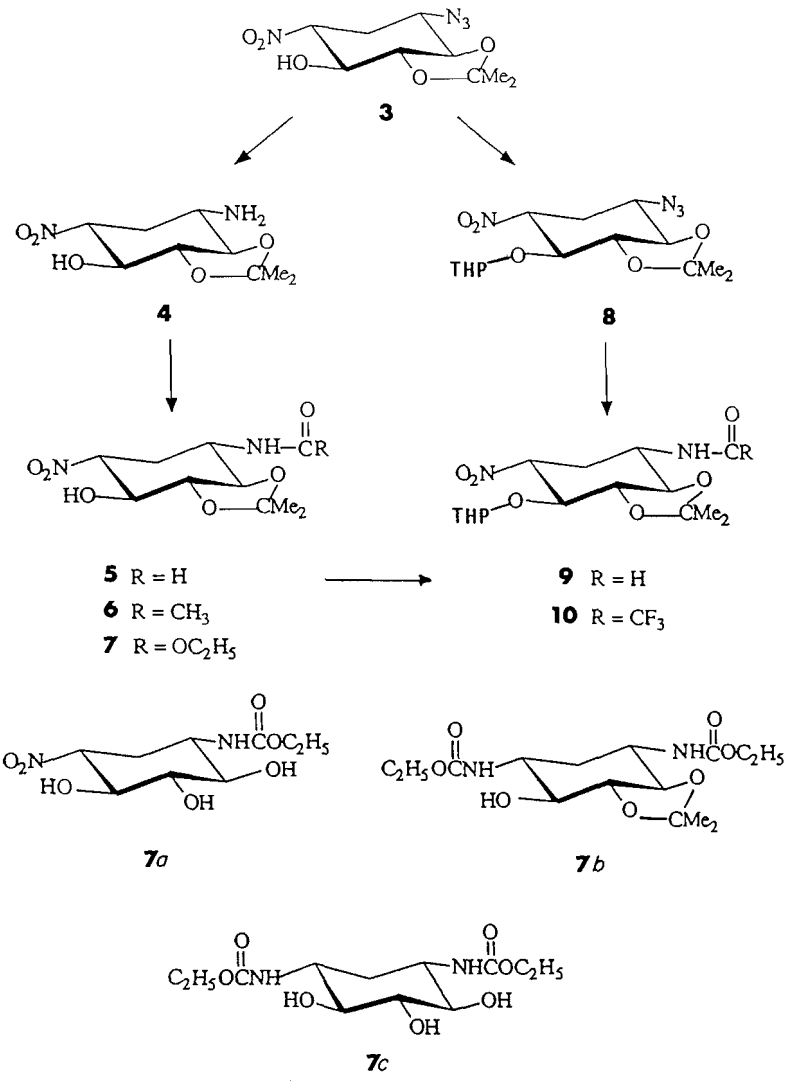
2
(−)-hyosamine



3

[1]Author to whom correspondence may be addressed.

Can. J. Chem. Downloaded from www.nrcresearchpress.com by 84.41.108.74 on 09/07/12
For personal use only.



SCHEME 1

economical D-mannose and proceeds to the (achiral) target via several chiral precursors and derivatives. The purpose of the enterprise was to obtain such chiral derivatives in a stereospecific manner, for potential use in syntheses of unsymmetrically substituted, and hence optically active, 2-deoxystreptamines (such as **1** and **2**, and others) without the need for racemate resolution at some stage. One key intermediate in that work (6) was 1L-(1,3/2,4,6)-6-azido-1,2-*O*-isopropylidene-4-nitro-1,2,3-cyclohexanetriol (**3**), the point of departure for the present study.

Results and discussion

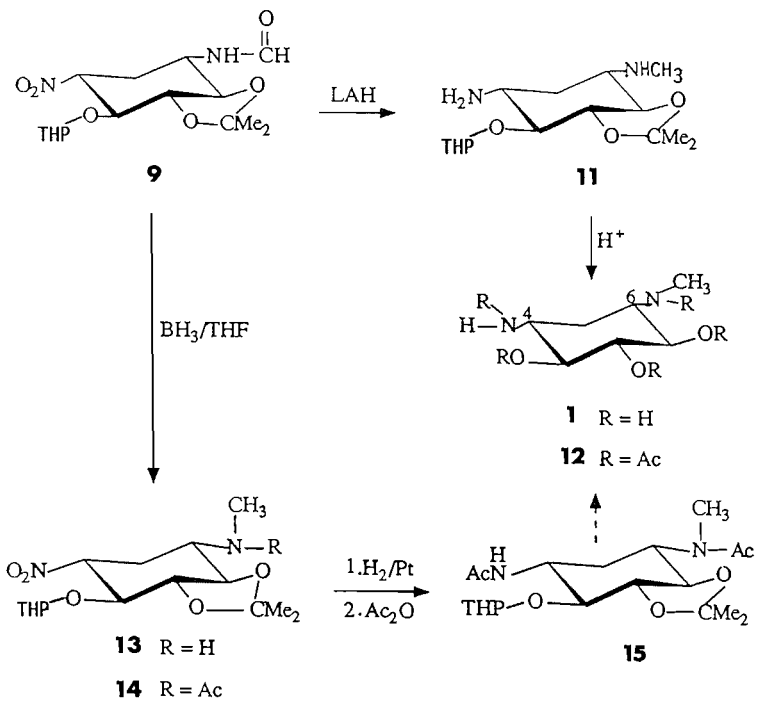
Compound **3** is available from D-mannose in eight facile preparative operations involving nitro sugar chemistry, with yields in the 80–90% range for each step except the last one, a Fischer-type cyclization (7), which gave a 67% yield of pure **3** (6). Compound **3** possesses two nitrogen and three oxygen functions in the same disposition and relative configurational relationship as the hyosamines, and it was reasoned that the two nitrogenous groups, being of different oxidation states, should be able to undergo sequential reduction to the amino stage so that appropriate manipulations should make possible an individual *N*-methylation of either, leading enantiospecifically to **1** and **2**. Several approaches to the realization of this concept are described.

Preparation of starting compounds

For the various designs of routes to **1** and **2** that follow, the cyclitol derivatives **5**–**10** were required as initial stepping stones. Their preparation from the azidonitro cyclitol **3** is illustrated in Scheme 1. Catalytic transfer hydrogenation of **3** over palladium on charcoal in the presence of 1,4-cyclohexadiene selectively reduced the azido group, to produce the aminonitro cyclitol **4**. Although the strained, *trans*-fused dioxolane ring in **3** is very prone to acid hydrolysis, it fortunately tolerates exposure to acetic acid in low concentration (and even to *p*-toluenesulfonic acid in catalytic amounts) for short periods of time, and acetic acid was therefore provided in the transfer hydrogenation medium in a quantity sufficient to neutralize the engendered amine **4** and thus prevent the medium from becoming basic. This precaution was deemed advisable because **3** (and **4**) can undergo base-catalyzed epimerization at C-3 through a retro nitroaldol reaction (6), and although **3** is thermodynamically preferred over its 3-epimer, epimerization occurring to even a minor extent would be most undesirable.[2] For the same reason of presumptive sensitivity, the nitroamine **4**

[2]Epimerization at C-4 is also theoretically possible but in practice poses no risk because of the well-established, great preference of nitro groups on six-membered sugar or cyclitol rings for adopting, or remaining in, an equatorial orientation (8).

Can. J. Chem. Downloaded from www.nrcresearchpress.com by 84.41.108.74 on 09/07/12
For personal use only.



SCHEME 2

was not isolated for characterization but was treated *in situ* with formyl acetate and so converted into the stable formamide **5**, isolated crystalline in 90% yield. Performance of the transfer hydrogenation of **3** in the presence of acetic acid and acetic anhydride furnished the crystalline acetamide **6** in 97% yield.

Crude nitroamine **4**, generated as for the preparation of **5**, was treated in aqueous solution with ethyl chloroformate in the presence of either pyridine or sodium hydrogen carbonate, to produce the carbamate **7**. Although high yields of crude **7** were obtained in several experiments, the product tended to be contaminated by more-polar by-products and required chromatographic purification, after which pure crystalline **7** was isolated in yields of 40–57%. One of the by-products, isolated in one instance in 10% yield, was found by microanalysis and spectroscopy to be the corresponding triol **7***a*, resulting from hydrolytic loss of the isopropylidene group. A second by-product (14%), separated chromatographically in the same experiment, had a polarity (tlc) intermediate beteen **7** and **7***a* and somewhat surprisingly turned out to be the bis-carbamate **7***b*, previously described as the racemic form (9); its deacetonation with 50% acetic acid gave known (9) *N,N'*-diethoxycarbonyl-2-deoxystreptamine (**7***c*). As far as **7***a* is concerned, it has not been clarified whether hydrolysis occurred during the reaction or during processing or chromatography, or whether an impure sample of **3** that had partially become deacetonated during storage was inadvertently used. More intriguing was the encounter with a fairly significant amount of **7***b* in at least one experiment. Although nitroarenes are readily reduced to aminoarenes in phase transfer hydrogenation under a variety of conditions, the same does not normally seem to be the case for nitroalkanes. A comprehensive review (10) of the method makes no mention of nitroalkane reduction, which is why we chose it for selective azide reduction, with obvious success. However, NO_2 *can* evidently undergo slow reduction to NH_2. No attempts were made to pinpoint the cause in the observed instance; this might be difficult because, for such a heterogeneous reaction, precise reproducibility of conditions is hard to achieve and the quality of the batch of catalyst used or the efficacy of agitation (by ultrasound) may have played a role. At any rate, the observations suggest that reactions with **3** need to be performed with circumspection.

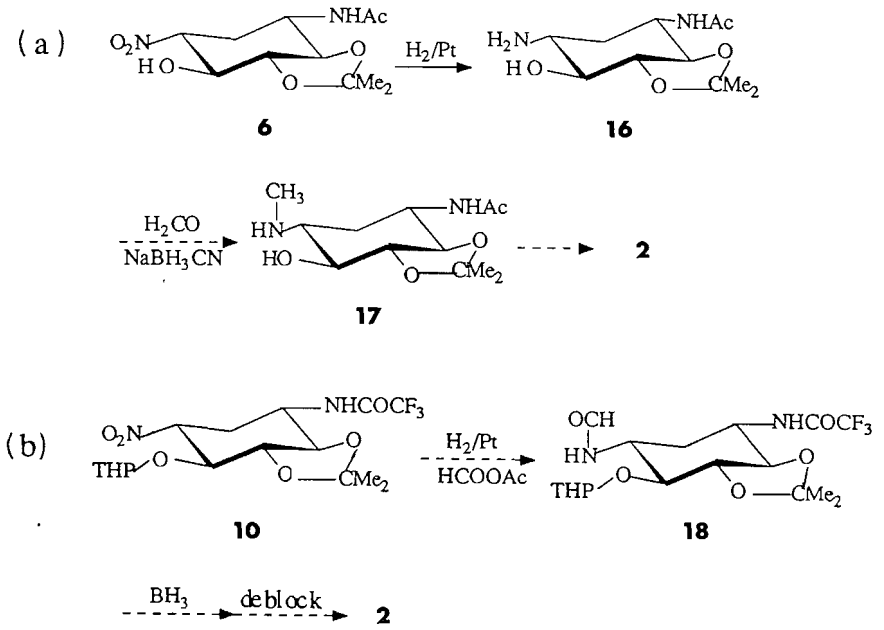
A further intermediate required for one of the planned syntheses was an O-3 protected derivative of **5**. The tetrahydropyranyl ether **9** was obtained in 93% yield by treatment of **5** with 2,3-dihydropyran. Alternatively, **3** was first tetrahydropyranylated to give its 3-THP ether **8**, which was subsequently hydrogenated and *N*-formylated, as for the preparation of **5**, to furnish an 86% yield of crystalline **9**. Finally, the trifluoroacetamide **10** was prepared from **8** by transfer hydrogenation followed by *N*-acylation of the resulting amine with trifluoroacetic anhydride. As was to be expected, the THP ethers **8**, **9**, and **10** (and products derived from them in later sections) arose as mixtures of epimers due to asymmetry at the acetalic C-2′ position. This was reflected in the nmr spectra of these compounds. Partial separation of epimers was observed in some cases after chromatography or fractional crystallization (see Experimental), but separation was not necessary for the conduct of further operations.

Synthesis of (+)-hyosamine

The synthesis of (+)-hyosamine was accomplished as shown in Scheme 2. The blocked formamidonitro compound **9** was treated with lithium aluminum hydride in refluxing 1,4-dioxane to effect concurrent reduction of the nitro and formamido groups.[3] The resulting, *O*-protected cyclitol **11** was not characterized other than by giving an immobile. ninhydrin-positive spot in tlc. It was deprotected by hydrolysis with trifluoroacetic acid to furnish the target compound **1**, m/z 177 for $[M + 1]^+$ as required (chemical ionization mass spectrum). For definitive characterization the product was peracetylated to give its crystalline penta-*N,O*-acetyl derivative **12**, m/z 387 ([M +

[3]This reduction was originally tried with the unprotected alcohol **5** but failed because of solubility problems. Upon addition of the hydride the starting material precipitated from the solution (ether or dioxane) as an insoluble alkoxide, and no reduction in heterogeneous phase was observed.

Can. J. Chem. Downloaded from www.nrcresearchpress.com by 84.41.108.74 on 09/07/12
For personal use only.



SCHEME 3

1]$^+$), in 23% yield based on **9**. Its melting point and specific rotation (but with opposite sign) agreed with the data recorded for the known enantiomer **22** (4, 5), and its ^{1}H nmr spectrum with data reported (2) for the synthetic racemate.

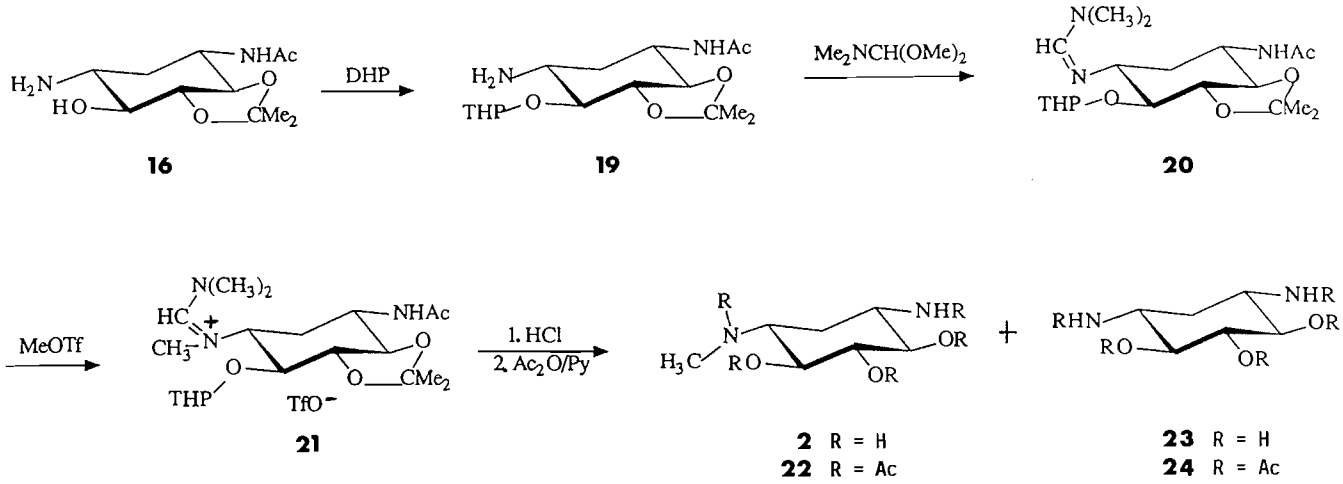
A second aproach to **1** was pursued in an exploratory way (Scheme 2). Treatment of **9** with borane–tetrahydrofuran complex effected reduction of the formamido group alone, leaving the nitro group intact. The crude methylamino derivative **13** so obtained was crystalline but gave a poor ^{1}H nmr spectrum, probably because of contamination by some boron complex; nevertheless, the spectrum confirmed a complete transformation of NHCHO into $NHCH_3$, which was also indicated by the mass spectrum showing a strong [M + 1]$^+$ peak for **13** at m/z 331. Upon *N*-acetylation of **13**, crystalline and well-characterized *N*-methylacetamide **14** was obtained, and platinum-catalyzed hydrogenation of the latter, followed by *N*-acetylation, afforded the amorphous, unsymmetrically blocked (+)-hyosamine derivatives **15**, charcaterized by ^{1}H nmr and mass spectra. It should no doubt be possible to remove all the blocking groups by standard procedures and thus arrive at **1**; more importantly, intermediates useful for generating regiospecifically substituted derivatives of **1** should be obtainable from **15** by applying selective deprotection procedures.

Syntheses of (−)-hyosamine

In first attempts to synthesize **2**, the strategies illustrated in Scheme 3 were pursued. It was considered that the acetamidonitro cyclitol **6** could be converted into the amine **16**, which after *N*-methylation to **17** and deprotection would furnish **2** (Scheme 3(a)). Hydrogenation of **6** over Adams catalyst proceeded very well, with consumption of the theoretical amount of hydrogen overnight at ordinary temperature and pressure. The amorphous amine **16** was characterized by its mass spectrum only, but was authenticated by its successful use in crude form in a subsequent experiment (see Scheme 4). Unfortunately, attempted monomethylation of **16** failed to provide **17** in a practical way. The method of reductive alkylation (11) with formaldehyde and sodium cyanoborohydride gave a complex pattern of products (tlc) that discouraged further efforts. In similar work, Suami *et al.* (5) had methylated an aminocyclitol by hydrogenation in formalin solution with a palladium catalyst, but the desired *N*-methyl derivative was obtained in only 28% yield, accompanied by 18% of *N,N*-dimethyl derivative and 37% of unmethylated product. This did not augur well for our project and we therefore turned to another approach (Scheme 3(b)). It was hoped that the formamido-trifluoroacetamido cyclitol **18**, to be produced from the nitro precursor **10** by catalytic hydrogenation followed by *N*-formylation, might be reducible by borane in the formamido group (compare the successful reduction of **9**) without undue reduction of the trifluoroacetamido group. Being a strong Lewis acid, borane is expected to attack preferentially at centers of high electron density; ordinary amides are readily reduced to alkylamines, but trichloroacetaldehyde is not attacked to any great extent, nor are acyl chlorides (12), and it appeared worthwhile to examine whether selective reduction is possible in **18**. The fact that trifluoroethylamines have been prepared by reduction of trifluoroacetamides by use of mixtures of sodium borohydride and aluminum trichloride (or boron trifluoride), in which borane is believed to be the active reductant (13), militated against the proposition, but, on the other hand, we were encouraged by a series of model experiments that we performed. 1-Formamido- and 1-trifluoroacetamido-1-deoxy-D-xylitol tetraacetates were treated with borane under identical conditions, and the results were evaluated by tlc and mass spectrometry. It was found that both amides were in fact reduced, but the former reacted about 10 times faster than the latter. This finding held promise for an acceptably selective reduction in **18** and prompted us to prepare its precursor **10**. However, the plan was brought to naught when **10** rather unexpectedly proved to be extraordinarily resistant to catalytic hydrogenation (with a 34% recovery of unchanged **10** after many days, and after multiple additions of fresh charges of platinum catalyst), and no pure **18** could be elaborated. This experience contrasted starkly with the facile hydrogenations of the nitro compounds **6** and **14** (and **7**; see below).

The first successful route to **2** is depicted in Scheme 4. Crude **16**, obtained from **6** as mentioned before, was tetrahydropyranylated to yield 83% (based on **6**) of its 3-THP ether **19**,

Can. J. Chem. Downloaded from www.nrcresearchpress.com by 84.41.108.74 on 09/07/12
For personal use only.



SCHEME 4

which without purification was subjected to *N*-methylation by the method of O'Donnell *et al.* (14). This one-pot procedure involves generation of a formamidine (**20**) by action of *N,N*-dimethylformamide dimethyl acetal, followed by reaction with methyl triflate (→**21**) and hydrolysis with boiling hydrochloric acid. The hydrolysis converts the amidinium function in **21** into a methylamino group and, of course, removes all blocking groups from the molecule, which emerges as **2**·dihydrochloride. The product obtained was not homogeneous in tlc, however. It showed two closely spaced, ninhydrin-positive spots, one identical with that of enantiomer **1** (hence attributable to **2**), and the other migrating like an authentic sample of 2-deoxystreptamine (**23**). Conventional peracetylation of the reaction mixture and column chromatography furnished the crystalline penta-*N,O*-acetyl derivative **22** of (+)-hyosamine in 20% yield from **19**, agreeing in its physical constants and ^{1}H nmr spectrum with literature data (2, 4, 5) and with the enantiomer **12**, and crystalline penta-*N,O*-acetyl-2-deoxystreptamine (**24**) (15) in 14% yield. Identification of the latter revealed that *N*-methylation of **19** by this procedure was incomplete, a circumstance that prompted us to seek yet another approach.

To that end, we returned to the concept of selective amide reduction by borane. The reagent has been shown to be capable of reducing amides without affecting carbamate functions present in the same molecule (12*c*, 16). Therefore, the reaction sequence depicted in Scheme 5 was devised. Like **6** and **14**, the nitrocarbamate **7** could be smoothly hydrogenated over Adams catalyst, and the amine engendered was *N*-formylated *in situ*, to give the crystalline formamido carbamate **25** in 76% yield. Treatment with borane in refluxing tetrahydrofuran for 5 h then reduced the formamido to a methylamino group, leaving the ethyl carbamate function intact. At the end of such a reduction it is necessary to decompose amine–boron complexes formed, which is normally done by acidification of the reaction mixture with hydrochloric acid (12*c*, 16). Adopting that work-up procedure in first experiments (and recognizing that this would also cleave off the isopropylidene protecting group[4]), we obtained what according to ^{1}H nmr and mass spectra of the crude product was the desired hyosamine ethyl carbamate (as hydrochloride). However, the product proved difficult to isolate and purify. When, instead, the processing was performed with water and a stream of carbon dioxide, the acetonide group was largely retained and the product was easier to handle. It required chromatographic purification, though, and pure **26** was obtained in 35% yield only. A substantial proportion of **26** (43%) emerged from the column as a syrup contaminated by a minor amount of deacetonated material that, we suspect, may have risen at least in part on the column under the influence of the silica gel. Acetylation of this fraction failed to give crystalline material but yielded a syrupy mixture of the *N,O*-diacetyl derivative **27** (major component) and the *N,O,O,O*-tetraacetyl derivative **30** as evaluated by ^{1}H nmr, ^{13}C nmr, and mass spectra.

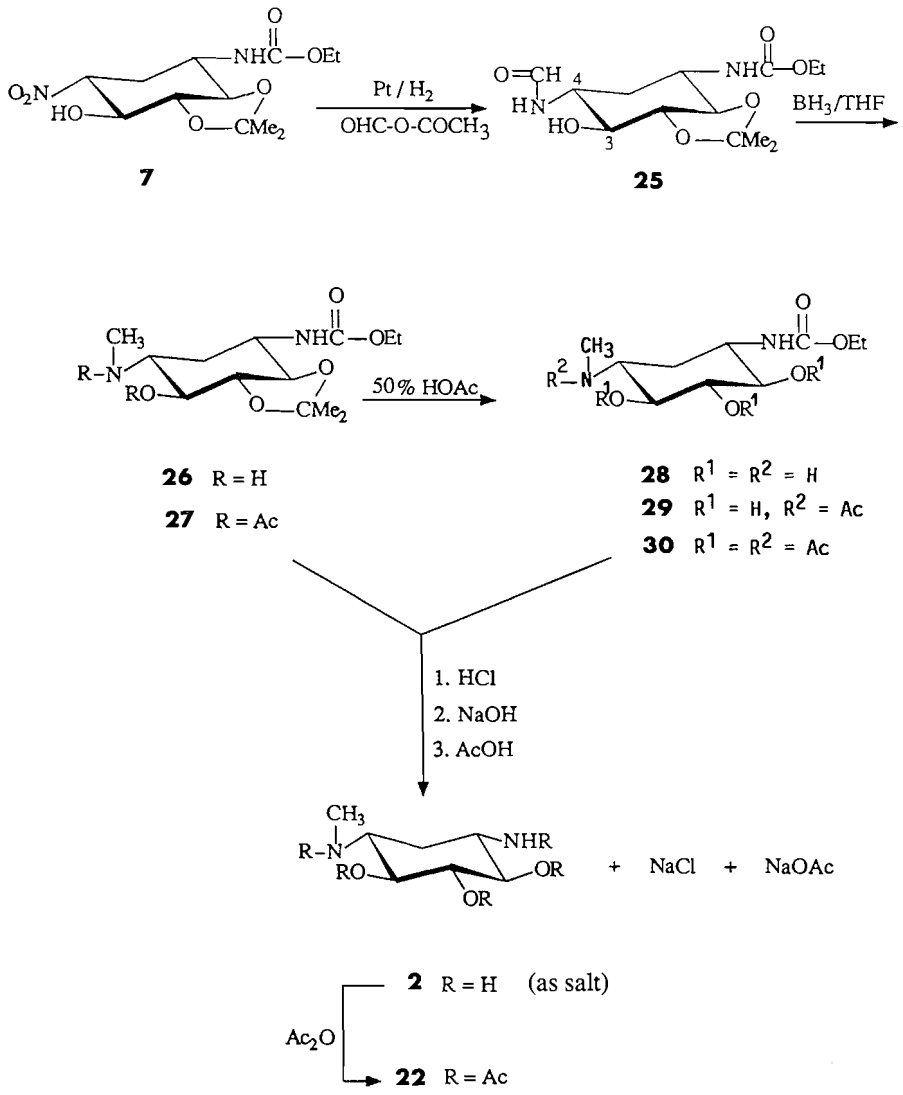
The acetonide **26** exhibited an nmr-spectral peculiarity (see below) which was felt to be possibly attributable to its strained bicyclic structure, and we were therefore interested in obtaining for comparison a pure sample of its product of deacetonation (**28**). Overnight treatment of pure **26** with 50% acetic acid at room temperature cleanly hydrolyzed the ketal, but the compound underwent *N*-acetylation in the process,[5] giving the methylacetamido triol **29**.

For completion of the synthesis, the mixture of blocked derivatives **27** and **30** was to be hydrolyzed. Whereas boiling with dilute hydrochloric acid (1–2 M) could be expected to effect *O*- and *N*-deacetylation (and of course deacetonation in **27**), cleavage of the carbamate was anticipated to require more-forcing conditions and the mixture was therefore heated at 100°C in 6 M HCl. The more-labile groups were split off rapidly, but the carbamate resisted completely under these drastic conditions for at least 2 h, according to the ^{13}C nmr spectrum of the hydrolyzate. Evidently, after an early cleavage of the *N*-acetyl group the compound exists as a methylammonium ion whose charge electrostatically impedes further protonation for carbamate hydrolysis. (For the same reason, glyco-

[4]At this stage of the synthesis the group had become dispensable. In the analogous borane reduction of **9** (Scheme 2), retention of the acetonide was desired and acid treatment was therefore omitted. Processing was performed with methanol instead, and some boron apparently remained in the product.

[5]Partial acetylation even of hydroxyl groups in carbohydrates with *hot* 50% acetic acid has been reported (17), and minor proportions of *O*-acetylated products were occasionally observed to arise under conditions of deacetalation with hot 80% acetic acid (18). The occurrence of (more facile) *N*-acetylation in the present instance should therefore not be surprising; possibly it took place during processing by evaporation of the acid at moderately elevated temperature.

Can. J. Chem. Downloaded from www.nrcresearchpress.com by 84.41.108.74 on 09/07/12
For personal use only.



SCHEME 5

sides of amino sugar hydrochlorides are extremely resistant to acid hydrolysis.) However, subsequent saponification with 2 M sodium hydroxide removed the ethoxycarbonyl substituent and produced **2**, extracted from the resulting salt mixture, after peracetylation, as crystalline pentaacetyl derivative **22** in 60% yield. The product was identical in every respect with **22** from the previous synthesis. Although not all operations have been optimized, the overall yield in the four steps from **3** was 20%.

Nuclear magnetic resonance spectra

Some of the nmr parameters for the compounds prepared (see the experimental section) deserve special comment. Thus, the ^1H spectra of the pentaacetylhyosamines **12** and **22** exhibited the phenomenon of signal multiplication already observed in the synthetic racemate (2). There were *two* *N*-methyl signals, namely, a broadened and a sharp singlet at δ 2.81 and 2.72, respectively, in an intensity ratio of ~3:2, integrating jointly to 3 protons,[6] and instead of the expected five 3-proton singlets for the acetyl groups around δ 2.0 there was a cluster of numerous singlets (13–14) with varying intensities but correctly integrating to five times the combined *N*-CH_3 signal intensity. Furthermore, *two* low-field doublets (δ 5.70 and 5.63, J = 8 Hz) integrating together to 1 proton were seen for the amidic NH. The phenomenon has been attributed "probably (to) the space requirement of the methylacetamido group" (2). It seems possible that free rotation of that group about the bond connecting it to the ring is sufficiently impeded by the neighboring acetoxyl for individual rotamers to become spectroscopically recognizable; however, it may also be a rotational-barrier effect in one or both of the amidic CO—N bonds, as is well known to occur in *N,N*-dimethylformamide. Conceivably both factors may contribute. The 4-acetamido-6-(*N*-methyl)-acetamido derivative **15** displayed the same phenomenon, showing two major *N*-CH_3 singlets in 2:1 intensity ratio (each being accompanied by a minor satellite at slightly lower field, presumably due to tetrahydropyranyl epimerism), and a cluster of several $COCH_3$ singlets integrating to 6 protons. Steric hindrance of the methylacetamido group would appear less plausible in this case, and the 4-nitro analog **14** gave only one sharp, 3-proton singlet each for the *N*-CH_3 and $COCH_3$ groups, thus revealing no rotamers. The same was true for the 4-(*N*-methyl)acetamido 6-carbamate **29**, for which homogeneity was moreover confirmed by a ^{13}C nmr spectrum.

[6]In one of the spectra taken, the broadened singlet was resolved into two sharp singlets at δ 2.84 and 2.81 whilst the singlet at δ 2.72 was unchanged. This was probably a temperature or concentration effect.

Can. J. Chem. Downloaded from www.nrcresearchpress.com by 84.41.108.74 on 09/07/12
For personal use only.

Can. J. Chem. Downloaded from www.nrcresearchpress.com by 84.41.108.74 on 09/07/12
For personal use only.

Surprisingly in light of the above observations, the nonacetylated *N*-methylamino compounds **13** and **27** displayed duplicate NH-CH_3 signals. These were doublets (J = 6.1 and 5.9 Hz) at δ 2.53 and 2.69 (ratio ~1:2), and δ 2.60 and 2.44 (ratio 1:1.2), respectively. While we refrain from further comment regarding **13** because this compound had not been isolated in entirely pure state, **27** was analytically pure and we conclude that it exists in solution as a mixture of stable, magnetically nonequivalent species. This was borne out by the ^{13}C nmr spectrum in which the peaks for *N*-CH_3 and all the ring carbon atoms (but not those for the ethyl carbamate and the isopropylidene methyl groups) were accompanied by satellites showing 75–90% intensities relative to the main peaks. Perhaps the phenomenon is due to the possibility of hydrogen bonding between the vicinal methylamino and hydroxyl groups, in $CDCl_3$ solution. It is to be noted that the ^{13}C nmr spectrum of hyosamine **1** in water contains only the seven resonances expected for the structure (1).

Finally, it is interesting to compare the ^1H spectra of the formamides **5**, **9**, and **25**. Whereas the nitroformamide **5** and (both 2′-epimers of) its 3-THP ether **9** in $CDCl_3$ solution showed one singlet (δ 8.18) for the formyl proton, in the formamido carbamate **25** in acetone-d_6 two rotameric forms apparently interconverted slowly enough to become manifest. The spectrum contained a slightly broadened singlet (δ 8.13, $J_{CHO,NH} < 1$ Hz) and a doublet (δ 8.03, $J_{CHO,NH}$ = 12 Hz) in a ratio of ~4:1, integrating to 1 proton of the formyl group, and the corresponding amidic NH signals (also ~4:1) appeared as a doublet (δ 7.3, $J_{NH,4}$ = 7 Hz, with slightly broadened lines) and a triplet (δ 6.7, $J_{NH,4} = J_{NH,CHO}$ = 12 Hz). Upon deuterium exchange the NH signals disappeared and the two formyl signals became sharp singlets. The ^{13}C spectrum likewise showed a major and a minor set of signals for the formyl and cyclitol ring carbon atoms, attributed to rotamers. Again, hydrogen bonding with the vicinal hydroxyl group could be responsible for the effect.

Experimental

Thin-layer chromatography (tlc) was performed on precoated silica gel plates, and spots were made visible by spraying the plates with 5% H_2SO_4 in EtOH or, for amines, with 2% ninhydrin in EtOH, and heating them on a hot plate. Column chromatography was performed with silica gel Merck 9385 (particle size 20–45 μm) or equivalent material. The following solvent combinations (v/v) were used for chromatography, unless otherwise specified: MeOH/$CHCl_3$ 1:1 (*A*), 1:5 (*B*), 1:9 (*C*), 1:19 (*D*), and 1:49 (*E*); EtOAc/hexane 3:1 (*F*), 3:2 (*G*), 1:1 (*H*), 1:3 (*I*), and 1:9 (*J*); Et_2O/hexane 1:1 (*K*) and 1:4 (*L*); MeOH/EtOAc 1:6 (*M*); MeCN/conc. aq. NH_3/water 3:2:1 (*N*) and 4:1:2 (*O*); MeOH/CH_2Cl_2 1:9 (*P*) and 1:49 (*Q*).

Melting points were determined in capillaries with a Gallenkamp electrothermal apparatus. Optical rotations were measured at room temperature in a Perkin Elmer 241 polarimeter. Infrared data (ν_{max}) refer to spectra obtained from Nujol mulls for solids, or from thin films for syrups, unless otherwise indicated; only bands of particular structural significance are listed. Mass spectral data (m/z) were obtained by the chemical ionization mode using ether as the ionizing gas. Nuclear magnetic resonance (nmr) data given without special notation refer to spectra taken from $CDCl_3$ solutions at 300 MHz (for ^1H) or 75.43 MHz (for ^{13}C) with a Varian XL-300 instrument. Data denoted by 200 MHz (for ^1H) or 50.3 MHz (for ^{13}C) were obtained with a Varian Gemini 200 instrument. Solvents other than $CDCl_3$ are stated.

*1L-(1,3/2,4,6)-6-Azido-1,2-*O*-isopropylidene-4-nitro-1,2,3-cyclohexanetriol (3)*

Compound **3** was prepared as described (6), and verified by its well-resolved ^1H nmr spectrum to be free from 3-epimer (6); ^{13}C nmr (50.3 MHz), not previously recorded, δ: 113.3 (O_2CMe_2), 86.4 (C-4), 79.0, 78.4 (C-1, 2), 71.5 (C-3), 57.0 (C-6), 32.9 (C-5), 26.4 (CMe_2).

*1L-(1,3/2,4,6)-6-Formamido-1,2-*O*-isopropylidene-4-nitro-1,2,3-cyclohexanetriol (5)*

To a solution of **3** (516 mg, 2 mmol) in MeOH (20 mL) containing AcOH (0.18 mL) was added 10% Pd-C (400 mg, suspended in a small amount of MeOH), followed by 1,4-cyclohexadiene (1.6 mL). An N_2 atmosphere was provided and the flask immersed in an ultrasonic bath at 45°C. After sonication until **3** (R_f 0.9, acid spray) was completely replaced by the amine **4** (R_f 0.2, ninhydrin spray; tlc with EtOAc), which normally took 30 but occassionally up to 120 min, the catalyst was filtered off and washed with MeOH, and to the filtrate was added 1 mL of formyl acetate (19). *N*-Formylation was complete after 30 min at 25°C when tlc (EtOAc) showed **5** as a single spot, R_f 0.65. The solvent was evaporated and several portions of added EtOH were evaporated from the syrupy residue to remove acid. The slightly turbid solution of the residue in EtOAc was clarified with Celite, and **5** was then obtained crystalline (470 mg, 90%) from EtOAc/$CHCl_3$/Et_2O; mp 167–168°C (unchanged after recrystallization from 2-propanol); $[\alpha]_D$ +31.3 (*c* 0.6, MeOH); ν_{max}: 3350 (br, OH and NH), 1675 (amide CO), 1550 (NO_2) cm^{-1}; ^1H nmr, δ: 8.18 (s, slightly broadened, CHO), 4.73 (br s, NH), 4.51 (m, H-4), 4.41 (t, $J_{2,3} = J_{3,4}$ = 9.2 Hz, H-3), 4.18 (m, H-6), 3.56 (t, $J_{1,2} = J_{1,6}$ = 9.2 Hz, H-1), 3.48 (t, $J_{1,2} = J_{2,3}$ = 9.2 Hz, H-2), 2.91 (dt, $J_{4,5eq} \approx J_{5eq,6} \approx$ 4.8 Hz, $J_{5ax,5eq}$ = 13.3 Hz, H-5eq), 2.78 (br s, OH), 1.87 (dt, $J_{4,5ax} = J_{5ax,6}$ = 12.2 Hz, $J_{5ax,5eq}$ = 13.3 Hz, H-5ax), 1.46 (s, 6H, CMe_2); m/z: 261 ($M^+ + 1$, base peak), 245 ($M^+ + 1 - O$), 243 ($M^+ + 1 - H_2O$), 203 ($M^+ + 1 - Me_2CO$), 185 ($M^+ + 1 - H_2O - Me_2CO$). Anal. calcd. for $C_{10}H_{16}N_2O_6$ (260.2): C 46.15, H 6.20, N 10.77; found: C 46.27, H 6.29, N 11.04.

*1L-(1,3/2,4,6)-6-Acetamido-1,2-*O*-isopropylidene-4-nitro-1,2,3-cyclohexanetriol (6)*

Compound **3** (516 mg) was subjected to transfer hydrogenation as described for the preparation of **5**, except that acetic anhydride (0.4 mL) was added to the medium, along with the AcOH (0.18 mL). The reaction was monitored by tlc (solvent *C*), which indicated that the conversion of **3** (R_f 0.7) into **6** (R_f 0.3) was virtually complete after sonication at 45°C for 20 min. Hydrogenation was stopped after 30 min, the catalyst was removed and washed exhaustively with MeOH, and the filtrate was concentrated with consecutive additions of three portions of fresh MeOH and then brought to dryness. Added EtOH and toluene were evaporated from the residue until a smell of acetic acid was no longer noticeable. The cloudy solution of the residue in EtOAc was clarified by passage through a plug of Celite/activated carbon, and concentrated, and **6** then crystallized upon addition of some $CHCl_3$ and, eventually, some hexane. Isolated and washed with a mixture of the same solvents, **6** (532 mg, 97%) had mp 175–177°C, raised to 185–186°C by recrystallization from 2-propanol; $[\alpha]_D$ +40.3 (*c* 0.5, MeOH); ν_{max}: 3390 (sharp , NH), 3260 (br, OH), 1650 (amide CO), 1545 (NO_2) cm^{-1}; ^1H nmr, δ: 5.58 (br d, $J_{6,NH}$ = 6.3 Hz, NH), 4.50 (m, H-4), 4.39 (t, $J_{2,3} = J_{3,4}$ = 9.0 Hz, H-3), 4.10 (m, H-6), 3.49 (AB-m, 2H, $J_{1,2} = J_{1,6} = J_{2,3}$ = 9 Hz, H-1,2), 2.92 (dt, $J_{4,5eq} = J_{5eq,6}$ = 5.1 Hz, $J_{5ax,5eq}$ = 13.3 Hz, H-5eq), 2.75 (br s, OH), 1.99 (s, 3H, Ac), 1.77 (dt, $J_{4,5ax} = J_{5ax,6}$ = 12.3 Hz, $J_{5ax,5eq}$ = 13.3 Hz, H-5ax), 1.44 and 1.45 (2s, 6H, CMe_2); m/z: 275 ($M^+ + 1$, base peak), 217 ($M^+ + 1 - Me_2CO$), 199 ($M^+ + 1 - H_2O - Me_2CO$). Anal. calcd. for $C_{11}H_{18}N_2O_6$ (274.3): C 48.17, H 6.62, N 10.21; found: C 48.28, H 6.65, N 10.26.

*1L-(1,3/2,4,6)-6-Ethoxycarbonylamido-1,2-*O*-isopropylidene-4-nitro-1,2,3-cyclohexanetriol (7) and derivatives 7a–7c*

Compound **3** (516 mg) was converted by catalytic transfer hydrogenation into the amine **4**, as described for the preparation of **5**. The catalyst was filtered off and washed well with MeOH, and the filtrate was evaporated to a syrup that was taken up in water (20 mL). Pyridine (0.23 mL, 1.44 mol. equiv.) was added and then, dropwise, ethyl chloroformate (0.23 mL, 1.2 mol. equiv.). The mixture was stirred at room temperature for 1 h, after which the conversion of **4** (R_f 0.2) into **7** (R_f 0.6) was complete (tlc, solvent *C*). The mixture was diluted with an equal volume of water and extracted with EtOAc (3 × 20 mL), with addition of brine to destabilize the emulsion that tended to form. The dried (Na_2SO_4) and concentrated extract gave a syrup that was passed through an SiO_2 column (2.3 × 20 cm) by means of solvent *I*, to give

Can. J. Chem. Downloaded from www.nrcresearchpress.com by 84.41.108.74 on 09/07/12
For personal use only.

crystalline **7**, (242 mg, 40%). A 57% yield was achieved in a similar experiment in which the ethoxycarbonylation was performed at 0°C in the presence of $NaHCO_3$ (1.2 mol. equiv.) instead of pyridine. Usually the crude product contained small amounts of by-products that migrated more slowly in tlc. Crystalline **7** had mp 76–78°C; $[\alpha]_D$ +24.1 (*c* 1.1, $CHCl_3$); ν_{max}: 3350 (br, NH and OH), 1700–1680 (urethane CO), 1545–1530 (NO_2 and urethane NH) cm^{-1}; ^1H nmr, (DMSO-d_6 at 55°C; assignments confirmed by COSY), δ: 7.14 (d, $J_{6,NH}$ = 8.8 Hz, NH), 5.95 (d, $J_{3,OH}$ = 5.8 Hz, OH-3), 4.71 (ddd, $J_{3,4}$ = 9.4, $J_{4,5eq}$ = 5.0, $J_{4,5ax}$ = 12.6 Hz, H-4), 4.08–3.96 (m, 3H, H-3 and OCH_2Me), 3.88 (crude octet with broadened center peaks, W = 35 Hz, H-6), 3.47 (sym. septet, 2H, W = 34.3 Hz with line separations of 9.15, 6.25, and 1.75 Hz, H-1,2), 2.34 (dt, $J_{4,5eq}$ = $J_{5eq,6}$ = 4.8 Hz, $J_{5ax,5eq}$ = 12.7 Hz, H-5eq), 1.86 (apparent q, W = 36.6 Hz, with splittings of 12.6, 11.4, and 12.6 Hz, consistent with $J_{4,5ax} \approx J_{5ax,5eq} \approx 12.6$ and $J_{5ax,6} \approx 11.4$ Hz, H-5ax), 1.38 and 1.37 (2s, 3H each, CMe_2), 1.17 (t, 3H, J = 7.1 Hz, ethyl CH_3 *m/z*: 305 ($M^+ + 1$), 260 ($M^+ + 1 - OEt$), 247 ($M^+ + 1 - Me_2CO$). Anal. calcd. for $C_{12}H_{20}N_2O_7$ (304.3): C 47.62, H 6.63, N 9.21; found: C 47.43, H 6.70, N 8.98.

In one experiment, performed on a 2-mmol scale in the presence of $NaHCO_3$ during *N*-acylation at 0°C, the slow-moving by-products seen in tlc of the crude **7** appeared especially prominent, and they were isolated for examination. Column chromatography was performed using 2:3 EtOAc/hexane, and after collection of pure **7** (350 mg, 57.5%) the elution was continued and sequentially gave crystalline **7***b* (95 mg, 13.7%) and crystalline **7***a* (55 mg, 10.4%), R_f 0.35 and 0.1 (tlc with solvent *C*).

1D(1,3/2,4,6)-4-Ethoxycarbonylamido-6-nitro-1,2,3-cyclohexanetriol[7] (7a) had mp 202–204°C; $[\alpha]_D$ +22.9 (*c* 0.6, MeOH); ν_{max} ($CHCl_3$): 3300 (br, OH and NH), 1675 (urethane CO), 1560–1540 (amide II and NO_2) cm^{-1}; ^1H nmr (DMSO-d_6), δ: 6.99 (d, $J_{4,NH}$ = 8.5 Hz, NH), 5.62, 5.23, 4.93 (3d, exchangeable, J = 5.6, 4.6, and 4.4 Hz, OH-1,2,3), 4.60 (ddd, $J_{5eq,6}$ = 4, $J_{1,6}$ = 10, $J_{5ax,6}$ = 12 Hz, H-6), 3.94 (q, 2H, J = 7 Hz, O-CH_2Me), 3.50–3.35 and 3.10 (2m, 4H total, H-1,2,3,4), 2.14 (dt, $J_{4,5eq} \approx J_{5eq,6} \approx 4$ Hz, $J_{5ax,5eq}$ = 12 Hz, H-5eq), 1.75 (~q, $J_{4,5ax} \approx J_{5ax,6} \approx J_{5ax,5eq} \approx 12$ Hz, H-5ax), 1.13 (t, 3H, J = 7 Hz, ethyl CH_3); ^{13}C nmr (50.3 MHz, DMSO-d_6), δ: 156.4 (CO), 86.7 (C-6), 75.3, 74.1, 74.0 (C-1,2,3), 59.9 (OCH_2), 50.7 (C-4), 32.7 (C-5), 14.8 (ethyl CH_3); *m/z*: 265 ($M^+ + 1$, weak), and no species of greater mass. Anal. calcd. for $C_9H_{16}N_2O_7$ (264.2): C 40.91, H 6.10, N 10.60; found: C 41.07, H 6.08, N 10.74.

1L-(1,3/2,4,6)-4,6-Di-(ethoxycarbonylamido)-1,2-O-isopropylidene-1,2,3-cyclohexanetriol (7b) had mp 188–190°C (lit. (9) for racemate, mp 199–200°C); $[\alpha]_D$ +10.8, $[\alpha]_{546}$ +13.3, $[\alpha]_{436}$ +21.6, $[\alpha]_{365}$ +28.4 (*c* 1.2, $CHCl_3$), and $[\alpha]_D$ +1.1, $[\alpha]_{365}$ −0.43 (*c* 1.2, MeOH); ν_{max} ($CHCl_3$): 3300 (br, OH and NH), 1670 (urethane CO), 1545 (amide II) cm^{-1}; ^1H nmr (200 MHz, DMSO-d_6), δ: 7.26 and 7.05 (2d, exchangeable, J = 8.6 and 7.7 Hz, 2NH), 5.12 (d, exchangeable, J = 4.8 Hz, OH-3), 3.97 (q, 4 H, J = 7 Hz, $2OCH_2$Me), 3.7–3.2 (complex m, unresolved, H-1,2,3,4,6), 1.85 (dt, $J_{5eq,5eq}$ = 12 Hz, H-5eq), 1.33 (s, 6H, CMe_2), 1.27 (m, overlapped by adjacent signals, H-5ax), 1.15 (t, 6H, J = 7 Hz, 2 ethyl CH_3); in $CDCl_3$ solution, the dt for H-5eq was at δ 2.24, CMe_2 gave two separate signals (δ 1.42, 1.40), and also the OEt groups gave separate (but overlapping) quartets at δ 4.08 and triplets at δ 1.20; ^{13}C nmr (50.3 MHz, DMSO-d_6), δ: 156.5 156.0 (2CO), 110.2 (O_2CMe_2), 81.2, 78.5, 71.6 (C-1,2,3), 60.0, 59.9 ($2OCH_2$), 53.3, 49.0 (C-4,6), 36.6 (C-5), 27.1, 27.0 (CMe_2), 14.8 (double intensity, 2 ethyl CH_3). Anal. calcd. for $C_{15}H_{26}N_2O_7$ (346.4): C 52.01, H 7.57, N 8.08; found: C 51.82, H 7.46, N 7.98.

[7]For **7** the rules of nomenclature (20) require that the triol system is numbered so as to give any *substituted* (by isopropylidene in this case) OH groups the lowest possible locant numbers. For **7***a*, however, with unsubstituted OH groups only, the sense of numbering is dictated by alphabetic precedence of other substituents present and must here be reversed because EtOCONH comes before NO_2. As a result, the configurational prefix 1D applies.

(1,3/2,4,6)-Di-(ethoxycarbonylamido),1,2,3-cyclohexanetriol (7c) was obtained by overnight treatment of **7***b* (95 mg) with 50% aqueous AcOH (10 mL) at room temperature, after which **7***b* (R_f 0.35) was seen replaced by immobile **7***c* (tlc with solvent *C*). The acid was evaporated with additions of EtOH, and the white residue was passed through an SiO_2 column (1.5 × 10 cm) by elution with solvent *P*, a solvent that was also used for monitoring the effluent by tlc. There was obtained 63 mg (75%) of crystalline **7***c*, mp 235–237°C (lit. (9) mp 321–232°C); ^1H nmr (DMSO-d_6) δ: 6.90 (d, 2H, J = 7.6 Hz, 2NH), 4.85 (d, J = 3.7 Hz, OH-2), 4.65 (d, 2H, J = 3.9 Hz, OH-1,3), 3.95 (q, 4H, J = 7.1 Hz, $2OCH_2$), 3.20 (m, 2H, H-4,6), 3.00 (m, 3H,H-1,2,3), 1.75 (dt, $J_{5ax,5eq}$ = 13 Hz, H-5eq), 1.15 (t, 6H, J = 7.1 Hz, ethyl CH_3; superimposed on m, 1H, for H-5ax); ^{13}C nmr (50.3 MHz, DMSO-d_6), δ: 156.3 (2CO), 77.1 (C-2), 74.2 (C-1,3), 59.6 ($2OCH_2$), 51.5 (C-4,6), 35.2 (C-5), 14.8 (2 ethyl CH_3); *m/z*: 307 ($M^+ + 1$, base peak), 261 ($M^+ + 1 - EtOH$), 215 ($M^+ + 1 - 2EtOH$). Anal. calcd. for $C_{12}H_{22}N_2O_7$ (306.3): C 47.05, H 7.24, N 9.20; found: C 47.29, H 6.82, N 9.11.

1L-(1,3/2,4,6)-6 Azido-1,2-O-isopropylidene-4-nitro-3-O-(tetrahydropyran-2-yl)-1,2,3-cyclohexanetriol (8)

A solution of **3** (747 mg, 3 mmol), 2,3-dihydropyran (1.4 mL, 15 mmol), and *p*-toluenesulfonic acid monohydrate (57 mg) in 1,4-dioxane (25 mL) was kept at 25°C for 1 h; tlc (solvent *I*) had revealed that conversion of **3** (R_f 0.3) into **8** (two epimers, R_f 0.7 and 0.65) was nearly complete after 30 min. Saturated aqueous $NaHCO_3$ (3 mL) was added and the mixture was evaporated. The residue was distributed between water and $CHCl_3$, and the organic phase washed with water, dried, and concentrated to a syrup of crude **8** (1.00 g, 97%) that could be used directly for preparing **9** or **10**. For analytical characterization, the crude **8** was chromatographed on an SiO_2 column (3.8 × 12 cm) by elution with hexane followed by solvent *J*. Early fractions contained pure, faster-moving epimer, which crystallized in fine needles upon concentration of the eluate and addition of hexane; yield, 522 mg; double mp at 97–99 and 112–113°C; $[\alpha]_D$ −118.6 (*c* 1, $CHCl_3$); ^1H nmr, δ: 5.11 (t, J = 2.4 Hz, H-2′), 4.57 (ddd, $J_{4,5eq}$ = 5.0, $J_{3,4}$ = 9.35, $J_{4,5ax}$ = 12.3 Hz, H-4), 4.48 (t, $J_{2,3}$ = $J_{3,4}$ = 9.35 Hz, H-3), 3.67 (ddd, $J_{5eq,6}$ = 4.7, $J_{5ax,6}$ = 11.4, $J_{1,6}$ = 9.9 Hz, H-6), 3.5 (m, 3H, containing H-6′,6″ signals and a t, J = 9.5 Hz, for H-1), 3.38 (t, $J_{1,2}$ = $J_{2,3}$ = 9.4 Hz, H-2), 2.56 (dt, $J_{4,5eq} \approx J_{5eq,6} \approx 4.7$ Hz, $J_{5ax,5eq}$ = 13.2 Hz, H-5eq), 2.05 (octet, $J_{4,5ax}$ = 12.5, $J_{5ax,6}$ = 11.5, $J_{5ax,5eq}$ = 13.2 Hz, H-5ax), 1.7–1.5 (m, 6H, H-3′,3″,4′,4″,5′,5″), 1.45 and 1.43 (2s, 3H each, CMe_2); *m/z*: 343 ($M^+ + 1$, base peak), 327 ($M^+ + 1 - O$), 315 ($M^+ + 1 - N_2$), 285 ($M^+ + 1 - Me_2CO$), 268 ($M^+ - O - Me_2CO$), 242 ($M^+ + 1 - C_5H_9O_2$ (tetrahydropyranyloxy)). Anal. calcd. for $C_{14}H_{22}N_4O_6$ (342.3): C 49.12, H 6.48, N 16.36; found: C 49.01, H 6.47, N 16.47.

Further elution of the column produced mixed fractions containing both epimers as well as slower-moving impurities. These latter were separated off by repeated chromatography but the second epimer could not be obtained free from the first one, even though the product crystallized from hexane; yield, 130 mg; mp 95–96°C; $[\alpha]_D$ −65.4 (*c* 1, $CHCl_3$). The ^1H nmr spectrum showed all the signals listed above for the first epimer (which in fact preponderated ~2:1), and most of the signals of the second epimer coincided with these, except for H-2′ (δ 4.67, t, J = 3.7 Hz), H-3 (δ 4.40, t, J ~ 9 Hz), H-6′ or H-6″ (δ 4.00, septet, J = 3.5, 9, and 11 Hz), CMe_2 (δ 1.47 and 1.45, 2s). The mass spectrum showed the same peaks, in almost the same intensity ratios, as that of the pure first epimer. The microanalytical data found were C 49.02, H 6.43, N 16.46.

1L-(1,3/2,4,6)-6-Formamido-1,2-O-isopropylidene-4-nitro-3-O-(tetrahydropyran-2-yl)-1,2,3-cyclohexanetriol (9)

From alcohol **5**

Compound **5** (260 mg, 1 mmol) in dry 1,4-dioxane (20 mL) was treated at 25°C with 2,3-dihydropyran (0.9 mL) in the presence of *p*-toluenesulfonic acid monohydrate (38 mg). The reaction was complete after 2 h as revealed by tlc (solvent *C*), which showed **9** (R_f 0.5) and no more **5** (R_f 0.3). The acid catalyst was neutralized with Et_3N,

Can. J. Chem. Downloaded from www.nrcresearchpress.com by 84.41.108.74 on 09/07/12
For personal use only.

the mixture concentrated, and a chloroform solution of the residue was washed with water, dried ($MgSO_4$), and evaporated. The crude crystalline material was chromatographed on SiO_2 (2.2 × 15 cm) with solvent *C*. The combined fractions containing **9** were evaporated, and EtOH was evaporated from the residue, whereupon **9** crystallized. The crystals were triturated with EtOAc and hexane, stored at 0°C, collected, and washed with hexane; yield, 165 mg (48%); mp 208–209°C; $[\alpha]_D$ −47.7 (*c* 0.9, $CHCl_3$); ^1H nmr, δ: 8.18 (s, CHO), 5.70 (d, $J_{6,NH}$ = 6 Hz, NH), 5.12 (t, *J* = 2 Hz, H-2′), 4.62 (m, H-4), 4.50 (t, $J_{2,3} = J_{3,4}$ = 9.5 Hz, H-3), 4.16 (m, H-6), 3.6–3.4 (m, 4H, containing 2 triplets with *J* = 9–10 Hz, H-1,2,6′,6″), 2.83 (dt, $J_{4,5eq}$ = $J_{5eq,6}$ = 4.7 Hz, $J_{5ax,5eq}$ = 13.1 Hz, H-5eq), 1.93 (~sextet, $J_{4,5ax} \approx J_{5ax,6} \approx$ 11.5 Hz, $J_{5ax,5eq}$ = 13 Hz, H-5ax), 1.65–1.45 (m, 6H, H-3′,3″,4′,4″,5′,5″), 1.42 and 1.41 (2s, 6H, CMe_2); *m/z*: 345 ($M^+ + 1$, base peak), 287 ($M^+ + 1 - Me_2CO$), 261 ($M^+ + 1 - C_5H_8O$ (dihydropyran)). Anal. calcd. for $C_{15}H_{24}N_2O_7$ (344.4): C 52.32, H 7.03, N 8.13; found: C 52.40, H 7.06, N 7.96.

The mother liquor of the crystalline **9** was concentrated and passed once more through a column as just described, to give a second crop of **9** (156 mg, 45%) that failed to crystallize. It gave the same mass spectrum as crystalline **9**, but the ^1H nmr spectrum indicated a mixture of epimers: All signals listed above were present, and there was a second set of similar or identical signals that partly coincided or overlapped with the first set, except for H-2′ (δ 4.68, narrow t), H-3 (δ 4.42, t, *J* ≈ 9 Hz), H-6′ or H-6″ (δ 4.00, m), and CMe_2 (δ 1.44 and 1.43, 2s). Epimer proportions varied somewhat in different preparations.

From tetrahydropyranyl ether ***8***

Compound **8** (342 mg, 1 mmol; epimer mixture) was dissolved in MeOH (15 mL) containing AcOH (0.06 mL, 1 mmol), 1,4-cyclohexadiene (0.5 mL), and 10% Pd-C (300 mg), and was sonicated under N_2 at 45°C for 30–60 min. The formation of ninhydrin-positive amine was indicated by tlc (R_f 0.0 with solvent *K*, 0.45 with solvent *C*). Formyl acetate (0.5 mL) was then added, and the conversion of the amine into ninhydrin-negative **9** (R_f 0.5, solvent *C*) was complete after 30 min. The catalyst was filtered off and washed with MeOH, the filtrate neutralized with Et_3N, and the solvent evaporated to give crude crystalline **9**. This was taken up in a little $CHCl_3$ and applied to an SiO_2 column (2.3 × 10 cm). Elution with hexane followed by solvent *I* (100 mL) produced fast-moving impurities, and subsequent elution with solvent *G* (200 mL) gave **9** (295 mg, 86%) as a crystalline mixture of epimers (2:1 according to ^1H nmr). The mass spectral data were identical with those given in the preceding section. A partial separation of epimers was observed when a sample was rechromatographed by use of solvent *E*. A nearly homogeneous epimer crystallized on concentration of some eluate fractions and, after trituration with ether–hexane and drying, melted at 196–197°C and showed $[\alpha]_D$ −64.7 (*c* 1, $CHCl_3$). Its ^1H nmr data were identical with those given above for crystalline **9**. Both crystalline preparations contained traces of the second epimer, as indicated by very minor signals in the spectra, with the product made from **5** appearing to contain slightly more of it. This may also explain the discrepancy in the $[\alpha]_D$ values; a chromatographic fraction consisting of approximately equal proportions of the epimers (^1H nmr evidence) had $[\alpha]_D$ −5, which indicated that the second epimer must be dextrorotatory.

*1L-(1,3/2,4,6)-1,2-*O*-Isopropylidene-4-nitro-3-*O*-(tetrahydropyran-2-yl)-6-trifluoroacetamido-1,2,3-cyclohexanetriol (**10**)*

Compound **3** (774 mg, 3 mmol) was tetrahydropyranylated, and the crude epimer mixture **8** obtained was subjected to transfer hydrogenation (see the preparation of **9**), but not subsequently treated with formyl acetate. Instead, the amine-containing hydrogenolysis solution was filtered, the catalyst washed well with MeOH, and the filtrate evaporated. To a solution of the residue in CH_2Cl_2 (25 mL) was added dry pyridine (1 mL) followed by trifluoroacetic anhydride (1 mL), at 0°C. The dark olive-colored mixture was concentrated, and several portions of added EtOH were evaporated from the crystalline residue, which showed two strong spots for epimers of **10**, R_f 0.43 and 0.35, accompanied by trace spots for **8** (R_f 0.65 and 0.55) that had resisted hydrogenolysis (tlc with solvent *I*). A solution of the material in $CHCl_3$ was washed with water, dried ($MgSO_4$), and evaporated, and the product purified by chromatography on a short column of SiO_2 by use of solvent *L*. The eluted product having R_f 0.43–0.35 (solvent *I*) was recrystallized from $CHCl_3$–hexane to give **10** (508 mg, 41%), mp 199–200°C. The ^1H nmr spectrum was practically identical with that of **9**, except for the absence of the low-field formyl proton singlet, a substantial downfield shift (to δ 6.42) of the NH signal, and a minor upfield shift (to δ 4.08) of the H-6 multiplet. Mass spectrum: *m/z*: 413 ($M^+ + 1$, base peak), 397 ($M^+ + 1 - O$), 355 ($M^+ + 1 - Me_2CO$), 329 ($M^+ + 1 - C_5H_8O$ (dihydropyran)), 313 ($M^+ + 1 - O - C_5H_8O$), 271 ($M^+ + 1 - Me_2CO - C_5H_8O$). Anal. calcd. for $C_{16}H_{23}F_3N_2O_7$ (412.3): C 46.60, H 5.62, N 6.79; found: C 46.71, H 5.34, N 6.46.

*1L-(1,3/2,4,6)-4-Acetamido-1,2,3-tri-*O*-acetyl-6-(*N*-methyl)acetamido-1,2,3-cyclohexanetriol (**12**)*

A solution of **9** (170 mg, 0.5 mmol) and $LiAlH_4$ (75 mg) in dry 1,4-dioxane (10 mL) was gently boiled inder reflux for 1.5 h. Celite was added to the cooled and vigorously stirred mixture, and the excess of hydride was decomposed by slow addition of MeOH followed by some water. The solids were filtered off and washed with MeOH. The filtrate showed a strong, immobile, ninhydrin-positive spot in tlc (solvent *C*), attributed to the *O*-protected diamine **11**; starting compound **9** (R_f 0.5) was absent. After solvent evaporation the product was treated overnight at room temperature with 90% trifluoroacetic acid (2 mL) in MeOH (10 mL). The mixture was concentrated at reduced pressure, and residual acid was removed by coevaporation with benzene. The brown, amorphous product dissolved in a little water was applied to a column (1 × 10 cm) of Dowex-50W(H^+) cation exchange resin, which was exhaustively washed with water and then eluted with aqueous, 3.5 M NH_3. Evaporation of the ammoniacal eluate gave crude (+)-hyosamine (**1**) as a light-brown, amorphous material, R_f 0.25 (ninhydrin-positive, with the brown impurities travelling with the solvent front; tlc with solvent *N*). An authentic sample of 2-deoxystreptamine (**23**) spotted for comparison had R_f 0.35. A small sample of **1** was purified on a small column of SiO_2 with solvent *O*, which readily eliminated the fast-moving impurities and gave **1** as a white solid; *m/z*: 177 ($M^+ + 1$) and 161 ($M^+ - CH_3$) in agreement with the composition $C_7H_{16}N_2O_3$. The bulk of the crude **1** was treated with 1:1 Ac_2O/pyridine (2 mL) for 16 h at 25°C. Processing by addition of excess MeOH, coevaporation of the solvent with toluene, and chromatography on SiO_2 (1.2 × 25 cm, solvent *C*) gave **12** (45 mg, 23.5%), mp 156–157°C (from EtOH–Et_2O–hexane) (lit. (5) mp 156.5–157°C for the enantiomer); $[\alpha]_D$ −4.4 (*c* 1, MeOH) (lit. (4) $[\alpha]_D$ −7.5 (MeOH)). It is noteworthy that the pentaacetyl derivative of (+)-hyosamine is levorotatory, and that of (−)-hyosamine is dextrorotatory (4); ^1H nmr, δ: 5.74 and 5.66 (2d, 1H total, $J_{NH,4} \approx$ 8 Hz, NH), 5.1–4.7 (m, 3H, ill-resolved, H-1,2,3), 4.2–3.8 (m, 2H, H-4,6), 2.81 and 2.72 (broadened s and s, ratio ~3:2, total 3H, *N*-CH_3), 2.05–1.89 (multiple s, 15H, 5 Ac); *m/z*: 387 ($M^+ + 1$), 343 ($M^+ - Ac$), 327 ($M^+ + 1 - AcOH$).

*Crude 1L-(1,3/2,4,6)-1,2-*O*-isopropylidene-6-methylamino-4-nitro-3-*O*-(tetrahydropyran-2-yl)-1,2,3-cyclohexanetriol (**13**)*

A solution of **9** (295 mg, 0.85 mmol, epimer mixture) in dry THF (12 mL) containing 2.2 mol. equiv. of BH_3 (added as 1.4 mL of 1.34 M BH_3–THF complex) was boiled gently under reflux, with exclusion of atmospheric moisture. After 30 min a complete replacement of **9** (R_f 0.5) by two new products, R_f 0.8 and 0.45, was indicated by tlc (solvent *C*). (A separate pilot experiment had shown that continued boiling with additional BH_3 did not change the pattern.) Excess MeOH was carefully added to the cooled mixture, which was then evaporated, and several portions of added MeOH were evaporated from the colorless, crystalline residue of crude **13**. After thorough drying it weighed 303 mg (i.e., 20 mg in excess of the theoretical yield, presumably due to incomplete removal of boron). The ^1H nmr spectrum was poorly resolved but clearly demonstrated that the formyl group of **9** (s at δ 8.18) had been replaced by an *N*-methyl group which gave 2 doublets (*J* 5.9 and 6.1 Hz) at δ 2.69 and 2.53, in an ~2:1 intensity ratio and integrating to 3 protons. Mass spectrum, *m/z*: 331 ($M^+ + 1$, strong), 273 ($M^+ + 1 - Me_2CO$), 247 ($M^+ + 1 - C_5H_8O$ (dihydropyran)).

Can. J. Chem. Downloaded from www.nrcresearchpress.com by 84.41.108.74 on 09/07/12
For personal use only.

*1L-(1,3/2,4,6)-1,2-O-Isopropylidene-6-(N-methyl)acetamido-4-nitro-3-O-(tetrahydropyran-2-yl)-1,2,3-cyclohexanetriol (**14**)*

Crude **13** (410 mg) was *N*-acetylated by treatment with Ac_2O in methanolic solution (2 h, 25°C). The solvent was evaporated, and a solution of the residue in $CHCl_3$ was washed with aqueous $NaHCO_3$ and water, dried ($MgSO_4$), and concentrated to give a crystalline mass that was inhomogeneous in tlc (solvent *H*), showing strong spots at R_f 0.75 and 0.2, and several intermediate trace spots. Column chromatography on SiO_2 (2.3 × 10 cm) yielded the less-polar (unidentified) product (120 mg) by elution with solvent *I* (200 mL), and crystalline **14** (R_f 0.2; 275 mg, 55%) by subsequent elution with solvent *G* (300 mL). End fractions containing some even more-polar material (R_f 0.1; 49 mg) were discarded. Compound **14** had mp 189–192°C (not recrystallized); ^{1}H nmr, δ: 5.13 (narrow t, H-2′), 4.68 (m, 2H, H-4,6), 4.48 (t, with small satellite t at 4.40 for epimer, $J_{2,3} = J_{3,4} = 9.7$ Hz, H-3), 3.64 (dd, $J_{1,2} = 8.8$, $J_{1,6} = 11$ Hz, H-1), 3.50 (m, 3H, H-2,6′,6″), 2.94 (s, with small satellite at 2.86, 3H, *N*-CH_3), 2.38 (m, H-5eq), 2.11 (s, 3H, Ac), 2.01 (~q, splittings 12–13 Hz, H-5ax), 1.65–1.45 (m, 6H, H-3′,3″,4′,4″,5′5″), 1.42 and 1.39 (2s, 3H each, CMe_2); *m/z*: 373 ($M^+ + 1$, base peak), 315 ($M^+ + 1 - Me_2CO$), 289 ($M^+ + 1 - C_5H_8O$), 231 ($M^+ + 1 - Me_2CO - C_5H_8O$); in accord with mol. wt. 372 for $C_{17}H_{28}N_2O_7$.

*1L-(1,3/2,4,6)-4-Acetamido-1,2-O-isopropylidene-6-(N-methyl)-acetamido-3-O-(tetrahydropyran-2-yl)-1,2,3-cyclohexanetriol (**15**)*

A solution of nitro compound **14** (268 mg, 0.72 mmol) in 99% EtOH (25 mL) was shaken with PtO_2 (227 mg, 1 mmol) under H_2 at ordinary pressure and room temperature. The required volume of H_2 (94 mL; calcd., 93 mL) was consumed overnight, and the solution showed a positive ninhydrin reaction. Acetic anhydride (1.5 mL) was added, and after 15 min the ninhydrin test was negative. The catalyst was filtered off and washed exhaustively with EtOH, and the evaporated filtrate gave a gel-like residue that showed **15** as a slow-moving (solvent *C*) or immobile (EtOAc) spot in tlc, and a contaminant migrating with the solvent front, but **14** (R_f 0.7 and 0.6, respectively) was absent. Chromatography on SiO_2 (2.3 × 10 cm) by elution with EtOAc (100 mL, to remove the nonpolar impurity) followed by solvent *M* furnished **15** as a colorless syrup that failed to crystallize and was dried on the oil pump to a hard glass (280 mg, quantitative); ^{1}H nmr, δ: 2.88 and 2.80 (2s, intensity ratio 2:1, total 3H, *N*-CH_3), 2.15–1.90 (multiple s, total 6H, 2Ac); each of the *N*-CH_3 signals was accompanied by a minor satellite at slightly lower field, probably due to 2′-epimerism. Mass spectrum, *m/z*: 385 ($M^+ + 1$), 327 ($M^+ + 1 - Me_2CO$), 301 ($M^+ + 1 - C_5H_8O$, base peak), 243 ($M^+ + 1 - Me_2CO - C_5H_8O$).

*1L-(1,3/2,4,6)-6-Acetamido-4-amino-1,2-O-isopropylidene-1,2,3-cyclohexanetriol (**16**)*

Nitro compound **6** (274 mg, 1 mmol) was dissolved in 99% EtOH (20 mL) containing AcOH (0.06 mL) and hydrogenated over Adams catalyst (114 mg of PtO_2, 0.5 mmol) at ambient temperature and pressure. After 18 h, the calculated volume (90 mL) of H_2 was consumed, and tlc showed a strong ninhydrin-positive spot (R_f 0.3) for **16**, while **6** (R_f 1.0) was absent (solvent *A*, double irrigation). The catalyst was washed exhaustively with EtOH, and evaporation of the filtrate gave syrupy **16** that was dried *in vacuo* to a colorless, hard glass (240 mg, 98%), homogeneous in tlc; *m/z*: 245 ($M^+ + 1$, base peak), 187 ($M^+ + 1 - Me_2CO$). It was used without further characterization for the preparation of **22**.

*Attempted preparation of the formamidotrifluoroacetamido derivative **18***

The nitrotrifluoroacetamido **10** (0.50 g) was hydrogenated over PtO_2 (0.1 g) as just described for the hydrogenation of **6**. Hydrogen uptake was very slow, and only a trace of ninhydrin-positive product was seen after 16 h (tlc with solvents *I* and *C*). Hydrogenation was continued for 6 days, with additions of fresh catalyst (3 × 0.1 g), after which reduction was still far from complete. Catalyst and solvent were removed, and the procedure was repeated with fresh catalyst for another 4 days, without satisfactory progress. Work-up then gave a crystalline but inhomogeneous material (tlc) containing some amine (ninhydrin test), which was *N*-formylated in MeOH solution (15 mL) with formyl acetate (1 mL) during 3 h. The processed mixture was chromatographed on SiO_2. Elution with solvent *I* produced unchanged **10** (173 mg, 34% recovery, mp 199–200°C), and subsequent elution with solvents *G*, *F*, and EtOAc gave three fractions of products having R_f 0.6 (31 mg), 0.3 (176 mg), and 0.2 (double spot; 116 mg) in tlc with solvent *H*. One of them may have been **18** but the matter was not pursued.

*1D-(1,3/2,4,6)-4-Acetamido-1,2,3-tri-O-acetyl-6-(N-methyl)acetamido-1,2,3-cyclohexanetriol (**22**) from **16***

Amine **16**, obtained as a glassy foam (~290 mg) by hydrogenation of **6** (330 mg, 1.2 mmol), was pulverized and suspended in 1,4-dioxane (25 mL) to which 2,3-dihydropyran (500 mg, 6 mmol) and *p*-TsOH · H_2O (250 mg, 1.3 mmol) were added. The mixture was stirred at room temperature, and DMF (2 mL) was added after 0.5 h to aid in dissolving the starting material; after 2 h the clear solution appeared free from **16** (R_f 0.2) and showed a strong spot for its 3-THP ether **19** (R_f 0.8, plus a weak spot at R_f 0.7 attributed to the 2′-epimer; tlc with solvent *A* and ninhydrin indication). The mixture was made slightly basic with Et_3N, and evaporated, with residual DMF being eliminated by coevaporation with toluene. The dry residue was purified on a column of SiO_2 (2.2 × 13 cm), which was irrigated first with $CHCl_3$ (to remove a yellow, fast-moving impurity) and then with solvents *D* (100 mL) and *A* (200 mL), to furnish ninhydrin-positive fractions that gave **19** (329 mg, 83.6% based on **6**) as a glassy foam; *m/z*: 329 ($M^+ + 1$) and 245 ($M^+ + ″\tau + + - C_5H_8O$ (dihydropyran)) in harmony with the composition $C_{16}H_{28}N_2O_5$.

The crude **19** (328 mg, 1 mmol) in CH_2Cl_2 (10 mL) was treated overnight at 25°C with *N,N*-dimethylformamide dimethyl acetal (0.2 mL). Solvent evaporation gave a pale yellow syrup presumed to contain the *N,N*-dimethylformamidine **20**; *m/z*: 384 ($M^+ + 1$, base peak). The syrup was redissolved in CH_2Cl_2 (10 mL) and treated overnight at 25°C with methyl trifluoromethanesulfonate (0.17 mL, 1.5 mmol) to generate the *N,N,N′*-trimethylformamidinium salt **21**. The mixture was evaporated to a syrup that was immediately boiled under reflux for 1.5 h with 6 M HCl (10 mL). The dark-colored hydrolyzate containing some tarry decomposition products was diluted with water and extracted with $CHCl_3$, which took out much of the color. The clear yellow aqueous phase was evaporated to give a brownish, crystalline residue of aminocyclitol hydrochlorides, R_f 0.3–0.4 (double spot; tlc with solvent *N*). The faster spot migrated like authentic 2-deoxystreptamine (**23**) spotted for comparison, and the slower one was attributed to (−)-hyosamine (**2**). Dissolved in a little aqueous MeOH, the material was applied to a small column of Dowex-50W(H^+) resin (~10 mL). Rinsing with MeOH and water eluted the brown impurities, and subsequent elution with 5% aqueous NH_3 produced the amines, without separation. The residue obtained by evaporation of the ammoniacal eluate was dried in a desiccator and then treated with Ac_2O and pyridine (16 h, 25°C). Processing by coevaporation of the reagents with added toluene gave a syrupy mixture of peracetyl derivatives **22** (R_f 0.4, like **12**) and **24** (R_f 0.3, migrating like an authentic sample; tlc with solvent *C*). Note that the relative mobilities were reversed in comparison to unprotected **2** and **23**. Column chromatography (SiO_2, 2.3 × 15 cm; solvent *D*) of the mixture yielded **22** (77 mg, 20% based on **19**) and **24** (52 mg, 14%), both as fine colorless needles from EtOH–Et_2O–hexane.

Compound **22** had mp 156–157°C as reported (5); $[\alpha]_D$ +4.6 (*c* 1, MeOH) (lit. $[\alpha]_D$ +5.4 (4) and +7.5 (5)); *m/z*: 387 ($M^+ + 1$, base peak), 373 ($M^+ + 2 - Me$), 345 ($M^+ + 2 - Ac$), 327 ($M^+ + 1 - AcOH$), 254 ($M^+ + 1 - AcNH_2 - AcNHMe$). The ^{1}H nmr spectrum was indistinguishable from that of **12**.

Compound **24** had mp 318–321°C (lit. (15) mp 322–323°C); $[\alpha]_D$ 0 (*c* 2, MeOH); ^{1}H nmr (2-deoxystreptamine numbering), δ: 5.68 (br d,

2H, NH-1,3), 5.23 (t, $J_{4,5} = J_{5,6} = 9.8$ Hz, H-5), 4.88 (t, 2H, splitting ~ 10 Hz, H-4,6), 4.17 (m, 2H, H-1,3), 2.42 (m, H-2eq), 2.03 (s, 6H, AcO-4,6), 1.99 (s, 3H, AcO-5), 1.90 (s, 6H, AcNH-1,3), 1.38 (m, H-2ax); *m/z*: 373 ($M^+ + 1$, base peak), 359 ($M^+ + 2 -$ Me), 331 ($M^+ + 2 -$ Ac), 313 ($M^+ + 1 -$ AcOH), 254 ($M^+ + 1 - 2AcNH_2$).

1L-(1,3/2,4,6)-6-Ethoxycarbonylamido-4-formamido-1,2-O-isopropylidene-1,2,3-cyclohexanetriol (25)

Platinum dioxide (550 mg) suspended in 99% EtOH (20 mL) containing AcOH (0.17 mL) was prehydrogenated, nitrocarbamate **7** (600 mg, 2 mmol) in EtOH (10 mL) was added, and the mixture vigorously shaken under H_2 at ambient temperature and pressure. After 30 h, **7** (R_f 0.5) was completely replaced by the corresponding amine, which gave an immobile, ninhydrin-positive spot (tlc with solvent *C*). The H_2 supply was disconnected, the mixture cooled (0°C), and formyl acetate (3 mL) was introduced, after which the mixture was stirred for 2 h at room temperature. Thin-layer chromatography then showed almost complete replacement of the amine spot by a single spot for **25**, R_f 0.15. Filtration and evaporation of the solution, with several additions of fresh EtOH, gave **25** as colorless crystals (460 mg, 76%). An analytical sample was freed from a trace of impurity (immobile) by passage through an SiO_2 column with $CHCl_3$ containing 3% of MeOH. Pure **25** had R_f 0.45 (solvent *B*), mp 127–129°C; $[\alpha]_D$ +6.1 (*c* 0.9, $CHCl_3$); ν_{max} ($CHCl_3$): 3300 (br, OH and NH), 1678 and 1543 (amide I and II) cm^{-1}; ^1H nmr (acetone-d_6) δ: 8.13 and 8.03 (slightly broadened s, and d with J = 12 Hz, intensity ratio ~4:1, 1H total, formyl), 7.3 and 6.7 (d with J = 7 and t with J = 11 Hz, both broadened, ratio 4:1, 1H total, formamido NH), 6.4 (br t, carbamate NH), 4.7 and 4.5 (2d with J = 4.7 Hz, ratio 1:4, total 1H, OH-3), 4.01 (q, 2H, OCH_2), 3.9–3.8, 3.7, 3.5–3.4 (3m, ill-resolved, 2, 1, and 2H, H-1,2,3,4,6), 2.24 (dt, $J_{4,5eq} = J_{5eq,6} = 4.5$ Hz, $J_{5ax,5eq} = 13.2$ Hz, H-5eq), 1.47 (~q, splittings 11–13 Hz, H-5ax), 1.36 and 1.33 (2s, 3H each, CMe_2), 1.16 (t, 3H, J = 7.1 Hz, ethyl CH_3). Upon D_2O exchange the NH and OH signals disappeared and the small doublet at δ 8.03 collapsed to a singlet while the broadened singlet at δ 8.13 became sharp; ^{13}C nmr (50.3 Mz, acetone-d_6), for the major rotamer, δ: 161.8 (formamido CO), 156.3 (carbamate CO), 110.7 (O_2CMe_2), 81.7, 79.0, 73.2, (C-1,2,3) 60.2 (OCH_2), 51.4, 49.4 (C-4,6), 36.2 (C-5), 26.6 and 26.5 (CMe_2), 14.3 (ethyl CH_3); small signals for the minor rotamer, δ: 164.8 (formamido CO), 110.9 (O_2CMe_2), satellites to above C-1,2,3 and C-5 signals, and 55.0 (presumably C-4). Mass spectrum, *m/z*: 303 ($M^+ + 1$, base peak), 258 ($M^+ + 1 -$ OEt), 285 ($M^+ + 1 - H_2O$), 245 ($M^+ + 1 - Me_2CO$), 227 ($M^+ + 1 - H_2O - Me_2CO$). Anal. calcd. for $C_{13}H_{22}N_2O_6$ (302.3): C 51.65, H 7.34, N 9.27; found: C 51.48, H 7.54, N 9.14.

1L-(1,3/2,4,6)-6-Ethoxycarbonylamido-1,2-O-isopropylidene-4-methylamino-1,2,3-cyclohexanetriol (26), and acetylated derivatives **27**, **29**, and **30**

A solution of **25** (653 mg, 2.15 mmol) in THF (10 mL, dried over Na) was added dropwise during 5 min to 1 M borane in THF (5 mL), maintained at 0°C under N_2 in a flask equipped with dropping funnel, reflux condenser, and gas inlet. The colorless solution was then heated at reflux for 5 h, under N_2. Replacement of **25** (R_f 0.2) by a ninhydrin-positive product (R_f 0.55) was seen in tlc (solvent *P*). The mixture was cooled to 25°C, a few drops of water were added, and a stream of CO_2 was passed through for 20 min. Evaporation of the solvent followed by evaporation of six portions of MeOH sequentially added to the syrupy residue gave crude **26**. Chromatographic purification (SiO_2, 2 × 20 cm) using solvent *Q* furnished pure **26** as a colorless, brittle glass (218 mg, 35%); ^1H nmr, δ: 4.09 and 1.22 (q, 2H, and t, 3H, respectively, J = 7.1 Hz, OCH_2CH_3), 2.60 and 2.44 (2d, J = 6.1 and 5.9 Hz, intensity ratio 1:1.2, 3H total, N-CH_3), 1.42 (s, 6H, CMe_2). The ^{13}C nmr spectrum showed, near most resonances, a second resonance (given in brackets) of 70–95% intensity; δ: 156.0 (CO), 112.2 [112.3] (O_2CMe_2), 80.5 [80.6], 78.5 [78.3], 69.7 [69.1] (C-1,2,3), 63.1 [63.9] (C-4), 61.2 (OCH_2), 49.2 [49.1] (C-6), 42.5 [42.6] (N-CH_3), 27.7 [27.55] (C-5), 26.7 (CMe_2), 1.44 (ethyl CH_3). Mass spectrum, *m/z*: 298 ($M^+ + 1$). Anal. calcd. for $C_{13}H_{24}N_2O_5 \cdot 0.5H_2O$ (297.4): C 52.51, H 8.47, N 9.42; found: C 52.40, H 8.63, N 9.19.

Further elution of the chromatographic column gave a fraction (268 mg, 43%) consisting apparently of **26** (major component) and its product of deacetonation (**28**). This mixture was acetylated by overnight treatment with 1:1 Ac_2O/pyridine (8 mL) at room temperature. After processing by dilution with CH_2Cl_2, washing of the solution with water, aqueous $NaHCO_3$, and water, drying (Na_2SO_4), and evaporation with added portions of toluene, a colorless syrup that failed to crystallize was obtained. It showed two spots, R_f 0.8 (major) and 0.95 (minor) in tlc (solvent *P*), and spectroscopic examination suggested that the material consisted mainly of the *N,O*-diacetyl derivative (**27**) of **26**, accompanied by a small proportion of the *N,O,O,O*-tetraacetyl derivative (**30**) of **28**. Thus, the ^1H nmr spectrum exhibited substituent resonances for carbamate OCH_2CH_3 (m at δ 4.09 and 1.22, intensity ratio 2:3), the N-CH_3 group (s at δ 2.89, 2.83, and 2.74, ratio 1:2:1, 3H total), the *N*- and *O*-acetyl groups (multiple singlets at δ 2.12–1.96), and the acetonide CH_3 groups (s at δ 1.43 and 1.41). Integration for the total of acetyl signals was somewhat greater than 6H, whereas it was somewhat less than 6H for the acetonide CH_3 groups. The ^{13}C nmr spectrum (ADEPT plot) showed CH_3 resonances (δ) for CH_3CH_2O (14.5), $OCOCH_3$ (20.9–20.4), $NCOCH_3$ (22.15–22.1), $O_2C(CH_3)_2$ (26.7–26.4), and N-CH_3 (32.0). The mass spectrum showed prominent peaks for **27** at *m/z* 373 (54%, $M^+ + 1$), 315 (100%, $M^+ + 1 - Me_2CO$), and 269 (12%, $M^+ + 1 - Me_2CO -$ EtOH) in accord with the composition $C_{17}H_{28}N_2O_7$, and small peaks for **30** at *m/z* 417 (9%, $M^+ + 1$) and 357 (2%, $M^+ + 1 -$ AcOH) in agreement with $C_{18}H_{28}N_2O_9$. Column chromatography with solvent *F* failed to separate the products.

1D-(1,3/2,4,6)-4-Ethoxycarbonylamido-6-(N-methyl)acetamido-1,2,3-cyclohexanetriol (**29**) was obtained when a sample of pure **26** was treated overnight at room temperature with 50% aqueous AcOH, whereby **26** (R_f 0.55) was converted into a product having R_f 0.1 (tlc, solvent *P*). The acid was evaporated with several additions of toluene and the syrupy **29** dried in a oil-pump vacuum over KOH; ^1H nmr (DMSO-d_6), δ: 6.19 (d, J = 8.5 Hz, carbamate NH), 3.96 (q, 2H, J = 7.1 Hz, OCH_2), 3.20 (m, $W \approx 35$ Hz, H-4), 3.1–2.9 (m, 3H, narrowed on D_2O exchange, H-1,2,3), 2.29 (s, 3H, NCH_3; superposed on m for H-6), 1.92 (dt, $J_{4,5eq} \approx J_{5eq,6} \approx 12.7$ Hz, H-5eq), 1.87 (s, 3H, *N*Ac), 1.15 (t, 3H, J = 7.1 Hz, ethyl CH_3), 0.99 (~q, splittings ≈ 12.3 Hz, H-5ax); ^{13}C nmr (DMSO-d_6, ADEPT plot), δ: 173.1 (amide CO), 156.2 (carbamate CO), 76.5 (C-2), 74.4 (double line seen on expansion, C-1,3), 59.8 (OCH_2), 58.9 (C-6), 51.5 (C-4), 32.6 (NCH_3), 31.9 (C-5), 22.3 (*N*Ac), 14.9 (ethyl CH_3).

1D-(1,3/2,4,6)-4-Acetamido-1,2,3-tri-O-acetyl-6-(N-methyl)acetamido-1,2,3-cyclohexanetriol (22) from **26**

A 30-mg sample of the mixture of acetylated compounds **27** (major componnt) and **30** obtained from **26** as described was heated for 2 h on a steam bath in 6 M HCl (2 mL). After dilution with water, the acid was evaporated *in vacuo* and the residue dried in a desiccator over KOH. The ^{13}C nmr spectrum (D_2O) indicated that the acetonide and all acetyl groups were cleaved off but the carbamate group was retained; δ: 158.1 (CO), 74.9, 73.5, 71.5 (C-1,2,3), 61.7 (OCH_2), 57.2, 50.6 (C-4,6), 29.6 (NCH_3), 27.5 (C-5), 13.6 (ethyl CH_3). To the aqueous solution of the product was added an equal volume of 4 M NaOH, the mixture was heated for 3 h on a steam bath, cooled, neutralized with AcOH, and evaporated to dryness. The white mass of NaCl, NaOAc, and **2** (in salt form) was dried in a desiccator, then covered with Ac_2O (3 mL), and agitated overnight at room temperature. Removal of the anhydride by repeated coevaporation with toluene, extraction of the desiccator-dried salt mass with $CHCl_3$, and evaporation of the colorless extract gave **22**, which crystallized from a small amount of EtOH upon careful addition of Et_2O and hexane, and storage at −18°C; yield, 18 mg (60%); mp 157–158°C (lit. (5) mp 156.5–157°C); $[\alpha]_D$ +6.8 (*c* 1.8, MeOH) (lit. $[\alpha]_D$ +7.5 (5) and +5.4 (4)); *m/z*: 387 ($M^+ + 1$, base peak), 373 ($M^+ + 2 -$ Me), 345 ($M^+ + 2 -$ Ac), 327 ($M^+ + 1 -$ AcOH). The

Can. J. Chem. Downloaded from www.nrcresearchpress.com by 84.41.108.74 on 09/07/12
For personal use only.

^{1}H nmr data (200 MHz) were the same as for **12** and for **22** prepared from **16**, except that the stronger of the two *N*-CH_3 signals (previously seen as a broadened singlet at δ 2.81) appeared as separate singlets at δ 2.84 and 2.81.

Acknowledgments

This work was financially supported by the Natural Sciences and Engineering Research Council of Canada and the United States Public Health Service (GM 35244). Dr. Bruno Radatus is thanked for preliminary experiments concerning the preparation of **5** and **6**.

1. N. Neuss, K. F. Koch, B. B. Molloy, W. Day, L. L. Huckstep, D. E. Dorman, and J. D. Roberts. Helv. Chim. Acta, **53**, 2314 (1970); H. Hashimoto, K. Asano, F. Fujii, and J. Yoshimura. Carbohydr. Res. **104**, 87 (1982).
2. M. Nakajima, A. Hasegawa, and N. Kurihara. Liebigs Ann. Chem. **689**, 235 (1965).
3. T. Suami, S. Ogawa, and H. Sano. Bull. Chem. Soc. Jpn. **43**, 1843 (1970).
4. N. Kurihara, K. Hayashi, and M. Nakajima. Agric. Biol. Chem. (Tokyo), **33**, 256 (1969).
5. T. Suami, S. Ogawa, N. Tanno, M. Suguro, and K. L. Rinehart, Jr. J. Am. Chem. Soc. **95**, 8734 (1973).
6. H. H. Baer, I. Arai, B. Radatus, J. Rodwell, and C. Nguyen. Can. J. Chem. **65**, 1443 (1987).
7. J. M. Grosheintz and H. O. L. Fischer. J. Am. Chem. Soc. **70**, 1479 (1948); M. L. Wolfrom, S. M. Olin, and W. J. Polglase. J. Am. Chem. Soc. **72**, 1724 (1950); H. H. Baer. Adv. Carbohydr. Chem. Biochem. **24**, 67 (1969); J. Kovář and H. H. Baer. Carbohydr. Res. **45**, 161 (1975), and earlier work cited therein.
8. H. H. Baer and J. Kovář. Can. J. Chem. **54**, 2038 (1976).
9. Y. Nishimura, T. Tsuchiya, and S. Umezawa. Bull. Chem. Soc. Jpn. **43**, 2960 (1970).
10. R. A. W. Johnstone, A. H. Wilby, and I. D. Entwistle. Chem. Rev. **85**, 129 (1985).
11. R. F. Borch, M. D. Bernstein, and H. D. Durst. J. Am. Chem. Soc. **93**, 2897 (1971).
12. (*a*) H. C. Brown and S. Krishnamurthy. Aldrichimica Acta, **12**, 3 (1979); (*b*) H. C. Brown and P. Heim. J. Am. Chem. Soc. **86**, 3566 (1964); (*c*) H. C. Brown and P. Heim. J. Org. Chem. **38**, 912 (1973).
13. E. R. Bissell and M. Finger. J. Org. Chem. **24**, 1256 (1959).
14. M. J. O'Donnell, W. A. Bruder, B. W. Daugherty, O. Liu, and K. Wojciechowsky. Tetrahedron Lett. 3651 (1984).
15. S. Ogawa, K. L. Rinehart, Jr., G. Kimura, and R. P. Johnson. J. Org. Chem. **39**, 812 (1974).
16. W. V. Curran and R. R. Angier. J. Org. Chem. **31**, 3867 (1966); M. J. Kornet, P. A. Thio, and S. I. Tan. J. Org. Chem. **33**, 3637 (1968).
17. R. B. Duff. J. Chem. Soc. 4730 (1957); L. Hough, J. K. N. Jones, and D. L. Mitchell. Can. J. Chem. **37**, 725 (1959).
18. H. H. Baer, B. Radatus, and J. Defaye. Can. J. Chem. **63**, 440 (1985); H. H. Baer and B. Radatus. Carbohydr. Res. **146**, 73 (1986).
19. L. I. Krimen. Org. Synth. Coll. Vol. **6**, 8 (1988).
20. Nomenclature of cyclitols. Issued by IUPAC–IUB Commissions on the Nomenclature of Organic Chemistry and Biochemical Nomenclature. Pure Appl. Chem. **37**, 285 (1974).

Can. J. Chem. Downloaded from www.nrcresearchpress.com by 84.41.108.74 on 09/07/12
For personal use only.

The dual pathway in photocycloaddition of 1,3-diketonatoboron difluorides: excimer reactions

YUAN L. CHOW AND XIANEN CHENG
Department of Chemistry, Simon Fraser University, Burnaby, B.C., Canada V5A 1S6
Received December 20, 1990

YUAN L. CHOW and XIANEN CHENG. Can. J. Chem. **69**, 1575 (1991).

The lowest singlet excited state of dibenzoylmethanatoboron difluoride $DBMBF_2$, a model compound of the BF_2 complexes of 1,3-diketones, reacted with various simple olefins to give regiospecific and stereospecific photocycloadducts of 1,5-diketones similar to those from the de Mayo type reaction. $DBMBF_2$ in acetonitrile exhibited two discrete fluorescences at 398 and 416 nm for the monomer and at 522 nm for the excimer; they were both quenched, but in different proportions, by a simple olefin. An "oxygen test" showed that the excimer of $DBMBF_2$ is formed irreversibly in acetonitrile. The quantum yields of the photocycloaddition were shown to be proportional not only to olefin concentrations but also to $DBMBF_2$ concentrations. Kinetic analysis has established that the total quantum yield is the sum of those arising from the interactions of the singlet excited $DBMBF_2$ and its excimer, respectively, with an olefin, i.e., the sum of the quantum yields of exciplex and triplex pathways. The contributions from the two pathways are determined by the type of olefins and the range of $DBMBF_2$ concentrations. For endocyclic olefins, the triplex pathway is more important and the corresponding photocycloaddition becomes very efficient as soon as the excimer starts to form in $[DBMBF_2] > 0.001$ M. For the monosubstituted olefins, on the contrary, the exciplex pathway is always more important than the triplex pathway; they react primarily from the singlet excited state of $DBMBF_2$.

Key words: singlet state photocycloaddition, irreversible excimer formation, excimer cycloaddition, triplex and exciplex reactions.

YUAN L. CHOW et XIANEN CHENG. Can. J. Chem. **69**, 1575 (1991).

L'état excité singulet le plus bas du difluorure de dibenzoylméthanatobore ($DBMBF_2$, un composé modèle des complexes du BF_2 avec les 1,3-dicétones) réagit avec diverses oléfines simples pour donner des photocycloproduits régiospécifiques et stéréospécifiques de 1,5-dicétones semblables à ceux obtenus lors des réactions observées par de Mayo. Dans l'acétonitrile, le $DBMBF_2$ présente deux bandes discrètes de fluorescence à 398 et à 416 nm pour le monomère et à 522 nm pour l'excimère; elles sont toutes les deux désactivées, mais à des degrés différents, par une oléfine simple. Un «test à l'oxygène» démontre que l'excimère du $DBMBF_2$ se forme d'une façon irréversible dans l'acétonitrile. On a démontré que les rendements quantiques de photocycloaddition ne sont pas seulement proportionnels aux concentrations d'oléfine mais aussi aux concentrations de $DBMBF_2$. Une analyse cinétique a permis d'établir que le rendement quantique total est égal à la somme de ceux résultant des interactions respectives de l'état excité singulet du $DBMBF_2$ et de son excimère avec une oléfine, soit la somme des rendements quantiques des voies impliquant l'exciplexe et l'état triplet. On a déterminé les contributions de ces deux voies par types d'oléfines et par plages de concentrations de $DBMBF_2$. Pour les oléfines endocycliques, la voie impliquant l'état triplet est plus importante et la photocycloaddition correspondante devient très efficace aussitôt que l'excimère commence à se former lorsque $[DBMBF_2] > 0{,}001$ M. Au contraire, pour les oléfines monosubstituées, la voie impliquant l'exciplexe est toujours plus importante que celle impliquant l'état triplet; elles réagissent principalement à partir de l'état excité singulet du $DBMBF_2$.

Mots clés : photocycloaddition par l'état singulet, formation irréversible d'un excimère, cycloaddition par un excimère, réactions des excimères et des états triplets.

[Traduit par la rédaction]

Introduction

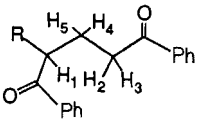
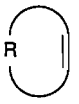
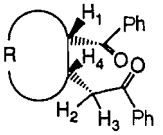
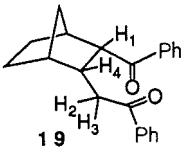
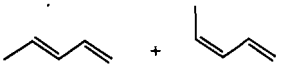
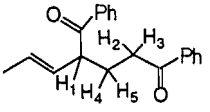
In a preliminary communication (1) we summarized various types of photoreactions displayed by dibenzoylmethanatoboron difluoride ($DBMBF_2$), a representative of the BF_2 complexes of 1,3-diketones; they involve photocycloaddition with olefins, sensitization of electron-rich olefins by electron transfer to form cation radicals, exciplex–excimer formations, and subsequent reactions therefrom. It was proposed that these photoreactions could be related to some degree of single electron transfer in the interaction of the singlet excited $DBMBF_2$ with substrates in which the former acted as an electron acceptor. We wish to describe the synthetic and mechanistic details of the [2 + 2] photocycloaddition of $DBMBF_2$ with simple olefins and the subsequent formation of 1,5-diketones, in which the role played by the $DBMBF_2$ excimer (2) is demonstrated by kinetic studies.

The [2 + 2] photocycloaddition (3–8) of β-diketones (from their enol form) with simple olefins is generally known as the de Mayo reaction (3) and has been suggested to take place from the triplet state of β-diketones (7). While this reaction is a very efficient methodology to construct carbon skeletons, it suffers from low quantum efficiencies. However, published results show that chemical yields are reasonable with long irradiation. The photocycloaddition described here, while it displays similar product patterns to the de Mayo reaction, involves the singlet excited state of $DBMBF_2$ and gives much higher quantum efficiency.

In the enol form, β-diketones are excellent ligands to form chelate complexes with all types of metal ions. While these metal β-diketonates show relatively few irreversible photochemical reactions, they do undergo efficient electron transfer reactions with excited state ketones (9). In aprotic solvent, β-diketones react rapidly with boron trifluoride to form tetracoordinated chelate complexes of boron difluorides that have been known for almost 65 years (10–19). Recently such BF_2 complexes have been patented as latent catalysts for epoxy resin polymerization (20, 21) and photoconducting sensitizers in polymeric films (22, 23). However, the extent of actual commercial applications is obscure. It has been suggested that the BF_2 complexes of β-diketones are good electron accep-

Can. J. Chem. Downloaded from www.nrcresearchpress.com by 84.41.108.74 on 09/07/12
For personal use only.

TABLE 1. The photocycloaddition of $DBMBF_2$ to olefins in CH_3CN[a]

Olefin	Irradiation times (h)	Product	Yield (%)
$RCH=CH_2$			
$R=CH_3(CH_2)_3$ (1)	2.2	11	78
$R=CH_2{:}CH(CH_2)_2$ (2)	3.5	12	92
$R=(CH_3)_3C$ (3)	3.5	13[b]	69
			
$R=(CH_2)_3$ (4)	7.5	14	58[c,d]
$R=(CH_2)_4$ (5)	8.0	15	69
$R=(CH_2)_5$ (6)	6.0	16	65
$R=(CH_2)_6$ (7)	2.2	17	68
$R=(CH_2)_2CH{:}CH(CH_2)_2$ (8)	3.0	18	50
 9	3.5	 19	45[c,d]
 10a 10b	6	 20a	32[c,e]

[a]The conditions of the preparations are described in the Experimental, and the % yields are those isolated from column chromatography and based on $DBMBF_2$ consumed.
[b]The products are liquid unless specified; **13**, mp 109–111°C, and **19**, mp 140–143°C.
[c]The isolated sample was contaminated with a small percentage of an isomer.
[d]By GC–MS, the second isomer (10%) was recorded.
[e]By GC–MS, three minor isomers (11%, <3%, and <3%) were recorded.

tors and can find their applications in photoimaging processes (22). Indeed such BF_2 complexes were shown to have lower reduction potentials (11) and more efficient fluorescence (2, 15–19) than the parent β-diketones.

Results

Photocycloadditions

The photocycloaddition of $DBMBF_2$ to acyclic olefins **1–3** was regiospecific, giving a single product **11–13** in each case (Table 1). Their structures were readily determined from their GC–MS, IR, and ^{13}C and ^1H NMR spectroscopic data as 1,5-diketones (see Tables 7–10, supplementary material).[1]

[1]Tables 7–10, which contain IR, GC–MS, and ^1H and ^{13}C NMR data of the products, may be purchased from the Depository of Unpublished Data, Document Delivery, CISTI, National Research Council Canada, Ottawa, Canada K1A 0S2.

The alternative regio-isomers could not be detected by GC–MS of the photolysates; if formed, they could be detected by GC in yields as low as 3% and would be readily recognized from their NMR spectra owing to their symmetry element. The photocycloaddition to cyclic olefins **4–8** also occurred just as efficiently to yield a single product in each case except that of cyclopentene, in which case 10% of the minor product was obtained in addition to the major product **14**. As **14** was shown to have the *cis* configuration, both from the vicinal coupling constant of the neighbouring methine protons (6.8 Hz) (23) as well as the consequence of a 5–4 ring fusion in the intermediate stage **21** (see Discussion), we assume the unisolated isomer to be the *trans* isomer derived from an acid-catalyzed isomerization of **14** during isolation. Indeed the GC peak of this minor *trans* isomer increased if a longer time elapsed in the isolation processes. While the stereochemistry of *vic*-disubstituted

Can. J. Chem. Downloaded from www.nrcresearchpress.com by 84.41.108.74 on 09/07/12
For personal use only.

Can. J. Chem. Downloaded from www.nrcresearchpress.com by 84.41.108.74 on 09/07/12
For personal use only.

TABLE 2. Experimental and computed vicinal coupling constants of the methine protons in 1,5-diketones **14–18**

Cycloadducts	Ring size	*J* values (Hz)		
		trans (calcd.)	*cis* (calcd.)	Found
14	5	11.9	7.2	6.8
15	6	12.2	3.7	6.8
16	7	10.5	6.3	3.8
17	8	11.8	5.5	4.2
18	8	11.7	2.8	4.0

diketones **14** and **15** could be judged to be *cis* orientation from the relevant ^1H coupling constant (23) of 6.8 Hz, that of higher member cycloalkanes **16–18** could not readily be decided. Therefore, the stereochemistry of diketone substituted cycloalkanes **14–18** was examined by calculating the vicinal coupling constants for *cis* and *trans* orientation using MM-2 minimized structures (24, 25). In the calculations, the effects of the dihedral angle of the substituted vicinal protons as well as the polar interactions of the substituents were taken into consideration to arrive at the calculated values shown in Table 2. As the observed values are much closer to the calculated values of the *cis* orientation than those of the *trans* orientation, we concluded that our products **14–18** possessed the *cis* configuration.

The major product from the photocycloaddition to norbornene was assigned to the *cis,endo* configuration as in **19** because of two observations, namely, (i) irradiation of H1 caused >20% enhancement of H4 and the *syn* bridge proton (26) and (ii) the *anti* bridge proton was not coupled to H1 and H4, as shown by decoupling experiments. The minor isomer (10%) was not obtained by an acid treatment of **19**, as shown by the GC monitor. This led us to suggest the unisolated minor product as the *cis,exo* isomer corresponding to **19**. The *cis,exo* isomer showed a very strong *m/e* 251 fragment arising from the McLafferty rearrangement followed by the loss of a cyclopentenyl moiety. In contrast, the *cis,endo* isomer **19** could not easily lose a cyclopentenyl moiety, but showed the alternative *m/e* 213 fragment arising from the facile loss of a C_6H_5CO moiety; the detailed mechanism is described in the Ph.D. thesis (27) submitted by one of us.

The photocycloaddition of $DBMBF_2$ to 1,3-pentadiene was an exception since similar irradiation processes in the presence of other electron-rich dienes (cyclohexadiene and 2,4-dimethyl-1,3-pentadiene) caused sensitization without cycloaddition (1). In this reaction, four 1:1 photoaddition products were obtained, as shown by GC–MS; two of them were in trace amounts (<3%, by GC) and probably regioisomeric to the other two. The two major products, **20** (*trans* isomer) and its *cis* isomer, were obtained in 32 and 11% yield, respectively, but could not be obtained in a pure state. The former showed that the CH_3 protons had allylic coupling of 1.8 Hz, much bigger than that of 1.0 Hz for the latter; this provided the rationale (23) for the assignment of the *trans* orientation to **20**.

Under the photolysis conditions used above, $DBMBF_2$ failed to react with 1-methylcyclohexene; careful GC examinations during photolysis showed that the starting materials were not consumed.

TABLE 3. The quantum yields of the photocycloaddition of $DBMBF_2$ (0.01 M) to olefins (1.0 M) in CH_3CN[a]

Olefin	IP (eV)	Quantum yields[b]
3,3-Dimethyl-1-butene (**3**)	9.45	0.18 (0.12)[c]
1-Hexene (**1**)	9.36	0.28
1,5-Hexadiene (**2**)	9.29	0.38
Cyclohexene (**5**)	8.94	0.03
Cycloheptene (**6**)	8.87	0.12 (0.20)[c]
Cyclooctene (**7**)	8.82	0.40

[a]CH_3CN solutions (5 mL) containing each olefin were irradiated in a merry-go-round.
[b]Standard deviations of 6%.
[c]These two figures are obtained at $[DBMBF_2] = 0.07$ M.

Quantum yields

The quantum yields of the product formations (Φ) of $DBMBF_2$ photocycloaddition to several olefins (1.0 M) were measured in a carousel under identical conditions for comparison. The quantum yields were essentially the same for nitrogen-purged or unpurged solutions, but were reduced drastically by the addition of quadricyclene. In agreement with this observation, it is noted that $DBMBF_2$ fluorescence was not reduced in the presence of oxygen (air). As shown in Table 3, for two separate series of monosubstituted acyclic and disubstituted cyclic olefins, Φ was higher for olefins with lower ionization potentials. Subsequently, the quantum yields of the product formations for 3,3-dimethyl-1-butene (**3**) and cycloheptene (**6**) were determined over the range of olefin concentrations [O] $\approx$ 0.05–1.00 M at $[DBMBF_2] = 1.0 \times 10^{-2}$ M; the usual Stern–Volmer plots of $1/\Phi$ vs. reciprocals of olefin concentrations (Fig. 1) gave the experimental quenching rates ($= k_q\tau_0$ = intercept/slope) of 0.38 M^{-1} for **3** and 5.13 M^{-1} for **6**, respectively (Table 4).

The quantum yields of the product formations for the photocycloaddition at increasing concentrations of $DBMBF_2$ over the range 0.01–0.07 M were determined in the presence of a fixed initial concentration of an olefin (1.0 M). Taking the Φ value at $[DBMBF_2] = 0.01$ M as the reference point, Φ/Φ_0 at various $[DBMBF_2]$ were plotted as shown in Fig. 2. For cyclic olefins **5**, **6**, and **7** the ratio characteristically increased with increasing $[DBMBF_2]$ as opposed to the decreasing trend exhibited by acyclic olefin **3**.

Fluorescence quenching

In the concentration range of $[DBMBF_2]$ 10^{-6}–10^{-2} M in CH_3CN, $DBMBF_2$ fluoresces (2) with two peaks at 398 and 416 nm from its monomeric excited state; the former becomes progressively weaker at higher concentration, registering only the latter emission peak at $[DBMBF_2]$ 10^{-3}–10^{-2} M. To eliminate internal filter effects, the fluorescence spectra were taken with a "front-face" configuration for those solutions with $[DBMBF_2] > 10^{-4}$ M. The emission intensities of these two peaks at a fixed $DBMBF_2$ concentration were reduced successively in the presence of increasing amounts of an olefin. The quenching of $DBMBF_2$ fluorescence by **3** was expressed by Stern–Volmer plots (I_0/I vs. concentrations of olefins) in Fig. 3. It was noted that the I_0/I points monitored at either 398 or 416 nm were correlated by a single straight line, and that the slopes ($=$ experimental $k_x\tau_0'$) decreased when quenching experiments were carried out at higher $DBMBF_2$ concentrations (Table 4). Similar patterns were observed for $DBMBF_2$ fluo-

Can. J. Chem. Downloaded from www.nrcresearchpress.com by 84.41.108.74 on 09/07/12
For personal use only.

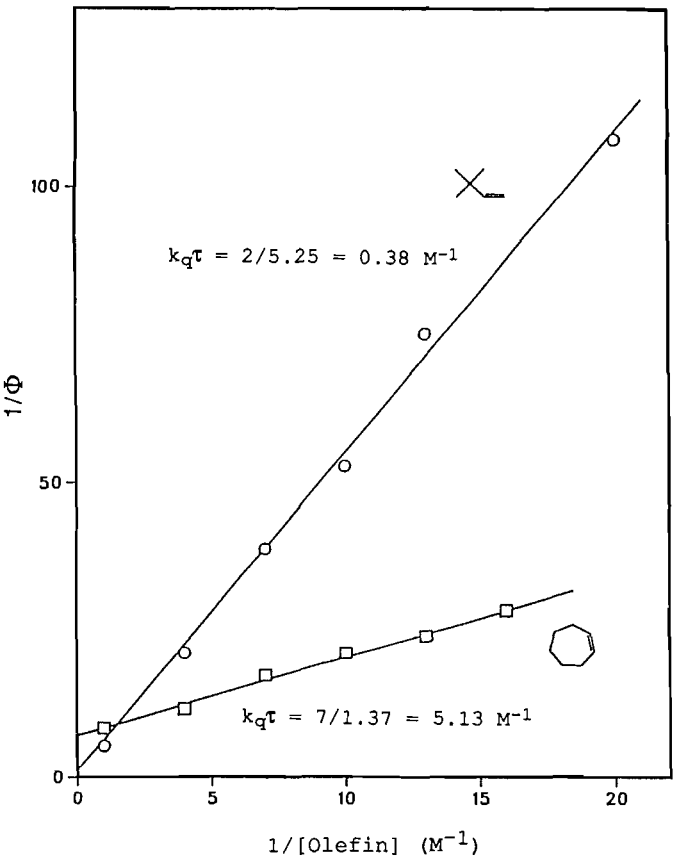


FIG. 1. Stern–Volmer plots of reciprocal quantum yields ($1/\Phi$) vs. reciprocal olefin concentrations (1/[O]) in the photocycloaddition of $DBMBF_2$ with 3,3-dimethyl-1-butene (**3**) (○) and cycloheptene (**6**) (□) in CH_5CN.

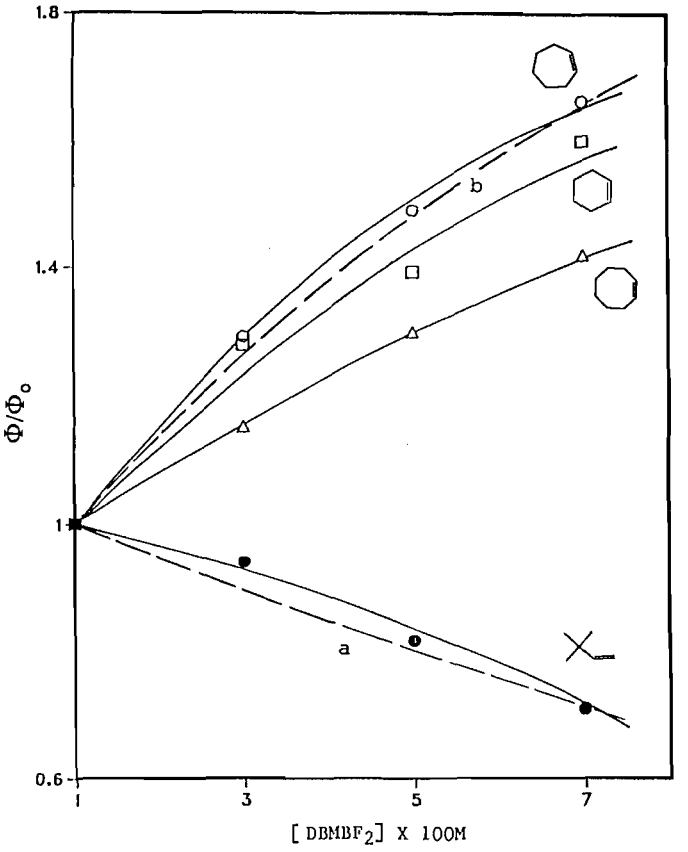


FIG. 2. The dependence of the quantum yields of the photocycloaddition on $DBMBF_2$ concentrations with reference to the quantum yield (Φ_0) at [$DBMBF_2$] = 1.0×10^{-2} M as unity: the dashed lines are computed from eqs. [5] and [6].

TABLE 4. The Stern–Volmer quenching rates of $DBMBF_2$ fluorescence ($k_x\tau_0'$) and the photocycloaddition with olefins **3** and **6** ($k_q\tau_0$)

	Stern–Volmer rate (M^{-1})	
[$DBMBF_2$] (M)	3,3-Dimethyl-1-butene (**3**)	Cycloheptane (**6**)
5×10^{-6}	0.57 ± 0.02^a	4.86 ± 0.08^a
1×10^{-3}	0.50 ± 0.02^b	4.49 ± 0.08^b
1×10^{-2}	0.42 ± 0.02^b	4.37 ± 0.08^b
1×10^{-2}	0.38 ± 0.05^c	5.13 ± 0.14^c

[a]The $DBMBF_2$ fluorescence quenching monitored at 398 and 416 nm with a 90° cell geometry.

[b]The $DBMBF_2$ fluorescence quenching monitored at 416 nm with a front-face geometry.

[c]The $k_q\tau_0$ was obtained from the monitor of cycloaddition quantum yields.

rescence quenching at 398 and 416 nm by cycloheptene, **6**. The decreases of slopes (= $k_x\tau_0'$) (in Table 4) were small, about 10% with 5000-fold decrease in $DBMBF_2$ concentration, but reproducible.

Taking advantage of the fact that in the region of [$DBMBF_2$] $> 5 \times 10^{-2}$ M a well-separated broad excimer fluorescence band could be observed (2), the possibility of the interaction of the excimer with olefins was investigated. From time-resolved fluorimetry,[2] the lifetime of the excimer was shown to be 50 ns in acetonitrile, more than an order of magnitude higher than the monomer lifetime. This suggested that the excimer was formed by an irreversible process, which was also supported by an "oxygen test" (28, 29); excimer fluorescence intensities were significantly reduced by oxygen in the presence of air while $DBMBF_2$ fluorescence remained unaffected. There are many cases of interactions of exciplexes or excimers with a substrate leading to termolecular photochemical and photophysical phenomena (30–39). Steady-state exciplex (excimer) fluorescence quenching has been analysed by Medinger and Wilkinson (30) as well as by Caldwell and coworkers (31–33) to follow a simple Stern–Volmer relation if the corrected intensity ratios of exciplex (excimer) fluorescence, $I_0(ex)/I(ex) \div I_0(mono)/I(mono)$, are plotted against quencher concentrations, where $I_0(ex)$ and $I_0(mono)$ are the exciplex (excimer) and monomer intensities in the absence of the quencher, i.e., [Q] = 0. The excimer intensities at 522 nm in the presence (I) and absence (I_0) of an olefin at the same $DBMBF_2$ concentration were used to calculate the quenching by the olefin (Fig. 4). Owing to the fact that the fluorescence intensity (i.e., concentration) of the excimer varies drastically in this $DBMBF_2$ concentration range, the latter reading (I') was obtained by normalizing with respect to the peak height at the 437-nm fluorescence peak (dashed curves); this peak corresponds to the monomer fluorescence at 416 nm observed in dilute solutions, which was red-shifted with the appearance of the excimer peak. This experimental manoeuvre essentially normalized excimer intensities to constant monomer intensity,

[2]J. Korppi-Tommola. University of Jyväskylä, Finland. Unpublished results.

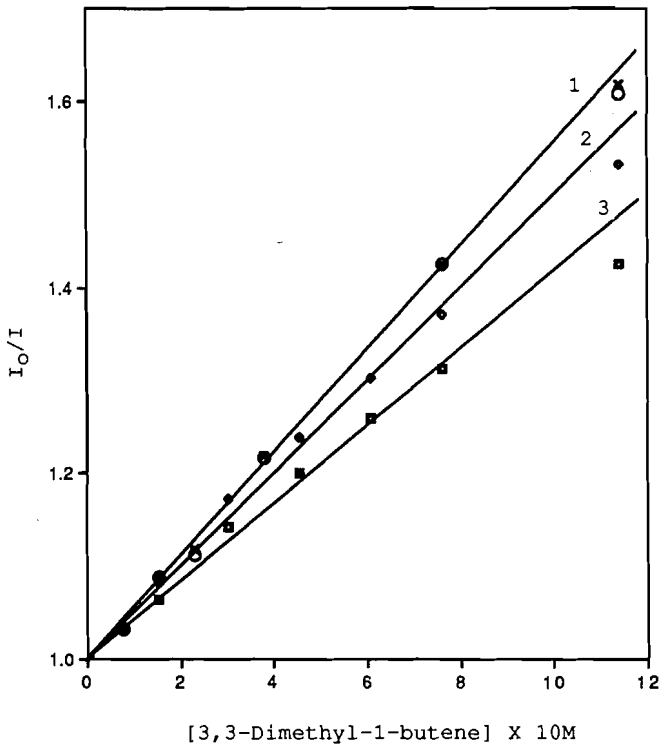


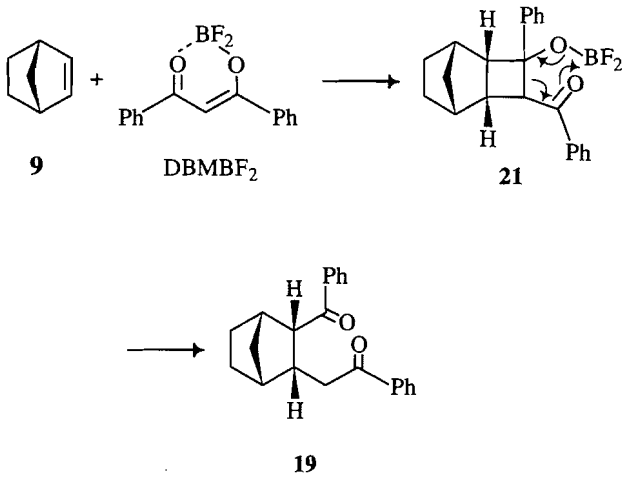
FIG. 3. Stern–Volmer plots of the quenching of $DBMBF_2$ fluorescence by 3,3-dimethyl-1-butene (**3**) in CH_3CN: plot 1, $[DBMBF_2] = 5 \times 10^{-6}$ M, and monitored at 398 and 416 nm; plots 2 and 3, $[DBMBF_2] = 10^{-3}$ and 10^{-2} M, and monitored at 416 nm.

i.e., I' is equivalent to the term of $I_0(\text{ex}) \div I_0(\text{mono})/I(\text{mono})$ (31). The plot of I'/I for cycloheptene revealed that the quenching efficiency of the excimer as represented by the slope was $k_t\tau_m = 6.77\ M^{-1}$ if the point of [**6**] = 0.329 M was ignored; at this high concentration, extensive quenching caused a large margin of error due to weak excimer emission. Under the same procedure, it was shown that the excimer intensities were feebly quenched by **3**; the slope was about 0.4 M^{-1}.

Discussion

The quenching of monomer fluorescence of $DBMBF_2$ at 398 and 416 nm by an olefin concurrent with the photoaddition of the olefin with $DBMBF_2$ can be regarded as a qualitative indication that $DBMBF_2$ reacts from its lowest singlet excited state with the olefins to yield 1,5-diketones **11–20** with excellent regiospecificity. The 1,5-diketones from the photoreaction are conveniently interpreted with a [2 + 2] photocycloaddition pattern shown below in analogy to the de Mayo reaction (3–8). However, the present photoaddition of $DBMBF_2$ with olefins is distinctly different from the de Mayo reaction in that the former is a singlet state reaction with much higher quantum efficiency than the latter. In fact, we showed that DBM does not add photolytically to these simple olefins by prolonged irradiation. Furthermore, we have shown that acetylacetone slowly adds photolytically to norbornene to give only the *cis,exo* adduct (27), in contrast to the major product of the *cis,endo* adduct **19** in the $DBMBF_2$ photocycloaddition. As the photocycloaddition probably involves a complex pattern, as suggested by the results of Figs. 2–4, it is premature to discuss its limitation, scope, and stereochemistry in detail as the reactive steps are being investigated.

However, the available data show that the overall consequence of the addition is stereospecific with the *cis*-addition mode and, probably, sensitive to steric hindrance. In the communication (1) it was concluded that an exciplex between the singlet excited state $DBMBF_2$ and an olefin is involved through partial electron transfer interactions, as suggested by the correlation of log k_q with the energy required to transfer a single electron to singlet excited state $DBMBF_2$ from a substrate. Subsequently we discovered that the kinetics of the interaction of the singlet state $DBMBF_2$ with an olefin are more complex, arising from the concurrent interaction of the $DBMBF_2$ excimer, particularly in a high $[DBMBF_2]$ region, as shown in the results.



The participation of the excimer in photocycloaddition is indicated by two observations. First of all, the measured quenching rates of monomer fluorescence intensities exhibit small but finite decreases with increases of $DBMBF_2$ concentrations (Table 4, Fig. 3); this trend hints at the presence of a competing reaction step that involves $DBMBF_2$. Secondly, the variations of the quantum yield of the photocycloaddition with $DBMBF_2$ concentrations (Fig. 2) suggest that the excimer is involved in the photocycloaddition. Scheme 1 is therefore proposed as a basis for kinetic analysis of chemical and physical events upon excitation of $DBMBF_2$ (A) in the presence of olefin (O), where $^*(A,O)$ is an exciplex and $^*(A,A,O)$ is a triple complex, analogies of which have been proposed in other photoreactions and have been referred to as triplexes (31–33). In this scheme, the excimer $^*(A,A)$ is formed from $^*A$ irreversibly as shown above. The quenching of exciplexes is a well-known phenomenon (31–39) and the involvement of a stilbene excimer in cycloaddition (40) has been suggested. The present case is the first well-established example of photoreactions originated by quenching of an excimer.

On the basis of Scheme 1, the quenching of $DBMBF_2$ fluorescence by an olefin can be expressed by the Stern–Volmer relation as shown in eq. [1]. This predicts the slope ($= k_x\tau_0'$) of the plots must be affected by the $k_m[A]$ term because the excimer $^*(A,A)$ is formed irreversibly, i.e., the slope is reduced at higher $DBMBF_2$ concentrations; this is what is found (Table 4). In a low concentration range of $[DBMBF_2] < 10^{-3}$ M where the excimer formation is insignificant (i.e., $k_m[A] \ll k_d$), the lifetime τ_0 ($= 1/k_d$) of singlet excited $DBMBF_2$ was previously estimated, by a biacetyl quenching experiment (2), to be 2.7 ns. Using this τ_0 value, the fluorescence quenching rate constants at $[DBMBF_2] = 5 \times 10^{-6}$ M (Fig. 3 and Table 4) are calculated to be $k_x = 2.1 \times 10^8\ M^{-1}\ s^{-1}$ for **3** and $k_x = 1.78 \times 10^9\ M^{-1}\ s^{-1}$ for **6**

Can. J. Chem. Downloaded from www.nrcresearchpress.com by 84.41.108.74 on 09/07/12
For personal use only.

Can. J. Chem. Downloaded from www.nrcresearchpress.com by 84.41.108.74 on 09/07/12
For personal use only.

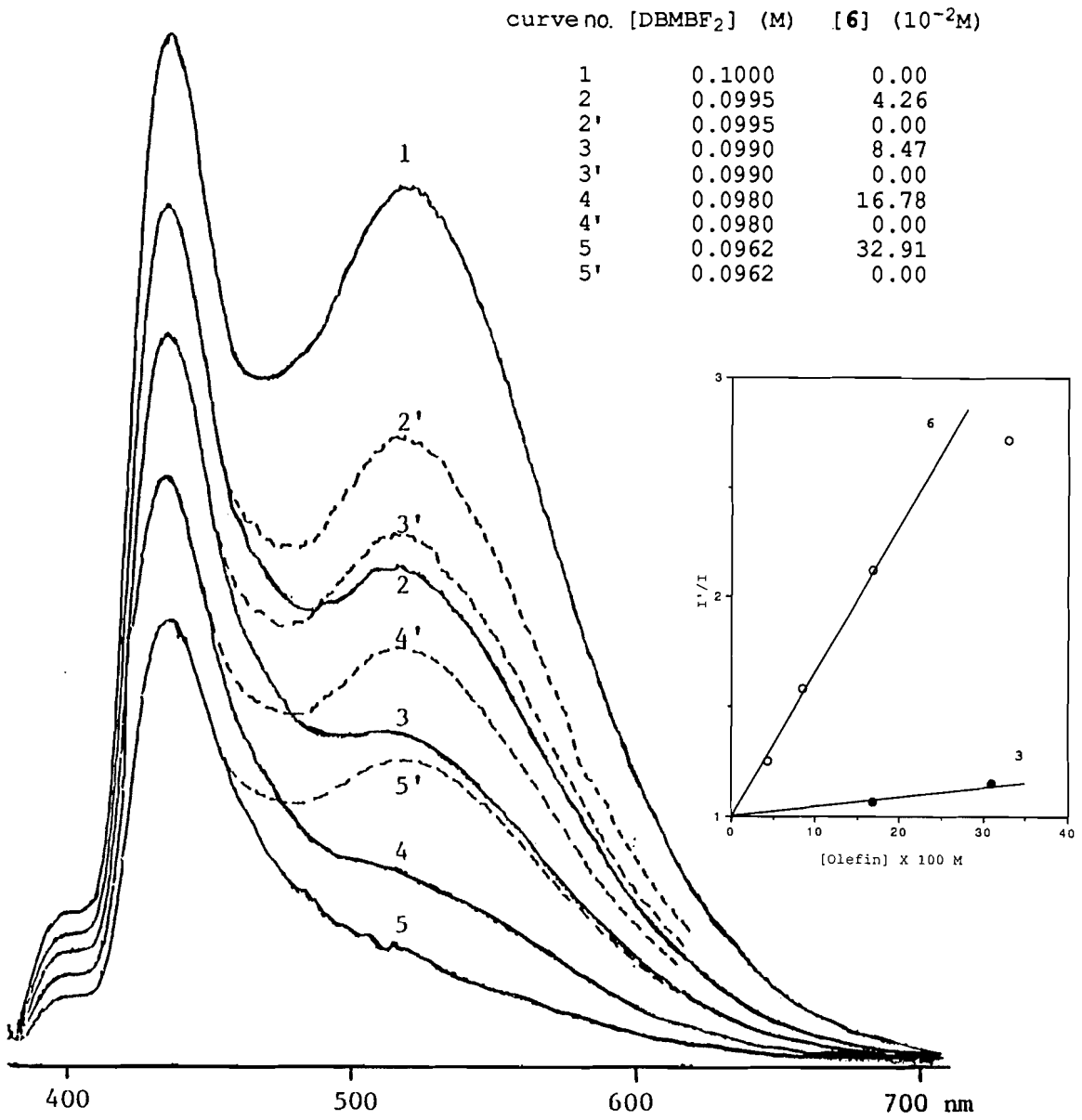
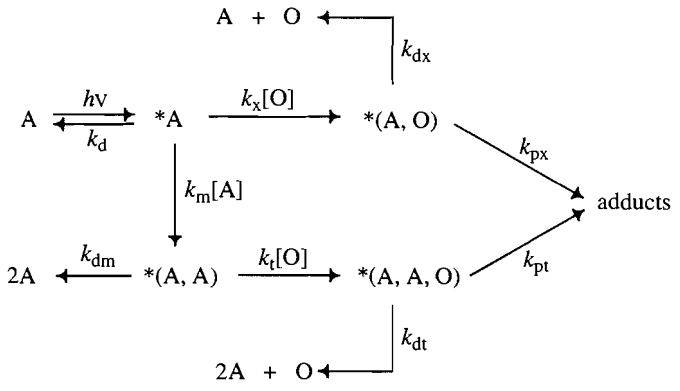


FIG. 4. The quenching of fluorescence intensities of $DBMBF_2$ (0.100–0.0962 M) excimer fluorescence intensities by cycloheptene **6** in CH_3CN, λ_{ex} 365 nm; the dashed curves were taken with the same [$DBMBF_2$] as these solid curves without **6** and were normalized with respect to the corresponding solid curves at 437 nm. Inset: The Stern–Volmer plots monitored at 522 nm.



SCHEME 1

(Table 5). These values can be regarded as the real quenching rate constants of monomeric singlet excited $DBMBF_2$ by the olefins, because we have established that $DBMBF_2$ does not form ground state aggregates (2) and that the excimer formation is feeble at [$DBMBF_2$] = 5×10^{-6} M. The fluorescence quenching pattern in the [$DBMBF_2$] 10^{-4}–10^{-1} M range can be expressed by eq. [1].

$$[1] \quad I_0/I = 1 + k_x[O]/(k_d + k_m[A]) = 1 + k_x\tau_0'[O]$$

The rate constant of the excimer formation k_m was estimated from the decrease of the 416-nm peak to 6×10^9 M^{-1} s^{-1}, assuming that at [$DBMBF_2$] = 0.06 M the peak intensity is halved. This value is in agreement with the fact that the photo-

TABLE 5. The reaction parameters of singlet excited state $DBMBF_2$ with olefins **3** and **6** at 1 M concentration

	3	**6**
k_x (M^{-1} s^{-1})[a]	0.21×10^9	1.78×10^9
M (eq. [3])	0.53	0.13
	$k_{px} = 1.13k_{dx}$	$k_{px} = 0.15k_{dx}$
M (1/intercept)[b]	0.5	0.14
N (eq. [4])	0.04	0.69
$k_t\tau_m$[c]	0.4	6.8
	$k_{pt} = 0.14k_{dt}$	$k_{pt} = 3.8k_{dt}$

[a]These values are obtained from the quenching of $DBMBF_2$ fluorescence in Table 4.
[b]The intercept of the plots in Fig. 1.
[c]Obtained from the plots in Fig. 4.

cycloaddition quantum yield began to be affected in the region of $[DBMBF_2] > 10^{-2}$ M as shown in Fig. 2.

On the basis of Scheme 1, the quantum yield of cycloadduct (Φ) can be represented by the sum of that from the exciplex (Φ_x) and that from the triplex (Φ_t) as in eq. [2]: Φ is the function of the concentrations of both olefin and $DBMBF_2$. A direct solution of eq. [2] is difficult unless some rate constants are known from other experiments, such as time-resolved fluorimetry.

$$[2] \quad \Phi = \Phi_x + \Phi_t = (Mk_x[O] + Nk_m[A])/(k_d + k_x[O] + k_m[A])$$

where

$$[3] \quad M = k_{px}/(k_{dx} + k_{px})$$

$$[4] \quad N = \{k_{pt}/(k_{dt} + k_{pt})\} \times \{k_t[O]/(k_{dm} + k_t[O]\}$$

However, under the limiting conditions of constant concentration of olefin [O] = 1 M, such as used in Fig. 2 and Table 3, it is possible to estimate the relative importance of the two pathways. From the first derivative ($d\Phi/d[A]$) of eq. [2], it can be shown that a plot of eq. [2] will have a positive slope when $N > (Mk_x[O])/(k_d + k_x[O])$, and vice versa. While the complex relation cannot easily be simplified, it essentially means that if the triplex pathway (k_t and k_{pt}) is faster than the exciplex pathway (k_x and k_{px}), a positive slope is obtained; the cases of **5**, **6**, and **7** in Fig. 2 are examples. In the opposite case, as for **3**, a negative slope is obtained.

A more quantitative analysis of the proposed mechanism with respect to eq. [2] can be made if k_m and k_x estimated for **3** and **6** above are substituted into eq. [2] at [O] = 1 M to give eqs. [5] and [6], respectively.

$$[5] \quad \Phi \text{ (for } \mathbf{3}) = (0.21M + 6N[A])/(0.58 + 6[A])$$

$$[6] \quad \Phi \text{ (for } \mathbf{6}) = (1.78M + 6N[A])/(2.15 + 6[A])$$

The values of M and N can be obtained by using the Φ values determined for **3** and **6** at $[DBMBF_2] = 0.01$ and 0.07 M given in Table 3, from which $M = 0.53$, $N = 0.04$ for **3**, and $M = 0.13$, $N = 0.69$ for **6** are obtained (see Table 5). Using these values, the calculated quantum yield ratios Φ/Φ_0 for **3** and **6** at $[DBMBF_2]$ 0.01–0.07 M are shown as the dashed lines in Fig. 2. The good coincidence with the experimental points for both olefins clearly supports dual photocycloaddition pathways for singlet excited state $DBMBF_2$ with olefins. The acceptability of these M and N values is tested by varying the values for drawing the curves by ±10%; as these test drawings deviate drastically from the experimental points, the calculated M and N values appear to be reasonable. Furthermore, from the definitions in eq. [3], M represents the limiting quantum yields and could be obtained from the reciprocals of the intercept in plots of $1/\Phi$ vs. $1/[O]$ in Fig. 1; 1/(intercept) for **3** is 1/2 = 0.5 and for **6** is 1/7 = 0.14. These values are very close to those M values calculated above.

TABLE 6. Calculated % contributions of the exciplex pathway (Φ_x) and the triplex pathway (Φ_t) to the quantum yield of photocycloaddition as a function of $DBMBF_2$ concentration[a]

Olefin	$[DBMBF_2]$ (M)					
	0.001	0.005	0.010	0.050	0.100	0.220
3 Φ_x(%)	99.8	98.9	97.9	90.3	82.3	67.8
Φ_t(%)	0.2	1.1	2.1	9.7	177	32.2
6 Φ_x(%)	98.2	91.8	84.8	52.8	35.9	20.3
Φ_t(%)	1.8	8.2	15.2	47.2	64.1	79.7

[a]The data are calculated from eq. [5] for **3** and from eq. [6] for **6** at the olefin concentration of 1.0 M.

The slopes of the plots (dashed lines) for **3** and **6** in Fig. 2 indicate the relative contribution of the exciplex pathway (Φ_x) versus the triplex pathway (Φ_t). The relative contributions of these two quantum yields can be calculated from the first and second terms, respectively, in eqs. [5] and [6] for these two olefins. As shown in Table 6, the photocycloaddition pattern for acyclic olefin **3** is clearly different from that for cyclic olefin **6**. For acyclic olefin **3**, the exciplex pathway remains the major pathway up to very high concentrations of $DBMBF_2$. In contrast, for cyclic olefin **6** the triplex pathway has started to show as early as $[DBMBF_2] = 5 \times 10^{-3}$ M (i.e., at the $[DBMBF_2]$ where the excimer barely started to show its presence (2)) and becomes dominant at about $[DBMBF_2] = 0.05$ M and above; other cyclic olefins should show a similar trend in view of the positive slopes of the Φ/Φ_0 vs. $[DBMBF_2]$ plots in Fig. 2. This reaction pattern is nicely confirmed by the strong quenching of the excimer fluorescence at 522 nm by **6** with the quenching rate ($k_t\tau_m$ where $\tau_m = 1/k_{dm}$ is the lifetime of the excimer) of 6.8 M^{-1} as opposed to the feeble quenching (0.04 M^{-1}) shown by **3**.

These data can be used to evaluate the relative importance of two decay modes of exciplex *(A,O) and triplex *(A,A,O) from the known numerical values of M and N at [O] = 1 M. According to eq. [3], direct substitution of M values gives $k_{px} = 1.13k_{dx}$ for **3** and $k_{px} = 0.15k_{dx}$ for **6**. Acyclic olefin **3** shows better efficiency than cyclic olefin **6** for the collapse of *(A,O) to the cycloadducts. In eq. [4], the second term is converted to $k_t\tau_m/(1 + k_t\tau_m)$ at [O] = 1 M. The substitution of N values gives $k_{pt} = 0.16k_{dt}$ for **3** and $k_{pt} = 3.8k_{dt}$ for **6**. These relations indicate that cyclic olefin **6** is more efficient than acyclic olefin **3** to convert triplex *(A,A,O) to the product. The kinetic parameters are summarized in Table 5 for comparison.

The foregoing discussion clearly indicates that the photocycloaddition of $DBMBF_2$ to simple olefins follows complex mechanisms that are dependent on the type of olefins (either cyclic disubstituted **6** or acyclic monosubstituted **3**) and the $DBMBF_2$ concentration. Table 5 shows that the exciplex path-

Can. J. Chem. Downloaded from www.nrcresearchpress.com by 84.41.108.74 on 09/07/12
For personal use only.

Can. J. Chem. Downloaded from www.nrcresearchpress.com by 84.41.108.74 on 09/07/12
For personal use only.

way is more important for the monosubstituted acyclic olefin **3**, for which the triplex pathway from the excimer is secondary under all conditions. Endocyclic olefins, such as **6**, primarily react with the $DBMBF_2$ excimer with high efficiency; as shown in Table 6 this reaction pathway becomes noticeable as soon as the excimer is being formed, at [$DBMBF_2$] as low as 0.005 M. Finally, it is useful to examine the slopes obtained in Fig. 1. The mechanism outlined in Scheme 1 dictates that $k_q\tau_0$ values obtained from the double reciprocal plots of $1/\Phi$ vs. 1/[olefin] (Fig. 1 and Table 4) must be a composite of two reaction pathways arising from the consequence that quantum yields determined are those of total Φ ($= \Phi_x + \Phi_t$). Qualitatively, depending on the extent of triplex pathway contributions to Φ, the calculated $k_q\tau_0$ is either smaller (as for **3**) or larger (as for **6**) than those determined from monomer fluorescence quenching as shown in Table 4 (top three rows).

Other factors influencing the importance of the dual reaction pathway are of course possible; e.g., the polarity of solvent and the temperature are two common factors that may be examined. However, such investigations should use the time-dependent fluorescence decay technique, a more efficient method for clear demonstration.

Experimental section

Materials and general conditions

Commercially available olefins were distilled before use. Unless specified otherwise the following conditions prevailed. The boron difluoride complex of dibenzoylmethane was prepared from the reaction of the ligand with BF_3 etherate in acetonitrile according to the published procedure; $DBMBF_2$ mp 192–194°C (lit. (11) mp 193–194°C). The IR and NMR spectra of $DBMBF_2$ have been reported (10).

Gas chromatographic (GC) analyses were performed on a Hewlett–Packard 5790 chromatograph equipped with a FID and an OV-1 (12 m × 0.20 mm) or HP-1 (25 m × 0.20 mm) capillary column, and connected to a Hewlett–Packard 3390A chart integrator. Preparative GC was conducted on a Varian 1700 chromatograph equipped with an OV-1 packed column (4 ft × 0.25 in., 15%, Chromsorb A, 60–80 mesh). Melting points were determined on a Fisher–Johns apparatus (uncorrected). Infrared (IR) spectra were recorded on a Perkin–Elmer 559B (neat film or KBr), and (or) a BOMEM Michelson 120 (FT-IR). Mass spectra (MS) and gas chromatography – mass spectra (GC–MS) were taken with a Hewlett–Packard 5985 GC–MS system by the electron-impact ionization (EI) and (or) chemical ionization (CI) mode. Nuclear magnetic resonance spectra were acquired on either a Bruker 100SY spectrometer equipped with Aspect 2000 software or a Bruker WH400 spectrometer. Two-dimensional (2D) NMR spectra were recorded on the latter. Chemical shifts (δ) for ^1H and ^{13}C spectra are reported in ppm with reference to tetramethylsilane. The coupling constants are reported in Hz. Ultraviolet and visible (UV/VIS) spectra were recorded on a Varian Cary 210 or a Philips PV8720 spectrophotometer. Emission spectra were obtained on a Perkin–Elmer MPF 44B spectrophotometer (uncorrected). The fluorescence spectra of $DBMBF_2$ in acetonitrile without degassing were taken with excitation at 365 nm in a right-angle arrangement for [$DBMBF_2$] $< 1 \times 10^{-4}$ M or in a front-face cell for [$DBMBF_2$] $> 10^{-4}$ M.

The photocycloaddition of $DBMBF_2$ and olefins

A solution of $DBMBF_2$ (1.5 mmol) and an olefin (15 mmol) in acetonitrile (30 mL) was distributed equally in six Pyrex test tubes (13 × 100 mm) that were placed in a "merry-go-round" mounted in a Rayonet photoreactor equipped with 3500 Å lamps. Without degassing, these samples were irradiated at about 31°C. Samples were taken at intervals for GC analysis, in which the appearance of products and (or) disappearance of $DBMBF_2$ were examined. If the reaction was slow, irradiation was stopped at about 80% consumption of $DBMBF_2$.

The photolysates were evaporated, and the residues were taken for flash chromatography using hexane – ethyl acetate as eluent. For photolysates with 80% completion of photoreaction, the residue was treated with hexane. Insoluble $DBMBF_2$ was filtered and the hexane solution was chromatographed. Olefins, products, and % yields based on consumed $DBMBF_2$ are given in Table 1. The IR, NMR, and GC data are given in Tables 7–10.[1] Compounds **11** and **19** were distilled and analysed. For **11**: Anal. calcd. for $C_{21}H_{24}O_2$: C 81.78, H 7.84; found: C 81.58, H 7.96. For **19**: Anal. calcd. for $C_{22}H_{22}O_2$: C 82.99, H 6.96; found: C 83.29, H 6.75.

Quantum yield measurement

The same air-cooled Rayonet photoreactor was used for the quantum yield determinations. Five millilitres each of sample and actinometry solutions were loaded into Pyrex test tubes (100 mm × 13 mm) that were evenly distributed on a rotary merry-go-round for irradiation at 31°C. Degassed benzene solutions of benzophenone (5×10^{-2} M) and benzhydrol (1×10^{-1} M) were used for actinometry, assuming a quantum yield of 0.74. The consumption of benzophenone was measured by the absorption at 340 nm. Octadecane (2.0×10^{-3} M) was added to the sample solution before photolysis to act as an internal standard for GC analysis. The conversion of $DBMBF_2$ was controlled to about 20% except for a few cases of 20–30% conversion.

Computation of vicinal proton coupling constant

The vicinal proton spin–spin coupling constants of the methine protons in **14–18** were computed using the MM-2 program, VAX/VMS Version 4.5, in which not only the dihedral angle of the vicinal protons but also the polar interactions of the substituents were considered. The conformers assumed were the "envelope" for cyclopentane, a chair for cyclohexane, a twisted chair for cycloheptane, and the "crown" for cyclooctane. Only the equatorial conformer was considered for *trans*-substituted compounds.

The quenching of $DBMBF_2$ excimer fluorescence

A 0.1 M $DBMBF_2$ solution in acetonitrile was prepared. Sample solutions were prepared by injecting the necessary amounts of cycloheptene **6** with a microsyringe. The corresponding reference solutions were prepared by injecting the same volumes of acetonitrile instead of **6**. First, a sample solution fluorescence was recorded as shown by the solid lines (Fig. 4). The corresponding reference solution fluorescence was taken by adjusting the pen to the height at 437 nm of the sample spectrum (shown as dashed lines). The fluorescence intensities at 522 nm for the samples corresponding to those for the reference (I/I') were plotted against the olefin concentrations (Fig. 4, insert). Front-face illumination was used in this experiment.

Acknowledgement

The authors are grateful to the Natural Sciences and Engineering Research Council of Canada for generous financial support.

1. Y. L. CHOW and X. E. CHENG. J. Chem. Soc. Chem. Commun. 1043 (1990).
2. Y. L. CHOW, X. E. CHENG, and C. I. JOHANSSON. J. Photochem. Photobiol. A: **51**, 247 (1990).
3. A. C. WEEDON. *In* Synthetic organic photochemistry. *Edited by* W. M. Horspool. Plenum, New York. 1984. p. 61.
4. P. DE MAYO and H. TAKESHITA. Can. J. Chem. **41**, 44 (1963).
5. H. HIKINO and P. DE MAYO. J. Am. Chem. Soc. **86**, 3582 (1984).
6. B. C. CHALLAND, G. KORNIS, G. LANGE, and P. DE MAYO. J. Org. Chem. **34**, 794 (1969).
7. H. NOZAKI, M. KURITA, T. MORI, and R. NOYORI. Tetrahedron, **24**, 1821 (1968).
8. M. TADA, H. HARADA, and K. MIURA. Bull. Chem. Soc. Jpn. **51**, 839 (1978).
9. Y. L. CHOW and G. E. BUONO-CORE. J. Am. Chem. Soc. **104**, 3770 (1982).
10. N. M. D. BROWN and P. BLADOM. J. Chem. Soc. (A), 526 (1969).
11. L. H. TOPORCER, R. E. DESSY, and I. E. GREEN. Inorg. Chem. **4**, 1649 (1965).

12. F. UMLAND, E. HOHAUS, and K. BRODIE. Chem. Ber. **106**, 2427 (1973).
13. H.-D. ILGE, D. FABLER, and H. HARTMANN. Z. Chem. **24**, 218 (1984).
14. H.-D. ILGE, D. FABLER, and H. HARTMANN. Z. Chem. **24**, 292 (1984).
15. H.-D. ILGE, E. BIRCKNER, D. FASSLER, M. V. KOZMENKO, M. G. KUZ'MIN, and H. HARTMANN. J. Photochem. **32**, 177 (1986).
16. H.-D. ILGE, E. BIRCKNER, D. FASSLER, M. V. KOZMENKO, M. G. KUZMIN, and H. HARTMANN. J. Photochem. **36**, 27 (1987).
17. V. E. KARASEV and O. A. KOROTKIKH. Russ. J. Inorg. Chem. (Engl. Transl.) **30**, 1290 (1985).
18. V. E. KARASEV and O. A. KOROTKIKH. Russ. J. Inorg. Chem. (Engl. Transl.) **31**, 493 (1986).
19. N. P. SHAPKIN, O. A. KOROTKIKH, and V. E. KARASEV. Russ. J. Inorg. Chem. (Engl. Transl.) **30**, 1069 (1985).
20. J. F. CHANDLER, B. DOBINSON, E. JOHNSTON, M. E. B. JONES, R. J. MARTIN, and B. P. STARK. Br. Polym. J. **1**, 208 (1969).
21. B. P. STARK and M. E. B. JONES. German Patent No. 1, 495,259 (1973).
22. (*a*) J. M. HALM. TAPPI, **60**, 90 (1977); (*b*) U.S. Patent No. 4,360,584 (1982).
23. (*a*) D. J. PASTO and C. R. JOHNSON. Laboratory text for organic chemistry. Prentice, Englewood Cliffs, NJ. 1979. pp. 180–264; (*b*) S. STERNHELL. Q. Rev. Chem. Soc. **23**, 236 (1969).
24. C. A. G. HAASNOOT, F. A. A. M. DE LEEUW, and C. ALTOONA. Tetrahedron, **36**, 2783 (1980).
25. C. STILL. Macromodel molecular modeling system, Version 2. Department of Chemistry, Columbia University, New York. 1988.
26. J. K. SAUNDERS and J. W. EASTON. *In* Determination of organic structure by physical methods. *Edited by* F. C. Nachod, J. J. Zuckerman, and E. M. Randall. Academic Press, New York. 1976. p. 271.
27. X.-E. CHENG. Ph.D. Dissertation, Simon Fraser University. 1990.
28. M. COHEN and B. K. SELINGER. Mol. Photochem. **1**, 371 (1969).
29. R. J. MCDONALD and B. K. SELINGER. Mol. Photochem. **3**, 99 (1971).
30. T. MEDINGER and F. WILKINSON. Trans. Faraday Soc. **62**, 1785 (1966).
31. R. A. CALDWELL, D. CREED, D. C. DEMARCO, L. A. MELTON, H. OHTA, and P. H. WINE. J. Am. Chem. Soc. **102**, 2369 (1980).
32. R. A. CALDWELL, D. CREED, and H. OHTA. J. Am. Chem. Soc. **97**, 3246 (1975).
33. D. CREED and R. A. CALDWELL. J. Am. Chem. Soc. **100**, 2905 (1978).
34. T. MIMURA and M. ITO. J. Am. Chem. Soc. **98**, 1095 (1976).
35. H. BEENS and A. WELLER. Chem. Phys. Lett. **2**, 140 (1968).
36. J. SALTIEL, D. E. TOWNSEND, B. D. WATSON, and P. SHANNON. J. Am. Chem. Soc. **97**, 5688 (1975).
37. S. OKAJIMA, B. T. LIM, and E. C. LIM. Chem. Phys. Lett. **122**, 82 (1985).
38. G. C. CALHOUN and G. B. SCHUSTER. J. Am. Chem. Soc. **108**, 8021 (1986).
39. N. C. YANG, D. M. SHOLD, and B. KIM. J. Am. Chem. Soc. **98**, 6587 (1976).
40. (*a*) F. D. LEWIS. Acc. Chem. Res. **12**, 152 (1979): Adv. Photochem. **13**, 165 (1986); (*b*) B. C. GREEN, M. REJTÖ, D. E. JOHNSON, C. E. HOYLE, T. I. HO, J. T. SIMPSON, and F. D. LEWIS. J. Am. Chem. Soc. **101**, 3325 (1979).

Can. J. Chem. Downloaded from www.nrcresearchpress.com by 84.41.108.74 on 09/07/12
For personal use only.

Thermal diffusion with hydrolysis in aqueous solutions of sodium carbonate

HUI LÜ AND DEREK G. LEAIST[1]

Department of Chemistry, University of Western Ontario, London, Ont., Canada N6A 5B7

Received February 5, 1991

HUI LÜ and DEREK G. LEAIST. Can. J. Chem. **69**, 1584 (1991).

A conductimetric technique is used to measure thermal diffusion in aqueous solutions of sodium carbonate. In dilute solutions hydrolysis produces significant amounts of sodium bicarbonate and sodium hydroxide: $Na_2CO_3 + H_2O = NaHCO_3 + NaOH$. The applied temperature gradient causes the various solutes to migrate to the cooler parts of the solution. NaOH is found to diffuse more rapidly than $NaHCO_3$, leading to the accumulation of excess NaOH (relative to $NaHCO_3$) at the cold plate. Binary $Na_2CO_3(m) + H_2O$ mixtures therefore separate into ternary $Na_2CO_3(m_1) + NaOH(m_2) + H_2O$ mixtures under nonisothermal conditions. The steady-state molality gradients dm_1/dT and dm_2/dT and the ternary heats of transport of aqueous Na_2CO_3 and NaOH are reported.

Key words: aqueous sodium carbonate, hydrolysis, mixed electrolytes, Soret coefficient, thermal diffusion.

HUI LÜ et DEREK G. LEAIST. Can. J. Chem. **69**, 1584 (1991).

On a utilisé un technique conductimétrique pour mesurer la diffusion thermique dans des solutions aqueuses de carbonate de sodium. En solutions diluées, l'hydrolyse conduit à la formation de quantités importantes de bicarbonate de sodium et d'hydroxyde de sodium : $Na_2CO_3 + H_2O = NaHCO_3 + NaOH$. Lorsqu'on applique un gradient de température, il y a migration des divers solutés vers les parties les plus froides de la solution. On a trouvé que le NaOH diffuse plus rapidement que le $NaHCO_3$; il en résulte une accumulation de l'excès du NaOH (relatif au $NaHCO_3$) au niveau de la plaque froide. Dans des conditions qui ne sont pas isothermes, les mélanges binaires de $Na_2CO_3(m) + H_2O$ se séparent donc en mélanges ternaires de $Na_2CO_3(m_1) + NaOH(m_2) + H_2O$. On a aussi déterminé les gradients de molalité de l'état stationnaire dm_1/dT et dm_2/dT ainsi que les chaleurs de transport ternaire des solutions aqueuses de Na_2CO_3 et de NaOH.

Mots clés : carbonate de sodium aqueux, hydrolyse; électrolytes mixtes; coefficient de Soret, diffusion thermique.

[Traduit par la rédaction]

1. Introduction

A concentration gradient develops when a temperature gradient is applied to a convection-free solution (1–4). Aqueous salts, for example, usually migrate to the cooler parts of a nonisothermal solution. The separation that is achieved is expressed by the Soret coefficient

$$[1] \quad \sigma = -m^{-1}(dm/dT)_{\infty \text{ or steady state}}$$

which gives the fractional change in solute molality per degree at steady state. Measured Soret coefficients can be used to calculate enthalpies of transport — the heat that must be absorbed to maintain constant temperature when solute diffuses out of an element of solution. Heats of transport can in turn provide fundamental information about solute–solvent and solute–solute interactions, including hydration.

The work reported here concerns the diffusion behavior of aqueous sodium carbonate, a hydrolyzing salt. The work was motivated by the practical importance of carbonates and other hydrolyzing salts (such as phosphate, sulfide, cyanide, iron, aluminum, and uranium salts). In addition, aqueous hydrogen and hydroxide ions, which are hydrolysis products, have unusually large heats of transport (5, 6), so the consequences for thermal diffusion might be significant, especially in dilute solutions where hydrolysis is extensive.

Equations are developed here for calculating the Soret coefficients of hydrolyzing salts from nonisothermal conductivity measurements. Soret coefficients and heats of transport are then reported for aqueous Na_2CO_3 at 25°C and salt molalities down to 0.001 mol kg^{-1}. This salt was chosen because isothermal diffusion data (7, 8) are available, which simplifies the analysis enormously. In the most dilute solutions that were studied, about 35% of the total carbonate ions were hydrolyzed.

2. Theory

2.1 Isothermal diffusion

Before the thermal diffusion of aqueous sodium carbonate is discussed, it is helpful to summarize briefly its unusual isothermal diffusion behavior (7, 8).

Only minor amounts of carbonate are hydrolyzed at Na_2CO_3 concentrations above *ca.* 0.05 mol dm^{-3}. There are two major solute species, Na^+ and CO_3^{2-}, but only one solute flux is independent because the electroneutrality condition guarantees that the two ions diffuse at the same speed. In this case the diffusion of the salt is a binary process described by Fick's equation

$$[2] \quad J_1 = -D\nabla C_1$$

with binary diffusion coefficient D. C_1 is the concentration of dissolved Na_2CO_3, in moles per unit volume, and J_1 is the molar flux density of the salt.

Dilute solutions

Dilute sodium carbonate solutions contain four major solute species: Na^+ and CO_3^{2-} ions together with HCO_3^- and OH^- ions produced by the hydrolysis reaction (7, 8)

$$[3] \quad CO_3^{2-}(aq) + H_2O = HCO_3^-(aq) + OH^-(aq)$$

$$K(25°C) = 2.15 \times 10^{-4}$$

Electroneutrality and local reaction equilibrium place two constraints on the ionic concentrations. At thermodynamic equilibrium, there is a third constraint: the concentrations of HCO_3^- and OH^- are identical. Only one solute concentration is therefore independent, which is consistent with the well-known result that aqueous Na_2CO_3 can be treated as a binary solution under equilibrium conditions.

[1]To whom correspondence should be addressed.

Can. J. Chem. Downloaded from www.nrcresearchpress.com by 84.41.108.74 on 09/07/12
For personal use only.

Can. J. Chem. Downloaded from www.nrcresearchpress.com by 84.41.108.74 on 09/07/12
For personal use only.

However, once a gradient in the concentration of Na_2CO_3 is formed, the various ions will begin to diffuse, at different speeds. In particular, the relatively mobile OH^- ions will diffuse more rapidly than the HCO_3^- ions, making the OH^- ions more abundant than HCO_3^- ahead of the diffusion boundary. Although electroneutrality and local reaction equilibrium still hold, the restriction of equal concentrations of HCO_3^- and OH^- no longer applies.

With two constraints on the four solute species, two nonequilibrium solute concentrations remain independent. Diffusion of dilute aqueous sodium carbonate is therefore a ternary process described by the extended Fick equations (7, 8)

$$[4] \quad J_1 = -D_{11}\nabla C_1 - D_{12}\nabla C_2$$

$$[5] \quad J_2 = -D_{21}\nabla C_1 - D_{22}\nabla C_2$$

C_1 represents the concentration of the total sodium carbonate component (hydrolyzed plus unhydrolyzed forms): $C_1 = [HCO_3^-] + [CO_3^{2-}]$. C_2 represents the concentration of "added" NaOH, *i.e.* the NaOH in excess of that produced by the carbonate hydrolysis: $C_2 = [OH^-] - [HCO_3^-]$ ([Y] denotes the concentration of species Y.)

Ternary diffusion coefficient D_{ik} gives the flux density J_i of component i produced by the gradient in the concentration of component k. The cross-coefficient D_{21} takes large positive values for dilute solutions owing to the relatively large coupled flow of the NaOH(2) component produced by the extensively hydrolyzed Na_2CO_3(1) component (7, 8).

Further details of the diffusion of aqueous $NaCO_3$, and other hydrolyzing solutes, can be found elsewhere (7–12).

2.2 Nonisothermal diffusion

What happens when a temperature gradient is applied to an aqueous solution of sodium carbonate? Following accepted practice (1, 3, 13), the description below employs salt molalities (m_i) (rather than molarities (C_i)) to avoid complications arising from differential thermal expansion of the solutions.

Consider a column of height a of uniform binary aqueous sodium carbonate solution at molality $\bar{m}_1$. The temperature gradient $\Delta T/a$ is established at time $t = 0$ by holding the base of the column ($x = 0$) at temperature T and the top of the column ($x = a$) at $T + \Delta T$. Warm-up corrections and convection are assumed to be negligible.

If hydrolysis is unimportant ($m_1 > 0.05$ mol kg^{-1}), the sodium carbonate molality along the column is given by the expression (13)

$$[6] \quad m_1(x,t) = \bar{m}_1 + \left(\frac{x}{a} - \frac{1}{2}\right)\Delta m_{1\infty} + \frac{4\Delta m_{1\infty}}{\pi^2}\sum_{n=1}^{\infty}\frac{1}{(2n-1)^2}\cos(b_n x)\exp(-b_n^2 Dt)$$

for the binary thermal diffusion of a single solute component. b_n is an abbreviation for $(2n - 1)\pi/a$.

The steady-state molality difference

$$[7] \quad \Delta m_{1\infty} = m_1(a,\infty) - m_1(0,\infty)$$

between the top and the bottom of the column is attained as $t \rightarrow \infty$.

From measured values of $\Delta m_{1\infty}$, the Soret coefficient

$$[8] \quad \sigma = -(\Delta m_{1\infty}/\bar{m}_1)\Delta T$$

and the molar heat of transport (1–4)

$$[9] \quad H_1^* = \nu RT^2(1 + \mathrm{d}\ln\gamma_\pm/\mathrm{d}\ln m_1)_T\sigma$$

can be derived. $\gamma_\pm$ is the stoichiometric mean molal ionic activity coefficient and ν is the number of moles of ions per mole of dissolved salt (3 for Na_2CO_3).

Dilute solutions

A temperature gradient applied to a dilute solution of sodium carbonate will generate gradients in the concentrations of each of the Na^+, CO_3^{2-}, HCO_3^-, and OH^- ions. Owing to the relatively large heat of transport of the OH^- ion (5), the thermally-induced gradient in the concentration of OH^- ions will exceed that of HCO_3^-, generating a ternary nonequilibrium system with gradients in both the Na_2CO_3(1) and the NaOH(2) components (14):

$$[10] \quad m_i(x,t) = \bar{m}_i + \left(\frac{x}{a} - \frac{1}{2}\right)\Delta m_{i\infty} + \frac{4}{\pi^2}\sum_{n=1}^{\infty}\sum_{k=1}^{2}\frac{A_{ik}\cos(b_n x)}{(2n-1)^2}\exp(-b_n^2 D_k t)$$

D_1 and D_2 are the eigenvalues of the diffusion coefficient matrix (evaluated at the mean cell temperature):

$$[11] \quad D_1 = [D_{11} + D_{22} + (D_{11} - D_{22})[1 + 4D_{12}D_{21}/(D_{11} - D_{22})^2]^{1/2}]/2$$

$$[12] \quad D_2 = [D_{11} + D_{22} - (D_{11} - D_{22})[1 + 4D_{12}D_{21}/(D_{11} - D_{22})^2]^{1/2}]/2$$

The A_{ik} parameters are abbreviations for

$$[13] \quad A_{11} = [(D_{11} - D_2)\Delta m_{1\infty} + D_{12}\Delta m_{2\infty}]/(D_1 - D_2)$$

$$[14] \quad A_{12} = [(D_1 - D_{11})\Delta m_{1\infty} - D_{12}\Delta m_{2\infty}]/(D_1 - D_2)$$

$$[15] \quad A_{21} = [-D_{21}\Delta m_{1\infty} + (D_2 - D_{22})\Delta m_{2\infty}]/(D_2 - D_1)$$

$$[16] \quad A_{22} = [D_{21}\Delta m_{1\infty} + (D_{22} - D_1)\Delta m_{2\infty}]/(D_2 - D_1)$$

The steady-state molality differences

$$[17] \quad \Delta m_{1\infty} = m_1(a,\infty) - m_1(0,\infty)$$

$$[18] \quad \Delta m_{2\infty} = m_2(a,\infty) - m_2(0,\infty)$$

are established as $t \rightarrow \infty$. The gradient in NaOH, $\Delta m_{2\infty}/a$, is generated even though the solution is free of added NaOH; the cool end of the cell will contain more OH^- than HCO_3^- ions ($m_2 > 0$), while the warm end contains more HCO_3^- than OH^- ions ($m_2 < 0$).

If $\Delta m_{1\infty}$ and $\Delta m_{2\infty}$ can be measured, the heats of transport of Na_2CO_3(1) and NaOH(2) can be calculated from the expression (15)

$$[19] \quad H_1^* = -(T/\Delta T)\left[\Delta m_{1\infty}\frac{\partial\mu_1}{\partial m_1} + \Delta m_{2\infty}\frac{\partial\mu_1}{\partial m_2}\right]$$

$$[20] \quad H_2^* = -(T/\Delta T)\left[\Delta m_{1\infty}\frac{\partial\mu_2}{\partial m_1} + \Delta m_{2\infty}\frac{\partial\mu_2}{\partial m_2}\right]$$

for a ternary mixed electrolyte. μ_1 and μ_2 are the chemical potentials of the components at the mean cell temperature and composition.

$$[21]\quad \mu_1 = \mu_1^0 + RT \ln (m_{Na}^2 m_{CO_3} \gamma_{Na}^2 \gamma_{CO_3})$$

$$[22]\quad \mu_2 = \mu_2^0 + RT \ln (m_{Na} m_{OH} \gamma_{Na} \gamma_{OH})$$

γ_i is the activity coefficient of species i. Defining $\beta = m_{HCO_3}/m_1$ as the extent of hydrolysis, the ionic molalities are given by $m_{CO_3} = (1 - \beta)m_1$, $m_{HCO_3} = \beta m_1$, $m_{OH} = \beta m_1 + m_2$ and $m_{Na} = 2m_1 + m_2$. β can be calculated from the relation

$$[23]\quad K = \frac{\beta(\beta m_1 + m_2)}{1 - \beta} \frac{\gamma_{HCO_3}\gamma_{OH}}{\gamma_{CO_3}}$$

3. Experimental

Reagent grade sodium carbonate and bicarbonate were used as received. Carbonate-free sodium hydroxide solutions were standardized potentiometrically. Distilled, deionized water was used to prepare the solutions.

The two Harned-type Soret cells (13) (heights 0.912 and 1.219 cm) used in this work were operated with a 10 K temperature difference. Changes in the molalities of the Na_2CO_3 and NaOH components during thermal diffusion were followed by measuring the corresponding changes in electrical resistance across small platinum electrodes at levels $a/6$ and $5a/6$ along the solution columns. Details of the equipment, procedure, and cell calibration are given elsewhere (13, 14, 16).

The problem is to calculate $\Delta m_{1\infty}$ and $\Delta m_{2\infty}$ from the resistance measurements. The first step is to convert the absolute resistances to the differential quantity

$$[24]\quad Y(t) = \frac{R(5a/6, t) - R(a/6, t)}{R(5a/6, t) + R(a/6, t)}$$

to correct for small but unavoidable drifts in the mean cell temperature.

The series expression for $Y(t)$ converges very rapidly. For the pseudo-binary solutions, the truncated expression

$$[25]\quad Y(t) = Y_\infty + Y_1 \exp(-t/\theta)$$

is accurate provided $t/\theta > 0.15$, where θ is the characteristic time, $a^2/\pi^2 D$. The Soret coefficient is given by

$$[26]\quad \sigma = -\pi^2 Y_1 / 2\sqrt{3} B \Delta T$$

where

$$[27]\quad B = -\mathrm{d} \ln R/\mathrm{d} \ln m_1 = \mathrm{d} \ln \Lambda/\mathrm{d} \ln m_1$$

Least-squares values of Y_1 together with published (17) molar conductivities (Λ), diffusion coefficients (7, 8), and activity coefficients (18, 19), all evaluated at the mean cell temperature and composition, were used to calculate σ and H^* for the pseudo-binary Na_2CO_3 solutions.

Dilute solutions

At 0.05 mol kg^{-1} and below, plots of $\ln |Y(t) - Y_\infty|$ were curved, rather than linear, indicating measurable departures from pseudo-binary behavior (see Fig. 1). For these ternary $Na_2CO_3(1)$ + NaOH(2) solutions, $Y(t)$ decayed as (14)

$$[28]\quad Y(t) = Y_\infty + Y_1 \exp(-t/\theta_1) + Y_2 \exp(-t/\theta_2)$$

with characteristic times $\theta_1 = a^2/\pi^2 D_1$ and $\theta_2 = a^2/\pi^2 D_2$. D_1 and D_2, and hence θ_1 and θ_2, were calculated from published D_{ik} values (8). The parameters Y_∞, Y_1, and Y_2 were then calculated by using linear least squares to fit $Y(t)$ to the variables $\exp(-t/\theta_1)$ and $\exp(-t/\theta_2)$ according to eq. [28].

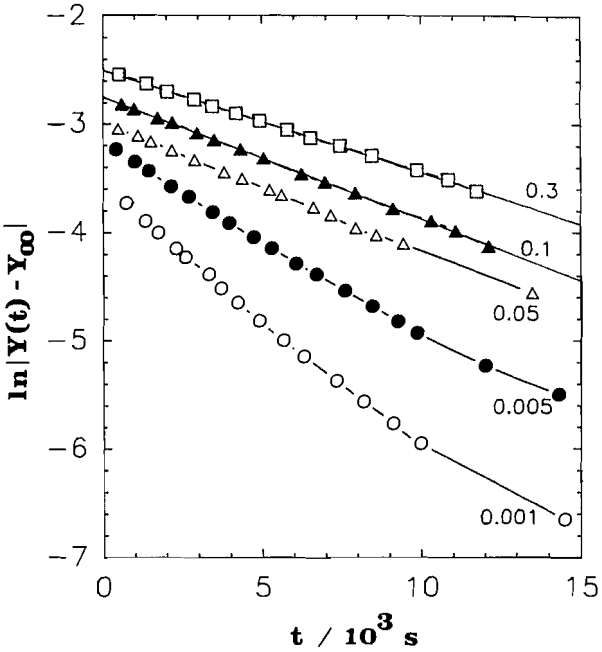


FIG. 1. Plots of $\ln |Y(t) - Y_\infty|$ against t for aqueous sodium carbonate at the molalities 0.001, 0.005, 0.05, 0.1, and 0.3 mol kg^{-1}.

TABLE 1. Soret coefficients and heats of transport of pseudo-binary aqueous $Na_2CO_3(\bar{m}_1)$ solutions at 25°C[a]

m_1	B	D	σ	$1 + \mathrm{d} \ln \gamma_\pm/\mathrm{d} \ln m_1$	H_1^*
0.10	0.833	0.943	8.46	0.774	14.5
0.30	0.758	0.834	7.56	0.707	11.9
0.50	0.706	0.745	8.21	0.654	11.9

[a]Units: m_1 in mol kg^{-1}, D in 10^{-9} m^2 s^{-1}, σ in 10^{-3} K^{-1}, H_1^* in kJ mol^{-1}.

$\Delta m_{1\infty}$ and $\Delta m_{2\infty}$ were evaluated by solving the linear equations

$$[29]\quad B_1'\Delta m_{1\infty} + B_2'\Delta m_{2\infty} = (\pi^2/2\sqrt{3})(Y_1 + Y_2)$$

$$[30]\quad [B_1'(D_{11} - D_{22}) + 2B_2'D_{21}]\Delta m_{1\infty} + [2B_1'D_{12} + B_2'(D_{22} - D_{11})]\Delta m_{2\infty} = (\pi^2/2\sqrt{3})(D_1 - D_2)(Y_1 - Y_2)$$

The parameters

$$[31]\quad B_i' = -(\partial \ln R/\partial m_i)_{T,m_k}$$

were measured by using an auxiliary conductance cell; B_1' was obtained from the conductivities of binary solutions of Na_2CO_3 above and below $\bar{m}_1$, while B_2' was obtained using solutions of composition $\bar{m}_1$ to which NaOH or $NaHCO_3$ had been added.

Finally, eqs. [19] and [20] gave the ternary heats of transport of the components. The ionic activity coefficients that were used were calculated from the expression (20)

$$[32]\quad \ln \gamma_{\pm i} = -1.17 z_i^2 I^{1/2}/(1 + I^{1/2})$$

which is sufficiently accurate for the present application. I, the ionic strength, equals $(3 - \beta)m_1 + m_2$.

Can. J. Chem. Downloaded from www.nrcresearchpress.com by 84.41.108.74 on 09/07/12
For personal use only.

TABLE 2. Heats of transport and steady-state molality gradients for ternary aqueous $Na_2CO_3(\bar{m}_1)$ + NaOH($\bar{m}_2 = 0$) solutions to 25°C[a]

m_1	β	$\frac{\partial\mu_1}{\partial m_1}$	$\frac{\partial\mu_1}{\partial m_2}$	$\frac{\partial\mu_2}{\partial m_1}$	$\frac{\partial\mu_2}{\partial m_2}$	$\frac{\Delta m_{1,\infty}}{\Delta T}$	$\frac{\Delta m_{2,\infty}}{\Delta T}$	H_1^*	H_2^*
0.001	0.352	75.70	37.85	37.87	54.12	−0.410	−1.01	20.7±0.8	21.0±1.0
0.002	0.260	36.27	18.13	18.15	32.90	−1.15	−1.41	20.0±1.0	20.0±1.0
0.005	0.167	13.67	6.835	6.851	18.27	−3.15	−2.67	18.3±0.7	21.0±0.8
0.010	0.116	6.509	3.254	3.268	12.30	−7.25	−3.53	17.5±0.5	20.0±0.5
0.050	0.0463	1.149	0.5744	0.5876	5.657	−46.1	−7.07	17.0±0.8	20.0±2.0

[a]Units: m_1 in mol kg^{-1}, $\partial\mu_i/\partial m_k$ in 10^5 J kg mol^{-2}, $\Delta m_{i\infty}/\Delta T$ in 10^{-5} mol kg^{-1} K^{-1}, H_i^* in kJ mol^{-1}.

TABLE 3. Supplementary data for ternary aqueous $Na_2CO_3(\bar{m}_1)$ + NaOH($\bar{m}_2 = 0$) solutions at 25°C[a]

$\bar{m}_1$	D_{11}	D_{12}	D_{21}	D_{22}	B_1'	B_2'
0.001	1.02	−0.44	0.35	3.30	920	734
0.002	1.03	−0.45	0.30	3.25	437	362
0.005	1.04	−0.53	0.22	3.06	198	158
0.010	1.05	−0.64	0.14	3.65	89.8	72.6
0.050	1.01	−0.53	−0.01	3.44	11.9	8.64

[a]Units: m_1 in mol kg^{-1}, D_{ik} in 10^{-9} m^2 s^{-1}, B_i' in kg mol^{-1}.

The analysis of the data for the ternary $Na_2CO_3(1)$ + NaOH(2) solutions closely resembles the treatment (14) developed previously for ternary NaCl(1) + NaOH(2) solutions. In the present study, however, the mean cell molality of the NaOH component, $\bar{m}_2$, is zero. The equations have therefore been rewritten to replace indeterminate terms such as d ln R/d ln m_2 or d ln m_2/dT with d ln R/dm_2 and dm_2/dT.

4. Results and discussion

Thermal diffusion was measured at the mean cell temperature 25.0 ± 0.1°C and total sodium carbonate molalities from 0.001 to 0.5 mol kg^{-1}.

Table 1 gives the measured Soret coefficients and heats of transport for "pseudo-binary" Na_2CO_3 solutions at the molalities 0.1, 0.3, and 0.5 mol kg^{-1}. Each reported σ value is the average of values from six runs. The standard deviation of the σ values was about 2%.

The "short" and the "tall" cells gave identical results within experimental precision, which suggests that convection was not a serious source of error. Table 1 includes the auxiliary values of B, D, and 1 + d ln $\gamma_\pm$/d ln m that were used in the calculations.

Table 2 gives the steady-state molality gradients and the derived heats of transport for the dilute ternary $Na_2CO_3(\bar{m}_1)$ + NaOH($\bar{m}_2 = 0$) solutions. In this case eight runs were made at each composition and the $\Delta m_{i\infty}/a$ values were averaged. The supplementary values of D_{ik}, B_i', β, and $\partial\mu_i/\partial m_k$ are listed in Tables 2 and 3. The two cells gave identical results.

$\Delta m_{1\infty}/\Delta T$ and $\Delta m_{2\infty}/\Delta T$ are negative, indicating that both the Na_2CO_3 and NaOH components diffuse to the cold plate. At 0.05 mol kg^{-1}, where only about 5% of the carbonate ions are hydrolyzed, the gradient in the NaOH component is about 15% as large as the Na_2CO_3 gradient. At 0.001 mol kg^{-1}, hydrolysis is only 35% complete, yet the thermally-induced gradient in the NaOH component is $2\frac{1}{2}$ times larger than the Na_2CO_3 gradient! It should be emphasized that the NaOH gradients represent gradients in "excess" NaOH, over and above the NaOH present to balance the $NaHCO_3$ produced by hydrolysis.

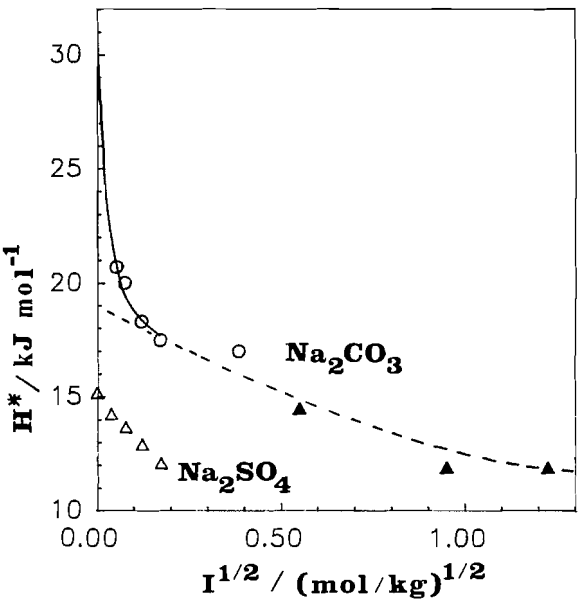


FIG. 2. Heats of transport of aqueous salts at 25°C plotted against the square root of the ionic strength. Na_2CO_3: ○, measured H_1^* values (this work); —, predicted values (eq. [33]); - - -, extrapolated pseudo-binary H_1^* values. Na_2SO_4: △, measured values (21).

The OH^- ions strongly seek the cooler parts of the solution because their heat of transport is so large. The substantial electric field that is generated to slow down these unusually mobile ions (and thereby maintain electroneutrality) will tend to drive the CO_3^{2-} ions in the opposite direction — to the warm plate. This may help account for the relatively small induced gradients in the Na_2CO_3 component at high dilution.

The results show that the gradient in the Na_2CO_3 component relative to that of the NaOH component decreases sharply with concentration. Below 0.001 mol kg^{-1} the Na_2CO_3 could conceivably change sign, signalling the reversed thermal diffusion of Na_2CO_3 to the warm plate. (Such behavior has been reported for NaCl in the analogous NaCl + NaOH solutions (14).) Unfortunately, reliable results could not be obtained at concentrations significantly below 0.001 mol kg^{-1} — the cell resistances were too large to be measured precisely.

In Fig. 2 the heat of transport of the Na_2CO_3 component, H_1^*, is plotted against the square root of the ionic strength, $I^{1/2}$. For comparison, the heat of transport of Na_2SO_4 (21) — a nonhydrolyzing 1:2 salt — is also plotted. The jump in $H_1^*(Na_2CO_3)$ at low ionic strength due to hydrolysis is evident.

Can. J. Chem. Downloaded from www.nrcresearchpress.com by 84.41.108.74 on 09/07/12
For personal use only.

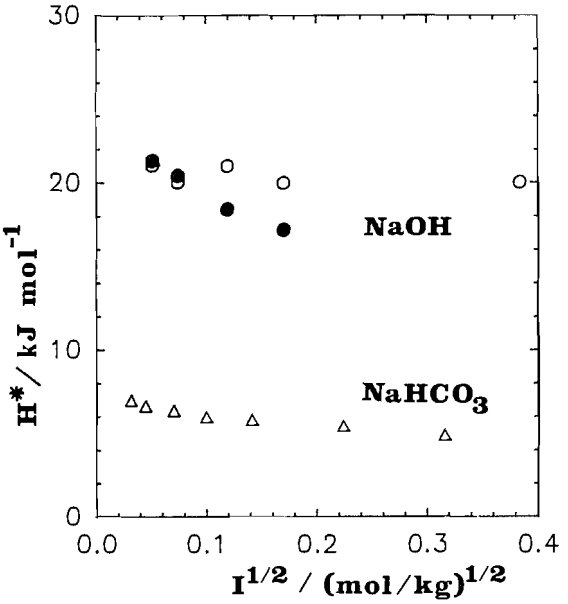


FIG. 3. Heats of transport of aqueous electrolytes at 25°C plotted against the square root of the ionic strength. NaOH: ○, measured H_2^* values for NaOH in aqueous N_2CO_3 solutions (this work); ●, measured binary values for NaOH in pure water (5). $NaHCO_3$: △, measured values (this work).

TABLE 4. Soret coefficients and heats of transport of binary aqueous $NaHCO_3(m)$ solutions at 25°C[a]

m	B	D	σ	$1 + d \ln \gamma_\pm / d \ln m$	H^*
0.001	0.990	1.237	4.78	0.983	6.95
0.002	0.943	1.232	4.51	0.975	6.50
0.005	0.911	1.222	4.44	0.961	6.31
0.010	0.906	1.198	4.22	0.951	5.93
0.020	0.898	1.186	4.31	0.929	5.92
0.050	0.892	1.158	4.03	0.909	5.42
0.100	0.876	1.132	3.74	0.884	4.89

[a]Units: m in mol kg^{-1}, D in 10^{-9} m^2 s^{-1}, σ in 10^{-3} K^{-1}, H^* in kJ mol^{-1}.

H_2^*, the ternary heat of transport of the NaOH component in aqueous Na_2CO_3 solutions, is plotted against $I^{1/2}$ in Fig. 3. The binary heat of transport of NaOH in pure water (5, 6, 14), H^*(NaOH), is also shown. Study of Fig. 3 shows that H_2^* and H^*(NaOH) become identical as the ionic strength drops. This result is hardly surprising in view of the additivity rule, but it does provide a valuable check that the experiments and the calculations were performed correctly.

To help interpret the results, a few thermal diffusion measurements were made on dilute aqueous $NaHCO_3$ solutions. Table 4 gives the results. In Fig. 3 the heat of transport of $NaHCO_3$ is plotted against $I^{1/2}$. Convection did not appear to be significant, as indicated by linear plots of $Y(t)$ against $\exp(-t/\theta)$. Although nonequilibrium $NaHCO_3$ solutions are strictly ternary systems owing to disproportionation ($NaHCO_3 = CO_2 + NaOH$), this feature was unimportant at the compositions that were used; no evidence was obtained for ternary thermal diffusion of this salt.

Although the theory of thermal diffusion with chemical reaction is well understood for binary solutions (22), the corresponding theory for ternary systems remains to be developed. In the meantime, the simple-minded expression

$$[33] \quad H_1^* = (1 - \beta)H^*(Na_2CO_3,unh) + \beta H^*(NaHCO_3) + \beta H^*(NaOH)$$

may provide a qualitative guide to the behavior of dilute aqueous Na_2CO_3 solutions. $H^*(NaHCO_3)$ and $H^*(NaOH)$ stand for the binary heats of transport of $NaHCO_3$ or NaOH in pure water (Fig. 3). $H^*(Na_2CO_3,unh)$, the hypothetical heat of transport per mole of *unhydrolyzed* sodium carbonate, may be obtained by extrapolation of H_1^* values from above 0.05 mol kg^{-1} where hydrolysis is unimportant (dashed curve, Fig. 2). The estimates of H_1^* obtained from eq. [33] are plotted in Fig. 2. Satisfactory agreement with the measured H_1^* values is obtained. The limiting heat of transport of infinitely dilute (and therefore completely hydrolyzed) aqueous Na_2CO_3, 31 ± 1 kJ mol^{-1}, equals the sum of the limiting heats of transport of aqueous $NaHCO_3$ and NaOH.

Acknowledgment

The authors thank the Natural Sciences and Engineering Research Council for the financial support of this research.

1. J. N. AGAR. *In* The structure of electrolytic solutions. *Edited by* W. J. Hamer. Wiley, New York. 1959. Chap. 13.
2. H. J. V. TYRRELL. Diffusion and heat flow in liquids. Butterworths, London. 1961.
3. J. N. AGAR. *In* Advances in electrochemistry and engineering. *Edited by* P. Delahay and C. W. Tobias. Interscience, New York. 1962. Chap. 2.
4. J. N. AGAR. Ann. Rev. Phys. Chem. **15**, 469 (1964).
5. P. N. SNOWDON and J. C. R. TURNER. Trans. Faraday Soc. **56**, 1409 (1960).
6. N. TAKEYAMA and K. NAKASHIMA. J. Solution Chem. **17**, 305 (1988).
7. D. G. LEAIST. Can. J. Chem. **61**, 1494 (1983).
8. D. G. LEAIST and R. A. NOULTY. Can. J. Chem. **63**, 2319 (1984).
9. D. G. LEAIST. J. Phys. Chem. **89**, 1486 (1985).
10. D. G. LEAIST. J. Solution Chem. **14**, 709 (1985).
11. D. G. LEAIST. J. Phys. Chem. **91**, 4635 (1987).
12. D. G. LEAIST. J. Chem. Soc. Faraday Trans. 1, **84**, 581 (1988).
13. J. N. AGAR and J. C. R. TURNER. J. Phys. Chem. **64**, 1000 (1960).
14. D. G. LEAIST and H. LU. J. Phys. Chem. **94**, 447 (1990).
15. D. G. LEAIST. J. Solution Chem. **19**, 1 (1990).
16. D. G. LEAIST. J. Solution Chem. **18**, 651 (1989).
17. International critical tables. McGraw-Hill, New York. 1929.
18. J. C. PEIPER and K. S. PITZER. J. Chem. Thermodyn. **14**, 613 (1982).
19. W. J. HAMER and Y.-C. WU. J. Phys. Chem. Ref. Data, **1**, 1047 (1972).
20. E. A. GUGGENHEIM and J. C. TURGEON. Trans. Faraday Soc. **51**, 747 (1955).
21. P. N. SNOWDON and J. C. R. TURNER. Trans. Faraday Soc. **56**, 1812 (1960).
22. J. N. AGAR and J. LIN. J. Solution Chem. **16**, 973 (1987).

Can. J. Chem. Downloaded from www.nrcresearchpress.com by 84.41.108.74 on 09/07/12
For personal use only.

An *ab initio* study of the H_2O-mediated 1,3-hydrogen rearrangement in the HX—CH=Y(H_2O) ⇌ X=CH—YH(H_2O) isoelectric series: X, Y = CH_2, NH, or O

RAYMOND A. POIRIER AND DAKE YU
Chemistry Department, Memorial University of Newfoundland, St. John's, Nfld., Canada A1B 3X7

AND

PETER R. SURJAN
Technical University, Budapest Institute of Physics, Quantum Theory Group, H-1521 Budapest, Hungary

Received February 22, 1991

RAYMOND A. POIRIER, DAKE YU, and PETER R. SURJAN. Can. J. Chem. **69**, 1589 (1991).

Ab initio calculations are performed to investigate the effect of water on the 1,3-intramolecular hydrogen rearrangement in the HX—CH=Y ⇌ X=CH—YH isoelectronic series, for X, Y = CH_2, NH or O, by modeling with a single H_2O molecule. The geometries for the complexes are optimized at both the 3-21G and 6-31G** basis set levels. MP2 and some MP4 calculations are performed to take into account the correlation effects, and ZPV corrections are calculated at the MNDO level. The results show that the water molecule has a significant effect on the molecules in which hydrogen bonds can be formed or partially formed. The "solvent effects" are also examined using the self-consistent reaction-field (SCRF) approach. A combination of supermolecule and SCRF approach appears to work well at predicting the effect of solvent on relative stabilities and barriers.

Key words: tautomerism, *ab initio*, 1,3-hydrogen rearrangement, solvent effects.

RAYMOND A. POIRIER, DAKE YU et PETER R. SURJAN. Can. J. Chem. **69**, 1589 (1991).

Utilisant un modèle impliquant une seule molécule de H_2O, on a effectué des calculs *ab initio* pour étudier l'effet de l'eau sur la réaction de transposition intramoléculaire-1,3 de l'hydrogène dans les séries isoélectroniques HX—CH=Y ⇌ X=CH—YH dans lesquelles X, Y = CH_2, NH ou O. On a optimisé les géométries des complexes aux niveaux des ensembles 3-21G et 6-31G**. On a aussi effectué des calculs MP2 et MP4 pour tenir compte des effets de corrélation et on a calculé les corrections ZPV au niveau MNDO. Les résultats montrent que la molécule d'eau a un effet important sur les molécules dans lesquelles il peut se former au moins partiellement des liaisons hydrogènes. On a aussi étudié les «effets de solvant» en utilisant une approche de champ de réaction auto-cohérent (SCRF). Il semble qu'une approche combinant une supermolécule et un champ de réaction auto-cohérent permet de bien prédire l'effet de solvant sur les stabilités relatives et sur les barrières des réactions.

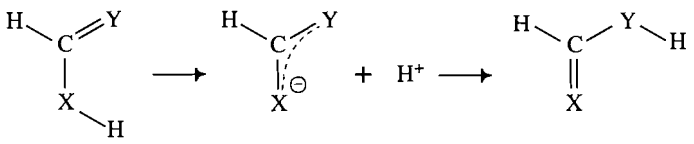
Mots clés : tautomérisme, *ab initio*, transposition-1,3 de l'hydrogène, effets de solvant.

[Traduit par la rédaction]

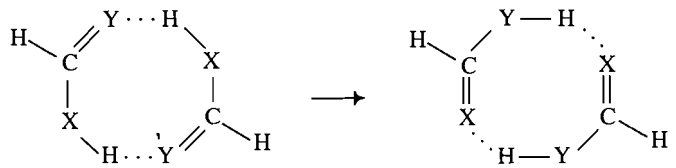
I. Introduction

Tautomerism is of interest to many areas of chemistry and biology (1–34). Understanding tautomerism is of great importance to chemistry and especially to biochemistry, where, for example, tautomerism of nucleic acid bases is relevant to the theory of spontaneous mutagenesis (1). Although there are, for example, many possible tautomeric forms of uracil, until recently only the diketo tautomer was known to exist. The keto–enol form of both uracil and thymine have now been detected by the fluorescence excitation method (11). For this reason and due to interest in the orbital symmetry rule a great deal of quantitative theoretical interest has also been given to tautomerism (13–34). Knowledge of the energetics of tautomerism in simple model molecules such as formamide – formamidic acid and amidine can provide useful information on the intrinsic stability of various tautomers of more complex molecules. These serve as prototypes for many biologically active molecules, a few of which have been tabulated in Table 1. Most of the calculations have focused on the relative stabilities of the tautomeric forms and have looked at barriers for the direct 1,3-intramolecular hydrogen rearrangement, which models the gas phase reaction. It is well known that the solvent plays an important role in both affecting the relative stabilities and the barriers, especially in protic solvents. In solution one can formulate a number of possible mechanisms (5):

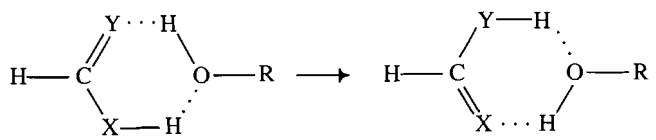
Mechanism A: Deprotonation/reprotonation



Mechanism B: Dimerization (self-catalysed)



Mechanism C: Solvent-catalysed



Measurements of the relative stabilities and even more so the barriers to the hydrogen shift are difficult experimentally since the equilibrium concentration of one or some of the less stable isomers can be very small. Often these values can only be estimated. For example, the pK method was used to

Can. J. Chem. Downloaded from www.nrcresearchpress.com by 84.41.108.74 on 09/07/12
For personal use only.

Can. J. Chem. Downloaded from www.nrcresearchpress.com by 84.41.108.74 on 09/07/12
For personal use only.

TABLE 1. Relative energies (kJ/mol) for related structures†

System	ΔE	Exptl/theoretical	Reference
Formamide – formamidic acid	44.6	6-31G**/CISD-DQ//6-31G**	31
	33	STO-3G//STO-3G	25
Formamide – formamidic acid (H_2O)	13	STO-3G//STO-3G	25
	69.8	6-31G//3-21G	19
Formamide – formamidic acid ($2H_2O$)	11	STO-3G//STO-3G	25
Formamide – formamidic acid dimer	117.5	3-21G//3-21G	22
Methyl imine – vinyl amine	50.7	6-31G**/CISD-DQ//6-31G**	31
Acetaldehyde – vinyl alcohol	66.8	6-31G**/CISD-DQ//6-31G**	31
	36	Exptl (aqueous)	12
N-phenylbenzamide	60	Exptl (gas)	10
Uracil			
kk	0.0	—	
ke 1-H	62.7	MBPT(2)/6-31G*//3-21G + ZPV	34
	52.5	AM1	33
	79 ± 25	Exptl (gas)	9
ke 3-H	58.3	AM1	33
ek 1-H	86.1	AM1	33
ek 3-H	39.0	AM1	33
	40–72.1	Exptl	11
ee	61.3	AM1	33
	88 ± 38	Exptl (gas)	9
Cytosine			
ka 3-H	0.0		
ki	5.8	MBPT(2)/6-31G*//3-21G + ZPV	34
	2.6	6-31G*//3-21G	32
	5.9	MP2/6-31G*//6-31G*	32
	0.1	6-31G*//3-21G + ZPV	32
	6.23	AM1	33
	~0	Exptl	32
ea	16		
	7.24	AM1	33
	1.0	MBPT(2)/6-31G*//3-21G + ZPV	34
ka 1-H	2.0	AM1	33
ei 3-H	68.1	AM1	33
ei 1-H	50.8	AM1	33
2-oxopyridine			
keto	0.0	—	
enol	2.3	6-31G*//3-21G	32
	0.42	6-31G*//6-31G*	32
	−6.74	MP2/6-31G*//6-31G*	32
	−0.75	6-31G*//3-21G + ZPV	32
	−2 to −3	Exptl (gas)	4,8
2-oxopyrimidine			
keto	0.0	—	
enol	−7.74	6-31G*//3-21G	32
	−10.4	6-31G*//3-21G + ZPV	32
	−10	Exptl (gas)	4

†See Fig. 1 for the structures.

estimate the relative free energies in solution of the diketo and keto–enol tautomers of uracil (2). Bensaude and Dubois (5, 6) have shown, using the T-jump relaxation technique, that 6-methoxy 2-oxopyridine in aqueous solvent undergoes a concerted 1,3-hydrogen rearrangement through a water bifunctional diffusion-controlled dimerization (Mechanism B). Under various other conditions competition between these mechanism can occur (6). The same authors (7) have also shown that the equilibria and therefore the relative stabilities can be significantly affected by the solvent. The keto/enol ratios of 6-chloro and 6-methoxy 2-oxopyridines, for example, have been shown to vary by several orders of magnitudes in going from polar

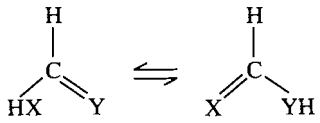
TABLE 2. Barriers (kJ/mol) for related structures

System	ΔE†	Theoretical	Reference
Amidine	247.3	4-31G//4-31G	23
Amidine (H_2O)	90.21	4-31G//STO-3G	23
	65.48	STO-3G//STO-3G	23
	87.5	6-31G//3-21G	20
Amide-dimer	66.9	3-21G//3-21G	22
Formamide – formamidic acid dimer	125.1/7.6	3-21G//3-21G	22
Formamide – formamidic acid (H_2O)	138.7	6-31G//3-21G	20
Formamide – formamidic acid	282/249	STO-3G//STO-3G	25
Formamide – formamidic acid (H_2O)	59.8/46.9	STO-3G//STO-3G	25
Formamide – formamidic acid ($2H_2O$)	21/9.6	STO-3G//STO-3G	25

†Barriers for the forward/reverse reaction.

aprotic solvents to water. The relative energies of these tautomers in different environments can give some insight into the influence of solvent effects on molecular stability and on the barriers. Another difficulty which arises with determining the position of tautomeric equilibrium experimentally is that in order to eliminate solvation effects of polar solvents, dilute solutions in nonpolar solvents have to be used. It has been shown that for 2-oxopyridine, for example, that only in very dilute solution ($<10^{-7}$ M) and high temperatures (>100°C) did the equilibrium constant become comparable to the gas phase value and this was shown to be due to the formation of dimers (3). Therefore, both solvation and the formation of dimers can affect significantly the position of the equilibrium.

A theoretical description of solvation is particularly difficult. In general, both an accurate statistical treatment and an exact solution of the Schrödinger equation for the solute–solvent complex, representing a many body system, remain an insoluble problem. The studies on solvent effect within theoretical calculations are carried out in two different kinds of approximate approaches, namely the discrete (35) and the continuum (36, 37) models. In the former model, individual solvent molecules interact with a solute and are explicitly dealt with. The solvent effect is included into the calculations by considering a "supermolecule" system, *i.e.*, a complex consisting of the solute molecule surrounded by one or more solvent molecules. The discrete approach is often used when specific interactions are prevailing. On the other hand, the continuum model studies the properties of a molecule situated in a cavity embedded in a dielectric medium and it is associated with the reaction-field concept (37). In the SCRF (self-consistent reaction field) approximation (38), the dielectric field generated by the polarized environment is described by the so-called reaction-potential and the polarization potentials are incorporated into the Schrödinger equation. The cavity radius is selected in such a way that the limitations imposed by the van der Waals radii are met. The continuum model describes well the mean properties of the environment but it does not account for specific effects. Studies (39, 40) show that calculations using a modified reaction-field approach on a series of important reactions gives qualitatively the same results as those obtained using the supermolecular approach for reactions in which only one or two water molecules are involved mechanistically. The SCRF approximation has been used successfully to predict the effect on tautomeric equilibria (41) and on radical formation energies (42). The discrete-continuum approach involves a combination of the above two methods. In this model, the solvent molecules in the first layer are treated individually, whereas those of the outer sphere are represented by a continuous dielectric field. In many cases, a discrete plus continuum model is better suited for describing complex systems (43).



SCHEME 1

As illustrated by Tables 1 and 2, there are few systematic studies which look at the relative tautomeric stabilities and there are even fewer mechanistic studies (barriers). Due to the difficulties mentioned, a systematic experimental study which looks at a number of related systems, takes into account solvent effect and carefully investigates mechanism, would be very difficult. Such systematic study is more amenable to a computational approach.

As a first step in a systematic study we looked at the direct 1,3-intramolecular hydrogen rearrangement in the following isoelectronic series of small molecules (31), as shown in Scheme 1.

The results indicated, for one, that the relative stabilities and barriers were in excellent agreement whether calculated using the 3-21G or 6-31G** optimized geometries. For example, the 6-31G**/CISD results did not differ by more than 1 or 2 kJ/mol in using the 3-21G geometry instead of the 6-31G** optimized geometry, representing less than 1% error. The work also further revealed the advantage of treating a series of the same type of molecules is that it clearly shows that the trends, in barriers for example, are independent of the level of calculation, although the individual barriers may vary significantly. The trends in relative stabilities and in the barriers of these simple compounds was explained using simple proton affinity arguments and bond order concepts.

The barriers for the 1,3-intramolecular hydrogen rearrangement reactions tend to be high and would model tautomeric

Can. J. Chem. Downloaded from www.nrcresearchpress.com by 84.41.108.74 on 09/07/12
For personal use only.

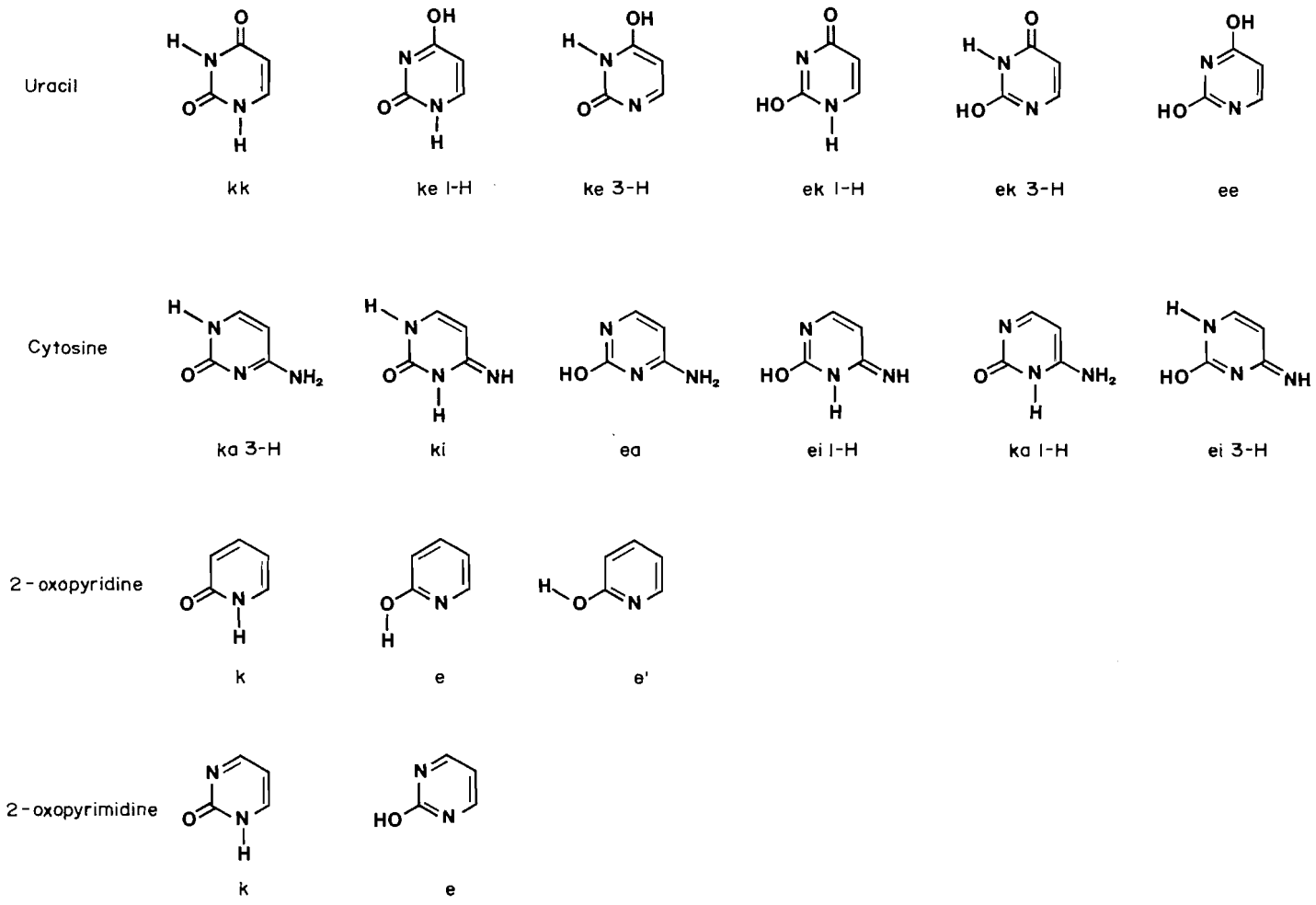


FIG. 1. Structures related to the model compounds studied in this work.

Can. J. Chem. Downloaded from www.nrcresearchpress.com by 84.41.108.74 on 09/07/12
For personal use only.

equilibrium in the gas phase. In the present work a systematic study similar to that in ref. 31 is made for the 1,3-intramolecular hydrogen rearrangement reaction in water, modeled with a single H_2O molecule. Through the remaining text, the direct 1,3-intramolecular hydrogen rearrangement will be referred to as the gas phase case and the 1,3-intramolecular hydrogen rearrangement via a H_2O molecule will be referred to as the H_2O-mediated or supermolecule case. The H_2O-mediated tautomeric mechanism in formamide, formamidic acid, and amidine have been studied in the past, but using the 3-21G basis set only, which favors planar structures at nitrogen and fails qualitatively in predicting relative energies (31). The SCRF method is also used to investigate the interactions between "solvent molecules" and the supermolecule. The effect of the reaction-potential on energies are examined with a number of values for k, which is a combination of the macroscopic dielectric constant ϵ of the solvent, and the so-called "cavity radius" R (36). The importance of correlation and ZPV (zero-point vibration) on relative stabilities and barriers is also examined.

II. Computational details

Calculations were performed with the MUNGAUSS (44) program on the Newfoundland and Labrador Computer Services (NLCS) AMDAHL 5880 and GAUSSIAN86 (45) on the VAX 8800 of Memorial University of Newfoundland. Structures for the supermolecules were optimized using analytical energy gradients at the 3-21G split valence shell basis set level (46) and the 6-31G** polarized basis set level (47, 48). Single-point calculations at the 3-21G geometries were also performed at the 6-31G** level for comparison. All minima and symmetrical transition states were optimized with the OC method (ref. 49, the algorithm is described in ref. 49) and the nonsymmetrical transition states were optimized using the minimization of sum of squares gradient technique VA05AD (50). All the bond orders were calculated using Mayer's definition (51). GAUSSIAN86 was used for MP2/6-31G*//6-31G** calculations for all the molecules, including the gas phase model molecules and the supermolecules to investigate the correlation effects. MP2/6-31G**//6-31G** and MP4/6-31G*//6-31G** calculations were also performed for the smallest system, HO—CH=O(H_2O). For the SCRF calculations, the effective Fock operator is expressed as $F = F_0 - k\hat{\mu}\langle\hat{\mu}\rangle$, where k can be given by $2(\epsilon - 1)/(2\epsilon + 1)R^3$ bohr^{-3} in the SCRF model suggested by Tapia (36), $\hat{\mu}$ is the dipole moment operator and F_0 is the standard SCF Fock operator. In the present study we assume k is a purely empirical parameter. The SCRF energy is defined as $E(\text{SCRF}) = E_0 - \frac{1}{2}k\langle\hat{\mu}\rangle^2$. It should be emphasized that this work represents the first application of the SCRF approximation to estimate the effect of solvation on barriers for reactions of this type. We are assuming that the thermodynamic formulation of the transition state theory will apply to the solution phase, as described by the SCRF. This is a reasonable assumption in this case since the barriers are high (52) and the reaction is an intramolecular arrangement in which little solvent reorganization is expected. The ZPV corrections were calculated with MNDO (53) at the

Can. J. Chem. Downloaded from www.nrcresearchpress.com by 84.41.108.74 on 09/07/12
For personal use only.

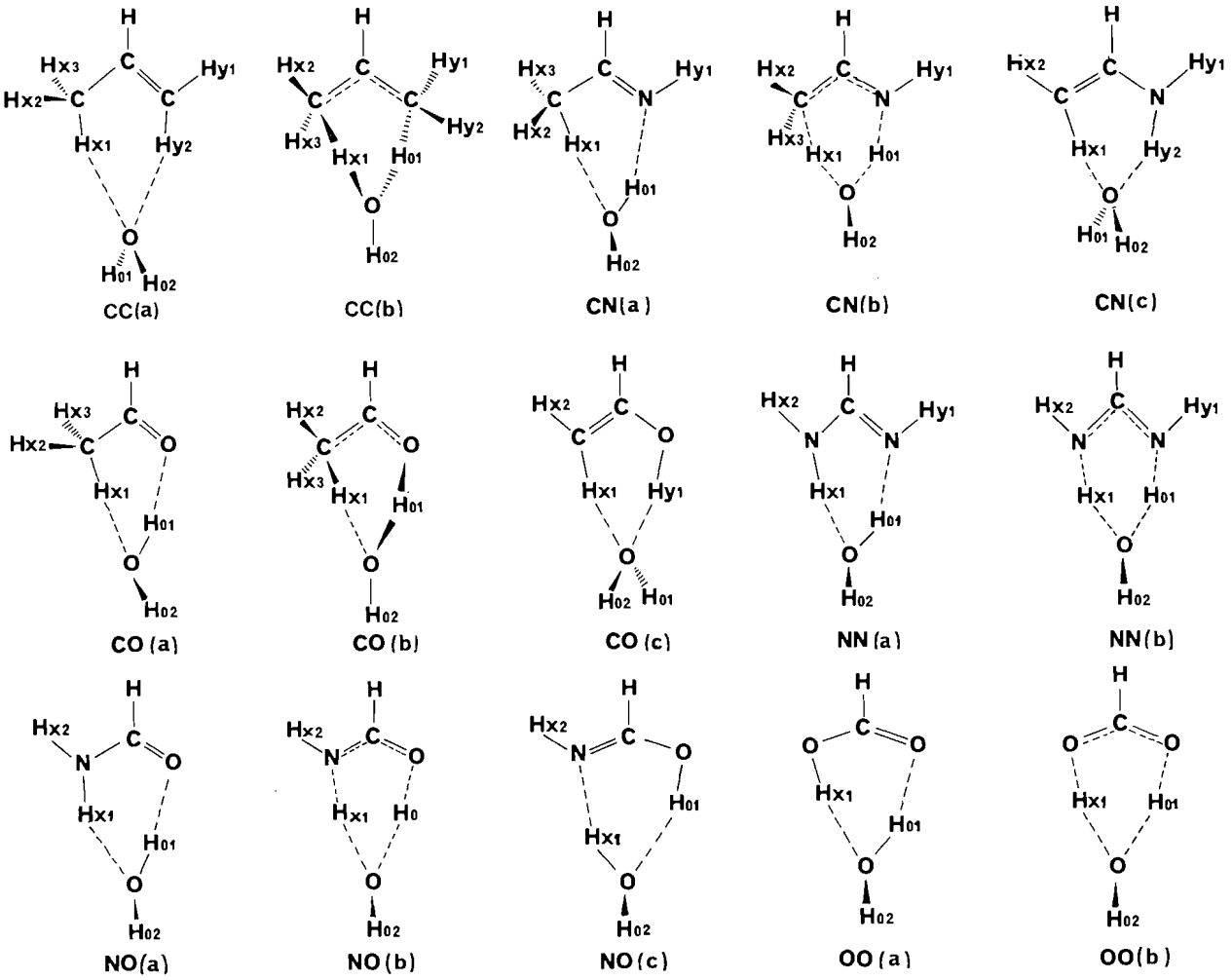


FIG. 2. Structures for the supermolecules studied in this work. The XY under the structures represent the terminal atoms and (**a**), (**b**), and (**c**) are for reactant (minimum), transition state (saddle point), and product (minimum), respectively.

6-31G** geometries. The gas phase model 3-21G//3-21G, 6-31G**//3-21G, and 6-31G**//6-31G** SCF results are from ref. 31.

III. Results and discussion

III.1 Geometries

The 3-21G and 6-31G** optimized structures for the supermolecules shown in Fig. 2 are summarized in Tables 3 and 4, respectively. The total energies corresponding to these structures, calculated with different basis sets at the SCF level and with MP2 corrections, are reported in Table 5.

For the 15 supermolecules studied in the present work, most of the optimized geometries yield "cyclic structures" for the reactants (**a**), transition states (**b**), and products (**c**). Except for the propene–H_2O case, which has a dipole moment of only 0.3 D compared with 1.0 to 4.1 D for other species, the cyclic structures show strong co-operative hydrogen bonding, indicated by the characteristic geometric parameter, the O—H_x and/or O—H_y distance, as shown in Fig. 2 and reported in Tables 3 and 4.

In all the unsymmetrical cases, the H_2O molecule in the supermolecules is preferentially bonded to the terminal atom which forms the double bond with the central carbon.

Similar to the results of the study on the gas model molecules (31), a number of trends appear when comparing some of the most important geometrical parameters of the 3-21G and 6-31G** optimized geometries. The C—X and C—Y 6-31G** bond lengths are generally shorter than the corresponding 3-21G bond lengths. The 3-21G and 6-31G** XCY bond angle differs by less than 1°, except for CH_3CHCH_2, in which the XCY angle changed by 1.2° in (**a**) and by 2.0° in (**b**). In contrast with the gas model molecule results, the supermolecule XCY angles decrease in going from 3-21G to 6-31G** (except for CH_2CHNH_2 (**a**), where 6-31G** XCY is larger than that of 3-21G by 0.4°). This reveals the role of polarization functions in cases where hydrogen bonding exists.

Comparing the optimized geometries for the reactants, transition states, and products, the most significant difference between the gas model molecules and the H_2O-mediated case is the change in the XCY angle in the transition state. For the H_2O-mediated case, the XCY angle increased only slightly (0.3 to 6°), compared to the 14 to 19° change for the gas model molecules (31). The changes in other geometric parameters from reactant to transition state and then to product are also smaller compared with those in the gas model molecules. This significant difference in the changes in geometry between the gas model molecules and the supermolecules is consistent with the lower barriers for the H_2O-mediated case.

III.2 Relative stabilities

Table 6 summarizes the relative stabilities for H_2O-mediated results for various levels of calculations, along with the direct

Can. J. Chem. Downloaded from www.nrcresearchpress.com by 84.41.108.74 on 09/07/12
For personal use only.

TABLE 3. Optimized 3-21G geometries for structures shown in Fig. 2 (bond lengths in Å and angles in degrees)

	CC		CN			CO			NN		NO			OO	
	a	**b**	**a**	**b**	**c**	**a**	**b**	**c**	**a**	**b**	**a**	**b**	**c**	**a**	**b**
HC	1.0767	1.0802	1.0820	1.0789	1.0754	1.0852	1.0807	1.0714	1.0798	1.0766	1.0820	1.0765	1.0749	1.0752	1.0759
XC	1.5117	1.4324	1.5050	1.4516	1.3280	1.5033	1.4046	1.3184	1.3492	1.3076	1.3362	1.2895	1.2603	1.3247	1.2681
YC	1.3170	1.4324	1.2602	1.2896	1.3700	1.2156	1.2764	1.3636	1.2718	1.3076	1.2286	1.2933	1.3363	1.2147	1.2681
$H_{x1}X$	1.0814	1.2520	1.0791	1.3626	1.0726	1.0794	1.5420	1.0713	1.0086	1.1758	1.0103	1.3251	1.8821	0.9973	1.3308
$H_{x2}X$	1.0870	1.0781	1.0855	1.0779	1.0702	1.0860	1.0727	1.0704	0.9933	0.9968	0.9948	1.0000	1.0070	—	—
$H_{x3}X$	1.0870	1.0945	1.0862	1.0876	—	1.0860	1.0829	—	—	—	—	—	—	—	—
$H_{y1}Y$	1.0745	1.0781	1.0124	1.0004	0.9932	—	—	0.9793	1.0069	0.9968	—	—	—	—	—
$H_{y2}Y$	1.0735	1.0946	—	—	1.0027	—	—	—	—	—	—	—	—	—	—
OH_{x1}	2.4311	1.3946	2.2360	1.2610	2.7582	2.2319	1.1624	2.6348	1.9024	1.3338	1.9003	1.1775	0.9849	1.6421	1.1257
$H_{o1}O$	0.9660	1.3946	0.9780	1.3619	0.9668	0.9716	1.1145	0.9645	0.9864	1.3338	0.9776	1.2306	1.6531	0.9738	1.1257
$H_{o2}O$	0.9660	0.9692	0.9667	0.9609	0.9668	0.9661	0.9632	0.9646	0.9664	0.9673	0.9655	0.9627	0.9646	0.9636	0.9615
YCH	120.17	119.45	122.45	118.36	114.26	119.79	116.88	111.21	123.53	120.24	120.95	116.39	111.34	123.34	118.34
XCH	116.32	119.45	115.78	121.34	119.00	115.46	119.42	121.50	114.23	120.24	114.35	121.89	125.30	111.69	118.34
$H_{x1}XC$	109.87	104.44	109.23	98.49	121.37	109.60	91.84	121.45	116.96	108.76	117.17	105.87	104.38	112.05	105.26
$H_{x2}XC$	110.73	115.57	110.02	113.65	121.13	109.54	117.28	120.51	121.72	120.76	121.88	119.63	116.09	—	—
$H_{x3}XC$	110.73	106.66	110.06	110.62	—	109.51	115.32	—	—	—	—	—	—	—	—
$H_{y1}YC$	121.49	115.57	115.45	121.16	120.52	—	—	112.70	115.33	120.76	—	—	—	—	—
$H_{y2}YC$	120.92	106.66	—	—	120.13	—	—	—	—	—	—	—	—	—	—
$OH_{x1}X$	155.90	137.55	145.55	144.58	126.78	142.04	142.76	122.69	143.58	149.28	140.87	145.93	139.47	151.86	146.69
$H_{o1}OH_{x1}$	107.68	92.60	71.06	89.65	70.96	75.90	92.58	103.60	80.22	84.38	83.66	89.10	88.02	93.92	92.78
$H_{o2}OH_{x1}$	107.68	133.70	108.16	128.30	70.96	117.84	116.81	105.97	115.28	116.32	122.77	119.16	110.68	130.49	121.49
XCHY	180.00	180.00	180.33	184.09	180.00	180.12	187.04	180.00	180.18	179.23	179.91	180.09	179.93	179.95	180.45
$H_{x1}XCH$	180.00	163.49	177.50	148.28	180.00	179.32	132.26	180.00	181.80	179.72	179.44	181.12	178.20	179.62	180.11
$H_{x2}XCH$	59.47	17.88	56.89	11.71	0.00	57.74	358.20	0.00	357.38	1.73	1.36	358.96	0.53	—	—
$H_{x3}XCH$	300.53	254.55	298.54	246.12	—	300.29	219.85	—	—	—	—	—	—	—	—
$H_{y1}YCH$	0.00	17.88	0.02	3.36	0.00	—	—	180.00	0.27	358.27	—	—	—	—	—
$H_{y2}YCH$	180.00	254.55	—	—	180.00	—	—	—	—	—	—	—	—	—	—
$OH_{x1}XC$	0.00	48.17	0.16	38.42	0.00	2.74	42.32	0.00	357.22	0.99	0.22	0.03	5.09	0.49	359.59
$H_{o1}OH_{x1}X$	238.56	329.70	357.14	339.12	120.79	1.80	340.49	122.65	6.48	359.40	355.86	359.38	355.64	357.82	0.18
$H_{o2}OH_{x1}X$	121.44	149.70	100.24	157.02	239.21	258.40	104.45	238.81	260.83	116.05	104.35	235.10	120.32	120.39	230.16

Can. J. Chem. Downloaded from www.nrcresearchpress.com by 84.41.108.74 on 09/07/12
For personal use only.

TABLE 4. Optimized 6-31G** geometries for structures shown in Fig. 2 (bond lengths in Å and angles in degrees)

	CC		CN			CO			NN		NO			OO	
	a	**b**	**a**	**b**	**c**	**a**	**b**	**c**	**a**	**b**	**a**	**b**	**c**	**a**	**b**
HC	1.0767	1.0802	1.0820	1.0789	1.0754	1.0852	1.0807	1.0714	1.0798	1.0766	1.0820	1.0765	1.0749	1.0752	1.0759
XC	1.5117	1.4324	1.5050	1.4516	1.3280	1.5033	1.4046	1.3184	1.3492	1.3076	1.3362	1.2895	1.2603	1.3247	1.2681
YC	1.3170	1.4324	1.2602	1.2896	1.3700	1.2156	1.2764	1.3636	1.2718	1.3076	1.2286	1.2933	1.3363	1.2147	1.2681
$H_{x1}X$	1.0814	1.2520	1.0791	1.3626	1.0726	1.0794	1.5420	1.0713	1.0086	1.1758	1.0103	1.3251	1.8821	0.9973	1.3308
$H_{x2}X$	1.0870	1.0781	1.0855	1.0779	1.0702	1.0860	1.0727	1.0704	0.9933	0.9968	0.9948	1.0000	1.0070	—	—
$H_{x3}X$	1.0870	1.0945	1.0862	1.0876	—	1.0860	1.0829	—	—	—	—	—	—	—	—
$H_{y1}Y$	1.0745	1.0781	1.0124	1.0004	0.9932	—	—	0.9793	1.0069	0.9968	—	—	—	—	—
$H_{y2}Y$	1.0735	1.0946	—	—	1.0027	—	—	—	—	—	—	—	—	—	—
OH_{x1}	2.4311	1.3946	2.2360	1.2610	2.7582	2.2319	1.1624	2.6348	1.9024	1.3338	1.9003	1.1775	0.9849	1.6421	1.1257
$H_{o1}O$	0.9660	1.3946	0.9780	1.3619	0.9668	0.9716	1.1145	0.9645	0.9864	1.3338	0.9776	1.2306	1.6531	0.9738	1.1257
$H_{o2}O$	0.9660	0.9692	0.9667	0.9609	0.9668	0.9661	0.9632	0.9646	0.9664	0.9673	0.9655	0.9627	0.9646	0.9636	0.9615
YCH	120.17	119.45	122.45	118.36	114.26	119.79	116.88	111.21	123.53	120.24	120.95	116.39	111.34	123.34	118.34
XCH	116.32	119.45	115.78	121.34	119.00	115.46	119.42	121.50	114.23	120.24	114.35	121.89	125.30	111.69	118.34
$H_{x1}XC$	109.87	104.44	109.23	98.49	121.37	109.60	91.84	121.45	116.96	108.76	117.17	105.87	104.38	112.05	105.26
$H_{x2}XC$	110.73	115.57	110.02	113.65	121.13	109.54	117.28	120.51	121.72	120.76	121.88	119.63	116.09	—	—
$H_{x3}XC$	110.73	106.66	110.06	110.62	—	109.51	115.32	—	—	—	—	—	—	—	—
$H_{y1}YC$	121.49	115.57	115.45	121.16	120.52	—	—	112.70	115.33	120.76	—	—	—	—	—
$H_{y2}YC$	120.92	106.66	—	—	120.13	—	—	—	—	—	—	—	—	—	—
$OH_{x1}X$	155.90	137.55	145.55	144.58	126.78	142.04	142.76	122.69	143.58	149.28	140.87	145.93	139.47	151.86	146.69
$H_{o1}OH_{x1}$	107.68	92.60	71.06	89.65	70.96	75.90	92.58	103.60	80.22	84.38	83.66	89.10	88.02	93.92	92.78
$H_{o2}OH_{x1}$	107.68	133.70	108.16	128.30	70.96	117.84	116.81	105.97	115.28	116.32	122.77	119.16	110.68	130.49	121.49
XCHY	180.00	180.00	180.33	184.09	180.00	180.12	187.04	180.00	180.18	179.23	179.91	180.09	179.93	179.95	180.45
$H_{x1}XCH$	180.00	163.49	177.50	148.28	180.00	179.32	132.26	180.00	181.80	179.72	179.44	181.12	178.20	179.62	180.11
$H_{x2}XCH$	59.47	17.88	56.89	11.71	0.00	57.74	358.20	0.00	357.38	1.73	1.36	358.96	0.53	—	—
$H_{x3}XCH$	300.53	254.55	298.54	246.12	—	300.29	219.85	—	—	—	—	—	—	—	—
$H_{y1}YCH$	0.00	17.88	0.02	3.36	0.00	—	—	180.00	0.27	358.27	—	—	—	—	—
$H_{y2}YCH$	180.00	254.55	—	—	180.00	—	—	—	—	—	—	—	—	—	—
$OH_{x1}XC$	0.00	48.17	0.16	38.42	0.00	2.74	42.32	0.00	357.22	0.99	0.22	0.03	5.09	0.49	359.59
$H_{o1}OH_{x1}X$	238.56	329.70	357.14	339.12	120.79	1.80	340.49	122.65	6.48	359.40	355.86	359.38	355.64	357.82	0.18
$H_{o2}OH_{x1}X$	121.44	149.70	100.24	157.02	239.21	258.40	104.45	238.81	260.83	116.05	104.35	235.10	120.32	120.39	230.16

TABLE 5. Total energies (hartrees) for the 3-21G and 6-31G** optimized geometries† at the 3-21G, 6-31G**, and MP2/6-31G* levels

		3-21G//3-21G	6-31G**//3-21G	6-31G**//6-31G**	MP2/6-31G*//6-31G**
CC	a	−192.018495	−193.104501	−193.107387	−193.653897
	b	−191.859694	−192.931010	−192.940902	−193.503367
CN	a	−207.929527	−209.114642	−209.118716	−209.699292
	b	−207.857195	−209.015304	−209.019060	−209.615583
	c	−207.927814	−209.100625	−209.103479	−209.679504
CO	a	−227.659846	−228.951608	−228.955618	−229.552649
	b	−227.586091	−228.853616	−228.857764	−229.474500
	c	−227.650172	−228.930135	−228.935038	−229.527022
NN	a	−223.853700	−225.124495	−225.129199	−225.740594
	b	−223.826323	−225.077074	−225.079385	−225.705964
NO	a	−243.599388	−244.975257	−244.979470	−245.607722
	b	−243.560461	−244.918512	−244.921578	−245.567991
	c	−243.576215	−244.954212	−244.961031	−245.588442
OO	a	−263.319454	−264.804718	−264.811137	−265.455572
	b	−263.296581	−264.763750	−264.769006	−265.430295

†See Fig. 2 for the structures.

TABLE 6. Relative stabilities (kJ/mol) for the H_2O-mediated 1,3-hydrogen shift compared with those of gas phase model†

	Col. 1	Col. 2	Col. 3	Col. 4	Col. 5	Col. 6	Col. 7	Col. 8
CN								
I	−9.0	28.2	29.5	38.5	39.6	—	30.3	34.5
II	4.5	36.8	40.0	49.2	52.0	48.0	46.1	89.0
CO								
I	35.4	58.3	56.7	71.2	69.8	—	60.0	82.1
II	25.4	56.4	54.0	68.3	67.3	73.6	52.5	41.1
NO								
I	73.7	57.4	53.1	59.6	58.3	—	59.6	101.4
II	60.8	55.3	48.4	54.4	50.6	59.4	50.5	64.5

†I for gas phase molecule and II for H_2O-mediated case. Column 1, 3-21G//3-21G; col. 2, 6-31G**//3-21G; col. 3, 6-31G**//6-31G**; col. 4, 6-31G*//6-31G**; col. 5, MP2/6-31G*//6-31G**; col. 6, MP2/6-31G*//6-31G** + ZPV(MNDO); col. 7, 6-31G**//6-31G** at k = 0.001 bohr^{-3}; col. 8, 6-31G**//6-31G** at k = 0.006 bohr^{-3}.

1,3-intramolecular hydrogen shift results of ref. 31. In most cases, the largest change in relative stabilities for both the gas phase results and the H_2O-mediated results occurs in going from the 3-21G//3-21G level to the 6-31G**//3-21G level. The results at the 6-31G**//3-21G level and higher are in good agreement. For example, the 6-31G**//3-21G and 6-31G**//6-31G** relative stabilities differ by an average of only 3 kJ/mol.

For the methyl imine – vinyl amine case (CN), the methyl imine is predicted to be more stable by 48 kJ/mol at the highest level. This is the only case for which the 3-21G//3-21G level fails qualitatively. Both the addition of a water molecule and the SCRF increases the stability of the methyl imine tautomer.

For acetaldehyde – vinyl alcohol (CO), the only case for which experimental results are available, the acetaldehyde tautomer is predicted to be more stable by 74 kJ/mol at the highest level. For the H_2O-mediated case the SCRF increases slightly the stability of the vinyl alcohol (column 3 vs. columns 7 and 8), whereas the opposite occurs for the gas phase. The gas phase and the H_2O-mediated case give similar results, where the relative stability differs by only 2 to 3 kJ/mol with the vinyl alcohol being consistently stabilized by the addition of a water molecule. Experimentally the relative stability in acidic aqueous solution is estimated to be 36 kJ/mol (10), indicating that the SCRF does correctly reduce the relative stability, predicting 41 kJ/mol for a value of k = 0.006 bohr^{-3}.

For the formamide – formamidic acid case (NO), formamide is predicted to be more stable, by 59 kJ/mol at the highest level. The addition of a water molecule and the SCRF to the gas phase both result in an increase in the stability of formamidic acid. Addition of the SCRF to the H_2O-mediated case on the other hand increases the stability of the formamide tautomer. These results can be compared to related systems, such as *N*-phenylbenzamide for which a relative stability in the gas phase is predicted to be 60 kJ/mol, in excellent agreement with the calculated gas phase values. This is also in good agreement with the MBPT(2)/6-31G*//3-21G+ZPV results (34) for the relative stability kk-ke tautomers of uracil of 63 kJ/mol (cf. Table 1). These results suggest that the relative stability in related structures is fairly consistent. The exceptions to the rule, such as 2-oxopyridine and 2-oxopyrimidine, where the relative stability between the keto and enol form are about

Can. J. Chem. Downloaded from www.nrcresearchpress.com by 84.41.108.74 on 09/07/12
For personal use only.

Can. J. Chem. Downloaded from www.nrcresearchpress.com by 84.41.108.74 on 09/07/12
For personal use only.

TABLE 7. Dipole moments (D) for the gas phase and H_2O-mediated molecules† calculated at 6-31G**//6-31G** level

		gas phase	H_2O-mediated
CC	a	0.32	2.57
	b	0.48	6.13
CN	a	2.20	3.92
	b	2.97	4.58
	c	1.71	1.02
CO	a	3.00	3.19
	b	1.80	2.69
	c	1.03	3.71
NN	a	2.98	2.98
	b	2.29	5.45
NO	a	4.09	3.21
	b	3.05	2.77
	c	1.19	2.34
OO	a	1.63	1.43
	b	1.45	2.30

†See Fig. 2 for the structures.

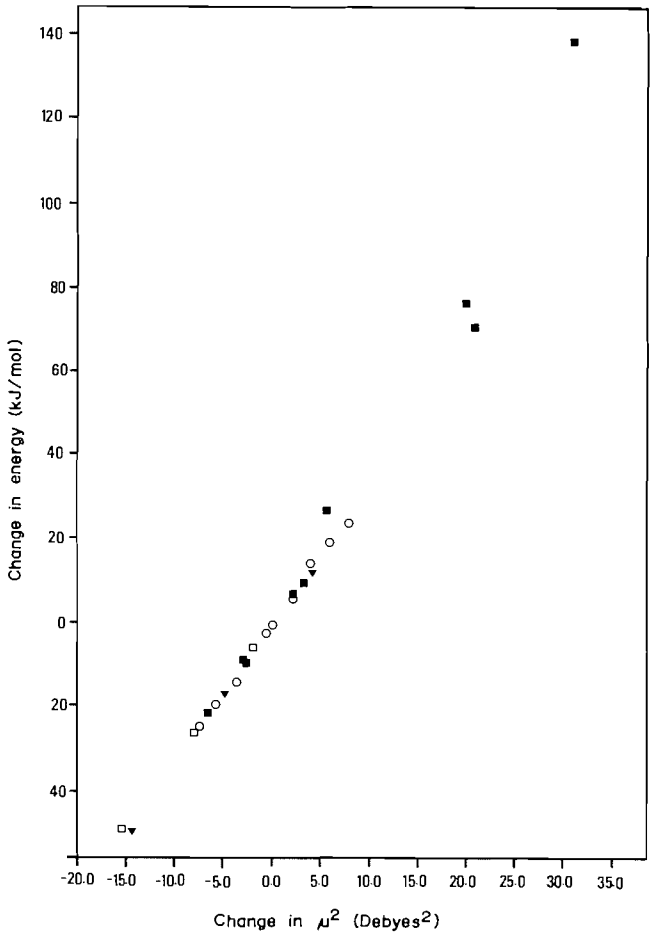


FIG. 3. The relationship between changes in barrier height and relative stability, and changes in the square of the dipole moment (○ gas phase barrier, ■ H_2O-mediated barrier, □ gas phase relative stability, and ▼ H_2O-mediated relative stability). The energies and dipole moment are for the 6-31G**//6-31G** level.

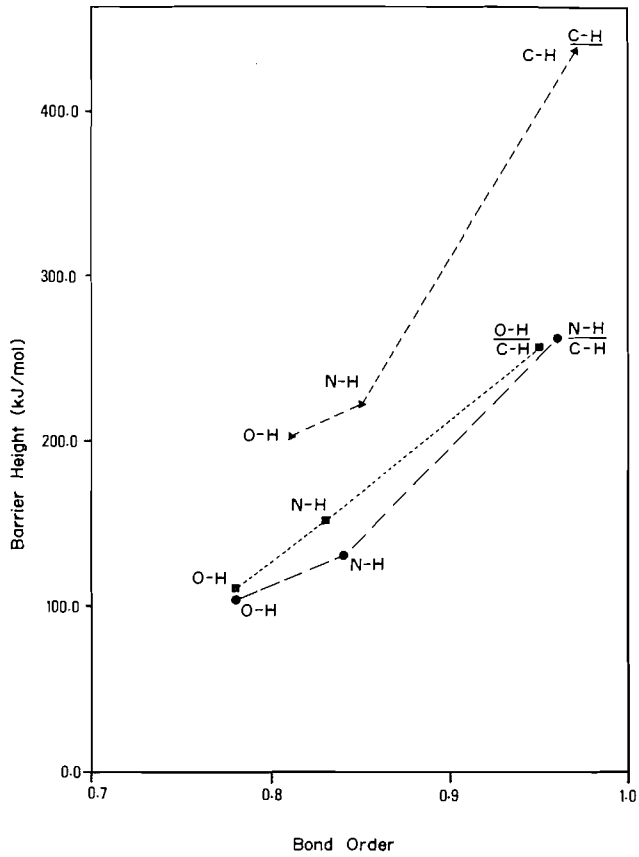


FIG. 4. The relationship between the barrier height and the bond order of the X—H bond being broken in going from reactant to transition state (6-31G**//6-31G**). The bonds beside the points are bonds being broken and the underlined bonds at the top of each curve are the bonds being formed.

−2.5 and −10 kJ/mol, respectively, can be explained by the increase resonance in the enol form relative to the keto form.

The effect of correlation on relative stability can be seen by comparing columns 4 and 5 of Table 6. For both the gas phase molecules and the supermolecules the change in relative stabilities due to correlation varies between 1.0 and 3.8 kJ/mol for MP2/6-31G*//6-31G**. Addition of ZPV correction represents a further change of between 4.0 and 8.8 kJ/mol.

Columns 3 and 7 or 8 represent the effect of a polar aprotic solvent. Addition of the SCRF consistently stabilizes the tautomer with the largest dipole (cf. Table 7 and Fig. 3). This is not too surprising since the SCRF adds a dipole–dipole interaction term to the Fock operator.

III.3 Barriers

Table 8 summarizes the barrier heights for the H_2O-mediated results for various levels of calculations, along with the direct 1,3-intramolecular hydrogen shift results of ref. 31. As can be seen from Table 2, no experimental results and few computational results are available in this case. As indicated in Table 8, the nine barriers predicted by 6-31G**//3-21G and 6-31G**//6-31G** only differ by an average of 6 kJ/mol. This encourages the use of 3-21G optimized structures on large systems for this kind of study.

The correlation has a much larger contribution on the transition states and therefore on the barriers. For the gas phase case, the lowering in the barriers heights at MP2 ranges from 54 to 65 kJ/mol compared to a range of 26 to 52 kJ/mol

TABLE 8. Barriers (kJ/mol) for the H_2O-mediated 1,3-hydrogen shift compared with those of gas phase model†

		Col. 1	Col. 2	Col. 3	Col. 4	Col. 5	Col. 6	Col. 7	Col. 8
CC									
	I	450.3	437.8	435.8	443.6	378.4	—	435.8	435.5
	II	416.9	455.5	437.1	430.9	395.2	373.9	423.4	299.4
CN									
	I	341.6	357.1	355.7	370.0	316.2	—	354.0	340.8
	II	189.9	260.8	261.7	267.2	219.8	187.4	259.1	234.4
CN‡									
	I	350.6	328.9	326.2	331.6	276.6	—	323.7	306.3
	II	185.4	224.0	221.6	218.0	167.8	141.4	213.0	145.4
CO									
	I	373.2	372.2	366.2	381.3	322.1	—	368.6	385.0
	II	193.6	257.3	256.9	273.5	205.2	186.7	258.2	264.9
CO‡									
	I	337.8	313.9	309.5	310.1	252.3	—	308.6	302.8
	II	168.2	200.9	202.9	205.2	137.9	131.1	205.7	223.7
NN									
	I	247.6	256.2	254.9	265.4	205.3	—	256.5	268.3
	II	71.9	124.5	130.8	134.9	90.9	60.9	121.9	60.2
NO									
	I	270.8	261.8	255.8	266.3	203.8	—	259.0	279.7
	II	102.2	149.0	152.0	165.3	104.3	79.8	153.1	160.8
NO‡									
	I	197.1	204.5	202.7	206.7	150.3	—	199.4	178.3
	II	41.4	93.7	103.6	110.9	53.7	20.4	102.7	96.3
OO									
	I	229.4	215.3	207.7	212.0	150.3	—	208.0	209.4
	II	60.1	107.6	110.6	119.1	66.4	39.5	109.3	100.3

†See the footnote of Table 6 for definition of I and II and the different levels of calculations (columns 1 to 8), and Fig. 2 for the structures.
‡Barriers for the reverse reaction.

Can. J. Chem. Downloaded from www.nrcresearchpress.com by 84.41.108.74 on 09/07/12
For personal use only.

at CISD-DQ/6-31G**//6-31G** (31). For the H_2O-mediated case MP2 lowers the barrier heights by 36 to 68 kJ/mol. Higher level calculations on formic acid at the MP2/6-31G**//6-31G** level further lowers the barrier by 7.3 kJ/mol, while MP4/6-31G*//6-31G** lowers the barrier by only 1.7 kJ/mol.

The SCRF term introduces both significant decreases and increases in the barrier heights. Again the species with the largest dipole is the most stabilized by the SCRF. This can be seen from Fig. 3, where the change in barrier is plotted against the change in the square of the dipole moment. When the transition state dipole increases relative to the reactant, the effect of a polar solvent (SCRF) is to lower the barrier and vice versa. Barrier heights should be further reduced by the addition of a second water molecule (cf. Table 2).

Figure 4 plots the barrier height as a function of the X—H bond order, which is being broken in going from reactant to product, and the lines connect the points with the same X. There is a general increase in barrier height in the order O—H, N—H, and C—H. This implies that the O—H bond is the easiest to break and that the C—H bond is the most difficult to break for a given series, when the terminal group Y is kept the same. For a group in which the bond being broken is held the same, the order of barrier heights are N—H, O—H, and C—H, that is, O—H and N—H is opposite to the gas phase results. These results indicate that the barriers in these systems are predominantly controlled by the type of bond being broken in the transition state and is consistent with product-like transition states (in this paper, we have chosen the more stable tautomers as the reactant (**a**)).

Table 8 shows that the barriers are reduced by 94 to 124 kJ/mol from the gas model molecules to the supermolecules except for X and Y = CH_2, where the barriers for both CH_3CHCH_2 and $CH_3CHCH_2(H_2O)$ are essentially the same, based on 6-31G** results.

IV. Conclusions

The results in this work indicate that for reliable results the lowest acceptable level is 6-31G*//3-21G. The water molecule plays a significant role in catalyzing the 1,3-intramolecular hydrogen rearrangement reaction for molecules in which some hydrogen bonding is possible. The combination of the supermolecule and self-consistent reaction field approach in predicting the effect of solvent on both relative stabilities and barriers appears to be quite promising. The results indicate that the effect of polar solvent can be qualitatively predicted based on changes in dipole moment.

Acknowledgements

The continuing support of the Natural Sciences and Engineering Research Council (NSERC) is acknowledged by R.A.P. and the support from the Dean of Science of Memorial University of Newfoundland is acknowledged by D.Y. We

would like to thank the Newfoundland and Laborator Computer Services (NLCS) and the University Computer Service at Memorial University for their generous allocation of computer time.

1. P. O. LOWDIN. Adv. Quantum Chem. **2**, 213 (1965).
2. C. D. POULTER and G. D. FREDERICK. Tetrahedron Lett. **26**, 2171 (1975).
3. P. BEAK, J. B. CORINGTON, and S. G. SMITH. J. Am. Chem. Soc. **98**, 8284 (1976).
4. P. BEAK, F. S. FRY, JR., J. LEE, and F. STEELE. J. Am. Chem. Soc. **98**, 171 (1976).
5. O. BENSAUDE and J.-E. DUBOIS. C.R. Acad. Sci. Paris C**285**, 503 (1977).
6. O. BENSAUDE, M. CHEVRIER, and J.-E. DUBOIS. J. Am. Chem. Soc. **78**, 7055 (1978).
7. O. BENSAUDE, M. CHEVRIER, and J.-E. DUBOIS. Tetrahedron Lett. **25**, 2221 (1978).
8. R. S. BROWN, A. TSE, and J. C. VEDERAS. J. Am. Chem. Soc. **102**, 1174 (1980).
9. P. BEAK and J. M. WHITE. J. Am. Chem. Soc. **104**, 7073 (1982).
10. G.-Q. TANG, J. MACINNIS, and M. KASHA. J. Am. Chem. Soc. **109**, 2531 (1987).
11. Y. TSUCHIYA, T. TAMURA, M. FUJII, and M. ITO. J. Phys. Chem. **92**, 1760 (1988).
12. J. R. KEEFFE, A. J. KRESGE, and N. P. SCHEPP. J. Am. Chem. Soc. **110**, 1993 (1988).
13. N. BODOR, M. J. S. DEWAR, and A. J. HARGET. J. Am. Chem. Soc. **92**, 2929 (1970).
14. B. PULLMAN and A. PULLMAN. Adv. Heterocycl. Chem. **13**, 77 (1971).
15. P. D. ADENEY, W. J. BOUMA, L. RADOM, and W. R. RODWELL. J. Am. Chem. Soc. **102**, 4069 (1980).
16. W. J. BOUMA, L. RADOM, and W. R. RODWELL. Theoret. Chim. Acta (Berl.) **56**, 149 (1980).
17. W. R. RODWELL, W. J. BOUMA, and L. RADOM. Int. J. Quantum Chem. **18**, 107 (1980).
18. T. J. ZIELINSKI, R. A. POIRIER, M. R. PETERSON, and I. G. CSIZMADIA. J. Comput. Chem. **3**, 477 (1982).
19. T. J. ZIELINSKI. J. Comput. Chem. **4**, 345 (1983).
20. T. J. ZIELINSKI, R. A. POIRIER, M. R. PETERSON, and I. G. CSIZMADIA. J. Comput. Chem. **4**, 419 (1983).
21. A. SYGULA and A. BUDA. J. Mol. Struct. **92**, 267 (1983).
22. T. J. ZIELINSKI and R. A. POIRIER. J. Comput. Chem. **5**, 466 (1984).
23. T. YAMABE, K. YAMASHITA, M. KAMINOYAMA, M. KOIZUMI, A. TACHIBANA, and K. FUKUI. J. Phys. Chem. **88**, 1459 (1984).
24. F. BERNARDI, M. A. ROBB, H. B. SCHLEGEL, and G. TONACHINI. J. Am. Chem. Soc. **106**, 1198 (1984).
25. A. LLEDOS and J. BERTRAN. J. Mol. Struct. (Theochem) **107**, 233 (1984).
26. M. J. SCANLAN and I. H. HILLIER. J. Am. Chem. Soc. **106**, 3737 (1984).
27. M. J. SCANLAN and I. H. HILLIER. J. Chem. Soc. Chem. Commun. 7 (1984).
28. A. LLEDOS and J. BERTRAN. J. Mol. Struct. (Theochem) **120**, 73 (1985).
29. M. BERNDT and J. S. KWIATKOWSKI. *In* Theoretical chemistry of biological systems. *Edited by* Naray-Szabo. Elsevier, Amsterdam. 1986. p. 349.
30. J. S. KWIATKOWSKI, T. J. ZIELINSKI, and R. REIN. Adv. Quantum Chem. **18**, 85 (1986).
31. R. A. POIRIER, D. MAJLESSI, and T. J. ZIELINSKI. J. Comput. Chem. **7**, 464 (1986).
32. P. CIEPLAK, P. BASH, U. C. SINGH, and P. A. KOLLMAN. J. Am. Chem. Soc. **109**, 6283 (1987).
33. U. NORINDER. J. Mol. Struct. (Theochem) **151**, 259 (1987).
34. J. S. KWIATKOWSKI, R. J. BARTLETT, and W. B. PERSON. J. Am. Chem. Soc. **110**, 2353 (1988).
35. A. PULLMAN. *In* Quantum theory of chemical reactions. Vol. II. *Edited by* R. Daudel, A. Pullman, L. Salem, and A. Veillard. Reidel, Dordrecht. 1981. p. 1.
36. O. TAPIA. *In* Quantum theory of chemical reactions. Vol. II. *Edited by* R. Daudel, A. Pullman, L. Salem, and A. Veillard. Reidel, Dordrecht. 1981. p. 25.
37. L. ONSAGER. J. Am. Chem. Soc. **58**, 1486 (1936).
38. O. TAPIA and G. JOHANNIN. J. Chem. Phys. **75**, 3624 (1981).
39. R. BONACCORSI, J. TOMASI, C. A. REYNOLDS, and C. THOMSON. J. Comput. Chem. **9**, 779 (1988).
40. M. HODOŠČEK, D. KOCJAN, and D. HADŽI. J. Mol. Struct. Theochem. **165**, 115 (1988).
41. A. R. KATRITZKY and M. KARELSON. J. Am. Chem. Soc. **113**, 1561 (1991).
42. M. KARELSON, A. R. KATRIZKY, and M. C. ZERNER. J. Org. Chem. **56**, 134 (1991).
43. A. RAUDINO, F. ZUCCARELLO, and G. BUEMI. Faraday Trans. II, **79**, 1759 (1983).
44. R. A. POIRIER, M. R. PETERSON, and A. YADAV. MUNGAUSS. Chemistry Department, Memorial University of Newfoundland, St. John's, Nfld., Canada.
45. M. J. FRISCH, J. S. BINKLEY, H. B. SCHLEGEL, K. RAGHAVACHARI, C. F. MELIUS, R. L. MARTIN, J. J. P. STEWART, F. W. BOBROWICZ, C. M. ROHLFING, L. R. KAHN, D. J. DEFREES, R. SEEGER, R. A. WHITESIDE, D. J. FOX, E. M. FLEUDER, and J. A. POPLE. Gaussian 86. Carnegie-Mellon Quantum Chemistry Publishing Unit, Pittsburgh PA. 1984.
46. J. S. BINKLEY, J. A. POPLE, and W. J. HEHRE. J. Am. Chem. Soc. **102**, 939 (1980).
47. W. J. HEHRE, R. DITCHFIELD, and J. A. POPLE. J. Chem. Phys. **56**, 2257 (1972).
48. P. C. HARIHARAN and J. A. POPLE. Theoret. Chim. Acta. (Berl.) **28**, 213 (1973).
49. (*a*) W. C. DAVIDON and L. NAZARETH. Technical Memos 303 and 306. 1977. Applied Mathematics Division, Argonne National Laboratories, Argonne, IL; (*b*) W. C. DAVIDON. Math. Prog. **9**, 1 (1975).
50. M. J. D. POWELL. Subroutine VAO5AD, AERE Subroutine Library, Harwell, Didcot, Berkshire, U.K.
51. I. MAYER. Chem. Phys. Lett. **97**, 270 (1983).
52. S. T. HAYNES. The theory of reactions in solution. *In* Theory of chemical reaction dynamics. Vol. IV. *Edited by* M. Baer. CRC Press. 1986. Chap. 4.
53. J. J. P. STEWART. QCPE Program No. 455, Chemistry Department, Indiana University.

Can. J. Chem. Downloaded from www.nrcresearchpress.com by 84.41.108.74 on 09/07/12
For personal use only.

Stereochemical requirements for the formation of vanadate complexes with peptides

JASWINDER S. JASWAL AND ALAN S. TRACEY[1]
Department of Chemistry, Simon Fraser University, Burnaby, B.C., Canada V5A 1S6
Received April 18, 1991

JASWINDER S. JASWAL and ALAN S. TRACEY. Can. J. Chem. **69**, 1600 (1991).

The condensation reactions occurring between vanadate and a number of amino acids and simple peptides have been studied by ^{51}V nuclear magnetic resonance. Vanadate and ligand stoichiometry has been established for the complexes formed and their formation constants determined. The amino acids were all found to undergo rather weak interactions with vanadate and in general provided two products with ^{51}V chemical shifts near −545 and −555 ppm. The peptides also gave minor products with NMR signals occurring with that of vanadate itself. However, in this case, the major products occur at approximately −510 ppm. These latter complexes are monovanadate, monoligand complexes which require the terminal amino, the carboxylate groups and an unsubstituted nitrogen in the peptide linkage in order for product formation to occur. Sidechains promote product formation, apparently by favouring a more readily complexed peptide conformation. Formation constants vary from about 20 to 50 M^{-1} depending on the sidechain. The carboxylate group can be replaced by a hydroxymethyl. This, however, leads to a significant decrease in product formation at pH 7. Hydrogen ion concentration studies showed that the complexes, when considered to be formed from $VO_4H_2^-$ and neutral peptide, did not require or give off protons. However, when the carboxylate was replaced by the alcohol functionality a proton was released. On the basis of this study the coordination of the vanadate/peptide complexes has been assigned.

Key words: peptide, vanadate, complexes, vanadium magnetic resonance.

JASWINDER S. JASWAL et ALAN S. TRACEY. Can. J. Chem. **69**, 1600 (1991).

Faisant appel à la rmn du ^{51}V, on a étudié les réactions de condensation qui se produisent entre le vanadate et un certain nombre d'acides aminés et de peptides simples. On a déterminé les stoechiométries du vanadate et du ligand dans les complexes formés ainsi que leurs constantes de formation. On a trouvé que tous les acides aminés n'établissent que des interactions faibles avec le vanadate et que, en général, ils conduisent à deux produits avec des déplacements chimiques du ^{51}V de près de −545 et −555 ppm. Les peptides fournissent aussi des produits mineurs avec des signaux de rmn apparaissant avec ceux du vanadate lui-même. Toutefois, dans ce cas, les produits majeurs présentent un signal près de −510 ppm. Ces derniers complexes sont des complexes monocoordinés du monovanadate qui ne peuvent se produire qu'en présence d'un groupement amino terminal, de groupements carboxylates et d'un azote non-substitué d'une liaison peptidique. Les chaînes latérales favorisent la formation du produit, apparemment en favorisant une conformation peptidique qui peut être complexée plus facilement. Les constantes de formation varient de 20 à 50 M^{-1} dépendant de la chaîne latérale. On peut remplacer un groupe carboxylique par un groupe hydroxyméthyle. À un pH de 7, cette modification conduit toutefois à une diminution importante dans la formation du produit. Des études sur la concentration en ions hydrogènes ont montré que, lorsqu'on considère que les complexes se forment à partir du $VO_4H_2^-$ et d'un peptide neutre, leur formation ne requière pas de protons et qu'elle ne donne pas lieu à une expulsion de protons. Toutefois, lorsqu'on remplace le carboxylate par une fonction alcool, il y a expulsion d'un proton. Sur la base de cette étude, on a attribué la coordination des complexes de vanadate/peptide.

Mots clés : peptide, vanadate, complexes, rmn du vanadium.

[Traduit par la rédaction]

Introduction

The past few years have seen an extraordinary expansion of interest in the aqueous chemistry and biochemistry of vanadium oxoanions, particularly of the V(IV) and V(V) oxidation states. Much of this interest has concentrated on the role of these ions as phosphate analogues principly because they are potent inhibitors of a variety of phosphate metabolizing enzymes and activators of a number of others (1, 2). Additionally, both vanadate (V(V)) and vanadyl (V(IV)) bind tightly to a number of proteins, particularly albumins (3, 4) and transferrins (5). Vanadium has a large number of other biochemical effects many of which have been discussed in a number of recent reviews concerning the biochemistry of vanadium. These have been published in the single volume referred to in ref. 1.

In view of the biological activity of vanadate, considerable work has gone into obtaining an understanding of the interactions of this ion with metabolites and other small molecules. Of particular interest in this regard is the interactions of vanadate with amino alcohols (6, 7), amino acids (8–10), and small peptides (9–12). A good understanding of the interactions of vanadate with such materials will provide a firm basis for extension into studies of more complex systems.

A study of the available information on vanadate/peptide interactions revealed a surprising lack in fundamental information concerning these systems and furthermore suggested that some reported results were not correct. In view of this it was decided to undertake a detailed investigation of vanadate interactions with a variety of amino acids and small oligopeptides. The main purpose of this study was to establish which functional groups were necessary for complex formation, whether complexes of differing coordination were formed, and the stoichiometry of and proton requirements for complex formation. This initial report concentrates mainly on the function of the peptide bond and the terminal groups in complex formation. An additional report will consider the role of functionalized side chains in complex formation.

Experimental section

Materials

All amino acids and peptides used in this study were purchased from Sigma Chemical Company except for the glycylglycine, gly-

[1]Author to whom correspondence should be addressed.

Can. J. Chem. Downloaded from www.nrcresearchpress.com by 84.41.108.74 on 09/07/12
For personal use only.

TABLE 1. Table of reactants and chemical shifts of products of complex formation between vanadate and a selection of amino acids and peptides[a,b]

Ligand[a]	^{51}V chemical shift	Reference	Ligand	^{51}V chemical shift	Reference
Glycine[c]	−523, −546, −560	9, 10	Alanine	−547, −557	
Serine	−541, −554	9	Arginine	−555	
Asparagine	−545, −556		Valine	−552	
Glycinamide	NP				
Glygly	−505	9, 10	Glyglygly	−505	10
GlyglyOEt	NP		GlyglyglyOEt	NP	
CBZ-glygly	NP		CBZ-glyglygly	NP	
Glyglyglygly	NP		Glyglycinamide	NP	
Glyser	−494, −504, −507	9	GlyserOEt	−494, −501	
Glypro	NP	9	Progly	−493	9
Glyval	−510		Valgly	−506	
Glyasp	−509	9	Valasp[c]	−513	9
Leuleu	−512		Glysar	NP	9

[a]The standard three letter abbreviations for amino acids have been used: NP, no product; CBZ, carbobenzoxy.
[b]All ligands in this table have been studied in our laboratory under conditions of μ = 1.0 M KCl, 20 mM HEPES buffer, pH 7, and variable vanadate or ligand concentrations.
[c]The results of this study are not in agreement with previously published reports.

Can. J. Chem. Downloaded from www.nrcresearchpress.com by 84.41.108.74 on 09/07/12
For personal use only.

cylglycylglycine, and glycylserine ethyl ester hydrochlorides which were prepared according to literature procedures (13). The latter compounds were characterized by ^1H NMR spectroscopy and by elemental analysis. ^1H NMR spectra of the purchased materials were obtained as deemed necessary; all were used as supplied. Vanadium pentoxide (99.99%) was purchased from Aldrich Chemical Company and the buffer, *N*-(2-hydroxyethyl)-piperazine-*N'*-ethane sulfonic acid (HEPES), was obtained from Boehringer Mannheim GmbH.

Solutions

The vanadate stock solution was prepared from vanadium pentoxide by adding 0.5 mol equiv. of V_2O_5 to a 1.0 M solution of NaOH and stirring until the solution became colourless (~24 h). The solution was then diluted with distilled water to provide a 0.1 M vanadate stock solution.

Except for leucylleucine and the tri- and tetraglycine final solutions, which were prepared by direct weighing, 1.0 M peptide stock solutions were prepared in distilled water. Suspensions were warmed slightly if needed for dissolution to occur. HEPES (1.0 M) and KCl (2.0 M) stock solutions were also prepared. As an intermediate step in the process, solutions containing peptide, vanadate, KCl, and HEPES were prepared so as to ascertain what pH the stock solutions needed to be adjusted to so that mixing them provided a resultant solution of pH about 6.0 to 6.5. For the final solutions the pH was adjusted upward with NaOH to pH 7.0. This process avoided the formation of decavanadate. The final solutions contained 20 mM HEPES, the appropriate amount of vanadate and peptide and the ionic strength was maintained at 1.0 M with KCl.

Freshly opened pH 10.0 and pH 4.0 standard buffer solutions were used for pH calibration and the calibration was confirmed using a pH 7 buffer.

Spectroscopy

All ^{51}V NMR spectra were obtained from a Bruker AMX-400 NMR spectrometer operating at 105 MHz and at ambient temperature (22 ± 1°C). Chemical shifts are relative to an external $VOCl_3$ reference assigned to 0.0 ppm. Spectral widths of 80 KHz, 60° pulse widths and 0.05 acquisition times were used throughout. A polynomial baseline correction was applied to all spectra before integrals were obtained.

Methods

The appropriate equilibria were considered as outlined in the text. The equations were put into their linear form and the results analyzed graphically. The slopes and, where non-zero, the intercepts were obtained by least-squares analysis. The errors in the parameters represent the 95% confidence levels (3σ).

Results

Vanadate tends to not react very strongly with amino acids. Products, however, are formed as indicated in Table 1. Apparently, there are three distinct types of products formed with ^{51}V chemical shifts near −525, −545, and −555 ppm. Chemical shifts near these positions are not observed for any of the peptides in this study. The peptides give rise to product NMR signals which are centred near −494, −506, and −511 ppm, depending on the peptide.

Under the conditions of this study, a number of peptides do not yield complexes with vanadate. These peptides fall into three classes. Peptides, which are protected at the *N*-peptide linkage as by the ring in proline or the methyl group of sarcosine do not give product complexes. This was observed for glycylproline and glycylsarcosine. Prolylglycine, however, does provide a product. Also, no products were observed if the terminal NH_2 group was protected with a carbobenzoxy (CBZ) group or if the carboxylate group was protected as the ethyl ester. These observations are in agreement with those of other workers (9).

In order to quantify the formation of the amino acid and peptide complexes it is necessary to take into account the formation of vanadate oligomers. The vanadate tetramer, V_4, in particular serves as a useful reference compound. The formation of the predominant products is represented in eqs. [1] through [3].

$$[1] \quad 4V_1 \overset{K_0}{\rightleftharpoons} V_4 \qquad [V_1]^4K_0 = [V_4]$$

$$[2] \quad 2V_1 \overset{K_1}{\rightleftharpoons} V_2 \qquad [V_1]^2K_1 = [V_2]$$

$$[3] \quad 5V_1 \overset{K_2}{\rightleftharpoons} V_5 \qquad [V_1]^5K_2 = [V_5]$$

It is of importance to establish whether any complexes are formed which are in rapid exchange with vanadate itself so that a time-averaged signal is being observed. This formation is given in eq. [4]. Tetravanadate can be used to examine this

TABLE 2. Formation constants for the vanadate complexes of selected amino acids[a,b]

Amino acid	^{51}V chemical shift	Formation constant	^{51}V chemical shift	Formation constant
Glycine[c]	−523	$0.5 \pm 0.2\ M^{-2}$	−560	$0.13 \pm 0.12\ M^{-1}$
	−546	$0.39 \pm 0.10\ M^{-1}$		
Alanine	−547	$0.19 \pm 0.14\ M^{-1}$	−557	$0.49 \pm 0.08\ M^{-1}$
Serine	−541	$0.75 \pm 0.24\ M^{-1}$	−554	$0.94 \pm 0.04\ M^{-1}$
Arginine			−555	$0.71 \pm 0.12\ M^{-1}$

[a]All formation constants were determined for $\mu = 1.0$ M KCl, pH 7.0, 20 mM HEPES buffer, and variable amounts of added vanadate or added amino acid.

[b]Single NMR spectra of asparagine and valine solutions were obtained and products observed to form. The ^{51}V chemical shifts were −545 and −556 ppm for the asparagine products and −552 ppm for that of valine.

[c]The formation constants determined in this study are two orders of magnitude smaller than those previously reported (10).

possibility so that combination of eq. [1] with eq. [4] and rearrangement gives eq. [5].

$$[4] \quad V_1 + l \overset{K_3}{\rightleftharpoons} Vl \qquad [V_1][l]K_3 = [Vl]$$

$$[5] \quad \frac{[V_1] + [Vl]}{[V_4]^{1/4}} = K_0^{-1/4} + K_0^{-1/4}K_3[l]$$

A graph of the term on the left of this equation versus the equilibrium concentration of the added ligand should give a straight line of intercept $K_0^{-1/4}$ and slope $K_0^{-1/4}K_3$. The possibility of formation of Vl was examined for the amino acids and for a variety of peptides, including glycylglycine, prolylglycine, glycylvaline, and glycylserine.

Of the amino acids studied, only with glycine was there an indication of formation of the Vl product. However, glycine does not give rise to a signal near −555 ppm. It is very likely that the Vl product observed for glycine corresponds to the −555 ppm products, perhaps occurring with the much more intense V_1 signal at −560 ppm by virtue of accidental degeneracy. This seems possible since the product formed with the closely related alanine has a chemical shift of −557 ppm, only 3 ppm from that of V_1. The formation constants that were determined are listed in Table 2. Of the products formed with glycine, the largest formation constant ($0.4\ M^{-1}$) is about a factor of 200 smaller than that determined under similar conditions by an enzyme assay technique (10). The reason for this discrepancy is not clear but the same assay procedure gave formation constants for di- and triglycine complexes which also were larger than those determined in this study; factors of 5 and 35, respectively. It may be that the amino acids or peptides interfere with the enzymic assay procedure. It is worth noting here that 3-hydroxybutanoic acid, ethanolamine, and 1,3-propanediol did not provide observable products which can be assigned to cyclic derivatives although, of course, vanadate esters will be formed at the hydroxyl positions (14).

Figure 1 shows a number of ^{51}V NMR spectra obtained from solutions containing glycylglycine or other peptides. In each case the formation of at least one product clearly is evident. Ligand and vanadate concentrations studies allowed the stoichiometry of the products to be established.

Initial examination of the results according to eq. [5] revealed that a product corresponding to Vl is formed as demonstrated in Fig. 2*A*. From the slope and intercept the constants $K_0^{-1/4} = (2.5 \pm 0.1) \times 10^{-3}\ M^{3/4}$ and $K_3 = 0.34 \pm 0.11\ M^{-1}$ were obtained. Values of K_3 similar to that for glycylglycine were measured for a number of dipeptides. They are given in Table 3 where the products are assigned a chemical shift of −560 ppm. They probably occur at this frequency by virtue of rapid exchange with vanadate. Glycylserine gives rise to the largest value for K_3 ($0.8 \pm 0.3\ M^{-1}$). However, this peptide has a hydroxyl group which will give rise to a vanadate ester with a formation constant of about $0.2\ M^{-1}$ (14). It is evident from these results that the formation of Vl must be taken into account when characterizing the other products.

Variation of the vanadate and ligand concentrations revealed that, for all cases studied, only one peptide and one vanadate were involved in product formation. Product formation can then be represented as in eq. [6] where the product is identified by its ^{51}V chemical shift (PPM) and V_1 is given by $[V_1] = K_0^{-1/4}[V_4]^{1/4}$ to allow for Vl formation or alternatively,

$$[6] \quad V_1 + l \overset{K_4}{\rightleftharpoons} PPM \qquad [V_1][l]K_4 = [PPM]$$

where $V_1 = (V_1 + Vl)/(1 + K_3[l])$. Having obtained V_1, K_4 can readily be obtained by plotting the relevant quantities of eq. [6]. The results obtained for glycylglycine are displayed in Fig. 2*B* from which it is evident that a good linear relationship is obtained. In this graph the open circles derive from fixed ligand studies with variable vanadate concentrations while the solid circles represent variable ligand concentration studies. Table 3 gives the formation constants obtained for the −505 ppm product of glycylglycine and the corresponding values for a number of other dipeptides. These studies with glycylglycine and the other peptides did not completely rule out the possibility of the formation of divanadobisligand products at high ligand concentrations. Such products, if they are formed, must be present in low concentrations for the conditions of this study. In this regard, it should, however, be noted that the studies with prolylglycine revealed some upward curvature in the plots. In view of the results obtained with the other peptides this curvature was attributed to non-ideal behaviour in solution, a result perhaps of attractive interactions between the hydrocarbon rings of different proline entities. Similar observations have been ascribed to based stacking interactions in the nucleoside/vanadate systems (15).

Unlike the other dipeptides studied, glycylserine gives rise to two major products, one occurring at −507 ppm the other at −494 ppm. Ligand and vanadate concentration studies clearly showed a 1:1 stoichiometry for both products. Good

Can. J. Chem. Downloaded from www.nrcresearchpress.com by 84.41.108.74 on 09/07/12
For personal use only.

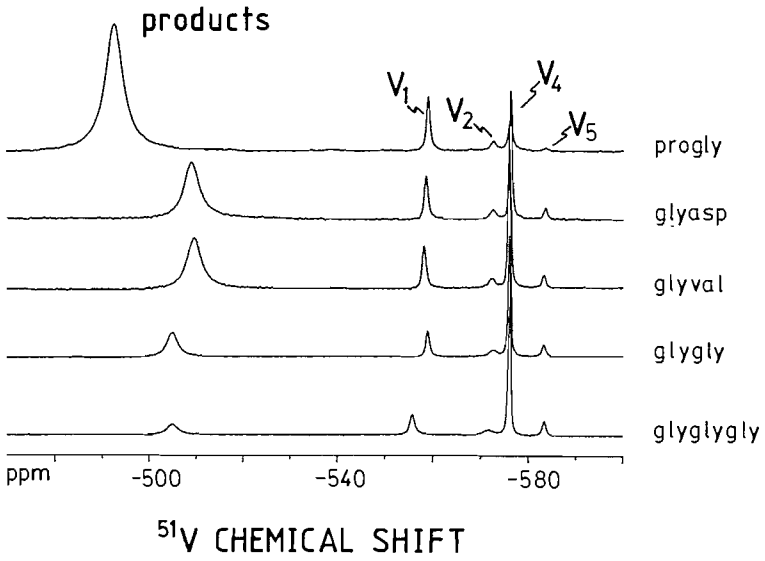


FIG. 1. ^{51}V NMR spectra showing the formation of various peptide complexes of vanadium (V). Conditions of the experiments were 3.0 mM vanadate, 20 mM HEPES buffer, μ = 1.0 M KCl, pH 7.0, 125 mM peptide.

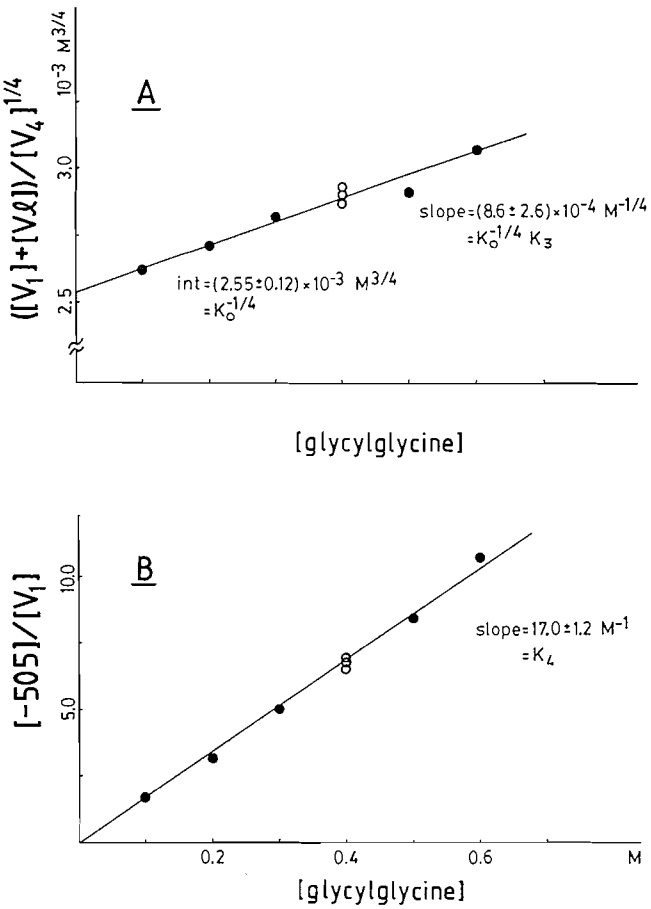


FIG. 2. Graphical display of the formation of glycylglycine/vanadate complexes plotted according to eq. [5] (top) and eq. [6] (bottom). Good linear relationships were obtained. The top graph indicates the presence of a product with an NMR signal occurring under that of vanadate. The bottom graph establishes the V_1l_1 stoichiometry of the −505 ppm product. Conditions of the experiments were pH 7.0, HEPES buffer 20 mM, μ = 1.0 M KCl; variable vanadate concentrations (○); variable glycylglycine concentrations (●).

linear plots were obtained for the products with the equilibrium constants being 7.5 ± 0.8 M^{-1} and 54 ± 3 M^{-1} for the −494 and −507 ppm products, respectively at pH 7.4.

The close correspondence between the −507 ppm signal of the glycylserine product compared to that of glycylglycine at −505 ppm suggests a similar structure for those products. Evidence in support of this was obtained from pH studies which allowed proton stoichiometry to be established. It was necessary to first determine the pK_a values for vanadate and the dipeptide under the conditions of the different pH studies which were 3.0 mM total vanadate, 20 mM HEPES buffer, μ = 1.0 M KCl, variable pH, 125 mM glycylserine or 400 mM glycylglycine. The chemical shift of the vanadate signal can be used to determine the second pK_a of vanadate

$$[7] \quad pH = pK_a + \log\left(\frac{\delta_L - \delta_0}{\delta_0 - \delta_H}\right)$$

according to eq. [7] where δ_0 is the observed chemical shift and δ_L = −560 ppm is the chemical shift of $VO_4H_2^-$ and δ_H = −537 ppm is that of VO_4H^{2-} (16–18). The values determined were 8.06 ± 0.08 and 7.90 ± 0.08, respectively, for the glycylserine and glycylglycine solutions. The first (18) and third (19) pK_a values of vanadate, approximately 3 and 12, respectively, are well outside the range of pH values utilized in this study. The pK_a's of glycylglycine and of glycylserine were determined by titration and found to be 8.1 ± 0.1 and 8.2 ± 0.1, respectively, for the conditions of this study. These pK_a values are for the equilibrium $RNH_3^+ \rightleftharpoons RNH_2 + H^+$ since only this is important for the present study.

Equation [6], when rewritten to take into account proton stoichiometry and the pK_a values of the reactants and products, gives eq. [8], where PPM is used to specify the product of interest by its chemical shift.

When the pH of a 3 mM vanadate 400 mM glycylglycine solution was increased in a stepwise manner from pH 6.5 to 9.5, it was found that product formation was increasingly disfavoured, while for the glycylserine only the formation of the −507 ppm product was disfavoured while the −494 ppm

Can. J. Chem. Downloaded from www.nrcresearchpress.com by 84.41.108.74 on 09/07/12
For personal use only.

Can. J. Chem. Downloaded from www.nrcresearchpress.com by 84.41.108.74 on 09/07/12
For personal use only.

TABLE 3. Formation constants determined for vanadate complexes of some simple peptides

(*a*) pH-dependent formation constants for pH 7.0[a,b]

Peptide	^{51}V chemical shift (ppm)	Formation constant (M^{-1})	^{51}V chemical shift (ppm)	Formation constant (M^{-1})
Glygly[e]	−560	0.34 ± 0.11	−505	17 ± 1
Glyglygly[c]	−560	0.1 ± 0.2	−505	5.0 ± 0.6
Glyasp[e]	−560	0.2 ± 0.4	−509	28 ± 2
Glyval	−560	0.6 ± 0.4	−510	26 ± 2
Valgly[e]			−506	26 ± 9
Valasp			−513	29 ± 3
Progly[e]	−560	0.5 ± 0.2	−493	52 ± 4
Leuleu			−512	65 ± 8
Glyser[c]	−560	0.8 ± 0.3	−507	63 ± 4
	−504	0.4 ± 0.2	−494	2.9 ± 0.8
GlyserOEt[c]	−501	34 ± 4	−494	2 ± 1

(*b*) pH-independent formation constants[a,d]

Equilibrium equation	^{51}V chemical shift	Equilibrium constant
$VO_4H_2^{1-}$ + glygly ⇌ $Vglygly^{1-}$	−505	19 ± 1 M^{-1}
$Vglygly^{1-}$ ⇌ $Vglygly^{2-}$ + H^+	−505	(1.3 ± 1.1) × 10^{-11} M
$VO_4H_2^{1-}$ + glyser ⇌ $Vglyser^{1-}$	−507	72 ± 6 M^{-1}
$Vglyser^{1-}$ ⇌ $Vglyser^{2-}$ + H^+	−507	(4.5 ± 1.1) × 10^{-10} M
$VO_4H_2^{1-}$ + glyser ⇌ $Vglyser^{2-}$ + H^+	−494	(3.3 ± 0.8) × 10^{-7}
$Vglyser^{2-}$ ⇌ $Vglyser^{3-}$ + H^+	−494	(1.5 ± 0.5) × 10^{-10} M
$VO_4H_2^{1-}$ + glyser ⇌ $Vglyser^{2-}$ + H^+	−504	(5.3 ± 0.6) × 10^{-8}
$VO_4H_2^{1-}$ + $glyserOEt^{1+}$ ⇌ $VglyserOEt^{1-}$ + H^+	−504	(2 ± 1) × 10^{-7}
$VO_4H_2^{1-}$ + $glyserOEt^{1+}$ ⇌ $VglyserOEt^{1-}$ + H^+	−501	(39 ± 4) × 10^{-7}

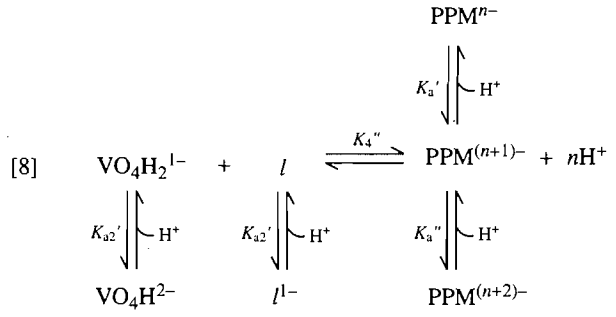
[a]Products are identified by their vanadium chemical shifts and the errors quoted for the formation constants are at the 95% confidence level.

[b]Formation constants are reported for the following conditions: μ = 1.0 M KCl, 20 mM HEPES buffer, pH 7.0, variable vanadate and peptide concentrations.

[c]The values reported were calculated for pH 7.0 from the pH independent formation constants according to eq. [10], the ligand and vanadate concentration studies were done at pH 7.4.

[d]Equilibrium constants were determined under conditions of μ = 1.0 M KCl, 20 mM HEPES buffer, 0.125 M glycylserine or 400 mM glycylglycine and variable pH, from pH 6.5 to 9.6.

[e]Equilibrium constants for solutions containing no added KCl were glygly, 19 ± 2 M^{-1}; glyasp, 21 ± 5 M^{-1}; valgly, 60 ± 3 M^{-1}; progly, 73 ± 5 M^{-1}.



product was initially favoured, then disfavoured at the higher pH levels. The results of the pH study for glycylserine are shown in Fig. 3. This figure clearly reveals a different proton stoichiometry for the −494 and −507 ppm products and also shows that there is an additional product (−504 ppm) formed that apparently has a proton stoichiometry similar to that of the −494 ppm product. Evidently the −494 and −504 ppm products lose a proton as the product is formed while the −507 ppm product does not, thus *n* (of eq. [8]) = 1, 1, and 0, respectively, for the three. The remaining question is whether the product itself has a pK_a near the range of pH values of this study. The formation constant K_4' is related to K_4'' of eq. [8] as shown in eq. [9] where

$$[9] \quad K_4' = K_4''(1 + [H^+]/K_a' + K_a''/[H^+])$$

$K_4' = [PPM]/[VO_4H_2^{1-}][l^0]$ and [PPM] represents the total observed product at that chemical shift. Calculation of this last ratio as a function of pH of the solution revealed that it increased slightly with increase in pH. This suggested that a proton was being lost at high pH, indicating the occurrence of the dissociation K_a'' of eq. [8] so that the term $[H^+]/K_a'$ in eq. [9] can be neglected. A plot of K_4' vs. $1/[H^+]$ gave a line of intercept $K_4'' = 72 \pm 6$ M^{-1} and slope $K_4''K_a'' = (3.2 \pm 0.8) \times 10^{-8}$ for the −507 ppm product and an intercept of $(3.3 \pm 0.8) \times 10^{-7} = K_4''$ and slope of $(4.9 \pm 1.7) \times 10^{-17}$ M $= K_4''K_a''$ for the −494 ppm product. These correspond to the pK_a'' values 9.4 and 9.8, for the −507 and −494 ppm products, respectively. These pK_a values are at the upper limit

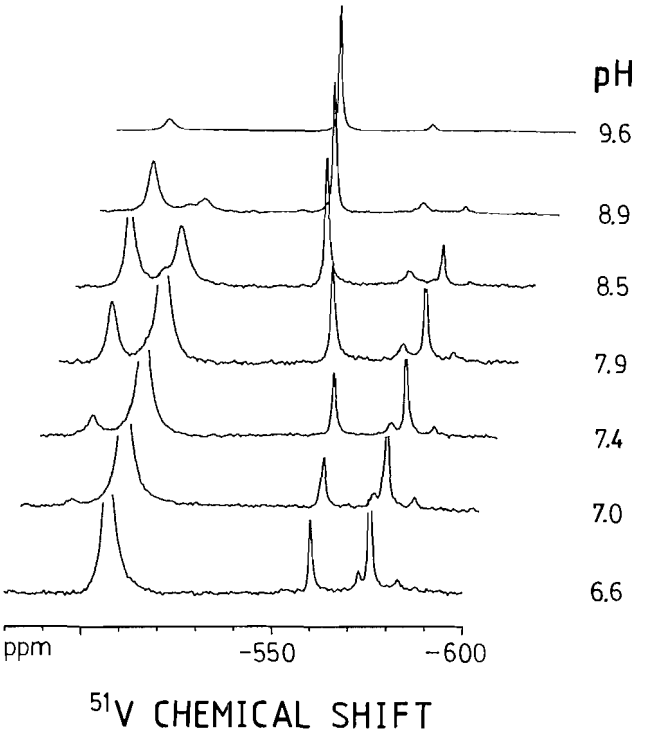


FIG. 3. ^{51}V NMR spectra of the vanadate/glycylserine system showing the dependence of product formation on the hydrogen ion concentration. The signals at −494 and −504 ppm are derived from the involvement of the hydroxymethyl in complex formation and that at −507 ppm results from the utilization of the terminal carboxylate. Conditions of the experiments were 3.0 mM vanadate, 125 mM glycylserine, 20 mM HEPES buffer, μ = 1.0 M KCl, variable pH.

of the pH levels of this study where little or no product is formed. At such high levels both $VO_4H_2^-$ and glyser^0 are lost to VO_4H^{2-} and glyser$^-$ because of their respective pK_a values. An additional proton would have to be given up as the product formed in order for product formation to be maintained. It did not prove possible to obtain a pK_a value for the −504 ppm product. Its value can not be significantly smaller than the pK_a's discussed above, therefore K_4'' can be assumed to be equal to the observed value of $K_4' = (5.3 \pm 0.6) \times 10^{-8}$ for pH values below about 9.

The pH variation studies of the glycylglycine/vanadate complex formation (−505 ppm) revealed that this product had a pH dependence similar to that of the −507 ppm product formed with glycylserine. This suggests a close structural analogy in agreement with very similar chemical shifts. On the other hand, the complexes formed with glycylserineOEt of chemical shifts −484 and −501 ppm had a pH dependence similar to that of the −494 and −504 ppm products formed with glycylserine. Table 3 provides all of the equilibrium constants determined in this study.

The pH independent formation constants, K_4'', of Table 3 can be used to calculate K_4 of eq. [6] for any pH value by utilizing eq. [10] which follows directly from eq. [8] with $n = 0$ or 1. This formula is useful if different equilibrium

$$[10]\quad K_4 = \frac{K_4''(1 + K_a''/[H^+])}{[H^+]^n(1 + K_{a2}/[H^+])(1 + K_{a2}'/[H^+])}$$

studies have not been done at the same pH and a direct comparison is desired. It also provides an internal check on K_4 and K_4'' since these constants are determined in separate experiments utilizing a different procedure.

Discussion

Amino acids undergo rather weak interactions with vanadate to form three types of products with characteristic ^{51}V chemical shifts of about −523, −545, and −556 ppm. The three signals were not observed for all the amino acids studied. Glycine, alanine, and serine gave products at approximately −545 ppm. Only glycine provided an observable signal at −523 ppm while the alanine, serine, and arginine products gave signals at −556 ppm. Although glycine did not give signals near −556 ppm this frequency is close to that of vanadate, −560 ppm, and there may be signal overlap. Utilization of tetravanadate for a reference signal supported this and indicated that the V_1 signal was a composite signal for the case of glycine but not for the other amino acids where a separate signal near −556 ppm was observed.

The stoichiometry established for the products giving rise to the −523, −545, and −556 ppm products was Vl_2, Vl, and Vl, respectively. If the two ligands of Vl_2 complex in a bidentate manner than Vl_2 is probably octahedral. Picolinic acid, a structural analogue of amino acids, gives products with NMR signals at −513 and −529 ppm (20). These apparently correspond to octahedral products. Picolinic acid also gives a product with a ^{51}V chemical shift of −550 ppm. It seems likely that this corresponds to the −545 ppm signals of the amino acids. In the picolinate case the signal was tentatively assigned to a trigonal bipyramidal product. This coordination about vanadate has been found from X-ray studies of the picolinate derivative, $VO_2(pic)(OP(N(CH_3)_2)_3)$ (21). It seems likely that a similar coordination occurs with the amino acids.

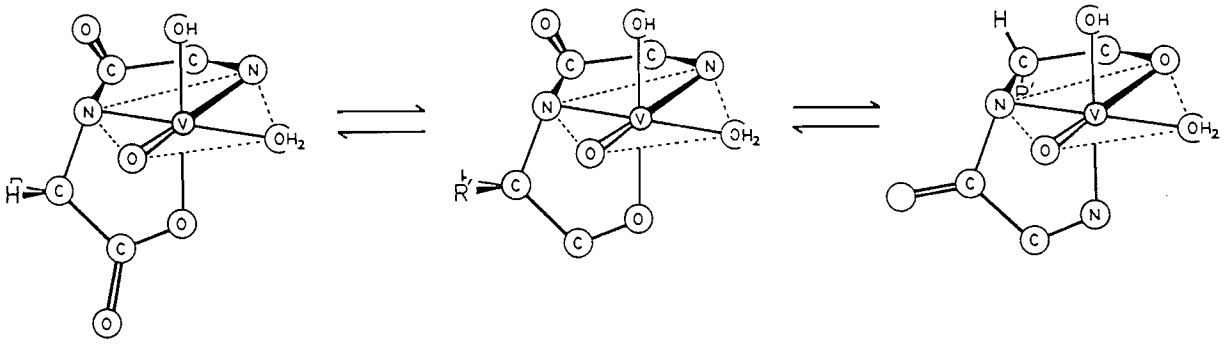
The −556 ppm products possibly derive from anhydride formation with the carboxylate group of the various amino acids. These complexes arise from the acid form of the carboxylate (22). Calculations based on the pK_a of the amino acid and the formation constant determined for acetic acid suggest that the formation constant should be negligibly small ($\sim$0.03 M^{-1}). However, the adjacent ammonium group could well interact positively to stabilize products. On the other hand, the peptides studied also give rise to complexes with formation constants similar to those of the amino acids and chemical shifts which occur with the V_1 signal. It seems more likely then that all these products arise from complex formation with the amino group to give tetrahedrally coordinated products. In any event, with the peptides these are minor products compared to the much more favourable reactions involving the peptides as multidentate ligands.

It is evident from Table 1 that the formation of vanadate peptide complexes follow a simple pattern. Diglycine and triglycine form products, tetraglycine does not, or at best only exceedingly weakly. Protection of either the *N*-terminal or *C*-terminal position prevents complex formation. Furthermore, if the nitrogen of the peptide linkage is substituted as in glycylsarcosine or glycylproline there also is no product formation. In addition, prolylglycine forms a product while glycylglycinamide does not.

Evidently in the absence of functionalized side chains the requirements for complex formations are three-fold: (*1*) a terminal primary or secondary amine, (*2*) an unsubstituted nitrogen in the peptide bond, and (*3*) a carboxylate group.

Non-functionalized sidechains or sidechains which are functionalized at a remote site as in valylaspartate were not ob-

Can. J. Chem. Downloaded from www.nrcresearchpress.com by 84.41.108.74 on 09/07/12
For personal use only.



SCHEME 1

Can. J. Chem. Downloaded from www.nrcresearchpress.com by 84.41.108.74 on 09/07/12
For personal use only.

served to form products additional to those discussed above. The sidechains however, did promote product formation, doubling or trebling the formation constants compared to glycylglycine as is evident from Table 3. Even if the dipeptide has bulky substituents in the sidechains of both of the amino acid residues, as in valylaspartate or leucylleucine, there is no diminution in the formation of products (Table 3). This probably occurs because the sidechain interaction favour a peptide conformation which more readily complexes vanadate. In this respect, preliminary studies of the effect of ionic strength on the equilibria established in these systems suggests that lower ionic strength favours product formation for some, but not all, peptides. The behaviour seems to depend on the presence of sidechains and also may simply be related to changes in conformer populations.

There is no necessity for the carboxylate carbonyl functionality to be present. In glycylserine the sidechain, $—CH_2OH$, provides an alternative to the $—CO_2^-$ as the third functional group necessary for strong complexation to occur. Indeed, two products, in addition to that occurring with the carboxylate functionality, as formed. Furthermore, they are retained when the glycylserine ethylester is utilized instead of glycylserine as the ligand.

The proton requirements for product formation suggest that the different types of ligands coordinate, similarly. The product obtained from glycylglycine (−505 ppm) does not release a proton as products are formed, that from glycylserine (−507 ppm) also does not. These are the products formed from $H_3N^+(—)NH(—)CO_2^-$. Those formed from $H_3N^+(—)NH(—)CH_2OH$ (−494 ppm, −504 ppm) both release protons as complexation occurs. Thus the charge on the complex centre is the same in either case, the extra negative charge on the second set of products derives from a free side-chain carboxylate group and is not present if the glycylserine ethyl ester is the ligand. The pK_a values of the product glycylserine complexes are also similar, being 9.4 for the carboxylate product and 9.8 for the hydroxymethyl-derived product.

Replacement of the peptide hydrogen by an alkyl group prevents product formation. Evidently, this proton is required for water production. Presumably one, if not two, of the ammonium protons are also required for water formation as the final coordination geometry is established. The coordination about vanadate in these peptide complexes is one of conjecture, although octahedral coordination has been proposed (9, 12). Little compelling evidence for this has been presented since the products as well could be trigonal bipyramidal, as proposed for a series of aminoalcohol multidentate ligands (6). Ligand and proton stoichiometry as well as the ability to lose a proton at high pH are consistent with either coordination, the difference between the two coordinations being the presence of an aquo ligand for the octahedral geometry.

Triglycine forms a −505 ppm complex only if neither the amino nor the carboxylate groups are protected while tetraglycine does not yield a product. This suggests that triglycine is acting as a tetradentate ligand. Tetradentate complexation suggests the coordination is octahedral as, for instance, found for the complex formed between ethylenediamine tetraacetic acid and vanadate (23). Perhaps the most compelling evidence for octahedral coordination is the observation of three products with glycylserine. The two involving the hydroxymethyl are separated by 10 ppm (−494 and −504 ppm). The product utilizing carboxylate (−507 ppm) is only separated by 3 ppm from the −504 ppm product. These chemical shifts suggest a close structural correspondence between the various products.

The orientation of the carboxylate and amide groups in octahedral geometry can be expected to be strongly directed by the electronic factors deriving from the V=O bond, the tendency being towards a 90° orientation (see ref. 24 for a compilation of structures). This would lead to a single product since proton transfer between —OH and $—OH_2$ will be rapid. Actually, with glycylserine two products could be formed because of the asymmetric centre. However, since the coordination at the vanadium will be virtually identical in either case, the ^{51}V chemical shift separation would be expected to be small and not observable, perhaps contributing to the linewidth of several ppm. When the complex forms with the hydroxyl group of the hydroxymethyl rather than with the carboxylate, the strong directing influence of the V=O will be absent and the hydroxyl groups could complex in either a 90 or 180° orientation. Scheme 1 depicts a simple equilibrium scheme based on the above arguments. Interestingly enough, inspection of molecular models indicates that sterically the ethyl ester of glycylserine will favour a peptide conformation in which the $—CH_2OH$ is rotated to the position normally occupied by the $—CO_2^-$. The large increase in the formation constant of the −504 ppm product (a factor of 100) is in accord with this, and by implication, the carboxylate and hydroxymethyl groups occupy structurally similar positions in the product complexes as depicted in Scheme 1.

It is not possible to form three trigonal bipyramidal products since the three rings produced in each product are all 5-membered and too small to accommodate the 120° angle required for an equatorially oriented ring. However, trigonal bipyramidal geometry can not be completely ruled out. The 10–12 ppm separation in chemical shift between the two

types of products may represent a difference in coordination geometry rather than the difference in ligand orientation in Scheme 1. This could explain the observation that the rotationally restricted prolylglycine gives a product at −494 ppm (see Table 2). More likely though, this +10 ppm shift compared to glycylglycine is a result of complexing a secondary rather than a primary nitrogen. In support of this, it has been observed that the chemical shift of the complex formed with the tertiary amine, *N*-methyldiethanolamine, is shifted +7 ppm with respect to that formed with diethanolamine (6).

It is evident from this work that complexation of vanadate by serum albumins and other proteins can not occur by random binding at accessible peptide linkages since in the absence of both terminal amino and carboxylate groups no complexation occurs. These requirements are for the simple peptides and can be bypassed if an amino acid segment which is accessible to vanadate contains an appropriately functionalized sidechain as in glycylserine and other peptides (8, 11, 12). Clearly, different sidechain substituents will apply different constraints to complex formation and this is a topic of continuing interest. In the systems investigated here, no evidence for complexation by vanadate oligomers was obtained and this also points out the importance of extending studies similar to this to more complex peptides.

Acknowledgements

Thanks are gratefully extended to the Medical Research Council of Canada for its financial support of this work.

1. M. J. GRESSER and A. S. TRACEY. *In* Vanadium in biological systems. *Edited by* N. D. Chasteen. Kluwer Academic Publishers, Dordrecht, Boston, London. 1990. p. 63–79.
2. M. J. GRESSER, A. S. TRACEY, and P. J. STANKIEWICZ. Adv. Prot. Phosphatases **4**, 35 (1987).
3. N. D. CHASTEEN, J. K. GRADY, and C. E. HOLLOWAY. Inorg. Chem. **25**, 2754 (1986).
4. S. M. ASHRAF and W. U. MALIK. J. Inorg. Biochem. **35**, 1 (1989).
5. W. R. HARRIS. Biochemistry, **24**, 7412 (1985).
6. D. C. CRANS and P. K. SHIN. Inorg. Chem. **27**, 1797 (1988).
7. A. S. TRACEY and M. J. GRESSER. Inorg. Chem. **27**, 1269 (1988).
8. A. S. TRACEY and M. J. GRESSER. Proc. Natl. Acad. Sci. USA, **83**, 609 (1986).
9. D. REHDER. Inorg. Chem. **27**, 4312 (1988).
10. D. C. CRANS, R. L. BUNCH, and L. A. THEISEN. J. Am. Chem. Soc. **111**, 7597 (1989).
11. D. REHDER, H. HOLST, R. QUAAS, W. HINRICHS, U. HAHN, and W. SAENGER. J. Inorg. Biochem. **37**, 141 (1989).
12. D. REHDER. *In* Vanadium in biological systems. *Edited by* N. D. Chasteen. Kluwer Academic Publishers, Dordrecht, Boston, London. 1990. pp. 173–197.
13. R. W. HAY and M. P. PUJARI. Inorg. Chim. Acta, **123**, 47 (1986).
14. A. S. TRACEY, B. GALEFFI, and S. MAHJOUR. Can. J. Chem. **66**, 2294 (1988).
15. A. S. TRACEY and C. H. LEON-LAI. Inorg. Chem. In press.
16. A. S. TRACEY, M. J. GRESSER, and K. M. PARKINSON. Inorg. Chem. **26**, 629 (1987).
17. A. S. TRACEY, J. S. JASWAL, M. J. GRESSER, and D. REHDER. Inorg. Chem. **29**, 4283 (1990).
18. E. HEATH and O. W. HOWARTH. J. Chem. Soc. Dalton Trans. 1105 (1981).
19. L. PETTERSSON, B. HEDMAN, A.-M. NENNER, and I. ANDERSSON. Acta Chem. Scand. A**39**, 499 (1985).
20. B. GALEFFI and A. S. TRACEY. Inorg. Chem. **28**, 1726 (1989).
21. H. MIMOUN, L. SAUSSINE, E. DAIRE, M. POSTEL, J. FISCHER, and R. WEISS. J. Am. Chem. Soc. **105**, 3101 (1983).
22. A. S. TRACEY, H. LI, and M. J. GRESSER. Inorg. Chem. **29**, 2267 (1990).
23. W. R. SCHEIDT, R. COUNTRYMAN, and J. L. HOARD. J. Am. Chem. Soc. **93**, 3878 (1971).
24. C. E. HOLLOWAY and M. MELNIK. Rev. Inorg. Chem. **7**, 75 (1985).

Can. J. Chem. Downloaded from www.nrcresearchpress.com by 84.41.108.74 on 09/07/12
For personal use only.

Infrared intensities of liquids VIII. Accurate baseline correction of transmission spectra of liquids for computation of absolute intensities, and the 1036 cm^{-1} band of benzene as a potential intensity standard

JOHN E. BERTIE and C. DALE KEEFE

Department of Chemistry, University of Alberta, Edmonton, Alta., Canada T6G 2G2

AND

R. NORMAN JONES

Steacie Institute for Molecular Sciences, National Research Council of Canada, Ottawa, Ont., Canada K1A 0R6

Received May 30, 1991

JOHN E. BERTIE, C. DALE KEEFE, and R. NORMAN JONES. Can. J. Chem. **69**, 1609 (1991).

FT-IR transmission spectra of liquids in well-made and firmly held cells with KBr or NaCl windows are usually very reproducible except that their baselines often show unexpected variations. To obtain absolute absorption intensities from these spectra such baseline differences must be corrected. The problem is illustrated with absorbance spectra of the 1036 cm^{-1} band of benzene and the absorption index spectra calculated from them via the National Research Council of Canada program 46. Distinction is made between the experimental absorbance spectrum, the ideal experimental absorbance spectrum, and the absorbance spectrum, and a soundly-based method to correct the baselines is presented. We describe a modification of the NRC program 46 that effects the correction and calculates, on a laboratory computer, the complex refractive indices from a transmission spectrum of a liquid.

The method is applied to 15 transmission spectra of the 1036 cm^{-1} band of benzene. It improves the agreement between the 15 peak absorption index values obtained from these spectra from 4% to 2.5%, and improves the agreement between the baseline absorption index values from 5% to 0.01%, all percentages being of the peak value. A table of the average real and imaginary refractive indices and molar absorption coefficients is given. The average peak absorption index value and the area under the band agree closely with those obtained in 1980, and with earlier values from transmission or ATR measurements. These areas are all distinctly lower than those calculated from early measurements of dispersion. These results form the basis for a possible recommendation to the International Union of Pure and Applied Chemistry for a secondary intensity standard. We encourage others to measure this band to help ascertain that systematic errors do not significantly influence our results.

To summarise our numerical results at 25 ± 1°C and 1.0 cm^{-1} nominal resolution: The average peak absorption index is 0.0710 with a 95% confidence limit of 0.0004, which is within 0.0001 of the less precise value measured in 1980 with a dispersive instrument that was calibrated against a primary intensity standard. The area under the absorption index band between 1095.8 and 912.6 cm^{-1} is 1.358 cm^{-1} with a 95% confidence limit of 0.009 cm^{-1}, and that under the molar conductivity band is 3.69 ± 0.03 km/mol. These areas convert to 15.64 ± 0.1 km/mol and 6.79 ± 0.05 km/mol for the more commonly used measures of integrated absorption, the areas under the Naperian and decadic molar absorption coefficients, respectively.

Key words: infrared, absorption intensity, optical constants, FT-IR spectroscopy, benzene (liquid), intensity standard.

JOHN E. BERTIE, C. DALE KEEFE et R. NORMAN JONES. Can. J. Chem. **69**, 1609 (1991).

Les spectres de transmission IR-TF des liquides dans des cellules bien faites et bien fermées, avec des fenêtres de KBr ou de NaCl, sont généralement très reproductibles, à l'exception du fait que leurs lignes de base donnent souvent lieu à des variations inattendues. Afin d'obtenir des intensités d'absorption absolues à partir de tels spectres, ces différences dans les lignes de base doivent être corrigées. Le problème est illustré par le spectre d'absorption de la bande à 1036 cm^{-1} du benzène et du spectre d'indice d'absorption calculé à partir de ceux-ci par le biais du programme 46 du Conseil National de Recherches du Canada. On fait un distinction entre le spectre d'absorption expérimental, le spectre d'absorption expérimental idéal, et le spectre d'absorption et on présente une méthode bien fondée pour corriger les lignes de base. On décrit un modification du programme 46 du CNRC qui effectue la correction et qui calcule, sur un ordinateur de laboratoire, les indices de réfraction complexes à partir d'un spectre de transmission d'un liquide.

On a appliqué la méthode à 15 spectres de transmission de la bande du benzène à 1036 cm^{-1}. On peut ainsi améliorer de 4% à 2,5% la correspondance entre les valeurs des indices d'absorption des bandes obtenues à partir de ces spectres et on améliore aussi de 5% à 0,01% la correspondance entre les valeurs de l'indice d'absorption de la ligne de base; tous les pourcentages sont relatifs à la valeur maximale. On rapporte une table des valeurs moyennes réelles et imaginaires des indices de réfraction et des coefficients molaires d'absorption. La valeur de l'indice moyen d'absorption du pic ainsi que la surface sous la bande sont en bon accord avec les valeurs obtenues en 1980 et avec des valeurs antérieures obtenues à partir de mesures de transmission ou de ATR. Ces surfaces sont plus basses que celles calculées antérieurement sur la base de mesures de dispersion. Ces résultats forment la base d'une recommandation potentielle à l'Union Internationale de Chimie Pure et Appliquée pour un étalon secondaire d'intensité. On invite les autres chercheurs à mesurer cette bande afin de s'assurer que des erreurs systématiques n'influencent pas nos résultats d'une façon importante.

Pour résumer nos résultats numériques à 25 ± 1°C et 1,0 cm^{-1} résolution nominale, l'indice d'absorption moyen du pic est égal à 0,0710 avec une limite de confiance de 95% de 0,0004; cette valeur à 0,0001 de la valeur moins précise mesurée en 1980 à l'aide d'un instrument de dispersion qui avait été calibré à l'aide d'un étalon primaire d'intensité; la surface sous la bande d'indice d'absorption qui s'étend de 1095,8 à 912,6 cm^{-1} est égale à 1,358 cm^{-1} avec une limite de confiance de 95% de 0,009 cm^{-1} et cette sous la band de conductivité molaire est égale à 3,69 ± 0,03 km/mol. Ces surfaces correspondent à 15,64 ± 0,1 km/mol et 6,79 ± 0,05 km/mol pour les mesures plus couramment utilisées pour l'absorption intégrée, respectivement les surfaces sous les coefficients molaires d'absorption napériens et décadiques.

Mots clès : infrarouge, intensité d'absorption, constantes optiques, spectroscopie IR-TF, benzène (liquide), étalon d'intensité.

[Traduit par la rèdaction]

Can. J. Chem. Downloaded from www.nrcresearchpress.com by 84.41.108.74 on 09/07/12
For personal use only.

Can. J. Chem. Downloaded from www.nrcresearchpress.com by 84.41.108.74 on 09/07/12
For personal use only.

Introduction

In work reported in earlier papers in this series about 5 years ago (1–3) we recorded transmission spectra of liquid benzene at 25°C and converted them to imaginary refractive index spectra using methods developed in the 1970s by Jones and coworkers (4–11). Our objective was to determine whether our FT-IR spectrometer, which had not been calibrated for intensity accuracy, gave the same absolute intensitiés at the peaks of the imaginary refractive index bands as had been found by Goplen, Cameron, and Jones (4) using a dispersive infrared spectrometer which was calibrated using the primary standard provided by rotating sectors. For the 1036 cm^{-1} band of benzene, the average of all our measurements gave (1, 2) the maximum value of $k(\tilde{\nu})$, the imaginary refractive index, equal to 0.0718, with a 90% confidence limit of 0.0004, at 1036.0 cm^{-1}, compared with 0.0711 with an estimated error (4, 5) of 0.0014 given by Goplen, Cameron, and Jones. Our measurements were made at 1 cm^{-1} nominal resolution (in fact 0.8 cm^{-1} resolution with the triangular apodisation function that was used (1, 2)). The measurements of Goplen, Cameron, and Jones (4) were made at 0.7 to 1.0 cm^{-1} resolution.

Our earlier calculations (1–3) were done on a mainframe computer using the programs 22, 45, and 46 from the National Research Council of Canada Bulletins "Computer programs for infrared spectrophotometry" (10, 11), and the imaginary refractive indices were obtained from numerical computer output lists. No provision existed at that time for superimposing all of the input absorbance spectra or all of the output $k(\tilde{\nu})$, spectra for visual comparison.

Since then we have connected the Aspect 2000 computer on our Bruker IFS 113V spectrometer to a Dell System 220, a computer which runs Microsoft DOS, and we can transfer our spectra and manipulate them using Spectracalc (Galactic Industries Corporation, Salem, New Hampshire, U.S.A.). Spectracalc allows, *inter al,* many spectra to be loaded and compared on the monitor. Comparison of many experimental spectra, and of the imaginary refractive index spectra calculated from them, revealed that baseline inconsistencies existed in the experimental spectra (1, 2) that were not fully corrected by the NRC program 46 which transformed the experimental spectra to imaginary refractive index spectra.

In the present paper we describe how the Bruker 113V spectrometer is connected to our DOS computer and how the baseline inconsistencies in the absorbance spectra may be removed with confidence. We report here what we now believe to be the best imaginary refractive index spectrum and the best molar absorption coefficient spectrum of the 1036 cm^{-1} band of benzene. The average peak intensity from these spectra agrees to within 0.2% with the less precise result (4) that was estimated (5) via rotating sector calibration to be accurate to better than ±2%.

At the end of the paper, we summarise a procedure and a Fortran computer program that can be conveniently used on a computer running the DOS operating system with a 16 MHz Intel 80286 or 80386 cpu, preferably with a math co-processor, to correct an experimental absorbance or transmission spectrum of a full liquid cell for baseline and reflection effects. Reliable absolute intensity data may be obtained if such corrected spectra are accompanied by an absorbance or transmission spectrum of the same cell empty which shows the interference fringes due to multiple reflections between the windows from which the sample thickness can be calculated. The procedure described is of general use, but will be particularly applied in these laboratories to the establishment of infrared secondary intensity standards, under the IUPAC program described elsewhere (12). The potential use of the 1036 cm^{-1} band of benzene as a secondary standard of infrared intensity is discussed.

The absolute intensity may be described by the imaginary refractive index, $k(\tilde{\nu})$, which is more briefly called the absorption index (13, 14). It may be equally well described by any other equivalent measure of absorption intensity, including the quantity usually preferred by chemists, the molar absorption coefficient, $E_m(\tilde{\nu})$. This is more properly (13, 14) called the molar decadic absorption coefficient, to indicate the use of the decadic logarithm, and is defined as

$$E_m(\tilde{\nu}) = (Cd)^{-1}\{-\log_{10}[I_t(\tilde{\nu})/I_o(\tilde{\nu})]\}$$

where C is the molar concentration and d is the pathlength. This paper uses these quantities as well as the linear (decadic) absorption coefficient, which is defined (13, 14) as

$$K(\tilde{\nu}) = d^{-1}\{-\log_{10}[I_t(\tilde{\nu})/I_o(\tilde{\nu})]\}$$

Method

Data transfer and format

The Aspect 2000 computer of our Bruker 113V FT-IR spectrometer communicates with the Dell system 220 computer through its ports for the high-speed-paper-tape punch and reader. A digital direct memory access interface card (model PDMA–16 from the Metrabyte Corporation, Taunton, MA, U.S.A.) was fitted to the Dell computer to allow it to communicate with the Aspect, and the two computers are linked by a 60 ft long, 40 conductor cable. The data transfer is controlled by the programs ASTOPC for the Dell and the Aspect computers. A data file of 6000 points transfers in about 2 s. This system was developed for the aspect 2000 and Aspect 3000 computers in the Chemistry Department at the University of Alberta by R. E. D. McClung and G. Bigam. The software is available from Professor McClung.

The spectra are transferred as Bruker ".DATA" files in the "ATS" data format, and are imported into Spectracalc as ".SPC" files via a data converter supplied by Galactic Industries Corporation. The programs we use can read and write the Spectracalc ".SPC" files, and can also read and write the ASCII ".Y" files which contain, in sequence, the first wavenumber, the last wavenumber, the number of points, and the ordinate values.

The NRC programs 22 (10), 45 (11), and 46 (11) were modified in this laboratory to provide this facility under the names RNJ22A, RNJ45A, and RNJ46A. The Kramers–Kronig transform routine in NRC program 46 (11) was modified to increase its speed and to incorporate the MacLaurin formula method of handling the singularity that has been described by Ohta and Ishida (15). Details of this modification will be published elsewhere (16).

Absorbance spectra, apparent absorbance, experimental absorbance spectra, and ideal experimental absorbance spectra

The problem in detail

An experimentalist usually obtains an absorbance spectrum of a cell full of liquid by measuring the transmission spectrum of the full cell relative to the empty sample compartment and taking the negative decadic logarithm of the transmittance. In FT-IR spectroscopy, this is usually done by recording separate intensity spectra, which were traditionally called single beam

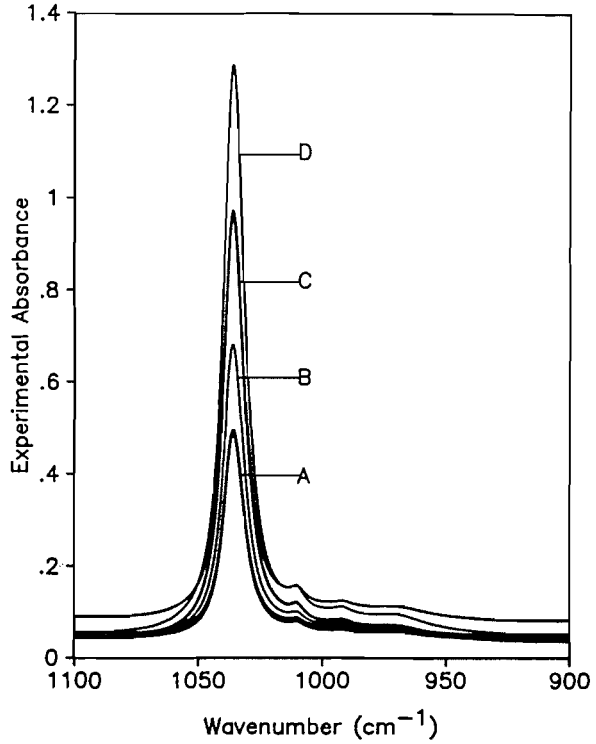


FIG. 1. Experimental absorbance spectra of C_6H_6(l) in cells with KBr or NaCl windows; 25°C and 1 cm^{-1} resolution. The number of spectra in each of the four groups of spectra labelled A to D and the approximate liquid layer thickness for each group are Group A, six spectra, 11 μm; Group B, one spectrum, 15 μm; Group C, seven spectra, 23 μm; Group D, one spectrum, 33 μm.

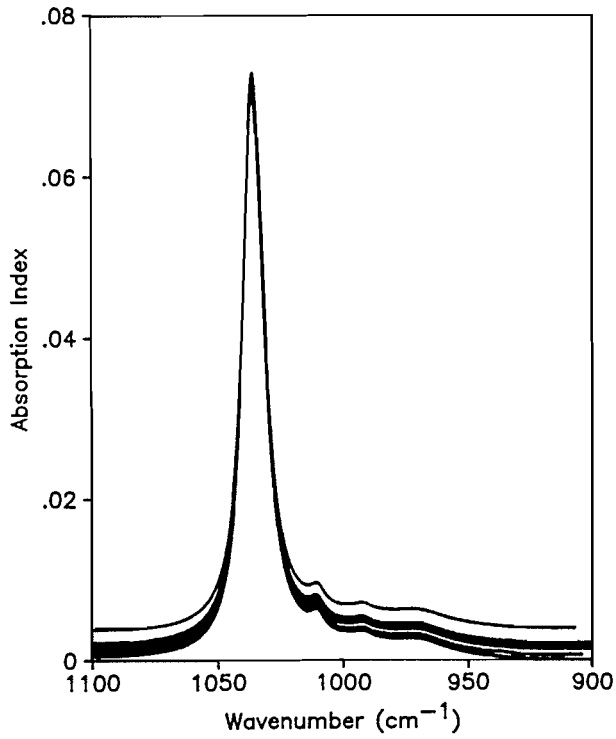


FIG. 2. The 15 absorption index spectra (imaginary refractive index spectra) calculated from the 15 spectra in Fig. 1.

spectra, of the full cell and of the empty sample compartment, ratioing them, and taking the negative logarithm. On a double-beam dispersive instrument, it is done by recording the spectrum of the full cell relative to that of the empty reference beam, and taking the negative logarithm.

It is important to note that neither method yields the absorbance spectrum as it is currently defined by IUPAC (13, 14). IUPAC defines *absorbance* to be a measure of the energy loss due only to absorption by the sample (13, 14). Absorbance does not include the energy loss due to reflection effects at the inner and outer window surfaces, nor does it include background energy loss due to attenuation by the cell or other mechanism. For this reason, we use the term *experimental absorbance spectrum* for the spectrum the experimentalist obtains by either of the above methods. We reserve the term *absorbance spectrum* for the spectrum that has been fully corrected for background effects and reflection losses so that it contains only the loss due to absorption. We use the term *apparent absorbance* for contributions to the experimental absorbance from effects other than absorption.

The *experimental absorbance* is, thus, the sum of the *absorbance* and the *apparent absorbance* due to reflection effects and other sources of energy loss.

Experimental absorbance spectra of liquid benzene and the absorption index, $k(\tilde{\nu})$, spectra calculated from them are shown in Figs. 1 and 2. These spectra are those reported earlier (1, 2), and will be further explored in this paper. Fifteen experimental absorbance spectra recorded in cells of four different path lengths are shown in Fig. 1. The inconsistencies in the baselines are clear, because the curves cross. In particular, two of the curves of set C clearly have very high baselines.

The NRC program 46, which transformed the experimental absorbance spectra to the $k(\tilde{\nu})$ spectra, corrects for reflection effects at the inner and outer window surfaces under certain ideal assumptions (7, 11) about the light beam, including the assumption of 90° incidence. All apparent absorbance due to reflection effects under these ideal assumptions should have been eliminated by the transformation of the experimental absorbance spectra to the $k(\tilde{\nu})$ spectra by the program, as should all effects of the different pathlengths. Thus the 15 spectra in Fig. 2 would be superimposed if the experimental absorbance spectra were recorded under the ideal conditions assumed by the NRC program 46. We define *ideal experimental absorbance spectra* as experimental absorbance spectra recorded under the ideal conditions assumed by NRC program 46.

The absorption index spectra, $k(\tilde{\nu})$ spectra, in Fig. 2 show the magnitude of the error. There is a spread at the peak of 4% and a spread at the baseline of 5%, both percentages of the peak k value. The spread at the baseline must result from differences between the real experimental conditions and the ideal ones assumed by the program, *i.e.* from differences between the experimental absorbance spectra and the ideal experimental absorbance spectra.

Differences in the baseline can arise from a variety of sources. A gross error occurs if the metal of the window holder blocks part of the beam. But even when, as usual, this is avoided, the angle of incidence of the infrared beam is very important, because marked variations are seen unless the cell is held very firmly in the infrared beam, and its position is very reproducible each time it is placed in the beam.

In the experiments we reported earlier (1, 2), the liquid cell was held by a leaf-spring in a massive brass holder which was pinned into holes in the bottom of the sample compartment.

Can. J. Chem. Downloaded from www.nrcresearchpress.com by 84.41.108.74 on 09/07/12
For personal use only.

This ensured that the position of the cell was very reproducible each time it was inserted, much more reproducible than is provided by the cell holders supplied by most manufacturers. This improved the reproducibility of the spectra immensely, but the baseline variations evident in Figs. 1 and 2 resulted in spite of this. We speculated (2) that they may arise from differences in the exact position of the infrared beam in the sample compartment each time the interferometer module is aligned which cause small differences in the angle of incidence.

The solution

Whatever be the source of the baseline variations, the position of the baseline in the ideal experimental absorbance spectrum can be calculated accurately. Thus the spurious, or non-ideal, contribution to the experimental baseline can be calculated and removed from the experimental absorbance spectrum with good accuracy, to yield the ideal experimental absorbance spectrum.

The apparent absorbance due to reflection effects under the ideal conditions of NRC program 46 can be calculated via the logic of program 46. We call this the *ideal apparent absorbance.*

The ideal experimental absorbance is simply the sum of the ideal apparent absorbance and the absorbance of the sample.

The absorbance of the sample in a cell of known pathlength can be calculated for the spectral regions of very weak absorption if the linear absorption coefficient, $K(\tilde{\nu})$, of the sample is known for these regions. The linear absorption coefficient can be found from measurements using long pathlength cells for which the absorbance of the sample in these regions of very weak absorption sufficiently exceeds the apparent absorbance due to non-ideal effects that the latter can be neglected.

The ideal experimental absorbances in the wings of the band, at one wavenumber on each side of the band, are then calculated as the sum of the absorbance of the sample and the ideal apparent absorbance at these wavenumbers.

The differences between the experimental absorbances and the ideal experimental absorbances at these two wavenumbers are the desired corrections to the baseline at these two wavenumbers. The correction to the baseline at other wavenumbers is obtained as a straight line through these two points, yielding a linear correction spectrum.

The correction spectrum is subtracted from the experimental absorbance spectrum to yield the ideal experimental absorbance spectrum.

The ideal experimental absorbance spectrum is then converted to the absorption index spectrum via NRC program 46.

Results

The detailed solution

Calculation of the ideal apparent absorbance

The ideal apparent absorbance is the absorbance due to reflection effects in a transmission cell full of liquid under the ideal assumptions described by Jones and colleagues (7) in eq. [26] of their paper. These assumptions are normal incidence for the central ray, optically flat windows, and uniform intensity distribution across the beam.

It is noteworthy, in passing, that the intensity distribution across the beam is not an important factor. This is shown by using program 46 to calculate the optical constants for different values of the half-cone angle of the convergent light in the focussed beam. The calculated results are the same to better than 0.1% for half-angles of 5.5°, as on our Bruker 113V spectrometer, and for 0°. This could not be so if the spatial intensity distribution across the beam was important.

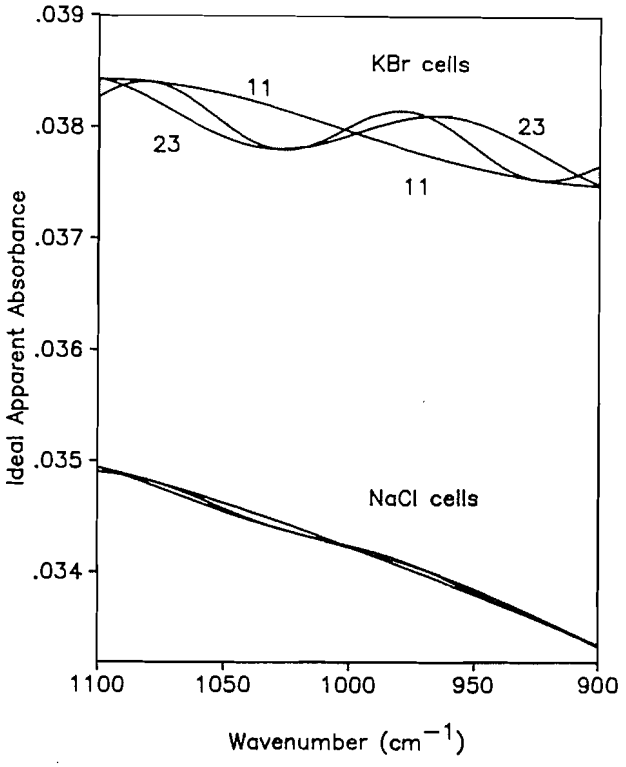


FIG. 3. Ideal apparent absorbance calculated by program Baseline for cells full of benzene. The window materials are shown and the pathlengths 11, 23, and 33 μm were used for each window material.

The Fortran programming to calculate the ideal apparent absorbance is provided as part of NRC program 46, and was extracted by us into a program BASELINE. The programs use the wavenumber-dependent real refractive index of the window material. They assume that the windows are sufficiently thick that interference fringes from within the windows are too closely spaced to be resolved, so that the effect of the multiple reflection can be calculated by neglecting the phases of the multiply reflected rays in each window (7).

The programs correctly calculate the interference fringes caused by multiple reflection within the thin liquid layer. For calculation of the baseline, absorption by the liquid was ignored, by assuming the absorption indices to be zero at all wavenumbers, and the real refractive index of the liquid was assumed constant at its value at the high wavenumber limit of the band. For the 1036 cm^{-1} band of benzene, the value at 1100 cm^{-1} was used, with $n = 1.475$.

Figure 3 shows the spectral baselines, i.e., the ideal apparent absorbance spectra, calculated by program BASELINE for benzene in cells fitted with KBr windows or with NaCl windows. The refractive index discontinuity at the window–benzene interface is so small that the amplitude of the interference fringes is small. It is clear that the baseline one would obtain by neglecting the fringes decreases in apparent absorbance from 1100 to 900 cm^{-1}. This is because the refractive indices of KBr (17, 18) and NaCl (19, 20) are larger at 1100 cm^{-1} than at 900 cm^{-1}, as is shown in Table 1. Table 1 also contains the numerical ideal apparent absorbances at 1100 and

Can. J. Chem. Downloaded from www.nrcresearchpress.com by 84.41.108.74 on 09/07/12
For personal use only.

TABLE 1. Infrared refractive index and apparent absorbance due to reflection effects for KBr and NaCl windows

	KBr windows		NaCl windows	
Wavenumber (cm^{-1})	1100	900	1100	900
Refractive index of windows				
	1.5282	1.5239	1.5006	1.4870
Apparent absorbance for pathlength				
(*a*) From BASELINE				
11 μm	0.0384	0.0375	0.0349	0.0333
23 μm	0.0384	0.0375	0.0349	0.0333
33 μm	0.0383	0.0377	0.0349	0.0333
(*b*) From eq. [1]				
Any pathlength	0.0379	0.0374	0.0348	0.0333

900 cm^{-1} for the KBr and NaCl windows and cells 11, 23, and 33 μm thick.

Alternatively this information can be obtained, with slightly lower accuracy, without invoking program BASELINE. To an accuracy of better than 0.0005 the ideal apparent absorbances calculated at 1100 and 900 cm^{-1} equal those expected from a single window in air. If the interference fringes are averaged by summing over the multiple reflections, the formulae for the apparent transmittance, $T = I_t/I_o$, at normal incidence which result from this treatment are (eq. [12] in ref. 7)

$$[1] \quad T = (1 - R)/(1 + R)$$

where $R = (n - 1)^2/(n + 1)^2$, therefore $T = 2n/(n^2 + 1)$. The ideal apparent absorbance due to these reflection losses is $-\log_{10}\{T\}$.

The values calculated from these equations are independent of the cell thickness. Equation [1] yields the ideal apparent absorbances shown at the bottom of Table 1. The agreement between these and the more accurate values given by program BASELINE ranges from 0.0001 to 0.0005.

The linear absorption coefficient of the liquid in the wings of the band

The true absorbance of the liquid at the extremes of a band is found from spectra of a liquid layer sufficiently thick that neglect of possible baseline inconsistencies has an acceptably small effect.

Figure 4 shows experimental absorbance spectra of benzene in nominally 500 μm thick KBr cells. The top spectrum, for example, was recorded in a 506.7 μm cell and shows experimental absorbances at 1095.8 and 912.2 cm^{-1} of 0.3430 and 0.3215. From program BASELINE, the ideal apparent absorbances are 0.0383 and 0.0376 at 1095.8 and 912.2 cm^{-1}. With the neglect of possible baseline inconsistencies, the difference between these two quantities at each wavenumber gives the absorbances of benzene as 0.3047 and 0.2839, and the *absorbances per cm path,* i.e., the linear absorption coefficients, as 6.01 cm^{-1} and 5.60 cm^{-1}. In fact, the average of 11 such spectra in 500 and 780 μm cells gave the linear absorption coefficients at 1095.8 and 912.2 cm^{-1} equal to 6.01 cm^{-1} and 5.57 cm^{-1} with 95% confidence limits of 0.09 cm^{-1}.

Ideal experimental absorbance, absorbance, and absorption index spectra

Table 2 summarises the calculation of the ideal experimental absorbances at 1095.8 and 912.2 cm^{-1} of a KBr cell full of 23 μm thickness of liquid benzene. The absorbance at 1095.8 cm^{-1} of a benzene layer 23.0 μm thick is $(6.01 \pm 0.09) \times 10^{-4}$ $\mu m^{-1} \times 23.0$ μm = 0.0138 ± 0.0002. The ideal apparent absorbance at 1095.8 cm^{-1} of a KBr cell filled with 23 μm thickness of benzene is 0.0384 ± 0.0001 from program BASELINE. The ideal experimental absorbance at 1095.8 cm^{-1} of this cell is the sum of these two numbers, 0.0522 ± 0.0003. At 912.2 cm^{-1}, the corresponding numbers are $(5.57 \pm 0.09) \times 10^{-4}$ $\mu m^{-1} \times 23.0$ μm = 0.0128 ± 0.0002, 0.0376 ± 0.0001 from BASELINE, and 0.0504 ± 0.0003.

Thus the ideal experimental absorbance at the extreme of the band can be calculated with a precision of about 0.6%.

The differences between these ideal experimental absorbances and the experimental absorbances must be removed before NRC program 46 is used.

To correct the experimental absorbance spectra to ideal experimental absorbance spectra, a straight line was interpolated between the differences found at 1095.8 and 912.2 cm^{-1} and was subtracted from the experimental absorbance spectrum. Program BASECORR performed this correction. The 15 ideal experimental absorbance spectra which resulted from this procedure are shown in Fig. 5, which should be compared with Fig. 1 to see the effect of the corrections.

The ideal experimental absorbance spectra were processed by our program RNJ46A to convert them to refractive index spectra by an iterative procedure (11). Once the absorption index spectrum is obtained, the true absorbance spectrum can be calculated from it by

$$\mathrm{Abs}(\tilde{\nu}) = \frac{4\pi\tilde{\nu}k(\tilde{\nu})d}{2.303}$$

Figure 6 shows for one sample the experimental absorbance spectrum, the ideal experimental absorbance spectrum, and the absorbance spectrum of benzene, the latter showing only energy loss due to absorption if our ideal assumptions are correct.

The absorption index spectra are shown in Fig. 7. They should be compared with those in Fig. 2 to see the marked improvement provided by this correction procedure. The spread of values at the peak is 2.5% of the peak value in Fig. 7 and 4% of the peak value in Fig. 2. At the edges of the band, the spread of values is 0.01% of the peak value in Fig. 7 and 5% in Fig. 2.

The average of the 15 absorption index spectra of Fig. 7 is presented in Fig. 8 with the real refractive index, $n(\tilde{\nu})$, spectrum calculated from it via Kramers–Kronig transformation and the value 1.475 for n at 1100 cm^{-1}. This value of n at 1100 cm^{-1} was found by the Kramers–Kronig transform of $k(\tilde{\nu})$ between 2131 and 804 cm^{-1}, using the value 1.474 for n at 2131 cm^{-1} which was taken from ref. 4. The spread of the 15 real refractive index spectra calculated from the absorption index spectra in Fig. 7 was ±0.045%, so the accuracy of the real refractive index values is largely determined by the value $n(1100\ cm^{-1}) = 1.475$.

Figure 8 also includes the molar absorption coefficient spectrum calculated from the absorption index spectrum. It is indistinguishable from the absorption index spectrum on the scale shown, and is defined by the right-hand ordinate scale.

Infrared intensities

The values of the real refractive indices, the absorption indices, and the molar absorption coefficients are tabulated in

Can. J. Chem. Downloaded from www.nrcresearchpress.com by 84.41.108.74 on 09/07/12
For personal use only.

TABLE 2. Calculation of ideal experimental absorbance for liquid benzene in a 23 μm KBr cell at 1095.8 and 912.2 cm^{-1}

Quantity	1095.8 cm^{-1}	912.2 cm^{-1}
Ideal apparent absorbance	0.0384±0.0001	0.0376±0.0001
Linear absorption coefficient[a]	(6.01±0.09) × 10^{-4}	(5.57±0.09) × 10^{-4}
Absorbance[b]	0.0138±0.0002	0.0128±0.0002
Ideal experimental absorbance[c]	0.0522±0.0003	0.0504±0.0003

[a]Units μm^{-1}.
[b]Absorbance = linear absorption coefficient times 23 μm pathlength.
[c]Ideal experimental absorbance = ideal apparent absorbance + absorbance.

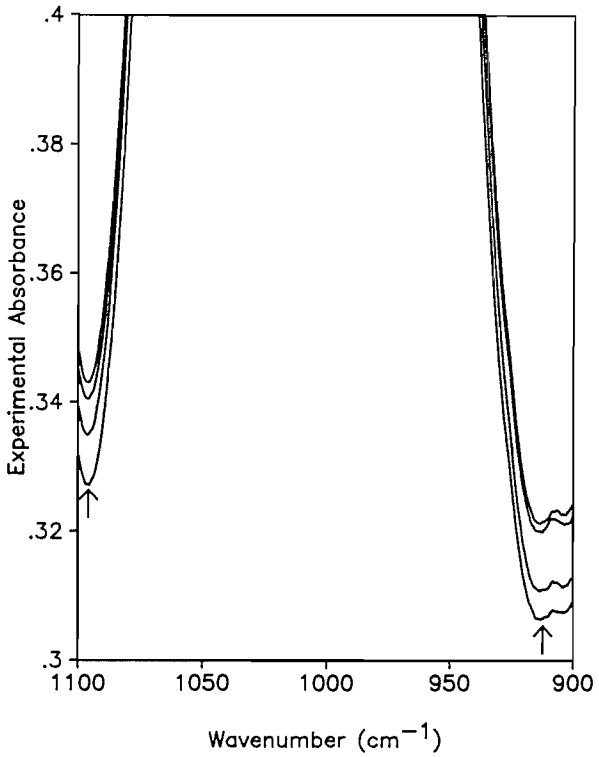


FIG. 4. Experimental absorbance spectra of C_6H_6(l) in KBr cells; 25°C and 1 cm^{-1} resolution. Pathlengths from top to bottom: 506.7, 506.9, 495.8, and 480.1 μm, all ±1 to 2 μm. The arrows are located at 1095.8 and 912.2 cm^{-1}.

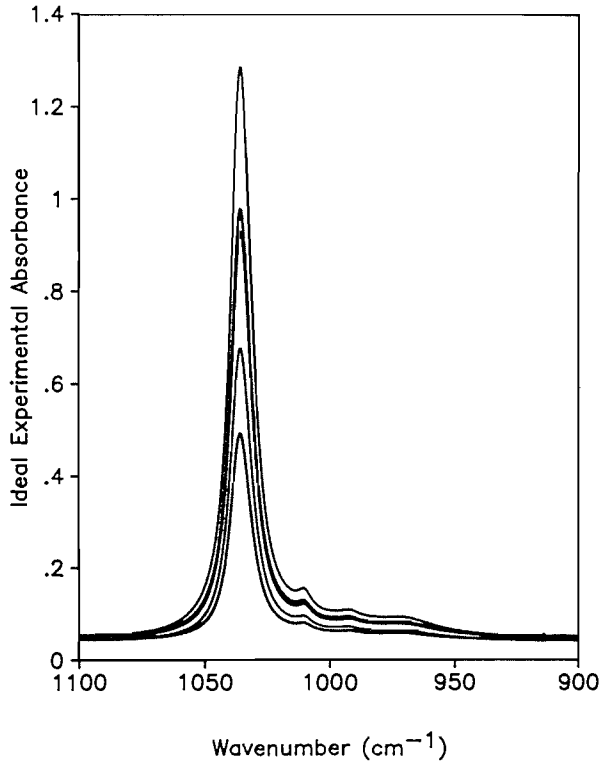


FIG. 5. The 15 ideal experimental absorbance spectra calculated from the experimental absorbance spectra in Fig. 1.

Table 3. The wavenumber intervals are 0.964 cm^{-1} rather than the 0.482 cm^{-1} intervals of the original spectrum to save space. The tabulated absorption index spectrum can be interpolated via a program that Fourier transforms, zero-fills, and inverse-Fourier transforms, such as INTERPOL in Spectracalc, to reproduce the original $k(\tilde{\nu})$ values to ≤0.00004. The instrumental resolution was 1 cm^{-1} and the temperature was 25°C.

The average absorption index value at the peak of the band is 0.0710 with a 95% confidence limit of 0.0003. Two points should be noted. First, this value is clearly to be preferred over our earlier (1, 3) value, 0.0718 with a 90% confidence limit of 0.0004, because the latter clearly includes baseline errors. Second, this result agrees to 0.0001 with the value given by Goplen, Cameron, and Jones (4) which was calibrated against a primary standard but is less precise. The average peak value of the molar absorption coefficient is 35.9 ± 0.2 L per mole-cm.

The area under the absorption index band between 1095.8 and 912.6 cm^{-1} is 1.358 ± 0.009 cm^{-1} where 0.009 is the 95% confidence limit. The area under the molar absorption coefficient band is 6.79 ± 0.05 km/mol. It is sometimes preferred to measure the area above a baseline through the data rather than above zero ordinate. We took a linear baseline through the average of 5 ordinates centered on 1095.8 cm^{-1} and the average of 5 ordinates centered on 912.6 cm^{-1}. The area between 1095.8 and 912.6 cm^{-1} above this baseline is 1.163 cm^{-1} for the absorption index and 5.84 km/mol for the molar absorption coefficient. The 6.79 ± 0.05 km/mol area under the molar absorption coefficient band will be used in the program IRYTRUE (12) as the secondary absolute intensity reference to facilitate the calibration of liquid cells for absolute intensities.

The molar conductivity spectrum is $V_m\tilde{\nu}\epsilon''(\tilde{\nu}) = 2V_m\tilde{\nu}n(\tilde{\nu})k(\tilde{\nu})$ where V_m is the molar volume and ϵ'' is the imaginary dielectric constant, also called the dielectric loss. The molar conductivity is used to calculate molecular properties, because the area under a molar conductivity band equals

Can. J. Chem. Downloaded from www.nrcresearchpress.com by 84.41.108.74 on 09/07/12
For personal use only.

Can. J. Chem. Downloaded from www.nrcresearchpress.com by 84.41.108.74 on 09/07/12
For personal use only.

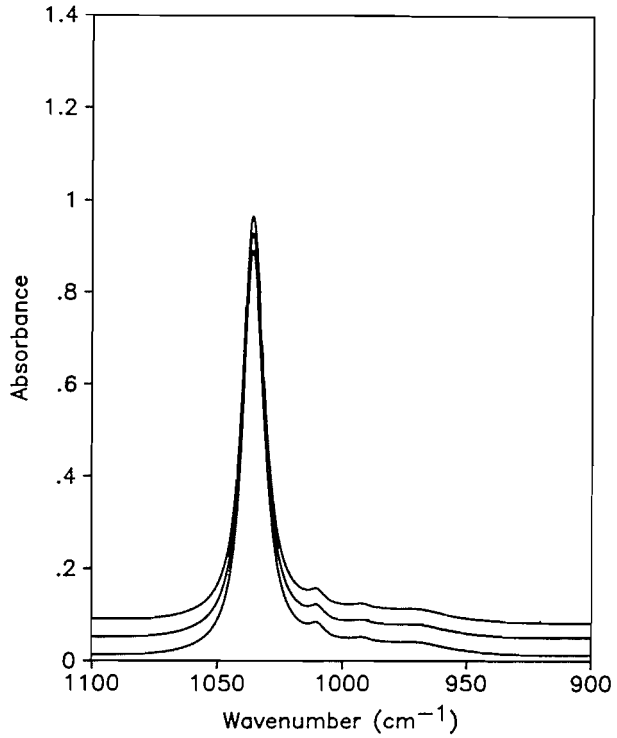


FIG. 6. From top to bottom, the experimental absorbance spectrum, the ideal experimental absorbance spectrum, and the absorbance spectrum of one sample of benzene.

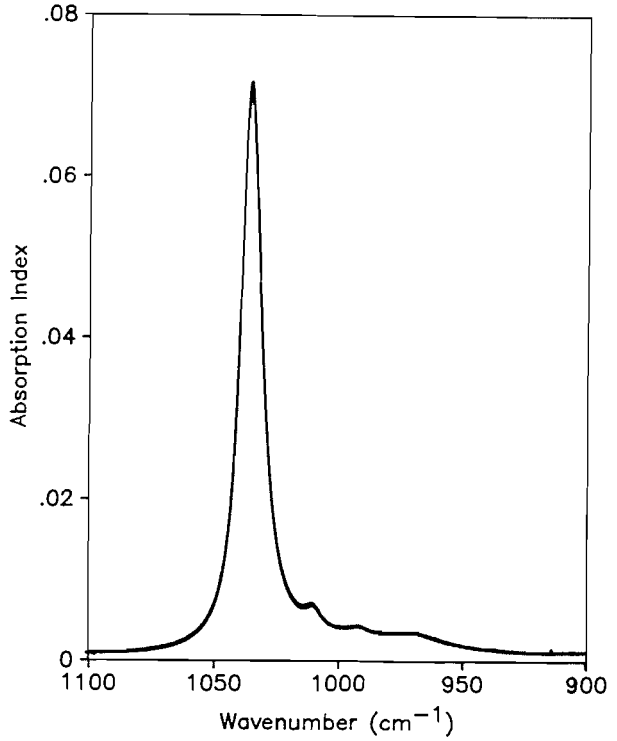


FIG. 7. The 15 absorption index (imaginary refractive index) spectra of benzene calculated from the spectra in Fig. 5.

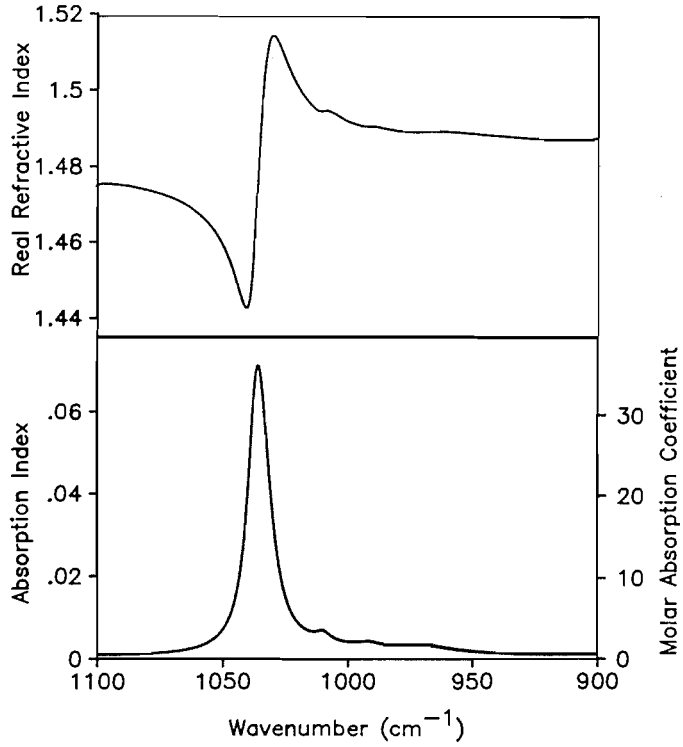


FIG. 8. Lower box, the average of the 15 absorption index spectra in Fig. 7 and, upper, the real refractive index spectrum calculated from it and $n(1100\ \text{cm}^{-1}) = 1.475$. The lower box contains the absorption index band defined by the left ordinate scale and also the molar absorption coefficient band defined by the right ordinate scale. The two curves are indistinguishable on this scale.

$(N_a/6c^2)\ (\partial\mu/\partial Q)_{eff}^2$, which equals $\{(0.1487)^{-1}\ (\partial\mu/\partial Q)_{eff}^2\}$ if $(\partial\mu/\partial Q)_{eff}^2$ is in (Debye/Å)^2/amu and the area is in km/mol. Here N_a and c are Avogadro's number and the velocity of light, respectively, and $(\partial\mu/\partial Q)_{eff}$ is the effective dipole moment derivative for a benzene molecule in the liquid. The area between 1095.8 and 912.6 cm^{-1} under the molar conductivity band is 3.69 km/mol above the zero ordinate, or 3.17 km/mol above the baseline described above. It is not clear which of these two areas should be used, because it is not clear to what extent the fundamental vibration contributes intensity to the baseline.

The 1036 cm^{-1} band of liquid benzene as a potential infrared secondary intensity standard

In a paper to be published elsewhere (12) we describe a project, set up under the auspices of the International Union of Pure and and Applied Chemistry, for the establishment of a set of calibration standards for quantitative infrared intensities. It is particularly desired that the standards be useful to the analytical community to facilitate quantitative infrared analysis of liquids. The 1036 cm^{-1} band of benzene is one of the bands to be included in this project, and the procedure described above will also be used to develop and evaluate the standard intensities.

The 1036 cm^{-1} band of benzene has been studied by many workers (1, 2, 4, 21–27) between 1960 and 1980 by different methods. Their values for the peak absorption index range from 0.069 to 0.072. The average of these values is 0.0705 ± 0.0015, so it seems clear that the absolute peak intensity of this

TABLE 3. Real and imaginary refractive indices and molar absorption coefficients of liquid benzene at 25°C between 1100 and 900 cm^{-1}

$\tilde{\nu}/cm^{-1}$	$n(\tilde{\nu})$	$k(\tilde{\nu})$	$E_m(\tilde{\nu})$	$\tilde{\nu}/cm^{-1}$	$n(\tilde{\nu})$	$k(\tilde{\nu})$	$E_m(\tilde{\nu})$	$\tilde{\nu}/cm^{-1}$	$n(\tilde{\nu})$	$k(\tilde{\nu})$	$E_m(\tilde{\nu})$
1100.2	1.475	0.0010	0.548	1028.8	1.514	0.0280	14.072	959.4	1.489	0.0026	1.234
1099.2	1.475	0.0010	0.545	1027.9	1.512	0.0237	11.890	958.5	1.489	0.0026	1.198
1098.3	1.475	0.0010	0.538	1026.9	1.511	0.0202	10.119	957.5	1.489	0.0025	1.152
1097.3	1.475	0.0010	0.533	1025.9	1.509	0.0174	8.700	956.5	1.489	0.0024	1.112
1096.3	1.475	0.0010	0.542	1025.0	1.508	0.0151	7.561	955.6	1.489	0.0023	1.074
1095.4	1.475	0.0010	0.539	1024.0	1.506	0.0133	6.650	954.6	1.489	0.0022	1.040
1094.4	1.475	0.0010	0.539	1023.1	1.505	0.0118	5.914	953.6	1.489	0.0022	1.004
1093.4	1.475	0.0010	0.541	1022.1	1.503	0.0107	5.322	952.7	1.489	0.0021	0.976
1092.5	1.475	0.0010	0.549	1021.1	1.502	0.0097	4.843	951.7	1.489	0.0020	0.946
1091.5	1.475	0.0010	0.553	1020.2	1.501	0.0089	4.454	950.7	1.488	0.0020	0.921
1090.6	1.475	0.0010	0.555	1019.2	1.500	0.0083	4.142	949.8	1.488	0.0019	0.892
1089.6	1.475	0.0011	0.565	1018.2	1.499	0.0078	3.895	948.8	1.488	0.0019	0.865
1088.6	1.475	0.0011	0.575	1017.3	1.498	0.0074	3.690	947.8	1.488	0.0018	0.839
1087.7	1.475	0.0011	0.583	1016.3	1.497	0.0071	3.541	946.9	1.488	0.0018	0.823
1086.7	1.475	0.0011	0.583	1015.3	1.496	0.0069	3.428	945.9	1.488	0.0017	0.796
1085.7	1.475	0.0011	0.588	1014.4	1.496	0.0068	3.367	945.0	1.488	0.0017	0.776
1084.8	1.474	0.0011	0.593	1013.4	1.495	0.0068	3.355	944.0	1.488	0.0016	0.756
1083.8	1.474	0.0011	0.606	1012.4	1.495	0.0069	3.396	943.0	1.488	0.0016	0.738
1082.8	1.474	0.0012	0.619	1011.5	1.494	0.0070	3.464	942.1	1.488	0.0016	0.723
1081.9	1.474	0.0012	0.629	1010.5	1.494	0.0071	3.503	941.1	1.488	0.0015	0.709
1080.9	1.474	0.0012	0.646	1009.6	1.494	0.0069	3.418	940.1	1.488	0.0015	0.698
1079.9	1.474	0.0013	0.661	1008.6	1.494	0.0065	3.211	939.2	1.488	0.0015	0.687
1079.0	1.473	0.0013	0.679	1007.6	1.494	0.0060	2.966	938.2	1.488	0.0015	0.671
1078.0	1.473	0.0013	0.697	1006.7	1.494	0.0056	2.745	937.2	1.488	0.0014	0.660
1077.1	1.473	0.0014	0.722	1005.7	1.494	0.0052	2.565	936.3	1.488	0.0014	0.646
1076.1	1.473	0.0014	0.748	1004.7	1.493	0.0049	2.417	935.3	1.488	0.0014	0.631
1075.1	1.473	0.0015	0.776	1003.8	1.493	0.0047	2.309	934.3	1.488	0.0014	0.618
1074.2	1.473	0.0015	0.797	1002.8	1.493	0.0045	2.224	933.4	1.488	0.0013	0.601
1073.2	1.472	0.0016	0.821	1001.8	1.492	0.0044	2.166	932.4	1.488	0.0013	0.594
1072.2	1.472	0.0016	0.847	1000.9	1.492	0.0044	2.129	931.5	1.487	0.0013	0.578
1071.3	1.472	0.0017	0.878	999.9	1.492	0.0043	2.103	930.5	1.487	0.0013	0.572
1070.3	1.472	0.0017	0.907	999.0	1.491	0.0043	2.091	929.5	1.487	0.0012	0.560
1069.3	1.471	0.0018	0.941	998.0	1.491	0.0043	2.080	928.6	1.487	0.0012	0.556
1068.4	1.471	0.0019	0.976	997.0	1.491	0.0043	2.080	927.6	1.487	0.0012	0.544
1067.4	1.471	0.0019	1.015	996.1	1.491	0.0043	2.085	926.6	1.487	0.0012	0.544
1066.4	1.470	0.0020	1.058	995.1	1.491	0.0043	2.096	925.7	1.487	0.0012	0.535
1065.5	1.470	0.0021	1.111	994.1	1.490	0.0044	2.122	924.7	1.487	0.0012	0.533
1064.5	1.470	0.0022	1.168	993.2	1.490	0.0044	2.142	923.7	1.487	0.0012	0.526
1063.6	1.469	0.0024	1.227	992.2	1.490	0.0044	2.150	922.8	1.487	0.0012	0.519
1062.6	1.469	0.0025	1.294	991.2	1.490	0.0044	2.125	921.8	1.487	0.0011	0.517
1061.6	1.468	0.0026	1.367	990.3	1.490	0.0043	2.068	920.8	1.487	0.0011	0.515
1060.7	1.468	0.0028	1.450	989.3	1.490	0.0041	1.997	919.9	1.487	0.0011	0.514
1059.7	1.467	0.0030	1.546	988.3	1.490	0.0040	1.926	918.9	1.487	0.0011	0.512
1058.7	1.467	0.0032	1.645	987.4	1.490	0.0039	1.866	918.0	1.487	0.0011	0.506
1057.8	1.466	0.0034	1.765	986.4	1.490	0.0038	1.823	917.0	1.487	0.0011	0.506
1056.8	1.466	0.0037	1.895	985.5	1.490	0.0037	1.789	916.0	1.487	0.0011	0.501
1055.8	1.465	0.0040	2.046	984.5	1.490	0.0037	1.765	915.1	1.487	0.0011	0.503
1054.9	1.464	0.0043	2.214	983.5	1.490	0.0036	1.744	914.1	1.487	0.0011	0.512
1053.9	1.464	0.0047	2.409	982.6	1.489	0.0036	1.729	913.1	1.487	0.0011	0.501
1052.9	1.463	0.0051	2.631	981.6	1.489	0.0036	1.710	912.2	1.487	0.0011	0.499
1052.0	1.462	0.0056	2.895	980.6	1.489	0.0035	1.696	911.2	1.487	0.0011	0.507
1051.0	1.461	0.0062	3.199	979.7	1.489	0.0035	1.689	910.2	1.487	0.0011	0.507
1050.1	1.459	0.0070	3.568	978.7	1.489	0.0035	1.689	909.3	1.487	0.0012	0.511
1049.1	1.458	0.0078	4.011	977.7	1.489	0.0035	1.684	908.3	1.487	0.0012	0.510
1048.1	1.457	0.0089	4.546	976.8	1.489	0.0035	1.689	907.3	1.487	0.0012	0.510
1047.2	1.455	0.0102	5.205	975.8	1.489	0.0036	1.693	906.4	1.487	0.0012	0.513
1046.2	1.453	0.0118	6.018	974.8	1.489	0.0036	1.697	905.4	1.487	0.0012	0.515
1045.2	1.452	0.0138	7.039	973.9	1.489	0.0036	1.704	904.5	1.487	0.0012	0.514
1044.3	1.449	0.0163	8.332	972.9	1.489	0.0036	1.703	903.5	1.487	0.0012	0.512
1043.3	1.447	0.0196	9.990	972.0	1.489	0.0036	1.705	902.5	1.487	0.0012	0.517
1042.3	1.445	0.0239	12.148	971.0	1.489	0.0036	1.697	901.6	1.487	0.0012	0.513
1041.4	1.443	0.0294	14.963	970.0	1.489	0.0036	1.688	900.6	1.487	0.0012	0.521
1040.4	1.443	0.0366	18.574	969.1	1.489	0.0035	1.668				
1039.4	1.444	0.0453	22.988	968.1	1.489	0.0035	1.643				

Can. J. Chem. Downloaded from www.nrcresearchpress.com by 84.41.108.74 on 09/07/12
For personal use only.

TABLE 3 (*concluded*)

$\tilde{\nu}$/cm^{-1}	$n(\tilde{\nu})$	$k(\tilde{\nu})$	$E_m(\tilde{\nu})$	$\tilde{\nu}$/cm^{-1}	$n(\tilde{\nu})$	$k(\tilde{\nu})$	$E_m(\tilde{\nu})$	$\tilde{\nu}$/cm^{-1}	$n(\tilde{\nu})$	$k(\tilde{\nu})$	$E_m(\tilde{\nu})$
1038.5	1.448	0.0550	27.903	967.1	1.489	0.0034	1.605				
1037.5	1.456	0.0641	32.469	966.2	1.489	0.0033	1.566				
1036.6	1.468	0.0699	35.359	965.2	1.489	0.0032	1.519				
1035.6	1.481	0.0709	35.857	964.2	1.489	0.0031	1.478				
1034.6	1.493	0.0676	34.130	963.3	1.489	0.0030	1.427				
1033.7	1.502	0.0615	31.017	962.3	1.489	0.0029	1.381				
1032.7	1.508	0.0541	27.296	961.3	1.489	0.0028	1.328				
1031.7	1.512	0.0466	23.466	960.4	1.489	0.0027	1.282				
1030.8	1.514	0.0395	19.876								
1029.8	1.514	0.0333	16.732								

band is known to at least ±2%. In fact the most recent values are probably the best, partly because one value was measured against a primary standard (4), and also because of the great improvements in instrumentation over the past 15 years. Thus we believe the current value, 0.0710 with a 95% confidence limit of 0.0003, is the best available for 25°C and a nominal resolution in the range 0.8–1.0 cm^{-1}.

The area under the average molar absorption coefficient band between 1095.8 and 912.6 cm^{-1} is 6.79 ± 0.05 km/mol. When multiplied by 2.303 this converts to 15.64 ± 0.10 km/mol for A_j, the Napierian-logarithmic equivalent measure of the integrated absorption. Previous workers have found similar values, namely 15.34 (24), 15.4 ± 1.1 (23), and 15.82 (26) km/mol between 1080 and 920 cm^{-1}) (we obtain 15.3 between 1080 and 920 cm^{-1}) and 15 (22) between 1080 and 1000 cm^{-1} (we obtain 13.0 between 1080 and 1000 cm^{-1}). Other workers (28, 29) have deduced the integrated intensity from measurements of the real refractive index, and have all found values nearer to 19 km/mol. Again, we believe the value obtained in this work is the best currently available for 25°C, although it should be noted that our values of the real refractive index are about 1.5% higher than the literature (4, 21–27, 29) values.

To help assess the reliability of peak heights and areas recommended to IUPAC as secondary intensity standards, we seek the assistance of the spectroscopic community. We plan to explore the intensities of benzene in the regions 3820 – 3525, 3320 – 2915, 2260 – 2125, 1905 – 1720, 1565 – 1335, 1100 – 905, and 915 – 800 cm^{-1}. We seek spectra of cells full of benzene recorded in other laboratories with peak experimental absorbances between 0.5 and 1.5 in these wavenumber regions, together with spectra of the cell exactly as it was used for the benzene but recorded either before filling or after removing all of the benzene. The reference for these spectra should be the empty sample compartment, not the empty cell. A nominal resolution 1 cm^{-1} is preferred, but 2 cm^{-1} is useful. We will process such spectra with the program RNJ46A in order to test the reliability of our results.

It should be noted that the thermal expansion of benzene (30) is sufficient to change the value of the absorption index by 0.0004 per 5°C change in temperature, even if no change in molecular transition moment occurs, because the molar volume changes from 88.86 mL/mol at 20°C to 89.41 mL/mol at 25°C. It is important, therefore, to maintain the temperature constant to about ±1°C, and preferably at 25°C, in order to obtain results to test the values reported in this paper.

Computer programs

Until this work was finished the only changes to the NRC program 46 that were incorporated in program RNJ46A were to allow the input and output to be in Spectracalc format or ASCII ".Y" format, and to use Bertie and Zhang's (16) much faster modification of the original Kramers–Kronig transform subroutine. Thus the following three steps were necessary to convert an experimental absorbance spectrum to an ideal experimental absorbance spectrum and then to the real and imaginary refractive index spectra. (1) Select a reference wavenumber on each side of the band and determine the ideal experimental absorbance at these reference wavenumbers using the cell thickness, the linear absorption coefficient obtained from thick cell measurements, and the ideal apparent absorbance as calculated by BASELINE. (2) Correct the experimental absorbance spectrum to the ideal experimental absorbance spectrum with BASECORR, using the ideal experimental absorbances calculated in (1) at the two reference wavenumbers. (3) Use this ideal experimental absorbance spectrum in RNJ46A to calculate the $k(\tilde{\nu})$and $n(\tilde{\nu})$ spectra.

However, since the logic of BASELINE is contained in NRC program 46, the above procedure can be done automatically by the program if the baseline correction procedure (i.e., the logic of BASECORR) is added to it and if the user supplies the linear absorption coefficient at the two reference wavenumbers.

Our latest version of NRC program 46 (RNJ46A, version 04/91) incorporates these features. Further, to reduce the execution time, the complex variables and complex arithmetic operations contained in the original NRC program 46 have been replaced by real variables and real arithmetic. Further, Ohta and Ishida's (31) correction to the logic has been included, although it has negligible effect for the 1036 cm^{-1} band of benzene.

These modifications to program RNJ46A were made for compilation under Microsoft Fortran 5.0 running under Microsoft DOS, Version 3.3 or 4.1, and execution on moderately fast laboratory computers such as 16 to 20 MHz 286- or 386-based computers, preferably with a math co-processor. For a file of 416 data points, the current version of RNJ46A requires approximately 1 min to compute converged optical constants.

The program RNJ46A is available from J.E.B. on request.

Acknowledgements

C.D.K. thanks the Natural Sciences and Engineering

Can. J. Chem. Downloaded from www.nrcresearchpress.com by 84.41.108.74 on 09/07/12
For personal use only.

Research Council of Canada for a graduate studentship and J.E.B. thanks the same body for its support of this work.

1. J. E. BERTIE, R. N. JONES, and V. BEHNAM. Appl. Spectrosc. **39**, 401 (1985).
2. J. E. BERTIE, R. N. JONES, and V. BEHNAM. Appl. Spectrosc. **40**, 427 (1986).
3. J. E. BERTIE, H. H. EYSEL, V. BEHNAM, and J. C. M. ZWINKELS. SPIE **553**, Fourier and computerized infrared spectroscopy. 1985. p. 34.
4. T. G. GOPLEN, D. G. CAMERON, and R. N. JONES. Appl. Spectrosc. **34**, 657 (1980).
5. T. G. GOPLEN, D. G. CAMERON, and R. N. JONES. Appl. Spectrosc. **34**, 652 (1980).
6. R. N. JONES, D. ESCOLAR, J. P. HAWRANEK, P. NEELAKANTAN, and R. P. YOUNG. J. Mol. Struct. **19**, 21 (1973)
7. J. P. HAWRANEK, P. NEELAKANTAN, R. P. YOUNG, and R. N. JONES. Spectrochim. Acta, **32A**, 75 (1976).
8. J. P. HAWRANEK, P. NEELAKANTAN, R. P. YOUNG, and R. N. JONES. Spectrochim. Acta, **32A**, 85 (1976).
9. J. P. HAWRANEK and R. N. JONES. Spectrochim. Acta, **32A**, 99 (1976).
10. R. N. JONES and R. P. YOUNG. Computer programs for infrared spectrophotometry XVI to XXII. National Research Council of Canada Bulletin 13. 2nd ed. 1976.
11. D. G. CAMERON, J. P. HAWRANEK, P. NEELAKANTAN, R. P. YOUNG, and R. N. JONES. Computer programs for infrared spectrophotometry XLII to XLVII. National Research Council of Canada Bulletin 16. 1977.
12. J. E. BERTIE, C. D. KEEFE, H. MANTSCH, D. G. MOFFAT, and R. N. JONES. Appl. Spectrosc. In press.
13. N. SHEPPARD, H. A. WILLIS, and J. C. RIGG. Spectrochim. Acta, **43A**, 1 (1987).
14. I. MILLS, T. CVITAS, K. HOMANN, N. KALLAY, and K. KUCHITSU. Quantities, units and symbols in physical chemistry. International Union of Pure and Applied Chemistry. Blackwell Scientific Publications, Oxford. 1988.
15. K. OHTA and H. ISHIDA. Appl. Spectrosc. **42**, 952 (1988).
16. J. E. BERTIE and S. ZHANG. To be published.
17. K. R. JUNE. Appl. Op. **11**, 1655 (1972).
18. R. E. STEPHENS, E. K. PLYLER, W. S. RODNEY, and R. J. SPINDLER. J. Opt. Soc. Am. **43**, 110 (1953).
19. W. W. COBLENTZ. J. Opt. Soc. Am. **4**, 432 (1920).
20. International critical tables of numerical data, physics, chemistry and technology 1926 Series. Vol. 7, 1930. pp. 13, 14, with k, the coefficient of λ^2 extended to 9.285837 from 9.28584 and the parameter β_1^2 changed to 0.025474707 instead of 0.02547407, as given in Program 46 of ref. 11.
21. D. G. CAMERON, D. ESCOLAR, T. G. GOPLEN, A. NADEAU, R. P. YOUNG, and R. N. JONES. Appl. Spectrosc. **34**, 646 (1980).
22. G. M. IRONS and H. W. THOMPSON. Proc. R. Soc. London, Ser. A, **298**, 160 (1967).
23. A. C. GILBY, J. BURR, JR., W. KRUEGER, and B. CRAWFORD, JR. J. Phys. Chem. **70**, 1525 (1966).
24. J. P. HAWRANEK and R. N. JONES. Spectrochim. Acta, **32A**, 111 (1976).
25. V. M. ZOLOTAREV. Sov. J. Opt. Technol. **43**, 494 (1976).
26. A. E. TCHMEL and V. L. VETTEGREN. Spectrochim. Acta, **29A**, 1681 (1973).
27. J. FAHRENFORT. Proc. 10th Colloquium Spectroscop. Internat. College Park Maryland, 1962, Spartan Books, Washington, DC (1963), p. 437, cited in ref. 26.
28. A. J. ZELANO and W. T. KING. J. Chem. Phys. **53**, 4444 (1970).
29. P. N. SCHATZ. J. Chem. Phys. **32**, 894 (1960).
30. International critical tables of numerical data, physics, chemistry and technology 1926 series. Vol. 3. 1928. p. 29.
31. K. OHTA and H. ISHIDA. Appl. Opt. **29**, 2466 (1990).

Can. J. Chem. Downloaded from www.nrcresearchpress.com by 84.41.108.74 on 09/07/12
For personal use only.

Vibrational circular dichroism of (*S*,*S*)-[2,3-$^2H_2$]oxirane in the gas phase and in solution

TERESA B. FREEDMAN,[1] KEVIN M. SPENCER, N. RAGUNATHAN, AND LAURENCE A. NAFIE
Department of Chemistry, Syracuse University, Syracuse, NY 13244-4100, U.S.A.

AND

JEFFREY A. MOORE AND JOHN M. SCHWAB
Department of Medicinal Chemistry and Pharmacognosy, School of Pharmacy and Pharmacal Sciences, Purdue University, West Lafayette, IN 47907, U.S.A.

Received April 9, 1991

This paper is dedicated to Dr. Richard Norman Jones

TERESA B. FREEDMAN, KEVIN M. SPENCER, N. RAGUNATHAN, LAURENCE A. NAFIE, JEFFREY A. MOORE, and JOHN M. SCHWAB. Can. J. Chem. **69**, 1619 (1991).

Vibrational circular dichroism (VCD) spectra of an exceptionally simple chiral three-membered ring molecule, (*S*,*S*)-[2,3-$^2H_2$]oxirane, have been obtained for samples in the gas phase and in C_2Cl_4 and CS_2 solution. The VCD band contours for the gas phase samples of this molecule with C_2 symmetry follow those of the absorption spectra, with the modes of *A* symmetry species giving rise to bands with two sharp Q-branch maxima on either side of a distinct minimum, and the modes of *B* symmetry species giving rise to bands with a strong central Q-branch. The signs and relative intensities of the VCD bands can be understood in terms of chiral perturbation by the deuterium substitution of the vibrational modes of the parent oxirane molecule, which mixes modes of A_1 and A_2 symmetry, and modes of B_1 and B_2 symmetry, thus introducing angular charge oscillation about the direction of linear charge oscillation.

Key words: vibrational circular dichroism, oxirane, chiral perturbation.

TERESA B. FREEDMAN, KEVIN M. SPENCER, N. RAGUNATHAN, LAURENCE A. NAFIE, JEFFREY A. MOORE et JOHN M. SCHWAB. Can. J. Chem. **69**, 1619 (1991).

Opérant en phase gazuese ainsi qu'en solutions dans le C_2Cl_4 ou le CS_2, on a déterminé les spectres de dichroïsme circulaire vibrationnel (DCV) d'une molécule cyclique chirale exceptionnellement simple, le (*S*,*S*)-[2,3-$^2H_2$]oxirane. Les bandes de contour du DCV des échantillons gazeux de cette molécule de symétrie C_2 sont semblables à celles du spectre d'absorption; les modes des espèces de symétrie *A* donnent lieu aux bandes comportant deux maxima aigus de la branche Q de chaque côté d'un minimum distinct alors que les espèces de symétrie *B* donnent lieu aux bandes qui possèdent une branche Q centrale forte. On peut comprendre les signes et les intensités relatives des bandes du DCV en fonction d'une perturbation chirale, causée par une substitution par du deutérium des modes vibrationnels de la molécule oxirane fondamentale, qui provoque un mélange des modes de symétrie A_1 et A_2 avec les modes de symétrie B_1 et B_2 et qui introduit une oscillation angulaire de charge autour de la direction de l'oscillation linéaire de charge.

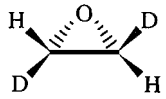
Mots clés : dichroïsme circulaire vibrational, oxirane, perturbation chirale.

[Traduit par la rédaction]

Introduction

The evaluation of theoretical formulations (1–8) and calculational approaches (9–16) for determining vibrational circular dichroism (VCD) intensities (17–21) requires small rigid molecules for which testing of methodological variables is practical. Simple three-membered ring molecules that are chiral due to isotopic substitution are ideal for this purpose. Calculations on such species (9–15, 22) have outpaced the generation of experimental data (23–26) with which theoretical results can be compared and evaluated. In addition, these simple chiral molecules provide the opportunity to investigate mechanisms for generating VCD intensity that can be applied to the interpretation of VCD spectra of complex molecules, in order to obtain information on solution conformations when calculations are not practical or desirable.

The smallest chiral molecule in this category, (*S*,*S*)-[2,3-$^2H_2$]-oxirane, **1**, has been the focus of recent theoretical investigations (12, 14, 15) using three different approaches to calculating VCD intensities. We previously reported the CH- and CD-stretching VCD spectra of **1** in CCl_4 solution (23). Mid-infrared spectra were not possible at the time of that study due to sample impurities. With the availability of higher purity samples of the *trans*-[$^2H_2$]oxirane enantiomers, we have undertaken a more extensive investigation of the VCD spectra of gas-phase (25) solution samples, in order to provide experimental data for comparison to the calculational approaches, and to gain a better understanding of the mechanisms for generating the VCD features.



(*S*,*S*)-[2,3-$^2H_2$]oxirane

1

Experimental

The (*S*,*S*) and (*R*,*R*) antipodes of [2,3-$^2H_2$]oxirane were synthesized by a modification of the published procedure (27). The benzene contaminant that had prevented observation of the mid-infrared bands in our earlier study of solution-phase samples (23) was largely eliminated by decreasing (to 1.1 equivalents) the amount of tetraethylammonium fluoride used in the desilylation of labeled (trimethylsilyl)-oxirane. The oxirane thus generated was trapped in a collection vessel cooled to −196°C. The enantiomeric excess values of both labeled oxirane enantiomers were estimated at 94% by 500 MHz ^1H NMR analysis of the Mosher ester derivatives (28) of the antipodal 3-(triphenylsilyl)[2,3-$^2H_2$]oxiranemethanol precursors. Small amounts (<5%) of benzene and diethyl ether impurities were revealed by the infrared absorption spectra of the oxirane samples.

[1]Author to whom correspondence may be addressed.

Printed in Canada / Imprimé au Canada

Can. J. Chem. Downloaded from www.nrcresearchpress.com by 84.41.108.74 on 09/07/12
For personal use only.

Can. J. Chem. Downloaded from www.nrcresearchpress.com by 84.41.108.74 on 09/07/12
For personal use only.

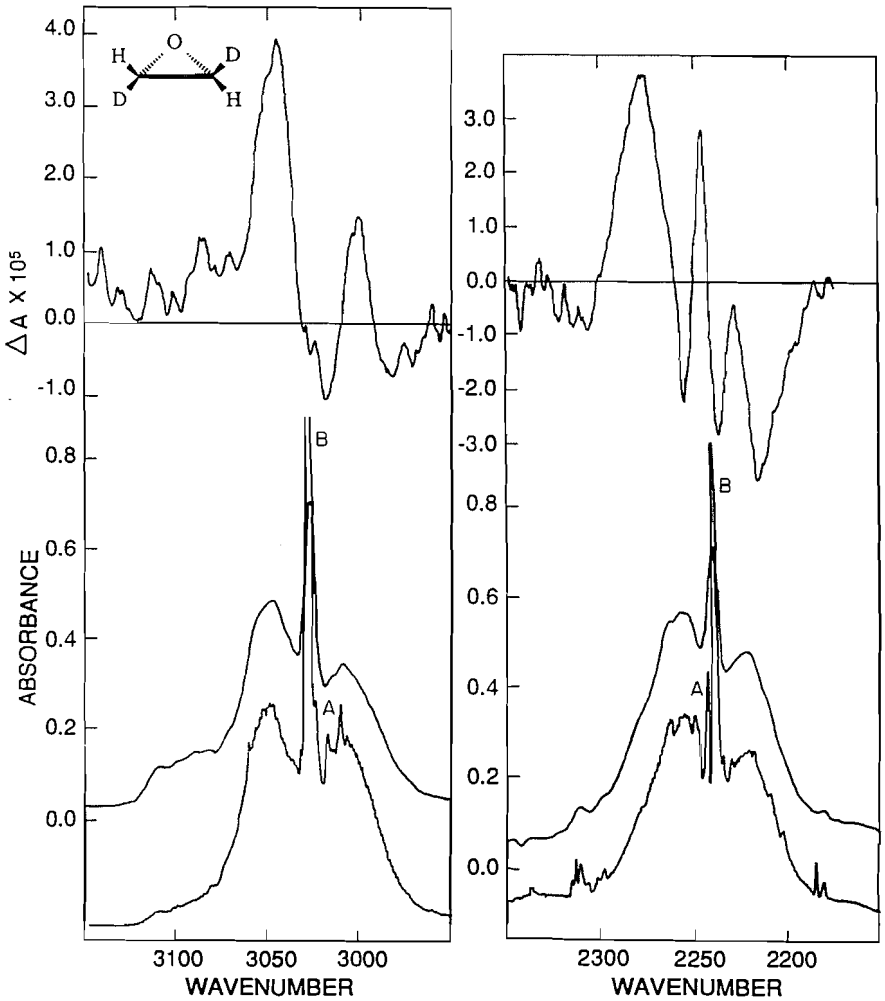


FIG. 1. Gas-phase absorption (middle traces) and VCD (upper traces) spectra of (*S,S*)-[2,3-$^2H_2$]oxirane in a 25.4-mL volume, 5-cm path length cell, in the (A) CH-stretching region, 7.2 cm^{-1} resolution, 8-mg sample and (B) CD-stretching region, 5.4 cm^{-1} resolution, 13-mg sample. Lower traces in both regions show spectra at 1 cm^{-1} resolution for a different sample (ordinate scale not displayed).

Infrared absorption and VCD spectra were obtained at Syracuse University for gas-phase samples in a 5-cm path length, 25.4-mL volume cell equipped with KBr windows and a sidearm for condensing the sample. For the solution-phase samples, a sealed cylindrical Pyrex cell (25 mm diameter and 8 mm path length) was constructed with BaF_2 windows, a sidearm for condensing the sample and solvent, and a vacuum line port. The amount of sample (or solvent) introduced into either cell was accurately determined by condensation from a known volume on a vacuum line equipped with a 1000-Torr High Accuracy Baratron gauge (MKS Instruments, Andover, MA) for measuring pressure (1 Torr = 133.3 Pa).

The CH- and CD-stretching VCD spectra for the gas-phase samples were recorded on a dispersive VCD instrument previously described (29), with resolutions of 7.2 cm^{-1} at 3000 cm^{-1} and 5.4 cm^{-1} at 2100 cm^{-1}. Prior to obtaining spectra of the solution-phase samples, this instrument was interfaced to an IBM XT computer equipped with a Data Translation 2811 data acquisition board and Spectra Calc software (Galactic Industries, Salem, NH), for data acquisition and manipulation. For the 1500–750 cm^{-1} region, VCD spectra were recorded on a modified Nicolet 7199FITIR spectrometer (30) at 4 cm^{-1} resolution with 12 288 AC and 800 DC scans (2.5 h per enantiomer) for the solution-phase sample. For the 4 cm^{-1} resolution gas-phase spectrum in this region, four sets of data at 4 cm^{-1} resolution, each consisting of 12 288 AC and 800 DC scans for each enantiomer, were collected on successive days and averaged. Absorption spectra were recorded on Nicolet 7199 or Bomem DA3 FTIR spectrometers. Sample sizes, ranging from 8 to 40 mg, were selected to maintain maximum absorbances below 0.8 in the region of interest. The final VCD spectra were obtained as one-half the difference between the spectra of the (*S,S*) and (*R,R*) enantiomers in order to remove baseline artifacts. Rotational and dipole strengths were determined by obtaining peak areas with the Spectra Calc curve-fitting software.

Results

Absorption and VCD spectra in the CH- and CD-stretching regions are shown in Fig. 1 for the gas-phase sample of (*S,S*)-[2,3-$^2H_2$]oxirane. The middle and upper traces show the absorption and corresponding VCD spectra at the maximum resolution obtainable with good signal quality on the dispersive instrument, 7.2 cm^{-1} in the CH-stretching region and 5.4 cm^{-1} in the CD-stretching region. The lower traces show the absorption spectra at 1 cm^{-1} resolution obtained for a different sample. The absorption intensity observed near 3100 cm^{-1} and extra intensity near 3050 cm^{-1} in the center trace of Fig. 1, which is absent in the lower trace, is due to some benzene contaminant in the sample of the (*R,R*)-[2,3-$^2H_2$]oxirane antipode used to obtain the absorption spectrum. The achiral benzene does not interfere with the VCD spectrum. The corresponding spectra for the sample in tetrachloroethylene (C_2Cl_4) solution with 8 cm^{-1} resolution are shown in Fig. 2. The CH-stretching spectra for a

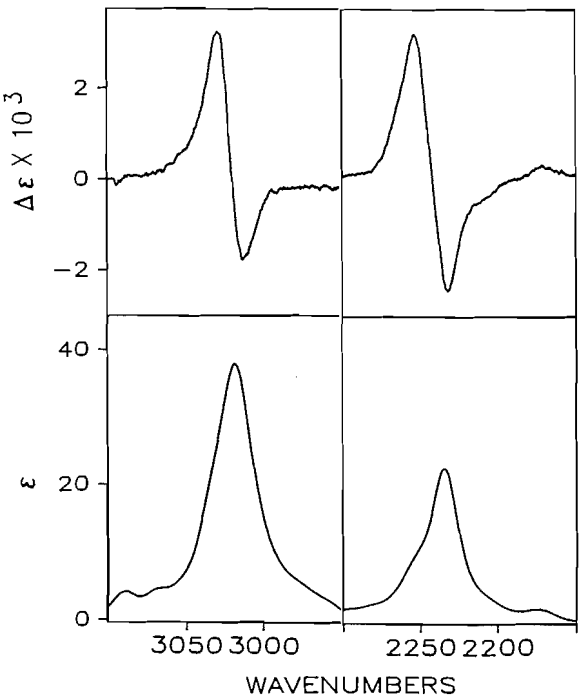


FIG. 2. CH- and CD-stretching absorption and VCD spectra of (*S,S*)-[2,3-$^2H_2$]oxirane 0.019 M in C_2Cl_4 solution, 0.8-cm path length, 8 cm^{-1} resolution.

sample at approximately the same concentration in carbon disulfide (CS_2) solution were nearly identical in anisotropy ratio to those in C_2Cl_4.

Spectra at 4 cm^{-1} resolution in the 700–1500 cm^{-1} region for a gas-phase sample (20 mg) are shown in Fig. 3. We previously presented gas-phase absorption and VCD spectra in the 1000–1500 cm^{-1} region for a larger sample (40 mg), with correspondingly improved signal-to-noise ratio for that region (25). The spectra shown in Fig. 3 include several bands below 1000 cm^{-1}, which could not be measured at the higher pressure. Mid-infrared spectra obtained at 1 cm^{-1} resolution displayed the expected sharper and more intense Q-branches, but did not exhibit any additional features (31). The lowest frequency band, observed at 673 cm^{-1} in the gas-phase absorption spectrum, is below the low frequency limit of our VCD instrument. The positive VCD signals for the 885 and 817 cm^{-1} modes occur at the Q-branch frequencies and are above the noise level, whereas any VCD for the 754 cm^{-1} could not be measured with our present detector. The spectra for a sample 0.052 M in CS_2 solution are presented in Fig. 4 for the 900–1350 cm^{-1} region; bands outside this region were obscured by interfering, intense solvent absorbance. The absorption feature at 1034 cm^{-1} and the shoulder at 1117 cm^{-1} are due to small amounts of benzene and diethyl ether impurities, respectively; these achiral impurities did not interfere with the VCD spectra.

The frequencies, absorption intensities, and VCD intensities are compiled in Table 1. The intensities are presented as dipole and rotational strengths, which were determined from the integrated band intensities.

Assignments

For gas-phase vibrational spectra, the rotational band contours provide information on the symmetry species of the vibrational modes (32). (*S,S*)-[2,3-$^2H_2$]Oxirane is an asymmetric top molecule in which the C_2 axis coincides with the intermediate moment of inertia. The smallest moment of inertia is approximately perpendicular to the plane of the three-membered ring, and the largest moment of inertia lies perpendicular to the C_2 axis approximately in the ring plane. The value of $\rho = B/A$ (where A and B are the rotational constants about the axes of the smallest and intermediate moments of inertia, respectively) is ~0.9. Calculations of band contours with these parameters (33) show that, under medium dispersion, the modes of A symmetry (dipole moment change along the C_2 axis) should have "type B" band contours, with two sharp Q maxima on either side of a distinct minimum, and weaker broad P- and R-branches. Modes of B symmetry (dipole moment change in the plane perpendicular to the C_2 axis) will have "type A" or "type C" band contours; for ρ near its limiting value of 1, "type A" and "type C" bands will both have a strong central Q-branch and weaker broad P- and R-branch maxima on either side. With the exception of some of the strongly overlapping bands, the absorption spectra of (*S,S*)-[2,3-$^2H_2$]oxirane display these types of band contours, and identical band contours are observed in the VCD spectra. The symmetry species of the normal modes listed in Table 1 were readily determined from the band contours.

To obtain additional information on the nature of the normal modes, a normal coordinate calculation was carried out in cartesian coordinates. The scaled *ab initio* force field (4-31G basis set) of Lowe *et al.* (34) and the experimental geometry of Hirose (35), both determined for the parent oxirane molecule, were employed. This force field yields normal mode frequencies quite close to those obtained with a 6-31G(ext) basis set (12); the latter force field is not yet available in the literature. The calculated cartesian displacement derivatives were then used to find distorted geometries at the two extremes of the vibrational cycle for each mode. These two geometries were overlaid, viewed from various angles, and plotted with ChemCad (C-Graph Software, Austin, TX). The 15 normal modes are shown in Figs. 5 and 6 as stereoprojections in a plane perpendicular to the C_2 axis.

The fundamental vibrational normal modes of the parent oxirane molecule can be described in terms of the 15 symmetry coordinates shown in Fig. 7. The symmetry species for this C_{2v} molecule can be characterized by the translation T_α along the α axis ($\alpha = x$, y, or z) and (or) rotation R_α about the α axis that transforms as that species. Oxirane has five modes of A_1 symmetry (T_z), three modes of A_2 symmetry (R_z), four modes of B_1 symmetry (T_x,R_y), and three modes of B_2 symmetry (T_y,R_x). Vibrational circular dichroism intensity is proportional to the rotational strength, $R = (\boldsymbol{\mu})_{01} \cdot (\boldsymbol{m})_{10}$, the scalar product of the electric dipole transition moment $\boldsymbol{\mu}$, which has the same transformation properties as a translation, and the magnetic dipole transition moment $\boldsymbol{m}$, which transforms like a rotation. In Fig. 7, the arrows designate the direction of displacement of the hydrogen or ring nuclei for one phase of the mode. We make the approximation that the nuclear displacement produces a local electric dipole transition moment, which we position along the hydrogen or oxygen displacement; electric or magnetic dipole transition moment contributions from charge flow away from the local nuclear displacement are ignored. For each coordinate, the $\oplus$ or $\ominus$ for T_α indicates the direction of the electric dipole transition moment, $\boldsymbol{\mu} = \boldsymbol{\mu}_\alpha$, along the α axis for the phase of nuclear displacement shown. In determining the electric dipole transition moment directions, we use the results of *ab initio* molecular orbital calculations, which show that for an aliphatic CH contraction, positive $\boldsymbol{\mu}$ is directed C → H, whereas for CH

Can. J. Chem. Downloaded from www.nrcresearchpress.com by 84.41.108.74 on 09/07/12
For personal use only.

Can. J. Chem. Downloaded from www.nrcresearchpress.com by 84.41.108.74 on 09/07/12
For personal use only.

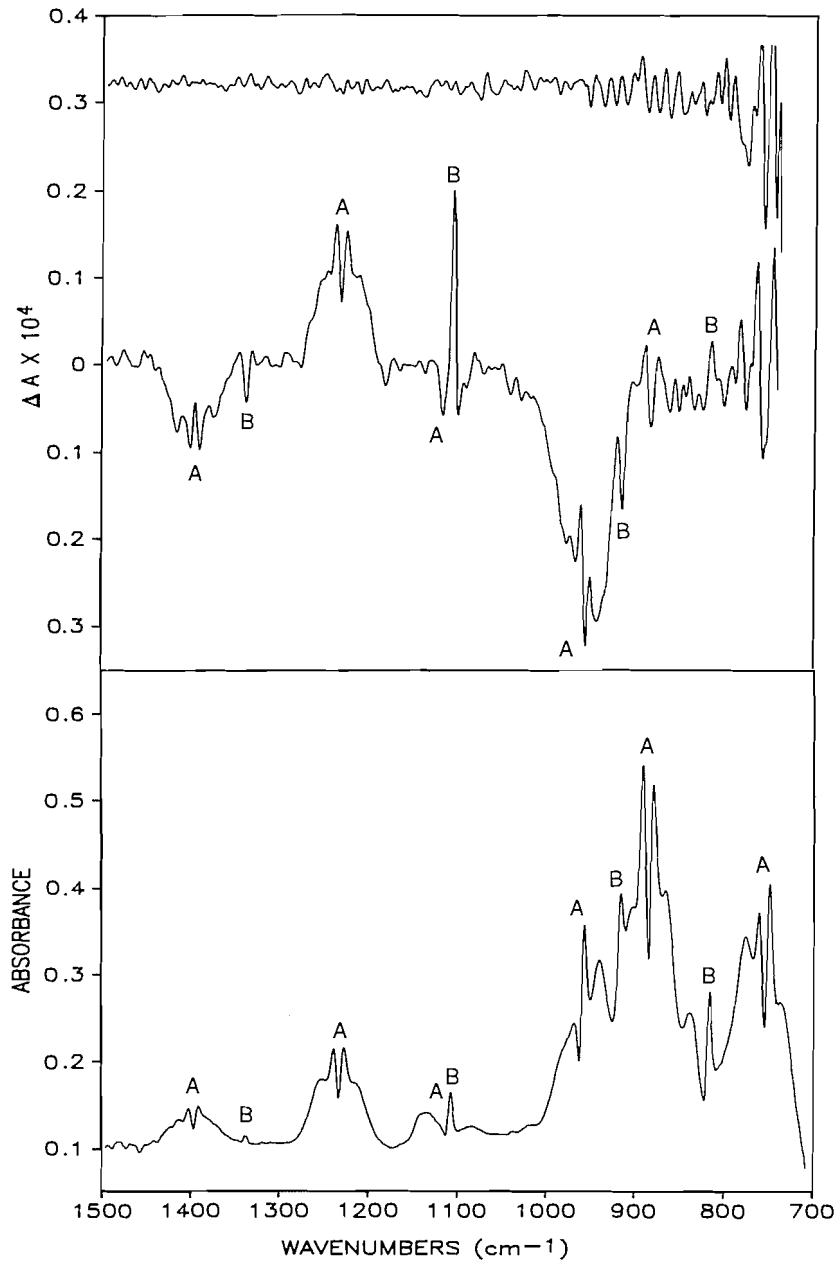


FIG. 3. Mid-infrared absorption and VCD spectra of a gas-phase sample of (*S,S*)-[2,3-$^2H_2$]oxirane; 20-mg sample, in a 5-cm path length, 25.4 mL volume cell, at 4 cm^{-1} resolution.

displacement perpendicular to the bond direction, positive μ is in the direction of hydrogen motion (36); for the ring modes, positive μ is in the direction opposite to that of the motion of the oxygen nucleus. The sign for each R_α indicates the direction of the magnetic dipole transition moment, $\boldsymbol{m} = \boldsymbol{m}_\alpha$, as determined by using the right-hand rule and the sense of circulation of positive charge. For the scissors, wag, rock, and twisting modes, the sense of charge circulation that defines the direction of $\boldsymbol{m}$ is readily determined from the sense of circulation of the displacement vectors, since the positive direction of each local electric dipole transition moment approximately coincides with the direction of the displacement vector for the hydrogen motion. For the CH stretches, the direction of $\boldsymbol{m}$ is deduced from the sense of circulation of the electric dipole transition moments (which are oposite in direction to the hydrogen displacements) about the coordinate axes placed at the center of mass. Although not forbidden by symmetry, the rotational character of the B_1 stretch and scissors modes (S_1 and S_8) is quite small and will be neglected. As expected for the achiral oxirane, none of the symmetry coordinates (or normal modes, which are linear combinations of coordinates of the same symmetry) can contribute to VCD intensity, since R_α and T_α, for the same direction α, do not transform as the same symmetry species.

Deuteriation of the *trans* CH bonds reduces the symmetry to the chiral point group C_2. The A_1 and A_2 species under C_{2v} symmetry both correlate to the A species (T_z,R_z) under C_2 symmetry; similarly, the B_1 and B_2 symmetry species both correlate to the B species (T_x,R_x,T_y,R_y). The normal modes of (*S,S*)-[2,3-$^2H_2$]oxirane can all be decomposed into linear combinations of the oxirane symmetry coordinates in Fig. 7. With this decomposition, the *trans* deuterium substitution can

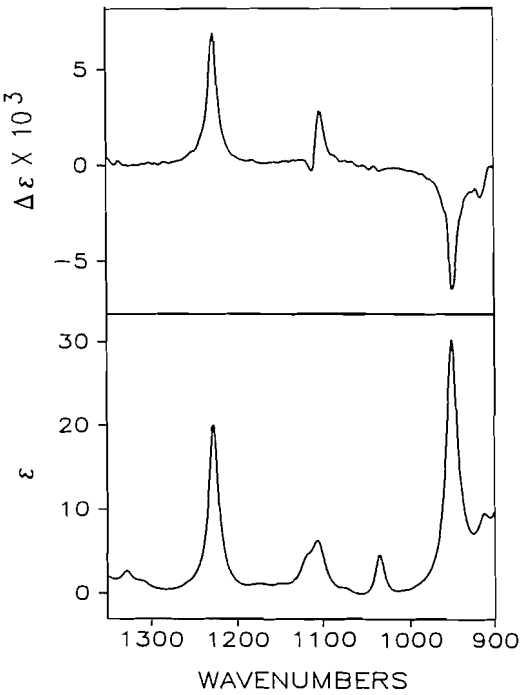


FIG. 4. Absorption and VCD spectra of (*S,S*)-[2,3-$^2H_2$]oxirane in the 900–1350 cm^{-1} region, 0.052 M in CS_2 solution, 0.8-cm path length, at 4 cm^{-1} resolution.

be considered as a chiral perturbation that mixes the A_1 and A_2 symmetry modes, or B_1 and B_2 symmetry modes, of the parent achiral oxirane. In Figs. 5 and 6, each (*S,S*)-[2,3-$^2H_2$]oxirane vibration is described by the oxirane symmetry coordinates, with relative phases indicated by + or −, that make the largest contributions to that mode. In addition, for each symmetry coordinate contribution, the translational and (or) rotational property and the directions of the electric and magnetic dipole transition moments are given. With this breakdown into translational (electric dipole) and rotational (magnetic dipole) contributions, the sign of the VCD for each (*S,S*)-[2,3-$^2H_2$]-oxirane mode is readily predicted from the directions of μ_α and m_α for each α, taking into account the relative sizes of opposing contributions. The decomposition of each mode into symmetry coordinate contributions can be deduced quantitatively from the calculated nuclear displacements. To assess opposing electric dipole moment contributions, we note that oxygen displacement results in a much larger electric dipole moment change than a comparable CH bending displacement. For unit displacements, the rocking displacement coordinates have larger projections than the twisting coordinates in the *xy* plane (Fig. 7) for the A_2 modes or in the *yz* plane for the B_2 modes, which result in a larger magnetic dipole transition moment due to local electric moment circulation from the rocking contributions to a mode, compared to a similar contribution from a twisting coordinate. In the following detailed descriptions, the modes are designated by our calculated frequencies.

The *B*-symmetry modes at 3040 and 2224 cm^{-1} arise from the in- and out-of-phase combinations of the B_1 and B_2 CH stretches, S_7 and S_{10}. The two modes are predicted to have similar VCD intensities of opposite sign, with the in-phase combination at 3040 cm^{-1} being positive. The *A*-symmetry modes at 3036 and 2239 cm^{-1} are the two linear combinations of the A_1 and A_2 symmetry coordinates S_1 and S_4. VCD intensities of similar magnitude but opposite sign, with the in-phase mode at 3036 cm^{-1} negative, are predicted. These predicted VCD intensity patterns agree with the observed CH- and CD-stretching spectra in Figs. 1 and 2.

The *A*-symmetry modes at 1397, 1235, and 947 cm^{-1} are found to be three linear combinations of the S_2 (A_1 CH_2-scissors) and S_5 (A_2 CH_2-rock), and either the S_{13} (A_1 in-phase ring stretch) or S_{14} (A_1 out-of-phase ring stretch) symmetry coordinates. In this case, the large electric dipole moment contribution from the ring stretch (due to the oxygen motion) dominates that from the CH_2-scissors. The A_2 CH_2-rock has a large rotational character. The modes at 1235 and 947 cm^{-1}, in which the electric dipole moment contributions from the ring stretch and CH_2-scissors are in the same direction, are predicted to have large absorption intensity (due to the ring motion) and large positive and negative VCD intensity (due to the relative phases of the ring stretch and CH_2-rock), respectively. In the mode at 1397 cm^{-1}, the electric dipole moment contributions from ring stretch and CH_2-scissors are in opposite directions, and the contribution from oxygen motion is smaller; these two factors reduce the magnitude of both the absorption and VCD intensity compared to the other two modes. The S_5 and S_{13} or S_{14} contributions have the same phase relationship in the 1397 and 947 cm^{-1} modes, and both are predicted to be negative. From Figs. 3 and 4, we observe that these three modes give rise to the three most dominant features in the VCD spectrum; the intensities follow the predicted sign and magnitude pattern, with the 1397 cm^{-1} mode being weaker than the other two.

The *B* mode at 1328 cm^{-1} is the in-phase combination of S_8 (B_1 CH_2-scissors) and S_{11} (B_2 CH_2-rock), and is predicted to have negative VCD intensity, as observed. This mode is much weaker in both absorbance and VCD than the *A* mode at 1397 cm^{-1} since there is no ring-stretching contribution. The S_8 and S_{11} symmetry coordinates contribute in small amounts to the lower frequency *B* modes; the lowest frequency mode at 646 cm^{-1} contains the out-of-phase combination of S_8 and S_{11}, in addition to a large contribution from S_{12} (B_2 CH_2-twist). With the assumption that the contributions from the rock dominate those from the twist, we predict weak positive VCD for the 646 cm^{-1} mode, which lies below the detection limit for our instrument. The absorption intensity is predicted to be small, since no oxygen motion is involved; the weak band observed at 673 cm^{-1} in the absorption spectrum (not shown) is comparable in intensity to the 1106 cm^{-1} band.

Four modes can be primarily described as linear combinations of CH_2 wag and twist. The pair of *A*-symmetry modes at 1123 and 726 cm^{-1} are the in- and out-of-phase combinations of S_3 (A_1 CH_2-wag) and S_6 (A_2 CH_2-twist), with the wag making the more dominant contribution to the higher frequency mode and the twist making the more dominant contribution to the lower frequency mode. When the modes are viewed as a projection in the *xz* plane, it is clear that the hydrogens are undergoing large displacement in the 1123 cm^{-1} mode, and the deuteriums in the 746 cm^{-1} mode. The 1123 cm^{-1} mode is predicted to be quite weak in absorbance, with negative VCD intensity, in agreement with observation. A contribution from S_{14} (A_1 ring stretch) to the 746 cm^{-1} mode should result in a large absorption intensity. This mode, predicted to have positive VCD, is observed as an intense absorption band at 754 cm^{-1}, at the detection limit of the VCD instrument where the VCD signal-to-noise ratio is poor. The pair of *B*-symmetry modes at 1117 and 918 cm^{-1} arise from in- and out-of-phase mixing of the S_9 (B_1 CH_2-wag) and S_{12} (B_2 CH_2-twist). The

Can. J. Chem. Downloaded from www.nrcresearchpress.com by 84.41.108.74 on 09/07/12
For personal use only.

Can. J. Chem. Downloaded from www.nrcresearchpress.com by 84.41.108.74 on 09/07/12
For personal use only.

TABLE 1. Comparison of observed and calculated frequencies and rotational and dipole strengths for (*S,S*)-[2,3-$^2H_2$]oxirane

	Frequencies (cm^{-1})			Rotational strengths ($esu^2\ cm^2 \times 10^{44}$)					Dipole strengths ($esu^2\ cm^2 \times 10^{39}$)				
	Observed		Calculated[a]	Observed[b]	Calculated[c]				Observed[b]	Calculated[c,d]			
	Gas	Solution[e]			MFP	LMO(I)	LMO(II)	VC		MFP	LMO(I)	LMO(II)	VC
B	3028	3027	3040	+11.4	+30.7	+10.6	+10.4	+14.4	5.3	5.65	5.00	4.52	5.06
A	3015	3014	3036	−8.9	−26.7	−18.2	−13.2	−11.8		0.89	0.90	0.49	0.61
A	2254	2252	2239	+12.1	+14.4	+7.9	+6.0	+13.2	0.57	1.06	1.05	0.56	0.72
B	2240	2232	2224	−10.4	−14.8	−2.9	−3.4	−12.0	2.7	5.11	4.55	4.01	4.48
A	1397		1397	(−15)	−10.0	−9.8	−9.5	−18.5	(1.2)	1.48	1.08	1.02	1.08
B	1339		1328	(−2.5)	−2.2	−2.6	−1.4	−0.9	0.23	0.19	0.12	0.08	0.12
A	1235	1226	1235	+24.1	+13.6	+17.4	+17.7	+19.2	2.96	3.26	2.87	2.59	2.87
A	1112	1109	1123	−4.9	+4.3	+3.3	+1.5	+3.3		0.10	0.07	0.06	0.07
B	1106	1102	1117	+11.1	+9.3	+7.8	+4.2	+14.1	0.86	1.09	0.93	0.90	0.93
A	961	948	947	−29.0	−40.8	−35.7	−34.3	−18.8	5.4	12.98	9.08	9.19	10.28
B	914	914	918	−6.2	−1.0	−4.1	−2.9	+5.7	0.63	2.42	2.30	1.88	2.09
A	885		871	(~+5)	+5.8	+30.5	+31.6	−5.5		16.29	14.53	11.71	12.99
B	817		820	(+)	+1.3	+2.7	+2.9	−2.1		6.09	5.75	4.17	4.52
A	754		751		+15.0	−6.7	−8.0	+2.1		15.68	19.00	12.76	14.03
B	673		646		+0.7	+0.2	+0.5	+3.4		0.12	0.11	0.27	0.18

[a]Calculated with *ab initio* force field of Lowe *et al.* (34) and experimental geometry of C. Hirose (35).

[b]Measured from integrated intensities for solution-phase sample for all bands except for values in parentheses, which were estimated from the relative intensities in the gas-phase spectrum.

[c]MFP = magnetic field perturbation, from ref. 12, with 6-31G(ext) basis; LMO(I) and LMO(II) = localized molecular orbital model, from ref. 14, with 6-31G(ext) and 6-31$\tilde{G}$(-2$\tilde{S}$,2$\tilde{P}$,2$\tilde{P}_H$) basis sets, respectively; VC = vibronic coupling, sum-over-states method, from ref. 15, 6-31$\tilde{G}$(-2$\tilde{S}$,2$\tilde{P}$,2$\tilde{P}_H$) basis.

[d]The dipole strength calculations are identified by the rotational strength method to which they correspond.

[e]C_2Cl_4 solution for CH- and CD-stretching modes; CS_2 solution for mid-infrared modes.

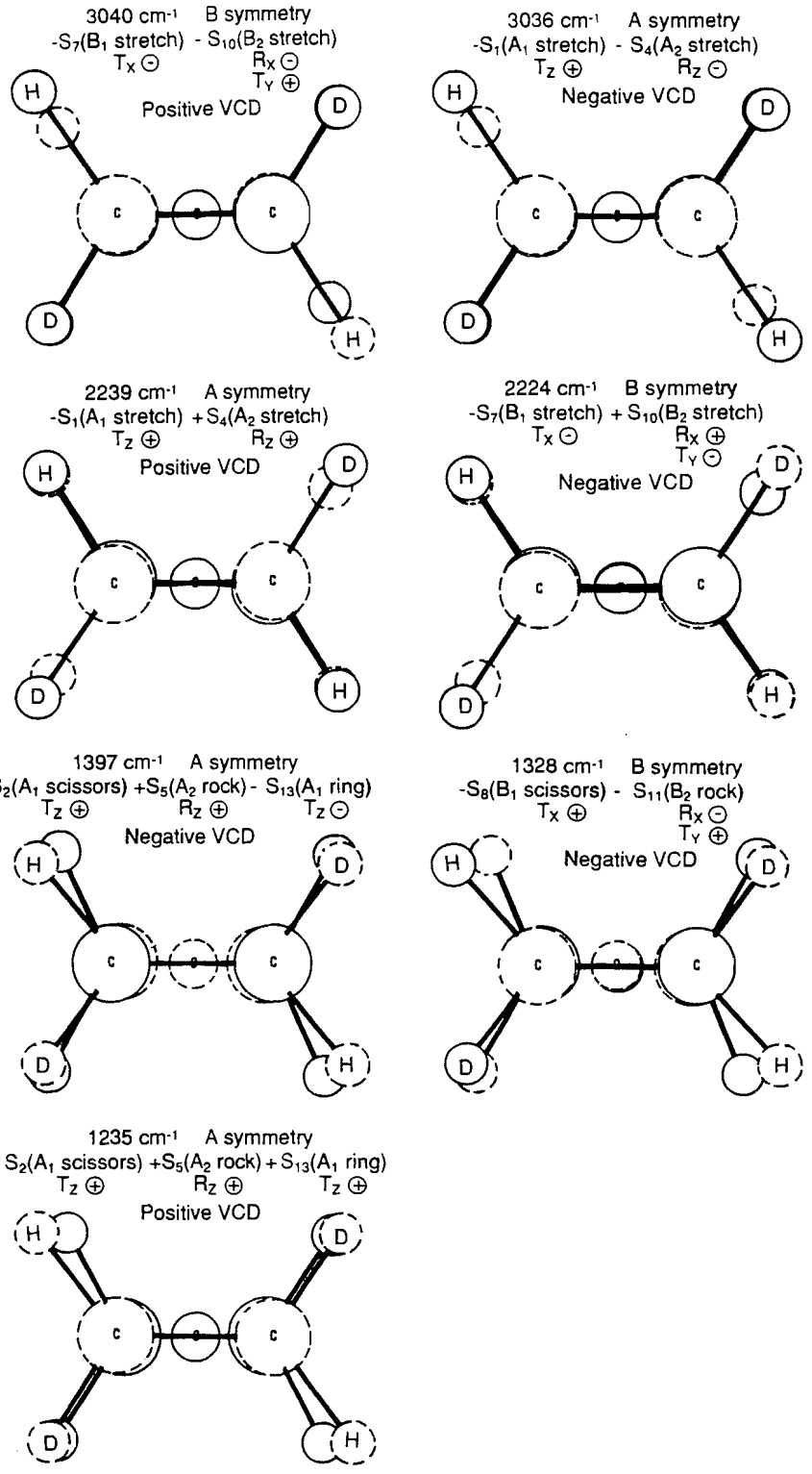


FIG. 5. Stereoprojections of the calculated vibrational normal modes of (*S*,*S*)-[2,3-$^2H_2$]oxirane between 3100 and 1200 cm^{-1}. Dotted and solid circles indicate nuclear positions at opposite extremes of the vibrational cycle. For each mode (in the phase of vibration from solid to dotted nuclear positions), the symmetry coordinates of the parent oxirane molecule (see Fig. 7), with phase indicated by + or −, that makes the largest contributions to the mode are identified. In addition, for each symmetry coordinate contribution, the translational (T_α) and (or) rotational (R_α) character is listed, and the direction of the electric dipole transition moment along the translational axis or magnetic dipole transition moment along the rotational axis is given.

Can. J. Chem. Downloaded from www.nrcresearchpress.com by 84.41.108.74 on 09/07/12
For personal use only.

Can. J. Chem. Downloaded from www.nrcresearchpress.com by 84.41.108.74 on 09/07/12
For personal use only.

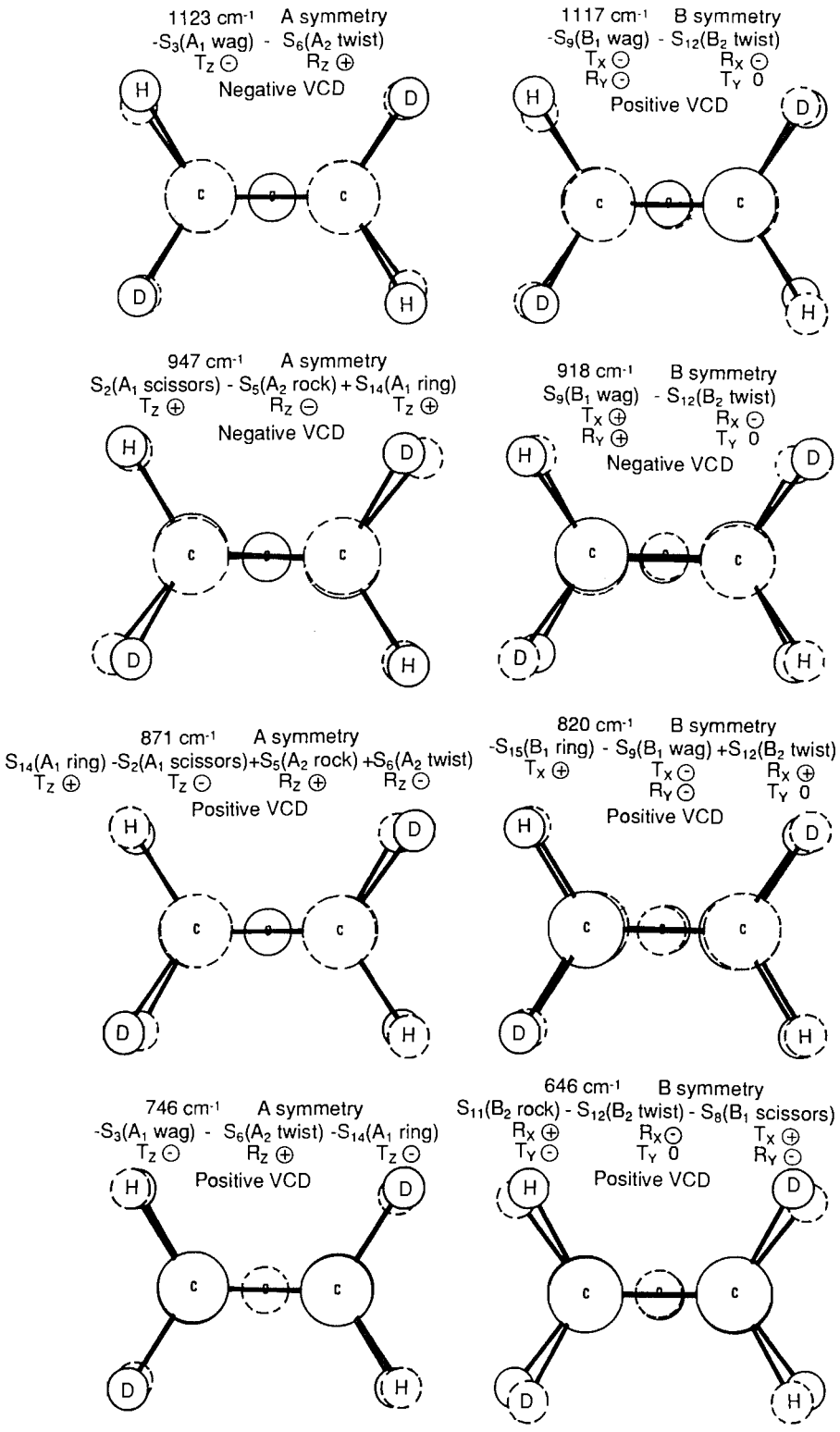


FIG. 6. Stereoprojections of the calculated vibrational normal modes of (*S*,*S*)-[2,3-$^2H_2$]oxirane between 1150 and 600 cm^{-1}. See Fig. 5 for description.

modes are predicted and observed to be a positive–negative VCD pair, with moderate absorption intensity.

The final two modes are primarily ring stretches. The most intense mode at 885 cm^{-1} corresponds to the calculated *A* mode at 871 cm^{-1}. In addition to the large contribution from the S_{14} (A_1 ring stretch) symmetry coordinate, small contributions from S_2 (A_1 CH_2-scissors), S_5 (A_2 CH_2-rock), and S_6 (A_2 CH_2-twist) are present. The magnetic dipole transition moment contributions from the A_2 rock and twist are in opposite directions, but since the rotational character of the rock is larger than that of the twist, we predict weak positive VCD, in agreement with the observed weak positive VCD at 880 cm^{-1}. The *B* ring stretch at

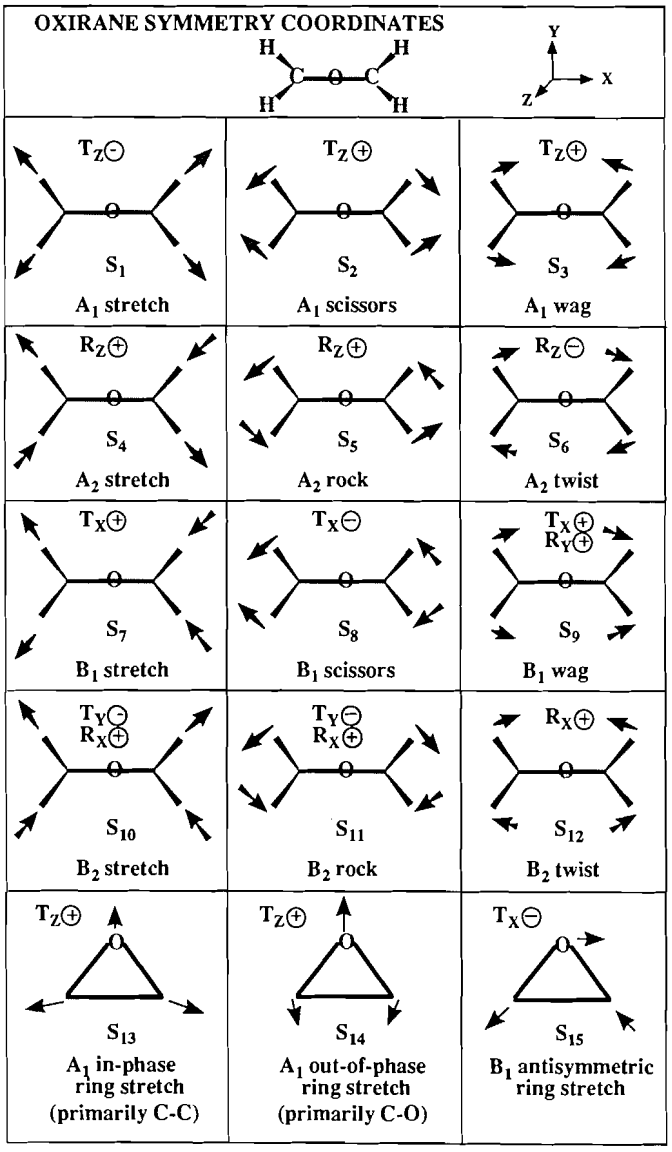


FIG. 7. Schematic diagram of symmetry coordinates for oxirane CH_2 stretch, scissors, wag, rock and twist, and ring stretching motion of symmetry species A_1, A_2, B_1, or B_2. T_α and R_α ($\alpha = x, y,$ or z) identify the translational and rotational character of the motion, respectively. The sign associated with T_α denotes the direction of the electric dipole transition moment due to linear displacement of positive charge along the α axis; the sign associated with R_α denotes the direction of the magnetic dipole transition moment due to positive charge circulation about the α axis.

820 cm^{-1}, primarily S_{15} (B_1 ring stretch), includes small amounts of S_9 (B_1 CH_2-wag) and S_{12} (B_2 CH_2-twist). Since S_{15} gives the predominant electric dipole transition moment contribution, weak positive VCD is predicted. Weak positive VCD intensity that coincides in frequency with the Q-branch of the 817 cm^{-1} mode is observed with signal-to-noise ratio ~2.

Discussion

Conceptualizing the vibrational modes of (*S,S*)-[2,3-$^2H_2$]-oxirane as arising from chiral perturbation of the modes of the parent oxirane molecule provides a lucid insight into the origin, sign, and relative magnitude of each VCD feature. With the vibrational force field employed here, and the approximation of local electric dipole moment contributions, we are able to predict all the observed VCD signs and relative intensities. The requirements for large VCD intensity are the presence of a large linear charge oscillation along an axis accompanied by a large amount of oscillating charge circulation about the same axis. For the most intense VCD features in (*S,S*)-[2,3-$^2H_2$]oxirane, the linear charge motion arises from oxygen displacement in the ring stretches; the charge circulation arises from the methylene group motions. The largest oxygen displacements occur in the mid-infrared modes of *A* symmetry, which are more intense than the *B*-symmetry modes. In contrast, in (*S,S*)-[1,2-$^2H_2$]-cyclopropane, where there is no oxygen in the ring, the *B* modes are more intense (24). The ring modes in (*S,S*)-[2,3-$^2H_2$]-oxirane at 885 and 817 cm^{-1}, which involve large oxygen displacement but only small contributions from angular methylene motion, exhibit small VCD anisotropy ratios. In the CH- and CD-stretching regions, the net linear charge oscillation is larger for the *B* modes, but the charge circulation is larger for the *A* modes. As a result, nearly conservative VCD couplets are observed in each region.

The approach taken in this study to understand the origin of the VCD features in molecules that are chiral due to isotopic substitution also serves to demystify the results of calculations of VCD intensities for (*S,S*)-[2,3-$^2H_2$]oxirane using various *ab initio* methods (12, 14, 15), and to provide insight into the discrepancies between observed and calculated VCD signs and intensities. Calculations on (*S,S*)-[2,3-$^2H_2$]oxirane using three different approaches have appeared in the recent literature: the magnetic field perturbation (MFP) method of Stephens and co-workers (6, 12, 13), the implementation for *ab initio* wavefunctions by Polavarapu and Bose (14) of the localized molecular orbital (LMO) method of Nafie and Walnut (1, 2), and the implementation by Dutler and Rauk (15) of the sum-over-states vibronic coupling formulation of Nafie and Freedman (3). In addition, the absorption and VCD intensities in the CH- and CD-stretching regions have been calculated with the random phase approximation (37), which gave results similar to, but slightly smaller than, the magnetic field perturbation method. We present in Table 1 a comparison of the observed intensities with the results of the three calculations (12, 14, 15) that reported all the normal modes. It must be noted that none of the three calculations or our analysis were carried out with precisely the same geometry and normal mode nuclear displacements. The LMO calculations were carried out with an unscaled force field, whereas both the MFP and VC calculations employed scaled force fields that give similar good agreement with experiment. Our analysis (4-31G basis set), and the MFP and LMO(I) calculation (6-31G(ext) basis) employed the experimental geometry; the LMO(II) and VC calculations employed the optimized geometry for the basis set used (6-31$\tilde{G}$(-2$\tilde{S}$,2$\tilde{P}$,2$\tilde{P}_H$)). In Table 1, we have identified each dipole strength calculation by the rotational strength calculational method with which it is associated. The dipole strength calculations are of course not model dependent; the differences in calculated dipole strength for a given mode reflect the differences in geometry, scaling, and basis set used.

Overall, all three calculations reproduce the VCD and absorption intensity patterns. There are some notable discrepancies. The *A* mode at 1112 cm^{-1} is calculated with the incorrect sign with all three approaches. Our analysis shows that this mode has a small electric dipole transition moment contribution from ring stretch that is opposite in direction to the contribution from S_3 (A_1 wag). The correct sign is obtained if the wag

Can. J. Chem. Downloaded from www.nrcresearchpress.com by 84.41.108.74 on 09/07/12
For personal use only.

Can. J. Chem. Downloaded from www.nrcresearchpress.com by 84.41.108.74 on 09/07/12
For personal use only.

contribution determines the net electric dipole moment direction. If the calculations are overestimating the contribution from oxygen motion, the incorrect sign would result. A comparison of the observed and calculated dipole strengths for the modes that involve ring stretches suggests that this may indeed be the case; for example, the calculated absorption intensity of the 961 cm^{-1} mode is much too large.

The rotational strengths for the two CH-stretching modes calculated with the MFP approach (12) are two to three times larger than both the observed values and those calculated by the other two methods, which agree well with experiment. Although a VCD couplet with the observed magnitude can be simulated from the MFP rotational strengths by decreasing the frequency separation between the two modes to allow extensive cancellation of two Lorentzian bands of opposite sign, the resulting band shapes in the simulated spectrum do not agree with the observed spectrum. In comparing the observed and calculated rotational strengths for (*S,S*)-cyclopropane-1,2-$^2H_2$, we have found a similar disagreement for the MFP calculations in the CH-stretching region.[2]

For the rotational strengths of the five lowest frequency modes, there are several differences in sign for the three calculations, and the magnitude for the 885 cm^{-1} ring mode calculated by the LMO method is much larger than that obtained by experiment. Unfortunately, our instrumentation does not allow observation of the VCD bands for the two lowest frequency modes, and the VCD features for the 885 and 817 cm^{-1} modes are only slightly above the noise level. From our analysis of the oxirane symmetry coordinate contributions to the (*S,S*)-[2,3-$^2H_2$]oxirane normal modes, we find that these five modes in general involve ring stretching and methylene motions that in some cases generate electric dipole transition moment contributions in opposite directions, and (or) two different methylene motions that produce magnetic dipole transition moment contributions in opposite directions. Since none of the calculations used precisely the same force field and geometry, some of the differences among the calculations may lie in the form of the normal modes used, reflected in differences among these opposing contributions to the modes. Alternatively, the three calculational approaches, as implemented, may place different importance on the various electronic contributions to the rotational strengths. Without employing the same normal mode nuclear displacement vectors with all three approaches, it is not possible to use the comparison with experiments as a way to rank the accuracy of the various calculational approaches.

The CH- and CD-stretching VCD couplets can also be calculated with the coupled oscillator model, $R^{\pm} = \mp\pi\nu_0 \boldsymbol{R}_{12} \cdot \boldsymbol{\mu}_1 \times \boldsymbol{\mu}_2$, where the + and − signs refer to the in- and out-of-phase modes, respectively; ν_0 is the unperturbed frequency of a single isolated oscillator; $\boldsymbol{R}_{12}$ is the separation vector between oscillators 1 and 2; and $\boldsymbol{\mu}_1$ and $\boldsymbol{\mu}_2$ are the electric dipole transition moments for the uncoupled oscillators. With $|\boldsymbol{\mu}_i| = (D/2)^{1/2}$, where D is the total dipole strength obtained from the integrated absorption intensity, we calculate $R^+ = -6.04 \times 10^{-44}$ esu^2 cm$_2$ for the *A*-symmetry CH stretch and $R^+ = -2.71 \times 10^{-44}$ esu^2 cm^2 for the *A*-symmetry CD stretch, if we assume that the electric dipole transition moment lies along the bond axis. These values agree in sign with the observed spectra, but are too small in magnitude. Stephens *et al.* (12) calculate an angle between the bond direction and electric dipole transition moment of 16.0° and 22.6° for the CH and CD stretch, respectively. Placing the electric dipole transition moment vector off the bond axis (which is reasonable for a charge flow contribution to the CH stretch from the adjacent CO bond) results in a larger coupled oscillator rotational strength, but introduces an uncertainty into the location of the separation vector (12). Although some adjacent *A* and *B* symmetry modes in the mid-infrared region appear to have in- and out-of-phase relationships between *trans* CH or CD motions (Figs. 5 and 6), these modes cannot be analyzed in terms of isolated coupled oscillators, due to the differing contributions from ring stretches.

The vibrational modes of (*S,S*)-[2,3-$^2H_2$]oxirane consist of coupled nuclear motion with translational and rotational characteristics. The electronic motion in this molecule for the most part appears to follow hae nuclear motion or to result in charge flow within a bond or two adjacent bonds. There is no extended region in the molecule for charge flow to occur in the absence of nuclear motion. It is reasonable, therefore, to obtain a satisfactory descriptive analysis of the VCD intensities based only on the arrangement of local electric dipole moment contributions as deduced from the nuclear displacements. For this type of normal mode, it is also reasonablle that all three calculational approaches should yield similar, satisfactory rotational strengths, since the calculated dipole strengths agree adequately with experiment. We previously postulated that the positive VCD intensity in the CH-stretching region of (*S,S*)-[2,3-$^2H_2$]oxirane resulted from vibrationally generated ring current in the three-membered ring (23). That proposal is not valid, The difference in intensity between the *A* and *B* symmetry CH stretches is adequately reproduced in the MFP and VC calculations and can be attributed to differences due to symmetry in the contributions from charge flow in the CO bonds (38).

Acknowledgments

We acknowledge support for this work from the National Institutes of Health via grant GM-23567 to T.B.F. and L.A.N. and grant GM-36285 to J.M.S. We are grateful to S. J. Cianciosi for his assistance in sample preparation.

1. L. A. Nafie and T. H. Walnut. Chem. Phys. Lett. **49**, 441 (1977).
2. T. H. Walnut and L. A. Nafie. J. Chem. Phys. **67**, 1491 (1977); **67**, 1501 (1977).
3. L. A. Nafie and T. B. Freedman. J. Chem. Phys. **78**, 7108 (1983).
4. L. A. Nafie. J. Chem. Phys. **79**, 4950 (1983).
5. T. B. Freedman and L. A. Nafie. J. Chem. Phys. **89**, 374 (1988).
6. P. J. Stephens. J. Phys. Chem. **89**, 748 (1985).
7. P. J. Stephens. J. Phys. Chem. **91**, 1712 (1987).
8. A. D. Buckingham, P. W. Fowler, and P. A. Galwas. Chem. Phys. **112**, 1 (1987).
9. M. A. Lowe, G. A. Segal, and P. J. Stephens. J. Am. Chem. Soc. **108**, 248 (1986).
10. R. D. Amos, N. C. Handy, K. J. Jalkanen, and P. J. Stephens. Chem. Phys. Lett. **133**, 21 (1987).
11. K. J. Jalkanen, R. W. Kawiecki, P. J. Stephens, and R. D. Amos. J. Phys. Chem. **94**, 7040 (1990).
12. P. J. Stephens, K. J. Jalkanen, and R. W. Kawiecki. J. Am. Chem. Soc. **112**, 6518 (1990).
13. K. J. Jalkanen, P. J. Stephens, R. D. Amos, and N. C. Handy. J. Am. Chem. Soc. **110**, 2012 (1988).
14. P. L. Polavarapu and P. K. Bose. J. Chem. Phys. **93**, 7524 (1990).

[2]T. B. Freedman, K. M. Spencer, N. Ragunathan, S. J. Cianciosi, and J. E. Baldwin. In preparation.

15. R. DUTLER and A. RAUK. J. Am. Chem. Soc. **111**, 6957 (1989).
16. A. RAUK, R. DUTLER, and D. YANG. Can. J. Chem. **68**, 258 (1990).
17. T. B. FREEDMAN and L. A. NAFIE. *In* Topics in stereochemistry. Vol. 17. *Edited by* E. Eliel and S. Wilen. Wiley, New York. 1987. pp. 113–206.
18. P. J. STEPHENS and M. A. LOWE, Annu. Rev. Phys. Chem. **36**, 213 (1985).
19. T. A. KEIDERLING. *In* Practical Fourier transform infrared spectroscopy. *Edited by* J. R. Ferraro and K. Krishnan. Academic Press, San Diego. 1990. pp. 203–283.
20. P. L. POLAVARAPU. *In* Vibrational spectra and structure. Vol. 13. *Edited by* J. R. Durig. Elsevier Publishing, Amsterdam. 1984. pp. 103–160.
21. L. A. NAFIE. *In* Advances in infrared and Raman spectroscopy. Vol 11. *Edited by* R. J. M. Clark and R. E. Hester. Wiley–Heyden, London. 1984. p. 49.
22. P. L. POLAVARAPU and P. K. BOSE. J. Phys. Chem. **95**, 1606 (1991).
23. T. B. FREEDMAN, M. G. PATERLINI, N.-S. LEE, L. A. NAFIE, J. M. SCHWAB, and T. RAY. J. Am. Chem. Soc. **109**, 4247 (1987).
24. S. J. CIANCIOSI, K. M. SPENCER, T. B. FREEDMAN, L. A. NAFIE, and J. E. BALDWIN. J. Am. Chem. Soc. **111**, 1913 (1989).
25. T. B. FREEDMAN, K. M. SPENCER, C. MCCARTHY, S. J. CIANCIOSI, J. E. BALDWIN, L. A. NAFIE, J. A. MOORE, and J. M. SCHWAB. Proc. SPIE-Int. Soc. Opt. Eng. **1145**, 273 (1989).
26. T. B. FREEDMAN, S. J. CIANCIOSI, N. RAGUNATHAN, J. E. BALDWIN, and L. A. NAFIE. J. Am. Chem. Soc. In press.
27. J. M. SCHWAB, T. RAY, and C.-K. HO. J. Am. Chem. Soc. **111**, 1057 (1989).
28. J. A. DALE, D. L. DULL, and H. S. MOSHER. J. Org. Chem. **34**, 2543 (1969).
29. (*a*) M. DIEM, P. J. GOTKIN, J. M. KUPFER, A. G. TINDALL, and L. A. NAFIE. J. Am. Chem. Soc. **99**, 8103 (1977); (*b*) M. DIEM, P. J. GOTKIN, J. M. KUPFER, and L. A. NAFIE. J. Am. Chem. Soc. **100**, 5644 (1978); (*c*) M. DIEM, E. PHOTOS, H. KHOURI, and L. A. NAFIE. J. Am. Chem. Soc. **101**, 6829 (1979).
30. E. LIPP and L. A. NAFIE. Appl. Spectrosc. **38**, 20 (1984).
31. K. M. SPENCER. Ph.D. thesis, Syracuse University, 1989.
32. G. HERZBERG. Infrared and Raman spectra of polyatomic molecules. Van Nostrand, Princeton, NJ. 1945. Chap. IV.
33. R. M. BADGER and L. R. ZUMWALT. J. Chem. Phys. **6**, 711 (1938).
34. M. A. LOWE, J. S. ALPER, R. KAWIECKI, and P. J. STEPHENS. J. Phys. Chem. **90**, 41 (1986).
35. C. HIROSE. Bull. Chem. Soc. Jpn. **47**, 1311 (1974).
36. K. B. WIBERG and J. J. WENDOLOSKI. J. Phys. Chem. **88**, 586 (1984).
37. K. J. JALKANEN, P. J. STEPHENS, P. LAZZERETTI, and R. ZANASI. J. Phys. Chem. **93**, 6583 (1989).
38. P. L. POLAVARAPU and P. K. BOSE. Chem. Phys. Lett. **143**, 337 (1988).

Can. J. Chem. Downloaded from www.nrcresearchpress.com by 84.41.108.74 on 09/07/12
For personal use only.

Molecular orbital studies of the singlet and triplet states of formylmethylene conformers

RATNAKAR K. GOSAVI, MANUEL TORRES, AND OTTO P. STRAUSZ[1]
Department of Chemistry, University of Alberta, Edmonton, Alta., Canada T6G 2G2

Received April 30, 1991

This paper is dedicated to Dr. Richard Norman Jones

RATNAKAR K. GOSAVI, MANUEL TORRES, and OTTO P. STRAUSZ. Can. J. Chem. **69**, 1630 (1991).

The energies and geometries of the low-lying electronic states of formylmethylene have been calculated at the SCF and CI levels using 6-31G** basis set. In agreement with previous reports and accumulated experimental observations, the ground state is the carbenoid triplet with a planar geometry. Also, in agreement with all previous single configuration SCF and CI calculations, the lowest excited singlet state is computed to be the nonplanar closed shell carbenoid structure. In contrast, accumulated experimental evidence along with previously reported MC–SCF results require this state to be planar. The present calculation predicts the existence of a (σ–σ) 1,3-diradical $^1A'$ state, which appears to be identical to the MC–SCF lowest singlet state, but this state lies some 11 kcal/mol above the closed shell carbenoid ^1A state. Apparently, single configuration SCF methods are inadequate for the correct description of the electronic manifold of formylmethylene.

Key words: formylmethylene, singlet and triplet states, *ab initio* MO calculations, conformers, molecular structure.

RATNAKAR K. GOSAVI, MANUEL TORRES et OTTO P. STRAUSZ. Can. J. Chem. **69**, 1630 (1991).

On a calculé les énergies et les géométries des états électroniques inférieurs du formylméthylène à des niveaux SCF et CI, en utilisant un ensemble de base 6-31G**. En accord avec les données rapportées antérieurement et les observations expérimentales accumulées, l'état fondamental est le triplet carbénoïde avec une géométrie plane. De plus, en accord avec tous les calculs SCF et CI de configuration unique, on a calculé que l'état singulet excité le plus bas possède la structure carbénoïde non planaire, à couche fermée. Par ailleurs, les données expérimentales accumulées ainsi que les résultats MC–SCF rapportés antérieurement indiquent que cet état est plan. Les calculs rapportés ici prédisent l'existence d'un état (σ–σ) 1,3-radicalaire, $^1A'$, qui semble être identique à l'état singulet le plus bas du MC–SCF; toutefois, l'énergie de cet état est 11 kcal/mol plus élevée que celle de l'état carbénoïde à couche fermée, ^1A. Apparemment, les méthodes SCF à configuration unique sont inadéquates pour décrire correctement des divers états électroniques du formylméthylène.

Mots clés : formylméthylène, états singulet et triplet, calculs d'OM *ab initio*, conformères, structure moléculaire.

[Traduit par la rédaction]

Introduction

Ketocarbenes and oxirenes have been postulated as intermediates in the Wolff rearrangement of α-diazoketones. There have been several theoretical studies reported in the literature (1–20) on the structures and electronic states of ketocarbenes and related oxirenes, and numerous attempts have been made to explain the mechanism of their reactions. All the *ab initio* molecular orbital calculations reported have been performed on the isomers of the parent C_2H_2O. All closed shell RHF–SCF geometry optimizations predicted a nonplanar geometry for the lowest singlet state of formylmethylene, with the hydrogen atom H_5 (Fig. 1a) on the carbene carbon, C_2, lying above the CCO plane. In contrast, photolysis and thermolysis studies (21–24) of α-diazoketones have shown that their ketocarbene decomposition products occur in geometric conformer pairs and therefore must have a planar geometry, and that the conformation of the more abundant conformer agrees with the conformation of the parent α-diazoketone and, thus, the conformation is maintained in the decomposition. The only *ab initio* calculation that has predicted the correct planar geometry for the lowest excited singlet state of formylmethylene is the recent multi-configuration SCF calculation by Robb and co-workers (15) indicating a σ–σ 1,3-diradical structure with an energy 5.5 kcal/mol higher than the cylic oxirene isomer.

After submission of the present article a paper by Schaefer and co-workers (20) came to our attention, reporting some coupled-cluster calculations on oxirene. The part of this paper that is relevant to the present work is the statement that in the b_2 ring deformation in oxirene leading in the direction of carbenoid closed shell singlet formylmethylene, where Radom and co-workers (11) were able to locate the transition state between oxirene and formylmethylene ^1A at the 4-31G SCF level of theory, Schaefer and co-workers found that formylmethylene is not a minimum at the double zeta plus polarization function with configuration interaction calculations involving single and double excitations.

ESR studies of several ketocarbenes (25–28) have shown that these carbenes have a triplet ground state with planar geometry and also that in most cases the conformation of the most abundant triplet ketocarbene is the same as that of the precursor diazoketone. Recently some highly strained ketocarbenes have been isolated in sufficiently high concentration so that their UV-visible and infrared spectra (27, 28) could be recorded. Earlier *ab initio* molecular orbital calculations (5) on formylmethylene with partially optimized geometry using STO-3G + 3*d* functions on the carbene carbon with the open shell RHF–SCF method predicted a planar triplet as the ground state. At the same level of calculations the closed shell lowest singlet state was 25 kcal/mol higher in energy than the triplet ground state.

Preliminary results of Tanaka and Yoshimine (9) have also shown that formylmethylene has a triplet ground state with a planar geometry and that the lowest singlet state, lying 20 kcal/mol above the triplet ground state, has a closed shell nonplanar geometry. Harding and Wagner (13) optimized the geometry for the low-lying $^3A''$ and $^3A'$ states of formylmethylene with double zeta plus polarization functions, at the RHF–SCF, CISD, and CISDQ levels and found that the $^3A''$ state is

[1]Author to whom correspondence may be addressed.

Can. J. Chem. Downloaded from www.nrcresearchpress.com by 84.41.108.74 on 09/07/12
For personal use only.

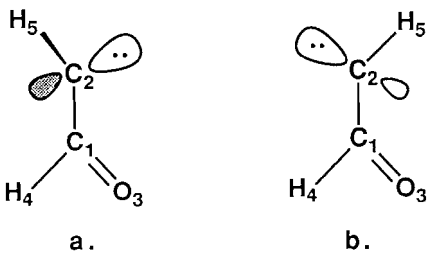


FIG. 1. Carbenoid closed shell structure of formylmethylene.

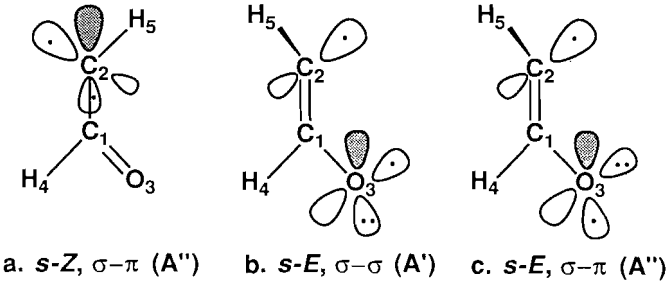


FIG. 2. Diradical structures of formylmethylene.

lower than the $^3A'$ state by 29 kcal/mol. The $^3A'$ state had a 1,3-diradical structure with a carbon–oxygen single bond and a carbon–carbon double bond, whereas the $^3A''$ state had a carbenoid structure with a carbon–oxygen double bond and a carbon–carbon single bond.

The MC–SCF computations (15) with 6-31G* basis set and complete geometry optimization, using reference space with only two active π orbitals and two active σ orbitals, predicted a σ–σ type diradical for the lowest singlet ($^1A'$) and triplet ($^3A'$) states. However, in calculations using five active orbitals (three π and two σ) the σ–π triplet ($^3A''$) state turned out to have a lower energy than the σ–σ triplet state, $^3A'$. These calculations also predicted the triplet to be the ground state for formylmethylene, and the σ–σ diradical ($^1A'$) singlet state to be the lowest singlet state, which is only 1.3 kcal/mol higher in energy than the $^3A'$ state.

Knowledge of the structure and conformation of the lowest singlet state of formylmethylene is important with respect to the interpretation of the mechanism of the decomposition of α-diazoketones and, as has recently been shown, to the reactivity of ketocarbenes (29). Since there are no calculations reported in the literature on the relative energies of the geometric conformers of singlet and triplet states of formylmethylene, we carried out a series of *ab initio* molecular orbital calculations on the conformer pairs of the low-lying electronic states of formylmethylene, including both the lowest singlet and triplet states.

Methods

The singlet state of formylmethylene can be represented either as a closed shell carbene, Fig. 1, or as an open shell diradical structure, Fig. 2. The open shell structures can be represented as either a carbene in which both unpaired electrons are localized on carbene carbon, C_2, with one electron in the σ and the other in the π orbital, giving an A'' state (Fig. 2a), or as a 1,3-diradical in which one electron is localized on the carbene carbon, C_2, in the σ orbital, and the other on the oxygen atom. Depending on the occupation of the single unpaired electron on the oxygen atom, namely, whether it is in the in-plane σ orbital, Fig. 2b, or in the perpendicular π orbital relative to the CCO plane, Fig. 2c, a (σ–σ) A' or (σ–π) A'' state will result, respectively. All molecular parameters were optimized at the SCF level by the energy gradient method with 6-31G** basis set (30). The RHF open shell SCF method was used for the lowest singlet and triplet-state energy calculations of the diradical isomers. It is known that the geometry optimization by the RHF–SCF open shell method tends to overestimate the stability of the extreme localized structures (31–33). This has been overcome by the geometry optimization at the CI level, which usually gives the delocalized structure with a global minimum. Configuration interaction calculations including singly and doubly excited configurations (CISD) with respect to the SCF configuration were performed using the direct CI method (34) at the SCF optimized geometry. Quadruple excitation correction was calculated by Davidson's formula (35) and added to the CI results (CISDQ). Only the lowest 30 orbitals ($24a' + 6a''$ in the C_s symmetry structures) were used in the CI calculations, with the lowest three orbitals corresponding to the carbon and oxygen 1*s* core orbitals kept doubly occupied and frozen. Partial optimization of the geometry at the CISDQ level was done by the stepwise method. All computations were performed with the modified version of the Gaussian 82 program (36), the Monstergauss Program (37).

Results and discussion

The optimized molecular parameters of all carbene and diradical isomers of formylmethylene at the SCF level are summarized in Table 1. Calculated total energies at the SCF and CI level of all isomers at the SCF optimized geometry are tabulated in Table 2, along with the relative energies at the CISDQ level with respect to the $^3A''$ ground state of the diradical structure of formylmethylene.

The computational results predict the triplet, $^3A''$, as the ground state of formylmethylene with an *s-Z* conformation and both unpaired electrons localized on the carbene carbon, C_2, one in the σ and the other in the π orbital (Fig. 2a). Earlier, Harding and Wagner (13) also reported a similar electronic structure for the $^3A''$ ground state and our optimized molecular parameters (Table 1) are in good agreement with their values optimized with double zeta plus polarization functions. The corresponding triplet *s-E* conformer with the same electronic configuration is only 1.4 kcal/mol higher in energy than the *s-Z* conformer. The energy barrier for *s-Z* to *s-E* isomerization in the triplet ground state is 9.0 kcal/mol, with the terminal H atom being linear with the C—C bond. The molecular parameters for the two conformers are quite similar (Table 1). The next excited triplet state has an A', σ–σ structure with the two unpaired electrons localized on different centers, C_2 and O, with an *s-Z* configuration, which is 26.1 kcal/mol above the ground state triplet ($^3A''$). The optimized molecular parameters (Table 1) are in good agreement with earlier reported values (13), and the $^3A'' - {}^3A'$ energy difference calculated at the CISDQ level with SCF optimized geometry (26.1 kcal/mol) is very close to the value of 29.1 kcal/mol obtained with the geometry optimization at the CISDQ level (13). The $^3A'$ *s-E* conformer is isoenergetic with the *s-Z* conformer, and their optimized molecular parameters are also very close to one another (Table 1) and in agreement with the MC–SCF optimized values (15). The energy barrier for the *s-Z* to *s-E* isomerization in the $^3A'$ state is 5.2 kcal/mol, which is smaller than in the $^3A''$ ground state. These results are consistent with the experimental (25–28) and earlier theoretical (5, 7, 9, 13, 15) prediction that formylmethylene and its substituted derivatives have a triplet ground state. MC–SCF calculations reported by Novoa *et al.* (15) also predicted that the lowest triplet state has a σ–π structure, but the authors did not report the total energy and electronic configuration of this state, nor the energies for the *s-Z* conformers. All the calculations they reported were for the *s-E* conformers with σ–σ structure (A' states).

Can. J. Chem. Downloaded from www.nrcresearchpress.com by 84.41.108.74 on 09/07/12
For personal use only.

TABLE 1. Optimized molecular parameters of formylmethylene conformers, with 6-31G** basis set at the SCF level. Bond distances are in (Å) and bond angles are in degrees

State	Conformer	$R(C_1—C_2)$	$R(C_1—O_3)$	$R(C_1—H_4)$	$R(C_2—H_5)$	$<C_2C_1O_3°$	$<C_2C_1H_4°$	$<H_5C_2C_1°$
Carbenoid closed shell								
^1A		1.443	1.192	1.108	1.091	128.94	108.30	111.01[a]
($^1A'$	*s-E*	1.524	1.189	1.095	1.097	119.67	120.69	106.29)[b]
($^1A'$	*s-Z*	1.528	1.191	1.090	1.094	122.97	116.52	103.72)[b]
($^1A'$	Linear	1.358	1.208	1.111	1.061	132.07	105.06	180.00)[b]
Carbenoid double open shell								
($^1A''$	*s-E*	1.411	1.205	1.097	1.071	125.24	113.69	135.69)[c]
($^1A''$	*s-Z*	1.416	1.208	1.088	1.071	121.71	116.68	135.81)[c]
($^1A''$	Linear	1.413	1.204	1.092	1.059	124.18	115.27	180.00)[c]
$^3A''$	*s-E*	1.458	1.191	1.096	1.073	124.04	114.90	128.85
$^3A''' \pm$	*s-Z*	1.458	1.193	1.092	1.074	122.96	115.59	128.09
$^3A''$	Linear	1.443	1.192	1.092	1.059	124.28	114.89	180.00
1,3-Diradical								
$^1A'$	*s-E*	1.304	1.347	1.080	1.068	125.78	123.38	132.63
$^1A'$	*s-Z*	1.304	1.349	1.079	1.069	127.62	122.23	136.48
$^1A'$	Linear	1.292	1.354	1.081	1.055	127.15	123.64	180.00
$^1A''$	*s-E*	1.312	1.347	1.080	1.071	121.63	121.36	133.83
$^1A''$	*s-Z*	1.312	1.351	1.077	1.071	120.59	122.28	134.59
$^1A''$	Linear	1.303	1.351	1.080	1.057	122.08	122.00	180.00
$^3A'$	*s-E*	1.302	1.342	1.081	1.067	125.43	123.53	133.95
$^3A'$	*s-Z*	1.301	1.347	1.080	1.068	127.76	122.25	137.50
$^3A'$	Linear	1.288	1.351	1.083	1.055	127.18	123.84	180.00

[a]Out-of-plane $<H_4C_1C_2O_3 = 175.82°$, $<H_5C_2C_1O_3 = 95.37°$.
[b]Saddle points with critical point order one.
[c]Disappear on geometry optimization at the CISDQ level.

TABLE 2. Total energies (au) and relative energies (kcal/mol) of formylmethylene conformers at SCF optimized geometry with 6-31G** basis set

State	Conformer	E_{SCF}	E_{CISD}	E_{CISDQ}	ΔE_{CISDQ}
Carbenoid closed shell					
^1A		−151.611630	−151.845280	−151.867797	18.07
($^1A'$	*s-E*	−151.589896	−151.825963	−151.849605	29.49)[a]
($^1A'$	*s-Z*	−151.593377	−151.828409	−151.851682	28.18)[a]
($^1A'$	Linear	−151.587099	−151.819267	−151.841244	34.73)[a]
Carbenoid double open shell					
($^1A''$	*s-E*	−151.592074	−151.821884	−151.843906	33.06)[b]
($^1A''$	*s-Z*	−151.592277	−151.822778	−151.845172	32.27)[b]
($^1A''$	Linear	−151.582567	−151.809939	−151.831551	40.82)[b]
$^3A''$	*s-E*	−151.649769	−151.873743	−151.894362	1.40
$^3A''$	*s-Z*	−151.650828	−151.875644	−151.896597	0.00
$^3A''$	Linear	−151.630007	−151.860125	−151.882288	8.98
1,3-Diradical					
$^1A'$	*s-E*	−151.609574	−151.828856	−151.849771	29.38
$^1A'$	*s-Z*	−151.608068	−151.827923	−151.848927	29.91
$^1A'$	Linear	−151.596819	−151.817940	−151.839072	36.10
$^1A''$	*s-E*	−151.610458	−151.830983	−151.852166	27.88
$^1A''$	*s-Z*	−151.609648	−151.830219	−151.851740	28.15
$^1A''$	Linear	−151.597616	−151.820334	−151.842060	34.22
$^3A'$	*s-E*	−151.612774	−151.833519	−151.854733	26.27
$^3A'$	*s-Z*	−151.611852	−151.833604	−151.855015	26.09
$^3A'$	Linear	−151.601871	−151.825190	−151.846785	31.26

[a]Saddle points with critical point order one.
[b]Disappear on geometry optimization at the CISDQ level.

Can. J. Chem. Downloaded from www.nrcresearchpress.com by 84.41.108.74 on 09/07/12
For personal use only.

TABLE 3. Bond order of formylmethylene conformers

State	Conformer	C_1—C_2	C_1—O_3	C_1—O_3	C_1—H_4	C_2—H_5
Carbenoid closed shell						
^1A		1.094	1.839	0.050	0.907	0.935
($^1A'$	*s-E*	1.014	1.919	0.024	0.926	0.933)[a]
($^1A'$	*s-Z*	1.005	1.905	0.015	0.936	0.948)[a]
($^1A'$	Linear	1.337	1.727	0.104	0.904	0.896)[a]
Carbenoid double open shell						
($^1A''$	*s-E*	1.234	1.727	0.137	0.930	0.932)[b]
($^1A''$	*s-Z*	1.201	1.727	0.147	0.945	0.937)[b]
($^1A''$	Linear	1.184	1.777	0.115	0.945	0.912)[b]
$^3A''$	*s-E*	1.027	1.859	0.054	0.932	0.946
$^3A''$	*s-Z*	1.017	1.856	0.063	0.938	0.950
$^3A''$	Linear	1.062	1.871	0.056	0.943	0.917
1,3-Diradical						
$^1A'$	*s-E*	1.931	0.904	0.053	0.941	0.956
$^1A'$	*s-Z*	1.930	0.910	0.051	0.945	0.958
$^1A'$	Linear	2.020	0.904	0.045	0.937	0.922
$^1A''$	*s-E*	1.891	0.961	0.065	0.953	0.945
$^1A''$	*s-Z*	1.868	0.968	0.067	0.961	0.949
$^1A''$	Linear	1.923	0.983	0.055	0.960	0.913
$^3A'$	*s-E*	1.943	0.917	0.060	0.932	0.956
$^3A'$	*s-Z*	1.942	0.916	0.060	0.939	0.957
$^3A'$	Linear	2.040	0.913	0.057	0.927	0.922

[a]Saddle points with critical point order one.
[b]Disappear on geometry optimization at the CISDQ level.

Can. J. Chem. Downloaded from www.nrcresearchpress.com by 84.41.108.74 on 09/07/12
For personal use only.

The single configuration RHF–SCF level geometry optimization gives the close shell carbene with nonplanar structure as the lowest singlet state, which is 18.1 kcal/mol higher in energy than the $^3A''$ ground state at the CISDQ level. All the earlier closed shell RHF–SCF calculations (3–5, 7–9, 11) predicted the nonplanar geometry for the lowest singlet state, with the exception of the MC–SCF calculations of Novoa *et al.* (15), which gave the σ–σ 1,3-diradical planar structure ($^1A'$) as the lowest singlet state for formylmethylene. Since their calculations were performed to explore the role of the lowest triplet state of formylmethylene in the Wolff rearrangement and the ring closure reaction in the lowest singlet state formylmethylene to form the oxirene, they did not investigate the energies of other conformers of formylmethylene or of the A″ state.

Open shell RHF–SCF geometry optimization of the diradical configuration of formylmethylene gave three structures, Fig. 2, corresponding to three local minima, which were verified by the calculation of eigenvalues of the Hessian matrix. Of the three structures, the *s-E* conformer of the $^1A''$ 1,3-diradical state with the σ–π configuration is the lowest singlet state for the diradical structure and is 9.8 kcal/mol above the closed shell singlet with a nonplanar carbene structure, and 27.9 kcal/mol above the ground state $^3A''$ with an *s-Z* conformation. The $^1A'$ state *s-E* and *s-Z* conformers with a 1,3-diradical structure are close, 1.5 and 1.8 kcal/mol, respectively, above the $^1A''$ state. The *s-E* and *s-Z* conformers are nearly isoenergetic (Table 2), the *s-E* conformation being slightly more stable in both the $^1A''$ and $^1A'$ states with the 1,3-diradical structure. The third local minimum corresponds to the carbenoid $^1A''$ state. This state is also fairly close to the lowest $^1A''$ state with 1,3-diradical structure, only 5.2 and 4.1 kcal/mol above the respective conformers. In the carbenoid structure, the *s-Z* conformer is slightly more stable than the *s-E* conformer. For comparison, the planar closed shell carbene geometry (Fig. 1b) was optimized for the $^1A'$ state. But this turned out to be a saddle point on the surface with a critical point order of one. Recently, Schaefer and co-workers (20), in their study on the oxirene b_2 ring deformation leading to formylmethylene, did not find a minimum that corresponds to formylmethylene at the DZP–CISD level theory. Surprisingly, the total energy (Table 2) of this planar carbene structure at the CISDQ level is very close to those of the $^1A'$ 1,3-diradical conformers.

In the carbenoid structures, both closed shell as well as open shell, the SCF optimized bond distance (Table 1) and the calculated bond order (Table 3) show that the C—C bond distance is slightly shorter than the single bond value and the C—O bond distance is close to the C=O double bond value. In the 1,3-diradical structure, the C—C bond distance is close to the C=C double bond value and the C—O bond distance is close to the C—O single bond value. The $^1A'$ optimized molecular parameters (Table 1) are in good agreement with the MC–SCF optimized values (15).

It has been recognized (31–33) that in open shell molecules containing multiple bond(s), the geometry optimization at the RHF–SCF level tends to overestimate the stability of the extreme, localized structures. This problem is overcome by the geometry optimization at the CI level, which usually results in a delocalized structure with a global minimum. For this reason we carried out a partial geometry optimization at the CISDQ level with C_1—C_2 and C_1—O_3 bond distances and $C_2C_1O_3$ bond angle, on the closed shell carbene (^1A) and the lowest energy conformers of the $^3A''$, $^1A''$, and $^1A'$ states. Optimized molecular parameters with the CISDQ level energy are tabulated in Table 4. In the $^3A''$ state we obtained only one minimum

TABLE 4. Optimized molecular parameters, total energies (au), and relative energies (kcal/mol) of formylmethylene conformers, with 6-31G** basis set at the CISDQ level. Bond distances are in (Å) and bond angles are in degrees

State	Conformer	$R(C_1—C_2)$	$R(C_1—O_3)$	$<C_2C_1O_3°$	E_{CISDQ}	ΔE_{CISDQ}
Carbenoid closed shell						
^1A		1.465	1.238	128.56°	−151.870714	18.44
Carbenoid double open shell						
$^3A''$	*s-Z*	1.470	1.245	121.91°	−151.900105	0.00
1.3-Diradical						
$^1A'$	*s-E*	1.342	1.372	126.03°	−151.851665	30.40
$^1A''$	*s-E*	1.350	1.346	121.48°	−151.853847	29.03

TABLE 5. Total energies (au) of formylmethylene conformers at the SCF optimized geometry with 6-31G** basis set

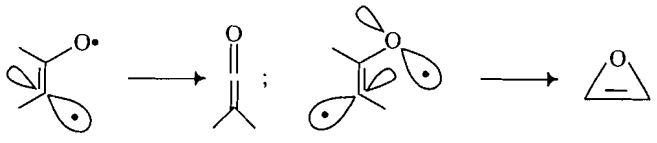
State[a]	Conformer	E_{UHF}	E_{RHF}	ΔE(RHF − UHF)[b]	Spin (S)	$S(S+1)$
$^1A'$	*s-E*	−151.624035	−151.609574	9.07	0.208	0.252
$^1A''$	*s-E*	−151.634633	−151.610458	15.17	0.150	0.173
^1A			−151.611630[c]	14.43		
$^3A'$	*s-E*	−151.625511	−151.612774	7.99	1.075	2.229
$^3A''$	*s-E*	−151.663985	−151.649769	8.92	1.067	2.205
$^3A''$	*s-Z*	−151.664884	−151.650828	8.82	1.065	2.199

[a]The $^1A''$ (RHF optimized geometry) and both $^1A'$ and $^3A'$ states have a 1,3-diradical structure while the ^1A, $^1A''$ (UHF optimized geometry) and $^3A''$ states have a carbenoid structure.
[b]In kcal/mol.
[c]Energy value of closed shell carbene isomer.

corresponding to the carbenoid structure. Even the partial geometry optimization of the $^1A''$ state resulted in only one minimum corresponding to the 1,3-diradical structure. The minimum found in the RHF–SCF geometry optimization corresponding to the carbenoid structure (Fig. 2a) in the $^1A''$ state vanishes. The optimized bond distances at the CISDQ level are slightly longer that the SCF optimized values, and there is not much change in the total and relative energies.

The question of the low-lying electronic states of formylmethylene and their substituted derivatives is of primary importance in the photochemistry of α-diazoketones, the associated Wolff rearrangement reactions, and in the chemistry of ketocarbenes, oxirenes, and their isomeric structures. According to the results of the present calculations, in agreement with all previous *ab initio* SCF, CI, and MC–SCF calculations, the ground state of formylmethylene is the *s-Z* conformer of the planar ($\sigma-\pi$) carbenoid A″ state. The *s-E* conformer of this state lies 1.40 kcal/mol above the *s-Z* conformer. These theoretical results are supported by the experimental observation of a series of triplet state ketocarbenes in low-temperature crystals and matrices that, at sufficiently low temperatures, are stable indefinitely. Evidence for the existence of *s-Z*–*s-E* conformerism also comes from esr spectroscopy. It has been found that most ketocarbenes can assume two conformer geometries, one major and one minor, and their esr spectra suggest that these are *s-Z*–*s-E* conformers and therefore they must have a planar structure.

With regard to the nature of the lowest singlet state of formylmethylene, the theoretical results are not as concordant. All available *ab initio* single configuration SCF, SCF–CI calculations including the present results predict a closed shell, nonplanar carbenoid structure for the lowest singlet state. However, the prediction of the only available MC–SCF calculations is different in that it gives for the lowest singlet state the planar ($\sigma-\sigma$) 1,3-diradical A′ state. Yet according to the double zeta plus polarization function with CISD calculation by Schaefer and co-workers (20), formylmethylene is not a minimum on the C_2H_2O surface. The available experimental results on the chemistry of ketocarbenes suggest that the lowest state is indeed a planar ($\sigma-\sigma$) state that exists in two close-lying conformations. In the absence of complicating secondary effects, one of the conformers readily undergoes Wolff rearrangement while the other conformer prefers oxirene formation (29):



s-E *s-Z*

Thus, the accumulated experimental data support the MC–SCF result. Therefore, we can tentatively conclude that for formylmethylene, a small molecule with several available orbital occupancies and many close-lying electronic states, the single configuration SCF method is inadequate for the correct description of the electronic manifold of the molecule, and MC–SCF calculations must be employed. It must also be stated that the single configuration SCF–CI calculation produces a $^1A'$ state with the same geometry and orbital occupancy as the MC–SCF calculation but this state occurs as one of the low-lying excited singlet states and not as the lowest singlet state. Also, the

Can. J. Chem. Downloaded from www.nrcresearchpress.com by 84.41.108.74 on 09/07/12
For personal use only.

carbenoid ^1A state computed here must correspond to an excited singlet state, as probably does the diradical $^1A''$ state. Therefore, the main inadequacy of the SCF–CI method in the computing of the electronic manifold of formylmethylene does not appear to be the generation of spectroscopic states that do not correspond to physical reality but rather to the incorrect energy ordering of the generated states.

We further performed some UHF–SCF calculations with geometry optimization on a few diradical isomers, the results of which are tabulated in Table 5. Spin contamination is evident in both singlet and triplet states and the UHF–SCF total energies obtained are lower than the RHF–SCF values, which conforms to the known performance of the UHF calculations leading to low values for total energies. The UHF–SCF results also predict the carbenoid $^3A''$ state to be the ground state, as do the RHF results. But for the singlet state the calculations predict the carbenoid $^1A''$ state to lie lower in energy than the closed shell carbene structure, Table 5. These UHF–SCF results along with the calculated energies of the RHF–SCF optimized geometry of all planar conformers, which are very close to each other, clearly manifest the inadequacy of single configuration calculations for the singlet states.

The closed shell reaction surfaces for the interconversion of C_2H_2O isomers have been reported in the literature (4, 8, 9, 11–13, 18, 19). MC–SCF calculations (15) have been reported only for the reaction of the diradical form of formylmethylene to give oxirene along with the singlet–triplet state crossing in formylmethylene. The present results reveal the existence of other close-lying conformer pair singlet states in formylmethylene, which undoubtedly play some role in the photochemistry of α-diazoketones, in the Wolff rearrangement reactions, and in the chemistry of formylmethylene and its isomers.

Acknowledgement

The authors are grateful to the Natural Sciences and Engineering Research Council of Canada for continuing financial support.

1. I. G. CSIZMADIA, H. E. GUNNING, R. K. GOSAVI, and O. P. STRAUSZ. J. Am. Chem. Soc. **95**, 133 (1973).
2. M. J. S. DEWAR and C. A. RAMSDEN. J. Chem. Soc. Chem. Commun. 688 (1973).
3. A. C. HOPKINSON. J. Chem. Soc. Perkin Trans. 2, 794 (1973).
4. O. P. STRAUSZ, R. K. GOSAVI, A. S. DENES, and I. G. CSIZMADIA. J. Am. Chem. Soc. **98**, 4784 (1976); O. P. STRAUSZ, R. K. GOSAVI, and H. E. GUNNING. J. Chem. Phys. **67**, 3057 (1977); O. P. STRAUSZ, R. K. GOSAVI, and H. E. GUNNING. Chem. Phys. Lett. **54**, 510 (1978).
5. N. C. BAIRD and K. F. TAYLOR. J. Am. Chem. Soc. **100**, 1333 (1978).
6. C. E. DYKSTRA. J. Chem. Phys. **69**, 4244 (1978).
7. K. S. KIM and H. F. SCHAEFER III. J. Am. Chem. Soc. **102**, 5389 (1980).
8. J. BARGON, K. TANAKA, and M. YOSHIMINE. Computational methods in chemistry. *Edited by* J. Bargon. Plenum Press, New York. 1980.
9. K. TANAKA and M. YOSHIMINE. J. Am. Chem. Soc. **102**, 7655 (1980).
10. L. B. HARDING. J. Phys. Chem. **85**, 10 (1981).
11. W. J. BOUMA, R. N. NOBES, L. RADOM, and C. E. WOODWARD. J. Org. Chem. **47**, 1869 (1982).
12. S. SCHRÖDER and W. THIEL. J. Am. Chem. Soc. **107**, 4422 (1985); **108**, 7985 (1986); J. Mol. Struct. (Theochem), **138**, 141 (1986).
13. L. B. HARDING and A. F. WAGNER. J. Phys. Chem. **90**, 2974 (1986).
14. O. MO, J. L. G. DE PAZ, and M. YANEZ. J. Phys. Chem. **91**, 6484 (1987).
15. J. J. NOVOA, J. J. W. MCDOUALL, and M. A. ROBB. J. Chem. Soc. Faraday Trans. 2, **83**, 1629 (1987).
16. M. ALCAMI, J. L. G. DE PAZ, and M. YANEZ. J. Mol. Struct. (Theochem), **165**, 99 (1988).
17. H. BOGEL. Anal. Chim. Acta, **206**, 233 (1988).
18. M. YOSHIMINE. J. Chem. Phys. **90**, 378 (1989).
19. C. BACHMANN, T. Y. N'GUESSAN, F. DEBU, M. MONNIER, J. POURCIN, J. P. AYCARD, and H. BODOT. J. Am. Chem. Soc. **112**, 7488 (1990).
20. G. VACEK, B. T. COLEGROVE, and H. F. SCHAEFER III. Chem. Phys. Lett. **177**, 468 (1991).
21. F. KAPLAN and G. K. MELOY. J. Am. Chem. Soc. **88**, 950 (1966).
22. F. KAPLAN and M. L. MITCHELL. Tetrahedron Lett. 759 (1979).
23. M. TORRES, J. RIBO, A. CLEMENT, and O. P. STRAUSZ. Can. J. Chem. **61**, 996 (1983).
24. C. MARFISI, P. VERLAQUE, G. DAVIDOVICS, J. POURCIN, L. PIZZALA, J. P. AYCARD, and H. BODOT. J. Org. Chem. **48**, 533 (1983).
25. M. TORRES, I. SAFARIK, H. MURAI, and O. P. STRAUSZ. Rev. Chem. Intermed. **7**, 243 (1986), and references therein.
26. H. D. ROTH and R. S. HUTTON. Tetrahedron, **41**, 1578 (1985).
27. R. A. HAYES, T. C. HESS, R. J. MCMAHON, and O. L. CHAPMAN. J. Am. Chem. Soc. **105**, 7786 (1983).
28. R. J. MCMAHON, O. L. CHAPMAN, R. A. HAYES, T. C. HESS, and H. P. KRIMMER. J. Am. Chem. Soc. **107**, 7597 (1985).
29. M. TORRES, R. K. GOSAVI, E. M. LOWN, E. J. PIOTRKOWSKI, B. KIM, J. L. BOURDELANDE, J. FONT, and O. P. STRAUSZ. *In* Structure, interactions and reactivity. *Edited by* S. Fraga. Elsevier Science Publishers, The Netherlands. In press.
30. P. C. HARIHARAN and J. A. POPLE. Theor. Chim. Acta, **28**, 213 (1973).
31. J. F. HARRISON, A. DENDRAMIS, and G. E. LEROI. J. Am. Chem. Soc. **100**, 4352 (1978).
32. E. R. DAVIDSON and W. T. BORDEN. J. Am. Chem. Soc. **99**, 2053 (1977).
33. N. C. BAIRD, R. R. GUPTA, and K. F. TAYLOR. J. Am. Chem. Soc. **101**, 4531 (1979).
34. N. C. HANDY, J. D. GODDARD, and H. F. SCHAEFER III. J. Chem. Phys. **71**, 426 (1979).
35. S. R. LANGHOFF and E. R. DAVIDSON. Int. J. Quantum Chem. **8**, 61 (1974).
36. J. S. BINKLEY, M. J. FRISCH, K. RAGHAVACHARI, D. J. DEFREES, H. B. SCHLEGEL, R. A. WHITESIDE, E. FLUDER, R. SEEGER, and J. A. POPLE. GAUSSIAN 82. Department of Chemistry, Carnegie Mellon University, Pittsburgh, PA. 1982.
37. M. R. PETERSON. MONSTERGAUSS. Department of Chemistry, University of Toronto, Toronto, Ontario. 1988.

Can. J. Chem. Downloaded from www.nrcresearchpress.com by 84.41.108.74 on 09/07/12
For personal use only.

Theoretical studies of peptidic structures. Conformation of the tetrapeptide *N*-acetyl-Asp-Glu-Lys-Ser-NH-CH_3

S. E. THORNTON AND S. FRAGA

Department of Chemistry, University of Alberta, Edmonton, Alta., Canada T6G 2G2

Received April 19, 1991

This paper is dedicated to Dr. Richard Norman Jones

S. E. THORNTON and S. FRAGA. Can. J. Chem. **69**, 1636 (1991).

The peptide Asp-Glu-Lys-Ser has been studied using the software package ALTA:maPS, with simulation of the pH conditions and the influence of the solvent, in order to investigate the possible stabilization of its structure by a hydrogen bond and a salt-bridge. The theoretical results confirm the existence of a salt-bridge, between the side chains of the Glu and Lys residues, in aqueous solution at neutral pH but not at acid pH, in agreement with the observation from NMR studies. On the other hand the calculations indicate that no hydrogen bond exists in aqueous solution at either pH. The fact that an in-vacuum simulation shows the existence of a hydrogen bond between the peptidic CO group of the Asp residue and the peptidic NH group of the Ser residue suggests that a molecular dynamics study might confirm that a small percentage (less than 25%) of the peptide molecules may exist as an H-bonded conformer, as postulated from the NMR results.

Key words: peptides, conformation, theoretical prediction.

S. E. THORNTON et S. FRAGA. Can. J. Chem. **69**, 1636 (1991).

Afin d'évaluer la possibilité de stabilisation de sa structure par une liaison hydrogène et un pont de sel, on a étudié le peptide Asp-Glu-Lys-Ser en utilisant le programme ALTA:maPS simulant les conditions de pH et l'influence du solvant. Les résultats théoriques confirment que, en solutions aqueuses, à des pH neutres mais non acides, il existe un pont de sel qui relie les chaînes latérales des portions Glu et Lys; ces conclusions sont en accord avec les observations faites par des études RMN. Par ailleurs, les calculs indiquent que, en solutions aqueuses, à tous les pH, il n'existe pas de liaisons hydrogènes. Le fait qu'une simulation sous vide démontre l'existence d'une liaison hydrogène entre le groupe CO peptidique du résidu Asp et le groupe NH peptidique du résidu Ser suggère qu'une étude de dynamique moléculaire pourrait confirmer qu'un faible pourcentage (moins que 25%) des molécules peptidiques peuvent exister sous la forme d'un conformère comportant une liaison hydrogène, comme on peut le déduire des résultats de RMN.

Mots clés : peptides, conformation, prédictions théoriques.

[Traduit par la rédaction]

Can. J. Chem. Downloaded from www.nrcresearchpress.com by 84.41.108.74 on 09/07/12
For personal use only.

Introduction

The practical significance of being able to predict the spatial conformation of peptides "from scratch" (i.e., from their amino acid sequences or primary structure) has motivated the dedication of considerable efforts to this task. A variety of potentials have been developed for this purpose and implemented in corresponding software packages, such as AMBER, CHARMM, ECEPP, MMPEP, etc. (for details and references, see the recent works in ref. 1).

At this laboratory, work in this area was developed in various stages. First, a potential was proposed (2) for the study of molecular interactions and associations. This potential was expressed as a summation of all the atom–atom pair potentials (AAPP) for the two interacting molecules, with the AAPP's given as $1/R$ expansions (with terms in $1/R$, $1/R^4$, $1/R^6$, and $1/R^{12}$). The coefficients of those terms were obtained by fitting of the accurate self-consistent field results of Clementi and co-workers (3–5) for the interaction of biomolecules (amino acids, purines, and pyrimidines) with water, with some semi-empirical considerations and modification by inclusion of a dispersion contribution. Later on, the above potential was adapted to the study of protein structures (6). Independently of these developments, and taking into account the difficulties in the theoretical prediction of the tertiary structure of proteins from their amino acid sequences, some effort was dedicated to the prediction of secondary structures (7–9). Finally, the complete formulation for the prediction of secondary structures, the determination of tertiary structures, and the molecular interactions was implemented in the software package ALTA:maPS (hereafter abbreviated as maPS) for the modelling and analysis of protein structures, either by themselves or in interaction with other systems (10).

The theoretical study of protein structures is based on a minimum energy criterion, with the goal of determining the global minimum in the conformational energy hypersurface. The considerable number of degrees of freedom in large peptidic structures may pose serious difficulties, which is not the case for short peptides. An additional advantage in the study of the latter is the possible availability of more complete experimental information, which allows for a more detailed evaluation of the theoretical procedure and of its results.

The tetrapeptide Asp-Glu-Lys-Ser (hereafter denoted in short as DEKS) corresponds to the sequence positions 7 through 10 of the collagen type I α-1 chain *N*-telopeptide (16 amino acids long) (11). The interest in this peptide arises from the fact that its conformation may correspond to a β-I turn and that β-turns have been postulated to play a significant role in the initiation of protein folding (12). Consequently, DEKS represents a very appropriate system for the test of both experimental and theoretical techniques.

Recently, DEKS has been studied (13) under varying conditions of solvent and pH, using several one- and two-dimensional NMR techniques for both proton and ^{13}C (such as COSY, ROESY, proton–carbon shift correlation, and selective

COLOC). The experimental results were interpreted using the software package ECEPP/2 (14), checking for consistency with the patterns of ROE's and the coupling constants.

This work presents the results obtained in the theoretical study of DEKS.

Calculations

The calculations were performed, on an IBM RISC System/6000, using the software package maPS.

Crystallographic structures of the individual amino acids were used in the initial construction of the peptidic chain, whose N and C termini were then protected with the groups H_3C-CO- and -HN-CH_3, respectively, in order to simulate the experimental conditions (13). (It must be noted that in the experiments the C terminus was protected by an -NH_2 group. The protection groups used in the theoretical calculations were chosen and incorporated into the program in the belief that they better simulate the situation in the complete peptide, eliminating or at least reducing unwanted interactions between the extremes of the chain in such short, test peptides as the one considered in this work.) In all the calculations described below, the backbone dihedral angles ϕ and ψ as well as the first side-chain dihedral angles χ_1 were optimized to one degree under a minimum energy criterion; the peptidic dihedral angles, ω, however, were set to, and maintained at, 180°, as usual.

Two sets of calculations were first performed for the isolated peptide. The sequence $D^-E^-K^+S$ (i.e., with ionized carboxyl groups in the side chains of the Asp and Glu residues and with the amino group in the side chain of the Lys residue in protonated form) was used for the modelling of the conformation of the peptide at an approximately neutral pH. On the other hand, the sequence DEK^+S was used for the simulation of the conformation at a low (acid) pH.

In each case the isolated peptide was constructed by successive formation of each peptidic bond, with optimization in each case of the ψ angle of the residue preceding the peptidic bond and of the ϕ and χ_1 angles of the residue following it. After the tetrapeptide was constructed, its termini were then protected, with optimization of the first ϕ angle and the last ψ angle of the peptidic chain. Then, the tertiary structure just obtained was fully optimized until convergence to one degree was reached for each angle. As a representative example, Fig. 1 presents schematically the structure obtained for $D^-E^-K^+S$, showing the H-pattern postulated from the experimental work (13). (See below for the quantitative discussion of the results.)

The resulting, optimized structures were then re-optimized in the presence of the solvent. The procedure used in this study is as follows. A solvent molecule is placed in the presence of the peptide, whose conformation is then re-optimized with consideration of the interaction with the solvent molecule. The latter is then allowed to approach the peptide, in a controlled manner, along the path of decreasing energy for the molecular association; only a maximum, preset displacement is allowed in this procedure in order to permit the solute to fully adapt to the existence of the solvent. Next, the peptide is re-optimized again, and the process is repeated until both the conformation of the peptide and of the molecular association peptide–solvent have stabilized (with mimimum energy). The solvent molecule is then incorporated into the peptide, as if it formed part of the closest residue; that is, it is included in the listing of atoms of the peptide, with the coordinates it had at the moment of stabilization. The procedure is then repeated for successive solvent

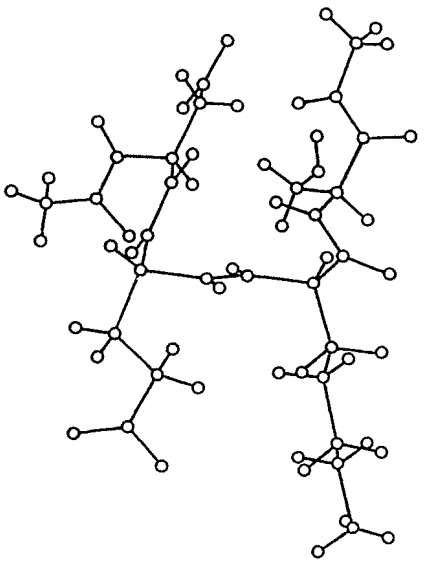


FIG. 1. Schematic representation of the structure obtained for *N*-acetyl-$D^-E^-K^+S$-NH-CH_3. The salt-bridge is established between the side chains of the Glu and Lys residues, which form the lower arms of the H-pattern. See, for comparison, the figure postulated from the experimental results (13).

molecules. As the number of solvent molecules added increases, their stabilization positions will lie farther and farther from the peptide, with less and less effect on its conformation. For that reason, the present calculations were carried out until a total of only six solvent molecules had been incorporated.

This simulation will allow for the consideration, to a certain extent, of the influence of the solvent on the conformation of the solute. Comparison of the resulting conformations for the peptide (structure $D^-E^-K^+S$, alone and in the presence of solvent, and structure DEK^+S, alone and in the presence of solvent) will yield the necessary information for a discussion of the effect of both the pH and solvent on the conformation of the peptide. It must be emphasized, however, that the procedure adopted in this work, with successive instead of simultaneous addition of the solvent molecules, will provide only an approximate simulation of the solvation process.

Although the experimental results were obtained in both aqueous and CD_3OH/H_2O (60:40) solutions, the calculations were performed only with water. It is expected that, in terms of molecular interactions, the situation will be very similar for both types of solutions, given the high percentage of water.

Results and discussion

The experimental observations of Otter *et al.* (13) yielded information on the possible existence of a salt-bridge and a hydrogen bond, depending on the experimental (pH and solvent) conditions.

In particular, a clear correlation was observed between the existence of the salt-bridge and the pH of the solution. At approximately neutral pH, both in aqueous and in CD_3OH/H_2O (60:40) solutions, the evidence indicated the existence of a salt-bridge between the side chains of the Glu and Lys residues (i.e., between the respective -COO^- and -NH_3^+ groups). At a pH below the pK_a of the carboxyl groups, in aqueous solution, no evidence was obtained for the existence of a salt-bridge.

It seems, however, that the H-bond does not constitute a fundamental characteristic of the peptide conformation. An

Can. J. Chem. Downloaded from www.nrcresearchpress.com by 84.41.108.74 on 09/07/12
For personal use only.

indication of the existence of such a bond between the peptidic -NH group of the Ser residue and the peptidic -CO group of the Asp residue was obtained only in CD_3OH/H_2O (60:40) solution, at about neutral pH, being estimated[1] that less than 25% of the peptide molecules may exist as an H-bonded conformer. No evidence of the H-bond was observed in the other two cases (i.e., in aqueous solution at about neutral pH and in CD_3OH/H_2O (60:40) solution at acid pH).

The existence of the salt-bridge (or, equivalently, the dependence of the conformation on the pH) is confirmed by the theoretical calculations. Inspection of the conformations obtained for the isolated peptides shows that the distance between the (hydroxyl) oxygen of the $-COO^-$ group of the Glu residue and the nitrogen of the $-NH_3^+$ group of the Lys residue is 4.86 Å (in $D^-E^-K^+S$) and 9.81 Å (in DEK^+S); that is, a salt-bridge exists in $D^-E^-K^+S$ (at neutral pH) but not in DEK^+S (at acid pH). The corresponding distances, in the conformations obtained in the calculations performed in the presence of solvent (with six molecules added as described above) are 4.81 Å (in $D^-E^-K^+S$) and 8.05 Å (in DEK^+S); that is, the solvent will not destroy the salt-bridge.

On the other hand, analysis of the conformations obtained for the isolated peptides shows that the distance between the oxygen in the peptidic -CO group of the Asp residue and the hydrogen of the peptidic -NH group of the Ser residue is 2.67 Å (in $D^-E^-K^+S$) and 1.82 Å (in DEK^+S); that is, an H-bond exists in the isolated DEK^+S molecules (at acid pH) and a close-to-H-bond exists in $D^-E^-K^+S$ (at neutral pH). The interesting fact, however, is that in the presence of solvent (see above) no H-bond is observed in either case; the corresponding distances are 5.41 Å (in $D^-E^-K^+S$) and 3.87 Å (in DEK^+S).

These results confirm that in aqueous solution the peptide adopts, at neutral pH, a conformation stabilized by a salt-bridge, which does not exist in acid pH. A static calculation, as the present one, indicates that no H-bond exists in solution but it is possible, taking into account the results obtained for the isolated peptide, that a molecular dynamics study would show the possible existence of an H-bonded conformer.

Regarding the possible existence of a β-I turn, the results show that such is not the case. The dihedral angles φ and ψ for the Glu and Lys residues should have in such a case the values −60, −30, −90, and 0°, respectively, but the values obtained in the calculations are as follows:

	Isolated peptide	Solvated peptide
DEK^+S	−63, −21, −70, −17	−97, −51, −99, −3
$D^-E^-K^+S$	−57, −28, −158, 28	−160, −44, −140, 34

[1]G. Kotovych. Private communication.

These results show, taking into account the confirmed existence of the salt-bridge, that stabilization by the latter may be obtained with a conformation that is not necessarily that of a β-I turn.

In concluding, it may be mentioned that the relevance of considering solvation effects, even though in an approximate manner, has been confirmed in this work, which in addition shows the usefulness of maPS in the study of protein structures.

1. (*a*) S. Wolfe, D. F. Weaver, and K. Yang. Can. J. Chem. **66**, 2687 (1988); (*b*) S. Wolfe, S. Bruder, D. F. Weaver, and K. Yang. Can. J. Chem. **66**, 2703 (1988); (*c*) S. Wolfe, M. Khalil, and D. F. Weaver. Can. J. Chem. **66**, 2715 (1988); (*d*) S. Wolfe, K. Yang, and M. Khalil. Can. J. Chem. **66**, 2733 (1988); (*e*) S. Wolfe, R. J. Bowers, H. S. Shin, C. K. Sohn, D. F. Weaver, and K. Yang. Can. J. Chem. **66**, 2751 (1988); (*f*) I. K. Roterman, K. D. Gibson, and H. A. Scheraga. J. Biomol. Struct. Dyn. **7**, 391 (1989); (*g*) I. K. Roterman, M. H. Lambert, K. D. Gibson, and H. A. Scheraga. J. Biomol. Struct. Dyn. **7**, 421 (1989).
2. S. Fraga. J. Comput. Chem. **3**, 329 (1982); S. Fraga. Comput. Phys. Commun. **29**, 351 (1983).
3. E. Clementi, F. Cavallone, and R. Scordamaglia. J. Am. Chem. Soc. **99**, 5531 (1977).
4. R. Scordamaglia, F. Cavallone, and E. Clementi. J. Am. Chem. Soc. **99**, 5545 (1977).
5. B. Bolis and E. Clementi. J. Am. Chem. Soc. **99**, 550 (1977).
6. B. Coghlan and S. Fraga. Comput. Phys. Commun. **36**, 391 (1985).
7. S. Thornton, E. San Fabian, S. Fraga, J. M. R. Parker, and R. S. Hodges. J. Molec. Struct. (Theochem), **226**, 87 (1991).
8. S. Fraga, E. San Fabian, S. Thornton, and B. Singh. J. Mol. Recognit. **3**, 65 (1990).
9. S. Thornton, E. San Fabian, S. Fraga, J. M. R. Parker, and R. S. Hodges. J. Molec. Struct. (Theochem). In press.
10. Software package ALTA:maPS. Protein Software Inc., Box 60499, University of Alberta Postal Outlet, Edmonton, Alta., Canada T6G 2S7.
11. D. A. D. Parry and A. S. Craig. *In* Ultrastructure of the connective tissue matrix. *Edited by* A. Ruggeri and P. M. Molta. Martinus Nijhoff, Boston. 1984.
12. P. N. Lewis, F. A. Momany, and H. S. Scheraga. Proc. Natl. Acad. Sci. U.S.A. **68**, 2293 (1971); S. S. Zimmerman and H. A. Scheraga. Proc. Natl. Acad. Sci. U.S.A. **74**, 4126 (1977); K. S. Schoemaker, P. S. Kim, E. Y. York, J. M. Stewart, and R. L. Baldwin. Nature, **326**, 563 (1987).
13. A. Otter, P. G. Scott, X. Liu, and G. Kotovych. J. Biomol. Struct. Dyn. **7**, 455 (1989).
14. G. Nemethy, M. S. Pottle, and H. A. Scheraga. J. Phys. Chem. **87**, 1883 (1983).

Can. J. Chem. Downloaded from www.nrcresearchpress.com by 84.41.108.74 on 09/07/12
For personal use only.

Protein secondary structure from FT-IR spectroscopy: correlation with dihedral angles from three-dimensional Ramachandran plots[1]

MICHAEL JACKSON AND HENRY H. MANTSCH
Steacie Institute for Molecular Sciences, National Research Council Canada, Ottawa, Ont., Canada K1A 0R6
Received May 28, 1991
This paper is dedicated to Dr. Richard Norman Jones

MICHAEL JACKSON and HENRY H. MANTSCH. Can. J. Chem. **69**, 1639 (1991).

The frequency of the so-called "amide I" band (amide C=O stretching vibration, νC=O) of proteins is discussed in terms of the dihedral angles of the various secondary structures present within proteins. We propose that in the case of intra- or intermolecular hydrogen-bonded amide carbonyl groups the frequency of this absorption can be directly related to the ϕ, ψ angles of the amide moieties for the major secondary structures. Amide I bands at frequencies above those found for non-hydrogen bonded amide carbonyl groups are rationalized in terms of a change in the third dihedral angle, ω. Rotation around the amide C—N bond in sterically demanding structures, such as turns where ω deviates from 180°, is expected to cause an increase in the electron density of the amide carbonyl groups and so increase νC=O to frequencies greater than that seen for unperturbed carbonyl groups.

Key words: FT-IR spectroscopy, proteins, structure, dihedral angles.

MICHAEL JACKSON et HENRY H. MANTSCH. Can. J. Chem. **69**, 1639 (1991).

On discute de la fréquence de la bande dite « amide I » (vibration d'élongation C=O de l'amide, νC=O) des protéines en fonction des angles dièdres de diverses structures secondaires présentes dans les protéines. On suggère que, dans les cas de groupes carbonyles d'amides impliqués dans des liaisons intra- ou intermoléculaires, la fréquence de cette absorption peut être reliée directement avec les angles ϕ et ψ des portions amides des structures secondaires principales. Les bandes amide I observées à des fréquences situées au-dessus de celles que l'on retrouve pour des groupes carbonyles d'amides qui ne sont pas impliqués dans des liaisons hydrogènes peuvent être rationalisées en fonction d'un changement du troisième angle dièdre, ω. On s'attend à ce que des rotations autour de la liaison amide C—N dans des structures implicant de fortes demandes stériques, comme dans les cas où ω s'éloigne de 180°, vont provoquer une augmentation dans la densité électronique des groupes carbonyles des amides et par la suite une augmentation de νC=O vers des fréquences plus élevées que celles observées avec des groupes carbonyles non-pertubés.

Mots clés : spectroscopie FT-IR, protéines, structure, angles dièdres.

[Traduit par la redaction]

The amide I band

The amide groups of proteins give rise to a prominant infrared absorption band, νC=O, which involves the amide carbonyl stretching vibration and is commonly referred to as the amide I band; it covers the range 1600–1700 cm^{-1}. Elliot (1) first demonstrated an empirical correlation between the frequency of the maximum of the νC=O band and the secondary structure of a range of proteins as determined by X-ray diffraction. These studies were extended by Susi *et al.* (2) and together with theoretical predictions (3) identified infrared spectroscopy as a potentially powerful tool for the structural characterization of proteins and polypeptides. Two major problems restricted the application of IR spectroscopy to the conformational analysis of proteins. The first was the almost blanket absorption of water in the spectral regions of interest. This problem is alleviated by the use of short pathlengths and digital subtraction routines, and (or) the use of ^2H_2O as solvent. The second problem was more difficult to overcome. No naturally occurring protein contains only one secondary structural motif. Each protein is composed of varying proportions of a number of commonly occurring secondary structures, namely α-helices, β-sheets and turns, together with polypeptide segments having little order. Each of these structures gives rise to a νC=O band, and the relative widths and peak separations are such that these individual bands cannot be resolved by increasing the instrumental resolution. The result is a broad νC=O band, from which relatively little information (apart from the overall peak maximum) can be gained. Obviously, the substructure of the νC=O band could provide important structural information. To this end, a number of band narrowing (often also called resolution enhancement) methodologies have been developed.

Fourier self-deconvolution

The most widely used band narrowing technique in IR spectroscopy of biological materials is Fourier self-deconvolution (4). Any absorption in an IR spectrum can be considered to be the result of the convolution of a line that has position but no shape (i.e., the Dirac δ function) with a lineshape (which has width but no position), to produce an absorption with both position and shape. In the Fourier domain this may be expressed as the multiplication of a cosine wave, whose period is determined by the frequency of the line, and a decaying exponential, the rate of decay being determined by the width of the lineshape, to produce an exponentially decaying cosine function. The more rapid the rate of decay, the wider the absorption profile. Obviously, if we could reduce the rate of decay of the cosine function we would reduce the width of the IR absorption band. This is achieved by multiplying the Fourier transform of the absorption band with an increasing exponential function. The inverse Fourier transform of the product then yields an absorption band of reduced width. Successful application of Fourier deconvolution to overlapping absorption bands can significantly enhance peak separation.

The application of deconvolution to the amide I band of

[1]Issued as NRCC No. 32839.

Can. J. Chem. Downloaded from www.nrcresearchpress.com by 123.30.183.119 on 09/07/12
For personal use only.

proteins reveals the existence of considerable fine structure for most proteins. The newly visualized bands may then be assigned to specific secondary structures within the protein.

Assignment of amide I bands to specific secondary structures

Although by now hundreds of papers have been published on the FT-IR spectroscopic analysis of protein secondary structure (see refs. 5–7 for reviews), correlations between the position of the νC=O bands and a particular type of secondary structure remain on a semi-empirical basis. A large number of proteins, polypeptides, and peptides whose structures have been determined by X-ray have been examined by FT-IR spectroscopy and correlations made between the frequency of νC=O and the principle components of the protein secondary structure deduced from X-ray diffraction.

Correlation of structure with νC=O is relatively straightforward for proteins which have a high β-sheet or α-helical character. Thus absorptions in the regions 1630–1640 cm^{-1} and 1648–1657 cm^{-1} are generally attributed to β-sheet and α-helices respectively. However, assignment of absorptions outside these ranges is highly variable. Particular problems are encountered in the 1660–1700 cm^{-1} region of the spectrum. Absorptions in this region are often attributed to turns although this is complicated by the presence of the high-frequency component of the anti-parallel β-sheet absorption, which arises as a result of coupling of neighbouring amide C=O transition dipoles (such coupling is only apparent for β-sheet structures and does not produce splitting of bands associated with other secondary structural motifs). Attributing absorptions above 1660 cm^{-1} on a semi-empirical basis to individual secondary structures has thus met with less success than the assignment of the major bands. Herein we propose a different approach to correlating νC=O with structure. The first step is to correlate relative hydrogen bond strengths, which may be correlated with the dihedral angles φ and ψ from the well-known two-dimensional Ramachandran plot, with νC=O. In addition, we suggest that the Ramachandran plot should be extended to include the third dihedral angle, ω. With reference to this three-dimensional Ramachandran plot, the effect of variations in ω upon νC=O is then considered.

Correlation of νC=O with dihedral angles

An example of a 2-D Ramachandran plot is shown in Fig. 1. Two features are immediately apparent. Firstly, the appearance of two main clusters on the plot indicates that certain sets of dihedral angles, corresponding to the commonly occurring protein secondary structres, are favoured. Secondly, although certain sets of dihedral angles are favoured, the areas between clusters are still relatively well populated, that is, there is a continuum. We shall now show that the major populations of dihedral angles may be related to specific νC=O frequencies.

Values of the dihedral angles φ,ψ of −180°,180° correspond to an extended polypeptide chain such as those found upon thermal denaturation of a protein. In such an extended structure intramolecular hydrogen bonding is not possible. However, a planar, extended chain will be able to align extremely well with neighbouring chains, which will allow the formation of strong intermolecular hydrogen bonds. The formation of such very strong hydrogen bonds would be expected to result in a low νC=O frequency. In Fig. 2a we show the spectrum of

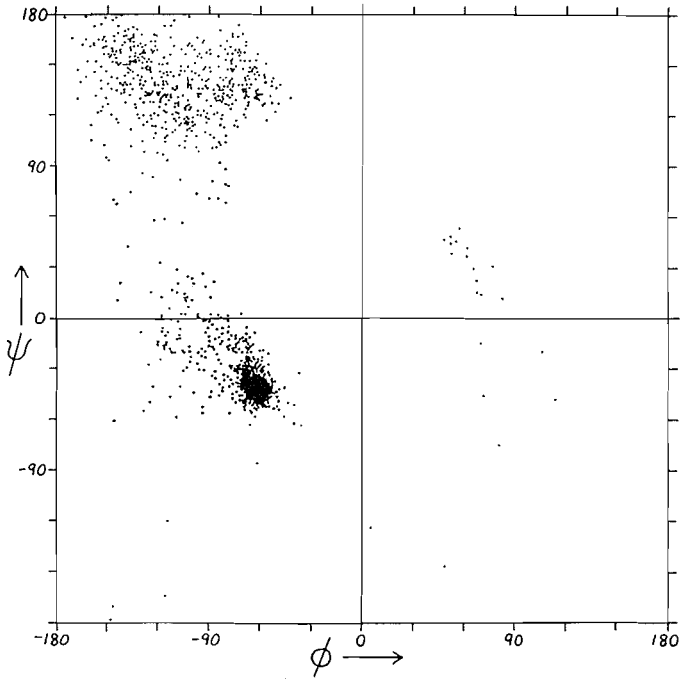


FIG. 1. Two-dimensional Ramachandran plot of the φ and ψ values found in a representative sample of X-ray structures (resolution 1.2–1.8 Å). Reproduced from J. S. Richardson and D. C. Richardson. *In* Prediction of protein structure and the principles of protein conformation. *Edited by* G. D. Fasman. Plenum Press, New York. 1990.

poly-L-lysine in its extended, intermolecularly hydrogen bonded form. As predicted, a low amide I maximum is seen (1612 cm^{-1}). Formation of strong intermolecular hydrogen bonds between extended strands (often referred to as an intermolecular β-sheet) has been suggested to account for the appearance of bands between 1610 and 1625 cm^{-1} in thermally and solvent denatured proteins (8, 9).

A reduction in φ,ψ to −120°,140° brings us to one of the more highly populated regions of the Ramachandran plot. Dihedral angles in this range still form structures of an extended type, although the reduction in the dihedral angles will now favour intramolecular hydrogen bonding between extended chains, forming the standard β-sheet structures. Packing constraints obviously mean that the strength of these intramolecular hydrogen bonds is less than those seen in the intermolecular β-sheet. We should therefore expect to see the νC=O for intramolecular β-sheet structures at a higher frequency, although still reflecting the presence of relatively strong hydrogen bonds. In Fig. 2b we show the spectrum of concanavalin A, a protein known from X-ray diffraction data to be predominantly β-sheet in structure. The νC=O maximum is indeed observed at a higher frequency than for poly-L-lysine, i.e., 1636 cm^{-1} compared to 1612 cm^{-1}.

Further changes in φ,ψ to −60°,−40°, bring us to the second main cluster of points in the 2-D Ramachandran plot. Successive φ,ψ angles of −60°,−40° produce a structure in which the C=O group of residue *n* is so aligned as to be able to form an almost linear hydrogen bond with the N—H group of residue *n* + 4, forming the well-known α-helix. The length of the hydrogen bond formed by this arrangement will be greater than that in intramolecular β-sheets, and we may expect to observe

Can. J. Chem. Downloaded from www.nrcresearchpress.com by 123.30.183.119 on 09/07/12
For personal use only.

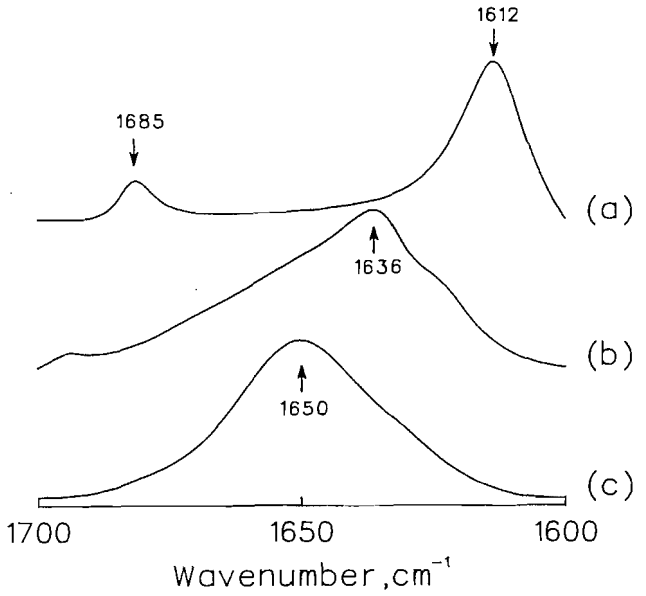


FIG. 2. FT-IR spectra in the νC=O region of poly-L-lysine in ^2H_2O, pD 12 at 60°C (a), of concanavalin A in ^2H_2O, pD 7.4 at 25°C (b), and of myoglobin in ^2H_2O pD 7.4 at 25°C (c).

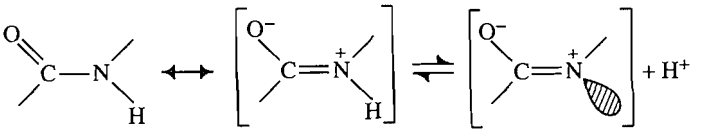
the νC=O maximum at a higher frequency. Examination of the spectrum of the α-helical protein myoglobin in Fig. 2c shows this to be the case, νC=O occurring at 1650 cm^{-1}. Other helical structures have been proposed, including the 3_{10}-helix and the α_{II}-helix. The 3_{10}-helix has φ,ψ angles of −70°,−5°, which results in the $^{\alpha}C$ atoms of residues *n* and *n* + 3 being exactly in line rather than the C=O and N—H groups. The result of this is that hydrogen bonds formed between C=O and N—H groups are nonlinear, which reduces their strength. We may therefore confidently expect distorted helical structures such as 3_{10}-helices to absorb at higher frequencies than α-helices. This has recently been demonstrated experimentally (10), 3_{10}-helices exhibiting an absorption band at 1660–1666 cm^{-1} in chloroform solution.

A non-repetitive sequence of φ,ψ angles for consecutive amino acid residues results in the formation of irregular hydrogen bonding patterns, that is, so-called random structures. As there exists a range of hydrogen bonding strengths and degrees of linearity, a broad absorption profile characterizes such structures; in ^2H_2O solution this is centered at 1644 cm^{-1}. This frequency is lower than that observed for hydrogen-bonded helical structures in the same solvent, which reflects the greater degree of hydrogen bond formation with solvent in disordered proteins.

Under certain circumstances, extended structures with a range of dihedral angles and no intramolecular hydrogen bonding are formed. We have recently shown this to be the case for all proteins and polypeptides dissolved in dimethyl sulfoxide (11). The νC=O band is observed at 1663 ± 2 cm^{-1} for every protein we have so far examined in this solvent. The appearance of this absorption is due to hydrogen bonding of the DMSO to all amide N—H groups, which totally disrupts the native structure of the protein. As all N—H groups are hydrogen bonded to the solvent and DMSO has no hydrogen bond donor capability, the amide carbonyl groups must be non-hydrogen bonded. We believe therefore that νC=O for free C=O groups in proteins and peptides occurs in the 1660–1665 cm^{-1} region of the spectrum.

We have shown above that absorptions appearing in the spectral region 1610–1665 cm^{-1} can be confidently assigned to intermolecular associations (1610–1625 cm^{-1}), β-sheet (1630–1640 cm^{-1}) and α-helical (1648–1652 cm^{-1}) structures, and free amide carbonyls (1660–1665 cm^{-1}), and that the frequencies of these various absorptions can be related to φ,ψ angles, which determine hydrogen bonding schemes. This still leaves a number of consistently reported (although relatively minor) absorptions between 1665 and 1695 cm^{-1} that are generally difficult to assign. It would not be expected that C=O bands should be seen at frequencies above that assigned to the free stretching C=O vibration, as any hydrogen bonding effects would tend to lower νC=O due to reductions in electron density of the C=O bond. To explain increases in frequency above that seen for the free C=O in DMSO, we envisage two mechanisms by which electron density in the C=O bond may be increased.

Firstly, a reduction in the dielectric constant of the environment will decrease the degree of polarization of the carbonyls and will result in an increase in electron density in the double bond. This will result in an increase in νC=O and may account for absorptions above 1665 cm^{-1}. The second way in which the electron density of the amide carbonyl can be increased relates to the planarity of the amide group. The amide group is planar due to resonance and tautomerism:



These structures are stabilized by hydrogen bonding and result in the C—N bond assuming partial double bond character due to a flow of electrons from the C=O to the C—N bond. Free rotation around this bond is therefore restricted, the planarity of the amide group is enforced, and the third dihedral angle, ω, is 180°. In other words the amide group is in a *trans* configuration. A reduction in the planarity of the amide groups will have the opposite effect, that is, electron flow from the C—N bond may restore the electron density in the carbonyl groups and so increase the νC=O maximum. Thus while we believe that free amide C=O groups in proteins and peptides generally exhibit an absorption in the range 1660–1665 cm^{-1}, this frequency may be increased by rotation around the C—N bond of the amide group. Such a situation may result from steric constraints imposed upon peptide groups in such rigid and conformationally restricted structures as turns.

In conclusion, we postulate herein that the major absorption bands arising from hydrogen-bonded amide C=O groups of proteins in the region 1610–1660 cm^{-1} are related to the dihedral angles φ,ψ, whereas we interpret absorptions above 1665 cm^{-1} as arising from non-hydrogen bonded amide C=O groups with distorted C—N bonds, in which the third dihedral angle, ω, deviates from 180°. In addition, a reduction in the dielectric constant of the environment of C=O groups may also increase the frequency.

1. A. ELLIOT. Proc. 3rd Int. Congress on Biochemistry. New York 1956. Academic Press, New York.
2. H. SUSI, S. N. TIMASHEFF, and L. STEVENS. J. Biol. Chem. **242**, 5460 (1967).
3. S. KRIMM. J. Mol. Biol. **4**, 528 (1962).

Can. J. Chem. Downloaded from www.nrcresearchpress.com by 123.30.183.119 on 09/07/12
For personal use only.

4. J. K. KAUPPINNEN, D. J. MOFFATT, H. H. MANTSCH, and D. G. CAMERON. Appl. Spectrosc. **35**, 271 (1981).
5. H. SUSI and D. M. BYLER. Methods Enzymol. **130**, 290 (1986).
6. W. K. SUREWICZ and H. H. MANTSCH. Biochim. Biophys. Acta, **952**, 115 (1988).
7. M. JACKSON, P. I. HARIS, and D. CHAPMAN. J. Mol. Struct. **214**, 329 (1989).
8. A. H. CLARK, D. H. P. SAUNDERSON, and S. SUGGETT. Int. J. Peptide Protein Res. **17**, 353 (1981).
9. E. J. AMBROSE and A. ELLIOTT. Proc. R. Soc. London, A: **208**, 75 (1951).
10. D. F. KENNEDY, M. CRISMA, C. TONIOLO, and D. CHAPMAN. Biochemistry. In press.
11. M. JACKSON and H. H. MANTSCH. Biochim. Biophys. Acta, **1078**, 231 (1991).

Can. J. Chem. Downloaded from www.nrcresearchpress.com by 123.30.183.119 on 09/07/12
For personal use only.

Time-resolved ESR study on photochemical formation of radical pair in cyclodextrin cavities

HISAO MURAI[1]

Department of Chemistry, Faculty of Science, Osaka University, Toyonaka, Osaka 560, Japan

AND

YOSHINORI YAMAMOTO AND YASUMASA J. I'HAYA

Department of Applied Physics and Chemistry, The University of Electro-Communications, Chofu, Tokyo 182, Japan

Received April 24, 1991

This paper is dedicated to Dr. Richard Norman Jones

HISAO MURAI, YOSHINORI YAMAMOTO, and YASUMASA J. I'HAYA. Can. J. Chem. **69**, 1643 (1991).

The photoreduction of xanthone with diethylaniline in cyclodextrin cavities was studied at 77 K and room temperature by a time-resolved ESR technique. The radical pair observed in β- and γ-cyclodextrins showed inverted spin polarization compared to that of precursor excited triplet xanthone. This result is rationalized by taking account of the fixed orientation of the radical ion pair in the cyclodextrins. Frozen aqueous solutions and dried powder-like samples provided similar results. The spectrum of the radical pair was also detected in an aqueous solution of β-cyclodextrin at room temperature.

Key words: cyclodextrins, xanthone, spin polarization, radical ion-pair, time-resolved ESR.

HISAO MURAI, YOSHINORI YAMAMOTO et YASUMASA J. I'HAYA. Can. J. Chem. **69**, 1643 (1991).

Utilisant une technique de RPE résolue en fonction du temps et opérant à 77 K, on a étudié la photoréduction de la xanthone, par la diéthylaniline, dans des cavités de cyclodextrine. La paire de radicaux observée dans des β- et γ-cyclodextrines présente une polarisation de spin inversée par rapport à celle du triplet excité de la xanthone précurseur. On rationalise ce résultat en prenant en considération l'orientation déterminée de la paire d'ions radicalaire dans les cyclodextrines. Des solutions aqueuses congelées et des solutions séchées sous forme de poudre fournissent des résultats similaires. On a aussi détecté le spectre de la paire de radicaux dans une solution aqueuse de β-cyclodextrine, à température ambiante.

Mots clés : cyclodextrines, xanthone, polarisation de spin, paire d'ions radicalaire, RPE résolue en fonction du temps.

[Traduit par la rédaction]

Introduction

Cyclodextrins (CD) can be used to model enzymes, and their cavities provide unique reaction fields for specific physical and (or) chemical events (1). To explore these reaction fields, spin polarization transfer along with triplet–triplet energy transfer has been studied by a time-resolved ESR (TRESR) technique (2, 3). When xanthone and naphthalene were dissolved in γ-CD, excitation of xanthone led to the formation of the spin polarized triplet excited state of naphthalene. On the basis of this observation, a fixed conformation of the two molecules in the CD cavity was proposed. The chemical reaction in the CD cavity is of great interest and the observation of TRESR should provide important information about the reactivity and the conformation of the intermediate radical pair in the cavity.

In a series of TRESR studies of the excited states of aromatic compounds and intermediate radical pairs, low temperature organic glasses were employed as matrices (4–8). In glassy solution, an anisotropic dipole interaction between the two spins that are known to form a triplet state appears in the spectrum. The spin polarization pattern of the excited triplet state and the intermediate radical pair provides information about intersystem crossing and (or) polarization transfer during the reaction.

In glassy media, the photoreduction of benzophenone with *N*,*N*-diethylaniline produced a spin-polarized radical pair along with the excited triplet state of benzophenone (9). Both the radical pair and the excited triplet state showed a similar polarization pattern. Therefore, it was concluded that the hydrogen abstraction reaction took place from the excited triplet state of benzophenone and the direction of the active principal axis of the radical pair was nearly parallel to the C=O direction of precursor benzophenone. A similar study has been reported for the system acridine/acridan, where the TRESR spectrum of inverted spin polarization compared to the precursor excited triplet state of acridine appeared (10). The polarization of the radical pair is rationalized by taking account of the fixed relative conformation of the principal axes of the excited triplet state of acridine and that of the resultant radical pair.

In this paper, a TRESR study of the direct chemical reaction of photoexcited xanthone and *N*,*N*-diethylaniline inside β- and γ-CD cavities is reported, and its polarization transfer mechanism is briefly discussed. Dried CDs are shown to work as a good reaction field and an isolation matrix even at room temperature.

Experimental

A conventional X-band ESR spectrometer (Varian E-109), with minor modification, was used for the TRESR measurement. No field modulation was employed, so the TRESR spectra shown in the present paper are all given by the absorption and emission of the microwave signal (upward absorption and downward emission throughout). A nitrogen gas laser (Molectron UV24, $\lambda = 337.1$ nm) was used as the source of the excitation light pulse. The signals in several fixed time regions were accumulated by a boxcar integrator (NF, BX531) (3).

Commercially available xanthone (Xn) was recrystallized from ethanol and then purified by multiple zone refining. GR grade *N*,*N*-diethylaniline (DEA) was used immediately after distillation under reduced pressure. Commercially available GR grade α-, β-, and γ-CDs were used as received. The concentration of both Xn and DEA in aqueous solutions of CDs were 2×10^{-3} mol dm^{-3}. The concentration of CDs was changed from 2×10^{-2} to 2×10^{-3} mol dm^{-3} to investigate whether CDs possibly reveal an aggregated environment.

[1]Author to whom correspondence may be addressed.

Printed in Canada / Imprimé au Canada

Can. J. Chem. Downloaded from www.nrcresearchpress.com by 84.41.108.74 on 09/07/12
For personal use only.

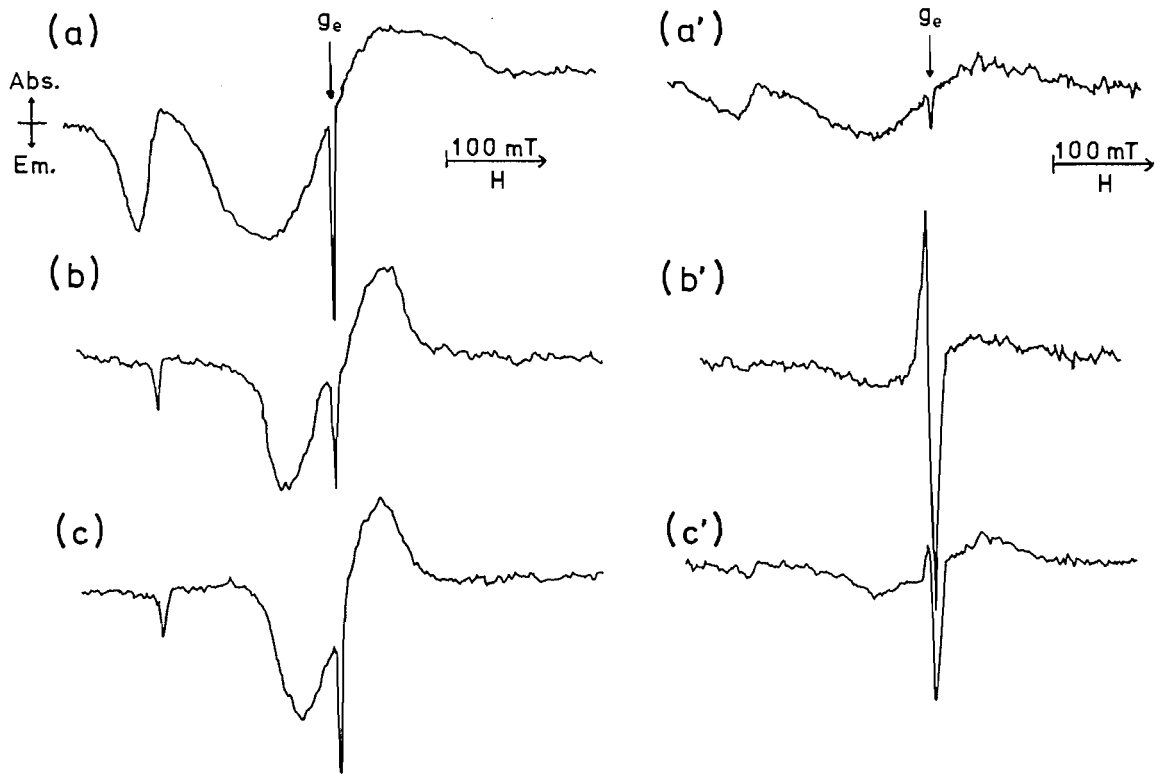


FIG. 1. Time-resolved ESR spectra observed for the systems of xanthone in (a) α-CD, (b) β-CD, and (c) γ-CD in the absence of DEA, and also in (a′) α-CD, (b′) β-CD, and (c′) γ-CD in the presence of DEA at 77 K. The observation time is 0.8–1.0 μs after laser excitation.

Measurement of the frozen aqueous solution of CDs was carried out at 77 K in a 5 mm o.d. quartz tube after degassing the sample. The powder sample was prepared by drying aqueous solutions of Xn, DEA, and CDs by passing dry nitrogen gas and degassing in vacuum. The TRESR measurements of the powder sample were carried out at 77 K and room temperature. The TRESR measurement of the liquid phase sample at the above concentration was performed by a flow method (11) at room temperature.

Results and discussion

Frozen solution of CDs

Figures 1a, b, and c show the TRESR spectra observed in the photolysis of the frozen aqueous solution of Xn and respective CDs at 77 K. These spectra were assigned to the excited triplet state of Xn (12). The differences in these spectra reflect the different environments in the respective CD cavities. The spectrum in α-CD is explained by the nonhydrated excited triplet state of Xn, while the spectra in β- and γ-CDs are explained by the hydrated Xn in the CD cavity. Especially in γ-CD, inclusion of two Xn molecules is possible. When DEA was added to the above solutions, either a similar or a different spectrum appeared, depending on the CD used. Figure 1a′ shows the spectrum observed for the system of Xn and DEA in α-CD. This spectrum is almost identical to that observed in the absence of DEA except for the signal intensity. This implies that the xanthone and the DEA molecules are not included in the same cavity or, if they are included, they do not interact. Figures 1b′ and c′ show the appearance of certain paramagnetic species with spin polarization in the presence of DEA, and the excited triplet state of Xn is still observed. The latter may be due to isolated Xn that does not interact with DEA under the influence of CDs.

Figure 2a shows the center portion of Fig. 1b′, which indicates that a spin-polarized radical pair is produced in the photolysis of Xn/DEA in β-CD. The computer-simulated TRESR spectrum of randomly oriented triplets (7) is shown in Fig. 2c for zfs (zero-field splitting) parameters $D = -9.7$ mT, $E = 0.8$ mT, with the highest population assumed to be in the middle spin-sublevel (Y′) which is located close to the lowest one. The use of a negative D value is rationalized by the assumption that a radical pair can be approximated in terms of a point dipole model. A small bump observed near the g_e field in Fig. 2a may be due to a small amount of stabilized radicals. The assignment of this radical pair and the cause of the spin polarization will be discussed later.

Figure 3a shows the center portion of the TRESR spectra observed in the photolysis of Xn/DEA in γ-CD (Fig. 1c′). The spectral line shape is asymmetrical compared to that observed in β-CD. The sharp emissive peak is located near the g_e field. This means that the spectrum is composed of both the radical pair and the product radical; in other words, there exist two different reaction modes in the γ-CD environment.

To see what happens for high concentrations of CDs, the following experiments were carried out. CD aggregate formation was confirmed for the β-CD system above a concentration of 2×10^{-3} mol dm^{-3} by observing the CD concentration dependence of the optical density of Xn. Therefore, aggregate formation must be the cause of the complication of the data. A quite interesting result was obtained when samples with low concentration of β- and γ-CDs (2×10^{-3} mol dm^{-3}) were passed through a micro-filter with 0.45 μm i.d. The observed TRESR spectra of the radical pairs were much clearer than those observed in high concentration CDs, that is, the spectra of excited Xn and stabilized radical had almost vanished. In the case of β-CD, no drastic spectral change of the radical pair occurred. There was only a slight decrease of the emissive signal of the radical near the g_e field as shown in Fig. 2b. In the case of γ-CD, however, the spectrum of the radical pair

Can. J. Chem. Downloaded from www.nrcresearchpress.com by 84.41.108.74 on 09/07/12
For personal use only.

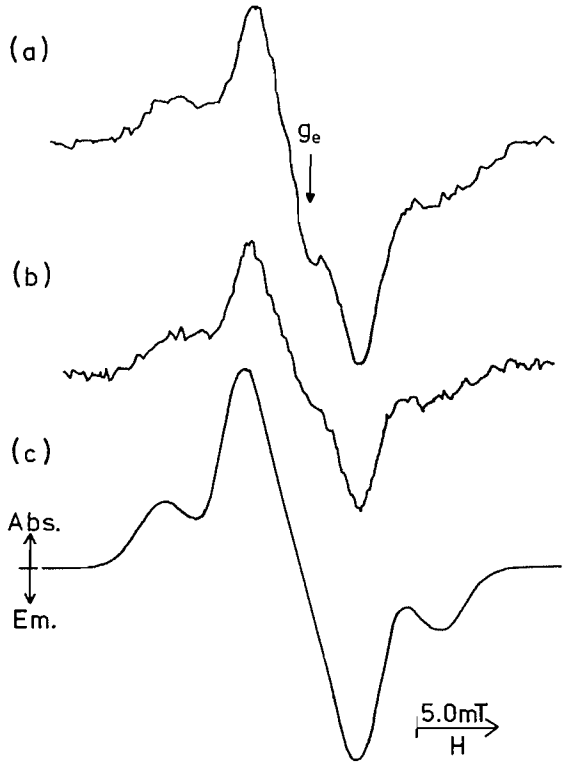


FIG. 2. Time-resolved ESR spectra observed at 0.8–1.0 μs after laser excitation for the system of xanthone/DEA in β-CD. (a) [β-CD] $= 2 \times 10^{-2}$ mol dm^{-3}, (b) [β-CD] $= 2 \times 10^{-3}$ mol dm^{-3} (see text), and (c) simulated spectrum (the relative population rates $P_{x'}/P_{y'}/P_{z'}$ = 0.1/0.9/0).

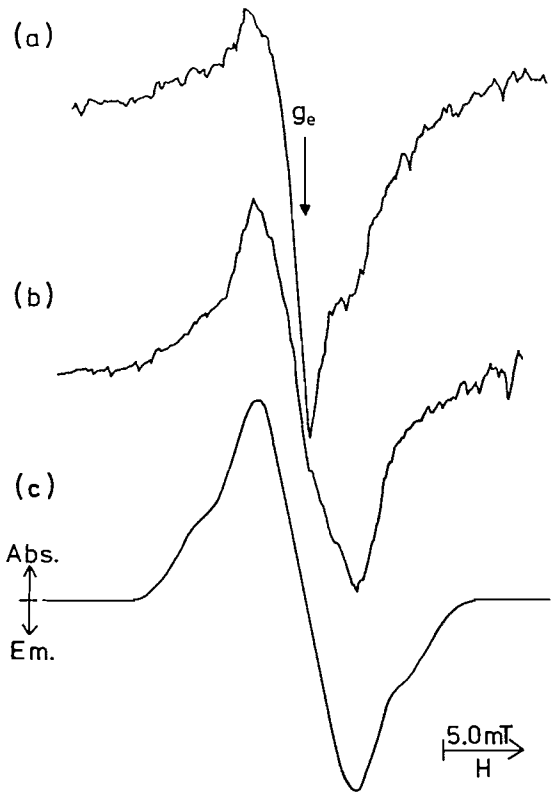


FIG. 3. Time-resolved ESR spectra observed at 0.8–1.0 μs after laser excitation for the system of xanthone/DEA in γ-CD. (a) [γ-CD] $= 2 \times 10^{-2}$ mol dm^{-3}, (b) [γ-CD] $= 2 \times 10^{-3}$ mol dm^{-3} (see text), and (c) simulated spectrum (the relative population rates $P_{x'}/P_{y'}/P_{z'}$ = 0.1/0.9/0).

became sharper and the emissive component of a stabilized radical was not observed. These results lead to an important conclusion. Most CD molecules exist as aggregates under high concentration conditions and the many xanthone molecules in the CD cavity are isolated in the aggregate. Under these conditions, the excited triplet state of xanthone is observable. Under low concentration conditions, the Xn molecule in the unaggregated CDs can react with DEA located close to, or included with, the Xn. In γ-CD, whose cavity size is larger than that of β-CD, the effect of CD aggregation is significant. The trapped Xn in the aggregate of γ-CD may react with γ-CD or DEA located nearby to produce a stabilized radical with an emissive polarization as in the triplet mechanism of CIDEP (Chemically Induced Dynamic Electron Polarization) (13).

Figures 3b and c show the observed and simulated TRESR spectra of Xn/DEA in the γ-CD system for low concentrations of γ-CD. From the simulated spectrum, zfs parameters of $D = -7.4$ mT and $E = 0.3$ mT are determined. The Y′ sublevel is also the most actively populated level in this system, just as in β-CD. The smaller D value, compared to that in β-CD, implies that the distance between two dipoles is larger. This may reflect the relative cavity sizes.

In the photolysis of the homogeneous solution of Xn in 2-propanol in the presence of DEA, a Xn anion radical with an emissive pattern was observed.[2] A similar experiment was carried out in an SDS micellar solution in the presence of DEA, and the emissive Xn anion radical was also observed in this special system.[2] These results suggest that charge transfer between photoexcited Xn and DEA takes place, and the excited triplet state of Xn with the highest population of the upper sublevel is the precursor of this reaction. In the present system of CDs, no clear evidence for the assignment of the radical species forming the radical pair was obtained. However, the photochemical reaction in the homogeneous and micellar systems shown above and the theoretical consideration that will be discussed later suggest the formation of a radical ion pair composed of a Xn anion radical and a DEA cation radical under the influence of β- and γ-CDs.

The inside diameters of α-, β-, and γ-CDs are known to be about 0.45, 0.7, and 0.85 nm, respectively (1). The different size of these CD cavities may be one of the crucial points that determine the inclusion conditions. In α-CD, only a single molecule can be included because of the small size of the cavity. In β- and γ-CDs, partial and (or) complete inclusion (see below) of the two molecules may be possible. The distances of the two spins of the radical pair in β- and γ-CDs are estimated to be 0.66 and 0.72 nm, respectively, in terms of the point-dipole approximation. This difference may reflect the diameters of the respective CD cavities.

In the experiment of triplet–triplet energy transfer in γ-CD reported previously, inclusion of two molecules, Xn and naphthalene, that keep their molecular plane parallel, was proposed to explain the spin polarization transfer (2, 3). In β-CD, the observation of a reproducible triplet–triplet energy transfer failed because of the smaller cavity size compared to γ-CD. In the present case, we assume that a similar inclusion of Xn and DEA to those in the energy transfer experiment occurs and that charge transfer takes place between the two molecules. The observation of the radical pair in β-CD implies that com-

[2]N. Ishiwata. Unpublished data.

Can. J. Chem. Downloaded from www.nrcresearchpress.com by 84.41.108.74 on 09/07/12
For personal use only.

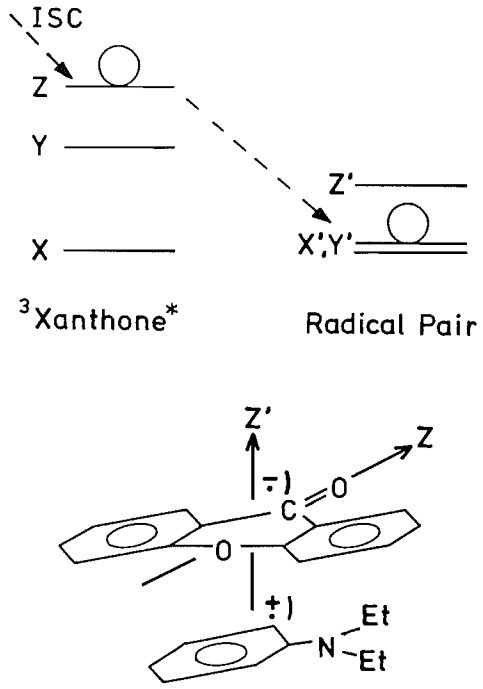


FIG. 4. Conceptual diagram of radical pair formation and polarization transfer in a CD cavity.

plete inclusion of the two molecules in the cavity is unlikely, but that partial inclusion of the coupled two molecules should occur. Observation and comparison of the optical absorption spectra of Xn in β-CD with and without DEA in aqueous solution showed no band shift of the absorption spectrum of Xn.[3] This indicates that there is no strong contribution of a charge transfer (CT) complex of Xn and DEA in β-CD.

The spin polarization of the radical pair is apparently inverted compared to that of the excited triplet state of Xn. To explain this, the following two mechanisms are postulated. (1) Excitation of a local electronic state of Xn, leading to the lowest excited triplet state by intersystem crossing (ISC) from the excited singlet state. This spin-polarized triplet state reacts with DEA located nearby to form a radical ion pair. (2) Excitation of the weak CT complex of Xn and DEA, which leads to the lowest excited triplet state of the complex by ISC from its excited singlet state, prior to charge separation. In the first model, the spin polarization is induced through ISC in locally excited Xn, and the conversion of the principal axes of the excited triplet state sublevels of Xn into those of the radical ion pair takes place during the very fast charge transfer reaction. The active Z-axis of the excited state of Xn becomes roughly perpendicular to the Z'-axis of the radical ion pair after the fast charge separation. This situation is illustrated in Fig. 4. This interpretation of the spin polarization transfer through the interconversion of the principal axes has been applied to T–T energy transfer (2, 3) and radical pair formation (8–10). In the second model, ISC of the excited CT complex may induce the characteristic spin polarization of the resultant radical pair. When the CT character of this excited complex is not strong enough, the local electronic state of Xn induces a similar spin polarization in the excited triplet state of the complex. Therefore, the same mechanism of inversion of the spin sublevel during the charge separation may be anticipated. In any case, the local excitation of Xn plays an important role for the induction of the spin polarization of the radical pair.

In addition, the use of triethylamine or diphenylamine or dimethylaniline instead of DEA did not provide a radical pair spectrum such as that observed in the system of Xn and DEA in β-CD.[3] They provided only an emissive spectrum without any special structure, probably because of the formation of the intermediate radical species or the radical pair, in which the two radicals involved are oriented randomly so that an exclusively emissive spectral pattern is expected just as for triplet–triplet energy transfer in glassy media (14). Therefore, the systems of Xn and DEA in β- and γ-CDs are very specific.

Powder condition of CDs

Figure 5 shows the TRESR spectra observed in the photolysis of a powdered β-CD sample at 77 K and room temperature. The spectrum observed at 77 K is almost identical to that of the frozen solution at 77 K (Fig. 2a). This indicates that the condition of Xn and DEA in the CD cavity and (or) in the CD aggregate is about the same as that in the frozen aqueous solution. The spectrum of the powdered sample at room temperature is very similar to that at 77 K. The spectral change with time indicates that the signal decay of this radical pair is almost independent of temperature. The polarization pattern gradually alters with time; that is, the intensity ratio of the center portion to the side peaks of the spectrum gradually decreases with time in favor of the totally emissive component. The decay of this signal is thought not to be due to ordinary spin lattice relaxation, but may be due to anisotropic ISC followed by a chemical reaction such as back charge transfer through the singlet manifold. The spectral change may be interpreted as depopulation of one of the spin sublevels of the in-plane principal axes and also the superposition of the signal due to the emissively polarized radicals.

Figure 6 shows the TRESR spectra similarly observed in the photolysis of the powdered γ-CD sample at 77 K and room temperature. The spectrum observed at 77 K is also similar to that observed in the γ-CD system of the frozen aqueous solution (Fig. 3a) except for the intensity of the emissive signal of the radical species near g_e. In this case, the spectrum at room temperature is a bit different from that observed for the same timing at 77 K, but similar to that observed at a later time at 77 K. This indicates that the spectrum of the radical pair deforms much faster at room temperature than that at 77 K. This difference may be ascribed to the larger diameter of the cavity and (or) the rough packing of the γ-CD aggregate compared to that of β-CD.

Since the powdered sample of β- and γ-CDs works like the frozen solution, the two molecules, Xn and DEA, are thought to be tightly restrained even without the aqueous medium. Therefore, it may safely be concluded that CD powders can be used for the observation of the excited molecules and (or) the intermediate radical pair even at room temperature.

Aqueous solution at room temperature

The TRESR measurement of the aqueous solution was carried out by the flow technique at room temperature. Only the β-CD solution provided a CIDEP-like A/E pattern as shown in Fig. 7. This spectrum seems to be easily assigned to some intermediate radical with the singlet precursor RPM (Radical Pair Mechanism) (13), but it is realized that it is almost identical to that observed in the frozen condition. In other words, the triplet-state radical pair is an apparent anomaly in aqueous solution at room temperature. We know that, for high concen-

[3]Y. Yamamoto. Unpublished data.

Can. J. Chem. Downloaded from www.nrcresearchpress.com by 84.41.108.74 on 09/07/12
For personal use only.

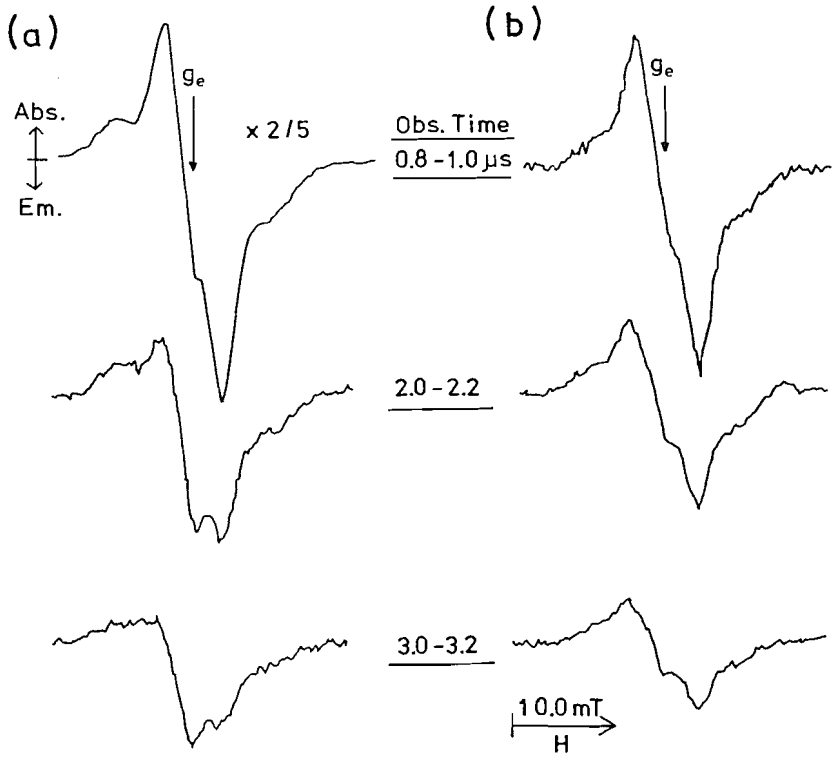


FIG. 5. Time-resolved ESR spectra observed at three different observation times for the system of the powdered sample of xanthone/DEA in β-CD at (a) 77 K and (b) room temperature.

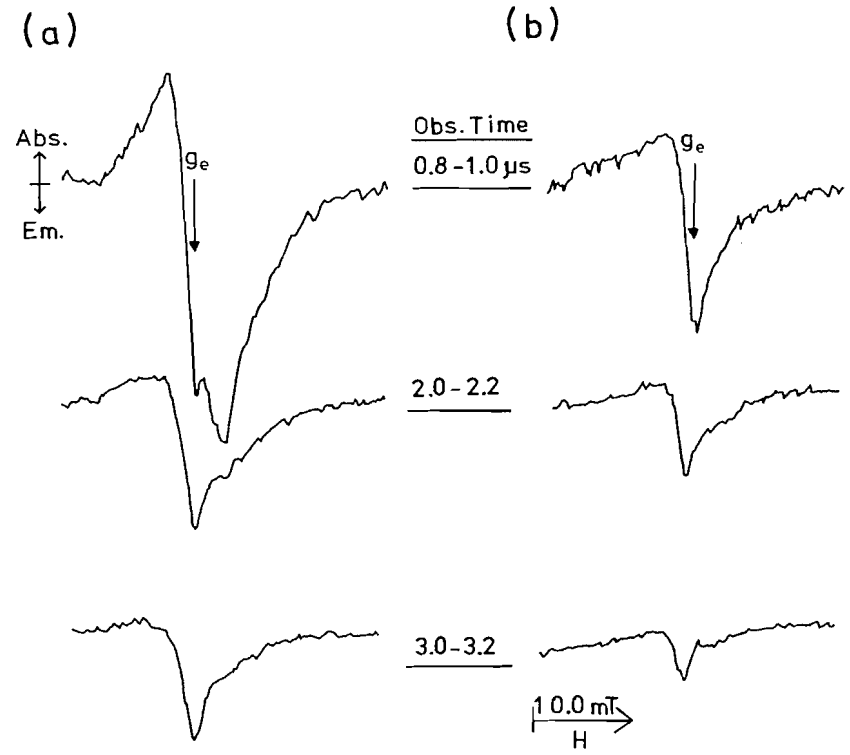


FIG. 6. Time-resolved ESR spectra observed at three different observation times for the system of the powdered sample of xanthone/DEA in γ-CD at (a) 77 K and (b) room temperature.

Can. J. Chem. Downloaded from www.nrcresearchpress.com by 84.41.108.74 on 09/07/12
For personal use only.

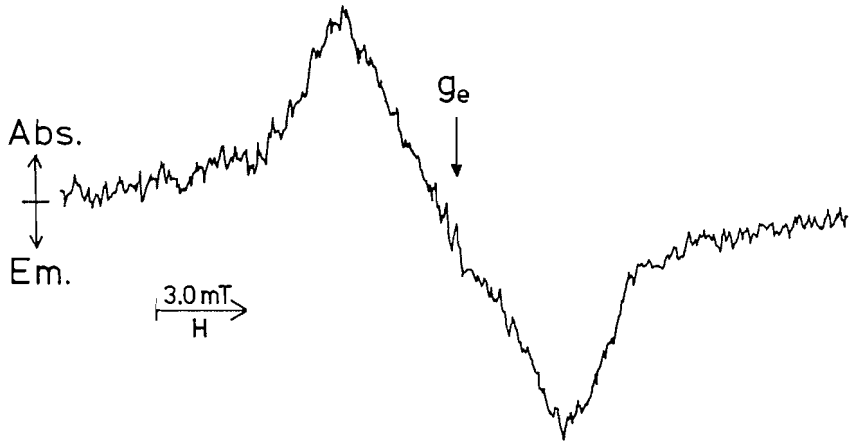


FIG. 7. Time-resolved ESR spectrum observed at 0.8–1.0 μs after laser excitation of the aqueous solution of β-CD at room temperature.

trations of CDs, they form aggregates that may be too large to tumble freely under this condition. The restrained molecular motion makes it possible to observe the radical pair directly as a triplet state. In fact, the observation of this spectrum failed for low concentrations of β-CD (ca. 1×10^{-3} mol dm^{-3}) where no aggregate formation was expected.

Conclusion

The spin-polarized radical pair between the Xn anion and DEA cation radicals with a fixed orientation was produced under the influence of β- and γ-CDs in both frozen solution at 77 K, and dried powder at both 77 K and room temperature. The spin polarization patterns of these radical pairs were inverted compared to that in the excited triplet state of Xn. This inversion may be interpreted as the interconversion of the principal axes between the excited triplet state of Xn and the radical ion pair. The liquid sample of the β-CD system showed the same spectrum of the radical ion pair as that observed at 77 K, probably because of aggregate formation of β-CD in water.

Acknowledgement

The authors would like to thank Professor K. Kuwata and Mr. N. Ishiwata, Osaka University, for measurements of the CIDEP spectra[2] in the liquid phase.

1. M. L. BENDER and M. KOMIYAMA. Cyclodextrin chemistry. Springer-Verlag, Berlin. 1978.
2. H. MURAI, Y. MIZUNUMA, K. ASHIKAWA, Y. YAMAMOTO, and Y. J. I'HAYA. Chem. Phys. Lett. **114**, 417 (1988).
3. H. MURAI and Y. J. I'HAYA. Chem. Phys. **135**, 131 (1989).
4. H. MURAI, T. IMAMURA, and K. OBI. Chem. Phys. Lett. **87**, 295 (1982).
5. H. MURAI, T. HAYASHI, and Y. J. I'HAYA. Chem. Phys. Lett. **106**, 139 (1984).
6. T. IMAMURA, O. ONITSUKA, H. MURAI, and K. OBI. J. Phys. Chem. **89**, 4921 (1985).
7. H. MURAI, M. MINAMI, T. HAYASHI, and Y. J. I'HAYA. Chem. Phys. **93**, 333 (1985).
8. Y. YAMAMOTO, H. MURAI, and Y. J. I'HAYA. Chem. Phys. Lett. **112**, 559 (1984).
9. K. MIYAGAWA, H. MURAI, and Y. J. I'HAYA. Chem. Phys. Lett. **109**, 97 (1984).
10. S. NIIZUMA, K. AKIYAMA, and J. K. S. WAN. Chem. Phys. Lett. **150**, 429 (1988).
11. H. HAYASHI, Y. SAKAGUCHI, H. MURAI, and Y. J. I'HAYA. J. Phys. Chem. **90**, 4403 (1986).
12. H. MURAI, M. MINAMI, and Y. J. I'HAYA. J. Phys. Chem. **92**, 2120 (1988).
13. K. A. MCLAUCHLAN. Advanced EPR: applications in biology and biochemistry. *Edited by* A. J. Hoff. Elsevier, Amsterdam. 1989. p. 345.
14. T. IMAMURA, O. ONITSUKA, H. MURAI, and K. OBI. J. Phys. Chem. **88**, 4028 (1984).

Can. J. Chem. Downloaded from www.nrcresearchpress.com by 84.41.108.74 on 09/07/12
For personal use only.

The effect of added salts on carbon monoxide adsorption on platinum and palladium hydrosols: an FTIR study

MICHAEL R. MUCALO AND RALPH P. COONEY[1]

Chemistry Department, University of Auckland, Private Bag, Auckland, New Zealand

Received April 2, 1991

This paper is dedicated to Professor Richard Norman Jones

MICHAEL R. MUCALO and RALPH P. COONEY. Can. J. Chem. **69**, 1649 (1991).

Fourier transform infrared spectroscopy has been used to investigate the effect of added cations and anions on CO adsorption on platinum and palladium hydrosols. In general, anion effects on CO adsorption may be classified into three categories. In the first category, poisoning anions (*e.g.* CN^-, SH^-) block the surface against CO adsorption so that infrared spectra exhibit either no $\nu(CO)_{ads}$ bands or $\nu(CO)_{ads}$ bands at lower frequencies (<2070 cm^{-1}). In the second category, inert anions (*e.g.* the halides, citrate, $EDTA^{2-}$) have no apparent effect on $\nu(CO)_{ads}$. The third category is characterised by anions such as PO_4^{3-}, CO_3^{2-}, or stearate ion which affect $\nu(CO)_{ads}$ via the pH change that the dissolved anions cause in the metal hydrosol dispersion medium. Infrared spectra of platinum and palladium hydrosols in cyanide media were found to exhibit bands due to cyanate, tetracyanoplatinate(II), and tetracyanopalladate(II) arising from cyanide corrosion of the metal hydrosols. Ultraviolet/visible spectra of iodide ion in platinum hydrosols indicated that iodoplatinate(II) species had been produced. The band shape of $\nu(CO)_{ads}$ at 2070 cm^{-1} in platinum hydrosols is found to be sensitive to the state of dispersion of the hydrosol particles. Bands due to CO adsorbed on hydrosol particles in either a completely or partially aggregated state are weaker and broader with a decreased value of $\nu(CO)_{ads}$ relative to that of the unaggregated hydrosol.

Key words: platinum hydrosols, palladium hydrosols, CO adsorption, infrared spectroscopy, added salts.

MICHAEL R. MUCALO et RALPH P. COONEY. Can. J. Chem. **69**, 1649 (1991).

On a utilisé la spectrométrie infrarouge avec transformation de Fourier pour rechercher l'influence de l'addition des cations et des anions sur l'adsorption de la molécule de CO sur les hydrosols de platine et de palladium. En général, on peut classifier les effets des anions sur l'adsorption du monoxyde de carbone dans trois catégories. Dans la première catégorie se trouvent les anions empoisonnants (par exemple, CN^-, SH^-) qui bloquent la surface contre l'adsorption du CO en causant la disparition de la bande $\nu(CO)_{ads}$ du spectre infrarouge ou l'apparition de la bande $\nu(CO)_{ads}$ à une fréquence plus basse (<2070 cm^{-1} pour les hydrosols de platine). La catégorie secondaire se caractérise par des anions qui sont apparemment inertes (par exemple, les halogénures, le citrate et le tétra-acétate éthylènediamine). L'addition de ces anions aux hydrosols métalliques n'influencent pas la fréquence de la bande $\nu(CO)_{ads}$. Dans la troisième catégorie se trouvent les anions PO_4^{3-}, CO_3^{2-} et l'ion stéarate. L'influence de ces anions sur la bande $\nu(CO)_{ads}$ est le résultat du changement de pH qui est causé par la dissolution des anions dans le milieu de dispersion. Quand on introduit les hydrosols dans un milieu de cyanure, il est possible d'observer des bandes dans les spectres infrarouges de ces solutions, que l'on a assignées aux espèces cyanate, platinotétracyanure et palladotétracyanure. Ces espèces sont les produits formés par la corrosion des hydrosols dans le milieu de cyanure. Le spectre ultra-violet/visible de l'iodure dissous dans les hydrosols de platine a indiqué la présence du platinotétraiodure. On a noté que l'état de la dispersion du hydrosol de platine influe sur la forme de la bande $\nu(CO)_{ads}$ à 2070 cm^{-1}. Les bandes dues au CO adsorbé sur la surface des particules colloïdales dans un état complètement ou partiellement agrégé sont plus faibles et plus larges avec une valeur inférieure de $\nu(CO)_{ads}$ relative à celle de l'hydrosol non-agrégé.

Mots clés : hydrosols de platine, hydrosols de palladium, adsorption du CO, spectrométrie infrarouge, sels ajoutés.

1. Introduction

The study of adsorption processes occurring at metal sol particles has been facilitated by Fourier transform infrared spectra of adsorbed carbon monoxide which serves as a convenient spectroscopic surface probe molecule for this purpose (1–3) since the vibrational spectra of CO adsorbed at electrode, catalyst, and single crystal surfaces are well-documented (4, 5). The application of electric double-layer theory to explain (6) the stabilisation achieved by metal hydrosols implies that the particles in such systems may be considered as microelectrodes. The addition of electrolytes to negatively charged metal hydrosols affects double-layer properties and hence hydrosol surface properties. For example, aggregation of the colloid may occur if, above a critical electrolyte concentration, the Debye length of the hydrosol particle double-layers is sufficiently diminished (6). Changes in the vibrational surface spectra of CO adsorbed on colloidal platinum surfaces reflect the effects of added electrolytes on the surface properties of the platinum hydrosols. Both linear and 2-fold bridging CO have been detected for colloidal platinum in dichloromethane (7) and for colloidal palladium in methylcyclohexane media (8). An *ab initio* SCF study (9) of the Pd–CO chemisorption system has demonstrated that bond weakening in CO due mainly to $d_\pi(Pd)—\pi^*(CO)$ backbonding, leads to a calculated frequency ($\nu(CO)$) reduction of -72 cm^{-1} with an increase in C—O bond length of *ca.* 0.7 pm. The band due to CO adsorbed linearly on platinum (at *ca.* 2070 cm^{-1}) is used to study surface processes in platinum hydrosols and the band due to the two-fold bridging mode, B_2, of adsorbed CO (at *ca.* 1950 cm^{-1}) is used in studies of palladium hydrosols. In X-ray photoelectron spectra of the deposited hydrosols (10), there is evidence for thin layers or patches of platinum(II) oxides on the platinum hydrosols and palladium(II) and palladium(IV) oxides on the palladium hydrosols. Observed $\nu(CO)_{ads}$ values for CO adsorbed on platinum and palladium hydrosols are characteristic of CO adsorbed on platinum and palladium metal (4) thus the oxide layer is not believed to intervene between adsorbed CO and the metal. However, the extent of surface oxidation may influence the amount of metal available for CO adsorption as illustrated in a recent FTIR study of the influence of pH on CO adsorption on

[1]Author to whom correspondence may be addressed.

Can. J. Chem. Downloaded from www.nrcresearchpress.com by 123.30.183.119 on 09/07/12
For personal use only.

Can. J. Chem. Downloaded from www.nrcresearchpress.com by 123.30.183.119 on 09/07/12
For personal use only.

platinum and palladium hydrosols (2). In particular, increasing the pH of the medium was found to lead to a decrease in $\nu(CO)_{ads}$ caused by a reduction in CO coverage which was believed to result from oxide film growth on the platinum and palladium particles.

In the present study, the effect of the presence of added electrolytes (cyanide, halides, hydrosulfide, and others) on carbon monoxide adsorption on platinum and palladium hydrosols has been monitored by infrared spectroscopy.

2. Experimental

Reagents

Unprotected borohydride-generated platinum hydrosols were the principal colloidal substrates used in this study. Borohydride-generated palladium hydrosols were studied to a lesser extent since the unprotected sols are colloidally stable for only a few hours after preparation whereas the platinum sols are colloidally stable for an indefinite period under ambient conditions. The use of unprotected hydrosols over protected poly (vinyl alcohol) hydrosols is favoured since the protecting agent is found to influence CO adsorption (3). The preparation, purification, and characterisation of the hydrosols by densimetry, ultraviolet/visible and X-ray photoelectron spectroscopy have been described in previous studies (2, 10). The potassium cyanide, potassium chloride, cesium chloride, and barium chloride (all analytical reagents), sodium stearate, and disodium hydrogen citrate (both laboratory reagents) were all supplied by BDH Chemicals and the trisodium phosphate ($Na_3PO_4 \cdot 12H_2O$), lithium chloride, potassium bromide (laboratory reagent grade), sodium chloride, potassium iodide, and anhydrous potassium carbonate (all Pronalys analytical reagents) were supplied by May and Baker Chemicals. Potassium fluoride, rubidium chloride, and strontium chloride (analytical grade) were supplied by Reidel-De-Haën and the anhydrous sodium acetate, sodium hydrosulfide, and calcium chloride hexahydrate (analytical reagents) were supplied, respectively, by Merck Chemicals, Aldrich Chemicals, and Koch-Light Laboratories. Disodium EDTA (ethylenediamine tetraacetate) and magnesium chloride (analytical reagents) were supplied by Ajax Chemicals. These salts were used without further purification. Millipore water, obtained by passing singly distilled water through a Milli-Q Continental Water System, was used for the preparation of the stock solutions of inorganic salts. The CO gas used (minimum purity, 99.5%) was supplied by New Zealand Industrial Gases Ltd.

Spectroscopy

All infrared spectra were recorded at 4 cm^{-1} resolution using a Digilab FTS-60 Fourier transform infrared spectrometer. Ultraviolet/visible spectra were recorded on a Hewett Packard 8452A diode-array ultraviolet/visible spectrophotometer. Platinum or palladium sol/inorganic salt solutions for infrared analysis were usually prepared by adding 0.2 cm^3 of inorganic salt stock solution (in general, 10^{-3} to 2 mol dm^{-3}) to 1.8 cm^3 of platinum or palladium sol to yield a salt concentration that was ten times less than that of the stock solution (10^{-4} to 0.2 mol dm^{-3}). Samples (*ca.* 0.15 cm^3) of these solutions were saturated with CO gas in a gas-bubbling vessel for 10 min and then examined by infrared spectroscopy as a thin film between calcium fluoride windows using the spectrum of the windows as a background. A spectrum of water was then subtracted from the resultant spectrum until water bands in the vicinity of $\nu(CO)_{ads}$ were suppressed. Asymmetric $\nu(CO)_{ads}$ band profiles were subjected to smoothing (Savitsky-Golay) and sub-band analysis based on Gaussian sub-bands using Spectra-Calc (Galactic Industries) curve-fitting software. The sum of the sub-band absorbances ($\Sigma(A_{CO})_i$, $i = 1$–3) obtained from bandfitting was then used (2) to calculate the CO coverage given by $\theta(CO)_{ads}$.

3. Results and discussion

Stability of hydrosol towards added electrolytes

In general, the bulk of the infrared data arises from spectral analysis of platinum sol/inorganic salt solutions in which the concentration of the inorganic salt was less than 10^{-2} mol dm^{-3} and the platinum sol was colloidally stable. Monovalent salt concentrations exceeding 0.02 mol dm^{-3} in platinum sols usually induced aggregation. Salts containing divalent or trivalent anions (*e.g.* Na_3PO_4 and K_2CO_3) normally caused aggregation of the platinum sol at salt concentrations of ≥ 0.01 mol dm^{-3} whereas salts containing divalent cations like $MgCl_2$ caused aggregation at salt concentrations of $\geq$ *ca.* 10^{-4} mol dm^{-3}. The aggregation concentrations observed in this study for the various inorganic salts are in agreement with critical coagulation concentrations reported in the study of platinum sol stability toward salts by Furlong *et al.* (11). Palladium hydrosol samples, on the other hand, were already aggregated prior to adding the inorganic salt. However, CO treatment was found to cause colloidal redispersal (2) of the palladium, so that $\nu(CO)_{ads}$ which was observed for such systems was related to spectra of a dispersed colloid.

Effect of salt addition on $\nu(CO)_{ads}$

Previous studies of carbon monoxide adsorption on platinum and palladium hydrosols as a function (2) of pH have demonstrated that surface adsorption of anions (viz., OH^-) reduces CO coverage and hence the value of $\nu(CO)_{ads}$ by the effective loss of dipolar coupling between the adsorbed CO molecules on the surface. Figure 1 represents the $\nu(CO)_{ads}$–θ data accumulated in this study arising from the addition of electrolytes which come under three categories (see later discussion) to platinum hydrosols. In general, Fig. 1 demonstrates that $\nu(CO)_{ads}$ decreases with decreasing θ which confirms that a loss of dipolar coupling is responsible for the reduction in $\nu(CO)_{ads}$ values. Figure 2 illustrates how the various anions studied affected $\nu(CO)_{ads}$ for CO adsorbed on platinum hydrosols. Tables 1 and 2 give salt concentrations, $\theta(CO)_{ads}$, $\nu(CO)_{ads}$, and pH values for some selected platinum and palladium hydrosol/inorganic salt systems. In general, the effects of anions on CO adsorption on platinum and palladium hydrosols have been summarised into three broad categories: (*i*) anionic poisons which completely block CO adsorption on the sol particles, (*ii*) inert anions which have no apparent effect on $\nu(CO)_{ads}$, and (*iii*) anions which affect $\nu(CO)_{ads}$ via the pH change brought about in the sol dispersion medium by the introduction of dissolved anions. The influence of the alkali and alkaline earth cations on $\nu(CO)_{ads}$ was found to be negligible except where the cations induced sol aggregation.

(i) Poisoning anions (SH^-, CN^-)

Cyanide and hydrosulfide anions are known to exhibit strong specific adsorption on platinum and it is well documented that sulfides are catalyst poisons (12). It is therefore not surprising that CO adsorption is completely blocked by these anions. In the case of the Pt sol/NaSH system, $\nu(CO)_{ads}$ was not observed for the CO-treated hydrosols for a series of NaSH concentrations starting from 0.013 to 0.00013 mol dm^{-3} (pH = 7.90). At this lower concentration limit, $\theta(CO)_{ads}$ is reduced leading to a lower $\nu(CO)_{ads}$ value of *ca.* 2065 cm^{-1} (see Fig. 2(*b*) and Table 1), indicating that either the residual poisoning effect of the SH^- ion or the effect of dispersion pH may be the dominant factor (see later). Bonzel and Ku (13) have shown that pre-adsorbed sulfur affects both the adsorption energy and the total amount of CO adsorbed on Pt(111) surfaces. In the case of the Pd sol/SH^- (0.01 mol dm^{-3}) system, CO treatment of the flocculated sol did not result in sol redispersal and no $\nu(CO)_{ads}$ was observed in the infrared spectrum of the CO-treated flocculated palladium. This indicated that CO was not able to displace the strongly adsorbed hydrosulfide anion.

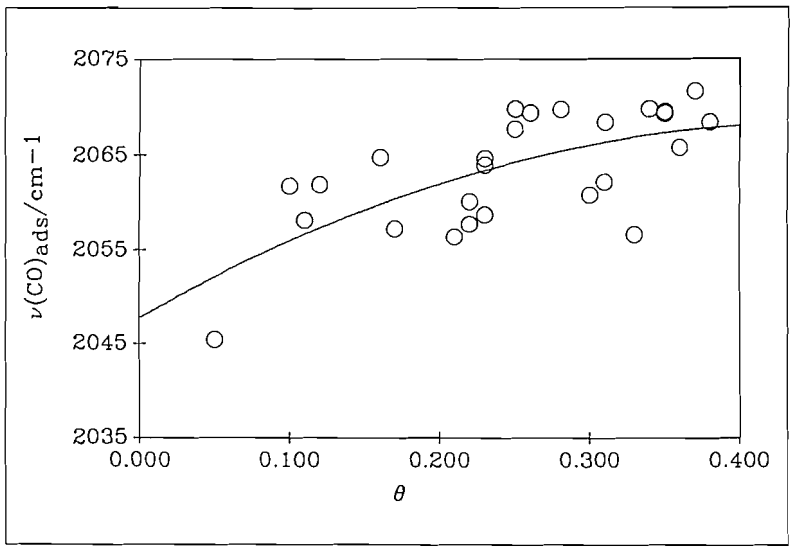


FIG. 1. Correlation of $\nu(CO)_{ads}$ with CO coverage (given by $\theta(CO)_{ads}$) for CO adsorbed on platinum sols in the presence of various added anions (collated data from many experiments).

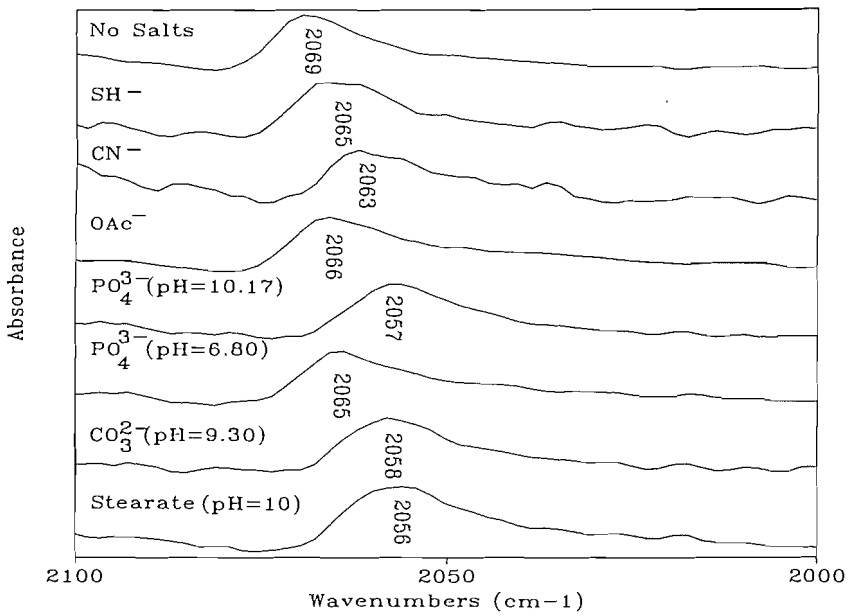


FIG. 2. Infrared spectra of CO adsorbed on a platinum hydrosol in the presence of various anions. Top to bottom: no anions added, 1.3×10^{-4} mol dm^{-3} NaSH, 1×10^{-4} mol dm^{-3} KCN, 1×10^{-2} mol dm^{-3} NaOAc, 2.2×10^{-3} mol dm^{-3} Na_3PO_4 (pH = 10.2), 2.2×10^{-3} mol dm^{-3} Na_3PO_4 (adjusted to pH = 6.8 using $HClO_4$), 2.2×10^{-3} mol dm^{-3} K_2CO_3 (pH = 9.3), and (*h*) 1 cm^3 of platinum sol saturated with sodium stearate (*ca.* 10^{-5} mol dm^{-3}, pH = 10.1).

Cyanide is recognised as being a better σ-donor ligand than carbon monoxide in the reactive and synthetic chemistry of discrete metal complexes. Infrared spectra of CO-treated Pt sol/KCN (0.1, 0.01, and 0.001 mol dm^{-3}) did not exhibit $\nu(CO)_{ads}$ bands, suggesting poisoning by preferential adsorption of cyanide. However, at a potassium cyanide concentration of 0.0001 mol dm^{-3} (pH = 7.28), $\nu(CO)_{ads}$ was detected at *ca.* 2063 cm^{-1} (see Table 1 and Fig. 2(*c*)) which is lower than the expected (2) value (*ca.* 2067 cm^{-1}) in the absence of cyanide at this pH (see later). This observation implies coverage of adsorbed CO as a result of surface poisoning by cyanide. The relatively low pH (7.28) of this system suggests that some cyanide ions may be removed from the solution hydrolysis equilibrium by adsorption. Infrared spectra of CO-treated palladium hydrosols in the presence of cyanide (0.1 mod dm^{-3}) also exhibited no $\nu(CO)_{ads}$ bands.

Infrared spectra of the aggregated Pt sol/KCN (0.1 mol dm^{-3}) samples revealed two relatively weak bands at 2133 and 2169 cm^{-1} in addition to the more intense band at 2080 cm^{-1} due to bulk solution cyanide (see Fig. 3(*b*), the 2133 cm^{-1} band is due (14) to the ν(CN) stretching mode of $[Pt(CN)_4]^{2-}$(aq) and the 2169 cm^{-1} band has been assigned (15–17) to the ν(CN) band of bulk cyanate (NCO^-)). These species are believed to arise from the enhanced corrosion of the platinum particles in the (pH ~ 11) cyanide medium. Indeed, this was confirmed when the same bands were observed for cyanide addition to platinum hydrosols from different preparations *viz.*, citrate- and electric-arc-generated (Bredig) sols. In contrast, spectro-

Can. J. Chem. Downloaded from www.nrcresearchpress.com by 123.30.183.119 on 09/07/12
For personal use only.

TABLE 1. FTIR studies of the influence of anions on CO adsorption on platinum hydrosols

Pt sol system	[salt]/mol dm^{-3}	$\nu(CO)_{ads}/cm^{-1}$	$\theta(CO)_{ads}$[a]	pH
SH^-	1.3×10^{-4}	2065.0	0.17 (0.30)	7.90
CN^-	1.0×10^{-4}	2062.0	0.11 (0.30)	7.28
F^-	1.0×10^{-3}	2070.0	0.41 (0.69)	6.00
Cl^-	2.6×10^{-3}	2067.0	0.61 (0.72)	5.15
Br^-	1.0×10^{-3}	2072.0	0.43 (0.69)	5.53
I^-	1.0×10^{-3}	2070.0	0.57 (0.69)	6.29
OAc^-	1.0×10^{-2}	2065.8	0.36 (0.35)	6.56
OAc^-	1.1×10^{-2}	2065.8	0.31 (0.69)	6.02
Citrate	1.0×10^{-3}	2072.0	0.37 (0.35)	5.42
Stearate	Saturated	2056.0	0.24 (0.31)	10.08
PO_4^{3-}	2.2×10^{-3}	2057.2	0.20 (0.30)	10.17
PO_4^{3-}	2.2×10^{-3}	2064.7	0.32 (0.30)	6.80[b]
CO_3^{2-}	2.0×10^{-4}	2068.0	0.29 (0.31)	7.62
CO_3^{2-}	2.2×10^{-3}	2058.0	0.25 (0.31)	9.30

[a]Value in parentheses refers to the coverage of adsorbed CO on a platinum sol in the absence of added salts.
[b]Adjusted with 0.025 mol dm^{-3} $HClO_4$.

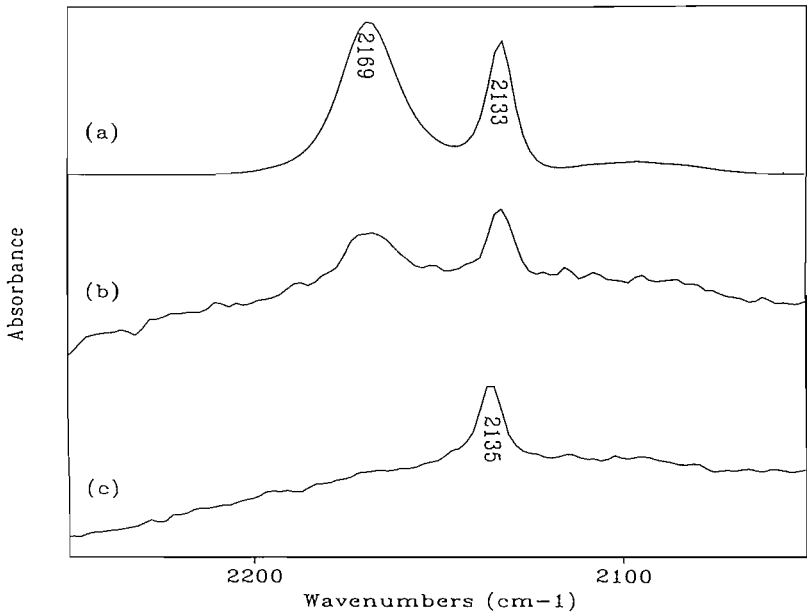


FIG. 3. Infrared spectra of the solution from (*a*) $PtO_2 \cdot xH_2O$ suspension in 0.1 mol dm^{-3} KCN, (*b*) platinum hydrosol (aggregated in 0.1 mol dm^{-3} KCN, and (*c*) clear solution arising from complete dissolution of palladium hydrosol in 0.1 mol dm^{-3} KCN. In all spectra the band due to bulk solution cyanide ($\nu(CN) = 2080\ cm^{-1}$) has been suppressed by subtraction.

electrochemical studies of cyanide corrosion of platinum electrodes have shown little (17) or no evidence (16) for tetracyanoplatinate(II) species. There was no evidence for bands due to $\nu(CO)_{ads}$ as reported in a spectroelectrochemical study of cyanide electrosorption at platinum electrodes (16). The infrared spectra of the species arising from cyanide corrosion of platinum hydrosols was found to be identical to that of platinum dioxide in the presence of cyanide (Fig. 3(*a*)) suggesting that the species observed in the spectra of the Pt sol/KCN system had arisen from cyanide interaction with an oxidised platinum surface.

In contrast, flocculated palladium sol particles dissolve quickly in 0.1 mol dm^{-3} KCN. The infrared spectrum of the resultant clear solution exhibits a single band (Fig. 2(C)) at *ca.* 2135 cm^{-1} which has been assigned (14) to the $\nu(CN)$ stretching mode of $[Pd(CN)_4]^{2-}(aq)$. The complete dissolution of platinum hydrosol particles in the 0.1 mol dm^{-3} KCN as opposed to the slow corrosion of the platinum hydrosol particles in the same medium supports the general observation that palladium is more reactive than platinum (18).

(ii) Inert anions (halides, citrate, acetate)

When platinum sol samples containing halide ions (F^-, Cl^-, Br^-, and I^-) in the concentration range 0.001 to 0.002 mol dm^{-3} were treated with CO, $\nu(CO)_{ads}$ was found to be insensitive to the presence of halide ion. Coverages given by $\theta(CO)_{ads}$ also show no clear trend (see Table 1). However, it was noted that the pH values of the platinum sol/KI samples were higher than for the iodide solution background whereas the other halides exhibited the opposite result. For example, the pH of a platinum sol/0.01 mol dm^{-3} KI solution was higher (7.62) than the pH of a straight 0.01 mol dm^{-3} KI solution prepared in the absence of the platinum hydrosol (6.25). This indicates a

Can. J. Chem. Downloaded from www.nrcresearchpress.com by 123.30.183.119 on 09/07/12
For personal use only.

TABLE 2. FTIR studies of the influence of anions on CO adsorption on palladium hydrosols

Pd sol system	[salt]/mol dm^{-3}	$\nu(CO)_{ads}$/cm^{-1}	$\theta(CO)_{ads}$[a]	pH
CO[b]	—	1954	0.07	5.89
OAc^-	0.01	1953	0.09	7.15
PO_4^{3-}	0.01	1944	0.05	11.83

[a]Spectra represent colloidal palladium redispersed by CO treatment.
[b]Control system (no inorganic salts added to sol).

possible reaction of iodide (see reaction [1]) with the surface layer of platinum(II) oxide:

[1] $Pt(OH)_2 + 4I \rightarrow [PtI_4]^{2-} + 2OH^-$

The surface hydroxide/oxide film has been detected (10) on the platinum sol surface by XPS (see Introduction). Indeed, when the concentration of KI in the dispersion medium is *ca.* 0.2 mol dm^{-3}, the platinum sol aggregates ($\nu(CO)_{ads}$, 2058 cm^{-1}), and an orange–pink colour is apparent in the clear solution after the flocculated particles have settled. Ultraviolet/visible spectra of this solution yielded bands at 338, 388, and 494 nm as well as a shoulder at 442 nm. The series of bands at 338 and 388 nm and shoulder at 442 nm agree approximately in position and relative intensity to those observed for the ultraviolet/visible spectrum of an aqueous solution (19) of $[PtI_4]^{2-}$(aq). The band at 494 nm has not been assigned as the wavelength does not correspond to any simple complex or polyiodide species (20). The ultraviolet/visible spectrum of the aquo complex $[PtI_3(H_2O)]^-$ has also been reported in the literature (19) but this species exhibits bands which differ from those observed in ultraviolet/visible spectra discussed in this study. It is possible that mixed iodohydroxo complexes ($[PtI_{4-x}(OH)_x]^{2-}$) contribute to the ultraviolet/visible spectrum.

Infrared spectra of a CO-treated platinum sol samples containing *ca.* 0.01 mol dm^{-3} sodium acetate exhibit $\nu(CO)_{ads}$ at *ca.* 2066 cm^{-1} at a pH in the range 6–7 (see Table 1). Thus the acetate ion appears to have a slight effect on CO adsorption, although the onset of aggregation of the hydrosol at the acetate concentration studied may be responsible for the decrease in $\nu(CO)_{ads}$ (see later). Radiotracer studies show that acetate adsorbs significantly on platinum electrode surfaces (21) at higher electrode potentials where appreciable oxidation of the electrode has occurred. The platinum sol is believed (10) to possess a thin oxide layer (*ca.* 2.07 nm) as measured from X-ray photoelectron spectroscopy so that acetate adsorption on this layer may be responsible for the slight decrease in $\nu(CO)_{ads}$. No bands due to adsorbed acetate were detected since the molar extinction coefficients (22) of carbonyl stretching frequencies ($\nu(CO)$) are in general smaller (by 2 to 6 times) than the value for CO adsorbed (23) on platinum (1200 dm^3 cm^{-1} mol^{-1}). The infrared spectrum of CO-treated palladium sol in 0.01 mol dm^{-3} sodium acetate (pH = 7.15) shows $\nu(CO)_{ads}$ to be at 1953 cm^{-1} (see Table 2) which is similar to $\nu(CO)_{ads}$ for this system in the absence of acetate (2) at pH 7.2.

When solutions of disodium hydrogen citrate are added to platinum sols, infrared spectra of the CO-treated sol samples show no anion-induced change in the position of $\nu(CO)_{ads}$ or in CO coverage (see Table 1). The result is not surprising since disodium hydrogen citrate is commonly used (11, 24) as a reductant for the preparation of metallic hydrosols from H_2PtCl_6 solutions. Moreover, infrared spectra of citrate-generated platinum hydrosols treated with CO have been reported by the authors (1) to exhibit $\nu(CO)_{ads}$ bands in the same region (2065–2070 cm^{-1}) as that observed for CO adsorbed on the borohydride-generated platinum hydrosols. Infrared spectra of CO-treated platinum sol solutions containing 0.001 mol dm^{-3} disodium EDTA and sodium oxalate also show negligible changes in the position of $\nu(CO)_{ads}$ (2070 cm^{-1}) and $\theta(CO)_{ads}$.

(iii) Anions affecting $\nu(CO)_{ads}$ via pH (PO_4^{3-}, CO_3^{2-})

Inorganic salts such as Na_3PO_4, K_2CO_3, and sodium stearate dissolved in platinum sols often cause significant pH changes in the dispersion medium. The increase in pH is thus believed to be the major factor responsible for the decrease in $\nu(CO)_{ads}$ observed when metal hydrosol samples containing these inorganic salts are treated with CO gas. This effect can be observed most clearly when frequency–pH data from anion addition to platinum or palladium hydrosols are superimposed on the $\nu(CO)_{ads}$ vs. pH plots reported (2) in an earlier publication (see Fig. 4) dealing with the influence of pH on CO adsorption on the hydrosols. For example, saturation of a 1.0 cm^3 sample of platinum sol with sodium stearate (pH = 10) was found to cause $\nu(CO)_{ads}$ to decrease from 2070 to *ca.* 2060 cm^{-1} (see Fig. 2(h)). The saturation of the sol was evident when further addition of solid sodium stearate led to no further increase in pH and no further decrease in $\nu(CO)_{ads}$. Therefore, dispersion pH appears to be a more important factor in the decrease in $\nu(CO)_{ads}$ than adsorption of stearate ion. This assumption is supported by Fig. 4, where the data relating to sodium stearate lies on the polynomial fitted to the frequency–pH data from ref. 2.

Trisodium phosphate concentrations of 0.001 to 0.002 mol dm^{-3} (pH = 10–11) in platinum hydrosols cause $\nu(CO)_{ads}$ to decrease to values in the range 2050–2060 cm^{-1} (see Fig. 2(*e*) and Table 1) while concentrations of 0.01 mol dm^{-3} lead to aggregation and to the appearance of $\nu(CO)_{ads}$ bands at 2038 cm^{-1}. For palladium sols in 0.01 mol dm^{-3} Na_3PO_4 (pH = 11.83, $\nu(CO)_{ads}$ decreases from 1953 cm^{-1} to 1944 cm^{-1} (see Table 2) as expected at this pH on the basis of earlier studies (2). Indeed, when a platinum sol in 0.002 mol dm^{-3} trisodium phosphate (pH = 10.2, $\nu(CO)_{ads}$ = 2057 cm^{-1}) is adjusted to pH 6.8 by perchloric acid addition, $\nu(CO)_{ads}$ increased to 2065 cm^{-1} (see Fig. 2(*f*) and Table 1) which illustrates the importance of pH in determining $\nu(CO)_{ads}$ in the platinum sol/phosphate ion system. This hypothesis is supported by the observation (Fig. 4) that phosphate systems appear to follow the frequency–pH curve closely. Platinum sol solutions containing 0.001–0.01 mol dm^{-3} potassium carbonate appear to cause similar decreases in $\nu(CO)_{ads}$ in infrared spectra as does phosphate (see Table 1 and Fig. 2(g)). Frequency–pH data for carbonate media also follow the curve in Fig. 4 except for some divergence at high pH. This may be attributable (23) to carbonate adsorption on a platinum oxide surface.

The frequency–pH data from the poisoning anions (CN^-, SH^-) and acetate have also been included in Fig. 4. In general, the poisoning of the platinum sol surface by cyanide is indicated

Can. J. Chem. Downloaded from www.nrcresearchpress.com by 123.30.183.119 on 09/07/12
For personal use only.

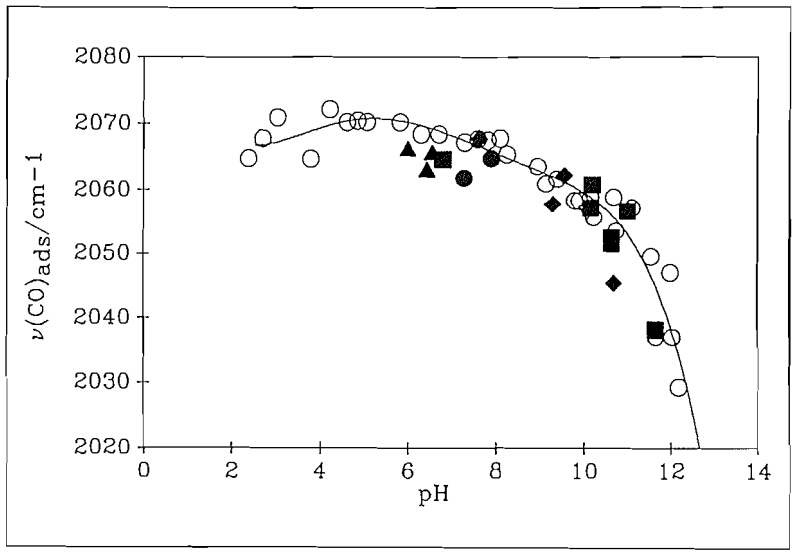


FIG. 4. $\nu(CO)_{ads}$–pH data from infrared spectra of CO adsorbed on platinum hydrosols in the presence of various anions superimposed on the frequency–pH data (open circles) for CO adsorbed on platinum hydrosols from ref. 2. Legend: phosphate (filled squares), carbonate (filled diamonds), acetate (filled triangles), cyanide, hydrosulfide (filled circles), and stearate (obscured by phosphate point at pH ~ 10).

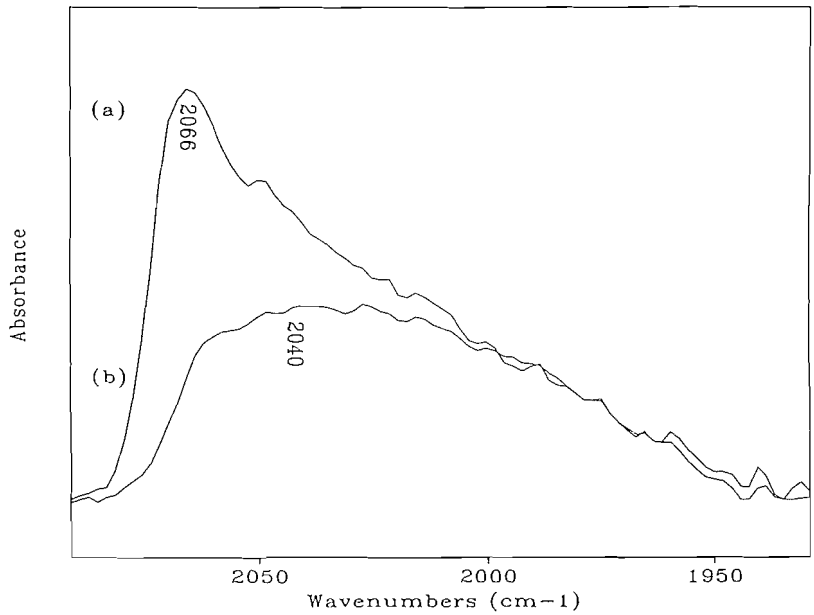


FIG. 5. Infrared spectra of CO adsorbed on a platinum hydrosol in the presence of calcium chloride: (*a*) 10^{-5} mol dm^{-3} $CaCl_2$ (hydrosol stable) and (*b*) 10^{-3} mol dm^{-3} $CaCl_2$ (hydrosol aggregated).

by the deviation of $\nu(CO)_{ads}$ observed for the 10^{-4} mol dm^{-3} cyanide system from the platinum sol frequency–pH curve. The decrease in $\nu(CO)_{ads}$ for the 1.3×10^{-4} mol dm^{-3} NaSH/platinum sol solution, in contrast, appears to yield a value of $\nu(CO)_{ads}$ which would be expected at a pH of 7.90. The absence of significant deviation of acetate frequency–pH data from the curve in Fig. 4 also reveals the insensitivity of CO adsorption on platinum sols in the presence of this anion.

Frequency–pH data relating to CO adsorption on palladium hydrosols in the presence of acetate and phosphate have been superimposed on the plot of $\nu(CO)_{ads}$ vs. pH (consisting of two straight lines) for the palladium hydrosol/CO system from ref. 2. The negligible deviation of this data from the plot supported the suggestion that these anions only exert a pH effect.

Effect of aggregation on the $\nu(CO)_{ads}$ band

In general, the shape of the $\nu(CO)_{ads}$ band is sensitive to aggregation processes in the platinum hydrosol. For CO adsorbed on platinum metal in a colloidally dispersed state, $\nu(CO)_{ads}$ is in general relatively narrow as depicted in Fig. 2(*a*) for CO adsorbed on platinum in the absence of added salts. However, CO treatment of platinum sols in the presence of inorganic salts close to critical coagulation concentrations leads to lower frequency $\nu(CO)_{ads}$ bands which are weaker and considerably broadened. For example, CO-treated solutions of platinum hydrosols in 0.01 mol dm^{-3} KCl have produced broad $\nu(CO)_{ads}$ bands at *ca.* 2055 cm^{-1} even though the colloid appears to be stable. The bulk solution from which the platinum sol/KCl (0.01 mol dm^{-3}) sample for infrared analysis was withdrawn was observed to aggregate on standing. The $\nu(CO)_{ads}$

Can. J. Chem. Downloaded from www.nrcresearchpress.com by 123.30.183.119 on 09/07/12
For personal use only.

band of a CO-treated platinum sol solution in 0.01 mol dm^{-3} sodium acetate appears weaker and broader than the $\nu(CO)_{ads}$ band for CO adsorbed on platinum in the absence of acetate. Given that the value for $\nu(CO)_{ads}$ is slightly lower than that expected at the dispersion pH (see Fig. 4), it is possible that the partial aggregation in the colloid sample induced by the concentration of sodium acetate used (*ca.* 0.01 mol dm^{-3}, see Effect of salt addition on $\nu(CO)_{ads}$) is responsible for the slight effect caused by acetate on CO adsorption (see earlier).

Presumably, the aggregation of the platinum sol induces surface heterogeneity and loss of surface area so that the $\nu(CO)_{ads}$ band broadens and weakens in intensity. Broadening of $\nu(CO)_{ads}$ for flocculated hydrosols has been noted in earlier work referring to aggregation of platinum hydrosols by $HClO_4$ (2) and by extraction of such sols into aliphatic alcohols (3).

The effects of cations on CO adsorption on platinum hydrosols have also been investigated. However, infrared spectra of CO adsorption on colloidally stable platinum hydrosols in the presence of the alkali (10^{-3} mol dm^{-3}) or alkaline earth metal chlorides (10^{-5} mol dm^{-3}) revealed no detectable differences in $\nu(CO)_{ads}$. Alkali and alkaline-earth metal chloride concentrations of 10^{-2} and 10^{-4} mol dm^{-3}, respectively, were observed to induce aggregation of the platinum sols. The difference in aggregation concentrations between the monovalent and divalent cations is indicative of the Schultze–Hardy Rule which states (6) that the valency of the cation is important in determining the critical coagulation concentration. Irrespective of the aggregating cation, CO-treatment of the flocculated platinum sol particles leads to the loss of the relatively sharp peak at 2070 cm^{-1} and the appearance of the expected broad $\nu(CO)_{ads}$ bands which are centered at *ca.* 2040 cm^{-1} (see Fig. 5). Other cations such as Pb^{2+} (as lead(II) acetate) added to platinum sols cause negligible changes in $\nu(CO)_{ads}$ for $[Pb^{2+}]$ in the dispersion medium below the coagulation concentration. Amphiphilic cations such as the cetyl trimethyl ammonium cation cause an initial decrease in $\nu(CO)_{ads}$ from 2070 to 2065 cm^{-1}. The invariance of $\nu(CO)_{ads}$ with further addition of CTAB suggests that a saturation limit for CTAB has been reached. The spectroscopic behaviour of this system is thus similar to that of the platinum sol/sodium stearate system although the pH (5.0) of platinum sol/CTAB samples differs negligibly from the natural pH of the hydrosol in the absence of CTAB. This is consequently reflected by the smaller deviation of $\nu(CO)_{ads}$ from 2070 cm^{-1}.

The following infrared spectroscopic study in this series will involve the adsorption of CO on rhodium hydrosols (25).

Can. J. Chem. Downloaded from www.nrcresearchpress.com by 123.30.183.119 on 09/07/12
For personal use only.

Acknowledgements

The authors are grateful to the New Zealand University Grants Committee for funding to purchase the Fourier transform infrared spectrometer as well as for the awarding of a Postgraduate and William Georgetti Scholarship to M.R.M.

1. M. R. MUCALO and R. P. COONEY. J. Chem. Soc. Chem. Commun. 94 (1989).
2. M. R. MUCALO and R. P. COONEY. J. Chem. Soc. Faraday Trans., **87**, 1221 (1991).
3. M. R. MUCALO and R. P. COONEY. J. Chem. Soc. Faraday Trans. To be published.
4. N. SHEPPARD and T. T. NGUYEN. *In* Advances in infrared and Raman spectroscopy. Vol. 5. *Edited by* R. J. H. Clark and R. E. Hester. Wiley, Heyden, London. 1978. p. 106.
5. A. BEWICK and S. PONS. *In* Advances in infrared and Raman spectroscopy. Vol. 12. *Edited by* R. J. H. Clark and R. E. Hester. Wiley, Heyden, London. 1985. p. 1.
6. D. H. EVERETT. Basic principles of colloid science. Royal Society of Chemistry, London. 1988. pp. 36, 129.
7. L. N. LEWIS and N. LEWIS. J. Am. Chem. Soc. **108**, 7228 (1986).
8. J. S. BRADLEY, J. MILLAR, E. W. HILL, and M. MELCHIOR. J. Chem. Soc. Chem. Commun. 705 (1990).
9. P. SCHWERDTFEGER, J. S. MCFEATERS, J. J. MOORE, D. M. MCPHERSON, R. P. COONEY, G. A. BOWMAKER, M. DOLG, and D. ANDRAE. Langmuir, **7**, 116 (1991).
10. M. R. MUCALO, R. P. COONEY, and J. B. METSON. Colloids Surf. In press.
11. D. N. FURLONG, A. KAUNIKONIS, W. H. F. SASSE, and J. V. SAUNDERS. J. Chem. Soc. Faraday Trans. 1. **80**, 571 (1984).
12. C. H. BARTHOLOMEW, P. K. AGRAWAL, and J. R. KATZER. Adv. Catal. **31**, 136 (1982).
13. H. P. BONZEL and R. KU. J. Chem. Phys. **58**, 4617 (1973).
14. K. NAKAMOTO. Infrared spectra of inorganic and coordination compounds. Wiley, New York. 1986.
15. A. Y. TSIVADZE, Y. Y. KHARITOVNOV, and G. V. TSINTSADZE. Russ. J. Inorg. Chem. **17**, 1417 (1972).
16. F. KITAMURA, M. TAKAHASHI, and M. ITO. Chem. Phys. Lett. **130**, 181 (1986).
17. A. S. HINMAN, R. A. KYDD, and R. P. COONEY. J. Chem. Soc. Faraday Trans. I. **82**, 3525 (1986).
18. F. R. HARTLEY. The chemistry of platinum and palladium. Applied Science, London. 1973. p. 5.
19. B. CORAIN and A. J. POË. J. Chem. Soc. (A), 1318 (1967).
20. M. MIZUNO, J. TANAKA, and I. HARADA. J. Phys. Chem. **85**, 1789 (1981).
21. V. E. KAZARINOV and G. P. GIRINA. Élektrokhimiya, **3**, 107 (1967).
22. C. J. W. BROOKS, G. EGLINTON, and J. F. MORMAN. J. Chem. Soc. 106 (1961).
23. L. H. LITTLE. Infrared spectra of adsorbed species. Academic Press, London. 1966. p. 78.
24. K. AIKA, L. L. BAN, I. OKURA, S. NAMBA, and J. TURKEVICH. J. Res. Inst. Catal. Hokkaido Univ. **24**, 54 (1976).
25. M. R. MUCALO and R. P. COONEY. Chem. Mater. To be published.

Thermal lensing and photoacoustic spectra of gaseous acetylene by pulsed tunable infrared laser

MAKOTO TAKAHASHI, YASUO OKUZAWA, MASAAKI FUJII, AND MITSUO ITO
Department of Chemistry, Faculty of Science, Tohoku University, Sendai 980, Japan

Received April 19, 1991

This paper is dedicated to Dr. Richard Norman Jones

MAKOTO TAKAHASHI, YASUO OKUZAWA, MASAAKI FUJII, and MITSUO ITO. Can. J. Chem. **69**, 1656 (1991).

Thermal lensing and photoacoustic spectra of ν_3, $\nu_1 + \nu_3$, and $\nu_1 + \nu_2 + \nu_3$ vibrational transitions of gaseous acetylene were observed by a tunable pulsed IR laser converted from a pulsed dye laser. Application of a pulsed IR laser to photothermal spectroscopy is demonstrated.

Key words: thermal lensing spectra, photoacoustic spectra, pulsed tunable infrared laser.

MAKOTO TAKAHASHI, YASUO OKUZAWA, MASAAKI FUJII et MITSUO ITO. Can. J. Chem. **69**, 1656 (1991).

Utilisant un laser IR pulsé et accordable, dérivé d'un laser à colorant pulsé, on a observé les spectres photo-acoustiques et d'effet de lentille thermique des transitions vibrationnelles ν_3, $\nu_1 + \nu_3$ et $\nu_1 + \nu_2 + \nu_3$ de l'acétylène gazeux. On a mis en évidence les applications possibles d'un laser IR pulsé à la spectroscopie photothermique.

Mots clés : les spectres lentille thermique, les spectres photo-acoustiques, laser infrarouge pulsé et accordable

[Traduit par la rédaction]

Introduction

Recent developments in laser techniques enable us to convert tunable visible dye laser light into tunable light in the IR region. Raman shifting in H_2 and differential frequency mixing are typical techniques for frequency conversion to the IR region. Though the bandwidth of the converted IR light is greater (typically $0.1 \sim 1\ cm^{-1}$) than that of a diode laser, it has a wider tunable range, higher peak power ($0.1 \sim 1$ MW) and shorter duration (<10 ns). These factors give us several possibilities in the study of the spectroscopy and dynamics of molecules. For example, pump–probe experiments with pulsed IR lasers allow ultrafast time-resolved spectroscopy in the IR region as the poor time resolution of typical IR detectors is overcome (1). The high peak power allows efficient generation of vibrationally excited molecules so that it is possible to observe their electronic transitions. Since with IR laser light we can populate particular vibrational levels that cannot be reached at room temperature, the observed electronic transitions may lead to new information on vibrational levels of the excited electronic state (2) and also to the study of the dissociation dynamics from high vibrational states of the excited electronic state (3–13). Another application of this type of laser is in photothermal spectroscopy (photoacoustic and thermal lensing spectroscopies). Since in photothermal spectroscopy a transition is detected by a thermal effect, this technique may be applied to nonemissive molecules and states. The high overtone vibrations of acetylene were observed by the photoacoustic spectroscopy with visible output of a dye laser (14). However, for IR transitions, the heat generated is small because of the small transition energy. It is desirable, therefore, to use a high sensitivity detection method and a tunable IR laser with high peak power. In this paper, we demonstrate the application of the pulsed tunable IR laser and photothermal spectroscopy to the measurement of the infrared spectrum of gaseous acetylene. The original aim of our study is the observation of electronic transitions of acetylene from particular vibrational levels of the electronic ground state rather than the observation of the infrared spectrum itself. The results obtained here provide an important step towards our final aim.

The following three techniques were used to generate pulsed IR laser light depending on the wavelength region: (I) 3100–3500 cm^{-1}: The difference wave produced by frequency mixing of the fundamental of a Nd^{3+}:YAG laser-pumped dye laser and the second harmonic of the Nd^{3+}:YAG laser (532 nm) with a $LiIO_3$ (LIO) crystal. (II) 5800–7700 cm^{-1}: The difference wave generation of (I), in which the 532 nm beam was replaced by the fundamental of the YAG laser (1.064 μm). (III) 7400–9700 cm^{-1}: The second Stokes stimulated Raman lines excited by the Nd^{3+}:YAG laser-pumped dye laser by using a H_2 Raman shifter.

Our experimental setup is shown in Fig. 1. A Nd^{3+}:YAG laser (Quantel YG 581-10) was operated at 10 Hz repetition rate. In method (I), the output of a dye laser was mixed with the 532 nm beam of the YAG laser in a LIO crystal mounted on an automatically tracked, angle-tuned stage (Inrad, IR Autotracker). In the case of (II), the setup was almost the same as (I) except that the dye laser beam was mixed with a fundamental of YAG laser. In method (III), the dye laser beam was passed through a H_2 Raman shifter which contained H_2 gas at a pressure of 20 atm. The IR laser light produced by these three methods was separated from the dye laser beam, 1.064 μm beam, or 532 nm beam by a visible-cut filter and a 1.064 μm reflection mirror. For photoacoustic spectroscopy, shown in Fig. 1(*a*), a cell was equipped with a home-made ribbon microphone and the sample gas pressure was ~200 Torr. For thermal lensing spectroscopy, shown in Fig. 1(*b*), the IR laser beam was passed through a 40 cm-long cell which contained sample gas at about 470 Torr. From the opposite side of the cell, a He–Ne laser beam was passed collinearly. The density of the transmitted He–Ne beam was monitored by a photodiode. The signal from the microphone or the photodiode was amplified by gains of 10 and 2000, respectively. The amplified signal was integrated by a digital boxcar integrator (PAR 4402/4420), and recorded on a microcomputer. Acetylene gas was used after passing through a Dry Ice/methanol trap for purification.

The observed spectra are shown in Fig. 2. Figure 2(*a*) shows the photoacoustic spectrum of ν_3 (CH anti-symmetric stretching 3287 cm^{-1}) region of gaseous acetylene. The IR laser light of 37 μJ energy per pulse was generated by method (I) using a DCM dye laser. The spectrum shows sharp rovibrational lines.

Printed in Canada / Imprimé au Canada

Can. J. Chem. Downloaded from www.nrcresearchpress.com by 84.41.108.74 on 09/07/12
For personal use only.

Can. J. Chem. Downloaded from www.nrcresearchpress.com by 84.41.108.74 on 09/07/12
For personal use only.

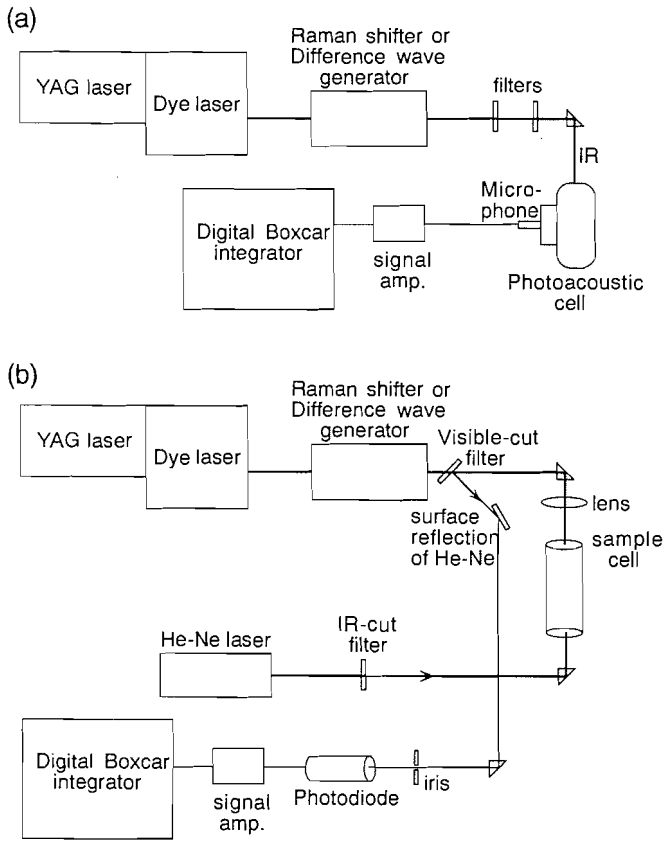


FIG. 1. Schematic diagram of the experimental setup for (*a*) photoacoustic spectroscopy and (*b*) thermal lensing spectroscopy.

The observed structures are complicated by Fermi resonance of ν_3 with several combination bands ($\nu_2 + \nu_4 + \nu_5$...see ref. 15). Figure 2(*b*) shows the photoacoustic spectrum of the $\nu_1 + \nu_3$ combination band (ν_1: CH symmetric stretching 3373 cm^{-1}). The IR laser light was generated by method (II) also using DCM. The energy of the IR laser was 1.0 mJ per pulse. The spectrum shows the regular rovibrational structure of a Σ–Σ transition. No extra lines due to vibrational mixing are observed. Assignments of the rotational lines are indicated in the figure. Both spectra are consistent with the known IR absorption spectrum of acetylene (15–20). The observation of well-resolved rovibrational structure is a good demonstration that the tunable IR laser is useful for detecting vibrational spectra with high sensitivity when combined with photoacoustic spectroscopy.

We have also used the tunable pulsed IR laser in thermal lensing spectroscopy. Figure 2(*c*) shows the thermal lensing spectrum of gaseous acetylene in the region of $\nu_1 + \nu_2 + \nu_3$ (ν_2: CC stretching 1974 cm^{-1}). Infrared laser light of 1.3 mJ per pulse was generated by method (III). The spectrum again shows the well-resolved rovibrational structure of a Σ–Σ transition, showing that combination of thermal lensing spectroscopy with a tunable IR laser is also useful for gaseous vibrational spectroscopy. We have also measured the photoacoustic spectrum for the same combination band, which yields a similar spectrum. The photoacoustic signal is about 100 times more intense than the signal from thermal lensing spectroscopy, giving a better signal-to-noise ratio for the photoacoustic spectrum. Despite the lower signal intensity, thermal lensing spectroscopy may still be useful because it does not require any special equipment such as a microphone or a specially designed cell.

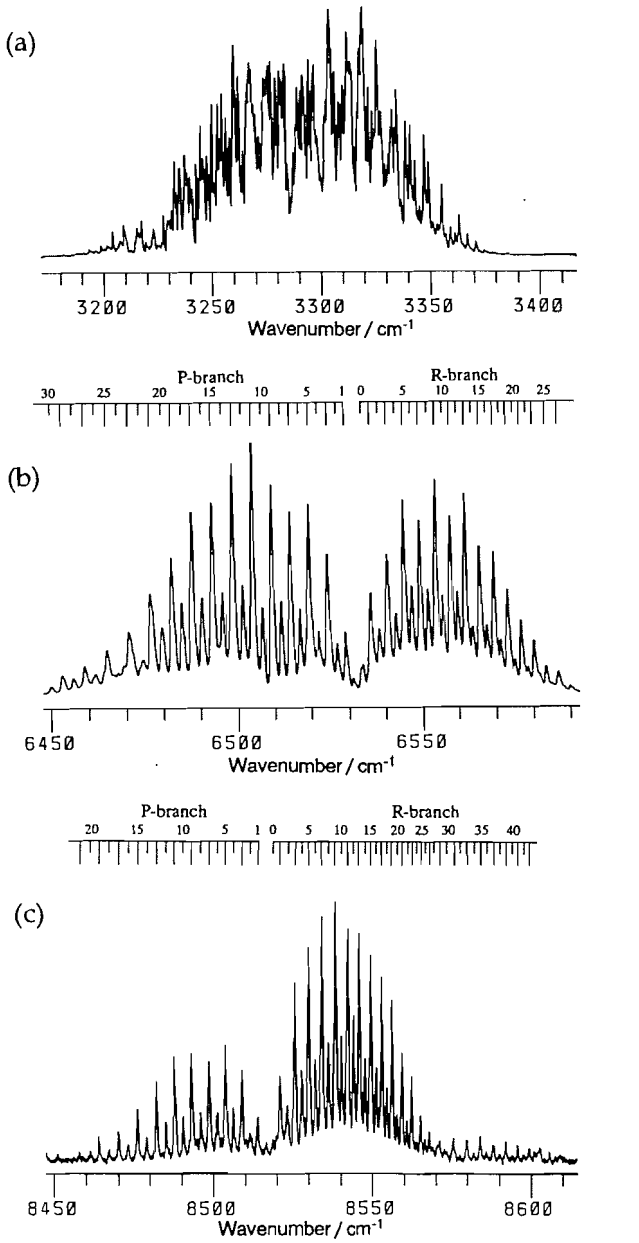


FIG. 2. Photoacoustic spectra of ν_3 (*a*), $\nu_1 + \nu_3$ (*b*) and a thermal lensing spectrum of $\nu_1 + \nu_2 + \nu_3$ (*c*) for gaseous acetylene.

In this paper, we have presented vibrational spectra of acetylene observed using a tunable pulse IR laser derived from a visible dye laser. The combination of this laser with photoacoustic and thermal lensing spectroscopies has proved useful for the measurement of vibrational spectra in the gas phase.

1. M. P. CASASSA, J. C. STEPHENSON, and D. S. KING. J. Chem. Phys. **89**, 1966 (1988).
2. R. H. PAGE, Y. R. SHEN, and Y. T. LEE. J. Chem. Phys. **88**, 5362 (1988).
3. T. M. TICICH, M. D. LIKAR, H.-R. DÜBAL, L. J. BUTLER, and F. F. CRIM. J. Chem. Phys. **87**, 5820 (1987).
4. A. SINHA, R. L. VANDER WAL, L. J. BUTLER, and F. F. CRIM. J. Phys. Chem. **91**, 4645 (1987).

5. M. D. LIKAR, J. E. BAGGOT, A. SINHA, T. M. TICICH, R. L. VANDER WAL, and F. F. CRIM. J. Chem. Soc. Faraday Trans. 2, **84**, 1483 (1988).
6. M. D. LIKAR, A. SINHA, T. M. TICICH, R. L. VANDER WAL and F. F. CRIM. Ber. Bungsenges. Phys. Chem. **92**, 289 (1988).
7. M. D. LIKAR, J. E. BAGGOTT, and F. F. CRIM. J. Chem. Phys. **90**, 6266 (1989).
8. A. SINHA, R. L. VANDER WAL, and F. F. CRIM. J. Chem. Phys. **91**, 2929 (1989).
9. A. SINHA, R. L. VANDER WAL, and F. F. CRIM. J. Chem. Phys. **92**, 401 (1990).
10. R. L. VANDER WAL, and F. F. CRIM. J. Phys. Chem. **93**, 5331 (1989).
11. R. L. VANDER WAL, J. L. SCOTT, and F. F. CRIM. J. Chem. Phys. **92**, 803 (1990).
12. E. CARRASQUILLO M., A. L. UTZ, and F. F. CRIM. J. Chem. Phys. **88**, 5976 (1988).
13. M. BROUARD, M. T. MARTINEZ, J. O'MAHONY, and J. P. SIMONS. Chem. Phys. Lett. **150**, 6 (1988).
14. G. J. SCHERER, K. K. LEHMANN, and W. KLEMPERER. J. Chem. Phys. **78**, 2817 (1983).
15. B. C. SMITH, and J. S. WINN. J. Chem. Phys. **89**, 4638 (1988).
16. S. GHERSETTI, J. E. ADAMS, K. N. RAO. J. Mol. Spectrosc. **64**, 157 (1977).
17. L. W. RICHARDS. J. Chem. Educ. **43**, 644 (1966).
18. H. C. ALLEN, JR., E. D. TIDWELL, and E. K. PLYLER. J. Res. NBS, **57**, 213 (1956).
19. A. BALDACCI, S. GHERSETTI, and K. N. RAO. J. Mol. Spectrosc. **68**, 183 (1977).
20. R. M. TALLEY, and A. H. NIELSEN. J. Chem. Phys. **18**, 1680 (1950).

Can. J. Chem. Downloaded from www.nrcresearchpress.com by 84.41.108.74 on 09/07/12
For personal use only.

The infrared emission spectra of LiF and HF

H. G. HEDDERICH,[1] C. I. FRUM, R. ENGLEMAN, JR., AND P. F. BERNATH[1]
Department of Chemistry, The University of Arizona, Tucson, AZ 85721, U.S.A.
Received March 20, 1991
This paper is dedicated to Dr. Richard Norman Jones

H. G. HEDDERICH, C. I. FRUM, R. ENGLEMAN, JR., and P. F. BERNATH. Can. J. Chem. **69**, 1659 (1991).

The high resolution infrared spectrum of LiF has been measured in emission with the McMath Fourier transform interferometer at Kitt Peak. A total of 800 lines with $v = 1 \rightarrow 0$ to $v = 8 \rightarrow 7$ of the main isotopomer, ^{7}LiF, and 250 lines with $v = 1 \rightarrow 0$ to $v = 3 \rightarrow 2$ of the minor isotopomer, ^{6}LiF, were observed. These ro-vibrational transitions and the pure rotational transitions from the literature were fit to a set of Dunham coefficients Y_{ij} and a set of mass-reduced Dunham coefficients U_{ij}. The same spectrum shows 13 pure rotational emission transitions of HF in the vibrational ground state with $J = 13 \rightarrow 12$ to $J = 25 \rightarrow 24$. These transitions were used to determine an improved set of rotational constants for HF.

Key words: infrared spectra, LiF, HF.

H. G. HEDDERICH, C. I. FRUM, R. ENGLEMAN, JR. et P. F. BERNATH. Can. J. Chem. **69**, 1659 (1991).

On a mesuré les spectres d'émission infrarouge à haute résolution du LiF à l'aide d'un interféromètre à transformation de McMath Fourier au niveau Kitt Peak. On a observé 800 raies avec des valeurs de v allant de $v = 1 \rightarrow 0$ à $v = 8 \rightarrow 7$ pour l'isotopomère principal, ^{7}LiF, et on a observé 250 raies avec des valeurs de v allant de $v = 1 \rightarrow 0$ à $v = 8 \rightarrow 7$ pour l'isotopomère minoritaire. On a adapté ces transitions de vibration-ro et les transitions de rotation pure répertoriées dans la littérature à un ensemble de coefficients de Dunham Y_{ij} et à un ensemble de coefficients U_{ij} de masse réduite Dunham. Ces mêmes spectres montrent 13 transitions d'émission de rotation pure du HF dans l'état fondamental de vibration avec $J = 13 \rightarrow 12$ à $J = 25 \rightarrow 24$. On a utilisé ces transitions pour déterminer un ensemble amélioré de constantes de rotation pour le HF.

Mots clés : spectres infrarouge, LiF, HF.

[Traduit par la rédaction]

I. Introduction

The infrared spectra of alkali halides have been of interest to spectroscopists for a long time (1, 2). However, high-resolution infrared data for these molecules have only become available after the introduction of diode laser and Fourier transform infrared spectrometers. Nevertheless, the first infrared data on LiF was obtained by Vidale (3) as early as 1959 with a Perkin-Elmer grating spectrometer. He observed the spectrum of LiF both in absorption and emission. However, the resolution was not high enough to obtain an unambiguous rotational assignment and, therefore, the correct band center. Vidale gave three possible assignments. Only after the microwave measurements on ^{6}LiF by Wharton *et al.* (4) did the correct assignment become apparent. Several additional papers report the infrared spectrum of LiF trapped in low temperature matrices (5–10).

The first high-resolution infrared data on LiF was published by Maki (11). He used a tunable diode laser system for the observation of ro-vibrational transitions with $v = 1 \leftarrow 0$ to $v = 8 \leftarrow 7$ for ^{7}LiF and ^{6}LiF. Diode lasers display many gaps in their spectral coverage. Therefore, only a few lines of each vibrational band were accessible. In this paper the complete emission spectra of ^{7}LiF and ^{6}LiF between 630 and 1030 cm^{-1} are published (Figs. 1, 2).

HF is an important gas for use as an absolute wavenumber standard. In 1987 Jennings *et al.* (12) published rotational constants for HF calculated from measurements in four different laboratories. Highly accurate data in the far infrared ($J = 1 \leftarrow 0$ to $J = 4 \leftarrow 3$) were obtained with a tunable far-infrared spectrometer at the National Bureau of Standards laboratory in Boulder. Transitions with $J = 5 \leftarrow 4$ to $J = 7 \leftarrow 6$ were measured with a commercial high-resolution Fourier transform spectrometer at the National Research Council, Ottawa, Canada. Lines with $J = 17$ to $J = 21$ were observed with a vacuum grating spectrograph (13) and lines with $J = 26$ to $J = 32$ with a tunable diode laser spectrometer at the University of Lille, France. In 1988 Jennings and Wells (14) remeasured the $J = 27 \leftarrow 26$ and $J = 33 \leftarrow 32$ transitions by using a tunable diode laser heterodyne spectrometer (15). Except for these two lines, the mid-infrared transitions are relatively inaccurate. Unfortunately the uncertainties in the molecular constants in this publication seem to be a factor of 10 too small. As a by-product of our work with LiF, we publish thirteen rotational transitions of HF in the range 500 to 900 cm^{-1}. A new fit including the far-infrared data and the diode laser measurements provide an improved set of rotational constants for HF.

II. Experimental

The high resolution infrared emission spectra of ^{6}LiF, ^{7}LiF, and HF between 500 and 1400 cm^{-1} were observed with the McMath Fourier transform spectrometer at Kitt Peak. The unapodized resolution was 0.0055 cm^{-1} with a liquid helium cooled As:Si detector and a KCl beamsplitter. The upper wavenumber limit was set by a wedged InSb filter while the lower limit was given by the transmission of the KCl beamsplitter and by the detector response. The spectrum of LiF was taken accidentally during an attempt to observe the infrared spectrum of MgF_2.

Solid MgF_2 was heated to about 1500 K in an alumina tube furnace. The apparatus used for the experiment was described in detail earlier (16). The heating rate was about 5 K/min. The temperature of the furnace was measured with a chromel–alumel thermocouple placed between the heating elements and the alumina tube. Deposition of solid material onto the windows was avoided by pressurizing the cell with 5 Torr of argon. A series of spectra were taken as the furnace heated up and then cooled down. Initially a globar was placed behind the tube furnace and its image was focused on the 8 mm aperture of the Fourier transform spectrometer. No absorption spectra were observed, but when the globar was shut off (at a temperature of about 1300 K) an emission spectrum was monitored. The inten-

[1]Also affiliated with Centre for Molecular Beams and Laser Chemistry, Department of Chemistry, The University of Waterloo, Waterloo, Ont., Canada N2L 3G1.

Printed in Canada / Imprimé au Canada

Can. J. Chem. Downloaded from www.nrcresearchpress.com by 84.41.108.74 on 09/07/12
For personal use only.

TABLE 1. Ro-vibrational transitions of ^{7}LiF and ^{6}LiF

	J''	Obs./cm^{-1}	Obs. − calc. /10^{-5} cm^{-1}	J''	Obs./cm^{-1}	Obs. − calc. /10^{-5} cm^{-1}
^{7}LiF				P4	883.42268(50)	−16
$v = 1 \rightarrow 0$	P67	643.22499(50)[a]	−32	P3	886.21112(50)	−15
	P66	647.79186(50)	−14	P2	888.96043(50)	−16
	P65	652.34367(100)	11	P1	891.67033(50)	−19
	P64	656.87691(50)	3	R0	896.97099(50)	−10
	P63	661.39365(50)	5	R1	899.56097(50)	−19
	P62	665.89322(50)	21	R2	902.11051(50)	−23
	P61	670.37521(50)	56	R3	904.61936(50)	−17
	P60	674.83778(50)	−20	R4	907.08707(50)	−21
	P59	679.28310(50)	52	R5	909.51355(50)	−17
	P58	683.70808(50)	60	R6	911.89840(50)	−18
	P57	688.11522(150)	130	R7	914.24140(50)	−20
	P56	692.49965(50)	−11	R8	916.54237(50)	−16
	P55	696.86537(50)	1	R10	921.01692(50)	−16
	P54	701.21006(50)	22	R11	923.19005(50)	−16
	P53	705.53328(50)	5	R12	925.32007(50)	−17
	P52	709.83535(50)	38	R13	927.40677(50)	−17
	P51	714.11486(50)	21	R14	929.44992(50)	−13
	P50	718.37200(50)	12	R15	931.44921(50)	−14
	P49	722.60630(50)	6	R16	933.40445(50)	−16
	P48	726.81744(50)	10	R17	935.31541(50)	−18
	P47	731.00488(50)	10	R18	937.18186(50)	−20
	P46	735.16819(50)	2	R19	939.00368(50)	−12
	P45	739.30720(50)	9	R20	940.78049(50)	−11
	P44	743.42133(50)	12	R21	942.51208(50)	−16
	P43	747.51018(50)	9	R22	944.19838(50)	−11
	P42	751.57345(50)	10	R23	945.83905(50)	−11
	P41	755.61069(50)	7	R24	947.43398(50)	−5
	P40	759.62154(50)	3	R25	948.98282(50)	−9
	P39	763.60582(50)	18	R26	950.48550(50)	−8
	P38	767.56266(50)	1	R27	851.94180(50)	−7
	P37	771.49217(50)	3	R28	953.35151(50)	−5
	P36	775.39382(50)	6	R29	954.71447(50)	−1
	P35	779.26714(50)	1	R30	956.03041(50)	−3
	P34	783.11189(50)	1	R31	957.29927(50)	1
	P33	786.92762(50)	−4	R32	958.52075(50)	−1
	P32	790.71410(50)	1	R33	959.69477(50)	1
	P31	794.47076(50)	−5	R34	960.82113(50)	3
	P30	798.19745(50)	−3	R35	961.89967(50)	6
	P29	801.89368(50)	−4	R36	962.93020(50)	8
	P28	805.55917(50)	−3	R37	963.91257(50)	9
	P27	809.19351(50)	−5	R38	964.84670(50)	16
	P26	812.79639(50)	−5	R39	965.73172(50)	−42
	P25	816.36742(50)	−9	R40	966.56926(50)	13
	P24	819.90638(50)	−4	R41	967.35751(50)	13
	P23	823.41278(50)	−5	R42	968.09690(50)	16
	P22	826.88635(50)	−4	R43	968.78722(50)	14
	P21	830.32668(50)	−10	R44	969.42838(50)	10
	P20	833.73363(50)	−3	R45	970.02040(50)	20
	P19	837.10660(50)	−9	R46	970.56296(50)	23
	P18	840.44548(50)	−8	R47	971.05594(50)	19
	P17	843.74986(50)	−6	R48	971.49941(50)	27
	P16	847.01934(50)	−11	R49	971.89296(50)	16
	P15	850.25377(50)	−7	R50	972.23690(50)	27
	P14	853.45267(50)	−10	R51	972.53012(50)	−41
	P13	856.61580(50)	−11	R52	972.77459(50)	20
	P12	859.74286(50)	−9	R53	972.96841(50)	26
	P11	862.83347(50)	−11	R54	973.11156(50)	−14
	P10	865.88735(50)	−14	R55	973.20486(50)	−11
	P9	868.90424(50)	−14	R58	973.18288(50)	−9
	P8	871.88380(50)	−13	R59	973.07410(50)	28
	P7	874.82572(50)	−13	R60	972.91472(50)	5
	P6	877.73041(50)	57	R61	972.70458(50)	−28
	P5	880.59549(50)	−11	R62	972.44380(100)	−56

Can. J. Chem. Downloaded from www.nrcresearchpress.com by 84.41.108.74 on 09/07/12
For personal use only.

TABLE 1 (*continued*)

	J''	Obs./cm^{-1}	Obs. − calc. /10^{-5} cm^{-1}		J''	Obs./cm^{-1}	Obs. − calc. /10^{-5} cm^{-1}
	R63	972.13208(100)	−103		P4	867.67416(50)	−17
	R64	971.76979(150)	−131		P3	870.42072(50)	−25
	R66	970.88707(1000)	−757		P2	873.12879(50)	−32
	R67	631.22869(50)	−31		P1	875.79864(50)	17
$v = 2\rightarrow1$	P66	635.72007(50)	−54		R0	881.01967(50)	−9
	P65	640.19664(50)	12		R1	883.57101(50)	−11
	P64	644.65580(50)	−49		R2	886.08249(50)	−11
	P63	649.09925(50)	−24		R3	888.55365(50)	−28
	P62	653.52568(50)	−2		R4	890.98463(50)	−21
	P61	657.93478(50)	30		R5	893.37488(50)	−19
	P60	662.32515(50)	−27		R6	895.72416(50)	−20
	P59	666.69846(50)	30		R7	898.03226(50)	−19
	P58	671.05195(50)	−10		R8	900.29890(50)	−19
	P57	675.38687(50)	−4		R9	902.52385(50)	−17
	P56	679.70218(50)	−7		R10	904.70683(50)	−17
	P55	683.99744(50)	−21		R11	906.84760(50)	−18
	P54	688.27260(50)	−9		R12	908.94670(50)	59
	P53	692.52716(50)	18		R13	911.00160(50)	−16
	P52	696.76022(50)	12		R14	913.01435(50)	−15
	P51	700.97172(50)	6		R15	914.98392(50)	−16
	P50	705.16135(50)	11		R16	916.91013(50)	−15
	P49	709.32807(50)	−39		R18	920.63150(50)	−13
	P48	713.47301(50)	10		R19	922.42624(50)	−10
	P47	717.59424(50)	4		R20	924.17663(50)	−16
	P46	721.69209(50)	16		R21	925.88263(50)	−12
	P45	725.76575(50)	3		R22	927.54388(50)	−13
	P44	729.81524(50)	6		R23	929.16031(50)	−7
	P43	733.83991(50)	−1		R24	930.73159(50)	−6
	P42	737.83964(50)	8		R25	932.25754(50)	−8
	P41	741.81377(50)	5		R26	933.73800(50)	−9
	P40	745.76208(50)	7		R27	935.17279(50)	−8
	P39	749.68415(50)	7		R28	936.56172(50)	−5
	P38	753.57956(50)	3		R29	937.90461(50)	1
	P37	757.44812(50)	13		R30	939.20117(50)	−2
	P36	761.28913(50)	2		R31	940.45135(50)	−1
	P35	765.10256(50)	5		R32	941.65492(50)	0
	P34	768.88784(50)	2		R33	942.81174(50)	2
	P33	772.64482(50)	14		R34	943.92159(50)	0
	P32	776.37275(50)	1		R35	944.98457(50)	21
	P31	780.07159(50)	−4		R36	945.99995(50)	8
	P29	787.38047(50)	−3		R37	946.96804(50)	7
	P28	790.98979(50)	1		R38	947.88866(50)	15
	P27	794.56839(50)	−9		R39	948.76142(50)	8
	P26	798.11622(50)	−4		R40	949.58641(50)	9
	P25	801.63268(50)	−9		R41	950.36345(50)	14
	P24	805.11760(50)	−8		R42	951.09230(50)	12
	P23	808.57063(50)	−2		R43	951.77288(50)	9
	P22	811.99123(50)	−10		R44	952.40513(50)	11
	P21	815.37936(50)	−4		R45	952.98891(50)	15
	P20	818.73443(50)	−9		R46	953.52413(50)	26
	P19	822.05627(50)	−10		R47	954.01031(50)	5
	P18	825.34455(50)	−6		R48	954.44802(50)	21
	P17	828.59880(50)	−12		R49	954.83642(50)	1
	P16	831.81897(50)	−1		R50	955.17610(50)	12
	P15	835.00440(50)	−8		R51	955.46643(50)	2
	P13	841.27036(50)	−12		R52	955.70813(100)	52
	P12	844.35032(50)	−5		R53	955.89976(50)	26
	P11	847.39426(50)	−17		R55	956.13526(50)	22
	P10	850.40221(50)	−15		R58	956.11660(50)	−6
	P9	853.37365(50)	−21		R60	955.85520(100)	−71
	P8	856.30845(50)	−17		R61	955.65116(50)	32
	P7	859.20616(50)	−18		R62	955.39582(50)	−8
	P6	862.06649(50)	−24		R63	955.09177(50)	69
	P5	864.88929(50)	−20	$v = 3\rightarrow2$	P63	637.08050(50)	47

Can. J. Chem. Downloaded from www.nrcresearchpress.com by 84.41.108.74 on 09/07/12
For personal use only.

TABLE 1 (*continued*)

J''	Obs./cm^{-1}	Obs. − calc. /10^{-5} cm^{-1}		J''	Obs./cm^{-1}	Obs. − calc. /10^{-5} cm^{-1}
P62	641.43448(50)	38		R4	875.21320(50)	−9
P61	645.77142(50)	23		R5	877.56817(50)	27
P60	650.09061(50)	−26		R6	879.88235(50)	15
P59	654.39259(50)	−14		R7	882.15584(50)	−10
P58	658.67705(50)	71		R8	884.38874(50)	−11
P57	662.94016(100)	−114		R9	886.58060(50)	−10
P56	667.18712(50)	−7		R10	888.73113(50)	−10
P55	671.41350(50)	−10		R11	890.84013(50)	−8
P54	675.62027(50)	14		R12	892.90734(50)	−6
P53	679.80640(50)	4		R13	894.93247(50)	−8
P52	683.97197(50)	6		R14	896.91535(50)	−9
P51	688.11522(100)	−114		R15	898.85576(50)	−7
P50	692.23944(50)	12		R16	900.75346(50)	−5
P49	696.34045(50)	7		R17	902.60817(50)	−6
P48	700.41927(50)	10		R18	904.41976(50)	−4
P47	704.47535(50)	7		R19	906.18792(50)	−6
P46	708.50834(50)	1		R20	907.91254(50)	−3
P45	712.51815(50)	23		R21	909.59335(50)	0
P44	716.50367(50)	−1		R22	911.23010(50)	−2
P43	720.46523(50)	1		R23	912.82266(50)	−2
P42	724.40076(150)	−140		R24	914.37083(50)	1
P41	728.31423(50)	11		R25	915.87433(50)	−2
P40	732.20075(50)	2		R26	917.33306(50)	−1
P39	736.06160(50)	−1		R27	918.74679(50)	−2
P38	739.89648(50)	9		R28	920.11539(50)	3
P37	743.70475(50)	4		R29	921.43861(50)	5
P36	747.48629(50)	11		R30	922.71629(50)	7
P35	751.24050(50)	4		R31	923.94823(50)	7
P34	754.96726(50)	8		R32	925.13427(50)	5
P33	758.66554(50)	−44		R33	926.27433(50)	10
P32	762.33658(50)	9		R34	927.36815(50)	12
P31	765.97844(50)	7		R35	928.41551(50)	5
P30	769.59128(50)	1		R36	929.41649(50)	12
P29	773.17489(50)	7		R37	930.37073(50)	14
P28	776.72871(50)	3		R38	931.27823(50)	24
P27	780.25263(50)	11		R39	932.13854(50)	12
P25	787.20868(50)	−3		R40	932.95179(50)	4
P24	790.64043(50)	4		R41	933.71793(50)	9
P23	794.04065(50)	−2		R42	934.43673(50)	18
P22	797.40920(50)	−3		R43	935.10785(50)	8
P21	800.74569(50)	−3		R44	935.73142(50)	6
P20	804.04978(50)	−4		R45	936.30716(50)	−6
P19	807.32117(50)	−4		R46	936.83529(50)	6
P18	810.55952(50)	−4		R47	937.31524(50)	−4
P17	813.76451(50)	−3		R48	937.74720(50)	−7
P16	816.93581(50)	−3		R49	938.13106(50)	−3
P15	820.07305(50)	−8		R50	938.46692(50)	26
P14	823.17607(50)	−5		R51	938.75398(50)	11
P13	826.24442(50)	−5		R54	939.32502(50)	44
P12	829.27779(50)	−10		R55	939.41816(100)	58
P11	832.27601(50)	−5		R58	939.40280(100)	−116
P10	835.23860(50)	−9	$v = 4 \rightarrow 3$	P61	633.87765(50)	−1
P8	841.05602(50)	−7		P60	638.12641(100)	−83
P7	843.91016(50)	−11		P59	642.35907(50)	−35
P6	846.72833(100)	62		P58	646.57356(50)	−25
P5	849.50808(50)	−4		P57	650.76959(50)	−38
P4	852.25109(50)	−11		P56	654.94728(50)	−24
P3	854.95662(50)	−6		P55	659.10622(50)	19
P2	857.62348(100)	−79		P54	663.24355(150)	−156
P1	860.25368(50)	−1		P53	667.36412(50)	−24
R0	865.39691(50)	−1		P52	671.46338(50)	1
R1	867.90996(50)	−21		P51	675.54147(50)	−27
R2	870.38398(50)	−18		P50	679.59883(50)	−27
R3	872.81853(50)	−10		P49	683.63493(50)	−10

Can. J. Chem. Downloaded from www.nrcresearchpress.com by 84.41.108.74 on 09/07/12
For personal use only.

TABLE 1 (*continued*)

J''	Obs./cm^{-1}	Obs. − calc. /10^{-5} cm^{-1}		J''	Obs./cm^{-1}	Obs. − calc. /10^{-5} cm^{-1}
P48	687.64923(50)	8		R18	888.53957(50)	4
P47	691.64100(50)	−7		R19	890.28173(50)	6
P46	695.61031(50)	−9		R20	891.98095(50)	6
P45	699.55677(50)	1		R21	893.63709(50)	11
P44	703.47971(50)	−7		R22	895.24986(50)	13
P43	707.37895(50)	−11		R23	896.81903(50)	9
P42	711.25435(50)	12		R24	898.34452(50)	11
P41	715.10502(50)	10		R25	899.82602(50)	6
P40	718.93082(50)	7		R26	901.26345(50)	6
P39	722.73143(50)	8		R27	902.65654(50)	3
P38	726.50642(50)	7		R28	904.00516(50)	0
P37	730.25548(50)	8		R29	905.30926(50)	12
P36	733.97812(50)	1		R30	906.56825(50)	−3
P35	737.67426(50)	13		R31	907.78243(50)	2
P34	741.34315(50)	4		R33	910.07504(50)	5
P33	744.98473(50)	5		R34	911.15319(50)	8
P32	748.59889(50)	40		R35	912.18567(50)	9
P31	752.18426(50)	7		R36	913.17222(50)	−2
P30	755.74152(50)	10		R37	914.11269(50)	−26
P28	762.76918(50)	8		R38	915.00775(50)	19
P27	766.23995(100)	110		R39	915.85593(50)	−1
P26	769.67877(50)	0		R40	916.65813(50)	19
P25	773.08856(50)	6		R41	917.41343(50)	−2
P24	776.46786(50)	14		R42	918.12241(50)	9
P23	779.81612(50)	4		R44	919.40004(50)	34
P22	783.13355(50)	29		R45	919.96811(50)	14
P21	786.41897(50)	4		R46	920.48895(50)	−20
P20	789.67280(50)	4		R47	920.96316(50)	3
P19	792.89451(50)	9		R48	921.39014(50)	34
P18	796.08353(50)	−6		R49	921.76922(50)	13
P17	799.23978(50)	−18		R50	922.10129(50)	41
P16	802.36319(50)	−2		R52	922.62144(50)	−22
P15	805.45303(50)	1		R54	922.95179(50)	29
P14	808.50912(50)	4	$v = 5 \rightarrow 4$	P57	638.86621(50)	31
P13	811.53103(50)	−5		P56	642.97601(50)	−20
P12	814.51865(50)	−6		P55	647.06761(50)	−31
P11	817.47133(50)	−35		P54	651.14147(100)	84
P10	820.38974(50)	7		P53	655.19459(50)	64
P9	823.27215(50)	−24		P52	659.22747(50)	−2
P8	826.11958(50)	4		P51	663.24355(300)	271
P7	828.93075(50)	−8		P50	667.23339(50)	−22
P6	831.70600(50)	3		P49	671.20542(50)	−1
P5	834.44486(50)	19		P48	675.15624(50)	35
P4	837.14646(50)	−17		P47	679.08464(50)	3
P3	839.81170(50)	11		P46	682.99066(100)	−56
P2	842.43925(50)	0		P45	686.87564(50)	31
P1	845.02984(50)	49		P44	690.73652(50)	−3
R0	850.09554(50)	−19		P43	694.57445(50)	−8
R1	852.57155(50)	7		P42	698.38898(50)	11
R2	855.00854(50)	−3		P41	702.17991(100)	70
R3	857.40662(50)	−14		P40	705.94515(50)	−3
R4	859.76600(50)	24		P39	709.68645(50)	4
R5	862.08542(50)	9		P38	713.40242(50)	−12
R6	864.36526(50)	5		P37	717.09308(50)	−12
R7	866.60519(50)	4		P36	720.75821(50)	19
R8	868.80486(50)	−5		P34	728.00889(50)	13
R9	870.96427(50)	5		P33	731.59387(50)	−8
R10	873.08284(50)	−2		P32	735.15166(50)	−24
R11	875.16049(50)	−10		P31	738.68227(50)	3
R12	877.19718(50)	2		P30	742.18469(50)	6
R13	879.19241(50)	7		P29	745.65885(50)	12
R15	883.05771(50)	8		P28	749.10425(50)	6
R16	884.92738(50)	9		P27	752.52062(50)	−5
R17	886.75478(50)	12		P26	755.90785(50)	1

Can. J. Chem. Downloaded from www.nrcresearchpress.com by 84.41.108.74 on 09/07/12
For personal use only.

TABLE 1 (*continued*)

	J''	Obs./cm^{-1}	Obs. − calc. /10^{-5} cm^{-1}		J''	Obs./cm^{-1}	Obs. − calc. /10^{-5} cm^{-1}
	P24	762.59288(50)	1		R45	903.96352(50)	16
	P23	765.89020(50)	12		R46	903.47840(50)	45
	P22	769.15714(50)	5		R47	904.94617(50)	9
	P21	772.39227(50)	4		R48	905.36761(50)	−6
	P20	775.59618(50)	−34		R49	905.74250(50)	−12
	P29	778.76916(50)	−3		R50	906.07049(50)	−35
	P18	781.90999(50)	6		R51	906.35198(50)	−27
	P17	785.01842(50)	2		R55	907.00830(50)	7
	P16	788.09442(50)	11	$v = 6 \rightarrow 5$	P56	631.26624(50)	0
	P15	791.13745(50)	11		P54	639.29894(100)	−76
	P14	794.14719(50)	2		P52	647.25691(50)	−39
	P13	797.12355(50)	4		P51	651.20753(100)	85
	P12	800.06611(50)	6		P50	655.13622(50)	30
	P11	802.97466(50)	18		P49	659.04535(100)	71
	P10	805.84856(50)	5		P46	670.64369(50)	−18
	P9	808.68758(50)	−26		P45	674.46635(50)	−35
	P8	811.49219(50)	2		P44	678.26686(50)	−25
	P6	816.99486(50)	15		P43	682.04524(50)	51
	P5	819.69328(100)	95		P42	685.79951(50)	32
	P4	822.35384(50)	3		P41	689.53022(50)	9
	P3	824.98004(150)	118		P40	693.23728(50)	12
	P2	827.56823(100)	101		P39	696.91967(50)	−27
	R1	837.54801(50)	−17		P38	700.57774(50)	−35
	R2	839.94955(50)	58		P37	704.21097(50)	−29
	R3	842.31126(50)	−19		P36	707.81909(50)	1
	R4	844.63543(50)	6		P35	711.40128(50)	7
	R5	846.92047(50)	0		P34	714.95743(50)	14
	R6	849.16668(50)	19		P33	718.48678(50)	−18
	R7	851.37325(50)	5		P32	721.99000(50)	11
	R8	853.54035(50)	1		P31	725.46568(50)	−3
	R9	855.66776(50)	9		P30	728.91460(50)	51
	R11	859.80190(50)	−5		P29	732.33460(50)	−9
	R12	861.80857(50)	14		P28	735.72725(50)	9
	R13	863.77432(50)	15		P27	739.09118(50)	1
	R14	865.69880(50)	−13		P26	742.42629(50)	−8
	R15	867.58258(50)	10		P25	745.73224(50)	−21
	R16	869.42471(50)	9		P23	752.25605(50)	17
	R17	871.22522(50)	9		P22	755.47261(50)	3
	R18	872.98382(50)	4		P20	761.81424(50)	−10
	R19	874.70051(50)	14		P19	764.93689(200)	−187
	R20	876.37479(50)	9		P18	768.03182(50)	5
	R21	878.00655(50)	0		P17	771.09320(50)	12
	R22	879.59579(50)	6		P16	774.12229(50)	−7
	R24	882.64532(50)	3		P15	777.11933(50)	2
	R25	884.10528(50)	−1		P13	783.01522(50)	24
	R26	885.52187(50)	2		P12	785.91301(50)	−9
	R27	886.89474(50)	−5		P11	788.77891(150)	124
	R28	888.22390(50)	−3		P10	791.60833(50)	−8
	R29	889.50909(50)	−1		P9	794.40495(50)	−6
	R30	890.75008(50)	−4		P8	797.16733(50)	15
	R31	891.94677(50)	−6		P7	799.89493(50)	28
	R32	893.09916(50)	10		P6	802.58730(50)	19
	R33	894.20679(50)	13		P5	805.24087(350)	−342
	R34	895.26944(50)	−2		P4	807.86617(50)	26
	R35	896.28763(50)	31		P2	813.00221(100)	87
	R36	897.26012(50)	3		R2	825.19847(50)	−3
	R37	898.18763(50)	1		R3	827.52599(50)	14
	R38	899.07002(50)	25		R4	829.81527(50)	2
	R39	899.90634(50)	−7		R5	832.06651(50)	8
	R40	900.69714(50)	−26		R6	834.27886(50)	−30
	R41	901.44250(50)	−12		R8	838.58819(50)	−5
	R42	902.14189(50)	−5		R9	840.68389(50)	−23
	R43	902.79536(50)	11		R10	842.74058(50)	1
	R44	903.40252(50)	9		R11	844.75707(50)	−30

Can. J. Chem. Downloaded from www.nrcresearchpress.com by 84.41.108.74 on 09/07/12
For personal use only.

TABLE 1 (*continued*)

	J''	Obs./cm^{-1}	Obs. − calc. /10^{-5} cm^{-1}		J''	Obs./cm^{-1}	Obs. − calc. /10^{-5} cm^{-1}
	R12	846.72833(600)	−594		P21	745.21175(50)	−23
	R13	848.67116(50)	10		P20	748.31931(50)	−12
	R14	850.56750(50)	0		P19	751.39546(100)	−86
	R15	852.42330(50)	−9		P18	754.44228(50)	−7
	R16	854.23959(50)	10		P17	757.44812(1000)	−908
	R17	856.01250(50)	−11		P16	760.44010(50)	−47
	R18	857.75264(700)	712		P15	763.39169(50)	−45
	R19	859.43674(50)	−27		P14	766.31080(100)	−82
	R20	861.08708(50)	18		P13	769.19877(50)	7
	R21	862.69487(50)	−9		P12	772.05255(50)	−53
	R22	864.26104(50)	2		P11	774.87448(50)	1
	R23	865.78496(50)	10		P10	777.66275(50)	17
	R24	867.26622(50)	−9		P9	780.41688(50)	−23
	R25	868.70521(50)	3		P8	783.13355(500)	−423
	R26	870.10125(50)	−3		P7	785.82366(100)	−63
	R27	871.45421(50)	−22		R0	806.05185(200)	−178
	R28	872.76452(50)	6		R3	813.04233(100)	−76
	R29	874.03130(50)	10		R6	819.69328(300)	−302
	R30	875.25442(50)	−6		R7	821.83811(50)	−6
	R31	876.43369(50)	−44		R9	826.00653(50)	−11
	R32	877.56817(200)	−183		R10	828.03300(50)	22
	R33	878.66191(50)	−1		R11	830.02000(50)	13
	R34	879.70976(50)	2		R12	831.96699(100)	−71
	R35	880.71316(50)	−16		R13	833.87574(50)	−29
	R36	881.67234(50)	−17		R14	835.74396(50)	−69
	R37	882.58714(50)	−3		R15	837.57308(50)	−26
	R38	883.45736(50)	20		R16	839.36132(100)	−56
	R39	884.28195(50)	−40		R17	841.10989(50)	−18
	R40	885.06264(50)	4		R18	842.81765(50)	−3
	R41	885.79740(50)	−41		R19	844.48452(50)	−1
	R42	886.48648(150)	−136		R20	846.11019(50)	−22
	R44	887.73275(100)	85		R21	847.69396(150)	−116
	R45	888.28561(50)	−12		R22	849.23796(50)	−51
	R47	889.25732(100)	89		R23	850.74056(50)	29
	R50	890.36885(50)	14		R24	852.20033(50)	1
	R51	890.64793(50)	48		R25	853.61839(50)	−6
	R54	891.20663(50)	8		R26	854.99312(150)	−136
$v = 7 \rightarrow 6$	P49	647.14517(100)	−58		R27	856.33010(200)	188
	P48	650.97177(50)	−19		R28	857.62348(400)	396
	P47	654.77918(200)	187		R29	858.86836(50)	17
	P46	658.56125(50)	−20		R30	860.07412(50)	5
	P45	662.32515(100)	116		R31	861.23685(50)	−16
	P44	666.06510(100)	54		R33	863.43413(100)	72
	P42	673.47846(50)	12		R34	864.46643(50)	−14
	P41	677.15168(100)	88		R35	865.45592(50)	−25
	P40	680.79849(150)	−134		R36	866.40256(50)	49
	P39	684.42469(50)	−38		R37	867.30403(50)	−11
	P38	688.02566(50)	−50		R38	868.16397(200)	173
	P37	691.60208(100)	−66		R39	868.97640(50)	16
	P36	695.15490(50)	45		R40	869.74394(250)	−208
	P35	698.68078(50)	−17		R41	870.47184(50)	40
	P34	702.17991(200)	−197		R42	871.15340(100)	100
	P33	705.65682(50)	−8		R43	871.78846(50)	−32
	P32	709.10513(50)	−52		R44	872.38031(50)	−17
	P31	712.51815(1000)	−965		R46	873.42902(50)	−37
	P30	715.92281(50)	−19		R49	874.66493(50)	−19
	P29	719.29063(50)	−29	$v = 8 \rightarrow 7$	P42	661.42085(150)	141
	P28	722.63170(50)	49		P38	675.74003(50)	10
	P27	725.94266(100)	−89		P35	686.23006(100)	98
	P26	729.23121(350)	362		P33	693.09693(50)	−3
	P25	732.48296(50)	−5		P32	696.49270(50)	31
	P24	735.70932(50)	−17		P30	703.20429(50)	−28
	P23	738.90654(50)	−15		P28	709.80945(50)	−11
	P22	742.07481(50)	52		P27	713.07091(50)	−12

Can. J. Chem. Downloaded from www.nrcresearchpress.com by 84.41.108.74 on 09/07/12
For personal use only.

TABLE 1 (*continued*)

	J''	Obs./cm^{-1}	Obs. − calc. /10^{-5} cm^{-1}		J''	Obs./cm^{-1}	Obs. − calc. /10^{-5} cm^{-1}
	P26	716.30457(50)	−14		P15	896.44556(50)	26
	P25	719.51041(50)	14		P14	900.06386(50)	8
	P24	722.68777(50)	38		P13	903.64038(50)	27
	P23	725.83593(50)	19		P12	907.17407(50)	17
	P22	728.95561(50)	61		P11	910.66485(50)	11
	P21	732.04517(50)	30		P9	917.51612(50)	8
	P20	735.10512(50)	11		P8	920.87587(50)	14
	P19	738.13524(50)	12		P6	927.46149(50)	22
	P18	741.13479(50)	−10		P5	930.68665(50)	29
	P17	744.10391(50)	−10		P4	933.86603(50)	18
	P15	749.95028(150)	121		P3	936.99984(50)	47
	P14	752.82567(150)	126		P2	940.08696(50)	42
	R3	798.85770(150)	142		R1	951.96648(200)	178
	R4	801.07990(150)	160		R2	954.81511(50)	26
	R8	809.60458(1000)	1080		R3	957.61714(50)	58
	R9	811.62911(100)	81		R4	960.36968(50)	19
	R10	813.62541(100)	79		R5	963.07337(50)	7
	R13	819.37905(300)	−305		R7	968.33239(50)	14
	R14	821.22278(100)	−59		R8	970.88707(50)	32
	R15	823.02561(50)	29		R9	973.39100(50)	16
	R19	829.83516(100)	−69		R10	975.84433(50)	13
	R25	838.83764(50)	−28		R11	978.24675(50)	23
	R27	841.50984(100)	91		R12	980.59770(50)	20
	R28	842.78178(50)	−6		R13	982.89712(50)	29
	R29	844.01424(150)	146		R14	985.14439(50)	17
	R30	845.20204(50)	44		R15	987.33946(50)	9
	R31	846.34856(50)	42		R16	989.48225(50)	25
	R32	847.45203(50)	−21		R17	991.57200(50)	18
	R34	849.53230(50)	−24		R18	993.60879(50)	25
	R37	852.33205(100)	97		R19	995.59199(50)	9
	R38	853.17689(100)	−64		R20	997.52168(50)	7
^{6}LiF					R21	999.39761(50)	19
$v = 1 \rightarrow 0$	P49	751.39546(200)	174		R22	1001.21912(50)	6
	P48	756.18469(100)	−82		R23	1002.98612(50)	−15
	P47	760.94616(500)	−442		R24	1004.69906(50)	27
	P46	765.68855(50)	13		R25	1006.35654(50)	15
	P45	770.39839(50)	−14		R26	1007.95899(50)	18
	P44	775.08005(50)	−37		R27	1009.50605(50)	24
	P43	779.73328(50)	−30		R28	1010.99719(50)	2
	P42	784.35734(50)	−19		R29	1012.43284(50)	19
	P41	788.95138(50)	−40		R30	1013.81195(50)	−7
	P40	793.51789(250)	206		R31	1015.13504(50)	−3
	P38	802.55164(50)	21		R32	1016.40130(50)	−28
	P37	807.02133(100)	−68		R33	1017.61128(50)	−7
	P36	811.46031(50)	−19		R34	1018.76427(50)	11
	P35	815.86652(50)	12		R35	1019.85968(50)	−14
	P34	820.23918(50)	−8		R36	1020.89828(50)	14
	P33	824.57866(50)	5		R37	1021.87841(50)	−52
	P32	828.88382(50)	−17		R38	1022.80178(50)	−22
	P31	833.15515(50)	22		R39	1023.66705(50)	−13
	P30	837.39117(50)	18		R40	1024.47393(50)	−36
	P29	841.59199(50)	28		R41	1025.22300(50)	−17
	P28	845.75658(50)	−6		R42	1025.91354(50)	−12
	P27	849.88539(50)	5		R43	1026.54473(100)	−88
	P26	853.97776(50)	40		R44	1027.11936(100)	50
	P25	858.03243(50)	16		R45	1027.63336(50)	9
	P24	862.04978(50)	17		R46	1028.08907(50)	36
	P23	866.02906(50)	8		R47	1028.48432(50)	−72
	P22	869.96988(50)	−4		R48	1028.82102(100)	−113
	P21	873.87216(50)	15		R49	1029.09819(150)	−171
	P19	881.55813(50)	15		R50	1029.31757(50)	−62
	P18	885.34109(50)	9		R51	1029.47703(50)	11
	P17	889.08367(50)	16		R52	1029.57530(50)	−67
	P16	892.78527(500	20	$v = 2 \rightarrow 1$	P45	755.43538(100)	−67

Can. J. Chem. Downloaded from www.nrcresearchpress.com by 84.41.108.74 on 09/07/12
For personal use only.

TABLE 1 (*continued*)

J''	Obs./cm^{-1}	Obs. − calc. /10^{-5} cm^{-1}		J''	Obs./cm^{-1}	Obs. − calc. /10^{-5} cm^{-1}
P43	764.61478(50)	−45		R28	992.16338(50)	−8
P41	773.67949(50)	−60		R29	993.57652(50)	−9
P40	778.16834(50)	−10		R30	994.93450(50)	−6
P39	782.62662(50)	−13		R31	996.23725(50)	15
P38	787.05450(50)	−6		R32	997.48431(50)	29
P37	791.45148(50)	9		R33	998.67506(50)	−5
P36	795.81657(50)	−19		R34	999.81007(50)	−11
P35	800.14984(50)	−37		R35	1000.88915(50)	12
P34	804.45136(50)	8		R36	1001.91146(50)	−1
P33	808.71805(150)	−145		R37	1002.87728(50)	−5
P32	812.95455(50)	13		R38	1003.78611(50)	−30
P31	817.15543(50)	−15		R39	1004.63850(50)	−5
P30	821.32216(50)	−37		R40	1005.43360(50)	1
P29	825.45465(50)	−16		R41	1006.17163(50)	27
P28	829.55201(50)	3		R42	1006.85155(50)	−16
P27	833.61364(50)	3		R43	1007.47425(50)	−24
P26	837.63928(50)	4		R44	1008.03932(50)	−23
P25	841.62865(50)	20		R45	1008.54547(150)	−129
P24	845.58079(50)	0		R46	1008.99703(150)	105
P23	849.49399(200)	−185		R47	1009.38662(50)	−47
P21	857.21231(50)	−5		R48	1009.71917(50)	−80
P20	861.01304(50)	5	$v = 3 \rightarrow 2$	P41	758.75890(100)	99
P19	864.77476(50)	13		P40	763.17149(50)	−22
P18	868.49715(50)	28		P38	771.91079(50)	14
P17	872.17929(50)	−2		P37	776.23471(50)	−13
P16	875.82136(50)	−17		P36	780.52789(50)	−33
P15	879.42319(50)	6		P34	789.02044(50)	−25
P14	882.98366(50)	−4		P33	793.21835(50)	−52
P13	886.50302(50)	16		P32	797.38225(250)	−214
P12	889.98011(50)	−9		P31	801.51430(250)	−252
P11	893.41533(50)	0		P30	805.61544(50)	−25
P9	900.15735(50)	−7		P29	809.68058(50)	1
P8	903.46399(50)	37		P28	813.71070(50)	−31
P7	906.72608(50)	0		P27	817.70707(50)	50
P6	909.94425(50)	−18		P26	821.66970(300)	289
P5	913.11846(50)	17		P25	825.59133(50)	2
P4	916.24665(100)	−66		P24	829.47955(50)	−7
P3	919.33092(50)	−18		P22	837.14646(50)	45
R1	934.05897(50)	−45		P21	840.92343(50)	19
R2	936.86533(100)	83		P19	848.36390(50)	22
R3	939.62222(50)	29		P18	852.02613(50)	7
R4	942.33100(50)	−36		P17	855.64945(50)	11
R6	947.60494(50)	−1		P16	859.23324(50)	13
R7	950.16843(50)	−2		P15	862.77709(50)	11
R8	952.68273(50)	7		P14	866.28072(50)	19
R9	955.14718(50)	−9		P13	869.74394(50)	55
R10	957.56191(50)	−6		P12	873.16500(50)	−15
R11	959.92643(50)	−2		P11	876.54562(50)	19
R12	962.24050(50)	8		P9	883.18000(50)	−2
R13	964.50353(50)	−3		P8	886.43358(50)	1
R14	966.71581(50)	21		P7	889.64414(50)	3
R15	968.87667(50)	44		P6	892.81130(50)	1
R16	970.98505(50)	−13		P5	895.93473(50)	0
R17	973.04232(50)	15		P4	899.01544(150)	136
R18	975.04697(50)	6		P2	905.04087(200)	184
R19	976.99921(50)	8		R3	922.01884(50)	5
R20	978.89871(50)	13		R4	924.68524(50)	−24
R21	980.84527(50)	29		R5	927.30477(50)	14
R22	982.53819(50)	11		R7	932.39898(50)	−8
R23	984.27761(50)	−2		R8	934.87365(50)	−5
R24	985.96322(50)	−14		R9	937.29833(150)	−121
R25	987.59499(50)	−6		R10	939.67647(50)	19
R26	989.17244(50)	−2		R11	942.00368(50)	7
R27	990.69572(50)	39		R12	944.28135(50)	11

Can. J. Chem. Downloaded from www.nrcresearchpress.com by 84.41.108.74 on 09/07/12
For personal use only.

TABLE 1 (*concluded*)

J''	Obs./cm^{-1}	Obs. − calc. /10^{-5} cm^{-1}	J''	Obs./cm^{-1}	Obs. − calc. /10^{-5} cm^{-1}
R13	946.50882(50)	−5	R28	973.73717(50)	−32
R14	948.68641(50)	19	R29	975.12887(50)	2
R15	950.81344(50)	45	R30	976.46613(50)	22
R16	952.88892(50)	0	R31	977.74904(100)	58
R17	954.91365(50)	−6	R32	978.97634(50)	4
R18	956.88709(50)	−2	R33	980.14903(50)	−19
R19	958.80858(50)	−26	R34	981.26726(50)	22
R20	960.67877(50)	14	R35	982.32871(100)	−85
R21	962.49611(50)	−13	R36	983.33625(50)	−34
R22	964.26116(50)	−24	R38	985.18360(50)	9
R23	965.97345(50)	−43	R39	986.02215(100)	−91
R24	967.63365(50)	23	R40	986.80581(50)	−63
R25	969.23974(50)	−4	R41	987.53253(100)	−98
R26	970.79251(50)	−22	R43	988.81787(50)	−23
R27	972.29165(50)	−39			

[a]Numbers in parentheses are estimated uncertainties.

sities of the emission lines increased with higher temperature. The maximum temperature which is accessible with our current system is about 1500 K and it was at this temperature that the best emission spectrum was obtained. All emission signals decreased rapidly as the furnace cooled and disappeared at about 1200 K.

III. Results

The emission features were observed in the region where the infrared spectrum of MgF_2 was expected (Figs. 1, 2). However, the high resolution spectrum showed a pattern typical of a diatomic molecule. After some thought and a literature search we found that the emission spectrum belonged to LiF (11). The presence of Li in our system was puzzling but in a previous experiment the alumina tube was used to vaporize LiNC. Despite careful cleaning of the cell, some Li remained on the walls of the alumina tube. At higher temperatures the MgF_2 could react with water (which is always present in the system) and form HF. The HF can react with the Li impurities and produce LiF. Direct reduction of MgF_2 with Li is also possible but MgF was not detected. An additional reaction of HF with the alumina tube took place to form AlF. The emission of AlF was observed in the spectrum (17).

The spectral analysis program PC-DECOMP, developed by J. W. Brault, was used for data analysis. The rotational line profiles were fit to Voigt lineshape functions. The strong lines show a "ringing" caused by the $(\sin x/x)$ lineshape function of the Fourier transform spectrometer. The ringing was eliminated by using the "filter fitting" routine available in PC-DECOMP. The signal-to-noise ratio for the strong lines was better than 1000 and the resulting resolution-enhanced line width was 0.0005 cm^{-1}. The HF lines were used for absolute calibration (+/−0.0002 cm^{-1}) of the spectrum. For this calibration the HF absorption lines, taken in a spectrum at lower temperature, were calibrated against CO_2 (18).

The assignment of the vibrational bands of the main isotopomer ^{7}LiF was straightforward (Table 1). Data reduction was made by using Dunham's equation (19)

$$[1] \quad T(v,J) = \sum_{i,j} Y_{ij} \left(v + \frac{1}{2}\right)^i [J(J+1)]^j$$

Pure rotational transitions reported by Pearson and Gordy (20) were included in the fit. The Dunham coefficients obtained from this fit are shown in Table 2.

TABLE 2. Dunham constants for LiF (in cm^{-1})[a]

Constant	Value	
	^{7}LiF	^{6}LiF
Y_{10}	910.57272(10)	964.30621(22)
Y_{20}	−8.207956(46)	−9.19819(12)
Y_{30}	0.569166(82)	0.64808(20)
Y_{40}	−0.28437(49)E−3	
Y_{01}	1.34525715(57)	1.5087385(14)
Y_{11}	−0.02028749(19)	−0.02409773(41)
Y_{21}	0.156247(64)E−3	0.19766(15)E−3
Y_{31}	−0.3860(88)E−6	−0.736(21)E−6
Y_{41}	−0.870(45)E−8	
Y_{02}	−0.1174389(33)E−4	−0.147719(13)E−4
Y_{12}	0.113878(98)E−6	0.15246(29)E−6
Y_{22}	0.720(23)E−9	0.619(33)E−9
Y_{32}	−0.306(13)E−10	
Y_{03}	0.30449(55)E−10	0.4300(35)E−10
Y_{13}	0.836(15)E−12	0.1120(70)E−11
Y_{23}	−0.270(27)E−13	

[a]Each isotopomer was fit independently. One standard deviation in parentheses.

The assignment of the vibrational bands of the minor isotopomer, ^{6}LiF, was carried out by comparing predicted line positions with the unassigned lines in the spectrum. The line positions for ^{6}LiF are also shown in Table 1. The mass-dependent Dunham coefficients Y_{ij} are listed in Table 2.

Finally, all infrared and microwave data for LiF was combined and fit to the mass-reduced Dunham expression including Watson's correction due to the breakdown of the Born–Oppenheimer approximation (21, 22)

$$[2] \quad Y_{ij} = \mu^{[(i+2j)/2]} U_{ij} \left[1 + \left(\frac{m_e}{m_{Li}}\right) \Delta_{ij}\right]$$

where μ is the reduced mass, U_{ij} are the mass-independent parameters, m_{Li} is the atomic mass of Li (23), m_e is the electron mass, and Δ_{ij} is the mass scaling factor for the Li atom. The

Can. J. Chem. Downloaded from www.nrcresearchpress.com by 84.41.108.74 on 09/07/12
For personal use only.

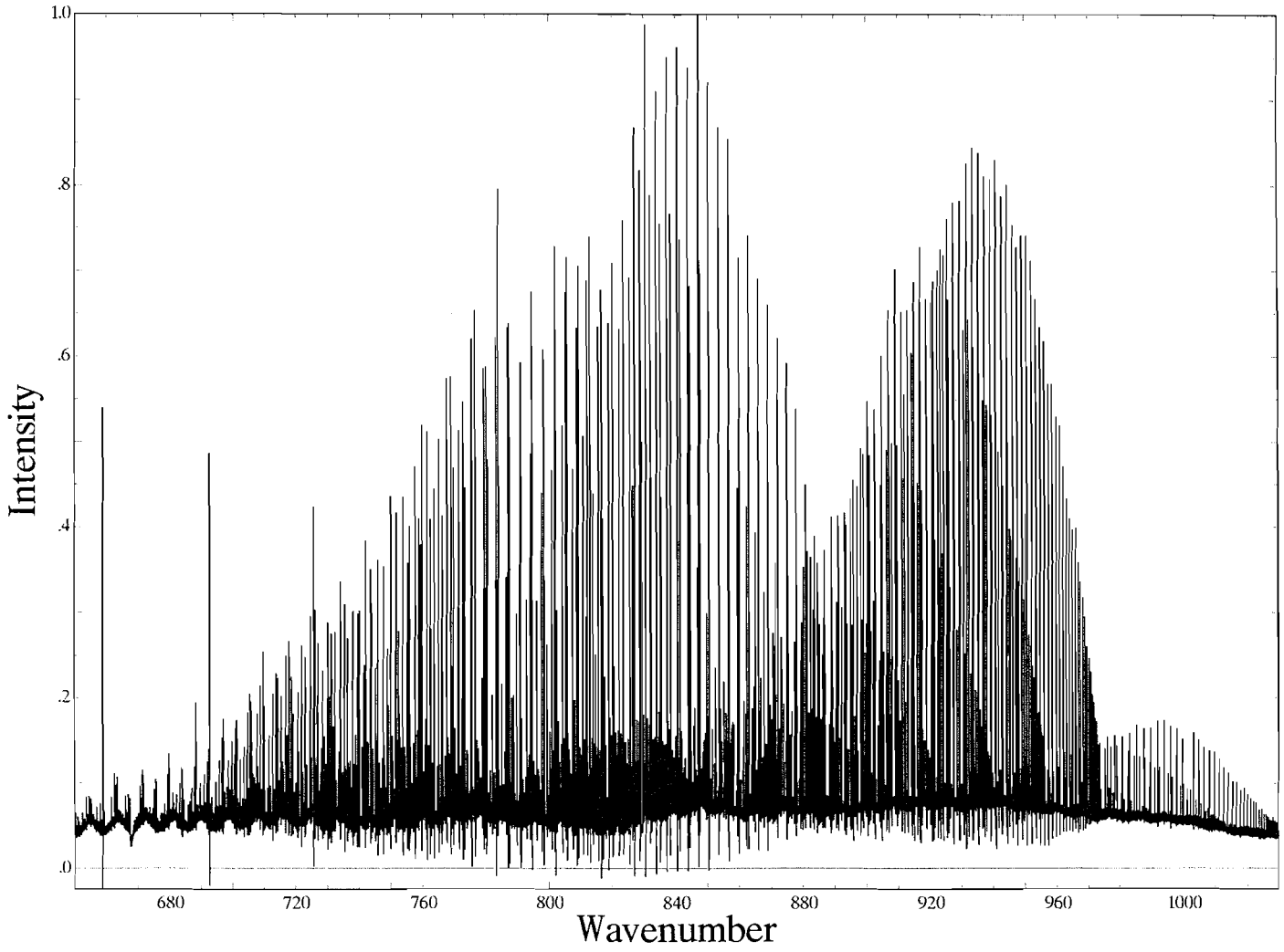


FIG. 1. Infrared spectrum of ^{7}LiF.

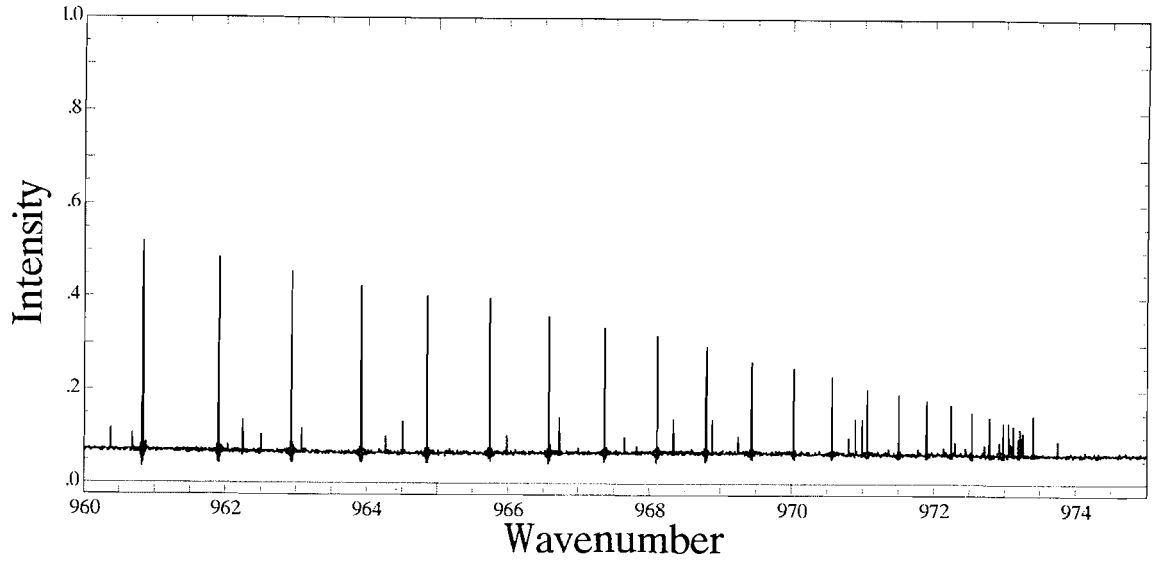


FIG. 2. Infrared spectrum of ^{6}LiF.

Can. J. Chem. Downloaded from www.nrcresearchpress.com by 84.41.108.74 on 09/07/12
For personal use only.

Can. J. Chem. Downloaded from www.nrcresearchpress.com by 84.41.108.74 on 09/07/12
For personal use only.

TABLE 3. Mass-reduced Dunham constants for LiF (in cm^{-1})[a]

Constant	Our work
U_{10}	2061.15184(33)
U_{20}	−42.05641(19)
U_{30}	0.660241(80)
U_{40}	−7.480(11)E−3
U_{01}	6.8926542(36)
U_{11}	−0.2352993(16)
U_{21}	4.1016(14)E−3
U_{31}	−0.2259(44)E−4
U_{41}	−0.1199(52)E−5
U_{02}	−0.3083223(30)E−3
U_{12}	0.67650(42)E−5
U_{22}	0.991(25)E−7
U_{32}	−0.995(32)E−8
U_{03}	0.40964(30)E−8
U_{13}	0.2566(34)E−9
U_{23}	−0.186(17)E−10
Δ_{10}	0.0417(17)
Δ_{01}	0.3595(58)

[a]One standard deviation in parentheses.

TABLE 4. Pure rotational transitions of HF

J'	J''	Observed/cm^{-1}	Obs. − calc. /10^{-5} cm^{-1}	Uncertainty (1σ) /10^{-5} cm^{-1}
1	0	41.1109832[a]	0.181	0.15
2	1	82.1711179[a]	0.139	0.3
3	2	123.12967[a]	−1	0.5
4	3	163.93616[a]	0	0.5
5	4	204.54045[b]	1	10
6	5	244.89283[b]	0	10
7	6	284.94444[b]	23	15
13	12	516.28061[c]	−14	20
14	13	552.92046[c]	9	20
15	14	588.89904[c]	−1	20
16	15	624.17733[c]	11	20
17	16	658.71682[c]	4	20
18	17	692.48121[c]	8	20
19	18	725.43557[c]	38	20
20	19	757.54540[c]	−13	20
21	20	788.78013[c]	−15	20
22	21	819.10918[c]	−8	20
23	22	848.50386[c]	−8	20
24	23	876.93745[c]	−5	20
25	24	904.38481[c]	5	20
27	26	956.22816[d]	−3	13
28	27	980.5832[e]	74	75
29	28	1003.8672[e]	62	50
31	30	1047.1570[e]	−169	125
32	31	1067.1377[e]	−11	50
33	32	1085.98903[d]	0	13

[a]Tunable far infrared spectroscopy (ref. 12).
[b]Fourier transform spectroscopy (ref. 12).
[c]Fourier transform spectroscopy (our work).
[d]Diode laser heterodyne spectroscopy (ref. 14).
[e]Diode laser spectroscopy (ref. 12).

TABLE 5. Rotational constants of ground state HF[a]

Constant	Our work /cm^{-1}	Jennings *et al.* (12) /cm^{-1}
B_0	20.5597298(8)	20.5597300(25)
D_0	2.119901(36)E−3	2.11991(14)E−3
H_0	0.163483(116)E−6	0.16334(50)E−6
L_0	−0.14974(132)E−10	−0.1473(66)E−10
M_0	0.1052(50)E−14	0.94(27)E−15

[a]Two standard deviations in parentheses.

data required two Δ's, one for U_{10} ("ω_e") and one for U_{01} ("B_e"). The final mass-independent coefficients and the Δ's are listed in Table 3.

The energy levels of HF were fit to the expression (24)

$$[3]\quad E_v(J) = B_vJ(J+1) - D_v[J(J+1)]^2 + H_v[J(J+1)]^3 + L_v[J(J+1)]^4 + M_v[J(J+1)]^5$$

The fit includes all lines listed in Table 4 and Table 5 shows the determined constants.

IV. Conclusion

The high-resolution infrared emission spectra of LiF and HF were observed with a Fourier transform instrument. The ro-vibrational transitions of the fundamental band and of seven hot bands for ^{7}LiF and of three bands for ^{6}LiF were rotationally analyzed. Pure rotational transitions for HF were also observed and enabled us to calculate an improved set of molecular constants. The accuracy of the line positions allows the use of HF as an absolute wavenumber standard.

Acknowledgements

The National Solar Observatory is operated by the Association of Universities for Research in Astronomy, Inc., under the contract with the National Science Foundation. We would like to thank J. W. Brault and J. Wagner for assistance in recording the spectra. This work was supported by the Astronautics Laboratory, Edwards Air Force Base, CA. Acknowledgement is made to the Petroleum Research Fund, administered by the American Chemical Society, for partial support of this work. One of us (H.G.H.) thanks the Deutsche Forschungsgemeinschaft for a postdoctoral scholarship.

1. S. E. VEAZEY and W. GORDY. Phys. Rev. A, **138**, 1303 (1965).
2. A. J. HEBERT, F. J. LOVAS, C. A. MELENDRES, C. D. HOLLOWELL, T. L. STORY, JR., and K. STREET, JR. J. Chem. Phys. **48**, 2824 (1968).
3. G. L. VIDALE. J. Phys. Chem. **64**, 314 (1960).
4. L. WHARTON, W. KLEMPERER, L. P. GOLD, R. STRAUCH, J. J. GALLAGHER, and V. E. DERR. J. Chem. Phys. **38**, 1203 (1963).
5. M. J. LINEVSKY. J. Chem. Phys. **34**, 587 (1961).
6. M. J. LINEVSKY. J. Chem. Phys. **38**, 658 (1963).
7. A. SNELSON and K. S. PITZER. J. Phys. Chem. **67**, 882 (1963).
8. S. SCHLICK and O. SCHNEPP. J. Chem. Phys. **41**, 463 (1964).
9. A. SNELSON. J. Chem. Phys. **46**, 3652 (1967).
10. S. ABRAMOWITZ, N. ACQUISTA, and I. W. LEVIN. J. Res. Nat. Bur. Stand. Sect. A, **72**, 487 (1968).
11. A. MAKI. J. Mol. Spectrosc. **102**, 361 (1983).
12. D. A. JENNINGS, K. M. EVENSON, L. R. ZINK, C. DEMUYNCK, J. L. DESTOMBES, B. LEMOINE, and J. W. C. JOHNS. J. Mol. Spectrosc. **122**, 477 (1987).

13. U. K. SENGUPTA, P. K. DAS, and K. N. RAO. J. Mol. Spectrosc. **74**, 322 (1979).
14. D. A. JENNINGS and J. S. WELLS. J. Mol. Spectrosc. **130**, 267 (1988).
15. J. S. WELLS, F. R. PETERSON, A. G. MAKI, and D. J. SUKLE. Appl. Opt. **20**, 1676 (1981).
16. C. I. FRUM, R. ENGLEMAN, JR., and P. F. BERNATH. J. Chem. Phys. **93**, 5457 (1990).
17. H. G. HEDDERICH, C. I. FRUM, R. ENGLEMAN, JR., and P. F. BERNATH. To be published.
18. G. GUELACHVILI and K. N. RAO. Handbook of infrared standards. Academic Press, Orlando, FL. 1986.
19. J. L. DUNHAM. Phys. Rev. **41**, 721 (1932).
20. E. F. PEARSON and W. GORDY. Phys. Rev. **177**, 52 (1969).
21. J. K. G. WATSON. J. Mol. Spectrosc. **45**, 99 (1973).
22. J. K. G. WATSON. J. Mol. Spectrosc. **80**, 411 (1980).
23. H. S. PEISER, N. E. HOLDEN, P. DE BIEVRE, I. L. BARNES, R. HAGEMANN, J. R. DE LAETER, T. J. MURPHY, E. ROTH, M. SHIMA, and H. G. THODE. Pure Appl. Chem. **56**, 695 (1984).
24. W. GORDY and R. L. COOK. Microwave molecular spectra. Wiley, New York, NY. 1984.

Can. J. Chem. Downloaded from www.nrcresearchpress.com by 84.41.108.74 on 09/07/12
For personal use only.

On vibrational force field calculations[1]

W. F. MURPHY

Steacie Institute for Molecular Sciences, National Research Council of Canada, Ottawa, Ont., Canada K1A 0R6

Received April 22, 1991

This paper is dedicated to Dr. Richard Norman Jones

W. F. MURPHY. Can. J. Chem. **69**, 1672 (1991).

A series of computer routines for performing normal coordinate calculations of harmonic vibrational frequencies is described. These are designed for operation on current-generation computers having direct-access storage. Example results are given for the chain isomer of disulfur difluoride.

Key words: vibrational force field calculations, normal coordinate calculations, harmonic force fields.

W. F. MURPHY. Can. J. Chem. **69**, 1672 (1991).

On décrit une série de routines d'ordinateur permettant de calculer les coordonnées normales des fréquences vibrationnelles harmoniques. Elles ont été développées pour être utilisées avec les ordinateurs de la présente génération possédant un accès direct aux données enregistrées. On rapporte des résultats types obtenus avec la chaîne isomère du difluorure de disulfure.

Mots clés : calculs de champs de force vibrationnelle, calculs de coordonnées normales, champs de force harmonique.

[Traduit par la rédaction]

Can. J. Chem. Downloaded from www.nrcresearchpress.com by 123.30.183.119 on 09/07/12
For personal use only.

Introduction

One of the principal themes of R. N. Jones' scientific career has been his interest in the development of computer programs for the analysis of vibrational spectroscopic data, and in making these programs available for the use of the spectroscopic community. Many of these have been distributed as N.R.C. Bulletins, in which some eight bulletins contain descriptions, operating instructions, and listings of over 55 programs implemented by Jones and his co-workers.

One of the more popular bulletins (1) describes the programs CART, GCALC, and FPERT, used for the calculation of vibrational frequencies and fitting harmonic vibrational potentials by means of the Wilson **GF** matrix procedure (2). These programs, implementations and improvements of earlier routines due to Hilderbrandt (3) and Schachtschneider (4), were designed for batch operation on the main frame computers used during the 1960's and 70's. Thus, each program's output was required as input for the succeeding program in the series, and the operator had to be concerned with incorporating this information correctly with the input data for the next program. However, with modern computers having on-line storage, this mode of operation is not very convenient.

In the past few years, I have developed a series of programs to perform vibrational force field and intensity calculations on such computer systems, and it seems appropriate to include a description of them in this special issue honoring Norman Jones. These routines are noteworthy in that output data are stored in machine readable form in auxiliary data files where they may be automatically accessed by subsequent programs. The force field program itself is designed explicitly to scale *ab initio* calculated force fields to fit vibrational wavenumbers (5). In addition, several enhancements have been incorporated in these programs, which should be of interest to others making such calculations. Among alternative routines are two available from the Quantum Chemistry Program Exchange: NORCRD (6), which carries out the calculation in cartesian coordinates, and a "General Vibrational Analysis System" (7), which can automatically exploit the molecular symmetry to simplify the calculation.

[1]Issued as NRCC No. 33243.

The procedures and background for normal coordinate calculations have been considered in detail in the book by Wilson, Decius, and Cross (2). There have been several more recent review articles treating various aspects of such calculations; among them refs. 8–11. In this article, I will assume that the reader is familiar with the general concepts of normal coordinate calculations as provided in these references.

The remainder of this paper includes a description of the utility DATIO routines, followed by a discussion of our implementation of programs for calculating the **B** and **G** matrices required for the kinetic term in the problem. Then the programs for calculating and fitting the potential are described. Finally, the operation of these programs is demonstrated by a sample calculation chosen to verify the operation in the case where the molecular coordinates include a torsional coordinate.

Method

These programs are implemented on the NRC VM/CMS system (IBM model 3090) in the FORTRAN 77 language. The IMSL mathematical subroutine library (12) has been used extensively for numerical routines. (Use of the current version of the IMSL library (Edition 10.0; IMSL MATH/LIBRARY Version 1.0) would require significant revision of several of the programs.) The underlying approach used in formulating these programs is that storage size is not an appreciable problem in modern machines, so that I have chosen to minimize the input/output carried out by the programs. The fundamental constants used in these routines are those given in the recent IUPAC compilation (13).

Auxiliary data routine: DATIO

This routine is used to store arrays calculated by one program for access and use by other programs at a later time. When the DATIO routine is used in a program, it is first initialized through a prologue entry. Here, the input/output file name is passed to the routine, where the file is opened and read into memory.

The stored information is as follows: the first record is a list of array labels, used to identify the stored arrays. The second record is an integer array that contains the dimensions of these arrays. The following records contain the arrays, in machine

readable IBM double precision words (FORTRAN unformatted I/O), in the order given by the labels. The current version is dimensioned for ten arrays, each having a maximum of 4000 elements. The dimensions are easily modified, if necessary.

To access an array from a program, the array label and the maximum dimensions of the target array are passed to DATIO. If the label matches one of the stored labels, and the dimensions are valid, the internal array is copied to the target in single or double precision, as requested. If the expected array dimensions are provided from the calling program, the actual dimensions are checked for validity; otherwise, the actual dimensions are passed back to the calling program.

To store an array, the label, dimensions, and array itself are passed to DATIO. If the array is not currently stored, the routine checks that free space is available; if it is stored, the new version will replace it. In either case, the dimensions are checked and, if valid, the single or double precision array elements are stored in double precision format.

When ending a program, a DATIO epilogue entry is called; if any changes have been made to the stored information, the entire data file is rewritten.

Two types of files are maintained: those containing data that are mass independent, such as the geometry; these files are designed as MOLECULE files in the following discussion. The ones containing mass dependent data are designated as SPECIES files.

Molecular geometry

There are several existing routines for converting molecular bond lengths and angles to cartesian coordinates, such as CART (1, 3), XYZ (6), EUCLID (14), and ATCOOR (15). We make use of one of these, as appropriate, or use the cartesian coordinates determined in an *ab initio* calculation. A simple routine reads the cartesian geometry, permutes the axes and atom numbering, if desired, and stores these coordinates in the DATIO MOLECULE file.

***B* matrix/*U* matrix:** *UBMAT*

The routine UBMAT, the first calculation routine of the group, reads the cartesian geometry from the designated MOLECULE file. Then, the various internal coordinates are defined as specified in the input data file: first the bond stretches, in terms of the atoms involved, and then the various types of deformations, in terms of the bonds involved. The deformation coordinates are implicitly normalized by a length of 1 Å to maintain consistent units for the force constant matrix.

Then, for each of the internal coordinates, the elements of the **B** matrix, relating the internal and cartesian coordinates, are generated. For bond stretches and nonlinear bond angle deformations, the relations given by Wilson, Decius, and Cross (2) are used. For several of the deformation coordinates, the displacement vectors s_{ti} (2), where t indicates the internal coordinate and i the atom, can be conveniently expressed in terms of the unit vector

$$[1] \qquad \hat{\boldsymbol{h}}_{12} = \frac{\hat{\boldsymbol{e}}_1 \times \hat{\boldsymbol{e}}_2}{\sin \phi_{12}}$$

where $\hat{\boldsymbol{e}}_1$ and $\hat{\boldsymbol{e}}_2$ are unit vectors directed toward the terminal atoms of bonds 1 and 2, away from their common atom, 3, and ϕ_{12} is the angle between the bonds, which have lengths of r_1 and r_2. The relation between the s_{ti} vectors and the **B** matrix elements is straightforward (2).

Thus, for a nonlinear bend coordinate

$$[2] \qquad \boldsymbol{s}_{t1} = \frac{\hat{\boldsymbol{e}}_1 \times \hat{\boldsymbol{h}}_{12}}{r_1}$$

$$\boldsymbol{s}_{t2} = \frac{\hat{\boldsymbol{e}}_2 \times \hat{\boldsymbol{h}}_{21}}{r_2}$$

and

$$\boldsymbol{s}_{t3} = -\boldsymbol{s}_{t1} - \boldsymbol{s}_{t2}$$

For the out-of-plane deformation of a bond with respect to the plane formed by two other bonds, the recommended coordinate (16) is equivalent to the change in the quantity

$$[3] \qquad \hat{\boldsymbol{e}}_1 \cdot \hat{\boldsymbol{e}}_2 \times \hat{\boldsymbol{e}}_3$$

where the three bonds, 1, 2, and 3, share a common atom, 4. This coordinate has the advantage that it is invariant, to within a change of sign, to permutation of the bond labels. It differs from the coordinate, θ, defined by Wilson, Decius, and Cross (2),

$$[4] \qquad \sin \theta = \hat{\boldsymbol{h}}_{23} \cdot \hat{\boldsymbol{e}}_1$$

by the factor $\sin \phi_{23}$. In terms of these quantities, the $\boldsymbol{s}$ vectors are for the out-of-plane deformation coordinate (eq. [3])

$$\boldsymbol{s}_{t1} = \frac{\sin \phi_{23}}{r_1 \cos \theta}(\hat{\boldsymbol{h}}_{23} - \sin \theta \hat{\boldsymbol{e}}_1)$$

$$[5] \qquad \boldsymbol{s}_{t2} = \frac{1}{r_2 \cos \theta}(\sin \phi_{31} \hat{\boldsymbol{h}}_{31} - \sin \theta \hat{\boldsymbol{e}}_3 \times \hat{\boldsymbol{h}}_{23})$$

$$\boldsymbol{s}_{t3} = \frac{1}{r_3 \cos \theta}(\sin \phi_{12} \hat{\boldsymbol{h}}_{12} + \sin \theta \hat{\boldsymbol{e}}_2 \times \hat{\boldsymbol{h}}_{32})$$

and

$$\boldsymbol{s}_{t4} = -\boldsymbol{s}_{t1} - \boldsymbol{s}_{t2} - \boldsymbol{s}_{t3}$$

For the torsional coordinate of two bonds 1 and 3, attached to either end of bond 2, the $\boldsymbol{s}$ vectors may be given in terms of the $\hat{\boldsymbol{h}}$ vectors by

$$\boldsymbol{s}_{t1} = \frac{\hat{\boldsymbol{h}}_{12}}{r_1 \sin \phi_{12}}$$

$$\boldsymbol{s}_{t2} = \frac{(r_1 \cos \phi_{12} - r_2)\hat{\boldsymbol{h}}_{12}}{r_1 r_2 \sin \phi_{12}} - \frac{\cos \phi_{32} \hat{\boldsymbol{h}}_{32}}{r_2 \sin \phi_{32}} \qquad [6]$$

$$\boldsymbol{s}_{t3} = \frac{(r_3 \cos \phi_{32} - r_2)\hat{\boldsymbol{h}}_{32}}{r_2 r_3 \sin \phi_{32}} - \frac{\cos \phi_{12} \hat{\boldsymbol{h}}_{12}}{r_2 \sin \phi_{12}}$$

$$\boldsymbol{s}_{t4} = \frac{\hat{\boldsymbol{h}}_{32}}{r_3 \sin \phi_{32}}$$

The torsional coordinates have been discussed several times in the literature, and the error in the standard reference (2) has been pointed out (17, 18). In our work, we have used the coordinate defined (16, 19, 20) as the sum of all of the three-bond combinations that involve the central bond, 2, where the (summed) **B** matrix elements are then divided by the total number of these combinations.

Can. J. Chem. Downloaded from www.nrcresearchpress.com by 123.30.183.119 on 09/07/12
For personal use only.

Can. J. Chem. Downloaded from www.nrcresearchpress.com by 123.30.183.119 on 09/07/12
For personal use only.

Finally, the linear bend coordinate **B** matrix elements are calculated as defined by Ferigle and Meister (21).

It is often convenient to consider the problem in terms of symmetry coordinates, made up of linear combinations of internal coordinates that transform according to the various representations of the molecular point group. The elements of the **U** matrix, which transforms the internal coordinates to symmetry coordinates, and labels for the various symmetry coordinates, used for convenience in the printed output, are read from the input file. The coefficients for each coordinate are normalized by the program, and then their orthogonality is checked. The redundancy relations, which may exist among internal coordinates, need not be removed by the operator at this step.

The **B**, **U**, and **UB** matrices, along with the symmetry coordinate labels, are stored in the MOLECULE file upon completion of this program.

G Matrix calculation: GCALC

This routine begins by retrieving the **UB** matrix from the MOLECULE file. Then, a list of symbols for the atoms is read from the input file, and the appropriate atomic masses (22) are obtained from a look-up table. If required, i.e., if the **G** matrix is being calculated for a lower symmetry isotopic species, an additional blocking matrix may be included in the input file, as well.

The procedure followed in this routine is governed by the method used for solving the **GF** matrix eigenvalue problem. The **G** matrix is conventionally obtained from

$$[7] \quad \mathbf{G} = (\mathbf{UB})\mathbf{M}^{-1}(\mathbf{UB})^T$$

where **M** is the diagonal mass matrix, and ^{T} denotes the matrix transpose. However, since the eigenvalue problem will be solved by means of the Choleski decomposition of $\mathbf{G}^{-1}$ (8), this latter matrix is the principal result calculated in this routine. A check is made whether symmetry coordinates have been used to block the **G** matrix and, if so, the calculations outlined here are carried out separately for each of the symmetry blocks. Also, a check is made for redundant coordinates and, optionally, they may be removed.

We proceed as follows: The **G** matrix may be given as eq. [7] above, or equivalently,

$$[8] \quad \mathbf{G} = (\mathbf{UBM}^{-1/2})(\mathbf{UBM}^{-1/2})^T$$

Then, the singular value decomposition (23) of $(\mathbf{UBM}^{-1/2})^T$ can be determined as

$$[9] \quad (\mathbf{UBM}^{-1/2})^T = \mathbf{PSV}^T$$

where **P** and **V** are orthogonal matrices, and **S** is diagonal. In terms of these matrices, **G** is given by

$$[10] \quad \mathbf{G} = (\mathbf{PSV}^T)^T(\mathbf{PSV}^T) = \mathbf{VS}^2\mathbf{V}^T$$

or

$$[11] \quad \mathbf{GV} = \mathbf{VS}^2$$

so the elements of the diagonal $\mathbf{S}^2$ matrix are the eigenvalues of **G**, and **V** are the eigenvectors. This provides a means of eliminating redundant coordinates, if any are present.

If **G** has zero eigenvalues, the corresponding eigenvectors give (combinations of) the redunancy relations, and the remaining eigenvectors are orthogonal combinations of the symmetry coordinates with the redundancies removed (24). By means of an interactive procedure, suitable orthogonal transformations are applied to the remaining eigenvectors, in order to generate symmetry coordinates of the desired structure. For example, deformation coordinates for methyl and methylene groups have been given (25), as well as a complete set of recommended coordinates (5). If redundancies are removed, the transformed eigenvector matrix, **V′**, is used to transform the **U** matrix to the new set of coordinates, and revised coordinate labels are requested from the operator. Finally, the revised **UB** product matrix is calculated.

For the solution of the **GF** eigenvalue problem, we require the Choleski decomposition of the inverse of **G**, i.e., the lower triangular matrix, **R**, satisfying

$$[12] \quad \mathbf{G}^{-1} = \mathbf{RR}^T$$

To accomplish this, note from eq. [10] that, since **V** is orthogonal,

$$[13] \quad \mathbf{G}^{-1} = \mathbf{VS}^{-2}\mathbf{V}^T$$

Thus, **R**, the Choleski factor of **G**, is obtained by applying the Givens' reduction (23) to transform $\mathbf{VS}^{-1}$ to triangular form.

The Choleski matrix, **R**, the atomic masses, and the auxiliary blocking matrix are stored in the SPECIES file and, if redundant coordinates have been removed, the revised **U** and **UB** matrices and the revised coordinate labels are stored in the MOLECULE file. Finally, the **G** matrix is calculated and printed out, for reference.

Normal coordinate calculation: FCALC

The **GF** eigenvalue problem can be expressed in the form of the generalized symmetric eigenvalue problem (23)

$$[14] \quad \mathbf{FL} = \mathbf{G}^{-1}\mathbf{L}\Lambda$$

As stated earlier, this problem may be transformed into a simple symmetric matrix eigenvalue problem, if the Choleski decomposition of the $\mathbf{G}^{-1}$ matrix (eq. [12]) is used.

$$[15] \quad (\mathbf{R}^{-1}\mathbf{FR}^{-T})(\mathbf{R}^T\mathbf{L}) = (\mathbf{R}^T\mathbf{L})\Lambda$$

or

$$[16] \quad \mathbf{ZW} = \mathbf{W}\Lambda$$

The symmetric matrix **Z** is obtained from **F** by two applications of the Choleski forward substitution routine (23) to obtain the intermediate matrix **Y**

$$[17] \quad \mathbf{RY} = \mathbf{F}$$

and then **Z**

$$[18] \quad \mathbf{ZR}^T = \mathbf{Y}$$

while the eigenvectors, **L**, are obtained from the eigenvectors of eq. [16] by Choleski back substitution (23)

$$[19] \quad \mathbf{R}^T\mathbf{L} = \mathbf{W}$$

The vibrational frequencies, ν_i, are obtained from the eigen-

values, λ_i, by means of

[20] $\nu_i = \lambda_i^{1/2}/2\pi c$

where the factors required for conversion of units have been suppressed.

Thus, to perform a calculation of the vibrational frequencies from a given force field, the program reads the **R** matrix from the SPECIES file, as well as the auxiliary blocking matrix, if needed. The **F** matrix, expressed in internal or symmetry coordinates, may be input in one of three formats: element by element, as blocks of a symmetrized **F** matrix, or the entire matrix may be read in from an additional file. The **U** matrix, if needed to transform the **F** matrix from internal to symmetry coordinates, is read from the MOLECULE file, along with the symmetry coordinate labels for use in the printed output.

The eigenvalue problem is solved as outlined above, and the phase of each eigenvector is arbitrarily adjusted so the largest element is positive. The potential energy distribution is calculated for the diagonal **F** matrix elements using the usual relations (1). The **L** matrix elements are expressed in the mass weighted representation (2), and also in the dimensionless representation (26). The vibrational frequencies and both representations of the **L** matrices are stored in the SPECIES file at the completion of the program.

Force field scaling: FFIT

In our recent work, we have not required a procedure for deriving an empirical force field by performing a best fit of observed vibrational frequencies, but such a routine could be easily implemented (8) by means of standard library routines. In general, however, such an approach is of limited value for larger molecules; the numerical system is often underdetermined, at least in a practical, if not a strict mathematical, sense (8). In our work, we have used extensively a routine to scale *ab initio* force fields (5) to fit observed frequencies, to compensate for basis set deficiencies and the neglect of electron correlation in the *ab initio* calculation. Such an empirical procedure will be needed until high-level *ab initio* force field calculations, including electron correlation, can be carried out for larger molecules of interest to chemical spectroscopists. If frequency data from a sufficient number of isotopic species are available, we have obtained better fits when relating scale factors to different types of symmetry coordinates (17, 28) (CH stretch, methyl symmetric deformation, methyl and methylene asymmetric deformation, methyl and methylene rocking, etc., for alkane molecules, for example). This behavior may be understood by noting that, for the molecules we have considered, the force constant matrix is more nearly diagonal when expressed in symmetry coordinates, as compared to internal coordinates. Thus, the empirical scaling procedure has a more limited effect upon the smaller interaction force constants in the symmetry coordinate representation. It is also important to allow for the correlation of anharmonic observed frequencies to harmonic ones (29).

On each iteration of the nonlinear fitting routine, the fitting parameters are allocated to appropriate elements of a diagonal scaling matrix, **D**, and then the scaled *ab initio* $\mathbf{F}_{sai}$ matrix is given by

[21] $\mathbf{F}_{sai} = \mathbf{D}\mathbf{F}_{ai}\mathbf{D}$

This procedure has the effect of multiplying diagonal force constants by the square of a scale factor, and off-diagonal ones by the product of the related scale factors. Thus, the scale factors determined in our work are the square of those used by other workers (5).

In the fitting procedure, $\mathbf{F}_{sai}$ is used to calculate vibrational eigenvalues, and the minimization routine then varies the scaling parameters to minimize the sum of squares of the weighted differences from the observed ones. The weights, w, for each eigenvalue, λ_{calc}, can be chosen to be

[22] $$w = \frac{1}{2\lambda_{obs}}$$

which is equivalent to fitting the percent frequency difference:

[23] $$w(\lambda_{calc} - \lambda_{obs}) = \frac{\nu_{calc}^2 - \nu_{obs}^2}{2\nu_{obs}^2} \simeq \frac{\nu_{calc} - \nu_{obs}}{\nu_{obs}}$$

or, alternatively,

[24] $$w = \frac{\nu_{obs}}{2\lambda_{obs}}$$

which is equivalent to fitting the frequency difference, itself:

[25] $$w(\lambda_{calc} - \lambda_{obs}) \simeq \nu_{calc} - \nu_{obs}$$

In fact, for the determination of the scaled *ab initio* force field, there is little difference between the fitted results with the two types of weights.

The fitting is carried out using the IMSL nonlinear least-squares routine ZXSSQ (12), with the convergence criterion that each parameter estimate agrees to a specified number of significant digits on successive iterations. The standard errors of the scale factors are calculated (30) from the standard error of the fit.

For each isotopic species considered in the calculation, the frequencies and the two forms of the **L** matrix are saved in the SPECIES file for use in subsequent calculations.

Auxiliary routines

Ab initio force field calculations normally yield a force constant matrix in cartesian coordinates, $\mathbf{F}_X$, which must be transformed to internal or symmetry coordinates for use in our calculations. This transformation requires either the generalized inverse of **B** or that of **UB** for these two cases. This inverse is the non-unique matrix that satisfies, for the symmetry coordinate case,

[26] $(\mathbf{UB})\mathbf{A} = \mathbf{E}$

where **E** is the unit matrix. In terms of quantities already calculated in our routines, a convenient form of **A** may be given as (5)

[27] $\mathbf{A} = \mathbf{M}^{-1}(\mathbf{UB})^T\mathbf{G}^{-1}$

The inverses of the **M** and **G** matrices are those for a selected parent isotopic species; the latter matrix, expressed in symmetry coordinates, can be obtained from the Choleski decomposition matrix, **R** (see eq. [12]). Then the $\mathbf{F}_S$ matrix, in symmetry coordinates, is given by

[28] $\mathbf{F}_S = \mathbf{A}^T\mathbf{F}_X\mathbf{A}$

Permutations can be applied to the cartesian axes and atom numbering, to maintain consistency with any such permutations performed earlier on the geometry.

Can. J. Chem. Downloaded from www.nrcresearchpress.com by 123.30.183.119 on 09/07/12
For personal use only.

TABLE 1. UBMAT program output. Geometry and **B** matrix for FS—SF[a]

(*a*) Cartesian coordinates

Atom	*X*	*Y*	*Z*
1	1.550463	0.000000	−1.459771
2	0.000000	0.000000	−0.944000
3	0.000000	0.000000	0.944000
4	0.067630	1.548988	1.459771

(*b*) Internal coordinate definitions (INPUT)

Number	Type	Atoms/bonds		Equilib. value
1	Bond str.	2	3	1.8880
2	Bond str.	2	1	1.6340
3	Bond str.	3	4	1.6340
4	Def (bent)	2	1	108.40
5	Def (bent)	3	1	108.40
6	Torsion		1	87.5

(*c*) Transpose of **B** matrix (symmetry coordinates)

	1 SF s str	2 SS str	3 SSF s def	4 Tors	5 SF a str	6 SSF a def
X 1	0.670957	0.000000	−0.136596	0.000000	0.670957	−0.136596
Y 1	0.000000	0.000000	0.000000	−0.644968	0.000000	0.000000
Z 1	−0.223198	0.000000	−0.410622	0.000000	−0.223198	−0.410622
X 2	−0.670957	0.000000	0.494786	−0.176027	−0.670957	0.527459
Y 2	0.000000	0.000000	−0.374170	0.828849	0.000000	0.374170
Z 2	0.223198	−1.000000	0.410622	0.000000	0.223198	0.410622
X 3	−0.029267	0.000000	−0.352232	0.820382	0.029267	−0.396822
Y 3	−0.670318	0.000000	0.510636	−0.212013	0.670318	−0.510636
Z 3	−0.223198	1.000000	−0.410622	0.000000	0.223198	0.410622
X 4	0.029267	0.000000	−0.005958	−0.644355	−0.029267	0.005958
Y 4	0.670318	0.000000	−0.136466	0.028133	−0.670318	0.136466
Z 4	0.223198	0.000000	0.410622	0.000000	−0.223198	−0.410622

[a]Geometry taken from ref. 39. Units: cartesian coordinates and bond lengths in angstroms, angles in degrees.

Example

The operation of these routines has been demonstrated in several publications from our laboratory over the past few years, including force field determinations for hexafluoroacetone (31), propane (32), cyclohexane (33), trimethylphosphine (27), and *n*-butane (28), and the results of such calculations have also been used in our absolute Raman intensity studies (28, 33–36). For this reason, it is felt that there is no need to carry out a complete force field determination as part of this description of the computational capability of these programs.

However, when writing a program to carry out normal coordinate calculations, it is useful to have detailed example results available, for testing purposes. Such examples are contained in a IUPAC publication of test data for normal coordinate calculations (37). There, input data for testing normal coordinate analysis programs and the results of the calculation are given for four representative molecules. These data were used to verify the operation of the present routines.

There is one situation that is not checked in these examples: the proper consideration of the torsional coordinate. The sign error for the torsion **B** matrix elements, mentioned above, has

TABLE 2. GCALC program output. **G** matrix for FS—SF[a]

(*a*) Masses of atoms

Atom 1	18.998398
Atom 2	31.972076
Atom 3	31.972076
Atom 4	18.998398

(*b*) **G** matrix (symmetry coordinates)

Block 1				
	1	2	3	4
1 SF s str	0.083913			
2 SS str	−0.013962	0.062555		
3 SSF s def	−0.015034	−0.025686	0.054334	
4 Tors	0.007388	0.000000	−0.024848	0.088704
Block 2				
	5	6		
5 SF a str	0.083913			
6 SSF a def	−0.016405	0.056423		

[a]Units: masses in u (atomic mass units) and **G** matrix elements in u^{-1}.

Can. J. Chem. Downloaded from www.nrcresearchpress.com by 123.30.183.119 on 09/07/12
For personal use only.

TABLE 3. FCALC program output. Force field, vibrational frequencies, and normal coordinates for FS—SF[a]

(*a*) **F** matrix (symmetry coordinates)

	1	2	3	4	5	6
1 SF s str	3.560000					
2 SS str	0.879000	4.035000				
3 SSF s def	0.000000	0.285000	1.042000			
4 Tors	0.084000	0.000000	−0.048400	0.364400		
5 SF a str	0.000000	0.000000	0.000000	0.000000	3.216000	
6 SSF a def	0.000000	0.000000	0.000000	0.000000	0.158000	1.153700

(*b*) Eigenvalues, frequencies, and eigenvectors (mass weighted coordinates)

Eigenvalue	0.298191	0.234182	0.052466	0.019700	0.268480	0.061297
Frequency	711.414	630.451	298.410	182.853	675.042	322.547
Assignment	SF s str	SS str	SSF s def	Tors	SF a str	SSF a def
PED	88	105	53	65	100	99
Assignment		SF s str	Tors	SSF s def		
PED		14	36	42		
1 SF s str	0.271981	−0.096853	−0.023626	−0.000890	0.000000	0.000000
2 SS str	0.036107	0.247348	−0.007504	0.003688	0.000000	0.000000
3 SSF s def	−0.103059	−0.095092	−0.163611	0.088891	0.000000	0.000000
4 Tors	0.046469	−0.002720	0.226301	0.187951	0.000000	0.000000
5 SF a str	0.000000	0.000000	0.000000	0.000000	0.289609	0.006313
6 SSF a def	0.000000	0.000000	0.000000	0.000000	−0.061646	0.229396

(*c*) Potential energy distribution

Frequency	711.414	630.451	298.410	182.853	675.042	322.547
1 SF s str	88.31	14.26	3.79	0.01	0.00	0.00
2 SS str	1.76	105.42	0.43	0.28	0.00	0.00
3 SSF s def	3.71	4.02	53.16	41.80	0.00	0.00
4 Tors	0.26	0.00	35.57	65.34	0.00	0.00
5 SF a str	0.00	0.00	0.00	0.00	100.47	0.21
6 SSF a def	0.00	0.00	0.00	0.00	1.63	99.04

(*d*) Eigenvectors (dimensionless coordinates)

Frequency	711.414	630.451	298.410	182.853	675.042	322.547
1 SF s str	0.059209	−0.022398	−0.007941	−0.000382	0.000000	0.000000
2 SS str	0.007860	0.057200	−0.002522	0.001583	0.000000	0.000000
3 SSF s def	−0.022436	−0.021990	−0.054994	0.038170	0.000000	0.000000
4 Tors	0.010116	−0.000629	0.076066	0.080706	0.000000	0.000000
5 SF a str	0.000000	0.000000	0.000000	0.000000	0.064723	0.002041
6 SSF a def	0.000000	0.000000	0.000000	0.000000	−0.013777	0.074166

[a]Force constants taken from ref. 39. Units: **F** matrix elements in aJ $Å^{-1}$, eigenvalues in aJ $Å^{-1}$ u^{-1}, frequencies in cm^{-1}, the eigenvectors (**L** matrix elements) for the mass weighted normal coordinates in $u^{-1/2}$, the eigenvectors (**L** matrix elements) for the dimensionless normal coordinates in Å, and P.E.D. in percent.

no effect if the three bonds involved are in the same plane. In addition, if the torsional coordinate about a bond is defined in terms of all three-bond combinations involving the central bond, the sign errors cancel if the central bond lies in a plane of symmetry. Thus a torsional coordinate not satisfying such symmetry conditions should be considered in order to check the correct determination of the **B** matrix elements for this case.

Therefore, the present programs may be demonstrated by performing an example calculation for such a situation; the case of the FS—SF chain isomer of disulfur difluoride has been chosen. This is an interesting molecule; it rearranges to form a more stable pyramidal S=SF_2 isomer at room temperature (38). The vibrational analysis of this molecule was recently described (39). The atom numbering, geometry, and internal and symmetry coordinates are given in Table III of ref. 39. The output from the UBMAT routine is shown in Table 1, and from the GCALC routine in Table 2. If the sign error is present in the **B** matrix routine, the (x,y,z) elements for the torsional coordinate become (0.176027, 0.813478, 0) for atom 2, and (0.820382, 0.140376, 0) for atom 3. These values then give (−0.007388, 0, −0.013592, 0.087125) for row 4 of the **G** matrix. The output from the FCALC routine is shown in Table 3.

Can. J. Chem. Downloaded from www.nrcresearchpress.com by 123.30.183.119 on 09/07/12
For personal use only.

Conclusion

The program system outlined here has been used satisfactorily for several years in this laboratory for the calculation of vibrational force fields and normal coordinates. The ability to store intermediate results in auxiliary data files has proven to be very convenient, and has simplified the transfer of the results of one program for use in another. Several unique numerical procedures have been incorporated into these programs, to enhance their operation. Finally, the example calculation for disulfur difluoride should prove useful for anyone wishing to check other versions of routines for performing such calculations.

1. H. FUHRER, V. B. KARTHA, K. G. KIDD, P. J. KRUEGER, and H. H. MANTSCH. Normal coordinate analysis — computer programs for infrared spectrophotometry XXXIX–XLI. Bulletin 15. National Research Council of Canada, Ottawa, Canada. 1976.
2. E. B. WILSON, JR., J. C. DECIUS, and P. C. CROSS. Molecular vibrations: the theory of infrared and Raman vibrational spectra. McGraw–Hill, New York. 1955.
3. R. L. HILDERBRANDT. J. Chem. Phys. **51**, 1654 (1969).
4. J. H. SCHACHTSCHNEIDER. Technical report 57-65. Shell Development Co., Emeryville, CA. 1966.
5. G. FOGARASI and P. PULAY. *In* Vibrational spectra and structure. Vol. 14. *Edited by* J. R. Durig. Elsevier, New York. 1985. pp. 125–219.
6. W. D. GWINN. J. Chem. Phys. **55**, 477 (1971); Program NORCRD. QCPE 176/177. Program XYZ. QCPE 178. Quantum Chemistry Program Exchange. Indiana University, Bloomington, IN.
7. D. F. MCINTOSH, K. H. MICHAELIAN, and M. R. PETERSON. Can. J. Chem. **56**, 1289 (1978); General vibrational analysis system. QCPE 342/576. Quantum Chemistry Program Exchange. Indiana University, Bloomington, IN.
8. P. GANS. *In* Advances in infrared and Raman spectroscopy. Vol. 3. *Edited by* R. J. H. Clark and R. E. Hester. Heyden, London. 1977. pp. 87–126.
9. J. F. BLANKE and J. OVEREND. *In* Vibrational spectra and structure. Vol. 7. *Edited by* J. R. Durig. Elsevier, New York. 1978. pp. 269–315.
10. D. F. MCINTOSH and K. H. MICHAELIAN. Can. J. Spectrosc. **24**, 1 (1979); **24**, 35 (1979); **24**, 65 (1979).
11. H. MATSUURA and M. TASUMI. *In* Vibrational spectra and structure. Vol. 12. *Edited by* J. R. Durig. Elsevier, New York. 1983. pp. 69–143.
12. IMSL, Inc., Houston, TX. IMSL Library — user's manual, Edition 9.2. 1984.
13. I. MILLS (*Editor*). Quantities, units and symbols in physical chemistry. IUPAC Commission on Physicochemical Symbols, Terminology, and Units, Blackwell, London. 1988.
14. H. ESSÉN. J. Comput. Chem. **4**, 136 (1983); Program EUCLID. QCPE 452. Quantum Chemistry Program Exchange. Indiana University, Bloomington, IN.
15. J. E. NORDLANDER, A. F. BOND IV, and M. BADER. Comput. Chem. **9**, 209 (1985).
16. Y. MORINO and T. SHIMANOUCHI. Pure Appl. Chem. **50**, 1707 (1978).
17. T. MIYAZAWA and K. FUKUSHIMA. J. Mol. Spectrosc. **15**, 308 (1965).
18. I. H. WILLIAMS and J. MCKENNA. J. Mol. Struct. **55**, 147 (1979).
19. R. L. HILDERBRANDT. J. Mol. Spectrosc. **44**, 599 (1972).
20. I. H. WILLIAMS. J. Mol. Spectrosc. **66**, 288 (1977).
21. S. M. FERIGLE and A. G. MEISTER. J. Chem. Phys. **19**, 982 (1951).
22. A. H. WAPSTRA and K. BOS. At. Data Nucl. Data Tables, **19**, 177 (1977).
23. J. C. NASH. Compact numerical methods for computers: linear algebra and function minimization. Wiley, New York. 1979.
24. C. E. SUN, R. G. PARR, and B. CRAWFORD, JR. J. Chem. Phys. **17**, 840 (1949).
25. T. SHIMANOUCHI, H. MATSUURA, Y. OGAWA, and I. HARADA. J. Phys. Chem. Ref. Data, **7**, 1323 (1978).
26. J. K. G. WATSON. *In* Vibrational spectra and structure. Vol. 6. *Edited by* J. R. Durig. Elsevier, New York. 1977. pp. 1–89.
27. D. C. MCKEAN, G. P. MCQUILLAN, W. F. MURPHY, and F. ZERBETTO. J. Phys. Chem. **94**, 4820 (1990).
28. W. F. MURPHY, J. M. FERNÁNDEZ-SÁNCHEZ, and K. RAGHAVACHARI. J. Phys. Chem. **95**, 1124 (1991).
29. J. L. DUNCAN, D. C. MCKEAN, F. TULLINI, G. D. NIVELLINI, and J. PEREZ PEÑA. J. Mol. Spectrosc. **69**, 123 (1978).
30. A. A. CLIFFORD. Multivariate error analysis. Applied science, New York. 1975.
31. D. A. C. COMPTON, J. D. GODDARD, S. C. HSI, W. F. MURPHY, and D. M. RAYNER. J. Phys. Chem. **88**, 356 (1984).
32. K. M. GOUGH, W. F. MURPHY, and K. RAGHAVACHARI. J. Chem. Phys. **87**, 3332 (1987).
33. K. M. GOUGH and W. F. MURPHY. J. Chem. Phys. **87**, 1509 (1987).
34. K. M. GOUGH and W. F. MURPHY. J. Chem. Phys. **85**, 4290 (1986).
35. K. M. GOUGH, W. F. MURPHY, T. STROYER-HANSEN, and E. N. SVENDSEN. J. Chem. Phys. **87**, 3341 (1987).
36. K. M. GOUGH and W. F. MURPHY. J. Mol. Struct. **224**, 73 (1990).
37. M. TASUMI and M. NAKATA. Pure Appl. Chem. **57**, 121 (1985).
38. R. D. BROWN and G. P. PEZ. Aust. J. Chem. **20**, 2305 (1967).
39. R. W. DAVIS and S. FIRTH. J. Mol. Spectrosc. **145**, 225 (1991).

Can. J. Chem. Downloaded from www.nrcresearchpress.com by 123.30.183.119 on 09/07/12
For personal use only.

Fourier-transform infrared and circular dichroism studies on temperature dependence of the secondary structure of troponin C from bullfrog skeletal muscle

TATSUYUKI YAMAMOTO[1] AND MITSUO TASUMI[2]

Department of Chemistry, Faculty of Science, The University of Tokyo, Bunkyo-ku, Tokyo 113, Japan

AND

MASARU TANOKURA

Department of Biochemistry and Biophysics, Faculty of Science, The University of Tokyo, Bunkyo-ku, Tokyo 113, Japan

Received April 19, 1991

This paper is dedicated to Dr. Richard Norman Jones

TATSUYUKI YAMAMOTO, MITSUO TASUMI, and MASARU TANOKURA. Can. J. Chem. **69**, 1679 (1991).

The infrared spectra and circular dichroism of bullfrog (*Rana catesbeiana*) skeletal muscle troponin C with and without Ca^{2+} have been measured in aqueous solution at temperatures between 24 and 80°C at pH 7.0. Infrared spectral changes with increasing temperature, particularly in the amide I region, have been extensively examined by using the techniques of thermal difference spectrum and deconvolution. Ca^{2+}-free troponin C seems to be denatured at about 70°C, but its denaturation proceeds gradually without an abrupt structural change. Ca^{2+} binding causes a considerable change in the secondary structure of the whole protein. Consequently, Ca^{2+}-bound troponin C has a higher α-helix content and is thermally more stable than the Ca^{2+}-free protein. Both the deconvolved amide I bands and circular dichroism data indicate that there are similarities between the secondary structure (and probably the tertiary structure as well) of the Ca^{2+}-bound protein at 80°C and that of the Ca^{2+}-free protein at room temperature.

Key words: bullfrog skeletal muscle troponin C, Fourier transform infrared and circular dichroism studies.

TATSUYUKI YAMAMOTO, MITSUO TASUMI et MASARU TANOKURA. Can. J. Chem. **69**, 1679 (1991).

Opérant en solutions aqueuses, à un pH de 7,0, en présence et en l'absence d'ions Ca^{2+} et à des températures allant de 24 à 80°C, on a mesuré les spectres infrarouges et le dichroïsme circulaire de la troponine C des muscles du squelette de la grenouille taureau (*Rana catesbeiana*). Utilisant les techniques de déconvolution et de différences spectrales causées par la chaleur, on a examiné avec attention les variations des spectres infrarouges avec une augmentation de la température, particulièrement dans la région amide I. Il semble que la troponine C sans ions Ca^{2+} soit dénaturée à environ 70°C; cette dénaturation se fait toutefois graduellement, sans changement structural abrupt. Une liaison avec le Ca^{2+} provoque un changement important dans la structure secondaire de la protéine dans son ensemble. On peut en déduire que la troponine C liée au Ca^{2+} soit plus riche en hélice α et thermiquement plus stable que la protéine sans Ca^{2+}. Les données tant du dichroïsme circulaire que des bandes amide I soumises à une déconvolution indiquent qu'il existe des similarités entre la structure secondaire (et probablement la structure tertiaire) de la protéine liée au Ca^{2+}, à 80°C, et celle de la protéine sans Ca^{2+} à la température ambiante.

Mots clés : troponine C des muscles du squelette de la grenouille taureau, spectres infrarouges et de dichroïsme circulaire.

[Traduit par la rédaction]

Introduction

Troponin C (abbreviated as TnC) is one of Ca^{2+}-binding proteins and is known to be involved in regulation of muscle contraction (1–3). A TnC molecule binds up to four Ca^{2+} ions in two kinds of Ca^{2+} binding sites called the high and low affinity sites (4, 5). Binding of Ca^{2+} by TnC removes inhibition of interaction between actin and myosin, thus causing muscle contraction (6, 7).

X-ray analyses of crystalline TnCs from skeletal muscles of turkey and chicken (8–11) have revealed a rather peculiar "dumbbell" like structure of the TnC molecule, which consists of two globular domains interconnected by an α-helical rod. Each globular domain contains two Ca^{2+} binding sites. The content of α-helix in the TnC molecule calculated on the basis of the structure determined by X-ray analysis is about 60% (8).

Although the amino acid sequence of bullfrog skeletal muscle TnC has not been determined yet, it is expected to be quite similar to that of TnC from another frog species *Rana esculenta* (12) because the amino acid compositions of TnCs from the two frog species are almost identical (13). Both frog and chicken skeletal muscle TnCs are composed of 162 amino acid residues, of which only 15 residues are different between them. The residues in the Ca^{2+}-binding loops are mostly preserved. Therefore, it is reasonable to assume that the three-dimensional structure of bullfrog TnC under study would be analogous to that of chicken TnC, if the former could be crystallized.

It has been pointed out from fluorescence measurements (14, 15) and an X-ray small-angle scattering study (16) that the three-dimensional structures in crystal (prepared from solutions at pH 5.5) may be different from those in aqueous solution at pH 7.0. Thermal denaturation processes of TnC in aqueous solution have been studied by ^1H nuclear magnetic resonance (17), circular dichroism (18), and calorimetric measurements (19–21). The results of these studies have indicated that, broadly speaking, thermal denaturation of TnC gradually occurs in contrast with globular proteins which usually have well-defined denaturation temperatures. All the above studies cited in this paragraph have been done by using rabbit skeletal muscle TnC. On the other hand, a group including one of the present authors has suggested that differences may exist in thermodynamic properties between rabbit and frog skeletal muscle TnCs (22). In the present paper, we have studied thermal denaturation processes of TnC from bullfrog skeletal muscle in H_2O solution

[1]Present address: Department of Biological Sciences, Faculty of Bioscience and Biotechnology, Tokyo Institute of Technology, Ohokayama 2-12-1, Meguro-ku 152, Japan.

[2]Author to whom correspondence may be addressed.

Printed in Canada / Imprimé au Canada

Can. J. Chem. Downloaded from www.nrcresearchpress.com by 84.41.108.74 on 09/07/12
For personal use only.

at neutral pH with and without Ca^{2+} by Fourier-transform infrared and circular dichroism (CD) measurements.

Experimental

Sample preparation

Bullfrog skeletal muscle TnC was prepared by the method described previously (22). Contaminating Ca^{2+} was removed by the trichloroacetic acid treatment. To obtain a Ca^{2+}-free sample, freeze-dried TnC (20 mg) was dissolved in an aqueous solution (2 mL) containing 0.1 M KCl and 10 mM EGTA. Similarly, a Ca^{2+}-bound sample was prepared by dissolving freeze-dried TnC in an aqueous solution containing 0.1 M KCl and 0.2 M $CaCl_2$. A small quantity of dithiothreitol (about 1 mM) was added to each solution to suppress aggregation of TnC. The pH value was adjusted to 7.0. These solutions were concentrated to about 10% (w/v) by centrifugation and were used for infrared measurements.

For circular dichroism measurements, a Ca^{2+}-free TnC sample was prepared by dissolving freeze-dried TnC into a solution containing 2 mM KCl, 1mM EGTA, and 1 mM PIPES buffer (pH 7.0). A Ca^{2+}-bound TnC sample was prepared by dissolving freeze-dried TnC in an aqueous solution, in which 0.5 mM $CaCl_2$ was contained instead of 1 mM EGTA. The concentration of TnC was adjusted to 46 mg/L in each solution. A small quantity of dithiothreitol was added in this case also.

Measurements of infrared spectra

Infrared spectra were observed on a JEOL JIR-100 Fourier-transform infrared spectrophotometer equipped with an MCT detector (Judson J15D12). Spectral measurements were carried out at 2 cm^{-1} resolution in a temperature range from 24 to 80°C at intervals of 4°C. Interferograms from 500 scans were averaged to obtain one spectrum. This required about 10 min. The temperature of the sample was changed with a ribbon heater wound around the cell holder, and monitored by a copper–constantan thermocouple inserted in the cell. The sample was kept at a constant temperature for 10 min before performing a spectral measurement at this temperature. Dry air was continuously flowed into the spectrophotometer during spectral measurements. About 10 μL of the protein solution was set between two CaF_2 disks using a 15 μm Teflon spacer. The gap between the two CaF_2 disks was sealed with glue to avoid evaporation of water. Infrared spectra of the buffer solutions were similarly observed at various temperatures. To eliminate the contribution of absorptions due to water from the spectrum of the protein solution, the spectrum of the buffer solution was subtracted, after multiplying an appropriate factor (approximately 0.9), from the spectrum of the protein solution observed at the same temperature (23).

No smoothing procedure was employed for the observed infrared spectra. Deconvolution was performed according to the method described by Jones and Shimokoshi (24). A Lorentz bandshape function and a triangle^2 apodizing function were used with deconvolving parameters as follows: $2\sigma = 28$ cm^{-1} and $L = 0.18$ cm. To examine the reproducibility, the same spectral measurements were repeated at least three times.

Measurements of circular dichroism spectra

Circluar dichroism spectra of Ca^{2+}-free and Ca^{2+}-bound TnC were observed on a JASCO J-600 CD spectropolarimeter. A cell of 2 mm path length was placed in a holder through which temperature-controlled water was circulated. The temperature of the sample, monitored by a thermometer directly fixed to the cell holder, was raised from 25 to 80°C at intervals of 5°C. Circular dichroism spectra were observed from 200 to 250 nm under continuous flow of nitrogen gas.

The α-helix content of TnC was estimated using the following equations (25–27). Even if the α-helix contents estimated in this way may not be completely reliable per se, their relative values are useful for confirming infrared results, as described later.

$$\alpha\text{-helix content} = \frac{4880 - [\Theta_{222}]}{45400}$$

$$[\Theta_{222}] = \frac{M\Theta_{222}}{100cl}$$

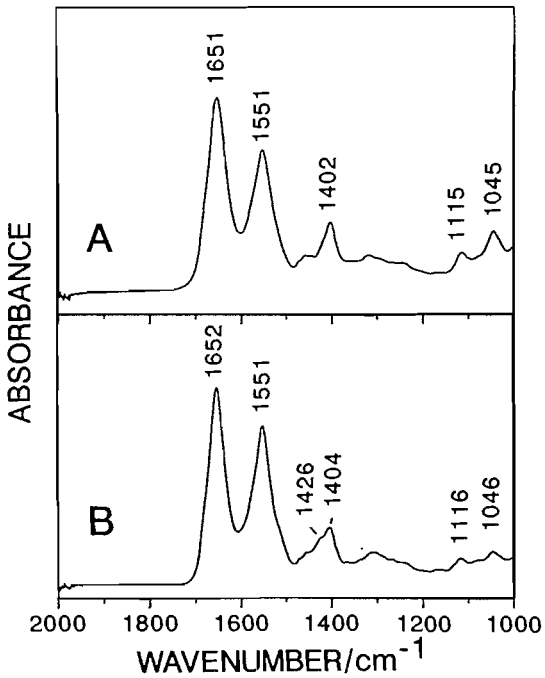


FIG. 1. Infrared spectra of Ca^{2+}-free (*A*) and Ca^{2+}-bound (*B*) bullfrog skeletal muscle troponin C in H_2O solution at 24°C; 4 cm^{-1} resolution. The intensities of the amide I bands at 1651 cm^{-1} in *A* and at 1652 cm^{-1} in *B* are about 0.5 in absorbance unit.

where Θ_{222} is the ellipticity observed at 222 nm, M is the mean molecular weight of the amino acid residues of the protein under study (112 for TnC), c is the protein concentration in g/mL, and l is the thickness in dm of the sample solution.

Results and discussion

Comparison of the infrared spectra of Ca^{2+}-free and Ca^{2+}-bound troponin C

The infrared spectra (2000–1000 cm^{-1}) of Ca^{2+}-free and Ca^{2+}-bound TnC at room temperature are shown in Fig. 1, where strong absorptions of solvent water have already been subtracted. At first glance, the spectra of the Ca^{2+}-free and Ca^{2+}-bound proteins are similar. It is noted, however, that the widths of the intense amide I and II bands at about 1650 and 1550 cm^{-1}, respectively, are different before and after Ca^{2+}-binding, although their peak positions remain almost unchanged. The full widths at half maximum of the amide I bands in Figs. 1*A* and 1*B* are 50 and 40 cm^{-1}, respectively. Since it is well known that the amide I bands due to α-helices and random coils are closely located (28–30), the present results suggest that both the Ca^{2+}-free and Ca^{2+}-bound proteins contain α-helices and random coils, but the Ca^{2+}-bound protein has a higher content of α-helix.

A closer look at the two spectra in Fig. 1 leads us to find small but nevertheless significant differences between them, particularly in the region around 1400 cm^{-1}. The band at 1402 cm^{-1} in the spectrum of Ca^{2+}-free TnC (Fig. 1*A*) is assignable to the symmetric stretch of the free carboxylate groups of aspartic and glutamic acid residues. In the spectrum of Ca^{2+}-bound TnC, on the other hand, two bands are observed at 1426 and 1404 cm^{-1} (Fig. 1*B*). A more extensive examination of the effects of Ca^{2+} binding on this region of the infrared spectrum may shed new light on the mechanism of Ca^{2+} binding and accompanying structural changes, to which a Raman study (31) has not given a definite answer. In the present study, however, we will confine

Can. J. Chem. Downloaded from www.nrcresearchpress.com by 84.41.108.74 on 09/07/12
For personal use only.

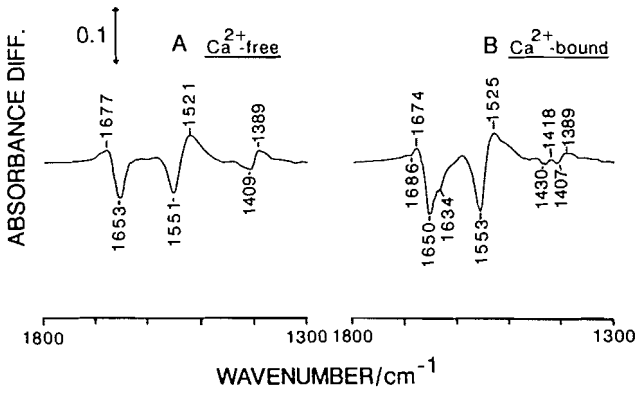


FIG. 2. Infrared thermal difference spectra of Ca^{2+}-free (*A*) and Ca^{2+}-bound (*B*) troponin C between 80 and 24°C; 2 cm^{-1} resolution.

our attention to temperature dependences of the infrared spectra of the Ca^{2+}-free and Ca^{2+}-bound proteins.

Infrared difference spectra

Differences between the infrared spectra observed at 80 and 24°C has been computed for both Ca^{2+}-free and Ca^{2+}-bound TnC without multiplying a factor to either of the spectra observed at the two temperatures, and the results are shown in Fig. 2. The strong negative bands are observed at 1653 and 1551 cm^{-1} in the difference spectrum of Ca^{2+}-free TnC (Fig. 2*A*), and likewise at 1650 and 1551 cm^{-1} in the difference spectrum of Ca^{2+}-bound TnC (Fig. 2*B*). These negative bands are reasonably assigned to α-helical parts, which are destroyed and converted into random coil as the temperature is raised. The random coil is considered to have very broad absorptions centering around 1660 and 1530 cm^{-1}, which should appear in the positive side but are largely cancelled by the overlapping negative bands. Therefore, the positive peaks at 1677 and 1674 cm^{-1} in Figs. 2*A* and 2*B*, respectively, should not be treated as true ones corresponding to a certain secondary structure.

In Fig. 2*B*, a small negative feature is observed at 1686 cm^{-1}. This negative feature is considered to arise from overlapping of a weak negative absorption and the tail of the broad positive absorption due to the random coil. The presence of this weak negative absorption at 1686 cm^{-1} is supported by the fact that a band located at about 1682 cm^{-1} in the deconvolved spectra (see below) seems to decrease in intensity at high temperatures. Moreover, in the case of ribonuclease A, a similar band has been observed at 1690 cm^{-1} and assigned to β-sheet (32, 33). An NMR study (34) has shown that a short β-sheet structure is formed in the C-terminal region of rabbit skeletal muscle TnC upon Ca^{2+} binding. According to X-ray diffraction studies (8–11), the TnC molecules from skeletal muscle of turkey and chicken have β-turns in the Ca^{2+}-binding loops. Since β-turns are also known to give rise to an absorption in the region of 1690–1680 cm^{-1} (30), it is highly probable that the negative 1686 cm^{-1} band of Ca^{2+}-bound TnC arises from the β-sheet and/or β-turns which are destroyed or become loose with increasing temperature. In the thermal difference spectrum of Ca^{2+}-free TnC (Fig. 2*A*), it is not clear whether a corresponding band exists.

From the absorbance difference of the negative band at 1653 cm^{-1} and the absorbance at 1651 cm^{-1} in Fig. 1*A*, the percentage absorbance change at 80°C for the amide I band of Ca^{2+}-free TnC can be calculated. The results of such calculation are plotted against temperature in Fig. 3, together with the results for the negative band of Ca^{2+}-bound TnC at 1650 cm^{-1}.

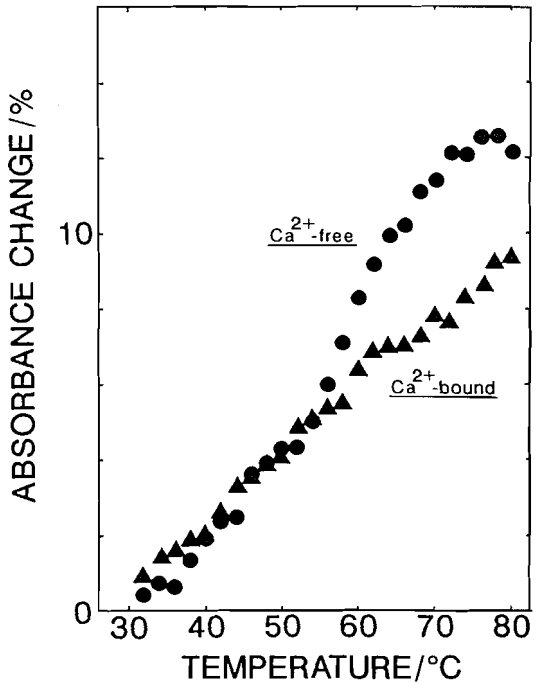


FIG. 3. Absorbance change vs. temperature plot for the amide I band at 1653 cm^{-1} of Ca^{2+}-free troponin C (●) and for that at 1650 cm^{-1} of Ca^{2+}-bound troponin C (▲).

Similar results for the amide II bands are shown in Fig. 4. The percentage absorbance changes thus calculated are always underestimated because, in measuring the absorbance difference of a negative band, an offset arising from the broad positive absorption due to the random coil is not taken into account. Then, the peak-to-peak differences (for example, the distance between the positive absorbance at 1677 cm^{-1} and the negative absorbance at 1653 cm^{-1} in Fig. 2*A*) are used to calculate the percentage absorbance changes. The results obtained in this way change the slopes of the curves (or lines), but do not change the shapes of the curves (or lines) which are most important in the following discussion.

The following points may be noted in Figs. 3 and 4. (*1*) No abrupt absorbance change occurs when the temperature is raised. This means that the secondary structure of the protein changes gradually with increasing temperature. The absorbance changes shown in Figs. 3 and 4 present a marked contrast with those observed for ribonuclease A, which shows an abrupt absorbance change corresponding to a cooperative structural change (32, 33). (*2*) In the case of Ca^{2+}-free TnC, the slope of the absorbance change of the amide I band becomes greater at about 55°C, and the change itself seems to level off in the temperature range above 75°C. The intensity of the amide II band changes almost linearly with temperature until about 75°C and then levels off. These results indicate that Ca^{2+}-free TnC is denatured at about 75°C. (*3*) In the case of Ca^{2+}-bound TnC, both amide I and II bands change in intensity almost linearly over the entire temperature range of 24–78°C, giving no sign of levelling off. Thus, Ca^{2+}-bound TnC, being thermally more stable than the Ca^{2+}-free proteins, is not fully denatured at 78°C.

The above three points are mostly in agreement with the results previously reported by ^1H nuclear magnetic resonance (17), circular dichroism (18), and calorimetric measurements (19–21), although there are minor deviations which are prob-

Can. J. Chem. Downloaded from www.nrcresearchpress.com by 84.41.108.74 on 09/07/12
For personal use only.

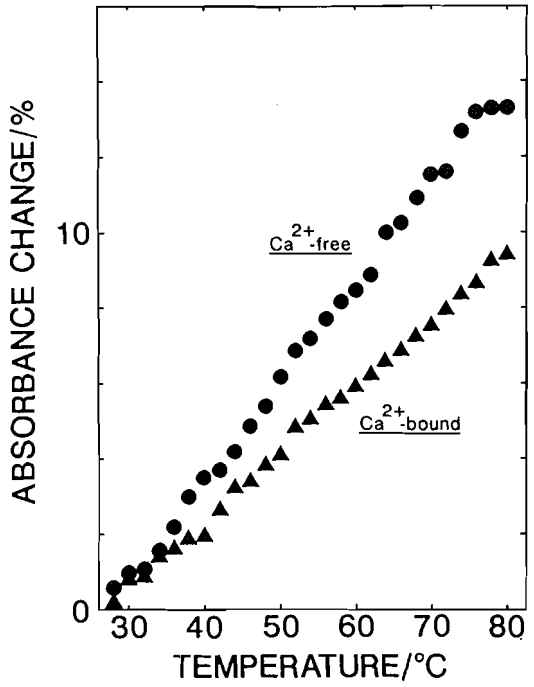


FIG. 4. Absorbance change vs. temperature plot for the amide II band at 1551 cm^{-1} of Ca^{2+}-free troponin C (●) and for that at 1553 cm^{-1} of Ca^{2+}-bound troponin C (▲).

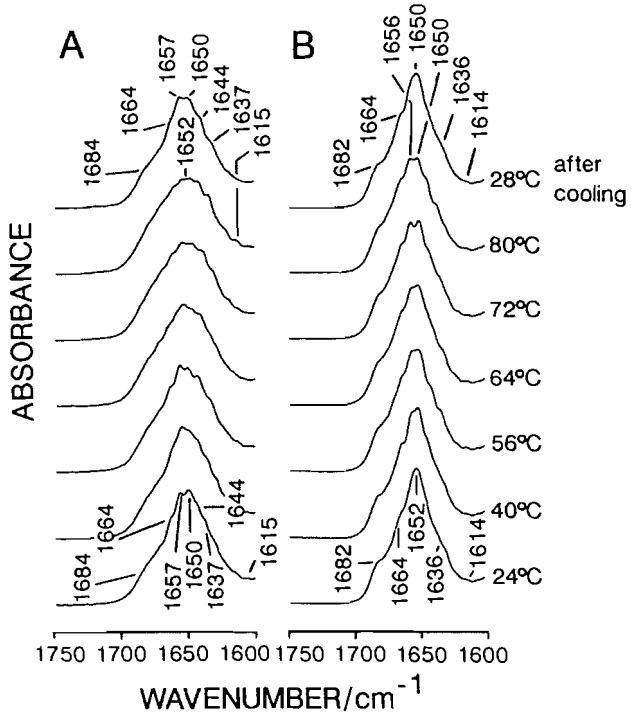


FIG. 5. Temperature dependence of the deconvolved amide I bands of Ca^{2+}-free (*A*) and Ca^{2+}-bound (*B*) troponin C; 2 cm^{-1} resolution.

ably due to differences in measuring conditions (concentration, etc.)

Deconvolved infrared spectra

The deconvolved infrared spectra in the amide I region of Ca^{2+}-free and Ca^{2+}-bound TnC are shown in Fig. 5. Compared with the deconvolved spectra of ribonuclease A (31, 32), the deconvolved spectra in Fig. 5 seem to have a broad background absorption extending from 1700 to 1600 cm^{-1}, which must be associated with more or less random structures. On top of this broad background absorption, each spectrum has peaks which are made less broad by the deconvolution procedure. For example, the spectrum of the Ca^{2+}-free protein at 24°C (Fig. 5*A*) has a doublet at 1657 and 1650 cm^{-1}, which undoubtedly corresponds to the negative band at 1653 $^{-1}$ in Fig. 2*A*. The spectrum of the Ca^{2+}-bound protein at 24°C (Fig. 5*B*) has a prominent single peak at 1652 cm^{-1}, which again corresponds to the negative band at 1650 cm^{-1} in Fig. 2*B*.

In the deconvolved spectrum of Ca^{2+}-bound TnC from rabbit sketetal muscle in D_2O solution, Trewhella *et al.* (35) have observed two intense peaks at 1647 and 1637 cm^{-1} (Fig. 4*a* of ref. 35). (In the text of ref. 35, the wavenumber of the former peak is referred to as 1644 cm^{-1}.) It is possible that both of these peaks derive upon deuteration from the 1652 cm^{-1} band of the Ca^{2+}-bound protein in Fig. 5*B*, although the sources of TnCs used by Trewhella *et al.* and in the present study are different. Trewhella *et al.* seem to assign the 1647 cm^{-1} band to "distorted" α-helix without touching on the origin of the 1637 cm^{-1} band. Our own data, which were obtained in H_2O solution, are not useful for discussing the validity of their band assignment.

Although it is not possible to make a definite assignment of each peak in the doublet of the Ca^{2+}-free protein, both of the two peaks are most probably associated with α-helical parts, because, as mentioned above, these peaks correspond very well to the negative band at 1650 cm^{-1} in Fig. 2*A*. The two peaks are merged into the prominent, rather sharp peak at 1652 cm^{-1} of the Ca^{2+}-bound protein (Fig. 5, 24°C). This spectral change upon Ca^{2+} binding is rather small in wavenumber but very clear in bandshape. Therefore, it is inferred that Ca^{2+} binding to the globular domains gives a significant perturbation to the three-dimensional structure of the whole protein, e.g., an increase in α-helix content (this point will be discussed later) and modifications of α-helical structures not only in the globular domains but also in the interconnecting rod. A ^1H nuclear magnetic resonance study (34) and an optical rotatory dispersion study (36) have also shown that the Ca^{2+} binding causes significant conformational changes to the rabbit skeletal muscle TnC molecule.

In the deconvolved spectrum of the Ca^{2+}-bound protein at 24°C, a shoulder exists at 1682 cm^{-1} (as mentioned earlier) but only a broad band is seen in the corresponding region (around 1684 cm^{-1}) of the Ca^{2+}-free protein.

With increasing temperature the doublet at 1657 and 1650 cm^{-1} of the Ca^{2+}-free protein becomes less apparent. On the contrary, the 1652 cm^{-1} band of the Ca^{2+}-bound protein gradually splits into a doublet as the temperature is raised. At 80°C this doublet appears to be quite similar to that of the Ca^{2+}-free protein at 24°C. Indeed, the overall spectral pattern of the Ca^{2+}-bound protein at 80°C resembles that of the Ca^{2+}-free protein at 24°C. This indicates that similarities exist between the three-dimensional structure of the Ca^{2+}-bound protein at 80°C and that of the Ca^{2+}-free protein at 24°C. It should be emphasized that Ca^{2+} is still bound to the apoprotein at 80°C, although the number of Ca^{2+} per apoprotein is not clear. If the protein has no Ca^{2+} at 80°C, the deconvolved spectrum at 80°C in Fig. 5*B* must be identical to that of the Ca^{2+}-free protein at 80°C in Fig. 5*A*.

The shoulder at 1682 cm^{-1} of the Ca^{2+}-bound protein at 24°C appears to become broader at higher temperatures. This is consistent with the presence of the negative feature at 1686 cm^{-1} in Fig. 2*B*.

Can. J. Chem. Downloaded from www.nrcresearchpress.com by 84.41.108.74 on 09/07/12
For personal use only.

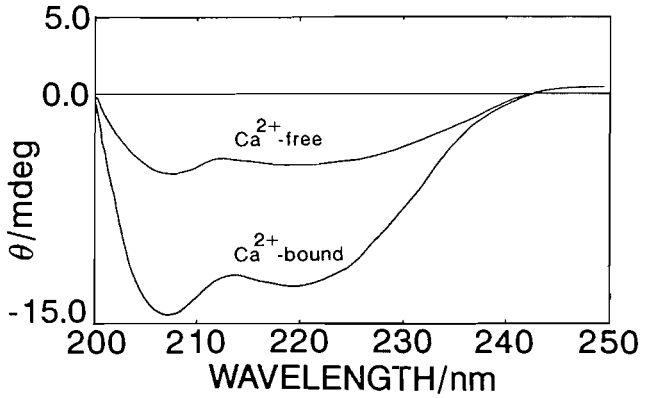


FIG. 6. CD spectra of Ca^{2+}-free (top) and Ca^{2+}-bound (bottom) troponin C at room temperature.

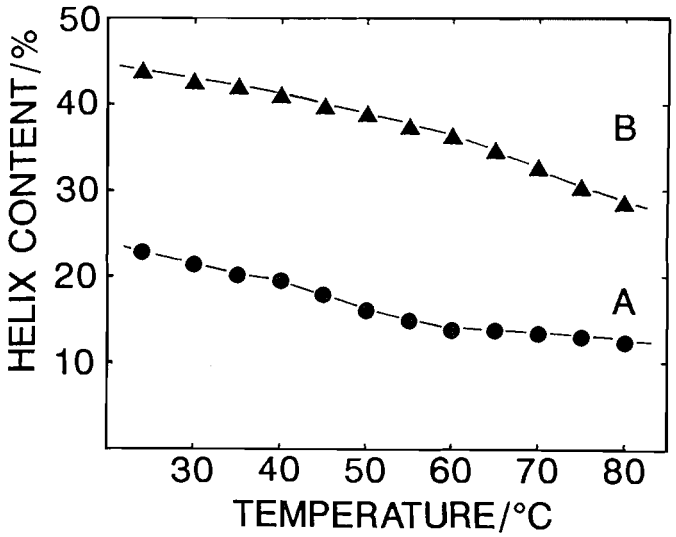


FIG. 7. Helix content vs. temperature plot for Ca^{2+}-free (●) and Ca^{2+}-bound (▲) troponin C.

Circular dichroism and the α-helix content

Circular dichroism (CD) spectra of Ca^{2+}-free and Ca^{2+}-bound TnC observed at 25°C are shown in Fig. 6. The α-helix contents calculated from the values of Θ_{222} using the equations given earlier are plotted against temperature in Fig. 7.

The α-helix contents thus estimated (44 and 23% for the Ca^{2+}-bound and Ca^{2+}-free proteins, respectively, at room temperature) are considerably lower than the value (60%) obtained for the Ca^{2+}-bound proteins in crystal, even if we admit that the accuracy of such estimation is not completely dependable. This is consistent with the existence of a very broad background absorption mentioned earlier for the deconvolved infrared spectra. Such spectral evidence suggests that the three-dimensional structure of TnC determined by X-ray analysis does not persist in aqueous solution, particularly for the Ca^{2+}-free protein. Such a view is consistent with the conclusion derived from fluorescence measurements (14, 15) and an X-ray small-angle scattering study (16) that the distance between the two globular domains in Ca^{2+}-bound TnC from rabbit skeletal muscle is smaller in aqueous solution at neutral pH than that in crystal. A higher α-helix content in Ca^{2+}-bound TnC than in the Ca^{2+}-free protein has been shown from optical rotatory dispersion measurements (36).

It is clearly seen in Fig. 7 that the α-helix contents of both the Ca^{2+}-free and Ca^{2+}-bound proteins decrease gradually with increasing temperature. The slope of the curve for the Ca^{2+}-free protein appears to change at about 60°C. This is consistent with the trend observed in the absorbance change of the amide I band in the difference spectra (Fig. 3) and also with the results obtained from CD measurements (18). However, the slope of the α-helix content vs. temperature relationship in Fig. 7 becomes smaller above 60°C, whereas that of the amide I absorbance change becomes larger in the same temperature range. The origin of this discrepancy is not clear.

In the case of the Ca^{2+}-bound protein, the helix content vs. temperature relationship in Fig. 7 has a moderate curvature over the entire temperature range. It should be noted the the α-helix content of the Ca^{2+}-bound protein at 80°C is about 28%, a value close to that of the Ca^{2+}-free protein at 25°C. This result obtained from the CD spectra is consistent with the above-mentioned similarity of the deconvolved infrared spectra between the Ca^{2+}-bound protein at 78°C and the Ca^{2+}-free protein at 24°C.

In going from 25 to 80°C, the α-helix content of the Ca^{2+}-free protein decreases from 23 to 13% (10% decrease), and that of the Ca^{2+}-bound protein from 44 to 28% (16% decrease). These decreases in α-helix content are not far from the percentage absorbance changes of the amide I and II bands in going from 24 to 78°C (Figs. 3 and 4), although the percentage absorbance change of the Ca^{2+}-free protein is greater than that of the Ca^{2+}-bound protein.

Thus, it may be said that, apart from some discrepancies in detailed aspects, there is a good correspondence between the results obtained independently from the infrared and CD spectra, despite the fact that these two kinds of spectra have been observed at very different concentrations.

Conclusion

Fourier-transform infrared techniques, viz., thermal difference spectrum and deconvolution, are useful for obtaining information on conformational changes occurring in thermal denaturation processess of Ca^{2+}-free and Ca^{2+}-bound TnCs.

The present infrared and circular dichroism studies have collectively shown the following points so far expressed separately by other authors. (*1*) Ca^{2+}-free TnC seems to be denatured at about 75°C, although the denaturation proceeds gradually without an abrupt structural change. Ca^{2+}-bound TnC is thermally more stable than the Ca^{2+}-free protein. (*2*) The secondary structure (and the tertiary structure as well) of Ca^{2+}-bound TnC in aqueous solution at neutral pH is different from either that in crystal or that of Ca^{2+}-free TnC. (*3*) Ca^{2+}-bound TnC in aqueous solution has a rather high α-helix content (about 44%) at room temperature. Its α-helix content decreases with increasing temperature. (*4*) The α-helix content in Ca^{2+}-free TnC in aqueous solution is much lower than that in the Ca^{2+}-bound protein at room temperature, and decreases further with increasing temperature.

In addition to the above points, it has been convinvingly shown that the secondary structure (and probably the tertiary structure also) of Ca^{2+}-bound TnC at 80°C resembles that of the Ca^{2+}-free protein at room temperature.

Acknowledgement

We are grateful to Dr. F. Inagaki, Tokyo Metropolitan Institute of Medical Science, for his cooperation in circular dichroism measurements.

Can. J. Chem. Downloaded from www.nrcresearchpress.com by 84.41.108.74 on 09/07/12
For personal use only.

1. S. EBASHI and A. KODAMA. J. Biochem. **58**, 107 (1965).
2. S. EBASHI and M. ENDO. Progr. Biophys. Mol. Biol. **18**, 123 (1968).
3. M. L. GREASER and J. GERGELY. J. Biol. Chem. **246**, 4226 (1971).
4. R. H. KRETSINGER and C. D. BARRY. Biochim. Biophys. Acta, **405**, 40 (1975).
5. J. D. POTTER and J. GERGELY. J. Biol. Chem. **250**, 4628 (1975).
6. S. EBASHI. Essays Biochem. **10**, 1 (1974).
7. I. OHTSUKI, K. MARUYAMA, and S. EBASHI. Adv. Protein Chem. **38**, 1 (1986).
8. O. HERZBERG and M. N. G. JAMES. Nature (London), **313**, 653 (1985).
9. O. HERZBERG and M. N. G. JAMES. FEBS Lett. **199**, 279 (1986).
10. M. SUNDARALINGAM, R. BERGSTROM, G. STRASSBURG, S. T. RAO, P. ROYCHOWDHURY, M. GREASER, and B. C. WANG. Science, **227**, 945 (1985).
11. K. A. SATYSHUR, S. T. RAO, D. PYZALSKA, W. DRENDEL, M. GREASER, and M. SUNDARALINGAM. J. Biol. Chem. **263**, 1628 (1988).
12. J-P. VAN EERD, J-P. CAPONY, C. FERRAZ, and J-F. PECHERE. Eur. J. Biochem. **91**, 231 (1978).
13. M. TANOKURA. Unpublished results.
14. C.-L. A. WANG, Q. ZHAN, T. TAO, and J. GERGELY. J. Biol. Chem. **262**, 9636 (1987).
15. H. C. CHEUNG, C. K. WANG, I. GRYCZYNSKI, W. WICZK, G. LACZKO, R. F. STEINER, J. R. LAKOMICZ, and M. L. JOHNSON. Biophys. J. **55**, 122*a* (1989).
16. D. B. HEIDORN and J. TREWHELLA. Biochemistry, **27**, 909 (1988).
17. B. A. LEVINE, D. MERCOLA, D. COFFMAN, and J. M. THORNTON. J. Mol. Biol. **115**, 743 (1977).
18. H. BRZESKA, S. VU. VENYAMINOV, Z. GRABAREK, and W. DRABIKOWSKI. FEBS Lett. **153**, 169 (1983).
19. T. N. TSALKOVA and P. L. PRIVALOV. Biochim. Biophys. Acta, **624**, 196 (1980).
20. T. N. TSALKOVA and P. L. PRIVALOV. J. Mol. Biol. **181**, 533 (1985).
21. R. H. INGRAHAM and C. A. SWENSON. Eur. J. Biochem. **132**, 85 (1983).
22. M. IMAIZUMI, M. TANOKURA, and K. YAMADA. J. Biol. Chem. **262**, 7963 (1987).
23. D. G. CAMERON, H. L. CASAL, and H. H. MANTSCH. J. Biochem. Biophys. Methods, **1**, 21 (1979).
24. R. N. JONES and K. SHIMOKOSHI. Appl. Spectrosc. **37**, 59 (1983).
25. N. GREENFIELD and G. D. FASMAN. Biochemistry, **8**, 4108 (1969).
26. I. STAPRANS and S. WATANABE. J. Biol. Chem. **245**, 5962 (1970).
27. J. T. YANG, C.-S. C. WU, and H. M. MARTING. Methods Enzymol. **130**, 208 (1986).
28. T. MIYAZAWA and E. T. BLOUT. J. Am. Chem. Soc. **83**, 712 (1961).
29. S. KRIMM. J. Mol. Biol. **4**, 528 (1962).
30. D. M. BYLER and H. SUSI. Biopolymers, **25**, 469 (1986).
31. E. B. CAREW, P. C. LEAVIS, H. E. STANLEY, and J. GERGELY. Biophys. J. **30**, 351 (1980).
32. T. YAMAMOTO and M. TASUMI. Can. J. Spectrosc. **33**, 133 (1988).
33. T. YAMAMOTO and M. TASUMI. J. Mol. Struct. **242**, 235 (1991).
34. S. TSUDA, Y. HASEGAWA, M. YOSHIDA, K. YAGI, and K. HIKICHI. Biochemistry, **27**, 4120 (1988).
35. J. TREWHELLA, W. K. LIDDLE, D. B. HEIDORN, and N. STRYNADKA. Biochemistry, **28**, 1294 (1989).
36. J-P VAN EERD and Y. KAWASAKI. Biochem. Biophys. Res. Commun. **47**, 859 (1972).

Can. J. Chem. Downloaded from www.nrcresearchpress.com by 84.41.108.74 on 09/07/12
For personal use only.

Calorimetric study of the digestion of gibbsite, $Al(OH)_3$(cr), and thermodynamics of aqueous aluminate ion, $Al(OH)_4^-$(aq)

QIYUAN CHEN,[1] YUMING XU,[2] AND LOREN G. HEPLER
Department of Chemistry and Department of Chemical Engineering, University of Alberta, Edmonton, Alta., Canada T6G 2G2

Received January 29, 1991

This paper is dedicated to Dr. Richard Norman Jones

Can. J. Chem. Downloaded from www.nrcresearchpress.com by 84.41.108.74 on 09/07/12
For personal use only.

QIYUAN CHEN, YUMING XU, and LOREN G. HEPLER. Can. J. Chem. **69**, 1685 (1991).

We have made calorimetric measurements of the enthalpies of solution of gibbsite, $Al(OH)_3$(cr), in aqueous sodium hydroxide solutions at five temperatures from 100 to 150°C. Results of these measurements have been used to obtain the standard enthalpies of formation of Na^+(aq) + $Al(OH)_4^-$(aq) at the experimental temperatures. These results have also led to values of ΔC_p^0 for the reaction represented concisely by $Al(OH)_3$(cr) + OH^-(aq) = $Al(OH)_4^-$(aq), from which we have obtained standard state partial molar heat capacities of Na^+(aq) + $Al(OH)_4^-$(aq). Combination of our results with those from earlier investigations has permitted calculation of thermodynamic properties of Na^+(aq) + $Al(OH)_4^-$(aq) over a wide range of temperature and thence some generalizations about the usefulness of various equations for representing or predicting these thermodynamic properties.

Key words: gibbsite, enthalpy of solution; sodium aluminate (aqueous), thermodynamic properties; heat capacities, Na^+(aq) + $Al(OH)_4^-$(aq).

QIYUAN CHEN, YUMING XU et LOREN G. HEPLER. Can. J. Chem. **69**, 1685 (1991).

Nous avons mesuré, par calorimétrie, les enthalpies de solution de la gibbsite, $Al(OH)_3$(cr), dans des solutions aqueuses d'hydroxyde de sodium à 5 températures différentes allant de 100 à 150°C. Ces résultats ont permis d'obtenir les enthalpies standards de formation des ions Na^+(aq) + $Al(OH)_4^-$(aq) à ces températures. Ces résultats ont également permis d'obtenir les valeurs de ΔC_p^0 de la réaction représentée de façon concise par l'équation : $Al(OH)_3$(cr) + OH^-(aq) = $Al(OH)_4^-$(aq), à partir de laquelle nous avons obtenu les capacités molaires partielles de l'état standard des ions Na^+(aq) + $Al(OH)_4^-$(aq). En combinant nos résultats à ceux provenant d'études précédentes, nous avons pu calculer les propriétés thermodynamiques des ions Na^+(aq) + $Al(OH)_4^-$(aq) dans un large intervalle de températures et de faire une généralisation relative à l'utilité de diverses équations pour représenter ces propriétés thermodynamiques.

Mots clés : gibbsite, enthalpies de formation; $NaAl(OH)_4$(aq), les propriétés thermodynamiques; capacités calorifiques, Na^+(aq) + $Al(OH)_4^-$(aq).

[Traduit par la rédaction]

Introduction

The present calorimetric investigations of the enthalpy of solution of the mineral gibbsite, $Al(OH)_3$, in aqueous sodium hydroxide (several concentrations and several temperatures) have been carried out for two reasons. One specific reason has been to obtain thermochemical data that can be useful in connection with the Bayer process for treating gibbsite prior to processes leading directly to the production of metallic aluminum. A more general reason for the research described here has been to obtain thermodynamic data for the aqueous aluminate ion, $Al(OH)_4^-$, over a range of temperatures; these thermodynamic data can be useful in fields as varied as the geochemistry of aluminum-containing minerals and the corrosion of metallic aluminum. Results from these calorimetric measurements also permit testing earlier predictions of the temperature dependence of thermodynamic properties of $Al(OH)_4^-$(aq).

We already have some thermodynamic data for $Al(OH)_3$(gibbsite, cr), $Al(OH)_4^-$(aq), Al^{3+}(aq), and related species such as OH^-(aq) for 298 K. There are also some equilibrium data for higher temperatures. Most directly related to the results of this research are calorimetrically determined partial molar heat capacities for Na^+(aq) + $Al(OH)_4^-$(aq) over the temperature ranges 10–55°C (1) and 53–245°C (2).

In this work we have made calorimetric measurements of the enthalpy (ΔH) of the reaction represented by

[1] $Al(OH)_3$(gibbsite) + OH^-(aq) = $Al(OH)_4^-$(aq)

in which the non-reactive Na^+(aq) is not shown.

Experimental

Synthetic gibbsite was prepared according to a procedure established by Yin *et al.* (3). The procedure of Yin *et al.* involved dissolving certified (Fisher, Lot 765051) aluminum hydroxide in concentrated aqueous sodium hydroxide to obtain a solution with molar ratio Na/Al = 1.7. This solution was diluted with distilled water until the concentration of NaOH was 3.5 mol/L. Then this solution was seeded with small crystals of gibbsite (confirmed by X-ray analysis) that were kindly supplied by Yin. The seeded solution, initially at 32°C, was stirred slowly for 72 h while the temperature declined to 24°C. The resulting precipitate of gibbsite was washed with dilute sodium hydroxide and then with distilled water for several hours after the wash water became neutral. The washed $Al(OH)_3$ was dried at 60°C and then at 105°C to constant weight. Finally, sieving led to a sample of synthetic gibbsite that was 325–500 mesh to be used for analysis and calorimetric measurements. Heating to drive off all water led to 65.38 ± 0.05% Al_2O_3, as compared with 65.36% calculated from atomic masses.

[1]Visiting Professor from Department of Chemistry, Central-South University of Technology, Changsha, Hunan 410083, People's Republic of China.

[2]Present address: Alberta Research Council, Edmonton, Alta., Canada.

TABLE 1. Enthalpies of solution of gibbsite in aqueous sodium hydroxide (eq. [1])

Molality of $NaAl(OH)_4$ in final solution (mol kg^{-1})	ΔH (kJ mol^{-1})	Molality of $NaAl(OH)_4$ in final solution (mol kg^{-1})	ΔH (kJ mol^{-1})
t = 150.3°C		t = 125.7°C	
Ionic strength = 5.00 mol kg^{-1}		Ionic strength = 5.00 mol kg^{-1}	
3.598	35.18	3.564	32.53
3.266	35.18	3.043	32.63
2.620	35.16	2.754	32.52
2.036	35.17	2.008	32.74
1.831	35.23	0.969	32.95
1.152	35.19	0.578	32.85
0.788	35.34	0.296	32.90
0.441	35.77		
0.221	35.75	Ionic strength = 3.00 mol kg^{-1}	
		1.749	33.23
Ionic strength = 3.00 mol kg^{-1}		1.180	33.12
2.017	35.87	0.614	33.17
1.942	35.78	0.380	33.25
1.322	35.81		
0.934	35.91	Ionic strength = 1.00 mol kg^{-1}	
0.601	35.79	0.556	33.08
0.423	35.88	0.490	33.11
		0.357	33.15
Ionic strength = 1.00 mol kg^{-1}		0.211	33.33
0.683	35.78		
0.653	35.80	t = 112.9°C	
0.579	35.93		
0.314	36.00	Ionic strength = 5.00 mol kg^{-1}	
0.285	36.25	3.229	31.26
		2.803	31.33
t = 138.6°C		2.288	31.40
		1.674	31.54
Ionic strength = 5.00 mol kg^{-1}		1.179	31.59
3.727	34.07	0.549	31.56
3.223	33.72	0.417	31.76
2.798	34.24		
2.090	34.04	Ionic strength = 3.00 mol kg^{-1}	
1.521	33.18	1.740	31.65
1.074	34.97	1.232	31.83
0.967	34.22	0.836	31.69
0.578	34.13	0.378	31.70
0.333	34.67		
0.065	34.38	Ionic strength = 1.00 mol kg^{-1}	
		0.447	31.71
Ionic strength = 3.00 mol kg^{-1}		0.338	31.71
2.225	34.54	0.329	31.35
2.084	34.44	0.244	31.77
1.684	34.41		
1.483	34.46	t = 100.1°C	
1.290	34.66		
0.843	34.83	Ionic strength = 5.00 mol kg^{-1}	
0.621	34.56	2.596	30.07
0.426	34.83	2.083	30.17
		1.679	30.21
Ionic strength = 1.00 mol kg^{-1}		1.251	30.15
0.649	34.40	0.734	30.39
0.599	34.59	0.442	30.53
0.454	34.55	0.153	30.29
0.323	34.42		

TABLE 1 (*concluded*)

Molality of $NaAl(OH)_4$ in final solution (mol kg^{-1})	ΔH (kJ mol^{-1})	Molality of $NaAl(OH)_4$ in final solution (mol kg^{-1})	ΔH (kJ mol^{-1})
		Ionic strength = 3.00 mol kg^{-1}	
		1.285	30.20
		1.116	30.21
		0.690	30.24
		0.439	30.45
		0.289	30.34
		Ionic strength = 1.00 mol kg^{-1}	
		0.405	29.86
		0.370	30.16
		0.316	30.11
		0.305	30.39

Sodium hydroxide solutions were prepared from Assured Reagent (BDH, Lot 103769/14850) NaOH and distilled water, with care being taken to exclude CO_2. Weight titrations with standard potassium hydrogen phthalate led to the temperature-independent molalities (mol/kg) of the NaOH solutions. Separate titrations with hydrochloric acid solutions permitted establishment of the upper limit of carbonate contamination as 0.2% of the NaOH concentration.

A Tian-Calvet heat-flow calorimeter (Setaram, Model C-80) was used for our calorimetric measurements. Calibration and testing of this calorimeter has been described in detail by Xu (4). On the basis of Xu's testing and our own experience, we estimate that accuracy of the ΔH values reported here is about 0.5%.

Times required for complete reaction of gibbsite with excess NaOH ranged from about 45 to 75 min, depending on the temperature and the concentration of the NaOH solution.

To minimize thermal effects due to corrosion of the cells, four preliminary calorimetric measurements were carried out with concentrated NaOH (5 molal) at 150°C. These preliminary experiments led to formation of a "tight" layer of corrosion product on the cell walls and effectively stopped further corrosion. Blank runs with NaOH solutions (no gibbsite) confirmed the absence of a further thermal effect due to corrosion.

Results

Results (ΔH values) of all the calorimetric measurements of heats of solution of gibbsite in aqueous sodium hydroxide are reported in Table 1. Because the reaction, as represented concisely by equation [1], is electrically symmetrical, the initial molality of NaOH is equal to the final molal ionic strength of the solution as listed in Table 1.

It is possible to obtain ΔH^0 and $C_p{}^0$ values corresponding to infinite dilution as follows. First we recognize that ΔH (at any one temperature) of an electrically symmetrical reaction is independent of ionic strength in the Debye–Hückel range of concentration, and that initial dependence on ionic strength will be proportional to the ionic strength and also related to the composition of the constant ionic strength solution. The ΔH values in Table 1 are clearly dependent on temperature ($\Delta C_p \neq 0$), so we express the enthalpies of reaction as a quadratic function of temperature. All of this is summarized by the equation

$$[2] \quad \Delta H = (a_1 + a_2 m_{Al} + a_3 I + a_4 m_{Al} I) + (a_5 + a_6 m_{Al} + a_7 I + a_8 m_{Al} I)T + (a_9 + a_{10} m_{Al} + a_{11} I + a_{12} m_{Al} I)T^2$$

Can. J. Chem. Downloaded from www.nrcresearchpress.com by 84.41.108.74 on 09/07/12
For personal use only.

TABLE 2. Coefficients of eqs. [2]–[4]

$a_1 = -9.50987 \times 10^0$	$a_7 = -1.373631 \times 10^{-3}$
$a_2 = -1.105191 \times 10^1$	$a_8 = -5.852004 \times 10^{-3}$
$a_3 = +8.514732 \times 10^{-1}$	$a_9 = +2.715057 \times 10^{-5}$
$a_4 = +1.174895 \times 10^0$	$a_{10} = -6.544641 \times 10^{-5}$
$a_5 = +9.591291 \times 10^{-2}$	$a_{11} = -1.870039 \times 10^{-6}$
$a_6 = +5.439204 \times 10^{-2}$	$a_{12} = +6.80837 \times 10^{-6}$

TABLE 3. ΔH^0 and $\Delta C_p{}^0$ of reaction [1]

t (°C)	ΔH^0 (kJ mol^{-1})	$\Delta C_p{}^0$ (J K^{-1} mol^{-1})
100.1	30.07	116.2
112.9	31.56	116.9
125.7	33.06	117.6
138.6	34.59	118.3
150.3	35.97	118.9

Then we have

[3] $\Delta H^0 = a_1 + a_5 T + a_9 T^2$

and

[4] $\Delta C_p{}^0 = a_5 + 2a_9 T$

Values of the parameters in eqs. [2]–[4] are listed in Table 2.

We have used the values of the parameters listed in Table 2 to calculate the values of ΔH corresponding to each calorimetric measurement. The standard deviation, $S = [(y_i - y)^2/(n - 1)]^{1/2}$, associated with these calculated values is 0.14 kJ mol^{-1}.

Derived values of ΔH^0 and $\Delta C_p{}^0$ for the reaction represented by eq. [1] are listed in Table 3.

Thermodynamic calculations and discussion

A principal aim of this research has been to obtain thermodynamic properties of aqueous sodium aluminate: $Na^+(aq) + Al(OH)_4{}^-(aq)$. To obtain these thermodynamic properties, we combine our experimental results with the already known thermodynamic properties of gibbsite and aqueous sodium hydroxide as follows.

Hemingway *et al.* (5) have measured the heat capacities of gibbsite from 13 to 480 K. Their results lead to $S^0 = 68.44$ J K^{-1} mol^{-1} for $Al(OH)_3$(cr,gibbsite) at $T = 298.15$ K and also to values of $(H^0{}_T - H^0{}_{298.15})$ for this substance. Hemingway and Robie (6) have applied hydrofluoric acid calorimetry to determine $\Delta_f H^0 = -1293.13 \pm 1.19$ kJ mol^{-1} for gibbsite at $T = 298.15$ K. We have combined all of these properties with those of the elements (7) to obtain the thermodynamic properties of gibbsite that are listed in Table 4.

For NaOH(aq) at $T = 298.15$ K we select $\Delta_f H^0 = -470.355 \pm 0.072$ kJ mol^{-1} and $S^0 = 47.55 \pm 0.25$ J K^{-1} mol^{-1} from the CODATA critical compilation (8). Standard state partial molar heat capacities of NaOH(aq) have been selected from results of five calorimetric investigations (9–13). All of these results fit together smoothly and apparently reliably over the temperature range of interest to us. We have combined these properties with those of the elements (7) to obtain the thermodynamic properties of NaOH(aq) that are listed in Table 5.

We have combined our enthalpies of reaction (Table 3) of gibbsite with NaOH(aq) with the enthalpies of formation of gibbsite (Table 4) and aqueous NaOH (Table 5) to obtain the enthalpies of formation of aqueous sodium aluminate, $Na^+(aq) + Al(OH)_4{}^-(aq)$, listed in the second column in Table 6. The values of $\Delta_f(H^0{}_T - H^0{}_{298.15})$ listed in the third column in Table 6 are calculated from heat capacities of the elements (7) and the partial molar heat capacities of $NaAl(OH)_4$(aq) from this work as discussed in the following paragraphs. Finally, the fourth column in Table 6 lists our values for the standard state enthalpy of formation of aqueous sodium aluminate at $T = 298.15$ K: the average is $\Delta_f H^0 = 1743.11 \pm 0.24$ kJ mol^{-1}, where the $\pm$ indicates the *standard deviation*. The *uncertainty* in this $\Delta_f H^0$ is much larger than the standard deviation. Considerations of uncertainties in auxiliary data (other standard enthalpies of formation and heat capacities) and our measurements lead us to estimate that the *total* uncertainty in our $\Delta_f H^0$ values in Table 6 is about ± 1.5 kJ mol^{-1}.

To obtain values for the standard state partial molar heat capacities of aqueous sodium aluminate, we start with the $\Delta C_p{}^0$ values listed in Table 3 for the reaction represented by eq. [1]. Combinations of these $\Delta C_p{}^0$ values with heat capacities at the same temperatures for gibbsite (Table 4) and aqueous NaOH (Table 5) lead to the standard standard state heat capacities of $NaAl(OH)_4$(aq) that are list in the last column of Table 6.

In addition to our heat capacities of $NaAl(OH)_4$(aq) for five temperatures (100–150°C) listed in Table 6, we have experimental heat capacities at four temperatures (10–55°C) from Hovey *et al.* (1) and at five temperatures (53–245°C) from Caiani *et al.* (2). As our first step toward assessing and then using these standard state heat capacities for $NaAl(OH)_4$(aq) at 14 temperatures from 10 to 245°C, we have made a graph of $C_p{}^0$ against T (Fig. 1) and observed that 13 of the results fall on a reasonably smooth curve. We have therefore proceeded with analysis, omitting the $C_p{}^0$ from Caiani *et al.* (2) for 53°C, which seems to be inconsistent with the other 13 heat capacities from three independent investigations.

An equation proposed by Holmes and Mesmer (14) has been used by them and others for convenient representation of standard state heat capacities of aqueous electrolytes. We have fitted their equation to the results of Hovey *et al.* (1), Caiani *et al.* (2), and the present results to obtain

[5] $C_p{}^0 = -1451.041 - 7.758518/(T - 470) + 8.993519T - 1.235584 \times 10^{-2} T^2$

for $NaAl(OH)_4$(aq). For this fitting we have weighted the direct heat capacities (1, 2) twice as heavily as we have our own heat capacities (obtained by differentiation of ΔH^0 values). The standard deviation of the fit of eq. [5] is 12 J K^{-1} mol^{-1}, which is very good. We have also used the same heat capacities of $NaAl(OH)_4$(aq) for fitting the HKF equation (15) and find that the standard deviation of the fit is twice as large as the 12 J K^{-1} mol^{-1} found above for the Holmes–Mesmer equation.

The Holmes–Mesmer equation fits the experimental data better than does the HKF equation, but it should be noted that the former equation has more adjustable parameters than does the latter. Because the fit of the Holmes–Mesmer equation is better, we use this equation in some further calculations.

Although we are using the Holmes–Mesmer equation here, let us point out that the HKF equation has a substantial value.

Can. J. Chem. Downloaded from www.nrcresearchpress.com by 84.41.108.74 on 09/07/12
For personal use only.

TABLE 4. Thermodynamic properties of gibbsite, $Al(OH)_3$

t (°C)	C_p^0 ($J\,K^{-1}\,mol^{-1}$)	S^0 ($J\,K^{-1}\,mol^{-1}$)	$H^0_T - H^0_{298.15}$ ($kJ\,mol^{-1}$)	ΔfH^0 ($kJ\,mol^{-1}$)
0	84.79	60.71	−2.207	−1292.56
10	87.62	63.81	−1.345	−1292.81
25	91.69	68.44	0.000	−1293.13
40	95.58	73.04	1.405	−1293.40
60	100.52	79.11	3.366	−1293.69
80	105.20	85.10	5.424	−1293.89
100	109.61	91.02	7.572	−1294.02
120	113.76	96.85	9.807	−1294.07
140	117.71	102.59	12.122	−1294.05
160	121.59	108.25	14.515	−1293.96
200	130.13	119.35	19.542	−1293.58
250	147.49	133.18	26.432	−1292.56
100.1	109.63	91.05	7.583	−1294.02
112.9	112.31	94.79	9.004	−1294.06
125.7	114.91	98.50	10.458	−1294.07
138.6	117.44	102.19	11.957	−1294.05
150.3	119.71	105.52	13.344	−1294.01

TABLE 5. Thermodynamic properties of NaOH(aq)

t (°C)	C_p^0 ($J\,K^{-1}\,mol^{-1}$)	S^0 ($J\,K^{-1}\,mol^{-1}$)	$H^0_T - H^0_{298.15}$ ($kJ\,mol^{-1}$)	ΔfH^0 ($kJ\,mol^{-1}$)
0	−239.6	61.75	4.034	−464.90
10	−170.6	54.46	2.001	−467.50
25	−102.3	47.55	0.000	−470.355
40	−64.78	43.55	−1.222	−472.44
60	−45.61	40.24	−2.283	−474.66
80	−46.16	37.64	−3.177	−476.74
100	−55.87	34.86	−4.189	−481.57
120	−69.92	31.57	−5.445	−484.05
140	−87.96	27.68	−7.001	−486.83
160	−113.4	23.00	−9.006	−490.05
200	−211.2	9.30	−15.213	−498.69
250	−497.3	−24.12	−31.978	−518.50
100.1	−55.97	34.85	−4.190	−481.57
112.9	−64.55	32.80	−4.961	−483.13
125.7	−74.54	30.53	−5.850	−484.80
138.6	−86.54	27.99	−6.886	−486.63
150.3	−99.84	25.36	−7.977	−488.43

TABLE 6. Enthalpies of formation and partial molar heat capacities of $NaAl(OH)_4$(aq)

T (°C)	$\Delta_f H^0_T$ ($kJ\,mol^{-1}$)	$\Delta_f H^0_T - \Delta_f H^0_{298.15}$ ($kJ\,mol^{-1}$)	$\Delta_f H^0_{298.15}$* ($kJ\,mol^{-1}$)	C_p^0 ($J\,K^{-1}\,mol^{-1}$)
100.1	−1745.52	−2.739	−1742.78	169.8
112.9	−1745.62	−2.649	−1742.97	164.6
125.7	−1745.81	−2.656	−1743.15	157.9
138.6	−1746.09	−2.806	−1743.29	149.2
150.3	−1746.47	−3.114	−1743.36	138.8

*Average $\Delta_f H^0_{298.15} = -1743.11 \pm 0.24\ kJ\,mol^{-1}$.

Hovey *et al.* (1) used their heat capacities over the relatively narrow range from 10 to 55°C to evaluate the parameters in the HKF equation and thence estimated standard heat capacities of $NaAl(OH)_4$(aq) at much higher temperatures. Although the experimental results from the present investigation and from Caiani *et al.* (2) for high temperatures are to be preferred to the values estimated by Hovey *et al.* (1), it should be recognized that the estimated values are close enough to the better experimental values to be useful for a variety of thermodynamic calculations.

On the basis of the calculations summarized above and a few similar calculations for other electrolytes, we offer the following generalizations. (*i*) The Holmes–Mesmer equation is usually better than the HKF equation for accurate represen-

Can. J. Chem. Downloaded from www.nrcresearchpress.com by 84.41.108.74 on 09/07/12
For personal use only.

TABLE 7. Thermodynamic properties of $NaAl(OH)_4(aq)$

t (°C)	C_p^0 ($J\,K^{-1}\,mol^{-1}$)	S^0 ($J\,K^{-1}\,mol^{-1}$)	$H^0 - H^0_{298.15}$ ($kJ\,mol^{-1}$)	$\Delta_f H^0$ ($kJ\,mol^{-1}$)	$\Delta_f G^0$ ($kJ\,mol^{-1}$)
0	83.7	150.41	−2.729	−1741.64	−1581.66
10	104.9	153.81	−1.784	−1742.37	−1575.78
25	132.1	159.94	0.000	−1743.11	−1566.94
40	153.7	166.97	2.150	−1743.50	−1558.06
60	173.9	177.15	5.442	−1743.62	−1546.21
80	184.1	187.63	9.038	−1743.47	−1534.37
100	184.5	197.83	12.741	−1745.85	−1522.51
120	175.1	207.27	16.353	−1745.75	−1510.55
140	155.7	215.52	19.678	−1745.94	−1498.58
160	126.5	222.23	22.516	−1746.63	−1486.59
200	35.67	229.89	25.956	−1750.27	−1462.44
250	−127.9	226.00	23.952	−1761.18	−1431.54

TABLE 8. Thermodynamic properties of $Al(OH)_4^-(aq)$

t (°C)	C_p^0 ($J\,K^{-1}\,mol^{-1}$)	S^0 ($J\,K^{-1}\,mol^{-1}$)	$H^0 - H^0_{298.15}$ ($kJ\,mol^{-1}$)	$\Delta_f H^0$ ($kJ\,mol^{-1}$)	$\Delta_f G^0$ ($kJ\,mol^{-1}$)
0	104.7	94.08	−2.116	−1501.03	−1321.51
10	80.8	97.26	−1.231	−1501.68	−1314.92
25	89.6	101.49	0.000	−1502.77	−1305.00
40	106.1	106.30	1.471	−1503.63	−1295.02
60	123.0	113.42	3.773	−1504.45	−1281.68
80	132.8	120.91	6.343	−1505.02	−1268.29
100	135.6	128.34	9.039	−1505.48	−1254.87
120	131.0	135.33	11.717	−1505.97	−1241.42
140	119.3	141.57	14.233	−1506.63	−1227.95
160	100.3	146.79	16.440	−1507.62	−1214.44

Can. J. Chem. Downloaded from www.nrcresearchpress.com by 84.41.108.74 on 09/07/12
For personal use only.

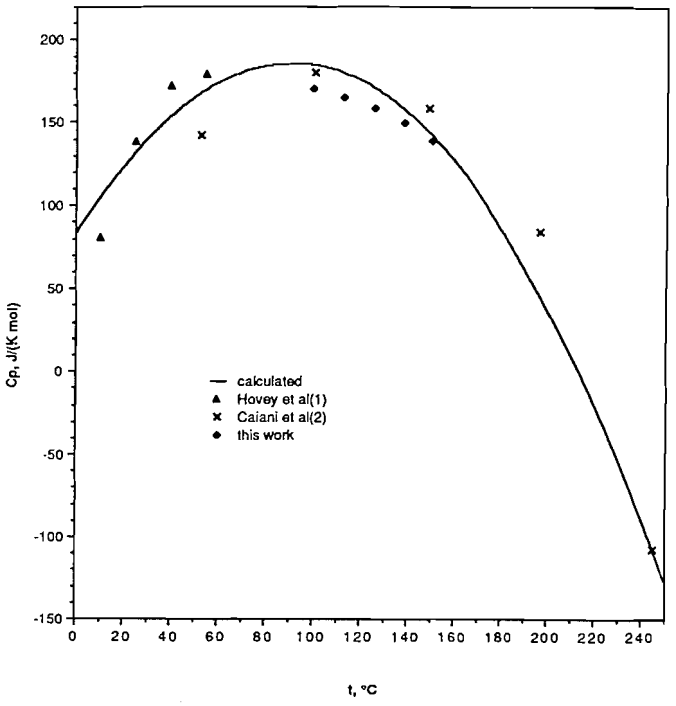


FIG. 1. Standard state partial molar heat capacities of $NaAl(OH)_4$-(aq) from various sources.

tation of experimental heat capacities of aqueous electrolytes over a wide range of temperatures. (*ii*) The HKF equation is most useful in the common case where one has heat capacities for a narrow range of temperatures (say 10–55°C) and wants to estimate heat capacities for higher temperatures.

In Table 7 we summarize the thermodynamic properties of $NaAl(OH)_4(aq)$. Calculations leading to the tabulated quantities have made use of properties already cited and the smoothed heat capacities obtained from the Holmes–Mesmer equation [5].

Next we use the thermodynamic properties for $NaAl(OH)_4$-(aq) that are listed in Table 7 with the thermodynamic properties of HCl(aq) and NaCl(aq) to calculate the conventional thermodynamic properties of $Al(OH)_4^-(aq)$ that are listed in Table 8. All of these tabulated properties are based on the commonly used convention that $\Delta_f G^0$, $\Delta_f H^0$, S^0, and C_p^0 of $H^+(aq)$ are zero at every temeprature. For these calculations we have used thermodynamic properties from this investigation and from refs. 8, 16–18.

Thermodynamic properties listed in Tables 7 and 8 are related to the earlier work by Chang (19, 20), Kuyunko *et al.* (21), and Apps *et al.* (22, 23). It is a convincing indication of thermodynamic consistency of a variety of experimental results that the Gibbs energies of $Al(OH)_4^-(aq)$ reported by Apps *et al.* (22, 23) are in good agreement with our values that are based on calorimetric measurements. It appears (24) that

consideration of all of these results together leads to selection of "best" $\Delta_f H^0$ and S^0 values that are closer to those we have selected here than to those selected earlier (23) by Apps *et al.*

Acknowledgements

We thank the Natural Sciences and Engineering Research Council of Canada for support of this and related research. We also thank A. Yin for providing seed crystals of gibbsite and advice about chemical preparation. Finally, we thank J. K. Hovey for useful advice on our calculations.

1. J. K. HOVEY, L. G. HEPLER, and P. R. TREMAINE. J. Phys. Chem. **92**, 1323 (1988).
2. P. CAIANI, G. CONTI, P. GIANNI, and E. MATTEOLI. J. Solution Chem. **18**, 447 (1989).
3. A. YIN *et al.* To be published.
4. Y. XU. Thesis, University of Alberta. 1990.
5. B. S. HEMINGWAY, R. A. ROBIE, J. R. FISHER, and W. H. WILSON. J. Res. U.S. Geol. Survey, **5**, 797 (1977).
6. B. S. HEMINGWAY and R. A. ROBIE. J. Res. U.S. Geol. Survey, **5**, 413 (1977).
7. M. W. CHASE *et al.* JANAF thermochemical tables, 3rd ed. (J. Phys. Chem. Ref. Data, **14**, Supplement No. 1 (1985)). 1985.
8. J. D. COX, D. D. WAGMAN, and V. A. MEDVEDEV. CODATA key values for thermodynamics. Hemisphere Publishing Corporation, New York. 1989.
9. P. P. SINGH, E. M. WOOLLEY, K. G. MCCURDY, and L. G. HEPLER. Can. J. Chem. **54**, 3315 (1976).
10. G. C. ALLRED and E. M. WOOLLEY. J. Chem. Thermodyn. **13**, 147 (1981).
11. A. H. ROUX, G. PERRON, and J. E. DESNOYERS. Can. J. Chem. **62**, 878 (1984).
12. G. CONTI, P. GIANNI, A. PAPINI, and E. MATTEOLI. J. Solution Chem. **17**, 481 (1988).
13. J. M. SIMONSON, R. E. MESMER, and P. S. Z. ROGERS. J. Chem. Thermodyn. **21**, 561 (1989).
14. H. F. HOLMES and R. E. MESMER. J. Phys. Chem. **87**, 1242 (1983).
15. H. C. HELGESON, D. H. KIRKHAM, and G. C. FLOWERS. Am. J. Sci. **281**, 1249 (1981).
16. P. R. TREMAINE, K. SWAY, and J. A. BARBERO. J. Solution Chem. **15**, 1 (1986).
17. K. S. PITZER and J. C. PEIPER. J. Phys. Chem. Ref. Data, **13**, 1 (1984).
18. B. S. HEMINGWAY, R. A. ROBIE, and J. A. KITTRICK. Geochim. Cosmochim. Acta, **42**, 1533 (1978).
19. B.-T. CHANG. Bull. Chem. Soc. Jpn. **54**, 1960 (1981).
20. B.-T. CHANG. Bull. Chem. Soc. Jpn. **55**, 1949 (1982).
21. N. S. KUYUNKO, S. D. MALININ, and I. L. KHODAKOVSKY. Geochim. Int. **20**, 76 (1983).
22. J. A. APPS and J. M. NEIL. Am. Chem. Soc. Symp. Ser. **416**, 414 (1990).
23. J. A. APPS, J. M. NEIL, and C.-H. JUN. Lawrence Berkeley Laboratory, LBL-21482. 1988.
24. Q. CHEN and L. G. HEPLER. To be published.

Can. J. Chem. Downloaded from www.nrcresearchpress.com by 84.41.108.74 on 09/07/12
For personal use only.

Molecular orientation in thin Langmuir–Blodgett films of dipalmitoylphosphatidylcholine as studied by FTIR transmission and reflection–absorption spectroscopy

EMIKO OKAMURA, JUNZO UMEMURA, AND TOHRU TAKENAKA[1]
Institute for Chemical Research, Kyoto University, Uji, Kyoto-fu 611, Japan

Received April 19, 1991

This paper is dedicated to Dr. Richard Norman Jones

EMIKO OKAMURA, JUNZO UMEMURA, and TOHRU TAKENAKA. Can. J. Chem. **69**, 1691 (1991).

Langmuir–Blodgett (LB) films of DPPC were prepared by the horizontal lifting technique at various surface pressures encompassing the plateau region of its surface pressure (π) – area (A) isotherm. Molecular orientation in the LB films was quantitatively evaluated by a method recently proposed by Umemura *et al.* (J. Phys. Chem. **94**, 62 (1990)) using Fourier transform infrared (FTIR) transmission and reflection–absorption (RA) spectra. From the results obtained, it is apparent that (*i*) in the LB films deposited at higher surface pressures above the plateau, the hydrocarbon chains are of all-*trans* conformation and well oriented at the tilting angle of *ca.* 20° from the surface normal; (*ii*) at lower surface pressures below the plateau, the chain segments are almost randomly oriented (like in a liquid-crystalline state) with an increased amount of the *gauche* conformers; and (*iii*) in the films deposited within the plateau, the hydrocarbon chains are in an intermediate state between the above two states. It is therefore concluded that the plateau corresponds to a process of the reorientation of the hydrocarbon chains from an almost randomly-oriented state to a highly-oriented one with the increase in the number of the all-*trans* conformers.

Key words: dipalmitoylphosphatidylcholine, Langmuir–Blodgett film, molecular orientation, infrared reflection–absorption spectra, surface pressure–area isotherm.

EMIKO OKAMURA, JUNZO UMEMURA et TOHRU TAKENAKA. Can. J. Chem. **69**, 1691 (1991).

Utilisant la technique du soulèvement horizontal à diverse pressions superficielles couvrant la région du plateau de son isotherme de la pression superficielle (π) – surface (A), on a préparé des films de Langmuir–Blodgett (LB) de la DPPC. Utilisant la méthode proposée récemment par Umemura et ses collaborateurs (J. Phys. Chem. **94**, 62 (1990)) et basée sur les spectres infrarouges par transformation de Fourier de transmission (IRTF) et de réflexion–absorption (RA), on a évalué d'une façon quantitative l'orientation moléculaire dans les films de LB. À partir des résultats obtenus, il est apparent que, dans les films LB déposés : (*i*) à des pressions superficielles supérieures à celle du plateau, les chaînes hydrocarbonées possèdent toutes la conformation complètement *trans* et elles sont toutes orientées à un angle d'environ 20° par rapport à la surface normale; (*ii*) à des pressions inférieures à celles de la pression du plateau, les segments de chaînes sont pratiquement orientés au hasard (état semblable à celui d'un cristal-liquide) avec une quantité plus importante des conformères *gauches*; et (*iii*) à des pressions correspondant à celles du plateau, les chaînes hydrocarbonées sont dans un état intermédiaire entre les deux états mentionnés plus haut. On en conclut donc que le plateau correspond à un processus de réorientation des chaînes hydrocarbonées d'un état orienté pratiquement au hasard vers un état hautement orienté avec une augmentation du nombre des conformères complètement *trans*.

Mots clés : dipalmitoylphosphatidylcholine, film de Langmuir–Blodgett, orientation moléculaire, spectre infrarouge de réflexion–absorption; isotherme de la pression superficielle–surface.

[Traduit par la rédaction]

Introduction

Langmuir–Blodgett (LB) films of phospholipids have been of great interest as highly organized assemblies mimicking biomembranes. As far as we know, however, the structure and molecular orientation in the thin LB films have scarcely been investigated mainly for two reasons.

One reason is the difficulty of depositing phospholipid LB films on solid substrates by vertical dipping (or LB) technique. In the case of dipalmitoylphosphatidylcholine (DPPC), for example, only the single monolayer has so far been deposited with a transfer ratio of unity (1–3). Peng *et al.* (3) have overcome this difficulty by using an aqueous uranyl acetate solution as the subphase. However, the uranyl ion may affect the structure of the LB films of DPPC, since the surface pressure (π) – area (A) isotherm of the spread monolayer on this subphase differs from that on pure water (3). Another improvement of the film deposition of DPPC has recently been achieved by Okahata and co-workers (4). They have succeeded in depositing multibilayer LB films from pure water surface at higher surface pressures, using the horizontal lifting (HL) technique without a frame for removing the residual monolayer from the water surface at the pulling-up stage of the solid substrate. The transfer ratio was found to be 2.0 (4). Usefulness and characteristics of this technique for the deposition of the LB films of stearic acid have also been pointed out by our laboratory (5). Futhermore, in the present study, we found that the multilayer LB films of DPPC could be deposited by this technique from the water surface even at lower surface pressures, as will be described later in detail.

The other reason is that the convenient technique for quantitative analyses of molecular orientation in thin organic films has not been established. Recently, however, Umemura *et al.* have proposed a useful method for the quantitative evaluation of molecular orientation in thin LB films using infrared reflection–absorption (RA) and transmission spectroscopy (6).

In this paper, using the same method, we quantitatively evaluated the molecular orientation in thin LB films of DPPC deposited by the HL technique at various surface pressures. Since it has been known that the spread monolayer of DPPC on the water surface has a clear plateau region in the π–A isotherm ascribable to a liquid-expanded (LE) to liquid-condensed (LC) phase transition (7–11), special attention was paid to the difference in molecular structure and orientation in the LB films

[1]Author to whom correspondence should be addressed.

Printed in Canada / Imprimé au Canada

Can. J. Chem. Downloaded from www.nrcresearchpress.com by 84.41.108.74 on 09/07/12
For personal use only.

prepared at the surface pressures below and above the plateau pressure.

Experimental

L-DPPC was purchased from Sigma Chemical Co. and used without further purification. Chloroform used as the spreading solvent was a specially prepared reagent from Nacalai Tesque, Kyoto. Water was purified as described previously (12). The DPPC monolayers were spread from a 1.3×10^{-3} M chlorofrom solution on water at 20°C. The surface pressure of the monolayers was measured by the Wilhelmy method using a Shimadzu model ST-1 surface tensometer equipped with a ground-glass plate. As the solid substrates for infrared transmission measurements, CaF_2 plates (25 mm in diameter) were employed. Glass slides on which a 100-nm thick silver film had been vacuum-evaporated were used for RA measurements. Since the surfaces of both substrates are hydrophilic, the first DPPC monolayer was transferred using the vertical dipping technique and the following monolayers were deposited by the HL technique without a frame for removing the residual monolayer from the water surface at the pulling-up stage of the solid substrates. The dipping speed of the substrates was 5 mm min^{-1}. The transfer ratios were found to be 1.0 ± 0.1 for the first monolayer and 1.9 ± 0.2 for the following monolayers at all the surface pressures examined.

The infrared spectra were recorded on a Nicolet model 6000C FTIR spectrophotometer equipped with an MCT detector with a resolution of 4 cm^{-1}. Five thousand interferograms were accumulated for both RA and transmission measurements. The accuracy of frequency readings was better than ± 0.2 cm^{-1}. For the RA measurements, a Harrick model RMA-00G reflection attachment was used at an angle of incidence of 85°. Two wire-grid polarizers were placed in parallel with each other just after the reflection attachment to improve the degree of polarization.

Results and discussion

The π–A isotherm of the DPPC monolayer on the water surface is given in Fig. 1, being in good agreement with those reported previously (9–13). There is a clear plateau region between *ca.* 0.6 and 0.8 nm^2 $molecule^{-1}$. The LB films were deposited at (*a*) 1.5, (*b*) 5.5, (*c*) 30, and (*d*) 45 mN m^{-1}, with points (*a*) and (*b*) being below and around the plateau pressure, respectively, and (*c*) and (*d*) being above it.

Infrared transmission and RA spectra of DPPC LB films

Figure 2 shows the infrared transmission spectra of the 9-monolayer LB films of DPPC deposited on a CaF_2 substrate at the above four points. In this figure, increase in band intensities, which is due to the surface-density increase of DPPC on the monolayer compression, was corrected and normalized to the value at 1.5 mN m^{-1}. Assignments of the absorption bands are summarized in Table 1. Frequency changes of the antisymmetric and symmetric CH_2 stretching (ν_aCH_2 and ν_sCH_2) bands on the monolayer compression are shown in Table 2. Both bands shift to lower frequencies with the increase in the surface pressure, suggesting the increase in the amount of all-*trans* conformers of the hydrocarbon chain (14–16). These frequency shifts are very similar to the recent results of FTIR external reflection spectroscopy by Dluhy *et al.* (17, 18) for DPPC monolayers spread on the water surface. This fact implies the similarity of the structure between the spread monolayer and the LB films. The CH_2 scissoring band of the DPPC LB films is observed at 1468 cm^{-1} irrespective of the surface pressure, indicating that the hydrocarbon chains are predominantly packed in the hexagonal subcell lattice (6, 14, 15).

As shown in Fig. 2, the intensities of the CH_2 stretching and scissoring bands are largely enhanced at 30 and 45 mN m^{-1}. Although the intensities of the polar group bands are relatively weak as compared to these hydrocarbon bands, the intensity

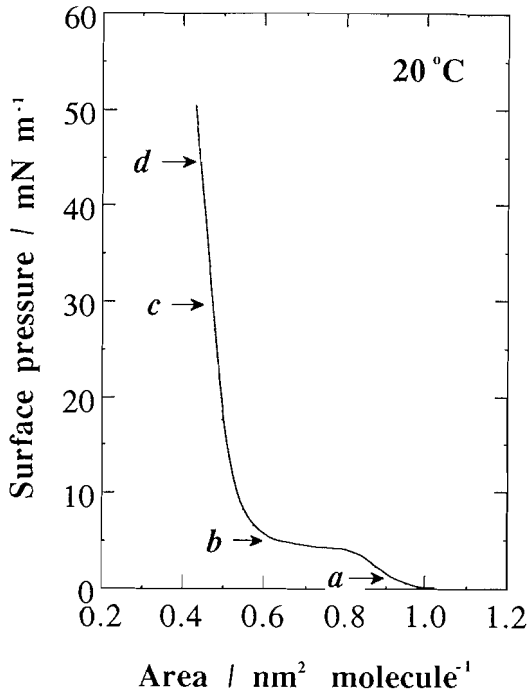


FIG. 1. Surface pressure (π) – area (A) isotherm of a DPPC monolayer at the air/water interface at 20°C. The arrows *a*, *b*, *c*, and *d* represent the surface pressures at which the LB films were transferred.

enhancements are also found for the C=O stretching (1737 cm^{-1}), antisymmetric and symmetric PO_2^- stretching (1257 and 1093 cm^{-1}), symmetric C—O—C stretching (1058 cm^{-1}), and asymmetric $N^+(CH_3)_3$ stretching (969 cm^{-1}) bands at 30 and 45 mN m^{-1}.

Figure 3 represents the infrared RA spectra of the 9-monolayer LB films of DPPC deposited on a Ag-evaporated glass slide at the points (*a*), (*b*), (*c*), and (*d*) in Fig. 1. Increase in intensities caused by the surface-density increase was also corrected. Evidently, the intensity of the ν_aCH_2 and ν_sCH_2 bands is decreased with increasing the surface pressure, being accompanied by the same frequency shifts as that shown in Table 2. The decrease in intensity of these bands makes a striking contrast to the above-mentioned fact for the transmission spectra (Fig. 2). This clearly indicates that the transition moments of these bands tend to orient parallel to the film surface at higher surface pressures above the plateau. In other words, the hydrocarbon chain of DPPC tends to orient perpendicular to the film surface at these pressures. This is also ascertained by the fact that the CH_2 wagging band at 1200 cm^{-1} appears at 30 and 45 mN m^{-1} in the RA spectra, while it is absent at the same pressures in the transmission spectra. The spectral change for the polar group bands is rather complex, but the intensities of the symmetric PO_2^- stretching and symmetric C—O—C stretching bands are enhanced at 30 and 45 mN m^{-1}. However, the asymmetric $N^+(CH_3)_3$ stretching band cannot be detected at these pressures.

Quantitative evaluation of the molecular orientation

Using our new method (6), the orientation of the hydrocarbon chain and the polar groups of DPPC in the LB films deposited at (*a*), (*b*), (*c*), and (*d*) points was quantitatively evaluated from the transmission and RA spectra shown in Figs. 2 and 3, under the confirmed condition of an uniaxial orientation with respect to the surface normal. The orientation

Can. J. Chem. Downloaded from www.nrcresearchpress.com by 84.41.108.74 on 09/07/12
For personal use only.

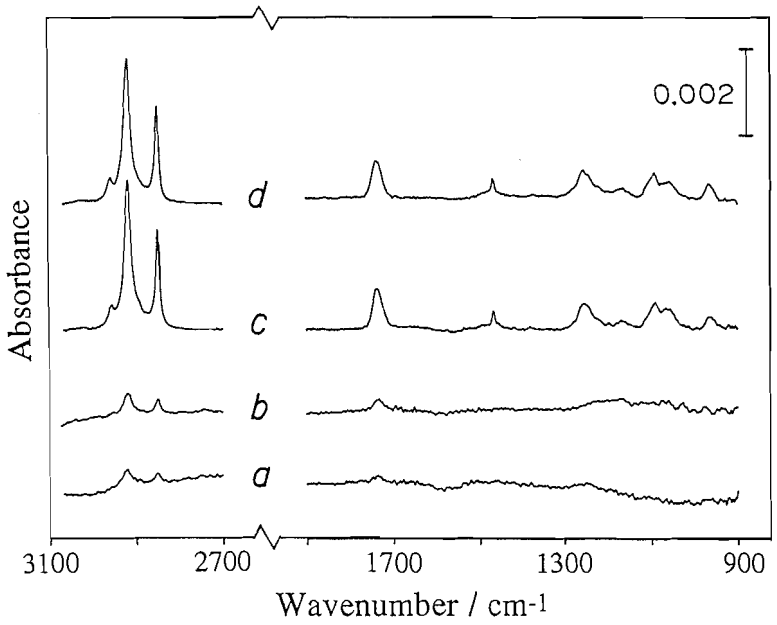


FIG. 2. Infrared transmission spectra of 9-monolayer LB films of DPPC deposited on both sides of a CaF_2 substrate at (*a*) 1.5, (*b*) 5.5, (*c*) 30, and (*d*) 45 mN m^{-1}.

TABLE 1. Assignments of the major absorption bands of DPPC in the 9-monolayer LB film

Wavenumber/cm^{-1}	Assignment
2957	Asymmetric CH_3 stretching
2920	Antisymmetric CH_2 stretching
2875	Symmetric CH_3 stretching
2850	Symmetric CH_2 stretching
1737	Ester C=O stretching
1468	CH_2 scissoring
1379	Symmetric CH_3 bending
1257	Antisymmetric PO_2^- stretching
1200	CH_2 wagging of the *trans* conformer
1166	Antisymmetric C—O—C stretching
1093	Symmetric PO_2^- stretching
1058	Symmetric C—O—C stretching
969	Asymmetric $N^+(CH_3)_3$ stretching

angles of the transition moments of the ν_aCH_2 and ν_sCH_2 bands (α and β, respectively) thus obtained are listed in Table 2, together with the orientation angle of the hydrocarbon chain axis (γ) calculated from the α and β values by the orthogonal relation (6)

$$\cos^2\alpha + \cos^2\beta + \cos^2\gamma = 1$$

In the 9-monolayer LB films deposited at 30 and 45 mN m^{-1} (above the plateau), the transition moments of both ν_aCH_2 and ν_sCH_2 bands are oriented with the angle of 76–78° from the surface normal. By using these values, the orientation angle of the hydrocarbon chain axis (γ) is calculated to be 18–20° from the surface normal, in a good agreement with that (19°) estimated by Akutsu *et al.* (1) from the transmission infrared dichroism for thick LB films of DPPC (~120 layers on each side of a ZnS substrate coated with a ferric stearate layer) deposited at 29.5 mN m^{-1}. From these γ values, the order parameter $f = (3\langle\cos^2\gamma\rangle - 1)/2$ of the hydrocarbon chain is calculated to be 0.8–0.9 at 30 and 45 mN m^{-1}, suggesting the highly ordered state of the chain.

TABLE 2. Frequencies and orientation angles α, β, and γ of DPPC in the 9-monolayer LB films deposited at various surface pressures

		ν_aCH_2		ν_sCH_2		
Point	π/mN m^{-1}	ν/cm^{-1}	α^a	ν/cm^{-1}	β^a	γ^b
d	45	2918	76°	2850	76°	20°
c	30	2918	77°	2850	78°	18°
b	5.5	2919	59°	2851	64°	42°
a	1.5	2922	56°	2853	57°	51°

[a]Tilt angle of the transition moments from the surface normal.
[b]Orientation angle of the hydrocarbon chain axis derived from the orthogonal relation.

At 1.5 mN m^{-1} (below the plateau), however, the hydrocarbon chain axis is found to be tilted with the angle of *ca.* 50°, which corresponds to the order parameter of *ca.* 0.1. These values mean that the hydrocarbon-chain segments are almost randomly oriented with large proportion of the *gauche* conformers (like in a liquid-crystalline state) below the plateau. The orientation angle and the order parameter of the chain axis ($\gamma \approx 40°$ and $f \approx 0.3$) at 5.5 mN m^{-1} (around the plateau) are the intermediates between the above two cases. This fact suggests that the hydrocarbon chain in the LB film prepared around the plateau region is in the gel to liquid-crystalline transition state. These results agree well with those of electron microscopic observations by Neuman *et al.* (13, 19) for the monomolecular DPPC films deposited on a mica substrate at the plateau surface pressure.

The orientation angles (φ's) were also calculated for the polar bands at 30 and 45 mN m^{-1}, as shown in Table 3. The intensity of these bands at 1.5 and 5.5 mN m^{-1} was very weak and the angles hard to estimate. The results in Table 3 are also compatible with those obtained at 29.5 mN m^{-1} by Akutsu *et al.* (64° for the C=O stretching band and 55–90° for the symmetric PO_2^- stretching band) (1); they mean that the transition moments of the polar bands lie rather parallel to the film surface. The weak intensities of these bands at 1.5 and 5.5 mN m^{-1} in the

Can. J. Chem. Downloaded from www.nrcresearchpress.com by 84.41.108.74 on 09/07/12
For personal use only.

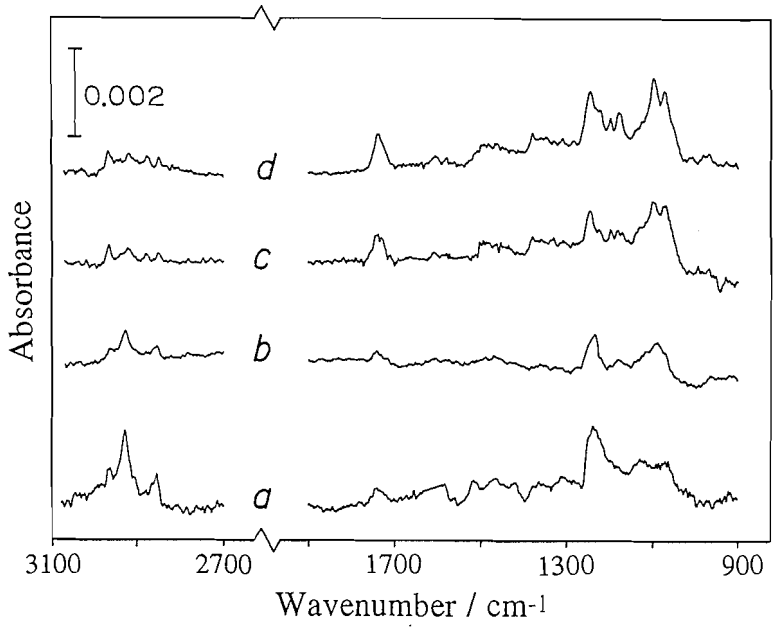


FIG. 3. Infrared RA spectra of 9-monolayer LB films of DPPC deposited on a Ag-evaporated glass substrate at (*a*) 1.5, (*b*) 5.5, (*c*) 30, and (*d*) 45 mN m^{-1}.

TABLE 3. Orientation angle φ of the polar groups of DPPC in the 9-monolayer LB films deposited at higher surface pressures

	φ	
	π/mN m^{-1}	
Assignment	30	45
C=O stretching	68°	65°
Antisymmetric PO_2^{-1} stretching	68°	65°
Symmetric PO_2^{-1} stretching	64°	61°
Symmteric C—O—C stretching	61°	58°

transmission and RA spectra imply that a different type of orientation of the polar groups takes place at these low surface pressures.

Conclusions

Using the horizontal lifting technique, we deposited the multilayer LB films of DPPC on solid substrates from the water surface at various surface pressures. FTIR transmission and RA spectra were recorded for these LB films deposited on CaF_2 and Ag substrates, respectively. From the intensity ratio of the major absorption bands between the RA and transmission spectra, we quantitatively evaluated the molecular orientation in the LB films. The hydrocarbon-chain segments of DPPC in the LB films transferred at lower surface pressures below the plateau of the π–*A* isotherm were almost randomly oriented as in a liquid-crystalline state. The chains in the films transferred at higher surface pressures above the plateau were found to be highly oriented with the all-*trans* conformation. The orientation angle of the hydrocarbon chain axis was obtained to be *ca.* 20° from the surface normal. For the films transferred at the surface pressures around the plateau, the hydrocarbon chains were in the intermediate state between the above two cases. It is, therefore, concluded that the plateau in the π–*A* isotherm corresponds to a process of the reorientation of the hydrocarbon chains from an almost randomly-oriented state to a highly-oriented one with the increase in the number of the all-*trans* conformers.

1. H. AKUTSU, M. IKEMATSU, and Y. KYOGOKU. Chem. Phys. Lipids, **28**, 149 (1981).
2. D. M. TAYLOR, and M. G. B. MAHBOUBIAN-JONES. Thin Solid Films, **87**, 167 (1982).
3. J. B. PENG, M. PRAKASH, R. MACDONALD, P. DUTTA, and J. B. KETTERSON. Langmuir, **3**, 1096 (1987).
4. K. TANAKA, K. ARIGA, and Y. OKAHATA. Proceedings of the 59th Annual Meeting of the Chemical Society of Japan. 1990. Vol. I. p. 76 (1A2 30).
5. T. KAMATA, J. UMEMURA, and T. TAKENAKA. Chem. Lett. 1231 (1988).
6. J. UMEMURA, T. KAMATA, T. KAWAI, and T. TAKENAKA. J. Phys. Chem. **94**, 62 (1990).
7. M. C. PHILIPS and D. CHAPMAN. Biochim. Biophys. Acta, **163**, 301 (1968).
8. H. TRAUBLE, H. EIBL, and H. SAWADA. Naturwissenschaften, **61**, 344 (1974).
9. O. ALBRECHT, H. GRULER, and E. SACKMAN. J. Phys. **39**, 313 (1978).
10. F. VILALLONGA. Biochim. Biophys. Acta, **163**, 290 (1968).
11. A. BLUME. Biochim. Biophys. Acta, **557**, 32 (1979).
12. E. OKAMURA, J. UMEMURA, and T. TAKENAKA. Biochim. Biophys. Acta, **856**, 68 (1986).
13. R. D. NEUMAN and S. FERESHTEHKHOU. J. Colloid Interface Sci. **125**, 34 (1988).
14. H. L. CASAL, and H. H. MANTSCH. Biochim. Biophys. Acta, **779**, 381 (1984).
15. E. OKAMURA, J. UMEMURA, and T. TAKENAKA. Biochim. Biophys. Acta, **1025**, 94 (1990).
16. H. H. MANTSCH and R. N. MCELHANEY. J. Mol. Struct. **217**, 347 (1990).
17. M. L. MITCHELL, and R. A. DLUHY. J. Am. Chem. Soc. **110**, 712 (1988).
18. R. D. HUNT, M. L. MITCHELL, and R. A. DLUHY. J. Mol. Struct. **214**, 93 (1989).
19. R. D. NEUMAN, S. FERESHTEHKHOU, and R. OVALLE. J. Colloid Interface Sci. **101**, 309 (1984).

Can. J. Chem. Downloaded from www.nrcresearchpress.com by 84.41.108.74 on 09/07/12
For personal use only.

Anomalous temperature-dependent Raman scattering in lithium hydrazinium sulfate

ROGER FRECH AND SCOTT H. BROWN
Department of Chemistry and Biochemistry, University of Oklahoma, Norman, OK 73019, U.S.A.

Received April 23, 1991

This paper is dedicated to Dr. Richard Norman Jones

ROGER FRECH and SCOTT H. BROWN. Can. J. Chem. **69**, 1695 (1991).

Results of a polarized Raman scattering study of single crystal lithium hydrazinium sulfate, $LiN_2H_5SO_4$, over a temperature interval from 11 to 300 K are discussed. Unusual temperature dependence of the band center scattering intensity is observed in a few intramolecular hydrazinium modes, intramolecular sulfate ion modes, and lattice modes. The intensity of these modes increases with increasing temperature from 11 K to about 175 K, then abruptly decreases over a small interval between 175 and 200 K. Above 200 K the band center intensity then exhibits normal behavior, slowly decreasing with increasing temperature. Possible explanations for this anomalous behavior are discussed.

Key words: lithium hydrazinium sulfate, proton conductor, Raman spectroscopy.

ROGER FRECH et SCOTT H. BROWN. Can. J. Chem. **69**, 1695 (1991).

On discute des résultats obtenus lors d'une étude de diffusion Raman polarisée sur un cristal unique du sulfate de lithium et d'hydrazinium, $LiN_2H_5SO_4$, réalisée dans l'intervalle de températures allant de 11 à 300 K. On a observé une relation inhabituelle entre la température et l'intensité de la diffusion du centre de la bande de quelques modes intramoléculaires de l'hydrazinium, de quelques modes intramoléculaires de l'ion sulfate et dans quelques modes du réseau. Les intensités de ces modes augmentent avec une augmentation de la température de 11 K à environ 175 K; elles diminuent alors rapidement sur un petit intervalle entre 175 et 200 K. Au-dessus de 200 K, l'intensité du centre de la bande se comporte normalement; elle diminue lentement avec une augmentation de la température. On discute de diverses explications possibles pour ce comportement anormal.

Mots clés : sulfate de lithium et d'hydrazinium; conducteur protonique; spectroscopie Raman.

[Traduit par la rédaction]

Can. J. Chem. Downloaded from www.nrcresearchpress.com by 84.41.108.74 on 09/07/12
For personal use only.

Introduction

The coarse features of the proton conductivity of lithium hydrazinium sulfate, $LiN_2H_5SO_4$, can be explained in part by the structure of a crystallographic unit cell. The crystal is orthorhombic (1–4) with a tetramolecular cell characterized by the space group $Pna2_1$ ($C_{2v}{}^9$). The sulfur and lithium atoms are tetrahedrally coordinated by oxygen atoms, forming a three-dimensional framework through which channels run parallel to the c axis. The hydrazinium ions, $N_2H_5{}^+$, lie in these channels and are linked by an extended hydrogen-bonded network between NH_2 groups with the N—N axis perpendicular to the channels, *i.e.* perpendicular to the c axis. The $NH_3{}^+$ ends of the hydrazinium ions are hydrogen bonded to the surrounding sulfate ions.

The protonic conductivity is anisotropic, with the highest value along the c axis (5). Therefore, it is assumed that the extended hydrogen-bonded network of hydrazinium ions is implicated in the ionic transport mechanism. Two models have been invoked to describe the mechanism of proton transport in this compound. In the first, a Grotthuss-like mechanism (6), proton transport is described (7) as a hop along the extended hydrogen-bonded network, perhaps assisted by tunneling, from a polyatomic donor to an adjacent polyatomic acceptor species. Following the hop, the donor ion reorients to receive another proton. In this model, the charge-carrying species is the proton and the donor/acceptor ions are part of a relatively rigid framework. Reorientational degrees of freedom of the donor/acceptor ions play a significant role in the proton transport mechanism. In the Vehicle Model (8) the charge-carrying species is a polyatomic species to which a proton is attached. The protonated species is mobile within the framework defined by other charged species occupying fixed lattice sites. Therefore in lithium hydrazinium sulfate, the mobile species is assumed to be the $N_2H_5{}^+$ hydrazinium ion (5).

The X-ray and neutron diffraction analyses describe the structural features of the unit cell of lithium hydrazinium sulfate and this, combined with the conductivity data, implicate the extended hydrogen-bonded network of the NH_2 portion of the hydrazinium ions as playing a role in the conductivity mechanism. However, dynamical measurements are required to extend this picture. To this end there have been few infrared (9) and Raman (10, 11) spectroscopic studies, as well as NMR studies (12–14). We recently reported the results of a temperature-dependent Raman study of an oriented single crystal (15); these data argued against the Vehicle mechanism as significantly contributing to the conductivity below room temperature. In the course of these and subsequent measurements, a pattern of anomalous behavior was noted in a number of vibrational modes. That behavior is the subject of this paper.

Experimental

Reagent grade $N_2H_6SO_4$ and Li_2CO_3 were mixed in a 2:1 molar ratio in water. Large single crystals of optical quality were obtained by slow evaporation of the aqueous solution at 40°C. Typical crystals were elongated along the c axis with prominent (010), (110), and (011) faces. The crystal used for the spectroscopic measurements was cut into a parallelpiped whose axes corresponded to the crystallographic axes as verified by X-ray diffraction measurements.

Polarized Raman spectra were recorded at a spectral bandpass of 3 cm^{-1} on a system based on a 0.85 meter Czerny-Turner double monochromator with a cooled C31034 photomultiplier tube. The incident radiation was provided by the 488.0 nm line of a Spectra Physics model 165/265 argon ion laser operating with an output power of 300 mW. The sample was cooled in an Air Products Displex model CSA-202E closed cycle helium refrigeration system equipped with a DMX-1E vacuum shroud sample chamber. The high optical quality of the sample prevented secondary laser emission lines from appearing in the Raman spectra, necessitating the use of a neon calibration lamp to calculate the frequencies of the various bands. The uncertainty in the band positions is estimated to be ± 1 cm^{-1}.

Printed in Canada / Imprimé au Canada

Can. J. Chem. Downloaded from www.nrcresearchpress.com by 84.41.108.74 on 09/07/12
For personal use only.

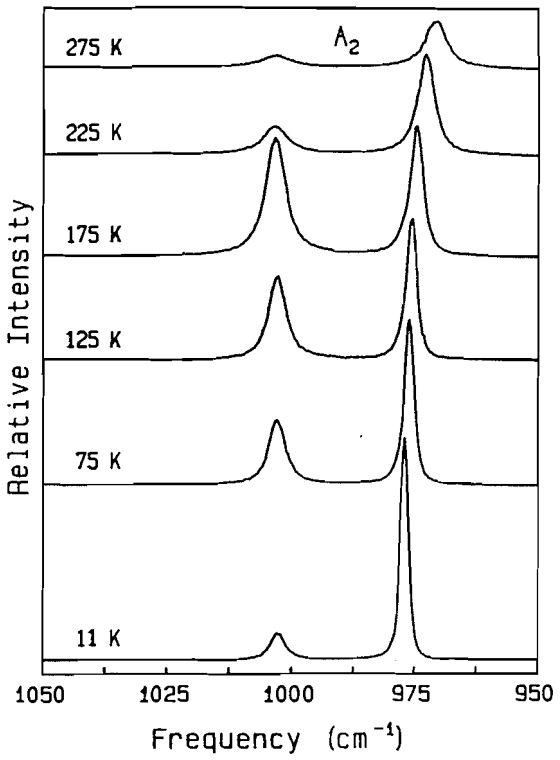


FIG. 1. Temperature-dependent Raman scattering spectra for the hydrazinium ion ν(N—N) mode and the anomalous sulfate ion ν_1 mode in an A_2 scattering geometry.

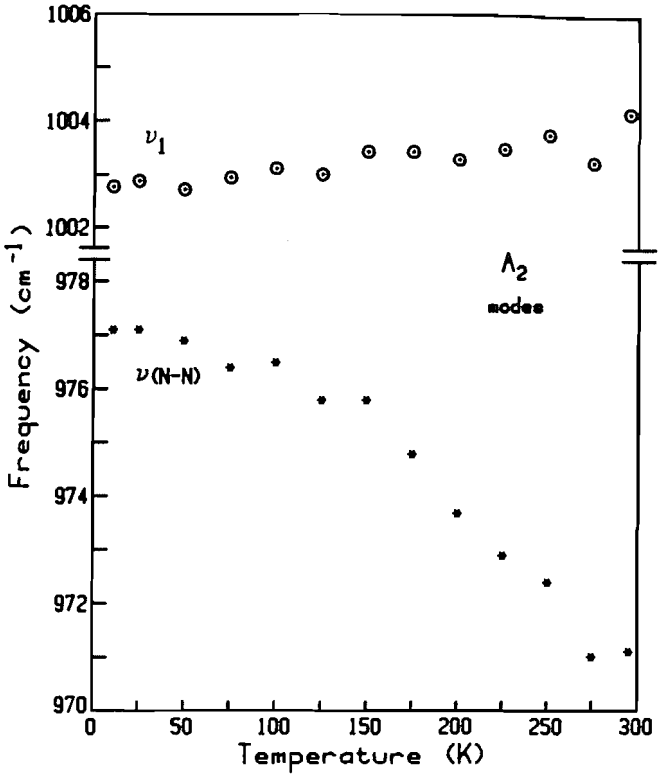


FIG. 2. The temperature dependence of the hydrazinium ion ν(N—N) and the anomalous sulfate ion ν_1 stretching frequencies.

Results

Figure 1 shows the temperature dependence of the ν(N—N) mode at 977 cm^{-1} and the $\nu_1(SO_4^{2-})$ at 1004 cm^{-1} in a scattering geometry which allows modes belonging to the A_2 irreducible representation. The ν(N—N) mode shows the expected trends in intensity, frequency, and bandwidth over the entire temperature range. In particular, the peak intensity slowly decreases with increasing temperature. By contrast, the $\nu_1(SO_4^{2-})$ component shows two distinct types of anomalous intensity behavior in this range. First, the intensity at the band center gradually *increases* with temperature over the range 11–175 K. Second, the intensity decreases dramatically and abruptly over the small temperature interval between 175 and 200 K. Then, above 200 K, the peak intensity gradually decreases with increasing temperature as expected for a typical vibrational mode.

The frequency and bandwidth behavior of this mode were carefully measured, primarily to examine these spectral parameters for breaks or anomalies which might coincide with the surprising intensity behavior. The spectral bandwidth (FWHM) was deconvoluted assuming a triangular instrumental slit function and was found to increase from 3.6 cm^{-1} at 11 K to 7.9 cm^{-1} at 295 K. The rate of increase of the bandwidth with temperature is small at low temperatures, but increases at about 100 K and appears to be linear from 100 to 300 K. This bandwidth behavior is quite similar to most of the other modes in lithium hydrazinium sulfate and is not unusual. The bandwidths of the ν_1 components belonging to other irreducible representations was also examined and the temperature dependence was found to be quite similar to the A_2 component.

The temperature dependence of the frequencies of both the

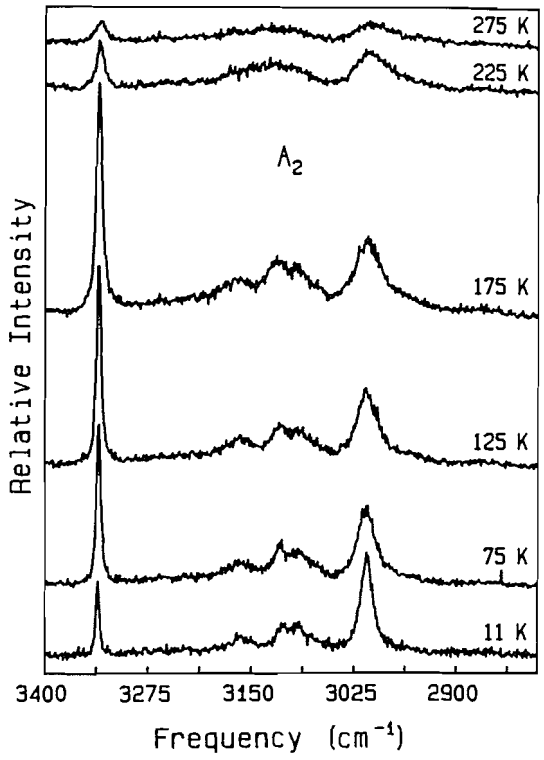


FIG. 3. Temperature-dependent Raman spectra for the NH stretching modes of the hydrazinium ion in an A_2 scattering geometry. Note the anomalous intensity behavior of the mode at 3336 cm^{-1}.

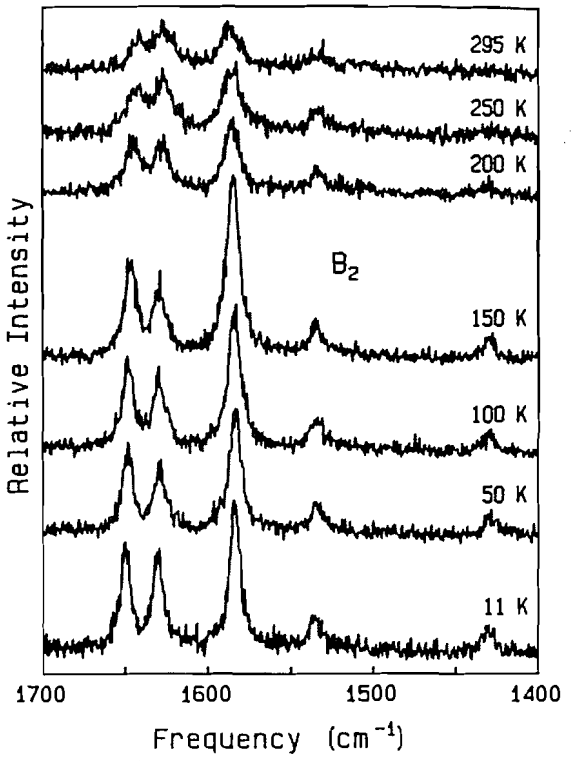


FIG. 4. Temperature-dependent Raman spectra of the HNH angle deformation modes of the hydrazinium ion in a B_2 scattering geometry, illustrating the anomalous mode at 1583 cm^{-1}.

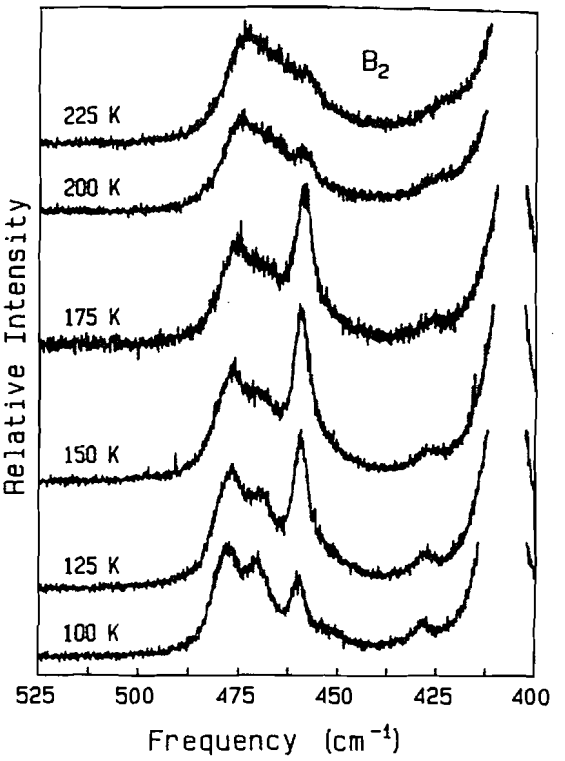


FIG. 5. Raman spectra of the sulfate ion ν_2 mode and the lithium ion lattice modes from 100 to 225 K, illustrating the anomalous mode at 461 cm^{-1}.

ν(N—N) mode and $\nu_1(SO_4^{2-})$ is shown in Fig. 2. The ν_1 mode is only slightly dependent on temperature, which is not unusual for the totally symmetric stretching motion of the sulfate anion. However, it is unusual that there is a slight increase of the frequency with increasing temperature. These data show that there are no abrupt changes in either the frequency or the bandwidth of the $\nu_1(SO_4^{2-})$ mode at 175–200 K in spite of the abrupt change in peak intensity.

Behavior similar to the A_2 component of $\nu_1(SO_4^{2-})$ is noted in a small number of other modes. Figure 3 shows the N—H stretching region in an A_2 scattering geometry. The symmetry-based assignments of these bands have been previously given (10). The mode at 3336 cm^{-1} shows exactly the same pattern of intensity dependence on temperatures as did the $\nu_1(SO_4^{2-})$ mode. It should be noted that all other N—H stretching modes show no unusual temperature dependent behavior.

Although the previous two bands displaying anomalous intensities occurred in an A_2 scattering geometry, such behavior is not restricted to that irreducible representation. Figure 4 shows a rather complicated spectral region containing bands primarily from the HNH angle deformation modes which belong to the B_2 symmetry species. The intensity of the band at 1583 cm^{-1} exhibits the previously described anomalous pattern with increasing temperature.

Another striking example is the B_2 mode at 461 cm^{-1} illustrated in Fig. 5. This mode is predominantly the ν_2 bending motion of the sulfate ion, although it is possible that there is some contribution from lithium ion translatory motion mixed in. It is particularly interesting that the other ν_2 components at slightly higher frequencies show no unusual temperature-dependent intensity behavior.

Finally the external optic modes from 320 to 20 cm^{-1} are shown in Fig. 6. Here the modes at 199, 126, and 115 cm^{-1} exhibit the previously described anomalous behavior. The latter two modes are especially striking, since at 25 K they appear as high and low frequency shoulders around the lattice mode at 121 cm^{-1}. As the temperature increases, the mode at 121 cm^{-1} slowly decreases in peak intensity, while the two flanking anomalous modes grow in intensity. Between 175 and 225 K these modes collapse into an asymmetric band whose peak intensity continues to decrease with increasing temperature.

Discussion

Abrupt intensity changes in the Raman scattering spectrum with temperature are often associated with phase transitions. Indeed there is evidence that Raman spectroscopy is more sensitive to minute displacements of atoms than are X-ray diffraction methods (16). In lithium hydrazinium sulfate, any structural change responsible for the anomalous modes would be expected to be small since such a small percentage of the modes is affected. No major structural phase transitions have been reported for lithium hydrazinium sulfate in the range of 11–300 K; in fact the temperature-dependent spectroscopic data in this study argue against any major transitions in this range.

One dynamical change in the lithium hydrazinium sulfate crystal which occurs in the temperature range of interest originates in the reorientational motions of the $—NH_2$ and $—NH_3^+$ ends of the hydrazinium ion. The oscillations of the $—NH_3^+$ entity are reported to increase in amplitude with temperature throughout the entire 11–300 K range (17, 18). It is conceivable that the changes in the dynamics of the hydrazinium ion

Can. J. Chem. Downloaded from www.nrcresearchpress.com by 84.41.108.74 on 09/07/12
For personal use only.

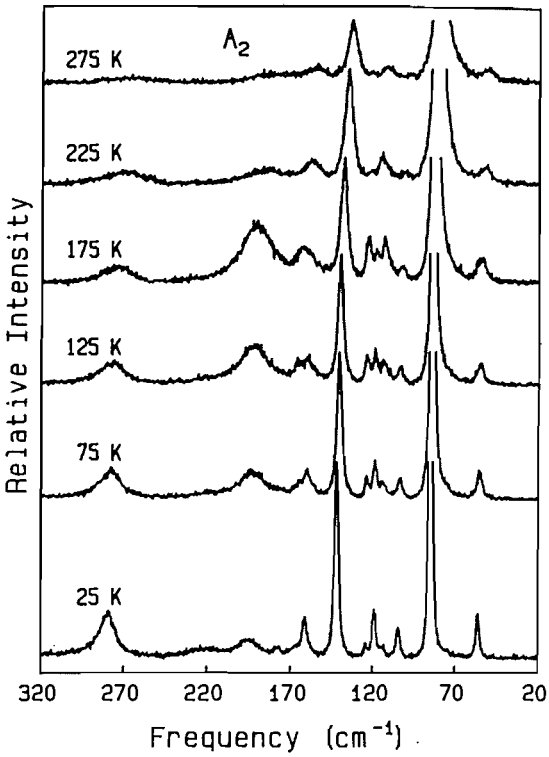


FIG. 6. Temperature dependence of the Raman active lattice modes in an A_2 scattering geometry. Note the anomalous modes at 199, 126, and 115 cm^{-1}.

could cause the intensities of several hydrazinium ion internal modes to correspondingly vary with temperature. However, using this picture to justify the anomalous behavior observed in several sulfate ion internal modes and lattice modes is difficult and would require a substantial degree of coupling between the hydrazinium modes and the other sulfate and lattice modes which display unusual temperature-dependent behavior. This degree of coupling seems unlikely since the sulfate internal modes are relatively unaffected by deuterium substitution, indicating a low degree of coupling between the hydrazinium and sulfate ion sublattices (11).

Though the structural change responsible for the anomalous mode behavior must be small, the fact that both intramolecular sulfate and hydrazinium ion modes and intermolecular lattice modes are involved suggests that the origin of this anomalous behavior is global in nature, *i.e.* associated with the entire unit cell. One possible origin for this behavior is the unusual temperature dependence of the unit cell dimensions. The thermal expansion coefficients for lithium hydrazinium sulfate have been measured (19) and are anisotropic in nature, with a very erratic coefficient along the *c* axis from 130 to 200 K. Possibly the anomalous behavior can be explained in terms of vibrational modes which are very sensitive to the anisotropic nature of the orthorhombic cell expansion. In the case of NH_4ReO_4, anomalous Raman spectroscopic and heat capacity data were determined to be due solely to changes in the unit cell parameters with temperature rather than a first or second order phase transition (20–22). This suggests that a careful study of the lithium hydrazinium sulfate lattice dimensions and unit cell structure as a function of temperature might afford some insight into the origin of the anomalous modes.

1. I. D. BROWN. Acta Crystallogr. **17**, 654 (1964).
2. J. H. VAN DEN HENDE and H. BOUTIN. Acta Crystallogr. **17**, 660 (1964).
3. M. R. ANDERSON and I. D. BROWN. Acta Crystallogr. B**30**, 831 (1974).
4. V. M. PADMANABHAN and R. BALASUBRAMANIAN. Acta Crystallogr. **22**, 532 (1967).
5. K. D. KREUER, W. WEPPNER, and A. RABENAU. Solid State Ionics, **3/4**, 353 (1981).
6. C. J. D. VON GROTTHUSS. Mémoire sur la décomposition de l'eau et des corps, qu'elle tient en solution, à l'aide de l'électricité galvanique. Rome, Italy (1805); Ann. Chim. **LVIII**, 54 (1806).
7. J.-O. LUNDGREN, R. LIMINGA, and I. OLOVSSON. Arkiv Kemi, **30**, 81 (1968).
8. K. D. KREUER, A. RABENAU, and W. WEPPNER. Angew. Chem. Int. Ed. Engl. **21**, 208 (1982).
9. A. V. R. WARRIER and P. S. NARAYANAN. Proc. Indian Acad. Sci. **64**, 254 (1964).
10. R. S. KRISHNAN and K. KRISHNAN. Proc. Indian Acad. Sci. **61**, 122 (1965).
11. S. H. BROWN and R. FRECH. Spectrochim. Acta, **44**A, 1 (1988).
12. F. L. HOWELL and V. H. SCHMIDT. J. Chem. Phys. **51**, 1983 (1969).
13. R. R. KNISPEL and H. E. PETCH. Can. J. Phys. **49**, 870 (1971).
14. R. S. PARKER and V. H. SCHMIDT. J. Mag. Res. **6**, 507 (1972).
15. R. FRECH and S. H. BROWN. Solid State Ionics, **35**, 127 (1989).
16. J. F. SCOTT. *In* Molecular spectroscopy of dense phases. Proceedings of the 12th European Congress on Molecular Spectroscopy. *Edited by* M. Grossmann, S. G. Elkomoss, and J. Ringeissen. Elsevier. 1976. pp. 203–213.
17. W. D. MACCLEMENT, M. PINTAR, and H. E. PETCH. Can. J. Phys. **45**, 3257 (1967).
18. R. N. HASTINGS and T. OJA. J. Chem. Phys. **57**, 2139 (1972).
19. S. DEVANARAYANAN and K. R. K. EASWARAN. Proc. Indian Acad. Sci. **64**, 173 (1966).
20. R. J. C. BROWN and S. L. SEGEL. J. Chem. Phys. **67**, 3163 (1971).
21. Y. S. PARK, H. F. SHURVELL, and R. J. C. BROWN. J. Raman Spectrosc. **17**, 351 (1986).
22. R. J. C. BROWN, J. E. CALLANAN, R. D. WEIR, and E. F. WESTRUM. J. Chem. Phys. **85**, 5963 (1986).

Can. J. Chem. Downloaded from www.nrcresearchpress.com by 84.41.108.74 on 09/07/12
For personal use only.

Pressure effect on hydrogen isotope exchange kinetics in chymotrypsinogen investigated by FT-IR spectroscopy[1]

P. T. T. WONG

Steacie Institute for Molecular Sciences, National Research Council of Canada, Ottawa, Ont., Canada K1A 0R6

Received April 4, 1991

This paper is dedicated to Dr. Richard Norman Jones

Can. J. Chem. Downloaded from www.nrcresearchpress.com by 123.30.183.119 on 09/07/12
For personal use only.

P. T. T. WONG. 1991. Can. J. Chem. **69**, 1699 (1991).

Hydrogen/deuterium (H/D) exchange rate constants in chymotrypsinogen have been determined at several pressures up to 28.9 kbar by FTIR spectroscopy. The secondary structure of the protein molecules was monitored simultaneously at the corresponding pressures by the intensity redistribution of the infrared amide I band at these pressures. As in other proteins, the labile protons on the amide groups in chymotrypsinogen can, to a good approximation, be separated into two classes, each with distinct first order H/D exchange rates constants in the time period from 10 min to ~24 h. The fast exchange rate constant increases while the slow exchange rate constant decreases with increasing pressure. The increase in the fast exchange rate constant at high pressure is largely associated with the pressure-induced unfolding of the protein molecules. At extremely high pressure (12.8 kbar), in addition to the unfolding of protein molecules, pressure induced a distortion and weakening of the hydrogen bonds of the fold protein segments also contribute to an increase in the overall H/D exchange rate. The present results confirm that when chymotrypsinogen is dissolved in D_2O, a considerable amount of D_2O molecules is bound to the protein molecules on the surface as well as in the interior cavities of the molecules. The H/D exchange takes place between these bound D_2O and the protons in the protein molecules. The mechanism of the H/D exchange and the interior dynamics in proteins are discussed on the basis of the present results.

Key words: hydrogen/deuterium exchange, exchange kinetics, rate constant, pressure effects, infrared spectroscopy, protein, conformation structure, bound water.

P. T. T. WONG. 1991. Can. J. Chem. **69**, 1699 (1991).

Faisant appel à la spectroscopie ir par transformation de Fourier, on a déterminé les constantes de vitesse d'échange hydrogène/deutérium (H/D) du chymotrypsinogène, à plusieurs pressions allant jusqu'à 28,9 kbar. En se basant sur la redistribution de l'intensité de la bande infrarouge amide I aux diverses pressions, on a déterminé simultanément la structure secondaire des molécules de protéines aux pressions correspondantes. Comme dans d'autres protéines, les protons labiles des groupes amides du chymotrypsinogène peuvent être séparés, en première approximation, en deux classes possédant chacune des constantes (allant de 10 min à environ 24 h) distinctes pour les vitesses d'échange H/D du premier ordre. Lorsqu'on augmente la pression, la constante de vitesse pour l'échange rapide augmente alors que celle de l'échange lent diminue. L'augmentation observée à des pression élevées de la constante de vitesse de l'échange rapide est principalement associée à un déploiement des protéines qui serait induit par la pression. À des pressions extrêmement élevées (12,8 kbar), la pression, en plus de provoquer un déploiement des molécules de protéines, induit aussi une distorsion et un affaiblissement des liaisons hydrogènes des segments repliés de la molécule qui contribuent à augmenter la vitesse globale de l'échange H/D. Les résultats présentés ici confirment que, lorsque le chymotrypsinogène est dissous dans du D_2O, il y a un grand nombre de molécules de D_2O qui sont liées aux molécules de protéines, tant à la surface que dans les cavités intérieures des molécules. L'échange H/D se produit entre ces molécules de D_2O liées et les protons des molécules de protéines. On discute du mécanisme d'échange H/D et de la dynamique intérieure des protéines en fonction des résultats obtenus dans cette étude.

Mots clés : échanges hydrogène/deutérium, cinétique des échanges, constante de vitesse, effets de pression, spectroscopie à l'infrarouge, protéine, structure de conformation, eau liée.

[Traduit par la rèdaction]

Introduction

The hydrogen/deuterium (H/D) exchange method has been widely used to investigate the internal dynamics of globular proteins (1–4). It has been shown from these studies that in general, exchange of labile protons of peptides and side chain protons which are located on the surface of the protein and are exposed to the bulk water is extremely rapid, whereas peptide and side chain protons in the interior of folded protein exchange with much slower rates.

Three distinct theories for the mechanism of H/D exchange in proteins have been proposed, i.e., (*1*) local unfolding, (*2*) solvent penetration, and (*3*) regional melting (2,5–8). The local unfolding model suggested that H/D exchange in proteins is controlled by the localized cooperative unfolding of segments of proteins, which leads to an extrusion of the chains with labile protons into the bulk solvent where exchange takes place. The penetration model assumes that H/D exchange takes place within the protein interior as a result of diffusion of solvent molecules into the buried exchangeable sites by small amplitude fluctuations or mobile defects in the protein packing. The regional melting mechanism suggests that H/D exchange takes place within solvent-filled clefts in the protein surface formed by localized disruption of the conformational structure arising from the cooperative breaking of several hydrogen bonds.

Hydrostatic pressure is known to enhance hydrogen bonding (9–11) and to damp molecular fluctuation (9–12). Pressure is also known to induce a dramatic change in conformational structure in globular proteins (10, 13, 14). Therefore, a study of

[1]NRC No. 31532.

Can. J. Chem. Downloaded from www.nrcresearchpress.com by 123.30.183.119 on 09/07/12
For personal use only.

pressure effects on the H/D exchange rate in globular proteins would certainly shed some light on the mechanism of the H/D exchange and thus the interior dynamics of globular proteins. The conformational state of a globular protein is also altered by changes in temperature or pH. However, in addition to a change in the conformational structure, a kinetic energy change is associated with a change in temperature. The H/D exchange rate is also altered by different acid/base catalyzing mechanisms at different pHs (1–4).

Infrared spectroscopy is a classical technique for the study of H/D exchange in proteins (15), which became a powerful and rapid technique for this purpose after the development of Fourier transform infrared spectrometers. One of the advantages of infrared spectroscopy over other physical methods for the study of H/D exchange in proteins is that the conformational structure of the protein under study can be monitored concomitantly during the measurement of the H/D exchange rate constants.

In the present work, the H/D exchange rate constants of chymotrypsinogen at several pressures up to 28.9 kbar have been measured. The study of pressure effects on the structure of proteins has gained considerable interest in recent years (10, 13, 14, 16–28). A number of experimental techniques have been used. In most of these investigations, changes in the properties of proteins were observed below 5 kbar. Recent advances in the high pressure infrared spectroscopic technique for aqueous systems developed in our laboratory allows us for the first time to combine the pressure parameter with infrared spectroscopy to determine pressure effects on both the conformational structure and the H/D exchange rate constant simultaneously in a globular protein, chymotrypsinogen, in the pressure range up to 28.9 kbar. Consequently, the correlation between the H/D exchange rate and the conformational state of the protein can be established, which in turn may reveal the mechanism of H/D exchange and the internal dynamic properties in globular proteins.

Experimental methods

High-purity chymotrypsinogen A from bovine pancreas was purchased from Sigma Chemical Co. Solutions of 100 mg/mL were prepared in Tris-HCl D_2O buffer (pD = 7.6). Protein solutions were placed at room temperature together with powdered α-quartz in a 0.37 mm diameter hole on a 0.23 mm thick stainless steel gasket mounted on a diamond anvil cell. The α-quartz was used as internal pressure calibrant (29). All the protein solutions were prepared immediately prior to the infrared measurements. The maximum time required between the preparation of the solution and the recording of the first infrared spectrum is less than 10 min.

Infrared spectra of samples were measured as a function of time at room temperature and at a constant pressure on a Bomem model DA3.02 Fourier transform spectrometer using a liquid-nitrogen cooled mercury cadmium telluride detector. The infrared beam was condensed by a sodium chloride lens system onto the sample in the diamond anvil cell. For each spectrum 512 interferograms were co-added at a spectral resolution of 4 cm^{-1}.

For each pressure, infrared spectra of the protein solutions were measured at intervals of 10 min for the first 3 to 4 h and then at intervals of 30 min set by the computer of the spectrometer. The zero time of the H/D exchange was taken as the time when the solid protein was first mixed with D_2O buffer.

The H/D exchange rate in proteins were measured by following the decrease in the amide II peak at 1550 cm^{-1} with time (15), which takes advantage of the fact that this infrared absorption peak shifts to a frequency of about 1450 cm^{-1} when the proton atom is replaced by deuterium atom. The base line of the spectra was obtained from the spectrum of a fully exchanged sample which was prepared by three months incubation in D_2O followed by heating to 40°C for 6 h or alternately followed by pressurizing to 8 kbar. In the infrared spectrum of the fully exchange sample, the intensity of the amide II band is diminished and only the wings of the deuterated amide II band at 1450 cm^{-1} and the shoulder band of the side chains at 1570 cm^{-1} remain (13). Data reduction was performed with software developed in this laboratory.

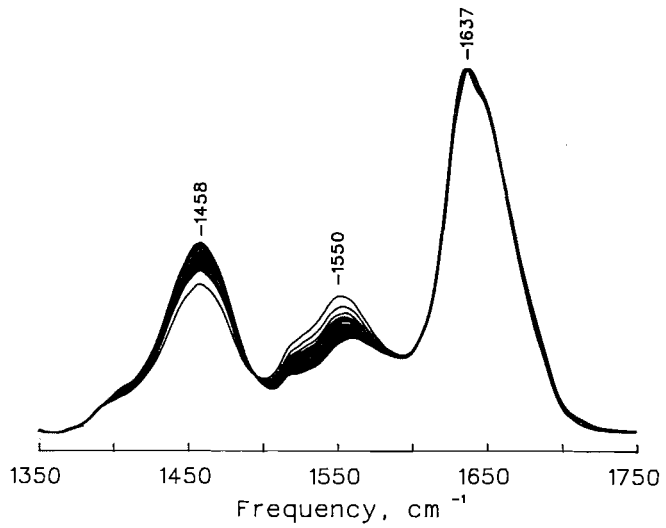


FIG. 1. A stack plot of the infrared spectra of chymotrypsinogen in the frequency region 1350–1750 cm^{-1} as a function of time up to 13 h.

Results and discussion

Infrared spectra of chymotrypsinogen solution in D_2O buffer (pD, 7.6) have been measured as a function of time at several pressures. Typical infrared spectra measured at 3.5 kbar and in a time period of 13 h are shown in Fig. 1. The strong amide I band at 1637 cm^{-1} is due to the in-plane C=O stretching vibration weakly coupled with C—N stretching and in-plane N—H bending and the band at 1550 cm^{-1} is due to the amide II mode which is a mixed vibration involving N—H in-plane bending and C—N stretching (30). It is evident from Fig. 1 that as a result of H/D exchange, the intensity of the amide II band at 1550 cm^{-1} decreases while that of the deuterated amide II band at 1447 cm^{-1} increases with increasing time. The peak intensity ratios between the amide II band and the amide I band ($A_{\text{amide II}}/A_{\text{amide I}}$) are plotted versus time for several pressures in Fig. 2. Taking this intensity ratio before exchange begins as 0.45 (15, 31) the percentage of the hydrogen exchanged in the protein can be calculated as a function of time for various pressures.

I. H/D exchange at ambient conditions

At atmospheric pressure, about 17% of the labile protons in chymotrypsinogen are exchanged within 10 min. It has been generally assumed that these extremely rapidly exchanging protons are those located on the surface of protein molecules and hence are in direct contact with the solvent (1–4). After 10 min, the exchange becomes slower and the $A_{\text{amide II}}/A_{\text{amide I}}$ ratio decreases exponentially with time. The decreasing rate of this intensity ratio and thus the H/D exchange rate becomes much slower after about 4 h. It has been shown that in a period of 17 days the H/D exchange in chymotrypsinogen is still far from completion (13). If those protons which do not exchange with solvent after 24 h are considered as the "hard to exchange" protons in the protein molecule, they represent more than 50% of the amide protons in chymotrypsinogen at atmospheric pressure (see Table 1).

TABLE 1. H/D exchange rate constants of two classes of labile protons in chymotrypsinogen and percentages of "hard-to-exchange" protons and extremely fast exchanging protons at several pressures

Pressure (kbar)	Hard-to-exchange protons (%)	Protons exchanged within 10 min (%)	Slow exchange k (min)	Fast exchange k (min)
0.001	52	17	4.3×10^3	3.7×10^{-2}
2.3	42	26	4.6×10^3	4.0×10^{-2}
3.5	31	30	2.1×10^3	4.8×10^{-2}
4.8	11	36	1.8×10^3	7.2×10^{-2}
12.8	1	75	1.3×10^3	1.9×10^{-1}
28.9	32	47	1.3×10^3	8.9×10^{-2}

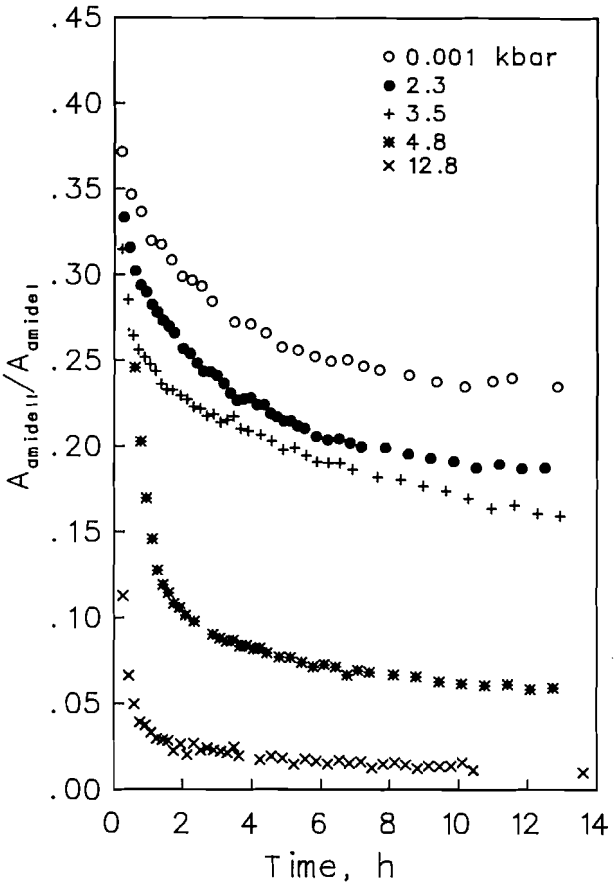


FIG. 2. Time dependences of infrared intensity ratio between the amide II band and amide I band of chymotrypsinogen at several pressures.

According to the graphic method (32, 33), in addition to the extremely fast exchange which occurs within 10 min, the first order H/D exchange rate can be distributed into two regions in many proteins, i.e., the fast and slow exchange regions. The semilogarithmic plots of the $A_{amide\ II}/A_{amide\ I}$ ratios of chymotrypsinogen at atmospheric pressure as well as at various pressures versus time in the time period between 10 min and 24 h also show two distinct portions which are related to the fast and slow exchange regions, each with distinct first order H/D rate constants. These fast and slow exchange rate constants of chymotrypsinogen at several pressures are given in Table 1. Therefore, according to the H/D exchange characteristics, labile protons in chymotrypsinogen can be classified into four categories: (*1*) extremely fast exchange (within 10 min) (*2*) fast exchange (in 10 min to ~4 h), (*3*) slow exchange (in ~4 to 24 h), and (*4*) hard to exchange (longer than 24 h).

II. Pressure effects on H/D exchange

As shown in Fig. 2 and Table 1, in general, the overall H/D exchange rate in chymotrypsinogen is increased by hydrostatic pressure. However, effects of pressure on the H/D exchange in chymotrypsinogen are significant different in three pressure ranges, i.e. below 3.5 kbar, between 3.5 and 12.8 kbar, and above 12.8 kbar.

Below 3.5 kbar, the pressure-induced changes in both the fast and slow exchange rate constants are very small (Table 1). However, the number of "hard-to-exchange" protons is significantly reduced by pressure (10% at 2.3 kbar). In the meantime, almost the same number of "extremely fast exchange" protons which exchange within 10 min is increased by pressure. These results suggest that the main pressure effect in the pressure range below 3.5 kbar is to convert small amount of labile protons (10% at 2.3 kbar) from the "hard-to-exchange" state to the "extremely fast exchange" state.

In the pressure range between 3.5–12.8 kbar, pressure induces a significant increase in the fast exchange rate constant (more than double at 4.8 kbar, see Table 1). On the other hand, pressure also induces a significant decrease in the slow exchange rate constant (more than half at 4.8 kbar, see Table 1). In this pressure range, not all those "hard-to-exchange" protons disappeared at high pressure are converted into "extremely fast exchange" protons. For instance, at 4.8 kbar only 11% of the total labile protons remain as "hard-to-exchange" protons, but the "extremely fast exchange" protons only increase slighly from 30% of the total labile protons at 3.5 kbar to 36% at 4.8 kbar (see Table 1). Apparently, some of the disappeared "hard-to-exchange" protons contribute to the increase in the fast exchange rate constant.

At 12.8 kbar, the "hard-to-exchange" protons have almost disappeared, the fast exchange rate constant increases more than double of that at 4.8 kbar, and the slow exchange rate constant again has decreased slightly. The most dramatic pressure effect at 12.8 kbar is that about 75% of the labile protons become "extremely fast exchange" protons which complete the H/D exchange within 10 min (Fig. 2 and Table 1).

III. Pressure effects on conformational structure in chymotrypsinogen

The infrared spectrum of the amide I band of chymotrypsinogen in D_2O buffer solution has been reported previously (13). Apparently, this amide I band consists of several overlap-

Can. J. Chem. Downloaded from www.nrcresearchpress.com by 123.30.183.119 on 09/07/12
For personal use only.

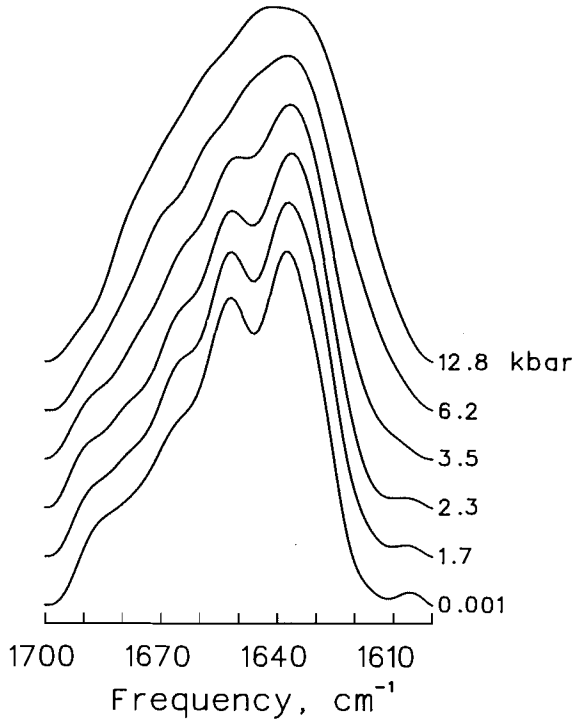


FIG. 3. Deconvolved infrared spectra of chymotrypsinogen in the amide I band region at several pressure using a band width of 15 cm^{-1} and a resolution enhancement factor of 1.7.

ping bands with maxima at 1636, 1654, 1667, and 1686 cm^{-1}, which are more clear in the slightly deconvolved spectra as shown in Fig. 3. It is well recognized that for various types of conformational structure of the amide backbone in polypeptides and proteins, the peak maxima of the amide I band are at different frequencies. Thus, the amide I band in the infrared spectra of polypeptides and proteins has been widely used for determination of the conformational structure in these systems (15, 30, 34). The infrared spectra of the amide I band in Fig. 3 clearly indicate that the amide backbone in chymotrypsinogen consists of segments in the β-sheet, α-helical, and unordered conformations, which give rise to the amide I bands at 1636 (1686), 1654, and 1667 cm^{-1}, respectively (15, 30, 34). The strongest component band is at 1636 cm^{-1}, which indicates that the β-sheet conformation of the amide groups predominates over other structures in chymotrypsinogen at atmospheric pressure.

It is known that considerable changes in conformational structure in globular proteins can be induced by external pressure in the pressure range above about 3 kbar (10, 13, 14). In chymotrypsinogen below 3.5 kbar no significant redistribution of intensity of the amide I band is induced by pressure (Fig. 3). Starting from 3.5 kbar, the intensities in the frequency region between 1640 and 1650 cm^{-1} (random coil) and that near 1667 cm^{-1} (turns) increase with increasing pressure. On the other hand, the intensities of the component bands at 1636, 1686 (β-sheet), and 1654 cm^{-1} (α-helix) decrease as pressure increases. These results indicate that a pressure-induced denaturation associated with changes in conformational structure in aqueous chymotrypsinogen starts at 3.5 kbar. In this denaturation process, the contributions of the unorderd random coil and turn structures increase at the expense of the β-sheet and α-helical structures. Moreover, in the denatured chymotrypsinogen the α-helical structure is largely distorted as evident from the broadening of the component band at 1654 cm^{-1}. This pressure-induced denaturation is irreversible as shown by the irreversible changes in the infrared spectrum.

IV. Effects of conformational changes on H/D exchange

Below 3.5 kbar, the fine features on the amide I band are the same as those at atmospheric pressure. Therefore, there is no significant change in conformational structure in chymotrypsinogen in this pressure range.

It is well known (35) that in the pressure range up to 3 kbar, globular proteins are subject to a pressure-induced dissociation from oligomers to monomers. In this process, some interacting side chains are ionized and the labile protons in these ionized side chain are in contact with bulk solvent. In the meantime, some of the interior labile protons of the amide backbone in oligomers become exposed to bulk solvent when they are dissociated into monomers. Consequently, some "hard-to-exchange" protons in oligomeric chymotrypsinogen become "extremely fast exchange" protons in monomers. The present results show that about 10% of the labile protons take part in this conversion at 2.3 kbar.

The conformational structure of chymotrypsinogen starts to change at 3.5 kbar. The amunt of random coil segments and unordered turns increase slightly at 3.5 kbar and further increase with increasing pressure at the expense of β-sheet and α-helical segments. It is well established that the rate of H/D exchange of random coil segments and unordered turns in protein molecules is the fastest, whereas that of β-sheet segments is the slowest (2, 5, 15, 36–38). Therefore, a 50% increase in the fast exchange rate constant at 4.8 kbar from that at 3.5 kbar is the result of pressure-induced conversion of a large portion of the amide backbone in the protein molecules from α-helical and β-sheet conformation into the unordered random coil and turns. The slow H/D exchange process must be involved in the exchange reaction of "hard-to-exchange" protons which are buried in the interior of the β-sheet segments of the protein molecules (5). This is further supported by the fact that the slow rate constant decreases slightly with decreasing amount of "hard-to-exchange" protons in the protein molecules as pressure increases (see Table 1).

At 12.8 kbar, chymotrypsinogen is almost completely denatured, most of the amide backbones of the protein molecules are in the random coil and unordered turn structure, and the remaining α-helical and β-sheet segments are distorted (13). The disappearance of the "hard-to-exchange" protons and the dramatic increase in the fast exchange rate constant at 12.8 kbar imply that at such a high pressure, pressure not only induces more protein segments into the fast exchange unordered state, it also gives rise to a significant distortion and a weakening of hydrogen bonds of the protein segments with "hard-to-exchange" conformation.

V. H/D exchange in the ice VII state

Figure 4 compares the time dependence of $A_{\text{amide II}}/A_{\text{amide I}}$ ratio of chymotrypsinogen between 28.9 and 12.8 kbar. Apparently the H/D exchange rate at 28.9 kbar becomes much slower than that at 12.8 kbar and is even slower than that at 4.8 kbar (Fig. 2 and Table 1). This abnormal trend of the pressure effect on the H/D exchange rate at 28.9 kbar is the result of a phase transition in the solvent. Liquid D_2O transforms into ice VII at about 25 kbar pressure (39). The mobility of D_2O molecules in the ice VII state is much smaller than that in the liquid state and thus the H/D exchange of labile protons in chymotrypsinogen with D_2O molecules in ice VII at 28.9 kbar is expected to be prohibited if the H/D exchange only takes place between labile protons and bulk D_2O. However, at 28.9 kbar even though the bulk D_2O is

Can. J. Chem. Downloaded from www.nrcresearchpress.com by 123.30.183.119 on 09/07/12
For personal use only.

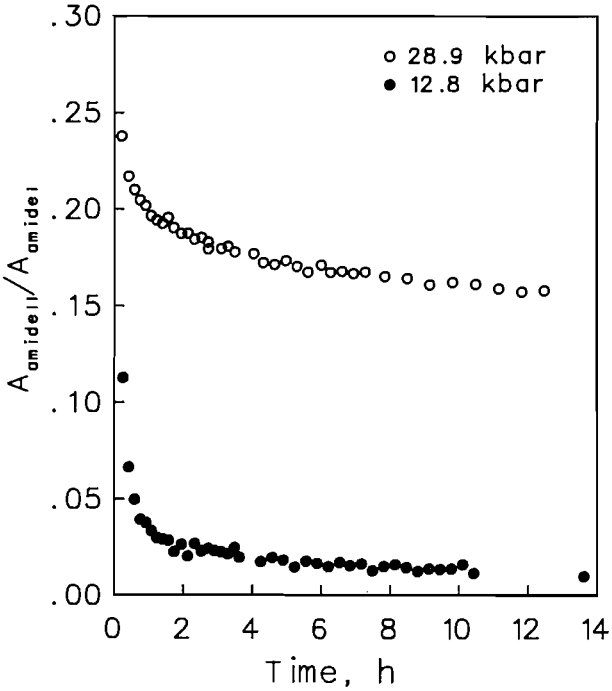


FIG. 4. Time dependences of infrared intensity ratio between the amide II band and amide I band of chymotrypsinogen at 12.8 and 28.9 kbar.

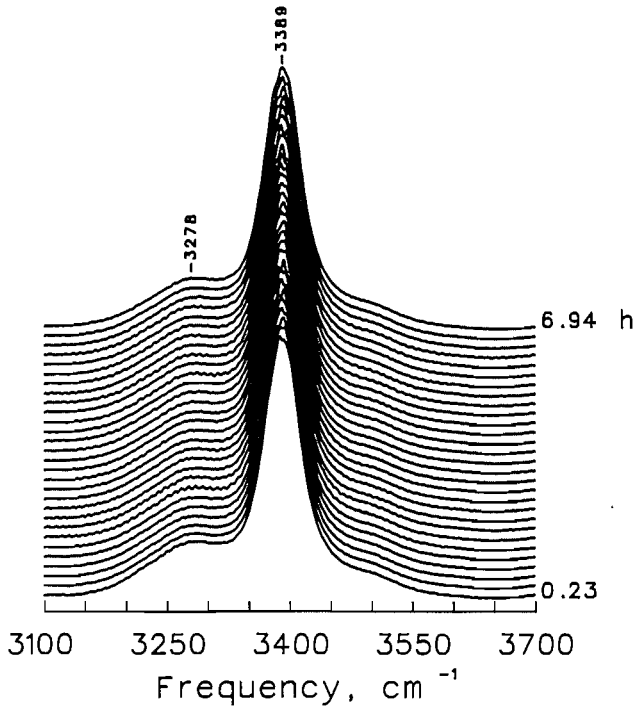


FIG. 5. A stack plot of the uncoupled OH stretching band of a D_2O solution of chymotrypsinogen at 28.9 kbar as a function of time.

in the ice VII state, the H/D exchange still takes place continuously with time, which is evident from the decrease in the $A_{amide\ II}/A_{amide\ I}$ ratio with increasing time (Fig. 4). The general pattern of the H/D exchange at low pressure, i.e., fast in the first several hours and then tapering off, still remains at 28.9 kbar. Therefore, there must be some D_2O molecules in chymotrypsinogen which do not take part in the formation of ice VII at 28.9 kbar and the H/D exchange at 28.9 kbar takes place between these D_2O molecules and the labile protons in chymotrypsinogen. Indeed, this is evident from the infrared spectrum at 28.9 kbar of the uncoupled OH stretching mode of HOD molecules which are present in the commercial D_2O samples as impurities as shown in Fig. 5. It is known that the uncoupled OH stretching mode of ice VII appears as a very sharp band at about 3390 cm^{-1} and that of the bound HOD molecules gives rise to a broad band extending from 3100 to 3700 cm^{-1} (40). As seen in Fig. 5, both the sharp ice VII band and the broad bound water band coexist in the infrared spectrum of the chymotrypsinogen solution in D_2O at 28.9 kbar. Since the integrated intensity of the broad band of bound HDO is comparable with that of the sharp ice VII band of bulk HDO at 28.9 kbar, a significant amount of D_2O molecules are bound to chymotrypsinogen when the protein is dissolved in D_2O. Therefore, in addition to the surface bound D_2O, some D_2O molecules penetrate into the interior cavities of the protein where they are separated from bulk D_2O, which is consistent with the results from X-ray study (5). All these surface and interior bound D_2O molecules do not take part in the formation of ice VII in bulk D_2O at 28.9 kbar and the H/D exchange takes place between labile protons of protein molecules and these bound D_2O molecules. The fact that about 70% of total labile protons are exchanged in about 7 h (see Fig. 4) also indicates that in this ice VII system quite a large amount of D_2O penetrates into the protein interior and binds to the protein molecules when solid chymotrypsinogen is dissolved in D_2O. These results indicate that the H/D exchange picture in chymotrypsinogen is close to that described by the regional melting mechanism (5). Apparently, no collective small amplitude fluctuations or mobile defects are required for this penetration process as suggested by the penetration mechanism of H/D exchange. Moreover, since the H/D exchange takes place in the interior of the protein molecules, no movement of the unfolded segment into bulk solvent on the surface of the protein molecules is necessary for the H/D exchange as suggested by the local unfolding hypothesis. At 28.9 kbar, chymotrypsinogen is denatured, and thus the H/D exchange should be fast and all the "hard-to-exchange" protons should be converted into "easy-to-exchange" protons similar to that observed at 18.9 kbar. However, the fast exchange rate constant at 28.9 kbar is smaller than that at 12.8 kbar and 32% of the labile protons remain unexchanged after 24 h (see Table 1). These results suggest that the availability of the exchangeable D_2O molecules decreases with time at 28.9 kbar and imply that the diffusion and exchange between bound D_2O and bulk D_2O which is in the ice VII state at 28.9 kbar is extremely slow.

1. F.-R. N. GURD and T. M. ROTHGEB. Adv. Protein Chem. **33**, 73 (1979).
2. C. K. WOODWARD and B. D. HILTON. Ann. Rev. Biophys. Bioeng. **8**, 99 (1979).
3. S. W. ENGLANDER, N. W. DOWNER, and H. TEITELBAUM. Rev. Biochem. **41**, 903 (1972).
4. R. G. GREGORY and A. ROSENBERG. Methods Enzymol. **131**, 448 (1986).
5. A. A. KOSSIAKOFF. Nature, **296**, 713 (1982).
6. A. D. BARKSDATL and A. ROSENBERG. Methods Biochem. Anal. **28**, 1 (1982).
7. C. K. WOODWARD, I. SIMON, and E. TCHSEN. Mol. Cell. Biochem. **48**, 135 (1982).
8. S. W. ENGLANDER and J. J. ENGLANDER. *In* Structure and dynamics: nucleic acids and proteins. *Edited by* I. Clementi and R. H. Sarma. Academic Press, New York. 1983.
9. P. T. T. WONG. *In* High pressure chemistry and biochemistry.

Can. J. Chem. Downloaded from www.nrcresearchpress.com by 123.30.183.119 on 09/07/12
For personal use only.

Edited by R. Van Eldik and J. Jonas. NATO ASI Ser. C. Reidel, Dordrecht. 1987. pp. 381-400.
10. P. T. T. WONG. *In* Current perspective in high pressure biology. *Edited by* H. W. Jannasch, R. E. Marquis, and A. M. Zimmerman. Academic Press, New York. 1987.
11. P. T. T. WONG. *In* Vibrational spectra and structure. Vol. 16. *Edited by* J. R. Durig. Elsevier, Amsterdam. 1987. pp. 357–445.
12. P. T. T. WONG. Ann. Rev. Biophys. Bioeng. **13**, 1 (1984).
13. P. T. T. WONG, and K. HEREMANS. Biochem. Biophys. Acta, **956**, 1 (1988).
14. P. T. T. WONG, I. S. GIROUS, Y. GUILLON, G. N. COHEN, O. BRZU, and H. H. MANTSCH. Biochem. Biophys. Acta, **996**, 260 (1989).
15. F. S. PARKER. Application of infrared spectroscopy in biochemistry, biology and medicine. Plenum Press, New York 1971.
16. S. A. HAWLEY. Biochemistry, **10**, 2436 (1971).
17. T. M. LI, J. W. HOOK, H. G. DRICKAMER, and G. WEBER. Biochemistry, **15**, 5571 (1976).
18. G. S. CHRYSOMALLIS, P. M. TORGERSON, H. G. DRICKAMER, and G. WEBER. Biochemistry, **20**, 3955 (1981).
19. K. HEREMANS. Ann. Rev. Biophys. Bioeng. **11**, 1 (1982).
20. K. HEREMANS. *In* Current perspective in high pressure biology. *Edited by* H. W. Jannasch, R. E. Marquis, and A. M. Zimmerman. Academic Press, New York. 1987. pp. 224–234.
21. G. WEBER and H. G. DRICKAMER. Quant. Rev. Biophys. **16**, 89 (1983).
22. J. F. BRANDTS, R. J. OLIVERA, and C. WESTORT. Biochemistry, **9**, 1038 (1970).
23. A. ZIPP and W. KAUZMANN. Biochemistry, **12**, 4217 (1973).
24. S. J. GILL and R. I. GLOGOVSKY. J. Phys. Chem. **69**, 1515 (1965).
25. R. K. WILLIAMS, C. A. FYFE, D. BRUCK, and L. V. VEEN. Biochemistry, **18**, 757 (1979).
26. B. NYSTROM and J. ROOTS. Makromol. Chem., **185**, 1441 (1984).
27. K. HEREMANS and P. T. T. WONG. Chem. Phys. Lett., **118**, 101 (1985).
28. C. E. KUNDROT and F. M. RICHARDS. J. Mol. Biol. **193**, 157 (1987).
29. P. T. T. WONG, D. J. MOFFATT, and F. L. BAUDAIS. Appl. Spectrosc. **39**, 733 (1985).
30. H. SUSI. *In* Structure and stability of biological macromolecules. *Edited by* S. N. Timasheff and G. D. Fasman. Marcel Dekker, New York. 1969.
31. L. WILLUMSEN. Compt. Rend. Trav. Lab. Carlsberg, **36**, 327 (1968).
32. A. HVIDT. Compt. Rend. Trav. Lab. Carlsberg, **33**, 475 (1963).
33. K. R. BHASKAR and F. S. PARKER. J. Biol. Chem. **245**, 3302 (1970).
34. F. S. PARKER. Application of infrared Raman and resonance Raman spectroscopy in biochemistry. Plenum Press, New York. 1983.
35. G. WEBER. 1987. *In* High pressure chemistry and biochemistry. *Edited by* R. Van Eldik and J. Jonas. NATO ASI Ser. C. Reidel, Dordrecht. 1987. pp. 401–420.
36. H. B. BENSUSAN and S. O. NIELSEN. Biochemistry, **3**, 1367 (1964).
37. E. R. BLOUT, C. DELOZE, and A. ASADOURIAN. J. Am. Chem. Soc. **83**, 1895 (1961).
38. G. WAGNER and K. WTHRICH. J. Mol. Biol., **134**, 75 (1979).
39. P. T. T. WONG and D. J. MOFFATT. Appl. Spectrosc., **41**, 1070 (1987).
40. P. T. T. WONG and C. H. HUANG. Biochemistry, **8**, 99 (1989).

Can. J. Chem. Downloaded from www.nrcresearchpress.com by 123.30.183.119 on 09/07/12
For personal use only.

Infrared spectra of tautomers and rotamers of 9-methylguanine. An experimental and theoretical study[1]

K. SZCZEPANIAK, M. SZCZESNIAK, W. SZAJDA,[2] AND W. B. PERSON[3]
Department of Chemistry, University of Florida, Gainesville, FL 32611-2046, U.S.A.

AND

J. LESZCZYNSKI
Department of Chemistry, Jackson State University, Jackson, MS 39217, U.S.A.

Received May 24, 1991

This paper is dedicated to Dr. Richard Norman Jones

K. SZCZEPANIAK, M. SZCZESNIAK, W. SZAJDA, W. B. PERSON, and J. LESZCZYNSKI. Can. J. Chem. **69**, 1705 (1991).

Both amino-oxo and amino-hydroxy tautomeric forms of 9-methylguanine have been identified in approximately equal abundance in infrared studies of these molecules isolated in the hydrophobic environment of an argon matrix at 12 K. The amino-hydroxy tautomer occurs in two different rotamers correlated with the rotation of the OH group. The ratio of concentrations of the two rotamers is sensitive to UV irradiation, and this ratio then relaxes to an equilibrium value after irradiation is stopped. This sensitivity allows us to separate the experimental spectra related to the oxo tautomer and to each of the rotamers of the hydroxy tautomer. The relative concentrations of the amino-oxo and amino-hydroxy tautomers ([a-o]/[a-h] = K(o-h) = 1.0 ± 0.3) and of the two rotamers (K(h1-h2) = 0.31 ± 0.10 in an argon matrix at 12 K and about 30 ± 15 in the vapor at 470 K) are estimated from the observed relative infrared absorbances. From these relative concentrations the differences between the free energies of the tautomers (ΔG_{470} (o-h) = 0 ± 0.5 kJ mol^{-1}) and of the two rotamers (ΔG(h1-h2) = 0.12 ± 0.03 kJ mol^{-1} in the argon matrix at 12 K and ΔG_{470} between +2 and −13 kJ mol^{-1} in the vapor at 470 K) have been estimated. The electronic absorption spectrum of 9-methylguanine isolated in the argon matrix at 12 K and the effect of brief ultraviolet irradiation on it have also been studied. In an effort to interpret the experimental results, *ab initio* calculations of the infrared spectra have been made for 9-methylguanine at the 3-21G//3-21G level. Comparison with the experimental spectra is of some help with the assignment of the infrared spectra for the different tautomers.

Key words: 9-methylguanine, tautomerism, infrared and ultraviolet spectra, matrix isolation, *ab initio* calculation.

K. SZCZEPANIAK, M. SZCZESNIAK, W. SZAJDA, W. B. PERSON et J. LESZCZYNSKI. Can. J. Chem. **69**, 1705 (1991).

Des études infrarouges effectuées dans un environnement hydrophobe, dans une matrice d'argon, à 12 K, on permis de mettre en évidence des quantités pratiquement égales des formes tautomères amino-oxo et amino-hydroxy de la 9-méthylguanine. Le tautomère amino-hydroxy se retrouve dans deux rotamères différents reliés à la rotation du groupe OH. Le rapport des concentrations des deux rotamères est sensible à l'irradiation UV; ce rapport retourne vers une valeur d'équilibre lorsqu'on cesse l'irradiation. Cette sensibilité nous permet de séparer le spectre expérimental relié au tautomère oxo et à chacun des rotamères du tautomère hydroxy. En se basant sur les absorptions relatives observées dans l'infrarouge, on a évalué les concentrations relatives des tautomères amino-oxo et amino-hydroxy ([a-o]/[a-h] = K(o-h) = 1,0 ± 0,3) et deux rotamères (K(h1-h2) = 0,31 ± 0,10 dans une matrice d'argon à 12 K et d'environ 30 ± 15 en phase vapeur à 470 K). Sur la base de ces concentrations relatives, on a évalué les différences entre les énergies libres des tautomères (ΔG_{470}(o-h) = 0 ± 0,5 kJ mol^{-1}) et des deux rotamères (ΔG(h1-h2) = 0,12 ± 0,03 kJ mol^{-1} dans la matrice d'argon à 12 K alors que le ΔG_{470}, en phase vapeur à 470 K, se situe entre +2 et −13 kJ mol^{-1}). On a aussi étudié le spectre d'absorption électronique de la 9-méthylguanine isolée dans la matrice d'argon à 12 K ainsi que l'effet d'une brève irradiation avec de l'ultraviolet. Dans le but d'interpréter les résultats expérimentaux, on a effectué des calculs *ab initio* au niveau 3-21G//3-21G des spectres infrarouges de la 9-méthylguanine. Une comparaison des résultats de ces calculs avec les spectres expérimentaux est utile pour attribuer les spectres infrarouges des divers tautomères.

Mots clés : 9-méthylguanine, tautomérie, spectres infrarouge et ultraviolet, isolement dans une matrice, calculs *ab initio*.

[Traduit par la rédaction]

Introduction

There are at least two reasons for studying infrared (IR) spectra of nucleic acid bases isolated in an inert environment such as that provided by isolation in an argon matrix. First, such studies are necessary to obtain data for testing the reliability of predictions from quantum mechanical *ab initio* calculations with different basis sets of properties (particularly the vibrational spectra) for these molecules. Such calculations are at present possible only for individual isolated molecules, so that their predictions *must* be tested with data from studies of molecules unperturbed by intermolecular interactions. Matrix isolation studies of the nucleic acid bases provide uniquely such experimental data. If the quantum mechanical calculations with a given basis set predict accurate values for vibrational properties and relative energies of smaller isolated bases, one can hope that similar calculations might also successfully predict vibrational properties, energies, and conformations for the larger biomolecules.

The second reason for studies of the spectra of isolated molecules is to determine spectra, for non-interacting molecules, that serve as a reference for comparison with corresponding spectra of molecules incorporated in DNA or RNA from studies of solutions or solids where the vibrations of the nucleic acid bases are affected by their mutual interactions and by interactions with the solvent or in the crystal (e.g., see refs. 1–6

[1]We believe that our extensive use of the computer in analyzing the data for this paper makes it especially appropriate for this special issue dedicated to Dr. Norman Jones. We have certainly kept in mind his cautionary advice in our analysis, so that he has always been in our minds as we wrote it.

[2]On leave of absence from the Department of Chemistry, A. Mickiewicz University, Poznań, Poland.

[3]Author to whom correspondence may be addressed.

Printed in Canada / Imprimé au Canada

Can. J. Chem. Downloaded from www.nrcresearchpress.com by 84.41.108.74 on 09/07/12
For personal use only.

and references given there). Such comparisons are expected to provide valuable information concerning the nature of these interactions and their effects on the vibrations of molecules.

A number of studies of tautomerism have been made for nucleic acid bases and their analogues (see refs. 7*a*–*d* and references therein), including studies of molecules isolated in the gas phase (see ref. 8, and references therein) and in inert noble gas matrices (see refs. 9, 10, and references therein). In addition there have been several studies concerning the effect of UV irradiation on the matrix-isolated nucleic acid bases (see ref. 10, and references therein).

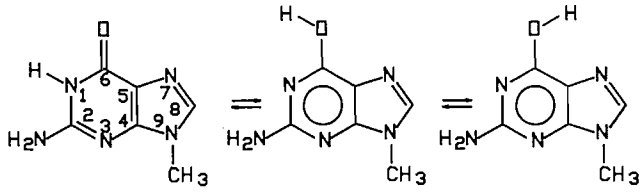
Guanine and 9-methyl- (or 9-ethyl) guanine are the only nucleic acid bases of biological significance for which high concentrations of the "rare" amino-hydroxy tautomer have been found to occur in the gas phase (8*h*) and in an inert hydrophobic environment formed by condensation of a thermal molecular beam of these molecules in a large excess of argon (i.e., in a low-temperature argon matrix held on a cold window at 12 K) (11–14). The most recent *ab initio* quantum mechanical calculations (15, 16) performed for guanine with a 6-31G (d, p) basis set at the MBPT2 level (single point calculation), with zero point vibrational energy included, confirm the results from the experimental observations that the energy of the amino-hydroxy (a-h) tautomer is nearly the same as that of the amino-oxo (a-o) tautomer ($E_{a\text{-}o} - E_{a\text{-}h} = -5.1$ kJ mol^{-1} (16*a*)). *Ab initio* calculations of the vibrational spectra of the a-o tautomer of guanine had been made before, using STO-3G (17) and 3-21G (12) basis sets. As far as we know there have been no published results from *ab initio* calculations of the vibrational frequencies and intensities for the amino-hydroxy tautomers of guanine or 9-methylguanine (9MG).

In our previous study (13) we showed that the relative concentration of the tautomers of 9MG can be changed by ultraviolet (UV) irradiation of the matrix over a long period of time (about 12 h), which probably causes photodecomposition of the a-o and a-h tautomers at different rates. In the present paper we report results of a recent experimental study of the infrared (IR) absorption spectra and rotational isomerism observed for the hydroxy tautomer as well as the effect of brief (2–5 min) UV irradiation on the relative concentrations of the rotational isomers. The results from our previous study (13) of the effect of long-lasting UV irradiation provided additional help with the analysis of the spectra of the different tautomers and rotamers and with the vibrational assignment of the experimentally observed bands to the normal modes of the a-o and a-h forms. The spectrum of the a-h tautomer discussed in ref. 13 corresponds to that of the hydroxy form in the relaxed state (a-h2) discussed here.

Methods

Experimental

The experimental procedure and conditions for preparing the low-temperature matrix and recording the IR spectra with the Nicolet model 740 FTIR spectrometer were the same as those described elsewhere (18). The spectra were studied at a spectral resolution of 1 cm^{-1}. The sample of 9MG was kindly provided to us by Professor Nelson Leonard of the University of Illinois (for a description of the synthesis see ref. 8*h*). It was additionally purified by vacuum sublimation in the process of preparing the matrix sample. The temperature of the sublimation was about 200°C, much below the melting point. There was no indication of any thermal decomposition of samples heated to this temperature, as shown by IR spectra from the solid films remaining on the window after evaporating the argon that were *identical* with spectra from KBr pellets of the original unheated solid 9MG sample.



SCHEME 1

The matrix sample was obtained by passing argon gas over the subliming sample and condensing the resulting gaseous mixture (with 9MG:Ar ratio of about 1:1000) onto a cold CsI window mounted in a closed cycle He cryostat (Displex model CSA 202E) and cooled to about 12 K.

The matrix sample was irradiated for 2–5 min by focussed UV light, which passed through a water filter 7 cm thick. The source of the UV light was a 100-W medium-pressure mercury lamp. The IR spectrum of a solid film of 9MG remaining after evaporation of the argon from the matrix after the UV irradiation (2–5 min) did not show any measurable new features when compared with the spectrum of solid 9MG (in KBr) that had not been irradiated with UV light. From this observation it follows that the *2–5 min* UV irradiation through this filter does not cause measurable photodecomposition of the matrix-isolated sample, as had been observed for long-lasting UV irradiation.

The electronic absorption spectrum of 9MG isolated in the argon matrix was studied using a Nicolet model 9420 UV/VIS spectrophotometer, with the same technique for forming the matrix-isolated sample and UV irradiation as described above for the infrared study.

Calculation

An *ab initio* LCAO calculation (19) was carried out using the GAUSSIAN 86 program (20) with a split valence 3-21G basis set (19). The geometries of the tautomers and rotamers were optimized by the gradient procedure (21). To simplify the calculation, it was assumed that all molecules were planar (C_s symmetry) and the geometry optimization was performed within this restriction. The calculated structures are shown in Scheme 1.

The force constants for the optimized structures gave positive frequencies for all modes except for the torsion of the methyl group about the CN9 bond, indicating that the conformation of the CH_3 group for our calculations did not correspond to the minimum energy value. It is expected that this error will have no effect on any of the other normal modes of the molecule. All optimized structures were characterized by analysis of the harmonic vibrational frequencies obtained by diagonalizing the force-constant matrices. To account for the errors due to the small basis set and for anharmonicity of the vibrations, the calculated frequencies for in-plane modes were multiplied by a scaling factor of 0.90 (22), the OH stretch by 0.918 (23), and those for the out-of-plane modes (excluding the modes involving the CH_3 group, which used the 0.9 factor) by a factor of 0.81 (see ref. 24) for comparison with the experimental spectra. The calculated intensities are compared with the relative intensities measured in the experimental spectra.

Results and discussion

Tautomerism and rotational isomerism of 9MG

The most easily derived information about hydroxy ↔ oxo tautomerism and about the rotational isomerism in the hydroxy tautomer of the 9MG molecule is obtained from the spectral region related to the characteristic stretching vibrations of the OH, NH, and CO bonds involved in these transformations. Other vibrational modes, although very important from the

Can. J. Chem. Downloaded from www.nrcresearchpress.com by 84.41.108.74 on 09/07/12
For personal use only.

Can. J. Chem. Downloaded from www.nrcresearchpress.com by 84.41.108.74 on 09/07/12
For personal use only.

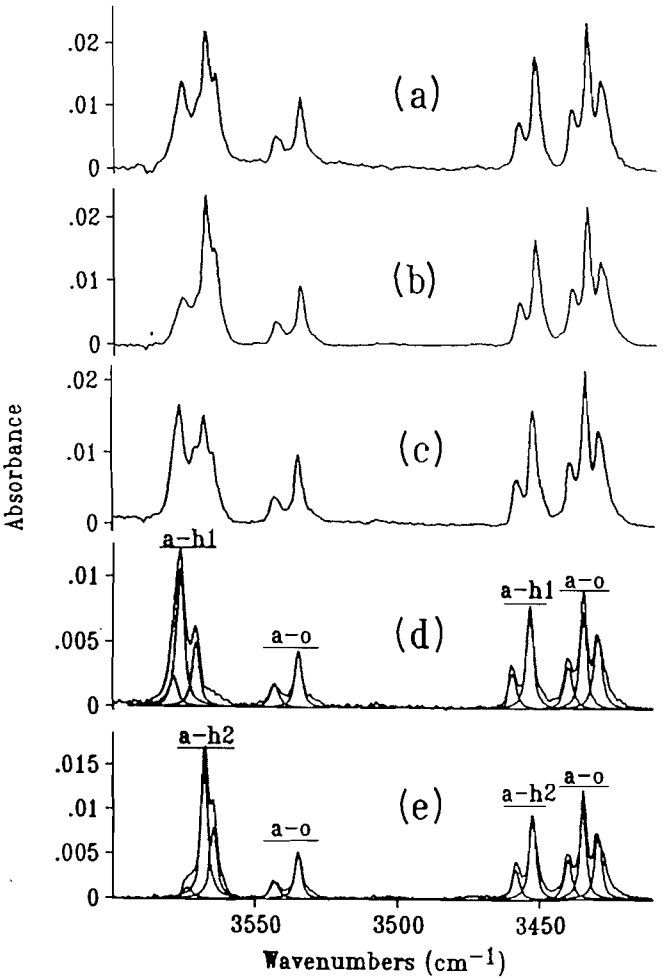


FIG. 1. The infrared spectrum in the OH and NH stretching region for 9MG isolated in an argon matrix at about 12 K. (a) Spectrum recorded just after deposition, recorded using only 5 scans to minimize the effect of relaxation during the scan time. (b) Spectrum of the same matrix as in (a), but after 2 hours relaxation, recorded using 200 scans. (c) Spectrum from the same sample as in (b) after 5 min of UV irradiation, recorded using 32 scans to mimimize relaxation during the scans. (d) The difference spectrum obtained from the subtraction (c − b = d). Spectrum (d) corresponds to that from a mixture of rotamer a-h1 and the a-o tautomer. (e) The difference spectrum obtained from the subtraction (b − c = e). Spectrum (e) corresponds to that from a mixture of rotamer a-h2 and tautomer a-o. Both spectra (d) and (e) show the separated components for the overlapping bands obtained from the deconvolution procedure. The weak band at 3572 cm^{-1} is due to the water dimer impurity.

spectroscopic and analytical points of view, provide much less straightforward information about these particular phenomena, especially because they are made up of strongly coupled motions of several atoms in the molecule. The entire experimental IR spectrum is discussed at the end of this paper where we propose a vibrational assignment base on *ab initio* calculations of different tautomers and rotamers of 9MG.

For now, let us focus on the IR spectrum of 9MG in the characteristic region related to the OH and NH stretching vibrations shown in Fig. 1.

The spectrum of the matrix sample of 9MG obtained immediately after deposition is shown in Fig. 1(a), while spectrum (b) is from the same matrix at the same temperature after a period of 2 hours relaxation. The only visible difference between these two spectra is the drastic change in the intensity distribution in the region between 3580 and 3560 cm^{-1}, where the OH and NH_2 asymmetric stretching modes occur (see ref. 11).

The original intensity distribution can be restored or even reversed by brief (2–5 min) irradiation of the matrix sample by UV light to produce the spectrum shown as (c) in Fig. 1. When the UV irradiated matrix sample is allowed to relax in the dark, the intensity distribution gradually changes until, after about 2 h, it returns to the same spectrum originally observed before UV irradiation (Fig. 1(b)). This process can be repeated over and over again. We interpret the changes in the intensity distribution in this region as due to changes in the relative concentrations of rotamers of the a-h tautomer: the high frequency band in the OH stretch due to a-h1 and the low frequency band to the a-h2 species. Our intuitive expectation for the conformation of these two rotamers was that indicated in Scheme 1 showing the conformations used in the *ab initio* calculations. The first rotamer (a-h1) was expected to have the OH group directed towards the C6—N1 bond (RN1) and the second rotamer (a-h2) to have the OH bond directed towards the C5—N7 bond (RN7). Here we use a different notation (a-h1 or a-h2) to describe the rotamers responsible for the changes in the experimental spectrum from that used to describe the rotamers considered in the calculation (RN1 or RN7) to stress the possibility that they might not be the same. As we shall see below in the discussion of the vibrational assignment of the IR spectrum, other possible conformations (for example with the OH bond out of the plane) might be responsible for the experimental spectra attributed to the rare a-h tautomer of 9MG.

The effect of the UV irradiation on the distribution of intensity in the spectrum from the different rotamers isolated in the low-temperature matrix and the relaxation in the dark observed here is very similar to observations for a number of other molecules reported previously (25–28).

To check whether the change in the intensity distribution during the relaxation process is induced by exposure of the matrix sample to irradiation by the infrared source in the spectrometer, as has been observed for rotational isomers of other smaller molecules isolated in low-temperature matrices (29–37), we observed the relaxation of the matrix in the IR beam as compared with that in the dark (i.e., with the sample cut off from the infrared and UV beams) for the same period of time after UV irradiation. There was no significant difference between the relaxation occurring in the dark and that occurring in the sample exposed to the infrared source.

The IR spectrum of matrix-isolated 9MG is a superposition of the spectra of three species: a-o, a-h1, and a-h2. To obtain the spectrum of each component separately, we utilized the selective effect provided by brief UV irradiation on the distribution of the intensity in the infrared spectra of rotamers a-h1 and a-h2, combined with the subroutines from the SpectraCalc (Galactic Industries Corp.) software for subtraction, multiplication, deconvolution, and integration of the overlapping bands of the multicomponent spectrum. This procedure and the level of uncertainty involved are demonstrated in Figs. 1(d) and 1(e) for that part of the spectrum related to the OH, NH, and NH_2 stretching modes.

Step 1 of the procedure is subtraction of the "relaxed" spectrum obtained before UV irradiation (shown in Fig. 1(b)) from that obtained after brief UV irradiation (shown in Fig. 1(c)) using a multiplication factor that reduces to zero in the

Can. J. Chem. Downloaded from www.nrcresearchpress.com by 84.41.108.74 on 09/07/12
For personal use only.

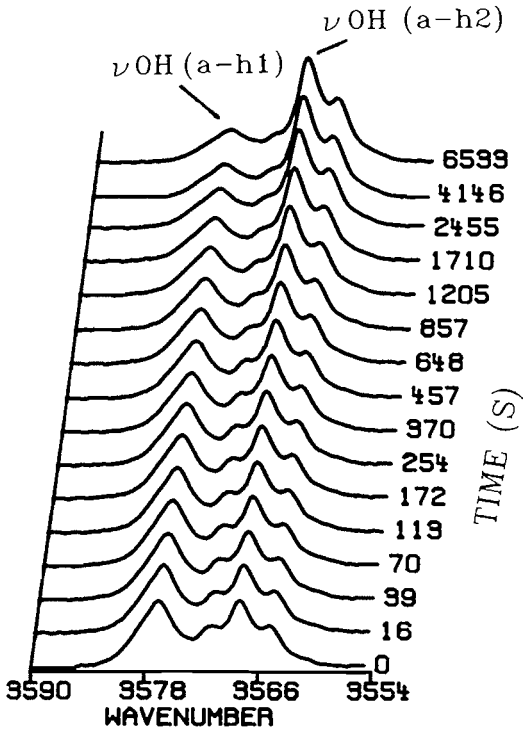


FIG. 2. Time dependence of the intensity distribution in the OH stretching region corresponding to rotamers a-h1 and a-h2 of 9MG isolated in an argon matrix at about 12 K. The spectrum at time $t = 0$ was obtained using 1 scan after UV irradiation of the matrix for 5 min. The number of scans for succeeding traces increases as $N + 1$ for the Nth scan, up to a maximum of 10 scans.

difference spectrum the absorbance of the low-frequency component of the OH stretch related to the a-h2 species. The resulting difference spectrum (Fig. 1(d)) contains only absorption bands due to the a-o and a-h1 species.

Step 2 of the procedure is to subtract the spectrum in Fig. 1(c) from that in Fig. 1(b) using a multiplication factor that reduces to zero the absorbance of the high frequency component of the OH stretch related to the a-h1 species. This difference spectrum (Fig. 1(e)) contains bands corresponding to the a-o and a-h2 species.

Step 3 now applies the band deconvolution subroutine for the bands that overlap in Figs. 1(d) and 1(e), using a band shape that is a mixture of Lorentzian (75%) and Gaussian (25%) functions and allowing the widths and intensities to be optimized, to give the separated absorption components related to the a-o, a-h1, and a-h2 species.

Figure 2 shows the time dependence of the intensity distribution in the OH stretching region for the two bands at 3568 and 3576 cm^{-1}. Because the absorbance, A, at 3576 cm^{-1} attributed to the a-h1 rotamer (and that at 3568 cm^{-1} for the a-h2 rotamer) is proportional to its concentration, the plot in Fig. 3(a) shows the kinetics of the relaxation process. A plot of $\ln(A_t - A_\infty)$, where A_t is the absorbance of either species at time t and A_∞ is the absorbance of that species extrapolated to infinite time, against time will be linear if the relaxation from one rotamer to the other follows first-order kinetics. As can be seen in Fig. 3(b) this plot is exactly linear both for the species whose concentration decreases in the relaxation process and for the species whose concentration increases.

The observed changes in the intensity distribution in the OH stretching region allow us to estimate the difference in the

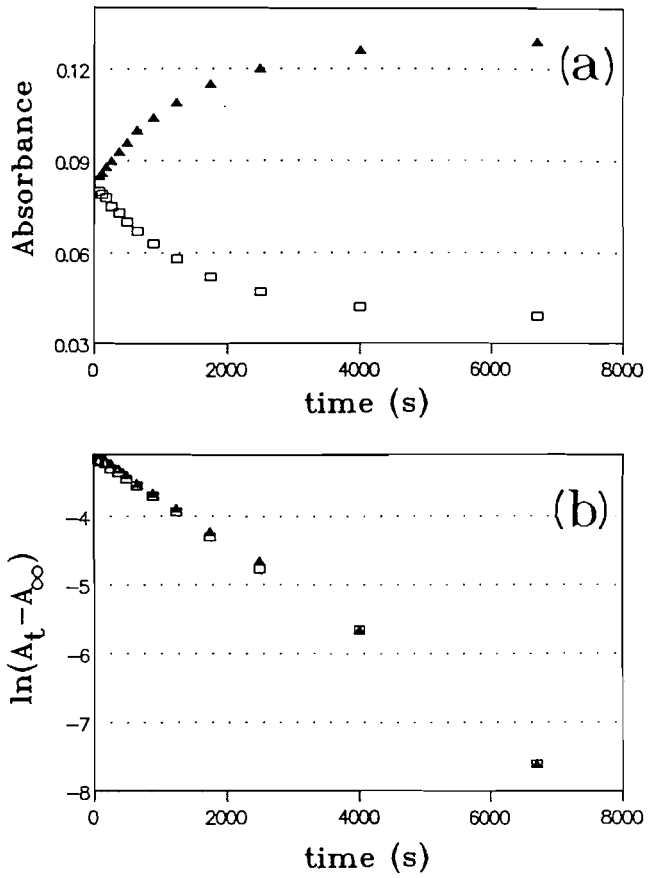


FIG. 3. (a) A graph showing the intensities of the OH stretching modes for the a-h1 and a-h2 rotamers of 9MG as a function of the time after UV irradiation of the matrix sample. (b) A graph showing the dependence of $\ln|A_t - A_\infty|$ on the time after UV irradiation of the matrix sample. Here A_t is the maximum absorbance for the band at time t, and A_∞ is the maximum absorbance of that band at infinite time. This correlation is for the band at 3576 cm^{-1} (Δ) for the a-h1 rotamer and for the band at 3568 cm^{-1} (□) for the a-h2 rotamer. The correlation is given by: $\ln|A_t - A_\infty| = 6.7 \times 10^{-4}t - 3.1$.

stabilization energies for the a-h1 and a-h2 rotamers. We believe that the spectrum of the relaxed matrix sample (shown in Fig. 1(b)) corresponds to the equilibrium concentrations of the rotamers at the matrix temperature (about 12 K). The ratio of the integrated absorbance of the OH band for the a-h1 rotamer at 3576 cm^{-1} to that of the a-h2 rotamer at 3568 cm^{-1} is measured to be $A_{h1}/A_{h2} = K_{12}(h1\text{-}h2) = [a\text{-}h1]/[a\text{-}h2] = 0.31 \pm 0.10$. The error is mainly due to the uncertainty of the decomposition of the overlapping bands. From this value of K, the standard free energy difference at 12 K can be obtained:

$$\Delta G_{12}^0 = -RT\ln K_{12}(h1\text{-}h2) = +0.12 \pm 0.03 \text{ kJ mol}^{-1}$$

with the a-h1 rotamer slightly *less* stable than the a-h2 rotamer. This standard free energy difference is between rotamers isolated in argon at equilibrium.

We have also estimated the free energy difference between rotamers in the vapor phase by looking at the intensity ratio of these same two bands in the spectrum of the "unrelaxed" sample recorded immediately after deposition (spectrum (a) in Fig. 1). For this unrelaxed sample the value of $K(h1\text{-}h2) = 0.62$. If this value of $K(h1\text{-}h2)$ is used as a measure of the equilibrium in the vapor at 470 K, $\Delta G_{470}^0 = +2$ kJ mol^{-1}. Since the deposition occurs over some period of time, the spectrum recorded

immediately after deposition contains contributions from molecules that have partially relaxed as well as from those that have just been deposited without time for any relaxation. We have corrected the absorbances shown in Fig. 1(a) using the relaxation parameters (the rate constant from the slope of the plot shown in Fig. 3(b)): slope = -6.7×10^{-4} and intercept = -3.1. Correction of the original intensity ratio ($A_{h1}/A_{h2} = 0.62$) by extrapolation to the time for the beginning of the deposition (about 39 min) gives an estimated upper limit for the equilibrium constant, for the vapor at 470 K, of K_{470}(h1-h2) = 30. If we use this value for K_{470} in the equation for ΔG^0, we find that our estimate for the standard free energy change from the a-h2 rotamer to the a-h1 rotamer in the gas phase is $\Delta G_{470}{}^0$ (h1-h2) = -13 kJ mol^{-1}. The "true" value of $\Delta G_{470}{}^0$(h1-h2) thus lies between +2 and -13 kJ mol^{-1}.

Finally, we should note here that we have remeasured the equilibrium constant for the hydroxy ↔ oxo tautomeric equilibrium in the same way as is described above for the rotameric equilibria. The result is K(o-h) = [a-o]/[a-h] = 1.0 ± 0.3, agreeing with our previous estimate (K(o-h) = 1.25 (ref. 13)) within the experimental error. Assuming that the appropriate temperature for this equilibrium is 470 K, the standard free energy change for this tautomerization is $\Delta G_{470}{}^0 = 0 \pm 0.5$ kJ mol^{-1}. There is no time "relaxation" effect on this equilibrium.

The experimental estimates of the values of ΔG, both for the tautomeric equilibrium and for the rotameric equilibrium, may be compared with the relative internal energy differences, ΔE (including zero point energies, ZPE). calculated at the HF/6-31G(d)//3-21G level for these equilibria:

$$\Delta E_1 = E_{a\text{-}o} - E_{RN7} = -9.8 \text{ kJ mol}^{-1}$$
$$\Delta E_2 = E_{a\text{-}o} - E_{RN1} = -5.2 \text{ kJ mol}^{-1}$$
$$\Delta E_3 = E_{RN1} - E_{RN7} = -4.6 \text{ kJ mol}^{-1}$$

These predictions are to be compared with the experimental estimates, at 470 K for the vapor:

$$G_{a\text{-}o} - G_{a\text{-}h} = 0 \text{ kJ mol}^{-1}$$
$$G_{a\text{-}h1} - G_{a\text{-}h2} = (\text{from } +2 \text{ to } -13) \text{ kJ mol}^{-1}$$

and in the matrix at 12 K:

$$G_{a\text{-}h1} - G_{a\text{-}h2} = 0.12 \text{ kJ mol}^{-1}$$

The calculated energy differences include the difference in zero point vibrational energies at the 3-21G level. We believe that the agreement between the experimental and theoretically predicted values may be within the uncertainty of the calculation, although it is possible that the equilibria studied experimentally are for different species than for the calculation (see below).

Vibrational assignment of the infrared spectra

Figure 4a shows the infrared spectrum (3600–400 cm^{-1}) measured for 9MG isolated in an Ar matrix recorded just after deposition and relaxation of the matrix. Figure 4b presents the spectrum of the same matrix after short (5 min) irradiation with the UV light. Comparison of these two spectra shows that brief UV irradiation causes changes in many spectral regions. The most clearly visible changes are observed in the 3580–3560 cm^{-1} and 1350–1150 cm^{-1} regions. When a UV-irradiated matrix is left for some time to relax, its spectrum converts back to the original one (Fig. 4a).

Subtracting the spectrum in Fig. 4(a) from that in Fig. 4(b) leads to the spectrum shown in Fig. 4(c). Here, the lower part (negative) shows all absorption bands (related to a-h1) that increase their absorbance as a result of UV irradiation, while the upper part (positive) indicates all bands (related to a-h2) for which the relative absorbance decreases with the UV irradiation. All bands that are not affected by UV irradiation cancel out and do not appear in the difference spectrum. Also bands with the same frequency for each rotamer cancel, as for example the bands at 3459 and 3453 cm^{-1}.

The main features of the difference spectrum in Fig. 4(c) are (1) a total absence of absorption from the C=O stretching mode (near 1740 cm^{-1}); and (2) the appearance of the well-resolved features in the positive and negative parts of the spectra in many regions, particularly in that of the OH stretching modes (near 3576 and 3568 cm^{-1}) and in the region of COH bending modes 1350–1150 cm^{-1}). These observations confirm the suggestion above based upon the changes in the OH, NH, and NH_2 region that this brief UV irradiation affects only the hydroxy tautomer of 9MG, and it seems most likely that this irradiation affects only the rotation of the OH group. Applying the subtraction procedure with different multiplication factors and the band decomposition procedure as described above for the OH and NH spectral region, we were able to obtain the separated spectra over the entire IR region for the two rotamers a-h1 and a-h2 of the amino-hydroxy tautomer and the amino-oxo tautomer (a-o).

These results are summarized in Table 1, where the first two columns collect "unprocessed" frequencies and maximum absorbances for all bands observed in the experimental spectrum of the relaxed matrix. The next six columns give the integrated intensities of the particular bands, obtained from the experimental spectrum using the subtraction, decomposition, and integration routines as mentioned above, together with the vibrational assignments of these bands.

Comparison of the experimental and calculated spectra

Table 2 summarizes the frequencies, intensities, and descriptions of the normal modes (potential energy distributions, PEDs) obtained from the *ab initio* calculations for the RN1 and RN7 rotamers of the a-h tautomer, and the results for the a-o tautomer. The definition of the symmetry coordinates needed to interpret the PEDs is given in Table 3.

Figure 5 shows a comparison of the experimental (a-o, a-h1, and a-h2) and calculated (a-o, RN1, and RN7) spectra. A more detailed comparison of the frequencies and intensities in the experimental and calculated spectra for each normal mode of each species can be obtained by comparing data listed in Tables 1 and 2. As seen in Table 1, there are several spectral regions where frequencies of the different tautomers and rotamers are very similar or even identical. In attempting to separate the absorption bands for the different species in these regions we rely strongly on the *relative intensities* of the bands in the difference spectra corresponding to the mixture of a-o and a-h1 and (or) of a-o and a-h2 species obtained after using the subtraction procedure described above and shown in Figs. 1(d), (e) so that we were able to identify which species was responsible for which absorption.

There could be several reasons for discrepancies between experimental and calculated spectra; some of these are suggested below.

1. The limitations involved in the calculation of spectra for this large molecule using this small 3-21G basis set are expected to cause discrepancies. This limitation might be particularly important in the vibrational assignment of ring modes, for which contributions from different atoms are known to depend relatively strongly on the basis set used, and it is known

Can. J. Chem. Downloaded from www.nrcresearchpress.com by 84.41.108.74 on 09/07/12
For personal use only.

Can. J. Chem. Downloaded from www.nrcresearchpress.com by 84.41.108.74 on 09/07/12
For personal use only.

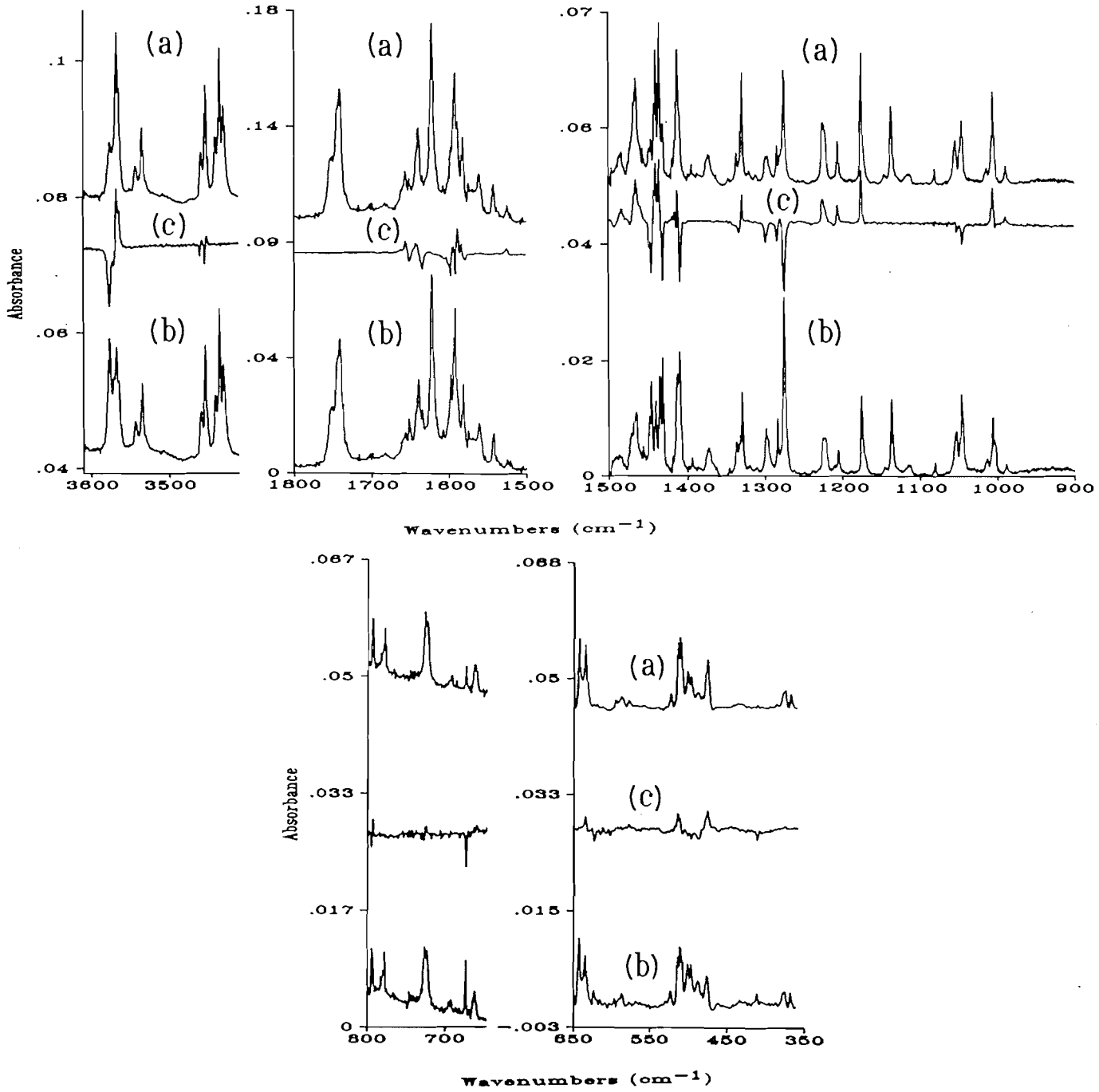


FIG. 4. Infrared spectrum of 9MG isolated in an argon matrix at about 12 K. (Regions where no (or only very low) absorption was observed are not shown.) (a) Spectrum obtained after the sample had relaxed for about 2 h after deposition, using 200 scans. (b) Spectrum obtained (using 32 scans) after sample a was irradiated by UV light for 5 min. (c) The difference spectrum (a − b) corresponding to the spectrum from a mixture of the a-h1 rotamer (negative bands) and the a-h2 tautomer (positive bands).

to be important for the out-of-plane modes (e.g., near 500–450 cm^{-1}) because these modes are predicted with intensities too high and also with frequencies too high after scaling by the factor of 0.9. The calculated frequencies for the out-of-plane modes are found to agree better with the experimental values when they are scaled by 0.81 rather than 0.9. This effect from the use of the 3-21G basis set is seen clearly in the comparison of the experimental spectra of uracil with the calculated vibrational spectra using 3-21G, 6-31G(d), and 6-31G(d,p) basis sets (38)).

2. The harmonic approximation made in calculating the spectra does not account for anharmonic effects, particularly Fermi resonance splittings, which are likely to be present in experimental spectra (e.g., in the carbonyl stretching region (40)).

3. Restricted rotation of the NH_2 group probably results in splitting each of the NH_2 stretching modes into two components (see the experimental spectra in Figs 1. and 4 in the region around 3540 and 3450 cm^{-1}, related, respectively, to the

Can. J. Chem. Downloaded from www.nrcresearchpress.com by 84.41.108.74 on 09/07/12
For personal use only.

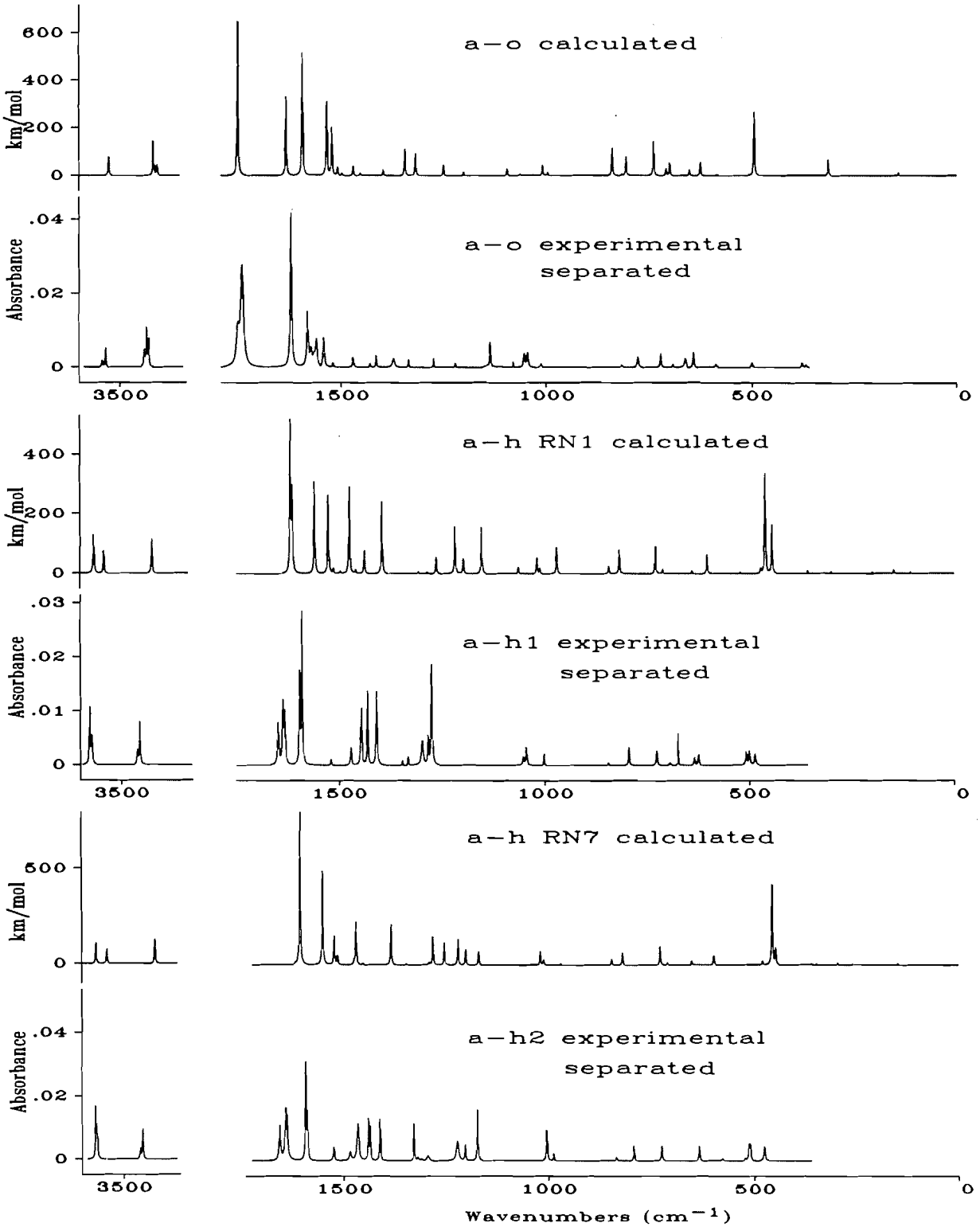


FIG. 5. Comparison of the separated experimental infrared spectra for the a-o tautomer and the a-h1 and a-h2 rotamers of 9MG isolated in an argon matrix at 12 K and with the spectra calculated using a 3-21G basis set for the a-o tautomer and for the RN1 and RN7 rotamers shown in Scheme 1. The simulation of the calculated spectra is made by setting the intensity at the maximum equal to the value of the calculated absolute intensity, choosing the band contour to be a mixture of Lorentzian (75%) and Gaussian (25%) shapes, and using a value of 3 cm^{-1} for the full width of the band at half the maximum intensity.

TABLE 1. Experimental frequencies (FREQ), absorbances at maxima (ABS), relative intensities (INT) and vibrational assignment for the amino-oxo tautomer (a-o) and for two rotamers of the amino-hydroxy tautomer (a-h1) and (a-h2) of 9-methylguanine isolated in Ar matrix at 12 K

Experimental spectrum (relaxed)		Amino-oxo		Amino-hydroxy			
				a-h1		a-h2	
FREQ	ABS[a]	INT[b]	MODE[c]	INT[d]	Assignment[e]	INT[f]	Assignment[e]
3576	0.007			125	OH st		
3571sh	0.008			56	Am a st		
3568	0.024					157	OH st
3565	0.015					84	Am a st
3544	0.004	44	1				
3535	0.009						
3459	0.007			118*	Am s st	128*	Am s st
3453	0.017						
3440	0.009	85	2				
3435	0.022						
3430	0.013	46	3				
3157	0.001	3	4	2	C8H st	2	C8H st
2988	0.001	4	5	3	Me a st	3	Me a st
2961	0.001	10	6	4	o Me a st	7	o Me a st
2925	0.002	4	7	5	Me s st	2	Me s st
1752	0.023	662*	8				
1741	0.050						
1657	0.015					164	R st
1652	0.013			112	R st		
1643sh	0.022			169		398	HNH be
1640	0.033						
1635	0.014			115	HNH be		
1622	0.075	381	9				
1598	0.027			182	R st		
1593	0.056					302	R st
1591sh	0.045			294	R st		
1589	0.037					118	R st
1584sh	0.024					60	R st
1582	0.031	77	10				
1575	0.013	163	11				
1566	0.011						
1561	0.018						
1542	0.014	78	12				
1524	0.006					58	R st
1520	0.002	7	14	13	R st		
1493	0.002					58	R st
1485	0.005						
1471	0.007	22	15	46	R st		
1465	0.018					239	R st
1448	0.006			51	R st		
1445	0.007			90			
1441	0.014					135	R st
1440	0.022						
1435	0.027					137	
1431	0.010			123	R st		
1429sh	0.008	7	16				
1418	0.005	10	17				
1415sh	0.007						
1412	0.023					146	R st
1409sh	0.011			172	R st		
1372	0.005	32	18				
1346	0.001			8	Me sci		
1336	0.005	10	19				
1332	0.003			20	R st, HOC be		

Can. J. Chem. Downloaded from www.nrcresearchpress.com by 84.41.108.74 on 09/07/12
For personal use only.

TABLE 1 (*concluded*)

Experimental spectrum (relaxed)		Amino-oxo		Amino-hydroxy a-h1		Amino-hydroxy a-h2	
FREQ	ABS[a]	INT[b]	MODE[c]	INT[d]	Assignment[e]	INT[f]	Assignment[e]
1329	0.018					95	R st, C8H be
1320	0.002					16	
1310	0.002					10	
1298	0.004			92	R st, C8H be		
1295	0.005					41	C8H be
1283	0.006			44	R st, C8H be		
1275	0.019	9	21	257	R st, HOC be		
1225	0.010	6	22			150	
1221sh	0.009	6	22			49	R st, C8H be, HOC be
1205	0.007						
1174	0.021					168	
1145	0.002						
1136	0.013	45	24				
1113	0.002						
1080	0.003	4	25				
1053	0.008	32	26	19	NH2 ro, R st, R de		
1046	0.011	41	27	47			
1012	0.003	8	28				
1005	0.015					118	R de
1002	0.005			17	R st		
988	0.003					20	R st, R de
844	0.001			3	o R de, o C8H wag		
834	0.001					6	o R de, o C8H wag
817	0.002	5	29				
813	0.005	2	32				
794sh	0.004			35	o C8H wag, o R de		
792	0.008					45	o C8H wag, o R de
777	0.007	29	30				
725	0.010			35	o C2NAm wag, o R de	59	o C2NAm wag, o R de
722	0.009	28	31				
695	0.001			10	o R de		
691	0.002	5	33				
686	0.002						
674	0.004			28	o R de		
661	0.004	32	36				
644sh	0.005	29	35				
642	0.010						
634	0.009					55	R de, CO be
632sh	0.004			18	R de		
623	0.001			23	R de		
586	0.002	9	38				
577	0.001					14	CO be, R str
522	0.002					11	R de
513	0.010					54	o OH tor
511	0.010					55	
508sh	0.006			34	o C2NAm wag		
500	0.006			37	R de		
496	0.005	10	39				
487	0.002			33	o C2NAm wag, o OH tor		
475	0.008					71	o C2NAm wag
377	0.003	12	41				
368	0.002	5	43				

[a]Absorbances at maxima in experimental spectrum of the 9MG in Ar before UV irradiation (relaxed sample).

[b]Relative integrated intensities obtained from the band separation and integration procedures (see description in text). The experimental integrated absorbance assigned to the well-separated C=O stretching vibration (marked by *) was assumed to be the same as the calculated intensity of this mode (see Table 2, for a-o).

[c]Normal mode according to numbering in Table 2 for this tautomer.

[d]Relative integrated intensity as in (*b*), only related to the calculated intensity of the vibration Am s st of the a-h1 tautomer (see Table 2, for RN1 tautomer).

[e]Abbreviations for description of vibrations as in Table 3. Note that de = De.

[f]Relative integrated intensity as in (*b*), only related to the calculated intensity of the vibration Am s st of the a-h2 tautomer (see Table 2, for RN7 tautomer).

Can. J. Chem. Downloaded from www.nrcresearchpress.com by 84.41.108.74 on 09/07/12
For personal use only.

TABLE 2. Comparison of the frequencies (FREQ, in cm^{-1}) absolute intensities (INT, in km mol^{-1}), and potential energy distributions (PEDs) from *ab initio* calculations at the HF level, using a 3-21G basis set, for the amino-oxo (a-o) and the rotamers (RN7 and RN1) of the amino-hydroxy (a-h) tautomeric forms of 9-methylguanine

	a-o Form			a-h RN1 Form			a-h RN7 Form		
Q_i[a]	FREQ[b]	INT	PEDs[c]	FREQ[b]	INT	PEDs[c]	FREQ[b]	INT	PEDs[c]
1	3526	79	AmNH15 st (54+) AmNH14 st (46−)	3541	76	AmNH15 st (52−) AmNH14 st (49+)	3540	79	AmNH14 st (51+) AmNH15 st (49−)
				3567	131	OH st (100+)	3564	110	OH st (100+)
2	3417	145	AmNH14 st (43+) AmNH15 st (35+) N1H st (22+)	3422	118	AmNH14 st (51−) AmNH15 st (48−)	3420	128	AmNH15 st (50−) AmNH14 st (49−)
3	3408	46	N1H st (78+) AmNH14 st (11−) AmNH15 st (11−)						
4	3121	2	C8H st (99−)	3115	2	C8H st (99+)	3116	2	C8H st (99+)
5	2971	13	a Me st (100−)	2968	13	a Me st (100+)	2969	12	a Me st (100+)
6	2964	18	o a Me st (100+)	2961	18	o a Me st (100+)	2963	16	o a Me st (100+)
7	2903	29	s Me st (100−)	2901	30	s Me st (100−)	2901	29	s Me st (100+)
8	1752	662	C6O st (70+) C6C5 st (13−)	1618	515	C6C5 st (34+) N3C4 st (13−) HOC be (10−)	1618	8	HNH be (46+) N3C4 st (12−) N1C6 st (11−)
9	1633	336	HNH be (90+)	1615	266	HNH be (84+)	1605	829	HNH be (40−) N3C4 st (13−) N1C6 st (12−)
10	1593	530	C2N3 st (34−) N1H be (25−) C2NAm st (13+)						
11	1534	313	N3C4 st (23−) Me sci (18−) C5C4 st (16+) N9C4 st (13+)	1561	314	N3C4 st (19+) C5C4 st (15−)	1551	505	C6C5 st (29+) C5C4 st (20−)
12	1521	201	C5C4 st (15+) Me umb be (12−)	1525	267	N7C8 st (18+) C2NAm st (10−) C8H be (10+)	1522	151	N7C8 st (13+) C2NAm st (12−) R6 De 1 (10+) N9C4 st (10−)
13	1507	33	Me sci (66−) C5C4 st (11−)	1514	17	Me sci (84−)	1514	47	Me sci (75−)
14	1497	8	o Me sci (91+)	1496	8	o Me sci (91−)	1495	9	o Me sci (91−)
15	1469	41	N7C8 st (19+) Me umb be (15−) N1C2 st (12−)	1475	294	C2NAm st (21+) N7C8 st (17+) Me umb be (16−)	1475	22	Me umb be (25−) N1C6 st (13−) C6O st (13+)
16	1452	9	Me umb be (61−) N7C8 st (29−)	1459	13	Me umb be (63+) N7C8 st (23+)	1470	223	N7C8 st (15−) C2NAm st (14−) Me umb be (13+) R5 De 2 (10+)
17	1395	26	N7C8 st (21+) N9C4 st (18+) C5C4 st (12−)	1437	77	N1C6 st (24−) C6O st (19+) C2N3 st (11+)	1452	9	Me umb be (44−) N7C8 st (32−)
18	1343	113	C2NAm st (13−) HNH ro (13−) N1C2 st (11+) N1H be (10−) C6C5 st (10+) R5 De 2 (10−)	1396	246	N9C4 st (21−) C5C4 st (11+) Me umb be (11+) N7C8 st (10−)	1385	213	N9C4 st (21+) N7C8 st (14+) N9C(Me) st (11−) C5C4 st (10−)
19	1319	94	N1H be (28+) C2NAm st (14+) R5 De 2 (11−)	1307	8	HOC be (27+) N9C(me) st (14+) C8N9 st (11−) R5 De 2 (11−)	1291	12	C8H be (25−) C5C4 st (13+) HNH ro (12+)
20	1274	4	Me ro (31−) C8N9 st (25−)	1285	5	C8H be (31+) Me ro (12+) C5C4 st (12−)	1282	150	C8N9 st (19−) Me ro (15−)
21	1249	45	C8H be (42−) C5N7 st (16−) N7C8 st (13+)	1261	58	Me ro (19−) C8H be (14+) HOC be (12−) C5N7 st (11+) C8N9 st (11−) N9C4 st (11+)	1254	117	HOC be (42+) Me ro (16−)
22	1199	18	C8H be (19−) C5N7 st (16+)	1217	160	HNH ro (14−) N3C4 st (13+)	1221	135	C8H be (20+) N9C(Me) st (16−)

Can. J. Chem. Downloaded from www.nrcresearchpress.com by 84.41.108.74 on 09/07/12
For personal use only.

TABLE 2 (*continued*)

	a-o Form			a-h RN1 Form			a-h RN7 Form		
Q_i[a]	FREQ[b]	INT	PEDs[c]	FREQ[b]	INT	PEDs[c]	FREQ[b]	INT	PEDs[c]
			N9C(Me) st (15+) N3C4 st (11−) R5 De 1 (10−)			C5N7 st (12−)			C6O st (13−) C5C4 st (12+) HNH ro (11+)
				1198	53	C8H be (22−) C5C4 st (18−) N9C(Me) st (16+) C5N7 st (16+)	1203	84	C5N7 st (28+) C8H be (13−) N3C4 st (10−)
				1152	159	HOC be (23−) N1C6 st (22+) C6O st (13+)	1171	74	N1C6 st (32+) HOC be (17+)
23	1149	1	o Me ro (89−)	1149	1	o Me ro (89−)	1149	1	o Me ro (89−)
24	1092	29	HNH ro (24−) C2N3 st (21+) N1C6 st (20+) C5N7 st (11−)						
25	1062	8	NH2 ro (20+) C2N(Am) st (11−) Me ro (11+) N1C6 st (10+)	1063	23	NH2 ro (36−) C2N3 st (20+) N1C2 st (10−)	1061	0	HNH ro (37+) C2N3 st (22−) N1C2 st (12+)
26	1031	4	N1C2 st (17+) R5 De 1 (14−) N1C6 st (14−) Me ro (12−) R6 De 1 (10−)	1018	55	R5 De 1 (17+) C6O st (15+) R6 De 1 (12+)	1018	73	R5 De 1 (19+) C6O st (16+) R6 De 1 (10+)
27	1007	45	C8N9 st (29−) Me ro (16+) R5 De 1 (16+) N1C2 st (12+) N1C6 st (12−)	1011	20	C8N9 st (38+) Me ro (28−) R5 De 1 (10−)	1012	29	C8N9 st (39−) Me ro (30+)
28	996	12	HNH ro (18+) N1C2 st (12+) C6O be (12+) N9C4 st (11−)	969	92	N1C2 st (23−) N9C4 st (10+) R5 De 1 (10−)	970	9	N1C2 st (22+) C2N3 st (13+) C2NAm st (12+) R5 De 1 (10+) N9C4 st (10−)
29	833	115	o R5 De 1 (36−) o R5 De 2 (28+) C6O wag (28−) C8H wag (12−)	842	27	C8H wag (43+) o R5 De 1 (27+) o R5 De 2 (22−)	846	32	C8H wag (36−) o R5 De 1 (30−) o R5 De 2 (24+) C6O wag (10−)
30	805	81	C8H wag (88+)	817	83	C8H wag (59−) o R5 De 2 (15−) o R5 De 1 (10+)	821	67	C8H wag (67−) o R5 Def 2 (12−)
31	738	147	o R5 De 2 (41+) N1H wag (34+) C2NAm wag (23−) o R5 De 1 (14−)	727	91	C2NAm wag (66+) o R6 De 1 (15+) o R5 De 1 (12+) o R5 De 2 (10−)	728	100	C2NAm wag (68−) o R6 Def 1 (15−) o R5 Def 1 (10−)
32	815	7	R6 De 1 (24−) C5N7 st (19+) R5 De 2 (10−)	808	1	R6 De 1 (23+) C5N7 st (21−) R5 De 2 (10+) C5C4 st (10−)	810	1	R6 De 1 (23+) C5N7 st (22−) R5 De 2 (10+)
33	700	55	C2NAm wag (43−) o R5 De 2 (20−) C6O wag (28−) o R6 De 2 (19+)	681	0	o R5 De 2 (52+) C6O wag (48+)	678	0	o R5 De 2 (57−) C6O wag (49−)
34	708	30	R5 De 1 (29−) N9C(Me) st (25−) R6 De 3 (13+) C6C5 st (11+)	710	16	R5 De 1 (30+) N9C(Me) st (23+) R6 De 3 (15−) C6C5 st (10−)	711	14	R5 De 1 (29+) N9C(Me) st (22+) R6 De 3 (14−) C6C5 st (11−)
35	625	58	o R5 De 1 (30+) N1H wag (24−) o R5 De 2 (24+) C2NAm wag (11−)	602	67	o R5 De 1 (53+) o R5 De 3 (27+)	598	47	o R5 De 1 (49−) o R5 De 3 (34+)
36	652	26	C6O be (24−) C2N be (18−) R5 De 2 (15+)	640	12	R5 De 2 (19+) C2N be (14−) R6 De 1 (13−) C6O be (11−)	651	24	R5 De 2 (22−) C6O be (16+) C2N be (16+)

Can. J. Chem. Downloaded from www.nrcresearchpress.com by 84.41.108.74 on 09/07/12
For personal use only.

TABLE 2 (*concluded*)

	a-o Form			a-h RN1 Form			a-h RN7 Form		
Q_i[a]	FREQ[b]	INT	PEDs[c]	FREQ[b]	INT	PEDs[c]	FREQ[b]	INT	PEDs[c]
37	583	5	N1H wag (32−) o R5 De 3 (30−) o R5 De 1 (15−) C6O wag (14+)						
38	585	2	N1C6 st (16−) N1C6 st (11−) R6 De 1 (10−)	591	2	C6O st (17−) C6O be (10+) N1C2 st (10−)	598	9	C6O st (18−) R6 De 1 (11−)
39	493	270	o NH14 wag (92−)	472	16	o NH14 wag (46+) o NH15 wag (36+) OH tor (17621)	478	21	o NH15 wag (67−) o NH14 wag (31−)
40	504	0	R6 De 3 (28−) R6 De 2 (23−)	522	7	R6 De 2 (27−) R6 De 3 (20−) N9C(Me) st (12−) N9C4 st (12−)	521	6	R6 De 2 (26+) R6 De 3 (21+) N9C(Me) st (12+) N9C4 st (12+)
				461	338	OH tor (63+) o NH14 wag (30+)	446	83	OH tor (96−)
				443	167	o NH15 wag (60−) o NH14 wag (22+) OH tor (11−)	455	427	o NH14 wag (66+) o NH15 wag (25−)
41	475	2	R6 De 2 (47+) R6 De 3 (15−)	489	0	R6 De 2 (40−) R6 De 3 (22+) C5N7 st (10−)	496	2	R6 De 2 (40−) R6 De 3 (22+) C5N7 st (10−)
42	351	4	o R5 De 3 (38−) o R6 De 1 (30+) o R6 De 3 (27−) o R5 De 1 (26+)	345	1	o R5 De 3 (34−) o R6 De 1 (32+) o R6 De 3 (27−) o R5 De 1 (24+)	346	7	o R5 De 3 (35−) o R6 De 1 (33+) o R6 De 3 (28−) o R5 De 1 (27+)
43	364	3	N9Me be (27−) C2NAm be (26−) C6C5 st (12−)	359	11	C2NAm be (43−) N9Me be (23−)	358	6	C2NAm be (48−) N9Me be (21−)
44	312	70	o NH15 wag (90−)						
45	325	4	C6O be (36−) C2NAm be (30+)	300	5	C6O be (52+) C2NAm be (18−)	294	11	C6O be (49−) C2NAm be (15+)
46	242	1	o R5 De 3 (44+) N9Me wag (42−) o R6 De 2 (12−)	256	1	o R5 De 3 (47+) o R6 De 3 (29−) N9Me wag (26−) o R6 De 2 (15−)	257	5	o R5 De 3 (52+) N9Me wag (27+) o R6 De 3 (25−) o R6 De 2 (15−)
47	200	3	N9Me be (46−) R6 De 3 (14−)	200	5	N9Me be (46−) R6 De 3 (12−) R5 De 2 (10+)	196	3	N9Me be (43−) R6 De 3 (14−) R5 De 2 (11+)
48	180	4	o R6 De 3 (68+) o R6 De 1 (20+)	220	1	o R6 De 3 (38+) C6O wag (21+) N9Me wag (15−) o R6 De 1 (15+)	219	2	o R6 De 3 (43+) C6O wag (20+) N9Me wag (13−) o R6 De 1 (15+)
49	141	14	o R5 De 2 (24+) o R6 De 2 (18−) N9Me wag (14−) o R6 De 3 (13+) o R6 De 1 (10−)	146	11	o R6 De 2 (25−) o R5 De 2 (19+) N9Me wag (14−) C2NAm wag (10+)	147	8	o R6 De 2 (30−) o R5 De 2 (16+) N9Me wag (11−) C2NAm wag (10+)
50	107	0	o R6 De 2 (78−) o R6 De 1 (20+) N9Me wag (21+)	105	4	o R6 De 2 (72−) N9Me wag (25+) o R5 De 2 (10−)	107	2	o R6 De 2 (70−) N9Me wag (28+) o R5 De 2 (14−)
51	−76	0	Me tor (88−) N9Me wag (13+)	−72	0	Me tor (88−) N9Me wag (13+)	−69	0	Me tor (89−) N9Me wag (13+)
Total intensity		3764			3899			3949	

[a]Numbering of the normal modes for the a-o tautomeric form, in order of the calculated unscaled frequencies.

[b]Frequencies scaled by a factor of 0.90, except for the OH stretch (0.918, based on studies of other systems (23)) and for the out-of-plane modes, which are scaled by a factor of 0.81 (all op modes except for the stretch, scissors bend, and rock of the CH_3 group). These scaling factors have been chosen because of experience with previous calculations for uracils (38) and thiouracils (24). The negative frequency for the Me tor is, of course, imaginary; it is the eigenvalue that is negative, indicating that calculated geometry is not correct for the orientation of the CH_3 group.

[c]The potential energy distributions (PEDs) are as defined by Morino and Kuchitsu (39*a*), using the procedure suggested by Keresztury and Jalsovszky (39*b*). Abbreviations and symmetry coordinates are defined in Table 3.

Can. J. Chem. Downloaded from www.nrcresearchpress.com by 84.41.108.74 on 09/07/12
For personal use only.

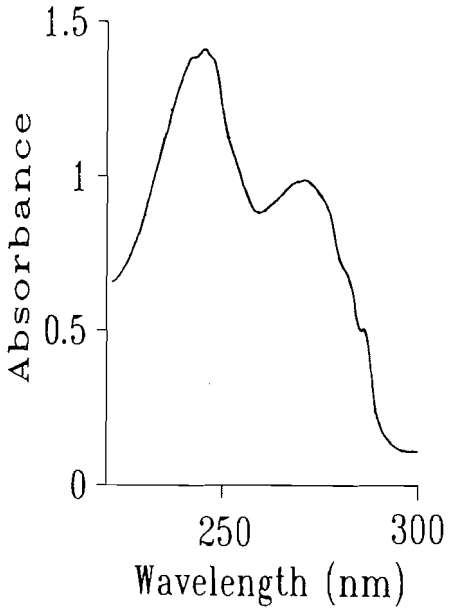


FIG. 6. Ultraviolet absorption spectra of 9MG isolated in an argon matrix at about 12 K, before and after a 5-min UV irradiation by the medium-pressure Hg lamp. Both spectra are identical and overlap exactly.

asymmetric NH_2 stretch of the a-o form and NH_2 symmetric stretch of the a-h1 and a-h2 rotamers).

As seen in Fig. 5, the agreement between the general patterns of the experimental and calculated spectra for the a-o tautomer is reasonably good, as can be expected for a calculation at this level of theory (see also Tables 1 and 2 for details).

For the a-h1 and a-h2 rotamers the agreement is very poor, particularly for the intensities, as can be seen in Fig. 5. Although it is possible to find bands in the experimental spectra for a-h1 and a-h2 that correspond reasonably well in frequency to the calculated spectra for RN1 and RN7, the corresponding relative intensities found in the experimental spectra are often drastically different from those predicted by the calculation (compare data in Tables 1 and 2). For this reason we do not believe that a reliable detailed vibrational assignment of the experimental spectrum to the calculated modes can be made at this time for the a-h rotamers; consequently in Table 1 we have proposed very tentative and general assignment of the vibrational absorption bands observed for the a-h1 and a-h2 species. It should be pointed out, however, that we believe that the separation given in Table 1 between the bands due to the oxo tautomer and also between the bands from the two hydroxy rotamers is valid and useful, and that the correct assignment of the observed absorption bands for the hydroxy tautomers to the normal modes will not differ greatly from that given in Table 1.

These very large discrepancies between the experimental spectra for a-h2 and a-h1 and the spectra calculated for the RN7 and RN1 conformation of the a-h tautomer might indicate nonplanarity of the OH group for one or both rotamers in the experimental study. To be able to carry out the calculation at this level for such a large molecule, we were forced to assume planar RN1 and RN7 conformations, so that it is not possible at present to test whether calculated spectra for nonplanar conformations would, in fact, agree better with the experimental spectra. One may expect that a nonplanar configuration of the OH group might well result in a different spectrum than for a planar configuration, particularly in the intensity pattern.

Finally, we should comment on the hypothetical possibility that the hydroxy-imino tautomer might be present in our experimental spectrum, rather than the amino-hydroxy rotamers. The observed spectrum in the OH, NH stretching region is not totally inconsistent with such a tautomer instead of the amino-hydroxy form. Unfortunately, we do not have any idea at present what spectrum could be expected in other regions for the hydroxy-imino form.

To investigate the hypothesis concerning the possibility of the appearance of the hydroxy-imino tautomer we have optimized the geometry for this tautomer at the 3-21G level. This calculation predicts the energy of the hydroxy-imino tautomer to be 120 kJ mol^{-1} *higher* than that of the a-o form. The calculations at the same level quoted above predict the RN1 tautomer to be only 19 kJ mol^{-1} and RN7 only 22 kJ mol^{-1} less stable than the a-o tautomer. Although it is known that calculations with a 3-21G basis set do not predict stabilization energies well, the very high value predicted for the hydroxy-imino tautomer certainly indicates that this tautomer is less likely to be present in our experiment.

Additional support for the interpretation of the observed IR spectrum as due to the presence of the rotamers a-h1 and a-h2 and not due to the presence of additional tautomers, such as the imino-hydroxy tautomer, comes from the studies of the electronic absorption spectrum of the matrix-isolated 9MG sample and the effect on this spectrum of brief irradiation by UV light from a mercury lamp, similar to the study reported above for the IR spectrum.

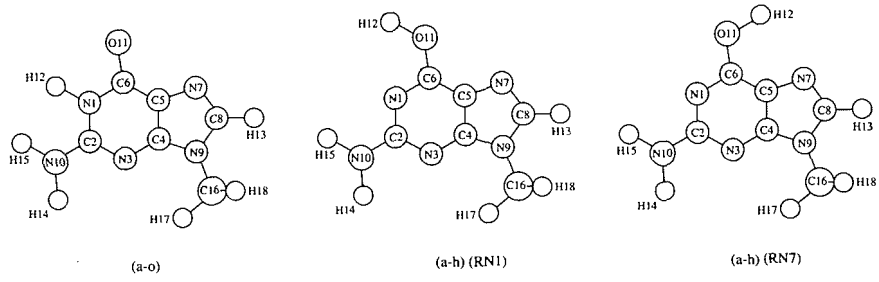
The electronic absorption spectrum from this study is shown in Fig. 6. The spectra of the matrix sample before and after UV irradiation lasting the same period of time as in the IR experiment are identical. If the UV irradiation caused any changes in the equilibrium between tautomers, one might expect visible changes in the electronic absorption, as has previously been observed for the case of cytosines (see ref. 41).

Conclusion

In summary, the use of the changes induced by the UV irradiation, aided by the SpectraCalc computer analysis of our experimental IR spectra, has allowed us to separate the infrared spectrum observed for 9MG isolated in an argon matrix into contributions from three species. One species is surely the amino-oxo tautomer; the most likely interpretation of the other two species is that they are rotamers of the amino-hydroxy tautomer. However, the infrared spectra calculated with a 3-21G basis set for the two planar rotamers of the amino-hydroxy tautomer do not agree very well with the observed spectra attributed to these forms. Because spectra calculated at this level of theory for the amino-oxo tautomer of 9MG and for most other molecules in our experience generally have better resemblance in pattern to the experimental spectra than we found between the experimental spectra of a-h1 and a-h2 and the spectra calculated for RN1 and RN7, we suspect that the structures for the molecules a-h1 and a-h2 studied in our experiment may be different from those assumed for the calculation. We believe that the most likely explanation for the discrepancy between the 3-21G calculated spectra and the experimental spectra is the planar configuration assumed for the OH bond in the calculation for this tautomer. We cannot rule out the possibility that the 3-21G basis is simply much less adequate for calculations for the hydroxy tautomer than it is for the oxo

Can. J. Chem. Downloaded from www.nrcresearchpress.com by 84.41.108.74 on 09/07/12
For personal use only.

TABLE 3. Symmetry coordinates for 9-methylguanine amino-oxo (a-o) and amino hydroxy (a-h) tautomers[a]



Symmetry coordinates[b]	Description[c]
In-plane coordinates	
$S_1 = \Delta r_1$	C5C4 st
$S_2 = \Delta r_2$	C5N7 st
$S_3 = \Delta r_3$	N7C8 st
$S_4 = \Delta r_4$	C8N9 st
$S_5 = \Delta r_5$	N9Cr st
$S_6 = \Delta r_6$	N3Cr st
$S_7 = \Delta r_7$	C2N3 st
$S_8 = \Delta r_8$	N1C2 st
$S_9 = \Delta r_9$	N1C6 st
$S_{10} = \Delta r_{10}$	C6C5 st
$S_{11} = \Delta r_{11}$	C6O st
$S_{12} = \Delta r_{12}$	N1H st (a-o)
$S'_{12} = \Delta r'_{12}$	OH st (a-h)
$S_{13} = \Delta r_{13}$	N9C(Me) st
$S_{14} = \Delta r_{14}$	C8H st
$S_{15} = \Delta r_{15}$	C2NAm st
$S_{16} = \Delta r_{16}$	AmNH15 st
$S_{17} = \Delta r_{17}$	AmNH14 st
$S_{18} = \Delta r_{18} + \Delta r_{19} + \Delta r_{20}$	s Me st
$S_{19} = 2\Delta r_{18} + \Delta r_{19} + \Delta r_{20}$	a Me st
$S_{20} = \Delta\alpha_1 - \Delta\alpha_2 + \Delta\alpha_3 - \Delta\alpha_4 + \Delta\alpha_5 - \Delta\alpha_6$	R6 De 1
$S_{21} = 2\Delta\alpha_1 - 2\Delta\alpha_2 + \Delta\alpha_3 - 2\Delta\alpha_4 + \Delta\alpha_5 - \Delta\alpha_6$	R6 De 2
$S_{22} = \Delta\alpha_2 - \Delta\alpha_3 + \Delta\alpha_5 - \Delta\alpha_6$	R6 De 3
$S_{23}{}^d = \Delta\alpha_8 - a\Delta\alpha_9 + b\Delta\alpha'_4 - b\Delta\alpha'_5 - a\Delta\alpha_7$	R5 De 1
$S_{24}{}^d = c\Delta\alpha_9 + d\Delta\alpha'_4 - d\Delta\alpha'_5 + c\Delta\alpha_7$	R5 De 2
$S_{25} = \Delta\beta_{65} - \Delta\beta_{61}$	C6O be
$S_{26} = \Delta\beta_{16} - \Delta\beta_{12}$	N3H be (a-o)
$S'_{26} = \Delta\theta$	HOC be (a-h)
$S_{27} = \Delta\beta_{21} - \Delta\beta_{23}$	C2NAm be
$S_{28} = \Delta\beta_{94} - \Delta\beta_{98}$	N9Me be
$S_{29} = \Delta\beta_{89} - \Delta\beta_{87}$	C8H be
$S_{30} = 2\Delta\phi_1 - \Delta\phi_2 - \Delta\phi_3$	HNH be
$S_{31} = \Delta\phi_2 - \Delta\phi_3$	HNH ro
$S_{32} = \Delta\phi_4 + \Delta\phi_5 + \Delta\phi_6 - \Delta\phi_7 - \Delta\phi_8 - \Delta\phi_9$	Me umb be
$S_{33} = 2\Delta\phi_4 - \Delta\phi_5 - \Delta\phi_6$	Me ro
$S_{34} = 2\Delta\phi_7 - \Delta\phi_8 - \Delta\phi_9$	Me sci
Out-of-plane coordinates	
$S_{35} = \Delta\gamma_{Co}$	C6O wag
$S_{36} = \Delta\gamma_{N1H}$	N1H wag (a-o)
$S'_{36} = \Delta\tau_{CO}$	OH tor (a-h)
$S_{37} = \Delta\gamma_{C8H}$	C8H wag
$S_{38} = \Delta\gamma_{C2N}$	C2NAm wag
$S_{39} = \Delta\gamma_{N9Me}$	N9Me wag
$S_{40} = \Delta r_{19} - \Delta r_{20}$	o a Me st
$S_{41} = \Delta\phi_5 - \Delta\phi_6$	o Me ro
$S_{42} = \Delta\phi_8 - \Delta\phi_9$	o Me sci
$S_{43} = \Delta\tau_{H14N}$	o NH14 wag

Can. J. Chem. Downloaded from www.nrcresearchpress.com by 84.41.108.74 on 09/07/12
For personal use only.

TABLE 3. (*concluded*)

Symmetry coordinates[b]	Description[c]
$S_{44} = \Delta\tau_{H15N}$	o NH15 wag
$S_{45} = \Delta\tau_{H17C} + \Delta\tau_{H18C} + \Delta\tau_{H19C}$	Me tor
$S_{46} = \Delta\tau_{12} - \Delta\tau_{23} + \Delta\tau_{34} - \Delta\tau_{45} + \Delta\tau_{56} - \Delta\tau_{61}$	o R6 De 1
$S_{47} = \Delta\tau_{12} - \Delta\tau_{34} + \Delta\tau_{45} - \Delta\tau_{61}$	o R6 De 2
$S_{48} = \Delta\tau_{12} + 2\Delta\tau_{23} - \Delta\tau_{34} - \Delta\tau_{45} + 2\Delta\tau_{56} - \Delta\tau_{61}$	o R6 De 3
$S_{49} = \Delta\gamma_{N9C4}$	o R5 De 1
$S_{50} = \Delta\gamma_{N7C5}$	o R5 De 2
$S_{51} = \Delta\tau_{49} - \Delta\tau_{57}$	o R5 De 3

[a]The symmetry coordinates are the same for all three molecules (the a-o tautomer and the two rotamers (RN1 and RN7) of the a-h tautomer) except for those coordinates involved in the tautomerism (namely, the N1H bond in the a-o tautomer and the OH bond in the a-h form). These coordinates appear in pairs in the table and have the same numbers, but those for the a-h tautomer are designated by a prime: e.g., S_{12} and S'_{12} for the N1H st of a-o and for the OH st of the a-h forms, respectively.

[b]Unnormalized linear combinations of internal coordinates, defined to be orthogonal to the redundancy conditions, and with the appropriate symmetry (see Pulay *et al.* (42)). The Δr bond stretching internal coordinates are defined by their descriptions; the $\Delta\alpha_i$ bending coordinates describe the changes in the internal ring angles with apex at atom i (e.g., $\alpha_1 = <$C6N1C2, etc.); the $\Delta\beta_{ij}$ coordinates describe the bending of the external angles with apex at atom i and with the j subscript giving the ring atom on the other arm of the angle (e.g., $\beta_{65} = <$OC6C5, and $\beta_{61} = <$OC6N1, etc.); $\Delta\theta$ is defined by the description; $\Delta\phi_i$ (i = 1–3) are deformations of the angles in the NH_2 group (e.g., ϕ_1 is the HNH angle); $\Delta\phi_i$ (i = 4–9) are deformations of the angles in the CH_3 group; the $\Delta\gamma$ out-of-plane wagging coordinates are given by their descriptions; and the $\Delta\tau$ out-of-plane torsions are designated by a subscript that describes either the end bond that is being twisted out of plane or by two numbers that give the center bond in the ring about which the torsion is taking place. Definitions of the internal coordinates follow those given by S. Califano (43).

[c]Abbreviations are st, stretch; s, symmetric; a, asymmetric; Me, methyl; Am, amino; R6, the six-membered pyrimidine ring; De, deformation; R5, the five-membered imidazole ring; be, bend; ro, rock; sci, scissors bend; umb, umbrella; tor, torsion; and o, out-of-plane.

[d]The coefficients are $a = 0.80902$, $b = 0.30902$, $c = 1.11803$, and $d = 1.80902$.

form for this molecule. Possibly future calculations of the vibrational spectra for a nonplanar a-h tautomer of 9MG at the 3-21G level or with a better basis set may help to interpret further the experimental results obtained from this study.

Acknowledgements

We are extremely grateful to Professor Nelson Leonard and to Dr. S. Kumar of the University of Illinois for supplying the sample of 9-methylguanine. We also wish to thank Dr. Pierre LeBreton (University of Illinois, Chicago Circle) for valuable discussions. Support of the experimental study by NIH Research Grant No. GM32988 is gratefully acknowledged, as is support for the computing by the University of Alabama at Birmingham.

Registry No. 9MG, 5502-78-3.

1. (*a*) K. A. HARTMAN, R. C. LORD, and G. J. THOMAS, JR. *In* Physico-chemical properties of nucleic acid bases. Vol. 2. *Edited by* J. Duchesne. Academic Press, London. 1983. Chap. 10. (*b*) M. TSUBOI, S. TAKAHASHI, and I. HARADA. *In* Physico-chemical properties of nucleic acid bases Vol. 2. *Edited by* J. Duchesne. Academic Press, London. 1983. Chap. 11.
2. (*a*) H. H. MANTSCH, H. L. CASAL, and R. N. JONES. *In* Advances in infrared and Raman spectroscopy. Vol. 13. Spectroscopy of biological systems. *Edited by* R. J. H. Clark and R. E. Hester. Wiley, Chichester. 1986. Chap. 1; (*b*) E. TAILLANDIER, J. LIQUIER, and J. A. TABOURY. *In* Advances in infrared and Raman spectroscopy. Vol. 12. *Edited by* R. J. H. Clark and R. E. Hester. Wiley, Chichester. 1985. Chap. 2; (*c*) E. TAILLANDIER, J. LIQUIER, and M. GHOMI. J. Mol. Struct. **214**, 185 (1989).
3. (*a*) W. L. PETICOLAS, W. I. KUBASEK, G. A. THOMAS, and M. TSUBOI. *In* Biological applications of Raman spectroscopy. Vol. 1. *Edited by* T. Spiro. Wiley, Chichester. 1987. Chap. 3; (*b*) W. L. PETICOLAS, Z. DAI, and G. A. THOMAS. J. Mol. Struct. **242**, 135 (1991); (*c*) J. M. BENEVIDES and G. J. THOMAS, JR. Nucleic Acids Res. **11**, 5747 (1983); (*d*) J. M. BENEVIDES, A. H.-J. WANG, G. A. VAN DER MAREL, J. H. VAN BOOM, A. RICH, and G. J. THOMAS, JR. Nucleic Acids Res. **12**, 5913 (1984).
4. A. TOYAMA, H. TAKEUCHI, and I. HARADA. J. Mol. Struct. **242**, 87 (1991).
5. J. M. DELABAR and M. MAJOUBE. Spectrochim. Acta, Part A; **34A**, 129 (1978).
6. (*a*) Y. NISHIMURA, M. TSUBOI, T. NAKATA, S. HIGUCHI, T. SATO, T. SHIDA, S. UESUGI, E. OHTSUKA, and M. IKEHARA. Nucleic Acids Res. **11**, 1579 (1983); (*b*) Y. NISHIMURA, M. TSUBOI, and S. SATO. Nucleic Acids Res. **12**, 6901 (1984).
7. (*a*) J. ELGUERO, C. MARZIN, A. R. KATRITZKY, and P. LINDA. *In* The tautomerism of heterocycles. *Edited by* A. R. Katritzky and A. J. Boulton. Academic Press, London. 1976; (*b*) J. S. KWIATKOWSKI and B. PULLMAN. Adv. Heterocycl. Chem. **18**, 199 (1975); (*c*) J. S. KWIATKOWSKI, T. J. ZIELINSKI, and R. REIN. Adv. Quantum Chem. **18**, 85 (1985); (*d*) D. SHUGAR and A. PSODA. *In* Landolt–Bornstein New Series Biophysics. Part I. Nucleic acids. VII/1D. Springer, Berlin. 1990. pp. 308–348.
8. (*a*) C. N. RADINOVA and E. S. LEVIN. Dokl. Acad. Nauk SSSR, **174**, 1132 (1967) (Russian); (*b*) P. BEAK. Acc. Chem. Res. **10**, 186 (1977); (*c*) M. J. NOWAK, K. SZCZEPANIAK A. BARSKI, and D. SHUGAR. Z. Naturforsch. C: Biosci. **33**, 876 (1978); (*d*) A. MAQUESTIAU, Y. V. HAVERBEKE, R. FLAMMANG, H. MISPREUVE, A. R. KATRITZKY, J. ELLISON, J. FRANK, and Z. MESZAROS. J. Chem. Soc. Chem. Commun. 888 (1979); (*e*) A. R. KATRITZKY and M. SZAFRAN. J. Chem. Soc. Perkin Trans. 2, 871 (1990); (*f*) H. ROSTKOWSKA, A. BARSKI, K. SZCZEPANIAK, M. SZCZESNIAK, and W. B. PERSON. J. Mol. Struct. **176**, 137 (1988); (*g*) H. ROSTKOWSKA, K. SZCZEPANIAK, M. J. NOWAK, J. LESZCZYNSKI, K. KUBULAT, and W. B. PERSON. J. Am. Chem. Soc. **112**, 2147 (1990); (*h*) P. R. LEBRETON, XU YANG, S. URANO, S. FETZER, MIN YU, N. J. LEONARD, and S. KUMAR. J. Am. Chem. Soc **112**, 2138 (1990).

Can. J. Chem. Downloaded from www.nrcresearchpress.com by 84.41.108.74 on 09/07/12
For personal use only.

9. (*a*) W. B. PERSON, K. SZCZEPANIAK, M. SZCZESNIAK, J. S. KWIATKOWSKI. L. HERNANDEZ, and R. CZERMINSKI. J. Mol. Struct. **194**, 239 (1989); (*b*) J. S. KWIATKOWSKI and W. B. PERSON. *In* Theoretical biochemistry and molecular biophysics. Vol. I. DNA. *Edited by* D. L. Beveridge and R. Lavery. Adenine Press, Guilderland, NY. 1991; (*c*) YU. P. BLAGOI, E. D. RADCHENKO, S. G. STEPANIAN, and G. G. SHEINA. *In* Laser scattering spectroscopy of biological objects. *Edited by* J. Stepanek, P. Anzenbacher, and B. Sedlacek. Elsevier, Amsterdam. 1987.
10. (*a*) M. SZCZENIAK, K. SZCZEPANIAK, J. S. KWIATKOWSKI, K. KUBULAT, and W. B. PERSON. J. Am. Chem. Soc. **110**, 8319 (1988); (*b*) M. J. NOWAK. L. LAPINSKI, and L. FULARA. Spectrochim. Acta, Part A: **45A**, 229 (1989); (*c*) L. LAPINSKI, M. J. NOWAK, J. FULARA, A. LES, and L. ADAMOWICZ. J. Phys. Chem. **94**, 6555 (1990).
11. K. SZCZEPANIAK and M. SZCZESNIAK. J. Mol. Struct. **156**, 29 (1986).
12. Z. LATAJKA, W. B. PERSON, and K. MORUKUMA. J. Mol. Struct. (Theochem), **135**, 253 (1986).
13. K. SZCZEPANIAK, M. SZCZESNIAK, and W. B. PERSON. Chem. Phys. Lett. **153**, 39 (1988).
14. (*a*) G. G. SHEINA, E. D. RADCHENKO, and YU. P. BLAGOI. Dokl. Acad. Nauk SSSR, **282**, 1407 (1985) (Russian); (*b*) G. G. SHEINA, S. G. STEPANIAN, E. D. RADCHENKO, and YU. P. BLAGOI. J. Mol. Struct. **158**, 275 (1987).
15. (*a*) I. R. GOULD and I. H. HILLIER. Chem. Phys. Lett. **161**, 185 (1989); (*b*) M. SABIO, S. TOPIOL, and W. C. LUMMA, JR. J. Phys. Chem. **94**, 1366 (1990).
16. (*a*) J. LESZCZYNSKI. Chem. Phys. Lett. **174**, 347 (1990); (*b*) J. S. KWIATKOWSKI and J. LESZCZYNSKI. J. Mol. Struct. (Theochem), **208**, 350 (1990).
17. Y. NISHIMURA, M. TSUBOI, and K. MOROKUMA. Bull. Chem. Soc. Jpn. **58**, 638 (1985).
18. W. B. PERSON, J. E. DEL BENE, W. SZAJDA, K. SZCZEPANIAK, and M. SZCZESNIAK. J. Phys. Chem. **95**, 2770 (1991).
19. W. J. HEHRE, L. RADOM, P.V.R. SCHLEYER, and J. A. POPLE. Ab initio molecular orbital theory. Wiley, New York. 1986.
20. M. J. FRISCH, J. S. BINKLEY, H. B. SCHLEGEL, K. RAGHAVACHARI, C. F. MELIUS, L. MARTIN, J. J. P. STEWART, F. W. BOBROWICZ, C. M. ROHFING, L. R. KAHN, D. J. DEFREES, R. SEEGER, H. B. WHITESIDES, D. J. FOX, E. M. FLUDER, and J. A. POPLE. Carnegie–Mellon Quantum Chemistry Publishing Unit, Pittsburgh, PA. 1984.
21. H. B. SCHLEGEL. J. Comput. Chem. **3**, 314 (1982).
22. (*a*) J. A. POPLE, H. B. SCHLEGEL, R. KRISHNAN, D. J. DEFREES, J. S. BINKLEY, M. J. FRISCH, R. A. WHITESIDE, R. F. HOUT, JR., and W. J. HEHRE. Int. J. Quantum Chem. Symp. **15**, 269 (1981); (*b*) D. J. DEFREES and A. D. MCLEAN. J. Chem. Phys. **82**, 33 (1985).
23. M. SZCZESNIAK, W. SZAJDA, K. SZCZEPANIAK, J. LESZCZYNSKI, and W. B. PERSON. Manuscript in preparation.
24. H. ROSTKOWSKA, K. SZCZEPANIAK, M. J. NOWAK, J. LESZCZYNSKI, K. KUBULAT, and W. B. PERSON. J. Am. Chem. Soc. **112**, 2147 (1990).
25. C. Y. LIN, A. KRANTZ, and T. D. GOLDFARB. J. Am. Chem. Soc. **94**, 9282 (1972).
26. A. KRANTZ, T. D. GOLDFARB, and C. Y. LIN. J. Am. Chem. Soc. **94**, 4022 (1972).
27. C. BLOM, R. P. MULLER, and H. H. GUNTHARD. Chem. Phys. Lett. **73**, 483 (1980).
28. A. J. BARNES, H. F. HALLAM, and S. WARING. J. Chem. Soc. Faraday 2, 72 (1976).
29. H. FREI and G. C. PIMENTEL. Annu. Rev. Phys. Chem. **36**, 491 (1985).
30. A. J. BARNES. *In* Matrix isolation spectroscopy. *Edited by* A. J. Barnes, W. J. Orville-Thomas, A. Muller, and R. Gaufries. Reidel, Dordrecht. 1981. p. 351.
31. M. RASANEN, G. P. SCHWARTZ, and V. E. BONDYBEY. J. Chem. Phys. **84**, 59 (1986).
32. T. BEECH, R. GUNDE, P. FELDER, and H. GUNTHARD. Spectrochim. Acta, Part A: **41A**, 319 (1985).
33. H. H. GUNTHARD. Chem. Phys. **136**, 463 (1989).
34. M. PERTTILA, J. MURTO, A. KIVINEN, and K. TURUNEN. Spectrochim. Acta, Part A: **34A**, 99 (1978).
35. T. LOTTA, J. MURTO, M. RASANEN, and A. ASPIALA. J. Mol. Struct. **114**, 333 (1984).
36. A. J. BARNES. J. Mol. Struct. **113**, 161 (1984).
37. M. TASUMI and M. NAKATA. J. Mol. Struct. **126**, 111 (1985).
38. K. SZCZEPANIAK, J. LESZCZYNSKI, and W. B. PERSON. Manuscript in preparation.
39. (*a*) Y. MORINO and K. KUCHITSU. J. Chem. Phys. **20**, 1809 (1952); (*b*) G. KERESZTURY and G. JALSOVSZKY. J. Mol. Struct. **10**, 304 (1973).
40. (*a*) M. SZCZESNIAK, M. J. NOWAK, H. ROSTKOWSKA, K. SZCZEPANIAK, W. B. PERSON, and D. SHUGAR. J. Am. Chem. Soc. **106**, 5969 (1983); (*b*) M. J. WOJCIK, H. ROSTKOWSKA, K. SZCZEPANIAK, and W. B. PERSON. Spectrochim. Acta, **45A**, 499 (1989); (*c*) A. J. BARNES, M. A. STUCKEY, and L. LEGALL. Spectrochim. Acta, **40A**, 419 (1984); (*d*) M. GRAINDOURZE, J. SMETS, TH. ZEEGERS-HUYSKENS, and G. MAES. J. Mol. Struct. **222**, 345 (1990).
41. M. SZCZESNIAK and W. B. PERSON. Manuscript in preparation.
42. S. PULAY, G. FOGARASI, F. PANG, and J. F. BOGGS. J. Am. Chem. Soc. **101**, 2550 (1979).
43. S. CALIFANO. *In* Vibrational states. Wiley, London. 1976.

Can. J. Chem. Downloaded from www.nrcresearchpress.com by 84.41.108.74 on 09/07/12
For personal use only.

Amino acid/zwitterion equilibria II: vibrational and NMR studies of substituted thiazolidine-4-carboxylic acids

H. E. HOWARD-LOCK,[1] C. J. L. LOCK, AND M. L. MARTINS

Laboratories for Inorganic Medicine, Departments of Chemistry and Pathology, McMaster University, Hamilton, Ont., Canada L8S 4M1

Received July 5, 1991

This paper is dedicated to Dr. Richard Norman Jones

H. E. HOWARD-LOCK, C. J. L. LOCK, and M. L. MARTINS. Can. J. Chem. **69**, 1721 (1991).

Infrared and Raman spectra (4000–100 cm) of solid samples of seven different 2-phenyl-, *N*-benzoyl-, and 2-ethyl-2 methyl derivatives of L-cysteine and D-penicillamine have been observed and assigned. Proton and ^{13}C nuclear magnetic resonance spectra for the compounds have also been measured. Amino acid/zwitterion equilibria are discussed with reference to p*K* values and the vibrational spectra

Key words: amino acid/zwitterion equilibria, thiazolidine carboxylic acids.

H. E. HOWARD-LOCK, C. J. L. LOCK et M. L. MARTINS. Can. J. Chem. **69**, 1721 (1991).

On a déterminé les spectres infra-rouge et Raman (4000–100 cm) d'échantillons solides de sept dérivés différents des 2-phényl-, *N*-benzoyl- et 2-éthyl-2-méthyl- de la L-cystéine et D-pénicillamine et on rapporte les attributions qui en découlent. On a aussi déterminé les spectres de résonance magnétique nucléaire du ^{1}H et du ^{13}C de ces composés. On discute des équilibres acide aminé/zwitterion par rapport aux valeurs de p*K* et aux spectres de vibration.

Mots clés : équilibres acide aminé/zwitterion, acides carboxyliques de thiazolidine.

[Traduit par la rédaction]

Introduction

The modes of action and adverse side effects of the drug D-penicillamine depend on several reactions, an important one being the condensation with aldehydes and ketones to form thiazolidine rings. Penicillamine might compete successfully with cysteine in vivo in this type of reaction (1). Both bind specifically to free aldehydes on collagen. Penicillamine inhibits cross-linking and depolymerizes incomplete cross-links of collagen, where these linkages are of the aldimine type. Thus, the effects of penicillamine are mainly upon skin collagen, giving rise to several side effects and some benefits (in scleroderma) as well.

The formation of thiazolidine rings is the basis for the suggested use of D-penicillamine as an alcohol detoxicant, and for treatment of scleroderma, morphea, keloid formation, and of vitreous and scleral scarring of the eye. Formation of thiazolidine rings is also the probable mode of action of D-penicillamine as vitamin B6 antagonist, and we have fully characterized the complex between pyridoxal and D-penicillamine (2).

Recently, we showed that methyl substitution at the C2 and C5 positions of thiazolidine-4-carboxylic acid affects the amino acid/zwitterion equilibrium (3). A downward shift of amino group p*K* and an upward shift of COOH group p*K* with increasing number of CH_3 groups was noted, although it was evident that other factors, such as the change in ring conformation and the degree of hydrogen bonding, played a role. The nature of the carbonyl-containing group affects the substitution at the C2 thiazolidine ring position and this in turn can affect the amino acid/zwitterion equilibrium and thus the hydrogen bonding behaviour in vivo.

A further process occurs in vivo, which may affect thiazolidine ring formation and which will affect zwitterion formation. This is substitution at the amine group. A new drug, which is used in the treatment of respiratory diseases, is *N*-acetylcysteine. This introduces a new variable, namely substitution at the N3 position. Thus we have extended our previous studies of how substitution affects these equilibria by considering a series of 2-phenyl, 2-methyl-2-ethyl-, and *N*-benzoyl-substituted thiazolidine-4-carboxylic acids.

[1]Author to whom correspondence may be addressed.

Materials and methods

All the starting materials were reagent grade and were used as received, after checking the NMR spectrum. D-(−)-Penicillamine free base and L-(+)-cysteine hydrochloride monohydrate were supplied by Sigma Chemical Company, St. Louis, MO. Formaldehyde, 37% v/v, was supplied by Sargent–Welsh Scientific Co., Skokie, IL. Acetaldehyde was distilled from paraldehyde, reagent grade, supplied by BDH Chemicals, Toronto, Ont. Benzaldehyde was obtained from Eastern Chemical, Hauppauge, NY, acetone from BDH Chemicals, Toronto, Ont., 2-butanone from Aldrich Chemical Company, Milwaukee, WI, and benzoyl chloride from Eastman Kodak Company, Rochester, NY. Elemental analyses were provided by Guelph Chemical Laboratories, Guelph, Ont. Melting points were determined on a Gallenkamp capillary melting point apparatus, and are not corrected. The preparation of the various substituted thiazolidine-4-carboxylic acids was carried out as indicated schematically in Table 1 and outlined in detail as follows.

2-Phenylthiazolidine-4-carboxylic acid **1**

The method of Riemschneider and Hoyle (4) was followed with modification: 1.2 g (0.01) mol of L-cysteine hydrochloride monohydrate, A, was added to a mixture of 1.08 g (0.0105 mol) of benzaldehyde in 30 mL of water at pH 8.0. The mixture was stirred at room temperature and a precipitate started appearing within 30 min. The mixture was filtered to yield 1.35 g (65%) of white solid, $C_{10}H_{11}NO_2S$, mp 154–155°C (lit. (4) mp 159–160°C).

3-Benzoyl-2-phenylthiazolidine-4-carboxylic acid **2**

The method of Clarke *et al.* (5a) was followed with modification: 0.42 g (0.002 mol) of **1** was dissolved in 20 mL of pyridine. The solution was cooled on ice and it became a light suspension. Benzoyl chloride (0.3 g, 0.0025 mol) was added dropwise to the stirred mixture, which slowly turned yellow as the solid gradually dissolved. The reaction was allowed to proceed in the refrigerator overnight. The product was recovered as follows: The mixture was evaporated under reduced pressure to leave a yellow oil and some white solid. This was dissolved in 80 mL dichloromethane, then extracted twice with 20 mL water. The combined aqueous layers were extracted once with a small

Can. J. Chem. Downloaded from www.nrcresearchpress.com by 84.41.108.74 on 09/07/12
For personal use only.

TABLE 1. Nomenclature and preparation scheme for some substituted thiazolidine-4-carboxylic acids[a]

Reactants	Benzaldehyde	2-Butanone	Benzoyl chloride
L-Cysteine	**1**[b]	**3**	
1			**2**
3			**4**
D-Pencillamine	**5**	**6**	
6			**7**

Nomenclature: The products are secondary amino acids that are 5-membered heterocyclic rings containing a sulfur atom at position 1, a nitrogen atom at position 3, carbon atoms at 2, 4, and 5, and a COOH group attached to C4.

[a]Reflux overnight at room temperature or gentle heat (~80°C).

[b]**1**, 2-phenylthiazolidine-4-carboxylic acid; **2**, 3-benzoyl-2-phenylthiazolidine-4-carboxylic acid; **3**, 2-ethyl-2-methylthiazolidine-4-carboxylic acid; **4**, 3-benzoyl-2-ethyl-2-methylthiazolidine-4-carboxylic acid; **5**, 2-phenyl-5,5-dimethylthiazolidine-4-carboxylic acid; **6**, 2-ethyl-2,5,5-trimethylthiazolidine-4-carboxylic acid; **7**, 3-benzoyl-2-ethyl-2,5,5-trimethylthiazolidine-4-carboxylic acid.

volume of CH_2Cl_2. The combined organic layer was dried with anhydrous sodium sulfate, filtered, and evaporated in the rotoevaporator. The yellow solid recovered, which had only a faint pyridine odour at this stage, was dissolved in 20 mL methanol and was acidified to pH 2–3 with aqueous HCl. Water was added dropwise until the solution turned slightly cloudy. The mixture was allowed to stand at room temperature until crystals formed. These were recrystallized from hot methanol to give a pale yellow solid. Yield 0.35 g (60%), mp 128-129°C (lit. (5*a*) mp 153–154°C). Anal. calcd. for $C_{17}H_{15}NO_3S$: C 65.2, H 4.8, N 4.5, S 10.2, O 15.3; found: C 62.5, H 5.7, N 4.3, S 9.8, O 18.2. Anal. calcd. for **2**·0.7 H_2O: C 62.6, H 5.1, N 4.3, S 9.8, O 18.2.

2-Ethyl-2-methylthiazolidine-4-carboxylic acid 3

A published procedure (5*b*) was used as follows: 1.5 g (0.0125 mol) L-cysteine was added to 22 mL of 2-butanone and the mixture was refluxed for 5 h. The mixture was filtered while hot. Most of the cysteine remained undissolved and unreacted. White solid, 0.6 g, was recovered after evaporation of the filtrate, followed by recrystallization from hot 2-butanone; $C_7H_{13}NO_2S$, mp 130–132°C (lit. (5*b*) mp 132–133°C).

3-Benzoyl-2-ethyl-2-methylthiazolidine-4-carboxylic acid 4

Compound **3** (1.0 g, 0.006 mol), 30 mL of pyridine, and 0.8 g of benzoyl chloride were reacted in a flask cooled by an ice bath. Thirty minutes later a white solid started precipitating out of the pale yellow solution. The work-up procedure was identical to that reported in the preparation of **2**; 0.6 g (40%) of a white solid was obtained, mp 133–134°C. Anal. calcd. for $C_{14}H_{17}NO_3S$: C 60.2, H 6.1, N 5.0, S 11.5, O 17.2; found: C 60.5, H 6.3, N 4.8, S 11.3, O 17.2.

2-Phenyl-5,5-dimethylthiazolidine-4-carboxylic acid 5

A published procedure (5*a*) was followed: 1.0 g (0.0066 mol) of D-penicillamine was added to 1.0 mL benzaldehyde and 10 mL ethanol, and the mixture was heated for 30 min. The almost clear mixture was filtered while hot and as the filtrate cooled a white precipitate started separating. The cooled solution was filtered to obtain 1.3 g (80%) of a white solid, $C_{12}H_{15}NO_2S$, mp 141–142.5°C (lit. (5*a*) mp 145–146°C).

2-Ethyl-2,5,5-trimethylthiazolidine-4-carboxylic acid 6

To 1.5 g (0.01 mol) of D-penicillamine was added 25 mL 2-butanone and the mixture was refluxed for 4 h. The clear solution was allowed to cool but no crystallization occurred. Evaporation produced 1.5 g (70%) of white solid, recrystallized from 2-butanone, mp 117–119°C (lit. (5*c*) mp 183–183.5°C). Anal. calcd. for $C_9H_{17}NO_2S$: C 53.2, H 8.4, N 6.9, O 15.7, S 15.8; found: C 53.7, H 8.6, N 6.8, O 15.4, S 15.4.

3-Benzoyl-2-ethyl-2,5,5-trimethylthiazolidine-4-carboxylic acid 7

Compound **6** (0.20 g, 0.00125 mol) was dissolved in 15 mL pyridine and 0.15 g benzoyl chloride was added. The mixture was left in the refrigerator overnight. A yellow oil was recovered after evaporation and yielded a yellow crystalline solid after cyrstallization from methanol–water. The crystals were filtered and washed with ether to give a white solid, 0.15 g (40%), mp 182–183°C. Anal. calcd. for $C_{16}H_{21}NO_3S$: C 62.5, H 6.9, N 4.6, O 15.6, S 10.4; found: C 62.4, H 7.0, N 4.6, O 15.6, S 10.8.

Almost all of the compounds were purified by recrystallization and their melting points are close to the reported values, except for **2** and **6**. Elemental analyses were obtained for those compounds for which no mp was found in the literature, **4** and **7**. Most of these compounds had been previously prepared but very little is known about their structure and spectroscopic properties. Many of the thiazolidines known today were synthesized before 1949 from *dl*-penicillamine, so that the products obtained consisted of mixtures of stereoisomers. This might explain the melting point disparity between the published values and the values obtained here for 3-benzoyl-2-phenylthiazolidine-4-carboxylic acid **2** (128–129°C vs. 153–154°C). It is much more likely that the material described here is at least partly hydrated; the analytical figures are poor for the anhydrous material but agree fairly well with a 0.7 hydrate. An even larger disparity occurs for the melting point of **6**: 117–119°C versus 183–183.5°C published, for which no apparent explanation arises. The narrow range of observed mp's suggests the compounds are relatively pure; moreover, their proton and carbon-13 spectra were obtained and are consistent with the structure proposed, and the vibrational spectra agree with those of closely related structures.

No literature mp values could be found for 3-benzoyl-2-ethyl-2-methylthiazolidine-4-carboxylic acid **4** (mp 133–134°C) and 3-benzoyl-2-ethyl-2,5,5-trimethylthiazolidine-4-carboxylic acid **7** (mp 182–183°C), and we believe we are reporting their preparation and characterization for the first time. The elemental analyses of **4** and **7** indicate purity and stability.

Spectral measurements

Infrared spectra were recorded on both Nicolet 7199 FT-IR and Perkin–Elmer model 283 spectrophotometers. The samples were ground with KBr at a concentration of approximately 1% by weight and then pressed into pellets. Spectra were calibrated with polystyrene. Raman spectra were excited by means of λ5145 Å radiation from a Spectra-Physics model 164-02 argon ion laser and recorded on a Spex 14018 double monochromator. Solid samples were contained in glass melting point tubes, and solutions in NMR tubes. The spectrometer was calibrated regularly against an indene standard and had previously been calirtated with a neon lamp; the wavelength readout scale was found not to change (±1–2 cm).

Solutions for NMR studies were prepared in D_2O and concentrations were about 100 mg (solid)/mL of solvent. External tetramethylsilane was used as the reference. Proton NMR spectra were recorded on a Varian T60 spectrometer, and ^{13}C NMR spectra were recorded on a Bruker WP-80 spectrometer operating at 20.115 MHz.

The p*K* values of some of the water-soluble thiazolidine-4-carboxylic acids **3**, **6**, and **7** were obtained by titration of aqueous solutions with 0.01 N NaOH and 0.01 N HCl. The pH values were measured with a Corning model 130 pH meter, which was standardized with Scientific Products potassium hydrogen phthalate pH 4.00 buffer, BDH pH 7.00 buffer, and Scientific Products boric acid/potassium hydroxide pH 10.00 buffer. The pH measurements are reliable to ±0.03.

Results and discussion

The vibrational spectra

In the *N*-benzoyl compounds and in the thiazolidine compounds derived from benzaldehyde there are peaks that result from aromatic and C—H bond stretches. These give rise to multiple absorption peaks in the 3100–3000 cm region of

Can. J. Chem. Downloaded from www.nrcresearchpress.com by 84.41.108.74 on 09/07/12
For personal use only.

Can. J. Chem. Downloaded from www.nrcresearchpress.com by 84.41.108.74 on 09/07/12
For personal use only.

the spectrum, while aliphatic C—H bond stretches occur at 3000 cm or lower. For a monosubstituted aromatic ring, carbon–carbon stretching frequencies have been assigned to bands in the regions 1608–1600, 1589–1580, 1495–1490, and 1452–1446 cm. Bands at 1240 ± 8, 1177 ± 6, 1156 ± 5, 1073 ± 4, and 1027 ± 3 cm have contributions from the bending vibrations of aromatic C—H bonds (6). We observe these bands and find that they are slightly sharper than neighbouring bands in the infrared spectra. Also we have allowed our assignments slightly wider frequency ranges than in benzene alone because of contributions from both phenyl and benzoyl groups. Medium strong bands at 751 ± 15 and 697 ± 11 cm are also characteristic of monosubstituted benzene rings. The frequency of these bands is variable because of the interaction with out-of-plane ring bending. Raman bands expected for monosubstituted benzene rings are 1620–1565, 1005–90 (very strong), 625–605, and 415–400 (very weak) cm (6).

The C—S stretching frequency has been assigned in D-penicillamine and β,β-dimethylcysteic acid to 548 cm, a very strong Raman band. In L-cysteine it has been assigned to 678 cm and it has been concluded that substituents on carbon atoms adjacent to sulfur cause a decrease in the stretching frequency of the C—S bond (7). Bands in the region of 680 and 600 cm, and 630 and 540 cm, are so assigned.

Thiazolidine ring modes have been assigned in the past as follows: 1150–1110 cm arise from CCN stretches; 380, 330, 280, and 191 cm bands result from CNC, CCS, NCS, and CSC deformations, respectively. Deformations involving sulfur usually have been found to be intense in the Raman, and showed isotopic shifts caused by the adjacent CD_3 groups in tetramethylthiazolidine-4-carboxylic acid prepared from deuterated acetone (7). The ring assignments are consistent with previous findings. The detailed spectra have been deposited.[2]

Table 2 shows selected vibrational bands that pertain to the amino acid/zwitterion equilibria, and we will discuss in detail only these features. Characteristic O—H stretching bands are present in the infrared at 3460–3400 cm for all compounds containing COOH functional groups. There are also fairly intense broad bands at about 3000 cm for some of the compounds as well as distinct bands between 2500 and 1940 cm. These broad absorptions at lower frequency are a result of moderately strong hydrogen bonds in some of these compounds. In cysteine and D-penicillamine the hydrogen bond absorptions are so strong that they mask the CH_2 and CH_3 absorptions almost completely (3).

Three types of hydrogen bonds can occur in thiazolidine-4-carboxylic acid derivatives: O—H...O, O—H...N, and N—H...O bonds. The first type can be much shorter than the other two: Hamilton and Ibers (8) have discussed correlations between the frequency of anti-symmetric stretching modes and the O...O or N...O distance in such bonds. A lowering of OH frequency correlates with a lower force constant and a longer OH bond. The O—H bond length actually increases as the O...O bond length decreases. Thus lower O—H stretching frequencies correlate with formation of stronger O—H...O hydrogen bonds. Increase of band width and intensity enhancement occur at the same time. Similar effects occur for the O—H...N and N—H...O bonds (8).

Hydrogen bonds of the type O—H...O are expected to have infrared bands between 3500 and 2600 cm for O...O distances of 2.90–2.60 Å. Hydrogen bonds between oxygen and nitrogen atoms have lower stretching frequency bands in the region of 2600–1900 cm (8).[3] All compounds in Table 2 show hydrogen bonding bands in the range 3450–3000 cm. Some compounds show splitting of bands and others have additional bands at lower wave numbers. These observations imply that there are moderate O...O hydrogen bonds, in the range of 2.88–2.65 Å (8). Hydrogen bonds of the O...N or N...O type only exist for the non-*N*-benzolyated compounds, and are characterized by two bands in the regions 2500–2350 cm and 1990–1900 cm, as observed by us for *S*-2,2,5,5-tetramethylthiazolidine-4-carboxylic acid (7).

The two *N*-benzoyl derivatives of L-cysteine **2** and **4**, and the compounds **5**, **6**, and **7** in Table 2 are all amino acids, having C=O stretching frequencies around 1725 cm. Compounds **1**, 2-phenylthiazolidine-4-carboxylic acid, and **3**, 2-ethyl-2-methylthiazolidine-4-carboxylic acid, are zwitterions; there are no bands in the C=O region of 1740–1725 cm or in the C—O region (1215–1190 cm). COO^- stretching bands are very intense in the infrared at 1625 cm, and weaker in the Raman at 1630 and 1603 cm, for **3**, and at 1572 cm in the infrared for **1**. The latter is an unusually low frequency, but it is probaby caused by the proximity of the phenyl group, and there are three Raman bands between 1621 and 1580 cm. The symmetric vibrations of COO^- in both zwitterions are assigned to the bands at 1388–1376 cm. The amide C=O band was assigned to 1660–1620 cm, typical of disubstituted amides.

The NMR spectra

The proton NMR spectra of thiazolidine-4-carboxylic acids derived by condensation of D-penicillamine and L-cysteine with benzaldehyde and 2-butanone and their *N*-benzoyl derivatives are shown in Table 3 and the coupling constants in Table 4. Peaks at 7.42 ppm are assigned to the aromatic protons, a multiplet being observed because the protons are not equivalent. The protons on C4 have chemical shifts between 3.56 and 4.90 ppm depending on the overall structure of the molecule. The lowest chemical shift is caused by the C4 proton in 2-phenyl-5,5-dimethylthiazolidine-4-carboxylic acid, **5**, and the greatest deshielding of a C4 proton is in 3-benzoyl-2-phenylthiazolidine-4-carboxylic acid, **2**. In general the chemical shift of the C4 proton is higher in the *N*-benzoyl derivatives than in the other thiazolidine compounds. C5 protons are mostly unaffected by the presence of the benzoyl group, since they are spatially removed from the nitrogen atom, although some deshielding is noticed if there is a phenyl group on C2. Protons on C2 are markedly deshielded compared to protons on other ring carbon atoms, probably because of the presence of the phenyl ring on the same carbon atom. Deshielding is especially pronounced in the *N*-benzoyl-2-phenylthiazolidine compound, **2**, because of the proximity of the carbonyl of the amide, which attracts electron density from neighbouring atoms. The spectrum of the 2-phenylthiazolidine compound, **1**, is similar to that of the 2-methylthiazolidine compound in that both are mixtures of stereoisomers and each proton type in the molecule gives rise

[2]Tables containing the complete listing of infrared and Raman wave numbers and the approximate mode descriptions and assignments for compounds **1–7** may be purchased from: The Depository of Unpublished Data, Document Delivery, CISTI, National Research Council Canada, Ottawa, Canada K1A 0S2.

[3]I. D. Brown, personal communication.

TABLE 2. Selected vibrational bands[a]

1[b] Z[d] *RR,SR*[e]	**2** AA *RR,SR*	**3** Z,Z* *RR,SR*	**4** AA *RR,SR*	**5** AA *RS,SS*	**6** AA,Z* *RS,SS*	**7** AA *RS,SS*	Assignment[c]
2665(70) br,ir	2670(30),ir 2560(30),ir	2650,w br,ir	2505(50) br,ir			3000–2200,ir br.wing	O—H...O
		2350(55) br,ir		2490(70), br,ir	2480(70) br,ir		O—H...N
	1747(92),ir 1725,R		1733(95),ir 1727,R 1700(70),ir	1727(94),ir 1700,R	1720(95),ir 1705,R	1744(87),ir 1740,R	νC=O
1621,R		1625(100),ir 1630,R					$\nu_a CO_2$
1376,ir 1380,R		1388(93),ir 1388(25),R					$\nu_s CO_2$
	1338,ir 1212(35),ir		1326(70),ir 1215(86),ir	1328(100),ir 1222(70),ir	1324(99),ir 1232(91),ir	1318(50),ir 1213(69),ir	δ OH νC—O

[a]Infrared, ir, and Raman, R, bands, cm, relevant to the amino acid/zwitterion equilibria; intensities of some of the stronger bands in parentheses relative to strongest band = 100.
[b]Compounds **1–8** as defined in Table 1.
[c]ν = stretching frequency, a = antisymmetric, s = symmetric, δ = deformation, br = broad, w = weak.
[d]Forms present in the solid: Z, zwitterion; AA, amino acid; Z*, zwitterion in solution deduced from p*K* values.
[e]Diastereomers present.

TABLE 3. ^{1}H NMR spectra of substituted thiazolidine-4-carboxylic acids[a,b]

Compound	C_6H_5	(C-4)H	(C-5)H	(C-2)H	CH_3(C-5)	CH_3(C-2)	CH_3CH_2(C-2)
1	7.42, m, 50	3.92, t 4.22, t } 10	3.26, m, 50	5,50, s 5.68, s } 10			
2	7.30, m, 60	4.90, t, 7	3.45, m, 12	6.28, s, 6			
3		4.46, t, 7	3.36, m, 14			1.62, s, 20	1.92, dq 0.90, t } 35
4	7.35, m, 50	4.72, dd, 9	3.15, m, 25			1.83, s, 31	2.45, m, 20 0.90, t, 30
5	7.45, m, 25	3.56, s 3.67, s } 6		5.62, s 5.83, s } 6	1.63, s 1.51, s } 15 1.32, s 1.29, s } 15		
6		3.80, s 3.70, s } 16			1.45, s 1.50, s } 48 1.20, s 1.25, s } 46	1.60, s 1.57, s } 48	1.80, q, 30 1.00, t, 46
7	7.40, m, 30	4.30, s 4.38, s } 6			1.30, s 1.27, s } 20 1.60, s 1.64, s } 20	1.95, s, 20	0.93, q 1.00, t } 30

[a]Concentrated solution in DMSO-d_6.
[b]The chemical shift in ppm is followed by peak multiplicity (s = singlet, d = doublet, t = triplet, q = quartet, m = multiplet) and by the integrated area.

to two signals. The chemical shift difference is probably very small, however, since no splitting was observed. The three-line signal of the proton at C4 was expected to be a four-line signal.

Compound **2** had some new aromatic peaks in a multiplet at 7.30 ppm, and the downfield shift of the proton at C2 was increased significantly, probably because of the proximity of the amide carbonyl group, which attracts electron density from neighbouring atoms. Even though the compound is a mixture of diastereomers, only one signal was observed for each type of proton.

The C4 proton of 2-ethyl-2-methythiazolidine-4-carboxylic acid, **3**, gives a triplet at low field and the C5 protons cause overlapping doublets of doublets. A singlet at 1.62 ppm results from the resonance of the methyl protons on C2. The ethyl

Can. J. Chem. Downloaded from www.nrcresearchpress.com by 84.41.108.74 on 09/07/12
For personal use only.

TABLE 4. Coupling constants of ^{1}H NMR spectra of thiazolidine-4-carboxylic acids

	Compound	$^2J_{H\text{-}C5,H\text{-}C5}$	$^3J_{H\text{-}C4,H\text{-}C5}$	$^2J_{H\text{-}CC2,H\text{-}CC2}$
1	2-Phenyl-	6.4	1.6	—
2	3-Benzoyl-2-phenyl-	7.8	—	—
3	2-Ethyl-2-methyl-	6.4	1.2	6.0
4	3-Benzoyl-2-ethyl-2-methyl-	6.6	2.2	7.2
5	2-Phenyl-5,5-dimethyl-	—	—	—
6	2-Ethyl-2,5,5-trimethyl-	—	—	4.4
7	3-Benzoyl-2-ethyl-2,5,5-trimethyl-	—	—	4.4

[a] *J* values in Hz; ^{1}H NMR spectra recorded at 25°C.

TABLE 5. Carbon-13 chemical shifts of substituted thiazolidine-4-carboxylic acids[a]

Compound	COOH	CO(N)	C_6H_5	C-5	C-4	C-2	CH_3(C-5)	CH_3(C-2)	CH_3CH_2(C-2)
1	173.24	—	128.76	38.30	71.11	65.88	—	—	—
	172.58		128.50	37.20	71.38	65.23	—	—	—
			127.84						
			127.53						
			127.19						
2	171.21	145.07	136.99	40.02	64.69	63.58	—	—	—
		143.89	132.95		64.28				
			129.86						
			129.36						
			128.22						
			127.32						
			126.96						
			126.68						
			125.41						
3	172.77	—	—	37.73	64.34	80.51	—	38.17	29.44
					64.18			36.29	26.59
4	171.84	138.80	132.91	32.90	67.41	76.72	—	32.90	27.22
	171.60		129.20						
			128.46						
			125.88						
5	170.79	—	128.95	61.53	74.19	69.12	29.15	—	—
	170.48	—	128.56	60.83	73.32	67.81	28.26		
			128.26				27.83		
			127.42				26.82		
			126.95						
			126.34						
6	170.64	—	—	77.22	60.20	72.69	30.77	37.70	28.69
					59.71	72.15		36.09	27.66
7	170.73	138.94	129.86	78.09	77.24	78.09	27.99	33.09	33.76
	169.64	138.69	129.22	77.91	77.01	77.01		32.78	26.71
			129.05						25.81
			128.69						
			125.70						
			125.22						

[a] Concentrated solutions in DMSO-d_6.

group shows two set of peaks: the methyl group is a triplet, and the methylene protons are nonequivalent and form part of an ABC_3 system.

The spectrum of 3-benzoyl-2-ethyl-2-methylthiazolidine-4-carboxylic acid, **4**, is essentially the same as the previous one with additional aromatic peaks. Both NMR spectra show two closely spaced signals for each type of proton, like all the other compounds in this table, because of the presence of a new asymmetric center at C2.

The 2-phenyl-5,5-dimethylthiazolidine-4-carboxylic acid, **5**, has two methyl groups, each of which gives two singlets, since they can be in one of two possible positions that are nonequivalent. Otherwise the spectrum is similar to that of the L-cysteine analogue.

Can. J. Chem. Downloaded from www.nrcresearchpress.com by 84.41.108.74 on 09/07/12
For personal use only.

TABLE 6. pK values of L-cysteine, D-penicillamine, and some thiazolidine-4-carboxylic acids

Compound	pK_1[a]	pK_2[b]	ΔG°[c]	Isoelectric point[d]
L-cysteine	1.96	8.18	−4.23	5.07
D-Penicillamine	1.8	7.9	−4.14	4.85
Thiazolidine-4-carboxylic acid	1.51	6.21	−3.19	3.86
2-Methyl-	2.8	6.0	−2.17	4.4
2,2-Dimethyl-	2.7	5.7	−2.04	4.2
5,5-Dimethyl-	2.7	5.8	−2.11	4.25
2,5,5-Trimethyl-	2.6	5.6	−2.04	4.1
2,2,5,5-Tetramethyl-	2.8	5.5	−1.83	4.15
2-Ethyl-2-methyl-	2.7	7.8	−3.50	5.25
2-Ethyl-2,5,5-trimethyl-	2.9	7.4	−3.07	5.15

[a] pK_1 is pK of the carboxylic group.
[b] pK_2 is pK of the amino group.
[c] Calculated in kcal mol, from $\Delta G = -RT \ln (K_2/K_1)^{1/2}$.
[d] $(1/2)(pK_1 + pK_2)$.

The carbon-13 chemical shifts of the componds are shown in Table 5. Some of the peak assignments, especially those of the carbon atoms in the ring, were difficult to make. Spin-sorted spectra were obtained and compared, and it is believed the peaks are assigned correctly. Only general trends of the data listed in Table 5 will be noted here.

The carboxyl carbon atoms have very consistent chemical shifts, near 170 ppm, and thus this group is very little affected by other ring substituents. The next most deshielded carbon atom is in the amide carbonyl of the benzoylated compounds, the signal occurring at 138.7–145 ppm. The aromatic carbon atoms all have values between 125 and 137 ppm, with the two nearest the C=O being the most deshielded.

The carbon atom in the thiazolidine ring with the highest chemical shift is usually C4 except when C2 is doubly substituted. The highest-field ring carbon atom is C5, which has low chemical shift values unless there are methyl substituents directly bonded to it. Methyl groups on C5 give peaks around 30 ppm and those on C2 have slightly higher chemical shifts, 33–38 ppm. Ethyl group carbon atoms are not assigned specifically in Table 5, but the terminal methyl carbon atom gives a peak of higher field than the methylene carbon atom.

The amino acid/zwitterion equilibria

The amino acid/zwitterion equilibria are independent of the pH of solution and the presence of the cation and anion. The vibrational spectra, on the other hand, are capable of showing the presence of all three species — the cation, the neutral species, and the anion.

The pK values represent the extent of protonation of ionizable groups, and are presented in Table 6. There is a downward shift of amino group pK with increasing methyl group substitution, especially on C2. Increase of COOH group pK with methyl substitution is partly caused by inductive effects of the methyl group; also with increasing substitution the anion cannot be solvated so effectively. Thus the equilibrium $AH \rightleftarrows A^- + H^+$ is shifted to the left-hand side.

From the equation relating the Gibbs standard free energy to the equilibrium constant relationship for a given reaction in solution, we have calculated the free energy of conversion from the amino acid to the zwitterion form. The values of ΔG°, also shown in Table 6, vary between −4.23 and −1.83 kcal mol^{-1} for L-cysteine and *S*-2,2,5,5-tetramethylthiazolidine-4-carboxylic acid. The isoelectric point is the pH at which the concentration of the zwitterion is at a maximum, and the concentrations of anion and cation are equal. Below the isoelectric point, the molecule is positively charged; above it, negatively. Thus at physiological pH these thiazolidine-4-carboxylic acids would all be negatively charged.

Compounds **3** and **6** have the highest values for amino group pK in this series. The carboxyl group pK values of 2.7 and 2.9 are similar to the rest of the series. The ΔG° values of −3.50 and −3.07 are closer to the value for the unsubstituted thiazolidine-4-carboxylic acid, and higher than the values for the methyl-substituted compounds.

The pK values for some compounds could not be measured because of poor solubility, but their form in the solid state can be assigned as either amino acid or zwitterion from the vibrational spectra. The compounds that exist in the amino acid form in the solid are **2**, **4**, **5**, **6**, and **7** (which includes all the *N*-benzoyl derivatives). Compounds **1** and **3** are zwitterions in the solid. Although **6** has pK values typical of the zwitterion in solution, the solid shows the characteristic C=O and C—O infrared bands of the amino acid.

The ^{13}C NMR spectra show a correlation related to these equilibria: The chemical shifts of the carboxylate carbon atoms in **1** and **3** are greater than those for the other compounds, and are close to the values for the unsubstituted thiazolidine-4-carboxylic acid. These compounds are all zwitterions in the solid.

The zwitterion forms of D-penicillamine and L-cysteine become the amino acid forms in the thiazolidine complexes because of marked changes in the pK values of the amino and carboxylic acid groups.

The amino acid/zwitterion equilibria depend both on structural variations in the ring and on the number and type of substituents on the ring (with changes at the C2 position having greater effect than those at C5). In all cases, however, the changes are large enough that they will markedly affect the hydrogen bonding behaviour in vivo, and thus this is an important feature of thiazolidine formation in biological milieu.

Acknowledgments

Financial support from NSERC, the Medical Research Council of Canada, Atomic Energy of Canada Ltd., and

Can. J. Chem. Downloaded from www.nrcresearchpress.com by 84.41.108.74 on 09/07/12
For personal use only.

McMaster University Science and Engineering Research Board is gratefully acknowledged.

1. H. E. HOWARD-LOCK, C. J. L. LOCK, A. MEWA, and W. F. KEAN. Semin. Arthritis Rheum. **15**, 261 (1986).
2. R. FAGGIANI, H. E. HOWARD-LOCK, C. J. L. LOCK, and R. ORGIAS. Can. J. Chem. **69**, 1 (1991).
3. H. E. HOWARD-LOCK, C. J. L. LOCK, M. L. MARTINS, P. S. SMALLEY and R. A. BELL. Can. J. Chem. **64**, 1215 (1986).
4. V. R. RIEMSCHNEIDER and G. A. HOYLE. Z. Naturforsch. **176**, 765 (1962).
5. H. T. CLARKE, J. R. JOHNSON, and R. ROBINSON. The chemistry of penicillin. Princeton University Press, Princeton, NJ. 1949. (*a*) p. 962; (*b*) p. 959; (*c*) p. 961.
6. N. B. COLTHUP, L. H. DALY, and S. E. WIBERLEY. Introduction to infrared and Raman spectroscopy. Academic Press, New York, NY. 1964.
7. H. E. HOWARD-LOCK, C. J. L. LOCK, and P. S. SMALLEY. Can. J. Chem. **63**, 2411 (1985).
8. W. C. HAMILTON and J. A. IBERS. Hydrogen bonding in solids, W. A. Benjamin, Inc., New York, NY. 1968.

Can. J. Chem. Downloaded from www.nrcresearchpress.com by 84.41.108.74 on 09/07/12
For personal use only.

Energy transfer between Langmuir–Blodgett monolayers of organic dyes

E. JOHNSON AND R. AROCA[1]

Department of Chemistry and Biochemistry, University of Windsor, Windsor, Ont., Canada N9B 3P4

Received May 28, 1991

This paper is dedicated to Dr. Richard Norman Jones

E. JOHNSON and R. AROCA. Can. J. Chem. **69**, 1728 (1991).

The Langmuir–Blodgett technique has been used to prepare multilayer structures in order to investigate the distance dependence of the nonradiative transfer of electronic energy from a donor plane of molecules to an acceptor plane. The distance between well-separated donor molecules and acceptor molecules was carefully controlled by spacer layers of arachidic acid. New systems for energy transfer studies are considered that use *N*-hexyl-*N'*-ethyl-3,4:9,10-perylenetetracarboxyldiimide (HPTCDE) and *N*-hexyl-3,4:9,10-perylenetetracarboxylmonoimide (HPTCO) as donors and lutetium diphthalocyanine ($LuPc_2$) as acceptor. The limitations of the Förster dipole theory of energy transfer from a donor monolayer of point dipoles to an acceptor layer are discussed.

Key words: energy transfer, Langmuir–Blodgett, diphthalocyanine, perylene.

E. JOHNSON et R. AROCA. Can. J. Chem. **69**, 1728 (1991).

Afin d'étudier la relation entre la distance et l'énergie électronique de transferts non-radiatifs de molécules d'un plan donneur à un plan accepteur on a préparé des structures multicouches à l'aide de la technique de Langmuir–Blodgett. Pour contrôler avec précision la distance entre des molécules de donneur et des molécules d'accepteur bien séparées, on a utilisé des couches d'acide arachidique. On a considéré de nouveaux systèmes pour les études de transfert d'énergie; ils utilisent le *N*-hexyl-*N'*-éthyl pérylène-3,4:9,10-tétracarboxyldiimide (HPTCDE) et le *N*-hexyl pérylène-3,4:9,10-tétracarboxylmonoimide (HPTCO) comme donneurs et le diphtalocyanine de lutécium ($LuPc_2$) comme accepteur. On discute des limitations de la théorie dipolaire de Förster du transfert d'énergie d'une monocouche de dipôles ponctuels agissant comme donneur à une couche agissant comme accepteur.

Mots clés : transfert d'énergie, Langmuir–Blodgett, diphtalocyanine, pérylène.

[Traduit par la rédaction]

Introduction

Langmuir–Blodgett (LB) monolayers of strongly absorbing and fluorescent dyes represent an important type of model systems where the increase and direction of photon absorption can be studied. The nontrivial transfer of electronic excitation energy between well-separated donor molecules and acceptor molecules occurs before the emission takes place. Förster's dipole theory of energy transfer (ET) predicts that when the corresponding optical transitions in both molecules are allowed, the probability of ET decreases with the sixth power of the distance (1). A parallel can be drawn between the trivial and nontrivial ET between molecules and the transfer of power in the far-zone and the near-zone fields of oscillating dipoles in classical electrodynamics (2). Hans Kuhn (3) applied the dipole–dipole model to a number of practical systems with restricted geometries. In particular, he derived the basic equations for the luminescence quenching of a dipole emitter by a monolayer of oriented dipoles. The latter approach has been used by several groups to explain the results for the distance dependence of nontrivial ET between well-separated monomolecular layers (4–6). Recently, the dynamics of the Förster-type energy transfer in organic systems of restricted geometries has been reviewed by Yamazaki *et al.* (7). There exists, however, a very limited amount of data for energy transfer between neat LB monolayers of strongly absorbing dye molecules. Only very recently, Penner reported steady-state energy transfer for donor and acceptor layers of concentrated J-aggregated cyanine dyes (5). In the present report, the excimer emissions of two perylene derivatives: *N*-hexyl-*N'*-ethyl-3,4:9,10-perylenetetracarboxyldiimide (HPTCDE) and *N*-hexyl-3,4:9,10-perylenetetracarboxylmonoimide (HPTCO), that were in resonance with the red absorption of lutetium bis-phthalocyanine ($LuPc_2$) were used to study the distance dependence of the energy transfer between LB layers. The separation between the two dye layers was controlled by interposing fatty acid layers. A critical discussion of the results and Kuhn's model is presented. The possibility of a competitive quenching from electron transfer processes has also been examined experimentally, and the perylene–phthalocyanine interactions were followed for a number of perylene derivatives.

[1]Author to whom correspondence may be addressed.

Experimental

The spectroscopic characterization of HPTCDE, HPTCO, and $LuPc_2$ has previously been reported (8, 9). Reproducible isotherms of all three dyes have been recorded at 20°C. Both perylene derivatives possess two limiting areas. HPTCO has limiting areas of 0.24 and 0.84 nm^2. HPTCDE has limiting areas of 0.64 and 0.94 nm^2. $LuPc_2$ has a limiting area of 0.75 nm^2. Moreover, all three dyes have collapse pressures above 35 mN/m. The acceptor layer of $LuPc_2$ was first deposited on to a Corning 7056 glass slide. Spacer layers of arachidic acid were then deposited on top of the acceptor layer. Finally, the desired perylene derivative was placed above the previously deposited matrix as well as on a bare glass section of the slide. The latter section of the slide was used as a fluorescence reference layer. Z deposition was used in all cases. All film materials were dissolved in chloroform for film spreading. HPTCO was the least soluble. Its final concentration in $CHCl_3$ was 1.9×10^{-4} M. The concentration of HPTCDE, $LuPc_2$, and arachidic acid was 1.2×10^{-4} M, 8.3×10^{-5} M, and 1.8×10^{-3} M respectively. Approximately 6×10^{16} chromophore molecules were spread onto an aqueous subphase containing $CdCl_2$ at a concentration of 2.5×10^{-4} M. Films were prepared in a Lauda Langmuir film balance equipped with an electronically controlled dipping device, Lauda Filmlift FL-1. Monolayers of the perylene dyes were transferred at a constant speed of 3 mm/min, and at surface pressures of 15 mN/m. Monolayers of $LuPc_2$ were transferred at 10 mN/m. In all cases, the transfer ratio was near unity. Spectra Physics model 2020 Kr^+ and Ar^+ ion lasers were used. Typical spectral bandpass and laser power were 5 cm^{-1} and 200 mW

Can. J. Chem. Downloaded from www.nrcresearchpress.com by 84.41.108.74 on 09/07/12
For personal use only.

respectively. Raman shifts and steady-state fluorescence were measured with a Spex-1403 double monochromator and the Ramanor U-100 with microscope attachment. Electronic absorption spectra were recorded on a Response UV–VIS spectrophotometer interfaced with an IBM PC computer.

Results and discussion

Electronic spectra and excimer emission

The electronic absorption spectrum of $LuPc_2$ (in a 1:1 molar ratio solution of HPTCDE and $LuPc_2$ in $CHCl_3$), and the fluorescence spectrum of HPTCDE obtained from the same solution are shown in Fig. 1. A dip in the 650–680 nm region of the emission spectrum of HPTCDE is due to trivial and nontrivial energy transfer between the two dye molecules. It can be seen that the molecular monomer emission of perylene and perylene derivatives does not have a strong fluorescence band in resonance with the absorption Q (667 nm) band of the $LuPc_2$. However, perylene and perylene derivatives show a structureless band about 5000 cm^{-1} to the red of the lowest absorption band, which has been associated with excimer or exciplex emission (10, 11). The strong excimer emission in the 650-nm region is observed in crystal, thin solid evaporated films, pellets, and LB layers of perylene derivatives (12). The exciplex formation is well documented in Birks' book (9), and is obtained by dissolving a perylene derivative in certain aromatic solvents such as *N*,*N*-dimethylaniline (DMA). For instance, solution experiments with HPTCDE, HPTCO, and PDCI (*N*-octyl-3,4-perylenedicarboximide) in DMA provided a clear example of exciplex formation with a characteristic broad emission in the 600–700 nm region of the visible spectrum. Azumi and McGlynn (13) have explained the formation of stable excited perylene dimers (excimers) using molecular exciton and charge resonance states, and concluded that a number of excimers could be formed by perylene molecules in a geometrical arrangement where the molecular planes are parallel. It is the strong excimer emission of perylene derivatives in LB monolayers, which is in resonance with the Q-absorption band of the $LuPc_2$ molecule, that was used to monitor the energy transfer between the two LB monolayers. Typical results of steady-state measurements of the excimer fluorescence of an HPTCO LB monolayer of the neat material and separated from one LB of $LuPc_2$ by arachidic acid monolayers are illustrated in Fig. 2. The emitter monolayer was facing the collection optics to avoid the contribution of trivial emission–absorption transfer in the intensity measurements.

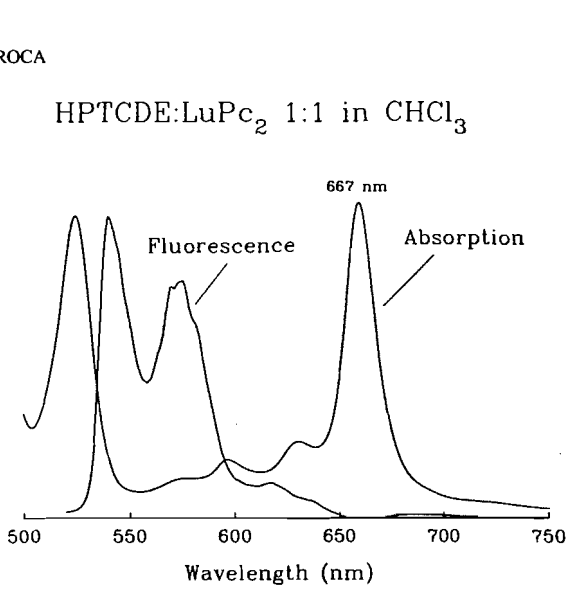


FIG. 1. Absorption spectrum of $LuPc_2$ and fluorescence spectrum of HPTCDE in a 1:1 molar ratio in $CHCl_3$.

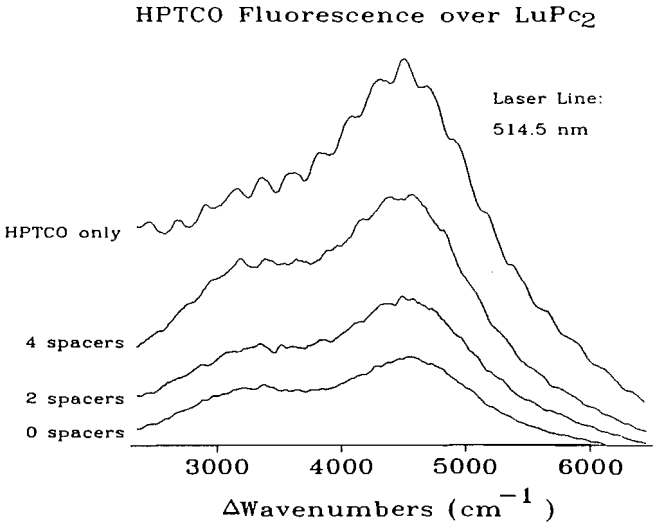


FIG. 2. Fluorescence intensity of the HPTCO excimer emission in a HPTCO/AA/$LuPc_2$ system.

Distance dependence of the energy transfer

The $LuPc_2$ monolayer is the acceptor layer and the perylene derivative forms the donor layer. The physical model in Förster's dipole theory of energy transfer is a donor monolayer of point dipoles interacting with an acceptor layer of dipoles, in a case where the corresponding electronic transitions are allowed. The limitations of the model have been recently discussed by Chang (14). It was found that the Förster dipole approximation for energy transfer would be applicable for donor–acceptor distances large compared to their sizes and when an angular average of the dipolar orientations may be taken. The latter condition implies that the approximation would not be suitable for ordered layers if the rotational relaxation time is greater than the fluorescence lifetime.

The quenching of luminescence of a dipole emitter in the donor layer by absorbing dipoles in the acceptor layer is proportional to the power of the electric field. In Kuhn's model the emitter is an oscillating dipole perpendicular to the donor layer plane located at a distance d from the acceptor layer with dipoles parallel to the layer plane (3). The power of the classical field contains three terms proportional to r^{-2}, r^{-4}, and r^{-6}, which after integration to calculate the power absorbed produces Kuhn's equation for the distance dependence of the energy transfer

$$[1]\quad q/q_d = 1 + (d_0/d)^4 + \eta(d_0/d)^2$$

where q is the quantum yield of the emitter in the absence of the acceptor layer, and q_d is the quantum yield for an acceptor layer at a distance d; d_0 is the critical transfer distance, or distance where the energy transfer and deactivation through other paths are equal. A simplification of eq. [1] is obtained by dropping the quadratic dependence, and the energy transfer decreases as the fourth power of the interlayer separation (5). Application of the latter approximation to the interpretation of experimental data has not always been successful, and Fromherz and Reinbold (15) have found that the dependence of the energy transfer on the distance of the dye layers, for their experiments, was better fit by a cubic power.

Can. J. Chem. Downloaded from www.nrcresearchpress.com by 84.41.108.74 on 09/07/12
For personal use only.

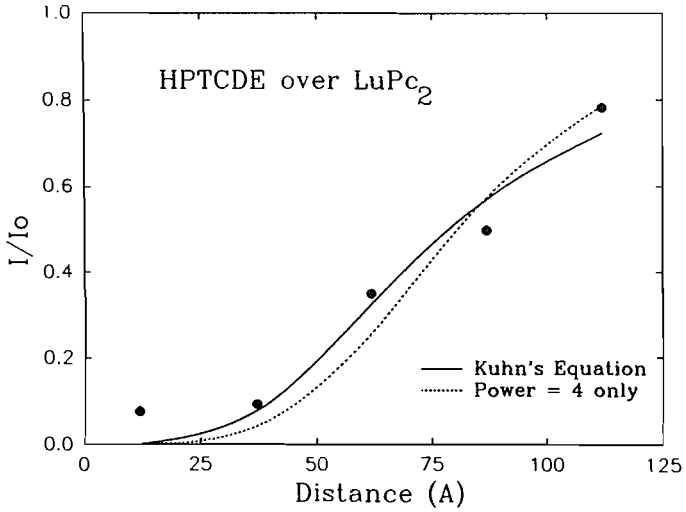


FIG. 3. Fluorescence intensity ratio I/I_0 of the HPTCDE excimer emission as a function of the distance from one LB of neat $LuPc_2$.

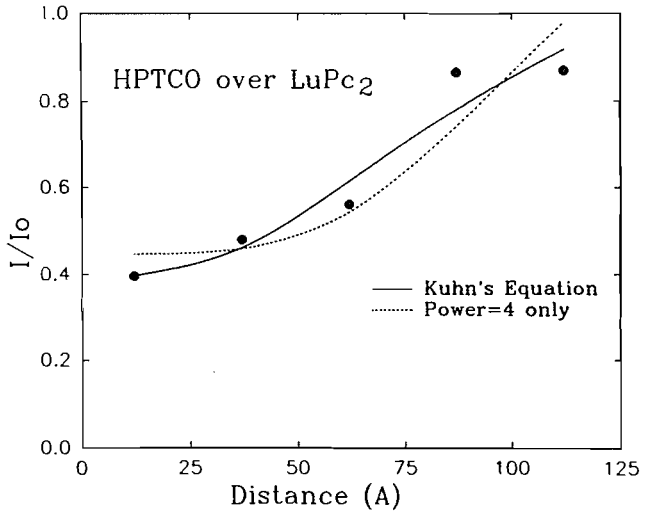


FIG. 4. Fluorescence intensity ratio I/I_0 of the HPTCO excimer emission as a function of the distance from one LB of neat $LuPc_2$.

In general, the information accumulated on ET between LB monolayers seems to indicate: (a) the fourth power term alone (in eq. [1]) may not provide a good fitting of the experimental results, (b) the most significant ET between LB layers (d_0 values) takes place on a scale of 10 nm.

Langmuir–Blodgett monolayer samples for the present study were prepared by Z deposition of the acceptor layer, spacer, and donor monolayer. The thickness of one spacer layer has been reported to be 2.7 nm (16). The results of the ET experiments for HPTCDE/spacer/$LuPc_2$ and HPTCO/spacer/$LuPc_2$ are presented in Figs. 3 and 4 respectively. Equation [1] gave the best fit for the present set of experimental points. The critical distance values obtained are given in Table 1, where the results produced by the fourth power fitting are also included for comparison. The d_0 values given by Kuhn's full equation gave results in agreement with Fromherz and Reinbold (15), who reported d_0 values between 6.2 and 6.4 nm for their monomethine–oxacyanine–monomethine–thiacyanine system. The fourth power approximation seems to overestimate the critical transfer distance. The η coefficient, which depends strongly on molecular orientation, changes considerably for the two molecules, 1 for HPTCDE and 3 for HPTCO. In this respect it would be interesting to carry out experiments with LB monolayers fabricated with well-defined molecular orientations to study the orientational effect on the energy transfer measurements.

TABLE 1. Critical transfer distances

	Kuhn's full equation		Power = 4 term only
	d_0 (Å)	η	d_0 (Å)
HPTCDE	65	1	81
HPTCO	58	3	108

Electron transfer versus energy transfer

Dr. R. O. Loutfy of the Xerox Research Centre of Canada was concerned with the extent of electron-transfer contribution to the fluorescence quenching of HPTCDE and HPTCO. To distinguish electron transfer from energy transfer, a number of experiments were carried out. First, solutions with different relative concentrations of HPTCO, HPTCDE, and $LuPc_2$ were prepared. The solution containing $LuPc_2$ mixed with HPTCDE showed no changes in any of the absorption bands of either component. However, at a high relative concentration of HPTCO with $LuPc_2$, a new band at 700 nm appears. This new band has been assigned in the literature to the Q-band of oxidized $LuPc_2$ (17). However, the 700-nm band was not observed for a HPTCO/$LuPc_2$ bilayer assembly or any other LB assemblies used in this study of energy transfer. The latter results would indicate that the electron transfer complex formed between $LuPc_2$ and HPTCO has geometric requirements that are not satisfied by the molecular arrangement in the LB films. The mixed solution of HPTCO/$LuPc_2$ in $CHCl_3$ was unique in forming aggregates that precipitated out of solution. This reaction is limited to the perylene derivatives containing an anhydride group, and was not observed in a series of solutions of perylene dicarboximide derivatives and $LuPc_2$. The absorption spectrum of the solution and that of the precipitate are shown in Fig. 5. In solution the absorptions of the HPTCO and $LuPc_2$ are clearly observed. The Q-band of $LuPc_2$ showed the presence of the 700-nm band, which corresponds to the oxidized form of $LuPc_2$. The spectrum of the precipitate indicated the formation of an aggregate with very broad bands of the phthalocyanine unit and a weak absorption in the spectral region of the HPTCO. The nature of the aggregate is not known. In a second set of experiments, an aliquot of an aqueous solution containing the strong electron acceptor, 1,1′-diheptyl-4,4′-bipyridinium dibromide (HBP) (18) was spread over 1 LB of $LuPc_2$. After the solvent had evaporated, the absorption spectrum of this slide was recorded. Again, no bands corresponding to either the reduced or oxidized form of $LuPc_2$ were observed. In conclusion, there was no evidence of electron transfer for the HPTCDE/$LuPc_2$ system. The HPTCO and $LuPc_2$ formed, in solution, aggregates or a change transfer complex that contains oxidized $LuPc_2$. However, the formation of these aggregates or the oxidation of $LuPc_2$ was not observed in LB bilayers with adjacent LB monolayers of each dye. Furthermore, the quenching of HPTCO for the latter system was less effective than in the HPTCDE/$LuPc_2$ case (see Figs. 3 and 4), ruling out the extra quenching due to electron transfer.

Can. J. Chem. Downloaded from www.nrcresearchpress.com by 84.41.108.74 on 09/07/12
For personal use only.

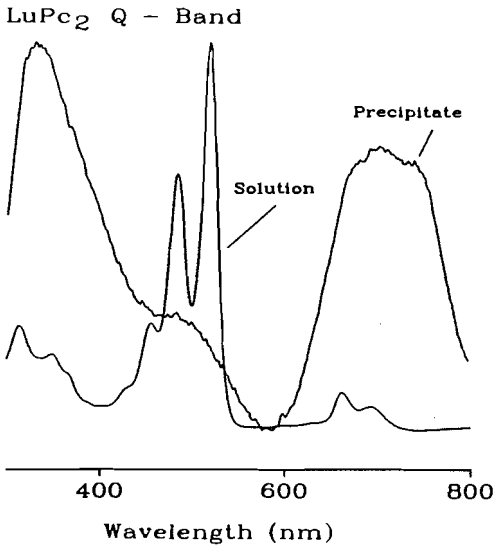


FIG. 5. Absorption spectrum of the HPTCO–LuP_2 mixture in $CHCl_3$, and absorption spectrum of the precipitate obtained from insoluble aggregates.

Conclusion

An important new system of perylene–phthalocyanine dyes has been used for energy transfer studies involving the excimer emission of the perylene derivative. The critical distance observed for energy transfer in the new system indicated that the ET occurs mainly on the 10-nm scale, which is in agreement with previous observations with different dyes. The possibility of electron transfer contributions to the fluorescence quenching was found to be negligible. Further studies of energy transfer between LB monolayers with well-defined molecular orientation could help to clarify the limitations of the equations obtained using the dipole theory.

Acknowledgment

The financial support of the NSERC of Canada is gratefully acknowledged.

1. T. FÖRSTER. Discuss. Faraday Soc. **27**, 1 (1959).
2. R. P. CLAYTON and A. N. SYED. Introduction to electromagnetic fields. McGraw–Hill, New York. 1987.
3. H. KUHN. J. Chem. Phys. **53**, 101 (1970).
4. H. KUHN, D. MOBIUS, and H. BUCHER. *In* Physical methods of chemistry. Vol. I. Part IIIB. *Edited by* A. Weissberger and W. B. Rossiter. Wiley, New York. 1972. pp. 577–702.
5. T. L. PENNER. Thin Solid Films, **160**, 241 (1988).
6. R. E. CLAVIJO and R. AROCA. Raman Spectrosc. Proc. Int. Conf. 12th. *Edited by* J. R. Durig and J. F. Sullivan. John Wiley & Sons, Chichester. 1990. p. 256.
7. I. YAMAZAKI, N. TAMAI, and T. YAMAZAKI. J. Phys. Chem. **94**, 516 (1990).
8. R. AROCA and E. JOHNSON. SPIE v1336. Raman Lumin. Spectrosc. Technol. 2, 291 (1990).
9. R. AROCA, R. E. CLAVIJO, C. A. JENNINGS, G. J. KOVACS, J. M. DUFF, and R. O. LOUTFY. Spectrochim. Acta, **45A**, 957 (1989).
10. J. B. BIRKS. Photophysics of aromatic molecules. John Wiley & Sons Ltd., London. 1970.
11. R. M. HOCHSTRASSER and C. A. NYI. J. Chem. Phys. **72**, 2591 (1980).
12. R. AROCA, U. GUHATHAKURTA-GHOSH, R. O. LOUTFY, and Y. NAGAO. Spectrochim. Acta, **46A**, 717 (1990).
13. T. AZUMI and S. P. MCGLYNN. J. Chem. Phys. **42**, 1675 (1965).
14. J. C. CHANG. J. Chem. Phys. **67**, 3901 (1977).
15. P. FROMHERZ and G. REINBOLD. Thin Solid Films, **160**, 347 (1988).
16. M. C. PETTY. *In* Langmuir–Blodgett films. *Edited by* G. G. Roberts. Plenum Press, New York. 1990.
17. G. A. CORKER, B. GRANT, and N. J. CLECAK. J. Electrochem. Soc. **126**, 1339 (1979).
18. R. STEIGER and F. ZBIDEN. J. Imaging Sci. **32**, 64 (1988).

Can. J. Chem. Downloaded from www.nrcresearchpress.com by 84.41.108.74 on 09/07/12
For personal use only.

Polarized and depolarized continuum resonance Raman scattering of molecular iodine: accurate determination of repulsive states

J. STREMPEL AND W. KIEFER

Institut für Physikalische Chemie der Universität Würzburg, Marcusstrasse 9-11, D-8700 Würzburg, Federal Republic of Germany

Received April 18, 1991

This paper is dedicated to Dr. Richard Norman Jones

J. STREMPEL and W. KIEFER. Can. J. Chem. **69**, 1732 (1991).

We have recorded high-resolution polarized and depolarized resonance Raman spectra of molecular iodine with excitation by argon-ion laser lines at 496.5, 488.0, and 476.5 nm up to the seventh, and with 457.9 nm up to the fifth, overtone. These spectra were also calculated numerically applying second-order perturbation theory. In contrast to earlier publications on this subject, special emphasis was put on obtaining highly reliable polarized and depolarized spectra. The variations of the spectral band shapes and depolarization ratios obtained at different excitation wavelengths could be explained by means of the specific contributions of the two excited electronic states $^3\Pi_{0^+u}$ and $^1\Pi_{1u}$. About 60 different experimentally obtained spectra were finally used to derive the positions of the two excited-state potentials involved in this type of light scattering. The derivation was done by comparison of the experimental and theoretically simulated spectra where parameters of the $^1\Pi_{1u}$ as well as of the $^3\Pi_{0^+u}$ state potentials were varied.

Key words: resonance Raman scattering, diatomic molecules, potentials, excited electronic states.

J. STREMPEL et W. KIEFER. Can. J. Chem. **69**, 1732 (1991).

Utilisant une excitation par les raies d'un laser ion-argon (à 496,5, 488,0 et 476,5 nm jusqu'à septième harmonique et par celle à 457,9 nm jusqu'à la cinquième harmonique), on a enregistré les spectres Raman de résonance polarisée et dépolarisée, à haute résolution, de l'iode moléculaire. On a aussi calculé ces spectres d'une façon numérique en appliquant la théorie du deuxième ordre de perturbation. Par opposition aux publications antérieures sur ce sujet pointu, on a mis l'accent sur l'obtention de spectres polarisés et dépolarisés très fiables. On peut expliquer les variations des formes des bandes des spectres et des rapports de dépolarisation avec les longueurs d'onde d'excitation à l'aide de contributions spécifiques des deux états électroniques excités $^3\Pi_{0^+u}$ et $^1\Pi_{1u}$. On a finalement utilisé 60 spectres expérimentaux différents pour évaluer les positions des potentiels des deux états excités impliqués dans ce type de diffusion de la lumière. On a réalisé cette évaluation en comparant les spectres expérimentaux et théoriques qui avaient été simulés en faisant varier les paramètres de $^1\Pi_{1u}$ ainsi que les potentiels de l'état $^3\Pi_{0^+u}$.

Mots clés : diffusion Raman de résonance, molécules diatomiques, potentiels, états électroniques excités.

[Traduit par la rédaction]

Introduction

Since the first observation of the resonance Raman effect in halogen gases (1) at the National Research Council in Ottawa, Canada, the molecules bromine and iodine have been extensively examined experimentally. Kiefer and Bernstein (2) measured the Raman spectra of iodine excited in the resonant region with high resolution and explained the various features of the fundamental and overtone bands by means of Fortrat parabolas and the thermal distribution of the states as S-, Q-, and O-branches. Theoretical calculations were performed in order to simulate the spectra (3–8). In the case of bromine, Baierl and Kiefer (6–8) showed that two excited electronic states, the repulsive $^1\Pi_{1u}$ and the bound $^3\Pi_{0^+u}$ state, have to be taken into account in order to calculate the spectra. The influence of these two states appears in very specific band shapes and depolarization ratios of the fundamental Q-branch for excitation with different laser frequencies. In the case of iodine, Williams and Rousseau (3) measured and calculated depolarized spectra with 488.0, 476.5, and 457.9 nm lines and $\Delta v = 3$ and $\Delta v = 8$ but neglected the contribution of discrete levels of the $^3\Pi_{0^+u}$ and the contribution of the $^1\Pi_{1u}$ state. No spectra were calculated for excitation with 496.5 nm where the intermediate Raman level is just above the dissociation limit of the $^3\Pi_{0^+u}$ state. In a further investigation Williams *et al.* (5) included, in their calculations of the $\Delta v = 3$ and 8 Raman transitions, the $^1\Pi_{1u}$ state as well as the discrete $^3\Pi_{0^+u}$ levels and measured polarized and depolarized spectra. With the new experimental data they optimized the potential position but they had difficulty in simulating the spectra excited with 496.5 nm. Furthermore the $^3\Pi_{0^+u}$ potential was held at a fixed position.

In this paper we report for the first time polarized and depolarized spectra with all vibrational transitions from $\Delta v = 1$–8 excited with the laser lines 496.5, 488.0, and 476.5 nm and with $\Delta v = 1$–6 excited with 457.9 nm. The theoretical calculations consider both the $^1\Pi_{1u}$ state as well as the continuous and discrete vibrational levels of the $^3\Pi_{0^+u}$ state. Both potentials have been varied in order to achieve a good agreement with all experimental spectra. The huge amount of experimental data allowed us to derive what we think to be very accurate data for the excited state potentials.

Theoretical calculation of continuum resonance Raman band intensities

Because the theory employed in this paper has been described earlier in detail (6, 8), only a short summary with the essential ideas is presented here.

The standard expression for the scattering intensity of a space-fixed scattering arrangement is given by

$$[1] \quad I_{\rho z}^{if} \propto \omega_f^4 N_i g_i |(\alpha_{\rho z})_{if}|^2$$

where i and f designate the initial and final states, respectively, and ρ the direction of polarization x or z of the scattered light. The incident light is chosen to be linearly polarized in the z-direction. ω_f is the frequency of scattered light. The population

Printed in Canada / Imprimé au Canada

Can. J. Chem. Downloaded from www.nrcresearchpress.com by 84.41.108.74 on 09/07/12
For personal use only.

Can. J. Chem. Downloaded from www.nrcresearchpress.com by 84.41.108.74 on 09/07/12
For personal use only.

of initial states N_i is calculated with the assumption of thermal equilibrium in the scattering region. The intensity dependence from the nuclear spin quantum number is expressed by the nuclear spin factor g_i.

$(\alpha_{\rho z})$ is the polarizability tensor, which can be calculated using second-order perturbation theory (Kramers–Heisenberg–Dirac relation) and the dipole approximation. In the case of resonance excitation one obtains

$$[2] \quad (\alpha_{\rho z})_{if} = \sum\!\!\!\!\!\!\int_r \frac{\langle f|\mu_\rho|r\rangle\langle r|\mu_z|i\rangle}{\hbar\omega_{ri} - \hbar\omega_0}$$

with the dipole operators μ_ρ, the incident energy $\hbar\omega_0$, and the energy difference $\hbar\omega_{ri}$ between the initial state i and the unperturbed eigenstates r. The sum sign stands for summation over discrete states and the integral sign for the integration over continuous levels. In the integral the density of states factor is omitted for clarity. The damping factor that would appear in the denominator of eq. [2] has been set to zero according to ref. 4.

The state of a diatomic molecule is characterized by the quantum numbers e (electronic), v (vibronic), J (total angular momentum), k (projection of J on the molecular axis), and m (magnetic). Because no external field is applied one has in addition to sum over the degenerate quantum numbers m_i and m_f.

The polarizability tensor is transformed into spherical space-fixed coordinates. This space-fixed frame is changed into a molecular-fixed frame by using the formula of rotation matrices. Now the rotational part is separated from the matrix elements. The matrix elements are calculated in the molecular rest frame by transforming the coordinate system to a molecular fixed cartesian one.

The Raman transitions occur between the rovibronic levels of the ground state $^1\Sigma_g^+$ ($e_f = e_i = 0$, $k_f = k_i = 0$) via excited electronic states and therefore one obtains for the polarizability tensor (without the rotational part):

$$[3] \quad (\bar{\alpha}_{\bar{\rho}\bar{z}})_{if} = \sum_{e,k} \sum\!\!\!\!\!\!\int_{v_r^e} \frac{\langle 0 v_f 0|\bar{\mu}_{\bar{\rho}}|e\, v_r^e\, k\rangle\langle e\, v_r^e\, k|\bar{\mu}_{\bar{z}}|0 v_i 0\rangle}{\hbar\omega_{ri} - \hbar\omega_0}$$

The overlined quantities are expressed in the molecular rest frame. The sum and (or) integration must be taken over the two upper excited electronic states $^3\Pi_{0^+u}$ (abbreviated as B) and $^1\Pi_{1u}$ (abbreviated as Π) with all their involved discrete and continuous vibronic levels and the possible orientations of the total angular momentum k. For the $^3\Pi_{0^+u}$ state there is only one orientation of J ($k = 0$) but the $^1\Pi_{1u}$ state is double degenerate with respect to k ($k = \pm 1$).

By applying the Born–Oppenheimer approximation one obtains for a single matrix element

$$[4] \quad \langle e'v'k'|\bar{\mu}_\xi|e\,v\,k\rangle \approx \langle e'k'|\bar{\mu}_\xi|ek\rangle\langle v'|v\rangle$$

Using only the first term of the Herzberg–Teller expansion, the electronic matrix element is calculated with the electronic wave functions at equilibrium distance of the nuclei and treated as a constant factor:

$$[5] \quad \langle e'k'|\bar{\mu}_\xi|ek\rangle \approx \langle e_0'k'|\bar{\mu}_\xi|e_0k\rangle = M_{e'e}$$

This approximation causes only a small error in the resulting Raman intensities because the change in the value of the electronic transition moment M_{B-X} for a fixed incident wavelength is only about 2% between the $v_i = 0$ and $v_i = 19$ states with respect to the value for the $v_i = 9$ state using the linear function given by Tellinghuisen (9)

$$[6] \quad M_{B-X}(\bar{R}) = 0.884\bar{R} + 1.388$$

With $\bar{R}$ as the R centroid. The units of M_{B-X} are debye (D) and $\bar{R}$ is in angstrom (Å). Because only the relative intensity ratios of the various bands within the Raman transitions belonging to the same Δv will be taken into account, and not the intensity ratios between the Raman bands excited with different wavelengths (where in fact the variation of M_{B-X} with the incident energy is remarkable), the error in neglecting the energy dependence of M_{B-X} is small compared to the error introduced through the uncertainty in determining the spectroscopic temperature.

Additionally, Tellinghuisen (9, 10) has assumed the electronic transition moment between the states $^1\Pi_{1u}$ and $^1\Sigma_g^+$ to be constant, which leads to correct theoretical results within experimental error in calculating the absorption coefficient. However, it has been mentioned (9) that this assumption is not absolutely correct. Since the contribution of the $^1\Pi_{1u}$–$^1\Sigma_g^+$ transition to the absorption coefficient in the region above 21 000 cm^{-1} is even greater than that of the $^3\Pi_{0^+u}$–$^1\Sigma_g^+$ transition, the error in treating M_{B-X} as a constant is even smaller and therefore negligible in our case. In addition it should be mentioned that the degeneracy of the $^1\Pi_{1u}$ state is contained in the rotational part and not involved in the electronic transition moment.

The selection rule of J for a single dipole transition is $\Delta J = \pm 1$. This results in a total selection rule $\Delta J = 0, \pm 2$ and gives rise to three different branches, which are designated by O ($\Delta J = -2$), Q ($\Delta J = 0$), and S ($\Delta J = +2$).

The polarizability tensor can now be written as

$$[7] \quad (\alpha_{\rho z})_{if} = \sum_{e=B,\Pi} M_e^2 D_e(J_i, \Delta J, \rho) \underbrace{\sum\!\!\!\!\!\!\int_{v_r^e} \frac{\langle v_f|v_r^e\rangle\langle v_r^e|v_i\rangle}{\hbar\omega_{ri} - \hbar\omega_0}}_{=:\ \chi_e^{v_f v_i}}$$

The factors M_e represent the electronic matrix elements between the ground state $^1\Sigma_g^+$ and the two excited electronic states $^3\Pi_{0^+u}$ and $^1\Pi_{1u}$. The factors $D_e(J_i, \Delta J, \rho)$ contain the change between the different coordinate systems. The second sum and integral is abbreviated by $\chi_e^{v_f v_i}$. It has the meaning of a scattering amplitude and is a complex function since the integral has to be calculated over the singularity at $\omega_{ri} = \omega_0$ (4).

After summation over the magnetic quantum numbers m_i and m_f, the intensity of a Raman transition between rovibronic levels of the ground state is now given by:

$$[8] \quad I_{\rho z}^{if} \propto \omega_f^4 g_i N_i \{ M_B^4 R_B(J_i, \Delta J, \rho)|\chi_B^{v_f v_i}|^2 + M_\Pi^4 R_\Pi(J_i, \Delta J, \rho)|\chi_\Pi^{v_f v_i}|^2 + 2M_B^2 M_\Pi^2 R_{B+\Pi}(J_i, \Delta J, \rho)|\chi_B^{v_f v_i}\chi_\Pi^{v_f v_i}| \}$$

where R_B, R_Π, and $R_{R+\Pi}$ are the rotational factors for the states B and Π and for the interference term, respectively, after summation over m_i and m_f.

Equation [8] clearly shows that the intensity of a rovibronic transition is composed of the contributions of the two excited states as well as an interference term. Each term involves an

electronic, a rotational, and a vibrational part. In the electronic part the ratio $\mathcal{R} = \frac{M_\Pi^2}{M_B^2}$ determines the relative electronic contribution of the two excited states. Because it is only possible to determine the ratio $\mathcal{R}$ and not the single electronic transition moments M_Π and M_B, we have set M_B^2 to unity. For the two directions of polarization, the three rotational branches, and the three intensity terms given in eq. [8] one has to calculate 18 algebraic rotational factors (6). The complex functions $\chi_e^{v_f v_i}$ are calculated numerically by iteration of the wavefunctions and integration of the product of the wavefunctions. The integral over the singularity is calculated using Cauchy's law of integration.

In the low energy region the $^1\Sigma_g^+$ ground state is known with satisfactory accuracy and corresponding data were therefore taken from the literature (11, 12). The RKR values of the $^1\Sigma_g^+$ ground state potential have been taken from Coxon (11). Between these values the ground state potential has been interpolated with cubic splines. The spectroscopic parameters have been taken from Barrow and Yee (12). From these data the line positions of the rovibronic transitions are calculated using the standard expression

$$[9]\quad \frac{E_{evJ}}{hc} = \omega_e\left(v+\frac{1}{2}\right) - \omega_e x_e\left(v+\frac{1}{2}\right)^2 + \omega_e y_e\left(v+\frac{1}{2}\right)^3 + \ldots + \left(B_e - \alpha_e\left(v+\frac{1}{2}\right)\right)(J+1)J + \ldots$$

where ω_e, $\omega_e x_e$, and $\omega_e y_e$ are the vibrational constants, B_e the rotational constant, and α_e the coupling coefficient. Higher order expressions can be neglected because the spectral resolution is only about 1 cm^{-1}.

In the experiment the absorption of the molecules leads to a high temperature in the laser focus, with the consequence that many rovibronic levels are populated. Therefore in a numerical calculation one has to consider a high number of rotational and vibrational occupied levels. We have used 400 rotational and 20 vibrational levels of the ground state. For three rotational branches a Raman band then consists of 24 000 rovibronic transitions. The δ-like intensities are folded with an appropriate gaussian function in order to simulate the restricted spectral conditions (resolving power of the spectrometer). The proportionality factor is used to scale the calculated intensity to the experimental data.

The specific appearance of a Raman band is determined, first, by the exact position of the electronic potential curves of the contributing states via the Franck–Condon factors and, second, parametrically by the rotational intensity factors, which depend only on the symmetry of the involved states and the ratio of the square of the two electronic transition moments.

The depolarization ratio ρ of a Raman signal is defined as the ratio between the depolarized and polarized intensity, I_{xz} and I_{zz}, respectively:

$$[10]\quad \rho = \frac{I_{xz}}{I_{zz}}$$

The depolarization ratio of O- and S-bands is 0.75 and depends neither on the excitation wavelengths nor on the different electronic transitions. Q-branches are polarized ($\rho < 0.75$) and the exact value depends on the square of the electronic transition moments as well as on the Franck–Condon factors of the different transitions (8). The depolarization of overlapping S- and Q-bands can be used to determine the ratio $\mathcal{R}$ although the Q-branches are not resolved. The latter lower the depolarization ratio of the combined band, depending upon their relative contributions.

Experimental

The continuum resonance Raman spectra of iodine were excited with an argon-ion laser (Spectra Physics, model 171). No foreign gas was added in the iodine cell. To achieve approximately the same spectroscopic temperature for different excitation wavelengths, the laser output power was set to 1 W for each of the laser lines used. The spectra were recorded with a Spex model 1403 double monochromator using a photon counting system. The polarized and depolarized Raman spectra were obtained simultaneously, applying the two-channel technique developed by Kiefer and Topp (13). The correct adjustment of the system with respect to polarization was checked first, by recording the polarized 459 cm^{-1} and depolarized 214 cm^{-1} and 318 cm^{-1} lines of liquid carbon tetrachloride.

The spectral resolution was chosen to about 0.3 cm^{-1} for the fundamental bands, and 1.0 cm^{-1} for lower, and 1.5 cm^{-1} for higher overtones.

The iodine cell was heated just above the melting point of iodine (≈387 K). This results in a vapor pressure of about 120 hPa. Kiefer and Bernstein (2) determined the spectroscopic temperature under similar conditions by the Stokes/Anti-Stokes ratio of the fundamental band and found a value of 1150 K. This method is acceptable for the case of iodine because the Franck–Condon factors vary only slightly between the Stokes and Anti-Stokes bands. Methods described elsewhere (3, 14) do not measure the rovibronic temperature directly. The relatively high spectroscopic temperature in the iodine cell in comparison to the temperatures reported elsewhere (3, 5) is due to the fact that no N_2 was added. Therefore no cooling effect due to collisions with the cold foreign gas N_2 occurs.

The influence of different spectroscopic temperatures on the band shape of an overtone (e.g., $\Delta v = 3$) can be seen in Fig. 1, where sharp S-band heads occur. In the calculated spectrum B a temperature of 1000 K was used and the S-band heads are sharp and high. With a temperature of 650 K (spectrum C), as reported by Williams and Rousseau (3), the calculated S-band heads are lower compared to spectrum B. The bands have an appearance similar to the data reported in ref. 3. This behaviour is due to the fact that at low temperatures the maximum of the Maxwell–Boltzmann distribution is far away from the maximum of the Fortrat parabola (2) and therefore only weak S-band heads are formed. There is no strong effect of the temperature on the intensity distribution for the various bands. Therefore all other spectra have been calculated with a temperature of 1000 K.

Results and discussion

Contribution from discrete levels of the $^3\Pi_{0^+u}$ state

The sum over states in eq. [7] contains the sum over the discrete levels of the $^3\Pi_{0^+u}$ state as well as the integrals over the continuum of the $^3\Pi_{0^+u}$ and $^1\Pi_{1u}$ states. The sum over states is weighted with the energy difference between incident energy and the energy difference between the initial and intermediate states. The discrete sum therefore makes a significant contribution to the scattering intensity only if the laser energy is very close to the dissociation limit of the $^3\Pi_{0^+u}$ state. In the case of the 496.5-nm excitation the laser energy added to the lowest initial ($v = 0$, $J = 0$) level of the ground state reaches the continuum of the $^3\Pi_{0^+u}$ state about 92 cm^{-1} above the dissociation limit. Therefore a non-negligible contribution of the discrete states to the scattering intensity has to be taken into account in the calculated spectra.

As an example of how the discrete levels contribute to the intensity of the $\Delta v = 1$ band excited with the 496.5-nm argon-

Can. J. Chem. Downloaded from www.nrcresearchpress.com by 84.41.108.74 on 09/07/12
For personal use only.

Can. J. Chem. Downloaded from www.nrcresearchpress.com by 84.41.108.74 on 09/07/12
For personal use only.

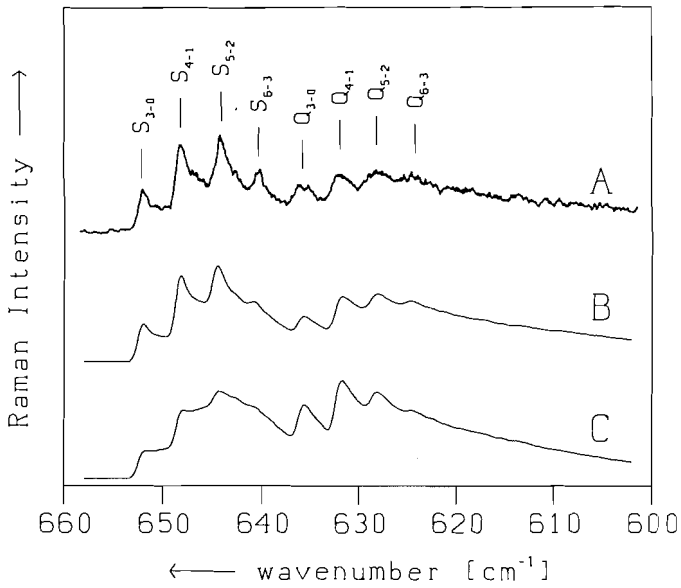


FIG. 1. Depolarized (I_{xz}) continuum resonance Raman spectrum of the second overtone region in iodine with excitation at $\lambda = 488.0$ nm. A: experimental; B: calculated using $T = 1000$ K; C: calculated using $T = 650$ K.

ion laser line, we show this band in Fig. 2 together with calculations in which the contributions of the discrete levels have been included (spectrum B) and excluded (spectrum C). The contribution of the discrete levels is significant only for the Q_{1-0}-band because here the energy dominators in the sum over the discrete levels are low enough. In this case the Q_{1-0}-band is decreased because the sign of the interference term is negative and the additional contribution from the discrete levels therefore lowers the overall intensity. The hot bands have a larger energy difference than the discrete levels and are therefore not influenced by these levels. For all spectra excited with higher energy the contribution of the discrete $^3\Pi_{0^+u}$ levels is very low and essentially can be neglected in the calculated spectra.

Contribution from the $^1\Pi_{1u}$ state

In most previous work (3, 7) the $^1\Pi_{1u}$ state was not taken into account because its square of the electronic transition moment is small relative to that for $^3\Pi_{0^+u}$ state. To achieve a better agreement between simulated and experimental spectra we also included the contribution from the repulsive $^1\Pi_{1u}$ state.

In Fig. 3 we clearly demonstrate this contribution for the case of $\Delta v = 8$ transitions excited with 496.5 nm. Including the $^1\Pi_{1u}$ state in the calculation, we observe a notable decrease of all Q-branch intensities and an increase of the S_{8-0} band intensity. This is a nice example of the interference being effected by the mixed term in eq. [8]. The interferences for the Q- and S-branches are in opposite directions because the rotational intensity factors in the interference term for I_{zz} have different signs for each branch while all other terms have the same signs.

In Fig. 4 (experiment) and Figs. 5 and 6 (theory) an example of nearly complete overlapping bands is shown. Here the S-band heads with $v_f \leftarrow v_i$ transitions overlap in frequency with $(v_f - 1) \leftarrow (v_i - 1)$ transitions of the Q-branches. Spectrum A of Fig. 4 was obtained for parallel laser and observation polarization (I_{zz}) whereas spectrum B represents I_{xz} where laser and observation polarization are perpendicular. Spectrum C is a direct recording (13) of the isotropically scattered Raman light

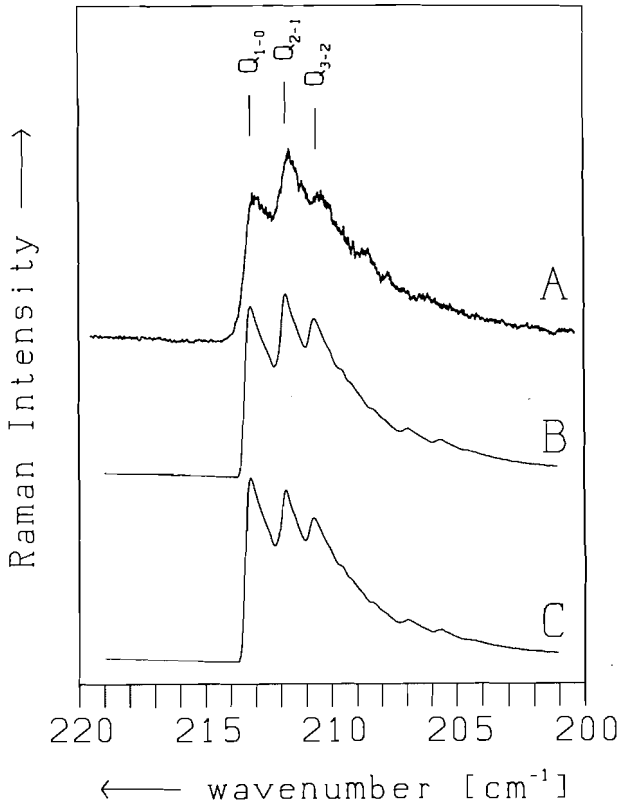


FIG. 2. Contributions from discrete levels of the $^3\Pi_{0^+u}$ state to the scattering intensity with excitation wavelength 496.5 nm demonstrated for the $\Delta v = 1$ transition in iodine. A: experimental spectrum (I_{zz}); B: calculated spectrum (I_{zz}) including the contributions from the discrete levels; C: same as B, but excluding the contributions from the discrete levels.

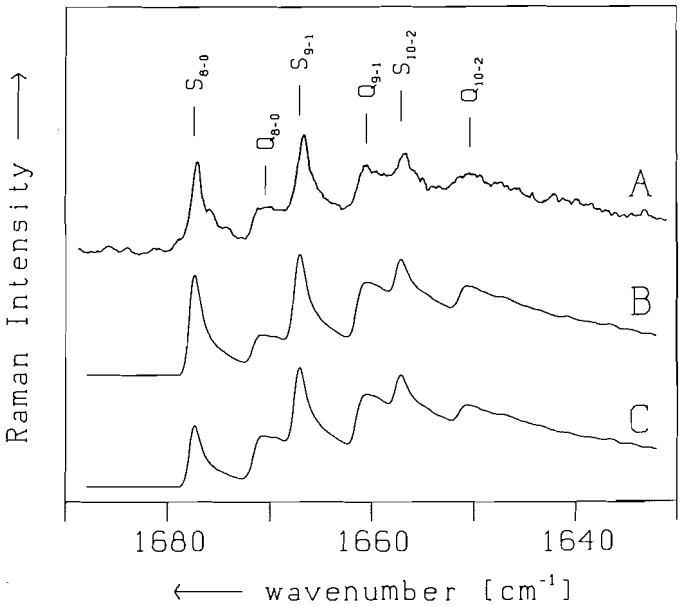


FIG. 3. Contributions from the $^1\Pi_{1u}$ state to the scattering intensity demonstrated for the $\Delta v = 8$, I_{zz} transitions in iodine excited with 496.5 nm. A: experimental spectrum (I_{zz}); B: calculated spectrum including the contribution of the $^1\Pi_{1u}$ state; C: same as B, but excluding the contribution of the $^1\Pi_{1u}$ state.

Can. J. Chem. Downloaded from www.nrcresearchpress.com by 84.41.108.74 on 09/07/12
For personal use only.

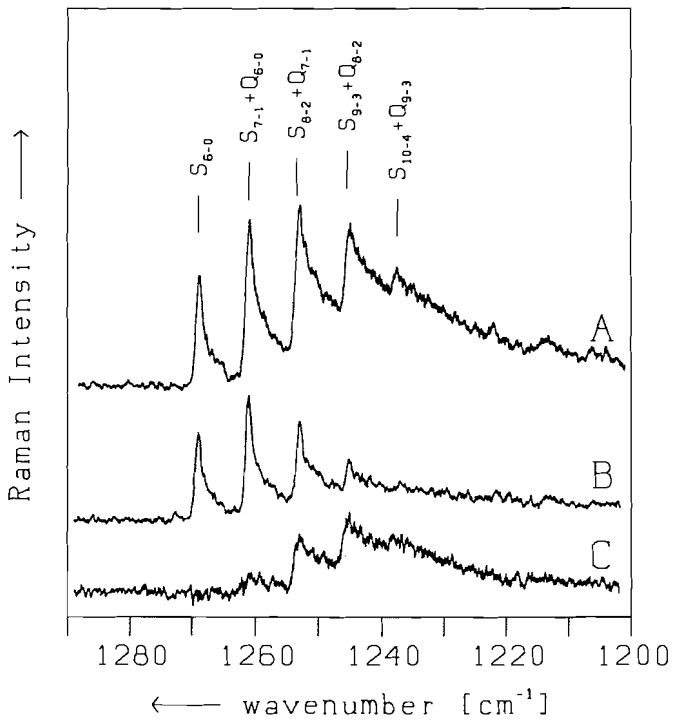


FIG. 4. Experimentally obtained continuum resonance Raman spectrum of the fifth overtone ($\Delta v = 6$) of iodine for 488.0-nm excitation. A: I_{zz}; B: I_{xz}; C: $I_{zz} - \frac{4}{3}I_{xz}$.

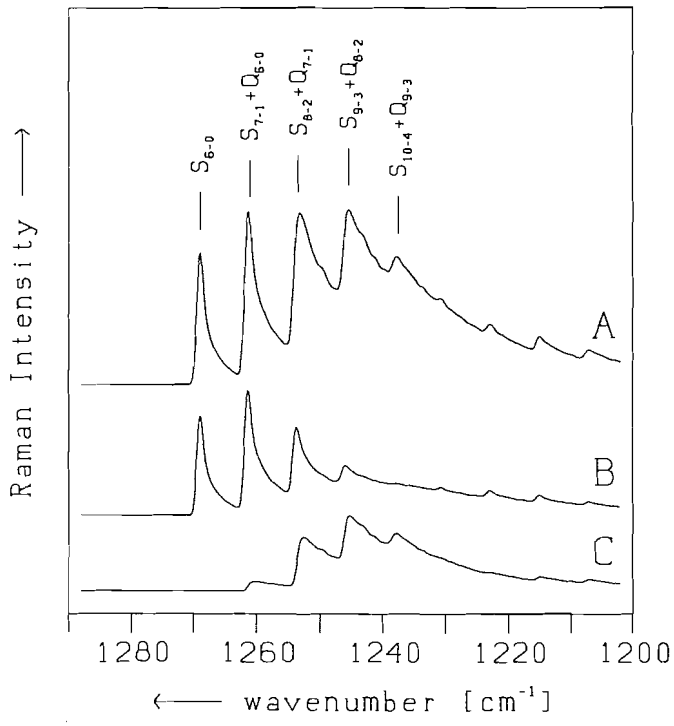


FIG. 5. Calculated continuum resonance Raman spectrum of the fifth overtone ($\Delta v = 6$) of iodine for 488.0-nm excitation. Contribution from the $^1\Pi_{1u}$ state are included. A: I_{zz}; B: I_{xz}; C: $I_{zz} - \frac{4}{3}I_{xz}$.

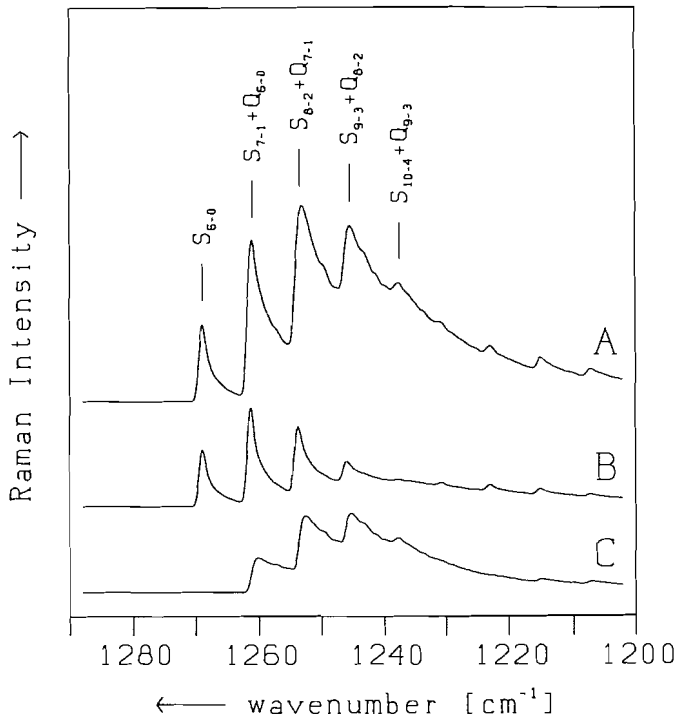


FIG. 6. Same as Fig. 5 but with exclusion of the $^1\Pi_{1u}$ state contributions.

($I_{zz} - \frac{4}{3}I_{xz}$). Spectrum C therefore contains only Q-branch scattering, while spectrum B shows the whole depolarized band intensity. The calculations including and excluding the $^1\Pi_{1u}$ state contribution, Figs. 5 and 6, respectively, reveal that the $^1\Pi_{1u}$ state cannot be neglected. Compare for instance the calculated S_{6-0} transition with the experiment: inclusion of the repulsive state reproduces the experimentally observed intensity much better. The same holds for the Q-bands. This fine comparison could only be made because of the experimental possibility of scanning directly the isotropically pure scattering, i.e., the Q-branches.

The influence of the $^1\Pi_{1u}$ state can be seen at overlapping Q- and S-bands by determining the depolarization ratios of the different bands, because the rotational intensity factors of the Q-branches and the scattering amplitudes for transitions via the two electronic states are different for the two states and the interference term. In Table 1 the calculated depolarization ratios for 488.0-nm excitation for the $\Delta v = 6$ transition with and without inclusion of the $^1\Pi_{1u}$ state for the $6 \leftarrow 0$ transition and various hot bands are compared with experimental data. The experimental values have an accuracy of about 10%. It is obvious that the $^1\Pi_{1u}$ state has a remarkable influence on the depolarization ratio although this is not clearly visible from the relative peak intensities. Again the $^1\Pi_{1u}$ contribution via the Q-branches is destructive and enhances the depolarization ratio because the depolarization ratios for the $^1\Pi_{1u}$ and interference terms alone are lower than for the single $^3\Pi_{0^+u}$ term.

We have found for the ratio $\mathcal{R}$ defined above a value of 0.16 with an uncertainty of about 25%, which has been estimated in the following way: first, the Raman spectra were calculated using temperatures associated with the maximum and minimum temperatures within the error limit. These spectra were compared to the observed ones. In a second calculation, which has been performed for $T = 1000$ K, we varied the ratio $\mathcal{R}$.

TABLE 1. Calculated and observed depolarization ratios for $\Delta v = 6$ transitions in iodine for 488.0-nm excitation

	S_{6-0}	$S_{7-1} + Q_{6-0}$	$S_{8-2} + Q_{7-1}$	$S_{9-3} + Q_{8-2}$
Experiment	0.75	0.73	0.53	0.36
Calculated including $^1\Pi_{1u}$	0.75	0.71	0.51	0.29
Calculated excluding $^1\Pi_{1u}$	0.75	0.61	0.40	0.26

For the extreme values of $\mathcal{R}$ we took the ones that led to a similar deviation from the observed spectra as was the case for the calculated spectra with the extreme values of temperature.

The values of $\mathcal{R} = 0.19$ and 0.20 as given by Tellinghuisen in refs. 9 and 10, respectively (which were derived for 470 nm), as well as the value (0.18) reported by Brith *et al.* (15) are within this error limit. The value 5.0 as reported by Williams *et al.* (5) is probably due to a printing mistake in the definition of $\mathcal{R}$. The reciprocal would be 0.2 and this value would be in good agreement with the others mentioned.

Sensitivity to position of excited state potentials

The spectral feature in continuum resonance Raman scattering is very sensitive to the relative position between ground and excited states. The ground state position was determined by Coxon (11) using the Rydberg–Klein–Rees (RKR) method. The accuracy of turning points for the $^1\Sigma_g^+$ state in the range of interest of low ($v < 40$) vibrational levels is below 2×10^{-14} m. The ground state potential was not varied because its position is very well known and therefore the error is much lower than that of the excited states. The potential in the bound region of the $^3\Pi_{0^+u}$ state was calculated by Barrow and Yee using the same method (12). In our case the important turning points are those near the dissociation limit and here the method is less accurate. The accuracy of turning points in this region has been estimated to be $\pm 2 \times 10^{-13}$ m (9). In a more recent analysis Gerstenkorn *et al.* (16) have given new values for the eigenenergies and turning points, which differ about 0.08 cm^{-1} and 5×10^{-14} m, respectively, from the values given in ref. 12 for high values of v. These new values are within the estimated error limit of the previous values.

The repulsive part of the $^3\Pi_{0^+u}$ state and the potential for the pure repulsive $^1\Pi_{1u}$ state have been determined from absorption data by Child and Bernstein (17) applying an exponential form. In the continuous region between 20 000 and 22 000 cm^{-1} both the $^3\Pi_{0^+u}$ and $^1\Pi_{1u}$ states show continuous absorption bands and the determination of potential functions is less accurate than in bound regions.

In this paper the repulsive parts of the potentials are calculated using an exponential function of the form

$$[11] \quad V(R) = V_e + Ce^{-\gamma(R-r_e)}$$

A set of parameters given by Child and Bernstein (17) was used as a first approximation. The final set of parameters was achieved by alternate variation of the single parameters and comparison of the resultant calculated spectra with the experimental data.

To demonstrate how the position of the excited potentials influences the intensities of the various bands in the continuum resonance Raman spectra, we demonstrate in Figs. 7–9 various calculations and compare them to the observed ones. Excellent agreement between calculation (spectra B) and experiment

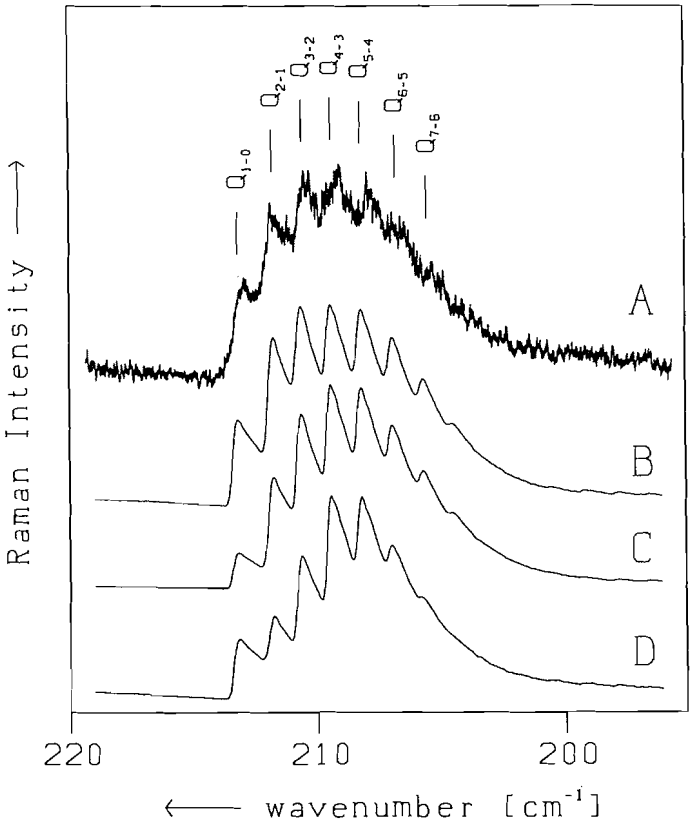


FIG. 7. Observed (A) and calculated (B–D) continuum resonance Raman spectra (I_{zz}) of the fundamental region ($\Delta v = 1$) of iodine for 457.9-nm excitation. B: calculated with optimized parameter using an exponential form given in eq. [11]; C: same as B, except that the $^3\Pi_{0^+u}$ and $^1\Pi_{1u}$ potentials have been shifted by -4×10^{-13} m and -3.25×10^{-12} m, respectively; D: same as B, except that the $^3\Pi_{0^+u}$ and $^1\Pi_{1u}$ potentials have been shifted by $+5 \times 10^{-13}$ m and $+2.75 \times 10^{-12}$ m, respectively.

(spectra A) has been obtained for the fundamental and all observed overtones for one set of parameters. Besides the fundamental vibrational region (Fig. 7), we show as additional examples the first ($\Delta v = 2$) and third ($\Delta v = 4$) overtones (Figs. 8 and 9, respectively). The set of parameters that led to the best agreement between experiment and theory is listed in Table 2. It was obtained by a combined variation of the parameters.

In Figs. 7–9 we show in addition calculated spectra C and D, where the excited-state potentials have been shifted by a small amount to either smaller (spectra C) or larger (spectra D) nuclear distances. For exact values see the caption for Fig. 7. Again these small shifts demonstrate the high sensitivity of continuum resonance Raman band shapes to the position of excited-state potentials.

Can. J. Chem. Downloaded from www.nrcresearchpress.com by 84.41.108.74 on 09/07/12
For personal use only.

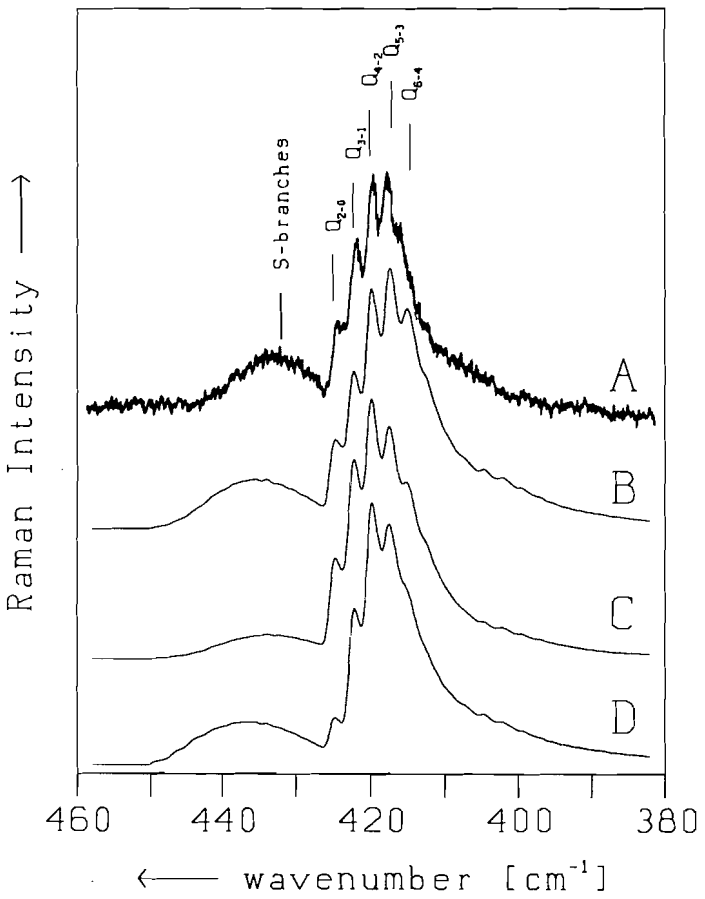


FIG. 8. Same as Fig. 7, except for $\Delta v = 2$ and excitation wavelength 476.5 nm.

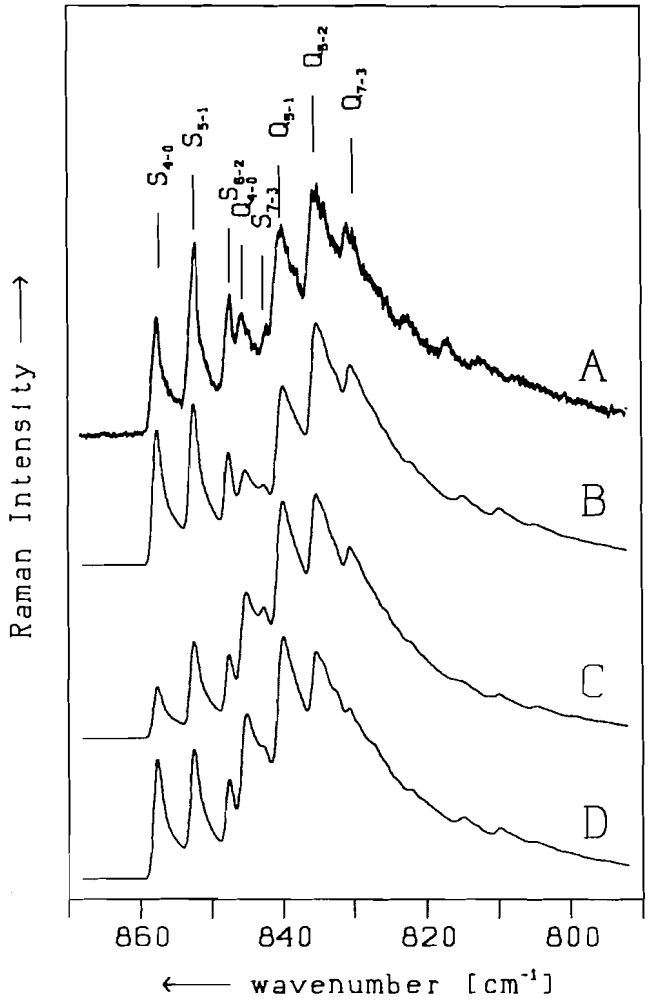


FIG. 9. Same as Fig. 7, except for $\Delta v = 4$ and excitation wavelength 488.0 nm.

Finally, we want to compare our potential curves with those obtained by means of other methods. The deviation of our $^1\Pi_{1u}$ potential curve at about 22 000 cm^{-1} from the curve obtained by Chapman and Bunker (18) by means of predissociation measurements is -2.4×10^{-12} m. The deviation in the same region of the $^1\Pi_{1u}$ potential curve given by Tellinghuisen (9) (obtained from absorption measurements) is -3.2×10^{-12} m. If we continue the pure repulsive $^3\Pi_{0^+u}$ potential curve into the bound region, it turns out that near the dissociation limit the repulsive turning points given by Barrow and Yee (12) as well as those from Gerstenkorn *et al.* (16) differ by about -2.3×10^{-12} m from the extrapolated repulsive values. To attach the bound potential curve to the repulsive part without discontinuity, we shifted the turning points of the bound part by this amount. The inaccuracy to the Raman band shapes involved in this procedure is not critical because the contribution of the bound states is significant but rather low only with the excitation wavelength 496.5 nm and can be neglected for higher incident energies. The reason for the different results obtained with absorption, predissociation, and continuum resonance Raman measurements is that in each method important simplifications, e.g., truncating of even low Herzberg–Teller terms, still have to be used in order to derive the potential data within acceptable computation time. Therefore one would expect some differences between the different methods. If one takes a look at the calculated absorption spectra in Fig. 2 of ref. 9, which were computed using two different sets of parameters having the same order of deviations as those mentioned above, one remarks that both absorption curves do not differ much more than the given experimental uncertainty. For this reason we conclude that the method of deriving potential data via the calculation of continuum resonance Raman band shapes serves as an additional approach with a similar accuracy to the conventional methods.

TABLE 2. Parameters for the excited states $^3\Pi_{0^+u}$ and $^1\Pi_{1u}$ of iodine as derived from the comparison of simulated to experimentally observed continuum resonance Raman spectra

State	M_e^2/M_B^2	C/cm^{-1}	γ/nm^{-1}	r_e/nm	V_e/cm^{-1}
$^1\Pi_{1u}$	0.16	7470	34.4	0.26825	12547.2
$^3\Pi_{0^+u}$	1.00	3340	63.5	0.26655	15769.1

Because our calculations refer only to the pure repulsive branches of the potential curves, we want to emphasize that the values given in this work are valid only above the dissociation limit of the $^3\Pi_{0^+u}$ state, that is, in the region of pure continuous absorption bands.

Conclusion

In this paper we have shown that continuum resonance Raman spectroscopy delivers a huge amount of spectroscopic data in the form of vibrational–rotational bands (fundamental,

Can. J. Chem. Downloaded from www.nrcresearchpress.com by 84.41.108.74 on 09/07/12
For personal use only.

hot bands, overtones) that can be excited with various lines of ion lasers. The simulation of these bands using time-independent (perturbation) theory as applied in this paper or applying time-dependent theory (19, 20) allows the determination of positions of repulsive potentials or repulsive parts of bound states. To demonstrate the accuracy inherent in this method we have measured many polarized and depolarized continuum resonance Raman spectra in iodine. It turned out that the experimental method, where the isotropically scattered Raman light can be directly recorded (13), was of great help for this purpose. To improve the values of the potential curves it would be useful to undertake a sophisticated comparison between the calculations of continuous absorption coefficients and continuum resonance Raman spectra. Similar work on other (isotopically pure) halogen and interhalogen molecules is presently in progress in our laboratory.

Acknowledgement

The authors gratefully acknowledge financial support by the Fond der Chemischen Industrie.

1. W. HOLZER, W. F. MURPHY, and H. J. BERNSTEIN. J. Chem. Phys. **52**, 399 (1970).
2. W. KIEFER and H. J. BERNSTEIN. J. Mol. Spectrosc. **43**, 366 (1972).
3. P. F. WILLIAMS and D. L. ROUSSEAU. Phys. Rev. Lett. **30**, 951 (1973).
4. D. L. ROUSSEAU and P. F. WILLIAMS. J. Chem. Phys. **64**, 3519 (1976).
5. P. F. WILLIAMS, A. FERNANDEZ, and D. L. ROUSSEAU. Chem. Phys. Lett. **47**, 150 (1977).
6. P. BAIERL and W. KIEFER. J. Raman Spectrosc. **10**, 197 (1981).
7. P. BAIERL and W. KIEFER. J. Raman Spectrosc. **11**, 393 (1981).
8. P. BAIERL and W. KIEFER. J. Raman Spectrosc. **15**, 360 (1984).
9. J. TELLINGHUISEN. J. Chem. Phys. **76**, 4736 (1982).
10. J. TELLINGHUISEN. J. Chem. Phys. **58**, 2821 (1973).
11. J. A. COXON. J. Quant. Spectrosc. Radiat. Transfer, **11**, 443 (1971).
12. R. F. BARROW and K. Y. YEE. J. Chem. Soc. Faraday Trans. 2, **69**, 684 (1973).
13. W. KIEFER and J. A. TOPP. Appl. Spectrosc. **28**, 26 (1974).
14. P. BAIERL and W. KIEFER. J. Raman Spectrosc. **3**, 353 (1975).
15. M. BRITH, O. O. SCHNEPP, and P. STEPHENS. Chem. Phys. Lett. **26**, 549 (1974).
16. S. GERSTENKORN, P. LUC, and C. AMIOT. J. Phys. **46**, 355 (1985).
17. M. S. CHILD and R. B. BERNSTEIN. J. Chem. Phys. **59**, 5916 (1973).
18. G. D. CHAPMAN and P. R. BUNKER. J. Chem. Phys. **57**, 2951 (1972).
19. B. HARTKE. Chem. Phys. Lett. **160**, 538 (1989).
20. M. GANZ, B. HARTKE, W. KIEFER, J. MANZ, and J. STREMPEL. Vib. Spectrosc. **1**, 119 (1990).

Can. J. Chem. Downloaded from www.nrcresearchpress.com by 84.41.108.74 on 09/07/12
For personal use only.

Solubility of domoic acid in water and in non-aqueous solvents[1]

MICHAEL FALK, PING F. SETO, AND JOHN A. WALTER

Institute for Marine Biosciences, National Research Council of Canada, 1411 Oxford Street, Halifax, N.S., Canada B3H 3Z1

Received June 24, 1991

This paper is dedicated to Dr. Richard Norman Jones

MICHAEL FALK, PING F. SETO, and JOHN A. WALTER. Can. J. Chem. **69**, 1740 (1991).

The solubility of domoic acid (DA) in H_2O and D_2O, in aqueous NaCl solution and in several non-aqueous solvents was measured by NMR and UV spectroscopies. The solubility in water is comparable with that of aminoacids such as glutamic acid and aspartic acid. It is markedly pH-dependent, passing through a minimum at the isoelectric point, the increase towards both higher and lower pH values indicating that the anionic and cationic forms are more soluble than the neutral form. The effect of NaCl on the solubility of DA in water is negligible. The solubility of DA in alcohols is lower than in water but it is much higher than the solubility of glutamic acid or aspartic acid. The octanol–water partition coefficient for DA at pH 5.32, $K_{ow} = 0.0037$, was obtained by a direct UV measurement. The low value of K_{ow} indicates that aquatic organisms cannot take up DA directly from the water and bioaccumulation may proceed only through dietary intake.

Key words: solubility of domoic acid, NMR of domoic acid, UV spectra of domoic acid, octanol–water partition coefficient of domoic acid.

MICHAEL FALK, PING F. SETO et JOHN A. WALTER. Can. J. Chem. **69**, 1740 (1991).

On a determiné la solubilité de l'acide domoïque (AD) dans H_2O et D_2O, dans une solution aqueuse de NaCl et dans plusieurs solvents non-aqueux par les spectroscopies RMN et UV. La solubilité dans l'eau est comparable à celle des acides aminés tels que l'acide glutamique ou aspartique. Elle dépend du pH et passe par un minimum au point isoélectrique. L'accroîssement de solubilité lorsque le pH est supérieur ou inférieur au point isoélectrique indique que les formes anionique et cationique sont plus solubles que sa forme neutre. L'effet du NaCl sur la solubilité de l'acide domoïque dans l'eau est négligeable. La solubilité dans les alcools est moins grande que celle dans l'eau, mais elle est beaucoup plus grande que la solubilité de l'acide glutamique ou aspartique. Le coefficient de partition octanol–eau à pH 5,32, $K_{ow} = 0{,}0037$, a été determiné directement par la spectroscopie UV. La basse valeur de K_{ow} indique que les organismes aquatiques ne peuvent pas absorber l'acide domoïque dissous dans l'eau mais peuvent l'accumuler seulement par leur régime alimentaire.

Mots clés : solubilité de l'acide domoïque, spectre RMN de l'acide domoïque, spectre UV de l'acide domoïque, coefficient de partition de l'acide domoïque entre l'octanol et l'eau.

Can. J. Chem. Downloaded from www.nrcresearchpress.com by 123.30.183.119 on 09/07/12
For personal use only.

Introduction

The solubilities of domoic acid (DA, Fig. 1) in different media are important parameters for the understanding of the biological action and environmental behaviour of this newly discovered and seasonally dangerous marine toxin (1, 2). Knowledge of solubilities of DA is also important in the development of suitable conditions of separation, purification, and analysis. The objective of the present study was to determine the solubility of DA in water and in organic solvents and to compare it with the solubilities of related compounds.

A limited quantity of material, about 50 mg, was available for this study. This and the need to recycle it precluded the use of the very accurate classical gravimetric methods of solubility measurement (3, 4), necessitating the use of the somewhat less accurate spectroscopic methods, ultraviolet spectoscopy (UV) and ^1H nuclear magnetic resonance spectroscopy (NMR). These two methods are complementary: NMR works best at concentrations above 1 mM, and is well suited to studies of DA in water and methanol, in which DA has a relatively high solubility. The more sensitive UV method works best at lower concentrations and is well suited to studies of DA in such solvents as octanol or acetonitrile. The UV method enabled us to measure directly the octanol–water partition coefficient, a parameter widely used in estimating pollutant partitioning between water and sediments, bio-concentration factors and toxicity relationships (5, 6). The NMR measurements of DA solubility in water were performed

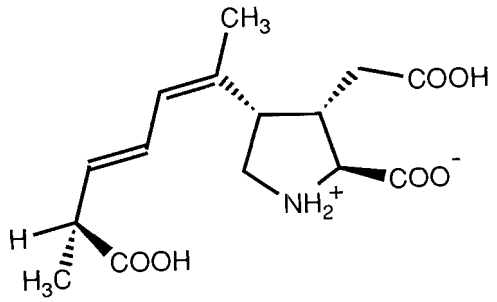


FIG. 1. Molecular structure of neutral domoic acid in its most stable zwitterion form.

both in H_2O and D_2O, the measurements in the latter being more accurate for reasons discussed below. The solubilities of DA in H_2O and in D_2O are expected to be almost the same, as are the solubilities of most organic molecules (7, 8).

Experimental

Materials

The same stock of crystalline DA dihydrate was used as in our earlier work (9, 10). The non-aqueous solvents were of spectroscopic grade and were thoroughly dried with molecular sieve. 1-Octanol was Aldrich HPLC grade, glass-distilled and filtered through 0.5 micron pore filters. The amount of water that could have entered these solvents by the dissolution of DA dihydrate crystals during the experiments was calculated to be about 66 ppm for methanol, 6 ppm for 1-octanol, and less than 1 ppm for the other solvents.

NMR spectroscopy

The experiments were performed at 20°C. DA crystals were added

[1]NRCC No. 33340. Presented in part at the Second Canadian Workshop on Harmful Marine Algae, Bedford Institute of Oceanography, Dartmouth, N.S., October 2–4, 1990.

Can. J. Chem. Downloaded from www.nrcresearchpress.com by 123.30.183.119 on 09/07/12
For personal use only.

to D_2O in a high-precision NMR tube (Wilmad 535-pp, nominal i.d. 4.200 to 4.213 mm; measured i.d. of 5 tubes 4.20 ± 0.01 mm) until the solution was saturated, as indicated by undissolved crystals remaining after vigorous agitation of the solution. This yielded the saturated solution at the isoelectric point. Thereafter, pD was adjusted by the addition of small amounts of 0.1 M NaOD or DCl. The pH and pD measurements were made with a Fisher Accumet model 610A pH meter and an Ingold 6030 combination electrode, calibrated with standard Anachemia buffers. Values of pD were obtained by adding 0.4 to the meter readings (11).

^{1}H NMR spectra of the solutions were recorded at 300.13 MHz on a Bruker MSL-300 spectrometer, care being taken to ensure that the probe tuning was optimized and that the degree of probe damping was not detectably altered by changes to the DA solution or by the use of a separate sucrose standard. Acquisitions used single 45° pulses separated by 10 s delays to ensure complete spin–lattice relaxation between transients. The average integrated intensity per proton type, I_D, of the DA resonances was calibrated by comparison with the average area I_S obtained under the same conditions from a standard 12.49 mM solution of sucrose contained in an identical NMR tube. The concentration of the DA solution was obtained as $C = 12.49 \times I_D/I_S$ (mM). This method allows a direct measurement of the saturation concentration of DA without the need to dilute an aliquot of the solution, and circumvents the possibility of errors due to the suspended small crystals in an aliquot, as the NMR spectrum of solid DA would be too broad to be detectable in these experiments. The validity of the method rests on the assumption that the physical distribution of the sample in the probe, the response of the probe, the excitation pulse, and the signal amplification are constant, and that complete relaxation occurs between transients. Ancillary experiments showed that errors resulting from these sources were not significant compared to those due to integration.

An identical procedure was used for the NMR determination of the solubility of DA in D_2O containing 3.5 wt% NaCl. Standard sucrose solutions for these experiments were prepared in D_2O having the same NaCl concentration. Similarly, measurements of DA solubility in CD_3OD utilized the same procedure and type of tube, the standard being an 18.3 mM solution of glucose in CD_3OD.

In the pD range 4.8 to 5.2, the solubility of DA in D_2O increased to the point where there was insufficient material to prepare a saturated solution in a 5 mm NMR tube. The measurement at pD 5.38, the highest pD for which a saturated solution was attainable with the amount of DA at our disposal, utilized a Wilmad 520-1 tube, which has a 2.5 mm o.d. portion containing *ca.* 80 μL of solution in the active region of the NMR probe. The same tube was used in successive measurements with identical volumes of DA or sucrose solution in D_2O, the tube being positioned reproducibly in the probe. It was not possible to use the pH meter with such a small amount of solution, so pD was determined from the chemical shifts of proton resonances which are sensitive to pD (10). Small but undetermined concentration dependences of chemical shifts reduce the accuracy of this method of pD determination: the pD measured by pH meter (11) on the solutions in the pD range 3.45 to 5.15, in a 5 mm tube, was 0.10 lower on the average than that calculated from the chemical shifts.

One set of measurements was also made at the isoelectric point in H_2O solution, in which case the prominent water resonance was presaturated before data accumulation. The level of irradiation used for presaturation was shown in preliminary experiments to have no influence on the intensity of the DA resonances. The need to presaturate with H_2O solution was the reason for our use of D_2O for the remainder of the experiments. Presaturation reduced the accuracy with which integrals could be measured, and was particularly difficult to perform satisfactorily with the small sample tube needed at high pD.

Ultraviolet spectroscopy

The experiments were performed at 20°C. Chloroform, tetrahydrofuran, and acetone were insufficiently transparent at 241 nm to observe the spectrum of dissolved DA. Water, alcohols, dichloromethane, acetonitrile, and cyclohexane did have sufficient transparency. Saturated solutions of DA in these solvents were prepared by placing a few small crystals of DA in a small quantity of solvent in a stoppered glass tube. After several days of equilibration, a small amount of the solution was drawn off (taking care to avoid including any of the crystals), diluted if necessary, and its absorbance at 241 nm measured in a 1-cm cuvette on a CA/McPherson EU-700 spectrophotometer as in ref. 9. The concentration of DA in non-aqueous solvents was determined by assuming its peak molar absorptivity at 241 nm to be $\epsilon_{max} = 2.44 \times 10^4$ L mol^{-1} cm^{-1}, the value for the uncharged molecule (9). In a preliminary experiment we have established that ϵ_{max} of neutral DA is the same to within about 2% in pure water and in a mixture of 100 parts methanol and 1 part water. We have thereupon assumed that ϵ_{max} is also the same for the other non-aqueous solvents. The uncertainty of this assumption is probably only a minor source of error, more likely sources being the possibly incomplete saturation of the non-aqueous solutions and the difficulties attending the many-fold dilutions necessary in the case of saturated aqeuous or methanolic solutions. For the saturated 1-octanol solutions, the peak absorbance A_{241}, too high to be measured directly, was calculated from the much lower absorbance at 260 nm, A_{260}, using the ratio $A_{241}/A_{260} = 4.57$, based on DA spectra of more dilute solutions.

TABLE 1. Solubility of domoic acid in H_2O and D_2O

pH or pD*	Solubility mmol/L	Solubility g/L
H_2O results		
UV, pH 3.09±0.01	22.8±3.0	7.1±1.0
NMR, pH 3.15±0.03	24.5±1.0	7.6±0.6
D_2O results		
NMR, pD 2.26±0.04	46.9±1.8	14.6±0.4
NMR, pD 3.45±0.03	24.3±1.0	7.6±0.6
NMR, pD 4.85±0.02	43.7±1.7	13.6±0.3
NMR, pD 5.15±0.10†	67.6±2.7	21.0±0.9
NMR, pD 5.38±0.10†	367±15	114±6

*A constant 0.4 has been added to pH meter readings in D_2O to provide the pD value (11).

†Estimated from the positions of the 5′- and 1′-CH_3 proton signals (1).

Measurement of K_{ow}

The octanol–water partition coefficient of DA, K_{ow}, was measured by placing in a tightly stoppered vial a lower layer of 4 mL of water initially containing about 2 μmol DA and an upper layer of 12 mL of 1-octanol. The initial concentration of DA in water corresponded to about 2% of its solubility limit and was chosen to be directly measurable in a 1-mm UV cuvette. The bottle was gently agitated on a mechanical shaker, stopped intermittently in order to measure A_o, the peak absorbance of the octanol layer at 241 nm in a 1-cm cuvette. When the A_o readings reached a stationary level, which took several days, the peak absorbance of the water layer, A_w, was measured in a 1-mm cuvette and its pH was determined. The octanol–water partition coefficient was obtained as $K_{ow} = A_o/10A_w$.

Results

The solubility of DA in H_2O at the isoelectric point was measured independently by NMR and UV. The NMR result, 24.5 ± 1.0 mM at pH 3.15 ± 0.03, was in good agreement with the mean UV result, 22.8 ± 3.0 mM at pH 3.09 ± 0.01. The solubility of DA in D_2O at different pD values is recorded in Table 1. At the isoelectric point, pD 3.45, the solubility of DA in D_2O, 24.3 ± 1.0 mM, is essentially the same as the NMR-measured value for H_2O. This close agreement and the general observation that solubilities of organic molecules in D_2O and in H_2O differ by only a few percent (7, 8) lead us to assume that the

TABLE 2. Solubility of domoic acid in water, saline solution, and non-aqueous solvents

Solvent (method)	Absorbance in a 1 cm cell†	Solubility mmol/L	Solubility g/L	Ratio*
D_2O at isoelectric point (NMR)	—	24.3±1.0	7.6	1
3.5% NaCl in D_2O at isoelectric point (NMR)	—	25.4±1.0	7.9	1
Methanol (NMR)	—	2.1±0.2	0.66	12
1-Octanol (UV)	4.8	0.20	0.062	118
Dichloromethane (UV)	0.186	0.0076	0.0023	3050
Acetonitrile (UV)	0.090	0.0037	0.0011	6330
Cyclohexane (UV)	<0.0005	<0.00002	<0.000006	>1000000

*Ratio of solubility in water at isoelectric point to solubility in solvent.
†Estimated standard error of the UV measurements is 4%.

Can. J. Chem. Downloaded from www.nrcresearchpress.com by 123.30.183.119 on 09/07/12
For personal use only.

variation of the solubility of DA in H_2O with pH and with salt content is essentially the same as for DA in D_2O, which we could measure more accurately. The solubility of DA in 3.5 wt.% NaCl solution in D_2O (which corresponds roughly to the salinity of seawater) was found to be 25.4 ± 1.0 mM, the same within the experimental error as in pure D_2O (Table 2). Table 2 also lists the measured solubilities of DA in non-aqueous solvents. The solubility in methanol could be measured by NMR or UV (NMR giving the more accurate value), but the solubility in the other organic solvents was too low for an NMR measurement. The solubility of DA diminishes in the series water – methanol – octanol–dichloromethane–acetonitrile–cyclohexane. The solubility in cyclohexane is too low to be measurable even by UV, signifying that it must be below 2.0×10^{-5} mM.

The value of the octanol–water partition coefficient was obtained by a direct UV measurement at pH 5.32 as K_{ow} = 0.00374, or $\log K_{ow} = -2.43$. Because of the marked variation of DA solubility with pH, the value of K_{ow} is likely to be pH-dependent and probably passes through a maximum near the isoelectric point. This does not affect the *order of magnitude* of K_{ow} or conclusions which we draw from it.

Discussion

Solubility in water at the isoelectric point

Solubilities of aminoacids in water at room temperature vary widely, from the highly soluble glycine (250 g/kg) and L-proline (162 g/kg) to the relatively insoluble L-tyrosine (0.45 g/kg) (12). The solubility of DA in water, 7.6 g/L, is intermediate between these extremes, and is comparable with the solubilities of the structurally related glutamic acid and of aspartic acid (Table 3). An aminoacid related even more closely to domoic acid is the neurotoxin kainic acid, occurring in marine algae (15). A recent measurement of the solubility of kainic acid in water at its isoelectric point (pH 3.27) yielded the solubility 11.0 g/L or 51.6 mmol/L at 20° (16). Thus, DA is slightly less soluble in water than kainic acid, probably due to the longer olefinic side-chain of DA.

Effect of pH

The solubility of aminoacids in water passes through a minimum near their isoelectric point but increases towards both lower and higher pH values, since both the anionic and cationic forms are more water-soluble than the uncharged form. This behaviour has been reported for tyrosine (17, 18), glycine (19), and phenylalanine (20), and has also been observed for glutamic acid (16). The solubility of DA in water follows the same pattern.

A simple linear model of DA solubility

We made an attempt to fit the pD-dependence of the solubility of DA in D_2O to an equation based on the following linear model. As discussed in our earlier paper (9), DA molecules occur in aqeuous solution in one of five possible protonation forms, whose proportions vary with pH: the fully protonated cation (**A**), the neutral molecule (**B**, see Fig. 1), the singly charged anion (**C**), the doubly charged anion (**D**), and the triply charged anion (**E**). In analogy with other physico-chemical parameters of DA (9), its total solubility S may be expressed at any pH as a linear combination of the individual solubilities of the five DA species, S_a to S_e:

$$[1] \qquad S = aS_a + bS_b + cS_c + dS_d + eS_e$$

where a to e are the mole fractions of the five species. At every pH, the mole fractions can be calculated from the known pK_a values of domoic acid (10), so that the data in Table 1 can be fitted to eq. [1] by optimization. Using an optimization technique previously used to fit the variation of UV and NMR spectral parameters of DA with pH and pD (9, 10), we have found that the data points between pD 2.26 and 5.15 could be fitted to the model (Fig. 2). On the other hand, attempts to include the very large value of solubility at pD 5.38 led to physically unacceptable negative values for some of the solubility parameters. The linear model is based on the assumption that the dissolved DA molecules function as independent entities and the failure of this model signals the occurrence of strong molecular interactions between DA molecules or ions in solution. Such interactions are also apparent from the observed variation of the NMR chemical shifts with DA concentration (10). At the moment, the molecular basis of these interactions is not clear, but since we have found that the analogous linear model similarly fails to fit the dependence of the solubility of glutamic acid with pH (16), the phenomenon is not specific to DA and could be of a more general nature. It is likely that strong interactions and a steep rise of solubility could also occur at low pH, so that extrapolation of the measured solubilities to the region below pD 2.26, based on the linear model, cannot be trusted.

Effect of temperature

We have no data for DA, but other aminoacids show only a very moderate increase of aqueous solubility with rising temperature. The rates of increase that have been reported vary from

TABLE 3. Solubility (g/kg solvent) of selected L-aminoacids in water and alcohols at 25°C

Solvent	Solubility					
	Domoic acid[a]	Glycine	Alanine	Valine	Aspartic acid	Glutamic acid
Water	7.6	250[b,c]	167[b]	88.5[b,c]	5.00[b]	8.64[b]
Methanol	0.66	0.41[b]	0.80[c]	0.050[c]	—	—
Ethanol	—	0.037[b]	0.45[c]	0.029[c]	0.0020[b]	0.0035[b]
2-Propanol	—	0.0011[c]	0.27[c]	0.026[c]	—	—
t-Butanol	—	0.00097[c]	0.22[c]	0.023[c]	—	—
1-Octanol	0.062	—	—	—	—	—

[a]This work (g/L; 20°C).
[b]Reference 12.
[c]References 13 and 14.

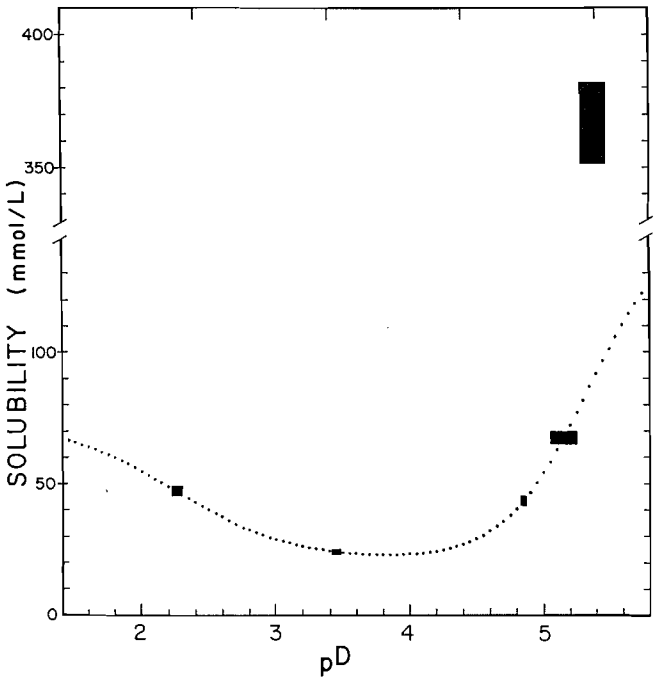


FIG. 2. Solubility of domoic acid in D_2O as a function of pD. Rectangles: NMR measurements. Dotted curve: eq. [1] fitted to the data points between pD = 2.26 and pD = 5.15.

0.3% per degree for phenylalanine to 1% per degree for glycine (21).

Effect of salinity

The effect of salinity on the solubility of DA in water, at levels corresponding to seawater, is small enough to be neglected in most practical considerations.

Solubility in alcohols

The solubility of DA in alcohols is less than in water. Though the data are very limited, it is clear that solubility diminishes with increasing length of the hydrocarbon chain: the solubility of DA in methanol and in 1-octanol is, respectively, 1/12 and 1/118 of its solubility in water at the isoelectric point. Aminoacids such as glutamic acid, aspartic acid, or glycine, appear to exhibit an even more drastic diminution of solubility with increasing length of hydrocarbon chain (Table 3). However, such comparisons are complicated by the uncertain degree of hydration of solvents used in such studies, which has led to serious discrepancies in the literature. For example, the solubility of glycine in ethanol at 25°C has been reported to be 0.39 mM by McMeekin *et al.* (22) and 8.5 mM by Dey and Lahiri (13).

Solubility in alcohol–water mixtures

The solubility of DA in alcohol–water mixtures was not investigated, but one should not assume that the solubility varies linearly or even monotonically as a function of alcohol concentration, complex behaviour having been observed for some aminoacids. For example, the solubility of phenylalanine in mixtures of water and 1-propanol increases at first, passes through a maximum at about 0.2 mole fraction alcohol, then decreases sharply at higher alcohol concentrations (23).

Bioaccumulation

Aquatic organisms, including molluscs, crustaceans, and fish, may take up organic chemicals either directly from the water or through the food chain (24). The tendency of such uptake for various substances is measured by bioconcentration factors, K_B, which have been found to correlate linearly with octanol–water partition coefficients, K_{ow} (25–27). The K_{ow}/K_B correlations have been specifically shown (28) to apply to the bioconcentration of many organic compounds by *Mytilus edulis*, the mussel responsible for the original human intoxications in 1987 that first led to the discovery of DA as the amnesic shellfish toxin (1, 2). The value of log $K_{ow} = -2.43$, obtained in the present work and the K_{ow}/K_B correlations of refs. 25–28 imply that log K_B is negative, i.e. K_B is less than unity, indicating little tendency of DA to be bioconcentrated.

While the low value of K_{ow} and K_B implies that passive transport of DA across biological membranes is negligible, active uptake of DA by the epithelial cells of the digestive system might be expected to occur, these cells being involved in the active uptake of aminoacids. However, it has been observed during toxic outbreaks that DA present in contaminated shellfish is found largely (or perhaps exclusively) in their digestive systems and not in muscles or other body tissues (29). It thus appears that DA does not efficiently pass across body membranes by either passive or active transport mechanisms.

Acknowledgments

A part of this research was carried out by Paul W. Wiseman, summer assistant at this Institute, 1988 and 1989. Some of the NMR measurements were carried out by D. M. Leek. We are

Can. J. Chem. Downloaded from www.nrcresearchpress.com by 123.30.183.119 on 09/07/12
For personal use only.

indebted to Dr. A. S. W. de Freitas for suggesting the measurement of K_{ow} and for critical comments on the manuscript. Helpful discussions with Mr. A. J. Windust are also acknowledged.

1. J. L. C. WRIGHT, R. K. BOYD, A. S. W. DE FREITAS, M. FALK, R. A. FOXALL, W. D. JAMIESON, M. V. LAYCOCK, A. W. MCCULLOCH, A. G. MCINNES, P. ODENSE, V. P. PATHAK, M. A. QUILLIAM, M. A. RAGAN, P. G. SIM, P. THIBAULT, J. A. WALTER, M. GILGAN, D. J. A. RICHARD, and D. DEWAR. Can. J. Chem. **67**, 481 (1989).
2. J. L. C. WRIGHT, M. FALK, A. G. MCINNES, and J. A. WALTER. Can. J. Chem. **68**, 22 (1990).
3. E. J. COHN, T. L. MCMEEKIN, J. T. EDSALL, and J. H. WEARE. J. Am. Chem. Soc. **56**, 2270 (1934).
4. Y. NOZAKI and C. TANFORD. J. Biol. Chem. **246**, 2211 (1971).
5. D. MACKAY, A. BOBRA, W. Y. SHIU, and S. H. YALKOWSKI. Chemosphere, **9**, 701 (1980).
6. R. A. RAPAPORT and S. J. ELSENREICH. Environ. Sci. Technol. **18**, 163 (1984).
7. A. BEN-NAIM, J. WILF, and M. YAACOBI. J. Phys. Chem. **77**, 95 (1973).
8. P. BACKX and S. GOLDMAN. J. Phys. Chem. **85**, 2975 (1981).
9. M. FALK, J. A. WALTER, and P. W. WISEMAN. Can. J. Chem. **67**, 1421 (1989).
10. J. A. WALTER, D. M. LEEK, and M. FALK. NMR studies of the protonation of domoic acid. To be published.
11. P. K. GLASOE and F. A. LONG. J. Phys. Chem. **64**, 188 (1960).
12. Handbook of chemistry and physics. 66th edition. CRC Press, Boca Raton, FL. 1986. C-704.
13. B. P. DEY and S. C. LAHIRI. Indian J. Chem. **25A**, 136 (1986).
14. A. PAL, B. P. DEY, and S. C. LAHIRI. Indian J. Chem. **25A**, 322 (1986).
15. M. V. LAYCOCK, A. S. W. DE FREITAS, and J. L. C. WRIGHT. J. Appl. Phycol. **1**, 113 (1989).
16. M. FALK. Gravimetric determination of the solubilities of glutamic acid and kainic acid in water. Unpublished results.
17. K. K. NASS. AIChE J. **34**, 1257 (1988).
18. C. C. Chen, Y. Zhu, and L. B. Evans. Biotechnol. Prog. **5**, 111 (1989).
19. R. B. GUPTA and R. A. HEIDEMANN. AIChE J. **36**, 333 (1990).
20. A. B. HERMAN, V. V. TSIBANOV, L. T. KUSHASHVILI, A. K. ZHURAVLEV, A. D. NYEKLYUDOV, and N. N. SUVOROV. Khim. Farm. Zh. **23**, 749 (1989).
21. B. P. DEY and S. C. LAHIRI. Indian J. Chem. **27A**, 297 (1988).
22. T. L. MCMEEKIN, E. J. COHN, and J. H. WEARE. J. Am. Chem. Soc. **58**, 2173 (1936).
23. C. J. ORELLA and D. J. KIRWAN. Biotechnol. Prog. **5**, 89 (1989).
24. R. J. NORDSTROM, A. E. MCKINNON, and A. S. W. DE FREITAS. J. Fish. Res. Board Can. **33**, 248 (1976).
25. W. B. NEELY, D. R. BRANSON, and G. E. BLAU. Environ. Sci. Technol. **8**, 1113 (1974).
26. C. T. CHIOU, V. H. FREED, D. W. SCHMEDDING, and R. L. KOHNERT. Environ. Sci. Technol. **11**, 475 (1977).
27. D. MACKAY. Environ. Sci. Technol. **16**, 274 (1982).
28. H., GEYER, P. SHEEHAN, D. KOTZIAS, D. FREITAG, and F. KORTE. Chemosphere, **11**, 1121 (1982).
29. S. S. BATES, C. J. BIRD, A. S. W. DE FREITAS, R. FOXALL, M. W. GILGAN, L. A. HANIC, G. E. JOHNSON, A. W. MCCULLOCH, P. ODENSE, R. POCKLINGTON, M. A. QUILLIAM, P. G. SIM, J. C. SMITH, D. V. SUBBA RAO, E. C. D. TODD, J. A. WALTER, and J. L. C. WRIGHT. Can. J. Fish. Aquat. Sci. **46**, 1203 (1989).

Can. J. Chem. Downloaded from www.nrcresearchpress.com by 123.30.183.119 on 09/07/12
For personal use only.

Measurements of far-infrared optical constants of liquids with a synchrotron radiation source

YOSHITAKA FUJITA, TETSUHIKO OHBA,[1] AND SHUN-ICHI IKAWA[2]
Department of Chemistry, Faculty of Science, Hokkaido University, Sapporo 060, Japan
Received April 17, 1991
This paper is dedicated to Dr. Richard Norman Jones

YOSHITAKA FUJITA, TETSUHIKO OHBA, and SHUN-ICHI IKAWA. Can. J. Chem. **69**, 1745 (1991).

The far-infrared optical constants of liquid acetonitrile, carbon disulfide, and carbon tetrachloride were determined from transmission measurements with a synchrotron radiation source at the Institute for Molecular Science (Okazaki). The small size of the synchrotron radiation source was of benefit to measurements of transmittances that were suited for an analysis based on an optical theory. From the transmittances of liquid acetonitrile at temperatures ranging from 238 to 343 K, both the absorption coefficients and the refractive indices were obtained by using the subtractive Kramers–Kronig relation proposed by Jones and co-workers. The dipole moment of liquid acetonitrile calculated from the optical constants, 4.5 ± 0.1 D, is nearly independent of temperature. The spectra of carbon disulfide and carbon tetrachloride were measured at pressures in the ranges 1–1800 bar and 1–1100 bar, respectively. The absorption coefficients were obtained from the transmittances by neglecting the dispersion of the refractive indices. The zeroth and second moments of the collision-induced absorption bands were obtained as a function of pressure, after resolving the overlap of intramolecular vibrational bands.

Key words: far-infrared, optical constants, pressure, liquid, synchrotron radiation source.

YOSHITAKA FUJITA, TETSUHIKO OHBA et SHUN-ICHI IKAWA. Can. J. Chem. **69**, 1745 (1991).

Utilisant des mesures de transmission effectuées avec une source de radiation synchrotron, à l'Institute for Molecular Science (Okazaki), on a déterminé les constantes optiques dans l'infrarouge lointain de l'acétonitrile, du disulfure de carbone et du tétrachlorure de carbone liquides. La petite taille de la source de radiation synchrotron était utile dans la mesure des transmissions appropriées pour une analyse basée sur une théorie optique. À partir des transmissions de l'acétonitrile liquide, à des températures allant de 238 à 343 K, et utilisant la relation soustractive de Kramers–Kronig proposée par Jones et ses collaborateurs, on a obtenu les coefficients d'absorption ainsi que les indices de réfraction. Le moment dipolaire de l'acétonitrile liquide calculé à partir des constantes optiques, 4,5 ± 0,1 D, est pratiquement indépendant de la température. On a mesuré les spectres du disulfure de carbone et du tétrachlorure de carbone à des pressions respectives de 1 à 1800 bar et de 1 à 1100 bar. On a obtenu les coefficients d'absorption à partir des coefficients de transmission, en négligeant la dispersion des indices de réfraction. Après avoir résolu le recouvrement des bandes vibrationnelles intramoléculaires, on a pu déterminer les moments d'ordre zéro et second des bandes d'absorption induites par les collisions en fonction de la pression.

Mots clés : infrarouge lointain, constantes optiques, pression, liquide, source de radiation synchrotron.

[Traduit par la rédaction]

Introduction

Band shapes of far-infrared absorption of liquids are informative about the dynamics and interactions of liquid molecules. If the molecules have permanent dipole moments, the absorption is caused primarily by the reorientational motion of the dipole moments, and the band shape, providing a spectral density of the motion, tells about how the orientation of the molecules fluctuates in the liquid state. On the other hand, non-dipolar liquids show far-infrared absorption that arises from transient dipole moments induced through molecular collisions. The band shape of this collision-induced absorption is given by the fluctuation of both the orientation and the magnitude of the induced dipole moments.

For analyzing the band shapes (1, 2), we need the optical constants or the complex refractive indices by which spectra of liquids are fully characterized. However, measurements of the optical constants of liquids in the far-infrared region are scarce. Most of them were performed by Dispersive Fourier-Transform Spectrometry (3), but the procedure for data analysis by this method is not straightforward. In the previous study (4, 5), we measured attenuated total reflection (ATR) of liquids with an optically pumped far-infrared laser as a source and obtained fairly precise values of the optical constants of some liquids. However, the precise measurements of ATR could be performed only at spot frequencies where strong laser lines were available.

The present paper reports the determination of continuous spectra of the optical constants of liquids from transmission measurements with the synchrotron orbital radiation (hereafter referred to as SOR) as a far-infrared source. The SOR facilities are usually intended to produce high-intensity photon beams in the range of extreme ultraviolet to X-ray. However, the SOR is also a promising light source in the far-infrared region (6–8) where intense broad-band sources are lacking. At present, the radiative intensity of the SOR in the far-infrared is not very remarkable. At a typical operating current of 100 mA, it is only in the region below 30 cm^{-1} (8) that the SOR provides a greater intensity than the high-pressure mercury lamp, the conventional far-infrared source. In spite of this, the SOR has advantages over the mercury lamp in its brightness, its high degree of polarization, and its pulsed nature. Particularly, the brightness of the SOR coming from its very small source and small beam divergence is of benefit for precise measurement of the optical constants. For instance, the source is about 0.5 mm in diameter and the acceptance angles are 60 (vertical) and 80 (horizontal) mrad (9) at the far-infrared beam line of the UVSOR facility of the Institute for Molecular Science (IMS, Okazaki). Therefore, the SOR makes it easier to obtain a par-

[1]Present address: Advantest Laboratories Ltd., 250-1, Hoshino, Otaru, 047-02, Japan.

[2]Author to whom correspondence may be addressed.

Printed in Canada / Imprimé au Canada

Can. J. Chem. Downloaded from www.nrcresearchpress.com by 84.41.108.74 on 09/07/12
For personal use only.

allel or near-parallel beam of a moderate diameter and to control the angle of incidence of light into the liquid cell within a small tolerance.

Though the transmission measurements are conventional and simple, we must carefully analyze observed transmittances, which are usually deformed by interference fringes due to multiple reflection inside a cell and by errors due to spread of incident angle of light and uncertainty in the sample thicknesses and so on. A good guide for dealing with these effects has been given by Jones and co-workers (10–12). They have established a standard way to control or treat the errors associated with the transmission measurements and to obtain the optical constants in the infrared region. In the present study, we have consulted their scheme of analysis, which is also applicable in the far-infrared region.

In this paper, we report two extreme cases of transmission measurements. One is measurement of a liquid film of acetonitrile of about 30 μm thickness. Acetonitrile is one of the most heavily absorptive liquids in the far-infrared region and its optical constants have been difficult to measure without large uncertainty (5). The other case concerns measurements of liquid carbon tetrachloride and carbon disulfide under pressure. The thicknesses of these liquid layers were 4–6 mm, since the collision-induced absorption (hereafter referred to as CIA) of the non-dipolar liquids is roughly two orders of magnitude smaller than that of liquid acetonitrile. To obtain the optical constants from the observed transmittances, we applied an optical theory in somewhat different ways to the thin and thick liquid layers.

Recently, after we started this study, Marteau *et al.* (13) reported measurements of the CIA of the same liquids under pressure. Their method of processing experimental data is different from ours and, we believe, it is worthwhile to compare the results of the two studies, since high-pressure measurements of CIA are very scarce, although they would provide an important clue to the mechanism of CIA and also to the local structure of the liquids.

Experimental method and results

Spectroscopic grade acetonitrile, carbon tetrachloride, and carbon disulfide from Nacalai Tesque were used as received. Spectral measurements were performed at the FIR beam line (BL6A1) of UVSOR by use of a SPECAC Martin–Puplett interferometer. The detectors used were Infrared Laboratories Ge and InSb bolometers operated at liquid helium temperature. Spectral resolution was 3 cm^{-1}. An observed interferogram was corrected for the time decay of the beam current before being transformed to a spectrum. Windows of the cell used for measuring thin liquid films of acetonitrile were hyper-pure silicon disks with thickness of 3 mm and the opening of the cell was 15 mm. Thicknesses of liquid films were adjusted to be about 30 μm with an aluminum spacer. The temperature of the cell was controlled by use of an electric heater and liquid nitrogen in the 238–343 K range, with a precision of ±0.5 K during a spectral scan. Figure 1 shows an example of apparent transmittances of liquid acetonitrile, which were obtained as a ratio of the transmission intensity of the filled cell to that of a silicon disk of 6 mm thickness as reference. Because of absorption by a quartz window used as a radiation shield in the detector housing, the signal-to-noise ratio is fairly low on the high frequency side. Two types of interference fringes are involved in the observed transmittance. Waving with a period of about 30 cm^{-1} is attributed to interference fringes arising from about a 50-μm difference in thickness between front and rear windows of the cell. This type of interference fringe has not been reported so far, to our knowledge, and indicates the uniformity of the angle of incidence. The collection angle of the optics used was less than 5°, which is several times smaller than that of conventional optics with a high-pressure

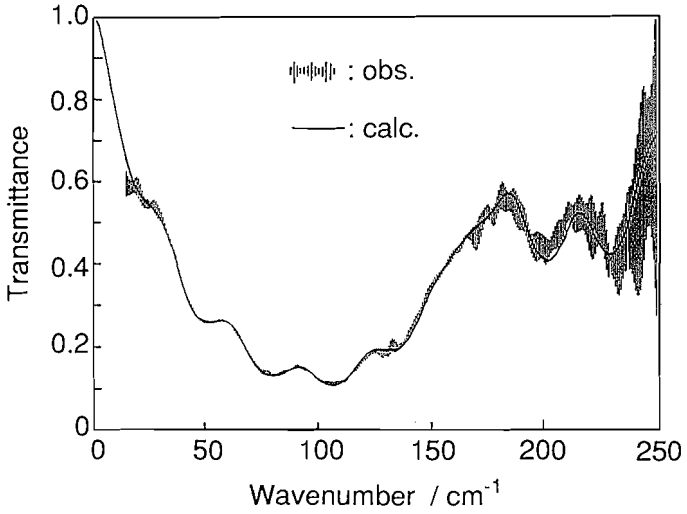


FIG. 1. Observed (||||||||||||) and calculated (—) transmittances of an acetonitrile liquid film of about 30 μm thickness at 298 K, obtained as a ratio of transmission intensity of a filled cell to that of a silicon disk as reference. The vertical bars of the observed transmittance indicate uncertainty estimated from standard deviation of the transmission intensities.

mercury lamp. Another type of interference fringe involved in Fig. 1, though not obvious, has about a 130-cm^{-1} period. This is due to the multiple reflection within the liquid film of about 30-μm thickness.

A schematic of the high-pressure cell used is shown in Fig. 2. The cell body is made of precipitation-hardened stainless steel SUS630; its effective aperture for optical transmission is 4 mm and the path length, including windows, is 30 mm. The windows are hyper-pure silicon crystals of 10 mm diameter and 10–14 mm thick, by which the path length of a sample can be adjusted in the 2–10 mm range. Oil pressure is generated by a hand pump and intensified by about 20 times to pressurize the liquid specimen. The pressure is measured by a semiconductor strain gauge with a precision of a few percent. Spectra of carbon tetrachloride were measured at pressures ranging from 1 to 1100 bar at 298 K and those of carbon disulfide in the range 1–1800 bar. The reference was taken to be transmission intensity of the empty high-pressure cell. Figure 3 shows examples of observed transmittances of carbon disulfide.

Theory of transmittance

We shall consider transmission of light through a three-layer (vacuum–window–vacuum) system and a five-layer (vacuum–window–liquid–window–vacuum) system. The transmittances are generally given by the method of the characteristic matrix (14) and, for the normal incidence of light, the results are

$$[1]\quad T_3(\nu) = \left| \frac{\hat{t}_{12}\hat{t}_{23}\exp(i\hat{\beta}_2)}{1+\hat{r}_{21}\hat{r}_{32}\exp(2i\hat{\beta}_2)} \right|^2$$

and

$$[2]\quad T_5(\nu) = \left| \frac{\hat{t}_{12}\hat{t}_{23}\hat{t}_{34}\hat{t}_{45}\exp[i(\hat{\beta}_2+\hat{\beta}_3+\hat{\beta}_4)]}{1+\hat{Q}} \right|^2$$

for the three- and five-layer systems, respectively, where

$$[3]\quad \hat{Q} = \hat{r}_{12}\hat{r}_{23}\exp(2i\hat{\beta}_2) + \hat{r}_{23}\hat{r}_{34}\exp(2i\hat{\beta}_3) + \hat{r}_{34}\hat{r}_{45}\exp(2i\hat{\beta}_4) + \hat{r}_{12}\hat{r}_{34}\exp[2i(\hat{\beta}_2+\hat{\beta}_3)] + \hat{r}_{23}\hat{r}_{45}\exp[2i(\hat{\beta}_3+\hat{\beta}_4)] + \hat{r}_{12}\hat{r}_{23}\hat{r}_{34}\hat{r}_{45}\exp[2i(\hat{\beta}_2+\hat{\beta}_3+\hat{\beta}_4)] + \hat{r}_{12}\hat{r}_{45}\exp[2i(\hat{\beta}_2+\hat{\beta}_3+\hat{\beta}_4)]$$

Can. J. Chem. Downloaded from www.nrcresearchpress.com by 84.41.108.74 on 09/07/12
For personal use only.

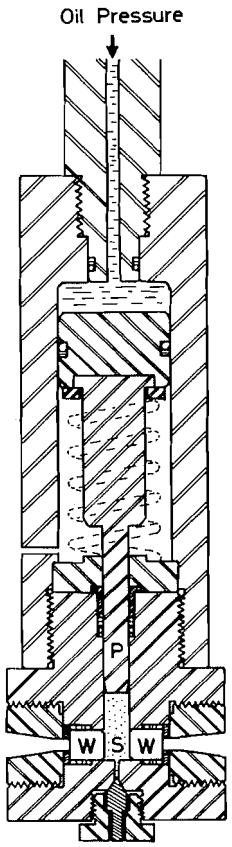


FIG. 2. A schematic of the high-pressure cell for measuring far-infrared spectra of liquids. P: piston; S: liquid sample; W: silicon windows of 10 mm diameter and 10–14 mm thickness by which the path length of a sample is adjusted in the 2–10 mm range. Oil pressure is generated by a hand pump and intensified by about 20 times to pressurize the liquid sample.

Here, $\hat{r}_{ij}$ and $\hat{t}_{ij}$ are the complex coefficients of reflection and transmission, respectively, at an interface between layers i and j, and $\hat{\beta}_i$ is the complex propagation coefficient of the layer i. These coefficients are given by

$$[4] \quad \hat{r}_{ij} = \frac{\hat{n}_i - \hat{n}_j}{\hat{n}_i + \hat{n}_j}$$

$$[5] \quad \hat{t}_{ij} = \frac{2\hat{n}_i}{\hat{n}_i + \hat{n}_j}$$

$$[6] \quad \hat{\beta}_i = 2\pi\nu d_i \hat{n}_i$$

where $\hat{n}_i = n_i + ik_i$ is the complex refractive index of layer i and d_i its thickness. Equations [1] and [2] can be rewritten as

$$[7] \quad T_3(\nu) = \exp(-\alpha_W d_W)\left|\frac{1-\hat{R}_{VW}}{1-\hat{R}_{VW}\exp(2i\hat{\beta}_W)}\right|^2$$

$$[8] \quad T_5(\nu) = \exp[-\alpha_W(d'_W + d''_W) - \alpha_L d_L] \times \left|\frac{(1-\hat{R}_{VW})(1-\hat{R}_{WL})}{1+\hat{Q}}\right|^2$$

where suffixes V, W, L indicate vacuum, window, and liquid, respectively, and

$$[9] \quad \alpha_i = 4\pi\nu k_i$$

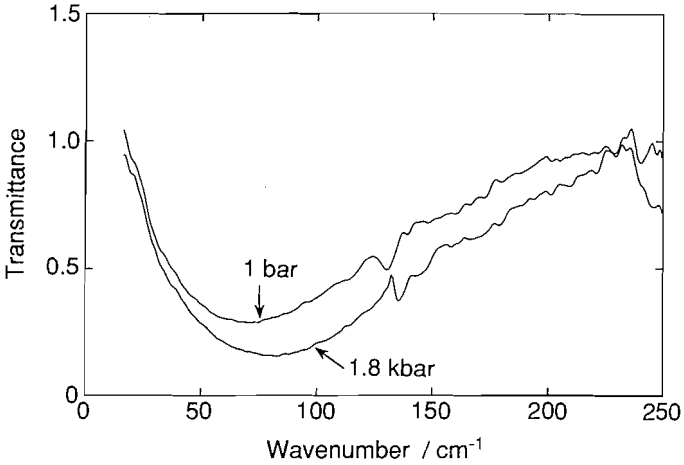


FIG. 3. Observed transmittances of liquid carbon disulfide at 1 bar and 1.8 kbar at 298 K, obtained as ratios of transmission intensities of a filled and an empty high-pressure cell.

is the absorption coefficient of layer i, and

$$[10] \quad \hat{R}_{ij} = \hat{r}_{ij}^2$$

Transmittances given by eqs. [7] and [8] would show complicated interference fringes. However, the fringes are largely smeared in the observed transmittance, which is given by a convolution of $T_n(\nu)$ with an instrumental line-shape (ILS) function, $F(\nu)$, as (15)

$$[11] \quad \langle T_n(\nu)\rangle_{ILS} = \int_0^\infty T_n(\nu')F(\nu-\nu')d\nu'$$

where $F(\nu)$ is given by the Fourier transform of an apodization function $f(x)$, x being the optical path difference between two arms of the interferometer (16). In the present experiment, we used $f(x) = \cos^2(\pi x/2L)$, where L is the maximum of x, and then

$$[12] \quad F(\nu) = \frac{1}{1-(2\nu L)^2}\cdot\frac{\sin\pi\nu L}{2\pi\nu L}$$

The measurements were performed with $L = 3.2$ mm, which provides 3.1 cm^{-1} full-width of $F(\nu)$. At this condition, the interference fringes of $T_3(\nu)$ are completely leveled out in $\langle T_3(\nu)\rangle_{ILS}$, which is given by

$$[13] \quad \langle T_3(\nu)\rangle_{ILS} = \exp(-\alpha_W d_W)\frac{|1-\hat{R}_{VW}|^2}{1-|\hat{R}_{VW}|^2\exp(-2\alpha_W d_W)}$$

On the other hand, the interference fringes will partially remain in $\langle T_5(\nu)\rangle_{ILS}$. In general, far-infrared absorption of liquids is very broad and featureless, and both n_L and k_L are slowly varying functions of ν. As a result, eq. [11] for $n = 5$ can be reduced to

$$[14] \quad \langle T_5(\nu)\rangle_{ILS} = \exp[-\alpha_W(d'_W + d''_W) - \alpha_L d_L] \times |(1-\hat{R}_{VW})(1-\hat{R}_{WL})|^2 N(Q)$$

where

$$[15] \quad N(Q) = \int_0^\infty \frac{F(\nu-\nu')}{|1+\hat{Q}(\nu')|^2}\,d\nu'$$

Can. J. Chem. Downloaded from www.nrcresearchpress.com by 84.41.108.74 on 09/07/12
For personal use only.

Can. J. Chem. Downloaded from www.nrcresearchpress.com by 84.41.108.74 on 09/07/12
For personal use only.

Optical constants of liquid acetonitrile at various temperatures

The observed apparent transmittance of liquid acetonitrile, $T^{obs}(\nu)$, shown in Fig. 1, is represented by a ratio of eq. [14] to eq. [13]. Since $d'_W + d''_W$ is approximately equal to d_W and absorption coefficients of hyper-pure silicon used for the windows are very small in the far-infrared region (17), the effects of absorption of the silicon windows are partially cancelled in $T^{obs}(\nu)$, which is given by

$$[16]\quad T^{obs}(\nu) = \exp(-\alpha_L d_L)|1 - \hat{R}_{WL}|^2 \times \{1 - |\hat{R}_{VW}|^2 \exp(-2\alpha_W d_W)\}N(Q)$$

$T^{obs}(\nu)$ is a function of the complex refractive indices of the liquid. To determine both the real and imaginary parts, we have used the subtractive Kramers–Kronig relation proposed by Jones and co-workers (10*b*),

$$[17]\quad n(\nu) - n(\nu_r) = \frac{2}{\pi} P \int_0^\infty \frac{\mu k(\mu)}{\mu^2 - \nu^2} d\mu - \frac{2}{\pi} P \int_0^\infty \frac{\mu k(\mu)}{\mu^2 - \nu_r^2} d\mu = \frac{2(\nu^2 - \nu_r^2)}{\pi} P \int_0^\infty \frac{\mu k(\mu)}{(\mu^2 - \nu^2)(\mu^2 - \nu_r^2)} d\mu$$

where P denotes the Cauchy principal value of the integral, frequency ν_r is called the anchor point, and the refractive index at this point, $n(\nu_r)$, is assumed to be known. The $n(\nu_r)$ value at 298 K was taken from the result of the laser ATR method (4) and values at other temperatures were calculated by utilizing the Lorenz–Lorentz equation (18).

For a practical calculation, we have assumed the following analytical expression for the absorption coefficient:

$$[18]\quad \alpha(\nu) = \frac{\nu^2}{P_0 + P_1\nu^2 + P_2\nu^4 + \cdots + P_N\nu^{2N}}$$

An advantage of using eq. [18] is that the integral in the subtractive Kramers–Kronig relation, eq. [17], can be analytically carried out by the following equation:

$$[19]\quad \frac{2}{\pi} P \int_0^\infty \frac{\mu k(\mu)}{\mu^2 - \nu^2} d\mu = \frac{1}{4\pi^2\nu} P \int_{-\infty}^\infty \frac{\alpha(\mu)}{\mu - \nu} d\mu = \frac{1}{4\pi\nu} \sum_{i=1}^{N} \mathrm{Re}\left\{ \frac{Z_i^2}{(Z_i - \nu)\mathrm{Im}(Z_i)} \prod_{j(\neq i)}^{N} \frac{1}{(Z_i - Z_j)(Z_i - Z_j^*)} \right\}$$

where Z_i is the ith pole of eq. [18] with a positive imaginary part and Z_i^* its complex conjugate. The parameters $\{P_n\}$ were adjusted by least-squares fitting of the theoretical transmittance to the observed spectrum. For the present spectra, $N = 6$ was found to be enough. The result of the least-squares fitting is shown by a solid curve in Fig. 1 and the resulting optical constants are plotted in Figs. 4 and 5.

Using the sum rule (19, 20), we can estimate the internal dipole moments of the liquid molecules from the optical constants. The dipole moment μ is given by

$$[20]\quad \mu^2 = \frac{3c^2 I_\perp}{2\pi\rho} \int_0^\infty n(\nu)\alpha(\nu)D(\nu)d\nu$$

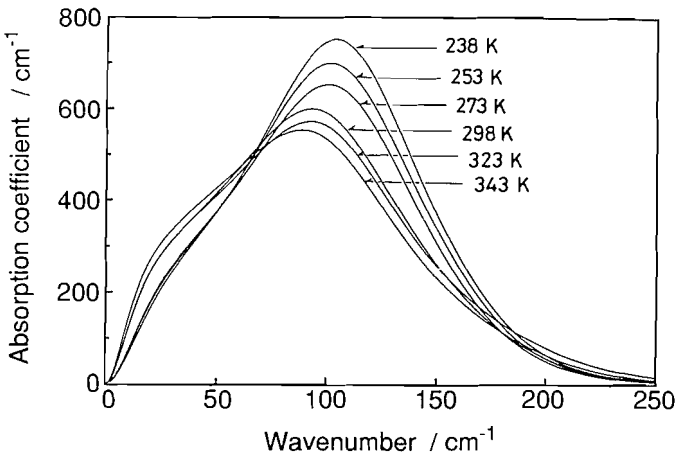


FIG. 4. Absorption coefficients of liquid acetonitrile at various temperatures.

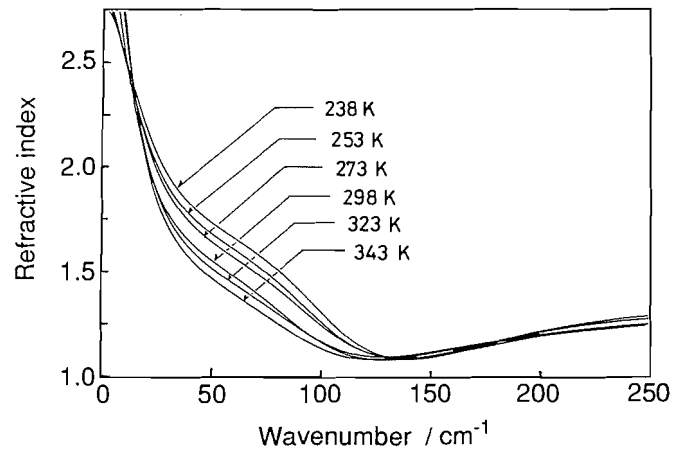


FIG. 5. Refractive indices of liquid acetonitrile at various temperatures.

where ρ is the number density of the molecules, $I_\perp$ the moment of inertia about the axis perpendicular to the dipole moment, and $D(\nu)$ a correction factor for the internal-field effect given by (21)

$$[21]\quad D(\nu) = 3\frac{2(n^2 + k^2)^2 + n_\infty^4}{(n_\infty^2 + 2)^2(n^2 + k^2)^2}$$

where n_∞ is the refractive index related to the molecular polarizability. The calculated dipole moments of liquid acetonitrile were 4.5 ± 0.1 D in the 238–343 K range and almost independent of temperature. This result supports the basic assumption that most of the far-infrared absorption of liquid acetonitrile comes from rotational motion of the dipole moments. An increase of the dipole moment from the gas-phase value, 3.92 D (22), is attributed to the intermolecular induction effect by the dipole–dipole interaction in the liquid state (23).

Absorption coefficients of liquid carbon disulfide and carbon tetrachloride under pressure

Transmittance of the empty high-pressure cell is given by eq. [14] with $\alpha_L = 0$ and $n_L = 1$, and the observed apparent transmittance of liquids, examples of which are shown in Fig. 3, is given by

$$[22]\quad T^{obs}(\nu) = \exp(-\alpha_L d_L)\frac{|1-\hat{R}_{WL}|^2 N(Q)}{|1-\hat{R}_{VW}|^2 N_{empty}(Q)}$$

All of the optical path lengths, $n_i d_i$, of the three layers in the high-pressure cell were thick enough and different from each other. Therefore, all the oscillating terms must disappear in the observed transmittances and $N(Q)$ is reduced to

$$[23]\quad N(Q) = \sum_k (QQ^*)^k$$

Since the aperture of the high-pressure cell is limited to 4 mm while its optical path length is considerably longer, components of multiple reflection are easy to lose from the optical axis owing to the spread of the angle of incidence and the possible wedge shape of the layers. In this case, the summation on the right-hand side of eq. [23] must be limited to a certain order. If we limit to the first order, eq. [22] is reduced to

$$[24]\quad T^{obs}(\nu) = \exp(-\alpha_L d_L)\left|\frac{1-\hat{R}_{WL}}{1-\hat{R}_{VW}}\right|^2 \times \frac{(1+|\hat{R}_{VW}\hat{R}_{WL}|)^2 + (|\hat{R}_{VW}| + |\hat{R}_{WL}|)^2 \exp(-2\alpha_L d_L)}{1+6|\hat{R}_{VW}|^2 + |\hat{R}_{VW}|^4}$$

where eqs. [3]–[6], [9], and [10] were used. For both hyper-pure silicon and non-dipolar liquids, the imaginary parts of the refractive indices are negligibly small as compared with the real parts, $k_W \ll n_W$ and $k_L \ll n_L$, in the far-infrared region, and the dispersion of both n_W and n_L will be very small. Therefore, $\hat{R}_{WL}$ and $\hat{R}_{VW}$ in eq. [24] can be approximated as real constants given by

$$[25]\quad R_{WL} = \left(\frac{n_W - n_L}{n_W + n_L}\right)^2$$

$$[26]\quad R_{VW} = \left(\frac{1-n_W}{1+n_W}\right)^2$$

The magnitude of the dispersion of the refractive index of hyper-pure silicon from 10 to 150 cm^{-1} is about 0.002 (24) and the value of n_W is taken to be the average in this range, 3.418. No refractive indices of carbon tetrachloride and carbon disulfide in the far-infrared region have been reported so far and the values of n_L were estimated from the static dielectric constants, ε_L, by the Maxwell relation

$$[27]\quad n_L^2 = \varepsilon_L$$

Using these values, we calculate the absorption coefficients of the liquid specimens from the observed transmittances by eq. [24]. The results from two kinds of measurement with the InSb detector and the Ge detector were joined at 30 cm^{-1} for carbon disulfide and 50 cm^{-1} for carbon tetrachloride where the lower frequency ranges were given by the InSb detector. The resulting absorption coefficients of liquid carbon disulfide and carbon tetrachloride are plotted in Figs. 6 and 7. Uncertainty at high frequencies is particularly large for the spectra of carbon tetrachloride. This is due to absorption by a thick quartz window for separating vacuums between the storage ring and the interferometer. The quartz window had been set

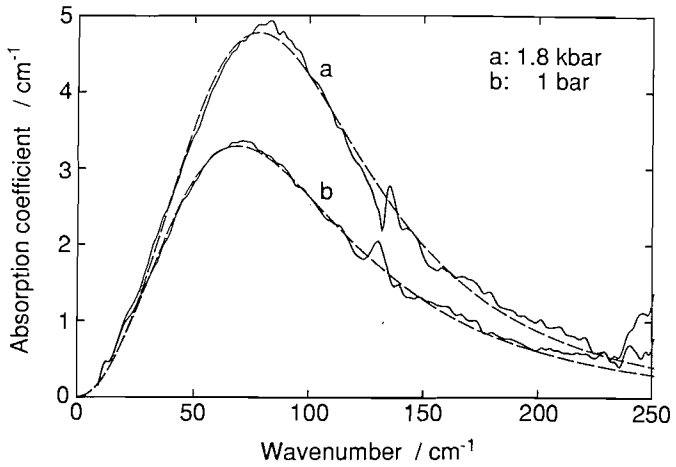


FIG. 6. Absorption coefficients of liquid carbon disulfide at 1 bar and 1.8 kbar at 298 K, obtained by applying eq. [24] to the observed transmittances. Broken lines represent calculated collision-induced absorption bands.

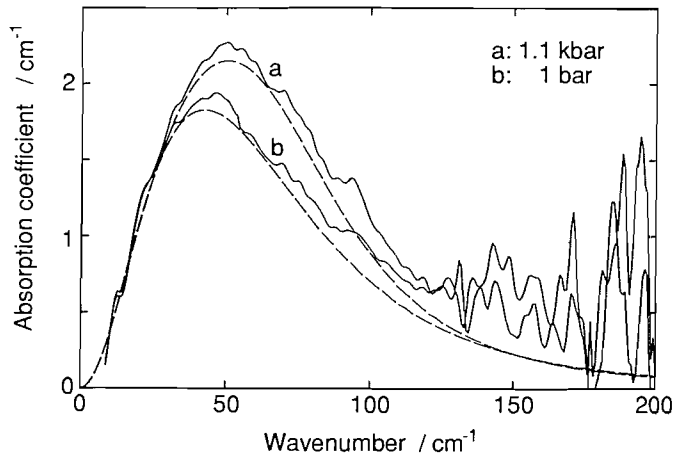


FIG. 7. Absorption coefficients of liquid carbon tetrachloride at 1 bar and 1.1 kbar at 298 K, obtained by applying eq. [24] to the observed transmittances. Broken lines represent calculated collision-induced absorption bands.

in place of a silicon window when carbon tetrachloride was measured.

For a test of the validity of the above method, we analyzed the transmittance observed at 1 bar (100 kPa) with an ordinary liquid cell, which had a sufficient opening of 15 mm diameter and shorter path length of 9–13 mm, including 3 and 4 mm thicknesses of the silicon windows. The transmittance was obtained as a ratio of transmission intensities at 2 and 6 mm thicknesses of the liquid layers. The absorption coefficients were obtained by applying eq. [22] with the expansion of eq. [23]. It was found that even when the expansion was limited to the first order, the result was within 1–2% of the convergent value, which was reached at expansion to the fourth order. The result agrees within a few percent to that obtained with the high-pressure cell at 1 bar, and also agrees well with the literature values (13, 25).

To analyze the band shape of the collision-induced absorption (CIA), we must resolve overlap of a few intramolecular vibrational bands on the high frequencies. However, the signal-to-noise ratio of the present high-pressure measurements was too low at the high frequencies. Therefore, we obtained a spec-

Can. J. Chem. Downloaded from www.nrcresearchpress.com by 84.41.108.74 on 09/07/12
For personal use only.

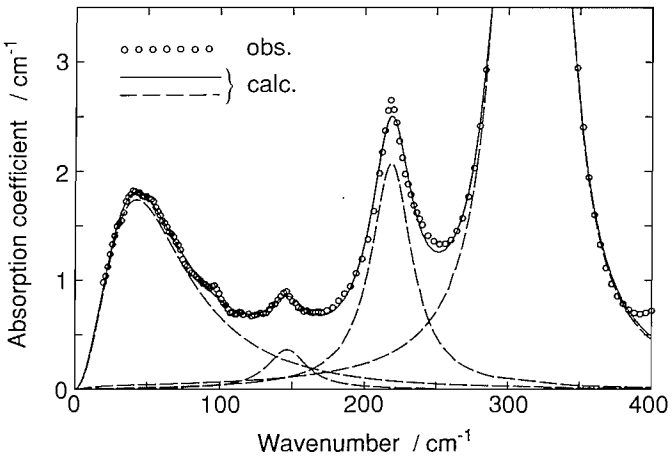


FIG. 8. A joined spectrum of carbon tetrachloride at 1 bar. (○○○): observed; (—): calculated total; and (– – –): calculated component bands.

trum at higher frequencies at 1 bar with a conventional FT-FIR spectrometer and joined this spectrum to that measured with the high-pressure cell at 1 bar. The resulting spectrum of carbon tetrachloride is shown in Fig. 8. Bands at 96, 147, 219, and 311 cm^{-1} are assigned to the ν_4–ν_2, ν_1–ν_4, ν_2, and ν_4 transitions, respectively (26). The overlap was resolved by least-squares fitting, where the CIA band was represented by eq. [18] with $N = 3$, while the intramolecular bands were given by Lorentzian functions that were modified so as to be zero at zero wavenumber, i.e.,

$$[28]\quad F(\nu) = \frac{hb^2}{b^2 + (\nu - \nu_0)^2} - \frac{hb^4}{(\nu^2 + b^2)(\nu_0^2 + b^2)}$$

Fairly good fit was obtained, as shown in Fig. 8. To analyze the spectra at the high pressures, the parameters of the intramolecular bands were fixed at values for 1 bar except for a correction of h for change in the density. The resulting bands of the CIA are shown by broken lines in Fig. 7.

For carbon disulfide, overlap of intramolecular bands is less heavy than that for carbon tetrachloride. The CIA band was separated from bands with peaks at 263 cm^{-1} (ν_1–ν_2) and 396 cm^{-1} (ν_2) in a similar way to the above for carbon tetrachloride. The results are shown by broken lines in Fig. 6.

Moments of the collision-induced bands calculated by the equations

$$[29]\quad A_0 = \int_0^\infty \frac{\alpha(\nu)}{\nu^2} d\nu$$

and

$$[30]\quad A_2 = \int_0^\infty \alpha(\nu) d\nu$$

are plotted against pressure in Figs. 9 and 10, for carbon tetrachloride and carbon disulfide, respectively. These moments are related to the molecular multipole moments that give the collision-induced dipole moments, and to the local structure of the liquids (27). The A_0 and A_2 values of carbon tetrachloride at 1 bar, i.e., 0.134 and 156 cm^{-2} respectively, are in good agreement with recent literature values, i.e., 0.148 (13), 0.189 (25), 0.145 (28), and 149 cm^{-2} (13), 145 cm^{-2} (25), and 154 cm^{-2} (28), respectively. The value of A_0 is only slightly dependent

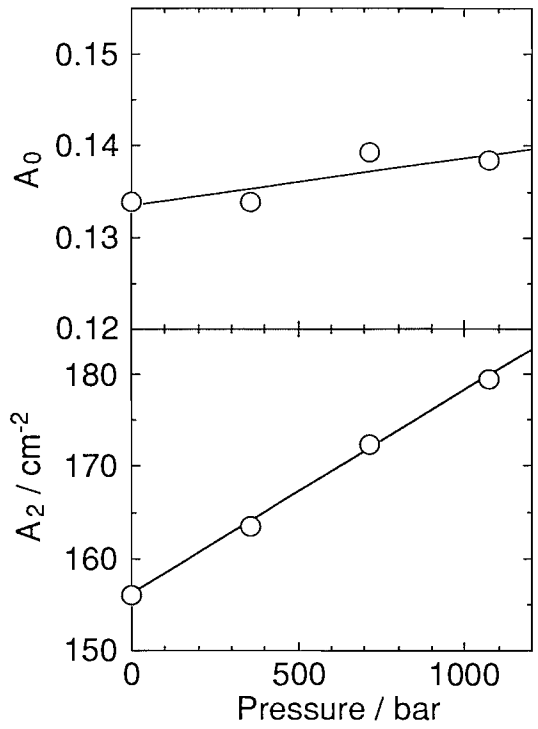


FIG. 9. The zeroth and second moments of the collision-induced absorption bands of carbon tetrachloride plotted against pressure.

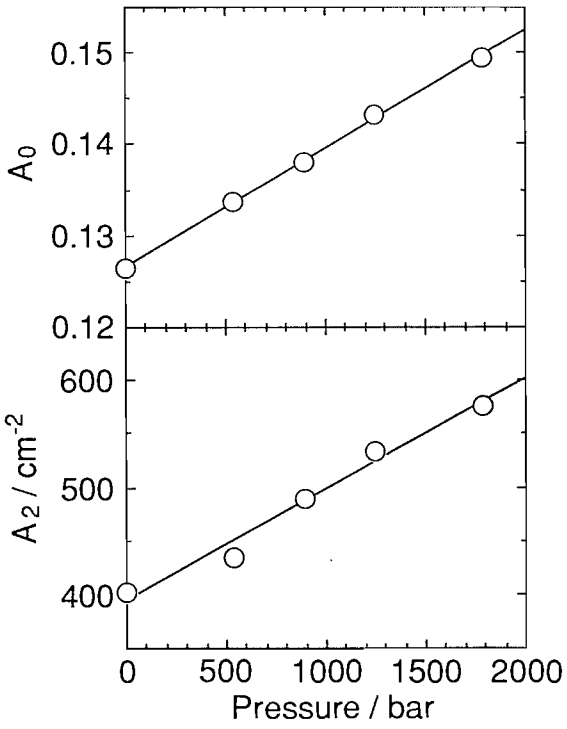


FIG. 10. The zeroth and second moments of the collision-induced absorption bands of carbon disulfide plotted against pressure.

on the pressure, while the A_2 value increases about 15% as the pressure increases from 1 bar to 1.1 kbar. On the other hand, the A_0 value calculated from the result by Marteau *et al.* (13) increased definitely with increasing pressure, and the rate of increase of their A_2 value was about double that of the present result. The discrepancy between the two studies is probably

Can. J. Chem. Downloaded from www.nrcresearchpress.com by 84.41.108.74 on 09/07/12
For personal use only.

due to the different ways of dealing with the high-frequency wing of the CIA band, where Marteau *et al.* assumed an exponential decay instead of separating the intramolecular bands. For carbon disulfide, the present A_0 value at 1 bar, 0.126, is distinctly smaller than the literature values, which are 0.190 (13) and 0.175 (28), while the A_2 value, 402 cm^{-2}, is somewhat larger than the previous values, which are 322 cm^{-2} (13), 357 cm^{-2} (28), and 386 cm^{-2} (29). This is probably also due to the difference in dealing with the high-frequency wing of the CIA band. In spite of this, the slopes of A_0 and A_2 against the pressure agree moderately well with those of Marteau *et al.* (13). Further studies are required to clarify the "true" property of the CIA. A molecular dynamics calculation, as well as further experiments, would be useful.

An average magnitude of the collision-induced dipole moment is calculated by (28)

$$[31] \quad \langle \mu^2 \rangle = (3\varepsilon_0 k_B T/\pi^2 \rho) n D_{pw} A_0$$

where ε_0 is the permittivity of free space, k_B the Boltzmann constant, and nD_{pw} the Polo–Wilson correction factor (30),

$$[32] \quad nD_{pw} = \frac{9n}{(n^2+2)^2}$$

where D_{pw} is given by eq. [21] with $k = 0$ and $n_\infty = n$. The value of n under pressure was calculated by the Tait equation (31). The calculated root-mean-square values of the induced dipole moments are 0.093 and 0.124 D for carbon tetrachloride and carbon disulfide, respectively, being almost independent of pressure. These values agree moderately well with the previous values (28, 29).

Acknowledgements

The authors wish to thank Prof. Shigehiro Konaka for valuable discussion. This work was supported by the Joint Studies Program (1986–1990) of the Institute for Molecular Science. Financial support by the Kurata Research Grant is greatly appreciated. The calculations were performed on a HITAC M-682H at the Hokkaido University Computing Center.

1. R. G. GORDON. J. Chem. Phys. **43**, 1307 (1965).
2. J. H. R. CLARKE. *In* Advances in infrared and Raman spectroscopy. Vol. 4. *Edited by* R. J. H. Clark and R. E. Hester. Heyden, London. 1978. pp. 109–193.
3. J. R. BIRCH and T. J. PARKER. *In* Infrared and millimeter waves. Vol. 2. *Edited by* K. J. Button. Academic Press, New York. 1979. pp. 137–271.
4. S. IKAWA, T. OHBA, S. TANAKA, Y. MORIMOTO, K. FUKUSHI, and M. KIMURA. Int. J. Infrared Millimeter Waves, **6**, 287 (1985).
5. T. OHBA, S. IKAWA, and M. KIMURA. Chem. Phys. Lett. **117**, 397 (1985).
6. J. YARWOOD, T. SHUTTLEWORTH, J. B. HASTED, and T. NANBA. Nature, **312**, 742 (1984).
7. J. YARWOOD. Chem. Br. **22**, 423 (1986).
8. T. NANBA, J. YARWOOD, T. SHUTTLEWORTH, and J. B. HASTED. Int. J. Infrared Millimeter Waves, **7**, 759 (1986).
9. T. KASUGA and M. WATANABE. *In* UVSOR Activity Report. 1984/1985. Institute for Molecular Science, Okazaki. 1986.
10. (*a*) J. P. HAWRANEK, P. NEELAKANTAN, R. P. YOUNG, and R. N. JONES. Spectrochim. Acta, **32A**, 75 (1976); (*b*) Spectrochim. Acta, **32A**, 85 (1976); (*c*) J. P. HAWRANEK and R. N. JONES. Spectrochim. Acta, **32A**, 99 (1976); (*d*) Spectrochim. Acta, **32A**, 111 (1976).
11. (*a*) D. G. CAMERON, D. ESCOLAR, T. G. GOPLEN, A. NADEAU, R. P. YOUNG, and R. N. JONES. Appl. Spectrosc. **34**, 646 (1980); (*b*) T. G. GOPLEN, D. G. CAMERON, and R. N. JONES. Appl. Spectrosc. **34**, 652 (1980); (*c*) Appl. Spectrosc. **34**, 657 (1980).
12. J. E. BERTIE, R. N. JONES, and V. BEHNAM. Appl. Spectrosc. **39**, 401 (1985).
13. PH. MARTEAU, J. OBRIOT, R. OCCELLI, T. K. BOSE, A. GHERFI, and J. M. ST ARNAUD. J. Mol. Liq. **43**, 193 (1989).
14. M. BORN and E. WOLF. Principles of optics. Pergamon Press, Oxford. 1970.
15. K. S. SESHADRI and R. N. JONES. Spectrochim. Acta, **19**, 1013 (1963).
16. R. J. BELL. Introductory Fourier transform spectroscopy. Academic Press, New York. 1972.
17. T. OHBA and S. IKAWA. J. Appl. Phys. **64**, 4141 (1988).
18. T. OHBA and S. IKAWA. Mol. Phys. In press.
19. R. G. GORDON. J. Chem. Phys. **38**, 1724 (1963).
20. S. IKAWA, S. YAMAZAKI, and M. KIMURA. Chem. Phys. **58**, 275 (1981).
21. D. D. KLUG, D. E. KRANBUEHL, and W. E. VAUGHAN. J. Chem. Phys. **50**, 3904 (1969).
22. Landolt-Börnstein. Numerical data and functional relationships. New Series, II/4. Springer. 1967.
23. T. OHBA and S. IKAWA. Mol. Phys. In press.
24. T. OHBA and S. IKAWA. Infrared Phys. **29**, 27 (1989).
25. J. K. VIJ. J. Chem. Phys. **87**, 3357 (1987).
26. H. R. WYSS, R. D. WERDER, and HS. H. GÜNTHARD. Spectrochim. Acta, **20**, 573 (1964).
27. (*a*) C. G. JOSLIN, S. SINGH, and C. G. GRAY. Mol. Phys. **55**, 1075 (1985); (*b*) C. G. JOSLIN and C. G. GRAY. Chem. Phys. Lett. **154**, 369 (1989).
28. L. POTTHAST, J. SAMIOS, and T. DORFMÜLLER. Chem. Phys. **102**, 147 (1986).
29. G. J. DAVIES, J. CHAMBERLAIN, and M. DAVIES. J. Chem. Soc. Faraday Trans. 2, **69**, 1223 (1973).
30. S. R. POLO and M. K. WILSON. J. Chem. Phys. **23**, 2376 (1955).
31. N. S. ISAACS. Liquid phase high pressure chemistry. Wiley, Chichester. 1981.

Can. J. Chem. Downloaded from www.nrcresearchpress.com by 84.41.108.74 on 09/07/12
For personal use only.

Infrared and Raman microscopy of fowl feather barb

MASAMICHI TSUBOI
Faculty of Science and Engineering, Iwaki-Meisei University, Iwaki, Fukushima 970, Japan

FUMIKO KANEUCHI AND TERUKI IKEDA
Japan Spectroscopic Co., Ltd., 2967-5 Ishikawa, Hachioji, Tokyo 192, Japan

AND

KISO AKAHANE
Department of Chemistry, Faculty of Science, Josai University, Sakado, Saitama 350-02, Japan

Received April 29, 1991

This paper is dedicated to Dr. Richard Norman Jones

MASAMICHI TSUBOI, FUMIKO KANEUCHI, TERUKI IKEDA, and KISO AKAHANE. Can. J. Chem. **69**, 1752 (1991).

A fowl feather barb 10 μm in thickness was subjected to a polarized infrared spectroscopic measurement by the use of a microscopic device. Nearly 50% of its peptide groups were found to give the 1633 and 1684 cm^{-1} bands characteristic of the antiparallel-chain pleated sheet structure, and the remaining 50% gave the 1659 cm^{-1} band assignable to unordered polypeptide chains. The orientation of the pleated sheet was determined to be on average $\theta = 52°$ and $\chi = 39°$, where θ and χ are the angles for the transformation of the *XYZ* coordinate system fixed on the pleated sheet and the *abc* coordinate system fixed on the sample barb. The Raman spectra of the barb were also examined with another microscopic device and a 488.0-nm laser beam. A sharp *aa* component of the Raman scattering tensor was observed at 1667 cm^{-1}. Based on this fact, a revised set of parameters for the vibrational couplings among the peptide groups in the pleated sheet has been proposed. Some discussions have been made on the amide I Raman tensor of the antiparallel-chain pleated sheet.

Key words: fowl feather barb, Raman microscope, infrared microscope, antiparallel-chain pleated sheet, Raman scattering tensor.

MASAMICHI TSUBOI, FUMIKO KANEUCHI, TERUKI IKEDA et KISO AKAHANE. Can. J. Chem. **69**, 1752 (1991).

Utilisant un appareil microscopique, on a soumis la barbette d'une plume d'oiseau d'une épaisseur de 10 μm à une mesure de spectroscopie infrarouge polarisé. On a trouvé que près de 50% des groupes peptidiques donnent lieu à des bandes à 1633 et 1684 cm^{-1} caractéristiques de la structure à feuillets plissés avec des chaînes antiparallèles; l'autre 50% donne lieu à une bande à 1659 cm^{-1} que l'on peut attribuer à des chaînes de polypeptides qui ne sont pas ordonnées. On a déterminé que l'orientation du feuillet plissé est en moyenne $\theta = 52°$ et $\chi = 39°$, où θ et χ sont les angles de la transformation du système de coordonnées *XYZ* fixé sur le feuillet plissé et du système de coordonnées *abc* fixé sur l'échantillon de barbette. On a aussi examiné le spectre Raman de la barbette à l'aide d'un autre appareil microscopique et d'un faisceau de laser de 488,0 nm. On a observé une forte composante *aa* du tenseur de diffusion Raman à 1667 cm^{-1}. Sur la base de ce résultat, on propose un ensemble révisé des paramètres de couplages vibrationnels parmi les groupes peptidiques du feuillet plissé. On présente aussi quelques discussions du tenseur Raman de l'amide I du feuillet plissé avec des chaînes antiparallèles.

Mots clés : barbette d'une plume d'oiseau, microscope Raman, microscope infrarouge, feuillets plissés avec des chaînes antiparallèles, tenseur de diffusion Raman.

[Traduit par la rédaction]

Introduction

Spectroscopic studies of feather keratin have so far been made mostly with samples prepared from the calamus or rachis section of avian feathers (1, 2). Their barbs, in which the crystallite alignment looks better under a polarizing microscope, are too thin for conventional infrared and Raman spectroscopic measurements. Due to recent developments in infrared and Raman microscopy (3, 4), however, even such a thin barb (10 μm in diameter, for example) can now be subjected to these vibrational spectroscopic examinations. If, in such spectroscopic examinations, a comparative study is possible of the infrared and Raman data for the same barb sample, it may yield additional benefits. For each polypeptide conformation, an infrared transition moment caused by its characteristic vibration (the amide I vibration, for example) is well understood as a vector sum of the localized transition moments at the constituent peptide groups. On the other hand, our knowledge of the corresponding Raman scattering tensor is still quite limited. For example, the amide I Raman tensor localized at a peptide group has not yet been established. The contribution of such a localized Raman tensor to the tensor of the antiparallel-chain pleated sheet has never been examined. Such an examination would be facilitated by structural knowledge derived from infrared data on the same sample.

In the present paper, the infrared and Raman spectra of a single barb from fowl feather are reported, and a combined interpretation is described.

Experimental

Fowl feathers were scoured with a dilute, non-ionic detergent solution, rinsed in tap water and then in distilled water, air-dried, and degassed repeatedly by soaking in fresh dry acetone and then air-drying again. These were refluxed with diethyl ether (50°C) for 48 h to remove waxes. A single barb from this was found to be a long cylinder with a diameter of 10 μm and with small lumps arranged at intervals of 75 μm along its elongation direction (see Fig. 1). Under a polarizing microscope it showed a marked positive birefringence. The retardation looked rather homogeneous all over the cylinder.

Its infrared spectra were observed with an infrared microscope,

Printed in Canada / Imprimé au Canada

Can. J. Chem. Downloaded from www.nrcresearchpress.com by 84.41.108.74 on 09/07/12
For personal use only.

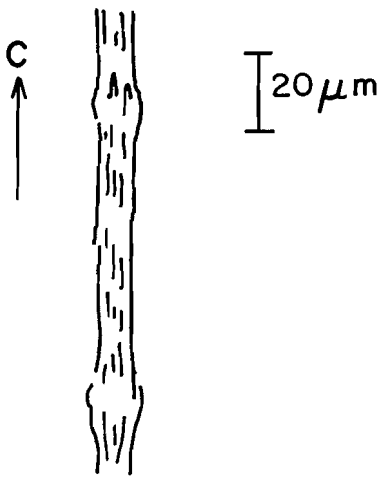


FIG. 1. Fowl feather barb.

Jasco Micro FTIR-100, in its transmission mode. By the use of four aperture plates, all the beams were cut except those going through a rectangular field of 10 × 120 μm, which covered the sample barb. By the use of an infrared polarizer placed in front of the detector, two spectra were recorded, with the electric vector of the infrared radiation both parallel and perpendicular to the elongation direction (*c* axis) of the barb. The results of these observations are shown in Fig. 2.

Raman spectra were observed with a Jasco R-MPS-11 Raman microscope connected with a Jasco NR-1100 Raman spectrophotometer system. For excitation, the 488.0-nm beam of an NEC GLG 3200 Ar ion laser was used. The exciting laser beam came down through the objective (50×) onto the sample barb placed on the microscope stage. First, its elongation direction (*c* axis) was placed parallel to the electric vector of the incident laser beam ($E \parallel c$). Raman scatterings with the *cc* and *ca* components from it were collected by the same objective (in a back-scattering mode), and sent through a beam splitter and a mirror system into the Raman spectrophotometer. The sample barb was found to be fluorescent, but irradiation with a relatively weak laser beam for 1 or 2 h rendered it less fluorescent to the extent that a Raman spectroscopic measurement became possible. The signal-to-noise ratio, however, did not yet become sufficiently high to observe the two components, *cc* and *ca*, separately with a polarizer. Thus, only the Raman scattering intensity, $I_{cc} + I_{ca}$, was obtained, and the result is shown in the upper portion of Fig. 3. Next, the sample barb was rotated on the stage by 90° around the vertical axis, so that the electric vector of the exciting laser beam was now perpendicular to the elongation direction of the barb. The Raman scattering intensity, $I_{aa} + I_{ac}$, was examined, and the result is given in the lower portion of Fig. 3.

Results and discussion

1. Interpretation of the infrared spectra

The observed spectra (Fig. 2) were analyzed by a least-squares procedure into component bands, each of which was assumed to have a Lorentz function profile. Both of the $E \parallel c$ and $E \perp c$ amide I bands were found to consist of three components, with peaks at 1684, 1659, and 1633 cm^{-1}. The 1659 cm^{-1} component is assignable to the unordered polypeptide chains, which probably involve a number of turns. This assignment is supported by the fact that its shape and height are exactly the same for the $E \parallel c$ spectrum as for the $E \perp c$ spectrum. Following Miyazawa's analysis (5), the two components at 1684 and 1633 cm^{-1} are assigned to the antiparallel-chain pleated sheet structure (6), whose unit cell contains four peptide groups (see Fig. 4). The 1684 cm^{-1} component must have a vector-sum transition moment along the *Z* axis (defined as the extending direction of the zigzag polypeptide chain; see Fig. 4), whereas the 1633 cm^{-1} component has a moment along the *Y* axis (perpendicular to *Z* in the sheet plane; nearly parallel to the C═O bond; see Fig. 4).

From the area–intensity measurements of these components of the amide I band, an estimate of the relative amounts of these polypeptide structures was made. It was found that (unordered polypeptide)/(antiparallel-chain pleated sheet) = 51:49.

2. Orientation of the antiparallel-chain pleated sheet

With its external appearance in mind, let us assume that the barb has a cylindrical symmetry, or that it is a uniaxial crystal. The crystal is considered to involve a number of antiparallel-chain pleated sheets as well as the unordered polypeptide chains. Let us next assume that one of these pleated sheets (*XYZ*) is oriented in the crystal (*abc*) as illustrated in Fig. 5. Then, other pleated sheets must be oriented so that all the sheets have the same θ and χ values, whereas the ϕ values are distributed evenly over 360° to keep the axial symmetry around the *c* axis.

The $E \parallel c / E \perp c$ intensity ratio of the 1684 cm^{-1} component is found to be 1.3 (from Fig. 2), and therefore the *Z* axis must be inclined from the *c* axis by $\theta = 52°$ (because $\parallel / \perp = 2 \cos^2 \theta / \sin^2 \theta$). The $E \parallel c / E \perp c$ intensity ratio of the 1633 cm^{-1} component is found to be 0.69, and therefore the *Y* axis must be inclined by 60° from the *c* axis. The set of these data determines uniquely the orientation angles: $\theta = 52°$, $\chi = 39°$.

3. Interpretation of the Raman spectra

As seen in Fig. 3, a sharp Raman peak is found to rise at 1667 cm^{-1} in the broad-background Raman scattering covering the 1690–1640 cm^{-1} range. This 1667 cm^{-1} Raman band is assigned the amide I vibration of the antiparallel-chain pleated sheet, in which all the peptide groups vibrate in-phase ($\nu(0,0)$, in the following section).

4. Proposed revision of the set of the vibrational coupling constants in the antiparallel-chain pleated sheet

Miyazawa and Blout (7) derived an equation for the frequency of the amide I vibration of the antiparallel-chain pleated sheet:

$$[1] \qquad \nu(\delta, \delta') = \nu_0 + D1 \cos \delta + D1' \cos \delta'$$

where the first term ν_0 is the unperturbed frequency, and the second and third terms are due to the intrachain and interchain vibrational interactions, respectively. δ is the phase angle between adjacent peptide group motions in the chain ((1) and (2), or (3) and (4) in Fig. 4) and $D1$ is determined by the potential and kinetic energy interactions between them; δ' and $D1'$ pertain to the interaction through interchain hydrogen bonds (between (1) and (4) in Fig. 4, for example) and have meanings similar to those of δ and $D1$. Miyazawa and Blout (7) gave the following set of values

$$[2] \qquad \nu_0 = 1658, \quad D1 = 8, \quad D1' = -18 \text{ cm}^{-1}$$

This leads to the following frequencies:

Can. J. Chem. Downloaded from www.nrcresearchpress.com by 84.41.108.74 on 09/07/12
For personal use only.

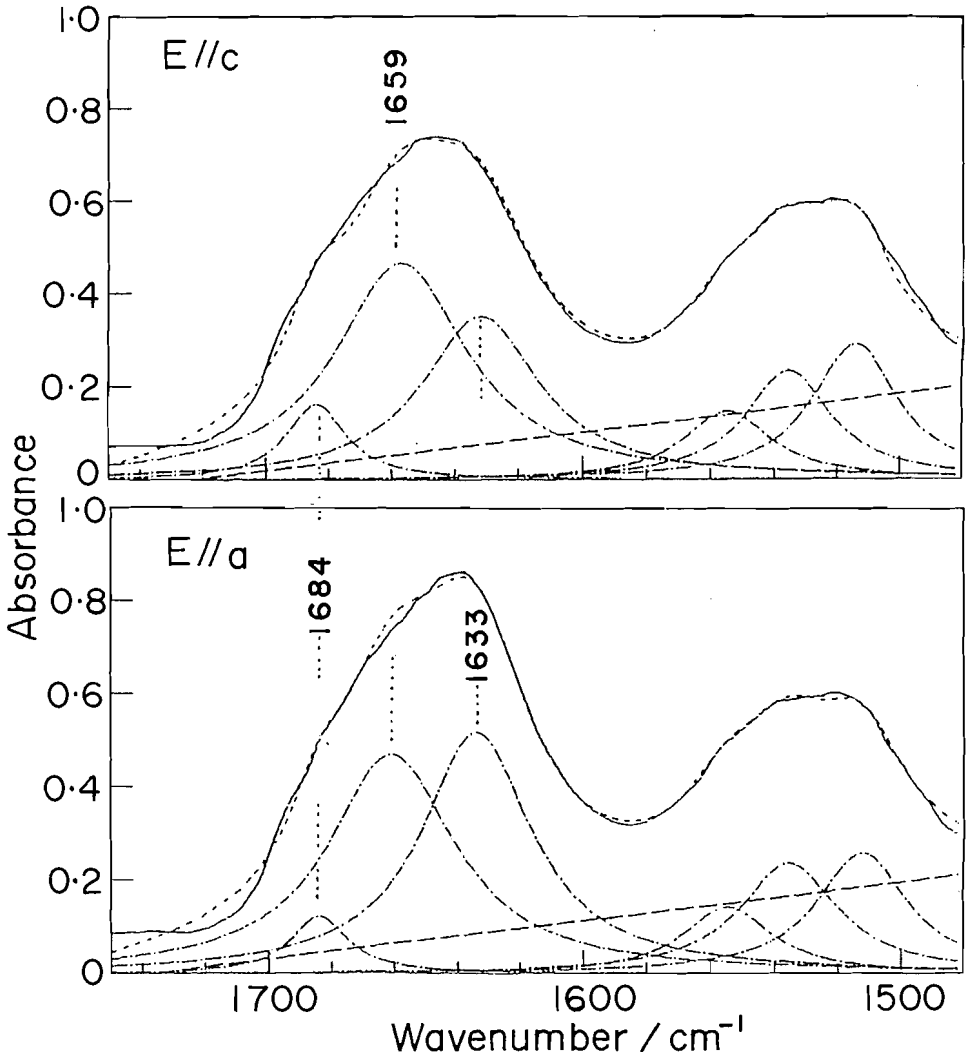


FIG. 2. Infrared absorption spectra (full line) of single barb from fowl feather. Upper spectra, electric vector (E) of the incident radiation is parallel to the elongation direction (c axis) of the barb. Lower spectra, E is perpendicular to the c axis. Resolved components of the amide I band around 1650 cm^{-1} are shown by the chain line (-·-·-·-). The broken line indicates the assumed background, and the dotted line gives the calculated spectrum, which is the sum of the resolved components, and which should fit the observed spectrum (full line).

$$[3]\quad \begin{cases} \nu(0,\pi) = \nu_0 + D1 - D1' = 1684\ cm^{-1}\ (1684\ cm^{-1})\ \text{IR-}Z \\ \nu(\pi,0) = \nu_0 - D1 + D1' = 1632\ cm^{-1}\ (1633\ cm^{-1})\ \text{IR-}Y \\ \nu(0,0) = \nu_0 + D1 + D1' = 1648\ cm^{-1}\ (1667\ cm^{-1})\ \text{Raman} \end{cases}$$

for the observed frequencies given in parentheses. Thus, the calculated frequency, 1648 cm^{-1}, for the Raman-active vibration, now in question, does not agree with the observed frequency (1667 cm^{-1}). To improve this point, we propose to change the set of parameters as follows:

$$[4]\quad \nu_0 = 1658,\quad D1 = 18,\quad D1' = -8\ cm^{-1}$$

This leads to the following frequencies:

$$[5]\quad \begin{cases} \nu(0,\pi) = \nu_0 + D1 - D1' = 1684\ cm^{-1}\ (1684\ cm^{-1})\ \text{IR-}Z \\ \nu(\pi,0) = \nu_0 - D1 + D1' = 1632\ cm^{-1}\ (1633\ cm^{-1})\ \text{IR-}Y \\ \nu(0,0) = \nu_0 + D1 + D1' = 1668\ cm^{-1}\ (1667\ cm^{-1})\ \text{Raman} \end{cases}$$

Can. J. Chem. Downloaded from www.nrcresearchpress.com by 84.41.108.74 on 09/07/12
For personal use only.

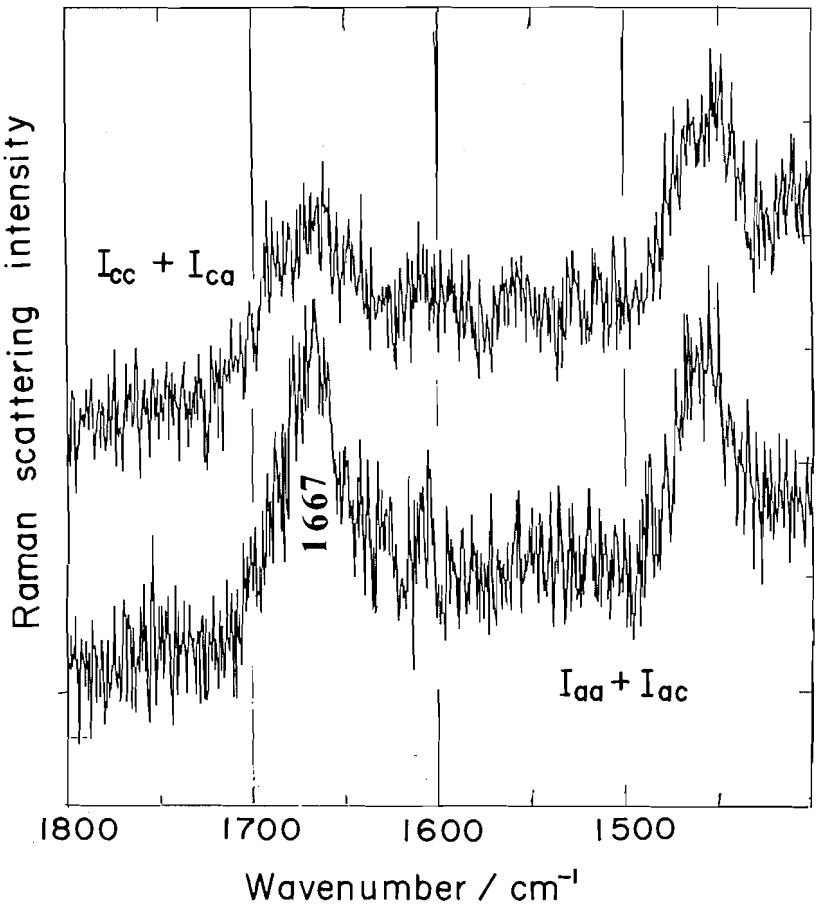


FIG. 3. Raman spectra of single barb from fowl feather. Upper spectrum, the electric vector of the exciting laser beam (Ar^+, 488.0 nm) was placed parallel to the elongation direction of the barb (*c* axis). The Raman scattering beam is considered to involve *cc* and *ca* components. Lower spectrum, the exciting laser beam is polarized perpendicularly to the *c* axis, so that the Raman scattering beam consists of the *aa* and *ac* components.

Can. J. Chem. Downloaded from www.nrcresearchpress.com by 84.41.108.74 on 09/07/12
For personal use only.

with nearly perfect agreement with the observed frequencies given in the parentheses.

5. Raman scattering tensor for the amide I vibration of the antiparallel-chain pleated sheet

On the basis of the Raman spectroscopic measurement on a single crystal of a dipeptide (aspartame), whose molecule involves only one peptide group, Tsuboi *et al.* (4) derived the shape and orientation of the amide I Raman tensor ($\boldsymbol{\alpha}'$) excited at 488.0 nm. The orientation of the principal axes, *x*, *y*, and *z*, of the tensor is reproduced in Fig. 6. The relative amounts of the tensor components are $\alpha'_{xx}/\alpha'_{xx} = 0.05$ ($= r_1'$) and $\alpha'_{yy}/\alpha'_{zz} = 0.2$ ($= r_2'$). If this tensor is placed at every peptide group (see Fig. 4), the Raman scattering tensor $\boldsymbol{\alpha}$ of an antiparallel-chain pleated sheet is given as

$$[6] \qquad \boldsymbol{\alpha} = \sum_{i=1}^{4} \tilde{\boldsymbol{L}}_i \boldsymbol{\alpha}' \boldsymbol{L}_i$$

$\boldsymbol{L}_i$ is calculated from the atomic coordinates given by Pauling and Corey (6) as

$$[7] \qquad L_1 = \begin{pmatrix} 0.0052 & -0.3735 & 0.9276 \\ 0.5877 & -0.7494 & -0.3051 \\ 0.8090 & 0.5468 & 0.2156 \end{pmatrix}$$

$$[8] \qquad L_2 = \begin{pmatrix} 0.0052 & 0.3735 & 0.9276 \\ -0.5877 & -0.7494 & 0.3051 \\ -0.8090 & 0.5468 & -0.2156 \end{pmatrix}$$

$$[9] \qquad L_3 = \begin{pmatrix} -0.0052 & 0.3735 & 0.9276 \\ -0.5877 & 0.7494 & -0.3051 \\ -0.8090 & -0.5468 & 0.2156 \end{pmatrix}$$

$$[10] \qquad L_4 = \begin{pmatrix} -0.0052 & -0.3735 & 0.9276 \\ 0.5877 & 0.7494 & 0.3051 \\ 0.8090 & -0.5468 & -0.2156 \end{pmatrix}$$

The principal axes of the synthetic Raman tensor $\boldsymbol{\alpha}$ come out to be the *X*, *Y*, and *Z* axes shown in Fig. 4, as expected, and its tensor components are calculated to be

$$[11] \qquad \alpha_{XX}/\alpha_{ZZ} = 0.2585 \qquad (= r_1)$$

$$[12] \qquad \alpha_{YY}/\alpha_{ZZ} = 1.7300 \qquad (= r_2)$$

6. Raman scattering intensities of the barb and the orientation of the antiparallel-chain pleated sheet in it

The relation of the polarized Raman spectra of a crystal and the orientation of the molecules in it is not as simple as the relation of its polarized infrared spectra and the molecular orientation. If the crystal is uniaxial, and if the molecule in it,

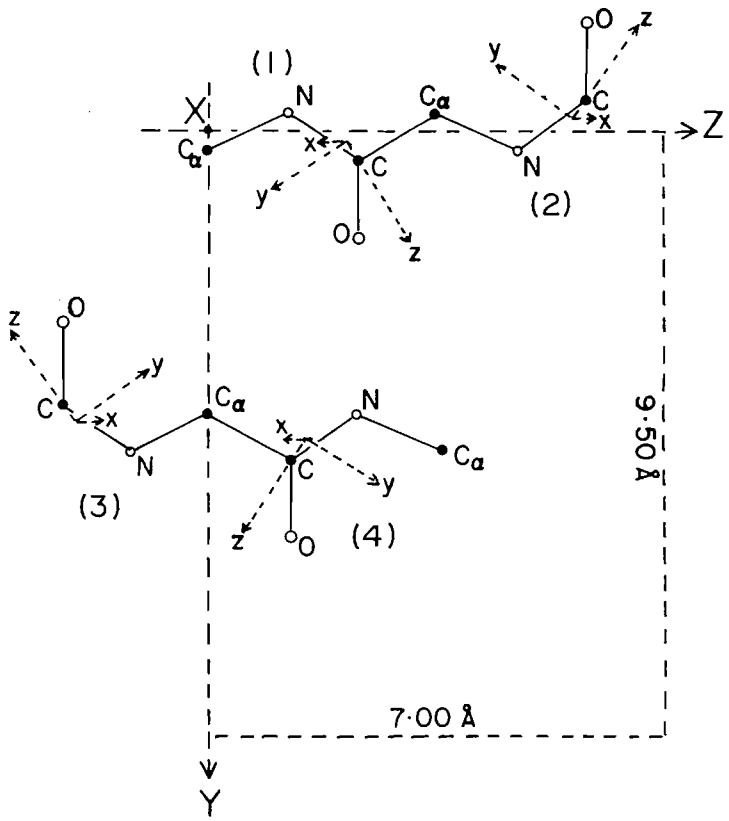


FIG. 4. Antiparallel-chain pleated sheet structure of polypeptide, drawn on the basis of the coordinates given by Pauling and Corey (6). Its X, Y, and Z axes are defined as given here. Its unit cell involves four peptide groups, and the principal axes, x, y, and z, of the amide I Raman tensor (for 488.0 nm excitation) localized on each peptide group are also shown here.

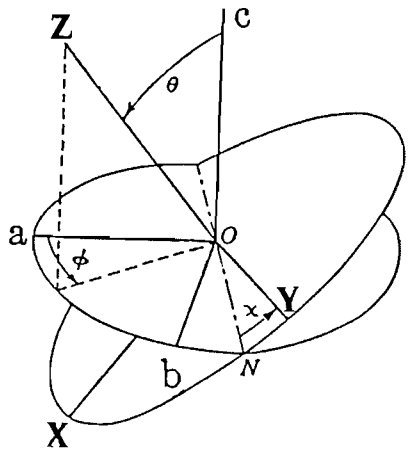


FIG. 5. Definitions of the angles, θ, φ, and χ. These angles are for designating the orientation of the XYZ rectangular axes system of the antiparallel-chain pleated sheet (see Fig. 4) with respect to the crystallographic abc rectangular axes system.

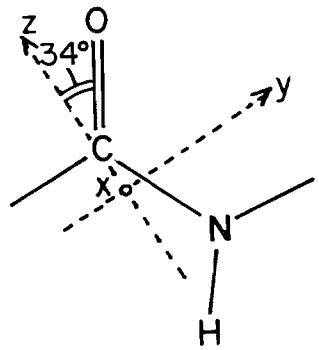


FIG. 6. Amide I Raman tensor (excited at 488.0 nm) of a single peptide group. Its principal axis x is perpendicular to the peptide plane, y and z axes are in the plane, and z axis makes a 34° angle from the C=O bond. $r_1 = \alpha_{xx}/\alpha_{zz} = 0.05$ and $r_2 = \alpha_{yy}/\alpha_{zz} = 0.2$, where α_{xx}, etc., are the Raman tensor components.

with the Raman tensor of $\alpha_{XX}/\alpha_{ZZ} = r_1$ and $\alpha_{YY}/\alpha_{ZZ} = r_2$, is placed with the orientation angles θ and χ (see Fig. 5), then the Raman scattering intensities I_{cc}, I_{aa}, and I_{ac} are given as (5)

$$[13]\quad \frac{I_{cc}}{I_{aa}} = \frac{I_{cc}}{I_{bb}} = 4\left(\frac{\sin^2\theta(r_1\cos^2\chi + r_2\sin^2\chi) + \cos^2\theta}{\cos^2\theta(r_1\cos^2\chi + r_2\sin^2\chi) + (r_1\sin^2\chi + r_2\cos^2\chi) + \sin^2\theta}\right)^2$$

$$[14]\quad \frac{I_{ac}}{I_{aa}} = \frac{I_{bc}}{I_{bb}} = 2\,\frac{\sin^2\theta\cos^2\theta(r_1\cos^2\chi + r_2\sin^2\chi - 1)^2 + \sin^2\theta\sin^2\chi\cos^2\chi(r_1 - r_2)^2}{(\cos^2\theta(r_1\cos^2\chi + r_2\sin^2\chi) + (r_1\sin^2\chi + r_2\cos^2\chi) + \sin^2\theta)^2}$$

In our present case of antiparallel-chain pleated sheet, it has been concluded that $r_1 = 0.2585$ and $r_2 = 1.7300$ (Sect. 5). By replacing these values in eqs. [13] and [14], I_{cc}/I_{aa} and I_{ac}/I_{aa} have been calculated for various θ and χ values. The results are shown in Fig. 7. By the help of such a diagram one should be able, in principle, to determine the orientation (θ and χ) of the antiparallel-chain pleated sheet in the barb from Raman data alone. In the present case, however, the ac component cannot be resolved from the aa component, and the spectral separation of the unordered portion of the polypeptide chain from the antiparallel-chain pleated sheet portion also seems difficult (see Fig. 3). In addition, the orientation has already been determined from the infrared data (in Sect. 2). Let us therefore examine whether this orientation is consistent with the Raman data now in question.

The set of angles, $\theta = 52°$ and $\chi = 39°$, corresponds to $I_{cc}/I_{aa} = 0.75$ and $I_{ac}/I_{aa} = 0.15$ (from Fig. 7), and therefore $(I_{cc} + I_{ca})/(I_{aa} + I_{ac}) = 0.78$. The actually observed Raman spectra (Fig. 3) definitely indicate that $(I_{cc} + I_{ca})/(I_{aa} + I_{ac}) < 1$ at 1667 cm^{-1}, and hence it is concluded that the orientation predicted from the infrared data is qualitatively consistent with the Raman data. A slightly more quantitative examination, however, suggests that χ is smaller than 39° because $(I_{cc} + I_{ca})/(I_{aa} + I_{ac})$ seems smaller than 0.7. In this connec-

Can. J. Chem. Downloaded from www.nrcresearchpress.com by 84.41.108.74 on 09/07/12
For personal use only.

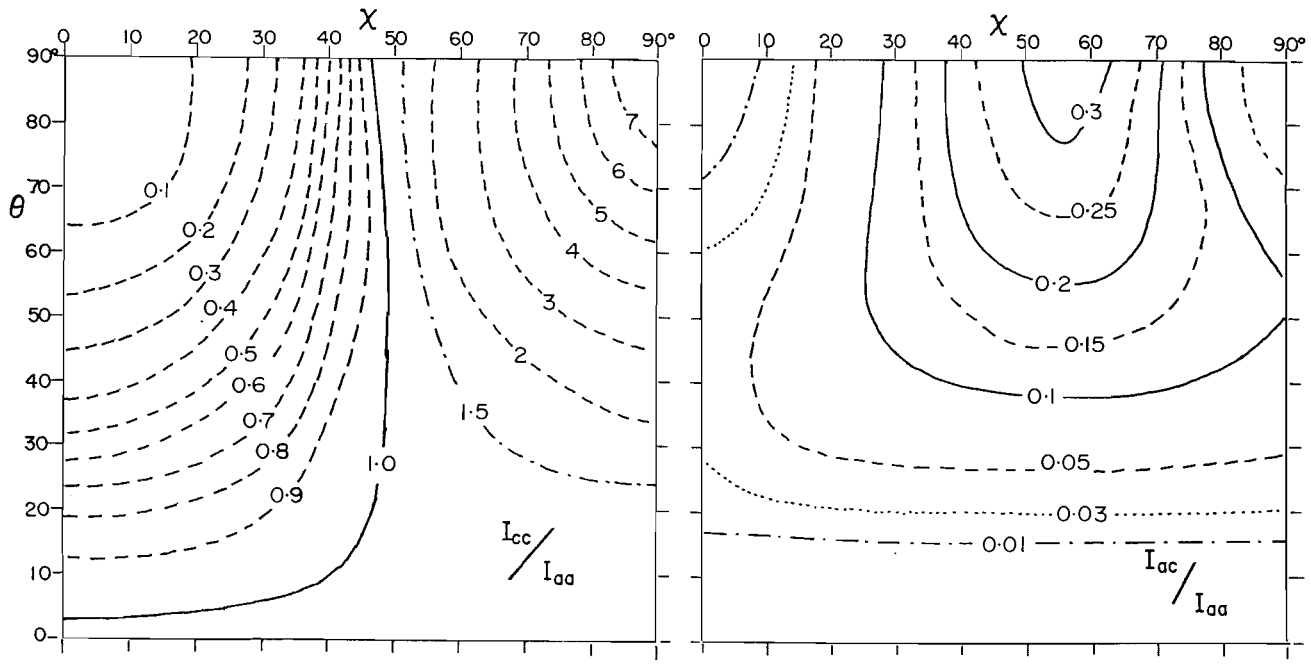


FIG. 7. The Raman scattering intensity ratios, I_{cc}/I_{aa} and I_{ac}/I_{aa}, expected from the orientations (θ and χ) of the antiparallel-chain pleated sheet whose principal axes are X, Y, and Z as shown in Fig. 4. Here, it was assumed that $\alpha_{XX}/\alpha_{ZZ} = 0.2585$ and $\alpha_{YY}/\alpha_{ZZ} = 1.7300$, as calculated in Sect. 5 in the text.

tion, we should pay attention to the following two conditions in our experiments: First, we are observing a much greater area (10 × 120 μm) of the sample barb in the infrared microscopy than in the Raman microscopy (a circle only 2 μm in diameter). Second, we are rotating the sample barb on going from the Raman spectroscopic measurement of the $I_{cc} + I_{ca}$ component to that of the $I_{aa} + I_{ac}$ component, which does not ensure that exactly the same area of the barb sample is subjected to the $I_{cc} + I_{ca}$ measurement as to the $I_{aa} + I_{ac}$ measurement. In the infrared dichroism measurement, on the other hand, the sample barb was never moved, and therefore it is certain that our $E \parallel c$ spectrum came from exactly the same sample area as the $E \perp c$ spectrum. Taking these two factors into account, we may conclude that, in our sample barb, there is an appreciable heterogeneity (with a scale of 2 μm) in the orientation of the pleated sheet, and that the values derived from the infrared data ($\theta = 52°$, $\chi = 39°$) represent the average of such a heterogeneous orientation.

Acknowledgement

The work carried out at Iwaki-Meisei University was partly supported by Grant No. 02670985 from the Ministry of Education, Science, and Culture of Japan.

1. R. D. B. FRASER, T. P. MACRAE, D. A. D. PARRY, and E. SUZUKI. Polymer, **12**, 35 (1971).
2. S. L. HSU, W. H. MOOR, and S. KRIMM. Biopolymers, **15**, 1513 (1976).
3. Y. MITSUTSUKA, T. AOYAMA, S. OHBA, Y. SAITO, F. KANEUCHI, and M. TSUBOI. Bull. Chem. Soc. Jpn. **64**, 1743 (1991).
4. M. TSUBOI, T. IKEDA, and T. UEDA. J. Raman Spectrosc. In press.
5. T. MIYAZAWA. J. Chem. Phys. **32**, 1647 (1960).
6. L. PAULING and R. B. COREY. Proc. Natl. Acad. Sci. U.S.A. **39**, 253 (1953).
7. T. MIYAZAWA and E. R. BLOUT. J. Am. Chem. Soc. **83**, 712 (1961).

Can. J. Chem. Downloaded from www.nrcresearchpress.com by 84.41.108.74 on 09/07/12
For personal use only.

Phase transitions in adamantane derivatives: 1-fluoroadamantane

NANCY T. KAWAI, DENIS F. R. GILSON,[1] AND IAN S. BUTLER[1]

Department of Chemistry, McGill University, 801 Sherbrooke St. W., Montreal, P.Q., Canada H3A 2K6

Received April 23, 1991

This paper is dedicated to Dr. Richard Norman Jones

NANCY T. KAWAI, DENIS F. R. GILSON, and IAN S. BUTLER. Can. J. Chem. **69**, 1758 (1991).

The solid-state phase behaviour of 1-fluoroadamantane (1-$C_{10}H_{15}F$) has been investigated by differential scanning calorimetry, and by infrared and Raman spectroscopy. The phase transition occurs at 227 K on cooling and at 231 K upon heating, with average ΔH_t and ΔS_t of 1.65 kJ mol^{-1} and 7.3 J K^{-1} mol^{-1}. The transition was also apparent in the low-temperature IR and Raman spectra by a sudden line narrowing, and characteristic spectral features of each phase were identified. Both phases I and II were disordered, and further cooling of phase II resulted in the formation of a glass. Attempts to induce a glass transition (predicted to occur at ~90 K) by slow heating were unsuccessful. Vibrational spectroscopic studies at high pressures showed a phase transition at 3.3 ± 1.0 kbar, upon compression. The phases formed under pressure were the same as those induced by lowering temperature.

Key words: high-pressure infrared and Raman spectroscopy, phase transition, plastic crystal, orientational disorder.

NANCY T. KAWAI, DENIS F. R. GILSON et IAN S. BUTLER. Can. J. Chem. **69**, 1758 (1991).

Faisant appel à la calorimétrie de balayage différentiel et aux spectroscopies infrarouge et Raman, on a étudié le comportement de phase de l'état solide du 1-fluoroadamantane (1-$C_{10}H_{15}F$). La transition de phase se produit à 227 K lors du refroidissement et à 231 K lors du chauffage; les valeurs moyennes du ΔH_t et du ΔS_t sont 1,65 kJ mol^{-1} et 7,3 J K^{-1} mol^{-1}. On peut aussi détecter la transition dans les spectres IR et Raman à basses températures grâce à un amincissement soudain des raies; on a identifié les caractéristiques spectrales de chaque phase. Les phases I et II sont toutes les deux désordonnées et un refroidissement plus poussé de la phase II conduit à la formation d'un verre. Aucun des essais tentés pour induire une transition de verre (qui devrait se produire à environ 90 K) par un chauffage lent n'a été couronné de succès. Des études de spectroscopie vibrationnelle à pressions élevées ont montré que, lors de la compression, il se produit une transition de phase à 3,3 ± 1,0 kbar. Les phases qui se forment sous pression sont les mêmes que celles qui sont induites par un abaissement de la température.

Mots clés : spectroscopies infrarouge et Raman à haute pression, transition de phase, cristal plastique, désordre orientationnel.

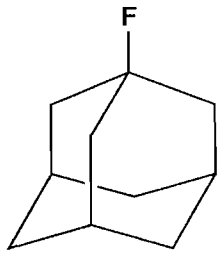
[Traduit par la rédaction]

Can. J. Chem. Downloaded from www.nrcresearchpress.com by 123.30.183.119 on 09/07/12
For personal use only.

Introduction

A large number of organic cage compounds exhibit orientational disorder in the solid state (1–3), and investigations of many derivatives of adamantane, tricyclo[3.3.1.1]decane, have been reported with the aim of correlating phase behaviour with molecular structure. There are two positions on the adamantane cage where single substitution can occur: the 1-position, where the molecule retains a threefold rotation axis, and the 2-position, where a plane of symmetry remains intact. The phase behaviour of the 1-adamantanes varies according to the substituent. Among the halo-adamantanes, 1-chloro and 1-bromoadamantane exhibit one- and two-phase transitions, respectively, to ordered phases (4). The 1-iodo derivative also exhibits a solid–solid phase transition; however, the high-temperature phase is not plastically crystalline (4, 5). The behaviour of 1-cyanoadamantane is drastically different from the halo derivatives (6). Upon cooling, the plastic crystal, phase I, undergoes a transition to phase II, which can be quenched to a glassy crystal, phase I_g. Upon heating, this glassy phase can be annealed to form a metastable phase, phase I′, which will then undergo an irreversible transition to phase II.

Several studies have been reported specifically on the phase behaviour of 1-fluoroadamantane. Differential scanning calorimetric measurements (4) revealed a phase transition at 222 K, with an enthalpy and entropy of transition of 1.50 kJ mol^{-1} and 6.77 J K^{-1} mol^{-1}, respectively. The melting temperature in a sealed tube was measured to be 525 K, but the entropy of fusion was not measured. Single-crystal X-ray diffraction (7)



1-fluoroadamantane

was used to determine the structure of the high-temperature phase as face-centred cubic (*Fm3m*), with four molecules per unit cell, with a = 9.535(4) Å. Although the entropy of fusion is not known, the cubic structure suggests that the high-temperature phase of fluoroadamantane is plastic. The molecular motions in this phase were investigated by ^{1}H, ^{19}F, and ^{13}C NMR spectroscopy, by measuring T_1 relaxation times (8), by incoherent quasielastic neutron scattering (9), from dielectric properties (10), and by Raman scattering from a single crystal (11). The reorientational motions of fluoroadamantane could be separated into two components: rotation about the threefold molecular axis, and a tumbling motion of the molecular axis about eight distinguishable equilibrium orientations along the ⟨111⟩ directions of the cubic lattice. The results of the different techniques agreed very well with each other; the correlation times of the motions could be described by Arrhenius laws (9):

[1] $\tau_{C4} = 9.3 \times 10^{-13} \exp(2960/T)$ s

[1]Authors to whom correspondence may be addressed.

[2] $\tau_{M3} = 5.9 \times 10^{-13} \exp(1560/T)$ s

where τ_{C4} is the correlation time of the tumbling motion, and τ_{M3} is that of molecular rotation. The activation energies for the tumbling and rotational motions are therefore 24.6 and 13.0 kJ mol^{-1}, respectively. These barriers are comparable to those in the plastic phase of 1-chloroadamantane (12), reflecting the structural similarities of the two solids. Only the ^{1}H wideline NMR and dielectric experiments were successfully carried out below the phase transition temperature. According to proton second-moment measurements, the phase transition does not qualitatively change the reorientational motions, which slow down progressively until a rigid lattice is formed near 80 K (8). The crystal structure of the phase below 222 K could not be determined precisely because the single crystals cracked upon cooling through the transition; however, the low-temperature phase was shown to be non-cubic even at 4 K (10). The dielectric measurements suggested that the low-temperature lattice is tetragonal, as in adamantane (13, 14), with one of the ⟨001⟩ directions of the cubic lattice remaining as a fourfold axis. The barriers to reorientation below and above the phase transition were determined by dielectric relaxation to be 29.1 and 19.0 kJ mol^{-1}, respectively. The knowledge of the structure and the degree of order of fluoroadamantane below 222 K, therefore, remains elusive.

Recently, a "symmetry departure" model was used to explain glass transitions in molecular crystals such as cyclohexanol and 1-cyanoadamantane (15), and an analysis of the available data on fluoroadamantane led to the prediction of a glass transition, upon heating, near 90 K. The IR spectrum, measured in solution, has been reported, but with virtually no assignments (16), and, except for the few bands measured from the single crystal (11), the full Raman spectrum has yet to be described. The behaviour of fluoroadamantane under pressure also remains unexplored, and, due to the apparent disorder down to 4 K, the effect of pressure may be different from the effects that result from lowering the temperature. Thus, as an extension of previous studies on the chloro and bromo derivatives (17–19), the phase behaviour of fluoroadamantane was investigated by low-temperature and high-pressure vibrational spectroscopy.

Experimental

Sublimed crystals of 1-fluoroadamantane were provided by Ms. K. Khougaz and Professor P. G. Farrell (McGill University). Proton NMR analysis (200 MHz) did not reveal the presence of any impurities, and the sample was used without additional purification.

Differential scanning calorimetry (DSC) was performed on a Perkin–Elmer DSC-7 calorimeter with liquid nitrogen as the coolant. Both the temperature and enthalpy of the calorimeter were calibrated by using the phase transition of cyclohexane (Aldrich, Gold Label). The sample, typically 5–10 mg, was weighed on a Cahn microbalance and hermetically sealed in an aluminium pan. Thermograms were obtained on cooling and on heating at a scanning rate of 5 K min^{-1}.

Infrared spectra were acquired on a Nicolet 6000 FT-IR spectrometer with a liquid nitrogen cooled MCT-B (mercury cadmium telluride) detector. A spectral resolution of 1 cm^{-1} was employed. Raman spectra were recorded on an Instruments S.A. spectrometer with a Jobin–Yvon Ramanor U-1000 double monochromator, with an IBM PS/2 model 60 computer for data collection and processing. The excitation source was the 514.532-nm line of a Spectra Physics model 165-5W argon ion laser. In the variable-temperature experiments, the sample temperature was maintained with a Cryodyne Cryocooler model 21 cryostat (Cryogenics Technology Inc.) and measured using a silicon diode thermocouple attached to a Cryophysics model 4025 controller. Infrared and Raman spectra were measured over a wide temperature range (60–295 K) on both cooling and heating, and at every 5 K near the phase transition. In the Raman spectroscopic experiments, the sample was sealed in a glass capillary tube and mounted onto the cold finger in the cryostat with indium foil as a conducting junction. Typically, the laser power at the sample was 300 mW and a resolution of between 1 and 2.5 cm^{-1} was obtained. For the IR spectra, the sample was sublimed onto a KBr window attached to the cold finger. The sample was then annealed through the phase transition until the spectra of the two phases remained consistent. Although the cryostat was usually operated under vacuum, a nitrogen atmosphere was also used to prevent sublimation of phase I from the window.

Variable-pressure Raman spectra were obtained using a diamond anvil cell (DAC) from Diacell Products, Leicester, England, equipped with type IIA diamonds. The sample, together with a ruby chip as a pressure calibrant (20), was placed in the 300-μm hole of a 380 μm thick stainless steel gasket between the diamonds. The DAC was placed under the 4× objective of the Nachet optical microscope coupled to the spectrometer. Typically, a resolution of 4 cm^{-1} was employed and about 50 mW of laser power at the sample were used. Spectra were measured upon compression every 1–5 kbar up to 60 kbar (1 bar = 100 kPa).

The DAC used in the IR experiments was from High Pressure Diamond Optics (Tucson, Arizona), and was also equipped with type IIA diamonds. A 200 μm thick stainless steel gasket was used between the diamonds. The pressure calibrant chosen was the antisymmetric stretching mode of NO_3^- in $NaNO_3$ diluted in a NaBr matrix (0.1–0.3 wt.%) (21). The DAC was mounted onto an XYZ stage, which was aligned on a Spectra-Bench 4× beam condenser (Spectra-Tech). Infrared spectra were obtained upon compression and decompression at 1–3 kbar intervals up to 22 kbar.

Results and discussion

Differential scanning calorimetric measurements of fluoroadamantane confirmed the presence of a single phase transition (phase I ⟶ phase II) at 227 K on cooling, with enthalpy and entropy changes of 1.7 kJ mol^{-1} and 7.6 J K^{-1} mol^{-1}. Upon heating, the transition displayed a slight hysteresis, occurring at 231 K, with ΔH_t and ΔS_t of 1.6 kJ mol^{-1} and 6.9 J K^{-1} mol^{-1}. This transition temperature is higher than the value of 222 K (on heating) reported in the literature (4). No other phase transitions were observed by DSC, and repeated cycling of the sample between 298 and 123 K did not affect the phase I ⟶ phase II transition temperature.

Variable-temperature IR and Raman spectra were measured at every 5 K on cooling and on heating between 250 and 200 K, i.e., through the phase I ⟶ phase II transition temperature. Spectra of each phase are shown in Figs. 1 and 2. Upon comparison of these spectra, very few differences are apparent, but a definite narrowing of peaks did occur suddenly at the transition point. Figure 3 is a plot of linewidths (FWHH) of two isolated bands versus temperature, in the cooling direction. In both cases, there is a distinct decrease in the linewidths at the phase transition, and the C–H stretching region showed the most pronounced changes. In both the IR and Raman spectra, phase I is characterized by a peak at 2857 cm^{-1} and then a broad envelope of peaks centred at about 2928 cm^{-1}. In phase II, the narrowing of peaks is sufficient to resolve the band at 2891 cm^{-1}, and the other higher-frequency C—H stretching bands appear as a more rounded band centred at about 2930 cm^{-1}. The Raman spectra of both phase I and phase II do not contain any discrete peaks below 100 cm^{-1}, indicating that, on the timescale of the Raman measurements, the molecular motions are isotropic. This agrees well with the reorientational correlation times reported in the literature

Can. J. Chem. Downloaded from www.nrcresearchpress.com by 123.30.183.119 on 09/07/12
For personal use only.

Can. J. Chem. Downloaded from www.nrcresearchpress.com by 123.30.183.119 on 09/07/12
For personal use only.

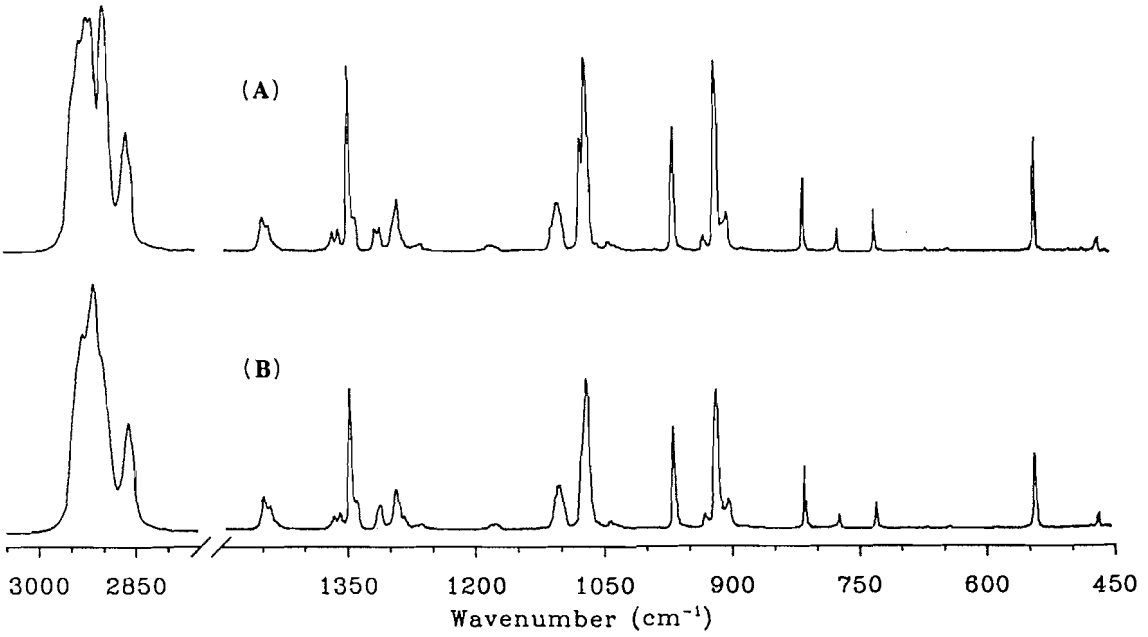


FIG. 1. Infrared spectra of 1-fluoroadamantane at (A) 200 and (B) 250 K.

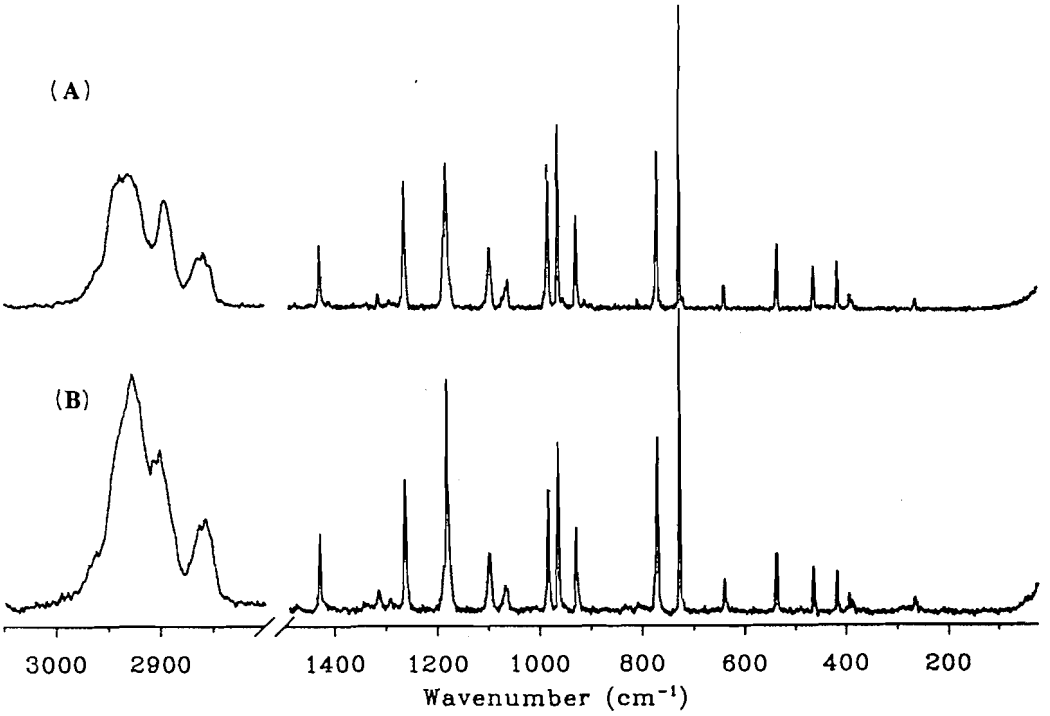


FIG. 2. Raman spectra of 1-fluoroadamantane at (A) 205 and (B) 250 K.

(17). Further cooling of phase II down to 60 K did not induce any other observable phase transitions. To see if the glassy crystalline structure would anneal to an ordered crystal, the temperature of the sample was increased from 60 to 120 K by approximately 5 K every hour. If the glassy phase transformed to an ordered, crystalline phase, line narrowing and the appearance of sharp external modes would be expected. Such effects, however, were not observed in the Raman spectrum.

The vibrational peaks of phases I and II of fluoroadamantane are listed in Table 1. Raman polarization measurements were measured in CS_2 solution. While the spectra of adamantane itself have been assigned according to force-field calculations (22), other 1-substituted derivatives have been assigned simply by comparison with other molecules. The vibrational spectra of fluoroadamantane, $C_{10}H_{15}F$, should contain 72 normal modes. Under C_{3v} molecular symmetry, however, these transform as $\Gamma_{vib}{}^{int} = 17a_1 + 7a_2 + 24e$, where only the a_1 and e modes are IR and Raman active, and the a_2 modes are totally inactive. These can be separated into 15 C—H stretching modes ($\Gamma_{\nu(CH)} = 4a_1 + a_2 + 5e$), and 57 non-CH modes ($\Gamma_{non\text{-}CH} = 13a_1 +$

TABLE 1. Vibrational data (cm^{-1}) for 1-F-adamantane

Solution/CS_2 Raman[a] (295 K)	Phase I Raman (250 K)	Phase I IR (250 K)	Phase II Raman (205 K)	Phase II IR (200 K)	Assignment
264 dp	267 vw		266 w		C—C—F bend, *e*
	391 vw		391 vw		
	396 vw		395 vw		
420 pp	420 w	419 w	420 w	419 w	
		463 w		463 w	
465 dp	467 w		467 w		C—C—C def.
540 p	540 w	539 s	539 m	538 s	
	642 w	640 vw	643 w	641 vw	
		668 vw		668 vw	
			724 vw		
730 p	731 s	729 w	731 vs	729 w	C—F str., a_1
774 p	775 m	773 w	775 s	773 w	C—C str., a_1
		814 m	814 vw	814 m	
		904 m		904 m	
920 pp		918 s	918 vw	918 s	
931 dp	934 w	932 w	935 m	933 w	
			959 vw		
		969 s		968 s	
970 dp	970 m		970 s	970 m,sh	
988 dp	989 m		990 s		
		1044 vw		1045 vw	
			1070 w		
1076 dp	1072 vw	1072 s	1074 vw,sh	1072 s	
			1080 vw,sh	1079 s	C—C str.
1102 dp	1105 w	1105 m	1105 m	1105 m	+ CH_2 and CH def.
		1111 w,sh		1113 w,sh	
		1183 vw,br		1184 vw,br	
1180 dp	1189 s		1190 s		
	1195 w,sh		1195 m,sh		
1265 dp	1271 m	1268 vw	1273 m	1268 vw	
		1290 w			
		1297 m		1295 m	
	1301 vw		1302 vw	1299 w,sh	
		1318 m		1316 w	
	1323 w		1324 w	1322 w	
		1345 m		1346 m	
		1353 s		1354 s	CH_2 and CH def.
		1366 w		1366 w	
		1373 w		1373 w	
1439 dp	1439 w		1439 m		
		1449 w		1449 w	CH_2 scissor
		1456 m		1456 m	
2851 p	2852 m,sh		2852 m,sh	2851 m,sh	C—H str., CH_2, a_1
2857 pp	2857 m	2857 s	2858 m	2857 s	CH_2, *e*
2864 dp	2863 m,sh		2863 m,sh	2862 m,sh	CH_2, *e*
2886 p					($2 \times 1456\ cm^{-1}$, A_1)
2901	2901 m	2898 s,sh	2896 m	2891 vs	CH, a_1
2909	2907 m	2910 vs		2911 vs	CH, *e*
				2917 vs	CH_2, *e*
2925 p	2928 s,br	2928 vs,sh	2931 m	2930 vs	CH_2, a_1
			2938 m,sh		CH_2, *e*
2958 p	2962 w,sh		2959 w,sh		CH_2, a_1

[a]dp = depolarized, pp = partially polarized, and p = polarized.

$6a_2 + 19e$). Therefore, there should be a total of 41 peaks coincident in the IR and Raman spectra, with nine of these in the C—H stretching region. A total of 50 bands were observed in the IR and Raman spectra of phase II, which should not display any solid-state effects, but where the linewidths are narrowed sufficiently to resolve close-lying bands. The vibrational spectrum was assigned with the aid of assignments for adamantane (23, 26) and other 1-substituted derivatives (23), and seven a_1 bands could be identified from the polarization measurements. Although C—F stretching bands usually occur between 1000

Can. J. Chem. Downloaded from www.nrcresearchpress.com by 123.30.183.119 on 09/07/12
For personal use only.

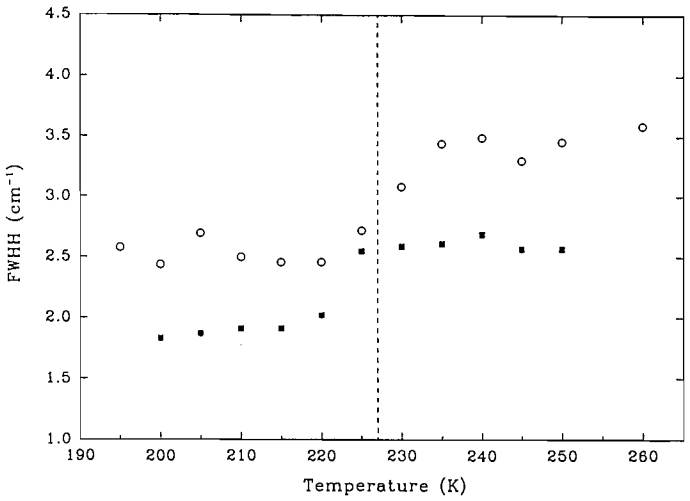


FIG. 3. Full width at half height (FWHH) of two vibrational peaks of 1-fluoroadamantane: ○, 420 cm^{-1} Raman band; ■, 731 cm^{-1} IR band. The dashed line represents the phase transition temperature as measured by DSC (227 K on cooling).

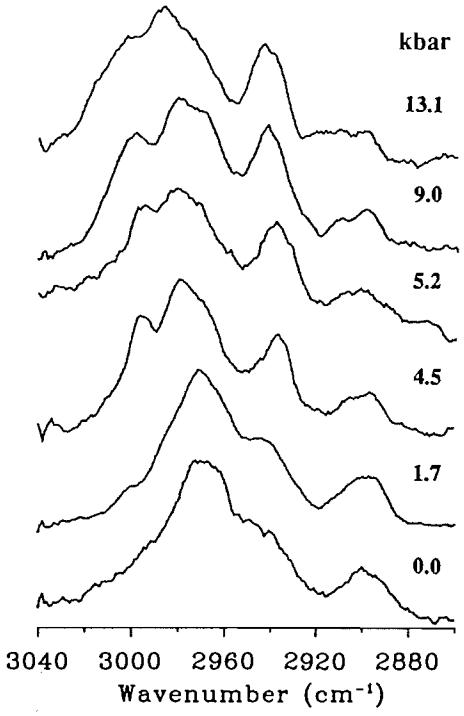


FIG. 4. The C—H stretching region of the Raman spectrum of 1-fluoroadamantane at the indicated pressures upon compression.

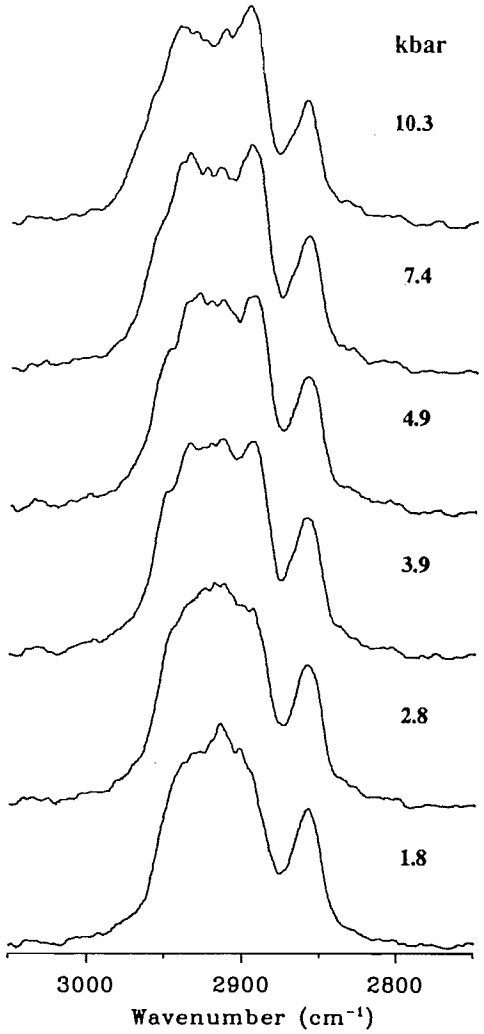


FIG. 5. Infrared spectra of the C—H stretching region of 1-fluoroadamantane at the indicated pressures upon compression.

and 1400 cm^{-1} (24), it has been reported that, when adjacent to a C—C single bond, the C—F and C—C stretching vibrations become mixed and the lower frequency band is higher in C—F character (25). For example, in $(CH_3)_3CF$, the C—F stretching band occurs at 751 cm^{-1} whereas the symmetric and antisymmetric C—C stretches are observed at 892 and 1260 cm^{-1}, respectively (26). From comparisons with other 1-substituted adamantanes, the symmetric cage-breathing mode was assigned to the strong, polarized band at 774 cm^{-1}. Therefore, the C—F stretching vibration could be assigned to the polarized band at 730 cm^{-1}, and the peak at 1265 cm^{-1} is probably a skeletal stretching mode having *e* symmetry. As a consequence of the cage structure, the majority of the other bands between 800 and 1400 cm^{-1} are coupled, and involve contributions from skeletal stretching, and from methylene and methine C—C—H deformations. Based on valence force-field calculations for adamantane (22), the symmetric and antisymmetric methine C—H stretching modes are assigned to the bands occurring at 2891 and 2911 cm^{-1}, respectively. The remaining C—H stretches were assigned to the methylene hydrogens, and their symmetries were determined according to the polarization measurements.

In the cases of adamantanone (27), 2-chloroadamantane (17), and 1-chloroadamantane (17), the behaviour of the compounds under pressure mimicked their low-temperature results. These molecules, however, all displayed phase transitions to ordered, crystalline solids. The effects of pressure on fluoroadamantane, therefore, may or may not be analogous to the low-temperature experiments. Initially, Raman spectra were measured over a wide pressure range of 59 kbar. Figure 4 shows the C—H stretching region through a range of moderate pressures. Below 1.7 kbar, the spectrum resembles those observed for phase I in the variable-temperature experiments. Between 1.7 and 4.5 kbar, however, the shoulder at about 2945 cm^{-1} becomes better separated from the remainder of the higher-frequency C—H bands. This is analogous to the observations of the phase I → phase II transition under low-temperature conditions. The additional application of pressure,

Can. J. Chem. Downloaded from www.nrcresearchpress.com by 123.30.183.119 on 09/07/12
For personal use only.

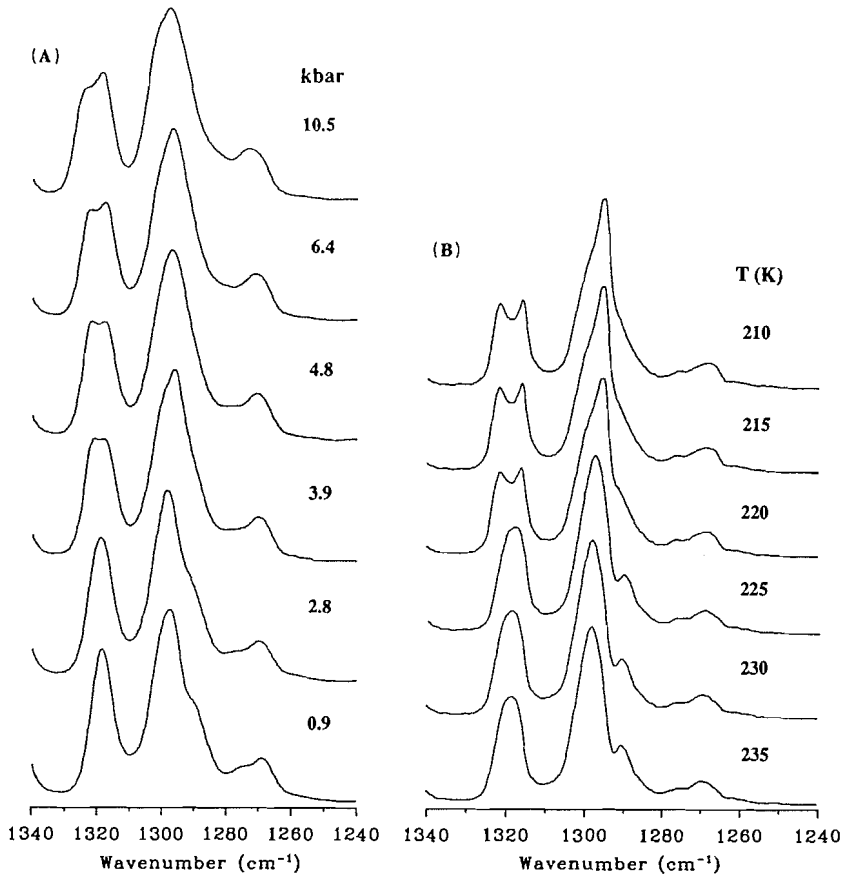


FIG. 6. The resolution of the 1318 cm^{-1} IR band into two bands at 1316 and 1322 cm^{-1} at the phase transition of 1-fluoroadamantane, (A) under pressure, and (B) at low temperature.

TABLE 2. Pressure dependences of vibrational peaks of 1-F-adamantane[a]

Phase I			Phase II			
ν (cm^{-1})	$d\nu/dp$ (cm^{-1} $kbar^{-1}$)	d ln ν/dp ($kbar^{-1} \times 10^4$)	ν (cm^{-1})	$d\nu/dp$ (cm^{-1} $kbar^{-1}$)	d ln ν/dp ($kbar^{-1} \times 10^4$)	Assignment
			419	0.2	4	C—C—C def.
			463	0.1	2	
			538	0.2	3	
640	0.2	3	641	0.18	2.8	
729	0.46	6.2	729	0.42	5.8	C—F str.
773	0.71	9.2	773	0.54	7.0	C—C str.
814	0.78	9.6	814	0.57	6.9	C—C str. + CH_2 and CH def.
904	0.2	2	904	0.47	5.2	
			918	0.32	3.5	
932	0.64	6.9	933	0.35	3.7	
969	0.4	4	968	0.2	2	
970 (R)	0.31	3.2				
989 (R)	0.3	3	990 (R)	0.6	6	
1044	0.60	5.7	1045	0.58	5.6	
1072	0.2	2	1071	0.1	1	
1105	0.8	7	1105	0.5	5	
1183	1	11	1184	0.38	3.2	
1268	0.44	3.4	1268	0.47	3.7	
			1295	0.3	2	
1318	0.29	2.2	1316	0.23	1.7	
			1322	0.5	4	
1353	0.37	2.8	1354	0.26	1.9	
1366	0.40	2.9	1366	0.38	2.8	
1373	0.56	4.1	1373	0.48	3.5	
2857	1	4	2857	0.2	0.7	methylene C—H str.
			2891	0.3	1	methine C—H str.

[a]All peaks are from the IR spectrum, except for those marked with an R.

Can. J. Chem. Downloaded from www.nrcresearchpress.com by 123.30.183.119 on 09/07/12
For personal use only.

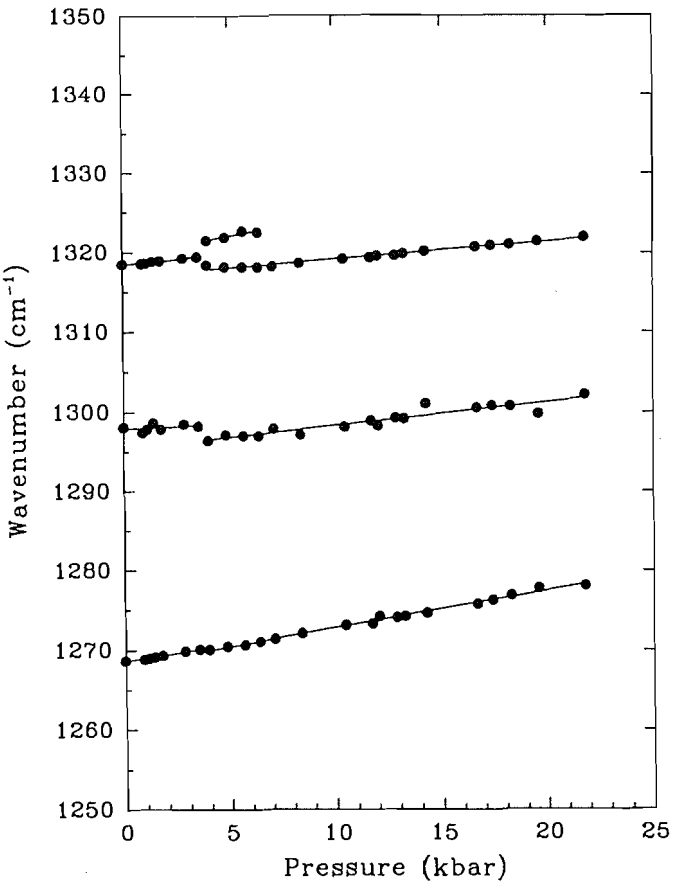


FIG. 7. Pressure dependences of selected IR bands of 1-fluoroadamantane.

even as high as 59 kbar, did not induce any other phase transitions. It is concluded, therefore, that the glassy phase also forms upon compression, and will not spontaneously crystallize even under very high pressure.

High-pressure IR experiments were performed, but at smaller pressure increments and over a narrower range of pressures. Figure 5 shows the C—H stretching region of the IR spectrum at various pressures. Although the line-narrowing effect is not as obvious as in the Raman spectra, the phase I → phase II transition can be observed between 2.8 and 3.9 kbar. The IR experiments were also used to measure the spectral changes that occur to the peak at 1318 cm^{-1}, which is a combination of C—C stretching and various C—C—H and CH_2 bending modes. In Fig. 6(A), the splitting of this peak into two due to sudden line narrowing is observed between 2.8 and 3.9 kbar, which is analogous to the effect that occurred upon lowering the temperature (Fig. 6(B)), and offers further proof of the occurrence of the phase transition at 3.3 ± 1.0 kbar. In another attempt to induce the second phase transition, the sample was left under 22 kbar of pressure for a period of 36 h, and then left at 18 kbar for an additional 36 h. From our experience, these pressures correspond roughly to cooling the sample at 20 K and then around 80 K, respectively. As in the low-temperature experiments, a crystalline phase of fluoroadamantane did not form.

The pressure dependences of several modes were measured in both the IR and Raman spectra. Since more points were obtained in the IR spectra at moderate pressures, the dv/dp values were measured from the IR rather than the Raman spectra whenever possible. Figure 7 shows the pressure dependences of selected peaks in the IR spectrum, and Table 2 lists the pressure dependences of all the vibrational bands measured. Overall, the dln ν/dp values of both phases are quite high, which is consistent with the disordered nature of phases I and II. The pressure dependences of several Raman bands of adamantane itself have been reported (28), and these dln ν/dp values are also very high, ranging from −0.5 to 14×10^{-4} $kbar^{-1}$ for the skeletal modes, and from 1.1 to 3.2×10^{-4} $kbar^{-1}$ for the C—H stretching vibrations. The totally symmetric, cage-breathing vibration in adamantane, occurring at 759 cm^{-1}, has the highest pressure dependence of 14×10^{-4} $kbar^{-1}$. These pressure dependences can be compared to the dln ν/dp values for the 773 cm^{-1} peak of fluoroadamantane (9.2×10^{-4} and 7.0×10^{-4} $kbar^{-1}$ in phases I and II, respectively). The disordered phases of these adamantanes belong to the same space group, *Fm3m*, $Z = 4$, where $a = 9.445$ Å for adamantane (29), and $a = 9.53$ Å for fluoroadamantane (7). From these unit cell dimensions, the densities of these solids are calculated to be 1.07 and 1.18 g cm^{-3}, respectively. It is reasonable, therefore, that the pressure dependence of the cage-breathing mode of fluoroadamantane has a lower value compared to that in adamantane, because its crystal density is higher, and its lattice should be less compressible.

Upon examination of the pressure dependences within the fluoroadamantane molecule, those of the 729 and 773 cm^{-1} peaks are particularly high. This is expected since these bands have been assigned in the variable-temperature section as the symmetric C—F and C—C stretching modes, respectively, and stretching vibrations generally have higher pressure dependences than bending motions (30, 31). The C—C stretching mode has a higher pressure dependence compared to the C—F stretch in both phases I and II; the C—F bond length in fluoroadamantane was reported to be 1.370 ± 0.004 Å by microwave spectroscopy (32), and the C—F stretching force constant is typically 6.0×10^{-5} dyn cm^{-1} (33). Thus, the higher force constant causes the C—F bond to be less compressible, and the pressure dependence is slightly lower than that of C—C vibrations, even though the former also has a shorter bond length. The peaks at 814, 904, and 1045 cm^{-1} also have relatively large pressure dependences, and these bands can therefore be assigned to modes that also have significant contributions from skeletal stretching vibrations. The peaks that have very low dln ν/dp values are largely deformation modes, i.e., those at 1316 and 1354 cm^{-1} are CH_2 twisting or wagging vibrations. Although the C—H stretching region could not be fully explored, due to the extensive overlap of these peaks, the two bands that were measured suggest that their pressure dependences are relatively low, compared with, for example, the data obtained for the smaller cage molecules norbornadiene (30) and norbornylene (31). This can be attributed to the absence of ring strain in the fluoroadamantane molecule.

Conclusion

The phase behaviour of 1-fluoroadamantane has been explored by DSC, and by vibrational spectroscopy at low temperatures and at elevated pressures. The phase transition which occurs under pressure is the same as that which occurs upon lowering the temperature. Below the phase transition temperature, or above the corresponding transition pressure, the formation of a glassy-crystalline phase was observed. This behaviour is similar to that of cyanoadamantane, and it sets 1-

Can. J. Chem. Downloaded from www.nrcresearchpress.com by 123.30.183.119 on 09/07/12
For personal use only.

fluoroadamantane apart from the other halo derivatives. It is interesting to note that, upon changing the halogen substituent from F to Cl to Br to I, the number of ordered and disordered phases also changes. This trend may be due to differences in dipole moment, size of the substituent, or other molecular properties. This substituent effect may be further expanded by considering the halo-adamantanes substituted at the 2-position. In this case, the bromo derivative exhibits one phase transition, whereas the chloro derivative undergoes two solid–solid transitions (17). No investigations of the solid-state phase behaviour of either 2-fluoro or 2-iodoadamantane have been reported up to the present time.

Acknowledgements

This research was supported by grants from NSERC (Canada) and FCAR (Quebec). N.T.K. also acknowledges the award of a postgraduate scholarship from NSERC.

1. N. G. PARSONAGE and L. A. K. STAVELEY. Disorder in crystals. Clarendon Press, Oxford. 1978.
2. J. TIMMERMANS. J. Chim. Phys. **35**, 25 (1938).
3. J. N. SHERWOOD (*Editor*). The plastically crystalline state (orientationally disordered crystals). Wiley–Interscience, Chichester. 1979.
4. T. CLARK, T. MC. O. KKNOX, H. MACKLE, and M. A. MCKERVEY. J. Chem. Soc. Faraday Trans. 1, **73**, 1224 (1977).
5. M. FOULON and C. GORS. Acta Crystallogr. Sect. B: Struct. Sci. **B44**, 156 (1988).
6. M. FOULON, J. P. AMOUREUX, J. L. SAUVAJOL, J. LEFEBVRE, and M. DESCAMPS. J. Phys. C: Solid State Phys. **16**, L265 (1983).
7. J. P. AMOUREUX, M. BEE, and J. L. SAUVAJOL. Acta Crystallogr. Sect. B: Struct. Crystallogr. Cryst. Chem. **B38**, 1984 (1982).
8. J. P. AMOUREUX, R. DECRESSAIN, and M. CASTELAIN. *In* Dynamics of molecular crystals. Studies in physical and theoretical chemistry. Vol. 46. *Edited by* J. Lascombe. Elsevier Science Publishers B.V., Amsterdam. 1987. p. 559.
9. M. BEE and J. P. AMOUREUX. Mol. Phys. **50**, 585 (1983).
10. J. P. AMOUREUX, M. CASTELAIN, M. BEE, M. D. BENADDA, and M. MORE. Mol. Phys. **55**, 241 (1985).
11. Y. GUINET, J. L. SAUVAJOL, and M. MULLER. Mol. Phys. **65**, 723 (1988).
12. M. BEE and J. P. AMOUREUX. Mol. Phys. **48**, 63 (1983).
13. C. E. NORDMAN and D. L. SCHMITKONS. Acta Crystallogr. **18**, 764 (1965).
14. J. DONOHUE and S. H. GOODMAN. Acta Crystallogr. **22**, 352 (1967).
15. H. SZWARC. Thermochim. Acta, **109**, 91 (1986).
16. T. J. BROXTON, L. W. DEADY, M. KENDALL, and R. D. TOPSOM. Appl. Spectrosc. **25**, 600 (1971).
17. R. M. PAROLI. Ph.D. Thesis, McGill University, Montreal, Quebec, Canada. 1988.
18. R. M. PAROLI, N. T. KAWAI, I. S. BUTLER, and D. F. R. GILSON. Can. J. Chem. **66**, 1973 (1988).
19. Y. HUANG, D. F. R. GILSON, I. S. BUTLER, and F. A. MORIN. J. Phys. Chem. **95**, 2151 (1991).
20. G. J. PIERMARINI, S. BLOCK, J. D. BARNETT, and R. A. FORMAN. J. Appl. Phys. **46**, 2774 (1975).
21. D. D. KLUG and E. WHALLEY. Rev. Sci. Instrum. **54**, 1205 (1983).
22. R. G. SNYDER and J. H. SCHACHTSCHNEIDER. Spectrochim. Acta, **21**, 169 (1965).
23. R. T. BAILEY. Spectrochim. Acta, **27A**, 1447 (1971).
24. F. L. DOLLISH, W. G. FATELEY, and F. F. BENTLEY. Characteristic Raman frequencies of organic compounds. Wiley–Interscience, New York. 1974. p. 23.
25. E. C. TUAZON, W. G. FATELEY, and F. F. BENTLEY. Appl. Spectrosc. **25**, 374 (1971).
26. W. HUTTNER and W. ZEIL. Spectrochim. Acta, **22**, 1007 (1966).
27. P. D. HARVEY, I. S. BUTLER, D. F. R. GILSON, and P. T. T. WONG. J. Phys. Chem. **90**, 4546 (1986).
28. G. BURNS, F. H. DACOL, and B. WELBER. Solid State Commun. **32**, 151 (1979).
29. J. P. AMOUREUX, M. BEE, and J. C. DAMIEN. Acta Crystallogr. Sect. B: Struct. Crystallogr. Cryst. Chem. **B36**, 2633 (1980).
30. N. T. KAWAI, D. F. R. GILSON, and I. S. BUTLER. J. Phys. Chem. **94**, 5729 (1990).
31. N. T. KAWAI, I. S. BUTLER, and D. F. R. GILSON. J. Phys. Chem. **95**, 634 (1991).
32. D. CHADWICK, A. C. LEGON, and D. J. MILLEN. J. Chem. Soc. A, 1116 (1968).
33. G. HERZBERG. Molecular spectra and molecular structure. Vol. II. Infrared and Raman spectra of polyatomic molecules. D. Van Nostrand Company, Princeton, NJ. 1945. p. 193.

Can. J. Chem. Downloaded from www.nrcresearchpress.com by 123.30.183.119 on 09/07/12
For personal use only.

A Raman spectral study of solvation and ion association in the systems $LiAsF_6/CH_3CO_2CH_3$ and $LiAsF_6/HCO_2CH_3$

ZHONGYI DENG AND DONALD E. IRISH

Guelph–Waterloo Centre for Graduate Work in Chemistry, Department of Chemistry, University of Waterloo, Waterloo, Ont., Canada N2L 3G1

Received April 19, 1991

This paper is dedicated to Dr. Richard Norman Jones

ZHONGYI DENG and DONALD E. IRISH. Can. J. Chem. **69**, 1766 (1991).

The structure of the solvated lithium cation in methyl acetate (MA) solutions has been investigated using Raman spectroscopy. Two bands at 844 and 864 cm^{-1} have been assigned to two different types of MA: the former is from the bulk solvent and the latter arises from MA molecules solvating the lithium cation. From measurement of changes in intensity of these bands with increasing salt concentration a solvation number of four for Li^+ in MA has been inferred. Changes in the Raman bands at ca. 1740 cm^{-1} suggest that solvation occurs through the carbonyl group. Evidence for contact ion pairing between Li^+ and AsF_6^- is also presented. An equilibrium between solvent-shared ion pairs and contact ion pairs is proposed for which an equilibrium constant is estimated. The system $LiAsF_6$/methyl formate (MF) is similar in structure.

Key words: Raman, ion pair formation, lithium and hexafluoroarsenate ions, methyl acetate and formate, lithium ion solvation.

ZHONGYI DENG et DONALD E. IRISH. Can. J. Chem. **69**, 1766 (1991).

Faisant appel à la spectroscopie Raman, on a étudié la structure du cation de lithium solvaté dans des solutions d'acétate de méthyle (AM). On a attribué les deux bandes observées à 844 et à 864 cm^{-1} à deux types différents d'AM; la première est attribuée à la masse de la solution alors que la deuxième est attribuée à l'AM solvaté par le cation lithium. En se basant sur des mesures de changement dans l'intensité de ces bandes avec une augmentation de la concentration du sel, on peut déduire que le nombre de solvatation du Li^+ dans l'AM est égal à quatre. Des changements dans les bandes Raman aux environ de 1700 cm^{-1} suggèrent que la solvatation se produit par le biais du groupe carbonyle. On présente aussi des données suggérant l'existence de paires d'ions de contact entre le Li^+ et le AsF_6^-. On suggère qu'il existe un équilibre entre les paires d'ions partagées par le solvant et les paires d'ions de contact; on en a évalué la constante d'équilibre. La structure du système $LiAsF_6$/formiate de méthyle (FM) est semblable.

Mots clés : Raman, formation des paires d'ions, ions de lithium et hexafluoroarsénate, acétate et formiate de méthyle, solvatation du ion de lithium.

[Traduit par la rédaction]

Introduction

The search for new electrolyte–solvent systems capable of providing improved performance of both primary and secondary lithium cells and batteries is ongoing. Aprotic solvents, such as ethers, esters, amides carbonates, nitriles, and dimethyl sulfoxide, either alone or mixed, have received extensive study (1). Effort has been focused on overcoming the inferior conductivity of the electrolyte, relative to aqueous systems. Recently methyl formate (MF) and methyl acetate (MA) were identified as possible solvents (2–5). Conductance measurements (3–5) and, for MA/$LiAsF_6$ and MA/$LiClO_4$, microwave relaxation spectroscopy and some infrared spectra (5) have been reported. Solutions of MA have a surprisingly high conductance over a wide temperature range. Despite evidence for ion pairing, strong ion–solvent interactions were also suggested in these studies.

Raman spectroscopy has proved to be a powerful technique for probing ion–ion and ion–solvent interactions. Recently Hyodo and Okabayashi studied local structure in $LiClO_4$/EC (ethylene carbonate) and mixed solvent systems (6). We have reported Li^+ solvation in CH_3CN solutions, and adsorption of the species at silver electrode surfaces (7). In anticipation of surface Raman studies of the electrode systems Ag/MA, $LiAsF_6$ and Li/MA, $LiAsF_6$, the present investigation was undertaken to gain knowledge of the solvation number of Li^+ in MA (and MF), the extent of ion pair formation, and the spectral changes that could be expected because of such phenomena. $LiAsF_6$ has been regarded favourably as an electrolyte salt because of its high conductivity and apparent stability towards lithium (8). We chose $LiAsF_6$ for this study because of the previous work done with $LiAsF_6$/MA (5). Future work will focus on the new class of imide and methide salts (9).

Experimental

Reagents and solution preparation

The following chemicals were used without further purification: lithium hexafluoroarsenate ($LiAsF_6$) electrochemical grade (Lithco, Lithium Corp. of America); methyl acetate (MA) and methyl formate (MF) anhydrous, 99+% (Aldrich Chemical Co.); 18-crown-6, 99% (Aldrich Chemical Co.). Solutions were prepared by weight and concentrations are expressed as moles per kilogram of solvent. The lithium salt was slowly added to the solvent in a dry-box with an argon atmosphere.

Raman spectra

All Raman spectra were recorded using a Jarrell–Ash 25-100 1.0-m Czerny–Turner monochromator equipped with a model 129 digital cosecant stepping drive, an RCA 31034 selected photomultiplier tube, and an SSR model 1104/1120 photon-counting system. This spectrometer operates under microcomputer control. Data can be transmitted to a DEC PRO 380 microcomputer, interfaced to a VAX 11/785. On this system programs for baseline correction and spectral bandfitting are available; the program used is an adaptation of the one developed by Pitha and Jones (10) and subsequently modified by Murphy and Bernstein (11).

Results and discussion

Raman spectra of pure MA and $LiAsF_6$/MA

The Raman spectrum of pure methyl acetate in the 150–1850 cm^{-1} range is presented in Fig. 1(a). The observed Raman frequencies and assignments are given in Table 1. The Raman

Can. J. Chem. Downloaded from www.nrcresearchpress.com by 84.41.108.74 on 09/07/12
For personal use only.

TABLE 1. The fundamental frequencies for methyl acetate, observed Raman frequencies, and assignments

Symmetry	Mode	Approximate description	$\nu_{calc.}$[a]	$\nu_{obs.}$	Assignment[b]
a'	ν_1	CH_3O asym. stretch	3027	3028	ν_1
	ν_2	CH_3C asym. stretch	2985		
	ν_3	CH_3O sym. stretch	2972	2953	ν_3 or ν_{19}
	ν_4	CH_3C sym. stretch	2907	2942	ν_4
				2847	$2\nu_8 = 2870$
				2722	$\nu_5 + \nu_{13} = 2722$
	ν_5	C=O stretch	1747	1740	ν_5
	ν_6	CH_3O asym. bend	1520		
	ν_7	CH_3O sym. bend	1487		
	ν_8	CH_3 asym. bend	1435		
	ν_9	CH_3 sym. bend	1382	1372	ν_9
	ν_{10}	C—O stretch	1259	1252	ν_{10}
	ν_{11}	CH_3O rock	1158	1159	ν_{11}
	ν_{12}	H_3C—O stretch	1039	1046	ν_{12}
	ν_{13}	CH_3C rock	975	979	ν_{13}
	ν_{14}	H_3C—C stretch	858	844	ν_{14}
	ν_{15}	O—C—O bend	639	640	ν_{15}
	ν_{16}	CCO bend	440	434	ν_{16}
	ν_{17}	C—O—C bend	303	305	ν_{17}
a''	ν_{18}	CH_3O asym. stretch	3023	3002	ν_{18}
	ν_{19}	CH_3C asym. stretch	2983		
	ν_{20}	CH_3O asym. bend	1487	1447	ν_{20}
	ν_{21}	CH_3C asym. bend	1487		
	ν_{22}	CH_3O rock	1127	1188	ν_{22}
	ν_{23}	CH_3C rock	1063		
	ν_{24}	CH_3—CO_2 out-of-plane bend	628	610	ν_{24}
	ν_{25}	COC out-of-plane bend	215		
	ν_{26}	C—CH_3 torsion	124		
	ν_{27}	O—CH_3 torsion	120		

[a]From refs. 12 and 19.
[b]From refs. 13 and 14.

Can. J. Chem. Downloaded from www.nrcresearchpress.com by 84.41.108.74 on 09/07/12
For personal use only.

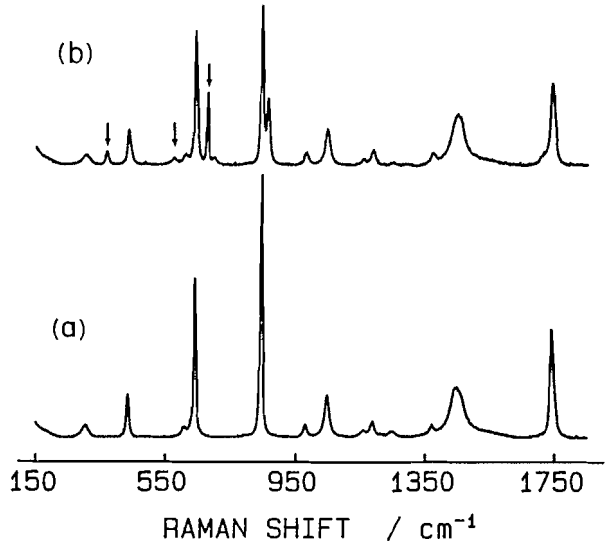


FIG. 1. Raman spectra of (a) pure MA and (b) 1 *m* $LiAsF_6$/MA in the 150–1850 cm^{-1} region. Arrows designate bands of AsF_6^-. Here and hereafter the vertical axis indicates the intensity in arbitrary units unless otherwise specified.

spectrum of 1 *m* $LiAsF_6$/MA is shown in Fig. 1(b). Raman bands of AsF_6^- are marked by arrows. The Raman bands of methyl acetate show little change of frequency or shape on addition of $LiAsF_6$, except for Raman bands at ca. 844 cm^{-1} and at ca. 1740 cm^{-1}. The Raman band at 844 cm^{-1} has been assigned to the C—C symmetric stretching mode (12, 13). A second band at 864 cm^{-1} increases in intensity as the concentration of solute increases. The Raman band at about 1740 cm^{-1} has been assigned to the C=O stretching vibration (12–14). A shoulder at 1720 cm^{-1} also increases with the increase of concentration of solute.

The AsF_6^- anion has octahedral symmetry (O_h) and thus its 15 normal modes of vibration span the representation:

$$\Gamma = A_{1g} + E_g + 2F_{1u} + F_{2g} + F_{2u}$$

Of these $\nu_1(A_{1g})$, $\nu_2(E_g)$, and $\nu_5(F_{2g})$ are Raman active, $\nu_3(F_{1u})$ and $\nu_4(F_{1u})$ are infrared active, and the F_{2u} mode is inactive. The Raman and infrared spectra of AsF_6^- in polycrystalline $CsAsF_6$ have been reported (15). Raman bands at 685, 576, and 372 cm^{-1} have been assigned to ν_1, ν_2, and ν_5, respectively. Infrared bands at 699 and 392 cm^{-1} were assigned to ν_3 and ν_4, respectively. The ν_6 band position was estimated as 322 cm^{-1} (15); it has been observed at 252 cm^{-1} for $O_2^+AsF_6^-$ (16), in which the O_h symmetry is lowered to T_h.

In MA the Raman bands of AsF_6^- occur at 676, 572, and 366 cm^{-1}. A shoulder at about 696 cm^{-1} can be seen in Fig. 1(b). Farber *et al.* (17) attributed this weak band to the Raman forbidden ν_3 mode, made active by perturbations from the solvent.

Inoue *et al.* (18) have studied the ν_3 infrared band region of $LiAsF_6$ in several organic solvents. They observed three bands in this region. A band at 702 cm^{-1} was assigned to the "spectroscopically free" AsF_6^-, including solvent-separated ion pairs $Li^+SAsF_6^-$ (and possibly dimers). A band at 717 cm^{-1} was

Can. J. Chem. Downloaded from www.nrcresearchpress.com by 84.41.108.74 on 09/07/12
For personal use only.

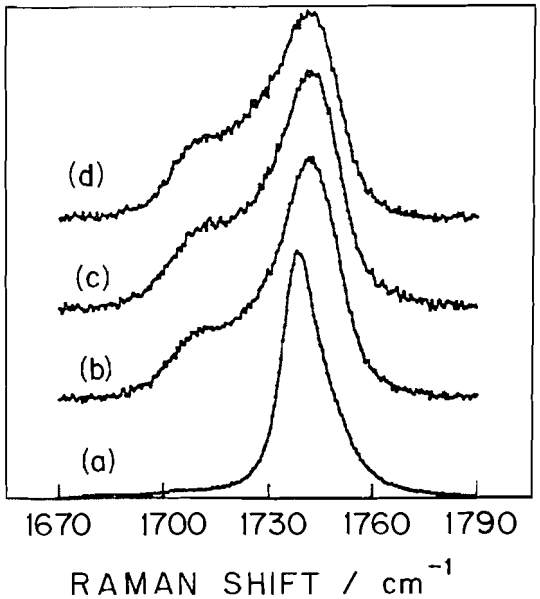


FIG. 2. The dependence on the concentration of $LiAsF_6$ of the Raman intensity in the C=O stretching region, 1670–1790 cm^{-1}. Concentrations are (a) 0; (b) 1.5; (c) 2.8; (d) 4.1 *m* respectively.

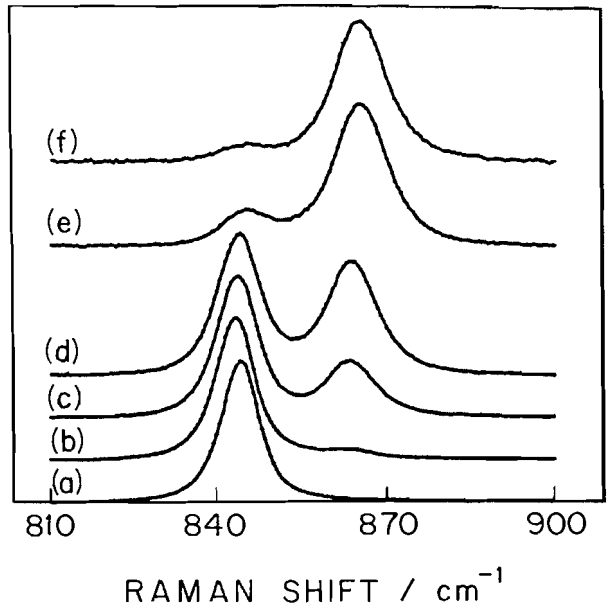


FIG. 3. The dependence on the concentration of $LiAsF_6$ of the Raman intensity in the H_3C—C stretching region, 810–900 cm^{-1}. Concentrations are (a) 0; (b) 0.2; (c) 1.0; (d) 1.5; (e) 2.8; (f) 4.1 *m* respectively.

assigned to a contact ion pair $Li^+AsF_6^-$, and the 676 cm^{-1} band was assigned to a combination $\nu_5 + \nu_6$.

We shall discuss the new features in the spectra in detail.

The C=O stretching mode spectral region of methyl acetate

Three new bands occur in addition to the Raman-active bands of methyl acetate and lithium hexafluoroarsenate in Fig. 1(b). First we discuss the shoulder (1720 cm^{-1}) of the C=O stretching vibration mode of methyl acetate ($\nu_5 \cong 1740$ cm^{-1}). Figure 2 illustrates how the Raman spectra in the C=O stretching vibration region of MA change as the concentration of $LiAsF_6$ increases. Figure 2(a) is the spectrum of pure MA; Figs. 2(b), (c), and (d) are the spectra of 1.5 *m*, 2.8 *m*, and 4.1 *m* $LiAsF_6$/MA, respectively. The band of pure MA is asymmetrical on the high-wavenumber side of the peak maximum but otherwise it has a simple contour. For the electrolyte solution there is obviously a new band at ca. 1720 cm^{-1}, which increases in intensity when the concentration of $LiAsF_6$ increases. These bands suggest that two kinds of methyl acetate coexist in the electrolyte solution. One kind, from the bulk solvent, described as "free", generates the 1740 cm^{-1} band. The other kind solvates the lithium cation and gives the 1720 cm^{-1} band. The lithium cation probably binds through the carbonyl functional group of methyl acetate, because the C=O stretching vibration has been very strongly affected by solvating with lithium cation. None of the other vibrational modes, except the C—C stretching vibration (to be discussed below) of methyl acetate, was significantly affected by the solvation.

The C—C stretching mode spectral region of methyl acetate

Raman spectra in the 810–900 cm^{-1} region of methyl acetate (a) and $LiAsF_6$/MA solutions ((b)–(f)) are presented in Fig. 3. As the concentration of $LiAsF_6$ increases from 0.2 to 4.1 *m*, a new band at 864 cm^{-1} increases in intensity at the expense of the 844 cm^{-1} band.

The ratio of the intensity of the Raman band at 864 cm^{-1} (I_{864}) to the intensity of the Raman band at 844 cm^{-1}, ν_{14} of methyl acetate (I_{844}), I_{864}/I_{844}, changes from 0.059 for 0.2 *m* to 12.19 for 4.1 *m* $LiAsF_6$. The relative intensities of these two bands depend

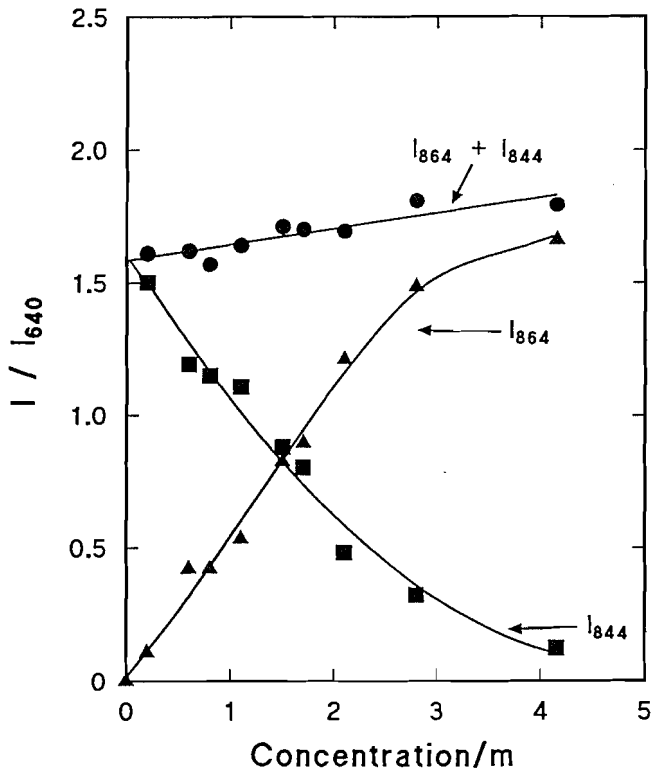


FIG. 4. Relative integrated intensities of the 844 and 864 cm^{-1} bands and their sum versus the concentration of $LiAsF_6$.

on the concentrations of the solutions, but the total combined intensity of these two bands ($I_{864} + I_{844}$) is almost constant, as shown in Fig. 4. The band at 844 cm^{-1} is assigned to the C—C stretching vibration of "free" methyl acetate and the band at 864 cm^{-1} is assigned to the C—C stretching vibration of the species solvating the lithium cations. It may be significant that the 864 cm^{-1} band has a larger full width at half-peak maximum (FWHM) than the 844 cm^{-1} band. The difference diminishes

from about 3.7 cm^{-1} for 0.2 *m* solution to about 0.8 cm^{-1} for 4.1 *m* solution. The larger FWHM for the band from MA molecules in the lithium ion solvation sphere suggests a shorter lifetime for MA in the solvation shell of Li^+; such lability is expected for a solvent complex. The enhanced FWHM decreases as the amount of bulk solvent decreases.

In the discussion above, the ν_{14} mode has been described as C—C stretch, in accordance with an early assignment by Wilmshurst (13). The normal coordinate analysis of Matzke *et al.* (19) suggests that this is a mixed mode with 39.5% H_3C—C stretch, 24.3% C—O stretch, 16.7% O—C—O bend, and 11.5% C=O stretch. In a later report by George *et al.* (14) the ν_{14} mode is assigned to the CH_3—O stretch. In recent publications dealing with metal ion – acetate ion complexing (20, 21) we have observed that the C—C stretch of acetate ion is sensitive to the addition of a cation; it shifts from 926 cm^{-1} to 939 cm^{-1} on binding to Mg^{2+}, Pb^{2+}, or Zn^{2+}. The present shift for the ester–lithium interaction is somewhat comparable. In the absence of more extensive normal coordinate calculations we shall continue to designate ν_{14} as a C—C stretch but recognise the probability that there can be a significant contribution from the C—O stretch in the normal mode. Probably in solution and particularly when binding to a cation the ester would adopt the *cis* conformation.

The addition of crown ethers

Crown ethers and cryptands are good macrocyclic ligands for alkali-metal cations (22–24). It has also been reported that charge transport of a lithium salt in a solid electrolyte is enhanced by addition of crown ethers (25, 26). It is interesting to observe the effect of adding a crown ether or cryptand to the present system. In view of the cavity size of the macrocyclic ligands, the most suitable for sequestering the lithium ion should be 12-crown-4 and Kryptofix 211. Unfortunately, white precipitates formed when these were added to concentrated $LiAsF_6$/MA solutions. A precipitate also formed when 15-crown-5 was added to the system. Surprisingly, no precipitate formed when 18-crown-6 was added to the system, even at a concentration equal to half of the concentration of $LiAsF_6$.

The effect of addition of 18-crown-6 is illustrated in Fig. 5 and Table 2. Figures 5(a), (b), and (c) show Raman spectra of 2 *m* $LiAsF_6$/MA, 2 *m* $LiAsF_6$/MA + 1 *m* 18-crown-6, and 1.1 *m* $LiAsF_6$/MA, respectively. It is clear that the intensity of the C—C stretching vibrational mode, 844 cm^{-1}, is lower than that of the solvation band, 864 cm^{-1}, for 2 *m* $LiAsF_6$/MA. The reverse is true for 2 *m* $LiAsF_6$/MA + 1 *m* 18-crown-6. The ratio of the intensities of the two bands I_{844}/I_{864} in 2 *m* LiAsF6 + 1 *m* 18-crown-6 is almost the same as that in 1.1 *m* $LiAsF_6$/MA (Fig. 5 and Table 2). Also note that the intensity of the new band at 696 cm^{-1} in Fig. 5(b) is much lower than the intensity in 5(a). I_{696} in the former system is almost the same as that in 1.1 *m* $LiAsF_6$/MA. The intensity data are listed in Table 2.

The interpretation of these results is as follows. One molecule of 18-crown-6 sequesters one lithium cation, thus lowering the concentration of $Li^+(CH_3CO_2CH_3)_x$ and so reducing the intensity of the 864 cm^{-1} band to that of a 1.1 *m* solution. Thus the observation supports the assignment of the 864 cm^{-1} band to molecules in the first solvation sphere of Li^+. The observation of diminished intensity of the 696 cm^{-1} band will be dealt with below.

The determination of the solvation number of lithium cation

To calculate the concentrations of the free methyl acetate and the complexed species from the measured Raman intensities of different salt concentrations, an intensity standard is required. An internal standard should ideally be sufficiently soluble in the solvent, should not have Raman bands that interfere with the bands being measured, and should not compete by complexation. We found the band of methyl acetate (solvent of the system) at 640 cm^{-1} (the O—C—O bend) to be satisfactory. It retained a single, symmetrical band profile on addition of the salt to MA and its integrated intensity appears to be a faithful measure of the total MA concentration.

One band that was studied at 696 cm^{-1} is quite weak when the concentration of $LiAsF_6$ is less than 1 *m*. To measure its intensity it was desirable to have an internal standard with comparable intensity; thus the 610 cm^{-1} band (the CH_3—CO_2 out-of-plane bend) was chosen. The ratio of the intensities I_{610} to I_{640} was found to be essentially constant over the concentration range 0.2–2.8 *m* $LiAsF_6$; the value was 0.0596 ± 0.0058. Thus both of these bands can serve as standards to obtain relative integrated intensities.

In Fig. 4 the relative intensities I_{844}/I_{640}, I_{864}/I_{640}, and $I_{total}/I_{640} = (I_{864} + I_{844})/I_{640}$ are plotted versus the concentration of $LiAsF_6$. The intensity of the band at 864 cm^{-1} increases and the intensity of the band at 844 cm^{-1} decreases as the concentration of salt increases. The total intensity, $(I_{864} + I_{844})/I_{640}$, remains almost constant over a quite wide concentration range. The increase of the intensity of the 864 cm^{-1} band with increasing concentration

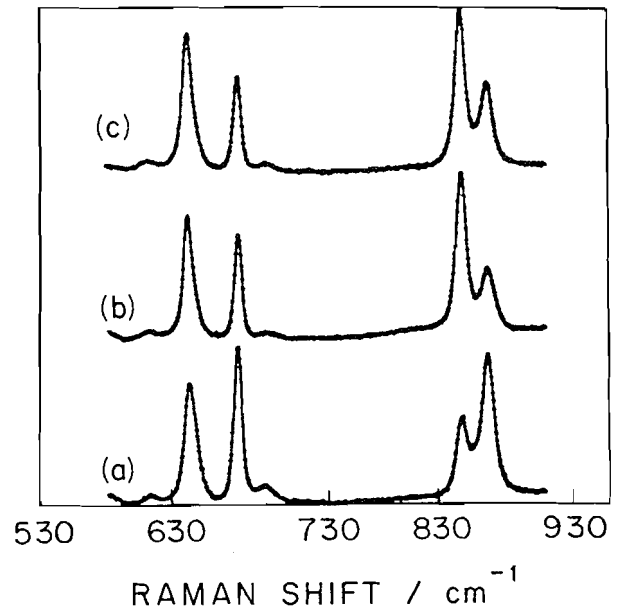


FIG. 5. Raman spectra of (a) 2 *m* $LiAsF_6$/MA; (b) 2 *m* $LiAsF_6$/MA + 1 *m* 18-crown-6, and (c) 1.1 *m* $LiAsF_6$/MA in the 590–900 cm^{-1} region.

TABLE 2. Raman intensity ratios for the system of $LiAsF_6$/MA with and without 18-crown-6

System	I_{676}/I_{640}	I_{696}/I_{640}	I_{844}/I_{640}	I_{864}/I_{640}
2.0 *m* $LiAsF_6$/MA	0.81	0.256	0.628	1.21
2.0 *m* $LiAsF_6$/MA +1.0 *m* 18-crown-6	0.53	0.063	1.21	0.52
1.06 *m* $LiAsF_6$/MA	0.44	0.058	1.06	0.67
1.5 *m* $LiAsF_6$/MA	0.53	0.081	0.085	0.77
1.5 *m* $LiAsF_6$/MA +0.5 *m* 18-crown-6	0.48	0.052	1.19	0.56

Can. J. Chem. Downloaded from www.nrcresearchpress.com by 84.41.108.74 on 09/07/12
For personal use only.

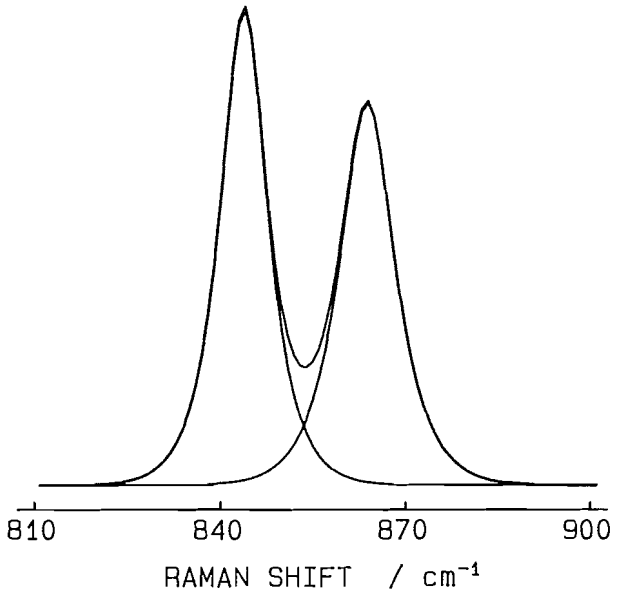


FIG. 6. The application of BNDFT to the spectrum of 1.5 *m* $LiAsF_6$/MA in the 810–900 cm^{-1} region.

of lithium cations is consistent with the assignment of the band to molecules in the primary solvation sphere of Li^+. The decrease in the intensity of the 844 cm^{-1} band is consistent with the assignment to the "free" methyl acetate molecules. The greater the concentration of lithium cations, the less is the amount of free methyl acetate left in the system. This fact supports the assignment of the two bands to the two different classes of solvent, viz., bulk (or free) and solvating.

Figure 6 illustrates the result of applying the BNDFT program to the spectrum of 1.5 *m* $LiAsF_6$/MA solution.

We designate the relative integrated intensity of the free species as I_f and its concentration as C_f; similarly for the bound species we define I_b and C_b. Assuming proportionality between intensity and concentration we can write

$$[1] \quad I_f = J_f C_f$$

and

$$[2] \quad I_b = J_b C_b$$

where J_f and J_b are the molar scattering coefficients for the two species.

Material balance requires that

$$[3] \quad C_{MA} = C_f + C_b$$

The total intensity is given by

$$[4] \quad I_T = I_b + I_f = J_b C_b + J_f C_f$$

If the molar scattering coefficients of the 864 and the 844 cm^{-1} bands are equal, and are set equal to J, then eq. [4] becomes

$$[5] \quad I_T = J(C_b + C_f) = JC_{MA}$$

On a molality scale of concentration, C_{MA} is constant and thus I_T should be independent of the concentration of salt. As Fig. 4 illustrates, this is not quite true; the slope of I_T vs. C_{Li} is not quite zero. There is indication that J_b may be somewhat larger than J_f.

Equation [4] can be rearranged to give

$$[6] \quad I_T = (J_b - J_f)C_b + J_f C_{MA}$$
$$= (1 - J_f/J_b)I_b + J_f C_{MA}$$

TABLE 3. Composition, relative integrated intensities, and solvation numbers of lithium

$LiAsF_6$/mol kg^{-1}	I_b	I_T	C_b/mol kg^{-1}	$\bar{n}_s$
4.1	1.551	1.678	12	2.8
2.8	1.485	1.808	11	3.9
2.2	1.333	1.866	9.8	4.5
1.7	0.8962	1.700	6.6	3.9
1.5	0.8264	1.708	6.1	4.1
1.3	0.7198	1.719	5.3	4.1
1.1	0.5854	1.645	4.3	3.9
0.79	0.4424	1.644	3.3	4.1
0.64	0.4227	1.616	3.1	4.9
0.18	0.1064	1.608	0.79	4.4

A plot of I_T versus I_b should be linear with a slope of $(1 - J_f/J_b)$ and an intercept of $J_f C_{MA}$, where C_{MA} is known and constant. The data give the equation

$$[7] \quad I_T = 0.129\, I_b + 1.59$$

with a correlation coefficient of 0.755. Thus $J_f = 0.118$ and $J_b = 0.135$, where $C_{MA} = 13.5$ mol kg^{-1}.

The solvation number of the lithium cation, equivalent to the average ligand number of lithium, $\bar{n}_s$, is defined as

$$[8] \quad \bar{n}_s = C_b/C_{Li} = I_b/(C_{Li}J_b)$$

This value is tabulated in Table 3 for each concentration of $LiAsF_6$. A solvation number of four for the lithium cation is suggested. This value is commonly found for the lithium cation in ionic crystals (27, 28) and aqueous solutions (29), and it has also been reported for solutions of $LiClO_4$ in ethylene carbonate (6). The lower values at higher salt concentrations are attributed to some ion pairing between Li^+ and AsF_6^-. At concentrations of salt greater than 3.4 *m* there is insufficient solvent to allow for a complete solvation sphere of four molecules of MA and thus some ion pairing and solvent-shell distortion must occur. Other evidence for ion pairing is presented below.

Raman spectral evidence for contact ion pairing in $LiAsF_6$/MA

Shown in Fig. 7 are Raman spectra of five concentrations of $LiAsF_6$/MA solutions in the 580–720 cm^{-1} region. The band with a maximum at ca. 610 cm^{-1} is ν_{24}, the $H_3C—O_2$ out-of-plane bending vibration mode of MA, a very weak band. The band with a maximum at 640 cm^{-1} is ν_{15}, the O—C—O bending mode of MA, which has been chosen as an internal standard as discussed above. The two bands at 676 and 696 cm^{-1} originate from the AsF_6^- ion. In this spectral region the infrared spectrum contains three bands at 717, 703, and 677 cm^{-1} (5). The assignments must rationalize both the Raman and infrared spectra. The Raman band at 676 cm^{-1} corresponds closely to the ν_1 (A_{1g}) mode of AsF_6^- (Table 4). For a 2.5 *m* aqueous solution of $LiAsF_6$ we observe this band at 682 cm^{-1}. Ion pairs are unlikely in aqueous solution and thus it is reasonable, based solely on spectroscopy, to assign this band to the "free" anion. However, from microwave dielectric relaxation and electrical conductivity measurements Salomon *et al.* (5) concluded that virtually no free ions exist in $LiAsF_6$/MA solutions, because of the low permittivity (6.67); solvent-separated ion pairs and possibly dimers, referred to as "spectroscopically free" because their vibrational signals are essentially indistinguishable from those of free ions, and contact ion pairs were proposed (5). Thus we will assign the 676 cm^{-1} Raman band to the ν_1 (A_{1g}) mode of solvent-shared ion

Can. J. Chem. Downloaded from www.nrcresearchpress.com by 84.41.108.74 on 09/07/12
For personal use only.

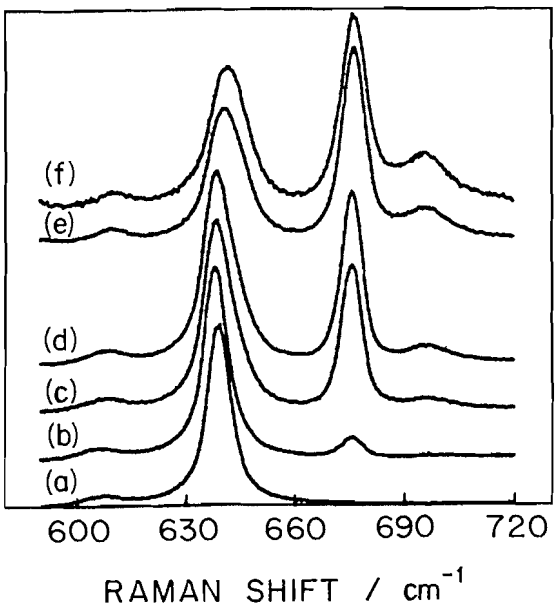


FIG. 7. Raman spectra of $LiAsF_6$/MA solutions in the region 580–720 cm^{-1}. Concentrations are (a) 0; (b) 0.2; (c) 1.0; (d) 1.5; (e) 2.8; (f) 4.1 *m* $LiAsF_6$.

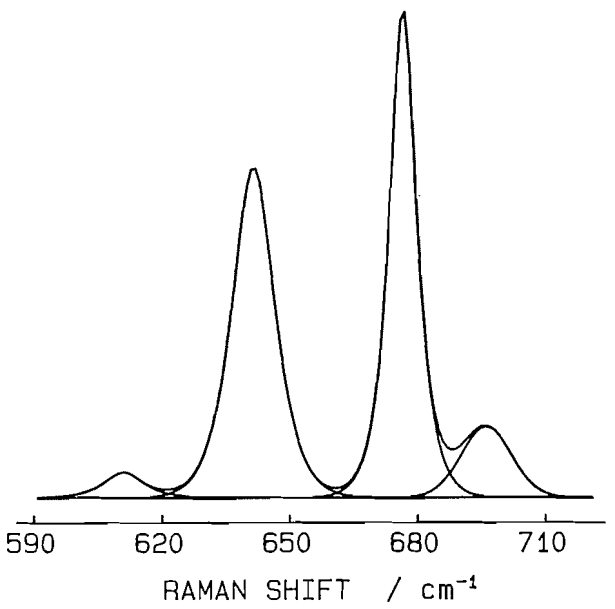


FIG. 8. The application of BNDFT to the spectrum of 2.8 *m* $LiAsF_6$/MA in the 590–720 cm^{-1} region.

TABLE 4. Raman bands of AsF_6^-

	$\nu_1(A_{1g})$	$\nu_2(E_g)$	$\nu_5(F_{2g})$	
$CsAsF_6$ (solid)[a]	685	576	372	
$O_2^+AsF_6^-$ (solid)[b]	689	573	375	
$KAsF_6$ (solid)[c]	679	565	372	
$KAsF_6$/MeCN[d]	676	574	372	
$LiAsF_6$/MF[e]	678	—	344	
$LiAsF_6$/MF[f]	675(m)	572(w)	365(w)	696 (ion pair)
$LiAsF_6$/MF[f]	676(m)	572(w)	366(w)	696 (ion pair)

[a]From ref. 15.
[b]From ref. 16.
[c]From ref. 32.
[d]From ref. 33.
[e]From ref. 30.
[f]Present work.

pairs. The 703 cm^{-1} infrared band is assigned to the ν_3 (F_{1u}) mode of the same species.

The 696 cm^{-1} Raman band is assigned to the ν_1 (A_{1g}) mode (under O_h symmetry and selection rules) of a contact ion pair. This band increases in intensity relative to the 676 cm^{-1} band as the concentration of $LiAsF_6$ increases. Shown in Fig. 8 is a typical example of the result of bandfitting the 580–720 cm^{-1} region for 2.8 *m* $LiAsF_6$/MA. The relationship between the intensity of the 676 cm^{-1} band and the 696 cm^{-1} band is illustrated in Fig. 9. The corresponding F_{1u} mode of the ion pair must be the 717 cm^{-1} infrared band. Its intensity increases with salt concentration in a manner analogous to the intensity of the 696 cm^{-1} Raman band, although it was only studied in dilute solutions (5). There is no trace of this band in the Raman spectrum, and it is forbidden by selection rules.

The remaining band to be assigned is the 676 cm^{-1} infrared band. Salomon *et al.* (5) assigned this band to the ($\nu_5 + \nu_6$) combination ($F_{2g} \times F_{2u} = A_{1u} + E_u + F_{1u} + F_{2u}$; active in infrared, inactive in Raman). We place the ν_5 (F_{2g}) mode at 366 cm^{-1}. Thus the forbidden F_{2u} mode would occur at ca. 311 cm^{-1}. This position is consistent with the estimate of Begun and Rutenberg

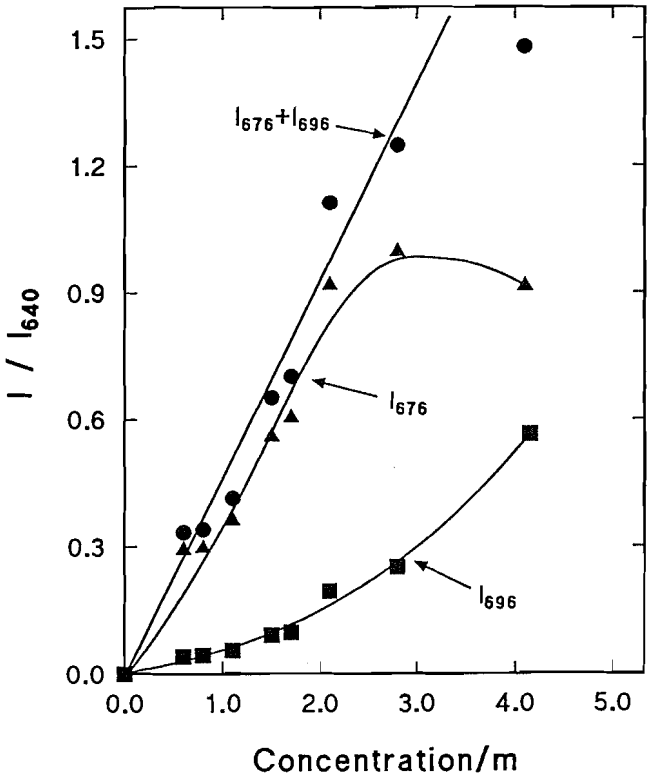


FIG. 9. Concentration versus the relative integrated intensities, I_{676}/I_{640} (▲) of the ν_1 band of the AsF_6^-, I_{696}/I_{640} (■) of the 696 cm^{-1} band attributed to the contact ion pair, and $(I_{676} + I_{696})/I_{640}$ (●).

(15). Because it is forbidden in the Raman spectrum and because combinations have weak Raman intensity, no contribution from this combination is expected under the intense 676 cm^{-1} Raman band. The assignments are summarized in Table 5.

Further evidence that the 696 cm^{-1} band originates from a contact ion pair is presented in Fig. 5 and Table 2. For a MA solution containing $LiAsF_6$ (2 *m*) and 18-crown-6 (1 *m*) the intensity of the 696 cm^{-1} band decreased markedly. Thus when

Can. J. Chem. Downloaded from www.nrcresearchpress.com by 84.41.108.74 on 09/07/12
For personal use only.

TABLE 5. Assignments of bands of AsF_6^- in methyl acetate

Spectroscopically free	Assignment[a]	Contact ion pair
—	ν_6 (F_{2u}) ia	—
366 (w)[b]	ν_5 (F_{2g}) R	*
ns	ν_4(F_{1u}) IR	ns
572 (w)[b]	ν_2 (E_g) R	*
677 (w)[c]	$\nu_5 + \nu_6$ IR	
676 (s)[b]	ν_1 (A_{1g}) R	696 (m)[b]
703 (s)[c]	ν_3 (F_{1u}) IR	717 (s)[c]

[a]ia: inactive; w: weak; s: strong; m: medium; ns: not studied; *: too weak to be detected.
[b]Present work.
[c]From ref. 5.

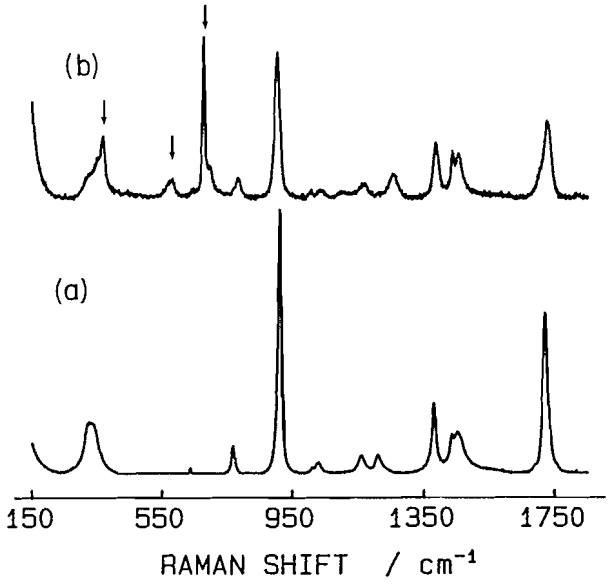


FIG. 10. Raman spectra of (a) pure MF and (b) 4.4 *m* $LiAsF_6$/MF in the 250–1800 cm^{-1} region. Arrows designate bands of AsF_6^-.

lithium is made unavailable such that ion pairing is diminished, the band intensity is diminished; the conclusion is that the band arises from ion pairing. An equilibrium of the following type is proposed:

[9] $Li(MA)_4^+AsF_6^- = Li(MA)_3^+AsF_6^- + MA$

Inoue *et al.* (18) have reported infrared spectra for $LiAsF_6$ in several organic solvents: acetone, 1,2-dimethoxyethane, tetrahydrofuran, 2-methyltetrahydrofuran, and dimethyl carbonate. In all cases three infrared bands were observed for AsF_6^-, and their assignments are as described above. The intensity of the 717 cm^{-1} band was found to be dependent on the permittivity of the solvent and the concentration. It was very weak in the case of acetone, a result also confirmed by our Raman measurements. Acetone has a permittivity of 20.7 compared to values of less than 7 for the other solvents. Thus the evidence for contact ion pairs in solvents of low permittivity from both Raman and infrared spectra is strong, despite the fact that experience has shown that the perturbations of the highly symmetrical anions (with T_d or O_h symmetry) by ion association are rarely sufficient to alter the symmetric vibrations significantly.

An estimate of the value of the equilibrium constant for process [9] can be arrived at from the intensity data in Fig. 9 if the following assumptions are made: the molar scattering factor of the 676 cm^{-1} band is equal to that of the 696 cm^{-1} band (this is probably true within 10% if the mode of vibration is the same and only the environment has changed); the concentration of free MA is given by

[10] $C_{MA} = C_{MA(TOTAL)} - 4(C_{MA,ssip}) - 3(C_{MA,cip})$

Here ssip refers to solvent-shared ion pair and cip refers to contact ion pair. The concentration quotient for process [9] is then

[11] $K = C_{cip}C_{MA}/C_{ssip}$

where the mole fraction of the contact ion pair is $X_{cip} = I_{696}/(I_{696} + I_{676})$ and $C_{cip} = X_{cip}C_{salt}$. The value of K is 1.2 ± 0.3 over the concentration range 0.64–2.8 *m* (average of seven values). In an independent experiment using reagents that were not dried, a value of K equal to 1.1 ± 0.2 was obtained over the concentration range 0.86–2.5 *m* (average of nine points). Thus a value of 1.2 ± 0.3 at ca. 25°C is within the present accuracy for the given model.

Extensions to the methyl formate (MF)/$LiAsF_6$ system

Methyl formate has also been identified as a possible battery electrolyte, despite its limited liquid range (mp −99°C; bp 34°C). Spectra of 4.4 *m* and 1.0 *m* solutions of MF/$LiAsF_6$ were measured for comparison with those of methyl acetate. Shown in Fig. 10 are spectra of pure MF and the 4.4 *m* $LiAsF_6$ solution in the 150–1850 cm^{-1} range. Three Raman-active bands of the AsF_6^- ion were observed (Table 4), contrary to the report of Venkatasetty (30) who observed only the ν_1 and ν_5 bands at 678 and 344 cm^{-1} respectively. In addition, the 696 cm^{-1} band, attributed to the ion pair, is clearly visible as a shoulder on the 675 cm^{-1} band.

The Raman band at 1718 cm^{-1}, assigned to the ν_4 C=O stretching vibration of MF (31), develops a distinct shoulder on the low-frequency side when $LiAsF_6$ is present (Fig. 10). This shoulder can be attributed to those MF molecules which are solvating the lithium cation, by analogy to the MA case. Because of the weakness of this shoulder, quantitative study was not undertaken.

Summary

From Raman spectra of $LiAsF_6$ in MA, a solvation number of four for the lithium cation has been inferred. Bonding through the carbonyl group is suggested. As the concentration of salt increases, the concentration of a contact ion pair also increases. An equilibrium between solvent-shared ion pairs and contact ion pairs is proposed. The equilibrium constant has been estimated as 1.2 ± 0.3 at 25°C. Spectral comparisons suggest that similar chemistry occurs in $LiAsF_6$/MF solutions.

Acknowledgements

This work was supported by grants from the Natural Sciences and Engineering Research Council of Canada and the Office of Naval Research (U.S.A.). D.E.I. also expresses his appreciation to Dr. Norman Jones for his advice, encouragement, and friendship over many years.

1. M. SALOMON. J. Power Sources, **26**, 9 (1989).
2. E. PLICHTA, M. SALOMON, S. SLANE, M. UCHIYAMA, D. CHUA, W. B. EBNER, and H. W. LIN. J. Power Sources, **21**, 25 (1987).
3. E. PLICHTA, M. SALOMON, S. SLANE, and M. UCHIYAMA. J. Solution Chem. **16**, 225 (1987).

Can. J. Chem. Downloaded from www.nrcresearchpress.com by 84.41.108.74 on 09/07/12
For personal use only.

4. M. SALOMON, S. SLANE, E. PLICHTA, and M. UCHIYAMA. J. Solution Chem. **18**, 977 (1989).
5. M. SALOMON, M. UCHIYAMA, M. XU, and S. PETRUCCI. J. Phys. Chem. **93**, 4374 (1989).
6. S. HYODO and K. OKABAYASHI. Electrochim. Acta, **34**, 1551 (1989); **34**, 1557 (1989).
7. D. E. IRISH, I. R. HILL, P. ARCHAMBAULT, and G. F. ATKINSON. J. Solution Chem. **14**, 221 (1985).
8. V. R. KOCH. J. Electrochem. Soc. **126**, 181 (1979).
9. L. A. DOMINEY. Fifth International Seminar on Lithium Battery Technology and Applications, March 4–6, 1991, Deerfield Beach, Florida.
10. J. PITHA and R. N. JONES. Can. J. Chem. **44**, 3031 (1966); **45**, 2347 (1967); Optimization methods for fitting curves to infrared band envelopes. NRC Bulletin No. 12, National Research Council of Canada, Ottawa, 1968.
11. W. F. MURPHY and H. J. BERNSTEIN. J. Phys. Chem. **76**, 1147 (1972).
12. E. M. POPOV, G. A. KOGAN, M. I. STRUCHKOVA, and V. N. ZHELTOVA. J. Struct. Chem. USSR, **12**, 61 (1971).
13. J. K. WILMSHURST. J. Mol. Spectrosc. **1**, 201 (1957).
14. W. O. GEORGE, T. E. HOUSTON, and W. C. HARRIS. Spectrochim. Acta, **30A**, 1035 (1974).
15. G. M. BEGUN and A. C. RUTENBERG. Inorg. Chem. **6**, 2212 (1967).
16. C. NAULIN and R. BOUGON. J. Chem. Phys. **64**, 4155, (1976).
17. H. FARBER, D. E. IRISH, and S. PETRUCCI. J. Phys. Chem. **87**, 3515 (1983).
18. N. INOUE, M. XU, and S. PETRUCCI. J. Phys. Chem. **91**, 4628 (1987).
19. P. MATZKE, O. CHACON, and C. ANDRADE. J. Mol. Struct. **9**, 255 (1971).
20. M. M. YANG, D. A. CRERAR, and D. E. IRISH. Geochim. Cosmochim. Acta, **53**, 319 (1989).
21. J. SEMMLER, D. E. IRISH, and T. OZEKI. Geochim. Cosmochim. Acta, **54**, 947 (1990).
22. Y. INOUE and G. W. GOKEL (*Editors*). Cation binding by macrocycles: complexation of cationic species by crown ethers. Marcel Dekker, New York. 1990.
23. A. J. SMETANA and A. I. POPOV. J. Solution Chem. **9**, 183 (1980).
24. K. OZUTSUMI, M. NATSUHARA, and H. OHTAKI. Bull. Chem. Soc. Jpn. **62**, 2807 (1989).
25. M. L. KAPLAN, E. A. RIETMAN, R. J. CAVA, L. K. HOLT, and E. A. CHANDROSS. Solid State Ionics, **25**, 37 (1987).
26. D. P. COBRANCHI, G. R. PHILLIPS, D. E. JOHNSON, R. M. BARTON, D. J. ROSE, E. M. EYRING, L. J. RODRIGUEZ, and S. PETRUCCI. J. Phys. Chem. **93**, 1396 (1989).
27. R. D. SHANNON and C. T. PREWITT. Acta Crystallogr. Sect. B: Struct. Crystallogr. Cryst. Chem. **B25**, 925 (1969).
28. R. D. SHANNON. Acta Crystallogr. Sect. A: Cryst. Phys. Diffr. Theor. Gen. Crystallogr. **A32**, 751 (1976).
29. J. C. HINDMAN. J. Chem. Phys. **36**, 1000, (1962).
30. H. V. VENKATASETTY. J. Electrochem. Soc. **122**, 245 (1975).
31. W. C. HARRIS, D. A. COE, and W. O. GEORGE. Spectrochim. Acta, **32A**, 1 (1976).
32. J. WEIDLEIN and K. DEHNICKE. Z. Anorg. Chem. **337**, 113 (1965).
33. J. A. EVANS and D. A. LONG. J. Chem. Soc. A: **5**, 1688 (1968).

Can. J. Chem. Downloaded from www.nrcresearchpress.com by 84.41.108.74 on 09/07/12
For personal use only.

The polymorphism of alkali metal formates. Part 4. A Raman study of the phase transition in KHCOO

A. M. HEYNS
Department of Chemistry, University of Pretoria, 0002 Pretoria, South Africa
AND
K.-J. RANGE AND K. MÜLLER
Institute of Inorganic Chemistry, University of Regensburg, D8400 Regensburg, Germany

Received April 23, 1991

This paper is dedicated to Dr. Richard Norman Jones

A. M. HEYNS, K.-J. RANGE, and K. MÜLLER. Can. J. Chem. **69**, 1774 (1991).

KHCOO II is orthorhombic at ambient conditions and it is shown that traces of moisture affect the polymorphism of these very hygroscopic crystals. Dry KHCOO II transforms into phase I at 417 K (144°C), and this phase can be supercooled to room temperature, remaining metastable for several days before transforming back to the orthorhombic phase II. The Raman spectra of phases I and II, as well as of supercooled phase I, are reported in the present study. The absence of some prominent translational modes in the Raman spectra of KHCOO II, compared to NaHCOO II, can be explained on the basis of a group-theoretical treatment. From the temperature dependence of the linewidths of various Raman-active librational and internal modes, activation energies are obtained for intramolecular motions of the formate ions. Fermi resonance occurs between the overtone of the bending mode $2\nu_5$ and the C—H stretching mode ν_1 in KHCOO II and the coupling constant W increases with temperature. The Raman and X-ray data show that KHCOO I is structurally different from NaCHOO I, but it is not possible to assign a definite structure to this phase on the basis of a Raman spectrum alone.

Key words: Potassium formate, phase transition, Raman spectra.

A. M. HEYNS, K.-J. RANGE et K. MÜLLER. Can. J. Chem. **69**, 1774 (1991).

À la température ambiante, le KHCOO II est orthorhombique; on a montré que des traces d'humidité affectent le polymorphisme de ces cristaux très hygroscopiques. À 417 K (144°C), le KHCOO II sec se transforme en phase I que l'on peut surgeler jusqu'à la température ambiante; il peut être maintenu dans cette forme métastable pendant plusieurs jours avant sa retransformation en phase II orthorhombique. Dans ce travail, on a mesuré les spectres Raman des phases I et II ainsi que de la phase surgelée. Pour expliquer l'absence de modes translationnels remarquables dans le spectre Raman de la phase II du KHCOO, par comparaison avec celui de la phase II du NaHCOO, on fait appel à un traitement théorique des groupes. Sur la base de la relation entre la température et les largeurs de bande des divers modes librationnels et internes actifs en spectroscopie Raman, on a déterminé les énergies d'activation des mouvements intramoléculaires des ions formiates. Dans le KHCOO II, il se produit de la résonance de Fermi entre l'harmonique du mode de vibration angulaire $2\nu_5$ et le mode d'élongation C—H ν_1; la constante de couplage W augmente avec la température. Les spectres Raman et les données de la diffraction des rayons-X démontrent que le KHCOO I est structurellement différent du NaHCOO I; il n'est toutefois pas possible d'attribuer un structure définie à cette phase uniquement sur la base d'un spectre Raman.

Mots clés : formiate de potassium, transition de phase, spectre Raman.

[Traduit par la rédaction]

Introduction

The polymorphism of NaHCOO (1–3), $LiHCOO \cdot H_2O$, and LiHCOO (4) has been investigated in our laboratories and it was found that these alkali metal formates exhibit complex behaviour as far as the variety of phases and their crystal structures are concerned. NaHCOO, in particular, undergoes a series of phase transitions upon the application of pressure (1) as well as upon heating to 500 K (227°C) at ambient pressures (2). Upon cooling the high-temperature phase I of NaHCOO, an intermediate phase is obtained that can be supercooled to room temperature, requiring an induction period of several days before transforming back to phase II, the modification stable at ambient conditions (3).

KHCOO has not been studied so thoroughly. It is known to be orthorhombic, belonging to the space group $Cmcm$ (D_{2h}^{16}) (5, 6). It undergoes a first-order phase transition at 418 K (145°C) with $\Delta H_{tr} = 0.1$ kcal mol^{-1} and $\Delta S_{tr} = 0.4$ cal mol^{-1} K^{-1} and melts at 441 K (168°C) (7). The Raman spectra of KHCOO have been reported at ambient temperatures (1); however, in the present paper we report the temperature dependence of its Raman spectra and these results are supplemented by DTA/DTG and X-ray powder diffraction measurements of the changes that occur at the phase transition and melting point temperatures during heating and cooling cycles.

Experimental

KHCOO has been prepared according to the equation:

$$2HCOOH + K_2CO_3 \rightarrow 2KHCOO + CO_2 + H_2O$$

Accordingly, formic acid was added to K_2CO_3 and the product formed was filtered off. The KHCOO so obtained was handled in a glove-box under an argon atmosphere. The crystals were heated at 423 K to remove the excess of formic acid. The product was then recrystallized from methanol and long, transparent needles were obtained. These crystals were dried under vacuum and kept in a desiccator under dry P_2O_5.

The Raman spectra were recorded on a Dilor Z-24 spectrometer using the 514.5-nm line of Coherent Innova-5 Ar^+-laser to excite the spectra. The samples of KHCOO were sealed in glass capillary tubes and were then placed in a heating oven obtained from Dilor Industries, Lille, France, for Raman measurements at ambient and higher temperatures. The resolution of the Raman bands quoted in this study is approximately 2 cm^{-1}.

Powder diffraction patterns at variable temperatures have been obtained on an Enraf–Nonius Delft Guinier–Simon camera, model FR 553. For these measurements the KHCOO samples were sealed in

Printed in Canada / Imprimé au Canada

Can. J. Chem. Downloaded from www.nrcresearchpress.com by 84.41.108.74 on 09/07/12
For personal use only.

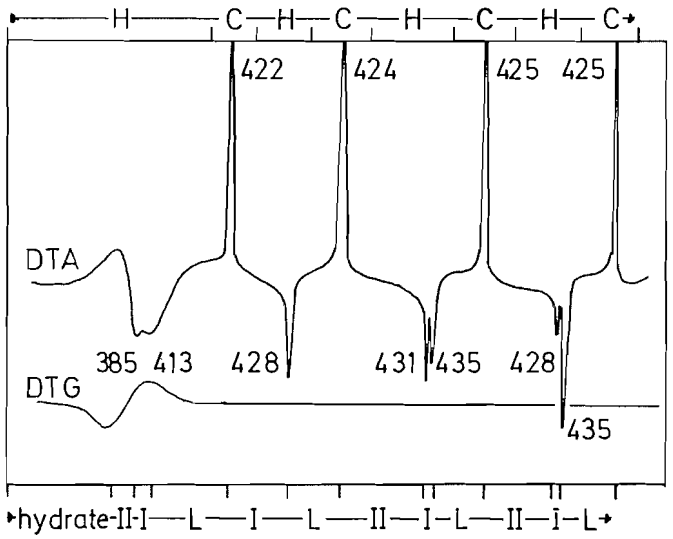


FIG. 1. DTA/DTG recordings of a KHCOO sample that has absorbed moisture during the sample preparation. The heating (H) and cooling (C) cycles are indicated at the top of the figure. At the bottom the two phases (I and II), and the liquid (L) are shown.

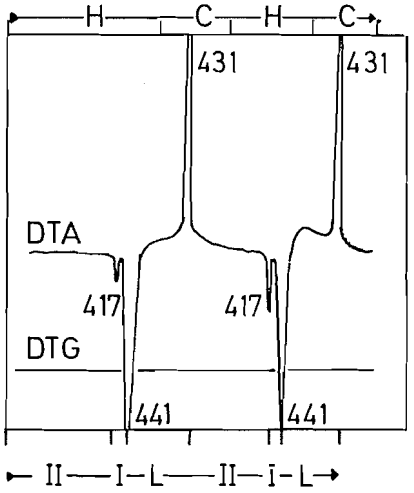


FIG. 2. DTA/DTG recordings of a dry sample of KHCOO. The heating (H) and cooling (C) cycles are indicated, as well as the temperature stability regions of phases I and II and those of the melt (L).

Lindemann tubes. A heating or cooling rate of 3 K min^{-1} was used in these experiments.

The DTA-TG recordings were made on a thermogravimetric-differential thermal analyser obtained from Rigaku, model 8076 D1. Great care had to be exercised to prevent the absorption of any moisture by the very hygroscopic KHCOO crystals, and the samples were thus sealed from the atmosphere after the containers and sampling area had been thoroughly dried and kept under a dry argon atmosphere. The heating and cooling rate in these experiments was approximately 10 K min^{-1}.

Results

The polymorphism of KHCOO

The influence of traces of moisture on the polymorphism of KHCOO is shown in Fig. 1. Upon heating a sample that was exposed to the atmosphere for a very short time, a mass loss, starting at 346 K (73°C) was observed. This can be attributed to the loss of water. Two peaks are further evident at 385 K (112°C) and 413 K (140°C), the latter being the melting point and the former the phase transition temperature in KHCOO. Upon cooling, the melt solidifies at 422 K and, upon heating, the solid melts at 428 K. When the melt is cooled down once again, the freezing point shifts to 424 K and a new heating cycle shows two peaks at 431 and 435 K respectively. They once again represent the phase transition and the melting points respectively.

However, upon using a thoroughly dried sample of KHCOO and taking the necessary precautions to exclude moisture during the experiments, the results shown in Fig. 2 are obtained. The phase transition occurs at 144°C (417 K), agreeing very well with the temperature of 145°C (418 K) reported elsewhere (7). The melting point occurs at 168° (441 K). As is evident in Fig. 2, these temperatures could be reproduced, within experimental error, in subsequent measurements.

Powder diffraction patterns that were obtained of KHCOO at various temperatures indicate that, from 300 K up to approximately 415 K, the spectrum obtained is of the room temperature phase only. Then, until the solid melts at 441 K, the lines of the high-temperature modification (phase I) are obtained. After the melt has been kept at a temperature of ca. 448 K for approximately 1 h, freezing occurs at 432 K and the spectrum of the room temperature phase is obtained upon further cooling. However, when the samples are heated to temperatures just below that of the melting point, KHCOO I is obtained and, upon cooling, the high-temperature phase I remains metastable, even at room temperature for several days, before it transforms into the room temperature phase II. When the supercooled phase I at room temperature was heated again to the melting point, only the room temperature phase II of KHCOO was obtained upon cooling. It must also be noted that heating to its melting point does not always ensure the formation of phase II upon solidification; in some cases the high-temperature modification was observed in this process as well.

To summarize, the high-temperature modification of KHCOO (phase I) can be supercooled, sometimes from the melt, and this metastable phase then takes up to 5 days before it is transformed completely to the room temperature phase II. The powder diffraction patterns that were obtained of KHCOO I could be indexed by means of the programmes GUIN and VISSER and indicate a possible monoclinic crystal system for this phase with $a = 10.145(7)$, $b = 12.781(5)$, and $c = 7.581(3)$ Å and $\beta = 103.893(2)°$. However, exact structural details of this phase can only be obtained from a single-crystal X-ray diffraction analysis.

Vibrational selection rules and Raman spectra (Phase II)

The different fundamental vibrations of the formate ion are as follows: $\nu_1(A_1)$, the symmetric C—H stretching mode, occurs at 2750–2850 cm^{-1}, $\nu_2(A_1)$, the symmetrical C—O stretching mode, occurs at 1380–1410 cm^{-1}, $\nu_3(A_1)$, the symmetric O—C—O bending mode, occurs at 750–800 cm^{-1}; ν_4, the asymmetric C—O stretching mode, occurs at 1530–1600 cm^{-1}; $\nu_5(B_1)$, the in-plane C—H bending mode, is usually observed between 1330 and 1380 cm^{-1}; and ν_6, the out-of plane bending mode, occurs at 1050–1080 cm^{-1} (1). Under *Cmcm* (D_{2h}^{17}) symmetry, the formate groups are located on the sites of C_{2v} symmetry and the following splitting of fundamental modes can be expected, viz. $\nu_1(A_1)$, $\nu_2(A_1)$, and $\nu_3(A_1)$ under C_{2v} will split into $A_g(R) + B_{2u}(ir)$ mode under D_{2h}; $\nu_4(B_1)$ and $\nu_5(B_1)$ will split into $B_{3g}(R) + B_{1u}(ir)$; and, finally, $\nu_6(B_2)$ will split into $B_{1g}(R) + B_{3u}(ir)$ components. In other words, each fundamental vibrational mode will split into a Raman- and an infrared-active component. The vibrational spectra of KHCOO are summarized in Table 1. (It should be noted that the correct

Can. J. Chem. Downloaded from www.nrcresearchpress.com by 84.41.108.74 on 09/07/12
For personal use only.

Can. J. Chem. Downloaded from www.nrcresearchpress.com by 84.41.108.74 on 09/07/12
For personal use only.

TABLE 1. The vibrational spectra of KHCOO at various temperatures

KHCOO II 25°C			KHCOO I 150°C	KHCOO I 25°C	
IR,[a] cm^{-1}	Raman, cm^{-1}	Assignment	Raman, cm^{-1}	Raman, cm^{-1}	Assignment
2808	2809	ν_1-B_{2u} + A_g	2807	2870	ν_1
			2783	2784	ν_1
			—	2753	$2\nu_5$
2730	—		—	2274	$2\nu_5$
	2713		2714	2716	$2\nu_5$
	—		2695	2697	$2\nu_5$
			1391	1396	ν_5
			1382	1387	ν_5
1389	1366	ν_5-B_{1u} + B_{3g}	1368	1369	ν_5
			1360	1360	ν_2
			1348	1348	ν_2
1357	1345	ν_2-B_{2u} + A_g	1346	1346	ν_2
1062	1070	ν_6-B_{3u} + B_{1g}			
			768	760	ν_3
772	759	ν_3-B_{2u} + A_g	758	758	ν_3
			753	750	ν_3
—	206	ν_{R_x}	~190	201	ν_{R_x}
—	—		—	~198sh	ν_{R_x}
—	156sh	ν_T	—	~158sh	ν_{R_y}
—	—		—	~141sh	ν_{R_y}
—	131sh	ν_{R_y}	—	—	ν_{R_y}
—	125	ν_{R_z}	125	125	ν_{R_z}
—	~100sh		92sh	93sh	ν_T
—	—		72	70	ν_T
—	—		38	39	ν_T

[a]Reference 6.

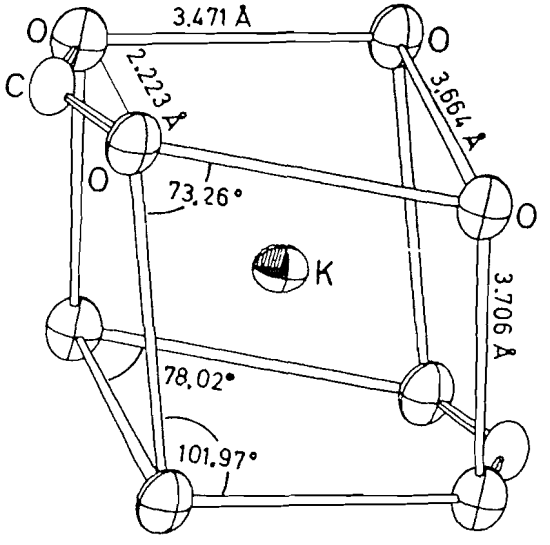


FIG. 3. The eightfold coordination of the K^+ ion in KHCOO. The orientation of the two formate ions with respect to the crystal axes is also clearly shown.

correlation between the C_{2v} site group and the D_{2h} factor is obtained by choosing the $C_{2(y)}$ axis to correlate C_{2v} with D_{2h} under *Cmcm* symmetry. Our results therefore differ from those of Mentzen and Oddon (6) who used a different correlation.) The K^+ ion is eightfold coordinated to oxygen atoms as shown in Fig. 3, and this polyhedron is of C_{2h} symmetry (6). Under this symmetry, the A_u and $2B_u$ translational modes of the K^+ ions split into $A_u(—)$ + $B_{3u}(ir)$ + $2B_{1u}(ir)$ + $2B_{2u}(ir)$ modes. The

TABLE 2. The symmetry operators (R/t) of *Cmcm* (D_{2h}^{17}) and their effect on the K and C atoms in KCHOO[a]

R/t	(R/t)K	(R/t)C
$\{E/000\}$	(1)→(1); (2)→(2)	(1)→(1); (2)→(2)
$\{C_{2x}/000\}$	(1)→(1); (2)→(2)	(1)→(2)
$\{C_{2y}/00½\}$	(1)→(2)	(1)→(1); (2)→(2)
$\{C_{2z}/00½\}$	(1)→(2)	(1)→(2)
$\{i/000\}$	(1)→(1); (2)→(2)	(1)→(2)
$\{\sigma_h/00½\}$	(1)→(2)	(1)→(1); (2)→(2)
$\{\sigma_v(xz)/00½\}$	(1)→(2)	(1)→(2)
$\{\sigma_v(yz)/000\}$	(1)→(1); (2)→(2)	(1)→(1); (2)→(2)

[a](1)→(1) shows that atom 1 is transformed into itself and (1)→(2) that atom 1 is transformed into atom 2.

A_1, B_1, and B_2 translational modes of the $HCOO^-$ groups under C_{2v} symmetry split into $A_g(R)$ + $B_{2u}(ir)$ + $B_{3g}(R)$ + $B_{1u}(ir)$ + $B_{1g}(R)$ + $B_{3u}(ir)$ modes under D_{2h}. Subtracting the acoustic modes B_{1u} + B_{2u} + B_{3u}, the following translational modes are predicted for KHCOO, viz. $\Gamma_{transl} = A_g(R) + B_{1g}(R) + B_{3g}(R) + A_u(-) + 2B_{1u}(ir) + 2B_{2u}(ir) + B_{3u}(ir)$.

The symmetry operators (R/t) of *Cmcm* and their effect on the K and C atoms in KHCOO are shown in Table 2.

Using the information in Table 2, schematic representations of the translatory lattice modes can be made as is shown in Fig. 4 (the acoustic modes are not included in this figure). It can be noted that no modes involving motions of the K^+ ions are Raman active in KHCOO and that the Raman-active translatory vibrations therefore involve motions of the $HCOO^-$ groups only. "Molecular" translational modes, the term used by Maas

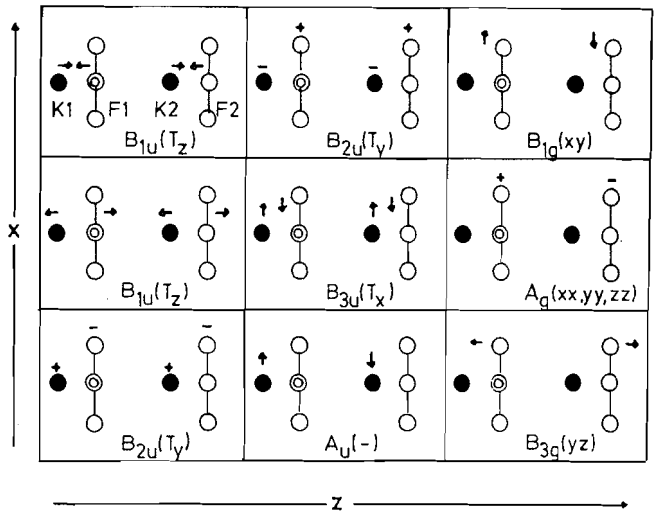


FIG. 4. A schematic representation of the translatory lattice modes in KHCOO in the $x-z$ plane. K1,F1 and K2,F2 denote the potassium and formate ions 1 and 2 respectively.

(8, 9) to describe motions in which the Na^+ and $HCOO^-$ groups of one molecule in NaHCOO move in the same direction, while the second molecule moves in an opposite direction, are not allowed in KHCOO.

In addition to the above-mentioned lattice modes, the $A_2 + B_1 + B_2$ rotational modes of the $HCOO^-$ groups under C_{2v} site group symmetry in KHCOO will split into $B_{1g}(R) + B_{2g}(R) + B_{3g}(R) + A_u(-) + B_{1u}(ir) + B_{2u}(ir)$ components under D_{2h} symmetry.

As far as the internal formate vibrations are concerned, the infrared and Raman bands of KHCOO are in agreement with the group-theoretical predictions. Each fundamental mode is split into a Raman- and an infrared-active component. These bands are summarized in Table 1. The assignment of the bands is rather obvious and has been discussed elsewhere in detail for the Raman-active modes (1).

The low-frequency Raman spectrum of KHCOO II is shown in Fig. 5 at various temperatures. At ambient conditions, the bands at 206, 131 (shoulder), and 125 cm^{-1} can be assigned to the $R_x(B_{3g})$, $R_y(B_{2g})$, and $R_z(B_{1g})$ rotational modes, by analogy to NaHCOO II (9). These bands closely resemble their counterparts in NaHCOO II, as far as their frequencies, bandshapes, and relative intensities are concerned. The sequence of frequencies of the rotational bands is in agreement with the magnitude of the moments of inertia of the formate ion, which vary in the order of $I_x << I_y \simeq I_z$. A weak shoulder at 156 cm^{-1} and a very weak feature at ~100 cm^{-1} once again resemble bands that have been observed in NaHCOO II (1, 8, 9). These features can be assigned to translational modes involving the formate groups.

The major difference between the Raman spectra of KHCOO II and NaHCOO II is the absence of the most intense Raman band at ~75 cm^{-1} in NaHCOO II in the spectrum of KHCOO II. This vibration has been assigned (8, 9) to a molecular vibration in NaHCOO in which the two molecular units move in opposite directions along the x-axis. It is not allowed for KHCOO II, as is evident from Fig. 4, but is, however, activated in phase I of KHCOO, as can be seen in Fig. 5.

Temperature dependence of modes, II–I phase transition

The temperature dependence of the major bands of KHCOO is shown in Fig. 6. The occurrence of the II–I phase transition at

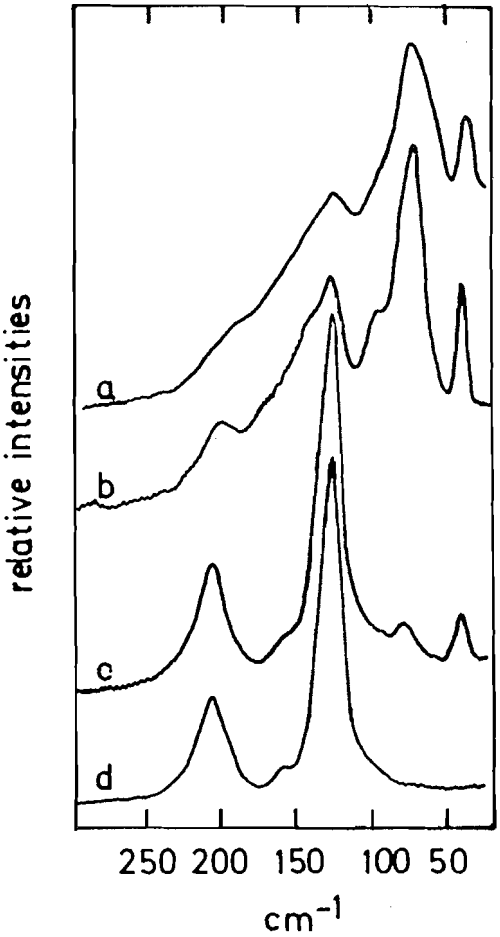


FIG. 5. The Raman-active lattice modes of KHCOO at (a) 425 K (phase I); (b) 300 K (phase I at 300 K); (c) supercooled phase I at 300 K after 72 h; (d) phase II at 300 K.

417 K in this compound is clearly evident. The results shown in Fig. 6 have been obtained during heating cycles only and do not reflect the results obtained during the cooling cycles. It was already shown in Fig. 5 that phase I can be supercooled, the room-temperature phase only being recovered after the elapse of a few days. Hysteresis, as shown by KHCOO I, is a common feature of first-order phase transitions (10) and was also observed in the cases of NaHCOO (1, 2) and LiHCOO (4). It is controlled by the strain energy stored in hybrid crystals and (or) kinetic barriers preventing nucleation (10). The magnitude of the hysteresis width is affected by factors such as particle size, rate of heating, and impurities (10). As was already shown, the presence of traces of moisture affects the polymorphism of KHCOO and, although the crystals were carefully dried and sealed in glass tubes, it is possible that traces of moisture were present and could affect the hysteresis width in the Raman measurements.

The majority of frequencies of the Raman modes graphically represented in Fig. 6 show downward shifts upon an increase in the sample temperature. A few modes, like ν_3, ν_2, and ν_5 are only marginally affected by an increase in the sample temperature. The rotational modes are particularly sensitive towards temperature. Figure 6 shows the variation in the frequencies of Raman modes; many of them also show a decrease in their half-widths with temperature. The linewidth can be expressed by the equation $\Delta = \Delta_0 + A_0 e^{-E/RT}$, where Δ is the linewidth of a band at a particular temperature T and Δ_0 is the linewidth at a

Can. J. Chem. Downloaded from www.nrcresearchpress.com by 84.41.108.74 on 09/07/12
For personal use only.

Can. J. Chem. Downloaded from www.nrcresearchpress.com by 84.41.108.74 on 09/07/12
For personal use only.

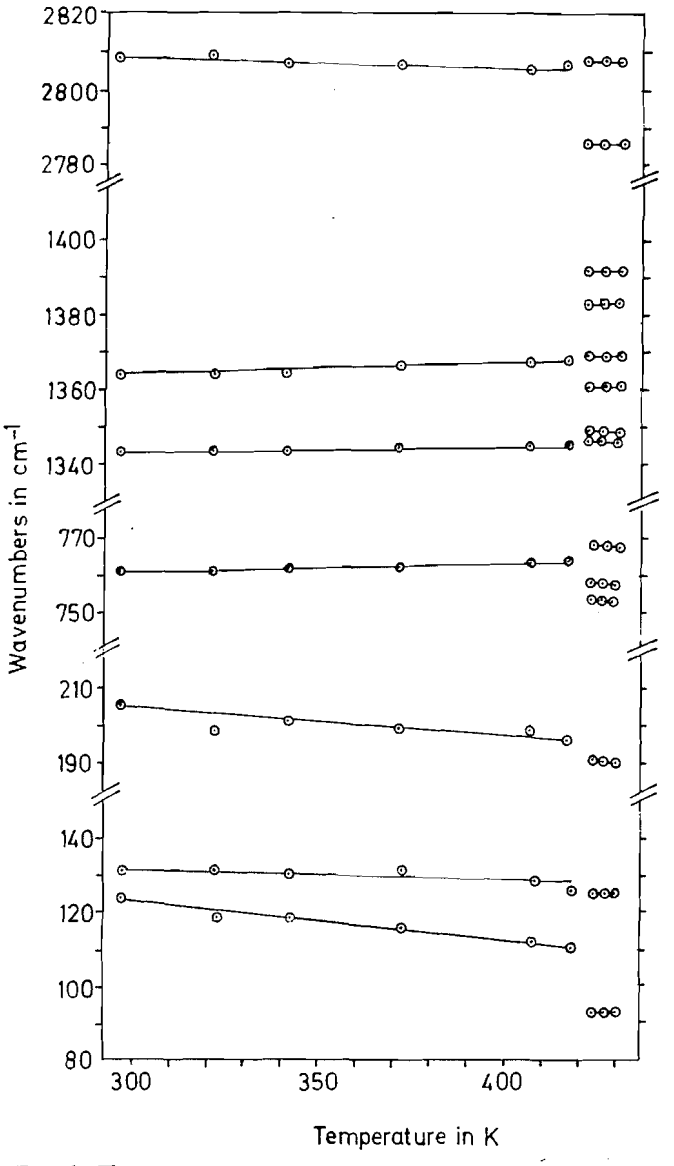


FIG. 6. The temperature dependence of the major Raman bands of KHCOO. The occurrence of the phase transition at 417 K is clearly evident.

very low temperature where molecular motions no longer influence the linewidth; A_0 is a constant and E is the activation energy (11). A plot of $\ln(\Delta-\Delta_0)$ vs. $1/T$ should give rise to a straight line with a slope of $-E/R$. The result of such a plot for the librational mode ν_{R_z} at 125 cm^{-1} is shown in Fig. 7. An activation energy of 5.6 kJ mol^{-1} is accordingly obtained. The activation energies calculated from other bands are summarized in Table 3.

It is known that the formate ion has several resonance structures and it was shown that in the case of NaHCOO these structures contribute towards the final one (12). It was also shown that both internal and external bands of KHCOO are broadened at high temperatures and the activation energy of 6.0 kJ mol^{-1} or less represents a low barrier to molecular motions that cannot be ascribed to rapid reorientations of the formate ions. Calculations involving the moments of inertia of the formate ions show that these orientations have much higher activation energies than 6.0 kJ mol^{-1}, and the well-defined librational bands observed in the Raman spectra of KHCOO are

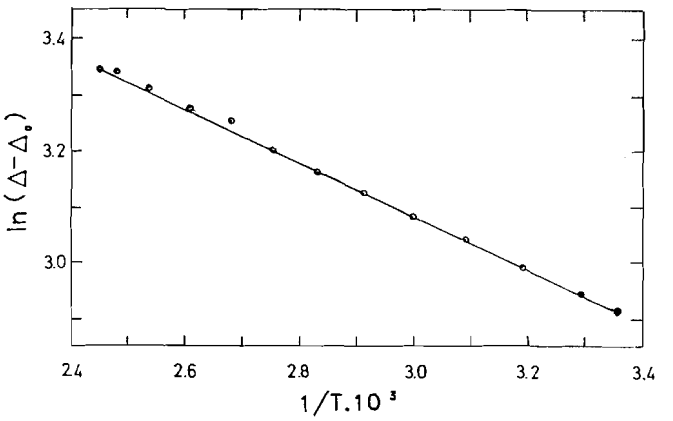


FIG. 7. The variation of $\ln(\Delta-\Delta_0)$, where Δ is the half-width at a particular temperature T and Δ_0 the very value at a very low temperature, against $1/T$ for the librational band ν_{R_x} at 206 cm^{-1}.

TABLE 3. Activation energies for the reorientational motions of the formate groups in KHCOO

Mode	cm^{-1}	E, kJ/mol^{-1}
ν_1	2810	5.7±0.10
ν_{R_z}	125	5.6±0.10
ν_{R_x}	206	4.0±0.05
ν_2	1345	6.0±0.20

also not in accordance with a great deal of reorientational freedom for the formate ions. There are, therefore, other motions that must affect the linewidths of the Raman-active formate groups, which could possibly be ascribed or partly ascribed to intramolecular motions reflecting the various structures that the formate ion can adopt.

It was shown that ν_5 is of $B_{3g}(R) + B_{1u}(ir)$ symmetry, and $2\nu_5$ should split into $2A_g(R) + 2B_{2u}(ir)$ components under D_{2h} symmetry. $2\nu_5$ occurs at 2713 cm^{-1} in the Raman spectrum of KHCOO II, showing that only one of the predicted A_g components is observed. ν_1 is also of A_g symmetry and occurs at 2809 cm^{-1} and it could therefore be expected that Fermi resonance will occur between these modes. It can be assumed that the ratio of the intensities of ν_5 and ν_1 are related by the equation (13)

$$R = I_a/I_b = \frac{\Delta\nu - \Delta\nu^0}{\Delta\nu + \Delta\nu^0}$$

where $\Delta\nu$ is the observed frequency separation between $2\nu_5$ and ν_1, and $\Delta\nu^0$ is the frequency separation between the unperturbed modes. $\Delta\nu^0$ can be obtained accordingly. R was found to vary linearly with temperature for KHCOO II and the variation of $\Delta\nu^0$ with temperature could therefore be determined. If the intensity of the unperturbed overtone, $2\nu_5$, is assumed to be neglible with respect to ν_1, the Fermi coupling constant, W, can be calculated from the following equation (ref. 13):

$$W^2 = \frac{(\Delta\nu)^2 - (\Delta\nu^0)^2}{4}$$

W has been calculated accordingly and its value at various temperatures are summarized in Table 4.

It can be seen from these results that the unperturbed energy

TABLE 4. The variation of W, the Fermi resonance coupling constant, with temperature for $2\nu_5$ and ν_1 in KHCOO

T, K	W, cm^{-1}
298	39.14
323	40.20
373	41.63
408	42.71

levels of ν_1 and $2\nu_5$, which are separated by 56 cm^{-1} at ambient conditions, will be coupled by Fermi resonance, pushing the energy levels further apart. W increases slightly with temperature, as is evident in Fig. 8 where the perturbed and unperturbed energy levels of ν_1 and $2\nu_5$ are graphically represented against temperature. These corrected values of $2\nu_5$ can also be used to calculate harmonic frequencies for ν_5 and it becomes evident immediately that this fundamental mode is largely harmonic in nature. This is also reflected by its temperature dependence, as is shown in Fig. 6.

At a first glance, the Raman spectra of phase I in KHCOO and NaHCOO are identical, as has already been reported (1). However, a closer scrutiny reveals a number of differences between these spectra. Firstly, KHCOO I has a Raman band at 38 cm^{-1}, which is not present in NaHCOO I (this feature does, however, develop in the intermediate phase I′ of NaHCOO (3)). No intermediate phase has been observed upon cooling down KHCOO; either the metastable phase I is obtained or the room temperature phase II forms directly. It is, however, difficult to say whether the supercooled phase I of KHCOO does not invariably contain traces of phase II since so many Raman bands of these two phases occur at identical frequencies (this is evident in Fig. 6). ν_3, which is observed in a frequency range where other bands do not occur, is split into two components in NaHCOO I and into three components in KHCOO I (Table1). Then, finally, six components are observed in the frequency range of 1300–1400 cm^{-1} and three, viz. the ones at 1346, 1348, and 1360 cm^{-1}, can be assigned to the C—O stretching mode ν_2, and the ones at 1369, 1387, and 1396 cm^{-1} are most probably due to components of the C—H bending mode ν_5.

It is more difficult to identify all of the individual components of the lattice modes of supercooled KHCOO I at room temperature. It is abundantly clear, however, that the bands are much broader than the ones of KHCOO II at the same temperatures (Fig. 5). For example, the half-width of the librational mode ν_{R_x} at 201 cm^{-1} in KHCOO I is 43 cm^{-1} compared to 23 cm^{-1} of the corresponding band in KHCOO II. It is also clear from Fig. 5 that the librational band ν_{R_z} at 125 cm^{-1} in KHCOO I could have several components that are not clearly resolved at room temperature. It is also clear from Fig. 5 that the "molecular" translation mode at ~70 cm^{-1} in phase I of KHCOO is the most intense band in the Raman spectra of both phase I at 423 K and the supercooled phase at 300 K. If this mode does indeed represent the motions of the molecules in the x-direction, then the band at 39 cm^{-1}, which is also rather prominent in the Raman spectrum of KHCOO I, can be assigned to the corresponding mode in either the y- or z-directions of the crystals. This mode has previously been assigned to a difference band in NaHCOO, viz. 112–74 cm^{-1} (1), but its temperature dependence shows that this assignment is highly unlikely in the case of KHCOO I.

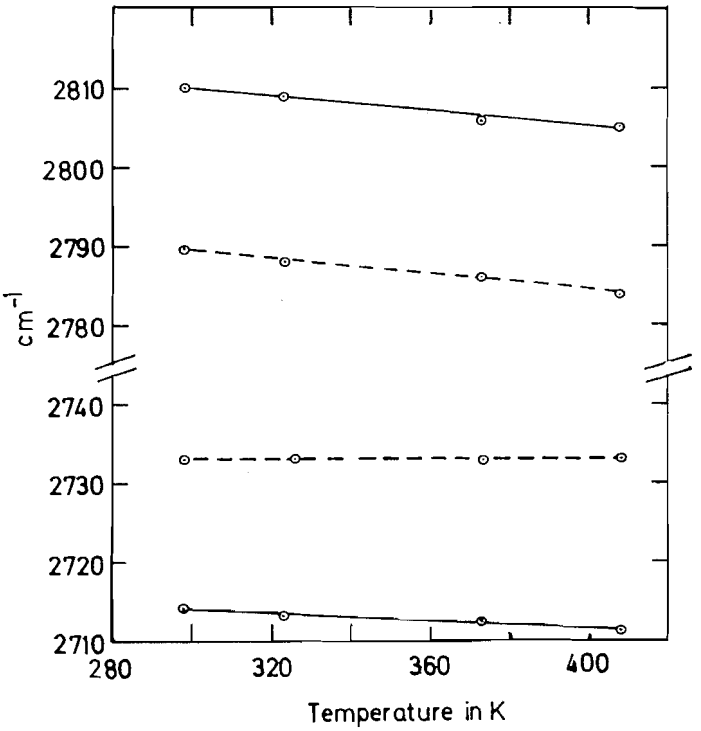


FIG. 8. The temperature dependence of the observed frequencies of ν_1 and $2\nu_5$ (solid lines) and the corrected frequencies for Fermi resonance (broken lines) in KHCOO.

The structural differences between NaHCOO I and KHCOO I were also evident from the powder diffraction patterns of these two compounds. The pattern obtained for NaHCOO I could be indexed on the basis of an orthorhombic unit cell with $a = 10.715$, $b = 13.007$, and $c = 3.4477$ Å compared to the monoclinic system of KHCOO I mentioned earlier. Not too much value can be attached to these assignments and only an exact crystal structure determination of single crystals will give an unambiguous assignment to the correct space group. But in view of the results obtained with both Raman spectroscopy and X-ray crystallography, there is little doubt that the crystal structures of these two compounds in phase I are indeed different.

Monoclinic structures are known for the alkali metal formates. NH_4HCOO belongs to the monoclinic space group Pc (C_s^2) with $Z = 2$ (14) and each internal formate mode is split into A' (ir,R) and A'' (ir,R) components. This space group can therefore be excluded as a possible candidate for KHCOO I. The monoclinic high-temperature phase of LiHCOO belongs to the space group $C2/c(C_{2h}^6)$ with $Z = 32$ (15). In this structure there are four independent formate groups and each formate mode can theoretically be split into four components. This will, of course, depend on the extent of differences in the bond lengths and angles. For example, the C—H bond lengths are equal to 1.03, 1.01, 1.00, and 0.99 Å in LiHCOO and four closely spaced C—H symmetric stretches (ν_1) have indeed been observed in the Raman spectra of this compound (4). On the other hand, only two C—O stretching modes have been observed in its Raman spectra (4), and it is obvious that the C—O bond lengths of 1.232, 1.235, 1.237, 1.238, 1.239, 1.241, 1.243, and 1.245 Å (15) are not sufficiently different to give rise to separate components for each bond length. A possible explanation for this is that the C—O stretching modes are broader in this compound than the C—H modes. This could

Can. J. Chem. Downloaded from www.nrcresearchpress.com by 84.41.108.74 on 09/07/12
For personal use only.

be due to molecular motions in the crystal. However, it was impossible to resolve all the predicted C—O components, even using a resolution of less than 0.5 cm^{-1}. It can therefore lead to serious misconceptions if the number of modes in the Raman spectra are simply counted and a structure is assigned accordingly. It can also be noted that the number of lattice modes and their frequencies closely correspond in LiHCOO I and KHCOO I. The structure of LiHCOO I can therefore not be excluded as a possible candidate for the structure of KHCOO I.

Acknowledgment

One of the authors (A.M.H.) wishes to thank the Council of the University of Pretoria and the Foundation of Research Development, Pretoria, for financial support.

1. A. M. HEYNS. J. Chem. Phys. **84**, 3610 (1986).
2. A. M. HEYNS, O. T. VAN NIEKERK, P. W. RICHTER, and K.-J. RANGE. J. Phys. Chem. Solids, **49**, 1133 (1988).
3. A. M. HEYNS and K.-J. RANGE. Mater. Res. Bull. **26**, 589 (1991).
4. K.-J. RANGE, K. MÜLLER, and A. M. HEYNS. Z. Naturforsch. In press.
5. J. W. BATS and H. FUESS. Acta Crystallogr. Sect. B: Struct. Crystallogr. Cryst. Chem. **B36**, 1940 (1980).
6. B. F. MENTZEN and Y. ODDON. Inorg. Chim. Acta, **43**, 237 (1980).
7. P. FERLONI, M. SANESI, and P. FRANZOSINI. Z. Naturforsch. A: Phys. Phys. Chem. Kosmophys. **30A**, 1477 (1975).
8. J. P. M. MAAS. Spectrochim. Acta, Part A: **33A**, 761 (1977).
9. J. P. M. MAAS and F. KELLENDONK. Spectrochim. Acta, Part A: **35A**, 87 (1979).
10. C. N. R. RAO and K. J. RAO. Phase transitions in solids. McGraw–Hill, New York. 1978.
11. S. D. ROSS. Inorganic infrared and Raman spectra. McGraw–Hill, London. 1972.
12. P. L. MARKILA, S. J. RETTIG, and J. TROTTER. Acta Crystallogr. Sect. B: Struct. Crystallogr. Cryst. Chem. **B31**, 2927 (1975).
13. G. D. TEWARI, D. P. KHANDELWAL, H. D. BIST, and V. P. TAYAL. Can. J. Chem. **61**, 2745 (1983).
14. I. NAHRINGBAUER. Acta Crystallogr. Sect. B: Struct. Crystallogr. Cryst. Chem. **B24**, 565 (1968).
15. J. KANSIKAS and K. HERMANSSON. Acta Crystallogr. Sect. C: Cryst. Struct. Commun. **C45**, 187 (1989).

Can. J. Chem. Downloaded from www.nrcresearchpress.com by 84.41.108.74 on 09/07/12
For personal use only.

Computers and infrared spectroscopy: evolution and revolution[1]

D. J. MOFFATT, J. K. KAUPPINEN,[2] AND H. H. MANTSCH

Steacie Institute for Molecular Sciences, National Research Council of Canada, Ottawa, Ont., Canada K1A 0R6

Received May 28, 1991

This paper is dedicated to Dr. Richard Norman Jones

D. J. MOFFATT, J. K. KAUPPINEN, and H. H. MANTSCH. Can. J. Chem. **69**, 1781 (1991).

A brief history of the relationship between computer and infrared spectroscopist is given with emphasis on the use of the Fourier transform. Subsequently, an algorithm is developed that may be used to devise an objective Fourier self-deconvolution procedure which depends only on the input data and is not subject to the biases that are often introduced in such subjective techniques.

Key words: deconvolution, Fourier transform, maximum entropy method.

D. J. MOFFATT, J. K. KAUPPINEN et H. H. MANTSCH. Can. J. Chem. **69**, 1781 (1991).

Mettant l'accent sur l'utilisation de la transformation de Fourier, on présente un résumé de l'histoire de la relation entre les ordinateurs et les practiciens de la spectroscopie infrarouge. Par la suite, on propose un algorithme qui peut être utilisé pour développer une méthode objective d'auto-déconvolution de Fourier qui ne dépend que sur les données fournies et qui n'est pas sujette aux déviations qui sont souvent introduites dans de telles techniques subjectives.

Mots clés : déconvolution, transformation de Fourier, méthode d'entropie maximale.

[Traduit par la rèdaction]

Can. J. Chem. Downloaded from www.nrcresearchpress.com by 84.41.108.74 on 09/07/12
For personal use only.

Preamble

Shortly after the digital computer became available to scientists some 30 years ago, enterprising spectroscopists started to harness it to the task of solving problems in infrared spectroscopy. One such spectroscopist was Dr. R. Norman Jones, who was among the first to utilize computers for processing of IR spectral data. As Norman put it then to his friend, he was out "to marry the computer to infrared spectroscopy", and what a successful marriage it became! He began the production of computer software in the early 60s here in Ottawa and, along with a number of dedicated co-workers, produced a compilation of modular computer programs that are still in use today in many laboratories throughout the world. They were collated into the National Research Council of Canada Bulletin series entitled "Computer programs for infrared spectroscopy" (1), and were disseminated to the spectroscopic community at large for a token fee that barely covered the cost of the magnetic tape on which they were distributed.

The 50 individual programs cover such diverse areas as (*i*) organization, sorting and error-checking of raw spectral data; (*ii*) simple conversion and scale changes (e.g., transmittance/absorbance and wavenumber/wavelength); (*iii*) basic analysis of spectral curves including smoothing, differentiation, peak and valley location, integration; (*iv*) band simulation and band contour analysis including the damped harmonic oscillator model and Cauchy (Lorentzian)–Gauss functions; (*v*) instrument calibration including wavenumber calibration, correction for slit width distortion and evaluation of cell path length; (*vi*) programs for normal coordinate analysis; (*vii*) calculation of optical properties including determination of optical constants from transmission and ATR measurements. Some of the former programs will appear somewhat rudimentary by today's standards but at that time the spectroscopist who wished to work with digitized data was forced to write his own programs for virtually *everything*. Moreover, it was the era of the punched card, when a gust of wind or an unfortunate slip of the hand could undo hours of tedious data encoding. Careful attention to error-checking and data organization was necessary to limit the extent of such catastrophies.

The bond between computer and spectroscopist that was fomented by Norman Jones is totally consummated today. The keypunch has been replaced by the keyboard, paper tape by the floppy disk, and endless columns of numbers have given way to lines of glowing phosphor on computer monitors. Few of us foresaw the explosive advances that were to become the hallmark of the computer industry, but thanks to men like Norman Jones we were well prepared to embrace them.

Revolution

In the period 1975–1985 the infrared spectroscopist saw the quality of his instrumentation increase by roughly three orders of magnitude[3] with the introduction of the Fourier transform infrared (FT-IR) spectrometer. Fortunately for the spectroscopist, there grew in tandem a technology that was ideally suited to manage the enormous amount of information flowing from this instrumentation — the microcomputer industry. It would be lamentable indeed were we forced to record as traces of ink on paper spectra having a signal-to-noise (S/N) ratio exceeding 10 000.

The many characteristics of the Fourier transform IR spectrometer that brought about this revolution have been detailed elsewhere (2–4), so only a few major ones will be noted here: (*i*) higher energy throughput (no slits) and multiplexed data, both leading to significant improvements in S/N; (*ii*) an abscissa scale linear in wavenumber, constant in resolution, and accurate to within 0.01 wavenumber (and even better in high resolution instruments); (*iii*) perforce, the collection of raw data in *digitized* form on a relatively powerful computer, eliminating the laborious hand-digitization process that had to be applied to data from older instruments.

---

[1]NRCC No. 32844.

[2]On leave of absence from the University of Turku, Department of Applied Physics, Turku, Finland.

[3]It may be argued that it is the quality of the data and not the instruments themselves that had undergone this dramatic improvement.

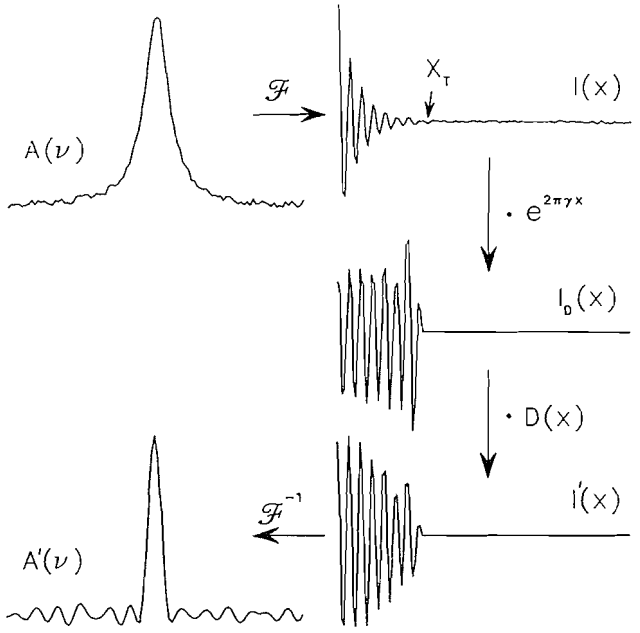


FIG. 1. Illustration of the FSD procedure applied to a single noisy Lorentzian band. In this illustration $D(x)$ is the Fourier transform of a Bessel function, the output lineshape of $A'(\nu)$.

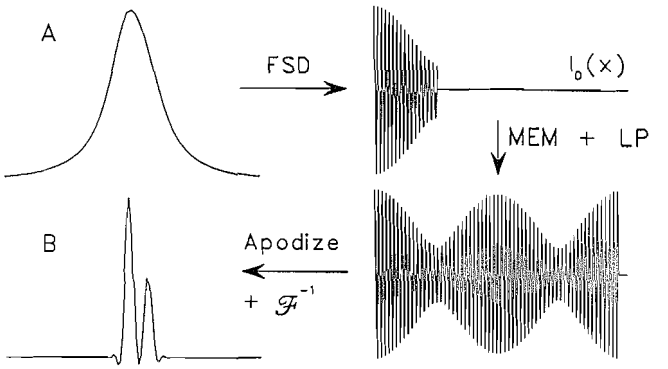


FIG. 2. Illustration of the LOMEP procedure applied to a Lorentzian doublet.

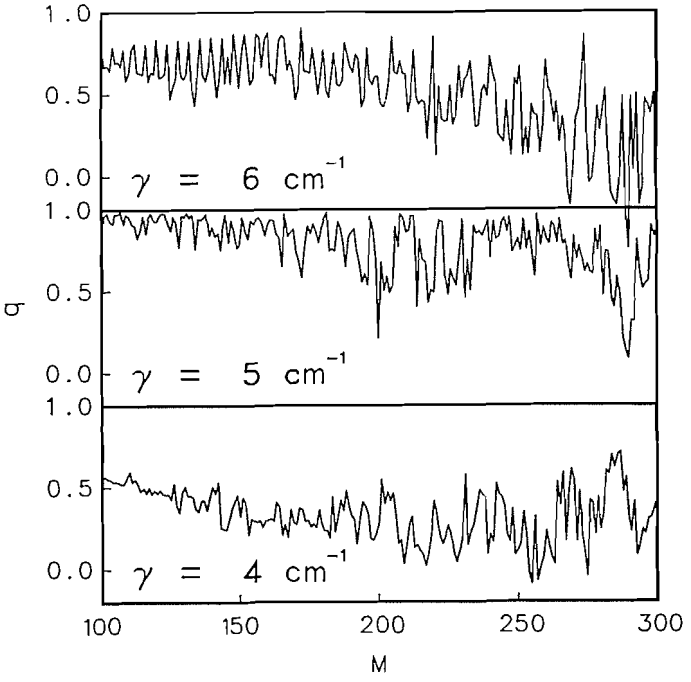


FIG. 3. Behavior of q as a function of M for three values of γ in the FSD step of LOMEP.

The Fourier transform — a digression

Apart from the pragmatic advantages, another perhaps less recognized benefit of the FT-IR technology was that it forced many spectroscopists to familiarize themselves with a mathematical tool that has found an application in virtually all fields of scientific investigation (5, 6), the Fourier transform. Like the NMR spectroscopist a decade earlier, the IR spectroscopist who made the effort to learn the relationship between data in the frequency and time domains gave himself a powerful new perspective in interpreting the data presented by his spectrometer. With a mastery of the Fourier transform comes a *clear* understanding of such common and useful data processing procedures as smoothing, interpolation, differentiation, apodization, and data sampling. A good example of this is the process of digital smoothing involving convolution with a set of coefficients, e.g., the method of Savitzky and Golay (7). Viewed in the time domain, this conceptually complicated procedure of convolution is reduced to the trivial multiplication by a weighting function (8).

Another common problem in IR spectroscopy that may benefit from the use of the Fourier transform is the choice of "optimal resolution", *i.e.*, the lowest instrumental resolution that may be used without degrading the spectrum. The choice of this value has been the source of some controversy, with many spectroscopists choosing to err on the side of caution using a higher resolution than necessary and paying a price in terms of computation time, data storage/transfer and, above all, signal-to-noise ratio. The Fourier transform is quite useful in this context; for a given spectrum, the point in the time domain where signal falls below the noise level can be used to accurately calculate this resolution value.

Evolution

With the widespread availability of digitized spectra came a demand for software to process this large quantity of data. Programs initially made available by the instrument manufacturers performed such mundane tasks as data collection, plotting/display, scaling, baseline correction, and addition/subtraction. Shortly thereafter more sophisticated routines appeared including smoothing, interpolation, differentiation, integration, and interactive subtraction (digital spectral stripping). Then there evolved programs directed at specific applications. The analytical spectroscopist in particular benefited from routines that performed quantitative analysis on multi-component samples. Also developed were libraries containing thousands of digitized spectra that could be scanned in a matter of seconds. Such customized software became more and more commonplace as spectroscopists became familiar with this new technology and became aware of what the computer could (and could not) do for them.

While the software tools evolved, so too did the tools accessible for spectroscopy itself. The new technology made possible such low energy techniques as photoacoustic, diffuse reflectance, and aqueous solution studies. However, there was somewhat of a dilemma with the more routine high energy spectra, i.e. neat liquids, KBr pellets, or organic solutions. Such spectra were being routinely obtained with an S/N of 4000 or more while for

Can. J. Chem. Downloaded from www.nrcresearchpress.com by 84.41.108.74 on 09/07/12
For personal use only.

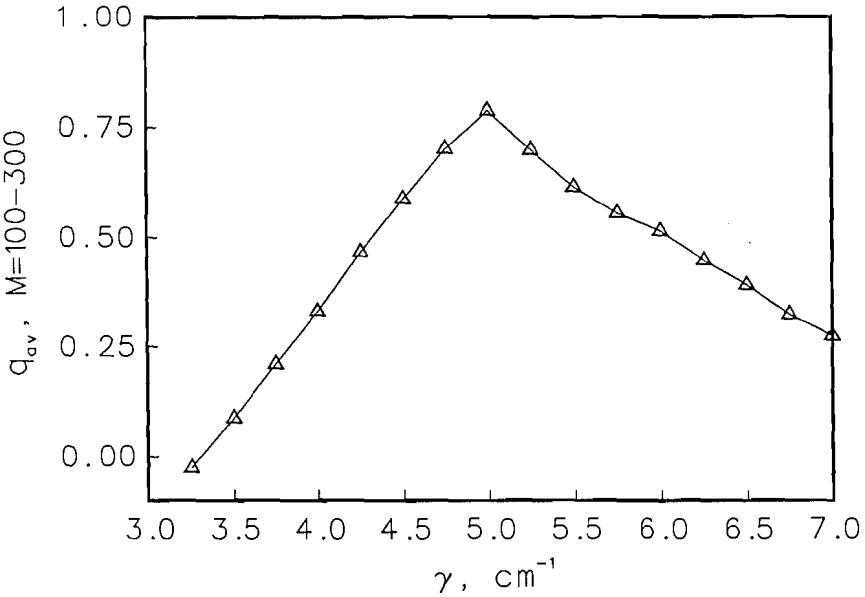


FIG. 4. Average value of q ($100 \geq M \geq 300$) as a function of γ in the FSD step of LOMEP, applied to the doublet in Fig. 2*A*.

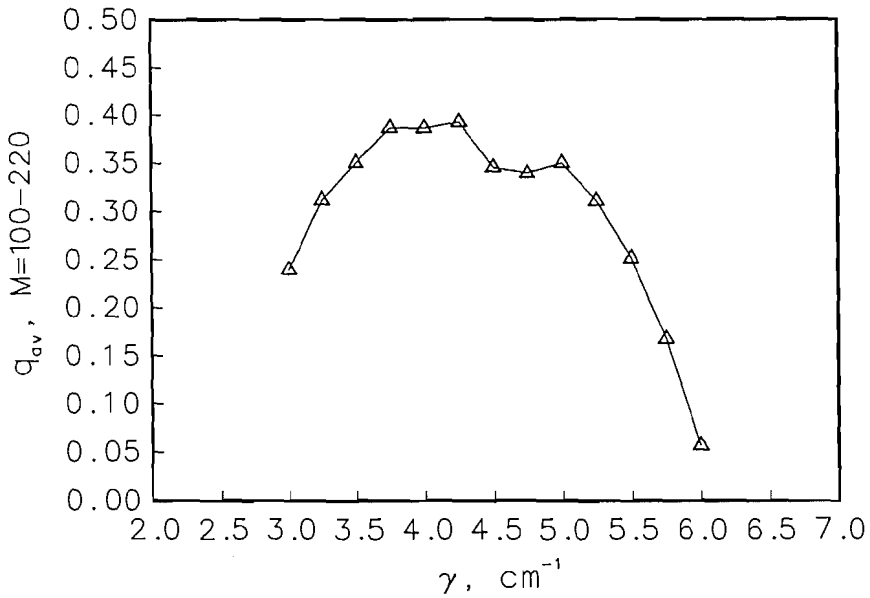


FIG. 5. Average value of q ($100 \geq M \geq 220$) as a function of γ in the FSD step of LOMEP applied to the C=O stretching region of the IR spectrum of a commercial sample of dairy cream (see top trace in Fig. 6).

Can. J. Chem. Downloaded from www.nrcresearchpress.com by 84.41.108.74 on 09/07/12
For personal use only.

most applications 400 was utterly sufficient. How to make use of the excess S/N, i.e. *information*? Once again as we shall see the computer comes to the rescue.

Deconvolution

One of the NRC computer programs mentioned above (9) deals with corrections for the distortion introduced by the finite slit width of a dispersive spectrometer, which is accomplished by deconvolving this distortion from the experimental data. In 1981, this procedure was taken a step further with the introduction of the technique of Fourier Self-Deconvolution (FSD) to IR spectroscopy (10). Essentially this was an attempt to correct for a "distortion" that nature imposes on infrared absorption bands — the Lorentzian lineshape.

To illustrate the principles of FSD let us consider a single infrared absorbance band, $A(\nu)$, with a Lorentzian lineshape. The absorbance value, A, at a given wavenumber, ν, is given by:

$$[1] \qquad A(\nu) = A_0\gamma^2/[\gamma^2 + (\nu - \nu_0)^2]$$

where A_0 is the maximum absorbance, ν_0 is the wavenumber corresponding to A_0, and γ is the half-width at halfheight (HWHH) of the band. The cosine Fourier transform of $A(\nu)$ is given by

$$[2] \quad I(x) = \mathcal{F}\{A(\nu)\} = \int_{-\infty}^{+\infty} A(\nu)\cos(2\pi\nu x)d\nu = A_0\gamma\pi\cos(2\pi\nu_0 x)e^{-2\pi\gamma|x|}$$

where x has the unit of cm with ν given in wavenumbers. The

Can. J. Chem. Downloaded from www.nrcresearchpress.com by 84.41.108.74 on 09/07/12
For personal use only.

exponential decay term, $\exp(-2\pi\gamma|x|)$, in eq. [2] is controlled by γ, that is, the wider the band, the more rapidly its Fourier transform decays. A point, x_T, in the time domain is then chosen beyond which the data are set to zero; this is often the point where the signal falls below the noise level. (In practice, this position is arrived at empirically, based on the noise level that may be tolerated in the deconvolution result.) Then, for a Lorentzian bandshape, FSD is performed by multiplying eq. [2] by the quantity $\exp(2\pi\gamma|x|)$ yielding an undamped cosine wave. This time domain function, $I_D(x)$, may then be multiplied by one of several suitable weighting functions, $D(x)$ (11), to yield a new signal, $I'(x)$, before inverse Fourier transformation to give the deconvolved band $A'(\nu)$. A typical choice for $D(x)$ is $(1 - (x/x_T)^2]^2$ which becomes a Bessel function on Fourier transformation. Figure 1 illustrates the steps involved in the FSD procedure.

FSD accomplishes a narrowing of all individual lines in a given spectrum with subsequent improvement of the information content to the spectroscopist, i.e., line positions, intensities and, most importantly, number. The practical restrictions on the method are non-uniform distribution of lineshape in the spectrum and the signal-to-noise ratio (note the higher noise level in $A'(\nu)$ compared to $A(\nu)$. Thus it is evident that this technique provides a practical use for the excess S/N made available to us by the FT-IR spectrometer.

Though it has found a niche in the spectroscopist's array of data processing tools, a major drawback of FSD has been its subjectivity (12); the output of the method depends somewhat on the practitioner since the values of γ and x_T have to be estimated and can greatly affect the output $A'(\nu)$.

Beyond deconvolution

Recently (13), we introduced a procedure of line-narrowing which we named LOMEP (from Lineshape Optimized Maximum Entropy linear Prediction), a combination of the procedures of Fourier Self-Deconvolution (FSD), Maximum Entropy Method (MEM), and Linear Prediction (LP). Given a spectrum consisting of lines all having the same (known) lineshape with only their position and intensity changing (a situation to which we refer as the LOMEP criterion), FSD is first performed but is stopped at step 2 ($I_D(x)$ in Fig. 1), which leads, in the time domain, to a signal consisting of undamped cosine waves. The impulse response of a prediction error filter (required by LP) is then computed using Burg's MEM and this time domain signal is extrapolated using LP. The Fourier transform of this extended signal leads to higher resolution in the frequency domain, hence to narrower lines in the output spectrum. Figure 2 illustrates this procedure applied to a synthetic double of Lorentzian lines (A in Fig. 2). The lines have a separation of 4 cm^{-1} with intensities 1.0 and 0.5, respectively; both lines have halfwidths at half height of 5.0 cm^{-1} and an S/N (peak-to-peak) of ~500. Application of the LOMEP procedure leads ot the separation of the two lines as per B in Fig. 2.

In a subsequent study (14), in which we explored the practical application of LOMEP, we introduced a value q, the quality factor, for estimating the accuracy of the linear prediction step in LOMEP. The q factor uses the property of a signal consisting only of undamped cosine waves that LP should work equally well in both directions. A corollary to this observation is that the data used in the calculation of the a_k coefficients (in the MEM step of LOMEP) should accurately predict themselves. This value, q, essentially gives an indication of how well the time domain signal can be modelled with a small number of undamped cosine waves.

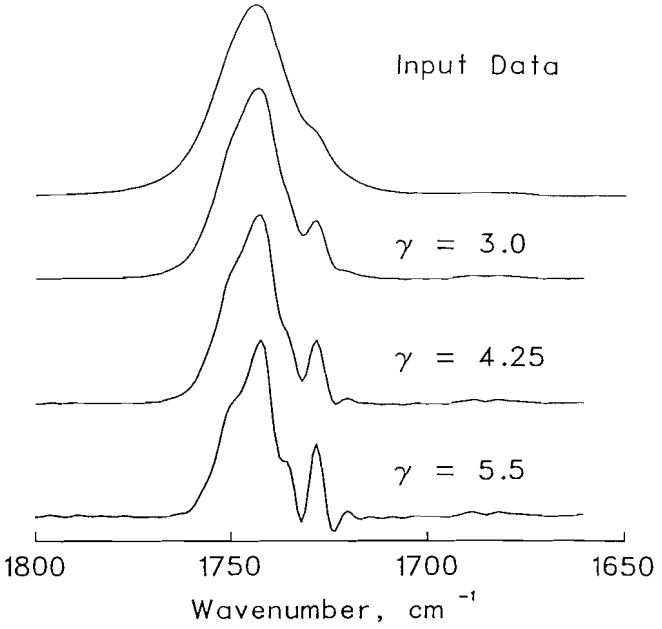


FIG. 6. FSD, at three γ values, applied to the C=O stretching region of the infrared spectrum of dairy cream (neat).

Hence, a by-product of the development of the LOMEP procedure is the feasibility of developing an objective FSD algorithm the output of which depends only on the input data. In theory, one merely varies the FSD halfwidth parameter, γ, to maximize q. The present study investigates such a procedure applied to a model system of Lorentzian lines containing random noise (trace A in Fig. 2).

In LOMEP the value of q depends not only on the FSD lineshape parameters, but also, and rather chaotically, on the number of points, M, used in the MEM part of the LOMEP procedure. Figure 3 illustrates this problem for three FSD halfwidth values when LOMEP is applied to the Lorentzian doublet in Fig. 2. There are various solutions to this difficulty; in this study we will take the simple approach of merely averaging the value of q between certain values of M, i.e., $M_1 \leq M \leq M_2$. Hence we can define

$$[3] \quad q_{av} = \frac{\sum_{i=M_1}^{M_2} q_i}{M_2 - M_1 + 1}$$

Figure 4 illustrates a plot of q_{av} versus FSD halfwidth when LOMEP is applied to the model doublet. In this example $M_1 \geq 100$, $M_2 \geq 300$. It is apparent that the q value goes through a distinct maximum at the halfwidth of the input Lorentzian lines.

Figure 5 shows the result of same procedure applied to some experimental IR spectroscopic data — the region of the carbonyl stretching band of a sample of commercial table cream. The maximum q_{av} occurs at approximately $\gamma = 4.25$ cm^{-1}. Figure 6 illustrates the results of applying FSD to the same data using this value for γ, along with two other γ values that differ by approximately ±30%. A sampling of the literature will reveal this to be a reasonable value for the range of FSD halfwidths applied to similar experimental spectroscopic data. Because of the subjective nature of FSD, any of the traces in Fig. 6 can be argued as a correct FSD result. The power of this new procedure, then, is to remove this ambiguity, by limiting the range of γ halfwidths applied to a set of data in the FSD procedure.

Epilog

The algorithm presented above is a symbolic product of the "marriage" that Norman Jones had arranged several decades ago. This marriage has now become a synergy as one is often hard-pressed today to decide where the spectrometer ends and the computer begins. The challenge is, as infrared spectrometers present us with yet better spectra, to find new approaches that allow us to extract additional information from the experimental spectra by means of data processing.

1. R. N. JONES (*Editor*). Computer programs in infrared spectrophotometry. NRC Bull. 11, 12 (1968); NRC Bull. 13 (1969); NRC Bull. 14, 15 (1976); NRC Bull. 16, 17 (1977).
2. P. R. GRIFFITHS. Chemical infrared Fourier transform spectroscopy. Wiley and Sons. New York. 1975.
3. J. DE HASETH. *In* Fourier, Hadamard, and Hilbert transforms in chemistry. *Edited by* A. G. Marshall. Plenum Press, New York. 1982. pp. 387–421.
4. D. R. SCHEUING. *In* Fourier transform infrared spectroscopy in colloid and interface science. *Edited by* D. R. Scheuing Am. Chem. Soc. Symp. Ser. 447, 1990 pp. 1–21.
5. A. G. MARSHALL and F. R. VERDUN. Fourier transforms in NMR, optical, and mass spectrometry: a user's handbook. Elsevier, New York. 1990.
6. R. BRACEWELL. The Fourier transform and its applications. McGraw-Hill, New York. 1965.
7. A. SAVITZKY and M. J. E. GOLAY. Anal. Chem. **36**, 1627 (1964).
8. J. K. KAUPPINEN, D. J. MOFFATT, H. H. MANTSCH, and D. G. CAMERON. Appl. Opt. **21**, 1866 (1982).
9. R. N. JONES and J. PITHA. Program XII in NRC Bull. 12, (1968).
10. J. K. KAUPPINEN, D. J. MOFFATT, H. H. MANTSCH, and D. G. CAMERON. Appl. Spectosc. **35**, 271 (1981).
11. J. K. KAUPPINEN, D. J. MOFFATT, D. G. CAMERON, and H. H. MANTSCH. Apl. Opt. **20**, 1866 (1981).
12. H. H. MANTSCH, H. L. CASAL and R. N. JONES. *In* Advances in spectroscopy. Vol. 13. *Edited by* R. J. H. Clark and R. E. Hester. Wiley and Sons, New York. 1986.
13. J. K. KAUPPINEN, D. J. MOFFATT, M. R. HOLLBERG, and H. H. MANTSCH. Appl. Spectrosc. **45**, 411 (1991).
14. J. K. KAUPPINEN, D. J. MOFFATT, M. R. HOLLBERG, and H. H. MANTSCH. Appl. Spectrosc. In press.

Can. J. Chem. Downloaded from www.nrcresearchpress.com by 84.41.108.74 on 09/07/12
For personal use only.

Diffuse reflectance infrared spectra of kaolinite and kaolinite/alkali halide mixtures. Curve-fitting of the OH stretching region

K. H. MICHAELIAN AND W. I. FRIESEN

Energy, Mines and Resources Canada, CANMET, Coal Research Laboratories, P.O. Bag 1280, Devon, Alta., Canada T0C 1E0

AND

S. YARIV AND A. NASSER

Department of Inorganic and Analytical Chemistry, The Hebrew University of Jerusalem, 91904 Jerusalem, Israel

Received May 17, 1991

This paper is dedicated to Dr. Richard Norman Jones

K. H. MICHAELIAN, W. I. FRIESEN, S. YARIV, and A NASSER. Can. J. Chem. **69**, 1786 (1991).

Diffuse reflectance infrared spectra of kaolinite and binary mixtures of this clay with alkali halides have been analysed using curve-fitting and deconvolution. For caesium chloride and caesium bromide, decomposition of the hydroxyl stretching region has made it possible to correlate the positions and intensities of bands due to structural hydroxyl groups of kaolinite, or to intercalated water, with the degree of intercalation. One of these bands, arising from uncoupled inner surface OH stretching in kaolinite, is not identifiable in spectra of the uncomplexed clay or mixtures where intercalation did not occur. A new band revealed by curve-fitting spectra of intercalated samples is attributed either to water at the interface between the clay and the alkali halide, or to an FeO—H impurity in the kaolinite.

Key words: kaolinite, infrared, curve-fitting.

K. H. MICHAELIAN, W. I. FRIESEN, S. YARIV et A. NASSER. Can. J. Chem. **69**, 1786 (1991).

Faisant appel à un ajustement de courbes et à la déconvolution, on a analysé les spectres infrarouges de réflexion diffuse de la kaolinite et de mélanges binaires de cet argile avec des halogénures alcalins. Pour le chlorure ainsi que le bromure de césium, il a été possible de décomposer la région d'élongation de l'hydroxyle afin d'établir une corrélation entre les positions et les intensités des bandes dues aux groupes structuraux hydroxyles ou à l'eau intercalée et le degré d'intercalation. Il n'a pas été possible d'identifier l'une de ces bandes, provenant de l'élongation du OH non couplé de la surface interne de la kaolinite, dans l'argile non complexée ou dans les mélanges où il ne s'est pas produit d'intercalation. On attribue une nouvelle bande, révélée par l'ajustement des bandes des spectres des échantillons intercalés, soit à l'eau qui se trouve à l'interface entre l'argile et l'halogénure alcalin ou à une impureté de FeO—H qui serait présente dans la kaolinite.

Mots clés : kaolinite, infrarouge, ajustement de courbes.

[Traduit par la rédaction]

Can. J. Chem. Downloaded from www.nrcresearchpress.com by 84.41.108.74 on 09/07/12
For personal use only.

Introduction

Curve-fitting and deconvolution (resolution enhancement) are two of the many numerical methods for the analysis of infrared spectra to which Dr. R. Norman Jones has contributed during his distinguished career. Many spectroscopists now use these techniques on a daily basis in order to increase the amount of information discernible in their data: as an example, this paper describes an infrared study of clay intercalation, where the identification of several bands would not have been possible without the use of both curve-fitting and deconvolution. In addition, second-derivative calculations were carried out using a program derived from one published in the NRC bulletins on infrared spectrophotometry.

Recently, we described diffuse reflectance ("DRIFT") and photoacoustic infrared spectra of binary mixtures of kaolinite, $Al_2Si_2O_5(OH)_4$, with several alkali halides (1). These spectra show that caesium chloride intercalates kaolinite when the two are either mixed, ground in air, or ground in the presence of a small amount of water. The data may be interpreted in terms of a complex in which a water molecule is hydrogen bonded to both a siloxane oxygen and an inner surface hydroxyl group, while being coordinated to the Cs^+ and Cl^- ions. For caesium bromide, intercalation occurred only when the mixture of the two solids was kept moist during grinding.

The OH stretching region of the DRIFT spectra of these complexes shows substantial changes with respect to that of kaolinite (Figs. 1a and 2a, ref. 1). Four new bands are visible: two arise from the symmetric (ν_1) and the antisymmetric (ν_3) vibrations of the intercalated water; one is due to uncoupled stretching vibrations of inner surface hydroxyl groups; and the remaining band arises from a new AlO—H stretching vibration. Moreover, the positions and relative intensities of the four well-known hydroxyl stretching bands of kaolinite are also modified as a result of the intercalation. The complexity of these spectra makes it desirable to separate the individual bands numerically so that the spectra can be fully characterized. To achieve this objective, we have performed curve-fitting and deconvolution calculations, the results of which are presented in this paper.

Spectra and calculations

Details regarding sample preparation and measurement of spectra have been reported previously (1). Before the curve-fitting was carried out, the spectra were baseline-linearized using standard software of the infrared spectrometer (Bruker IFS 113v). This adjustment to the data creates a horizontal baseline by subtracting a straight line from the spectrum over the selected region. The OH stretching region was arbitrarily assumed to extend from 3500 cm^{-1} to 3800 cm^{-1} for kaolinite and the mixtures whose spectra resemble that of the natural clay. The lower limit was changed to 3200 cm^{-1} for spectra displaying a broad low-frequency tail.

Our treatment of the spectra incorporated curve-fitting and deconvolution in the three-step approach previously employed for analysis of infrared spectra of coal (2, 3). According to this strategy, the measured spectrum is first deconvolved to increase the resolution of the bands, thereby providing better initial estimates of their number and peak

TABLE 1. Curve-fitting analysis of OH stretching bands (cm^{-1}) in DRIFT spectra of kaolinite and its complexes with CsCl and CsBr

Band assignment	Symbol[a]	Natural clay	CsCl mixture			CsBr mixture
			Mixed	Air ground	Wet ground	Wet ground
Intercalated HOH	ν_1	—	3524	3522	3509	3547
HOH or FeO—H		—	3561	3561	3548	3589
Intercalated HOH	ν_3	—	3583	3582	3578	3609
FeO—H		3596	—	—	—	—
AlO—H	A′	—	3601	3601	3599	3595
Inner OH	D	3623	3617	3616	3614	3620
Inner surface OH	C	3653	3636	3631	3628	3658[c]
Inner surface OH	B	3668	—	—	—	—
Uncoupled inner surface OH	Z	3686[b]	3672	3670	3668	—
Inner surface OH	A	3692	3691	3687	3683	3690

[a]Kaolinite band designation A, B, C, and D from ref. 4; A′ and Z from ref. 1.
[b]Frequency from Raman (9) and photoacoustic infrared (10, 11) spectra.
[c]Contains contributions from both B and C.

positions. After curve-fitting is completed, the resulting synthesized spectrum is also deconvolved. Consistency between the two deconvolved spectra is then made the essential criterion for accepting the curve-fitting parameters. In cases where doubt about the validity of certain features remained after these calculations, second derivatives of the observed spectra were computed; the results supported our conclusions regarding the existence of the bands.

Results and discussion

Our results are summarized in Figs. 1–5 and Table 1, and discussed in detail for kaolinite, kaolinite/CsCl, and kaolinite/CsBr in the following paragraphs.

The kaolinite bands A, B, C, D, Z, and A′ were fit satisfactorily with Lorentzian functions. Both Lorentzian and Gaussian shapes were tried for the water ν_1 and ν_3 bands, with Gaussian bands producing the superior fit. This observation is not surprising, as Gaussian bands generally reproduce both infrared and Raman spectra of water more accurately than Lorentzian bands.

Kaolinite

Figure 1 shows the results obtained for natural kaolinite from Makhtesh Ramon, Israel. Curve a represents the fitted spectrum, while b shows the individual bands making up the spectrum. Curve c is the difference between the fitted and measured (baseline-linearized) spectra.

The positions of the individual bands are listed in Table 1, together with their assignments and accepted symbols (4). According to the results of intercalation and deuteration studies (5), it is generally accepted that bands A, B, and C arise from inner surface hydroxyl groups, whereas D is due to the less accessible inner hydroxyl. In contrast, the 3596 cm^{-1} band occurs only for kaolinites that contain iron (6), but is not relevant in the following discussion of alkali halide mixtures because it is masked by another, much stronger, band.

The only ambiguity regarding the interpretation of the kaolinite spectrum involves the possible existence of band Z, which is observed in Raman (7–9) and photoacoustic infrared (10, 11) spectra of kaolinite, and arises from uncoupled inner surface hydroxyl stretching (12, 13). Deconvolution of the measured spectrum only hinted at a band at the appropriate frequency (3686 cm^{-1}). To check whether this band might contribute to the measured spectrum, the curve-fitting calculation

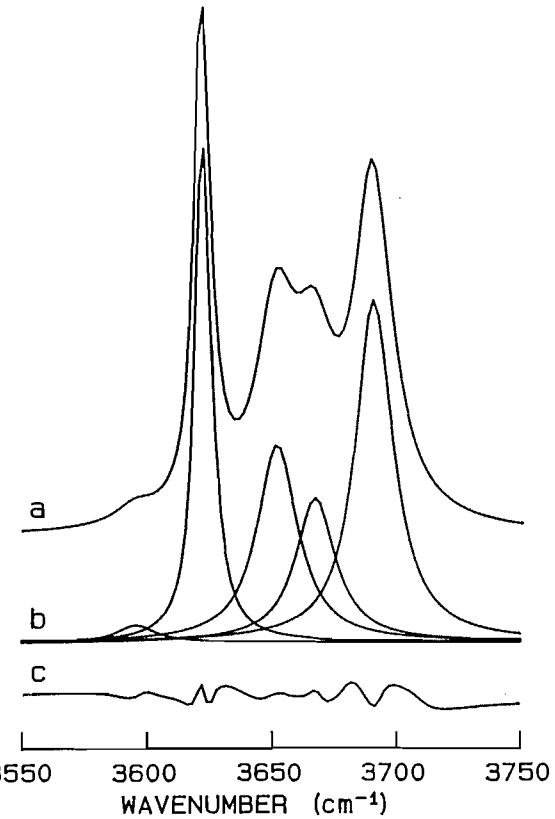


FIG. 1. Curve-fitting results for natural kaolinite. Curve a: fitted spectrum; curve b: component bands (cf. Table 1); curve c: difference between fitted and measured spectra.

was repeated by adding it to the five shown in Fig. 1. The resulting calculated spectrum was in slightly better agreement with the measured one; however, deconvolution of this new fitted spectrum did not verify the presence of the extra band. Moreover, the fitted intensity and width of the band varied with the starting values of these parameters. Since we require consistency between the results of the curve-fitting and deconvolution calculations, the occurrence of band Z is not confirmed. There-

Can. J. Chem. Downloaded from www.nrcresearchpress.com by 84.41.108.74 on 09/07/12
For personal use only.

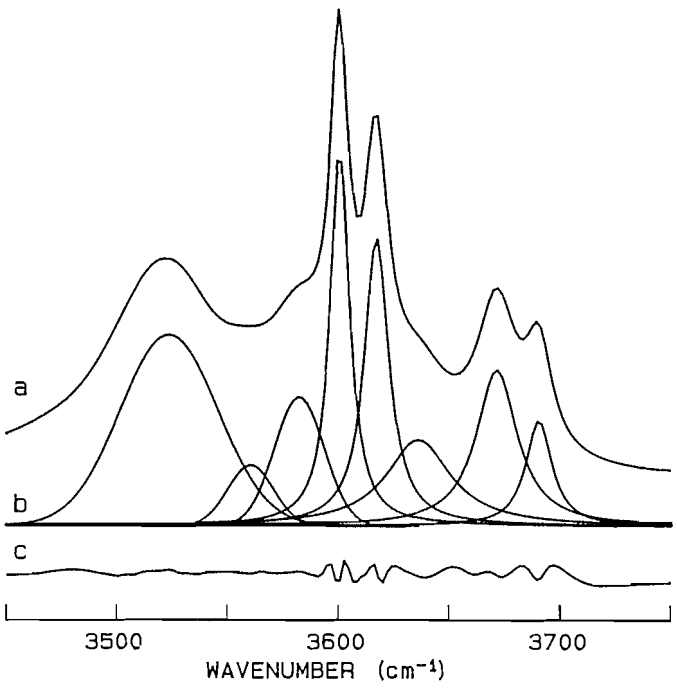


FIG. 2. Curve-fitting results for mixed kaolinite/CsCl. a–c as in Fig. 1.

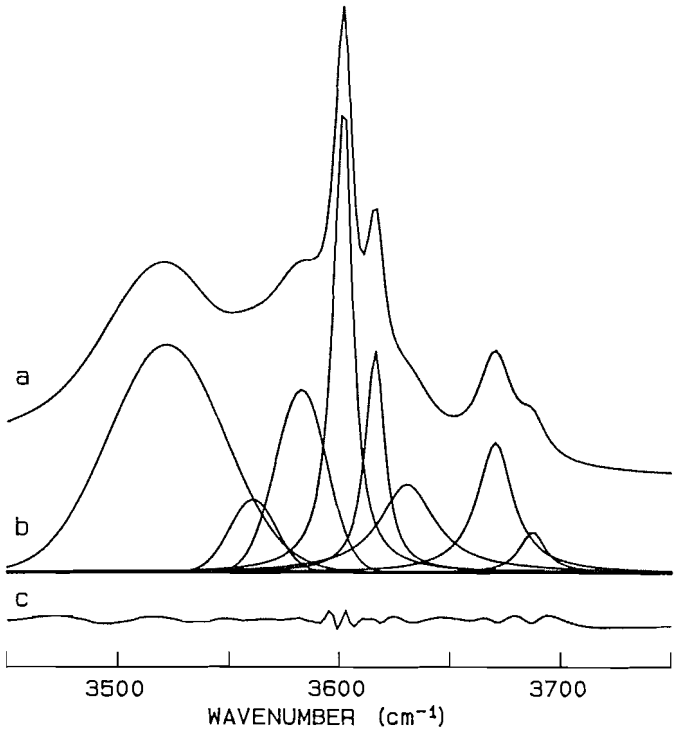


FIG. 3. Curve-fitting results for air-ground kaolinite/CsCl. a–c as in Fig. 1.

fore, we conclude that it contributes little or no intensity to the DRIFT spectrum of kaolinite.

Kaolinite/CsCl

All of the kaolinite/CsCl mixtures yield spectra that differ substantially from that of kaolinite. As shown in our previous work (1), the degree of intercalation in these mixtures varies in the sequence: mixed < air ground < wet ground. A qualitative indication of the different degrees of intercalation is provided by comparing the fitted spectra in Figs. 2–4 (corresponding to the measured spectra in Fig. 2a, ref. 1). The availability of three samples also makes it possible to monitor trends in frequencies and (or) intensities of individual bands and to achieve a consistent set of assignments.

Considering first the structural hydroxyl groups of kaolinite, the calculations reveal a progressive decrease in the frequencies and intensities of bands A, C, D, and Z as intercalation increases. Some of the weaker bands in the fitted spectra are not visible in the measured spectra, with the result that Table 1 in this work is more complete than Table 2 in ref. 1 with regard to hydroxyl stretching frequencies. Furthermore, the frequencies obtained from curve-fitting can be considered to be more accurate than the apparent maxima in the original spectra. It should also be emphasized that the curve-fitting results in no way contradict our previous conclusions (1).

The occurrence of band D in the spectra of the air-ground and wet-ground mixtures deserves further comment. Because this band is due to inner OH groups (5), it should not be affected by the intercalation. However, the peak positions listed in Table 1 indicate that band D shifts to slightly lower frequency as the degree of intercalation increases. As discussed previously (1), this frequency shift might be attributable to delamination of the tactoid and reduction of the symmetry of the alumino-silicate layer (perhaps through curling, which also occurs in halloysite). Such structural changes could also cause some reduction in the intensity of this band. This appears to be the case according to Figs. 2–4 but, since the intensity scale in each figure depends on the maximum of the sharp, narrow band A′, comparisons of absolute intensities for a particular band are difficult.

The OH stretching frequencies of the intercalated water also decrease systematically as the degree of intercalation increases. These bands are noticeably broader than those of kaolinite, reflecting greater participation of the hydroxyl groups of water in hydrogen bonding; as mentioned above, they are Gaussian, whereas the bands due to kaolinite are all Lorentzian. Intuitively, the water bands in the spectrum of the wet-ground sample (Fig. 4) should be more intense than those for the air-ground sample (Fig. 3). This expectation seems to be supported by the fact that the H_2O bands account for a greater proportion of the integrated intensity in Fig. 4, although it must be reiterated that the intensity scale differs from one figure to the next.

An unexpected result of the curve-fitting calculations is their prediction of a third Gaussian component between the ν_1 and ν_3 water bands: a satisfactory fit could not be obtained in the region below 3600 cm^{-1} until a band was introduced near 3560 cm^{-1}. Its existence is also suggested by the second-derivative spectra, particularly for the wet-ground kaolinite/CsCl complex. As shown in Table 1, the behaviour of this band is similar to that of bands of both kaolinite and intercalated water, thus providing at least circumstantial support for its authenticity. Therefore, it is plausible that this newly detected band arises from an intercalated water molecule in an environment different from that described previously (1), i.e., one where coordination to both alkali halide ions does not occur. One candidate is the water, possibly located at the interface between kaolinite and the alkali halide, that yields the endothermic DTA peak near 100°C (14). If the band is due to the ν_3 vibration of such a water molecule, then the ν_1 band would fall below 3500 cm^{-1} and contribute to the broad low-frequency wing that extends to the beginning of the OH stretching region.

Can. J. Chem. Downloaded from www.nrcresearchpress.com by 84.41.108.74 on 09/07/12
For personal use only.

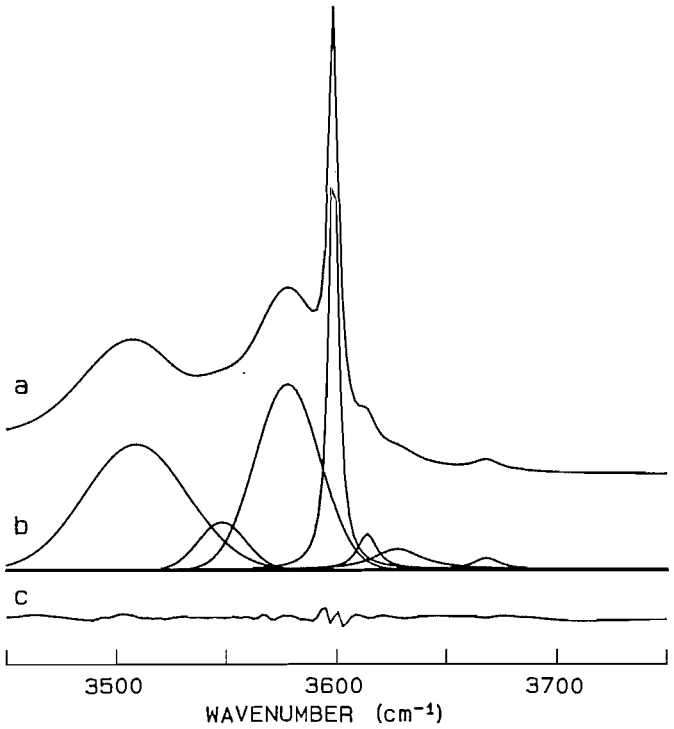


FIG. 4. Curve-fitting results for wet-ground kaolinite/CsCl. a–c as in Fig. 1.

Another explanation of the third Gaussian band is that it arises from FeO—H stretching. To check this possibility, we recently recorded the infrared spectrum of a freshly prepared wet-ground mixture of the Fe-free Georgia kaolinite with CsCl (the absence of Fe is inferred from the lack of a 3596 cm^{-1} band in the spectrum of the uncomplexed clay). Because this mixture had not been aged like the others (1), its spectrum differed from that in Fig. 4, resembling instead the result for the mixed sample in Fig. 2. The curve-fitting results indicate that three Gaussian bands are present, although no band appears in the vicinity of 3560 cm^{-1}. Hence this experiment does not permit a definite assignment of the third Gaussian band to either intercalated water or FeO–H stretching. The spectrum of this sample will be measured after a suitable period for intercalation, in a further attempt to establish the origin of this band.

The remaining band in these rather complex spectra, designated A′, arises from a new inner surface hydroxyl stretching vibration (1) that does not occur in kaolinite. Unlike many of the bands discussed above, its frequency hardly varies with the extent of intercalation. The clear definition of band A′ in the original spectra is such that curve-fitting yields no significant new information about it.

Kaolinite/CsBr

The results for the wet-ground mixture of kaolinite and caesium bromide are plotted in Fig. 5 and summarized in the last column of Table 1. Bands A and D are visible in the measured spectrum, which also appears to contain very weak bands corresponding to B and C; with regard to the latter two bands, however, our curve-fitting analysis yielded only a single band at 3658 cm^{-1}. Since A and D have frequencies about the same as those of the natural clay, the fact that the 3658 cm^{-1} frequency is intermediate between bands B and C suggests that it contains contributions from both. More importantly, these results imply the existence of some uncomplexed kaolinite in the mixture.

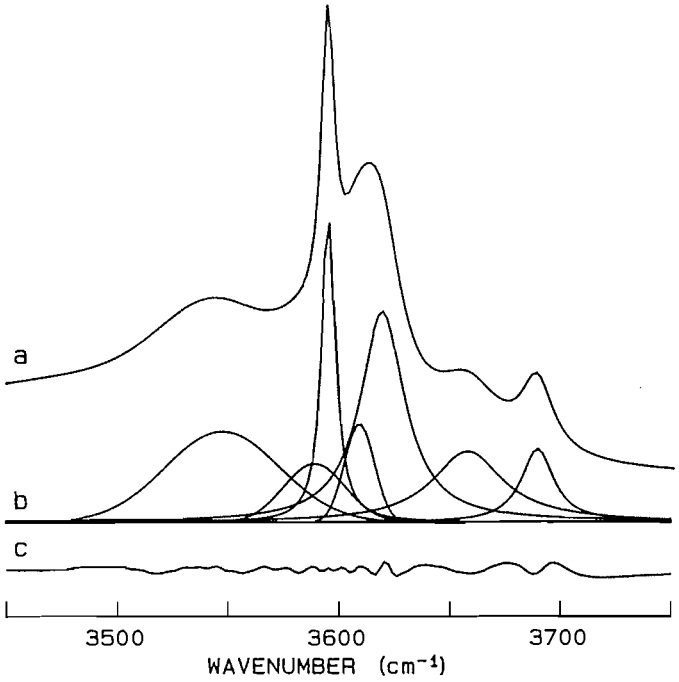


FIG. 5. Curve-fitting results for wet-ground kaolinite/CsBr. a–c as in Fig. 1.

The ν_1 and ν_3 vibrations of the intercalated water in kaolinite/CsBr occur at higher frequencies than for any of the caesium chloride mixtures (cf. Table 1). Taken together with the fact that band A′ occurs at slightly lower frequency in the CsBr complex, the result is that ν_3 now falls on the high-frequency side of A′. Curve-fitting for this spectrum suggested a third Gaussian band between ν_1 and ν_3, similar to that found for kaolinite/CsCl; as discussed above for kaolinite/CsCl, this can be attributed either to a second type of water molecule or to an FeO—H group.

Other mixtures

Finally, we mention results for three other air-ground mixtures: kaolinite/CsBr, kaolinite/KBr, and kaolinite/KI. All three yielded spectra similar to that of uncomplexed kaolinite (Fig. 1); hence the only pertinent question again concerns the presence of band Z. In fact, the curve-fitting results for these three mixtures were also inconclusive: the parameters of the fitted bands depended on their initial values, and the fit was only marginally improved by adding the extra band. These results lead to the conclusion that band Z is so weak that its contribution to the spectra cannot be verified by these calculations.

Conclusions

This paper has described the use of curve-fitting and other numerical methods for the analysis of diffuse reflectance infrared spectra of mixtures of kaolinite and alkali halides. Progressive decreases in the frequencies (and, in some cases, the intensities) of the hydroxyl stretching bands of kaolinite or intercalated water were monitored for kaolinite/caesium chloride mixtures. Furthermore, a new band was identified in the spectra of kaolinite/CsCl and kaolinite/CsBr mixtures, and attributed either to a water molecule at the clay/alkali halide interface or to FeO—H stretching. For kaolinite and its mixtures where intercalation does not occur, the presence of the band arising from uncoupled inner surface hydroxyl stretching was not confirmed by curve-fitting and deconvolution.

Can. J. Chem. Downloaded from www.nrcresearchpress.com by 84.41.108.74 on 09/07/12
For personal use only.

NOTE ADDED IN PROOF: The spectrum of the wet-ground mixture of Georgia kaolinite and CsCl, measured after an ageing period of 3 months, was fit using Gaussian bands at 3524, 3565, and 3592 cm^{-1}. These results support the assignment of the 3565 cm^{-1} band to intercalated water rather than to FeO—H.

1. K. H. MICHAELIAN, S. YARIV, and A. NASSER. Can. J. Chem. **69**, 749 (1991).
2. K. H. MICHAELIAN and W. I. FRIESEN. Fuel, **69**, 1271 (1990).
3. W. I. FRIESEN and K. H. MICHAELIAN. Appl. Spectrosc. **45**, 50 (1991).
4. J. G. MILLER and T. D. OULTON. Clays Clay Miner. **18**, 313 (1970).
5. R. L. LEDOUX and J. L. WHITE. Science, **143**, 244 (1964).
6. E. MENDELOVICI, S. YARIV, and R. VILLALBA. Clay Miner. **14**, 323 (1979).
7. A. WIEWIORA, T. WIECKOWSKI, and A. SOKOLOWSKA. Arch. Mineral. **35**, 5 (1979).
8. C. T. JOHNSTON, G. SPOSITO, and R. R. BIRGE. Clays Clay Miner. **33**, 483 (1985).
9. K. H. MICHAELIAN. Can. J. Chem. **64**, 285 (1986).
10. W. I. FRIESEN and K. H. MICHAELIAN. Infrared Phys. **26**, 235 (1986).
11. K. H. MICHAELIAN. Infrared Phys. **30**, 181 (1990).
12. P. G. ROUXHET, N. SAMUDACHEATA, H. JACOBS, and O. ANTON. Clay Miner. **12**, 171 (1977).
13. K. H. MICHAELIAN, K. BUKKA, and D. N. S. PERMANN. Can. J. Chem. **65**, 1420 (1987).
14. S. YARIV, A. NASSER, Y. DEUTSCH, and K. H. MICHAELIAN. J. Thermal Anal. In press.

Can. J. Chem. Downloaded from www.nrcresearchpress.com by 84.41.108.74 on 09/07/12
For personal use only.

Relative cross section and time-resolved fluorescence of porphyrin–DNA complexes

YIXIAN LIU AND J. A. KONINGSTEIN
The Ottawa–Carleton Institute of Chemistry, Department of Chemistry, Carleton University, Ottawa, Ont., Canada K1S 5B6

AND

Y. YEVDOKIMOV
Institute for Molecular Biology of the Academy of Science of the USSR, 32 Ul. Vavilova, Moscow, USSR

Received April 23, 1991

This paper is dedicated to Dr. Richard Norman Jones

YIXIAN LIU, J. A. KONINGSTEIN, and Y. YEVDOKIMOV. Can. J. Chem. **69**, 1791 (1991).

Relative values have been obtained for the cross section of fluorescence of tetrakis(4-*N*-methylpyridyl)porphine and the zinc(II) complex with DNA. Time-resolved fluorescence spectra have been used to assign fluorescence of porphyrins which intercalate at or are externally bound to DNA. The experimental data suggest that an equilibrium distribution for intercalated and externally groove-bound to DNA of porphyrin is reached for $r \simeq 200$ complexes. Radiative lifetimes of the various porphyrin species have been determined and evidence is found suggesting the contribution of non-linear effects to the intensity of laser induced fluorescence of $r > 1000$ complexes.

Key words: cross section, fluorescence, porphyrin–DNA complexes, intercalation, outside bound.

YIXIAN LIU, J. A. KONINGSTEIN et Y. YEVDOKIMOV. Can. J. Chem. **69**, 1791 (1991).

On a déterminé les valeurs relatives des sections efficaces de fluorescence de la tétrakis(4-*N*-méthylpyridyl)porphyrine et du complexe du zinc(II) avec l'ADN. On a utilisé les spectres de fluorescence résolus en fonction du temps pour attribuer la fluorescence des porphyrines intercalées à ou liées à l'extérieur de l'ADN. Les données expérimentales suggèrent qu'on atteint une distribution à l'équilibre entre les porphyrines intercalées à ou liées à l'extérieur de l'ADN lorsqu'on approche de $r \simeq 200$ complexes. On a déterminé les temps de radiation des diverses espèces de porphyrines et on a trouvé des données suggérant la contribution des effets non-linéaires à l'intensité de la fluorescence induite par un laser des complexes avec $r > 1000$.

Mots clés : section transversale, fluorescence, complexes porphyrine–ADN, intercalation.

[Traduit par la rédaction]

I. Introduction

There is a large body of information available in the literature on the complexation of water-soluble, substituted, and cationic porphyrins and metalloporphyrins with nucleic acids in solution (1–10). These studies indicate that tetrakis(4-*N*-methylpyridyl)porphine [H_2TMpyP] and its zinc derivative display different affinities for GC and AT rich regions of DNA. Various spectroscopic techniques, including absorption, circular and linear dichroism have been employed in the past to study the complexation and it is well known that intercalation takes place in H_2TMpyP at the GC sites while in addition this molecule can also attach itself to the AT sites of DNA. The Zn–porphyrin molecule does not intercalate but is believed to bind externally (5, 10).

The porphyrins exhibit fluorescence in the red part of the spectrum between 580 and 800 nm (9) (Fig. 1). The emission spectrum of H_2TMpyP changes upon the addition of DNA to the solution, in particular the width of the bands. Such changes, however, are not observed for the zinc(II) derivative molecule.

In this paper we discuss the results of a spectroscopic study of the emission spectra of H_2TMpyP and ZnTMpyP in a buffer solution with and without DNA. We have taken advantage of an experimental situation that the fluorescence signal of the porphyrin molecule and that due to the Raman shift of water at ~3500 cm^{-1} are separated if these emissions are induced with laser radiation of an argon ion laser tuned to a wavelength at 476.5 nm (Fig. 1). The intensity of the Raman band of water can be used as an internal standard and the relative value for the cross section of fluorescence can be determined as a function of the concentration of porphyrin molecules in solution. These results, in combination with those of a picosecond time-resolved fluorescence study which includes polarization anisotropy measurements, permit the assignment of spectra that belong to two sites where the H_2TMpyP molecules are either intercalated or externally bound to DNA.

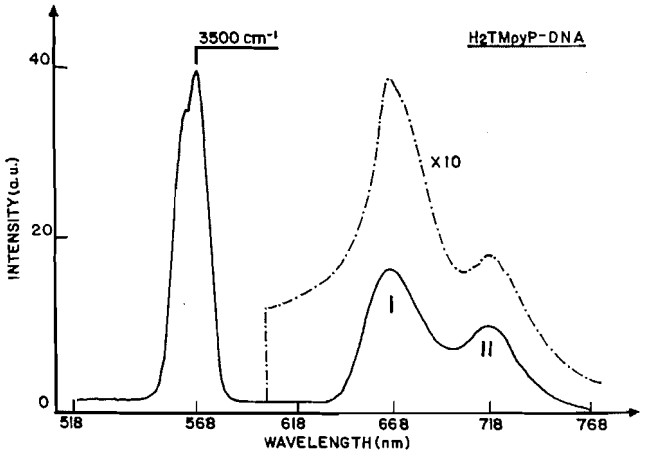


FIG. 1. Typical Raman and fluorescence spectra of water and H_2TMpyP–DNA complexes; — fresh sample; ····· used sample after 20 days; $r = 800$.

From the concentration-dependent value of the cross section for molecular fluorescence, the distribution of the H_2TMpyP molecule over the two sites of DNA as a function of r number of the porphyrin–DNA complexes has been determined (r is the concentration of base pairs of DNA/total concentration of porphyrins).

Can. J. Chem. Downloaded from www.nrcresearchpress.com by 84.41.108.74 on 09/07/12
For personal use only.

Can. J. Chem. Downloaded from www.nrcresearchpress.com by 84.41.108.74 on 09/07/12
For personal use only.

II. Experimental

A. Instrumental

Emission spectra (Raman and fluorescence) of buffer solutions (pH = 7) of H_2TMpyP and its zinc derivative, together with those of such solutions to which DNA was added, were recorded with a Raman spectrometer. The spectra were dispersed with a Jovin-Yvon double monochromator and the signals emerging from the exit slit were detected with a cooled RCA 31034 A photomultiplier tube. The output of this tube was processed by a photon counting system, spectral data could also be stored in a PC.

Raman and fluorescence spectra were excited with radiation of 476.5 nm of an argon ion laser (power level ~ 30 mW). A typical experimental run is displayed in Fig. 1, and the intensity of the polarized Raman shift at ~3500 cm^{-1} of water is proportional to $45\alpha^2 + 7\beta^2$. Because the integrated intensity of the fluorescence band of the porphyrin molecule is compared to that of the intensity of the Raman band of water (internal standard), one could in principle obtain an absolute value for the cross section of fluorescence band if the cross section for the Raman band of water would be known. The cross section for the Raman shift has recently been determined for excitation wavelength in the uv and vuv but a disagreement exists in the literature (12, 13) on the exact value of the intensity. Extrapolation of these results by intensity calculations for the spectrum of water excited with 476.5 nm is at present thought to yield only approximate results.

Of importance to this work is the ratio $I(fl)/I(Raman)$ where $I(fl)$ and $I(Raman)$ are the integrated intensity of the red fluorescence bands of the porphyrin and the integrated intensity of the Raman shift of water, see Fig. 1. For the solutions used in the present experiments we found that the ratio $I(fl)/I(Raman)$ was proportional to the cross section for fluorescence of the porphyrins and is therefore referred to as the cross section for fluorescence.

Time-resolved spectra were obtained using a 6 ps dye laser as an excitation source where the wavelength could be tuned to the region of 560–650 nm. If tuned to 590 nm one finds that this wavelength is in resonance with a weak absorption band of the porphyrins in solution. The molecular emission was detected by a cooled Hamamatsu R 1564U multichannel plate photomultiplier which is attached to a Jarrell-Ash double monochromator. This monochromator operates in the subtractive mode. The signal generated by the multichannel photomultiplier was processed by a time correlated single photon counting system with the time response of the optical detection system being 42 ps (11).

B. Sample handling

Emission spectra were measured from solutions which were prepared from stock buffer solutions containing H_2TMpyP or its zinc derivative and of a stock buffer solution of chicken blood erythrocytes DNA (B-form), the O.D. = 1.0 at 256 nm. The pH = 7 buffer solutions contained 0.01 M sodium phosphate and 0.3 M NaCl and the concentration of H_2TMpyP and ZnTMpyP was 1.47×10^{-3} and 1.096×10^{-3} M, respectively. Fresh samples were made before each series of measurements and the spectra were taken from solutions in air-tight Raman cells.

III. Results

A. Cross sections for molecular emission of H_2TMpyP and its zinc derivative in buffer solutions

Figures 2*A* and *B* show the concentration-dependent value of the cross section of the red fluorescence band of H_2TMpyP and its zinc derivative in a buffer solution. The fluorescence band extends from about 600 to 780 nm and the signal is well separated from the Raman shift of water at ~3500 cm^{-1} and this shift occurs at ~568 nm, see also Fig. 1. The signal/noise of fluorescence for solutions containing the Zn–porphyrin is higher than that of the H_2TMpyP molecule and fluorescence cross sections could be determined for Zn–porphyrin solutions which are $< 3 \times 10^{-7}$ M. The value of the cross section of

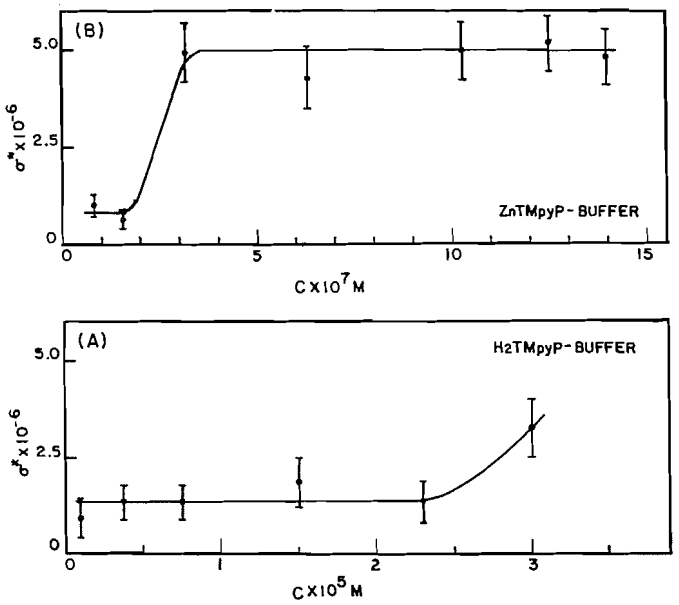


FIG. 2. Relative cross section σ* of fluorescence of H_2TMpyP and ZnTMpyP in buffer solution versus concentration C of H_2TMpyP and ZnTMpyP, respectively; (*A*) H_2TMpyP in buffer solution; (*B*) ZnTMpyP in buffer solution.

TABLE 1. A comparison of relative cross section and radiation lifetime for fluorescence of porphyrin complexes

Compounds	Cross section† $\sigma^* \times 10^{-6}$	Lifetime τ (ns)	Remarks
H_2TMpyP	1.5±0.3	5.0±0.5	Monomer in buffer
H_2TMpyP	>3	<4.5	Aggregate in buffer
H_2TMpyP–DNA	‡	1.7±0.3	Porphyrin binding site I
H_2TMpyP–DNA	‡	10±0.5	Porphyrin binding site II
ZnTMpyP	5.0±0.5	1.3±0.3	Monomer
ZnTMpyP–DNA	70±5	1.8±0.5	Bound externally

†Relative to the cross section of the Raman of H_2O at 3500 cm^{-1} excited with λ = 476.5 nm.
‡σ^*(site I) >> σ^*(site II).

fluorescence for the H_2TMpyP porphyrin molecules is independent of concentration for solutions which are $< 2.5 \times 10^{-5}$ M. The cross section increases in value for solutions which are $> 2.5 \times 10^{-5}$ M. The rotational correlation time of monomeric H_2TMpyP is ~300 ps, but if measured for solutions which are $> 7.4 \times 10^{-5}$ M, the rotational relaxation time increases suggesting that the concentration of aggregates of this molecule increases (14).

The data shown in Fig. 2*B* are for the Zn–porphyrin molecule in the buffer solution. For solutions which are $< 3 \times 10^{-7}$ M one finds that the cross section decreases. The decrease in the value of the cross section for concentrations $< 3 \times 10^{-7}$ M is the result of effective population saturation of the electronic excited state in which the spontaneous fluorescence originates. The fluorescence intensity for solutions $< 3 \times 10^{-7}$ M is non-linear in laser intensity. In Table 1 are given the relative values of the cross section for emission of fluorescence of aggregates of H_2TMpyP and its zinc derivative.

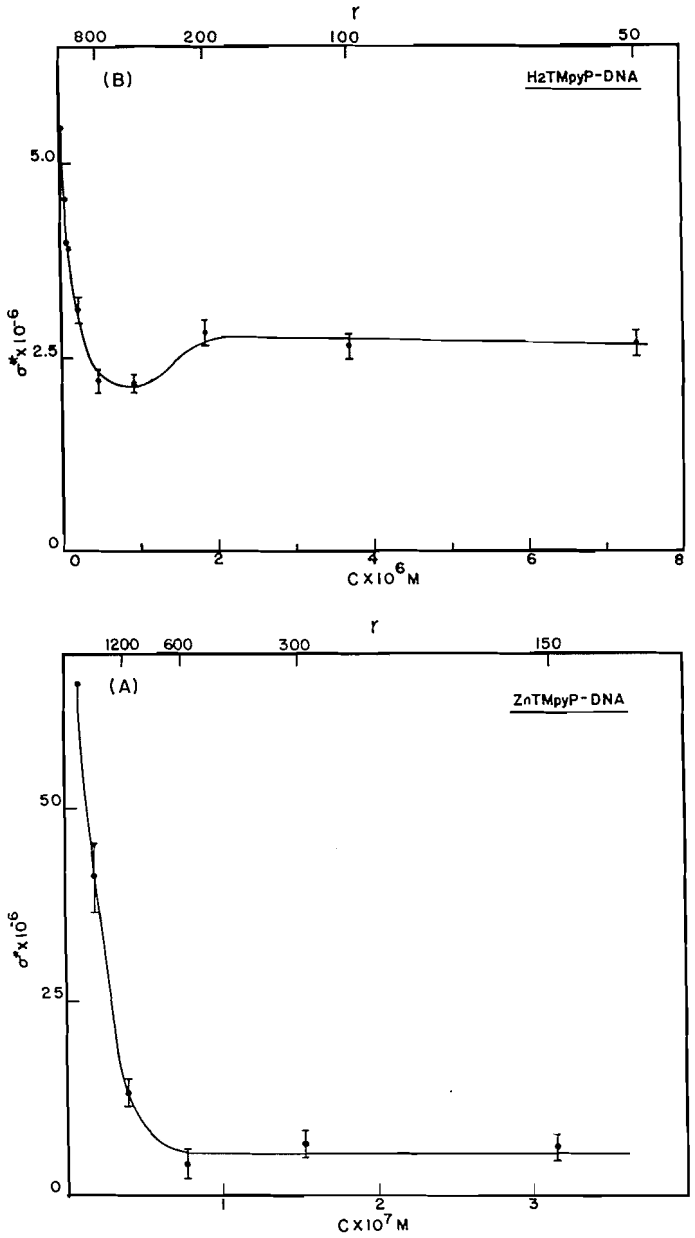


FIG. 3. Relative cross section σ^* of fluorescence of H_2TMpyP–DNA and ZnTMpyP–DNA complexes in buffer solution versus concentration C of H_2TMpyP and ZnTMpyP respectively; (*A*) ZnTMpyP–DNA in buffer solution; (*B*) H_2TMpyP–DNA in buffer solution.

B. Fluorescence of porphyrin–DNA complexes

In Fig. 3*A* is shown the concentration-dependent value of the cross section of fluorescence originating in the Zn–porphyrin molecule complexed to DNA with r values between 5000 and 150. For $r < 600$ complexes, the value of the cross section of fluorescence is within experimental error and equals the value for the cross section of emission of Zn–porphyrin, see Fig. 2*B*.

A sharp increase occurs for the cross section of fluorescence of ZnTMpyP–DNA and H_2TMpyP–DNA complexes takes place in solutions with $r > 600$, see Fig. 3*A* and 3*B*. It is shown in section IV that the sharp increases are the result of the onset of non-linear effects. If the increases are neglected, the data points (Fig. 3*B*) indicate that the cross section for fluorescence for $r > 800$ complexes approaches a value which could be close to the cross section for emission of monomeric H_2TMpyP. On the other hand, for $200 > r > 50$ complexes, the value of the cross section is independent of the concentration of the porphyrin molecule.

IV. Assignment of fluorescence of H_2TMpyP–DNA complexes

The interpretation of the concentration-dependent value of the cross section of fluorescence of H_2TMpyP–DNA complexes in terms of concentration of fluorescence of various species is facilitated if the results (11) of a time-dependent fluorescence study are considered. In these experiments, fluorescence from the porphyrin–DNA complexes are induced with a 6 ps pulse at 590 nm. An analysis of the fluorescence decay at 668 and 718 nm of solutions with $r = 50$ complexes shows that to a first approximation this decay is biexponential with decay times of 2.0 ± 0.5 and 10.0 ± 0.5 ns. There is evidence that another fluorescence process contributes to the overall intensity for solution with $r = 5$ complexes. The decay time of this process is estimated to be 5.0 ± 1.5 ns and the fluorescence is assigned to that of the porphyrin molecule unbound to DNA because the value of the decay time is within the experimental error equal to the decay of 5.0 ± 0.5 ns measured for fluorescence of H_2TMpyP in the buffer solution which does not contain DNA. The presence of fluorescence from unattached porphyrin becomes more clear if the value of r decreases. The rotational relaxation time of monomeric H_2TMpyP in the buffer solution, obtained from time-resolved polarization anisotropy measurements, is 300 ± 50 ps.

The rotational correlation times of the two species for fluorescence with decay time of 2.0 ± 0.5 and 10.0 ± 0.5 ns, within experimental error, are the same and longer than 10 ns. The long rotation time indicates that the emissions originate in excited states of the H_2TMpyP molecule which occupy different sites, designated by site I (nonintercalation) and II (intercalation), respectively (see also section V) for porphyrin molecules attached to DNA. The time-resolved spectrum of the two different sites is shown in Fig. 4, see also Table 1.

In the fluorescence experiments, the laser radiation is focussed on a cell with a 10 cm lens and the path length of the beam inside the cell is 1 cm. For a 10^{-7} M solution, there are $\sim 2 \times 10^7$ porphyrin molecules in the irradiated volume. Assuming a diameter of $d = 200$ μm for the focussed blue laser beam, these molecules are exposed to a flux of $\sim 10^{17}$ photons/s for a power level of 40 mW. Assuming that 10% of the photons are absorbed by H_2TMpyP molecules with the longer lifetime (site II) of the excited state from which the fluorescence originates, we find that during one lifetime of 10 ns, the ratio of photons/porphyrin molecules $\simeq 5$. This suggests that conditions are favorable for effective population saturation of an excited state of porphyrin and hence stimulated emission may contribute to the intensity of the fluorescence. Also, the excited state absorption spectrum of porphyrin molecules may replace in part that of the ground state and the intensity of the Raman band of water could change as a result of absorption of the Raman emitted light by the excited state of porphyrin molecule (15). The observed behaviour of the value of the cross section for ZnTMpyP and H_2TMpyP–DNA complexes with $r \geq 800$ is thought to be mainly caused by the onset of stimulated emission. The results obtained for ZnTMpyP in the buffer solution and for ZnTMpyP–DNA complexes suggest that differences exist in their energy level diagrams and value of transition moments for transition from the ground and (populated) first excited state in the spectral region of 580–720 nm.

Can. J. Chem. Downloaded from www.nrcresearchpress.com by 84.41.108.74 on 09/07/12
For personal use only.

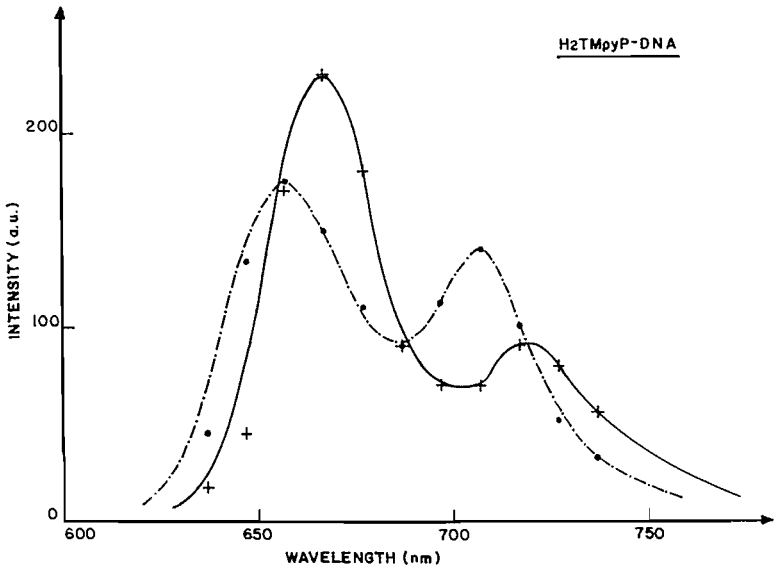


FIG. 4. Time-resolved fluorescence spectra of H_2TMpyP–DNA in buffer solution; — lifetime 1.7 ± 0.3 ns and bound to site I of DNA; ----- lifetime is of 10 ± 0.5 ns and bound to site II of DNA.

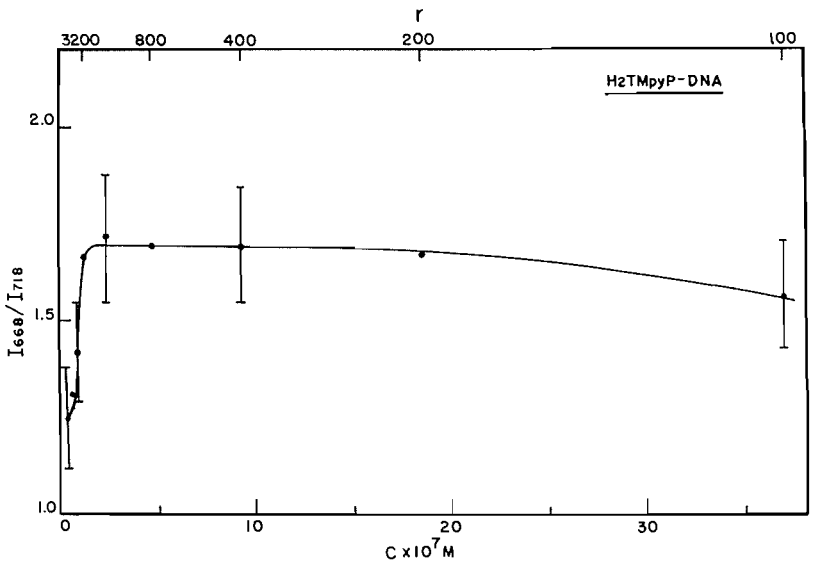


FIG. 5. Amplitude ratio I_{668}/I_{718} of fluorescence peaks of H_2TMpyP–DNA in buffer solution versus concentration C of H_2TMpyP.

Shown in Fig. 5 is the concentration-dependent value for the intensity ratio $I(668)/I(718)$ for peak intensities at 668 and 718 nm. The ratio decreases for solutions with $r > 800$ complexes and approaches the value for fluorescence observed in the time-resolved spectrum of site II.

From the discussion above, the increase in the value of the cross section for fluorescence (Fig. 3*B*) for $r > 800$ complexes is associated with the onset of non-linear effect of porphyrin molecules which occupy site II. This information, combined with the observation (Fig. 3*B*) that the cross section for emission of H_2TMpyP–DNA decreases for $800 > r > 200$ complexes, suggests that for $r > 200$ complexes preferential occupation of site II over site I takes place. For the $r = 200$ complexes, however, an equilibrium distribution has been reached.

Assuming that for $r > 200$ all porphyrin molecules are attached to the DNA, the ratio of molecules occupying site II/site I = 3.0 ± 0.3 as determined from the data points of Figs. 4 and 5. However, for the $r < 200$ complexes, the concentration of unattached porphyrin to the fluorescence signal becomes more evident.

V. Conclusions

Shown in Table 1 are the values of the cross section for emission of the various species. The (relative) values of the cross section were obtained from the data displayed in Figs. 3, 4, and 5. It is well known from circular (3) and linear dichroism (10) and absorption spectra, that H_2TMpyP molecules intercalate at the GC sites of DNA for $r = 200$. Our results suggest that H_2TMpyP molecules binding to DNA are intercalating dominantly for the $r \geq 3200$. For smaller r values another species contributes to the absorption signal and this species has been identified in terms of H_2TMpyP which is externally bound to DNA. Thus the emission spectrum of site II is due

Can. J. Chem. Downloaded from www.nrcresearchpress.com by 84.41.108.74 on 09/07/12
For personal use only.

to the intercalated H_2TMpyP molecules while the porphyrin molecules occupying site I are externally bound to DNA. Upon storage of solutions containing porphyrins which are intercalated and externally bound to DNA it is observed that fluorescence originating in the intercalated porphyrin gradually disappears while that of externally bound porphyrin remains observable, although the intensity of the fluorescence has decreased in time, see Fig. 1. The disappearance of the spectrum of intercalated H_2TMpyP is thought to be the result of splitting of the DNA sugar–phosphate chains.

Solution of ZnTMpyP–DNA complexes reveals the emission of a complex with a decay time which, within the experimental error, equals that of externally groove-bound H_2TMpyP. The Zn complex is $5 \sim 6$ coordinated with H_2O which has led in earlier work to the suggestion that steric hindrance prevents intercalation (4, 5).

We believe that the results given above can be used in any study of the drug molecules — DNA complexes as long as the position of the Raman shift of water, used as an internal standard for intensity measurements, does not overlap with that of the fluorescence spectrum of the drug molecules. However, by using the radiation of tunable lasers, experimental conditions can always be found to satisfy this requirement. This is particularly true if the molecular emission is induced with laser light tuned to the position of the strong Soret band of porphyrin molecules in solution.

Acknowledgements

The authors wish to thank Dr. P. Myslinski and Ms. Yizhong Shen for discussions and advice. This research is in part supported by a grant from the National Science and Engineering Research Council of Canada (NSERC). One of us (Y.L.) is a visiting scientist funded by the Network of Centers of Excellence Programme in association with NSERC.

1. R. J. FIEL, J. C. HOWARD, E. H. MARK, and N. DATTA GUPTA. Nucleic Acids Res. **6**, 3093 (1979).
2. R. J. FIEL and B. R. MUNSON. Nucleic Acids Res. **8**, 2835 (1980).
3. M. J. CARVLIN, E. MARK, and R. J. FIEL. Nucleic Acids Res. **11**, 6141 (1983).
4. M. J. CARVLIN and R. J. FIEL. Nucleic Acids Res. **11**, 6121 (1983).
5. R. F. PASTERNACK, E. J. GIBBS, and J. J. VILLAFRANCA. Biochemistry, **22**, 2406 (1983).
6. R. F. PASTERNACK, E. J. GIBBS, and J. J. VILLAFRANCA. Biochemistry, **22**, 5409 (1983).
7. R. F. PASTERNACK, A. ANTEBI, B. EHRLICH, D. SIDNEY, E. J. GMIBBS, S. L. BASSNER, and L. M. DEPOY. J. Mol. Catal. **23**, 235 (1984).
8. R. F. PASTERNACK, E. J. GIBBS, A. GAUDEMER, A. ANTEBI, S. L. BASSNER, L. M. DEPOY, D. H. TURNER, A. WILLIAMS, F. LAPLACE, M. H. LANSARD, C. MERIENNE, and M. PERRE-FAUVET. J. Am. Chem. Soc. **107**, 8179 (1985).
9. J. M. KELLY, M. J. MURPHY, D. J. MCCONNEL, and C. OHUIGIN. Nucleic Acids Res. **13**, 167 (1985).
10. N. E. GEACINTOV, V. IBANEZ, M. ROUGEE, and R. V. BENSASSON. Biochemistry, **26**, 3087 (1987).
11. P. MYSLINSKI, Y. SHEN, and J. A. KONINGSTEIN. To be published.
12. B. LI and A. B. MYERS. J. Phys. Chem. **94**, 4051 (1990).
13. S. P. A. FODOR, R. A. COPELAND, C. A. GRYGON, and T. G. SPIRO. J. Am. Chem. Soc. **111**, 5509 (1989).
14. R. F. PASTERNACK, P. R. HUBER, P. BOYD, G. ENGASSER, L. FRANCESCONI, E. GIBBS, P. FASELLA, G. C. VENTURO, and L. DE C. HINDS. J. Am. Chem. Soc. **94**, 4511 (1972).
15. J. A. KONINGSTEIN. J. Raman Spectrosc. **20**, 83 (1989).

Can. J. Chem. Downloaded from www.nrcresearchpress.com by 84.41.108.74 on 09/07/12
For personal use only.

TABLE 1. Experimental determinations of heat capacities of *n*-heptanoic acid (R = 8.3145 J K^{-1} K^{-1} mol^{-1})

T/K	$C_{p,m}/R$	T/K	$C_{p,m}/R$	T/K	$C_{p,m}/R$	T/K	$C_{p,m}/R$	T/K	$C_{p,m}/R$
Series I		$\Delta_{trs}H$ Detn. A		246.68	27.46	77.40	9.556	206.71	20.11
203.57	19.83	224.59	22.56	249.43	28.33	81.14	9.555	212.99	20.89
209.86	20.59	226.15	23.06	257.32	29.54	85.12	10.363	216.75	21.21
215.93	21.52	231.20	23.96	255.29	31.57	89.37	10.762	218.08	21.86
219.11	410	236.14	24.79	258.02	35.56	93.87	11.147	219.35	25.56
220.40	41.4	237.48	24.88	260.38	45.33	98.39	11.509	219.821	—
225.10	23.14	$\Delta_{fus}H$ Detn. F		262.17	69.18	103.17	11.892	219.611	—
230.63	23.97	$\Delta_{fus}H$ Detn. G		263.30	122	108.20	12.309	219.586	451
235.66	24.91	272.43	30.30	264.06	190	113.23	12.706	219.624	305
240.52	25.97	273.99	31.02	264.53	270	118.28	13.079	219.704	270
247.52	27.82			264.80	490	123.34	13.446	219.826	181
256.00	33.77	Series V		265.21	1070	128.41	13.829	220.042	110
261.88	70.6	207.31	20.28	265.456	2960	133.50	14.179	220.490	33.6
264.36	230	212.31	20.92	265.458	6270	138.58	14.552	221.14	26.94
265.22	330	$\Delta_{trs}H$ Detn. B		265.475	1740	143.65	14.924	221.93	23.02
265.46	1090	224.63	23.09	265.495	1460	148.75	15.24	222.77	22.78
265.49	6690	228.58	23.54	265.516	1630	153.84	15.61	223.63	22.60
265.51	1690	232.45	24.17	265.535	2190	158.94	15.95	224.48	23.02
265.54	3550	236.87	25.11	265.580	899	164.04	16.325		
265.60	1550	$\Delta_{fus}H$ Detn. H		268.19	30.55			Series XIII	
269.17	36.81	$\Delta_{fus}H$ Detn. I		271.27	30.64	Series XII		215.03[a]	19.28
277.01	30.84	274.63	30.86	274.35	30.77	5.99	0.052	219.77	26.61
		280.28	31.13	277.41	30.88	6.74	0.070	224.18	22.70
Series II				280.46	31.06	7.49	0.101	228.82	23.50
213.33	21.23	Series VI		283.49	31.23	8.26	0.136	233.32	24.30
214.84[b]	21.42	207.81	20.22	286.57	31.38	9.04	0.178	237.68	25.30
224.44	23.02	212.80	20.90			9.93	0.232		
234.03	24.72	$\Delta_{trs}H$ Detn. C		Series X		10.89	0.300	Series XIV	
235.42	24.98	223.89	22.88	160.20	16.05	11.87	0.379	217.01[b]	21.73
239.87	25.99	226.20	23.08	165.62	16.46	12.87	0.469	221.46[b]	22.41
247.15	28.02			170.71	16.82	13.83	0.563	225.80[b]	23.06
253.83	31.47	Series VII		175.81	17.23	14.89	0.684	230.02	23.80
259.43	43.53	207.32[a]	20.14	180.90	17.67	16.09	0.826	234.13	24.52
262.90	101	212.35[a]	20.76	185.99	18.10	17.31	0.978	238.14	25.31
264.33	302	$\Delta_{trs}H$ Detn. D		191.10	18.50	18.54	1.143	252.52	48.01
264.86	634	223.41	23.00	196.18	19.03	19.79	1.318	265.14	1740
265.11	1020	225.72	23.00	201.27	19.60	21.10	1.510	265.49	1050
265.27	1630	229.15	23.50	206.35	20.14	22.46	1.720		
265.38	2340	233.65	24.39	211.42	20.83	23.83	1.936	Series XV	
265.46	2570	$\Delta_{fus}H$ Detn. J		214.68	21.29	25.22	2.161	265.44	746
265.53	3810	$\Delta_{fus}H$ Detn. K		216.14	21.46	26.61	2.390	265.48	1020
265.67	440	268.68	190	217.58	21.75	28.02	2.626	265.52	1440
266.59	82	275.24	30.80	218.87	40.7	29.49	2.871	265.552	2060
269.05	30.71	280.88	31.08	219.006	21.83	31.00	3.127	265.537	8180
271.94	30.44			219.022	47.6	32.52	3.389	265.447	750
274.78	30.68	Series VIII		219.085	44.7	34.06	3.649	265.548	1140
277.62	30.98	209.82	20.40	219.592	—	35.60	3.912	265.561	1190
280.47	30.84	213.63	21.14	219.771	48.8	37.24	4.187	265.574	1190
		220.62	36.84	221.33	24.85	38.98	4.468	265.90	980
Series III		227.25	23.46	222.93	22.75	40.73	4.752	265.679	270
212.74	20.90			224.65	22.87	42.48	5.031	266.44	30.49
214.25	21.23	Series IX		226.36	23.12	44.24	5.307	267.79	30.51
216.95	58.59	207.83	20.30	228.06	23.31	46.11	5.599	269.14	30.62
218.84	47.01	212.83	20.88			48.07	5.898	270.49	30.62
220.71	35.23	$\Delta_{trs}H$ Detn. E		Series XI		50.04	6.186	275.16	30.75
223.54	22.88	223.88	22.92	56.37	7.084	52.02	6.479	283.10	31.20
225.11	22.80	226.19	23.12	58.59	7.381	54.24	6.784	290.95	31.62
		229.61	23.72	61.37	7.740	56.71	7.119	298.70	32.05
Series IV		234.09	24.55	64.23	8.104	81.28	9.976	306.46	32.54
213.15	20.96	238.43	25.44	67.21	8.454	127.41	13.724	314.48	33.04
214.74	21.16	241.76	25.96	70.44	8.809	173.56	16.941	322.69	33.57
		244.11	26.66	73.92	9.188	200.21	19.355	330.89	34.21
								339.08	34.85
								344.74	35.14
								347.83	35.48

[a]Note used in fitting procedure.
[b]Undercooling points (metastable Phase I).

Can. J. Chem. Downloaded from www.nrcresearchpress.com by 84.41.108.74 on 09/07/12
For personal use only.

Can. J. Chem. Downloaded from www.nrcresearchpress.com by 84.41.108.74 on 09/07/12
For personal use only.

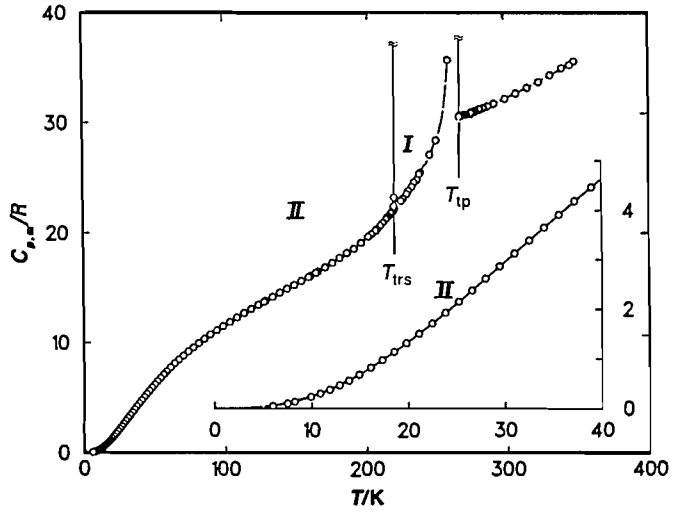


FIG. 1. Heat capacity versus temperature curve of heptanoic acid. Phase designations are given by Roman numbers.

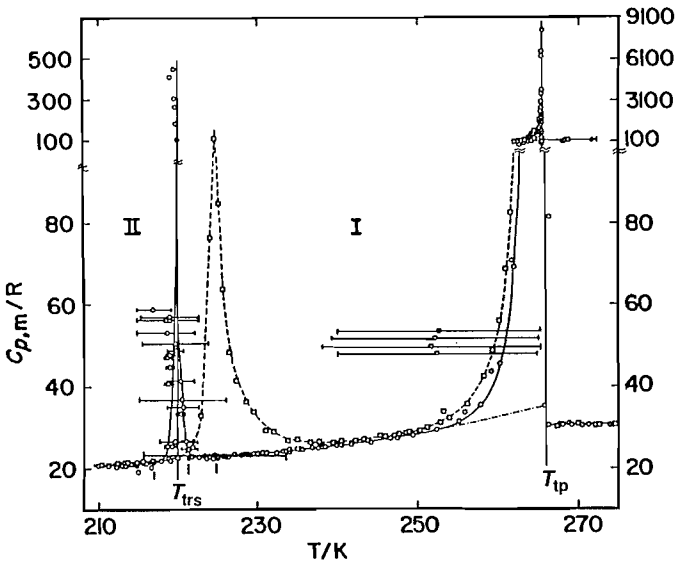


FIG. 2. Expanded heat-capacity curve of heptanoic acid in the transition/fusion regions. —○—, this work; ---□--- ref. 3. Lattice heat-capacity contributions are indicated by dashed line. The three undercooled (metastable) Phase I points of Series XIV are indicated by ●. Horizontal bars designate the temperature range of enthalpy-type determinations.

tion, is presumably occasioned by their failure to cool their sample low enough to convert between enantiotropic forms of the acid.

In our measurements on cooling slowly to 212 K (Series II), no excess transitional enthalpy was observed on an enthalpy determination. Subsequently, we cooled rapidly to 215 K (Series XIV) and were able to make heat capacity measurements on the Phase I over its region of metastability below the transition. These (three) metastable values are displayed in Fig. 2. These values coincide with those of Phase II and hence provide a firm basis for devising a lattice heat-capacity trend smoothly through the transition region despite the fact that the transition by its sharpness, high heat-capacity values ($\approx 400R$), and undercooling phenomena is characteristically first-order. The sharpness of our transition is noticeably more pronounced than that of Schaake *et al.* (3) as seen in Fig. 2.

Fusion

Five sets of runs were made through the melting region; these results also are shown in Table 2. The lattice line for Phase I, drawn through the transition region in Series XIV, is extrapolated to continue the lattice curve to T_{tp}. The enthalpy of fusion is $(1820 \pm 1)R$ K and corresponds to an entropy of fusion $(6.891 \pm 0.004)R$.

Fractional fusion

The nonlinearity of the curve of equilibrium melting temperatures from the Series II determinations (Table 1) as further delineated in Table 3 versus the reciprocal of the fraction melted ($1/F$) are treated by the approach of Mastrangelo and Dornte (10) for solid-soluble/liquid-soluble contaminates. The curvature of the T versus $1/F$ plot for this sample, shown in Fig. 4, suggests that at least part of the impurities are certainly present to some extent in solid solution with heptanoic acid. The form of the melting equation suitable in the presence of solid solution formation is (10):

$$T = T_{tp} - x_2 R T_{tp}^2 \{\Delta_{fus} H_m^0 [F + K(1 - K^{-1}]\}^{-1}$$

in which x_2 is the mole fraction of impurity, T_{tp} is the triple-point temperature, T is the equilibrium temperature of the determinations, $\Delta_{fus}H_m^0$ is the enthalpy of fusion, F is the fraction melted, and K is the partition coefficient. The $K(1 - K)^{-1}$ factor corrects the upward concavity of the otherwise linear plot of T versus $1/F$ (if $K = 0$) in the absence of solubility of the impurity in the solid phase and rectifies the plot for $0 < K < 1$. To determine K, values at $T_{1.00}$, $T_{0.50}$, and $T_{0.25}$

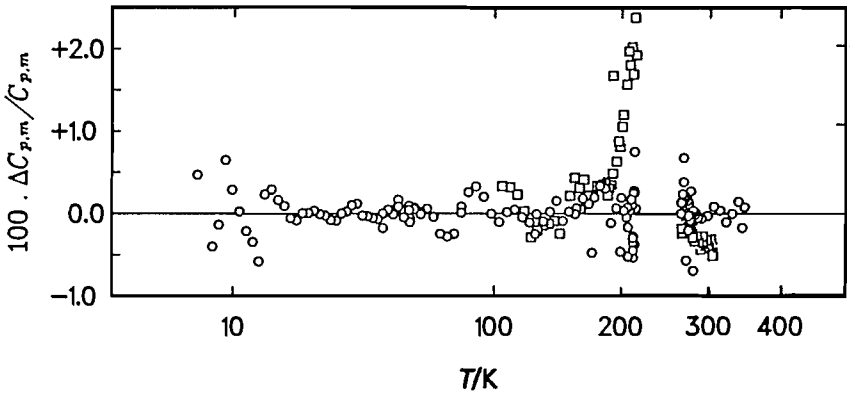


FIG. 3. Deviation plot for heptanoic acid sample with respect to our smoothed curve. ○, this work; □, ref. 3 (a $T^{1/3}$ scale was used to arbitrarily spread the individual data points.)

Can. J. Chem. Downloaded from www.nrcresearchpress.com by 84.41.108.74 on 09/07/12
For personal use only.

TABLE 2. Summary of transition and fusion thermophysical quantities for heptanoic acid (R = 8.3145 J K^{-1} mol^{-1})

Detn. and Series	No. of Detns.	T_1/K	T_2/K	$\Delta_{T_1}^{T_2}H_m^0/R$ K	$\Delta_{215\text{ K}}^{225\text{ K}}H_m^0/R$ K	$\Delta_{215\text{ K}}^{225\text{ K}}S_m^0/R$
Transition II → I						
I	4	212.95	228.07	582.9	469.2[a]	
III	5	215.00	225.90	489.6	468.9[a]	
Detn. A(IV)	2	215.54	225.37	454.8	463.5[a]	
Detn. B(V)	2	214.8	226.63	513.2	470.9[a]	
Detn. C(VI)	2	215.30	225.055	474.9	480.6	
Detn. D(VII)	2	214.82	224.57	482.2	481.6	
Detn. E(IX)	2	215.32	225.04	475.2	481.7	
XII	16	216.06	224.90	451.5	482.1	
Graphical integration					469.9[a]	2.138 ± 0.002
Mean value					481.5 ± 0.6	
Lattice contribution					221.3 ± 1	1.006 ± 0.006
				$\Delta_{trs}H_m^0$(II–I)/R K =	260.2 ± 1	$\Delta_{trs}S_m^0$(II–I)/R = 1.132 ± 0.006
$\Delta_{II}^{I}H_m^0/R$ K = 260.2 ± 1 $\Delta_{II}^{I}S_m^0/R$ = 1, 132 ± 0.004						
Fusion						
I	11	242.91	271.79	2733.6	2452.02	
II	13	243.63	270.48	2641.8	2451.4	
Detns. F and G (IV)	2	238.11	271.69	2821.9	2450.6	
Detns. H and I (V)	2	239.36	271.79	2795.9	2451.8	
Detns. J and K (VII)	2	240.13	272.40	2794.4	2451.0	
Graphical integration					2450.5[a]	9.320 ± 0.002
Mean value					2451.4 ± 0.6	
Lattice contribution					631.7 ± 1	2.429 ± 0.004
				$\Delta_{fus}H_m^0/R$ K =	1819.7 ± 1	$\Delta_{fus}S_m^0/R$ = 6.891 ± 0.004

[a]These values were not used in determination of the mean for reasons indicated in text.

TABLE 3. Series II fractional melting data for heptanoic acid (R = 8.3145 J K^{-1} mol^{-1})

T/K	$C_{p,m}/R$	ΔT/K	$\Sigma\Delta H/R$ K	T^a/K	F^{-1} [b]	$[F + K(1 - K)^{-1}]^{-1}$
264.32	980	0.749	400	264.70	4.545	3.0668
264.86	2030	0.320	593	265.02	3.067	2.3139
265.11	3420	0.190	791	265.21	2.299	1.8485
265.27	4070	0.131	991	265.34	1.835	1.5357
265.38	7360	0.089	1193	265.43	1.524	1.3127
265.46	8860	0.073	1396	265.50	1.303	1.1447
265.53	12100	0.054	1598	265.55	1.138	1.0157
265.57	13000	0.025	1697	265.58	1.072	0.9622
	Triple point of sample			265.60 ± 0.01		
	Triple point of pure compound			265.98 ± 0.01		
	Mole fraction impurity			0.0103 + 0.0003		
	Partition coefficient, K			0.093 + 0.003		

[a]Equilibrium temperature.
[b]F = fraction melted.

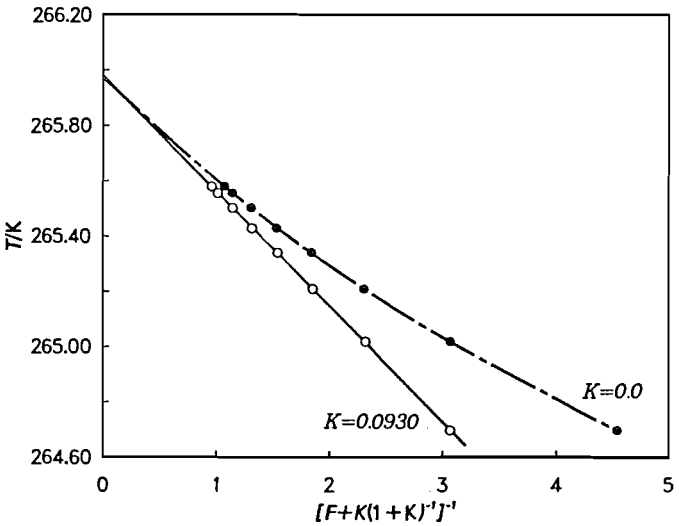


FIG. 4. Plot of the equilibrium temperature versus functions of the fraction melted for heptanoic acid. F is the fraction melted and K is the partition coefficient. The experimental values with $K = 0$ are represented by ● 's and the - - - line. The same values with $K = 0.0930$ for the solid-solution approach are shown as ○ 's with a continuous line.

are read off the ordinary curve at $1/F$ values of 1, 2, and 4 and are then substituted in the expression for K and the process is reiterated until K and T_{tp} values converge.

In this treatment, the T_{tp} and x_2 values obtained from the expressions $T_{tp} = T_{1.00} + (T_{1.00} - T_{0.50})(1 + K)(1 - K)^{-1}$ and $x_2 = (\Delta_{fus}H_m^0)/(RT_{tp}^2)(T_{1.00} - T_{0.50})(1 + K)(1 - K)^{-2}$ are $K = 0.093 \pm 0.003$, $x_2 = 0.0103 \pm 0.0003$, and $T_{tp} = (265.98 \pm 0.01)K$. The literature values for the triple point of **C7H** are 265.83 K (3), 261.75 K (1, 2), 266.02 K (5), 266.05 K (12), and 265.69 K (13).

The summary of fractional melting data is shown in Table 4. In Table 5, a comparison of observed transition and fusion temperatures and thermodynamic property increments with literature values is provided. Although our sample is purer than that of Schaake *et al.* (3) the similarity of the K values suggests similarity in the nature of the impurities.

The solubility of the impurity in the solid phase revealed by the value of K and the somewhat higher purity of our sample judged by the same criterion may explain the observed slightly higher fusion temperature and the much lower transition temeprature than those reported by Schaake *et al.* (3).

As noted by previous investigators (2–4) the thermodynamic sums of thermophysical enthalpies (or entropies) of fusion and solid/solid transition for odd n n-alkanoic acids (neglecting small temperature effects) nearly match the trend of the same properties of fusion for the even acids. Since our Phases II and I are identified as α- and β-phases, respectively, in earlier literature, it can be seen readily in Fig. 5 (in which the solid lines essentially represent the $\Delta_{trs}H_m^0$) that the enthalpies of fusion of the even compounds are well represented by the sums for the odd compounds. The trends as n gets small are attributed to hydrogen bonding (11).

In Fig. 6, the enthalpies of fusion of the odd acids and those of transition for the odd acids are plotted separately against the total number n of carbon atoms. The increment in the entropies of fusion of odd members with increasing length of the carbon chain is probably related to the packing of the methylene groups in the crystalline Phase I state (1, 2), but the magnitude of enthalpies of transition of the Phase I to the Phase II form of the odd acids are not as smoothly dependent on n as are the enthalpies of fusion at the triple point. This

TABLE 4. Thermodynamic properties of heptanoic acid (R = 8.3145 J K^{-1} mol^{-1})

T/K	$C_{p,m}/R$	$\Delta_0^T S_m^0(T)/R$	$\Delta_0^T H_m^0(T)/R$ K	$\phi_m^0(T,0)/R$
		Phase II		
0	0	0	0	0
5	0.030	0.010	0.038	0.002
10	0.236	0.080	0.599	0.020
15	0.694	0.254	2.828	0.066
20	1.349	0.540	7.871	0.146
25	2.125	0.923	16.519	0.262
30	2.960	1.384	29.218	0.410
35	3.808	1.904	46.140	0.585
40	4.636	2.466	67.26	0.785
45	5.428	3.059	92.44	1.004
50	6.180	3.670	121.48	1.240
60	7.565	4.922	190.36	1.749
70	8.764	6.180	272.13	2.292
80	9.841	7.422	365.24	2.856
90	10.806	8.638	468.58	3.431
100	11.656	9.821	581.0	4.011
120	13.199	12.084	829.7	5.170
140	14.646	14.229	1108.4	6.312
160	16.04	16.27	1415.1	7.431
180	17.58	18.25	1750.9	8.524
200	19.41	20.19	2119.9	9.594
215[a]	21.36	21.66	2424.8	10.38
219.99[b]	(450)	(22.16)	(2533.5)	(10.65)
	[22.13]	[22.16]	[2533.5]	[10.65]
		Phase I		
219.99[b]	(450)	(23.29)	(2780.7)	(10.65)
	[22.13]	[22.16]	[2533.5]	[10.65]
225	22.94	(23.80)	(2893.1)	(10.94)
	[22.94]	[22.67]	[2646.2]	[10.91]
230	23.79	(24.31)	(3010.2)	(11.22)
	[23.79]	[23.18]	[2763.0]	[11.17]
240	23.79	(25.36)	(3257.6)	(11.79)
	[23.79]	[24.23]	[3010.4]	[10.69]
250	25.77	(26.47)	(3528.7)	(12.36)
	[25.77]	[25.34]	[3281.5]	[12.22]
265.98[c]	(35.29)	(28.44)	(4037.6)	(13.26)
	[35.23]	[27.31]	[3790.4]	[13.06]
		Liquid		
265.98[c]	(30.47)	(35.33)	(5857.3)	(13.26)
	[35.23]	[27.31]	[3790.4]	[13.06]
270	30.60	35.79	5980.1	13.64
280	31.04	36.91	6165	14.89
298.15	32.15	38.89	6737	16.29
300	32.15	39.09	6769	16.53
325	33.78	41.72	7593	18.36
350	(35.67)	(44.29)	(8459)	(20.12)

[a]Quantities in square brackets represent estimated heat capacities at indicated temperature.

[b]Quantities in parentheses represent estimated heat capacities or other thermodynamic functions estimated on the assumption that the transition is truly isothermal at the transition temperature indicated.

[c]Assuming the melting is truly isothermal at the triple point.

Can. J. Chem. Downloaded from www.nrcresearchpress.com by 84.41.108.74 on 09/07/12
For personal use only.

TABLE 5. Summary of transition and fusion thermophysics for heptanoic acid (R = 8.3145 J K^{-1} mol^{-1})

Transition			Fusion				
T_{trs}/K	$\Delta_{trs}H_m^0/R$ K	$\Delta_{trs}S_m^0/R$	T_{tp}/K	$\Delta_{fus}H_m^{0\,a}/R$ K	$\Delta_{fus}S_m^0/R$	10^2x	Reference
$219.9_9 \pm 0.2$	260.2 ± 1	1.132 ± 0.004	265.98 ± 0.01	1820.7 ± 1.5	6.89 ± 0.01	1.03 ± 0.03	This work
224.8 ± 1	245.1 ± 4.6	1.09 ± 0.02	265.83 ± 0.01	1856.7 ± 6.6	6.98 ± 0.03	1.54	3
— No transition found —			261.75	1802	6.88		1,2
— No transition found —			266.02 ± 0.10	1744 ± 70	6.55 ± 0.26	0.1	5
			266.05				9
			265.69				10

[a] x is the mole fraction of impurity in the sample on the basis of fractional fusion (see text).

Can. J. Chem. Downloaded from www.nrcresearchpress.com by 84.41.108.74 on 09/07/12
For personal use only.

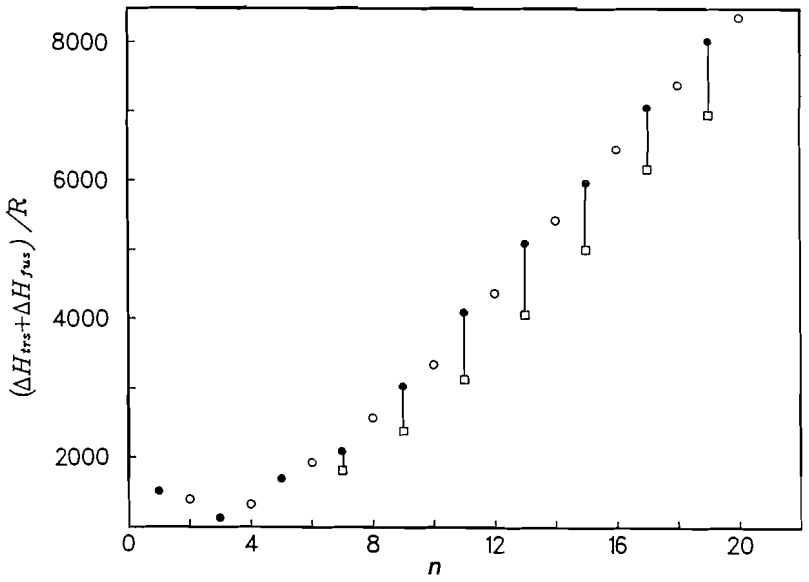


FIG. 5. Experimental $\Delta_{fus}H_m^0/R$ (even acids), ○, or $(\Delta_{fus}H_m^0 + \Delta_{trs}H_m^0)/R$ (odd acids $n > 3$), ●. The □'s (representing the transitions) are plotted relative to the fusion curve, thus the length of the solid lines indicate the magnitude of $\Delta_\beta{}^\alpha H_m^0/R$ (transition values), rather than their position relative to the abscissa. References: for $n = 7$, this work; for $n \neq 7$, ref. 3.

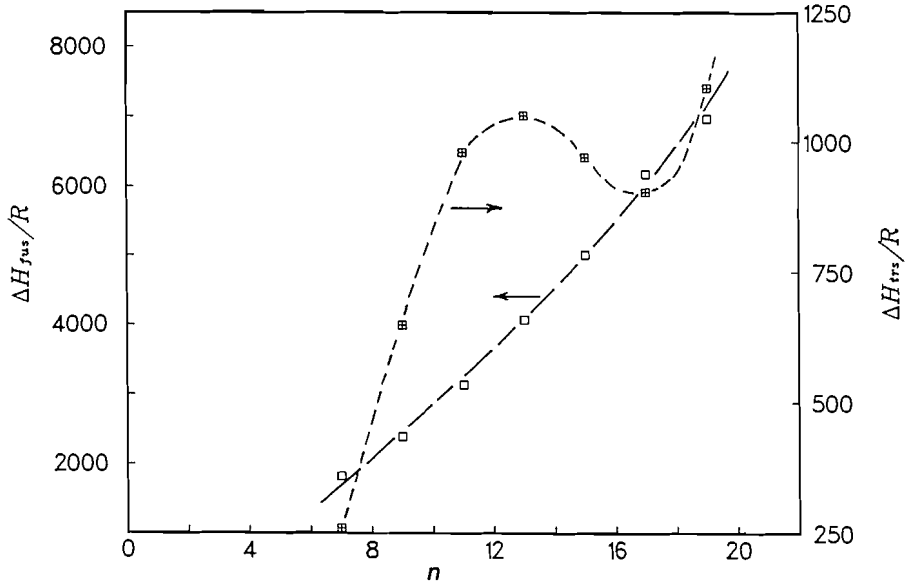


FIG. 6. Experimental enthalpies of transition ⊞ and fusion □ for odd normal alkanoic acids plotted against the total number n of carbon atoms. (□) $\Delta_{fus}H^0/R$ (see left abscissa) and (⊞) $\Delta_{trs}H^0/R$ (α and β conversion) (see right abscissa) (references as in Fig. 5.)

may possibly be the consequence of the freedom of the alkane chain or the presence of a disturbing factor (1, 2).

1. W. E. GARNER, F. C. MADDEN, and J. E. RUSHBROOKE. J. Chem. Soc. **127**, 2491 (1926).
2. W. E. GARNER and F. C. RANDALL. J. Chem. Soc. **125**, 881 (1924).
3. R. C. F. SCHAAKE, J. C. VAN MILTENBURG, and C. G. DE KRUIF. J. Chem. Thermodyn. **14**, 763 (1982).
4. R. C. F. SCHAAKE, J. C. VAN MILTENBURG, and C. G. DE KRUIF. J. Chem. Thermodyn. **14**, 771 (1982).
5. N. ADRIAANSE, H. DEKKER, and J. COOPS. Recl. Trav. Chim. Pays-Bas, **83**, 557 (1964).
6. A. K. LABBAN, F. L. LOPEZ DE LA FUENTE, J. A. R. CHEDA, E. F. WESTRUM, JR., and F. FERNANDEZ-MARTIN. J. Chem. Thermodyn. **21**, 375 (1989).
7. F. FERNANDEZ-MARTIN, F. L. LOPEZ DE LA FUENTE, J. A. R. CHEDA, and E. F. WESTRUM, JR. XXI Bienal Real Sociedad Exp. Quim. 1986.
8. E. F. WESTRUM, JR., G. T. FURUKAWA, and J. P. MCCULLOUGH. *In* Experimental thermodynamics. Vol. I. *Edited by* J. P. McCullough and D. W. Scott. Butterworths, London. 1968. p. 133.
9. E. F. WESTRUM, JR. Proceedings NATO Advanced Study Institute on Thermochemistry, Viana do Castello. 1983. *Edited by* M. A. V. Ribeiro da Silva. Reidel, New York. 1984. p. 745.
10. S. V. R. MASTRANGELO and R. W. DORNTE. J. Am. Chem. Soc. **77**, 6200 (1955).
11. J. L. DERISSEN. Ph.D. Thesis, Rijksuniversiteit, Utrecht. 1970.
12. E. S. LUTTON. *In* Fatty acid. Part 4. 2nd ed. *Edited by* K. S. Markley. Wiley, New York. 1967. p. 2585.
13. R. BILTERYS and J. GISSELEIRE. Bull. Soc. Chim. Belg. **44**, 567 (1935).

Can. J. Chem. Downloaded from www.nrcresearchpress.com by 84.41.108.74 on 09/07/12
For personal use only.

Heat capacity and thermophysical properties of *n*-heptanoic acid from 5 to 350 K

ABDUL KARIMEH LABBAN[1] AND EDGAR FRANCIS WESTRUM, JR.[2]
Department of Chemistry, University of Michigan, Ann Arbor, MI 48109, U.S.A.

AND

JOSE ANTONIO RODRIGUEZ CHEDA
Physical Chemistry Department, Chemical Faculty, Universidad Complutense, 28040 Madrid, Spain

Received May 31, 1991

This paper is dedicated to Dr. Richard Norman Jones

ABDUL KARIMEH LABBAN, EDGAR FRANCIS WESTRUM, JR., and JOSE ANTONIO RODRIGUEZ. Can. J. Chem. **69**, 1796 (1991).

The sub-ambient heat capacity of heptanoic acid is characterized by a first order transition at 219.99 K which shows a $C_{p,m}$ maximum greater than $400R$ and $\Delta_{trs}S_m^0$ of $1.132R$. The acid melts at the triple point 265.98 K and shows a $C_{p,m}$ maximum greater than $8200R$ and $\Delta_{fus}S_m^0$ of $6.891R$. At 298.15 K the values of $\Delta_0^{T\ K}S_m^0$, $\Delta_0^{T\ K}H_m^0$, and $\Phi_m(T,0)$ are $38.89R$, $6737R$ K, and $16.29R$. Prior measurements by Adriaanse *et al.* (1964) with a micro calorimeter between 173 and the melting point did not reveal the transition, nor did the method-of-mixtures ("drop") calorimetry of Garner *et al.* (1924) between 213 K and the melting point although they claim to have confirmed the presence of both distinct crystalline phases. The somewhat greater measurement range of Schaake *et al.* (1982) — from 104 to 304 K — by adiabatic calorimetry on a characterized sample did reveal the transition albeit at a temperature 4.8 K higher and with 4% less entropy of transition (double the combined estimated standard deviation).

Key words: *n*-heptanoic acid, heat capacity, transitions, triple point.

ABDUL KARIMEH LABBAN, EDGAR FRANCIS WESTRUM, JR. et JOSE ANTONIO RODRIGUEZ. Can. J. Chem. **69**, 1796 (1991).

La capacité calorifique de l'acide heptanoïque à des températures inférieures à la température ambiante est caractérisée par une transition du premier ordre à 219,99 K qui présente un $C_{p,m}$ maximum qui est supérieur à $400R$ et un $\Delta_{trs}S_m^0$ de $1,132R$. L'acide fond au point triple de 265,98 K et présente un $C_{p,m}$ supérieur à $8200R$ et du $\Delta_{fus}S_m^0$ de $6,891R$. À 298,15 K, les valeurs du $\Delta_0^{T\ K}S_m^0$, $\Delta_0^{T\ K}H_m^0$ et $\Phi_m(T,0)$ sont égales à $38,89R$, $6737R$ K et $16,29R$. Des mesures antérieures effectuées par Adiaanse *et al.* (1964), à l'aide d'un microcalorimètre, à des températures allant de 173 au point de fusion, n'ont pas permis de détecter la transition; il en a été de même pour la calorimétrie des méthodes de mélange («abaissement») de Garner *et al.* (1924) réalisée entre 213 K et le point de fusion, même s'ils ont affirmé avoir confirmé la présence des deux phases cristallines distinctes. Les résultats de Schaake *et al.* (1982), obtenus à partir de mesures s'étalant de 104 à 304 K effectuées à l'aide de la calorimétrie adiabatique sur un échantillon caractérisé, ont révélés la transition même si sa transition est 4,8 K plus élevée et que l'entropie de transition est 4% plus faible (deux fois les écarts types combinés calculés).

Mots clés : acide *n*-heptanoïque, capacité calorifique, transitions, point triple.

[Traduit par la rédaction]

Introduction

Heptanoic acid — $CH_3(CH_2)_5COOH$ hereafter (**C7H**) — has special relevance in biology, industry, and environmental pollution and its fusion and the transition processes in the acid have been previously studied. The heat capacity of heptanoic acid was studied by Garner *et al.* (1, 2) by drop (method of mixtures) calorimetry from 213 K to its melting point, but no transition was found below the melting point. They claim, however, to have confirmed the presence of two (α- and β-) enantiotropic forms seen in the other odd acids of this series. These forms have different enthalpies of crystallization as a consequence of the differences in the crystal structure. Schaake *et al.* (3, 4) studied several odd- and even-linear alkanoic acids and the low-temperature heat capacity of heptanoic acid from 104 to 304 K by equilibrium adiabatic calorimetry and found a solid/solid transition at 224.8 K. The heat capacity of a 99.9% pure heptanoic acid has been measured from 173 K to the melting point by Adriaanse *et al.* (5) with a microcalorimeter; they found no transition between 173 K and the melting point.

Although the prevailing discrepancy in the thermophysical properties of heptanoic acid in the region of the transition can possibly be explained by the failure of both Garner and Adriaanse to cool the sample to a temperature low enough to convert it to the α-enantiotropic form stable at lower temperatures, our heat-capacity measurements are extended to cover the entire range between 5 and 350 K, to complete the morphology of heat capacity curve, to provide more reliable thermodynamic values, to explore the nature of the transition, and to provide data for comparison with planned subsequent measurements on the acid (**C7H**)/salt(**C7Tl**) complex (6, 7).

A sharp solid/solid, first-order, phase transition is observed in this study (the phases designated here as II and I correspond to α-, β-forms in the literature) and new and more precise values of the transition temperature and increments T_{trs}, $\Delta_{trs}H^0$, $\Delta_{trs}S^0$, and the corresponding values for the triple point (tp) are determined as well as the thermophysical properties derived from smoothed values C_p from 5 to 350 K.

Experimental

Sample provenance

The sample used in this study was prepared from commercial (Fluka Company) heptanoic acid; their assay of the purity indicated 98%. The acid was subsequently purified by the following procedure. First it was freed from neutral and basic impurities by dissolving it in aqueous KOH and extracting with dry diethyl ether. The aqueous phase was acidified with HCl, again extracted with dry diethyl ether, and the extract washed several times with distilled water. The basifi-

[1]Present address: Department of Chemistry, Hebron University, Hebron, Israel.

[2]Author to whom correspondence may be addressed.

Can. J. Chem. Downloaded from www.nrcresearchpress.com by 84.41.108.74 on 09/07/12
For personal use only.

cation and acidification processing was done on an equimolar basis. This extract was dried over magnesium sulphate for several days and the diethyl ether removed by distillation. Then the acid was fractionally distilled at 1.8 kPa; the boiling point at this pressure is 337 K.

The acid was stored under an argon atmosphere to prevent the absorption of water. The purity determined by gas–liquid chromatography with mass spectrometric sensor technique (University of Michigan, Mass Spectrometry Laboratory) indicated a value of (99.72 ± 0.02)% purity, and about (0.30 ± 0.02)% of organic impurities, such as 0.1% in each of the following: acetate, diethyl ether, and hexanoic acid or isomeric heptanoic acids. In addition, the sample analyzed by d.s.c. indicated a value of 99.5% purity. The loading process was done in a dry He atmosphere to avoid contamination and absorption of water.

Calorimetric technique

The sample (mass = 49.637 g) was loaded into a gold-plated, OFHC copper calorimeter, laboratory designation W-AB. This corresponds to an amount-of-substance factor of 2.62287 mol^{-1} with a molar mass of 130.1090 g mol^{-1} on the basis of the 1978 IUPAC relative atomic masses. The buoyancy corrections were calculated assuming a density of 0.916 g cm^{-3}. Following evacuation, 5.1 kPa of purified helium were added to the calorimeter to enhance thermal equilibration. The calorimeter was sealed within the vacuum chamber by a screw cap (activated by a remotely operating hexagonal wrench) which pressed a gold gasket against the circular knife edge on the stainless-steel neck of the calorimeter.

The calorimetric measurements were made in the Mark XIII cryostat described previously (8). This calorimeter uses intermittent-heating, adiabatic, equilibrium methods. The programming, data logging, and calorimetry were done by computerization as described elsewhere (9). All measurements of mass, time, resistance, etc., were referred to calibrations of the National Bureau of Standards.

To achieve approximate thermal equilibration in mapping runs, the sample was kept for at least two hours after the heating periods at each determination in the region of transition and fusion for Series XII and II; even so, at best semi-equilibration was achieved. The enthalpy increments are, however, based on (equilibrium) enthalpy-type runs across the entire transition region.

The thermal history of the C7H sample is shown by the linear array (solid arrows indicate cooling and dashed arrows indicate data acquisition ranges for various series of heat capacity or enthalpy increment measurements when so specified or more rarely simply a heating period):

$$310\ \text{K} \xrightarrow{16\ \text{h}} 156\ \text{K} \xrightarrow[\text{Series I}]{12\ \text{h}} 281\ \text{K} \xrightarrow{16.7\ \text{h}} 212\ \text{K} \xrightarrow[\text{Series II}]{27\ \text{h}} 282\ \text{K} \xrightarrow{19.5\ \text{h}} 150\ \text{K} \dashrightarrow[\text{Series III}]{4\ \text{h}} 225\ \text{K} \xrightarrow{17\ \text{h}} 211\ \text{K} \dashrightarrow[\text{Series IV}]{9.3\ \text{h}} 275\ \text{K}$$

$$\xrightarrow{13\ \text{h}} 108\ \text{K} \dashrightarrow[\text{Series V}]{11.5\ \text{h}} 283\ \text{K} \xrightarrow{10.7\ \text{h}} 196\ \text{K} \dashrightarrow{12\ \text{h}} 205\ \text{K} \dashrightarrow[\text{Series VI}]{3\ \text{h}} 227\ \text{K} \xrightarrow{9.4\ \text{h}} 170\ \text{K} \dashrightarrow{2\ \text{h}} 205\ \text{K}$$

$$\dashrightarrow[\text{Series VII}]{10\ \text{h}} 284\ \text{K} \xrightarrow{10.5\ \text{h}} 194\ \text{K} \dashrightarrow{2\ \text{h}} 204\ \text{K} \dashrightarrow[\text{Series VIII}]{4\ \text{h}} 228\ \text{K} \xrightarrow{18\ \text{h}} 162\ \text{K} \dashrightarrow{1\ \text{h}} 205\ \text{K} \dashrightarrow[\text{Series IX}]{20\ \text{h}} 228\ \text{K}$$

$$\xrightarrow{52\ \text{h}} 262\ \text{K} \dashrightarrow{3.5\ \text{h}} 301\ \text{K} \xrightarrow{20.5\ \text{h}} 157\ \text{K} \dashrightarrow[\text{Series X}]{14\ \text{h}} 228\ \text{K} \xrightarrow{30\ \text{h}} 55\ \text{K} \dashrightarrow[\text{Series XI}]{12\ \text{h}} 166\ \text{K} \xrightarrow{29\ \text{h}} 5.7\ \text{K} \dashrightarrow[\text{Series XII}]{56\ \text{h}} 225\ \text{K}$$

$$\xrightarrow{7\ \text{h}} 212\ \text{K} \dashrightarrow[\text{Series XIII}]{3\ \text{h}} 240\ \text{K} \xrightarrow{2\ \text{h}} 215\ \text{K} \dashrightarrow[\text{Series XIV}]{7.7\ \text{h}} 265.5\ \text{K} \dashrightarrow{10.4\ \text{h}} 300\ \text{K} \xrightarrow{6.4\ \text{h}} 265.4\ \text{K} \dashrightarrow[\text{Series XV}]{21\ \text{h}} 349\ \text{K}$$

Results and discussion

Heat capacity

The values of $C_{p,m}/R$ at the mean temperature of each measurement (arranged in chronological order so the magnitude of ΔT employed usually can be inferred from the increments in mean temperatures) are listed in Table 1 and diagrammed in Fig. 1. Details of the heat capacity peaks are shown in Fig. 2. Apart from transition and melting regions, the numerical data have been fitted to appropriate orthogonal polynomials on the basis of which the relevant smoothed heat capacities were calculated at selected temperatures. The heat capacity of the sample at low temperature ranged from 93% of that of sample plus calorimeter at 10 K, to a minimum of 78% at 118 K, and gradually increased to 86% above 300 K, except in the transition and melting regions. The standard deviations in the heat-capacity values are 3.0% at 6 K and decrease to 0.2% at 20 K and to less than 0.1% above 50 K.

Schaake *et al.* (3) reported the heat capacity of heptanoic acid only from 104 to 304 K. The deviation of their data from the smoothed curve of the present measurement is shown in Fig. 3. No significant difference below the transition and above the melting point between our sample and their relatively less pure sample is observed, except in the region near transition and fusion as shown in Figs. 2 and 3.

II–I transition

In the present measurements, the II–I transition in the heat capacity was observed at 219.99 K, a temperature substantially lower than the 224.8 K value observed by Schaake *et al.* (3). The magnitude of $\Delta_{trs}H_m^0$ is (260.2 ± 1)R K for the present work, and about 6% higher than the reported value of (245.1 ± 4.6)R K for the previous work (3). These differences can be attributed to the higher purity of the sample in the present work. The enhanced maximum heat capacity observed at the peaks in our measurements, as well as the more nearly isothermal nature of our transition further reinforce this point. The solid/solid transition occurs reproducibly at equilibrium (on heating) at a temperature lower by 4.8 K than their reported value.

In the course of the measurements eight sets of heat-capacity and enthalpy-type determinations were made through the anomalous region from an initial temperature, T_1, to a final temperature, T_2, as summarized in Table 2. Series I, III, IV, and V are not included in the average even though the measurements were taken at different cooling rates through the transition, and some (Series I, III, and V) to relatively low temperatures. The low results found are probably accounted for by some inadequacy in the phase conversion. That Garner *et al.* (1, 2) and Adriaanse *et al.* (5) did not find the transi-

Can. J. Chem. Downloaded from www.nrcresearchpress.com by 84.41.108.74 on 09/07/12
For personal use only.

TABLE 1. Experimental determinations of heat capacities of *n*-heptanoic acid (R = 8.3145 J K^{-1} K^{-1} mol^{-1})

T/K	$C_{p,m}/R$	T/K	$C_{p,m}/R$	T/K	$C_{p,m}/R$	T/K	$C_{p,m}/R$	T/K	$C_{p,m}/R$
Series I		$\Delta_{trs}H$ Detn. A		246.68	27.46	77.40	9.556	206.71	20.11
203.57	19.83	224.59	22.56	249.43	28.33	81.14	9.555	212.99	20.89
209.86	20.59	226.15	23.06	257.32	29.54	85.12	10.363	216.75	21.21
215.93	21.52	231.20	23.96	255.29	31.57	89.37	10.762	218.08	21.86
219.11	410	236.14	24.79	258.02	35.56	93.87	11.147	219.35	25.56
220.40	41.4	237.48	24.88	260.38	45.33	98.39	11.509	219.821	—
225.10	23.14	$\Delta_{fus}H$ Detn. F		262.17	69.18	103.17	11.892	219.611	—
230.63	23.97	$\Delta_{fus}H$ Detn. G		263.30	122	108.20	12.309	219.586	451
235.66	24.91	272.43	30.30	264.06	190	113.23	12.706	219.624	305
240.52	25.97	273.99	31.02	264.53	270	118.28	13.079	219.704	270
247.52	27.82			264.80	490	123.34	13.446	219.826	181
256.00	33.77	Series V		265.21	1070	128.41	13.829	220.042	110
261.88	70.6	207.31	20.28	265.456	2960	133.50	14.179	220.490	33.6
264.36	230	212.31	20.92	265.458	6270	138.58	14.552	221.14	26.94
265.22	330	$\Delta_{trs}H$ Detn. B		265.475	1740	143.65	14.924	221.93	23.02
265.46	1090	224.63	23.09	265.495	1460	148.75	15.24	222.77	22.78
265.49	6690	228.58	23.54	265.516	1630	153.84	15.61	223.63	22.60
265.51	1690	232.45	24.17	265.535	2190	158.94	15.95	224.48	23.02
265.54	3550	236.87	25.11	265.580	899	164.04	16.325		
265.60	1550	$\Delta_{fus}H$ Detn. H		268.19	30.55			Series XIII	
269.17	36.81	$\Delta_{fus}H$ Detn. I		271.27	30.64	Series XII		215.03[a]	19.28
277.01	30.84	274.63	30.86	274.35	30.77	5.99	0.052	219.77	26.61
		280.28	31.13	277.41	30.88	6.74	0.070	224.18	22.70
Series II				280.46	31.06	7.49	0.101	228.82	23.50
213.33	21.23	Series VI		283.49	31.23	8.26	0.136	233.32	24.30
214.84[b]	21.42	207.81	20.22	286.57	31.38	9.04	0.178	237.68	25.30
224.44	23.02	212.80	20.90			9.93	0.232		
234.03	24.72	$\Delta_{trs}H$ Detn. C		Series X		10.89	0.300	Series XIV	
235.42	24.98	223.89	22.88	160.20	16.05	11.87	0.379	217.01[b]	21.73
239.87	25.99	226.20	23.08	165.62	16.46	12.87	0.469	221.46[b]	22.41
247.15	28.02			170.71	16.82	13.83	0.563	225.80[b]	23.06
253.83	31.47	Series VII		175.81	17.23	14.89	0.684	230.02	23.80
259.43	43.53	207.32[a]	20.14	180.90	17.67	16.09	0.826	234.13	24.52
262.90	101	212.35[a]	20.76	185.99	18.10	17.31	0.978	238.14	25.31
264.33	302	$\Delta_{trs}H$ Detn. D		191.10	18.50	18.54	1.143	252.52	48.01
264.86	634	223.41	23.00	196.18	19.03	19.79	1.318	265.14	1740
265.11	1020	225.72	23.00	201.27	19.60	21.10	1.510	265.49	1050
265.27	1630	229.15	23.50	206.35	20.14	22.46	1.720		
265.38	2340	233.65	24.39	211.42	20.83	23.83	1.936	Series XV	
265.46	2570	$\Delta_{fus}H$ Detn. J		214.68	21.29	25.22	2.161	265.44	746
265.53	3810	$\Delta_{fus}H$ Detn. K		216.14	21.46	26.61	2.390	265.48	1020
265.67	440	268.68	190	217.58	21.75	28.02	2.626	265.52	1440
266.59	82	275.24	30.80	218.87	40.7	29.49	2.871	265.552	2060
269.05	30.71	280.88	31.08	219.006	21.83	31.00	3.127	265.537	8180
271.94	30.44			219.022	47.6	32.52	3.389	265.447	750
274.78	30.68	Series VIII		219.085	44.7	34.06	3.649	265.548	1140
277.62	30.98	209.82	20.40	219.592	—	35.60	3.912	265.561	1190
280.47	30.84	213.63	21.14	219.771	48.8	37.24	4.187	265.574	1190
		220.62	36.84	221.33	24.85	38.98	4.468	265.90	980
Series III		227.25	23.46	222.93	22.75	40.73	4.752	265.679	270
212.74	20.90			224.65	22.87	42.48	5.031	266.44	30.49
214.25	21.23	Series IX		226.36	23.12	44.24	5.307	267.79	30.51
216.95	58.59	207.83	20.30	228.06	23.31	46.11	5.599	269.14	30.62
218.84	47.01	212.83	20.88			48.07	5.898	270.49	30.62
220.71	35.23	$\Delta_{trs}H$ Detn. E		Series XI		50.04	6.186	275.16	30.75
223.54	22.88	223.88	22.92	56.37	7.084	52.02	6.479	283.10	31.20
225.11	22.80	226.19	23.12	58.59	7.381	54.24	6.784	290.95	31.62
		229.61	23.72	61.37	7.740	56.71	7.119	298.70	32.05
Series IV		234.09	24.55	64.23	8.104	81.28	9.976	306.46	32.54
213.15	20.96	238.43	25.44	67.21	8.454	127.41	13.724	314.48	33.04
214.74	21.16	241.76	25.96	70.44	8.809	173.56	16.941	322.69	33.57
		244.11	26.66	73.92	9.188	200.21	19.355	330.89	34.21
								339.08	34.85
								344.74	35.14
								347.83	35.48

[a]Note used in fitting procedure.
[b]Undercooling points (metastable Phase I).

Can. J. Chem. Downloaded from www.nrcresearchpress.com by 84.41.108.74 on 09/07/12
For personal use only.

Can. J. Chem. Downloaded from www.nrcresearchpress.com by 84.41.108.74 on 09/07/12
For personal use only.

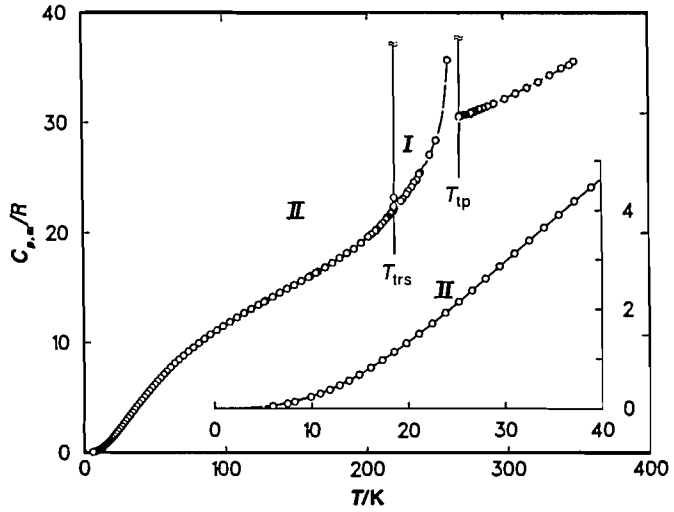


FIG. 1. Heat capacity versus temperature curve of heptanoic acid. Phase designations are given by Roman numbers.

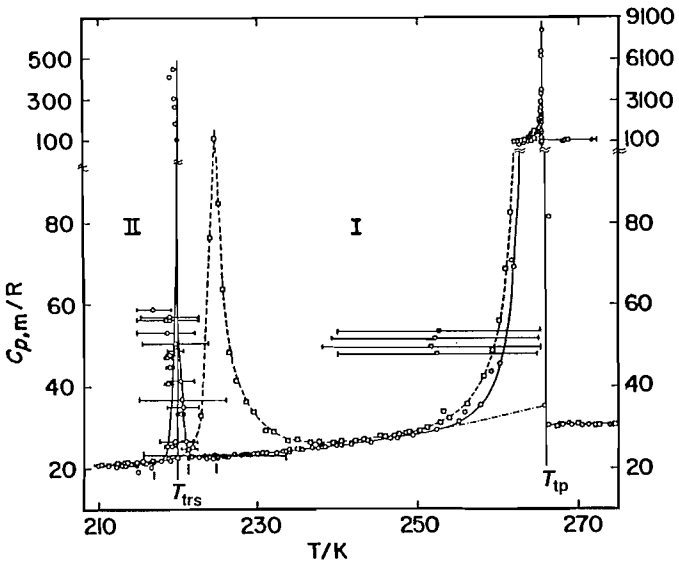


FIG. 2. Expanded heat-capacity curve of heptanoic acid in the transition/fusion regions. —○—, this work; ---□--- ref. 3. Lattice heat-capacity contributions are indicated by dashed line. The three undercooled (metastable) Phase I points of Series XIV are indicated by ●. Horizontal bars designate the temperature range of enthalpy-type determinations.

tion, is presumably occasioned by their failure to cool their sample low enough to convert between enantiotropic forms of the acid.

In our measurements on cooling slowly to 212 K (Series II), no excess transitional enthalpy was observed on an enthalpy determination. Subsequently, we cooled rapidly to 215 K (Series XIV) and were able to make heat capacity measurements on the Phase I over its region of metastability below the transition. These (three) metastable values are displayed in Fig. 2. These values coincide with those of Phase II and hence provide a firm basis for devising a lattice heat-capacity trend smoothly through the transition region despite the fact that the transition by its sharpness, high heat-capacity values ($\approx 400R$), and undercooling phenomena is characteristically first-order. The sharpness of our transition is noticeably more pronounced than that of Schaake *et al.* (3) as seen in Fig. 2.

Fusion

Five sets of runs were made through the melting region; these results also are shown in Table 2. The lattice line for Phase I, drawn through the transition region in Series XIV, is extrapolated to continue the lattice curve to T_{tp}. The enthalpy of fusion is $(1820 \pm 1)R$ K and corresponds to an entropy of fusion $(6.891 \pm 0.004)R$.

Fractional fusion

The nonlinearity of the curve of equilibrium melting temperatures from the Series II determinations (Table 1) as further delineated in Table 3 versus the reciprocal of the fraction melted ($1/F$) are treated by the approach of Mastrangelo and Dornte (10) for solid-soluble/liquid-soluble contaminates. The curvature of the T versus $1/F$ plot for this sample, shown in Fig. 4, suggests that at least part of the impurities are certainly present to some extent in solid solution with heptanoic acid. The form of the melting equation suitable in the presence of solid solution formation is (10):

$$T = T_{tp} - x_2 R T_{tp}^2 \{\Delta_{fus} H_m^0 [F + K(1 - K^{-1}]\}^{-1}$$

in which x_2 is the mole fraction of impurity, T_{tp} is the triple-point temperature, T is the equilibrium temperature of the determinations, $\Delta_{fus}H_m^0$ is the enthalpy of fusion, F is the fraction melted, and K is the partition coefficient. The $K(1 - K)^{-1}$ factor corrects the upward concavity of the otherwise linear plot of T versus $1/F$ (if $K = 0$) in the absence of solubility of the impurity in the solid phase and rectifies the plot for $0 < K < 1$. To determine K, values at $T_{1.00}$, $T_{0.50}$, and $T_{0.25}$

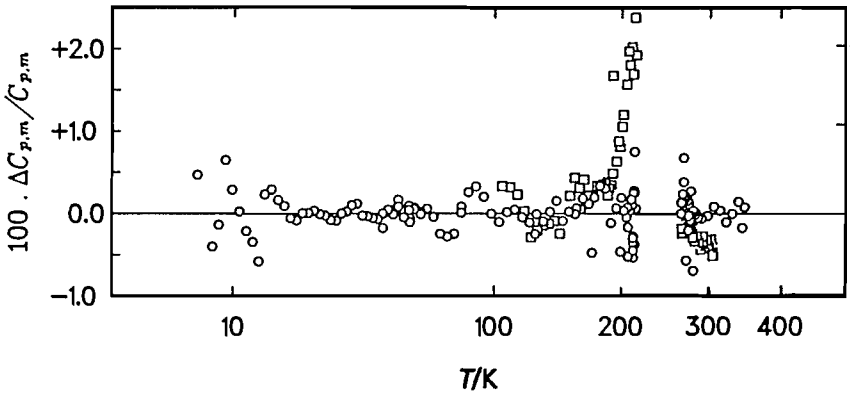


FIG. 3. Deviation plot for heptanoic acid sample with respect to our smoothed curve. ○, this work; □, ref. 3 (a $T^{1/3}$ scale was used to arbitrarily spread the individual data points.)

Can. J. Chem. Downloaded from www.nrcresearchpress.com by 84.41.108.74 on 09/07/12
For personal use only.

TABLE 2. Summary of transition and fusion thermophysical quantities for heptanoic acid (R = 8.3145 J K^{-1} mol^{-1})

Detn. and Series	No. of Detns.	T_1/K	T_2/K	$\Delta_{T_1}^{T_2}H_m^0/R$ K	$\Delta_{215\text{ K}}^{225\text{ K}}H_m^0/R$ K	$\Delta_{215\text{ K}}^{225\text{ K}}S_m^0/R$
Transition II → I						
I	4	212.95	228.07	582.9	469.2[a]	
III	5	215.00	225.90	489.6	468.9[a]	
Detn. A(IV)	2	215.54	225.37	454.8	463.5[a]	
Detn. B(V)	2	214.8	226.63	513.2	470.9[a]	
Detn. C(VI)	2	215.30	225.055	474.9	480.6	
Detn. D(VII)	2	214.82	224.57	482.2	481.6	
Detn. E(IX)	2	215.32	225.04	475.2	481.7	
XII	16	216.06	224.90	451.5	482.1	
Graphical integration					469.9[a]	2.138 ± 0.002
Mean value					481.5 ± 0.6	
Lattice contribution					221.3 ± 1	1.006 ± 0.006
				$\Delta_{trs}H_m^0$(II–I)/R K =	260.2 ± 1	$\Delta_{trs}S_m^0$(II–I)/R = 1.132 ± 0.006
$\Delta_{II}^{I}H_m^0/R$ K = 260.2 ± 1 $\Delta_{II}^{I}S_m^0/R$ = 1, 132 ± 0.004						
Fusion						
I	11	242.91	271.79	2733.6	2452.02	
II	13	243.63	270.48	2641.8	2451.4	
Detns. F and G (IV)	2	238.11	271.69	2821.9	2450.6	
Detns. H and I (V)	2	239.36	271.79	2795.9	2451.8	
Detns. J and K (VII)	2	240.13	272.40	2794.4	2451.0	
Graphical integration					2450.5[a]	9.320 ± 0.002
Mean value					2451.4 ± 0.6	
Lattice contribution					631.7 ± 1	2.429 ± 0.004
				$\Delta_{fus}H_m^0/R$ K =	1819.7 ± 1	$\Delta_{fus}S_m^0/R$ = 6.891 ± 0.004

[a]These values were not used in determination of the mean for reasons indicated in text.

TABLE 3. Series II fractional melting data for heptanoic acid (R = 8.3145 J K^{-1} mol^{-1})

T/K	$C_{p,m}/R$	ΔT/K	$\Sigma\Delta H/R$ K	T^a/K	F^{-1} [b]	$[F + K(1 - K)^{-1}]^{-1}$
264.32	980	0.749	400	264.70	4.545	3.0668
264.86	2030	0.320	593	265.02	3.067	2.3139
265.11	3420	0.190	791	265.21	2.299	1.8485
265.27	4070	0.131	991	265.34	1.835	1.5357
265.38	7360	0.089	1193	265.43	1.524	1.3127
265.46	8860	0.073	1396	265.50	1.303	1.1447
265.53	12100	0.054	1598	265.55	1.138	1.0157
265.57	13000	0.025	1697	265.58	1.072	0.9622
	Triple point of sample			265.60 ± 0.01		
	Triple point of pure compound			265.98 ± 0.01		
	Mole fraction impurity			0.0103 + 0.0003		
	Partition coefficient, K			0.093 + 0.003		

[a]Equilibrium temperature.
[b]F = fraction melted.

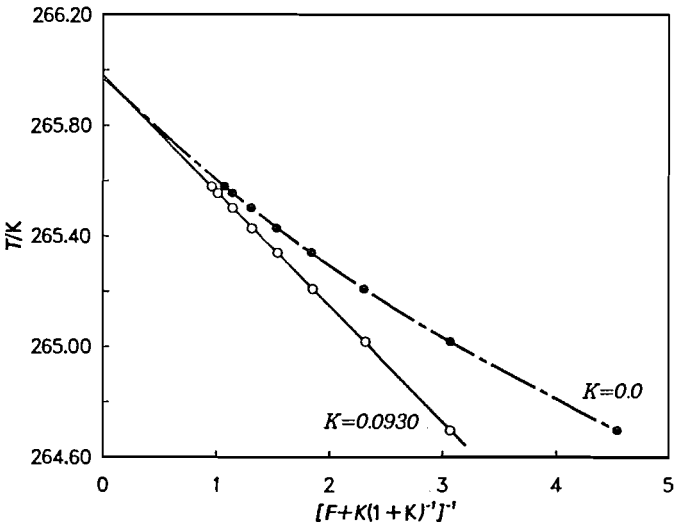


FIG. 4. Plot of the equilibrium temperature versus functions of the fraction melted for heptanoic acid. F is the fraction melted and K is the partition coefficient. The experimental values with $K = 0$ are represented by ● 's and the - - - line. The same values with $K = 0.0930$ for the solid-solution approach are shown as ○ 's with a continuous line.

are read off the ordinary curve at $1/F$ values of 1, 2, and 4 and are then substituted in the expression for K and the process is reiterated until K and T_{tp} values converge.

In this treatment, the T_{tp} and x_2 values obtained from the expressions $T_{tp} = T_{1.00} + (T_{1.00} - T_{0.50})(1 + K)(1 - K)^{-1}$ and $x_2 = (\Delta_{fus}H_m^0)/(RT_{tp}^2)(T_{1.00} - T_{0.50})(1 + K)(1 - K)^{-2}$ are $K = 0.093 \pm 0.003$, $x_2 = 0.0103 \pm 0.0003$, and $T_{tp} = (265.98 \pm 0.01)K$. The literature values for the triple point of **C7H** are 265.83 K (3), 261.75 K (1, 2), 266.02 K (5), 266.05 K (12), and 265.69 K (13).

The summary of fractional melting data is shown in Table 4. In Table 5, a comparison of observed transition and fusion temperatures and thermodynamic property increments with literature values is provided. Although our sample is purer than that of Schaake *et al.* (3) the similarity of the K values suggests similarity in the nature of the impurities.

The solubility of the impurity in the solid phase revealed by the value of K and the somewhat higher purity of our sample judged by the same criterion may explain the observed slightly higher fusion temperature and the much lower transition temeprature than those reported by Schaake *et al.* (3).

As noted by previous investigators (2–4) the thermodynamic sums of thermophysical enthalpies (or entropies) of fusion and solid/solid transition for odd n n-alkanoic acids (neglecting small temperature effects) nearly match the trend of the same properties of fusion for the even acids. Since our Phases II and I are identified as α- and β-phases, respectively, in earlier literature, it can be seen readily in Fig. 5 (in which the solid lines essentially represent the $\Delta_{trs}H_m^0$) that the enthalpies of fusion of the even compounds are well represented by the sums for the odd compounds. The trends as n gets small are attributed to hydrogen bonding (11).

In Fig. 6, the enthalpies of fusion of the odd acids and those of transition for the odd acids are plotted separately against the total number n of carbon atoms. The increment in the entropies of fusion of odd members with increasing length of the carbon chain is probably related to the packing of the methylene groups in the crystalline Phase I state (1, 2), but the magnitude of enthalpies of transition of the Phase I to the Phase II form of the odd acids are not as smoothly dependent on n as are the enthalpies of fusion at the triple point. This

TABLE 4. Thermodynamic properties of heptanoic acid (R = 8.3145 J K^{-1} mol^{-1})

T/K	$C_{p,m}/R$	$\Delta_0^T S_m^0(T)/R$	$\Delta_0^T H_m^0(T)/R$ K	$\phi_m^0(T,0)/R$
		Phase II		
0	0	0	0	0
5	0.030	0.010	0.038	0.002
10	0.236	0.080	0.599	0.020
15	0.694	0.254	2.828	0.066
20	1.349	0.540	7.871	0.146
25	2.125	0.923	16.519	0.262
30	2.960	1.384	29.218	0.410
35	3.808	1.904	46.140	0.585
40	4.636	2.466	67.26	0.785
45	5.428	3.059	92.44	1.004
50	6.180	3.670	121.48	1.240
60	7.565	4.922	190.36	1.749
70	8.764	6.180	272.13	2.292
80	9.841	7.422	365.24	2.856
90	10.806	8.638	468.58	3.431
100	11.656	9.821	581.0	4.011
120	13.199	12.084	829.7	5.170
140	14.646	14.229	1108.4	6.312
160	16.04	16.27	1415.1	7.431
180	17.58	18.25	1750.9	8.524
200	19.41	20.19	2119.9	9.594
215[a]	21.36	21.66	2424.8	10.38
219.99[b]	(450)	(22.16)	(2533.5)	(10.65)
	[22.13]	[22.16]	[2533.5]	[10.65]
		Phase I		
219.99[b]	(450)	(23.29)	(2780.7)	(10.65)
	[22.13]	[22.16]	[2533.5]	[10.65]
225	22.94	(23.80)	(2893.1)	(10.94)
	[22.94]	[22.67]	[2646.2]	[10.91]
230	23.79	(24.31)	(3010.2)	(11.22)
	[23.79]	[23.18]	[2763.0]	[11.17]
240	23.79	(25.36)	(3257.6)	(11.79)
	[23.79]	[24.23]	[3010.4]	[10.69]
250	25.77	(26.47)	(3528.7)	(12.36)
	[25.77]	[25.34]	[3281.5]	[12.22]
265.98[c]	(35.29)	(28.44)	(4037.6)	(13.26)
	[35.23]	[27.31]	[3790.4]	[13.06]
		Liquid		
265.98[c]	(30.47)	(35.33)	(5857.3)	(13.26)
	[35.23]	[27.31]	[3790.4]	[13.06]
270	30.60	35.79	5980.1	13.64
280	31.04	36.91	6165	14.89
298.15	32.15	38.89	6737	16.29
300	32.15	39.09	6769	16.53
325	33.78	41.72	7593	18.36
350	(35.67)	(44.29)	(8459)	(20.12)

[a]Quantities in square brackets represent estimated heat capacities at indicated temperature.

[b]Quantities in parentheses represent estimated heat capacities or other thermodynamic functions estimated on the assumption that the transition is truly isothermal at the transition temperature indicated.

[c]Assuming the melting is truly isothermal at the triple point.

Can. J. Chem. Downloaded from www.nrcresearchpress.com by 84.41.108.74 on 09/07/12
For personal use only.

TABLE 5. Summary of transition and fusion thermophysics for heptanoic acid (R = 8.3145 J K^{-1} mol^{-1})

Transition			Fusion				
T_{trs}/K	$\Delta_{trs}H_m^0/R$ K	$\Delta_{trs}S_m^0/R$	T_{tp}/K	$\Delta_{fus}H_m^{0\,a}/R$ K	$\Delta_{fus}S_m^0/R$	10^2x	Reference
$219.9_9 \pm 0.2$	260.2 ± 1	1.132 ± 0.004	265.98 ± 0.01	1820.7 ± 1.5	6.89 ± 0.01	1.03 ± 0.03	This work
224.8 ± 1	245.1 ± 4.6	1.09 ± 0.02	265.83 ± 0.01	1856.7 ± 6.6	6.98 ± 0.03	1.54	3
— No transition found —			261.75	1802	6.88		1,2
— No transition found —			266.02 ± 0.10	1744 ± 70	6.55 ± 0.26	0.1	5
			266.05				9
			265.69				10

[a] x is the mole fraction of impurity in the sample on the basis of fractional fusion (see text).

Can. J. Chem. Downloaded from www.nrcresearchpress.com by 84.41.108.74 on 09/07/12
For personal use only.

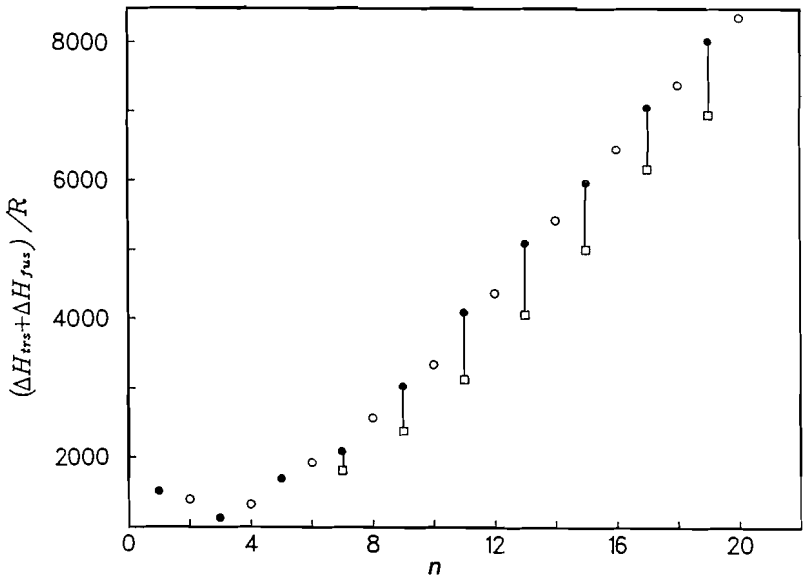


FIG. 5. Experimental $\Delta_{fus}H_m^0/R$ (even acids), ○, or $(\Delta_{fus}H_m^0 + \Delta_{trs}H_m^0)/R$ (odd acids $n > 3$), ●. The □'s (representing the transitions) are plotted relative to the fusion curve, thus the length of the solid lines indicate the magnitude of $\Delta_\beta{}^\alpha H_m^0/R$ (transition values), rather than their position relative to the abscissa. References: for $n = 7$, this work; for $n \neq 7$, ref. 3.

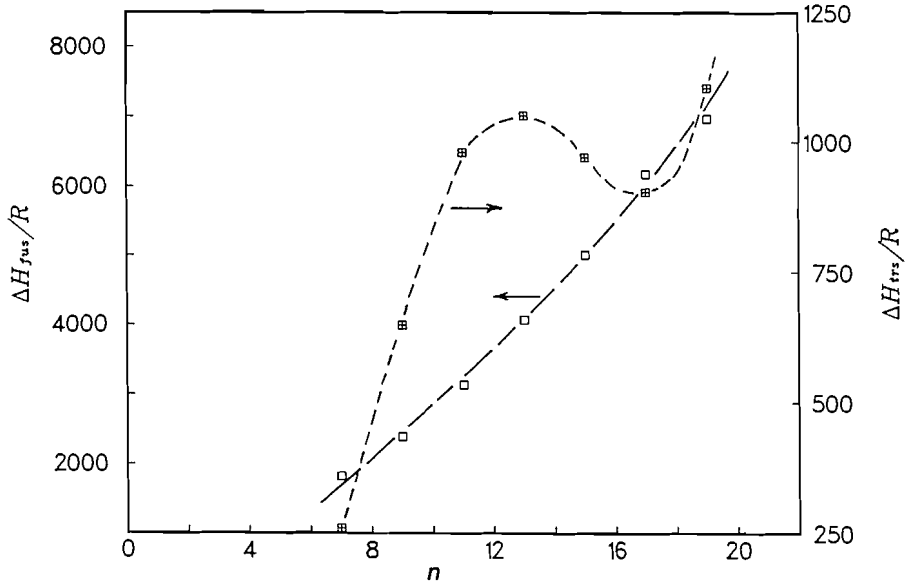


FIG. 6. Experimental enthalpies of transition ⊞ and fusion □ for odd normal alkanoic acids plotted against the total number n of carbon atoms. (□) $\Delta_{fus}H^0/R$ (see left abscissa) and (⊞) $\Delta_{trs}H^0/R$ (α and β conversion) (see right abscissa) (references as in Fig. 5.)

may possibly be the consequence of the freedom of the alkane chain or the presence of a disturbing factor (1, 2).

1. W. E. GARNER, F. C. MADDEN, and J. E. RUSHBROOKE. J. Chem. Soc. **127**, 2491 (1926).
2. W. E. GARNER and F. C. RANDALL. J. Chem. Soc. **125**, 881 (1924).
3. R. C. F. SCHAAKE, J. C. VAN MILTENBURG, and C. G. DE KRUIF. J. Chem. Thermodyn. **14**, 763 (1982).
4. R. C. F. SCHAAKE, J. C. VAN MILTENBURG, and C. G. DE KRUIF. J. Chem. Thermodyn. **14**, 771 (1982).
5. N. ADRIAANSE, H. DEKKER, and J. COOPS. Recl. Trav. Chim. Pays-Bas, **83**, 557 (1964).
6. A. K. LABBAN, F. L. LOPEZ DE LA FUENTE, J. A. R. CHEDA, E. F. WESTRUM, JR., and F. FERNANDEZ-MARTIN. J. Chem. Thermodyn. **21**, 375 (1989).
7. F. FERNANDEZ-MARTIN, F. L. LOPEZ DE LA FUENTE, J. A. R. CHEDA, and E. F. WESTRUM, JR. XXI Bienal Real Sociedad Exp. Quim. 1986.
8. E. F. WESTRUM, JR., G. T. FURUKAWA, and J. P. MCCULLOUGH. *In* Experimental thermodynamics. Vol. I. *Edited by* J. P. McCullough and D. W. Scott. Butterworths, London. 1968. p. 133.
9. E. F. WESTRUM, JR. Proceedings NATO Advanced Study Institute on Thermochemistry, Viana do Castello. 1983. *Edited by* M. A. V. Ribeiro da Silva. Reidel, New York. 1984. p. 745.
10. S. V. R. MASTRANGELO and R. W. DORNTE. J. Am. Chem. Soc. **77**, 6200 (1955).
11. J. L. DERISSEN. Ph.D. Thesis, Rijksuniversiteit, Utrecht. 1970.
12. E. S. LUTTON. *In* Fatty acid. Part 4. 2nd ed. *Edited by* K. S. Markley. Wiley, New York. 1967. p. 2585.
13. R. BILTERYS and J. GISSELEIRE. Bull. Soc. Chim. Belg. **44**, 567 (1935).

Can. J. Chem. Downloaded from www.nrcresearchpress.com by 84.41.108.74 on 09/07/12
For personal use only.

A study of the phase transition in semiconducting 1:2 tetracyanoquinodimethane charge transfer complexes with dipropylamine derivatives: X-ray structure and polarized reflection spectra[1]

KIM D. TRUONG, CLAUDE PÉPIN, AND ANDRÉ D. BANDRAUK
Laboratoire de chimie théorique, Faculté des sciences, Université de Sherbrooke, Sherbrooke (Québec), Canada J1K 2R1

MARC DROUIN AND ANDRÉ MICHEL
Laboratoire de chimie structurale, Faculté des sciences, Université de Sherbrooke, Sherbrooke (Québec), Canada J1K 2R1

AND

MARCEL BANVILLE
Département de physique, Faculté des sciences, Université de Sherbrooke, Sherbrooke (Québec), Canada J1K 2R1

Received June 6, 1991

This paper is dedicated to Dr. Richard Norman Jones

KIM D. TRUONG, CLAUDE PÉPIN, ANDRÉ D. BANDRAUK, MARC DROUIN, ANDRÉ MICHEL, and MARCEL BANVILLE. Can. J. Chem. **69**, 1804 (1991).

The donors dipropylamine (DPA), methyldipropylamine (MDPA), and ethyldipropylamine (EDPA) from 1:2 charge transfer complexes with the acceptor tetracyanoquinodimethane (TCNQ). All crystals in the above series are semiconductors and undergo a first-order phase transition at the temperature around 210 K as obtained from conductivity measurements. The X-ray structure of DPA–$(TCNQ)_2$ was obtained as a function of temperature, and shows a distinct order–disorder transition in the hydrogen-bond network between donors and acceptors. Polarized reflection spectra on single crystals of these compounds were measured as a function of temperature in the frequency range from 400 to 4000 cm^{-1}. A detailed study of the C≡N modes of TCNQ indicates this mode is strongly influenced by the transition due to it being hydrogen bonded to the donors. The reflection coefficients of the IR active A_g modes of TCNQ also undergo a sharp discontinuity at the transition temperature. These results are interpreted as due to a cooperative order–disorder and electronic spin – Peierls transition.

Key words: organic semiconductors, X-ray structure, polarized reflection spectra, phase transition, cooperative order–disorder transition, spin–Peierls transition.

KIM D. TRUONG, CLAUDE PÉPIN, ANDRÉ D. BANDRAUK, MARC DROUIN, ANDRÉ MICHEL et MARCEL BANVILLE. Can. J. Chem. **69**, 1804 (1991).

La dipropylamine (DPA), la méthyldipropylamine (MDPA) et l'éthyldipropylamine (EDPA) agissent comme donneurs pour former des complexes de transfert de charge 1 : 2 avec le tétracyanoquinométhane (TCNQ) qui agit comme accepteur. Tous les cristaux des séries sus-mentionnées sont des semi-conducteurs et, d'après les mesures de conductivité, ils subissent une transition de phase du premier ordre à une température d'environ 210 K. Faisant appel à la diffraction des rayons-X, on a déterminé la structure du complexe DPA–$(TCNQ)_2$ en fonction de la température; on observe une transition distincte ordre/désordre dans le réseau des liaisons hydrogènes entre donneurs et accepteurs. On a mesuré le spectre de réflexion polarisée de cristaux uniques en fonction de la température entre 400 et 4000 cm^{-1}. Une étude détaillée des modes C≡N du TCNQ indique que ce mode est fortement influencé par la transition; cet effet est dû au fait que cette liaison est impliquée dans une liaison hydrogène avec les donneurs. Les coefficients de réflexion des modes A_g du TCNQ actifs en infrarouge subissent aussi une discontinuité importante au niveau de la température de transition. On interprète ces résultats en fonction d'une transition coopérative ordre/désordre et spin électronique/Peierls.

Mots clés : semiconducteurs organiques, structure aux rayons-X, spectres de polarisation, transition de phase, transition coopérative ordre–désordre, transition spin–Peierls.

[Traduit par la rédaction]

Introduction

Organic low-dimensional materials attract much attention due to the extensive π-electron delocalization along 1D or 2D stacks of anions or cations. Some of these materials become superconductors. In general these materials exhibit Peierls or spin–Peierls transitions that strongly affect the optical, magnetic, and electrical properties of such systems (1, 2). Recently, these materials were examined for large optical nonlinearities (3).

In previous papers we examined the effect of hydrogen bonding between donors and acceptors (4–6). In particular, a 1:2 charge transfer series of crystals with dipropylamine (DPA) and its derivatives as donors and 7,7′,8,8′-tetracyanoquinodimethane (TCNQ) as acceptor exhibited unique electric, magnetic, and thermoelectric power (TEP) behaviour (7, 8). A dominant transition around the temperature T_c = 210 K showed an abrupt change of these properties. Measurements of the electrical conductivity and magnetic properties suggested the occurrence of an "inverse spin – Peierls" transition (8) because the lower temperature phase exhibited an increase in conductivity. Preliminary infrared (IR) spectra showed that A_g modes of the TCNQ anion became IR active and split into multiplets below the phase transition temperature T_c (7).

In the present paper we present both X-ray data and polarized reflection spectra in order to elucidate the nature of the transition in single crystals of these materials. The crystal structure of DPA–$(TCNQ)_2$ was obtained above and below T_c, leading to the conclusion that an order–disorder transition occurs in the hydrogen-bond network between donors

[1]Contribution from le Groupe de Recherches sur les Semiconducteurs et Diélectriques.

Can. J. Chem. Downloaded from www.nrcresearchpress.com by 84.41.108.74 on 09/07/12
For personal use only.

TABLE 1. Crystallographic parameters

Parameters	Value	
	293 K	193 K
Formula	$C_{30}H_{24}N_9$	$C_{30}H_{24}N_9$
Formula wt.	510.58	510.58
Space group	*P-1*	*P-1*
a, Å	6.5589(3)	12.896(1)
b, Å	7.9184(3)	7.8207(7)
c, Å	13.9179(6)	13.958(1)
α (°)	96.005(3)	95.603(7)
β (°)	98.779(3)	98.222(7)
ν (°)	103.331(3)	102.891(8)
Vol, Å^3	687.74(5)	1345.9(2)
D_c, g/cm	1.233	1.260
F(000)	275.92	533.85
Radiation	MoKα (0.71069)	MoKα (0.71069)
Monochromator	Graphite	Graphite
Temperature, deg K	293(1)	193(1)
Scan speed, deg/min^{-1}	2.7	2.7
Max, deg	22.5	22.5
No. unique reflections collected	1803	3460
No. reflections observed	1204	2335
Crystal dimensions	0.15 × 0.25 × 0.40	0.15 × 0.25 × 0.40
μ (MoKα), mm^{-1}	0.07	0.08
No. variables	190	361
Max (Δ/σ)	0.066	0.001
Secondary ext. coeff.	0.23(3)	0.14(2)
Goodness of fit	2.829	2.304
Agreement factors: *R*	0.057	0.047
Rw	0.037	0.034

and acceptors as the temperature is lowered below T_c. Detailed reflection spectra are presented for single crystals of DPA–$(TCNQ)_2$, MDPA–$(TCNQ)_2$, and EDPA–$(TCNQ)_2$, as a function of polarization. The changes in the reflectivity connected with the phase transition around 210 K are examined as a function of temperature. Transverse and longitudinal frequencies in the TCNQ anion stacks have been determined from the reflectance spectra by means of a Kramers–Kronig analysis. Correlation of the structural and spectral data suggests a cooperative order–disorder transition in the H-bond network and an electronic spin – Peierls transition in the conduction stack of TCNQ anions.

Experimental

Preparation and spectra

Single crystals of the materials were prepared by methods described elsewhere (7). Chemical analysis showed 1:2 stoichiometry. The crystals are triclinic (see below) and form in needles, the needle axis being *a*, the stacking axis of the TCNQ chains. In our spectral measurements, the light was polarized parallel and perpendicular to the TCNQ stacks. All measurements were taken as total reflectance, the standard used being evaporated aluminium. An FT-IR spectrometer BOMEM model DA3 was used for spectral measurements with a cooled detector of Ge doped with Cu in the frequency range 400 to 4000 cm^{-1}. A Perkin–Elmer polarizer (gold grid on AgBr) was used for polarization experiments. All measurements were done on single crystals a few mm long and up to 0.5 mm wide, with a very good S/N ratio for polarization parallel to the *a* axis.

Low-temperature spectra were obtained by thermally anchoring the sample to a controlled cold finger. The temperature was measured with thermocouples (Au chromel) with an accuracy of ±3 K.

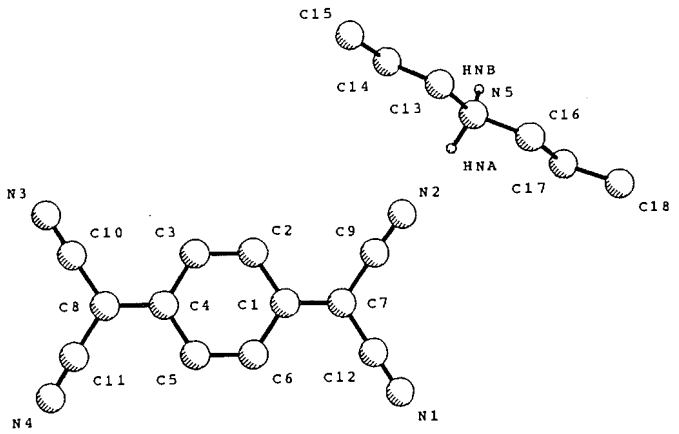


FIG. 1. TCNQ and DPA atom labelling.

X-ray crystallography[2]

The crystal data and experimental details are given in Table 1. The cell parameters were determined by least-squares refinement of the

[2]Tables of bond lengths and angles, atomic parameters for H and non-H atoms, and anisotropic thermal parameters for non-H atoms may be purchased from: The Depository of Unpublished Data, Document Delivery, CISTI, National Research Council Canada, Ottawa, Canada K1A 0S2.

Tables of bond lengths and angles and atomic parameters have also been deposited with the Cambridge Crystallographic Data Centre, and can be obtained on request from The Director, Cambridge Crystallographic Data Centre, University Chemical Laboratory, Lensfield Road, Cambridge CB2 1EW, U.K.

Can. J. Chem. Downloaded from www.nrcresearchpress.com by 84.41.108.74 on 09/07/12
For personal use only.

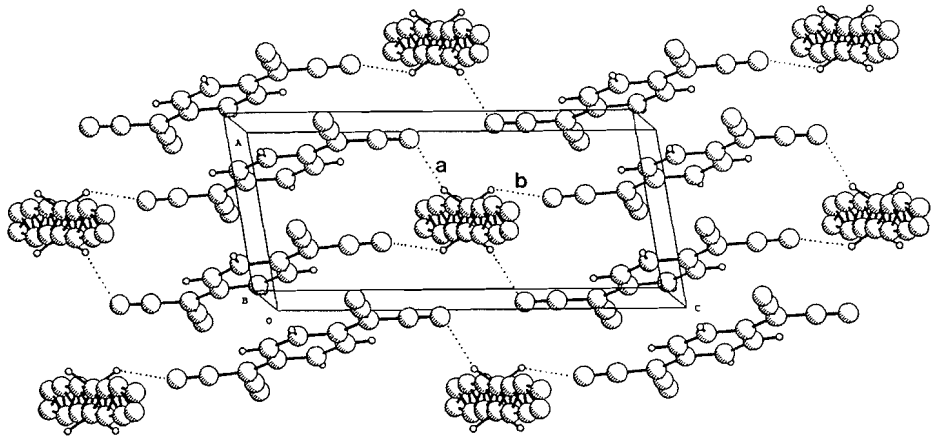


FIG. 2. Crystal structure at 293 K showing hydrogen bonds a,b. a(A) is the stacking axis.

TABLE 2. Bond distances (Å) and angles (deg) related to the hydrogen bonding

Bond N—H···N	Distances (esd's) N···N		H···N		Angles (esd's) N—H—N	
Temperature (K):	293	193	293	193	293	193
(a) N(5)—HNA···N(2)	3.058(8)	2.937(5)	2.20(6)	2.04(5)	136(4)	138(4)
(b) N(5)—HNB···N(4)	3.272(8)	3.021(5)	2.33(6)	1.95(5)	160(5)	168(4)

diffraction geometry of 24 accurately centered reflections. Data were collected at 293 and 193 K on an Enraf–Nonius CAD4 automated diffractometer using $\omega/2\theta$ scan technique. Two standard reflections were monitored every 60 min without significant deviation. The data were corrected for Lorentz and polarization effects. No correction was made for absorption. The structure was solved using direct methods. At 293 K, the DPA molecule is disordered. The N5 atom (Fig. 1) is located near the center of symmetry. The four hydrogens on the TCNQ molecule were located by Fourier difference, whereas those on the DPA that could not be located were geometrically placed. We decided to keep fixed the atomic parameters x, y, z, and u of DPA H atoms, since refinement gives unrealistic distances and angle values. All non-H atoms of the TCNQ were refined anisotropically and treated isotropically for the DPA. The structure at 193 K shows no disorder on the DPA. All hydrogens were geometrically placed and refined. The final cycles of the refinement process were carried out by full-matrix least squares on F, minimizing the function $\Sigma\omega\,(|F_o| - |F_c|)^2$ where ω is defined as $1/\sigma^2$ (F).

The NRCVAX system was used for all calculations (9). Scattering factors were those of Cromer and Waber (10). The highest peaks of residual electron density were respectively 0.28 and 0.18 e/Å^3 at 293 and 193 K. The secondary extinction coefficient was 0.23(3) and 0.14(2) at 293 and 193 K respectively (11, 12). Full detailed structures will be published in Acta Crystallographica (Sect. C).

X-ray structure of DPA–TCNQ$_2$

Above the critical temperature $T_c = 210$ K, the acceptor TCNQ's are stacked along the a(A) axis at equal distances of 3.27(3) Å. The donor DPA molecules are disordered by the thermal motions. Each DPA shares its two hydrogen bonds with four equivalent TCNQ's (Fig. 2). The N(5) atom (Fig. 1) is located at the inversion center. The two cyanide nitrogens N(2) and N(4) are H-bonded to N(5). Table 2 shows the H-bond distances and angles at two different temperatures, 293 and 193 K.

Below T_c, the DPA donor molecule is ordered. The asymmetric unit is doubled as well as the unit cell. The inversion center located at N(5) is lost because of the nonsymmetric DPA (Fig. 3). The TCNQ's are not equivalent as in the phase above T_c. The acceptor molecules stack as NMMN·NMMN tetramers. The MM planes are parallel. The distances separating MM and NN are 3.20(3) and 3.30(3) Å respectively. The former are H-bonded, the latter are not. The NM planes are not parallel, forming an angle of 2.22(5)°. In the unit cell, the two DPA's are oriented in such a way to H-bond only the M-TCNQ's. The M planes are linked together via two H-bonds from separate DPA's. Each DPA links two separate M-TCNQ's, so that two neighbouring sheets of H-bonded TCNQ's and DPA's are separated by two adjacent sheets of non H-bonded (isolated) N-TCNQ's. The DPA H-bonds in neighbouring sheets point towards each other, whereas in the high-temperature, disordered phase, these are randomly distributed.

Reflectance spectra

In Fig. 4 we present the reflectance spectra of DTA–(TCNQ)$_2$ for polarization parallel to the a stacking axis as a function of temperature. The broad features at 295 K are identical to those found in many other TCNQ organic conductors (13–16). We observe five distinct large TCNQ vibration bands around 700, 1200, 1300, 1600, and 2200 cm^{-1}, which are usually associated with IR active A_g modes of the TCNQ anion (4, 14). These bands appear at almost the same frequency in the case of the deuterated compound DPA$_d$–(TCNQ)$_2$, and the derivatives MDPA–(TCNQ)$_2$ and EDPA–(TCNQ)$_2$ (Figs. 5–7). For cations of bigger size, such as MDPA and EDPA, we observe that at 210 K the bands seem larger than in the case of DPA. The coefficient of reflection at this polarization is almost 40% in the case of DPA–(TCNQ)$_2$, diminishing to 18% for EDPA and 30% for DPA$_d$ and MDPA. For the electric field polarized perpendicular to the a stacking axis, the reflectivity is much lower, thus confirming the free electron delocalization along the stacking axis.

The low reflectivity along the a axis indicates a markedly high electron–phonon scattering rate, which is related to the low electrical conductivity observed at room temperature in these complexes (7). Below 210 K, the spectra of all these complexes change dramatically, many bands splitting below T_c as in the case of TEA–(TCNQ)$_2$ (14, 17). In Tables 3 and 4 we report all the vibrational frequencies of DPA–(TCNQ)$_2$ above and below the phase transition, $T_c \sim 212$ K. These were calculated from the conductivity obtained from the reflectance spectra by a Kramers–Kronig inversion. This spectral con-

Can. J. Chem. Downloaded from www.nrcresearchpress.com by 84.41.108.74 on 09/07/12
For personal use only.

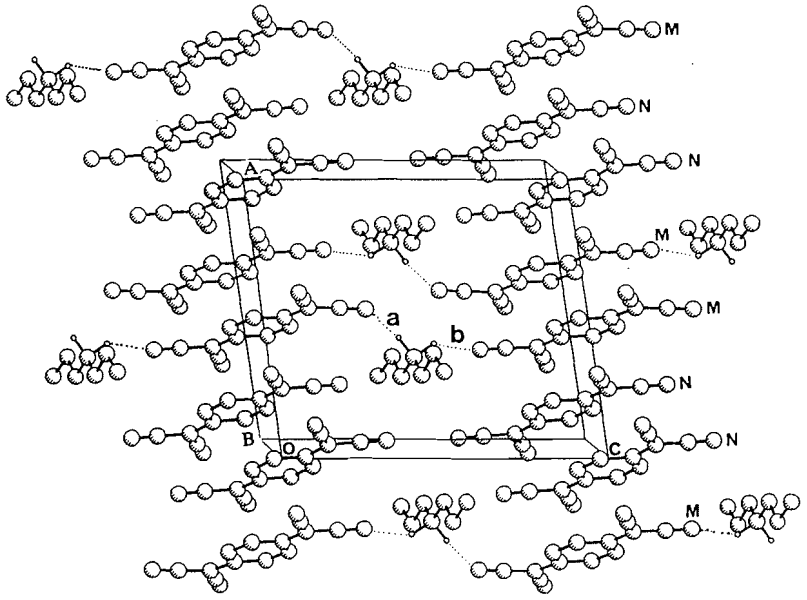


FIG. 3. Crystal structure at 193 K showing hydrogen bonds a,b, hydrogen bonded M-TCNQ's, and nonbonded N-TCNQ's. a(A) is the stacking axis.

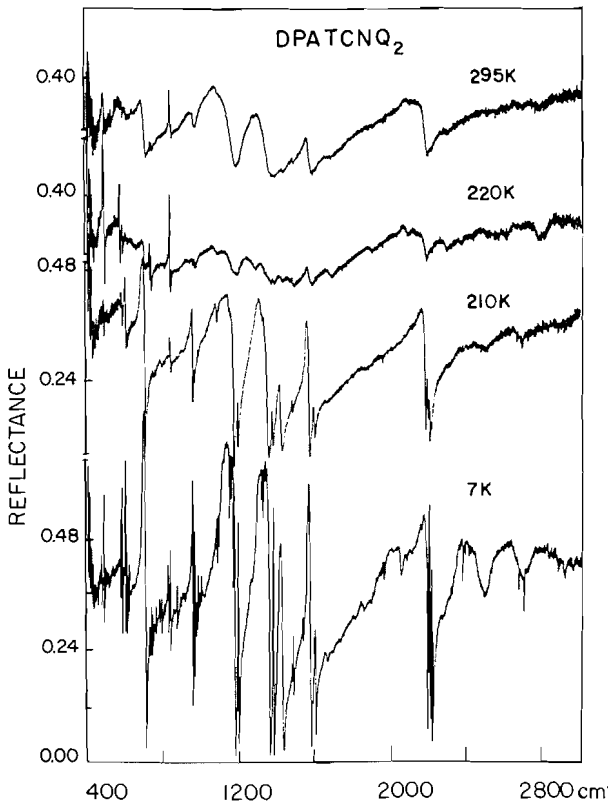


FIG. 4. IR reflectance spectra of DPA–$(TCNQ)_2$ at different temperatures and at polarization $\|a$.

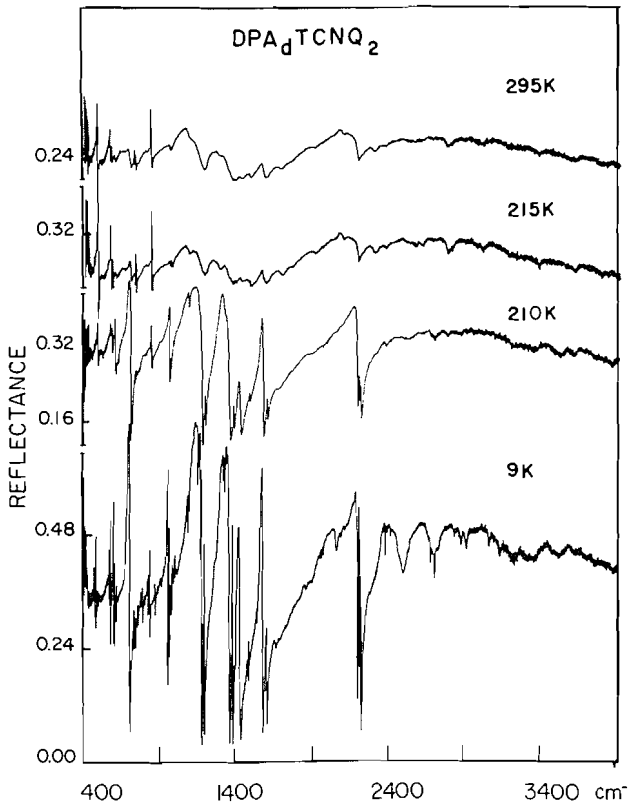


FIG. 5. IR reflectance spectra of deuterated DPA_d–$(TCNQ)_2$ at different temperatures ($\vec{E}\|a$).

ductivity is fitted with the dielectric factorized function model (18),

$$[1] \quad \epsilon(\omega) = \epsilon(\infty)\prod_j \frac{(\omega_{Lj}^2 - \omega^2 - i\gamma_j\omega)}{(\omega_{Tj}^2 - \omega^2 - i\gamma_j\omega)}$$

Formula [1] describes transverse (T) and longitudinal (L) phonons where ω_{Tj} is the transverse frequency, ω_{Lj} the longitudinal frequency, and γ_j a general damping parameter, assumed to be the same for the j'th mode. These frequencies are obtained from a least-squares fitting procedure. The oscillator strength parameters S_j (proportional to the square of effective charges) reported in Tables 3 and 4 are calculated from a generalized Lyddane–Sachs–Teller relation (18).

$$[2] \quad S_j' = \epsilon(\infty)\left[\left(\frac{\omega_{Lj}}{\omega_{Tj}}\right)^2 - 1\right]\prod_{M\neq j}\frac{(\omega_{LM}^2 - \omega_{Tj}^2)}{(\omega_{TM}^2 - \omega_{Tj}^2)}$$

Can. J. Chem. Downloaded from www.nrcresearchpress.com by 84.41.108.74 on 09/07/12
For personal use only.

Can. J. Chem. Downloaded from www.nrcresearchpress.com by 84.41.108.74 on 09/07/12
For personal use only.

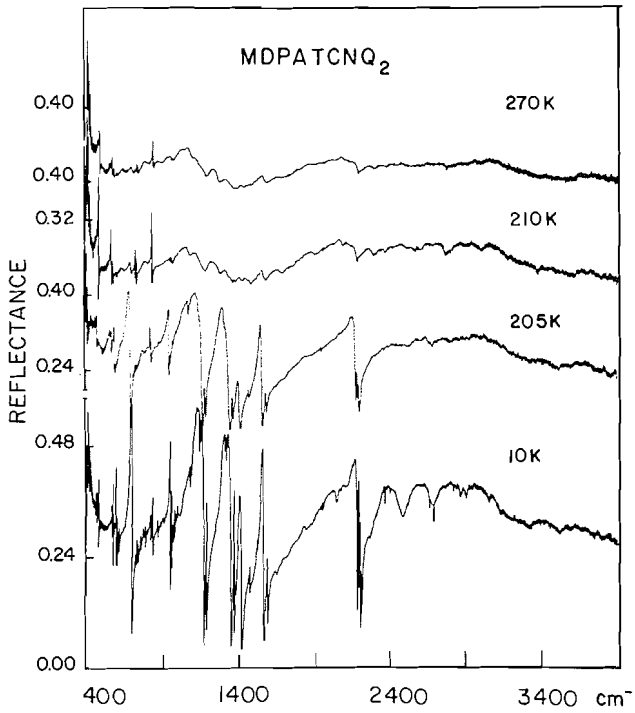


FIG. 6. IR reflectance spectra of MDPA–$(TCNQ)_2$ at different temperatures ($\vec{E} \| a$).

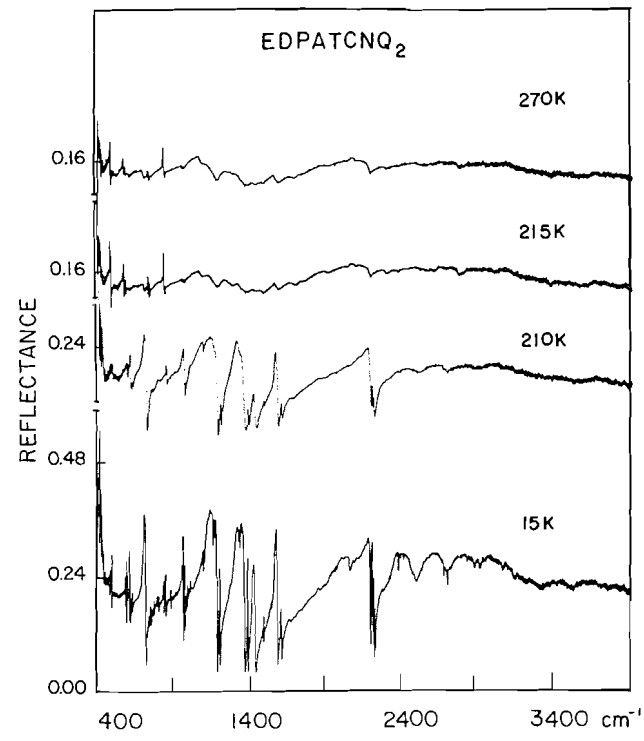


FIG. 7. IR reflectance spectra of EDPA–$(TCNQ)_2$ at different temperatures ($\vec{E} \| a$).

This expression requires the detection of all the infrared active phonons and $\epsilon(\infty)$ is the dielectric constant at infinity treated as a constant.

In Figs. 8 and 9, we show the spectral conductivity spectrum fitted with the phonon parameters of Tables 3 and 4. The parameters determined by minimizing the χ^2 function between the model and the phonon conductivity yield the full line in Figs. 8 and 9.

TABLE 3. Vibrational frequency parameters for DPA–$(TCNQ)_2$ at 220 K

ω_T (cm^{-1})	ω_L (cm^{-1})	γ_j (cm^{-1})	S_j	Assignment (Refs. 4, 19)
486	492	7	0.26	B_u C—CN bend
570	572	5	0.10	A_g C—CN bend
583	585	7	0.05	
604	608	30	0.10	B_u ring bend
692	696	25	0.12	B_u ring and external C—C stretchings
728	729	31	0.02	B_u ring and external C—C stretchings
735	736	3	0.01	A_g
806	808	60	0.06	
833	834	2	0.03	B_u CH out-of-plane bend
854	856	50	0.04	
950	952	28	0.04	A_g ring and external C—C stretching
1064	1073	91	0.19	
1137	1153	90	0.25	B_u
1254	1266	90	0.18	A_g
1333	1350	91	0.19	B_u ring stretching
1422	1430	70	0.08	A_g ring and external C=C stretching
1480	1482	20	0.01	A_g
1567	1571	25	0.04	B_u
1681	1692	100	0.09	A_g
2164	2180	75	0.13	B_u C≡N stretching
2282	2294	90	0.09	A_g
2364	2368	60	0.03	

In general, we observe that the IR active A_g broad vibrations at 220 K appear as multiplets at 210 K. These results suggest that the symmetry at low temperatures is lower, in accordance with a loss of inversion symmetry. We calculated the oscillator strength parameter S (Tables 3 and 4) and found out that at 210 K, the S values are generally higher than those at 220 K for most vibrations. These results indicate that the effective charges increase in the low-temperature phase, in accordance with the thermoelectric power results (8) at the low temperatures. The phase transition also clearly affects the C≡N stretch (Fig. 10) and deformation vibrations (Fig. 11). With the polarization parallel to the a axis, the C≡N in-plane stretching vibration at 2198 cm^{-1} appears as a strong band at the phase transition temperature T_c = 210 K (Fig. 10). The same results were obtained with MDPA–$(TCNQ)_2$ and EDPA–$(TCNQ)_2$. We can explain this result as a strong interaction between the conduction electrons along the a axis with the C≡N vibrations at the lower temperature due to the large electronegativity of these groups. Similarly in Fig. 11, the C≡N in-plane deformation at 700 cm^{-1} becomes more intense in the low-temperature phase. We reiterate that in this phase there is a higher conductivity due to a lower activation energy for the electron hopping. Thus increased conductivity correlates here with stronger C≡N IR activity. The appearance of this C≡N stretching mode at 2198 cm^{-1} for polarization parallel to the conduction (stacking) axis a has been previously associated with dimerization in TCNQ salts (19). We are thus observing the same phenomenon here. Conversely, in Fig. 11, the C—C—N out-of-plane deformation at 486 cm^{-1} disappears at 210 K, indicating a reduction of electron vibration interaction for this mode below the phase transition. The same effect occurs for the 820 cm^{-1} CH out-of-plane bend. We conclude that *in-plane* vibrations acquire intensity in the low-temperature phase, whereas *out-of-plane* vibrations become much less intense in this new phase.

In general, with the polarization parallel to the a axis, the coefficients of reflection of TCNQ A_g modes are around 30%. This coefficient is very small (about 3%) for the polarization perpendicular to the stacking a axis, confirming thus that TCNQ A_g modes

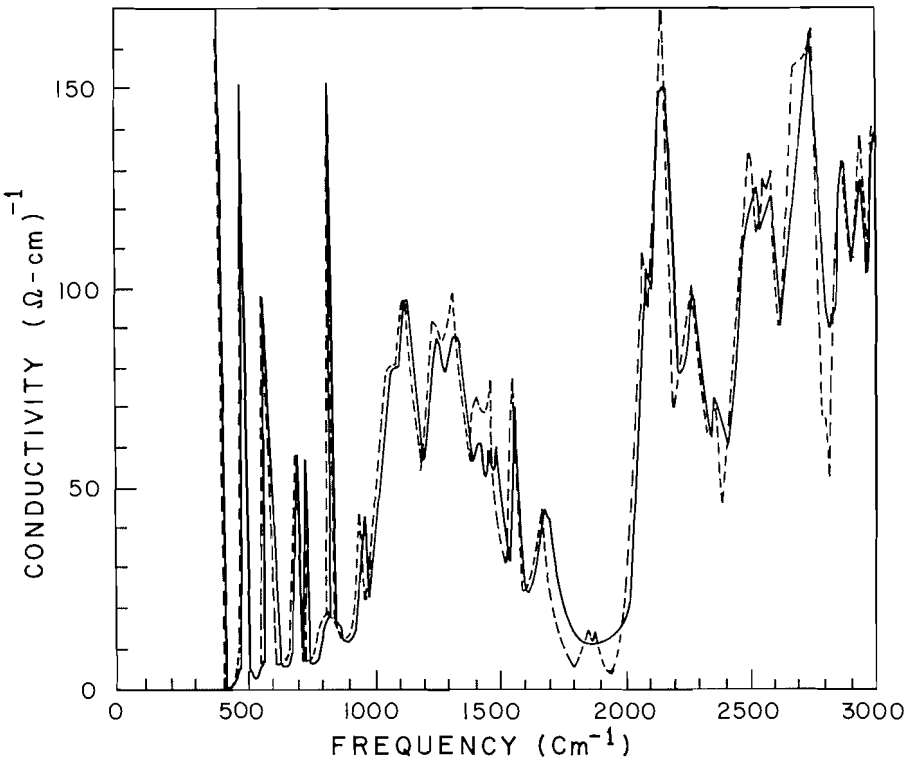


FIG. 8. Frequency-dependent conductivity, determined by Kramers–Kronig analysis of the reflectance of DPA–$(TCNQ)_2$ at 220 K. The dashed curve is from the model (eq. [1]).

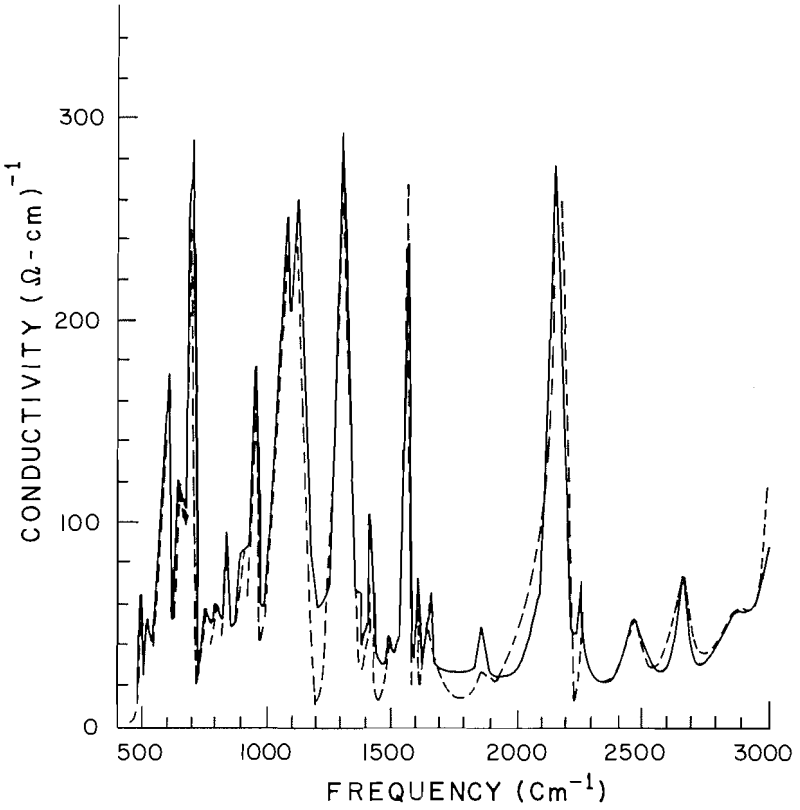


FIG. 9. Frequency-dependent conductivity, determined by Kramers–Kronig analysis of the reflectance of DPA–$(TCNQ)_2$ at 210 K. The dashed curve is from the model (eq. [1]).

Can. J. Chem. Downloaded from www.nrcresearchpress.com by 84.41.108.74 on 09/07/12
For personal use only.

Can. J. Chem. Downloaded from www.nrcresearchpress.com by 84.41.108.74 on 09/07/12
For personal use only.

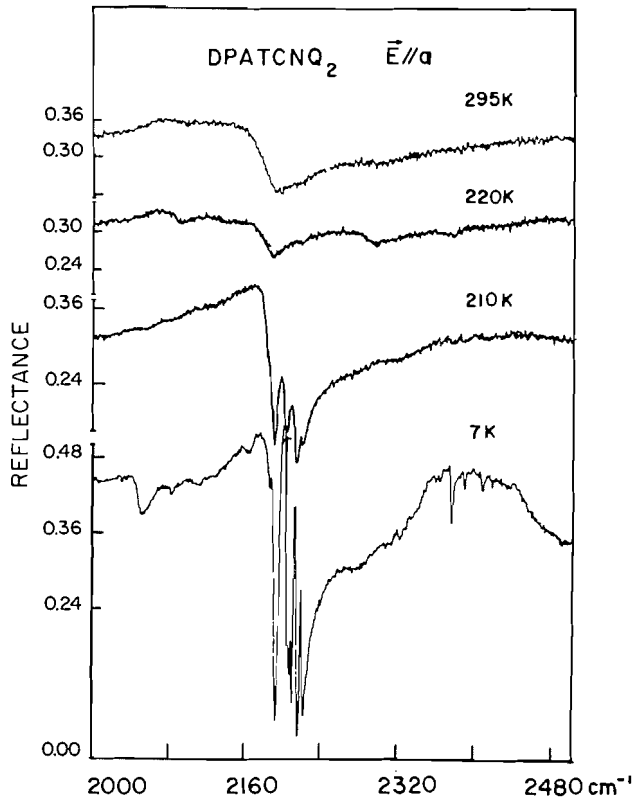


FIG. 10. Reflectance spectra at different temperatures in the C≡N stretching region showing the appearance of the C≡N mode at 2195 cm^{-1} in the low-temperature phase (210 K) with the polarization $\|a$.

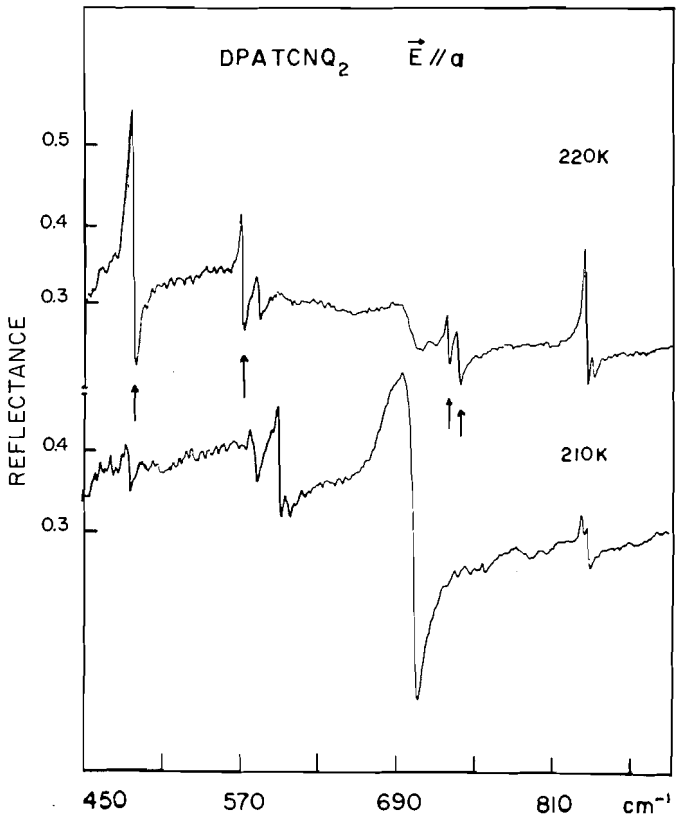


FIG. 11. Low-frequency reflectance spectra showing the disappearance of C—N deformation in the low-temperature phase (210 K) with the polarization $\|a$.

TABLE 4. Vibrational frequency parameters of DPA–$(TCNQ)_2$ at 210 K

ω_T	ω_L	γ_j	S_j
486	487	7	0.09
550	554	30	0.37
578	585	30	0.50
599	603	10	0.18
639	647	30	0.45
687	702	12	0.40
746	752	40	0.18
793	798	42	0.15
835	839	20	0.16
901	913	80	0.39
949	956	20	0.16
1029	1037	55	0.26
1072	1081	36	0.30
1116	1161	60	0.68
1296	1342	57	0.59
1374	1375	5	0.003
1412	1419	21	0.05
1556	1566	18	0.12
1596	1598	8	0.02
1653	1655	20	0.055
2143	2172	60	0.227
2195	2196	6	0.004
2252	2254	20	0.0118

gain intensity via coupling to the delocalized charge density at the TCNQ site in these complexes.

Discussion

Previously reported electrical and magnetic properties of these semiconductors (7, 8) pointed to an unusual phase transition, which we termed an inverse spin – Peierls transition. Sharp decreases in resistivity, thermoelectric power, and magnetic susceptibility all occurred simultaneously at around 210 K for the DPA and its derivative series.

The X-ray structure, Figs. 2 and 3, reveals that these discontinuities in physical properties are manifestations of the disorder-to-order phase transition occurring in the hydrogen-bond network to be found in these materials. The donor molecules have two protons accessible for hydrogen bonding, with the highly electronegative C≡N groups of the stacked acceptor TCNQ's responsible for the conductivity. In the high-temperature phase, all TCNQ's are equivalent, with an approximate 1/2 charge by stoichiometry. This corresponds to the 1/4-filled band, which in the limit of weak electronic correlation can be expected to undergo an electronic spin – Peierls transition, a tetramerization in this case, leading to a metal–semiconductor phase transition upon lowering the temperature (1, 2). The transition observed at 210 K is of the semiconductor–semiconductor type since only a change in the activation energy occurs. Both electron–electron repulsion and the disorder induced by the H-bonds scatter the conduction electron sufficiently to maintain the high-temperature phase semiconducting (20).

The tetramerization expected for the present compounds, which is a signature of an electronic spin – Peierls, is strongly coupled to the order–disorder H-bond transition upon lowering the temperature. Two different types of TCNQ dimers are formed in the stack: hydrogen-bonded M-TCNQ dimers and nonhydrogen-bonded N-TCNQ dimers (Fig. 3), resulting

in a NMMN tetrameric system. This is therefore a cooperative order–disorder and electronic spin – Peierls transition. In the ordered phase, the protons induce an extra electrostatic potential of periodicity $4k_F$, where k_F is the Fermi wave vector, which therefore reinforces the Peierls transition, i.e., tetramerization of the TCNQ's. The increase in complexity of the IR active A_g mode spectrum also correlates strongly with this picture. In particular, the increase in oscillator force of these vibrations is now explainable as an increase in electron-vibration coupling in the tetramer (21). Furthermore, the C≡N vibrations show the greatest spectral change in crossing the phase transition (Figs. 10 and 11). These changes corroborate this interpretation, which is reflected in the abrupt increase in H-bonding to these highly electronegative groups upon lowering the temperature to $T_c = 210$ K.

We conclude by reiterating that the present results point to a cooperative disorder–order proton transition and an electronic spin – Peierls transition enhancing the tetramerization of these 1/4-filled band organic conductors as one lowers the temperature to $T_c = 210$ K.

Acknowledgments

We thank the Natural Sciences and Engineering Research Council of Canada and the Department of National Defence (contract 8SD8-00313) for supporting this research.

1. J. S. MILLER. Extended linear chain compounds. Vol. 2. Plenum Press, New York. 1982.
2. D. JEROME and L. CARON. Low dimensional conductors and superconductors. NATO ASI Vol. B155, Plenum Press, New York. 1987.
3. S. R. MARDER, J. W. PERRY, and W. P. SCHAEFFER. Science, **245**, 626 (1989).
4. A. D. BANDRAUK, K. D. TRUONG, C. CARLONE, S. JANDL, and K. ISHII. J. Phys. Chem. **89**, 434 (1985).
5. A. D. BANDRAUK, K. ISHII, K. D. TRUONG, M. AUBIN, and A. W. HANSON. J. Phys. Chem. **89**, 1478 (1985).
6. A. D. BANDRAUK, K. D. TRUONG, C. CARLONE, and A. W. HANSON. J. Phys. Chem. **91**, 2063 (1987).
7. A. D. BANDRAUK, K. D. TRUONG, and M. AUBIN. Can. J. Chem. **66**, 938 (1988).
8. K. D. TRUONG, A. D. BANDRAUK, and M. AUBIN. Solid State Commun. **72**, 1145 (1989).
9. E. J. GABE, F. L. LEE, and Y. LEPAGE. *In* Crystallographic computing: data collection, structure determination, proteins and database. *Edited by* G. M. Sheldrick, C. Kruger, and R. Goddard. Clarendon Press, Oxford. 1985. pp. 167–174.
10. D. J. CROMER and J. T. WABER. International tables for X-ray crystallography. Vol. IV. *Edited by* J. A. Iber and W. C. Hamilton. Kluwer Academic Publishers, Dordrecht. 1974.
11. A. C. LARSON. Acta Crystallogr. **23**, 664 (1967).
12. W. H. ZACHARIASEN. Acta Crystallogr. **16**, 1139 (1963).
13. R. M. GRANT, R. L. GREENE, G. C. WRIGHTON, and G. CASTRO. Phys. Rev. Lett. **31**, 1311 (1973).
14. A. BRAU, P. BRÜESCH, J. P. FARGES, W. HINZ, and K. KUSE. Phys. Status Solid B: **62**, 615 (1974).
15. D. B. TANNER, J. E. DEIS, A. J. EPSTEIN, and J. S. MILLER. Solid State Commun. **31**, 671 (1979).
16. C. S. JACOBSEN, D. B. TANNER, and K. BECHGAARD. Phys. Rev. B, **28**, 7019 (1983).
17. E. F. STEIGMEIR, H. ANDERSET, D. BAERISWYL, and M. ALMEIDA. Mol. Cryst. Liq. Cryst. **120**, 163 (1985).
18. L. MARTEN and G. LAMPRECHT. Phys. Stat. Sol. **39**, 573 (1970).
19. Z. IQBAL, C. W. CHRISTOE, and D. K. DAWSON. J. Chem. Phys. **63**, 4485 (1975).
20. K. D. TRUONG, A. D. BANDRAUK, J. ZAUHAR, and M. AUBIN. Synth. Met. **27**, B439 (1988).
21. K. D. TRUONG, A. D. BANDRAUK, J. ZAUHAR, and C. CARLONE. Can. J. Chem. **69**, 901 (1991).

Can. J. Chem. Downloaded from www.nrcresearchpress.com by 84.41.108.74 on 09/07/12
For personal use only.

An infrared spectroscopic study of 2-methylpropene (isobutene) adsorbed on a Pt/SiO_2 catalyst before and after hydrogenation

GULERANA SHAHID[1] AND NORMAN SHEPPARD
School of Chemical Sciences, University of East Anglia, Norwich NR4 7TJ, U.K.

Received April 22, 1991

This paper is dedicated to Dr. Richard Norman Jones

GULERANA SHAHID and NORMAN SHEPPARD Can. J. Chem. **69**, 1812 (1991).

The infrared spectrum from 2-methylpropene (isobutene) adsorbed at room temperature on a Pt/SiO_2 catalyst is interpreted, with the help of the metal-surface selection rule, in terms of the presence of a mixture of π-bonded, di-σ, and alkylidyne (2-methylpropylidyne) surface species. Heating and evacuation at 100°C retains the original alkylidyne, which occurs together with another surface species probably containing multiple $-CH_2Pt$ groups. Heating to 200 and then to 300°C leads to progressive and strong reductions in the absorptions from alkyl-type surface species, which are replaced by increasing absorptions at ca. 3060 cm^{-1} from unsaturated alkene groups. Hydrogenation at room temperature, after the removal of gas-phase and physically adsorbed 2-methylpropane (isobutane) by evacuation, leaves a methyl-rich spectrum, probably from a partially hydrogenated surface species. Hydrogenation and evacuation at 100°C give a much weaker residual spectrum from saturated hydrocarbon surface species. Subsequent hydrogenation at 200°C gives a spectrum suggesting the presence of a surface *n*-butyl group, clearly the result of a skeletal surface isomerisation. At 300°C in hydrogen the surface species is from a longer *n*-alkyl chain and occurs together with gas-phase methane implying the operation of a disproportionation reaction on the surface. Evacuation of hydrogen at 200 or 300°C leads to virtually total removal of the *n*-alkyl absorptions, which are, however, completely restored by re-addition of H_2. In agreement with a similar study by Avery on a Pd/SiO_2 catalyst, we conclude that after evacuation C—H bonds are largely replaced by C—Pt bonds at stepped-type surface sites.

Key words: 2-methylpropene adsorbed on Pt/SiO_2, infrared spectrum.

GULERANA SHAHID and NORMAN SHEPPARD Can. J. Chem. **69**, 1812 (1991).

Faisant appel à la règle de sélection des surfaces métalliques, on interprète le spectre infrarouge du 2-méthylpropène (isobutène) adsorbé à la température ambiante sur un catalyseur de Pt/SiO_2 en fonction de la présence à la surface d'un mélange d'espèces avec des liaisons-π, des adsorptions di-σ et d'alkylidyne (2-méthylpropylidyne). Par chauffage et mise sous vide à 100°C, l'alkylidyne original est conservé avec une autre espèce présente à la surface qui contient probablement plusieurs groupes $-CH_2Pt$. Par chauffage à 200°C, puis à 300°C, il y a une forte perte progressive des espèces alkyles présentes à la surface; elles sont remplacées par des absorptions croissantes aux environs de 3060 cm^{-1}, causées par des groupes alcènes. Après une hydrogénation à la température ambiante, suivie d'une élimination de la phase gazeuse et du 2-méthylpropane (isobutane) adsorbé, on observe un spectre riche en groupes méthyles qui est probablement dû à une espèce partiellement hydrogénée présente à la surface. Une hydrogénation, suivie d'une élimination des espèces par chauffage à 100°C, fournit un spectre contenant, à la surface, un résidu contenant une quantité beaucoup plus faible d'hydrocarbures saturés. Une hydrogénation subséquente à 200°C donne un spectre suggérant la présence à la surface d'un groupe *n*-butyle qui serait la résultat d'une isomérisation du squelette à la surface. À 300°C, en présence d'hydrogène, l'espèce à la surface est due à une chaîne carbonée beaucoup plus longue et elle se retrouve en même temps que du méthane dans la phase gazeuse; ces résultats suggèrent qu'il se produit une réaction de dismutation sur la surface. L'évacuation de l'hydrogène à 200 ou à 300°C conduit à une élimination pratiquement complète des absorptions de groupes *n*-alkyles qui sont toutefois complètement réintroduits par une ré-addition de H_2. En accord avec les conclusions d'Avery, basées sur une étude semblable impliquant un catalyseur de Pd/SiO_2, on conclut que, après l'évacuation, les liaisons C—H sur des sites superficiels à gradin sont en grande partie remplacées par des liaisons C—Pt.

Mots clés : 2-méthylpropène adsorbé sur Pt/SiO_2, spectre infrarouge.

[Traduit par la rédaction]

Introduction

In a previous paper we interpreted the infrared spectra of propene adsorbed on a silica-supported platinum Pt/SiO_2 catalyst as a function of temperature and hydrogenation in terms of the structures of the adsorbed species present under the various conditions (1). As the Pt/SiO_2 catalyst had fairly large metal particles, typically 5–15 nm in diameter, the use of the metal-surface selection rule (MSSR) gave effective insight in the interpretive process (1). A similar study, confined to straight adsorption at room temperature, has also been described for the three linear butenes, but-1-ene and *cis*- and *trans*-but-2-ene, adsorbed on Pt/SiO_2 (2). The latter results were compared with those obtained by reflection–absorption infrared spectroscopy (RAIRS) from the same alkenes adsorbed on the Pt(111) face of a metal single crystal (2). In the present paper we describe the spectra from 2-methylpropene (isobutene) adsorbed on Pt/SiO_2 over a wide range of temperature and hydrogenation conditions. Comparisons are made with the results of 2-methylpropene adsorbed on Pt(111) as a function of temperature as studied by RAIRS[2] and by vibrational electron energy loss spectroscopy (VEELS) (3).

Earlier room temperature studies of 2-methylpropene adsorbed on silica-supported Ni (4), Pd (5), Pt (4), and Ir (6) catalysts gave similar spectra, dominated by absorptions from methyl-rich species, to those obtained in the present study before and after the addition of hydrogen.

Experimental

The detailed procedure for the preparation of the Pt/SiO_2 discs for infrared transmission study from $H_2PtCl_6 \cdot xH_2O$ and finely-divided Cabosil (SiO_2) by reduction with hydrogen has been reported else-

[1]Present address: Department of Chemistry, University of the Punjab, Lahore, Pakistan.

[2]M. A. Chester, P. Gardner, and P. Pudney. Unpublished work.

Printed in Canada / Imprimé au Canada

Can. J. Chem. Downloaded from www.nrcresearchpress.com by 84.41.108.74 on 09/07/12
For personal use only.

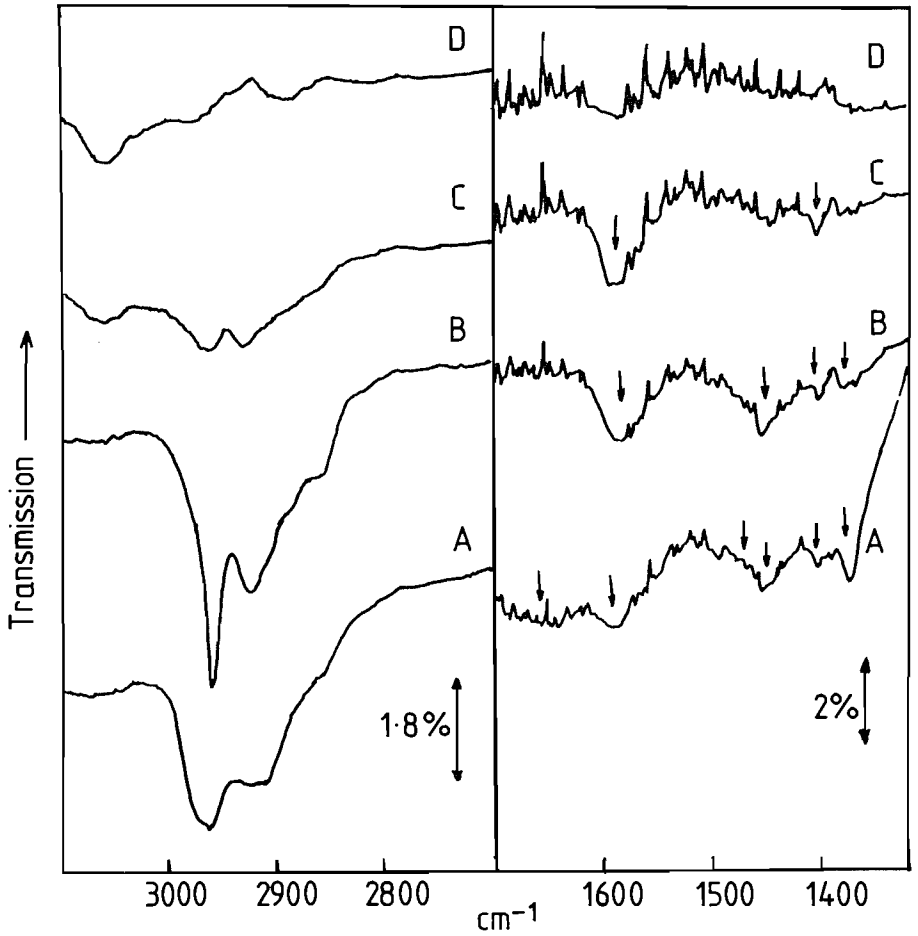


FIG. 1. Infrared spectra in the $\nu CH_3/\nu CH_2$ and $\delta CH_3/\delta CH_2$ regions after adsorption of 2-methyl propene on Pt/SiO_2 at room temperature (A); followed by successive heating to (B) 100°C; (C) 200°C; and (D) 300°C. All spectra were recorded at room temperature after evacuation of the gas phase at the temperatures indicated, and are ratioed against the spectrum of the catalyst in vacuum prior to the adsorption of propene. Sharp features in the 1700–1320 cm^{-1} region additional to those indicated by arrows and discussed in the text are due to poor cancellation of absorption from water vapour in the optical path.

Can. J. Chem. Downloaded from www.nrcresearchpress.com by 84.41.108.74 on 09/07/12
For personal use only.

where (1). All infrared spectra were measured *at room temperature* at 4 cm^{-1} resolution using a Digilab FTS 20V Fourier-transform spectrometer. Transmission spectra were ratioed against that of a clean Pt/SiO_2 disc obtained prior to carrying out the adsorption experiments and, where appropriate, against the gas-phase spectrum obtained by lifting the Pt/SiO_2 disc out of the infrared beam.

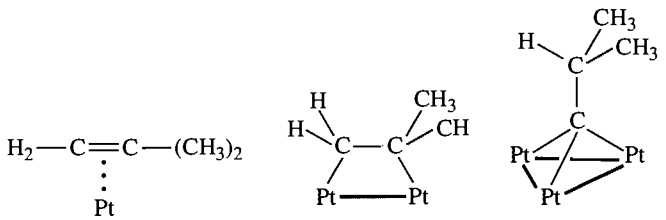
2-Methylpropene (isobutene), stated purity of 99.0%, was obtained from Messer Griesheim of Germany.

Results and discussion

Room temperature adsorption and evacuation

The spectrum obtained after adsorption at ca. 300 K followed by evacuation is shown in the starting spectra, labelled A, of Figs. 1, 2, and 3. There was some variability of the relative intensities of absorption bands, showing that more than one species is present. The positions, in cm^{-1}, and relative intensities of the absorption bands are as follows: ca. 2970 (m, sh), 2960 (s), ca. 2925 (w to m), 2910 (m), 2865 (mw), ca. 1660 (m, vbd), 1600 (m, bd), 1475 (mw), 1450 (m), 1405 (mw), 1375 (m), where the abbreviations are s, strong; ms, medium strong; m, medium; mw, medium weak; w, weak; sh, shoulder; bd, broad; vbd, very broad. The ca. 2970 and 2925 cm^{-1} absorptions were strongest in Fig. 1A, and only that spectrum possibly had a very broad and weak absorption at ca. 3070 cm^{-1}. Figures 1A and 3A showed the very broad absorption between 1700 and 1620 cm^{-1}, centred at about 1660 cm^{-1}. No sharp absorptions were present that could be attributed to 2-methylpropene adsorbed on the silica support (7).

Following our successful analysis of the spectra from ethene (8–10) and propene (1) adsorbed on the same type of Pt/SiO_2 catalyst, we shall consider the spectra of the initially adsorbed species in terms of possible contributions from the π-bonded species (**1**), the di-σ adsorbed species (**2**), and the 2-methylpropylidyne (isobutylidyne) surface species (**3**). Each



1 **2** **3**

of these surface complexes could retain a plane of symmetry to give an overall symmetry of C_s. In the case of the di-σ species this requires the atoms in the C_2M_2 ring to be coplanar: if this is not the case the symmetry is C_1. The metal-surface selection rule (MSSR) (11, 12) states that only the completely symmetrical A′ vibrational modes will be infrared active through

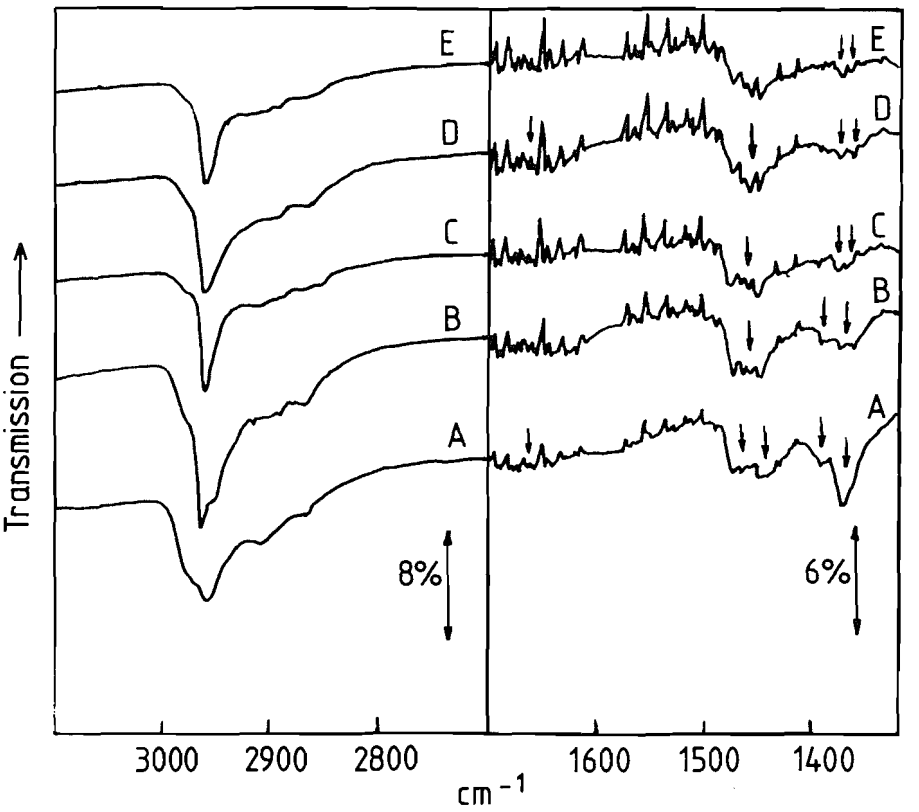


FIG. 2. Infrared spectra of 2-methyl propene (A) adsorbed at room temperature on Pt/SiO_2; followed in succession by (B) addition of 1 Torr H_2; (C) evacuation; (D) addition of 2 Torr H_2; and (E) evacuation. All spectra are ratioed against that of the evacuated catalyst prior to propene adsorption.

having components of their vibrational dipole moments perpendicular to the surface. The A″ antisymmetric modes have dipole changes parallel to the surface and are therefore MSSR-forbidden. For each of the structures **1–3** we identify below the expected strongest allowed A′ modes that could occur down to 1300 cm^{-1}. The latter is the experimental cut-off limit due to effectively black-out absorption by the SiO_2 lattice modes of the catalyst. The intensity predictions take into account the expected directions of the vibrational dipoles with respect to the surface, and also the relative intensities of the functional-group absorptions in the absence of preferred molecular orientations, as measured in the liquid state.

The approximate wavenumbers to ±20 cm^{-1} and relative intensities of some relevant group modes in the absence of the MSSR are as follows (13): 2965, νCH_3as (s); 2915, νCH_3s in $CH_3CH{=}C$ (s); 2870, νCH_3s in alkanes (m); 1450, δCH_3as (m); 1375, δCH_3s (s); 2890, νCH in alkanes (w); 1340, δCH in alkanes (m).

The values for the absorptions of other relevant groups as actually measured on metal surfaces, i.e., also incorporating the effects of the MSSR, are as follows (9, 10): 3015, νCH_2s in $C{=}CH_2$ (mw); 1600–1500, νC=C in π-complexes (mw); 1415, δCH_2 in $C{=}CH_2$ (m); 2920, νCH_2s in $-CH_2M$ (M = metal) (m); 1430, δCH_2 in $-CH_2M$ (w,bd).

Taking into account the above data, modified where necessary by the requirements of the MSSR (allowed vibrational dipoles approximately perpendicular to the surface strong, and those near parallel to the surface weak) we can predict the following positions for the most prominent absorptions from structures **1–3**.

1, The π-complex: 2965, νCH_3as and 1450, δCH_3as.

2, The di-σ complex: 2920, νCH_2s; 2870, νCH_3s; 1375, δCH_3s. In the RAIR spectrum of this complex[2] on Pt(111) at 90 K, the strongest absorption at 2895 cm^{-1} probably is from the νCH_3s mode.

3, 2-Methylpropylidyne (isobutylidyne): 2965, νCH_3as and 1450 δCH_3as. The strongest absorptions in the RAIR spectrum at room temperature on Pt(111), where this species is expected to predominate, are at 2968 and 1445 cm^{-1},[2] in very good agreement with the above predictions.

It is seen that on the above criteria alone it is not possible to distinguish between the π-complex and the alkylidyne. No strong absorptions occur in Figs. 1A, 2A, or 3A that can be attributed to $\nu H_2C{=}C$ or νC=C modes of a π-complex, although a pair of weak absorptions at ca. 3070 and 1600 cm^{-1} in Fig. 1A may denote the presence of a small amount of this surface species. In general, however, we shall assume, as also in the propene case (1), that the νCH_3 and δCH_3 absorptions from the 2-methylpropylidyne predominate in the spectrum. We hence assign the absorption bands of the initially adsorbed species as set out in Table 1. It is noted that the MSSR restricts the number of split-degeneracy CH_3 modes that can be observed.

The great breadth of the ca. 1660 cm^{-1} absorption in Figs. 1A, 2A, and 3A is such that it is unlikely to be attributable to a νC=C mode. At elevated temperatures, as shown in Figs. 1B and 1C, another strong absorption occurs at 1590 cm^{-1}. This persists in Fig. 1C where the absorptions from surface hydrocarbon species are much weakened. Based on the band positions (14) and breadths we tentatively assign the ca. 1660 and the 1590 cm^{-1} absorptions to νPtHPt*s* modes from adsorbed hydrogen on 2-fold bridged sites, possibly on different crystalline facets. Further work with the perdeutero hydrocarbon is needed to confirm this structural assignment. The adsorbed hy-

Can. J. Chem. Downloaded from www.nrcresearchpress.com by 84.41.108.74 on 09/07/12
For personal use only.

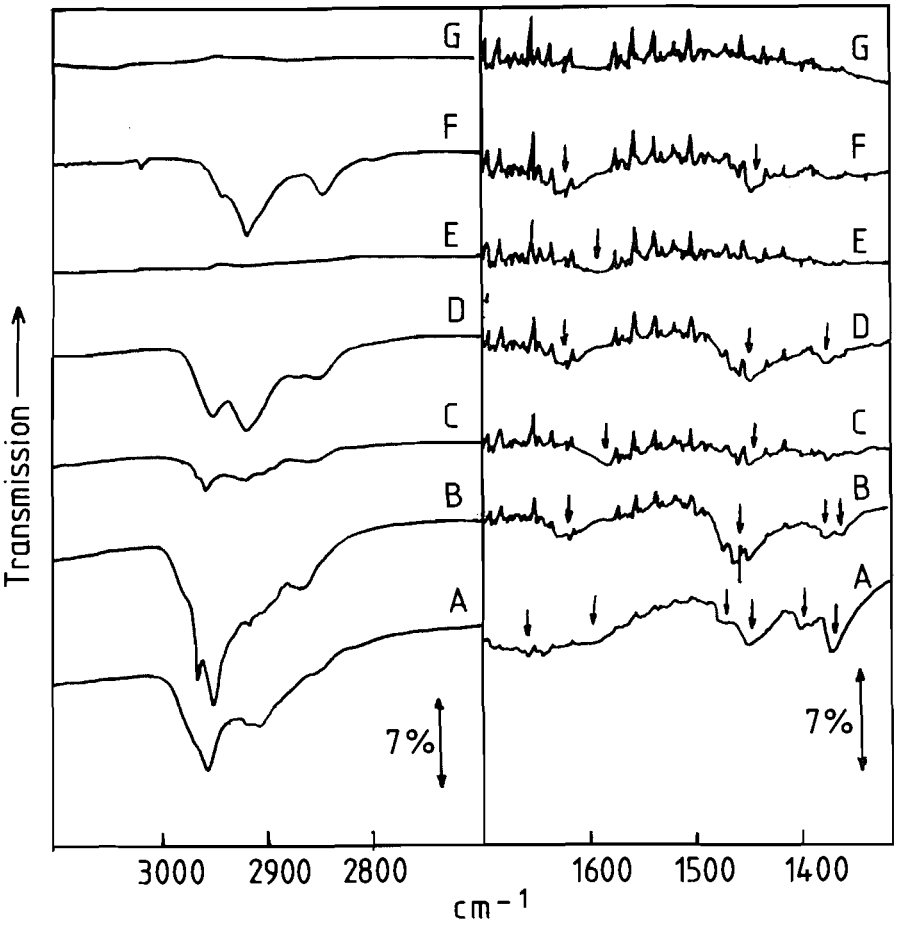


FIG. 3. Infrared spectra of 2-methyl propene (A) adsorbed at room temperature on Pt/SiO_2; followed successively by (B) addition of H_2 at 100°C; (C) evacuation at 100°C; (D) addition of H_2 at 200°C; (E) evacuation at 200°C; (F) addition of H_2 at 300°C; and (G) evacuation at 300°C. All spectra were measured after cooling to room temperature and are ratioed against that of the evacuated catalyst prior to propene adsorption.

TABLE 1. The assignments of the observed absorption bands (cm^{-1}) from the room temperature adsorption of 2-methylpropene (isobutene) on Pt/SiO_2 catalysts

Band position	Assignment[a]		Band position	Assignment	
ca. 3060 (w,bd)	$\nu H_2C=$	1?	ca. 1660 (m,vbd)	νPtHPt*s*	
ca. 2970 (m,sh)	νCH_3as	1	1600 (m,bd)	$\nu C=C$	1?
2960 (s)	νCH_3as	3	1475 (mw)	δCH_3as	1
ca. 2925 (w to m)	νCH_2Ms	2	1450 (m)	δCH_3as	3
2910 (m)	νCH_3s	2	1405 (mw)	δCH_2 of CH_2M	2
2865 (mw)	νCH_3s	3	1375 (m)	δCH_3s	2

[a] **1** the π-bonded species; **2** the di-σ species; **3** 2-methylpropylidyne (isobutylidyne). s, strong; ms, medium strong; m, medium; mw, medium weak; w, weak; sh, shoulder; bd, broad; vbd, very broad.

drogen at room temperature could arise from the dissociative adsorption of 2-methylpropene as 2-methylpropylidyne and at elevated temperatures from further CH-bond dissociation.

Heating and evacuation at elevated temperatures

Figure 1B shows the spectrum obtained after heating and evacuation at 100°C followed by cooling to room temperature. A strong spectrum is retained but with a greatly modified profile relative to that obtained at room temperature. The absorptions were observed at ca. 2970 (w,sh); 2960 (vs); 2922 (s); ca. 2910 (w,sh); 2890 (w,sh); 2860 (m); 1590 (ms,bd); 1450 (ms); 1405 (m); 1375 (m). Compared with the room temperature spectrum, the weakening of the 2970 and 1475 cm^{-1} absorptions is consistent with the removal of some of the π-species on heating. Likewise the substantial weakening of the 2910 and 1375 cm^{-1} absorptions can be interpreted in terms of a reduction in the amount of the di-σ species present. Conversely the strengthening of the 2960 and 1450 cm^{-1} absorptions suggests an increase in the amount of the 2-methylpropylidyne species. The alkylidyne species are frequently found to persist to higher temperatures than the others (3, 16). In the specific case of ethene on Pt/SiO_2 (10) and Pt/Al_2O_3 (17), di-σ com-

Can. J. Chem. Downloaded from www.nrcresearchpress.com by 84.41.108.74 on 09/07/12
For personal use only.

Can. J. Chem. Downloaded from www.nrcresearchpress.com by 84.41.108.74 on 09/07/12
For personal use only.

plexes were found to be converted to ethylidyne on heating from lower temperatures to room temperature.

Additional to the expected absorptions of 2-methylpropylidyne, there remain prominent hydrocarbon bands in the spectrum of Fig. 1B at ca. 2920 and 1405 cm^{-1}. In the case of ethene on Pt/SiO_2, nearby νCH_2s absorptions were observed from two distinct di-σ species, presumably occurring on different surface sites or crystal facets, only one of which was converted to ethylidyne at room temperature. The persistence of the 2920 and 1405 cm^{-1} absorption could therefore be attributed to a remaining more stable di-σ species, of which the 2920 cm^{-1} band represents νCH_2s and the 1405 cm^{-1} δCH_2 of CH_2M. The considerable strength of the 2920 cm^{-1} band, however, suggests the possibility of the presence of alternative structures containing multiple CH_2M groups (which are expected to absorb at ca. 2920 cm^{-1} (νCH_2s) and ca. 1430 cm^{-1} (δCH_2) (10) derived from further dehydrogenation of CH_3 groups.

After heating to 200°C followed by evacuation and then cooling, a much weakened spectrum occurs in the region 3000–2800 cm^{-1} characteristic for alkane-type groups, but a broad new absorption occurs at ca. 3060 cm^{-1}, which is typical of alkene absorption of the C═CH or C═CH_2 types (13). Clearly a mixture of saturated and unsaturated species now occurs on the surface. The great weakening of the νCH_3as absorption, now shifted to ca. 2965 cm^{-1}, is paralleled by a strong reduction in intensity of the δCH_3as absorption near 1450 cm^{-1}. The second alkane absorption, shifted to ca. 2930 cm^{-1}, is also weakened by at least a factor of two relative to the spectrum of Fig. 1B. The ca. 1405 cm^{-1} band retains its intensity but the δCH_2 mode of a C═CH_2 group could now also be contributing intensity at this position (13). The ca. 1590 cm^{-1} absorption retains its intensity, but is now accompanied by a weak absorption at ca. 2200 cm^{-1} (not illustrated), which can be attributed to a νPtH vibration of a "linear" or "on-top" PtH group. On a bare Pt/SiO_2 surface such modes absorb at 2130 cm^{-1} (15, 18, 19), but the coadsorption of hydrocarbon species may well cause a wavenumber shift.

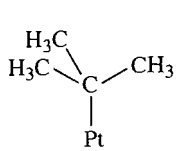
After heating to 300°C the 3060 cm^{-1} absorption becomes more prominent and the alkane absorptions weaker again, showing that the one replaces the other. The "negative" features at ca. 2920 and 2850 cm^{-1} may well arise from weak features from hydrocarbon contamination in the spectrum of the Pt/SiO_2 background used for ratioing purposes. Although the earlier VEEL study of 2-methylpropene was not taken to such a high temperature, such spectra from propene, but-1-ene, and pent-1-ene, taken in the range 230–330°C, all showed a single νCH absorption between 3050 and 3070 cm^{-1} (3). These absorptions were accompanied by strong low-energy loss features between 850 and 830 cm^{-1}, which are found in many high-temperature VEEL spectra from hydrocarbon adsorption residues. They are usually attributed to C_2H or CH surface species (3, 20). The low wavenumber feature is suggestive of an out-of-plane δCH deformation mode of a substituted ethylene (13), or of a tilted CH group interacting with several metal atoms by a combination of σ and π bonding (3). The considerable strength of the 3060 cm^{-1} νCH absorption suggests that the CH bond is oriented at an angle to the surface of the metal particles so as not to be weakened by the operation of the MSSR (3). Overall there is very satisfactory agreement between the results on Pt/SiO_2 and the VEELS evidence on Pt(111) about the general types of hydrocarbon species present on the Pt surface in the different temperature ranges.

After heating at 300°C both the absorptions at 2200 cm^{-1} (νPtH) and 1590 cm^{-1} ($\nu PtHPt$) have gone in agreement with a second burst of hydrogen desorption in this temperature range from 2-methylpropene adsorbed on Pt(111) (3). The only absorptions additional to those shown in Fig. 1 are at 2020 and 1820 cm^{-1}, which can clearly be assigned to the presence of small proportions of adsorbed CO on on-top (linear), and bridging, sites respectively (21). The bridging CO species occurs at an early stage but does not subsequently grow, whereas the linear species gradually increases in amount during the consecutive experiments at higher temperatures.

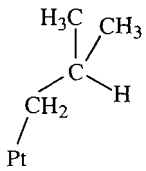
Hydrogenation at room temperature

The effect of the addition of 1 Torr H_2 (1 Torr = 133.3 Pa) at room temperature (ca. 25°C) on the spectrum obtained on initial adsorption, Fig. 2A, is shown in Figs. 2B and 2C before and after evacuation respectively. The substantial reduction of intensity between Figs. 2B and 2C on evacuation, and particularly the weakening of absorptions at 2950, 1465, and near 1370 cm^{-1}, implies the removal of physically adsorbed species formed by the hydrogenation. These absorptions are consistent with the presence of the expected hydrogenation product, 2-methylpropane (isobutane), which is also detected in the gas phase. However, after evacuation (Fig. 2C) a substantial methyl-rich spectrum is retained, showing that there are stable chemisorbed species that resist hydrogenation. Essentially the same spectra were obtained after addition of 2 Torr H_2 followed by evacuation, Figs. 2D and 2E.

The two likely partially hydrogenated surface species are **4** and **5** below. Possibly one of these is hydrogenated to isobutane while the other stays chemisorbed at room temperature. The absorptions in Fig. 2C occur at ca. 2980 (w,sh); 2960 (s); 2910 (w,bd,sh); 2870 (w); ca. 1470 (m,bd); ca. 1380 (w); and 1365 (w). Taking into account the MSSR, the intensity distribution suggests the structural assignment to the adsorbed species of either residual 2-methylpropylidyne or the partially hydrogenated structure **5**. Of these two alternatives, **5** is preferred because of the occurrence of two δCH_3s absorptions at 1380 and 1365 cm^{-1}. These are typical of the presence of $(CH_3)_2CH$- groups, but for the more rigid 2-methylpropylidyne structure one of these would be forbidden by the MSSR. Structure **5** could be most readily produced by hydrogenation of the 2-methylpropylidyne adsorbed species and **4** from the di-σ or π initial species.



4



5

Further addition of gas-phase hydrogen leads, Fig. 2D, to only minor changes in the spectrum of the adsorbed species, mainly a thickening of the 2960 cm^{-1} absorption on the low wavenumber side and some background intensification in the 2930 cm^{-1} region. It seems that there is a minor proportion of adsorbed species that are susceptible to hydrogenation on the surface. Further evacuation and rehydrogenation cycles lead to no further changes so the surface species in question are very stable at room temperature.

No appreciable ca. 1600 cm^{-1} absorptions occur in the spectra of Figs. 1A, 2A, and 3A, but the very broad band

centred near 1660 cm^{-1} occurs more consistently. It persists after hydrogenation but is weaker in intensity in spectra obtained after evacuation, which is consistent with its association with hydrogen chemisorption.

Hydrogenation at elevated temperatures

The spectra are illustrated in Fig. 3 and all were obtained at room temperature after the higher temperature treatments. Spectra were taken in both the presence and absence, i.e., after evacuation, of gas-phase hydrogen.

Addition of hydrogen at 100°C led to 2-methylpropane (isobutane) in the gas phase and, on cooling, a larger amount of the physically adsorbed species compared with hydrogenation at room temperature. This is shown by the greater strength of absorptions at 2950 and 1470 cm^{-1} and is confirmed by evacuation at 100°C, Fig. 3C, where only a weak residual spectrum is retained with bands at 2960, 2915, 2870, 2855, 1580, ca. 1450, and 1380 cm^{-1}. However, subsequent addition of hydrogen at 200°C led to a much stronger spectrum of an *n*-alkyl species and the relative intensities within the 2950/2915 and 2870/2850 cm^{-1} band-pairs is close to what would be expected from the CH_3/CH_2 ratio of an *n*-butyl group bonded to the surface (5, 22). This provides clear evidence that isomerisation of the C_4 skeleton to a straight chain has occurred under the influence either of the high temperature or hydrogenation, or both.

On evacuation at 200°C this spectrum virtually disappears, Fig. 3E, but is restored in a modified form on rehydrogenation at 300°C, Fig. 3F. Such a very remarkable loss of intensity of all the bands from the adsorbed species on evacuation was observed previously at lower temperatures by Avery (5) for alkyl groups bonded to Pd/SiO_2 catalysts. As the removal of CH bonds from the substituted alkane is accompanied by the appearance of only an extremely weak absorption band (if any), in the 3100–3000 cm^{-1} characteristic of alkenes, it seems that CH bonds must be largely replaced by CPt bonds on evacuation. Avery has suggested that this may occur for the linear alkane groups that can become multiply CPt-bonded on evacuation along the edges of steps in the surfaces of the metal particles. For geometrical reasons, some sort of grooved metal surface feature seems to be necessary for the formation of many CPt bonds. A notable difference between the Pt/SiO_2 and Pd/SiO_2 cases is that in the former the phenomenon occurs above 100°C, but in the latter case at room temperature.

The addition of hydrogen at 300°C, Fig. 3F, again indicates the presence of *n*-alkyl groups bonded to the surface, but with much weaker relative absorptions from CH_3 groups at ca. 2940 (shoulder) and near 1380 cm^{-1}, implying the presence of longer alkyl chains. At the same time a weak and sharp gas-phase absorption at ca. 3020 cm^{-1} denotes the presence of gas-phase methane. Overall, compared with the results at 200°C, a disproportionation reaction has clearly occurred. Finally, evacuation at 300°C, Fig. 3G, leads once again to the disappearance of all the alkyl hydrocarbon absorptions. At 300°C the spectra are indistinguishable from those obtained either before or after evacuation from the adsorption of any of the linear butenes (15).

The absorptions assigned to the PtHPt groups alternate in position between 1620 and 1590 cm^{-1} in the presence or absence respectively of hydrogen in the gas phase. When hydrogen is present, weak absorption bands at 2130 cm^{-1} from surface PtH species are also present (18, 19). Absorption bands from adsorbed CO increase in intensity with increasing high-temperature treatments of the sample, giving a weak doublet at ca. 1890 and 1850 cm^{-1} in the CO-bridging region, and stronger absorptions from the linear adsorbed species moving from ca. 1980 to 2030 cm^{-1}.

Conclusions

Through application of the MSSR for vibrational spectra on these Pt/SiO_2 catalysts with fairly large metal particles it has proved possible to account for the room temperature infrared spectrum from the adsorption of 2-methylpropene in terms of the presence of π-, di-σ adsorbed, and 2-methylpropylidyne species. At higher temperatures, up to 300°C, the adsorbed species gradually transform from alkane to alkene in type.

Hydrogenation at room temperature leads some of the adsorbed species to leave the surface as 2-methylpropane and others, of a branched alkyl type, to remain chemisorbed. Hydrogenations at high temperatures up to 300°C provide spectroscopic evidence for isomerisation of the C_4 skeleton to a straight chain and for surface disproportionation reactions leading to gas-phase methane with longer alkyl chains remaining on the surface. The alkyl-type spectra in the presence of hydrogen virtually completely disappear on evacuation but are regenerated by a renewed dose of hydrogen. As suggested earlier for such spectroscopic adsorption phenomena on Pd/SiO_2 (5), this must imply the replacement of many CH groups by CPt bonds to the surface. This probably occurs along steps or similar features in the surfaces of the metal particles.

NOTE ADDED IN PROOF: A recent paper (23) has reported the VEEL spectra of 2-methyl propene adsorbed on Ni(111) between 80 and 150 K. The di-σ form is found at low temperatures, decomposing to a di-σ/π adsorbed species. This could be a precursor of room temperature 2-methyl propylidene.

Acknowledgements

We thank Professor M. A. Chesters and Drs. P. Gardner and P. Pudney[2] for making available to us their unpublished RAIRS results on Pt(111). One of us (G.S.) thanks the Ministry of Education of the Government of Pakistan for a studentship; the other (N.S.) thanks the British SERC for equipment and support of his work on the spectra of adsorbed species.

1. G. SHAHID and N. SHEPPARD. Spectrochim. Acta, **46A**, 999 (1990).
2. M. A. CHESTERS, C. DE LA CRUZ, P. GARDNER, E. M. MCCASH, P. PUDNEY, G. SHAHID, and N. SHEPPARD. J. Chem. Soc. Faraday Trans. **86**, 2757 (1990).
3. N. R. AVERY and N. SHEPPARD. Proc. R. Soc. London, **A405**, 1 (1986).
4. J. W. WARD. Ph.D. Thesis, University of Cambridge. 1962.
5. N. R. AVERY. J. Catal. **19**, 15 (1970).
6. A. RAVI and N. SHEPPARD. J. Phys. Chem. **76**, 2699 (1972).
7. G. BUSCA, G. RAMIS, and V. LORENZELLI. J. Chem. Soc. Faraday Trans. 1, **85**, 137 (1989).
8. N. SHEPPARD, D. I. JAMES, A. LESIUNAS, and J. D. PRENTICE. Commun. Dept. Chem. Bulg. Acad. Sci. **17**, 95 (1984).
9. B. J. BANDY, M. A. CHESTERS, D. I. JAMES, G. S. MCDOUGALL, M. E. PEMBLE, and N. SHEPPARD. Phil. Trans. R. Soc. London, **A318**, 141 (1986).
10. C. DE LA CRUZ and N. SHEPPARD. J. Chem. Soc. Chem. Commun. 1854 (1987).
11. H. A. PEARCE and N. SHEPPARD. Surf. Sci. **59**, 205 (1976).
12. R. G. GREENLER, D. R. SNIDER, D. WITT, and R. S. SORBELLO. Surf. Sci. **118**, 415 (1982).
13. L. J. BELLAMY. Infrared spectra of complex molecules. 3rd ed. Vol. 1. Chapman and Hall, London. 1975.
14. U. A. JAYASOORIYA, M. A. CHESTERS, M. W. HOWARD, S. F.

Can. J. Chem. Downloaded from www.nrcresearchpress.com by 84.41.108.74 on 09/07/12
For personal use only.

A. KETTLE, D. B. POWELL, and N. SHEPPARD. Surf. Sci. **93**, 526 (1980).
15. G. SHAHID. M.Phil. Thesis, University of East Anglia. 1987.
16. H. STEININGER, H. IBACH, and S. LEHWALD. Surf. Sci. **117**, 685 (1982).
17. S. B. MOHSIN, M. TRENARY, and H. J. ROBOTA. J. Phys. Chem. **92**, 5229 (1988).
18. D. D. ELEY, D. M. MORAN, and C. H. ROCHESTER. Trans. Faraday Soc. **64**, 2168 (1968).
19. M. PRIMET, J. M. BASSET, M. V. MATHIEU, and M. PRETTRE. J. Catal. **28**, 368 (1973).
20. N. SHEPPARD. Annu. Rev. Phys. Chem. **39**, 589 (1988).
21. N. SHEPPARD and T. T. NGUYEN. Adv. Infrared Raman Spectrosc. **5**, 67 (1978).
22. B. A. MORROW and N. SHEPPARD. Proc. R. Soc. London, **A311**, 391 (1969).
23. L. HAMMER, B. DÖTSCH, F. BRANDENSTEIN, A. FRICKE, and K. MÜLLER. J. Electron Spectrosc. Relat. Phenom. **54**, 687 (1990).

Can. J. Chem. Downloaded from www.nrcresearchpress.com by 84.41.108.74 on 09/07/12
For personal use only.

Semiclassical model calculations of weak, strong, and short O—H···O H-bonds

WERNER A. P. LUCK AND THOMAS WESS
Universität Marburg, D-W-3550 Marburg, Germany

Received March 8, 1991

This paper is dedicated to Dr. Richard Norman Jones

WERNER A. P. LUCK and THOMAS WESS. Can. J. Chem. **69**, 1819 (1991).

The OH potentials of the complexes $(HOH\cdots OH)^-$ are calculated by an *ab initio* MO-LCAO-SCF-CISD method with a 6-31G** basis set for 30 different O···O distances. The resulting OH vibration levels are calculated by the so-called semiclassical Planck–Sommerfeld phase integral. The experimental H-bond effects on vibration spectra, and their anomalies, could be established by calculations of H-bond energies, OH frequencies, anharmonicities, the Badger–Bauer rule, correlation between OH and O···O distances, isotopic effects, and the Ubbelohde effect. For very short H-bonds new properties could be predicted. There seem to exist three classes of H-bond: (1) weak or medium-strong, (2) strong, and (3) very short. The simple phase integral method could demonstrate the anomalous effects of strong H-bonds solely by the transition from two separated minima to one, without necessarily assuming tunnel effects.

Key words: strong H-bonds, IR spectra and theory, tunnel effects.

WERNER A. P. LUCK et THOMAS WESS. Can. J. Chem. **69**, 1819 (1991).

Utilisant une méthode MO-LCAO-SCF-CISD *ab initio* avec un ensemble de base 6-31G** et 30 distances O···O différentes, on a calculé les potentiels OH des complexes $(HOH\cdots OH)^-$. On a calculé les niveaux vibrationnels OH qui en découlent par la méthode semi-classique d'intégrale de phase de Planck–Sommerfeld. Grâce à ces calculs, on a pu déterminer les effets des liaisons hydrogènes expérimentales sur les spectres de vibration ainsi que leurs anomalies, comme : les énergies des liaisons H, fréquences des OH, les anharmonicités, la règle de Badger–Bauer, la corrélation entre les distances OH et O···O, les effets isotopiques et l'effet Ubbelohde. Pour des liaisons H très courtes, on a prédire de nouvelles propriétés. Il semble qu'il existe trois classes de liaisons H : (1) des liaisons faibles ou moyennement fortes; (2) des liaisons fortes et (3) des liaisons très courtes. La méthode simple d'intégrale de phase permet de démontrer les effets anormaux des liaisons H fortes grâce à la transition de deux minima séparés vers un, sans pour cela faire l'hypothèse de l'existence d'effets tunnels.

Mots clés : liaisons H fortes, spectres et théorie IR, effets tunnels.

[Traduit par la rédaction]

Introduction

In our group, Schiöberg (1, 2) recently demonstrated again, for the H-atom, Morse potentials, and harmonic oscillators, the agreement of quantized energy levels of known potentials between the modern Schrödinger method and the older Planck–Sommerfeld phase integral (3, 4).

$$[1] \qquad \oint p_v(r)\,\mathrm{d}r = (v + 1/2)\,h \qquad v = 0, 1, 2, \cdots$$

where $p_v(r) = (2\mu\ E_{\mathrm{kin},v}(r))^{1/2} = (2\mu)^{1/2}\ (E_v - V(r))^{1/2}$; p_v: momentum; $E_{\mathrm{kin},v}$, E_v, and $V(r)$: kinetic, total, and potential energies; and μ: reduced mass.

The Schrödinger method should include eq. [1], which is related to the de Broglie equation. For instance, for the H-atom with mv = constant, and assuming a periodic orbit $\oint \mathrm{d}q = 2\pi r$ at wavelength λ, eq. [1] is parallel to the de Broglie relation $\lambda = h/mv$. Applying eq. [1] means that the areas between the potential curve and the vibration levels have to be set as multiples of h. This requires only short computer times. It gives the possibility of intuition as a supplement to quantum mechanical calculations. Colleagues who like it may find consolation in the word of the Nobel prize winner Max Born (5): "Renouncing such interpretations would make impossible every insight and bring to a standstill the intuition as a basis of research." With this method we were recently able to demonstrate (6) nearly quantitatively the temperature (T) constancy of the density $\rho = \rho_0$ of rare gas crystals from $T = 0$ K to a limiting temperature T_g, and the experimental linear relation $\rho = \rho_0 - bT$ for $T > T_g$. This simple approximation not only brings a deep understanding of intermolecular interactions in the condensed phase up to the T-linearity of the heat of vaporization but can also give intuitive understanding of the continuum of Debye's quantized specific heat frequencies or Planck's black body radiation (6). Equation [1] could also be applied with some success to H-bonds $(ClH\cdots Cl)^-$ (7).

There is some interest in applying eq. [1] to important problems in the mechanism of proton transfer. Certain anomalous behaviour of strong H-bonds has been interpreted as caused by tunnel effects. We were interested in testing whether the properties of strong H-bonds are a conclusive and unique argument for tunnel effects. We were also interested in testing whether this simple method of eq. [1] could give a consistent model of the complicated results of H-bond spectroscopy. Surprisingly, this seems to be possible.

It was of special interest to determine if the semiclassical approximation would be able to calculate experimental isotope ratios $(OH\cdots O)/\nu(OD\cdots O)$ significantly lower than 1, which wave-mechanics calculations did not do (8–12). Also it would be interesting to find out if a result of quantum mechanics (9–12) could be established that a small disturbance of a symmetric double-well potential induces strong different transitions.

1. Results

1. Calculation of the OH potential

Lippincott and Schroeder (13) described OH···O complexes with a double minimum potential. Other authors used different polynomials (8–15), namely Morse potentials (16), exponential functions (9), parabolic functions (9), etc. Janoschek, Weidemann, Zundel, *et al.* (17–19) and Scheiner (20, 21) used quantum chemical energies of models $(H_2O—H\cdots OH_2)^+$ of $(H_3N—H\cdots NH_3)^+$. Our model $(HOH\cdots OH)^-$ was calculated with the *ab initio* MO-LCAO-SCF-CISD method with a 6-31G** basis set using a CONVEX C230 computer. The Cl procedure is extensive but it is necessary to take into account the electron–electron correlations for the potential in strong

Can. J. Chem. Downloaded from www.nrcresearchpress.com by 84.41.108.74 on 09/07/12
For personal use only.

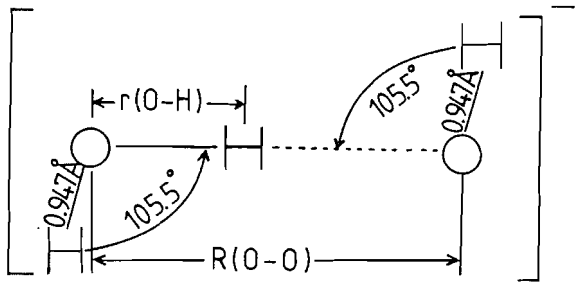


FIG. 1. Assumed geometry of a linear H-bonded $(HOH\cdots OH)^-$ complex. (Geometry of the monomer H_2O optimized with the Hartree–Fock method).

H-bonds (22–26). The geometry of the H_2O monomer has been estimated with the simple Hartree–Fock method neglecting the electron–electron correlations, which are less important for the geometry. We assume the geometry of $(HOH\cdots OH)^-$ to be as shown in Fig. 1.

Figure 2 shows some examples of OH potentials obtained by the *ab initio* method (black points in Fig. 2). The whole potential curve has been represented between points 1 and 2 by polynomials $ar^2 + br^3 + cr^4$ determined by points 1–3 and in the next step between points 2 and 3 by a similar polynomial with varying a, b, and c determined by points 2–4, etc. It was necessary to add r^3 terms to get normal potential curves. The zero point of the potential scale in Fig. 2 is the potential minimum of the monomeric OH group (Fig. 2 on the left). Starting at $R_{O\cdots O} = 3.8$ Å, the potential of the complex is noticeably negative on this scale as a consequence of H-bond interaction (Fig. 2 on the right). Potential curves have been calculated for 30 different $R_{O\cdots O}$ distances in the region $3.8 \text{ Å} \geq R_{O\cdots O} \geq 2.2$ Å (47).

The maximum of the H-bond interaction (the most negative value of V in curves in Figs. 2–5) has been found as 120.65 kJ mol^{-1} at $R_{O\cdots O} = 2.44$ Å, in a region where the double minimum changes to a single one. In this region the distance of the centred H-atom is going to be equal to both O-atoms and is called a symmetric H-bond.

2. Semiclassic calculation of the OH vibration levels

The 30 different potentials described in the last section have been treated with eq. [1], integrating from the smallest OH distance r_{OH} to the largest one along the potential curves and multiplying for a full oscillation by a factor 2 to get the allowed vibration levels with the whole phase integral. The value of the integral, calculated by iterations with a DEC VAX 11/750 computer, increases monotonically with increasing energy level. After about 10–20 steps the quantized vibration levels and the values of the two turning amplitudes were obtained. These levels are given as full lines in Figs. 2–5. The same procedure was repeated for OD (dotted lines in Figs. 2–5). We calculated H or D oscillations assuming non-moving O-atoms. This means we took $\mu(H) = 1.008$ g mol^{-1} or $\mu(D) = 2.014$ g mol^{-1}.

Our monomer OH model ($R_{O\cdots O} = \infty$ gives an OH frequency $\nu = 3740.4$ cm^{-1} in fairly good agreement with $\nu(HOD_{vapour}) = 3707$ cm^{-1} (27). The frequencies with H-bond interactions will be discussed later in Figs. 7–10.

At large $R_{O\cdots O}$ distances with a double minimum the phase integral obviously has to be applied to just one minimum. Two possibilities could be discussed for H-bond cases near a *symmetric H-bond:*

1. In a double minimum potential with oscillations below the potential barrier between the two minima we apply the phase integral to only one minimum. Near symmetric H-bonds at some $R_{O\cdots O}$ (for instance 2.76 Å and $\upsilon = 1, 2$; 2.72 Å, $\upsilon = 1$; 2.66 Å, $\upsilon = 1$) it happens that the admitted value $(\upsilon + 1/2)h$ is, on the one hand, too large compared with the area of one minimum to allow oscillations within only one potential well, but on the other hand too small for oscillations above the potential barriers including the two minima in eq. [1]. In such cases certain quantum numbers υ could be impossible. This effect is mass dependent and could therefore induce the anomalous isotope effect for $\nu(OH)/\nu(OD)$. $\upsilon = 1$ could be possible for OD at 2.76 and 2.72 A (Fig. 3).

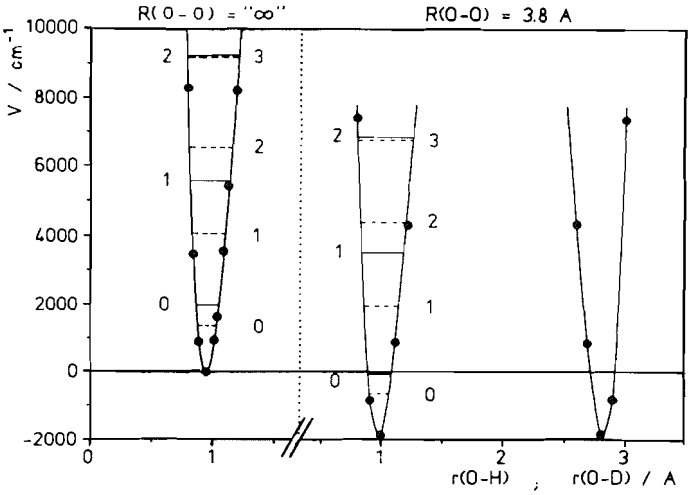


FIG. 2. (●) Potential V values calculated with the 6-31G** basis set. (—) Allowed OH vibration levels υ_H calculated with the phase integral on one minimum (υ_H values on the left side). (----) Allowed OD vibration levels υ_D calculated with the phase integral (υ_D values on the right side). From left to right: $R(O\cdots O)$/Å: ∞; 3.8.

2. We admit total "tunneling" and apply the phase integral immediately to both minima, integrating both areas. For the region $3.8 \text{ Å} > R_{O\cdots O} > 2.52$ Å eq. [1] has therefore also been applied to both minima (corresponding allowance of unlimited tunneling). Figure 5 for example shows the results for $R_{O\cdots O}$: 2.76, 2.72, and 2.66 Å. For 2.76 Å, vibrations up to $\upsilon = 2$ are possible below the potential barrier and for $R_{O\cdots O} = 2.72$ Å, $\upsilon_H = 1$ is included in oscillations below the potential well. All calculations are done only for $\upsilon \leq 4$, excluding high T.

As an approximation, we decided to exclude case 2 (quantization including areas of two partial potential minima). But, if the theoretical vibration level is not far from the potential barrier, $O\cdots O$ vibrations or environmental influences could change the height of the barrier a little for the proton transfer and also change the condition of quantization. Therefore the following discussion for such selected cases is based on the results of such calculations as the examples of Fig. 5 (integrating over the two minima of the double minimum). Case 2 has been assumed for all $R_{O\cdots O} < 2.66$ Å as well (Fig. 4). This procedure could also be an indication of a tunnel effect in such cases.

The theoretical coupling with $O\cdots O$ vibrations is neglected in our method, studying the head lines on a first approximation. This seems to be possible in regard to the large change of $\nu(OH)$ from 3740 to 700 cm^{-1} in Fig. 7, etc.

As one result, Figs. 3–5 demonstrate that the allowed level distances increase with the quantum number υ in case of an overlapping of two minima with vibration levels in symmetric potential parts. That means they are neither harmonic with constant level distances nor anharmonic with decreasing distances but "superharmonic" with increasing distances (negative

Can. J. Chem. Downloaded from www.nrcresearchpress.com by 84.41.108.74 on 09/07/12
For personal use only.

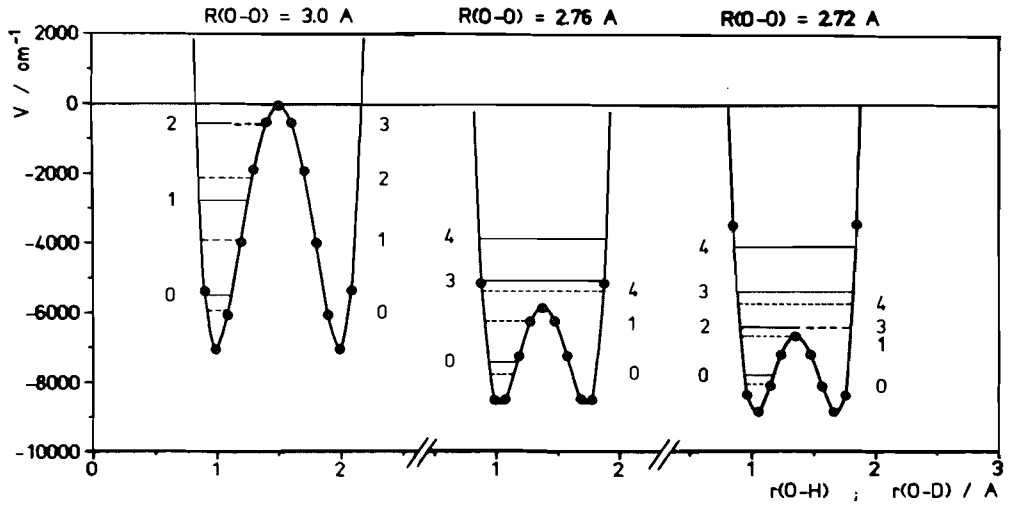


FIG. 3. Potential V calculated with the 6-31G** basis set and OH; OD vibration levels (detailed caption, see Fig. 2). $R(O\cdots O)/Å$: 3, 2.76, and 2.72.

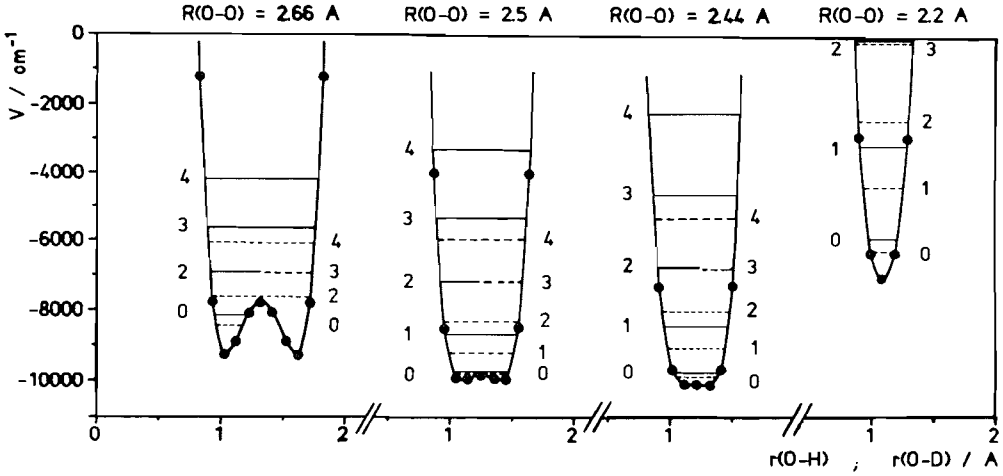


FIG. 4. Potential V calculated with the 6-31G** basis set and OH; OD vibration levels (detailed caption see Fig. 2). $R(O\cdots O)/Å = 2.66$ quantized with only one maximum; $R(O\cdots O)/Å = 2.5$, 2.44, and 2.2 quantizied with the full potential curves.

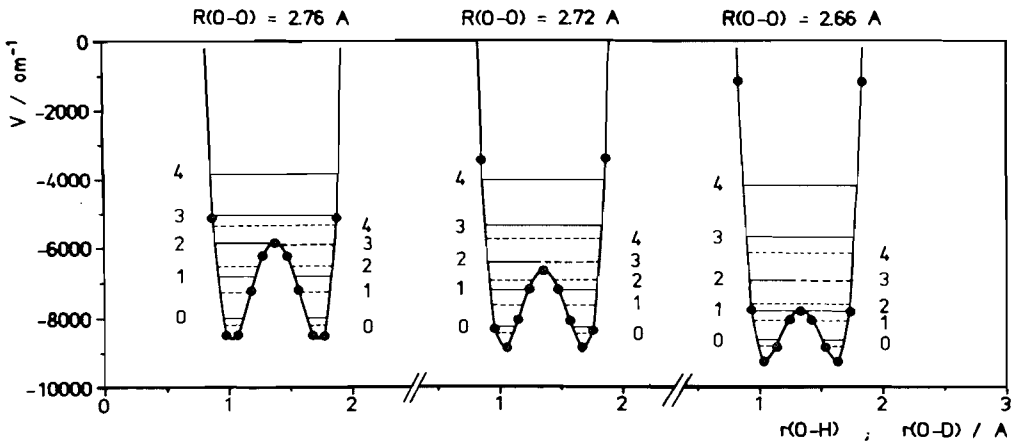


FIG. 5. Potential V calculated with the 6-31G basis set and OH; OD vibration levels (detailed caption, see Fig. 2) quantized with the phase integral and the two minima.

Can. J. Chem. Downloaded from www.nrcresearchpress.com by 84.41.108.74 on 09/07/12
For personal use only.

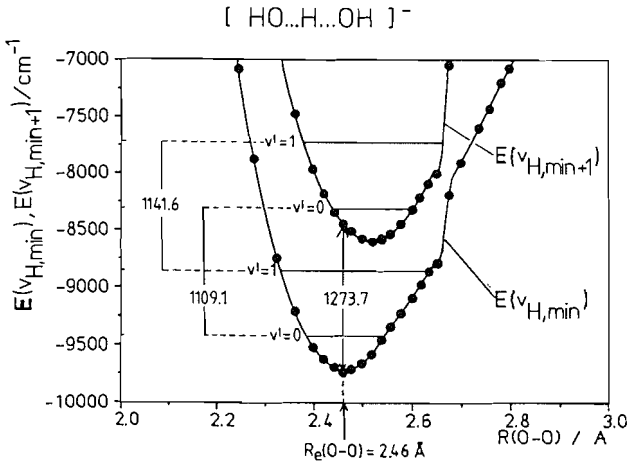


FIG. 6. Below: The lowest OH energy levels allowed $E(0, H)$ (zero point) for curves of the type of Figs. 2–5. Top: The allowed vibration levels next $E(1, H)$ above the zero-point energies of Fig. 2, etc. Levels v': Allowed O···O vibration levels.

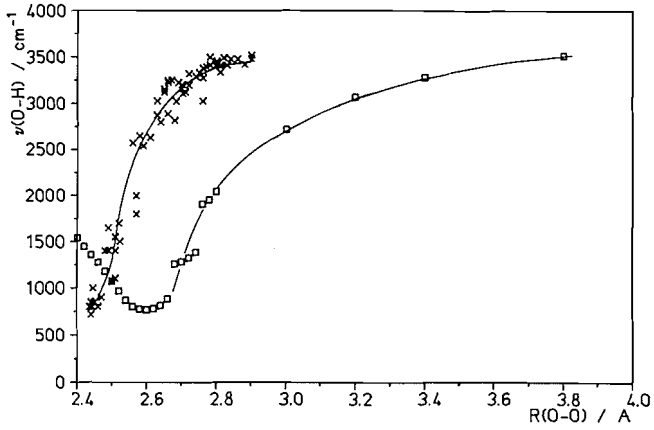


FIG. 7. (×) Experimental OH frequencies (32) as $f[R(O\cdots O)]$. (□) Calculated OH frequencies based on Figs. 2–5, etc.

$x_e\omega_e$ in Fig. 9). We had found (6) a similar superharmonic case with the sum of intermolecular Lennard–Jones potentials of nearest neighbours in condensed phases, and Millen and co-workers were able to establish this effect experimentally with H-bond vibrations (57). The first, meanwhile more or less forgotten, theoretical "superharmonic" example was given by Pöschel and Teller (58) in 1933.

2. Discussion

1. H-bond energies

Figure 6 shows the energy levels $E(v_{H,min})$ and $E(v_{H,min} + 1)$ in units of cm^{-1} of all 30 cases calculated at a certain constant $R_{O\cdots O}$ ($v_{H,min}$: smallest allowed level of our procedure discussed above). These levels would correspond to the zero-point vibrations. The calculated black points in Fig. 6 are connected with a polynomial $ax^2 + bx^3 + cx^4$. The two curves of Fig. 6 correspond as energies for different $R_{O\cdots O}$ to potential curves of the O···O vibrations. Applying the phase integral of eq. [1] to these curves yields information about the possible vibrational levels of the H-bond stretching ($\mu_{(0)} = 8$ g mol^{-1} is used). We define them by the quantum numbers v'. The minimum of the lower "potential curve" of the O···O vibrations was found at $R_{O\cdots O} = 2.46$ Å with $E(v_{H,min}) = -139.58$ kJ mol^{-1}. If we similarly plot V_{min} for the 30 curves of the types in Figs. 2–5, and assuming, as in Fig. 2, V_{min} of the monomer as the zero point, we get the minimum of the O···O potential curve at $R_{O\cdots O} = 2.44$ Å and $V_{min}(O\cdots O) = -120.65$ kJ mol^{-1} (see above). In a first approximation this value would be the calculated H-bond dissociation energy. Our value is similar to the quantum-mechanics calculation (24): -118.07 kJ mol^{-1} at 2.465 Å. Experimental data give values of -94.2 kJ mol^{-1} (28), -100 kJ mol^{-1} (29), and -144 kJ mol^{-1} (30). A comparison between these experimental values and the theoretical value has to take into account corrections for the zero-point energies of other vibrations and rotations or librations, respectively (22, 24, 31). The shortest known strong H-bonds are given in the literature (32) as 2.44 Å, a value not far from our model, minimum value 2.46 Å in Fig. 6. H-bond energies ΔU_H for the strongest O—H···O H-bonds (33) are given as about -130 kJ mol^{-1}, similar to our prediction. These comparisons are extended to different types of O···O H-bonds, not only the same type as our model, with different charge distributions (HOH···OH)$^-$, so these could be only half-quantitative comparisons of the size of order.

The limited comparison of our charged model complex with medium strong uncharged H-bonds is demonstrated by the H-bond energy value $\Delta U_H = -85$ kJ mol^{-1} (7100 cm^{-1}) of Fig. 3 at $R_{O\cdots O} = 3$ Å, a region in which the known $\nu(OH) = f(R_{O\cdots O})$ diagrams (32) already give $\nu(OH)$ values not far from monomers. Therefore, comparisons between our charged model and real neutral H-bonds seem to give mainly theoretical $R_{O\cdots O}$ values that are a little too large. That means the potential of real non-charged H-bonds corresponding to Fig. 6 would be expected to become a little steeper at larger $R_{O\cdots O}$ values. But the general view of our theoretical results seems to be quite good.

For the strong H-bonded equilibrium configuration of our model complex (HOH···OH)$^-$ around $R_{O\cdots O} = 2.46$ Å, Fig. 6 indicates, for $\nu(OH)$, for the O···O quantum state $v' = 0$ a value of 1109.1 cm^{-1}, and for $v' = 1$ a value of 1141.6 cm^{-1}. OH transitions with a change of the quantum number v' of the O···O vibrations are not very probable for strong H-bonds (1, 2).

The minimum in Fig. 6 corresponds to a change of this potential curve in Figs. 2–5 from two minima into one; the "kink" around 2.6 Å corresponds to the change of vibration levels with areas in only one potential minimum to levels containing both minima.

2. The OH stretching frequencies

Figure 7 compares the experimental values (32) of $\nu(OH) = f(R_{O\cdots O})$ with the result of our changed model complex (HOH···OH)$^-$. The experimental curve for mainly neutral OH···OH bonds has a similar relation, but a shift to smaller $R_{O\cdots O}$. The theory predicts a minimum at about 2.6 Å. This distance corresponds to the case of a $v_H = 0$ near the potential barrier in Fig. 4; therefore case 2 (Sect. 1.2) has been assumed. The smallest $\nu(OH)$ in the theoretical minimum of Fig. 7 is about 750 cm^{-1}, which is in good agreement with the smallest experimental value (720 cm^{-1}) in Novak's (32) review. The appearance of the predicted minimum is unknown; perhaps it could be proved by high pressure measurements, which often show red shifts in a similar way in not too large pressure regions, for ROH systems, as the decreasing temperature corresponds to shorter distances (36, 37). In the case of self-association of 2,2,3,3,4,4,4-heptafluoro-1-butanol (HFB) in perfluoroheptane (PFHP) as solvent, our research group found (37) really experimental OH ν-minima. But they do have much smaller

Can. J. Chem. Downloaded from www.nrcresearchpress.com by 84.41.108.74 on 09/07/12
For personal use only.

depth at pressures $p \approx 3$ GPa. This p corresponds to a density increase of about 55%. We found a similar ν-minimum for the OH vibration of perfluoro-*tert*-butanol (PFTB) H-bonded to dioxane or to tetrahydrofuran (37) with poly-monochlorotrifluoroethene (PCFE) as solvent. In this case the minimum of the density change is about 30%.

Similarly, we observed small OH ν-minima at $p \approx 2$–3 GPa for monomeric OH (36) induced by van der Waals interactions between OH and solvents. Such minima could be observed for the systems HFB/PFHP/PCFE or PFTB/PFHP/PCFE. In these cases we could also calculate these minima at 3.8 Å (HFB/PFHP), at 3.6 Å (PFTB/PFHP), at 3.55 Å (HFB/PCFE), or at 3.4 Å (PFTB/PCFE) with the semiclassical phase integral method, overlapping the Morse potential with the Lennard–Jones potential. We were able to establish similar minima with other methods (60, 61) as well. This is another example of the efficiency of the phase integral method.

With the assumption of a correlation (34) between the half-width $\Delta\nu_{1/2}$ and a thermal distribution of O···O distances, the theoretical curve in Fig. 7 would predict a proportionality between $\Delta\nu_{1/2}$ and the H-bond induced shift $\Delta\nu$, as it is observed in many experiments (35, 37). In the region of short H-bonds (minimum in Fig. 7) $\Delta\nu_{1/2}$ could be reduced. There are also some indications of the reality of these predictions (14, 32). High pressure spectroscopy (36, 37) has also shown an increase of $\Delta\nu_{1/2}$ (OH) with increasing pressure p. It has been difficult to understand these effects until now, but they could be related to the curve of Fig. 7 in the sense that smaller $R_{O\cdots O}$ values are induced by high p. On the other hand $\Delta\nu_{1/2}$ decreases with reduced T (reduced $R_{O\cdots O}$ distribution) and does not change much at a low T. ν becomes nearly constant at $T \leq 90$ K (59).

3. *The anharmonicity $x_e\omega_e$ of the OH stretching vibration in dependence on the O···O distance*

The calculated frequencies of our model complex for the fundamental vibration $\nu_{min} \rightarrow (\nu_{min} + 1)$ and the first and second overtones $\rightarrow(\nu_{min} + 2)$ and $\rightarrow(\nu_{min} + 3)$ are plotted in Fig. 8.

The irregularities near the minimum depend on uncertainties in our calculations at higher transitions of the O—H excitations. Here in the critical region we could not decide clearly whether the quantization for the higher quantum numbers ($\nu = 2, 3\ldots$) must be done within only one minimum of the double minimum potential or whether areas of both minima have to be considered in the sense of an effect induced by O···O vibrations or tunneling. In the region of strong H-bonds near $R_{O\cdots O} \approx 2.8$ Å the overtone frequencies come near to the fundamental ones (Fig. 8). This could be related to the broad bands of strong H-bonds, called "continuum" by Zundel (17–19, 38–41). This "continuum" could not really be a continuum because the more precise overtone spectra of acids (34, 42) or NaOH (43, 44) show the broad absorption only at the low frequency sides of the OH bands (42, 43). The presented results also make improbably the assumption that the broad bands of strong acids could be induced by an H_3O^+ absorption region (44, 45). This conclusion has already been questioned because OH^- solutions show similar broad bands in the liquid state (42, 43).

Instead of the continuum, we would prefer the nomenclature: very broad OH band or "partial continuum". The increasing $\Delta\nu_{1/2}$, meaning uncertain spectroscopic results, vindicates the use of approximate calculations also for strong H-bonds.

The calculated strong reduction of overtone frequencies (Fig. 8) could also be related to the discussed "triplet structure" of

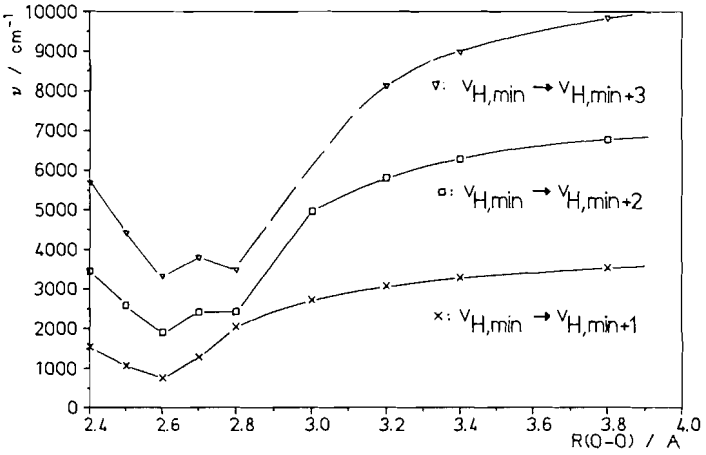


FIG. 8. Calculated OH frequencies based on Figs 2–5 of the fundamental, first, and second overtones (from the bottom to the top).

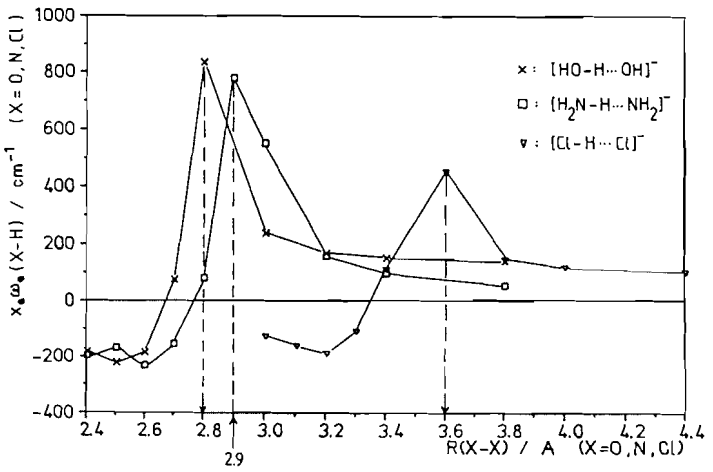


FIG. 9. Anharmonicities $x_e\omega_e$ calculated with the theoretical fundamental and first overtone. OH, NH, and ClH bands calculated with the same method (47) in dependence on the H-bond lengths.

strong OH bands. This effect has been interpreted occasionally by tunnel effects (8). As Fig. 8 demonstrates, this conclusion seems not to be necessary in this case.

In the case of medium-strong H-bonds, $\Delta\nu$ of the first overtone has been observed to be nearly double compared with $\Delta\nu_{(fundamental)}$ (46). This is in agreement with the calculated results but this rule may be not valid for strong H-bonds, a region that is not so easy to measure by the strong increase in $\Delta\nu_{1/2}$.

The strong change of the anharmonicity in the case of strong H-bonds is demonstrated in Fig. 9, which is based on the comparison between the first overtone and fundamental frequencies. Figure 9 includes similar calculations for NH···N and ClH···Cl H-bonds (47). For the predicted behaviour of very short H-bonds, $R_{O\cdots O} < 2.7$ Å, the anharmonicity becomes superharmonic already for the first overtone, an effect that has already been recognized for higher overtones as shown in Figs. 2–5.

4. *H-bond energies and frequency shifts (Badger–Bauer rule)*

Figure 10 shows the relation between the OH stretching frequencies calculated in our approximation in dependence on the potential minima V_{min} (minima in the series of Figs. 2–5).

Can. J. Chem. Downloaded from www.nrcresearchpress.com by 84.41.108.74 on 09/07/12
For personal use only.

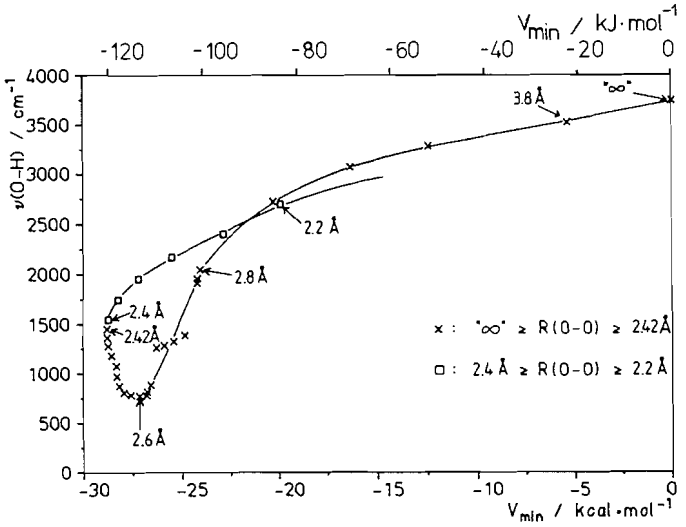


FIG. 10. Calculated fundamental OH stretching frequency of the $(HOH\cdots OH)^-$ complex as a function of the potential minimum V_{min} in the series of Figs. 2–5.

For weak H-bonds the diagram demonstrates an approximate proportionality between $\Delta\nu$ and V_{min}, a relation often discussed by experimentalists as the Badger–Bauer rule. Sometimes this relation has been questioned by theoreticians because of the relation claimed by Buckingham (48): $\Delta\nu \sim \partial V/\partial R$. Both relations could be true if $V_{min} \sim \partial V/\partial R$ is valid (36, 49).

Figure 10 demonstrates strong anomalies at very short O···O distances. Because of the decrease of V_{min} at very short H-bond length, we propose the following nomenclature: 1. long H-bonds, 2. short H-bonds, and 3. very short H-bonds or 1. weak, 2. strong, and 3. short H-bonds. Very short H-bonds are not necessarily strong H-bonds. In this region the repulsion forces have more influence on V_{min}. In the region of strong H-bonds, small influences by the environment (solvent effect, temperature or pressure changes) could induce in addition fairly strong frequency shifts and changes of $\Delta\nu_{1/2}$. This has to be taken into account in discussions of the so-called "continuum" of strong H-bonds.

The minimum in Fig. 10 at about 2.6 Å corresponds to an $R_{O\cdots O}$ at which the zero-point level is extended on both potential minima (Fig. 4); $R_{O\cdots O} \approx 2.4$ Å corresponds to a transition from a flat minimum (as in Fig. 4), which appears for 2.46 Å $> R_{O\cdots O} >$ 2.42 Å, to a more parabola-like potential curve (47).

5. *Correlation between OH distances r_{OH} and O···O distances $R_{O\cdots O}$*

Hamilton and Ibers (50) have given collected neutron-scattering data for the relation $r_{OH} = f(R_{O\cdots O})$. Figure 11 shows these data with a jump in the $R_{O\cdots O}$ region at about 2.48 Å, while cases with angle deviations >10° from a linear H-bond are excluded. In Fig. 11 theoretical results of our calculation for the $(HOH\cdots OH)^-$ complex under discussion are included. These results are in good agreement with the experimental data for neutral OH···O H-bonds with the exception of a change of the shift to higher O···O distances similar to that discussed in Fig. 7. In cases of calculated minima, the position of the lower one of the two minima nearest to oxygen has been taken for r_{OH}. In cases of symmetric potentials of the OH vibration, r_{OH} has been taken at $0.5R_{O\cdots O}$. At about $R \lesssim 2.55$ Å the double minimum changes to one in the series of Figs. 1–5 (47).

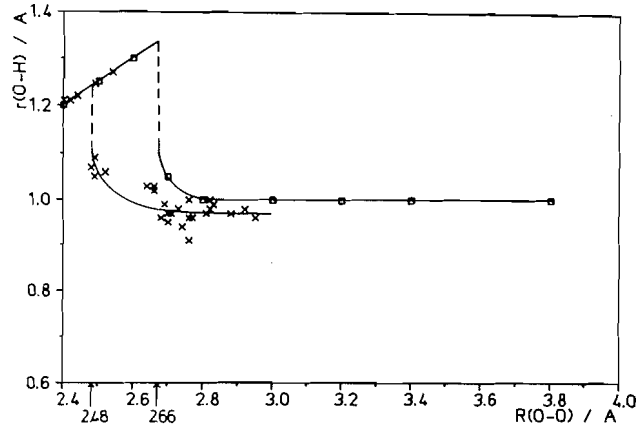


FIG. 11. (×) Neutron scattering results for $r_{OH} = f(R_{O\cdots O})$ (50). (□) Our theoretical values.

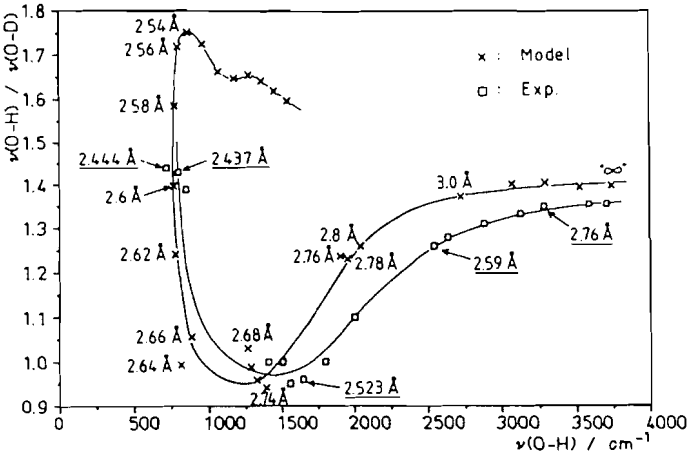


FIG. 12. Experimental (□) and theoretical (×) model isotope ratio $y = \nu(OH)/\nu(OD)$ of the fundamental stretching vibrations in different frequency ranges.

6. *Ratio of the frequencies* $\nu(OH)/\nu(OD)$

The experimental ratio $y = \nu(OH)/\nu(OD)$ of the fundamental OH band gives experimental anomalies in the region of the transition between the double minima to a single minimum (8–13, 32, 51–54) (Fig. 12, squares). Our calculated values of the charged complex agree with these results but give again a shift of the minimum position (Fig. 12). The curves in Fig. 12 consist of three parts:

1. Weak H-bonds with $R_{O\cdots O} >$ 2.76 Å (theory) or >2.6 Å (experiments) with $1.2 \lesssim y \lesssim 1.4$ and $r_{OH} = 1$ Å (Fig. 11).

2. Strong H-bonds with 2.74 Å $\gtrsim R_{O\cdots O}$ (theory) $\gtrsim$ 2.68 Å or 2.55 Å $\gtrsim R_{O\cdots O}$ (exp.) $\gtrsim$ 2.5 Å with a sharp decrease of y from about 1.2 to 0.9 and a kink in r_{OH} (Fig. 11).

3. Short OH-bonds with $R_{O\cdots O} \leq$ 2.68 Å (theory), $R_{O\cdots O}$ (exp.) < 2.5 Å with a sharp increase of y experimentally up to about $(2)^{1/2}$ or theoretically predicted to about 1.75 for very short H-bonds.

Papers on wave mechanics describe the second region with low y-values as caused by tunneling effects (8, 16). The three regions of Fig. 12 are caused in our model calculation by the three regions of Fig. 11: 1. weak H-bonds with constant r_{OH} distance; 2. small increase of r_{OH} from 1 to 1.1 Å; 3. short H-bonds with enlarged r_{OH}. The anomalous isotope ratio (case 2) does not require tunnel effects in our description.

Can. J. Chem. Downloaded from www.nrcresearchpress.com by 84.41.108.74 on 09/07/12
For personal use only.

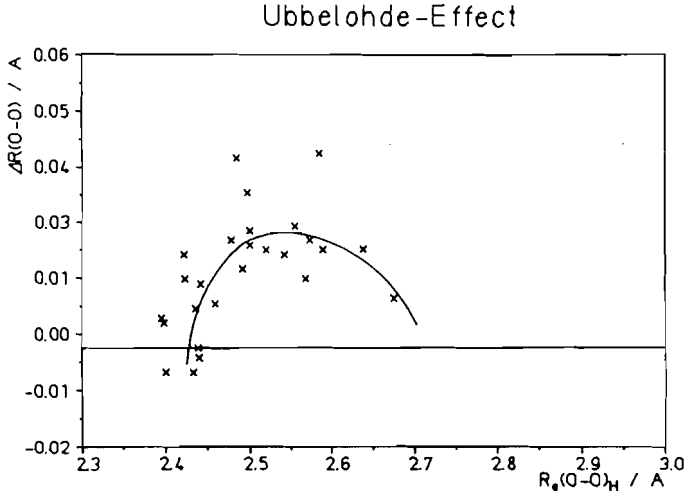


FIG. 13. The increase $\Delta R_{O\cdots O}$ of the O···O distances by deuteration (Ubbelohde effect) (56).

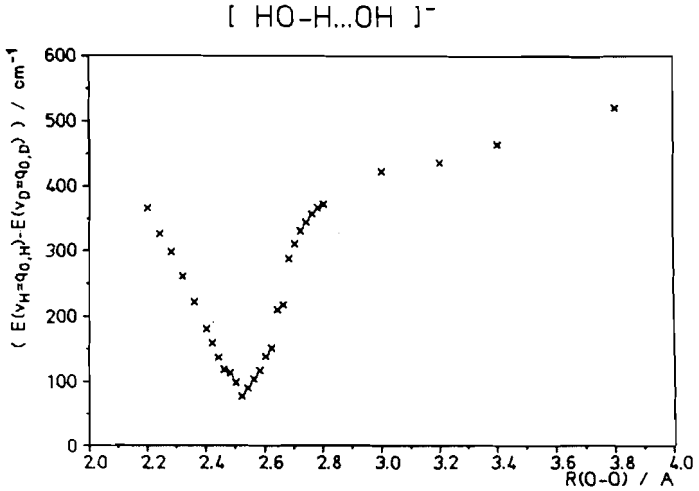


FIG. 14. The difference of the calculated zero-point energy levels of OH and OD as $f(R_{O\cdots O})$.

7. *The Ubbelohde effect, the increase of O···O distances in OD complexes*

The larger vibration amplitudes of OH compared with OD would lead one to expect smaller O···O distances after deuteration. But on the contrary, Ubbelohde (55) demonstrated that deuteration increases the O···O distances in the region between about 2.43 and 2.7 Å (Fig. 13). For shorter H-bonds, $R_{O\cdots O} < 2.43$ Å, the O···O distance may decrease for OD.

We now consider our model complex $(HO—H\cdots OH)^-$ in equilibrium (RO···O = 2.46 Å) as example of an O—H···O bond where the Ubbelohde effect is still to be expected with regard to Fig. 13. Varying the O···O distance, the OD vibration levels are below the OH levels (see Figs. 2–5). The difference of the lowest allowed zero-point energy level for OH minus OD is given in Fig. 14 (data Fig. 2, etc.). Starting at a large O···O distance for our model complex $(HO—H\cdots OH)^-$, this difference decreases with decreasing $R_{O\cdots O}$ to at least a minimum of about 60 cm^{-1} and increases again for shorter O···O distances. The cause of the so-called Ubbelohde effect for our model complex is based on the O···O vibration around its equilibrium distance 2.46 Å, which is near the maximum of the observed Ubbelohde effect at $R_{O\cdots O} = 2.5$ Å: If we discuss the H-bond potential as $f(R_{O\cdots O})$ (Fig. 6) the corresponding OD curve for our calculation would be obtained by subtracting, for every $R_{O\cdots O}$, the values of Fig. 14. As a result the OD curve would become more flat (higher anharmonicity) than the OH curve. Consequently the mean value of $R_{O\cdots O}$ averaged on one O···O oscillation would be larger for OD than for OH and the Ubbelohde effect could be understood based on the calculation for Fig. 14.

$R_{O\cdots O} \approx 2.52$ Å in Fig. 14 corresponds to the case in which the second possible vibration level ($v = 1$) for OH starts to contain areas of both potential minima (Fig. 3) (47) but the second level for OD contains an area of just one potential minimum (Fig. 3). The maximum of about 2.54 Å corresponds to the first potential area in which the zero-point level contains areas of the two minima.

3. Conclusion

The discussed charged H-bond complex $(HOH\cdots OH)^-$ applying the simple semiclassical Planck–Sommerfeld phase integral gives a consistent picture of many anomalous spectroscopic H-bond observations. For mainly O—H···O neutral H-bond complexes experimental anomalies appear only at smaller O···O distances of about 0.2 Å compared with the calculated charged complex. The anomalies are based mainly on the transition from a double-minimum potential to a single-minimum one. They appear even without taking a tunnel effect into account. The calculations can be discussed with the separation of three different types of H-bonds: weak, strong, and short. For short H-bonds some predictions can be given. Experiments with the high pressure technique should be done in this region of repulsion forces for testing the given predictions. Analogous calculations done of $(HN—H\cdots NH_2)^-$ and $(Cl—H\cdots Cl)^-$ give similar results, except that the H-bond distances for the anomalous effects increase (47).

Acknowledgements

We thank Mrs. M. Buchner, Marburg, for translation help and Dipl.-Ing. B. Weber for some drawings.

1. D. SCHIÖBERG. Mol. Phys. **59**, 1123 (1986).
2. D. SCHIÖBERG. Habilitationsschrift, Universität Marburg, AG Luck, 1986.
3. M. PLANCK. Ann. Phys. **50**, 385 (1916).
4. A. SOMMERFELD. Ann. Phys. **51**, 1 (1916); Atombau und Spektrallinien, Bd. II. Friedr. Vieweg & Sohn, Braunschweig. 1944.
5. M. BORN. Lecture at the Nobel prize winner meeting 1964, Lindau, Germany; Physik im Wandel meiner Zeit. 4. Aufl. Vieweg, Braunschweig. 1966, p. 267.
6. W. A. P. LUCK and T. WESS. J. Mol. Liq. Lett. **179**, 303 (1991).
7. H. KLEEBERG, V. VIDENOVA-ADRABINSKA, and T. WESS. J. Mol. Liq. **46**, 305 (1990).
8. T. SAITOH, K. MORI, and R. ITOH. Chem. Phys. **60**, 161 (1981).
9. J. LAANE. J. Chem. Phys. **55**, 2514 (1971).
10. V. A. SAVEL'EV and N. D. SOKOLOV. Chem. Phys. Lett. **34**, 281 (1975).; N. D. SOKOLOV and V. A. SAVEL'EV. Chem. Phys. **22**, 383 (1977).
11. H. ROMANOWSKI and L. SOBCZYK. Chem. Phys. **19**, 361 (1977).
12. Y. GUISSAN and H. RATAJCZAK. Chem. Phys. **62**, 319 (1981).
13. E. R. LIPPINCOTT and R. SCHROEDER. J. Chem. Phys. **23**, 1099 (1955).
14. S. BRATOS and H. RATAJCZAK. J. Chem. Phys. **76**, 77 (1982).
15. E. A. PSHENICHNOV and N. D. SOKOLOV. Opt. Spectrosc. **17**, 183 (1964).
16. E. MATSUSHITA and T. MATSUBARA. Prog. Theor. Phys. **67**, 1 (1982).
17. R. JANOSCHEK, E. G. WEIDEMANN, H. PFEIFFER, and G. ZUNDEL. J. Am. Chem. Soc. **94**, 2387 (1972).

Can. J. Chem. Downloaded from www.nrcresearchpress.com by 84.41.108.74 on 09/07/12
For personal use only.

18. R. JANOSCHEK, E. G. WEIDEMANN, and G. ZUNDEL. J. Chem. Soc. Faraday Trans. 2, **69**, 505 (1973).
19. R. JANOSCHEK, A. HAID, E. WEIDEMANN, M. LEUCHS, and G. ZUNDEL.J. Chem. Soc. Faraday Trans. 2, **74**, 1238 (1978).
20. S. SCHEINER. J. Phys. Chem. **86**, 376 (1982).
21. S. SCHEINER. J. Chem. Phys. **77**, 4039 (1982).
22. A. STOGARD, A. STRICH, J. ALMÖF, and B. ROOS. Chem. Phys. **8**, 405 (1975).
23. W. MEYER, W. JAKUBETZ, and P. SCHUSTER. Chem. Phys. Lett. **21**, 97 (1973).
24. B. O. ROOS, W. P. KRAMER, and G. H. F. DIERCKSEN. Theor. Chim. Acta, **42**, 77 (1976).
25. S. SCHEINER and L. B. HARDING. J. Am. Chem. Soc. **103**, 2169 (1981).
26. S. SCHEINER and L. B. HARDING. Chem. Phys. Lett. **79**, 39 (1981).
27. W. A. P. LUCK and W. DITTER. Z. Naturforsch. B: Anorg. Chem. Org. Chem. Biochem. Biophys. Biol. **24B**, 482 (1969).
28. M. ARSHADI and P. KEBARLE. J. Phys. Chem. **74**, 1483 (1970).
29. J. D. PAYZANT, R. YAMDAGNI, and P. KEBARLE. Can. J. Chem. **49**, 3308 (1971).
30. M. DE PAZ, A. GUIDONI GIARDINI, and L. FRIEDMANN. J. Chem. Phys. **52**, 687 (1970).
31. J. A. IBERS. J. Chem. Phys. **41**, 25 (1964).
32. A. NOVAK. Structure Bonding, **18**, 177 (1974).
33. T. ZEEGERS-HUYSKENS. J. Mol. Struct. **177**, 125 (1988).
34. C. BUANAM-OM, W. A. P. LUCK, and D. SCHIÖBERG. Z. Phys. Chem. NF, **117**, 19 (1979).
35. W. A. P. LUCK. J. Mol. Struct. **217**, 281 (1990); W. A. P. LUCK, S. PEIL, L. SCHRIVER, and A. SCHRIVER. J. Mol. Struct. **224**, 185 (1990).
36. T. F. MENTEL and W. A. P. LUCK. J. Phys. Chem. **94**, 1059 (1990); T. F. MENTEL. Thesis, Universität Marburg, AG Luck (1988).
37. W. A. P. LUCK, W. KÜMMEL, and T. MENTEL. J. Mol. Struct. **237**, 233 (1990); T. F. MENTEL and W. A. P. LUCK. J. Phys. Chem. **95**, 68 (1991).
38. G. ZUNDEL. Hydration and intermolecular interaction. Academic Press, New York. 1969.
39. D. SCHIÖBERG and G. ZUNDEL. J. Chem. Soc. Faraday Trans. 2, **69**, 771 (1973).
40. M. LEUCHS and G. ZUNDEL. J. Chem. Soc. Faraday Trans. 2, **73**, 2256 (1977); J. Phys. Chem. **82**, 1632 (1978).
41. G. ZUNDEL. *In* The hydrogen bond, recent developments. Vol. II. *Edited by* P. Schuster, G. Zundel, and C. Sandorfy. North Holland, Amsterdam. 1976.
42. W. A. P. LUCK. Fortschr. Chem. Forsch. **4**, 653 (1964).
43. W. A. P. LUCK. Ber. Bunsen-ges. Phys. Chem. **67**, 186 (1963).
44. T. ACKERMAN. Z. Phys. Chem. **27**, 253 (1961).
45. E. WICKE, M. EIGEN, and T. ACKERMANN. Z. Phys. Chem. **1** 348 (1945).
46. W. LUCK and W. DITTER. Ber. Bunsen-ges. Phys. Chem. **72**, 365 (1968).
47. T. WESS. Thesis, Universität Marburg, AG Luck (1991).
48. A. D. BUCKINGHAM. Proc. R. Soc. London, A: **248**, 169 (1958); **255**, 31 (1960); Trans. Faraday Soc. **56**, 753 (1960).
49. G. HEINJE, W. A. P. LUCK, and P. BOPP. Chem. Phys. Lett. **152**, 358 (1988).
50. W. C. HAMILTON and J. A. IBERS. Hydrogen bonding in solids. W. A. Benjamin, Inc., New York, Amsterdam. 1968.
51. Y. GUISSANI and H. RATAJCZAK. Chem. Phys. **62**, 319 (1981).
52. S. ODINOKOV, A. NABIULLIN, A. MASHKOVSKY, and V. GLAZUNOV. Spectrochim. Acta, **39A**, 1055 (1983).
53. E. GRECH, Z. MARLARSKI, and L. SOBCZYK. Chem. Phys. Lett. **128**, 259 (1986).
54. TH. ZEEGERS-HUYSKENS. Chem. Phys. Lett. **157**, 105 (1989).
55. A. R. UBBELOHDE. Proc. R. Soc. London, **173**, 417 (1939).
56. N. D. SOKOLOV, M. V. VENER, and V. A. SAVEL'EV. J. Mol. Struct. **177**, 93 (1988).
57. Z. KISIEL, A. C. LEGON, and D. J. MILLEN. Proc. R. Soc. A, **381**, 419 (1982).
58. G. PÖSCHEL and E. TELLER. Z. Phys. **83**, 143 (1933).
59. W. A. P. LUCK. J. Mol. Struct. **217**, 285 (1990).
60. A. M. BENSON and H. G. DRICKAMER. J. Chem. Phys. **27**, 1164 (1957); R. R. WIEDERKEHR and H. G. DRICKAMER. J. Chem. Phys. **28**, 311 (1958).
61. F. G. DIJKMAN and J. H. VAN DER MAAS. J. Chem. Phys. **66**, 3871 (1977).

Can. J. Chem. Downloaded from www.nrcresearchpress.com by 84.41.108.74 on 09/07/12
For personal use only.

Conformational stability, barriers to internal rotation, *ab initio* calculations, and vibrational assignment of 2-butanone

J. R. DURIG,[1] F. S. FENG, AIYING WANG, AND H. V. PHAN[2]
Department of Chemistry, University of South Carolina, Columbia, SC 29208, U.S.A.

Received July 9, 1991

This paper is dedicated to Dr. Richard Norman Jones

J. R. DURIG, F. S. FENG, AIYING WANG, and H. V. PHAN. Can. J. Chem. **69**, 1827 (1991).

The Raman (3200–10 cm^{-1}) and infrared spectra (3200–30 cm^{-1}) have been recorded for 2-butanone (ethyl methyl ketone), $CH_3CH_2C(O)CH_3$, for the gas and solid. Additionally, the Raman spectrum and qualitative depolarization ratios have been obtained for the liquid. Evidence for the existence of two conformations in the gas and liquid is observed, with the *trans* form (the two CH_3 moieties oriented *trans* about the central C—C bond) much more abundant than the high-energy form, presently identified tentatively to be the *gauche* rotamer. The *trans* form is the only form remaining in the spectrum of the solid. A very weak infrared band at 65 cm^{-1} has been assigned to the asymmetric torsion of the *trans* conformer. Using this frequency, ΔH, and the dihedral angle of the *gauche* rotamer, a potential function is proposed for the conformational interchange. Spectral features observed at 195.5 and 181.0 cm^{-1} in the far infrared spectrum of the gas have been assigned to the $1^{\mp} \leftarrow 0^{\pm}$ and $2^{\mp} \leftarrow 1^{\pm}$ of the methyl torsion of the ethyl group of the *trans* form, from which a barrier of 868 ± 3 cm^{-1} (2.48 ± 0.01 kcal/mol) is calculated. Similarly, the fundamental CH_3—C(O) torsion has been observed at 94.5 cm^{-1} for the *trans* conformer from which a threefold barrier to internal rotation has been calculated to be 233 cm^{-1} (666 cal/mol). Utilizing the rotational constants for two isotopic species, which were reported in an earlier microwave study, the heavy atom r_0 structural parameters have been determined. A complete vibrational assignment is proposed, which is supported with the results from a normal coordinate analysis performed with the force fields calculated with the 3-21G basis set. Full geometry optimizations have been carried out at the 6-31G* basis set for both the *trans* and *gauche* conformations as well as for the transition states to determine the structural parameters, energy difference, and barriers to internal rotation about the central C—C bond.

Key words: 2-butanone, vibrational spectrum; *ab initio* calculations, 2-butanone; conformational stability, 2-butanone.

J. R. DURIG, F. S. FENG, AIYING WANG et H. V. PHAN. Can. J. Chem. **69**, 1827 (1991).

On a déterminé les spectres Raman (3200–10 cm^{-1}) et infrarouge (3200–30 cm^{-1}) de la butan-2-one (éthyl méthyl cétone), $CH_3CH_2COCH_3$, tant à l'état gazeux que solide. On a aussi déterminé le spectre Raman et les rapports qualitatifs de dépolarisation du liquide. On a obtenu des données qui suggèrent l'existence de deux conformations tant en phase gazeuse que liquide; l'abondance de la forme *trans* (dans laquelle les deux portions CH_3 sont orientées en *trans* par rapport à la liaison C—C centrale) est beaucoup plus grande que celle de la forme plus riche en énergie que l'on croit être le rotamère *gauche*. La forme *trans* est la seule présente dans le spectre du solide. On a attribué une très faible bande, présente à 65 cm^{-1} du spectre infrarouge, à une torsion asymétrique du conformère *trans*. Utilisant cette fréquence, le ΔH et l'angle dièdre du rotamère *gauche*, on propose une fonction de potentiel qui permet de déterminer le changement conformationnel. On a observé des caractéristiques spéciales à 195,5 et 181,0 cm^{-1} dans le spectre infrarouge lointain du produit gazeux; on les a attribuées aux torsions $1^{\mp} \leftarrow 0^{\pm}$ et $2^{\mp} \leftarrow 1^{\pm}$ du méthyle présent dans la forme *trans* du groupe éthyle; à partir de ces données, on a pu calculer que la barrière à cette torsion est égale à 868 ± 3 cm^{-1} (2,48 ± 0,01 kcal/mol). De la même manière, on a observé la torsion fondamentale CH_3—C(O) à 94,5 cm^{-1} pour le conformère *trans*; on en a déduit que la barrière triple à la rotation interne est égale à 233 cm^{-1} (666 cal/mol). Utilisant les constantes rotationnelles des deux espèces isotopiques qui ont été antérieurement sur la base d'une étude par micro-ondes, on a déterminé les paramètres structuraux r_0 de l'atome lourd. On propose une attribution vibrationnelle complète qui est en accord avec les résultats obtenus à partir d'une analyse des coordonnées normales réalisée avec des champs de force calculés avec un ensemble de base 3-21G. Dans le but de déterminer les paramètres structuraux, les différences d'énergie et les barrières à la rotation interne autour de la liaison centrale C—C et utilisant un ensemble de base 6-31G*, on a effectué une optimisation complète de la géométrie des conformations *trans* et *gauche* ainsi que des états de transition.

Mots clés : butan-2-one, spectre vibrationnel; calculs *ab initio*, butan-2-one; stabilité conformationnel, butan-2-one.

[Traduit par la rédaction]

Introduction

We recently completed investigations on the rotational isomerism in a series of compounds having the general formula $CH_3CH_2C(O)X$, where X is F (1), Cl (2), and Br (3) utilizing Raman and infrared spectroscopy. All of these molecules were shown to exist in *trans/gauche* equilibria in the gaseous and liquid phases, with the *trans* conformer (CH_3 moiety is *trans* to the halogen atom) being the more stable form in both of these phases and the only conformer present in the annealed solid. While exclusive evidence for the existence of the second conformer in these molecules was abundantly observed with Raman and infrared spectroscopy (1–3), microwave spectroscopy proved to be useful in the observation of the high-energy rotamer only in the case of propionyl fluoride (4), although the electron diffraction technique has been utilized to determine the structure of the *gauche* form of propionyl bromide (5). As a continuation of our studies of this series of compounds, we extend our investigation to 2-butanone (ethyl methyl ketone), $CH_3CH_2C(O)CH_3$, where the CH_3 moiety rather than the halogen atom is the substituent.

Although ethyl methyl ketone has been studied by microwave spectroscopy (6, 7), the detection of the second conformer has not been made with this technique. In the first (6) of these two microwave investigations of the *trans* form,

[1]Author to whom correspondence may be addressed.
[2]Permanent address: Ethyl Corporation, P.O. Box 1028, Orangeburg, SC 29115, U.S.A.

Printed in Canada / Imprimé au Canada

Can. J. Chem. Downloaded from www.nrcresearchpress.com by 84.41.108.74 on 09/07/12
For personal use only.

the barrier of the methyl group attached to the sp^2 carbon was determined to be 518 ± 1 cal/mol (181 ± 0.3 cm^{-1}) and 497 ± 1 cal/mol (174 ± 0.3 cm^{-1}) for the normal and the $CH_3CD_2C(O)CD_3$ species, respectively. Additionally, the total dipole moments of 2.779 ± 0.015 and 2.771 ± 0.015 D were determined for the normal and d_5 species, respectively. In the second microwave investigation (7), a similar value of 183 cm^{-1} was determined for the internal rotation barrier for the same methyl group for the *trans* form. For the other CH_3 group, the authors of the second microwave investigation obtained a value of 795 ± 10 cm^{-1} for the barrier to internal rotation. A rough estimate of 5500 cm^{-1} was proposed for the barrier of the asymmetric torsional rotation, which, according to the authors (7), would yield a fundamental frequency of 80.4 cm^{-1} for this vibration. In neither of these two microwave studies were structural parameters determined, although in the first study (6) parameters were suggested that were transferred from acetone and propane.

The electron diffraction technique has also been utilized to study rotational isomerism in ethyl methyl ketone (8). With a *trans/gauche* equilibrium in the gas, the population of the *trans* form was estimated to be 95 ± 3%, which corresponds to a ΔG of 2.1 ± 0.4 kcal/mol. The r_α structure was given with the *gauche* form having a dihedral angle of 110°, which was estimated from that of 2-methyl-1-butene (the *trans* is presently defined to be at 0°).

Infrared spectra of ethyl methyl ketone in various phases have been studied (9) previously. With the results of a normal coordinate analysis, the authors concluded that the *gauche* rotamer was the higher energy form. Values of 1070 ± 100 and 2020 ± 100 cal/mol, respectively, were obtained for enthalpy differences for the liquid and gas from variable-temperature studies of the infrared bands.

Ab initio calculations have also been utilized to investigate the barriers to internal rotation about the C—C bond in ethyl methyl ketone (10–12). In the first study (10), however, complete geometry optimizations were carried out only with the RHF/STO-3G and RHF/3-21G basis sets, and energies at higher basis set levels (RHF/6-31G* and MP3/6-31G*) were obtained using RHF/3-21G geometries. The energies so obtained at the RHF/6-31G* basis set failed to predict a second conformer, although an abundance of evidence was previously observed in the infrared spectra (9) for the second conformer. In a subsequent study (11), full optimizations were carried out at the RHF/6-31G*//6-31G*, MP2/6-31G*//6-31G*, MP3/6-31G*//6-31G*, and MP4/6-31G*//6-31G* levels. However, the authors again performed calculations at fixed conformations rather than searching for the "true" *gauche* minimum and *trans*-to-*gauche* transition state. This method once again failed to locate the *gauche* conformation with basis sets higher than RHF/3-21G. The similar procedure was employed in the third investigation (12) where the 4-21G basis set was used. The calculations were carried out for conformations at 30° intervals and from the calculated energies a second stable conformer was not predicted.

We are presently utilizing Raman spectroscopy along with infrared data as a means to study rotational isomerism in $CH_3CH_2C(O)CH_3$. In addition, we also carry out restricted Hartree–Fock *ab initio* calculations with the 3-21G and 6-31G* basis sets with complete geometry optimizations at all maxima and minima on the potential surface. These results are compared to those obtained for the propionyl halides and also to the corresponding quantities of some other similar molecules.

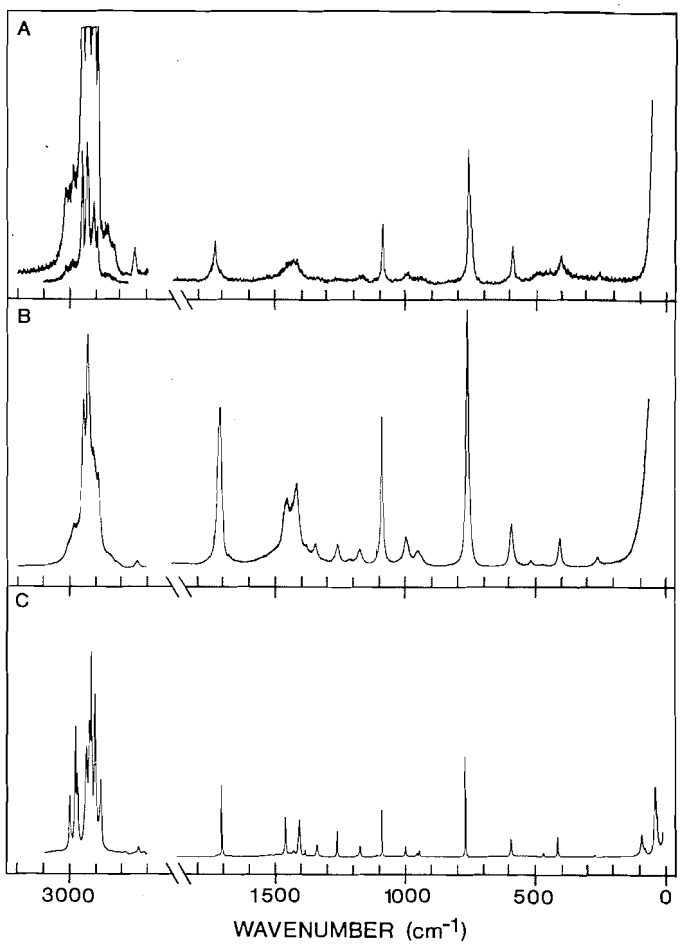


FIG. 1. Raman spectra of (A) gaseous, (B) liquid, and (C) solid ethyl methyl ketone.

Experimental

A sample of ethyl methyl ketone was obtained commercially from Fisher Scientific (Fair Lawn, NJ). Further purification was accomplished by using a low-temperature vacuum fractionation column. The pure sample was stored under vacuum and in a slush of *n*-propanol and Dry Ice. All sample handling and manipulation was carried out under vacuum racks.

The Raman spectra (Fig. 1) were recorded on a Cary model 82 spectrophotometer. This instrument is equipped with a Spectra-Physics model 171 argon ion laser operating on the 5145 Å line. The spectrum of the vapor (Fig. 1A) was recorded with the standard Cary multipass accessory. The spectrum of the liquid (Fig. 1B) was obtained with the sample sealed in a spherical cell (13). The spectrum of the solid (Fig. 1C) was recorded by depositing the sample onto a blackened brass block that was housed in a cell fitted with quartz windows and cooled by boiling liquid nitrogen. The annealing process was accomplished by repeatedly warming and freezing the sample until the line observed at 519 cm^{-1} completely disappeared.

The mid-infrared spectra of the gas (Fig. 2A) and annealed solid (Fig. 2B) were recorded on a Digilab model FTS-14C Fourier transform interferometer equipped with a Ge/KBr beamsplitter and a TGS detector. For the spectrum of the gas, the sample was contained in a 12-cm cell fitted with CsI windows. The spectrum of the solid was obtained by depositing the sample onto a CsI plate, which was cooled by boiling liquid nitrogen and housed in a cell fitted with CsI windows. The annealing process was the same as described above.

The far infrared spectrum of the gas (Fig. 3A) was collected with a Nicolet model SVX 200 Fourier transform interferometer from a sample contained in a 1-m cell fitted with polyethylene windows. The instrument was equipped with a vacuum bench and a liquid

Can. J. Chem. Downloaded from www.nrcresearchpress.com by 84.41.108.74 on 09/07/12
For personal use only.

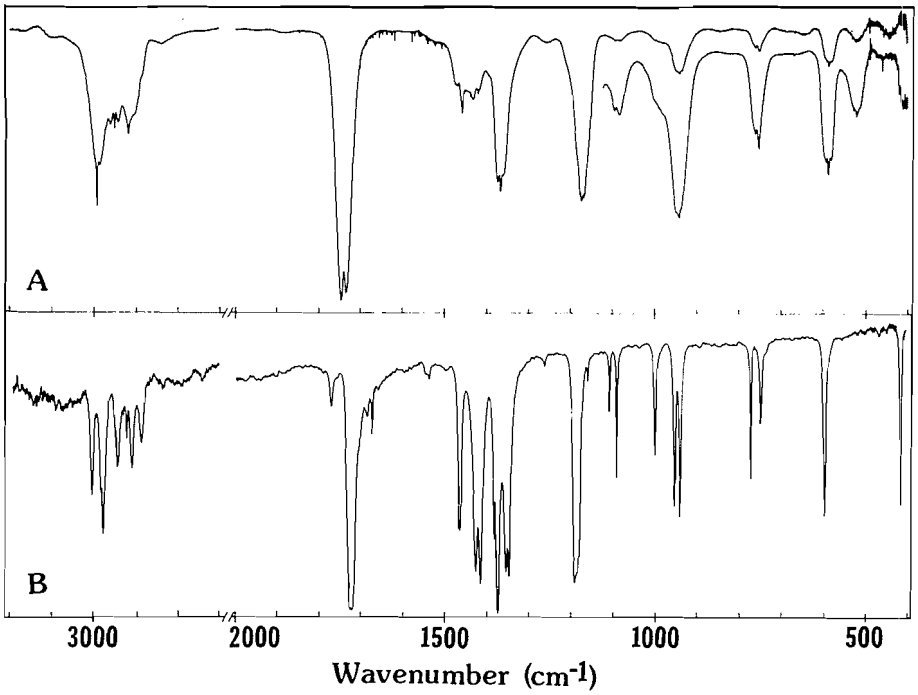


FIG. 2. Mid-infrared spectra of (A) gaseous and (B) solid ethyl methyl ketone.

TABLE 1. Comparison of potential coefficients (cm^{-1}) and barriers (cm^{-1}) to interconversion of the conformers of ethyl methyl ketone as determined from far infrared spectral data and *ab initio* calculations

	Far infrared[a]		*Ab initio*	
	Calc. 1	Calc. 2	3-21G	6-31G*
V_1	816 ± 58	652 ± 68	1013	718
V_2	—	70 ± 50	22	9
V_3	338 ± 8	356 ± 25	447	297
trans/gauche barrier	594 ± 29	611 ± 24	776	527
gauche/gauche barrier	589 ± 29	485 ± 77	708	491
gauche/trans barrier	29 ± 8	88 ± 10	24	3
Energy difference	565 ± 66	514 ± 93	752	524
Dihedral angle of the *gauche* conformer (deg)	102.8	110.3	90.8	85.6
Torsional fundamental (cm^{-1})				
trans	64.5	64.5	56	
gauche	(59.5)[b]	(44.5)[b]	55	

[a]Calculated with F_0 = 1.109811, F_1 = 0.007084, F_2 = 0.046600, F_3 = −0.005652, F_4 = 0.002077, F_5 = 0.000372, and F_6 = 0.000109 (cm^{-1}). The listed uncertainties are statistical uncertainties.
[b]See text.

helium cooled Ge bolometer containing a wedged sapphire filter and a polyethylene window. The resolution was 0.10 cm^{-1} and a 25-μm Mylar beamsplitter was used. The spectrum of the annealed solid (Fig. 3B) was obtained with a Digilab model FTS-15B Fourier transform interferometer equipped with a 6.25-μm Mylar beamsplitter and a TGS detector. The sample was deposited onto a silicon plate cooled by boiling liquid nitrogen and contained in a cell fitted with polyethylene windows.

Asymmetric and methyl torsions

Asymmetric torsion

In our recent studies of propionyl halides (1–3) and fluoroacetone (14) an abundance of evidence was found in the far infrared spectra of the gas for the asymmetric torsional mode of the stable conformers. In some cases, Q-branches were observed arising from transitions near the top of the potential wells, and these prominent Q-branches allowed the determination of an accurate potential function from which barriers to internal rotation were obtained. Therefore, it was hoped that the corresponding spectrum of gaseous ethyl methyl ketone would contain Q-branches for the asymmetric torsion arising from both the *trans* and *gauche* conformers so that a potential function could be calculated.

Unfortunately, even at very high vapor pressure, no prominent Q-branches were observed in the appropriate region (100–30 cm^{-1}) in our spectrum (Fig. 3A) that could be definitively

Can. J. Chem. Downloaded from www.nrcresearchpress.com by 84.41.108.74 on 09/07/12
For personal use only.

Can. J. Chem. Downloaded from www.nrcresearchpress.com by 84.41.108.74 on 09/07/12
For personal use only.

assigned to the asymmetric torsion. However, there is a weak band occurring at about 65 cm^{-1} and we confidently assigned it to the asymmetric torsional mode of one of the conformers. Since the *trans* conformer is so much more abundant, we assigned it to this conformer.

Utilizing this frequency, along with the ΔH (706 $cm^{-1} \cong \Delta E$) for the gas (9) as a forbidden transition between the lowest energy levels in each of the conformer wells and the dihedral angle for the *gauche* conformer from the *ab initio* calculation, we have calculated the first three terms of the potential function for the conformational interchange. The barriers to internal rotation may be obtained by using the sum of cosine functions for the potential energy:

$$V(\phi) = \frac{1}{2}\sum_{i=1}^{3} V_i(1 - \cos i\,\phi)$$

Since the structural parameters are different for the two conformers, the calculations for the kinetic energy term, which is also a function of the dihedral angle, ϕ, of the rotating top, included "relaxation" of the structural parameters. Therefore, the structural parameters obtained from the *ab initio* calculations with the 6-31G* basis set were utilized to calculate the kinetic energy term, or the "*F*-series", of the Hamiltonian according to:

$$F(\phi) = F_0 + \sum_{i=1}^{6} F_i \cos i\,\phi$$

With this calculated "*F*-series" and the potential coefficients given in Table 1, a reasonable fit of the observed transition was obtained with a *gauche* dihedral angle of 102.8° and an energy difference of 565 ± 66 cm^{-1}. Although the fundamental asymmetric torsion of the *trans* conformer has been assigned, the corresponding vibration of the high-energy *gauche* form was not observed in our far infrared spectrum of the gas, and an attempt to locate the $1^{\mp} \leftarrow 0^{\pm}$ and $2^{\mp} \leftarrow 0^{\pm}$ transitions in the Raman spectrum of the gas proved to be unsuccessful. In the calculations of the potential function, we used the frequency of 59.5 cm^{-1} for the *gauche* form. This rough estimate for this quantity was based on the separation of about 4 cm^{-1} between the fundamental frequencies for the asymmetric torsions for the two conformers for fluoroacetone (14) (the only ketone for which we have observed the asymmetric torsional mode for both rotamers). It should be noted that a dihedral angle less than 102.8 leads to a *gauche* well with a barrier too low to accommodate a torsional energy level with the zero point energy. Similarly, a ΔH ($\sim \Delta E$) greater than 565 cm^{-1} leads to a well with a barrier lower than the zero point energy (Table 1). This calculation initially gave a V_2 term of 3 cm^{-1} with an uncertainty of about 10 times the value so the V_2 term was dropped.

A second calculation (Table 1, calc. 2) was carried out utilizing the energy difference obtained from the *ab initio* calculation with the 6-31G* basis set and the *gauche* dihedral angle estimated in the electron diffraction study (8). The torsional frequency for the *gauche* conformer was put into the calculation with a very low weight. This calculation gives a more realistic *gauche*-to-*trans* barrier of 88 ± 10 cm^{-1} but the predicted *gauche*-to-*gauche* barrier is about 100 cm^{-1} higher than the value predicted from the *ab initio* calculations with the 6-31G* basis set. Also, the asymmetric torsional frequency for the *gauche* conformer is predicted at 44.5 cm^{-1}, which seems very low compared to the predicted *ab initio* value. Nevertheless, it appears that this potential function is a more realistic one than that of calculation 1. However, since the *ab initio* calculation gives a *gauche* torsional frequency of 55 cm^{-1}, which implies a zero point level of approximately 23 cm^{-1}, the first potential function is physically satisfactory.

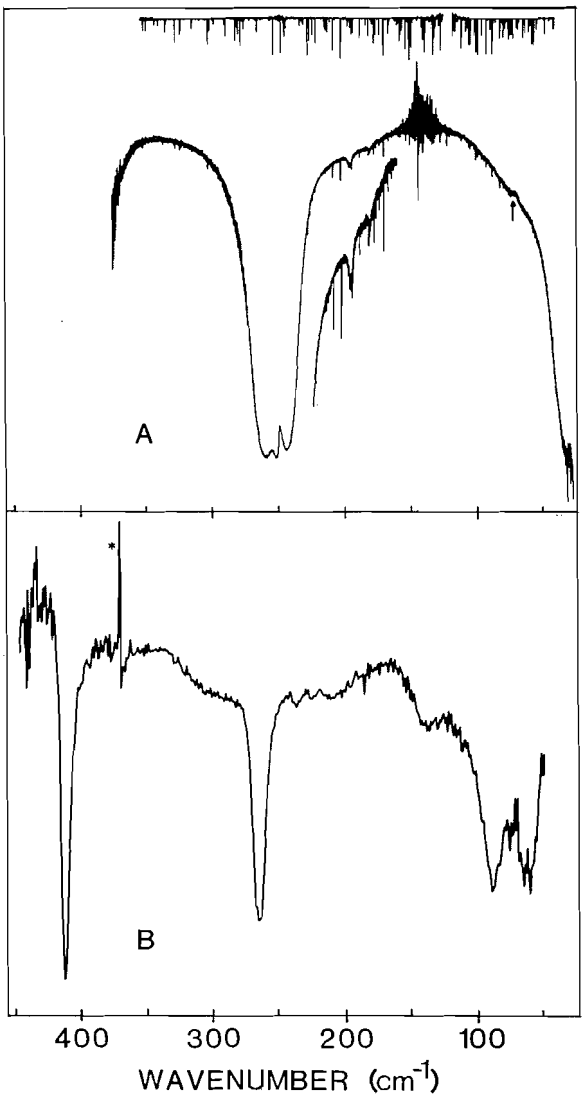


FIG. 3. Far infrared spectra of (A) gaseous and (B) solid ethyl methyl ketone. The top spectrum in (A) is the spectrum of water in the vapor phase. The sharp line indicated with an asterisk (*) is an instrumental artifact.

Methyl torsions

In the far infrared spectrum of the gas (Figs. 3A and 4) there are two weak bands of apparent C-type band contour. Based on the microwave study (7) and our recent investigations of propionyl halides (1–3), the higher frequency feature at 195.5 cm^{-1} is assigned to the fundamental transition of the CH_3—CH_2 torsional mode of the *trans* conformer. Using an *F* number of 5.613 cm^{-1} this frequency was fitted to a threefold potential and the preliminary results indicated that the C-type band at 181.0 cm^{-1} was due to the first excited state transition. With the inclusion of this second feature in the calculations, the barrier to internal rotation of the CH_3—CH_2 torsion was

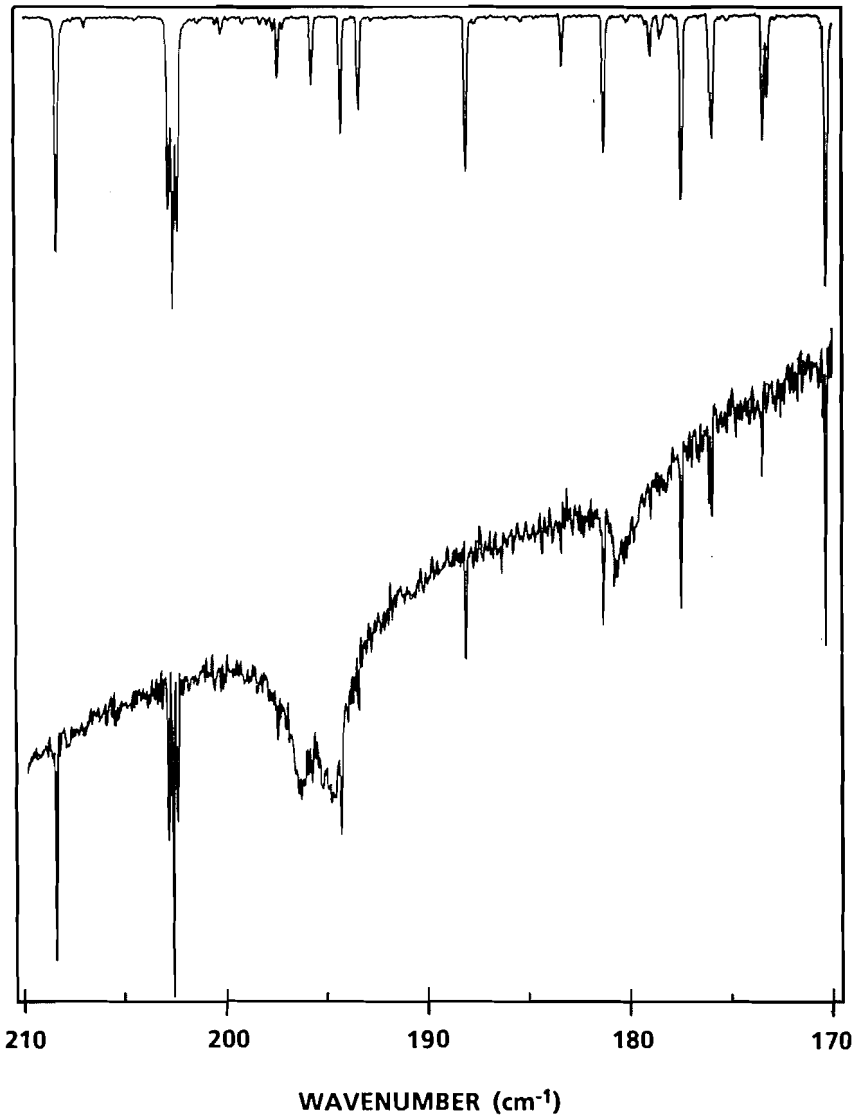


FIG. 4. Far infrared spectrum of gaseous ethyl methyl ketone in the region of the methyl torsion from 205 to 175 cm^{-1}.

TABLE 2. Comparison of the barriers (cm^{-1}) to internal rotation of the CH_3 moieties for ethyl methyl ketone as determined by microwave (MW) and infrared (IR) spectroscopy and *ab initio* calculations

	trans conformer					*gauche* conformer	
Torsion	MW[a]	MW[b]	IR[c]	3-21G	6-31G*	3-21G	6-31G*
CH_3—CH_2		795 ± 10	868 ± 3	860(806)[d]	1030(1036)	1225(1213)	1247(1220)
CH_3—C(O)	181 ± 0.3	183	233	324(303)	248(283)	493(506)	520(504)

[a]Value taken from ref. 6. This value is for the d_0 isotopic species. Value of 184 ± 0.3 cm^{-1} was reported for $CH_3CD_2C(O)CD_3$.
[b]Values taken from ref. 7.
[c]This study.
[d]Values in parentheses were obtained with hydrogens in each moiety reoptimized as equivalent to each other. See text.

determined to be 868 ± 3 cm^{-1}. Our present value is about 10% higher than the value of 795 ± 10 cm^{-1} previously determined in the microwave study (7). For the corresponding fundamental of the *gauche* form we could not find any infrared band in the appropriate region, despite a very extensive search.

Values of 181 ± 0.3 and 183 cm^{-1} have been determined for the barrier to internal rotation of the CH_3—C(O) torsion of the *trans* form in the microwave investigations (6, 7). With the latter value the authors (7) in the second study proposed a value of 85 cm^{-1} for the fundamental torsional vibration. There appears to be no such feature in this region of our infrared spectrum of the gas. However, there appears to be a very weak band at 94.5 cm^{-1} and this feature is tentatively assigned to the $1^{\mp} \leftarrow 0^{\pm}$ transition of the CH_3—C(O) torsion of the *trans* form. Again using a threefold periodic cosine-

Can. J. Chem. Downloaded from www.nrcresearchpress.com by 84.41.108.74 on 09/07/12
For personal use only.

TABLE 3. Observed[a] infrared and Raman frequencies (cm^{-1}) and vibrational assignment for ethyl methyl ketone

Infrared				Raman						Assignment	
Gas	Rel. int.	Solid	Rel. int.	Gas	Rel. int.	Liquid	Rel. int. and depol.	Solid	Rel. int.	ν_i[b]	Approximate description
3022	sh,w									ν'	CH_3 antisymmetric stretch
3014	sh,m			3015	sh,m					ν'	CH_2 antisymmetric stretch
2998	sh,vw	3002	s			3000	sh,w,dp	3002	s	ν_{21}, ν_{22}	CH_3 antisymmetric stretch
		2981	sh,s					2982	vs		
2992 Q,C	vs	2974	vs	2986	bd,m	2978	sh,m,dp	2974	sh,s	ν_{23}	CH_2 antisymmetric stretch
2985 P											
2960 R											
2950 Q,A	m	2942	m	2952	vs	2940	s,p	2940	vs	ν_1	CH_3 antisymmetric stretch
2942 P											
				2933	vs	2924	vs,p	2928	sh,vs	ν_2	CH_3 antisymmetric stretch
2919 Q,C(?)	m	2920	m	2915	sh,s			2920	vs	ν_3	CH_3 symmetric stretch
2902	sh,m	2908	m	2908	vs	2907	sh,m,p	2907	vs	ν_4	CH_3 symmetric stretch
2892	sh,m	2885	m	2895	s	2886	sh,m,p	2885	s	ν_5	CH_2 symmetric stretch
2838	bd,vw			~2850	bd,w	2842	vw,p				$2 \times 1420 = 2840$
				2750	w	2739	vw,p	2737	vw		$1383 + 1348 = 2731$
1745 R											
1739 min,B	vs	1716	vs	1741	w	1712	s,p	1704	s	ν_6	C=O stretch
1734 P											
		1680	sh,w								$937 + 745 = 1682$
		1668	m					1668	vw		
		1553	w								$2 \times 768 = 1536$
1470	sh,m									ν'	CH_3 antisymmetric deformation
		1463	s								
1457 Q,C	m	1460	s			1456	m,p(?)	1458	m	ν_7, ν_{24}	CH_3 antisymmetric deformation
1430 R											
1425 min,B	w	1422	vs	1437	bd,vw	1420	m,p(?)	1426	w	ν_8, ν_{25}	CH_3 antisymmetric deformation
1420 P											
		1412	vs					1406	m	ν_9	CH_2 deformation
		1379	sh,s			1383	sh,w,dp(?)	1384	w	ν_{10}	CH_3 symmetric deformation
1374 R											
1367 Q,A	s	1371	vs					1369	vw	ν_{11}	CH_3 symmetric deformation
1360 P											
		1352	vs								
		1344	vs			1348	w,p	1338	m	ν_{12}	CH_2 wag
1256	bd,vw	1259	w			1258	w,dp	1260	m	ν_{26}	CH_2 twist
						~1212	vw,dp(?)			ν'	CH_2 twist
1186	sh,m									ν'	CH_3 in-plane rock
1178 R		1186	vs								
1175 Q,A(?)	vs	1181	vs			1173	w,dp(?)	1173	m	ν_{13}	CH_3 in-plane rock
1167 P											
		1156	sh,w								$745 + 411 = 1156$
1098	sh,vw	1104	m					1107	vw	ν_{27}	CH_3 out-of-plane rock
1084	vw	1087	s	1092	m	1088	s,p	1090	s	ν_{14}	CH_3 in-plane rock
990	sh,vw	995	s	992	bd,vw	996	w,p	998	m	ν_{15}	$C_1C_2C_3$ antisymmetric stretch
948 R											
941 Q,A(?)	m	950	s	942	vw	949	w,p	953	w	ν_{16}	C_1C_4 stretch
935 P											
		937	s					944	w	ν_{28}	CH_3 out-of-plane rock
844	bd,vw									ν'	CH_2 rock
761	sh,w	768	s	760	s	764	vs,p	768	vs	ν_{17}	$C_1C_2C_3$ symmetric stretch
752	sh,m			748	sh,m	~750	sh,m,p			ν'	$C_1C_2C_3$ symmetric stretch
		745	m					743	vw	ν_{29}	CH_2 rock
687	bd,vw										$941 - 252 = 689(?)$
644	bd,vw									ν'	CO out-of-plane bend
592 R											
588 Q,A	m	594	s	589	w	592	m,p	592	m	ν_{18}	CO in-plane bend
580 P											
520	bd,m					519	vw,p			ν'	CO in-plane bend
								471	w	ν_{30}	CO out-of-plane bend
442	bd,w									ν'	CC(O)C deformation
		411	vs	409	w	409	m,p	415	m	ν_{19}	CC(O)C deformation

Can. J. Chem. Downloaded from www.nrcresearchpress.com by 84.41.108.74 on 09/07/12
For personal use only.

TABLE 3 (*concluded*)

Infrared				Raman						Assignment	
Gas	Rel. int.	Solid	Rel. int.	Gas	Rel. int.	Liquid	Rel. int. and depol.	Solid	Rel. int.	ν_i[b]	Approximate description
260 R											
252 Q,A	vs	265	m	252	vw	262	w,p	270	w	ν_{20}	CCC bend
244 P											
195.5 Q,C	vw							~227	vvw	ν_{31}	$1^{\pm} \leftarrow 0^{\mp}$ CH_3 torsion
181.0 Q,C	vw										$2^{\pm} \leftarrow 1^{\mp}$ CH_3 torsion
		137	sh,w					~150	vvw	ν_{32}, ν_{33}	CH_3 torsion, asymmetric torsion
		89	s					90	m		
								70	sh,w		Lattice modes
		62	s								
								40	vs		

[a]Abbreviations used: s, strong; m, moderate; w, weak; sh, shoulder; bd, broad; p, polarized; dp, depolarized; P, Q, and R refer to vibrational–rotational branches. A, B, and C refer to infrared band contours.
[b]ν' denotes assignment modes for the *gauche* conformer.

based function and an F number of 5.488 cm^{-1}, a value of 233 cm^{-1} was obtained. Although the observed feature is very weak, and hence the assignment tentative, the calculated value of 233 cm^{-1} for the barrier is very reasonable based on the barrier of 292 cm^{-1} determined (15) for acetone, and a lower barrier is expected for ethyl methyl ketone. The presently determined barriers for the CH_3 rotors are compared to those obtained with microwave spectroscopy and *ab initio* calculations in Table 2.

Vibrational assignment

With the results obtained from the normal coordinate analysis, the assignment of the carbon–hydrogen stretching modes of the *trans* rotamer is straightforward, with all of the antisymmetric stretches predicted and assigned to frequencies higher than those of the symmetric stretches. However, the depolarization ratios of the two lines observed at 3000 and 2978 cm^{-1} in the Raman spectrum of the liquid necessitate the assignment of the former to ν_{21} and ν_{22} as degenerate and the latter to ν_{23}, respectively. This assignment does not agree entirely with the order predicted by *ab initio* calculations. Infrared bands observed as shoulders at 3022 and 3014 cm^{-1} in the spectrum of the gas are found to be absent from the spectrum of the solid. Based on the calculated frequencies, we tentatively assign these to the CH_3 antisymmetric stretch (ν'_1) and CH_2 antisymmetric stretch (ν'_{23}), respectively, of the *gauche* form. All of the carbon–hydrogen bending fundamentals are assigned as predicted from the *ab initio* calculations, with the exception of the CH_2 rocking mode of the *trans* form. This particular bending fundamental is calculated to occur at a higher frequency than the $C_1C_2C_3$ symmetric stretch; however, we observe a strong line at 768 cm^{-1} and a very weak feature at 743 cm^{-1} in the Raman spectrum of the solid. The relative intensity of these features necessitates the present assignment of the higher frequency line to the $C_1C_2C_3$ symmetric stretching mode and that at 743 cm^{-1} to the CH_2 rocking fundamental. A similar situation was also encountered in the study of propionyl fluoride (1).

The C=O stretching vibration (ν_6) of ethyl methyl ketone is observed to occur, as expected, at a much lower frequency at 1739 cm^{-1} in the infrared spectrum of the gas than the corresponding vibration in the propionyl halides (1–3). The observation of the only B-type band indicates that the C=O stretches of the *trans* and *gauche* conformers are degenerate or nearly degenerate. The carbon–carbon stretches of the *trans* form are assigned to intense infrared bands at 995 ($C_1C_2C_3$ antisymmetric stretch, ν_{15}), 950 (C_1C_4 stretch, ν_{16}), and 768 cm^{-1} ($C_1C_2C_3$ antisymmetric stretch, ν_{17}). For the *gauche*, the shoulder of medium intensity occurring at 748 cm^{-1} in the Raman spectrum of the gas is observed for the $C_1C_2C_3$ symmetric stretch.

The present assignment of the low-frequency skeletal bending modes of both isomers is very much in agreement with that proposed in the previous study (9). For the *trans* form, prominent features are observed at 594, 411, and 265 cm^{-1} for the CO in-plane bend (ν_{18}), CC(O)C deformation (ν_{19}), and CCC (ν_{20}) bend, whereas the weak line at 471 cm^{-1} in the Raman spectrum of the solid is assigned to the CO out-of-plane bend (ν_{30}). For the *gauche* conformation, weak featureless bands are observed at 644 (CO out-of-plane bend), 520 (CO in-plane bend), and 442 cm^{-1} (CC(O)C deformation) in the spectrum of the gas. The details of the complete assignment of ethyl methyl ketone are listed in Table 3.

Ab initio calculations

As mentioned above, *ab initio* calculations have previously been carried out for ethyl methyl ketone (10–12); however, full geometry optimizations for fixed conformations failed to predict a higher energy form. This failure is undoubtedly due to lack of relaxation of the structural parameters. In other words, the values of the structural parameters of ethyl methyl ketone at the RHF/6-31G* basis set, for example, must be at least slightly different from the corresponding quantities with the RHF/3-21G basis set. Therefore, we have carried out full optimizations at the RHF/6-31G* basis set for the *trans* and *gauche* forms, as well as for the transition states, in order to obtain better determination of the energy differences and barriers to internal rotations.

The LCAO-MO-SCF restricted Hartree–Fock calculations were performed with the GAUSSIAN-86 program (16) using Gaussian-type basis functions. The calculations were carried out wtih the 3-21G and 6-31G* basis sets. Based on the results of the microwave investigations (6, 7) and our own studies of propionyl halides (1–3), we initially performed optimization

Can. J. Chem. Downloaded from www.nrcresearchpress.com by 84.41.108.74 on 09/07/12
For personal use only.

TABLE 4. Structural parameters[a] and dipole moments for ethyl methyl ketone as determined experimentally and by *ab initio* calculations

	s-trans					*gauche*		
		This study						
Parameter	MW[b]	r_0	E.D.[c]	3-21G	6-31G*	E.D.[c]	3-21G	6-31G*
r(C=O)	1.222	1.218±0.003	1.218±0.001	1.211	1.192	1.218±0.001	1.212	1.193
r(C_1—C_2)	1.507	1.512±0.007	1.518[d]	1.518	1.518	1.518[d]	1.516	1.519
r(C_1—C_4)	1.507	1.507±0.007	1.518[d]	1.516	1.515	1.518[d]	1.514	1.513
r(C_2—C_3)	1.526	1.531±0.009	1.531[d]	1.533	1.524	1.531[d]	1.550	1.535
r(C—H_5)	1.094	1.095	1.102[d]	1.083	1.085	1.102[d]	1.083	1.084
r(C—H_6)	1.094	1.093	1.102[d]	1.082	1.083	1.102[d]	1.083	1.084
r(C—H_7)	1.094	1.093	1.102[d]	1.082	1.083	1.102[d]	1.084	1.085
r(C—H_8)	1.085	1.098	1.102[d]	1.087	1.088	1.102[d]	1.082	1.083
r(C—H_9)	1.085	1.098	1.102[d]	1.087	1.088	1.102[d]	1.083	1.086
r(C—H_{10})	1.085	1.091	1.102[d]	1.080	1.081	1.102[d]	1.080	1.081
r(C—H_{11})	1.085	1.096	1.102[d]	1.085	1.086	1.102[d]	1.084	1.086
r(C—H_{12})	1.085	1.096	1.102[d]	1.085	1.086	1.102[d]	1.086	1.087
∠(C_2C_1O)	121.40	122.9±0.9	121.3±0.7	122.12	122.08	121.3±0.7	121.98	120.96
∠($C_2C_1C_4$)	177.20	116.3±0.20		115.46	116.44		115.53	117.38
∠($C_1C_2C_3$)	112.40	113.8±0.6	113.4±0.6	112.13	113.61	113.4±0.6	109.76	110.80
∠(CCH_5)		110.4	113.1±0.9	110.64	110.40	113.1±0.9	110.26	110.42
∠(CCH_6)		111.0	113.1±0.9	110.43	111.00	113.1±0.9	109.86	110.48
∠(CCH_7)		111.0	113.1±0.9	110.43	111.00		111.24	111.66
∠(H_6CH_7)	107.05	107.6		107.72	107.55		108.65	108.19
∠($C_1C_2H_8$)		107.9	113.1±0.9	108.26	107.86	113.1±0.9	108.32	107.67
∠($C_1C_2H_9$)		107.9	113.1±0.9	108.26	107.86	113.1±0.9	110.42	110.45
∠(H_8CH_9)	108.13	105.4	108.8[d]	106.60	105.44	108.8[d]	109.28	108.32
∠(CCH_{11})		109.7	113.1±0.9	109.63	109.72	113.1±0.9	109.88	109.97
∠(CCH_{12})		110.4	113.1±0.9	110.15	110.42	113.1±0.9	110.85	111.12
∠(CCH_{13})		110.4	113.1±0.9	110.15	110.42	113.1±0.9	109.37	109.39
dih ($CCCH_5$)		180.0		180.00	180.00		178.68	178.58
dih ($OC_1C_2C_3$)		0.0		0.00	0.00	110.0	90.81	85.64
dih (C_4CCO)		180.0		180.00	180.00		181.20	180.85
dih ($H_{10}CCO$)		0.0		0.00	0.00		−7.72	−9.53
A (MHz)		9544.7[e]		9543	9758		7535	7788
B (MHz)		3597.5		3638	3596		3836	3774
C (MHz)		2745.4		2767	2760		3042	3028
μ_a (D)	0.079±0.025			0.239	0.159		0.026	0.086
μ_b (D)	2.778±0.015			2.995	2.995		2.614	2.841
μ_c (D)	0.0			0.000	0.000		1.690	1.169
μ_t (D)	2.779±0.015			3.004	2.999		3.113	3.073
$-(E + 229)$ (hartrees)				0.7093494	1.9980483		0.7059207	1.9956588

[a]Distances in Å and angles in degrees.
[b]Values for the structural parameters were assumed values. Taken from ref. 6.
[c]Taken from ref. 8.
[d]Assumed values.
[e]Experimental values: A = 9544.63, B = 3596.85, and C = 2746.51 MHz.

for the *trans* conformation having a plane of symmetry containing all of the heavy atoms. The structural parameters for this form are given in Table 4. To make good predictions on the form of the high-energy conformation, a potential surface scan was carried out by only varying the dihedral angle $OC_1C_2C_3$ from 0° (*trans* position) to 180° (*cis* position) and keeping the remaining parameters at the optimized values obtained for the *trans* form. The resulting potential surface obtained with the 6-31G* basis set is given by the dashed line in Fig. 5. The potential surface obtained in this manner predicts a second stable form at about 100° and 712 cm^{-1} higher in energy than the *trans* form. At the 3-21G basis set level the *gauche* form is also at 100° and 904 cm^{-1} less stable. From the potential surface at the 6-31G* basis set, values of 727 and 917 cm^{-1}, respectively, are calculated for the *trans*-to-*gauche* and *gauche*-to-*gauche* barriers. It can be seen that the *gauche*-to-*trans* barrier is calculated extremely low at 15 cm^{-1}. With the 3-21G basis set, values of 958 and 1227 cm^{-1} were obtained for the *trans*-to-*gauche* and *gauche*-to-*gauche* barriers, respectively, and a small value of 53 cm^{-1} for the *gauche*-to-*trans* barrier was calculated.

In addition to the *gauche* minimum, the *trans*-to-*gauche* and *gauche*-to-*gauche* transition states were further optimized by relaxation of all geometric parameters to produce more meaningful potential surfaces. The potential surface obtained with the 6-31G* basis set is indicated by the solid line curve in Fig. 5. Structural parameters for the *gauche* conformer are also given in Table 4. With these additional calculations, the *trans*-to-*gauche*, *gauche*-to-*gauche*, and *gauche*-to-*trans* barriers are 527, 491, and 3 cm^{-1}, respectively, with the larger

Can. J. Chem. Downloaded from www.nrcresearchpress.com by 84.41.108.74 on 09/07/12
For personal use only.

TABLE 5. Symmetry coordinates for ethyl methyl ketone

Species	Approximate description	Symmetry coordinate[a]
A′	CH_3 antisymmetric stretch[b]	$S_1 = 2a_1' - a_2' - a_3'$
	CH_3 antisymmetric stretch	$S_2 = 2a_1 - a_2 - a_3$
	CH_3 symmetric stretch	$S_3 = a_1 + a_2 + a_3$
	CH_3 symmetric stretch[b]	$S_4 = a_1' + a_2' + a_3'$
	CH_2 symmetric stretch	$S_5 = r_1 + r_2$
	C=O stretch	$S_6 = T$
	CH_3 antisymmetric deformation	$S_7 = 2\alpha_1 - \alpha_2 - \alpha_3$
	CH_3 antisymmetric deformation[b]	$S_8 = 2\alpha_1' - \alpha_2' - \alpha_3'$
	CH_2 deformation	$S_9 = (\sqrt{6}+2)\delta - (\sqrt{6}-2)\mu - \sigma_1 - \sigma_2 - \varepsilon_1 - \varepsilon_2$
	CH_3 symmetric deformation	$S_{10} = \alpha_1 + \alpha_2 + \alpha_3 - \beta_1 - \beta_2 - \beta_3$
	CH_3 symmetric deformation[b]	$S_{11} = \alpha_1' + \alpha_2' + \alpha_3' - \beta_1' - \beta_2' - \beta_3'$
	CH_2 wag	$S_{12} = \sigma_1 + \sigma_2 - \varepsilon_1 - \varepsilon_2$
	CH_3 in-plane rock[b]	$S_{13} = 2\beta_1' - \beta_2' - \beta_3'$
	CH_3 in-plane rock	$S_{14} = 2\beta_1 - \beta_2 - \beta_3$
	$C_1C_2C_3$ antisymmetric stretch	$S_{15} = d_1 - d_2$
	C_1C_4 stretch	$S_{16} = d_3$
	$C_1C_2C_3$ symmetric stretch	$S_{17} = d_1 + d_2$
	CO in-plane bend	$S_{18} = \omega - \theta$
	CC(O)C deformation	$S_{19} = 2\phi - \omega - \theta$
	$C_1C_2C_3$ bend	$S_{20} = (\sqrt{6}-2)\delta - (\sqrt{6}+2)\mu + \sigma_1 + \sigma_2 + \varepsilon_1 + \varepsilon_2$
	CH_3 redundancy[b]	$S_{1R} = \alpha_1' + \alpha_2' + \alpha_3' + \beta_1' + \beta_2' + \beta_3'$
	CH_3 redundancy	$S_{2R} = \alpha_1 + \alpha_2 + \alpha_3 + \beta_1 + \beta_2 + \beta_3$
	CH_2 redundancy	$S_{3R} = \delta + \mu + \sigma_1 + \sigma_2 + \varepsilon_1 + \varepsilon_2$
	CO redundancy	$S_{4R} = \phi + \omega + \theta$
A″	CH_3 antisymmetric stretch	$S_{21} = a_2 - a_3$
	CH_3 antisymmetric stretch[b]	$S_{22} = a_2' - a_3'$
	CH_2 antisymmetric stretch	$S_{23} = r_1 - r_2$
	CH_3 antisymmetric deformation	$S_{24} = \alpha_2 - \alpha_3$
	CH_3 antisymmetric deformation[b]	$S_{25} = \alpha_2' - \alpha_3'$
	CH_2 twist	$S_{26} = \sigma_1 - \sigma_2 - \varepsilon_1 + \varepsilon_2$
	CH_3 out-of-plane rock	$S_{27} = \beta_2 - \beta_3$
	CH_3 out-of-plane rock[b]	$S_{28} = \beta_2' - \beta_3'$
	CH_2 rock	$S_{29} = \sigma_1 - \sigma_2 + \varepsilon_1 - \varepsilon_2$
	CO out-of-plane bend	$S_{30} = \eta$
	CH_3 torsion	$S_{31} = \tau_1$
	CH_3 torsion[b]	$S_{32} = \tau_2$
	Asymmetric torsion	$S_{33} = \tau_3$

[a]Not normalized.
[b]These fundamentals belong to the CH_3 moiety closest to the carbonyl moiety.

6-31G* basis set and 776, 708, and 24 cm^{-1}, respectively, with the 3-21G basis set. The total energies for the *trans* and *gauche* conformers were calculated at the 6-31G* basis set to be −230.9980483 and −230.9956588 hartrees, respectively, which corresponds to an energy difference of 524 cm^{-1}. The energies obtained from the smaller basis set give a larger difference of 752 cm^{-1} also with the *trans* conformer as the low-energy form.

In our investigations of propionyl chloride (2) and propionyl bromide (3), the barrier to internal rotation of the CH_3 group was reproduced very well by *ab initio* calculations (within 20% in the worst case). Therefore, for the present case of ethyl methyl ketone, similar agreement is also expected and similar calculations were performed. Using the optimized structural parameters obtained for the *trans* and *gauche* forms at both the 3-21G and 6-31G* basis sets, the CH_3 moieties were rotated 60° with no additional optimizations. With this procedure, the barrier for the CH_3—CH_2 torsion of the *trans* conformer is calculated to be 860 and 1030 cm^{-1} at the 3-21G and 6-31G* basis sets, respectively. The corresponding quantities for the *gauche* rotamer are much higher at 1220 and 1247 cm^{-1}. The same procedure was carried out for the CH_3—C(O) torsion and values of 324 and 248 cm^{-1}, respectively, with the 3-21G and 6-31G* basis sets were obtained for the *trans* form, whereas barriers of 493 and 520 cm^{-1} were calculated for the *gauche* conformer. These values are listed and compared to those obtained experimentally in Table 2.

A comparison of the barriers for the CH_3 moieties for the *trans* form calculated with *ab initio* calculations and those derived from experimental data shows conflicting results. For example, the value of 860 cm^{-1} at the 3-21G basis set for the CH_3—CH_2 torsion is in excellent agreement with the value of 868 ± 3 cm^{-1} calculated with our far infrared data. However, the value of 1030 cm^{-1} obtained with the 6-31G* basis set is almost 20% too high (compared to the value of 868 ± 3 cm^{-1}). The opposite trend is obtained for the CH_3—C(O) torsion, with the 6-31G* basis set giving a value in much better agreement than the 3-21G basis set.

Subsequently, the conformations were reoptimized with hydrogen atoms in each moiety being held equivalent to each other in order to have a "true" threefold potential. As before, each CH_3 moiety was then rotated 60° to determine the

Can. J. Chem. Downloaded from www.nrcresearchpress.com by 84.41.108.74 on 09/07/12
For personal use only.

Can. J. Chem. Downloaded from www.nrcresearchpress.com by 84.41.108.74 on 09/07/12
For personal use only.

TABLE 6. Harmonic force constants (mdyn/Å) for the *trans* conformer of ethyl methyl ketone

	a_1	a_2	a_3	r_1	r_2	d_2	d_1	T	d_3	a_1'	a_2'	a_3'	α_1	α_2	α_3	β_1	β_2	β_3	μ
a_1	5.827	0.060	0.060	0.013	0.013	0.078	−0.004	−0.012	0.009	0.001	0.000	0.000	−0.094	0.099	0.099	0.072	−0.087	−0.087	0.048
a_2		5.891	0.061	0.012	−0.014	0.076	−0.025	0.027	0.000	0.001	0.000	−0.001	0.101	0.084	−0.077	−0.080	0.057	−0.079	−0.057
a_3			5.891	−0.014	0.012	0.076	−0.025	0.027	0.000	0.001	−0.001	0.000	0.101	−0.077	0.084	−0.080	−0.079	0.057	−0.057
r_1				5.707	0.071	0.081	0.081	0.007	0.007	0.000	0.018	−0.002	−0.004	−0.003	−0.006	−0.009	−0.010	0.031	−0.086
r_2					5.707	0.081	0.081	0.007	0.007	0.000	−0.002	−0.018	−0.004	−0.006	−0.003	−0.009	0.031	−0.010	−0.086
d_2						4.686	0.162	−0.014	0.000	0.004	0.000	0.000	−0.179	−0.176	−0.176	0.154	0.179	0.179	0.267
d_1							4.471	0.614	0.213	−0.002	0.006	0.006	−0.004	0.002	0.002	0.026	−0.013	−0.013	0.372
T								14.675	0.615	0.024	0.009	0.009	0.001	−0.017	−0.017	0.000	0.016	0.016	−0.075
d_3									4.379	0.039	0.072	0.072	−0.004	−0.001	−0.001	0.016	−0.006	−0.006	0.045
a_1'										5.980	0.045	0.045	−0.001	−0.001	−0.001	0.004	0.000	0.000	0.012
a_2'											5.789	0.062	0.000	0.001	0.001	0.002	0.001	−0.003	0.004
a_3'												5.789	0.000	0.001	0.001	0.002	−0.003	0.001	0.004
α_1													0.597	−0.105	−0.105	−0.122	−0.123	−0.123	−0.010
α_2														0.667	−0.185	−0.121	−0.090	−0.155	−0.007
α_3															0.667	−0.121	−0.155	−0.090	−0.007
β_1																0.669	−0.164	−0.164	0.090
β_2																	0.695	−0.172	−0.034
β_3																		0.695	−0.034
μ																			1.082

Can. J. Chem. Downloaded from www.nrcresearchpress.com by 84.41.108.74 on 09/07/12
For personal use only.

TABLE 6 (*concluded*)

	δ	σ_1	σ_2	ε_1	ε_2	ω	ϕ	θ	α_1'	α_2'	α_3'	β_1'	β_2'	β_3'	η	τ_1	τ_2	τ_3
a_1	−0.010	−0.012	−0.012	−0.008	−0.008	−0.001	0.007	−0.006	−0.001	0.000	0.000	0.004	−0.001	−0.001	0.000	0.000	0.000	0.000
a_2	0.005	−0.001	0.046	−0.002	0.013	−0.023	0.016	0.008	0.000	0.000	0.001	0.001	−0.001	−0.001	0.005	−0.016	0.000	−0.007
a_3	0.005	0.046	−0.001	0.013	−0.002	−0.023	0.016	0.008	0.000	0.001	0.000	0.001	−0.001	−0.001	−0.005	0.016	0.000	0.007
r_1	0.105	0.070	−0.094	0.110	−0.094	0.041	−0.031	−0.010	−0.001	−0.011	0.010	0.003	−0.001	0.001	0.014	0.003	−0.009	0.012
r_2	0.105	−0.094	0.070	−0.094	0.110	0.041	−0.031	−0.010	−0.001	0.010	−0.011	0.003	0.001	−0.001	−0.014	−0.003	0.009	−0.012
d_2	−0.164	0.128	0.128	−0.196	−0.196	−0.085	0.073	0.012	−0.001	0.000	0.000	0.012	−0.006	−0.006	0.000	0.000	0.000	0.000
d_1	−0.217	−0.188	−0.188	0.102	0.102	0.239	0.098	−0.336	−0.002	−0.023	−0.023	0.025	0.011	0.011	0.000	0.000	0.000	0.000
T	−0.016	−0.008	−0.008	0.057	0.057	0.220	−0.416	0.196	−0.024	−0.016	−0.016	−0.044	0.050	0.050	0.000	0.000	0.000	0.000
d_3	−0.008	−0.028	−0.028	0.009	0.009	−0.294	0.147	0.148	−0.173	−0.129	−0.129	0.155	0.134	0.134	0.000	0.000	0.000	0.000
a_1'	−0.001	0.000	0.000	−0.006	−0.006	0.010	0.064	−0.074	−0.082	0.082	0.082	0.080	−0.081	−0.081	0.000	0.000	0.000	0.000
a_2'	−0.001	0.001	−0.002	0.004	−0.006	−0.012	−0.032	0.044	0.095	0.073	−0.077	−0.086	0.080	−0.083	0.008	0.000	−0.020	0.005
a_3'	−0.001	−0.002	0.001	−0.006	0.004	−0.012	−0.032	0.044	0.095	−0.077	0.073	−0.086	−0.083	0.080	−0.008	0.000	0.020	−0.005
α_1	0.007	−0.005	−0.005	0.007	0.007	0.000	−0.002	0.002	0.001	0.000	0.000	−0.001	0.000	0.000	0.000	0.000	0.000	0.000
α_2	0.005	−0.013	0.005	−0.015	0.027	0.011	−0.010	−0.001	0.000	0.000	0.000	−0.002	0.001	0.002	0.001	0.075	0.000	−0.003
α_3	0.005	0.005	−0.013	0.027	−0.015	0.011	−0.010	−0.001	0.000	0.000	0.000	−0.002	0.002	0.001	−0.001	−0.075	0.000	0.003
β_1	0.002	−0.045	−0.045	−0.003	−0.003	−0.036	0.034	0.001	−0.001	−0.002	−0.002	0.009	−0.002	−0.002	0.000	0.000	0.000	0.000
β_2	−0.009	−0.055	0.113	−0.010	−0.005	0.007	−0.007	−0.001	0.000	−0.001	0.003	−0.002	0.000	0.000	0.008	0.027	−0.002	−0.004
β_3	−0.009	0.113	−0.055	−0.005	−0.010	0.007	−0.007	−0.001	0.000	0.003	−0.001	−0.002	0.000	0.000	−0.008	−0.027	0.002	0.004
μ	−0.206	−0.242	−0.242	−0.228	−0.228	−0.018	0.072	−0.054	−0.004	0.000	0.000	0.030	−0.013	−0.013	0.000	0.000	0.000	0.000
δ	0.621	−0.082	−0.082	−0.106	−0.106	−0.039	0.016	0.023	0.005	−0.001	−0.001	−0.005	0.001	0.001	0.000	0.000	0.000	0.000
σ_1		0.664	−0.121	−0.122	−0.105	−0.016	−0.010	0.026	−0.001	−0.001	0.008	−0.001	−0.007	0.003	0.007	−0.013	−0.007	−0.005
σ_2			0.664	−0.105	−0.122	−0.016	−0.010	0.026	−0.001	0.008	−0.001	−0.001	0.003	−0.007	−0.007	0.013	0.007	0.005
ε_1				0.671	−0.089	0.045	−0.036	−0.009	0.001	−0.010	0.004	−0.012	0.026	−0.008	0.071	−0.027	−0.005	−0.015
ε_2					0.671	0.045	−0.036	−0.009	0.001	0.004	−0.010	−0.012	−0.008	0.026	−0.071	0.027	0.005	0.015
ω						0.841	−0.386	−0.455	0.013	0.010	0.010	0.014	−0.023	−0.023	0.000	0.000	0.000	0.000
ϕ							0.715	−0.329	0.010	−0.021	−0.021	0.122	−0.045	−0.045	0.000	0.000	0.000	0.000
θ								0.784	−0.023	0.012	0.012	−0.135	0.069	0.069	0.000	0.000	0.000	0.000
α_1'									0.569	−0.102	−0.102	−0.113	−0.122	−0.122	0.000	0.000	0.000	0.000
α_2'										0.637	−0.175	−0.116	−0.073	−0.166	0.005	0.000	0.054	−0.009
α_3'											0.637	−0.116	−0.166	−0.073	−0.005	0.000	−0.054	0.009
β_1'												0.625	−0.148	−0.148	0.000	0.000	0.000	0.000
β_2'													0.659	−0.151	0.089	0.000	0.055	−0.002
β_3'														0.659	−0.089	0.000	−0.055	0.002
η															0.554	0.006	−0.011	0.005
τ_1																0.076	0.000	−0.006
τ_2																	0.032	−0.010
τ_3																		0.015

Can. J. Chem. Downloaded from www.nrcresearchpress.com by 84.41.108.74 on 09/07/12
For personal use only.

TABLE 7. Harmonic force constants (mdyn/Å) for the *gauche* conformer of ethyl methyl ketone

	a_1	a_2	a_3	r_1	r_2	d_2	d_1	T	d_3	a_1'	a_2'	a_3'	α_1	α_2	α_3	β_1	β_2	β_3	μ
a_1	5.836	0.062	0.057	0.012	0.011	0.078	−0.020	0.003	0.001	0.000	−0.001	0.000	−0.090	0.105	0.098	0.056	−0.080	−0.084	0.036
a_2		5.804	0.059	0.012	−0.016	0.084	−0.011	0.006	0.009	0.001	0.016	−0.001	0.105	0.107	−0.093	−0.084	0.051	−0.083	−0.028
a_3			5.855	−0.016	0.011	0.085	−0.007	0.025	0.000	0.001	−0.001	−0.001	0.099	−0.099	0.103	−0.085	−0.085	0.071	−0.019
r_1				5.837	0.052	0.092	0.046	0.021	0.020	−0.003	−0.004	0.015	−0.004	−0.005	−0.004	−0.010	−0.010	0.034	−0.079
r_2					5.895	0.081	0.050	0.025	0.002	0.004	−0.001	0.001	−0.003	−0.005	−0.003	−0.010	0.029	−0.010	−0.076
d_2						4.361	0.178	−0.013	0.005	0.000	0.003	−0.004	−0.169	−0.186	−0.172	0.169	0.161	0.178	0.224
d_1							4.411	0.616	0.193	−0.002	0.003	0.006	0.005	0.009	0.008	0.021	−0.002	−0.040	0.130
T								14.625	0.638	0.025	0.009	0.005	−0.009	−0.005	−0.017	0.029	−0.007	0.008	0.013
d_3									4.386	0.039	0.060	0.084	−0.002	−0.006	−0.007	0.007	0.014	−0.006	0.015
a_1'										5.981	0.044	0.047	0.000	−0.001	0.000	0.001	−0.002	0.001	−0.016
a_2'											5.831	0.062	−0.001	−0.004	0.004	0.003	−0.002	0.000	−0.001
a_3'												5.754	0.000	0.001	0.002	0.000	0.000	−0.002	−0.006
α_1													0.600	−0.125	−0.103	−0.129	−0.124	−0.109	0.002
α_2														0.667	−0.169	−0.103	−0.086	−0.176	−0.016
α_3															0.656	−0.121	−0.163	−0.078	−0.011
β_1																0.663	−0.154	−0.166	0.103
β_2																	0.699	−0.188	−0.026
β_3																		0.705	−0.054
μ																			0.797

Can. J. Chem. Downloaded from www.nrcresearchpress.com by 84.41.108.74 on 09/07/12
For personal use only.

TABLE 7 (*concluded*)

	δ	σ_1	σ_2	ε_1	ε_2	ω	ϕ	θ	α_1'	α_2'	α_3'	β_1'	β_2'	β_3'	η	τ_1	τ_2	τ_3
a_1	−0.007	−0.011	−0.010	−0.003	−0.005	0.005	−0.003	−0.003	0.001	0.000	0.000	0.000	0.000	0.000	0.004	0.003	0.000	0.002
a_2	−0.001	−0.008	0.040	−0.007	0.005	0.013	−0.009	−0.004	−0.003	0.000	0.000	0.003	0.000	−0.001	0.013	0.003	0.002	0.011
a_3	−0.002	0.035	−0.010	0.002	−0.007	0.001	0.001	−0.002	0.000	0.000	0.001	0.001	−0.001	0.000	0.002	−0.012	−0.001	−0.005
r_1	0.097	0.041	−0.063	0.073	−0.071	0.062	−0.049	−0.013	0.000	0.005	−0.011	−0.001	0.006	0.001	−0.004	0.001	0.009	−0.014
r_2	0.091	−0.068	0.046	−0.072	0.084	−0.069	0.060	0.009	−0.002	0.000	0.001	0.010	−0.009	−0.001	−0.015	−0.002	−0.001	0.009
d_2	−0.174	0.151	0.163	−0.186	−0.180	−0.009	0.007	0.001	−0.002	−0.011	0.006	0.002	0.018	−0.013	0.037	−0.005	−0.005	−0.017
d_1	−0.124	−0.164	−0.184	0.189	0.152	0.134	0.156	−0.290	−0.005	−0.033	−0.008	0.031	0.011	0.003	−0.005	0.002	−0.015	0.003
T	−0.019	−0.022	−0.015	0.080	−0.037	0.194	−0.396	0.202	−0.025	−0.020	−0.014	−0.043	0.060	0.041	−0.012	0.002	−0.002	−0.004
d_3	−0.020	−0.017	−0.019	0.008	0.033	−0.286	0.136	0.151	−0.176	−0.116	−0.138	0.151	0.148	0.122	−0.019	0.004	0.005	−0.012
a_1'	0.002	0.000	−0.002	−0.009	0.009	0.009	0.064	−0.074	−0.082	0.083	0.081	0.079	−0.080	−0.083	0.009	−0.001	0.004	0.001
a_2'	0.001	0.005	0.003	0.005	0.002	−0.008	−0.045	0.053	0.096	0.071	−0.069	−0.084	0.065	−0.079	0.011	−0.003	−0.025	0.013
a_3'	−0.001	−0.002	0.002	0.004	0.005	−0.011	−0.024	0.035	0.096	−0.082	0.076	−0.088	−0.085	0.090	−0.010	−0.001	0.018	0.001
α_1	0.003	−0.007	−0.010	0.007	0.005	0.002	−0.003	0.001	−0.001	0.001	0.001	0.000	−0.001	0.000	−0.052	−0.014	−0.001	0.000
α_2	0.008	−0.013	0.008	−0.020	0.034	0.004	−0.006	0.002	0.002	0.000	0.001	−0.002	−0.002	0.002	−0.008	0.085	−0.001	0.004
α_3	0.006	0.008	−0.014	0.033	−0.023	−0.001	−0.002	0.004	0.001	0.004	−0.002	0.001	−0.005	0.001	0.001	−0.077	0.004	0.009
β_1	0.000	−0.050	−0.047	−0.003	−0.004	0.012	−0.005	−0.008	0.000	−0.002	0.001	0.002	0.002	−0.003	0.021	0.010	−0.001	0.005
β_2	−0.010	−0.062	0.117	−0.020	0.002	0.004	0.006	−0.009	−0.002	−0.005	0.000	−0.002	0.010	0.000	−0.018	0.049	−0.001	−0.010
β_3	−0.007	0.124	−0.056	0.004	−0.14	−0.021	0.010	0.010	0.000	0.002	0.000	0.001	−0.004	0.000	0.007	−0.055	0.001	−0.007
μ	−0.152	−0.180	−0.178	−0.143	−0.149	0.000	0.005	−0.006	−0.001	−0.014	0.007	−0.007	0.036	−0.022	0.073	0.002	−0.010	−0.028
δ	0.594	−0.105	−0.094	−0.138	−0.100	0.011	−0.019	0.008	−0.002	0.005	0.002	0.002	−0.006	−0.002	0.006	0.000	0.002	0.001
σ_1		0.677	−0.153	−0.112	−0.140	−0.024	0.006	0.018	0.002	0.002	0.002	0.000	−0.003	−0.002	−0.005	−0.017	0.002	0.012
σ_2			0.711	−0.162	−0.111	0.020	−0.033	0.014	0.002	0.005	−0.002	−0.004	−0.004	0.003	0.001	0.017	0.003	−0.011
ε_1				0.718	−0.172	0.098	−0.056	−0.041	0.003	−0.004	−0.002	−0.013	−0.007	0.024	−0.035	−0.036	−0.003	0.016
ε_2					0.683	−0.107	0.099	0.009	−0.004	0.006	−0.007	0.023	−0.017	−0.001	−0.040	0.037	0.005	0.010
ω						0.754	−0.347	−0.407	0.014	0.012	0.005	0.011	−0.031	−0.011	0.023	0.004	0.006	0.009
ϕ							0.703	−0.356	0.008	−0.022	−0.017	0.125	−0.052	−0.045	−0.017	−0.002	−0.003	−0.00
θ								0.764	−0.022	0.009	0.013	−0.136	0.081	0.058	−0.017	−0.002	−0.003	0.010
α_1'									0.571	−0.105	−0.098	−0.111	−0.127	−0.119	0.006	−0.001	−0.001	−0.001
α_2'										0.633	−0.185	−0.105	−0.079	−0.165	0.014	−0.003	0.061	0.004
α_3'											0.657	−0.126	−0.168	−0.064	−0.017	0.002	−0.069	0.002
β_1'												0.617	−0.147	−0.147	0.021	−0.002	0.009	0.005
β_2'													0.661	−0.150	0.076	0.004	0.054	−0.011
β_3'														0.651	−0.102	0.000	−0.057	0.001
η															0.572	−0.009	0.002	0.019
τ_1																0.107	−0.003	−0.002
τ_2																	0.045	0.001
τ_3																		0.011

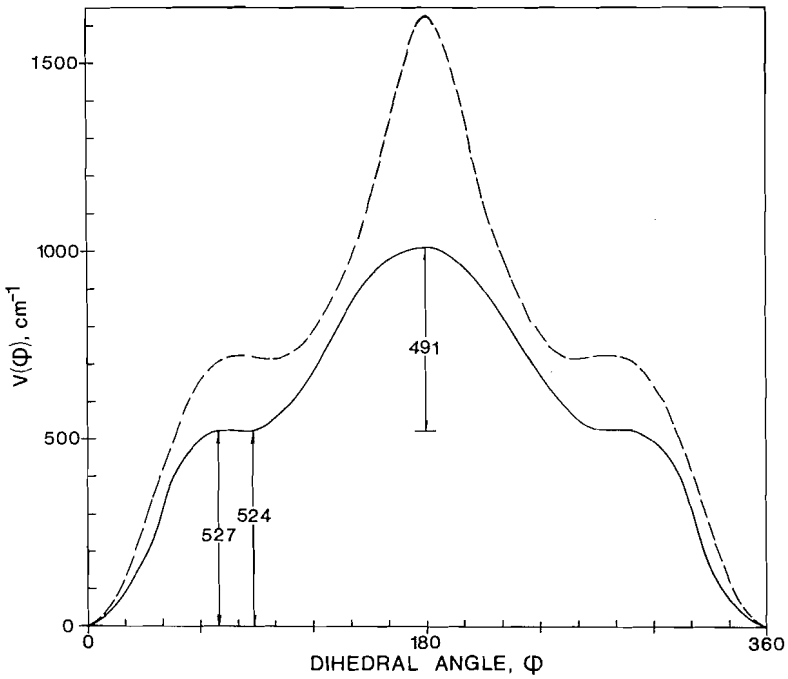


FIG. 5. Potential function governing internal rotation about the central C—C bond in ethyl methyl ketone as determined by *ab initio* calculations with the 6-31G* basis set. The potential surface given by the dashed line was obtained by allowing the torsional dihedral angle to vary by 10° increments from the *trans* position (0°) to the *cis* position (180°) while all other structural parameters were held fixed at the optimized values obtained for the *trans* conformer. The potential surface given by the solid line was obtained by additional optimizations at the *gauche* minimum and at the transition states by relaxation of all the geometric parameters.

barrier. With the exception of the value for the CH_3—CH_2 torsion with the 6-31G* basis set, the barriers show significant effects of forcing the hydrogen atoms to be equivalent, as seen in Table 2. For the *gauche* conformation, the barriers are essentially non-sensitive to the levels of calculations and the calculated values appear to be too large in all cases, although one can only speculate in the absence of derived values from experimental data.

Normal coordinate analysis

Normal coordinate analyses for both the *trans* and *gauche* conformers of ethyl methyl ketone were carried out using the force fields calculated with the GAUSSIAN-86 program (16) with the RHF/3-21G basis set. The optimized structural parameters (Table 4) and the symmetry coordinates (Table 5) were used to calculate the *G* and *B* matrices according to the Wilson method (17) and the computer programs written by Schachtschneider (18). The *B* matrix was then utilized to convert the force fields in cartesian coordinates into the force fields in internal coordinates (Fig. 6). The force fields in internal coordinates are given in Tables 6 and 7 for the *trans* and *gauche* conformers, respectively. The *G* matrix was used along with the force fields in internal coordinates to calculate the "pure" *ab initio* vibrational frequencies with scaling factors of 1.0. These frequencies, as well as the potential energy distribution (P.E.D.), are summarized in Tables 8 and 9 for the *trans* and *gauche* conformers, respectively.

A comparison of the calculated frequencies and the observed values for both conformers shows that the calculated frequencies are overestimated by 10.7 and 9.3% overall average error for the *trans* and *gauche* conformers, respectively. Subsequently, we scaled the force constants for the stretching coordinates by 0.90, those for the bending coordinates by 0.80,

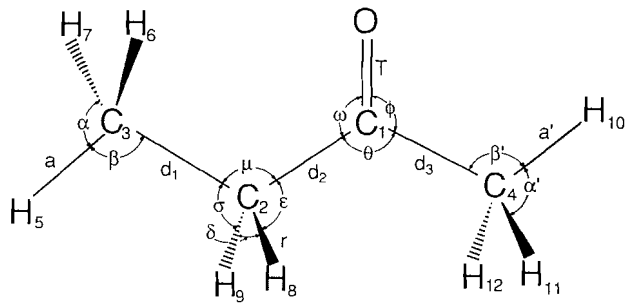


FIG. 6. Internal coordinates for ethyl methyl ketone. Torsional internal coordinates are not included.

those for the torsional coordinates by 1.0, and those for the interaction coordinates by geometric averages. With this procedure, we obtained overall average errors of 3.8 and 3.5%, respectively, for the *trans* and *gauche* rotamers. These "fixed scale" frequencies are also summarized in Tables 8 and 9.

Discussion

For all of the compounds with the general formula CH_3CH_2-C(O)X, where X is F, Cl, Br, and CH_3, a *trans/gauche* equilibrium is observed in the gas and liquid, with the *trans* conformer being the more stable form in both states. It is also the *trans* form that exists in the solid. One can assume that substitution on the sp^2 carbon does not affect significantly the conformational behavior. We have just completed similar studies on haloacetones, $XCH_2C(O)CH_3$, where X is F (14), Cl (19), and Br.[3] For these latter molecules, it is the *cis* (in fluoroacetone) or *gauche* (in chloroacetone and bromoace-

[3] J. R. Durig, Jie Lin, and H. V. Phan. To be published.

Can. J. Chem. Downloaded from www.nrcresearchpress.com by 84.41.108.74 on 09/07/12
For personal use only.

TABLE 8. Comparison of observed and calculated frequencies (cm^{-1}) for the *trans* conformer of ethyl methyl ketone

Species	Fundamental	*Ab initio*[a]	Fixed scaled[b]	IR intensity[c]	Obsd.[d]	P.E.D.
A′	CH_3 antisymmetric stretch[f]	3305	3137	9.35	2952	$95S_1$
	CH_3 antisymmetric stretch	3276	3110	23.40	2933	$97S_2$
	CH_3 symmetric stretch	3217	3053	19.30	2919	$95S_3$
	CH_3 symmetric stretch[f]	3205	3042	15.40	2908	$67S_4$, $28S_5$
	CH_2 symmetric stretch	3196	3033	5.49	2895	$68S_5$, $28S_4$
	C=O stretch	1936	1828	109.80	1739	$83S_6$
	CH_3 antisymmetric deformation	1669	1493	8.56	1457	$89S_7$
	CH_3 antisymmetric deformation[f]	1630	1459	23.70	1425	$81S_8$, $11S_9$
	CH_2 deformation	1620	1449	6.86	(1412)[e]	$86S_9$, $10S_8$
	CH_3 symmetric deformation	1585	1418	10.50	(1379)[e]	$96S_{10}$
	CH_3 symmetric deformation[f]	1557	1394	32.30	1367	$94S_{11}$
	CH_2 wag	1500	1350	21.80	(1344)[e]	$72S_{12}$, $15S_{15}$
	CH_3 in-plane rock[f]	1283	1173	85.60	1175	$29S_{13}$, $22S_{18}$, $20S_{10}$, $11S_{15}$
	CH_3 in-plane rock	1213	1096	11.90	1092	$54S_{14}$, $10S_{20}$
	$C_1C_2C_3$ antisymmetric stretch	1073	990	1.88	990	$42S_{15}$, $19S_{13}$, $15S_{14}$
	C_1C_4 stretch	1010	944	9.77	941	$32S_{16}$, $31S_{17}$, $18S_{13}$, $12S_{15}$
	$C_1C_2C_3$ symmetric stretch	803	751	0.41	760	$39S_{17}$, $15S_{15}$, $12S_{20}$, $11S_{17}$
	CO in-plane bend	627	570	12.10	588	$52S_{18}$, $23S_{16}$, $11S_{20}$
	CC(O)C deformation	433	391	6.72	409	$42S_{19}$, $20S_{18}$, $13S_{13}$, $13S_{20}$
	$C_1C_2C_3$ bend	276	247	6.67	252	$50S_{20}$, $41S_{19}$
A″	CH_3 antisymmetric stretch	3288	3120	25.00	2998	$96S_{21}$
	CH_3 antisymmetric stretch[f]	3255	3089	11.20	2998	$96S_{22}$
	CH_2 antisymmetric stretch	3225	3061	4.31	2992	$93S_{23}$
	CH_3 antisymmetric deformation	1670	1491	7.57	1457	$85S_{24}$
	CH_3 antisymmetric deformation[f]	1651	1472	15.50	1425	$89S_{25}$
	CH_2 twist	1430	1283	0.03	1256	$75S_{26}$, $14S_{27}$
	CH_3 out-of-plane rock	1264	1153	0.67	1098	$28S_{27}$, $22S_{28}$, $19S_{29}$, $11S_{30}$
	CH_3 out-of-plane rock[f]	1086	971	6.22	(937)[e]	$45S_{28}$, $22S_{27}$, $20S_{26}$
	CH_2 rock	846	763	5.01	745	$50S_{29}$, $26S_{27}$, $13S_{28}$
	CO out-of-plane bend	533	513	0.05	(471)[e]	$64S_{30}$, $20S_{29}$, $11S_{28}$
	CH_3 torsion	216	216	0.09	195	$91S_{31}$
	CH_3 torsion[f]	124	124	0.001	(137)[e]	$68S_{32}$, $12S_{28}$
	Asymmetric torsion	56	56	0.15	64	$40S_{33}$, $38S_{32}$

[a]Calculated at the 3-21G basis set.
[b]Frequencies determined after force constants were scaled, see text.
[c]Units are in km/mol. These are calculated values with the 3-21G basis set by Gaussian-86 program.
[d]Observed frequencies from the Raman and (or) infrared spectra of the gas unless otherwise noted.
[e]Observed in the spectra of the solid.
[f]Fundamentals belonging to the CH_3 moiety closest to the carbonyl moiety.

Can. J. Chem. Downloaded from www.nrcresearchpress.com by 84.41.108.74 on 09/07/12
For personal use only.

tone) conformer that is thermodynamically more stable than the *trans* form. However, in the liquid phase the abundance of the *trans* form increased and it becomes the lower energy species. Then in the solid phase, the *gauche* isomer completely disappeared upon annealing of the samples and the *trans* conformer exclusively remained. The increased stability of the *trans* isomeric form upon condensation can be attributed to dipole–dipole interactions, which can be at least in part correlated with the total dipole moment (20, 21). Therefore, it is evident that for these simple molecular systems it is not only the degree of substitution that affects the conformational behavior, but the positions of substitution also play a major role in the equilibrium between the stable forms. It would be interesting to investigate the conformational composition and behavior of the compounds with the general formulas $CH_3CX_2C(O)Y$ and $YCX_2C(O)CH_3$, where X and Y are halogen atoms.

The presently proposed potential function governing the asymmetric torsion for ethyl methyl ketone must be considered as tentative. However, it is worthwhile to note that in our studies of propionyl halides (1–3), excellent agreement was achieved between the values determined from *ab initio* calculations and those derived from the asymmetric potential functions. Therefore, in view of these points, the uncertainties in the barriers to internal rotation (Table 1) may be underestimated. Nevertheless, the barriers are in fair agreement with those calculated theoretically. Lastly, the *gauche*-to-*trans* barrier for ethyl methyl ketone is very small compared to the corresponding quantities for the propionyl halides (1–3). It is not surprising that in the earlier studies (10–12) the authors "missed" the *gauche* potential minimum as well as the *trans*-to-*gauche* transition state at the 6-31G* basis set because of their procedures in carrying out the calculations. In several cases we found that the smaller 3-21G basis set gives better predictions on conformational stabilities than the larger 6-31G* basis set.

Among the structural parameters determined by *ab initio* calculations only four are significantly different between the two conformers of ethyl methyl ketones: $r(C_2—C_3)$, $\angle(C_1C_2C_3)$, $\angle(C_1C_2C_9)$, and $\angle(H_8CH_9)$. With the 6-31G* basis set, the $C_2—C_3$ distance increases by about 0.01 Å from 1.524 Å in the *trans* form to 1.535 Å in the *gauche* form. In the electron diffraction study (8), this parameter was held fixed at

TABLE 9. Comparison of observed and calculated frequencies (cm^{-1}) for the *gauche* conformer of ethyl methyl ketone

Fundamental	*Ab initio*[a]	Fixed scaled[b]	IR intensity[c]	Obsd.[d]	P.E.D.
CH_3 antisymmetric stretch[f]	3306	3138	10.48	3022	$94S_1$
CH_2 antisymmetric stretch	3293	3125	27.91	3014	$73S_{23}$, $23S_{21}$
CH_3 antisymmetric stretch	3274	3107	21.52		$76S_2$, $12S_{21}$
CH_3 antisymmetric stretch	3263	3096	14.03		$54S_{21}$, $16S_2$, $15S_{23}$, $13S_{22}$
CH_3 antisymmetric stretch[f]	3254	3089	10.36		$81S_{22}$
CH_2 symmetric stretch	3233	3068	9.98		$93S_5$
CH_3 symmetric stretch	3206	3042	19.75		$93S_3$
CH_3 antisymmetric stretch[f]	3201	3038	2.96		$86S_4$
C=O stretch	1935	1827	131.90		$83S_6$
CH_3 antisymmetric deformation	1675	1502	11.51	1470	$72S_7$, $13S_{24}$
CH_3 antisymmetric deformation	1672	1497	11.76	1470	$73S_{24}$, $10S_{31}$
CH_3 antisymmetric deformation[f]	1651	1474	18.46	1437	$71S_{25}$, $14S_9$
CH_2 deformation	1643	1468	1.07		$68S_9$, $21S_{25}$
CH_3 antisymmetric deformation[f]	1627	1456	14.45		$86S_8$
CH_3 symmetric deformation	1574	1407	4.73		$93S_{10}$
CH_3 symmetric deformation[f]	1556	1393	37.33		$91S_{11}$
CH_2 wag	1474	1324	11.03		$75S_{12}$, $10S_{15}$
CH_2 twist	1424	1279	11.28	(1212)[e]	$70S_{26}$, $13S_{27}$
CH_3 in-plane rock[f]	1313	1199	60.03	1186	$10S_{13}$, $18S_{18}$, $15S_{16}$, $15S_{27}$, $13S_{29}$
CH_3 out-of-plane rock	1239	1125	5.45		$13S_{27}$, $17S_{14}$, $13S_{28}$, $11S_{29}$
CH_3 in-plane rock	1225	1105	16.98		$12S_{14}$, $20S_{13}$, $19S_{28}$
CH_3 out-of-plane rock[f]	1109	996	7.67		$36S_{28}$, $33S_{14}$, $11S_{12}$
$C_1C_2C_3$ antisymmetric stretch	1041	967	15.34		$41S_{15}$, $19S_{13}$, $13S_{16}$
C_1C_4 stretch	994	925	9.34		$31S_{16}$, $15S_{17}$, $24S_{15}$
CH_2 rock	878	792	0.90	844	$45S_{29}$, $31S_{27}$
$C_1C_2C_3$ symmetric stretch	791	744	1.36	752	$27S_{17}$, $36S_{16}$, $11S_{15}$
CO out-of-plane bend	659	624	0.48	644	$44S_{30}$, $24S_{28}$, $11S_{17}$, $10S_{20}$
CO in-plane bend	544	493	18.50	520	$69S_{18}$
CC(O)C deformation	414	375	1.45	442	$74S_{19}$, $11S_{13}$
CCC bend	264	242	0.71		$62S_{20}$, $26S_{30}$
CH_3 torsion	237	233	0.64		$84S_{31}$
CH_3 torsion[f]	142	144	0.10		$81S_{32}$
Asymmetric torsion	55	55	3.09		$71S_{33}$, $10S_{20}$

[a]Calculated at the 3-21G basis set.
[b]Frequencies determined after force constants were scaled, see text.
[c]Units are in km/mol. These are calculated values with the 3-21G basis set by Gaussian-86 program.
[d]Observed frequencies from the Raman and (or) infrared spectra of the gas unless otherwise noted.
[e]Observed in the Raman spectrum of the liquid.
[f]Fundamentals belonging to the CH_3 moiety closest to the carbonyl moiety.

TABLE 10. Fit of the experimentally observed rotational constants (MHz) for the *trans* conformer of ethyl methyl ketone

	Rotational constant	Obsd.[a]	Calcd.[b]	Δ[c]	*Ab initio* 3-21G	*Ab initio* 6-31G*
$CH_3CH_2C(O)CH_3$	*A*	9544.63	9544.72	−0.09	9543	9758
	B	3596.85	3597.48	−0.63	3638	3596
	C	2746.51	2745.43	1.08	2767	2760
$CH_3CD_2C(O)CD_3$	*A*	8006.73	8006.83	−0.10	8022	8180
	B	3185.14	3185.77	−0.63	3217	3183
	C	2452.00	2450.93	1.07	2469	2462

[a]Values taken from ref. 6. These values do not include the effects of coupling of internal and overall rotation.
[b]Calculated with diagnostic least-squares adjustment of the structural parameters indicated in Table 3. Also see text.
[c]Obsd. − Calcd.
[d]The rotational constants for the d_5 species were obtained using *ab initio* calculated structural parameters.

Can. J. Chem. Downloaded from www.nrcresearchpress.com by 84.41.108.74 on 09/07/12
For personal use only.

Can. J. Chem. Downloaded from www.nrcresearchpress.com by 84.41.108.74 on 09/07/12
For personal use only.

1.531 Å for both conformers, which is not quite the average of our 6-31G* *ab initio* predicted values. For the $C_1C_2C_3$ angle, a difference of 2.81° was calculated with the 6-31G* basis set with that of the *trans* being larger. The difference in the $\angle(C_1C_2C_3)$ of the two forms was not observed in the case of the halides (1, 2). The decrease in the value of this parameter when the molecule rotates from the *trans* to the *gauche* conformation is probably at the expense of the $\angle(C_1C_2H_9)$ and $\angle(H_8CH_9)$ angles, both of which increase significantly from the values of the *trans* to those for the *gauche* conformation.

With the 6-31G* basis set, the C—H and C=O bonds are expected to be about 0.010 and 0.02 Å too short, respectively. Using the microwave (6) rotational constants obtained for the *trans* conformer of $CH_3CH_2C(O)CH_3$ and $CH_3CD_2C(O)CD_3$, we calculated the r_0 parameters by adjusting $r(C_1—C_2)$, $r(C_2—C_3)$, and $r(C_1—C_4)$, and $\angle(C_2C_1O)$, $\angle(C_2C_1C_4)$, and $\angle(C_1C_2C_3)$. As initial values, we utilized structural parameters predicted with the 6-31G* basis set with the above adjustment for the C—H and C=O bond lengths. Excellent reproducibility of the experimental rotational constants was obtained, as evident in Table 10. However, the values of the $C_1—C_2$ and $C_1—C_4$ distances, which were varied, decreased, and the $C_1—C_4$ distance is essentially equal to the value for acetone (22) (1.507 ± 0.003 Å). The reported (22) C=O distance in acetone is 1.222 ± 0.003 Å. Since the C=O distance is expected to have the same value for both acetone and ethyl methyl ketone we used the electron diffraction (8) value of 1.218 Å, which is, within experimental error, the same value as that for acetone. The difference in the $C_1—C_2$ and $C_1—C_4$ distances is larger than expected since the *ab initio* results indicate the difference should be 0.003 Å, but $r(C_1—C_2)$ and $r(C_2—C_3)$ are strongly correlated so the final results are somewhat dependent on the initial starting values for these parameters. The determined angles are in good agreement with those predicted with the 6-31G* basis set except for $\angle C_2C_1O$, which is 0.8° larger than the *ab initio* value. The r_0 structural parameters obtained from the microwave data are compared to those obtained experimentally and theoretically in Table 4. It is believed that the r_0 parameters obtained are closer to the actual ones than any of those previously proposed.

Of the three bond distances between heavy atoms that are common in propionyl fluoride, propionyl chloride, and ethyl methyl ketone, only the C=O bond distance in both conformations is affected by the substitution of the CH_3 moiety for a halogen atom. The value for this parameter calculated with the 6-31G* basis set increases from about 1.168 Å in the two halides (1, 2) to 1.192 Å in the ketone. This sharp increase is accompanied by a significant decrease in the C_2C_1O bond angle, which goes from 128.7° (*trans*) and 128.5° (*gauche*) for propionyl fluoride (1), to 127.4° (*trans*) and 126.8° (*gauche*) in propionyl chloride (2), and finally to 122.1° (*trans*) and 121.0° (*gauche*) in ethyl methyl ketone. Presumably, these changes are due to the electron-withdrawing ability of the substituents in $CH_3CH_2C(O)X$. These trends were also observed in our studies of fluoroacetone (16) and chloroacetone (19).

Finally, the *ab initio* dihedral angle for the *gauche* form is as much as 25° smaller than the value estimated from 2-methyl-1-butene and kept constant in the electron diffraction study (8). The deviation of this structural parameter from the expected value of 120° reflects the repulsive interactions between the two methyl groups.

Among the diagonal force constants, only four force constants are different between the two conformers, with values of 1.082 and 0.797 mdyn/Å calculated for the $C_1C_2C_3$ bending coordinate for the *trans* and *gauche* form, respectively. The difference reflects the difference in the calculated values for the $\angle C_1C_2C_3$ angle. However, the corresponding calculated frequencies for this motion are not significantly affected by these different force constants. Likewise, the force constants for both of the CH_3 torsional coordinates increase by 41% from the *trans* to the *gauche* form, but the calculated frequencies for the torsions change only slightly. Similarly, the asymmetric torsional force constants of 0.011 and 0.015 mdyn/Å are calculated for the *trans* and *gauche* conformer, respectively, which represent a 36% difference, but the asymmetric torsional fundamental frequencies for both forms are predicted to have the same value of 55 cm^{-1}.

As evident from Tables 8 and 9, extensive mixing of the normal modes are predicted for fundamental frequencies below 1500 cm^{-1}. For the *trans* form, mixing is calculated between the C—C stretching and the in-plane skeletal bending vibrations in the A′ symmetry block, whereas the carbon–hydrogen rocking modes are predicted to be coupled in the A″ block. For the *gauche* conformer, mixing occurs among the same normal modes as those for the *trans* conformer. The degree of mixing in both conformers made it difficult to assign several of the spectral features observed in the spectra of the gas and liquid, especially those arising from the *gauche* rotamer, because the bands are already nondescript, featureless, and weak. In several instances the assignment could not have been made without the calculated potential energy distributions among the symmetry coordinates.

The vibrational data clearly show that there is a substantial well at the *gauche* conformation. To obtain a better theoretical value for the relative barriers for conformational interchange a very large basis set must be used with electron correlation. We plan to carry out such a calculation in the near future.

1. J. R. DURIG, G. A. GUIRGIS, and H. V. PHAN. J. Raman Spectrosc. **21**, 359 (1990).
2. J. R. DURIG, A. Q. MCCARVER, H. V. PHAN, and G. A. GUIRGIS. J. Phys. Chem. **95**, 539 (1991).
3. J. R. DURIG, G. A. GUIRGIS, and H. V. PHAN. J. Mol. Struct. **244**, 139 (1991).
4. O. L. STIEFVATER and E. B. WILSON. J. Chem. Phys. **50**, 5385 (1969).
5. S. J. SKJÖRHOLM and K. HAGEN. J. Phys. Chem. **91**, 3977 (1987).
6. L. PIERCE, C. K. CHENG, M. HAYASHI, and R. NELSON. J. Mol. Spectrosc. **5**, 449 (1969).
7. N. M. POZDEEV, A. KB. MAMTEER, L. N. GUNDEROVA, and R. V. GALEEV. Zh. Strukt. Khim. **29**, 62 (1988).
8. M. ABE, K. KUCHITSU, and T. SHIMANOUCHI. J. Mol. Struct. **4**, 245 (1969).
9. T. SHIMANOUCHI, Y. ABE, and M. MIKAMI. Spectrochim. Acta, **24A**, 1037 (1968).
10. K. B. WIBERG and E. MARTIN. J. Am. Chem. Soc. **107**, 5035 (1985).
11. K. B. WIBERG and M. A. MURCKO. J. Comput. Chem. **9**, 488 (1987).
12. L. SCHÄFER, K. SIAM, and J. D. EWBANK. J. Mol. Struct. (Theochem), **200**, 189 (1989).
13. K. FURIC and J. R. DURIG. Appl. Spectrosc. **42**, 175 (1988).
14. J. R. DURIG, J. A. HARDIN, H. V. PHAN, and T. S. LITTLE. Spectrochim. Acta, **45A**, 1239 (1989).
15. P. GRONER, G. A. GUIRGIS, and J. R. DURIG. J. Chem. Phys. **86**, 565 (1987).
16. M. J. FRISCH, J. S. BINKLEY, H. B. SCHLEGEL, K. RAGHAVACHARI, C. F. MELIUS, R. L. MARTIN, J. J. P. STEWART, F. W. BOBROWICZ,

C. M. ROHLFING, L. R. KAHN, D. J. DEFREES, R. SEEGER, R. A. WHITESIDE, D. J. FOX, E. M. FLEUDER, and J. A. POPLE. GAUSSIAN-86, Carnegie–Mellon Quantum Chemistry Publishing Unit, Pittsburgh, PA. 1986.
17. E. B. WILSON, J. C. DECIUS, and P. C. CROSS. *In* Molecular vibrations. McGraw–Hill, New York. 1955.
18. J. H. SCHACHTSCHNEIDER. *In* Vibrational analysis of polyatomic molecules. Parts V and VI. Technical Reports Nos. 231 (1964) and 57 (1965), Shell Development Company, Houston, TX.
19. J. R. DURIG, JIE LIN, C. L. TOLLEY, and T. S. LITTLE. Spectrochim. Acta, **47A**, 105 (1991).
20. I. M. WATANABE, S. MIZUSHIMA, and Y. MASIKO. Sci. Pap. Inst. Phys. Chem. Res. Jpn. **40**, 425 (1943).
21. A. WADA. J. Chem. Phys. **22**, 198 (1954).
22. R. NELSON and L. PIERCE. J. Mol. Spectrosc. **18**, 344 (1965).

Can. J. Chem. Downloaded from www.nrcresearchpress.com by 84.41.108.74 on 09/07/12
For personal use only.

The vibrational spectrum, barrier to internal rotation, and *ab initio* calculations of 2-chloropropane[1]

J. F. SULLIVAN,[2] AIYING WANG, MEI-SHIOW CHENG, AND J. R. DURIG
Department of Chemistry, University of South Carolina, Columbia, SC 29208, U.S.A.

Received July 15, 1991

This paper is dedicated to Dr. Richard Norman Jones

J. F. SULLIVAN, AIYING WANG, MEI-SHIOW CHENG, and J. R. DURIG. Can. J. Chem. **69**, 1845 (1991).

The Raman spectra (3200–50 cm^{-1}) of gaseous, liquid, and solid 2-chloropropane-d_3 (isopropyl-d_3 chloride), $CH_3(CD_3)$-CHCl, and the infrared spectra (3200–50 cm^{-1}) of the gas and solid have been recorded. The torsional transitions observed in the far infrared spectrum of the gaseous sample recorded at a resolution of 0.10 cm^{-1} between 265 and 135 cm^{-1} were analyzed in terms of the semirigid rotor model. An effective barrier of 1378 ± 4 cm^{-1} (3.94 ± 0.01 kcal/mol), cosine–cosine coupling term of 166 ± 10 cm^{-1} (0.47 ± 0.03 kcal/mol), and sine–sine coupling term of −173 ± 1 cm^{-1} (−0.49 ± 0.01 kcal/mol) were determined by fitting ten observed frequencies arising from the CH_3 and CD_3 torsions. The assignment of the 27 fundamentals is given and discussed. A complete equilibrium geometry, barrier to internal rotation, and vibrational frequencies have been determined by *ab initio* Hartree–Fock gradient calculations employing either 3-21G* or 6-31G* basis sets for both the d_0 and d_3 species. These calculated results are compared to the experimental values as well as to the corresponding quantities for some similar molecules.

Key words: 2-chloropropane, vibrational spectrum; *ab initio* calculations; barrier to internal rotation.

J. F. SULLIVAN, AIYING WANG, MEI-SHIOW CHENG et J. R. DURIG. Can. J. Chem. **69**, 1845 (1991).

On a enregistré les spectres Raman (3200–50 cm^{-1}) d'échantillons gazeux, liquide et solide du 2-chloropropane-d_3 (chlorure d'isopropyle-d_3), $CH_3(CD_3)CHCl$, ainsi que les spectres infrarouges (3200–50 cm^{-1}) du gaz et du solide. On a analysé les transitions de torsion, observées dans le spectre infrarouge lointain de l'échantillon gazeux enregistré à une résolution de 0,10 cm^{-1} entre 265 et 135 cm^{-1}, en fonction du modèle du rotor semi-rigide. On a déterminé une barrière effective de 1378 ± 4 cm^{-1} (3,94 ± 0,01 kcal/mol), terme de couplage cosinus/cosinus de 166 ± 10 cm^{-1} (0,47 ± 0,03 kcal/mol) et un terme de couplage sinus/sinus de −173 ± 1 cm^{-1} (−0,49 ± 0,01 kcal/mol) en ajustant dix fréquences observées pour les torsions de CH_3 et de CD_3. On fait les attributions de 27 fondamentales et on en discute. En se basant sur des calculs *ab initio* de gradient de Hartree–Fock utilisant des ensembles de base soit 3-21G* ou 6-31G* tant pour les espèces d_0 et d_3, on a déterminé une géométrie d'équilibre complète, la barrière à la rotation interne et les fréquences de vibration. On compare les résultats de ces calculs avec les valeurs expérimentales ainsi qu'avec les valeurs correspondantes pour des molécules semblables.

Mots clés : 2-chloropropane, spectre vibrationnel; calculs *ab initio*; barrière à la rotation interne.

[Traduit par la rédaction]

Introduction

The barriers to internal rotation of two methyl groups bonded to a common carbon atom have been the subject of a number of investigations. Recently, the microwave and far-infrared spectra, structure, and barriers to internal rotation for 2-fluoropropane were reported (1). Based on the magnitude of the sine–sine ($V'_{33} = -92$ cm^{-1}) and cosine–cosine coupling terms ($V_{33} = 107$ cm^{-1}) determined for the parent and two isotopic species of 2-fluoropropane, it was concluded that top–top coupling is significant in this molecule. A similar study (2) has also been carried out on 2-chloropropane (isopropyl chloride) where the average effective V_3 barrier was found to be 1380 ± 3 cm^{-1} (3.95 ± 0.01 kcal/mol) based on the observation of six Q-branches observed between 270 and 230 cm^{-1} in the infrared spectrum, and a second series of double jumps observed in the Raman spectrum and assigned to the lower energy series. Because the structure of this molecule results in *B*-type infrared band contours for the A″ methyl torsion, no Q-branches were observed in the far-infrared spectrum for this series. Consequently, only two double-jump transitions from the Raman spectrum could be used in the calculations. Because of the uncertainty in the assignment of the A″ methyl torsional series, we decided to record the far-infrared spectrum of the 2-chloropropane-d_3 molecule, $(CH_3)(CD_3)CHCl$, as deuteration of one of the methyl groups would lower the symmetry to trivial C_1, where all fundamentals would give rise to $A/B/C$ hybrid bands. Deuteration in this position would also shift the CD_3 methyl torsion out of the region of the CH_3 torsion, which should aid in the assignment.

For comparison with the previous vibrational assignment (3) for the 2-chloropropane-d_0 molecule, the infrared and Raman spectra of the -d_3 molecule have also been recorded, and *ab initio* Hartree–Fock gradient calculations employing both 3-21G* and 6-31G* basis sets were carried out to obtain the equilibrium geometry and potential energy distributions. The r_0 structure has also been calculated based on the rotational constants for eight isotopic species from the previously reported microwave study (4) from which r_s structural parameters were determined. The results of this study are reported herein.

Experimental

The sample of 2-chloropropane-d_3 was synthesized via the reaction of isopropanol-d_3 (Merck, Sharp and Dohme, Quebec, Canada) with phosphorus trichloride at a ratio of 3:1. It was then purified by a low-temperature, low-pressure fractionation column.

Mid-infrared spectra of the gas and solid from 3200 to 400 cm^{-1} were obtained with a Digilab model FTS-14C Fourier transform interferometer equipped with a Ge/KBr beamsplitter and a TGS detector. Far-infrared spectra (480–50 cm^{-1}) of the gas and solid were obtained with a Digilab model FTS-15B Fourier transform interfero-

[1]Taken in part from the thesis of Mei-Shiow Cheng which was submitted to the Department of Chemistry in partial fulfillment of the requirements for a Ph.D. degree.

[2]Author to whom correspondence may be addressed.

Printed in Canada / Imprimé au Canada

Can. J. Chem. Downloaded from www.nrcresearchpress.com by 84.41.108.74 on 09/07/12
For personal use only.

meter equipped with a 6.25-μm beamsplitter and a TGS detector. The gaseous sample was contained in a 1-m cell fitted with polyethylene windows for the far-infrared studies and in a 10-cm cell equipped with CsI windows for the mid-infrared study. For the gas phase, the data were collected at a resolution of 0.5 cm^{-1}. For the solid phase, the sample was condensed onto a silicon or cesium iodide plate, which was maintained under vacuum and cooled with liquid nitrogen. The resolution used for the solid phase was 1 cm^{-1}. The far-infrared spectra at a resolution of 0.1 cm^{-1} below 270 cm^{-1} were also recorded on a Nicolet model 200 SXV Fourier transform interferometer equipped with a vacuum bench and a liquid helium cooled Ge bolometer containing a wedged sapphire filter and polyethylene windows.

The Raman spectra were recorded on a Cary model 82 spectrophotometer equipped with a Spectra-Physics model 171 argon ion laser operating on the 5145 Å line. The spectrum of the gas was recorded by using a standard Cary multipass accessory and the laser power at the sample was 1 W. The spectrum of the liquid was recorded from the sample sealed in a glass capillary. The spectrum of the solid was obtained by annealing the sample sealed in a glass capillary using a Cryogenic Technologies, Inc. cryostat connected to a Lake Shore Cryogenics Inc. model DTC-500 temperature controller. Reported frequencies are expected to be accurate to ±2 cm^{-1}.

Results

Methyl torsion

The infrared spectrum of gaseous 2-chloropropane-d_3 recorded at 0.10 cm^{-1} resolution between 265 and 135 cm^{-1} is shown in Fig. 1. Though the water absorption bands exist at relatively the same intensity as the torsional transitions, there is no difficulty in recognizing either the $-CH_3$ or the $-CD_3$ torsional transitions. The strongest Q-branch at 250.2 cm^{-1} is assigned to the $1 \leftarrow 0$ transition for the methyl torsion whereas the second strongest Q-branch at 178.9 cm^{-1} is assigned to the $1 \leftarrow 0$ transition for the CD_3 torsion. The other three Q-branches with medium intensity at 237.2, 172.7, and 166.5 cm^{-1} were assigned to be the $2 \leftarrow 1$ transition for the $-CH_3$ torsion, and the $2 \leftarrow 1$ and $3 \leftarrow 2$ transitions for the $-CD_3$ torsion, respectively.

The torsional problem in 2-chloropropane may be treated on the basis of the semi-rigid $C_{3v}(T)$-$C_s(F)$-$C_{3v}(T)$ or $C_s(e)$ model (T = top; F = frame; e = two equivalent tops). Its internal Hamiltonian was derived by Groner and Durig (5) and is given by

$$H_1 = \tfrac{1}{2}[g^{44}\hat{p}_0^2 + 2g^{45}\hat{p}_0\hat{p}_1 + g^{55}\hat{p}_1^2] + \tfrac{1}{2}[V_{30}(1 - \cos 3\tau_0) + V_{06}(1 - \cos 6\tau_0) + V_{03}(1 - \cos 3\tau_1) + V_{06}(1 - \cos 6\tau_1) + V_{33}(\cos 3\tau_0 \cos 3\tau_1 - 1) + V'_{33} \sin 3\tau_0 \sin 3\tau_1]$$

with symmetry restrictions $V_{30} = V_{03}$ and $V_{60} = V_{06}$. The symmetry group of this internal Hamiltonian is of order 18, $C_3 \otimes \Theta_3$, and is isomorphous to the direct product of cyclic group, C_3, of order 3 with dihedral group Θ_3, of order 6. Its character table has been given by Durig *et al.* (6) and is available elsewhere in the same notations. The high barrier torsional energy levels split into sublevels according to:

$$\Gamma^{00\sigma} \otimes \Gamma^{10} \otimes \Gamma^{11} \otimes \Gamma^{12\sigma}$$

where σ is + or − for $\bar{v}$ even or odd, respectively, and where $\bar{v}$ is the limiting vibrational quantum number of the antisymmetric mode in the C_s point group with respect to the symmetry plane of the molecular frame. $\Gamma^{00\sigma}$ are one-dimensional representations and Γ^{11} is the two-dimensional representation. $\Gamma^{12\sigma}$ are the symbols for two complex conjugate pairs of one-dimensional representations. Γ^{10} represents a complex conjugate pair of two-dimensional representations and, thus, leads to fourfold degenerate energy levels. The selection rules have been derived and summarized elsewhere (6).

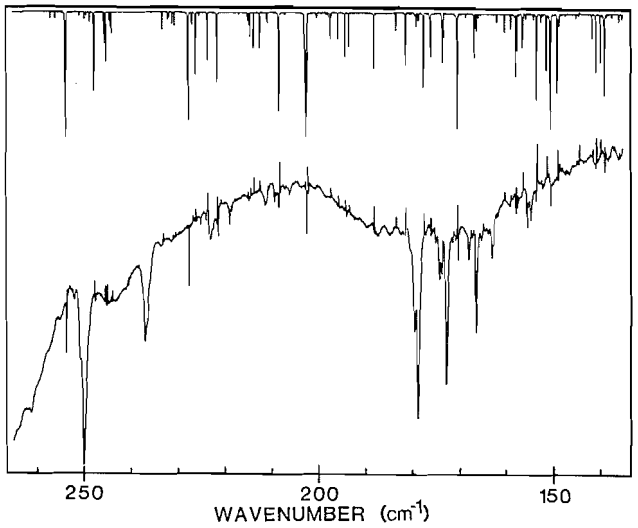


FIG. 1. Far infrared spectrum of gaseous CH_3CD_3CHCl at a resolution of 0.12 cm^{-1}.

TABLE 1. Observed torsional data (cm^{-1}) and assignments for 2-chloropropane-d_3

Obsd.	Assignment	Obsd. − Calcd.[a]
252.2	$2,1 \leftarrow 2,0$	−0.02
251.0	$1,1 \leftarrow 1,0$	0.10
250.2	$0,1 \leftarrow 0,0$	−0.14
237.2	$0,2 \leftarrow 0,1$	0.15
223.1	$4,0 \leftarrow 0,2$	0.02
179.5	$1,1 \leftarrow 0,1$	0.18
178.9	$1,0 \leftarrow 0,0$	0.14
174.2	$2,1 \leftarrow 1,1$	−0.15
172.7	$2,0 \leftarrow 1,0$	−0.33
166.5	$3,0 \leftarrow 2,0$	0.02

[a]Calculated by using the potential coefficients in Table 2.

As shown by Groner and Durig (5), the potential parameter set commonly used for this potential function presented above is not the best one in terms of determinability since some of the coefficients are strongly correlated. There exist linear combinations that are considerably less correlated than V_{30}, V_{03}, and V_{33}. These new parameters have generally lower

$$\begin{bmatrix} V_{3s} \\ V_{3d} \\ V_{\text{eff}} \end{bmatrix} = \begin{bmatrix} \frac{1}{2} & \frac{1}{2} & 0 \\ \frac{1}{2} & -\frac{1}{2} & 0 \\ \frac{1}{2} & \frac{1}{2} & -1 \end{bmatrix} \begin{bmatrix} V_{30} \\ V_{03} \\ V_{33} \end{bmatrix}$$

dispersions than the original ones. In the case of the potential function for equivalent tops, $V_{3s} = V_{03} = V_{30}$ and $V_{3d} = 0$, and the effective barrier is given directly by V_{eff}.

The initial calculations were carried out by using five of these transitions together with the potential constants for the

Can. J. Chem. Downloaded from www.nrcresearchpress.com by 84.41.108.74 on 09/07/12
For personal use only.

TABLE 2. Torsional[a] potential constants (cm^{-1}) and kinetic coefficients (cm^{-1}) for 2-chloropropane-d_3

Parameter	CH_3CD_3CHCl Value	Dispersion	$(CH_3)_2CHCl$ Ref. 2
V_{30}	1544	10	1589 ± 8
V_{03}	1544	10	1589 ± 8
V_{60}	−0.8	1.5	−7.0 ± 3.0
V_{06}	−0.8	1.5	−7.0 ± 3.0
V_{33}	166	10	209 ± 12
V'_{33}	−173	3	−171 ± 2
$\frac{1}{2}(V_{30} + V_{03}) - V_{33}$	1378	4	1380 ± 3
$\hbar^2 g^{44} = 2F_1$	10.907		10.950
$\hbar^2 g^{45} = 2F'$	−0.094		−0.102
$\hbar^2 g^{55} = 2F_2$	5.655		10.950

[a]Standard deviation of the frequency fit is 0.20 cm^{-1}.

2-chloropropane-d_0 compound provided earlier (2). Five more weak transitions were located, based on the calculated eigenvalues and eigenfunctions from the output of the initial calculations. The observed bands and their assignments are listed in Table 1. The calculations were continued as an iterative process until the difference between the observed and calculated frequencies, as well as the dispersions in the potential constants, were minimized. The final fit of the calculation gives rise to an average effective barrier of 1378 ± 4 cm^{-1} (3.94 ± 0.01 kcal/mol) for 2-chloropropane-d_3. This result is in excellent agreement with the value of 1380 ± 3 cm^{-1} (3.95 ± 0.01 kcal/mol) obtained for 2-chloropropane-d_0 by Durig and Guirgis (2). In addition to the effective barrier, both the cosine–cosine coupling term, V_{33}, and the sine–sine coupling term, V'_{33}, were evaluated and these constants were found to have values of 166 ± 10 cm^{-1} and −173 ± 3 cm^{-1}, respectively. The values should be contrasted with the values of V_{33} = 209 ± 12 cm^{-1} and V'_{33} = −171 ± 2 cm^{-1} for the d_0 molecule (2). The torsional potential constants and kinetic coefficients for the -d_3 compound are listed in Table 2.

Vibrational assignment

The 2-chloropropane-d_3 has C_1 symmetry and the 27 normal modes should show $A/B/C$ hybrid-type infrared band contours. The Raman spectra, mid-infrared, and far-infrared spectra of this compound are shown in Figs. 2, 3, and 4, respectively. The proposed vibrational assignment is listed in Table 3. In the CH stretching region, five bands with relatively consistent intensity and frequencies are observed for both the -d_3 and -d_0 compounds, whereas only four fundamental modes are expected for the -d_3 compound in this region. The band at 2888 cm^{-1} is assigned as an overtone of the fundamental frequency at either 1464 or 1455 cm^{-1}. This band was assigned as a fundamental mode in the previous study by Klaboe (3). The *ab initio* calculations predict the CH stretch to be higher in frequency than the two CH_3 antisymmetric stretches, and was, thus, initially considered to be at 2996 cm^{-1}, which is the highest observed frequency. However, this assignment is not consistent with that given by McKean *et al.* (7) for $(CD_3)_2CHCl$ where a band at 2962 cm^{-1} had to be assigned to the CH stretch. Since an isolated CH stretch provides a definitive assignment for this mode, we likewise assign the band at 2958 cm^{-1} to the secondary CH stretch.

There are two CD_3 antisymmetric stretches and one CD_3 symmetric stretch to be assigned around 2000 cm^{-1}. They

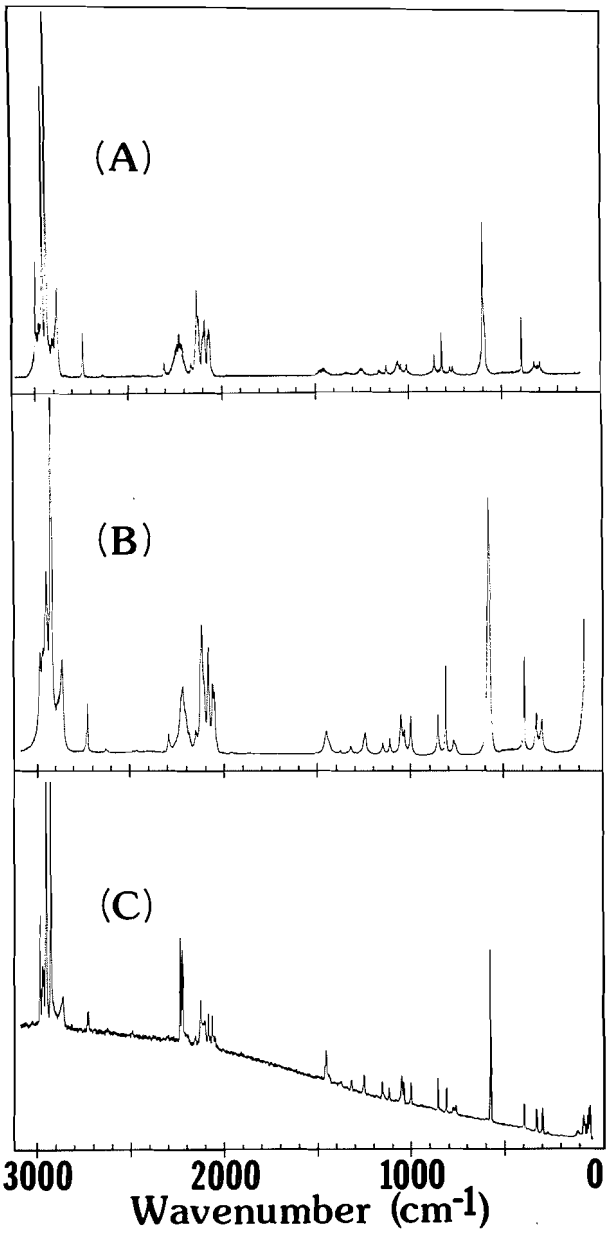


FIG. 2. Raman spectra of CH_3CD_3CHCl: (A) gaseous phase; (B) liquid phase; (C) solid phase.

were assigned at 2242, 2231, and 2130 cm^{-1}, respectively, in the mid-infrared spectrum of the gas. There are two more peaks with medium intensity in the Raman spectra of both the gas and liquid around 2000 cm^{-1}. Since they are too low in frequency to be CD_3 stretching fundamentals, they are assigned as overtone bands.

The two CH_3 antisymmetric deformations, CH_3 symmetric deformation, two HCCl bends, one of the CH_3 rocks, and the CCC antisymmetric stretch are assigned to bands that are close in frequencies to the similar fundamentals of the -d_0 compound. The comparison between the fundamental frequencies from experiments (3) and *ab initio* calculations for the -d_0 compound is given in Table 4. The CH_3 deformations occur around 1400 cm^{-1} as expected, whereas the CD_3 deformations shift to much lower frequencies around 1000 cm^{-1}, which is close to the CH_3 rocking region. The CH_3 rock of the -d_3 compound is forced down to 1010 cm^{-1} from 1066 cm^{-1} for

Can. J. Chem. Downloaded from www.nrcresearchpress.com by 84.41.108.74 on 09/07/12
For personal use only.

TABLE 3. Observed[a] frequencies (cm^{-1}) and vibrational assignment of isopropyl chloride-d_3

Infrared				Raman						Assignment	
Gas	Rel. int.	Solid	Rel. int.	Gas	Rel. int.	Liquid	Rel. int.	Solid	Rel. int.	ν_i[b]	Approximate description
2996 Q 2988 P	vs	2989	m	2994	s	2996	m,sh	2990	ms	ν_1	CH_3 antisymmetric stretch
2978 Q 2971 P	vs	2975 2970	m m	2976	sh			2975 2969	m m	ν_2	CH_3 antisymmetric stretch
2958 Q 2946 R	s,sh	2957	w	2956	vvs	2954	ms	2956	vvs	ν_3	CH stretch
2938 Q 2930 P	s	2930	m	2938	vvs	2930	vvs	2932	vvs	ν_4	CH_3 symmetric stretch
2888	m,bd	2867	w	2879	s	2870	m	2866	m		$2\nu_6$
2744 Q	vvw			2742	m	2735	m	2734 2728	w w		$2\nu_7$
2640 Q	vvw			2310	w	2303	w				$2\nu_{22}$
2242 Q 2238 P	s	2238	m	2240	m,sh			2238	ms	ν_{16}	CD_3 antisymmetric stretch
2231 Q	s	2228 2222	m m	2230	m,bd	2226	m,bd	2228 2221	ms ms	ν_{17}	CD_3 antisymmetric stretch
2130	w	2126	w	2131 2090	s m	2125 2089	ms ms	2126 2088	m m	ν_{18}	CD_3 symmetric stretch $2\nu_{21}$
2076	w	2078	w	2069	m	2064	m	2066	m		$2\nu_{19}$
1464 Q	m	1464	s	1466	vw,bd					ν_5	CH_3 antisymmetric deformation
1455 Q	m	1450	m,sh	1458	vw,bd	1458	m,bd	1454	m	ν_6	CH_3 antisymmetric deformation
1442 Q 1388 R	sh										$\nu_{24} + \nu_{12}$
1384 Q 1379 P	m	1380 1374	s s	1382	vvw	1382	vw	1374	vvw	ν_7	CH_3 symmetric deformation
1332 R 1328 Q 1318 P	w	1322	m	1330	vvw	1326	vw	1320	w	ν_{22}	HCCl out-of-plane wag
1265 Q 1256 Q 1249 Q	s	1250	s	1254	vw,bd	1250	m	1252	w	ν_8	HCCl in-plane deformation
1162 R 1158 Q 1148 P	m	1154 1148	s s	1156	vvw	1157	w	1154	w	ν_9	CH_3 rock
1128 R 1120 Q 1112 P	m	1120	s	1119	vw	1119	w	1120	w	ν_{23}	Antisymmetric skeletal stretch
1065 R 1058 Q 1047 P	m	1054	s	1056	w	1059	m	1050	m	ν_{21}	CD_3 symmetric deformation
1043 Q 1019 R	m,sh	1037	s	1042	w	1042	m	1043	m	ν_{19}	CD_3 antisymmetric deformation
1015 Q	s	1014	sh					1014	m	ν_{20}	CD_3 antisymmetric deformation
1010 Q 1001 P	s	1003	s	1008	w	1006	m			ν_{10}	CH_3 rock
870 R 861 Q 852 P	m	860	s	860	w	860	m	860	m	ν_{11}	Symmetric skeletal stretch
830 R 822 Q 813 P	s	814	s	820	m	818	ms	813	m	ν_{24}	CD_3 rock
778 Q	vw	774	m	778	vw	774	w,bd	776	vw		$2\nu_{14}$
764 Q 608 Q	vw	759	m	764	vw			760	vw	ν_{25}	CD_3 rock
599 Q	s	576 572	vs vs	598	s	583	s	578	s	ν_{12}	CCl stretch
400 R 390 Q 382 P	vw	397 393	m m	390	m	393	ms	398	m	ν_{14}	Skeletal bend
330 R 325 Q 316 P	vw	330	m	326	w	328	m	332	m	ν_{13}	HCCl rock

Can. J. Chem. Downloaded from www.nrcresearchpress.com by 84.41.108.74 on 09/07/12
For personal use only.

TABLE 3 (*concluded*)

Infrared				Raman						Assignment	
Gas	Rel. int.	Solid	Rel. int.	Gas	Rel. int.	Liquid	Rel. int.	Solid	Rel. int.	ν_i[b]	Approximate description
304 R											
295 Q	vw	299	m	294	w	297	m	300	m	ν_{26}	HCCl twist
290 P											
250.0	vvw	272	vw							ν_{15}	CH_3 torsion
178.8	vvw	196	vw							ν_{27}	CD_3 torsion
		104	w								
		83	w								
		72	m					76	m		
								72	m		
								56	m		
								49	m		
								42	m		

[a]Abbreviations used: s, strong; m, medium; w, weak; v, very; sh, shoulder; bd, broad; P, Q, and R refer to vibrational–rotational branches.
[b]This is the same numbering used in Table 4, which is consistent with the numbering for the d_0 compound.

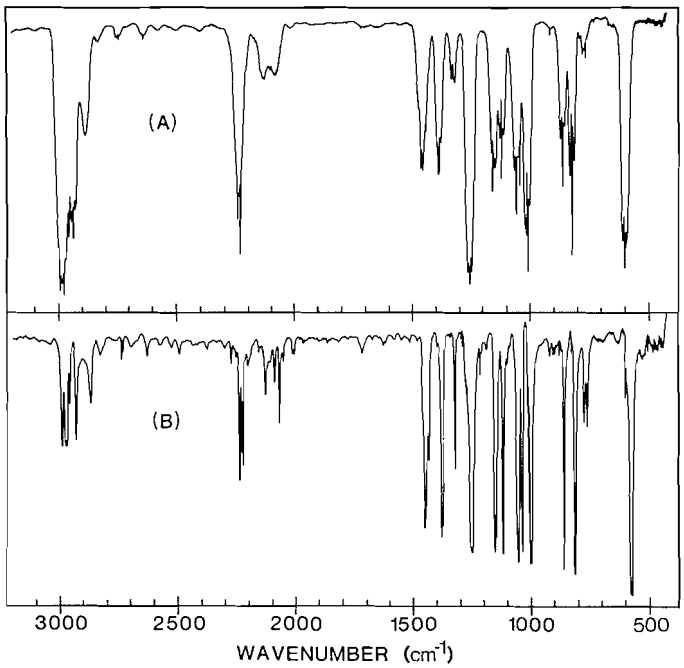


FIG. 3. Mid-infrared spectra of CH_3CD_3CHCl: (A) gaseous phase; (B) solid phase.

the CH_3 rock in the -d_0 compound by three CD_3 deformations. It should be noted that the band at 1010 cm^{-1} has extensive mixing with other normal modes that are higher in frequency. The CD_3 symmetric deformation is calculated to be higher in frequency than two of the CD_3 antisymmetric deformations whereas the CH_3 antisymmetric deformations are almost always higher than the CH_3 symmetric deformation. Deuteration of the BH_3 group shows the same tendency (8, 9).

The two CD_3 rocks are assigned at 822 and 764 cm^{-1}. The shift factors of 1.10 and 1.23, respectively, appear too low but these two modes mix with the CH_3 rocking and CC stretching modes, which should not shift with deuteration of the methyl group. Presumably, this is part of the reason for the low shift factors for these two modes.

All the skeletal modes are assigned in agreement with the assignment of these modes made by Klaboe (3). The assignment of the -CH_3 and -CD_3 torsions has already been addressed. The antisymmetric (A″) methyl torsion for 2-chloropropane-d_0 should have a *B*-type band contour and a depolarized Raman line. Unfortunately, the methyl torsions for this compound were not observed in the Raman spectrum. From the far-infrared spectrum previously reported (2), along with the present *ab initio* calculations, it can be concluded that the A′ methyl torsion should be assigned higher in frequency than the A″ methyl torsion for the 2-chloropropane-d_0 species. This is the exact opposite of the previously proposed (2, 3) assignments for these two fundamentals. The comparison of the assignment by Klaboe (3) with the present normal coordinate analysis will be discussed in detail in the Discussion.

Ab initio *calculations*

The program GAUSSIAN-82 using Gaussian-type basis functions (10) was utilized to perform the LCAO-MO-SCF restricted Hartree–Fock calculations. The energy minima with respect to nuclear coordinates were obtained by simultaneous relaxation of all geometric parameters using the gradient method of Pulay (11, 12). The calculated structural parameters for 2-chloropropane determined with both the 3-21G* and 6-31G* basis sets are listed in Table 5.

To obtain a more complete distribution of the molecular motions involved in the normal modes of 2-chloropropane, we carried out normal coordinate analyses. The force field obtained from the *ab initio* program (10) is in cartesian coordinates. Basis sets typically used for this purpose are at the 3-21G, 3-21G*, 4-21G, or 4-21G* level, but from previous studies it has been found that for most molecules the values in the force constants and frequencies are not significantly different when a smaller, as opposed to a larger, basis set is used. For this study the 3-21G* basis set was used to obtain the force field, and the normal coordinate analysis was performed by using the Wilson matrix method (13) and the computer program written by Schachtschneider (14).

The following procedure was followed for the normal coordinate analysis. The cartesian coordinates obtained for the optimized structure were input into the *G*-matrix program together with the complete set of 30 internal coordinates (Fig. 5). This set of internal coordinates was used to form the 27 symmetry coordinates with the three redundancies that are given in Table 6. With the deuteration of one of the methyl groups, the

Can. J. Chem. Downloaded from www.nrcresearchpress.com by 84.41.108.74 on 09/07/12
For personal use only.

Can. J. Chem. Downloaded from www.nrcresearchpress.com by 84.41.108.74 on 09/07/12
For personal use only.

TABLE 4. Comparison of observed and calculated frequencies (cm^{-1}) and potential energy distribution (P.E.D.) for 2-chloropropane-d_0 and -d_3

Species	Vib.[a] No.	Fundamentals	2-Chloropropane-d_0				2-Chloropropane-d_3			
			Ab initio[b]	Fixed scaled[c]	Obsd.[d]	P.E.D.	*Ab initio*[b]	Fixed scaled[c]	Obsd.[e]	P.E.D.
A′	ν_1	CH_3 antisymmetric stretch	3283	3115	3005	$68S_1$, $18S_3$, $14S_2$	3268	3101	2996	$87S_1$
	ν_2	CH_3 antisymmetric stretch	3268	3101	2989	$80S_2$, $8S_1$, $9S_3$	3285	3117	2978	$77S_2$, $16S_3$
	ν_3	CH stretch	3312	3142	2955	$73S_3$, $25S_1$	3308	3138	2958	$81S_3$, $18S_2$
	ν_4	CH_3 symmetric stretch	3208	3043	2927	$95S_4$	3205	3042	2938	$94S_4$
	ν_5	CH_3 antisymmetric deformation	1676	1499	1472	$84S_5$, $9S_{10}$	1667	1490	1464	$88S_5$, $8S_{23}$
	ν_6	CH_3 antisymmetric deformation	1664	1489	1454	$84S_6$, $9S_9$	1659	1483	1455	$87S_6$, $8S_9$
	ν_7	CH_3 symmetric deformation	1589	1421	1390	$100S_7$	1582	1414	1384	$100S_7$
	ν_8	HCCl deformation	1419	1267	1270	$56S_8$, $26S_{13}$, $12S_{10}$	1405	1255	1256	$65S_8$, $24S_{14}$
	ν_9	CH_3 rock	1310	1176	1163	$64S_9$, $12S_{14}$, $8S_6$	1262	1145	1158	$26S_9$, $23S_{21}$, $10S_{11}$, $10S_{23}$
	ν_{10}	CH_3 rock	1207	1081	1065	$62S_{10}$, $28S_8$	1108	1015	1010	$43S_{10}$, $15S_{24}$
	ν_{11}	Skeletal stretch	922	870	888	$85S_{11}$, $9S_9$	940	860	861	$26S_{11}$, $28S_{25}$, $23S_9$
	ν_{12}	CCl stretch	638	598	633	$75S_{12}$, $16S_{13}$	609	572	599	$74S_{12}$, $9S_{24}$, $9S_{14}$
	ν_{13}	HCCl rock	453	408	418	$33S_{13}$, $38S_{14}$, $8S_8$, $8S_9$	422	380	390	$39S_{14}$, $27S_{13}$, $9S_{24}$
	ν_{14}	Skeletal bend	366	332	336	$45S_{14}$, $26S_{13}$, $14S_{12}$	354	321	325	$36S_{13}$, $19S_{26}$, $14S_{22}$, $11S_{14}$
	ν_{15}	CH_3 torsion	290	261	276	$97S_{15}$	278	249	250	$94S_{15}$
A″	ν_{16}	CH_3/CD_3 antisymmetric stretch	3288	3120	2997	$97S_{16}$	2439	2312	2242	$99S_{16}$
	ν_{17}	CH_3/CD_3 antisymmetric stretch	3265	3098	2975	$91S_{17}$	2420	2295	2231	$98S_{17}$
	ν_{18}	CH_3/CD_3 symmetric stretch	3202	3038	2947	$93S_{18}$	2303	2184	2130	$99S_{18}$
	ν_{19}	CH_3/CD_3 antisymmetric deformation	1656	1481	1472	$93S_{19}$	1200	1074	1043	$92S_{19}$
	ν_{20}	CH_3/CD_3 antisymmetric deformation	1652	1478	1454	$91S_{20}$, $8S_{25}$	1185	1061	1015	$62S_{20}$, $21S_{23}$
	ν_{21}	CH_3/CD_3 symmetric deformation	1573	1406	1377	$100S_{21}$	1230	1081	1058	$29S_{21}$, $24S_{10}$, $18S_9$
	ν_{22}	HCCl out-of-plane wag	1491	1337	1334	$48S_{22}$, $33S_{26}$, $12S_{25}$	1481	1327	1328	$49S_{22}$, $33S_{26}$
	ν_{23}	Skeletal stretch	1034	1121	1123	$55S_{23}$, $34S_{24}$, $10S_{23}$	1207	1116	1120	$27S_{23}$, $30S_{20}$, $26S_{21}$
	ν_{24}	CH_3/CD_3 rock	1220	956	972	$47S_{24}$, $39S_{23}$, $9S_{26}$	914	826	822	$53S_{24}$, $18S_9$, $10S_{23}$
	ν_{25}	CH_3/CD_3 rock	1066	949	936	$69S_{25}$, $12S_{22}$	839	769	764	$40S_{25}$, $46S_{11}$
	ν_{26}	HCCl twist	352	317	317	$52S_{26}$, $40S_{22}$	322	289	295	$32S_{26}$, $24S_{22}$, $17S_{13}$, $10S_{14}$
	ν_{27}	CH_3/CD_3 torsion	263	239	253	$97S_{27}$	198	177	179	$97S_{27}$

[a]These are in observed frequency number for the -d_0 compound.
[b]Calculated with the 3-21G* basis set.
[c]Scaled *ab initio* calculations with factors of 0.9 for stretches and torsions, and 0.8 for bends.
[d]From ref. 3 by Klaboe.
[e]From the present study.

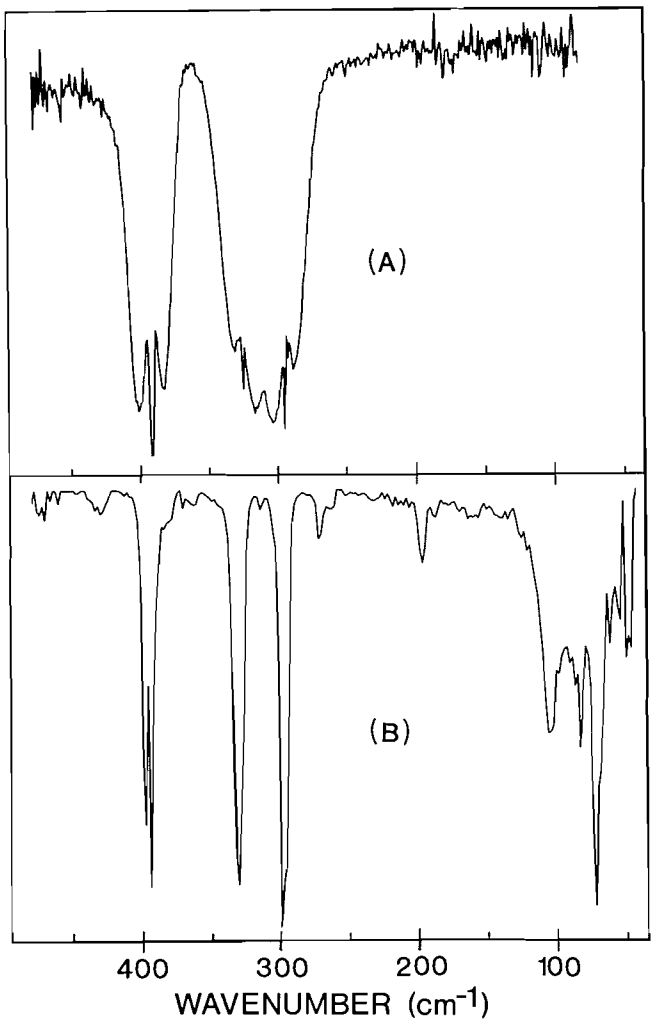


FIG. 4. Far infrared spectra of CH_3CD_3CHCl: (A) gaseous phase; (B) solid phase.

$-d_3$ molecule does not possess a symmetry plane as the $-d_0$ compound does. Therefore, there may be less coupling between the two rotors in the $-d_3$ molecule compared to that in the $-d_0$ species. The output of this *G*-matrix program consists of the *B* matrix as well as the unsymmetrized and symmetrized *G* matrices. The *B* matrix was used to convert the force field in cartesian coordinates from the *ab initio* calculations to a force field in terms of the desired internal coordinates. The resulting force field for 2-chloropropane is given in Table 7. This force field was then input, along with the unsymmetrized *G* matrix and scaling factors, into the perturbation program by Schachtschneider (14). All diagonal elements of the obtained force fields in internal coordinates were assigned scaling factors. Initially all scaling factors were kept fixed at a value of 1.0 to produce the pure *ab initio* calculated vibrational frequencies. Subsequently, scaling factors of 0.9 for stretching coordinates, 0.8 for bending coordinates, and 1.0 for torsional coordinates, and the geometric average of scaling factors for the interaction force constants were used to obtain the "fixed scaled" force field and resultant frequencies. A total of 30 symmetry coordinates were used to determine the potential energy distributions (P.E.D.), which are given in Table 4 for the $-d_0$ and $-d_3$ species, respectively.

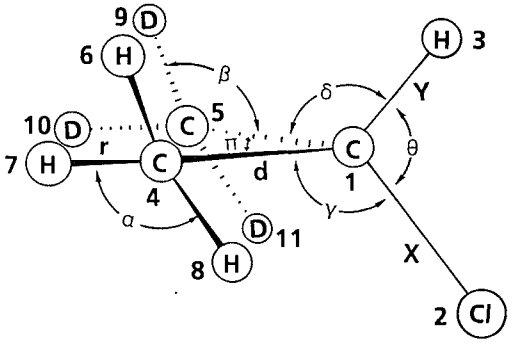


FIG. 5. Internal coordinates of CH_3CD_3CHCl.

Structure

The r_0 structure for the 2-chloropropane molecule has been determined with the previously reported (4) rotational constants using a program (15) developed in our laboratory. It consists of direct iterative adjustments of structural parameters to the observed rotational constants. With the availability of 24 moments of inertia determined for 2-chloropropane from the assignment of the microwave spectrum (4), the calculation of the r_0 structure presents no difficulties.

As input to the program, we utilized the *ab initio* calculated parameters with an adjustment of 0.010 Å added to the calculated methyl C—H distances from the 6-31G* basis set. The secondary C—H distance was fixed at 1.095 Å according to the experimentally determined value (7). With only these adjusted C—H distances fixed, we then calculated the heavy atom bond distances and all bond angles and dihedral angles. The determined values agree well with the previously reported r_s structures (Table 5), with the exception of the C—Cl bond distance. Our value of 1.806 ± 0.003 Å for the C—Cl bond distance is larger than the r_s value of 1.798 ± 0.006 Å; however, considering the uncertainty on the r_0 and r_s values for this parameter, the two values are within experimental error of each other. Nevertheless, the discrepancy between the r_0 and r_s values is greater than expected although the *ab initio* results indicate that the C—Cl distance should be longer than the reported r_s value.

The rotational constants are readily reproduced with only four of the 24 parameters having errors a little larger than 0.5. The weighted least-squares fit of the rotational constants gives relatively small uncertainties for most of the parameters. Only the $<H_3C_1C_4$ angle, which is equal to the $<H_3C_1C_5$ angle for the $-d_0$ compound, is calculated to have an uncertainty of 0.3° and the C—Cl distance has a relatively larger uncertainty of 0.003 Å. The relatively large uncertainty on the $H_3C_1C_4$ angle may be accounted for by the relatively larger calculated uncertainty on the rotational constant *A* of the $-H_3$ substituted species, $CH_3CDClCH_3$. However, this angle had the exact same value as that from the r_s structure, and most of the other HCC angles agreed with the *ab initio* calculated and r_s values except for the $<H_6C_4H_8$, which is off by more than 1.0°.

To determine the reliability of the resultant r_0 structures, we attempted a few more similar calculations. The r_0 values listed in Table 5 were obtained by inputting uncertainties of 0.015 Å for bond distances and 1.5° for bond angles. We tried a similar iterative calculation by changing the uncertainties to 0.030 Å and 3.0° for the bond distances and angles. The resultant bond angles are only different from those listed in Table 5 by ±0.1°.

Can. J. Chem. Downloaded from www.nrcresearchpress.com by 84.41.108.74 on 09/07/12
For personal use only.

TABLE 5. Structural parameters[a] for 2-chloropropane

Parameter[b]	3-21G*	6-31G*	r_s[c]	r_0[d]	r_0[e]
$r(C_1—Cl)$	1.831	1.816	1.798 ± 0.008	1.806 ± 0.003	1.801 ± 0.002
$r(C_1—H_3)$	1.078	1.080	1.091 ± 0.003	1.095(fixed)	
$r(C_1—C_4) = r(C_1—C_5)$	1.529	1.520	1.521 ± 0.004	1.521 ± 0.001	1.521 ± 0.001
$r(C_4—H_6) = r(C_5—H_9)$	1.085	1.086	1.092 ± 0.008	1.096(fixed)	
$r(C_4—H_7) = r(C_5—H_{10})$	1.083	1.084	1.092 ± 0.008	1.094(fixed)	
$r(C_4—H_8) = r(C_5—H_{11})$	1.082	1.083	1.092 ± 0.008	1.093(fixed)	
$\measuredangle C_4C_1Cl = \measuredangle C_5C_1Cl$	108.9	109.1	109.4 ± 0.3	109.3 ± 0.1	109.4 ± 0.1
$\measuredangle H_3C_1Cl$	104.7	104.5	105.3 ± 0.7	105.1 ± 0.1	
$\measuredangle CCC$	112.6	113.2	112.7 ± 0.5	113.3 ± 0.2	113.0 ± 0.1
$\measuredangle H_3C_1C_4 = \measuredangle H_3C_1C_5$	110.7	110.2	109.9 ± 0.4	109.9 ± 0.3	
$\measuredangle H_6C_4C_1 = \measuredangle H_9C_5C_1$	109.3	109.4	109.7 ± 0.6	108.6 ± 0.1	
$\measuredangle H_7C_4C_1 = \measuredangle H_{10}C_5C_1$	110.2	110.8	109.7 ± 0.6	109.4 ± 0.1	
$\measuredangle H_8C_4C_1 = \measuredangle H_{11}C_5C_1$	111.0	111.2	110.9 ± 0.7	110.7 ± 0.1	
$\measuredangle H_7C_4H_8 = \measuredangle H_{10}C_5H_{11}$	108.8	108.5	108.5 ± 0.8	109.1 ± 0.2	
$\measuredangle H_6C_4H_7 = \measuredangle H_9C_5H_{10}$	108.8	108.3	109.1 ± 0.7	108.8 ± 0.1	
$\measuredangle H_6C_4H_8 = \measuredangle H_9C_5H_{11}$	108.8	108.5	109.1 ± 0.7	110.1 ± 0.1	
dih $\measuredangle H_6C_4C_1Cl$ = dih $\measuredangle H_9C_5C_1Cl$	178.1	177.5		176.7 ± 0.2	
A	8049.9	8080.1	8108.9	8068.3	
B	4487.6	4546.4	4584.3	4571.0	
C	3167.2	3194.8	3220.9	3207.7	
μ_a	2.568	2.474			
μ_b	0.000	0.000			
μ_c	0.476	0.482			
μ_t	2.612	2.520			
$-E$ (hartree)	574.4409448	577.1693633			

[a]Bond lengths in Å, angles in degrees, rotational constants in MHz, dipole moments in debye, and energy in hartrees.
[b]For atom numbering, see Fig. 5.
[c]From ref. 4. The rotational constants listed in this column are presently calculated using the r_s structure.
[d]Calculated using the rotational constants given in ref. 4 with an adjustment of 0.010 Å added to the calculated methyl C—H distances from the 6-31G* basis set. The C—H distance for $C_1—H_3$ is fixed at 1.095 which was determined from ref. 7. Microwave determined values, A = 8069.09, B = 4570.82, and C = 3207.57 MHz.
[e]Calculated using only the rotational constants of molecules with heavy atom substitution.

The two heavy atom bond distances are strongly correlated with each other for all of the r_0 calculations. With the larger input uncertainty, the C—C distance increased by 0.001 Å whereas the C—Cl distance decreased by the same amount.

We tried another calculation in which we utilized only the rotational constants reported (4) for the heavy atom isotopic species. Twelve moments of inertia of this type were used to calculate only the heavy atom structures with all the bond distances and angles associated with the carbon–hydrogen bonds held fixed. The results of this calculation were dramatically different, i.e., the carbon–carbon distance increased to 1.521 ± 0.001 Å and the carbon–chlorine distance was reduced to 1.801 ± 0.002 Å. The fit to the rotational constants was excellent and this value for the C—Cl distance agrees very well with the r_s value of 1.798 ± 0.008 Å for this bond.

For the 2-chloropropane-d_0 compound, the two methyl tops are equivalent. The two hydrogens, -H_6 and -H_9, which are oriented approximately 180° to the chlorine atom, are calculated to have longer CH bond distances than the other hydrogens. The corresponding angles, $<H_6C_4C_1$ and $<H_9C_5C_1$, are calculated to be smaller than the other HCC angles from all the methods, i.e., *ab initio*, r_s, and r_0 structural calculations. Compared to the other hydrogens, these two are further away from the chlorine atom, which is a weak electron donor. This may then partially account for the unique property of the two hydrogens. All the bond angles from the r_0 structural calculations are in excellent agreement with those from the r_s structural determination and *ab initio* calculations. We believe the determined r_0 structural parameters should be within the listed uncertainties of the actual values.

Discussion

The barriers to internal rotation of the methyl rotors are essentially the same for the two isotopic species of 2-chloropropane, i.e., for CH_3CD_3CHCl, V_3 = 1378 ± 4 cm^{-1}, and for $(CH_3)_2CHCl$, V_3 = 1380 ± 3 cm^{-1} (Table 2). This value is considerably larger than the V_3 value of 1149 ± 69 cm^{-1} (3.29 ± 0.12 kcal/mol) for the corresponding fluoride molecule (1), $(CH_3)_2CHF$. However, it is consistent with the methyl barriers of other chlorine-substituted hydrocarbons compared to the corresponding fluorine-substituted molecules. The chlorine-containing compounds always have much larger methyl barriers than the fluorides.

The values for the sine–sine coupling term for the two isotopomers are essentially identical where $V'_{33} = -173 \pm 3$ cm^{-1} for CH_3CD_3CHCl and −171 ± 2 cm^{-1} for $(CH_3)_2CHCl$. Because of the agreement this potential constant appears to be well determined. However, for the cosine–cosine coupling term there is a difference of approximately 15% between the two values, i.e., V_{33} = 166 ± 10 cm^{-1} for CH_3CD_3CHCl and V_{33} = 209 ± 12 cm^{-1} for $(CH_3)_2CHCl$. Since the cosine–cosine coupling term is expected to have essentially the same value

Can. J. Chem. Downloaded from www.nrcresearchpress.com by 84.41.108.74 on 09/07/12
For personal use only.

TABLE 6. Symmetry coordinates[a] for 2-chloropropane

Description	Symmetry coordinate[b]
A′ CH_3 antisymmetric stretch	$S_1 = 2r_1 - r_2 - r_3 + 2r_4 - r_5 - r_6$
CH_3 antisymmetric stretch	$S_2 = r_2 - r_3 + r_5 - r_6$
CH stretch	$S_3 = Y$
CH_3 symmetric stretch	$S_4 = r_1 + r_2 + r_3 + r_4 + r_5 + r_6$
CH_3 antisymmetric deformation	$S_5 = 2\alpha_1 - \alpha_2 - \alpha_3 + 2\alpha_4 - \alpha_5 - \alpha_6$
CH_3 antisymmetric deformation	$S_6 = \alpha_2 - \alpha_3 + \alpha_5 - \alpha_6$
CH_3 symmetric deformation	$S_7 = \alpha_1 + \alpha_2 + \alpha_3 - \beta_1 - \beta_2 - \beta_3 + \alpha_4 + \alpha_5 + \alpha_6 - \beta_4 - \beta_5 - \beta_6$
HCCl in-plane deformation	$S_8 = (\sqrt{6} + 2)\theta - (\sqrt{6} - 2)\pi - \delta_1 - \delta_2 - \gamma_1 - \gamma_2$
CH_3 rock	$S_9 = \beta_2 - \beta_3 + \beta_5 - \beta_6$
CH_3 rock	$S_{10} = 2\beta_1 - \beta_2 - \beta_3 + 2\beta_4 - \beta_5 - \beta_6$
Skeletal stretch	$S_{11} = d_1 + d_2$
CCl stretch	$S_{12} = X$
HCCl rock	$S_{13} = \gamma_1 + \gamma_2 - \delta_1 - \delta_2$
Skeletal bend	$S_{14} = (\sqrt{6} + 2)\pi - (\sqrt{6} - 2)\theta - \delta_1 - \delta_2 - \gamma_1 - \gamma_2$
CH_3 torsion	$S_{15} = \tau_1 - \tau_2$
Redundancy	$S_{1R} = \alpha_1 + \alpha_2 + \alpha_3 + \beta_1 + \beta_2 + \beta_3 + \alpha_4 + \alpha_5 + \alpha_6 + \beta_4 + \beta_5 + \beta_6$
Redundancy	$S_{2R} = \theta + \delta_1 + \delta_2 + \gamma_1 + \gamma_2 + \pi$
A″ CH_3 antisymmetric stretch	$S_{16} = r_2 - r_3 - r_5 + r_6$
CH_3 antisymmetric stretch	$S_{17} = 2r_1 - r_2 - r_3 - 2r_4 + r_5 + r_6$
CH_3 symmetric stretch	$S_{18} = r_1 + r_2 + r_3 - r_4 - r_5 - r_6$
CH_3 antisymmetric deformation	$S_{19} = 2\alpha_1 - \alpha_2 - \alpha_3 - 2\alpha_4 + \alpha_5 + \alpha_6$
CH_3 antisymmetric deformation	$S_{20} = \alpha_2 - \alpha_3 - \alpha_5 + \alpha_6$
CH_3 symmetric deformation	$S_{21} = \alpha_1 + \alpha_2 + \alpha_3 - \beta_1 - \beta_2 - \beta_3 - \alpha_4 - \alpha_5 - \alpha_6 + \beta_4 + \beta_5 + \beta_6$
HCCl out-of-plane wag	$S_{22} = \gamma_1 - \gamma_2 + \delta_1 - \delta_2$
Skeletal stretch	$S_{23} = d_1 - d_2$
CH_3 rock	$S_{24} = 2\beta_1 - \beta_2 - \beta_3 - 2\beta_4 + \beta_5 + \beta_6$
CH_3 rock	$S_{25} = \beta_2 - \beta_3 - \beta_5 + \beta_6$
HCCl twist	$S_{26} = \gamma_1 - \gamma_2 - \delta_1 + \delta_2$
CH_3 torsion	$S_{27} = \tau_1 + \tau_2$
Redundancy	$S_{3R} = \alpha_1 + \alpha_2 + \alpha_3 + \beta_1 + \beta_2 + \beta_3 - \alpha_4 - \alpha_5 - \alpha_6 - \beta_4 - \beta_5 - \beta_6$

[a]For 2-chloropropane-d_3, which has no symmetry, the symmetry coordinates for the -CH_3 top are taken as the "first half" of the A′ symmetry block whereas those for the -CD_3 top are taken as the "second half" of the A″ block.
[b]Not normalized.

Can. J. Chem. Downloaded from www.nrcresearchpress.com by 84.41.108.74 on 09/07/12
For personal use only.

as the sine–sine coupling term except opposite in sign, we believe the lower value of 166 ± 10 cm^{-1} obtained in the present study is probably a better value than the larger value reported (2) earlier.

In the recent study (1) of 2-fluoropropane, the V_{33} and V'_{33} values for the d_0 and d_7 isotopic species are about 95 and −95 cm^{-1}, respectively, whereas for the d_3 molecule the values are more than twice these values. Since the potential coupling is expected to be smaller in the fluoride, it is probable that the lower values are closer to the actual values. However, it would be of interest to determine these potential coupling parameters by *ab initio* calculations for the fluoride. Similarly there have not been any determinations of these parameters for the corresponding bromide and the determination of these potential terms from the low frequency data would be of interest for comparison to the values for the chlorides.

Initially we did not expect the 6-31G* basis set to give such a poor prediction for the C—Cl bond distance. For example this basis set gives (16) a value for the C–Cl bond of 1.785 Å for the CH_3Cl molecule with the experimental value determined (17) to be 1.775 ± 0.002 Å. Therefore, one would expect the calculated value of 1.815 Å to be too large by 0.010 Å but probably not by 0.014 Å. Nevertheless, we believe the smaller C—Cl distance is closer to the actual value. The fact that the C—D distance is shorter by 0.007 Å than the corresponding C—H distance may skew the results to a longer C—Cl distance when the rotational constants for the deuterium-substituted molecules are used. To determine the correct value for the C—Cl distance it would be useful to carry out *ab initio* calculations for chloroethane and compare the calculated parameters to the experimental ones (18). Similar *ab initio* calculations for tertiary butyl chloride could be used to see if the theoretical results reproduce the observed elongation of the C—Cl bond with substitution of an increased number of methyl groups on the carbon atom (19).

In Table 8, the structural data for propane and 2-halopropanes are listed for comparison. Definite trends exist among the parameters considered, despite the differences between the method of least-squares fitting of the present study and the isotopic substitution method of Kraitchman (20) used to calculate the r_s structural parameters of the remaining molecules listed in Table 8. The progressive increase in the CCX angle and the C—X bond distance from propane to 2-iodopropane parallels the systematic increase in the size of X. The trend in the CCC angle is not so well defined and, in fact, this parameter appears to be relatively constant for the 2-halopropane molecules. The difference in the C—C distance in propane and that for 2-fluoropropane is within the experimental uncertainties but, based on data from the other 2-halopropanes, it is clear that the C—C distance is shorter for the halosubstituted molecules than in propane. In fact, a slight decrease in the C—C distance is found with an increase in the size of the

TABLE 7. *Ab initio* calculated

	X	Y	d_1	d_2	r_1	r_2	r_3	r_4	r_5	r_6	θ	γ_1	γ_2	π	δ_1
X	3.007	0.078	0.230	0.230	−0.003	0.018	0.014	−0.003	0.018	0.014	0.278	0.323	0.323	−0.305	−0.275
Y		5.993	0.085	0.085	0.013	−0.017	0.011	0.013	−0.017	0.011	−0.008	−0.041	−0.041	−0.065	0.077
d_1			4.626	0.146	0.076	0.074	0.065	0.003	0.012	−0.008	−0.152	0.171	−0.186	0.182	0.144
d_2				4.624	0.003	0.012	−0.008	0.076	0.076	0.065	−0.152	−0.186	0.171	0.182	−0.183
r_1					5.775	0.055	0.055	0.016	−0.001	−0.001	−0.009	0.072	0.006	−0.032	−0.015
r_2						5.873	0.054	−0.001	0.011	−0.002	0.010	−0.039	−0.010	−0.023	0.049
r_3							5.902	−0.001	−0.002	0.003	−0.009	−0.041	0.002	0.052	−0.007
r_4								5.775	0.055	0.055	−0.009	0.006	0.072	−0.032	−0.018
r_5									5.873	0.054	0.010	−0.010	−0.039	−0.023	0.013
r_6										5.902	−0.009	0.002	−0.041	0.052	−0.002
θ											0.813	−0.196	−0.196	−0.227	−0.063
γ_1												1.087	−0.172	−0.219	−0.221
γ_2													1.087	−0.219	−0.245
π														0.924	−0.175
δ_1															0.739
δ_2															
β_1															
β_2															
β_3															
β_4															
β_5															
β_6															
α_1															
α_2															
α_3															
α_4															
α_5															
α_6															
τ_1															
τ_2															

halogen atom in the halopropanes. A similar trend is observed in other haloalkanes (21–25).

The vibrational assignment for the -d_3 species was supported by the *ab initio* calculations and the Teller–Redlich product rule. The theoretical value for the entire A block is 18.47 whereas the experimental value is 17.92, which leads to an acceptable error of 3%. For many compounds (26, 27) containing the CD_3 group, frequently the CD_3 symmetric deformation and the CD_3 rock have a smaller shift factor compared to the expected value, ~1.37, whereas the CD_3 antisymmetric deformations have relatively large shift factors. The skeletal modes in the region below 650 cm^{-1} shift down for the -d_3 compound and are mainly due to the change in mass of the methyl groups from 15 amu to 18 amu for the perdeuterated methyl group. Results from the fixed scale *ab initio* calculations of the low frequency skeletal modes are in excellent agreement with the observed bands. The light and heavy methyl torsions are calculated within 1 and 2 cm^{-1}, respectively, of the calculated values. It is interesting that even though the CD_3 torsion shifts only by a factor of 1.3, when it is multiplied by the shift factor of the CH_3 torsion, 1.05, the product is the expected shift factor of 1.37 for the CD_3 methyl group.

For the -d_0 species, the 27 fundamentals span the irreducible representations 15A′ + 12A″. The 15A′ modes should give rise to polarized Raman lines and A/C-type band contours in the infrared spectrum of the gas, whereas the 12A″ fundamental vibrations should have depolarized Raman lines and show B-type band contours in the infrared spectrum of the gas. The assignments made by Klaboe (3) according to the band contours and depolarization ratios are in fair agreement with the calculated results from the present study with a few exceptions.

In the C—H stretching region, we expect three A″ fundamentals and they are thus assigned to two depolarized lines and one B-type band as previously proposed (3) even though it is not totally consistent with the frequency order from the *ab initio* calculations. For the four A′ carbon–hydrogen stretches, however, the CH_3 symmetric stretch (ν_4) was misassigned at 2878 cm^{-1}, which is too low to be a fundamental. This mode is assigned to a strong band at 2927 cm^{-1}, which was previously assigned (3) to the CH stretching motion. The corresponding C—H stretch (ν_3) and CH_3 antisymmetric stretch (ν_2) are assigned to a weak band at 2955 cm^{-1} and a strong band at 2989 cm^{-1}. Similar to the assignment for the -d_3 compound, the C—H stretch is assigned as the third frequency even though it is calculated as the highest frequency. It is interesting that by adding 0.010 Å to the *ab initio* calculated value for this secondary carbon–hydrogen distance, one would obtain a distance of 1.090 Å, whereas the experimental value is 1.095 ± 0.001 Å. Therefore, the *ab initio* calculations give a considerably shorter distance for this C—H bond than those for the C—H bonds of the methyl group. This significant difference in the calculated distance is the apparent reason why the *ab initio* predicted frequency for this C—H bond is the highest predicted value.

The A′ and A″ CH_3 torsions are calculated to occur at 261 and 236 cm^{-1}, respectively, and they are thus assigned at 276 and 253 cm^{-1}. As mentioned earlier, these two torsions have been (2, 3) assigned just the opposite. Similarly, the HCCl rock (ν_{13}) is assigned at 418 cm^{-1}, which is higher than the skeletal bend (ν_{14}) at 336 cm^{-1}. These two fundamentals were in the opposite order. It should be mentioned that these two modes mix extensively according to the P.E.D. from *ab initio* cal-

Can. J. Chem. Downloaded from www.nrcresearchpress.com by 84.41.108.74 on 09/07/12
For personal use only.

force constants for 2-chloropropane

δ_2	β_1	β_2	β_3	β_4	β_5	β_6	α_1	α_2	α_3	α_4	α_5	α_6	τ_1	τ_2
−0.275	0.097	−0.038	−0.031	0.097	−0.038	−0.031	−0.012	−0.008	−0.007	−0.012	−0.008	−0.007	0.003	−0.003
0.077	−0.004	0.029	−0.011	−0.004	0.029	−0.011	−0.003	−0.007	−0.004	−0.003	−0.007	−0.004	0.000	0.000
−0.183	0.105	0.207	0.188	−0.009	−0.029	0.048	−0.160	−0.173	−0.180	−0.003	−0.002	−0.006	−0.001	0.002
0.144	−0.009	−0.029	0.048	0.105	0.207	0.188	−0.003	−0.002	−0.006	−0.160	−0.173	−0.180	−0.002	0.001
−0.018	0.078	−0.088	−0.086	0.004	−0.001	0.001	−0.093	0.096	0.098	0.000	−0.001	−0.004	0.001	−0.002
0.013	−0.082	0.069	−0.084	−0.002	0.010	0.000	0.095	0.092	−0.088	−0.006	−0.001	−0.001	0.003	0.002
−0.002	−0.080	−0.083	0.064	−0.005	−0.006	0.011	0.094	−0.087	0.092	0.001	−0.002	0.001	−0.004	0.000
−0.015	0.004	−0.001	0.001	0.078	−0.088	−0.086	0.000	−0.001	−0.004	−0.093	0.096	0.098	0.002	−0.001
0.049	−0.002	0.010	0.000	−0.082	0.069	−0.084	−0.006	−0.001	−0.001	0.095	0.092	−0.088	−0.002	−0.003
−0.007	−0.005	−0.006	0.011	−0.080	−0.083	0.064	0.001	−0.002	0.001	0.094	−0.087	0.092	0.000	0.004
−0.063	−0.007	−0.002	−0.007	−0.007	−0.002	−0.007	0.006	−0.001	0.011	0.006	−0.001	0.011	−0.015	0.015
−0.245	0.119	−0.058	−0.047	−0.014	0.001	−0.008	0.005	−0.012	−0.007	0.009	0.010	0.001	0.010	−0.018
−0.221	−0.014	0.001	−0.008	0.119	−0.058	−0.047	0.009	0.010	0.001	0.005	−0.012	−0.007	0.018	−0.010
−0.175	−0.038	−0.050	0.113	−0.038	−0.050	0.113	−0.017	0.006	−0.015	−0.017	0.006	−0.015	0.006	−0.006
−0.048	−0.048	0.112	−0.051	−0.006	−0.002	−0.010	−0.006	−0.008	0.001	0.004	0.005	0.009	−0.012	0.006
0.739	−0.006	−0.002	−0.010	−0.048	0.112	−0.051	0.004	0.005	0.009	−0.006	−0.008	0.001	−0.006	0.012
	0.674	−0.162	−0.161	0.010	0.002	−0.011	−0.125	−0.114	−0.116	0.000	0.002	−0.003	−0.002	0.000
		0.694	−0.165	0.002	0.006	−0.008	−0.123	−0.124	−0.129	−0.002	0.000	0.002	0.001	0.001
			0.685	−0.011	−0.008	0.029	−0.122	−0.127	−0.124	−0.003	−0.004	−0.003	0.001	−0.001
				0.674	−0.162	−0.161	0.000	0.002	−0.003	−0.125	−0.114	−0.116	0.000	0.002
					0.694	−0.165	−0.002	0.000	0.002	−0.123	−0.124	−0.129	−0.001	−0.001
						0.685	−0.003	−0.004	−0.003	−0.122	−0.127	−0.124	0.001	−0.001
							0.587	−0.108	−0.109	0.005	−0.001	0.001	0.000	−0.001
								0.592	−0.102	−0.001	0.004	0.000	0.001	0.000
									0.590	0.001	0.000	0.005	−0.001	0.000
										0.587	−0.108	−0.109	0.001	0.000
											0.592	−0.102	0.000	−0.001
												0.590	0.000	0.001
													0.016	−0.001
														0.016

TABLE 8. Comparison of the heavy atom structural parameters of propane and 2-halopropane molecules

Molecule	r_{C-C}, Å	r_{C-X}, Å	∢CCX, deg	∢CCC, deg	∢CCH_{sec}, deg	Reference
Propane	1.526±0.002	1.096±0.002	106.1 ±2	112.4 ±0.2	111.8 ±1.0	21
2-Fluoropropane	1.522±0.007	1.398±0.013	108.19±0.41	113.37±0.79	110.20±0.08	1
2-Chloropropane	1.521±0.001	1.801±0.002	109.4 ±0.1	113.0 ±0.1	109.9 ±0.3	22, this study
2-Bromopropane	1.518±0.010	1.962±0.006	109.25±0.72	113.27±1.65	110.33±1.23	23
2-Iodopropane	1.517±0.005	2.167±0.002	109.73±0.28	113.42±0.75	110.02±0.62	23

culations. For the -d_3 compound, the one at higher frequency (380 cm^{-1}) has more skeletal bend (39%) than the HCCl rock (27%) from the P.E.D. predictions.

One can also note that the A″ skeletal stretch is calculated lower in frequency than the two A″ CH_3 rocking modes before scaling. Since we scale the stretching modes by 0.9 and bendings by 0.8, the A″ skeletal stretch then occurs higher in frequency at 1121 cm^{-1} than the two CH_3 rocks (956 and 949 cm^{-1}) after scaling. This frequency order is consistent with that proposed by Klaboe (3), who assigned the stretch and the two CH_3 rocks at 1123, 972, and 936 cm^{-I}, respectively. The switching after scaling is also the case for the -d_3 species for the antisymmetric skeletal stretch with the CD_3 symmetric deformation.

Finally it should be noted that the determined force constants (Table 7) are very similar in value to those obtained for the corresponding fluoride (1) except for those associated with the C—X bond. It should be possible to use these force constants with adjustment for the C—Br or C—I bonds to predict the normal frequencies for 2-bromo- and 2-iodopropane.

1. G. A. GUIRGIS, H. NANAIE, and J. R. DURIG. J. Chem. Phys. **93**, 3837 (1990).
2. J. R. DURIG and G. A. GUIRGIS. Chem. Phys. **44**, 309 (1979).
3. P. KLABOE. Spectrochim. Acta, **26A**, 87 (1970).
4. F. L. TOBIASON and R. H. SCHWENDEMAN. J. Chem. Phys. **40**, 1014 (1979).
5. P. GRONER and J. R. DURIG. J. Chem. Phys. **66**, 1856 (1977).
6. J. R. DURIG, M. G. GRIFFIN, and P. GRONER. J. Phys. Chem. **81**, 554 (1977).
7. D. C. MCKEAN, O. SAUR, J. TRAVERT, and J. C. LAVALLEY. Spectrochim. Acta, **31A**, 1713 (1975).
8. J. D. ODOM, A. E. STANLEY, MEI-SHIOW CHENG, and J. R. DURIG. J. Raman Spectrosc. **18**, 25 (1987).
9. J. R. DURIG, J. J. RIZZOLO, J. F. SULLIVAN, MEI-SHIOW CHENG, T. J. HIZER, and J. D. ODOM. J. Mol. Struct. **156**, 267 (1987).
10. J. S. BINKLEY, M. J. FRISCH, D. J. DEFREES, K. RAGHAVACHARI, R. A. WHITESIDE, H. B. SCHLEGEL, E. M. FLEUDER, and J. A. POPLE. GAUSSIAN-82, Carnegie–Mellon Quantum Chemistry Publishing Unit, Pittsburgh, PA. 1982.
11. P. PULAY. Mol. Phys. **17**, 197 (1969).
12. G. FOGARASI and P. PULAY. *In* Vibrational spectra and structure. Vol. 14. *Edited by* J. R. Durig. Elsevier, Amsterdam. 1985.

Can. J. Chem. Downloaded from www.nrcresearchpress.com by 84.41.108.74 on 09/07/12
For personal use only.

13. E. B. WILSON, J. C. DECIUS, and P. C. CROSS. Molecular vibrations. McGraw–Hill, New York. 1955.
14. J. H. SCHACHTSCHNEIDER. Vibrational analysis of polyatomic molecules. Parts V and VI. Technical Report Nos. 231 and 57, Shell Development Company, Houston, TX. 1964 and 1965.
15. P. GRONER, J. S. CHURCH, Y. S. LI, and J. R. DURIG. J. Chem. Phys. **82**, 3894 (1985).
16. W. J. HEHRE, L. RADOM, P. V. R. SCHLEYER, and J. A. POPLE. *Ab initio* molecular orbital theory. John Wiley & Sons, New York. 1986.
17. M. IMACHI, T. TANAKAN, and E. HIROTA. J. Mol. Spectrosc. **63**, 265 (1976).
18. R. H. SCHWENDEMAN and G. D. JACOBS. J. Chem. Phys. **36**, 1245 (1962).
19. J. R. DURIG, G. A. GUIRGIS, and Y. S. LI. J. Chem. Phys. **74**, 5946 (1981).
20. J. KRAITCHMAN. Am. J. Phys. **21**, 17 (1953).
21. D. R. LIDE, JR. J. Chem. Phys. **33**, 1514 (1960).
22. R. H. SCHWENDEMAN and F. L. TOBIASON. J. Chem. Phys. **43**, 201 (1965).
23. C. IKEDA, T. INAGUSA, and M. HAYASHI. J. Mol. Spectrosc. **135**, 334 (1989).
24. L. PIERCE. J. Chem. Phys. **34**, 498 (1961).
25. C. FLANAGAN and L. PIERCE. J. Chem. Phys. **38**, 2693 (1963).
26. J. F. SULLIVAN, D. T. DURIG, J. R. DURIG, and S. CRADOCK. J. Phys. Chem. **91**, 1770 (1987).
27. J. N. GAYLES, JR. and W. T. KING. Spectrochim. Acta, **21**, 543 (1965).

Can. J. Chem. Downloaded from www.nrcresearchpress.com by 84.41.108.74 on 09/07/12
For personal use only.

Vibrational spectra and force field studies of $[PtCl_3(CO)]^-$ anion labelled with $^{13}C^{16}O$, $^{12}C^{18}O$, and radioactive $^{14}C^{16}O$

J. MINK

Institute of Isotopes of the Hungarian Academy of Sciences, H-1525 Budapest, P.O.B. 77, Hungary

AND

P. L. GOGGIN

Department of Inorganic Chemistry, University of Bristol, Bristol BS8 1TS, United Kingdom

Received April 29, 1991

This paper is dedicated to Dr. Richard Norman Jones

J. MINK and P. L. GOGGIN. Can. J. Chem. **69**, 1857 (1991).

Detailed infrared and Raman studies are reported for $[PtCl_3(^{12}C^{16}O)]^-$, $[PtCl_3(^{13}C^{16}O)]^-$, $[PtCl_3(^{12}C^{18}O)]^-$, and $[PtCl_3(^{14}C^{16}O)]^-$ together with assignments. Bands observed for the $^{14}C^{16}O$ species at 2005, 483, 507, and 466 cm^{-1} are assigned to CO and PtC stretching, PtCO in-plane and out-of-plane linear bending modes, respectively. Force constants have been calculated using a modified valence force field, with constrained off-diagonal force constants based on $[PtCl_4]^{2-}$ and $[PtX_3(CO)]^-$ (X = Br, I). The effective **G**-matrix method (EGM) has been used for approximate calculation of CO and PtC stretching force constants for some other square-planar platinum–carbonyl complexes. The results are discussed with the assistance of stretching force constants for some of the simpler complexes.

Key words: vibrational spectra, force constant calculation, ^{13}C, ^{14}C, and ^{18}O labelled $[PtCl_3(CO)]^-$.

J. MINK et P. L. GOGGIN. Can. J. Chem. **69**, 1857 (1991).

On a réalisée des études ir et Raman détaillées des anions $[PtCl_3(^{12}C^{16}O)]^-$, $[PtCl_3(^{13}C^{16}O)]^-$, $[PtCl_3(^{12}C^{18}O)]^-$ et $[PtCl_3(^{14}C^{16}O)]^-$ et on rapporte les attributions qui en découlent. Les bandes observées à 2005, 483, 507 et 466 cm^{-1} pour l'espèce $^{14}C^{16}O$ sont attribuées respectivement aux modes de d'élongation du CO et du PtC et aux modes de déformation angulaire linéaire dans le plan et hors-du-plan du PtCO. On a calculé les constantes de force en utilisant un champ de force de valence modifié avec des constantes de force contraintes, décalées par rapport à la diagonale et basées sur les anions $[PtCl_4]^{2-}$ et $[PtX_3(CO)]^-$ (X = Br, I). On a utilisé la méthode de matrice-**G** effective (MGE) pour faire des calculs approximatifs des constantes de force pour l'élongation du CO et du PtC dans quelques autres complexes plans carrés du platine-carbonyle. On discute des résultats à l'aide de constantes de force d'élongation de quelques complexes plus simples.

Mots clés : spectres vibrationnels, calculs de constantes de force, $[PtCl_3(CO)]^-$ marqué avec du ^{13}C, du ^{14}C et du ^{18}O.

[Traduit par la rédaction]

Introduction

Carbon monoxide is known to form complexes with almost every transition element. The bonding in metal carbonyls has attracted a number of experimental and theoretical scientists. Important information about the nature of bonding lies in the value of the force constants. Apart from the fact that the vibrational spectra of isotopic species give additional data for force constant calculation, the isotope shifts provide a great help in the assignment of the vibrational bands.

The CO stretching bands observed in the infrared and Raman spectra are usually strong, sharp, and sensitive to the environment. The vibrational spectra outside the CO stretching region are also informative though their interpretation is less easy. The M—C stretching and M—CO bending modes are usually very close to each other (near 600–400 cm^{-1}) and it is difficult to assign them without additional information. That is another important reason for studying the vibrational spectra of metal carbonyls labelled with carbon or oxygen isotopes. Labelled carbon monoxide, $^{14}C^{16}O$, has not — until now — been used in metal carbonyls for studying vibrational spectra and structure.

We have made extensive studies by means of rotational and vibrational spectroscopy of carbon-14 labelled compounds, involving pure rotational spectra of $^{14}C^{16}O$ (1), rotational–vibrational spectra of $^{14}C^{16}O$ (2), $^{14}C^{16}O_2$ (3, 4), $^{14}C_2H_2$ (5, 6), $^{14}C_2H_6$ (7), $^{14}C^{12}CH_2$ (7), and $^{14}C_6H_6$ (3).

Vibrational spectral measurements and in most of the cases force field studies of simple square-planar carbonyl complexes of platinum metals have been carried out for $[M_2X_4(CO)_2]^{2-}$ (M = Pt(I), Pd(I), X = Cl, Br) (8, 9); *cis*-$[MX_2(CO)_2]^{n-}$ (for $n = 0$, MX = PtCl, PtBr (8, 9); for $n = 1$, MX = RhCl, RhBr, or IrCl) (10, 11). Infrared and Raman spectra of $[MX_3(CO)]^-$ (MX = PdCl, PdBr, PtCl, PtBr, or PtI) (10) and force constants for planar vibrations (12) have been reported.

In this paper we report the results of detailed analysis of the vibrational spectra of $[PtCl_3(^{13}C^{16}O)]^-$, $[PtCl_3(^{12}C^{18}O)]^-$, and $[PtCl_3(^{14}C^{16}O)]^-$ and force constant calculations involving out-of-plane vibrations as well.

Experimental

The salts $[NPr_4^n][PtCl_3(CO)]$ were prepared as previously reported (10). The $^{13}C^{16}O$ and $^{12}C^{18}O$ gases used for the preparation were purchased from the Prochem division of BOC in the U.K. The $^{14}C^{16}O$ gas was prepared on a usual vacuum line equipped with mercury manometer, liquid N_2 traps, and a Töppler pump for gas manipulation. The starting material for producing $^{14}C^{16}O$ was $Ba^{14}CO_3$ and $^{14}CO_2$ was eliminated by adding H_2SO_4 and then carbon dioxide was reduced on a Zn catalyst at 385°C to carbon monoxide.

The infrared spectra were recorded partly on a Digilab FTS-20C spectrometer equipped with TGS detector and KBr supported Ge-beamsplitter and on a Perkin-Elmer 580 B spectrometer. Far-infrared spectra were measured with a Grubb-Parsons I.R.I.S. interferometer using 0.01 and 0.04 mm Mylar beam splitters.

The Raman spectra of solid and dissolved samples of ^{14}C-labelled species were produced with a Jobin Yvon Ramanor HG-25 spectrom-

Printed in Canada / Imprimé au Canada

Can. J. Chem. Downloaded from www.nrcresearchpress.com by 84.41.108.74 on 09/07/12
For personal use only.

Can. J. Chem. Downloaded from www.nrcresearchpress.com by 84.41.108.74 on 09/07/12
For personal use only.

TABLE 1. Infrared and Raman spectra (cm^{-1}) of different isotopic species for $[PtCl_3(CO)]^-$ complexes[a,b]

$[NPr_4^n][PtCl_3(^{12}C^{16}O)]$				$[NBu_4^n][PtCl_3(^{13}C^{16}O)]$			$[NBu_4^n][PtCl_3(^{12}C^{18}O)]$			$[NBu_4^n][PtCl_3(^{14}C^{16}O)]$				
Infrared		Raman		Infrared		Raman	Infrared		Raman	IR	Raman			
Mull	Solution	Solid	Solution	Mull	Solution	Solid	Mull	Solution	Solid	Solution	Solid	Solution	Assignment	
2088 vs	2097 vs	2083 vs	2095 vs,p	[c]	2048 vs	[c]	[c]	2052 vs	[c]	2005 vs	1995 m	2005 w,p	CO stretch.	a_1
543 s	540 s		539 vvw	525 s	523 s		539 s	537 ms		507 s			PtCO i.p. bend.	b_1
504 sh		507 m	497 m,p	500 vw		499 w	497 mw	492 mw	488 w	484 m	496 m	483 m,p	PtC stretch.	a_1
508 m	496 m,w			483 mw	481 ms		490 w			466 m			PtCO o.o.p. bend.	b_2
		348 s	345 s,p			344 ms			343 ms		348 vs	345 s,p	$PtCl_2$ sym. stretch.	a_1
344 s	344 s			343 vs	343 vs		343 vs	343 vs					$PtCl_2$ asym. stretch.	b_1
325 m	322 m	324 m	322 m,p	324 mw	322 mw	323 mw	325 mw	322 mw	322 mw		326 m	321 m,p	PtCl(trans) stretch.	a_1
164 w	~170 vw	163 s	166 m								166 vs	165 m,dp	$PtCl_2$ deform.	b_1
151 wm	152 w	150 vw	152 vw,p?									152 vw	$PtCl_2$ deform.	a_1
129 m	131 s											137 vvw	CPtCl i.p. deform.	b_1
		105 m	105 m,dp										ClPtCl o.o.p. def.	b_2
(30)	(80)	(50)	(100)	(200)	(200)	(20)	(200)	(200)	(20)	(400)	112 s (10)	100 w,dp (80)	CPtCl o.o.p. bend.	b_2
													Limit of study (cm^{-1})	

[a]Cation and unassigned (not fundamental) bands omitted.
[b]Infrared spectra measured in CH_2Cl_2 or in $CHCl_3$, Raman spectra in C_6H_6 solution. More precise frequency values are listed in Table 4.
[c]Spectral range is not measured.

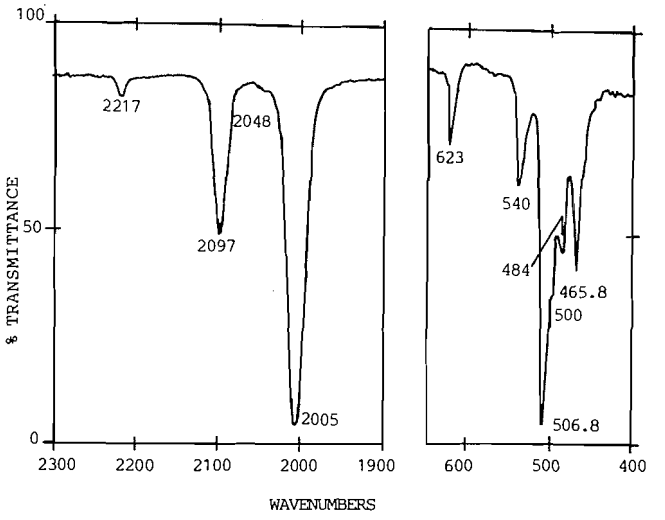


FIG. 1. Selected ranges of infrared spectrum for $[NBu_4^n][PtCl_3(^{14}C^{16}O)]$ measured in CH_2Cl_2 solution. The extra bands belong to the following species: 2217 w, $^{14}CO_2$ dissolved in CH_2Cl_2; 2097 m, $^{12}C^{16}O$ stretching; 2048 vw, sh, $^{13}C^{16}O$ stretching of natural abundance; 623 w, cation band; 540 m, ~500 sh band of $Pt^{12}C^{16}O$.

eter by using the 488 and 514.5 nm lines of an ILA 120 Ar^+ laser (Karl Zeiss, Jena). The other isotope derivatives were measured on a Coderg T800 triple monochromator spectrometer with excitation from Coherent Radiation Laboratories model 52 krypton- or argon-ion lasers.

Assignment of the spectra

The spectra features in the 2300–1700 and below 650 cm^{-1} regions recorded for solutions as well as the solid state are presented in Table 1. The infrared spectrum of $[PtCl_3(^{14}C^{16}O]^-$ in CH_2Cl_2 solution is shown in Fig. 1, whilst its Raman spectrum of the solid in the 550–25 cm^{-1} region is given in Fig. 2. The largest isotope shifts ever observed for metal carbonyls have been detected, namely 92, 33, 31, and 14 cm^{-1} for CO stretching, PtCO in-plane, PtCO out-of-plane bendings, and PtC stretching modes, respectively. The relative integrated intensities of the two CO stretching bands (2097 and 2005 cm^{-1}) in Fig. 1 correspond exactly to 86% isotopic purity calculated from the specific activity of the starting $Ba^{14}CO_3$.

The assignment discussed below is generally based on our earlier publications (10, 12), although additional experimental data of three isotopic species have led to slight modifications of the previous assignments.

For C_{2v} symmetry there should be three vibrations in the 600–400 cm^{-1} region: PtC stretching, in-plane and out-of-plane PtCO deformations. The polarized Raman line must relate to the PtC stretching mode and the strong infrared band can be assigned to the PtCO in-plane deformation which is close to those of *cis*-$[PtCl_2Me(CO)]^-$ where it was observed as a polarized Raman line (13). Fortunately, the carbon isotope sensitivity of the PtCO out-of-plane mode produces 16 and 31 cm^{-1} isotope shifts for $^{13}C^{16}O$ and $^{14}C^{16}O$ species, respectively, which is considerably stronger than those for the PtC stretching mode (6 and 14 cm^{-1}, respectively). Therefore, the accidentally degenerate PtC stretching and PtCO out-of-plane modes of $[PtCl_3(^{12}C^{16}O)]^-$ appear as well-separated pairs at 499/481 and 483/466 cm^{-1} for the $^{13}C^{16}O$ and $^{14}C^{16}O$ species, respectively. It is interesting to note that for $C^{18}O$ the PtC mode is lower than either of the PtCO bending modes.

The assignments of PtCl stretching vibrations basically

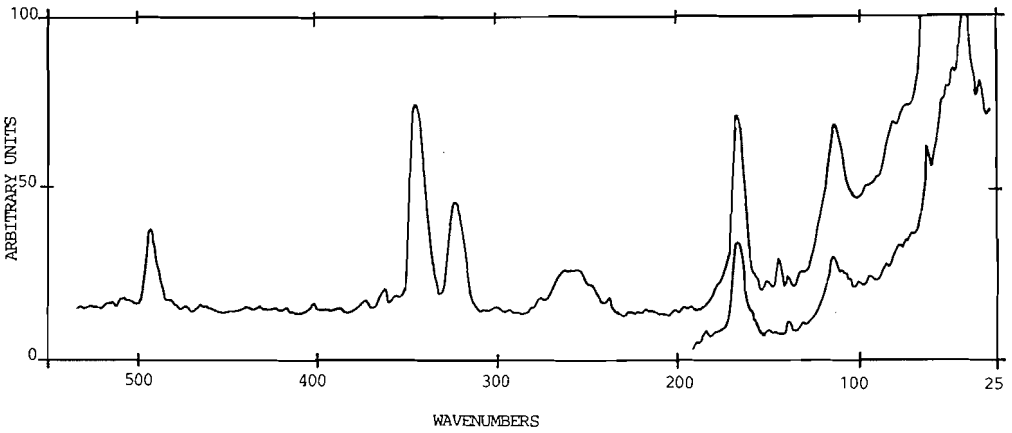


FIG. 2. Raman spectrum of $[NBu_4^n][PtCl_3(^{14}C^{16}O)]$ in solid state. Excitation by 40 mW at 514.5 nm line of argon laser.

follow from the patterns that we have previously established for $[PtCl_3L]^-$ (14, 15). For all isotope species only two Raman lines were observed around 345 and 320 cm^{-1}, and two infrared bands basically at the same positions. Since both were polarized in the Raman spectra the assignment for a_1 species is obvious. Therefore, the more intense infrared band was assigned to $PtCl_2$ asymmetric stretching of b_1 species at 343 cm^{-1}.

The in-plane and out-of-plane deformation modes below 170 cm^{-1} are assigned on the basis of $[PtCl_4]^{2-}$ (16). The strong infrared feature at 131 cm^{-1} in solution is probably an out-of-plane deformation related to b_2, which coincides with CPtCl in-plane deformation mode of b_1 species, whilst the lowest feature (105 cm^{-1}) is close to the frequency calculated for the inactive b_{2u} mode of $[PtCl_4]^{2-}$ (16). The feature near 150 cm^{-1}, which is possibly polarized in the Raman, corresponds to the e_u in-plane vibration of $[PtCl_4]^{2-}$ and maybe to the a_1 mode for the carbonyl complex. The remaining highest frequency band at about 170 cm^{-1} can be related to the b_{2g} mode of $[PtCl_4]^{2-}$ appearing at 172 cm^{-1}. The above discussed correlation is summarized in Table 2.

TABLE 2. Correlation between low frequency deformation modes (cm^{-1}) of $[PtCl_4]^{2-}$ and $[PtCl_3(CO)]^-$ anions[a]

D_{4h}	$[PtCl_4]^{2-}$		C_{2v}	$[PtCl_3(CO)]^-$
b_{2g}	173 m,dp	—	b_1	166 m,dp
e_u	167 w(IR)	—	a_1	152 vw,p?
		\	b_1	(130)
a_{2u}	150 m(IR)	—	b_2	131 s(IR)
b_{2u}	(112)	—	b_2	105 m,dp

[a]Calculated frequencies in parentheses; data for $[PtCl_4]^{2-}$ are taken from ref. 16.

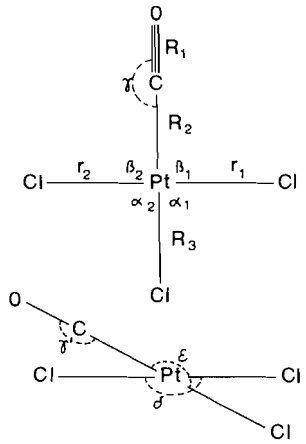


FIG. 3. Internal coordinates of the square-planar $[PtCl_3(CO)]^-$ complex.

Calculation of force constants

Force constant calculation of $[PtCl_3(CO)]^-$ was first performed by Norton (17). Reinvestigation of the vibrational spectra with a slightly modified assignment and the evaluation of ^{13}C isotopic species in the CO stretching region (in natural abundance) gave a reason for recalculating the force constants for planar modes (12).

Now we have spectroscopic data for four pure or highly enriched isotopic species of CO and we are able to extend our force field studies.

The ten in-plane and three out-of-plane internal coordinates are defined with reference to Fig. 3. Square-planar molecular geometry with linear PtCO bonding has been assumed. The equilibrium interatomic distances (pm) are in CO, 114; PtC, 176; PtCl(*cis*), 230; PtCl(*trans*), 232. These values were adopted from the molecular parameters of similar structures, e.g. from $[PtCl_4]^{2-}$. The *trans*-PtCl bond of the CO group was estimated to be 2 pm longer than in the *cis*-ClPtCl bonds (18). The program system used for normal coordinate treatment and force constant calculations is described elsewhere (19).

The $[PtCl_3(CO)]^-$ anion belongs to the C_{2v} symmetry group. The non-redundant internal valence symmetry coordinates were used as published earlier (12), and the additional out-of-plane species (b_2) involve $S_{10} = \gamma'$, $S_{11} = \delta$, and $S_{12} = \epsilon$ symmetry coordinates. The relationship between the force constants in symmetry coordinate terms and those in internal coordinate terms is shown in Table 2 of ref. 12.

There are nine in-plane vibrations, $5a_1 + 4b_1$, and three out-of-plane modes, $3b_2$. For four isotopic species we have formally 48 frequencies, but a number of them are not carbon- or oxygen-isotope sensitive (they are not independent). We are restricted to determining 12 diagonal and one non-diagonal terms. Initially we ignored all interaction constants of the CO group and thus entries F_{12}, F_{13}, F_{14}, F_{15}, F_{67}, F_{68}, F_{69}, and $F_{10,11}$ are set to zero. This constraint is identical to that used

Can. J. Chem. Downloaded from www.nrcresearchpress.com by 84.41.108.74 on 09/07/12
For personal use only.

Can. J. Chem. Downloaded from www.nrcresearchpress.com by 84.41.108.74 on 09/07/12
For personal use only.

earlier (12). Six other interaction constants were taken from ref. 12 without further refinement.

Initial values for the force constant refinements were taken from previous calculations (12). The final refined values in symmetry coordinate terms are listed in Table 3. The agreement between the wavenumbers calculated from the force constants and the experimental assignments is evident from Table 4. It can be seen that the wavenumber correspondence is good for the available experimental frequencies. We have used estimated experimental wavenumbers for ν_{11} and ν_{12} for some of the isotopic species so the force field for the out-of-plane vibrations must be considered as a preliminary result: the evidence from the $^{12}C^{16}O$ and $^{14}C^{16}O$ cases shows little wavenumber sensitivity to isotopic substitution.

When comparing the force constants in Table 3 with earlier ones (12) it is important to mention that from the isotope-sensitive frequencies we were able to determine more accurate force constants F_{11}, F_{22}, F_{66} but the others are close to the earlier results. The PtCl (*trans* to CO) stretching mode, ν_4, showed some carbon and oxygen isotope sensitivity, that is why the new value of F_{44} slightly differs from the earlier one. The PED and eigenvector calculations proved that there is some contribution from the PtC stretching mode in this PtCl stretching one.

For the ν_1 and ν_2 frequencies we have eight independent isotope-sensitive wavenumbers. Taking into account that $F_{12} = 0$, we have eight experimental data for three force constants (F_{11}, F_{12}, and F_{22}). The results of this calculation are presented in Table 5. The stretching force constants of the PtCO group are very much distorted by introducing an extra F_{12} interaction term, especially for the calculation based on experimental data only for two ^{12}CO and ^{13}CO isotopes (last column in Table 5). It should be pointed out that there is no reason for introducing an extra force constant for the stretch–stretch interaction of the PtCO group. The fit was found better for $F_{12} = 0$ and the force constants became more comparable with the literature results.

TABLE 3. Force constants of $[PtCl_3(CO)]^-$ complex

Force constant		Goggin, Norton, and Mink (12)	Present work[a]	
a_1	F_{11}	16.445	16.467 ± 0.027	a
	F_{22}	3.905	3.802 ± 0.026	a
	F_{23}	0.281	0.281	a+
	F_{24}	0.107	0.107	a+
	F_{25}	−0.107	−0.107	b+
	F_{33}	2.127	1.973 ± 0.058	a
	F_{34}	0.107	0.107	a+
	F_{35}	0.142	0.142	b+
	F_{44}	2.209	2.496 ± 0.074	a
	F_{55}	0.983	0.966 ± 0.019	b
b_1	F_{66}	0.596	0.612 ± 0.054	b
	F_{77}	1.828	1.845 ± 0.015	a
	F_{78}	0.198	0.198	c+
	F_{88}	0.898	0.722 ± 0.019	b
	F_{89}	0.107	0.173 ± 0.041	b
	F_{99}	0.922	0.928 ± 0.030	b
b_2	$F_{10,10}$		0.565 ± 0.148	b
	$F_{11,11}$		0.653 ± 0.221	b
	$F_{12,12}$		0.565 ± 0.131	b

[a]Units: a = 10^2 N m^{-1}; b = 10^{-18} N m rad^{-2}; c = 10^{-8} N rad^{-1}; +, constrained values.

Discussion

Table 6 lists the internal coordinate force constants which may be evaluated from Table 3. All diagonal in-plane terms have been fitted with low dispersion except the PtCO linear bending mode. The relatively high inaccuracy of the H(PtCO) in-plane force constant can be explained by the bad fit of ν_6 for the $^{14}C^{16}O$ isotope species. The observed isotope shift (33 cm^{-1}) for this molecule is much higher than the calculated one (24 cm^{-1}).

The relatively high dispersion of the out-of-plane force constants (b_2 species) is not surprising since only the ν_{10} mode shows carbon and oxygen isotope sensitivity in our series. This picture did not change significantly by the introduction of additional $F_{10,12}$ and $F_{11,12}$ force constants into the refinement.

The *trans*-influence of the CO ligand can be clearly recognised by slight lowering of the *trans*-PtCl force constant.

We have already reported results of force constant calculation for *cis*-$[PtX_2(CO)_2]$ (X = Cl, Br) (11) and $[PtX_3(CO)]^-$ (X = Br, I) (12). Some characteristic spectroscopic data for these molecules are presented in Table 7.

Since the coupling of PtC and especially CO stretching modes to other motions in these molecules should not significantly differ in a series of platinum monocarbonyls, these stretching force constants can be approximately reproduced by the following so-called effective **G**-matrix (EGM) method.

Using the experimental CO and PtC stretching frequencies (ν in cm^{-1}) and the corresponding force constants (K in N cm^{-1}) obtained from the full solution of the vibrational problem for $[PtX_3(CO)]^-$ series (where X = Cl, Br, I) and with the simplified relation:

$$\Lambda = 0.5891(\nu/1000)^2 \sim G_e K$$

where Λ is the eigenvalue, the effective **G** matrix elements (G_e) have been calculated.

Using the averaged G_e values obtained for $[PtX_3(CO)]^-$ anions, the expressions for approximate calculation of force constants of related molecules have been obtained:

$$[1] \quad K(^{12}CO) = 3.7404(\nu/1000)^2$$

$$[2] \quad K(^{13}CO) = 3.9191(\nu/1000)^2$$

$$[3] \quad K(PtC) = 15.8280(\nu/1000)^2$$

where ν is the corresponding stretching frequency in wavenumbers and the parameters 3.7404, 3.9191, and 15.8280 refer to the relation $0.5891/G_e$. On the basis of the above approximate expressions, CO and PtC stretching force constants (in N cm^{-1}) can be predicted for other platinum monocarbonyls without performing full normal coordinate treatment for all of them, as listed in Table 7.

The calculated CO stretching force constants for different isotopic species can be slightly different (e.g. for *cis*-$[PtCl_2(CO)(PMe_3)]$ 16.61/16.55 N cm^{-1} for ^{12}CO and ^{13}CO, respectively), therefore averaged values are listed in Table 7.

It is well known that for CO stretching force constants the factored force field parameter referring to eq. [1] is 4.0383 calculated on the basis of the isolated diatomic approximation. It is important to note that the EGM method presumably gives more comparable approximate force constants with the refined

TABLE 4. Experimental[a] and calculated frequencies (cm^{-1})

Assignment				$[PtCl_3(^{12}C^{16}O)]^-$		$[PtCl_3(^{13}C^{16}O)]^-$		$[PtCl_3(^{12}C^{18}O)]^-$		$[PtCl_3(^{14}C^{16}O)]^-$	
				Obs.	Calc.	Obs.	Calc.	Obs.	Calc.	Obs.	Calc.
a_1	ν_1	CO	Stretching	2097	2098.3	2048	2046.5	2051.5	2055.4	2005	2001.2
	ν_2	PtC	Stretching	497	498.3	491	492.3	489.7	482.5	483	486.6
	ν_3	$PtCl_2$	Sym. stretching	345.7	344.9	344	347.0	344.0	346.3	345	346.5
	ν_4	PtCl	(*trans*)stretching	321.8	321.9	322	319.2	322.5	319.2	320.5	319.2
	ν_5	$PtCl_2$	Deformation	152	150.3	152	152.5	152	152.5	152	152.5
b_1	ν_6	PtCO	In-plane bending	540.3	540.4	522.7	523.0	536.5	536.4	506.8	516.7
	ν_7	$PtCl_2$	Asym. stretching	342.0	343.1	343.2	343.0	343.0	343.1	345	343.0
	ν_8	$PtCl_2$	Asym. deformation	170	168.7	166	161.2	165	168.5	165	168.7
	ν_9	CPtCl	Deformation	132	129.3	(130)	133.7	(130)	124.8	(130)	128.7
b_2	ν_{10}	PtCO	Out-of-plane bending	496.3	496.3	480.5	480.6	492.3	491.7	465.8	466.2
	ν_{11}	ClPtCl	Out-of-plane bending	131	130.1	(130)	130.1	(130)	128.8	(120)	129.9
	ν_{12}	ClPtC	Out-of-plane bending	105	103.7	(100)	103.5	(100)	102.3	100	103.2

[a]In Table 1 experimental frequencies are rounded off, here we give more precise data; estimated values are in parentheses. For observed frequencies solution data were used where available.

TABLE 5. Comparison of force constants for different sets of refinement[a]

		$F_{12} = 0$[b]	$F_{12} \neq 0$[b]	$F_{12} \neq 0$[c]	Unit
a_1	F_{11} (CO)	16.467 ± 0.027	17.756 ± 0.424	18.921	a
	F_{12} (PtC,CO)	0	1.030 ± 0.352	2.042	a
	F_{22} (PtC)	3.802 ± 0.026	3.592 ± 0.048	3.578	a
	F_{33} (PtCl-*trans*)	1.973 ± 0.058	2.041 ± 0.045	2.139	a
	F_{44} ($PtCl_2$)	2.496 ± 0.074	2.412 ± 0.057	2.208	a
	F_{55} (ClPtCl)	0.966 ± 0.019	0.960 ± 0.014	0.984	b

[a](F_{11} ... F_{44}) are stretching force constants, F_{55} is bending force constant (see Tables 3 and 4).
[b]Values for four isotopes.
[c]Values for two isotopes ^{12}C and ^{13}C.
[d]Units a = 10^2 N m^{-1}; b = 10^{-18} N m rad^{-2}.

TABLE 6. Force constants for $[PtCl_3(CO)]^-$ complex in internal coordinate representation

Force constant	Coordinates involved	Force constant values[a]	Unit[b]
K(CO)	R_1	16.467(27)	a
K(PtC)	R_2	3.802(26)	a
K(PtCl) *trans*	R_3	1.973(58)	a
K(PtCl) *cis*	r	2.170(44)	a
F(PtCl,PtCl)	$r_1 r_2$	0.325(29)	a
H(CPtCl)	β	0.527(22)	b
H(CPtCl,CPtCl)	$\beta\beta$	−0.150(37)	b
H(CPtCl,CPtCl)	$\alpha\beta$	−0.078(25)	b
H(PtCO) in plane	γ	0.612(54)	b
H(PtCO) out-of-plane	γ'	0.565(148)	b
H(ClPtCl)	δ	0.653(221)	b
H(ClPtC)	ϵ	0.565(131)	b
Constrained values			
F(PtC,PtCl)	R_2R_3	0.281	a
F(PtC,PtCl)	R_2r	0.076	a
F(PtCl,PtCl)	R_3r	0.076	a
h(PtC,CPtCl)	$R_2\beta$	0.107	c
h(PtCl,ClPtCl)	$R_3\alpha$	0.142	c
$h_{r\alpha} = h_{r\beta}$	$r\alpha, r\beta$	0.140	c
H(ClPtCl)	α	1.211	b
H(ClPtCl,ClPtCl)	$\alpha\alpha$	0.188	b

[a]Dispersion of force constants in parentheses.
[b]Units: a = 10^2 N m^{-1}; b = 10^{-18} N m rad^{-2}; c = 10^{-8} N rad^{-1}.

values obtained from the full solution. The other advantage of the EGM method is that PtC stretching force constants can also be predicted by eq. [3].

The relationship between the square of CO stretching frequencies and force constants is presented in Fig. 4. Basically all monocarbonyls (one CO group per platinum atom) lie close to a line but the two dicarbonyls, namely *cis*-$[PtX_2(CO)_2]$ (X = Cl, Br), are out from this relation.

The relationship between CO and PtC stretching force constants is presented in Fig. 5.

Of course, the PtC stretching mode is more strongly coupled with other vibrations of the complex and so we cannot expect the almost linear correlation as in Fig. 4. In spite of the slightly scattered picture, it is clearly seen that the type of halide ligands always determines the metal–carbon bond strengths in the order: iodide < bromide < chloride, independent of the sequence of CO stretching frequency or force constant. Generally, it can be concluded that the PtC force constants are more sensitive to the coordination sphere, oxidation state, or overall charge of platinum.

The force constants calculated for PtC stretching in *cis*-$[PtX_2(CO)_2]$ are the lowest for the series presented in Table 7. In mononuclear dicarbonyls the two CO ligands have to share the back donation from the in-plane d orbital of the metal, consequently the Pt—C bond is weakened. The lower (zero) charge of the complex enhances the trend in the same direction. Conversely, the CO stretching force constants show the opposite trend, being at their highest in $[PtX_2(CO)_2]$. This

Can. J. Chem. Downloaded from www.nrcresearchpress.com by 84.41.108.74 on 09/07/12
For personal use only.

TABLE 7. Characteristic spectroscopic data for some square-planar platinum carbonyls

Compounds	CO stretching[a] cm^{-1}		PtC stretching cm^{-1}		Force constants[b] K(CO)	K(PtC)	cation anion	Remarks	Reference
cis-$PtCl_2(CO)_2$	2175/2148	2134/2093	459.5	430	17.63	3.06		[c]	11
cis-$PtBr_2(CO)_2$	2163/2130	2121/2086	454	421	17.43	2.93		[c]	11
$[PtCl_3(CO)]^-$	2097/2048		497		16.47	3.91[e]	$[NPr^n_4]$	[c]	This work
$[PtBr_3(CO)]^-$	2090/2043		496		16.33	3.90	$[NBu^n_4]^+$	[c]	12
$[PtI_3(CO)]^-$	2075/2029		492		16.13	3.83	$[NBu^n_4]^+$	[c]	12
cis-$[PtCl_2Bu^n(CO)]^-$	2052/ —		522		15.75	4.31	$[NPr^n_4]^+$	[d]	13
cis-$[PtCl_2Me(CO)]^-$	2061/ —		528		15.89	4.41	$[NPr^n_4]^+$	[d]	13
cis-$[PtCl_2(CO)(PMe_3)]$	2107/2055		490		16.58	3.80	—	[d]	10
cis-$[PtBr_2(CO)(PMe_3)]$	2103/2054		486		16.53	3.74	—	[d]	10
cis-$[PtI_2(CO)(PMe_3)]$	2094/2055		475		16.47	3.57	—	[d]	10
$[PtCl(CO)(PMe_3)_2]^+$	2111/ —		502		16.57	3.99	$[BF_4]^-$	[d]	10
$[PtBr(CO)(PMe_3)_2]^+$	2111/2050		494		16.57	3.86	$[BF_4]^-$	[d]	10
$[Pt_2Cl_4(CO)_2]^{2-}$	2047/1993	2027/1985	529*	512	15.48	4.29	$[NPr^n_4]^+$	[d]	8
$[Pt_2Br_4(CO)_2]^{2-}$	2028*/1971*	2010*/ —	516*	503	15.21	4.11	$[NPr^n_4]^+$	[d]	8

[a]All frequencies taken from solution spectra except those marked with asterisks; for CO stretchings the $^{12}CO/^{13}CO$ frequency pairs are listed.
[b]Force constants unit is 10^2 N m^{-1}.
[c]Calculated force constants by full solution refinement.
[d]Calculated force constants by EGM method (20).
[e]For a better comparability K(PtC) is taken from ref. 12, where the refinement is based on a single PtC stretching frequency for all chloride, bromide, and iodide anions as well.

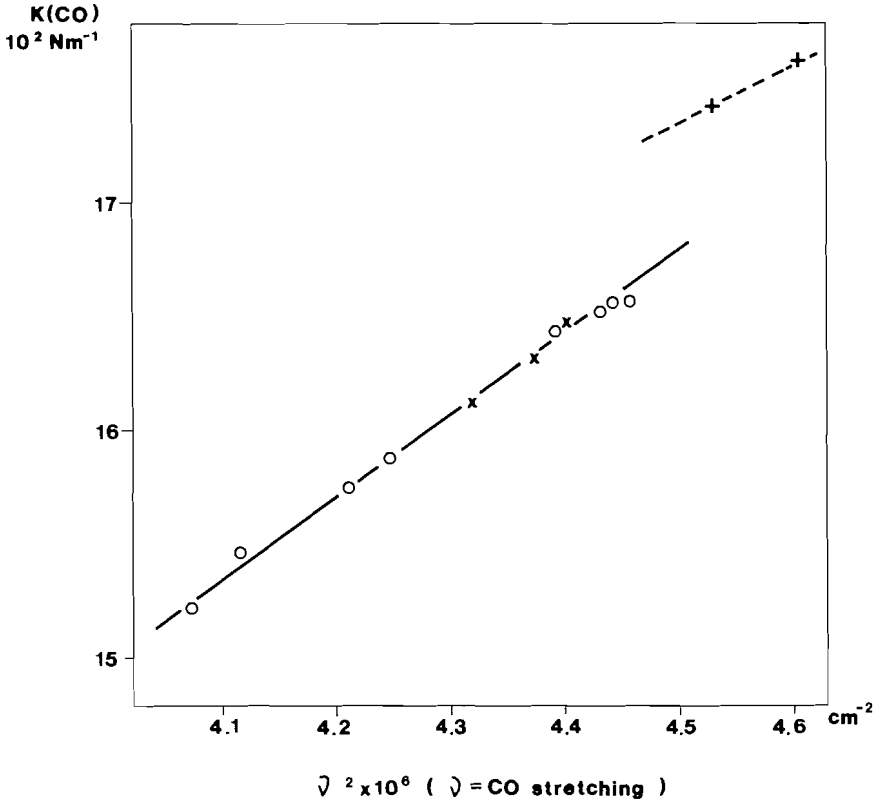


FIG. 4. Relationship between square of the ^{12}CO wavenumbers and CO stretching force constants for square-planar platinum carbonyls (see Table 7): +, *cis*-$PtX_2(CO)_2$ full solution (average frequency); ×, $[PtX_3(CO)]^-$ full solution; ○, calculated by EGM method (for dicarbonyls averaged frequency used).

Can. J. Chem. Downloaded from www.nrcresearchpress.com by 84.41.108.74 on 09/07/12
For personal use only.

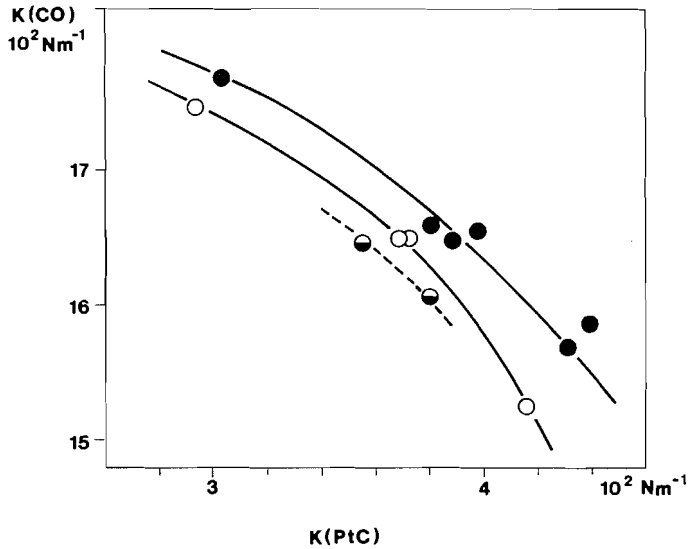


FIG. 5. Relationship between CO and PtC stretching force constants for square-planar platinum carbonyls (see Table 7): ●, chlorides; ○, bromides; ◒, iodides.

is presumably the consequence of the lower σ-overlap of the metal in the uncharged complex.

The other zero-charged representatives are the *cis*-$[PtX_2(CO)(PMe_3)]$ compounds, but the PMe_3 ligand is a strong electron donor; on this basis the PtC stretching force constant increases by about 25%, as compared to those in dicarbonyls.

Among the negative charged complexes the strongest PtC bond is formed in *cis*-$[PtX_2R(CO)]^-$ anions (where R = Me, Bu^n) indicating again a strong electron donor character of alkyl ligands.

The charge independence and close similarity of PtC force constants in $[PtX_3(CO)]^-$, *cis*-$[PtX_2(CO)(PMe_3)]$, and $[PtX(CO)(PMe_3)_2]^+$ can result from the superposition of several effects. As the number of X decreases the metal becomes more positive as a consequence of the decrease in overall charge, but this effect is compensated by the strongly electron donor PMe_3 ligand, and the π-component of the metal—carbon bond remains relatively constant, as does the strength of the Pt—C bond.

The relatively large PtC force constants for Pt(I) dimer complexes agree with the very low CO stretching force constants. The trend of averaged PtC force constants for

$$[PtX_2(CO)_2]^0 \quad [PtX_3(CO)]^- \quad [Pt_2X_4(CO)_2]^{2-}$$
$$3.1 \quad < \quad 3.8 \quad < \quad 4.2 \text{ N cm}^{-1}$$

shows that changes in overall charge of the complex and changes in oxidation state affect the Pt—C bond strength in the same way.

Acknowledgements

We thank Dr. F. Kling for the preparation of $^{14}C^{16}O$, the late Dr. A. T. Ayoub for his contribution in force field calculations, Dr. M. Gál for recording Raman spectra of the $^{14}C^{12}O$ complex, Mr. C. Webber for experimental assistance, and the Royal Society and Hungarian Academy of Sciences for supporting our cooperation.

1. J. MINK, A. AYOUB, G. KEMÉNY, R. KREMÓ, and F. KLING. Spectrochim. Acta, **36**A, 151 (1980).
2. J. MINK, A. AYOUB, G. KEMÉNY, and F. KLING. J. Mol. Spectrosc. **86**, 258 (1986).
3. A. AYOUB. Ph.D. Thesis. Institute of Isotopes of the Hung. Acad. Sci., Budapest. 1982.
4. S. DOBOS, G. WINNEWISSER, F. KLING, and J. MINK. Z. Naturforsch. **44**A, 633 (1989).
5. J. MINK and G. KEMÉNY. Spectrochim. Acta, **33**A, 277 (1977).
6. S. DOBOS, F. KLING, G. WINNEWISSER, and G. KERESZTURY. Z. Naturforsch. **44**A, 640 (1989).
7. A. AYOUB, J. MINK, and M. GAL. J. Mol. Spectrosc. **60**, 243 (1980).
8. P. L. GOGGIN and R. J. GOODFELLOW. J. Chem. Soc. Dalton, 2355 (1973).
9. P. L. GOGGIN and J. MINK. J. Chem. Soc. Dalton, 2355 (1974).
10. J. BROWNING, P. L. GOGGIN, R. J. GOODFELLOW, M. G. NORTON, A. J. M. RATTRAY, B. F. TAYLOR, and J. MINK. J. Chem. Soc. Dalton, 206 (1977).
11. P. L. GOGGIN and J. MINK. Inorg. Chim. Acta, **34**, 225 (1979).
12. P. L. GOGGIN, M. G. NORTON, and J. MINK. Inorg. Chim. Acta, **26**, 125 (1978).
13. J. BROWNING, P. L. GOGGIN, R. J. GOODFELLOW, N. W. HURST, L. G. MALLISON, and M. MURRAY. J. Chem. Soc. Dalton, 872 (1978).
14. D. A. DUDDELL, P. L. GOGGIN, R. J. GOODFELLOW, M. G. NORTON, and J. G. SMITH. J. Chem. Soc. A, 545 (1970).
15. J. MINK and P. L. GOGGIN. Kémiai Közlemények, **57**, 275 (1982).
16. P. L. GOGGIN and J. MINK. J. Chem. Soc. Dalton, 1479 (1974).
17. M. G. NORTON. Ph.D. Thesis. Bristol University, England. 1968.
18. F. R. HARTLEY. The chemistry of platinum and palladium. Applied Sciences, London. 1973.
19. J. MINK, L. MINK, and G. KEMÉNY. Report of Cent. Res. Ins. Phys. KFKI-76-47, Budapest. 1976.

Can. J. Chem. Downloaded from www.nrcresearchpress.com by 84.41.108.74 on 09/07/12
For personal use only.

Can. J. Chem. Downloaded from www.nrcresearchpress.com by 123.30.183.119 on 09/08/12
For personal use only.

Étude potentiométrique de la stabilité de complexes tensioactif–β-cyclodextrine

D. JEZEQUEL, A. MAYAFFRE ET P. LETELLIER[1]

Laboratoire d'énergétique et réactivité aux interfaces, Université Pierre et Marie Curie, Bât. F, 8, rue Cuvier, 75231 Paris CEDEX 05, France

Reçu le 22 février 1991

D. JEZEQUEL, A. MAYAFFRE et P. LETELLIER. Can. J. Chem. **69**, 1865 (1991).

Les valeurs des constantes de dissociation des complexes formés entre la β-cyclodextrine (β-CD) et 13 agents tensio-actifs cationiques de type alkylammonium ont été déterminées par potentiométrie au moyen d'électrodes sélectives aux amphiphiles. Les résultats suggèrent, pour les plus longues chaînes (C12, C14 et C16), l'existence de deux complexes successifs (β-CD)M^+ et (β-CD)$_2M^+$, dont les valeurs relatives des constantes de dissociation sont dans un rapport voisin de 600. Ce comportement n'est pas modifié lorsque l'on change la nature de la «tête polaire», les valeurs des constantes de dissociation étant très peu influencées par ce paramètre. Pour les chaînes carbonées alkyles comportant moins de 12 atomes de carbone, on constate une stabilisation des complexes 1 : 1 lorsque la chaîne s'allonge. Jusqu'à $n = 12$, les valeurs des pK_1 des complexes 1 : 1 varient linéairement avec le nombre de carbones, n, de la chaîne alkyle. Ensuite, pour $n = 14$ et $n = 16$, l'augmentation de pK_1 est moins importante et parallèlement l'intervention d'un deuxième complexe s'avère indispensable pour décrire convenablement le comportement des surfactifs en solution. La connaissance des valeurs des constantes de dissociation de ces complexes permet d'envisager la constitution de «solutions tampons» formées d'agents tensio-actifs permettant de maintenir une concentration fixe de l'amphiphile en solution, lors d'une réaction.

Mots clés : agent tensio-actif, β-cyclodextrine, électrodes sélectives, constantes de complexation, potentiométrie.

D. JEZEQUEL, A. MAYAFFRE, and P. LETELLIER. Can. J. Chem. **69**, 1865 (1991).

The complexation constants K of β-cyclodextrine with 13 ammonium surfactants were determined by a potentiometric method using electrodes selective to amphiphilic ions. Especially for C12, C14, and C16 tails, a model that provides for the formation of a second complex (β-CD)$_2M^+$, with a K_1/K_2 ratio of about 600, provides a good fit with the experimental curves. Results show a poor influence of the polar group, for example in the case of the dodecyl chain. On the other hand, the pK_1 values and the hydrophobic tail length are linked by a linear relation up to $n = 12$ carbon atoms; beyond, pK_1 tends to be proportionally smaller and pK_2 more important.

Key words: surfactant, β-cyclodextrin, selective electrodes, complexation constants, potentiometric study.

Introduction

Les propriétés complexantes des cyclodextrines vis-à-vis des agents tensio-actifs (surfactifs) neutres ou chargés (anioniques et cationiques) ont été mises en évidence et étudiées par de nombreux auteurs (1–9). Les valeurs des constantes de complexation ont été le plus souvent mesurées pour les espèces chargées par une méthode conductimétrique et leur précision dépend essentiellement de l'estimation de la différence de mobilité entre l'espèce tensio-active monomère et celle du complexe formé (4–9). Si dans le cas des surfactifs anioniques cette différence est notable, il faut constater que pour les cationiques elle est faible, et souvent insuffisante pour obtenir des valeurs précises des constantes d'équilibre. Pour cette raison, nous avons abordé l'étude de la complexation des tensio-actifs cationiques par une voie *potentiométrique*, en utilisant des *électrodes sélectives indicatrices de surfactif.*

Nous avons borné notre étude aux propriétés de la β-cyclodextrine (CD) vis-à-vis de six surfactifs cationiques dont les têtes polaires sont des ammonium totalement substitués :

décyltriméthylammonium	DTA
dodécyltriméthylammonium	DDTA
tétradécyltriméthylammonium	TDTA
hexadécyltriméthylammonium	HDTA
hexadécylpyridinium	HDP
dodécyldiméthylallylammonium	DDDAA

et de sept ammonium acides obtenus par la protonation d'une amine à longue chaîne aliphatique :

octylammonium	OA
décylammonium	DA
dodécylammonium	DDA
tétradécylammonium	TDA
hexadécylammonium	HDA
dodécyldiméthylammonium	DDDA
cyclododécylammonium	CDDA

On cherchera donc, dans cette étude, à comparer les valeurs des constantes de dissociation des complexes selon la nature de leur groupement polaire, la longueur et la nature de leur chaîne aliphatique.

Partie expérimentale

1. Produits

La β-cyclodextrine est un produit Orsan. Les bromure d'alkyltriméthylammonium ainsi que ceux d'hexadécylpyridinium et de cyclododécylammonium sont des produits Aldrich. Le bromure de dodécyldiméthylallylammonium a été synthétisé selon la procédure décrite dans la référence 10.

Nous avons préparé les chlorure et acétate d'alkylammonium et de dodécyldiméthylammonium, à partir des amines correspondantes (produits Fluka (C_{10}); Janssen (C_{12}, C_{14}); Aldrich (C_{16}, cycloC_{12}). On neutralise par de l'acide chlorhydrique ou acétique, un système hétérogène constitué d'amine pure en présence de sa solution aqueuse saturée.

Les chlorure d'ammonium peu solubles dans l'eau précipitent à froid. Ils sont lavés et recristallisés dans l'eau en dessous de la température de Kraft. Les solutions d'acétate correspondant à la solution neutralisée ramenée à un pH légèrement acide par ajout d'une très faible quantité d'acide acétique, sont lyophilisées (l'acide acétique en excès est éliminé au cours de la lyophilisation).

1. Auteur à qui adresser toute correspondance.

Printed in Canada / Imprimé au Canada

Can. J. Chem. Downloaded from www.nrcresearchpress.com by 123.30.183.119 on 09/08/12
For personal use only.

Can. J. Chem. Downloaded from www.nrcresearchpress.com by 123.30.183.119 on 09/08/12
For personal use only.

2. Technique expérimentale

2.1. Électrodes sélectives de surfactif

Pour les alkyltriméthyl ammonium : Les électrodes indicatrices d'alkyltriméthylammonium mettent en jeu des membranes polymériques rendues sélectives à l'amphiphile cationique. Elles ont été réalisées au laboratoire (11) selon une méthode proche de celle décrite dans la littérature par différents auteurs (12, 13).

La membrane polymérique a été préparée en effectuant la suite d'opérations suivantes : (*a*) 0,4 g de PVC de très haut poids moléculaire (Janssen) et 1,6 g de dinonylphtalate, DNP (Merck), sont dissous dans 10 mL de tétrahydrofurane, THF (R.P. Prolabo); (solution *a*). (*b*) L'ion tétraphénylborure (TPB) est utilisé comme «transporteur» de l'amphiphile cationique dans la membrane polymérique. On prépare le tétraphénylborure du surfactif cationique par précipitation dans l'eau en mélangeant en quantités stoechiométriques du tétraphénylborure de sodium et du bromure de l'amphiphile cationique. Le précipité est lavé et purifié par, au minimum, trois extractions successives liquide–liquide (eau–CH_2Cl_2). Le sel est ensuite recristallisé deux fois dans un mélange éther éthylique – dichlorométhane. On prépare une solution 0,01 mol dm^{-3} du complexe TPB–amphiphile dans du THF. (*c*) On mélange 0,5 mL de la solution précédente à 3 mL de la solution contenant le PVC et le plastifiant. (*d*) La solution est mise à évaporer à l'atmosphère ambiante pendant 24 h dans un récipient à fond plat (aire = 25 cm^2).

La membrane ainsi obtenue, d'une épaisseur de 0,2 mm environ, est découpée et collée sur un embout en verre préalablement trempé dans la solution *a*.

La référence interne est constituée par la chaîne électrochimique suivante :

électrode calomel, solution de KCl saturée dans l'eau	KCl aq saturé	gel de KCl : $C = 2$ mol dm^{-3}	solution d'amphiphile cationique : $C = 10^{-3}$ mol dm^{-3}

Pour les alkylammonium : Nous avons réalisé des électrodes indicatrices d'ions alkylammonium en employant une méthode de préparation identique à la précédente, l'ion transporteur étant également l'ion tétraphénylborure. Pour un milieu donné, ces électrodes présentent en général une réponse nernstienne convenable au surfactif étudié. Cependant, le groupement ammonium étant acide, le complexe tétraphénylborure d'alkylammonium est susceptible de se dissocier à la surface de la membrane selon le niveau d'acidité de son environnement. Il en résulte que les électrodes ainsi constituées sont sensibles au pH du milieu, ce qui constitue un inconvénient majeur lorsque les espèces à doser possèdent par elles-mêmes des propriétés acides. Ces électrodes n'ont donc été utilisées que dans des milieux de pH fixé.

Il est connu que la spécificité des électrodes indicatrices de surfactifs vis-à-vis de composés possédant des groupements chargés hydrophiles *de nature voisine et de chaînes de longueurs comparables* reste très faible (14), alors qu'elle est excellente par rapport aux ions inorganiques. Si cette caractéristique limite généralement l'emploi de ces électrodes indicatrices aux milieux qui ne contiennent qu'un seul surfactif, elle présente également l'avantage de permettre le dosage de différents surfactifs avec une réponse nernstienne dans une certaine zone de concentration. Nous avons ainsi utilisé des électrodes incluant des complexes d'alkyltriméthylammonium (indépendantes du pH) pour doser des alkylammonium, après avoir déterminé leur domaine de réponse linéaire. Les valeurs des concentrations des ammonium suivants ont pu être mesurées au moyen d'électrodes indicatrices d'alkyltrimélthylammonium, incluant un complexe

de DA	pour doser le	CDDA
de DTA	pour doser le	DDA
de DDTA	pour doser le	DDDA
de TDTA	pour doser le	TDA, HDA et DDDAA

Pour les autres surfactifs, l'électrode indicatrice faisait intervenir un complexe de l'amphiphile dosé.

2.2. Pile de mesure

L'électrode spécifique est opposée à une électrode de référence :

Ag | AgCl | KCl gel 2 mol dm^{-3} |

protégée de la diffusion de l'amphiphile par un pont salin (KCl 2 mol dm^{-3}) gélifié contenu dans un fin tuyau en Téflon. Cette configuration a été adoptée pour retarder au maximum la diffusion rapide du surfactif dans l'électrode. Il est important de renouveler très souvent le gel en contact avec la solution. On réalise donc la chaîne électrochimique suivante :

référence interne | membrane | solution étudiée | référence

dont la f.é.m. peut s'écrire sous la forme :

$$[1] \quad \Delta E = \Delta E^0 + 2{,}3\,\frac{RT}{F}\log(M^+) = \Delta E^0 - 2{,}3\,\frac{RT}{F}\,\mathrm{p}M$$

Les mesures de f.é.m. ont été effectuées à l'aide d'un millivoltmètre Tacussel, Minisis 8000, la température des solutions étant maintenue constante et égale à (298 ± 0,1) K par un bain thermostaté.

À titre d'exemple, les courbes d'étalonnage pour les surfactifs DDTA, HDA et CDDA sont reportées sur la figure 1. On observe sur les courbes la présence de points anguleux (exemple des courbes DDTA et HDA, figure 1) correspondant aux concentrations micellaires critiques (cmc), dont les valeurs sont regroupées dans le tableau 1.

Ces électrodes présentent une réponse nernstienne (pente égale à 0,059 V par décade) pour une gamme de concentrations en surfactif (obtenues par dilution d'une solution concentrée) pouvant aller de $5\cdot10^{-7}$ mol dm^{-3} jusqu'à la cmc. Cet étalonnage permet également d'obtenir le paramètre ΔE^0 de l'équation [1]. Les f.é.m. sont stables à ±0,1 mV.

Par ailleurs, ces graphes montrent que pour une concentration inférieure à la cmc, les amphiphiles se trouvent essentiellement sous la forme monomère et que l'on ne peut mettre en évidence la présence d'éventuels dimères (15, 16). Pour des solutions de titre inconnu en surfactif, on détermine le pM correspondant :

$$[2] \quad \mathrm{p}M = \frac{\Delta E^0 - \Delta E}{0{,}059}$$

La technique que nous mettons en oeuvre conduit à une excellente reproductibilité des courbes expérimentales. Ceci prouve la fiabilité de la chaîne électrochimique utilisée et, en conséquence, le bon fonctionnement de ses éléments constitutifs. Cependant, un tel résultat ne peut être obtenu que si l'on apporte un soin particulier à protéger l'électrode de référence de la diffusion du surfactif.

3. Détermination des constantes de complexation des surfactifs

3.1. Conditions expérimentales

La détermination potentiométrique des constantes de complexation a été effectuée à 298 K à partir des courbes de titrage de l'amphiphile par une solution de β-cyclodextrine

TABLEAU 1. Valeurs des concentrations micellaires critiques des acétates d'alkylammonium, et d'alkyltriméthylammonium, dans l'eau à 298 K, déterminées par potentiométrie. Le nombre de carbones de la chaîne aliphatique est n

Acétates d'alkylammonium							
Composé	OA	DA	DDA	TDA	HDA	DDDA	CDDA
Carbones, n	8	10	12	14	16	12	12
cmc/mol dm^{-3}	$1{,}75\cdot10^{-1}$	$4\cdot10^{-2}$	$1{,}4\cdot10^{-2}$	$3{,}4\cdot10^{-3}$	$8\cdot10^{-4}$	$1{,}6\cdot10^{-2}$	—

Acétates d'alkyltriméthylammonium						
Composé	DTA	DDTA	TDTA	HDTA	HDP	DDDAA
Carbones, n	10	12	14	16	16	12
cmc/mol dm^{-3}	$6\cdot10^{-2}$	$1{,}4\cdot10^{-2}$	$3{,}5\cdot10^{-3}$	10^{-3}	$7\cdot10^{-4}$	$1{,}1\cdot10^{-2}$

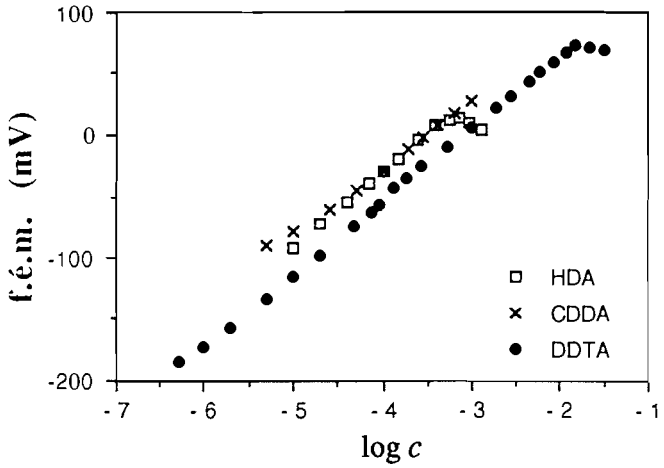


FIG. 1. Exemples d'étalonnages d'électrodes indicatrices de surfactifs.

10^{-2} mol dm^{-3}. Nous avons exploité ces courbes à partir de la fonction $\Delta E = f(r)$, où r est, pour chaque point de la courbe, défini comme le rapport du nombre total de moles de cyclodextrine n_{CD} ajoutées, au nombre total de moles de surfactif n_M introduites :

$$[3] \quad r = \frac{n_{CD}}{n_M}$$

Les concentrations de surfactif utilisées ont toujours été choisies inférieures à la concentration micellaire critique. Les solutions d'acétate d'alkylammonium ont été acidifiées par une faible quantité d'acide acétique afin d'éviter une éventuelle dissociation du sel acide. L'ensemble de ces dosages a été réalisé par pilotage automatique permettant l'obtention d'un grand nombre de points expérimentaux (pilote Tacussel TT-P2 couplé à un micro-ordinateur).

3.2. *Résultats expérimentaux*

À titre d'exemple nous présentons dans les tableaux 2–5 une série de résultats caractéristiques des différents comportements observés que nous commenterons dans la discussion. ΔE (mV) est la valeur de la f.é.m. mesurée, ΔE_1 et ΔE_2 sont les valeurs de f.é.m. calculées à partir des modèles présentés dans le paragraphe suivant.

3.3. *Modèles de complexation*

L'exploitation des fonctions $\Delta E = f(r)$ exige que l'on se fixe un modèle de complexation du surfactif par la cyclodextrine. On peut ainsi envisager deux possibilités :

TABLEAU 2. Titrage de DTA$^+$ (ΔE^0 = 205,0 mV)

r	pM	ΔE (mV)	ΔE_1 (mV)	ΔE_2 (mV)
0,000	3,00	28,0	28,0	28,0
0,024	3,01	27,5	27,4	27,4
0,212	3,09	23,0	22,9	22,9
0,452	3,19	17,0	16,8	16,8
0,691	3,30	11,0	10,5	10,5
0,912	3,40	5,0	4,6	4,6
1,150	3,50	−0,5	−1,2	−1,2
1,390	3,59	−6,5	−6,6	−6,6
1,628	3,67	−11,0	−11,4	−11,4
1,880	3,74	−16,0	−15,9	−15,9
2,150	3,82	−20,5	−20,1	−20,1
2,420	3,88	−24,0	−23,8	−23,8
2,690	3,93	−27,5	−27,1	−27,1
2,960	3,98	−30,5	−30,0	−30,1
3,230	4,03	−33,0	−32,7	−32,8
3,522	4,08	−35,5	−35,3	−35,4
3,805	4,11	−38,0	−37,7	−37,8
3,992	4,14	−39,0	−39,1	−39,2

(a) Modèle à un complexe

On suppose que la cyclodextrine CD et le surfactif M$^+$ conduisent à un complexe 1 : 1 (CDM$^+$). L'équilibre de dissociation du complexe s'écrit :

$$[4] \quad CDM^+ \Longleftrightarrow CD + M^+$$

La constante d'équilibre est égale à :

$$[5] \quad K = \frac{[CD][M^+]}{[CDM^+]}$$

en faisant intervenir les valeurs des concentrations des espèces en solution. On supposera que l'on se place toujours en solution suffisamment diluée pour ne pas avoir à tenir compte de l'intervention des coefficients d'activité. La conservation des masses s'écrit :

$$[6] \quad \begin{aligned} [M^+]_{total} &= [M^+] + [CDM^+] = C \\ [CD^+]_{total} &= [CD] + [CDM^+] = rC \end{aligned}$$

Pour chaque point du dosage, on calcule la valeur de la constante de complexation par la relation :

$$[7] \quad K = \frac{10^{-2pM} + C(r-1)10^{-pM}}{C - 10^{-pM}}$$

Can. J. Chem. Downloaded from www.nrcresearchpress.com by 123.30.183.119 on 09/08/12
For personal use only.

Can. J. Chem. Downloaded from www.nrcresearchpress.com by 123.30.183.119 on 09/08/12
For personal use only.

TABLEAU 3. Titrage de $DDTA^+$ (ΔE^0 = 212,5 mV)

r	pM	ΔE (mV)	ΔE_1 (mV)	ΔE_2 (mV)
0,000	3,00	35,5	35,5	35,5
0,032	3,01	35,0	34,6	34,6
0,349	3,18	25,5	24,7	24,7
0,632	3,38	15,0	13,1	13,1
0,881	3,59	3,0	0,5	0,7
1,133	3,81	−9,0	−12,5	−12,3
1,385	4,00	−21,0	−23,5	−23,3
1,662	4,16	−30,5	−32,8	−32,7
1,955	4,29	−38,5	−40,3	−40,3
2,267	4,40	−45,5	−46,6	−46,8
2,608	4,49	−51,5	−52,1	−52,5
2,968	4,58	−57,0	−57,0	−57,6
3,328	4,65	−61,5	−61,0	−61,8
3,700	4,71	−65,0	−64,7	−65,6
3,968	4,76	−67,5	−67,0	−68,1
4,000	4,76	−68,0	−67,3	−68,4

TABLEAU 4. Titrage de TTA^+ (ΔE^0 = 203,5 mV)

r	pM	ΔE (mV)	ΔE_1 (mV)	ΔE_2 (mV)
0,000	3,00	26,5	26,5	26,5
0,072	3,03	24,5	24,5	24,5
0,550	3,34	7,5	6,2	6,3
0,870	3,68	−10,0	−13,9	−13,7
1,126	4,01	−29,0	−33,5	−32,9
1,376	4,26	−46,5	−48,3	−47,7
1,676	4,47	−60,5	−60,3	−60,0
2,064	4,65	−72,5	−70,8	−71,0
2,549	4,82	−82,0	−79,9	−80,6
3,102	4,95	−91,0	−87,5	−88,8
3,696	5,07	−97,5	−93,8	−95,6
4,344	5,17	−103,0	−99,2	−101,6
4,993	5,26	−108,0	−103,7	−106,6
5,641	5,33	−112,0	−107,5	−110,9
6,308	5,39	−115,5	−110,9	−114,7
6,978	5,45	−119,0	−113,9	−118,1
7,668	5,50	−122,0	−116,7	−121,3
8,359	5,55	−124,5	−119,2	−124,1
8,991	5,59	−127,0	−121,3	−126,5

On détermine ainsi une valeur moyenne de pK à ±0,05 unité sur l'ensemble des points expérimentaux. Cette valeur étant connue, on peut alors recalculer la concentration de M^+ en fonction de r en résolvant l'équation du second degré :

$$[8] \quad [M^+]^2 + (K + C(r-1))[M^+] - KC = 0$$

puis calculer à l'aide de la relation [1] la f.é.m. ΔE_1 de la pile (cf. tableaux 2–5). Ce modèle simple permet de décrire parfaitement les résultats expérimentaux pour le traitement des courbes relatives aux surfactifs de C8–C12.

En revanche en ce qui concerne les composés en C14 et C16, on constate que l'expression [7] conduit à des valeurs de pK qui varient avec r principalement lorsque ce paramètre prend des valeurs élevées. Les valeurs de ΔE_1 calculées à partir d'une valeur moyenne de pK obtenue sur le domaine $1 < r < 2$ par exemple, s'écartent nettement des valeurs expérimentales pour le domaine où $r \geq 3$ (tableaux 4 et 5, et figure 2, courbe E1).

TABLEAU 5. Titrage de $HDTA^+$ (ΔE^0 = 273,2 mV)

r	pM	ΔE (mV)	ΔE_1 (mV)	ΔE_2 (mV)
0,000	3,13	88,5	88,5	88,5
0,099	3,18	86,5	85,7	85,7
0,664	3,58	64,5	61,8	61,9
0,980	3,99	42,5	36,9	37,6
1,232	4,33	22,0	16,4	17,4
1,518	4,60	3,0	1,2	1,9
1,949	4,85	−12,0	−12,8	−12,8
2,504	5,05	−25,0	−24,1	−25,1
3,144	5,22	−35,5	−32,9	−35,0
3,872	5,37	−43,5	−40,3	−43,5
4,695	5,49	−51,0	−46,7	−51,0
5,549	5,60	−57,5	−52,0	−57,3
6,413	5,69	−63,0	−56,4	−62,7
7,312	5,77	−67,5	−60,3	−67,4
8,212	5,84	−71,5	−63,7	−71,6
9,112	5,91	−75,0	−66,7	−75,3
10,041	5,96	−78,5	−69,5	−78,7
11,020	6,02	−81,5	−72,1	−81,9
11,977	6,07	−84,5	−74,4	−84,8
12,421	6,09	−85,5	−75,5	−86,1

Ceci suggère la présence d'un complexe d'ordre supérieur, à deux cyclodextrines, dont l'existence a été déjà signalée par J. W. Park et H. J. Song dans le cas de surfactifs anioniques (2) pour la β-CD, et par R. Palepu et V. C. Reinsborough (8) pour la α-CD et la β-CD. Nous avons donc envisagé cette hypothèse et effectué l'analyse de nos résultats à partir du système d'équations suivant :

(b) Modèle à deux complexes

$$[9] \quad CDM^+ \Longleftrightarrow CD + M^+ \qquad K_1 = \frac{[CD][M^+]}{[CDM^+]}$$

$$CD_2M^+ \Longleftrightarrow CDM^+ + CD \qquad K_2 = \frac{[CDM^+][CD]}{[CD_2M^+]}$$

La conservation des masses s'écrit alors :

$$[10] \quad [M^+]_{total} = [M^+] + [CDM^+] + [CD_2M^+] = C$$

$$[CD]_{total} = [CD] + [CDM^+] + 2[CD_2M^+] = rC$$

soit :

$$[11] \quad C = [M^+]\left(1 + \frac{[CD]}{K_1} + \frac{[CD]^2}{K_1K_2}\right)$$

et

$$[12] \quad rC = [CD] + [M^+]\left(\frac{[CD]}{K_1} + \frac{2[CD]^2}{K_1K_2}\right)$$

À partir de ce système d'équations, on ajuste les valeurs de pK_1 et pK_2 de manière à obtenir le meilleur accord possible entre les courbes expérimentales et calculées. On constate que les valeurs de pK_1 restent voisines de celles que l'on obtient pour le domaine où $r < 3$, en supposant l'existence d'un seul complexe, ce qui confirme la prédominance du complexe 1 : 1.

Les résultats expérimentaux sur l'ensemble des valeurs de r sont parfaitement décrits pour les C14 et C16 à l'aide du

TABLEAU 6. Valeurs des constantes de dissociation des complexes formés entre la cyclodextrine et les amphiphiles cationiques

Alkyltriméthylammonium						
Composé	DTA	DDTA	TDTA	HDTA	HDP	DDDAA
Carbones, *n*	10	12	14	16	16	12
pK_1	3,60	4,25	4,60	4,85	4,85	4,20
pK_2	<0,5[a]	<1,4[a]	1,75	2,10	2,25	<1,5[a]
pK_1 (litt.)		3,69 (5) 3,39 (6)	4,07 (8)	3,35 (9) 4,30 (4)	4,60 (4)	

Alkylammonium							
Composé	OA	DA	DDA	TDA	HDA	DDDA	CDDA
Carbones, *n*	8	10	12	14	16	12	12
pK_1	2,85	3,55	4,15	4,60	4,85	4,15	3,45
pK_2	<1[a]	<1,2[a]	<1,5[a]	1,70	2,20	<1,5[a]	<1,3[a]
pK_1 (litt.)			3,11 (8) 3,68 (5)				

[a]Pour les composés en C8, C10 et C12, le modèle à un complexe permet de décrire correctement les courbes expérimentales, en particulier lorsque les concentrations en surfactif restent faibles. Cependant l'exploitation des résultats à l'aide du modèle à deux complexes est également possible de manière aussi satisfaisante pour C8 et C10. L'introduction du deuxième complexe devient indispensable pour C12, lorsque les concentrations en surfactif sont supérieures à 10^{-2} mol L^{-1}.

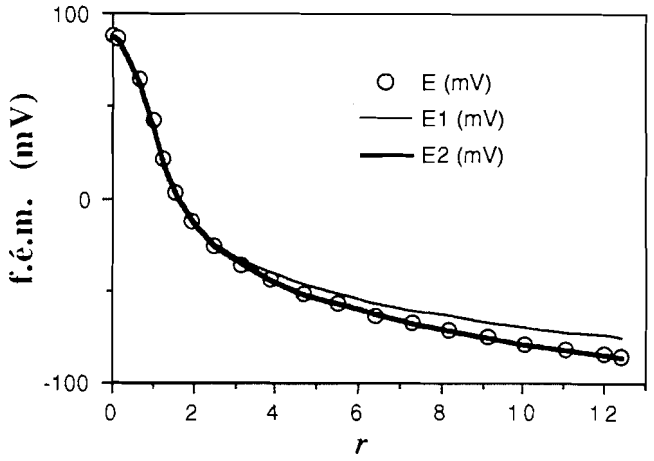


FIG. 2. Courbes de titration de HDTABr par la β-cyclodextrine. La courbe calculée au moyen du modèle à deux complexes (ΔE2) passe par l'ensemble des points expérimentaux. La courbe calculée au moyen du modèle à un complexe (ΔE1) ne parvient pas à décrire le comportement du surfactif en présence de cyclodextrine.

modèle à deux complexes (cf. valeurs de ΔE_2 dans les tableaux 4 et 5, et la courbe E2 sur la figure 2).

Les valeurs de pK_1 et pK_2 pour tous les amphiphiles étudiés sont regroupées dans le tableau 6 et sont données avec une incertitude absolue de l'ordre de 0,05 unité logarithmique.

(c) Influence de la concentration du surfactif

Pour l'écriture et le calcul des constantes d'équilibre K_1 et K_2, nous avons toujours considéré que les solutions étaient suffisamment diluées pour ne pas avoir à tenir compte des coefficients d'activité. Si l'on considère leur intervention dans l'expression de ces constantes (équations [5] et [9]), on obtient :

$$[5'] \quad K_1 = \frac{[CD][M^+]}{[CDM^+]} \frac{\gamma_{CD}\gamma_{M^+}}{\gamma_{CDM^+}}$$

$$[9'] \quad K_2 = \frac{[CDM^+][CD]}{[CD_2M^+]} \frac{\gamma_{CDM^+}\gamma_{CD}}{\gamma_{CD_2M^+}}$$

Les coefficients d'activité sont définis alors dans le modèle des solutions diluées. La cyclodextrine étant une espèce électriquement neutre, de concentration maximum de 10^{-2} mol L^{-1}, il est raisonnable de poser $\gamma_{CD} = 1$. En ce qui concerne les rapports $\gamma_{M^+}/\gamma_{CDM^+}$ et $\gamma_{CDM^+}/\gamma_{CD_2M^+}$, même en admettant qu'individuellement les valeurs des coefficients sont différents de 1, on peut supposer en se référant au modèle de Debye et Hückel, que leur rapport doit être très proche de l'unité, et ceci quelle que soit la force ionique du milieu.

En revanche, la mise en évidence d'un éventuel deuxième complexe doit s'avérer d'autant plus aisée que la concentration du surfactif est plus grande. Afin de vérifier ces hypothèses, nous avons effectué le dosage du DDTA à plusieurs concentrations de surfactif. Pour les concentrations élevées ($C = 10^{-2}$ mol dm^{-3}) l'introduction d'une deuxième constante (pK_2 de l'ordre 1,4) s'avère effectivement indispensable pour décrire avec précision le comportement du surfactif. On vérifie d'autre part que les valeurs de pK_1 et pK_2 sont indépendantes de la force ionique du milieu.

4. Discussion

Comme on peut le constater sur le tableau 6, les valeurs de pK déterminées au moyen de mesures conductimétriques sont dans la littérature, selon les auteurs, très différentes les unes des autres. Ceci tient au fait que les conductivités équivalentes des amphiphiles et des complexes sont relativement proches pour les surfactifs cationiques et que l'analyse des courbes exige que l'on détermine simultanément la conductivité du complexe et sa constante de dissociation.

Il n'en est pas de même pour les mesures potentiométriques. Dès lors que l'on dispose d'une chaîne électrochimique fiable (voir partie expérimentale), on peut déterminer avec précision pM, *pour tous les points expérimentaux*, et en conséquence, calculer à l'aide de l'équation [7] autant de valeurs de pK que

Can. J. Chem. Downloaded from www.nrcresearchpress.com by 123.30.183.119 on 09/08/12
For personal use only.

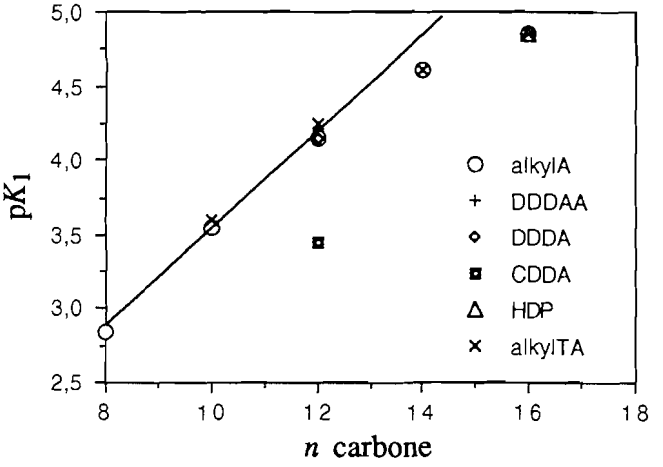


FIG. 3. Valeurs de pK_1 en fonction de la longueur de la chaîne carbonée.

de points. La constance des valeurs obtenues et leur dispersion autour d'une valeur moyenne permet alors de conclure sans ambiguïté sur la valeur du pK retenue ainsi que sur la validité du modèle utilisé pour exploiter les courbes. C'est une démarche de ce type qui nous a conduit à proposer une exploitation des résultats à l'aide d'un modèle à deux complexes dans les cas où, au lieu d'observer une distribution *aléatoire* des valeurs de la constante autour d'une valeur moyenne, on observe une variation continue en fonction de r, de la constante calculée avec le modèle à un complexe.

À titre de comparaison, nous avons introduit les valeurs de constantes trouvées par conductimétrie dans les équations des courbes de dosage potentiométriques. Nous avons constaté que, pour nombre d'entre elles, il est impossible de décrire convenablement les résultats expérimentaux. À l'inverse, les valeurs que nous proposons permettent de retrouver les courbes de conductimétrie publiées, en modifiant légèrement les paramètres de conductivité. Il semble donc qu'il faille considérer avec prudence les valeurs d'un certain nombre de constantes de dissociation des complexes surfactif–cyclodextrine publiées dans la littérature.

L'analyse des valeurs de constantes de dissociation déterminées par potentiométrie confirme et précise un certain nombre de propriétés déjà mises en évidence par différents auteurs pour d'autres complexes β-cyclodextrine–surfactif (4, 5, 7–9).

Importance de la nature du groupement polaire

On constate (tableau 6 et figure 3) que les valeurs des constantes de dissociation des complexes pour les alkyltriméthylammonium et alkylammonium diffèrent très peu pour des longueurs de chaînes identiques. Ainsi, on trouve un pK_1 de 4,20 ± 0,05 pour les quatre surfactifs possédant une chaîne linéaire à 12 carbones. Le groupement ionique constituant la tête polaire du surfactif ne semble donc pas influencer notablement le phénomène de complexation (6). Seul le cyclododécylammonium possède un comportement particulier, dû, bien évidemment, à la présence du cycle dans la molécule.

En revanche, si l'on compare ces valeurs à celles publiées dans la littérature concernant les complexes de surfactifs anioniques de même longueur de chaîne (détermination par conductimétrie (5)), on remarque qu'elles sont différentes et que l'on devrait en conclure que les complexes anioniques, à même longueur de chaîne, sont plus dissociés que les complexes cationiques. Une telle affirmation est cependant téméraire car on ne peut pas affirmer que cette différence est totalement attribuable à une spécificité des interactions surfactif anionique – cyclodextrine, et qu'elle n'est pas due plus simplement à une incertitude sur les constantes de dissociation inhérente à la méthode employée.

Complexation en fonction de la longueur de la chaîne

On remarque que les valeurs des pK de dissociation augmentent de façon sensiblement linéaire avec la longueur de la chaîne jusqu'à $n = 12$, ce qui implique que les complexes deviennent de plus en plus stables au fur et à mesure que la chaîne s'allonge. L'accroissement moyen de pK_1 par carbone est de 0,33 unité environ.

En revanche, pour les composés en C14 et C16, on observe que la variation de pK_1 par carbone devient moins importante que pour les surfactifs de chaîne plus courte. Ceci est à mettre sur le compte de l'apparition du complexe 1:2 qui implique une seconde molécule de cyclodextrine.

Ce comportement diffère de celui observé pour les surfactifs anioniques, comme les alcanesulfonates pour lesquels les valeurs des constantes de dissociation (complexes 1:1) deviennent invariantes dès que le nombre de carbones de la chaîne linéaire dépasse 10 (5). L'accroissement moyen de pK est inférieur à celui que nous observons pour les alkylammonium (0,2 unité pour les alcanesulfonates). Là encore, il est difficile de conclure sur cette différence de comportement basée sur des valeurs de constantes obtenues par des techniques expérimentales différentes qui ne conduisent pas aux mêmes analyses. Ainsi, on peut s'interroger sur l'éventuelle formation d'un complexe à deux cyclodextrines pour les surfactifs anioniques où $n \geq 14$.

Conclusion

Les résultats qui viennent d'être exposés montrent l'intérêt de la mise en oeuvre d'une méthode potentiométrique basée sur la fabrication d'une électrode indicatrice de surfactif pour étudier la stabilité des complexes entre la β-cyclodextrine et les surfactifs.

La possibilité de déterminer précisément des valeurs de constantes de dissociation dans l'eau, mais également dans des milieux réactionnels complexes, permet d'envisager différents types d'applications aux complexes surfactif–cyclodextrine et en particulier la réalisation de «solutions tampons». En général, les surfactifs sont utilisés au cours d'opérations industrielles, dans des milieux comportant de nombreux solutés susceptibles d'interagir avec eux, et entre autres de les précipiter. Il se pose donc très souvent le problème du maintien à une concentration donnée et fixe du surfactif en solution tout au long de l'opération envisagée. Ceci est rendu possible par l'utilisation de solutions tampon de surfactifs dont la fabrication et l'utilisation peut être calquée strictement sur celles des «solutions tampon de protons». Les valeurs reportées dans le tableau 6 montrent que selon le surfactif employé, il est possible de maintenir la concentration d'un surfactif dans la gamme 10^{-4}–10^{-5} mol dm^{-3}. L'utilisation d'autres formes de la cyclodextrine permet sans aucun doute d'étendre encore ce domaine. Un travail sur ce thème est en cours au laboratoire.

Remerciements

Nous remercions particulièrement C. Tribet pour la synthèse de l'allyldiméthyldodécylammonium (DDDAA) ainsi que la société Orsan pour la fourniture de la β-cyclodextrine et sa contribution générale à nos travaux de recherches.

Can. J. Chem. Downloaded from www.nrcresearchpress.com by 123.30.183.119 on 09/08/12
For personal use only.

1. T. OKUBO, Y. MAEDA et H. KITANO. J. Phys. Chem. **93**, 3721 (1989).
2. J. W. PARK et H. J. SONG. J. Phys. Chem. **93**, 6454 (1989).
3. M. OPALLO, N. KOBAYASHI, T. OSA, H. YAMADA et S. ONODERA. Bull. Chem. Soc. Jpn. **62**, 2995 (1989).
4. R. PAPELU, J. E. RICHARDSON et V. REINSBOROUGH. Langmuir, **5**, 218 (1989).
5. I. SATAKE, S. YOSHIDA, K. HAYAKAWA, T. MAEDA et Y. KUSOMOTO. Bull. Chem. Soc. Jpn. **59**, 3991 (1986).
6. I. SATAKE, T. IKENOUE, T. TAKESHITA, K. HAYAKAWA et T. MAEDA. Bull. Chem. Soc. Jpn. **58**, 2746 (1985).
7. R. PALEPU et V. C. REINSBOROUGH. Can. J. Chem. **67**, 1550 (1989).
8. R. PALEPU et V. C. REINSBOROUGH. Can. J. Chem. **66**, 325 (1988).
9. T. OKUBO, H. KITANO et N. ISE. J. Phys. Chem. **80**, 2661 (1976).
10. C. M. PALEOS, P. DAIS et A. MALLIARIS. J. Polym. Sci. **22**, 3383 (1984).
11. D. JEZEQUEL, A. MAYAFFRE et P. LETELLIER. J. Chim. Phys. **88**, 391 (1991).
12. T. SHINBO, N. KAMO, K. KURIHARA et Y. KOBATAKE. Arch. Biochem. BioPhys. **187**, 414 (1978).
13. G. J. MOODY, R. B. OKE et J. D. R. THOMAS. Analyst, **95**, 910 (1970).
14. T. MAEDA, M. IKEDA, M. SHIBAHARA, T. HARUTA et I. SATAKE. Bull. Chem. Soc. Jpn. **54**, 94 (1981).
15. P. SOMASUNDARAN et K. P. ANANTHAPADMANABHAN. Solution chemistry of surfactants. Vol. 2. *Éditeur* : K. L. Mittal. Plenum Press, New York. 1978. p. 777.
16. P. MUKERJEE. Adv. Colloid Interface Sci. **1**, 241 (1967).

Can. J. Chem. Downloaded from www.nrcresearchpress.com by 123.30.183.119 on 09/08/12
For personal use only.

Metallometallation of allenes: an exploratory study[1]

SHANKAR M. SINGH AND ALLAN C. OEHLSHLAGER
Department of Chemistry, Simon Fraser University, Burnaby, B.C., Canada V5A 1S6
Received March 11, 1991

SHANKAR M. SINGH and ALLAN C. OEHLSHLAGER. Can. J. Chem. **69**, 1872 (1991).

Reaction of either *n*-$Bu_3SnCu(CN)Li$ (**8**) or $(n\text{-}Bu_3Sn)_2Cu(CN)Li_2$ (**9**) with 1,2-undecadiene gave 71–92% of a (*Z*/*E*) mixture of 1-tri-*n*-butylstannyl-2-undecene (**27**) accompanied by 8–32% of a mixture of (*E*)-2-tri-*n*-butylstannyl-2-undecene (**28**) and 2-tri-*n*-butylstannyl-1-undecene (**29**). When the above reactions were warmed to 0°C, **28** and **29** were the major products. The mixed cuprates, **10–14**, gave the mixtures rich in vinylstannanes, **28** and **29**, along with **27**. Addition of Sn—Al reagents, **15** and **16**, or Sn—B reagents, **18** and **19**, to 1,2-undecadiene in the presence of 5 mol% of CuCN or $CoCl_2\cdot(PPh_3)_2$ provided mixtures rich in vinylstannanes, **28** and **29**. However, with 1 equiv. of CuCN, mixtures rich in allylstannanes **27** were obtained. Reaction of 5-hydroxy-1,2-pentadiene with the Sn—Al reagents, **15** and **16**, gave 53–61% of a single 5-hydroxy-2-tri-*n*-butylstannyl-1-pentene (**32**) in the presence of 5 mol% of $CoCl_2\cdot(PPh_3)_2$. The stannylcopper adducts generated in the reaction of 1,2-undecadiene and **8** or **9** were treated with iodomethane to give 55–78% of a (*Z*/*E*: 67/33) mixture of 1-tri-*n*-butylstannyl-2-methyl-2-undecene (**33**). Addition of mixed silylcuprates, **21**, **22**, and **23**, to 1,2-undecadiene gave mixtures rich in (*E*)-2-dimethylphenylsilyl-2-undecene (**35**) and 2-dimethylphenylsilyl-1-undecene (**36**). A rationale for the putative adducts' formation is also presented.

Key words: Sn—Cu, Sn—Al, Sn—B reagents; putative adducts.

SHANKAR M. SINGH et ALLAN C. OEHLSHLAGER. Can. J. Chem. **69**, 1872 (1991).

La réaction du *n*-$Bu_3SnCu(CN)Li$ (**8**) ou du $(n\text{-}Bu_3Sn)_2Cu(CN)Li_2$ (**9**) avec le undéca-1,2-diène fournit de 71 à 92% d'un mélange (*Z*/*E*) de 1-tri-*n*-butylstannylundéc-2-ène (**27**) accompagné de 8 à 32% d'un mélange de (*E*)-2-tri-*n*-butylstannylundéc-2-ène (**28**) et de tri-*n*-butylstannylundéc-1-ène (**29**). Les cuprates mixtes, **10–14**, fournissent des mélanges riches en vinylstannanes (**28** et **29**) aux côtés du produit **27**. L'addition des réactifs Sn—Al, **15** et **16**, ou des réactifs Sn—B, **18** et **19**, au undéca-1,2-diène, en présence de 5 mol% de CuCN ou de $CoCl_2\cdot(PPh_3)_2$ conduit à des mélanges riches en vinylstannanes, **28** et **29**. Toutefois, avec un équivalent de CuCN, on obtient des mélanges riches en allylstannanes **27**. La réaction du 5-hydroxypenta-1,2-diène avec les réactifs Sn—Al, **15** et **16**, en présence de 5 mol% de $CoCl_2\cdot(PPh_3)_2$, fournit de 53 à 61% d'un seul 5-hydroxy-2-tri-*n*-butylstannylpent-1-ène (**32**). Les adduits de stannylcuivre générés au cours de la réaction du undéca-1,2-diène avec **8** ou **9** ont été traités avec l'iodométhane pour fournir de 55 à 78% d'un mélange (*Z*/*E*: 77/33) de 1-tri-*n*-butylstannyl-2-méthylundéc-2-ène (**33**). L'addition de silylcuprates mixtes, **21**, **22** et **23**, au undéca-1,2-diène fournit des mélanges riches en (*E*)-2-diméthylphénylsilylundéc-2-ène (**35**) et 2-diméthylphénylsilylundéc-1-ène (**36**). On présente aussi une rationalisation pour la formation des adduits putatifs.

Mots clés : Sn—Cu, Sn—Al, Sn—B réactifs; adduits putatifs.

[Traduit par la rédaction]

Can. J. Chem. Downloaded from www.nrcresearchpress.com by 123.30.183.119 on 09/08/12
For personal use only.

Introduction

Metallometallations of unsaturated organic compounds proceed well for silyl and stannyl containing dimetallic reagents (e.g. Sn—M; Al, Zn, B, Mg, Mn, Sn, Si and Si—M; Al, Zn, B, Mg, Sn). These reactions are catalyzed by transition metals and copper(I) has emerged as a catalyst of choice (1). The reactions are presumed to involve silyl- or stannylcupration followed by transmetallation of the vinyl copper bond by the electrophilic metal accompanying the silyl or stannyl anion. When conducted under controlled conditions these processes can proceed with high regio- and stereospecificity to provide easily functionalized dimetallic intermediates (2).

Recently Oshima and co-workers reported the copper(I)- or palladium-catalyzed addition of Si—M (M = Mg, Al, Zn) reagents to symmetrical allenes (3). Silylcuprations of allene as well as mono-, di-, and trisubstituted allenes with **1** have been reported by Fleming and co-workers (4). The products were either vinylsilanes, **2**, or allylsilanes, **3**, depending on the degree of substitution of the allenes (Scheme 1).

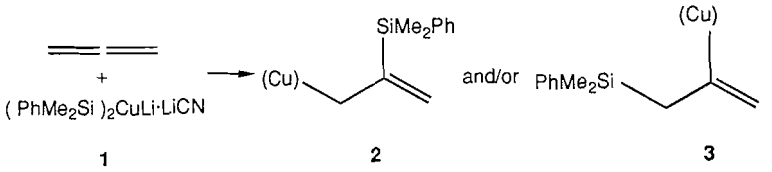
Recent work by Barbero and co-workers (5), summarized in the Table 1, has shown that the regiochemistry of the reaction depends upon the temperature and the nature of the stannylcuprate reagents. Stannylcupration of 1,2-propadiene gave only vinylstannane, **6**, in the presence of LiCl at −76 to 0°C (Table 1, entry 1) while at −100°C only allylstannane, **7**, was formed (Table 1, entry 2). The formation of **6** at the higher temperature and **7** at the low temperature suggests that the former is a product of thermodynamic control and the latter is a product of kinetic control. Effects of salts were also studied. When the halide-free stannylcuprate was reacted with allene at −78°C, only **7** was obtained (Table 1, entry 5) whereas the stannylcuprate in the presence of LiCl (*in situ*) gave **6** as the major product at this temperature (Table 1, entry 3).

Both vinyl and allylstannanes are important intermediates in organic synthesis due to their ability to undergo stereospecific C—C bond formation under mild conditions (6). Our continuing interest in the metallometallations led us to explore the reactions of dimetallic reagents with allenes. In this paper, we describe the reactions of Sn—Cu, Sn—Al, and Sn—B as well as Si—Cu reagents with allenes. We also have briefly investigated the mechanism of these reactions.

Results and discussion

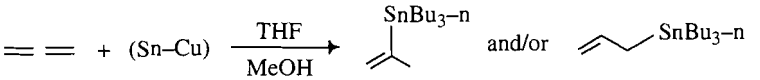
Tri-*n*-butylstannyllithium (**5**) was prepared by deprotonation of Bu_3SnH with lithium diisopropylamide or by cleavage of *n*-Bu_3Sn—$SnBu_3$-*n* with alkyllithium (7). Treatment of 1 equiv. of *n*-Bu_3SnLi (**5**) with 1 equiv. of CuCN gave the lower order cuprate, *n*-$Bu_3SnCu(CN)Li$ (**8**), while 2 equiv. of **5** gave the higher order cuprate, $(n\text{-}Bu_3Sn)_2Cu(CN)Li_2$ (**9**). Reaction of **5** with CuCN in the presence of 2-thienyllithium gave *n*-Bu_3Sn(2-thienyl)$Cu(CN)Li_2$ (**10**). Reaction of **5** with

[1]This paper is dedicated to Professor Herbert C. Brown on the occasion of his 80th birthday.



SCHEME 1

TABLE 1. Addition of Sn—Cu reagents to 1,2-propanediene



Entry	*n*-Bu_3SnLi	Sn—Cu reagent	Reaction conditions (°C, h)	Product ratio (%) 6	7	Yield (%)
1	*n*-Bu_3SnCl + Li	(*n*-$Bu_3Sn)_2Cu(CN)Li_2$ + LiCl	−78 → 0, 1	100	—	92
2	"	"	−100, 1	—	100	100
3	"	"	−100 → −78, 1	82	18	98
4	"	(*n*-$Bu_3Sn)_2CuLi$ + LiBr·Me_2S	−78, 1	100	—	100
5	(*n*-$Bu_3Sn)_2$ + *n*-BuLi	(*n*-$Bu_3Sn)_2Cu(CN)Li_2$	−78, 1	—	100	100

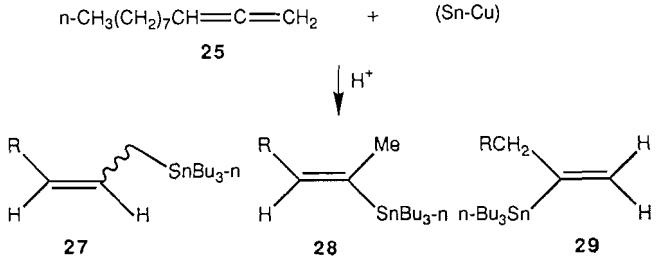
CuBr·DMS in the presence of lithium diisopropylamide or lithium dicyclohexylamide gave *n*-Bu_3Sn(N-*i*-Pr_2)CuLi (**11**) and *n*-Bu_3Sn(N-Cy_2)CuLi (**12**), respectively. Mixed stannylalkylcuprates, *n*-Bu_3Sn(*n*-Bu)Cu(CN)Li_2 (**13**) and *n*-Bu_3Sn(*sec*-Bu)Cu(CN)Li_2 (**14**) were prepared by the reaction of **5** with CuCN followed by the addition of the appropriate alkyllithium.

Addition of Et_2AlCl or Me_3Al to **5** at −78°C gave *n*-Bu_3Sn—$AlEt_2$ (**15**) and *n*-Bu_3Sn—$AlMe_3^-Li^+$ (**16**), respectively. Similarly, reaction of *B*-methoxy-9-BBN (**17**) or tri-*n*-butylborane with **5** provided *n*-Bu_3Sn—$BBN^-(OMe)Li^+$ (**18**) and *n*-Bu_3Sn—$BBu_3^-Li^+$ (**19**), respectively.

Silylcuprates $PhMe_2SiCu(CN)Li$ (**20**), $(PhMe_2Si)_2Cu(CN)Li_2$ (**1**), $PhMe_2Si$(*n*-Bu)Cu(CN)Li_2 (**21**), $PhMe_2Si$(*sec*-Bu)Cu(CN)Li_2 (**22**), and $PhMe_2Si$(*t*-Bu)Cu(CN)Li_2 (**23**) were prepared by reaction of $PhMe_2SiLi$ (**24**) with solutions containing 1 equiv. each of CuCN and the appropriate lithium reagent. 1,2-Undecadiene (**25**) was chosen as a substrate because of its low volatility that facilitated detection of unreacted starting material. It was prepared by alkylation of allene with 1-octylbromide (8). 5-Hydroxy-1,2-pentadiene (**26**) was employed to determine if the polar functional group would exhibit a directive effect on the regiochemistry of the additions.

Reaction of 2 equiv. of *n*-$Bu_3SnCu(CN)Li$ (**8**) with 1,2-undecadiene (Scheme 2) in tetrahydrofuran (THF) at −78°C followed by quenching with aqueous NH_4Cl/MeOH gave 91% of a (*Z*/*E*:65/35) mixture of 1-tri-*n*-butylstannyl-2-undecene (**27**) accompanied by 9% of a mixture of (*E*)-2-tri-*n*-butylstannyl-2-undecene (**28**) and 2-tri-*n*-butylstannylstannyl-1-undecene (**29**) (Table 2, entry 1). Structures of **27**, **28**, and **29** were determined by analysis of their ^1H nmr spectra.

Thus, in the ^1H nmr spectrum of *Z*-**27**, signals in between 5.31 and 5.39 ppm (dtt, 1 H, J = 10, 7, 1 Hz) were assigned to



SCHEME 2

the vinyl hydrogen attached to C-3 while the vinyl hydrogen at C-3 in *E*-**27** gave signals between 5.43 and 5.51 ppm (dtt, 1 H, J = 15, 7, 1.5 Hz). The signals between 5.71 and 5.85 ppm in the spectrum of *Z*-**27** (dtt, 1 H, J_{trans} = 15, 7, 1.5 and J_{cis} = 10, 7, 1 Hz) were attributed to a vinyl hydrogen at C-2 of this isomer. The ^1H nmr spectrum of **28** exhibited a signal at 5.85 ppm (tq, 1 H, J = 7, 1 Hz and $^3J_{Sn—H}$ = 64 Hz) attributed to the vinyl hydrogen attached to C-3. The Sn—H coupling (64 Hz) indicates these two nuclei possess a *cis* arrangement (1 h). The *Z*- and *E*-vinyl hydrogens of **29** resonated at 5.36 ppm (dt, 1 H, J = 2.9, 1 Hz and $^3J_{Sn—H}$ = 64 Hz) and 5.91 ppm (dt, 1 H, J = 2.9, 1.5 Hz and $^3J_{Sn—H}$ = 146 Hz), respectively.

Reaction of homostannylcuprates **9** and **8** with **25** (Table 2, entries 1–6) revealed that these reagents gave mixtures rich in allylstannane, **27**.[2] To improve the stereoselectivity of allylstannane formation we examined a variety of proton sources

[2]THF solutions containing 2 equiv. of trialkylstannyllithium and 1 equiv. of CuCN have been shown by NMR to contain nearly equivalent amounts of $(R_3Sn)_2CuCNLi_2$, $(R_3Sn)_3CuLi_2$, and $(R_3Sn)_3Cu_2Li$, ref. 9.

Can. J. Chem. Downloaded from www.nrcresearchpress.com by 123.30.183.119 on 09/08/12
For personal use only.

TABLE 2. Reaction of Sn—Cu reagents with 1,2-undecadiene[a]

Entry	Sn—Cu reagent	Reaction conditions (°C, h)	Product ratio, (%)[b]			Yield (%)
			27	**28**	**29**	
1	n-$Bu_3SnCu(CN)Li$ (2 eq)	−78, 3	65 (*Z*) 35 (*E*) 91	3	6	91
2	(1 eq)	−78 → 20, 18	14 (*Z*) 86 (*E*) 71	19	10	71
3	$(n$-$Bu_3Sn)_2Cu(CN)Li_2$	−78, 2	99 (*Z*) 75	18	7	86
4	$(n$-$Bu_3Sn)_2Cu(CN)Li_2$/HMPA	−78, 1	63 (*Z*) 37 (*E*) 68	24	8	85
5	$(n$-$Bu_3Sn)_2Cu(CN)Li_2$	−100, 1	60 (*Z*) 40 (*E*) 88	5	6	87
6	$(n$-$Bu_3Sn)_2Cu(CN)Li_2$/HMPA	−100, 1	70 (*Z*) 30 (*E*) 92	4	4	94
7	$(n$-$Bu_3Sn)_2Cu(CN)Li_2$	−100 → 0, 2	41 (*Z*) 59 (*E*) 44	36	20	75
8	$(n$-$Bu_3Sn)_2Cu(CN)Li_2 \cdot 2LiCl$	−100 → 0, 2	40 (*Z*) 60 (*E*) 39	49	12	77
9	n-Bu_3Sn(2-Th)$Cu(CN)Li_2$	−78 → 10, 12	99 (*E*) 40	55	5	69[c]
10	n-$Bu_3Sn(N—Cy_2)CuLi$	−78, 3	99 (*Z*) 49	5	16	58[c]
11	n-$Bu_3Sn(N$-i-$Pr_2)CuLi$	−78, 3	80 (*Z*) 20 (*E*) 50	20	30	59[c]
12	n-$Bu_3Sn(n$-Bu$)Cu(CN)Li_2$	−78, 2	66 (*Z*) 34 (*E*) 14	59	27	79
13	n-$Bu_3Sn(sec$-Bu$)Cu(CN)Li_2$	−78 → 0, 9	10	52	38	69

[a]Reactions were conducted in THF.
[b]The ratios were determined by capillary gc.
[c]Yields refer to gc, *n*-dodecane was used as the internal standard.

to quench the presumptive stannylcopper intermediates. On the assumption that neither aqueous NH_4Cl nor MeOH provide products of kinetic control (e.g. *Z*-**27**), we employed more active hydrogen ion sources such as acetic and trifluoroacetic acids. These did not alter the stereochemistry of **27**, but decreased yields of the stannyl products to 63–65% and nearly 30% of **25** was recovered. No undecenes were detected in these reaction mixtures. Reaction of 1 equiv. of cuprate **8** with **25** required 18 h to yield **27** which was a mixture of *E* and *Z* isomers (Table 2, entry 2). In contrast, reaction of **9** with **25** gave *Z*-**27** stereospecifically. Thus, reaction of 2 equiv. of $(n$-$Bu_3Sn)_2Cu(CN)Li_2$ (**9**) with **25** provided 75% of *Z*-**27**, along with 25% of **28** and **29** (Table 2, entry 3). Use of HMPA as a coordinating solvent did not alter the regioselectivity of the reaction (Table 2, entry 4). However, when **9** was treated with **25** at −100°C the regioselectivity of the reaction improved significantly (Table 2, entries 5, 6). Thus reaction in THF/HMPA gave 92% of **27** along with 8% of **28** and **29**. Quenching the above reactions after warming to 0°C gave 56% of **28** and **29** together with 44% of **27** (Table 2, entry 7). While our work was in progress, Barbero and co-workers (5) reported that presence of the salts in these reactions catalyzes the isomerization of the initially formed adduct to a more stable isomer (Table 1). We studied the effect of the salt and found that it had little effect on the regioselectivity of the reaction (Table 2, compare entries 7 and 8). Thus, it appears that the stannylcuprations that occur at higher temperature yield vinylstannanes, **28** and **29** (e.g. thermodynamic control), while at low temperature the reactions yield allylstannane, **27** (e.g. kinetic control).

Homostannylcuprates, **8** and **9**, are inherently unstable and their reactions with **25** are accompanied by the formation of numerous stannyl-containing byproducts due to the excess of reagent required to achieve complete consumption of allene (even in the presence of methanol). To circumvent these problems we examined the reactions of several heterostannylcuprates with **25**. Heteroalkylcuprates containing phosphido, amido and 2-thienyl groups react with organic substrates via exclusive transfer of the alkyl group (10). Furthermore, both 2-thienyl (10*c*) and alkylstannylcuprates (11) exclusively transfer trialkylstannyl ligands. Fleming and Newton have shown an identical preference for the transfer of silyl with $PhMe_2Si(Me)Cu(CN)Li_2$ (12). Stannylcuprates containing 2-thienyl (**10**) or amino ligands (**11** and **12**) react with **25** to give nearly equal amounts of vinyl and allyl stannane products (Table 2, entries 9–11). Mixed alkylstannylcuprates, **13** and **14**, gave mixtures rich in vinylstannanes, **28** and **29** (Table 2, entries 12, 13).

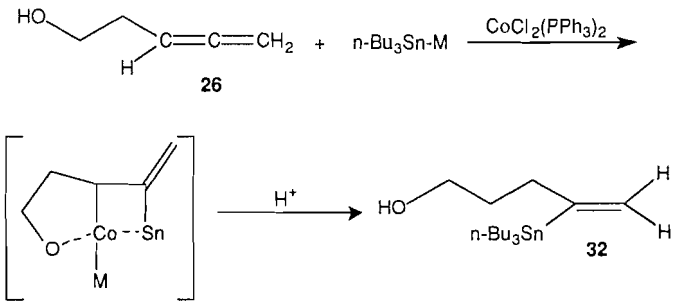
It is evident from recent work in our laboratory that dialkylaluminum and boron cations act as *in situ* transmetallation agents in stannylcuprations to provide intermediates containing reactive C—Al and C—B bonds in place of relatively unreactive C—Cu bonds (1 h, ref. 2). These transmetallations can be achieved by the copper-catalyzed addition of preformed reagents such as n-$Bu_3Sn—AlEt_2$ (**15**), n-$Bu_3Sn—AlMe_3^-Li^+$ (**16**), n-$Bu_3Sn—BBN^-(OMe)Li^+$ (**18**) or n-$Bu_3Sn—BBu_3^-Li^+$ (**19**). Alternatively, addition of Et_2AlCl or *B*-methoxy-9-BBN (**17**) to stannylcuprations will result in C—Cu transmetallation (2). Reaction of n-$Bu_3Sn—AlEt_2$ (**15**), n-$Bu_3Sn—AlMe_3^-Li^+$ (**16**), n-$Bu_3Sn—BBN^-(OMe)Li^+$ (**18**) or n-$Bu_3Sn—BBu_3^-Li^+$ (**19**) with **25** in the presence of 5 mol% CuCN gave mixtures rich in vinylstannane, **29** (Table 3, entries 1, 4, 7, 10). With 1 equiv. of catalyst mixtures rich in allylstannane, **27**, were obtained (Table 3, entries 2, 5, 8, 11). Use of $CoCl_2 \cdot (PPh_3)_2$ as a catalyst gave mixtures of allyl and vinylstannanes, **27** and

Can. J. Chem. Downloaded from www.nrcresearchpress.com by 123.30.183.119 on 09/08/12
For personal use only.

TABLE 3. Addition of Sn—Al and Sn—B reagents to 1,2-undecadiene[a]

Entry	Sn—M	Catalyst	Reaction conditions (°C, h)	Product ratio, (%)[c] 27	28	29	Yield (%)
1	n-Bu_3Sn—$AlEt_3$	CuCN 5 mol%	−40 → rt, 16	90 (*Z*), 10 (*E*) 35	—	65	80
2	"	1 equiv.	−78, 1.5	55 (*Z*), 45 (*E*) 82	6	12	46
3	"	$CoCl_2(PPh_3)_2$ 5 mol%	−50 → −15, 6	57 (*Z*), 43 (*E*) 17	—	83	53
4	n-Bu_3Sn—$\bar{A}lMe_3\overset{+}{L}i$	CuCN 5 mol%	−78 → −40, 6	5	14	81	78
5	"	1 equiv.	−78, 1	89 (*Z*), 11 (*E*) 83	—	16	90
6	"	$CoCl_2(PPh_3)_2$ 5 mol%	−50 → −15, 6	55 (*Z*), 45 (*E*) 53	—	47	37
7	n-Bu_3Sn—$\bar{B}BNL\overset{+}{i}$[c]	CuCN 5 mol%	−78 → −50, 3	70 (*Z*), 30 (*E*) 21	9	70	51[d]
8	"	1 equiv.	−78, 1.5	45 (*Z*), 55 (*E*) 69	—	31	47
9	"	$CoCl_2(PPh_3)_2$ 5 mol%	−78 → −50, 4	70 (*Z*), 30 (*E*) 11	7	82	61[d]
10	n-Bu_3Sn—$\bar{B}Bu_3\overset{+}{L}i$	CuCN 5 mol%	−30, 2	69 (*Z*), 31 (*E*) 12	—	88	25[d]
11	"	1 equiv.	−78, 2	76 (*Z*), 24 (*E*) 84	6	10	41[d]
12	"	$CoCl_2(PPh_3)_2$ 5 mol%	−78 → −50, 4	65 (*Z*), 35 (*E*) 48	15	37	49

[a]Reactions were conducted in THF.
[b]The ratios were determined by capillary gc.
[c]n-Bu_3Sn—$\bar{B}BNL\overset{+}{i}$ was prepared from n-Bu_3SnLi and B-methoxy-9-BBN.
[d]Yields refer to gc, n-dodecane was used as the internal standard.



SCHEME 3

29, respectively (Table 3, entries 3, 6, 9, 12). Regioselectivity of these reactions depends upon the temperature and the nature of Sn—Al and Sn—B reagents. With 1 equiv. of catalyst, reactions conducted at −78°C provided mixtures rich in **27** while with 5 mol% of the catalyst higher temperatures were required to complete the reaction and gave mixtures rich in **28** and **29**.

Metallometallation of hydroxyallene, **26**, was studied in the hope that the hydroxyl group would direct the regiochemistry of addition of Sn—M reagents (Scheme 3). Addition of both lower and higher order homostannylcuprates (**9** and **8**) gave mixtures of allyl and vinylstannanes, **30–32** (Table 4, entries 9 and 10). Addition of Sn—Al and Sn—B reagents in the presence of CuCN also gave mixtures (Table 4, entries 2, 4, 6, 8). Only use of oxyphilic $CoCl_2 \cdot (PPh_3)_2$ as a catalyst with **15–19** gave a single vinylstannane product (**32**) in high regiochemical purity (Table 4, entries 1, 3, 5, 7). The ^1H nmr spectrum of **32** in the vinyl region was very similar to that of **29**.

Stannylcopper adducts generated in the reactions of **8** and **9** with **25** were reacted with MeI, Et_2AlCl, and *B*-Br—BBN in the hope that electrophilic capture would provide single isomers. Indeed, the adducts generated from either **8** or **9** and **25** reacted with MeI to give only allylstannane, **33** (Table 5, entries 1 and 2). The isomer distribution obtained is, within experimental error, that obtained upon quenching with a solution of MeOH and aq. NH_4Cl (Table 2, entries 1 and 4). The structure of **33** was confirmed by NMR spectroscopy. A signal at 1.73 ppm was assigned to the hydrogens of *E*-methyl carbon while the hydrogens of *Z*-methyl carbon resonanted at 1.81 ppm. Signals at 1.91 ppm (bs) and 1.93 ppm (bs) were attributed to the hydrogens at C-1 of *Z*- and *E*-isomers, respectively. The hydrogen on the *Z*-vinylic carbon resonated at 5.12 ppm (bt, $J = 7$ Hz) while the hydrogen of the *E*-vinylic carbon resonated at 5.26 ppm (bt, $J = 7$ Hz). Irradiation of the signals at 5.12 ppm resulted in enhancement of the signal at 1.81 ppm. Hence, the hydrogen of the vinylic carbon and the hydrogens of the methyl carbon at 1.81 ppm are *cis*. The reaction with the higher order cuprate provides a higher yield of product in a shorter time than reaction with the lower order cuprate. Quenching the reaction of **8** or **9** and **25** by addition of Et_2AlCl or B-Br-9-BBN followed by protonolysis gave allylstannane, **27**, and vinylstannanes, **28** and **29** (Table 5, entries 3–6). Yields of stannanes are again higher from the reaction with the higher order cuprate.

We also studied silylcupration of **25** with $PhMe_2SiCu(CN)Li$ (**20**), $(PhMe_2Si)_2Cu(CN)Li_2$ (**1**), $PhMe_2Si(n\text{-}Bu)Cu(CN)Li_2$ (**21**), $PhMe_2Si(sec\text{-}Bu)Cu(CN)Li_2$ (**22**), and $PhMe_2Si(t\text{-}Bu)Cu(CN)Li_2$ (**23**). Reaction of homosilylcuprates **1** and **20** gave

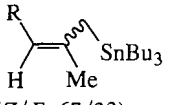
Can. J. Chem. Downloaded from www.nrcresearchpress.com by 123.30.183.119 on 09/08/12
For personal use only.

TABLE 4. Reaction of n-Bu_3Sn—M reagents with 5-hydroxy-1,2-pentadiene[a]

Entry	Sn—M	Catalyst[b]	Reaction conditions (°C, h)	Product (%)[c] 30	31	32	Product (%)
1	n-Bu_3Sn—$AlEt_2$	$CoCl_2(PPh_3)_2$	−78 → rt, 18	—	—	>99	53
2	"	CuCN	−78 → rt, 15	36 (*Z*) 64 (*E*) 68	20	12	57
3	n-Bu_3Sn—$\bar{A}lMe_3\dot{Li}$	$CoCl_2(PPh_3)_2$	−78 → 0, 4	—	—	>99	61
4	"	CuCN	−78 → −50, 3	66 (*Z*) 34 (*E*) 22	—	78	66
5	n-Bu_3Sn—$\bar{B}BN\dot{Li}$	$CoCl_2(PPh_3)_2$	−60 → −20, 4	—	—	>99	30[d]
6	"	CuCN	−78 → −20, 4	66 (*Z*) 34 (*E*) 43	—	57	15[d]
7	n-Bu_3Sn—$\bar{B}Bu_3\dot{Li}$	$CoCl_2(PPh_3)_2$	−60 → −20, 4	—	—	>99	27[d]
8	"	CuCN	−70 → −20, 4	61 (*Z*) 39 (*E*) 46	—	54	25[d]
9	n-$Bu_3SnCu(CN)Li$	—	−78 → −70, 2	61 (*Z*) 39 (*E*) 85	—	15	57
10	$(n$-$Bu_3Sn)_2Cu(CN)Li_2$	—	−78, 1.5	59 (*Z*) 40 (*E*) 68	14	18	63

[a]Reactions were conducted in THF.
[b]5 mol% of catalyst was used.
[c]The ratios were determined by capillary gc.
[d]Yields refer to gc, n-dodecane was used as the internal standard.

TABLE 5. Quenching of the adducts from lower order and higher order cuprates with the electrophiles[a]

Entry	Adduct (from)	Electrophile	Reaction conditions (°C, h)	Product[b] (R = n-$CH_3(CH_2)_7$)		Yield[c] (%)
1	L.O. Cuprate	MeI	−78 → 15 15	 **33** (*Z*/*E*: 67/33)		55
2	H.O. Cuprate	"	−78, 1 0, 1	**33** (*Z*/*E*: 67/33)		78
3	L.O. Cuprate	Et_2AlCl	−78, 1	**27** (*Z*/*E*: 70/30) **29**	(95) (5)	46
4	H.O. Cuprate	"	−78, 1	**27** (*Z*/*E*: 70/30) **28** **29**	(73) (19) (8)	75
5	L.O. Cuprate	B—Br-9-BBN	−78, 1	**27** (*Z*/*E*: 64/36) **29**	(88) (12)	24
6	H.O. Cuprate	"	−78, 1	**27** (*Z*/*E*: 53/47) **28** **29**	(77) (8) (15)	53

[a]Reactions were conducted in THF.
[b]The ratios were determined by capillary gc.
[c]Yields refer to isolated.

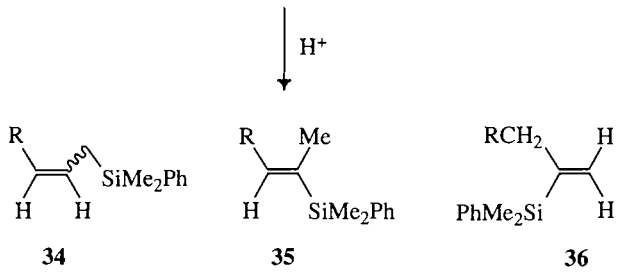
mainly allylsilane, **34**, while mixed silylalkylcuprates, **21–23**, provided vinylsilanes, **35** and **36** (Table 6).

In reactions in which cuprous ion is present in catalytic quantities the higher order stannyl or silylcuprates are considered to be the active species regardless of the presence of electrophilic aluminum or boron counter ions (1 h). A catalytic role for cuprous ion in the additions of Sn—M reagents to allenes is described in Scheme 4 (1 h) in which the first step is the oxidative addition (*a*) of the Sn—M reagent to Cu^+ to generate a three-coordinate Cu^+ species. This is followed by complexation (*b*) and stannylcupration (*c*) of the allene. Another equivalent Sn—M reagent oxidatively adds (*d*) to the vinyl copper species to give a higher order cuprate which undergoes reductive elimination with the assist of solvent (*e*) to regenerate the initial complex and a Sn—M adduct. The oxidative state of copper remains +1 throughout the reaction sequence. Examination of Tables 3 and 5 reveals that the outcome of stannylmetallations of **25** is not influenced by the order of addition of reagents. Essentially the same compositions of allylstannane **27** are obtained from reactions in which aluminum or boron reagents are added before or after the allene.

Addition of Sn—M reagents to the least substituted double bond of 1,2-allenes would give intermediates **37** and **38**, while

Can. J. Chem. Downloaded from www.nrcresearchpress.com by 123.30.183.119 on 09/08/12
For personal use only.

TABLE 6. Reaction of silylcuprates with 1,2-undecadiene[a]

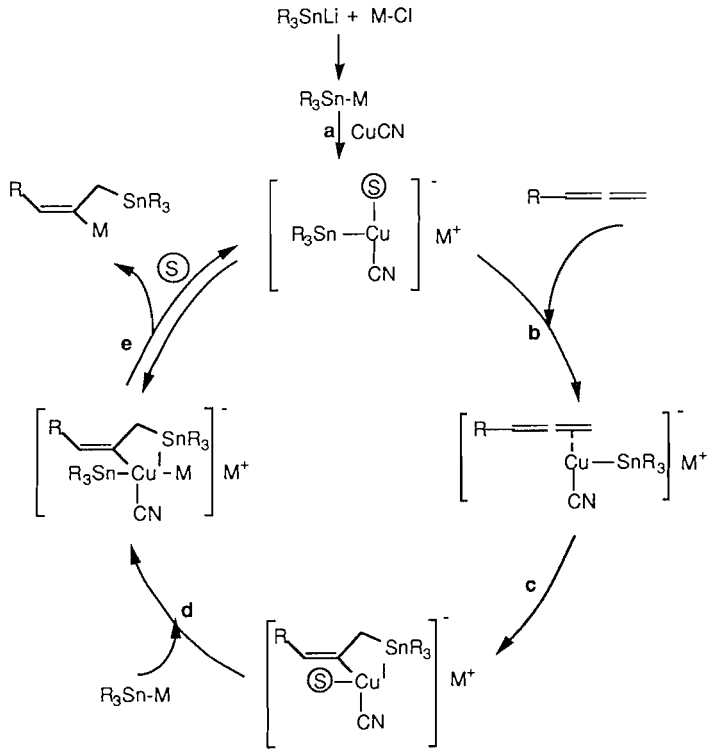


34 35 36

Entry	Si—Cu reagent	Reaction conditions (°C, h)	Product ratio, (%)[b] 34	35	36	Yield[c] (%)
1	$PhMe_2SiCu(CN)Li$	−78, 1	95 (*Z*) 5 (*E*) 87	9	4	80
2	$(PhMe_2Si)_2Cu(CN)Li_2$	−78, 1	90 (*Z*) 10 (*E*) 82	14	4	78
3	$PhMe_2Si(n\text{-}Bu)Cu(CN)Li_2$	−78, 1	2	55	45	83
4	$PhMe_2Si(sec\text{-}Bu)Cu(CN)Li_2$	−78, 1	4	72	24	71
5	$PhMe_2Si(t\text{-}Bu)Cu(CN)Li_2$	−78, 1	10	50	50	90

[a]Reactions were conducted in THF.
[b]The ratios were determined by capillary gc.
[c]Yields refer to isolated products.

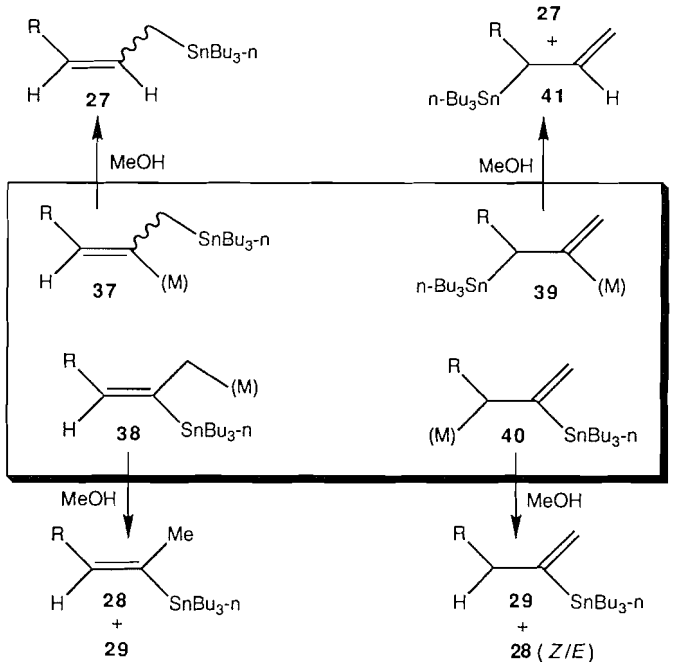
addition to the internal double bond would give intermediates **39** and **40**. The formation of allylstannanes is undoubtedly via **37** and **39**. Allylstannane, **27**, derived from most additions of Sn—Cu, Sn—Al, and Sn—B reagents is predominantly, but not exclusively, *Z*. Notable exceptions (Table 2, entries 2 and 9) in which *E*-**27** predominated were reactions quenched after warming above 0°C. Intermediate, **37**, would be expected to give predominantly *Z*-**27** since stannylcupration should occur in *cis* fashion (13) from the least hindered side of the allene. To rule out the involvement of **39** as an intermediate we conducted the work-up and isolation of **27** under conditions which would be expected (14) to allow the isolation of **41**. Under carefully controlled work-up conditions and using ^1H nmr analysis we found no evidence of **41**.[3] This militates against the involvement of **39** as an intermediate in the formation of **27** and suggests **37** as the intervening species. The formation of both *E*- and *Z*-**27** in the reactions described in Tables 2 and 3 is thus due to either *Z* to *E* isomerization during workup or nonstereoselective attack of **25** by the organometallic reagents. Allylstannane, **27**, was shown to be stable under both work-up and analysis conditions (14). Intermediates **38** and **40** are presumptive precursors of vinylstannanes, **28** and **29**. *In situ* transmetallation of the C—Cu bonds of **38** and **40** by electrophilic aluminum or boron followed by the protonolysis of allylmetal increases the proportion of **29** relative to **28**. This course of events requires that **38** (M = Al, B) be converted to **29** by SE′ protonolysis. Indeed, it is known that both allylaluminums (16) and allylborons (17) undergo protonolysis by SE′ processes. Thus it appears that the vinylstannanes are formed via **38** and not **40**. Overall the weight of evidence suggests stannylcupration of 1,2-allenes occurs at the external olefin linkage to yield **37** and **38** which ultimately give rise to **27–29**. The relative proportions of allyl to vinylstannane



SCHEME 4

[3]Crotyltrimethylstannanes undergo facile equilibration between the 1-stannyl and 3-stannyl isomers with the latter being sufficiently unstable in polar solvents that it is difficult to isolate. Kinetically controlled isomerization of 1-buten-3-yltrimethylstannane in methanol gives a 3:1 mixture of *Z*- and *E*-2-butenyltrimethylstannanes which equilibrates to an approximate 1:1 mixture upon standing, ref. 14. However, in non-polar aprotic solvents allylstannanes are stable to 1,3 shift, ref. 15.

Can. J. Chem. Downloaded from www.nrcresearchpress.com by 123.30.183.119 on 09/08/12
For personal use only.



SCHEME 5

products are thus a function of the regiochemistry of addition. Homocuprates **8** and **9** give **37** while heterostannylcuprates, **10–12**, and mixed alkylstannylcuprates favor **38**. Only in the case of an allene containing a proximal polar functional group **26** are the reactions clean (Table 4).

Reaction of **25** with homosilylcuprates, **20** and **1**, gave predominantly allylsilane (*Z*-**34**, Table 6). This result parallels the stannylcuprations of this allene (Table 2). Addition of mixed silylalkylcuprates, **21–23**, to give **25** gave mixtures rich in vinylsilane, again paralleling the stannyl system. It is attractive to attribute the products formed in these reactions to the intermediacy of the silyl analogs of **37** (M = Cu) and **38** (M = Cu).

Experimental

Gas–liquid chromatographic analyses were conducted on either a Hewlett-Packard 5880A or 5890A gas chromatographs fitted with capillary inlet systems, flame-ionization detectors and WCOT columns (7, 15, and 30 m × 0.25 mm i.d.) of glass or fused silica. Columns were coated with OV-101, SP-2100, or DB-1 liquid phases. Injection port and detector temperatures were 260 and 275°C, respectively. Helium was the carrier gas. Dodecane was used as the internal standard for quantitative analyses.

Low resolution mass spectra were obtained on a Hewlett-Packard 5985B gas chromatograph – mass spectrometer and high resolution mass spectra were recorded with Kratos/AEI MS 50 or MS 902 spectrometers. ^{1}H nmr spectra were recorded in $CDCl_3$ or C_6D_6 Bruker 100 or 400 WM spectrometers. Signal positions are given in δ units and the tin–hydrogen coupling constants ($J_{Sn—H}$) are given as an average of the ^{117}Sn and ^{119}Sn values. Infrared spectra were determined on a Perkin-Elmer 599B spectrometer.

All reactions requiring anhydrous and/or oxygen-free conditions were conducted with a positive pressure of argon or nitrogen in flame-dried glassware. Tetrahydrofuran (THF) was freshly distilled from sodium or potassium metal with benzophenone as an indicator. CuCN, 9-BBN, *n*-Bu_3SnCl, $(n\text{-}Bu_3Sn)_2$, $PhMe_2SiCl$, and Et_2AlCl were purchased from Aldrich Chemical Co.

*Preparation of 1,2-undecadiene (**25**)*

This was prepared in 93% yield by the method of Brandsma (8); bp 55°C (3 Torr); ir (film): 2959, 2928, 2872, 1957.9, 1660.8, 1466, 1377.5, 1093.7, and 841 cm^{-1}; ^{1}H nmr ($CDCl_3$) δ: 0.86 (3 H, t, *J* = 6 Hz), 1.2–1.62 (12 H, m), 1.86–2.21 (2 H, m), 4.62–4.86 (2 H, dt, *J* = 6, 3 Hz), 5.0–5.32 (1 H, tt, *J* = 6, 6 Hz).

*Preparation of 5-hydroxy-1,2-pentadiene (**26**)*

Ethyl 3,4-pentadienoate (18) (6.3 g, 50 mmol) in 10 mL of ether was added dropwise to a suspension of LAH (2 g, 50 mmol) in 50 mL of ether at 0°C. The mixture was stirred for 1.5 h. Ice-cold 2 N HCl was added to hydrolyze excess LAH. The aq. layer was extracted with ether (3 × 30 mL) and the etheral layer was washed with brine, dried ($MgSO_4$), and concentrated *in vacuo* to give a crude product which was distilled to give 3.1 g of **26** (74%), bp 50–53°C at 12 Torr; ir (film): 3346.7, 2957.1, 2928.2, 2854.8, 1957.9, 1735.4, 1466, 1377.3, 1180.5, 1093.7, and 841 cm^{-1}; ^{1}H nmr ($CDCl_3$) δ: 1.67 (1 H, bs), 2.10–2.43 (2 H, m), 3.72 (2 H, bs), 4.62–4.89 (2 H, dt, *J* = 6, 3 Hz), 5.99–5.27 (1 H, tt, *J* = 6, 6 Hz).

*Preparation of tri-*n*-butylstannyllithium (**5**)*

From n-*Bu_3SnH*: To a mixture of diisopropylamine (0.7 mL, 5 mmol) in 10 mL of THF was added *n*-BuLi (2.1 mL, 5 mmol) at −40°C. After 30 min, *n*-Bu_3SnH (1.35 mL, 5 mmol) was added and the solution was stirred for 40 min to give 5 mmol of *n*-Bu_3SnLi.

From n-*Bu_3SnH—$SnBu_3$*-n: *n*-Butyllithium (2.1 mL, 5 mmol) was added to a solution of bis tri-*n*-butylstannane (2.53 mL, 5 mmol) in 10 mL of THF and the reaction mixture was stirred for 20 min to yield *n*-Bu_3SnLi (5 mmol).

Preparation of n-*$Bu_3SnCu(CN)Li$ (**8**)*

Copper(I) cyanide (0.45 g, 5 mmol) was added to a THF solution of tri-*n*-stannyllithium (prepared as above) (5 mmol) at −78°C to give **8**.

Preparation of $(n\text{-}Bu_3Sn)_2Cu(CN)Li_2$ (**9**)

CuCN (0.225 g, 2.5 mmol) was added to **5** (5 mmol) at −78°C to afford **9**.

*Preparation of mixed cuprates, **10–14***

Addition of lithium 2-thienylcyanocuprate (20 mL, 5 mmol) to **8** (5 mmol) in THF at −78°C gave the mixed cuprate, **10**. Similarly, other mixed cuprates were prepared by mixing 1 equiv. of the organolithium with an equivalent of **8** in THF at −78°C.

Preparation of n-*$Bu_3Sn—AlEt_2$ (**15**) and* n-*$Bu_3Sn—AlMe_3^-Li^+$ (**16**)*

Diethylaluminum chloride (5 mmol) was added to a THF solution of *n*-Bu_3SnLi (5 mmol) at −78°C and the mixture was stirred for 30 min to give **15**. Similarly, reaction of trimethylaluminum with **5** at −78°C gave **16**.

Preparation of n-*$Bu_3Sn—BBN(OMe)^-Li^+$ (**18**) and* n-*$Bu_3Sn—BBu_3^-Li^+$ (**19**)*

Addition of B-methoxy-9-BBN (5 mmol) to a THF solution of 5 mmol of tri-*n*-butylstannyllithium (**5**) at −78°C provided **18**. Similarly, reaction of tri-*n*-butylborane with **5** gave **19**.

*Preparation of dimethylphenylsilyllithium (**24**)*

Small pieces of lithium wire (0.45 g, 64 mmol) were added to dimethylphenylsilyl chloride (3.6 g, 21 mmol) in 20 mL of THF at −5°C. The mixture was stirred overnight at 0°C and the reagent was titrated by following the method of Fleming *et al.* (19).

*Preparation of $PhMe_2SiCu(CN)Li$ (**20**) and $(PhMe_2Si)_2Cu(CN)Li_2$ (**1**)*

Addition of 1 equiv. of $PhMe_2SiLi$ in THF as prepared above to 1 equiv. of CuCN at −78°C gave **20** whereas reaction of 2 equiv. of $PhMe_2Si$ with 1 equiv. of CuCN at −78°C gave **1**.

Preparation of $CoCl_2{\cdot}(PPh_3)_2$

This complex was prepared according to the reported method (20). A solution of triphenylphosphine (38 g, 145 mmol) in 250 mL of benzene was refluxed with anhydrous cobalt chloride (8.64 g, 66 mmol) for 1 h. The blue precipitate which formed melted at 100–102°C (lit. (21) mp 102°C).

Reaction of n-*$Bu_3SnCu(CN)Li$ (**8**) with 1,2-undecadiene (**25**) (Table 2, entry 1)*

The following procedure is representative: To a mixture of 10

Can. J. Chem. Downloaded from www.nrcresearchpress.com by 123.30.183.119 on 09/08/12
For personal use only.

Can. J. Chem. Downloaded from www.nrcresearchpress.com by 123.30.183.119 on 09/08/12
For personal use only.

mmol of **8** in 20 mL of THF was added allene **25** (0.95 mL, 5 mmol) at −78°C. After the addition, the mixture was stirred for 1 h and quenched by the addition of a solution of MeOH and aq. NH_4Cl. The aqueous layer was extracted with hexanes (4 × 50 mL). The combined organic layer was washed twice with brine (30 mL), dried ($MgSO_4$), and the solvent removed *in vacuo* to give crude products (3.7 g). The crude isolate was treated with silver acetate (2.8 g, 16 mmol) in 100 mL of ethyl acetate in the open air at room temperature. After 13 h, the mixture was filtered through Celite, then washed with ice-cold water (2 × 50 mL) and brine (2 × 50 mL), dried ($MgSO_4$), and the solvents removed. The crude products were purified on silica gel (pretreated with Et_3N) by elution with hexanes to give a mixture of **27**, **28**, and **29** in 91% yield (2 g). Isomer ratios were determined by gc analysis.

Attempted isolation of ***41*** *under the control experiment*

To a suspension of **9** (2.5 mmol) in 20 mL of THF, was added allene **25** (0.2 mL, 1.25 mmol) at −78°C. After I h the reaction mixture was quenched with saturated $NaHCO_3$ at −78°C and work up as usual. The products obtained were subjected to nmr analysis immediately.

(E)- and (Z)-1-Tri-n-*butylstannyl-2-undecene (27)*

^{1}H nmr ($CDCl_3$) δ: 0.9–1.08 (18 H, m), 1.25–1.51 (18 H, m), 1.56–1.66 (6 H, m), 1.89 (2 H_{trans}, d, J = 7 Hz, $J_{Sn—H}$ = 49.95, 66.6 Hz), 1.96 (2 H_{cis}, d, J = 7 Hz, $J_{Sn—H}$ = 53.28, 59.94), 2.16 (2 H_{trans}, dt, J = 7, 6.5 Hz), 2.24 (2 H_{cis}, dt, J = 7, 6.5 Hz), 5.31–5.39 (1 H_{cis}, dtt, J = 10, 7, 1 Hz), 5.43–5.51 (1 H_{trans}, dtt, J = 16, 7, 1.5 Hz), 5.71–5.85 (1 H_{trans} and 1 H_{cis}, dtt, J_{trans} = 16, 7, 1.5 and J_{cis} = 10, 7, 1 Hz); gc/ms, m/e (%, rel. int.): 387 (M^+ − 57, 30.3%). Exact Mass calcd. for $C_{19}H_{39}Sn$ (M^+ − Bu): 387.2073; found: 387.2080.

(E)-2-Tri-n-*butylstannyl-2-undecene (28)*

^{1}H nmr (C_6D_6) δ: 0.85–1.25 (18 H, m), 1.28–1.56 (18 H, m), 1.59–1.84 (6 H, m), 2.02 (3 H, d, J = 1.5 Hz and $J_{Sn—H}$ = 49.95 Hz), 2.29 (2 H, dt, J = 7, 6.5 Hz), 5.85 (1 H, tq, J = 7, 1.5 Hz and $J_{Sn—H}$ = 70 Hz); gc/ms, m/e (%, rel. int.): 387 (M^+ − 57, 92.85%). Exact Mass calcd. for $C_{19}H_{39}Sn$ (M^+ − Bu): 387.2073; found: 387.2080.

2-Tri-n-*butylstannyl-1-undecene (29)*

^{1}H nmr (C_6D_6) δ: 0.9–1.08 (18 H, m), 1.25–1.51 (20 H, m), 1.56–1.83 (6 H, m), 2.46 (2 H, t, J = 6.5 Hz), 5.36 (1 H, d, J = 2.9 Hz and $J_{Sn—H}$ = 65 Hz), 5.91 (1 H, dt, J = 2.9, 1.5 Hz and $J_{Sn—H}$ = 140 Hz); gc/ms, m/e (%, rel. int.): 387 (M^+ − 57, 66.66%). Exact Mass calcd. for $C_{19}H_{39}Sn$ (M^+ − Bu): 387.2073; found: 387.2082.

Addition of (n-$Bu_3Sn)_2Cu(CN)Li_2$ ***(9)*** *to* ***25*** *(Table 2, entry 3)*

The following method is representative: Allene **25** (0.45 mL, 2.5 mmol) was added to a mixture of **9** (5 mmol) in 20 mL of THF at −78°C. The reaction mixture was stirred for 1.5 h and quenched by the addition of a solution of MeOH and aq. NH_4Cl. The organic layer was separated and the aqueous solution was extracted with hexanes (4 × 50 mL) and dried ($MgSO_4$). Removal of the solvents gave the crude products which were treated with silver acetate and purified as above to give a mixture of **27**, **28**, and **29** in 86% yield (0.95 g).

Addition of n-$Bu_3Sn(2\text{-}Th)Cu(CN)Li_2$ ***(10)*** *to* ***25*** *(Table 2, entry 9)*

The following method is representative: To a solution of *n*-$Bu_3Sn(2\text{-}Th)Cu(CN)Li_2$ (5 mmol, prepared as above) in THF was added 1,2-undecadiene (0.45 mL, 2.5 mmol) at −78°C. The reaction was warmed to 10°C over a period of 12 h. Gas chromatographic (quantitative, dodecane as the internal standard) analysis of an aliquot revealed the product distribution given in Table 2 in an overall 69% yield.

Reaction of n-$Bu_3Sn—AlEt_2$ ***(15)*** *with* ***25*** *(Table 3, entry 1)*

The following procedure is representative: To reagent **15** (5 mmol) prepared as above in 20 mL of THF was added **25** (0.45 mL, 2.5 mmol) followed by CuCN (0.025 g, 0.27 mmol) at −40°C. The reaction mixture was warmed to room temperature over a period of 16 h and quenched by addition of a mixture of MeOH and aq. NH_4Cl. After the usual work-up as above, the crude product was treated with silver acetate and subjected to flash chromatography to yield allylstannane **27** and vinylstannane **29** in 80% yield (0.83 g).

Reaction of n-$Bu_3Sn—AlMe_3^-Li^+$ ***(16)*** *with* ***25*** *(Table 3, entry 5)*

The following method is representative: 1,2-Undecadiene (0.34 g, 2.3 mmol) and CuCN (0.45 g, 5 mmol) were added to a solution of **16** in 20 mL of THF at −78°C. After 2 h, the mixture was hydrolyzed by addition of an ice-cold solution of MeOH and aq. NH_4Cl. The aq. solution was extracted with hexanes (4 × 30 mL). The combined organic layer was washed with brine (2 × 30 mL), dried ($MgSO_4$), and concentrated *in vacuo* to provide crude product which was purified by flash chromatography to give **27** and **29** in 90% yield (0.9 g).

Addition of n-$Bu_3Sn—AlEt_2$ ***(15)*** *to 5-hydroxy-1,2-pentadiene* ***(26)*** *in presence of* $CoCl_2{\cdot}(PPh_3)_2$ *(Table 4, entry 1)*

The following procedure is representative: To a solution of **15** (5 mmol) in 20 mL of THF was added allene **26** (0.22 mL, 2.5 mmol) followed by $CoCl_2{\cdot}(PPh_3)_2$ (0.163 g, 5 mol%) at −78°C. The mixture was warmed to room temperature over a period of 18 h and quenched by addition of an ice-cold solution of MeOH and aq. NH_4Cl. After the usual work-up, the crude product was flash chromatographed (ethyl acetate:*n*-hexane, 1:9) to provide 5-hydroxy-2-tri-*n*-butylstannyl-1-pentene (**32**) in 53% yield (0.5 g).

Addition of n-$Bu_3Sn—AlEt_2$ ***(15)*** *to 5-hydroxy-1,2-pentadiene* ***(26)*** *in presence of CuCN (Table 4, entry 2)*

The following method is representative: To a solution of **15** (5 mmol) in 20 mL of THF was added **26** (0.2 mL, 2.5 mmol) followed by CuCN (0.026 g, 5 mol%) at −78°C. The mixture was warmed to room temperature over a period of 15 h and hydrolyzed by the addition of a mixture of MeOH and aq. NH_4Cl. After the extractive work-up with ether, the crude product was purified as above to give (*E*)- and (*Z*)-5-hydroxy-1-tri-*n*-butylstannyl-2-pentene (**30**), (*E*)-5-hydroxy-2-tri-*n*-butylstannyl-2-pentene (**31**) and **32** in 57% yield (0.54 g).

(E)- and (Z)-5-Hydroxy-1-tri-n-*butylstannyl-2-pentene (30)*

Infrared (film): 3340 (OH) cm^{-1}; ^{1}H nmr (C_6D_6) δ: 0.94–1.03 (15 H, m), 1.39 (2 H, sextet, J = 6.5 Hz), 1.53–1.66 (3 H, m), 1.81 (2 H_{trans}, d, J = 6.5 Hz, and $J_{Sn—H}$ = 46.62, 59.94 Hz), 1.86 (2 H_{cis}, d, J = 6.5 Hz and $J_{Sn—H}$ = 39.96, 46.62 Hz), 2.18 (2 H_{trans}, dt, J = 7, 6.5 Hz), 2.29 (2 H_{cis}, dt, J = 7, 6.5 Hz), 3.48 (2 H_{trans}, q, J = 6 Hz), 3.51 (2 H_{cis}, q, J = 6 Hz), 5.14–5.29 (2 H, dtt, J_{cis} = 10, 7, 1 Hz and J_{trans} = 15, 7, 1.5 Hz), 5.69–5.78 (1 H_{trans}, dtt, J = 15, 7, 1.5 Hz), 5.79–5.86 (1 H_{cis}, dtt, 10, 7, 1 Hz); gc/ms, m/e (%, rel. int.): 319 (M^+ − 57, 9.5%). Anal. calcd. for $C_{17}H_{36}OSn$: C 54.25, H 9.57; found: C 54.12, H 9.77.

(E)-5-Hydroxy-2-tri-n-*butylstannyl-2-pentene (31)*

^{1}H nmr (C_6D_6) δ: protons of *n*-Bu_3Sn group resonate at same frequency as for **30**, 1.94 (3 H, d, J = 1 Hz and $J_{Sn—H}$ = 46.6 Hz), 2.34 (2 H, dt, J = 7, 6.5 Hz), 3.43 (2 H, q, J = 6 Hz), 5.75 (1H, tq, 6.5, 1 Hz); gc/ms, m/e (%, rel. int.): 319 (M^+ − 57, 28.57%).

5-Hydroxy-2-tri-n-*butylstannyl-1-pentene (32)*

Infrared (film): 3350 (OH) cm^{-1}; ^{1}H nmr (C_6D_6) δ: 0.95–1.08 (15 H, two triplet, J = 6.5 Hz), 1.43 (2 H, sextet, J = 6.5 Hz), 1.49–1.66 (3 H, m), 2.41 (2 H, t, J = 7 Hz), 3.44 (2 H, dt, J = 4.5, 6.5 Hz), 5.34 (1 H, dt, J = 2.9, 1 Hz, and $J_{Sn—H}$ = 64 Hz), 5.88 (1 H, dt, J = 2.9, 1 Hz, and $J_{Sn—H}$ = 140 Hz); gc/ms, m/e (%, rel. int.): 319 (M^+ − 57, 9.79%). Anal. calcd. for $C_{17}H_{36}OSn$: C 54.25, H 9.57; found: C 54.11, H 9.79.

Quenching of the adducts from reaction of cuprate ***8*** *and allene* ***25*** *with iodomethane (Table 5, entry 1)*

Allene **25** (0.45 mL, 2.5 mmol) was added to a solution of **8** (5 mmol) in 20 mL of THF at −78°C. After 2.5 h, MeI (1 mL, 16 mmol) was added and the reaction mixture was allowed to warm to 15°C over a period of 15 h. The mixture was quenched by the addition of a solution of MeOH and aq. NH_4Cl. The aqueous solution was extracted with hexanes (4 × 50 mL). The organic layer was washed with brine (2 × 30 mL), dried ($MgSO_4$), and solvents removed *in vacuo* to give the crude product, which was purified by preparative tlc

(neutral alumina, *n*-hexanes as an eluent) to give a (*Z*/*E*:67/33) mixture of 1-tri-*n*-butylstannyl-2-methyl-2-undecene (**33**) in 55% yield (0.629 g).

Quenching of the adducts from reaction of cuprate **9** *and allene* **25** *with iodomethane (Table 5, entry 2)*

To a solution of reagent **9** (2.5 mmol) in 20 mL of THF was added **25** (0.45 mL, 2.5 mmol) at −78°C. After 1.5 h, iodomethane (1 mL, 16 mmol) was added and the mixture was stirred for 1 h at −78°C, followed by 1 h at 0°C. The usual work-up followed by purification as above gave **33** in 78% yield (0.9 g).

(E)- and (Z)-1-Tri-n-*butylstannyl-2-methyl-2-undecene (33)*

^{1}H nmr (C_6D_6) δ: 0.89–1.08 (18 H, m), 1.24–1.54 (18 H, m), 1.58–1.68 (6 H, m), 1.73 (3 H_{trans}, bs), 1.81 (3 H_{cis}, d, J = 1.5 Hz), 1.91 (2 H_{cis}, bs), 1.93 (2 H_{trans}, bs), 2.11–2.19 (4 H, m), 5.12 (1 H_{cis}, bt, J = 7 Hz), 5.26 (1 H_{trans}, bt, J = 7 Hz); gc/ms, *m*/*e* (%, rel. int.): for *cis*-**33**: 401 (M^+ − 57, 100%), for *trans*-**33**: 458 (M^+, 12.5%). Exact Mass calcd. for $C_{24}H_{50}Sn$: 458.2934; found: 458.2929.

Addition of $PhMe_2SiCu(CN)Li$ (20) to allene **25** *(Table 6, entry 1)*

The following method is representative: To a mixture of **20** in 15 mL of THF was added allene **25** (0.17 mL, 1 mmol) at −78°C. After 1 h, the reaction mixture was quenched by addition of MeOH followed by aq. NH_4Cl. The aqueous solution was extracted with hexanes (4 × 30 mL). The organic layer was washed with brine (2 × 30 mL), dried ($MgSO_4$), and the solvent removed *in vacuo* to give a crude product, which was purified on preparative tlc (silica gel, *n*-hexane as an eluent) to provide 1-dimethylphenylsilyl-2-undecene (**34**), *E*-2-dimethylphenylsilyl-2-undecene (**35**) and 2-dimethylphenylsilyl-1-undecene (**36**) in 80% yield (0.23 g).

Addition of $PhMe_2Si$(n-Bu)$Cu(CN)Li_2$ (21) to **25** *(Table 6, entry 3)*

The following procedure is representative: Allene **25** (0.35 mL, 2 mmol) was added to a solution of $PhMe_2$(*n*-Bu)$SiCu(CN)Li_2$ (2.5 mmol) in 20 mL of THF at −78°C. After 1 h, the usual work-up followed by purification gave **34**, **35**, and **36** in 83% yield (0.48 g).

(E)- and (Z)-1-Dimethylphenylsilyl-2-undecene (34)

^{1}H nmr (C_6D_6) δ: 0.30 (6 H, s), 0.96 (3 H, t, J = 6.5 Hz), 1.21–1.43 (12 H, m), 1.71 (2 H_{trans}, d, J = 8 Hz), 1.76 (2 H_{cis}, d, J = 8 Hz), 2.02 (4 $H_{trans\ and\ cis}$, q, J = 6.5 Hz), 5.34–5.41 (1 H_{trans}, dtt, J = 15, 7, 1.5 Hz, other *trans*-vinyl hydrogen signal overlaps with *cis*-vinyl hydrogen signal), 5.43–5.49 (1 H_{cis}, dtt, J = 10, 7, 1 Hz), 5.51–5.59 (1 H_{cis}, dtt, J = 10, 7, 1 Hz); gc/ms, *m*/*e* (%, rel. int.): 288 (M^+, 13.33%). Anal. calcd. for $C_{19}H_{32}Si$: C 79.08, H 11.17; found: C 78.81, H 10.76.

(E)-2-Dimethylphenylsilyl-2-undecene (35) and 2-dimethylphenylsilyl-1-undecene (36)

^{1}H nmr (C_6D_6) δ: 0.41 (6 H, s), 0.97 (3 H, t, J = 6.5 Hz), 1.19–1.51 (12–14 H, m), for **35** 1.74 (3 H, dt, J = 2, 1 Hz), for **35** (2 H, dt, J = 7, 6.5 Hz), for **36** 2.23 (2 H, t, J = 7 Hz), for **36** 5.56 (1 H, dt, J = 3, 1 Hz), for **36** 5.81 (1 H, dt, J = 3, 1.5 Hz), for **35** 6.03 (1 H, tq, J = 7, 2 Hz); gc/ms, *m*/*e* (%, rel. int.): 288 (M^+, 29%). Anal. calcd. for $C_{19}H_{32}Si$: C 79.08, H 11.17; found: C 78.87, H 11.05.

Acknowledgement

This work was supported through a Natural Sciences and Engineering Research Council of Canada Operating Grant to ACO.

1. (*a*) S. MATSUBARA, J. HIBINO, K. OSHIMA, and H. NOZAKI. J. Organomet. Chem. **285**, 163 (1985); (*b*) K. WAKAMATSU, T. NONAKA, Y. OKUDA, W. TUCHMANTEL, K. OSHIMA, K. UTIMOTO, and N. NOZAKI. Tetrahedron, **42**, 4427 (1986); (*c*) K. NOZAKI, K. WAKAMATSU, T. NONAKA, W. TUCKMANTEL, K. OSHIMA, and K. UTIMOTO. Tetrahedron Lett. **27**, 2007 (1986); (*d*) E. PIERS and R. D. TILLYER. J. Org. Chem. **53**, 5366 (1988) and references therein; (*e*) E. PIERS and M. CHONG. Can. J. Chem. **66**, 1425 (1988); (*f*) B. L. CHENARD and C. M. VAN ZYL. J. Org. Chem. **51**, 3561 (1986); (*g*) S. SHARMA and A. C. OEHLSCHLAGER. Tetrahedron Lett. **27**, 6161 (1986); (*h*) S. SHARMA and A. C. OEHLSCHLAGER. J. Org. Chem. **54**, 5064 (1989) and references therein; (*i*) T. NONAKA, Y. OKUDA, S. MATSUBARA, K. OSHIMA, K. UTIMOTO, and H. NAZAKI. J. Org. Chem. **51**, 4716 (1986); (*j*) H. HAYAMA, M. SATO, S. KANEMOTO, Y. MORIZAWA, K. OSHIMA, and H. NOZAKI. J. Am. Chem. Soc. **105**, 4497 (1983); (*k*) Y. OKUDA, Y. MORIZAWA, K. OSHIMA, and H. NOZAKI. Tetrahedron Lett. **25**, 2483 (1984); (*l*) J. HIBINO, K. FUGAMI, S. MATSUBARA, K. OSHIMA, and H. NOZAKI. J. Am. Chem. Soc. **107**, 6416 (1985); (*m*) K. FUGAMI, J. HIBINO, S. NAKATSUKASA, S. MATSUBARA, K. OSHIMA, K. UTIMOTO, and H. NOZAKI. Tetrahedron, **44**, 4277 (1988); (*n*) E. PIERS and R. T. SKERLJ. J. Chem. Soc. Chem. Commun. 627 (1986); (*o*) T. N. MITCHELL, A. AMARIA, H. KILLING, and D. J. RUTSCHOW. J. Organomet. Chem. **304**, 257 (1986); (*p*) T. N. MITCHELL, H. DILLING, R. DICKE, and R. WICKENKAMP. J. Chem. Soc. Chem. Commun. 354 (1985); (*q*) T. N. MITCHELL, R. WICKENKAMP, A. AMAMRIA, R. DICKE, and U. SCHNEIDER. J. Org. Chem. **52**, 4868 (1987); (*r*) R. RITTER. Synthesis, 218 (1989).
2. S. SHARMA and A. C. OEHLSCHLAGER. Tetrahedron Lett. **29**, 261 (1988).
3. Y. MORIZAWA, H. ODA, K. OSHIMA, and H. NOZAKI. Tetrahedron Lett. **25**, 1163 (1984).
4. (*a*) I. FLEMING and F. J. PULIDO. J. Chem. Soc. Chem. Commun. 1010 (1986); (*b*) I. FLEMING and M. ROWLEY. Tetrahedron, **45**, 413 (1989).
5. A. BARBERO, P. CUADRADO, I. FLEMING, A. M. GONZALEZ, and F. J. PULIDO. J. Chem. Soc. Chem. Commun. 1030 (1990).
6. (*a*) M. PEREYRE, J.-P. QUINTARD, and A. RAHM. *In* Tin in organic synthesis. Butterworths. 1987; (*b*) B. M. TROST and J. W. HERNDON. J. Am. Chem. Soc. **106**, 6835 (1984); (*c*) Y. YAMAMOTO. Aldrichim. Acta, **20**, 45 (1987); (*d*) E. W. COLVIN. *In* Silicon in organic synthesis. Butterworths. 1981.
7. W. C. STILL. J. Am. Chem. Soc. **99**, 4836 (1977).
8. L. BRANDSMA and H. D. VERKRUIJSSE. *In* Synthesis of acetylenes, allenes and cumulenes. Elsevier, New York, NY. 1981.
9. S. SHARMA and A. C. OEHLSCHLAGER. Unpublished results.
10. (*a*) S. H. BERTZ, G. DABHAGH, and G. M. VILLACORTA. J. Am. Chem. Soc. **104**, 5824 (1982); (*b*) B. H. LIPSHUTZ, M. KOERNER, and D. A. PARKER. Tetrahedron Lett. **28**, 945 (1987); (*c*) J. R. BEHLING, K. A. BABIAK, J. S. NG, A. L. CHAMPBELL, R. MORETTI, M. KOERNER, and B. H. LIPSHUTZ. J. Am. Chem. Soc. **110**, 2641 (1988).
11. (*a*) A. C. OEHLSCHLAGER, M. W. HUTZINGER, R. AKSELA, S. SHARMA, and S. M. SINGH. Tetrahedron Lett. **31**, 165 (1990); (*b*) B. H. LIPSHUTZ and D. C. REUTER. Tetrahedron Lett. **30**, 4617 (1989); B. H. LIPSHUTZ, E. L. ELLSWORTH, S. H. DIMOCK, and D. C. REUTER. Tetrahedron Lett. **30**, 2065 (1989).
12. I. FLEMING and T. W. NEWTON. J. Chem. Soc. Perkin Trans. 1, 1805 (1984).
13. E. PIERS and J. M. CHONG. J. Chem. Soc. Chem. Commun. 934 (1983).
14. J. A. VERDONE, J. A. MANGRAVITE, N. M. SCARPA, and H. G. KUIVILA. J. Am. Chem. Soc. **97**, 843 (1975).
15. (*a*) V. J. JEPHCOTE and E. J. THOMAS. Tetrahedron Lett. **26**, 5327 (1985); (*b*) D. YOUNG, M. JONES, and W. KITCHING. Aust. J. Chem. **39**, 563 (1986).
16. (*a*) M. MONTURY and J. GORE. Tetrahedron Lett. **21**, 51 (1980); (*b*) J. J. EISCH and G. R. HUSK. J. Organomet. Chem. **4**, 415 (1965).
17. H. C. BROWN and S. M. SINGH. Unpublished results.
18. J. K. CRANDALL and G. L. TINDELL. J. Chem. Soc. Chem. Commun. 1411 (1970).
19. I. FLEMING, T. W. NEWTON, and F. ROESSLER. J. Chem. Soc. Perkin Trans. 1, 2527 (1981).
20. J. RIMBAULT and R. HUGEL. Inorg. Nucl. Chem. Lett. **9**, 1 (1973).
21. J. RIMBAULT and R. HUGEL. Rev. Chim. Minerale. **10**, 773 (1973).

Can. J. Chem. Downloaded from www.nrcresearchpress.com by 123.30.183.119 on 09/08/12
For personal use only.

Electrochemically oxidized carbon fibres as an adsorbent for the attachment of dissolved substances. Adsorption of nitro compounds and ion-exchange of heavy metals

E. THEODORIDOU, A. D. JANNAKOUDAKIS, P. D. JANNAKOUDAKIS, AND S. ANTONIADOU
Laboratory of Physical Chemistry, Aristotelian University of Thessaloniki, Greece
Received November 12, 1990[1]

E. THEODORIDOU, A. D. JANNAKOUDAKIS, P. D. JANNAKOUDAKIS, and S. ANTONIADOU. Can. J. Chem. **69**, 1881 (1991).

The adsorption of several aromatic nitro compounds and the ion-exchange of heavy metal ions on electro-oxidized carbon fibres have been investigated using cyclic voltammetric and polarographic techniques. Electro-oxidation is performed by potentiostatic double pulse application. This procedure results in the generation of many functional —OH and —COOH groups with adsorptive and ion-exchanging properties.

Multimolecular layers of adsorbed substances may be formed through a procedure of successive adsorption of the nitro-compound and electro-reduction to the corresponding amine, resulting in the attachment of considerable amounts of the nitro-compound to the carbon fibres.

The ion-exchange capacity is estimated to be ca. 1 mequiv. g^{-1} and with slight deviations it follows the rank Ag, Cu, Cd, Pb, Hg. After the electro-reduction of the exchanged metal ions, the ion-exchange process can be repeated several times. This procedure is of importance for the removal of significant amounts of heavy and toxic metals from industrial waste waters.

Key words: electro-oxidized carbon fibres, adsorption of aromatic nitro compounds, cation-exchange of heavy metals.

E. THEODORIDOU, A. D. JANNAKOUDAKIS, P. D. JANNAKOUDAKIS et S. ANTONIADOU. Can. J. Chem. **69**, 1881 (1991).

Faisant appel à des techniques de polarographie et de voltampérométrie cyclique, on a étudié l'adsorption de plusieurs composés aromatiques nitrés et l'échange ionique d'ions de métaux lourds sur des fibres de carbone électro-oxydées. On a réalisé l'électro-oxydation en appliquant une double pulsation potentiostatique. Cette méthode permet de générer plusieurs groupes fonctionnels —OH et —COOH possédant des propriétés d'adsorption et d'échange ionique.

Si on utilise une technique d'adsorptions successives des composés nitrées suivies d'électroréductions en amines correspondantes, on peut former des couches multimoléculaires de substances adsorbées; il en résulte un attachement de quantités considérables de composés nitrés sur les fibres de carbone.

On a évalué que la capacité d'échange ionique est d'environ 1 mequiv. g^{-1} et, avec des déviations légères, l'ordre est le suivant : Ag, Cu, Cd, Pb et Hg. Après l'électroréduction des ions métalliques échangés, on peut répéter le processus d'échange ionique plusieurs fois. Cette procédure est importante pour l'enlèvement de quantités importantes de métaux lourds et toxiques d'eaux usées industrielles.

Mots clés : fibres de carbone électro-oxydées, adsorption de composés nitrés aromatiques; échange cationique de métaux lourds.

[Traduit par la rédaction]

Introduction

Carbon fibre sorption materials represent a species of carbonaceous adsorbents. They are in many respects similar to activated charcoal (1).

Studies on the application of carbon fibres as adsorbents for several gases (such as NO, NH_3, CH_3NH_2, and benzene vapour) have been reported in the literature. It was found that the adsorption ability of the carbon fibre material is enhanced through activation with metal or metal salt additives (2–4).

PAN-based activated carbon fibres pretreated with sulfuric acid and annealed at 350°C have been used for the adsorption of NO_x (5).

Activated carbon fibres have also been used for the removal of organic molecules of a comparatively large size from liquid media. For this purpose, adsorbents with a developed supermicro- and mesopore structure proved to be the most effective (6). As it has been reported in the literature (7), commercial carbon fibre adsorbents are very effective for the removal of toxic chlorine compounds from aqueous solutions.

Carbon fibres have also been used for the preparation of ion-exchangers. Oxidative treatment of the fibres is the most frequently used approach for this purpose. Various reagents have been used as oxidizers: solutions of nitric acid at different concentrations (8), mixtures of concentrated nitric and sulfuric acid (8, 9), hydrogen peroxide (10), and $K_2Cr_2O_7$ or $KMnO_4$ in concentrated acidic solutions (11). However, chemical pretreatment of the carbon fibres reduces their mechanical stability and electronic conductivity and therefore restricts their application in electrochemical procedures.

On the contrary, electrochemically oxidized PAN-based carbon fibres are characterized by good mechanical stability, high electronic conductivity, and a porous hydrophilic structure (12). These fibres bear hydroxylic and carboxylic groups and show remarkable ability for the attachment of several species dissolved in solutions. This property enables the use of the electro-oxidized fibres for chromatographic determinations and ion-exchange procedures.

The application of repetitive anodic oxidation and cathodic reduction by potentiostatic double pulses favours the generation of numerous —OH and —COOH groups on the carbon fibre surface without affecting the mechanical properties and electronic conductivity of the graphitic material (12–14).

The effective area of pulse oxidized fibres is of the order of $m^2\ g^{-1}$. These fibres have already been employed as supports for noble metal catalysts (12, 14, 15), for metalloporphyrin redox mediators (16–18), and for chemically modified electrodes (19).

The present study is focused on the adsorptive and ion-exchanging properties of the electrooxidized fibres and their utility as convenient substrates for the attachment of several

[1]Revision received May 29, 1991.

Printed in Canada / Imprimé au Canada

Can. J. Chem. Downloaded from www.nrcresearchpress.com by 123.30.183.119 on 09/08/12
For personal use only.

Can. J. Chem. Downloaded from www.nrcresearchpress.com by 123.30.183.119 on 09/08/12
For personal use only.

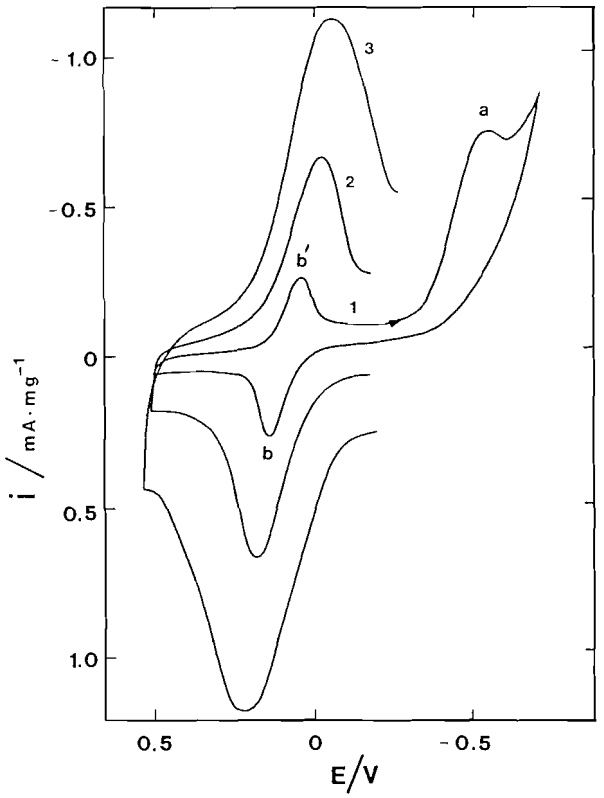


FIG. 1. Cyclic voltammograms (v = 10 mV s^{-1}, pH = 4) of 2-nitro-1-naphthol adsorbed on electrooxidized carbon fibres. (*1*), (*2*), and (*3*): first, second, and third successive adsorption procedure. Start potential: −0.1 V vs. SCE.

substances dissolved in solutions. The adsorption experiments were carried out with various nitro and nitroso compounds, while for the ion-exchange processes heavy and toxic metals have been used. The choice of these substances was based on our previous knowledge on their electrochemical behaviour on pristine, not electro-oxidized fibres (20–24) and especially on the possible ecological demand for their removal from technical waste waters.

Experimental

The PAN-based carbon fibres used in this study were produced by Celanese Corp. (type GY-70). They are formally arranged in bundles containing an average of 384 filaments. These fibres are highly oriented and mechanically stable with the following technical characteristics: density 2 g cm^{-3}, filament diameter 7 μm, specific resistance 7×10^{-4} Ω m, and Young modulus 5.15×10^{11} N m^{-2} (25).

The oxidation of the fibres was performed by potentiostatic double pulse application for a 6-min period in aqueous 0.05 M Na_2SO_4 solution. The applied potential range extended from +2.3 up to −0.3 V vs. S.C.E. and the duration of the oxidative pulse was six times longer than that of the reductive pulse (12). The effective area of the pristine bundle of fibres is 1.7 cm^2 mg^{-1}, while the corresponding value for the electro-oxidized fibres is 6.8 cm^2 mg^{-1}, i.e., four times larger (16). The electro-oxidation procedure enhances the widening of the fibres and thus facilitates inner planes of the bundles to be directly accessible to the solution.

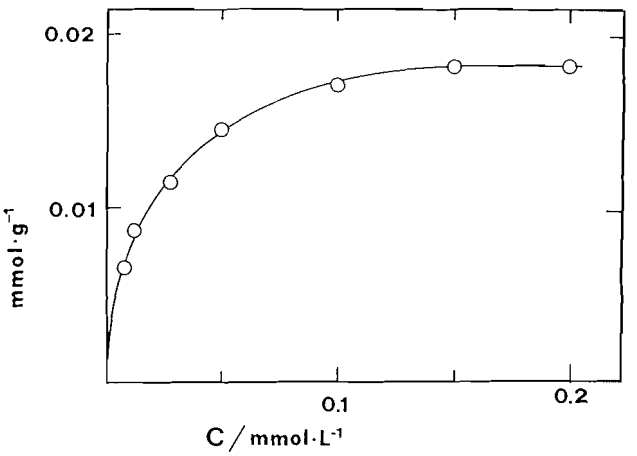


FIG. 2. Adsorption isotherm of 2-nitro-1-naphthol on electro-oxidized carbon fibres, for the first adsorption procedure (T = 25°C).

The electrical connection is performed by pressing one end of the fibre bundle painted with conductive carbon paste between two platinum sheets, which are then put to a metallic conjunction plugged into the electrical circuit.

The adsorption of nitro compounds was accomplished by dipping the electro-oxidized fibre bundles in aqueous methanolic solutions (50% v/v in methanol) of these compounds. The adsorption equilibrium was attained approximately after 3 h. The quantity of the nitro compound adsorbed on the fibres was estimated from the data obtained by cyclic voltammetric measurements on these fibres in aqueous buffered solutions. The same series of experiments were repeated on large bundles of carbon fibres. After the adsorption of the nitro compound, polarographic measurements were taken to estimate the remaining unadsorbed quantity of nitro compound in the solution. The results verified the values obtained from the cyclic voltammetric measurements.

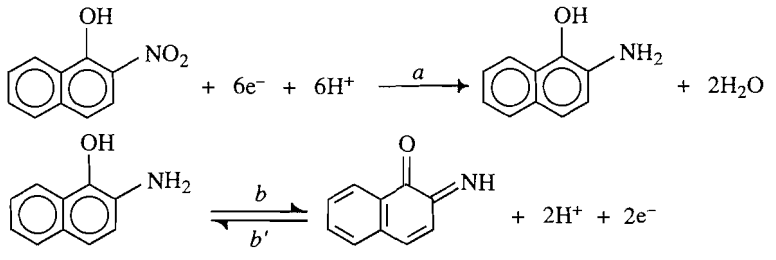
The ion-exchange of the heavy metal ions was accomplished by dipping the electrooxidized fibres in aqueous solutions of varying metal salt concentrations. The equilibrium was attained in a 2-h period. The ion-exchanged quantity of the metal was determined by cyclic voltammetric measurements of the carbon fibres bearing metal ions in aqueous buffered solutions. By means of cyclic voltammetry on a hanging mercury electrode the amount of the unexchanged metal remaining in solution after the establishment of equilibrium was also estimated.

Results and discussion

(a) Adsorption of nitro compounds

Figure 1 (curve *1*) presents, as an example, the cyclic voltammogram of carbon fibres bearing adsorbed 2-nitro-1-naphthol (2N1N). The adsorption was carried out in a 10^{-3} M 2N1N solution and the adsorption procedure follows a typical adsorption isotherm as shown in Fig. 2.

Peaks *a*, *b*, and *b'* in Fig. 1 correspond to the following reactions (20):



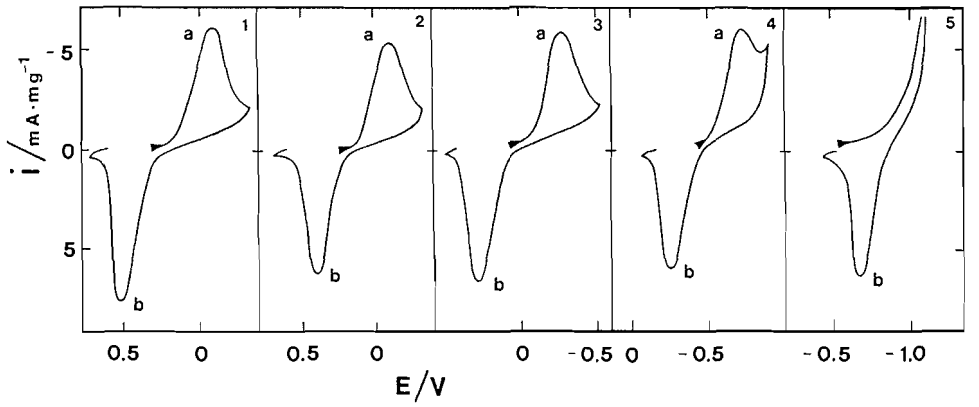


FIG. 3. Cyclic voltammograms (v = 20 mV s^{-1}, pH = 4) of electro-oxidized carbon fibres after ion-exchange with Ag^+ (*1*), Hg^{2+} (*2*), Cu^{2+} (*3*), Pb^{2+} (*4*), and Cd^{2+} (*5*).

The charge under peak *a* is almost three times larger than that under peak *b*, supporting the reaction scheme presented above. The peak currents depend linearly on the potential scan rate as it is expected for species immobilized on the electrode surface (26). The shape of peaks *b* and *b'* is unaffected through successive potential scans. This means that the reduction product, *i.e.*, aminonaphthol, remains strongly adsorbed on the electro-oxidized carbon fibres.

The amount of the adsorbed 2N1N was accurately evaluated from the charge under peak *b* more preferably than under peak *a*, since the reduction of 2N1N to the corresponding amine (peak *a*) is followed by the reduction of the surface functional groups (13, 14). The estimated values were used in Fig. 2. Figure 2 indicates that the maximum amount of 2N1N adsorbed on the electro-oxidized fibres during the first adsorption procedure is 0.018 mmol g^{-1}.

After the electro-reduction of the adsorbed 2N1N to the corresponding amine, it was found that the carbon fibres retain the ability to adsorb considerable amounts of additional nitro compound. This procedure can be performed repeatedly and the product of the electro-reduction (*i.e.* the corresponding aminonaphthol) still remains adsorbed on the electro-oxidized fibres. This is schematically presented in Fig. 1, where curves *2* and *3* refer to the 2nd and 3rd successive adsorption procedure, respectively.

The deposition of the limiting amount of 2N1N on the electro-oxidized fibres is achieved after four successive adsorption experiments, and measures 0.3 mmol g^{-1}. This indicates that the attached quantity of 2N1N is almost 17 times larger than that in the first adsorption procedure. Taking into account that 1 g of electro-oxidized fibres exhibits 6800 cm^2 of effective electrode area, it is estimated that the total amount of 2N1N deposited on the fibres is 4.4×10^{-8} mol cm^{-2}. Since it is known that in the case of electro-sorption of β-naphthol from aqueous solution onto graphite powder, the monolayer coverage is 2.5×10^{-10} and 6.4×10^{-10} mol cm^{-2} for planar and perpendicular orientation, respectively (27), it is concluded that the entire amount of 2N1N deposited on the fibres corresponds to a multilayer coverage.

The stable multimolecular layer that is finally formed indicates that during the successive adsorption procedures the nitro compound is attached to the previously subdeposited layers of the corresponding amino compound. This fact suggests that the reduced form of the nitro compound exhibits intensive adsorption properties.

After the series of experiments, it was found that dipping a 50 mg bundle of electro-oxidized fibres in 30 mL of a 10^{-3} M 2N1N solution, 90% of the total amount of the dissolved nitro compound could be withdrawn from the solution. This argument resulted from cyclic voltammetric measurements on the fibres as well as from polarographic determination of the remaining unadsorbed nitro compound in the solution.

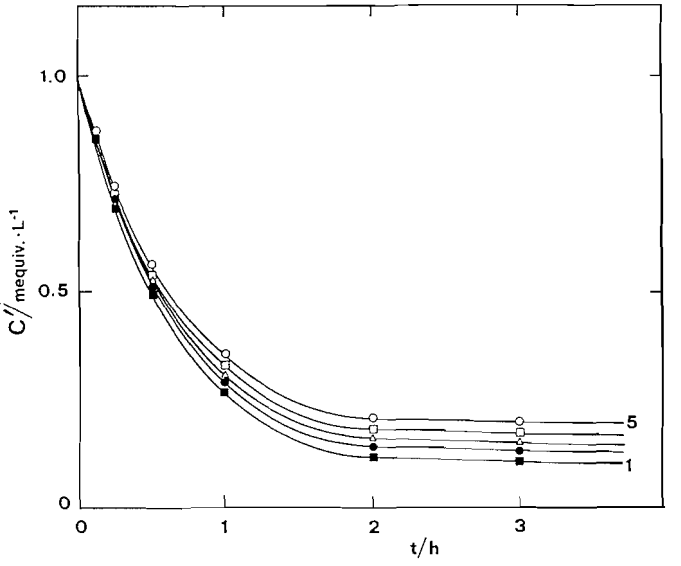


FIG. 4. Concentration of the metal ions remaining in the solution after the ion-exchange of electrooxidized carbon fibres with Ag^+ (*1*), Cu^{2+} (*2*), Cd^{2+} (*3*), Pb^{2+} (*4*), and Hg^{2+} (*5*) as a function of time.

Similar experiments for various nitro and nitroso compounds confirmed that adsorption on electro-oxidized fibres somewhat follows chemisorption, resulting in the formation of multimolecular layers. This conclusion implies that considerable amounts of the nitro compound can be attached to the fibres.

In the case of 1-nitro-2-naphthol, 1-nitroso-2-naphthol, and 2-nitroso-1-naphthol, the total amount adsorbed is approximately the same as in the case of 2-nitro-1-naphthol. As for the dinitrobenzene isomers, the adsorbed amount varies between 0.05 and up to 0.08 mmol g^{-1}.

(b) Ion-exchange of heavy metals

Figure 3 presents the cyclic voltammogram of electro-oxidized carbon fibres after the ion-exchange of heavy metal ions, accomplished in a rather concentrated solution of the corresponding metal salt (c = 10^{-2} M).

Can. J. Chem. Downloaded from www.nrcresearchpress.com by 123.30.183.119 on 09/08/12
For personal use only.

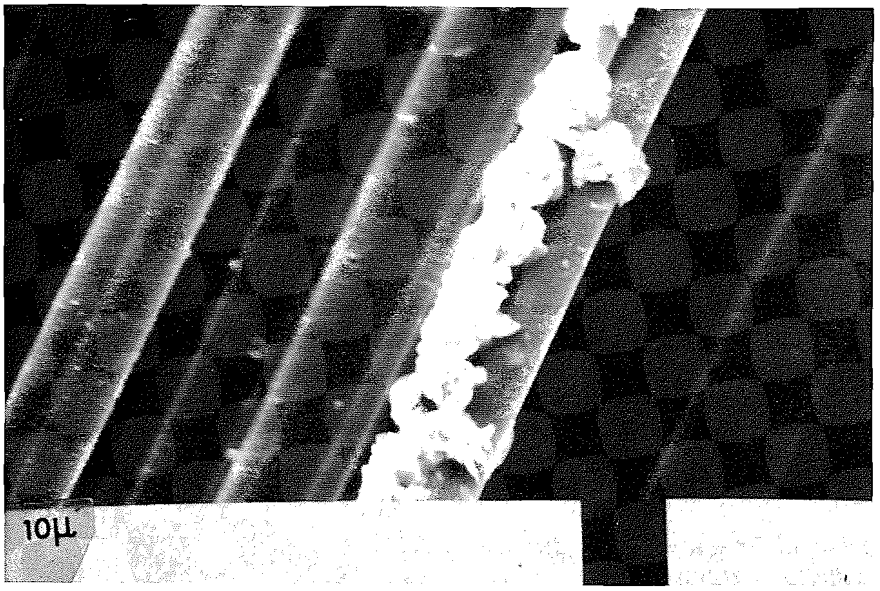


FIG. 5. SEM-micrograph of electrooxidized carbon fibres bearing Ag clusters after 25 successive ion-exchange procedures with Ag^+.

This figure shows that the electrochemical reduction of Ag^+, Hg^{2+}, Cu^{2+}, and Pb^{2+} ions (peak *a*) occurs before the reduction of the functional groups of the electro-oxidized fibres, whereas the reduction of Cd^{2+} takes place concurrently with the reduction of the functional groups. In all cases the ion-exchanged quantity was estimated from the integrated area under peak *b*, which corresponds to the dissolution of the respective ion-exchanged metal quantity. These results were confirmed by ion-exchange experiments on large bundles of electro-oxidized fibres under stationary conditions and further polarographic determination of the quantity not ion-exchanged in the solution. The values obtained in correlation with the time required for the ion-exchange equilibrium resulted in a plot in Fig. 4, which implies that 85–95% of the dissolved metal ions can be attached to 30 mg of electro-oxidized fibres dipped in 30 mL of a 10^{-3} M solution for a period of approximately 2 h.

The ion-exchange capacity is of the order of 1 mequiv. g^{-1} and with slight variations follows the order Ag, Cu, Cd, Pb, Hg. Similar range was obtained for heavy metal ion-exchange on natural cellulose (28).

After a quantitative electro-reduction of the ion-exchanged metal on the adsorptive material, further repetitive attachment of additional quantities is possible. This fact is of great importance for the removal of significant quantities of heavy and toxic metal ions from industrial waste waters. The total quantity of the metal ion that can be ion-exchanged using repeatedly the same electro-oxidized fibre bundle exceeds the primarily estimated value (1 mequiv. g^{-1}) during the first ion-exchange procedure.

Figure 5 illustrates a SEM-micrograph of electro-oxidized fibres after 25 successive Ag^+ ion-exchange procedures. It shows that large metal clusters are sparsely situated on the carbon fibre surface, while functional groups of the oxidized carbon matrix are directly exposed to metal ions of the solution, indicating that Ag^+ ion-exchange may still occur.

Cadmium ion-exchange experiments were carried out in addition to the experiments under stationary conditions, using a column filled with trimmed electro-oxidized fibres as adsorptive material. The most favourable conditions for the attachment of 90% of the metal ions dissolved in a 10^{-3} M solution as follows were: flow velocity 5 mL min^{-1}, column diameter 12 mm, and column height 60 cm.

For these experiments carbon fibres electro-oxidized for periods larger than 6 min were also used, since they exhibit enhanced ion-exchange properties because of an increased number of —OH and —COOH groups. It was found that carbon fibres oxidized for 15 min have ion-exchange capacity 2.5 mequiv. g^{-1}. The prolonged oxidation reduces the conductivity of the fibres; however, this fact does not interfere in their application as adsorptive material.

From our series of experiments it was found that the fibres exhibit ion-exchange capacity parallelling the electrooxidation time.

Ion-exchange capacity of heavy metal ions proved to be independent on pH in the range 4 to 8, and unaffected by significant concentrations of NaCl (up to 0.5 M).

The displacement of heavy metal ions is successfully accomplished through relatively concentrated solutions of $Ca(NO_3)_2$ (0.1–0.5 M), confirming the ion-exchanging properties of the oxidized graphitic material.

Blank measurements were performed on unelectro-oxidized fibres. The results showed that the amount of the attached nitro compound is ca. 15 times less than the corresponding amount on electro-oxidized fibres during the first adsorption procedure. The primary deposited quantity on the pristine fibres is not increased upon successive adsorption experiments due to the absence of functional groups.

The ion-exchange of heavy metals on initial carbon fibres was negligible.

Acknowledgement

We are obliged to the "Alexander von Humboldt Stiftung" for a grant of scientific instruments to the Laboratory of Physical Chemistry.

1. I. N. ERMOLENKO, I. P. LYUBLINER, and N. V. GULKO. *In* Chemically modified carbon fibres. *Edited by* VCH, Weinheim. 1990. p. 60.
2. I. N. ERMOLENKO, T. G. IVANOVA, N. V. GULKO, and I. P. LUYBLINER. Proceedings of the 4th International Carbon Conference. Baden-Baden. June 1986, pp. 382–383.

Can. J. Chem. Downloaded from www.nrcresearchpress.com by 123.30.183.119 on 09/08/12
For personal use only.

3. F. A. P. MAGGS, A. CAPON, and M. E. SMITH. Proceedings of the 13th Biennial Conference on Carbon. Irvine, CA. 1977. p. 386.
4. L. DJURICIC and M. POLONIVA. Proceedings of the 14th Biennial Conference on Carbon. University Park, Philadelphia. 1979. p. 260.
5. Y. KOMALSUBARA, S. IDA, and H. FUJITSU. Fuel, **63**, 1738 (1984).
6. G. D. PARFITT and C. H. ROCHESTER. *In* Adsorption from solution at the solid/liquid interface. *Edited by* Academic Press, London. 1983.
7. H. SIMANO and J. P. KOKAI. Tokkyo Koho 84-199819 (1983). Chem. Abstr. **102**, 100590 (1985).
8. S. BLAZEWICZ, J. CHLOPEK, M. BLAZEWICZ, and R. PAMPUCH. Proceedings of the 4th International Carbon Conference. Baden-Baden. June 1986. pp. 716–717.
9. A. SUZUKI, S. TOKUDA, Y. KANAYA, K. SHIMZU, and J. P. KOKAI. Tokkyo Koho 79-26287 (1977). Chem. Abstr. **90**, 122493 (1979).
10. J. PAWLOCZYK and H. SOBEZAK. Acta Pol. Pharm. **37**, 655 (1980).
11. E. THEODORIDOU, A. D. JANNAKOUDAKIS, and D. JANNAKOUDAKIS. Z. Phys. Chem. N.F. **134**, 227 (1983).
12. E. THEODORIDOU, A. D. JANNAKOUDAKIS, J. O. BESENHARD, and R. F. SAUTER. Synth. Met. **14**, 125 (1986).
13. A. D. JANNAKOUDAKIS, P. D. JANNAKOUDAKIS, E. THEODORIDOU, and J. O. BESENHARD. J. Appl. Electrochem. **20**, 619 (1990).
14. E. THEODORIDOU, A. D. JANNAKOUDAKIS, P. D. JANNAKOUDAKIS, J. O. BESENHARD, and A. KURTZE. *In* Carbon '88. *Edited by* B. McEnanay and T. J. Mays. 1988. p. 537.
15. E. THEODORIDOU, A. D. JANNAKOUDAKIS, J. O. BESENHARD, and R. F. SAUTER. Proceedings of the 4th International Carbon Conference. Baden-Baden. June 1986. pp. 623–625.
16. S. ANTONIADOU, A. D. JANNAKOUDAKIS, and E. THEODORIDOU. Synth. Met. **30**, 283 (1989).
17. S. ANTONIADOU, A. D. JANNAKOUDAKIS, and E. THEODORIDOU. Synth. Met. **30**, 295 (1989).
18. S. ANTONIADOU, A. D. JANNAKOUDAKIS, P. D. JANNAKOUDAKIS, and E. THEODORIDOU. Synth. Met. **32**, 309 (1989).
19. P. D. JANNAKOUDAKIS, A. D. JANNAKOUDAKIS, E. THEODORIDOU, and J. O. BESENHARD. J. Appl. Electrochem. **19**, 341 (1989).
20. E. THEODORIDOU, P. KARABINAS, and D. JANNAKOUDAKIS. Z. Naturforsch. **37**b, 97 (1982).
21. E. THEODORIDOU, P. KARABINAS, and D. JANNAKOUDAKIS. Z. Naturforsch. **37**b, 112 (1982).
22. P. D. JANNAKOUDAKIS and E. THEODORIDOU. Z. Phys. Chem. N.F. **130**, 49 (1982).
23. S. ANTONIADOU, A. D. JANNAKOUDAKIS, P. KARABINAS, and E. THEODORIDOU. J. Electroanal. Chem. **207**, 203 (1986).
24. E. THEODORIDOU, A. D. JANNAKOUDAKIS, and D. JANNAKOUDAKIS. Synth. Met. **9**, 19 (1984).
25. D. J. JOHNSON. *In* Chemistry and physics of carbon. *Edited by* P. A. Thrower. M. Dekker, New York. 1987. p. 1.
26. A. J. BARD and L. R. FAULKNER. *In* Electrochemical methods. *Edited by* J. Wiley & Sons, New York. 1980. p. 220.
27. R. S. EISINGER and R. C. ALKIRE. J. Electroanal. Chem. **112**, 327 (1980).
28. P. BURBA and P. G. WILMER. Wasser, **59**, 139 (1982).

Can. J. Chem. Downloaded from www.nrcresearchpress.com by 123.30.183.119 on 09/08/12
For personal use only.

Physical characteristics and polarographic reduction mechanism of some oxazolones

M. I. ISMAIL

Department of Chemistry, Faculty of Science, Ain-Shams University, Abbassia, Cairo, Egypt

Received April 12, 1990

M. I. ISMAIL. Can. J. Chem. **69**, 1886 (1991).

The redox potential ($\Delta E_{1/2}$), electron affinity (EA), ionization potential (IP), coulomb repulsion integral (J_{12}), and electronic transition energy (E_{CT}) of several oxazolone derivatives in DMF were computed. A linear correlation was shown to exist between $\Delta E_{1/2}$ and E_{CT}. The polarographic reduction was investigated in ethanolic-Theil buffer solutions. At pH $\leq$ 7.2, two waves were obtained representing the uptake of 2- and 4-electron steps respectively. In alkaline media, a third wave appeared seemingly a result of the hydrolysis of oxazolones. The rate of hydrolysis was determined and the electrode mechanism was elucidated and confirmed via spectrophotometric and coulometric analysis.

Key words: oxazolones, polarography, electrochemistry, electrode reaction, spectrophotometry, redox potential.

M. I. ISMAIL. Can. J. Chem. **69**, 1886 (1991).

On a calculé le potentiel rédox ($\Delta E_{1/2}$), l'affinité électronique (AE), le potentiel d'ionisation (PI), l'intégrale de répulsion coulombique (J_{12}) et l'énergie de transition électronique (E_{CT}) de plusieurs dérivés de l'oxazolone dans le DMF. On a démontré qu'il existe une corrélation linéaire entre $\Delta E_{1/2}$ et E_{CT}. On a étudié la réduction polarographique dans des solutions éthanoliques du tampon de Theil. À des pH inférieurs à 7,2, on a observé deux vagues correspondant respectivement à l'absorption de 2 et de 4 électrons. En solutions alcalines, une troisième vague apparaît; elle semble être causée par une hydrolyse des oxazolones. On a déterminé les vitesses d'hydrolyse des oxazolones, on a élucidé le mécanisme à l'électrode et on l'a confirmé par analyses spectrophotométriques et coulométriques.

Mots clés : oxazolones, polarographie, électrochimie, réaction à l'électrode, spectrophotométrie, potentiel rédox.

[Traduit par la rédaction]

Introduction

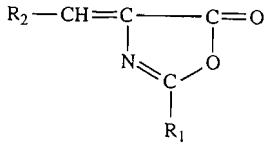
Numerous studies have been devoted to the chemistry, electrochemistry, and spectroscopy of heterocyclic compounds, specially those exhibiting applications in biological and medicinal researches (1, 2). On the other hand, the polarographic behaviour of the oxazole ring, structurally a heterocyclic system, has attracted only minor attention in literature (3, 4) as compared to major spectroscopic investigations (5–10). Consequently, in the present investigation our attention was devoted mainly to oxazolones possessing wide applications in the electrosyntheses of various amino alcohols, thiamine, and amino acids (11, 12). The study was focussed on the polarographic behaviour of some oxazolones (1–15), in Thiel buffer – ethanolic solutions of different pH values as well as in DMF. The electrode reaction mechanism and various physical properties of these compounds were also investigated.

An ultimate goal of this investigation was to establish the relationship between the spectroscopic data (E_{CT}) and the absolute difference in the electrochemical oxidation and reduction potentials ($\Delta E_{1/2}$) for the studied compounds. The study was extended to estimate the true $E^{OX}_{1/2}$ and/or $E^{R}_{1/2}$ as well as the coulomb repulsion integral J_{12}.

Experimental

Oxazolones (1–15) were prepared according to recommended procedure (13). The purity and structures of the compounds were checked by measurements of mp, nmr, mass spectra, and elemental analysis. The polarograms were recorded by Radiometer PO_4 type recording polarograph using a dropping mercury electrode with $m = 2.12$ mg/s and $t = 3.65$ s at h = 52 cm Hg. Depolarizer concentrations studied were 5×10^{-4} M in 50% (v/v) ethanolic – Theil buffer mixtures and in DMF – 0.1 M of *N*-tetrabutylammonium perchlorate. The electrolytic cell used was the same as that described by Peltier *et al.* (14).

The UV absorption spectra of oxazolones reaction in 50% ethanol – 0.1 M acid or base solution and in DMF were recorded on a Pye Unicam SP 1800 spectrophotometer attached to a temperature regulated cell holder.



2-alkyl (or aryl)-4-arylidene oxazolin-5-one derivatives

	Substituent			Substituent	
Compound	R_1	R_2	Compound	R_1	R_2
1	Ph	Ph	**9**	Ph	2-Furyl
2	Ph	4-$CH_3C_6H_4$	**10**	Ph	4-$(CH_3)_2NC_6H_4$
3	Ph	4-FC_6H_4	**11**	Ph	3,5-diiodo-4-(4-methoxyphenoxy)phenyl
4	Ph	2-ClC_6H_4	**12**	Me	Ph
5	Ph	4-ClC_6H_4	**13**	Me	4-FC_6H_4
6	Ph	4-$CH_3OC_6H_4$	**14**	Me	2-ClC_6H_4
7	Ph	4-OHC_6H_4	**15**	Me	4-ClC_6H_4
8	Ph	2-OHC_6H_4			

Can. J. Chem. Downloaded from www.nrcresearchpress.com by 123.30.183.119 on 09/08/12
For personal use only.

Printed in Canada / Imprimé au Canada

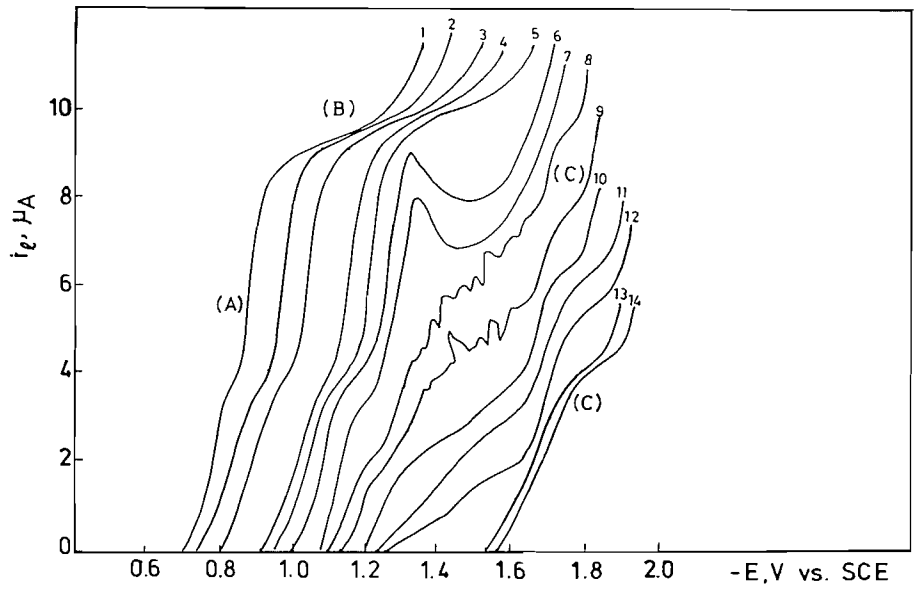


FIG. 1. Polarograms of 5×10^{-4} M of **1** in 50% ethanolic – Thiel buffer solutions at 25 ± 0.1°C, run and pH: (*1*) 2.2; (*2*) 3.2; (*3*) 4.4; (*4*) 6.5; (*5*) 7.2; (*6*) 7.5; (*7*) 7.9; (*8*) 8.2; (*9*) 8.4; (*10*) 9.1; (*11*) 10.5; (*12*) 11.5; (*13*) 11.5 after 25 min; (*14*) 0.1 M NaOH and after 25 min.

Results and discussion

1. The polarographic behaviour and spectrophotometry of 2-alkyl (aryl)-4-arylidene-oxazolin-5-one (1–15)

Figure 1 represents the polarographic reduction of 5×10^{-4} M of compound **1** in Theil buffer – 50% ethanolic solution of varying pH as a typical representative example for the studied series. At pH $\leq$ 7.2, the polarogram consists of two waves (A and B) with a height ratio 1:2. The limiting current (i_l) of the two waves is sustained constant and the whole polarogram shows a marked shift to more negative potentials throughout this pH range. When the pH is increased up to 7.5–7.9, the limiting current of the two waves starts to decrease while the second wave (B) becomes characterized by a small maximum. At pH $\geq$ 8.2, a third wave (C) starts to appear at more negative potential (−1.68 V) where its limiting current shows an increase by increasing the pH value (or by increasing the time at a constant pH). At these pH values, the current of waves A and B seems to be unstable and consequently an irregular shaped-polarogram is produced. This can be attributed to a change in the concentration of the electroactive species near the electrode surface with time. Such a change may be caused by hydrolysis of the oxazolones being catalysed by the alkali to form the corresponding acid (3, 9, 10, 15).

The effect of time on the electroreduction of compound **1** in 50% ethanol – 0.1 M NaOH is shown in Fig. 2. At zero time, two waves A and B are observed. As the time increases, the total limiting current decreases, followed by the formation of wave C. The limiting current of wave C increases with time; after 25 min, the produced polarogram shows only one well developed wave C where its i_l is quite similar to that of wave A.

Figure 3 represents the UV spectra of 1×10^{-4} M of compound **1** in presence of 50% ethanol – 0.1 M HCl (Fig. 3*a*) and 50% ethanol – 0.1 M NaOH (Fig. 3*b*). It is quite clear that this class of compounds shows a reasonable stability in acidic medium up to 35 min whereas in the basic medium, the hydrolysis starts a few minutes after the addition. In acidic conditions, hydrolysis tends to complete in 130 min and in basic conditions it takes only 15 min. These findings reflect the minor catalytic hydrolyzing effect of the acid as compared to that of the alkali. This indicates the stability of the compounds under study in acidic solutions within the time of polarographic measurements. It is known that oxazolones exhibit an absorption band at 366 nm which decreases in intensity with time with the appearance of a new band at 280 nm, representing the corresponding acid (during hydrolysis) or its ester (during alcoholysis). The composition of the medium used favours the hydrolysis of oxazalones but not alcoholysis since the latter requires a higher percentage of the alcohol and a lower concentration of the catalyst (10). The previously reported data (15–18) revealed that these compounds are

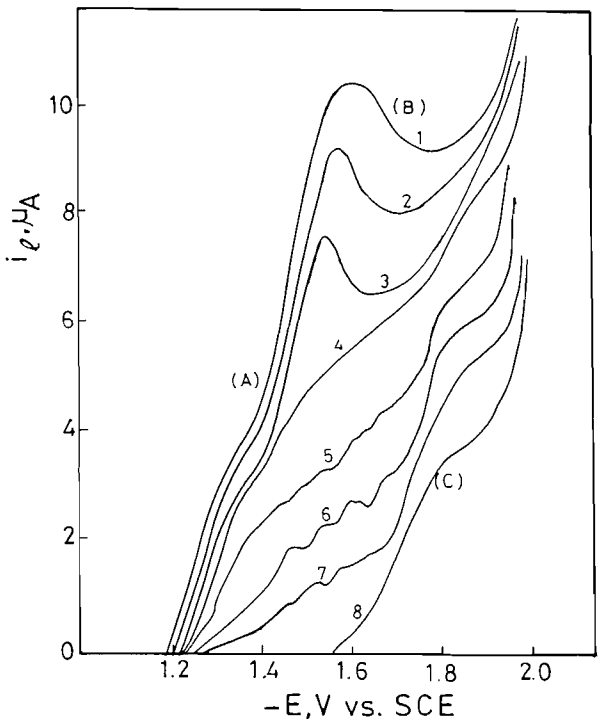


FIG. 2. Polarograms of 5×10^{-4} M of **1** in 50% ethanolic – 0.1 M NaOH after various times: (*1*) 0.0 min; (*2*) 1 min; (*3*) 4 min; (*4*) 5 min; (*5*) 8 min; (*6*) 13 min; (*7*) 20 min; (*8*) 25 min.

Can. J. Chem. Downloaded from www.nrcresearchpress.com by 123.30.183.119 on 09/08/12
For personal use only.

Can. J. Chem. Downloaded from www.nrcresearchpress.com by 123.30.183.119 on 09/08/12
For personal use only.

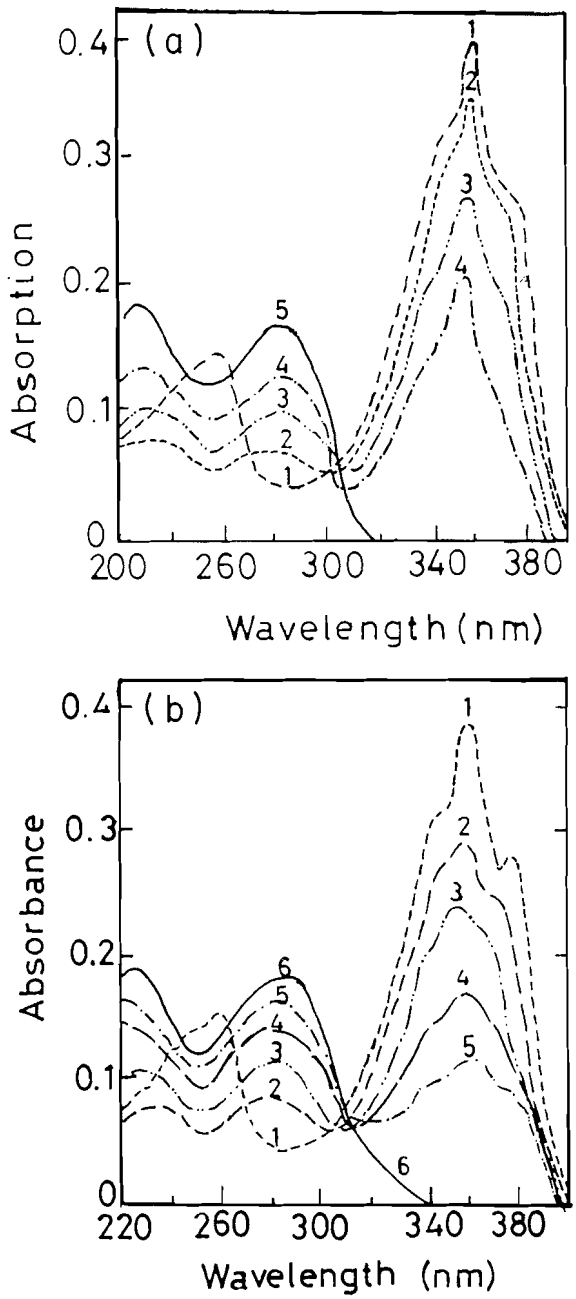


FIG. 3. (*a*) Ultraviolet absorption spectra of 1×10^{-4} M of **1** in 50% ethanol – 0.1 M HCl after various times: (*1*) 2 min; (*2*) 38 min; (*3*) 55 min; (*4*) 75 min; (*5*) 130 min. (*b*) Ultraviolet absorption spectra of 1×10^{-4} M of **1** in 50% ethanol – 0.1 M NaOH after various times: (*1*) 2 min; (*2*) 4 min; (*3*) 6 min; (*4*) 8 min; (*5*) 10 min; (*6*) 15 min.

considered the most stable oxazolones, resisting hydrolysis in cold water. The presence of phenyl group in position 2 was assumed to increase their stability towards acids.

The measurement of the polarographic reduction and the UV spectra of 2-benzoylaminocinnamic acid becomes essential to confirm that wave C represents the reduction of the hydrolysis product of the oxazolone studied. The experimental polarogram of this compound exhibited only one wave at −1.67 V, and its spectrum in ethanol displayed only one band at 280 nm. These results indicate that wave C does not represent a stepwise reduction of oxazolones moiety but may reflect the electroreduction of the hydrolysis product. Moreover, the

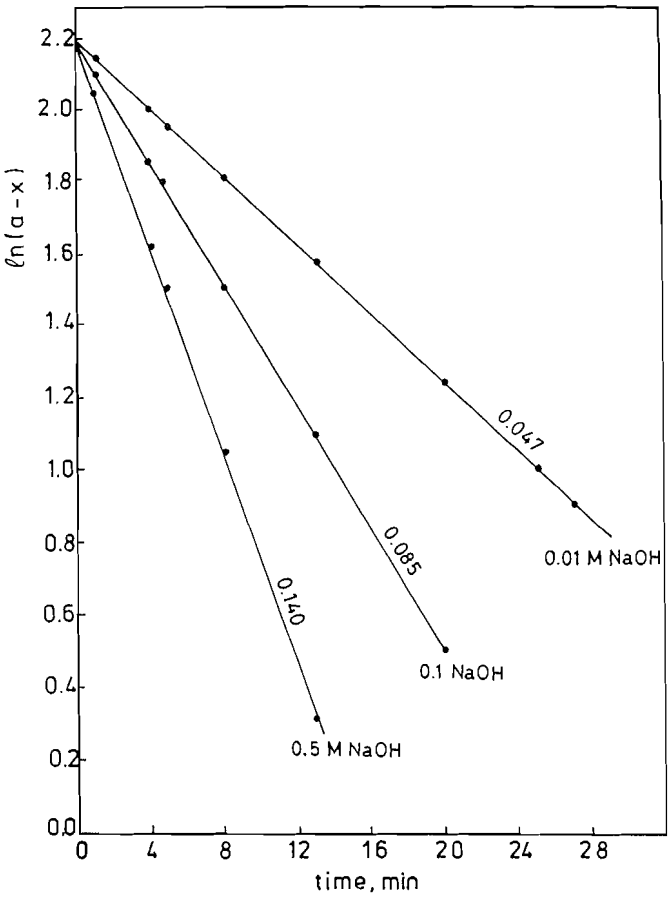


FIG. 4. First order Plots for the hydrolysis of (1) in 50% ethanol – NaOH at 25°C.

hydrolysis of oxazolones in alkaline ethanolic solution is found to be first order with respect to oxazolones (Fig. 4). The rate constant k increases *viz.*, 0.047, 0.085, and 0.14 min^{-1} as the concentration of NaOH is increased from 0.01, 0.1, to 0.5 M, respectively. In other words, the reaction rate is accelerated by the presence of OH^- ions.

2. Nature of waves

Coulometric analysis of compound **1** was carried out under controlled potential, *viz.* −1.1 V at ionic strength of 0.1 M in 50% ethanol – 0.05 M HCl as well as in ethanolic buffer solution of pH 3.2. The two solutions are the proper media since the compound studied showed reasonable stability. The total number of electrons transfered in the electrode process was found to be approximately six. From the height ratio of the two waves (1:2), one may assume that wave A represents a two-electron reduction step, whereas wave B corresponds to the uptake of four electrons. Using the Ilkovic equation the number of electrons could also be evaluated. The number of electrons obtained by both approaches were quite close. The diffusion coefficient (D) of the depolarizer was determined experimentally (19) by applying the Stokes–Einstein equation [1]. The obtained values are listed in Table 1.

$$[1] \quad D_0 = 3.31 \times 10^{-5}(D/M)^{1/3}/\eta \text{ cm}^2/\text{s}$$

The effect of mercury pressure on limiting current at pH < 7.2 reveals that the two waves are diffusion controlled. The applicability of Ilkovic equation at different pH shows that the values of i_l/C obtained at pH > 7 are not constant, evidently

TABLE 1. Polarographic results[a] obtained for oxazolone derivatives

Compound	pH	$-E_{1/2}$	Y^b	$D \times 10^6$ (cm^2/s)	αn_a	n_a	$\frac{\Delta E_{1/2}}{\Delta pH}$	Z_{H^+}	K_c^0 (cm/s)	ΔG^* (kJ/mol)
1	2.2	0.78[c]	12.82	6.355	0.756	0.38	0.05[c]	0.64	4.12×10^{-9}	347.82
		0.90[d]	13.14		0.775	0.19	0.057[d]	0.75	6.22×10^{-15}	513.77
	4.4	0.89[c]	11.99		0.707	0.35		0.60	3.62×10^{-10}	388.28
		1.035[d]	13.36		0.788	0.20		0.76	8.11×10^{-16}	541.69
	7.2	1.031[c]	10.89		0.643	0.32		0.54	2.83×10^{-11}	454.87
		1.198[d]	12.19		0.719	0.18		0.70	4.31×10^{-17}	550.84
2	2.2	0.82[c]	12.61	7.243	0.743	0.37	0.055[c]	0.69	2.14×10^{-10}	401.99
		0.96[d]	12.96		0.765	0.19	0.081[d]	1.05	1.12×10^{-16}	549.75
	4.4	0.92[c]	12.18		0.719	0.36		0.67	8.52×10^{-10}	475.48
		1.06[d]	13.11		0.714	0.18		0.98	3.61×10^{-17}	582.11
	7.2	1.07[c]	11.56		0.682	0.34		0.64	2.53×10^{-11}	536.09
		1.27[d]	12.21		0.720	0.18		0.99	1.97×10^{-18}	592.14
5	2.2	0.72[c]	11.22	7.136	0.662	0.33	0.051[c]	0.57	2.71×10^{-9}	308.53
		0.81[d]	12.43		0.733	0.18	0.071[d]	0.88	3.52×10^{-14}	458.17
	4.4	0.83[c]	10.87		0.641	0.32		0.55	6.97×10^{-9}	382.51
		0.99[d]	12.16		0.717	0.18		0.86	2.81×10^{-15}	496.88
	7.2	0.98[c]	10.63		0.627	0.31		0.54	2.74×10^{-10}	490.56
		1.14[d]	11.65		0.687	0.17		0.83	3.17×10^{-16}	524.29
6	2.2	0.8[c]	11.77	7.612	0.694	0.35	0.048[c]	0.56	5.12×10^{-9}	358.18
		0.88[d]	12.95		0.764	0.19	0.051[d]	0.66	7.17×10^{-15}	517.36
	4.4	0.87[c]	11.18		0.659	0.33		0.54	2.93×10^{-10}	380.00
		0.91[d]	12.89		0.761	0.19		0.66	1.23×10^{-16}	539.05
	7.2	1.01[c]	10.87		0.641	0.32		0.52	3.26×10^{-11}	423.56
		1.11[d]	12.74		0.752	0.19		0.65	4.34×10^{-17}	581.65
7	2.2	0.84[c]	11.91	6.875	0.702	0.35	0.065[c]	0.77	9.33×10^{-8}	304.76
		0.98[d]	12.62		0.745	0.19	0.062[d]	0.78	7.26×10^{-14}	461.14
	4.4	0.92[c]	11.24		0.663	0.33		0.73	2.91×10^{-9}	372.56
		1.05[d]	12.52		0.739	0.18		0.77	3.72×10^{-15}	508.12
	7.2	1.13[c]	10.71		0.632	0.32		0.70	5.11×10^{-10}	398.31
		1.31[d]	12.27		0.724	0.18		0.76	7.97×10^{-15}	543.78
10	2.2	0.9[c]	10.43	7.702	0.615	0.31	0.061[c]	0.64	2.11×10^{-10}	407.76
		1.05[d]	11.81		0.696	0.17	0.058[d]	0.68	3.81×10^{-15}	533.70
	4.4	1.02[c]	10.16		0.599	0.30		0.62	6.15×10^{-11}	478.74
		1.24[d]	11.27		0.665	0.17		0.65	3.18×10^{-16}	545.87
	7.2	1.25[c]	9.98		0.589	0.29		0.61	3.97×10^{-12}	540.31
		1.43[d]	10.96		0.647	0.16		0.64	5.43×10^{-17}	590.76
12	2.2	0.67[c]	11.28	1.883	0.666	0.33	0.051[c]	0.58	7.52×10^{-8}	298.16
		0.81[d]	12.53		0.739	0.18	0.05[d]	0.63	3.81×10^{-14}	436.94
	4.4	0.78[c]	11.75		0.693	0.35		0.60	1.22×10^{-9}	352.66
		0.94[d]	12.68		0.748	0.19		0.63	2.97×10^{-15}	497.29
	7.2	0.91[c]	10.85		0.640	0.32		0.55	3.36×10^{-10}	382.80
		1.02[d]	11.39		0.672	0.17		0.57	4.73×10^{-15}	536.67
15	2.2	0.62[c]	10.97	3.584	0.647	0.32	0.048[c]	0.53	2.93×10^{-8}	277.51
		0.80[d]	11.38		0.671	0.17	0.053[d]	0.60	3.14×10^{-14}	410.85
	4.4	0.76[c]	11.01		0.650	0.32		0.53	2.01×10^{-9}	330.14
		0.91[d]	12.21		0.720	0.18		0.65	1.55×10^{-15}	432.71
	7.2	0.87[c]	10.84		0.640	0.32		0.52	2.18×10^{-10}	375.87
		0.97[d]	11.29		0.666	0.17		0.60	3.97×10^{-15}	450.85

[a]The values of x in the relation $i_l = Kh^x$ are equal to 0.5–0.53 at different pH's.
[b]The slope of the correlation of log $i/(i_l - i)$ with E; the slopes are calculated by the least-squares method.
[c]Wave A.
[d]Wave B.

due to the hydrolysis of the oxazolones. An excellent linear relationship passing through the origin is obtained for the total limiting current of the two waves at pH < 7. Accordingly, it seemed that the polarographic determination of oxazolone derivatives should be performed only in acidic media.

The thermodynamic reversibility (20) of the waves can be tested from the correlation of E with log $(i/i_l - i)$ at pH < 7.5. The results show straight lines with somewhat varying slopes. The listed data in Table 1 indicate that the waves proceed irreversibly and this trend increases as the pH is increased. This is substantiated by a shift of $E_{1/2}$ towards more negative values as the concentration of the depolarizer is increased (21).

Can. J. Chem. Downloaded from www.nrcresearchpress.com by 123.30.183.119 on 09/08/12
For personal use only.

Can. J. Chem. Downloaded from www.nrcresearchpress.com by 123.30.183.119 on 09/08/12
For personal use only.

The irreversibility is further supported by the lower values of the electron rate constant, K_e^0, and the higher values of the free energy of activation, ΔG^*; both being calculated by applying the Delahay (22, 23) and Koutecky (24) equations as modified by Issa and Tharwat (25) for irreversible waves;

$$[2] \quad \log K_e^0 = \left(\frac{i_{irr}}{i_{rev} - i_{irr}}\right)_{E=0} + \log \frac{1}{0.886}\left(\frac{d}{t}\right)^{1/2}$$

$$[3] \quad \Delta G^* = 5778.8\left(5.097 + \frac{\alpha n_a}{0.059}E - \log K_e^0\right)$$

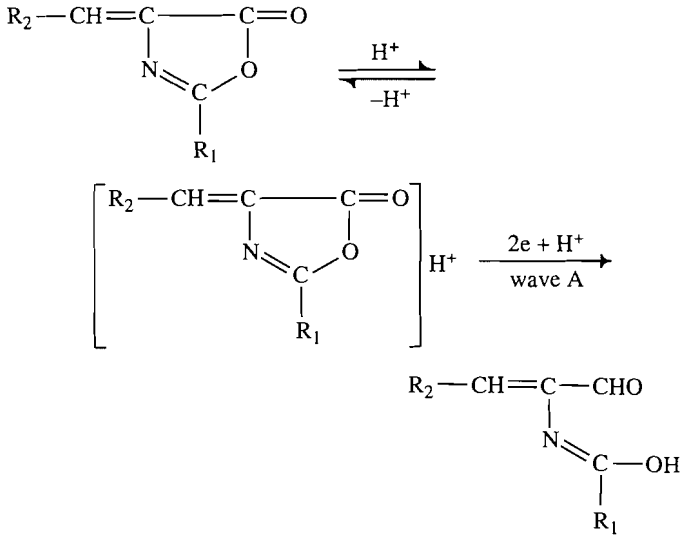
The correlation between limiting current of waves A, B, and C and pH is shown in Fig. 5. The first two waves (A and B) show dissociation curves (26). For wave C, however, i_l increases as pH is increased. The relationship between $E_{1/2}$ (for waves A and B) and pH gives straight lines (Fig. 5), the slope of each indicates the consumption of hydrogen ions (Z_{H^+}) in the reduction process (20). For wave C, $E_{1/2}$ is practically pH independent.

3. Reduction mechanism

The available data in the present study allow the following conclusions:

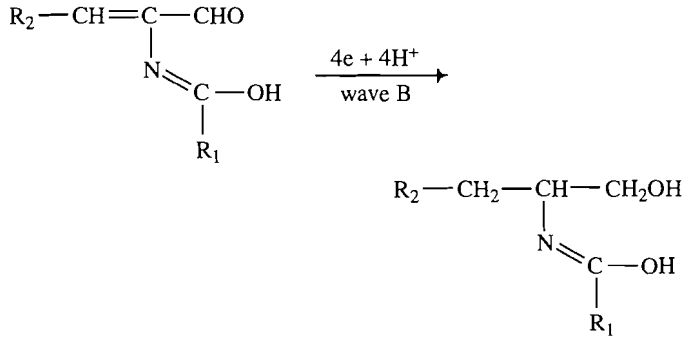
(a) At pH ≤ 7.2 (waves A and B)

Wave A represents the uptake of two electrons corresponding to the cleavage of the protonated oxazolone ring-oxygen (4) to give the corresponding aldehyde (**I**)



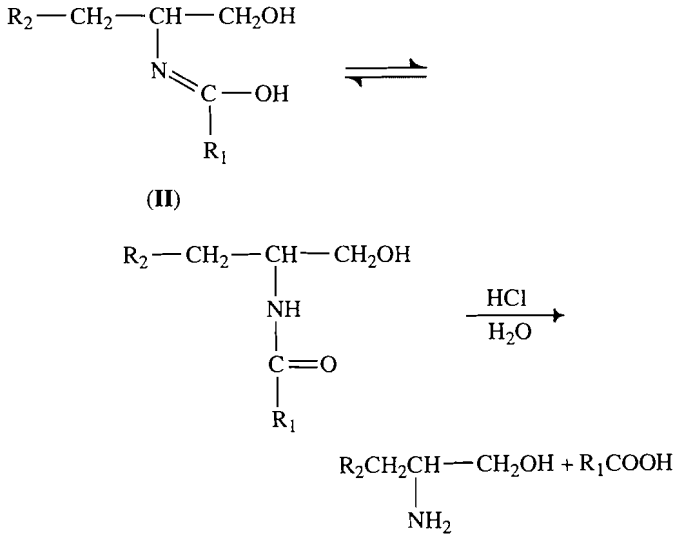
(**I**)

Wave B corresponds to a 4-electron reduction step, representing the reduction of α,β-unsaturated aldehyde (27, 28) to produce the corresponding saturated alcohol (**II**),



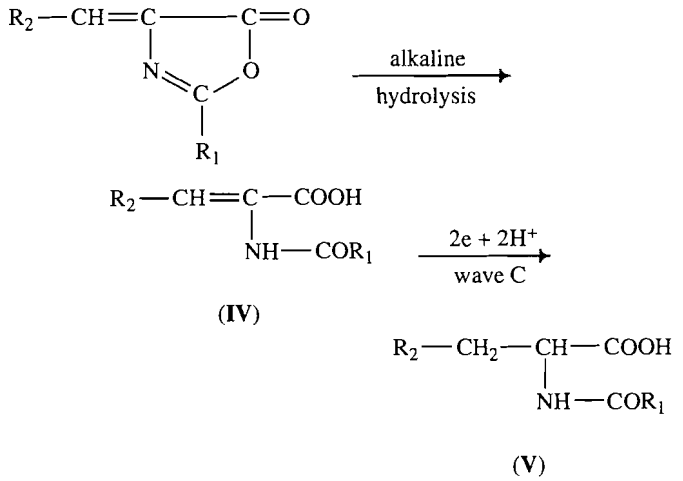
(**II**)

The proposed reduction mechanism was further supported by coulometric analysis of compound **1** in 50% ethanol – 0.05 M HCl carried out on the total limiting current. The main electrolysis product, 2-amino-3-phenylpropanol (**III**) could be identified by its mp and IR spectra (4, 11). Such electrolysis product can only be obtained through acid hydrolysis of benzoyl derivative of 2-amino-3-phenylpropanol (**II**) which is formed along wave B.



(b) At pH > 7.2 (wave C)

Based on the foregoing findings, oxazolones undergo hydrolysis in alkaline medium to form 2-benzoylaminocinnamic acid (**IV**) which is reduced at the DME via a two-electron step to form benzoyl derivative of phenyl alanine (**V**) (3).



4. Determination of electron affinities and ionization potentials of oxazolones

The half-wave reduction ($E_{1/2}^R$) and oxidation ($E_{1/2}^{OX}$) potentials for oxazolone derivatives under investigation were measured in DMF vs. SCE. The $E_{1/2}^R$ of the first wave A was taken as a measure of the electron affinity (EA) of the compound according to eq. [4] (29–31):

$$[4] \quad EA = -E_{1/2}^R + 2.49 \pm 0.26$$

The ($E_{1/2}^{OX}$) of organic compounds were directly related to the ionization potentials (IP) according to eq. [5] (32, 33):

$$[5] \quad IP = (1.478 \pm 0.027)E_{1/2}^{OX} + (5.821 \pm 0.009)$$

TABLE 2. Physical characteristic of oxazolone derivatives in DMF

Compound	$-E^{R}_{1/2}$ (V)	$E^{OX}_{1/2}$ (V)	$\Delta E_{1/2}$ (V)	EA (eV)	IP (eV)	E_{CT} (eV)	$-J_{12}$ (eV)
1	0.87	−0.156	0.714	1.62	5.59	3.39	2.676
2	0.92	−0.210	0.710	1.57	5.51	3.38	2.67
3	0.88	−0.157	0.723	1.61	5.59	3.43	2.70
4	0.83	−0.112	0.718	1.66	5.66	3.41	2.69
5	0.84	−0.125	0.715	1.65	5.64	3.40	2.69
6	0.89	−0.32	0.659	1.60	5.35	(3.18)[a] (3.19)[b]	2.52
7	0.95	−0.242	0.708	1.54	5.46	3.37	2.66
8	1.070	−0.361 −(0.366)[a]	0.709	1.42	5.29	(3.35)[b]	2.64
9	0.93	−0.262	0.665	1.56	5.43	3.22	2.56
10	1.05	−0.554	0.496	1.44	5.00	(2.62)[a] (2.59)[b]	2.15
11	1.03	−0.361	0.669	1.46	5.29	3.34	2.67
12	0.78	+0.030	0.808	1.71	5.87	3.73	2.92
13	0.77	+0.029	0.799	1.72	5.86	(3.70)[a] (3.72)[b]	2.90
14	0.75	+0.048	0.798	1.74	5.89	3.70	2.90
15	0.73	+0.064	0.794	1.76	5.92	3.63	2.89

[a]Calculated using eq. [6].
[b]Values taken from ref. 9.

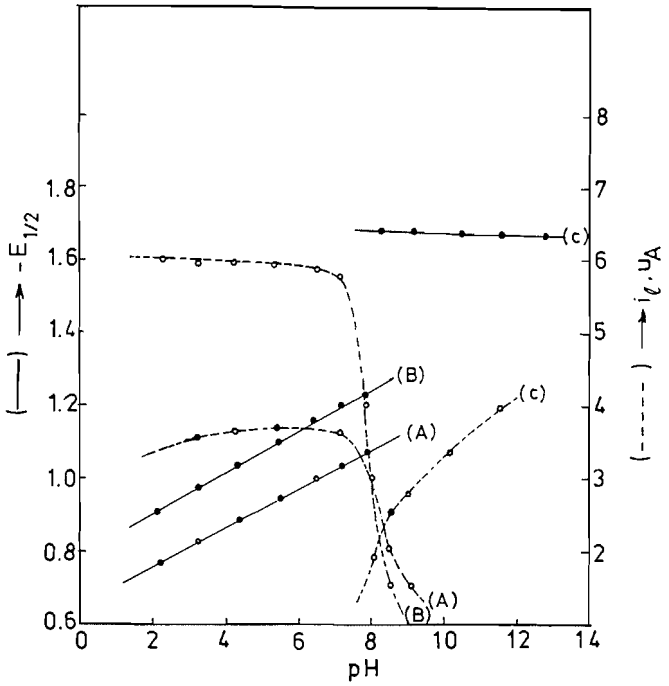


FIG. 5. The correlation of $E_{1/2}$ (—) and i_1 (···) with pH.

The values of $E^{R}_{1/2}$, $E^{OX}_{1/2}$, EA, and IP are listed in Table 2. It is worthy to mention that the polarographic behaviour of oxazolones in DMF, which is an aprotic solvent exhibiting no interaction with the oxazolones, is close to that in ethanolic buffer solutions at pH < 7.2 (Tables 1, 2). This may confirm that the obtained polarographic data in acidic media are confined to the compounds of interest and certainly not related to the hydrolytic product.

5. Effect of molecular structure on $E^{R}_{1/2}$ *and* E_{CT}

The electronic transition band (E_{CT}) of the studied oxazolones were measured in DMF (Table 2). From the obtained half-wave reduction potentials ($E^{R}_{1/2}$) and E_{CT} of oxazolone derivatives, one can conclude that the electron-donating substituents render the reduction process difficult and shifts the $E^{R}_{1/2}$ to more negative values and decreases the value of E_{CT}. However, the electron-attracting groups facilitate the reduction process leading to a decrease in delocalization within the oxazolone ring. On the other hand, the electroreduction of those compounds, when R_1 is the phenyl group, requires more energy than the electroreduction of the compounds containing a methyl group linked to a phenyl ring with donor character and steric effect. Thus, the $E^{R}_{1/2}$ of the former compounds should occur at more negative values and possess lower E_{CT} than the latter compounds.

The use of electrochemical redox potential data to interpret photochemical reactions, where the excited states undergo electron or charge transfer processes, was developed only recently (34–36). Accordingly, it was found interesting to correlate E_{CT} with the absolute difference between $E^{OX}_{1/2}$ and $E^{R}_{1/2}$. This runs in good harmony with the general correlation reported in literature for other types of molecules (36, 37). Analysis of our experimental data of $\Delta E_{1/2}$ and E_{CT} by the least-square sequential simplar method results in a linear equation [6], with an excellent correlation coefficient of 0.994.

$$[6]\quad \Delta E_{1/2}(E^{OX}_{1/2}-E^{R}_{1/2}) = -0.23(\pm 0.03)+0.279(\pm 0.009)E_{CT}$$

The validity of eq. [6] was tested by measuring and calculating either $E^{R}_{1/2}$, $E^{OX}_{1/2}$, or E_{CT} for some other oxazolone derivatives. The results show a good agreement between the calculated values and those measured experimentally as illustrated in Table 2. A trail was also made to compute the coulomb repulsion integral (36, 38) J_{12} according to eq. [7] (adopting the derived values of E_{CT} and $\Delta E_{1/2}$ in our present work),

$$[7]\quad E_{CT} = \Delta E_{1/2} - J_{12}$$

The data obtained are summarized in Table 2. It seems that the method of estimation of the parameter J_{12} given in this work

Can. J. Chem. Downloaded from www.nrcresearchpress.com by 123.30.183.119 on 09/08/12
For personal use only.

is much more direct and easier than the known complicated method based on semi-empirical molecular orbital theories.

1. O. MANOUSK, J. VOLKE, and J. HLAVATY. Electrochim. Acta, **25**, 515 (1980).
2. S. DARWISH, H. FAHMY, M. ABDEL AZIZ, and A. EL-MAGHRABY. J. Chem. Soc. Perkin II, **2**, 344 (1981).
3. P. B. BERNTSON, F. VASTRA, T. O. GORDER, and B. B. LAMM. (Aktie belag Hassle) German Offen. **2**, 243 665 (Cl. C070) (1973); Swedish Appl. **11**, 582/71, **6**, 12 (1971).
4. H. FAHMY, H. DABOUN, M. HUSSEIN, and M. ELNAGDI. J. Chem. Tech. Biotechnol. **32**, 489 (1982).
5. B. M. KRASOVITSKII, I. V. LYSOVA, and L. AFENASIDI. Khim. Geterotsikl. Soedin. **7**, 909 (1980).
6. B. M. KRASOVITSKII, A. V. YUDASHKIN, I. V. LYSOVA, L. AFENASIDI, and A. LIPKIN. Khim. Geterotsikl. Soedin. **12**, 1624 (1979).
7. J. D. MARGERUM and L. J. MILLER. Photochromic processes by tantomerism in photochromism. *Edited by* G. H. Brown. Wiley Interscience, New York. 1971.
8. R. PAETZOLD, M. REICHENBACHER, and K. APPENROTH. Z. Chem. **21**, 421 (1981).
9. M. ANTONIOUS, M. HABASHY, and Y. ELSAYED. J. Prakt. Chem. **330**, 563 (1988).
10. E. L. BENNETT and E. HOERGER. J. Am. Chem. Soc. **74**, 5975 (1952).
11. A. R. KATRITZKY and A. J. BOULTON. Advances in heterocyclic chemistry. Vol. 17. Academic Press, New York. 1974.
12. V. D. BEZUGLYI and N. P. SKIMANSKAYA. Z. Oeshch. Khim. **31**, 3160 (1961).
13. A. VOGEL. A text book of practical organic chemistry including qualitative analysis. 3rd ed. Longman, London. p. 910.
14. D. PELTIER, M. LEGUYADER, and J. TACUSSEL. Bull. Soc. Chim. Fr. **11**, 2609 (1963).
15. B. ERLENMEYER. Ann. **276**, 8 (1893).
16. B. ERLENMEYER and W. STADLIN. Ann. **337**, 283 (1904).
17. N. KRZYSZTOF and J. HANS. J. Chem. Soc. **17**, 1679 (1975).
18. S. BRONISLAW, W. JOLAUTA, and L. TACHLEUSZ. Rocz. Chem. **47**, 1281 (1973).
19. R. A. ROBINSON and R. H. STOKES. Electrolyte solutions. Butterworths, London. 1970. p. 256.
20. L. MEITES. Polarographic techniques. 2nd ed. Interscience Publishers, New York – London – Sydney. 1965.
21. M. SUZUKI and P. J. ELVING. J. Phys. Chem. **65**, 391 (1961).
22. P. DELAHAY. J. Am. Chem. Soc. **73**, 4944 (1951).
23. J. E. STRASSNER and P. DELAHAY. J. Am. Chem. Soc. **74**, 6232 (1952).
24. J. KOUTECKY. Chem. Listy, **47**, 323 (1953).
25. I. M. ISSA and M. THARWAT. Electrochim. Acta, **17**, 1065 (1972).
26. P. ZUMAN. Elucidation of organic electrode processes. *Edited by* L. Meites. Academic Press, New York. 1969. Chap. 11. p. 20.
27. D. BARNES and P. ZUMAN. Trans. Faraday Soc. **65**, 1668 (1969).
28. D. BARNES and P. ZUMAN. J. Electroanal. Chem. **16**, 575 (1968).
29. K. M. C. DAVIS, P. R. HAMMOND, and M. E. PEOVER. Trans. Faraday Soc. **61**, 1516 (1965).
30. A. H. MAKI and D. H. GESKE. J. Am. Chem. Soc. **83**, 1852 (1961).
31. S. H. ETAIW, M. I. ISMAIL, and M. ELBORAI. Can. J. Chem. **58**, 263 (1980).
32. A. STREITWIESER. Molecular orbital theory for organic chemistry. Wiley, New York. Chap. 7, 1961.
33. M. E. WOCKS and V. H. DIBELER. J. Chem. Phys. **21**, 1357 (1959).
34. R. F. LARGE. Photographic sensitivity. *Edited by* R. J. Cox. Academic Press, New York. 1973. p. 241.
35. M. HABASHY, F. ELZAWAWI, M. ANTONIOUS, and M. ABDEL-MOTTALEB. Indian J. Chem. **24**A, 908 (1985).
36. R. O. LOUTFY and R. O. LOUTFY. Can. J. Chem. **54**, 1454 (1976).
37. O. GURTLER and S. DAHNE. Z. Phys. Chem. (Leipzig), **255**, 3 (1974).
38. R. DITCHFIELD, J. E. DEL-BENF, and J. A. POPLE. J. Am. Chem. Soc. **94**, 703 (1972).

Can. J. Chem. Downloaded from www.nrcresearchpress.com by 123.30.183.119 on 09/08/12
For personal use only.

Concerning the distant polar interaction in free energies of transfer. An explanation and an estimation procedure

J. Peter Guthrie

Department of Chemistry, University of Western Ontario, London, Ont., Canada N6A 5B7

Received December 20, 1990[1]

J. Peter Guthrie. Can. J. Chem. **69**, 1893 (1991).

For polyfunctional compounds, free energies of transfer from gas to aqueous solution require corrections for the interactions of polar groups (Distant Polar Interactions). These corrections can be made with very few adjustable parameters by using a model of the solvation process assuming hydrogen bonding is the major source of the effect on free energy of transfer for polar groups, and that hydrogen bonding is perturbed by polar effects, measured by Taft σ^*. Parameters evaluated for polyfluoro, polychloro, and polybromo compounds successfully predicted the free energies of transfer for mixed polyhalogen compounds. Preliminary parameters have been evaluated for ethers, amines, phenyl groups, nitriles, and esters.

Key words: free energy of transfer, distant polar interaction, hydrogen bonding, solvation.

J. Peter Guthrie. Can. J. Chem. **69**, 1893 (1991).

Avec les composés polyfonctionnels, il est nécessaire de corriger les énergies libres de transfert de la phase gazeuse à des solutions aqueuses pour les interactions des groupements polaires (Interactions dipolaires à distance). On peut effectuer ces corrections avec un nombre limité de paramètres ajustables en utilisant un modèle du processus de solvatation basé sur l'hypothèse que les ponts hydrogènes sont la source principale de l'effet sur l'énergie libre de transfert pour les groupes polaires et que ces ponts hydrogènes sont perturbés par les effets polaires que l'on peut mesurer par le σ^* de Taft. Les paramètres évalués pour les composés polyfluorés, polychlorés et polybromés ont permis de prédire correctement les énergies de transfert de composés contenant un mélange d'halogènes. On a évalué les paramètres préliminaires pour les éthers, les amines, les groupes phényles, les nitriles et les esters.

Mots clés : énergie libre de transfert, interaction dipolaire à distance, liaison hydrogène, solvatation.

[Traduit par la rédaction]

Introduction

A longstanding goal of physical organic chemistry has been to explain chemical reactivity in terms of the structures of the reacting molecules. One way of approaching this goal is to look for ways to estimate enthalpies and free energies of formation of the species involved in reaction, so that the thermodynamics of the reaction can be used as a starting point for the explanation and prediction of reactivity. It has been found that thermodynamic quantities can be estimated quite reliably in terms of structural additivity (1–3). However, these quantities are estimated for the gas phase, and most organic reactions are carried out in solution. It was a major step forward when Hine and Mookerjee showed that free energies of transfer from the gas phase to aqueous solution could also be estimated in terms of structural additivity (4). A remaining problem, to which Hine and Mookerjee called attention, was that their scheme was only satisfactory for monofunctional compounds, because calculated free energies of transfer for polyfunctional compounds generally deviated from the experimental values by amounts much larger than were found for monofunctional compounds. This was attributed to distant polar interactions (DPI), which it was proposed were determined by hydrogen bonding interactions (4), but no way was suggested to estimate these interactions. Thus a large number of empirical corrections appeared necessary, and the usefulness of the estimation procedure for molecules of interesting complexity was severely restricted.

We wish now to report that a straightforward application of the assumption that the DPI is a linear function of the electron-withdrawing properties of other substituents on the molecule leads not only to a reliable way to estimate the DPI corrections, but allows an important reduction in the number of parameters needed to estimate the free energy of transfer. At least for the class of molecules with no hydrogens directly bonded to electronegative atoms, this means that the DPI problem is solved.

Results

We begin with an examination of the implications of the assumption that free energies of transfer are determined by relatively small and constant (i.e., independent of environment) contributions from hydrophobic solvation of the hydrocarbon moieties of a molecule and relatively large contributions from solvation of the electronegative atoms, by hydrogen bonding or other polar interactions. These polar contributions to solvation are assumed to be sensitive to the environment. In support of this analysis we quote the group contributions reported by Hine and Mookerjee for groups which can be represented by $[CH_2(X)_2]$, $[CH(X)_3]$, and $[C(X)_4]$, together with a few additional contributions based on measurements since this work. The values in Table 1 show that for X = C, in various bonding states, or for no more than one X being an electronegative atom, the group contribution is essentially constant, while if more than one X is an electronegative atom, the contributions are drastically different. This is a consequence of making the standard assumption, namely that all $[O(C)_2]$ groups are the same. This pushes all effects of the presence of more than one electronegative atom into the $[CH_n(X)_{4-n}]$ group contribution. We list the group contributions both as contributions to log γ ($\gamma = c_w/c_g$ (4)) and as contributions to ΔG_t (the free energy of transfer from gas at 1 atm (1 atm = 101.3 kPa) to aqueous solution at 1 M), which is directly applicable to the problem of calculating free energies of formation in solution. It is necessary to allow for the change in concentration units from gas to aqueous solution, so the calculation is:

$$\Delta G_t = 1.90 + \Sigma(\text{group contributions}) + \Sigma(\text{DPI})$$

First we examined the available data for haloalkanes to see

[1]Revision received July 12, 1991.

Can. J. Chem. Downloaded from www.nrcresearchpress.com by 123.30.183.119 on 09/07/12
For personal use only.

TABLE 1. Group contributions to log γ and ΔG_t, showing the constancy of the value for $[CH_n(X)]_{4-n}$ when no more than one electronegative atom is present[a]

Group	Value		Group	Value		Group	Value	
	log γ	ΔG_t		log γ	ΔG_t		log γ	ΔG_t
$[CH_2(C)_2]$	−0.15	0.20	$[CH(C)_3]$	0.24	−0.33	$[C(C)_4]$	0.71	−0.97
$[CH_2(C)(C_t)]$	−0.29	0.40	$[CH(C)_2(C_B)]$	0.29	−0.40	$[C(C)_3(C_B)]$	0.93	−1.27
$[CH_2(C)(C_d)]$	−0.23	0.31	$[CH(C)_2(O)]$	0.12	−0.16	$[C(C)_3(O)]$	0.78	−1.07
$[CH_2(C)(C_B)]$	−0.19	0.26	$[CH(C)(O)_2]$	−1.35	1.84	$[C(C)(O)_3]$	−3.11	4.25
$[CH_2(C)(O)]$	−0.13	0.18	$[CH(O)_3]$	−3.70	5.05			
$[CH_2(C)(CO)]$	−0.15	0.20						
$[CH_2(C)(N)]$	−0.08	0.11						
$[CH_2(O)_2)]$	−2.54	3.47						

[a]Group contributions from ref. 4; $[CH(O)_3]$ and $[C(C)(O)_3]$ calculated from data in ref. 43.

TABLE 2. Free energies of transfer for fluorine compounds[a]

Compound	ΔG_t obsd.	$\Sigma_F\sigma^*$	ΔG_t^b calcd. (fluorine only)	Errors	ΔG_t^b calcd. (all compounds)	Errors
CH_3-F	1.68[c]		1.69	−0.01	1.75	0.07
CH_3CH_2-F	1.85[d]		1.90	−0.04	1.96	−0.11
$CH_3CH_2CH_2F$	1.65[e,j]		2.10	−0.46	2.17	−0.52
CH_3CHFCH_3	1.70[f,j]		2.20	−0.50	2.27	−0.57
CH_3CHF_2	1.79[g]	6.42	1.70	0.09	1.81	−0.02
CHF_3	2.71[c]	19.26	2.63	0.08	2.76	−0.05
CF_4	5.01[c,h]	38.52	5.16	−0.15	5.29	−0.28
CF_3-CF_3	5.83[h]	54.18	5.52	0.31	5.73	0.10
CF_3-CH_2F	3.10[f]	25.17	2.44	0.66	2.62	0.48
$CF_3CF_2CF_3$	5.60[h,i]	70.74	6.06	−0.46	6.35	−0.75

[a]Free energies of transfer, ΔG_t, from the gas at 1 atm to 1 M aqueous solution at 25°C, unless otherwise stated. Free energies are in kcal/mol.

[b]$\Delta G_t = \Sigma[CH_n(X)_{4-n}] + [F]n_F + r_F\Sigma_F\sigma^*$; $[F] = -1.065$, $r_F = 0.221$, fluorine only; $[F] = -1.095$, $r_F = 0.228$, all compounds.

[c]Reference 4.

[d]Calculated from the solubility of the gas, at a pressure of 1 atm, in water at 25°C (5).

[e]Calculated from the solubility of the gas, at a pressure of 1 atm, in water at 14°C (5).

[f]Calculated from the solubility of the gas, at a pressure of 1 atm, in water at 15°C (5).

[g]Reference 24.

[h]Reference 25.

[i]Extrapolated from data at 10 and 15°C. These points defined a reasonable ΔH; if the data at 5°C were used as well, both ΔH and ΔC_p were needed and the values were not in reasonable accord with those for CF_4 and CF_3CF_3.

[j]Based on solubility data at a temperature other than 25°C; not included in the final least-squares fit.

whether such a treatment would work. Halocarbon data are relatively abundant because of the interest in their effects on the environment (5), and provide a convenient test set. We have found that what is, in effect, a two-parameter correlation for each halogen is sufficient. The two parameters were the number of halogen atoms and the sum of the Taft σ* values for substituents on the carbon bearing each halogen. Here we have in effect altered the parameterization from that used by Hine and Mookerjee, who made the normal assumption that univalent substituents should be incorporated into the group for the carbon bearing the substituents, as for example $[CHF_2(C)]$. If we assume that each halogen will affect the solvation of the other halogens or polar groups in the molecule, then we must treat each halogen as a group with a contribution, and a perturbation caused by the DPI. Here we are using the term DPI even for interactions of halogens bonded to the same carbon: while this is not really distant it allows us to continue using the accepted descriptor rather than inventing a new one. Thus in place of $[CHF_2(C)]$ we will use $2[F(C)] + [CH(X)_3]$. For each compound we calculated the sum of the contributions from the groups for C and H only, and then fitted the difference between this and the observed value to:

$$\delta\Delta G_t = n_F[F] + r_F\Sigma_F\sigma^*$$

The data are found in Table 2 and the quality of the fit is shown in Fig. 1. For other halogens analogous fits were obtained: chlorine, Table 3 and Fig. 2; bromine, Table 4 and Fig. 3; iodine, Table 5 and Fig. 4. For iodo compounds there are not enough data for a reliable determination of r_I.

A test of the general validity of these correlations is possible by examination of compounds with more than one kind of halogen. What we did was to use the parameters evaluated for compounds containing only fluorine, or only chlorine, or only bromine, along with the literature parameters for carbon groups, $[CH_n(X)_{4-n}]$, and calculate the free energy of transfer

Can. J. Chem. Downloaded from www.nrcresearchpress.com by 123.30.183.119 on 09/07/12
For personal use only.

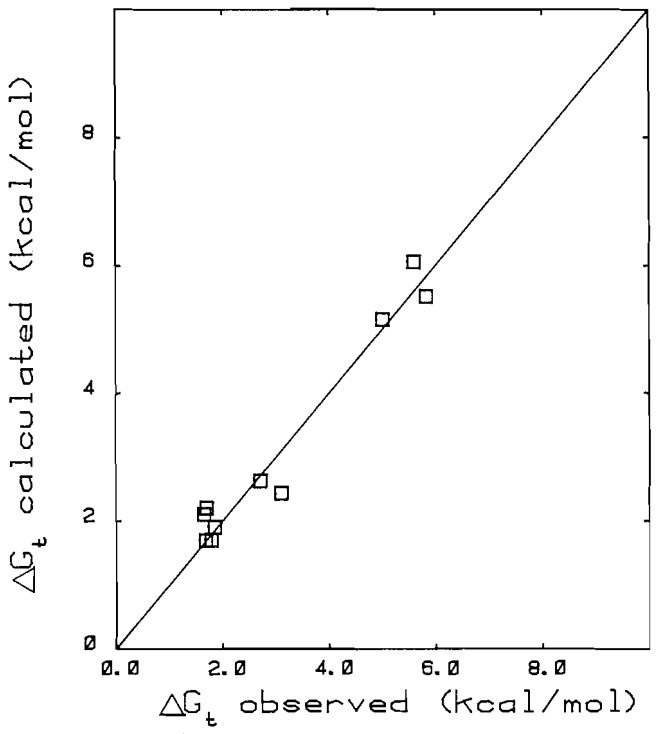


FIG. 1. Calculated vs. observed free energies of transfer for fluorine compounds.

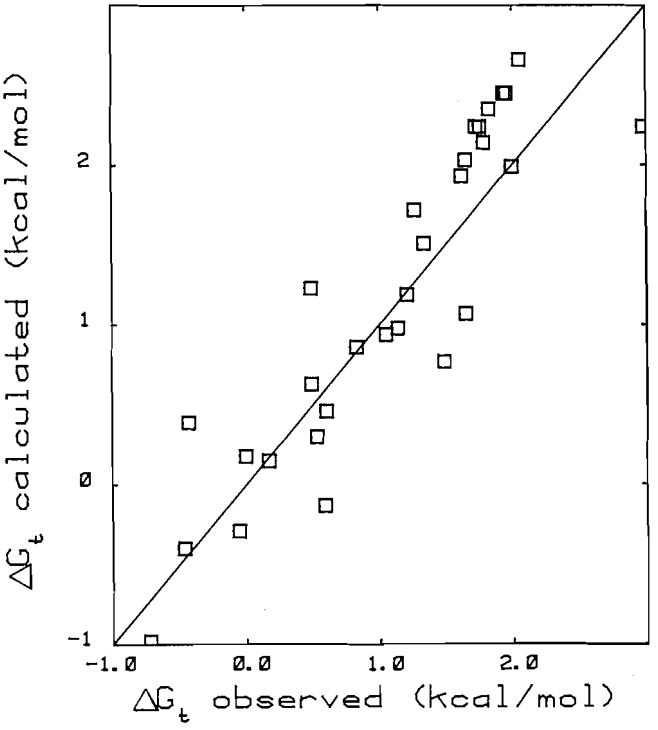


FIG. 2. Calculated vs. observed free energies of transfer for chlorine compounds.

for the mixed halogen compounds, with no adjustment of parameters.

The equation used to calculate these free energies of transfer is

$$\Delta G_t = n_3[CH_3(X)_1] + n_2[CH_2(X)_2] + n_1[CH_1(X)_3] + n_0[C(X)_4] + n_F[F] + r_F\Sigma_F\sigma^* + n_{Cl}[Cl] + r_{Cl}\Sigma_{Cl}\sigma^* + n_{Br}[Br] + r_{Br}\Sigma_{Br}\sigma^*$$

The quality of the match of calculated to experimental data, shown in Table 6 and Fig. 5, shows that we are indeed able to describe the free energies of transfer in terms of our DPI treatment with no additional parameters beyond those needed for compounds with only one kind of halogen. The rms deviation is 0.77, and as we will see when we consider possible sources of the larger deviations, in the Discussion, this may be higher than the true value.

Having demonstrated that the approach we are using provides not just a suitable correlation but also has good predictive powers, we now turn to other functional groups. For these the available body of data is more restricted. There has been, to date, insufficient motivation for gathering these data, which could not be satisfactorily correlated, even though polyfunctional molecules are likely to be the sorts of compounds where free energies of formation will be most useful.

The available body of data for non-halogen functional groups is collected in Table 7. We have limited ourselves to compounds where the interactions are through at least one sp^3 carbon. The problems of polysubstituted arenes or alkenes remain to be solved. To make maximum use of the meagre body of data, we have fitted all of the compounds at once, except for the iodo compounds where there is no overlap, since no free energies of transfer could be found for compounds containing iodine and another functional group. We have included the

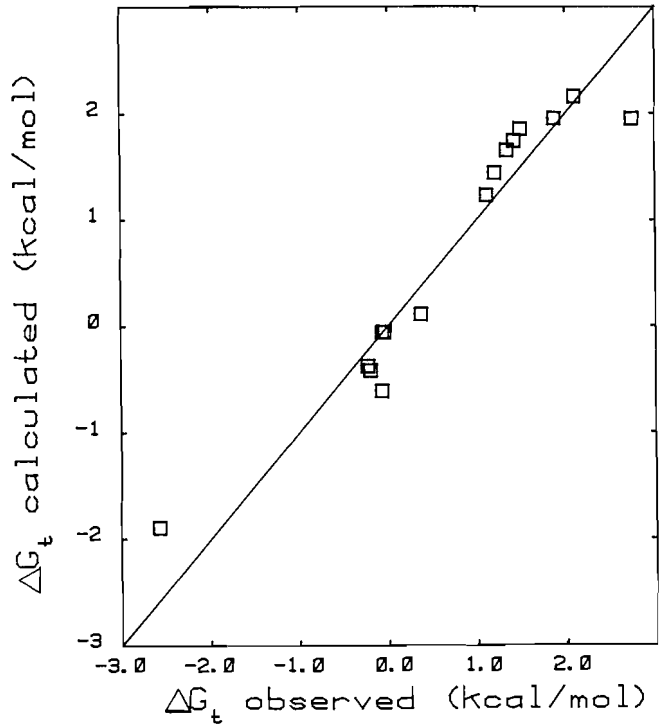


FIG. 3. Calculated vs. observed free energies of transfer for bromine compounds.

phenyl group in this treatment, using the published group contributions for aromatic C and H (4), but correcting for the effect of polar substituents. Obviously this can only apply for non-conjugated and unsubstituted phenyl substituents. The contributions from carbon groups, $[CH_n(C)_{4-n}]$, and from $[C_BH]$ and $[C_B(C)]$ were subtracted, and the remainders fitted by least

Can. J. Chem. Downloaded from www.nrcresearchpress.com by 123.30.183.119 on 09/07/12
For personal use only.

Can. J. Chem. Downloaded from www.nrcresearchpress.com by 123.30.183.119 on 09/07/12
For personal use only.

TABLE 3. Free energies of transfer for chlorine compounds[a]

Compound	ΔG_t	$\Sigma\sigma^*$	ΔG_t^b calcd. (chlorine only)	Errors	ΔG_t^b calcd. (all compounds)	Errors
Chloromethane	1.34[c]		1.51	−0.17	1.53	−0.19
Chloroethane	1.27[c]		1.72	−0.45	1.74	−0.47
1-Chloropropane	1.62[c]		1.93	−0.31	1.95	−0.33
2-Chloropropane	1.65[c]		2.03	−0.38	2.05	−0.40
$(CH_3)_3CCl$	2.98[f]		2.24	0.74	2.26	0.72
$CH_3CH_2CH_2CH_2Cl$	1.79[c]		2.14	−0.35	2.16	−0.37
$(CH_3)_2CH\text{-}CH_2Cl$	1.76[d]		2.24	−0.48	2.26	−0.50
$CH_3CH_2CHClCH_3$	1.73[e]		2.24	−0.51	2.26	−0.53
$CH_3(CH_2)_4Cl$	1.83[c]		2.35	−0.52	2.37	−0.54
$CH_3(CH_2)_2CHClCH_3$	1.96[c]		2.45	−0.49	2.47	−0.51
$(CH_3CH_2)_2CHCl$	1.94[c]		2.45	−0.51	2.47	−0.53
$(CH_3CH_2)(CH_3)_2CCl$	2.06[e]		2.66	−0.60	3.11	−1.05
Dichloromethane	0.49[c]	5.92	0.63	−0.14	0.67	−0.18
1,1-Dichloroethane	1.05[c]	5.92	0.94	0.11	0.98	0.07
1,2-Dichloroethane	0.17[c]	1.88	0.15	0.02	0.20	−0.03
$CH_3CHClCH_2Cl$	0.60[c]	1.88	0.46	0.14	0.51	0.09
$CH_2ClCH_2CH_2Cl$	0.00[c]	0.76	0.18	−0.18	0.22	−0.22
$CH_3CH_2CH_2CHCl_2$	1.21[c]	4.92	1.19	0.02	1.23	−0.02
$CH_3CHClCHClCH_3$	1.49[d]	1.78	0.77	0.72	0.82	0.67
$CH_2ClCH_2CH_2CH_2Cl$	−0.43[f]	0.30	0.39	−0.82	0.35	−0.78
$CH_3CCl(CH_3)CHClCH_3$	1.14[e]	1.68	0.98	0.16	1.03	0.11
Chloroform	0.83[c]	17.76	0.86	−0.03	0.93	−0.10
1,1,1-Trichloroethane	1.65[c]	17.76	1.07	0.58	1.14	0.51
1,1,2-Trichloroethane	−0.05[c]	9.75	−0.29	0.24	−0.22	0.17
$CH_2ClCHClCH_2Cl$	−0.72[d]	4.52	−0.98	0.26	−0.91	0.19
Carbon tetrachloride	2.00[c]	35.52	1.99	0.01	2.07	−0.07
1,1,2,2-Tetrachloroethane	−0.46[c]	19.60	−0.40	−0.06	−0.32	−0.14
CH_2ClCCl_3	0.59[d]	21.84	−0.13	0.72	−0.04	0.63
Pentachloroethane	0.53[c]	34.81	0.30	0.23	0.40	0.13
Hexachloroethane	0.49[c]	51.42	1.23	−0.74	1.36	−0.87

[a]Free energies of transfer, ΔG_t, from the gas at 1 atm to 1 M aqueous solution at 25°C, unless otherwise stated. Free energies are in kcal/mol.

[b]$\Delta G_t = \Sigma[CH_n(X)_{4-n}] + [Cl]n_{Cl} + r_{Cl}\Sigma_{Cl}\sigma^*$; [Cl] = −1.244, r_{Cl} = 0.170, chlorine only; [Cl] = −1.221, r_{Cl} = 0.170, all compounds.

[c]Reference 4.

[d]Calculated from the solubility of the liquid in water at 25°C (5) and the vapor pressure at 25°C, interpolated from data at other temperatures (8).

[e]Calculated from the solubility of the liquid in water at 25°C (5) and the vapor pressure at 25°C (26).

[f]Reference 13.

squares to:

$$\delta\Delta G_t = n_F[F] + r_F\Sigma_F\sigma^* + n_{Cl}[Cl] + r_{Cl}\Sigma_{Cl}\sigma^* + n_{Br}[Br] + r_{Br}\Sigma_{Br}\sigma^* + n_O[O(C)_2] + r_O\Sigma_O\sigma^* + n_N[N(C)_3] + r_N\Sigma_N\sigma^* + r_{Ph}\Sigma_{Ph}\sigma^* + n_{CN}[CN] + r_{CN}\Sigma_{CN}\sigma^* + n_{COO}[COO] + r_{CO_{COO}}\Sigma_{CO}\sigma^* + r_{O_{COO}}\Sigma_{O_{COO}}\sigma^*$$

where [ ] are the fixed contributions for the different groups and $\Sigma_X\sigma^*$ are the sums of the Taft σ^* values for the substituents on the carbon bonded to X. The ester group was initially assigned two polar contributions, the sums of the Taft σ^* values for the substituents on the carbon bonded to the carbonyl, and of the Taft σ^* values for the substituents on the carbon bonded to the oxygen. Least-squares evaluation of these parameters gave a good fit with only one deviation more than 1 kcal/mol, and an rms deviation of 0.539, but $r_{CO_{COO}}$ was undefined, i.e., the calculated uncertainty of the parameter was greater than its value. The least-squares fit was repeated with this parameter deleted from the model, and the resulting fit was essentially as good, but all parameters were now defined. The rms deviation was now 0.542. The revised model is

$$\delta G = n_F[F] + r_F\Sigma_F\sigma^* + n_{Cl}[Cl] + r_{Cl}\Sigma_{Cl}\sigma^* + n_{Br}[Br] + r_{Br}\Sigma_{Br}\sigma^* + O(C)_2]n_O + r_O\Sigma_O\sigma^* + N(C)_3]n_N + r_N\Sigma_N\sigma^* + r_{Ph}\Sigma_{Ph}\sigma^* + r_{CN}\Sigma_{CN}\sigma^* + COO]n_{COO} + r_{O_{COO}}\Sigma_{O_{COO}}\sigma^*$$

The quality of the fit is shown in Table 7 and Fig. 6.

All the σ^* values used in these correlations are given in Table 8. The final set of parameters is given in Table 9. It should be noted that the DPI can be quite large relative to the observed ΔG_t. For instance, from Table 2, $CF_3CF_2CF_3$, $\Sigma_F\sigma^*$ = 70.74, ΔG_t = 5.60; since r_F = 0.217 (Table 9), the DPI is 15.35, while the sum of group contributions (including the term for standard state adjustment) is −9.00, for a calculated value of 6.35. Clearly the DPI can have a major impact on the observable value, though it is often relatively small.

TABLE 4. Free energies of transfer for bromine compounds[a]

Compound	ΔG_t obsd.	$\Sigma\sigma^*$ calcd.	ΔG_t^b calcd. (bromine only)	Errors	ΔG_t^b calcd. (all compounds)	Errors
CH_3Br	1.11[c]		1.23	−0.11	1.36	−0.25
CH_3CH_2Br	1.20[c]		1.44	−0.24	1.57	−0.37
$CH_3CH_2CH_2Br$	1.34[c]		1.65	−0.30	1.78	−0.44
$CH_3CHBrCH_3$	1.42[c]		1.74	−0.32	1.88	−0.46
$CH_3CH_2CH_2CH_2Br$	1.49[c]		1.85	−0.36	1.99	−0.50
$(CH_3)_2CHCH_2Br$	1.87[c]		1.95	−0.08	2.09	−0.22
$(CH_3)_3CBr$	2.74[e]		1.95	0.79	2.09	0.65
$(CH_3)_2CHCH_2CH_2Br$	2.10[c]		2.16	−0.06	2.30	−0.20
CH_2Br_2	−0.07[c]	5.68	−0.06	−0.01	0.10	−0.17
CH_2BrCH_2Br	−0.20[c]	2.00	−0.42	0.22	−0.19	−0.01
$CHBr_2CHBr_2$	−2.57[c]	19.20	−1.89	−0.68	−1.72	−0.85
$CH_3CHBrCH_2Br$	−0.04[c]	2.26	−0.06	0.02	0.16	−0.20
$CH_2BrCH_2CH_2Br$	−0.07[c]	0.80	−0.61	0.54	−0.35	0.28
$CHBr_3$	−0.23[c]	17.04	−0.38	0.15	−0.30	0.07
CBr_4	0.37[d]	34.08	0.11	0.26	−0.02	0.39

[a]Free energies of transfer, ΔG_t, from the gas at 1 atm to 1 M aqueous solution at 25°C, unless otherwise stated. Free energies are in kcal/mol.

[b]$\Delta G_t = \Sigma[CH_n(X)_{4-n}] + [Br]n_{Br} + r_{Br}\Sigma_{Br}\sigma^*$; [Br] = −1.525, r_{Br} = 0.155, bromine only; [Br] = −1.388, r_{Br} = 0.135, all compounds.

[c]Reference 4.

[d]Calculated from the solubility of the solid in water at 25°C (5) and the vapor pressure at 25°C, interpolated from data at other temperatures (27).

[e]Reference 13.

TABLE 5. Free energies of transfer for iodine compounds[a]

Compound	ΔG_t obsd.	$\Sigma\sigma^*$	ΔG_t^b calcd.	Error
CH_3I	1.02[c]		1.00	0.01
CH_3CH_2I	1.18[c]		1.21	−0.04
$CH_3CH_2CH_2I$	1.31[c]		1.42	−0.11
CH_3CHICH_3	1.44[c]		1.52	−0.08
$CH_3CH_2CH_2CH_2I$	1.64[c]		1.63	0.01
CH_2I_2	−0.66[d]	2.46	−1.12	0.46
CHI_3	−3.39[e]	4.92	−3.16	−0.23

[a]Free energies of transfer, ΔG_t, from the gas at 1 atm to 1 M aqueous solution at 25°C, unless otherwise stated. Free energies are in kcal/mol.

[b]$\Delta G_t = \Sigma[CH_n(X)_{4-n}] + [I]n_I + r_I\Sigma_I\sigma^*$; [I] = −1.749, r_I = 0.106.

[c]Reference 4.

[d]Calculated from the solubility of the liquid in water at 25°C (5) and the vapor pressure at 25°C (26).

[e]Calculated from the solubility of the solid in water at 25°C (5) and the vapor pressure at 25°C, interpolated from data at other temperatures (27).

Discussion

We tested our model for the DPI by calculating values for mixed halogen compounds using only the parameters evaluated for compounds containing only fluorine or only chlorine or only bromine. This test was successfully passed, in that the observed and calculated values showed an rms deviation of 0.77. Nonetheless there were some disturbingly large deviations and we have examined these carefully. In most cases it seems likely that there are problems with the experimental results, because the values reported do not seem to be consistent with other data in the literature. Our approach in this examination is based on the assumption that one should have relatively smooth changes in ΔG_t for simple successive replacements of one halogen by another.

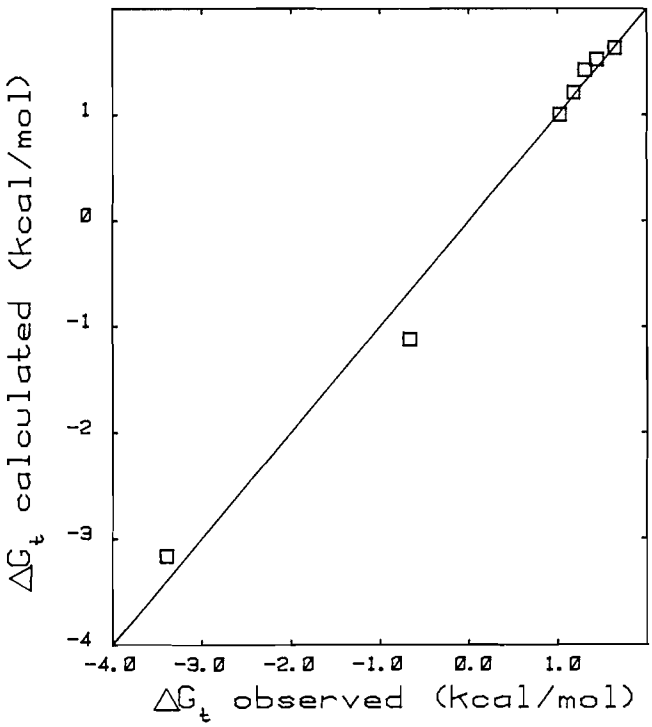


FIG. 4. Calculated vs. observed free energies of transfer for iodine compounds.

The first deviating compound was $CBrClF_2$. We look for a simple pattern in the series $CBrF_3$, $CBrClF_2$, $CBrCl_2F$, $CBrCl_3$, but cannot directly test the idea because values are only reported for the first two (Table 6) and the second is being examined. We can try the assumption that the series $CClF_3$, CCl_2CF_2, CCl_3F, CCl_4 should be similar, and here we have values of 4.17, 3.54, 2.85, and 2.00 respectively, for

Can. J. Chem. Downloaded from www.nrcresearchpress.com by 123.30.183.119 on 09/07/12
For personal use only.

TABLE 6. Free energies of transfer for mixed halogen compounds[a]

Compound	ΔG_t obsd.	$\Sigma\sigma^*F^b$	$\Sigma\sigma^*Cl^c$	$\Sigma\sigma^*Br^d$	ΔG_t^l calcd. (halogen only)	Error	ΔG_t^l (all compounds)	Error
$CBrClF_2$	1.28[e]	18.02	9.26	9.38	3.04	−1.76	3.08	−1.80
$CBrClH_2$	0.32[f]		2.84	2.96	0.28	0.04	0.38	−0.06
$CBrF_3$	3.18[g]	27.78		9.63	3.83	−0.65	3.88	−0.70
CBr_3F	1.87[h]	8.52		26.67	1.29	0.58	1.22	0.65
CH_2ClF	1.11[g]	2.96	3.21		1.01	0.10	1.08	0.03
$CHClF_2$	2.01[g]	12.34	6.42		2.00	0.01	2.11	−0.10
$CClF_3$	4.17[g]	28.14	9.63		4.32	−0.15	4.44	−0.27
$CHCl_2F$	0.99[e]	5.92	12.34		1.41	−0.42	1.50	−0.68
CCl_2F_2	3.54[g]	18.26	18.76		3.54	−0.00	3.66	−0.12
CCl_3F	2.90[i,m]	8.88	27.39		2.75	0.10	2.86	−0.01
CH_2ClCH_2F	0.06[h]	0.94	1.10		0.40	−0.34	0.48	−0.42
$CHClBrCF_3$	1.80[h]	25.08	5.45	5.57	1.97	−0.17	2.13	−0.33
CH_2BrCH_2Cl	−0.08[g]		1.00	0.94	−0.14	0.06	0.00	−0.08
$CHBrF\text{-}CF_3$	3.77[j,m]	31.02		5.82	2.55	1.08	2.73	0.90
CH_2ClCHF_2	−0.20[h]	8.30	2.05		0.59	−0.79	0.72	−0.92
$CH_2Cl\text{-}CF_3$	1.95[g]	22.08	2.61		2.02	−0.07	2.16	−0.21
$CClF_2CF_3$	5.98[h]	43.93	9.03		4.60	1.38	4.80	1.18
$CClF_2CClF_2$	4.68[g]	34.16	17.58		3.73	0.95	3.92	0.76
CCl_2FCF_3	4.41[g]	35.44	17.56		4.01	0.40	4.20	0.21
CCl_2FCClF_2	3.72[g]	25.37	25.87		3.04	0.68	3.22	0.50
CCl_2FCCl_2F	2.81[g]	16.58	34.16		2.33	0.48	2.49	0.32
$CH_2Br\text{-}CH_2\text{-}CH_2Cl$	−0.31[k]		0.40	0.38	−0.11	−0.20	0.04	−0.35
$CH_2BrCHBrCH_2Cl$	0.50[h]		1.40	3.32	−1.56	2.06	−1.33	1.83
$CH_2ClCH_2CF_3$	2.14[h]	20.40	1.04		1.58	0.56	1.73	0.41

[a]Free energies of transfer, ΔG_t, from the gas at 1 atm to 1 M aqueous solution at 25°C, unless otherwise stated. Free energies are in kcal/mol.

[b]Sum of the sums of the Taft σ^* values of substituents on a carbon bearing a fluorine, for all fluorines.

[c]Sum of the sums of the Taft σ^* values of substituents on a carbon bearing a chlorine, for all chlorines.

[d]Sum of the sums of the Taft σ^* values of substituents on a carbon bearing a bromine, for all bromines.

[e]Calculated from the solubility of the gas at a total pressure of 1 atm (5).

[f]Calculated from the solubility of the liquid (5), and the vapor pressure (26).

[g]Reference 24.

[h]Calculated from the solubility of the liquid (5), and the vapor pressure (27).

[i]Calculated from the solubility of the gas at a total pressure of 1 atm (5); the solubility was measured at 30°C.

[j]Calculated from the solubility of the gas at a total pressure of 1 atm (5); the solubility was measured at 37°C.

[k]Calculated from the solubility of the liquid (5), and the vapor pressure (27). Horvath (5) gives two values for the solubility; we have used the value from a report by Imperial Chemical Industries (28); the value from Dreisbach (26) seems 10 times too high by comparison with solubilities of $Cl(CH_2)_3Cl$ and $Br(CH_2)_3Br$.

[l]$\Delta G_t = \Sigma[CH_n(X)_{4-n}] + [F]n_F + r_F\Sigma_F\sigma^* + [Cl]n_{Cl} + r_{Cl}\Sigma_{Cl}\sigma^* + [Br]n_{Br} + r_{Br}\Sigma_{Br}\sigma^*$; $[F] = -1.065$, $r_F = 0.221$, $[Cl] = -1.244$, $r_{Cl} = 0.170$, $[Br] = -1.525$, $r_{Br} = 0.155$, halogens only; $[F] = -1.095$, $r_F = 0.228$, $[Cl] = -1.221$, $r_{Cl} = 0.170$, $[Br] = -1.388$, $r_{Br} = 0.135$, all compounds.

[m]Based on solubility data at a temperature other than 25°C; not included in the final least-squares fit.

an increment, on replacing F by Cl, of −0.63, −0.69, and −0.85 respectively. Then from the value for $CBrF_3$, ΔG_t = 3.18 kcal/mol, one expects that ΔG_t for $CBrClF_2$ will be about 2.55 rather than the value of 1.28 derived from published data. The value calculated by the least-squares parameters is 2.78.

The next one to be examined is $CHBrF\text{-}CF_3$. The literature value for $CHBrCl\text{-}CF_3$ is 1.80 kcal/mol; using the increment for replacement of Cl by F deduced above we get an expected value of about 2.4 kcal/mol instead of the value of 3.63 derived from literature data. The value calculated using the least-squares parameters is 2.18.

Next we examine $CClF_2CF_3$. In the series CF_3CF_3; $CClF_2\text{-}CF_3$; $CClF_2CClF_2$; CCl_2FCF_3; CCl_2FCClF_2; CCl_2FCCl_2F; CCl_3CCl_3; we observe only one exception to a monotonic decrease in ΔG_t as F is replaced by Cl, namely $CClF_2CF_3$. The increment by which ΔG_t decreases as F is replaced by Cl gets larger as the replacement process continues, but clearly we expect a ΔG_t value closer to 5 than to 6 kcal/mol for $CClF_2CF_3$. This in fact is also predicted by our model.

Now we turn to $CH_2Br\text{-}CH_2Br\text{-}CH_2Cl$. We observe that the change from $CH_2Cl\text{-}CH_2Cl$ (ΔG_t = 0.17 kcal/mol) to $CH_2Br\text{-}CH_2Br$ (ΔG_t = −0.20 kcal/mol) is accompanied by a change in ΔG_t of −0.37 kcal/mol. Similarly the change from $CH_3\text{-}CHCl\text{-}CH_2Cl$ (ΔG_t = 0.60 kcal/mol) to $CH_3\text{-}CHBr\text{-}CH_2Br$ (ΔG_t = −0.04 kcal/mol) is accompanied by a change in ΔG_t of −0.64 kcal/mol. Thus we expect that ΔG_t will decrease on going from $CH_2Cl\text{-}CHCl\text{-}CH_2Cl$ (ΔG_t = −0.72 kcal/mol) to $CH_2Br\text{-}CH_2Br\text{-}CH_2Cl$ to perhaps −1.2 kcal/mol, and not to be 0.50 as calculated from the solubility and vapor pressure data in the literature. The value calculated using the least-squares parameters is −1.32 kcal/mol.

We conclude that the literature data are in many cases imprecise, and that errors have been propagated from one compilation to another, in considerable measure because there has

Can. J. Chem. Downloaded from www.nrcresearchpress.com by 123.30.183.119 on 09/07/12
For personal use only.

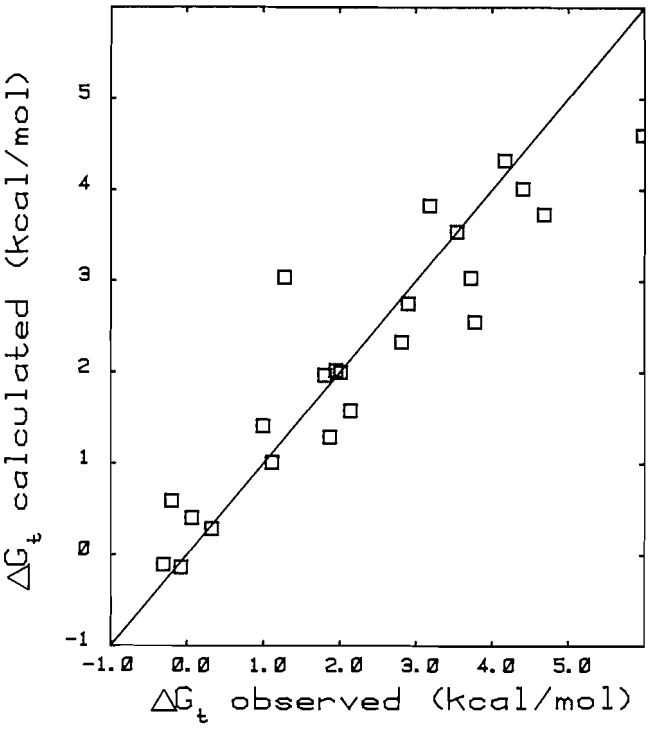


FIG. 5. Calculated vs. observed free energies of transfer for mixed halogen compounds.

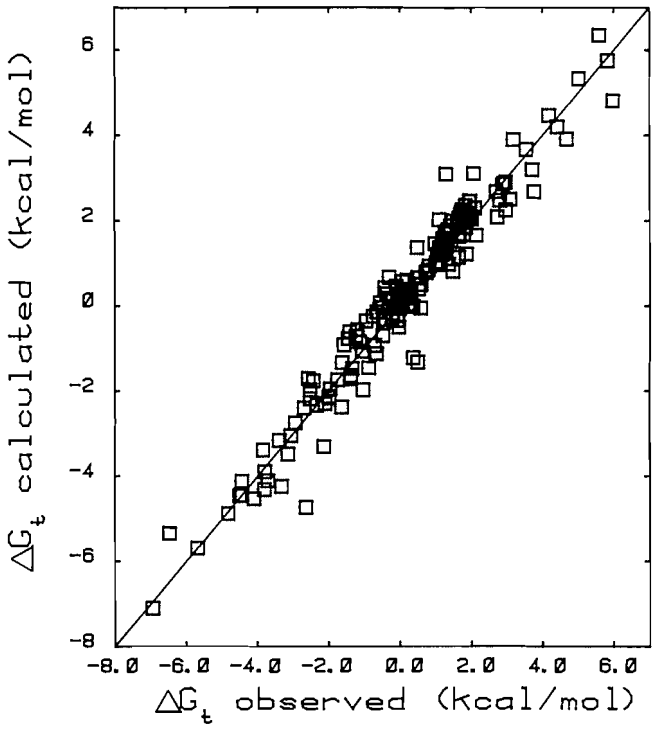


FIG. 6. Calculated vs. observed free energies of transfer for all compounds considered in this paper.

been no easy way to test values for reasonableness. Such a test is now feasible and it should be possible to avoid this class of errors in future.

Our treatment requires 17 parameters to fit 151 free energy of transfer values, with only 4 deviations greater than 1 kcal/mol. Three of these serious deviations represent compounds examined above, with the conclusion that the values reported are probably incorrect. Hine's treatment (4) would require 36 group contributions and 35 distant polar interactions (many based on only one compound) to fit the same set of data, and 32 compounds would have to be excluded as being unique within the group contributions framework. Cabani *et al.* published a different group contribution scheme (24), which for our set of 151 free energy of transfer values would require 14 group contributions and 70 corrections for polar interactions, most of them based on only one compound. The advantage of our treatment seems obvious.

There have been previous attempts, in addition to the schemes of Hine and Mookerjee (4) or Cabani *et al.* (24), to predict either solubility or free energies of transfer of organic compounds. Since, for sparingly soluble compounds, the solubility and vapor pressure permit the calculation of the free energy of transfer, and vapor pressures are relatively accessible (6–8), a reliable way to estimate solubility would be almost as valuable as a reliable way to estimate free energies of transfer. There would remain the problem of estimating the free energy of transfer for highly soluble compounds. Solubility has been successfully correlated with partition coefficient (9), with atomic and structural contributions (for halogenated hydrocarbons) (10), and with the surface areas of the polar groups (11, 12). Free energies of transfer have been fitted to the solvatochromic model (13). In the present context the deficiency in all of these efforts is in treating compounds with more than one nearby polar functional group. Although the partition coefficient is an additive constitutive property (14–16) it too is subject to distant polar interactions (17), for which there is not a good predictive method. Solubilities could be predicted successfully using surface areas and dipole moments, but the compounds fitted included few that were polyfunctional. Similarly the use of the solvatochromic method has concentrated on monofunctional compounds and it may be non-trivial to obtain values of the input parameters π, α, and β.

Recently there have been reports of calculational methods that hold promise of still more general solutions to the problem of calculating free energies of formation (18, 19). Both methods are computationally intensive, and although the algorithms are described, the programs to carry out the calculations are not widely available. Furthermore the data set used for initial testing has included almost entirely monofunctional compounds, so that at present it is not clear whether the promise of a general solution will be realized.

One advantage of our method is that it allows us to estimate, with some confidence, free energies of transfer for molecules for which direct measurement is not possible, because the compound of interest reacts rapidly with water. This is a problem that we have encountered (20, 21), and continue to encounter, in our research on analogs of tetrahedral intermediates and other metastable reaction intermediates.

Our treatment successfully handles ethers and tertiary amines, but does not fit alcohols or primary or secondary amines. These are, in polyfunctional compounds, likely to engage in intramolecular hydrogen bonding in the gas phase, and this will strongly perturb the free energy of transfer. Our approach could be used if one could calculate the equilibrium constant for formation of such intramolecular hydrogen bonds in the gas phase, but this is not yet possible.

The results presented above show that we have been able to account for DPI in substituted alkanes in terms of a simple

Can. J. Chem. Downloaded from www.nrcresearchpress.com by 123.30.183.119 on 09/07/12
For personal use only.

Can. J. Chem. Downloaded from www.nrcresearchpress.com by 123.30.183.119 on 09/07/12
For personal use only.

TABLE 7. Free energies of transfer for other polar functional groups[a]

(*a*) Oxygen compounds

Compound	ΔG_t obsd.	$\Sigma_O\sigma^*$	ΔG_t^b calcd.	Errors
MeOMe	0.00[c]		−0.06	0.06
EtOEt	0.15[c]		0.36	−0.21
MeOPr	0.23[c]		0.36	−0.13
MeO*i*Pr	−0.11[c]		0.46	−0.57
THF	−1.57[c]		−0.92	−0.65
EtOPr	0.08[c]		0.57	−0.49
MeO*t*Bu	−0.31[c]		0.67	−0.98
2-Me-THF	−1.41[c]		−0.61	−0.80
THP	−1.23[c]		−0.71	−0.52
PrOPr	0.74[c]		0.78	−0.04
*i*PrO*i*Pr	1.37[c]		0.98	0.39
BuOBu	1.07[c]		1.20	−0.13
$MeOCH_2CH_2OMe$	−2.94[c]	1.32	−2.75	−0.19
$EtOCH_2CH_2OEt$	−1.64[c]	1.16	−2.37	0.73
$CH_2(OEt)_2$	−1.62[g]	3.36	−1.34	−0.04
$(EtO)_2CH\text{-}Me$	−1.38[c]	3.36	−1.65	0.03
$(MeO)_2CH_2$	−1.04[c]	3.62	−1.99	0.95
$HC(OMe)_3$	−2.52[o]	11.04	−2.21	−0.31
$MeC(OMe)_3$	−2.52[o]	11.04	−2.00	−0.52
$MeOCH_2\text{-}C(OMe)_3$	−3.33[d]	13.8	−4.26	0.93
$CH_3\text{-}CH_2\text{-}C(OCH_3)_3$	−2.43[d]	11.04	−1.79	−0.65
$(CH_3)_2CH\text{-}C(OCH_3)_3$	−0.88[d]	11.04	−1.48	0.60
1,4-Dioxane	−3.15[c]	2.64	−3.48	0.33

(*b*) Compounds with oxygen and other heteroatoms

Compound	ΔG_t obsd.	$\Sigma_O\sigma^*$	$\Sigma_{Cl}\sigma^*$	$\Sigma_F\sigma^*$	$\Sigma_{CN}\sigma^*$	ΔG_t^b calcd.	Errors
$(ClCH_2CH_2)_2O$	−2.33[h]	1.88	1.28			−2.34	0.01
$(ClCH_2CH(CH_3))_2O$	−1.38[h]	1.88	1.08			−1.72	0.34
$Cl\text{-}CH_2\text{-}C(OCH_3)_3$	−2.69[d]	11.04	1.98			−2.42	−0.27
$NC\text{-}CH_2\text{-}C(OCH_3)_3$	−4.50[d]	14.76			2.0	−4.45	−0.05
$CF_3C(OMe)_3$	1.1[b]	18.87		25.20		2.00	−0.90

(*c*) Nitrogen compounds

Compound	ΔG_t obsd.	$\Sigma_O\sigma^*$	$\Sigma_N\sigma^*$	ΔG_t^b calcd.	Errors
Me_3N	−1.34[c]			−1.48	0.14
Et_3N	−1.13[c]			−0.85	−0.28
N-Methyl piperidine	−1.99[c]			−2.13	0.14
N-Methyl morpholine	−4.44[b]	1.00	1.32	−4.44	0.00
N,*N*'-Dimethyl piperazine	−5.68[b]		2.00	−5.68	−0.00

(*d*) Phenyl compounds

Compound	ΔG_t obsd.	$\Sigma_{Ar}\sigma^*$	$\Sigma_O\sigma^*$	$\Sigma_{Cl}\sigma^*$	$\Sigma_F\sigma^*$	$\Sigma_{Br}\sigma^*$	ΔG_t^b calcd.	Errors
$CH_2(Ph)_2$	0.37[c]	0.75					−1.17	0.25
$C(Ph)_4$	−6.47[i]	2.25					−5.07	−1.40
$Ph\text{-}CH_2CH_2\text{-}Ph$	−1.06[j]	0.54					−1.05	−0.01
$m(CF_3)_2C_6H_4$	2.97[k]	19.3			43.86		3.30	−0.33
$Ph\text{-}CH_2Cl$	−0.03[h]			0.75			−0.40	0.37
$Ph\text{-}CH_2Br$	−0.48[h]					0.75	−0.62	0.14
$Ph\text{-}C(OMe)_3$	−2.14[f]		13.1				−3.16	1.02

TABLE 7 (*concluded*)

(*e*) Cyano compounds

Compound	ΔG_t obsd.	ΔG_t^b calcd.	Errors
CH_3-CN	−1.99[c]	−2.17	0.18
CH_3CH_2CN	−1.95[c]	−1.96	0.01
$CH_3CH_2CH_2CN$	−1.75[c]	−1.75	0.00

(*f*) Acetate esters

Compound	ΔG_t obsd.	$\Sigma_{O_{COO}}\sigma^*$	ΔG_t^b calcd.	Errors
CH_3-OAc	−1.45[c]		−0.77	−0.68
CH_3CH_2-OAc	−1.19[c]		−0.56	−0.63
$CH_3CH_2CH_2$-OAc	−0.95[c]		−0.35	−0.60
$(CH_3)_2CH$-OAc	−0.75[c]		−0.25	−0.50
$CH_3(CH_2)_3$-OAc	−0.65[c]		−0.14	−0.51
$(CH_3)_2CHCH_2$-OAc	−0.49[c]		−0.04	−0.45
$CH_3(CH_2)_4$-OAc	−0.56[c]		0.07	−0.63
$(CH_3)_2CH(CH_2)_2$-OAc	−0.31[c]		0.17	−0.48
$CH_3(CH_2)_5$-OAc	−0.37[c]		0.28	−0.65
AcO-CH_2-CH_2-OAc	−4.44[l]	2.00	−4.11	−0.33
CH_3-$CH(OAc)_2$	−3.07[m]	5.12	−3.05	−0.02
CH_2(OAc)-CH(OAc)CH_2-OAc	−6.94[n]	4.80	−7.10	0.16

(*g*) Esters with polar substituents in the acyl group

Compound	ΔG_t obsd.	$\Sigma_O\sigma^*$	$\Sigma_F\sigma^*$	$\Sigma_{Cl}\sigma^*$	$\Sigma_{CO_{COO}}\sigma^*$	$\Sigma_{CN}\sigma^*$	ΔG_t^b calcd.	Errors
$(CH_2)_2(COOMe)_2$	−2.65[n]				1.60		−4.73	1.41
$(CH_2)(COOEt)_2$	−4.10[n]				4.52		−4.52	0.42
$(CH_2)_2(COOEt)_2$	−3.81[n]				1.81		−4.31	0.50
$(CH_2)_3(COOEt)_2$	−3.71[n]				0.72		−4.10	0.39
$(CH_2)_4(COOEt)_2$	−3.80[n]				0.29		−3.89	0.09
MeO-CH_2-COOMe	−3.84[f]	2.00			1.81		−3.38	−0.46
Cl-CH_2-COOMe	−2.10[f]			2.00	2.96		−2.30	0.20
NC-CH_2-COOMe	−4.82[f]				3.30	2.0	−4.85	0.03
CF_3-COOMe	0.80[e]		25.26		9.63		0.85	−0.05

[a]Free energies of transfer, ΔG_t, from the gas at 1 atm to 1 M aqueous solution at 25°C, unless otherwise stated. Free energies are in kcal/mol.

[b]$\Delta G_t = \Sigma[CH_n(X)_{4-n}] + [F]n_F + r_F\Sigma_F\sigma^* + [Cl]n_{Cl} + r_{Cl}\Sigma_{Cl}\sigma^* + [Br]n_{Br} + r_{Br}\Sigma_{Br}\sigma^* + n_O[O(C)_2] + r_O\Sigma_O\sigma^* + n_N[N(C)_3] + r_N\Sigma_N\sigma^* + r_{Ph}\Sigma_{Ph}\sigma^* + n_{CN}[CN] + r_{CN}\Sigma_{CN}\sigma^* + n_{COO}[COO] + r_{O_{COO}}\Sigma_{O_{COO}}\sigma^*$; [F] = −1.095, r_F = 0.228, [Cl] = −1.241, r_{Cl} = 0.170, [Br] = −1.388, r_{Br} = 0.135, $[O(C)_2]$ = −3.660, r_O = 0.423, $[N(C)_3]$ = −5.930, r_N = 0.872, r_{Ph} = 0.0934, [CN] = −4.923, r_{CN} = 0.742, [COO] = −4.373, $r_{O_{COO}}$ = 0.309.

[c]Reference 24.

[d]Calculated from solubility (29) and vp (30) data.

[e]Reference 31.

[f]Reference 32.

[g]Calculated from solubility (29) and vp (8) data.

[h]Reference 13.

[i]Calculated from the solubility (33) and the vapor pressure (34) at 25°C.

[j]Calculated from the solubility (35) and the vapor pressure (27).

[k]Calculated from the solubility (36) and an estimated vapor pressure; since the boiling point is the same (116°C) (8) as for *m*-fluorotoluene, and heat of vaporization is predictable as a function of boiling point (37, 38), we assume the vapor pressure for 1,3-bis(trifluoromethyl)benzene will be the same as for *m*-fluorotoluene, i.e., 22 Torr (1 Torr = 133.3 Pa) (by interpolation from data in ref. 8).

[l]Calculated from the solubility (39) and a vapor pressure extrapolated from data in ref. 8.

[m]Calculated from the solubility (40) and vapor pressure (41).

[n]Calculated from the solubility (29) and vapor pressure (27).

[o]Reference 43.

Can. J. Chem. Downloaded from www.nrcresearchpress.com by 123.30.183.119 on 09/07/12
For personal use only.

Can. J. Chem. Downloaded from www.nrcresearchpress.com by 123.30.183.119 on 09/07/12
For personal use only.

TABLE 8. σ* values used in calculations[a]

Substituent	σ*	Substituent	σ*
Br	2.84	$CHBrCH_2Cl$	(1.38)[f]
Cl	2.96	$CHClCH_2Cl$	(1.32)[g]
F	3.21	$COOCH_3$	2.00
CN	3.30	$OCOCH_3$	2.56
CF_3	2.61	CH_2CH_2Br	(0.40)[h]
CCl_3	2.65	$CHClCH_3$	(0.84)[i]
CBr_3	2.43	CH_2CH_2Cl	(0.38)[j]
$CClF_2$	2.37	CH_2OCH_3	0.66
CCl_2F	(2.37)[b]	OCH_2CH_3	1.68
$CHBr_2$	1.96	$COOCH_2CH_3$	2.26
$CHCl_2$	1.94	CH_2OCOCH_3	1.00
CHF_2	2.05	$CH_2CH_2CH_2Cl$	(0.15)[k]
CHBrCl	(1.94)[c]	$CCl(CH_3)_2$	(0.75)[l]
CHBrF	(2.10)[d]	$CH_2OCH_2CH_2Cl$	(0.64)[m]
CH_2Br	1.00	$CH_2COOC_2H_5$	0.82
CH_2Cl	0.94	$C(OCH_3)_3$	(1.98)[n]
CH_2F	1.10	$(CH_2)_2COOC_2H_5$	(0.54)[o]
OCH_3	1.81	$CH(CH_3)OCH(CH_3)CH_2Cl$	(0.54)[p]
CF_2CF_3	2.56	3-(CF_3)-C_6H_4	0.89[q]
CH_2CF_3	0.87	C_6H_5	0.75
CH_2CN	1.30	$(CH_2)_3COOC_2H_5$	(0.16)[r]
$CHBrCH_2Br$	(1.40)[e]	$CH(OCOCH_3)CH_2OCOCH_3$	(1.40)[s]

[a]Taft σ* values, taken from ref. 23 unless otherwise noted.
[b]Estimated as equal to $\sigma^*(CClF_2)$, because σ*(F) and σ*(Cl) are very similar, and there is a saturation effect for trihalomethyl groups.
[c]Estimated by a recommended procedure (23) as $\sigma^*(CH_2Br) + \sigma^*(CH_2Cl)$.
[d]Estimated by a recommended procedure (23) as $\sigma^*(CH_2Br) + \sigma^*(CH_2F)$.
[e]Estimated by a recommended procedure (23) as $\sigma^*(CH_2Br) + \sigma^*(CH_2CH_2Br)$.
[f]Estimated by a recommended procedure (23) as $\sigma^*(CH_2Br) + \sigma^*(CH_2CH_2Cl)$.
[g]Estimated by a recommended procedure (23) as $\sigma^*(CH_2Cl) + \sigma^*(CH_2CH_2Cl)$.
[h]Estimated by a recommended procedure (23) as $0.4 \times \sigma^*(CH_2Br)$.
[i]Estimated by a recommended procedure (23) as $\sigma^*(CH_2Cl) + \sigma^*(CH_2CH_3)$.
[j]Estimated by a recommended procedure (23) as $0.4 \times \sigma^*(CH_2Cl)$.
[k]Estimated by a recommended procedure (23) as $0.4^2 \times \sigma^*(CH_2Cl)$.
[l]Estimated by a recommended procedure (23) as $\sigma^*(CH_2Cl) + \sigma^*(CH(CH_3)_2)$.
[m]Estimated as $\sigma^*(CH_2OCH_3) + 0.4^3 \times \sigma^*(CH_2Cl)$.
[n]Estimated by a recommended procedure (23) as $3 \times \sigma^*(CH_2OCH_3)$.
[o]Estimated by a recommended procedure (23) as $0.4 \times \sigma^*(CH_2COOC_2H_5)$.
[p]Estimated as $\sigma^*(CH_2OCH_2CH_3) + \sigma^*(CH_2CH_3) + 0.4^3 \times \sigma^*(CH_2Cl)$.
[q]Reference 42.
[r]Estimated by a recommended procedure (23) as $0.4^2 \times \sigma^*(CH_2COOC_2H_5)$.
[s]Estimated by a recommended procedure (23) as $\sigma^*(CH_2COOC_2H_5) + 0.4 \times \sigma^*(CH_2COOC_2H_5)$.

TABLE 9. Parameters for the group contribution scheme predicting ΔG_t[a]

(*a*) Group contributions

Group	ΔG_t
$[CH_3(X)]$	0.85[b]
$[CH_2(X)_2]$	0.21[b]
$[CH(X)_3]$	−0.33[b]
$[C(X)_4]$	−0.97[b]
$[C_BH]$	−0.15[b]
$[C_B(C)]$	−0.96[b]
[Ph]	−1.71[c]
[F]	−1.00 ± 0.19
[Cl]	−1.23 ± 0.08
[Br]	−1.39 ± 0.11
[I]	−1.75 ± 0.11
$[O(C)_2]$	−3.66 ± 0.11
$[N(C)_3]$	−5.93 ± 0.32
[COO]	−4.37 ± 0.10
[CN]	−4.92 ± 0.33

(*b*) Parameters correlating DPI with Σσ*

Polar group	Slope
F	0.217 ± 0.022
Cl	0.171 ± 0.012
Br	0.135 ± 0.019
I	0.106 ± 0.082
Ph	0.094 ± 0.027
CN	0.742 ± 0.265
O	0.423 ± 0.030
N	0.872 ± 0.038
O_{COO}	0.309 ± 0.093

[a]All at 25°C; free energies of transfer from ideal gas at 1 atm to ideal 1 M aqueous solution with an infinitely dilute reference state. Unless otherwise noted, parameters were evaluated by least squares as described in the text.
[b]Calculated from the parameters in ref. 4.
[c]Contribution for the phenyl substituent, calculated from the contributions for the groups making it up as $5[C_BH] + [C_B(C)]$.

model with a very limited number of parameters. Moreover, we have been able to diminish very markedly the number of parameters required to predict ΔG_t for this class of compounds. The parameterization scheme proposed by Hine and Mookerjee was very successful in fitting the available data for monofunctional compounds, for which 22 group contributions were evaluated, but less successful for di- or polyfunctional compounds, where it was clear that a large number of DPI parameters would be needed; 13 could be evaluated from the data available then. However, this scheme included only a small fraction of the parameters that would be needed to cover all possible types of compound with 1, 2, 3, or 4 substituents on a central carbon, the substituents being C, N, O, F, Cl, Br, or I; in fact 336 group contributions would be needed, and a very large number of DPI terms. This combinatorial explosion makes some simpler method for estimating ΔG_t very important.

Hine and Mookerjee (4) suggested that DPI were often attributable to effects on hydrogen bonding, and we used hydrogen bonding as the mental model for the DPI in developing our approach. It must be remembered that, particularly for the polyhalogenated compounds, this may not be the correct description; by the empirical test of successful prediction there exists some polar effect upon the free energy of transfer. Jencks has suggested that hydrogen bond strength should follow basicity measured by pK_a with a Brønsted slope of approximately 0.2 (22). Since basicity depends on substituent effects at the carbon bearing the basic atom with a Taft ρ* of approximately 1.8 (23), we expect a slope of free energy of hydrogen bonding vs. Σσ* of $1.366 \times 0.2 \times 1.8 = 0.49$, which is approximately the value found: see Table 9. The behavior that we observe seems consistent with expectation for hydrogen bonds. That the DPI for halogens have some hydrogen bonding component may be indicated by the decreasing sensitivity to polar effects as the atom becomes larger.

We explored the possibility that the solvent-accessible surface area for the functional groups in a molecule would provide a measure of steric hindrance to solvation. It seemed plausible

that such hindrance might modulate the solubilizing effect of polar groups. However, we found that the coefficients for such areas were all undetermined when this more elaborate parameterization was used for least-squares fitting, i.e., the errors calculated by the least-squares program were larger than the parameters. Thus there was no advantage to including solvent-accessible surface areas, which required some computational effort to determine.

We conclude that it is now possible to estimate the free energy of transfer for a wide range of polyfunctional organic compounds that are derivatives of alkanes, with phenyl treated as a special kind of univalent substituent. Although the predictions are not as precise as were achieved for monofunctional compounds by the schemes of Hine and Mookerjee (4) or Cabani *et al.* (24), the ability to treat polyfunctional compounds with confidence and with a much smaller set of parameters more than compensates. Further efforts should lead to improved predictive schemes.

Acknowledgments

We thank the Natural Sciences and Engineering Research Council of Canada for financial support of this work.

1. S. W. BENSON and J. H. BUSS. J. Chem. Phys. **29**, 546 (1958).
2. S. W. BENSON, F. R. CRUICKSHANK, D. M. GOLDEN, G. R. HAUGEN, H. E. O'NEAL, A. S. RODGERS, R. SHAW, and R. WALSH. Chem. Rev. **69**, 279 (1969).
3. S. W. BENSON. Thermochemical kinetics. Wiley, New York. 1976.
4. J. HINE and P. K. MOOKERJEE. J. Org. Chem. **40**, 292 (1975).
5. A. L. HORVATH. Halogenated hydrocarbons: solubility–miscibility with water. Dekker, New York. 1982.
6. D. R. STULL. Ind. Eng. Chem. **39**, 517 (1947).
7. J. P. GUTHRIE. Can. J. Chem. **64**, 635 (1986).
8. R. C. WEAST (*Editor*). Handbook of chemistry and physics. 48th ed. Chemical Rubber Co., Cleveland, OH. 1967.
9. C. HANSCH, J. E. QUINLAN, and G. L. LAWRENCE. J. Org. Chem. **33**, 347 (1968).
10. F. IRMANN. Chem. Ing. Tech. **37**, 789 (1965).
11. S. C. VALVANI, S. H. YALKOWSKY, and G. L. AMIDON. J. Phys. Chem. **80**, 829 (1976).
12. G. L. AMIDON, S. H. YALKOWSKY, S. T. ANIK, and S. C. VALVANI. J. Phys. Chem. **79**, 2239 (1975).
13. M. H. ABRAHAM, G. S. WHITING, R. FUCHS, and E. J. CHAMBRA. J. Chem. Soc. Perkin Trans. 2, 291 (1990).
14. T. FUJITA, J. IWASA, and C. HANSCH. J. Am. Chem. Soc. **86**, 5175 (1964).
15. J. IWASA, T. FUJITA, and C. HANSCH. J. Med. Chem. **8**, 150 (1965).
16. C. HANSCH and S. M. ANDERSON. J. Org. Chem. **32**, 2583 (1967).
17. C. HANSCH, A. LEO, and D. NIKAITANI. J. Org. Chem. **37**, 3090 (1972).
18. Y. K. KANG, G. NEMETHY, and H. A. SCHERAGA. J. Phys. Chem. **91**, 4109 (1987).
19. W. C. STILL, A. TEMPCZYK, R. C. HAWLEY, and T. HENDRICKSON. J. Am. Chem. Soc. **112**, 6127 (1990).
20. J. P. GUTHRIE. J. Am. Chem. Soc. **96**, 3608 (1974).
21. J. P. GUTHRIE. J. Am. Chem. Soc. **99**, 3991 (1977).
22. W. P. JENCKS. Acc. Chem. Res. **9**, 425 (1076).
23. D. D. PERRIN, B. DEMPSEY, and E. P. SERJEANT. pK_a prediction for organic acids and bases. Chapman and Hall, London. 1981.
24. S. CABANI, P. GIANNI, V. MOLLICA, and L. LEPORI. J. Solution Chem. **10**, 563 (1981).
25. W.-Y. WEN and J. A. MUCCITELLI. J. Solution Chem. **8**, 225 (1979).
26. R. R. DREISBACH. Physical properties of chemical compounds III. Adv. Chem. Ser. **29**, 1961.
27. R. M. STEPHENSON and S. MALINOWSKI. Handbook of thermodynamics of organic compounds. Elsevier, Amsterdam. 1987.
28. Imperial Chemical Industries, Brixham Laboratory Report BL/B/1417, Brixham England; referred to in ref. 5.
29. N. C. DENO and H. BERKHEIMER. J. Chem. Eng. Data, **5**, 1 (1960).
30. J. A. DEAN (*Editor*). Lange's handbook of chemistry. 12th ed. McGraw–Hill, New York. 1972.
31. J. P. GUTHRIE. Can. J. Chem. **54**, 202 (1976).
32. J. P. GUTHRIE and P. A. CULLIMORE. Can. J. Chem. **58**, 1281 (1980).
33. B. G. COX and A. J. PARKER. J. Am. Chem. Soc. **94**, 3674 (1972).
34. A. S. KANA'AN. J. Chem. Thermodyn. **4**, 893 (1972).
35. L. J. ANDREWS and R. M. KEEFER. J. Am. Chem. Soc. **72**, 5034 (1950).
36. A. S. KERTES (*Editor*). Solubility data series. Vol. 20. Pergamon, London. 1985.
37. I. WADSO. Acta Chem. Scand. **20**, 544 (1966).
38. J. P. GUTHRIE. Can. J. Chem. **64**, 635 (1986).
39. M. WINDHOLZ (*Editor*). The Merck index. 9th ed. Merck & Co., Rahway, NJ. 1976.
40. J. C. SMITH. J. Phys. Chem. **46**, 229 (1942).
41. G. O. MORRISON and T. P. G. SHAW. Trans. Electrochem. Soc. **63**, 443 (1933).
42. Y. NAGAI, H. MATSUMOTO, T. NAKANO, and H. WATANABE. Bull. Chem. Soc. Jpn. **45**, 2560 (1972).
43. J. P. GUTHRIE. J. Am. Chem. Soc. **95**, 6999 (1973).

Can. J. Chem. Downloaded from www.nrcresearchpress.com by 123.30.183.119 on 09/07/12
For personal use only.

Dihydroxyacids from the chlorination of ketones: an unexpected process

J. PETER GUTHRIE,[1] JOHN COSSAR, AND JINQIAO LU
Department of Chemistry, University of Western Ontario, London, Ont., Canada N6A 5B7

Received January 18, 1991

J. PETER GUTHRIE, JOHN COSSAR, and JINQIAO LU. Can. J. Chem. **69**, 1904 (1991).

Chlorination of propiophenone in aqueous alkali at room temperature, with low concentrations of hypochlorite, leads to 2-phenylglyceric acid as the major product. This acid is formed by further oxidation of 1-phenyl-1,2-propanedione, which is an intermediate in the oxidation of propiophenone. Formation of this acid is reasonable in the light of other halogenation chemistry. Analogous reactions are observed for butyrophenone, which yields 2,3-dihydroxy-2-phenylbutanoic acid, and for cycloheptanone, which yields 1,2-dihydroxycyclohexanecarboxylic acid.

Key words: 2-phenylglyceric acid, propiophenone, chlorination, hydrolysis, rearrangement, cycloheptanone, 1,2-dihydroxycyclohexanecarboxylic acid.

J. PETER GUTHRIE, JOHN COSSAR et JINQIAO LU. Can. J. Chem. **69**, 1904 (1991).

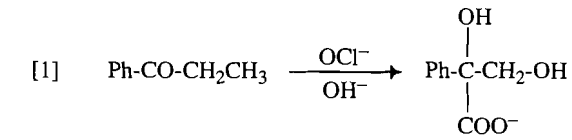
La chloration de la propiophénone, en solution aqueuse alcaline, à température ambiante, à faibles concentrations d'hypochlorite, conduit à la formation d'acide 2-phénylglycérique comme produit principal. Cet acide se forme par une oxydation subséquente de la 1-phényl-propane-1,2-dione qui se forme comme intermédiaire lors de l'oxydation de la propiophénone. La formation de cet acide peut être attendue à la lumière d'autres résultats obtenus dans la chimie des halogénations. Des réactions analogues ont été observées avec la butyrophénone qui conduit à l'acide 2,3-dihydroxy-2-phénylbutanoïque et avec la cycloheptanone qui conduit à l'acide 1,2-dihydroxycyclohexanecarboxylique.

Mots clés : acide 2-phénylglycérique, propiophénone, chloration, hydrolyse, réarrangement, cycloheptanone, acide 1,2-dihydroxycyclohexanecarboxylique.

[Traduit par la rédaction]

Can. J. Chem. Downloaded from www.nrcresearchpress.com by 123.30.183.119 on 09/08/12
For personal use only.

Chlorination of ketones is a well-known reaction, which has been used for many years. Nevertheless it can still give rise to unexpected products even with simple ketones: for example, acetone can give major amounts of lactic acid (1). The halogenation of propiophenone has been reported to give rise to benzoic acid (2, 3) and acetic acid (3). We wish to report that under some conditions the major product of the chlorination of propiophenone is 2-phenylglyceric acid, reaction [1], and that this appears to be a general reaction.



Results

2-Phenylglyceric acid was the major product when propiophenone in 1 M aqueous NaOH was treated with 4.05 equivalents of NaOCl solution. The hypochlorite was added slowly over 5 h, then excess oxidant was destroyed by adding $NaHSO_3$ solution. Acidification and extraction gave a product mixture shown by NMR analysis to contain small amounts of benzoic, mandelic, and atrolactic acids, but to be principally 2-phenylglyceric acid. This identification is based on comparison of NMR spectra with those of an authentic sample prepared by the literature route (4–6). ^1H NMR spectra in D_2O (Na salt) or CD_3OD were identical for both samples. The crude product mixture upon crystallization from 1:1 ethyl acetate – petroleum ether gave phenylglyceric acid of mp 146.5–148°C (lit. mp 145–146°C (7), 149°C (8), 146–148°C (9); mixture mp with an authentic sample, 148°C). The yield of 2-phenylglyceric acid was 75% by NMR analysis, 64% based on crystalline product.

In the early stages of the investigation, before yields had been improved by rational variation of the reaction conditions, we found that formation of the methyl ester and acetylation gave material that was better suited to column chromatography and separation of the various products.

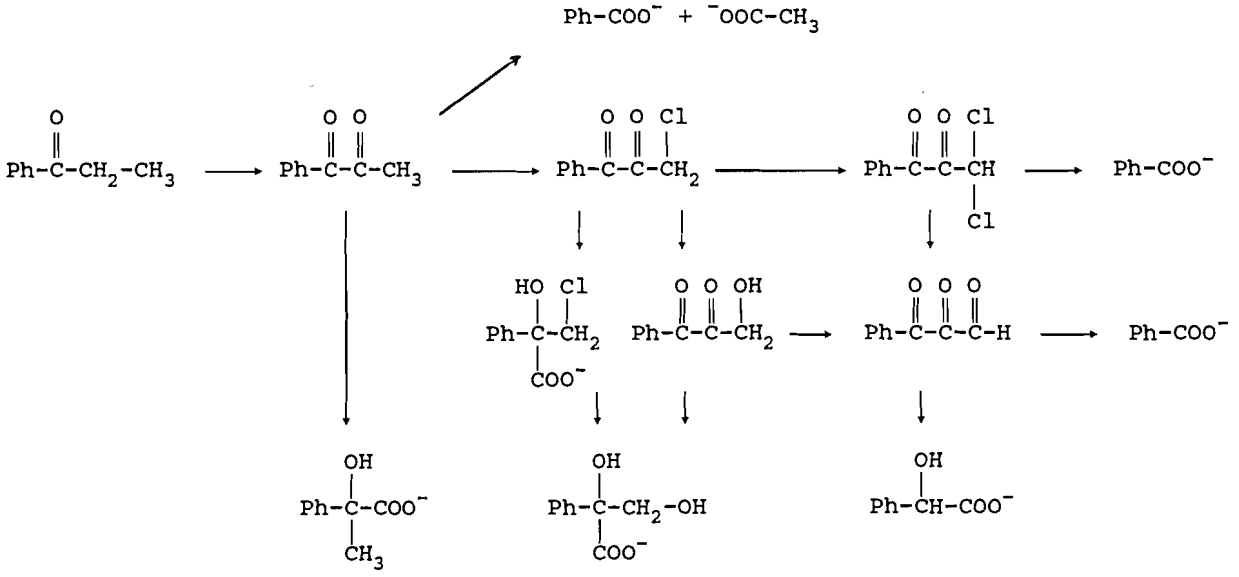
The reaction appears to be general. When we used butyrophenone as substrate, the major product crystallized from the acid extract, mp 125–133°C. The yield based on NMR analysis was 51%, and 32% based on crystalline material. This product had a 200 MHz ^1H NMR consistent with a mixture of diastereomeric 2,3-dihydroxy-2-phenylbutyric acids.

Oxidation of cycloheptanedione by lead tetraacetate has been reported to give, as a minor by-product, a compound identified as 1,2-dihydroxycyclohexanecarboxylic acid, although no rigorous structure proof was reported (10). We have found that chlorination of cycloheptanone by aqueous alkaline hypochlorite, with a high ratio of $[HO^-]$ to $[OCl^-]$, gives a useful yield of 1,2-dihydroxycyclohexanecarboxylic acid in one step. This reaction is more complex than the oxidations of alkyl aryl ketones, because of the possibility of Favorskii rearrangement, and the greater likelihood of aldol condensations because of the inherently greater reactivity of dialkyl ketones (11). Although the yield of 1,2-dihydroxycyclohexanecarboxylic acid was improved by lowering the hypochlorite concentration, preferably by use of a motor-driven syringe to add sodium hypochlorite solution, too low a concentration of hypochlorite led to decreased yields of acidic products, and a greater yield of neutrals, presumably the result of coupling reactions. Favorskii rearrangement leading to cyclohexanecarboxylic acid was a major side reaction, as was cleavage to pimelic acid. Nonetheless, under the best conditions that we found (1 g of cycloheptanone in 1 L 1 N aqueous NaOH, to which 60 mL "Javex" was added at a rate of 0.15 mL/min), 1,2-dihydroxycyclohexanecarboxylic acid would crystallize from the crude reaction product.

Discussion

We believe that the reaction of propiophenone proceeds via 1-phenyl-1,2-propanedione as an intermediate: see Scheme 1. That this dione is an intermediate in the halogenation of propio-

[1]Author to whom correspondence may be addressed.



SCHEME 1

phenone has been proposed before (2). Consistent with this mechanistic proposal, 1-phenyl-1,2-propanedione also gives 2-phenylglyceric acid upon chlorination in alkali. Reaction in 0.5 N NaOH, 0.012 N NaOCl, leads to 2-phenylglyceric acid in 67% yield based on NMR analysis, 48% based on crystalline product.

We propose that 1-phenyl-1,2-propanedione undergoes halogenation followed by a benzilic acid rearrangement to give 3-chloro-2-hydroxy-2-phenylpropanoate, which then undergoes hydrolysis to form 2-phenylglycerate. Consistent with this proposal, the yield of 2-phenylglyceric acid is increased by raising the hydroxide concentration, and lowering the hypochlorite concentration, i.e., by increasing the $[OH^-]/[OCl^-]$ ratio: see Table 1. This could be done by lowering the initial hypochlorite concentration or by adding the hypochlorite slowly rather than all at the start of the reaction. The competing pathways, whether the key intermediate is the hydroxy- or chloro-phenylpropanedione, are further chlorination or rearrangement. Chlorination will be first order (or zero order) in hydroxide (1) because the enolate reacts with hypochlorite ion; rearrangement may be first or second order in hydroxide depending on whether the mono- or di-anion of the tetrahedral adduct rearranges. Thus raising the ratio $[OH^-]/[OCl^-]$ should give more rearrangement and improve the yield, which it does.

Initially we suspected that the rearrangement involved the α-hydroxy derivative of the dione, i.e., 3-hydroxy-1-phenyl-1,2-propanedione. We now favor the involvement of the precursor to this hydroxy compound, i.e., 3-chloro-1-phenyl-1,2-propanedione, as the key intermediate which rearranges. A chloro substituent is likely to be better at stabilizing a "methide" migrating group than is a hydroxyl. In any event, it seemed of interest to determine whether 3-hydroxy-1-phenyl-1,2-propanedione would give rise to 2-phenylglyceric acid. 3-Hydroxy-1-phenyl-1,2-propanedione has been reported (12) but never purified; we thought it plausible that 3-hydroxy-1-phenyl-1-propanone might give rise to 3-hydroxy-1-phenyl-1,2-propanedione and that in alkaline solution 3-dimethylamino-1-propanone might give rise to 3-hydroxy-1-phenyl-1-propanone. In the event, reaction of 3-dimethylamino-1-phenyl-1-propanone with alkaline hypochlorite gave rise to phenylglyceric acid. This is a permissive rather than a conclusive experiment, but certainly suggests that 3-hydroxy-1-phenyl-1,2-propanedione is capable of forming 2-phenylglyceric acid under our reaction conditions.

TABLE 1. Effect of reagent concentrations upon 2-phenylglycerate yield[a]

$[OH^-]$	$[OCl^-]$	$[OH^-]/[OCl^-]$	Yield of 2-PGA (%)
0.46	0.03	15.	41
0.46	0.01	46.	57
1.0	<0.01[b]	>100.	75

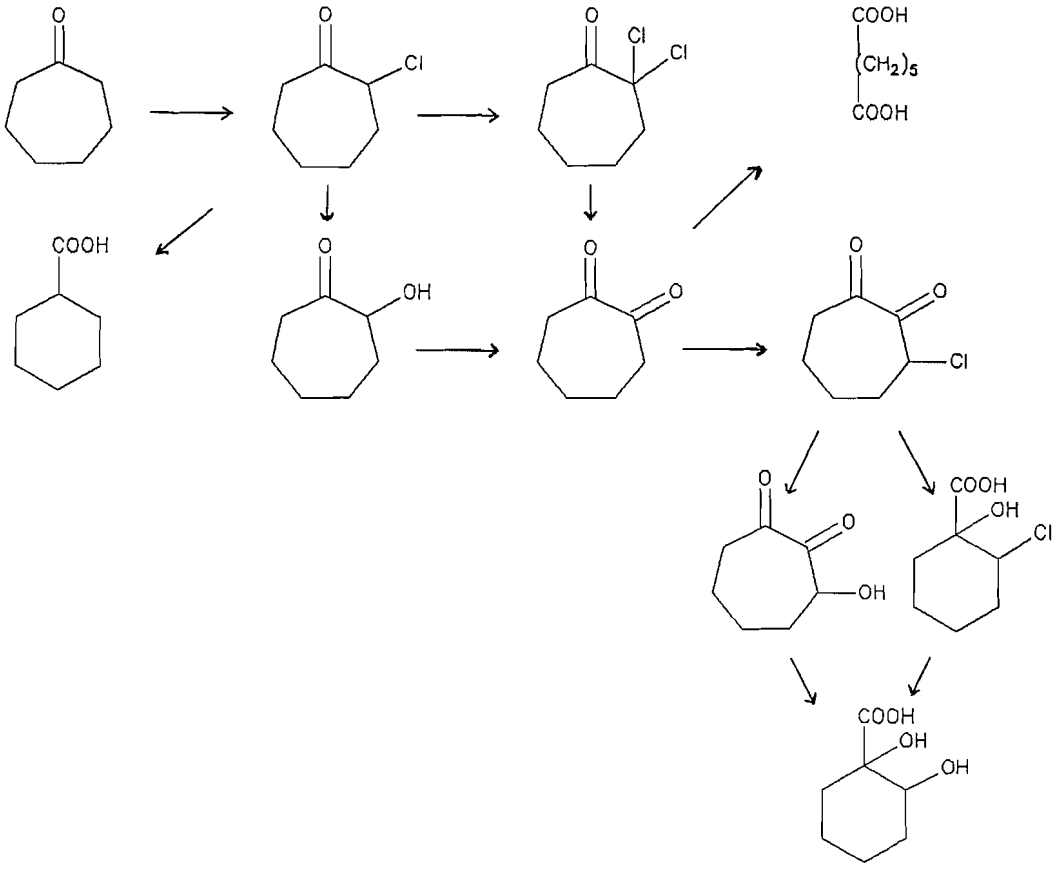
[a]Reactions carried out in water at 25°C.

[b]NaOCl solution added gradually: concentration would have been 0.01 M had it been added all at once.

Atrolactic acid is known to form by hydroxide-catalyzed rearrangement of phenylpropanedione (3). Benzoic acid can arise in various ways, including direct oxidative cleavage of phenylpropanedione by hypochlorite. Extensive oxidation of phenylpropanedione can also plausibly lead to benzoic acid. Mandelic acid is likely to arise from phenylglyoxal (13), which in turn might arise in various ways, most plausibly from phenylpropanetrione; see Scheme 1. Further investigations to unravel this complicated network of reactions are currently underway.

The stereochemistry of the 1,2-dihydroxycyclohexanecarboxylic acid produced from cycloheptanone is not rigorously defined by the ^{13}C NMR although comparison of the observed chemical shifts with values calculated from those for cyclohexanecarboxylic acid by additivity rules (14) suggest that the two OH groups are *trans*. Mechanistic arguments, assuming rearrangement of the chloride, suggest that the product should have the OH groups *trans*. If the conversion of CH-Cl to CH-OH takes place after rearrangement, then it must involve displacement of axial Cl by an internal nucleophile. If this is OH (or O^-), then diaxial opening leads to the isomer with the two OH groups *trans*. If the internal nucleophile is COO^-, then for it to have been axial while Cl was also axial requires the OH on carbon 1 to have been *cis* to the Cl. After internal displacement the OH will be *trans* to the oxygen of the β-lactone. This will open by

Can. J. Chem. Downloaded from www.nrcresearchpress.com by 123.30.183.119 on 09/08/12
For personal use only.



SCHEME 2

$B_{AC}2$ attack on the carbonyl, leading to the isomer with the OH groups *trans*.

The reaction of cycloheptanone with alkaline hypochlorite has numerous possible paths, Scheme 2, and it is not surprising that a number of products are formed. Complete optimization would require considerable investigation, but we have been able to demonstrate that the yield of the dihydroxyacid can be increased to the point of being useful with a modest amount of rational variation.

The reaction reported here represents the simplest preparation of either 2-phenylglyceric acid or 1,2-dihydroxycyclohexanecarboxylic acid reported to date, and appears to be a general way to effect the unusual transformation:

$$\text{R-CO-CH}_2\text{-CH}_2\text{-R'} \longrightarrow \text{R-C(OH)(COOH)-CH-R'}$$

An important restriction on the generality of this process is the requirement that the rest of the molecule be resistant to attack by alkaline hypochlorite, which is a powerful oxidant.

Experimental

Materials

Propiophenone (Aldrich), butyrophenone (Aldrich), cycloheptanone (Aldrich), 1-phenyl-1,2-propanedione (Aldrich), and cyclohexanecarboxylic acid (Eastman) were commercial materials. β-Dimethylaminopropiophenone · HCl was prepared by the literature route (15). Sodium hypochlorite solution was either Baker 5% reagent or Javex.

Methods

The presence of hypochlorite in a reaction mixture was tested for, using starch–iodide paper. Carboxylic acid products were detected on TLC plates by spraying with bromocresol green solution. Preparative layer chromatography of acids was carried out using solvents containing acetic acid to prevent tailing. The solvent was driven off after development by heating the plate at 50°C for 16 h. Bands could then be visualized by spraying with bromocresol green solution.

Propiophenone to 2-phenyl-2,3-dihydroxypropanoic acid

Propiophenone, 204 mg (1.50 mmol), was dissolved in a small amount of methanol (5 mL) and added with stirring to 1 L of 0.46 M NaOH, 0.54 M KCl, 0.01 M NaOCl and allowed to react at room temperature for 3 h. Reaction was stopped by the addition of $NaHSO_3$ (1.1 g) and the basic solution was extracted with ether (3 × 100 mL). Drying (Na_2SO_4) and evaporation gave 2 mg of oil, which had no distinct signals in proton NMR. The aqueous solution was cooled in ice, made acidic with concentrated HCl (45 mL), and extracted with ether (3 × 200 mL). Drying and evaporation gave 116 mg of oil, which partially crystallized on standing. Since only about 60% of the expected product had been recovered it was assumed that the remainder might be extracted by a more polar solvent. A further extraction with ethyl acetate (400 mL) yielded 62 mg of a colorless oil, which crystallized on standing and which was not soluble in chloroform. A third extraction of the aqueous solution with ethyl acetate (2 × 250 mL) gave another 60 mg with a proton spectrum similar to the second extract. Analysis by ^{1}H NMR, using integration of appropriate peaks, after the major product had been identified as 2-phenylglyceric acid, showed that the combined crude product consisted of 15% benzoic, 24% mandelic, and 57% phenylglyceric acids.

A similar product study starting with mandelic acid exposed for 1 h to aqueous 0.5 M OH^-, 0.03 M OCl^-, treated with sulphite, acidified and extracted with EtOAc resulted in 92% recovery of mandelic acid with no other products detectable by ^{1}H NMR (1:3 CD_3OD–$CDCl_3$), δ (TMS): 5.14 (s, -C*H*(OH)-COOH), 5.13 (s, -O*H*), 7.32 (m, C_6H_5).

Propiophenone to 2-phenyl-2,3-dihydroxypropanoic acid

Propiophenone, 643 mg (4.79 mmol), was dissolved in a small

Can. J. Chem. Downloaded from www.nrcresearchpress.com by 123.30.183.119 on 09/08/12
For personal use only.

amount of methanol (15 mL) and added with stirring to 1 L of 0.46 M NaOH, 0.54 M KCl, 0.03 M NaOCl and allowed to react at room temperature for 3 h. Reaction was stopped by addition of $NaHSO_3$ (4.5 g) and the basic solution was extracted with ether (3 × 100 mL) to remove any neutral products.

The aqueous solution was concentrated to 350 mL, cooled in ice, made acidic with concentrated HCl (45 mL) and extracted with ethyl acetate (5 × 100 mL), dried (Na_2SO_4), and evaporated, yielding 915 mg white solid. ^1H NMR analysis revealed a similar composition to the first product study. Aromatic signals for benzoic acid at 8.02 and 8.06 ppm made up only 11.5% of the total of aromatic signals, indicating only 29 mol% benzoic acid in the product mixture. A signal at 5.20 indicated 18 mol% mandelic acid, and the pair of doublets at 3.76 and 4.29 (J = 11) indicated 41 mol% (assuming 1H per doublet) of 2-phenylglyceric acid.

The UV spectrum in water showed short-wavelength absorption with no pronounced maximum. From the absorption at 225 nm (λ_{max} for benzoate in water, ϵ_{max} = 10 000) we calculated a maximum yield of 32 wt.% of benzoate in the crude product. Since ^1H NMR revealed 29 mol% benzoic acid, the other products cannot have much absorbance at this wavelength.

The entire product (915 mg) was refluxed in methanol containing 5 vol.% H_2SO_4 for 90 min, poured into ice water (100 mL), and extracted with ethyl acetate (3 × 100 mL). The extract was dried (Na_2SO_4) and evaporated, yielding 849 mg liquid. TLC with 15% EtOAc – petroleum ether gave four spots (UV-active), R_f's 0.7, 0.6, 0.3, and 0.25. The fastest moving spot had the same R_f as methyl benzoate.

The entire batch of methyl ester was treated with excess Et_3N – acetic anhydride (3 mL, 2.5 mL) with 15 min heating on a steam-bath followed by addition of methanol (3 mL) and extraction, drying, and evaporation as before, yielding 866 mg. Column chromatography (silica, 40 g; 0–25% EtOAc–hexanes) on the esterification mixture gave the following fractions: 104 mg methyl benzoate; 144 mg methyl *O*-acetylmandelate; 425 mg material later identified as methyl 3-acetoxy-2-hydroxy-2-phenylpropanoate. This material was crystallized from ether – petroleum ether, mp 59.5–60°C; ^1H NMR ($CDCl_3$), δ: 2.07 (3H, s, CH_3-CO), 3.82 (3H, s, CH_3O), 4.0 (1H, br, O*H*), 4.38 and 4.71 (2H, doublets of an AB quartet, J = 11 Hz, CH_2), 7.32–7.63 (5H, C_6H_5); ^{13}C NMR, δ: 20.71 (CH_3-CO), 53.46 (CH_3-O), 68.83 (CH_2-OAc), 77.63 (quaternary C), 125.60, 128.52, 128.58 (aromatic), 170.60 (CH_3-*CO*), 173.14 (*CO*-OCH_3). A 200 MHz proton spectrum in $CDCl_3$ revealed one *O*-methyl (3H, s) at 3.82 ppm, one *O*-acetyl group (3H, s) at 2.07, one broad OH group signal at 4.0 ppm, two doublets (J = 11.4) centred at 4.71 and 4.38 ppm, 3H aromatic (m) 7.32–7.40, and 2H aromatic (m) 7.58–7.63 ppm.

O-*Acetylmandelic acid methyl ester* (ref. 16)

Mandelic acid, 1.3 g, was refluxed 90 min in 5% H_2SO_4 in methanol, 50 mL, the solution poured into 150 mL ice water, and extracted with ethyl acetate, 3 × 100 mL. After evaporation, the product was treated with a mixture of 3 mL acetic anhydride, 3 mL Et_3N, heated on a steam bath 15 min, diluted with methanol, 5 mL, washed into a separatory funnel with water, 100 mL, and extracted with ethyl acetate, 300 mL. The organic layer was washed first with dilute acid (0.1 M H_3PO_4), then with dilute base (0.1 M NaOH) dried (Na_2SO_4), and evaporated, yielding 0.86 g oily liquid (48%). ^1H NMR spectrum ($CDCl_3$), δ (TMS): 7.40–7.48 (2H, m), 7.32–7.40 (3H, m), 5.93 (1H, s), 3.69 (3H, s), 2.17 (3H, s).

Propiophenone to 2-phenyl-2,3-dihydroxypropanoic acid

Propiophenone, redistilled, 647 mg (4.82 mmol), was dissolved in 5 mL methanol and added to 500 mL deoxygenated 1 M aqueous NaOH with vigorous stirring. A solution of NaOCl (0.3 M) was slowly added (65 mL, (19.5 mmol) over a period of 5 h). In the first 30 min, 35 mL was added, whereupon all of the ketone dissolved and the solution became deep yellow. In the second 30 min, 5 mL was added, followed by 10 mL the second hour, 5 mL after 4 h, and another 10 mL after 5 h. The reaction temperature was 28°C. The yellow colour began to fade after the last addition of hypochlorite. After 8 h, OCl^- was still present (iodide test), and was destroyed by reaction with $NaHSO_3$ (0.5 g). An ether extract of the basic solution (3 × 100 mL) yielded 20 mg brown oil (3%).

Half the water was evaporated from the basic solution before acidifying with concentrated HCl (45 mL). The ethyl acetate extract (4 × 200 mL) yielded 852 mg, which by ^1H NMR analysis was estimated to contain: 75% 2-phenylglyceric acid, doublets at 3.73 and 4.26 ppm; 7% atrolactic acid, singlet at 1.78 ppm; 7% benzoic acid, multiplets at 8.0–8.05 ppm; 9% mandelic acid, singlet at 5.18 ppm. The presence of atrolactic acid was confirmed by addition of 5 mg of authentic sample, which caused the sharp singlet at 1.78 ppm to double in intensity, thus confirming the proton assay.

Crystallization from 1:1 ethyl acetate – petroleum ether gave 564 mg 2-phenylglyceric acid (3.10 mmol, 64%), mp 146.5–148°C (lit. mp (7) 145–147°C; (8) 149°C; (9) 146–148°C; mixture mp with an authentic sample, 148°C). ^1H NMR (CD_3OD), δ (TMS): 3.73 and 4.26 (AB quartet), 7.24–7.66 (multiplet), and comparison with an authentic sample prepared by the literature route (4–6). ^1H NMR spectra in D_2O (Na salt) or CD_3OD were identical for both samples.

1-Phenyl-1,2-propanedione to 2-phenyl-2,3-dihydroxypropanoic acid

1-Phenyl-1,2-propanedione, 710 mg (4.79 mmol), was dissolved in a small amount of methanol (5 mL) and added with stirring to 1 L of 0.50 M NaOH, 0.5 M KCl, 0.012 M NaOCl and allowed to react for 3 h at room temperature. The initial yellow colour disappeared within 2 min. Reaction was stopped by addition of $NaHSO_3$ (1.1 g) and the basic solution was extracted with ether (3 × 100 mL). Evaporation gave no detectable products by TLC. The aqueous solution was cooled in ice, made acidic with concentrated HCl (45 mL), and extracted with ethyl acetate (3 × 200 mL). Drying and evaporation gave 933 mg of oil, which partially crystallized on standing. TLC (2% AcOH, 10% MeOH, 88% $CHCl_3$) showed a spot with the same R_f, 0.6, as benzoic acid. A 200 MHz proton spectrum of the acid extract (in $CDCl_3$ – 10% CD_3OD) indicated 22% benzoic, 14% mandelic, and 58% phenylglyceric acids by integration. The mixture of acids was dissolved in a minimum amount of methanol and crystallized from 88% benzene, 10% hexanes, 2% methanol, yielding 416 mg of almost pure 2-phenylglyceric acid (2.28 mmol, 47.6%), mp 143–145.5°C. ^1H NMR (CD_3OD), δ: 3.71 (1H, d, J = 11.3), 4.23 (1H, d, J = 11.3), 4.98 (4H, b, OH), 7.3–7.4 (3H, m), 7.6–7.7 (2H, m). A recrystallization from 1:1 ethyl acetate – pet. ether gave 279 mg (32%), mp 147–148.5°C (lit. mp (7) 145–147°C; (8) 149°C; (9) 146–148°C). The acids from the mother liquor were esterified with methanol – 5% H_2SO_4 (50 mL) with 3 h refluxing, diluted with ice-water (50 mL), and extracted with ethyl acetate (3 × 50 mL), yielding 490 mg (85–90% of expected), which was estimated by proton NMR to contain 41% benzoate (signals at 8.0–8.05), 21% mandelate (singlet at 5.19), and 38% 2-phenylglycerate (doublet at 4.32). Total assay: 2-phenylglyceric acid, 3.23 mmol (67%); benzoic acid, 1.03 mmol (21%); mandelic acid, 0.53 mmol (11%).

β-Dimethylaminopropiophenone · HCl to 2-phenyl-2,3-dihydroxypropanoic acid

β-Dimethylaminopropiophenone · HCl (15), 450 mg (2.11 mmol), was dissolved in a small amount of water (5 mL) and added to 500 mL 1 M NaOH, 0.02 M NaOCl with rapid stirring at room temperature. Initially, organic material began to oil out but redissolved within 1 min. A yellow colour appeared in the first minute but disappeared within 5 min. An acrid odour, probably of *N*-chlorodimethylamine, was produced. The vapors above the reaction solution produced a quick reaction with starch–iodide paper. Reaction was stopped after 3 h by addition of $NaHSO_3$ (1.0 g) and the solution brought to pH 7 by addition of 4 M H_3PO_4 (100 mL). The neutral solution was extracted with ether (3 × 100 mL); the evaporated ether extracts (15 mg) gave no signals in the proton NMR corresponding to likely products. The aqueous solution was acidified with 6 M HCl (100 mL) and extracted with ethyl acetate (4 × 200 mL). The extract was dried (Na_2SO_4) and evaporated, yielding 283 mg of a mixture of benzoic, mandelic, and 2-phenylglyceric acids (2-PGA). ^1H NMR spectrum (70:30 $CDCl_3$–CD_3OD), δ (TMS): 1.99 (s, acetic acid), 3.76 (d, J = 11.4, CH_2 of 2-PGA), 4.30 (d, J = 11.2, CH_2 of 2-PGA), 5.19 (s, CH of mandelic acid), 6.1 (s, b, OH), 7.2–7.7 (m, aromatic), 8.0–8.1 (m, aromatic *ortho* to COOH). Assay based on

Can. J. Chem. Downloaded from www.nrcresearchpress.com by 123.30.183.119 on 09/08/12
For personal use only.

integration: 28% benzoic; 44% mandelic; 28% 2-phenylglyceric acids. Based on the proton assay and the weight of product, the acids recovered represent 1.86 mmol, 89% of starting material.

Butyrophenone to 2,3-dihydroxy-2-phenylbutanoic acid

Butyrophenone, 744 mg (5.02 mmol) was dissolved in methanol (5 mL) and added with stirring to an aqueous solution of 1 M NaOH, 0.03 M NaOCl, 1 L (30 mmol, sixfold excess). After 3 h with vigorous stirring, the ketone was completely dissolved and most of the hypochlorite was gone. Hypochlorite solution (0.3 M), 20 mL (6 mmol), was added, and after an additional 2 h hypochlorite was still present. The excess was destroyed by addition of $NaHSO_3$ (2.0 g) and the basic solution was extracted with ether (3 × 200 mL), yielding 15 mg semi-solid, which had only one spot by TLC (10% EtOAc – 90% petroleum ether) with R_f value 0.24, not the same as butyrophenone, R_f 0.54. No further attempt was made to identify this product.

After acidifying with concentrated HCl (45 mL), the solution was extracted with ethyl acetate (4 × 150 mL), which, after drying (Na_2SO_4) and evaporation, yielded 684 mg colorless syrupy liquid. Crystallization from CCl_4 (20 mL) yielded 311 mg (1.59 mmol, 31.6%), mp 125–133°C; 200 MHz ^1H NMR ($CDCl_3$ – 10% CD_3OD), δ (TMS): 0.97 and 1.26 (3H, 2 methyl doublets indicating two diastereomers, J = 6.4 Hz and J = 6.2 Hz, with an integral ratio of 3.0:1.0), 4.58 (q, J = 6.4 Hz), larger, near 4.5, smaller and partly hidden under the OH signal (a pair of quadruplets, C*H*(OH)(CH_3)), 7.35 (3H, m), 7.69 (2H, m, aromatic protons); lit. (17) (mixture of diastereomers, ratio not stated) mp 158–165°C, ^1H NMR (acetone-d_6), δ: 0.9 and 1.2 (3H, 2d), 4.5 (1H, q, CH), 7.3 (3H, m, aromatic), 7.7 (2H, m, aromatic).

The mother liquor from crystallization, 373 mg, was dried and analysed by proton NMR (10% CD_3OD – 90% $CDCl_3$): 2,3-dihydroxy-2-phenylbutanoic acid was still present; a singlet at 5.15 indicated the presence of mandelic acid and the downfield aromatic signals of benzoic acid (8.04, 8.08) were clearly present. A proton assay indicated 32% benzoic, 25% mandelic, and 43% 2,3-dihydroxy-2-phenylbutanoic acid.

The total assay, based on both crystalline product and NMR analysis of the mother liquors is as follows: 2,3-dihydroxy-2-phenylbutanoic acid, 51.4%; benzoic acid, 14.7%; and mandelic acid, 11.5%, for a total yield of acids of 77.6%.

Cycloheptanone to 1,2-dihydroxycyclohexanecarboxylic acid

Cycloheptanone, 0.245 g (2.1 mmol), was added to 0.5 M aqueous NaOH solution, 500 mL, to which was added, at 0, 18, and 22 h, three equal portions of NaOCl solution, 5 mL, 0.44 M, 2.2 mmol each. Nearly all of the hypochlorite had been consumed before the second and third addition. The reaction was stopped after 42 h. No significant amount of material was recovered from extraction of the basic reaction solution. Acidification followed by extraction with ether (4 × 75 mL) gave 200 mg of light-yellow viscous liquid. Preparative layer chromatography, developed with 10% AcOH – 90% $CHCl_3$, gave cyclohexanecarboxylic acid, 43.6 mg, 0.34 mmol (16%), R_f 0.69; pimelic acid, 55.2 mg, 0.34 mmol (16%), R_f 0.51, mp 104–105°C (lit. (18) mp 106°C); 1,2-dihydroxycyclohexanecarboxylic acid, 28.0 mg, 0.175 mmol (8%), R_f 0.16, mp 113–114°C (lit. (10) mp 104–105°C); unidentified: 18.3 mg, R_f 0.38 and 0.58.

The apparent yield of cyclohexanecarboxylic acid may be lower than in the actual product mixture because it is sufficiently volatile to have evaporated during evaporation of solvent at 0.2 Torr[2] and during drying of the preparative layer plate at 50°C for 16 h after development. A control experiment in which 100 mg of the pure acid was put through the same procedure (dissolving in ether, evaporating to 0.2 Torr, running on a preparative layer plate, oven drying, extracting with ether, and evaporating again) yielded 81% by weight by the acid.

The identification of purified 1,2-dihydroxycyclohexanecarboxylic acid, mp 112–113°C, depends upon its spectroscopic properties. Exact Mass calcd. for $C_7H_{12}O_4$: 160.7386; found: 160.7361. ^1H NMR (90% $CDCl_3$ – 10% CD_3OD), δ (TMS): 1.6 (br m, 8H, CH_2), 3.88 (d of d, 1H, CH(OH)). ^{13}C NMR (CD_3OD), δ (TMS): 178.98 (COOH), 77.75 (quaternary, C-1), 73.34 (methyne, C-2), 34.93 (methylene, C-6), 30.44 (methylene, C-3), 25.08 (methylene, C-5), 20.76 (methylene, C-4). The acid was converted to the methyl ester using diazomethane. ^{13}C NMR (CD_3OD), δ (TMS): 176.67 (COOR), 76.89 (quaternary, C-1), 72.26 (methyne, C-2), 52.96 (*O*-methyl), 34.22 (methylene, C-6), 30.01 (methylene, C-3), 24.10 (methylene, C-5), 19.86 (methylene, C-4). The methyl ester was acetylated using acetic anhydride – pyridine to give methyl 2-acetoxy-1-hydroxycyclohexanecarboxylate. ^{13}C NMR (CD_3OD), δ (TMS): 175.34 (COOR), 169.96 (acetyl CO), 75.45 (C-1), 75.01 (C-2), 52.96 (*O*-methyl), 34.05 (C-6), 26.37 (C-3), 23.77 (C-5), 20.98 (acetyl methyl), 19.47 (C-4).

Pimelic acid and cyclohexanecarboxylic acid were identified by comparison of ^1H NMR spectrum and TLC behavior with authentic samples.

Cycloheptanone to 1,2-dihydroxycyclohexanecarboxylic acid

Cycloheptanone, 1.00 g, was dissolved in ice-cold water, 500 mL, and then a solution of NaOH, 40 g, in ice-cold water, 500 mL, was added slowly. Then Javex, 60 mL, was added using a motor-driven syringe at a rate of 0.15 mL/min. The solution was stirred for a further 70 h after the addition of all the Javex, and then excess hypochlorite was destroyed by adding $NaHSO_3$, 2.2 g. The solution was extracted (ether, 3 × 400 mL) and the extracts were evaporated to 50 mL, then washed (aqueous 2 N HCl, 2 × 50 mL; water, 2 × 50 mL), dried (Na_2SO_4), and evaporated to dryness: 40 mg. The aqueous product solution was acidified using concentrated HCl, 100 mL; NaCl was added, 250 g, and the resulting solution was extracted using ethyl acetate (5 × 400 mL). The extract was evaporated to 200 mL, washed with water (2 × 50 mL), dried (Na_2SO_4), and evaporated: 829 mg. From 671 mg of this crude product, crystallization (ether–hexane) gave 107 mg of 1,2-dihydroxycyclohexanecarboxylic acid, mp 112–114°C. Preparative layer chromatography on the mother liquor from crystallization gave cyclohexanecarboxylic acid, 236 mg; pimelic acid, 56 mg; unknown, 43 mg; and further 1,2-dihydroxycyclohexanecarboxylic acid, 110 mg.

[2]1 Torr = 133.3 Pa.

Acknowledgments

We thank the Natural Sciences and Engineering Research Council of Canada for financial support of this work.

1. J. P. GUTHRIE and J. COSSAR. Can. J. Chem. **64**, 1250 (1986).
2. M. W. FARRAR and R. LEVINE. J. Am. Chem. Soc. **71**, 1496 (1949).
3. R. LEVINE and J. R. STEPHENS. J. Am. Chem. Soc. **72**, 1642 (1950).
4. P. A. LEVENE and G. M. MEYER. Org. Synth. Coll. Vol. 2. Academic, New York. 1943. p. 288.
5. G. R. AMES and W. DAVEY. J. Chem. Soc. 1794 (1958).
6. J. A. FEE, G. D. HEGEMAN, and G. L. KENYON. Biochemistry, **13**, 2533 (1974).
7. C. A. KERR. J. Chem. Soc. 1943 (1927).
8. W. C. CRAIG and H. R. HENZE. J. Org. Chem. **10**, 16 (1945).
9. C. P. WHITMAN, J. C. CRAIG, and G. L. KENYON. Tetrahedron, **41**, 1183 (1985).
10. G. HESSE and G. KREHBIEL. Justus Liebigs Ann. Chem. **593**, 42 (1955).
11. J. P. GUTHRIE. Can. J. Chem. **56**, 962 (1978).
12. T. S. CANTRELL and A. C. ALLEN. J. Org. Chem. **54**, 135 (1989).
13. J. HINE and G. F. KOSER. J. Org. Chem. **36**, 3591 (1971).
14. F. WEHRLI and T. WIRTHLIN. Interpretation of carbon-13 NMR spectra. Heyden & Son, Philadephia, PA. 1976. p. 45.
15. C. E. MAXWELL. Org. Synth. Coll. Vol. 3, Academic, New York. 1955. p. 305.
16. G. PRACEJUS. Justus Liebigs Ann. Chem. **622**, 10 (1959).
17. A. CLERICI and O. PORTA. J. Org. Chem. **47**, 2852 (1982).
18. R. C. WEAST (*Editor*). CRC handbook of chemistry and physics. 52nd ed. Chemical Rubber Co., Cleveland, OH. 1971–72. p. C-322.

Can. J. Chem. Downloaded from www.nrcresearchpress.com by 123.30.183.119 on 09/08/12
For personal use only.

Synthesis of (+/−) arthrographol[1]

WILLIAM A. AYER[2] AND PETER A. CRAW
Department of Chemistry, University of Alberta, Edmonton, Alta., Canada T6G 2G2

Received May 8, 1991

WILLIAM A. AYER and PETER A. CRAW. Can. J. Chem. **69**, 1909 (1991).

A total synthesis of (+/−) arthrographol (**1**) in seven steps from vanillin is reported. Key steps in the synthesis are a single-step conversion of 5-allylvanillin (**2**) into the benzofuranmethanol **6**, alkylation of the chloride **25** with the lithium anion of crotyl phenyl sulfide to give the sulfide **26**, and formation of the 1(*E*),3(*E*)-1,3-pentadienyl side chain of arthrographol (**1**) via oxidation of the sulfide **26** and subsequent elimination of phenylsulfenic acid. The synthetic (+/−) arthrographol (**1**) inhibits the growth of *Ophiostoma clavigerum* (Robin.-Jeff. & Davids.) Harrington, the most pathogenic of the fungi associated with the blue stain disease of lodgepole pine (*Pinus contorta* Dougl. var *latifolia* Engelm.).

Key words: arthographol, alkylation, 2-butenyl phenyl sulfide, polyketide.

WILLIAM A. AYER et PETER A. CRAW. Can. J. Chem. **69**, 1909 (1991).

On rapporte une synthèse totale du (+/−)-arthrographol (**1**) impliquant sept étapes à partir de la vanilline. Les étapes clés de la synthèse sont une conversion en une étape de la 5-allylvanilline (**2**) en benzofuraneméthanol **6**, une alkylation du chlorure **25** avec le sel de lithium de l'anion du sulfure de crotyle et de phényle qui conduit au sulfure **26** et la formation de la chaîne latérale 1(*E*),3(*E*)-penta-1,3-diènyle de l'arthrographol (**1**) par oxydation du sulfure **26** et l'élimination subséquente de l'acide phénylsulfénique. Le (+/−)-arthrographol (**1**) de synthèse inhibe la croissance du *Ophiostoma clavigerum* (Robins.-Jeff & Davids.) Harrington, le plus pathogène des champignons associés avec la maladie de la teinte bleue du pin (*Pinus contorta* Dougl. var *latifolia* Engelm.).

Mots clés : arthographol, alkylation, sulfure de 2-butényle et de phényle, polyketide.

[Traduit par la rédaction]

Introduction

The blue stain disease of lodgepole pine (*Pinus contorta* Dougl. var *latifolia* Engelm.) is caused by a number of fungi vectored by the mountain pine beetle (*Dendroctonus ponderosae* Hopk.) (1). Recently we examined the metabolites produced in liquid cultures of the fungus *Arthrographis pinicola* Sigler and Yamaoka (2), which shows inhibitory activity against *Ophiostoma clavigerum* (Robin.-Jeff. & Davids.) Harrington, a fungus strongly associated with tree mortality caused by the blue stain fungi. Our investigations with *Arthrographis pinicola* led to the isolation of (−) arthrographol (**1**), which we believe to be responsible for the strong inhibitory activity of this fungus. Since (−) arthrographol (**1**) is produced in very small amounts (~0.2 mg/L) in liquid cultures, an efficient total synthesis of this compound was desirable to permit further testing of **1** as a potential control agent for the blue stain fungi. We report herein the results of our synthetic investigations, which culminated in a successful synthesis of (+/−) arthrographol (**1**).

Discussion

The successful synthesis of (+/−) arthrographol (**1**) began with *O*-allylation of vanillin and subsequent thermal Claisen rearrangement to give 5-allyl-4-hydroxy-3-methoxybenzaldehyde (**2**) (3). Epoxidation of **2** with 2.5 equivalents of *m*-chloroperbenzoic acid gave the unstable epoxyformate **3** resulting from concomitant epoxidation of the 5-allyl group and Baeyer–Villiger oxidation of the benzaldehyde (Scheme 1). The epoxyformate **3** suffered considerable decomposition when exposed to silica gel for any longer than brief periods during chromatography. Intramolecular cyclization (4) to give the benzofuran formate **4** occurred readily when the epoxyformate **3** was distilled at reduced pressure in a Kugelrohr oven. Cyclization to give **4** was also accompanied by some *trans*-esterification to give the bisformate **5** and decarbonylation to give the phenolic benzofuran **6**. If the epoxyformate **3** was not chromatographed, attempted thermal cyclization to give the benzofuran **4** gave only polymeric material. The combined yield of **4**–**6** for the two steps from **2** was 63%. A more efficient synthesis of the benzofuran **6** was achieved by epoxidation/Baeyer–Villiger oxidation of **2** and subsequent brief treatment of the crude, unchromatographed epoxyformate **3** with potassium carbonate in methanol. This procedure gave the benzofuran **6** in 71% yield.

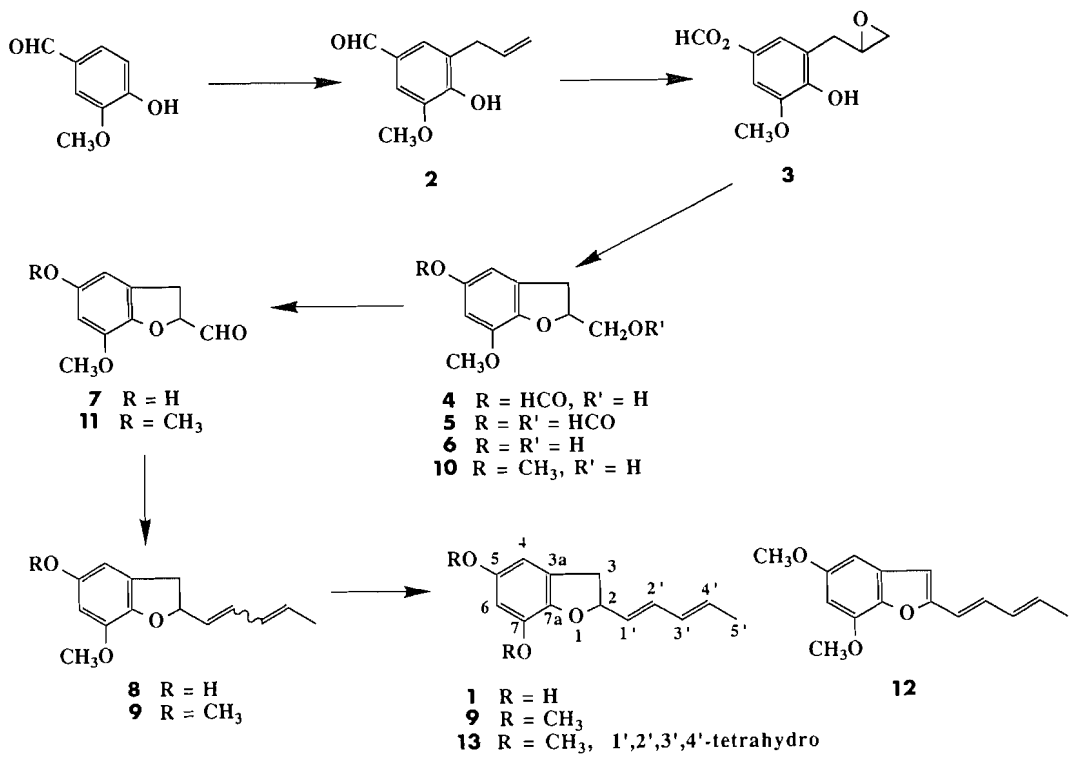
We now anticipated that oxidation of the primary alcohol of **6** to give the aldehyde **7** and subsequent Wittig reaction with the lithium anion of (2-butenyl)triphenylphosphonium bromide would give the diene **8**, which bears the C2-(1,3-pentadienyl) side chain of arthrographol (**1**). However, all attempts to oxidize the alcohol **6** using either pyridinium chlorochromate or dichromate in dichloromethane, or Swern conditions (5), failed to give the aldehyde **7**, possibly due to the low solubility of **6** in dichloromethane. Since it would be necessary to deprotect the C8-methoxy group of **8** in order to complete the synthesis of (+/−) arthrographol (**1**), we felt that the conditions for monodemethylation of **8** would equally well be applicable to bis-demethylation of a dimethyl ether of (+/−) arthrographol (**9**). In the event, **6** was methylated to give the dimethyl ether **10**, which was readily oxidized under Swern conditions to the aldehyde **11**. Interestingly, the Ftir spectrum of a chloroform cast of **11** displayed only a very weak $\nu_{C=O}$ band at 1732 cm^{-1} and a strong ν_{O-H} band at 3400 cm^{-1}, which suggests that **11** exists, at least when cast on a NaCl plate, as an equilibrium mixture of aldehyde and enol tautomers. The ^{13}C nmr spectrum of pure **11** contained the expected 10 signals for the aldehyde tautomer (δ_{CO} 201.6, δ_{C2} 85.0) and additional weaker and somewhat broadened signals that might be due to the enol tautomer.

The aldehyde **11** was converted into a mixture of dienes **9** upon reaction with the lithium anion of crotyl triphenylphosphonium bromide. However, ^1H nmr analysis indicated that the

[1]Presented in part at the 73rd Canadian Chemical Conference, Halifax, Nova Scotia, Canada. July 15–20, 1990.

[2]Author to whom correspondence may be addressed.

Can. J. Chem. Downloaded from www.nrcresearchpress.com by 123.30.183.119 on 09/08/12
For personal use only.



SCHEME 1

desired (*E,E*)-diene, as in arthrographol (**1**), was only a minor component of the inseparable mixture of dienes. The major diene in the mixture displayed signals in the ^{1}H nmr spectrum ($J_{H1'-H2'}$ = 10.0 Hz, $J_{H3'-H4'}$ = 14.9 Hz) that suggested it was the 1(*Z*),3(*E*)-pentadiene isomer arising from an unstabilized betaine formed by reaction of the crotyl triphenylphosphonium anion with the aldehyde **11**, and subsequent elimination of triphenylphosphine oxide to generate mainly a *Z* double bond. The mixture of dienes was isomerized to predominantly the 1(*E*),3(*E*)-diene (>80% by ^{1}H nmr) by refluxing with a catalytic amount of iodine (6) in carbon tetrachloride. The reaction with iodine also gave a small amount of the corresponding furan **12** (*m/z* 244 (M^+), δ_{H3} 6.47, s) possibly arising from dihydrofuran iodination (either benzylic or allylic) and subsequent dehydroiodination. Crystallization of the mixture of dienes containing mainly the (*E,E*) isomer gave the pure (*E,E*)-diene whose ^{1}H nmr spectrum was identical with that of dimethylarthrographol prepared by methylation of natural (−) arthrographol. Hydrogenation of the mixture of dienes obtained from the Wittig reaction gave tetrahydrodimethylarthrographol (**13**), which was identical (^{1}H nmr) with the product of methylation and hydrogenation of natural (−) arthrographol (**1**).

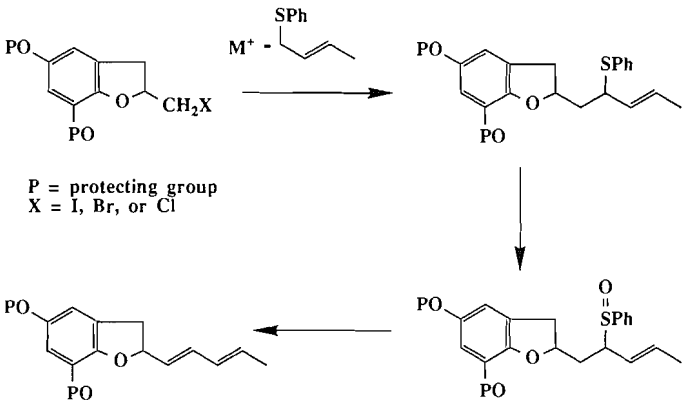
To complete the synthesis of (+/−) arthrographol (**1**) it was now necessary to address the anticipated difficult problem of demethylation of (+/−) dimethylarthrographol **9**. This was not expected to be an easy transformation as the (+/−) dimethyl ether **9** also contains a reactive *O*-allyl ether. Thus, we were not completely surprised when attempted demethylation with either trimethylsilyl iodide (7), boron tribromide (8), or lithium diphenylphosphide (9) failed to give any (+/−) arthrographol (**1**), and instead led to extensive decomposition of the starting material.

As a result of the inability to demethylate (+/−) dimethylarthrographol **9** we decided to investigate the possibility of unmasking the offending 3-methoxy group derived from vanillin prior to formation of the 1,3-pentadiene side chain at C2 of the benzofuran. Initially we were encouraged when 5-allyl vanillin (**2**) was smoothly demethylated with boron tribromide in dichloromethane to give 5-allyl-3,4-dihydroxybenzaldehyde. However, attempted epoxidation/Baeyer–Villiger oxidation and cyclization of this catechol did not give any 2,3-dihydro-5,7-dihydroxy-2-benzofuranmethanol (**14**), presumably due to facile oxidation to an *o*-benzoquinone, which then decomposed. As a result our attention shifted to cleavage of the methoxy group of the phenolic benzofuran **6**. At this stage we also wished to investigate an alternative procedure of forming the C2-1,3-pentadienyl side chain of arthrographol (**1**) in which alkylation of a C2-halomethylbenzofuran with the anion of crotyl phenyl sulfide followed by sulfur oxidation and elimination of phenylsulfenic acid would generate predominantly an (*E*)-1,2-double bond in the pentadienyl side chain (Scheme 2). A similar alkylation–oxidation–elimination sequence was used to form the (*E,E*)-1,3-pentadienyl unit of the sex pheromone of the codling moth, 8(*E*),10(*E*)-dodecadien-1-ol, from 8-bromo-1-octanol (10).

Cleavage of the methoxy group of **6** with boron tribromide failed to give a good yield of the desired resorcinol **14**. Accordingly, we converted the alcohol into the corresponding iodide **15**, bromide **16**, and chloride **17**. The iodide **15** and chloride **17** were prepared in high yield from reaction of the alcohol **6** with iodine–imidazole–triphenylphosphine in benzene (11) and acetonitrile,[3] and *N*-chlorosuccinimide–triphenylphosphine in tetrahydrofuran (THF) (12), respectively. Attempts to form the bromide **16** with either *N*-bromosuccinimide–triphenylphosphine in THF or carbon tetrabromide – triphenylphosphine in THF or dichloromethane (13) did not give more than 40%

[3]I. Paterson and P. Haley. Cambridge University, England, personal communication.

Can. J. Chem. Downloaded from www.nrcresearchpress.com by 123.30.183.119 on 09/08/12
For personal use only.



SCHEME 2

conversion to the bromide **16** even after prolonged reaction or use of excess of the brominating reagent.

Attempts to convert the iodide **15** into the resorcinol **18** with boron tribromide in dichloromethane led to decomposition, while the bromide **16** gave a low yield of the corresponding resorcinol **19** but this material was contaminated with considerable amounts of dibromo impurities (hreims, cims). Finally, cleavage of the methyl ether of the chloride **17** was investigated and it was found that reaction with 2 equivalents of boron tribromide in dichloromethane at room temperature gave nearly quantitative yields of the resorcinol **20**. Attention now turned to protection of the two phenolic groups in **20** prior to alkylation with the anion of crotyl phenyl sulfide. Initially we chose to protect the resorcinol **20** as its bismethoxymethyl ether **21** (74% yield), as the MOM protecting groups should be easily removable by mild acid treatment (14). Next, alkylation of the bismethoxymethyl ether **21** with the lithium anion of crotyl phenyl sulfide was investigated. After several attempts it was found that the allyl phenylsulfide **22** could be prepared in good yield using an excess of the lithium anion of crotyl phenyl sulfide in the presence of sodium iodide in a solvent mixture of tetrahydrofuran and 1,3-dimethyl-3,4,5,6-tetrahydro-2(1*H*)-pyrimidinone (DMPU) (15). The absence of either or both sodium iodide and DMPU from the reaction led to poor yields of **22** and many unwanted by-products. The allyl phenyl sulfide **22** was oxidized with *m*-chloroperbenzoic acid to the sulfoxide **23**. The sulfoxide **23** readily eliminated phenylsulfenic acid when refluxed in benzene containing triethylamine to give a mixture of bismethoxymethyldienes **24** (46% from sulfide **22**), which contained mainly the desired (*E,E*) isomer (>80% by ^{1}H nmr). Unfortunately, deprotection of the bismethoxymethyl ether **24** to give (+/−) arthrographol (**1**) using HCl (cat.) – *i*PrOH–THF–H_2O, HCl (cat.) – CH_3OH, pyridinium-*p*-toluenesulfonate (cat.) – CH_2Cl_2–H_2O, trifluoroacetic acid (cat.) – CH_2Cl_2, or silica gel – CH_2Cl_2–H_2O either failed to give any reaction or led to decomposition.

As an alternative to the use of MOM protecting groups for the resorcinol **20** we prepared the bistrimethylsilyl, and bis-*tert*-butyldimethylsilyl ethers of **20** but neither of these compounds underwent successful alkylation with the lithium anion of crotyl phenyl sulfide in the presence of sodium iodide – DMPU, probably due to iodide-promoted desilylation. Finally, the bisethoxyethyl ether **25** was prepared in high yield from resorcinol **20**. The ethoxyethyl group has been used extensively as a protecting group for alcohols, but not for phenols. Before proceeding with the alkylation of **25** we briefly examined the conditions for deprotection of the two bisethoxyethyl protecting groups and found that the bisethoxyethyl ether **25** could be deprotected in high yield to the resorcinol **20** using a mixture of acetic acid – methanol–water (1:50:50).

The bisethoxyethyl ether **25** was alkylated with the lithium anion of crotyl phenyl sulfide in THF–DMPU containing sodium iodide to give the allyl phenyl sulfide **26**, which was a complex mixture of diastereoisomers (^{1}H nmr) due to the additional asymmetric centres of the ethoxyethyl groups, in 71% yield. However, the ^{1}H nmr and hreims of **26** fully support the structure of this compound. The allyl phenyl sulfide **26** was oxidized with *m*-chloroperbenzoic acid to the sulfoxide **27**, which in turn was refluxed in benzene–triethylamine, and to our pleasure the crude diene **28** so obtained was readily deprotected with acetic acid in aqueous methanol to give (+/−) arthrographol (**1**) in 32% yield from the sulfide **26**. The reaction also gave a lesser amount (18%) of a by-product to which we have provisionally assigned the cyclopropane structure **29** on the basis of ^{1}H nmr and hreims data.

The synthetic (+/−) arthrographol (**1**) was contaminated with minor amounts of other diene isomers but these were readily removed by fractional crystallization to give pure (+/−) arthrographol (**1**). The ^{1}H nmr, Ftir, hreims, tlc behaviour, and mp of this material were in excellent agreement with those of natural (−) arthrographol (**1**). The synthetic (+/−) arthrographol (**1**) inhibited the growth of the blue stain fungus *Ophiostoma clavigerum* at concentrations of 50 and 100 μg in the filter paper disc bioassay (2).

Experimental

For general experimental details see ref. 16. The following solvents were distilled immediately prior to use: tetrahydrofuran (THF) and benzene were distilled under argon from sodium – benzophenone ketyl; 1,3-dimethyl-3,4,5,6-tetrahydro-2(1*H*)-pyrimidinone (DMPU) was distilled from calcium hydride at reduced pressure (85–90°C, 3 Torr (1 Torr = 133.3 Pa); dichloromethane, triethylamine, and diisopropylamine were distilled from calcium hydride under argon. Imidazole and triphenylphosphine were purified by sublimation at reduced pressure. *N*-Chlorosuccimide was recrystallized from benzene. *N*-Bromosuccinimide was recrystallized from water and dried *in vacuo* over silica gel. Sodium iodide was dried *in vacuo* at 100°C for 4 h and stored in a desiccator. *m*-Chloroperbenzoic acid was purified according to Fieser and Fieser (17). Crotyl phenyl sulfide was prepared according to Babler and Haack (10), and crotyl triphenylphosphonium bromide according to Bohlmann and Mannhardt (18). All other solvents and liquid reagents were distilled prior to use.

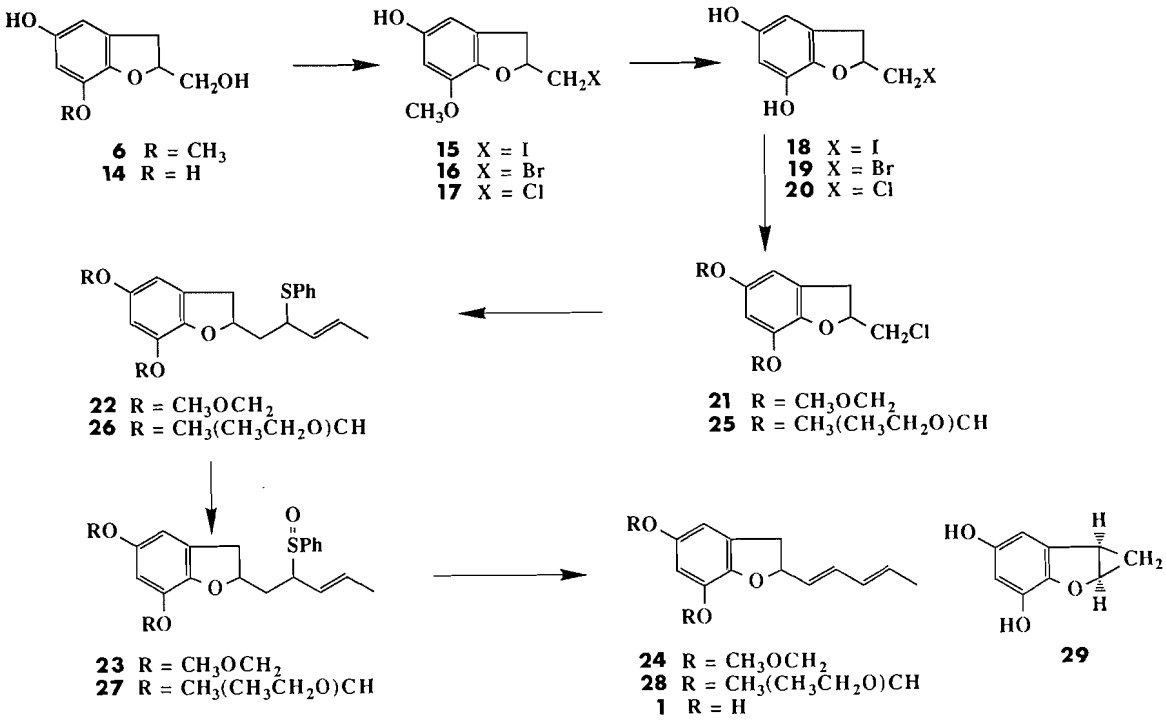
4-Allyloxy-3-methoxybenzaldehyde (3)

A mixture of vanillin (12.2 g, 80.3 mmol), potassium carbonate (10.0 g, 72.5 mmol), and allyl bromide (6.8 mL, 78.6 mmol) in dimethyl formamide (20 mL) was stirred under an argon atmosphere for 44 h, then further allyl bromide (0.5 mL) and potassium carbonate (1.0 g) were added and stirring continued for a futher 24 h. The mixture was poured into water (200 mL) and acidified to pH 5–6 (litmus) with 2 M hydrochloric acid. The aqueous mixture was extracted with ether (3 × 100 mL) and the combined extracts were washed successively with saturated sodium hydrogen carbonate solution and brine. The dried ether extract was evaporated to a pale yellow oil, which was chromatographed on silica gel, eluting with ethyl acetate – Skellysolve B (1:5) to give 4-allyloxy-3-methoxybenzaldehyde as a clear liquid (15.06 g, 98%); Ftir ($CHCl_3$ cast): 1684, 1594, 1585, 1508, 1276, 1136 cm^{-1}; ^{1}H nmr ($CDCl_3$) δ: 9.84 (1H, s), 7.40–7.46 (2H, m), 6.96 (1H, d, J = 8.1 Hz), 6.02–6.13 (1H, m), 5.43 (1H, d, J = 17.0 Hz), 5.33 (1H, d, J = 10.5 Hz), 4.69 (2H, d, J = 5.2 Hz), 4.00 (3H, s).

5-Allyl-4-hydroxy-3-methoxybenzaldehyde (2)

4-Allyloxy-3-methoxybenzaldehyde (0.63 g) was heated under an

Can. J. Chem. Downloaded from www.nrcresearchpress.com by 123.30.183.119 on 09/08/12
For personal use only.



SCHEME 3

atmosphere of argon at 195–205°C in a Kugelrohr oven for 15 min. The resulting orange-brown liquid, which crystallized upon cooling, was chromatographed on silica gel. Elution with ethyl acetate – Skellysolve B (1:4) gave 5-allyl-4-hydroxy-3-methoxybenzaldehyde (0.50 g, 79%), which crystallized from Skellysolve B as needles, mp 81–82°C (lit. (3) mp 83–84°C); Ftir ($CHCl_3$ cast): 3185, 1670 cm^{-1}; ^1H nmr ($CDCl_3$) δ: 9.82 (1H, s), 7.31 (2H, br s), 6.29 (1H, s), 5.94–6.06 (1H, m), 5.13 (1H, ddd, J = 3.6, 1.5, 1.5 Hz), 5.09 (1H, br s), 3.96 (3H, s), 3.46 (2H, d, J = 6.8 Hz).

2,3-Dihydro-5-hydroxy-7-methoxy-2-benzofuranmethanol (6)

A solution of 5-allyl-4-hydroxy-3-methoxybenzaldehyde (**2**) (1.00 g, 5.21 mmol) and *m*-chloroperbenzoic acid (80–85% assay, 2.5 g, 11.6–12.3 mmol) was stirred in dichloromethane (100 mL) under argon for 18 h, then transferred to a separatory funnel and washed with a 1:1 mixture of 10% w/v sodium sulfite and saturated sodium hydrogen carbonate. Evaporation of the dried dichloromethane solution gave an oil, which was dissolved in methanol (10 mL) and added to a stirred suspension of potassium carbonate (2.0 g, 14.5 mmol) in methanol (90 mL). The brown mixture was stirred for 1 h, then concentrated at reduced pressure to approximately 20 mL and diluted with water (100 mL). The aqueous mixture was extracted with ethyl acetate (5 × 50 mL) and the combined extracts were dried and evaporated to a brown oil. Flash chromatography, eluting with ethyl acetate – Skellysolve B (2:1), gave the benzofuran **6** as a pale brown oil (0.724 g, 71%), which crystallized on standing. Recrystallization from ethyl acetate gave small prisms, mp 126–127°C; Ftir (KBr): 3362, 3139, 3134, 1626, 1613, 1499, 1201, 1146, 1094 cm^{-1}; ^1H nmr (CD_3OD) δ: 6.13 (2H, s, H4, H6), 4.59–4.69 (1H, m, H2), 3.64 (3H, s, OCH_3), 3.54 (2H, d, J = 4.5 Hz, CH_2OH), 3.01 (1H, dd, J = 15.5, 9.5 Hz, H3), 2.80 (1H, dd, J = 15.8, 7.7 Hz, H3); ^{13}C nmr (CD_3OD) δ: 153.0, 145.5, 142.3, 129.2, 104.7, 101.0, 84.7, 65.0, 56.5, 33.3; hreims (probe 120°C), m/z calcd. for $C_{10}H_{12}O_4$ (M^+): 196.0736; found: 196.0740 (100), 165 ($M^+ - CH_2OH$, 30), 153 (22), 152 (24).

Epoxidation of 5-allyl-4-hydroxy-3-methoxybenzaldehyde (2)

A solution of 5-allyl-4-hydroxy-3-methoxybenzaldehyde (1.00 g, 5.21 mmol) and *m*-chloroperbenzoic acid (80–85% assay, 2.6 g, 12.0–12.8 mmol) was stirred in dichloromethane (100 mL) under argon for 25 h, then transferred to a separatory funnel and washed with a 1:1 mixture of 10% w/v sodium sulfite and saturated sodium hydrogen carbonate. Evaporation of the dried dichloromethane solution gave an oil, which was quickly flash chromatographed. Elution with ethyl acetate – Skellysolve B (2:3) gave the crude epoxyformate **3** (0.918 g), which was used in the next step without further purification; Ftir ($CHCl_3$ cast): 3445, 1738, 1620, 1600, 1496, 1466, 1438, 1360, 1290, 1234, 1185, 1152, 1102 cm^{-1}; ^1H nmr ($CDCl_3$) δ: 8.23 (1H, s), 6.56 (2H, br s), 6.08 (1H, s), 3.80 (3H, s), 3.16–3.21 (1H, m), 2.89 (1H, dd, J = 14.0, 5.0 Hz), 2.83 (1H, dd, J = 14.1, 6.0 Hz), 2.75 (1H, dd, J = 4.5, 3.5 Hz), 2.56 (1H, dd, J = 5.0, 2.6 Hz); hreims (probe 120°C), m/z calcd. for $C_{11}H_{12}O_5$ (M^+): 224.0685; found: 224.0687 (100), 196 (29), 181 (19), 177 (17), 168 (22), 166 (19), 165 (19), 153 (31), 152 (28), 135 (17), 123 (20), 107 (15).

Thermal rearrangement of the epoxyformate 3

The crude epoxyformate **3** (0.918 g) was distilled in a Kugelrohr oven (155–160°C, 1.0 Torr) and the distillate chromatographed on silica gel. Elution with ethyl acetate – Skellysolve B (1:1) gave successively the bisformate **4** (49.7 mg, 4% from **2**), then the hydroxy formate **5** (0.547 g, 42% from **2**). Further elution with ethyl acetate – Skellysolve B (2:1) gave the phenolic alcohol **6** (0.172 g, 17% from **2**). The bisformate **4** was obtained as an oily solid; Ftir ($CHCl_3$ cast): 1750 (sh), 1728, 1627, 1600, 1496, 1466, 1322, 1201, 1153, 1104, 1086 cm^{-1}; ^1H nmr ($CDCl_3$) δ: 8.25 (1H, s, HCO_2), 8.09 (1H, s, HCO_2), 6.58 (1H, d, J = 1.8 Hz, H4 or H6), 6.51 (1H, d, J = 2.2 Hz, H4 or H6), 5.06–5.14 (1H, m, H2), 4.43 (1H, dd, J = 12.5, 3.6 Hz, CH_2O_2CH), 4.34 (1H, dd, J = 12.2, 6.3 Hz, CH_2O_2CH), 3.83 (3H, s, OCH_3), 3.34 (1H, dd, J = 15.8, 9.7 Hz, H3), 3.05 (1H, dd, J = 16.0, 8.0 Hz, H3); ^{13}C nmr ($CDCl_3$) δ: 160.6, 159.7, 145.6, 144.4, 143.9, 127.0, 109.6, 105.1, 80.6, 64.7, 56.1, 32.4; hreims (probe 120°C), m/z calcd. for $C_{12}H_{12}O_6$ (M^+): 252.0634; found: 252.0631 (100), 224 (67), 178 (48), 177 (36), 165 (28), 152 (17), 137 (15), 135 (28), 107 (15), 77 (16). The hydroxy formate **5** crystallized on standing as fine needles, mp 91–92°C; Ftir ($CHCl_3$ cast): 3335, 1703, 1692, 1630, 1613, 1496, 1220, 1201, 1146 cm^{-1}; ^1H nmr ($CDCl_3$) δ: 8.07 (1H, s, HCO_2), 6.30 (1H, d, J = 2.5 Hz, H4 or H6), 6.28 (1H, d, J = 2.5 Hz, H4 or H6). 5.52–5.63 (1H, m, OH), 4.97–5.05 (1H, m, H2), 4.38 (1H, dd, J = 12.2, 3.9 Hz, CH_2OH), 4.32 (1H, dd, J = 12.2, 6.2 Hz, CH_2OH), 3.78 (3H, s, OCH_3), 3.24 (1H, dd, J = 16.0, 9.6 Hz, H3),

Can. J. Chem. Downloaded from www.nrcresearchpress.com by 123.30.183.119 on 09/08/12
For personal use only.

Can. J. Chem. Downloaded from www.nrcresearchpress.com by 123.30.183.119 on 09/08/12
For personal use only.

2.72 (1H, dd, J = 15.8, 7.7 Hz, H3); ^{13}C nmr ($CDCl_3$) δ: 161.1, 150.8, 144.3, 141.0, 126.8, 103.4, 99.7, 79.8, 65.0, 55.8, 32.6; hreims (probe 100°C), m/z calcd. for $C_{11}H_{12}O_5$ (M^+): 224.0685; found: 224.0683 (100), 178 (47), 177 (33), 165 (21), 153 (12), 152 (12), 137 (14), 135 (27), 107 (14), 77 (13), 65 (12), 39 (19). The phenolic alcohol **6** crystallized from ethyl acetate as prisms, mp 126–127°C (correct ^{1}H nmr spectrum).

*2,3-Dihydro-5,7-dimethoxy-2-benzofuranmethanol (**10**)*

Iodomethane (1.5 mL, 24.1 mmol) was added to a suspension of the phenol **6** (0.50 g, 2.55 mmol) and potassium carbonate (4.0 g) in acetone (25 mL). The mixture was stirred at room temperature under argon for 3 h, then further iodomethane (0.5 mL) was added and stirring continued for a further 17 h. The mixture was diluted with water and extracted with dichloromethane (3 × 30 mL). Evaporation of the dried combined extracts and flash chromatography of the oily product, eluting with ethyl acetate – Skellysolve B (3:2), gave an oily forerun followed by the dimethyl ether **10** (0.511 g, 95%), which crystallized as an amorphous solid on standing, mp 66–68°C; Ftir ($CHCl_3$ cast): 3400, 1618, 1606, 1499, 1203, 1148 cm^{-1}; ^{1}H nmr ($CDCl_3$) δ: 6.35 (2H, br d, J = 2.0 Hz, H4, H6), 4.88–4.96 (1H, m, H2), 3.89 (1H, dd, J = 12.4, 3.1 Hz, CH_2OH), 3.84 (3H, s, OCH_3), 3.75 (3H, s, OCH_3), 3.73 (1H, dd, J = 12.3, 6.0 Hz, CH_2OH), 3.21 (1H, dd, J = 15.8, 9.6 Hz, H3), 3.08 (1H, dd, J = 15.5, 8.0 Hz, H3); ^{13}C nmr ($CDCl_3$) δ: 154.7, 144.2, 141.5, 127.5, 101.1, 98.9, 83.6, 64.3, 55.8, 55.7, 32.1; hreims (probe 110°C), m/z calcd. for $C_{11}H_{14}O_4$ (M^+): 210.0891; found: 210.0891 (100), 182 (16), 179 (25), 167 (27), 166 (21).

*2,3-Dihydro-5,7-dimethoxy-2-benzofurancarboxaldehyde (**11**)*

Dimethyl sulfoxide (0.20 mL, 2.82 mmol) was added dropwise to a stirred solution of oxalyl chloride (0.15 mL, 1.72 mmol) in dichloromethane (5 mL) at −78°C under argon. The solution was stirred at −78°C for 5 min, then a solution of the alcohol **10** (0.242 g, 115 mmol) in dichloromethane (2 mL) was added dropwise. The resulting slurry was stirred at −78°C for 30 min, then triethylamine (1.0 mL, 7.2 mmol) was added and the mixture stirred at 0°C for 10 min. The slurry was transferred to a separatory funnel using dichloromethane and washed successively with 0.5 M hydrochloric acid and brine. Evaporation of the dried extract and flash chromatography of the product, eluting with ethyl acetate – Skellysolve B (1:1), gave the aldehyde **11** as a pale yellow oil (0.225 g, 94%); Ftir ($CHCl_3$ cast): 3400, 1732 (w), 1622, 1610, 1499, 1201, 1148 cm^{-1}; ^{1}H nmr ($CDCl_3$) δ: 9.88 (1H, d, J = 1.2 Hz, CHO), 6.38 (1H, d, J = 2.6 Hz, H4 or H6), 6.35 (1H, d, J = 2.6 Hz, H4 or H6), 5.04 (1H, ddd, J = 10.8, 6.5, 1.2 Hz, H2), 3.88 (3H, s, OCH_3), 3.75 (3H, s, OCH_3), 3.44 (1H, dd, J = 16.0, 10.5 Hz, H3), 3.33 (1H, dd, J = 16.0, 6.5 Hz, H3); ^{13}C nmr ($CDCl_3$) δ: 201.6, 155.6, 144.6, 141.1, 125.8, 100.9, 99.6, 85.0, 55.9, 55.8, 32.3; hreims (probe 150°C), m/z calcd. for $C_{11}H_{12}O_4$ (M^+): 208.0736; found: 208.0731 (100), 180 (13), 179 (99), 151 (24), 121 (23), 77 (12), 51 (10).

2,3-Dihydro-5,7-dimethoxy-2-[1-(1,3-pentadienyl)]benzofuran

n-Butyllithium (0.46 mL of a 1.6 M solution in hexanes) was added to a suspension of crotyl triphenylphosphonium bromide (0.29 g, 0.74 mmol) in THF (10 mL) at 0°C to give an orange-red solution of the phosphonyl anion. The solution was cooled to −78°C and a solution of the aldehyde **11** (57.6 mg) in THF (1.2 mL) was added dropwise. The mixture was stirred at −78°C for 2 h, then warmed to room temperature and quenched with water. The solution was transferred to a separatory funnel and diluted with water, acidified with 1 M hydrochloric acid, and extracted with dichloromethane (3 × 25 mL). Evaporation of the dried combined extracts and flash chromatography of the product, eluting with ethyl acetate – Skellysolve B (1:10), gave an inseparable mixture of the isomeric dienes (60.8 mg, 89%), which crystallized on standing; ^{1}H nmr ($CDCl_3$, major diene) δ: 6.35 (2H, br s, H4, H6), 6.11 (1H, dd, J = 11.0, 11.0 Hz, H2′), 5.80 (1H, dq, J = 14.9, 6.9 Hz, H4′), 5.67–5.80 (1H, m, H3′), 5.67 (1H, br dd, J = 9.0, 9.0 Hz, H2), 5.54 (1H, br dd, J = 10.0, 10.0 Hz, H1′), 3.83 (3H, s, OCH_3), 3.74 (3H, s, OCH_3), 3.36 (1H, dd, J = 15.5, 8.9 Hz, H3), 2.98 (1H, dd, J = 15.2, 8.9 Hz, H3), 1.79 (3H, dd, J = 7.0, 1.4 Hz, H5′); ^{13}C nmr ($CDCl_3$, major diene) δ: 154.6, 144.3, 141.7, 132.3, 131.4, 127.6, 127.3, 126.2, 101.0, 99.1, 79.2, 55.7 (2), 37.0, 18.1; hreims (probe 100°C), m/z calcd. for $C_{15}H_{18}O_3$ (M^+): 246.1256; found: 246.1260 (100), 231 (15), 191 (32), 167 (30), 166 (33).

*Isomerization to 1′(E),3′(E)-2,3-dihydro-5,7-dimethoxy-2-[1-(1,3-pentadienyl)]benzofuran (**9**)*

A very small crystal of iodine (<1 mg) was dissolved in carbon tetrachloride (2 mL) and 0.1 mL of the iodine solution was added to a stirred solution of the isomeric dienes (50.0 mg) in carbon tetrachloride (5 mL). The solution was refluxed under argon for 18 h, then evaporated to dryness and the product flash chromatographed. Elution with ethyl acetate – Skellysolve B (1:10) gave the furan (1.5 mg) followed by a mixture of the isomeric dienes (48.0 mg), which consisted mainly (^{1}H nmr) of the desired (*E,E*) isomer. Recrystallization of the mixture of dienes from dichloromethane – Skellysolve B gave the pure (*E,E*)-diene **9** as flaky needles, mp 101–103.5°C; ^{1}H nmr ($CDCl_3$,(*E,E*)-diene) δ: 6.35 (2H, br s, H4, H6), 6.28 (1H, dd, J = 15.0, 10.2 Hz, H2′), 6.05 (1H, ddq, J = 15.0, 10.2, 1.5 Hz, H3′), 5.76 (1H, dq, J = 15.0, 7.0 Hz, H4′), 5.74 (1H, dd, J = 15.0, 7.5 Hz, H1′), 5.21 (1H, br ddd, J = 8.5, 8.5, 8.5 Hz, H2), 3.83 (3H, s, OCH_3), 3.74 (3H, s, OCH_3), 3.31 (1H, dd, J = 15.6, 9.2 Hz, H3), 2.99 (1H, dd, J = 15.4, 8.8 Hz, H3), 1.76 (3H, dd, J = 6.8, 1.5 Hz, H5′); ^{13}C nmr ($CDCl_3$) δ: 154.7, 144.4, 141.9, 132.9, 131.1, 130.5, 129.0, 127.7, 101.2, 99.2, 84.1, 55.97, 55.92, 37.2, 18.1. The furan **12** was obtained as a pale yellow solid; ^{1}H nmr ($CDCl_3$) δ: 6.96 (1H, dd, J = 15.5, 10.5 Hz, H2′), 6.54 (1H, d, J = 2.5 Hz, H4 or H6), 6.47 (1H, s, H3), 6.41 (1H, d, J = 2.5 Hz, H4 of H6), 6.27 (1H, br d, J = 16.0 Hz, H1′), 6.20 (1H, br ddq, J = 15.0, 10.5, 1.0 Hz, H3′), 5.92 (1H, dq, J = 15.0, 7.0 Hz, H4′), 3.98 (3H, s, OCH_3), 3.82 (3H, s, OCH_3), 1.83 (3H, dd, J = 7.0, 1.0 Hz, H5′); hreims (probe 140°C), m/z calcd. for $C_{15}H_{16}O_3$ (M^+): 244.1099; found: 244.1098 (100), 229 (54), 214 (10), 115 (15).

Methylation of natural (−) arthrographol

Iodomethane (30 μL) was added to a suspension of (−) arthrographol (2.5 mg) and potassium carbonate (0.10 g) in acetone (1 mL). The mixture was stirred at room temperature under argon for 36 h, then diluted with dichloromethane and washed with water. Evaporation of the dried dichloromethane solution gave an oil, which was filtered through a plug of silica gel using ethyl acetate – Skellysolve B (1:5). Removal of the solvents gave the dimethyl ether of (−) arthrographol (2.8 mg); ^{1}H nmr ($CDCl_3$) δ: 6.35 (2H, s, H4, H6), 6.29 (1H, dd, J = 15.1, 10.5 Hz, H2′), 6.06 (1H, ddq, J = 15.0, 10.5, 1.5 Hz, H3′), 5.76 (1H, dq, J = 15.0, 7.0 Hz, H4′), 5.74 (1H, dd, J = 15.0, 7.5 Hz, H1′), 5.21 (1H, ddd, J = 8.5, 8.5, 8.5 Hz, H2), 3.83 (3H, s, OCH_3), 3.74 (3H, s, OCH_3), 3.31 (1H, dd, J = 15.5, 9.0 Hz, H3), 2.99 (1H, dd, J = 15.5, 8.5 Hz, H3), 1.76 (3H, dd, J = 7.0, 1.0 Hz, H5′).

Hydrogenation of the dimethyl ether of (−) arthrographol

5% Palladium – charcoal (5 mg) was added to a solution of (−) arthrographol dimethyl ether (2.8 mg) in ethyl acetate (0.5 mL) and the mixture was stirred under an atmosphere of hydrogen for 2 h. The mixture was filtered and the catalyst washed with ethyl acetate. The filtrate was evaporated and the product filtered through a plug of silica gel using ethyl acetate – Skellysolve B (1:20) to give 2,3-dihydro-5,7-dimethoxy-2-pentylbenzofuran (**13**) (*tetrahydrodimethoxyarthrographol*) as an oil (1.9 mg); ^{1}H nmr ($CDCl_3$) δ: 6.36 (2H, s, H4, H6), 4.79 (1H, ddt, J = 9.0, 9.0, 6.8 Hz, H2), 3.84 (3H, s, OCH_3), 3.75 (3H, s, OCH_3), 3.23 (1H, dd, J = 15.5, 9.2 Hz, H3), 2.85 (1H, dd, J = 15.6, 8.8 Hz, H3), 1.25–2.00 (8H, m), 0.89 (3H, t, J = 6.5 Hz, H5′); hreims (probe 140°C), m/z calcd. for $C_{15}H_{22}O_3$ (M^+): 250.1568; found: 250.1565 (100), 168 (24), 167 (46), 166 (20), 161 (14).

Hydrogenation of the mixture of synthetic dimethoxy dienes

Hydrogenation of a mixture of the dienes (5.2 mg) obtained from the Wittig reaction of the aldehyde and crotyl triphenylphosphonium bromide as for hydrogenation of the dimethyl ether of (−) arthrographol

Can. J. Chem. Downloaded from www.nrcresearchpress.com by 123.30.183.119 on 09/08/12
For personal use only.

(see above) gave (+/−) tetrahydrodimethoxyarthrographol (**13**) (4.5 mg) (^{1}H nmr ($CDCl_3$) identical with that above).

*2,3-Dihydro-5-hydroxy-2-iodomethyl-7-methoxybenzofuran (**15**)*

Iodine (56 mg, 0.221 mmol) was added in one portion to a suspension of triphenylphosphine (75 mg, 0.286 mmol) and imidazole (20 mg, 0.294 mmol) in acetonitrile (0.7 mL). The resulting yellow solution was stirred under argon at 10°C for 15 min, then benzene (2 mL) was added to give a pale yellow suspension to which was added a solution of the alcohol **6** (20 mg, 0.111 mmol) in acetonitrile (0.3 mL). The mixture was stirred under argon at room temperature for 21 h (tlc indicated the reaction was almost complete after 2 h). The mixture was diluted with dichloromethane and washed successively with 1 M sodium sulfite and brine. Evaporation of the dried solution gave an oil, which was flash chromatographed, eluting with ethyl acetate – Skellysolve B (1:3) to give the iodide **15** (29.6 mg, 87%), which crystallized on standing. Recrystallization from ethyl acetate – Skellysolve B – dichloromethane gave fine needles, mp 146.5–147.5°C; Ftir ($CHCl_3$ cast): 3350, 1622, 1605, 1510, 1492, 1467, 1451, 1435, 1335, 1195, 1140, 1087 cm^{-1}; ^{1}H nmr ($CDCl_3$) δ: 6.30 (1H, d, J = 2.2 Hz, H4 or H6), 6.28 (1H, d, J = 2.2 Hz, H4 or H6), 4.88 (1H, dddd, J = 10, 9, 7, 4 Hz, H2), 4.53 (1H, s, OH), 3.83 (3H, s, OCH_3), 3.49 (1H, dd, J = 10.0, 4.0 Hz, CH_2I), 3.36 (1H, dd, J = 16.1, 9.0 Hz, H3), 3.33 (1H, dd, J = 10.0, 10.0 Hz, CH_2I), 3.04 (1H, dd, J = 16.1, 7.0 Hz, H3); ^{13}C nmr ($CDCl_3$) δ: 150.5, 144.4, 141.7, 127.0, 103.5, 99.8, 82.1, 56.0, 36.9, 8.8; hreims (probe 120°C), m/z calcd. for $C_{10}H_{12}O_3I$ ($M^+ + H^+$): 306.9831; found: 306.9819 (15); m/z calcd. for $C_{10}H_{11}O_3$ ($M^+ - I$): 179.0708; found: 179.0708 (100), 147 (32), 127 (HI, 4), 126 (I, 4), 119 (30), 91 (19); cims: 324 ($M^+ + NH_4^+$, 100).

*2,3-Dihydro-2-bromomethyl-5-hydroxy-7-methoxybenzofuran (**16**)*

A solution of triphenylphosphine (0.267 g, 1.02 mmol) in THF (2 mL) was added dropwise to a stirred solution of *N*-bromosuccinimide (0.182 g, 1.02 mmol) in THF (10 mL) under argon to give a sticky precipitate. After 5 min a solution of the alcohol **6** (100 mg, 0.51 mmol) in THF (3 mL) was added and the resulting pale orange mixture was stirred for 26 h. The mixture was diluted with dichloromethane and washed with 1 M sodium sulfite. Evaporation of the dried solution and flash chromatography of the resulting red-brown oil, eluting with ethyl acetate – Skellysolve B (1:2), gave the bromide **16** (40.6 mg, 30.7%). Further elution with ethyl acetate – Skellysolve B (2:1) gave unreacted alcohol **6** (68.8 mg, 68.8%). The bromide crystallized from ethyl acetate as prisms, mp 126–127°C; Ftir ($CHCl_3$ cast): 3400, 1628, 1609, 1494, 1458, 1341, 1185, 1140, 1088, 948, 840 cm^{-1}; ^{1}H nmr ($CDCl_3$) δ: 6.30 (2H, br s, H4, H6), 5.07 (1H, br s, OH), 4.98 (1H, m, H2), 3.81 (3H, s, OCH_3), 3.62 (1H, dd, J = 10.4, 4.5 Hz, CH_2Br), 3.47 (1H, dd, J = 10.5, 7.6 Hz, CH_2Br), 3.31 (1H, dd, J = 15.8, 9.2 Hz, H3), 3.09 (1H, dd, J = 15.9, 7.2 Hz, H3); hreims (probe 120°C), m/z calcd. for $C_{10}H_{11}O_3{}^{81}Br$ (M^+): 259.9872; found: 259.9873 (75.2); m/z calcd. for $C_{10}H_{11}O_3{}^{79}Br$ (M^+): 257.9892; found: 257.9894 (73.2), 180 (13), 179 (M^+ − Br, 100), 151 (15), 149 (17), 147 (43), 119 (35), 91 (21), 77 (14), 65 (17), 53 (11), 51 (11).

*2,3-Dihydro-2-chloromethyl-5-hydroxy-7-methoxybenzofuran (**17**)*

A solution of triphenylphosphine (0.67 g, 2.56 mmol) in THF (4 mL) was added to a stirred solution of *N*-chlorosuccinimide (0.34 g, 2.55 mmol) in THF (10 mL) at room temperature under argon. The thick cream-colored suspension was stirred for 5 min, then a solution of the alcohol **6** (0.245 g, 1.25 mmol) in THF (6 mL) was added dropwise. The suspension was stirred for 7.5 h, then poured into water and extracted with dichloromethane (3×) (a small amount of 1 M hydrochloric acid (approx. 0.5 mL) was added to disperse an emulsion that formed upon shaking). Evaporation of the dried combined extracts gave an oil, which was flash chromatographed. Elution with ethyl acetate – Skellysolve B (1:2) gave unreacted triphenylphosphine, and further elution with ethyl acetate – Skellysolve B (1:1) gave the chloride **17** (0.265 g, 99%), which crystallized on standing. Recrystallization from ethyl acetate – Skellysolve B gave needles, mp 112.5–113°C; Ftir ($CHCl_3$ cast): 3360, 1628, 1610, 1495, 1457, 1342, 1196, 1140, 1090 cm^{-1}; ^{1}H nmr ($CDCl_3$) δ: 6.30 (2H, m, H4, H6), 5.01 (1H, m, H2), 3.83 (3H, s, OCH_3), 3.78 (1H, dd, J = 11.1, 5.0 Hz, CH_2Cl), 3.65 (1H, dd, J = 11.1, 6.9 Hz, CH_2Cl), 3.32 (1H, dd, J = 15.9, 9.1 Hz, H3), 3.12 (1H, dd, J = 16.1, 6.9 Hz, H3); ^{13}C nmr ($CDCl_3$) δ: 150.6, 144.3, 141.4, 126.9, 103.5, 99.8, 81.7, 55.9, 45.7, 34.2; hreims (probe 120°C), m/z calcd. for $C_{10}H_{11}O_3Cl$ (M^+): 214.0397; found: 214.0398 (100), 216/214 (100:32), 179 (16), 165 (33), 147 (53).

*2,3-Dihydro-2-chloromethyl-5,7-dihydroxybenzofuran (**20**)*

Boron tribromide (2.94 mL of a 1.0 M solution in dichloromethane) was added to a stirred solution of the chloride **17** (0.315 g, 1.47 mmol) in dichloromethane (30 mL) and the initially blue solution stirred under argon at room temperature for 6 h. The solution was poured into ethyl acetate (100 mL) and the organic layer washed successively with water, saturated sodium hydrogen carbonate, and brine. Evaporation of the dried solution and flash chromatography of the resultant brown oil, eluting with ethyl acetate – Skellysolve B (2:3), gave the resorcinol **20** (0.293 g, 99%), which crystallized on standing. Recrystallization of a portion of this material from dichloromethane gave fine needles, mp 117–118°C; Ftir (KBr): 3526, 3382, 1634, 1618, 1505, 1485, 1187, 1127, 854 cm^{-1}; ^{1}H nmr ($CDCl_3/CD_3OD$) δ: 6.25 (2H, br d, J = 2.0 Hz, H4, H6), 4.90 (1H, m, H2), 3.67 (1H, dd, J = 11.7, 6.2 Hz, CH_2Cl), 3.58 (1H, dd, J = 11.7, 6.2 Hz, CH_2Cl), 3.23 (1H, dd, J = 16.2, 9.0 Hz, H3), 2.96 (1H, dd, J = 16.2, 6.5 Hz, H3); ^{13}C nmr ($CDCl_3$) δ: 150.9, 140.2, 139.6, 127.0, 103.2, 102.8, 81.7, 45.9, 34.1; hreims (probe 150°C), m/z calcd. for $C_9H_9O_3Cl$ (M^+): 200.0240; found: 200.0242 (100), 202/200 (100:32), 165 (20), 163 (20), 151 (25), 147 (36), 138 (59), 123 (22), 19 (21).

*Bis(methoxymethyl) ether of 2,3-dihydro-2-chloromethyl-5,7-dihydroxybenzofuran (**21**)*

Methoxymethyl chloride (0.28 mL, 3.50 mmol) was added to a stirred solution of the resorcinol **20** (0.172 g, 0.86 mmol) and di-(isopropyl)ethylamine (0.61 mL, 3.50 mmol) in dichloromethane (15 mL). The solution was stirred at room temperature under argon for 22 h, then transferred to a separatory funnel and washed successively with 0.01 M hydrochloric acid and saturated sodium hydrogen carbonate. Evaporation of the dried dichloromethane solution and flash chromatography, eluting with ethyl acetate – Skellysolve B (1:3), gave the bis(methoxymethyl) ether **21** as a clear oil (0.184 g, 74%); Ftir ($CHCl_3$ cast): 1621, 1607, 1488, 1152, 1135, 1061, 1018 cm^{-1}; ^{1}H nmr ($CDCl_3$) δ: 6.71 (1H, d, J = 2.6 Hz, H6), 6.61 (1H, ddd, J = 2.4, 1.0, 1.0 Hz, H4), 5.20 (2H, s, OCH_2O), 5.08 (2H, s, OCH_2O), 5.02 (1H, dddd, J = 9.4, 6.8, 6.3, 4.5 Hz, H2), 3.78 (1H, dd, J = 11.5, 4.5 Hz, CH_2Cl), 3.66 (1H, dd, J = 11.5, 6.3 Hz, CH_2Cl), 3.50 (3H, s, OCH_3), 3.49 (3H, s, OCH_3), 3.36 (1H, br dd, J = 15.5, 9.4 Hz, H3), 3.16 (1H, br dd, J = 15.5, 6.8 Hz, H3); ^{13}C nmr ($CDCl_3$) δ: 152.3, 143.4, 141.3, 127.3, 106.7, 105.8, 95.5, 95.4, 81.9, 56.3, 55.9, 45.7, 34.2; hreims (probe 150°C), m/z calcd. for $C_{13}H_{17}O_5Cl$ (M^+): 288.0765; found: 288.0765 (24), 290/288 (24:8), 45 (100). Further elution gave a mono-(methoxymethyl) ether of the resorcinol (25 mg, 12%); ^{1}H nmr ($CDCl_3$) δ: 6.53 (1H, d, J = 2.2 Hz), 6.37 (1H, ddd, J = 2.2, 1.0, 1.0 Hz), 5.19 (2H, s), 4.95 (1H, dddd, J = 9.1, 7.0, 7.0, 4.5 Hz), 4.61 (1H, s), 3.77 (1H, dd, J = 11.5, 5.0 Hz), 3.66 (1H, dd, J = 11.2, 6.9 Hz), 3.50 (3H, s), 3.33 (1H, br dd, J = 16.0, 9.1 Hz), 3.14 (1H, dd, J = 16.0, 7.0 Hz).

Alkylation of the bis(methoxymethyl) ether of 2,3-dihydro-2-chloromethyl-5,7-dihydroxybenzofuran

n-Butyllithium (0.40 mL of a 1.6 M solution in hexanes) was added to a stirred solution of diisopropylamine (90 μL, 0.643 mmol) in THF (6 mL) at 0°C under argon. The solution of lithium diisopropyl amide was cooled to −78°C and crotyl phenyl sulfide (10) (107 μL, 0.652 mmol) was added. The yellow solution was stirred at −78°C for 25 min, then a solution of sodium iodide (20 mg, 0.133 mmol) and the bis(methoxymethyl) ether **21** (46 mg, 0.16 mmol) in THF (1 mL) and DMPU (0.5 mL) was added slowly via a cannula. The flask containing the bis(methoxymethyl) ether and sodium iodide was rinsed into the reaction vessel using further THF (0.5 mL) and the resulting orange

Can. J. Chem. Downloaded from www.nrcresearchpress.com by 123.30.183.119 on 09/08/12
For personal use only.

solution was stirred at −78°C for 1.5 h. The solution was then brought to 0°C, quenched with water, diluted with ethyl acetate, and washed successively with 0.05 M hydrochloric acid, water, and saturated sodium hydrogen carbonate. Evaporation of the dried solution and flash chromatography of the product, eluting with ethyl acetate – Skellysolve B (1:5), gave successively unreacted crotyl phenyl sulfide, the bis(methoxymethyl) ether of 2,3-dihydro-5,7-dihydroxy-2-[1-(2-phenylthio-3-pentenyl)]benzofuran **22** (52.1 mg, 95% based on recovered **21**), and unreacted bis(methoxymethyl) ether **21** (8.3 mg).

The alkylation product **22** was obtained as an oil; ^{1}H nmr ($CDCl_3$) δ: 7.36–7.43 (2H, m, PhS), 7.18–7.33 (3H, m, PhS), 6.68 (1H, d, J = 2.3 Hz, H6), 6.58 (1H, dd, J = 2.5, 1.3 Hz, H4), 5.26–5.51 (2H, m, H3′, H4′), 5.19, 5.202, 5.205 (2H, 3 s, OCH_2O), 5.06 (2H, s, OCH_2O), 4.81–5.04 (1H, m, H2), 3.90 (<1H, ddd, J = 9.5, 8.7, 5.0 Hz, H2′), 3.74 (<1H, dd, J = 15.0, 7.5 Hz, H2′), 3.47, 3.49, 3.51 (6H, 3 s, OCH_3), 3.25, 3.26 (1H, 2 br dd, J = 15.5, 9.0 Hz, H3), 2.82, 2.83 (1H, 2 dd, J = 15.5, 8.0 Hz, H3), 2.18–2.32 (1H, m, H1′), 1.94 (<1H, ddd, J = 13.8, 6.9, 6.9 Hz, H1′), 1.84 (<1H, ddd, J = 14.5, 9.8, 4.7 Hz, H1′), 1.72 (<1H, br dd, J = 5.0, 5.0 Hz, H1′), 1.59, 1.62 (3H, 2 dd, J = 6.4, 1.0 Hz, H5′); hreims (probe 150°C), m/z calcd. for $C_{23}H_{28}O_5S$ (M^+): 416.1658; found: 416.1658 (36), 306 (M^+ − PhSH, 2), 262 (7), 239 (36), 45 (100).

*2,3-Dihydro-5,7-bis[(methoxy)methyleneoxy]-2-[1-(1,3-pentadienyl)]benzofuran (**24**) ((+/−)Bismethoxymethylarthrographol)*

A solution of *m*-chloroperbenzoic acid (27 mg, 0.133 mmol) in dichloromethane (1.5 mL) was added to a solution of the sulfide **22** (52.1 mg, 0.125 mmol) in dichloromethane (5 mL) and the reaction mixture stirred at 0°C for 2.5 h. The solution was then diluted with ethyl acetate, washed with saturated sodium hydrogen carbonate, and evaporated to give an oil. Flash chromatography, eluting with ethyl acetate – Skellysolve B (1:1), gave the sulfoxide **23** (45.2 mg), which was used in the next step without further purification; hreims (probe 150°C), m/z calcd. for $C_{17}H_{24}O_6$ (M^+ − C_6H_5S): 324.1573; found: 324.1575 (3), 306 (M^+ − PhSOH, 21), 126 (PhSOH, 10), 125 (10), 78 (17), 45 (100). A solution of the sulfoxide **23** (45.2 mg, 0.104 mmol) and triethylamine (0.15 mL, 1.08 mmol) in benzene (5 mL) was stirred and refluxed under argon for 27 h. Removal of solvents and chromatography of the resulting pale brown oil, eluting with ethyl acetate – Skellysolve B (1:5), gave the diene **24** as a clear oil (17.8 mg, 46% from the sulfide **22**); ^{1}H nmr ($CDCl_3$, major diene) δ: 6.70 (1H, br d, J = 2.5 Hz), 6.60 (1H, br s), 6.28 (1H, dd, J = 15.0, 10.5 Hz, H2′), 6.05 (1H, br ddq, J = 15.0, 10.5, 1.5 Hz, H3′) 5.75 (1H, dq, J = 15.0, 7.0 Hz, H4′), 5.72 (1H, dd, J = 15.3, 7.5 Hz, H1′), 5.23 (1H, ddd, J = 8.2, 8.2, 8.2 Hz, H2), 5.19 (2H, s, OCH_2O), 5.07 (2H, s, OCH_2O), 3.47 (3H, s, OCH_3), 3.45 (3H, s, OCH_3), 3.31 (1H, dd, J = 15.5, 9.5 Hz, H3), 2.98 (1H, dd, J = 15.5, 8.6 Hz, H3), 1.76 (3H, br d, J = 7.0 Hz, H5′); ^{13}C nmr ($CDCl_3$, major diene) δ: 151.9, 143.7, 141.2, 133.0, 131.2, 130.5, 128.8, 106.7, 105.8, 95.6, 95.4, 84.3, 56.2, 55.9, 37.0, 18.1 (1 signal obscured); hreims (probe 150°C), m/z calcd. for $C_{17}H_{22}O_5$ (M^+): 306.1467; found: 306.1474 (24), 229 (11), 207 (8), 45 (100).

*Bis(ethoxyethyl) ether of 2,3-dihydro-2-chloromethyl-6,8-dihydroxybenzofuran (**25**)*

A solution of ethyl vinyl ether (0.25 mL, 2.6 mmol), the resorcinol **20** (50 mg, 0.25 mmol), and a small crystal of pyridinium *p*-toluenesulfonate in dichloromethane (5 mL) was stirred under argon for 20 h, then filtered through a short (2 cm) plug of silica gel, eluting with ethyl acetate – Skellysolve B (1:5, 100 mL). Removal of solvents gave the bis(ethoxyethyl) ether of 2,3-dihydro-2-chloromethyl-6,8-dihydroxybenzofuran (**25**) (86 mg, 99%) as a clear oil; Ftir ($CHCl_3$ cast): 1607, 1482, 1382, 1192, 1152, 1135, 1110, 1076, 1052 cm^{-1}; ^{1}H nmr ($CDCl_3$) δ: 6.64, 6.62 (1H, 2 m), 6.55 (1H, m), 5.40, 5.39 (1H, 2 overlapping q, J = 5.5 Hz, $OCH(CH_3)OCH_2CH_3$), 5.29 (1H, q, J = 5.4 Hz, $OCH(CH_3)OCH_2CH_3$), 4.98 (1H, m, H2), 3.94–3.74 and 3.72–3.52 (6H, 2 m, CH_2Cl, and OCH_2CH_3), 3.34 (1H, br dd, J = 16.0, 9.0 Hz, H3), 3.12 (1H, ddd, J = 16.0, 6.6, 2.9 Hz, H3), 1.48, 1.47 (3H, 2 d, J = 5.3 Hz, $OCH(CH_3)OCH_2CH_3$), 1.43 (3H, d, J = 5.3 Hz, $OCH(CH_3)CH_2CH_3$), 1.21, 1.20, 1.19 (6H, 3 t, J = 7.0 Hz, OCH_2CH_3); hreims (probe 150°C), m/z calcd. for $C_{17}H_{25}O_5Cl$ (M^+): 344.1390; found: 344.1390 (3), 299 (3), 272 (4), 227 (5), 202 (33), 201 (11), 200 (100), 73 (39).

Alkylation of the bis(ethoxyethyl) ether of 2,3-dihydro-2-chloromethyl-5,7-dihydroxybenzofuran

n-Butyllithium (0.54 mL of a 1.12 M solution in hexanes, 0.605 mmol) was added to a stirred solution of diisopropylamine (85 μL, 0.608 mmol) in THF (6 mL) at 0°C under argon. The solution of lithium diisopropyl amide was cooled to −78°C and crotyl phenyl sulfide (95 μL, 0.579 mmol) was added dropwise. The yellow solution was stirred at −78°C for 35 min, then a solution of sodium iodide (90 mg, 0.60 mmol) and the bis(ethoxyethyl) ether **25** (100 mg, 0.291 mmol) in THF (1 mL) and DMPU (1.0 mL) was added slowly via a cannula. The flask containing the bis(ethoxyethyl) ether and sodium iodide was rinsed into the reaction vessel using further THF (0.5 mL) and the resulting orange solution was stirred at −78°C for 35 min. The solution was then brought to 0°C, quenched with water (1 mL), diluted with ethyl acetate, and washed successively with 0.05 M hydrochloric acid, water, and saturated sodium hydrogen carbonate. Evaporation of the dried solution and flash chromatography of the product, eluting with ethyl acetate – Skellysolve B (1:10), gave unreacted crotyl phenyl sulfide, followed by the bis(ethoxyethyl) ether of 2,3-dihydro-5,7-dihydroxy-2-[1-(2-phenylthio-3-pentenyl)]benzofuran (**26**) (97.6 mg, 71%); ^{1}H nmr ($CDCl_3$) δ: 7.15–7.50 (5H, m, PhS), 6.57–6.65 (1H, m), 6.54 (1H, br s), 5.26–5.51 (2–3H, m), 5.19 (1H, q, J = 5.5 Hz), 4.97–5.10 (<1H, m), 4.76–4.92 (<1H, m), 3.71–3.97 (2H, m), 3.50–3.64 (2H, m), 3.20–3.32 (1H, m), 2.76–2.90 (1H, m), 2.14–2.30 (1H, m), 1.77–2.05 (1H, m), 1.63 (<3H, br d, J = 6.3 Hz), 1.58 (<3H, br d, J = 6.5 Hz), 1.47–1.51 (6H, m), 1.43 d, J = 5.5 Hz), 1.21 (6H, br t, J = 7.5 Hz); hreims (probe 160°C), m/z calcd. for $C_{27}H_{36}O_5S$ (M^+): 472.2284; found: 472.2274 (6), 329 (14), 328 (65), 219 (37), 218 (100), 189 (14), 163 (30), 151 (89), 150 (19), 139 (21), 110 (11), 73 (51), 45 (92), 44 (14), 43 (15).

1′(E),3′(E)-2,3-Dihydro-5,7-dihydroxy-2-[1-(1,3-pentadienyl)] benzofuran ((+/−) arthrographol)

A solution of *m*-chloroperbenzoic acid (63 mg, 95% assay, 0.346 mmol) in dichloromethane (4 mL) was added to a solution of the sulfide **26** (150 mg, 0.318 mmol) in dichloromethane (10 mL) and the reaction mixture stirred at 0°C under argon for 30 min. The solution was then diluted with further dichloromethane and washed with saturated sodium hydrogen carbonate. Evaporation of the dried solution gave the crude sulfoxide **27** (153.6 mg), which was used immediately without further purification. A solution of the crude sulfoxide **27** and triethylamine (0.50 mL, 3.59 mmol) in benzene (10 mL) was stirred and refluxed under argon for 4 h, then allowed to stand at room temperature overnight. The mixture was diluted with ethyl acetate and washed successively with 1 M hydrochloric acid, water, and saturated sodium hydrogen carbonate. Evaporation of the dried solution gave an oil, which was chromatographed, eluting with ethyl acetate – Skellysolve B (1:5), to afford a mixture of the bis(ethoxyethyl) ethers of 2,3-dihydro-5,7-dihydroxy-2-[1-(1,3-pentadienyl)]benzofuran (**28**) as an oil; hreims (probe 120°C), m/z calcd. for $C_{21}H_{30}O_5$ (M^+): 362.2093; found: 362.2116 (4), 219 (15), 218 (100), 163 (11), 138 (20), 73 (37), 45 (71). The mixture of bis-(ethoxyethyl) ethers **28** was stirred in a solution of acetic acid – methanol–water (1:50:50, 10 mL) for 1 h, then poured into saturated sodium hydrogen carbonate. The aqueous mixture was extracted (3×) with ethyl acetate and the combined extracts were dried and evaporated to an oil, which was flash chromatographed. Elution with ethyl acetate – Skellysolve B (1:3) gave an oily forerun that was discarded, followed by (+/−) arthrographol (22.2 mg, 32% from the sulfide **26**), which was contaminated with minor amounts of other diene isomers. The impure (+/−) arthrographol was recrystallized from ethyl acetate – Skellysolve B – dichloromethane to give pure (+/−) arthrographol (**1**) as needles (13.2 mg), mp 124–126°C (lit. (2) mp of (−)-**1**, 122°C); Ftir (KBr): 3440, 3420, 1660, 1641, 1615, 1503, 1489, 1471, 1163, 1130, 1047, 991, 850, 838, 810 cm^{-1}; ^{1}H nmr ($CDCl_3$) δ: 6.30 (1H, dd, J = 15.5, 10.5 Hz, H2′), 6.27 (1H, d, J = 2.5 Hz, H6), 6.25 (1H,

distorted dd, J = 2.0, 1.0 Hz, H4), 6.08 (1H, ddq, J = 15.0, 10.5, 1.5 Hz, H3′), 5.79 (1H, dq, J = 15.1, 7.0 Hz, H4′), 5.72 (1H, dd, J = 15.0, 7.8 Hz, H1′), 5.20 (1H, ddd, J = 8.3, 8.3, 8.3 Hz, H2), 4.90 (1H, s, OH), 4.43 (1H, s, OH), 3.30 (1H, dd, J = 15.5, 8.8 Hz, H3), 2.98 (1H, br dd, J = 15.5, 8.5 Hz, H3), 1.77 (3H, dd, J = 7.0, 1.5 Hz, H5′); hreims (probe 120°C), m/z calcd. for $C_{13}H_{14}O_3$ (M^+): 218.0943; found: 218.0941 (100), 203 (17), 185 (11), 164 (11), 163 (65), 139 (30), 138 (57), 91 (12), 80 (11), 79 (16), 77 (16), 65 (10), 41 (12), 39 (16).

Further elution of the column with ethyl acetate – Skellysolve B (1:1) gave the cyclopropane **29** as an oil (9.3 mg, 18%); ^{1}H nmr ($CDCl_3$–CD_3OD) δ: 6.34 (1H, d, J = 2.5 Hz, H4 or H6), 6.13 (1H, d, J = 2.5 Hz, H4 or H6), 4.71 (1H, ddd, J = 5.5, 5.5, 2.0 Hz, H2), 2.47 (1H, ddd, J = 9.0, 5.5, 4.0 Hz, H3), 0.89 (1H, ddd, J = 9.0, 5.5, 5.5 Hz, CH_2), 0.28 (1H, ddd, J = 5.5, 4.2, 2.0 Hz, CH_2); hreims (probe 80°C), m/z calcd. for $C_9H_8O_3$ (M^+): 164.0474; found: 164.0463 (100), 165 (67), 163 (47), 136 (10), 121 (10), 108 (10), 93 (10), 80 (14), 79 (13), 78 (10), 77 (15), 67 (13), 65 (11), 43 (15), 39 (13).

Acknowledgements

The financial support of the Natural Sciences and Engineering Research Council of Canada is gratefully acknowledged.

1. L. Sigler, Y. Yamaoka, and Y. Hiratsuka. Can. J. Microbiol. **36**, 77 (1990).
2. W. A. Ayer and K. Nozawa. Can. J. Microbiol. **36**, 83 (1990).
3. S. K. P. Sinha and D. N. Chaudhury. J. Indian Chem. Soc. **46**, 31 (1969).
4. W. F. Hoffman, O. W. Woltersdorf, F. C. Novello, E. J. Cragoe, J. P. Springer, L. H. Watson, and G. M. Fanelli. J. Med. Chem. **24**, 865 (1981).
5. S. L. Hwang, A. J. Mancuso, and D. J. Swern. J. Org. Chem. **63**, 2480 (1978).
6. T. R. Kelly, S. H. Bell, N. Ohashi, and R. J. Armstrong-Chong. J. Am. Chem. Soc. **110**, 6471 (1988).
7. G. A. Olah, S. C. Narang, B. G. B. Gupta, and R. Malhotra. J. Org. Chem. **44**, 1247 (1979).
8. J. F. W. McOmie and D. E. West. Org. Synth. Coll. Vol. V, 412 (1973).
9. R. E. Ireland and D. M. Walba. Org. Synth. **56**, 44 (1977).
10. J. H. Babler and R. A. Haack. J. Org. Chem. **47**, 4801 (1982).
11. K. C. Nicolaou, M. E. Duggan, and C.-K. Hwang, J. Am. Chem. Soc. **111**, 6676 (1989).
12. A. K. Bose and B. Lal. Tetrahedron Lett. 3937 (1973).
13. R. G. Weiss and E. I. Snyder. J. Org. Chem. **36**, 403 (1971).
14. J. P. Yardley and H. Fletcher. Synthesis, 244 (1976).
15. T. Mukhopadhyay and D. Seebach. Helv. Chim. Acta, **65**, 385 (1982).
16. W. A. Ayer, P. A. Craw, T. J. Stout, and J. Clardy. Can. J. Chem. **67**, 773 (1989).
17. L. F. Fieser and M. Fieser. Reagents for organic synthesis. John Wiley and Sons, Inc. NY. 1967. p. 135.
18. F. Bohlmann and H.-J. Mannhardt. Chem. Ber. **89**, 1307 (1956).

Can. J. Chem. Downloaded from www.nrcresearchpress.com by 123.30.183.119 on 09/08/12
For personal use only.

The proton affinities and deprotonation enthalpies of β-D-fructopyranose and α-L-sorbopyranose

ROBERT J. WOODS, WALTER A. SZAREK,[1] AND VEDENE H. SMITH, JR.[1]
Department of Chemistry, Queen's University, Kingston, Ont., Canada K7L 3N6

Received June 4, 1990[2]

This paper is dedicated to Professor Ross Stewart on the occasion of his 65th birthday

ROBERT J. WOODS, WALTER A. SZAREK, and VEDENE H. SMITH, JR. Can. J. Chem. **69**, 1917 (1991).

The proton affinities (PAs) and deprotonation enthalpies (DPEs) were calculated for the pyranoid forms of two naturally occurring sugars, D-fructose and L-sorbose. In both molecules the PAs of the primary hydroxyl group (HO-1), the anomeric hydroxyl group (HO-2), and the ring-oxygen atom (O-6) were calculated, as were the DPEs of HO-1 and HO-2. The stabilities of the conjugate acids and bases of these sugars are enhanced by the presence of intramolecular hydrogen bonding, a feature that is significant in explaining the differences in sweetness and the rates of mutarotation of the title compounds, as well as the differences in the rates of acid-catalyzed hydrolysis of ketopyranosides.

Key words: proton affinity, deprotonation enthalpy, *ab initio* calculations, AM1, hexuloses.

ROBERT J. WOODS, WALTER A. SZAREK et VEDENE H. SMITH, JR. Can. J. Chem. **69**, 1917 (1991).

On a calculé les affinité protoniques (AP) et les enthalpies de déprotonation (EDP) des formes pyranoïdes de deux sucres naturels, le D-fructose et le L-sorbose. Dans les deux molécules, on a calculé les AP du groupe hydroxyle primaire (OH-1), du groupe hydroxyle anomérique (OH-2) et de l'atome d'oxygène du cycle (O-6) ainsi que les EDP du HO-1 et du HO-2. Les stabilités des acides et des bases conjugués de ces sucres sont augmentées par la présence d'une liaison hydrogène intramoléculaire, une caractéristique qui est importante pour expliquer les différences dans la douceur et les vitesses de mutarotation des composés mentionnés dans le titre ainsi que dans les vitesses d'hydrolyses acido-catalysées des cétopyranosides.

Mots clés : affinité protonique, enthalpie de déprotonation, calculs *ab initio*, AM1, hexyloses.

[Traduit par la rédaction]

Introduction

The most direct computational approach to the measurement of atomic and molecular acidities and basicities is through evaluation of the deprotonation enthalpies (DPEs) and proton affinities (PAs) of the acids and bases, respectively. *Ab initio* computational methods are well suited for the evaluation of the PAs and DPEs of small molecules, and have been employed extensively for such calculations (1). Del Bene (2) has reported the effects of basis set choice and electron correlation on *ab initio* calculations of the PAs of several oxygen and nitrogen bases, consisting of compounds containing no more than two non-hydrogen atoms. The most accurate results reported by her were within 1–3 kcal/mol of the experimental values, and were obtained from calculations employing a triple-split valence basis set (6-311G) with two sets of polarization functions and one set of diffuse functions on all non-hydrogen atoms, and one set of polarization functions on the hydrogen atoms. It should be noted that it has been recently reported (3) that the 6-311G basis set is actually of valence double-zeta (ζ) quality. Corrections for electron correlation and zero-point vibrational energy were included by Del Bene (2), and the calculations were performed on geometries optimized with a 6-31G* basis set. It has been reported that the inclusion of electron correlation may lead to an incorrect prediction of the sign of the correlation contribution (4), unless a sufficiently large basis set is employed. Calculations performed without diffuse functions, such as at the 6-31G* level, have been shown to predict proton affinities less accurately by 1–3 kcal/mol (2). As might be expected, smaller basis sets do not predict absolute PAs satisfactorily; however, estimates of relative PAs may be made with some success, even with minimal STO-3G level calculations (5).

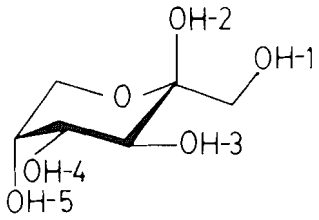
The calculation of accurate DPEs is somewhat more challenging, as it is necessary to allow the extra electrons, associated with the deprotonated species, to be distributed farther from the nuclei than are the electrons in the neutral species. Consequently, it has been reported that the use of basis sets incorporating diffuse functions is required (5).

Unfortunately, in calculations of the energies of larger molecules such as monosaccharides, it is often unfeasible to perform full geometry optimizations at the *ab initio* level. Moreover, to obtain meaningful values it would be necessary to choose a basis set that could not only provide the required accuracy in the calculation of the PAs and DPEs, but could reproduce also the energies associated with intramolecular hydrogen bonding and the stereoelectronic *exo*-anomeric effect (6). With current computational limitations, such calculations are not practical at the *ab initio* level; however, in a study of the conformational preferences of hexuloses, such as β-D-fructopyranose (**1**) and α-L-sorbopyranose (**2**), we (7) found that the AM1 semi-empirical molecular orbital method (8) performed well. Moreover, Dewar and Dieter (9) recently reported an examination of the application of AM1 in the calculation of the PAs and DPEs of a large selection of carbon, nitrogen, and oxygen bases and acids.

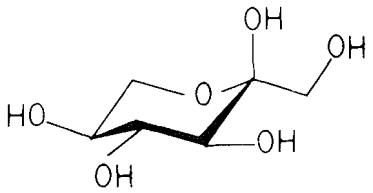
In the case of the PAs, Dewar and Dieter compared the AM1 results to experimental values, and to *ab initio* values calculated using a 6-31G* basis set employing geometries optimized at the 3-21G level. In the case of the DPEs, the AM1 results were compared to experimental values, and to *ab initio* values calculated at the 4-31+G level with, and without, second-order Møller–Plesset electron correlation, using geometries optimized at the 4-31+G level. The average error in the AM1-calculated PAs of the oxygen bases was reported to be 6.8 kcal/mol, while for the oxygen acids the average error in the DPEs was 7.6 kcal/mol. Those authors reported also that, for

[1]Authors to whom correspondence may be addressed.
[2]Revision received April 1, 1991.

Can. J. Chem. Downloaded from www.nrcresearchpress.com by 123.30.183.119 on 09/08/12
For personal use only.



β-D-Fructopyranose (**1**)



α-L-Sorbopyranose (**2**)

the oxygen bases, experimental trends in PAs were reproduced accurately by AM1. However, in the case of some of the oxygen acids, for example, the aliphatic alcohols, the calculated DPEs failed to reproduce the experimental trends, largely because of an observed increase in the error associated with the DPEs as a function of both the size of the alkyl group and the localization of the negative charge. Of relevance is the finding by those authors that, in the case of bifunctional bases, high PAs were obtained, in agreement with experiment, when intramolecular hydrogen bonds were able to stabilize the conjugate acids, and, moreover, that AM1 effectively reproduced this intramolecular hydrogen bonding.

For monosaccharides **1** and **2** it was not practical to perform *ab initio* calculations, and AM1 was selected as an alternative computational method for estimating the PAs and DPEs of these hexuloses.

Hydroxyl groups HO-1 and HO-2 in **1** and **2** are believed to bind to the sweet taste receptor through hydrogen bonding, in which the anomeric hydroxyl group has been considered to act as a proton donor (AH) group while the primary hydroxyl group has been considered to act as a proton acceptor (B) group (10). However, previous work by us indicated that the traditional assignment of the AH and B functionalities in **1** should be reversed (11, 12). A calculation of the PAs and DPEs of HO-1 and HO-2 was undertaken to address this question as well as to help explain the observation (10, 13) that **1** is significantly sweeter than **2**.

Presented in this paper are the calculated PAs of the primary hydroxyl group (HO-1), the anomeric hydroxyl group (HO-2), and the ring-oxygen atom (O-6), as well as the DPEs of HO-1 and HO-2, for both **1** and **2**. The errors associated with the DPEs were minimized in this study by limiting the calculations to molecules that had identical molecular formulas and differed in configuration at only one of the carbon nuclei. Furthermore, the anomeric effect (6) (in the case of deprotonation of HO-2) and intramolecular hydrogen bonding (in the cases of deprotonation of HO-1 and HO-2) should serve to delocalize the anionic charge.

TABLE 1. Calculated heats of formation and proton affinities for AM1 optimized conformers of β-D-fructopyranose (**1**)[a]

Molecule[b]	Conjugate acid[b]	Calcd. ΔH_f Molecule[c]	Calcd. ΔH_f Conjugate acid	Proton affinities
$\mathbf{1}_{g-}$	$\mathbf{1H}_{1g-}$	−303.21	−120.90	184.9
$\mathbf{1}_{g+}$	$\mathbf{1H}_{1g+}$(i)	−303.89	−120.66	184.0
$\mathbf{1}_{g+}$	$\mathbf{1H}_{1g+}$(ii)	−303.89	−119.76	183.1
$\mathbf{1}_{ap}$	$\mathbf{1H}_{1ap}$	−302.13	−115.06	180.1
Mean value				183.0
CH_3OH	$H[CH_3OH]^+$	−57.0[d]	138.3[d]	171.9[d]
$\mathbf{1}_{g-}$	$\mathbf{1H}_{2g-}$	−303.21	−126.04	190.0
$\mathbf{1}_{g+}$	$\mathbf{1H}_{2g+}$	−303.89	−126.46	189.8
$\mathbf{1}_{ap}$	$\mathbf{1H}_{2ap}$(i)	−302.13	−119.20	184.3
$\mathbf{1}_{ap}$	$\mathbf{1H}_{2ap}$(ii)	−302.13	−121.64	186.7
Mean value				188.0[e]
$CH_2(OH)_2$	$H[CH_2(OH)_2]^+$	−114.2[f]	83.7[f]	169.3[f]
$\mathbf{1}_{g+}$	$\mathbf{1H}_{6g+}$(i)	−303.89	−121.64	185.0
$\mathbf{1}_{g+}$	$\mathbf{1H}_{6g+}$(ii)	−303.89	−120.06	183.4
$\mathbf{1}_{ap}$	$\mathbf{1H}_{6ap}$(i)	−302.13	−117.76	182.8
$\mathbf{1}_{ap}$	$\mathbf{1H}_{6ap}$(ii)	−302.13	−115.40	180.5
Mean value				182.9

[a]Energies are in kcal/mol.
[b]The definition of the symbols is given in the legend for Fig. 1.
[c]Values taken from ref. 7.
[d]Values taken from ref. 9.
[e]The mean value does not include the PA of structure $\mathbf{1H}_{2ap}$(ii).
[f]See footnote 4.

Methodology

All calculations reported in this article were performed using the AM1 method, as provided in the AMPAC[3] package of computer programs, employing the keywords PRECISE, to lower all calculational tolerances by a factor of 100, and PULAY, to invoke Pulay's method (15) for achieving SCF convergence.

Starting geometries were defined using standard bond lengths and angles (16), and staggered torsion angles. Initially all of the C—O—H bond angles were defined, through the use of dummy atoms, as being linear. We found that optimization of these starting geometries consistently leads to low-energy, chemically reasonable, conformations, which often correspond to global energy minima (7). Other intramolecular hydrogen bond patterns were generated through manipulation of the hydroxyl groups in these optimized conformations, followed by reoptimization. While we found AM1 to perform well in the case of intramolecular hydrogen bonding, weaknesses associated with the AM1 calculated intermolecular hydrogen bonds were noted (17). In the case of the starting geometries of the protonated species, the protons were located about the oxygen atoms so as to generate planar trigonal geometries. For each structure the three staggered rotamers of the hydroxymethyl group (+gauche, *G*+; −gauche, *G*−; and anti-periplanar, *AP*; O-1 to O-2) were examined.

Discussion

Proton affinities

The calculated PAs of **1** and **2** are listed in Tables 1 and 2, respectively. The value reported by Stull and Prophet (18) for the heat of formation of H^+ (367.2 kcal/mol) was used in the calculation of all of the PAs and DPEs. Included for comparison

[3]AMPAC (QCPE Program No. 527) is described in the Quantum Chemistry Program Exchange newsletter (14).

Can. J. Chem. Downloaded from www.nrcresearchpress.com by 123.30.183.119 on 09/08/12
For personal use only.

TABLE 2. Calculated heats of formation and proton affinities for AM1 optimized conformers of α-L-sorbopyranose (**2**)[a]

Molecule[b]	Conjugate acid[b]	Calcd. ΔH_f Molecule[c]	Calcd. ΔH_f Conjugate acid	Proton affinities
$\mathbf{2}_{g-}$	$\mathbf{2H}_{1g-}$	−302.36	−120.30	185.1
$\mathbf{2}_{g+}$	$\mathbf{2H}_{1g+}$	−303.56	−119.33	183.0
$\mathbf{2}_{ap}$	$\mathbf{2H}_{1ap}$	−301.82	−112.59	178.0
Mean value				182.0
$\mathbf{2}_{g-}$	$\mathbf{2H}_{2g-}$	−302.36	−124.15	189.0
$\mathbf{2}_{g+}$	$\mathbf{2H}_{2g+}$	−303.56	−124.65	188.2
$\mathbf{2}_{ap}$	$\mathbf{2H}_{2ap}$(i)	−301.82	−117.56	182.9
$\mathbf{2}_{ap}$	$\mathbf{2H}_{2ap}$(ii)	−301.82	−116.97	182.3
Mean value				185.6
$\mathbf{2}_{g-}$	$\mathbf{2H}_{6g-}$	−302.36	−112.50	177.3
$\mathbf{2}_{g+}$	$\mathbf{2H}_{6g+}$(i)	−303.56	−119.72	183.4
$\mathbf{2}_{g+}$	$\mathbf{2H}_{6g+}$(ii)	−303.56	−119.12	182.8
$\mathbf{2}_{g+}$	$\mathbf{2H}_{6g+}$(iii)	−303.56	−118.84	182.5
$\mathbf{2}_{ap}$	$\mathbf{2H}_{6ap}$(i)	−301.82	−116.31	181.7
$\mathbf{2}_{ap}$	$\mathbf{2H}_{6ap}$(ii)	−301.82	−114.24	179.6
Mean value				181.2

[a]Energies are in kcal/mol.
[b]The definition of the symbols is given in the legend for Fig. 1.
[c]Values taken from ref. 7.

are the PAs of methanol (9) and methanediol.[4] The average PA of the anomeric oxygen atom (O-2) for the three rotamers of **1** was calculated to be 188 kcal/mol, whereas the average PA of O-1 for the same conformers was 183 kcal/mol. In each of the conformers of **1** the PA of O-2 was consistently higher than that of O-1. However, in both the case of protonation at O-1 and protonation at O-2, the *G*+ and *G*− rotamers gave rise to PAs that were approximately 5.5 kcal/mol higher than those calculated for the *AP* rotamers. This dependence of the PAs on the orientation of the hydroxymethyl group may be explained by an examination of the heats of formation of **1** and its protonated forms (see Table 1). The protonated *G*+ and *G*− rotamers of **1** were calculated to be more stable than the *AP* rotamers by approximately 6.5 kcal/mol for protonation at O-1 or O-2 whereas, in the case of the neutral species, the *G*+ and *G*− rotamers were calculated to be more stable than the *AP* rotamers by approximately 1 kcal/mol. Thus, the increased PAs for the *G*+ and *G*− conformations of **1** arise from corresponding increases in the stabilities of the protonated forms of these conformers. Methanediol has been studied (20) as a simple model for the anomeric effect (see ref. 6), and it is noteworthy that the PA of methanediol as calculated using AM1 is slightly lower than that of methanol. In the cases of HO-1 and HO-2 in **1** and **2**, the reverse trend in PAs is found, namely, the PA of the anomeric hydroxyl group is higher than that of the primary hydroxyl group.

The calculated PAs of **2** listed in Table 2 indicate the same general trends as observed for **1**. The PA of O-2 (185.6 kcal/mol) is higher on average than the PA of O-1 by approximately 3.5 kcal/mol. The *G*+ and *G*− rotamers again have the highest PAs, being higher by approximately 6 kcal/mol for protonation at O-1 or O-2 than calculated for protonation of the *AP* rotamers. Analogously to the case of **1**, the trends in the PAs of **2** reflect trends in stabilities of the protonated species. Of relevance is the observation that, for all conformers of **1** and **2**, the PA of O-2 in **1** was calculated to be higher than the PA of O-2 in **2** by 1–4 kcal/mol, whereas, the PAs of O-1 in both **1** and **2** are approximately equal for each corresponding rotamer, the difference in the average PAs being approximately 1 kcal/mol.

The average PAs for protonation at O-6 in both **1** and **2** were calculated to be approximately equal to the corresponding average PAs for protonation at O-1. However, unlike the case of protonation at O-1 or O-2, the lowest PAs calculated for O-6 occurred for conformations of **1** and **2** in which the hydroxymethyl groups adopted *G*− orientations. The PAs of the *G*− conformations were found to be lower by approximately 6 kcal/mol than those calculated for the *G*+ conformers. The *G*+ conformers were found to exhibit the highest PAs, which were higher by approximately 2 kcal/mol than predicted for the *AP* conformers.

The AM1 optimized geometries of the protonated forms of **1** and **2** are presented in Figs. 1 and 2, respectively. A summary of the intramolecular hydrogen bond geometries predicted for **1** and **2** is given in Tables 3 and 4, respectively. An examination of Figs. 1 and 2 indicates that the *G*+ and *G*− rotamers of **1** and **2**, when protonated at either O-1 or O-2, exhibit stabilizing interactions between the protonated hydroxyl groups and neighboring oxygen atoms. In the case of protonation at O-1 in the *G*+ rotamers, stabilizing interactions between $H(HO\text{-}1)^+$ and both O-2 and O-6 are present. The interaction of $H(HO\text{-}1)^+$ with O-2 in the *G*+ conformers of both **1** and **2** is facilitated by an orientation of HO-2 such that HO-2 adopts a torsion angle with respect to the ring-oxygen atom (O-6) of approximately 180°. We have previously used the term "anti-*exo*-anomeric" to describe this orientation of HO-2 (7). In this orientation hydrogen bonds extend between HO-2 and O-3, HO-3 and O-4, and HO-4 and O-5. In the case of **1**, HO-5 may be hydrogen bonded to the ring oxygen atom O-6, an interaction that was found also to be present in the neutral species (7). However, in the protonated form, the interaction between $H(HO\text{-}1)^+$ and O-6 has the effect of destabilizing any interaction between HO-5 and O-6, as indicated by the energy difference of approximately 1 kcal/mol between structures $\mathbf{1H}_{1g+}$(ii), which contains an interaction between HO-5 and O-6, and $\mathbf{1H}_{1g+}$(i), in which this interaction is absent.

Protonation of O-1 in **1** and **2**, in conformers in which O-1 adopts a *G*− orientation, led to the formation of hydrogen bonds between $H(HO\text{-}1)^+$ and both O-2 and O-3. An *exo*-anomeric orientation of HO-2 enabled the formation of a hydrogen bond between $H(HO\text{-}1)^+$ and O-2, and was accompanied by the formation of hydrogen bonds extending between HO-3 and O-4, HO-4 and O-5, and between HO-5 and O-6. Unlike the case of the *G*+ conformers of **1**, the most stable orientation of HO-5 in the *G*− conformers was that in which a hydrogen bond was present between HO-5 and O-6.

In the *AP* conformers of **1** and **2**, protonation of O-1 led to the generation of structures containing bifurcated hydrogen bonds between $H(HO\text{-}1)^+$ and O-6. In both **1** and **2**, an *exo*-anomeric orientation of HO-2 was preferred, with hydrogen bonds predicted between HO-3 and O-2. In the case of **2**, hydrogen bonds were predicted to exist also between HO-4 and O-3, and

[4]The values of the PA and DPE of methanediol were generated through protonation and deprotonation of the lowest energy conformer of methanediol as defined by constraining the H—O—C—O torsion angles to values of 60°. Details of these and related calculations at the *ab initio* level have been reported (19).

Can. J. Chem. Downloaded from www.nrcresearchpress.com by 123.30.183.119 on 09/08/12
For personal use only.

Can. J. Chem. Downloaded from www.nrcresearchpress.com by 123.30.183.119 on 09/08/12
For personal use only.

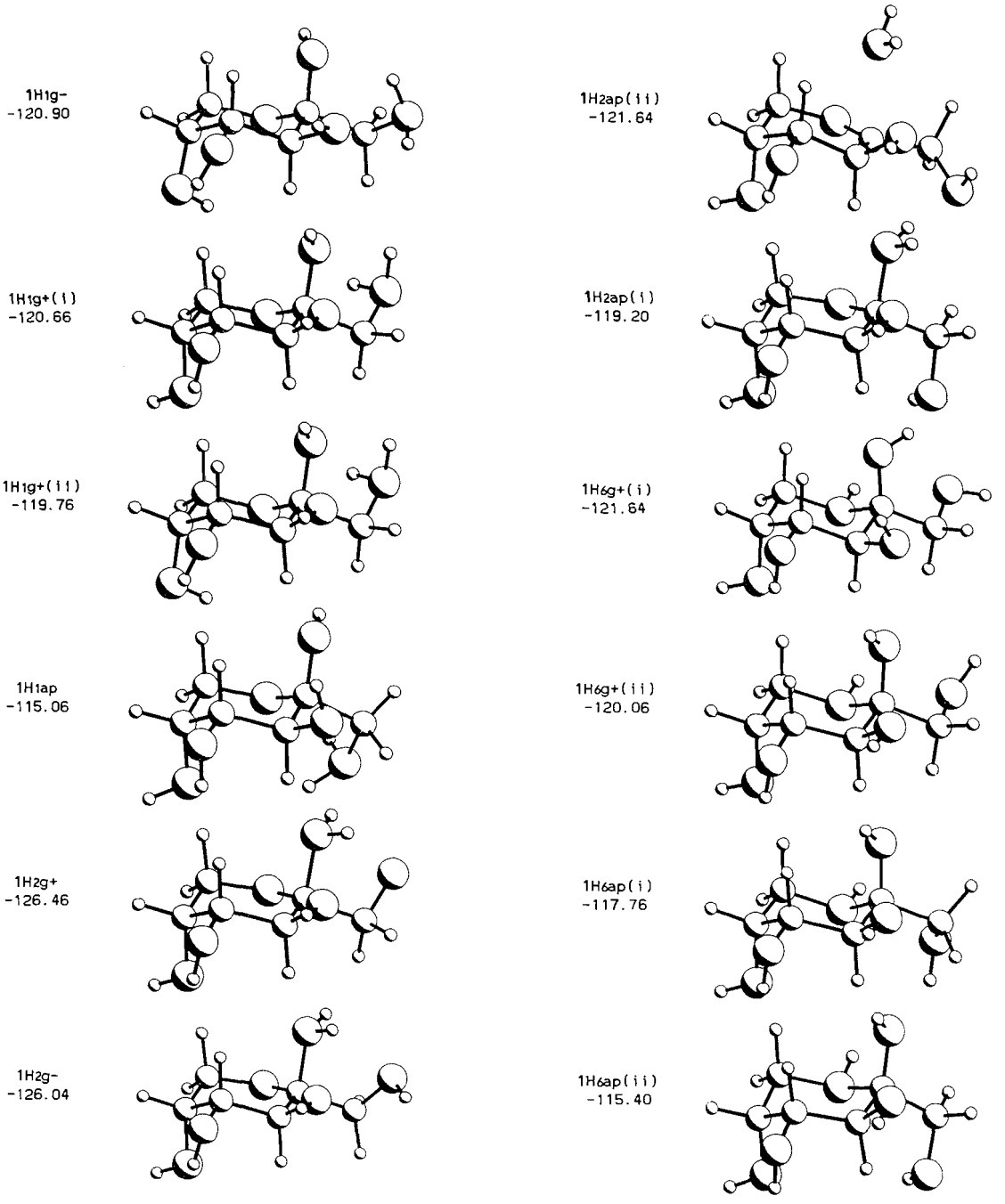


FIG. 1. AM1 optimized geometries and heats of formation (kcal/mol) of protonated β-D-fructopyranose (**1H**). Structures are listed in order of increasing energy for protonation at O-1, O-2, and O-6, respectively. Protonated species are indicated by "**H**" after the symbol for the neutral molecule, whereas deprotonated species are indicated by "−". Sites of protonation or deprotonation are indicated by a subscript numeral, indicating the relevant oxygen atom. The three staggered orientations of the hydroxymethyl groups are indicated by the symbols "g+" (+gauche), "g−" (−gauche), and "ap" (anti-periplanar), O-1 to O-2.

HO-5 and O-4 whereas, in the case of **1**, a hydrogen bond between HO-4 and O-5 was formed. These hydrogen bond patterns were predicted also to be present in the neutral forms of **1** and **2** (7). In the case of **1** protonated at O-1, the interaction between $H(HO\text{-}1)^+$ and O-6 precludes the possibility of hydrogen bonding between HO-5 and O-6.

Protonation of O-2 in both **1** and **2** led to structures in which hydrogen bonds were predicted to exist between $H(HO\text{-}2)^+$ and O-3, HO-3 and O-4, and HO-4 and O-5, regardless of the orientation of the hydroxymethyl group. In the case of **1**, there were no instances in which a hydrogen bond was predicted between HO-5 and O-6, an observation that is reflective of a reduced negative charge at O-6, presumably owing to a transfer of charge through the anomeric center to O-2. Moreover, the ring conformations of **1** and **2**, in conformers protonated at O-2, approach that of a half chair, as would be expected to arise from a depletion of electron density at C-2.

Both the *G*+ and *G*− conformers of **1** and **2**, when protonated at O-2, were found to exhibit hydrogen bonds between $H(HO\text{-}2)^+$ and O-1. Furthermore, in the *G*− conformers of both

Can. J. Chem. Downloaded from www.nrcresearchpress.com by 123.30.183.119 on 09/08/12
For personal use only.

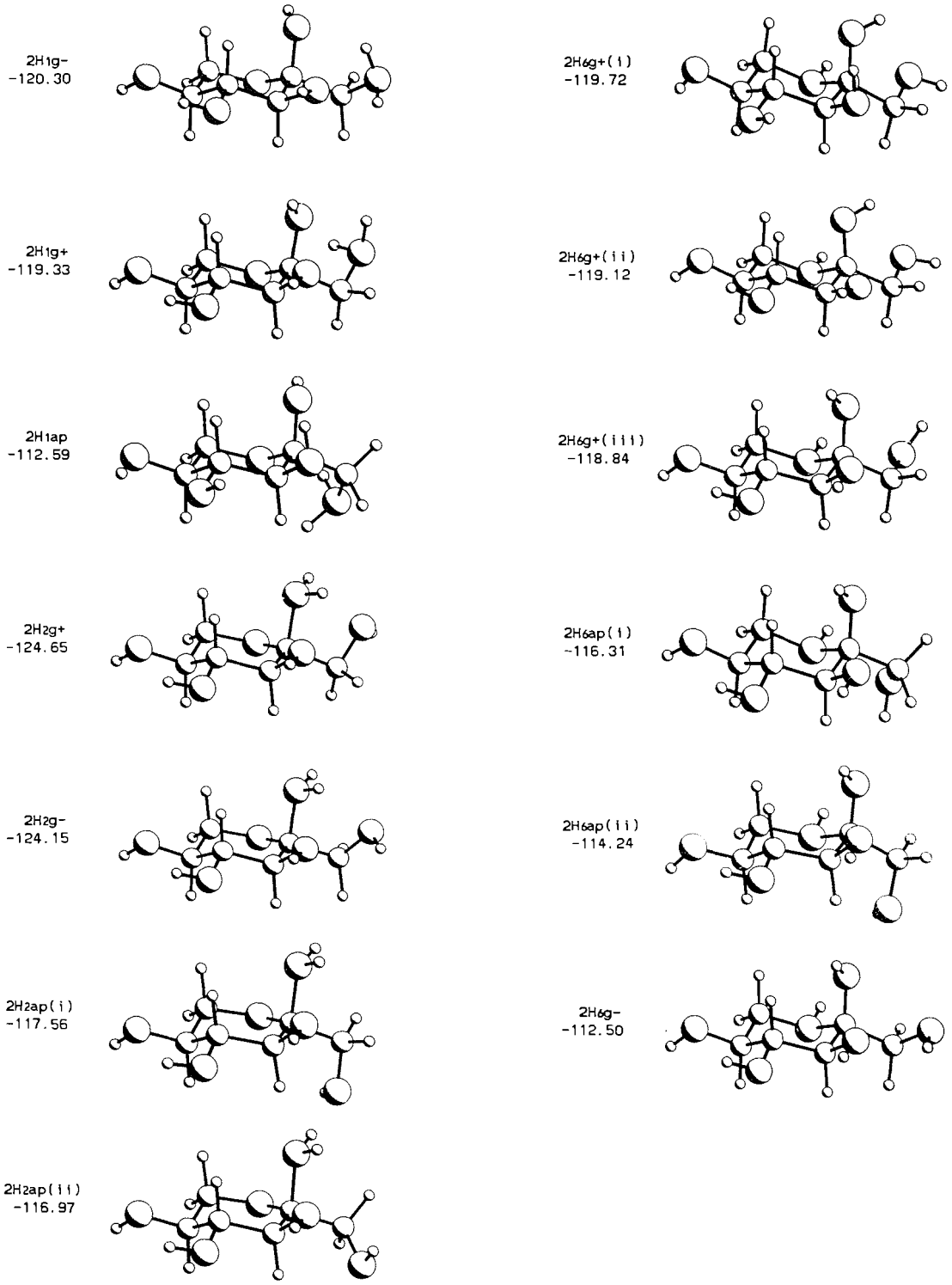


FIG. 2. AM1 optimized geometries and heats of formation (kcal/mol) of protonated α-L-sorbopyranose (**2H**). Structures are listed in order of increasing energy for protonation at O-1, O-2, and O-6, respectively. The definition of the symbols is given in the legend for Fig. 1.

1 and **2**, HO-1 was found to form a hydrogen bond with O-3. Weak hydrogen bonds between HO-1 and O-6 were predicted to form in the *AP* conformers of **1** and **2** when these conformers were protonated at O-2. The average HO-1—O-6 separation in structures $\mathbf{1H}_{2ap}$(i) and $\mathbf{2H}_{2ap}$(i) was 2.86 Å (see Tables 3 and 4), which may be compared to a corresponding value (7) of 2.34 Å for the neutral species. Lacking the ability to form hydrogen bonds between H(HO-2)$^+$ and O-1, the *AP* rotamers were predicted to be less stable by approximately 7 kcal/mol than the corresponding *G*+ or *G*− rotamers.

While conformer $\mathbf{2H}_{2ap}$(ii) indicated the possibility of a hydrogen bond existing between HO-1 and O-3, this structure was predicted to be slightly less stable than conformer $\mathbf{2H}_{2ap}$(i), in which a hydrogen bond existed between HO-1 and O-6. No conformer analogous to $\mathbf{2H}_{2ap}$(ii) was found for **1**, but rather, upon optimization, the corresponding rotamer of **1** gave rise

TABLE 3. Hydrogen bond distances (Å) and angles (deg) for the AM1 optimized geometries of protonated β-D-fructopyranose (**1H**)

Conformation[a] (ΔH_f)[b]	D—H···A	D—H	D···A	H···A	∠DHA
$\mathbf{1H}_{1g-}$	O-1—HO-1···O-2	1.014	2.680	2.118	112.93
(−120.90)	O-1—HO-1···O-3	1.005	2.439	2.001	103.40
	O-1—HO-1···O-3	1.014	2.439	2.236	88.97
	O-3—HO-3···O-4	0.971	2.901	2.447	108.25
	O-4—HO-4···O-5	0.971	2.797	2.281	112.19
	O-5—HO-5···O-6	0.966	3.058	2.641	106.40
	Mean values	0.990	2.719	2.287	105.36
$\mathbf{1H}_{1g+}$(i)	O-1—HO-1···O-2	1.008	2.436	2.059	101.22
(−120.66)	O-1—HO-1···O-6	1.004	2.883	2.388	105.40
	O-2—HO-2···O-3	0.969	2.733	2.298	106.30
	O-3—HO-3···O-4	0.971	2.915	2.473	107.45
	O-4—HO-4···O-5	0.970	2.779	2.311	108.76
	Mean values	0.984	2.749	2.306	105.83
$\mathbf{1H}_{1g+}$(ii)	O-1—HO-1···O-2	1.008	2.436	2.061	99.32
(−119.76)	O-1—HO-1···O-6	1.004	2.883	2.462	104.52
	O-2—HO-2···O-3	0.971	2.743	2.327	104.98
	O-3—HO-3···O-4	0.972	2.917	2.480	107.01
	O-4—HO-4···O-5	0.971	2.800	2.285	112.14
	O-5—HO-5···O-6	0.966	2.993	2.565	106.96
	Mean values	0.982	2.795	2.363	105.82
$\mathbf{1H}_{1ap}$	O-1—HO-1···O-6	1.002	2.372	2.151	89.94
(−115.06)	O-1—HO-1···O-6	1.006	2.372	2.244	84.69
	O-3—HO-3···O-2	0.970	2.768	2.658	86.20
	O-4—HO-4···O-5	0.968	2.867	2.504	102.06
	Mean values	0.987	2.595	2.389	90.72
$\mathbf{1H}_{2g-}$	O-1—HO-1···O-3	0.969	2.872	2.568	98.31
(−126.04)	O-2—HO-2···O-1	0.998	2.415	2.151	92.78
	O-2—HO-2···O-1	0.990	2.415	2.362	81.07
	O-2—HO-2···O-3	0.998	2.584	2.136	105.22
	O-3—HO-3···O-4	0.972	2.939	2.511	106.53
	O-4—HO-4···O-5	0.970	2.807	2.349	108.13
	Mean values	0.983	2.672	2.346	98.67
$\mathbf{1H}_{2g+}$	O-2—HO-2···O-1	0.996	2.447	2.071	99.92
(−126.46)	O-2—HO-2···O-3	0.994	2.548	2.175	100.33
	O-3—HO-3···O-4	0.971	2.958	2.544	105.68
	O-4—HO-4···O-5	0.970	2.801	2.344	108.00
	Mean values	0.983	2.689	2.283	103.48
$\mathbf{1H}_{2ap}$(i)	O-1—HO-1···O-6	0.969	2.980	2.864	87.26
(−119.20)	O-2—HO-2···O-3	0.991	2.525	2.081	104.89
	O-3—HO-3···O-4	0.971	2.976	2.594	103.61
	O-4—HO-4···O-5	0.970	2.792	2.336	107.96
	Mean values	0.975	2.818	2.489	106.55
$\mathbf{1H}_{2ap}$(ii)	O-1—HO-1···O-3	0.971	2.728	2.216	111.64
(−121.64)	O-2—HO-2···O-3[c]	0.965	2.764	2.369	103.90
	O-3—HO-3···O-4	0.972	2.984	2.604	103.50
	O-4—HO-4···O-5	0.970	2.825	2.382	107.15
	Mean values	0.969	2.825	2.393	106.55
$\mathbf{1H}_{6g+}$(i)	O-2—HO-2···O-1	0.978	2.676	2.202	108.43
(−121.64)	O-3—HO-3···O-4	0.971	2.848	2.598	94.76
	O-4—HO-4···O-5	0.970	2.813	2.426	103.32
	O-6—HO-6···O-1	0.993	2.735	2.323	103.76
	Mean values	0.978	2.768	2.387	102.57
$\mathbf{1H}_{6g+}$(ii)	O-1—HO-1···O-2	0.968	2.730	2.710	80.96
(−120.06)	O-2—HO-2···O-3	0.974	2.806	2.478	99.36
	O-3—HO-3···O-4	0.972	2.889	2.478	105.20
	O-4—HO-4···O-5	0.971	2.774	2.328	107.12
	O-6—HO-6···O-1	1.002	2.640	2.197	105.04
	Mean values	0.977	2.768	2.438	99.54

Can. J. Chem. Downloaded from www.nrcresearchpress.com by 123.30.183.119 on 09/08/12
For personal use only.

TABLE 3 (*concluded*)

Conformation[a] (ΔH_f)[b]	D—H···A	D—H	D···A	H···A	∠DHA
1H_{6ap}(i)	O-2—HO-2···O-3	0.974	2.842	2.519	99.14
(−117.76)	O-3—HO-3···O-4	0.972	2.880	2.456	105.99
	O-4—HO-4···O-5	0.971	2.767	2.319	107.22
	O-6—HO-6···O-1	1.001	2.368	2.141	90.29
	Mean values	0.979	2.714	2.359	100.66
1H_{6ap}(ii)	O-1—HO-1···O-6	0.967	2.911	2.747	89.96
(−115.40)	O-2—HO-2···O-3	0.976	2.698	2.306	102.92
	O-3—HO-3···O-4	0.971	2.917	2.561	101.71
	O-4—HO-4···O-5	0.970	2.805	2.379	105.92
	Mean values	0.971	2.833	2.498	100.13

[a]The definition of the symbols is given in the legend for Fig. 1.
[b]Energies are in kcal/mol.
[c]Intermolecular hydrogen bond.

to a cyclic oxocarbenium ion – water complex, **1**H_{2ap}(ii) (see Fig. 1). While this complex was predicted to be more stable than **1**H_{2ap}(i) by approximately 2.5 kcal/mol, it was still less stable than the *G*+ and *G*− species by approximately 5 kcal/mol. Similar oxocarbenium ions have been shown to be produced during the gas-phase decomposition of protonated methyl 2,3,4,6-tetra-*O*-methyl-α- and β-D-galactopyranosides (21) and permethylated deoxyhexopyranosides (22), and are believed to be intermediates in glycoside hydrolysis (23, 24). The spontaneous generation of a cyclic oxocarbenium ion resulting from protonation of O-2 in **1** may be relevant to the mechanism of the mutarotation of ketopyranoses, in that protonation of the anomeric oxygen atom, rather than of the ring oxygen atom, may be the first step; however, it is recognized that mutarotation is a solution phenomenon. The mechanism by which aldopyranoses mutarotate has been well studied, and is believed to proceed through an acyclic aldehyde intermediate arising from protonation of the ring oxygen atom (25, 26). However, in the cases of both the acid-catalyzed anomerization and hydrolysis of aldopyranosides, a cyclic oxocarbenium ion, derived from protonation of the anomeric oxygen atom, has been indicated as an intermediate (26). That this cyclic oxocarbenium ion was found in the present study for **1** and not for **2** may be of relevance as regards both the rates of mutarotation of **1** and **2** and the rates of acid-catalyzed hydrolysis of the corresponding glycosides. It is well known that **1** exhibits rapid mutarotation while **2** does not (27), and that methyl β-D-fructopyranoside is hydrolyzed at a significantly faster rate than is methyl α-L-sorbopyranoside (28, 29). The implications of these calculations, as concerns the mechanisms of mutarotation of ketopyranoses and of ketopyranoside hydrolysis, will be the subject of a future study.

Arguments analogous to those presented above may be used to explain the differences in the PAs for protonation at O-6. Both the *G*+ and *AP* rotamers of **1** and **2** were predicted to provide stabilizing interactions between O-1 and $H(O\text{-}6)^+$, in the cases of protonation at the ring oxygen atom. No corresponding interactions were possible in the *G*− rotamers. These stabilizing interactions had the effect of lowering the heats of formation of the protonated *G*+ and *AP* conformers, relative to that of the *G*− species, by approximately 3.5 kcal/mol. Thus, for both **1** and **2** the difference between the PAs of O-6 in the *G*+ and *AP* rotamers, and the PA of O-6 in the *G*− rotamers, is related to the additional stabilizations present in the *G*+ and *AP* conformers.

The PAs given in Tables 1 and 2, and discussed above, indicate that the anomeric hydroxyl groups in **1** and **2** are more basic than either the hydroxymethyl groups or the ring oxygen atoms in these sugars, and may be assigned to the proton acceptor (B) unit of the saporous group (10). Moreover, the PA of HO-2 in **1** was found to be higher than the PA of HO-2 in **2**, by an average value of approximately 2.5 kcal/mol.

Deprotonation enthalpies

The calculated DPEs for HO-1 and HO-2 in **1** and **2** are listed in Tables 5 and 6, respectively. Included for comparison are the DPEs of methanol (9) and methanediol.[4] The average DPE for the anomeric hydroxyl groups in **1** and **2** is 352 kcal/mol, while that for the hydroxymethyl groups is 360 kcal/mol, features that confirm the expected trends in the acidities of these hydroxyl groups. The absolute values of the DPEs for HO-1 in both **1** and **2** do not differ significantly from one another, regardless of the orientations of the hydroxymethyl groups. Similarly, the DPEs for HO-2 in **1** and **2** are approximately equal for all conformers. The higher acidity of the acetal hydroxyl proton than the primary hydroxyl proton was further confirmed by the values for the DPEs of methanediol (378.8 kcal/mol) and methanol (385.4 kcal/mol).

It is noteworthy that fewer stable conformations of the deprotonated structures were found than of either the neutral or protonated species. The hydrogen bond geometries for the AM1 optimized geometries of deprotonated **1** and **2** are given in Tables 7 and 8, respectively. In the case of deprotonation at HO-1, in both **1** and **2**, only the *G*− rotamers formed stable structures, a feature likely arising from repulsions between O-6 and $(O\text{-}1)^-$. In structures **1**$-_{1g-}$ and **2**$-_{1g-}$, hydrogen bonds were predicted to exist between HO-2 and $(O\text{-}1)^-$, HO-3 and $(O\text{-}1)^-$, and HO-3 and O-2 (see Figs. 3 and 4). The two conformers differed in the orientations preferred by HO-4 and HO-5. In **1**$-_{1g-}$, hydrogen bonds were formed between HO-4 and O-5, and between HO-5 and the ring oxygen atom, O-6, while in rotamer **2**$-_{1g-}$, hydrogen bonds were found between HO-4 and O-3, and between HO-5 and O-4. This reversal in the direction of the intramolecular hydrogen bonds in the cases of **1** and **2** was predicted to be present in the neutral molecules (7).

Only in the case of **1** was a stable *AP* rotamer found in the species deprotonated at O-1, namely **1**$-_{1ap}$ (see Fig. 3). In this structure the pyranose ring was found to prefer a $^{3,6}B$(D) boat conformation, stabilized by the formation of hydrogen bonds

Can. J. Chem. Downloaded from www.nrcresearchpress.com by 123.30.183.119 on 09/08/12
For personal use only.

TABLE 4. Hydrogen bond distances (Å) and angles (deg) for the AM1 optimized geometries of protonated α-L-sorbopyranose (**2H**)

Conformation[a] (ΔH_f)[b]	D—H···A	D—H	D···A	H···A	∠DHA
$\mathbf{2H}_{1g-}$	O-1—HO-1···O-2	1.014	2.669	2.104	113.05
(−120.30)	O-1—HO-1···O-3	1.014	2.445	2.259	88.06
	O-2—HO-2···O-6	0.970	2.287	2.269	78.73
	O-3—HO-3···O-4	0.971	2.869	2.423	107.60
	O-4—HO-4···O-5	0.970	2.860	2.465	104.09
	Mean values	0.988	2.626	2.304	98.31
$\mathbf{2H}_{1g+}$	O-1—HO-1···O-2	1.008	2.440	2.062	99.49
(−119.33)	O-1—HO-1···O-6	1.004	2.859	2.428	105.14
	O-2—HO-2···O-3	0.970	2.725	2.318	104.30
	O-3—HO-3···O-4	0.971	2.895	2.489	104.92
	O-4—HO-4···O-5	0.969	2.860	2.461	104.32
	Mean values	0.985	2.756	2.352	103.63
$\mathbf{2H}_{1ap}$	O-1—HO-1···O-6	1.003	2.357	2.185	87.06
(−112.59)	O-1—HO-1···O-6	1.002	2.357	2.175	87.65
	O-3—HO-3···O-2	0.970	2.743	2.451	96.92
	O-4—HO-4···O-3	0.968	2.960	2.643	99.45
	O-5—HO-5···O-4	0.969	2.848	2.461	103.52
	Mean values	0.983	2.653	2.383	94.92
$\mathbf{2H}_{2g-}$	O-1—HO-1···O-3	0.970	2.825	2.491	99.94
(−124.15)	O-2—HO-2···O-1	0.999	2.436	2.147	94.35
	O-2—HO-2···O-1	0.990	2.436	2.421	79.07
	O-2—HO-2···O-3	0.999	2.577	2.134	104.77
	O-3—HO-3···O-4	0.972	2.918	2.523	104.22
	O-4—HO-4···O-5	0.970	2.846	2.452	103.93
	Mean values	0.983	2.673	2.361	97.71
$\mathbf{2H}_{2g+}$	O-2—HO-2···O-1	0.997	2.414	2.069	97.70
(−124.65)	O-2—HO-2···O-3	0.996	2.541	2.176	99.69
	O-3—HO-3···O-4	0.971	2.937	2.561	103.03
	O-4—HO-4···O-5	0.970	2.849	2.461	103.58
	Mean values	0.983	2.685	2.317	101.00
$\mathbf{2H}_{2ap}$(i)	O-1—HO-1···O-6	0.969	2.917	2.825	85.69
(−117.56)	O-2—HO-2···O-3	0.992	2.526	2.082	104.90
	O-3—HO-3···O-4	0.971	2.943	2.592	101.50
	O-4—HO-4···O-5	0.970	2.845	2.451	103.95
	Mean values	0.976	2.808	2.487	99.01
$\mathbf{2H}_{2ap}$(ii)	O-1—HO-1···O-3	0.970	2.836	2.345	110.64
(−116.97)	O-2—HO-2···O-3	0.988	2.552	2.128	103.87
	O-3—HO-3···O-4	0.971	2.933	2.562	102.74
	O-4—HO-4···O-5	0.970	2.846	2.450	104.04
	Mean values	0.975	2.792	2.371	105.32
$\mathbf{2H}_{6g-}$	O-1—HO-1···O-3	0.971	2.916	2.326	118.42
(−112.50)	O-2—HO-2···O-3	0.975	2.835	2.520	98.64
	O-3—HO-3···O-4	0.972	2.840	2.442	104.12
	O-4—HO-4···O-5	0.970	2.855	2.514	100.55
	Mean values	0.972	2.862	2.450	105.43
$\mathbf{2H}_{6g+}$(i)	O-2—HO-2···O-1	0.978	2.682	2.207	108.41
(−119.72)	O-3—HO-3···O-2	0.970	2.859	2.639	93.03
	O-4—HO-4···O-3	0.969	2.940	2.602	100.70
	O-5—HO-5···O-4	0.971	2.825	2.449	102.69
	O-6—HO-6···O-1	0.995	2.704	2.293	103.46
	Mean values	0.976	2.802	2.438	101.66
$\mathbf{2H}_{6g+}$(ii)	O-2—HO-2···O-1	0.978	2.678	2.211	107.91
(−119.12)	O-3—HO-3···O-4	0.972	2.819	2.343	109.32
	O-4—HO-4···O-5	0.969	2.848	2.518	99.85
	O-6—HO-6···O-1	0.993	2.734	2.318	104.03
	Mean values	0.978	2.770	2.348	105.28
$\mathbf{2H}_{6g+}$(iii)	O-1—HO-1···O-2	0.968	2.729	2.715	80.58
(−118.84)	O-2—HO-2···O-3	0.975	2.801	2.502	97.50
	O-3—HO-3···O-4	0.972	2.851	2.484	102.17

Can. J. Chem. Downloaded from www.nrcresearchpress.com by 123.30.183.119 on 09/08/12
For personal use only.

TABLE 4 (*concluded*)

Conformation[a] (ΔH_f)[b]	D—H···A	D—H	D···A	H···A	∠DHA
	O-4—HO-4···O-5	0.970	2.857	2.512	100.81
	O-6—HO-6···O-1	1.001	2.634	2.191	104.99
	Mean values	0.977	2.775	2.481	97.21
2H$_{6ap}$(i)	O-2—HO-2···O-3	0.974	2.837	2.544	97.29
(−116.31)	O-3—HO-3···O-4	0.972	2.843	2.464	102.89
	O-4—HO-4···O-5	0.970	2.870	2.534	100.26
	O-6—HO-6···O-1	1.000	2.367	2.147	89.88
	Mean values	0.979	2.729	2.422	97.58
2H$_{6ap}$(ii)	O-1—HO-1···O-6	0.967	2.831	2.761	84.18
(−114.24)	O-2—HO-2···O-3	0.976	2.721	2.361	100.95
	O-3—HO-3···O-4	0.971	2.858	2.533	99.48
	O-4—HO-4···O-5	0.970	2.830	2.475	101.29
	Mean values	0.971	2.810	2.532	96.47

[a]The definition of the symbols is given in the legend for Fig. 1.
[b]Energies are in kcal/mol.

TABLE 5. Calculated heats of formation and deprotonation enthalpies for the AM1 optimized conformers of β-D-fructopyranose (**1**)[a]

		Calcd. ΔH_f		
Molecule[b]	Conjugate base[b]	Molecule[c]	Conjugate base	Deprotonation enthalpies
1$_{g-}$	**1**$-_{1g-}$	−303.21	−309.50	360.9
1$_{ap}$	**1**$-_{1ap}$	−302.13	−310.06	359.3
Mean value				360.1
CH_3OH	CH_3O^-	−57.0[d]	−38.8[d]	385.4[d]
1$_{g+}$	**1**$-_{2g+}$	−303.89	−319.52	351.6
1$_{ap}$	**1**$-_{2ap}$	−302.13	−317.08	352.2
Mean value				351.9
$CH_2(OH)_2$	$CH_2(OH)O^-$	−114.2[e]	−102.6[e]	378.8[e]

[a]Energies are in kcal/mol.
[b]The definition of the symbols is given in the legend for Fig. 1.
[c]Values taken from ref. 7.
[d]Values taken from ref. 9.
[e]See footnote 4.

TABLE 6. Calculated heats of formation and deprotonation enthalpies for the AM1 optimized conformers of α-L-sorbopyranose (**2**)[a]

		Calcd. ΔH_f		
Molecule[b]	Conjugate base[b]	Molecule[c]	Conjugate base	Deprotonation enthalpies
2$_{g-}$	**2**$-_{1g-}$	−302.36	−309.49	360.1
2$_{g+}$	**2**$-_{2g+}$	−303.56	−318.19	352.6
2$_{ap}$	**2**$-_{2ap}$	−301.82	−315.81	353.2
Mean value				352.9

[a]Energies are in kcal/mol.
[b]The definition of the symbols is given in the legend for Fig. 1.
[c]Values taken from ref. 7.

between HO-4 and (O-1)$^-$, and HO-5 and (O-1)$^-$. No such structure was found for **2**, since in **2** no analogous hydrogen bond between HO-5 and (O-1)$^-$ could form.

Deprotonation of the anomeric hydroxyl groups in **1** and **2** led to the formation of stable conformers in which O-1 adopted only the *AP* or *G*+ orientations. The *G*− conformers that

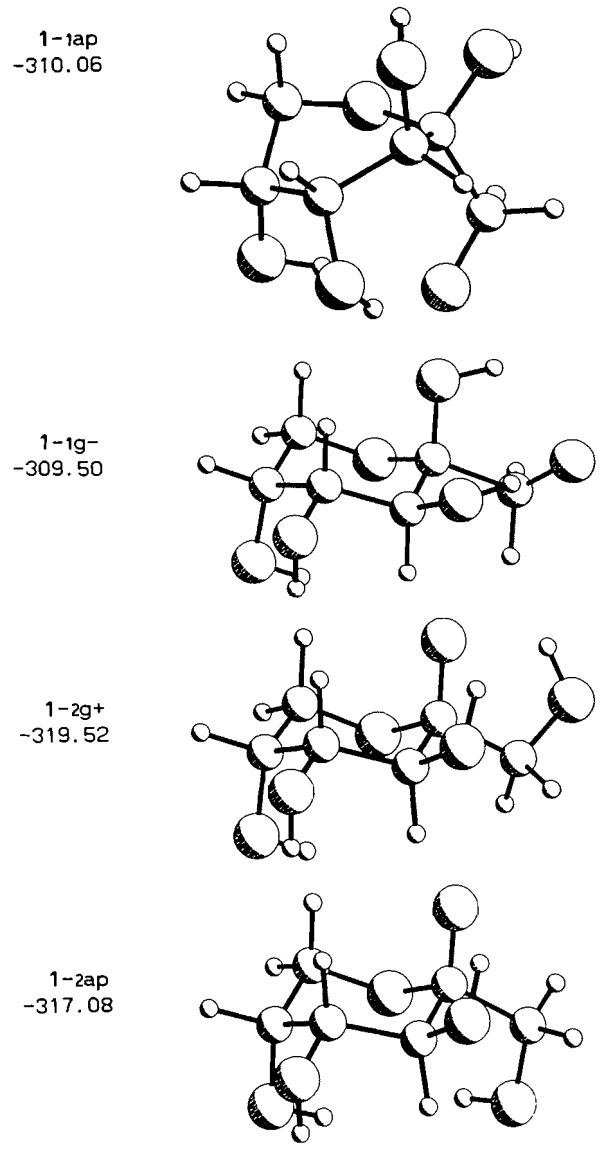


FIG. 3. AM1 optimized geometries and heats of formation (kcal/mol) of deprotonated β-D-fructopyranose (**1**−). Structures are listed in order of increasing energy for deprotonation at O-1, O-2, respectively. The definition of the symbols is given in the legend for Fig. 1.

Can. J. Chem. Downloaded from www.nrcresearchpress.com by 123.30.183.119 on 09/08/12
For personal use only.

TABLE 7. Hydrogen bond distances (Å) and angles (deg) for the AM1 optimized geometries of deprotonated β-D-fructopyranose (**1**−)

Conformation[a] (ΔH_f)[b]	D—H···A	D—H	D···A	H···A	∠DHA
1−$_{1g-}$	O-2—HO-2···O-1	0.974	2.654	2.076	116.20
(−309.50)	O-3—HO-3···O-1	0.978	2.925	2.067	145.36
	O-3—HO-3···O-2	0.978	2.819	2.631	90.75
	O-4—HO-4···O-5	0.965	2.793	2.438	101.32
	O-5—HO-5···O-2	0.968	2.897	2.434	108.95
	Mean values	0.973	2.818	2.329	112.52
1−$_{1ap}$	O-3—HO-3···O-2	0.964	2.594	2.154	106.19
(−310.06)	O-3—HO-3···O-2	0.964	3.194	2.851	102.03
	O-4—HO-4···O-5	0.978	2.655	2.450	91.05
	O-5—HO-5···O-2	0.981	2.876	2.562	98.47
	Mean values	0.972	2.830	2.504	99.44
1−$_{2g+}$	O-1—HO-1···O-2	0.974	2.646	2.036	118.75
(−319.52)	O-3—HO-3···O-2	0.971	2.797	2.259	113.92
	O-4—HO-4···O-5	0.965	2.793	2.396	104.13
	O-5—HO-5···O-2	0.968	2.839	2.348	110.74
	Mean values	0.969	2.769	2.260	111.88
1−$_{2ap}$	O-1—HO-1···O-2	0.964	2.687	2.160	112.96
(−317.08)	O-3—HO-3···O-2	0.972	2.749	2.197	114.76
	O-4—HO-4···O-5	0.965	2.799	2.416	103.24
	O-5—HO-5···O-2	0.968	2.811	2.323	110.34
	Mean values	0.967	2.761	2.274	110.33

[a]The definition of the symbols is given in the legend for Fig. 1.
[b]Energies are in kcal/mol.

TABLE 8. Hydrogen bond distances (Å) and angles (deg) for the AM1 optimized geometries of deprotonated α-L-sorbopyranose (**2**−)

Conformation[a] (ΔH_f)[b]	D—H···A	D—H	D···A	H···A	∠DHA
2−$_{1g-}$	O-2—HO-2···O-1	0.974	2.666	2.097	115.55
(−309.49)	O-3—HO-3···O-1	0.979	2.886	2.028	144.99
	O-3—HO-3···O-2	0.979	2.857	2.667	90.98
	O-4—HO-4···O-3	0.965	2.871	2.385	110.64
	O-5—HO-5···O-4	0.965	2.854	2.370	110.47
	Mean values	0.973	2.827	2.309	114.53
2−$_{2g+}$	O-5—HO-5···O-4	0.965	2.855	2.371	110.47
(−318.19)	O-4—HO-4···O-3	0.965	2.891	2.403	110.89
	O-1—HO-1···O-2	0.974	2.643	2.032	118.76
	O-3—HO-3···O-2	0.971	2.797	2.250	114.55
	Mean values	0.969	2.796	2.264	113.67
2−$_{2ap}$	O-1—HO-1···O-6	0.965	2.709	2.170	113.96
(−315.81)	O-3—HO-3···O-2	0.972	2.764	2.207	115.15
	O-4—HO-4···O-3	0.965	2.902	2.418	110.63
	O-5—HO-5···O-4	0.965	2.850	2.363	110.65
	Mean values	0.967	2.806	2.290	112.60

[a]The definition of the symbols is given in the legend for Fig. 1.
[b]Energies are in kcal/mol.

were predicted for the neutral and protonated species all have exhibited preferences for intramolecular hydrogen bonding in which O-1 acted as a proton acceptor. However, in the case of the deprotonated species, this rotamer would be expected to contain an unfavorable O-1···$(O\text{-}2)^-$ interaction that would inhibit the formation of stable *G*− conformations. In the *G*+ conformers hydrogen bonds were predicted to exist between HO-1 and $(O\text{-}2)^-$ and between HO-3 and $(O\text{-}2)^-$ for both **1** and **2**. In the case of **1**, further hydrogen bonding was observed between HO-4 and O-5, and HO-5 and O-6, whereas in the case of **2**, hydrogen bonds between HO-4 and O-3, and HO-5 and O-4, were preferred.

The *AP* conformers of **1** and **2**, deprotonated at O-2, gave rise to similar hydrogen bonding involving HO-3, HO-4, and HO-5, as seen in the *G*+ rotamers. Hydrogen bonds in the *AP* conformers, **1**−$_{2ap}$ and **2**−$_{2ap}$, were predicted to exist between HO-1 and O-6 as found in the neutral molecule (7).

Neither the geometries, nor the energies, of the conformers

Can. J. Chem. Downloaded from www.nrcresearchpress.com by 123.30.183.119 on 09/08/12
For personal use only.

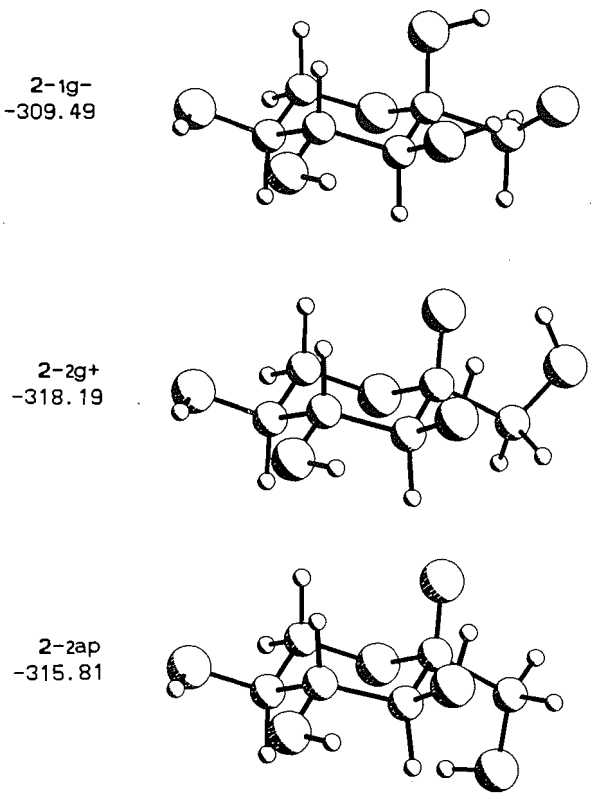


FIG. 4. AM1 optimized geometries and heats of formation (kcal/mol) of deprotonated α-L-sorbopyranose (**2**−). Structures are listed in order of increasing energy for deprotonation at O-1, O-2, respectively. The definition of the symbols is given in the legend for Fig. 1.

of the deprotonated forms of **1** and **2** exhibited any significant differences (with the exception of the formation of boat conformer $\mathbf{1}-_{1ap}$), an observation that indicates it is unlikely, at least in the gas phase, that the acidities of HO-1 or HO-2 in **1** and **2** are reflective of the different sweetness of these two sugars. However, the DPEs given in Tables 5 and 6, and discussed above, do indicate that, for both **1** and **2**, the anomeric hydroxyl group is more acidic than the hydroxymethyl group, HO-2 having an average DPE that was lower by approximately 8 kcal/mol than that of HO-1.

Conclusions

Based on the above analysis of the PAs and DPEs of **1** and **2**, it appears that the anomeric hydroxyl group is both more basic and more acidic than the hydroxymethyl group, and more basic than the ring heteroatom. The difference between the PAs of HO-1 and HO-2 was predicted to be approximately 5 kcal/mol in favor of the protonation of HO-2, whereas the difference between the DPEs of these groups was calculated to be approximately 8 kcal/mol in favor of the deprotonation of HO-2. Although these energies are not identical, their similarity indicates that the anomeric hydroxyl groups in **1** and **2** may be viewed as being amphiprotic. The higher acidity of HO-2 arises from a delocalization of the negative charge on O-2 in a manner equivalent to that responsible for the anomeric effect, namely, through an ($n_{O\text{-}2}$–$\sigma^*_{C—O\text{-}6}$) interaction, and results in an enhanced stabilization of the conjugate base. However, in the case of protonation, the basicity of HO-2 is enhanced by the presence of intramolecular hydrogen bonds in the conjugate acid between $H(HO\text{-}2)^+$ and other suitably located hydroxyl groups. The extent to which the conjugate acid is also stabilized through an ($n_{O\text{-}6}$–$\sigma^*_{C—O\text{-}2}$) anomeric interaction is not known; however, it has been reported that the protonation of sugars, in which the anomeric hydroxyl group is replaced by an amino group, leads to an attenuation of the anomeric effect, which is known as the "reverse anomeric effect" (6). Unlike the anomeric effect, in which an axial orientation is preferred at the anomeric center, the reverse anomeric effect is characterized by a preference for an equatorial orientation at that center.

The difference in the PAs of HO-2 in **1** and **2** suggests an explanation for the difference in the rates of mutarotation of these sugars and, moreover, may have broad implications as concerns the analysis of the rates of acid-catalyzed hydrolysis and anomerization of glycosides, it being recognized that these processes are solution phenomena.

The high PAs of HO-2 in both **1** and **2** indicate that the traditional assignment (10) of the proton donor (AH) unit to hydroxyl group HO-2, and the proton acceptor (B) unit to hydroxyl group HO-1, of the saporous group, should be reversed. That is, the anomeric hydroxyl group (HO-2) may be viewed as the proton acceptor unit, while the primary hydroxyl group (HO-1) may be the proton donor unit. Furthermore, the difference in the sweetness of **1** and **2** may be related to the difference in the PAs of the anomeric hydroxyl groups. The sugar is believed to bind to the taste receptor through a reciprocal hydrogen bond between the proton acceptor unit (B, HO-2) (11) and a proton donor unit in the receptor, and between the proton donor group (AH, HO-1) (11) and a proton acceptor unit in the receptor (10). The sweetness of the sugar would depend in part on the strength of this binding, a feature that would be reflected by the PA of HO-2 and the DPE of HO-1. In **1** and **2**, the DPEs of HO-1 were predicted to be approximately equal; however, the high PA of HO-2 in **1** would be expected to enhance the binding of **1** to the receptor, and may be responsible for the higher sweetness of **1**. The availability of low energy orientations of HO-2, which could facilitate hydrogen bond formation with the receptor, must be assumed to also play a significant role.

Acknowledgements

The authors wish to thank the Natural Sciences and Engineering Research Council of Canada for the award of grants (to V.H.S. and W.A.S.) and a scholarship (to R.J.W.).

1. (*a*) J. CHANDRASEKHAR, J. G. ANDRADE, and P. V. R. SCHLEYER. J. Am. Chem. Soc. **103**, 5609 (1981); **103**, 5612 (1981); (*b*) G. W. SPITZNAGEL, T. CLARK, J. CHANDRASEKHAR, and P. V. R. SCHLEYER. J. Comput. Chem. **3**, 363 (1982); (*c*) J. E. DEL BENE, D. D. METTE, M. J. FRISCH, B. T. LUKE, and J. A. POPLE. J. Phys. Chem. **87**, 3279 (1983); (*d*) S. IKUTA. J. Comput. Chem. **5**, 374 (1984); (*e*) L. L. LOHR, H. B. SCHLEGEL, and K. MOROKUMA. J. Phys. Chem. **88**, 1981 (1984); (*f*) M. SCARLETT and P. R. TAYLOR. Chem. Phys. **101**, 17 (1986).
2. J. E. DEL BENE. J. Comput. Chem. **6**, 296 (1985).
3. R. S. GREV and H. F. SCHAEFER III. J. Chem. Phys. **91**, 7305 (1989).
4. (*a*) M. J. FRISCH, J. E. DEL BENE, K. RAGHAVACHARI, and J. A. POPLE. Chem. Phys. Lett. **83**, 240 (1981); (*b*) J. E. DEL BENE, M. J. FRISCH, R. KRISHNAN, and J. A. POPLE. J. Phys. Chem. **86**, 1529 (1982).
5. W. J. HEHRE, L. RADOM, P. V. R. SCHLEYER, and J. A. POPLE. Ab initio molecular orbital theory. Wiley, New York. 1985. p. 310.
6. (*a*) R. U. LEMIEUX and S. KOTO. Tetrahedron, **30**, 1933 (1974); (*b*) R. U. LEMIEUX, S. KOTO, and D. VOISIN. *In* Anomeric effect, origin and consequences. *Edited by* W. A. Szarek and D. Horton. ACS Symp. Ser. **87**, 17 (1979); (*c*) S. WOLFE,

Can. J. Chem. Downloaded from www.nrcresearchpress.com by 123.30.183.119 on 09/08/12
For personal use only.

A. RAUK, L. M. TEL, and I. G. CSIZMADIA. J. Chem. Soc. B. 136 (1971); (*d*) A. J. KIRBY. The anomeric effect and related stereoelectronic effects at oxygen. Springer-Verlag, New York. 1983. p. 32.
7. R. J. WOODS, W. A. SZAREK, and V. H. SMITH, JR. J. Am. Chem. Soc. **112**, 4732 (1990).
8. M. J. S. DEWAR, E. G. ZOEBISCH, E. F. HEALY, and J. J. P. STEWART. J. Am. Chem. Soc. **107**, 3902 (1985).
9. M. J. S. DEWAR and K. M. DIETER. J. Am. Chem. Soc. **108**, 8075 (1986).
10. (*a*) G. G. BIRCH. Crit. Rev. Food Sci. Nutr. **8**, 57 (1976); (*b*) M. G. LINDLEY and G. G. BIRCH. J. Sci. Food Agric. **26**, 117 (1975); (*c*) R. S. SHALLENBERGER and T. E. ACREE. Nature, **216**, 480 (1967).
11. R. J. WOODS, V. H. SMITH, JR., W. A. SZAREK, and A. FARAZDEL. J. Chem. Soc. Chem. Commun. 937 (1987).
12. R. J. WOODS, M. KHALIL, W. PELL, S. H. MOFFAT, and V. H. SMITH, JR. J. Comput. Chem. **11**, 297 (1990).
13. (*a*) Y. TSUZUKI and J. YAMAZAKI. Biochem. Z. **323**, 525 (1953); (*b*) R. S. SHALLENBERGER. *In* Carbohydrates in solution. *Edited by* H. S. Isbell. Adv. Chem. **117**, 256 (1973).
14. M. J. S. DEWAR, E. G. ZOEBISCH, E. F. HEALY, and J. J. P. STEWART. QCPE Bulletin, **7**, 85 (1987).
15. P. PULAY and W. MEYER. J. Chem. Phys. **57**, 3337 (1972).
16. J. A. POPLE and M. GORDON. J. Am. Chem. Soc. **89**, 4253 (1967).
17. K. KHALIL, R. J. WOODS, D. F. WEAVER, and V. H. SMITH, JR. J. Comput. Chem. **12**, 584 (1991).
18. D. R. STULL and J. PROPHET. JANAF thermochemical tables, NBS37. 1971.
19. R. J. WOODS, W. A. SZAREK, and V. H. SMITH, JR. J. Chem. Soc. Chem. Commun. 334 (1991).
20. (*a*) G. A. JEFFREY, J. A. POPLE, and L. RADOM. Carbohydr. Res. **25**, 117 (1972); (*b*) S. WOLFE, M.-H. WHANGBO, and D. J. MITCHELL. Carbohydr. Res. **69**, 1 (1979).
21. (*a*) A. A. SOLOV'EV, E. I. KADENTSEV, and O. S. CHIZHOV. Bull. Acad. Sci. USSR, Div. Chem. Sci. (Engl. Transl.) **25**, 2105 (1976); Izv. Akad. Nauk SSSR, Ser. Khim. **25**, 2256 (1976); (*b*) A. A. SOLOV'EV, V. I. KADENTSEV, and O. S. CHIZHOV. Bull. Acad. Sci. USSR, Div. Chem. Sci. (Engl. Transl.) **25**, 2110 (1976); Izv. Akad. Nauk SSSR, Ser. Khim. **25**, 2261 (1976).
22. A. A. SOLOV'EV, V. I. KADENTSEV, and O. S. CHIZHOV. Bull. Acad. Sci. USSR, Div. Chem. Sci. (Engl. Transl.) **25**, 2328 (1976); Izv. Akad. Nauk SSSR, Ser. Khim. **25**, 2500 (1976).
23. A. F. BOCHKOV and G. E. ZAIKOV. Chemistry of the *O*-glycosidic bond, formation and cleavage. Pergamon, New York. 1979. p. 177.
24. J. N. BEMILLER. Adv. Carbohydr. Chem. **22**, 25 (1967).
25. H. S. ISBELL and W. PIGMAN. Adv. Carbohydr. Chem. **24**, 13 (1969).
26. K. GOTO and T. CHITANI. Bull. Chem. Soc. Jpn. **16**, 403 (1941).
27. W. PIGMAN and H. S. ISBELL. Adv. Carbohydr. Chem. **23**, 11 (1968).
28. C. B. PURVES and C. S. HUDSON. J. Am. Chem. Soc. **59**, 1170 (1937).
29. R. L. WHISTLER and R. M. HIXON. J. Am. Chem. Soc. **60**, 563 (1938).

Can. J. Chem. Downloaded from www.nrcresearchpress.com by 123.30.183.119 on 09/08/12
For personal use only.

An NMR study of the structure and reactivity of phosphonium ylides stabilized by a carbonyl function

MARGARET M. KAYSER[1] AND KRISTA L. HATT
Department of Chemistry, University of New Brunswick, P.O. Box 5050, Saint John, N.B., Canada E2L 4L5
AND
DONALD L. HOOPER
Department of Chemistry, Dalhousie University, Halifax, N.S., Canada B3H 4J3

Received March 26, 1991

MARGARET M. KAYSER, KRISTA L. HATT, and DONALD L. HOOPER. Can. J. Chem. **69**, 1929 (1991).

The structures of five stabilized phosphonium ylides **1–5** were studied by ^1H, ^{13}C, and ^{31}P NMR. Various trapping experiments were followed by investigation of the relative reactivities of these ylides vis-à-vis benzaldehyde. A novel effect of some significance, the influence of acidic contaminants (conjugate acids, H_2O, etc.) on the structure and reactivity of these compounds, is discussed.

Key words: stabilized phosphoranes, Wittig condensations, acid catalysis.

MARGARET M. KAYSER, KRISTA L. HATT et DONALD L. HOOPER. Can. J. Chem. **69**, 1929 (1991).

Faisant appel à la RMN du ^1H, du ^{13}C et du ^{31}P, on a étudié les structures de cinq ylures de phosphonium stabilisés (**1–5**). Après diverses expériences de piégeage, on a aussi examiné les réactivités relatives des ces ylures vis-à-vis du benzaldéhyde. On discute d'un nouvel effet qui a une certaine importance : l'influence des contaminants acides (acides conjugués, H_2O, etc.) sur la structure et la réactivité des ces composés.

Mots clés : phosphoranes stabilisés, condensations de Wittig, catalyse acide.

[Traduit par la rédaction]

Introduction

Stabilized phosphoranes such as methyl (triphenylphosphoranylidene)acetate **1** or 1-triphenylphosphoranylidene-2-propanone **4** derive much of their importance from their utility in the synthesis of α,β-unsaturated esters and ketones. As a result, numerous studies on the mechanism and stereochemistry of these condensations have been conducted over the years (1, 2). In spite of considerable efforts no experimental evidence of any, even transient, intermediates has so far been reported, and the course of these reactions still remains largely speculative (3).

In the course of our studies of the condensations of stabilized phosphoranes with various cyclic anhydrides by ^{31}P NMR, we noted small but persistent downfield drifts of ylide signals. As it was not clear whether the drifts were related to the temperature variation or to some transformation of the ylide during the reactions, we decided to conduct a background study of the temperature-related behaviour of selected stabilized ylides prior to the investigation of their condensations with carbonyl compounds.

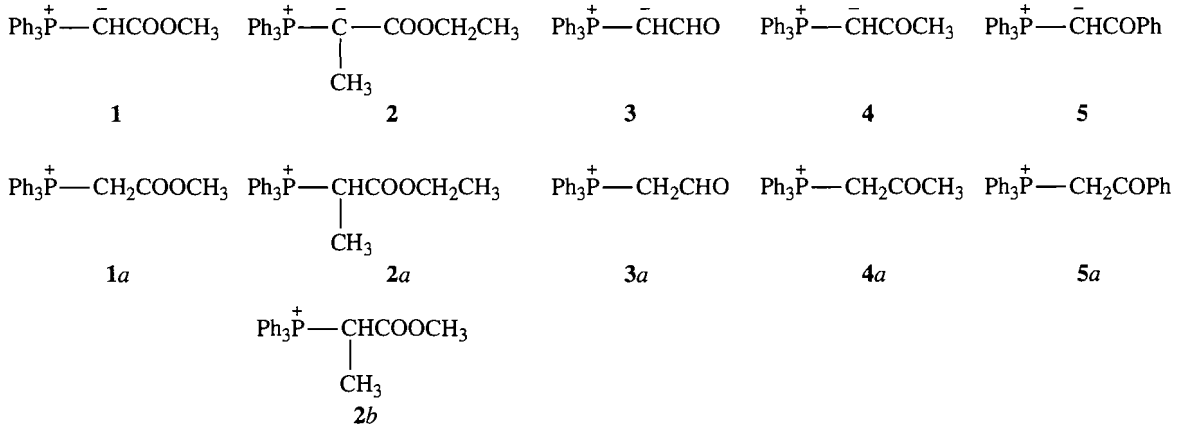
This paper reports a variable-temperature ^1H, ^{13}C, and ^{31}P NMR study of five commonly used ylides **1–5**, the subsequent investigation of their structures, and a base-line comparison of their reactivities vis-à-vis benzaldehyde.

Results

Our ^1H NMR study of ylide **1**, discussed extensively in the previous communication (7), supported the earlier findings (4–6). More complete data on the ^1H, ^{13}C, and ^{31}P chemical shifts and nuclear spin coupling constants for the five ylides under investigation are listed in Tables 1 and 2.

Methyl (triphenylphosphoranylidene)acetate 1

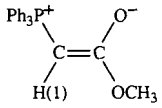
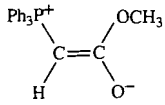
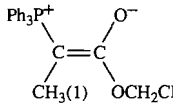
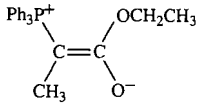
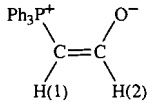
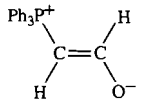
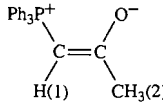
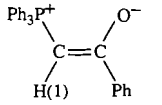
As the spectroscopic data for ylide **1** have been discussed previously (7) only the main points are reiterated here. The ^1H NMR spectrum of phosphorane **1** at room temperature shows two sharp signals corresponding to the protons of the methoxy group at 3.50 ppm and the methine proton at 2.95 ppm. No proton–phosphorus coupling is observed since the highly labile proton exchanges rapidly with traces of acidic contaminants



[1]Author to whom correspondence may be addressed.

Can. J. Chem. Downloaded from www.nrcresearchpress.com by 123.30.183.119 on 09/08/12
For personal use only.

TABLE 1. ^1H chemical shifts (ppm) and coupling constants (Hz)

Structure	No.	$t = +22°C$ H(1) $CH_3(2)$	OCH_3	OCH_2—CH_3	H(2) $CH_3(2)$	$t = -40°C$ H(1) $CH_3(1)$	OCH_3	OCH_2—CH_3	H(2) $CH_3(2)$
	**1**-*cis*					3.046 J_{PH}21.1	3.565		
		2.903 br	3.508 br						
	**1**-*trans*					2.86 J_{PH}20.9	3.360		
	**2**-*cis*					1.64 J_{PH}13.96		4.07 J_{HH}7.0	1.281 J_{HH}7.0
		1.630 J_{PH}14.0		3.775	0.720				
	**2**-*trans*					1.64 J_{PH}13.96		3.73 J_{HH}7.0	0.373 J_{HH}7.0
	**3**-*cis*	3.660 J_{HH}3.5 J_{PH}24.5			9.00 J_{HH}3.5 J_{PH}38.0	3.660 J_{HH}3.5 J_{PH}24.5			9.00 J_{HH}3.5 J_{PH}38.5
	**3**-*trans*	4.071 J_{HH}10.8 J_{PH}24.5			8.27 J_{HH}10.8 J_{PH}3.5	4.071 J_{HH}10.8 J_{PH}19.5			8.27 J_{HH}10.8 J_{PH}3.5
	**4**-*cis*	3.70 J_{PH}26.0			210 J_{PH}3.0	3.70 J_{PH}26.0			2.10 J_{PH}3.0
	**5**-*cis*	4.43 J_{PH}24.5				4.43 J_{PH}24.5			

(conjugate acid, atmospheric water, traces of DCl from solvent) at room temperature. When care is taken to minimize atmospheric moisture, both signals broaden significantly. When the ylide and the solvent $CDCl_3$ are treated to remove traces of water, and the spectra recorded under anhydrous conditions, further broadening is observed. At low temperatures, proton exchange slows sufficiently for the phosphorus–hydrogen coupling to be observable; moreover, as the proton exchange is slowed it becomes evident that the ylide exists in two distinct isomeric forms, *cis* (*E*) and *trans* (*Z*).

When a trace amount of BuLi is added to the $CDCl_3$ solution of the ylide, to remove conjugate acid and all other sources of acidic protons, the two isomeric structures become sharply distinct even at room temperature, their stability increased by the complexation of the enolate ions **1**-*cis* and **1**-*trans* (in the ratio 3:1) with available lithium cations.

It should be pointed out, however, that the lithium cation, although apparently stabilizing, is not essential for the room temperature stability of **1**-*cis* and **1**-*trans*. When other "proton sponges" such as CaH_2 or 1,1,1,3,3,3-hexamethyldisilazane are employed, the spectra of **1** are very similar to those obtained after treatment with BuLi. The ^{13}C and ^{13}P NMR studies of ylide **1** confirm the above findings (7).

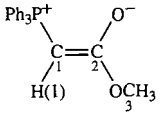
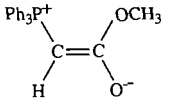
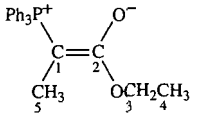
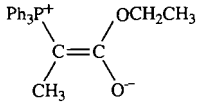
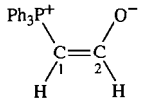
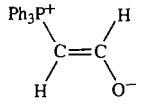
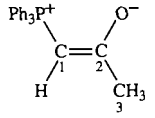
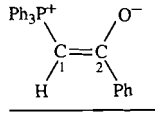
(Carboethoxyethylidene) triphenylphosphorane **2**

At −40°C ylide **2** also exists in two isomeric forms, with the **2**-*trans* (*Z*) configuration being the more abundant (75%) according to Crouse *et al.* (8). At this temperature the signals for the methylene protons (-OCH_2CH_3) show as two sharp quartets at 3.73 ppm *trans* and 4.07 ppm *cis* and the two methyl triplets are at 0.37 ppm *trans* and 1.28 ppm *cis*, Fig. 1. On warming to +35°C the methylene protons collapse to a single distinct quartet while the methyl group gives a broad poorly defined triplet. The two isomeric forms, however, become clearly distinguishable at this temperature when the sample is treated with a drop of BuLi.

The ^{13}C shift and coupling data for **2** at −40°C indicate the presence of a mixture of *cis* and *trans* structures. At room temperature, only a single form is observable, with chemical shifts corresponding closely to those described by Gray (9). This spectrum resolves to that of the two forms upon addition of BuLi.

Can. J. Chem. Downloaded from www.nrcresearchpress.com by 123.30.183.119 on 09/08/12
For personal use only.

TABLE 2. ^{13}C and ^{31}P chemical shifts (ppm) and coupling constants (Hz)

Structure	No.	$t = +24°C$ C_1	C_2	C_3	C_4	C_5	$t = -40°C$ C_1	C_2	C_3	C_4	C_5	^{31}P +24°C	^{31}P −40°C
	**1**-*cis*	29.78 J_{PC}127	171.6	49.73			29.76 J_{PC}129.7	171.57	50.12			17.83 br	17.58 sh
	**1**-*trans*						30.55 J_{PC}120.3	171.74	49.62			16.30 br	16.20 sh
	**2**-*cis*	32.30 J_{PC}122	171.0	57.30	14.12	12.82	32.75 J_{PC}128	sh	57.98	15.15	12.3 J_{PC}12.4	23.18	23.48 br
	**2**-*trans*						32.21 J_{PC}120.9	170.53	57.38	13.84	12.71 J_{PC}12.4		
	**3**-*cis*	54.86 J_{PC}99.5	181.48				54.86 J_{PC}99.5	181.48				13.99	13.98
	**3**-*trans*	56.55 J_{PC}110.7	181.58				56.55 J_{PC}110.7	181.58				18.03	18.00
	**4**-*cis*	51.54 J_{PC}107.7	190.61	28.38 J_{PC}15.8			52.12 J_{PC}107.6	190.6	28.53 J_{PC}14.2			13.23	13.21
	**5**-*cis*	50.54 J_{PC}112	184.80 J_{PC}3.5									21.6	

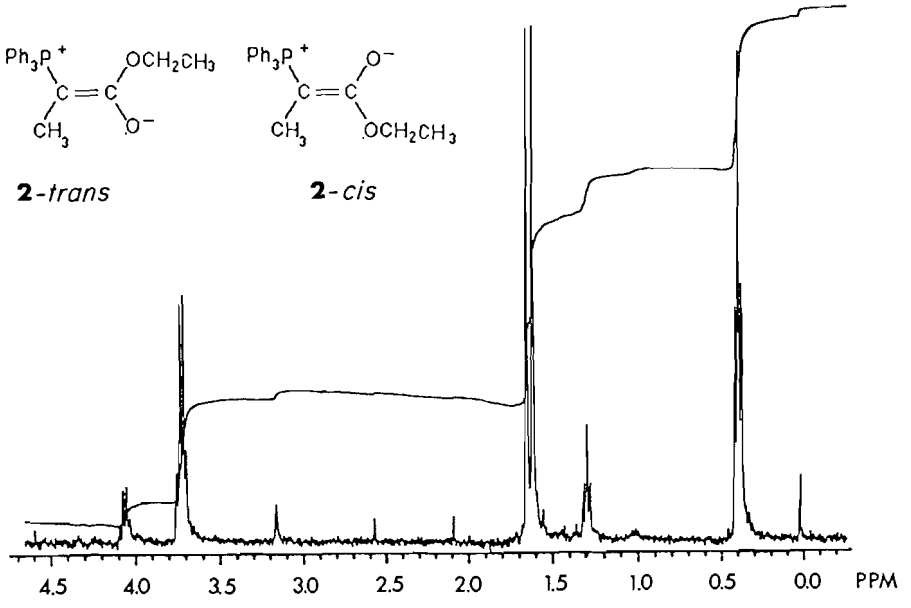


FIG. 1. ^{1} NMR spectrum of phosphorane **2** recorded at −40°C. The **2**-*trans* is the major product.

Can. J. Chem. Downloaded from www.nrcresearchpress.com by 123.30.183.119 on 09/08/12
For personal use only.

Can. J. Chem. Downloaded from www.nrcresearchpress.com by 123.30.183.119 on 09/08/12
For personal use only.

In the low temperature ^{31}P spectrum, a commercial sample of ylide **2** gives a broad peak at 23.48 ppm, and a small signal corresponding to its conjugate acid, **2***a*, at 26.29 ppm. Even on treatment with BuLi, which removes the conjugate acid, the peak at 23.48 ppm ($\nu_{\frac{1}{2}}$ = 65 Hz) is not resolved, indicating that the ^{31}P signals of the two isomers overlap. This is confirmed by the fact that as the temperature is raised to +20°C the signal becomes considerably narrower ($\nu_{\frac{1}{2}}$ = 34 Hz).

(Triphenylphosphoranylidene)acetaldehyde 3

NMR shows that a sample of ylide **3**, dried but not treated with BuLi, is a mixture of isomeric forms **3**-*cis* (*Z*) and **3**-*trans* (*E*) in the ratio 3:2 even at room temperature. Coalescence of the signals occurs above 80°C, which, along with the low temperature limiting frequency difference, corresponds well to the $\Delta G^{\neq}$ = 17.6 kcal/mol calculated by Snyder and Bestmann (10).

At low temperature (−40°C), spectra of **3** are identical to those run at room temperature, Fig. 2. When precautions are not taken to prevent the exposure of ylide **3** to air and moisture, the ^{1}H NMR spectrum at +30°C shows broad singlets without distinguishing features for all protons. The conjugate acid **3***a* is unstable; we were unable to prepare it or even to observe its signals in the NMR spectra.

1-Triphenylphosphoranylidene-2-propanone 4

Only a single structure is discernible for ylide **4** in NMR spectra at −40°C, as well as at room temperature. In the ^{1}H spectrum the methine proton is a doublet centered at 3.70 ppm with J_{PH} = 26 Hz. Methyl protons show as a doublet at 2.10 ppm with the coupling constant to ^{31}P of 3 Hz. In the presence of traces of conjugate acid both methine and methyl signals collapse to singlets. The ^{31}P spectra of **4** at room temperature and at −40°C show only a sharp singlet at 13.23 ppm ($\nu_{\frac{1}{2}}$ = 4.96 Hz).

Benzoylmethylene triphenylphosphorane 5

In a room temperature ^{1}H spectrum of a commercial sample of ylide **5**, the methine proton shows as a broad doublet. On adding a drop of butyl lithium the two peaks sharpen, but with no significant shift in the position of the doublet centered at 4.55 ppm with J_{PH} = 25 Hz. The spectrum corresponding to a single structural form is temperature invariant between +25 and −40°C. ^{13}C and ^{31}P spectra confirm that only one structural form can be detected by NMR. These results are in agreement with the earlier reports (4, 11–14).

The geometries of isomeric conformers in stabilized ylides

Assignment of the preferred *cisoid* conformation for ylides **1**, **3**, **4**, and **5** was based on the patterns of methine proton absorptions and the effects of diamagnetic shielding on the chemical shifts of the -OCH_3 or -OCH_2CH_3 groups in the *cis* form (4). The latter effect was invoked also to assign the *trans* conformation to the predominant isomeric structure in ylide **2** (8).

We confirmed these assignments in a series of trapping experiments. In general, triethyloxonium tetrafluoroborate was used for trapping reactions at low temperatures (−78 to −30°C), while trimethyloxonium tetrafluoroborate, which is insoluble in organic solvents at low temperatures, was reserved for the reactions carried out at room temperature. The ^{1}H and ^{13}C NMR shifts for the trapped ylides are shown in Table 3.

Ylide **1** trapped with triethyloxonium tetrafluoroborate at −78°C gave a mixture of two isomeric products **6**-*cis* and **6**-*trans* corresponding to the original ratio of **1**-*cis* (*E*) and **1**-*trans* (*Z*) observed at low temperatures. The major product showed a highly shielded methyl triplet (-OCH_2CH_3) with δ 0.728 indicating that the newly introduced ethyl group was in the region of diamagnetic shielding of the phenyl substituent on the phosphorus atom.

When the trapping experiment was carried out with trimethyloxonium tetrafluoroborate at 0°C, no *O*-alkylation could be detected in the crude reaction mixture; the product obtained consisted of a mixture of *C*-alkylated compound **2***b* and the conjugated acid **1***a*. The identities of the two products were confirmed by the two-dimensional $^{1}H/^{13}C$ chemical shift correlation spectrum shown in Fig. 3.

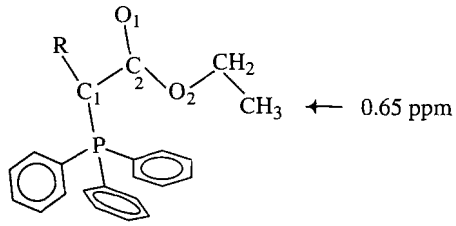
By analogy with phosphorane **1**-*cis* (*E*) and **1**-*trans* (*Z*), the assignment of the *trans* (*Z*) configuration to the predominant structure in **2** was based on the fact that the major isomer possessed a highly shielded methyl triplet at 0.373 ppm. When **2** was treated with triethyloxonium tetrafluoroborate at −78°C, the two ethoxy groups became clearly visible, with the methyl of the new ethoxy group appearing at the lower field (1.469 ppm), **7**, Table 3.

Ylide **3**, which exists in two forms at room temperature, was trapped with triethyloxonium tetrafluoroborate at 0°C. The ratio of salts **8**-*cis* and **8**-*trans* was found to correspond exactly to the ratio of isomeric forms **3**-*cis* and **3**-*trans* observed at room temperature. The major isomeric form **3**-*cis* gave the major compound **8**-*cis* with the more highly shielded methyl of the ethoxy group (methyl triplet at 0.937 ppm).

The NMR spectra of anhydrous **4** in $CDCl_3$ were invariant over the range of −30 to +40°C. This suggested that ylide **4** is essentially biased toward one conformation **4**-*cis* (*Z*), according to the trapping experiment with triethyloxonium tetrafluoroborane. The ^{1}H spectrum of the trapped product showed a highly shielded methyl triplet at 0.685 ppm belonging to an ethoxy group *cis* to the phosphorus atom.

Ylide **5** was trapped cleanly with triethyloxonium tetrafluoroborate at 0°C to give only one vinylic ether identified as **10**-*cis*. The methyl group of the new ethoxy group is diamagnetically shielded by the phenyl rings on the phosphorus (0.60 ppm), confirming the original structural assignment.

Additional support for geometry assignments for the two forms of ylides comes from the crystallographic study of a related ylide **11** (15). In **11** the ethoxy group *cis* to the phosphorus atom is located within the shielding region of one of the phenyl rings. In the ^{1}H NMR spectrum its methyl triplet appears, as expected, at higher field with δ 0.65 (16), suggesting that in the solution as in the crystalline state the same conformation is preferred energetically.



11, R = —CCH_2CH_2COOH (O)

Reactions of ylides with benzaldehyde

A low-temperature condensation monitored by ^{31}P NMR showed that when a solution of benzaldehyde in $CDCl_3$ cooled to −30°C was added to a frozen $CDCl_3$ solution of **1** and the temperature was subsequently maintained at −30°C the ylide's

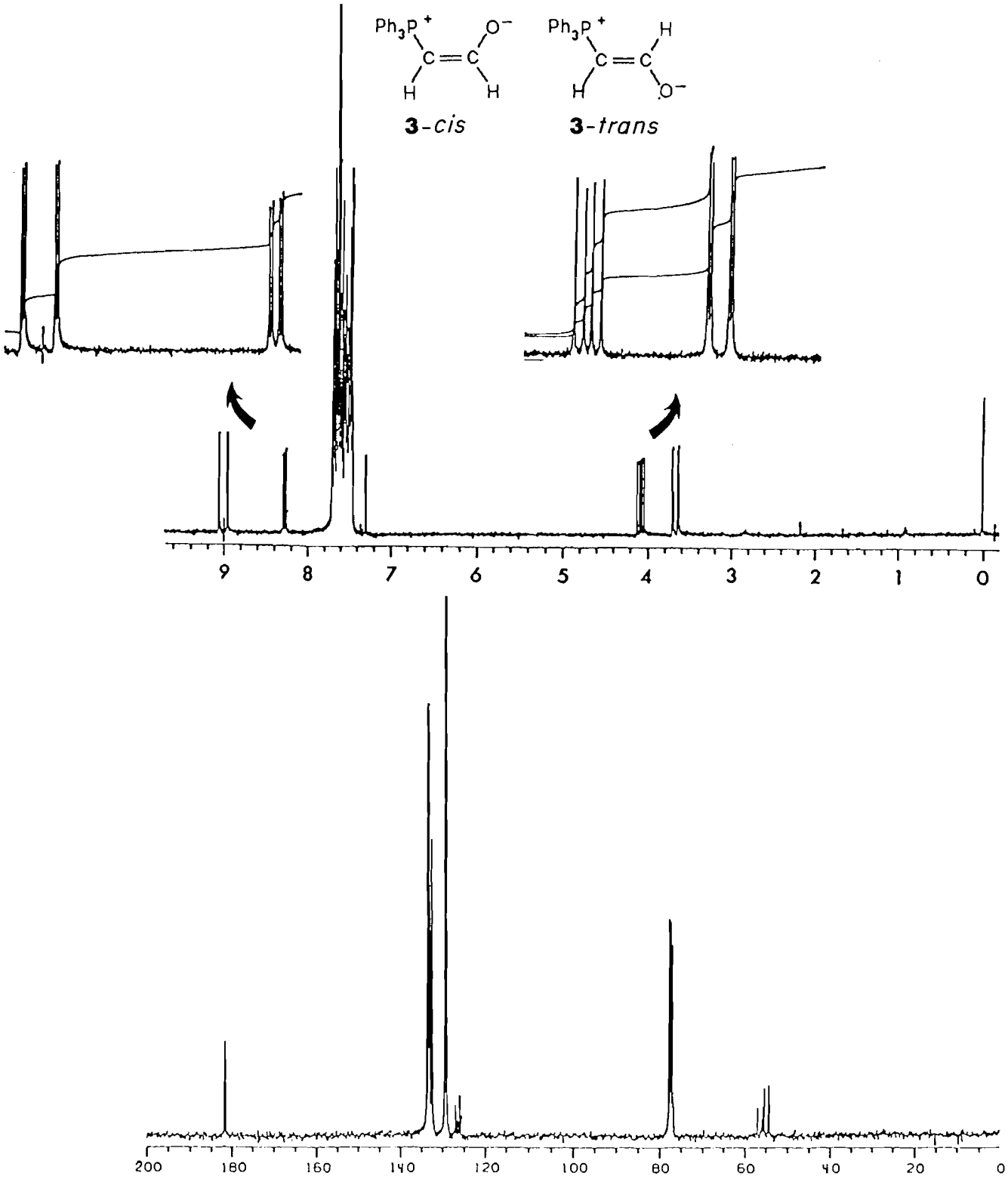


FIG. 2. ^{1}H and ^{13}C room temperature NMR spectra for ylide **3**.

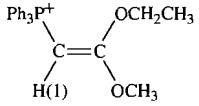
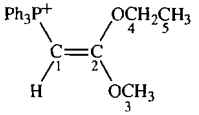
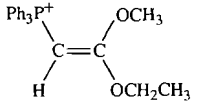
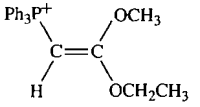
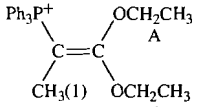
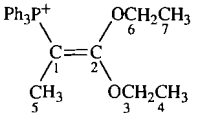
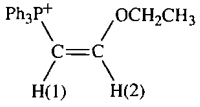
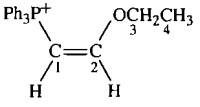
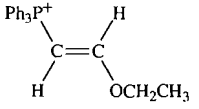
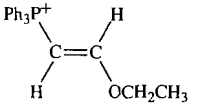
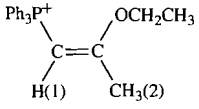
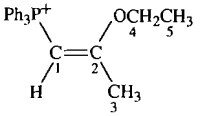
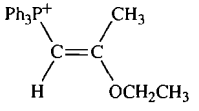
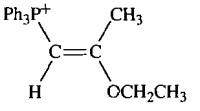
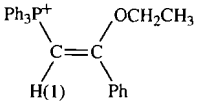
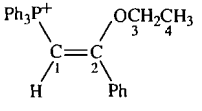
two signals at 17.99 and 16.43 ppm collapse instantaneously to a sharp singlet at 17.87 ppm. As the temperature was raised to −20°C the product (triphenylphosphine oxide) peak appeared. The reaction proceeded rapidly and after 90 min most of benzaldehyde was consumed, as shown by proton NMR. The product, methyl cinnamate, was contaminated with some conjugate acid **1***a*, indicating that acidic impurities originally present in the reaction mixture converted part of the ylide into its conjugate acid.

In the course of the reaction the new signal at 17.87 ppm corresponding to the "reactive" ylide diminished as the product peak grew. It also drifted slightly toward lower field. We

Can. J. Chem. Downloaded from www.nrcresearchpress.com by 123.30.183.119 on 09/08/12
For personal use only.

Can. J. Chem. Downloaded from www.nrcresearchpress.com by 123.30.183.119 on 09/08/12
For personal use only.

TABLE 3. ^{1}H and ^{13}C chemical shifts (ppm) and coupling constants (Hz) for ylides trapped with $(CH_3CH_2)_3OBF_4$

Structure	No.	t = +24°C H(1) CH_3(2)	OCH_3	OCH_2CH_3	H(2) CH_3(2)	Structure	No.	t = +24°C C1	C2	C3	C4	C5
	**6**-*cis*	4.282 J_{PH}11.1	4.138	4.023 0.728			**6**-*cis*	47.50 J_{PC}115.5	172	65.20	59.12	13.77
	**6**-*trans*	4.249 J_{PH}11.2	3.550	4.463 1.479			**6**-*trans*	48.0 J_{PC}117	168	55.26	68.94	23.07
	**7**	1.727 J_{PH}14.7		A 3.569 A 0.490 B 4.439 B 1.469			**7**	67.34 J_{PC}99.9	168.72 J_{PC}11.1	C6 65.33 C3 70.89	C7 15.2 C4 19.90	30.47
	**8**-*cis*	5.367 J_{PH}16.0 J_{HH}6.9		4.093 0.937	*a*		**8**-*cis*	78.70 J_{PC}105.8	170	66.14	14.89	
	**8**-*trans*	5.909 J_{PH}13.3 J_{HH}12.0		4.336 1.377	6.779 J_{PH}13.2 J_{HH}12.0		**8**-*trans*	77.86 J_{PC}93.9	168.67 J_{PC}24.5	68.82	14.54	
	**9**-*cis*	5.193 J_{PH}18.1		3.985 0.685	2.416		**9**-*cis*	75.61 J_{PC}101.5	178.85	19.83 J_{PC}11.0	65.84	13.84
	**9**-*trans*	5.088 J_{PH}11.7		4.251 1.417	1.704		**9**-*trans*					
	**10**-*cis*	5.485 J_{PH}17.6		3.636 0.603			**10**-*cis*	83.16	178.28	68.38	13.88	

[a] H(2) hidden under aromatic protons.

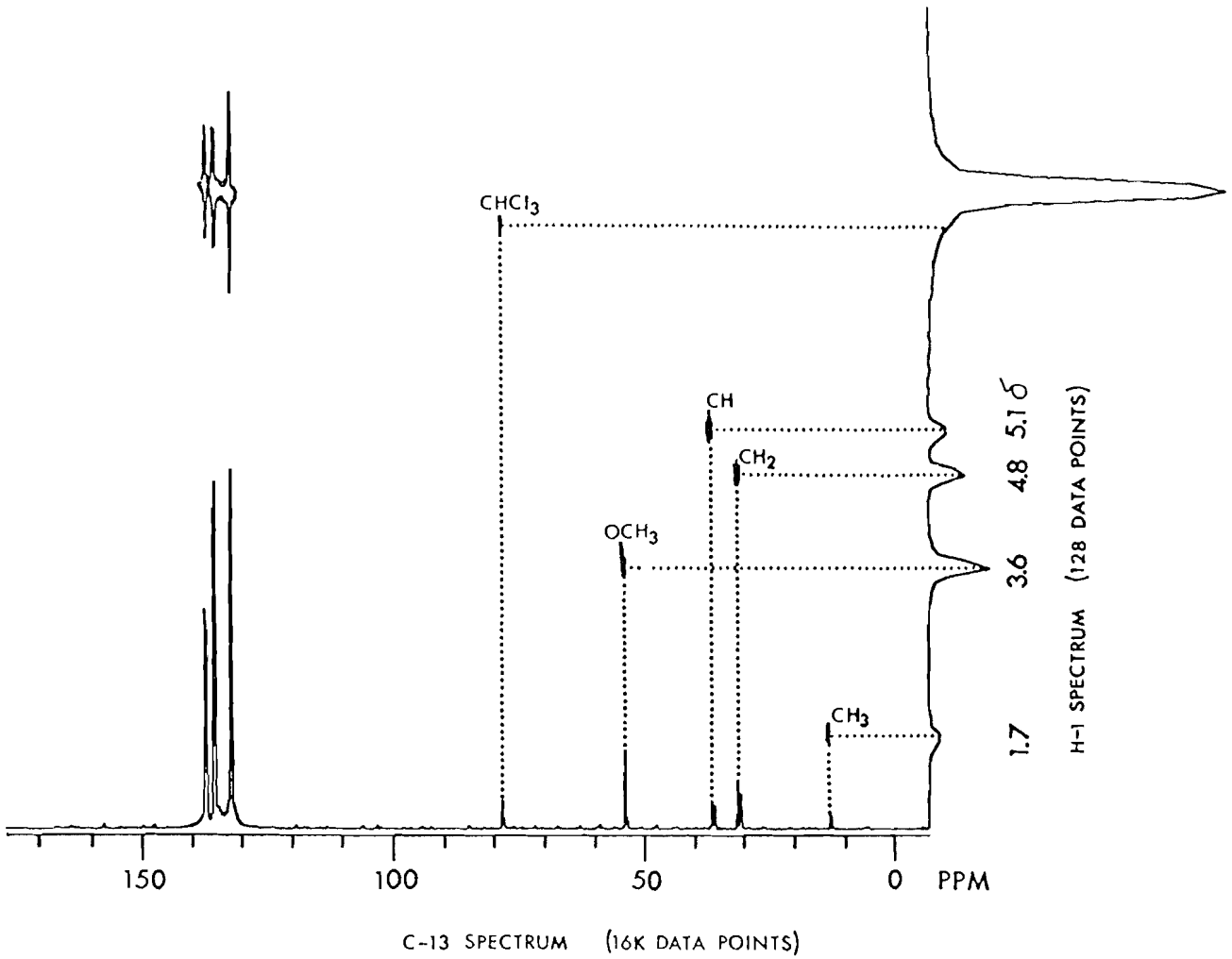


FIG. 3. Two-dimensional $^{1}H-^{13}C$ chemical correlation spectrum for the product of the reaction of the ylide **1** with trimethyloxonium tetrafluoroborate at 0°C.

suppose that the observed downfield drift is due to the continuously changing proportion of the rapidly exchanging ylide – conjugate acid pair as the ylide is consumed during the reaction. This view is supported by the fact that if a reaction, containing an excess of the ylide, is allowed to stand for several days at room temperature, the remaining ylide is slowly hydrolyzed by traces of atmospheric moisture and the only peak observable, other than that of the product, is the signal for the conjugate acid **1***a* at 21.42 ppm.

When the $CDCl_3$ solution of the ylide was treated with BuLi prior to the reaction with freshly distilled benzaldehyde at −30°C, the *cis* and *trans* signals persisted throughout the reaction, which was, in this case, quite slow. After 90 min at −20°C, less than 5% triphenylphosphine oxide showed in the ^{31}P spectrum. After standing for over 15 h at room temperature, the two signals of the ylide were small but clearly distinct, while a trace of benzaldehyde could be still be detected in the proton spectrum of the reaction mixture.

Phosphorane **2** is comparable in behaviour and reactivity to **1**. Both ylides react faster with benzaldehyde in the presence of traces of acidic contaminants and are significantly slower when a proton sponge is added to the reaction mixture.

Ylides **1** and **2** are considerably more reactive than **3**, **4**, and **5**. To illustrate this we compared room temperature condensations of the five phosphoranes, recrystallized but not otherwise treated, with freshly distilled benzaldehyde. Starting with a 1:1 ratio of the two reactants dissolved in $CDCl_3$, we monitored the time required to consume 50% of the ylide. Under the identical experimental and atmospheric conditions[2] the reactions with ylides **1** and **2** reached a half-time within 5 to 8 min, the reaction with **4** took 100 min, while the reaction with **5** required approximately 4 h. The condensation of benzaldehyde with **3** was much slower and no appreciable progress could be detected even after 4 h.

Room temperature condensations of benzaldehyde with ylides **1**, **4**, and **5** in presence of a small quantity of a proton sponge (hexamethyldisilazane) were noticeably slower, taking roughly twice as much time to reach the 50% point as the reactions described above.

Discussion

In an effort to better understand the structure/reactivity relationship in stablized ylides, we attempted to correlate the

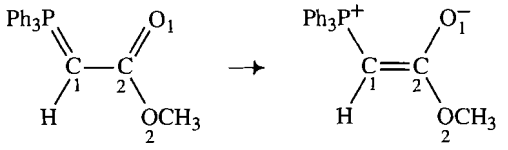
[2]It should be pointed out that since the rates of these reactions are highly variable, depending on how anhydrous are the reaction conditions, the same condensations carried out with highly purified ylides on a very dry day would all take a longer time, but their relative rates would be comparable.

Can. J. Chem. Downloaded from www.nrcresearchpress.com by 123.30.183.119 on 09/08/12
For personal use only.

Can. J. Chem. Downloaded from www.nrcresearchpress.com by 123.30.183.119 on 09/08/12
For personal use only.

results from our NMR study with available crystal structures. A search of the literature showed that although many phosphoranes have been investigated by X-ray crystallography (17), only two of the ylides included in our study, **1** and **5**, are among them (18, 19). Pertinent bond lengths, ^{13}C chemical shifts, and pK_a values for a series of ylides are listed in Table 4.

X-ray analysis of **1** showed the $PCHC(O)CH_3$ fragment to be almost planar, with both a short P—C bond and a significant double bond character in the C—C bond, Table 4. Thus, it was suggested that the best representation for ylide **1** appears to be a resonance hybrid between forms **1**-"ylide" and **1**-*cis* (18).



1-"ylide" **1**-*cis*

Although in ylides **1**, **5**, and **11** the P—C1 bonds are quite short (20), the ^{13}C chemical shifts show that there is a considerable negative charge localized on the C1 carbon of each ylide. Hence, the small P—C1 separation may be largely due to an important electrostatic attraction between P^+ and C^-. This conclusion is supported by the ^{31}P spectra of the ylides, which show P atoms highly deshielded, with chemical shifts very similar to those of their conjugate acids.[3]

Extended Hückel calculations for model compounds H_3PCH_2 and $CH_2PH_3CH_2$ show that, although including the 3*d* orbitals on phosphorus results in reduction of charge separation and an increase in P–C overlap population, there is essentially no barrier to rotation of the PH_3 group, and the ylide carbon remains quite negative (21).

In view of the high negative charge concentration on the carbon atom of the ylide, one might expect that in stabilized ylides an important charge delocalization should occur toward the electron-attracting or conjugating groups substituted on the carbon.

The fact that in several stabilized ylides two isomeric forms are observable by NMR, and the facility with which these ylides can be trapped as vinylic ethers, provides experimental evidence for the concentration of a significant negative charge on the carbonyl oxygen atom, particularly in compounds such as **3**, **4**, and **5** that are so easily *O*-alkylated.

The bond lengths from the crystal structures confirm an important contribution from the enolate forms in ylides **1** and **5**, Table 4. Thus, in **1** the C1—C2 bond is closer in length to a normal C_{sp2}—C_{sp2} double bond (1.34 Å) than to a C_{sp2}—C_{sp2} single bond (1.46 Å), while the C2—O1 bond seems to be largely a single bond. In compound **5** the length of the corresponding C1—C2 bond also suggests significant double bond character, but the C2—O1 bond is somewhat shorter. The apparent C2—O1 single bond character in **1** is enhanced by electron delocalization within the carboalkoxy group. Since such delocalization diminishes the contribution of enolate forms in compound **1**, it thereby increases the relative contribution of the $Ph_3P^+C^-HCOOCH_3$ form,[4] making it a more reactive ylide, and more difficult to trap as an enolate.

These conclusions are in agreement with the pK_a values and ^{13}C chemical shifts for C1 atoms. Thus, it is the ylide with the highest negative charge on its C1 carbon atom that has the lowest barrier to rotation and the highest reactivity.

Alkyl triphenylphosphonium salts are deprotonated only by very strong bases such as lithium alkyls or aryls or sodium amide in liquid ammonia. In phosphonium salts substituted with electron-attracting or conjugating groups, the acidity of the α-protons is considerably increased and the corresponding ylides are much weaker bases. Within the series of ylides studied, **1** is a stronger base (pk_a 8.8) than either **4** (pK_a 6.6) or **5** (pK_a 6.0). Kinetic studies have demonstrated that the rate of the reaction between benzaldehyde and a series of stabilized ylides increases logarithmically with their basicity (22). It may be anticipated, therefore, that ylide **1** (and the related ylide **2**) exchanges with protic acids more rapidly than **4** or **5**. This, in fact, is the key to their structure as well as their reactivity.

In view of the above, we propose the scenario illustrated, for ylide **1**, in Scheme 1. In the absence of a catalytic amount of acidic protons, ylide **1** is best represented by slowly (on the NMR time scale) interconverting *cis* and *trans* enolate forms. The observed 3:1 ratio reflects the relative stabilities of the two structures. When a source of acidic hydrogen atoms is introduced, proton exchange between the ylide and the protic acid occurs. This rapid exchange involves the reactive ylide, i.e., the form best represented by the resonance structure in which the negative charge is highly concentrated on the carbon atom of the ylide during the rotation about the C1—C2 bond. If a reactive carbonyl compound such as an aldehyde or a cyclic anhydride is available, addition to the carbonyl can occur instead of proton exchange. At low temperatures the coexistence of the two enolate forms is due to a slower rate of methine proton exchange (7).

Addition of BuLi removes all traces of acids, including the conjugate acid, and hence the low-energy route for the conversion of the two isomers. As a result, even at room temperature on the NMR time scale each of the isomers becomes more stable, further fixed in its enolate form by complexation with lithium cations. It should be pointed out that the complexation of the enolate(s) by Li cations has no effect on the ^{13}C chemical shifts. There is no increase in the enolate's contribution to the hybrid, it simply becomes more stable. An ylide "trapped" as an enolate will react preferentially with "hard acids" at the oxygen atom.

The less basic ylides **3**, **4**, and **5** are not nearly as sensitive to traces of acidic protons and under reasonably anhydrous conditions exist at room temperature in largely delocalized form(s). However, here also, addition of excess acid and (or) raising the temperature promotes proton exchange and faster rotation about the C1—C2 bond.[5]

The conclusions derived from this study may be summarized as follows:

1. The general description of stabilized ylides is not adequately represented by the resonance hybrid shown in **1**-"ylide"/**1**-*cis*. Depending on the nature of the ylide, the possibility of having two isomeric forms, each a hybrid in its own right, must be examined. This is important not only to the understanding of the structure of stabilized ylides, but also to the understanding of their reactivities.

2. Within a series of stabilized ylides, ^{13}C chemical shifts for

[3]Chemical shifts for conjugate acids vary slightly depending on the counterions present. However, in all cases the signals in these salts are quite close to those of the corresponding ylides. For example, the chemical shift for $Ph_3PCH_2COOCH_3Br$ **1***a* ia 21.42 versus 17.99 ppm in **1**.

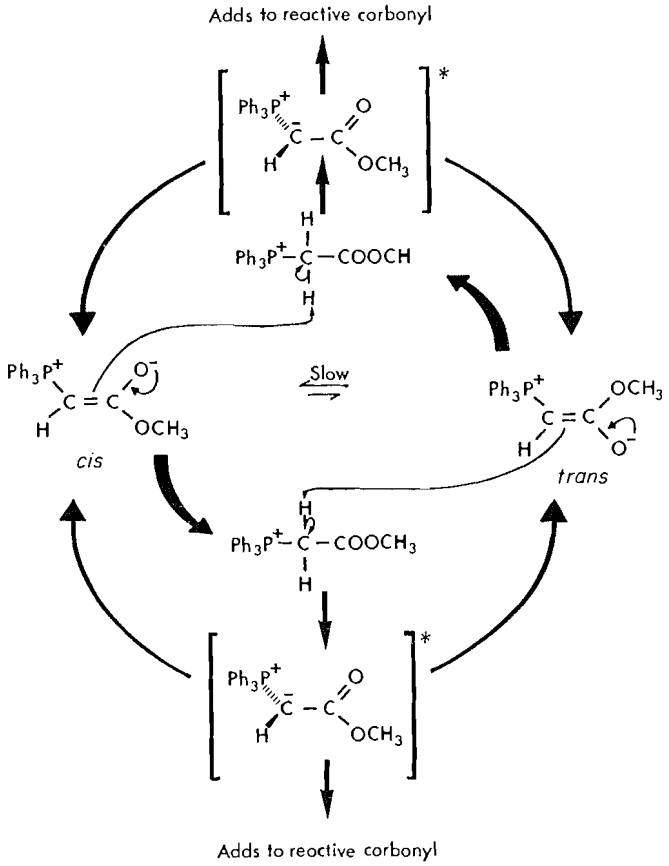
[4]This view is supported by the fact that Ph_3P-CH-C(O)-NH_2 is considerably more basic (pK_a 11) and more reactive than **1** (22, 23).

[5]Ylide **3** is moisture and light sensitive, hence it should be recrystallized from acetone and used under reasonably anhydrous conditions.

TABLE 4. Comparison of ^{13}C chemical shifts (ppm), bond lengths (Å), and pK_a values for a series of four ylides

Ylides	No.	C1	Ph—P	P—C1	C1—C2	C2—O1	pK_a of conjugate acid	Ref.
$Ph_3\overset{+}{P}-\underset{1}{\overset{-}{C}}H_2$	**12**	−4.1	1.823(5)	1.661(8)	—	—	>25	20
$Ph_3\overset{+}{P}-\underset{1}{\overset{-}{C}}H-\underset{2}{\overset{O1}{\overset{\|\|}{C}}}-OCH_3$	**1**	29.8	1.81	1.69(3)	1.378(3)	1.33(2)	8.8	18
$Ph_3\overset{+}{P}-\underset{1}{\overset{-}{C}}H-\underset{2}{\overset{O1}{\overset{\|\|}{C}}}-Ph$	**5**	50.5	1.81	1.71	1.390	1.26	6.0	19
$Ph_3\overset{+}{P}-\underset{1}{\overset{-}{C}}(\underset{3}{\overset{O3}{\overset{\|\|}{C}}}-CH_2CH_2COOH)-\underset{2}{\overset{O1}{\overset{\|\|}{C}}}-OCH_2CH_3$	**11**	73.0	1.807(3)	1.750(3)	1.452(5) C1—C3 1.425(4)	1.205(5) C3—O3 1.256(4)	Too weak to measure	15

Standard bond lengths: P=C, 1.66 Å; P—C, 1.87 Å; C=C, 1.34 Å; C3—C3, 1.46 Å; C=O, 1.22 Å; C3—O, 1.36 Å (ref. 24).



SCHEME 1

Cl atoms serve as an excellent indicator of the ylides' reactivity, as do the pK_a values of the corresponding conjugate acids.

3. It is not necessary to carry out condensations with stabilized ylides under strictly anhydrous conditions or with highly purified ylides, since traces of moisture or conjugate acid actually catalyze these reactions. The presence of "hard" cations such as Li^+ stabilizes the unreactive enolate forms, thus slowing the addition of an ylide to the reactive carbonyl groups. On the other hand, large excesses of moisture or other proton sources convert ylides into their conjugate acids, hence lowering the yields.[6]

[6]In the presence of moisture, ylide **1** is converted into its conjugate acid **1***a*, which slowly decomposes to Ph_3PO and methyl acetate.

Experimental

Nuclear magnetic resonance spectra were recorded at 361 MHz (^1H), 91 MHZ (^{13}C), and 146 MHz (^{31}P) on the Nicolet 360NB spectrometer of the Altantic Region Magnetic Resonance Centre, and some ^{31}P spectra were recorded at 81 MHz on the Varian XL-200 spectrometer of the University of New Brunswick. All spectra were recorded for $CDCl_3$ solutions. Calibration of the spectra was done with respect to TMS as the internal reference (^1H and ^{13}C) or 85% H_3PO_4 as external standard (^{31}P). Temperature control was by the usual Nicolet method. Calibration of the thermocouple showed an estimated error of less than 1° in the temperature range used. Line widths were measured by the Nicolet LF routine.

All the ylides used in this study were obtained from Aldrich or Lancaster Chemical Companies. For the reactions carried out under anhydrous conditions the ylides were dried by azeotropic treatment with benzene while $CDCl_3$ was dried over molecular sieves. The NMR tubes were heated at 150°C for at least 3 h and cooled under dry nitrogen. The reactions were run under argon.

General procedure for low temperature alkylation with triethyloxonium tetrafluroborate

Ylide (1.5 mmol) dissolved in 10 mL CH_2Cl_2 (dried over CaH_2 and distilled) was placed in an oven-dried 25-mL three-necked round bottom flask equipped with a dropping funnel and maintained under dry nitrogen. The stirred solution was cooled to −78°C and triethyloxonium tetrafluoroborate (1.5 mmol, 1.0 M in CH_2Cl_2) was added dropwise over 5 min to the vigorously stirred solution. The solution was stirred for an additional hour at −30°C, then allowed to warm slowly to room temperature. The solvent was removed under reduced pressure. The resulting reaction mixture was analyzed by ^1H and ^{13}C NMR.

General procedure for 0°C alkylation with trimethyloxonium tetrafluoroborate

Ylide (1.5 mmol) in 10 mL CH_2Cl_2 (dried over CaH_2 and distilled) was placed in an oven-dried 50-mL three-necked round bottom flask equipped with a dropping funnel and maintained under dry nitrogen. The solid trimethyloxonium tetrafluoroborate (1.6 mmol) was suspended in 20 mL CH_2Cl_2 and transferred into the dropping funnel. The suspension was added slowly to the stirred solution of the ylide cooled to 0°C. The stirring was continued for an additional hour and then the reaction mixture was allowed to warm to room temperature. Upon removing the solvent under reduced pressure the reaction product was analyzed by ^1H and ^{13}C NMR.

*Trapping of methyl (triphenylphosphoranylidene)acetate **1** at −78°C with triethyloxonium tetrafluoroborane*

The crude product was composed of the two isomers **6**-*cis* and **6**-*trans* in the ratio of 3:1. The major product **6**-*cis*: ^1H NMR δ: 0.728 (t, 3H, OCH_2CH_3), 4.023 (q, 2H, OCH_2CH_3), 4.138 (s, 3H, OCH_3),

Can. J. Chem. Downloaded from www.nrcresearchpress.com by 123.30.183.119 on 09/08/12
For personal use only.

Can. J. Chem. Downloaded from www.nrcresearchpress.com by 123.30.183.119 on 09/08/12
For personal use only.

4.282 (d, 1H, PC*H*, $^2J_{PH}$ = 11 Hz), 7.810–7.416 (aromatic H's); ^{13}C NMR δ: 13.77 (C5), 47.50 (C1, $^1J_{PC}$ = 115.5 Hz), 59.12 (C4), 65.20 (C3), aromatic, 172 (C2); the minor product **6**-*trans*: ^{1}H NMR δ: 1.479 (t, 3H, OCH_2CH_3), 3.550 (s, 3H, OCH_3), 4.249 (d, 1H, PC*H*, $^2J_{PH}$ = 11.2 Hz), 4.463 (q, 2H, OCH_2CH_3), 7.810–7.416 (aromatic H's); ^{13}C NMR δ: 23.07 (C5), 48.0 (C1, $^1J_{PC}$ = 117 Hz), 55.26 (C3), 68.94 (C4), aromatic, 168 (C2).

Trapping of methyl (triphenylphosphoranylidene)acetate ***1*** *at 0°C with trimethyloxonium tetrafluoroborane*

The crude mixture consisted of two products, *C*-alkylated ylide **2***b* and the conjugate acid **1***a*. Compound **2***b*: ^{1}H NMR δ: 1.67 (dd, 3H, $PCCH_3$, $^3J_{PH}$ = 18.4 Hz, $^3J_{HH}$ = 7.2 Hz), 3.55 (s, 3H, OCH_3), 5.06 (m, 1H, PC*H*), 7.58–7.84 (aromatic H's); ^{13}C NMR δ: 12.93, 36.06, 53.34, aromatic, 164.45; ^{31}P NMR δ: 28; conjugate acid **1***a*: ^{1}H NMR δ: 3.57 (s, 3H, OCH_3), 4.58 (d, 2H, PCH_2, $^2J_{PH}$ = 13.8 Hz), 7.58–7.84 (aromatic H's); ^{13}C NMR δ: 30.79, 53.34, aromatic, 164.45, ^{31}P NMR δ: 21.6.

Trapping of (carboethoxyethylidene) triphenylphosphorane ***2***

Ylide **2** (571 mg, 1.6 mmol) was dissolved in 20 mL CH_2Cl_2 (distilled from CaH_2) and cooled to −78°C in a dry, three-necked flask under nitrogen. Triethyloxonium tetrafluoroborate (300 mg, 1.6 mmol) was previously dissolved in a minimum amount of CH_2Cl_2. The ethylating agent was added to the ylide solution at −78°C and the mixture was stirred for 30 min before it was allowed to slowly warm to room temperature. The solvent was evaporated to give compound **7** containing some conjugate acid **2***a*. Trapped ylide **7**: ^{1}H NMR δ: 0.490 (t, 3H, OCH_2CH_3-A), 1.469 (t, 3H, OCH_2CH_3-B),1.727 (d, 3H, $PCCH_3$, $^3J_{PH}$ = 14.7 Hz), 3.569 (q, 2H, OCH_2CH_3-A), 4.439 (q, 2H, OCH_2CH_3-B), 8.10–7.60 (aromatic H's); ^{13}C NMR δ: 15.20 (C7), 19.90 (C4),30.47 (C5), 65.33 (C6), 67.34 (C1, $^1J_{PC}$ = 99.9 Hz), 70.89 (C3), aromatic, 168.72 (C2, J_{PC} = 11.1 Hz).

Trapping of triphenylphosphoranylidene acetaldehyde ***3***

Ylide **3** (240 mg, 0.8 mmol) was dissolved in 25 mL CH_2Cl_2 (distilled from CaH_2) at room temperature in a dry, three-necked flask under nitrogen. Triethyloxonium tetrafluoroborate (150 mg, 0.8 mmol) was previously dissolved in a minimum amount of CH_2Cl_2. The ethylating agent was added to the ylide solution at room temperature and the mixture was stirred for 30 min before the solvent was evaporated to give a mixture of two isomers **8**-*cis* and **8**-*trans* in the ratio 2:1. The major isomer **8**-*cis*: ^{1}H NMR δ: 0.937 (t, 3H, OCH_2CH_3), 4.093 (q, 2H, OCH_2CH_3), 5.367 (dd, 1H, PC*H*, $^2J_{PH}$ = 16.0 Hz, $^3J_{HH}$ = 6.9 Hz), 7.87–7.51 (aromatic H's); ^{13}C NMR δ: 14.89 (C4), 66.14 (C3), 78.70 (C1, $^1J_{PC}$ = 105.8 Hz), aromatic, 170 (C2); the minor isomer **8**-*trans*: ^{1}H NMR δ: 1.377 (t, 3H, OCH_2CH_3), 4.336 (q, 2H, OCH_2CH_3), 5.909 (dd, 1H, PC*H*, $^2J_{PH}$ = 13.3 Hz, $^3J_{HH}$ = 12.1 Hz), 6.779 (dd, 1H, PCC*H*, $^3J_{PH}$ = 13.2 Hz, $^3J_{HH}$ = 12.0 Hz), 7.87–7.51 (aromatic H's); ^{13}C NMR δ: 14.54 (C4), 68.82 (C3), 77.86 (C1, $^1J_{PC}$ = 93.9), aromatic, 168.67 (C2, $^2J_{PC}$ = 19.1 Hz).

Trapping of 1-triphenylphosphoranylidene-2-propanone ***4***

Ylide **4** (503 mg, 1.6 mmol) was dissolved in 20 mL of CH_2Cl_2 (distilled from CaH_2) and cooled to 0°C in a dry, three-necked flask under nitrogen. Triethyloxonium tetrafluoroborate (300 mg, 1.6 mmol) was previously dissolved in a minimum amount of CH_2Cl_2. The ethylating agent was added to the ylide solution at 0°C and the mixture stirred for 30 min before it was allowed to slowly warm to room temperature. The solvent was evaporated to give **9**-*cis*: ^{1}H NMR δ: 0.685 (t, 3H, OCH_2CH_3), 2.416 (s, 3H, CH_3), 3.985 (q, 2H OCH_2CH_3), 5.193 (d, 1H, PC*H*, $^1J_{PH}$ = 18.1 Hz), 7.85–7.50 (aromatic H's); ^{13}C NMR δ: 13.84 (C5), 19.83 (C3, $^3J_{PC}$ = 11.0 Hz), 65.84 (C4), 75.61 (C1, $^1J_{PC}$ = 101.5 Hz), aromatic, 178.85 (C2).

Trapping of benzoylmethylene triphenylphosphorane ***5***

Ylide **5** (609 mg, 1.6 mmol) was dissolved in 15 mL of CH_2Cl_2 (distilled from CaH_2) and cooled to 0°C in a dry, three-necked flask under nitrogen. Triethyloxonium tetrafluoroborate (300 mg, 1.6 mmol) was previously dissolved in a minimum amount of CH_2Cl_2. The ethylating agent was added to the ylide solution at 0°C and the mixture stirred for 30 min before it was allowed to warm to room temperature. The solvent was evaporated to give the trapped ylide **10**-*cis*: ^{1}H NMR δ: 0.603 (t, 3H, OCH_2CH_3), 3.636 (q, 2H, OCH_2CH_3), 5.485 (d, 1H, PC*H*, $^2J_{PH}$ = 17.7 Hz), 7.827–7.340 (aromatic H's); ^{13}C NMR δ: 13.88 (C4), 68.38 (C3), 83.16 (C1, $^1J_{PC}$ = 94.7 Hz), aromatic, 178.28 (C2); ^{31}P NMR δ: 17.38.

The conjugate acid **1***a* was purchased from Aldrich as the bromine salt. The other conjugate acids were prepared by treating the $CHCl_3$ solution of the corresponding ylide with concentrated HCl, drying, and evaporating the solvent. To introduce BF_4^- as the counterion, the solution of conjugate acid was treated with a slight excess of $AgBF_4$. The silver halide salt was removed by filtration and the solvent was evaporated to the new phosphonium salt, **1***a*: ^{1}H NMR δ: (PCH_2) 5.531 ($^2J_{PH}$ = 13.6 Hz) (Br^-) and 4.60 ($^2J_{PH}$ = 14.0 Hz) (BF_4^-); ^{13}C NMR δ: (PCH_2) 32.33 ($^1J_{PC}$ = 59.0 Hz) (Br^-) and 31.07 ($^1J_{PC}$ = 58.61 Hz) BF_4^-); **2***a*: ^{1}H NMR δ: ($PCHCH_3$) 6.850 (dq) (Cl^-) and 5.047 (dq) (BF_4^-); ($PCHCH_3$) 1.682 ($^3J_{PH}$ = 18.6 Hz, $^3J_{HH}$ = 7.1 Hz) (Cl^-) and 1.662 ($^3J_{PH}$ = 18.2 Hz, $^3J_{HH}$ = 7.1 Hz) (BF_4^-); ^{13}C NMR δ: (PC*H*) 36.11 ($^1J_{PC}$ = 52.2 Hz), ($PCHCH_3$) 12.91; **3***a*: ^{1}H NMR δ: (PCH_2) 6.10 ($^1J_{PC}$ = 11 Hz) (Cl^-) and 4.977 ($^2J_{PC}$ = 11.8 Hz); ^{13}C NMR δ: (PC*H*) 38.27 ($^1J_{PC}$ = 60.3 Hz), (CH_3) 31.10 (BF_4^-).

Acknowledgements

We would like to thank Drs. M. F. Richardson and S. Cameron for searching the Cambridge File, and Dr. C. K. Tompkins for helpful discussion of the manuscript. We acknowledge gratefully the assistance of the Atlantic Regional Magnetic Resonance Centre in recording NMR spectra and the Natural Sciences and Engineering Council of Canada for financial support of this research.

1. I. Gosney and A. G. Rowley. *In* Organophosphorus reagents in organic synthesis. *Edited by* J. I. G. Cadogan. Academic Press, New York. 1979. pp. 7–153.
2. S. Trippett. Q. Rev. Chem. Soc. **17**, 406 (1963); A. W. Johnson. Ylide chemistry. Academic Press, New York. 1966; J. Boutagy and R. Thomas. Chem. Rev. **74**, 87 (1974); B. E. Maryanoff and A. B. Reitz. Chem. Rev. **90**, 863 (1989), and references cited therein.
3. B. E. Maryanoff, A. B. Reitz, H. S. Mutter, R. R. Inners, H. R. Almond Jr., R. R. Whittle, and R. A. Olafson. J. Am. Chem. Soc. **108**, 7664 (1989); E. Vadejs and T. J. Fleck. J. Am. Chem. Soc. **111**, 5861 (1989).
4. F. J. Randall and A. W. Johnson. Tetrahedron Lett. **24**, 2841 (1968).
5. P. Crews. J. Am. Chem. Soc. **90**, 2961 (1968).
6. H. J. Bestmann and J. P. Snyder. J. Am. Chem. Soc. **89**, 3963 (1967).
7. M. M. Kayser and D. Hooper. Can. J. Chem. **68**, 2123 (1990).
8. D. M. Crouse, A. T. Wehman, and E. E. Schweizer. Chem. Commun. 866 (1986).
9. G. A. Gray. J. Am. Chem. Soc. **95**, 7736 (1973).
10. J. P. Snyder and H. J. Bestmann. Tetrahedron Lett. 3317 (1970).
11. A. J. Speziale and K. W. Ratts. J. Am. Chem. Soc. **85**, 2790 (1963).
12. P. Froyen and D. G. Morris. Acta Chem. Scand. B, **30**, 790 (1976).
13. A. W. Johnson and R. T. Amel. Can. J. Chem. **46**, 461 (1968).
14. K. W. Ratts and A. N. Yao. J. Org. Chem. **31**, 1185 (1966).
15. A. D. Abell, B. M. Clark, and W. T. Robinson. Aust. J. Chem. **41**, 1243 (1988).
16. A. D. Abell and R. A. Massey-Westrop. Aust. J. Chem. **35**, 2077 (1982).
17. Cambridge Structural Database System.
18. V. D. Cherepinskii-Malov, G. G. Alexandrov, A. I. Guser, and Y. T. Struchkov. Zh. Strukt. Khim. **13**, 298 (1972).

19. M. SHAO, X. YIN, and Y. TANG. Tetrahedron Lett. **23**, 5343 (1982).
20. C. J. BART. J. Chem. Soc. (B), 350 (1969).
21. R. HOFFMANN, D. B. BOYD, and S. Z. GOLDBERG. J. Am. Chem. Soc. **92**, 3929 (1970).
22. S. FLISZAR, R. H. HUDSON, and G. SALVADORI. Helv. Chim. Acta, **46**, 1580 (1963).
23. R. F. HUDSON. Structure and mechanism in organo-phosphorus chemistry. Organic Chemistry, A. Series of Monographs. Vol. 6, Academic Press, London. 1965.
24. L. PAULING. The nature of the chemical bond. 3rd ed. Cornell University Press, Ithaca, NY. 1960. Interatomic distances and configurations in molecules and ions. Spec. Publ.—Chem. Soc. No. 11. 1958.

Can. J. Chem. Downloaded from www.nrcresearchpress.com by 123.30.183.119 on 09/08/12
For personal use only.

Thermo- and photochromic dyes: indolino-benzospiropyrans. Part 1. UV–VIS spectroscopic studies of 1,3,3-spiro(2*H*-1-benzopyran-2,2′-indolines) and the open-chain merocyanine forms; solvatochromism and medium effects on spiro ring formation

SAM-ROK KEUM[1,2] AND MUN-SUK HUR
Department of Chemistry, Korea University, Chochiwon, Chung-Nam, Korea, 339-800
PETER M. KAZMAIER
Xerox Research Centre of Canada, Mississauga, Ont., Canada L5K 2L1
AND
ERWIN BUNCEL[2]
Department of Chemistry, Queen's University, Kingston, Ont., Canada K7L 3N6

Received October 4, 1990[3]

SAM-ROK KEUM, MUN-SUK HUR, PETER M. KAZMAIER, and ERWIN BUNCEL. Can. J. Chem. **69**, 1940 (1991).

A kinetic and ultraviolet–visible study of a series of thermo- and photochromic dyes is reported. Ultraviolet irradiation of the indolino-benzospiropyran derivatives **1′–4′** leads to their transformation to the open-chain, colored merocyanine forms, which undergo thermal ring closure into the colorless spiro forms. The rate of this ring closure has been determined in different solvents. Plots of log (rate) vs. the solvent parameter E_T are linear but are dependent on the nature of the substituent in the phenyl moiety, which yields information on the electronic character of the ground state (IIa ↔ IIb) and the transition state. The ring-closure process is characterized by a zwitterionic type transition state, TS_3. The merocyanine dyes exhibit a significant solvatochromic effect, which unexpectedly shows sensitivity to substituents on the phenyl group. This observation finds explanation through semi-empirical molecular orbital (MOPAC) calculations. The MOPAC calculations also predict that the most stable configurational isomer of the merocyanines is the CTTC form.

Key words: indolino-benzospiropyran–merocyanine interconversion, photochromic–solvatochromic dyes.

SAM-ROK KEUM, MUN-SUK HUR, PETER M. KAZMAIER et ERWIN BUNCEL. Can. J. Chem. **69**, 1940 (1991).

On rapporte une étude basée sur la cinétique ainsi que sur l'UV–VIS d'une série de colorants thermo- et photochromiques. Une irradiation par l'UV des dérivés indolino-benzospiropyranes **1′–4′** conduit à leur transformation en chaînes ouvertes, des formes colorées de la mérocyanine qui subissent une cyclisation thermique conduisant aux formes spiro incolores. On a déterminé la vitesse de cette cyclisation dans différents solvants. Les courbes du log (vitesse) vs. le paramètre E_T du solvant sont linéaires, mais elles dépendent de la nature des substituants présents sur la portion phényle; cete dépendance fournit de l'information sur le caractère électronique de l'état fondamental (IIa ↔ IIb) et de l'état de transition. Le processus de cyclisation est caractérisé par un état de transition de type zwitterionique. ET_3. Les colorants mérocyanines présentent un effet solvatochromique important qui présente d'une façon inattendue une sensibilité vis-à-vis des substituants présents sur le groupe phényle. Cette observation peut être expliquée à l'aide de calculs semi-empiriques d'orbitales moléculaires (MOPAC). Ces calculs permettent aussi de prédire que l'isomère des mérocyanines configurationnellement le plus stable est la forme CTTC.

Mots clés : interconversion indolino-benzospiropyrane–mérocyanine, colorants photochromiques–solvatochromiques.
[Traduit par la rédaction]

Introduction

Thermo- and photochromic compounds (1–3) are among the most interesting of functional dyes, since they form colored species upon heating or irradiation with ultraviolet light. A typical example of an organic thermo- and photochromic compound currently being studied is the spiropyran derivative, 6′-nitro-1,3,3-trimethylspiro-(indolino-2,2′-benzopyran), **4′**.

Spiropyran–merocyanine transformations have been studied extensively since these reversible photo processes were first discovered by Fischer and Hirshberg in 1952 (5), and independently by Chaude and Rumpf in 1953 (6). Basically, the spiropyran dyes consist of two π-systems linked by a tetrahedral spiro carbon, while substituents modify the stability of the spiropyran as well as the long wavelength absorption associated with the π-system. Spiropyrans are known to be in equilibrium with their metastable colored forms (2). Absorption of ultraviolet light shifts the equilibrium towards the merocyanine colored form, **II**, while the reverse process to the colorless form, **I**, is induced by visible light, heat, or can occur spontaneously.

A number of authors (7–10) have reported important advances towards understanding the detailed photochemical processes involved in the photochromism and the reverse photochromism of spiropyrans. As well, various practical applications, such as in recording, copying, and display materials, have highlighted the potential usefulness of such compounds (11–16).

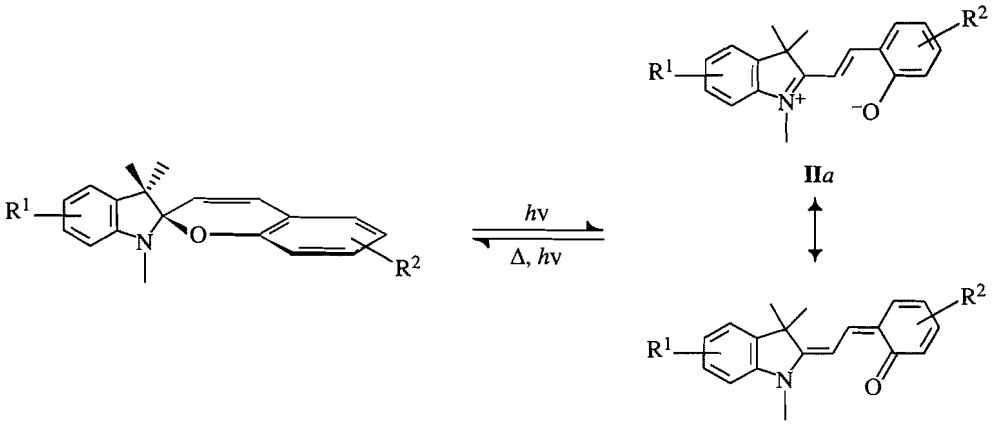
It is generally assumed that a thermo- and photo-sensitive equilibrium exists between the spiropyran (**I**) and a planar, colored, metastable, species resulting from scission of the bond between the spiro carbon and the pyran oxygen. Many unsolved problems remain, however, such as the identity and exact structure of the photochemically produced colored species, the formation of reaction intermediates, and the detailed mechanistic processes involved in the equilibrium between the two species. The colored species is generally accepted to have the electronic configuration of a resonance hybrid, i.e., zwitterionic (**II***a*)↔ quinoidal (**II***b*), depending on structure, substituents, solvent environment, etc. (17).

Our prime interest in these materials was the potential application for color imaging on synthetic materials. Use of the

[1]Present address: Department of Chemistry, Queen's University, Kingston, Ont., Canada K7L 3N6.
[2]Authors to whom correspondence may be addressed.
[3]Revision received June 27, 1991.

Printed in Canada / Imprimé au Canada

Can. J. Chem. Downloaded from www.nrcresearchpress.com by 123.30.183.119 on 09/08/12
For personal use only.



State **I**
Colorless spiro form

State **II**
Colored merocyanine form

photochemical system for these materials requires that states **I** and **II** should be reasonably stable at ordinary temperatures, in the absence of exciting illumination, and that the photochemical interconversion of states **I** and **II** should be feasible at ordinary temperatures. A number of studies are proceeding to develop spiropyrans that are photochemically active at room temperature and above. It has been found in our work that the thermal stability of state **II** can be markedly affected by careful choice of substituents on the photochemical process.

Continuing our studies of these thermo- and photochromic indolino-benzospiropyrans (4), in this paper we describe various UV–VIS spectroscopic studies to determine the influence of solvent on the equilibrium. Thus the aim of the present work is to evaluate the influence of solvent on UV–VIS spectral absorption (solvatochromism) (18), the electronic effects of substituents on thermo- and photochromism, and the kinetics of spiro ring formation of the open-chain merocyanine form of the indolino-benzospiropyrans. The influence of substituents in the benzopyran ring on the kinetics of the ring-closure reaction in different solvent systems is of particular interest since it could yield mechanistic information on the nature of the spiro ring formation process.

Experimental section

Materials and solvents

All compounds in this work have been prepared by literature procedures (2). Acetone and chloroform were dried over calcium sulfate and calcium chloride, respectively, and distilled. Dimethylformamide (DMF) and dimethyl sulfoxide (DMSO) were dried over molecular sieves (Type 4A) and calcium hydride, respectively, and distilled under reduced pressure. All other solvents were of spectroscopic grade.

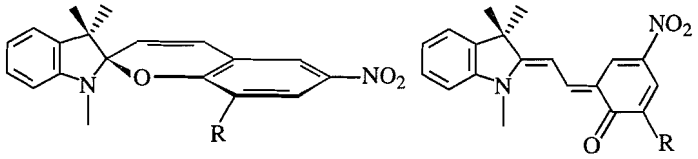
UV–VIS spectroscopy and kinetic measurements

The thermo- and photochromic spiropyran was dissolved in dry DMSO ($(1.0–10) \times 10^{-2}$ M) and kept in the dark. An aliquot (1–10 μL) was delivered to a quartz cuvette containing the solvent and allowed to come to thermal equilibrium. After half an hour, the cell was exposed to UV light from a 4-W "Blak-Ray" (Ultra-violet Products Inc., San Gabriel, CA) for 4–5 min and immediately placed in a Perkin–Elmer Lambda 5 or Perkin–Elmer 552 spectrophotometer. The disappearance of the colored form of the spiropyran was followed at the wavelength of maximum absorption (500–600 nm). The absorbance at equilibrium, A_e, was taken as the absorbance after 10 half-lives. First-order rate constants (k_{obs}) were calculated from linear log $(A_t - A_e)$ vs. time plots.

Results and discussion

Analysis of UV–VIS and kinetic data

The electronic absorption spectra of the spiropyrans in state **I** show no absorbance in the visible region, while in state **II**, formed on irradiation, a strong absorption at 500–600 nm with high extinction coefficients is observed. The rate of reversion to the colorless spiro ring (**II** → **I**) was measured after UV irradiation in various solvents for four 8′-substituted-6′-nitro-1,3,3-trimethylindolino-benzospiropyrans (**1′–4′**) by following the



1′–4′ **1–4**

1′, 1; R = H
2′, 2; R = Br
3′, 3; R = I
4′, 4; R = OMe

disappearance of the absorption band in the 500–600 nm region. A sample kinetic run for the ring closure reaction of **1**, the open-chain form of **1′**, in dimethyl sulfoxide after irradiation with UV light is shown in Fig. 1, while the corresponding absorbance vs. time data are given in Table 1.[4] The decay rate of the photoinduced colored transients obeyed good first-order kinetics for all substrates examined in this work.

The kinetic data for the ring-closure reactions of the four spiropyrans after UV irradiation are given in Table 2. The rate constants are independent of the initial spiropyran concentration in the range of 10^{-3} M to 5×10^{-5} M. The data in Table 2 demonstrate that the rate of the spiro ring formation is drastically reduced as the solvent polarity is increased.

Rate constants vs. solvent polarity parameters

Various attempts have been made to find a relationship between rate processes and solvent polarity parameters in related systems (18). Flannery (19) observed rather poor linearity on plotting log(rate) versus Kosower's *Z* or Brownstein's *S*

[4]Although only one configuration is shown for **1–4** it is understood that several conformers would be in equilibrium (*vide infra*).

Can. J. Chem. Downloaded from www.nrcresearchpress.com by 123.30.183.119 on 09/08/12
For personal use only.

Can. J. Chem. Downloaded from www.nrcresearchpress.com by 123.30.183.119 on 09/08/12
For personal use only.

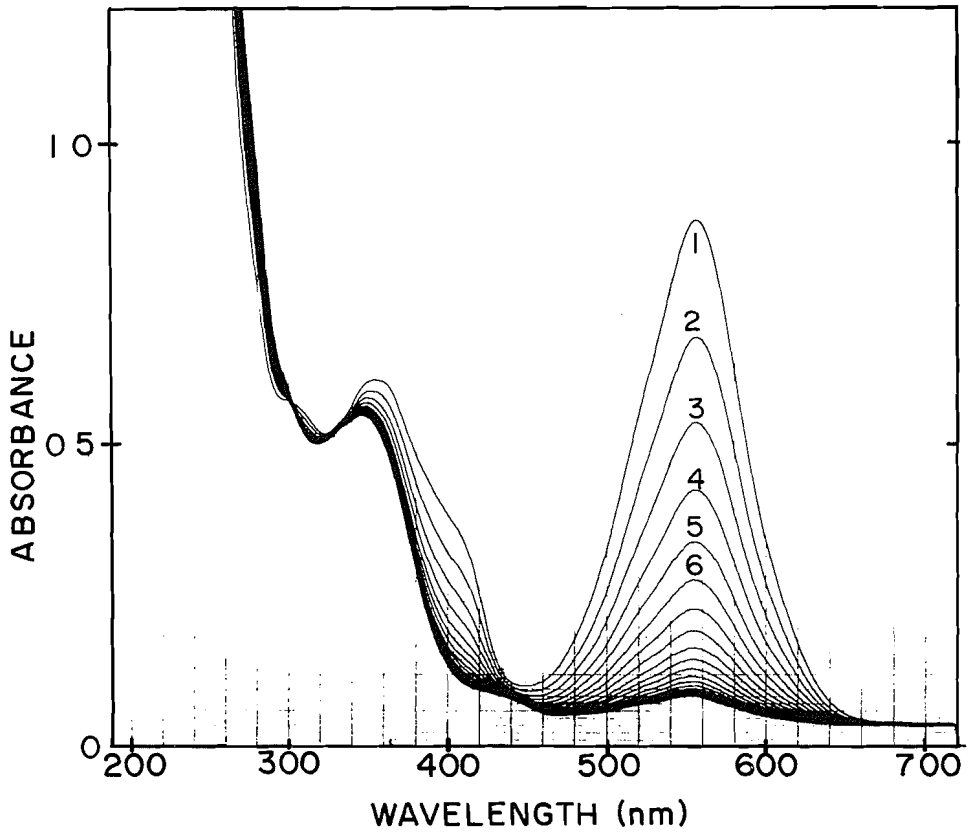


FIG. 1. Spectral scans as function of time (10-min intervals) for representative kinetic run for the ring-closure reaction of the open-chain merocyanine formed on UV irradiation of 6′-nitro-1,3,3-trimethylindolino-benzospiropyran (**4′**) in DMSO.

TABLE 1. Time-dependent absorbance data at 558 nm for 6′-nitro-1,3,3-trimethylindolino-benzospiropyran **1′** in DMF after irradiation with UV light

Times (s)	Absorbance	$-\log (A_e - A_t)^a$
0	1.52	−0.147
180	0.994	0.059
360	0.662	0.268
540	0.438	0.500
720	0.308	0.730
900	0.234	0.952
1200	0.170	1.321
1500	0.142	1.669

[a]The equilibrium value (A_e) was obtained experimentally from the absorbance at 558 nm after 10 half-lives.

TABLE 2. Kinetic data for spiro-ring formation of the open merocyanine form of substituted 1,3,3-trimethylindolino-benzospiropyrans, **1′–4′**, in various solvents

			$10^3 k_{obs}$ (s^{-1})			
No.	Solvent	E_T[a]	**1′**	**2′**	**3′**	**4′**
1	CCl_4	32.5	—	—	20.7	—
2	Toluene	33.9	122	—	14.3	44.2
3	Benzene	34.5	109	22.8	7.60	—
4	Ether	34.6	103	22.6	6.16	—
5	1,4-Dioxane	36.0	63.9	10.9	5.30	—
6	THF	37.4	26.8	7.83	2.29	20.2
8	$CHCl_3$	39.1	23.5	2.63	1.46	15.0
9	CH_2Cl_2	41.1	8.15	1.70	0.968	—
10	Acetone	42.2	7.30	0.542	0.374	—
12	DMF	43.8	2.85	—	—	5.98
13	DMSO	45.0	—	—	—	3.45

[a]From ref. 21.

parameters (20) for the ring-closure reaction of **2**. However, the choice of these scales is somewhat arbitrary and a more general solvent parameter would seem to be more appropriate.

In the present work, on plotting log(rate) versus the solvent parameter E_T (21) reasonably good linear plots were obtained (Fig. 2). It is apparent that the rate of the ring closure from the open-chain merocyanine form depends markedly on the substituents present in the series **1–4**. The sensitivity of rate on medium polarity is highest (slope = 0.17) for compounds **2** and **3**, which are halogen substituted in the 8′-position, whereas it is lowest (slope = 0.10) for **4**, which has a methoxy group in the 8′-position. The results for the latter are comparable to the sensitivity of **1** for which the slope value is 0.16. The slope and correlation-coefficient parameters on plotting log(rate) versus E_T for **1–4** are given in Table 3.

Another interesting observation is that there is a crossover in the lines for **1** and **4**, while the series **1**, **2**, and **3** exhibit practically parallel lines. This implies that reactivity comparison studies could be misleading. Thus the order of reactivity will be different in the region below and above E_T = 41–42. If a solvent

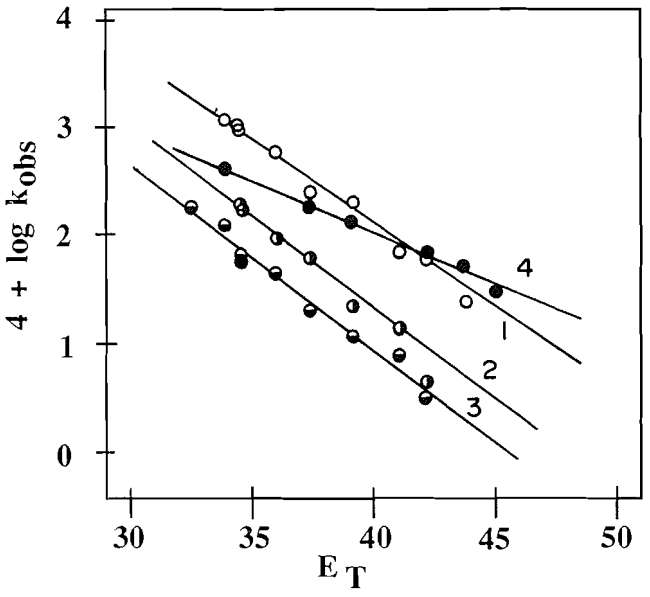


FIG. 2. Plots showing correlation between k_{obs} and E_T for the ring-closure reactions of merocyanines from UV irradiation of 8′-substituted 6′-nitro-1,3,3-trimethylindolino-benzospiropyrans in various solvents: **1**, (○); **2**, ◑; **3**, (◒); **4** (●).

TABLE 3. Slope and correlation-coefficient parameters in plotting −log (rate) versus E_T for ring closure after UV irradiation of spiropyrans **1′–4′**

Spiropyran	Slope	Corr. coeff.
1′	0.16±0.01	0.998
2′	0.17±0.01	0.988
3′	0.17±0.01	0.978
4′	0.10±0.01	0.998

of relatively low value of E_T is used for the reaction, the reactivity order is **1** > **4** > **2** > **3**, whereas for a solvent of higher E_T value the order could be changed to **4** > **1** > **2** > **3**.

Solvent effect on LFER for reaction rate vs. substituents

The Hammett linear free energy correlation between reaction rate and the substituent parameter $\Sigma\sigma$ (22) as a function of solvent polarity is of interest. Such a relationship was found previously in absolute ethanol (19) and is now extended to two solvent systems other than alcohols, namely to acetone and dimethylformamide.

The rate constants of the thermal ring-closure reaction of the open form of spiropyrans in the two solvent systems as a function of σ value are given in Table 4 and plotted in Fig. 3. The slopes derived from Fig. 3 are given in Table 5, including the literature data for ethanol (23). An interesting aspect is that the sensitivity (absolute value of slope) increases as the medium polarity is decreased (Fig. 4), which implies that a charge–dipole interaction is important in the reaction.

Mechanism of spiro ring closure

Three different mechanisms involving three corresponding transition states have been suggested for the thermal ring-closure reaction of the merocyanine open form of spiropyrans. TS_1 applies to a concerted electrocyclic process as suggested by Dürr

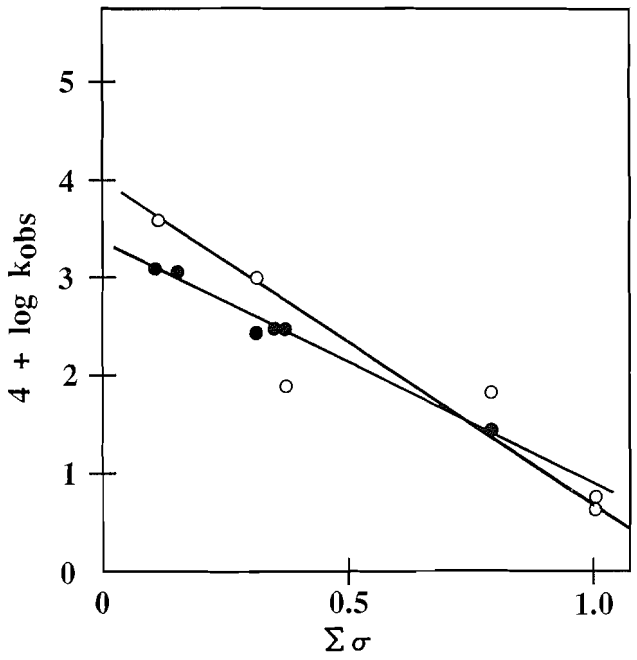


FIG. 3. Plots of log k_{obs} vs. $\Sigma\sigma$ for the ring-closure reactions of merocyanines from irradiation of substituted 1,3,3-trimethylindolino-benzospiropyrans in different solvents: acetone (○); DMF (●).

TABLE 4. Rate constants as function of σ values of substituents in 1,3,3-trimethylindolino-benzopyrans following UV irradiation in acetone and dimethylformamide

	$10^3\ k_{obs}\ (s^{-1})$		
Substituents	Acetone	DMF	$\Sigma\sigma^a$
6′-Nitro	7.30	2.85	0.79
6′-Chloro	398[b]	147[b]	0.11
6′-Bromo		121[b]	0.15
6′,8′-Dibromo		31.7[b]	0.36
6′8′-Dichloro		28.7[b]	0.35
6′8′-Diiodo	105[b]	44.6[b]	0.31
6′-Nitro-8′-methoxy	7.83		0.37
6′-Nitro-8′-bromo	0.542		1.00
6′-Nitro-8′-chloro	0.374[b]		1.00

[a]For substituents in the 6′-position, σ^+ values are chosen (22*a*), while for substituents in the 8′-position Taft's σ^* values (22*b*) for *ortho*-substituted benzene derivatives are used.
[b]Values obtained from ref. 33.

TABLE 5. Slope values from plot of log k_{obs} vs. $\Sigma\sigma$ (Fig. 3) for various solvents

Medium	E_T	−Slope	−log k_o
Acetone	42.2	2.95	0.30
DMF	43.8	2.54	0.57
EtOH	51.9	1.84	2.29

[a]From ref. 5.

(24) and Ollis *et al.* (25). TS_2 applies to the diradicaloid mechanism formed through homolytic cleavage of the C2—O bond and is favored by Sueishi *et al.* (26). TS_3 pertains to the ionic mechanism via a merocyanine-type zwitterionic species, as suggested by Flannery (19) and others (2).

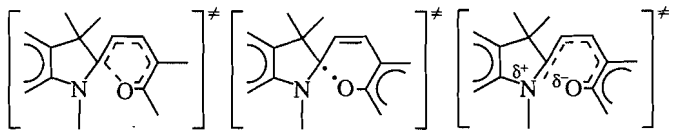
Can. J. Chem. Downloaded from www.nrcresearchpress.com by 123.30.183.119 on 09/08/12
For personal use only.

TABLE 6. UV data (λ_{max}, ν) of the open-chain merocyanine forms of 1,3,3-trimethylindolino-benzospiropyrans **1'**, **2'**, and **4'** in various solvents

			1'	**2'**	**4'**
No.	Solvent	E_T	λ_{max} (ν cm^{-1})	λ_{max} (ν cm^{-1})	λ_{max} (ν cm^{-1})
1	CCl_4	32.5	—	604 (16 600)	—
2	Toluene	33.9	603 (16 600)	596 (16 800)	620 (16 100)
3	Benzene	34.5	600 (16 700)	592 (16 900)	—
4	Ether	34.6	595 (16 800)	585 (17 100)	—
5	1,4-Dioxane	36.0	590 (16 900)	583 (17 200)	—
6	THF	37.4	585 (17 100)	575 (17 400)	—
7	Ethyl acetate	38.1	—	570 (17 500)	—
8	$CHCl_3$	39.1	581 (17 200)	567 (17 800)	—
9	CH_2Cl_2	41.1	579 (17 300)	560 (17 800)	—
10	Acetone	42.2	561 (17 800)	—	—
11	DMAA	43.7	563 (17 800)	550 (18 200)	588 (17 000)
12	DMF	43.8	558 (17 900)	—	590 (16 900)
13	DMSO	45.0	555 (18 000)	545 (18 300)	582 (17 200)
14	CH_3CN	46.0	557 (18 000)	—	583 (17 200)
15	EtOH	51.9	538 (18 600)	537 (18 600)	570[a] (17 500)
16	MeOH	55.5	—	—	545 (18 300)

[a]Double peaks at 550 and 570 nm.

It is apparent that the electrocyclic reaction is not expected to show marked sensitivity to medium polarity, in accordance with an isopolar, six-membered activated complex (ref. 2, pp. 160–170). The free-radical mechanism had been ruled out on the grounds that the colored solutions were unchanged on treatment with oxygen, hydrogen, and hydroquinone (27), although Sueishi (26) recently favored this from a pressure study of **1**. As well, a radical mechanism would not be expected to exhibit appreciable sensitivity to substituents, unlike the findings in the present study.



TS_I TS_2 TS_3

The large decrease in rate on increasing the solvent polarity (Fig. 2) is in accord with a process in which charge is dissipated on going from the ground state to the transition state. Clearly this supports TS_3 as the transition state which is operative in our system.

It is also interesting that the sensitivity of the reaction rate to solvent effect, i.e., the slope of the log k_{obs} vs. E_T plots in Fig. 2, is dependent on the nature of the substituent R; the slope is higher for electron-withdrawing substituents (Cl, Br) than for electron-releasing (OCH_3). This finds explanation in that an electron-withdrawing group will stabilize the dipolar structure **II***a* in the ground state. The more dipolar the character, the greater the sensitivity to solvent polarity of the reaction rate, and conversely for electron-donating substituents. Thus the observed trends of the slopes in Fig. 4 (see Table 5) provide further support for the dipolar structure of the merocyanines formed on ring opening of the spiropyrans.

Solvatochromism

The UV–VIS spectral data of the open form of the spiropyrans **1'**, **2'**, and **4'** in various solvents are collected in Table 6, while

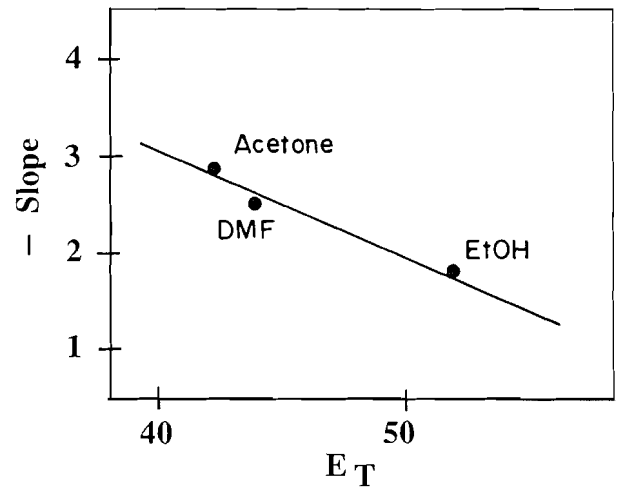


FIG. 4. Plot of slope parameter in log k_{obs} vs. $\Sigma\sigma$ plots vs. the solvent polarity parameter E_T for the thermal ring-closure reaction of the merocyanines formed on irradiation of 1,3,3-trimethylindolino-benzospiropyrans.

in Fig. 5 the results are plotted as frequency (ν) versus the solvent polarity parameter E_T.

The results show that a marked solvatochromism (18, 28–32) is exhibited by the merocyanines derived from spiropyrans **1'**, **2'**, and **4'**. As the solvent polarity is increased, a hypsochromic shift is observed. Figure 5 shows that there is a fairly good relationship between ν_{max} and the solvent polarity parameter E_T, with the following relationships:

[1] Compound **1**: $\nu_{max} = 113\ E_T + 12\ 800$ $r = 0.987$; $n = 13$

[2] Compound **2**: $\nu_{max} = 135\ E_T + 12\ 300$ $r = 0.985$; $n = 11$

[3] Compound **4**: $\nu_{max} = 94\ E_T + 12\ 900$ $r = 0.976$; $n = 7$

The striking feature about the present results, as displayed in Table 6 and Fig. 5, is the marked hypsochromic shift that is exhibited with increasing solvent polarity (i.e., negative solvato-

Can. J. Chem. Downloaded from www.nrcresearchpress.com by 123.30.183.119 on 09/08/12
For personal use only.

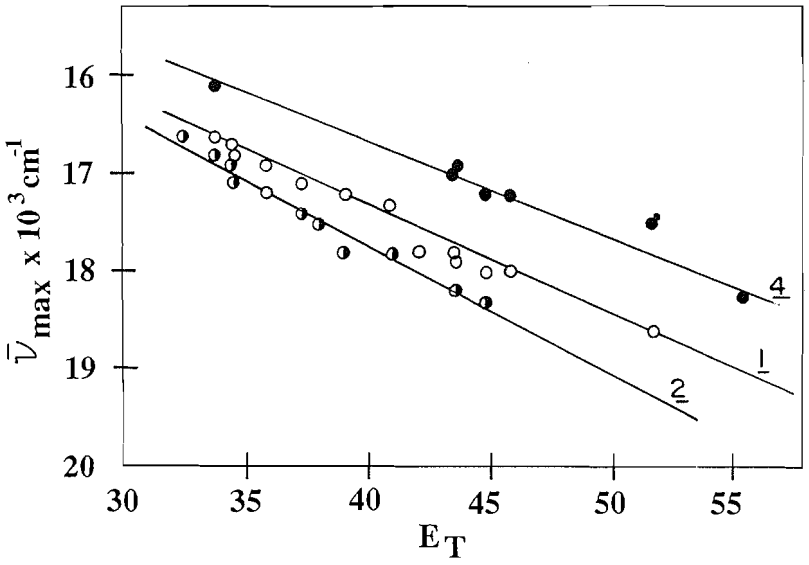


FIG. 5. Plots of frequency $\bar{\nu} \times 10^3$ vs. E_T for the open-chain merocyanine form of 1,3,3-trimethylindolino-benzospiropyrans: **1** (○); **2** (◑); **4** (●), in various solvents.

TABLE 7. Energies of the merocyanine configurational isomers

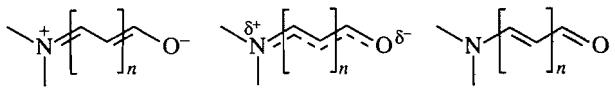
Substituent (X)	Configuration[a]	Heat of formation[b]
X = H	TTCC	63.73
	TTTC	62.51
	CTTC	61.61
	CTCC	63.03
X = Br	TTCC	71.70
	TTTC	70.30
	CTTC	69.37
	CTCC	71.06
X = OCH_3	TTCC	27.89
	TTTC	26.76
	CTTC	25.85
	CTCC	27.19

[a]See Fig. 6 for description of configurations.
[b]In kcal/mol.

chromism). It is known that the nature of the observed solvent effect for a given dye molecule, i.e., bathochromic or hypsochromic shift with increasing solvent polarity, depends largely on the change in dipolar characteristics between ground and excited states (18). For a weakly polar molecule, with low polarity in the ground state and increased polarity in the excited state, a bathochromic shift results. Conversely, for a highly polar molecule in the ground state and reduced polarity in the excited state, a hypsochromic shift is observed.

In principle, a merocyanine dye could exhibit either a bathochromic or a hypsochromic shift since the ground state could have an electronic configuration corresponding largely to the nonpolar quinoid form **II***b*, or to the dipolar, zwitterionic form **II***a*, or an in-between character. The observation of a hypsochromic shift (negative solvatochromism) in the present system is hence indicative of a highly polar ground state, i.e., approaching the configuration of the zwitterionic form **II***a*, and an excited state with decreased polarity.

In general terms, we may represent the ground state of the merocyanines as a polyene-like structure **A** and the excited state as a polymethine-like structure **B**, a situation that will result in a hypsochromic shift. Conversely, a bathochromic shift would have resulted if the ground state had the quinoidal structure **C** and the excited state the dipolar structure **B**.



MOPAC calculations of structural effects on solvatochromism

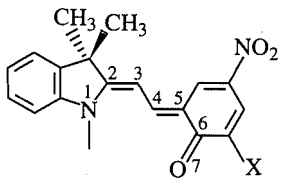
Since the solvatochromic evidence described above clearly showed a stabilization of the dipolar form as the aromatic ring substituents were varied from methoxy to bromo, i.e., **4** to **2**, it was of interest to see if molecular orbital calculations could provide additional insight into the origin of this substituent effect. Semi-empirical calculations have proven useful in interpreting the behavior of merocyanines (29, 34) and thus the question of substituent effects appeared tractable in light of the past success of calculations at this level of sophistication.

Accordingly, calculations have been performed to analyze the substituent effects observed for the solvatochromic behavior of merocyanines **1**, **2**, and **4**. To investigate the effect of ring substituents on the electronic configuration of the ground state, it was first necessary to calculate the predicted minimum energy configuration for this system, which is structurally different from those considered in earlier work (34). Figure 6 describes the configurations in the ring-open form that were considered, and the energy for each was fully optimized using MOPAC 5.0 (35) incorporating the AM1 Hamiltonian. Table 7 summarizes the results on the energies of the isomers investigated. Clearly, from a consideration of the energies, the CTTC stereoisomer is predicted to be the most stable for compounds **1**, **2**, and **4**. Table 8 summarizes the atomic charges, total bond orders, π bond orders, and bond lengths predicted for **1**, **2**, and **4**.

The results of the MOPAC-AM1 calculations are shown in Table 8. From a consideration of both the bond orders and the π

Can. J. Chem. Downloaded from www.nrcresearchpress.com by 123.30.183.119 on 09/08/12
For personal use only.

TABLE 8. Atomic charges and bond orders for **1**, **2**, and **4**



	N-1	C-2	C-3	C-4	C-5	C-6	O-7
Compound **1** (X = H)							
Charges	−0.2013	−0.1470	−0.3116	0.0839	−0.2542	0.2975	−0.3375
Bond order		1.1484	1.5610	1.1798	1.5469	0.9743	1.8038
π Bond order		0.2527	0.6169	0.2264	0.5920	0.0942	0.8322
Bond distances (Å)		1.3901	1.3698	1.4139	1.3720	1.4781	1.2448
Compound **2** (X = Br)							
Charges	−0.1966	0.1553	−0.3184	0.0936	−0.2597	0.3090	−0.3193
Bond order		1.1666	1.5348	1.1999	1.5178	0.9737	1.8217
π Bond orders		0.2712	0.5911	0.2461	0.5636	0.0952	0.8498
Bond distances (Å)		1.3870	1.3725	1.4107	1.3791	1.4791	1.2429
Compound **1** (X = OCH_3)							
Charges	−0.2030	−0.1412	−0.3061	0.0748	−0.2401	0.0345	−0.2991
Bond order		1.1382	1.5763	1.1687	1.5651	0.9764	1.8405
π Bond orders		0.2421	0.6319	0.2153	0.6106	0.0959	0.8684
Bond distances (Å)		1.3921	1.3683	1.4159	1.3741	1.4761	1.2398

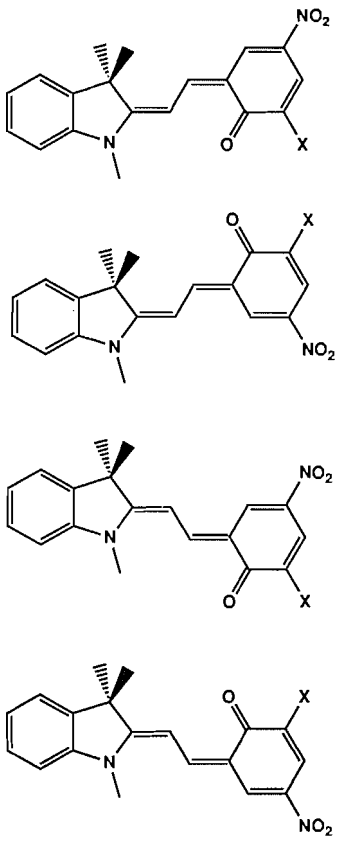


FIG. 6. Geometrical configurations of the indolino merocyanines. The TTCC, etc., designations refer to the geometry (*trans*, T, or *cis*, C) about the 2–3, 3–4, 4–5, and 5–6 bonds (see Table 8).

bond orders, it is clear that our calculations predict a quinoid ground state for **1**, **2**, and **4**. This is in agreement with other theoretical investigations (29, 34) applicable to the isolated molecules in the gas phase and in the absence of specific solute–solvent interactions. However, it is noteworthy that as the substituent on the chromophore is changed from an electron-donating group (**4**) to an electron-withdrawing group (**2**), the bond orders reflect a shift to a more dipolar electronic configuration. For example, the π bond order for the carbon–nitrogen bond is 0.2421 for the methoxy substituent while it is 0.2712 for the bromo substituent. Thus the consequence of chromophore substitution (**4** → **2**) is to stabilize the zwitterionic form.

Typically, solvatochromic compounds can be described by two extreme resonance-contributing structures: one a quinoidal, nonpolarized, formally nonaromatic structure; the other a zwitterionic, polarized, formally aromatic structure. The change in absorption band with solvent arises from a variation in the contribution of these canonical forms to the overall resonance hybrid (18, 29, 36). The present work shows that, just as increasing solvent polarity predisposes the ground state toward the zwitterionic contributing structure, progressively more powerful electron-withdrawing substituents also perturb the electronic ground state in the same direction and the observed solvatochromic effect is the superposition of these two perturbations. This is in agreement with the change in slope observed for the three merocyanines as shown in Fig. 5.

A second interesting consequence of the molecular orbital calculations on **1**, **2**, and **4** is the observation that the π bond order of the C15—C17 bond is very low. It has generally been assumed that aromaticity is an important contributor to the stability of the zwitterionic form. The π bond order for the C15—C17 bond only increases from 0.0942 for R = H to 0.0959 for R =

Can. J. Chem. Downloaded from www.nrcresearchpress.com by 123.30.183.119 on 09/08/12
For personal use only.

OCH_3 and this trend (π bond order (R = OCH_3) > (R = Br) > (R = H)) does not follow the trend observed for the substituent effect on the solvatochromism ((R = Br) > (R = H) = (R = OCH_3)). The implication of this result is that the substituent effect observed is stabilizing the zwitterionic form directly by enhancing the electron-accepting capacity of the oxygen anion and not by increasing the aromatic stabilization energy of the phenyl group.

In conclusion, substituents affect the solvatochromic behavior of merocyanine dyes by increasing the sensitivity of the chromophore to solvation effects. The molecular orbital calculations show that substituents introduce perturbations into the chromophore that are very similar, but not identical, to the perturbations caused by solvent effects themselves. The ultimate solvatochromic behavior is a superposition of these two effects. Although electronegative substituents increase the relative contribution of the dipolar canonical form to the overall ground state resonance hybrid, substituents do so without increasing the aromaticity of the aromatic pendent group.

Acknowledgements

Research funding by the Korean Ministry of Education and the Han-Wan Fine Chemicals Company is gratefully acknowledged. We also thank the Natural Sciences and Engineering Research Council of Canada for the award of an International Collaborative Research Grant for sabbatical leave (S.R.K.) at Queen's University.

1. H. DÜRR and H. BOUAS-LAURENT (*Editors*). Photochromism — molecules and systems. Elsevier, Amsterdam. 1990.
2. G. H. BROWN (Editor). Photochromism. *In* Techniques of chemistry. Vol. 3. Wiley, New York. 1971.
3. (*a*) R. DESSAUER and J. P. PARIS. Advances in photochemistry. Vol. 1. *Edited by* W. A. Noyes, Jr., G. S. Hammond, and J. N. Pitts, Jr. Interscience, New York. 1963; (*b*) R. EXELBY and R. GRINTER. Chem. Rev. **65**, 247 (1965).
4. S. R. KEUM. Thermo- and photochromism of 1.3.3-trimethylindolino-benzopyrans. *Presented at* The Institute of Industrial Development, Korea University. 1989.
5. E. FISCHER and Y. HIRSHBERG. J. Chem. Soc. 4522 (1952).
6. O. CHAUDE and P. RUMPF. C. R. Hebd. Séances Acad. Sci. **236**, 697 (1953).
7. S. DAEHNE. Z. Wiss. Photogr. Photophys. Photochem. **62**, 183 (1969).
8. L. D. WEISS, T. R. EVANS, and P. H. LEERMAKERS. J. Am. Chem. Soc. **90**, 6115 (1968).
9. E. FISHER. Forschr. Chem. Forsch. **7**, 605 (1967).
10. E. INQUE, H. KOKADO, I. SHIMIZU, H. KOBAYASHI, and Y. TAKAHASHI. Bull. Chem. Soc. Jpn. **45**, 1951 (1972).
11. S. ARAKWA, H. KONDO, and J. SETO. Chem. Lett., 1805 (1985).
12. D. A. HOLDEN, H. RINGSDORF, V. DEBLAUWE, and G. SMETS. J. Phys. Chem. **88**, 716 (1984).
13. T. TAMAKI and K. ICHIMURA. J. Chem. Soc. Chem. Commun. 1477 (1989).
14. (*a*) F. P. SHVARTSMAN, I. R. CABRERA, A. L. WEIS, E. J. WACHTEL, and A. KRONGAUZ. J. Phys. Chem. **89**, 3941 (1985); (*b*) I. CABRERA, V. KRONGAUZ, and H. RINGSDORF. Angew. Chem. Int. Ed. Engl. **26**, 1178 (1977).
15. D. LEVY and D. AVNIR. J. Phys. Chem. **92**, 4734 (1988).
16. E. MEIROVITCH, F. P. SHVARTSMAN, V. A. KRONGAUZE, and H. ZIMMERMANN. J. Phys. Chem. **89**, 5522 (1985).
17. E. BUNCEL and S. R. KEUM. Tetrahedron, **39**, 1091 (1983).
18. (*a*) E. BUNCEL and S. RAJAGOPAL. Acc. Chem. Res. **23**, 226 (1990); (*b*) J. Org. Chem. **54**, 798 (1989).
19. J. B. FLANNERY, JR. J. Am. Chem. Soc. **90**, 5660 (1968).
20. (*a*) E. M. KOSOWER. J. Am. Chem. Soc. **80**, 3253 (1958); (*b*) S. BROWNSTEIN. Can. J. Chem. **38**, 1590 (1960).
21. C. REICHARDT. Solvents and solvent effects in organic chemistry. 2nd ed. VCH, Weinheim. 1988. pp. 339–405.
22. (*a*) N. S. ISAACS. Physical organic chemistry. Longman, U.K. 1987. pp. 129–209; (*b*) R. W. TAFT. *In* Steric effects in organic chemistry. *Edited by* M. S. Newman. Wiley, New York. 1956.
23. E. BERMAN, R. E. FOX, and F. D. THOMSON. J. Am. Chem. Soc., **81**, 5605 (1959).
24. H. DÜRR. Angew. Chem. Int. Ed. Engl. **28**, 413 (1989).
25. W. O. OLLIS, K.L. ORMAND, and I. O. SUTHERLAND. Chem. Commun. 1697 (1968).
26. Y. SUEISHI, M. OHCHO, and N. NISHIMURA. Bull. Chem. Soc. Jpn. **58**, 2608 (1985).
27. W. DILTHEY and R. WIZINGER. Chem. Ber. **59**, 1856 (1926).
28. B. S. BRUNSCHWIG, S. EHRENSON, and N. SUTIN. J. Phys. Chem., **91**, 4714 (1987).
29. A. BOTREL, A. LEBEUZE, P. JACQUES, and H. STRAUB. J. Chem. Soc. Faraday Trans. 2, **80**, 1235 (1984).
30. J. FABIAN and H. HARTMANN. J. Mol. Struct. **27**, 667 (1975).
31. J. GRIFFITHS. Colour and constitution of organic molecules. Academic Press, London. 1976.
32. S. DAHNE and F. MOLDENHAUR. Progr. Phys. Org. Chem., **15**, 1 (1985).
33. S. R. KEUM and K. B. LEE. Unpublished results from M.Sc. Thesis of K. B. Lee, Korea University. 1988.
34. F. DIETZ, R. THIEME, and C. WEISS. J. Signalaufzeichnungsmater. **10**, 321 (1983).
35. J. P. STEWART. J. Comput.-Aided Mol. Des. **4**, 1 (1990).
36. H. W. GIBSON. Tetrahedron, **77**, 6789 (1977).

Can. J. Chem. Downloaded from www.nrcresearchpress.com by 123.30.183.119 on 09/08/12
For personal use only.

Preparation and characterization of a series of bromodiphenyl(*N*,*N*-dialkyldithiocarbamato)tellurium(IV) compounds where R = Me, Et, *i*-Pr, Bu, and of chlorodiphenyl(*N*,*N*-dibutyldithiocarbamato)tellurium(IV) and diphenylbis(*N*,*N*-dibutyldithiocarbamato)tellurium(IV). Crystal structure of $Ph_2TeBr[S_2CNEt_2]$ and $Ph_2Te[S_2CNBu_2]_2$

JANE H. E. BAILEY, JOHN E. DRAKE, and MARIA L. Y. WONG

Department of Chemistry and Biochemistry, University of Windsor, Windsor, Ont., Canada N9B 3P4

Received April 18, 1991

JANE H. E. BAILEY, JOHN E. DRAKE, and MARIA L. Y. WONG. Can. J. Chem. **69**, 1948 (1991).

The series $Ph_2TeBr[S_2CNR_2]$, where R = Bu, Pr, *i*-Pr, Et, and Me, as well as $Ph_2TeCl[S_2CNR_2]$ and $Ph_2Te[S_2CNR_2]_2$, where R = Bu, Pr, have been synthesized and characterized by elemental analysis and vibrational spectroscopy. Comparisons of the effect of changing R groups and halogen atoms can be made based on the two crystal structures determined herein along with earlier work. The geometry about tellurium is consistent with that of a distorted sawhorse structure where the dithiocarbamate groups are monodentate (or anisobidentate). The crystal structures of $Ph_2TeBr[S_2CNEt_2]$, **4**, and $Ph_2Te[S_2CNBu_2]_2$, **7**, were completed. The cell parameters for **4** are $a = 11.204(3)$ Å, $b = 14.106(11)$ Å, $c = 13.867(10)$ Å, $\alpha = 99.62(6)°$, $\beta = 102.76(5)°$, $\gamma = 87.73(4)°$, $V = 2107$ Å^3, $Z = 4$, $R = 0.0448$, and $R_w = 0.0489$ and for **7** are $a = 19.392(6)$ Å, $b = 9.622(2)$ Å, $c = 19.089(6)$ Å, $\beta = 104.70(2)°$, $V = 3445(2)$ Å^3, $Z = 4$, $R = 0.0397$, and $R_w = 0.0439$. Nuclear magnetic resonance spectra are not simple and indicate that several species are present in solution, as rearrangements and reductive elimination take place.

Key words: structure, tellurium, bromo, diphenyl, dialkyldithiocarbamato.

JANE H. E. BAILEY, JOHN E. DRAKE et MARIA L. Y. WONG. Can. J. Chem. **69**, 1948 (1991).

On a synthétisé la série $Ph_2TeBr[S_2CNR_2]$ dans laquelle R = Bu, Pr, *i*-Pr, Et et Me ainsi que les séries $Ph_2TeCl[S_2CNR_2]$ et $Ph_2Te[S_2CNR_2]_2$, dans lesquelles R = Bu et Pr et on les a caractérisées par leurs analyses élémentaires et les spectres de vibration. On peut faire des comparaisons de l'effet provoqué par le changement des groupes R et des atomes d'halogène en se basant sur des structures cristallines déterminées antérieurement ainsi que sur deux autres déterminées dans ce travail. La géométrie autour de tellure est en accord avec celle d'une structure en dent de scie déformée dans laquelle les groupes dithiocarbamates sont monocoordonnés (ou anisobicoordonnés). On a déterminé complètement les structures des composés $Ph_2TeBr[S_2CNEt_2]$ **4**, et $Ph_2Te[S_2CNBu_2]_2$ **7**. Pour le composé **4**, les paramètres sont $a = 11{,}204(3)$, $b = 14{,}106(11)$ et $c = 13{,}867(10)$ Å, $\alpha = 99{,}62(6)$, $\beta = 102{,}75(5)$ et $\gamma = 87{,}73(4)°$, $V = 2107$ Å^3, $Z = 4$, $R = 0{,}0448$, et $R_w = 0{,}0489$ alors que pour le composé **7**, les paramètres sont $a = 19{,}392(6)$ $b = 9{,}622(2)$ et $c = 19{,}089(6)$ Å, $\beta = 104{,}70(2)°$, $V = 3445(2)$ Å^3, $Z = 4$, $R = 0{,}0397$ et $R_w = 0.0439$. Les spectres rmn ne sont pas simples et ils indiquent que plusieurs espèces sont présentes en solution alors qu'il se produit des transpositions et des réactions d'éliminations réductrices.

Mots clés : structure, tellure, bromo, diphényle, dialkyldithiocarbamato.

[Traduit par la rédaction]

Introduction

Dithiocarbamate complexes have experienced extensive study (1–7). Dithiocarbamate groups usually act in a bidentate fashion (3–7); typical examples that have been observed range from transition metal complexes such as $Co[S_2CNMe_2]_2NO$, where the Co atom is at the centre of a square pyramid (8), and $Cu_4[(S_2CNEt_2)_2]_4$, where the dithiocarbamate group coordinates form the faces of the Cu_4 tetrahedron (9), to main group compounds such as $C_4H_9Sn[S_2CNEt_2]$, where the geometry around the tin atom is that of a pentagonal bipyramid (10). There are fewer examples of monodentate linkages, which usually occur in mixed ligand complexes such as $Pt[S_2CN\textit{i}\text{-}Bu_2]_2$-$[PMe_2Ph]_2$ (11).

Monodentate (or anisobidentate) bonding is consistently found in several, previously reported, dithiocarbamates of germanium (12–15). In some cases it has been noted that changes in the mode of attachment occur with the variation of the alkyl group of the dithiocarbamate ligand. Thus in $Zn[S_2$-$CNMe_2]_2$ (16), the dithiocarbamate groups are bidentate and bridging, whereas in $Zn[S_2CNEt_2]_2$ both dithiocarbamate groups are bidentate and the molecule is monomeric (17).

Previously, we reported the reactions of diphenyltellurium dichloride with the sodium salts of *N*,*N*-dimethyl-, *N*,*N*-diethyl-, and *N*,*N*-diisopropyldithiocarbamate in which the crystal structures, $Ph_2Te[S_2CNMe_2]_2$, $Ph_2Te[ClS_2CNEt_2]$, and Ph_2TeCl-$[S_2CN\textit{i}\text{-Pr}]$, were discussed (18). We now extend this study to include the series of bromo derivatives $Ph_2TeBr[S_2CNR_2]$, where R = Bu, Pr, *i*-Pr, Et, and Me, as well as $Ph_2TeCl[S_2CNR_2]$ and $Ph_2Te[S_2CNR_2]$ where R = Bu, Pr to complete the chloro- and bis-series of derivatives. Compounds were characterized by elemental analysis, vibrational and NMR spectroscopy, and two structural determinations were completed by X-ray crystallography. Studies were made by ^1H, ^{13}C, and ^{125}Te NMR spectroscopy of the mode of decomposition of these and related species in solution.

Experimental

Materials

$TeCl_4$, Ph_4Sn, Me_3SiBr, diisopropylamine, dipropylamine, dibutylamine, toluene, diethyl ether, and petroleum ether were obtained from Aldrich. All but toluene, which was distilled, were used as purchased. Carbon disulfide (BDH) was distilled from P_4O_{10} prior to use, whereas ethanol and methylene chloride were used as supplied by BDH. Both NaS_2CNMe_2 and NaS_2CNEt_2, obtained from Aldrich as hydrated salts, were dried in vacuum for 4–5 days prior to use.

Can. J. Chem. Downloaded from www.nrcresearchpress.com by 123.30.183.119 on 09/08/12
For personal use only.

Can. J. Chem. Downloaded from www.nrcresearchpress.com by 123.30.183.119 on 09/08/12
For personal use only.

Synthesis of NaS_2CNi-Pr_2, NaS_2CNPr_2, and NaS_2CNBu_2

An equimolar mixture of sodium hydroxide (3.96 g) and carbon disulphide (3.66 g) was mixed in ethanol (20 mL). Diisopropylamine was slowly added at 3 drops/s and the mixture was then heated for 1.5 h under a continuous N_2 stream of approximately 1–2 bubbles/s. The solid formed was washed with diethyl ether and dried under vacuum for 4–5 days. The butyl and propyl dithiocarbamate salts were similarly made with the substitution of dibutylamine and dipropylamine for diisopropylamine. The products were obtained in 60–80% yields.

Synthesis of Ph_2TeCl_2

An equimolar solution of tetraphenyltin (4.56 g) and tellurium tetrachloride (2.87 g) in toluene (20 mL) was refluxed at 60°C for 12 h and worked up in the manner previously described (19).

Synthesis of Ph_2TeBr_2

Diphenyltellurium dichloride (0.35 g) was dissolved in CS_2 (5 mL) and the system kept in an ice bath and purged under nitrogen. Bromotrimethylsilane (0.30 g) was added slowly to the mixture. Once addition was complete the mixture was stirred at ambient temperature for 3–4 h. The solution was then filtered and placed in the refrigerator to allow crystallization of Ph_2TeBr_2; 0.35 g; 80% yield; mp 196–198°C (lit. mp 196–198°C).

Synthesis of diphenylbis(N,N-*dialkyldithiocarbamato)tellurium(IV)*

Typically, sodium *N,N*-dibutyldithiocarbamate (1.02 g), previously dried *in vacuo* for 4–5 days, was added to a solution of Ph_2TeCl_2 (0.62 g) in CS_2 (15 mL). A continuous stream of N_2 at a rate of 3 bubbles/s was maintained throughout the procedure. The mixture was refluxed at 45°C for 3 h. The product solution was filtered to remove NaCl and any unreacted material. A couple of drops of petroleum ether were added and the solution was left in the refrigerator at −6°C until crystals formed. The crystals of $Ph_2Te[S_2CNBu_2]_2$ were washed with *n*-hexane and dried in vacuum for 2–3 days; 0.93 g; 77% yield; yellow crystals; mp 127–128°C. Anal. calcd. for $C_{30}H_{46}N_2S_4Te$: C 52.18, H 6.71, N 4.26; found: C 52.22, H 6.83, N 3.95. Similarly *N,N*-diphenylbis(*N,N*-dipropyldithiocarbamato)tellurium(IV) was prepared in 83% yield; yellow crystals; mp 76–77°C. Anal. calcd. for $C_{26}H_{38}N_2S_4Te$: C 49.24, H 6.04, N 4.42; found: C 48.88, H 5.97, N 4.23.

Synthesis of chlorodiphenyl(N,N-*dialkyldithiocarbamato)tellurium(IV)*

Typically, an equimolar mixture of sodium *N,N*-dibutyldithiocarbamate (0.57 g), previously dried, and Ph_2TeCl_2 (0.87 g) was refluxed in excess methylene dichloride or CS_2 (10 mL) at 45°C for 3 h. N_2 gas was bubbled through at a rate of 3 bubbles/s. The solution was then filtered to remove any solid materials and left in the refrigerator to crystallize. $Ph_2TeCl[S_2CNBu_2]$, 0.84 g; 65% yield; pale yellow crystals; mp 88–90°C. Anal. calcd. for $C_{21}H_{28}ClNS_2Te$: C 48.35, H 5.41, N 2.69; found: C 47.88, H 5.47, N 2.69.

Similarly prepared were $Ph_2TeCl[S_2CNR_2]$, R = Me, Et, Pr, and *i*-Pr for subsequent conversion to the four corresponding bromides.

Synthesis of bromodiphenyl(N,N-*dialkyldithiocarbamato)tellurium(IV)*

Typically, $Ph_2TeCl[S_2CNBu_2]$ (0.29 g) was dissolved in CS_2 (5 mL) and the system kept in an ice bath and purged under nitrogen. An equimolar amount of bromotrimethylsilane (0.075 mL) was added slowly to the mixture. Once addition was complete the mixture was stirred at ambient temperature for 3–4 h. The solution was then filtered and placed in a refrigerator to allow the crystallization of $Ph_2TeBr[S_2CNBu_2]$, 0.19 g; 60% yield; yellow crystals; mp 97–98°C. Anal. calcd. for $C_{21}H_{28}BrNS_2Te$: C 44.56, H 4.79, N 2.49; found: C 45.23, H 5.06, N 2.49. Similar methods were used to prepare pale lime-green crystals of $Ph_2TeBr[S_2CNPr_2]$, mp 93–94°C; of $Ph_2TeBr[S_2CNi\text{-}Pr_2]$, mp 143–147°C; $Ph_2TeBr[S_2CNEt_2]$,$\frac{1}{2}CS_2$, mp 192°C; and $Ph_2TeBr[S_2CNMe_2]$, mp 97°C.

Alternate synthesis of $Ph_2TeBr[S_2CNR_2]$

Typically, diphenyltellurium dibromide (0.82 g) was stirred in dried methylene chloride or CS_2 (10 mL) in a two-necked flask. The solution was cooled with an ice bath and purged under N_2. Sodium *N,N*-dibutyldithiocarbamate (0.53 g), previously dried *in vacuo* for 4–5 days, was added from a finger tube attached to the flask. The solution was stirred in an ice bath under nitrogen for 30 min. At this time the mixture was allowed to reach ambient temperature and stirred for 3–4 h. The product solution was filtered and placed in a refrigerator at −6°C until crystals formed. Crystals of $Ph_2TeBr[S_2CNBu_2]$ were washed with *n*-hexane and dried *in vacuo* for 2–3 days; 0.94 g; 71% yield; pale green crystals; mp 98°C. Anal. calcd. for $C_{21}H_{28}BrNS_2Te$: C 44.56, H 4.79,. N 2.49; found: C 44.29, H 4.78, N 2.21.

Physical measurements

All solvents were dried and distilled prior to use. Elemental analyses were performed by Galbraith Laboratories in Knoxville, TN, or M-H-W Laboratories in Phoenix, AR. Density measurements were performed by the flotation method in CCl_4/C_6H_6. The infrared spectra were recorded on a Nicolet 5DXFT spectrometer as KBr pellets and far infrared spectra on a Bohmem IR Spectrometer between polyethylene films. Samples for Raman spectroscopy were sealed in capillary tubes and the spectra recorded on a Ramanor U-1000 spectrometer using the 4880 Å exciting line. The ^1H NMR spectra were recorded on a Bruker AC300 spectrometer in CS_2 or $CDCl_3$ solutions using tetramethylsilane as the internal reference for CS_2 solutions. The same instrument was used to record the $^{13}C\{^1H\}$ NMR spectra. A Bruker AC200 spectrometer was used to record ^{125}Te spectra, referenced to dimethyl tellurium. The melting points were determined on a Fisher-Johns apparatus.

X-ray crystallographic analysis

X-ray diffraction data were collected on a Syntex P_21 diffractometer by the procedure already described in detail (13). In each case the crystal was sealed in a capillary and mounted along the largest dimension. The least-squares refinement of the setting angles of 35 reflections ($15 > 2\theta > 30$) led to the cell dimensions given in Table 1. The appropriate space group was used in both cases and later assumed correct because of successful refinement of the data. During data collection, the intensities of three monitor reflections measured after 200 reflections decreased in the range approximately 2–4% and the appropriate scaling factor was employed. Each set of data was corrected for Lorentz and polarization effects, and an empirical absorption correction was applied but resulted in no significant changes in refinement. The ranges of absorption correction factors were 0.92–0.90 for **4**, and 0.98–0.96 for **7**. A summary of crystal and refinement data are given in Table 1.

The position of the tellurium was determined by a sharpened Patterson synthesis. The remaining atoms were revealed using SHELX and difference maps. Te, S, N, and where appropriate Br were refined anisotropically. Limitations on data in one case allowed only the anisotropic refinement of carbon atoms other than those in the phenyl rings in which the carbon atoms were fixed as a hexagon and so we completed both refinements with the same restrictions. Hydrogen atoms were included at the idealized positions (C—H = 0.95 Å; HCH (for ethyl and butyl) = 109.5°; CCH = 120° (for phenyl rings)) with isotropic *U* values set at approximately 0.01 Å greater than the corresponding carbon atom. Complete refinement by full-matrix least-squares methods minimizing the function $\Sigma w(|F_o| - |F_c|)^2$ converged satisfactorily in both cases at $R = 0.0448$ and $R_w = 0.0489$ for **4**; and $R = 0.0397$ and $R_w = 0.0439$ for **7**. A weighting scheme of the form $w = 1/[\sigma(F) + \rho F^2]$ was employed with final ρ values of 0.00007 for **4** and 0.00012 for **7**, respectively. No evidence was found of reflections being affected by secondary extinctions. We also refined both structures without fixing the rings, which resulted in a NP/P of only 6.9 for **4** with convergence at $R = 0.0439$ and $R_w = 0.485$ for **4** and $R = 0.0391$ and $R_w = 0.0426$ for **7**. No bond distances or bond angles were significantly altered with the exception of those involving the connection of tellurium to the phenyl ring which changed marginally. Also because the phenyl rings were not fixed, the uncertainty on the Te—C bond lengths increased very slightly along

Can. J. Chem. Downloaded from www.nrcresearchpress.com by 123.30.183.119 on 09/08/12
For personal use only.

TABLE 1. Summary of crystal data, intensity collection and structural refinement for $Ph_2TeBr[S_2CNEt_2]\cdot\frac{1}{2}CS_2$, **4**, and $Ph_2Te[S_2CNBu_2]_2$, **7**

Parameter	$C_{17.5}H_{20}BrNS_3Te$ **4**	$C_{30}H_{46}N_2S_4Te$ **7**
Cell constants a (Å)	11.204(3)	19.392(6)
b (Å)	14.106(11)	9.622(2)
c (Å)	13.867(10)	19.089(6)
α (deg)	99.60(6)	90.0
β (deg)	102.74(4)	104.70(2)
γ (deg)	87.71(4)	90.0
Cell volume (Å)	2107(2)	3445(2)
Crystal system	Triclinic	Monoclinic
Space group	$P\bar{1}$	$P2/c$
Mol. wt. (g mol^{-1})	548.0	690.5
Z	4	4
ρ_{obsd}, ρ_{calcd} g cm^{-3}	1.68, 1.73	1.34, 1.33
Crystal dimensions (mm)	0.35 × 0.52 × 0.48	0.44 × 0.39 × 0.54
Abs. coeff. μ (cm^{-1})	34.39	10.32
Temperature (°C)	24±1	24±1
Radiation	MoKα 0.71069 Å	
Monochromator	Highly orientated graphite	
2θ	4-40	
Scan method	Coupled θ(crystal)/2θ(counter)	
Scan width	$K\alpha_1 - 1°$ to $K\alpha_2 + 1°$	
Background time/scan time	0.5	
Scan speed (deg min^{-1})	Variable, 2.02–4.88	
Total reflections measured	4050	4195
Unique data used	2980	1344
No. of parameters (NP)	256	126
$R = (\Sigma\|\|F_o\| - \|F_c\|\|/\Sigma\|F_o\|)$	0.0448	0.0397
$R_w = [\Sigma w(\|F_o\| - \|F_c\|)^2/\Sigma w\|F_o\|^2]^{\frac{1}{2}}$	0.0489	0.0439
Largest Δρ e Å^{-3}) shift/error max.	0.007	0.002
Largest residual electron density (e Å^{-3})	1.001	0.989
Atom associated with residual density	Te	Te

with the bond length: for **4**, Tel-C6 = 2.14(1) and Te2—C23 = 2.12(1) and for **7**, Te—C10 = 2.136(5).

The final fractional coordinates for non-hydrogen atoms of **4** and **7** are listed in Tables 2 and 3 respectively. Both molecules were subjected to the same degree of refinement and in both cases NP/P was greater than 10. Important bond lengths and angles are given in Tables 4 and 5. The molecular structures of both the compounds are given in Figs. 1 and 2. Tables of anisotropic Te, S, N, Br, and all C atoms not in the phenyl rings, final fractional coordinates and thermal parameters of hydrogen atoms, as well as tables of observed and calculated structure factors have been deposited.[1]

Results and discussion

The diphenylbromo(*N*,*N*-dialkyldithiocarbamato)tellurium-(IV) derivatives are made by either an essentially quantitative conversion of the corresponding chloro derivatives by an exchange reaction using bromotrimethylsilane or by direct reaction with diphenyltellurium dibromide. The chloro derivatives and diphenylbis(*N*,*N*-dibutyldithiocarbamato)tellurium-(IV) were made by the procedures described earlier (18). One typical method of characterizing such compounds is by NMR spectroscopy. However, it soon became apparent that although these species could all be recrystallized and their molecular formulation confirmed by analysis, they dissociated rapidly in solution. Thus assignments of NMR spectra to particular compounds (see Table 7) depended on selecting peaks in sequences of spectra which were changing with time. In this context it seemed appropriate to at least confirm the solid state structures of the new compounds when crystals of sufficient quality could be formed.

The crystal structure of $Ph_2Te[S_2CNBu_2]_2$, 7

Unlike that which was found for the analogous methyldithiocarbamate derivative, the compound crystallizes in the space group $P2/c$. However, the geometry around tellurium is again best described as a sawhorse structure typical of tellurium(IV) compounds based on a distorted trigonal bipyramid in which the lone-pair occupies an equatorial position. The organo substituent in the dithiocarbamate is a relatively long-chain alkane compared with other compounds of this type whose structures are known, namely, $Ph_2Te[S_2CNMe_2]_2$ (18) and $Ph_2Te[S_2CNEt_2]_2$ (20). Nevertheless, the structures are similar with the C—Te—C angles in the equatorial position being 95.3(2)° for **7** and 94.23(13) and 94.07(7)° for the two crystalline forms of $Ph_2Te[S_2CNEt_2]_2$ (20) and 99.4(1)° for $Ph_2Te[S_2CNMe_2]_2$ (18), and with the Te—C bond lengths being essentially identical in all three compounds. The exact length determined for the Te—C bond may vary depending on whether the structure is determined using fixed phenyl rings or not. Thus, with fixed rings, the value of the Te—C bond length in **7** is calculated to be 2.125(4) Å, which is close to the reported average value for tellurium – aryl carbon bonds (21). If, as was the case for $Ph_2Te[S_2CNMe_2]_2$, the carbon atoms in the ring are

[1]A complete set of material may be purchased from The Depository of Unpublished Data, Document Delivery CISTI, National Research Council Canada, Ottawa, Canada K1A 0S2.

TABLE 2. Final fractional coordinates for non-hydrogen atoms of $Ph_2TeBr[S_2CNET_2]$-(1/2)CS_2, **4**

Atom	*x*	*y*	*z*	Atom	*x*	*y*	*z*
Te1	0.53240(6)	0.50691(5)	0.82826(5)	Te2	0.02337(6)	0.03941(5)	0.69137(5)
Br1	0.5056(1)	0.6811(1)	0.7627(1)	Br2	0.2289(1)	−0.0208(1)	0.8194(1)
S1	0.5392(3)	0.3343(2)	0.8549(2)	S3	−0.1780(3)	0.0870(2)	0.5892(2)
S2	0.7077(3)	0.4540(2)	1.0261(2)	S4	0.0310(3)	0.1696(2)	0.5324(2)
N1	0.6707(9)	0.2656(7)	1.0089(7)	N2	−0.2001(9)	0.1833(7)	0.4401(7)
C1	0.6433(9)	0.3467(8)	0.9708(8)	C18	−0.119(1)	0.1522(8)	0.5142(8)
C2	0.754(1)	0.2634(9)	1.1087(8)	C19	−0.165(1)	0.2383(9)	0.3693(9)
C3	0.882(1)	0.240(1)	1.103(1)	C20	−0.154(1)	0.3477(9)	0.406(1)
C4	0.618(1)	0.1720(8)	0.958(1)	C21	−0.333(1)	0.160(1)	0.419(1)
C5	0.505(1)	0.150(1)	0.988(1)	C22	−0.400(2)	0.227(1)	0.476(1)
C6	0.6944(7)	0.4907(4)	0.7728(6)	C23	0.0391(5)	0.1718(5)	0.7901(6)
C7	0.7777(7)	0.5666(4)	0.8007(6)	C24	0.1550(5)	0.2123(5)	0.8281(6)
C8	0.8858(7)	0.5596(4)	0.7657(6)	C25	0.1683(5)	0.3001(5)	0.8928(6)
C9	0.9106(7)	0.4767(4)	0.7027(6)	C26	0.0658(5)	0.3474(5)	0.9196(6)
C10	0.8273(7)	0.4009(4)	0.6748(6)	C27	−0.0501(5)	0.3068(5)	0.8815(6)
C11	0.7192(7)	0.4079(4)	0.7098(6)	C28	−0.0634(5)	0.2190(5)	0.8168(6)
C12	0.4050(6)	0.4553(5)	0.6933(6)	C29	−0.0871(6)	−0.0336(5)	0.7619(4)
C13	0.4278(6)	0.4537(5)	0.5982(6)	C30	−0.1542(6)	−0.1124(5)	0.7041(4)
C14	0.3406(6)	0.4162(5)	0.5132(6)	C31	−0.2253(6)	−0.1650(5)	0.7472(4)
C15	0.2305(6)	0.3804(5)	0.5235(6)	C32	−0.2293(6)	−0.1388(5)	0.8480(4)
C16	0.2078(6)	0.3820(5)	0.6187(6)	C33	−0.1622(6)	−0.0600(5)	0.9057(4)
C17	0.2950(6)	0.4195(5)	0.7036(6)	C34	−0.0911(6)	−0.0074(5)	0.8627(4)
S5	0.3529(5)	0.1508(4)	0.6175(5)	C35	0.460(1)	0.092(1)	0.657(1)
S6	0.5707(4)	0.0290(4)	0.6989(5)				

TABLE 3. Final fractional coordinates for non-hydrogen atoms of $Ph_2Te[S_2CNBu_2]_2$, **7**

Atom	*x*	*y*	*z*	Atom	*x*	*y*	*z*
Te	0.0	0.05495(5)	0.25	C7	0.2551(4)	0.4616(6)	0.3858(4)
S1	0.1384(1)	0.0388(2)	0.2681(1)	C8	0.2897(6)	0.5601(8)	0.4464(5)
S2	0.1022(1)	0.2241(2)	0.3796(1)	C9	0.287(1)	0.707(1)	0.4198(7)
N1	0.2282(3)	0.2155(5)	0.3490(2)	C10	0.0068(2)	−0.0939(4)	0.3338(2)
C1	0.1617(3)	0.1681(6)	0.3355(3)	C11	−0.0288(2)	−0.0671(4)	0.3873(2)
C2	0.2797(4)	0.1760(7)	0.3079(4)	C12	−0.0230(2)	−0.1600(4)	0.4446(2)
C3	0.3251(4)	0.0538(7)	0.3414(5)	C13	0.0185(2)	−0.2796(4)	0.4484(2)
C4	0.3828(5)	0.022(1)	0.3031(4)	C14	0.0541(2)	−0.3063(4)	0.3949(2)
C5	0.4287(6)	−0.100(1)	0.3334(7)	C15	0.0483(2)	−0.2135(4)	0.3375(2)
C6	0.2571(4)	0.3155(7)	0.4092(3)				

not fixed then the Te—C bond length is calculated as 2.136(5) for **7** and 2.140(5), 2.143(2), and 2.142(2) for the methyl analogue (18) and the two forms of the ethyl analogue, respectively. The distortion from linear for the two axial S atoms bonded to tellurium is similar with an angle of 173.2(1)° for **7**, 175.11(3) and 178.94(2)° for the ethyl analogues, and 172.0(1)° for the methyl analogue. The Te—S distances are essentially identical, being 2.622(2) Å for **7**, 2.62(1) Å for $Ph_2Te[S_2CNMe_2]_2$ (18), and 2.6303(9) for $Ph_2Te[S_2CNEt_2]_2$ (20). Furthermore, not surprisingly, the positions of the non-bonded or partially "bonded" sulfur atoms are essentially the same, with distances of 3.195(2) Å for **7** and 3.186(2) Å and 3.1103(9) Å for the analogues; the sum of the van der Waals radii being ca. 4.0 Å (22). The similarity extends to the bite angles for the ligand of 61.0(2)° for **7** and 61.84(2)° for the *C*2/*c* form of $Ph_2Te[S_2CNEt_2]_2$ (20). If the longer tellurium–sulfur bonds are considered as part of the coordination shell about tellurium, then tellurium has an effective coordination number of seven and has close to a 1:2:2:2 geometry (23) as was described for the ethyl analogue (20) and $C_8H_8Te[S_2CNEt_2]_2$ (24). Presumably, the molecules are packed together in sufficiently discrete units so that the longer chains of the butyl groups provide no hindrance to crystallization in essentially identical arrangements, although it is notable that the nearest neighbour contact for tellurium is a terminal methyl group of a butyl chain.

The crystal structure of $Ph_2TeBr[S_2CNEt_2]\cdot\frac{1}{2}CS_2$, ***4***

This bromo derivative crystallizes out with CS_2 contained in the lattice as triclinic *P*1 and is essentially identical to that previously reported for the chloro derivative (18). The same distorted sawhorse structure is present around tellurium with the Te—Br bond now replacing an axial Te—S bond. The Te—Br bonds of 2.743(2) and 2.779 Å for the two asymmetric units are longer than the Te–Br bonds reported for Ph_2TeBr_2 of 2.682(3) Å (25) but by a lesser amount than was noted between Ph_2TeCl_2 and $Ph_2TeCl[S_2CNEt_2]$ (18). Other bond lengths and bond angles involving tellurium are essentially the same for the bromo and chloro derivatives. The similarity between $Ph_2TeCl[S_2CNEt_2]\cdot\frac{1}{2}CS_2$ and $Ph_2TeBr[S_2CNEt_2]\cdot\frac{1}{2}CS_2$ even ex-

Can. J. Chem. Downloaded from www.nrcresearchpress.com by 123.30.183.119 on 09/08/12
For personal use only.

TABLE 4. Interatomic distances (Å) in compounds **4** and **7**

$Ph_2TeBr[S_2CNEt_2]\cdot\frac{1}{2}CS_2$ **4**[a]				$Ph_2Te[S_2CNBu_2]_2$ **7**	
Atoms	Distance	Atoms	Distance	Atoms	Distance
Te1-Br1	2.743(2)	Te2-Br2	2.779(1)	Te-S1	2.622(2)
Te1-S1	2.518(3)	Te2-S3	2.516(3)	Te-S2	3.195(2)
Te1-S2	3.183(3)	Te2-S4	3.113(3)	Te-C10	2.125(4)
Te1-C6	2.113(7)	Te2-C23	2.111(7)	S1-C1	1.764(6)
Te1-C12	2.125(7)	Te2-C29	2.126(6)	S2-C1	1.681(6)
S1-C1	1.75(1)	S3-C18	1.74(1)	N1-C1	1.331(8)
S2-C1	1.69(1)	S4-C18	1.66(1)	N1-C2	1.469(8)
				N1-C6	1.494(8)
N1-C1	1.34(1)	N2-C18	1.34(1)	C2-C3	1.51(1)
N1-C2	1.49(1)	N2-C19	1.47(2)	C3-C4	1.52(1)
N1-C4	1.47(1)	N2-C21	1.50(2)	C4-C5	1.49(1)
C2-C3	1.48(2)	C19-C20	1.54(2)	C6-C7	1.472(8)
C4-C5	1.48(2)	C21-C22	1.42(2)	C7-C8	1.51(1)
Te1-S2″	3.678(3)	Te2-S4″	3.865(3)	C8-C9	1.50(1)
Te1-Te1″	5.008(3)	Te2-Te2″	5.151(3)		

[a]Symmetry-equivalent positions; double prime indicates 1-*x*, 1-*y*, 1-*z*.

TABLE 5. Bond angles (deg) in compounds **4** and **7** with standard deviations in parentheses and with fixed phenyl rings

$Ph_2TeBr[S_2CNEt_2]\cdot\frac{1}{2}CS_2$				$Ph_2Te[S_2CNBu_2]_2$[a]	
Bonds	Angle	Bonds	Angle	Bonds	Angle
Br1-Te1-S1	169.2(1)	Br2-Te2-S3	172.9(1)	S1-Te-S1′	173.2(1)
S1-Te1-C6	92.2(2)	S3-Te2-C23	92.4(2)	S1-Te-C10	89.7(1)
S1-Te1-C12	84.2(2)	S3-Te2-C29	84.4(2)	S1-Te-C10′	85.7(2)
Br1-Te1-C6	86.4(2)	Br2-Te2-C23	87.2(2)	S1′-Te-C10	84.7(2)
Br1-Te1-C12	85.5(2)	Br2-Te2-C29	88.6(2)	S1′-Te-C10′	89.7(2)
C6-Te1-C12	98.7(3)	C23-Te2-C29	98.1(3)	C10-Te-C10′	95.3(2)
Te1-S1-C1	98.7(4)	Te2-S3-C18	97.2(4)	Te-S1-C1	96.8(2)
C1-N1-C2	123(1)	C18-N2-C19	123(1)	C1-N1-C2	124.4(5)
C1-N1-C4	123(1)	C18-N2-C21	122(1)	C1-N1-C6	121.7(5)
C2-N1-C4	114(1)	C19-N2-C21	115(1)	C2-N1-C6	113.9(5)
S1-C1-S2	121.1(7)	S3-C18-S4	121.1(6)	S1-C1-S2	120.7(4)
S1-C1-N1	115.4(8)	S3-C18-N2	115.9(8)	S1-C1-N1	116.1(4)
S2-C1-N1	123.4(8)	S4-C18-N2	122.9(9)	S2-C1-N1	123.3(4)
N1-C2-C3	113(1)	N2-C19-C20	115(1)	N1-C2-C3	112.1(5)
N1-C4-C5	113(1)	N2-C21-C22	113(1)	N1-C6-C7	114.0(5)
Te1-C6-C7	117.8(2)	Te2-C23-C24	118.6(1)	Te-C10-C11	118.6(1)
Te1-C6-C11	122.2(2)	Te2-C23-C28	121.4(1)	Te-C10-C15	121.3(1)
Te1-C12-C13	123.5(2)	Te2-C29-C30	117.4(1)	C2-C3-C4	112.0(7)
Te1-C12-C17	116.4(2)	Te2-C29-C34	122.5(1)	C3-C4-C5	114.3(9)
				C6-C7-C8	113.2(6)
				C7-C8-C9	111.2(8)
S1-Te1-S2	62.2(3)	S3-Te2-S4	62.5(3)	S1-Te-S2	61.0(2)

[a]Symmetry-equivalent positions: prime indicates -*x*, *y*, 0.5-*z*.

tends to the location of the closest interaction between Te and an atom containing lone-pairs on an adjacent atom, the Te--S′ distances being 3.678(3), 3,865(3), 3.656(2), and 3.825(2), respectively, for **7** and its chloro analogue. By contrast, the packing in $Ph_2TeCl[S_2CN(i\text{-}Pr)_2]$ is such as to make the closest such interaction Te---Cl′ at a distance of 3.607(2) Å (18).

In all of these dithiocarbamates, as for the methyl and ethyl analogues, the S_2C—N bond clearly has partial double-bond character as it is considerably shorter (1.331(8) for **4** and 1.34(1) for **7**) than the shortest N—C bond to an organic group (1.469(8) for **4** and 1.47(2) for **7**). The similarity of the environment of the ligand itself is further emphasized by the short C—S(terminal) and long C—STe bonds in the two compounds which span the range 1.66(1)–1.69(1) for **7** and 1.681(6) for **4** for C=S and 1.74(1)–1.75(1) for **7** and 1.764(6) for **4** for C—STe. This situation is generally the case for all the ligands for the compounds reported or discussed herein. Thus the ligand is essentially unchanged whether it is in a bis-substituted compound or a chloro- or bromo-substituted derivative.

Can. J. Chem. Downloaded from www.nrcresearchpress.com by 123.30.183.119 on 09/08/12
For personal use only.

Can. J. Chem. Downloaded from www.nrcresearchpress.com by 123.30.183.119 on 09/08/12
For personal use only.

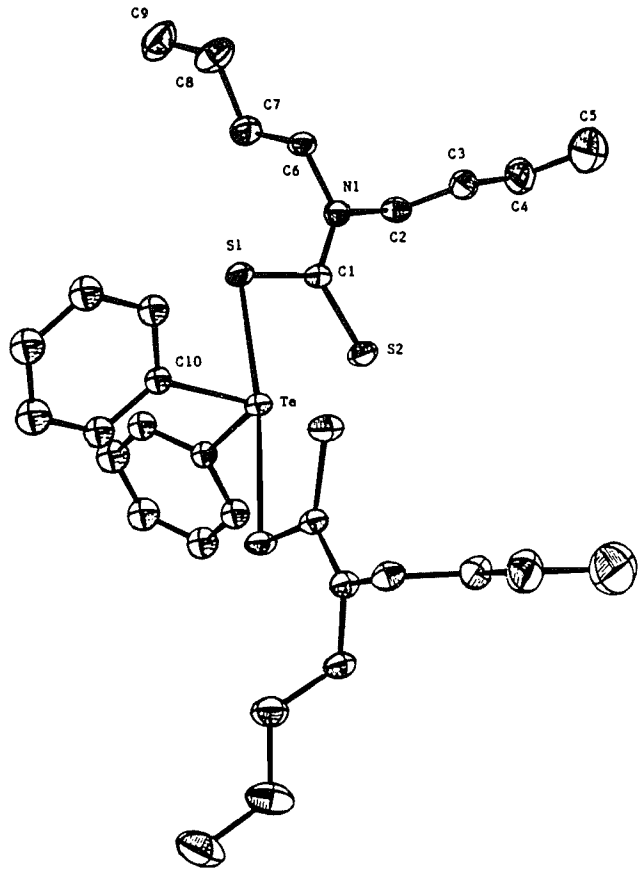


FIG. 1. ORTEP plot of the molecule $Ph_2Te[S_2CNBu_2]_2$, **7**. The atoms are drawn with 20% probability. Hydrogen atoms are omitted for clarity.

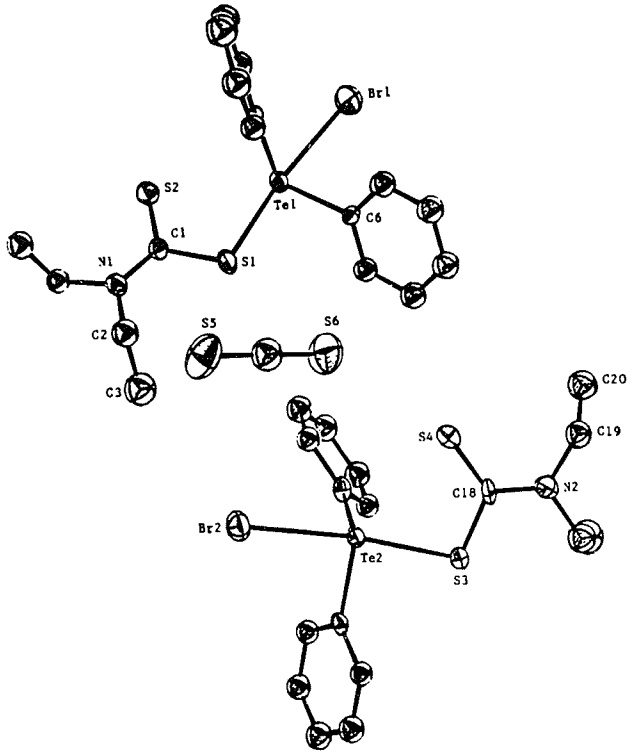


FIG. 2. ORTEP plot of the molecule $Ph_2TeBr[S_2CNEt_2]\cdot\frac{1}{2}CS_2$, **4**, showing the two independent molecules and CS_2. The atoms are drawn with 20% probability ellipsoids. Hydrogen atoms omitted for clarity.

Infrared and Raman spectra

As has been mentioned, these compounds all have a tendency to decompose when dissolved. Consequently, the vibrational spectra (Table 6) become more important in providing a characterization in the solid state. However, it soon becomes evident that those features attributed by previous workers to ν(C—NR_2), νC=S), and ν(C—SM) stretches in the regions 900–1500 cm^{-1} all occur in the same area as strong features in both the Raman and IR spectra of phenyl and alkyl groups so that their assignment is only possible by essentially circular arguments. Thus the infrared spectra, at least in this region, can provide little information to confirm the nature of the compound. However, the Raman spectrum shows a distinctive peak in the range 947–980 cm^{-1}, attributable to the NCS_2 group, close to and usually of comparable intensity to the definitive *p* and *b* phenyl vibrations (26) which are always seen at 998 ± 1 and 1018 ± 1 cm^{-1}. Another peak of comparable intensity appears consistently in all of these compounds in the 360–390 cm^{-1} region which is typical of many M—S containing compounds, and so it is assigned to the Te—S stretching mode. By contrast, in Ph_2TeCl_2, the two Te—Cl stretching vibrations are seen at 287 and 267 cm^{-1} (27) which is markedly to lower wave number than ν(Te—S), particularly as the Te—S bond is longer than the Te—Cl bond in Ph_2TeCl_2 of 2.48–2.54 Å (28). Another surprising feature is that in the bromo derivatives there is no very strong band in the region below 200 cm^{-1} in the Raman spectrum. This is in marked contrast to the Raman spectrum of Ph_2TeBr_2 where the band at 159 cm^{-1}, attributed to the symmetric Te—Br stretching vibration, is at least an order of magnitude more intense than any other feature in the whole spectrum (27). The most intense peak in this lower region of the Raman spectrum varies considerably from compounds **1**–**5** so that, rather disappointingly, ν(Te—Br) is not a distinctive Raman feature. However, in the far ir spectrum of compounds **1**–**5** there is a peak centred at ca. 169 cm^{-1} which is clearly more intense than any feature in this region in the spectra of compounds **6**–**8**. This is therefore assigned to ν(Te—Br) which places it at approximately the average value of the asymmetric (185 cm^{-1}) and symmetric (159 cm^{-1}) Te—Br stretching modes in Ph_2TeBr_2 (27).

Nuclear magnetic resonance spectra

The ^1H and ^{13}C NMR spectra recorded in Table 7 give the chemical shifts of compounds **1**–**8** recorded immediately after dissolution in $CDCl_3$ solution. Carbon disulfide was also used as solvent but in all cases the spectra recorded after a matter of days, in some cases only hours, showed no more than trace amounts of the original compound. The chemical shifts for all of the phenyl groups are very similar for all compounds **1**–**8** regardless of the nature of the attached dithiocarbamate or whether it is a bis-, chloro-, or bromo-substituted derivative. The shifts in the ^1H NMR spectrum are also close to those for Ph_2TeCl_2 and Ph_2TeBr_2 and significantly different from those of Ph_2Te, whose values are included for comparative purposes. The chemical shifts related to the alkyl groups of the dithiocarbamates are also virtually the same for a given ligand in the bis, chloro, or bromo derivatives, which is not surprising in view of the similarities within the X-ray structures that we report herein and that have been reported by us and others (18, 20). The typical H—H coupling associated with first-order spectra is clearly evident for the ethyl group and the terminal methyl groups in the isopropyl, propyl, and butyl compounds. For all of

TABLE 6. Selected features in the vibrational spectra (cm^{-1}) of compounds **1–8**

Compound	ν(C—S)		ν(Te—S)		ν(Te—X)	
	IR	Raman	IR	Raman	IR	Raman
$Ph_2TeBr[S_2CNBu_2]$, **1**	946(ms)	944(20)	382(m)	381(100)	168(m)	171(40)
$Ph_2TeBr[S_2CNPr_2]$, **2**	968(m)	966(25)	391(m)	390(85)	167(m)	171(100)
$Ph_2TeBr[S_2CNi\text{-}Pr_2]$, **3**	949(m)	946(20)	389(m)	387(100)	170(m)	
$Ph_2TeBr[S_2CNEt_2]$, **4**	964(m)	968(15)	387(m)	388(100)	169(m)	170(30)
$Ph_2TeBr[S_2CNMe_2]$, **5**	967(m)	960(50)	377(m)	376(100)	168(m)	167(90)
$Ph_2TeCl[S_2CNBu_2]$, **6**	946(m)	945(20)	378(m)	383(100)	181(ms)	192(50)
$Ph_2Te[S_2CNBu_2]_2$, **7**	973(m)	972(20)	360(m)	372(100)		*
$Ph_2Te[S_2CNPr_2]_2$, **8**	968(m)	968(25)	367(m)	375(100)		*
Ph_2TeBr_2					185m	
					159m	157(100)
Ph_2TeCl_2					287(m)	286(100)
					266(m)	267(75)

*Also have peaks in the Raman at ~174 cm^{-1} but none corresponding in the IR spectra.

the propyl and butyl compounds, the -CH_2 group attached to nitrogen has the expected triplet from H—H coupling, while the middle -CH_2 groups can be readily assigned as overlapping doublets of triplets in the case of propyl groups. For the butyl groups, the central -CH_2 groups are seen as doublets of triplets and doublets of quartets with very similar values of the coupling constants. It should be noted that in the diligands, e.g., $(CH_3CH_2CH_2CH_2)_2NCS_2S_2CN(CH_2CH_2CH_2CH_3)_2$, the NMR spectra indicate that the alkyl groups which are chemically equivalent are magnetically non-equivalent. Their NMR data are included in Table 7 for comparison.

While ^1H and ^{13}C NMR spectra can be obtained sufficiently rapidly to provide at least one spectrum that has essentially no extraneous peaks, the accumulation times involved in recording ^{125}Te NMR spectra of reasonable quality are such as to rarely show the presence of only the sample of compound **1–8** that was initially dissolved. In Table 8, the additional chemical shifts that are observed in the spectra of compounds **1–8** and other related derivatives are included to provide the background to indicate the mode of dissociation and/or rearrangement.

In the ^{125}Te NMR spectra of all bis compounds, $Ph_2Te[S_2CNR_2]_2$ peaks are seen in the range 703–712 ppm, compared to 765–780 ppm for all bromo-substituted compounds, $Ph_2TeBr[S_2CNR_2]_2$, and 918, 885, and 691 ppm respectively for Ph_2TeCl_2, Ph_2TeBr_2, and Ph_2Te. Based on the crystal structures and the similarities in the ^1H NMR spectra, the chemical shifts of $Ph_2Te[S_2CNR_2]_2$ species might well have been expected to be similar to those of the tellurium(IV), Ph_2TeX_2 (X = Cl, Br) species rather than the tellurium(II) species, Ph_2Te. Also, if the NMR is re-recorded after solutions of the bis compounds have been held at room temperature for more than 48 h, the only peak observed in the ^{125}Te NMR spectrum is that contributable to Ph_2Te. Thus, the overall reductive-elimination indicated for $Ph_2Te[S_2CNBu_2]_2$ [1] is a facile reaction for all $Ph_2Te[S_2CNR_2]_2$ species.

[1] $Ph_2Te[S_2CNBu_2]_2 \rightarrow Ph_2Te + Bu_2NCS_2S_2CNBu_2$

The presence of $Bu_2NCS_2S_2CNBu_2$ is readily confirmed by increases in the features attributable to it at 3.91 and 1.89, 1.72 ppm for NCH_2 and $NCCH_2$, respectively, in the ^1H NMR spectra and 57.82, 53.64 and 30.63, 28.55 ppm for NCH_2 and $NCCH_2$, respectively, in the ^{13}C NMR spectra of a solution of $Ph_2Te[S_2CNBu_2]_2$ as the corresponding peaks attributable to the bis compound decrease in intensity. Typically, if $CDCl_3$ is distilled onto freshly prepared $Ph_2Te[S_2CNBu_2]_2$ and held at liquid N_2 temperature until the solution is allowed to warm up in the spectrometer, all peaks can be initially assigned to the presence of only $Ph_2Te[S_2CNBu_2]_2$. However, these peaks progressively decrease in intensity until after 3 days the spectrum is dominated by peaks attributable to Ph_2Te and $Bu_2CNS_2NCBu_2$ although weak peaks are still present at room temperature at 134.5, 130.1, 129.7, ~54, and ~30 ppm which are similar to, but do not correspond to, those of the original compound but which are at least consistent with the presence of a second form of $Ph_2Te[S_2CNBu_2]_2$. The same general pattern is observed for all $Ph_2Te[S_2CNR_2]_2$ compounds so examined.

Thus, it seems reasonable to suppose that the bis compounds do exist in two forms in solution, one of which would be the favoured form at low temperature and so resembles the crystal structure with Te—S bonds at ca. 180° to each other (a "*trans*" form) and in which the closest approach of S-atoms on adjacent ligands would be approximately 5.50 Å even allowing for free rotation. The second form would be one in which at least one of the anisobidentate S-atoms of the crystal structure has become the more tightly bound S-atom of the ligand resulting in the presence of two dithiocarbamate groups with Te—S bonds at approximately 90° to one another (a "*cis*" form) and free rotation about these bonds would readily bring the pendant sulfur atoms into close contact leading to the ready formation of the diligand, as is demonstrated diagrammatically in Fig. 3*a*. The existence of S-ligands "*cis*" to one another is clearly seen in the structure of the dimeric species $\{Ph_3Te(S_2CNi\text{-}Pr)\}_2$ (29) although intramolecular monodentate–bidentate dithiolate exchange is an equally probale initiation step. The reductive-elimination might be expected to be reversible but if so the equilibrium must be very strongly towards the right hand side and we have been unable to obtain any unequivocal evidence of the formation of bis compounds from the reaction of diligand and Ph_2Te in solution.

The ^{125}Te NMR chemical shifts of the $Ph_2TeBr[S_2CNR_2]$ species, as mentioned earlier, are all in the range of 765–780 ppm and are approximately mid-way between those of Ph_2TeBr_2 and the bis compounds or Ph_2Te, again consistent with the thiocarbamate groups having a surprisingly small influence on the

Can. J. Chem. Downloaded from www.nrcresearchpress.com by 123.30.183.119 on 09/08/12
For personal use only.

TABLE 7. ^{1}H and $^{13}C^{a}$ chemical shifts in the NMR spectra of compounds **1–8**[a]

Compound	C_6H_5 [C_6H_5]	NCH_n [NCH_n]	$NCCH_n$ [$NCCH_n$]	$NCCCH_3$ [$NCCCH_3$]	$NCCCCH_3$ [$NCCCCH_3$]
$Ph_2TeBr[S_2CNBu_2]$, **1**	8.09–8.06; 7.48–7.44	3.71br(7.5)	1.64m(7.5,7.0)	1.31m(7.0,7.7)	0.91t(7.7)
	[135.1, 130.8, 129.9]	[54.6]	[29.1]	[20.1]	[13.8]
$Ph_2TeBr[S_2CNPr_2]$, **2**	8.08–8.06; 7.45–7.43	3.67br	1.69m(7.5,7.7)	0.88t(7.7)	
	[135.1, 130.8, 129.8]	[56.4]	[20.3]	[11.1]	
$Ph_2TeBr[S_2CNi\text{-}Pr_2]$, **3**	8.09–8.07; 7.46–7.41	3.17vbr	1.39d(7.5)		
	[135.1, 130.7, 129.8]	[n.o.]	[20.0]		
$Ph_2TeBr[S_2CNEt_2]$, **4**	8.08–8.06; 7.47–7.43	3.79br(7.1)	1.23t(7.1)		
	[134.8, 134.3, 130.8, 129.8]	[49.0]	[12.2]		
$Ph_2TeBr[S_2CNMe_2]$, **5**	8.09–8.05; 7.47–7.44	3.39s			
	[135.1, 130.9, 129.9]	[53.9]			
$Ph_2TeCl[S_2CNBu_2]$, **6**	8.09–8.05; 7.48–7.45	3.72br(7.4)	1.65m(7.4,7.5)	1.32m(7.5,7.0)	0.92t(7.0)
	[134.5, 134.0, 130.7, 129.7]	[54.4]	[28.9]	[20.0]	[13.8]
$Ph_2Te[S_2CNBu_2]_2$, **7**	8.07–8.03; 7.41–7.39	3.79t(7.2)	1.65m(7.2,7.7)	1.29m(7.7,7.8)	0.90t(7.8)
	[134.9, 129.7, 129.3]	[54.0]	[29.0]	[20.1]	[13.8]
$Ph_2Te[S_2CNPr_2]_2$, **8**	8.05–8.03; 7.40–7.38	3.72t(7.5)	1.68m(7.5,7.2)	0.85t(7.2)	
	[135.0, 129.8, 129.4]	[55.9]	[20.3]	[11.2]	
$Bu_2NCS_2S_2CNBu_2$		3.91m	1.89m, 1.72m	1.42m, 1.33m	1.0t, 0.94t
		[57.8, 53.6]	[30.6, 28.6]	[20.5] [14.1]	
$PrNCS_2S_2CNPr_2$		3.88q	1.90m, 0.98t		
		[59.2, 55.1]	[21.6, 19.5]		
$Et_2NCS_2S_2CNEt_2$		4.00m	1.45t, 1.27t		
		[52.4, 47.9]	[13.8, 11.8]		
$Me_2NCS_2S_2CNMe_2$		3.59, 3.56			
		[47.8, 42.4]			

[a] ^{13}C-NMR chemical chifts given in [ ].
[b] Coupling constnats given in ( ).

TABLE 8. ^{125}Te NMR chemical shifts in solutions of compounds **1–8** and selected related examples[a]

Compound	Ph_2TeX_2	Ph_2TeXL	Ph_2TeL_2	Ph_2Te
$Ph_2TeBr[S_2CNBu_2]$, **1**	884	775		691
$Ph_2TeBr[S_2CNPr_2]$, **2**	884	774		691
$Ph_2TeBr[S_2CNi\text{-}Pr_2]$, **3**	884	763		691
$Ph_2TeBr[S_2CNEt_2]$, **4**	884	774		691
$Ph_2TeBr[S_2CNMe_2]$, **5**	884	779		691
$Ph_2TeCl[S_2CNBu_2]$, **6**	917	779		691
$Ph_2Te[S_2CNBu_2]_2$, **7**			704	691
$Ph_2Te[S_2CNPr_2]_2$, **8**			703	691
Ph_2TeCl_2	917			
Ph_2TeBr_2	884			
$Ph_2TeClBr$	905			
Ph_2Te				691

[a] X = Cl, Br, L = dithiocarbamate.

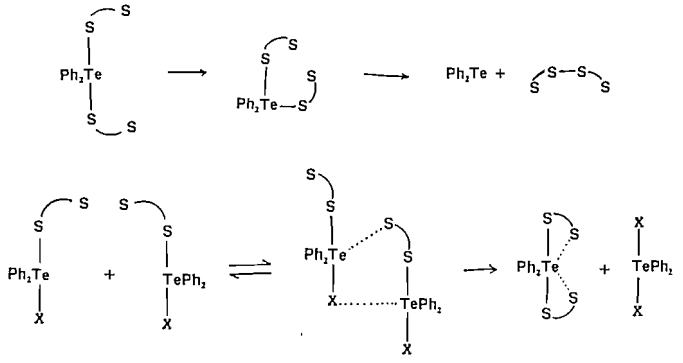


FIG. 3. Diagrammatical representation of (*a*) reductive-elimination of a bis compound and (*b*) disproportion and decomposition of a partially substituted halide.

[2] $Ph_2TeCl[S_2CNBu_2] \rightleftarrows Ph_2TeCl_2 + Ph_2Te[S_2CNBu_2]_2$

$$\downarrow$$

$$Ph_2Te + Bu_2NCS_2S_2CNBu_2$$

value of the chemical shift. It can be seen from Table 7 that the spectra of these halogenated derivatives also display features attributable to Ph_2TeX_2 and Ph_2Te.

Typically, the disappearance of the initial peak attributable to $Ph_2TeX[S_2CNR_2]$ species decreases at a much slower rate than was the case for the bis species. As the intensity of the initial peak decreases, so the intensities of those attributable to Ph_2TeX_2 and Ph_2Te increase. It is reasonable to assume that exchange takes place in accord with route [2] and that the bis species decompose as they form too rapidly for their presence to be picked up in these NMR spectra.

The transformation to Ph_2TeX_2 and $Ph_2Te[S_2CNR_2]_2$ could be by exchange involving the halide groups or the dithiocarbamate (as indicated in Fig. 3*b*) or both. Because of the propensity for bis compounds to undergo rapid reductive-elimination, it is difficult to obtain evidence of their ability to exchange. However, the presence of the dithiocarbamate as a bridging ligand in $\{Ph_3Te(S_2CNi\text{-}Pr)\}_2$ (29) with Te—S bond lengths of approximately 3.1 Å indicates that such a process is feasible, as does the crystal packing in $Ph_2TeCl[S_2CNEt_2]$, $Ph_2TeCl[S_2$-

Can. J. Chem. Downloaded from www.nrcresearchpress.com by 123.30.183.119 on 09/08/12
For personal use only.

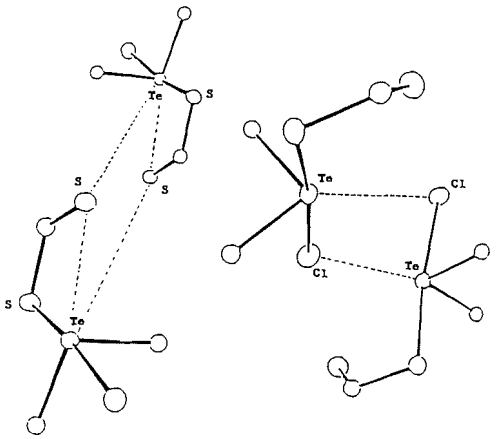


FIG. 4. Possible intermediates as suggested by a section of the packing diagrams of $Ph_2Te[S_2CNR_2]_2$ (*a*) and $Ph_2TeX[S_2CNR_2]_2$ (*b*) species showing the intermolecular interactions.

$CNi\text{-}Pr_2$] (18), and $Ph_2TeBr[S_2CNEt_2]$, which gives Te---S distances between molecules of ca 3.6 Å (Fig. 4*a*). Similarly, the crystal structure of $Ph_2TeCl[S_2CNi\text{-}Pr_2]$ also shows a Te---Cl′ interaction with an adjacent molecule of only ca. 3.6 Å (18) (Fig. 4*b*) and although no such interaction is observed between Cl or Br atoms in the crystal structures of the $Ph_2TeX[S_2CNEt_2]$ analogues, it is reasonable to suppose it is possible in solution. Indeed, the ^{125}Te NMR spectrum of a solution of Ph_2TeCl_2 and Ph_2TeBr_2 confirms that halogen exchange readily occurs with the formation of a peak at 905 ppm attributable to $Ph_2TeClBr$.

Acknowledgements

We thank the Natural Sciences and Engineering Research Council of Canada, the Ministry of Colleges and Universities of Ontario, and the University of Windsor for financial support.

1. G. D. THORN and R. A. LUDWIG. The dithiocarbamates and related compounds, Elsevier, Amsterdam. 1962.
2. D. COUCOUVANIS. Prog. Inorg. Chem. **11**, 233 (1970).
3. J. WILLEMSE, J. A. CRAS, J. J. STEGGERDA, and C. P. KEIJZERS. Struct. Bonding (Berlin), **28**, 83 (1976).
4. J. L. TEMPLETON and B. C. WARD. Inorg. Chem. **19**, 1753 (1980).
5. M. G. KANATZIDIS, D. COUCOUVANIS, A. SIMOPOULOS, A. KOSHKAS, and V. J. PAPAEFTHYMIOU. J. A. Chem. Soc. **107**, 4925 (1985).
6. (*a*) M. G. B. DREW, D. A. RICE, and D. M. WILLIAMS. J. Chem. Soc. Dalton Trans. 1821 (1985); (*b*) E. J. PETERSON, R. B. VON DREELE, and T. M. BROWN. Inorg. Chem. **17**, 1410 (1978).
7. (*a*) S. J. M. BURGMAYER and J. L. TEMPLETON. Inorg. Chem. **24**, 2224 (1985); (*b*) T. C. W. MAK, K. S. JASIM, and C. CHIEH. Inorg. Chem. **24**, 1587 (1985); (*c*) C. D. GARNER, N. C. HOWLADER, F. E. MABBS, A. T. MCPHAIL, R. W. MILLER, and K. D. ONAN. J. Chem. Soc. Dalton Trans. 1582 (1978).
8. P. R. H. ALDERMAN, P. G. OWSTON, and J. M. ROWE. J. Chem. Soc. 668 (1962).
9. R. HESSE. Ark. Kemi, **20**, 481 (1963).
10. J. S. MORRIS and E. D. SCHLEMPER. J. Cryst. Mol. Struct. **9**, 1 (1979).
11. I. J. B. LIN, H. W. CHEN, and J. P. FACKLER, JR. Inorg. Chem. **17**, 394 (1978).
12. R. K. CHADHA, J. E. DRAKE, and A. B. SARKAR. Inorg. Chem. **23**, 4769 (1984).
13. R. K. CHADHA, J. E. DRAKE, and A. B. SARKAR. Inorg. Chem. **25**, 2201 (1986).
14. R. K. CHADHA, J. E. DRAKE, and A. B. SARKAR. Inorg. Chim. Acta, **143**, 31 (1988).
15. R. K. CHADHA, J. E. DRAKE, A. B. SARKAR, and M. WONG. Acta Crystallogr. C, **45**, 37 (1989).
16. H. P. KLUG. Acta Crystallogr. **21**, 536 (1966).
17. M. BONAMICO, G. MAZZONE, A. VACIAGO, and L. ZAMBONELLI. Acta. Crystallogr. **19**, 898 (1965).
18. J. H. E. BAILEY, J. E. DRAKE, A. B. SARKAR, and M. L. Y. WONG. Can. J. Chem. **67**, 1735 (1989).
19. R. C. PAUL, K. K. BHASIN, and R. K. CHADHA. J. Inorg. Nucl. Chem. **37**, 2337 (1975).
20. D. DAKTERNIEKS, R. D. GIACOMO, R. W. GABLE, and B. F. HOSKINS. J. Organomet. Chem. **349**, 305 (1988).
21. F. H. ALLEN, O. KENNARD, D. G. WATSON, L. BRAMMER, A. G. ORPEN, and R. TAYLOR. J. Chem. Soc. Perkin Trans. II, S1 (1987).
22. A. J. BONDI. J. Phys. Chem. **68**, 441 (1964).
23. T. A. CLAXTON and G. C. BENSON. Can. J. Chem. **44**, 157 (1966).
24. D. DAKTERNIEKS, R. DIGIACOMO, R. W. GABLE, and B. F. HOSKINS. J. Am. Chem. Soc. **110**, 6753 (1988).
25. G. D. CHRISTOFFERSON and J. D. MCCULLOUGH. Acta. Crystallogr. **11**, 249 (1958).
26. D. H. WHIFFEN. J. Chem. Soc. 1350 (1956).
27. W. R. MCWHINNIE and G. P. Patel. J. Chem. Soc. Dalton Trans 199 (1972).
28. N. W. ALCOCK and W. D. HARRISON. J. Chem. Soc. Dalton Trans. 251 (1982).
29. J. E. DRAKE and M. L. Y. WONG. J. Organomet. Chem. **377**, 43 (1989).

Can. J. Chem. Downloaded from www.nrcresearchpress.com by 123.30.183.119 on 09/08/12
For personal use only.

A molecular mechanics study of conformational isomerism in 1- and 3-aryl hydantoins and 3-aryl-2-thiohydantoins

LAWRENCE D. COLEBROOK
Department of Chemistry and Biochemistry, Concordia University, 1455 de Maisonneuve Blvd. W., Montreal, P.Q., Canada H3G 1M8

Received November 2, 1990

LAWRENCE D. COLEBROOK. Can. J. Chem. **69**, 1957 (1991).

Energy profiles for internal rotation about the C—N pivot bond in a series of 1- and 3-aryl hydantoins and 3-aryl-2-thiohydantoins have been computed using the MMX molecular mechanics force field. Rotational ground and transition states have been identified and their energies calculated. Conformational preferences of diastereomeric rotamers have been investigated. Computed rotational energy barriers generally are within ±2 kcal/mol of the experimentally determined values.

Key words: conformational isomerism, hindered rotation, hydantoins, thiohydantoins, molecular mechanics.

LAWRENCE D. COLEBROOK. Can. J. Chem. **69**, 1957 (1991).

Utilisant des champs de force de la mécanique moléculaire MMX, on a calculé les profiles d'énergie pour la rotation interne autour de la liaison C—N d'une série de 1- et de 3-aryl hydantoïnes et de 3-aryl-2-thiohydantoïnes. On a identifié les états rotationnels fondamentaux et de transition et on a calculé leurs énergies. On a étudié les préférences conformationnelles des rotamères diastéréoisomères. Généralement les valeurs calculées pour les barrières à l'énergie de rotation sont à ±2 kcal/mol des valeurs expérimentales.

Mots clés : isomérie conformationnelle, rotation empêchée, hydantoïnes, thiohydantoïnes, mécanique moléculaire.

[Traduit par la rédaction]

Can. J. Chem. Downloaded from www.nrcresearchpress.com by 123.30.183.119 on 09/08/12
For personal use only.

Introduction

We have previously reported ^1H and ^{13}C nmr and X-ray crystallographic studies of a variety of aryl-substituted N-heterocyclic compounds which exhibit biphenyl-like isomerism. At equilibrium, these compounds form a mixture of enantiomeric or diastereomeric rotational isomers resulting from restricted internal rotation of the aryl and heterocyclic moieties about the C—N pivot bond connecting the two ring systems. The studies have included 1-arylhydantoins (1, 2), 3-arylhydantoins (1, 2), and 3-aryl-2-thiohydantoins (1, 3–5), with a number of different aryl group substituents and with various substitution patterns on the heterocyclic group.

It was shown that those compounds with diastereomeric rotational isomers usually exhibit room temperature nmr spectra that are the superimposition of the spectra of the two rotamers. The majority of the spectra are temperature dependent, collapsing to a single, time-averaged spectrum at sufficiently high temperature. Those compounds with enantiomeric rotational isomers (which have identical spectra in an achiral solvent) were synthesized with an internal chirality-sensitive probe that exhibited a spectrum dependent on the rate of internal rotation. Activation parameters for hindered rotation were obtained from the temperature-dependent ^1H nmr specrtra, from the coalescence points or by complete lineshape analysis when this proved feasible. Some of the rotational barriers were sufficiently high that time-averaged spectra could not be obtained at the highest attainable temperatures. In certain cases, the rotational barriers of compounds with diastereomeric rotational isomers were sufficiently high that a single rotational isomer could be isolated by careful crystallization, and its rate of isomerization followed by nmr methods. An X-ray crystallographic structure determination was carried out on one such isomer (5).

In the majority of cases in which the rotational isomers were disastereomers, it was observed that the isomers were present in unequal concentration at equilibrium. Although, in principle, this should always be the case for diastereomers, the mechanism by which stereochemical information was transmitted from one unsymmetrically substituted part of the molecule to another was not always clear. It was suggested that an unsymmetrical solvent shell could provide such a mechanism (5). The origin of ground state stereochemical preferences has been further investigated in the present study.

The temperature-dependent spectra of these compounds were originally interpreted in relation to conformational preferences and exchange processes with the aid of physical molecular models, using organic chemists' qualitative stereochemical intuition. There remained some uncertainty in the identification of the stereochemistry of the rotational ground states and the transition states, since two interconversion pathways are potentially available. We have now investigated the same structures using molecular mechanics calculations (6) to gain further insight into the ground and rotational transition state conformations, and to test the utility of these calculations to provide quantitative information on these systems. Energy profiles for rotation of the two ring systems about the central C—N bond have been computed, and the conformational isomers and possible rotational transition states have been identified. This quantitative treatment has led to a more complete understanding of the conformational preferences and the rotational transition states of these compounds.

Results and discussion

Rotational energy profiles and activation energies for rotation may readily be calculated using molecular mechanics methods. The parameters for molecular mechanics force fields are mainly derived from gas-phase results, so solute–solvent interactions are not evaluated. The experimental data reported for the compounds that are considered in this paper suggest that solvation influences rotational barriers and ground state conformations. Nevertheless, molecular mechanics calculations may provide insight into the conformational behaviour of these compounds, and aid our understanding of the significance of solvation.

The experimental measurements provided activation parameters for hindered rotation. In certain cases, it was only possible to measure $\Delta G^{\neq}$, but in others the complete set of Eyring

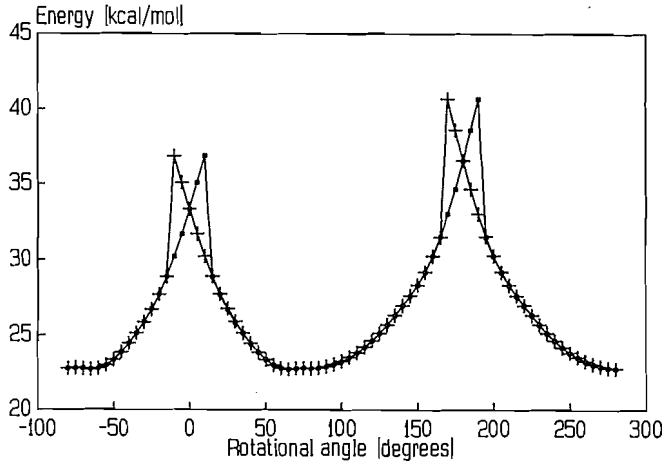


FIG. 1. Computed rotational energy profile for **1***b*, calculated at 5° intervals. The C2—N--C—C(CH_3) dihedral angle was driven. ■, increasing dihedral angle; +, decreasing dihedral angle.

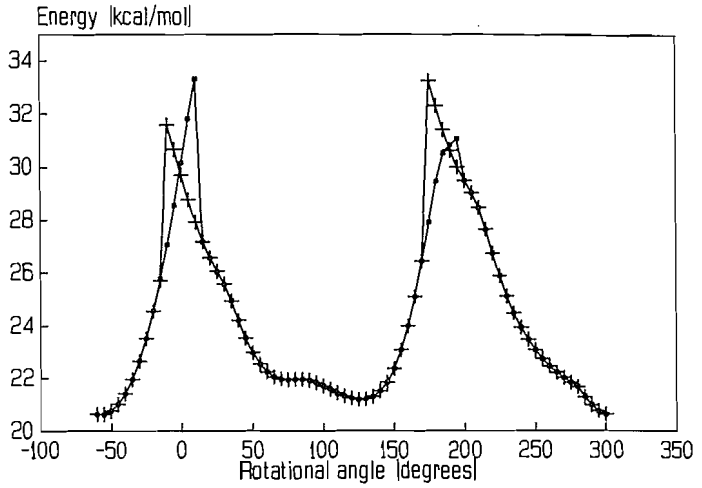


FIG. 2. Computed rotational energy profile for **1***i*, calculated at 5° intervals. The C2—N--C—C(CH_3) dihedral angle was driven. ■, increasing dihedral angle; +, decreasing dihedral angle.

activation parameters, $\Delta G^{\neq}$, $\Delta H^{\neq}$, and $\Delta S^{\neq}$, were calculated. The activation parameters obtained from molecular mechanics calculations correspond most closely to the enthalpy term, $\Delta H^{\neq}$.

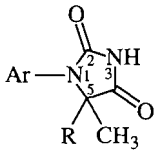
The dihedral driver option of PCMODEL 3.0, which was used to calculate the rotational energy profiles, writes an output file containing the coordinates of the energy-minimized structures corresponding to each selected dihedral angle about the C—N pivot bond. It is instructive to view the structures on the computer graphics screen in the vicinities of the energy minima (to identify the preferred conformations) and the energy maxima (the rotational transition states). The molecular mechanics calculations predict quite severe bond distortion near the rotational transition states of the more highly hindered compounds. The computed geometry of the distorted molecule near a transition state reflects the history of the molecule, i.e., the geometry depends on the geometries of the immediately preceding states. One aspect of this distortion is that there is a hysteresis effect in passing a high maximum: the computed energy maximum lags the change in dihedral angle, and the profiles differ depending on whether the dihedral angle is increasing or decreasing in passing through a maximum (the profiles are identical except near an energy maximum) (Figs. 1 and 2). This appears to be an artefact of the computational procedure. A further effect of the bond distortion is that the computed energy tends to increase relatively slowly as the maximum is approached, but it collapses rapidly as the maximum is passed. Examination of the predicted molecular structures at the rotational transition state shows the bulky *ortho*-aryl substituent bent away from the region of steric strain, out of the general plane of the ring, so that it lags behind the change in dihedral angle. At the energy maximum the *ortho* hydrogen atom has passed the general plane of the heterocyclic group, so that both *ortho*-aryl substituents lie on the same face of the molecule, which is very distorted. Further change in dihedral angle produces a sudden relief of steric strain, the bulky *ortho* substituent and the aryl group attaining a more normal geometry.

For those compounds which have enantiomeric rotational isomers, the skewed profiles in the vicinity of the energy maxima for increasing and decreasing dihedral angle are mirror images (Fig. 1). However, the 1-aryl-5-methylhydantoins, which have diastereomeric rotational isomers, show skewed profiles in the vicinity of the maxima that are not mirror images. Further, the corresponding increasing and decreasing computed maxima are not identical, since the rotational pathways remain diastereomeric up to, and including, the transition state maxima (Fig. 2). In effect, the computations predict that there are different (diastereomeric) rotational transition states (with different molecular geometries) in the directions of increasing and decreasing rotational angle, a consequence of the calculations following different (diastereomeric) pathways in the forward and the reverse directions. This prediction appears to violate the principle of microscopic reversibility. Similar problems have been noted in other force-field studies involving the interconversion of diastereomeric conformational isomers (7). Because of difficulties in interpretation, only a limited quantitative consideration of rotational barriers of the 1-aryl-5-methylhydantoins has been included in the discussion.

The 1-aryl-5-methylhydantoins have a strong steric interaction between the fixed chiral centre (at C-5) and the atropisomeric centre associated with the substituted biphenyl-like ring systems. In the 3-aryl-5-methylhydantoin series, the diastereomeric interactions between the aryl and heterocyclic moieties are much smaller, and the skewing of the profiles in the vicinity of the energy maxima does not show significant deviation from a mirror image relationship.

In this study, all of the rotational energy profiles were calculated starting near an energy minimum, where bond distortion should be negligible, with equal incrementation of the dihedral angle, so that the calculations approach and pass an energy maximum in a smooth progression of states. In addition, the energies near the maxima of **1***b* and **3***e* were investigated by starting with the molecules minimized to an unstrained low-energy conformation, rotating and then fixing the dihedral angle at a position near the energy maximum, then minimizing with a single dihedral angle constraint. In each case, the energy minimized to the corresponding point on the lower energy dihedral driver hysteresis curve (see figures), thus missing the hysteresis effect and finding a lower energy maximum than the dihedral driver procedure. Comparison of the energy barriers calculated by these two procedures with the experimental $\Delta H^{\neq}$ value for **3***e* showed that the dihedral driver method gave much better agreement. It was concluded that the dihedral driver method is the more realistic approach.

Can. J. Chem. Downloaded from www.nrcresearchpress.com by 123.30.183.119 on 09/08/12
For personal use only.



1

a Ar = phenyl, R = CH_3
b Ar = 2-methylphenyl, R = CH_3
c Ar = 2,3-dimethylphenyl, R = CH_3
d Ar = 2,4-dimethylphenyl, R = CH_3
e Ar = 2,5-dimethylphenyl, R = CH_3
f Ar = 2-chlorophenyl, R = CH_3
g Ar = α-naphthyl, R = CH_3
h Ar = phenyl, R = H
i Ar = 2-methylphenyl, R = H
j Ar = 2,3-dimethylphenyl, R = H
k Ar = 2-chlorophenyl, R = H
l Ar = α-naphthyl, R = H

1-Aryl-5,5-dimethylhydantoins

Studies of 1-aryl-5,5-dimethylhydantoins in both achiral (DMSO-d_6 and pyridine) and chiral (*S*-(+)-trifluoromethylphenylethanol) solvents have been reported (1,2).

The 5,5-dimethyl compounds have enantiomeric rotational isomers, which have indistinguishable spectra in an achiral solvent. However, the molecules contain a probe, the geminal dimethyl group, with a spectrum that is sensitive to the mean lifetimes of the conformational isomers. Reported activation parameters for restricted internal rotation were calculated from mean lifetimes obtained by complete lineshape analysis of the temperature-dependent ^{1}H nmr spectra of **1***b*, **1***c*, **1***f*, and **1***g*, and from the coalescence temperatures of signals of **1***d*–**1***e* in DMSO-d_6 solution. Free energies and enthalpies of activation for the 2-methylphenyl, 2,3-dimethylphenyl, 2,4-dimethylphenyl, 2,5-dimethylphenyl, 2-chlorophenyl, and α-naphthyl compounds (**1***b*–**1***g*) in various solvents are in the range 17.4–21.2 kcal/mol and 13.7–16.0 kcal/mol, respectively (Table 1) (1, 2, 8).

The computed rotational energy profile of 1-phenyl-5,5-dimethylhydantoin, **1***a*, shows a double energy minimum, with dihedral angles of 55° and 125° with respect to C-2, separated by a small barrier (0.4 kcal/mol) at a dihedral angle of 90°. The calculated rotational barrier is 2.8 kcal/mol. The computed rotational energy profiles of the substituted 1-aryl series show a broad, single potential well at a dihedral angle of 65–80°, with the *ortho* substituent inclined towards C-2. Compounds with substituted aryl groups are predicted to have less librational freedom than the phenyl compound, and to have much higher rotational barriers. There are two possible transition states for rotation, the *ortho*-aryl substituent passing either the substituents in the 5-position or the 2-carbonyl group. In the report of the experimental study (1), it was suggested, using a qualitative argument based on examination of Dreiding molecular models, that the bulky *ortho* substituent passes the 5-position in the preferred transition state. However, computation for the 5,5-dimethyl series predicts that the rotational transition state in which the more bulky 1-aryl group *ortho* substituent passes the carbonyl group in the 2-position rather than the geminal dimethyl group is preferred (by 0.6–3.9 kcal/mol). This prediction is supported by examination of the van der Waals surfaces of the carbonyl and geminal dimethyl groups, using molecular graphics.

Comparison of the computed rotational barriers of **1***b* and **1***c* supports the inferences that have been made on the buttressing effects of *ortho*-methyl groups. The 2,3-dimethylphenyl compound, **1***c*, has a higher computed and experimentally determined rotational enthalpy barrier than the 2-methyl compound, **1***b* (by 0.4 and 0.3 kcal/mol, respectively). This difference, which was originally observed during racemization studies of optically active biphenyls (9), has been attributed to the reduced ability of the 2-methyl group to bend in the rotational transition state because of steric interference from the 3-methyl group. Compounds **1***d* (2,4-dimethylphenyl) and **1***e* (2,5-dimethylphenyl), which lack this buttressing effect, have similar experimental and computed rotational energy barriers.

In the experimental paper, it was noted that the 2-methylphenyl compound, **1***b*, has a higher rotational barrier than the 2-chlorophenyl compound, **1***f*. Computation predicts a small difference in the opposite sense. Neglect of the influence of a polar solvent (DMSO-d_6) may be responsible for this discrepancy.

The computed rotational barriers (Table 1) show quite close agreement (within 1.0–2.4 kcal/mol) with the experimentally determined values of $\Delta H^{\neq}$ considering that the measurements may be subject to error (10), that solvation is not taken into account, and that further refinements in the force-field parameters used in the calculations are possible.

1-Aryl-5-methylhydantoins

The four compounds in this series, **1***i*–**1***l*, have diastereomeric rotational isomers, present in unequal concentration at equilibrium (equilibrium constants range from 1.1 to 1.3). The reported experimental rotational barriers are much lower than in the 5,5-dimethyl series ($\Delta G^{\neq}$ = 11.1–14.6 kcal/mol), so that time-averaged spectra are observed in the ^{1}H nmr spectra at normal temperatures. At sufficiently low temperatures, the separate spectra of the diastereomeric rotamers may be observed (1, 8).

1-Phenyl-5-methylhydantoin, **1***h*, shows a narrow computed energy minimum, the phenyl group being inclined away from the 5-methyl group at an angle of 35° (with respect to C-2). The computed rotational energy profiles of the substituted aryl compounds are complex, particularly in the range where the *ortho* substituent passes the substituents in the 5-position. In the predicted low-energy conformation of the preferred conformer of all the compounds examined, the aryl group is inclined at an angle of 60–70° (with respect to the *ortho* substituent and the 2-carbonyl group) to the plane of the hetero ring, the *ortho* substituent lying towards the 2-carbonyl group, on the same face of the molecule as the 5-methyl group. In the preferred conformation of the energetically less favoured conformer, the aryl group is inclined at an angle of 115–125°, with the *ortho* substituent lying towards the 5-hydrogen atom, on the face opposite the 5-methyl group. These computational predictions are of interest, since they indicate that the conformer with the bulky aryl substituent and the 5-methyl group *cisoid* is more stable (by 0.6–1.0 kcal/mol) than the conformer with these groups *transoid*. Inferences based on the use of physical molecular models led to the opposite conclusion in the experimental study (8). The similar placement of the aryl group in the two conformers is consistent with the observed small 5-methyl group ^{1}H nmr chemical shift difference, since the methyl groups experience similar deshielding effects from the aromatic ring current. Positive identification of the rotamers by ^{1}H nmr NOED measurements appears to be precluded by the very short rotamer lifetimes of these compounds, even at low temperatures.

Barriers to rotation by the lower energy path out of each of the two diastereomeric potential wells were calculated for **1***i*–**1***l*, using the energy profiles derived for increasing and decreasing

Can. J. Chem. Downloaded from www.nrcresearchpress.com by 123.30.183.119 on 09/08/12
For personal use only.

TABLE 1. Experimental and calculated activation and thermodynamic parameters for 1- and 3-arylhydantoins and 3-aryl-2-thiohydantoins

Compound	Solvent	Temperature[a]	$\Delta G^{\neq b}$	$\Delta H^{\neq b}$	Calc[c]	$\Delta G_0{}^d$	$K_{exp}{}^e$	K_{calc}	Reference
1*a*					2.8	—	—	—	
1*b*	DMSO-d_6	100	18.5	15.2	14.1	—	—	—	2
1*c*	DMSO-d_6	138.0	21.2	15.5	14.5	—	—	—	2
1*d*	DMSO-d_6	86.0	18.4		14.1	—	—	—	2
1*e*	DMSO-d_6	90.5	18.6		14.1	—	—	—	2
1*f*	DMSO-d_6	100	17.9	13.7	14.9	—	—	—	8
1*g*	DMSO-d_6	100	19.4	16.0	18.4	—	—	—	8
1*h*					3.3	—	—	—	
1*i*	Acetone-d_6/DMSO-d_6	−32	12.6		10.9 12.6	0.57	0.96		1
1*j*	Acetone-d_6/DMSO-d_6	−0.2	14.6		10.8 14.6	0.70	1.26		8
1*k*	Acetone-d_6/DMSO-d_6	−63	11.1		7.8 8.6	0.77	1.26		1
1*l*	Acetone-d_6/DMSO-d_6	−24	13.6		13.2 15.1	0.98	1.25		8
2*a*					5.0	—	—	—	
2*b*	Pyridine	100	18.2	13.1	13.9	—	—	—	2
2*c*	Pyridine	60	19.8	13.4	14.7	—	—	—	1
2*d*	2-Chloropyridine	25	21.3	18.3	16.1	—	—	—	11
2*e*	DMSO-d_6	70	19.3	11.1	13.7	0.11	1.00	1.2	1
2*f*	DMSO-d_6	25	19.9	13.7	14.5	0.11	1.17	1.2	12
2*g*	Pyridine	70	20.0	14.1	14.5	0.10	1.18	1.2	1
2*h*	1,1,2,2-tetrachloroethane	25	20.8	15.9	15.8	0.11	1.06	1.2	11
2*i*	DMSO-d_6	70	18.7	12.4	13.9	0.29	1.64	1.6	1
2*j*	DMSO-d_6	70	20.8	13.7	14.8	0.35	1.35	1.8	1
3*a*					7.4	—	—	—	
3*b*	Pyridine	57.5	24.8		16.8	0.14	1.4	1.3	13
3*c*	DMSO-d_6	86	19.7		11.4		1.1		13
3*d*	Pyridine	58.5	25.7		17.4	0.10	1.7	1.2	13
3*e*	Pyridine	25	25.2	17.6	18.9	0.16	1.9	1.3	5
3*f*	Pyridine	28.5	23.9		13.7		1.4		13
3*g*	Pyridine	25	25.7	20.5	18.8	0.13	1.2	1.2	3
3*h*	DMSO-d_6	97.5	21.7		7.7	0.0	0.0		4

[a]Temperature at which $\Delta G^{\neq}$ was calculated (°C).
[b]Measured activation parameter (kcal/mol).
[c]Calculated rotational barrier from the lowest energy conformation to the lower maximum (kcal/mol). For **1***i*–**1***l*, the rotational barrier from each of the diastereomeric minimum energy rotamers to the lower barrier is quoted.
[d]Measured free energy difference between rotamers (kcal/mol).
[e]Measured rotational equilibrium constant.

dihedral angles (Table 1). The computed rotational barriers are much lower in the 1-aryl-5-methylhydantoin series than for the corresponding compounds in the 5,5-dimethyl series, in agreement with the experimental observations. Because of experimental difficulties in obtaining reliable values for $\Delta H^{\neq}$, quantitative comparisons of the computed and experimentally determined barriers are not available.

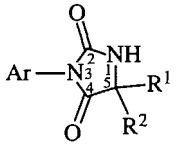
3-Aryl-5,5-dimethylhydantoins

Activation parameters for hindered internal rotation in the 3-aryl-5,5-dimethylhydantoin series (**2***b*–**2***d*) were obtained by complete lineshape analysis of the temperature-dependent 5-methyl spectra over a range of temperatures in pyridine or 2-chloropyridine solutions (1, 2, 11). All of the compounds were in the slow exchange region at ambient temperature. Free energies and enthalpies of activation are in the range 18.2–21.3 kcal/mol and 13.1–18.3 kcal/mol, respectively.

The computed rotational energy profile of 3-phenyl-5,5-dimethylhydantoin, **2***a*, shows the phenyl group inclined towards C-2 at a dihedral angle of 45° in the conformational ground state. The profiles of the 3-aryl-5,5-dimethyl series compounds (**2***b*–**2***d*) show two almost identical energy minima for each enantiomeric rotamer, with dihedral angles of about 60° and 120° from C-2, separated by a small barrier at 90° (about 1 kcal/mol). Hence there exists a broad range of dihedral angles available for librational motion between the two energy barriers to interconversion. Computation predicts that motional freedom in all of the aryl hydantoins and thiohydantoins is much more restricted in the rotational transition states than in the ground states, consistent with the large negative entropies of activation that have been measured (2, 11).

The original study was unable to provide detailed information on the nature of the conformational ground states or the transition states. In particular, it was not possible to make any inferences concerning the interconversion pathways, which involve apparently similar carbonyl groups. Interconversion of

Can. J. Chem. Downloaded from www.nrcresearchpress.com by 123.30.183.119 on 09/08/12
For personal use only.



2

a Ar = phenyl, $R^1 = R^2 = CH_3$
b Ar = 2-methylphenyl, $R^1 = R^2 = CH_3$
c Ar = 2-chlorophenyl, $R^1 = R^2 = CH_3$
d Ar = 2-bromophenyl, $R^1 = R^2 = CH_3$
e Ar = 2-methylphenyl, $R^1 = H$, $R^2 = CH_3$
f Ar = 2,3-dimethylphenyl, $R^1 = H$, $R^2 = CH_3$
g Ar = 2-chlorophenyl, $R^1 = H$, $R^2 = CH_3$
h Ar = 2-trifluoromethylphenyl, $R^1 = H$, $R^2 = CH_3$
i Ar = 2-methylphenyl, $R^1 = H$, $R^2 = C_6H_5$
j Ar = 2-chlorophenyl, $R^1 = H$, $R^2 = C_6H_5$

the enantiomeric rotational isomers could proceed via two possible transition states, in which the 3-aryl group *ortho* substituent passes either the 2- or the 4-carbonyl group oxygen atom. Computation indicates that these rotational transition states are very similar in energy, so that a distinct preference for one pathway over the other is unlikely.

The computed rotational barriers are in the order: phenyl << 2-methylphenyl < 2-chlorophenyl < 2-bromophenyl. There is satisfactory agreement with the computed barriers and the experimentally determined values of $\Delta H^{\neq}$ (Table 1).

3-Aryl-5-methyl- and 3-aryl-5-phenylhydantoins

Compounds **2***f*–**2***j*, with diastereomeric rotamers, have rotational barriers that are similar to those of the correspondingly substituted 5,5-dimethyl compounds, with reported (1, 11, 12) free energies of activation within the range 18.7–20.8 kcal/mol. Equilibrium constants range from about 1.0 to about 1.6, with the 5-phenyl compounds showing a somewhat greater deviation from unity than the 5-methyl compounds. The 2-chlorophenyl compounds have higher experimental rotational barriers ($\Delta G^{\neq}$), by 0.7–2.1 kcal/mol, than the corresponding 2-methylphenyl compounds. No significant differences between the rotational barriers of the 5-methyl and the 5-phenyl compounds were observed.

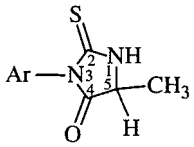
The computed rotational energy profiles of the 3-aryl-5-methyl- or 3-aryl-5-phenylhydantoins show two shallow minima of almost identical energy, separated by a barrier of less than 1 kcal/mol, for each rotational isomer, with dihedral angles of about 60° and 120°. The molecules are, therefore, free to undergo librational motion of large amplitude in their rotational ground states. Computation predicts that the diastereomeric rotamers have different ground state energies, so that the rotamers will be present in unequal concentration at equilibrium. Ground state energy differences between the rotamers are larger for the 5-phenyl compounds (0.29–0.35 kcal/mol) than for the 5-methyl compounds (0.10–0.11 kcal/mol), consistent with experimental data. The *ortho* aryl substituents are *cisoid* to the C-5 substituent (methyl or phenyl) in the energetically preferred rotamers.

The rotational barriers by the two available pathways (the *ortho* substituent passing either the 2- or the 4-carbonyl group) are very similar in energy, with perhaps a slight preference (≤0.5 kcal/mol) for the pathway past the 4-carbonyl group.

The computed rotational barriers are in the order 2-methylphenyl < 2,3-dimethylphenyl < 2-chlorophenyl < 2-trifluorophenyl. Computed barriers and experimental values of $\Delta H^{\neq}$ are close (Table 1).

3-Aryl-2-thiohydantoins

We previously reported (3, 5) that the equilibrium ratio of the diastereomeric rotational isomers of the 3-aryl-substituted 2-thiohydantoins, **3***e* and **3***g*, is non-unity, an observation that has been repeated for a number of other examples of 3-arylhydantoins and thiohydantoins unsymmetrically substituted at C-5 (1, 11–13). Equilibrium constants are in the range 1.2–1.9 for this series, the compound with the largest equilibrium constant, **3***e*, also having the largest rotational barrier. This observation was of particular interest since the sites of unsymmetrical substitution on the aryl and heterocyclic moieties are too far apart for a direct interaction that could transmit stereochemical information (5).



3

a Ar = phenyl
b Ar = 2-methylphenyl
c Ar = 2-fluorophenyl
d Ar = 2-chlorophenyl
e Ar = 2-bromophenyl
f Ar = 2-methoxyphenyl
g Ar = α-naphthyl
h Ar = β-naphthyl

With the exceptions of the 2-fluorophenyl (**3***c*) and the β-naphthyl (**3***h*) compounds, all of the members of this series have rotational barriers that are too high to measure by lineshape methods, so activation parameters were measured by equilibration in pyridine solution of one rotamer, isolated by careful crystallization (5, 13). Equilibration rates of **3***e* and **3***g* were measured over a range of temperatures so that $\Delta H^{\neq}$ could be calculated. Free energies of activation for rotation of **3***c* and **3***h* were measured for DMSO-d_6 solutions at the coalescence temperatures, 86° and 97.5°C, respectively (4, 13).

In the computed minimum energy conformation of 3-phenyl-5-methyl-2-thiohydantoin, **3***a*, the dihedral angle with respect to C-2 is 50°. There is a 7.4 kcal/mol rotational barrier at 0° and a 1.5 kcal/mol librational barrier at 90°. The computed profile for 3-(β-naphthyl)-5-methyl-2-thiohydantoin, **3***h*, is similar to that of the phenyl compound, with dihedral angles of 50° and 130°. The α-naphthyl compound shows a broad, flat minimum between about 50° and 130°, but the remaining compounds are predicted to have a stronger conformational preference, near 65°, in their conformational ground states.

An X-ray crystallographic study (5) of the thermodynamically *less* stable rotamer of **3***e*, isolated in >99% isomeric purity by careful crystallization, revealed that the bromine atom and the C-5 methyl group were *transoid*. The heterocyclic ring was found to be planar to within experimental error, while the dihedral angle between the heterocyclic rings was 82°, the bromine atom lying closer to the carbonyl oxygen atom than to the sulphur atom. This crystallographic study provided no evidence on how the unsymmetrically substituted aryl group could sense the stereochemistry at C-5 so that one rotamer is preferred. It was postulated that, in solution, the steric effect of the 5-methyl group might be transmitted to the bromine atom via an unsymmetrical solvent shell around the carbonyl and thiocarbonyl groups (5).

Computation of the rotational energy profile of **3***e* predicted

Can. J. Chem. Downloaded from www.nrcresearchpress.com by 123.30.183.119 on 09/08/12
For personal use only.

Can. J. Chem. Downloaded from www.nrcresearchpress.com by 123.30.183.119 on 09/08/12
For personal use only.

that the two rotational energy barriers differ by about 4.7 kcal/mol, the lower barrier, which is presumably involved in the interconversion process, requiring passage of the bromine atom past the oxygen rather than the sulphur atom. In the experimental study, the complete set of activation parameters was derived from rate constants for equilibration, measured over a range of temperatures. The computed barrier (from the less stable rotamer) of 18.9 kcal/mol is in good agreement with the 17.6 ± 1.7 kcal/mol experimental value of $\Delta H^{\neq}$.

Computation predicts ground state energies of the two rotamers differing by 0.16 kcal/mol, the isomer with the bromine atom and the 5-methyl group *cisoid* being the more stable. This is in complete agreement with experiment. Although the heterocyclic group was found to be planar to within the limits of refinement in the crystallographic study, the computational study predicts small deviations from planarity that transmit stereochemical information between C-5 and the aryl group. Assuming that the entropies of the two rotational isomers are very similar, the predicted equilibrium ratio is about 1.3 at normal temperatures, close to the observed value of 1.9 ± 0.1. Hence the computation suggests that it is not necessary to invoke an unsymmetrical solvent shell to explain that the equilibrium ratio differs from unity.

The dihedral angle at the energy minimum of the less stable (*transoid*) rotamer is predicted to be 113°. The energy trough is broad (with an additional shallow minimum at 80°) so that the angle is not well defined, and the angle determined crystallographically, 98°, falls within this range. The dihedral angle at the energy minimum of the preferred rotamer (*cisoid*) is 111°, with the bromine atom lying towards the 2-carbonyl group.

Overall, similar computed and solid state conformations of the thermodynamically less favoured isomers are predicted. The computed profiles of **3***b*, **3***c*, **3***d*, and **3***f* predict similar conformational behaviour to that of **3***e*.

We have reported (4) that 3-(β-naphthyl)-5-methyl-2-thiohydantoin, **3***h*, shows a ^{1}H nmr spectrum consisting of the superimposed spectra of two diasteromeric rotational isomers at room temperature, and a single, time-averaged, spectrum at higher temperatures. A value for $\Delta G^{\neq}$ of 21.7 kcal/mol was reported for the coalescence point (97.5°C, DMSO-d_6 solution).

Computation indicates no rotational ground state energy difference between the two diastereomeric rotational isomers of **3***h*, consistent with the experimental observation, and expected since the *ortho* substituents of the 3-aryl group are both hydrogen atoms. Further, no significant difference between the energies of the two rotational transition states is predicted, although a difference could be visualized as a result of buttressing of one of the *ortho* hydrogens of the 3-aryl group by the adjacent fused ring. This buttressed hydrogen atom must pass either a sulphur or an oxygen atom in the transition states. If buttressing effects exist, they are more likely to be seen in the strained transition states than in the ground states. Two, almost equal energy, conformational ground states for each diastereomeric rotamer are predicted, with dihedral angles of 49° and 131°, and separated by a barrier of 1.5 kcal/mol at a dihedral angle of 90°.

The rotational energy profile of 3-phenyl-5-methyl-2-thiohydantoin, **3***a*, was calculated for reference purposes. This was almost identical in appearance to that of 3-(β-naphthyl)-5-methyl-2-thiohydantoin, but the computed rotational barrier was slightly lower, 7.4 vs. 7.7 kcal/mol. It was earlier suggested (4) that the steric requirements of one of the *ortho* hydrogen atoms in β-naphthyl-substituted compounds might be increased by buttressing with the adjacent fused ring. These calculations indicate that such an effect is likely to be small. The large difference between the experimentally determined $\Delta G^{\neq}$ and the calculated rotational barrier of **3***h* is at present unexplained, but the role of the solvent (DMSO-d_6) may be important.

The computed rotational barriers are in the order: phenyl < β-naphthyl << 2-fluorophenyl < 2-methoxyphenyl < 2-methylphenyl < 2-chlorophenyl < α-naphthyl ≃ 2-bromophenyl (Table 1).

Computed rotational enthalpy barriers about 3 kcal/mol higher in the thiohydantoin series than in the corresponding oxygen analogues are predicted. The experimental free energy differences in corresponding compounds are about 5.5 kcal/mol.

Conclusions

This computational study has provided insight into the conformational ground and transition states of these compounds that was not available in the experimental studies. In the 3-aryl-5-methyl- or 3-aryl-5-phenylhydantoin and thiohydantoin series, with diastereomeric rotamers, it has shown that stereochemical information may be transmitted between the 3-aryl and the unsymmetrically substituted C-5 centre via small deviations from planarity of the ring systems, leading to unequal energies of the conformational ground states. It predicts that the bulky *ortho* substituent and the C-5 substituent prefer to be *cisoid* in the diastereomeric conformational ground states of both the 1-aryl and the 3-aryl series, contrary to what might be expected from a study of physical molecular models. It predicts the preferred conformational transition states where these are significantly different in energy. It predicts activation energies for conformational interconversion that are close to the experimentally determined enthalpy values, despite neglect of solvation effects. Molecular mechanics computation, therefore, provides a useful tool in interpreting the experimental data on these conformationally mobile molecules.

Computation

Molecular mechanics calculations were carried out on a Silicon Graphics, Inc., Personal IRIS 4D/25G workstation, using PCMODEL 3.0 software (Serena Software, Inc., Bloomington, IN, U.S.A.). Structures were minimized using the MMX force field (derived from the MM2 force field of Burkert and Allinger (6)) in combination with VESCF molecular orbital calculations on the aromatic π-electron systems. PCMODEL uses generalized force-field parameters if no standard MM2 parameters are available. Some generalized parameters were required in the calculations reported here. Absolute calculated energies will be less accurate if generalized, rather than exact, parameters are used, but geometries should be close. The default value was used for the dielectric constant.

Following identification of a low-energy conformation of each molecule, the dihedral driver software option was used to calculate a rotational energy profile. The dihedral angle about the C—N pivot bond between the two ring systems was driven in a stepwise fashion, with energy minimization at each step. Profiles were calculated for 5° increments (or decrements) in dihedral angle. Where knowledge of the transition state energies was important, the profiles in the immediate vicinity of the rotational transition states were calculated for 1° increments.

A plot of the minimized energy versus dihedral angle yielded a rotational energy profile. When the rotational ground state energies of diastereomeric rotamers were to be compared, the energies were minimized without constraints starting from dihederal angles corres-

ponding to the mimima established from the profiles. Dihedral angles are defined between C-2 and the *ortho* aryl carbon carrying a substituent.

Acknowledgments

This work was supported by an operating grant from the Natural Sciences and Engineering Research Council of Canada (NSERC). Thanks are due to Dr. T. J. Adley for his efforts in securing funding for the Personal IRIS computer.

1. L. D. COLEBROOK, H. G. GILES, A. GRANATA, S. ICLI, and J. R. FEHLNER. Can. J. Chem. **51**, 3635 (1973).
2. L. D. COLEBROOK, S. ICLI, and F. H. HUND. Can. J. Chem. **53**, 1556 (1975).
3. W. E. BENTZ, L. D. COLEBROOK, and J. R. FEHLNER. Chem. Commun. 974 (1970).
4. L. D. COLEBROOK, H. G. GILES, and A. ROSOWSKY. Tetrahedron Lett. **51**, 5239 (1972).
5. P. H. BIRD, L. D. COLEBROOK, A. R. FRASER, and H. G. GILES. Chem. Commun. 225 (1974).
6. U. BURKERT and N. L. ALLINGER. Molecular mechanics. ACS Monograph 177, American Chemical Society, Washington, DC. 1982.
7. F. A. L. ANET and F. KRANE. Tetrahedron Lett. 5029 (1973).
8. S. ICLI. PhD. Thesis, Sir George Williams University, Montreal. 1974.
9. F. H. WESTHEIMER. *In* Steric effects on organic chemistry. *Edited by* M. S. Newman. John Wiley and Sons, New York. 1956. pp. 543–554.
10. J. SANDSTROM. Dynamic NMR spectroscopy. Academic Press, New York. 1982. pp. 108–121.
11. J. R. FEHLNER. Ph.D. Thesis, University of Rochester, Rochester, New York. 1970.
12. A. GRANATA. M.Sc. Thesis, Sir George Williams University, Montreal. 1972.
13. H. G. GILES. Ph.D. Thesis, Sir George Williams University, Montreal. 1973.

Can. J. Chem. Downloaded from www.nrcresearchpress.com by 123.30.183.119 on 09/08/12
For personal use only.

The hydroxonium perchlorate complex of *cis-syn-cis*-dicyclohexano 18-crown-6 ether: conformational analysis in the solid state and in solution at low temperature as studied via ^{13}C NMR methods

G. W. BUCHANAN, C. MORAT,[1] AND R. A. KIRBY
Ottawa–Carleton Chemistry Institute, Department of Chemistry, Carleton University, Ottawa, Ont., Canada K1S 5B6

AND

J. S. TSE
Division of Chemistry, National Research Council of Canada, Ottawa, Ont., Canada K1A 0R9

Received April 12, 1991

Can. J. Chem. Downloaded from www.nrcresearchpress.com by 123.30.183.119 on 09/08/12
For personal use only.

G. W. BUCHANAN, C. MORAT, R. A. KIRBY, and J. S. TSE. Can. J. Chem. **69**, 1964 (1991).

From 100.6-MHz ^{13}C NMR coalescence temperature measurements, the title complex is shown to undergo a single degenerate ring inversion process with a free energy barrier of 49.4 ∓ 1.6 kJ/mol. This is ca. 5 kJ/mol higher than the barrier in the free crown. The solid state ^{13}C CPMAS spectrum is indicative of a totally unsymmetrical conformation and the shift trends in the solid are analyzed in terms of local torsional angle variations. Comparisons of experimental vs. calculated (GIAO) ^{13}C chemical shift ranges for the CH_2O carbons in the solid are made and satisfactory agreement with respect to the overall range and magnitude of the ^{13}C shielding differences is obtained.

Key words: crown ethers, stereochemistry, NMR.

G. W. BUCHANAN, C. MORAT, R. A. KIRBY et J. S. TSE. Can. J. Chem. **69**, 1964 (1991).

En se basant sur des mesures de température de coalescence en RMN du ^{13}C, à 100,6 MHz, on peut démontrer que le complexe mentionné dans le titre subit un seul processus dégénéré d'inversion de cycle avec une barrière d'énergie libre de 49,4 ∓ 1,6 kJ/mol. Cette valeur est environ 5 kJ/mol plus élevée que celle observée avec les éthers couronnes. Le spectre CPMAS du ^{13}C à l'état solide suggère l'existence d'une conformation complètement non-symétrique et on peut analyser les variations dans les déplacements dans le solide en fonction de variations locales de l'angle de torsion. On a effectué des comparaisons entre les plages des déplacements chimiques expérimentaux et calculés (GIAO) du ^{13}C des carbones CH_2O à l'état solide; on a obtenu une bonne correspondance pour l'ensemble des plages ainsi que pour l'amplitude des différences entre les blindages des ^{13}C.

Mots clés : éthers couronnes, stéréochimie, RMN.

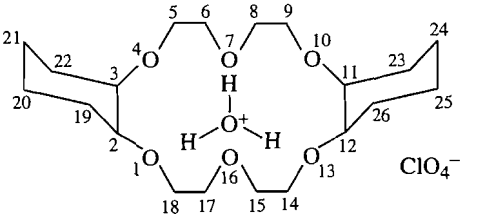
[Traduit par la rédaction]

Introduction

The hydroxonium perchlorate complex of *cis-syn-cis*-dicyclohexano-18-crown-6 (**1**) was first reported in the literature almost 20 years ago (1). More recently (2) the X-ray crystallographic structure was published. This material is of interest for several reasons, not the least of which is its hydrogen bonding characteristics involving three oxygens of the crown ether and the three H's of the H_3O^+ entity. Such stable hydrogen bonds might be expected to lead to increased stereochemical rigidity relative to the uncomplexed crown ether. In view of our general interest in the solution and solid phase stereochemical dynamics of 18-crown-6 systems (3–7), we now report the results of a 100.6 MHz ^{13}C NMR study of **1** as a function of temperature, as well as its solid phase ^{13}C NMR spectrum at 45.3 MHz. Results are compared with earlier findings on related systems.

Results and discussion

The structure and numbering scheme for **1** is illustrated in Fig. 1. The disposition of the cyclohexane rings is consistent with that determined by X-ray crystallography (2). In Fig. 2 are presented a series of 100.6 MHz ^{13}C spectra for **1** as a function of temperature, while Fig. 3 shows the solid phase spectrum. Table 1 contains the ^{13}C NMR chemical shift data in solution (at the limits of fast and slow conformational exchange) as well as the solid phase chemical shifts for **1**.



1

FIG. 1. Structure and numbering scheme for **1**.

The assignments of the solution ^{13}C shifts in the fast exchange limit are consistent with those reported earlier for the free *cis-syn-cis* isomer of dicyclohexano-18-crown-6 (8). There are only minor (less than 1.5 ppm) effects due to complexation of the H_3O^+ in the cavity. As the temperature is reduced, broadening begins to occur first in the low-field resonance (due to C2,3,11,12) since this is the site with the largest chemical shift difference (9.41 ppm or 936.8 Hz) in the slow exchange spectrum. Indeed, the spectrum at 295 K shows substantial evidence for this broadening effect. From coalescence temperatures (T_c) and the chemical shift differences in the slow exchange limit, one can use the Eyring equation to calculate $\Delta G^{\neq}$, the free energy of activation for ring reversal. In the present case, all five resonances in the fast exchange limit undergo coalescence behaviour, each at a unique temperature. Data are collected in Table 1. The similarity of $\Delta G^{\neq}$ values at different temperatures suggests that $\Delta S^{\neq}$ for the conformational processes involved cannot be substantially different

[1]Permanent address: LEDSS, Université Joseph Fourier (Grenoble I) BP 68, 38402, St. Martin-d'Hères, CEDEX, France.

TABLE 1. ^{13}C chemical shifts (δ_C from TMS)* and coalescence data

Carbon	δ_C (solid)	δ_C (sol'n, 313 K)	δ_C (sol'n, 173 K)	T_c (K)	$\Delta G^{\neq}$ (kJ/mol)
2	82.0	79.11	82.47		
12	81.0	79.11	82.47		
				285	51.5
3	(73.7)[a]	79.11	73.16		
11	(73.0)[a]	79.11	73.16		
5	(68.3)[b]	68.30	69.16		
9	(69.2)[c]	68.30	69.16		
				260	48.7
14	67.3	68.30	66.82		
18	(68.3)[b]	68.30	66.82		
6	(70.1)[d]	71.46	69.92		
8	(69.4)[c]	71.46	69.92		
				265	50.2
15	(70.1)[d]	71.46	72.72		
17	71.6	71.46	72.72		
22	26.0	26.66	26.13		
23	26.0	26.66	26.13		
				235	47.2
19	27.3	26.66	26.82		
26	27.3	26.66	26.82		
20	(25.6)[e]	22.06	24.63		
25	(25.7)[e]	22.06	24.63		
				268	49.6
21	(21.1)[f]	22.06	19.52		
24	(19.5)[f]	22.06	19.52		

*Solutions are 0.1 M in acetone-d_6.
[a–f]Denote possible interchange of assignments.

from zero. Hence one can calculate an average $\Delta G^{\neq}$ value of 49.4 kJ/mol with a standard deviation of 1.4 kJ/mol.

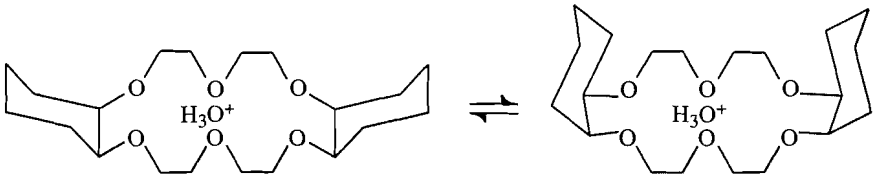
This value represents the free energy of activation for the degenerate double cyclohexane ring inversion process depicted below. The observation of 10 ^{13}C resonances in the slow exchange limit in solution is consistent with a conformation having a plane of symmetry that bisects O7 and O16. Of course the 18-membered central ring must also change its conformation as the cyclohexyl moieties invert; however, the rate-limiting process is almost certainly degenerate cyclohexane ring inversion since the activation energy for ring inversion of 18-crown-6 itself in solution is too low to be accessible via present NMR methods (6), while that for *cis*-1,2-disubstituted cyclohexanes is ca. 45 kJ/mol (9).

The value of $\Delta G^{\neq}$ for **1** is ca. 5 kJ/mol higher than the ring inversion barrier for disubstituted cyclohexanes as well as that for the free crown of **1** (3, 4), indicating that complexation with H_3O^+ indeed increases the effective rigidity of **1** relative to the free crown and hence renders the cyclohexane ring inversion process more difficult. Interestingly, the duality of conformational processes observed for the uncomplexed case is absent in the present H_3O^+ complex as well as the KOPh complex studied previously (3).

The chemical shift differences for the cyclohexyl carbons of **1** at 173 K are within 0.8 ppm of those for related molecules at low temperature (3) and reflect the now well-documented influence of axial vs. equatorial oxygen on the ^{13}C chemical shifts of carbons bearing α, β, and γ relationships to the oxygen atoms (10). Hence the C3,11 positions bearing axial oxygen are shielded (in this case by 9.31 ppm) relative to the C2,12 pair, which bear equatorial oxygen. The C21,24 sites, which bear *gauche*-γ relations to the axial oxygens O4 and O10 respectively, are shielded by 5.11 ppm relative to the C20,25 pair, which are *trans*-γ to the equatorial O1 and O13 sites respectively. Only small (0.69 ppm) β stereochemical differences are found for the C22,23 vs. C19,26 pairs of **1**.

The solid phase ^{13}C NMR spectrum of **1** (Fig. 3) shows the presence of a nonsymmetrical conformation in the solid in accord with the results from X-ray crystallography (2). Although some resonance overlap is present, there are 11 resolved oxygenated carbon resonances (out of 12 possible) in the range of 67–82 ppm. Since the torsional angles in the macrocyclic portion of **1** have been published (2), it is instructive to attempt an analysis of the 18-membered ring carbon shift pattern in terms of torsional angle influences on ^{13}C shieldings.

To this end, the experimental torsional angle data for these carbons of **1** are presented in Table 2. Using the Gauge Invariant Atomic Orbital (GIAO) approach (11, 12),



Can. J. Chem. Downloaded from www.nrcresearchpress.com by 123.30.183.119 on 09/08/12
For personal use only.

Can. J. Chem. Downloaded from www.nrcresearchpress.com by 123.30.183.119 on 09/08/12
For personal use only.

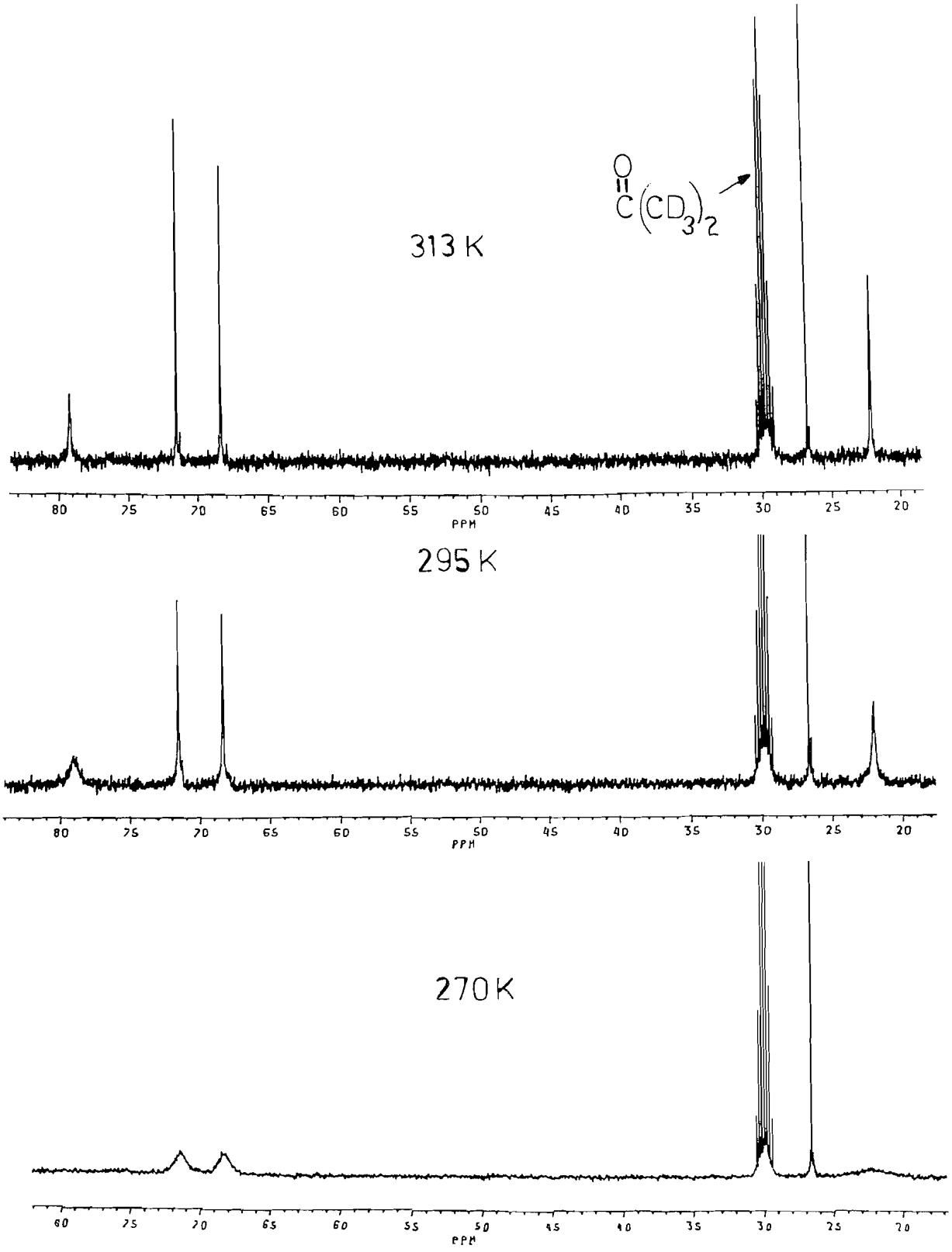


FIG. 2. 100.6 MHz ^{13}C NMR spectra of **1** as a function of temperature.

the ^{13}C NMR shielding for the O—C*—C—O network as a function of dihedral angle has been calculated using ethylene glycol as a model (Fig. 4) while shifts for the C*—C—O—C, C—O—C*—C, and C*—O—C—C networks as a function of dihedral angle are shown in Fig. 5. For the latter three networks, ethylmethyl ether was employed as a model compound. In these calculations, the absolute scale is employed wherein chemical shifts increase with increasing shielding. On this scale, CH_4 occurs at 221.0 ppm, whereas on the usual TMS scale it appears at −2.1 ppm.

For the latter three networks, the calculated dependence of the shielding on dihedral angle bears some similarity to the

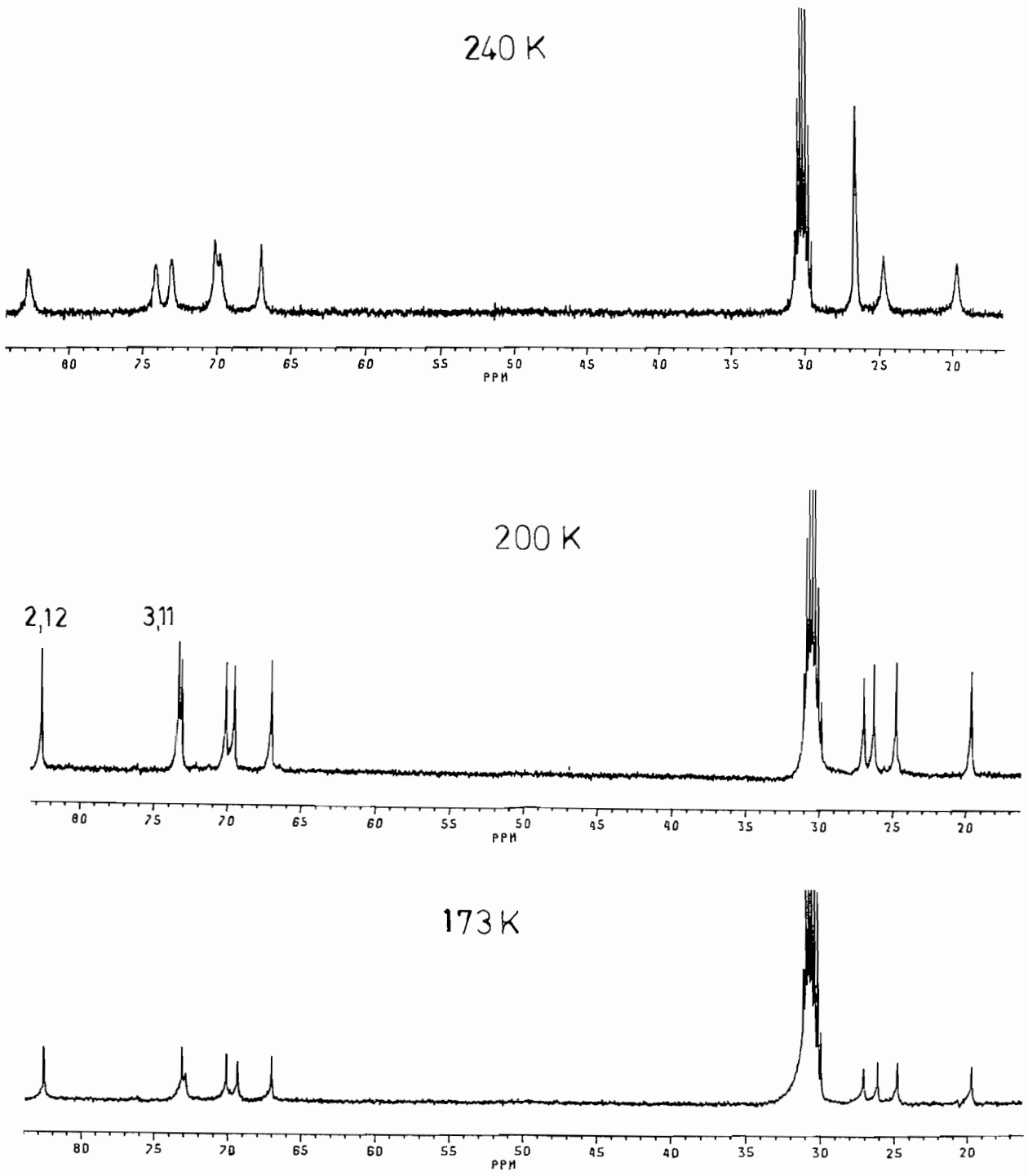


FIG. 2. (*concluded*)

INDO results for butane (13) in that maximum deshielding occurs near $\theta = 120°$ in each instance. A number of discussions have appeared in the literature (14, 15) regarding possible linear correlations between dihedral angle and experimental ^{13}C chemical shifts for terminal carbons of materials in which γ-steric shifts exist. The present calculations suggest that such correlations may indeed exist, but only in narrow ranges of dihedral angles.

To calculate the relative shielding for each of the CH_2-O carbons, the sum (Σ) of the four absolute chemical shifts was calculated using the four torsional network contributions as depicted in Figs. 4 and 5. The calculated range of Σ values was from 641.2 to 647.1. Hence a relative shielding for each carbon can be calculated by subtraction of the value of 641.2 from each Σ calculated. Using this approach, the C14 site is predicted to be the most shielded and has a relative shielding of 5.9 ppm. The most deshielded site is C17.

Accordingly, the most shielded CH_2-O resonance at 67.34 ppm in the ^{13}C CPMAS spectrum is attributed to C14. The next most shielded CH_2-O site is calculated to be C18 with a relative shielding of 5.6 ppm. Presumably this carbon is part of the intensity two resonance at 68.25 ppm. In a similar

Can. J. Chem. Downloaded from www.nrcresearchpress.com by 123.30.183.119 on 09/08/12
For personal use only.

Can. J. Chem. Downloaded from www.nrcresearchpress.com by 123.30.183.119 on 09/08/12
For personal use only.

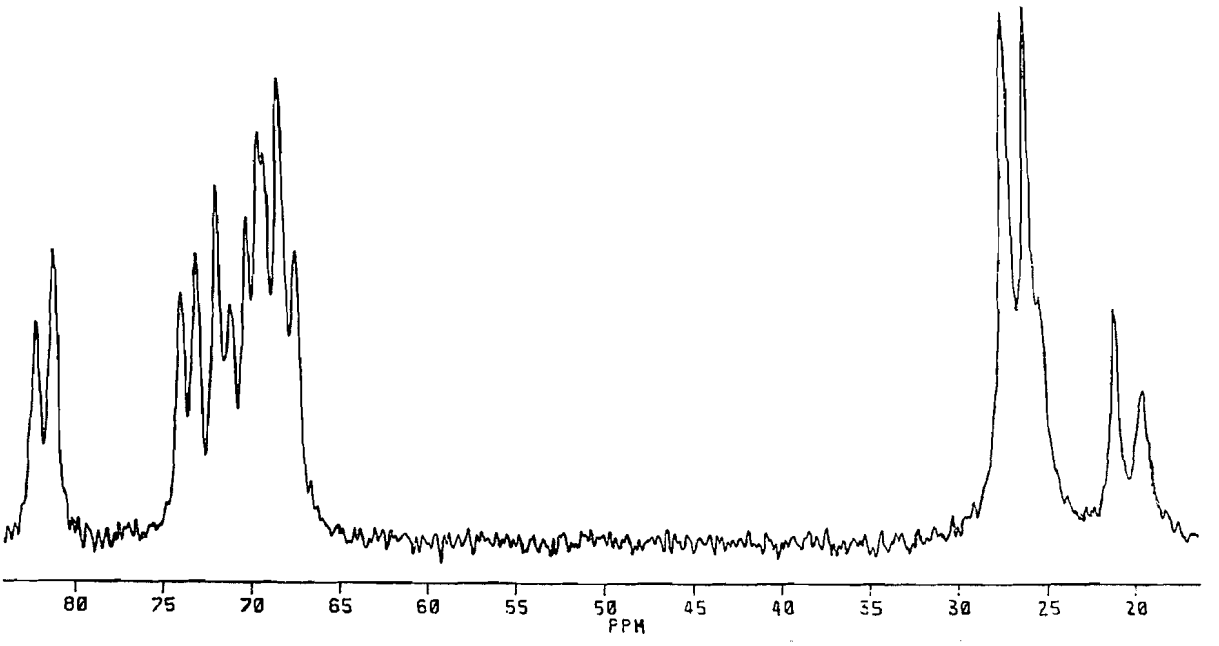


FIG. 3. 45.3 MHz ^{13}C CPMAS spectrum of **1**.

TABLE 2. Torsion angles (deg) in 18-crown-6 unit of **1** for CH_2-O sites (ref. 2)

Carbon	O—C*—C—O	C*—O—C—C	C—O—C*—C	C—O—C—C*
5	65.7	151.8	173.1	177.9
9	65.9	154.8	178.9	168.9
14	64.2	65.1	161.5	163.7
18	66.4	68.9	167.1	174.7
6	65.7	168.9	177.9	173.1
8	65.9	177.9	168.9	178.9
15	64.2	174.7	163.7	161.5
17	66.4	163.7	174.7	167.1

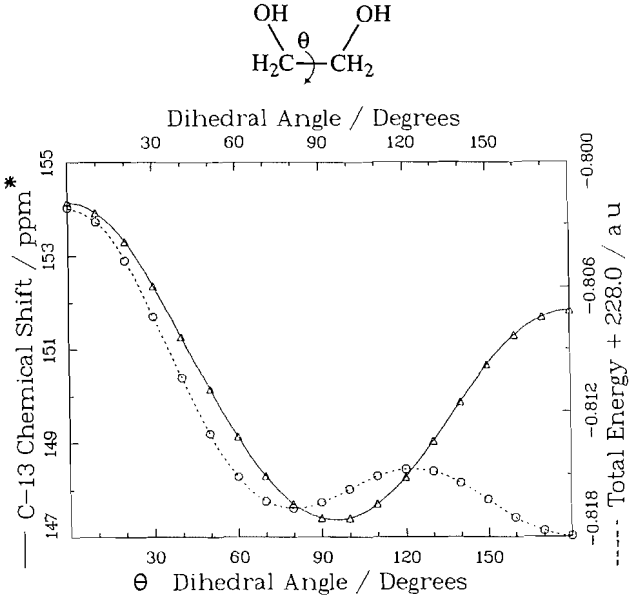


FIG. 4. GIAO calculated angular dependence of the isotropic ^{13}C NMR chemical shift of ethylene glycol as a function of dihedral angle (—). Total conformational energy as a function of dihedral angle (- - - -). (*) Absolute scale (CH_4 221 ppm) GIAO calcd.

fashion one can tentatively assign the remainder of the CH_2-O resonances of the solid as listed in Table 1.

The observed range of chemical shifts for these carbons in solid **1** is 4.3 ppm, while the range calculated from the GIAO treatment is 5.9 ppm. Given the fact that influences other than torsional environment (i.e., steric and electronic effects of the guest) may also play a significant role in determining the chemical shift, this level of agreement is deemed acceptable. Crystal packing forces may also be significant. In solution at 173 K, the range of CH_2-O ^{13}C shifts observed (5.9 ppm) is exactly that calculated via the GIAO approach.

One should, however, exercise some caution in strict application of the results of such theoretical chemical shift calculations for molecules in the gas phase to solution or solid phase spectra. Presently, efforts are underway in these laboratories to obtain experimental verification of these calculated, angularly dependent, ^{13}C shifts, especially in the case of ethylene glycol and some substituted derivatives.

Experimental

Materials

The complex **1** was prepared according to the published procedure (1). In acetone-d_6, there is no evidence of dissociation of the complex. The ^1H NMR chemical shift for the H_3O^+ protons of **1** is 9.858 ppm in acetone-d_6 solution.

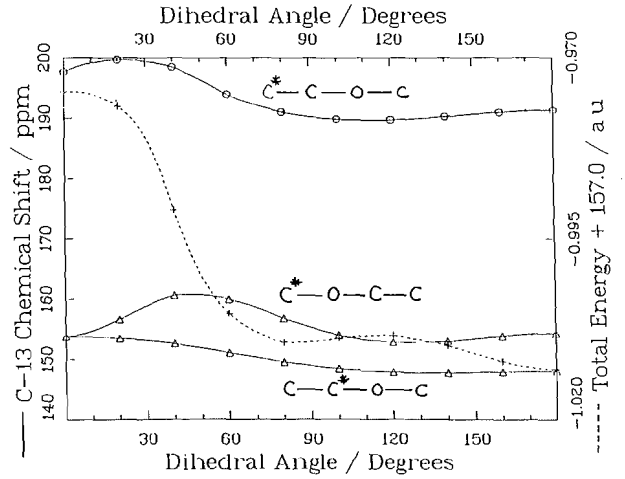


FIG. 5. GIAO calculated angular dependence of the isotropic ^{13}C NMR chemical shifts for the three carbons of ethylmethyl ether (—). Total conformational energy as a function of dihedral angle (- - - -).

Spectra

The solution phase ^{13}C NMR spectra were recorded at 100.6 MHz using a Bruker AM-400 spectrometer via techniques described previously (4). The ^{13}C CPMAS solid phase spectra were obtained on a Bruker CXP-180 instrument at 45.3 MHz. Experimental details have been described earlier (5, 6).

Computations

^{13}C chemical shifts were calculated using the NRC IBM-3090 computer system. For the GIAO calculations, standard geometries (16) were employed. The GAUSSIAN 86 program (17) was used to generate wavefunctions using a double zeta (DZ) basis set.

Acknowledgements

Access to the solid phase NMR facility at the National Research Council of Canada was provided by Dr. J. A. Ripmeester and Dr. C. I. Ratcliffe. G.W.B. acknowledges continuing financial support in the form of operating grants from NSERC. C.M. thanks the National Research Council of Canada for financial support via the Visiting Scientist program.

1. R. M. IZATT, B. L. HAYMORE, and J. J. CHRISTENSEN. J. Chem. Soc. Chem. Commun. 1308 (1972).
2. Y. A. SIMONOV, N. F. KRASNOVA, A. A. DVORKIN, V. V. YAKSHIN, V. M. ABASHKIN, and B. N. LASKORIN. Sov. Phys. Dokl. **28**, 823 (1983).
3. G. W. BUCHANAN, K. BOURQUE, J. W. BOVENKAMP, A. RODRIGUE, and R. A. B. BANNARD. Tetrahedron Lett. **25**, 3963 (1984).
4. G. W. BUCHANAN, K. BOURQUE, J. W. BOVENKAMP, and A. RODRIGUE. Can. J. Chem. **63**, 2747 (1985).
5. G. W. BUCHANAN, J. A. RIPMEESTER, J. W. BOVENKAMP, and A. RODRIGUE. Tetrahedron Lett. **27**, 2239 (1986).
6. G. W. BUCHANAN, R. A. KIRBY, J. A. RIPMEESTER, and C. I. RATCLIFFE. Tetrahedron Lett. **28**, 4783 (1987).
7. G. W. BUCHANAN, M. Z. KHAN, J. A. RIPMEESTER, J. W. BOVENKAMP, and A. RODRIGUE. Can. J. Chem. **65**, 2564 (1987).
8. M.-C. FEDARKO. J. Magn. Reson. **12**, 30 (1973).
9. S. WOLFE and J. R. CAMPBELL. Chem. Commun. 874 (1969).
10. H.-J. SCHNEIDER and V. HOPPEN. Tetrahedron Lett. 579 (1974).
11. R. DITCHFIELD. *In* MTP Int. Rev. Sci. Phys. Chem. Ser. I. Molecular structure and properties. Vol. II. Butterworths, London. 1972.
12. C. MCMICHAEL ROHLFING, L. C. ALLEN, and R. DITCHFIELD. Chem. Phys. **87**, 9 (1984).
13. K. SIEDMAN and G. E. MACIEL. J. Am. Chem. Soc. **99**, 659 (1977).
14. J. B. LAMBERT and A. R. VAGENAS. Org. Magn. Reson. **17**, 265 (1981).
15. H.-J. SCHNEIDER, U. BUCHEIT, V. HOPPEN, and G. SCHMIDT. Chem. Ber. **122**, 321 (1989).
16. R. C. WEAST, M. J. ASTLE, and W. H. BEYER (*Editors*). CRC handbook of chemistry and physics. 64th ed. CRC Press Inc., Boca Raton, FL. 1983–1984.
17. M. J. FRISCH, J. S. BINKLEY, H. B. SCHLEGEL, K. RAGHAVACHARI, C. F. MELIUS, R. L. MARTIN, J. J. P. STEWART, F. W. BOBROWICZ, C. M. ROHLFING, L. R. KAHN, D. J. DEFREES, R. SEEGER, R. A. WHITESIDE, D. J. FOX, E. M. FLEUDER, and J. A. POPLE. Carnegie–Mellon Quantum Chemistry Publishing Unit, Pittsburgh, PA. 1984.

Can. J. Chem. Downloaded from www.nrcresearchpress.com by 123.30.183.119 on 09/08/12
For personal use only.

Étude théorique (AM1) de l'affinité protonique des polyéthers cycliques (éthers couronnes) et non cycliques (glymes)

M'HAMED ESSEFFAR ET MOHAMED EL MOUHTADI[1]

Laboratoire de chimie théorique, Faculté des sciences, Université Cadi Ayyad, Avenue Prince My Abdellah, B.P. S15, Marrakech, Maroc

JOSÉ-LUIS M. ABBOUD

Consejo Superior de Investigaciones Cientificas, Instituto de quimica fisica Rocasolano, Serrano, 119, 28006 Madrid, Espagne

JOSÉ ELGUERO

Consejo Superior de Investigaciones Cientificas, Instituto de quimica medica, Calle Juan de la cierva 3, 28006 Madrid, Espagne

ET

DANIEL LIOTARD

Laboratoire de physicochimie théorique, Unité de recherche au Centre national de la recherche scientifique, n° 503, 351 Cours de la libération, 33405 Talence CEDEX, France

Reçu le 20 mars 1991

M'HAMED ESSEFFAR, MOHAMED EL MOUHTADI, JOSÉ-LUIS M. ABBOUD, JOSÉ ELGUERO et DANIEL LIOTARD. Can. J. Chem. **69**, 1970 (1991).

Des calculs semi-empiriques au moyen de la méthode AM1, ont été utilisés pour discuter de l'affinité protonique des molécules poly-oxygénées (dioxane, glymes et éthers couronne). Les valeurs calculées, bien que systématiquement plus faibles que les expérimentales, sont corrélées linéairement avec elles ($r = 0{,}993$). Étant donné les profondes modifications conformationnelles que subissent ces molécules quand on les protone, le résultat est très satisfaisant; il permet d'estimer les affinités protoniques, AP, du 9-éther-couronne-3 (206,5 kcal mol^{-1}) et du glyme-5 (231,1 kcal mol^{-1}). En plus, ce travail justifie le fait qu'à nombre égal d'atomes d'oxygène, les glymes sont plus basiques que les éthers couronne. Pour ces derniers l'affinité protonique dépend des tensions angulaires dans la base et des liaisons hydrogènes intramoléculaires dans le cation.

Mots clés : protonation, réactivité, glymes, éthers couronnes, coordination.

M'HAMED ESSEFFAR, MOHAMED EL MOUHTADI, JOSÉ-LUIS M. ABBOUD, JOSÉ ELGUERO, and DANIEL LIOTARD. Can. J. Chem. **69**, 1970 (1991).

Semi-empirical calculations at the AM1 level have been used to study the proton affinity (PA) of polyether compounds (dioxane, glymes, and crown ethers). The calculated values, although systematically lower than the experimental ones, are linearly correlated with eight experimental PA's ($r = 0.993$). Taking into account the considerable conformational changes that take place upon protonation, the result is highly satisfactory and provides an estimate of proton affinity for 9-ether-crown-3 (206.5 kcal mol^{-1}) and glyme-5 (231.1 kcal mol^{-1}). Moreover, this work provides a rationale for the fact that, for the same number of oxygen atoms, glymes are more basic than crown ethers. For the crown ethers, the proton affinity depends on angular strain in the base and on intramolecular hydrogen bonds in the cation.

Key words: protonation, reactivity, glymes, crown ethers, coordination.

Introduction

Les éthers macrocycliques $(CH_2CH_2O\text{-})_n$ originalement synthétisés par Pedersen (1) en 1967, ont connu une attention particulière au cours de ces deux dernières décenies. Ils présentent des propriétés aussi variées qu'intéressantes et sont susceptibles d'applications en catalyse, en synthèse organique et en biologie (2–4). À ce sujet un certain nombre de mises au point ont été publiées (5–8). Nous citons à titre d'exemple les structures cristallines du 18-éther-couronne-6 et ses complexes avec les sulfocyanures de divers métaux alcalins (9–14). Du point de vue théorique, peu d'études ont été réalisées. Seules les études structurales, du 12-éther-couronne-4 (15), la complexation du 18-éther-couronne-6 et du 12-éther-couronne-4 par NH_4^+, Na^+ et K^+, en CNDO/2 (16–18) sont connues.

Dans le but d'apporter une contribution exhaustive à ce sujet, nous nous proposons une étude quantitative de la protonation en phase vapeur de dix polyéthers : 6-éther-couronne-2, glyme-1, 9-éther-couronne-3, glyme-2, 12-éther-couronne-4, glyme-3, 15-éther-couronne-5, glyme-4, 18-éther-couronne-6 et glyme-5. La complexation de ces systèmes par les ions Li^+, Na^+ et K^+ sera examinée dans un prochain article.

Méthode de calcul et procédure

Pour obtenir des affinités protoniques bien précises, les méthodes *ab initio* avec des bases raisonablement étendues, constituent un moyen efficace et parfois inévitable. Mais souvent de telles méthodes ne peuvent pas être appliquées à des molécules organiques d'intérêt chimique et biologique. De ce fait, les méthodes semi-empiriques sont alors de grand intérêt dans l'approche de la réactivité de ces molécules. C'est dans ce cadre que nous avons fait appel à la méthode AM1. Cette méthode développée par le groupe de Dewar a trouvé des applications très variées aussi bien dans le domaine de la recherche fondamentale que dans le domaine de la recherche appliquée. Cette procédure implantée dans le programme AMPAC (19), s'est révélée d'une efficacité considérable. L'introduction d'une pseudodiagonalisation rapide au niveau des itérations SCF (20) et la précision des résultats obtenus rend cette méthode largement utilisée dans plusieurs domaines de la chimie.

Les affinités protoniques sont déterminées par différence des

[1]Auteur à qui adresser toute correspondance.

Printed in Canada / Imprimé au Canada

Can. J. Chem. Downloaded from www.nrcresearchpress.com by 123.30.183.119 on 09/08/12
For personal use only.

chaleurs de formations de la molécule neutre et de la molécule protonée de la réaction [1] en phase vapeur :

[1] $B + H^+ \rightarrow BH^+$

[2] $AP = -\Delta H = -[\Delta H_f(BH^+) - \Delta H_f(B) - \Delta H_f(H^+)]$

Dans le formalisme AM1, $\Delta H_f(H^+)$ est définie par la valeur paramétrisée U_{ss}, intégrale monocentrique électronique, choisie pour mieux reproduire les chaleurs de formation des hydrocarbures (21). Cette procédure conduit à une valeur empirique de U_{ss} qui diffère considérablement de celle appropriée à un atome d'hydrogène isolé. Par conséquent $\Delta H_f(H^+)$ calculée en AM1 (314,9 kcal mol^{-1}) est très faible devant la valeur expérimentale (367,2 kcal mol^{-1}) (22). Pour ce faire, nous avons basé nos calculs des AP sur la valeur expérimentale. L'utilisation de cette valeur est en accord avec la philosophie semi-empirique de la méthode et a l'avantage de limiter les erreurs des AP calculées uniquement aux erreurs dues aux chaleurs de formations des bases neutres et protonées. La méthode AM1 décrit alors de façon satisfaisante le phénomène de protonation des molécules oxygénées, tant sur le plan énergétique que conformationel (23).

Résultats et discussion

(a) Analyse des structures géométriques

Les molécules neutres et protonées présentent plusieurs conformations d'énergies très proches et les algorithmes d'optimisation convergent vers l'une d'entre elle, mais pas nécessairement la plus basse. Ce problème ne semble pas crucial pour les glymes dans la mesure où les minima sont probablement très voisins en énergie. Par contre les tensions de cycle dans les couronnes peuvent introduire des écarts énergétiques importants.

Une étude conformationnelle exhaustive (24) du dioxane et du glyme-1, dans les cas neutres et protonés, nous a fourni les motifs de base pour bâtir plusieurs conformations plausibles qui ont servi de points de départ pour les algorithmes d'optimisation. Les différentes conformations neutres ainsi obtenues ont, à leur tour, servi de points de départ pour les formes protonées, par ajout systématique du proton successivement placé sur les deux sites de protonation envisageables pour chaque oxygène.

Compte tenu de la taille des molécules envisagées et du nombre important des paramètres géométriques, nous ne décrirons dans cet articles que les structures géométriques les plus stables des éthers couronne (formes neutres et protonées). La stabilité de ces structures a été vérifiée par le procédé LTRD (25) implanté dans le programme AMPAC. Ce procédé permet de s'assurer de la fiabilité et de la nature de la structure. Si la structure correspond à un minimum sur la surface de potentiel, le nombre de valeurs propres négatives de la matrice des constantes de force (matrice de Hessien) est égal à 0.

9-Éther-couronne-3

Dans le 9-éther-couronne-3, bien qu'il soit supérieur au dioxane, la tension du cycle est encore non négligeable; ce qui réduit le nombre de possibilités conformationnelles. La structure la plus stable est celle représentée sur la figure 1(a) où les oxygènes s'alternent en dessus et en dessous du plan moyen du cycle. Les paramètres géométriques montrent que ces derniers sont disposés à environ 3 Å, les uns des autres réduisant ainsi les répulsions électroniques des paires libres. La protonation de cette molécule se fait sur l'un des trois oxygènes (les trois sites sont équivalents). La figure 1(b) montre que la protonation conduit à une déformation de la molécule par rapport à son état neutre. En effet, les motifs (OCH_2CH_2O) qui étaient disposés de façon à minimiser les interactions entre les paires libres, sont maintenant orientés de manière à favoriser la dicoordination du proton. La distance H^+–O calculée (1,01 Å) indique que le proton, bien qu'il

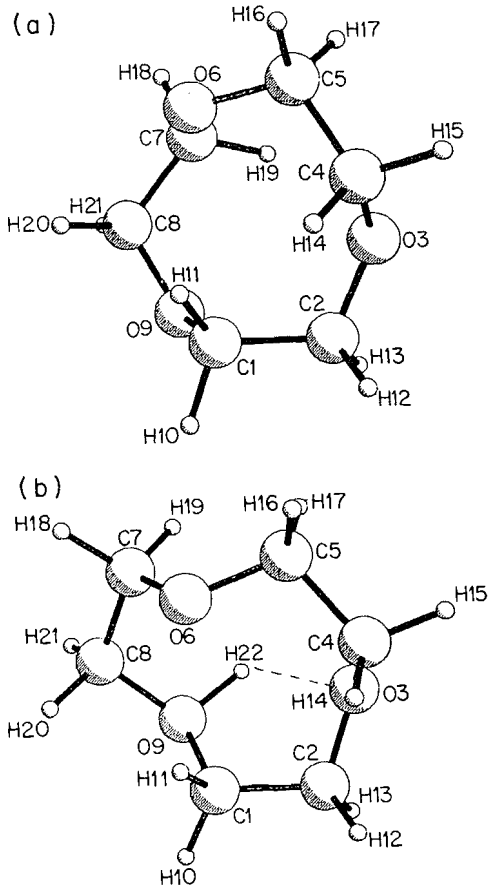


FIG. 1. (a) Structure du 9-éther-couronne-3; (b) structure du 9-éther-couronne-3 protoné.

soit lié à O_9 par une liaison covalente, crée une liaison hydrogène avec l'atome d'oxygène voisin (O_3) où la distance H^+—O_3 est de 2,08 Å.

12-Éther-couronne-4

Plusieurs conformations ont été mises en évidence pour cette molécule. La conformation la plus stable est celle qui présente une alternance plus ou moins régulière du motif chaise (OCH_2CH_2O) bien qu'on note l'apparition d'un motif à 120° pour fermer le cycle (figure 2(a)). Les longueurs de liaison C—C (1,52 Å) et C—O (1, 42 Å) sont pratiquement les mêmes, alors que les angles plans sont plus ou moins déviés de la valeur optimale (109°). Les angles dièdres qui sont caractéristiques de chaque conformation, montrent des déviations importantes des valeurs idéales (0°, 120° ou 180°). Ces valeurs présentent une alternance du motif chaise (OCH_2CH_2O) à ±60° à l'exception d'un seul qui apparaît à 116° rompant la symétrie de la molécule.

La fixation d'un proton sur chacun des sites actifs conduit à quatre conformations différentes du 12-éther-couronne-4 protoné et cela pour chacune des configurations probables de la molécule neutre. La conformation la plus stable est celle qui présente une liaison hydrogène intramoléculaire. Il est à signaler que la protonation depuis la conformation la plus stable de la molécule neutre ne conduit pas forcément au minimum le plus stable de la molécule protonée. En effet, parmi les différentes conformations de la molécule neutre, seule la protonation depuis l'optimum de symétrie C_{2v} conduit au minimum le plus stable représenté sur la figure 2(b). Il apparaît clairement que le proton est dicoordiné entre les oxygènes O_1 et O_2 formant ainsi une couronne bicyclique à huit chaînons. La liaison hydrogène ainsi obtenue

Can. J. Chem. Downloaded from www.nrcresearchpress.com by 123.30.183.119 on 09/08/12
For personal use only.

Can. J. Chem. Downloaded from www.nrcresearchpress.com by 123.30.183.119 on 09/08/12
For personal use only.

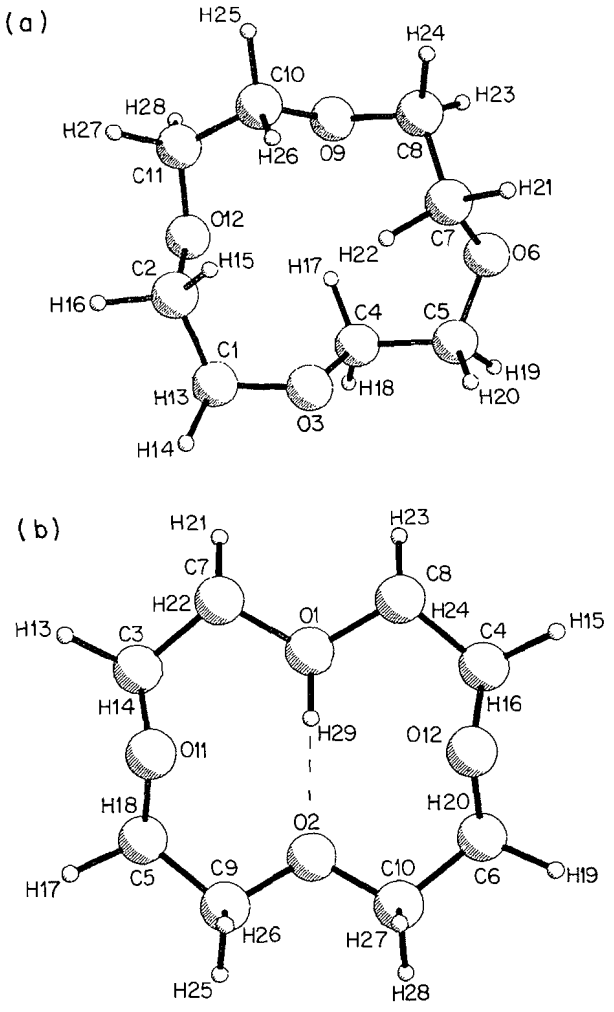


FIG. 2. (a) Structure du 12-éther-couronne-4; (b) structure du 12-éther-couronne-4 protoné.

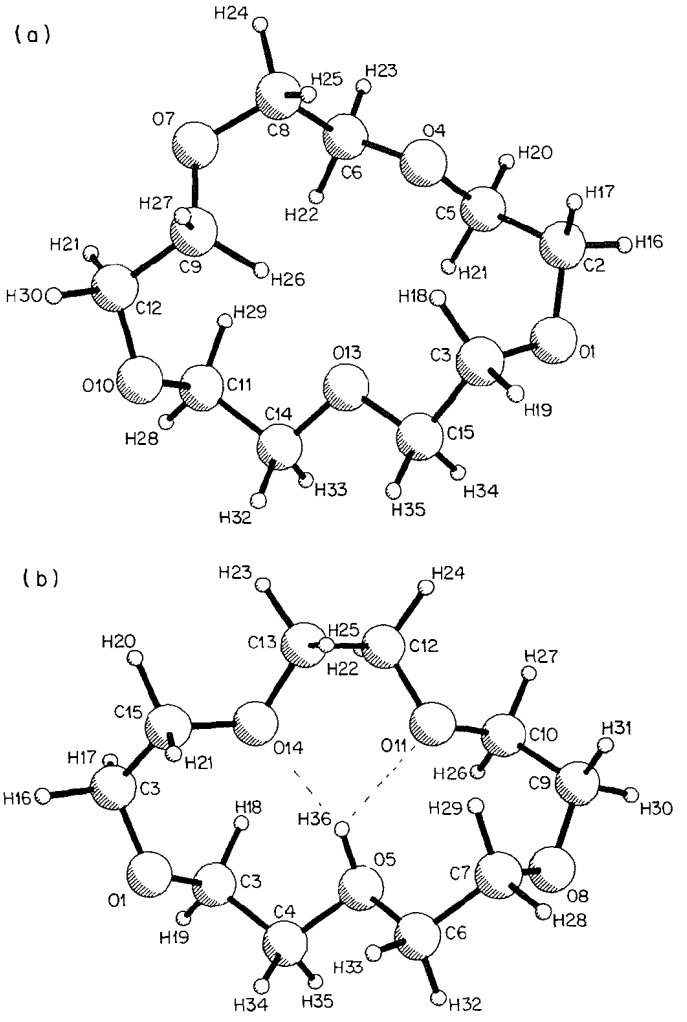


FIG. 3. (a) Structure du 15-éther-couronne-5; (b) structure du 15-éther-couronne-5 protoné.

n'est pas idéalement linéaire (O_1—H_{29}—$O_2 \cong 150°$). Cette faible déviation de la linéarité est imposée par la tension du cycle formé. Cette dicoordination peut être constatée également au niveau des angles plans des oxygènes en interactions ($C_7O_1C_8$) et ($C_9O_2C_{10}$) qui diminuent d'environ 3° par rapport aux autres. Il est à signaler également que contrairement à la conformation la plus stable de la molécule neutre où les motifs (OCH_2CH_2O) s'alternent de part et d'autre du plan moyen du cycle, tous les oxygènes sont du même côté et orientés de façon favorable à la dicoordination. Les deux oxygènes non impliqués dans la liaison hydrogène intramoléculaire sont à 4,3 Å l'un de l'autre.

15-Éther-couronne-5

Contrairement au 12-éther-couronne-4, le 15-éther-couronne-5 est beaucoup plus flexible et la régularité des motifs chaise et bateau n'est pas tout à fait respectée. La conformation la plus stable représentée sur la figure 3(a), montre que l'alternance des motifs (OCH_2CH_2O) chaise est très perturbée.

Les longueurs des liaisons et les angles plans sont identiques à ceux du 12-éther-couronne-4. Les angles dièdres des motifs (OCH_2CH_2O) sont alternés autour du plan moyen du cycle suivant la séquence (+ − + −) mais sont largement déformés par rapport aux valeurs idéales (±60° ou ±120°). Par conséquent, la structure du 15-éther-couronne-5 semble indiquer que les cinq sites basiques ne sont pas équivalents. La conformation protonée la plus stable est celle où l'orientation des dipôles (OCH_2CH_2O) permet une interaction par liaison hydrogène intramoléculaire. La structure représentée sur la figure 3(b) montre, encore une fois, que la dicoordination se fait préférentiellement entre les oxygènes opposés formant ainsi un cycle à huit membres à l'intérieur de la couronne. Les distances H^+–O indiquent qu'un faible pontage est possible entre le proton et les oxygènes O_{11} et O_{14} conduisant à une tricoordination. Cette interaction du proton avec les trois oxygènes empêche la linéarité connue de la liaison hydrogène. L'angle O_{14}—H—O_5 (155°) n'est que faiblement dévié de la valeur optimale, tandis que l'angle O_{11}—H—O_5 (120°) est franchement affecté. Les deux autres oxygènes (O_1 et O_8) sont dans des positions défavorables pour interagir avec le proton. Il est à noter que les distances H^+–O_{11} et H^+–O_{14} de 2,14 et 2,06 Å respectivement sont du même ordre de grandeur que dans le cas du 12-éther-couronne-4 protoné.

18-Éther-couronne-6

Le 18-éther-couronne-6 est la molécule la plus flexible de toute la série envisagée. Toutes les études rapportées sur cette molécule indiquent que sa structure la plus stable est de symétrie C_i (26). Celles effectuées au moyen de la mécanique moléculaire indiquent que les structures de symétrie C_i et D_{3d} sont de stabilité comparable (27). Le résultat de nos calculs réalisés au moyen de la méthode AM1 indique que la structure la plus stable est de symétrie D_{3d} (figure 4(a)). Sur cette structure, les motifs chaises

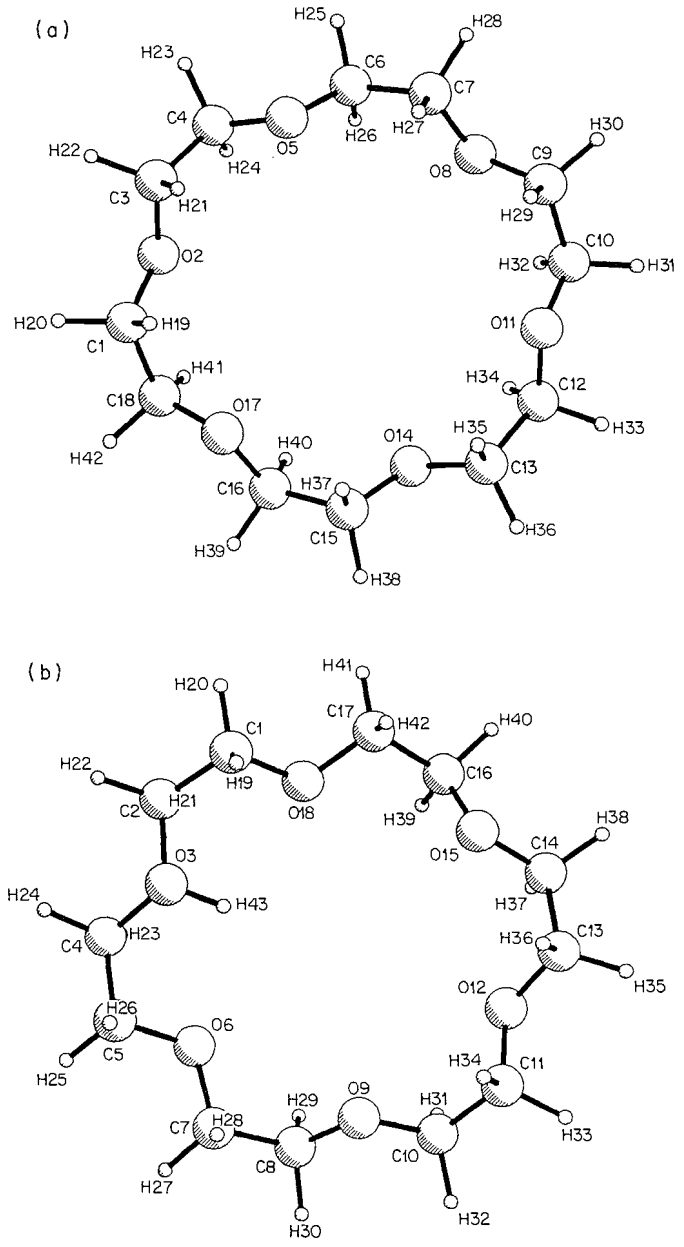


FIG. 4. (a) Structure du 18-éther-couronne-6; (b) structure du 18-éther-couronne-6 protoné.

sont bien alternés à ±0,3 Å autour du plan moyen du cycle. Les angles de torsion de ces motifs ne s'éloignent des valeurs optimales (120°) que d'environ 15°. Les oxygènes les plus proches sont ceux en position γ (3,2 Å). Les autres distances sont supérieures à 5 Å. Les plus éloignés sont à 6 Å l'un de l'autre déterminant ainsi le diamètre de la cavité de cette couronne.

La structure protonée la plus stable, parmi toutes les configurations, est celle représentée sur la figure 4(b). Bien que tous les motifs (OCH_2CH_2O) soient orientés de façon favorable, aucune des conformations mises en évidence n'a montré l'existence d'une liaison hydrogène intramoléculaire. Les distances H^+–O sont toutes supérieures à 2,5 Å, valeur optimale pour former une liaison hydrogène, excepté les oxygènes O_6 et O_{18} en position γ qui montrent une très faible interaction avec le proton (H^+–O_6 = 2,42 Å et H^+–O_{18} = 2,47 Å). Ceci est confirmé par le fait que la distance entre le proton et l'oxygène qui le fixe est inférieure à celle rencontrée dans les autres cas. Cette faible interaction par liaison hydrogène n'est sûrement pas suffisante pour stabiliser davantage la molécule protonée.

TABLEAU 1. Affinités protoniques expérimentales et calculées en AM1 des glymes et des éthers couronne[a]

N°	Composé	AP (AM1)[b]	AP (exp)[c]
1	Dioxane	181,9	192,6
2	9-Éther-couronne-3	190,3	205,0[d]
3	12-Éther-couronne-4	198,1	220,3
4	15-Éther-couronne-5	201,6	222,0
5	18-Éther-couronne-6	200,6	225,2
6	Glyme-1	188,9	204,6
7	Glyme-2	198,2	218,5
8	Glyme-3	200,8	223,3
9	Glyme-4	202,7	226,3
10	glyme-5	205,7	232,0[d]

[a]Toutes les valeurs sont en kcal mol^{-1}.
[b]Ce travail.
[c]Moyenne des valeurs des références 25 et 26.
[d]Valeur calculée au moyen de l'équation [3].

(b) Affinités protoniques

L'étude de la fixation d'un proton à l'intérieur d'un éther couronne, n'est qu'une première étape qui sera suivie par la complexation avec d'autres ions d'intérêt chimique pouvant conduire à des interactions au-delà de la dicoordination.

Les données expérimentales disponibles jusqu'à présent, concernant ces composés macrocycliques, sont celles de Meot-Ner (28) et de Kebarle et coll. (29). Les moyennes des valeurs de ces auteurs sont résumées dans le tableau 1.

L'énergie de complexation des polyéthers avec le proton est composée de deux contributions essentielles : électrostatique et covalente. Si la première est due à l'interaction ion–dipôle se produisant à grandes distances, la seconde est due au transfert de charges du ligand au cation. Dans les chaînes linéaires tels que les glymes, la protonation du premier groupe O-CH_3 est souvent suivie par une cyclisation induite par la formation d'une liaison hydrogène interne dans laquelle le proton est dicoordiné entre deux groupes basiques. À différence de la basicité, l'affinité protonique n'est pas affectée par le facteur entropique. L'examen des données du tableau 1 montre que l'AP des éthers couronne et des glymes croît régulièrement avec la taille de la molécule. Ceci traduit les effets stabilisateurs de la polarisation du squelette moléculaire (aussi bien à travers les liaisons qu'à travers l'espace) et de la liaison hydrogène intramoléculaire.

Une comparaison des AP (calculées et expérimentales), des glymes et des éthers couronne homologues indique que, sans exception, les glymes sont favorisés. La différence est maximale pour le dioxane et le 9-éther-couronne-3, atteint un minimum pour le 12-éther-couronne-4, puis augmente lentement avec la taille du cycle.

Le dioxane, relativement à son homologue ouvert, présente une tension du cycle importante. La protonation de ce dernier se fait préférentiellement sur la conformation bateau (24). Les répulsions dipolaires entre les oxygènes, qui sont importantes dans les formes neutres, ont disparu et l'orientation des groupes CH_2OCH_2 stabilise la charge positive beaucoup plus que dans la forme chaise. Le dipôle de ce motif, dans le cas de son homologue ouvert, le glyme-1, est dans une position encore plus favorable. Ce qui conduit à une forte AP relativement au dioxane bateau. La grande stabilité observée en passant du glyme-1 au glyme-2 est attribuée principalement à l'allongement de la

Can. J. Chem. Downloaded from www.nrcresearchpress.com by 123.30.183.119 on 09/08/12
For personal use only.

Can. J. Chem. Downloaded from www.nrcresearchpress.com by 123.30.183.119 on 09/08/12
For personal use only.

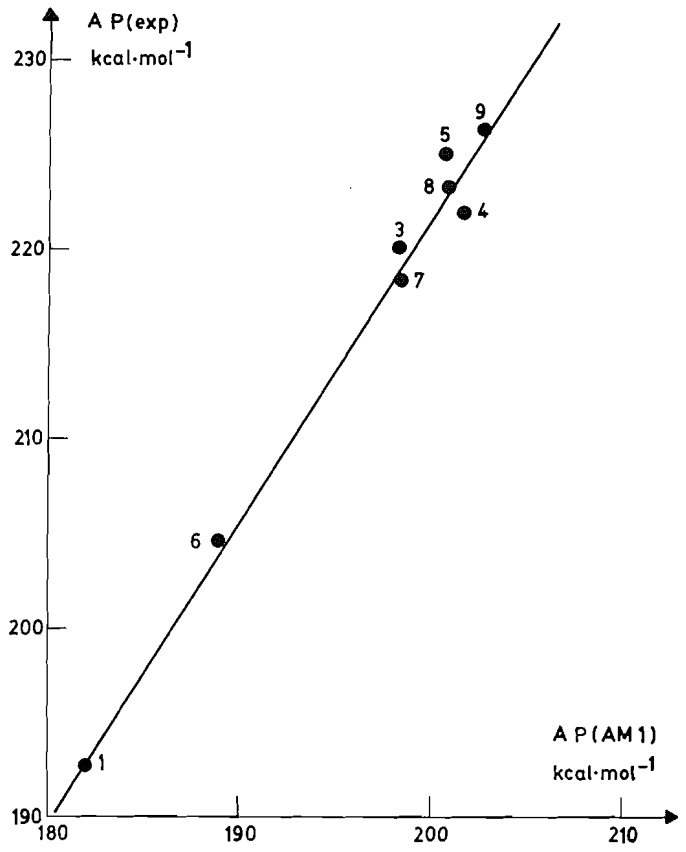


FIG. 5. Corrélation entre les affinités protoniques calculées et les valeurs expérimentales.

chaîne entre les deux oxygènes terminaux. La flexibilité de la chaîne linéaire est un facteur favorable à la dicoordination bien que l'oxygène du milieu défavorise la stabilisation dans certains cas.

La stabilité des couronnes est aussi très importante bien qu'elle soit inférieure à celle de leurs homologues ouverts. Dans le cas du 12-éther-couronne-4 protoné, deux oxygènes opposés dans le cycle peuvent atteindre une distance et une orientation favorables à la dicoordination. Les deux autres sont forcés être à des distances plus grandes. Le 15-éther-couronne-5 permet plus de flexibilité et une meilleure orientation dipolaire. En effet, les distances entre le proton et les cinq oxygènes de la molécule laissent supposer qu'une interaction au-delà de la dicoordination est possible. L'introduction du sixième groupe CH_2OCH_2 pour former le 18-éther-couronne-6 rend les distances entre les oxygènes relativement plus grandes. Seule l'interaction conduisant à un cycle hexagonal est possible, du moins dans le cadre de la méthode AM1. Ce qui explique probablement la faible AP de cette molécule par rapport à celle du 15-éther-couronne-5. Les différences entre les valeurs des AP calculées et mesurées varient entre 11 et 25 kcal mol^{-1}. Néanmoins, l'ordre de basicité est très bien reproduit, comme le montre la figure 5.

La relation entre AP(AM1) et AP(exp) est donnée par l'équation [3] :

$$[3] \quad AP(exp) = (-98{,}4 \pm 15{,}5) + (1{,}60 \pm 0{,}08)AP(AM1)$$

en kcal mol^{-1}; $n = 10$; $r^2 = 0{,}986$; d.s = 1,5 kcal mol^{-1}.

La pente de cette relation linéaire est importante (1,60). Ceci est à rapprocher des résultats obtenus dans une étude antérieure portant sur les effets de substituant sur l'affinité protonique des alcools et des éthers aliphatiques (23).

La qualité de la corrélation définie par l'équation [3] est cependant assez élevée pour montrer que la méthode AM1 est capable de décrire l'évolution de l'AP au sein de ces familles de composés d'une façon très satisfaisante et de conduire à des estimations fiables.

Conclusion

Dans ce travail nous avons présenté les structures géométriques les plus stables de quelques polyéthers sous leur forme neutre et protonée. Nous avons montré que la protonation à partir de la structure préférée de la molécule neutre ne conduit pas forcément à la conformation la plus stable de la molécule protonée. La dicoordination du proton n'apporte de stabilisation significative que si le pont hydrogène est formé entre deux oxygènes opposés conduisant à un cycle à huit membres. Dans le cas des glymes, la protonation de l'un des oxygènes des groupes extrêmes $-OCH_3$, est suivie d'une cyclisation par liaison hydrogène impliquant une stabilisation importante du système moléculaire.

La structure du 15-éther-couronne-5 protoné montre qu'une interaction par liaison hydrogène au-delà de la dicoordination, même en phase vapeur, n'est pas exclue. Ce comportement est probablement l'un des facteurs qui contribue à l'augmentation de l'AP de cette molécule par rapport à celle du 18-éther-couronne-6. La protonation de cette dernière n'a montré qu'un faible pontage entre deux oxygènes adjacents. La bonne corrélation obtenue entre nos valeurs calculées en AM1 et les valeurs expérimentales fournit une justification satisfaisante de nos résultats.

Ces résultats peuvent être utiles pour l'interprétation du phénomène de la protonation dans des solvants faiblement basiques où la stabilisation par tri- et tétra-coordination est fortement possible.

1. C. J. PEDERSEN. J. Am. Chem. Soc. **89**, 7017 (1967).
2. D. J. CRAM et K. N. TRUEBLOOD. Top. Curr. Chem. **98**, 43 (1981).
3. C. F. VÖGTLE. *Dans* The chemistry of ethers, crown ethers, hydroxyl groups and their sulfur analogues. Part I. Suppl. E. *Éditeur* : S. Patai. John Wiley & Sons, New York. 1980. p 1.
4. W. THIEL et A. SCHWEIG. Chem. Phys. Lett. **12**, 1 (1971); **16**, 2 (1972).
5. B. DIETRICH, M. W. HOSSIENI, J. M. LEHN et R. B. SESSIONS. J. Am. Chem. Soc. **103**, 1282 (1981).
6. W. SCHAFER et A. SCHWEIG. J. Chem. Soc. Chem. Commun. 824 (1972).
7. A. KATRIB, T. P. DEBIES, R. J. COLTON, T. H. LEE et J. W. RABALAIS. Chem. Phys. Lett. **22**, 196 (1973).
8. I. GOLDBERG. *Dans* Crown ethers and analogs. *Éditeurs* : S. Patai et Z. Rappoport. John Wiley, New York. 1989.
9. J. D. DUNITZ, M. DOBLER, P. SEILER, et R. P. PHIZACKERLEY. Acta Crystallogr. Sect. B: Struct. Crystallogr. Cryst. Chem. **B30**, 2733 (1974).
10. E. MAVERICK, P. SEILER, W. B. SCHWEIZER et J. D. DUNITZ. Acta Crystallogr. Sect. B: Struct. Crystallogr. Cryst. Chem. **B36**, 615 (1980).
11. P. GROTH. Acta Chem. Scand. **A36**, 109 (1982).
12. M. J. BOVILL, D. J. CHADWICK, I. O. SUTHERLAND et D. WATKIN. J. Chem. Soc. Perkin Trans. 2, 1529 (1980).
13. W. H. M. UITERWIJK, S. HARKEMA, B. W. VAN DE WAAL, F. GÖBEL et H. T. M. NIBBELING. J. Chem. Soc. Perkin Trans. 2, 1843 (1983).
14. B. BELAMRI, C. BAVOUX et A. THOZET. J. Inclusion Phenom. **8**, 383 (1990).
15. A. PULLMAN, C. GIESSNER-PRETTRE et YU. V. KRUGLYAK. Chem. Phys. Lett. **35**, 156 (1975).

16. K. HORI, H. YAMADA et T. YAMABE. Tetrahedron, **39**, 67 (1983).
17. T. YAMABE, K. HORI, K. AKAGI et K. FUKUI. Tetrahedron, **35**, 1065 (1979).
18. J. LESZCZYNSKI, A. NOWEK et W. WOJCIECHOWSKI. Theochem. **85**, 211 (1981).
19. (*a*) J. J. P. STEWART. Groupe de Dewar, Université de Texas, Austin, TX; (*b*) M. J. S. DEWAR, E. G. ZOEBISCH, E. F. HEALY et J. J. P. STEWART. J. Am. Chem. Soc. **107**, 3902 (1985); (*c*) QCPE, Indiana University Program N° 506.
20. J. J. P. STEWART, P. CSASZAR et P. PULAY. J. Comput. Chem. **3**, 227 (1982).
21. (*a*) M. J. S. DEWAR et W. THIEL. J. Am. Chem. Soc. **99**, 4899 (1977); (*b*) J. Am. Chem. Soc. **99**, 4907 (1977).
22. J. C. TRAEGER et R. G. MCLONGHLIN. J. Am. Chem. Soc. **103**, 3647 (1981).
23. J. L. M. ABBOUD, J. ELGUERO, D. LIOTARD, M. ESSEFFAR, M. EL MOUHTADI et R. W. TAFT. J. Chem. Soc. Perkin Trans. 2, 565 (1990).
24. M. ESSEFFAR, M. EL MOUHTADI et Y. G. SMEYERS. J. Mol. Struct. (Theochem), **208**, 179 (1990).
25. D. LIOTARD et J. P. PENOT. Springer Series dans Synergetics. Vol. 9 : Numerical methods in the study of critical phenomena. *Éditeurs* : J. Della Dora, J. Demongeot et B. Lacolle. Springer Verlag, Berlin. 1981. p. 213.
26. H. TAKEUCHI, T. ARAI et I. HARADA. J. Mol. Struct. (Theochem). **146**, 197 (1986).
27. W. H. WATSON, J. GALLOY, D. A. GROSSIE, F. VÖGTLE et M. MÜLLER. J. Org. Chem. **49**, 347 (1984).
28. M. MEOT-NER (Mautner). J. Am. Chem. Soc. **105**, 4906 (1983).
29. R. B. SHARMA, A. T. BLADES et P. KEBARLE. J. Am. Chem. Soc. **106**, 510 (1984).

Can. J. Chem. Downloaded from www.nrcresearchpress.com by 123.30.183.119 on 09/08/12
For personal use only.

An ion exchange atomic absorption method for the determination of ionized calcium at millimolar levels

AMITHA K. HEWAVITHARANA, VASANTHA MUTUCUMARANA,[1] AND BYRON KRATOCHVIL[2]
Department of Chemistry, University of Alberta, Edmonton Alta., Canada T6G 2G2

Received January 16, 1991

AMITHA K. HEWAVITHARANA, VASANTHA MUTUCUMARANA, and BYRON KRATOCHVIL. Can. J. Chem. **69**, 1976 (1991).

A quantitative ion exchange/atomic absorption method is described for measuring the fraction of free calcium in solution at millimolar levels. Sample solutions are equilibrated with a micro-column of strong-acid type cation-exchange resin under electrolyte concentrations (0.75 mol/L $NaNO_3$) high enough to provide conditions where the calcium sorbed on the resin is proportional to the free calcium in solution. After a water wash, the sorbed calcium is eluted from the resin with nitric acid directly into an atomic absorption spectophotometer. Free calcium levels were estimated using calibration curves obtained over the range 0–5 mM calcium with a precision of ±0.05 mM. The effect of magnesium, at concentrations twice that of calcium, on measured calcium levels is negligible. The method is pH insensitive over the range 5–7. Selectivity for free calcium in the presence of complexing ligands such as citrate and phosphate is high. The method shows promise for the determination of ionized calcium in biological systems.

Key words: ion exchange, atomic absorption, free calcium determination, ion speciation.

AMITHA K. HEWAVITHARANA, VASANTHA MUTUCUMARANA et BYRON KRATOCHVIL. Can. J. Chem. **69**, 1976 (1991).

On décrit une méthode quantitative d'échange ionique/absorption atomique permettant de mesurer le calcium libre, en solution à des niveaux millimolaires. On place les solutions d'échantillon dans une micro-colonne de résine échangeuse de cations de type acide fort, avec des concentrations d'électrolyte suffisamment élevées (0,75 mol/L de $NaNO_3$) pour qu'elles fournissent des conditions telles que la quantité de calcium adsorbé sur la résine est proportionnelle à la quantité de calcium à l'état libre dans la solution. Après un lavage à l'eau, le calcium adsorbé est élué de la résine à l'aide d'acide nitrique directement dans un spectrophotomètre d'absorption atomique. On évalue les niveaux de calcium en se basant sur des courbes de calibration obtenues entre 0 et 5 mM de calcium avec une précision de ± 0,05 mM. L'effet du magnésium sur les niveaux de calcium mesurés est négligeable jusqu'à des concentrations doubles de celles du calcium. Entre 5 et 7, la méthode n'est pas sensible au pH. En présence de ligands complexants comme le citrate et le phosphate, la sélectivité pour le calcium libre est élevée. La méthode est prometteuse pour la détermination de calcium ionisé dans des systèmes biologiques.

Mots clés : échange ionique, absorption atomique, détermination du calcium libre, spéciation ionique.

[Traduit par la rédaction]

Can. J. Chem. Downloaded from www.nrcresearchpress.com by 123.30.183.119 on 09/08/12
For personal use only.

Introduction

There is continuing interest in the measurement of ionized as opposed to total metal in environmental and clinical fields. Ionized calcium, in particular, is important in clinical applications (1–3) where it typically occurs at millimolar levels.

Calcium ion-selective electrode (ISE) potentiometry (4–6) and spectrophotometry with color-forming ligands (7, 8) are frequently used to measure ionic calcium at millimolar levels. ISE's are subject to several interferences, however, and require careful matching of samples and standards, while colorimetric methods have limitations in pH range and in application to colored samples. Another recently developed approach to ion speciation, an ion-exchange column-equilibration technique, has been used to determine free copper ion concentrations in natural waters (9) and free nickel ion concentrations in sewage (10). This method requires constant cation levels in the test solutions at concentrations such that the amount of analyte ion sorbed onto the resin is small compared to total sorbed cation. Under these conditions, called "trace conditions", the amount of analyte ion sorbed on the resin is directly proportional to the analyte ion concentration in solution.

In this paper the use of the ion-exchange column-equilibration technique for the determination of free calcium ion concentrations at millimolar levels is investigated. An ideal method for measuring individual species of a metal ion in solution will introduce little or no perturbation of the system. The ion exchange column equilibration method used here allows the column to come to equilibrium with fresh sample solution, so the concentration of calcium in the sample is not biased by sorption from the sample. The method does require that the fraction of resin in the calcium form be of the order of one percent or less. For the work described here this has been accomplished by making the samples to be analyzed about 0.75 mol/L in sodium nitrate.

[1]Present address: Department of Biochemistry, University of Oklahoma, Norman, OK, U.S.A.

[2]Author to whom correspondence may be addressed.

Experimental

Apparatus

A microcomputer-controlled data-acquisition/processing system, developed previously in this laboratory for ion speciation studies using the ion-exchange/atomic-absorption method (11), was used. The major components consist of a peristaltic multichannel pump and a Perkin Elmer model 4000 atomic absorption spectrophotometer, with data acquired by an IBM PC via an AST A to D converter. The construction of the micro resin column is described elsewhere (12). For this study a column containing 4.8 mg of resin was employed. pH measurements were made with a Fisher model 520 digital pH/ion meter and Fisher glass-calomel electrodes calibrated with Fisher standard buffers at pH 4 and 7.

Reagents

All chemicals used were reagent grade or better. The resin in the column was analytical grade 100–200 mesh Dowex 50W X8 strong-acid type cation exchanger (J. T. Baker Chemical Co.) treated as described in the literature (13). The ion exchange capacity of this resin is 5.1 mequiv./g on a dry basis.

Can. J. Chem. Downloaded from www.nrcresearchpress.com by 123.30.183.119 on 09/08/12
For personal use only.

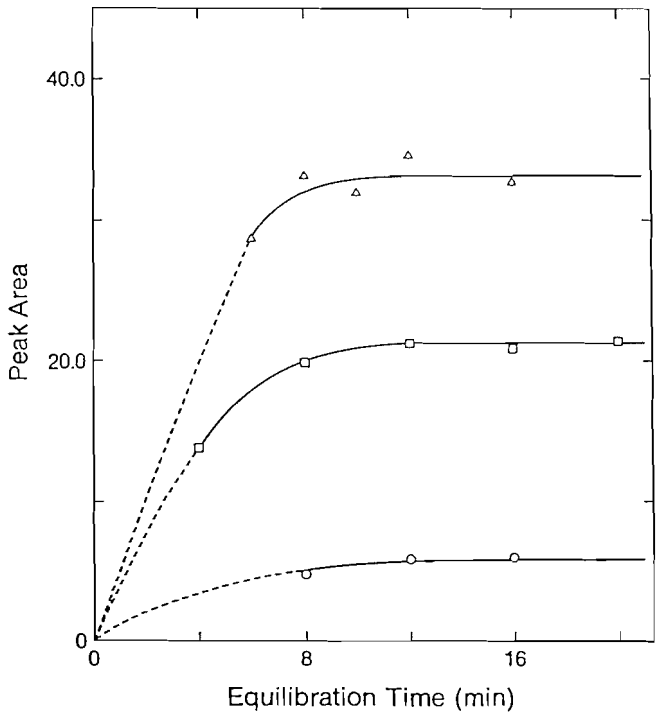


FIG. 1. Column equilibration curves at 0.1 mol/L Na^+: ○, 0.013 mM (0.5 mg/L) Ca^{2+}; □, 0.025 mM (1.0 mg/L) Ca^{2+}; △, 0.125 mM (5.0 mg/L) Ca^{2+}. Note: AA sensitivity was changed for the different solutions, so peak areas among plots are not directly comparable.

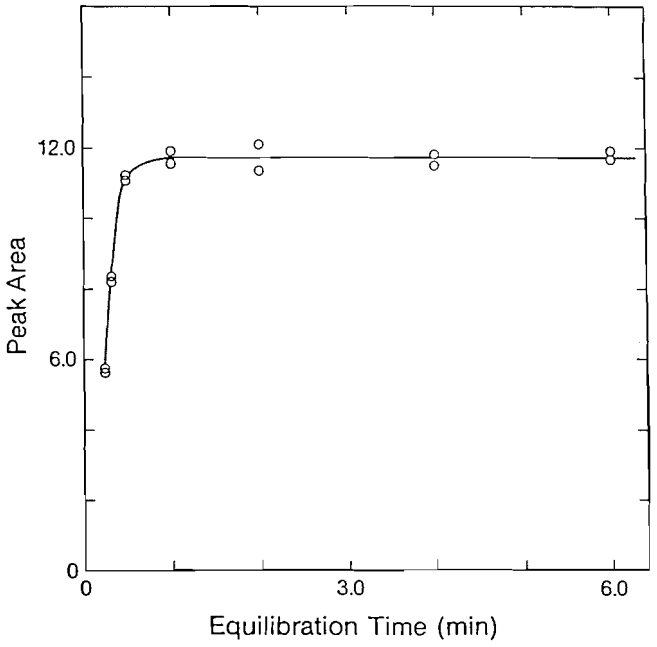


FIG. 2. Column equilibration curve for 0.625 mM (25 mg/L) Ca^{2+} solution in 0.75 mol/L Na^+.

Procedure

Standard solutions were prepared containing known concentrations of calcium as calcium nitrate (from calcium carbonate and HNO_3) and swamping electrolyte, $NaNO_3$. Some solutions were adjusted to pH 5 using HNO_3 or NaOH as required, others to pH 7 using HEPES buffer.

The column was thermostatted at 25 ± 1°C and the flow rate through it maintained at 4.5 mL/min with a peristaltic pump. A computer-controlled valve system described earlier (11) was used to perform the following operations.

The column was first washed by pumping water through it for 1 min. Next the solution of interest was passed through the column to waste until complete breakthrough was achieved (12). At breakthrough the composition of the column influent and effluent are the same and the resin is in equilibrium with the test solution. After the loading cycle, the column was backwashed with water for 3 min to remove any interstitial test solution. This washing cycle was followed by a 30 s elution of the sorbed ions with 2 M HNO_3 directly into the atomic absorption spectrophotometer. The column was washed with water before introduction of the next test solution. The data acquired from the AAS were stored in an IBM PC microcomputer, then processed to obtain peak heights and areas.

Results and discussion

Effect of calcium concentration on the time of equilibration

The time period required to achieve complete equilibration of resin with solution was examined with three concentrations of calcium at a constant electrolyte concentration of 0.1 mol/L and pH 5. The results, Fig. 1, show that the time required to achieve complete equilibration does not significantly change with the concentration of calcium at a constant electrolyte concentration. It was also determined that the time of equilibration was not affected by replacing sodium with potassium or by the presence of at least 4.1 mM (100 mg/L) magnesium or 0.65 mol/L of urea. For 0.1 mol/L electrolyte concentrations, the equilibration time is about 12 min. Therefore, for a series of Ca standards prepared with the same electrolyte concentration, measurement of the equilibration time of one standard is adequate to determine the equilibration time for the entire set.

Effect of electrolyte concentration on the time of equilibration

The equilibration time for 0.625 mM (25 mg/L) calcium solution in 0.75 mol/L sodium nitrate as electrolyte was found to be less than 1 min (Fig. 2). The corresponding time for 0.5 mol/L sodium nitrate was about 3 min. These data and the value of 12 min for 0.1 mol/L sodium nitrate reported in the previous section indicate that the time required for equilibrium between solution phase and resin phase decreases as the electrolyte concentration is increased.

Effect of electrolyte concentration on calibration curves

The effect on calibration plots for calcium of concentrations of $NaNO_3$ electrolyte ranging from 0.1 to 0.75 mol/L are shown in Fig. 3. The linearity of the plot depends on the closeness of the experimental conditions to trace conditions. The increase in the linear region with increasing concentration of electrolyte suggests that at lower levels of electrolyte the column is not operating under trace conditions. Table 1 gives the fraction of calcium present on the resin at equilibrium with sodium ion concentrations of 0.1 and 0.75 mol/L. The data show that the column is not operating at trace conditions at 0.1 mol/L electrolyte concentration, and explains the curvature of the calibration curve. A sodium ion concentration of 0.75 mol/L was found to provide a calibration curve which can be used to determine Ca^{2+} concentrations up to 5 mM (200 mg/L) with a standard deviation of the order of ±0.05 mM.

Tables of the affinity of DOWEX 50W X8 for cations show K^+ favored over Na^+ by a factor of about 1.5 (14). These affinities were measured at low ionic strengths, however. At the higher ionic strengths used here selectivity reversal is observed, such that sodium is better than potassium in providing trace conditions for calcium concentrations in the millimolar range. Therefore all subsequent measurements of calcium were made using 0.75 mol/L $NaNO_3$ as electrolyte.

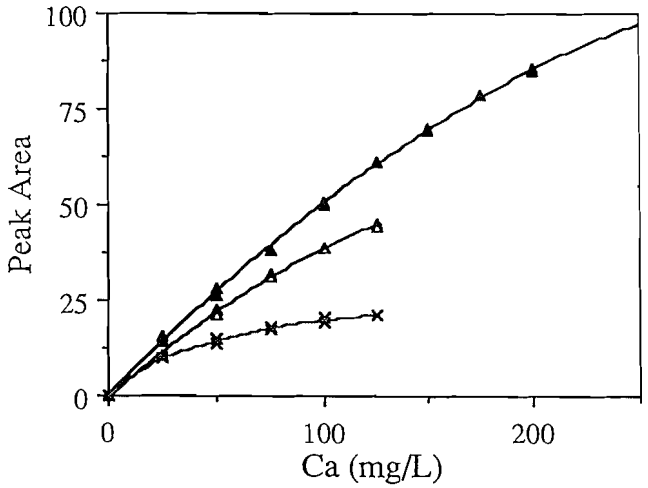


FIG. 3. Calibration curves for standard Ca^{2+} solutions. ×, at 0.1 mol/L Na^+; △, at 0.5 mol/L Na^+; ▲, 0.75 mol/L Na^+. Note: AA sensitivity was changed for different calibration curves, so peak area values are not directly comparable from plot to plot. All points were measured in duplicate.

TABLE 1. Fraction of resin in calcium form at equilibrium with 0.1 and 0.75 mol/L sodium ion in solution

Total Ca^{2+} mg/L (mM) in solution	Fraction resin in Ca form at	
	0.1 mol/L Na^+	0.75 mol/L Na^+
25 (0.625)	0.102	0.014
50 (1.25)	0.184	0.027
75 (1.88)	0.286	0.037
100 (2.50)	0.348	0.046
125 (3.13)	0.409	0.055

Effect of magnesium and pH on precision and accuracy of calcium measurements

The effect of magnesium, which often occurs at significant concentrations with calcium in biological systems (15), was evaluated by adding amounts ranging from 0 to 4.1 mM (100 mg/L) to a 1.87 mM (75 mg/L) solution of calcium and determining the free calcium levels. Although magnesium can be expected to sorb onto the resin, calcium peak areas are not significantly changed, indicating that magnesium does not interfere at these levels. This result suggests that column equilibrium between sodium and magnesium does not affect to any significant extent the equilibrium between calcium and sodium over the concentration range investigated.

The effect of pH over the range 5–7 on the calcium signal was also investigated. A solution of 1.87 mM (75 mg/L) calcium was taken as before, the pH adjusted to a value of 5, 6, or 7, and the sorbed calcium measured. The calcium signal was not affected, which suggests that the method is insensitive to pH over this range.

Selectivity of the method for free over bound calcium

The presence of complexing ligands results in the binding of metal ions and thereby lowers free metal ion concentrations in solution. Depending on ligand charge, the metal ligand complexes may be cationic, anionic, or neutral. In the ion-exchange column-equilibration method employed here, it is assumed that only free, hydrated, metal is sorbed onto the resin. However, sorption of cationic or neutral complexes might also occur (9), giving rise to falsely high free calcium values. To assess the extent to which this process occurs, the free calcium in solutions containing known concentrations of citrate and phosphate was measured by the ion exchange method. The fractions of free calcium in the solutions were also calculated from equilibrium-constant data by computer, using the program COMICS (16).

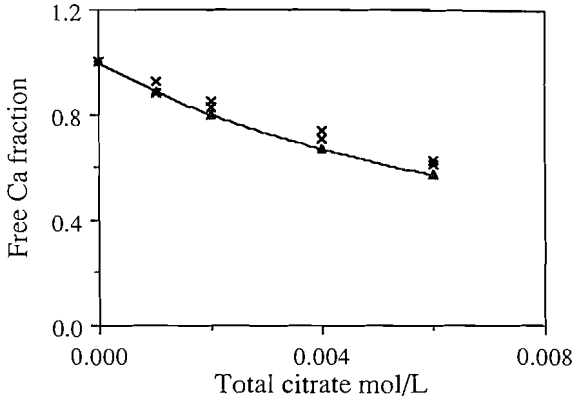


FIG. 4. Variation in fraction of free calcium with added citrate. ×, measured values; ▲, calculated values.

Results obtained for the fraction of free calcium in the presence of varying amounts of total citrate at pH 5 are shown in Fig. 4. Calculated values are based on complexes of the type $CaCit^-$, CaHCit, and CaH_2Cit^+ (Cit denotes the triply charged citrate anion). The stability constants at 0.1 ionic strength (17) were recalculated for 0.75 ionic strength using the Davies equation. Corrections were also made for the formation of $NaCit^{2-}$ (17) and $NaHCit^-$ (18) complexes. The agreement between the calculated and the measured calcium fractions is satisfactory, especially in light of uncertainties in equilibrium constants as a function of ionic strength. The results indicate that the column selectively sorbs free calcium in the presence of calcium–citrate species.

The variation of free calcium fraction in the presence of varying amounts of total phosphate at pH 5 is shown in Fig. 5. Calculated values are based on formation of the complexes $CaPO_4^-$, $CaHPO_4$, and $CaH_2PO_4^+$ (17) and ionic strength corrections were carried out as for the citrate system. Corrections were also made for the formation of $NaPO_4^{2-}$, $NaHPO_4^-$, and NaH_2PO_4 complexes (19). Here, too, agreement between the calculated and measured values is satisfactory. The small differences may be due to one or more of the following: (*1*) In the case of citrate, the possible formation of a neutral NaH_2Cit complex, which would also tie up citrate. A stability constant value for this species has not been reported. If such a complex were present, it would cause the calculated values of free calcium to be higher than shown in Fig. 4. (*2*) In the case of phosphate, stability constant values for $NaPO_4^{2-}$ and NaH_2PO_4 are reported for 37°C only (19), whereas all other stability constants used in these calculations were measured at 25°C. The stability constant for $NaHPO_4^-$, which has been measured at both temperatures, shows a slightly lower value for 25°C than for 37°C. The use of two stability constants measured at 37°C could cause calculated values of free calcium to be slightly higher than the actual ones. (*3*) The calculated values shown are for a pH of 5. Even small deviations in pH will cause a difference between calculated and observed free calcium values. (*4*) Small errors may be introduced in correction of activities to the high ionic strength used.

Can. J. Chem. Downloaded from www.nrcresearchpress.com by 123.30.183.119 on 09/08/12
For personal use only.

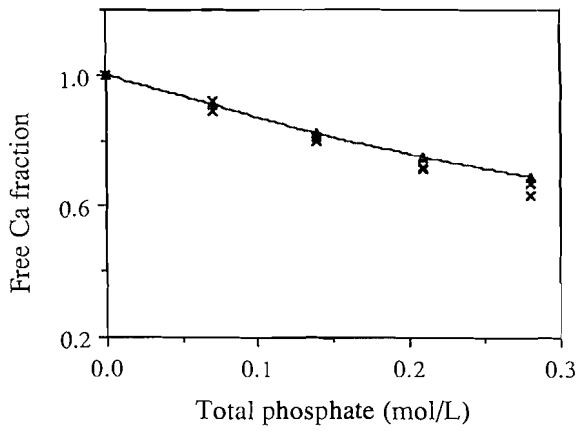


FIG. 5. Variation in fraction of free calcium with added phosphate. ×, measured values; ▲, calculated values.

TABLE 2. Results for the determination of free and total calcium in the urine of seven normal individuals; total measured by flame atomic absorption ($n = 3$), free by the ion exchange column equilibration method ($n = 2$) described in this study; uncertainties are ± one standard deviation

Free Ca^{2+}, mM	Total Ca, mM	% Free Ca
0.73±0.10	1.37±0.02	53
1.30±0.02	2.00±0.02	65
3.08±0.12	6.00±0.03	51
2.78±0.02	4.50±0.04	62
4.35±0.07	8.00±0.03	54
2.20±0.09	4.50±0.03	49
0.75±0.04	1.25±0.02	62

Despite these uncertainties, the method appears highly selective for free calcium. In the citrate system the fraction of neutral calcium-ligand species can be as high as 0.12, while in the phosphate system the fraction of neutral calcium-ligand species can be as high as 0.1 and that of the positively charged calcium-ligand species can be as high as 0.2. Thus even though, as mentioned earlier, the resin might be expected to sorb cationic and neutral calcium-ligand complexes, under the conditions studied such sorption processes appear to be negligible.

To provide a preliminary test of the method, the free urine calcium levels of seven normal individuals were determined by the procedure described. Total calcium levels were also measured by flame atomic absorption after 50-fold dilution of the urine samples. Percentages of free calcium in the range of 49–65% were found (Table 2). These levels are similar to those previously estimated for percent free calcium in urine (6).

In summary, this work describes a procedure for the estimation of free calcium at the millimolar level in the presence of ligands such as citrate and phosphate. The method can be used over the pH range normally seen in biological systems, and is unaffected by concentrations of magnesium twice that of calcium. It therefore shows promise for the estimation of ionized calcium in biological systems in the presence of a variety of ligands and interfering metal ions.

Acknowledgements

Financial support provided by the Natural Sciences and Engineering Research Council of Canada and by the University of Alberta is gratefully acknowledged.

1. B. E. C. NORDIN (*Editor*). Calcium, phosphate and magnesium metabolism: Clinical physiology and diagnostic procedures, Churchill Livingston, Edinburgh. 1976.
2. H. FLEISH, W. G. ROBERTSON, L. H. SMITH and W. VAHLENSIECK (*Editors*). Urolithiasis research. Plenum Press, New York. 1976.
3. M. RUBIN and A. E. MARTELL. Metal ions in biological systems. Vol. 16. *Edited by* H. Sigel. Marcel Dekker, New York. 1983. Chap 4.
4. S. F. SENA and G. N. BOWERS. Methods Enzymol. **158**, 320 (1988).
5. J. THODE, S. N. HOLMEGAARD, I. TRANSBOL, N. F. ANDERSON, and O. S. ANDERSON. Clin. Chem. **36**, 541 (1990).
6. A. L. JACOBSON, P. C. SINGHAL, H. MANDIN, and J. B. HYNE. Biochem. Med. **22**, 383 (1979).
7. B. E. CHAM. Clin. Chim. Acta, **37**, 5 (1972).
8. W. G. ROBERTSON. Ann. Clin. Biochem. **13**, 540 (1976).
9. J. A. SWEILEH, D. LUCYK, B. KRATOCHVIL, and F. F. CANTWELL. Anal. Chem. **59**, 586 (1987).
10. F. F. CANTWELL, J. S. NIELSON, and S. E. HRUDEY. Anal. Chem. **54**, 1498 (1982).
11. I. TABANI and B. KRATOCHVIL. Anal. Instrum. **14**, 169 (1985).
12. J. TREIT, J. S. NIELSON, B. KRATOCHVIL, and F. F. CANTWELL. Anal. Chem. **55**, 1650 (1983).
13. F. HELFFERICH. Ion exchange. McGraw-Hill, New York. 1962. p. 230.
14. F. HELFFERICH. Ion exchange. McGraw-Hill, New York. 1962. p. 169.
15. R. D. ESTHAM. Biochemical values in clinical medicine. 6th ed. John Wright and Sons Ltd., Bristol. 1978.
16. D. D. PERRIN and I. G. SAYCE. Talanta, **14**, 833 (1967).
17. A. E. MARTELL and R. M. SMITH. Critical stability constants. Vol. 3. Other organic ligands. Plenum Press, New York. 1977.
18. V. CUCINOTTA, P. G. DANIELE, C. RIGANO, and S. SAMMARTANO. Inorg. Chim. Acta, **56**, L45 (1981).
19. P. G. DANIELE, M. GRASSO, C. RIGANO, and S. SAMMARTANO. Ann. Chim. (Rome), **73**, 495 (1983).

Can. J. Chem. Downloaded from www.nrcresearchpress.com by 123.30.183.119 on 09/08/12
For personal use only.

A comparison of acetone and poly(propylene glycol) as solvents for lithium triflate and lithium perchlorate

JAMES R. STEVENS[1] AND PER JACOBSSON
Department of Physics, Chalmers University of Technology, S-412 96 Gothenburg, Sweden

Received March 18, 1991

JAMES R. STEVENS and PER JACOBSSON. Can. J. Chem. **69**, 1980 (1991).

Solutions of $LiCF_3SO_3$ and $LiClO_4$ in acetone and in poly(propylene glycol) (PPG 400 and PPG 4000) have been compared by studying the nondegenerate, symmetric stretch (A_1,SO_3) and (A_1,ClO_4) Raman modes. The Raman spectra contain bands due to the symmetric stretching motion of the "free" anion and due to the symmetric stretching motion of anions in ion aggregates. It is concluded that "free" ions, ion pairs, triplets, and aggregates are present. Although PPG has a much lower dielectric constant, it is a better solvent for these salts than the dipolar aprotic acetone. These findings have ramifications on the current controversy of whether "free" ions are present at all in polyether–salt complexes such as PPG 4000/$LiCF_3SO_3$.

Key words: acetone, poly(propylene glycol), lithium triflate, lithium perchlorate, Raman.

JAMES R. STEVENS et PER JACOBSSON. Can. J. Chem. **69**, 1980 (1991).

On a comparé des solutions de $LiCF_3SO_3$ et de $LiCl_4$ dans l'acétone et dans le poly(propylène glycol) (PPG 400 et PPG 4000) en étudiant les modes d'élongation symétrique non-dégénérés (A_1,SO_3) et (A_1,ClO_4) observés en spectroscopie Raman. Les spectres Raman contiennent des bandes qui sont dues au mouvement d'elongation symétrique de l'anion "libre"et d'autres qui sont dues au mouvement d'élongation symétrique des anions dans les agrégats d'ion. On en conclut que des ions "libres", des paires d'ions, des triplets et des agrégats sont présents. Pour ces sels, on observé que, même si la constante diélectrique du PPG est beaucoup plus faible, c'est un meilleur solvant que l'acétone aprotique et dipolaire. Ces observations ont des implications sur la question actuellement controversée concernant la présence des ions "libres" dans tous les complexes polyéther/sel, comme PPG 4000/$LiCF_3SO_3$.

Mots clés : acétone, poly(propylène glycol), triflate de lithium, perchlorate de lithium, Raman.

[Traduit par la rédaction]

Introduction

There has been an extensive study of the ion solvation and association of alkali and alkali earth metal perchlorates in a range of dipolar aprotic solvents using infrared and Raman spectroscopy. This was prompted, in large part, by the wide current interest in using these salts as dopants in polyethers and similar polymers to produce solid polymeric electrolytes for such applications as electrochromic devices, batteries, and fuel cells.

The most extensive studies have been carried out by Perelygin *et al.* (1–10). Raman studies are reported for perchlorates in acetone, acetonitrile, pyridine, and dimethylsulphoxide (1). Infrared studies are reported for perchlorates in propylene carbonate (2), ethyl acetate (3), tetrahydrofuran (4), dimethylformamide (5), dimethyl sulphoxide (6), acetone (7, 8), and acetonitrile (9, 10).

Generally the picture that emerges from the work of Perelygin and associates is that in an ion association equilibrium, we find such species as "free" ions, contact ion pairs (monodentate and bidentate), charged and neutral triplets, quadrupoles, and higher aggregates. In solvents with electron donicity (Gutmann's DN_{SbCl_5}, kcal mol^{-1}) values > 25 and relative permittivity (ϵ_r) values > 37 (e.g., dimethylformamide (5) and dimethyl sulphoxide (6)), the perchlorate salts are completely dissociated. (See Reichardt (11) for values of ϵ_r, DN, and dipole moments (μ)). For a series of solvents which have values of DN in the 15–35 range but values of ϵ_r in the range 8–37 (acetonitrile, acetone, pyridine, and tetrahydrofuran) "free" ions are found in equilibrium with associated species for the perchlorates (1, 4, 7–10). Ion association decreases in going from acetonitrile (ϵ_r = 35.9, DN = 14.1) to propylene carbonate (2) (ϵ_r = 64.9, DN = 15.1). In ethyl acetate (3) (ϵ_r = 6.0, DN = 17.1, $\mu = 6.1 \times 10^{-30}$ C m), the ions of these salts are completely associated even in dilute solutions with the largest assortment of different forms of associated ionic species being observed (3). In dilute solutions of $LiClO_4$ and $NaClO_4$ in ethyl acetate contact ion pairs are reported to be the most common species (3).

Wong *et al.* (12) carried out infrared, Raman, and NMR studies on solutions of various lithium and sodium salts in acetone. Cation–acetone vibrational bands were identified but were found to be independent of the anion for alkali metal salts with polyatomic anions. In disagreement with Perelygin *et al.* (1–10), Wong *et al.* (12) found that the symmetric stretch $\nu_1(A_1,ClO_4)$ band centred at 935 cm^{-1} remains unchanged when the acetone/$LiClO_4$ mole ratio is ≥4 but that below this ratio the band progressively broadens, shifting to higher frequency with increase in concentration.

By studying the splitting of the isotropic and anisotropic components of the Raman CO stretching vibration in acetone/perchlorate systems, Bukowska (13) identified both cation solvation and cation–acetone transient cross-links. Lalic *et al.* (14) studied the Raman spectra of solutions of $LiClO_4$ and $Sr(ClO_4)_2$ in acetone and acetonitrile with, in some cases, varying amounts of NaSCN. They observed a band at a lower frequency (911.5 cm^{-1}) than the ClO_4^- symmetric stretch and interpreted it as a $2\nu_2(A_1+E)$ overtone in Fermi resonance with $\nu_1(A_1)$. Lalic *et al.* (14) observed split bands related to the $\nu_1(A_1,ClO_4)$ symmetric stretch at 933, 939, and 948 cm^{-1} and citing the earlier Raman studies of Frost *et al.* (15) and Mayes *et al.* (16) of perchlorates in aqueous solutions (15) and in acetone (16) assigned these to, respectively, "free" anions, solvent separated ion-pairs, and contact ion pairs. Neither of these authors (13, 14) was, apparently, aware of the work of Perelygin and co-workers (1–10).

The solvation of $LiCF_3SO_3$ and $LiClO_4$ in polyethers is important in the synthesis of solid electrolytes. However, there

[1]Permanent address, Department of Physics, University of Guelph, Guelph, Ont., Canada N1G 2W1.

Printed in Canada / Imprimé au Canada

Can. J. Chem. Downloaded from www.nrcresearchpress.com by 123.30.183.119 on 09/07/12
For personal use only.

Can. J. Chem. Downloaded from www.nrcresearchpress.com by 123.30.183.119 on 09/07/12
For personal use only.

is a current controversy as to the nature of the charge carrying ion species in these systems. Gray (17) and MacCallum *et al.* (18) argue, based on the Fuoss triple ion interpretation (19), that charged triple ions are the mobile species which contribute to the ionic current for concentrations above 0.01 M. It should be noted that two adjustable parameters, the pair and triple ion formation constants, are used in fitting the "triple-ion" theory (19) to conductivity data. Cameron *et al.* (20) and Schanz (21) support the concept of the redissociation of ion pairs formed at low concentrations and argue that "free" ions are responsible for charge transport. The general contention of those in favour of the triple ion interpretation is that polyethers like poly(propylene oxide) have such a low dielectric constant that similar to ethyl acetate (3) and methyl acetate (22) ($\epsilon_r = 6.7$, DN = 16.5, $\mu = 7.9 \times 10^{-30}$ C m), for example, no free ions should be present for salt concentrations of the order of 1 M (also see ref. 18). They concur with Petrucci and co-workers (22) that salts like $LiClO_4$ and $LiAsF_6$ in low dielectric constant solvents can only be "spectroscopically free", by which they mean solvent separated (or loose) ion pairs.

This paper examines this contention by comparing the solubility of $LiClO_4$ and $LiCF_3SO_3$ in acetone and in PPG ($\epsilon_r = 4.7$ (23), $\mu = 28.0 \times 10^{-30}$ C m (24) for PPG 4000) as inferred from a study of the nondegenerate symmetric stretch (A_1,ClO_4) and (A_1,SO_3) modes in Raman spectra.

Acetone was selected since it is a dipolar, aprotic, electron-pair, oxygen donor solvent ($\epsilon_r = 20.6$, DN = 17.0, $\mu = 9.0 \times 10^{-30}$C m). According to Reichardt (11), both free and associated ions should exist in equilibrium for salts dissolved in acetone; the ratio between free and associated ions depends upon, *inter alia*, the solvent, ion sizes, charge distribution, and specific ion solvation. Persson *et al.* (25) have proposed a donor strength scale for hard acceptors (Li^+, Na^+) based on the Gibbs free energy of transfer of the sodium ion from a solvent to the same reference solvent as is used in the Gutmann DN scale. This scale indicates that hard oxygen donor solvents like acetone solvate hard acceptors particularly well (25). Although the electrostatic factor ($\mu \cdot \epsilon_r$) places acetone in the highest solvent classification, i.e., dipolar, non-hydrogen bond donor solvents (11), it is dangerous to rely totally on these macroscopic parameters since they are really unsuitable measures of microscopic molecular interactions. The state conditions which apply in these electrolytes are very complex. Potentials of higher order than ion–dipole or dipole–dipole are important (26).

Experimental

The preparation of poly(propylene glycol) (PPG) (Polyscience Inc.) included filtering through a 1 μm Millipore filter, heating in a vacuum oven for about 3 days at 120°C, and drying under a vacuum at pressures $<10^{-4}$ Torr using a freeze–thaw method. Anhydrous $LiCF_3SO_3$ and $LiClO_4$ (Ventron Division, Alpha) were vacuum dried at 125°C for 24 h and then at room temperature for 24 h. The salts were dissolved directly into the dried polyethers in a dry argon atmosphere using temperatures between 65 and 80°C. The prepared samples were stored under vacuum and measurements were made in a helium atmosphere. The PPG–$LiCF_3SO_3$ and PPG–$LiClO_4$ complexes were made for ether oxygen to lithium (O:Li) = 16:1 and molecular weights of 4000 and 400. The value of the ionic conductivity peaks for concentrations between O:Li = 16:1 and 30:1 (23). Karl Fischer titration (Metrohm 684) showed the water content to be of the order of 0.1% by weight.

We have measured the donicity of PPG 4000 using the ^1H NMR chloroform chemical shift technique of Hahn *et al.* (27). The observed shift of 0.1 M chloroform in PPG 4000 relative to tetramethylsilane (TMS) in *d*-chloroform was 8.00 ppm. The shift of pure chloroform relative to TMS in *d*-chloroform was 7.27 ppm. The observed shift of chloroform in PPG 4000 was corrected for the difference in the volume magnetic susceptibilities (K) of chloroform ($K = -0.740 \times 10^{-6}$ cgs (28)) and PPG 4000 ($K = -0.706 \times 10^{-6}$ cgs) giving a value of DN = 21. The K for PPG 4000 was estimated using Pascal's magnetochemical method (29).

Solutions of acetone/$LiCF_3SO_3$ (16:1) and acetone /$LiClO_4$ (16:1 and 1000:1) were prepared under a dry argon atmosphere by mixing pure anhydrous salt (dried as above) with dried reagent grade acetone. Since the acetone is completely miscible with water, great care was taken to dry the acetone using a freeze drying procedure under vacuum until there was no evidence of the infrared absorption bands of the valence vibrations of water molecules (3000–3600 cm^{-1}). Karl Fischer titration showed the water content to be less than 0.1% by weight.

The experimental setup includes an argon-ion laser operating at 488 nm, a Spex double monochromator (model 1403) with 1800 lines/mm holographic gratings, and a liquid nitrogen cooled charge coupled device (CCD) low signal to noise detector which gives a "readout" resolution of about 0.2 cm^{-1} with rapid recordings. The overall instrumental resolution, mainly restricted by the slitwidths, was set to give a value of 0.9 cm^{-1}. At all temperatures (250 K, 300 K, 350 K), a continuous flow cryostat (Oxford CF1204) with a temperature stability better than 0.1 K was used. The Raman spectrum of the pure dry acetone or pure dry PPG was subtracted from the spectra of the solutions. The remaining Raman profiles were then deconvoluted from the instrumental function using Jansson's method (30). The combination of better instrumental resolution, better samples, and much improved signal to noise ratios results in a standard error for the deconvoluted spectra which is an order of magnitude better than previous reports (15, 16).

Results and discussion

We begin with a brief report on the ν(A_1,ClO_4) symmetric stretch region of the ClO_4^- anion in acetone in order to relate to the previous work mentioned in the Introduction. The usual T_d symmetry of the ClO_4^- anion is reduced to C_{3v} and C_{2v} in association with cations and the symmetric stretch bands are observed for "free" anions and anions in ion aggregates, distinct band components indicating different ClO_4^- environments. Figures 1(*a*) and 1(*b*) show, respectively, the raw data and the deconvoluted spectra with fitted components at 300 K for those bands for acetone/$LiClO_4$ mole ratios of 1000 and 16. In agreement with Perelygin and Mikhailov (1), the feature at 911 cm^{-1} is attributed to an overtone of the deformational vibration $\nu_2(E)$ of the perchlorate ion; it is independent of concentration and is symmetric over a range of temperatures from 250 to 450 K. The feature at 938 cm^{-1} is attributed to contact ion pairs, $Li^+ClO_4^-$, monodentately coordinated; the frequency of this component is reported to shift on changing cations (1). We disagree with Frost *et al.* (15) and James *et al.* (16) who assigned this vibration to loose ion pairs for 1 M $LiClO_4$ (≈O:M = 16:1). The separation of the loose ion pair peak from the "free" ion peak at 932 cm^{-1} would not be as great as 6 cm^{-1}. As the temperature is increased, the relative intensity of the 938 cm^{-1} component for the 16:1 sample increases from 0.2 at 250 K to 0.3 at 350 K and the intensity of the 932 cm^{-1} component decreases. For an acetone/$LiClO_4$ mole ratio of 1000, we still find these 932 cm^{-1} and 938 cm^{-1} components present, the relative intensity of the contact ion pair component changing from 0.04 at 250 K to 0.1 at 350 K.

The feature at 932 cm^{-1} is independent of the cation (1) and is attributed to the "free" ClO_4^- anion. This assignment is justified in the following. James *et al.* (16) find the lowest (A_1ClO_4) band frequency to be 934 cm^{-1} for $LiClO_4$ in acetone. This group obtained the same frequency for $LiClO_4$ and $NaClO_4$ in aqueous solutions (>1 M) (15). These features are reported as narrow

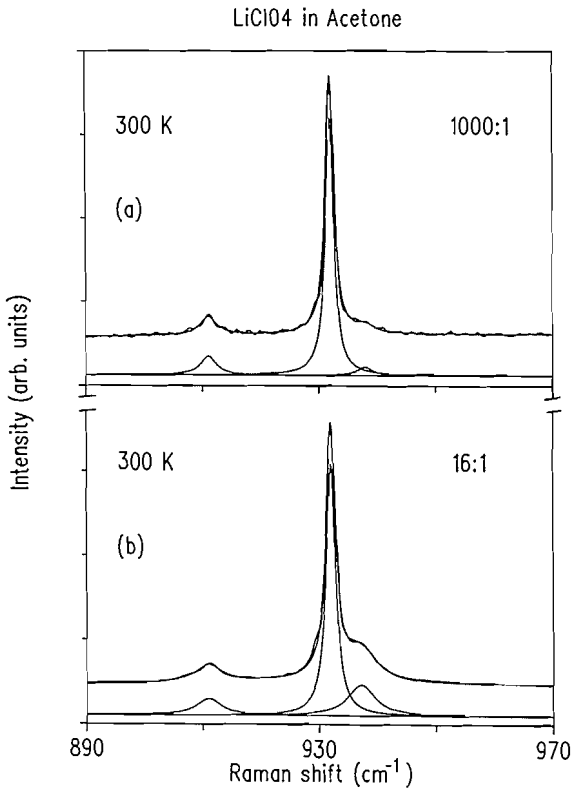


FIG. 1. (*a*) Acetone/$LiClO_4$ mole ratio 1000 at 300 K: raw Raman (A_1,ClO_4) spectrum above and deconvoluted, fitted Raman (A_1,ClO_4) spectra below. (*b*) Acetone/$LiClO_4$ mole ratio 16 at 300 K: raw spectrum above and deconvoluted, fitted Raman (A_1,ClO_4) spectra below.

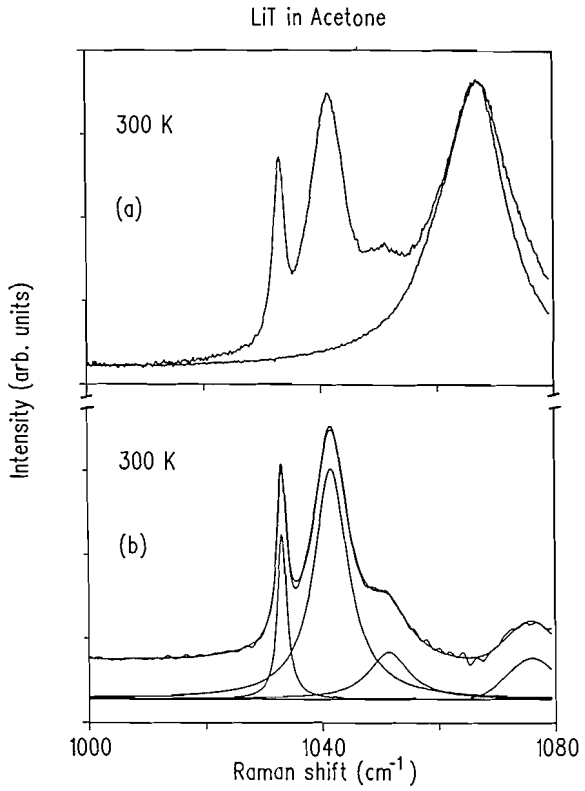


FIG. 2. (*a*) Acetone/$LiCF_3SO_3$ (LiT) mole ratio 16 at 300 K: raw Raman (A_1,SO_3) spectrum showing the acetone background. (*b*) Acetone/$LiCF_3SO_3$ mole ratio 16 at 300 K: background subtracted, deconvoluted, fitted Raman (A_1SO_3) spectrum.

Lorentzians (15). In a high permittivity solvent such as water, one should expect that a very high percentage of the salt is completely dissociated. We have observed this feature at 932 cm^{-1} with full width at half maximum (FWHM) = 1 cm^{-1}. In comparison with the Cary 82 used by Frost *et al.* (15) and James *et al.* (16), the signal-to-noise ratio of the CCD is much better and the resolution is also improved. Further, Perelygin *et al.* (1) have studied the $\nu_1(A_1,ClO_4)$ Raman spectra for the $(C_4H_9)_4NClO_4$ salt in acetone. They conclude that because the voluminous cation $(C_4H_9)_4N^+$ does not distort the symmetry of the anion even with incomplete dissociation, the 932 cm^{-1} feature must be attributed to vibrations of the free perchlorate ion of symmetry T_d (1). Finally, the hard oxygen donor acetone is an excellent solvent for a hard acceptor like Li^+ (25).

Figure 2(*a*) shows the raw data for the symmetric stretch Raman bands for an acetone/$LiCF_3SO_3$ mole ratio of 16 at 300 K. Figure 2(*b*) is the same band group with the background subtracted and the instrumental function deconvoluted. The fitted components are shown. The low frequency component is best fit with a Lorentzian at 1033 cm^{-1} with FWHM = 1 cm^{-1}. Schantz (21) studied a dilute (0.1 M) aqueous solution of $NaCF_3SO_3$ in which the $\nu_1(A_1SO_3)$ mode was detected as a one component band at 1033 cm^{-1} with FWHM = 5 cm^{-1} (Lorentzian). With a dilute salt concentration in such a high permittivity solvent almost all the ions should be "free". The component is not influenced by the change in cation from Na^+ to Li^+ and is assigned to "free" anions. The next band component (Gaussian) at 1042 cm^{-1} is shifted to higher frequencies by 9 cm^{-1} compared to the 5 cm^{-1} shift for the corresponding component for $NaCF_3SO_3$ in acetonitrile (31), a similar dipolar aprotic solvent. The fact that this component is sensitive to the cation suggests that it arises, at least in part, from contact ion pairs as was discussed by Perelygin and Mikhailov (1). The next highest frequency component (Lorentzian, Fig. 2(*b*)) at 1051 cm^{-1} is suggested to be due to $Li^+CF_3SO_3^-Li^+$ triplets. With Perelygin and Mikhailov (1), we infer from this the presence of the other triplet species $CF_3SO_3^-Li^+CF_3SO_3^-$ with an SO_3^- symmetric stretch vibration approximately the same as for contact ion pairs (1042 cm^{-1}). Finally, a broad (Gaussian) component is observed at 1076 cm^{-1} which we attribute to aggregates of ions. To confirm this we performed a Raman backscattering measurement on a compressed pellet of dried $LiCF_3SO_3$ and observed a narrower band centered at the same frequency. Although the amount of water contained in these complexes is extremely low, what is there may influence these ion associations.

Figure 3(*a*) shows the variation in the relative intensities of three of the four components in the $\nu_1(A_1,SO_3)$ region as a function of temperature for an acetone/$LiCF_3SO_3$ mole ratio of 16. Most of the ions are associated; only ~12% are "free". The concentration of "free" ions and aggregates decreases with increasing temperature. The proposed contact ion pair-triplet component at 1042 cm^{-1} is ~60% and increases very slightly with temperature. The overall triplet concentration is higher than the "free" ion concentration and increases with increasing temperature. Figure 3(*b*) shows that the frequencies on which these components are centered do not shift with changes in temperature.

Figure 4(*a*) shows the raw data and fitted components for the $\nu_1(A_1,SO_3)$ mode at 350 K for PPG 400/$LiCF_3SO_3$ (O:Li = 16:1). As for acetone/$LiCF_3SO_3$, the Lorentzian peak at

Can. J. Chem. Downloaded from www.nrcresearchpress.com by 123.30.183.119 on 09/07/12
For personal use only.

TABLE 1. The relative intensities of "free" ions and associated ions for $LiClO_4$ and $LiCF_3SO_3$ in PPG

PPG	Salt O:Li = 16:1	T (K)	Fraction "Free" ions	Contact pairs triplets	Triplets
400	$LiCF_3SO_3$	250	0.75	0.12	0.13
		350	0.75	0.20	0.05
	$LiClO_4$	250	~1.00		No triplets
		350	0.98	0.02	No triplets
4000	$LiCF_3SO_3$	250	0.41	0.44	0.15
		350	0.28	0.53	0.19
	$LiClO_4$	250	0.94	0.06	No triplets
		350	0.80	0.20	No triplets

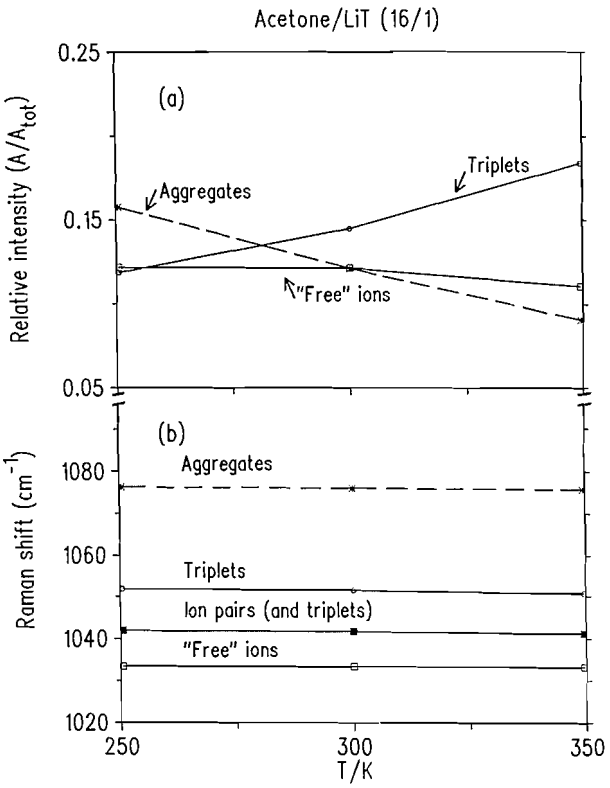


FIG. 3. (*a*) Acetone/$LiCF_3SO_3$ (LiT): relative intensities of the band profile of the Raman (A_1SO_3) spectrum as a function of temperature for "free" ions, triplets ($Li^+CF_3SO_3^-Li^+$) and aggregates. (*b*) Acetone/$LiCF_3SO_3$: peak frequencies of the band profile of the Raman (A_1, SO_3) spectrum as a function of temperature.

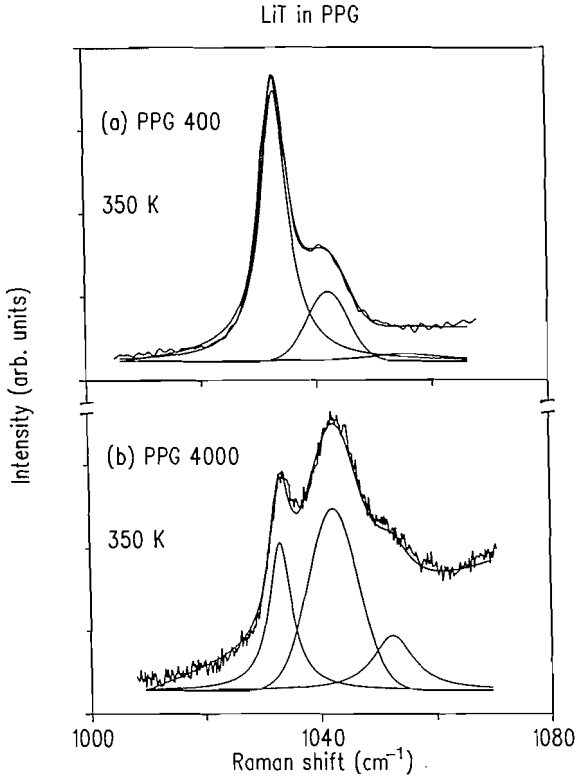


FIG. 4. (*a*) PPG 400/$LiCF_3SO_3$ (LiT) (O:Li = 6:1): Raman (A_1,SO_3) profile at 350 K; raw data above and background subtracted, deconvoluted below showing fitted components. (*b*) PPG 4000/$LiCF_3SO_3$ (O:Li = 16:1): Raman (A_1SO_3) profile at 350 K; raw data above and background subtracted, deconvoluted below showing fitted components.

1033 cm^{-1} (FWHM = 3 cm^{-1}) is suggested to be due to "free" ions. The Gaussian peak at 1042 cm^{-1} is assigned to contact ion pairs and $CF_3SO_3^-Li^+CF_3SO_3^-$ triplets and the very weak Lorentzian peak at 1055 ± 5 cm^{-1} is suggested to be due to $Li^+CF_3SO_3^-Li^+$ triplets. Figure 4(*b*) shows the $\nu_1(A_1,SO_3)$ profile at 350 K for PPG 4000/$LiCF_3SO_3$ (O:Li = 16:1). In Fig. 4(*b*) the lowest (Lorentzian, "free" ion) component peaks at 1032 cm^{-1} (FWHM = 2 cm^{-1}), the second (Gaussian) component at 1041 cm^{-1}, and the highest frequency (Lorentzian, triplet) component at 1052 cm^{-1}. As in Fig. 3(*b*), there is no change in these frequencies with temperature. Table 1 lists the relative intensities at 250 and 350 K for $LiCF_3SO_3$ and $LiClO_4$ in PPG 400 and PPG 4000 (O:Li = 16:1). The "free" ion component in $\nu_1(A_1,ClO_4)$ for the PPG/$LiClO_4$ complex peaks at 931 cm^{-1}.

From the experimental evidence (i.e., more "free" ions in PPG than in acetone for the same salt concentration), it is concluded that PPG is a better solvent for these salts than acetone, which is a very good solvent. This means that PPG should not be included in the class of apolar aprotic solvents like methyl acetate (22) and ethyl acetate (3) although they have about the same ϵ_r values as PPG (but much lower DN and μ values). (See Reichardt's Fig. 3.3 for defiinitions (11)). An explanation for this result is difficult; comments using values of ϵ_r, DN, and μ can be made but as pointed out above, probably gloss over the complex explanation. ϵ_r increases with

Can. J. Chem. Downloaded from www.nrcresearchpress.com by 123.30.183.119 on 09/07/12
For personal use only.

salt concentration in these PPG–salt complexes (23) as it does for most organic solvent/salt systems (≤0.3 M) (22). For PPG, DN is higher and μ is quite a bit higher. The orientation of dipolar aprotic solvent molecules around ions in the absence of specific ion–solvent interactions is determined largely by dipole moment (11). Here we also have the specific donor–acceptor relationship between the solvent and the cation. Since PPG is such a good solvent for these salts, since our spectral resolution is very good, and since there is good agreement between the frequencies of the low frequency peaks in the (A_1,ClO_4), and (A_1SO_3) Raman modes in water/salt solutions and solvent/salt solutions, we believe that these low frequency peaks are due to essentially free anions and not to solvent separated (or loose) ion pairs.

Conclusions

We conclude that "free" ions are present in PPG/$LiClO_4$ and PPG/$LiCF_3SO_3$ complexes and that PPG is a better solvent for these salts than acetone. Triple ions were not detected in PPG/$LiClO_4$ complexes but are suggested to be present in PPG/$LiCF_3SO_3$ and acetone/$LiCF_3SO_3$ systems. For PPG/$LiCF_3SO_3$ complexes, the fraction of "free" ions at room temperature is much greater than the fraction of triplets.

Acknowledgements

The authors wish to express their appreciation to Professor Lena Torell for her hospitality and the use of her excellent laboratory facilities. Appreciation is also expressed to M. Tchir for assistance in the DN measurement of PPG 4000 and to S. Schantz for consulations, and with M. Johansson and P. Pedersén for assistance in obtaining the PPG–$LiClO_4$ data in Table 1. P.J. wishes to acknowledge financial support from the Swedish National Research Council and J.R.S. wishes to acknowledge financial support from the Swedish Board for Technical Development for a visiting professorship.

1. I. S. Perelygin and G. P. Mikhailov. Zh. Prikl. Spektrosk. **49**, 65 (1988).
2. I. S. Perelygin, M. A. Klimchuck, and E. L. Smol'skava. Russ. J. Phys. Chem. **61**, 51 (1987).
3. I. S. Perelygin, M. A. Klimchuck, and A. A. Valeva. Russ. J. Phys. Chem. **58**, 1347 (1984).
4. I. S. Perelygin and S. Ya. Yanudanov. Russ. J. Phys. Chem. **52**, 741 (1978).
5. I. S. Perelgin and V. S. Osipov. Russ. J. Phys. Chem. **53**, 1036 (1979).
6. I. S. Perelygin and S. Ya. Yamudanov. Russ. J. Phys. Chem. **53**, 1354 (1979).
7. I. S. Perelygin and M. A. Klimchuck. Russ. J. Phys. Chem. **49**, 76 (1975).
8. I. S. Perelygin and M. A. Klimchuck. Russ. J. Phys. Chem. **48**, 1466 (1974).
9. I. S. Perelygin and M. A. Klimchuck. Russ. J. Phys. Chem. **47**, 1138 (1973).
10. I. S. Perelygin and M. A. Klimchuck. Russ. J. Phys. Chem. **47**, 1402 (1973).
11. C. Reichardt. *In* Solvents and solvent effects in organic chemistry. 2nd ed. VCH Verlagsgesellschaft mbH, Weinheim, Germany. 1988. pp.42–69.
12. M. K. Wong, W. J. McKinney, and I. Popov. J. Phys. Chem. **75**, 56 (1971).
13. J. Bukowska. J. Mol. Struct. **143**, 309 (1986).
14. M. Lalic, M. Terrmil, A. Antic-Tovanovic, and V. Bojovic. J. Mol. Liq. **39**, 105 (1988).
15. R. L. Frost, D. W. James, R. Appleby, and R. E. Mayes. J. Phys. Chem. **86**, 3840 (1982).
16. D. W. James and R. E. Mayes. Aust. J. Chem. **35**, 1775 (1982); **35**, 1785 (1982).
17. F. M. Gray. Solid State Ionics, **40/41**, 637 (1990).
18. J. R. MacCallum, A. S. Tomlin, and C. A. Vincent. Eur. Polym. J. **22**, 787 (1986).
19. R. M. Fuoss and C. A. Kraus. J. Am. Chem. Soc. **55**, 2387 (1933).
20. G. G. Cameron, J. L. Harvie, M. D. Ingram, and G. A. Sorrie. Br. Polym. J. **20**, 199 (1988).
21. S. Schantz. J. Chem. Phys. **94**, 6296 (1991).
22. M. Salomon, M. Uchijama, M. Xu, and S. Petrucci. J. Phys. Chem. **93**, 4374 (1989).
23. Y. Fu, K. Pathmanathan and J. R. Stevens. J. Chem. Phys. **94**, 6323 (1991).
24. R. J. W. LeFevre and K. M. S. Sundaram. J. Chem. Soc. Perkin. Trans. II, **2**, 2323 (1972).
25. I. Persson, M. Sandström, and P. L. Goggin. Inorg. Chim. Acta, **129**, 183 (1987).
26. C. G. Gray and K. E. Gubbins. *In* Theory of molecular fluids. Vol. 1. Clarendon Press, Oxford. 1984. p. 304.
27. S. Hahn, W. M. Miller, R. N. Lichtenthaler, and J. M. Prausnitz. J. Sol. Chem. **14**, 129 (1985).
28. R. C. Weast (*Editor*). CRC handbook of chemistry and physics. CRC Press Inc., Boca Raton, FL. 1987. pp. 1–125.
29. I. G. Dorman. *In* Diamagnetism and the chemical bond. Elsevier, New York. 1965. p. 22.
30. P. A. Jansson. *In* Deconvolution with applications in spectroscopy. Academic Press, New York. 1984. pp. 102–111.
31. S. Schantz, J. Sandhal, L.Börjesson, L. M. Torell, and J. R. Stevens. Solid State Ionics, **28–30**, 1047 (1988).

Can. J. Chem. Downloaded from www.nrcresearchpress.com by 123.30.183.119 on 09/07/12
For personal use only.

Solvation of the proton and the trifluoromethanesulfonate ion in eight solvents

ROBERT L. BENOIT AND DANIEL FIGEYS

Département de chimie, Université de Montréal, C.P. 6128, Succ "A", Montréal (Qué.), Canada H3C 3J7

Received February 25, 1991

ROBERT L. BENOIT and DANIEL FIGEYS. Can. J. Chem. **69**, 1985 (1991).

The enthalpies of solution of a sterically hindered aromatic diamine, 1,8-bis(dimethylamino)naphthalene (proton sponge, PS) and of its trifluoromethanesulfonate salt, and of trifluoromethanesulfonic acid have been determined in water, methanol (MeOH), ethanol (EtOH), pyridine (Py), dimethyl sulfoxide (Me_2SO), dimethylformamide (DMF), acetonitrile (MeCN), and sulfolane (Sul). Single ion enthalpies of transfer for $CF_3SO_3^-$ and H^+, from Me_2SO to the other solvents, have been calculated using two extrathermodynamic assumptions, namely the tetraphenylarsonium–tetraphenylborate one and the recently proposed assumption based on the equality of transfers of uncharged PS and its conjugated cation PSH^+. While both sets of transfer enthalpies using each assumption, for $CF_3SO_3^-$ and H^+, differ by some 12 kJ mol^{-1} for water and MeOH, the values are in satisfactory agreement for Py, DMF, Me_2SO, and Sul. These results support the validity of both extrathermodynamic assumptions for the nonprotogenic solvents, thus putting on firm ground the solvent basicity scale based on the enthalpy of transfer of H^+ (in kJ mol^{-1}): Py(−63) > DMF(−32) > Me_2SO(−27) > EtOH(−1) ~ H_2O(0) ~ MeOH(+2) > PC(+44) > MeCN(+55) > Sul(+68). These values correlate well with the enthalpies of complex formation with boron trifluoride.

Key words: solvation, proton, trifluoromethanesulfonate ion, proton sponge, extrathermodynamic assumption.

ROBERT L. BENOIT et DANIEL FIGEYS. Can. J. Chem. **69**, 1985 (1991).

On a déterminé les enthalpies de solution d'une diamine aromatique encombrée stériquement, la 1,8-bis(dimethylamino)-naphtalène (PS) et de son trifluorométhanesulfonate, et de l'acide trifluorométhanesulfonique dans l'eau, le méthanol (MeOH), l'éthanol (EtOH), la pyridine (Py), le diméthylformamide (DMF), le diméthylsulfoxyde (Me_2SO), l'acétonitrile (MeCN) et le sulfolane (Sul). On a calculé les enthalpies de transfert des ions $CF_3SO_3^-$ et H^+, du Me_2SO aux autres solvants, en utilisant deux hypothèses extrathermodynamiques, l'hypothèse tétraphénylarsonium–tétraphenylborate et l'hypothèse proposée récemment et basée sur l'égalité des transferts de la base neutre PS et de son cation conjugué PSH^+. Si les deux séries d'enthalpies de transfert utilisant chaque hypothèse pour $CF_3SO_3^-$ et H^+, différent d'environ 12 kJ mol^{-1} avec H_2O et MeOH, l'accord des valeurs est satisfaisant avec Py, DMF, Me_2SO and Sul. Ces résultats confirment la validité des deux hypothèses extrathermodynamiques pour les solvants non-protogéniques et permettent d'établir une échelle de basicité de solvants basée sur l'enthalpie de transfert de H^+ (en kJ mol^{-1}) : Py(−63) > DMF(−32) > Me_2SO(−27) > EtOH(−1) ~ H_2O(0) ~ MeOH(+2) > PC(+44) > MeCN(+55) > Sul(+68). Ces valeurs donnent une bonne corrélation avec les enthalpies de formation des complexes avec le trifluorure de bore.

Mots clés : solvatation, proton, trifluorométhanesulfonate, proton sponge, hypothèse extrathermodynamique.

Can. J. Chem. Downloaded from www.nrcresearchpress.com by 123.30.183.119 on 09/08/12
For personal use only.

Introduction

Single ion thermodynamics is a subject of considerable interest in its relation to the study of solvent effects on physicochemical properties and reactivity parameters. Efforts are currently being made to rationalize thermodynamic transfer functions of single ions (for example, the enthalpy of transfer) from a reference solvent to another solvent, in terms of properties of the ions and solvents (1). However, single ion transfer values can only be obtained with the help of a so-called extrathermodyamic assumption. Among the proposed assumptions (2) the tetraphenylarsonium–tetraphenylborate (TATB) assumption is widely preferred. It assumes the equality of the transfer functions, such as the enthalpy, for the related large symmetrical cation $As\Phi_4^+$ and anion $B\Phi_4^-$, $\Delta H_t^0(As\Phi_4^+) = \Delta H_t^0(B\Phi_4^-) = \frac{1}{2}\Delta H_t^0(As\Phi_4B\Phi_4)$. This assumption has nevertheless been criticized, mainly on spectroscopic grounds (3). It is clear that the validity of the TATB assumption would be considerably strengthened if a different assumption could be shown to give comparable values for the transfer functions of selected ions.

We have recently proposed and discussed (4) the basis and merits of such an assumption which calls, this time, for the equality of the transfer functions for an uncharged base, PS, and its conjugate cation, PSH^+, so that for example $\Delta H_t^0(PS) = \Delta H_t^0(PSH^+)$, where PS (proton sponge) stands for 1,8-bis(dimethylamino)naphthalene.

We are now reporting enthalpy data which lead us to compare values of the enthalpies of transfer between solvents for the ions $CF_3SO_3^-$ and H^+, as obtained using both the TATB assumption and the new PS/PSH^+ assumption. Our results demonstrate that both of these quite different hypotheses are compatible for transfers between five nonprotogenic solvents.

Experimental

Chemicals

Proton sponge (Aldrich) was recrystallised according to the procedure of De Groot and Sikkema (5). 1,8-Bis(dimethylamino)naphthalenium trifluoromethanesulfonate[1] was prepared by adding either an ethanol solution or pure trifluoromethanesulfonic acid[1] to an ethanol solution of 0.1–0.3 M proton sponge to reach the 1:1 equivalent point, as determined potentiometrically. The fine salt precipitate formed was filtered, washed with cold ethanol, and dried. pH measurements in water and Me_2SO showed the salt to be free of acidic or basic impurities. $SbCl_5$ (Aldrich 99.99%) and anhydrous HCl (Alpha gas 99.0%) were used as received. Acetonitrile (Fisher Scientific, optima grade, water ≤ 0.01%), pyridine (A&C reagent), dimethyl sulfoxide (BDH, analytical reagent), dimethylformamide (ACP, reagent), methanol (A&C, spectrograde), and ethanol (Anachemia) were used as received. Sulfolane (Aldrich) was vacuum distilled twice, the first time with CaH_2 (~3–5 g/L). Trifluoromethanesulfonic acid (Aldrich) was distilled under reduced pressure before use. The preparation of tetraethylammonium trifluoromethanesulfonate has already been described (6).

[1]Written as CF_3SO_3PSH rather than $PSHCF_3SO_3$ for easier comparison of data with trifluoromethanesulfonic acid which is written, as is customary, CF_3SO_3H.

Can. J. Chem. Downloaded from www.nrcresearchpress.com by 123.30.183.119 on 09/08/12
For personal use only.

Apparatus and procedure

Heats of solution were measured at 25.00 ± 0.01°C (30.00 ± 0.01°C for sulfolane) with an L.K.B. model 8721-1 isoperibol calorimeter as previously described (4). The calorimeter was connected to a home-made digital-analog circuit and a Zenith computer. A program was written in Basic to process the resistance–time signals of the calorimeter (7). The performance of the calorimeter was checked by determining the solution enthalpy of dried tris(hydroxymethyl)aminomethane (Aldrich) in 0.1 M aqueous HCl at 25.00 and 30.00°C. The values obtained were within 1% from literature data (8). This accuracy, although moderate, was adequate for our purpose. For each solute at least three measurements were made at different concentrations. Because of the unavoidable presence of some acidic or basic impurities at the 10^{-3} M level (3) in a few solvents, some measurements were made in these solvents using successive, instead of independent, additions of solutes and neglecting the first value. For example, with pyridine the heat of solution of CF_3SO_3PSH was found to be abnormally exothermic up to 5×10^{-3} M and this concentration corresponded exactly to the concentration of a strongly basic NH_3 impurity which neutralized PSH^+. With Me_2SO from Anachemia which contained a 1.9×10^{-3} M moderately strong acid (possibly HNO_3 since NO_2 is used as catalyst in the gas phase synthesis of Me_2SO) abnormal values were obtained for the enthalpies of solution of PS. Me_2SO from BDH had only 2×10^{-4} M acid and the enthalpy of solution of PS above this concentration was constant within the experimental errors. The possible influence of small concentrations of water present in some solvents on the enthalpy of solution of PS was also considered. This influence should be minimal since the enthalpies of solution of PS in water and the other solvents are not too different (Table 1) and the hydrolysis reaction of PS in solvent–water corresponds to $k_b \sim 10^{-1.8}$ and $\Delta H^0 \sim -11$ kJ mol^{-1} (4). Nevertheless, some experiments were carried out using the solvent MeCN, where the activity of water is high (20), and adding water up to 0.4 M. The solution enthalpy of PS, at the 5×10^{-3} M concentration level, was found to be +24.8 ± 0.4 kJ mol^{-1} (5 measurements) to be compared with +24.5 ± 0.3 kJ mol^{-1} (Table 1) so that the influence of water, if any, is well within our experimental errors.

Results

The molar enthalpies of solution of proton sponge (PS) and of its trifluoromethanesulfonate salt CF_3SO_3PSH, and of trifluoromethanesulfonic acid were determined in water, methanol (MeOH), ethanol (EtOH), pyridine (Py), dimethyl sulfoxide (Me_2SO), dimethylformanide (DMF), acetonitrile (MeCN), and sulfolane (Sul). Then, the enthalpies of transfer of PSH^+, $CF_3SO_3^-$, and H^+ were calculated.

1. Enthalpies of solution

Proton sponge

The plots of the heat of solution of PS against the number of moles dissolved (concentration range 0.8–7.5 $\times 10^{-3}$ M) are linear and the least-square slopes gave the molar enthalpy of solution of PS, which corresponds to reaction [1]:

[1] $\quad PS(c) = PS(s)$

The ΔH^0_{cs} values for the solvents, with their standard deviations, are given in Table 1 together with the value for water obtained indirectly (4).

Trifluoromethanesulfonate salt

The heats of solution of the salt CF_3SO_3PSH were plotted against the number of moles dissolved. The least-square slopes of the linear plots led to the molar enthalpy of solution $\Delta H_{csi}(CF_3SO_3^-\ PSH^+)$ for reaction [2].

[2] $\quad CF_3SO_3^-\ PSH^+(c) = PSH^+(s) + CF_3SO_3^-(s)$

In the concentration range studied ((0.8–5.3) $\times 10^{-3}$ M) the concentration dependence of the enthalpy of solution for a uni-univalent electrolyte is small (9) and masked by experimental errors. Possible ion-pairing effect at these low concentrations was also neglected on account of the nature of both anion and cation. The ΔH^0_{csi} values are listed in Table 1.

Trifluoromethanesulfonic acid

In the most basic solvents, H_2O, MeOH, EtOH, Me_2SO, and DMF, CF_3SO_3H is a strong electrolyte so that its solution corresponds to reaction [3] with its ΔH^0_{lsi}

[3] $\quad CF_3SO_3H(l) = H^+(s) + CF_3SO_3^-(s)$

However, in less basic MeCN and Sul the ionization of CF_3SO_3H is only partial, the pK's being respectively 2.5 (MeCN) (10) and 3.6 (Sul) (6) so that the solution of CF_3SO_3H involves both reactions [4] and [5] with their respective enthalpy changes ΔH^0_{ls} and ΔH^0_{si}.

[4] $\quad CF_3SO_3H(l) = CF_3SO_3H(s)$

[5] $\quad CF_3SO_3H(s) = H^+(s) + CF_3SO_3^-(s)$

Then we observe

[6] $\quad \Delta H_{obs} = \Delta H^0_{ls} + \alpha \Delta H^0_{si}$

where α the degree of ionization of CF_3SO_3H is obtained from the above pK values.

In order to calculate the enthalpy of transfer of the anion–cation pair $CF_3SO_3^-H^+$, we need to know the enthalpy change ΔH^0_{lsi} for reaction [3],

[7] $\quad \Delta H^0_{lsi} = \Delta H^0_{ls} + \Delta H^0_{si}$

We have already found that for moderately strong acids (chloroacetic acids in water (11)) it is not practical to determine ΔH^0_{ls} and ΔH^0_{si} from eq. [6] and values of ΔH_{obs} for different values α, i.e., of total acid concentrations. We have therefore determined ΔH^0_{ls} and ΔH^0_{si} separately. First, we approximate ΔH^0_{ls} by measuring the heat of solution of $CF_3SO_3H(l)$ in a 0.2 M CF_3SO_3H solution in MeCN or Sul. The correction for $\alpha \Delta H^0_{si}$ (eq. [6]) is negligible because α is small and $\Delta H^0_{si} < \Delta H^0_{ls}$. Second, we approximate $-\Delta H^0_{si}$. as the difference between the heat of solution of $CF_3SO_3NEt_4(c)$, first in the solvent containing 0.2 M HCl–$SbCl_5$, a strong acid (6), then in the solvent alone. This procedure, which has already been used in the case of sulfolane (6), was used for MeCN.

Values of ΔH^0_{lsi} for CF_3SO_3H in the most basic solvents of the series were obtained directly as described for $CF_3SO_3^-PSH^+$ and are reported in Table 1. For pyridine, with a 12.3 dielectric constant, although CF_3SO_3H is certainly a strong acid, like ClO_4H and HI (12), the ion-pair $CF_3SO_3^-PyH^+$ dissociation constant is estimated to be $\sim 10^{-3}$ (12). Since we did not observe a variation of the heat of solution of CF_3SO_3H between 0.009 and 0.05 M, we concluded that the enthalpy of dissociation of the ion-pair could be neglected.

2. Enthalpies of transfer

The enthalpy of transfer ΔH^0_t of a solute from a reference solvent (r) to a solvent (s) is equal to the molar enthalpy of solution of the solution in solvent (s) minus its enthalpy of solution in solvent (r). Thus for PS we have, from eq. [1],

TABLE 1. Enthalpies of solution of proton sponge PS, CF_3SO_3PSH, and CF_3SO_3H at 25°C

Solvent	ΔH_s^0 (kJ mol^{-1})			
	PS(c)[a]	CF_3SO_3PSH(c)[b]	$CF_3SO_3H(l)$[c]	$CF_3SO_3H(l)$[d]
H_2O	+30 ± 5[e]		−79.0 ± 0.4	—
MeOH	+20.7 ± 0.5	+37.7 ± 0.2	−73 ± 1	—
EtOH	+20.5 ± 0.6	+34 ± 1	−78.5 ± 0.4	—
Py	+17.35 ± 0.02	+22.9 ± 0.8	−136.3 ± 0.3	—
Me_2SO	+23.1 ± 0.5	+23.7 ± 0.5	−105.0 ± 0.4	—
DMF	+19.2 ± 0.6	+12.9 ± 0.3	−116.3 ± 0.4	—
MeCN	+24.5 ± 0.3	+26.3 ± 0.7	−22 ± 1	−20.2 ± 0.1
Sul[f]	+19.6 ± 0.5	+22.9 ± 0.8	−10 ± 1	−17.6 ± 0.1

[a] ΔH_{cs}^0 according to eq. [1].
[b] ΔH_{csi}^0 according to eq. [2].
[c] ΔH_{lsi}^0 according to eq. [3].
[d] ΔH_{ls}^0 according to eq. [4].
[e] Reference 4.
[f] Values obtained at 30°C.

TABLE 2. Ionic enthalpies of transfer from Me_2SO to other solvents at 25°C

Solvent	ΔH_t^0 (kJ mol^{-1})					
	PSH^+[a]	$CF_3SO_3^-$[a]	$CF_3SO_3^-$[b]	H^+[a]	H^+[c]	H^+[d]
H_2O	+6.9 ± 5.5	+9.6 ± 5.4	−1.2	+16.5 ± 4.6	+25.5	+27.2
MeOH	−2.4 ± 1.0	+16.4 ± 1.7	+3.2	+15.6 ± 3.1	—	+28.8
EtOH	−2.6 ± 1.1	+12.9 ± 2.6	—	+13.6 ± 3.4	—	~+26[e]
Py	−5.8 ± 0.5	+5.0 ± 1.8	—	−36.3 ± 2.5	—	—
Me_2SO	0	0	0	0	0	0
DMF	−3.9 ± 1.1	−6.9 ± 1.9	−4.6	−4.4 ± 2.7	−2.6	−6.7
MeCN	+1.4 ± 0.8	+1.2 ± 2.0	+1.3	+81.8 ± 3.4	+81.5	+82
Sul	−3.5 ± 1.0	+2.7 ± 2.3	—	+92.2 ± 3.7	+98.2	—

[a] Calculated from data in Table 1 and ref. 4 and $\Delta H_t^0(PS) = \Delta H_t^0(PSH^+)$.
[b] From data in ref. 13 using the TATB assumption.
[c] From data in ref. 14 for the transfer of H^+Cl^- and using the TATB assumption.
[d] From data in Table 1 for the transfer of $H^+CF_3SO_3^-$ and $\Delta H_t^0(CF_3SO_3^-)$ (column b) from ref. 13 using the TATB assumption.
[e] See text.

[8] $$\Delta H_t^0(PS) = \Delta H_{rs}^0(PS) = \Delta H_{cs}^0(PS) - \Delta H_{cr}^0(PS)$$

While water is usually selected as the reference solvent, particularly when dealing with ionic transfers (1), we found it more convenient here to take Me_2SO as the reference solvent (r) in part because the heat of solution of PS in water has a high ±5 kJ mol^{-1} margin of error.

Similarly, for the transfer of the salt CF_3SO_3PSH we have, according to eq. [2],

[9] $$\Delta H_{rs}^0(CF_3SO_3^-) + \Delta H_{rs}^0(PSH^+) = \Delta H_{csi}^0(CF_3SO_3PSH) - \Delta H_{cri}^0(CF_3SO_3PSH)$$

Using the extrathermodynamic assumption

[10] $$\Delta H_{rs}^0(PS) = \Delta H_{rs}^0(PSH^+)$$

we obtain

[11] $$\Delta H_{rs}^0(CF_3SO_3^-) = \Delta H_{csr}^0(CF_3SO_3PSH) - \Delta H_{cri}^0(CF_3SO_3PSH) - [\Delta H_{cs}^0(PS) - \Delta H_{cr}^0(PS)]$$

[12] $$\Delta H_{rs}^0(H^+) = \Delta H_{lsi}^0(CF_3SO_3H) - \Delta H_{lri}^0(CF_3SO_3H) - \Delta H_{rs}^0(CF_3SO_3^-)$$

The calculated enthalpies of transfer of PSH^+, $CF_3SO_3^-$, and H^+ with their corresponding errors are given in Table 2 together with the transfer values obtained from literature data with the TATB assumption (13, 14).

Discussion

The transfer enthalpies of $CF_3SO_3^-$ and H^+, derived from both extrathermodynamic assumptions (Table 2), can be compared for two hydroxylic solvents and three nonprotogenic solvents. First, we note that for H_2O and MeOH, the $\Delta H_{rs}^0(CF_3SO_3^-)$ or $\Delta H_{rs}^0(H^+)$ values corresponding to the PS/PSH^+ and TATB assumptions differ by some 12 kJ mol^{-1}. Second, for the solvents DMF and MeCN, the difference is now reduced to some 2 kJ mol^{-1}. We also see differences between the $\Delta H_{rs}^0(H^+)$ values obtained with the same TATB assumption but different experimental data, either based on the ionization of CF_3SO_3H or on that of HCl (14). Such differences, which come from experimental errors resulting from the many steps involved in the various thermochemical paths, give an idea of the margin of error on the transfer values. On this basis the agreement between the transfer values obtained with the PS/PSH^+ and TATB assumptions for the solvents Me_2SO, DMF, MeCN, and Sul can be considered satisfactory.

Both extrathermodynamic assumptions used here are quite different, assuming the equality of transfers either for a neu-

Can. J. Chem. Downloaded from www.nrcresearchpress.com by 123.30.183.119 on 09/08/12
For personal use only.

Can. J. Chem. Downloaded from www.nrcresearchpress.com by 123.30.183.119 on 09/08/12
For personal use only.

tral and a cation (PS/PSH^+) or for an anion and a cation ($B\Phi_4^-/As\Phi_4^+$) so that the agreement gives credence to both assumptions and the values obtained. The question remains as to why both assumptions are not compatible when considering hydroxylic solvents. We may assume that the PS/PSH^+ hypothesis is the faulty one with this solvent class. A possibility which comes to mind is that weak H-bonding may take place between these solvents and PS through the weakly basic $-NMe_2$ group. We are now making additional measurements of the heat of solution of PS in a larger number of solvents to try to isolate some H-bonding contributions on the basis of the correlation equation using the solvatochromic parameters of the solvents.

It is worth pointing out that the enthalpies of transfer of $CF_3SO_3^-$ obtained by combining the values obtained with the TATB and PS/PSH^+ assumptions (the latter for Py and Sul) are consistently low: using now H_2O as the reference solvent we have for ΔH^0_{ws}(kJ mol^{-1}), H_2O (0), MeOH (+4.4), Py (+6.2), Me_2SO (+1.2), DMF (−3.4), MeCN (+2.5), Sul (+3.9). This observation has an interesting consequence in that the enthalpy of transfer of CF_3SO_3H(l) can be used to approximate the enthalpy of transfer of H^+ for solvents when no data are available for the transfer of $CF_3SO_3^-$

$$[13]\quad \Delta H^0_{rs}(H^+) = \Delta H^0_{rs}(CF_3SO_3H) - \Delta H^0_{rs}(CF_3SO_3^-) \sim \Delta H^0_{rs}(CF_3SO_3H)$$

Thus for EtOH we estimate $\Delta H^0_{rs}(H^+) \sim +26$ kJ mol^{-1}. This latter value indicates that the basicities of bulk EtOH, and of MeOH and H_2O are indeed very close, a valuable result since there are apparently no $\Delta H^0_{ws}(H^+)$ data available for EtOH and MeOH (15).

By combining the TATB and PS/PSH^+ results in Table 2 (using the sixth column for H_2O, MeOH, EtOH, and averaging for the other solvents), the following basicity order for the solvents is deduced form the $\Delta H^0_{ws}(H^+)$ values in kJ mol^{-1} Py (−63) > DMF (−32) > Me_2SO (−27) > EtOH(−1) ~ H_2O(0) ~ MeOH(+2) > PC[2](+44) > MeCN(+55) > Sul(+69). We tried to correlate these enthalpies of transfer of H^+ with the solvents' solvatochromic parameters as was done before (1) but with, in our opinion, more reliable values. The correlation was poor but the number of solvents is still too limited for a good statistical evaluation of the data using the three relevant solvatochromic parameters, Π^*, α, and β.

The following interesting correlation has been found between the above enthalpies of transfer of H^+ and the enthalpies of complex formation with BF_3(g), which have been used as a measure of nonprotogenic solvent Lewis basicity (16):

$$[14]\quad \Delta H^0_{ws}(H^+) = (1.72 \pm 0.03)\Delta H^0_{gs}(BF_3) + (157 \pm 3)$$
$$N = 6, \qquad r = 0.999, \qquad \text{sd} = 2.2 \text{ kJ mol}^{-1}$$

The ranges covered for $\Delta H^0_{ws}(H^+)$ and $\Delta H^0_{gs}(BF_3)$ are, respectively, 132 and 77 kJ mol^{-1}. Considering that H^+ is a Brønsted acid and BF_3 a Lewis acid, although both may be considered "hard" acids, the results of the correlation are surprisingly good. As a matter of fact, the correlation is much better than that between $\Delta G^0_{ws}(H^+)$ and $\Delta H^0_{gs}(BF_3)$($N = 6, r = 0.891$, sd = 18 kJ mol^{-1}), one of the many relationships involving BF_3 already examined by Maria and Gal. Over and above its intrinsic interest (16), this correlation adds further support to the validity of our reported $\Delta H^0_{ws}(H^+)$ values for the nonprotogenic solvents.

Finally, it should be pointed out that conjugated B/BH^+ systems similar to PS/PSH^+ could also be used as the basis of related extrathermodynamic assumptions provided that BH^+ is a large cation with non-specific solvation (4), thus excluding for example Hammett-type bases (2). Macrocyclic ligands are clearly good candidates for such assumptions, and indeed they have been used to evaluate single-ion transfer parameters for ions such as Ag^+, Tl^+, K^+, Na^+ (see for example refs. 17 and 18). However, the present authors are not aware of any report on the use of macrocylic ligands to evaluate directly $\Delta H^0_t(H^+)$. It may be that the encapsulation of small species like H^+ in such ligands presents some particular problems (19).

[2]PC for propylene carbonate, value in ref. 14.

Acknowledgements

We wish to acknowledge a grant and a scholarship (D.F.) from the Natural Sciences and Engineering Research Council of Canada. We thank L. Bergeron for some of the early calorimetric determinations and C. Rio for her work on the influence of water in acetonitrile.

1. Y. Marcus, M. J. Kamlet, and R. W. Taft. J. Phys. Chem. **92**, 3613 (1988).
2. R. L. Benoit and C. Louis. *In* The chemistry of non-aqueous solvents. Vol. VA. *Edited by* J. J. Lagowski. Academic Press, New York. 1978, and references therein.
3. J. F. Coetzee, B. K. Deshmukh, and C. C. Liao. Chem. Rev. **90**, 827 (1990), and references therein.
4. R. L. Benoit, D. Lefebvre, and M. Frechette. Can. J. Chem. **65**, 996 (1987), and references therein.
5. R. L. De Groot and D. J. Sikkema. Recl. Trav. Chim. **95**, 10 (1976).
6. E. Milanova, S. Y. Lam, B. Desjardins, and R. L. Benoit. Adv. Chem. Ser. No 177, 145, (1979).
7. D. Figeys. M. Sc. Thesis, Université de Montréal, Montréal. (1991).
8. J. O. Hill, G. Öjelund, and I. Wadsö. J. Chem. Thermodyn. **1**, 111 (1969).
9. R. L. Benoit, M. Frechette, and D. Boulet. Can. J. Chem. **67**, 2148 (1989).
10. C. Louis. Ph.D. Thesis. Université de Montréal, Montréal. 1974.
11. R. L. Benoit, C. Louis, and M. Frechette. Thermochim. Acta, **176**, 221 (1991).
12. J. M. Nigretto and M. Jozefowicz. *In* The chemistry of non-aqueous solvents. Vol. VA. *Edited by* J. J. Lagowski. Academic Press, New York. 1978.
13. G. R. Hedwig and A. J. Parker. J. Am. Chem. Soc. **96**, 6589 (1974).
14. R. Domain, M. Rinfret, and R. L. Benoit. Can. J. Chem. **54**, 2101 (1976).
15. Y. Marcus. Pure Appl. Chem. **57**, 1103 (1985).
16. P. C. Maria and J. F. Gal. J. Phys. Chem. **89**, 1296 (1985).
17. J. Gutknecht, H. Schneider, and J. Stroka. Inorg. Chem. **17**, 3326 (1978).
18. M. -F. Lejaille, M. -H. Livertoux, C. Guidon, and J. Bessiere. Bull Soc. Chim. Fr. I-373 (1978).
19. R. W. Alder. Acc. Chem. Res. **16**, 321 (1983).
20. R. L. Benoit and S. Y. Lam. J. Am. Chem. Soc. **96**, 7385 (1974).

Microbial oxidation of benzyl sulfides and bibenzyl by *Mortierella isabellina* and *Helminthosporium* species

HERBERT L. HOLLAND, CYNTHIA G. RAND, PETER VISKI, AND FRANCES M. BROWN
Department of Chemistry, Brock University, St. Catharines, Ont., Canada L2S 3A1

Received April 25, 1991

HERBERT L. HOLLAND, CYNTHIA G. RAND, PETER VISKI, and FRANCES M. BROWN. Can. J. Chem. **69**, 1989 (1991).

The biotransformation of 1,2-diphenylethane by the fungus *Mortierella isabellina* ATCC 42613, and that of a series of alkyl benzyl sulfides by the fungi *M. isabellina* and *Helminthosporium species* NRRL 4671 have been studied. *Mortierella* hydroxylates 1,2-diphenylethane in low yield, giving (*S*)-1,2-diphenylethanol with an enantiomeric purity of 33%. Bioconversions of deuterium-labelled and racemic 1,2-diphenylethanol by *M. isabellina* demonstrate that this organism performs reversible oxidation/reduction of the alcohol. Biotransformations of *n*-alkyl benzyl sulfides by *H.* species give predominantly the (*S*) enantiomer of sulfoxide, with no sulfone formation, but *M. isabellina*, although showing a general preference for the oxidation of alkyl benzyl sulfides to (*R*) sulfoxides, also generates sulfones from *n*-alkyl benzyl sulfides in a time-dependent manner that suggests a stereoselective removal of (*R*) sulfoxide. The latter microorganism can be used, however, for the production of (*R*)-benzyl methyl and benzyl isopropyl sulfoxides, and gives (*S*)-benzyl *tert*-butyl sulfoxide in low yield.

Key words: biotransformation, enzymes, sulfoxides.

HERBERT L. HOLLAND, CYNTHIA G. RAND, PETER VISKI et FRANCES M. BROWN. Can. J. Chem. **69**, 1989 (1991).

On a étudié la biotransformation du 1,2-diphényléthane par le champignon *Mortierella isabellina* ATCC 42613 et celle d'une série de sulfures d'alkyle et de benzyle par les champignons *M. isabellina* et *Helminthosporium* NRRL 4671. Le *M. isabellina* provoque une hydroxylation du 1,2-diphényléthane avec un faible rendement conduisant au (*S*)-1,2-diphényléthanol, avec une pureté énantiomérique de 33%. Les bioconversions, par le *M. isabellina*, des 1,2-diphényléthanols racémiques et marqués au deutérium démontrent que cet organisme provoque une oxydoréduction réversible de l'alcool. Les biotransformations, par les espèces *H.*, des sulfures de *n*-alkyles et de benzyle conduisent principalement aux énantiomères (*S*) des sulfoxydes, sans formation de sulfone. Par ailleurs, même si le *M. isabellina* montre une préférence générale pour l'oxydation des sulfures d'alkyles et de benzyle en (*R*)-sulfoxydes, il conduit aussi à la formation de sulfones; la quantité de sulfone qui se forme en fonction du temps suggère qu'il y a un enlèvement stéréosélectif du sulfoxyde (*R*). On peut toutefois utiliser ce dernier micro-organisme pour produire, avec de faibles rendements, les sulfoxydes (*R*) de benzyle et de méthyle (ou de benzyle et d'isopropyle) et le sulfoxyde (*S*) de benzyle et de *tert*-butyle.

Mots clés : biotransformation, enzymes, sulfoxides.

[Traduit par la rédaction]

Introduction

Microbial biotransformation is now generally recognized as the simplest and most direct method for the preparation of a range of optically active sulfoxides of moderate to high enantiomeric purity (1), the most frequently studied group of substrates for this reaction being diaryl or alkyl aryl sulfides (1). Biotransformations or bioconversion has also been used as a method for the direct introduction of the hydroxyl group at the benzylic position of a range of unsubstituted and substituted aromatic hydrocarbons (2–4). Among the microorganisms most commonly employed for sulfoxidation are the fungi *Mortierella isabellina* NRRL 1757 (ATCC 42613), and *Helminthosporium* species NRRL 4671 (1, 5–7); the former organism has also been extensively examined for its ability to perform the benzylic hydroxylation reaction (2–4).

In spite of the widespread application of these fungi for asymmetric sulfoxidation, and the early demonstration that benzyl sulfides are good substrates for biotransformation by other organisms (8), and in the light of a renewed interest in the production of chiral benzyl sulfoxides (9), it is surprising that there has been no systematic study of the use of *M. isabellina* or *H.* species for the bioconversion of benzyl sulfides. We now present the results of the biotransformation of the series of benzyl sulfides **8**–**15** by both these microorganisms. An additional reason for this study was to assess the degree of competition (if any) between S and C oxidation when both atoms are in a benzylic position, and to this end we have also studied the biotransformation of the cyclic sulfide **16**, diphenyldisulfide **17**, and 1,2-diphenylethane (**1**) by *M. isabellina*.

Bioconversions of 1,2-diphenylethane (**1**) by *M. isabellina* (summarized in Table 1) proceeded very slowly, giving only a low yield of the corresponding alcohol **2** of moderate enantiomeric purity, assigned the (*S*) configuration on the basis of optical rotation measurements.

It was our intention to use the deuterium-labelled substrate **4** to study the intramolecular deuterium kinetic isotope effects associated with the benzylic hydroxylation reaction, but control experiments in which the expected product of such a reaction, the labelled alcohol **5**, was used as a substrate revealed that deuterium geminal to the hydroxyl group was lost to the extent of 75% over a 3-day period. That this loss was due was due to oxidation to the ketone **3** and subsequent reduction of the latter was confirmed following incubation of **3**, when a moderate yield of alcohol **2** was obtained. In confirmation of this, the use of racemic **2** as a substrate resulted in the isolation of the (*S*) enantiomer of **2** in high yield following 3 days in contact with *M. isabellina*.

The enantiomeric purity of **2** produced by carbonyl reduction (91%) is considerably higher than that obtained from biotransformation of the racemate (68%), or from hydroxylation of **1** (33%), a phenomenon attributable to incomplete processing of the racemic alcohol and an unknown stereoselectivity in the hydroxylation reaction, respectively. In the case of the labelled substrate **5** it was possible to assess both the overall optical purity of the product (by optical rotation), and the optical purity of that portion of the product which had lost deuterium (by ^{1}H nmr analysis in the presence of chiral shift reagent using the C*H*OH resonance). The results, listed in Table 2, clearly

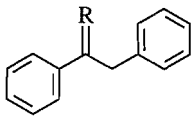
Can. J. Chem. Downloaded from www.nrcresearchpress.com by 123.30.183.119 on 09/08/12
For personal use only.

TABLE 1. Biotransformation of **1**–**5** by *M. isabellina*

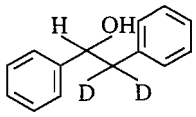
Substrate	Time (h)	Product	Yield (%)	Configuration	ee (%)
1	72	**2**	2	*S*	34
	120	**2**	5	*S*	32
	72[a]	—	—	—	—
3	72	**2**	51	*S*	91
(±)−**2**	72	**2**	96	*S*	68
(±)−**5**	72	**5**	25		
				S	65[b]
		2	75		88[c]
(±)−**7**	72	**7**	95	*S*	63

[a]Performed in the presence of autoclaved fungus.
[b]From rotation values.
[c]From ^{1}H nmr analysis, refers to component **2** only.

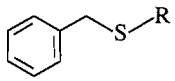
illustrate that the portion of the product which has undergone oxidation/reduction (and hence lost deuterium) has an enantiomeric purity (88%) identical (within experimental error) to that produced by carbonyl reduction (91%), confirming that the loss of label does indeed result from an oxidation/reduction process. The bioconversion of labelled substrate **7** without any loss of deuterium confirmed that no loss of label occurs from the α position (for example by carbonyl enolization), but in view of the potential complexity of the analysis of any results which might follow from biotransformation of **4**, this substrate was not investigated further.



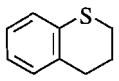
1; R = H_2
2; R = H,OH
3; R = O
4; R = D_2
5; R = D,OH
6; R = D,Cl



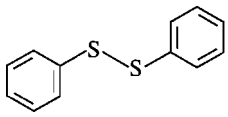
7



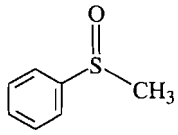
8; R = C_6H_5
9; R = C_6H_4-*para*-CH_3
10; R = CH_3
11; R = C_2H_5
12; R = *n*-C_3H_7
13; R = iso-C_3H_7
14; R = *n*-C_4H_9
15; R = *t*-C_4H_9



16



17



18

The results obtained from biotransformation of the sulfides **8**–**16** are listed in Tables 2 and 3. Table 2 presents product yields and enantiomeric excesses, from which it is apparent that, although yields are reasonable in most cases, sulfoxides are rarely formed with high enantiomeric purity. The absolute configurations of the sulfoxides listed in Tables 2 and 3 were determined by comparison of the sign of rotation values with those in the literature. This correlation is well established for benzyl alkyl sulfoxides, the relevant references being those listed in Table 3.

Helminthosporium species failed to oxidize the aryl benzyl sulfides **8** and **9**, the low isolated yields of racemic sulfoxide being possibly the result of autooxidation, but gave consistently the (*S*) enantiomer of alkyl benzyl sulfoxides, with the exception of benzyl isopropyl sulfoxide (**13**), which was formed as the racemate. In the case of oxidation of benzyl *n*-propyl sulfide (**12**), the low yield of close to racemic material prompted us to carry out a control incubation using autoclaved fungus, but no autooxidation was apparent. The ability of *H.* species to convert alkyl aryl sulfides to (*S*) sulfoxides is well documented (1), so that the formation of (*S*) alkyl benzyl sulfides by this microoganism is not unexpected.

Oxidations of benzyl sulfides by *H.* species were characterized by the absence of sulfone products, unlike many of the bioconversions of these substrates by *M. isabellina*, which were complicated by the formation of sulfone in a time-dependent manner. Although no sulfones were produced from the aryl benzyl sulfides **8** and **9**, the biotransformation of alkyl benzyl sulfides resulted in the formation of sulfone from all substrates except benzyl *tert*-butyl sulfide (**15**). *Mortierella isabellina* rarely produces sulfone products from bioconversion of alkyl aryl sulfides (1).

The absolute stereochemistry of the sulfoxides produced from *n*-alkyl benzyl sulfides was found to be dependent upon both the biotransformation time and the amount of sulfone produced. This dependence suggests that, although the initial oxidation of sulfide to sulfoxide may occur with a slight preference for the production of the (*R*) enantiomer (see Table 2, for example **11** after 10 h), consistent with the observation that alkyl aryl sulfides were converted predominantly to (*R*) sulfoxides by this fungus (1), subsequent oxidation of sulfoxide to sulfone involves a substantial preference for removal of the (*R*) enantiomer. After long bioconversions (e.g., 48 h for **11**), sulfoxide enriched in the (*S*) enantiomer remains, and in the case of substrates **12** and **14** this phenomenon is manifested as an increase in the proportion of the (*S*) enantiomer as the bioconversion period (and hence the production of sulfone) is increased.

In an attempt to investigate the stereochemistry of the sulfoxide–sulfone oxidation, racemic sulfoxides derived from the *n*-alkyl benzyl sulfides **10**–**12** and **14** were prepared and used as substrates for bioconversion by *M. isabellina*. In all cases the only isolable material consisted of racemic sulfoxide, recovered in almost quantitative amount: no sulfone products were detected. We considered that this may be attributable to the inability of sulfoxide to induce the necessary oxidative enzymes in *M. isabellina*, and therefore performed a series of incubations of sulfoxides in which the microorganism had been grown in the presence of a small amount of the corresponding sulfide, but again no sulfoxide oxidation was observed.

Can. J. Chem. Downloaded from www.nrcresearchpress.com by 123.30.183.119 on 09/08/12
For personal use only.

TABLE 2. Biotransformation of benzyl sulfides **8**–**15** and sulfide **16**

Substrate	Biocatalyst	Time (h)	Sulfone (%)	Sulfoxide		
				Yield (%)	Config.	ee (%)
8	Mi	48	—	45	*R*	58
	Hs	48	—	4	—	0
9	Mi	48	—	13	*R*	93
	Hs	48	—	3	—	0
10	Mi	30	5	87	*R*	48
		10	3	45	*R*	46
	Hs	30	—	68	*S*	62
11	Mi	48	50	41	*S*	24
		24	25	55	*R*	7
		10	9	40	*R*	15
	Hs	48	3	55	*S*	51
12	Mi	48	60	22	*S*	50
		10	12	28	*S*	12
	Hs	48	—	12	*S*	10
		48[a]	—	—	—	—
13	Mi	48	3	48	*R*	59
	Hs	48	—	22	—	0
14	Mi	48	82	6	*S*	86
		10	15	15	*S*	31
	Hs	48	—	38	*S*	25
15	Mi	48	—	14	*S*	72
	Hs	48	—	5	*S*	7
16	Mi	72	5	72	*R*	40

[a]Performed in the presence of autoclaved fungus.

TABLE 3. Specific rotations of sulfoxides from Table 2

Substrate	Fungus	Time (h)	Sulfoxide	
			$[\alpha]_D$ found	$[\alpha]_D$ reported (ref.)[a]
8	Mi	48	+147	254 (8) (acetone)
	Hs	48	0	
9	Mi	48	+232	250 (10) (acetone)
	Hs	48	0	
10	Mi	30	−45.7	96 (11)
		10	−44.3	
	Hs	30	+59.8	
11	Mi	48	+11.2	47 (11)
		24	−3.1	
		10	−7.3	
	Hs	48	+23.7	
12	Mi	48	+20.0	
		10	+5.3	
	Hs	48	+4	
13	Mi	48	+70.2	119 (11)
	Hs	48	0	
14	Mi	48	−90.2	105 (11) ($CHCl_3$)
		10	−33.1	
	Hs	48	−26.3	
15	Mi	48	−203	240 (11) ($CHCl_3$)
	Hs	48	−21.5	
16	Mi	72	−76	202 (12) (acetone)

[a]Solvent EtOH unless otherwise stated.

This inability of *M. isabellina* to convert sulfoxides to sulfones distinguishes this microorganism from many others (e.g., *Aspergillus niger*) that can be used to perform this bioconversion in a stereoselective manner (1). We were also unable to detect any sulfide products that may have arisen from sulfoxide reduction, a mode of biotransformation which is expressed by *M. isabellina* with other substrates (1).

We attribute the inability of *M. isabellina* to oxidize the sulfoxides used in this study to the failure of these sulfoxides to be accepted into the fungal cell, the location of the oxidative enzymes concerned (1). In this context it is noteworthy that, during sulfide biotransformation, the sulfoxide products are recovered exclusively from the aqueous bioconversion medium, suggesting that these materials, once excreted from the cell, do not reenter, and hence are not reoxidized from this environment. Oxidation of sulfoxide to sulfone during the biotransformation of sulfides must therefore occur immediately after formation of the former, and may take place even before dissociation of the sulfoxide from the enzyme's active site.

The general preference of *M. isabellina* for the production of (*R*) sulfoxides, established for the bioconversion of alkyl aryl sulfides (1), is seen in the bioconversion of benzyl isopropyl sulfide (**13**), where the (*R*) sulfoxide is obtained in an enantiomeric excess of 59%. Benzyl *tert*-butyl sulfide (**15**) is, however, oxidized to give predominantly the (*S*) enantiomer. This stereoreversal of benzyl sulfide oxidation in the presence of a *tert*-butyl substituent has also been observed for bioconversions carried out by *A. niger* (8), and oxidation by sodium metaperiodate in the presence of bovine serum albumin (13), and is rationalized by the assumption that the stereopreference for oxidation of benzyl alkyl sulfides is controlled by the relative sizes of the two substituents. Whereas the benzyl group is considered to be bulkier than *n*-alkyl or isopropyl substituents, the opposite holds in the case of benzyl *tert*-butyl sulfide (11).

It is interesting to note that in cases where the substrate presents the possibility of competitive benzylic S vs. C oxidation (e.g., **8**, **9**, and **16**) only the products of sulfoxidation were detected. In this respect, the oxidative enzymes of *M. isabellina* differ from those obtained from mammalian

Can. J. Chem. Downloaded from www.nrcresearchpress.com by 123.30.183.119 on 09/08/12
For personal use only.

sources, where both modes of oxidative metabolism are observed (14).

The final substrate used in the present study, diphenyldisulfide (**17**), was remarkable in that its biotransformation by *M. isabellina* represents a new type of bioconversion reaction. The only isolable product, formed in low yield, was **18**, the sulfoxide of thioanisole. This product was obtained predominantly as the (*R*) enantiomer, with an enantiomeric purity (48%) close to that obtained from the *M. isabellina* catalyzed oxidation of thioanisole (55%) (15), suggesting a route for the formation of **18** involving reductive cleavage and methylation of **17**, although the order in which these processes occur is not clear.

It is therefore apparent that, although *Helminthosporium* species NRRL 4671 can be used for the production of (*S*) *n*-alkyl benzyl sulfoxides of moderate enantiomeric purity, the corresponding (*R*) sulfoxides cannot be obtained routinely from sulfide bioconversions using *M. isabellina*. The latter microorganism can be used, however, for the production of (*R*)-benzyl methyl and benzyl isopropyl sulfoxides, and gives (*S*)-benzyl *tert*-butyl sulfoxide in low yield.

Experimental

Apparatus, materials, and methods

Melting points were determined on a Kofler heating stage. Infrared spectra were recorded with an Analect 6260FX spectrometer. The nmr spectra were recorded at 200 MHz (^{1}H) or 50 MHz (^{13}C) with a Bruker AC200 spectrometer, using $CDCl_3$ as solvent and $CHCl_3$ as internal standard. Enantiomeric ratios were determined where possible by ^{1}H nmr analysis in the presence of tris[3-(heptafluoropropylhydroxymethylene)-*d*-camphorato]europium(III). Mass spectra were obtained with a Kratos Concept 1S instrument. Thin-layer chromatography was performed on Merck silica gel 60F-254 and flash column chromatography used silica gel, Merck 9385, or equivalent. Optical rotations were obtained at 20°C with a Rudloph Autopol III polarimeter.

Maintenance of microorganisms

Mortierella isabellina ATCC 42613 (equivalent to NRRL 1757) and *Helminthosporium* species NRRL 4671 were maintained on malt agar slopes.

Preparation of substrates

With the exception of those listed below, the substrates used in this study were commerical samples. All substrates gave satisfactory spectral data (^{1}H nmr, ^{13}C nmr, ms, and ir).

1,2-Diphenylethane, 1,1-d_2 *(**4**)*

This was prepared from 1,2-diphenylethanol (**5**) (see below), via conversion using thionyl chloride to the chloride **6** and treatment of the latter with lithium triethylborodeuteride as described elsewhere (3). The reactions were carried out as described with the exception of the $LiEt_3BD$ treatment of **6**, which needed a reaction time of 7 days under refluxing conditions in order to achieve acceptable conversion. Under these conditions, **4** was obtained in an overall yield of 70% from alcohol **5**, and identified by comparison with authentic unlabelled material. Deuterium content ≥99% d_2 by ms and ^{1}H nmr.

*1,2-Diphenylethanol, 1-*d *(**5**)*

This was prepared in 85% isolated yield by lithium aluminum deuteride reduction of 1,2-diphenylethanone (**3**) as described elsewhere (3), and identified by comparison with authentic unlabelled material. Deuterium content ≥99% d_1 by ms and ^{1}H nmr.

1,2-Diphenylethanol-2,2-d_2 *(**7**)*

A solution of 1,2-diphenylethanone (**3**, 2 g) in dry toluene (100 mL) was treated with a solution of sodium deuteroxide in deuterium oxide as described (16). The mixture was stirred and refluxed for 3 days, and the toluene layer then separated, dried, and evaporated to give labelled 1,2-diphenylethanone having the following isotopic composition (by ms): d_2 85%, d_1 8%, d_0 7%. This material was subsequently treated without loss of deuterium label with lithium aluminium hydride as described (5) to give alcohol **7**, identified by comparison with authentic unlabelled material.

Benzyl p-*tolyl sulfide (**9**)*

This was prepared by adding 1 equivalent of benzyl chloride to a solution of 1 equivalent of *p*-thiocresol and 1 equivalent of potassium hydroxide in ethanol, and refluxing the mixture overnight. The product was obtained in high yield following a conventional work-up procedure, and gave satisfactory analytical data.

*Benzyl alkyl sulfides **11–14***

These compounds were prepared from benzyl mercaptan and the corresponding alkyl halide by the procedure described (17), and gave satisfactory analytical data.

Benzyl tert-*butyl sulfide (**15**)*

This was prepared from *tert*-butyl methyl sulfide and phenyl magnesium bromide by the route described (18). The final product had bp 130°C (24 Torr; 1 Torr = 133.3 Pa) (lit.(18) bp 129–131°C (21 Torr)) and exhibited satisfactory spectral data.

*Thiochroman (**16**)*

A mixture consisting of thiochromanone (5 g), potassium hydroxide (5 g), hydrazine (85%, 4 mL), and ethylene glycol (50 mL) was heated under reflux for 1.5 h, and then raised in temperature to 195°C and maintained at that temperature for a further 4 h. The reaction was then cooled, poured onto water, and the mixture extracted with ether. The extract was dried and evaporated to give a residue that was purified by chromatography (benzene/silica gel) to give **16** (1.8 g) as an oil, identified by comparison of spectral data with those reported (19, 20).

Preparation of sulfoxide standards

Sulfoxide standards were prepared from the corresponding sulfides using sodium metaperiodate as oxidant by the procedure described (21), and exhibited spectral and physical properties in accord with those reported.

Biotransformations

These are summarized in Table 1 for bibenzyl hydroxylations and Table 2 for sulfoxidations.

Mortierella isabellina: Two slopes of *M. isabellina* were used to inoculate 15 1-L Erlenmeyer flasks each containing 200 mL of a medium composed of glucose (40 g), yeast extract (5 g), sodium chloride (5 g), dibasic potassium phosphate (5 g), and soya flour (5 g) per litre of distilled water. The flasks were allowed to stand overnight at 27°C and then placed on a rotary shaker at 180 rpm, and growth continued for a further period of 72 h at 27°C. The fungus was then harvested by centrifugation, and resuspended in 15 1-L Erlenmeyer flasks each of which contained 200 mL of distilled water. Substrate (1 g in 30 mL 95% ethanol) was then distributed over the flasks, which were incubated at 180 rpm and 27°C for the time specified in the tables. The fungus and aqueous medium were then separated by centrifugation, and the latter extracted with dichloromethane (continuous extraction for 3–4 days). Concentration of this extract gave the crude material, which was examined as outlined below.

Helminthosporium species: The procedures were carried out exactly as described above, with the following modifications. The growth medium was composed of V-8 juice and calcium carbonate (200 mL and 3 g, respectively, per litre of water), adjusted to pH 7.2 by addition of 1 M sodium hydroxide, and separation of the fungus from its growth and incubation media was carried out by vacuum filtration.

Incubations with autoclaved fungus

These were performed as described above, with the exception that the fungal material was sterilized by autoclaving in distilled water at 121°C for 20 min, and then allowed to cool prior to addition of the substrate.

Attempted induction of sulfoxidizing enzymes in M. isabellina

This was performed by the addition of a solution of benzyl ethyl sulfide (**11**) (300 mg) in ethanol (95%, 15 mL) to a 48 h old growth of *M. isabellina* (15 1-L flasks), followed by growth for a further period of 24 h. Subsequent procedures were performed exactly as described above.

Can. J. Chem. Downloaded from www.nrcresearchpress.com by 123.30.183.119 on 09/08/12
For personal use only.

Isolation and characterization of products

The crude biotransformation extracts obtained as outlined above were examined by tlc, and submitted to flash chromatography using a benzene–ether 10% stepwise gradient, followed by an ether–methanol 10% stepwise gradient in the case of sulfoxides derived from **10–14**. The yields and ee values quoted in the tables refer to purified, homogeneous material, and arise from the combination of (only) homogeneous column fractions without further purification (e.g., crystallization) that could lead to alteration of stereochemical enrichment values. Products were identified by a combination of nmr, mass spectral, infrared, and optical rotation analysis. Specific rotation values for sulfoxides of Table 2, and references to values for homochiral sulfoxides, are listed in Table 3. Typical procedures are outlined below for 1,2-diphenylethane hydroxylation and for a sulfide biotransformation.

*Biotransformation of 1,2-diphenylethane (**1**) by* M. isabellina

Incubation of **1** (4 g) with 60 flasks of *M. isabellina* for a period of 72 h, followed by removal of the fungus by centrifugation and continuous extraction of the aqueous medium, resulted in an extract (0.54 g) that on chromatography afforded recovered 1,2-diphenylethane (0.4 g) followed by 1,2-diphenylethanol (80 mg), identified by comparison with authentic material, and having $[\alpha]_D$ −21 (*c* 0.5, EtOH) (lit. (22) $[\alpha]_D$ +60.6 (*c* 1.54, EtOH), lit. (23) $[\alpha]_D$ +52.8 (*c* 5.0, (EtOH)).

Biotransformation of benzyl methyl sulfide by H. *species*

Incubation of **10** (1 g) with *H.* species for a period of 30 h, followed by filtration and extraction of the aqueous medium, gave an extract (0.88 g) that on chromatography afforded benzyl methyl sulfoxide (0.76 g, 68%), identified by comparison with authentic racemic material, $[\alpha]_D$ +59.8 (*c* 1.08, EtOH) (lit. (11) $[\alpha]_D$ +96 (EtOH)).

*Biotransformation of diphenyldisulfide (**17**)*

Incubation of **17** (1 g) with 15 flasks of *M. isabellina*, followed by extraction and chromatography as described above, gave as the only isolable product thioanisole sulfoxide (**18**) (20 mg), identified by comparison with an authentic sample, $[\alpha]_D$ +85.25 (*c* 0.6, $CHCl_3$), ee 48%.

1. H. L. HOLLAND. Chem. Rev. **88**, 473 (1988).
2. H. L. HOLLAND, E. J. BERGEN, P. C. CHENCHAIAH, S. H. KHAN, B. MUNOZ, R. W. NINNISS, and D. RICHARDS. Can J. Chem. **65**, 502 (1987).
3. H. L. HOLLAND, F. M. BROWN, B. MUNOZ, and R. W. NINNISS. J. Chem. Soc. Perkin Trans. 2, 1557 (1988).
4. H. L. HOLLAND, F. M. BROWN, and M. CONN. J. Chem. Soc. Perkin Trans. 2, 1651 (1990).
5. B. J. AURET, D. R. BOYD, R. DUNLOP, and A. F. DRAKE. J. Chem. Soc. Perkin Trans. 1, 2827 (1988).
6. H. L. HOLLAND, M. J. CHERNISHENKO, M. CONN, A. MUNOZ, T. S. MANOHARAN, and M. A. ZAWADSKI. Can. J. Chem. **68**, 696 (1990).
7. M. MADESCLAIRE, A. FAUVE, J. METIN, and A. CARPY. Tetrahedron: Asymmetry, **1**, 311 (1990).
8. B. J. AURET, D. R. BOYD, H. B. HENBEST, and S. ROSS. J. Chem. Soc. C, 2371 (1968).
9. P. H. BUIST, D. M. MARECAK, E. T. PARTINGTON, and P. SKALA. J. Org. Chem. **55**, 5667 (1990).
10. C. J. M. STIRLING. J. Chem. Soc. 5741 (1963).
11. K. MISLOW, M. M. GREEN, and M. RABAN. J. Chem. Soc. **87**, 2761 (1965).
12. T. TAKATA, M. YAMAZAKI, K. FUJIMORI, Y. H. KIM, T. IYANAGI, and S. OAE. Bull. Chem. Soc. Jpn. **56**, 2300 (1983).
13. T. SUGIMOTO, T. KOKUBA, J. MIYAZAKI, S. TANIMOTO, and M. OKANO. J. Chem. Soc. Chem. Commun. 402 (1979).
14. Y. WATANABE, T. NUMATA, T. IYANAGI, and S. OAE. Bull. Chem. Soc. Jpn. **54**, 1163 (1981).
15. H. L. HOLLAND, H. PÖPPERL, R. W. NINNISS, and P. C. CHENCHAIAH. Can. J. Chem. **63**, 1118 (1985).
16. H. L. HOLLAND, F. M. BROWN, and L. TAN. J. Labelled Compd. Radiopharm. **27**, 629 (1989).
17. J. BÜCHI, M. PROST, H. EICHBERGER, and R. LIEBERHERR. Helv. Chim. Acta, **35**, 1527 (1952).
18. F. G. BORDWELL and B. M. PITT. J. Am. Chem. Soc. **77**, 572 (1955).
19. G. KRESZE and W. AMANN. Spectrochim. Acta, Part A: **26**, 637 (1970).
20. A. G. LOUDON, A. MACCOLL, and S. K. WONG. J. Chem. Soc. B, 1727 (1970).
21. N. J. LEONARD and C. R. JOHNSON. J. Org. Chem. **27**, 282 (1962).
22. V. M. POTAPOV and A. P. TERENT'EV. Zh. Obshch. Khim. **34**, 516 (1964).
23. W. GERRARD and J. KENYON. J. Chem. Soc. **131**, 2564 (1928).

Can. J. Chem. Downloaded from www.nrcresearchpress.com by 123.30.183.119 on 09/08/12
For personal use only.

Complexing behavior of rutin and quercetin[1]

GRACIELA M. ESCANDAR
Departamento de Química Analítica, Facultad de Ciencias Bioquímicas y Farmacéuticas, Universidad Nacional de Rosario, Suipacha 531. 2000, Rosario, Argentina

AND

LUIS F. SALA[2]
Departamento de Ciencias Exactas, Facultad de Ciencias Bioquímicas y Farmacéuticas, Universidad Nacional de Rosario, Suipacha 531. 2000, Rosario, Argentina

Received April 22, 1991

GRACIELA M. ESCANDAR and LUIS F. SALA. Can. J. Chem. **69**, 1994 (1991).

The equilibrium reactions between rutin, 3-[6-O-(6-deoxy-α-L-mannopyranosyl)-(β-D-glucopyranosyl)oxy]-2-(3,4-dihydroxyphenyl)-5,7-dihydroxy-4*H*-1-benzopyran-4-one, and quercetin (rutin aglycone) with iron(III), copper(II), cobalt(II), and nickel(II) have been studied by potentiometric and spectrophotometric methods in aqueous solution. All measurements were carried out at $t = 20°C$ and $\mu = 0.10$ M, and the corresponding stability constants were calculated by applying computational methods. The interactions between the proposed cations with both biological ligands and other related ones are compared, with simultaneous postulation of the probable structures.

Key words: chelate stability constants of rutin, chelate stability constants of quercetin, transition metal ion interaction with flavonoids, stability constant determinations, potentiometric and spectrophotometric studies.

GRACIELA M. ESCANDAR et LUIS F. SALA. Can. J. Chem. **69**, 1994 (1991).

Opérant en solutions aqueuses et faisant appel à des méthodes potentiométriques et spectrophotométriques, on a étudié les réactions d'équilibre de la rutine, 3-[6-O-(6-désoxy-α-L-mannopyranosyl)-(β-D-glucopyranosyl)oxy]-2-(3,4-dihydroxyphényl)-5,7-dihydroxy-4*H*-1-benzopyran-4-one, et de la quercétine (aglycone de la rutine) avec le fer(III), le cuivre(II), le cobalt(II) et le nickel(II). Toutes les mesures ont été effectuées à 20°C et à $\mu = 0{,}10$ M; on a calculé les constantes de stabilité correspondantes à l'aide de méthodes de calculs par ordinateurs. On a comparé les interactions des cations mentionnés plus hauts avec les deux ligands biologiques ainsi qu'avec d'autres substances apparentées; on a fait des hypothèses simultanées concernant leurs structures probables.

Mots clés : constantes de stabilité des chélates de la rutine, contantes de stabilité des chélates de la quercétine, interactions de ions des métaux de transition avec les flavonoïdes, déterminations des constantes de stabilité, études potentiométriques et spectrophotométriques.

[Traduit par la rédaction]

Introduction

Flavonoids are structures of recognized biological activity (1). Rutin (Scheme 1), one of the typical glucosides in the flavonoids series widely distributed in natural plants, is a potent inhibitor of lens aldose reductase (potentially useful for prevention of diabetic cataracts) (2). Pharmacologically, rutin as well as quercetin has a direct constructor action on the capillary bed and decreases the permeability and fragility of the vessels (3). We thought it of value to determine the stability constants of rutin and quercetin metal-ion complexes of biological interest, which have not yet been reported in the literature. The study was performed with the intention of applying the results to possible clinical and biological situations. For these reasons the chelate stability constants of rutin and quercetin with common divalent and trivalent metal ions have been determined.

Experimental section

Ligands

Rutin and quercetin were obtained commercially from Fluka. The purity of the ligands was checked by potentiometric titration. The ligand solutions were prepared just before each determination under nitrogen atmosphere to avoid oxidation of the ligand at high pH.

Reagents

Stock solutions of about 0.010 M of reagent grade metal nitrates were prepared in doubly distilled water, and their exact concentrations were determined by titration with previously standardized ethylenediaminetetraacetic acid (EDTA) solution in the presence of appropriate indicators (4). Fe(III) nitrate solution was prepared with 0.050 M HNO_3 to avoid the hydrolysis of this metal ion in the stock solution. The exact amount of excess acid was checked by the procedure used by Harris and Martell (5). Solutions of carbonate-free NaOH and HNO_3 were standardized against potassium hydrogen phthalate and sodium carbonate, respectively.

Potentiometric and spectrophotometric measurements

The procedures and apparatus used for potentiometric measurements have been described previously in detail (6). Briefly, measurements were made at 20.0 ± 0.1°C and 0.10 M ($NaNO_3$) ionic strength. The pH meter was standardized by titrations of HNO_3 and acetic acid to read $-\log [H^+]$ rather than hydrogen ion activity.

Since the acid form of the ligands is not sufficiently soluble, it was necessary to dissolve the ligands in standard base and develop the lower end of the equilibrium curves from a back titration, by stepwise addition of standard acid.

The spectrophotometric measurements were carried out with a Shimadzu UV-140-02(DB).

Competition equilibria

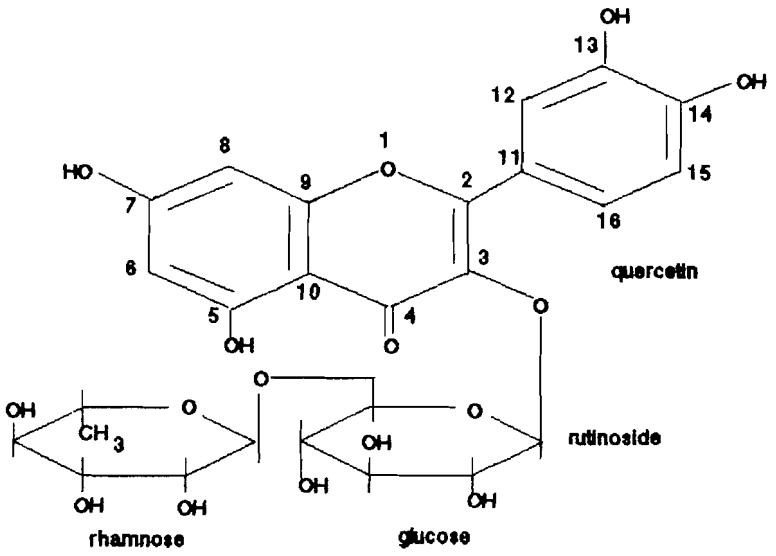
Since the rutin and quercetin–Fe(III) chelates are completely formed at low pH, spectrophotometric ligand–ligand competitions were performed by using a 1:1:1 molar ratio of the metal ion, ligand, and EDTA (reference ligand), employing a general method described on the literature (5). The pH and the wavelength for each competition had to be chosen so that only one ferric species absorbed. Protonation equilibria involving the free ligands and the ferric complexes were included in the calculations by using the protonation constants determined here or the literature values reported for EDTA. Duplicate reactions were run.

[1]Presented at the XIX Congreso Latinoamericano de Química, November 5–9, 1990, Buenos Aires, Argentina.

[2]To whom correspondence should be addressed.

Printed in Canada / Imprimé au Canada

Can. J. Chem. Downloaded from www.nrcresearchpress.com by 123.30.183.119 on 09/08/12
For personal use only.



SCHEME 1. Rutin or quercetin 3-β-D-rutinoside.

TABLE 1. Log protonation constants; μ = 0.10 M ($NaNO_3$), 20.0°C

	Value			
	Quercetin		Rutin	
Parameter	Potentiometric	Spectroscopic	Potentiometric	Spectroscopic
K_1	—	11.0	—	10.9
K_2	9.77	9.9	10.04	10.0
K_3	8.21	8.0	8.30	8.3
K_4	6.95	7.1	6.95	7.1
K_5	5.54	5.7		

Computations

The proton association constants for ligands, the protonation constants, and the stability constants of chelates were determined by using the FORTRAN program BEST (7).

Results and discussion

Protonation constants of ligands

The results of the equilibrium determinations on rutin and quercetin are presented in Table 1. The first protonation reaction of both ligands occurs above pH 10 where potentiometric measurements become insensitive. Therefore the high pH range was investigated spectrophotometrically. The absorption spectra of the ligands at several pH values are shown in Figs. 1 and 2. To calculate spectrophotometrically the protonation constants we performed a non-linear least-squares regression analysis on eq. [1], in the appropriate pH ranges.

$$[1] \quad A = T_L[(\epsilon_3\beta_3[H]^3 + \epsilon_2\beta_2[H]^2 + \epsilon_1\beta_1[H] + \epsilon)/(\beta_3[H]^3 + \beta_2[H]^2 + \beta_1[H] + 1)]$$

where A = absorbance, T_L = analytical concentration of ligand, ϵ_n = extinction coefficient, β_n = cumulative protonation constant.

Metal–ligand interaction

Due to the fact that the ligands under study present several positions where the selected metal ions can coordinate, different metal ion – ligand relationships were tried.

Iron(III) systems

Iron quercetin

The potentiometric equilibrium profile of pH vs. a (a: mol of NaOH added per mol of ligand or metal ion) for a 1:1 system shown in Fig. 3 has two breaks, one at $a = 3$ and the second one at $a = 6$. In the first buffer zone a fine precipitate was produced (probably the neutral species FeH_2L) and dissolved when the pH was increased. The equilibria are represented by eqs. [2]–[6]:

$$[2] \quad Fe^{3+} + L^{5-} + 2H_2O \rightleftharpoons Fe(OH)_2L^{4-} + 2H^+$$

$$[3] \quad Fe(OH)_2L^{4-} + H^+ \rightleftharpoons Fe(OH)L^{3-}$$

$$[4] \quad Fe(OH)L^{3-} + H^+ \rightleftharpoons FeL^{2-}$$

$$[5] \quad FeL^{2-} + H^+ \rightleftharpoons FeHL^-$$

$$[6] \quad FeHL^- + H^+ \rightleftharpoons FeH_2L$$

Of the three neutralized protons at the beginning of the potentiometric determination two of them were attributed to the catechol hydrogens and the third one to the deprotonation of the C-3 OH. It is facilitated by inductive presence of iron(III) through the conjugated network. We postulate the coordination to the catechol group by comparison of the absorption spectrum of our system with similar known simple models: catechol, tiron, salicylaldehyde. At pH = 4 the 1:1 Fe–quercetin system showed on its spectrum a smooth peak at λ 625–630 nm in the same zone in which 1:1 Fe–catechol (λ_{max} 680 nm) and 1:1

Can. J. Chem. Downloaded from www.nrcresearchpress.com by 123.30.183.119 on 09/08/12
For personal use only.

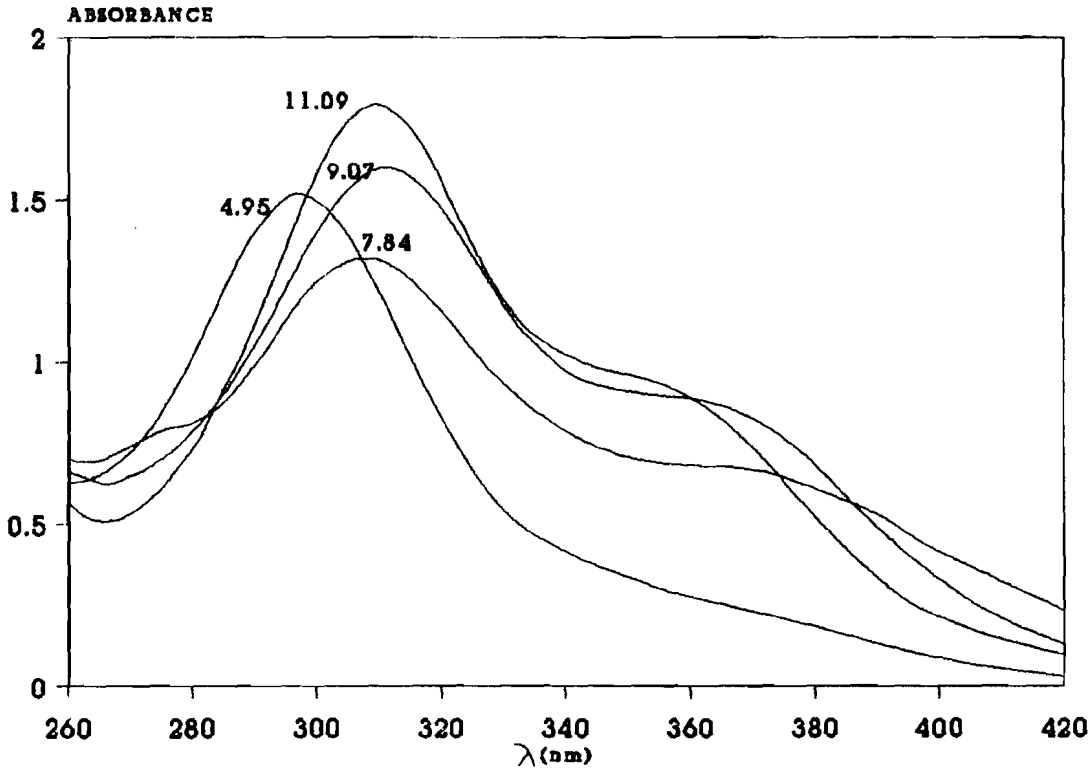


FIG. 1. Absorption spectra of quercetin as a function of pH. $\mu = 0.10$ M ($NaNO_3$), 1.00 mm cell, $t = 20.0$°C, [quercetin] = 5.00×10^{-5} M.

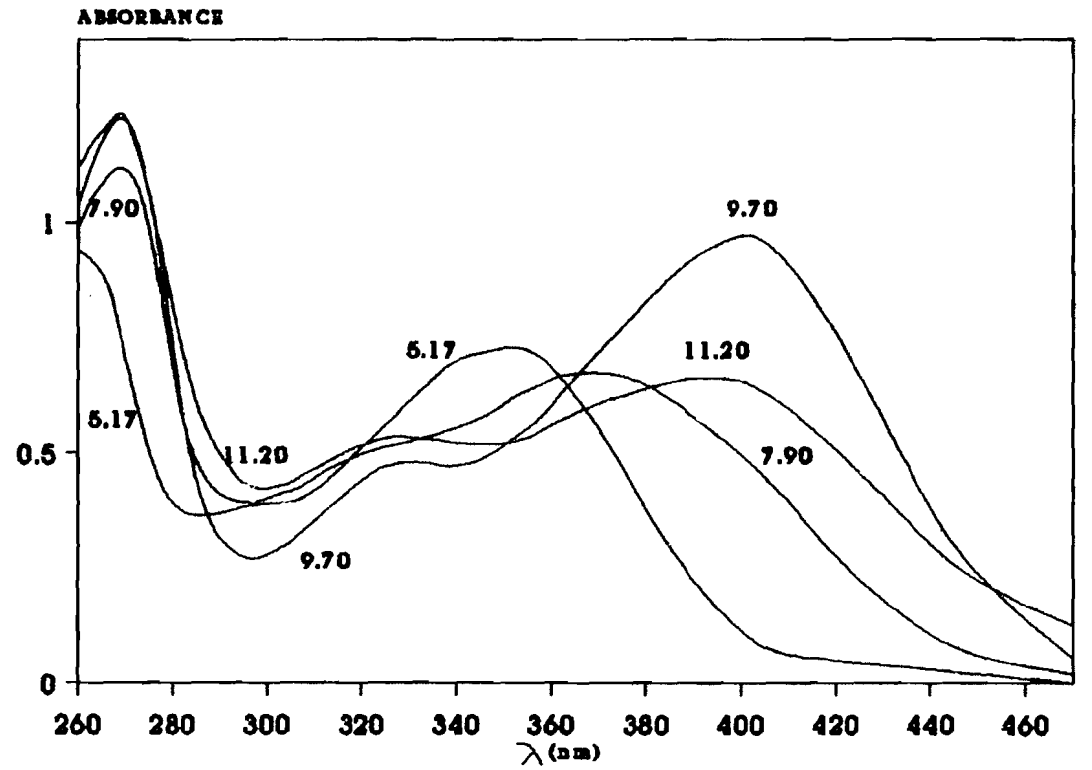


FIG. 2. Absorption spectra of rutin as a function of pH; $\mu = 0.10$ M ($NaNO_3$), 1 mm cell, t = 20.0°C, [rutin] = 4.95×10^{-5} M.

Can. J. Chem. Downloaded from www.nrcresearchpress.com by 123.30.183.119 on 09/08/12
For personal use only.

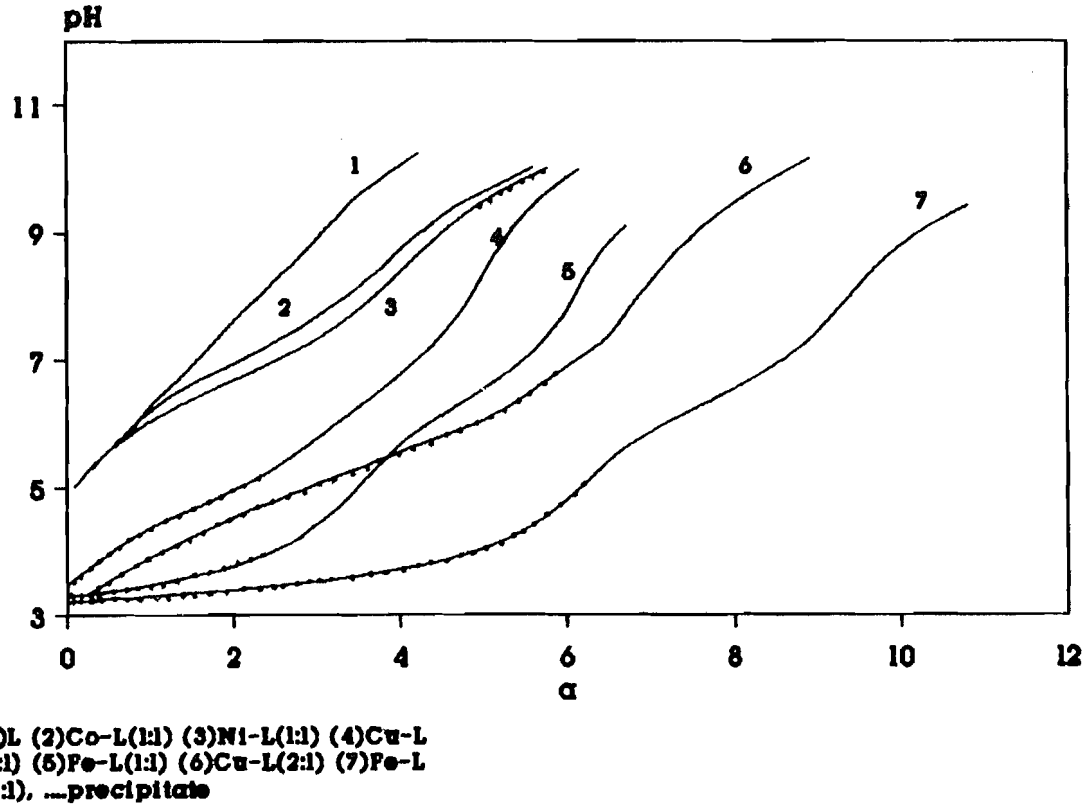


FIG. 3. Potentiometric equilibrium curves of quercetin in the absence and presence of metal ions; μ = 0.10 M ($NaNO_3$), t = 20.0°C.

Fe–tiron (λ_{max} 670–676 nm) absorb (8). The 1:1 Fe–salicylaldehyde system does not absorb at such wavelengths, a fact that allows us to assume the possibility of no coordination at the bottom of the molecule. All these results indicated that the coordination to the catechol group is the strongest possibility, in agreement with the high affinity of this bidentate group for Fe(III) (9). Due to the spatial constraints on the quercetin molecule, there is no opportunity for any other OH group to coordinate Fe(III) even if one dissociation does occur. The coordination number of this ion is fulfilled with water molecules with high polarization effect and consequent deprotonation of two water molecules, producing hydroxy complexes. The species diagram distribution of the system under study (Fig. 4) shows that the complex FeH_2L is completely formed at low pH. Its stability constant was calculated through a spectrophotometric competitive method, employing EDTA, at pH = 3.70, λ 625 nm (ϵ_{MH2L} 1883 cm^{-1} M^{-1}) working with dilute solutions to avoid complex precipitation. The metal chelate stability constant and the corresponding chelate protonation constants (calculated in the soluble region of the potentiometric curve) are listed in Table 2.

The potentiometric curve of the 2:1 iron–quercetin system (Fig. 3) showed the formation of the stable chelates with different degrees of protonation, with the neutral species being insoluble.

The coordination of the second Fe(III) to the quercetin molecule might be produced between the carbonyl oxygen and either the C-5 OH group or the C-3 OH group (Scheme 2). Although we are not able to decide between the two possible structures employing potentiometric data, the formation of a stable six-member chelate ring would suggest that 2a is the most likely structure.

TABLE 2. Stability constants and protonation constants of chelates between quercetin (H_5L) and Fe(III) at 20°C and μ = 0.10 M ($NaNO_3$)

Quotient[a]	log K	σfit
$[Fe(OH)_2L]/[Fe][L][OH]^2$	44.2	
$[Fe(OH)L]/[Fe](OH)_2L][H]$	8.88	
[FeL]/[Fe(OH)L][H]	6.76	0.03
[FeHL]/[FeL][H]	6.29	
$[FeH_2L]/[FeHL][H]$	4.95	
$[Fe_2(OH)_6L][H]^4/[Fe(OH)_2L][Fe]$	−17.16	
$[Fe_2(OH)_5L]/[Fe_2(OH)_6L][H]$	9.35	
$[Fe_2(OH)_4L]/[Fe_2(OH)_5L][H]$	8.24	
$[Fe_2(OH)_3L]/[Fe_2(OH)_4L][H]$	6.73	0.04
$[Fe_2(OH)_2L]/[Fe_2(OH)_3L][H]$	6.08	
$[Fe_2(OH)L]/[Fe_2(OH)_2L][H]$	5.50	
[FeTiron]/[Fe][Tiron]	20.4[b]	
[FeSal]/[Fe][Sal]	8.75[b]	

[a]Sal = Salicylaldehyde.
[b]25°C, μ = 0.1, ref. 10.

Equilibrium constants for the binuclear system were calculated from the data in the 2:1 pH profiles (keeping the values calculated on the 1:1 system constant). Figure 5 shows the distribution species diagram and Table 2 the corresponding results.

The formation of chelates containing a 1:2 metal-to-ligand

Can. J. Chem. Downloaded from www.nrcresearchpress.com by 123.30.183.119 on 09/08/12
For personal use only.

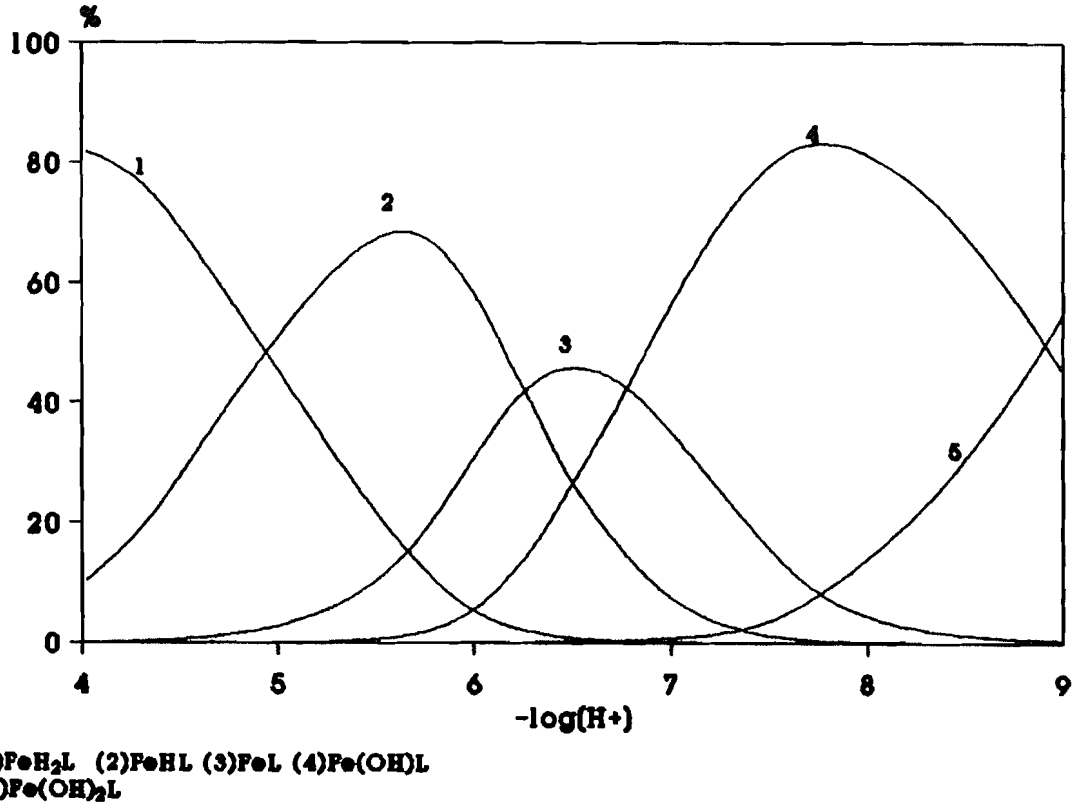
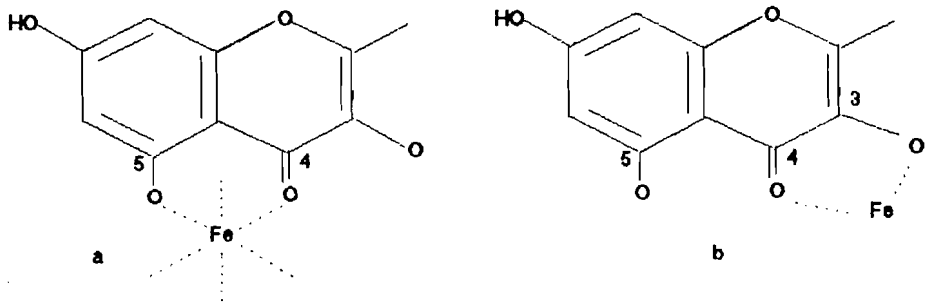


FIG. 4. Distribution of species as a function of $p[H^+]$ in a 1:1 Fe(III)–quercetin system; $\mu = 0.10$ M ($NaNO_3$), $t = 20.0$°C.



SCHEME 2

ratio could not be detected, and only 1:1 chelates were found in systems containing 1:2 ratio of reactants.

Iron rutin

The potentiometric curve of the 1:1 system (Fig. 6) could be explained with the formation of the same complexes proposed before for quercetin, with the difference that one less hydroxyl group was neutralized, the one involved on the glycosidic linkage. The first complex detected at low pH was the non-hydrolyzed species FeH_2L^+ whose formation constant was evaluated employing a competitive method with EDTA (pH = 3.00, λ 500 nm, ϵn_{MH2L} 2000 cm^{-1} M^{-1}). A relationship (2:1) M/L showed the existence of binuclear complexes. The coordination of the Fe(III) to the ligand would be established through the catechol group and between the carbonyl group and the free C-5 OH. The proposed equilibria for the 1:1 and 2:1 systems together with the corresponding equilibrium constants are shown in Table 3.

Cu(II) system

Cu quercetin

In the 1:1 solution the precipitation of the neutral species CuH_3L was observed at the beginning of the titration (Fig. 3). On increasing the pH the precipitate was dissolved with the production of a hydroxyl complex. The flattening of the curve after $a = 5$ suggests an additional equilibrium produced by the formation of the fully deprotonated complex. The proposed equilibria are

[7] $Cu^{2+} + L^{5-} + H_2O \rightleftharpoons Cu(OH)L^{4-} + H^+$

[8] $Cu(OH)L^{4-} + H^+ \rightleftharpoons CuL^{3-}$

[9] $CuL^{3-} + H^+ \rightleftharpoons CuHL^{2-}$

[10] $CuHL^{2-} + H^+ \rightleftharpoons CuH_2L^-$

The potentiometric curve of the 2:1 copper–quercetin system (Fig. 3) showed the formation of binuclear chelates. The

Can. J. Chem. Downloaded from www.nrcresearchpress.com by 123.30.183.119 on 09/08/12
For personal use only.

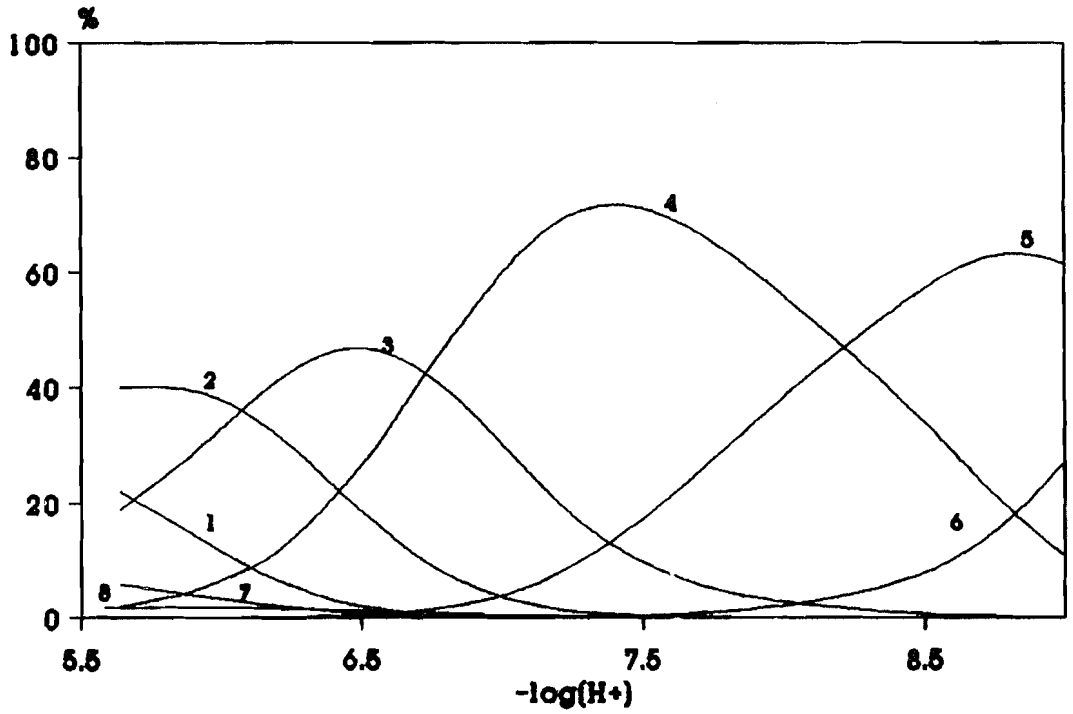


FIG. 5. Distribution of species as a function of $p[H^+]$ in a 2:1 Fe(III)–quercetin system; $\mu = 0.10$ M ($NaNO_3$), $t = 20.0$°C.

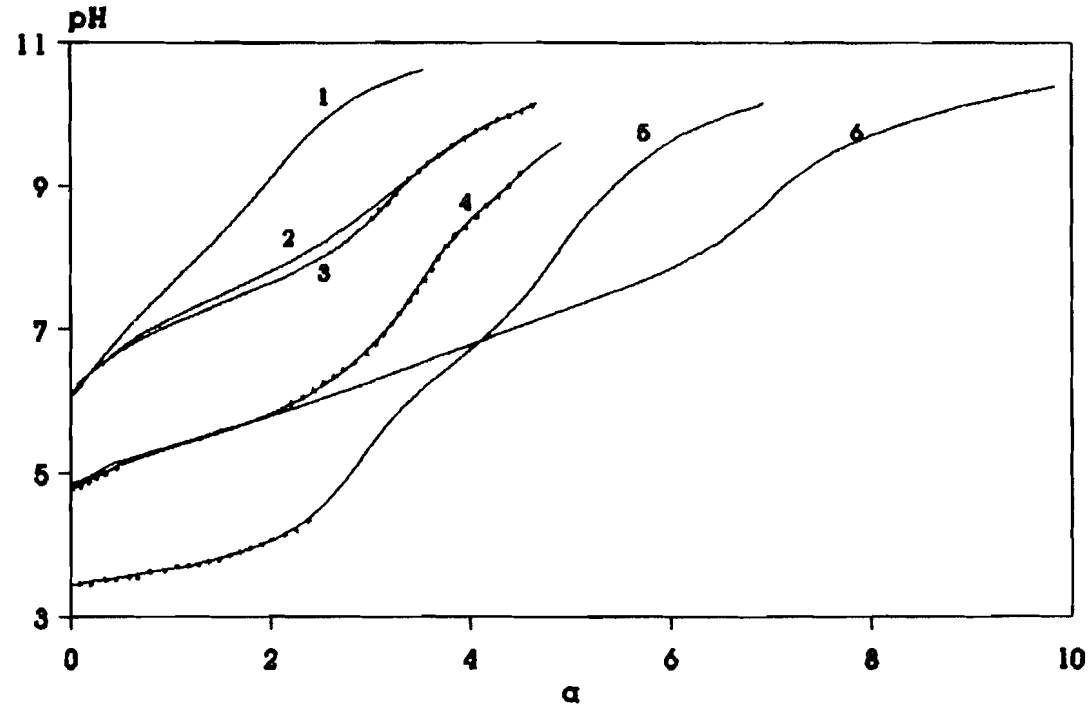


FIG. 6. Potentiometric equilibrium curves of rutin in the absence and presence of metal ions; $\mu = 0.10$ M ($NaNO_3$), $t = 20.0$°C.

Can. J. Chem. Downloaded from www.nrcresearchpress.com by 123.30.183.119 on 09/08/12
For personal use only.

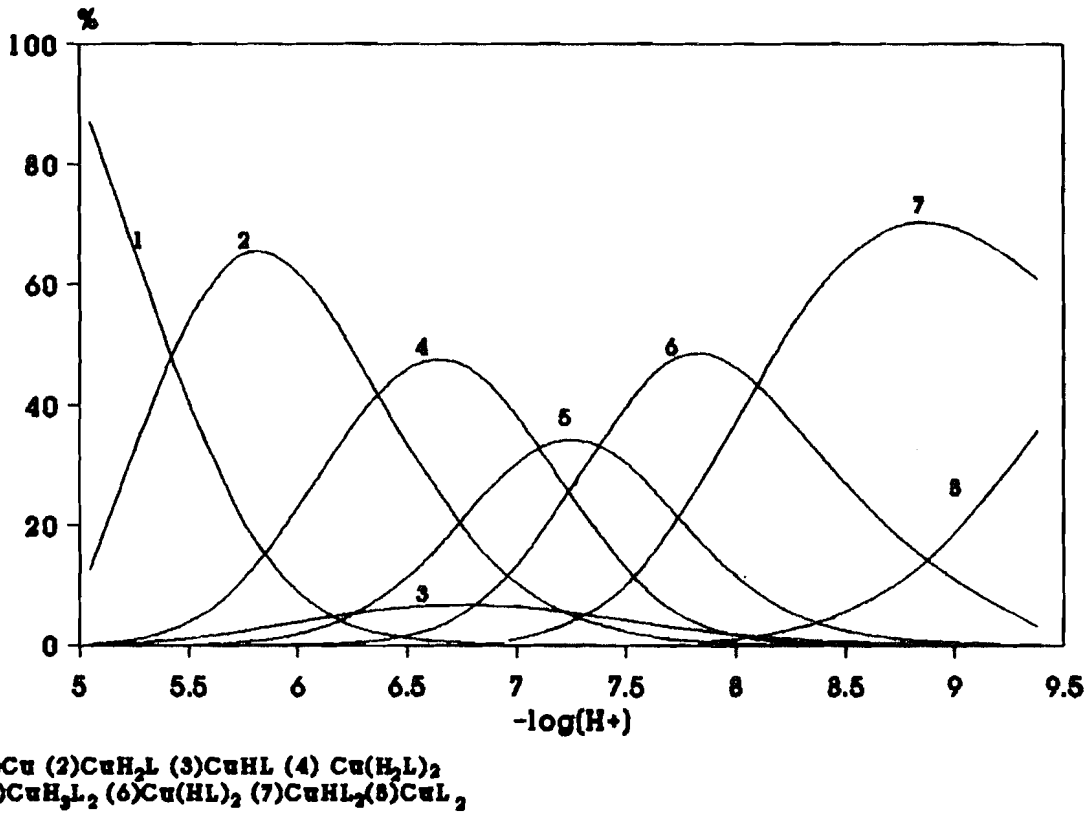


FIG. 7. Distribution of species as a function of p[H^+] in a 1:2 Cu(II)–rutin system; μ = 0.10 M ($NaNO_3$), t = 20.0°C.

TABLE 3. Stability constants and protonation constants of chelates between rutin (H_4L) and Fe(III) at 20°C and μ = 0.10 M ($NaNO_3$)

Quotient	log K	σfit
$[Fe(OH)_2L]/[Fe][L][OH]^2$	44.1	
$[Fe(OH)L]/[Fe](OH)_2L][H]$	9.28	
$[FeL]/[Fe(OH)L][H]$	7.34	0.04
$[FeHL]/[FeL][H]$	6.20	
$[FeH_2L]/[FeHL][H]$	3.84	
$[Fe_2(OH)_6L][H]^4/[Fe(OH)_2L][Fe]$	−17.08	
$[Fe_2(OH)_5L]/[Fe_2(OH)_6L][H]$	10.63	
$[Fe_2(OH)_4L]/[Fe_2(OH)_5L][H]$	9.02	0.03
$[Fe_2(OH)_3L]/[Fe_2(OH)_4L][H]$	7.32	
$[Fe_2(OH)_2L]/[Fe_2(OH)_3L][H]$	6.35	

TABLE 4. Stability constants of chelates between quercetin (H_5L) and Cu(II) at 20°C and μ = 0.10 M ($NaNO_3$)

Quotient[a]	log K	σfit
$[Cu(OH)L]/[Cu][L][OH]$	19.30	
$[CuL]/[Cu(OH)L][H]$	9.32	0.03
$[CuHL]/[CuL][H]$	7.37	
$[CuH_2L]/[CuHL][H]$	5.87	
$[Cu_2(OH)_4L][H]^3/[Cu(OH)L][Cu]$	−20.84	
$[Cu_2(OH)_3L]/[Cu_2(OH)_4L][H]$	10.22	
$[Cu_2(OH)_2L]/[Cu(OH)_3L][H]$	9.18	0.02
$[Cu_2(OH)L]/[Cu_2(OH)_2L][H]$	7.53	
$[Cu_2L]/[Cu_2(OH)L][H]$	5.75	
[CuTiron]/[Cu][Tiron]	14.27[b]	
[CuSal]/[Cu][Sal]	5.56[b]	

[a]Sal = salicylaldehyde.
[b]25°C, μ = 0.1, ref. 10.

complex produced at high pH with two hydroxyl groups coordinated at each Cu atom could explain the tendency of this metal to fulfill its coordination number producing square-planar complexes. Table 4 shows the equilibrium constants calculated from the 1:1 and 2:1 systems.

The treatment of the data for the 1:2 Cu–quercetin system did not show the existence of such complexes. It is likely that the open coordination sites on the metal ion can react with other partially coordinated ligand molecules.

Cu rutin

1:1 ratio: At the beginning of the titration the solution was clear, becoming turbid as the pH was increased (Fig. 6). The observed result could be explained as the early production of a 1:1 complex followed by a disproportionation process to produce $Cu(OH)_2$ and the 1:2 Cu–rutin complex. The above statement was confirmed through the absence of precipitate along the potentiometric curve of the 1:2 system. Table 5 shows the equilibrium constant value.

2:1 metal ion – ligand ratio: The potentiometric curve showed similar behavior to the 1:1 system up to an a value of 2.5, where a disproportionation process took place before the binuclear complexes could be detected. At pH above 9.30 the precipitate was dissolved to produce a mixture of stable complexes but in this narrow pH range measurements of useful potentiometric data were not possible.

Ni(II) and Co(II) systems

The potentiometric behavior of both cations with the ligands investigated in the 1:1 systems was found to be similar. The

Can. J. Chem. Downloaded from www.nrcresearchpress.com by 123.30.183.119 on 09/08/12
For personal use only.

TABLE 5. Stability constants of chelates between rutin (H_4L) and Cu(II) at 20°C and μ = 0.10 M ($NaNO_3$)

Quotient	log K	σfit
$[CuH_2L]/[Cu][L][H]^2$	28.51	
$[CuL_2]/[Cu][L]^2$	23.51	
$[CuHL_2]/[CuL_2][H]$	9.62	0.01
$[Cu(HL)_2]/[CuHL_2][H]$	8.10	
$[CuH_3L_2]/[Cu(HL)_2][H]$	7.38	
$[Cu(H_2L)_2]/[CuH_3L_2][H]$	7.11	

TABLE 6. Stability constants of chelates between quercetin and rutin with Co(II) and Ni(II) at 20°C and μ = 0.10 M ($NaNO_3$)

	Quercetin (H_5L)		Rutin (H_4L)	
Quotient[a]	log K	σfit	log K	σfit
[CoL]/[Co][L]	8.37		8.23	
[CoHL]/[CoL][H]	9.22	0.04	9.14	0.03
$[CoH_2L]/[CoHL][H]$	7.93		7.66	
[CoTiron]/[Co][Tiron]	9.49[b]			
[NiL]/[Ni][L]	9.53			
[NiHL)]/[NiL][H]	9.00	0.02	6.63	0.03
$[NiH_2L]/[NiHL][H]$	7.55		7.16	
[NiTiron]/[Ni][Tiron]	9.96[b]			
[NiSal]/[Ni][Sal]	3.58[b]			

[a]Sal = salicylaldehyde.
[b]25°C, μ = 0.1, ref. 10.

only difference lies in that the Co(II) complexes are stable enough to avoid the precipitation of the hydroxide. The analysis of the potentiometric curves (Figs. 3 and 6) showed a high coincidence with the potentiometric curves of the free ligands until $a \approx 1$. Precipitation of nickel(II) hydroxide took place at high pH, after the Ni(II) complexes were produced. Table 6 shows the stability constant values.

The ligands under study interact strongly with Fe(III), as shown through the stability constant values, with predominance of insoluble species at low pH values, and production of soluble hydroxo complexes at high pH. There are no possibilities of formation of complexes with several molecules of ligands such as catechol, probably due to the steric hindrance and the great hydrolytic tendency of the Fe(III) linked to rutin or quercetin which allow the production of very stable hydroxo complexes.

The interaction of rutin and quercetin is less strong with divalent ions of the transition series, the stability constant value of the complex produced between rutin and Cu(II) for a 1:2 M/L relationship being prominent.

The rigidity of these ligands would prevent simultaneous participation of other chelating donor groups within the ligand molecule. Therefore, it was decided to check the existence of binuclear complexes. The main coordination site was obviously the catechol group which was verified for the Fe(III)–L system by comparing the visible spectra with model systems. Moreover, the stability constant values were compared with those for the complexes with tiron and salicylaldehyde which appear at the end of each table.

Through the obtained results it can be observed that if the dissacharide present on the rutin molecule shows a possible interaction with the studied metal ions, it should be very weak, and its major influence should lie in increasing the solubility of the ligand.

Acknowledgments

We thank Dr J. R. Motekaitis, Chemistry Department, Texas A & M University, U.S.A., for helpful comments and CONICET and University of Rosario for financial support.

1. KLAUS FLOREY (*Editor*). Analytical profiles of drug substances. Vol. 12. Academic Press. 1983.
2. S. D. VARMA and J. H. KINOSHITA. Biochem. Pharmacol. **25**, 2505 (1976).
3. R. H. WILSON. J. Pharmacol. **90**, 120 (1947).
4. G. SCHWARZENBACH. Complex titrations. Interscience Publishers Inc., New York. 1960.
5. W. R. HARRIS and A. E. MARTELL. Inorg. Chem. **15**, 713 (1976).
6. G. M. ESCANDAR and L. F. SALA. An. Asoc. Quim. Argent. **78**, 37 (1990).
7. R. J. MOTEKAITIS and A. E. MARTELL. Can. J. Chem. **60**, 2403 (1982).
8. W. A. MCBRYDE. Can. J. Chem. **42**, 1917 (1964).
9. A. E. MARTELL *et al.* Inorg. Chim. Acta, **138**, 215 (1987).
10. A. E. MARTELL and R. M. SMITH. Critical stability constants. Vol. 3. Plenum Press, New York. 1989.

Can. J. Chem. Downloaded from www.nrcresearchpress.com by 123.30.183.119 on 09/08/12
For personal use only.

Ion–molecule reactions of transition-metal ions with nitriles in the gas phase: competitive formation of both "end-on" and "side-on" coordination

LIN-ZHI CHEN AND JACK M. MILLER[1]

Department of Chemistry, Brock University, St. Catharines, Ont., Canada L2S 3A1

Received March 6, 1991

LIN-ZHI CHEN and JACK M. MILLER. Can. J. Chem. **69**, 2002 (1991).

First field-free region B/E linked scan studies of metastable and particularly collision-induced dissociations show that two competitive coordination processes ("end-on" and "side-on") exist in the complexation of metal ions (Ni^+, Co^+, Fe^+, and Mn^+) with alkanenitriles in the FAB source of an E/B configuration mass spectrometer. Analysis of the B/E linked scan CA spectra gives approximate percentages of the end-on coordination mode in the reactive complexes. An unusual β-methyl migration, involved in the elimination of CH_4 from end-on complexes, may be in competition with β-H migration/elimination of H_2 and β-C—C bond cleavage/elimination of alkene. For the side-on complexes, the metal ions can insert into various C—C bonds followed by β-H transfer/competitive elimination of alkene and alkane or by a direct C—M^+ bond cleavage to give an alkyl radical.

Key words: FAB mass spectroscopy, metal-ion/nitrile reactions, collisional activation, coordination modes, ion–molecule reactions.

LIN-ZHI CHEN et JACK M. MILLER. Can. J. Chem. **69**, 2002 (1991).

Des études de dissociations unimoléculaires, en particulier des dissociations induites par des collisions, effectuées dans la première région sans champ d'un spectromètre de masse de configuration E/B, à l'aide de balayages couplés E/B, démontrent l'existence de deux processus compétitifs de coordination ("par le bout" et "par le côté") dans la complexation d'ions métalliques (Ni^+, Co^+, Fe^+ et Mn^+) par les nitriles aliphatiques. L'analyse des spectres d'activation fournit des pourcentages approximatifs du mode de coordination par le bout les espèces réactives. Il est possible qu'une migration inhabituelle β d'un méthyle, impliqué dans l'élimination de CH_4 à partir des complexes de coordination formés par le bout, soit en compétition avec une migration/élimination β d'un H de H_2 ainsi que le bris en β d'une liaison C—C avec élimination d'alcène. Dans les complexes formés par une attaque de côté, les ions métalliques peuvent subir des insertions dans diverse liaisons C—C, suivies par un transfert d'un H en β avec élimination compétitive d'alcène ou d'alcane ou par un bris direct d'une liaison C—M^+ conduisant à un radical alkyle.

Mots clés : spectroscopie de masse FAB, réactions ion métallique/nitrile, activation par collision, modes de coordination, réactions ion–molécule.

[Traduit par la rédaction]

Introduction

Ion–molecule reactions of transition-metal ions (both positive and negative, including cluster ions) with organic molecules in the gas phase have received considerable attention during the last decade (1). Ion cyclotron resonance (ICR), Fourier-transform ICR, quadrupole, and sector mass spectrometers have been successfully applied to this field. The discovery that selective functionalization of remote C—H and C—C bonds is caused by transition-metal ions in "end-on" complexes (1*a*, 2) is of particular importance, since they display a similarity to enzymes. This remote functionalization has also been found in other systems such as isonitriles (3), amines (4), alcohols (4*b*, 5), alkynes (6), allenes (6*e*), and ketones (7). In fact, the selective C—H or C—C bond activation is a reflection of the reactivity and coordination of the complexed metal ions. Another important reaction mechanism involves the insertion of a metal ion into a C—C (or C—H) bond followed by β-H transfer and the competitive elimination of the ligands (1*c*). This mechanism can explain reactions of metal ions in "side-on" complexes.

Recently, we demonstrated (8) a coexistence of both end-on and side-on coordinated complexes of short-chain alkanenitriles (**1** and **2**) with transition-metal ions, Ni^+, Co^+, Fe^+, and Mn^+. That is interesting because the results indicate a competition between the coordination processes. Further study of the system might give insight into the nature of the coordination process. In this paper we will present additional experimental evidence for the competition in the case of longer chain nitriles **3**–**7** with the transition-metal ions (Ni^+, Co^+, Fe^+, Mn^+). We will also discuss the distribution of both coordination modes. Finally, an unusual β-methyl migration is also proposed and discussed.

CH_3CN	CH_3CH_2CN	$CH_3(CH_2)_2CN$	$(CH_3)_2CHCH_2CN$
1	**2**	**3**	**4**

$CH_3(CH_2)_3CN$	$(CH_3)_2CH(CH_2)_2CN$	$CH_3(CH_2)_4CN$
5	**6**	**7**

Experimental

A Kratos Concept IS double-focusing mass spectrometer of E/B configuration (Kratos Analytical, Urmston, Manchester, UK) was used in this work. The instrument was controlled by a Kratos DS 90 Data General Eclipse based computer system. A Kratos Mach 3 data system running on a SUN SPARCstation was used for further data work-up. Ion–molecule adducts were prepared in a modified FAB source containing a small hole to accept the ligand vapour from a heated reservoir probe inserted via the EI/CI probe lock. A detailed description of the modified instrument, closed FAB source, and operating conditions are given elsewhere (8). Briefly, the instrument was fitted with an Ion Tech saddle field atom gun and xenon was used as the fast-atom source. The fast-atom-beam energy was 8 keV with a density corresponding to an emission current of about 1 mA. The source was operated at a temperature of 25°C, a pressure of about 10^{-5} Torr (measured in the source housing — not in the reaction region), and an accelerating voltage of 6 kV. We used a resolving power of 1000 for recording normal mass spectra. Metastable ion (MI) or

[1]For unknown reasons, complexation of Co^+ with valeronitrile was not observed by Schwarz and co-workers in their modified CI/FAB source coupled to a ZAB-HF-3F triple-sector mass spectrometer (2*b*), though we clearly detected the adduct in our system.

Can. J. Chem. Downloaded from www.nrcresearchpress.com by 123.30.183.119 on 09/08/12
For personal use only.

TABLE 1. B/E linked scan MI (in parentheses) and CA spectra of RCN/M^+ ions[a]

	7			5			3			6			4		
	Ni	Co	Fe	Ni	Co	Fe	Ni	Co	Fe	Ni	Co	Fe	Ni	Co	Fe
$1M^+$ (metal ions)	100	18	32	100	83	35	100	100	100	40	65	35	100	100	100
	(2)	(8)	(5)	(18)	(38)	(19)	(100)	(100)	(100)	(5)	(4)	(9)	(100)	(100)	(100)
Neutral loss[b]															
H_2	30	100	100	40	100	100	4	2	2	32	50	100	15	23	16
	(100)	(100)	(100)	(100)	(100)	(100)	(1)	(<1)		(34)	(46)	(100)			
CH_4	5	6	3	3	2	—	5	2	1	100	100	62	23	58	16
	(1)	(3)	(1)							(100)	(100)	(55)	(2)	(2)	(4)
C_2H_4	95	77	25	39	70	80	32	17	11						
	(40)	(60)	(35)	(70)	(62)	(79)									
$C_2H_5\cdot$	1	3	9	2	1	<1	10	8	5						
		(2)	(4)												
C_2H_6	4	<1	—	10	6	<1	—	—	—						
CH_3CHCH_2	8	2	<1	33	24	5	7	1	—	15	25	35	50	75	17
				(5)	(4)	(1)				(8)	(13)	(25)			
$CH_3CH_2CH_2\cdot$[c]	5	2	3	15	13	3	1	1	3						
$(CH_3)_2CH\cdot$										2	2	2	18	13	3
$(CH_3)_2CH_2$	15	2	<1	1	—	—				12	10	1	—	—	—
$C_2H_5CHCH_2$[c]	32	6	4	12	1	—									
$(CH_3)_2CCH_2$										8	2	8	22	8	—
$C_3H_7CH_2\cdot$[c]	28	4	4	<1	2					20	20	5	4	2	2
$C_3H_7CHCH_2$[c]	12	1	<1							8	3	—			
$C_4H_9CH_2\cdot$[c]	2	<1	1							1	3	4			

[a]For RCN/Mn^+ ions, the most abundant fragments are due to detachment and not listed here.
[b]Data given for the neutral loss as the abundances of corresponding charged fragments relative to the base peaks in the B/E linked scan spectra.
[c]Although linear and branched alkyl fragments with same carbon numbers cannot be distinguished in the experiments, we propose that they remain similar in skeletal combinations as in the complexes.

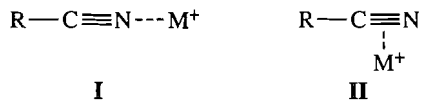
Can. J. Chem. Downloaded from www.nrcresearchpress.com by 123.30.183.119 on 09/08/12
For personal use only.

collision-induced dissociation (CID) in the first field-free region collision chamber behind the source slit was monitored by B/E linked scans. The collision gas was helium and its pressure in the collision chamber was maintained to reduce the main beam by 20% (corresponding to 1.1 collisions (9)). Since there was diffusion of gas from the source into the collision chamber region, metastable ions for recording the MI spectra might have been partially activated.

"Naked" metal ions were generated by sputtering from the solid salts, $FeSO_4\cdot 7H_2O$, $CoCl_2\cdot 6H_2O$, $NiCl_2\cdot 6H_2O$, and $MnCl_2\cdot 4H_2O$, which had been deposited by evaporation onto the FAB probe tip. Nitriles were introduced into the source via the reservoir probe. A 3-μL sample of the liquid reagent was typically injected into the reservoir probe whose temperature was 100°C. All samples were commerically available and used directly without further purification.

Results and discussion

Ion–molecule monoadducts, RCN—M^+, are the dominant products of the reactions between the transition-metal ions (Ni^+, Co^+, Fe^+, and Mn^+) and nitriles (**3**–**7**) in the closed FAB source.[1] We also observed diadduct ions, $(RCN)_2M^+$, and some fragments of the monoadducts. Stepnowski and Allison (10) have investigated these reactions in an ICR instrument. In most cases, however, the ion–molecule adducts were not dominant products. The fact that losses of small neutral species such as H_2, CH_4, and C_2H_2 remained significant may be due to the longer reaction time in ICR instruments vs. that in sector spectrometers. No reaction between acetonitrile and Co^+ and no diadduct ions, $(RCN)_2M^+$, were found in the ICR experiments.



I **II**

Fragmentations of adducts

In order to elucidate the structure and reaction mechansim of the monoadducts, metastable and collision-induced fragmentations of these species in the first field-free region were investigated using B/E linked scans (Table 1). Most of the fragments also exist in the normal mass spectra. Detailed description of the MI and CID fragmentations of **1** − M^+ and **2** − M^+ have been previously reported (8). Compared with the MI spectra of metal/nitrile (**3**–**7**) complexes, collisional activation induces additional fragmentation, consistent with the results obtained from **5** − M^+ and **7** − M^+ by Schwarz and co-workers (2). Schwarz's group described the most important processes, i.e. the losses of H_2 and C_2H_4, in terms of remote functionalization. However, the CA-induced fragmentations are of interest because they cannot be simply attributed to remote functionalization (see below). We will discuss these additional fragmentation processes and propose possible complexation modes.

By CA studies of the complexes of **5**, **7**, and unbranched longer-chain nitriles with Fe^+ and Co^+, Schwartz and co-workers demonstrated that the reactions of the end-on complexes involved an insertion of a metal ion into the C—H bond of a terminal methyl group of the nitrile, followed by both a β-hydrogen transfer to the metal centre and a β-C—C bond cleavage that produced, respectively, H_2 and C_2H_4 (2). Recently, however, a study combining FT-ICR and sector mass spectrometry suggested (11) that the reaction of **5**—M^+ is different from other long-chain nitrile complexes, and involved a degenerate isomerization to form a ferracyclobutane intermediate prior to any losses of neutral species. While the loss of one hydrogen was due to remote functionalization, ethylene was produced from internal chain positions. Loss of propene was

Can. J. Chem. Downloaded from www.nrcresearchpress.com by 123.30.183.119 on 09/08/12
For personal use only.

also observed in very low abundance. The difference was probably due to the ring strain in the intermediate formed during remote functionalization by **5**—Fe^+. Because of this special case, little of the following discussion relates to the **5**—M^+ complexes.

Remote functionalization reactions are also observed for complexes of **3** and **7** in our B/E linked scan experiments (MI and CA). These reactions are dominant and can be the sole reactions except for detachment in the metastable dissociations of RCN—M^+. For the complexes of **4** and **6** with branched alkyl chain, loss of propene instead of ethylene occurs (Table 1). Upon CA, however, some intense fragments due to losses of C_nH_{2n}, $\cdot C_nH_{2n+1}$, and C_nH_{2n+2} are observed. Figure 1 shows the MI and CA spectra of **7** − Ni^+. Compared with the MI spectrum, CA induces the losses of CH_4 (peak at *m/z* 139, 5% relative to losses of C_2H_4), C_2H_6 (*m/z* 125, 4%), C_3H_8 (*m/z* 111, 15%), C_3H_6 (*m/z* 113, 8%), C_4H_8 (*m/z* 99, 32%), C_5H_{10} (*m/z* 85, 12%), $\cdot C_2H_5$(*m/z* 126, 1%), $\cdot C_3H_7$ (*m/z* 112, 5%), $\cdot C_4H_9$ (*m/z* 98, 28%), and $\cdot C_5H_{11}$ (*m/z* 84, 2%).

In the end-on complex **I**, the approximately linear combination of atoms keeps M^+ so far from the nitrile chain that it attacks only the C—H or C—C bonds further out than the δ-position. Clearly, the end-on mode cannot account for the additional collision-induced fragments from RCN—M^+. One may suggest that an attack of the available C—H or C—C bonds by an electronically excited metal ion or a direct C—C bond cleavage contributes to these fragments. Although electron-impact ionization generates electronically excited M^+ ions (12), the FAB method generates ground-state metal ions (13, 14). Moreover, loss of alkane, alkyl radical, or alkene was found for other nitrile–metal complexes in sector (15), Fourier-transform ICR (2*d*, 16), and ICR (10) instruments, and described in terms of C—C bond insertion/C—M^+ bond cleavage sequence. Complexation of the metal ion with an organic substrate prior to insertion into a C—H or C—C bond is expected to be more favorable in energy and occurs in most ion–molecule reaction systems (1). If the initial complex is sufficiently long-lived, preferred coordination may play an important role in determining the final products (10). We thus suggest another coordination mode, which is in competition with the end-on mode, for the formation of the additional fragments from RCN—M^+.

The other coordination mode is probably the side-on, because side-on complexed metal ions are close enough to the α- and β-carbon to be able to insert (8). In fact, side-on coordination has been suggested by Schwarz *et al.* for the complexation of transition-metal ions with alkenenitriles (17), phosphaalkynes (18), and for the reaction of Cu^+ with nitriles (2*d*, 3*b*, 19). Moreover, the coordination mode of RNC—M^+ varies with the chain length of isonitrile. The side-on mode accounts for the complexes of short-chain isonitriles, corresponding to the losses of C_2H_4 and $\cdot C_2H_5$, while the end-on becomes competitive as the chain gets longer and even dominates when the methylene number in the chain is up to 5 (3). For α-branched nitrile (15, 16) and dinitrile (20), complexed metal ions insert into adjacent α-, β,- or γ-C—C bonds. These findings have led Schwarz *et al.* to propose the presence of the side-on coordination in addition to the end-on.

The traditional reaction mechanism of a side-on complex involves C—C bond insertion followed by β-H shift and competitive ligand elimination, as first suggested by Allison and Ridge (21, 22). A similar reaction mechanism has been established for the side-on complexes of RCN—Cu^+ (19). This also holds true for our side-on complexes RCN—M^+ (M = Ni, Co, Fe). When the metal ions insert into various C—C bonds, corresponding alkenes or alkanes are produced after hydrogen migration. Direct C—M^+ bond cleavage gives the alkyl radicals. In most cases, the loss of alkenes is much more intense than the loss of alkanes. This behavior has been interpreted by Schwarz *et al.* as due to a significant activation barrier and (or) a smaller frequency factor for the reductive elimination of alkanes (18). For complexes of **3**–**7** with the metal ions (Ni^+, Co^+, and Fe^+), almost all probable losses of alkenes and radicals except $CH_3\cdot$ are observed. The losses of the highest alkenes and radicals are accompanied by the formation of $[H,M,C,N]^+$ and M^+CN ions.[2] Ni^+ ions form $[H,M,C,N]^+$ rather than $M(CN)^+$ while the opposite case is observed for Fe^+. Co^+ behaves in a mode falling between Fe^+ and Ni^+. α-Disubstituted nitriles were also shown to give M^+/[H,C,N] ions (15, 23).

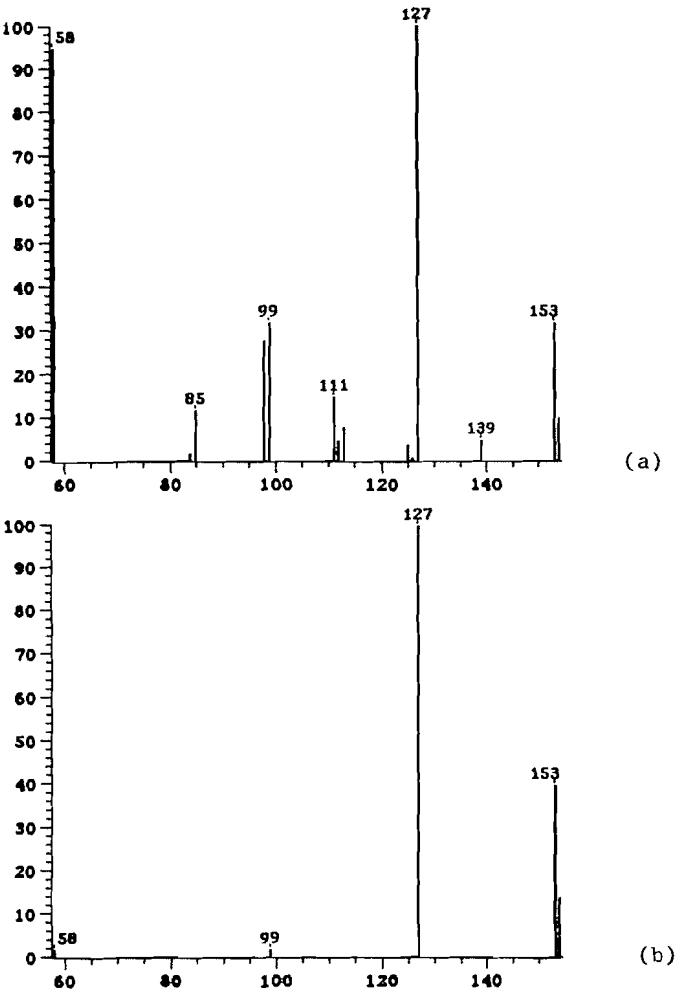


FIG. 1. B/E linked scan MI (*b*) and CA (*a*) spectra of **7**—Ni^+.

Most of the products generated by MI fragmentation of RCN—M^+ are expected from end-on coordination. This indicates that reaction from a side-on complex involves a higher activation energy than from an end-on complex, or that an activation energy is required for isomerization from "end-on" **I** to "side-on" **II** complexes prior to the dissociations.

The fragmentation of complexes formed from branched nitriles (**4**—M^+ and **6**—M^+) produces a considerable amount of methane. Figure 2 shows the MI and CA spectra of **6**—Co^+.

[2]In the experiment, we are unable to identify the structure of $[M,H,C,N]^+$ ions.

Can. J. Chem. Downloaded from www.nrcresearchpress.com by 123.30.183.119 on 09/08/12
For personal use only.

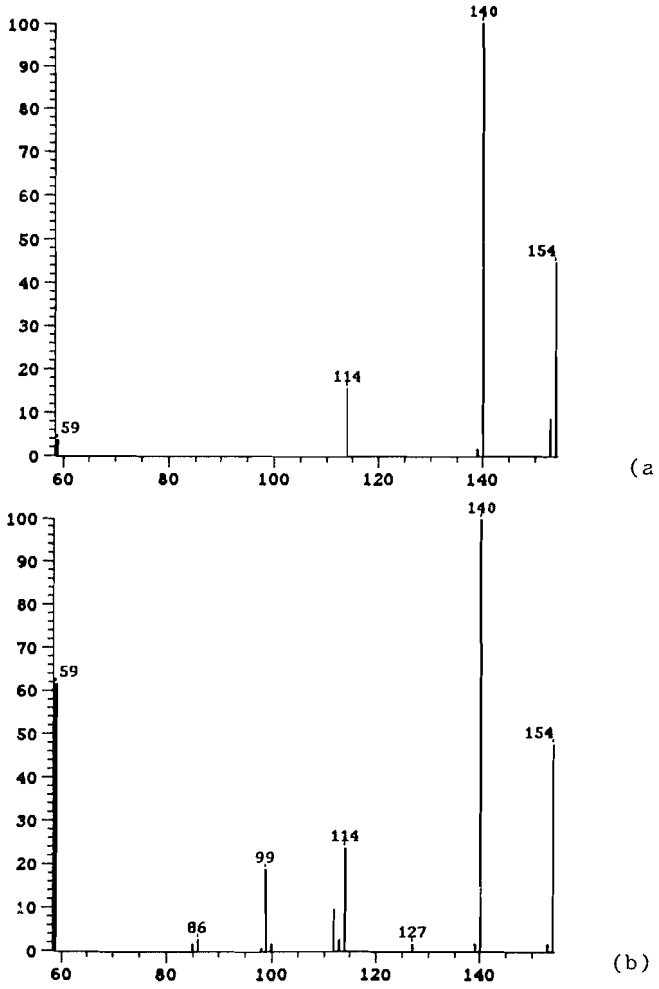


FIG. 2. B/E linked scan MI (*a*) and CA (*b*) spectra of **6**—Co^+.

The MI spectrum shows the fragment peaks at m/z 154 ($-H_2$, 45%), m/z 140 ($-CH_4$, base peak), m/z 114 ($-C_3H_6$, 16%), and m/z 59 (Co^+, 5%); more fragments are produced by collisional activation. For Ni^+ and Co^+, the loss of CH_4 corresponds to the base peaks. Uncertainties may still arise, e.g. which of the coordination modes is involved in the methane loss and by what mechanism. However, we postulate that the methane is produced from the terminal methyl groups, because corresponding unbranched nitriles give quite low intensities for the methane loss (<6% relative to the corresponding base peaks). Side-on coordination seems unreasonable for the methane loss for the following reasons: (*i*) it is expected that a methyl group attached to a primary or secondary carbon cannot make as much difference for the metal ion insertion in a π-complex; (*ii*) since internal C—C bonds are weaker than terminal C—C bonds and the strength of the M^+—R bond formed increases as R gets larger (24, 25), metal ions prefer to insert into an internal C—C bond (24); (*iii*) the CH_4 loss is present in the MI spectra of **6**—M^+ and **4**—M^+, whereas the corresponding unbranched nitrile complexes **3**—M^+ show only the products of the end-on coordination, C_2H_4 and H_2. Thus, the methane loss may be ascribed to the end-on complex. Two possible routes are depicted in Scheme 1.

Path *b* in Scheme 1 involves an initial insertion of the metal ion into the terminal C—C bond (**8–10**) followed by a β-hydrogen transfer to the metal centre (**10–11** and (or) **10–12**) and reductive elimination of CH_4. However, using labeled unbranched nitriles, Schwarz and co-workers (2*b*,*c*) have demonstrated that the CH_4 loss commenced with hexanenitrile for Ni^+ and Co^+ and with octanenitrile for Fe^+ after the insertion into the terminal C—C bond. Even for **7**—Co^+, a very low intensity for CH_4 loss (6% relative to H_2 elimination) was observed. Moreover, reactions involving an insertion of the bare metal ion (Ni^+, Co^+, or Fe^+) into a C—CH_3 bond is a minor process because of the high ionization energy of $\cdot CH_3$ (26).

Thus the initial step is more likely the insertion of the metal ions into the terminal C—H bond to give an intermediate **9** (path *a*) followed by β-methyl transfer (**9–11**)/elimination of CH_4. It has been reported that in certain cases the insertion of a complexed metal ion into a C—H bond in the gas phase preceded insertion into C—C bonds (27, 6*b*), although insertion of Fe^+ into C—C bonds occurred to a greater extent than attack of C—H bonds (28). β-Alkyl migration was found in solution for a few organometallic systems (29). This is rare in the gas phase but has been observed (30). It should be noted that by this method, C—C insertion/β-H transfer vs. C—H insertion/β-$CH_3\cdot$ migration for the elimination of CH_4 could not be clearly distinguished (31).

In fact, the initial step (**8–9**) is a selective functionalization of a remote C—H bond by the metal ion, as already described for the losses of H_2 and C_2H_4 from RCN − M^+ (2). Competition can thus be expected for the elimination of H_2, C_3H_6, and CH_4. For **6**—M^+, elimination of H_2 and CH_4 are more prominent than C_3H_6. Furthermore, Ni^+ and Co^+ ions prefer CH_4 loss over H_2 loss, whereas the opposite case is true for Fe^+. A high preference for the loss of CH_4 over H_2 (3:1, calculated from the CA spectrum) exists for Ni^+. However, a different situation is observed in the case of **4**—M^+. The relative intensity of the neutral loss is $C_3H_6 > CH_4 > H_2$ for Ni^+ and Co^+, while it is approximately equal for Fe^+. It can be seen that the relative kinetic yields of the three neutrals depend on both the metal ions and nitriles. Detailed descriptions of the competition may need further kinetic studies using labeled nitriles and related thermochemical data, which are very sparse at the moment.

Since an α-alkyl shift has been suggested in the reactions of Co^+ with labeled ketones to give CH_4 (32), one may suggest a third mechanism for the loss of CH_4 from **4**—M^+ and **6**—M^+, which involves an initial insertion of the metal ions into the $R(CH_3)_2C$—H bond followed by an α-$CH_3\cdot$ migration to produce CH_4. However, it seems unlikely because internal C—H insertion started at the position C(7) of the nitrile for Co^+ and Ni^+ and C(8) for Fe^+ (2). Moreover, α-methyl transfer was found to be unfavourable in the loss of 42 mass units from Fe^+/phosphaalkynes (18).

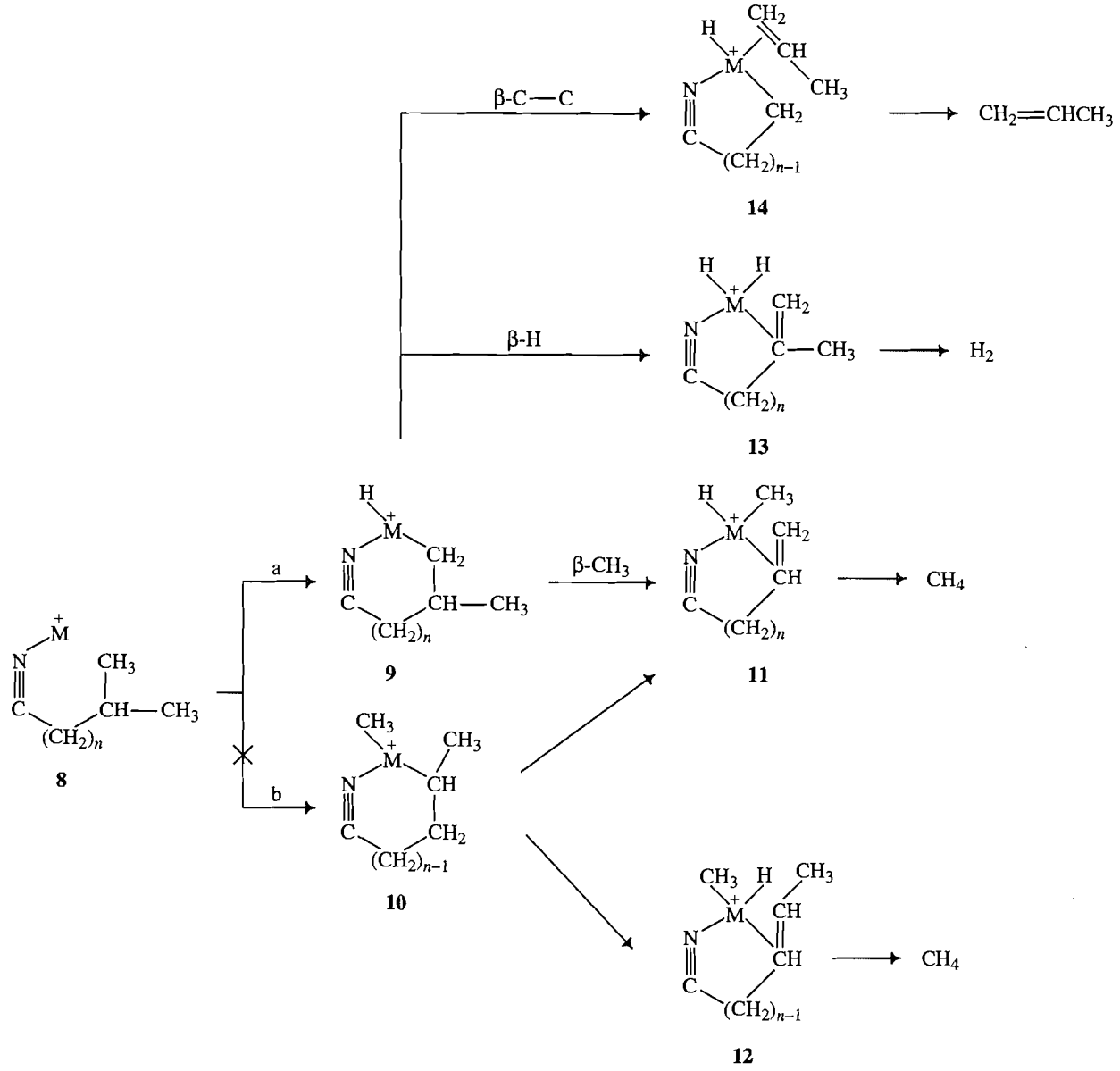
The fragmentations of diadduct ions, $(RCN)_2M^+$, have also been investigated. B/E linked scan MI spectra of the diadduct ions show monoadduct peaks. A few additional low intensity peaks may be observed only in the presence of collision gas. We are interested in these results because they indicate that diadducts with different ligands, R^1CN—M^+—NCR^2, may be useful to measure relative metal ion affinity of the nitriles.[3] This is one of our current projects (34).

Competitive coordinating processes

As we discussed above, products from either side-on or

[3]CI/MS/MS has been demonstrated to be successful in determining the relative PA of organic bases using the dimer ions B_1—H^+—B_2. See, for example, ref. 33. Our current work shows that a similar method can give at least a qualitative sequence of the metal ion affinity of nitriles.

Can. J. Chem. Downloaded from www.nrcresearchpress.com by 123.30.183.119 on 09/08/12
For personal use only.



SCHEME 1. Proposed mechanisms for methane loss from **4**—M^+ or **6**—M^+

TABLE 2. Relative percentage of end-on coordination in the reactive monoadduct[a]

RCN—M^+	Fe^+	Co^+	Ni^+
6—M^+	88	80	68
7—M^+	86	87	57

[a]The side-on adducts of **3** and **4** which may also give both H_2 and C_2H_4 (or C_3H_6) are not collected in this table. We think that the abundance of the detached metal ion may be attributed to both coordinations in a distribution approximately equal to the ratio of the abundance sum of fragments from each coordination mode.

end-on complexes may be approximately distinguished except for **5**—M^+; the end-on adduct produces H_2, C_2H_4 (C_3H_6 for **4**—M^+ and **6**—M^+) and CH_4 (**4**—M^+, **6**—M^+, and **7**—M^+ except for **7**—Fe^+) while most other fragments such as radicals may be ascribed to the side-on complexes. We are thus able to get the percentage of the end-on complex in the monoadduct, which is expressed as the ratio of the abundance sum of fragments from end-on complexes over the sum of the total product ions in the CA spectra (Table 2). The percentages reported below correspond to the reactive complexes. Non-dissociating complexes are not readily observable in these experiments.

It is clear that for Fe^+ and Co^+, end-on coordination dominates in the initial complexation (see Table 2) whereas Ni^+ shows a slight preference for end-on coordination. This may reflect the stability of the complex with different coordination modes and (or) the insertion ability of the metal ions. For RCN—Mn^+, almost all fragmentations are due to dissociative detachment. This indicates that the insertion ability of Mn^+ is much lower than the three other metal ions. In this case, it is impossible to estimate the portion of either end-on or side-on coordination.

There are a few experimental (35, 36) and theoretical (37) studies reported so far on the coordination of nitriles to metal ions but detailed descriptions of the potential surface of both coordination processes seem impossible for the moment.

Conclusion

Competitive formation of side-on and end-on coordinated adducts probably exists in the ion–molecule complexation of

transition-metal ions (Ni^+, Co^+. Fe^+ and Mn^+) with alkanenitriles. Approximate percentages of the end-on coordination can be obtained by analyzing the B/E linked scan spectra. Although β-CH_3· transfer is rare in the gas phase, it may occur for the loss of CH_4 from end-on RCN—M^+ complexes, and is in competition with β-H migration and β-C—C cleavage. For the side-on complexes, metal ions can insert into various C—C bonds, followed by β-H transfer and alkene or alkane loss or by direct C—M^+ bond cleavage to give alkyl radicals.

An essentially "analytical" mass spectrometer with slight modification has been shown to provide comparable results to those obtained from "reverse geometry" sector instrument or FT-ICR spectrometer usually used for such studies.

Acknowledgment

The authors wish to thank the Natural Sciences and Engineering Research Council of Canada for operating and equipment grants to J. M. Miller and to thank T. R. B. Jones and D. Vukmanic for experimental assistance. We also acknowledge the editor and reviewers for suggestions.

1. (*a*) H. SCHWARZ. Acc. Chem. Res. **22**, 282 (1989); (*b*) G. CZEKAY, T. DREWELLO, K. ELLER, C. B. LEBRILLA, T. PRUSSE, C. SCHULZE, S. STEINRUCK, D. SULZLE, T. WEISKE, and H. SCHWARZ. *In* Organometallics in organic synthesis. Vol. 2. *Edited by* H. Wernerand and G. Erker. Springer Verlag, Heidelberg, 1989. p. 203; (*c*) J. ALLISON. Prog. Inorg. Chem. **34**, 627 (1986); (*d*) R. H. CRABTREE. Chem. Rev. **85**, 245 (1985); (*e*) I. K. GREGOR and M. GUILHAUS. Mass Spectrom. Rev. **3**, 39 (1984); (*f*) B. S. FREISER. Chemtracts: Anal. Phys. Chem. **1**, 65 (1989); (*g*) P. B. ARMENTROUT AND J. L. BEAUCHAMP. Acc. Chem. Res. **22**, 315 (1989).
2. (*a*) C. B. LEBRILLA, C. SCHULZE, and H. SCHWARZ. J. Am. Chem. Soc. **109**, 98 (1987); (*b*) C. B. LEBRILLA, C. SCHULZE, and H. SCHWARZ. J. Am. Chem. Soc. **109**, 5639 (1987); (*c*) C. B. LEBRILLA, T. DREWELLO, and H. SCHWARZ. Int. J. Mass Spectrom. Ion Processes, **79**, 287 (1987); (*d*) K. ELLER and H. SCHWARZ. Int. J. Mass Spectrom. Ion Processes, **93**, 243 (1989).
3. (*a*) K. ELLER, C. B. LEBRILLA, T. DREWELLO, and H. SCHWARZ. J. Am. Chem. Soc. **110**, 3068 (1988); (*b*) K. ELLER and H. SCHWARZ. Chem. Ber. **123**, 201 (1990).
4. (*a*) S. KARRASS, K. ELLER, C. SCHULZE, and H. SCHWARZ. Angew. Chem. Int. Ed. Engl. **28**, 607 (1988); (*b*) S. KARRASS, T. PRUSSE, K. ELLER, and H. SCHWARZ. J. Am. Chem. Soc. **111**, 9018 (1989); (*c*) S. KARRASS, K. ELLER, and H. SCHWARZ. Chem. Ber. **123**, 939 (1990).
5. T. PRUSSE and H. SCHWARZ. Organometallics, **8**, 2851 (1989).
6. (*a*) C. SCHULZE and H. SCHWARZ. Chimia, **41**, 29 (1987); (*b*) C. SCHULZE, H. SCHWARZ, D. A. PEAK, and M. L. GROSS. J. Am. Chem. Soc. **109**, 2368 (1987); (*c*) C. SCHULZE and H. SCHWARZ. J. Am. Chem. Soc. **110**, 67 (1988); (*d*) C. SCHULZE, T. WEISKE, and H. SCHWARZ. Organometallics, **7**, 898 (1988); (*e*) N. STEINRUCK and H. SCHWARZ. Organometallics, **8**, 759 (1989).
7. D. SCHRODER and H. SCHWARZ. J. Am. Chem. Soc. **112**, 5947 (1990).
8. L. Z. CHEN and J. M. MILLER. J. Am. Chem. Soc. Mass Spectrom. **2**, 120 (1991).
9. J. L. HOLMES. Org. Mass Spectrom. **20**, 169 (1985).
10. R. M. STEPNOWSKI and J. ALLISON. Organometallics, **7**, 2097 (1988).
11. K. ELLER, W. ZUMMACK, H. SCHWARZ, L. M. ROTH, and B. S. FRIESER. J. Am. Chem. Soc. **113**, 833 (1991).
12. J. L. ELKIND and P. B. ARMENTROUT. J. Chem. Phys. **84**, 4862 (1986) and references therein.
13. M. BARBER, R. S. BORDOLI, G. T. ELLIOT, R. D. SEDGWICK, and A. N. TYLER. Anal. Chem. **54**, 645*A* (1982).
14. (*a*) R. B. FREAS, M. M. ROSS, and J. E. CHAMPANA. J. Am. Chem. Soc. **107**, 6195 (1985); (*b*) R. B. FREASE and J. E. CAMPANA. J. Am. Chem. Soc. **107**, 6202 (1985); (*c*) H. MESTDAGH, N. MORIN, and C. ROLANDO. Tetrahedron Lett. **27**, 33 (1986); (*d*) T. DREWELLO, K. ECKART, C. B. LEBRILLA, and H. SCHWARZ. Int. J. Mass Spectrom. Ion Proccesses, **76**, R1 (1987).
15. D. CZEKEY, T. DREWELLO, K. ELLER, W. ZUMMACK, and H. SCHWARZ. Organometallics, **8**, 2439 (1989).
16. K. ELLER, W. ZUMMACK, and H. SCHWARZ. J. Am. Chem. Soc. **112**, 621 (1990).
17. T. PRUSSE, T. DREWELLO, C. B. LEBRILLA, and H. SCHWARZ. J. Am. Chem. Soc. **111**, 2857 (1989).
18. K. ELLER, T. DREWELLO, Y. ZUMMACK, T. ALLSPACK, U. ANNEN, M. REGITY, and H. SCHWARZ. J. Am. Chem. Soc. **111**, 4228 (1989).
19. C. B. LEBRILLA, T. DREWELLO, and H. SCHWARZ. Organometallics, **6**, 2450 (1987).
20. T. PRUSSE, G. CZEKAY, and H. SCHWARZ. Chem. Ber. **124**, 141 (1991).
21. J. ALLISON and D. P. RIDGE. J. Am. Chem. Soc. **101**, 4998 (1979).
22. S. J. BALINEC and J. ALLISON. J. Am. Chem. Soc. **106**, 7718 (1984).
23. K. ELLER and H. SCHWARZ. Organometallics, **8**, 1820 (1989).
24. (*a*) D. B. JACOBSON and B. S. FREISER. J. Am. Chem. Soc. **105**, 736 (1983); (*b*) D. B. JACOBSON and B. S. FREISER. J. Am. Chem. Soc. **105**, 5197 (1983).
25. P. B. ARMENTROUT and J. L. BEAUCHAMP. J. Am. Chem. Soc. **103**, 784 (1981).
26. B. R. REDECKI and J. ALLISON. Organometallics, **5**, 411 (1986).
27. C. SCHULZE, T. WEISKE, and H. SCHWARZ. Chimia, **40**, 362 (1986).
28. (*a*) D. A. PEAK, M. L. GROSS, and D. P. RIDGE, J. Am. Chem. Soc. **106**, 4307 (1984); (*b*) D. B. JACOBSON and B. S. FREISER. J. Am. Chem. Soc. **105**, 7485 (1983).
29. P. L. WATSON and D. C. ROE. J. Am. Chem. Soc. **104**, 6479 (1982).
30. (*a*) P. B. ARMENTROUT and J. L. BEAUCHAMP. J. Am. Chem. Soc. **103**, 784 (1981); (*b*) L. F. HALLE, P. B. ARMENTROUT, and J. L. BEAUCHAMP. Organometallics, **1**, 963 (1982); (*c*) L. F. HALLE, P. B. ARMENTROUT, and J. L. BEAUCHAMP. Organometallics, **2**, 1818 (1983); (*d*) D. B. JACOBSON and B. S. FREISER. J. Am. Chem. Soc. **105**, 5197 (1983); (*e*) M. A. TOLBERT and J. L. BEAUCHAMP. J. Am. Chem. Soc. **106**, 8117 (1984); (*f*) R. TONKYN, M. RONAN, and J. C. WEISSHAAR. J. Phys. Chem. **92**, 92 (1988).
31. (*a*) T. PRUSSE, C. B. LEBRILLA, T. DREWELLO, and H. SCHWARZ. J. Am. Chem. Soc. **110**, 5986 (1988); (*b*) K. ELLER and H. SCHWARZ. Organometallics, **8**, 1820 (1989); (*c*) G. CZEKAY, T. DREWELLO, K. ELLER, W. ZUMMACK, and H. SCHWARZ. Organometallics, **8**, 2439 (1989).
32. L. F. HALLE, W. E. CROWE, P. B. ARMENTROUT, and J. L. BEAUCHAMP. Organometallics, **3**, 1694 (1984).
33. (*a*) R. G. COOKS and T. L. KRUGER. J. Am. Chem. Soc. **99**, 1279 (1977); (*b*) S. A. MCLUCKEY, D. CAMERON, and R. G. COOKS. J. Am. Chem. Soc. **103**, 1313 (1981); (*c*) L. Z. CHEN. Ph.D. thesis, University of Mons, Belgium. 1989; (*d*) L. Z. CHEN, R. FLAMMANG, A. MAQUESTIAU, R. W. TAFT, J. CATALAN, P. CABILDO, R. CLARAMUNT, and J. ELGUERO. J. Org. Chem. **56**, 179 (1991).
34. L. Z. CHEN and J. M. MILLER. To be published.
35. M. A. WEXLER and E. L. MUETTERTIES. J. Phys. Chem. **88**, 4037 (1984).
36. M. A. ANDREWS, C. B. KNOBLER, and H. D. KAESZ. J. Am. Chem. Soc. **101**, 7260 (1979).
37. (*a*) J. A. S. HOWELL, J. Y. SAILLARD, A. LE BEUZE, and G. JAOUEN. J. Chem. Soc. Dalton Trans., 2533 (1982); (*b*) E. SCHUSTOROVLCH. J. Phys. Chem. **87**, 14 (1983).

Can. J. Chem. Downloaded from www.nrcresearchpress.com by 123.30.183.119 on 09/08/12
For personal use only.

Efficient addition of cerium(III) enolate of ethyl acetate to ketones: application to the synthesis of β-ethoxycarbonylmethyl α, β-unsaturated ketones

HSING-JANG LIU[1] AND BING-YAN ZHU
Department of Chemistry, The University of Alberta, Edmonton, Alta., Canada T6G 2G2

Received May 31, 1991

HSING-JANG LIU and BING-YAN ZHU. Can. J. Chem. **69**, 2008 (1991).

The cerium(III) enolate derived from ethyl acetate was shown to undergo facile addition with ketones. With conjugated enones, 1,2-addition products were formed exclusively. Oxidative 1,3-oxygen transportation of these products provides an efficient route to synthetically useful β-ethoxycarbonylmethyl α,β-unsaturated ketones.

Key words: cerium(III) ester enolate, addition, ketones.

HSING-JANG LIU et BING-YAN ZHU. Can. J. Chem. **69**, 2008 (1991).

On montre que l'énolate de cérium(III) dérivé de l'acétate d'éthyle s'additionne facilement sur les cétones. Il se forme des produits d'addition 1,2 exclusivement avec les énones conjuguées. Le transfert oxydant d'oxygène-1,3 de ces produits fournit une voie d'accès efficace aux cétones α,β insaturées synthétiques très utiles β-éthoxycarbonylméthyles.

Mots clés : cérium(III), énolate d'ester, addition, cétones.

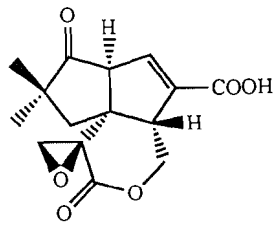
[Traduit par la rédaction]

Can. J. Chem. Downloaded from www.nrcresearchpress.com by 123.30.183.119 on 09/08/12
For personal use only.

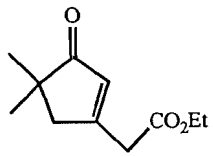
Introduction

In a projected total synthesis of pentalenolactone G (**1**) (1), enone ester **2** was required as an intermediate. Initial attempts to prepare this compound via the corresponding saturated ketone met with little success. Consequently, a synthetic approach involving addition of the enolate of ethyl acetate to enone **3** followed by oxidative 1,3-oxygen transportation of the resulting allylic alcohol **4** was explored. Although the addition of the lithium enolate of ethyl acetate to 2-cyclopentenone was found to proceed quite readily, giving the corresponding 1,2-adduct in 76% yield, the desired compound **4** could not be generated from enone **3** in more than 50% yield, regardless of the amount of reagent used, the reaction time, and temperature applied. This poor result could be attributed to the competing proton exchange process, which is an often encountered synthetic problem in aldol condensation reactions. To circumvent this problem, a reagent of lower basicity and (or) greater nucleophilicity is highly desirable. With regard to these properties, it has been demonstrated that organocerium(III) reagents in general are superior to the corresponding organolithium and magnesium reagents (2) that are commonly used. Under these considerations, the addition of the cerium(III) enolate of ethyl acetate to enone **3** was investigated. To our delight, treatment of enone **3** with slightly more than two equivalents of the cerium reagent under very mild conditions gave the desired 1,2-adduct **4** exclusively in virtually quantitative yield. Other than the reaction of the cerium enolate of *tert*-butyl acetate with acetophenones (3), the addition of the cerium(III) ester enolate to carbonyl is little known. The high efficiency observed for the transformation of **3** to **4** in terms of the yield (virtually quantitative) and regioselectivity (100% 1,2-addition) warranted further investigation on the addition of the cerium(III) ester enolate to conjugated enones, particularly in the context of preparation of β-alkoxycarbonylmethyl α,β-unsaturated ketones (e.g., **2**), which are useful synthetic intermediates for which efficient methods of preparation are rather limited.

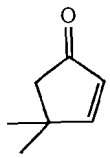
To determine the generality of the addition, a number of structurally diverse ketones were subjected to treatment with the cerium enolate, derived from the transmetallation reaction (3) of lithio ethyl acetate with anhydrous cerium(III) chloride (4). As



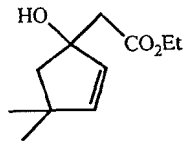
1



2



3



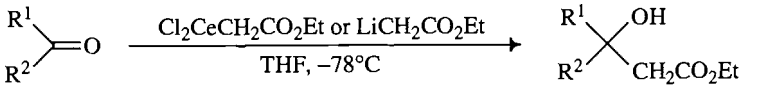
4

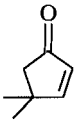
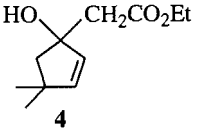
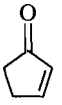
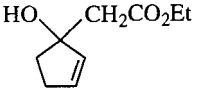
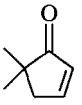
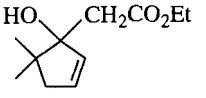
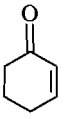
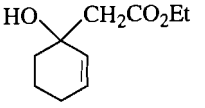
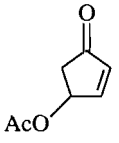
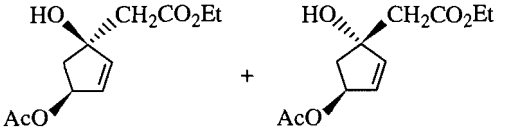
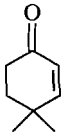
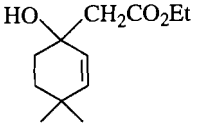
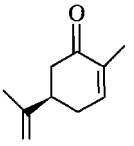
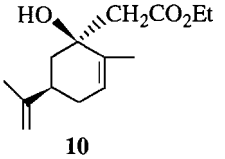
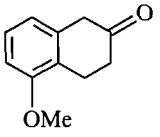
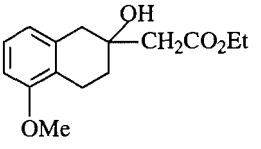
illustrated in Table 1, which summarizes the results, the addition reaction proceeded smoothly in all the cases examined and, without exception, products were obtained in yields greater than 90%. Several additional observations are noteworthy. (*i*) A minimum amount of two equivalents of the cerium(III) enolate is required in order to induce complete reaction. This is in agreement with the general observation for nucleophilic addition of cerium(III) reagents (3, 5). (*ii*) The addition of the cerium(III) enolate to conjugated enones (entries 1, 3, 5, 7, 9, 10, and 11) was shown to proceed with complete 1,2-regioselectivity. On the other hand, when the corresponding lithium reagent was applied in parallel experiments (entries 2, 4, 6, and 8), inferior yields of 1,2-adducts were obtained partly due to the formation of 1,4-addition product and recovery of the starting material. (*iii*) High yields of the desired addition products were also obtained from 4-acetoxy-2-cyclopentenone (entry 9), a highly unstable enone,[2] and 5-methoxy-β-tetralone (entry 12), a highly enolizable ketone. These results could be attributed to the mildness of reaction conditions applied, and to the low basicity and high nucleophilicity of the cerium(III) reagent. (*iv*) A high degree of stereoselectivity was observed for 4-acetoxy-2-cyclopentenone (entry 9), which gave an insepar-

[1]Author to whom correspondence may be addressed.

[2]This compound deteriorates readily on exposure to base or acid.

TABLE 1. Additions of cerium(III) and lithium enolates of ethyl acetate to ketones



Entry	Ketone	Enolate	Product	Time (h)	Yield (%)
1		$Cl_2CeCH_2CO_2Et$	 **4**	2	98
2		$LiCH_2CO_2Et$		2	50
3		$Cl_2CeCH_2CO_2Et$	 **5**	3.5	96
4		$LiCH_2CO_2Et$		3.5	76
5		$Cl_2CeCH_2CO_2Et$	 **6**	4	97
6		$LiCH_2CO_2Et$		4	60
7		$Cl_2CeCH_2CO_2Et$	 **7**	4	100
8		$LiCH_2CO_2Et$		4	30
9		$Cl_2CeCH_2CO_2Et$	 **8a** (9:1) **8b**	7	98
10		$Cl_2CeCH_2CO_2Et$	 **9**	3.5	96
11		$Cl_2CeCH_2CO_2Et$	 **10**	4	100
12		$Cl_2CeCH_2CO_2Et$	 **11**	15	92

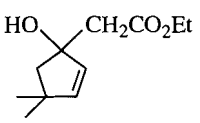
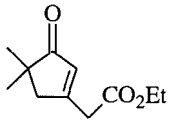
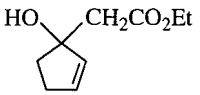
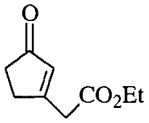
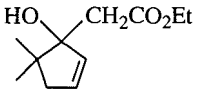
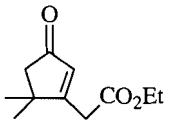
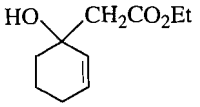
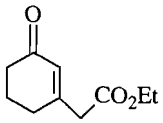
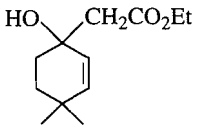
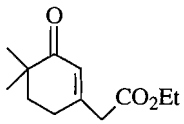
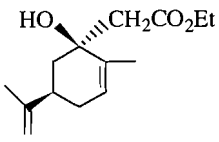
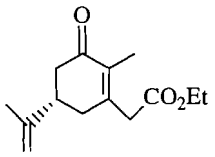
able mixture of two diastereomers **8***a* and **8***b* in a ratio of 9:1 as determined by ^{1}H NMR analysis. The stereochemistry of the major isomer **8***a* was confirmed by the nuclear Overhauser effect (NOE) detected as diagrammatically summarized in Fig. 1. The predominant formation of **8***a* could be attributed to the preferential addition of the cerium reagent from the sterically less hindered side of the starting enone. (*v*) The reaction of (−)-carvone (entry 11) gave rise to a single isomer **10**, presumably as a result of the stereoelectronically favored axial addition (6) of the cerium enolate to the carbonyl. The stereochemical assignment and the preferred conformation[3] depicted in Fig. 2 follow from several pieces of key information provided by the spin–spin decoupling, ^{1}H–^{13}C correlation 2D NMR and NOE studies, including the observed W-coupling

[3]The presence of an intramolecular hydrogen bonding was also indicated by the IR spectrum showing diagnostic absorption bands at 3509 and 3505 cm^{-1}.

Can. J. Chem. Downloaded from www.nrcresearchpress.com by 123.30.183.119 on 09/08/12
For personal use only.

Can. J. Chem. Downloaded from www.nrcresearchpress.com by 123.30.183.119 on 09/08/12
For personal use only.

TABLE 2. Oxidative 1,3-oxygen transportation of allylic alcohols

Entry	Allylic alcohol	Product	Time (h)[a]	Yield (%)
1	 **4**	 **2**	12	60
2	 **5**	 **12**	2.5	72
3	 **6**	 **13**	15	53
4	 **7**	 **14**	2	74
5	 **9**	 **15**	2	63
6	 **10**	 **16**	50	81

[a]All reactions were carried out in methylene chloride at room temperature using pyridinium chlorochromate.

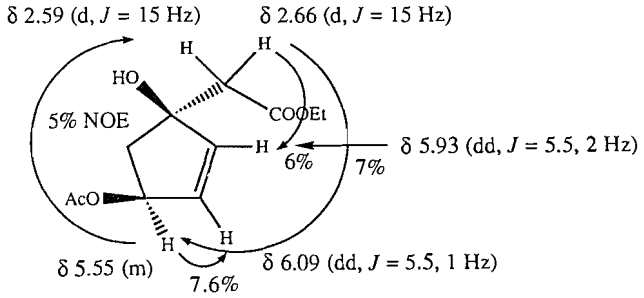


FIG. 1. NOE data for β-hydroxy ester **8***a*

(J = 1.5 Hz) between Ha and Hc, and a profound enhancement (10.9% NOE) of the multiplet at δ 2.28 due to Hd upon irradiation of the doublet at δ 2.58 for Hb (Fig. 2).

Oxidative 1,3-oxygen transportation was carried out on a large number of the allylic alcohols obtained in order to study the viability of using such a reaction in the formation of β-ethoxycarbonylmethyl α,β-unsaturated ketones. Treatment of alcohol **4** with pyridinium chlorochromate (2 mol. equiv.) in CH_2Cl_2 for 12 h at room temperature (7) gave a 60% yield of enone ester **2** required for our synthetic approach to pentalenolactone G (**1**). Similar treatment of several other allylic alcohols also resulted in their rearrangement to give the desired enone esters (Table 2). Thus, the combination of addition of the cerium(III) enolate of ethyl acetate to a conjugated enone and subsequent oxidative rearrangement provides an efficient means for the construction of β-ethoxycarbonylmethyl α,β-unsaturated ketones, useful synthetic intermediates that are otherwise difficult to prepare.

Experimental

General

All melting points were determined on a Köfler hot stage apparatus and are uncorrected. Elemental analyses were performed by the microanalytical laboratory of this department. Infrared spectra (IR) were recorded on a Perkin–Elmer model 457 or Nicolet 7-119 FT-IR spectrophotometer and were normally obtained in chloroform cast unless otherwise stated. High resolution mass spectra (HRMS) were

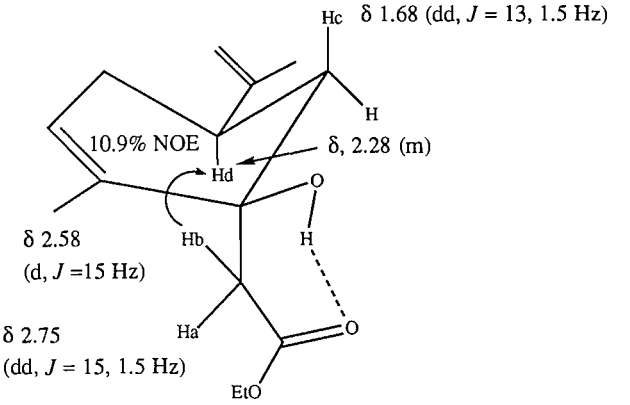


FIG. 2. The preferred conformation of alcohol **10**.

obtained using a Kratos AEI MS-50 high resolution mass spectrometer. Proton nuclear magnetic resonance specrtra (^{1}H NMR) were recorded on Bruker WH-300 (300 MHz) and WH-400 (400 MHz) spectrometers and were obtained on $CDCl_3$ solutions using tetramethylsilane as an internal reference. Carbon-13 nuclear magnetic resonance spectra (^{13}C NMR) were recorded on a Bruker WH-300 (75 MHz) spectrometer. The multiplicity of ^{13}C NMR signals was derived from off-resonance or Carr–Purcel–Meiboom–Gill spin echo J-modulated experiments (APT or Attached Proton Test) (8). Methyl and methine groups are shown as signals possessing an antiphase (doublet, quartet) with respect to the deuteriochloroform signal, whereas methylene groups, quaternary carbon atoms, and carbonyl groups appear in phase (singlet, triplet) with it. Nuclear Overhauser effects (NOE) were determined in the difference mode, in which a control (undecoupled) spectrum was computer-subtracted from the irradiated spectrum after Fourier transformation. Positive enhancements are defined as signals possessing an antiphase with respect to the irradiated signal. Samples for NOE measurements were deoxygenated with helium gas for 5 min prior to use. Optical rotations were otained on a Perkin–Elmer 24 polarimeter at the sodium D line using a 1.0 dm cell with a total volume of 1 mL.

All reactions were carried out under a positive pressure of argon gas. Argon was passed through a column of 4A molecular sieves and self-indicating silica gel. Reactions requiring anhydrous conditions were performed in oven-dried glassware that had then been assembled and allowed to cool while being purged with an inert gas. All reactions were monitored by analytical thin-layer chromatography (TLC). Analytical TLC was carried out on aluminium sheets precoated (0.20 mm layer thickness) with Merck silica gel 60F-254 containing a fluorescent indicator. Visualization was effected either by iodine or by dipping into an ethanol solution of vanillin (5%, w/v) in sulfuric acid (50%, v/v) followed by charring on a hot plate. Alternatively, an aqueous solution of phosphomolybdic acid (3%, w/v) containing ceric sulfate (0.5%, w/v) in sulfuric acid (3%, v/v) was used, followed by careful charring on a hot plate. Ultraviolet-active materials were detected by visualization under a UV lamp (254 or 350 nm). Flash chromatography (9) was used routinely for purification and separation of product mixtures using Merck silica gel of 230–400 mesh.

All solvents were distilled under an argon atmosphere prior to use. Tetrahydrofuran (THF) and diethyl ether were freshly distilled from a blue solution of sodium benzophenone ketyl. Diisopropylamine was distilled from sodium. Dichloromethane was distilled from calcium hydride. Hexane and ethyl acetate were purified by simple distillation. Cerium(III) chloride heptahydrate and pyridinium chlorochromate (PCC) were obtained from Aldrich. The following compounds were prepared according to the procedures in the literature: 5,5-dimethyl-2-cyclopenten-1-one (10), 4-acetoxy-2-cyclopenten-1-one (11), and 4,4-dimethyl-2-cyclohexen-1-one (12).

General procedure for the addition of cerium ester enolate to carbonyl compounds

(a) Anhyrdous cerium(III) chloride

Cerium(III) chloride heptahydrate (1.36 g, 3.64 mmol) was ground to a powder in a 30-mL round-bottomed flask with a magnetic stirring bar. The flask was heated gradually to 100°C under reduced pressure (ca. 0.1 Torr; 1 Torr = 133.3 Pa) in a Kugelrohr distillation apparatus. After 2 h at 100°C, the oven temperature was gradually increased to 150°C and cerium chloride was heated *in vacuo* for an additional 4–5 h. After the dried cerium chloride was cooled to room temperature under vacuum, argon and then THF (12 mL) were introduced. The resulting suspension was stirred for 2 h at room temperature prior to use for the prepartion of cerium ester enolate.

(b) Preparation of lithio ethyl acetate

To a stirred solution of diisopropylamine (405 mg, 4.0 mmol) in THF (5 mL), was added *n*-butyllithium (2.5 M in hexane, 1.6 mL, 4.0 mmol) dropwise at −78°C. The resulting solution was stirred at the same temperature for 20 min. A solution of ethyl acetate (326 mg, 3.7 mmol) in THF (2 mL) was then added and the reaction mixture stirred for 25 min at −78°C.

(c) Generation of cerium(III) enolate of ethyl acetate

The above suspension of cerium(III) chloride in THF was cooled to −78°C with stirring. The lithium ester enolate prepared from ethyl acetate was quickly transferred to this suspension via a cannula. The resulting mixture was vigorously stirred at −78°C for 2 h.

(d) Addition of cerium(III) ester enolate to carbonyl compounds

The carbonyl compound dissolved in a small amount of THF was added to the cerium ester enolate by syringe at −78°C. The reaction mixture was stirred at the same temperature until the starting material was no longer present as shown by TLC analysis. The reaction mixture was quenched with aqueous saturated NH_4Cl at −78°C and extracted with ether–hexane (1:1) (3 × 15 mL). The combined extracts were washed with water and brine and dried with magnesium sulfate. After filtration and concentration, the residue was subjected to flash chromatography on silica gel or bulb-to-bulb distillation under reduced pressure to afford the addition product.

*1-Carbethoxymethyl-4,4-dimethyl-2-cyclopenten-1-ol (**4**)*

According to the general procedure, 4,4-dimethyl-2-cyclopenten-1-one (170 mg, 1.55 mmol) was treated with the cerium(III) ester enolate (3.64 mmol) for 2 h. Flash chromatography of the crude product, using a solution of 15% ethyl acetate in hexane as an eluant, gave alcohol **4** (300 mg, 98% yield) as a colorless oil: IR: 3500 (OH), 1733, 1718 (C=O) cm^{-1}; ^{1}H NMR (300 MHz) δ: 5.70 (d, J = 5.5 Hz, 1H, CH=), 5.60 (d, J = 5.5 Hz, 1H, CH=), 4.19 (q, J = 7 Hz, 2H, OCH_2), 3.63 (s, 1H, OH), 2.68 (d, J = 16 Hz, 1H, C*H*HCO$_2$), 2.64 (d, J = 16 Hz, 1H, CH*H*CO$_2$), 1.92 (d, J = 14 Hz, 1H, C*H*H), 1.81 (d, J = 14 Hz, 1H, CH*H*), 1.29 (t, J = 7 Hz, 3H, CH_2CH_3), 1.19 (s, 3H, CH_3), 1.09 (s, 3H, CH_3); ^{13}C NMR δ: 172.81 (s, C=O), 144.97 (d, =CH), 131.70 (d, =CH), 83.35 (s, COH), 60.75 (t, OCH_2), 52.98 (t, CH_2), 45.89 (s, *C*Me$_2$), 44.78 (t, CH_2), 30.05 (q, CH_3), 29.19 (q, CH_3), 14.25 (q, CH_3); HRMS M$^+$: 198.1249 (calcd. for $C_{11}H_{18}O_3$: 198.1256). Anal. calcd. for $C_{11}H_{18}O_3$: C 66.67, H 9.09; found: C 66.60, H 9.02.

*1-Carbethoxymethyl-2-cyclopenten-1-ol (**5**)*

Following the general procedure, 2-cyclopenten-1-one (164 mg, 2.0 mmol) was reacted with the cerium(III) enolate (4.0 mmol) for 3.5 h. Alcohol **5** was isolated as a colorless oil in 96% yield (326 mg) after purification by flash chromatography on silica gel (15% EtOAc in hexane): IR: 3499, 3478 (OH), 1735 (C=O) cm^{-1}; ^{1}H NMR (300 MHz) δ: 5.92 (dt, J = 5.5, 2.2 Hz, 1H, C*H*=CH), 5.78 (dt, J = 5.5, 2.2 Hz, 1H, CH=C*H*), 4.20 (q, J = 7 Hz, 2H, OCH_2CH_3), 3.61 (s, 1H, OH), 2.66 (d, J = 15 Hz, 1H, C*H*HCO$_2$), 2.62 (d, J = 15 Hz, 1H, CH*H*CO$_2$), 2.50 (m, 1H), 2.30 (m, 1H), 2.00 (m, 2H), 1.28 (t, J = 7 Hz, CH_2CH_3); ^{13}C NMR δ: 172.72 (s, C=O), 135.07 (d, CH=), 134.13 (d, =CH), 83.15 (s, COH), 60.66 (t, OCH_2), 44.49 (t, CH_2CO_2), 37.76 (t, CH_2), 30.92 (t, CH_2), 14.16 (q, OCH_2CH_3); HRMS M$^+$: 170.0943 (calcd. for $C_9H_{14}O_3$: 170.0943). Anal. calcd. for $C_9H_{14}O_3$: C 63.53, H 8.24; found C 63.36, H 8.45.

*1-Carbethoxymethyl-5,5-dimethyl-2-cyclopenten-1-ol (**6**)*

Treatment of 5,5-dimethyl-2-cyclopenten-1-one (334 mg, 3.00 mmol) with the cerium(III) enolate (6.7 mmol) in THF for 4 h gave alcohol **6** as a colorless oil in 97% yield (576 mg) after purification by

Can. J. Chem. Downloaded from www.nrcresearchpress.com by 123.30.183.119 on 09/08/12
For personal use only.

Can. J. Chem. Downloaded from www.nrcresearchpress.com by 123.30.183.119 on 09/08/12
For personal use only.

flash chromatography (15% EtOAc in hexane): IR: 3500 (OH), 1716 (C=O) cm^{-1}; ^1H NMR (300 MHz) δ: 5.88 (dt, J = 5.5, 2.2 Hz, 1H, C*H*=CH), 5.79 (dt, J = 5.5, 2 Hz, 1H, CH=C*H*), 4.19 (m, 2H, OCH_2), 3.62 (s, 1H, OH), 2.58 (d, J = 15.6 Hz, 1H, C*H*HCO_2), 2.48 (d, J = 15.6 Hz, 1H, CH*H*CO_2), 2.34 (ddd, J = 16, 2, 2 Hz, 1H, C*H*HCH=), 2.09 (ddd, J = 16, 2, 2 Hz, 1H, CH*H*CH=), 1.30 (t, J = 7 Hz, 3H, OCH_2CH_3), 1.10 (s, 3H, CH_3), 0.98 (s, 3H, CH_3); ^{13}C NMR δ: 173.52 (s, C=O), 135.40 (d, CH=), 132.77 (d, =CH), 84.08 (s, C-OH), 66.95 (t, OCH_2), 60.73 (t, CH_2CO_2), 46.96 (t, CH_2CH=), 39.78 (s, CMe_2), 24.78 (q, CH_3), 22.98 (q, CH_3), 14.17 (q, OCH_2CH_3); HRMS M^+: 198.1257 (calcd. for $C_{11}H_{18}O_3$: 198.1256). Anal. calcd. for $C_{11}H_{18}O_3$: C 66.67, H 9.09; found: C 66.46, H, 8.95.

1-Carbethoxymethyl-2-cyclohexen-1-ol (7)

Using the above standard procedure, 2-cyclohexen-1-one (196 mg, 2.04 mmol) was reacted with the cerium(III) enolate (4.5 mmol) in THF at −78°C for 4 h. Alcohol **7** was obtained as a colorless oil in 100% yield (376 mg) after bulb-to-bulb distillation (40°C, 0.1 Torr). IR: 3500 (OH), 1732, 1716 (C=O) cm^{-1}; ^1H NMR (300 MHz) δ: 5.84 (dt, J = 10, 4 Hz, 1H, C*H*=CH), 5.68 (br dt, J = 10, 1.3 Hz, 1H, CH=C*H*), 4.19 (q, J = 7 Hz, 2H, OCH_2), 3.60 (s, 1H, OH), 2.56 (d, J = 16 Hz, 1H, C*H*HCO_2), 2.52 (d, J = 16 Hz, 1H, CH*H*CO_2), 1.6–2.1 (m, 6H, $CH_2CH_2CH_2$), 1.30 (t, J = 7 Hz, CH_2CH_3); ^{13}C NMR δ: 172.54 (s, C=O), 131.00 (d, CH=), 130.29 (d, =CH), 68.20 (s, C-OH), 60.66 (t, OCH_2), 45.52 (t, CH_2CO_2), 35.78 (t, CH_2), 25.05 (t, CH_2), 18.96 (t, CH_2), 14.21 (q, OCH_2CH_3); HRMS M^+: 184.1101 (calcd. for $C_{10}H_{16}O_3$: 184.1098). Anal. calcd. for $C_{10}H_{16}O_3$: C 65.22, H 8.70; found: C 65.09, H 8.75.

(1S,4S*)- (8a) and (1R*,4S*)-4-Acetoxy-1-(carbethoxylmethyl)-2-cyclopenten-1-ol (8b)*

4-Acetoxy-2-cyclopenten-1-one (322 mg, 230 mmol) was treated with the cerium(III) enolate (8.00 mmol) for 7 h according to the general procedure. After the usual work-up and flash chromatography on silica gel (40% EtOAc in hexane), an inseparable mixture of diastereoisomeric alcohols **8*a*** and **8*b*** (9:1) was isolated as a colorless oil in 98% yield (514 mg). IR: 3494, 3488, 3479, 3468 (OH), 1733 (C=O) cm^{-1}; ^1H NMR (300 MHz), major diastereomer **8*a***, δ: 6.09 (dd, J = 5.5, 1 Hz, 1H, CHC*H*=CH), 5.93 (dd, J = 5.5, 2 Hz, 1H, CHCH=C*H*), 5.55 (m, 1H, AcOCH), 4.19 (q, 2H, J = 7 Hz, OCH_2), 3.84 (s, 1H, OH), 2.66 (d, J = 15 Hz, 1H, C*H*HCO_2), 2.59 (d, J = 15 Hz, 1H, CH*H*CO_2), 2.55 (dd, J = 14, 7.5 Hz, 1H, CHC*H*H), 2.05 (s, 3H, CH_3CO_2), 2.00 (dd, J = 14, 4 Hz, 1H, CHCH*H*), 1.28 (t, J = 7 Hz, 3H, CH_2CH_3); minor diastereomer **8*b***, δ: 5.96 (dd, J = 6, 4.5 Hz, 1H, C*H*=CH), 5.76 (m, 1H, AcOCH), 3.89 (s, 1H, OH), 2.79 (d, J = 16 Hz, 1H, C*H*HCO_2), 2.72 (d, J = 16 Hz, 1H, CH*H*CO_2), 2.45 (dd, J = 12, 7 Hz, 1H, CHC*H*H), 2.04 (s, 3H, CH_3CO_2), other peaks were overlapped with those of the major diastereomer; ^{13}C NMR, major diastereomer **8*a***, δ: 172.22 (s, C=O), 170.84 (s, C=O), 140.22 (d, CH=), 131.87 (d, =CH), 80.99 (s, C-OH), 76.97 (d, *C*HOAc), 60.97 (t, OCH_2), 44.99 (t, CH_2CO_2), 44.36 (t, CH_2), 21.44 (q, CH_3CO_2), 14.15 (q, OCH_2CH_3); minor diastereomer **8*b***, δ: 173.80 (s, C=O), 140.94 (d, CH=), 132.13 (d, CH=). 78.32 (d, *C*HOAc), 45.15 (t, CH_2CO_2), other peaks were overlapped with those of the major diastereomer; HRMS M^+ was not observed; m/z: 211.0964 (M^+ − OH, calcd. for $C_{11}H_{15}O_4$: 211.0970). Anal. calcd. for $C_{11}H_{16}O_5$: C 57.89, H 7.01; found: C 58.30, H, 7.06.

1-Carbethoxymethyl)-4,4-dimethyl-2-cyclohexen-1-ol (9)

4,4-Dimethyl-2-cyclohexen-1-one (250 mg, 2.01 mmol) was treated with the cerium(III) enolate (5.60 mmol) at −78°C for 3.5 h, giving alcohol **9** as a colorless oil in 96% yield (405 mg) after flash chromatography (15% EtOAc in hexane): IR: 3500 (OH), 1732, 1717 (C=O) cm^{-1}; ^1H NMR (300 MHz) δ: 5.52 (s, 2H, CH=CH), 4.20 (q, J = 7 Hz, 2H, OCH_2), 3.58 (s, 1H, OH), 2.56 (d, J = 15 Hz, 1H, C*H*HCO_2), 2.54 (d, J = 15 Hz, 1H, CH*H*CO_2), 1.6–1.9 (m, 3H), 1.4–1.5 (m, 1H), 1.29 (t, J = 7 Hz, 3H, CH_2CH_3), 1.06 (s, 3H, CH_3), 0.98 (s, 3H, CH_3); HRMS M^+: 212.1413 (calcd. for $C_{12}H_{20}O_3$: 212.1413).

(1S,5R)-1-(Carbethoxymethyl)-2-methyl-5-(1-methylethenyl)-2-cyclohexen-1-ol (10)

Following the standard procedure, (−)-5*R*-carvone (300 mg, 2.00 mmol) was reacted with the cerium(III) enolate (4.02 mmol) in THF at −78°C for 4 h. After the usual work-up and flash chromatography (10% EtOAc in hexane), the optically active alcohol **10** was obtained as a colorless oil in 100% yield (476 mg): $[\alpha]_D^{22}$ −31.4 (*c* 1.46, $CHCl_3$); IR: 3509, 3505 (OH), 1715 (C=O), 1645 (C=C) cm^{-1}; ^1H NMR (300 MHz) δ: 5.48 (m, 1H, CH=C), 4.73 (m, 2H, CH_2=C), 4.20 (m, 2H, OCH_2), 3.86 (s, 1H, OH), 2.75 (dd, J = 15, 1.5 Hz, 1H, C*H*HCO_2), 2.58 (d, J = 15 Hz, 1H, CH*H*CO_2), 2.28 (m, 1H, CH_2CHCH_2) 1.90–2.14 (m, 3H, C*H*HCHCH_2), 1.73 (m, 6H, 2 × CH_3), 1.68 (dd, J = 13, 1.5 Hz, 1H, CH*H*$CHCH_2$), 1.29 (t, J = 7 Hz, 3H, CH_2CH_3); ^{13}C NMR δ: 172.73 (s, C=O), 148.31 (s, *C*=CH), 136.82 (s, *C*=CH_2), 124.30 (d, CH=), 109.08 (t, CH_2=), 72.54 (s, C-OH), 60.63 (t, OCH_2), 41.82 (t, CH_2CO_2), 40.94 (t, CH_2), 39.56 (d, CH_2CHCH_2), 30.74 (t, CH_2), 20.32 (q, CH_3), 16.92 (q, CH_3), 14.06 (q, OCH_2CH_3); HRMS M^+: 238.1570 (calcd. for $C_{14}H_{22}O_3$: 238.1569). Anal. calcd. for $C_{14}H_{22}O_3$: C 70.59, H 9.24; found: C 70.79, H 9.44.

2-(Carbethoxymethyl)-1,2,3,4-tetrahydro-5-methoxy-2-naphthol (11)

5-Methoxy-2-tetralone (400 mg, 2.27 mmol) was treated with the cerium(III) enolate (8 mmol) in THF at −78°C for 15 h. After work-up in the usual manner and purification by flash chromatography (20% EtOAc in hexane), alcohol **11** was obtained in 92% yield (551 mg) as a white solid: mp 25–30°C; IR: 3500 (OH), 1728, 1715 (C=O), 1578 (Ph) cm^{-1}; ^1H NMR (300 MHz) δ: 7.10 (dd, J = 8, 8 Hz, 1H, ArH), 6.68 (d, J = 8 Hz, 2H, ArH), 4.19 (q, J = 7 Hz, 2H, OCH_2), 3.80 (s, 3H, OCH_3), 3.74 (s, 1H, OH), 2.86 (m, 3H), 2.62–2.70 (m, 1H), 2.58 (d, J = 16 Hz, 1H, C*H*HCO_2), 2.54 (d, J = 16 Hz, 1H, CH*H*CO_2), 1.90–2.00 (m, 1H), 1.84 (m, 1H), 1.28 (t, J = 7 Hz, 3H, CH_2CH_3); ^{13}C NMR δ: 172.90 (s, C=O), 157.20 (s, Ph), 135.44 (s, Ph), 126.51 (d, Ph), 123.88 (s, Ph), 121.64 (d, Ph), 107.32 (d, Ph), 69.21 (s, C—OH), 60.75 (t, OCH_2), 55.24 (q, OMe), 43.42 (t, CH_2CO_2), 41.81 (t, CH_2), 33.60 (t, CH_2), 20.83 (t, CH_2), 14.22 (q, OCH_2CH_3); HRMS M^+: 264.1366 (calcd. for $C_{15}H_{20}O_4$: 264.1362). Anal. calcd. for $C_{15}H_{20}O_4$: C 68.18, H 7.58; found: C 67.92, H 7.44.

General procedure for the oxidation of tertiary allylic alcohols with PCC in CH_2Cl_2

To a magnetically stirred slurry of PCC (2.00 mmol) in CH_2Cl_2 (5–8 mL), was added in one portion a solution of tertiary allylic alcohol (1.00 mmol) in CH_2Cl_2 (2 mL) at room temperature. The resulting dark red-black mixture was stirred for several hours at room temperature. The progress of the reaction was monitored by the analytical TLC on silica gel. After the complete consumption of the starting material, the reaction mixture was diluted with Et_2O (15 mL). The ethereal solution was decanted from the black resinous residue, which in turn was washed with Et_2O (3 × 10 mL). The combined ethereal solutions were passed through a short column (ca. 10 cm) of Florisil to remove any black polar material. The column was washed with diethyl ether (3 × 10 mL) and the combined ethereal solutions were concentrated on a rotary evaporator. The residue was subjected to flash chromatography (EtOAc in hexane) to afford the desired enone.

3-Carbethoxymethyl-5,5-dimethyl-2-cyclopenten-1-one (2)

Treatment of allylic alcohol **4** (210 mg, 1.06 mmol) with PCC (457 mg, 2.12 mmol) in CH_2Cl_2 (5 mL) for 12 h according to the general procedure followed by flash chromatography (20% ethyl acetate in hexane) gave enone ester **2** (125 mg, 60% yield) as a light yellow liquid: IR: 1739 (C=O, ester), 1708 (C=O, ketone), 1622 (C=C) cm^{-1}; ^1H NMR (300 MHz) δ: 6.04 (m, 1H, CH=), 4.20 (q, J = 7 Hz, 2H, OCH_2), 3.42 (br d, J = 1 Hz, 2H, CH_2CO_2), 2.56 (m, 2H, CH_2), 1.29 (t, J = 7 Hz, 3H, CH_2CH_3), 1.12 (s, 6H, 2 × CH_3); ^{13}C NMR δ: 213.75 (s, C=O, enone), 169.35 (s, C=O, ester), 168.82 (s, *C*=), 129.82 (d, CH=), 61.35 (t, OCH_2), 48.17 (t, CH_2CO_2), 44.54 (s, O=C*C*), 38.85 (t, CH_2), 24.97 (q, CH_3), 24.77 (q, CH_3), 14.16 (q, CH_2CH_3); HRMS M^+: 196.1099 (calcd. for $C_{11}H_{16}O_3$: 196.1099). Anal. calcd. for $C_{11}H_{16}O_3$: C 67.35, H 8.16; found: C 67.30, H 8.04.

3-Carbethoxymethyl-2-cyclopenten-1-one (**12**)

Following the standard procedure, alcohol **5** (330 mg, 1.94 mmol) was treated with PCC (835 mg, 3.88 mmol) in CH_2Cl_2 (20 mL) at room temperature for 2.5 h. The enone ester **12** was obtained as a light brown oil in 72% yield (235 mg) after flash chromatography (20% EtOAc in hexane): IR: 1735 (C=O, ester), 1714 (C=O, enone), 1676, 1620 (C=C) cm^{-1}; ^1H NMR (300 MHz) δ: 6.12 (br s, 1H, CH=), 4.20 (q, J = 7 Hz, 2H, OCH_2), 3.47 (br s, 2H, CH_2CO_2), 2.70 (m, 2H, CH_2), 2.46 (m, 2H, CH_2), 1.30 (t, J = 7 Hz, OCH_2CH_3); ^{13}C NMR δ: 209.02 (s, C=O, ketone), 172.55 (s, C=O, ester), 168.59 (s, C=), 132.23 (d, CH=), 61.13 (t, OCH_2), 38.62 (t, CH_2), 35.25 (t, CH_2), 31.41 (t, CH_2), 13.95 (q, CH_3); HRMS M^+: 168.0785 (calcd. for $C_9H_{12}O_3$: 168.0786). Anal. calcd. for $C_9H_{12}O_3$: C 64.29, H 7.14; found: C 64.18, H 7.17.

3-Carbethoxymethyl-4,4-dimethyl-2-cyclopenten-1-one (**13**)

Treatment of allylic alcohol **6** (210 mg, 1.06 mmol) with PCC (457 mg, 2.12 mmol) in CH_2Cl_2 (10 mL) for 15 h afforded enone ester **13** in 53% yield (110 mg) as a light brown oil after purification by flash chromatography (15% EtOAc in hexane): IR: 1739 (C=O, ester), 1718 (C=O, enone), 1693, 1618 (C=C) cm^{-1}; ^1H NMR (300 MHz) δ: 6.04 (br t, J = 1.2 Hz, 1H, CH=), 4.20 (q, J = 7 Hz, 2H, OCH_2), 3.33 (d, J = 1.3 Hz, 2H, CH_2CO_2), 2.32 (s, 2H, CH_2C=O), 1.29 (t, J = 7 Hz, 3H, OCH_2CH_3), 1.22 (s, 6H, 2 × CH_3); ^{13}C NMR δ: 207.05 (s, C=O, ketone), 179.09 (s, C=O, ester), 169.28 (s, C=), 130.35 (d, CH =), 61.32 (t, OCH_2), 51.26 (t, CH_2CO_2), 43.17 (t, O=CCH_2), 33.98 (s, CMe_2), 26.66 (q, 2 × CH_3), 14.07 (q, CH_3); HRMS M^+: 196.1101 (calcd. for $C_{11}H_{16}O_3$: 196.1100). Anal. calcd. for $C_{11}H_{16}O_3$: C 67.35, H 8.16; found: C 67.15, H 8.22.

3-Carbethoxymethyl-2-cyclohexen-1-one (**14**)

Using the standard procedure, allylic alcohol **7** (340 mg, 1.85 mmol) was treated with PCC (997 mmol, 4.63 mmol) in CH_2Cl_2 (10 mL) for 2 h. The crude product was purified by flash chromatography on silica gel (15% EtOAc in hexane) to afford enone ester **14** as a light brown oil in 74% yield (250 mg): IR: 1736 (C=O, ester), 1673 (C=O, enone), 1631 (C=C) cm^{-1}; ^1H NMR (300 MHz) δ: 5.94 (br t, J = 1.2 Hz, 1H, CH=), 4.19 (q, J = 7 Hz, 2H, OCH_2), 3.22 (br s, 2H, CH_2CO_2), 2.40 (m, 4H), 2.04 (m, 2H), 1.28 (t, J = 7 Hz, 3H, OCH_2CH_3); ^{13}C NMR δ: 199.22 (s, C=O, ketone), 169.28 (s, C=O, ester), 157.18 (s, C=), 128.64 (d, CH =), 61.12 (t, OCH_2), 43.31 (t, CH_2CO_2), 37.03 (t, O=CCH_2), 29.50 (t, CH_2), 22.46 (t, CH_2), 14.05 (q, CH_3); HRMS M^+: 182.0943 (calcd. for $C_{10}H_{14}O_3$: 182.0943). Anal. calcd. for $C_{10}H_{14}O_3$: C 65.93, H 7.69; found: C 65.66, H 7.89.

3-Carbethoxymethyl-6,6-dimethyl-2-cyclohexen-1-one (**15**)

Treatment of alcohol **9** (330 mg, 1.58 mmol) with PCC (850 mg, 3.95 mmol) in CH_2Cl_2 (8 mL) at room temperature for 2 h gave the enone ester **15** as an oil in 63% yield (210 mg) after purification by flash chromatography (5% EtOAc in hexane): IR: 1737 (C=O, ester), 1673 (C=O, enone), 1637 (C=C) cm^{-1}; ^1H NMR (300 MHz) δ: 5.86 (br t, J = 1.2 Hz, 1H, CH=), 4.18 (q, J = 7 Hz, 2H, OCH_2), 3.20 (br s, 2H, CH_2CO_2), 2.42 (br t, J = 6 Hz, 2H, CH_2), 1.84 (t, J = 6 Hz, 2H, CH_2), 1.29 (t, J = 7 Hz, 3H, OCH_2CH_3) 1.10 (s, 2 × CH_3); ^{13}C NMR δ: 204.04 (s, C=O, ketone), 169.46 (s, C=O, ester), 154.90 (s, C=), 127.19 (d, CH=), 61.10 (t, OCH_2), 43.03 (t, CH_2CO_2), 40.37 (s, CC=O), 36.07 (t, =CCH_2), 27.04 (t, CH_2), 23.94 (q, 2 × CH_3), 14.09 (q, OCH_2CH_3); HRMS M^+: 210.1257 (calcd. for $C_{12}H_{18}O_3$: 210.1257). Anal. calcd. for $C_{12}H_{18}O_3$: C 68.57, H 8.57; found: C 68.25, H 8.53.

(+)-(5S)-3-Carbethoxymethyl-5-(1-methylethenyl)-2-methyl-2-cyclohexen-1-one (**16**)

Alcohol **10** (280 mg, 1.17 mmol) was oxidized with PCC (760 mg, 3.53 mmol) in CH_2Cl_2 (8 mL) for 50 h. Since the oxidation was quite slow, a large excess (3.0 mol. equiv.) of PCC was used in this case. After flash chromatography (10% EtOAc in hexane), the optically active enone **16** was obtained in 81% yield (224 mg) as a colorless oil: $[\alpha]_D^{22}$ +66.33 (*c* 1.71, $CHCl_3$); IR: 1736 (C=O, ester), 1671 (C=O, enone), 1639 (C=C) cm^{-1}; ^1H NMR (400 MHz) δ: 4.81 (m, 1H CHH=), 4.76 (m, 1H, CHH=), 4.19 (q, J = 7 Hz, 2H, OCH_2), 3.33 (d, J = 15 Hz, 1H, CHHCO$_2$), 3.28 (d, J = 15 Hz, 1H, CHHCO$_2$), 2.68 (m, 1H), 2.60 (ddd, J = 16, 4, 1.5 Hz, 1H, $CH_{eq}H_{ax}C$=O), 2.47 (m, 2H), 2.34 (dd, J = 16, 13 Hz, 1H, $CH_{eq}H_{ax}C$=O), 1.81 (br t, J = 2 Hz, 3H, CH_3C=CH_2), 1.76 (br s, 3H, CH_3C=C), 1.28 (t, J = 7 Hz, 3H, OCH_2CH_3); ^{13}C NMR δ: 198.99 (s, C=O, ketone), 169.63 (s, C=O, ester), 148.92 (s, =CCH_2CO_2), 146.51 (s, CH_3C=C), 133.35 (s, CH_3C=CH_2), 110.58 (t, CH_2=C), 61.18 (t, OCH_2), 42.51 (t, CH_2CO_2Et), 41.28 (d, CH_2CHCH_2), 40.70 (t, CH_2), 36.61 (t, CH_2), 20.50 (q, CH_3), 14.19 (q, CH_3), 11.01 (q, CH_3); HRMS M^+: 236.1415 (calcd. for $C_{14}H_{20}O_3$: 236.1412). Anal. calcd. for $C_{14}H_{20}O_3$: C 71.19, H 8.47; found: C 71.35, H 8.31.

Acknowledgements

We are grateful to the Natural Sciences and Engineering Research Council of Canada and the University of Alberta for financial support.

1. H. Seto, T. Sasaki, H. Yonehara, and J. Uzawa. Tetrahedron Lett. 923 (1978).
2. T. Imamoto, N. Takiyama, K. Nakamura, T. Hatajima, and Y. Kamiya. J. Am. Chem. Soc. **111**, 4392 (1989), and references cited therein.
3. K. Nagasawa, H. Kanbara, K. Matsushita, and K. Ito. Tetrahedron Lett. **26**, 6477 (1985).
4. T. Imamoto, Y. Sugiura, and N. Takiyama. Tetrahedron Lett. **25**, 4233 (1984).
5. S. E. Denmark, T. Weber, and D. W. Piotrowski. J. Am. Chem. Soc. **109**, 2224 (1987).
6. G. Stork and J. M. Stryker. Tetrahedron Lett. **24**, 4887 (1983).
7. W. G. Dauben and D. M. Michno. J. Org. Chem. **42**, 682 (1977).
8. S. K. Patt and J. N. Shoolery. J. Magn. Reson. **46**, 535 (1982).
9. W. C. Still, M. Khan, and A. Mitra. J. Org. Chem. **43**, 2923 (1978).
10. W. C. Agosta and A. B. Smith III. J. Am. Chem. Soc. **93**, 5513 (1971).
11. C. H. DePuy, M. Isaks, K. L. Eilers, and G. F. Morris. J. Org. Chem. **29**, 3503 (1964).
12. M. E. Flaugh, T. A. Crowell, and D. S. Farlow. J. Org. Chem. **45**, 5399 (1980).

Can. J. Chem. Downloaded from www.nrcresearchpress.com by 123.30.183.119 on 09/08/12
For personal use only.

Silylation de dérivés *gem*-dihalogénés bicycliques : synthèse de dihydro- et tétrahydro-oxépines siliciées

MICHELINE GRIGNON-DUBOIS,[1] MICHELLE FIALEIX ET CLAUDE BIRAN

Laboratoire de chimie organique et organométallique, Unité de recherche associée n° 35 du Centre national de la recherche scientifique, Université Bordeaux I, 351, Cours de la Libération, 33405 Talence CEDEX, France

Reçu le 1er mai, 1991

MICHELINE GRIGNON-DUBOIS, MICHELLE FIALEIX et CLAUDE BIRAN. Can. J. Chem. **69**, 2014 (1991).

La silylation du 2-oxa-7,7′-dichloronorcarane au moyen des systèmes $Me_3SiCl/Li/THF$ ou $Me_3SiCl/Mg/HMPT$ permet selon la nature du métal et du solvant d'accéder aux dérivés bicycliques siliciés correspondants ou à des dihydro- et tétrahydro-oxépines siliciées.

Mots clés : silylation, hydro-oxépines.

MICHELINE GRIGNON-DUBOIS, MICHELLE FIALEIX, and CLAUDE BIRAN. Can. J. Chem. **69**, 2014 (1991).

The silylation of 2-oxa-7,7′-dichloronorcarane has been studied. According to the reagent ($Me_3SiCl/Li/THF$ or $MeSi_3Cl/Mg/HMPT$), we observed significant differences in the reactivity, and silyloxabicyclonorcaranes or silylhydrooxepines were obtained. The influence of solvant and experimental conditions is discussed.

Key words: silylation, hydrooxepine skeleton.

Les cycles à sept chaînons occupent une place importante dans la chimie des produits naturels et en thérapeutique (1). En série oxygénée, ils sont bien répandus et se rencontrent tant dans des médicaments (doxépine, oxétorone, scopoline ... (1*a*)) que dans des phéromones (brevicomine, frontaline (1*b*)) ou des métabolites de végétaux inférieurs (palisadines (1*c*, 1*d*)). Ceci nous a conduits à nous intéresser au squelette de l'oxépine dont les dérivés ne sont pas toujours faciles d'accès. Nous avons tenté de l'obtenir à partir du dihydropyrane, via l'addition de dihalocarbène suivie d'une silylation. En effet, nous avions précédemment constaté que la silylation de systèmes bicycliques tendus pouvait s'accompagner d'une extension de cycle (2) et il est connu que la présence d'un atome d'oxygène en α d'un cyclopropane fragilise ce dernier (3); de plus, la présence d'un groupe triméthylsilyle sur la molécule permet d'envisager une fonctionnalisation ultérieure du composé cyclique obtenu (4).

Résultats et discussion

Afin de favoriser l'extension de cycle et d'apprécier l'effet de l'oxygène sur la réactivité des squelettes bicycliques, nous avons effectué la silylation des composés **1-3** avec le système $Me_3SiCl/Mg/HMPT$ (5) qui nécessite un chauffage prolongé à 80°C; le dérivé oxygéné **3** a également été soumis au réactif $Me_3SiCl/Li/THF$ à 0°C.

Silylation par $Me_3SiCl/Mg/HMPT$

La réaction est conduite à 80°C pendant 24 h avec 2 équivalents de magnésium et 2,6 équivalents de Me_3SiCl. La comparaison des résultats obtenus avec les substrats **1** et **2** (fig. 1) à ceux précédemment observés avec le système $Me_3SiCl/Li/THF$ (2) montre l'influence du solvant et du métal.

La silylation du 7,7′-dichlorobicyclo[3,1,0]hexane, **1**, est ici univoque et conduit au 2,6-bis(triméthylsilyl)cyclohexène (**4**, rdt 90%) résultant de l'extension de cycle. Ceci constitue une excellente méthode de préparation de ce dérivé qui n'était isolé jusqu'ici qu'avec 25% de rendement et dont nous avions montré les potentialités synthètiques (2).

De même, le 7,7′-dichloronorcarane **2** a un comportement différent selon l'agent silylant puisque le 7,7′-bis(triméthylsilyl)norcarane, précédemment isolé avec 80% de rendement (2), est ici absent du mélange réactionnel; cependant, la structure bicyclique est dans ce cas conservée et on isole le 7-chloro-7-triméthylsilylnorcarane (**5**, rdt 55%, *exo/endo* 90 : 10) et le 7-triméthylsilylnorcarane (**6**, rdt 15%, *exo/endo* 60 : 40); ce dernier provient de la réduction du composé **5** au sein du milieu, ce qui est à rapprocher des résultats décrits par Shimuzu et Tsuno (6) à partir du 7,7′-dibromonorcarane et de ceux observés par Oku *et al.* (7), par action du système $Me_3SiCl/K/NH_3$. Signalons que le composé chlorosilicié **5** avait également été isolé avec 62% de rendement par Seyferth et Hanson (8), mais par un procédé beaucoup plus long et délicat de mise en oeuvre.

Le 2-oxa-7,7′-dichloronorcarane, **3**, présente une réactivité intermédiaire puisque l'on isole un mélange de dérivés mono- et disiliciés bicycliques (**7** et **9**) et à sept chaînons (**8** et **10**), tous originaux. Le 2-oxa-7-triméthylsilylnorcarane (**7**, rdt 20%, isomère *exo*) et la 2,3-dihydro-6-triméthylsilyloxépine (**8**, rdt 40%) sont les produits principaux de la réaction. Le 2-oxa-7,7′-bis(triméthylsilyl)norcarane **9** et la 2,3,4,5-tétrahydro-5,6-bis(triméthylsilyl)oxépine **10** sont isolés avec un rendement global de 18% mais dans des proportions **9/10** variant de 40 : 60 à 5 : 95 selon les essais. Ceci suggère que la 2,3,4,5-tétrahydro-5,6-bis(triméthylsilyl)oxépine, **10**, proviendrait de l'ouverture de son isomère **9** au sein du mélange réactionnel, hypothèse qui est étayée par les observations suivantes : (*i*) la prolongation du chauffage (48 h au lieu de 24) favorise la formation du composé **10**, qui est alors isolé avec 25% de rendement; (*ii*) à l'état pur, le 2-oxa-7,7′-bis(triméthylsilyl)norcarane, **9**, évolue lentement, même à température ambiante, pour donner la tétrahydrooxépine **10** correspondante. L'addition de chloroforme accélère cette évolution qui devient totale en 3 jours; (*ii*) chauffé dans l'HMPT pendant 24 h à 80°C, l'oxadichlorononorcarane, **3**, conduit exclusivement à la 2,3-dihydro-6-chlorooxépine, **11**, et nous n'avons jamais isolé ainsi de 2,3,4,5-tétrahydro-5,6-dichlorooxépine dont la silylation aurait pu rendre compte de l'obtention du dérivé **10**.

Par contre, l'oxanorcarane silicié **7**, constitué du seul isomère *exo*, est thermiquement stable et ne donne pas lieu à un agrandissement de cycle qui conduirait au composé **8**; ceci suggère que ces deux dérivés se forment selon des processus différents et que la relative fragilité de l'oxanorcarane disilicié **9** est due à la gène stérique introduite par le groupe silyle en position

1. Auteur à qui adresser toute correspondance.

Printed in Canada / Imprimé au Canada

Can. J. Chem. Downloaded from www.nrcresearchpress.com by 123.30.183.119 on 09/08/12
For personal use only.

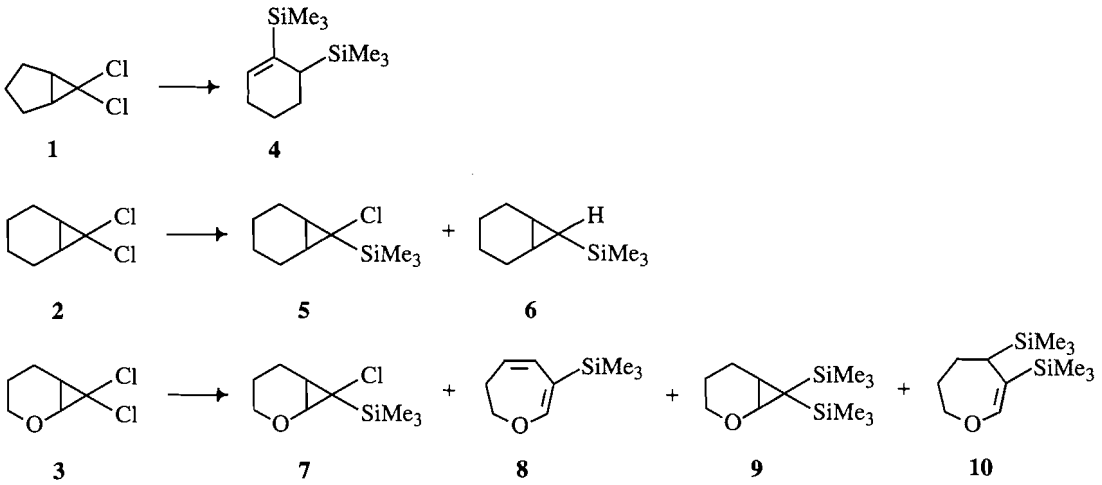


FIG. 1

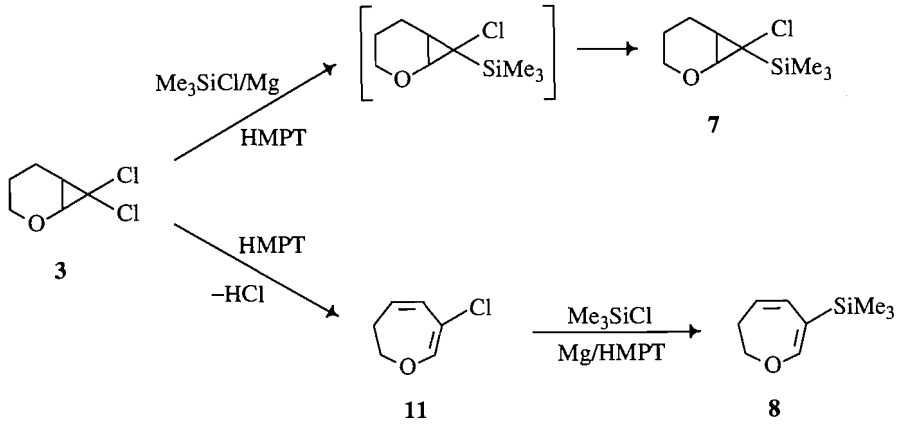


FIG. 2

endo. La 2,3-dihydro-6-triméthylsilyloxépine, **8**, résulterait de la silylation du dérivé chloré correspondant **11** (fig. 2); ce dernier proviendrait de la déchlorhydratation du substrat sous l'action de l'HMPT. En effet, lorsque la silylation est conduite avec la quantité stoechiométrique de magnésium, soit un équivalent, seule la 2,3-dihydro-6-chlorooxépine, **11**, est isolée. De plus, la silylation de cette dernière, préparée selon la référence 9, conduit dans les mêmes conditions (1 équiv. de Mg, 3 équiv. de Me_3SiCl, 24 h à 80°C) à l'oxépine siliciée **8**, isolée avec 65% de rendement.

La comparaison de ces résultats avec ceux observés à partir des dichlorobicycloalcanes **1** et **2** montre l'influence de l'atome d'oxygène puisqu'en son absence on n'isole pas de produit résultant d'une déchlorhydratation avec silylation. On note cependant l'analogie structurale entre les composés **7** et **5**–**6** d'une part et **10** et **4** d'autre part.

Silylation par $Me_3SiCl/Li/THF$

Le système $Me_3SiCl/Li/THF$ est un agent de silylation plus puissant que $Me_3SiCl/Mg/HMPT$ (4*c*, 5). La comparaison des résultats obtenus avec ces deux réactifs à partir du *gem*-dichloronorcarane en est une confirmation.

La silylation du 2-oxa-7,7′-dichloronorcarane, **3**, effectuée à 0°C avec 4 équivalents de lithium et 2,6 équivalents de Me_3SiCl, conduit, à côté des oxanorcaranes siliciés précédemment obtenus **7** (rdt 5%) et **9** (rdt 25%), aux 3-(triméthylsiloxy-3′-propyl)-1,2-bis(triméthylsilyl)cyclopropane (**12**, rdt 15%) et 3-(triméthylsiloxy-3′-propyl)-1,1,2-tris(triméthylsilyl)cyclopropane (**13**, rdt 5%) qui sont originaux (fig. 3). L'utilisation d'un excès de réactif (12 équiv. de Li, 6 équiv. de Me_3SiCl) permet d'augmenter le rendement en produits d'ouverture qui atteint alors 40% (**12**/**13** = 3 : 1). Ils résultent de la silylation de la liaison C(1)—O des composés **7** et **9** : elle s'effectue simultanément sur la face *endo* et *exo* du squelette bicyclique conduisant à un mélange d'isomères cyclopropaniques (proportion 70 : 30), qui ont été mis en évidence par chromatogra-

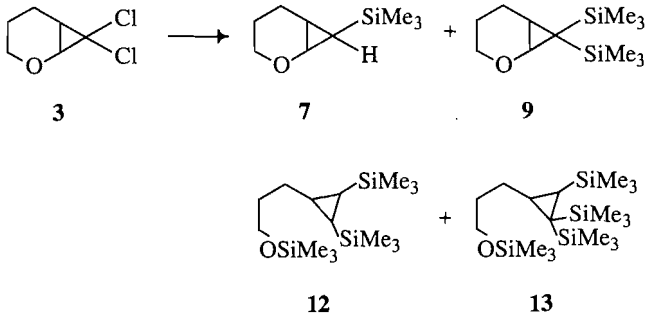
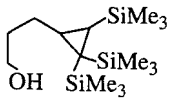


FIG. 3

Can. J. Chem. Downloaded from www.nrcresearchpress.com by 123.30.183.119 on 09/08/12
For personal use only.

phie en phase gazeuse reliée à un spectromètre de masse. La complexité des spectres RMN ^1H ne permet pas de préciser la nature de l'isomère prépondérant; cependant, il est vraisemblable qu'il s'agit dans les deux cas du 2,3-*trans*, stériquement moins encombré que le *cis*. En milieu acide, le composé **13** conduit quantitativement à l'alcool **14**, également constitué de deux isomères et qui résulte de l'hydrolyse de la liaison O—Si.



Composé **14**

L'extension de cycle n'intervient donc plus, ce qui confirme le mécanisme proposé pour rendre compte de la formation des oxépines : en effet, la déchlorhydratation de l'oxadichloronorcarane ne se produit pas à 0°C dans le THF.

L'ouverture du cycle oxygéné conduisant à la formation des composés **12** et **13** est comparable à celle décrite par ailleurs (10) dans le cas du benzofurane et du benzothiophène. Afin de limiter cette réaction secondaire, nous avons utilisé le système $Me_3SiCl/Li/Et_2O$ qui est un agent de silylation moins puissant, mais, dans ces conditions, aucune silylation n'intervient même si l'on prolonge le temps de contact entre les différents réactifs.

Conclusion

Cette étude montre l'influence de la structure du substrat et des conditions expérimentales sur l'orientation de la silylation en série bicyclique. Ainsi le 2-oxa-7,7′-dichloronorcarane réagit avec le système $Me_3SiCl/Mg/HMPT$ pour conduire à des hétérocycles oxygénés siliciés bicycliques ou heptagonaux tous originaux. L'enchaînement «addition de dichlorocarbène – silylation dans l'HMPT» permet donc de passer du squelette du dihydropyrane à celui des oxépines. La généralisation de cette méthodologie devrait ouvrir de nouvelles voies d'accès à d'autres hétérocycles siliciés à 7 chaînons.

Cette extension de cycle n'intervient pas lorsque la réaction met en jeu le lithium dans le THF. Par contre, on assiste alors à l'ouverture partielle du cycle oxygéné.

Partie expérimentale

Le THF est préalablement distillé sur sodium et benzophénone, l'HMPT sur CaH_2 et le Me_3SiCl sur Mg en poudre.

Les composés **1–3** ont été synthétisés par addition de dichlorocarbène respectivement sur le cyclopentène, le cyclohexène et le 2,3-dihydropyrane selon le procédé de Julia et Girebreda (11). Le composé **11** a été préparé selon la référence 9.

Silylation par le système $Me_3SiCl/Mg/HMPT$

À une suspension de 0,25 at.g de magnésium en poudre dans 60 mL d'HMPT et 0,25 mol de Me_3SiCl, on ajoute, goutte à goutte, le substrat (0,1 mol de **1–3** ou 0,2 mol de **11**), puis on porte le mélange à 90°C pendant 24 h. Après refroidissement, le produit réactionnel est versé sur un mélange pentane/eau glacée acidifiée. La phase organique est ensuite lavée jusqu'à neutralité et séchée sur Na_2SO_4 et les produits formés sont isolés par distillation à l'aide d'une colonne à bande tournante. Les proportions de réactifs sont indiquées dans la partie Résultats.

Silylation par le système $Me_3SiCl/Li/THF$

À une suspension de 0,4 at.g de lithium, finement granulé, dans 150 mL de THF et 0,26 mol de Me_3SiCl fraîchement distillé, on ajoute, goutte à goutte, 0,1 mol du composé **3**, en refroidissant de telle manière que la température du milieu réactionnel soit maintenue entre 0 et 5°C. L'addition terminée, l'agitation est poursuivie pendant 24 h en maintenant la température entre 0 et 5°C. Le mélange réactionnel est alors filtré pour éliminer LiCl qui a précipité et le filtrat est évaporé sous le vide de la trompe à eau. Dans le cas (fréquent) où LiCl précipite à nouveau, on effectue une deuxième filtration après addition de 50 mL de cyclohexane. Après élimination du solvant à la trompe à eau, on obtient une huile jaune clair, dont les constituants sont séparés par distillation à l'aide d'une colonne à bande tournante.

Caractéristiques physico-chimiques des produits siliciés obtenus

Les analyses centésimales ont été effectuées au service central d'analyse du CNRS (F-69390 Vernaison). Les spectres de masse (SM) ont été enregistrés sur un appareil VG micromass 16 F (70 eV) et les spectres IR sur un spectromètre Perkin–Elmer 1420; tous les dérivés siliciés isolés présentent en IR des bandes de très forte intensité à 1250 et 850 cm^{-1} caractéristiques des groupes $SiMe_3$ et qui peuvent masquer le reste du spectre. Les spectres de RMN ont été enregistrés sur un appareil Bruker AC 250 fonctionnant à 250 MHz dans le cas du proton et 62,9 MHz pour le ^{13}C (solvant, $CDCl_3$; C_6H_{12} ref. int. à 1,4 ppm (^1H) ou 27,08 ppm (^{13}C)).

Les cycloalcanes siliciés **4–6** sont identiques aux échantillons que nous avons isolés par ailleurs (2, 12).

2-Oxa-7-triméthylsilylnorcarane (7): il est isolé par distillation : Eb 102°C/30 Torr (1 Torr = 133,3 Pa), rdt 20%. IR (film NaCl, cm^{-1}) : 3020, 2960, 2900, 2860, 1250, 860, 850. RMN ^1H, δ ppm : 1,0 (t, 1H, H-7); 1,3–1,5 (m, 1H, H-6); 1,6–1,8 (m, 4H, H-4,4′ et H-5,5′); 3,3 (m, 1H, H-1); 3,8 (m, 2H, H-3,3′). RMN ^{13}C, δ ppm : $SiMe_3$ à −0,11; 3CH à 26,2, 28,1 et 53,5; $3CH_2$ à 15,8, 16,1 et 53,5. Anal. calc. pour $C_9H_{18}OSi$: C 63,47, H 10,65, Si 16,49; trouvée : C 63,52, H 10,63, Si 16,54.

2,3-Dihydro-6-triméthylsilyloxépine (8): Eb 95°C/30 Torr; rdt 40% à partir du 7,7′-dichloronorcarane (**3**), 65% à partir de la 3-chloro-2,6-dihydrooxépine (**11**). IR (film NaCl, cm^{-1}) : 3020, 2960, 2900, 1575, 1250, 1160, 840. RMN, ^1H, δ ppm : 0,1 (s, 9H); 2,55 (m, 2H, H-3,3′, $J_{2,3}$ 4,3 Hz, $J_{3,4}$ 5 Hz); 4,15 (t, 2H, H-2,2′, $J_{2,3}$ 4,3 Hz); 5,82 (m, 4H, H-4,4′ et H-5,5′, $J_{4,5}$ 10,7 Hz, $J_{4,7}$ 0,9 Hz, $J_{5,7}$ 0,8 Hz); 6,4 (signal large, 1H, H-7). RMN ^{13}C, δ ppm : $SiMe_3$ à −1,2; $2CH_2$ à 34,3 et 69,9; 3CH à 125,8, 130,3 et 152,1; C à 108,7. Anal. calc. pour $C_9H_{16}OSi$: C 64,22, H 9,58, Si 16,69; trouvée : C 63,93, H 9,72, Si 16,73.

2-Oxa-7,7′-bis(triméthylsilyl)norcarane (9): Eb 90–92°C/5 Torr. IR (film NaCl, cm^{-1}) : 3000, 2960, 2900, 2875, 1250, 1110, 1070, 890, 860, 845. RMN ^1H, δ ppm : 0,03 (s, 9H); 0,13 (s, 9H); 1,05 (m, 1H, H-6, $J_{6,5}$ 5,8 Hz, $J_{6,5'}$ 8,4 Hz); 1,5 (m, 4H, H-4,4′ et H-5,5′); 3,3 (d, 1H, H-1, $J_{1,6}$ 5,9 Hz); 3,7 (m, 2H, H-3,3′). RMN ^{13}C, δ ppm : $2SiMe_3$ à −0,8 et 2,9; $3CH_2$ à 18,4, 20,9 et 63,5; 2CH à 18,8 et 57,5; C à 5,2. Anal. calc. pour $C_{12}H_{26}OSi_2$: C 59,43, H 10,81, Si 23, 16; trouvée : C 59,48, H 10,77, Si 23,25.

2,3,4,5-Tétrahydro-5,6-bis(triméthylsilyl)oxépine (10): Eb 83–85°C/5 Torr. IR (film NaCl, cm^{-1}) : 2990, 2960, 2900, 2860, 1650, 1250, 1140, 870, 850, 770, 690. RMN ^1H, δ ppm : 0,03 (s, 9H); 0,13 (s, 9H); 1,4 (m, 1H, H-5); 1,47 et 1,58 (2m, 2H, H-4,4′); 1,8 et 1,86 (2m, 2H, H-3,3′); 3,9 (m, 2H, H-2,2′); 6,05 (s, 1H, H-7). RMN ^{13}C, δ ppm : $2SiMe_3$ à 0,2; $3CH_2$ à 22,8, 23,2 et 64,9; 2CH à 26,2 et 137,6; C à 112,6. Anal. calc. pour $C_{12}H_{26}OSi_2$: C 59,43, H 10,81, Si 23,16; trouvée : C 60,02, H 10,85, Si 23,29.

3-(Triméthylsiloxy-3′-propyl)-1,2-bis(triméthylsilyl) cyclopropane (12): il est isolé par distillation au moyen d'un four à boules avec un rendement de 15% lorsqu'on utilise 2,6 équiv. de Me_3SiCl pour 4 équiv. de Li et de 30% lorsqu'on utilise 6 équiv. de Me_3SiCl pour 12 équiv. de Li. IR (film NaCl, cm^{-1}) : 2990, 2960, 2900, 2860, 1250, 1100, 920, 870, 840, 760, 690. Le composé **12** est constitué de deux isomères (70 : 30). RMN ^1H (60 MHz), δ ppm : signal constitué de plusieurs singulets indicernables de 0,0 à 0,1 (27H, $SiMe_3$); 0,6–0,9 (m, 2H, H-1 et H-2); 1,1 à 1,8 (m, 5H, CH_2-CH_2 et H-3); 3,6 (m, 2H, CH_2O). Les spectres de masse de chacun des deux isomères ont été obtenus grâce à un spectromètre relié à un chromatographe en phase gazeuse (colonne SE 52, 5%, 2,5 m) : isomère prépondérant : SM, *m/e* (%) : 316 (0,8); 243 (0,6); 213 (2,18); 171 (3,7); 157 (3,7); 148 (4,56); 147 (29,1); 133 (21,06); 75 (17,9); 73 (100); isomère

Can. J. Chem. Downloaded from www.nrcresearchpress.com by 123.30.183.119 on 09/08/12
For personal use only.

mineur : SM, *m/e* (%) : 316 (1,19); 243 (0,6); 213 (2,3); 185 (1,58); 170 (0,94); 169 (1,68); 157 (3,66); 148 (4,5); 147 (23,67); 133 (16,5); 75 (17,4); 73 (100).

3-(Triméthylsiloxy-3'-propyl)-1,1,2-tris(triméthylsilyl)cyclopropane (13): il est isolé par distillation au moyen d'un four à boules avec un rendement de 5% lorsqu'on utilise 2,6 équiv. de Me_3SiCl pour 4 équiv. de Li et de 10% lorsqu'on utilise 6 équiv. de Me_3SiCl pour 12 équiv. de Li. Il est constitué de deux isomères. IR (film NaCl, cm^{-1}) : 2990, 2960, 2900, 2860, 1250, 1100, 920, 870, 840, 760, 690. RMN ^1H (60 MHz), δ ppm : signal constitué de plusieurs singulets indicernables de −0,01 à 0,1 (36H, $SiMe_3$); 0,6 (m, 1H, H-2); 1,2 à 1,8 (m, 5H, CH_2-CH_2 et H-3); 3,6 (m, 2H, CH_2O). Anal. calc. pour $C_{18}H_{44}OSi_4$: C 55,60, H 11,40, Si 28,89; trouvée : C 55,53, H 11,35, Si 28,79. Le spectre de masse des deux isomères a été obtenu par couplage avec un chromatographe en phase gazeuse (colonne SE 52, 5%, 2,5 m) : isomère prépondérant : SM, *m/e* (%) : 388 (0,7); 316 (0,4); 315 (0,5); 314 (1,5); 243 (1,0); 241 (1,2); 183 (2,19); 171 (0,95); 170 (1,7); 169 (1,7); 149 (4,7); 148 (9,2); 147 (59,7); 133 (6,4); 75 (4,2); 74 (8,1); 73 (100); isomère mineur : SM, *m/e* (%) : 354 (1,2); 298 (2,6); 270 (1,7); 243 (1,81); 183 (1,4); 171 (1,2); 170 (1,7); 169 (2,9); 149 (6,9); 148 (9,2); 147 (62,7); 133 (5,3); 75 (5,5); 74 (11,9); 73 (100).

3-(Propan-3'-ol)-1,1,2-tris(triméthylsilyl)cyclopropane (14): le composé **13** (1 g, 0,0025 mol) dissous dans 5 mL d'éthanol et 1 mL d'acide chlorhydrique 6 N est agité pendant 1 h à 0°C; après neutralisation du milieu et extraction au dichlorométhane, on isole l'alcool **14** (0,8 g, rdt quant.). IR (film NaCl, cm^{-1}) : 3500–3300, 2960, 2900, 2860, 1250, 1060, 900, 870, 850, 750, 680. RMN ^1H, δ ppm : 6s (27H) à −0,01; 0,07, 0,08 ($3SiMe_3$, isomère minoritaire) et à −0,015; 0,00 et 0,015 ($3SiMe_3$, isomère prépondérant); 0,8–1,4 (m, 2H, H-2 et H-3); 1,6 (m, 4H, CH_2–CH_2); 2,85 (signal large, 1H, OH); 3,55 (t, 2H, CH_2O). RMN ^{13}C, δ ppm : isomère prépondérant, $3SiMe_3$ à 0,9, 1,8 et 2,4; $C(Si)_2$ à 7,3; 2CH à 29,2 et 17,9; $3CH_2$ à 29,8, 34,0 et 62,5; isomère minoritaire, $3SiMe_3$ à −0,75, 1,7 et 3,8; $C(Si)_2$ à 7,3; 2CH à 14,4 et 28,25; $3CH_2$ à 27,2, 34,4 et 62,5. Anal. calc. pour $C_{15}H_{36}OSi_3$: C 56,89, H 11,46, Si 26,60; trouvée : C 56,97, H 11,43, Si 26,49.

1. (*a*) A. LESPAGNOL. Chimie des médicaments. Tome 1. Technique et Documentation, Paris. 1974; (*b*) J. APSIMON. The total synthesis of natural products. John Wiley, New York. vol. 2. 1973; vol. 4. 1981; vol. 5. 1983; (*c*) E. KUROSAWA, A. FUKURAURA et T. IRIE. Tetrahedron Lett. n° 42, 4135 (1973); (*d*) V. J. PAUL et W. FENICAL. Tetrahedron Lett. **21**, 2787 (1980).
2. M. LAGUERRE, M. GRIGNON-DUBOIS et J. DUNOGUÈS. Tetrahedron, **37**, 1161 (1981).
3. M. S. BAIRD, D. G. LINSAY et C. B. REESE. J. Chem. Soc. (C), 1173 (1969).
4. (*a*) E. W. COLVIN. Silicon reagents in organic synthesis. Academic Press, Londres. 1988; (*b*) W. P. WEBER. Silicon reagents for organic synthesis. Springer Verlag, Berlin. 1983; (*c*) J. DUNOGUÈS. L'Actualité chimique. 11 mars, 1986.
5. R. CALAS et J. DUNOGUÈS. J. Organomet. Chem. Libr. **2**, 277 (1976).
6. N. SHIMIZU et Y. TSUNO. Mem. Fac. Sci. Kyushu Univ. Ser. C: **12**, 95 (1979).
7. A. OKU, N. YOSHIURA et T. OKUDA. J. Org. Chem. **48**, 619 (1983).
8. D. SEYFERTH et E. M. HANSON. J. Organomet. Chem. **27**, 19 (1971).
9. E. E. SCHWEIZER et W. E. PARHAM. J. Am. Chem. Soc. **82**, 4085 (1960).
10. C. BIRAN, B. EFENDÉNÉ et J. DUNOGUÈS. J. Organomet. Chem. **253**, C13 (1983).
11. S. JULIA et A. GIREBREDA. Synthesis, 682 (1977).
12. (*a*) M. AHRA, M. GRIGNON-DUBOIS et J. DUNOGUÈS. J. Organomet. Chem. **271**, 15 (1984); (*b*) A. MARCHAND, P. GERVAL, M. AHRA et M. GRIGNON-DUBOIS. Spectrochim. Acta, **43A**, 539 (1987); (*c*) M. GRIGNON-DUBOIS, M. AHRA, M. LAGUERRE, B. BARBE et M. PÉTRAUD. Spectrochim. Acta, **45A**, 911 (1989).

Can. J. Chem. Downloaded from www.nrcresearchpress.com by 123.30.183.119 on 09/08/12
For personal use only.

Kinetics and mechanism of oxidation of DL-α-alanine by permanganate ion in acid perchlorate media

REFAT M. HASSAN
Department of Chemistry, Faculty of Science, Assiut University, Assiut, Egypt

Received June 22, 1990[1]

REFAT M. HASSAN. Can. J. Chem. **69**, 2018 (1991).

The kinetics of permanganate oxidation of DL-α-alanine in aqueous perchloric acid solution at a constant ionic strength of 2.0 mol dm^{-3} has been investigated spectrophotometrically. The reaction was found to show second-order kinetics overall with respect to each of the reactants in the slow initial stage; the second-order kinetics are not, however, maintained throughout the relatively fast final stage of reaction. The added salts lead to the prediction that Mn(III) and (or) Mn(IV) play a very important role in the reaction kinetics. A tentative mechanism consistent with the kinetics is discussed.

Key words: kinetics, oxidation, reduction, amino acids, permanganate.

REFAT M. HASSAN. Can. J. Chem. **69**, 2018 (1991).

Faisant appel à une méthode spectrophotométrique et opérant en solution aqueuse d'acide perchlorique à une force ionique constante de 2,0 mol dm^{-3}, on a étudié la cinétique de l'oxydation de la DL-α-alanine par le permanganate. On a trouvé que, dans sa phase initiale lente, la réaction est globalement du deuxième ordre impliquant chacun des réactifs; toutefois, cette cinétique n'est pas maintenue dans la phase finale, relativement rapide, de la réaction. L'effet des sels ajoutés laisse croire que les ions Mn(III) et (ou) Mn(IV) jouent des rôles très importants dans la cinétique de la réaction. On discute d'un mécanisme qui serait en accord avec la cinétique observée.

Mots clés : cinétique, oxydation, réduction, amino-acides, permanganate.

[Traduit par la rédaction]

Introduction

Although the extent of oxidation of organic compounds by permanganate ion depends on the nature of the substrate, the reactive species having the main role as the potential oxidant depends on the acidity of the medium (1).

The oxidation of DL-alanine by permanganate ion has been studied by Verma *et al.* (2) in concentrated solutions of sulphuric and perchloric acids (3–5 mol dm^{-3}). The mechanism proposed by them could not explain some of the experimental observations. Our preliminary experiments on this reaction at moderate $[H^+]$ suggested that the reaction mechanism is different from that proposed by Verma *et al.* The reaction was, therefore, reinvestigated in detail in an effort to put forward rate laws consistent with the experimental data, with a view to shedding more light on the mechanism of oxidation of amino acids by this oxidant as part of a series of investigations on amino acids carried out in our laboratory (3, 4).

Materials and method

Crystalline DL-α-alanine and potassium permanganate used were from Analar (BDH). All other reagents were of analytical grade and their solutions were prepared by dissolving the requisite amounts of the samples in doubly distilled conductivity water. The temperature is controlled within ±0.1°C.

The preparation and analysis of the stock solutions and the procedure for the kinetic runs were the same as described earlier (3, 4).

All kinetic measurements were conducted under pseudo-first-order conditions where the amino acid was maintained in a large excess over the permanganate ion concentration. The course of reaction was followed by monitoring the decrease in absorbance of permanganate ion at its absorption maximum, 525 nm, as a function of time. It was verified that there is no interference from other reagents at this wavelength.

Results

Stoichiometry and product analyses

The reaction mixtures containing varying ratios of the amino acid to MnO_4^- ion were mixed in the presence of 1.0 mol dm^{-3} $HClO_4$ adjusted to a constant ionic strength of 2.0 mol dm^{-3}, then equilibrated for 24 h at room temperature. Estimation of the unreacted $[MnO_4^-]$ showed that 1 mol of MnO_4^- consumed 2.5 ± 0.1 mol of the amino acid. Verma *et al.* (2) and Rao *et al.* (5) indicated that ammonia and acetaldehyde are two of the reaction products for the oxidation of DL-alanine by MnO_4^- ion. This result has been substantiated here by simple qualitative analyses (3, 6, 7) of the products conforming to the stoichiometric equation

$$[1]\quad 5CH_3CH(NH_2)COOH + 2MnO_4^- + 11H^+ = 5CH_3CHO + 5NH_4^+ + 2Mn^{2+} + 5CO_2 + 3H_2O$$

Similar reaction products have been observed during the oxidation of amino acids by MnO_4^- ion (3, 8–10) or by other oxidants (11, 12).

Reaction–time curves

The reaction–time curves were found to be of inverted S-shape throughout the entire range of reaction. The initial rates were relatively slow in the early stages, followed by an increase in the reaction rate over longer time periods. As the reaction is of autocatalytic nature, the oxidation obeys the rate expression $(A_t - A_\infty) = B_0 e^{-k_s t} + P_0 e^{-k_f t}$. Here, k_s and k_f are the first-order rate constants for the slow and fast reactions, while B_0 and P_0 represent the absorbance change for the slow and the fast reacting species, respectively. The rate constants, presented in Table 1, were obtained by drawing a straight line through the slow-time linear portion (k_s) of the first-order plot and extrapolating the line back to zero time (B_0). The rate of oxidation, k_f, for the fast oxidation reaction was obtained from plots of the form $-\ln [(A_t - A_\infty) - (A'_t - A_\infty)]$ vs. time. The quantity $(A_t - A_\infty)$ represents the experimental point and $(A'_t - A_\infty)$ represents the extrapolated point at time t' (13, 14) as shown in Fig. 1.

Dependence of reaction rate on $[MnO_4^-]$ and [amino acid]

The log (absorbance) – time plots for the initial stages of reaction indicate that the reaction is first order with respect to

[1]Revision received June 27, 1991.

Printed in Canada / Imprimé au Canada

Can. J. Chem. Downloaded from www.nrcresearchpress.com by 123.30.183.119 on 09/08/12
For personal use only.

TABLE 1. Rates of oxidation of DL-alanine by permanganate ion. $[MnO_4^-] = 2.8 \times 10^{-4}$ mol dm^{-3}; $[H^+] = 1.0$ mol dm^{-3}; $I = 2.0$ mol dm^{-3}; temperature = 25°C

10^2 [amino acid] (mol dm^{-3})	$10^4 k_s$ (s^{-1})	$10^4 k_f$ (s^{-1})	$10^3 k_s'$ (dm^3 mol^{-1} s^{-1})	$10^2 k_f'$ (dm^3 mol^{-1} s^{-1})
4.5	2.58	4.58	5.67	10.17
6.0	3.35	5.83	5.50	9.67
7.5	4.27	7.02	5.67	9.33
10.0	5.68	9.00	5.67	9.00
12.5	6.88	10.63	5.50	8.50
15.0	8.50	12.33	5.67	8.17

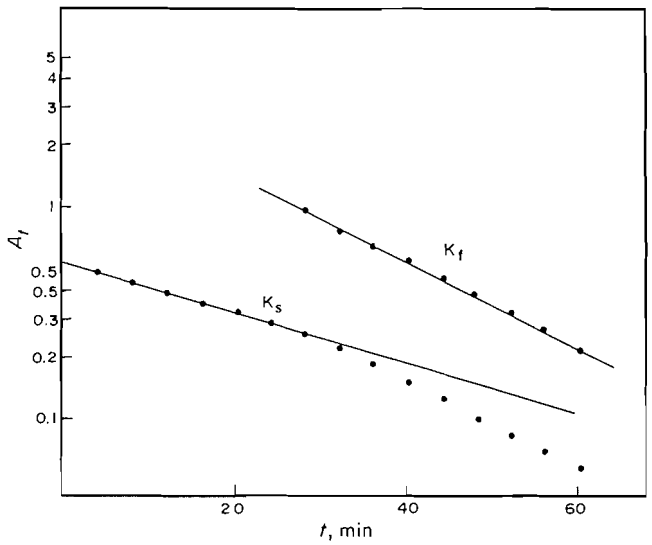


FIG. 1. Semi-log plot of A_t vs. time. $[MnO_4^-] = 2.8 \times 10^{-4}$; [DL-alanine] = 6×10^{-2}; $[H^+] = 1.0$; $I = 2.0$ mol dm^{-3}; temperature = 25°C.

permanganate ion. The order with respect to the amino acid in this initial stage was found from the measurements of the rates of several ratios of amino acid and fixed permanganate concentrations. The constancy of the second-order rate constants, k_s', derived from dividing k_s by [amino acid], indicates that the rate of oxidation is also first order in amino acid. The results are summarized in Table 1.

The second-order kinetics are, however, never maintained as the reaction proceeds throughout the autoacceleration period, and this behaviour is followed by a more complex kinetics.

Dependence of reaction rate on added salts

It is well known that acidified MnO_4^- is reduced by Mn^{2+} to give Mn^{3+} and Mn^{4+} ions (15)

$$[2] \quad MnO_4^- + 3Mn^{2+} + 8H^+ = 3Mn^{3+} + Mn^{4+} + 4H_2O$$

which are removed by fluoride ions through complex formation (16). If MnO_4^- ions are primarily responsible for the oxidation, a reduction in the initial rate should be observed in the presence of added Mn^{2+} ions, which reduce the concentration of MnO_4^- ions (17). If, on the other hand, intermediate manganese ions are the active oxidizing species, the addition of Mn^{2+} should cause an acceleration of the reaction rate. Similarly the addition of F^- ions should retard the reaction if the intermediate manganese ions are mainly responsible for the oxidation, but should cause no significant change if MnO_4^- ions are the principal oxidizing entities (3, 18).

TABLE 2. Effect of added salts on the autoacceleration rate of oxidation of DL-alanine by permanganate ion. $[MnO_4^-] = 2.8 \times 10^{-4}$ mol dm^{-3}; [DL-alanine] = 0.1 mol dm^{-3}; $[H^+] = 1.0$ mol dm^{-3}; $I = 2.0$ mol dm^{-3}; temperature = 25°C

10^3 [NaF] (mol dm^{-3})	$10^4 k_f$ (s^{-1})	10^3 [Mn^{2+}] (mol dm^{-3})	$10^4 k_f$ (s^{-1})
0.0	9.00	0.0	9.00
2.5	7.22	2.5	12.18
5.0	5.35	5.0	20.17
10.0	3.73	7.5	34.05

The experimental observations indicated that the reaction rate increased on increasing the Mn^{2+} ion, with the complete disappearance of the induction period even at low [Mn^{2+}], while a decrease in the rate was observed on addition of F^- ion. The results are summarized in Table 2.

Dependence of reaction rate on ionic strength

No primary effect was observed within the concentration limits demanded for the application of the Brønsted–Bjerrum equation. At higher concentrations of added $NaClO_4$, the values of k_s and k_f were found to increase with increasing ionic strength. The values of k_s and k_f at $I = 3.0$ and 4.0, and fixed values of $[H^+] = 1.0$, $[MnO_4^-] = 2.8 \times 10^{-4}$, and [DL-alanine] = 0.1 mol dm^{-3} at 30°C, are 6.83×10^{-4} and 7.83×10^{-4}, and 1.02×10^{-3} and 1.12×10^{-3} s^{-1}, respectively.

Dependence of reaction rate on [H^+]

To examine the influence of [H^+] on the rate of reaction, some kinetic runs were performed in $HClO_4$ solutions of 0.75–2.0 mol dm^{-3}. The ionic strength was kept constant at 2.0 mol dm^{-3} by adding sodium perchlorate as an inert electrolyte. It was found that the rate of oxidation increased with increasing [H^+]. The results are summarized in Table 3.

Oxidation of DL-alanine by manganese(III)

Manganese(III) perchlorate solutions are known to be reasonably stable in the presence of an excess of manganese(II), otherwise the Mn^{3+} disproportionates with the precipitation of manganese dioxide (7, 19).

Manganese(III) perchlorate solutions were prepared by addition of acid permanganate solution to sufficient acidified manganese(II) as described elsewhere (19). The prepared solutions were usually stable for a few days even when subsequently diluted so that the hydrogen ion concentration became about 1.5 mol dm^{-3}.

The kinetics of oxidation of DL-alanine by manganese(III)

Can. J. Chem. Downloaded from www.nrcresearchpress.com by 123.30.183.119 on 09/08/12
For personal use only.

TABLE 3. Effect of $[H^+]$ on the reaction rates of oxidation of DL-alanine by permanganate ion. $[MnO_4^-] = 2.8 \times 10^{-4}$ mol dm^{-3}; [DL-alanine] $= 7.5 \times 10^{-2}$ mol dm^{-3}; I = 2.0 mol dm^{-3}; temperature = 30°C

$[H^+]$ (mol dm^{-3})	$10^4 k_s$ (s^{-1})	$10^4 k_f$ (s^{-1})
0.75	5.63	9.55
1.00	6.13	10.50
1.25	6.75	11.55
1.50	7.38	12.65
1.75	8.15	13.87
2.00	9.00	15.27

TABLE 4. Rate constants for the oxidation of DL-alanine by manganese(III). $[Mn^{2+}] = 0.1$; $[Mn^{3+}] = 5.3 \times 10^{-4}$; $[H^+] = 1.0$; I = 2.0 mol dm^{-3}; temperature = 25°C

10^2[DL-alanine] (mol dm^{-3}):	5.00	7.50	10.00	15.00	20.00
$10^3 k_{obs}$ (s^{-1}):	2.35	3.22	4.10	5.35	6.18
$10^2 k$ (dm^3 mol^{-1} s^{-1}):	4.70	4.29	4.10	3.57	3.09

NOTE: k_{obs} is the observed pseudo-first-order rate constant and k is the second-order rate constant.

ion were followed spectrophotometrically under a nitrogen atmosphere at a wavelength of 290 nm, the absorption maximum of Mn^{3+} ion as a function of time. These kinetic measurements were carried out under pseudo-first-order conditions where the amino acid was present in a large excess over that of $[Mn^{3+}]$. The experimental results showed that the reaction was first order with respect to manganese(III) concentration, indicated by the linearity of log (absorbance) – time plots for more than three half-lives of reaction completion, while a fractional order was observed in [DL-alanine]. The results are summarized in Table 4.

Discussion

In acid solutions, amino acids tend to exist predominantly as the protonated species according to the following equilibria (20):

[3] $RCHNH_2CO_2H \rightleftharpoons RCH\overset{+}{N}H_3CO_2^-$ (zwitterion)

[4] $RCH\overset{+}{N}H_3CO_2^- + H^+ \overset{K_1}{\rightleftharpoons} RCH\overset{+}{N}H_3CO_2H$

By analogy with the chemistry of potassium permanganate under our experimental conditions (21), it is reasonable to assume that $HMnO_4$ species are generated as follows:

[5] $MnO_4^- + H^+ \overset{K_2}{\rightleftharpoons} HMnO_4$

where K_2 is the protonation constant (2.99×10^{-3} dm^3 mol^{-1} at 25°C) (21).

The hydrogen ion dependency of the reaction rate (non-integral order) suggests that at least one reaction path involving the protonated species is present in the slow stage of the reaction. Again, the positive salt effect further indicates that the reaction is between an ion and a neutral molecule (22).

In view of these facts and the experimental observations, a consistent mechanism involving two competitive reactions in the rate-determining step may be suggested for the induction period as follows:

[6] $MnO_4^- + LH^+ \xrightarrow{k_a} [*]$

[7] $HMnO_4 + LH^+ \xrightarrow{k_b} [*]$

where LH^+ represents the protonated species of DL-α-alanine. Hence the variation of the rate constant with change of the substrate and $[H^+]$ can be expressed by the following equation

$$[8] \quad \text{Rate} = \frac{k_a K_1 + k_b K_1 K_2 [H^+][LH^+][MnO_4^-]_T}{1 + K_2[H^+]}$$

where $[MnO_4^-]_T$ is the analytical total concentration of permanganate ion. Assuming that $K_2[H^+] \ll 1$ in eq. [8] under our experimental conditions, the second-order rate constant of the initial induction period can be rewritten as follows:

$$[9] \quad k_s' = k_a' + k_b'[H^+]^n$$

where $k_a' = k_a K_1$, $k_b' = k_b K_1 K_2$, and $n = 0.5$. Equation [9] requires that the plot of k_s' against $[H^+]^{0.5}$ be linear. The existing data satisfied this requirement, as shown in Fig. 2. The values of k_a' and k_b' were calculated by the least-squares method.

Unfortunately, the values of k_a and k_b could not be evaluated due to the non-availability of the protonation constants K_1 and K_2 at the various temperatures. Although some attempts were made to evaluate these constants at various temperatures from the experimental data, the results were not encouraging. The activation parameters of the k_a' and k_b' paths of the induction period were evaluated using Eyring's equation. The values calculated by the method of least squares are summarized in Table 5.

Several factors, such as the charge and the ordering of the solvent molecules around the activated complexes, may be responsible for the negative entropy of activation. In general, this ordering is affected by the charge on the activated complex. When the activated complex has zero charge, the ordering of the solvent molecules around the activated complex should be less than around the separate reactant ions; this will tend to make the entropy of activation less negative, and vice versa for the activated complex, which has a positive charge. It seems quite likely that the entropies of activation for the k_a' and k_b' paths are not consistent with this behaviour. Consequently, the less negative entropy of activation for the k_b' path compared with that for the k_a' path may be interpreted as the contribution of the positive ΔS^0 for the protonation of MnO_4^- ion in the former path, but not in the latter one, since $\Delta S^{\neq}$ values are composite quantities of entropy terms.

Moore and Hicks observed that the entropy of activation, $\Delta S^{\neq}$, for a group of MnO_4^- reactions, is negative for the reactions that proceed via complex formation, i.e., the inner-sphere mechanism (23, 24); while the $\Delta S^{\neq}$ values for the outer-sphere reactions tend to be more positive (25). The activation parameters for the oxidation of some organic substrates by MnO_4^- ion are summarized in Table 6. The entropy of activation for the MnO_4^-–DL-alanine reaction falls within the observed range of the former case. Again, Leffler and Grunwald (26) have pointed out that many reactions show an isokinetic relationship $\Delta H^{\neq} = C + B\Delta S^{\neq}$. As shown in Fig. 3, a plot of $\Delta H^{\neq}$ versus $\Delta S^{\neq}$ for the oxidation of some organic compounds by MnO_4^- ion (via similar reaction mechanisms) is fairly linear, with $C = 85$ kJ mol^{-1} and $B = 341$ K. The linearity and the slope of the curve obtained may confirm that the kinetics of these reactions follow similar reaction mechanisms, as previously suggested.

Can. J. Chem. Downloaded from www.nrcresearchpress.com by 123.30.183.119 on 09/08/12
For personal use only.

TABLE 5. Activation parameters of DL-alanine oxidation by permanganate ion

Pathway	$\Delta S^{\neq}$ (J K^{-1} mol^{-1})	$\Delta H^{\neq}$ (kJ mol^{-1})	$\Delta G^{\neq}$ (kJ mol^{-1})	Reference
k'_a	-123.91 ± 6.02	58.99 ± 1.74	95.91 ± 3.53	This work
k'_b	-55.15 ± 2.21	69.54 ± 1.77	86.02 ± 2.43	This work
k'_b	-55.13	70.35	86.18	2

TABLE 6. Activation parameters for some organic permanganate reactions

Reaction	$\Delta S^{\neq}$ (J K^{-1} mol^{-1})	$\Delta H^{\neq}$ (kJ mol^{-1})	$\Delta G^{\neq}$ (kJ mol^{-1})	Reference
DL-Alanine	-55	70	86	This work
β-Phenylalanine	-160	34	82	4
Glycine	-116	48	83	2
DL-Valine	-105	51	82	2
DL-Alanine	-53	70	86	2
L-Arginine	-127	50	88	8
Glycol	-120	41	77	24
Glycolic acid	-92	58	86	24
Tartaric acid	-119	45	80	29
Lactic acid	-58	59	76	30

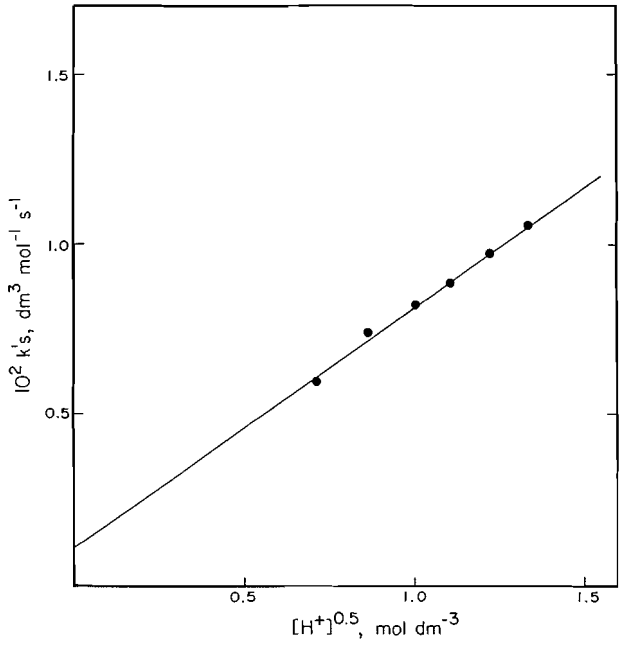


FIG. 2. Hydrogen ion dependency for the induction period. [MnO_4^-] = 2.8×10^{-4}; [DL-alanine] = 7.5×10^{-2}; I = 2.0 mol dm^{-3}; temperature = 30°C.

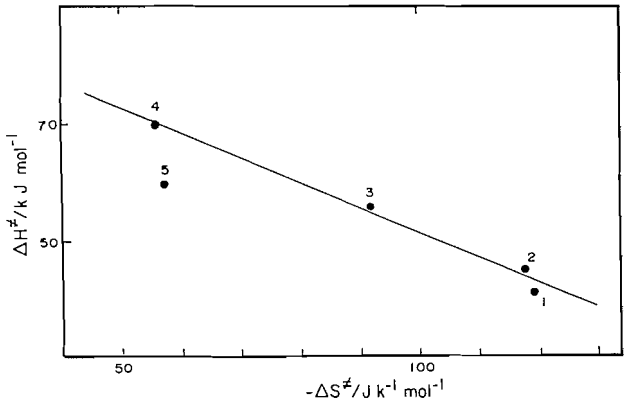


FIG. 3. Isokinetic relationship, $\Delta H^{\neq}$ vs. $\Delta S^{\neq}$, for oxidation of some organic substrates by MnO_4^- ion. (1) Glycol; (2) tartaric acid; (3) glycolic acid; (4) DL-alanine; (5) lactic acid.

Although the oxidation of DL-alanine by permanganate ion showed second-order overall kinetics, first order with respect to each of the reactants for the initial induction period, these kinetics are not maintained throughout the final, autoacceleration stage of reaction. Again, the complete disappearance of the induction period even at low [Mn^{2+}] and the decrease in the reaction rate on the addition of F^- ion may suggest that Mn^{3+} and (or) Mn^{4+} are the principle reactive species in the relatively fast final stage. But the oxidation of DL-alanine by manganese(III), as well as the continuous increase in oxidation rate with increasing the Mn^{2+} added to the MnO_4^-–alanine reaction mixture, indicates conclusively that Mn^{3+}, but not Mn^{4+}, is the sole oxidant throughout the autoacceleration stage.

Attempts were made to allow spectrophotometric detection of the Mn^{3+} ion intermediate as the reaction proceeded in the oxidation of DL-alanine by MnO_4^- ion. Unfortunately, the low concentration of the Mn^{3+} intermediate obtained under our experimental conditions made the detection unsuccessful.

Consequently, the most likely reaction mechanism that can be suggested for the autoacceleration period of the reaction involves the two competitive reactions [10] and [11]

$$[10] \quad Mn^{3+} + LH^+ \underset{}{\overset{K_3}{\rightleftharpoons}} MnL^{3+} + H^+ \xrightarrow[\text{slow}]{k_1} \text{product}$$

$$[11] \quad MnL^{3+} + LH^+ \overset{K_4}{\rightleftharpoons} MnL_2^{3+} + H^+ \xrightarrow[\text{slow}]{k_2} \text{product}$$

The intermediate complex ions, MnL^{3+} and MnL_2^{3+}, are formed and subsequently undergo further decomposition to give the reaction products. The variation of the rate constant either for the autoacceleration period or for the oxidation of

Can. J. Chem. Downloaded from www.nrcresearchpress.com by 123.30.183.119 on 09/08/12
For personal use only.

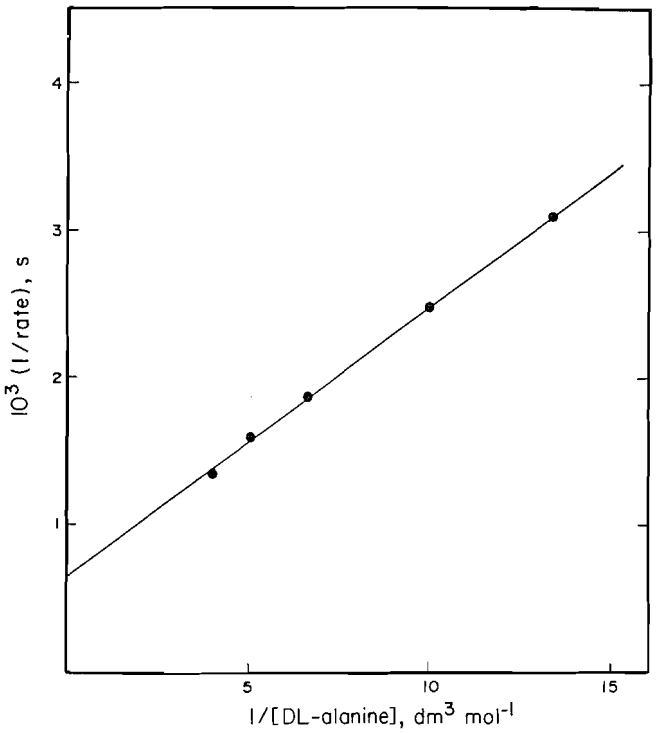


FIG. 4. Plot of 1/rate vs. 1/[DL-alanine] in the oxidation of DL-alanine by manganese(III). $[Mn^{3+}] = 5.3 \times 10^{-4}$; $[Mn^{2+}] = 0.1$; $[H^+] = 1.0$; $I = 2.0$ mol dm^{-3}; temperature = 25°C.

DL-alanine by manganese(III) with the change of the substrate and hydrogen ion concentrations may be expressed by the following relationship:

$$[12] \quad \text{Rate} = \frac{(k_1K_3[H^+]^{-1} + k_2K_3K_4[H^+]^{-2}) \cdot [LH^+][Mn^{3+}]_T}{1 + K_3[H^+]^{-1}[LH^+] + K_3K_4[H^+]^{-2}[LH^+]^2}$$

where $[Mn^{3+}]_T$ denotes the analytical total concentration of manganese(III)

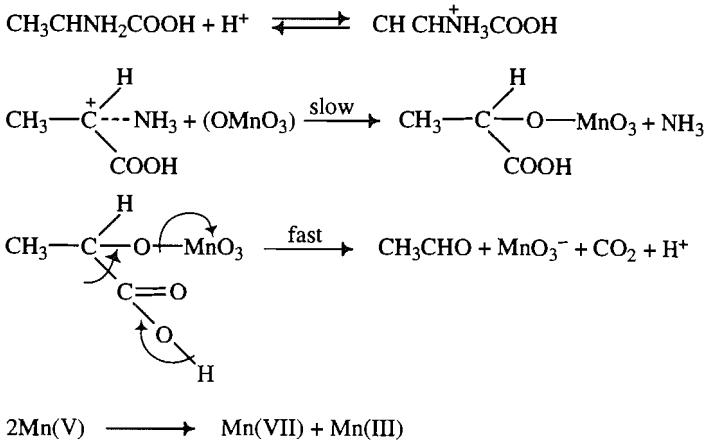
$$[13] \quad [Mn^{3+}]_T = [Mn^{3+}] + [MnL^{3+}] + [MnL_2^{3+}]$$

Under our experimental conditions of low $[LH^+]$, the factor $K_3K_4[H^+]^{-2}[LH^+]^2 \ll (1 + K_3[H^+]^{-1}[LH^+])$, and hence reaction [11] may be neglected. Then, reaction [10] is considered as the sole rate-determining step, and eq. [12] can be recast as

$$[14] \quad \text{Rate} = \frac{k_1K_3[H^+]^{-1}[LH^+][Mn^{3+}]}{1 + K_3[H^+]^{-1}[LH^+]}$$

According to eq. [14], at constant $[H^+]$ a plot of 1/rate versus 1/[DL-alanine] should be linear, as shown in Fig. 4. The good linearity obtained, in addition to the positive intercept on the 1/rate axis, may be considered as kinetic evidence for the formation of an intermediate complex ion in accordance with Michaelis–Menten kinetics (27). Again, the plot of 1/rate against $[H^+]$ at constant substrate should give a straight line, as is observed experimentally with respect to the oxidation of DL-alanine by MnO_4^- ion. Unfortunately, the latter plot could not be examined with respect to the oxidation of DL-alanine by manganese(III). Similar reaction mechanisms for the oxidation of some organic substrates by MnO_4^- have been reported elsewhere (28–30).

The positive catalytic effect of Mn^{2+} on the rate of reaction



SCHEME 1

may reflect the one-electron transfer mechanism. However, this pathway is not favoured from the energetic point of view for the Mn(VII)/Mn(VI) (+0.56 V) and Mn(VII)/Mn(V) (+1.1 V) couples (31). The protonation of permanganate ion shifts the Mn(VII)/Mn(VI) couple to a more positive value (+1.3 V), which makes $HMnO_4$ a stronger oxidizing agent than MnO_4^- ion.

In view of these facts and the experimental observations, it may be possible to suggest that the oxidation of DL-alanine by permanganate ion proceeds by a successive one-electron transfer mechanism of inner-sphere nature throughout two distinct stages. In the initial slow stage, manganese(III) is formed as a transient species. Then, the Mn(III) formed is attacked by the substrate to give the reaction products via intermediate complex formation throughout the autoacceleration period. The mechanism of oxidation is illustrated in Scheme 1.

It unfortunately does not appear possible to obtain direct evidence for detection of the intermediate complex ions; this failure is, however, not contrary to the proposed mechanism of this reaction since the subsequent oxidation of the intermediates is slow in comparison with their formation.

1. K. K. SENGUPTA, D. K. KHAMURI, and D. C. MUKHERJEE. Indian J. Chem. **13**, 348 (1975).
2. R. S. VERMA, M. J. REDDY, and V. R. SHASTRY. J. Chem. Soc. Perkin Trans. 2, 469 (1976).
3. M. M. GIRGIS, R. M. HASSAN, and A. S. EL-SHAHAWY. Bull. Fac. Sci. Assiut Univ. **16**, 41 (1987).
4. R. M. HASSAN, M. A. MOUSA, and M. H. WAHDAN. J. Chem. Soc. Dalton Trans. 605 (1988).
5. V. S. RAO, B. SETHURAM, and T. N. RAO. Indian J. Chem. Kinet. **11**, 165 (1975).
6. A. I. VOGEL. Practical organic chemistry. Longmans, London. 1962. p. 325.
7. A. I. VOGEL. A text book of quantitative inorganic analysis. Longman, London. 1962. p. 787.
8. U. D. MUDLIAR, V. R. CHOUREY, R. S. VERMA, and V. R. SHASTRY. J. Indian Chem. Soc. **60**, 561 (1983).
9. C. H. ASHRAF, I. AHMED, and F. K. N. LUGEMWA. Indian J. Chem. Sect A: **18A**, 373 (1979).
10. K. B. REDDY, B. SETHURAM, and T. N. RAO. Indian J. Chem. Sect. A: **20A**, 395 (1981).
11. M. Z. BARAKAT, M. F. ABDEL WAHAB, and M. M. ELSADAG. J. Chem. Soc. 4685 (1956).
12. M. S. RAMACHANDRAN and T. S. VIVEKANANDAM. Bull. Chem. Soc. Jpn. **60**, 3397 (1987).

Can. J. Chem. Downloaded from www.nrcresearchpress.com by 123.30.183.119 on 09/08/12
For personal use only.

13. K. W. HICKS and M. A. HURLESS. Inorg. Chem. Acta, **74**, 229 (1983).
14. R. M. HASSAN, M. H. WAHDAN, and A. HASSAN. Eur. Polym. J. **24**, 281 (1988).
15. W. A. WATERS. Q. Rev. Chem. Soc. **12**, 277 (1955).
16. H. F. LAUNER. J. Am. Chem. Soc. **54**, 2297 (1932).
17. P. S. RADHAKRISHNAMURTI and M. D. P. RAO. Indian J. Chem. Sect. A: **15A**, 524 (1977).
18. P. NATH, K. K. BANERJI, and G. V. BOKOVE. Ind. J. Chem. **8**, 1113 (1970).
19. D. R. ROSSEINSKY. J. Chem. Soc. 1181 (1963).
20. A. E. MARTELL and R. M. SMITH. Critical stability constants. Vol. I. Plenum Press, New York. 1974.
21. N. BAILEY, A. CARRINGTON, T. A. K. LOTT, and M. C. R. SYMONS. J. Chem. Soc. 290 (1960); Chem. Rev. **63**, 443 (1963).
22. C. H. ROCHESTER. Progress in reaction kinetics. Pergamon Press, Oxford. 1971. p. 145.
23. F. M. MOORE and K. W. HICKS. Inorg. Chem. **14**, 413 (1975).
24. K. W. HICKS. J. Inorg. Nucl. Chem. **38**, 1381 (1976).
25. F. FREES. J. Am. Chem. Soc. **103**, 1194 (1981).
26. L. LEFFLER and E. GRUNWALD. Rates and equilibria of organic reactions. Wiley, New York. 1963. pp. 324 and 342.
27. L. MICHAELIS and M. L. MENTEN. Biochem. Z. **49**, 333 (1918).
28. K. K. SENKUPTA, D. K. KHAMRUI, and D. C. MUKHERGEE. Indian J. Chem. **13**, 348 (1975).
29. G. V. BAKORE and R. SHANKER. Indian J. Chem. **1**, 108 (1963).
30. M. M. GIRGIS, S. A. EL-SHATOURY, and Z. H. KHALIL. Can. J. Chem. **63**, 3317 (1985).
31. G. MILLAZZO, S. CAROLL, and V. K. SHARMA. Tables of standard potentials. John Wiley and Sons, New York. 1978; W. LATIMER. Oxidation potentials. 2nd ed. Prentice–Hall, Englewood Cliffs, NJ. 1952.

Can. J. Chem. Downloaded from www.nrcresearchpress.com by 123.30.183.119 on 09/08/12
For personal use only.

Structural studies on 6-ethoxytetrahydropyrylium cations; stereoelectronic control in the reactions of lactonium salts

RONALD F. CHILDS,[1] MARIANNE D. KOSTYK, COLIN J. L. LOCK, AND MAILIVAGANAM MAHENDRAN
Department of Chemistry, McMaster University, Hamilton, Ont., Canada L8S 4M1
Received April 20, 1990[2]

RONALD F. CHILDS, MARIANNE D. KOSTYK, COLIN J. L. LOCK, and MAILIVAGANAM MAHENDRAN. Can. J. Chem. **69**, 2024 (1991).

The structures of 6-ethoxy-2,3,4,5-tetrahydropyrylium, **1**, 6-ethoxy-2-methyl-2,3,4,5-tetrahydropyrylium, **2**, and 2-ethoxy-3,4,4a,5,6,7,8,8a-octahydro-1-benzopyrylium, **3**, hexachloroantimonates have been determined by X-ray crystallography. In each case the tetrahydropyrylium rings exist in shallow half-chair conformations with the cationic centers C(6), C(5), O(1), and O(6) having a planar arrangement. The cations all have a *Z* conformation about the O(6)—C(7) bonds and it is shown that this conformation is also preferred in solution by comparison of narrow-line ^{13}C NMR spectra in the solid state and solution. The O(1)—C(2) and O(6)—C(7) bond distances in **1–3** are significantly longer than those of comparable bonds in neutral esters. The length of the O(1)—C(2) bond is very dependent on substitution at C(2) suggesting a considerable fraction of the positive charge resides on this carbon as well as C(7). The closest cation/anion interactions present in the crystal lattices of these salts are between the chlorine atoms of the anion and the cationic center, C(6). These interactions provide information on the origin of the stereoselectivity observed in nucleophilic attack on these cations. The conformations, details of the C—O bonding, and closest contacts between cation and anion are discussed in terms of the concept of stereoelectronic control.

Key words: 6-ethoxytetrahydropyrylium cations, lactonium salts, structure, X-ray, stereoelectronic control.

RONALD F. CHILDS, MARIANNE D. KOSTYK, COLIN J. L. LOCK et MAILIVAGANAM MAHENDRAN. Can. J. Chem. **69**, 2024 (1991).

Les structures des hexachloroantimonates des 6-éthoxy-2,3,4,5-tétrahydropyrylium (**1**), 6-éthoxy-2-méthyl-2,3,4,5-tétrahydropyrylium (**2**) et 2-éthoxy-3,4,4a,5,6,7,8,8a-octahydro-1-benzopyrylium (**3**) ont été déterminées par diffraction des rayons-X. Dans chaque cas, les cycles tétrahydropyrylium existent dans des conformations demi-chaises peu profondes dans lesquelles les centres cationiques C(6), C(5), O(1) et O(6) sont dans un arrangement planaire. Les cations possèdent tous une conformation *Z* autour des liaisons O(6)—C(7); par comparaison des bandes fines des spectres RMN du ^{13}C à l'état solide et en solution, on a aussi démontré que cette conformation est aussi la conformation privilégiée en solution. Les longueurs des distances O(1)—C(2) et O(6)—C(7) des composés **1–3** sont beaucoup plus longues que celles des liaisons comparables des esters neutres. La longueur de la liaison O(1)—C(2) dépend beaucoup de la substitution en C(2); ce résultat suggère qu'une fraction importante de la charge positive se trouve sur ce carbone ainsi que sur celui en C(7). Les interactions cation/anion le plus proches observées dans les réseaux cristallins de ces sels se retrouvent entre les atomes de chlore de l'anion et le centre cationique C(6). Ces interactions fournissent de l'information sur l'origine de la stéréosélectivité observée lors des attaques nucléophiles sur ces cations. On fait appel au concept de contrôle stéréoélectronique pour discuter des conformations, des détails de la liaison C—O et des contacts les plus près entre le cation et l'anion.

Mots clés : cations 6-éthoxytétrahydropyrylium, sels de lactonium, structure, rayons-X, contrôle stéréoélectronique.

[Traduit par la rédaction]

Introduction

Carbenium ions with two oxygen substituents (OR and (or) OH) at the positive center are commonly encountered intermediates in organic chemistry (1). They are formed, for example, during the acid-catalyzed reactions of carboxylic acids and esters, reactions that are fundamental transformations of these important functional groups. Collapse of these cations with solvent leads to the formation of tetrahedral intermediates such as ortho or hemi-ortho esters with three oxygen-containing substituents on a tetrahedral carbon (2).

The reaction of dialkoxy/hydroxy cations with nucleophiles and the corresponding ionization of the tetrahedral intermediates to form these cations can occur with remarkable selectivity. Deslongchamps and co-workers suggested that the ease in cleavage of a C—O bond of one of these tetrahedral intermediates is governed by the relative orientation of the lone pairs of electrons on the remaining oxygen atoms and they coined the term stereoelectronic control to describe this electronic effect (3–7). The concept of stereoelectronic control has become widely accepted as a result of a great deal of work particularly involving cyclic systems where the relative conformations of oxygen substituents are well defined (8). The operation of microscopic reversibility means that the reactions of a dialkoxy carbenium ion with nucleophiles should be governed by the same principles as the ionization reactions. Indeed this assumption has been made to account for the stereo- and regio-selectivities encountered in the reactions of these cations (4–7, 9, 10).

To fully understand these reactions, particularly those involving collapse of the cation with a nucleophile, it is important to know the structures of these intermediary ions. With the appropriate choice of conditions it is possible to generate alkoxy/hydroxy substituted carbenium ions as long-lived intermediates (1, 11). Despite the large number of studies describing the properties of these cations, there have been few reports of the determination of their structures using direct methods.[3] The conformational preferences of some acyclic dialkoxy/hydroxy carbenium ions have been determined by NMR studies (17), but, this methodology cannot be extended to the types of cyclic systems used in establishing the concept of stereoelectronic control.

[1]Author to whom correspondence may be addressed.
[2]Revision received July 2, 1991.

[3]The structures of protonated acetic acid, ref. 12, and several dioxolanylium salts, refs. 13–15, have been reported. For a review of the structure determination of carbenium ions see ref. 16.

Can. J. Chem. Downloaded from www.nrcresearchpress.com by 123.30.183.119 on 09/08/12
For personal use only.

TABLE 1. ^{13}C NMR spectra

Compound	Phase[a]	Chemical shift (ppm) C(2)	C(3)	C(4)	C(5)	C(6)	C(7)	C(8)	C(9)
4	A	64.2	28.5	21.8	34.2	173.5			
1	A	82.7	21.5	16.4	29.2	189.6	75.1	13.7	
1	B	82.7	21.6	17.1	30.3	189.7	74.6	15.7	
5	A	70.6	29.9	21.2	34.5	173.0			20.0
2	A	95.1	28.5	16.2	28.5	189.0	74.2	13.5	20.7
2	B	96.2	30.0	18.2	30.0	189.5	74.4	13.9	22.7
3	A	99.3	29.6[b]	24.7[b]	38.5	189.6	74.8	23.5[b]	31.5[b]

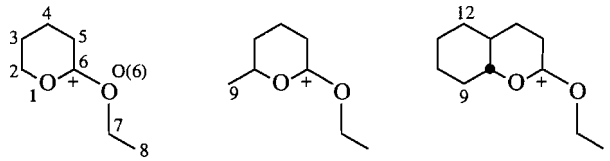
[a]A, CD_2Cl_2; B, solid state.
[b]Assignments may be reversed.

Can. J. Chem. Downloaded from www.nrcresearchpress.com by 123.30.183.119 on 09/08/12
For personal use only.

In this paper we describe the determination of the crystal structures of three dialkoxy carbenium ion salts derived by the alkylation of six-membered ring lactones.[4,5] These structures firmly establish the conformation of these cations and support the assumptions that have been made by previous workers.

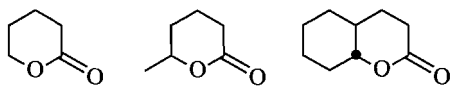
Results

The salts selected for study in this work were **1–3**. These materials were prepared by treatment of the corresponding lactones, **4–6** respectively, with triethyloxonium hexachloroantimonate (11). The salts **1** and **2** were characterized by comparison of their ^1H and ^{13}C NMR spectra in CD_2Cl_2 solutions with those previously reported (6).[6] Narrow-line ^{13}C NMR spectra of **1** and **2** as crystalline solids were obtained with use of magic angle spinning techniques. The NMR spectra of **3** were fully consistent with the assigned structure, Table 1. Single crystals of the three salts were obtained on recrystallization from CH_2Cl_2 at low temperature.



1 **2** **3**

The crystal structures of the three cations were determined by X-ray diffraction techniques. The diffraction data for **1** and **2** were collected at low temperatures while those for **3** were collected at room temperature with the samples being kept in sealed tubes to prevent reaction with atmospheric moisture.



4 **5** **6**

[4]A preliminary structure of **3** has previously been reported in a review, ref. 18.

[5]A variety of names have been used for these salts including "lactonium" and "dioxenium". In this paper the Chemical Abstracts names and numbering system have been used for **1** and **2**. The numbering system used for **3** is non-systematic, to allow easy comparison between the corresponding bonds of all three cations.

[6]Cation **1** was previously prepared as its BF_4^- salt, ref. 6.

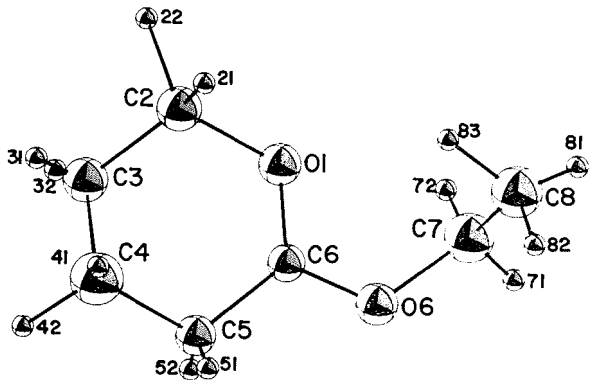


FIG. 1. The cation $C_7H_{13}O_2^+$ in compound **1**, showing the atom numbering. Hydrogen atoms are indicated by affixes only, in smaller print.

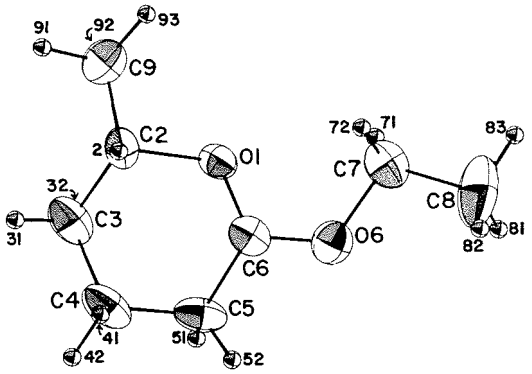


FIG. 2. The cation $C_8H_{15}O_2^+$ in compound **2**, showing the atom numbering. Hydrogen atoms are indicated by affixes only, in smaller print.

Selected bond distances and angles and atomic positional parameters of the three salts are given in Tables 2 and 3–5, respectively. The structures of **1–3** are shown in Figs. 1–3. Data on important planes in these cations are summarized in Table 6. Full details of the structure solutions are given in the experimental section and the supplementary material deposited with this paper.[7]

[7]Tables of supplementary data may be purchased from: The Depository of Unpublished Data, Document Delivery, CISTI, National Research Council Canada, Ottawa, Canada, K1A 0S2.

Can. J. Chem. Downloaded from www.nrcresearchpress.com by 123.30.183.119 on 09/08/12
For personal use only.

TABLE 2. Selected bond lengths (Å) and angles (°) of the cations in compounds **1**, **2**, and **3**

Bond	1	2	3
C(6)—O(1)	1.267(7)	1.270(8)	1.254(8)
C(6)—O(6)	1.273(8)	1.281(8)	1.257(8)
O(1)—C(2)	1.474(7)	1.520(7)	1.538(8)
O(6)—C(7)	1.488(7)	1.491(8)	1.500(10)
C(2)—C(3)	1.514(9)	1.492(9)	1.439(11)
C(3)—C(4)	1.504(9)	1.524(10)	1.491(12)
C(4)—C(5)	1.521(10)	1.512(10)	1.482(12)
C(5)—C(6)	1.483(8)	1.445(9)	1.516(10)
C(7)—C(8)	1.511(10)	1.473(11)	1.475(12)
C(2)—C(9)		1.491(10)	1.533(10)
C(9)—C(10)			1.495(11)
C(10)—C(11)			1.470(13)
C(11)—C(12)			1.472(12)
C(12)—C(3)			1.511(11)
Angle	**1**	**2**	**3**
C(2)—O(1)—C(6)	122.4(5)	121.6(5)	120.5(5)
C(6)—O(6)—C(7)	120.1(5)	119.5(5)	120.5(6)
C(3)—C(2)—O(1)	111.6(5)	110.4(6)	111.8(7)
C(2)—C(3)—C(4)	110.5(5)	110.6(6)	113.5(7)
C(3)—C(4)—C(5)	108.6(5)	109.7(5)	114.4(7)
C(4)—C(5)—C(6)	112.3(6)	113.8(6)	115.5(6)
C(5)—C(6)—O(1)	125.2(6)	125.8(6)	123.9(6)
C(5)—C(6)—O(6)	116.9(6)	116.4(6)	116.4(6)
O(1)—C(6)—O(6)	117.9(5)	117.8(6)	119.6(7)
O(6)—C(7)—C(8)	110.7(5)	107.9(7)	106.0(6)
O(1)—C(2)—C(9)		104.0(5)	104.1(5)
C(3)—C(2)—C(9)		116.0(6)	116.4(7)
C(2)—C(9)—C(10)			109.8(7)
C(9)—C(10)—C(11)			116.5(8)
C(10)—C(11)—C(12)			116.2(8)
C(11)—C(12)—C(3)			115.0(7)
C(2)—C(3)—C(12)			110.4(7)
C(4)—C(3)—C(12)			118.5(7)

TABLE 3. Atomic positional parameters ($\times 10^4$) and equivalent isotropic atomic displacement factors (Å^2) ($\times 10^3$) for non-hydrogen atoms in **1**

Atom	x	y	z	U_{eq}[a]
Sb(1)	0	0	0	11
Sb(2)	0	0	5000	11
Cl(11)	285 (2)	−2957 (2)	−1136 (1)	16
Cl(12)	165 (2)	972 (3)	−1228 (2)	18
Cl(13)	3307 (2)	2600 (3)	1480 (1)	16
Cl(21)	3224 (2)	1506 (3)	6078 (2)	20
Cl(22)	473 (3)	2399 (3)	6925 (2)	25
Cl(23)	703 (2)	2909 (3)	4896 (2)	22
O(1)	4050 (6)	−1392 (7)	7133 (4)	15
O(6)	6027 (6)	−153 (7)	6755 (4)	15
C(2)	3278 (10)	−1091 (12)	7870 (6)	21
C(3)	4705 (9)	1169 (12)	9201 (6)	18
C(4)	5559 (11)	3089 (12)	9217 (7)	23
C(5)	6574 (9)	2689 (10)	8607 (6)	16
C(6)	5463 (9)	275 (10)	7452 (6)	15
C(7)	5113 (10)	−2559 (11)	5653 (6)	20
C(8)	3379 (10)	−3404 (11)	4532 (6)	21

[a] $U_{eq} = 1/3(U_{11} + U_{22} + U_{33} + 2U_{12} \cos \gamma + 2U_{13} \cos \beta + 2U_{23} \cos \alpha)$.

TABLE 4. Atomic positional parameters ($\times 10^4$) and equivalent isotropic atomic displacement factors (Å^2) ($\times 10^3$) for non-hydrogen atoms in **2**

Atom	x	y	z	U_{eq}[a]
Sb(1)	2500	7029.3 (4)	1973.3 (4)	25.7
Sb(2)	2500	4086.9 (3)	7905.9 (4)	22.5
Cl(11)	4001 (1)	7026 (1)	1995 (1)	39
Cl(12)	2500	6227 (2)	545 (2)	42
Cl(13)	2500	5713 (2)	2865 (2)	41
Cl(14)	2500	7832 (2)	3421 (2)	43
Cl(15)	2500	8355 (2)	1108 (2)	47
Cl(21)	3998 (1)	4086 (1)	7917 (1)	33
Cl(22)	2500	5610 (1)	8158 (2)	38
Cl(23)	2500	4316 (2)	6244 (2)	52
Cl(24)	2500	3870 (2)	9576 (2)	55
Cl(25)	2500	2566 (1)	7686 (2)	57
O(1)	9455 (3)	8573 (3)	2858 (3)	37
O(6)	9815 (3)	9116 (3)	1469 (3)	45
C(2)	9534 (5)	8500 (4)	3941 (4)	41
C(3)	10418 (5)	8676 (4)	4247 (5)	50
C(4)	10733 (5)	9530 (4)	3813 (6)	52
C(5)	10698 (4)	9478 (4)	2731 (5)	43
C(6)	9958 (4)	9039 (4)	2369 (5)	34
C(7)	9055 (5)	8693 (5)	1046 (5)	54
C(8)	8976 (6)	8996 (7)	48 (5)	84
C(9)	9201 (5)	7610 (5)	4160 (5)	51

[a] $U_{eq} = 1/3(U_{11} + U_{22} + U_{33})$.

TABLE 5. Atomic positional parameters ($\times 10^4$) and equivalent isotropic atomic displacement factors (Å^2) ($\times 10^3$) for non-hydrogen atoms in **3**

Atom	x	y	z	U_{eq}[a]
Sb	−1263.4 (4)	2341.4 (2)	8879.0 (2)	24
Cl(1)	29 (2)	3808 (1)	8749 (2)	34
Cl(2)	−2511 (2)	850 (1)	9016 (2)	27
Cl(3)	−1552 (2)	2644 (1)	10485 (1)	44
Cl(4)	−1025 (2)	2060 (2)	7255 (1)	41
Cl(5)	695 (2)	1405 (1)	9166 (1)	36
Cl(6)	−3205 (2)	3260 (2)	8549 (2)	29
O(1)	2207 (4)	1833 (3)	6310 (3)	53
O(6)	905 (5)	633 (3)	5860 (4)	61
C(2)	2788 (9)	2899 (5)	6181 (5)	64
C(3)	1844 (9)	3562 (6)	5765 (6)	62
C(4)	1225 (9)	3162 (7)	4897 (7)	86
C(5)	741 (9)	2118 (6)	4974 (6)	73
C(6)	1339 (7)	1509 (5)	5761 (5)	55
C(7)	1383 (8)	−12 (6)	6647 (6)	68
C(8)	240 (11)	−634 (5)	6925 (7)	85
C(9)	3297 (8)	3170 (6)	7154 (5)	59
C(10)	3779 (10)	4229 (6)	7151 (7)	86
C(11)	2957 (14)	4958 (7)	6646 (8)	124
C(12)	2386 (8)	4616 (5)	5755 (6)	76

[a] $U_{eq} = 1/3(U_{11} + U_{22} + U_{33})$.

Discussion

Examination of the structures shown in Figs. 1–3 shows that in each case alkylation of the carbonyl oxygen atom of the lactone has taken place and that the structures are correctly represented as **1–3**. This alkylation is accompanied by a substantial change in the geometry of the salt with the C(6)–O(6) bond distance being significantly elongated and the O(1)—C(2) bond distance shortened as compared with those found

TABLE 6. Crystal data for **1–3**

Compound	**1**	**2**	**3**
	$[C_7H_{13}O_2]Cl_6Sb$	$[C_8H_{15}O_2]Cl_6Sb$	$[C_{11}H_{19}O_2]Cl_6Sb$
F.W.	464.68	477.68	517.45
Crystal size (mm)	0.3 × 0.3 × 0.5 parallelepiped	0.3 × 0.3 × 0.4 parallelepiped	0.3 × 0.3 × 0.3 rough cube
Systematic absences	None	$(h0l)$ $h + l = 2n$ $(hk0)$ $k = 2n$	$(0kl)$ $l = 2n$ $(h0l)$ $h = 2n$ $(00l)$ $l = 2n$
Space group	$P1$	$Pmnb$[a]	$Pca2_1$
Unit cell (Å and deg)	a = 9.285(2) b = 8.248(1) c = 15.034(3) α = 118.73(1) β = 108.98(1) γ = 109.30(1)	a = 15.888(5) b = 15.292(4) c = 13.945(3)	a = 10.081(3) b = 13.365(4) c = 14.331(3)
Volume (Å^3)	772.9(2)	3388(2)	1931(1)
Z	2	8	4
ρ_{calc} (g cm^{-3})	2.00	1.87	1.78
μ (cm^{-1})	28.13	25.71	22.01
Max. 2θ, reflections meas.	50°, $0 \le h \le 11$, $-9 \le k \le 9$, $-17 \le l \le 17$	45°, $0 \le h \le 13$, $0 \le k \le 16$, $-15 \le l \le 15$	50.15°, $0 \le h \le 8$, $0 \le k \le 15$, $-16 \le l \le 16$
Std. reflctns. (esd)	(−2, −3, 2) 1.6% (−3, 5, −3) 1.9%	(1, 5, 6) 3.5% (7, 5, 4) 3.6%	(1, 3, 6) 2.1% (1, −3, −5) 2.4%
Temperature (°C)	−65 ± 5	−65 ± 5	21 ± 1
Number of reflctns. meas.	2974	4579	3327
R_{merg}	0.0084	0.0127	0.0168
No. unique reflctns.	2674	2302	2853
No. used[b]	2674	1633	2853
Final R, R_w	0.041, 0.037	0.031, 0.033	0.036, 0.035
Final shift/error, max, ave	0.010, 0.002	0.011, 0.003	0.001, 0.000
x (secondary extinction)	0.00294	0.00005	0.00054
Final diff. map, max (e/Å^{-3})	0.74	0.91	0.47
location	−0.09, 0.15, −0.15	0.25, 0.41, −0.29	−0.08, 0.16, 0.74
min (e/Å^{-3})	−0.70	−0.76	−0.51
Weighting	$(\sigma_F^2 + 0.000034F_o^2)^{-1}$	$(\sigma_F^2 + 0.001939F_o^2)^{-1}$	$(\sigma_F^2 + 0.000413F_o^2)^{-1}$
Error in obs. of unit wt., S	3.407	0.811	1.204

$R = \Sigma||F_o| - |F_c||/\Sigma|F_o|$; $R_w = [\Sigma w(|F_o| - |F_c|)^2/\Sigma wF_o^2]^{1/2}$.
$S = [\Sigma w(|F_o| - |F_c|)^2/(n - m)]^{1/2}$; $\sigma_F = 1/2(k/\mathrm{Lp}^{1/2})(\sigma_I/I^{1/2})$ where k is the scale constant.
[a]This cell may be transformed into the standard cell, space group $Pnma$, a = 15.292(4), b = 15.888(5), c = 13.945(3) Å by the matrix (0 1 0 / 1 0 0 / 0 0 −1).
[b]Reflections with $I > 0$ used for **1** and **3**, with $I > 3\sigma_I$ for **2**.

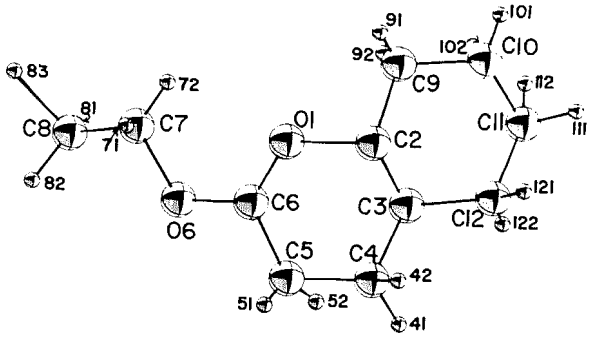


FIG. 3. The cation $C_{11}H_{19}O_2^+$ in compound **3**, showing the atom numbering. Hydrogen atoms are indicated by affixes only, in smaller print.

for six-membered ring lactones (19). There is no significant difference in the lengths of the O(1)—C(2) and C(6)—O(6) bonds of **1–3**, Table 2. Comparable C—O bond distances that are intermediate in length between C—O single and double bond lengths have been found in other oxygen-substituted carbenium ions (12–15, 18, 20, 21).

The geometry at the positively charged center of these salts is such that in each case atoms O(1), C(5), C(6), and O(6) lie in a plane, Plane A. Atoms C(2) and C(7) in **1** (−0.02(1) and 0.13(1) Å) and **3** (−0.06(1) and 0.06(1) Å) are also positioned close to Plane A. The C(2)—O(1)—C(6) and C(6)—O(6)—C(7) angles in each of these cations are close to 120°, as would be expected for sp^2-hybridized oxygen atoms. Overall, the structures are consistent with positive charge being delocalized over the O(1)C(6)O(6) fragment in these cations.

As a result of the near planar arrangement of the dialkoxy carbenium ion center, the six-membered rings of these cations are also forced to adopt relatively planar conformations. This can be seen, for example, on inspection of the edge view of **1**, shown in Fig. 4. The six-membered ring in **1** exists in a shallow pseudo-chair conformation with C(4) being above (−0.31(2) Å) and C(3) being below (0.43(2) Å) the plane defined by O(1), C(2), C(5), and C(6), Plane B. Cations **2** and **3** adopt similar pseudo-chair conformations with the C(2)-methyl group in **2** and the *trans*-fused six-membered ring in **3** occupying pseudo-equatorial positions on the lactonium ring.

The C(5)—C(6)—O(1) bond angles in these cations are significantly larger (125.2(6), 125.8(6), and 123.9(6)° in **1–3**, re-

Can. J. Chem. Downloaded from www.nrcresearchpress.com by 123.30.183.119 on 09/08/12
For personal use only.

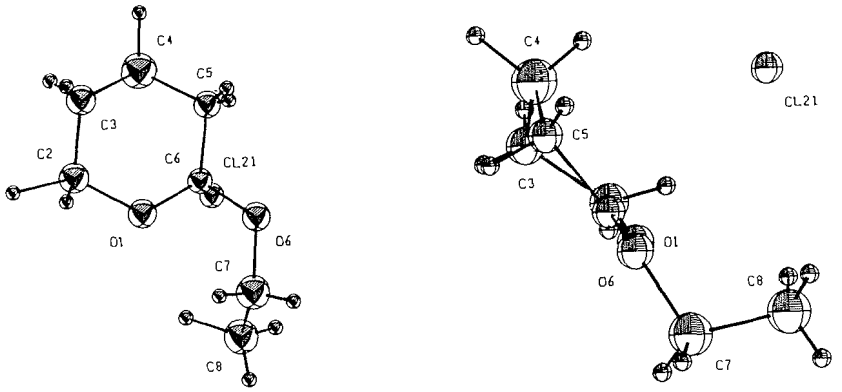


FIG. 4. The cation from **1**, showing the position of Cl(21). Left, top projection; right, side projection.

spectively) than is normally expected for a six-membered ring lactone (118.4(1.7)°) (19), (differences 3.8σ, 4.1σ, and 3.1σ respectively, where $\sigma = \sqrt{(\sigma_1^2 + \sigma_2^2)}$). Protonation of a ketone has been shown to result in an expansion of the C—C(=OH$^+$)—C bond angle from that encountered in the corresponding neutral ketone (21). Such an effect would seem to be unlikely in cations **1–3** where there are two oxygen substituents at C(6). Rather, the expansion in the C(5)—C(6)—O(1) bond angle is likely caused by the strain in the six-membered ring associated with the conformational requirements imposed by the planar arrangement of the four ring atoms.

It is interesting to consider the distances found for the O(1)—C(2) and O(6)—C(7) bonds in these structures and compare them with what normally would be expected for the corresponding O—C bonds in esters. In the first place the O—CH_2 bonds in **1–3** (O(1)—C(2) in **1** and O(6)—C(7) in **1–3**) are similar in length with an average distance of 1.489(5) Å.[8] This is significantly longer than the O—CH_2 distance (1.452(2) Å) found by Allen and Kirby in their detailed analysis of the structures of esters (22). It is clear that the presence of the positive charge in these lactonium salts causes an elongation of this O—CH_2 bond.[9] In **2** and **3** the O(1)—C(2) bonds are even longer (1.520(7) and 1.538(8) Å, respectively) than those of the O—CH_2 bonds and they represent some of the longest known C—O bonds. The difference between the O(1)—C(2) bonds in **2** and **3** as compared to **1** is that C(2) in the former cations has an extra carbon substituent. Within the ester series such a change in substitution at the carbon of a C—O bond leads on average to a small expansion of its length (1.460(2) as compared to 1.452(2) Å) (22). The elongation observed here is much larger than can be expected just on the basis of steric effects resulting from substitution at the carbon atom.

Allen and Kirby have shown that a C—O bond is lengthened as electron-withdrawing groups are attached to the O atom. This effect has been attributed to enhanced involvement of the ionic resonance contributor shown in eq. [1] (22, 24).

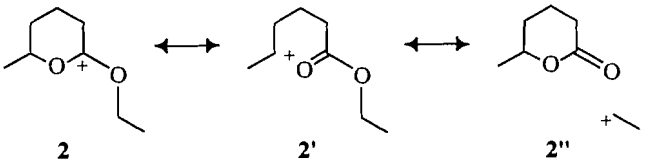
[1] R_3C—O—substituent ⟷ R_3C^+ O^--substituent

[8]The errors for mean bond lengths are given by

$$\sigma_D = \sqrt{(\Sigma_n (D - d_n)^2 / n(n-1))}$$

where D is the mean bond distance of n independent variables and d_n is the nth bond length.

[9]Corresponding O—C bond distances are found in the ethoxy group of the 1-ethoxyhomotropylium cation, ref. 23.



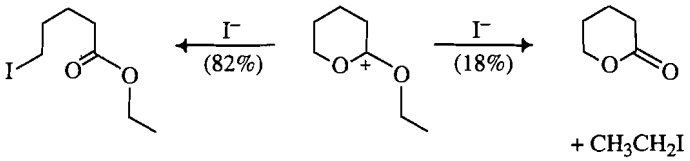
SCHEME 1

In the systems examined here the presence of the positive charge on C(6) means that there is a strongly electron-withdrawing group attached to O(1) and O(6). The elongation of the O(1)–C(2) and O(6)–C(7) bonds can be thought of as involving the structures shown in Scheme 1 with the transfer of the charge onto carbon atoms C(2) and C(7). Alkyl substitution at C(2), as in **2** and **3**, will enhance the contribution of the resonance form **2'** and cause a further elongation of this bond as compared to O(6)—C(6).

Examination of the bond angles at C(2) of **2** supports the suggestion of an enhanced ionic contribution to the O(1)—C(2) bond. Neglecting the bond angles involving hydrogen due to the large errors associated with them, it can be seen from the data in Table 2 that the C(3)—C(2)—C(9) and O(1)—C(2)—C(9) angles, 116.0(6) and 104.0(5)°, respectively, are significantly distorted from those expected for a carbon atom with a tetrahedral geometry. This distortion implies that the hybridization of C(2) is intermediate between sp^2 and sp^3 as would be expected to result from an elongation of the O(1)—C(2) bond and transfer of charge to C(2). Similar changes in bond angles as a function of the length of an O—C bond have been reported by Edwards, Jones, and Kirby in their mapping of the structural changes associated with the ionization of 1-arylethanol derivatives (25).

The $SbCl_6^-$ anions show no unusual features. They are very close to octahedral in all three compounds. In compound **1** there are two independent $SbCl_6^-$ anions, both sitting on inversion centres (000,00$\frac{1}{2}$). Although there are significant differences in the bond lengths and angles (Sb—Cl, ave. 2.367 Å, range 2.363(2)–2.378(1); *cis*-Cl—Sb—Cl, range 89.7(1)—91.3(1)), the differences are small and of no importance. In **2** there are again two independent $SbCl_6^-$ anions, both with the Sb atom and four chlorine atoms in the mirror planes at $\frac{1}{4}$,y,z and $\frac{3}{4}$,y,z. The variation in *cis* angles is similar to **1** (*cis*-Cl—Sb—Cl, range 89.4(1)–90.6(2)°) but the variation in Sb—Cl bond lengths is greater. In particular, the bonds out of the plane are longer than those in the plane (2.385(2) Å vs. a range of 2.339(2)–2.366(2) Å and 2.380(2) Å vs. a range of 2.344(2)–2.355(2) Å, although the average is very similar to

Can. J. Chem. Downloaded from www.nrcresearchpress.com by 123.30.183.119 on 09/08/12
For personal use only.



SCHEME 2

1 (2.363 Å). The $SbCl_6^-$ anion in **3** lies on a general position. The bond lengths and angles are similar to **1** and **2** (Sb—Cl ave. 2.363 Å, a range of 2.355(2)–2.373(2) Å; *cis*-Cl—Sb—Cl 88.3(1)–91.3(1)).

The large downfield shifts ($\Delta\delta$) observed for the solution ^{13}C chemical shifts of the C(2) resonances of **1–3** that occur on alkylation of these lactones indicates the presence of positive charge on these carbons in the cations, Table 1. Thus the downfield shifts of C(2) that accompany the conversion of **4** to **1** and **5** to **2** (18.5 and 24.5 ppm, respectively) are the largest shifts observed for any of the carbon atoms in these lactones. The downfield shift of C(2) resulting from the conversion of **5** to **2** is larger than that attending the formation of **1**, as would be expected on the basis of the greater C(2)—O(1) bond distance of **2**. A similar transfer of positive charge to the alkyl carbon atoms has been observed with the dioxolan-2-ylium cations (15).

The transfer of charge to C(2) and C(7) in these cations should be accompanied by contraction of the C(2)—C(3), C(2)—C(9), and C(7)—C(8) bonds (26). The errors associated with the structure determinations of **1–3** make this difficult to assess. For example, the average distance of the CH_2—CH_3 bond in these cations (1.486(12) Å) is not significantly different from the comparable bond in an ethyl group of an ester (1.503(2) Å) (difference 1.4σ) (22). It is clear that any contraction of this bond is small.

Beaulieu and Deslongchamps have shown that the reaction of **1** with iodide gives a high proportion of the ring-opened product as compared to cleavage of the ethyl group of the lactone, Scheme 2, and have accounted for this, at first sight surprising, regioselectivity on the basis of stereoelectronic effects (5). It was suggested that cleavage of the O(1)—C(2) or O(6)—C(7) bond would be facilitated when this breaking bond is anti-periplanar to the C(6)—O(6) or C(6)—O(1) bond, respectively. It was assumed that **1** existed in the *Z* conformation, Scheme 2, and, as such, cleavage of the O(1)—C(2) bond would be a low energy process.

The structures of **1–3** determined in this work fully support the assumption that these ions have a *Z* conformation about the C(6)—O(6) bond. As can be seen from Figs. 1–3, in each case these cations have adopted a *Z* conformation about this bond. Within each cation the -CH_2CH_3 group has a bisected arrangement with respect to the C(6)—O(6) bond. However, the CH_3 group of the ethyl substituent would seem to be able to adopt a variety of conformations, with it being closer to the plane of the ring (Plane B) in **2** (0.45(2) Å) and **3** (0.75(3) Å) than in **1** (−1.22(2) Å). The constraints imposed by the six-membered rings ensure that they have an *E* conformation about the C(6)—O(1) bonds. Acyclic dialkoxy carbenium ions have been shown to exist preferentially in an *E,Z* conformation about the two C^+—OR bonds. The present study demonstrates for the first time that this *E,Z* conformation is also preferred for cyclic cations.

It should be noted that the C(6)—O(6) *Z* conformational preference observed here for the cations **1–3** is for materials in their crystalline states. Reactions of these ions take place in solution and it could be argued that solvation might change the conformational preference about the C(6)—O(6) bond. While the occurrence of such a change in conformational preference in the two phases is extremely unlikely, given the uniformity in conformation found in the three separate examples of these cations studied here, this possibility is eliminated by the essentially identical ^{13}C NMR spectra observed for **1** and **2** in CD_2Cl_2 solution and in the solid state, Table 1. Overall, *the close similarity of the individual carbon atom resonances indicates that the conformation and charge distribution of these carbon atoms of the cation are the same in solution and the solid state.*

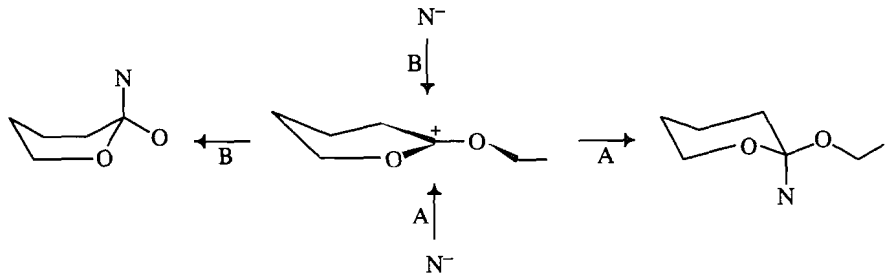
While the conformations found here for these cations fully support the assumptions made in explaining the regioselectivity of their reactions, examination of the various C—O bond distances fails to show evidence for the operation of stereoelectronic effects. It was suggested by Deslongchamps *et al.* that the reason for the *Z* conformation having a lower energy than the *E* form is due to the presence of a secondary electronic effect in which the lone pair of electrons on O(6) in the *Z* conformation is placed so as to interact with the antibonding orbital of the C(6)—O(1) σ bond. No such interaction is possible with the lone pair of electrons on O(1). As a result, the C(6)—O(6) bond should be shorter than the C(6)—O(1) bond. Examination of the data given in Table 2 shows no significant difference in the lengths of the C(6)—O(6) and C(6)—O(1) bonds in any of the cations. It is clear that any structural effect of the relative alignment of a lone pair and a C—O bond must be small. Similarly, one notes that attack at either C(2) or C(7) (Scheme 2) would be facilitated by the presence of positive charge on these carbon atoms and the lengthening and consequent weakening of the C(2)—O(1) and C(7)—O(6) bonds. However, the distances of these two bonds in each of the cations are the same within the error limits of the structure determinations (differences of 1.4σ, 2.5σ, and 3.0σ for **1–3** respectively) and as such there is no reason on this basis to expect a preference for attack at the C(2) position.

Crystal packing

It is of interest to consider the various cation/anion contacts present in the crystal lattices of these salts to see if the placement of the chlorine atoms of the $SbCl_6^-$ groups might correspond to the various types of reactions these cations can undergo with a nucleophile. For example, the long C(2)—O(1) and C(7)—O(6) bonds and positive charge on C(2) and C(7) could result from the presence of a chlorine atom in close proximity to these carbon atoms, situated to correspond to the commencement of nucleophilic attack as shown in Scheme 3 (27). However, examination of the long-range contacts in the crystal lattices of **1–3** shows that in each case the closest contacts occur at C(6) and that no other specific interactions seem to be present.

Cations **2** and **3** each have a chlorine atom above and below the O(1), C(5), C(6), O(6) plane. In **2** these chlorine atoms, Cl(21) and Cl(11), are situated 3.323(4) and 3.495(3) Å respectively from C(6), at internuclear distances that are less than the sum of the van der Waals radii of neutral C and Cl atoms (3.50 Å) (25). These Cl atoms are oriented as if they were undergoing a nucleophilic addition at C(6). The Cl(21)—C(6)—O(6) and Cl(21)—C(6)—O(1) angles are 93.7(5) and 94.1(5)°, respectively. In **3**, chlorine atoms Cl(4) and Cl(5) are found 3.279(7) and 3.766(7) Å respectively from C(6) and are sit-

Can. J. Chem. Downloaded from www.nrcresearchpress.com by 123.30.183.119 on 09/08/12
For personal use only.



SCHEME 3

uated approximately 90° to both the C(6)—O(6) and C(6)—O(1) bonds. The Cl(4)—C(6)—O(6) and Cl(4)—C(6)—O(1) angles are 83.0(7) and 91.3(7)°, while those corresponding to Cl(5) are 107.8(7) and 80.8(7)° respectively. The presence of counterions above and (or) below the carbonyl plane of a protonated or alkylated carbonyl group would seem to be a general phenomenon of the crystal packing of this type of organic salt (20).

Only one chlorine atom, Cl(21), is situated in close proximity to C(6) in the crystal lattice of **1**, Fig. 4. The C(6)—Cl(21) distance (3.200(6) Å) is significantly less than the sum of the van der Waals radii of the two atoms and the Cl(21)—C(6)—O(6) and Cl(21)—C(6)—O(1) angles are 88.5(3) and 97.3(4)°, respectively. In the other two known cases where only a single anion or other Lewis base is in close contact with the central carbon atom of a protonated or alkylated carbonyl group, this carbon atom is moved out of the carbonyl plane towards the Lewis base (20, 21). However, in **1** C(6) is not significantly displaced from the O(1), C(5), O(6) plane.

The addition of a nucleophile to C(6) of these tetrahydropyrylium salts takes place stereoselectively (2, 9). It has been suggested that the important feature of the reaction is that attack occurs on that face of the cation that leads directly to a chair, path A, rather than initially to a boat conformation, path B, of the six-membered ring, Scheme 3.

In the cations studied here both of these approaches are seen in the crystal lattice. With **1**, Cl(21) is situated in a position as if it were approaching by Path A, Scheme 3, to give the chair conformation. With both **2** and **3** the situation is more complicated, with two corresponding chlorine atoms perpendicular to C(6). However, the closest chlorine atom to C(6) in **2**, Cl(21), shows an approach angle corresponding to Path A. It should be noted that this path would give a chair conformation in which the C(2) methyl substituent would be in an equatorial position. Conversely, the closest chlorine atom contact in **3** is situated so as to approach by Path B.

It is perhaps not surprising that the cation/anion interactions present in the lattices of these salts show no clear preference for attack by Path A, Scheme 3, given the relatively low nucleophilicity of $SbCl_6^-$ and the consequent long C(6)—Cl distances involved.[10] However, as models for the cation in solution they are informative. It is clear that the environment of these cations in solution will be similar to that encountered in the crystal lattice. The near identity of the solid state and solution ^{13}C NMR spectra of **1** and **2** clearly demonstrates this point as does the general uniformity in relative anion–cation positions not only in the salts studied here, but also in the range of other known structures of alkoxy-substituted cations. In solution the anions could be replaced by solvent molecules depending on the nature and degree of ion-pairing present. However, the solvent molecules would in general be oriented in such a way that there would be interaction of a Lewis base in the solvent with C(6) as is found here within the crystal lattices. The results obtained here suggest that when the surrounding Lewis base atoms of anions, solvent, or nucleophiles are separated from C(6) by distances corresponding to somewhat less than the sum of the van der Waals radii of the two atoms involved, then no preference for attack by either of the two paths shown in Scheme 3 will be observed. For the chair/boat explanation shown in Scheme 3 to be correct, differentiation between Paths A and B must occur later in the reaction coordinate than those found here in the crystal lattices. However, the scope for delaying the transition states of these exothermic reactions is limited and relatively early transition states would be expected.

To examine these questions further it would be attractive to synthesize additional examples of these cations in which there is a closer, more specific interaction between the cationic center and a Lewis base. Such systems, while not easy to prepare and crystallize, offer the prospect of being able to map out the bonding changes associated with these reactions and would answer some of the questions raised in this work regarding the origin of the stereoselectivity of the reactions.

Experimental

NMR spectra were obtained on Varian EM-390, Bruker WM-250, WM-500, and MSL-100 spectrometers. All solution spectra were referenced with CD_2Cl_2. X-ray diffraction data for the crystals studied were collected on a Syntex $P2_1$ automatic diffractometer equipped with a low-temperature apparatus. Intensity measurements for **1** and **2** were made at low temperature (−65°C). The crystals were kept at low temperature by a stream of dry nitrogen, which had been cooled in a liquid nitrogen heat exchanger. Those for **3** were made at room temperature with the use of graphite monochromated MoK_α radiation ($\lambda = 0.71069$ Å).

Preparation of lactones

δ-Valerolactone (**4**) was commercially available and was distilled before use. Lactone **5** was obtained by Baeyer–Villiger oxidation of commercially available 5-methylcyclopentanone (28). *trans*-Octahydrocoumarin (**6**) was prepared according to the procedure of Graham and co-workers (29).

Preparation of hexachloroantimonate salts

Salts **1–3** were prepared from the corresponding lactones according to the procedure of Deslongchamps *et al.* (6). The salts were extremely hygroscopic and all manipulations were done under a controlled atmosphere. The salts were recrystallized from CH_2Cl_2 at −20°C to give single crystals suitable for X-ray diffraction studies.

6-Ethoxy-2,3,4,5-tetrahydropyrylium hexachloroantimonate, 1: mp 108–110°C (dec.). The ^1H NMR spectrum of **1** in CD_2Cl_2 at room

[10]While a chlorine atom remains in the nucleophile it is unlikely that examples of systems with extremely short C...Cl distances will be found.

Can. J. Chem. Downloaded from www.nrcresearchpress.com by 123.30.183.119 on 09/08/12
For personal use only.

temperature consisted of peaks at δ 1.40 (3H, t, J = 7.0 Hz, -CH_2-CH_3), 2.00 (4H, m, protons at C3 and C4), 3.42 (2H, m, protons at C5), 4.70 (2H, q, J = 7.0 Hz, -CH_2-CH_3), 5.04 (2H, m, protons at C2).

6-Ethoxy-2-methyl-2,3,4,5-tetrahydropyrylium hexachloroantimonate, 2: mp 127–128°C (dec.). The ^{1}H NMR spectrum of **2** in CD_2Cl_2 at room temperature displayed peaks at δ 1.44 (3H, t, J = 7.1 Hz, -CH_2-CH_3), 1.77 (3H, d, J = 6.5 Hz, -CH-CH_3), 2.0–2.5 (4H, m, protons at C3 and C4), 3.21 (2H, m, protons at C5), 4.90 (2H, dq, J = 7.1 Hz, $J_{H_aH_b}$ = 3.5 Hz, -CH_2-CH_3), 5.55 (1H, m, -CH-CH_3).

2-Ethoxy-3,4,4a,5,6,7,8,8a-octahydro-1-benzopyrylium hexachloroantimonate, 3: mp 120–122°C (dec.). The ^{1}H NMR spectrum of **3** in CD_2Cl_2 at room temperature displayed peaks at δ 1.45 (3H, t, J = 7.0 Hz, -CH_2-CH_3), 2.0–2.4 (13H, m, ring protons), 2.4–3.4 (1H, m, proton at C2), 4.90 (2H, q, J = 7.0 Hz, -CH_2-CH_3).

Crystallography

All crystals were handled under a dry nitrogen atmosphere at all times. Suitable single crystals were sealed in 0.3 mm diameter Lindemann capillary tubes with the use of a dry box equipped with a microscope. Buerger-type precession photographs were used to determine potential space groups and to establish approximate unit cell dimensions before the crystal was transferred to a Syntex $P2_1$ diffractometer. Crystal data for salts **1–3** are summarzed in Table 6.[11] For all crystals only reflections with $I > 0$ were used in the refinement. Scattering curves were taken from the International Tables and anomalous dispersion corrections applied to the curves for Sb and Cl. No absorption corrections were applied because the crystals were sealed in glass tubes.

6-Ethoxy-2,3,4,5-tetrahydropyrylium hexachloroantimonate, 1

Triclinic unit cell parameters for **1** were determined from a least-squares fit of χ, φ, and 2θ at −65°C for 15 reflections in the range 20° ≤ 2θ ≤ 29°. Intensity data were collected at low temperature in the space group $P\bar{1}$ by use of a coupled θ(crystal)–2θ(counter) scan. The XRAY76 (30) package and the XTAL program suite (31) were used for preliminary data treatment. The intensity data were corrected for Lorentz and polarization effects but not for absorption. This would lead to a maximum error on F_o of 3.6%.

The SHELX (32) program was used for structure determination and refinement. The antimony atom was found by direct methods with use of 2674 reflections with $|E| \geq 1.5$ and 20 sets of starting phases. Subsequent electron density difference maps revealed the positions of the remaining atoms. Temperature factors of all non-hydrogen atoms were made anisotropic and refined before hydrogen atom positions were located. Hydrogen atom positions and isotropic temperature factors were then varied through four full-matrix least-squares cycles before being fixed. Full-matrix least-squares refinement, which used a variable weighting scheme, minimized $\Sigma w(|F_o| - |F_c|)^2$ and was terminated when the maximum shift/error was ≤0.010.

6-Ethoxy-2-methyl-2,3,4,5-tetrahydropyrylium hexachloroantimonate, 2

The unit cell parameters for **2** were obtained at −65°C by a least-squares fit of χ, φ, and 2θ for 15 reflections in the range 20° ≤ 2θ ≤ 26°. The unit cell was found to be orthorhombic and intensity data were collected in the uniquely defined non-standard space group *Pmnb* by use of a coupled θ(crystal)–2θ(counter) scan. The XRAY76 (30) package and the XTAL program suite (31) were used for preliminary data treatment. Corrections were made for Lorentz and polarization effects but not for absorption. This would lead to a maximum error on F_o of 7.1%.

The position of the antimony atom was revealed by direct methods with use of 1633 reflections with $|E| \geq 1.5$ and 20 sets of starting phases. The remaining atoms were located from subsequent electron density difference maps. Temperature factors of all non-hydrogen atoms were made anisotropic and refined before hydrogen atoms were located. Hydrogen atom positional parameters and isotropic temperature factors were refined through four full-matrix least-squares cycles before being fixed. Full-matrix least-squares refinement, which employed a variable weighting scheme, minimized $\Sigma w(|F_o| - |F_c|)^2$ until the maximum shift/error was ≤0.011.

2-Ethoxy-3,4,4a,5,6,7,8,8a-octahydro-1-benzopyrylium hexachloroantimonate, 3

Unit cell parameter determination, data collection, and reduction were carried out as described above. The unit cell was found to be orthorhombic and data were collected in the uniquely defined space group $Pca2_1$. Corrections for Lorentz and polarization effects were applied to the measured intensities but not for absorption. This would lead to a maximum error on F_o of 8.4%. A SHELX (32) three-dimensional Patterson synthesis revealed the position of the antimony atom. All remaining atom positions were determined by subsequent electron density difference maps in conjunction with full-matrix least-squares refinement cycles. Hydrogen atoms were located once all non-hydrogen atoms had been anisotropically refined. Hydrogen atoms were given fixed positions and isotropic temperature factors. Full-matrix least-squares refinement with a variable weighting scheme minimized $\Sigma w(|F_o| - |F_c|)^2$ and refinement was terminated when the maximum shift/error was ≤0.001.

[11]Bond angles for the anions, anisotropic temperature factors, hydrogen atom positional parameters, isotropic temperature factors, bond lengths, and angles involving hydrogen atoms, and F_o and F_c tables are available as supplemental material, see footnote 7.

Crystal packing diagrams for **1–3** and tables of bond lengths and angles and hydrogen atom positional parameters have also been deposited with the Cambridge Crystallographic Data Centre and can be obtained on request from The Director, Cambridge Crystallographic Data Centre, University Chemical Laboratory, Lensfield Road, Cambridge CB2 1EW, U.K.

Acknowledgment

This work was supported by the Natural Sciences and Engineering Research Council of Canada and IBM Canada Ltd. through a collaborative project with McMaster University. Technical assistance of Mr. Romolo Faggiani is gratefully appreciated.

1. U. PINDER, J. MÜLLER, C. FLO, and H. WITZEL. Chem. Soc. Rev. **16**, 75 (1987); H. PERST. *In* Oxonium ions in organic chemistry. Academic Press, New York, NY. 1971; Carbonium Ions, **5**, 1961 (1976).
2. M. AHMAD, R. G. BERGSTROM, M. J. CASHEN, Y. CHIANG, A. J. KRESGE, R. A. MCCLELLAND, and M. F. POWELL. J. Am. Chem. Soc. **101**, 2669 (1979); R. A. MCCLELLAND and M. AHMAD. J. Am. Chem. Soc. **99**, 5356 (1977).
3. P. DESLONGCHAMPS. *In* Stereoelectronic effects in organic chemistry. Pergamon Press, New York, NY. 1983. Chap. 3; Tetrahedron, **31**, 2463 (1975).
4. P. DESLONGCHAMPS, P. ATLANI, D. FRÉHEL, and A. MALAVAL. Can. J. Chem. **50**, 3405 (1972); P. DESLONGCHAMPS, D. GUAY, and R. CHÊNEVERT. Can. J. Chem. **63**, 2493 (1985).
5. N. BEAULIEU and P. DESLONGCHAMPS. Can. J. Chem. **58**, 164 (1980).
6. P. DESLONGCHAMPS, R. CHÊNEVERT, R. J. TAILLEFER, C. MOREAU, and J. K. SAUNDERS. Can. J. Chem. **53**, 1601 (1975).
7. P. DESLONGCHAMPS, J. LESSARD, and Y. NADEAU. Can. J. Chem. **63**, 2485 (1985).
8. A. J. KIRBY. Acc. Chem. Res. **17**, 305 (1984); C. L. PERRIN and G. M. L. ARRHENIUS. J. Am. Chem. Soc. **104**, 2839 (1982).
9. E. L. ELIEL and F. W. NADER. J. Am. Chem. Soc. **92**, 584 (1970); **91**, 536 (1969).
10. F. F. KHOURI and M. K. KALOUSTIAN. J. Am. Chem. Soc. **108**, 6683 (1986).
11. H. MEERWEIN, P. BORNER, O. FUCHS, H. J. SASSE, H. SCHRODT, and J. SPILLE. Chem. Ber. **89**, 2060 (1956).
12. P.-G. JÖNSSON and I. OLOVSSON. Acta Crystallogr. Sect. B: Struct. Crystallogr. Cryst. Chem. **B24**, 559 (1968); A. KVICK, P.-G. JÖNSSON, and I. OLOVSSON. Inorg. Chem. **8**, 2775 (1969).

Can. J. Chem. Downloaded from www.nrcresearchpress.com by 123.30.183.119 on 09/08/12
For personal use only.

13. H. PAULSEN and R. DAMMEYER. Chem. Ber. **109**, 1837 (1976); **109**, 605 (1976); **106**, 2324 (1973); H. PAULSEN and E. SCHÜTTPELZ. Chem. Ber. **112**, 3214 (1979).
14. M. R. CAIRA and J. E. DE WET. Acta Crystallogr. Sect. B: Struct. Crystallogr. Cryst. Chem. **B37**, 709 (1981).
15. R. ORGIAS. M.Sc. Thesis, McMaster University. 1989.
16. M. SUNDARALINGHAM and A. K. CHWANG. Carbonium Ions, **5**, 2427 (1976).
17. B. G. RAMSEY and R. W. TAFT. J. Am. Chem. Soc. **88**, 3058 (1966); R. F. BORCH. J. Am. Chem. Soc. **90**, 5303 (1968); CH. H. V. DUSSEAU, S. E. SCHAAFSMA, H. STEINBERG, and TH. J. DE BOER. Tetrahedron Lett. 467 (1969); H. PAULSEN. Pure Appl. Chem. **41**, 69 (1975); G. A. OLAH, A. M. WHITE, and D. H. O'BRIEN. Carbonium Ions, **4**, 1697 (1973).
18. R. F. CHILDS, M. MAHENDRAN, S. ZWEEP, G. SHAW, S. CHADDA, N. BURKE, B. GEORGE, R. FAGGIANI, and C. J. L. LOCK. Pure Appl. Chem. **58**, 111 (1986).
19. W. B. SCHWEIZER and J. D. DUNITZ. Helv. Chim. Acta, **65**, 1547 (1982).
20. R. F. CHILDS. 74th Canadian Chemical Conference, Hamilton. 1991.
21. R. F. CHILDS, M. D. KOSTYK, C. J. L. LOCK, and M. MAHENDRAN. J. Am. Chem. Soc. **112**, 8912 (1990).
22. F. H. ALLEN and A. J. KIRBY. J. Am. Chem. Soc. **106**, 6197 (1984).
23. R. F. CHILDS, R. FAGGIANI, C. J. L. LOCK, and M. MAHENDRAN. J. Am. Chem. Soc. **108**, 3613 (1988).
24. P. G. JONES and A. J. KIRBY. J. Am. Chem. Soc. **106**, 6207 (1984); J. Chem. Soc. Chem. Commun. 444 (1986).
25. M. R. EDWARDS, P. G. JONES, and A. J. KIRBY. J. Am. Chem. Soc. **108**, 7067 (1986).
26. R. F. W. BADER. Can. J. Chem. **64**, 1036 (1986).
27. H. B. BÜRGI, J. D. DUNITZ, and E. SHEFTER. Acta Crystallogr. Sect. B: Struct. Crystallogr. Cryst. Chem. **B30**, 1517 (1974).
28. J. MEINWALD and E. FRAUENGLASS. J. Am. Chem. Soc. **82**, 5235 (1960).
29. C. S. DEAN, J. R. DIXON, S. H. GRAHAM, and D. O. LEWIS. J. Chem. Soc. (C), 1491 (1968).
30. J. M. STEWART. The XRAY76 system. Tech. Rept. TR-446. Computer Science Center, University of Maryland, College Park, MD. 1976.
31. J. M. STEWART and S. R. HALL. The XTAL system of crystallographic programs. Tech. Rept. TR-1364. University of Maryland, College Park, MD. 1976.
32. G. M. SHELDRICK. Program for crystal structure determination. University of Cambridge, England. 1976.

Can. J. Chem. Downloaded from www.nrcresearchpress.com by 123.30.183.119 on 09/08/12
For personal use only.

The crystal structure of $W(CO)_5$piperidine: Implications for photoreactivity of $W(CO)_5L$ complexes

CAROL MORALEJO, COOPER H. LANGFORD, AND PETER H. BIRD
Department of Chemistry and Biochemistry, Concordia University, 1455 de Maisonneuve Blvd. W., Montreal, P.Q., Canada H3G 1M8

Received November 19, 1990[1]

CAROL MORALEJO, COOPER H. LANGFORD, and PETER H. BIRD. Can. J. Chem. **69**, 2033 (1991).

The X-ray crystal structure of $W(CO)_5$piperidine is reported and assignments are given for the LF and CT band of $W(CO)_5$piperidine and $W(CO)_5$pyridine. The W---N, W---C (axial), and W---C (equatorial) bond lengths for $W(CO)_5$pip are 2.330(5), 1,963(6), and 2.04(7), respectively. The longer W---N bond length in $W(CO)_5$pip compared to $W(CO)_5$pyr corresponds to greater photoreactivity observed under LF triplet excitation for $W(CO)_5$pip but cannot account for the reverse trend observed under LF singlet irradiation. The structure also fails to support a model based on differences in π back donation from W. It is concluded that differences between singlet and triplet photoreaction originate in the relative rates of radiationless decay.

Key words: $W(CO)_5$piperidine, photoreactivity, crystal structure.

CAROL MORALEJO, COOPER H. LANGFORD et PETER H. BIRD. Can. J. Chem. **69**, 2033 (1991).

On a déterminé la structure cristalline du complexe $W(CO)_5$.pipéridine par diffraction des rayons-X et on a fait l'attribution des bandes LF et CT des complexes $W(CO)_5$.pipéridine et $W(CO)_5$.pyridine. Les longueurs des liaisons W---N, W---C(axial) et W---C(équatorial) du complexe $W(CO)_5$.pip sont respectivement 2,330(5), 1,963(6) et 2,04(7) Å. Le fait que la liaison W---N soit plus longue dans le complexe $W(CO)_5$.pip que dans le complexe $W(CO)_5$.pyr correspond à la plus grande photoréactivité observée lors de l'excitation LF du triplet du $W(CO)_5$.pip; elle ne peut toutefois pas expliquer le renversement de la tendance observée lors de l'irradiation LF du singulet. La structure ne permet pas non plus d'expliquer un modèle basé sur des différences dans la rétrocession d'électrons π par le W. On en conclut que les différences entre les photoréactions singlulet et triplet trouvent leur origine dans les vitesses relatives de la dégénérescence non radiative.

Mots clés : $W(CO)_5$.pipéridine, photoréactivité, structure cristalline.

[Traduit par la rédaction]

Introduction

Tutt and Zink (1) have elucidated the bond length changes characteristic of the vibrationally equilibrated low lying ^3E ligand field excited state of $W(CO)_5L$ (L = piperidine (pip) or pyridine (py)) using Heller's semi-classical time dependent theory of molecular spectroscopy (2). This provided an approach to the photochemical reactivity of the complexes, substitution of the L ligand. Recent results (3) show that the theoretical discussion of photoreactivity should include an appraisal of singlet behavior as well. In our recent work (3), we have observed that significant differences exist in the relative reactivities of $W(CO)_5$pyridine and $W(CO)_5$piperidine upon excitation into the LF singlet and triplet states. As a contribution to the understanding of the differences in reactivities between these two compounds, we have obtained a spectrum and a structure to evaluate the role of π back-donating in the pyridine complex. In this paper, the crystal structure of $W(CO)_5$pip is reported. The bond lengths are compared with reported bond lengths for $W(CO)_5$py and $W(CO)_6$ in an attempt to clarify whether a significant π back-bonding exists between W and pyridine which may account for observed differences in photochemical behavior between these two complexes under LF singlet irradiation. Other physical evidence such as the infrared frequencies and derived force constants for CO, and the positions of the LF bands in the deconvoluted electronic spectra do not support a very significant difference in W—N bonding between the py and pip complexes.

Experimental

Materials

$W(CO)_5$pip was prepared using a modification of the procedure proposed by Strohmeier and Gerlich (4). $W(CO)_6$ (0.65 g) and 5 mL of piperidine were mixed in 30 mL of THF. The solution was irradiated by exposure to cool-white fluorescent lab lights ($\lambda > 350$ nm) for 72 h. Prepurified N_2 was passed through a solvent bubbler into the solution to prevent solvent evaporation and to sweep out displaced CO. The reaction was monitored for unreacted $W(CO)_6$ by TLC on alumina plates. After 72 h, the THF was removed by rotary evaporation. The yellow residue was dissolved in benzene and mixed with 1–2 g of alumina. The benzene was evaporated overnight to encourage adsorption of the product onto the alumina. The adsorbed product was added to a column of neutral alumina in isoctane. Isooctane eluted unreacted $W(CO)_6$ and benzene eluted the product. Ethanol was used to elute the unreacted ligand. The crystals of $W(CO)_5$piperidine were grown by slow evaporation (2 weeks) in benzene/isooctane (2:1 v/v). $W(CO)_5$py (py = pyridine) was obtained as described in ref. 1.

The X-ray crystal structure determination

The chosen crystal was subjected to a preliminary photographic survey to check its quality and to determine the space group and approximate unit cell measurements. It was then transferred to a Picker Facs-1 diffractometer where more precise cell dimensions were obtained from 25 automatically centered reflections, and then intensity data were collected. Lorentz polarization and general absorption corrections were applied. The tungsten atom was located from a Patterson synthesis and the structure completed and refined routinely using anisotropic thermal parameters in the final stages. No attempt was made to include the hydrogen atoms. Details may be found in Table 1. Table 2 contains a listing of the final atomic coordinates, while listings of the anisotropic thermal parameters, observed and calculated structure factors, and a complete table of bond lengths and angles, are available as supplementary data.[2] All programs used for the data collection, structure solution, and refinement are part of the

[1]Revision received June 10, 1991.

[2]A complete set of material may be purchased from the Depository of Unpublished Data, Document Delivery, CISTI, National Research Council Canada, Ottawa, Canada K1A 0S2.

Can. J. Chem. Downloaded from www.nrcresearchpress.com by 123.30.183.119 on 09/08/12
For personal use only.

TABLE 1. Crystallographic data for $W(CO)_5$pip

(*a*) Crystal parameters

Formula: $C_{10}H_{11}NO_5W$	fw = 409.05
Crystal system: Monoclinic	Space group: $P2_1/c$
a = 11.127(6) Å	α = 90 deg
b = 10.269(4) Å	β = 110.51(5) deg
c = 12.325(9) Å	γ = 90 deg
V = 1319.01 Å^3	Z = 4
D_{calcd} = 2.060 g cm^{-1}	μ(Mo Kα) = 89.53 cm^{-1}
Colour: yellow	Transmission 33–43%
Crystal size: 0.2 × 0.1 × 0.5 mm	Temp = 21°C

(*b*) Data collection and structure refinement*

Diffractometer: Picker FACS-1	Radiation: Mo Kα
Monochromator: graphite	Scan method: $\theta/2\theta$
Scan speed: 2°/m	Data limits: $3.5 < 2\theta < 50°$
Octants collected: $\pm h, +k, +l$	Total reflections collected: 2316
Independant reflections collected: 2316	Unique data $F_0 > 3\sigma F_0$: 1865
Least-squares method: block diagonal	Absorption correction: yes
Parameters refined: 154	Data/parameter ratio = 12.1
R_1 = 0.028	R_2 = 0.046
Goodness of fit = 0.81	

*$R_1 = \Sigma[||F_0| - |F_c||]/\Sigma|F_0|$; $R_2 = [\Sigma w(||F_0| - |F_c||)^2/\Sigma w|F_0|^2]^{1/2}$, where $w = 1/\sigma(F_0)$; goodness of fit = $[\Sigma w(|F_0| - |F_c|)^2/(N_{obs} - N_{parm})]^{1/2}$.

X-ray crystallographic system for the PDP-8 minicomputer by Larson and Gabe (5).

Spectral band deconvolution

The electronic spectra of $W(CO)_5L$ (L = py, pip) in all solvents used in this study were deconvoluted using a Gaussian band least-squares minimization routine (6) employing a Marquardt algorithm (7). The program allows the band positions to be fixed and the best Gaussian fits for the W → pyr CT, ^1A and ^1E bands were determined when the band maxima of the ^3E bands were initially fixed between 446 and 448 nm, depending on the solvent.

Results and discussion

Electronic spectra

The band maxima determined from the curve-fitting program for different solvents are given in Table 3. The uv–vis absorption spectra of $W(CO)_6$, $W(CO)_5$py, and $W(CO)_5$pip in alkane solvents display characteristics which have been well documented (8–12). For $W(CO)_6$ in cyclohexane, the lowest energy absorption band at ~28 570 cm^{-1} (350 nm) is assigned as the spin-forbidden $^3T_{1g} \leftarrow {}^1A_{1g}$ transition (8, 9). The first LF (ligand field) singlet transition, $^1T_{1g} \leftarrow {}^1A_{1g}$ is observed at 32 258 cm^{-1} (310 nm) as a shoulder on the more intense M → π^* CO charge-transfer absorption at 34 485 cm^{-1} (290 nm). A higher energy absorption band observed as a shoulder at 37 037 cm^{-1} (270 nm) is assigned as the second LF $^1T_{2g} \leftarrow {}^1A_{1g}$ transition. The highest absorption observed at ~43 000 cm^{-1} (233 nm) is assigned as the second component of the M → π^* CO charge-transfer transition.

Substitution of a CO in $W(CO)_6$ by a pyridine or piperidine molecule reduces the symmetry of the complex from octahedral to C_{4v}. Reduction of the symmetry results in a splitting of the T_{1g} and T_{2g} states. The electronic spectra of $W(CO)_5$py and $W(CO)_5$pip exhibit similar features in alkane solvents. In isooctane, each compound exhibits a low energy band, near 22 625 cm^{-1} (442 nm) which has been previously assigned as a LF $^3E \leftarrow {}^1A_1$ transition and which appears as a shoulder on the more intense LF ^1E transition centered near 26 180 cm^{-1}

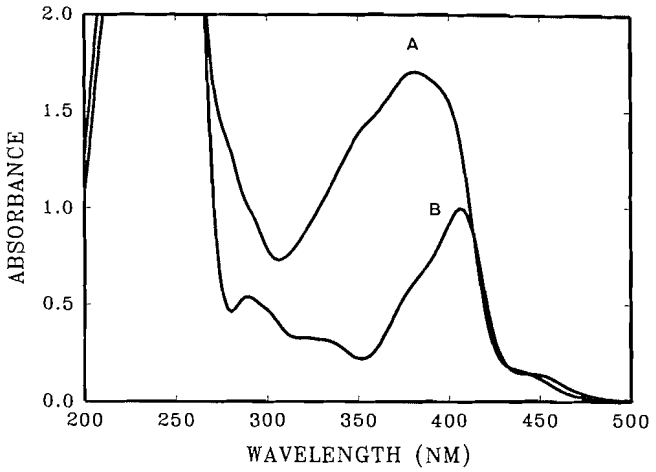


FIG. 1. Electronic spectra of (*a*) $W(CO)_5$pyridine and (*b*) $W(CO)_5$piperidine in isooctane. The concentration for both was 2.8 × 10^{-4} M.

(382 nm) for pyridine and 24 350 cm^{-1} (404 nm) for piperidine (Fig. 1) (10–12). Higher energy transitions have not been definitively assigned. The asymmetry of the band observed for piperidine at ~26 180 cm^{-1} (382 nm) suggests the presence of a second band. Based on the splitting of the $^1T_{1g}$ state from octahedral to C_{4v} symmetry, this asymmetry is probably due to a contribution from the orbitally forbidden, equatorially directed $^1A \rightarrow {}^1A_2$ transition (13). The intense absorption at 36 040 cm^{-1} (270 nm) observed for both complexes, by analogy to the MLCT assignment for $W(CO)_6$ is assigned as the W → π^* CO CT transition (8, 9). For $W(CO)_5$py in polar solvents, the asymmetry of the band observed near 28 570 cm^{-1} (350 nm) in non-polar solvents splits to reveal an absorption band which blue shifts and is resolved from the LF singlet band in more polar media (Fig. 2). This band has been assigned as a W → pyridine CT transition (14). Resolution of the CT and LF bands in the pyridine complex further reveals another transition at ~370 nm indicated by the asymmetry of the LF band.

Based on these assignments, the curve-fitting program previously described was used to deconvolute the bands in the 300–500 and 350–500 nm regions of the electronic spectra of $W(CO)_5$py and $W(CO)_5$pip, respectively. Four bands were assigned for the $W(CO)_5$py complex and three bands for the $W(CO)_5$pip complex. For $W(CO)_5$pyr, in order of decreasing energy, the four bands represent transitions to the W → pyr CT, ^1A, ^1E, and ^3E states, respectively. For $W(CO)_5$pip, the three bands represent, in order of decreasing energy, transitions to the ^1A, ^1E, and ^3E states, respectively.

X-ray data

Figure 3 shows the molecular structure. The important bond lengths for the $W(CO)_5$piperidine complex determined in this work are given in Table 4 together with the reported bond lengths for $W(CO)_6$ and $W(CO)_5$pyridine for comparison.

Photoreactivity

$W(CO)_5L$ (L = py, pip) are d^6 C_{4v} complexes which undergo efficient photochemical substitution of L by suitable donor molecules in solution (14–17). In mixed alkane/alkene solvents, LF singlet irradiation gives efficient substitution of L by alkene (3, 14–17) and the quantum yield is wavelength dependent for these complexes as was first reported by Wrighton, Hammond, and Gray (16). LF singlet excita-

Can. J. Chem. Downloaded from www.nrcresearchpress.com by 123.30.183.119 on 09/08/12
For personal use only.

TABLE 2. Atomic cordinates and equivalent isotropic thermal parameters for $W(CO)_5$pip*

Atom	x	y	z	B_{iso}
W	0.160139 (22)	0.156233 (24)	0.825398 (20)	2.971 (10)
C1	0.1182 (8)	0.0014 (6)	0.9120 (6)	3.9 (3)
C2	0.1994 (7)	0.3177 (7)	0.7458 (7)	4.3 (3)
C3	0.0954 (6)	0.2751 (6)	0.9170 (5)	3.52 (23)
C4	−0.0208 (7)	0.1399 (6)	0.7067 (7)	3.71 (3)
C5	0.3359 (8)	0.1628 (7)	0.9518 (7)	4.5 (3)
O1	0.0943 (7)	−0.0821 (6)	0.9620 (6)	6.0 (3)
O2	0.2200 (6)	0.4133 (5)	0.7062 (6)	6.1 (3)
O3	0.0568 (6)	0.3462 (5)	0.9711 (5)	4.97 (23)
O4	−0.1248 (6)	0.1294 (5)	0.6429 (6)	5.59 (24)
O5	0.4324 (6)	0.1655 (7)	1.0270 (6)	7.0 (3)
N	0.2352 (5)	0.0236 (5)	0.7094 (4)	3.15 (18)
C6	0.3569 (8)	0.0711 (8)	0.6961 (7)	4.8 (3)
C7	0.3918 (9)	−0.0084 (8)	0.6049 (8)	5.5 (4)
C8	0.4141 (11)	−0.1503 (9)	0.6449 (10)	7.2 (5)
C9	0.2905 (11)	−0.2064 (10)	0.6613 (8)	6.1 (4)
C10	0.2554 (8)	−0.1162 (7)	0.7488 (7)	4.5 (3)

*B_{iso} is the arithmetic mean of the principal axes of the vibration ellipsoids.
Esd's in parentheses refer to the least significant digit(s) printed.

TABLE 3. Band maxima for transitions of $W(CO)_5L$ (L = py, pip) determined from deconvolution of spectral bands

L	Solvent	Band maxima (2 nm) ^{1}MLCT	^1A	^1E	^3E
py	Isooctane	352	388	404	448
	Iso/hexene (2:1 v/v)	352	388	404	448
	1-Hexene	354	386	405	448
	CCl_4/1-hexene (2:1 v/v)	354	386	405	446
pip	Isooctane		388	410	448
	Iso/hexene (2:1 v/v)		388	409	448
	1-Hexene		388	409	448
	CCl_4/hexene (2:1 v/v)		389	410	448

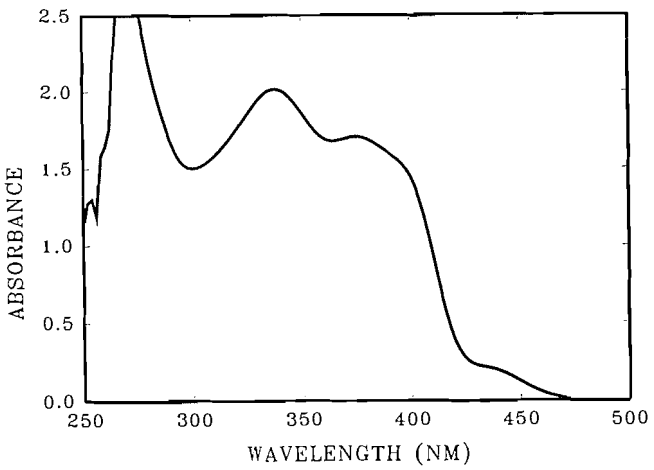


FIG. 2. Electronic spectrum of $W(CO)_5$pyridine in dichloromethane/1-hexane. The concentration was 2.8×10^{-4} M.

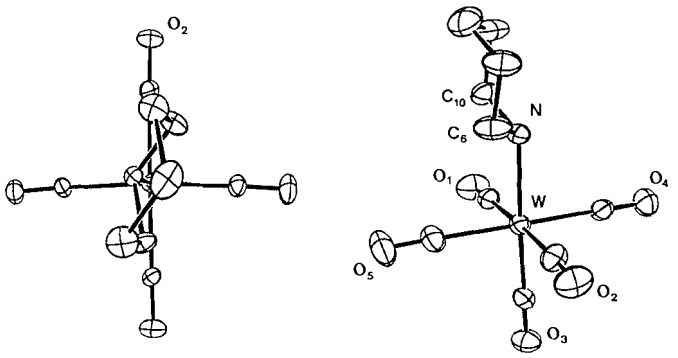


FIG. 3. Two views of $W(CO)_5$piperidine.

TABLE 4. Bond lengths in the ground electronic state of $W(CO)_5L$

Bond	Length (Å) L = Pip	L = Py (ref. 1)	L = CO (ref. 20)
W---C (axial)	1.963 (6)*	2.00 (1)	2.06 (5)
W---C (equatorial)	2.044 (11)†	2.04 (2)	
W---N	2.330 (5)*	2.26 (1)	
C---O (axial)	1.168 (8)*	1.13 (1)	1.13 (5)
C---O (equatorial)	1.149 (6)†	1.12 (2)	

*The figures in parentheses are in crystallographic esd.
†Averaged value and standard deviation from the average.

tion (365, 436 nm) produces larger photosubstitution quantum yields for $W(CO)_5$py than $W(CO)_5$pip (Table 5) (3). Quantum yields on irradiation into the LF triplet states of both complexes are lower than for LF singlet irradiation (3). Under direct LF triplet irradiation (488 nm), the quantum yields are larger for $W(CO)_5$pip than for $W(CO)_5$py. In solvents such as benzene and dichloromethane which resolve the W → pyr CT and LF states in $W(CO)_5$pyridine, the quantum yields decrease relative to solvents in which the W → pyr CT and LF states are mixed. There is a corresponding decrease for $W(CO)_5$pip as well, indicating the presence of a general solvent effect, not a role for charge transfer. In all solvents we have studied, the photochemical behavior is similar for both complexes. Under direct LF singlet irradiation, the photosubstitution quantum yields are greater for pyridine than for piperidine. Under direct LF triplet irradiation, the trend is reversed. The only significant difference between the two complexes is the presence of

Can. J. Chem. Downloaded from www.nrcresearchpress.com by 123.30.183.119 on 09/08/12
For personal use only.

TABLE 5. Photosubstitution quantum yields for $W(CO)_5L \rightarrow W(CO)_5$(1-hexene) in isooctane/1-hexene (2:1)*,†,‡,§

L		Wavelength (nm)				
		313‖	365‖	436‖	457.5	488.0
pyr	N_2	0.48 (2)[3]	0.53 (2)[4]	0.62 (2)[4]	0.44 (3)[7]	0.23 (3)[16]
	O_2	0.52 (3)[4]	0.54 (2)[11]	0.62 (4)[9]	0.44 (3)[7]	0.23 (1)[7]
		0.38 (4)¶	0.50 (5)¶	0.63 (6)¶		
pip	N_2		0.49 (3)[7]	0.54 (2)[2]	0.41 (2)[4]	0.37 (2)[8]
	O_2		0.48 (1)[8]	0.53 (2)[5]	0.44 (1)[6]	0.40 (2)[2]

*Concentrations of reactants are between $1.5–1.6 \times 10^{-4}$ M.
†Light intensities are between 3×10^{-10} and 2×10^{-6} Einsteins/s.
‡Numbers in parentheses represent standard deviations.
§Superscripts represent the number of trials.
‖Wavelengths are ±10 nm.
¶Reference 16, all other data are reproduced from ref. 3.

low-lying π^* orbitals on the pyridine in $W(CO)_5$py which may π-bond with the t_{2g} orbitals of W. In complexes where metal $d\pi$ – ligand π^* back-bonding is present, simultaneous depopulation of the $d\pi$-orbitals and population of a σ antibonding orbital may lead to enhanced photoreactivity.

Zink and Tutt have determined the excited state distortions of both complexes under LF triplet excitation using fluorescence, preresonance Raman spectroscopy, and time-dependent theory (1, 2). They observe that the W---N bond length in the piperidine complex is increased by as much as 0.3 Å while the W---N bond length in the pyridine complex is increased by 0.18 Å(1). This information may be used to interpret our photosubstitution results on the basis of bond strengths since quantum yields are higher for the piperidine complex than for the pyridine complex under LF triplet excitation (3). Reported CO stretching frequencies are lower for the monosubstituted complexes than they are for the hexacarbonyl, indicating more extensive metal-to-carbonyl π-bonding and stronger metal carbonyl bonds for the monosubstituted complexes (18, 19). Comparison of the W---C bond lengths of all three complexes confirms this (Table 4). The X-ray data obtained in this study shows that the W---N bond is longer in the piperidine complex than in the pyridine complex. The difference in bond lengths between these two complexes may be attributed to differences in the hybridization of the orbitals which are responsible for bonding in these complexes. The N orbitals in the pyridine complex are sp^2 hybridized due to the aromatic nature of the pyridine N. The N orbitals in the piperidine complex are sp^3 hybridized. Values obtained for the CO force constants of the pyridine complex do not differ significantly from those obtained for the piperidine complex (19). This suggests that no appreciable π-bonding exists between tungsten and the pyridine.

This appears to eliminate π back-bonding which is reduced in the excited state as a cause of enhanced photoreactivity in the pyridine complex upon LF singlet irradiation. It raises the question as to what other variable may account for both the observed differences under LF singlet irradiation and the reverse trend observed under LF triplet irradiation. Both the LF singlet and LF triplet reactive states have the same orbital configuration. As a consequence, MO arguments must lead to similar conclusions regarding the reactivity.

The structure reported in this paper is consistent with assignment of the difference between W---N bond distances in $W(CO)_5$py and $W(CO)_5$pip to differences in N hybridization. There is little reason to posulate π acceptor character for the py ligand. The lesser distortion of the W---N bond in the pyridine complex on excitation to the ^3E state with σ^* character cannot be attributed to residual π-bonding.

Tutt and Zink (1) have pointed out that the greater extension of the W---N bond in the pip complex can be seen as "explaining" the greater quantum yield for photosubstitution from the ^3E states. Unfortunately, no similar bonding factor is available to explain the reversal of reactivity from the ^1E states. This serves to emphasize that quantum yields are determined by a competition between reactive and non-reactive radiationless decay. The reactivity change between the ^1E and ^3E states must originate in the changes in the dynamics of the relaxation to the ground state. In a subsequent paper (21), an analysis of some solvent effects will hint as to the mechanisms of such relaxation processes.

Acknowledgement

We thank the Natural Sciences and Engineering Research Council of Canada for Financial Support.

1. L. TUTT and J. I. ZINK. J. Am. Chem. Soc. **108**, 5830 (1986).
2. E. J. HELLER. Acc. Chem. Res. **14**, 368 (1981).
3. C. MORALEJO, C. H. LANGFORD, and D. K. SHARMA. Inorg. Chem. **28**, 2205 (1989).
4. W. STROHMEIER and K. GERLICH. Chem. Ber. **94**, 398 (1961).
5. A. C. LARSEN and E. J. GABE. *In* Computing in crystallography. *Edited by* H. Schlenk, R. Olthof-Hazekamp, H. Van Koningsveld, and J. C. Bassi. Delft University Press, Delft, Holland. 1978. p. 81.
6. T. F. BELLIVEAU. Ph.D. Thesis. McGill University, Montreal. P.Q. 1988.
7. D. W. MARQUARDT. J. Soc. Ind. Appl. Math. **11**, 431 (1963).
8. N. A. BEACH and H. B. GRAY. J. Am. Chem. Soc. **90**, 5713 (1968).
9. H. B. GRAY and N. A. BEACH. J. Am. Chem. Soc. **85**, 2922 (1963).
10. M. WRIGHTON, G. S. HAMMOND, and H. B. GRAY. Inorg. Chem. **11**, 3122 (1972).
11. M. WRIGHTON, G. S. HAMMOND, and H. B. GRAY J. Am. Chem. Soc. **93**, 4336 (1971).
12. M. WRIGHTON and K. R. POPE. Inorg. Chem. **24**, 2792 (1985).
13. H. B. GRAY and V. M. MISKOWSKI. Inorg. Chem. **14**, 401 (1975).

Can. J. Chem. Downloaded from www.nrcresearchpress.com by 123.30.183.119 on 09/08/12
For personal use only.

14. M. WRIGHTON, H. B. ABRAMSON, and D. L. MORSE. J. Am. Chem. Soc. **98**. 4105 (1976).
15. M. WRIGHTON, G. S. HAMMOND, and H. B. GRAY. J. Organomet. Chem. **70**, 283 (1974).
16. M. WRIGHTON, G. S. HAMMOND, and H. B. GRAY. Mol. Photochem. **5**, 179 (1973).
17. M. WRIGHTON. Inorg. Chem. **13**, 905 (1974).
18. L. H. JONES. Spectrochim. Acta, **19**, 329 (1963).
19. R. A. BROWN and G. R. DOBSON. Inorg. Chim. Acta, **6**, 65 (1972).
20. M. S. WRIGHTON and D. L. MORSE. J. Organomet. Chem. **97**, 405 (1975).
21. C. MORALEJO and C. H. LANGFORD. Inorg. Chem. **30**, 567 (1991).

Can. J. Chem. Downloaded from www.nrcresearchpress.com by 123.30.183.119 on 09/08/12
For personal use only.

Formation of $C_6H_7^+$ ions in ion–molecule reactions in vinyl chloride

JAN A. HERMAN AND KAZIMIERA HERMAN
Département de chimie, Université Laval, Quebec (Qué.)., Canada G1K 7P4

AND

TERRY B. MCMAHON
Department of Chemistry and Guelph–Waterloo Center for Graduate Work in Chemistry, University of Waterloo, Waterloo, Ont., Canada N2L 3G1

Received June 21, 1991

JAN A. HERMAN, KAZIMIERA HERMAN, and TERRY B. MCMAHON. Can. J. Chem. **69**, 2038 (1991).

The formation of $C_6H_7^+$ species in ion/molecule reactions in gaseous vinyl chloride was studied in a high pressure photoionization mass spectrometer and in a Fourier transform ion cyclotron resonance (FT-ICR) spectrometer. Collision-induced dissociation (CID) mass spectra of $C_4H_5Cl^+$, $C_4H_6Cl^+$, and $C_6H_7^+$ species suggest a "butadiene-like" structure for the two former ions, and a non-benzenium structure for the last species. The $C_6H_7^+$ ions are formed in a two-step mechanism involving $C_4H_5^+$ as intermediate ions. These processes are in competition with condensation reactions leading to the formation of $C_6H_{7-9}Cl^+$ species.

Key words: ion–molecule reactions, gaseous vinyl chloride, collision-induced dissociation.

JAN A. HERMAN, KAZIMIERA HERMAN et TERRY B. MCMAHON. Can. J. Chem. **69**, 2038 (1991).

Utilisant un spectromètre de masse à photo-ionisation à haute pression et un spectromètre de résonance cyclotronique ionique par transformation de Fourier (FT-ICR), on a étudié la formation de l'espèce $C_6H_7^+$ dans des réactions ion/molécule du chlorure de vinyle gazeux. Les spectres de masse des dissociations induites par des collisions (DIC) des espèces $C_4H_5Cl^+$, $C_4H_6Cl^+$ et $C_6H_7^+$ suggèrent la présence d'une structure « ressemblant à un diène » pour les deux premiers ions et une structure qui ne correspond pas à un benzénium pour la dernière espèce. Les ions $C_6H_7^+$ se forment par un mécanisme en deux étapes impliquant les ions $C_4H_5^+$ comme intermédiaires. Ces processus sont en compétition avec les réactions de condensation conduisant à la formation d'espèce $C_6H_{7-9}Cl^+$.

Mots clés : réactions ion–molécule, chlorure de vinyle gazeux, dissociation induite par collision.

[Traduit par la rédaction]

Introduction

Ion/molecule reactions in gaseous vinyl chloride have been studied extensively. Both high pressure mass spectrometry (HPMS) and ion cyclotron resonance spectrometry (ICR) were used to unravel the complex ion/neutral processes occurring in this system (1–8). The main difference between the results found by these two techniques is the extent to which these ion/neutral processes can be followed. In HPMS the ion/neutral sequences up to the fourth generation of product ions could be followed (9). Moreover, the multiple collision conditions at high pressure allow a stabilization of excited collision complexes in three-body processes and formation of stabilized ion clusters. However, the increasing number of ion products formed in successive ion/molecule reactions which react in competition with the neutral constituent makes kinetic studies quite difficult due to the complexities of many processes taking place simultaneously in the system. On the other hand, the low pressure ($<10^{-5}$ Torr) in ICR experiments favours the study of events on a collision-by-collision time scale. However, this usually limits the measurements to the first generation of product ions. However, the capabilities characteristic of ICR spectrometry include the ability to carry out multiple-stage experiments involving the isolation of chosen ion species and the subsequent study of bimolecular ion/molecule reactions with the neutral gas target. Therefore, in order to unravel the complex details of the later ion/molecule reaction sequences in vinyl chloride it is desirable to prepare chosen product ions at high pressure, to selectively isolate them, and to allow them to react with neutrals at low pressure. In this manner the observed ion processes are unequivocally established without interferences from competing reaction channels.

The first sequence of ion/molecule reactions ([1] to [3]), providing the formation of $C_4H_5Cl^+$, $C_4H_6Cl^+$, and $C_3H_4Cl^+$ species has been observed both in HPMS or ICR experiments and is apparently well established (1–6):

$$[1]\quad C_2H_3Cl^+ + C_2H_3Cl \rightarrow [(C_2H_3Cl)_2]^{+*} \rightarrow C_4H_5Cl^+ + HCl$$

$$[2]\quad \rightarrow C_4H_6Cl^+ + Cl\cdot$$

$$[3]\quad \rightarrow C_3H_4Cl^+ + CH_2Cl\cdot$$

Ausloos and co-workers have reported the observation of the stabilized ion-dimer of vinyl chloride before its decomposition in reactions [1]–[3] (5), but this was not clearly substantiated in similar experiments by Neagu-Plesu (9). At higher pressure the next condensation step is observed with the formation of $C_6H_7Cl^+$, $C_6H_8Cl^+$, $C_6H_9Cl^+$, and $C_5H_6Cl^+$ species:

$$[4]\quad C_4H_5Cl^+ + C_2H_3Cl \rightarrow C_6H_7Cl^+ + HCl$$

$$[5]\quad \rightarrow C_6H_8Cl^+ + Cl\cdot$$

$$[6]\quad C_4H_6Cl^+ + C_2H_3Cl \rightarrow C_6H_8Cl^+ + HCl$$

$$[7]\quad \rightarrow C_6H_9Cl^+ + Cl\cdot$$

$$[8]\quad C_3H_4Cl^+ + C_2H_3Cl \rightarrow C_5H_6Cl^+ + HCl$$

In Fig. 1 the evolution of fractional intensities of these ion species as a function of pressure in experiments performed in a photoionization HPMS is shown. However, in addition to these ions, and with a far larger fractional intensity, is the formation of the $C_6H_7^+$ species, which seems to reach a steady state within the system (Fig. 1*A*). Evidently, this ion is formed in ion/molecule reactions involving C_4 ion species, and the reaction channel leading to its formation should reflect its structure. In order to elucidate the reaction channel through which the $C_6H_7^+$

Can. J. Chem. Downloaded from www.nrcresearchpress.com by 123.30.183.119 on 09/08/12
For personal use only.

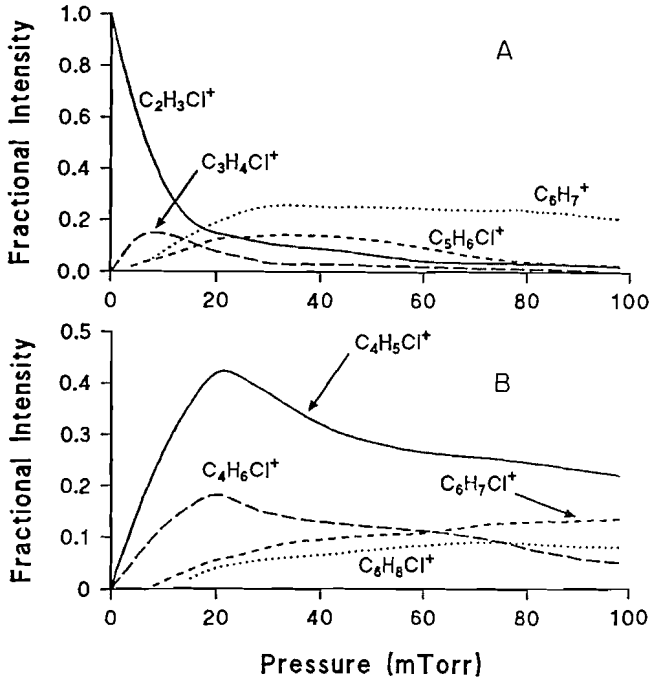


FIG. 1. Evolution of fractional intensities of ions in photoionized vinyl chloride at 10.64 eV as a function of pressure in high pressure mass spectrometer experiments.

is formed we have used the ICR ability to individually isolate the C_4 ion species and to react them with neutral vinyl chloride. An additional collision-induced dissociation (CID) experiment allowed the structure of this ion to be studied and, consequently, led to a proposal for the reactions sequence leading to its formation.

Experimental

The pressure dependence of fractional ion intensities was investigated in the photoionization high-pressure mass spectrometer already described (10, 11) A krypton resonance lamp very similar to those described by Ausloos and co-workers (12) was used as a photoionization source. The emitted light consists mainly of the 10.03 eV (~85%) and 10.64 eV (~15%) resonance lines. In these conditions about 70% of vinyl chloride ions are produced by absorption of 10.64 eV photons. The measurements were made under field-free conditions inside the collision chamber with an electric field of low intensity (~5 V cm^{-1}) applied in the ion optics. The distance in the collision chamber between the plane of formation of the parent ions by photon impact and the exit slit was 4.2 mm. The experiments were done at room temperature, 25 ± 2°C, as indicated by a thermocouple connected to the collision chamber.

The time evolutions of fractional intensities of selectively isolated $C_4H_5Cl^+$ and $C_4H_6Cl^+$ species and CID experiments on $C_6H_7^+$, $C_4H_5Cl^+$, and $C_4H_6Cl^+$ ions were carried out at ambient temperature (~23°C) on a Spectrospin CMS 47 FT-ICR spectrometer (13, 14). Pure vinyl chloride was introduced into the ICR cell through a heated inlet controlled by a manual precision leak valve. The pressure of vinyl chloride in the cell was maintained at ~3×10^{-8} mbar. After the ionizing electron pulse a delay of 4 s allowed for the formation of $C_4H_5Cl^+$ and $C_4H_6Cl^+$ ions. Thereafter the application of the radio-frequency resonance ejection technique to all undesired ion species allowed the isolation of a single ionic species, and the subsequent measurement of its disappearance rate through a variable time delay. The pulse sequence used in the present experiments is shown in Fig. 2. In Fig. 3 the selectivity of the ejection technique to isolate the $C_4H_5Cl^+$ species from all ions formed in the ICR cell is shown.

The collision-induced dissociation (CID) experiment on $C_6H_7^+$, $C_4H_5Cl^+$, and $C_4H_6Cl^+$ ions was also performed on the same FT-ICR spectrometer using argon gas at 3×10^{-8} mbar as the neutral target.

The gaseous vinyl chloride from Matheson was of the best available (>99.5%) and was used as such.

Results

HPMS experiments

Vinyl chloride photoionized by absorption of 10.64 eV photons fortunately does not fragment into $C_2H_3^+$ ion, which requires higher energy (A.P. = 12.4 ± 0.1 eV) (15, 16). Therefore, the mass spectrum obtained at low pressure (<2 mTorr) contains only $C_2H_3Cl^+$, $C_4H_5Cl^+$, $C_4H_6Cl^+$, and $C_3H_4Cl^+$ species. With increasing pressure (>10 mTorr) the next generation of ions starts to build up according to reactions [4]–[8]. However, it is important to note that the $C_6H_7^+$ species becomes visible at very short times, simultaneous with the chlorinated C_6 species, and its fractional intensity exceeds the intensities of these ions (Fig. 1). Moreover, the fractional intensity of $C_6H_7^+$ ions rapidly reaches a constant value around 0.25, while the intensities of the chlorinated C_6 ion species are still increasing. At pressures above 80 mTorr the intensity of $C_6H_7^+$ decreases and a new species $C_8H_9^+$, not shown on Fig. 1, starts to build up.

FT-ICR experiments

The time evolutions of isolated $C_4H_5Cl^+$ and $C_4H_6Cl^+$ species reacting with neutral vinyl chloride were followed in FT-ICR experiments and are shown in Figs. 4 and 5, respectively. In each case the only ion products found in the mass spectrum were $C_6H_7^+$ ions and, in very small amount (<3%), $C_4H_5^+$ species. The initial disappearance rates of $C_4H_5Cl^+$ and $C_4H_6Cl^+$ ions are relatively rapid but decrease markedly with time to reach more or less constant values when their fractional intensities drop to ~0.75. However, there are some differences in the behaviour of these two ions. The $C_4H_5Cl^+$ species reacts more slowly to form $C_6H_7^+$ ions and both ions do not reach true fractional intensity plateau values, while $C_4H_5^+$ ions do not disappear completely with time (Fig. 4). On the other hand, $C_4H_6Cl^+$ ions react more rapidly, attain well-characterized plateau intensity values for both primary and $C_6H_7^+$ species and the $C_4H_5^+$ ions disappear completely after 15 s (Fig. 5). It is also worthwhile to note that in these measurements $C_6H_7Cl^+$, $C_6H_8Cl^+$, and $C_6H_9Cl^+$ species were not formed at any time. This suggests, in relation to the results of HPMS experiments (Fig. 1), that a third-order process is probably required to stabilize the condensation products formed in reactions [4]–[7]. If that is the case, then these ions will not be formed in ICR experiments due to the very low pressure.

From the initial slopes of the plots of fractional intensities for disappearance of $C_4H_5Cl^+$ and $C_4H_6Cl^+$ ions one can calculate initial rate constants for the reactions with vinyl chloride neutrals (Figs. 4 and 5):

[9] $C_4H_5Cl^+ + C_2H_3Cl \rightarrow C_6H_7^+ + \text{neutrals}$

$k_{9,\text{init}} = 2.3 \times 10^{-11}\ \text{cm}^3\ \text{molecule}^{-1}\ \text{s}^{-1}$

[10] $C_4H_6Cl^+ + C_2H_3Cl \rightarrow C_6H_7^+ + \text{neutrals}$

$k_{10,\text{init}} = 4.4 \times 10^{-11}\ \text{cm}^3\ \text{molecule}^{-1}\ \text{s}^{-1}$

At longer time (>40 s) the rate constant for disappearance of $C_4H_5Cl^+$ ions decreases 10-fold to a value $k_9' = 2.0 \times 10^{-12}$ $\text{cm}^3\ \text{molecule}^{-1}\ \text{s}^{-1}$, while that for $C_4H_6Cl^+$ (k'_{10}) becomes unmeasurably slow.

Can. J. Chem. Downloaded from www.nrcresearchpress.com by 123.30.183.119 on 09/08/12
For personal use only.

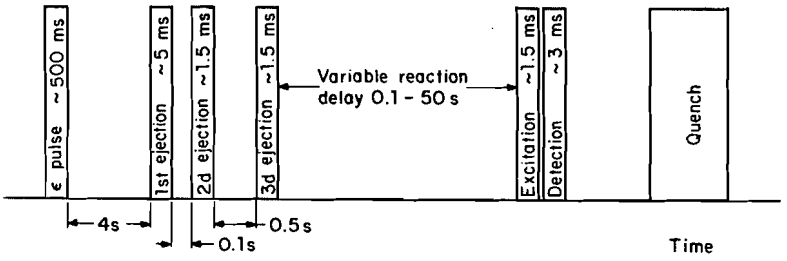


FIG. 2. Pulse sequence used with the pulsed valve to observe the reactions of isolated ion species.

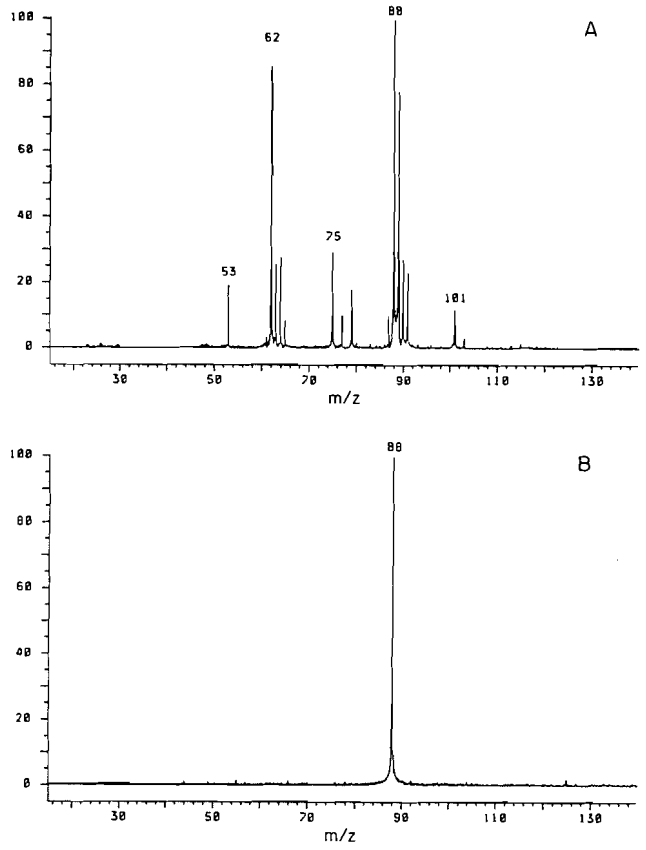


FIG. 3. The mass spectrum of selectively isolated $C_4H_5Cl^+$ ions: (*A*) before the isolation and (*B*) after selection.

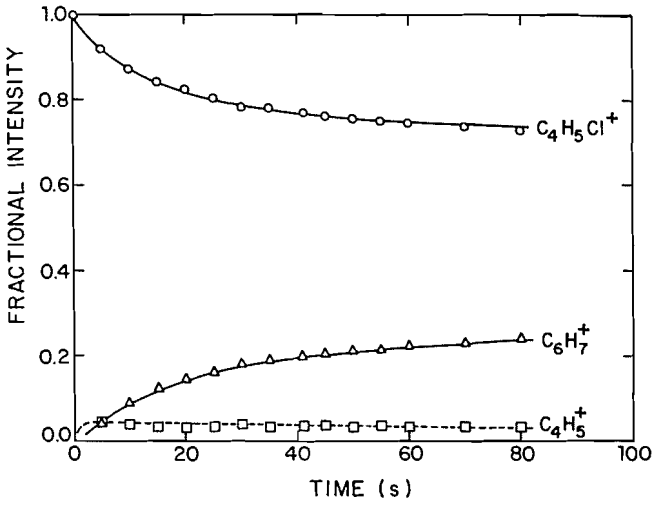


FIG. 4. Time evolution of fractional intensities of ions formed between $C_4H_5Cl^+$ and vinyl chloride in FT-ICR experiments.

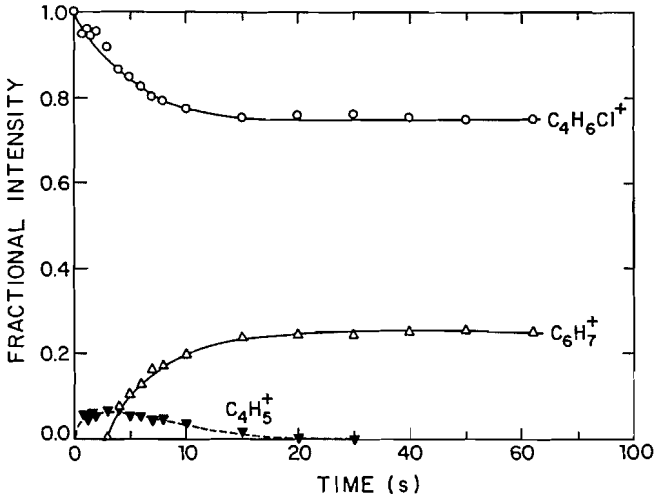


FIG. 5. Time evolution of fractional intensities of ions formed between $C_4H_6Cl^+$ and vinyl chloride in FT-ICR experiments.

CID experiments

Both $C_4H_5Cl^+$ and $C_4H_6Cl^+$ ions were examined in CID experiments. They were prepared in the same manner as in the above kinetic measurements and, after isolation, they were translationally excited by a RF pulse to ~16 eV energy and then allowed to collide with argon. In Fig. 6 the CID mass spectra of these ions under these conditions are shown. Both decomposition patterns are very similar with the main fragment being $C_4H_5^+$ (m/z 53) with two smaller $C_2H_3^+$ (m/z 27) and $C_3H_3^+$ (m/z 39) peaks. Other low intensity peaks (m/z 66 and 78) are probably ions formed in reaction with residual gases in the ICR cell.

In CID experiments $C_6H_7^+$ was prepared in the same manner as in the kinetic measurements, then selectively isolated and accelerated by a suitable RF pulse to an energy of ~16 eV and allowed to collide with argon atoms during a 0.15 s delay. The resulting CID mass spectrum is shown in Fig. 7*A*. It can be seen that the main fragment ions formed after collision are m/z 77 and 51, which correspond to $C_6H_5^+$ and $C_4H_3^+$ species. The origin of the low intensity m/z 67 peak is not clear. Formally it corresponds to a loss of one carbon atom from $C_6H_7^+$ species, but such a process seems unlikely at these low energies. It might be formed from some impurities present in the ICR cell.

In order to compare the structures of $C_6H_7^+$ ions with the same ions from different origin additional CID experiments were performed, the first on the protonated benzene ion (m/z 79) formed by reaction of benzene with CH_5^+ and $C_2H_5^+$:

[11] CH_5^+ (or $C_2H_5^+$) + $C_6H_6 \rightarrow C_6H_7^+ + CH_4$ (or C_2H_4)

Can. J. Chem. Downloaded from www.nrcresearchpress.com by 123.30.183.119 on 09/08/12
For personal use only.

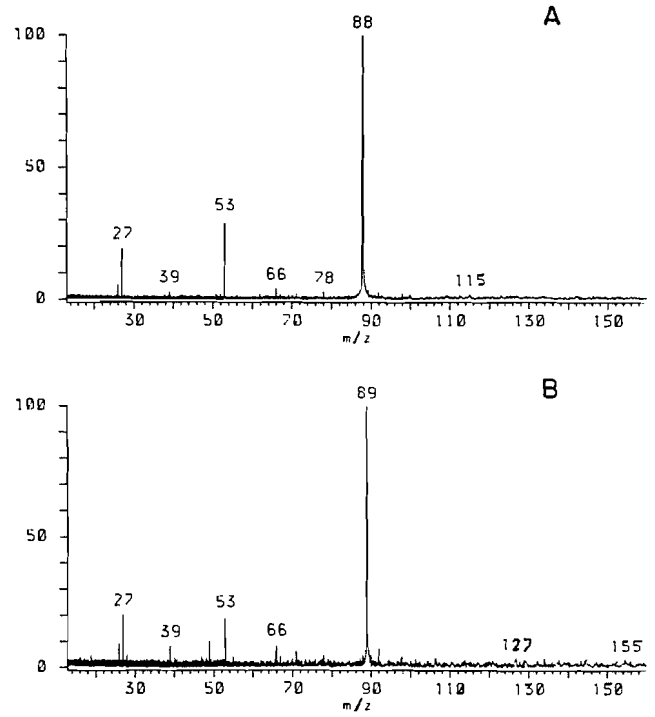


FIG. 6. Mass spectrum from collision-induced decomposition (CID) experiments of (*A*) $C_4H_5Cl^+$ and (*B*) $C_4H_6Cl^+$ ions.

and the second on the $(M - 1)^+$ fragment ion (m/z 79) of the 1,3,5-hexatriene formed in hydride abstraction with $C_2H_5^+$:

[12] $C_2H_5^+ + C_6H_8 \rightarrow C_6H_7^+ + C_2H_6$

In order to do this methane was introduced through a pulsed valve, ionized at the maximum pressure in the ICR cell, and allowed to form CH_5^+ and $C_2H_5^+$ species, and, after evacuation of the excess of methane, allowed to react with gaseous benzene or hexatriene at low pressure ($\sim 10^{-8}$ Torr) in the ICR cell. Once the $C_6H_7^+$ formed it was selectively isolated, activated, and allowed to collide with argon introduced to the ICR cell at 3×10^{-8} mbar.

Fig. 7*B* and *C* show the CID mass spectra on protonated benzene and on the $(M - 1)^+$ fragment ion of 1,3,5-hexatriene performed in the same conditions as for vinyl chloride system.

There are some differences between these three mass spectra: intensities of m/z 77 are not the same, and the absence of $C_2H_3^+$ (m/z 27) in Fig. 7*A*.

Discussion

The proposed reaction sequences leading to the $C_6H_7^+$ species formation must take into account the structure of this ion. The CID mass spectra experiments on $C_6H_7^+$ species formed, respectively, in vinyl chloride, benzene, or 1,3,5-hexatriene systems (Fig. 7), show distinct features to enable one to consider that the $C_6H_7^+$ from vinyl chloride compared to those formed in reactions [11] and [12] correspond to different structures.

The CID mass spectra of $C_6H_7^+$ formed in benzene or in 1,3,5-hexatriene are sufficiently similar to assume that to a large extent they may correspond to the same ion structure (Figs. 7*B* and *C*). Lias and Ausloos have shown that the $C_6H_7^+$ species formed in 1,3,5-hexatriene are a mixture of two ion populations composed of benzenium (~87%) and non-benzenium (~13%) isomers (19). This might account for the quantitative differences in peak intensities in Figs. 7*B* and *C*. On the other hand, the important m/z 77 peak and the absence of m/z 27 in the CID mass spectrum of $C_6H_7^+$ from vinyl chloride (Fig. 7*A*) point to another fragmentation pattern resulting from a different ion structure.

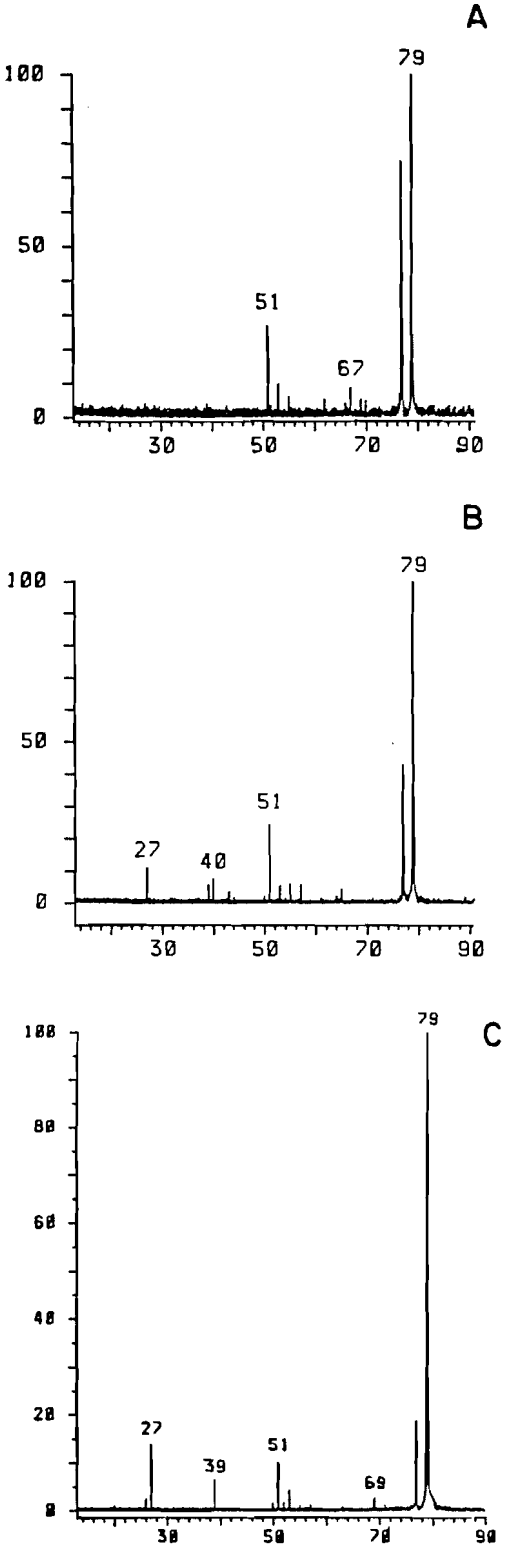


FIG. 7. Mass spectrum from collision-induced decomposition (CID) experiments of $C_6H_7^+$ ions: (*A*) formed in vinyl chloride system, (*B*) protonated benzene ion, and (*C*) from 1,3,5-hexatriene.

It is reasonable to assume that $C_6H_7^+$ ion species will react

Can. J. Chem. Downloaded from www.nrcresearchpress.com by 123.30.183.119 on 09/08/12
For personal use only.

Can. J. Chem. Downloaded from www.nrcresearchpress.com by 123.30.183.119 on 09/08/12
For personal use only.

with neutral bases in proton transfer processes only if their proton affinities (PA) are higher than that of the conjugate bases of the reactant ions. The PA of vinyl chloride is uknown, but it can be estimated to be ~172 kcal/mol (~719 kJ/mol) from the known heats of formation $\Delta H_f(H^+)$, $\Delta H_f(C_2H_3Cl)$, and $\Delta H_f(C_2H_4Cl^+)$ (20):

[13] $PA = \Delta H_f^0(C_2H_3Cl) + \Delta H_f(H^+) - \Delta H_f(C_2H_4Cl^+)$

The PA of benzene is 181.3 kcal/mol (21), while the PA of a "fulvene-like" structure of the same composition is estimated to be in the range 191–206 kcal/mol, and those of linear structures are PA = 196 kcal/mol (19). Therefore the absence of reactivity of $C_6H_7^+$ ions towards neutral vinyl chloride can be understood, and it is not surprising to see that this ion accumulates in the system with varying time and pressure (Fig. 1).

Whatever $C_6H_7^+$ structure is formed in the vinyl chloride system, its formation requires an ion-precursor species having a protonated butadiene structure. This ion is not observed in the HPMS experiment, but its transient presence is noted in the ICR mass spectrum (Figs. 4 and 5). The CID experiments for the $C_4H_5Cl^+$ and $C_4H_6Cl^+$ ions formed in reactions [1] and [2] suggest that the m/z 53 peak is an unsaturated four-carbon chain with the chlorine atom bound either on the first or second carbon atom (Fig.6). This is contrary to the condensation ion structures formed in ion/molecule reactions of alkyl chlorides which are those of the dialkylchloronium ions (17). The formation of such a carbon chain structure can be expected for the unsaturated radical ions, where condensation processes similar to those in addition polymerization might be operating. Ausloos *et al.* suggested that vinyl chloride ions may play the role of the chain initator in ionic polymerization of gaseous vinyl chloride (5).

FT-ICR experiments indicate clearly that $C_6H_7^+$ ions are originating from $C_4H_5Cl^+$ and $C_4H_6Cl^+$ species (Figs. 4 and 5). On the other hand, HPMS measurements suggest strongly that $C_6H_7Cl^+$, $C_6H_8Cl^+$, and $C_6H_9Cl^+$ ions also originate from the same chlorinated C_4 ion precursors (reactions [4]–[7]). It is not very likely that the collisional complexes, $(C_6H_{8\text{-}9}Cl_2)^+*$, will dissociate into $C_6H_7^+$ ions with elimination of two neutrals:

[14] $[C_6H_8Cl_2]^{+\cdot} \not\longrightarrow C_6H_7^+ + HCl + Cl^\cdot$

[15] $[C_6H_9Cl_2]^{+\cdot} \not\longrightarrow C_6H_7^+ + 2\,HCl$

It is, however, more likely that the formation of $C_6H_7^+$ species proceeds in two steps involving the $C_4H_5^+$ ions as intermediates. The first step probably involves thermoneutral or slightly endothermic reactions [16] and [17]:

[16] $C_4H_5Cl^+ + C_2H_3Cl \rightarrow [C_6H_8Cl_2]^+* \rightarrow C_4H_5^+ + C_2H_3Cl_2\cdot$

[17] $C_4H_6Cl^+ + C_2H_3Cl \rightarrow [C_6H_9Cl_2]^+* \rightarrow C_4H_5^+ + C_2H_4Cl_2$

followed by an exothermic reaction [18]:

[18] $C_4H_5^+ + C_2H_3Cl \rightarrow C_6H_7^+ + HCl$

The exothermicity of reaction [18] depends on the structures of $C_4H_5^+$ and $C_6H_7^+$ species. The available thermochemical data (19, 20) show that, if $C_4H_5^+$ ions have a "butadiene-like" structure and $C_6H_7^+$ is a benzenium ion, the reaction enthalpy might be as high as −70 kcal/mol, while for a $C_6H_7^+$ "fulvene-like" structure the heat of reaction drops to a range between −45 and −60 kcal/mol. On the other hand, if $C_4H_5^+$ has a methylcyclopropene structure, the reaction enthalpy is between −30 and −60 kcal/mol.

Reaction [18] has previously been observed, but at the same time it was shown that the formation of $C_4H_5^+$ ion requires the presence of vinyl ion, $C_2H_3^+$ (1):

[19] $C_2H_3^+ + C_2H_3Cl \rightarrow C_4H_5^+ + HCl$

However, in our HPMS experimental conditions the vinyl ion is not formed and in the FT-ICR experiment it is ejected. Therefore, we conclude that here $C_4H_5^+$ species originate in reactions [16] and [17].

In agreement with Bowers *et al.* the rate constant of $C_4H_5Cl^+$ in reaction [1] is 5.5×10^{-11} cm^3 molecule^{-1} s^{-1} (18), which is twice the measured rate constant of reaction [9]. This suggests, in relation to Figs. 4 and 5, that reactions [16] and [17] are slow processes determining the overall reaction rate. It follows that reaction [18] must be fast.

We believe that the mechanism of formation of $C_6H_7^+$ species in vinyl chloride is more closely related to those of formation of $C_6H_7^+$ isomers generated in propyne and allene than those in cyclohexadiene or hexatriene systems where only a loss of one hydrogen atom is involved. If this analogy holds, then it might be expected that an important fraction of $C_6H_7^+$ species has a non-benzenium structure. Moreover, the process leading to non-benzenium isomers increases in importance with increasing energy (19). Several different non-benzenium $C_6H_7^+$ isomers can be formed in the present conditions. In propyne and allene systems an examination of the energetics of proton transfer from the possible non-benzenium isomers, and the estimations of the proton affinities of possible C_6H_6 conjugate bases, point out that the most likely structures are the two protonated fulvenes **I** and **II** (19). It is probable that in vinyl chloride similar conditions prevail in order to form "fulvene-like" isomers, whose dissociation in CID experiments might possibly explain the absence of the $C_2H_3^+$ (m/z 27) and $C_3H_3^+$ (m/z 39) fragments.



I **II**

Experimental data from FT-ICR experiments indicate that only ~25% of the $C_4H_5Cl^+$ and $C_4H_6Cl^+$ species react to give $C_6H_7^+$ ions (Figs. 4 and 5). It is, therefore, tempting to assume that the above chlorinated C_4 ions are formed in different isomeric forms, one of which reacts to form $C_6H_7^+$ non-benzenium species (reactions [16] and [17]). The position of the chlorine atom on the first or the second carbon might determine the ability of the $C_4H_5Cl^+$ and $C_4H_6Cl^+$ ions to react either in addition processes [4]–[7] or in dissociation processes [16]–[17]. During the life-time of the collision complexes, $[H_{5,6}C_4Cl^+\cdot\cdot C_2H_3Cl]$, the chlorine atom in head (or tail) positions seems to be more accessible to transfer the chlorine atom or hydrogen chloride on the C=C double bond of the added neutral vinyl chloride with elimination of the $C_4H_5^+$ ion. On the other hand, the chlorine atom fixed on the second carbon atom seems to be less available, and the addition reactions to form $C_6H_{7-9}Cl^+$ species are more likely.

Conclusion

The CID mass spectra show evidence that the $C_6H_7^+$ species formed in the vinyl chloride system have predominantly non-benzenium structures. Owing to their higher proton affinities than vinyl chloride, they do not react further in proton transfer processes and accumulate in the system. The $C_6H_7^+$ species are formed from $C_4H_5Cl^+$ and $C_4H_6Cl^+$ precursor-ions in processes involving the $C_4H_5^+$ as intermediate species. These processes

are in competition with condensation reactions leading to $C_6H_{7-9}Cl^+$ ion products.

The rate constants of $C_6H_7^+$ formation and addition reactions to form higher condensation ion species are comparable and are of the order of 2×10^{-11} to 5×10^{-11} cm^3 molecule^{-1} s^{-1}. They are slow reactions.

The CID mass spectra of $C_4H_5Cl^+$ and $C_4H_6Cl^+$ species suggest that these ions have a "butadiene-like" structure. The time evolution of these ions points out that these species are formed in at least two isomeric forms, one of which reacts to form $C_6H_7^+$ species, while the other leads most probably to formation of $C_6H_7Cl^+$, $C_6H_8Cl^+$, and $C_6H_9Cl^+$ ions.

Acknowledgement

The authors acknowledge the financial assistance of the Natural Sciences and Engineering Research Council of Canada.

1. J. L. Beauchamp, L. R. Anders, and J. D. Baldeschwieler. J. Am. Chem. Soc. **89**, 4569 (1967).
2. J. A. Herman, J. J. Myher, and A. G. Harrison. Can. J. Chem. **47**, 647 (1969).
3. B. M. Hughes, T. O. Tiernan, and J. H. Futrell. J. Phys. Chem. **73**, 829, (1969).
4. V. G. Anicich and M. T. Bowers. Int. J. Mass Spectrom. Ion Phys. **12**, 231 (1973).
5. L. W. Sieck, R. Gorden Jr., S. G. Lias, and P. Ausloos. Int. J. Mass Spectrom. Ion Phys. **15**, 181 (1974).
6. V. G. Anicich and J. H. Futrell. Int. J. Mass Spectrom. Ion Phys. **21**, 383 (1976).
7. J. A. Herman, R. Neagu-Plesu, and L. Wojcik. Can. J. Chem. **67**, 97 (1989).
8. J. A. Herman, R. Neagu-Plesu, U. Krzemien, and K. Bederski. Can. J. Chem. **67**, 2196 (1989).
9. R. Neagu-Plesu. M.Sc. Thesis. Université Laval, Quebec, P.Q. 1987.
10. H. Wincel and J. A. Herman. J. Chem. Soc. Faraday Trans. I, **69**, 1799 (1973).
11. Z. Luczynski and J. A. Herman. Int. J. Mass Spectrom. Ion Phys. **31**, 237 (1979).
12. R. Gordon Jr., R. E. Rebbert, and P. Ausloos. NBS Technical Note no. 496 (1969).
13. M. Alleman, H. Kellerhalls, and K. P. Wanczek. Int. J. Mass Spectrom. Ion Processes, **98**, 139 (1983).
14. P. Kofel and T. B. McMahon. Int. J. Mass Spectrom. Ion Processes, **98**, 1 (1990).
15. F. P. Lossing. Can. J. Chem. **49**, 357 (1971).
16. D. Reinke, R. Kraessig, and H. Baumgartel. Z. Naturforsch. **28a**, 1021 (1973).
17. D. K. Sen Sharma and P. Kebarle. J. Am. Chem. Soc. (*a*) **100**, 5826 (1976); (*b*) **104**, 19 (1982).
18. V. G. Anicich and M. T. Bowers. Int. J. Mass Spectrom. Ion Phys. **11**, 329 (1973).
19. S. G. Lias and P. Ausloos. J. Chem. Phys. **82**, 3613 (1985).
20. S. G. Lias, J. E. Bartmess, J. F. Liebman, J. L. Holmes, R. D. Levin, and W. G. Mallard. J. Phys. Chem. Ref. Data, **17**, Suppl. 1 (1988).
21. S. G. Lias, J. F. Liebman, and R. D. Levin. J. Phys. Chem. Ref. Data, **13**, 695 (1984).

Can. J. Chem. Downloaded from www.nrcresearchpress.com by 123.30.183.119 on 09/08/12
For personal use only.

Mechanical and electrical anharmonicities of the linear hydrogen cyanide H-bonded trimer

WAGNER B. DE ALMEIDA[1]

Department of Chemistry, UMIST, P.O. Box 88, Manchester M6O 1QD, United Kingdom

Received March 8, 1991

WAGNER B. DE ALMEIDA. Can. J. Chem. **69**, 2044 (1991).

The anharmonicity of the hydrogen-bonded (N...H) and proton-donor (C—H) stretching modes of the linear $(HCN)_3$ species are calculated at the SCF level with the 4-31G and 6-31G** basis sets. Third and fourth energy derivatives and second and third dipole moment derivatives, which are needed to calculate the anharmonic terms, were evaluated by means of the one-dimensional Chebyshev polynomial fitting to the calculated *ab initio* points. Frequencies and intensities of overtone bands are reported and the effect of geometry relaxation on the polynomial fitted derivatives as well as mechanical anharmonicity on the vibrational intensities discussed.

Key words: H-bonding, anharmonicity, vibrational frequencies, intensities.

WAGNER B. DE ALMEIDA. Can. J. Chem. **69**, 2044 (1991).

Opérant au niveau auto-cohérent avec des ensembles de base 4-31G et 6-31**, on a calculé l'anharmonicité des modes d'élongation (N...H) impliqués dans une liaison hydrogène et (C—H) agissant comme donneur de proton des espèces linéaires $(HCN)_3$. Les troisième et quatrième dérivés de l'énergie et les deuxième et troisième moments dipolaires dérivés, nécessaires pour calculer les termes anharmoniques, ont aussi été évaluées en faisant appel à un ajustement unidimensionnel de polynôme de Chebyshev pour calculer les points *ab initio*. On a déterminé les fréquences et les intensités des harmoniques et on discute de l'effet de relaxation de géométrie sur les dérivés du polynôme ajusté ainsi que l'anharmonicité mécanique sur les intensités vibrationnelles.

Mots clés : liaison hydrogène, anharmonicité, fréquences vibrationnelles, intensités.

[Traduit par la rédaction]

Introduction

The subject of mechanical and electrical anharmonicity has increasingly attracted the attention of both theoreticians and experimentalists. The importance of the anharmonicity terms to our understanding of the infrared spectra of H-bond systems has been stressed by Sandorfy (1, 2). In ref. 1 anharmonicity constants have been determined for H-bonded complexes of the type dimethylether.....HX, X = F, Cl, from the measured overtones and combination bands. Also, the influence of mechanical and electrical anharmonicity on the intensity of X—H stretching vibrations (X = O or N in the most important cases) along with frequency and intensity of overtone bands, on the basis of the experimentally measured spectra, has been investigated (3–7).

Most theories of H-bonding have as their starting point the interaction of the fast X–H stretching motion (ν_1) and the slow X—H...Y bridge stretching motion (ν_σ),

$$\underset{\nu_1}{\text{X—H}}\text{.....}\underset{\nu_\sigma}{\text{Y}}$$

where X is a proton donor and Y is a proton acceptor. However, there are other low frequency H-bond vibrations with which ν_1 can interact. The X—H stretching is the most studied among the vibrations of the H-bonded species, its fundamental being characterized by its high intensity and great breadth compared to the free band. Anharmonicity plays an important role, with ν_1 in many cases being accompanied by a number of overtones and combination tones of vibrations of lower frequency whose intensity is boosted by Fermi resonance with ν_1. Ammonium and amine salts (8–11) and carboxylic acid dimers (12) are well-known examples of this. All available evidence from gas and solution spectra shows that H-bond formation increases the anharmonicity of the X—H stretching vibration and introduces appreciable anharmonic coupling between ν_1 and ν_σ modes. The importance of anharmonic coupling is highlighted by the appearance of combination bands. The great breadth of the infrared X—H stretching bands is thought to be due to combination bands of the type $(\nu_1 \pm \nu_\sigma)$ and $(\nu_1 \pm \nu_\beta)$, where ν_β is the H-bond bending mode X—H.....Y which accompanies ν_1 and under low resolution convolutes to it. Anharmonic coupling plays an essential role in making it possible for all these combination bands to appear. Sandorfy (1) has affirmed that both mechanical and electrical anharmonicity are needed to explain the observed intensities. It is also of interest to know the extent to which the anharmonicity of ν_1, χ_{11}, is affected by H-bond formation. It has been shown by Bernstein and co-workers (see ref. 1, table 3, p. 63) that, for a series of ethers, the χ_{11} values undergo a substantial increase upon H-bond formation, except for the weakest H-bonds.

The double harmonic approximation, in which terms higher than second energy and first dipole derivative in the energy and dipole moment expansion are respectively neglected, yields satisfactory values for frequency and intensity of fundamental bands. However, for the determination of overtones and combination bands which are forbidden in the harmonic approximation, the anharmonicity of the energy and dipole moment functions, determined through the anharmonicity of the wave function, need to be taken into account. A natural way of evaluating the anharmonic corrections consists of expanding the energy and dipole moment as a power series of the normal coordinates, Q, and then of calculating the higher energy and dipole derivatives, i.e., the expansion coefficients, by a polynomial fitting procedure or analytically (which means higher accuracy). The polynomial fitting approach has been applied for studying anharmonic effects on the vibrational spectra of the species $(HCN)_n$, $n = 1, 2, 3$ (14), HCN...HF and HF...HCN (15), and C_2H_2 (16). In the case of the hydrogen cyanide multimers and hydrogen cyanide – hydrogen fluoride complexes a least-squares one-dimensional Chebyshev polynomial fitting to the

[1]Permanent address: Departamento de Quimica – ICEx, U.F.M.G., Pampulha, CP 702, Belo Horizonte – MG30.161, Brazil.

Printed in Canada / Imprimé au Canada

Can. J. Chem. Downloaded from www.nrcresearchpress.com by 123.30.183.119 on 09/08/12
For personal use only.

Can. J. Chem. Downloaded from www.nrcresearchpress.com by 123.30.183.119 on 09/08/12
For personal use only.

calculated *ab initio* points has been done, while for the acetylene molecule a two-dimensional polynomial fitting in $r_{C—H}$ and $r_{C—C}$ has also been carried out.

The linear H-bonded hydrogen cyanide trimer has been much investigated. Most of the experimental and theoretical work can be found respectively in refs. 17–21 and 22–25, and references cited therein. However, the only study dealing with anharmonicity reported so far refers to the *ab initio* calculation of the anharmonicity of the ν_σ (H-bonding) stretching vibration, using the frozen monomer geometry approach (FMG), from ref. 14. In ref. 14 the effect due to geometry relaxation on the frequency and intensity parameters was examined for the HCN dimer. It was found that to keep the monomer geometry unchanged under complexation had considerable effect on higher dipole moment derivatives and, therefore, also on the intensity of the overtone bands. Moreover, the very high value found for the harmonic intensity for the H-bonded stretching mode of the HCN trimer, as compared to the value calculated using the dipole derivative evaluated analytically in ref. 25, suggested that geometry relaxation may be very important in large hydrogen-bonded clusters.

This work reports the calculation of higher energy and dipole moment derivatives along with mechanical and electrical anharmonic terms for the proton donor C—H (ν_1) and H-bonded N...H (ν_σ) stretching vibrations of the linear HCN trimer. A one-dimensional Chebyshev polynomial fitting to the 4-31G and 6-31G** *ab initio* points for the stretching coordinates ($r_{C—H}$ and $R_{N...H}$), with all other geometrical parameters being optimised in each case, has been performed. Frequency and intensity of the first and second overtone bands are given and the validity of the FMG approach in connection to the evaluation of the anharmonic terms discussed.

Method of calculation

The intensity of the kth non-degenerate vibrational normal mode of a molecule can be written as (26)

$$[1] \qquad \alpha_k = (8\pi^3 \nu_A N_A/3hc)|\langle v|\mu|v'\rangle|^2$$

where α_k is the intensity, ν_A the vibrational frequency, $\langle v|\mu|v'\rangle$ the matrix element between the two vibrational states v and v', and constants π, h, c, and N_A having their usual values. To express the intensity in km mol^{-1}, the unit in use here, eq. [1] may be rewritten as (14)

$$[2] \qquad A_k{}^T = K_a g_k |\langle v|\mu|v'\rangle|^2$$

where $A_k{}^T$ is the total vibrational intensity in km mol^{-1}, K_a is the conversion factor (in units of km mol^{-1} kg C^{-2}), g_k is the degeneracy, and $\langle v|\mu|v'\rangle$ the transition dipole moment (in units of C kg$^{-1/2}$). For convenience the vibrational frequency ν_A has been included in the term $|\langle v|\mu|v'\rangle|^2$. The total vibrational intensity, $A_k{}^T$, may be decomposed into the harmonic and anharmonic contributions.

$$[3] \qquad A_k{}^T = A_k[0;\, v \rightarrow v'] + A_k[1;\, v \rightarrow v']$$

the second term being ignored in the harmonic approximation.

To evaluate the matrix element $\langle v|\mu|v'\rangle$ the dipole moment is usually expanded as a Taylor series of the normal coordinates Q_k

$$[4] \qquad \mu = \mu^0 + (\partial\mu/\partial Q_k)_{eq} Q_k + (1/2!)(\partial^2\mu/\partial Q_k{}^2)_{eq} Q_k{}^2 + (1/3!)(\partial^3\mu/\partial Q_k{}^3)_{eq} Q_k{}^3$$

The dipole moment as given by eq. [4] is assumed to be a scalar quantity, i.e., only its magnitude has been considered. In this way the total intensity of the ν_k fundamental band, $v = 0 \rightarrow v' = 1$, acquires anharmonicity through the second and third dipole moment derivatives. By combining eqs. [2]–[4] it is found that for the fundamental band:

$$[5] \qquad A_k[0;\, 0 \rightarrow 1] = K_a g_k |(\partial\mu/\partial Q_k)_{eq} \langle 0|Q_k|1\rangle|^2$$

$$[6] \qquad A_k[1;\, 0 \rightarrow 1] = K_a g_k \{|(\partial^3\mu/\partial Q_k{}^3)_{eq} \langle 0|Q_k{}^3|1\rangle|^2 + 2(\partial\mu/\partial Q_k)_{eq} (\partial^3\mu/\partial Q_k{}^3)_{eq} \langle 0|Q_k|1\rangle\langle 0|Q_k{}^3|1\rangle\}$$

and for the overtones

$$[7] \qquad A_k[1;\, 0 \rightarrow 2] = K_a g_k |(\partial^2\mu/\partial Q_k{}^2)_{eq} \langle 0|Q_k{}^2|2\rangle|^2$$

$$[8] \qquad A_k[1;\, 0 \rightarrow 3] = K_a g_k |(\partial^3\mu/\partial Q_k{}^3)_{eq} \langle 0|Q_k{}^3|3\rangle|^2$$

The nth dipole moment derivative with respect to the normal coordinate Q, $\partial^n\mu/\partial Q^n$, is denoted $P^n{}_Q$ and, analogously, the corresponding derivative in internal coordinates is $P^n{}_R$. The relationships between the dipole derivatives in normal (Q) and internal (R) coordinates are given by (27).

$$[9] \qquad P_Q = P_R \mathbf{L}$$

where the $\mathbf{L}$ matrix is found by solving the well-known secular equations (28)

$$[10] \qquad \mathbf{GFL} = \mathbf{L}\lambda$$

and the $\mathbf{L}$ matrix is normalized according to

$$[11] \qquad \mathbf{L}\mathbf{L}^+ = \mathbf{G}$$

Values for $P^2{}_Q$ and $P^3{}_Q$ are obtained by taking successively the derivatives of eq. [9].

The mechanical anharmonicity is usually taken into account by expanding the vibrational potential energy as a Taylor series around the equilibrium position R_e

$$[12] \qquad U(R) = U_e + (1/2!)(\partial^2 U/\partial R_e{}^2)(R—R_e)^2 + (1/3!)(\partial^3 U/\partial R_e{}^3)(R—R_e)^3 + (1/4!)(\partial^4 U/\partial R_e{}^4)(R—R_e)^4$$

The transformation between internal and normal coordinates ($\partial^n U/\partial R^n \rightarrow \partial^n U/\partial Q^n$) follows the same procedure as in the case of dipole moment derivatives.

The vibrational energy of the kth vibrational mode may be written as

$$[13] \qquad E_{vib} = \omega_e(v_k + 1/2) + \chi_{kk}(v_k + 1/2)^2 + \alpha_e(v_k + 1/2)J_k(J_k + 1)$$

and the rotational contribution is

$$[14] \qquad E_{rot} = B_e J_k(J_k + 1) - \bar{D}_e J_k{}^2(J_k + 1)^2$$

where ω_e is the harmonic frequency, χ_{kk} the anharmonicity constant, α_e the vibration–rotation coupling constant, B_e the equilibrium rotational constant, and $\bar{D}_e$ the centrifugal-distortion constant. v_k and J_k are the vibrational and rotational quantum numbers for the kth mode respectively. For reasons of simplicity higher terms have been omitted in eqs. [13] and [14]. By neglecting vibration–rotation interaction and off-diagonal terms the observed frequency of the fundamental band and the first and second overtones can be written as (14)

$$[15] \qquad \nu^{01}{}_k = \omega_{ek} + 2\chi_{kk}$$

$$[16] \qquad \nu^{02}{}_k = 2\omega_{ek} + 6\chi_{kk}$$

$$[17] \qquad \nu^{03}{}_k = 3\omega_{ek} + 12\chi_{kk}$$

The spectroscopic parameters χ_{kk}, α_e, B_e, and $\bar{D}_e$, were

TABLE 1. The root-mean-square residual, S_n, for the least-square one-dimensional Chebyshev polynomial fitting of the energy (E) and dipole moment (μ) *ab initio* points

	S_n					
	4-31G				6-31G**	
	C_1—H_1		C_2—H_2		C_1—H_1	
n	E	μ	E	μ	E	μ
1	0.01410625	0.17033833	0.01415857	0.17579102	0.00298557	0.07721598
2	0.01243239	0.02190708	0.01243984	0.02196962	0.00306234	0.00495202
3	0.0025468	0.00408360	0.00254730	0.00398768	0.00032967	0.00072372
4	0.00034182	0.00090365	0.00034199	0.00068698	0.00002285	0.00036646
5	0.00003990	0.00049783	0.00003992	0.00029776	0.00000137	0.00039330
6	0.00000363	0.00049756	0.00000362	0.00026761	0.00000004	0.00028394
7	0.00000044	0.00051170	0.00000042	0.00027160	0.00000005	0.00022788
8	0.00000010	0.00052492	0.00000011	0.00026423	0.00000004	0.00025805
9	0.00000009	0.00049931	0.00000010	0.00027498	0.00000003	0.00031576
10	0.00000007	0.00051975	0.00000010	0.00024471	0.00000003	0.00022409

	S_n					
	4-31G				6-31G**	
	N_2...H_1		N_3...H_2		N_2...H_1	
n	E	μ	E	μ	E	μ
1	0.00029306	0.05337754	0.00027895	0.05492377	0.00005288	0.02299550
2	0.00026227	0.00384804	0.00025946	0.00438933	0.00005489	0.00096201
3	0.00003946	0.00073169	0.00003924	0.00042606	0.00000469	0.00020657
4	0.00000330	0.00038764	0.00000330	0.00043837	0.00000023	0.00019421
5	0.00000013	0.00039511	0.00000017	0.00043600	0.00000004	0.00020842
6	0.00000007	0.00035549	0.00000007	0.00039264	0.00000004	0.00019856
7	0.00000006	0.00030531	0.00000008	0.00036767	0.00000004	0.00022019
8	0.00000006	0.00030623	0.00000007	0.00036146	0.00000005	0.00019301
9	0.00000006	0.00031150	0.00000008	0.00033019	0.00000006	0.00023472
10	0.00000004	0.00028705	0.00000006	0.00034055	0.00000008	0.00002252

Can. J. Chem. Downloaded from www.nrcresearchpress.com by 123.30.183.119 on 09/08/12
For personal use only.

evaluated with the relationships derived by Levine (29) using second-order perturbation theory.

The energy and dipole moment derivatives with respect to the internal coordinates, R, were obtained via a one-dimensional Chebyshev polynomial fitting to the *ab initio* points calculated with an 4-31G (30) and 6-31G** (31) basis sets.

$$[18] \qquad E(r) \text{ or } \mu(r) = \sum_{k=1}^{n+1}{}' a_{k-1}T_{k-1}(r)$$

where a_{k-1} is a numerical coefficient which is found in a least-square fitting procedure of eq. [18] and $T_{k-1}(r)$ is a Chebyshev polynomial of degree $k-1$ (32).

The stretching variables used in the fitting procedure are shown below.

$$N_1—C_1\overset{r_1}{—}H_1\overset{R_1}{\text{-----}}N_2—C_2\overset{r_2}{—}H_2\overset{R_2}{\text{-----}}N_3—C_3—H_3$$

Four individual fittings (r_1, r_2, R_1, R_2) have been done. In each case 21 points were used with a grid of 2 pm (1 pm = 10^{-2} Å), which has been shown to give very good fitting results (14). In the one-dimensional fitting procedure a stretching coordinate, r_i^j, was varied as follows: r_i^1, r_i^2, ..., r_i^{21}. For each r_i^j value all the other geometrical parameters were optimised. This approach assures that the stretching coordinate r_i is varied along a one-dimensional minimum energy path in a multidimensional potential energy surface (PES). The full configurational space $|R^N$ may be decomposed into the components N internal coordinates and so, the process of optimising the $N-1$ variables, allowing one single stretching variable to assume distinct values (r_i^1, r_i^2, ..., r_i^{21}), appears to be a natural way of dealing with a multivariable problem. Perhaps this will give a more realistic picture than just freezing the other $N-1$ geometrical parameters. The energy and dipole derivatives were then evaluated by taking the derivative of the least-square fitted eq. [18] with respect to r_1, r_2, R_1, R_2 stretching coordinates.

In evaluating the dipole moment matrix elements, $<o|Q_k^n|v>$, $n = 1, 2, 3$ and $v = 1, 2, 3$, the harmonic oscillator wave functions (Hermite polynomials) have been used, a procedure which has been encouraged earlier (33). Another approach in which the wave functions Ψ_v and $\Psi_{v'}$ are written as linear combinations of the unperturbed harmonic oscillator wave functions, $\Psi^0_{v''}$, with the expansion coefficients $C_{v,v''}$ and $C_{v',v''}$ determined via second-order perturbation theory has been used for the CO molecule (34). In that approach the expansion coefficients depend on the energy derivatives, $\partial^n E/\partial Q_k^n$, which introduces a dependence between electric and mechanical anharmonicities.

The influence of mechanical anharmonicity on the intensity

TABLE 2. Energy derivatives, $\partial^n E/\partial R^n{}_k = F_{(k)n}$, in mdyn/Å^{n-1}

$\partial^n E/\partial R^n{}_k$	This work 4-31G	This work 6-31G**	Previous work[a] (FMG) (4-31G)	Kofranek *et al.*[b] (CPF)	Expt.[c]
F_{11}	7.047	6.639 (7.16)[d]		6.214[f]	
F_{111}	−41.40	−39.39 (−43.9)[d]			
F_{1111}	210.7	194.5 (228)[d]			
F_{σ}	0.144	0.120	0.290	0.127[f]	0.11
$F_{\sigma\sigma}$	−0.658	−0.552	−1.332		
$F_{\sigma\sigma\sigma}$	2.099	1.966	4.836		
F'_{11}	7.051				
F'_{111}	−41.40				
F'_{1111}	210.8				
$F'_{\sigma\sigma}$	0.156				
$F'_{\sigma\sigma\sigma}$	−0.699				
$F'_{\sigma\sigma\sigma\sigma}$	2.170				

[a] One-dimensional Chebyshev fitting results, using the FMG approach, from ref. 14.
[b] See ref. 23.
[c] See ref. 21.
[d] 6-31G** polynomial fitted values for the HCN free monomer from ref. 14.
[e] $\overset{\nu_1}{N_1}—C_1—H_1\cdots\overset{\nu_\sigma}{N_2}—C_2—\overset{\nu'_1}{H_2}\cdots\overset{\nu'_\sigma}{N_3}—C_3—H_3$.
[f] Scaled values.

of fundamental and overtone bands for the linear HCN trimer has also been examined in the present study. The expressions for $R_{v,v'}$, evaluated over anharmonic wave functions, derived by Herman and Shuler (34) using second-order perturbation theory were employed. The relationships for the fundamental band, $R_{1,0}$, first-overtone, $R_{2,0}$, and second-overtone, $R_{3,0}$, are as follows:

$$[19a]\quad R_{1,0} = (1/\sqrt{2})(1 - 3g/2 + 11b^2/4)P_q + (1/\sqrt{2})(-5b + 88bg - 715b^3/12)P^2{}_q + (3/\sqrt{2})P^3{}_q$$

$$[19b]\quad R_{2,0} = \sqrt{2}(b/2 - 111bg/8 - 71b^3/48)P_q + (1/\sqrt{2})(1 - 15g/4 + 3b^2/8)P^2{}_q + OP^3{}_q$$

$$[19c]\quad R_{3,0} = \sqrt{3}(g/4 + 3b^2/8)P_q + (\sqrt{3}/2)(2b - 84bg + 6573b^3/144)P^2{}_q + (\sqrt{3}/2)P^3{}_q$$

with $b = K_3/\omega_e$ and $g = K_4/\omega_e$, where K_3 and K_4 are, respectively, the third and fourth energy derivatives with respect to the normal coordinates in units of cm^{-1} and ω_e the harmonic frequency in cm^{-1}. $P^n{}_q$ are the dipole moment derivatives with respect to the dimensionless normal coordinates q, according to the dipole expansion.

$$\mu = P^0{}_q + P_q q + P^2{}_q q^2 + P^3{}_q q^3 + \ldots .$$

q is defined as

$$q = \alpha^{1/2}(r - r_e)$$

with $\alpha = 4\pi^2\omega_e cm/h$ in Å^{-2}, where ω_e is the harmonic frequency, m the reduced mass, and π, c, h have their common known values. The $P^n{}_q$ can be obtained from the dipole derivatives with respect to internal coordinates, P_R, using the relationship

$$P^n{}_q = P^n{}_R/(\alpha^{n/2}n!)$$

and P_Q may also be evaluated through eq. [9].

The transition dipole moments for the fundamental band, first and second overtone neglecting mechanical anharmonicities,

TABLE 3. Dipole moment derivatives, $\partial^n\mu/\partial R^n{}_k = \mu_{(k)n}$, in D/Å^n. $k = 1$ and $k = \sigma$ stand for C—H and N...H stretching, respectively $\mu_{(k)n}$ and $\mu'_{(k)n}$ values correspond to the stretching vibrations defined in Table 2

$\partial^n\mu/\partial R^n{}_k$	This work 4-31G	This work 6-31G**	Previous work[a] (FMG) (4-31G)	Kofranek *et al.*[b] (CPF)
μ_1	3.282	2.956 (1.408)[c]		1.99
μ_{11}	7.054	6.383 (0.388)[c]		
μ_{111}	40.86	43.72 (2.445)[c]		
μ_{σ}	−1.068	−0.881	−1.846	−0.82
$\mu_{\sigma\sigma}$	1.270	1.226	2.767	
$\mu_{\sigma\sigma\sigma}$	−6.427	−6.745	−13.48	
μ'_1	3.397			
μ'_{11}	7.252			
μ'_{111}	40.28			
μ'_{σ}	−1.121			
$\mu'_{\sigma\sigma}$	1.616			
$\mu'_{\sigma\sigma\sigma}$	0.0			

[a] One-dimensional Chebyshev fitting results, using the FMG approach, from ref. 14.
[b] See ref. 23.
[c] 6-31G** polynomial fitted values for the HCN free monomer from ref. 14.

Can. J. Chem. Downloaded from www.nrcresearchpress.com by 123.30.183.119 on 09/08/12
For personal use only.

Can. J. Chem. Downloaded from www.nrcresearchpress.com by 123.30.183.119 on 09/08/12
For personal use only.

TABLE 4. Frequencies and mechanical anharmonic contributions for the fundamental band; stretching vibrations ν_l and ν'_l (C—H) and ν_σ and ν'_σ (N...H) are as specified in Table 2, ω's are the harmonic frequencies and the ν's the observed vibrational frequencies, all frequency terms are in units of cm^{-1}

	This work		FMG[a] results	Kofranek *et al.*[b]	4-31G[c]	Expt.[d]
	4-31G	6-31G**				
ω_l	3599	3494 (3627)[e] (3653)[f]		3532	3577	
ν_l	3489	3377 (3504)[e]				
ω_σ	135	123	191	154	172	119
ν_σ	129	118	186			
ω'_l	3601					
ν'_l	3491					
ω'_σ	140					
ν'_σ	135					
χ_{ll}	−63.03	−67.01 (−70.47)[e]				
$\chi_{\sigma\sigma}$	−3.138	−2.908	−2.871			
χ'_{ll}	−62.91					
$\chi'_{\sigma\sigma}$	−3.057					

[a]FMG fitting results using the 4-31G basis set.
[b]See ref. 23.
[c]See ref. 25.
[d]See ref. 21.
[e]6-31G** polynomial fitted value for the HCN monomer.
[f]6-31G** value for the HCN monomer unit evaluated using analytic second energy derivative from ref. 36.

TABLE 5. Intensities and electrical anharmonic contributions (A'_l [1; $0 \rightarrow 1$] and A'_σ [1; $0 \rightarrow 1$]) for the fundamental band; stretching vibrations ν_l and ν'_l (C—H) and ν_σ and ν'_σ (N...H) are as specified in Table 2, A_l, A_σ, A'_l, A'_σ, correspond to ν_l, ν_σ, ν'_l, ν'_σ; all intensity terms are in km mol^{-1}

	This work		FMG[a] results	Kofranek *et al.*[b]	4-31G[c]
	4-31G	6-31G**			
A_l [0; $0 \rightarrow 1$]	478	387 (70.8)[d]		649	840
A_σ [0; $0 \rightarrow 1$]	3.42	2.33	10.39	2.0	3.0
A'_l [0; $0 \rightarrow 1$]	512				
A'_σ [0; $0 \rightarrow 1$]	3.79				
A_l [1; $0 \rightarrow 1$]	30.7	30.5 (0.652)[d]			
A_σ [1; $0 \rightarrow 1$]	0.194	0.184	0.502		
A'_l [1; $0 \rightarrow 1$]	31.3				
A'_σ [1; $0 \rightarrow 1$]	0.0				

[a]FMG fitting results calculated with the 4-31G basis set.
[b]See ref. 23.
[c]See ref. 25.
[d]6-31G** polynomial fitted value for the HCN monomer.

i.e., $b = g = 0$, are respectively

$$[20a] \quad R^0{}_{1,0} = (1/\sqrt{2})P_q + (3/\sqrt{2})P^3{}_q$$

$$[20b] \quad R^0{}_{2,0} = (1/\sqrt{2})P^2{}_q$$

$$[20c] \quad R^0{}_{3,0} = (\sqrt{3}/2)P^3{}_q$$

The intensities of the normal modes, $A_{v,v'}$ and $A^0{}_{v,v'}$, are evaluated with the appropriate expression for the transition dipole moment, $R_{v,v'}$ and $R^0{}_{v,v'}$.

TABLE 6. Vibrational frequencies and intensities (electrical anharmonicities A_i [1; $0 \rightarrow v$]) of the overtones; the notation and units are as specified in Table 4, frequencies in cm^{-1} and intensities in km mol^{-1}

	This work		FMG[a] results
Overtones	4-31G	6-31G**	
ν_l [$0 \rightarrow 2$]	6837	6602 (6849)[b]	
ν_σ [$0 \rightarrow 2$]	251	229	366
ν'_l [$0 \rightarrow 2$]	6839		
ν'_σ [$0 \rightarrow 2$]	262		
A_l [1; $0 \rightarrow 2$]	11.0	9.21 (0.0272)[b]	
A_σ [1; $0 \rightarrow 2$]	0.0437	0.0445	0.1498
A'_l [1; $0 \rightarrow 2$]	11.6		
A'_σ [1; $0 \rightarrow 2$]	0.0683		
ν_l [$0 \rightarrow 3$]	10058	9694 (10054)[b]	
ν_σ [$0 \rightarrow 3$]	367	335	539
ν'_l [$0 \rightarrow 3$]	10063		
ν'_σ [$0 \rightarrow 3$]	384		
A_l [1; $0 \rightarrow 3$]	0.916	1.106 (0.00286)[b]	
A_σ [1; $0 \rightarrow 3$]	0.00505	0.00665	0.0114
A'_l [1; $0 \rightarrow 3$]	0.890		
A'_σ [1; $0 \rightarrow 3$]	0.0		

[a]FMG fitting results calculated with the 4-31G basis set.
[b]6-31G** polynomial fitted value for the HCN monomer.

TABLE 7. Equilibrium geometries, in pm (1 pm = 10^{-2} Å), rotational and vibrational–rotational terms, in cm^{-1}; the stretching modes are as specified in Table 2

Source	r_{CN1}	r_{CH1}	r_{NH1}	r_{CN2}	r_{CH2}	r_{NH2}	r_{CN3}	r_{CH3}
This work								
6-31G**	113.4	106.5	225.5	113.2	106.5	224.9	113.1	106.0
4-31G								
(FOG)[e]	114.1	105.9	205.5	113.9	106.0	205.2	113.8	105.2
4-31G								
(FMG)[a]	113.8	105.0	206.3	113.8	105.0	205.8	113.8	105.0

Source	B_e	B_0	$\alpha_e/10^{-3}$	$\bar{D}_e/10^{-6}$
This work[c]				
4-31G	0.015829	0.015833	−0.009	0.0009
This work[c]				
6-31G**	0.015295	0.015300	−0.009	0.0009
Previous work[d]	0.01592	0.01592	−0.006	0.0004
Expt.[b]		0.01565		0.0027

[a]FMG results from ref. 14.
[b]See ref. 21.
[c]Values reported for the ν_σ mode ($N_2...H_1$).
[d]See ref. 14.
[e]See ref. 25.

Due to the nature of the polynomial fitting used here, off-diagonal energy and dipole moment derivatives have been neglected. Certainly the inclusion of off-diagonal terms (like crossing energy/dipole derivatives and anharmonicity constants) will improve the values of the spectroscopic parameters calculated. However, it is believed that the gross features may be satisfactorily predicted by the diagonal terms alone (14, 16).

It is worth saying that the interaction between ν_1(XH) and ν_σ(HY), which is very much wanted by spectroscopists, cannot be obtained from a one-dimensional treatment. It involves the calculation of cross-derivatives of the type $\partial^n E/\partial XH^s \partial Hy^t$ and $\partial^n \mu/\partial XH^s \partial HY^t$ with $s + t = n$. This may be achieved by expanding the energy and dipole moment functions as a two-dimensional polynomial in XH and HY. Also, for the calculation of the frequency and intensity of the bending mode ν_β (X—H...Y bending angle) a three-dimensional polynomial in XH, HY, and β would be needed. The evaluation of these stretching/bending energy and dipole derivatives would enable the calculation of frequencies and intensities of overtones and combination bands for vibrational modes relevant to hydrogen-bonded complexes. The procedure reported in this article is being extended to accommodate two- and three-dimensional expansions.

Results and discussion

The quality of the fitting procedure can be assessed by the root-mean-square residual values, S_n (35), from Table 1. It is seen that the degree of fitting varies considerably for each stretching coordinate. The best value for n in eq. [18] is given below.

	4-32G				6-31G**	
	r_1	r_2	R_1	R_2	r_1	R_1
E n	6	6	4	4	5	4
μ n	4	4	3	2	3	3

Energy and dipole moment derivatives are reported in Tables 2 and 3 along with other theoretical and experimental results available. These derivatives were previously evaluated (14) by means of a one-dimensional Chebyshev polynomial fitting of the H-bonded stretching coordinate R, using the frozen monomer geometry approach (FMG). It is seen that the FMG fitted derivatives are noticeably exaggerated and the present results, using the fully optimised geometry approach (FOG), are in satisfactory agreement with the experimental values available as well as with the *ab initio* calculations reported by Kofranek *et al.* (23). It is also noted that the dipole derivatives for the proton-donor C—H mode in the HCN trimer are considerably larger than the respective values for the free monomer unit. This reflects the fact that the C—H modes in the hydrogen cyanide trimer probably acquire part of their high intensity through electrical anharmonicity. Furthermore, concerning the H-bonded stretching mode, it is found that geometry relaxation affects significantly both energy and dipole derivatives and, in this sense, the FMG approach is of little value.

Tables 4 and 5 contain frequencies and intensities of the fundamental bands along with mechanical and electrical anharmonic contributions. The harmonic frequencies calculated with the FOG polynomial-fitted derivatives compare well with the other results available, which supports the validity of the approach used here. The present intensities of the fundamental band appear to be satisfactorily represented. The deviations from the values reported by Kofranek *et al.* (23) including electron correlation at the CPF (Coupled Pair Functional approach) level can be attributed to the small basis set employed rather than the methodology applied here.

The electrical anharmonic contribution to the intensity of the fundamental band can be assessed by eq. [6]. It is found that the non-linear behaviour of the dipole moment function accounts for ~7% of the intensity of the C—H proton-donor mode and ~6% of the intensity of the N...H hydrogen-bonded fundamental stretching vibration.

Frequencies and intensities of overtones are in Table 6. There

Can. J. Chem. Downloaded from www.nrcresearchpress.com by 123.30.183.119 on 09/08/12
For personal use only.

Can. J. Chem. Downloaded from www.nrcresearchpress.com by 123.30.183.119 on 09/08/12
For personal use only.

TABLE 8. Intensity data $A^0_{v,v'}$ and $A_{v,v'}$ in units of km mol^{-1}, transition dipole moments $R^0_{v,v'}$ and $R_{v,v'}$ in D, for the proton-donor C—H mode of the linear hydrogen cyanide trimer, $R_{v,v'}$ and $A_{v,v'}$ are evaluated including both mechanical and electrical anharmonicities

	4-31G		6-31G**	
C—H mode	$A^0_{1,0}$	$A_{1,0}$	$A^0_{1,0}$	$A_{1,0}$
C_1—H_1	478	598 (509)[a]	387	499 (417)[a]
C_2—H_2	512	637 (543)[a]		

	4-31G		6-31G**	
C—H mode	$A^0_{2,0}$	$A_{2,0}$	$A^0_{2,0}$	$A_{2,0}$
C_1—H_1	11.0	1.68	9.21	1.42
C_2—H_2	11.6	1.74		

	4-31G		6-31G**	
C—H mode	$A^0_{3,0}$ (10^{-1})	$A_{3,0}$ (10^{-1})	$A^0_{3,0}$ (10^{-1})	$A_{3,0}$ (10^{-1})
C_1—H_1	9.16	8.20	11.1	9.79
C_2—H_2	8.90	8.00		

	4-31G		6-31G**	
C—H mode	$\lvert R^0_{1,0}\rvert$	$\lvert R_{1,0}\rvert$	$\lvert R^0_{1,0}\rvert$	$\lvert R_{1,0}\rvert$
C_1—H_1	0.234	0.261	0.214	0.243
C_2—H_2	0.242	0.270		

	4-31G		6-31G**	
C—H mode	$\lvert R^0_{2,0}\rvert$	$\lvert R_{2,0}\rvert$	$\lvert R^0_{2,0}\rvert$	$\lvert R_{2,0}\rvert$
C_1—H_1	0.0253	0.00990	0.0236	0.00925
C_2—H_2	0.0260	0.0101		

	4-31G		6-31G**	
C—H mode	$\lvert R^0_{3,0}\rvert$	$\lvert R_{3,0}\rvert$	$\lvert R^0_{3,0}\rvert$	$\lvert R_{3,0}\rvert$
C_1—H_1	0.00603	0.00570	0.00674	0.00635
C_2—H_2	0.00594	0.00563		

[a]Intensity evaluated by adding the electrical anharmonic term (A'_1 [1; 0→ 1]), from Table 5, to the harmonic term $A^0_{1,0}$.

TABLE 9. Intensity data $A^0_{v,v'}$ and $A_{v,v'}$ in units of km mol^{-1}, transition dipole moments $R^0_{v,v'}$ and $R_{v,v'}$ in D, for the H-bonded N...H mode of the linear hydrogen cyanide trimer, $R_{v,v'}$ and $A_{v,v'}$ are evaluated including both mechanical and electrical anharmonicities

	4-31G		6-31G**	
N...H mode	$A^0_{1,0}$	$A_{1,0}$	$A^0_{1,0}$	$A_{1,0}$
N_2...H_1	3.42	3.63 (3.61)[a]	2.33	2.52 (2.51)[a]
N_3...H_2	3.79	3.54		

	4-31G		6-31G**	
N...H mode	$A^0_{2,0}$ (10^{-2})	$A_{2,0}$ (10^{-2})	$A^0_{2,0}$ (10^{-2})	$A_{2,0}$ (10^{-2})
N_2...H_1	4.37	14.2	4.45	11.3
N_3...H_2	6.83	19.1		

	4-31G		6-31G**	
N...H mode	$A^0_{3,0}$ (10^{-3})	$A_{3,0}$ (10^{-3})	$A^0_{3,0}$ (10^{-3})	$A_{3,0}$ (10^{-3})
N_2...H_1	5.05	29.8	6.65	31.7
N_3...H_2	0.0	12.6		

	4-31G		6-31G**	
N...H mode	$\lvert R^0_{1,0}\rvert$	$\lvert R_{1,0}\rvert$	$\lvert R^0_{1,0}\rvert$	$\lvert R_{1,0}\rvert$
N_2...H_1	0.103	0.106	0.0887	0.924
N_3...H_2	0.106	0.102		

	4-31G		6-31G**	
N...H mode	$\lvert R^0_{2,0}\rvert$	$\lvert R_{2,0}\rvert$	$\lvert R^0_{2,0}\rvert$	$\lvert R_{2,0}\rvert$
N_2...H_1	0.00833	0.0150	0.00879	0.0140
N_3...H_2	0.0102	0.0170		

	4-31G		6-31G**	
N...H mode	$\lvert R^0_{3,0}\rvert$	$\lvert R_{3,0}\rvert$	$\lvert R^0_{3,0}\rvert$	$\lvert R_{3,0}\rvert$
N_2...H_1	0.00234	0.00569	0.00281	0.00614
N_3...H_2	0.0	0.00361		

[a]Intensity evaluated by adding the electrical anharmonic term (A'_σ [1; 0→ 1]), from Table 5, to the harmonic term $A^0_{\sigma,0}$.

are no experimental results available or other *ab initio* calculations reported, apart from ref. 14 for comparison. However, it is seen that the first overtone of the proton-donor C—H mode should be the most easily assigned in the spectra of the $(HCN)_3$ species.

Table 7 reports the equilibrium geometries and rotational and vibrational–rotational terms. The effect of geometry relaxation is clearly seen. The present spectroscopic constant values are in closer agreement with the experiment than the previous calculation using the FMG approach (14).

It has been pointed out earlier (ref. 1, Table 3, p. 63) that the χ_{11} values increase substantially upon H-bond complexation except for weakly bound species. The change in χ_{11}, $\Delta\chi_{11} = (\chi_{11})_{assoc} - (\chi_{11})_{free}$, predicted for the weakest species in ref. 13 was $\Delta\chi_{11} = -12$ cm^{-1}. In this study a value of $\Delta\chi_{11} = 3.5$ cm^{-1} is reported for $(HCN)_3$ using the anharmonic constant for the free HCN monomer unit, $(\chi_{11})_{free}$, calculated at the 6-31G** level.

Tables 8 and 9 report the effect of mechanical anharmonicity on the intensity of the C—H proton donor and N...H H-bonded modes. $A^0_{v,v'}$ is the intensity value neglecting the mechanical anharmonicity contribution and $A_{v,v'}$ the intensity evaluated with transition dipole moments given by eqs. [19*a*]–[19*c*], which include mechanical anharmonic terms. The transition dipole moment is a more useful quantity than the intensity itself, since the experimental spectroscopic studies in general report

values for $R_{v,v'}$. Unfortunately, there are no other values for the transition moments reported so far for comparison. The values from Tables 8 and 9 exhibit a quite regular pattern with the $R_{v,v'}$, values decreasing in the sequence of transitions: $v = 1 \rightarrow v' = 0$; $v = 2 \rightarrow v' = 0$; $v = 3 \rightarrow v' = 0$, as would be expected.

The effects of including mechanical anharmonicity, through second-order perturbation theory, in the calculation of intensities of fundamental and overtone bands are as follows. For the C—H mode the intensity of the $(1 \rightarrow 0)$ fundamental is increased by ~27%, the $(2 \rightarrow 0)$ overtone decreased by a factor of ~6, and the $(3 \rightarrow 0)$ decreased by ~10%. For the N...H hydrogen-bonded stretching mode the situation is quite different. The intensity of the $(1 \rightarrow 0)$ fundamental is increased by ~7%, the $(2 \rightarrow 0)$ overtone increased by a factor of ~3, and the $(3 \rightarrow 0)$ overtone increased by a factor of ~5. The values in Tables 8 and 9 quoted in parentheses correspond to the intensity of the fundamental band including electrical anharmonic contribution alone. It is seen that for the C—H mode the electrical anharmonicity accounts for ~7% of the increase of the intensity value while for the N...H mode the non-linear behaviour of the dipole moment function accounts for 7% of the intensity of the fundamental band (which is the same amount as obtained taking into account mechanical anharmonicity) and therefore, in this case, the mechanical anharmonic correction appears not to be important. It is opportune to say that the decrease in the C—H $(2 \rightarrow 0)$ overtone intensity with the inclusion of mechanical anharmonicity appears to be counterintuitive. However, this result may be understood as a consequence of the relative contribution of each term in eq. [19*b*].

From Tables 8 and 9 it can be seen that the effect due to mechanical anharmonicity on the intensity values is more pronounced for the overtone bands. Moreover, the enhancement of the intensity of fundamental and overtone bands for the C—H proton-donor mode upon complexation can be seen from Tables 5 and 6. The intensity of the $(1 \rightarrow 0)$, $(2 \rightarrow 0)$, and $(3 \rightarrow 0)$ vibrational transitions of the C—H stretching mode of the HCN subunit upon complexation is increased respectively by factors of ~5, ~339, and ~387, as calculated with the 6-31G** basis set.

The problem of using a small (less expensive) basis set has been addressed. It is seen from Tables 2 and 3 that the 6-31G** basis set (including polarization function in both first and second row atoms) generally yields lower values for the polynomial fitted derivatives than the split-valence 4-31G, and agreement with the CPF and experimental values reported previously is improved when polarization functions are added. Also, the 6-31G** frequencies and intensities of the fundamental and overtone bands are significantly lower than the corresponding 4-31G ones. If electron correlation is added a further decrease in the frequency and intensity values would be expected, as it has been extensively reported in the literature.

In the light of the gas-phase experimental results reported so far for H-bonded complexes it can be seen that the approach used here for the determination of anharmonic terms yields satisfactory results, although anharmonic experimental data are not yet available for the hydrogen cyanide H-bonded trimer for comparison. The difficulties encountered for the assigning of the experimental spectra of H-bonded complexes in the gas phase have already been emphasized by Sandorfy (1).

For the determination of frequency and intensity of combination bands as well as anharmonic coupling between ν_1 and ν_σ, which are very much sought after by experimentalists, crossed derivatives need to be introduced in eqs. [4] and [12], which imply that a two-dimensional polynomial fitting is required. In addition, the matrix element $<v|\mu|v'>$ will have a more complex form, with a large number of interaction terms. Therefore the use of linear combinations of the unperturbed harmonic oscillator wave functions determined via second-order perturbation theory appear not to be a straightforward approach.

Finally, it is worthwhile to say that a two-dimensional polynomial fitting to the $r_{X—H}$ and $R_{H...Y}$ stretching coordinates of the $(HCN)_2$ H-bonded dimer has been carried out (13), with frequencies and intensities of overtones and combination bands along with anharmonic coupling been reported.

Conclusions

A least-square polynomial fitting procedure has been applied for the determination of the energy and dipole moment derivatives with respect to the internal stretching coordinates of the linear hydrogen cyanide H-bonded trimer, using the 4-31G and 6-31G** basis sets, making possible the evaluation of the mechanical and electrical anharmonic terms. The validity of the FMG approach has been investigated and, in the case of electrical anharmonicity, geometry relaxation was shown to be important. The agreement with the few experimental and theoretical results available was satisfactory, giving confidence to the approach used here.

The effect of the mechanical anharmonicity on the intensity of fundamental and overtone bands has been investigated. It is found that the mechanical contribution to the intensity is more pronounced for the overtone bands. The calculations revealed that the inclusion of mechanical anharmonicity, through second-order perturbation theory, decreases the intensity of the C—H overtone and increases the intensity of the N...H overtone bands.

Mechanical and electrical anharmonicity are doubtless of fundamental importance for the understanding of the spectra of H-bonded complexes. With regard to the intensity of overtones and combination bands, there is a shortage of data still to be supplied and the results reported in this work will, hopefully, help fill the gaps in our present knowledge concerning the spectra of H-bonded clusters.

Acknowledgements

The author wishes to thank the Conselho Nacional the Desenvolvimento Cientifico e Tecnologico (CNPq) for support and the Universidade Federal de Minas Gerais (UFMG, Depto. de Quimica, ICEx, Pampulha, Belo Horizonte-MG-30161, Brazil) for a leave of absence.

1. C. SANDORFY. Top. Curr. Chem. **120**, 42 (1984).
2. C. SANDORFY. The hydrogen bond. Vols. 1–3. *Edited by* P. Schuster, G. Zundel, and C. Sandorfy. North-Holland, Amsterdam. 1976.
3. T. DI PAOLO, C. BOURDERON, and C. SANDORFY. Can. J. Chem. **50**, 3161 (1972).
4. G. DUROCHER and C. SANDORFY. J. Mol. Spectrosc. **15**, 22 (1965).
5. C. BOURDERON and C. SANDORFY. J. Chem. Phys. **59**, 2527 (1973).
6. C. BERTHOMIEU and C. SANDORFY. J. Mol. Spectrosc. **15**, 15 (1965).
7. J. W. BEVAN, B. MARTINEAU, and C. SANDORFY. Can. J. Chem. **57**, 1341 (1979).
8. E. L. WAGNER and D. F. HORNIG. J. Chem. Phys. **18**, 296 (1950).
9. R. C. PLUMB and D. F. HORNIG. J. Chem. Phys. **23**, 947 (1955).
10. R. D. WALDRON. J. Chem. Phys. **21**, 734 (1953).
11. A. CABANA and C. SANDORFY. Spectrochim. Acta, **18**, 843 (1962).

Can. J. Chem. Downloaded from www.nrcresearchpress.com by 123.30.183.119 on 09/08/12
For personal use only.

12. S. BRATOS, D. HADZI, and N. SHEPPERD. Spectrochim. Acta, **8**, 249 (1956).
13. W. B. DE ALMEIDA. To be published.
14. W. B. DE ALMEIDA and A. HINCHLIFFE. Theochem, **204**, 153 (1990).
15. W. B. DE ALMEIDA, J. S. CRAW, and A. HINCHLIFFE. Theochem, **200**, 19 (1989).
16. W. B. DE ALMEIDA, A. HINCHLIFFE, and J. S. CRAW. Theochem, **209**, 247 (1990).
17. B. WALSH, A. J. BARNES, S. SUZUKI, and W. J. ORVILLE-THOMAS. J. Mol. Spectrosc. **72**, 44 (1978).
18. G. A. HOPKINS, M. MARONCELLI, J. W. NIBLER, and T. R. DYKE. Chem. Phys. Lett. **114**, 97 (1985).
19. M. MARONCELLI, G. A. HOPKINS, J. W. NIBLER, and T. R. DYKE. J. Chem. Phys. **83**, 2129 (1985).
20. K. W. JUCKS and R. E. MILLER. J. Chem. Phys. **88**, 2196 (1988).
21. R. S. RUOFF, T. EMILSSON, T. D. KLOTS, C. CHUANG, and H. S. GUTOWSKY. J. Chem. Phys. **89**, 138 (1988).
22. M. KOFRANEK, A. KARPFEN, and H. LISCHKA. Chem. Phys. **113**, 53 (1987).
23. M. KOFRANEK, H. LISCHKA, and A. KARPFEN. Mol. Phys. **61**, 1519 (1987).
24. W. B. DE ALMEIDA and A. HINCHLIFFE. J. Mol. Struct. **198**, 17 (1989).
25. W. B. DE ALMEIDA, J. S. CRAW, and A. HINCHLIFFE. Theochem, **184**, 381 (1989).
26. B. L. CRAWFORD and H. L. DINSMORE. J. Chem. Phys. **18**, 983 (1950).
27. W. B. DE ALMEIDA, J. S. CRAW, and A. HINCLIFFE. J. Mol. Struct. **220**, 279 (1990).
28. E. B. WILSON, JR., J. C. DECIUS, and P. C. CROSS. Molecular vibrations. McGraw-Hill, New York. 1955.
29. I. LEVINE. Molecular spectroscopy. Wiley, New York. 1975.
30. R. DITCHFIELD, W. J. HEHRE, and J. A. POPLE. J. Chem. Phys. **54**. 724 (1971).
31. M. J. FRISCH, J. A. POPLE, and J. S. BINKLEY. J. Chem. Phys. **80**, 3265 (1984) and references therein.
32. The National Physical Laboratory. Notes on applied science, Modern computing methods. No. 16, Her Majesty's Stationery Office, London. 1961.
33. L. A. WOODWARD. Introduction to the theory of molecular vibrations and vibrational spectroscopy. Oxford University Press, Oxford. 1972.
34. R. C. HERMAN and K. E. SHULER. J. Chem. Phys. **22**, 481 (1954).
35. A. D. BUCKINGHAM. Numerical methods. Sir Isaac Pitman and Sons Ltd., London. 1962.
36. W. B. DE ALMEIDA. Chem. Phys. Lett. **166**, 589 (1990).

Can. J. Chem. Downloaded from www.nrcresearchpress.com by 123.30.183.119 on 09/08/12
For personal use only.

Effect of methyl substitution on the intramolecular triplet deactivation of *p*-methoxy-β-phenylpropiophenone[1]

R. Boch
Department of Chemistry, Ottawa–Carleton Chemistry Institute, University of Ottawa Campus, Ottawa, Ont., Canada K1N 6N5

C. Bohne and J. C. Netto-Ferreira[2]
Steacie Institute for Molecular Sciences, National Research Council, Ottawa, Ont., Canada K1A 0R6

and

J. C. Scaiano
Department of Chemistry, Ottawa–Carleton Chemistry Institute, University of Ottawa Campus, Ottawa, Ont., Canada K1N 6N5
and Steacie Institute for Molecular Sciences, National Research Council, Ottawa, Ont., Canada K1A 0R6

Received June 3, 1991

R. Boch, C. Bohne, J. C. Netto-Ferreira, and J. C. Scaiano. Can. J. Chem. **69**, 2053 (1991).

The photochemistry of several methyl-substituted *p*-methoxy-β-phenylpropiophenones (**1–5**) has been examined by nanosecond laser flash photolysis using 337-nm laser excitation. The ketone triplets decay by intramolecular β-aryl quenching of the carbonyl in a well-known process that is believed to involve charge transfer. Surprisingly, methyl substitution at the β-methylene group, which is not a participant in the deactiviation mechanism, causes a dramatic decrease in the triplet lifetime; the effect is attributed to different conformational preferences in ketones **1–3** and is rationalized on the basis of MMX calculations. Methyl substitution in the β-aryl ring affects the ease of oxidation of this ring and as a result induces changes in the kinetics for intramolecular charge transfer. This conclusion is further supported by electrochemical studies of ketones **1**, **4**, and **5**.

Key words: laser flash photolysis, triplet ketones, intramolecular quenching, charge transfer.

R. Boch, C. Bohne, J. C. Netto-Ferreira et J. C. Scaiano. Can. J. Chem. **69**, 2053 (1991).

Faisant appel à la photolyse éclair au niveau de la nanoseconde utilisant une excitation laser de 337 nm, on a étudié la photochimie de plusieurs *p*-méthoxy-β-phénylpropiophénones substituées par des groupes méthyles (**1–5**). Les triplets des cétones décroissent par un piégeage intramoléculaire du carbonyle par un β-aryle par un processus bien connu qui impliquerait une transfert de charge. Il est surprenant qu'une substitution par un méthyle sur le groupe méthylène en β qui ne participe pas au mécanisme de désactivation provoque une diminution dramatique du temps de vie du triplet; on attribue l'effect à des préférences conformationnelles différentes dans les cétones **1–3** et on les rationalise à l'aide de calculs MMX. Une substitution par un groupement méthyle sur le cycle β-aryle affecte la facilité avec laquelle on peut oxyder ce cycle et, par conséquence, induit des changements dans la cinétique du transfert de charge intramoléculaire. Cette conclusion est en accord avec les études électrochimiques des cétones **1**, **4** et **5**.

Mots clés : photolyse éclair utilisant une excitation laser, triplets des cétones, piégeage intramoléculaire, transfert de charge.
[Traduit par la rédaction]

Introduction

Triplet states of ketones having aryl rings in the β-position, such as *p*-methoxy-β-phenylpropiophenone (**1**), decay through an intramolecular deactivation process involving the β-phenyl ring (1–6). This internal quenching mechanism has been known for over 20 years and is believed to involve the conformation shown in Chart 1. There has been extensive work using these ketones in mobility studies (7–10), taking advantage of the measurable slower deactivation when geometrical constraints are imposed on the movement of the β-phenyl ring. The mechanism of deactivation is not completely understood but it is generally accepted to involve movement of the phenyl ring above the carbonyl oxygen followed by charge transfer quenching involving the carbonyl n,π^* triplet state (1–4, 6), which may either be the lowest state, or be thermally populated (as in the examples herein).

Preliminary experiments with **2** indicated that methyl substitution away from the reaction centre had dramatic effects on the triplet lifetime compared to the unsubstituted ketone (**1**).

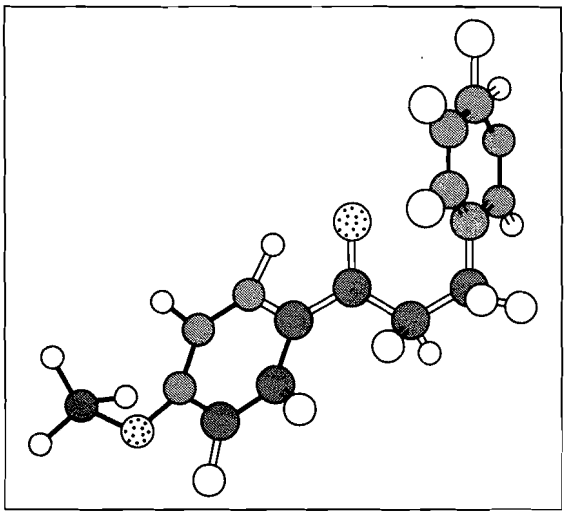


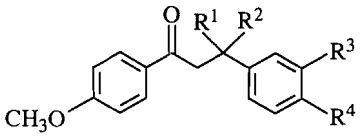
Chart 1

This observation prompted us to investigate various other methyl-substituted derivatives (**3–5**) in an attempt to understand the effects of methyl substitution on the triplet lifetimes. Substitutions were made either in the β-position or on the β-

[1]Issued as NRCC No. 32849.

[2]On leave from the Universidade Federal Rural do Rio de Janeiro, Itaguai, Rio de Janeiro, Brazil.

Can. J. Chem. Downloaded from www.nrcresearchpress.com by 123.30.183.119 on 09/07/12
For personal use only.



1: $R^1 = R^2 = R^3 = R^4 = H$
2: $R^1 = CH_3$; $R^2 = R^3 = R^4 = H$
3: $R^1 = R^2 = CH_3$; $R^3 = R^4 = H$
4: $R^1 = R^2 = R^4 = H$; $R^3 = CH_3$
5: $R^1 = R^2 = R^3 = H$; $R^4 = CH_3$

phenyl ring to explore the influence of steric and redox properties.

A previous study (6) using various ring-substituted β-arylpropiophenones indicated that triplet lifetimes were rather insensitive to substituent effects on the β-phenyl ring. The ketone triplets examined had short lifetimes (between 10 and 60 ns), which reflects their low-lying n,π^* triplet states. It is believed that movement of the β-phenyl ring into the correct orientation for quenching becomes the rate-determining step, rather than the dynamics for the charge transfer process (6). Thus, the corresponding analogs for **1**, **4**, and **5**, without the methoxy group, show essentially no differences in their triplet lifetimes (6). In constrast, compounds in the present study have β-phenyl ring substituents, but also contain a *p*-methoxy group on the chromophore side that serves to increase the triplet lifetime by leading to a low-lying π,π^* triplet state, thus facilitating readily observable substituent effects.

In this paper we report a combination of the results of photochemical studies employing laser flash photolysis techniques, electrochemical measurements, and molecular modelling calculations that, combined, allow us to rationalize the observed variations in triplet lifetimes.

Experimental

Materials

Solvents used for flash photolysis and synthesis (benzene, acetonitrile, cyclohexane, methanol) were obtained from BDH (Omnisolve, glass distilled) and were used without further purification.

Ketones **1** and **2** were prepared following a synthetic procedure (11) involving conversion of the corresponding carboxylic acids (from Aldrich) into the acid chlorides by reaction with thionyl chloride. After removal of excess thionyl chloride, a Friedel–Crafts reaction (11) was carried out on the acid chlorides using anisole (Aldrich). Removal of excess anisole under reduced pressure followed by recrystallization from ethanol gave the desired product. No *ortho*-substituted product — another possible product of the reaction — was observed.

Synthesis of ketone **3** involved the initial synthesis of neophyl chloride from 3-chloro-2-methylpropene (Aldrich) following a literature procedure (12). A standard Grignard reaction was then carried out, converting the neophyl chloride into its corresponding carboxylic acid (11). The remainder of the synthesis is the same as for ketones **1** and **2**. After removal of excess anisole, the crude yellow liquid was purified by TLC on a silica gel spinning plate (Chromatotron model 7924T).

Ketones **4** and **5** were synthesized from *p*-methoxyacetophenone and 3-methylbenzyl alcohol (for **4**) or 4-methylbenzyl alcohol (for **5**) by the method of Pratt and Evans (13).

p-*Methoxy*-β-*phenylpropiophenone* (*1*): mp 95–97°C; IR (KBr): 1669 cm^{-1}; ^1H NMR ($CDCl_3$) δ (ppm): 2.9–3.1 (t, 2H), 3.1–3.3 (t, 2H), 3.8 (s, 3H), 6.9 (d, 2H), 7.1–7.4 (m, 5H), 7.9 (d, 2H); ^{13}C NMR ($CDCl_3$) δ: 30.35 (CH_2), 40.16 (CH_2), 55.49 (CH_3), 113.74 (CH), 126.11 (CH), 128.45 (CH), 128.53 (CH), 129.94 (C), 130.32 (CH), 141.48 (C), 163.44 (C), 197.80 (CO); MS *m/z* (%): 240 (23, M^+), 136 (7), 135 (100), 107 (7), 92 (11), 77 (20).

p-*Methoxy*-β-*phenylbutyrophenone* (*2*): mp 86.5–87°C; IR (KBr): 1668 cm^{-1}; ^1H NMR ($CDCl_3$) δ (ppm): 1.3 (d, 3H), 3.0–3.3 (m, 2H), 3.4–3.6 (q, 1H), 3.9 (s, 3H), 6.9 (d, 2H), 7.1–7.4 (m, 5H), 7.9 (d, 2H); ^{13}C NMR ($CDCl_3$) δ: 21.64 (CH_3), 35.55 (CH), 46.51 (CH_2), 55.31 (CH_3), 113.67 (CH), 126.25 (CH), 126.89 (CH), 128.53 (CH), 128.71 (C), 130.39 (CH), 146.80 (C), 163.49 (C), 197.82 (CO); MS *m/z* (%): 254 (28, M^+), 239 (25), 150 (29), 135 (100), 105 (10), 92 (10), 77 (23).

p-*Methoxy-3,3-methyl-3-phenylpropiophenone* (*3*): IR (neat): 1674 cm^{-1}; ^1H NMR ($CDCl_3$) δ (ppm): 1.5 (s, 6H), 3.2 (s, 2H), 3.8 (s, 3H), 6.8 (d, 2H), 7.1–7.4 (m, 5H), 7.8 (d, 2H); ^{13}C NMR ($CDCl_3$) δ: 28.95 (CH_3), 37.39 (CC), 50.35 (CH_2), 55.29 (CH_3), 113.49 (CH), 125.49 (CH), 125.78 (CH), 128.20 (CH), 130.44 (CH), 131.27 (C), 149.18 (C), 163.26 (C), 197.75 (CO); MS *m/z* (%): 268 (4, M^+), 150 (100), 135 (92), 119 (24), 91 (24), 77 (24).

p-*Methoxy-(3′-methyl)-3-phenylpropiophenone* (*4*): mp 46–47°C; IR (KBr): 1669 cm^{-1}; ^1H NMR ($CDCl_3$) δ (ppm): 2.3 (s, 3H), 2.9–3.1 (t, 2H), 3.1–3.3 (t, 2H), 3.8 (s, 3H), 6.8–7.2 (m, 6H), 7.9 (d, 2H); ^{13}C NMR ($CDCl_3$) δ: 21.46 (CH_3), 30.26 (CH_2), 40.22 (CH_2), 55.46 (CH_3), 113.71 (CH), 125.41 (CH), 126.84 (CH), 128.43 (CH), 129.26 (CH), 130.31 (CH), 129.94 (C), 138.07 (C), 141.42 (C), 163.41 (C), 197.85 (CO); MS *m/z* (%): 254 (25, M^+), 135 (100), 77 (17).

p-*Methoxy-(4′-methyl)-3-phenylpropiophenone* (*5*): mp 64–66°C; IR (KBr): 1669 cm^{-1}; ^1H NMR ($CDCl_3$) δ (ppm): 2.3 (s, 3H), 2.9–3.1 (t, 2H), 3.1–3.3 (t, 2H), 3.8 (s, 3H), 6.9 (d, 2H), 7.0–7.3 (m, 4H), 7.9 (d, 2H); ^{13}C NMR ($CDCl_3$) δ: 21.0 (CH_3), 29.90 (CH_2), 40.29 (CH_2), 55.45 (CH_3), 113.69 (CH), 128.29 (CH), 129.17 (CH), 130.30 (CH), 129.95 (C), 135.55 (C), 138.35 (C), 163.39 (C), 197.85 (CO); MS *m/z* (%): 254 (25, M^+), 135 (100), 77 (18).

Laser flash photolysis

The samples, contained in 3 × 7 mm^2 Suprasil quartz cuvettes, were excited by pulses (337 nm; <10 mJ; ~8 ns) from a Molectron UV-24 nitrogen laser. Transient signals, initially acquired by a R-7912 Tektronix transient digitizer, were processed by a PDP-11/23+ computer, which also controlled the experiment and provided suitable storage and hardcopy facilities. Further details have been given elsewhere (14, 15).

Molecular modelling calculations

These calculations were carried out using a molecular modelling software program (PCMODEL version 4 from Serena Software) for the Macintosh II series of computers. The force field used is called MMX and is derived from the MM2 force field and MMP1 pi-VESCF routine of Allinger (16). A dihedral driver was utilized for the rotation of bonds and calculation of energies.

Cyclic voltammetry

Cyclic voltammograms were generated using an air-tight cell under nitrogen atmosphere and a Bioanalytical Systems CV-1B voltammograph instrument utilizing both platinum working (1 mm disk) and auxiliary electrodes and a silver/silver nitrate (0.1 M) reference electrode. Voltammograms were recorded on a calibrated Hewlett Packard X–Y recorder. The solutions for study consisted of 50 mL purified acetonitrile (passed through an activated alumina column), tetrabutylammonium perchlorate (1.71 g, 0.1 M) recrystallized 3 times from 90% ethyl acetate/10% hexane, and a mass of analyte equalling 1 mM. The solutions were degassed with nitrogen prior to the measurements. A standard solution of sublimed ferrocene gave a reversible signal with a potential of 0.05 V.

Results

Triplet lifetimes were determined at room temperature, employing laser flash photolysis techniques, as mentioned above. The decays showed clean monoexponential behavior, although a small amount of residual absorption was frequently observed following the completion of the triplet decay. Figure 1 shows a representative transient spectrum for **2** and a decay trace for the triplet monitored at 400 nm. The triplet spectra were virtually identical regardless of methyl substitution in the β-phenyl ring or in the methylene chain, and agree well with literature spectra for ketones with the *p*-methoxybenzoyl chro-

Can. J. Chem. Downloaded from www.nrcresearchpress.com by 123.30.183.119 on 09/07/12
For personal use only.

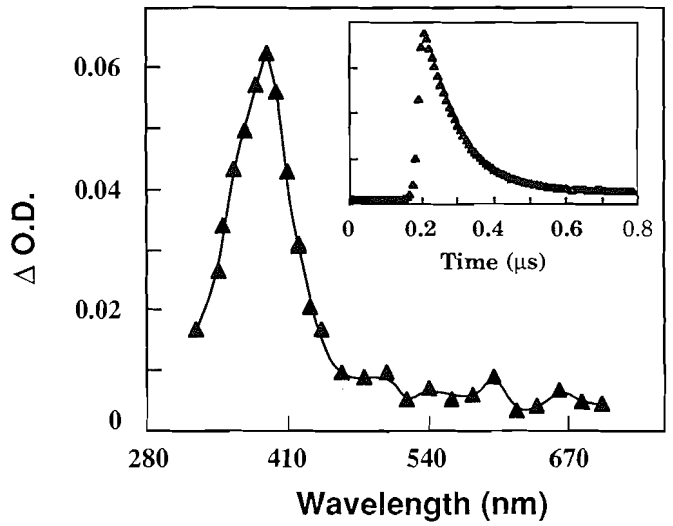


FIG. 1. Triplet–triplet absorption spectrum for **2** in methanol at room temperature monitored 20 ns after the laser pulse. *Inset*: Decay trace for **2** monitored at 400 nm following 337-nm laser excitation.

TABLE 1. Kinetic data for the decay of ketone triplets at room temperature[a]

	Lifetime[b] in nanoseconds in		
Ketone	Methanol	Acetonitrile	Benzene
1	239	50	
2	95	19	18
3	10		
4	151	29	28
5	31	9	12

[a]All decay traces monitored at 400 nm.
[b]Typical errors are about 5% for lifetimes of 50 ns or longer and ca. 10% for the shorter values.

mophore (6, 17). The triplet lifetimes recorded for ketones **1**–**5** are given in Table 1. The introduction of methyl groups in the β-position in ketones **2** and **3** had dramatic effects on the triplet lifetimes compared to the unsubstituted ketone **1**. We reasoned that since the mechanism of deactivation involves the interaction of the β-phenyl ring with the carbonyl oxygen, the introduction of methyl substituents may have induced changes in conformation and (or) the ring's freedom of movement. We note that since ketones **2** and **3** have γ-hydrogens, they can undergo the Norrish Type II reaction; Wagner *et al.* (2) showed that this process occurs with very low quantum yields in β-phenylbutyrophenone, thus supporting that the lifetimes are determined by β-phenyl quenching, and not chemical reactions.

Methyl substitutions in the *meta* and especially *para* positions on the β-phenyl ring also shorten the triplet lifetime (see Table 1). Shorter lifetimes could be the result of changes in the oxidation potential of the ring through methyl substitution, thereby facilitating easier transfer of electrons to the carbonyl n,π^* triplet during charge transfer. Electrochemical measurements (*vide infra*) were carried out in order to address this question.

While our studies center on methanol as solvent, a few exploratory measurements in acetonitrile and benzene (see Table 1) clearly suggest that our observations are quite general. The shorter lifetimes in non-hydroxylic solvents are believed to be due to entropic restrictions in hydroxylic media and have been discussed elsewhere (6).

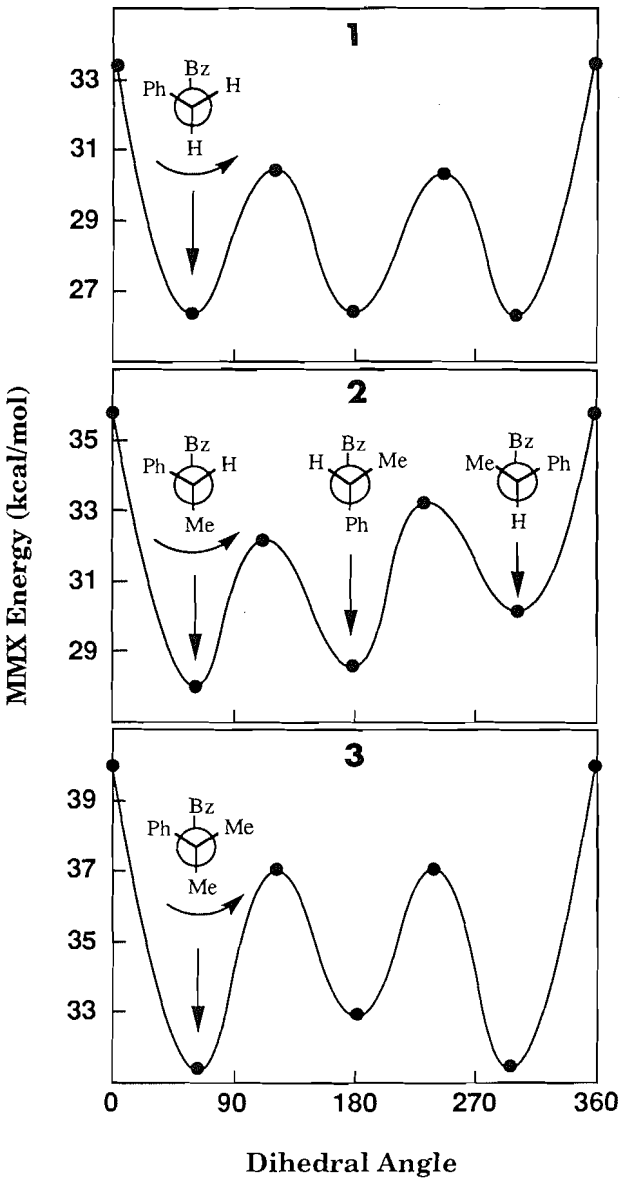


FIG. 2. Energy barriers calculated for key conformations using MMX (absolute MMX energies for different compounds are not comparable; only energy barriers can be compared). The energies were obtained by fixing the dihedral angle but minimizing the rest of the structure. "Bz" represents the *p*-methoxybenzoyl group; note that these are ground state structures.

Molecular mechanics calculations

In an attempt to understand the differences in triplet lifetimes (see Table 1), molecular mechanics calculations were performed using PCMODEL software to estimate the effects of conformational and steric factors of methyl substitution in the β-position. Dihedral drivers were used in which minimizations were performed for angle increments around 3° on ketones **1**–**3** for rotation about bond **b** as shown in the structure below. At the minimum and maximum energies the dihedral angle was fixed and the structure was reminimized; these positions were always very close (±2°) to the multiples of 60°. Figure 2 shows the results of these calculations. For example, ketone **1** has three lowest energy conformers having dihedral angles of about 60°, 180°, and 300° with respect to the car-

Can. J. Chem. Downloaded from www.nrcresearchpress.com by 123.30.183.119 on 09/07/12
For personal use only.

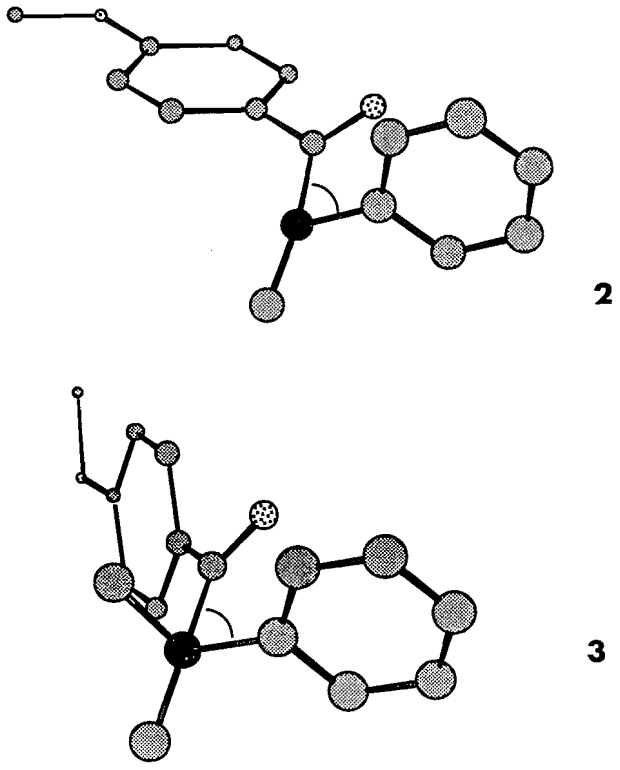
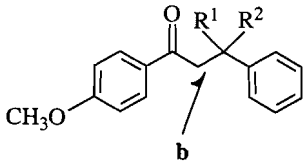


FIG. 3. Minimum energy conformations for **2** and **3** obtained using MMX calculations. Note that these are ground state structures. The solid black center displays two overlapping carbon atoms (as in a Newman projection) and the arc shows the angle displayed in Fig. 2.

bonyl group, each having approximately equal energies (180° being slightly higher). For ketone **2** the lowest energy conformer has a dihedral angle of about 60°. The preferred position of the deactivating phenyl ring in **2** now lies closer to the carbonyl (Fig. 3); this explains the reduction in lifetime between ketones **1** and **2**. For ketone **3**, the situation is quite similar; the β-phenyl ring now prefers to lie at either a 60° or 300° angle with respect to the carbonyl group. Combined with these conformational effects, increased methyl substitution in the β-position raises energy barriers of rotation, thus hindering movement of the phenyl group away from the carbonyl. Our calculations also suggested that in the case of **3** the distance



1–3

between the carbonyl oxygen and the ring (as measured by the distance to the *ortho*-carbons) was smaller than for **2**. However, it was clear that small changes in the position or tilt of the β-phenyl ring are not predicted very accurately at this level of calculation and any argument based on variations in this distance would be highly speculative.

Cyclic voltammetry

The electrochemistry of ketones **1**, **4**, and **5** was investigated in an attempt to establish to what degree different methyl substitutions on the phenyl ring can affect its electron-donating character. The oxidative properties of aromatic rings can be

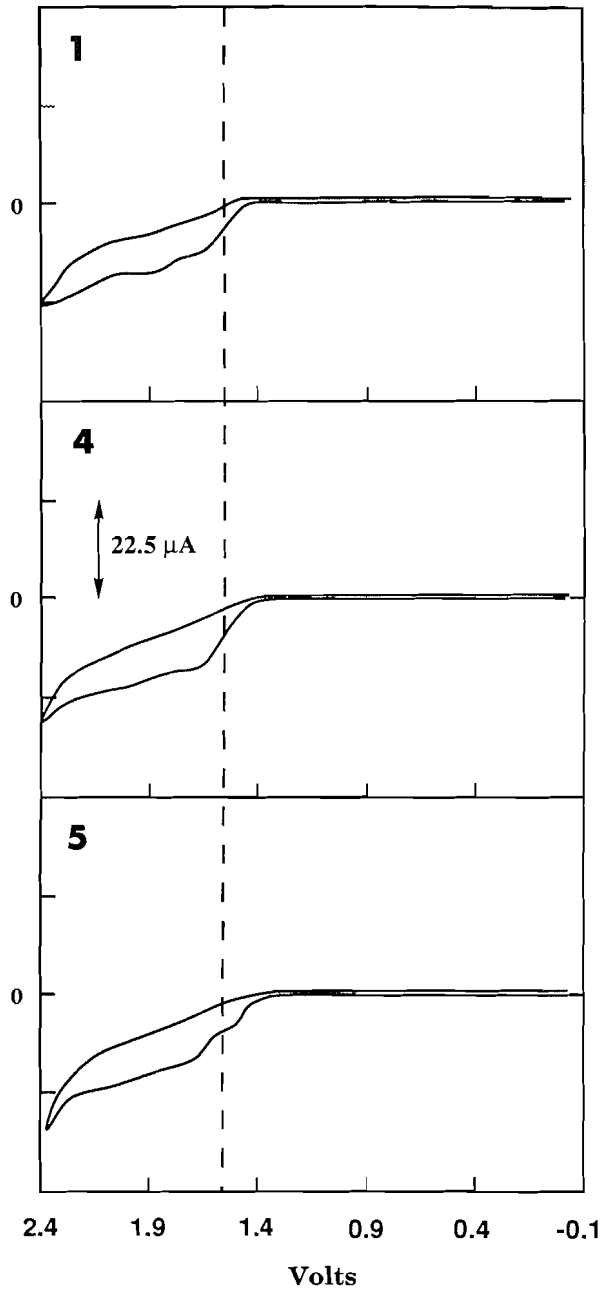


FIG. 4. Irreversible cyclic voltammograms of **1**, **4**, and **5** (the dashed line was added to facilitate comparison).

substantially altered by methyl substitution. In a related piece of work, differences in standard oxidation potentials for various alkylbenzene derivatives were reported by Kochi and coworkers (18), who recorded voltammograms under acid conditions with very fast scan rates and used microvoltammetric electrodes to measure the reversible reduction of the arene cation radicals. In our work, a more traditional cyclic voltammetry setup was sufficient since only relative irreversible oxidation voltammograms are adequate for our analysis.

Ketone **1**, **4**, and **5** all gave irreversible oxidative cyclic voltammograms, as expected. Representative voltammograms are shown in Fig. 4. For ketone **5**, which had the shortest triplet lifetime, the onset of oxidation was at a lower potential than for **1** or **4**. The same trend of oxidation potentials is also observed when comparing toluene to *m*- and *p*-xylene

Can. J. Chem. Downloaded from www.nrcresearchpress.com by 123.30.183.119 on 09/07/12
For personal use only.

Can. J. Chem. Downloaded from www.nrcresearchpress.com by 123.30.183.119 on 09/07/12
For personal use only.

(18). This lower potential is thought to be due to the *para*-substituted β-phenyl ring. Conclusions about oxidation potential differences concerning the β-phenyl ring for ketones **1** and **4** could not be easily drawn since the *p*-methoxyacetophenone moiety is oxidized at roughly the same potential as the β-phenyl ring, causing overlap of the signals. The faster onset of oxidation of ketone **5** suggests that the β-aryl ring is a better electron donor, thus resulting in the shorter triplet lifetime.

Discussion

It is well established that the mechanism for intramolecular β-aryl quenching of carbonyl triplets, like the Norrish Type I and II reactions (19), requires n,π^* triplet character (6) and adequate mobility so that the conformation for quenching can be achieved (see Chart 1). Conformational restrictions, imposed either by changes in the molecular structure (4), or by media (e.g., by inclusion in zeolite channels (7) or cyclodextrins (9, 10)) can lead to significant increases in triplet lifetime. All the ketones examined in this work have low-lying π,π^* triplets as a result of *p*-methoxy substitution of the benzoyl chromophore; this leads to triplet lifetimes that are sufficiently long to be amenable for study by nanosecond laser photolysis techniques. In addition, the lifetimes are sufficiently long that conformational and electronic factors can now lead to variations in these lifetimes. In contrast, in the case of β-phenylpropiophenone derivatives with no substitute on the benzoyl chromophore, the lifetimes are very short and are predominantly controlled by bond rotation (6).

Our initial work with **2** was motivated by our interest in systems with asymmetric centers. We were initially surprised by the unexpected shortening of the triplet lifetime upon introduction of a methyl group in the methylene chain. With hindsight we rationalize these results on the basis of conformational preferences. We note that earlier work comparing the lifetimes of β-phenylpropiophenones and α-phenoxyacetophenones also led to the conclusion that steric interactions involving the linkage between the chromophore and quencher can play a crucial role in determining the triplet lifetime (20, 21). Similarly, when the α- or β-carbon atoms in the linkage are part of a small ring system the triplet lifetimes are also increased significantly (4). In addition, conformational constraints imposed by substitution at the α-carbon of β-arylpropiophenones lead to reactivity differences towards triplet state intramolecular ϵ-hydrogen abstraction, which were interpreted as resulting from preferential population of the conformations necessary for reaction (22).

Our present studies reflect two distinct types of effects. In the case of compounds **1**, **2**, and **3**, the effects are of a conformational nature, since neither the properties of the chromophore nor those of the deactivating ring should be significantly affected by methyl substitution on the $-CH_2CH_2-$ link. Figures 2 and 3 show the results of MMX calculations, which even at this rather basic level illustrate the conformational preferences of these molecules. For ketone **1**, there are three preferred conformations with essentially the same predicted energy, whereas in the case of **2**, our MMX calculations indicate that the preferred conformation (see Figs. 2 and 3) places the β-phenyl ring at ~60° with respect to the carbonyl chromophore. The case of **3** is similar; now there are two energetically equivalent lowest energy conformations at 60° and 300°, increasing the probability of finding the β-phenyl ring close to the carbonyl. Besides analysing the preferred lowest energy conformations, one also has to take into account the energy barriers to approaching an eclipsed conformation. In a first approximation we assume that a fully eclipsed conformation (corresponding to the vertical axis in Fig. 2) between the β-phenyl and the carbonyl groups is required for quenching. The probability of obtaining the conformation required for quenching is a function of the energy barrier to obtain this eclipsed conformation but is also a function of the barriers observed for the other substituents. An increase of the rotational energy barrier required to move away from the preferred conformation is observed when substituting the β-hydrogens for methyl groups; this increase leads to a higher probability of the β-phenyl ring remaining close to the eclipsed conformation necessary for quenching. Clearly, not only are the chromophore and quencher closer in the case of **2** and **3**, but also the energy barriers predict easier quenching for these compounds, as observed.

It is generally believed that the mechanism for β-aryl quenching involves charge transfer from the quencher group to the excited carbonyl. Not surprisingly, in systems with low-lying π,π^* states quenching involves the more electrophilic and thermally populated n,π^* state (6). We reasoned that methyl substitution at the β-aryl ring should make oxidation easier and therefore result in a reduction of the triplet lifetimes. This prediction proved correct, as shown by the lifetimes for **4** and **5** given in Table 1. Cyclic voltammograms (see Fig. 4) also confirm this expectation, the largest effect on both the lifetime and the oxidation potential being induced by *para*-methyl substitution. It is interesting that, in the case of **5**, *p*-methyl substitutions essentially reverse the kinetic effect due to the low-lying π,π^* triplet in the *p*-methoxybenzoyl chromophore (compare the data in Table 1 with the unsubstituted substrate (6)); it is possible that, in the case of **5**, rotational control may play a role in determining the lifetime.

In conclusion, laser photolysis studies of the triplet states of **1–5** demonstrated the importance of conformational and redox properties in determining the kinetics for intramolecular charge transfer quenching in these molecules. The effects of substitution in the $-CH_2CH_2-$ link are quite dramatic but readily explained by MMX molecular modelling calculations. The results also confirm the earlier proposal (6) that in the absence of the *p*-methoxy substituent the lifetimes are too short to be amenable for direct study with nanosecond techniques and are largely controlled by bond rotation; this tends to mask other effects that are readily observable in the series studied herein.

Acknowledgements

Thanks are due to Dr. D. D. M. Wayner and Professor P. Wilde for their valuable advice in electrochemistry and to Mr. S. E. Sugamori and G. Charette for technical assistance. This work was supported by an operating grant (J.C.S.) from the Natural Sciences and Engineering Research Council of Canada.

1. D. G. WHITTEN and W. E. PUNCH. Mol. Photochem. **2**, 77 (1970).
2. P. J. WAGNER, P. A. KELSO, A. E. KEMPPAINEN, A. HAUG, and D. R. GRABER. Mol. Photochem. **2**, 81 (1970).
3. F. R. STERMITZ, D. E. NICODEM, V. P. MURALIDHARAN, and C. D. O'CONNELL. Mol. Photochem. **2**, 87 (1970).
4. J. C. SCAIANO, M. J. PERKINS, J. W. SHEPPARD, M. S. PLATZ, and R. L. BARCUS. J. Photochem. **21**, 137 (1983).
5. T. WISMONTSKI KNITTEL and T. KILP. J. Phys. Chem. **88**, 110 (1984).

6. J. C. NETTO-FERREIRA, W. J. LEIGH, and J. C. SCAIANO. J. Am. Chem. Soc. **107**, 2617 (1985).
7. J. C. SCAIANO, H. L. CASAL, and J. C. NETTO-FERREIRA. ACS Symp. Ser. **278**, 211 (1985).
8. W. J. LEIGH. J. Am. Chem. Soc. **107**, 6114 (1985).
9. H. L. CASAL. J. C. NETTO-FERREIRA, and J. C. SCAIANO. J. Inclusion Phenom. **3**, 395 (1985).
10. J. C. NETTO-FERREIRA and J. C. SCAIANO. J. Photochem. Photobiol. **45A**, 109 (1988).
11. A. VOGEL. Textbook of practical organic chemistry including qualitative organic analysis. Longman Group Limited, Essex. 1978.
12. F. C. WHITMORE, C. A. WEISBERGER, and A. C. STTABICA. J. Am. Chem. Soc. **65**, 1469 (1943).
13. E. F. PRATT and A. P. EVANS. J. Am. Chem. Soc. **78**, 4950 (1956).
14. J. C. SCAIANO. J. Am. Chem. Soc. **102**, 7747 (1980).
15. J. C. SCAIANO. M. TANNER, and D. WEIR. J. Am. Chem. Soc. **107**, 4396 (1985).
16. PCMODEL. Molecular Modelling Software, Serena Software, Bloomington, IN. 1990.
17. J. C. NETTO-FERREIRA and J. C. SCAIANO. Tetrahedron Lett. **30**, 443 (1989).
18. J. O. HOWELL, J. M. GONCALVES, C. AMATORE, L. KLASINC, R. M. WRIGHTMAN, and J. K. KOCHI. J. Am. Chem. Soc. **106**, 3968 (1984).
19. M. V. ENCINA, E. A. LISSI, E. LEMP, A. ZANOCCO, and J. C. SCAIANO. J. Am. Chem. Soc. **105**, 1856 (1983).
20. J. C. SCAIANO and J. C. NETTO-FERREIRA. J. Photochem. **32**, 253 (1986).
21. J. C. NETTO-FERREIRA, I. G. J. AVELLAR, and J. C. SCAIANO. J. Org. Chem. **55**, 89 (1990).
22. B. ZHOU and P. J. WAGNER. J. Am. Chem. Soc. **111**, 6796 (1989).

Can. J. Chem. Downloaded from www.nrcresearchpress.com by 123.30.183.119 on 09/07/12
For personal use only.

Alkylation of α-*tert*-butoxycarbonylamino ketone enolate anions. A useful synthesis of α-alkyl-α-amino ketones, 2-acylpyrrolidines, and 2-acylpiperidines[1]

ANGEL GUZMAN AND CLARA QUINTERO[2]
Syntex, S.A. de C.V., Division de Investigacion, Apartado Postal 10-820, Mexico 10, D.F., Mexico

AND

JOSEPH M. MUCHOWSKI[3]
Syntex Research, Institute of Organic Chemistry, 3401 Hillview Ave., Palo Alto, CA 94304, U.S.A.

Received April 2, 1991

ANGEL GUZMAN, CLARA QUINTERO, and JOSEPH M. MUCHOWSKI. Can. J. Chem. **69**, 2059 (1991).

A versatile synthesis of α-alkyl-α-amino ketones **5** and cyclic α-amino ketones **7** based on the selective mono-α-alkylation and $C(\alpha),N$-cycloalkylation of α-*tert*-butoxycarbonylamino ketones **2** and subsequent acidic hydrolysis is described.

Key words: α-*tert*-butoxycarbonylamino ketones, α-alkyl-α-amino ketones, 2-acylpyrrolidines, and 2-acylpiperidines.

ANGEL GUZMAN, CLARA QUINTERO et JOSEPH M. MUCHOWSKI. Can. J. Chem. **69**, 2059 (1991).

On décrit une synthèse versatile des α-alkyl-α-amino cétones de type **5** et des α-amino cétones cycliques de type **7**; ces synthèses sont basées sur la mono-α-alkylation sélective et la $C(\alpha),N$-cycloalkylation des α-*tert*-butoxycarbonylamino cétones de type **2**, suivie d'une hydrolyse acide subséquente.

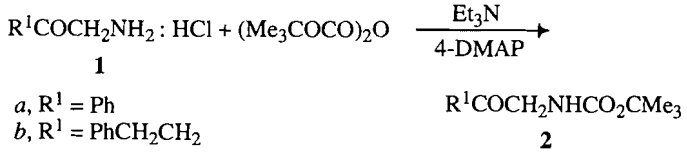
Mots clés : α-*tert*-butoxycarbonylamino cétones, α-alkyl-α-amino cétones, 2-acylpyrrolidines et 2-acylpipéridines.

[Traduit par la rédaction]

α-Amino ketones and the protected versions thereof are widely utilized as precursors of heterocyclic systems, ethanolamine derivatives of physiological interest, and peptidic natural products and congeners thereof. Numerous syntheses of these important starting materials have been devised (1) and new developments in this field continue apace (2–8). We recently demonstrated (9) that the monoanions of *N*-formylated α-amino ketones, like those of benzamidoacetone (10), are regioselectively alkylated on the α-carbon atom and that acidic hydrolysis of these products provided access to α-alkyl-α-amino ketones with satisfactory efficiency. A particular advantage of this process is that one substrate can serve as the progenitor of many new α-alkyl-α-amino ketones. This desirable characteristic is also found in the generation of such compounds based on the reaction of alkyl Grignard or alkyllithium reagents with N-protected α-amino acids (11–14) or with N-protected *O*,*N*-dialkyl-α-amino acid hydroxamates (15, 16) but is absent in many previously reported syntheses (e.g., see ref. 1 pp. 420–422, 431–432, 440–441, and 467). This paper describes studies on the mono- and dialkylation of α-*tert*-butoxycarbonylamino ketones, which show that they are also very useful substrates for the preparation of a variety of substituted α-amino ketone derivatives.

The *N*-*tert*-Boc-α-amino ketones **2** were prepared (Scheme 1) from the α-amino ketone hydrochlorides **1** and di-*tert*-butyl dicarbonate in the presence of a slight excess of triethylamine containing a catalytic amount of 4-dimethylaminopyridine.

As expected from the previous study with α-formamido ketones (9), reaction of **2** with an equivalent of sodium hydride in anhydrous dimethylformamide (DMF) generated the presumably thermodynamic, dipole-stabilized (10, 17) ketone enolates **3** (Scheme 2),[4] which on reaction with alkyl bromides or iodides led to the mono-α-alkyl derivatives **4** (Table 1) as the major products. In every case, a less polar by-product[5] was isolated and usually some starting material was recovered as well.



1 **2**

SCHEME 1

[1]Contribution no. 826 from the Syntex Institute of Organic Chemistry.

[2]Research completed in partial fulfillment of Licienciatura de Quimico Farmaceutico Biologo at the Escuela Nacional de Estudios Profesionales, Universidad Nacional Autonoma de Mexico, Zaragoza, D.F.

[3]Author to whom correspondence may be addressed.

[4]A referee has stated that "The structure of the α-*tert*-Boc-amino ketone enolate proposed in Scheme 2 (i.e., **3**) is virtually an impossible structure since the acidity of the NH there is very likely to be much higher than the activated methylene." The referee also suggests that alkylation is more likely to occur via a reactive dianion (i.e., $[R^1COCHNCO_2CMe_3]^{2-}$). While it is probable that such a dianion would undergo *C*-alkylation (18), and we have no evidence to exclude the presence of a small amount of this species, it is most instructive to note the following points. The monoanion **3** is undoubtedly formed under conditions of thermodynamic control. Bordwell and Algrim (19) have reported that the pK_a's of CH_3COCH_3 and CH_3CONH_2 in DMSO are 26.5 and 25.5, respectively. The inductive effect of the *N*-*t*-Boc moiety would increase the acidity of the methylene hydrogens. It is thus clear that the acidity of the NH is not likely to be "much higher" than that of the methylene hydrogens. Secondly, the pK_a of ketone enols is ca. 11 (20), which guarantees that the monoanion of **2** has structure **3** and not $R^1COCH_2NCO_2CMe_3$. Thus, there is no need to invoke the presence of a small amount of the dianion to rationalize the monoalkylation reactions described herein.

[5]For example, the alkylation of **2** (R^1 = Ph) with methyl iodide gave material which had ^1H nmr absorptions at δ 1.46, 1.53 (singlets, total ~9H), 3.26, 3.57 (singlets, total ~3H), 7.27 (s, ~4H), and 8.08 (q, ~1H) and infrared peaks at 3440 and 1700 cm^{-1}. Acidic hydrolysis under mild conditions (0.5 N HCl, room temperature) was without effect; more vigorous conditions (3 N HCl, reflux) caused resinification.

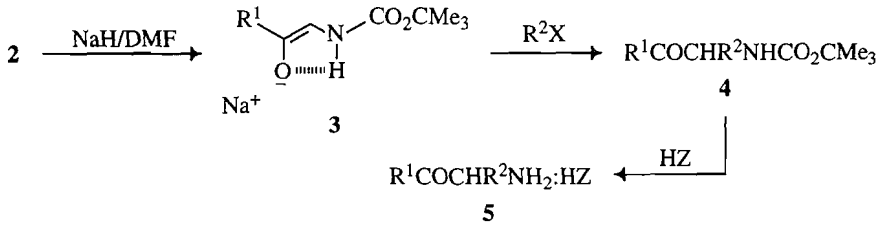
Printed in Canada / Imprimé au Canada

Can. J. Chem. Downloaded from www.nrcresearchpress.com by 123.30.183.119 on 09/07/12
For personal use only.

TABLE 1. Synthesis of α-alkyl-α-*tert*-butoxycarbonylamino ketones **4** and cyclic 2-acyl-*N*-*tert*-butoxycarbonylamines **6**

Alkylating agent	Product					Starting material, %
	Compound	R^1	R^2	*n*	% Yield[a]	
MeI	**4**	Ph	Me		83	
EtBr	**4**	Ph	Et		65	13
i-PrBr	**4**	Ph	*i*-Pr		37	23
n-BuBr	**4**	Ph	*n*-Bu		59	17
MeI	**4**	$PhCH_2CH_2$	Me		58	17
n-BuBr	**4**	$PhCH_2CH_2$	*n*-Bu		37	13
n-BuI	**4**	$PhCH_2CH_2$	*n*-Bu		60	ND[b]
$Br(CH_2)_3Br$	**6**	Ph		3	56	17
$Br(CH_2)_4Br$	**6**	Ph		4	41	20
$I(CH_2)_4I$	**6**	Ph		4	49	ND
$Br(CH_2)_3Br$	**4**	$PhCH_2CH_2$	$CH_2CH{=}CH_2$		19	
	6	$PhCH_2CH_2$		3	48	17
$Br(CH_2)_3Cl$	**4**	$PhCH_2CH_2$	$CH_2CH{=}CH_2$		14	
	6	$PhCH_2CH_2$		3	62	ND
$Br(CH_2)_4Br$	**6**	$PhCH_2CH_2$		4	39	32
$I(CH_2)_4I$	**6**	$PhCH_2CH_2$		4	47	ND

[a]Yield of product after column chromatographic purification.
[b]ND = not determined.



SCHEME 2

Removal of the *t*-Boc group from **4** was effected slowly with excess trifluoroacetic acid at ambient temperature or rapidly with excess methanolic hydrochloric acid at reflux temperature. The salts of the α-alkyl-α-amino ketones **5** were thus obtained in overall yields quite comparable to those reported for the α-formamido ketone process (Table 2).

The dialkylation of **2** was examined using an equivalent of a 1,3-dihalopropane or a 1,4-dihalobutane derivative in the presence of two equivalents of sodium hydride. The second alkylation took place on nitrogen to give the corresponding 2-acylpyrrolidine (**6**, $n = 3$, Scheme 3) or 2-acylpiperidine (**6**, $n = 4$). The efficiency of this cyclization was dependent, to a certain extent, on the α,ω-dihalide used (Table 1) but it was not improved by addition of the sodium hydride in two separate one-equivalent portions (i.e., stepwise alkylation). In the phenethyl series, the pyrrolidine derivative **6** (R^1 = $PhCH_2CH_2$, $n = 3$) was accompanied by appreciable amounts of the α-allyl compound **4** (R^1 = $PhCH_2CH_2$, R^2 = CH_2-$CH{=}CH_2$), which was presumably formed by dehydrohalogenation of the monoalkylated intermediate. The successful formation of the cyclic α-amino ketone derivatives **6** is not unique to the α-*tert*-butoxycarbonylamino ketones **2** since *N*-formylphenacylamine gave analogous cyclic products in comparable yields under conditions identical to those described herein.[6] Whereas *C*,*N*-cycloalkylation in these systems is synthetically useful, dialkylation in the intermolecular sense is not. For example, *N*-formylphenacylamine on attempted dialkylation with benzyl bromide gave a 1:2:3 mixture of α-mono-, α,α-di, and α,α,*N*-trialkylated compounds (9).

Deprotection of **6** with hot methanolic hydrochloric acid gave the cyclic α-amino ketones **7** (Table 2). Given the ready

[6]A. Guzman, C. Quintero, and J. M. Muchowski. Unpublished observations.

TABLE 2. Synthesis of acyclic and cyclic α-amino ketone salts **5** and **7**

Compound no.	R^1	R^2	*n*	HZ	% Yield[a]
5	Ph	Me		HCl	69
5	Ph	Me		TFA[b]	63
5	Ph	Et		HCl	65
5	Ph	Et		TFA	68
5	Ph	*i*-Pr		HCl	77
5	Ph	*i*-Pr		TFA	56
5	Ph	*n*-Bu		HCl	70
5	Ph	*n*-Bu		TFA	60
5	$PhCH_2CH_2$	Me		HCl	78
5	$PhCH_2CH_2$	*n*-Bu		HCl	67
7	Ph		3	HCl	68
7	Ph		4	HCl	78
7	$PhCH_2CH_2$		3	HCl	74
7	$PhCH_2CH_2$		4	HCl	71

[a]Yield after crystallization.
[b]Trifluoroacetic acid salt.

Can. J. Chem. Downloaded from www.nrcresearchpress.com by 123.30.183.119 on 09/07/12
For personal use only.

Can. J. Chem. Downloaded from www.nrcresearchpress.com by 123.30.183.119 on 09/07/12
For personal use only.

TABLE 3. Physical constants of α-*tert*-butoxycarbonylamino ketones and α-amino ketone salts

Compound no.	R^1	R^2	*n*	HZ	Melting point, °C	Cryst. solvent	Molecular formula	Calcd. C	Calcd. H	Calcd. N	Found C	Found H	Found N
4	Ph	Me			79–81	EtOAc–hex	$C_{14}H_{19}NO_3$	67.46	7.63	5.62	67.63	7.90	5.61
4	Ph	Et			64–65	EtOAc–hex	$C_{15}H_{21}NO_3$	68.44	7.98	5.32	68.41	8.05	5.25
4	Ph	*i*-Pr			95–96	EtOAc–hex	$C_{16}H_{23}NO_3$	69.31	8.30	5.05	69.23	8.49	4.99
4	Ph	*n*-Bu			Oil		$C_{17}H_{25}NO_3$	70.10	8.59	4.81	69.85	8.64	4.79
4	$PhCH_2CH_2$	Me			59–60	CH_2Cl_2–hex	$C_{16}H_{23}NO_3$	69.31	8.30	5.05	69.50	8.24	5.06
4	$PhCH_2CH_2$	*n*-Bu			50–51	CH_2Cl_2–hex	$C_{19}H_{29}NO_3$	71.44	9.15	4.38	71.47	8.93	4.23
4	$PhCH_2CH_2$	$CH_2CH{=}CH_2$			79–80	EtOAc–hex	$C_{18}H_{25}NO_3$	71.26	8.31	4.62	71.07	8.38	4.59
6	Ph		3		68–69	EtOAc–hex	$C_{16}H_{21}NO_3$	69.81	7.63	5.09	69.68	7.76	5.11
6	Ph		4		100–101	EtOAc–hex	$C_{17}H_{23}NO_3$	70.58	7.95	4.84	70.38	8.06	4.91
6	$PhCH_2CH_2$		3		Oil		$C_{18}H_{25}NO_3$[a]						
6	$PhCH_2CH_2$		4		80–81	EtOAc–hex	$C_{19}H_{27}NO_3$	71.89	8.57	4.41	71.65	8.39	4.35
5	Ph	Me		HCl	180–183[b]	MeOH–EtOAc	$C_9H_{12}ClNO$	58.22	6.46	7.54	58.05	6.49	7.49
5	Ph	Me		TFA[c]	150–153	EtOAc	$C_{11}H_{12}F_3NO_3$	50.19	4.56	5.32	49.92	4.65	5.29
5	Ph	Et		HCl	179–182[d]	MeOH–EtOAc	$C_{10}H_{14}ClNO$	58.82	7.16	6.86[e]	59.26	7.01	6.97
5	Ph	Et		TFA	123–126	EtOAc	$C_{12}H_{14}F_3NO_3$	51.98	5.05	5.05	51.87	5.22	4.94
5	Ph	*i*-Pr		HCl	205–207[f]	MeOH–EtOAc	$C_{11}H_{16}ClNO$	61.82	7.49	6.55	61.65	7.52	6.50
5	Ph	*i*-Pr		TFA	170–173	EtOAc	$C_{13}H_{16}F_3NO_3$	53.60	5.49	4.81	53.37	5.54	5.01
5	Ph	*n*-Bu		HCl	170–173	MeOH–EtOAc	$C_{12}H_{18}ClNO$	62.06	7.97	6.03[e]	61.92	7.83	6.12
5	Ph	*n*-Bu		TFA	95–98	EtOAc	$C_{14}H_{18}F_3NO_3$	54.28	6.02	4.52[e]	54.30	5.83	4.81
5	$PhCH_2CH_2$	Me		HCl	60–63	MeOH–EtOAc	$C_{11}H_{16}ClNO$	59.32	7.64	6.29[g]	59.14	7.40	6.19
5	$PhCH_2CH_2$	*n*-Bu		HCl	157–159	MeOH–EtOAc	$C_{14}H_{22}ClNO$	65.75	8.61	5.47	65.80	8.72	5.66
7	Ph		3	HCl	74–75	MeOH–EtOAc	$C_{11}H_{14}ClNO$	59.86	6.80	6.34[g]	60.00	6.54	6.48
7	Ph		4	HCl	225–227[h]	MeOH–EtOAc	$C_{12}H_{16}ClNO$	63.85	7.09	6.20	63.61	6.88	6.24
7	$PhCH_2CH_2$		3	HCl	149–152	MeOH–EtOAc	$C_{13}H_{18}ClNO$	65.13	7.51	5.84	64.86	7.30	5.87
7	$PhCH_2CH_2$		4	HCl	200–203	MeOH–EtOAc	$C_{14}H_{20}ClNO$	66.27	7.88	5.52	66.15	7.89	5.54

[a]Value of *m/e*: 303.1834 (calcd. for $C_{18}H_{25}NO_3$: 303.1835).
[b]Literature (24) mp 185–189°C; (25) mp 184°C.
[c]Trifluoroacetic acid salt.
[d]Literature (26) mp 178°C.
[e]Analysis calcd. for 0.25 H_2O.
[f]Literature (25) mp 208–209°C.
[g]Analysis calcd. for hemihydrate.
[h]Free base mp 89–91°C (EtOAc); lit. (21) mp 92°C.

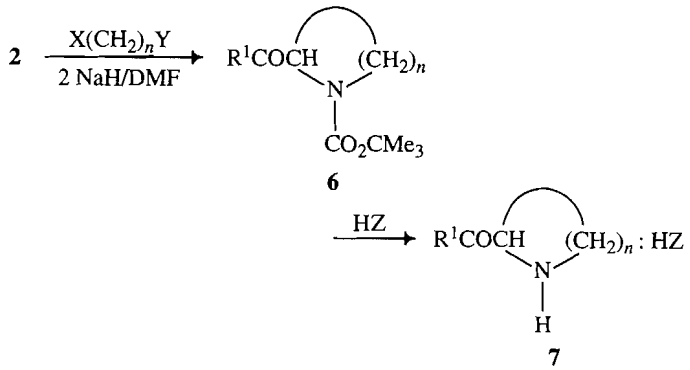
TABLE 4. Spectral properties of α-amino ketones and derivatives

Compound no.	R^1	R^2	HZ	n	Infrared (cm^{-1})[a]	Nuclear magnetic resonance (δ)[b]
4	Ph	Me			3513, 3413, 1711, 1691	1.41 (d, 2H, J = 7.15 Hz, Me), 1.46 (s, 9H, *t*-Bu), 5.30 (dd, 2H, J = 7.15 Hz, $J_{H,NH}$ = 7.5 Hz, CH), 5.58 (bd, 1H, $J \approx$ 7.5 Hz, NH), 7.46–7.65 (m, 3H), 7.98 (m, 2H)
4	Ph	*i*-Pr			3412, 1713, 1690	0.75 (d, 3H, J = 6.96 Hz, Me_2CH), 1.04 (d, 3H, J = 6.76 Hz, Me_2CH), 1.46 (s, 9H, *t*-Bu), 2.15 (m, 1H, Me_3CH), 5.23 (dd, 1H, J = 4.0 Hz, $J_{H,NH}$ = 4.0 Hz, CHNH), 5.44 (bd, 1H, NH), 7.47–7.65 (m, 3H), 7.98 (d, 1H, $J \approx$ 7.1 Hz)[c]
6	Ph			3	1698, 1683(sh)	1.27 (s, 5.4 H, *t*-Bu), 1.47 (s, 3.6 H, *t*-Bu), 1.94, 2.31 (multiplets, total 4H, CH_2CH_2), 3.42–3.77 (m, 2H, CH_2N), 5.21 (dd, 0.6 H, J_{AX} = 3.9 Hz, J_{BX} = 8.7 Hz, CHN), 5.35 (dd, 0.4H, J_{AX} = 3.2 Hz, J_{BX} = 8.9 Hz, CHN), 7.43–7.61 (m, 3H), 7.99 (m, 2H)
4	$PhCH_2CH_2$	Me			3334, 1712, 1674	1.11 (d, 3H, J = 7.3 Hz, Me), 1.44 (s, 9H, *t*-Bu), 2.66–3.03 (m, 1H, CH), 5.17 (bm, NH), 7.03–7.37 (m, 5H)[c]
6	$PhCH_2CH_2$			3	1723, 1687	1.38 (s, 5.4 H, *t*-Bu), 1.46 (s, 3.6 H, *t*-Bu), 1.80, 2.45 (multiplets, total 4H, CH_2CH_2), 2.71 (m, 4H, $PhCH_2CH_2$), 3.39–3.57 (m, 2H, CH_2N), 4.22 (dd, 0.6 H, J_{AX} = 5.3 Hz, J_{BX} = 8.4 Hz, CH), 4.33 (dd, 0.4 H, J_{AX} = 4.5 Hz, J_{BX} = 8.6 Hz, CH), 7.17–7.32 (m, 5H)
5	Ph	*n*-Bu	HCl		2635, 2525, 1701	0.78 (t, 3H, $J \approx$ 6.5 Hz, CH_3), 1.00–1.47 (Me, 4H, CH_2CH_2), 1.70–1.90 (m, 2H, $CHCH_2$), 5.08 (t, 1H, J = 5.7 Hz, CH), 7.49–7.52 (m, 3H), 8.04 (dd, 2H, J_o = 7.5 Hz, J_m = 1.2 Hz), 8.59 (bm, 3H, NH_3^+)
5	$PhCH_2CH_2$	Me	HCl		2659, 2584, 2478, 2442, 1722	1.39 (d, 3H, J = 7.0 Hz, Me), 2.69–3.08 (m, 4H, CH_2CH_2), 4.09 (q, 1H, J = 7.0 Hz, CH), 7.24 (s, 5H), 8.50 (bs, 3H, NH_3^+)
7	Ph		HCl	3	2738, 1687	1.75–2.09, 2.56 (multiplets, total 4H, CH_2CH_2), 3.28 (bt, 2H, $J \approx$ 5.7 Hz, CH_2N), 5.36 (bt, 1H, CHN), 7.59–7.81 (m, 4H), 8.10 (d, 2H, J = 8.2 Hz), 8.82 (bs, 2H, NH_2^+)
7	$PhCH_2CH_2$		HCl	3	2741, 2711, 2664, 2550, 2452, 1712	1.86, 2.33 (multiplets, total 4H, CH_2CH_2), 2.81–3.03 (m, 4H, $PhCH_2CH_2$), 3.17 (t, 2H, J = 6.6 Hz, NCH_2), 4.49 (t, 1H, J = 7.6 Hz, CHN), 7.22 (m, 5H)

[a]N-*t*-Boc compounds measured in $CHCl_3$; HCl salts obtained as dispersions in KBr.
[b]N-*t*-Boc compounds measured in $CDCl_3$; HCl salts in DMSO-d_6. Spectra measured at 200 MHz unless indicated otherwise.
[c]Measured at 90 MHz.

availability of **2**, this process constitutes a very useful route to such compounds for which few syntheses have been reported (21–23).

In summary, α-*tert*-butoxycarbonylamino ketones **2** are readily transformed into α-alkyl-α-amino ketones, 2-acylpyrrolidines, and 2-acylpiperidines. In this respect, they (i.e., **2**) are as synthetically useful as the corresponding formamido compounds and this fact adds flexibility to synthetic sequences in which the use thereof is contemplated.



SCHEME 3

Experimental

The melting points were determined in a Buchi model 510 melting point apparatus and are not corrected. The infrared spectra were measured with Perkin–Elmer 1720-X, 1420, or 197 infrared spectrophotometers. The ^1H nmr spectra were obtained with a Varian EM-390 or a Varian Gemini-200 nmr spectrometer and are expressed as parts per million (δ) from internal tetramethylsilane. The high-resolution mass spectra were obtained with a Finnigan MAT 311A mass spectrometer.

Phenacylamine hydrochloride (**1**, R^1 = Ph) and 1-amino-4-phenyl-2-butanone hydrochloride (**1**, $R^1 = PhCH_2CH_2$) were synthesized by the method of Ackrell *et al.* (9).

*2-N-tert-Butoxycarbonylaminoacetophenone (**2**, R^1 = Ph)*

Di-*tert*-butyl dicarbonate (10.36 g, 49.5 mmol), triethylamine (12.2 mL, 8.84 g, 87.5 mmol), and 4-dimethylaminopyridine (0.48 g, 3.9 mmol) were added to a stirred suspension of 2-aminoacetophenone hydrochloride (6.80 g, 39.6 mmol) in acetonitrile (100 mL). The mixture was stirred at room temperature for 0.5 h, the solvent was removed *in vacuo*, and the residue was subjected to column chromatographic purification on silica gel. The product (5.86 g, 63% yield) was eluted with hexane – ethyl acetate (95:5). After crystallization from dichloromethane–hexane it had mp 56–57°C; ir ($CHCl_3$): 3508, 3408, 1711, 1691 cm^{-1}; nmr ($CDCl_3$, 90) δ: 1.48 (s, 9H, *t*-Bu), 4.63 (d, 2H, J = 4.8 Hz, singlet after D_2O exchange, CH_2), 5.51 (bs,

Can. J. Chem. Downloaded from www.nrcresearchpress.com by 123.30.183.119 on 09/07/12
For personal use only.

Can. J. Chem. Downloaded from www.nrcresearchpress.com by 123.30.183.119 on 09/07/12
For personal use only.

1H, exchanged with D_2O, NH), 7.37–7.71 (m, 3H), 7.91–8.01 (m, 2H). Anal. calcd. for $C_{13}H_{17}NO_3$: C 66.38, H 7.23, N 5.95; found: C 66.29, H 7.25, N 5.93.

*1-N-tert-Butoxycarbonylamino-4-phenyl-2-butanone (**2**, $R^1 = PhCH_2CH_2$)*

This compound was prepared in the manner described above. It was obtained in 46% yield as an oil; ir ($CHCl_3$): 3434, 1703 cm^{-1}; nmr ($CDCl_3$, 90) δ: 1.43 (s, 9H, *t*-Bu), 2.59–2.99 (m, 4H, CH_2CH_2), 3.91 (d, 2H, J = 4.5 Hz, singlet after D_2O exchange, CH_2), 5.11 (s, 1H, exchanged with D_2O, NH), 7.08–7.24 (m, 5H, C_6H_5); *m/e*: 263.1521 (calcd. for $C_{15}H_{21}NO_3$: 263.1522).

*Monoalkylation of the α-tert-butoxycarbonylamino ketones **1***

A solution of the α-*tert*-butoxycarbonylamino ketone (2.0 mmol) in anhydrous DMF (5 mL) was added to a stirred suspension of sodium hydride (prepared from 0.10 g (2.1 mmol) of a 50% dispersion in mineral oil by washing with dry hexane) in dry DMF (5 mL) maintained in a nitrogen atmosphere at 0°C. After the addition was completed, stirring at 0°C was continued until hydrogen evolution was complete (0.25 h) and then the alkyl halide (2.4 mmol) was added. After a further 1 h at 0°C the reaction mixture was poured into saturated aqueous ammonium chloride solution, the product was extracted into ethyl acetate, the extract was washed with saturated salt solution, and then it was dried over sodium sulfate. The solvent was removed *in vacuo* and the residue was subjected to column chromatography on silica gel using hexane – ethyl acetate (95:5) as the eluting solvent. The less polar product of unknown structure was removed first, followed by the desired product and the starting material. The product yields are found in Table 1 and the physical constants in Table 3. The nmr and infrared spectra of selected compounds are found in Table 4. The remaining spectral data (Table 5) can be obtained from the Depository of Unpublished Data.[7]

*Alkylation of the α-tert-butoxycarbonylamino ketones **1** with α,ω-dihalides*

This alkylation reaction was carried out as described above except that 2.1 equivalents of sodium hydride were used.

*Synthesis of the alkylated α-amino ketone hydrochlorides of **5** and **7***

A solution of the alkylated α-*tert*-butoxycarbonylamino ketone (0.3 mmol) in methanol (15 mL) containing concentrated hydrochloric acid (0.14 mL, ~1.5 mmol) was heated at reflux temperature for 1 h. The solvent was removed *in vacuo* and the solid residue was crystallized from methanol – ethyl acetate. The product yields are found in Table 2 and the physical constants in Table 3. The spectroscopic data are compiled in Tables 4 and 5.

*Synthesis of the alkylated α-amino ketone trifluoroacetates of **5** and **7***

A solution of the alkylated α-*tert*-butoxycarbonylamino ketone (0.4 mmol) in dichloromethane (15 mL) containing trifluoroacetic acid (0.15 mL, 0.23 g, 2 mmol) was left at room temperature for 24 h. A further 2 mmol of the acid was added and after an additional 24 h the solvent was removed *in vacuo*. The solid residue was crystallized from ethyl acetate. The product yields are found in Table 2 and the physical constants are given in Table 3.

[7]This table may be purchased from: The Depository of Unpublished Data, Document Delivery, CISTI, National Research Council Canada, Ottawa, Canada K1A 0S2.

1. L. E. FISHER and J. M. MUCHOWSKI. Org. Prep. Proced. Int. **22**, 399 (1990).
2. Y.-L. HAN and H.-W. HU. Tetrahedron Lett. **30**, 5285 (1989); Synthesis, 122 (1990).
3. G. BRINGMANN and J.-P. GEISLER. Synthesis, 608 (1989).
4. P. MAGNUS and B. MUGRAGE. J. Am. Chem. Soc. **112**, 462 (1990).
5. W. O. MOSS, R. H. BRADBURY, N. J. HALES, and T. GALLAGHER. J. Chem. Soc. Chem. Commun. 51 (1990).
6. T. SHONO, Y. MATSUMURA, S. KATOH, K. TAKEUCHI, K. SASAKI, T. KAMADA, and R. SHIMIZU. J. Am. Chem. Soc. **112**, 2368 (1990).
7. B. BURNS, B. COATES, S. NEESON, and P. J. STEVENSON. Tetrahedron Lett. **31**, 4351 (1990).
8. S. SENGUPTA and V. SNIECKUS. J. Org. Chem. **55**, 5680 (1990).
9. J. ACKRELL, J. M. MUCHOWSKI, E. GALEAZZI, and A. GUZMAN. J. Org. Chem. **51**, 3374 (1986).
10. T. R. HOYE, S. R. DUFF, and R. S. KING. Tetrahedron Lett. **26**, 3433 (1985).
11. W. D. LUBELL and H. RAPOPORT. J. Am. Chem. Soc. **110**, 7447 (1988).
12. T. F. BUCKLEY and H. RAPOPORT. J. Am. Chem. Soc. **103**, 6157 (1981).
13. C. G. KNUDSON and H. RAPOPORT. J. Org. Chem. **48**, 2260 (1983).
14. P. J. MAURER, H. TAKAHATA, and H. RAPOPORT. J. Am. Chem. Soc. **106**, 1095 (1984).
15. M.-N. DUFOUR, P. JOUIN, J. PONCET, A. PANTALONI, and B. CASTRO. J. Chem. Soc. Perkin Trans. 1, 1895 (1986).
16. T. L. CUPPS, R. H. BOUTIN, and H. RAPOPORT. J. Org. Chem. **50**, 3972 (1985).
17. P. BEAK and D. B. REITZ. Chem. Rev. **78**, 275 (1978).
18. A. P. KRAPCHO and E. A. DUNDULIS. Tetrahedron Lett. 2205 (1976).
19. F. G. BORDWELL and D. ALGRIM. J. Org. Chem. **41**, 2507 (1976).
20. N. H. WERSTIUK and D. ANDREW. Can. J. Chem. **68**, 1467 (1990), and refs. therein.
21. J. HEER, E. SURY, and K. HOFFMANN. Helv. Chim. Acta, **38**, 134 (1955).
22. G. STORK, R. M. JACOBSON, and R. LEVITZ. Tetrahedron Lett. 771 (1979).
23. H.-P. KAISER and J. M. MUCHOWSKI. J. Org. Chem. **49**, 4203 (1984).
24. M. TIFFENEAU, J. LEVY, and E. DITZ. Bull. Soc. Chim. Fr. 1848 (1935).
25. H. ZINNER and G. BROSSMANN. J. Prakt. Chem. **5**, 91 (1957).
26. A. HILDESHEIMER. Ber. Dtsch. Chem. Ges. **43**, 2796 (1910).

Kinetics and mechanism of the hydrolysis of a (5,6)-spirophosphorane. Thermodynamics of the hydrolysis of cyclic five-membered and six-membered phosphonium ions

GLENN H. MCGALL AND ROBERT A. MCCLELLAND
Department of Chemistry, University of Toronto, Toronto, Ont., Canada M5S 1A1

Received March 27, 1991

GLENN H. MCGALL and ROBERT A. MCCLELLAND. Can. J. Chem. **69**, 2064 (1991).

The cyclic five-membered phosphonium ion **2***b* (2-(2′-hydroxyethoxy)-2-phenyl-1,3,2-dioxaphospholan-2-ylium) derived from ring-opening of the (5,5)-spirophosphorane **1***b* (5-phenyl-1,4,6,9-tetraoxa-5-phosphaspiro[4,4]nonane) has been observed in neat CF_3SO_3H and at >85% H_2SO_4. The cation undergoes hydrolysis in the latter solutions, and an extrapolation has been carried out to obtain an estimate for reactivity in 100% water. Hydrolysis rate constants for phenyltrialkoxyphosphonium ions in water are 10^7, 10^0, and 5×10^{-3} s^{-1} for cyclic five-membered, cyclic six-membered, and acyclic derivatives respectively; these show an excellent correlation with rate constants for a similar series of phosphate esters. An investigation of the hydrolysis of the (5,6)-spirophosphorane **5** (5-phenyl-8,8-dimethyl-1,4,6,10-tetraoxa-5-phosphaspiro[4,5]decane) provides a clue as to the origins of these rate differences. This phosphorane can in principle hydrolyze via two isomeric cyclic phosphonium ions, the six-membered **14** and the five-membered **15**. The former is thermodynamically more stable, being the only cation observed under equilibrating conditions of strong acid. However, the hydrolysis of the spirophosphorane, as well as the hydrolysis of fully formed **14**, channels through the cyclic five-membered **15**. A thermodynamic breakdown reveals that the 9.5 kcal mol^{-1} difference in activation free energy for the hydrolysis of five- and six-membered cyclic phosphonium ions is due to a combination of a *higher* free energy (2.5–4.5 kcal mol^{-1}) for the five-membered cation, and a *lower* free energy (7–5 kcal mol^{-1}) for the pentacoordinate transition state with the five-membered ring. This analysis also shows that a (5,6)-spirophosphorane is 6–8 kcal mol^{-1} more stable than a (6,6)-spirophosphorane. Thus, a five-membered ring has a significant stabilizing effect on a pentacoordinated phosphorus structure. The accelerated hydrolysis of cyclic phosphonium ions and phosphate esters with five-membered rings is caused by a combination of this stabilizing effect in the transition state and a destabilizing effect in the ground state associated with ring strain.

Key words: phosphorane, hydrolysis, phosphate, phosphonium.

GLENN H. MCGALL et ROBERT A. MCCLELLAND. Can. J. Chem. **69**, 2064 (1991).

L'ion phosphonium cyclique à cinq chaînons **2***b* ((2-(2′-hydroxyéthoxy)-2-phényl-1,3,2-dioxaphospholan-2-ylium), formé par une ouverture de cycle du (5,5)-spirophosphorane **1***b* (5-phényl-1,4,6,9-tétraoxa-5-phosphasiro[4,4]nonane), a pu être observé tant du CF_3SO_3H à l'état pur que dans du H_2SO_4 à >85%. Le cation subit une hydrolyse dans ces dernières solutions et on a effectué une extrapolation pour obtenir une évaluation de la réactivité dans de l'eau à 100%. Dans l'eau, les constantes de vitesse des réactions d'hydrolyse des ions phényltrialkoxyphosphonium cyclique à cinq chaînons, cyclique à six chaînons et aliphatique sont respectivement égales à 10^7, 10^0 et 5×10^{-3} s^{-1}; ces valeurs présentent une excellente corrélation avec les constantes de vitesse pour une série similaire d'esters de l'acide phosphorique. Une étude de l'hydrolyse du (5,6)-spirophosphorane **5** (5-phényl-8,8-diméthyl-1,4,6,10-tétraoxa-5-phosphaspiro[4,5]décane) fournit des indications sur les origines de ces différences dans les vitesses. En principe, ce phosphorane peut s'hydrolyser par le biais de deux ions phosphonium cycliques isomères, l'ion à six chaînons **14** et l'ion à cinq chaînons **15**. Le premier est thermodynamiquement plus stable; il est le seul cation à être observé dans des conditions fortement acides équilibrantes. Toutefois, l'hydrolyse du spirophosphorane, de même que l'hydrolyse de l'ion **14** complètement formé, passe par l'ion cyclique à cinq chaînons **15**. Une attribution thermodynamique révèle que la différence de 9,5 kcal mol^{-1} qui existe entre énergies libres d'activation pour les hydrolyses des ions phosphonium cycliques à cinq et à six chaînons est due à une combinaison d'une énergie libre *plus élevée* (2,5–4,5 kcal mol^{-1}) pour le cation à cinq chaînons et une énergie libre *plus faible* (7–5 kcal mol^{-1}) pour l'état de transition pentacoordiné du cycle à cinq chaînons. Cette analyse permet aussi de montrer qu'un (5,6)-spirophosphorane est de 6–8 kcal mol^{-1} plus stable qu'un (6,6)-spirophosphorane. Un cycle à cinq chaînons a donc comme effet de stabiliser une structure phosphorée pentacoordinée. L'hydrolyse plus rapide des ions phosphonium cycliques et des esters de l'acide phosphorique comportant des cycles à cinq chaînons est causée par une combinaison de cet effet stabilisant de l'état de transition et un effet déstablisant de l'état fondamental associé avec la tension de cycle.

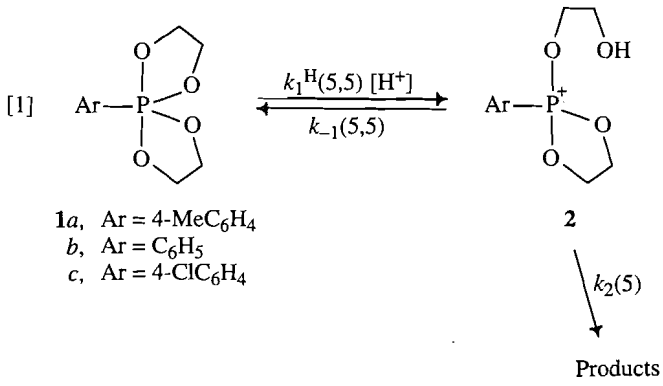
Mots clés : phosphorane, hydrolyse, phosphate, phosphonium.

[Traduit par la rédaction]

Oxyphosphoranes are the P=O analogs of acetals and ortho esters, and also model hydroxyphosphoranes, the pentavalent intermediates/transition states of phosphoryl group transfer. A variety of oxyphosphoranes have now been prepared, and their structural and fluxional characteristics subjected to considerable examination (1). However, kinetic and mechanistic studies of their hydrolysis reactions are limited (2–5), in marked contrast to the situation with acetals and ortho esters, which have been well studied in this respect (6, 7). With the initial objective to compare the carbonyl and phosphoryl derivatives, we have been studying mechanistic details of the hydrolysis of spirotetraalkoxyphosphoranes.

Our initial investigations focussed on (5,5)-spiro systems **1**, and revealed that there was hydrolysis throughout the pH range, with catalysis by H^+ and OH^-, as well as general acids and bases (8). The base reaction was proposed to follow an associative mechanism, with the base reacting at phosphorus to give a hexacoordinated intermediate. The acid reaction, on the other hand, appeared to involve a dissociative mechanism, with the formation of a phosphonium ion intermediate **2** and subse-

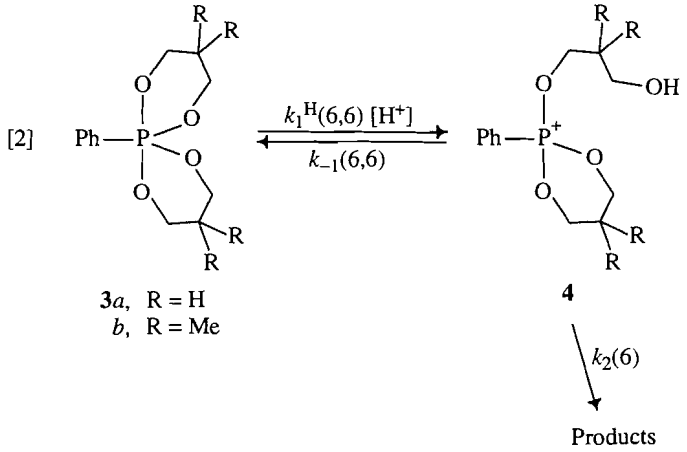
Can. J. Chem. Downloaded from www.nrcresearchpress.com by 123.30.183.119 on 09/08/12
For personal use only.



1*a*, Ar = 4-MeC_6H_4
b, Ar = C_6H_5
c, Ar = 4-ClC_6H_4

quent reaction with water. Analogous associative and dissociative mechanisms had previously been suggested by Archie and Westheimer, based upon observations with pentaaryloxyphosphoranes (2). The dissociative reaction is obviously analogous to the acid-catalyzed hydrolysis of acetals and ortho esters (6, 7).

With (6,6)-spirophosphoranes (9), no base reaction was observed, even at high pH. However, there was a very efficient dissociative reaction occurring throughout the pH range, with the ring-opened phosphonium ion **4** actually being observed as an intermediate in solutions with pH < ~8. The kinetic analysis revealed that this cation forms reversibly from the phosphorane in the hydrolysis, with an equilibrium constant, [**3***a*][H^+]/[**4***a*], of 3 × 10^{-9} M. The rate-limiting step in the



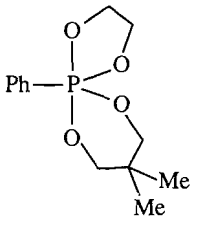
3*a*, R = H
b, R = Me

hydrolysis is the second step, the reaction of the cation with water, or at pH > 11, hydroxide ion. The reversibility results because the intramolecular reaction reforming the six-membered ring occurs with a rate constant $k_{-1}(6,6)$ 12 times greater than the rate constant $k_2(6)$ for the reaction of the cation with water.

Reversibility of the ring-opening step was considered for the acid hydrolysis of the (5,5)-spiro **1***a–c*, since this is consistent with the experimental data. This reaction exhibits a slightly positive entropy of activation, and this was originally taken as an indication of rate-limiting cation formation (8). A later study, however, demonstrated that, under non-hydrolytic conditions, addition of acid results in a rapid and reversible equilibrium (10). The phosphorane remains highly favored in the equilibrium, but the presence of small amounts of the phosphonium ion is indicated by an acid-catalyzed coalescence of ring protons in the ^1H NMR spectrum of the phosphorane associated with rapid opening and closing of the ring. A similar phenomenon is observed during the actual hydrolysis of an octamethyl analog of **1***b*, with the kinetic analysis showing that, with the octamethyl compound, $k_2(5)$ of eq. [1] is at least 2.5 × 10^6 smaller than $k_{-1}(5,5)$ (11). Moreover, this phosphorane also exhibits a positive entropy of activation for its overall hydrolysis, so that our use of this criterion to rule out reversibility with **1** had been incorrect. In consequence, our current interpretation is that ring-opening is probably reversible in the acid hydrolysis of **1***a–c* also (12).

In this paper we report the observation of the cyclic five-membered phosphonium ion **2***b* in strong acids, and extrapolate to arrive at an estimate of the rate constant $k_2(5)$ in 100% aqueous solution. This phosphonium ion is orders of magnitude more reactive than its cyclic six-membered analogs **4** as well as acyclic analogs, the same situation as observed in the hydrolysis of cyclic and acyclic phosphate esters (13). Rate constants for the phenyltrialkoxyphosphonium ions are in fact excellently correlated with rate constants for the hydrolysis of phosphate esters, with the conclusion that the same factors are determining reactivity in both series.

We then report an analysis of the hydrolysis of the (5,6)-spirophosphorane **5** that provides an evaluation of the relative



5

effects of five- and six-membered rings at stabilizing both reactant phosphonium ions and the transition states for their reactions with water. This phosphorane was originally chosen to see if the hydrolysis is similar to that of the (5,5)-spiro **1** or the (6,6)-spiro **3**. In fact it exhibits the interesting behavior of thermodynamically opening its 5-atom ring to give a cyclic six-membered phosphonium ion, while the overall hydrolysis proceeds essentially exclusively by way of the cyclic five-membered cation obtained on opening the (6)-atom ring. The two phosphonium ions and their transition states for reaction with water are isomers of each other, and it is this feature that allows free energies to be directly compared. What emerges is that there is a *higher* free energy of a cyclic five-membered cation but a *lower* free energy of the five-coordinate transition state, and it is the combination of the two factors that gives rise to the enormously accelerated hydrolysis of the five-membered system. That a five-membered ring has relative stabilizing effects in opposite directions in four-coordinated and five-coordinated phosphorus was suggested previously, based upon examination of crystal structures (14). However, most explanations for the enhanced reactivity of cyclic five-membered phosphates have focused on the starting state, and the relief of ring strain in the transition state for the cyclic five-membered compound (13, 15). The potential discrepancy between enthalpic strain energy and observed rate constants has, however, been noted (15).

Results

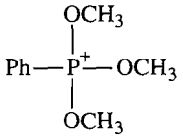
Observation of the cyclic five-membered phosphonium ion 2b

These experiments were carried out in an attempt to observe a cyclic five-membered phosphonium ion. Previously

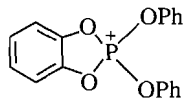
Can. J. Chem. Downloaded from www.nrcresearchpress.com by 123.30.183.119 on 09/08/12
For personal use only.

Can. J. Chem. Downloaded from www.nrcresearchpress.com by 123.30.183.119 on 09/08/12
For personal use only.

we had found that, whereas addition of a strong acid to a solution of (6,6)-spirophosphoranes **3** in CD_2Cl_2 or $CDCl_3$ leads to quantitative formation of cyclic six-membered phosphonium ions **4** (9), there is no observable reaction with (5,5)-spirophosphoranes other than the coalescence in the ^1H NMR spectrum (10). We now find that when dissolved in neat CF_3SO_3H **1***b* does exhibit NMR spectra consistent with the ring-opened phosphonium ion **2***b*. The most compelling evidence is the ^{31}P NMR chemical shift, which changes from −20.0 ppm in $CDCl_3$ to +59.7 ppm in the acid. The latter value is some 30 ppm more positive than the ^{31}P shifts of other phenyltrialkoxyphosphonium ions such as **4** (9) and **6** (16, 17). This is consistent with the formation of **2***b*, since a tetracoordinated phosphorus compound containing a five-membered ring is expected to exhibit a ^{31}P signal that is significantly downfield relative to acyclic and six-membered analogs (18–20). An example involving phosphonium ions involves a comparison of **7** (^{31}P = +12 ppm) and **8** (^{31}P = −18 ppm), where there is also a 30 ppm downfield shift caused by the presence of the five-membered ring (21).



6



7

$(PhO)_4P^+$

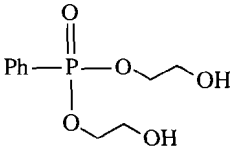
8

The cation **2***b* is not indefinitely stable in CF_3SO_3H, the ~60 ppm ^{31}P signal being completely replaced over 2–3 days by a cluster of signals around +34 ppm. The new products are likely oligomeric protonated phosphonate esters, forming by ring-opening of the cation in a reaction with an OH group of a second cation. Similar oligomerizations of spirophosphoranes under acidic conditions have been described previously (22).

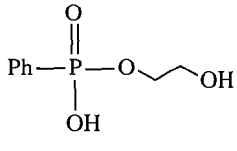
The cation **2***b* is also observed in concentrated sulfuric acid where it displays a ^{31}P resonance at +58.2 ppm. Decomposition also occurs here, with the half-life being about 30 min. This reaction is a hydrolysis, since the rate increases in more dilute acids, and the ^{31}P NMR of the product mixture shows two closely spaced signals near +35 ppm due to the two products of hydrolysis (see next section). These phosphonate esters are protonated under these strong acid conditions, and slowly undergo further hydrolyses themselves. First-order rate constants for the hydrolysis of the cation **2***b* were measured in three acids, 96.0, 90.0, and 85.0% H_2SO_4, as 4.8×10^{-4} s^{-1}, 1.0×10^{-2} s^{-1}, and 3.5×10^{-2} s^{-1} respectively.

*Products of the acid hydrolysis of the (5,5)-spirophosphorane 1*b

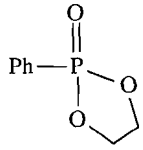
In our previous study, the hydrolysis of this phosphorane was found to give two phosphonate esters, **9** and **10**, plus ethylene glycol (8). The monoester **10** was presumed to arise from hydrolysis of the initially formed cyclic ester **11**. This has now



9



10



11

been confirmed by the direct observation of **11** in solutions where its hydrolysis is relatively slow. In 1:1 CD_3CN:D_2O containing a 1:1 mixture of CD_3COONa:CD_3COOD (0.01 M each) **1***b* rapidly hydrolyzes, producing a solution with two ^{31}P resonances, one at +21.3 ppm and a second at +39.3 ppm. The former is characteristic of phenylphosphonate diesters and corresponds to **9** (8). The latter is very similar to a literature shift reported for **11** (23). When this solution is acidified with a few drops of 6 M DCl, the downfield peak is completely replaced by a peak at +18.6 ppm, indicating that **11** has rapidly reacted to produce the ring-opened **10**. A small UV absorbance decrease accompanies this hydrolysis, thereby permitting rate measurements. This hydrolysis exhibits catalysis by both H^+ and OH^- with second-order rate constants of 0.37 M^{-1} s^{-1} and 6.0×10^2 M^{-1} s^{-1} respectively.

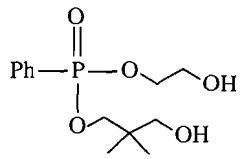
TABLE 1. Relative amount of the bis-phosphate ester **9** produced in the hydrolysis of the phosphorane **1***b*

Solution	pH	Percent **9**
3 M HCl	−1.0 (H_0)	53
1 M HCl	−0.25 (H_0)	58
0.1 M HCl	1.0	63
0.01 M HCl	2.0	67
Biphthalate buffer	3.0	84
Biphthalate buffer	4.0	90
Acetate buffer	5.0	99
Phosphate buffer	7.0	100
Phosphate buffer	8.0	100

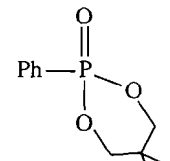
We have also investigated the pH dependency of the relative amounts of these products. As shown in Table 1 approximately 50% of the cyclic ester **11** or its hydrolysis product **10** is formed in acidic solutions, but this decreases as the pH is increased until at pH 7 the bis-ester **9** is the exclusive product (less than 1% **11**/**10**).

Products of the acid hydrolysis of the (5,6)-spirophosphorane 5

Hydrolysis of this phosphorane under acidic conditions yields two phosphonate esters, the bis-ester **12** and the monoester **10**, as well as 2,2-dimethyl-1,3-propanediol in an amount equivalent to the latter compound. The monoester **10** is also observed starting with the (5,5)-spirophosphorane **1***b*, and, as discussed in the previous section, arises from the cyclic ester **11**, which can be also observed with **5** in weakly acidic solutions. Two other products that could possibly have formed from the (5,6)-spirophosphorane are the cyclic six-membered phosphonate **13** and ethylene glycol. These were not detected



12



13

(less than 1%) in the ^{31}P and ^1H NMR spectra, as verified by the addition of authentic samples of these materials.

Yields of the bis-ester **12** as determined by integration of ^{31}P NMR signals were 80%, 3 M DCl; 83%, 1 M DCl; 85%, 0.1 M DCl; and 100%, pD 6 buffer.

Kinetics of the hydrolysis of the (5,6)-spirophosphorane 5

Kinetic studies were performed in aqueous solution at 25°C, with the ionic strength maintained at 1. First-order rate constants were measured between pH 12 and pH 5, the rates in

TABLE 2. Second-order rate constants for catalysis of the hydrolysis of the phosphorane **5** in aqueous solution at 25°C and an ionic strength of 1.0

Catalyst	k, M^{-1} s^{-1}
H_3O^+	$(3.65 \pm 0.05) \times 10^7$
$(CH_3)_2AsO_2H$	29 ± 4
$H_2PO_4^-$	9 ± 3
H_3BO_3	0.39 ± 0.02
HCO_3^-	0.005 ± 0.001
CO_3^{-2}	0.03 ± 0.01
OH^-	0.446 ± 0.001

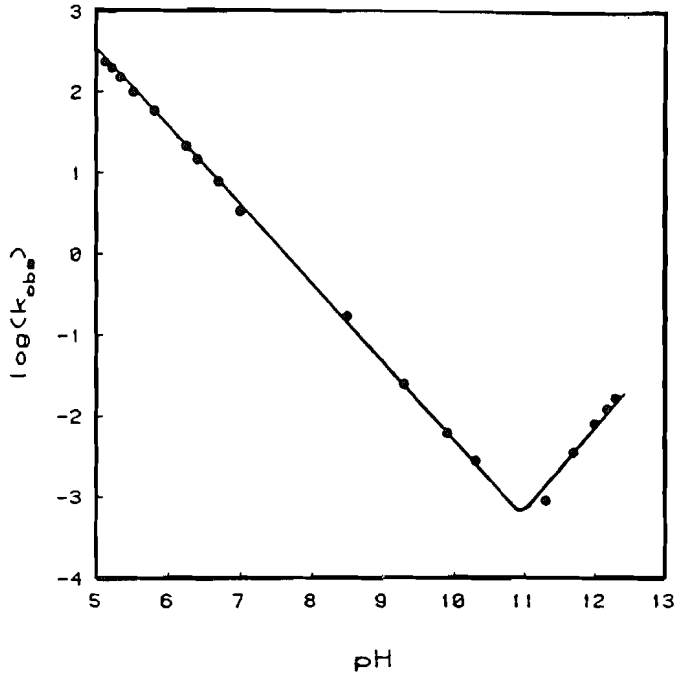


FIG. 1. Rate–pH profile for the hydrolysis of the (5,6)-spirophosphorane **5** in aqueous solution (25°C, ionic strength = 1.0).

more acidic solutions being too fast even for stopped-flow spectroscopy. These rate constants could be fit by the equation

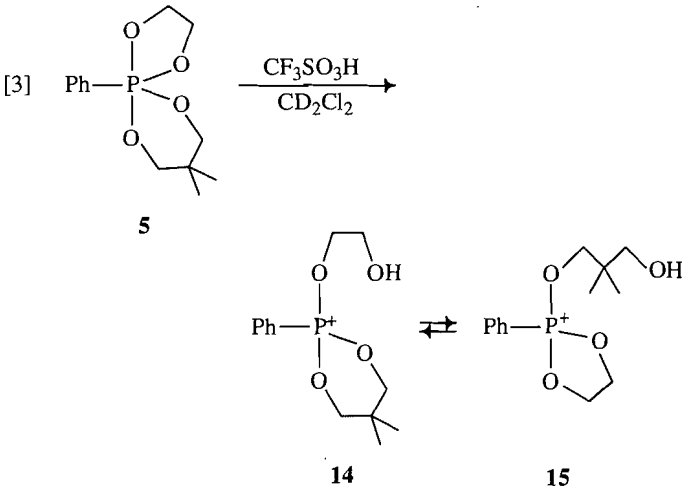
$$k(\text{obs}) = k_H[H^+] + k_{OH}[OH^-] + k_{HA}[HA] + k_B[A^-]$$

with catalysis by all acids and bases present in solution. Second-order rate constants are given in Table 2. This same kinetic pattern is observed with the (5,5)-spirophosphoranes **1** (8) and, as in the latter case, there is no pH-independent region with **5**, just a sharp break in the rate–pH profile at pH 11 from H_3O^+ to OH^- catalysis (Fig. 1). A Brønsted plot (not shown) for the four acid catalysts including H_3O^+ is linear, with a slope of 0.78 ± 0.05.

Phosphonium ions produced with the (5,6)-spirophosphorane 5

In behavior reminiscent of (6,6)-spirophosphoranes, treatment of **5** with one equivalent of CF_3SO_3H in CD_2Cl_2 quantitatively forms a phosphonium ion. This can be identified as the cyclic six-membered **14** from the ^1H NMR spectrum (see Fig. 2 and peak assignments indicated there) and the ^{31}P signal at +29.5 ppm. The latter is particularly indicative, being similar to the shift at +30.5 ppm observed with the analogous **4***b* (9). An isomeric cyclic five-membered phosphonium ion **15** can also form with this phosphorane but, as discussed previously, its ^{31}P signal is expected near +60 ppm, and no peak was observed in this region. Previous studies have shown that a spirophosphorane and a ring-opened phosphonium ion rapidly equilibrate under acidic conditions (9–11). Thus, the two cations **14** and **15** will be present in equilibrium amounts in this experiment, with equilibration occurring by way of the neutral phosphorane. Since a ^{31}P signal for the five-membered cation would have been detected if it were present in a 1% amount, we conclude that the equilibrium constant relating the two isomeric phosphonium ions ([**14**]/[**15**]) is greater than 100.

When a solution of **14** generated in acetonitrile with CF_3SO_3H is added to a weakly basic aqueous buffer, the phosphorane **5** is rapidly reformed. This is indicated by the observation of an absorbance *increase* characteristic of the hydrol-



ysis of the phosphorane, with a rate identical to that obtained starting with the phosphorane. Hydrolysis of the phosphonium ion would have appeared as an absorbance *decrease* (9, 17).

In acids with pH < 5, the hydrolysis of **5** is complete within 2 ms of mixing on a stopped-flow spectrophotometer, and in no solution up to and including 1 M HCl is there any indication of a phosphonium ion intermediate. The cation **14** is observed (and characterized by NMR) in concentrated H_2SO_4 solutions. It undergoes hydrolysis in these solutions with rate constants of 0.064, 0.011, 0.0016, and 0.000072 s^{-1} in 64.0, 70.0, 74.5, and 80.0% H_2SO_4 respectively.

Discussion

Lifetimes of phosphonium ions in water

With both phosphoranes **1** (8) and **5** the phosphonium ion intermediate cannot be detected during the hydrolysis in the normal pH range. This observation holds even under conditions where the overall hydrolysis of the phosphorane is complete within 2 ms, with the implication that the lifetime of the cation is shorter than this. We have described previously an approach for the oxocarbocation intermediates of acetal and ortho ester hydrolysis, where rate constants measured in strong acids were extrapolated to water with the assumption that differences between pairs of cations remain constant as the acidity is changed (24). This procedure was supported by observation of the required parallelism, albeit over a limited range in many cases, and through agreement with rate constants independently estimated by a "clock" approach (25). More recently, its validity

Can. J. Chem. Downloaded from www.nrcresearchpress.com by 123.30.183.119 on 09/08/12
For personal use only.

Can. J. Chem. Downloaded from www.nrcresearchpress.com by 123.30.183.119 on 09/08/12
For personal use only.

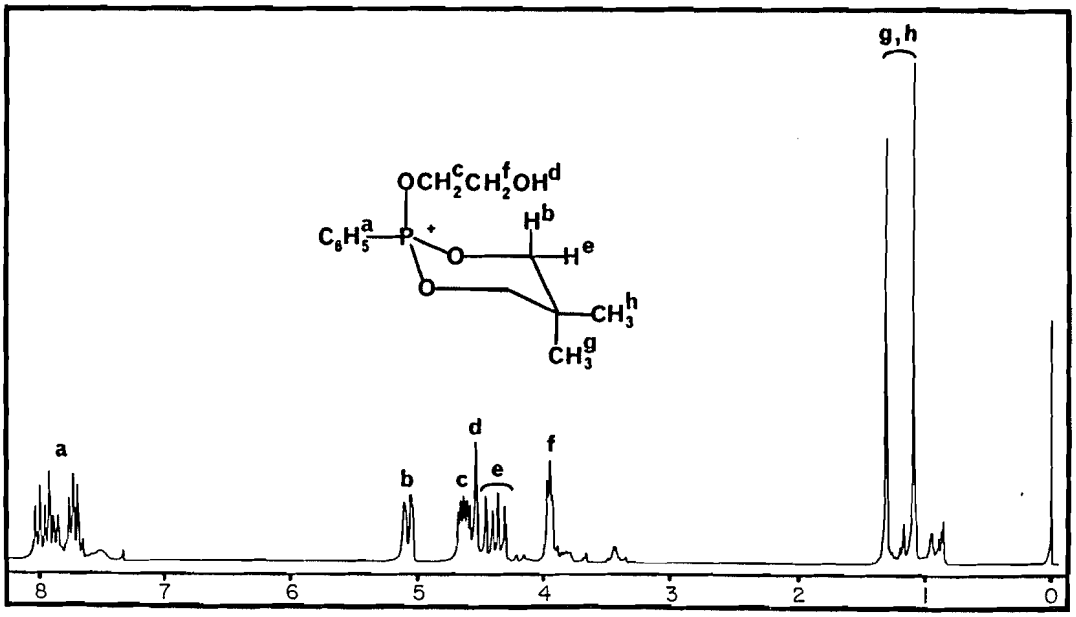


FIG. 2. ^{1}H NMR spectrum (200 MHz) of the cation **14** formed on the addition of CF_3SO_3H (0.11 M) to the phosphorane **5** (0.10 M) in CD_2Cl_2. The other unidentified small peaks in this spectrum are associated with impurities in the starting spirophosphorane.

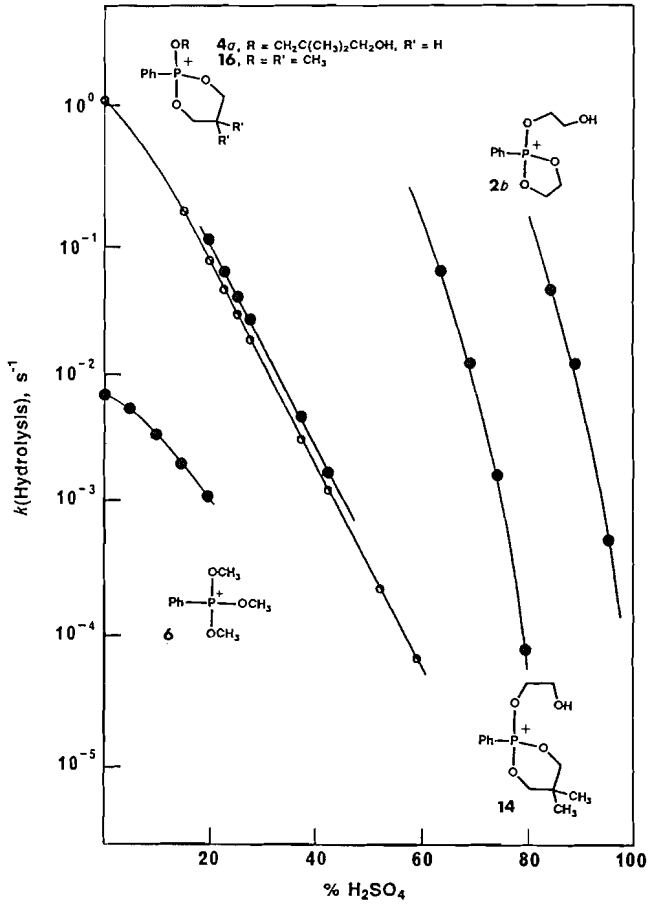


FIG. 3. Rate constants for the hydrolysis of phosphonium ions in sulfuric acid solutions (25°C). Data for **6** are from ref. 17, the point in water for **4***a* is from ref. 9, and the data for **4***a* and **16** in sulfuric acid solutions are from ref. 12.

has been conclusively established through direct measurement in water using the technique of laser flash photolysis (26, 27).

Figure 3 shows data for phosphonium ions that allow for such an extrapolation. For the acyclic **6** (17) and the cyclic six-membered **4***a* (9) rate constants have been measured directly in 100% aqueous solution, as 6.0×10^{-3} s^{-1} and 1.1 s^{-1} respectively. There is overlap of **4***a* and the more reactive **14** in 60–65% H_2SO_4, with a $10^{3.5}$ rate difference, and this leads to an estimate for the latter in water of $10^{3.5}$ s^{-1}. The assumption that is made is that the log k – acidity curve for this cation remains parallel to that of **4***a* on proceeding from solutions of this acidity to water. The cations **14** and **2***b* then overlap in 80–85% H_2SO_4, with a similar $10^{3.5}$ difference, and this leads to an estimate of 10^7 s^{-1} for the latter in water.

Incorporation of a ring into a trialkoxyphosphonium ion clearly has a significant effect, with the cyclic six-membered and five-membered cations being 200 times and 10^9 times more reactive than their acyclic analog. The accelerating effect of a five-membered ring in a phosphonium ion was observed previously, for the reaction of phenyltrialkylphosphonium salts with hydroxide ion (28). However, the rate enhancement, a factor of about 10^3, was considerably smaller than that observed in the present study, and there was no difference between the cyclic six-membered and acyclic cations. The trend with the phenyltrialkoxyphosphonium ions more closely parallels that seen in the hydrolysis of phosphate esters. Indeed, as shown in Fig. 4, there is an excellent quantitative correlation of rate constants for the three cations with rate constants for the base hydrolysis of similar phosphates (29). The phosphonium ions in fact show a slightly greater sensitivity to the structural change in this comparison, the slope of the correlation line being 1.3. Difference nucleophiles are, however, involved, and this could be part of the reason. What is apparent is that the very great reactivity of the five-membered cyclic system is observed in both the phosphonium ion and the phosphate

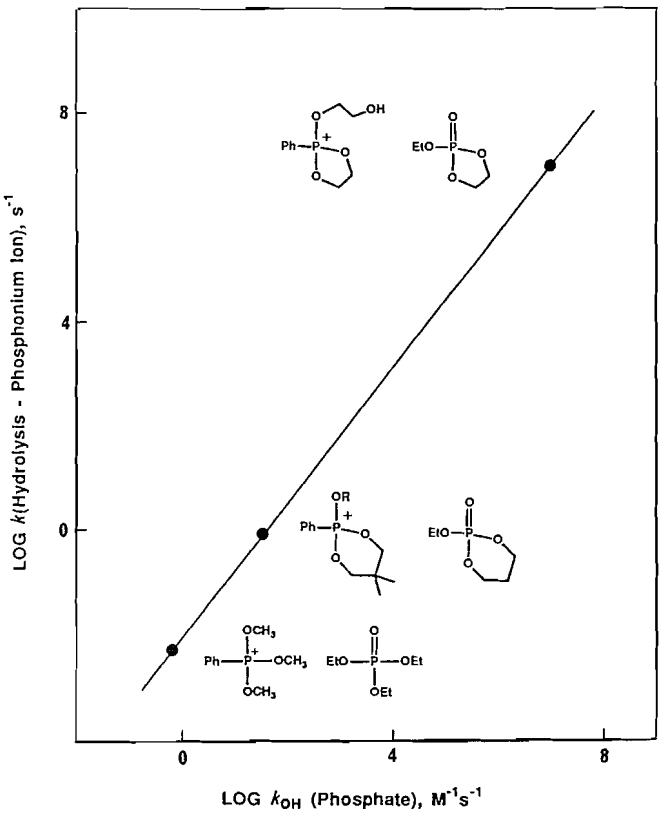


FIG. 4. Linear free energy correlation of rate constants for the hydrolysis of phosphonium ions with rate constants for phosphate esters reacting with hydroxide ion. Rate constants for the acyclic and cyclic six-membered phosphonium ions are directly measured in water (refs. 17 and 9 respectively). The rate constant for the cyclic five-membered phosphonium ion is based upon extrapolation from concentrated acid solutions. Data for the phosphates from ref. 29.

ester and, as demonstrated by the excellent linear free energy correlation, there must be a similar reason behind this.

The cation **14** is also interesting, since it reacts over three orders of magnitude more rapidly than **4***a* and **16**. This cannot represent a simple substituent effect since the three cations are very similar, and signals some unusual behaviour with **14**.

*Products of the acid hydrolysis of the (5,5)-spirophosphorane **1***

The analogy between cyclic five-membered phosphonium ions and phosphate esters is further illustrated by the pH dependency of the products obtained in the hydrolysis of each. Thus, the former, as an intermediate in the hydrolysis of **1**, exhibits a trend of giving only the bis-ester **9** in neutral solutions, with increasing amounts of the cyclic ester **11** as the acidity is increased (Table 1). This is exactly the same pattern as observed in the hydrolysis of methyl ethylene phosphate (30). In the latter case the explanation was advanced that the initially formed pentavalent intermediate can only undergo endocyclic cleavage, while a pseudorotation is required for exocyclic cleavage. The pH dependency was explained by a variation in the lifetime of the intermediate, with a very short lifetime at neutral pH so that breakdown occurs before pseudorotation. This same explanation must apply to the hydrolysis of the cyclic phosphonium ion. Here also the pentavalent intermediate **17′** that is formed initially on the addition of water would have a ring oxygen and an OH group in apical positions, so that only the bis-ester **9** derived from endocyclic cleavage can form. The cyclic ester **11** results only after pseudorotation to **17″** places the 2-hydroxyethoxy group in an apical position such that it also can be cleaved. As with methyl ethylene phosphate, the implication is that at neutral pH breakdown of **17′** occurs more rapidly than pseudorotation, so that only **9** is observed.

*Products of the acid hydrolysis of the (5,6)-spirophosphorane **5***

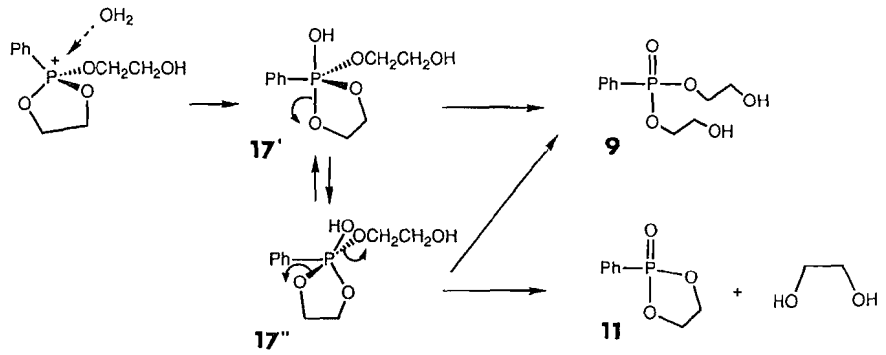
This phosphorane has aspects of the behaviour of both the (5,5)-spiro- and the (6,6)-spirophosphoranes. Like the latter, it reacts with strong acids in methylene chloride to quantitatively form a cyclic six-membered phosphonium ion. However, like the former, no phosphonium ion intermediate is observed during the hydrolysis in aqueous solutions. Moreover, the products **10** and **12** resemble those obtained from the (5,5)-spiro system, both in their nature and in their pH dependence. This suggests that these are forming by way of the cyclic five-membered phosphonium ion **15**, despite the fact that the six-membered isomer **14** is the more stable. The latter in fact can be ruled out as being the intermediate responsible for the final products, since its further reaction with water would result in significant quantities of the cyclic ester **13** and ethylene glycol, and these are not observed. This conclusion is supported by previous results with the (6,6)-spirophosphoranes **3**, where a cyclic six-membered phosphonium ion is the only intermediate that can form. With this system the appropriate cyclic six-membered phosphonate, and in this case a 1,3-diol, are indeed found as products (9).

*Thermodynamic analysis of the hydrolysis of the (5,6)-spirophosphorane **5***

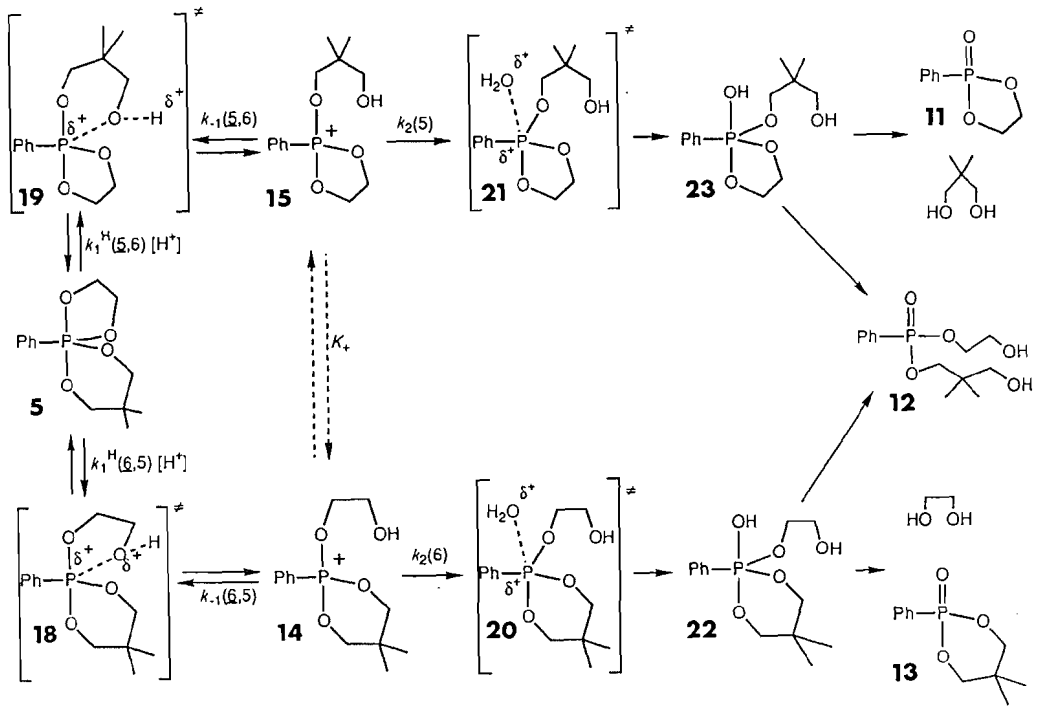
The general scheme for the acid-catalyzed hydrolysis of this phosphorane is given in Scheme 2, while a diagram depicting free energies of various species, including transition states, is shown as Fig. 5. The arguments behind this figure are somewhat complex, since the exact identity of rate-limiting steps cannot be stated unambiguously. Despite this uncertainty, however, relative free energies of a number of important species can be defined within a fairly narrow range.

This figure was based upon the following: (a) In aqueous solution in the range from pH 5 to 10, the phosphorane **5** undergoes hydrolysis with a strict dependency on H^+ concentration with a second-order rate constant, $k_H(5,6) = 3.7 \times 10^7$ M^{-1} s^{-1}. A phosphonium ion intermediate is not observed in the overall hydrolysis. (b) We assume that the hydroxyphosphoranes **22** and **23**, once formed, rapidly go on to products. This will be particularly true in less acidic solutions where there is an efficient base catalysis of this process (30). (c) The value for $k_H(5,6)$ corresponds to a $\Delta G^{\neq}$ of 7.1 kcal mol^{-1}. With assumption (b), this represents the free energy difference between **5** and either the transition state **19** or **21**, since the products demonstrate that more than 99% of the overall hydrolysis proceeds by way of the cyclic five-membered cation. (d) The equilibrium constant [**14**]/[**15**] is greater than 100, so that **15** is more than ~2.5 kcal mol^{-1} higher in energy than **14**. This result was obtained in CD_2Cl_2 and in strongly acidic solution, but it must also be true in 100% water, since these cations will have very similar solvation. (e) On addition to a slightly basic aqueous solution, the fully formed phosphonium ion **14** forms the phosphorane. This indicates that the

Can. J. Chem. Downloaded from www.nrcresearchpress.com by 123.30.183.119 on 09/08/12
For personal use only.



SCHEME 1



SCHEME 2

intramolecular cyclization in this cation is faster than its reaction with water. (f) In more concentrated acids, **14** reacts $10^{3.5}$ times faster than cyclic six-membered analogs that hydrolyze by a direct reaction with water. This is a key observation, since, coupled with the demonstration of reversibility and the product analysis, it indicates that the hydrolysis pathway followed by **14** must involve recyclization to the phosphorane, and reaction by way of **15**. The $10^{3.5}$ rate acceleration associated with this pathway indicates that its transition state is ~5 kcal mol^{-1} lower in energy than the transition state for the direct reaction of the cation **14** with water. (g) We assume that the rate constants $k_2(6)$ and $k_2(5)$ of Scheme 2 are 10^0 s^{-1} and 10^7 s^{-1} respectively, as with analogous cyclic phosphonium ions. These correspond to $\Delta G^{\neq}$ values of 17.5 and 8 kcal mol^{-1} respectively.

Figure 5 was then constructed in the following manner, with the cation **14** being assigned a relative ΔG of zero for comparison purposes. (h) From point (g), the free energy of the transition state **20** for the direct hydration of this cation is at +17.5 kcal mol^{-1}. (i) From point (f), the transition state for the actual hydrolysis of this cation is at +12.5 kcal mol^{-1}. This transition state is one of **18**, **19**, or **21** and, although it is not known which, *none of these can be higher in energy than this*. Thus the dashed line A in Fig. 5 represents the maximum position for each of these three transition states. (k) Point (d) permits the assignment of a minimum ΔG for the cation **15** at +2.5 kcal mol^{-1}, and this in turn places a minimum of +10.5 kcal mol^{-1} for the transition state **21**, which from point (g) is always 8 kcal mol^{-1} higher in energy than **15**. (l) From argument (i) the maximum for the transition state **21** is at +12.5 kcal mol^{-1}. This in turn means that the maximum for the cation **15** is 8 kcal mol^{-1} below this, i.e., at +4.5 kcal mol^{-1}. (m) The phosphorane **5** is 7 kcal mol^{-1} lower in energy than either the transition state **19** or **21** (point (c)), and since these cannot be higher than +12.5 kcal mol^{-1} (argument (i)), the maximum for **5** is +5.5 kcal mol^{-1}. (n) A minimum of +3.5 kcal mol^{-1} for **5** can also be assigned, based upon the minimum for **21** and the argument that **5** cannot be more than 7 kcal mol^{-1} lower in energy than this transition state. (o) Minimum positions for the transition states **18** and **19** cannot be unambiguously assigned.

Can. J. Chem. Downloaded from www.nrcresearchpress.com by 123.30.183.119 on 09/08/12
For personal use only.

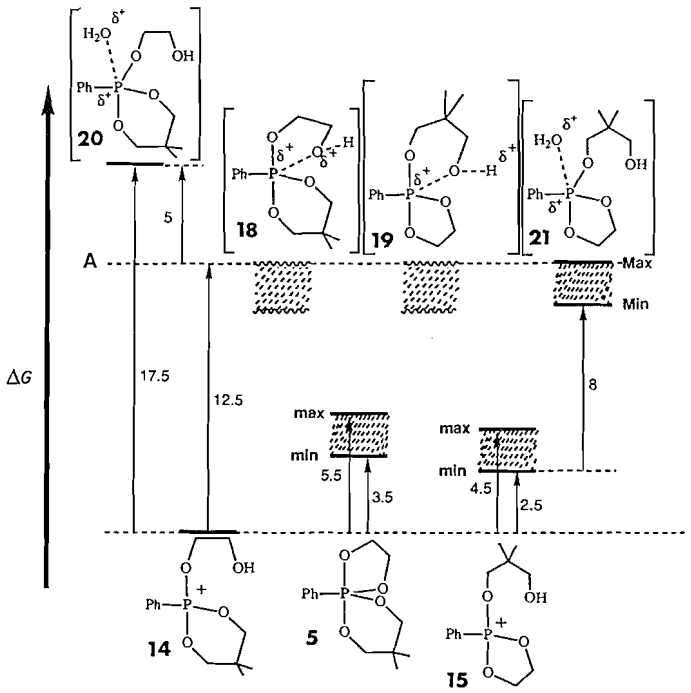


FIG. 5. Free energies for the hydrolysis of phosphonium ions. ΔG or ranges of ΔG have been determined as discussed in the text, and refer to 1 M H^+ as the standard state. In constructing this diagram, the values of ΔG have been rounded off to ± 0.5 kcal mol^{-1}.

Kinetic analysis of the hydrolysis of the phosphorane **5**

We consider in this section various possibilities for the rate-limiting steps in Scheme 2, and the consequences for the free energy diagram of Fig. 5.

(i) Cation **14** *and phosphorane* **5** *are rapidly equilibrating*

This is the model that we favor (see later), and it corresponds to a situation where the transition state **18** is lower in energy than the transition state **19**, or in kinetic terms $k_1^H(6,5) > k_1^H(5,6)$. With $k_{-1}(6,5)$ also greater than $k_2(6)$, **14** and **5** will therefore exist in a pH-dependent pseudo acid–base type of equilibrium during the hydrolysis, governed by an equilibrium constant that we define as before as $K_a(6,5) = [\mathbf{5}][H^+]/[\mathbf{14}]$. With the assumption that **15** is a steady-state intermediate, the following general rate expression is then obtained.

$$[4] \quad k(\text{obs}) = \left(\frac{k_1^H(5,6)\cdot k_2(5)[H^+]}{k_{-1}(5,6)+k_2(5)}\right) \times \left(\frac{K_a(6,5)}{K_a(6,5)+[H^+]}\right)$$

This derivation ignores any direct reaction of **14** with water, and makes no assumption as to the relative magnitudes of $k_{-1}(5,6)$ and $k_2(5)$. This equation describes two limiting conditions, phosphorane favored in the equilibrium ($K_a(6,5) > [H^+]$), with a linear dependency on $[H^+]$

$$[5] \quad k_H(5,6) = \left(\frac{k_1^H(5,6)\cdot k_2(5)}{k_{-1}(5,6)+k_2(5)}\right)$$

and phosphonium ion **14** favored in the equilibrium ($K_a(6,5) < [H^+]$), with k(obs) independent of pH

$$[6] \quad k(\text{cation}) = \left(\frac{k_1^H(5,6)\cdot k_2(5)}{k_{-1}(5,6)+k_2(5)}\right) K_a(6,5)$$

The former obviously represents the situation in the range from pH 10 to 5, where the required linear dependency on $[H^+]$ is observed, while the latter represents the situation in the concentrated sulfuric acid solutions where the cation is fully formed. Taking k(cation) as $10^{3.5}$ s^{-1}, the value obtained upon extrapolation from the latter solutions, $K_a(6,5)$ is calculated as 9×10^{-5} M by dividing eq. [6] by eq. [5]. Such a value is consistent with the observation that there is a linear dependency of k(obs) on $[H^+]$ in solutions with pH > 5. The value is also consistent with the observation that there are essentially *no* products derived from the direct reaction of **14** with water. For such a mechanism,

$$[7] \quad k(\text{obs}) = k_2(6) \times \left(\frac{K_a(6,5)[H^+]}{K_a(6,5)+[H^+]}\right)$$

and the second-order rate constant k_H in solutions where $K_a(6,5) > [H^+]$ is equal to $k_2(6)/K_a(6,5)$. Thus for this mechanism k_H can be calculated to be around 10^4 M^{-1} s^{-1}, using $k_2(6) = 1$ s^{-1} and the above $K_a(6,5)$. This number is over three orders of magnitude smaller than the observed k_H, which we have argued represents hydrolysis via **15**. In other words, the overall contribution to the products from a direct hydrolysis of **14** is less than 0.1%.

It can be noted that this model accurately defines the relative free energies of **14** and **5**, since it provides a numerical value for the equilibrium constant relating these species. This corresponds to $\Delta G = 5.5$, or the situation described in Fig. 5 by the maximum difference in free energy between **14** and **5**. The positions of the transition states **19** and **21** and the cation **15** then depend upon the relative magnitudes of $k_2(5)$ and $k_1(5,6)$.

(ia) Reaction of cation **15** *with water is rate limiting.* This corresponds to a situation where transition state **21** is higher in energy than transition state **19**, or $k_2(5) > k_1(5,6)$. In this sub-case of (i), transition state **21** represents the barrier in the overall hydrolysis of both **5** and **14**, and it has its free energy at the maximum position, +12.5 kcal mol^{-1}, in Fig. 5. Equations [5] and [6] simplify to

$$[8] \quad k_H(5,6) = \left(\frac{k_2(5)}{K_a(5,6)}\right)$$

$$[9] \quad k(\text{cation}) = \left(\frac{k_2(5)K_a(6,5)}{K_a(5,6)}\right)$$

where $K_a(5,6)$ is $[\mathbf{5}][H^+]/[\mathbf{15}]$, the equilibrium constant relating cation **5** and **15**. For this model, $K_a(5,6)$ is calculated as 3×10^{-1}, by substituting $k_2(5) = 10^7$ into eq. [8]. The equilibrium constant $[\mathbf{14}]/[\mathbf{15}]$ is also accurately determined as 3×10^3, from the ratio $K_a(5,6)/K_a(6,5)$. Thus these conditions also fix the free energy of the cation **15**, and this is at the maximum position indicated in Fig. 5.

(ib) Formation of cation **15** *from phosphorane* **5** *is rate limiting.* This corresponds to the opposite situation where $k_2(5) > k_{-1}(5,6)$, so that once **15** forms it proceeds on to products. For this sub-case, $k_H(5,6)$ is directly equal to $k_1^H(5,6)$ and the position of the transition state **18** lies at the maximum position in Fig. 5. The positions of the transition state **21** and the cation **15** are not precisely defined, although they must lie lower than the maximum indicated in the figure.

Although there is no unambiguous piece of experimental evidence distinguishing the two possibilities represented by

Can. J. Chem. Downloaded from www.nrcresearchpress.com by 123.30.183.119 on 09/08/12
For personal use only.

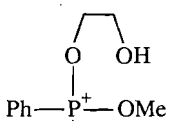
Can. J. Chem. Downloaded from www.nrcresearchpress.com by 123.30.183.119 on 09/08/12
For personal use only.

(ia) and (ib), consideration of the results with the (6,6)-spirophosphoranes suggests that the former is more likely. With the (6,6) compounds, there was the same competition, a ring closure at 3-hydroxypropoxy forming a six-membered ring versus a reaction with water, and the former was favored by more than one order of magnitude. The difference in the present case is that a much more reactive phosphonium ion is involved. This may attenuate the difference in the reactivity, but it would appear probable that ring closure would still be the faster process.

(ii) Ring closure to ***5*** *is rate limiting in the hydrolysis of preformed* ***14***

For this case, transition state **18** lies at its maximum position and both **19** and **20** are lower in energy. The cation **15** and the phosphorane **5** will also lie at positions lower than their maxima in Fig. 5, and $K_a(6,5)$ will be greater than the value obtained above since **14** and **5** will be closer in energy. In experiments that start with the phosphorane **5**, the cation **14** is never accessed since there is a lower barrier for overall hydrolysis through **15**. Starting with the cation **14**, reaction proceeds via the cation **15** but the initial cyclization step forming the phosphorane is rate limiting.

For this model, the rate constant for the reaction of the fully formed cation **14** is directly equal to the rate constant for cyclization $k_{-1}(6,5)$. At first glance, the number obtained, $10^{3.5}$ s^{-1}, is not unreasonable, since it signifies that the intramolecular reaction forming the five-membered ring is $10^{3.5}$ times faster than a reaction with a solvent water molecule. Similar comparisons have been well studied in 2-hydroxyethyl phosphate esters, and differences of this sort of magnitude are observed (31). However, in the following paper exactly the same competition arises in the phosphonium ion **24**, and the analysis conclusively establishes that cyclization is around 10^6 times faster than the reaction with water (32).



24

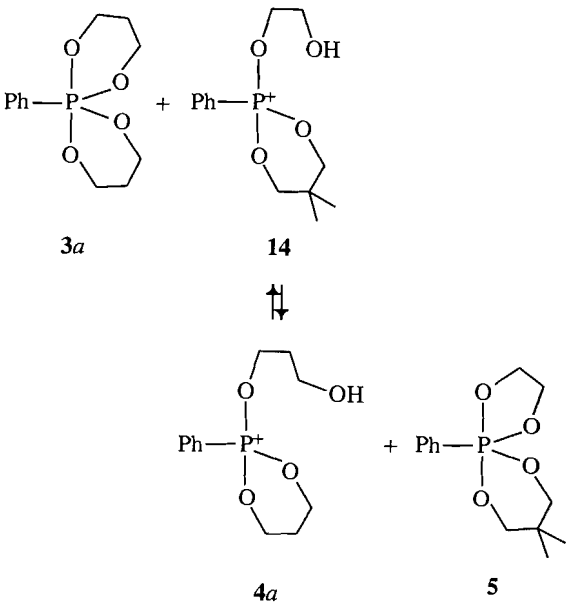
We believe that a similar difference is also likely to exist with **12**, and that $k_{-1}(6,5)$ is therefore greater than $10^{3.5}$. If this is true, **14** and **5** will exist in equilibrium and the arguments presented in case (i) apply.

In summary, the most likely situation is that described by case (ia). This has the phosphorane and the two cations in equilibrium in the overall hydrolysis, with the rate-limiting step the reaction of the five-membered cation with water, whether the starting point is the phosphorane or the cation **14**. For this situation the free energies of **5**, **15**, and **21** lie at the maximum position indicated in Fig. 5.

A five-membered ring stabilizes a spirophosphorane relative to a six-membered ring

One result that emerges from this analysis is that the equilibrium constant $K_a(6,5)$ is at least 10^4 times larger than the constant $K_a(6,6)$ for the similar equilibrium in a (6,6)-spirophosphorane (eq. [2]). This can be considered by placing the ions and phosphoranes that are involved into an isodesmic reaction.

This has an equilibrium constant that is the ratio of these two K_a values, and therefore lies in the range $3 \times 10^4 - 1 \times 10^6$.

[10] 

3a **14**

4a **5**

In other words, as written in this direction, the products are strongly favored in this equilibrium, with a ΔG of -6 to -8 kcal mol^{-1}. This cannot be due to a difference in thermodynamic stability of the reagent and product phosphonium ions, since these have very similar structure, both being cyclic six-membered phenyltrialkoxyphosphonium ions differing only in the presence or absence of remote methyl substituents and the length of the alkoxy chain. In consequence, the origin of the free energy change must lie in the relative energies of the two spirophosphoranes, with the conclusion that the (5,6)-spirophosphorane is considerably more stable, of the order of 6–8 kcal mol^{-1}, when compared to the (6,6)-spirophosphorane. This offers dramatic experimental confirmation that a five-membered ring has a significant stabilizing effect in a phosphorane structure.

Thermodynamics of the hydrolysis of cyclic phosphonium ions

A cyclic five-membered phosphonium ion is 10^7 times more reactive than a six-membered analog, a rate difference corresponding to a $\Delta\Delta G^{\neq}$ of 9.5 kcal mol^{-1}. Figure 5 shows how this $\Delta\Delta G^{\neq}$ is broken down into contributions from ground state and transition state. The cyclic five-membered phosphonium ion is indeed of higher energy than the six-membered cation. This is probably due to ring strain in the former (13), and it obviously provides for part of the accelerated hydrolysis of this cation. However, the free energy difference, 2.5–4.5 kcal mol^{-1}, is small and accounts for less than half of the overall $\Delta\Delta G^{\neq}$. The factor of greater importance is the lower free energy of the transition state having the five-membered ring. This difference, 5–7.5 kcal mol^{-1}, is in fact approaching the level of that observed between (5,5)- and (5,6)-spirophosphoranes, as discussed in the last section. The argument is normally made that the transition state for nucleophilic addition to tetracoordinated phosphorus resembles the pentacoordinate hydroxyphosphorane (13–15).

As noted in the introduction, there has been a previous suggestion that the accelerated hydrolysis of cyclic five-membered phosphates is due to a combination of destabilization in the starting phosphate and stabilization in the transition state (14), with the argument that ring strain is more important at tetracoordinated phosphorus, while intramolecular steric crowding is the principal factor at pentacoordinated phosphorus. While not pinpointing the actual origins of the effects, the data ob-

Can. J. Chem. Downloaded from www.nrcresearchpress.com by 123.30.183.119 on 09/08/12
For personal use only.

tained in the present study clearly provide strong support for a model of differential stabilization. In fact with the phenyltrialkoxyphosphonium ions the transition state stabilization is the more important factor.

Experimental section

Materials

5 - Phenyl - 8,8 - dimethyl - 1,4,6,10 - tetraoxa - 5 - phosphaspiro-[4,5]decane (**5**) was prepared by the reaction of 2-phenyl-1,3,2-dioxaphospholane (33), 2,2-dimethyl-1,3-propanediol, and *N*-chlorodiisopropylamine according to the method of Trippett and co-workers (34). The crude product was obtained as a colorless liquid, which, after distillation at 25°C, 0.5 Torr (1 Torr = 133.3 Pa), crystallized on standing. Recrystallization from hexane gave colorless crystals, mp 36–37°C; ^{31}P NMR δ : −34.9. The ^{1}H NMR spectrum of this compound has been reported (35).

5-Phenyl-1,4,6,9-tetraoxa-5-phosphaspiro[4.4]nonane (*1*b) was prepared in the same way as **5** using ethylene glycol. Physical data were in agreement with those obtained for a sample prepared by a different technique (8).

5,5 - Dimethyl - 2 - (2' - hydroxyethoxy) - 2 - phenyl - 1,3,2 - dioxaphosphorinan-2-ylium (*14*) *trifluoromethanesulfonate* was prepared by slowly adding 1 equivalent of trifluoromethanesulfonic acid to the phosphorane **5** in methylene chloride (or CD_2Cl_2) at −78°C under nitrogen. The mixture was then allowed to warm to room temperature. Attempts to obtain solid salt by adding dry ether resulted in the separation of an oil. The phosphonium ion in CD_2Cl_2 had ^{31}P NMR δ : +29.5; ^{1}H NMR δ : 8.05–7.65 (5H, mult.), 5.08 (2H, broad doublet of doublets, J_{P-H} = 2.4 Hz and J_{H-H} = 10.7 Hz), 4.64 (2H, doublet of triplets, J_{P-H} = 4.2 Hz and J_{H-H} = 3.7 Hz), 4.54 (1H, s), 4.39 (2H, doublet of doublets, J_{P-H} = 18.9 Hz and J_{H-H} = 10.7 Hz), 3.96 (2H, broad triplet, J_{H-H} = 3.7 Hz), 1.31 (3H, s), 1.10 (3H, s).

2-(2'-Hydroxyethoxy)-2-phenyl-1,3,2-dioxaphospholan-2-ylium (2b) *trifluoromethanesulfonate* was prepared by adding the phosphorane **1***b* to neat trifluoromethanesulfonic acid in an NMR tube under nitrogen at −10°C. In a similar manner **1***b* was added to 96% sulfuric acid-d_2 in an NMR tube at 5°C.

5,5-Dimethyl-2-oxo-2-phenyl-1,3,2-dioxaphosphorinane ***13*** was prepared as previously described (36).

Products

In general, hydrolyses were carried out under conditions very similar to those employed in the kinetic studies. Products were identified primarily by ^{31}P and ^{1}H NMR. Since complex and variable mixtures were usually obtained, no attempts were made to isolate or purify individual products, although in a few cases authentic samples were prepared by unambiguous routes. The relative amounts of individual products were determined by integration of ^{1}H and ^{31}P NMR spectra. For FT NMR spectra, a delay of 0.5 s between pulses was employed to minimize signal saturation effects. In cases where both ^{1}H and ^{31}P NMR were employed, the results agreed, within experimental error.

For the phosphorane **1***b*, NMR spectra were recorded directly on the aqueous solution employed for the hydrolysis, deuterated solvent and buffer being employed in the case where analysis involved ^{1}H NMR. The ^{1}H NMR spectra of products obtained in acidic D_2O have been reported elsewhere (8). Products are bis(2-hydroxyethyl) phenylphosphonate **9** (^{31}P +22.7 ppm), mono-(2-hydroxyethyl) phenylphosphonate **10** (^{31}P +18.4 at pH <2 and +16.3 at pH >3), and ethylene glycol. That **10** derives from an initially formed cyclic ester, 2-oxo-2-phenyl-1,3,2-dioxaphospholane **11**, was established by adding **1***b* to 1:1 CD_3CN:D_2O containing 0.01 M each of CD_3COOD and CD_3COONa, pD ~ 6. Two ^{31}P NMR signals were observed, one at +21.3 corresponding to **9**, and a second at +39.3 ppm. A synthetic sample of **11** has been reported to have a ^{31}P shift at +38.4 ppm (23).

For the phosphorane **5**, ^{31}P NMR were obtained directly in H_2O, and ^{1}H NMR specta were obtained in $CDCl_3$, after hydrolysis in D_2O and removal of the solvent by lyophilization. The major product, identified as the mixed diester 2-hydroxyethyl-(2,2-dimethyl-3-hydroxypropyl) phenylphosphonate **12**, had ^{31}P NMR δ : +22.2; ^{1}H NMR δ : 7.9–7.4 (5H, mult.), 4.15–4.05 (2H, mult.), 3.89 (1H, d, J_{P-H} = 7.0 Hz), 3.78 (2H, broad triplet, J_{H-H} = 4 Hz), 3.67 (1H, d, J_{P-H} = 7.0 Hz), 3.41 (1H, d, J_{H-H} = 11.4 Hz), 3.34 (1h, d, J_{H-H} = 11.3 Hz), 0.88 (3H, s), 0.87 (3H, s). Minor products were mono-(2-hydroxyethyl) phenylphosphonate **10** (^{31}P +18.1) and 2,2-dimethyl-1,3-propanediol. The former was identified by comparison with the same product obtained from **1***b*, the latter by direct comparison with an authentic sample. The absences of 5,5-dimethyl-2-oxo-2-phenyl-1,3,2-dioxaphosphorinane **13** and ethylene glycol were established by the addition of authentic materials.

Kinetics

Conventional kinetic measurements were carried out on a Cary 2390 spectrophotometer linked with an Apple IIe microcomputer. Stopped-flow kinetic measurements were conducted on a Durrum–Gibson apparatus linked to a Tektronix 4050 microcomputer. The cell compartments of both instruments were thermostated at 25.0 ± 0.1°C, unless otherwise noted. Rate constants slower than 0.10 s^{-1} were obtained on the Cary spectrophotometer, by adding a small quantity (1–2 μL) of a concentrated stock solution of the substrate in dichloromethane to a UV cuvette containing the solution of interest, pre-equilibrated at the desired temperature. Absorbance versus time data were transferred to the Apple IIe microcomputer, and the data fit by an iterative procedure to the general equation for an exponential reaction. Faster reactions were studied on the Durrum stopped-flow spectrometer, by first dissolving the substrate in a solution in which the substrate was fairly stable, and then mixing this with an appropriate solution to give the desired pH. Rate constants were calculated using a Tektronix microcomputer, by linear regression of plots of $\ln(A_\infty - A_t)$ or $\ln(A_t - A_\infty)$ versus time. Final concentrations of substrate in both types of experiments were of the order of 1 mM.

Rate constants for the hydrolysis of **5** in aqueous solution were obtained as previously described for the phosphoranes **1** (8), by following an absorbance increase at 265 mm. From pH 11 to pH 8.5, measurements were made with the Cary spectrometer. Below pH 8, the stopped-flow apparatus was employed, with the phosphorane dissolved in 1 mM NaOH being mixed with an appropriate buffer. In solution with pH > 11, where further hydrolysis of products complicates simple kinetic analysis, a pH jump method (8) was employed.

The kinetics of the hydrolysis of **11** were studied by first forming the cyclic ester *in situ* by hydrolyzing **1***b* in a dilute neutral buffer, and then mixing this solution with an appropriate HCl or NaOH solution on the stopped-flow spectrophotometer.

Rate constants for the hydrolysis of the phosphonium ion **2***b* in concentrated H_2SO_4 were obtained by following an absorbance decrease at 232 nm following addition of the phosphorane **2***b*. First-order kinetic plots were slightly nonlinear, probably due to further hydrolysis reactions.

Rate constants for the hydrolysis of the phosphonium ion **14** in 60–80% H_2SO_4 were measured by following an absorbance decrease at 275 nm following addition of the phosphorane **5**.

Acknowledgement

The continued financial support of the Natural Sciences and Engineering Research Council of Canada is gratefully acknowledged.

1. R. R. HOLMES. Pentacoordinated phosphorus. Vol. 1 and 2. ACS Monographs 175 and 176. American Chemical Society, Washington, DC. 1980.
2. W. C. ARCHIE and F. H. WESTHEIMER. J. Am. Chem. Soc. **95**, 5955 (1973).
3. A. QUEEN, A. E. LEMIRE, and A. F. JANZEN. Int. J. Chem. Kinet. **13**, 411 (1981).
4. V. E. BELSKII, L. A. KHISMATULLINA, T. G. BYKOVA, A. V. BURYKINA, and B. E. IVANOV. J. Gen. Chem. USSR, **49**, 298 (1979).

5. N. LOWTHER and C. D. HALL. J. Chem. Soc. Chem. Commun. 1303 (1985).
6. E. H. CORDES and H. G. BULL. Chem. Rev. **74**, 581 (1974).
7. T. H. FIFE. Acc. Chem. Res. **5**, 264 (1972).
8. R. A. MCCLELLAND, G. PATEL, and C. CIRRINA. J. Am. Chem. Soc. **103**, 6432 (1981).
9. G. H. MCGALL and R. A. MCCLELLAND. J. Am. Chem. Soc. **107**, 5198 (1985).
10. G. H. MCGALL and R. A. MCCLELLAND. J. Chem. Soc. Chem. Commun. 1222 (1982).
11. G. H. MCGALL and R. A. MCCLELLAND. J. Chem. Soc. Chem. Commun. 561 (1985).
12. G. H. MCGALL. Ph.D. Thesis, University of Toronto. 1987.
13. F. H. WESTHEIRMER. Acc. Chem. Res. **1**, 70 (1968).
14. P. GILLESPIE, F. RAMIREZ, I. UGI, and P. MARQUARDING. Angew. Chem. Int. Ed. Engl. **12**, 91 (1973).
15. G. R. J. THATCHER and R. KLUGER. Adv. Phys. Org. Chem. **25**, 99 (1989).
16. S. J. KUBISEN and F. H. WESTHEIMER. J. Am. Chem. Soc. **101**, 5985 (1979).
17. R. A. MCCLELLAND, G. H. MCGALL, and G. PATEL. J. Am. Chem. Soc. **107**, 5204 (1985).
18. D. I. PHILLIPS, I. SZELE, and F. H. WESTHEIMER. J. Am. Chem. Soc. **98**, 184 (1976).
19. D. B. DENNEY, D. Z. DENNEY, B. C. CHANG, and K. MARSI. J. Am. Chem. Soc. **91**, 5243 (1969).
20. D. B. DENNEY and S. D. PASTOR. Phosphorus Sulfur, **16**, 239 (1983); **22**, 183 (1985); **22**, 191 (1985).
21. J. GLEODE and SCHRAMM. Phosphorus Sulfur, **22**, 369 (1985).
22. S. KOBAYASHI and T. SAEGUSA. Pure Appl. Chem. **53**, 1663 (1981).
23. G. BERTRAND, J. P. MAJORAL, and A. BACEIRDO. Tetrahedron Lett. 5015 (1980).
24. R. A. MCCLELLAND and M. AHMAD. J. Am. Chem. Soc. **100**, 7031 (1978).
25. P. R. YOUNG and W. P. JENCKS. J. Am. Chem. Soc. **99**, 8238 (1977).
26. S. STEENKEN and R. A. MCCLELLAND. J. Am. Chem. Soc. **111**, 4967 (1989).
27. R. A. MCCLELLAND, V. M. KANAGASABAPATHY, and S. STEENKEN. Can. J. Chem. **68**, 375 (1990).
28. G. A. ASKNES and K. BERGESEN. Acta Chem. Scand. **19**, 931 (1965).
29. G. A. ASKNES and K. BERGESEN. Acta Chem. Scand. **20**, 2508 (1966).
30. R. KLUGER, F. COVITZ, E. DENNIS, L. D. WILLIAMS, and F. H. WESTHEIMER. J. Am. Chem. Soc. **91**, 6066 (1969).
31. A. J. KIRBY. Adv. Phys. Org. Chem. **17**, 183 (1980).
32. G. H. MCGALL and R. A. MCCLELLAND. Can. J. Chem. **69**, 2075 (1991).
33. A. FRANK. Organic phosphorus compounds. Vol. 4. *Edited by* G. M. Kosolapoff and L. Maier. John Wiley and Sons, New York. 1972, p. 255.
34. S. ANTCZAK, S. A. BONE, J. BRIERLEY, and S. TRIPPETT. J. Chem. Soc. Perkin Trans. 1, 278 (1977).
35. Y. KIMURA, M. MIYAMOTO, and T. SAEGUSA. J. Org. Chem. **47**, 916 (1982).
36. M. RAVEL, M. BON, and J. NAVECH, C. R. Seances, Acad. Sci. Ser. C: **274**, 430 (1972).

Can. J. Chem. Downloaded from www.nrcresearchpress.com by 123.30.183.119 on 09/08/12
For personal use only.

Hydrolysis of a monocyclic oxyphosphorane containing a five-membered ring

GLENN H. MCGALL AND ROBERT A. MCCLELLAND
Department of Chemistry, University of Toronto, Toronto, Ont., Canada M5S 1A1

Received March 27, 1991

GLENN H. MCGALL and ROBERT A. MCCLELLAND. Can. J. Chem. **69**, 2075 (1991).

A kinetic study is reported for the hydrolysis of 2,2-diphenyl-2-methoxy-1,3,2-dioxaphospholane **1**. This phosphorane exists in aqueous solution in a pseudo acid–base equilibrium with an observable phosphonium ion, the ring-opened (2′-hydroxyethoxy)diphenylmethoxyphosphonium ion **5**. The equilibrium constant K_a ([**1**][H^+]/[**5**]) is 9×10^{-9}, values determined by kinetic and spectroscopic methods being in good agreement. This phosphonium ion is, however, not involved in the overall hydrolysis reaction, which proceeds via the thermodynamically less stable cyclic five-membered phosphonium ion derived by loss of the exocyclic methoxy group from the phosphorane, the 2,2-diphenyl-1,3,2-dioxaphospholan-2-ylium ion **6**. This route for the overall hydrolysis is established by analysis of the products, and by the observation that the rate constant for the disappearance of **5** in acid solutions is 40 000 times greater than that for an analog that differs only in not being able to cyclize, the (2′-methoxyethoxy)diphenylmethoxyphosphonium ion **7**. At all pH, the phosphorane **1** and the ring-opened phosphonium ion **5** exist in equilibrium, and the rate-limiting step in the overall hydrolysis is the cleavage of the exocyclic methoxy group to give the cyclic phosphonium ion **6**, which is rapidly converted to products by reaction with water. The actual equilibration reaction involving **1** and **5** cannot be observed at any pH, even with stopped-flow spectroscopy. The non-catalyzed ring closure of the phosphonium ion **5** reforming the phosphorane **1** occurs with a rate constant of 200–500 s^{-1}, corresponding to an effective molarity of (2–5) $\times 10^7$ M for the intramolecular hydroxy group in this reaction. The rate-limiting exocyclic cleavage is assisted by H^+, with a very large rate constant 2×10^9 M^{-1} s^{-1}. Catalysis by general acids is also observed. The Brønsted plot has a slope α of 1.0 for the weaker acids, with a break for acids with $pK_a < 3$. This "Eigen"-type behavior is proposed to arise from a transition state with little phosphonium ion character, in which the proton is almost completely transferred for the weaker acids.

Key words: phosphorane, phosphate, phosphonium, hydrolysis.

GLENN H. MCGALL and ROBERT A. MCCLELLAND. Can. J. Chem. **69**, 2075 (1991).

On a effectué une étude cinétique de l'hydrolyse du 2,2-diphényl-2-méthoxy-1,3,2-dioxaphospholane, **1**. En solution aqueuse, ce phosphorane existe sous forme d'équilibre pseudo acide–base avec un ion phosphonium qui peut être observé, l'ion à cycle ouvert (2′-hydroxyéthyl)diphénylméthoxyphosphonium, **5**. Les valeurs de la constante d'equilibre K_a = [**1**][H^+]/[**5**] = 9×10^{-9} qui ont été déterminées par des méthodes cinétiques et spectroscopiques sont en bon accord. Toutefois, cet ion phosphonium n'est pas impliqué dans la réaction globale d'hydrolyse qui se produit par le biais de l'ion 2,2-diphényl-1,3,2-dioxaphospholan-2-ylium, **6**, comportant un cycle à cinq chaînons, qui est thermodynamiquement moins stable et qui est formé par la perte d'un groupe méthoxy exocyclique du phosphorane. On a établi que l'hydrolyse globale suit cette voie en examinant la nature des produits et en observant que la constante de vitesse pour la disparition du produit **5** en milieux acides est 40 000 fois plus grande que celle d'un analogue, l'ion (2′-méthoxyéthoxy)diphénylméthoxyphosphonium, **7**, qui ne diffère que par le fait qu'il ne peut pas se cycliser. À tous les pH, le phosphorane **1** et l'ion phosphonium à cycle ouvert **5** existent en équilibre et l'étape qui détermine la vitesse de la réaction de l'hydrolyse globale est la scission du groupement méthoxy exocyclique pour donner l'ion phosphonium cyclique **6** qui est transformé rapidement en produits par réaction avec l'eau. À aucun pH, même en faisant appel à la spectroscopie à flux stoppé, il n'est pas possible d'observer la réaction d'équilibre impliquant **1** et **5**. La clôture de cycle non-catalysée de l'ion phosphonium **5** pour redonner le phosphorane **1** se produit avec une constante de vitesse de 200–500 s^{-1} qui correspond à une molarité effective de (2–5) $\times 10^7$ M pour le groupe hydroxyle intramoléculaire impliqué dans cette réaction. La scission exocyclique qui détermine la vitesse de la réaction est aidée par les H^+ et la constante de vitesse est très élevée, 2×10^9 M^{-1} s^{-1}. On a aussi observé une catalyse générale par les acides. La pente α de la courbe de Brønsted est égale à 1,0 pour les acides plus faibles; on note un bris pour les acides avec un $pK_a < 3$. On propose que ce comportement de type « Eigen » est causé par un état de transition n'impliquant qu'un faible caractère d'ion phosphonium dans lequel le proton est pratiquement complètement transféré aux acides plus faibles.

Mots clés : phosphorane, phosphate, phosphonium, hydrolyse.

[Traduit par la rédaction]

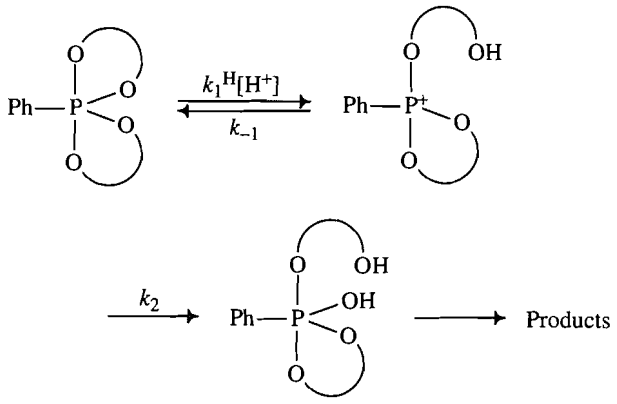
Introduction

In previous papers we have discussed the hydrolysis of spirotetraalkoxyphosphoranes comprising two five-membered rings (1, 2), two six-membered rings (3), and one five- and one six-membered ring (4). Throughout most of the pH region, these compounds undergo an acid-catalyzed dissociative hydrolysis involving a ring-opened phosphonium ion intermediate. This cation can be observed during the aqueous hydrolysis of the (6,6)-spirophosphoranes (3), while concentrated sulfuric acids are required to observe a cation with the other two. With all three types of phosphorane, ring-opening to the phosphonium ion is probably reversible. This has been unambiguously demonstrated with the (6,6)-spiro compound (3), with the (5,6)-spiro compound for ring-opening in one direction (4), and with an octamethyl-(5,5)-spiro derivative (2). Significant effects of ring size are observed on the thermodynamic and kinetic stabilities of phosphoranes and phosphonium ions, a cyclic five-membered phosphonium ion being 10^7 and 2×10^9 more reactive towards water than cyclic six-membered and acyclic analogs respectively (4). An analysis of the thermodynamics associated with the hydrolysis of the (5,6)-spirophosphorane revealed that part of the reason for the very much larger rate with the five-membered phosphonium ion is destabilization in the ground state, probably associated with ring strain (5). However, stabilization of the pentacoordinated transition state by the five-membered ring, probably due to relief of steric crowding (6), is equally, if not more important.

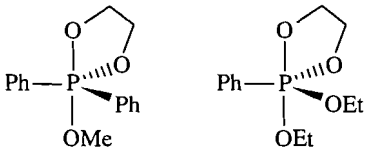
In this paper we discuss the hydrolysis of a phosphorane **1** that contains a single five-membered ring in addition to an exocyclic alkoxy group. A phosphorane of the type **2** had in fact been our

Can. J. Chem. Downloaded from www.nrcresearchpress.com by 123.30.183.119 on 09/08/12
For personal use only.

Can. J. Chem. Downloaded from www.nrcresearchpress.com by 123.30.183.119 on 09/08/12
For personal use only.

[1] 

first choice since this is a direct analog of the spiro compounds previously investigated. However, it proved difficult to maintain this compound in a pure state, since on standing it underwent disproportionation to phenyltetraethoxyphosphorane and the corresponding (5,5)-spirophosphorane. The contaminating material made analyses difficult, and **1**, which cannot disproportionate, was chosen for detailed studies.

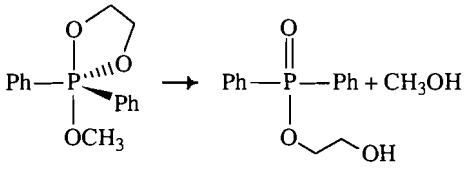


1 **2**

Results

Products

Phosphorane **1** undergoes hydrolysis at all pH to give 2-hydroxyethyl diphenylphosphinate **3** and methanol as the only observable products. Authentic samples of other possible products, methyl diphenylphosphinate **4** and ethylene glycol, were added to the product mixtures to ensure their absence. The esters **3** and **4** are easily distinguished by their ^{31}P NMR chemical shifts (+35.5 and +33.2 ppm respectively). There was no observable peak in the hydrolysis mixture at the latter position, and we conclude that there is less than one percent of **4** formed. A sample of **3** was in fact isolated after hydrolysis and evaporation of the solvent (and methanol) in essentially pure form, and, with no further purification, had the same melting point as one previously reported for this compound (7).

[2] 

1 **3**

Kinetics

Because of solubility problems in 100% aqueous media, kinetic experiments were carried out in 1:3 acetonitrile:water, with the temperature at 25°C and the ionic strength of 1.0 maintained with NaCl. Absorbance changes in the UV region between 260 and 280 nm were monitored. These changes were similar to ones previously observed with the spirophosphoranes (1–4). As illustrated in Fig. 1, addition of acid to a solution of phosphorane under anhydrous conditions is accompanied by a large absorbance increase, typical of the formation of a phosphonium ion (see NMR recorded under these conditions later). Addition of water to this solution results in an absorbance decrease, with the final spectrum corresponding to that of the phosphinate **3** lying intermediate between the spectra of the phosphonium ion and the phosphorane.

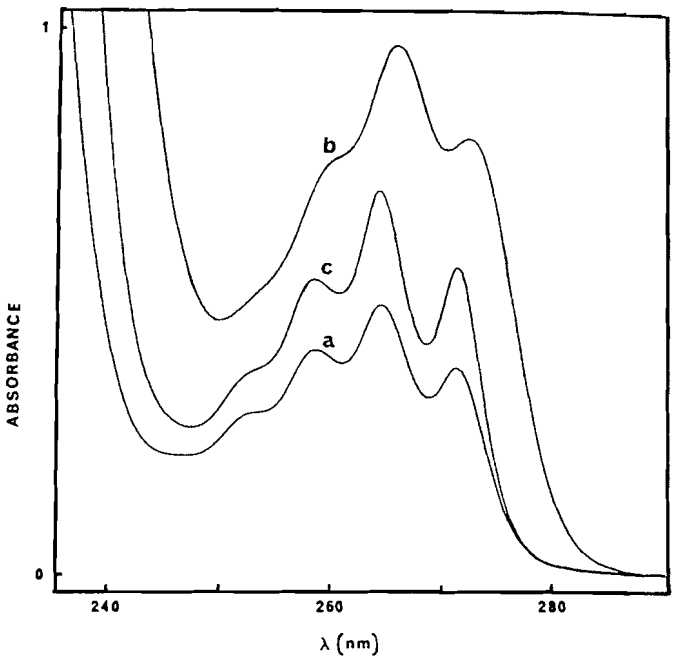


FIG. 1. UV spectra obtained with the phosphorane **1**. (a) 1 mM phosphorane in dioxane. (b) After the addition of one equivalent of CF_3SO_3H. (c) After the addition of water to the acidified solution.

Addition of the phosphorane to aqueous solution results in an absorbance *increase* at pH > 8, indicating direct conversion of the phosphorane to product, with an absorbance *decrease* at pH < 7, corresponding to the hydrolysis of a phosphonium ion. In both regions catalysis by added buffer is observed. At high pH the rate law is

$$[3] \quad k_B(obs) = k_B^H[H^+] + k_B^{OH}[OH^-] + k_B^0 + k_B^{HA}[HA]$$

where the first two terms represent H^+-catalyzed and OH^--catalyzed processes, the third a pH-independent reaction, and the fourth catalysis by added buffer acids. Rate constants are given in Table 1, and the rate–pH profile based upon extrapolation to zero buffer concentration is shown in Fig. 2. To ensure that the species undergoing reaction in these solutions was indeed the phosphorane, an ^1H NMR spectrum of a more concentrated solution of **1** was recorded as quickly as possible in 3:1 CD_3CN:D_2O containing 5 mM NaOD. In the initially recorded spectrum, the two doublets of the starting phosphorane were clearly visible. Later spectra showed the characteristic pattern of the products.

At pH < 7, where an absorbance decrease is observed, the rate law is

$$[4] \quad k_A(obs) = k_A^0 + k_A^B[A^-]$$

showing a pH-independent reaction (see Fig. 2) and a reaction catalyzed by the base component of the buffer. Rate constants obtained in this region are also given in Table 1.

Between pH 7 and pH 9, there is a transition between the two types of behavior that characterize the reactions at lower and higher pH. As illustrated in Fig. 3, a first-order absorbance change is observed in all solutions, but the absolute magnitude and direction change with pH, from the absorbance decrease observed at high pH to the decrease at low pH. Defining ΔAbs as

TABLE 1. Rate constants for the hydrolysis of the phosphorane **1** in 1:2 acetonitrile:water, at 25°C and ionic strength = 1.0. Units are $M^{-1}\,s^{-1}$, except for k_B^0 and k_A^0, which have units of s^{-1}

Obtained at pH > 8		Obtained at pH < 7	
$k_B^0(s^{-1})$	$(1.4\pm0.7)\times10^{-3}$	$k_A^0(s^{-1})$	15.4±1
k_B^{OH}	$(2\pm1)\times10^{-3}$	$k_A^B(CF_3CO_2^-)$	5±0.7
k_B^H	$(1.7\pm0.4)\times10^9$	$k_A^B(CCl_3CO_2^-)$	6.5±1
$k_B^{HA}(TrisH^+)$	15±3	$k_A^B(Cl_2CHCO_2^-)$	19±2
$k_B^{HA}(NH_4^+)$	5±1	$k_A^B(NCCH_2CO_2^-)$	42±5
$k_B^{HA}(Me_3NH_4^+)$	5±1	$k_A^B(CH_3OCH_2CO_2^-)$	86±4
$k_B^{HA}(HCO_3^-)$	1.0±0.5	$k_A^B(CH_3CO_2^-)$	127±4
		$k_A^B((CH_3)_3CCO_2^-)$	120±10
		$k_A^B((CH_3)_2AsO_2^-)$	91±8
		$k_A^B(HPO_4^{-2})$	130±15

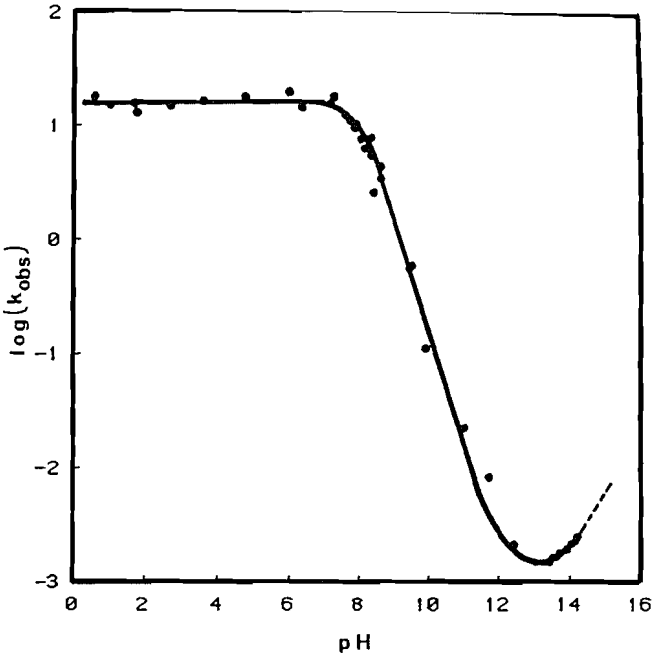


FIG. 2. Rate–pH profile for the hydrolysis of the phosphorane **1** in 1:3 acetonitrile:water at 25°C and ionic strength 1.0. See text for the significance of the various regions.

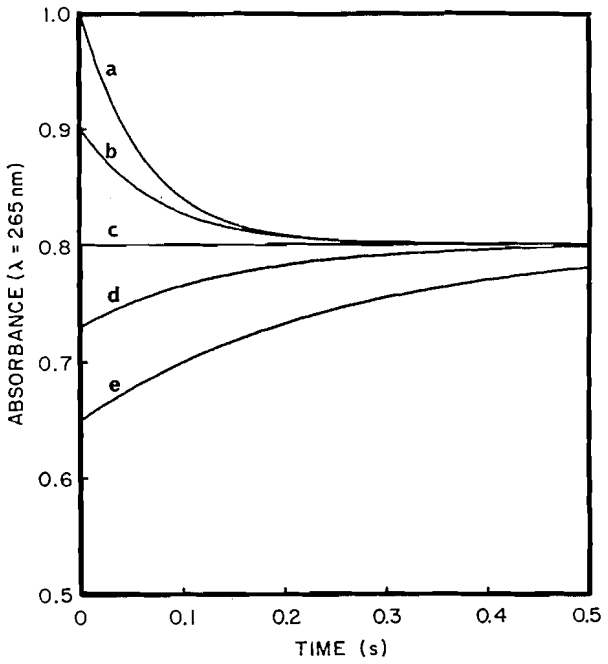


FIG. 3. Absorbance at 265 nm as a function of time for the hydrolysis of 1 mM phosphorane **1** at (a) pH 7.2; (b) pH 7.8; (c) pH 8.4; (d) pH 9.0; and (e) pH 9.6.

the initial absorbance minus the final absorbance, a plot of ΔAbs versus pH for a constant concentration of phosphorane is found to have the general form of an acid–base titration curve,

$$[5]\qquad \Delta Abs = \left(\frac{\Delta Abs(Acid)[H^+] + \Delta Abs(Base)K_a(Spect.)}{[H^+] + K_a(Spect.)}\right)$$

where ΔAbs(Acid) and ΔAbs(Base) are the absorbance changes that occur at low pH (<6) and high pH (>10.5) respectively. K_a(Spect.) is the apparent acidity constant; the value obtained from a fit of the experimental data is $(7 \pm 2)\times10^{-9}$.

The first-order rate constants obtained in this region connect the pH-independent region at low pH with the H^+-dependent region at high pH (see Fig. 2). These rate constants follow the rate law

$$[6]\qquad k_{Intermed.}(obs) = \left(\frac{k_A^0}{[H^+] + K_a(Kin.)}\right)$$

where $k_{Intermed.}$(obs) refers to rate constants obtained at zero buffer concentration, and K_a(Kin.) is a kinetic acidity constant. The constant k_A^0 is identical to the pH-independent rate constant observed in more acidic solutions (see eq. [4]), while the ratio k_A^0/K_a(Kin.) is the same as the constant k_B^H obtained at higher pH (see eq. [3]). Values of K_a(Kin.) were determined in two ways, from the ratio k_A^0/k_B^H as $(9 \pm 3)\times10^{-9}$, and from a fit to eq. [6] of the data in the intermediate range as $(10 \pm 2)\times10^{-9}$.

There must be an initial absorbance increase on adding the phosphorane to a solution with pH < ~9. This, however, could not be observed at any pH, even in experiments where the phosphorane in a basic solution (0.002 M NaOH) was mixed on a stopped-flow spectrophotometer. In these experiments a rapid increase in absorbance is expected, associated with the formation of the phosphonium ion, followed by the subsequent slower absorbance decrease that is illustrated in Fig. 3. All that was observed was the latter. We conclude that the rate of the initial process is beyond the limit of detectability of the stopped-flow apparatus, so that its rate constant must be greater than 500 s^{-1}.

Phosphonium ions

The ^1H NMR spectrum that results when **1** is reacted with an equivalent amount of CF_3SO_3H at −75°C in CD_2Cl_2 is shown in

Can. J. Chem. Downloaded from www.nrcresearchpress.com by 123.30.183.119 on 09/08/12
For personal use only.

Can. J. Chem. Downloaded from www.nrcresearchpress.com by 123.30.183.119 on 09/08/12
For personal use only.

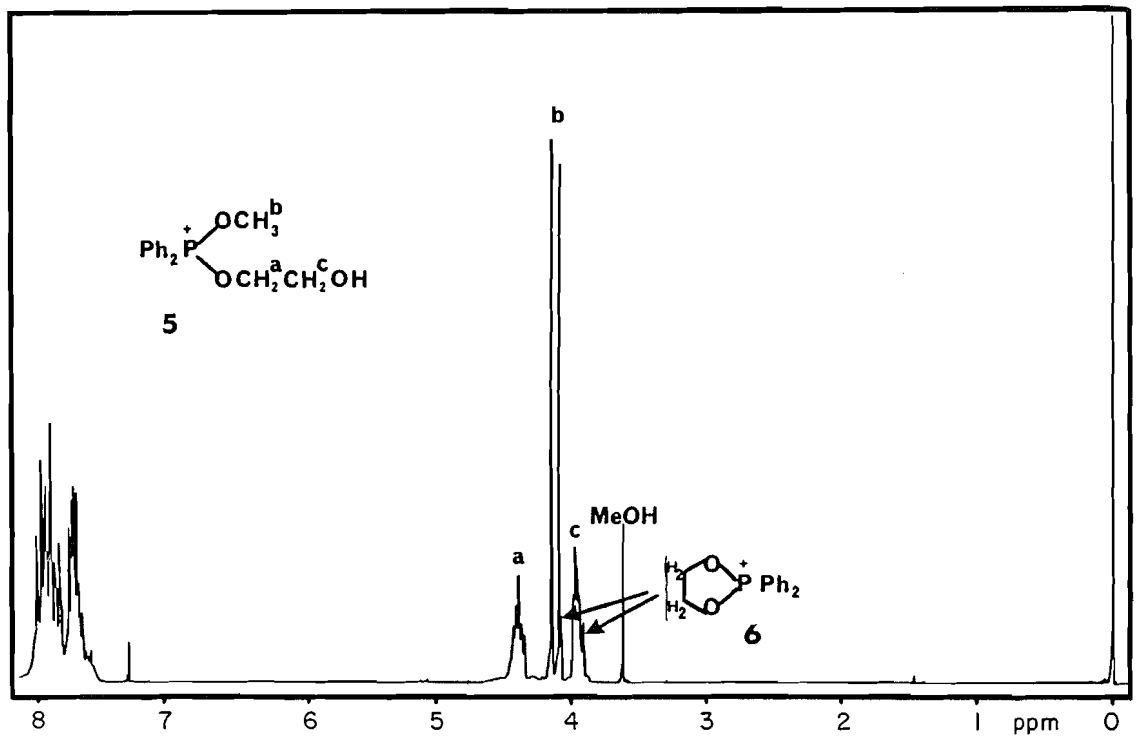
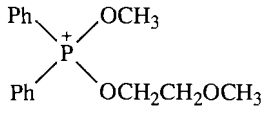


FIG. 4. ^1H NMR spectrum (200 MHz) of the phosphorane **1** (0.1 M) in CD_2Cl_2 after reaction at −70°C with one equivalent of trifluoromethanesulfonic acid.

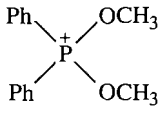
Fig. 4. For the most part, this spectrum is consistent with the formation of the ring-opened cation **5**. In particular, there is a doublet associated with the OCH_3 group still coupled with phosphorus, and complex multiplets due to the unsymmetrical $-CH_2CH_2-$ group. There is, however, a small amount of methanol also produced in this experiment, as verified by the addition of authentic alcohol. This suggests that some of the cyclic five-membered cation **6** is produced as well, and indeed two smaller peaks are visible in the ^1H NMR spectrum that are consistent with the doublet expected for the ethylene group of this cation. The situtation is more clearly revealed in the ^{31}P NMR spectrum, since here two resonances are clearly observed in a roughly 10:1 ratio, with the larger signal at +58.9 ppm and the smaller at +89.7 ppm. The 31 ppm difference strongly supports the assignment of the minor peak as the cyclic cation, since this is in line with the effect of the five-membered ring on the phosphorus chemical shift in a phosphonium ion (4).

It is possible to demonstrate that the ring-opened **5** is indeed the species observed in the hydrolysis of **1** in aqueous acid. When a solution of this cation in anhydrous acetonitrile is mixed with dilute aqueous HCl on a stopped-flow apparatus, an absorbance decrease is observed, with a rate constant of 25 s^{-1}. The same result is obtained when an acetonitrile solution of the phosphorane is mixed with the aqueous acid. When a similar experiment is carried out with the cation **5** in acetonitrile being mixed with aqueous borate buffer of pH 10, an absorbance increase is observed, again with a rate constant identical to that obtained with the phosphorane. This indicates that the phosphonium ion recyclizes in the more basic solutions, regenerating the phosphorane. The absorbance change associated with the cyclization cannot, however, be observed, being complete within the mixing time on the stopped-flow apparatus.

The cation **7** as its $CF_3SO_3^-$ salt was prepared as a model for **5** by reacting 2-methoxyethyl diphenylphosphinate with $CF_3SO_3CH_3$. This cation hydrolyzes in 1:3 acetonitrile:water (μ = 1.0, 25°C) with a rate constant of 4×10^{-4} s^{-1}. The analogous cation **8** has been previously studied, with the rate constant reported in 100% water (μ = 0.1, 25°C) of 5.0×10^{-4} s^{-1} (8).



7



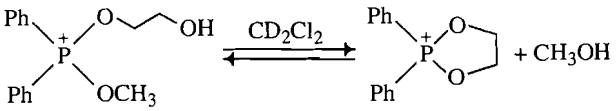
8

Discussion

Relative stability of cyclic five-membered and acyclic phosphonium ions

In the NMR experiment carried out in CD_2Cl_2 (Fig. 4), the two phosphonium ions would be present as a thermodynamic mixture of ion pairs, equilibrating by way of the phosphorane. This conclusion can be made since the rates should be very fast, the reaction in the forward direction involving a rapid cyclization (see later) and the reaction in the reverse direction the attack of a nucleophile on a very reactive cyclic five-membered cation (4). Based upon the ^{31}P NMR integration and the initial concentrations of the reagents, the equilibrium constant [**5**.CF_3SO_3-][CH_3OH]/[**6**·CF_3SO_3-] is approximately 10^{-3} M. This corresponds at −70°C to a difference in free energy of +2.7 kcal mol^{-1}.

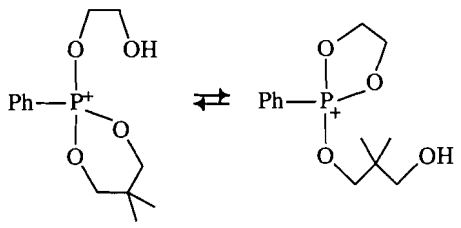
[7]



$CF_3SO_3^-$ $CF_3SO_3^-$

5 **6**

In the previous paper isomeric cyclic six-membered and five-membered phosphonium ions were compared. The conclusion was that for this equilibrium the free energy is +2.5 to +4.5 kcal/mol^{-1} at 25°C in water (4), with the higher number applying for the mechanistic model that we most favored.

[8] 

9 **10**

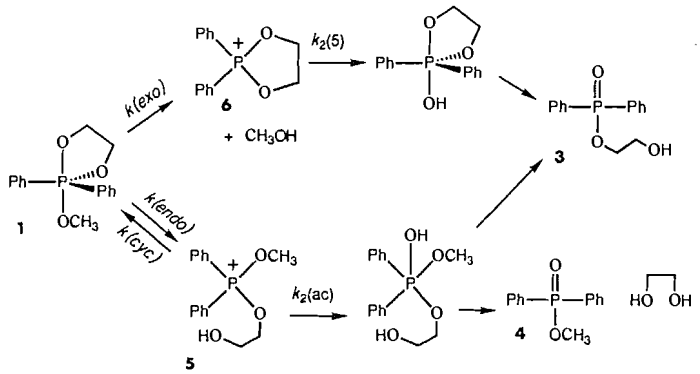
For this latter isomerization ΔG is probably fairly close to ΔH, since the rotational degrees of freedom in the reagent and product are similar, so that ΔS should be ~0. Thus ΔG is determined to a good approximation by the difference in potential energy between the six-membered and five-membered systems, associated with factors such as ring strain in the latter.

For the reaction in eq. [7], ΔS is not zero, but will contain a negative contribution associated with the loss of rotational degrees of freedom in the ethylene group as it forms the ring, offset by a positive contribution associated with the formation of two molecules from one. Estimates of these two effects are ~ −10 cal deg^{-1} mol^{-1} for the former and ~ +30 cal deg^{-1} mol^{-1} for the latter (9). Thus the overall ΔS should be ~ +20 cal deg^{-1} mol^{-1}, and ΔH is therefore about 7 kcal mol^{-1}. Considering the uncertainties in the analyses of the two equilibria of eqs. [7] and [8], it is perhaps risky to conclude that ΔH for the former is greater. What is clear is that in both cases there is an increase in potential energy associated with the formation of the cyclic five-membered phosphonium ion. However, this is not sufficient to entirely account for the enormously accelerated rate of hydrolysis of this type of cation. This was discussed in detail for a comparison of the two cyclic cations in the previous paper. Considering a comparison of a cyclic five-membered cation and an acyclic analog, the rate difference is around 10^8 (4), corresponding to $\Delta\Delta G^{\neq}$ of close to 11 kcal mol^{-1}. As the above calculation shows, this is greater than the difference in potential energy between the two cations.

Mechanism of acid hydrolysis of the monocyclic phosphorane 1

The mechanism for the acid-catalyzed hydrolysis of this phosphorane is shown in Scheme 1. Two different phosphonium ion intermediates can in principle be involved, as with the (5,6)-spirophosphorane discussed in the previous paper. In the latter case, both of the cations formed in ring-opening reactions that were in principle reversible. With the monocyclic derivative of the present study, the acyclic **5** also forms in a ring-opening reaction, and thus reversibility must be considered. However, the concentration of water is so much greater than that of methanol that **6**, if formed, would react with the former to go on to products. Thus for practical purposes the formation of this cation is irreversible.

As with the (5,6)-spiro derivatives the evidence points to the overall hydrolysis proceeding by way of the less thermodynamically stable cation. The first indicator of this is the products. As shown in Scheme 1, the reaction of the ring-opened **5** with water is expected to give rise to two phosphinate esters **3** and **4**, along with amounts of methanol and ethylene glycol equivalent to the former and latter respectively. In fact, neither **4** nor ethylene glycol were found (less than 1%), only **3**



SCHEME 1

and methanol, the products that would be expected of a hydrolysis proceeding by way of **6**. A further indication comes in the observation that the diphenylphosphonium ion **7** that models **5** actually undergoes hydrolysis orders of magnitude more slowly. Aside from a very small electronic effect associated with the 2-methoxy/2-hydroxy groups, the only difference between these two cations is the ability of **5** to cyclize and regenerate its phosphorane precursor. It is therefore concluded that no matter how far the ring-opening equilibrium lies toward **5**, the overall hydrolysis takes place via the strained cyclic cation, and not by a direct reaction of the former cation with water.

If the assumption is made that an equilibrium is maintained during the overall hydrolysis between the phosphorane and the ring-opened cation, then

$$[9] \quad k(\text{obs}) = (k_2(\text{ac}) + K^{\text{H}}(exo)K_a)\left(\frac{[\text{H}^+]}{[\text{H}^+] + K_a}\right)$$

where K_a is the equilibrium constant for the pseudo acid–base reaction involving **1** and **5** ([**1**][H$^+$]/[**5**]), k_2(ac) is the rate constant for the reaction of water with the cation **5**, and the exocyclic cleavage leading to **6** occurs with H$^+$-catalysis, so that $k(exo)$ of Scheme 1 is equal to $k^{\text{H}}(exo)$[H$^+$]. This equation is of the correct form to account for the observed rate–pH profile in solutions more acidic than pH 11 (see eq. [6] and Fig. 2). In acidic solutions where [H$^+$] > K_a, k(obs) is independent of pH, as is observed experimentally, and the pH-independent rate constant, $k_A{}^0$ of eq. [4], is equal to (k_2(ac) + $k^{\text{H}}(exo)K_a$). The direct reaction of **5** with water is modelled by the cation **7**, and thus k_2(ac) should be similar to the rate constant for the latter, i.e., around 4×10^{-4} s^{-1}. The actual observed $k_A{}^0$ is 15 s^{-1}, 40 000 times larger. Thus, as was concluded in the previous section, the contribution from k_2(ac) is negligible. Therefore, in acid solutions in the absence of buffer, k(obs) = $k_A{}^0 = k^{\text{H}}(exo)K_a$. The ring-opened **5** has formed essentially completely, but its hydrolysis proceeds by way of the phosphorane present in equilibrium in small amounts, with the rate-limiting step the H$^+$-catalyzed exocyclic cleavage. The rate is independent of pH since the phosphonium ion must first lose H$^+$ to form the neutral phosphorane. At higher pH where [H$^+$] < K_a and the phosphorane becomes the predominant species in the equilibrium, k(obs) becomes dependent on [H$^+$], with an observed second-order rate constant, $k_B{}^{\text{H}}$ of eq. [3], directly equal to $k^{\text{H}}(exo)$. The changeover from one behavior to the other occurs between pH 9 and pH 7; the K_a value is $(9 \pm 2) \times 10^{-9}$ (pK_a = 8.05), as determined both through an analysis of the kinetics and spectroscopically.

Can. J. Chem. Downloaded from www.nrcresearchpress.com by 123.30.183.119 on 09/08/12
For personal use only.

Can. J. Chem. Downloaded from www.nrcresearchpress.com by 123.30.183.119 on 09/08/12
For personal use only.

Reversibility of the ring-opening step

For the equilibrium assumption to be valid, two conditions must be met. The first is that $k_2(\text{ac}) < k(\text{cyc})$, that is, that hydration of the ring-opened cation is slower than its recyclization to the phosphorane. That this is true is demonstrated by the hydrolysis proceeding exclusively by way of the cyclic five-membered cation, even under acidic solutions where the ring-opened cation predominates. The ability of **5** to regenerate the phosphorane in basic solutions has also been demonstrated. Arguments will be presented shortly that $k(\text{cyc})$ is close to 10^6 times larger than $k_2(\text{ac})$, using for the latter the value expected from the comparison with the model **7**. The second requirement is that $k(endo) > k(exo)$; that is, starting with phosphorane the rate constant for ring-opening to form **5** is greater than the rate constant for exocyclic cleavage to **6**. That this condition is met is demonstrated by the fact that the observed rate constants do obey the rate law appropriate for the equilibrium situation. Moreover, the magnitude and direction of the absorbance changes exhibit the required dependency on H^+ concentration, and the spectroscopic K_a value so produced is in good agreement with the value determined in the kinetic analysis.

That the second condition is met can be further demonstrated for solutions around pH 8, on the basis that the actual equilibration process cannot be observed in these solutions while the exocyclic cleavage can still be seen. To illustrate the argument, we consider a pH 8.05 buffer containing 0.1 M $TrisH^+$. In this solution the measured rate of hydrolysis is 8.4 s^{-1}, with the buffer contributing about 10% (see later for a discussion of this buffer catalysis). Taking the model involving the equilibrium assumption, this solution contains a 50:50 mixture of phosphorane and **5**, and the actual value of $k(exo)$ is double that of $k(\text{obs})$, since half of the equilibrating mixture is unreactive. The approach to equilibrium occurs with a rate constant equal to the sum of the forward and reverse rate constants, $k(endo) + k(\text{cyc})$, and these are numerically equal at pH 8.05 because of the 50:50 equilibrium. The equilibration reaction is so fast that it cannot be observed even with the stopped-flow technique, leading to the conclusion that its rate constant is greater than 500 s^{-1}. Therefore the value of $k(endo)$ is greater than half this, which means that $k(endo)$ is greater than 15 times $k(exo)$.

The rate constant $k^{\text{H}}(exo)$ for H^+-catalyzed exocyclic cleavage is 1.7×10^9 M^{-1} s^{-1}, and the implication that $k(endo) > k(exo)$ means that $k^{\text{H}}(endo)$, the rate constant for H^+-catalyzed ring-opening, must be considerably larger. This is difficult to prove conclusively, but there is one important observation consistent with this interpretation, in that the kinetic and absorbance patterns consistent with reversible ring-opening are still observed in dilute HCl solutions where both endocyclic and exocyclic processes must occur with H^+-catalysis. In particular the magnitudes of the absorbance changes are consistent with those observed in buffer solutions, the absorbance change in dilute HCl being a decrease at the limit ($\Delta\text{Abs(Acid)}$) since phosphonium ion **5** fully forms. If $k^{\text{H}}(endo)$ were not significantly greater than $k^{\text{H}}(exo)$ some of the phosphorane would be immediately converted into products on addition to such a solution, less phosphonium ion **5** would therefore form, and the absorbance decrease associated with its reaction would be smaller.

Considering experimental uncertainties, $k^{\text{H}}(endo)$ must be greater than 10 times $k^{\text{H}}(exo)$, in other words, greater than 2×10^{10} M^{-1} s^{-1}. This number is in the range found for diffusion-controlled proton transfers involving H_3O^+, and is unlikely to exceed 5×10^{10} M^{-1} s^{-1}, the maximum observed for such processes (10). Thus we conclude that $k^{\text{H}}(endo)$ lies in the range $(2–5) \times 10^{10}$ M^{-1} s^{-1}. This also means that we can assign a value of 200–500 s^{-1} for the rate constant $k^0(\text{cyc})$ for the microscopic reverse process, the unassisted or water-catalyzed ring closure of **5** to reform the phosphorane. This conclusion arises since K_a is equal to the ratio $k^0(\text{cyc})/k^{\text{H}}(endo)$. The interesting feature of $k^0(\text{cyc})$ is that it is $\sim 10^6$ times $k_2(\text{ac})$, assuming that the latter will be the same as the rate constant obtained for the model **7** that cannot cyclize. This corresponds to a very large effective molarity of the internal hydroxy group in this cation, in the range $(2–5) \times 10^7$ M (converting $k_2(\text{ac})$ to bimolecular units). Effective molarities of 2-hydroxyethoxy groups in reactions at tetracoordinate phosphorus are generally large (11). The number obtained with the present system would appear at the upper end of ones previously measured.

These very large rate constants for $k^0(\text{cyc})$ and $k^{\text{H}}(endo)$ are also consistent with the failure to observe the kinetics of the pre-equilibrium stage at any pH. In the absence of catalysis by other species, the rate constant for the approach to equilibrium is given by $k^0(\text{cyc}) + k^{\text{H}}(endo)[\text{H}^+]$. With $k^{\text{H}}(endo)$ in the range $(2–5) \times 10^{10}$ M^{-1} s^{-1}, it can be easily seen that in acidic solutions the formation of the cation from the phosphorane is too fast to be observed by the stopped-flow technique, for example $k^{\text{H}}(endo)[\text{H}^+]$ being greater than 2×10^3 in a pH 7 solution. In more basic solutions, the rate of equilibration becomes dominated by $k^0(\text{cyc})$. At pH 8.5, for example, the approach to equilibrium will occur with a rate constant of greater than 260 s^{-1}, using the lower limits for these two rate constants. This corresponds to a half-life of 3 ms, which is just at the limit of detectability. Moreover, since at this pH there is about a 4:1 ratio of phosphorane and phosphonium in equilibrium, the actual absorbance "burst" associated with the approach to this equilibrium would be small, and thus very difficult to detect.

General acid catalysis

The buffer catalysis observed for the overall hydrolysis is explained by general acid catalysis of the exocyclic cleavage. This appears as true general acid catalysis at pH > 9, and general base catalysis at pH < 7, where the phosphonium ion **5** predominates in the initial equilibrium. In the latter case, a proton must be lost prior to the rate-limiting general acid step, and the observed rate constants for general base catalysis (k_A^B of eq. [4]) are related to the true rate constants for the general acid reaction $k^{\text{HA}}(exo)$ by the expression

$$[10] \qquad k^{\text{HA}}(exo) = \frac{k_A{}^B K_a(\text{HA})}{K_a}$$

where $k_a(\text{HA})$ is the acidity constant of the catalyzing acid, and K_a is the equilibrium constant previously defined relating the phosphorane and ring-opened phosphonium ion **5**. Figure 5 shows the Brønsted plot obtained for $k^{\text{HA}}(exo)$, combining the rate constants measured directly at high pH ($k^{\text{HA}}(exo) = k_B{}^{\text{HA}}$), along with ones calculated from eq. [10] for the data from low pH. This plot consists of a linear portion for acids with $pK_a(\text{HA}) > 3$, shared by oxygen acids and protonated amines alike, with a slope α of 1.00 ± 0.05. For acids with $pK_a(\text{HA}) < 3$ the plot curves, and it appears that α is approaching a limiting value of zero as $k^{\text{HA}}(exo)$ approaches the diffusion limit of $10^9–10^{10}$ M^{-1} s^{-1}. This break from linearity occurs with catalysts belonging to a single class, the carboxylic acids, so that it cannot be attributed to the presence of different structural types.

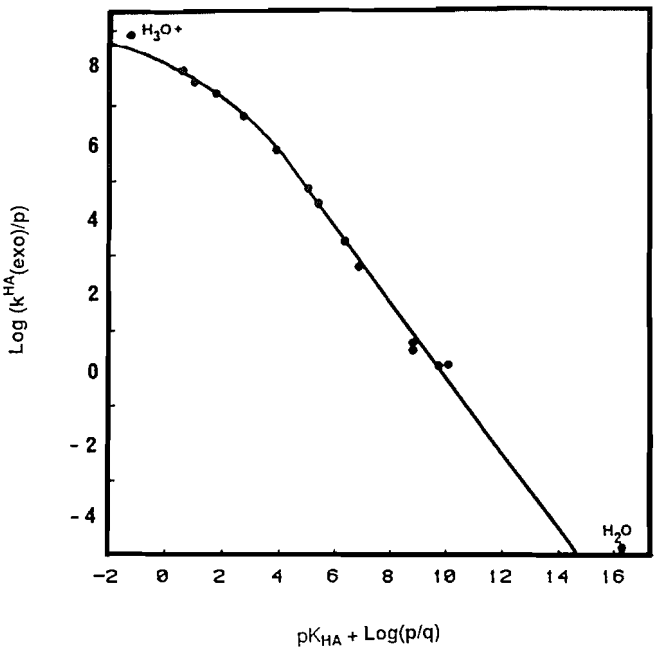


FIG. 5. Brønsted plot for general acid catalysis of exocyclic cleavage in the hydrolysis of the phosphorane **1**. The water rate constant has been converted to second-order units by dividing k_B^0 by the concentration of water in this solvent.

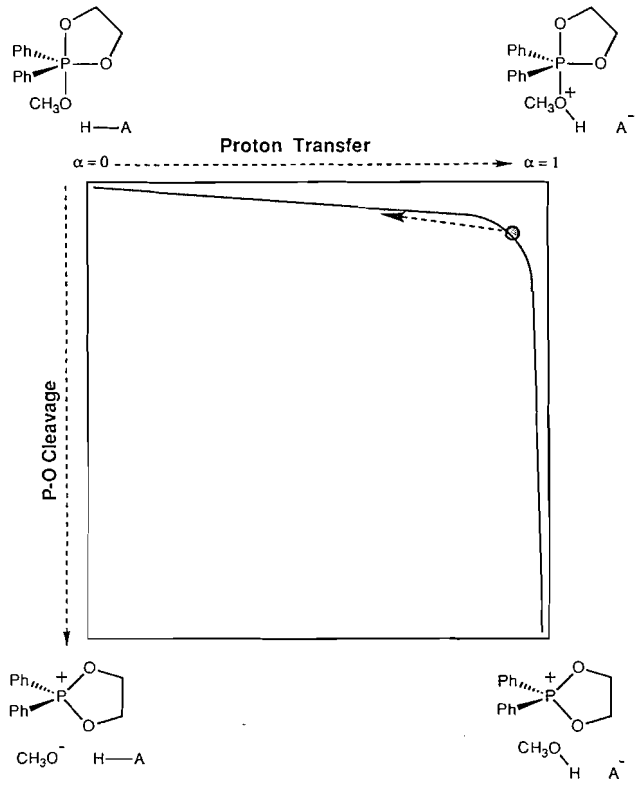
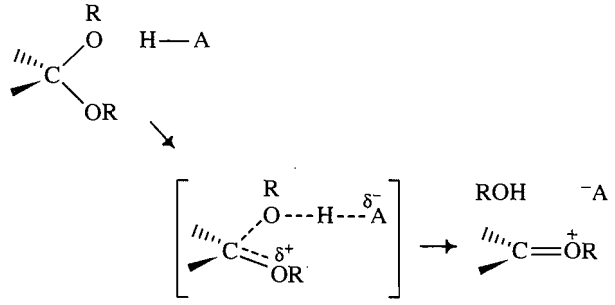


FIG. 6. Reaction coordinate diagram for the general acid-catalyzed exocyclic cleavage of the phosphorane **1**. The reaction is considered to be concerted, with almost complete proton transfer in the transition state, and only a small amount of phosphonium ion character. For strong acids, $pK_a < 3$, the transition state moves in the direction of the arrow toward the phosphorane corner, and the Brønsted value decreases.

This process is in some ways analogous to the general acid-catalyzed hydrolyses of acetals and ortho esters (12, 13), the C=O analogs of phosphoranes. With the acetal/ortho ester class there is now considerable evidence in favor of a mechanism with proton transfer and C—O bond breaking concerted (eq. [11]), with partial proton transfer to the departing alkoxide and partial oxocarbocation character in the transition state (14–18).

[11]

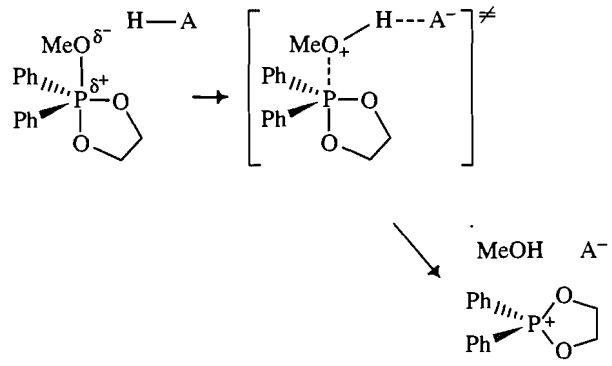


The picture with the phosphorane must, however, be different. The first noteworthy feature is the k^H value for H^+-catalysis, which is several orders of magnitude larger than any that have been observed with acetals and ortho esters, even with derivatives such as tropone diethyl ketal where very stable and observable (19) oxocarbocation intermediates are formed. With the acetals and ortho esters there is a general trend that the larger the k^H value, the smaller the Brønsted α. This is explained by a model where the more reactive systems have earlier transition states with less proton transfer. By analogy to the acetal system, the large k^H observed for the phosphorane leads to the expectation of a relatively low α. Exactly the opposite is observed, with the α value implying almost complete proton transfer in the transition state.

The Brønsted plot for the phosphorane in fact bears some resemblance to an "Eigen curve" for a simple proton transfer (20). This suggests a rate-limiting proton transfer to the exocyclic oxygen to form a protonated phosphorane, followed by a fast P—O cleavage to yield the phosphonium ion. We, however, feel that the mechanism cannot be as simple as this. A close comparison of the Brønsted plot of Fig. 5 and an "Eigen" Brønsted plot for a simple proton transfer shows that the former does not have exactly the same characteristics, a sharper "break" being observed with the Eigen plot. Moreover, the break with the phosphorane occurs near pH 2, implying that if the reaction were simple proton transfer, the conjugate acid of the phosphorane has a pK_a value of about +2. This is unlikely. Protonated phosphoranes have been argued to be very strong acids with large negative pK_a values (21), associated with the presence of the electron-withdrawing groups attached to phosphorus.

A reaction coordinate diagram for a general acid-catalyzed P—O cleavage is shown in Fig. 6. This has axes of P—O bond cleavage (y axis) and proton transfer (x axis). The α value is determined by the amount of proton transfer and is measured along the x axis. A similar diagram is drawn for the general acid-catalyzed C—O cleavage of acetals and ortho esters, and with these there is evidence from structure–activity correlations that the transition state lies towards the center of the diagram, showing significant amounts of both proton transfer and C—O bond cleavage (14–18). What we propose for the phosphorane, however, is a situation such as that described by the pathway indicated in Fig. 6, where the cleavage is concerted, but the transition state lies close to the protonated phosphorane

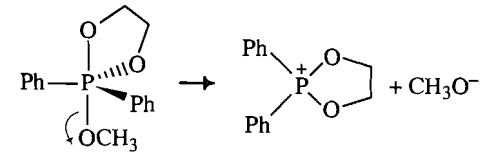
Can. J. Chem. Downloaded from www.nrcresearchpress.com by 123.30.183.119 on 09/08/12
For personal use only.

[12] 

corner. With weak acids, there is almost complete proton transfer in the transition state, so that the Brønsted α value is close to one. When the acids become sufficiently strong, around $pK_a(HA) < 3$, a Hammond effect results in movement of the transition state toward the phosphorane, and the α value decreases. It can be noted that the apical bonds in phosphoranes are highly polarized (22, 23). One can then imagine a model where, on encountering a weak acid, an almost complete proton transfer takes place before the P—O bond starts cleaving. We are currently conducting a detailed examination of this system, varying the aromatic substituent to provide a measure of phosphonium ion character in the transition state, and varying the basicity of the leaving alcohol to probe how this affects the amount of proton transfer.

pH-Independent hydrolysis

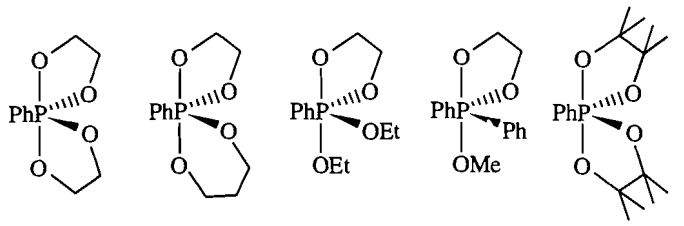
This section is concerned with the term k_B^0 of eq. [3], which becomes important around pH 12. At this pH the phosphorane is the dominant species present in the ring-opening equilibrium, and there are two possible mechanisms for a pH-independent hydrolysis, one involving a straightforward ionization of the exocyclic P—OCH_3 bond, and the second, a reaction in which water acts as a general acid catalyst to assist the cleavage, as in eq. [12] with HA = H_2O. As shown in Fig. 5, the pH-independent rate constant, after correcting to bimolecular units, lies above the Brønsted line for the other general acids. Similar findings are made with acetals and ortho esters that show pH-independent hydrolyses, and this has been argued as support for a non-assisted heterolysis (24). The deviation from the Brønsted line in the present case, however, is not great and, considering that water can be especially effective as a catalyst (25), the general acid mechanism probably cannot be eliminated.

[13] 

1 **6**

Hydroxide ion reaction

The catalysis by hydroxide ion observed at very high pH was not investigated in detail, but it is likely to involve an associative mechanism proceeding by way of a hexacoordinated anion, as has been suggested for the (5,5)-spirophosphoranes (1). A comparison of second-order rate constants for the hydroxide ion reaction is shown as follows:



0.062 (ref. 1) 0.44 (ref. 4) 0.38 (ref. 26) 0.001 $<10^{-4}$ (ref. 26)

The first three phenyltetraalkoxyphosphoranes react with hydroxide at similar rates. The relatively low reactivity of **1** is probably due to a steric effect exerted by the additional phenyl group. As shown by the last entry, an octamethyl derivative of the (5,5)-spirophosphorane undergoes an extremely slow OH^- hydrolysis, if at all, and this must be related to a steric effect.

Experimental section

Materials

2,2-Diphenyl-2-methoxy-1,3,2-dioxaphospholane (1) was prepared by the reaction of methyl diphenylphosphonite (27), ethylene glycol, and *N*-chlorodiisopropylamine (28) according to the method of Trippett and co-workers (29). The crude product was obtained as a viscous, colorless oil, which was further purified, albeit with substantial loss of material, by first dissolving in pentane, followed by washing with half of the volume of propylene carbonate at 0–5°C. This phosphorane had ^{31}P NMR ($CDCl_3$) δ: −26.4; ^1H NMR ($CDCl_3$) δ: 7.9–7.2 (10H, mult.), 3.8 (4H, d, J_{P-H} = 12 Hz), 3.1 (3H, d, J_{P-H} = 11 Hz).

2-Methoxyethyl diphenylphosphonate was prepared from diphenylphosphinyl chloride in dry ether through the addition of an ether solution of equivalent amounts of 2-methoxyethanol and triethylamine at 0°C under nitrogen. The triethylamine hydrochloride was removed by filtration, the ether was evaporated, and the ester recrystallized from benzene–hexane; mp 37.5–38.0°C; NMR ($CDCl_3$) δ: +32.4; ^1H NMR ($CDCl_3$) δ: 7.9–7.0 (10H, mult.), 4.2–3.8 (2H, mult.), 3.5 (2H, t, J_{H-H} = 5 Hz), 3.2 (3H, s).

The (2′-methoxyethoxy)diphenylmethoxyphosphonium ion (7) was prepared in methylene chloride solution (3 mL) by reacting 2-methoxyethyl diphenylphosphinate (1 mmol) with one equivalent of methyl trifluoromethanesulfonate. The reaction was monitored by ^{31}P NMR spectroscopy. The cation had ^{31}P NMR, δ: +58.7. Kinetic studies were performed directly on this solution.

Methyl diphenylphosphinate (4) (8) was prepared as previously described.

Products

The phosphoranes were dissolved in 1:1 D_2O:acetonitrile containing appropriate buffer or acid. After a short period of time, the solution was frozen, and the solvents removed by lyophilization. The products were dissolved in $CDCl_3$, and ^{31}P and ^1H NMR spectra recorded. A single product, 2-hydroxyethyl phenylphosphinate **3** was obtained at both neutral and acidic pH. This had ^{31}P NMR δ: +35.2; ^1H NMR δ: 8.0–7.2 (10H, mult.), 4.30–3.95 (2H, mult.), 3.90–3.60 (2H, mult.). A sample of **3** was obtained after hydrolysis as white crystals with mp 101–103°C (lit.(7) mp 103.5–104.5°C). Anal. calcd. for $C_{14}H_{14}O_3P$: C 64.12, H 5.72, P 11.82; found: C 64.32, H 6.06, P 11.95.

Kinetic methods

Rate constants were obtained in 1:3 CH_3CN:H_2O, with the ionic strength being maintained at 1.00 with NaCl. The procedures for the measurements have been described previously (1–4).

Spectroscopic acidity constants were obtained by adding a small quantity (5–10 μL) of a stock solution of the phosphorane in methylene chloride to 5 mL of 0.005 M NaOH, and then mixing this with an appropriate buffer on the stopped-flow spectrophotometer. The total absorbance change, $\Delta Abs = A_0 - A_\infty$, was measured. Special care was taken to insure that the concentration of phosphorane was the same

Can. J. Chem. Downloaded from www.nrcresearchpress.com by 123.30.183.119 on 09/08/12
For personal use only.

each time this was done. In addition, since the phosphorane is undergoing hydrolysis in the NaOH solution, the time interval between the intial preparation of this solution and the final mixing was kept constant.

Acknowledgement

The continued financial support of the Natural Sciences and Engineering Research Council of Canada is gratefully acknowledged.

1. R. A. McClelland, G. Patel, and C. Cirrina. J. Am. Chem. Soc. **103**, 6432 (1981)
2. G. H. McGall and R. A. McClelland. J. Chem. Soc. Chem. Commun. 561 (1985).
3. G. H. McGall and R. A. McClelland. J. Am. Chem. Soc. **107**, 5198 (1985).
4. G. H. McGall and R. A. McClelland. Can. J. Chem. **69**, 2064 (1991).
5. F. H. Westheimer. Acc. Chem. Res. **1**, 70 (1968).
6. P. Gillespie, F. Ramirez, I. Ugi, and P. Marquarding. Angew. Chem. Int. Ed. Engl. **12**, 91 (1973).
7. R. S. Edmunson and J. O. L. Wrigley. Tetrahedron, **23**, 283 (1969).
8. R. A. McClelland, G. H. McGall, and G. Patel. J. Am. Chem. Soc. **107**, 5204 (1985).
9. M. I. Page and W. P. Jencks. Proc. Natl. Acid. Sci. U.S.A. **68**, 1678 (1971).
10. J. E. Crookes. Comprehensive chemical kinetics. Vol. 8. *Edited by* C. H. Bamford and C. F. H. Tipper. Elsevier, New York. 1979. p. 197.
11. A. J. Kirby. Adv. Phys. Org. Chem. **17**, 183 (1980).
12. E. H. Cordes and H. G. Bull. Chem. Rev. **74**, 581 (1974).
13. T. H. Fife. Acc. Chem. Res. **5**, 264 (1972).
14. N. Gravitz and W. P. Jencks. J. Am. Chem. Soc. **96**, 507 (1974).
15. B. Capon and K. Nimmo. J. Chem. Soc. Perkin Trans. 2, 1113 (1974).
16. J. M. Sayer and W. P. Jencks. J. Am. Chem. Soc. **99**, 464 (1977).
17. W. P. Jencks. Acc. Chem. Res. **9**, 425 (1976).
18. R. G. Bergstrom, M. J. Cashen, Y. Chiang, and A. J. Kresge. J. Org. Chem. **44**, 1639 (1979).
19. R. A. McClelland and M. Ahmad. J. Am. Chem. Soc. **100**, 7027 (1978).
20. M. Eigen. Angew. Chem. Int. Ed. Engl. **3**, 1 (1964).
21. J. P. Guthrie. J. Am. Chem. Soc. **99**, 3991 (1977).
22. R. R. Holmes. Pentacoordinated phosphorus. Vols. 1 and 2. ACS Monographs 175 and 176, American Chemical Society, Washington, DC. 1980.
23. G. R. J. Thatcher and R. Kluger. Adv. Phys. Org. Chem. **25**, 99 (1989).
24. J. L. Jensen and W. P. Jencks. J. Am. Chem. Soc. **101**, 1476 (1979).
25. A. J. Kresge. Acc. Chem. Res. **8**, 354 (1975).
26. G. H. McGall. PhD. Thesis, University of Toronto, 1987.
27. L. A. Hamilton and S. Landis. Organic phosphorus compounds. Vol. 4. *Edited by* G. M. Kosolapoff and L. Maier. John Wiley and Sons, New York. 1972. p. 463.
28. H. Bock and K. L. Kompa. Chem. Ber. **99**, 1347 (1966).
29. S. Antczak, S. A. Bone, J. Brierley, and S. Trippett. J. Chem. Soc. Perkin Trans. 1, 278 (1977).

Can. J. Chem. Downloaded from www.nrcresearchpress.com by 123.30.183.119 on 09/08/12
For personal use only.

Kinetics of breakdown of aryl hemiacetals of α-bromoacetophenone. Effect of phenol leaving groups on the lifetimes of tetrahedral intermediates

ROBERT A. MCCLELLAND,[1] V. M. KANAGASABAPATHY, AND N. MATHIVANAN
Department of Chemistry, University of Toronto, Toronto, Ont., Canada M5S 1A1

Received May 3, 1991

ROBERT A. MCCLELLAND, V. M. KANAGASABAPATHY, and N. MATHIVANAN. Can. J. Chem. **69**, 2084 (1991).

The kinetics of breakdown of seven aryl hemiacetals of α-bromoacetophenone (TOH) have been examined, with aryl substituents 4-MeO, 4-Me, 3-Me, H, 3-MeO, 4-Cl, 3-Cl. The hemiacetals were generated as intermediates in the aqueous bromination of α-aryloxystyrenes, where the breakdown of the hemiacetal is the rate-limiting stage in the overall reaction. Base catalysis of the breakdown shows large Brønsted β values (0.8–1.0) and similarly large β_{lg} values (−0.8 to −1.0). These are argued to arise because of a preassociation mechanism in which the hydrogen-bonded intermediate $TO^- \cdots HA$ loses aryloxide faster than diffusional separation of the acid–base pair. This mechanism is enforced by lifetimes of the deprotonated hemiacetals TO^- in the 10^{10}–10^{12} s^{-1} range. Such lifetimes were estimated in two independent ways, by extrapolation of data previously obtained for alkyl hemiacetals of α-bromoacetophenone, and through a calculation based upon the experimental catalytic coefficients, and estimates of the acidity constants for TOH and the equilibrium constants for formation of hydrogen-bonded complexes. The pH-independent breakdown has $\beta_{lg} = -1.03$, and the point lies near the Brønsted line for the carboxylate catalysts. This, therefore, also occurs by a preassociation mechanism with water as the catalyst forming the intermediate $TP^- \cdots H_3O^+$, which loses aryloxide faster than diffusional separation. Catalysis by hydroxide ion occurs with rate constants of 8×10^9 M^{-1} s^{-1} independent of aryl substituent. This represents rate-limiting diffusional encounter of the hemiacetal and hydroxide ion, the hydrogen-bonded intermediate $TOH \cdots OH^-$ rapidly proceeding on to products. Acid catalysis of the hemiacetal breakdown occurs by a class "n" mechanism in which the acid assists departure of the substitued phenol. Alkyl hemiacetals of α-bromoacetophenone break down by a class "e" mechanism where the leaving group is fully protonated before bond cleavage. The class "e" mechanism can be excluded for the aryl derivatives, since rate constants much greater then diffusion are required to explain the observed catalytic coefficients. The different mechanism is followed in order to avoid the fully protonated hemiacetal, which, being of an O-protonated anisole structure, is of very high energy.

Key words: hemiacetal kinetics, preassociation, intermediate lifetime.

ROBERT A. MCCLELLAND, V. M. KANAGASABAPATHY et N. MATHIVANAN. Can. J. Chem. **69**, 2084 (1991).

On a étudié la cinétique de la décomposition de sept hémi-acétals aromatiques, portant les substituants 4-OMe, 4-Me, 3-Me, H, 3-OMe, 4-Cl et 3-Cl, de l'α-bromoacétophénone (TOH). On a formé les hémi-acétals comme intermédiaires par bromation d'α-aryloxystyrènes en milieu aqueux; dans ces conditions, la décomposition des hémi-acétals est l'étape qui limite la vitesse globale de la réaction. Une décomposition catalysée par les bases présente des valeurs β de Brønsted élevées (0,8 à 1,0) et, de la même manière, des valeurs β_{lg} élevées (−0,8 à −1,0). On suggère que ces résultats sont causés par un mécanisme de pré-association dans lequel la perte d'un arylate, par l'intermédiaire impliqué dans la liaison hydrogène $TO^- \cdots HA$ est plus rapide que la séparation causée par la diffusion de la paire acide–base. Ce mécanisme est imposé par des temps de vie des hémi-acétals déprotonés, TO^-, qui sont de l'ordre de 10^{10} à 10^{12} s^{-1}. On a évalué ces temps de vie de deux façons indépendantes : par une extrapolation de données obtenues antérieurement pour des hémi-acétals aliphatiques de l'α-bromoacétophénone suivie d'un calcul basé sur les coefficients catalytiques expérimentaux et par des évaluations des constantes d'acidité du TOH et des constantes d'équilibre pour la formation de complexes impliquant des liaisons hydrogènes. Pour la décomposition qui ne dépend pas du pH, la valeur de $\beta_{lg} = -1{,}03$ et ce point se trouve prés de la ligne de Brønsted pour les catalyseurs carboxylates. Cette réaction se produit donc par un mécanisme de pré-association dans lequel l'eau agit comme catalyseur conduisant à la formation de $TO^- \cdots H_3O^+$ pour lequel la perte d'un arylate est plus rapide que la séparation due à la diffusion. Quel que soit le substituant du noyau aromatique, les constantes de vitesse pour les réactions catalysées par l'ion hydroxyde sont toutes égales à 8×10^9 M^{-1} s^{-1}. Cette valeur est égale à une rencontre de l'hémi-acétal et d'un ion hydroxyde dont la vitesse serait limitée par la diffusion et dont l'intermédiaire $TOH \cdots OH^-$ se transforme rapidement en produits. La décomposition acido-catalysée des hémi-acétals se produit par un mécanisme de classe « n » dans lequel l'acide aide au départ du phénol. La décomposition des hémi-acétals aliphatiques de l'α-bromoacétophénone se produit par un mécanisme de classe « e » dans lequel le groupe nucléofuge est complètement protoné avant le bris de la liaison. On peut exclure le mécanisme de classe « e » pour les dérivés aromatiques car des constantes de vitesse beaucoup plus grandes que la diffusion sont nécessaires pour expliquer les coefficients catalytiques observés. Le mécanisme différent est suivi afin d'éviter l'hémi-acétal complètement protoné qui, possédant une structure d'anisole O-protoné, possède une énergie très élevée.

Mots clés : la cinétique de hémi-acétals, pré-association, intermédiaire, temps de vie.

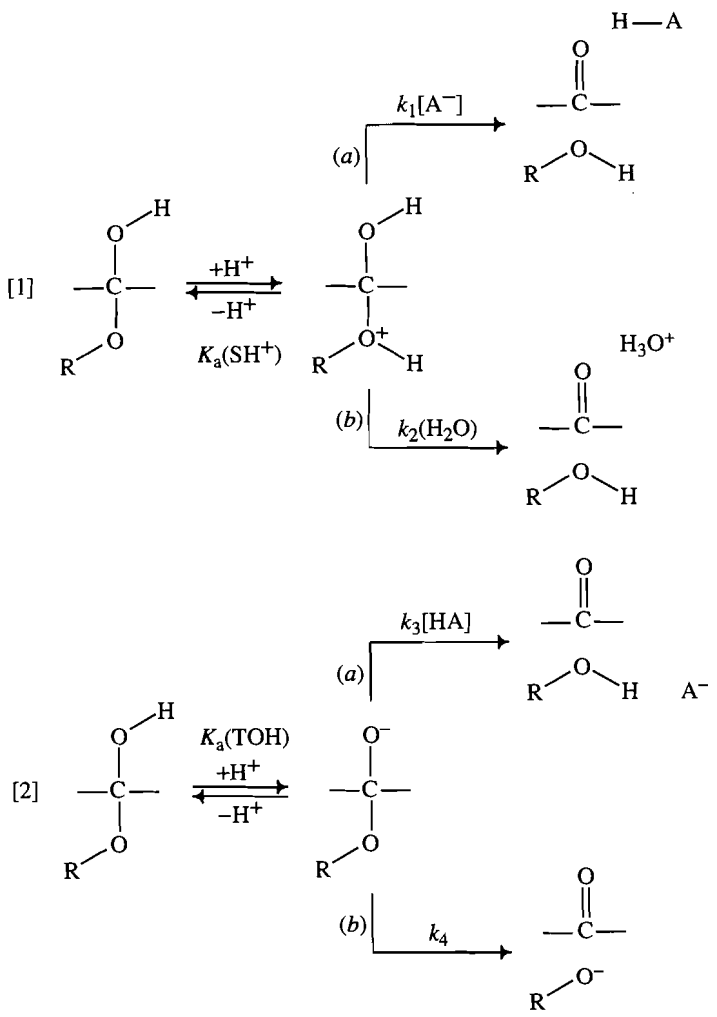
[Traduit par la rédaction]

Detailed kinetic studies of the general acid–base catalyzed breakdown of hydrates and hemiacetals have been carried out for a considerable period of time, and various kinetically equivalent mechanisms have been considered (1, 2). Based upon the analysis of structure–reactivity parameters, the general acid-catalyzed reaction has been suggested to proceed via the mechanism of eq. [1*a*], with base-catalyzed breakdown of the protonated hemiacetal as the rate-limiting step, while the general base reaction follows eq. [2*a*], with the rate-limiting step the acid-catalyzed breakdown of the hemiacetal conjugate base (3–5). These mechanisms are termed class "e" and class "n" respectively (2, 3), the catalyst acting on the electrophilic component, the carbonyl, in the acid reaction and the nucleophilic component, the alcohol, in the base reaction. Anal-

[1]Author to whom correspondence may be addressed.

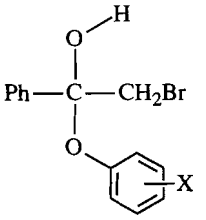
Can. J. Chem. Downloaded from www.nrcresearchpress.com by 123.30.183.119 on 09/08/12
For personal use only.

Can. J. Chem. Downloaded from www.nrcresearchpress.com by 123.30.183.119 on 09/08/12
For personal use only.



yses of energy contour diagrams (6), isotopic mapping (7), and vibrational calculations (8) have provided additional support for the general base mechanism, while the energy contour analysis suggests a slight modification in the acid mechanism (9). The hydroxide ion catalyzed reaction proceeds with pre-equilibrium deprotonation, as in the general base reaction, but RO^- likely departs with no assistance (eq. [2*b*]). The H_3O^+-catalyzed reaction likely follows the class e acid mechanism, with pre-equilibrium protonation and water acting as a general base (eq. [1*b*]]).

The above mechanisms were established through detailed studies of alkyl hemiacetals and hydrates of formaldehyde (3) and acetaldehyde (4), as well as hydrates of substituted benzaldehydes (5). We have been interested in the effect of structural changes that increase the free energy of the tetrahedral form relative to the breakdown products. Studies of the base-catalyzed breakdown of cyclic hemiacetals with phenol (10) and carboxylate (11) leaving groups have shown that the class n mechanism is no longer followed. With hemiorthoester tetrahedral intermediates derived from benzoic acid, the base-catalyzed reaction was found to still follow a class n type of mechanism, but with the proton transfer step rate-limiting (12, 13). This mechanism is enforced (2, 14) by the short lifetime of the anionic intermediate in respect to its breakdown by expulsion of RO^-, as in eq. [2*b*]. A situation similar to this was observed with the 2,2,2-trifluoroethyl hemiacetal of α- bromoacetophenone (15). With this system, a change in mechanistic behaviour from the normal type n reaction, with



X = 4-MeO, 4-Me, 3-Me, H, 3-MeO, 4-Cl, 3-Cl

the initial deprotonation rapid and reversible, to the mechanism with rate-limiting proton transfer occurred on changing the leaving alcohol from 2-chloroethyl to trifluoroethyl. This also was traced to the decreased lifetime of the anionic tetrahedral intermediate with trifluoroethoxide as the leaving group.

In this paper we report a further extension of the α-bromoacetophenone system to aryl hemiacetals. This structural change results in a further decrease in the lifetime of the deprotonated form of the hemiacetal, such that the general base-catalyzed breakdown nows occurs by a preassociation mechanism. It will also be argued that the acid reaction follows an alternative kinetically equivalent pathway, due to the high energy of the protonated tetrahedral intermediate of the class e mechanism.

Experimental section

α-Aryloxystyrenes were prepared by the reaction of aryl benzoates (16, 17) with Tebbe's reagent (18–20). In a typical procedure, titanocene dichloride (2.15 g, 8.6 mmol) and a toluene solution of trimethylaluminum (8.7 mL of 2 M solution, 17.2 mmol) were mixed and allowed to stand 3 days at room temperature under nitrogen. This solution was then transferred by syringe to a solution of the appropriate aryl benzoate (7.8 mmol) in 16 mL of rigorously dried toluene containing 80 μL of dry pyridine. The addition was carried out under nitrogen at −45°C; the reaction was maintained at this temperature for 45 min and then allowed to warm to room temperature. The reaction was quenched by the careful addition of 2.4 mL of 15% aqueous sodium hydroxide. The dark-red mixture was diluted with ether, dried over magnesium sulfate, and the solvent removed to furnish a dark oil. This oil was extracted three times with a small amount of hexane, the hexane fractions pooled, and the solvent removed. (Failure to perform this extraction resulted in difficulty in the chromatography, apparently due to the hexane-insoluble inorganic contaminants blocking the column.) The crude vinyl ether was purified on neutral alumina employing dry hexanes as eluant. The products were obtained as clear oils in yields ranging from 60 to 70%.

α-*(4-Methoxyphenoxy)styrene*. NMR ($CDCl_3$) δ: 3.80 (3H, s), 4.27 (1H, d, J = 2.5 Hz), 4.90 (1H, d, J = 2.5 Hz), 6.84 (2H, d, J = 9 Hz), 7.08 (2H, d, J = 9 Hz), 7.35 (3H, mult.), 7.75 (2H, mult.). High resolution MS, m/e for $C_{15}H_{14}O_2$, calcd.: 226.0994; observed: 226.1006.

α-*(4-Methylphenoxy)styrene*. NMR (CCl_4) δ: 2.30 (3H, s), 4.26 (1H, d, J = 2.5 Hz), 4.86 (1H, d, J = 2.5 Hz), 6.90 (4H, br s), 7.30 (3H, mult.), 7.60 (2H, mult.). High resolution MS, m/e for $C_{15}H_{14}O$, calcd.: 210.1045; observed: 210.1050.

α-*(3-Methylphenoxy)styrene*. NMR ($CDCl_3$) δ: 2.33 (3H, s), 4.44 (1H, d, J = 2.2 Hz), 5.04 (1H, d, J = 2.2 Hz), 6.90 (3H, mult.), 7.10 (1H, mult.), 7.35 (3H, mult.), 7.70 (2H, mult.). High resolution MS, m/e for $C_{15}H_{14}O$, calcd.: 210.1045; observed: 210.1045. Anal. calcd. for $C_{15}H_{14}O$: C 85.68, H 6.71; found: C 85.08, H 6.76.

α-*Phenoxystyrene* (see also ref. 21). NMR ($CDCl_3$) δ: 4.42 (1H, d, J = 2.5 Hz), 5.07 (1H, d, J = 2.5 Hz), 7.0–7.5 (8H, mult.), 7.6–7.8 (2H, mult.).

α-*(3-Methoxyphenoxy)styrene*. NMR (CCl_4) δ: 3.75 (3H, s), 4.44 (1H, d, J = 2.5 Hz), 4.96 (1H, d, J = 2.5 Hz), 6.60 (3H, mult.), 7.20 (4H, mult.), 7.60 (2H, mult.). High resolution MS, m/e for $C_{15}H_{14}O_2$, calcd.: 226.0994; observed: 226.1020.

α-(4-Chlorophenoxy)styrene. NMR (CCl_4) δ: 4.40 (1H, d, J = 2.5 Hz), 5.00 (1H, d, J = 2.5 Hz), 6.95 (2H, d, J = 10 Hz), 7.20–7.40 (5H, mult.), 7.60 (2H, mult.). High resolution MS, m/e for $C_{14}H_{11}ClO$, calcd.: 230.0498: observed: 230.0494.

α-(3-Chlorophenoxy)styrene. NMR ($CDCl_3$) δ: 4.57 (1H, d, J = 2.5 Hz), 5.16 (1H, d, J = 2.5 Hz), 7.70–7.74 (7H, mult.), 7.60 (2H, mult.). Anal. calcd. for $C_{14}H_{11}ClO$: C 72.89, H 4.81, found: C 72.51, H 5.02.

Kinetic experiments

A 2×10^{-5} M solution of the α-aryloxystyrene was dissolved in 0.002 M NaOH and mixed on a stopped-flow spectrophotometer with an equal volume of a solution containing 1.5×10^{-5} M bromine, 0.002 M HCl, and the appropriate buffer. The ionic strength was maintained at a concentration of 0.1 after mixing with NaCl, and the stopped-flow apparatus was thermostated at 25.0 ± 0.1°C. Since low concentrations of buffers were employed in many of the experiments, mixed samples were collected from the effluent of the stopped-flow apparatus and the pH recorded. Initial kinetic experiments were carried out with a Durrum–Gibson stopped-flow apparatus, as previously described (15). The later kinetic experiments were carried out with a High-Tech Scientific SF-51 stopped-flow apparatus interfaced with a Hewlett–Packard model 300 microcomputer. Increases in absorbance due to the formation of the product ketone α-bromoacetophenone were monitored at 250 nm. First-order rate constants were calculated from a least-squares fit to the general equation for an exponential process. Rate constants from replicate measurements agreed within ±3%.

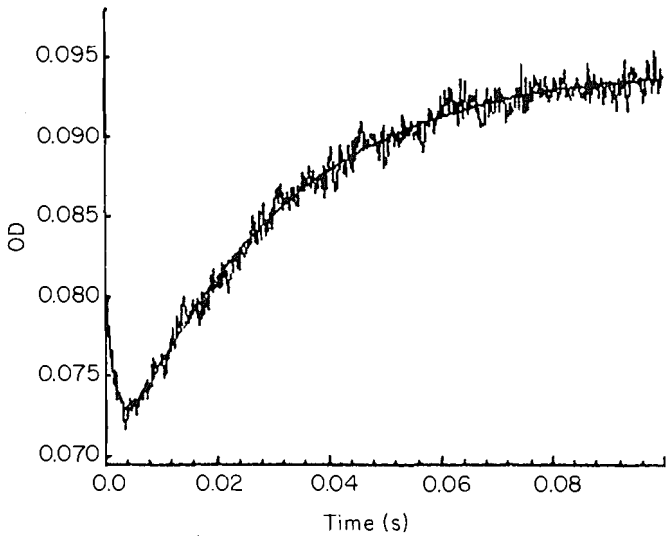
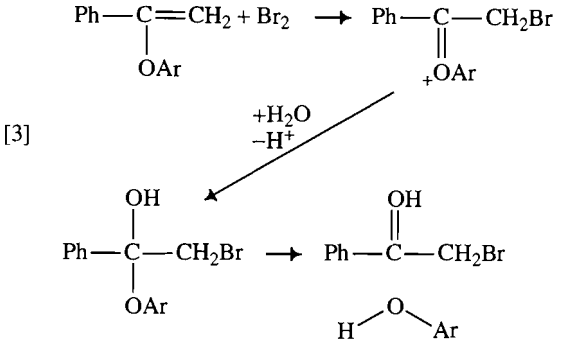


FIG. 1. Absorbance at 250 nm versus time on mixing a solution of 10 μM bromine, 0.002 M HCl, and a 1:1 HOAc:NaOAc buffer of total concentration 0.004 M with an equal amount of 20 μM α-(3-methoxyphenoxy)styrene in 0.002 M NaOH. The line drawn through the experimental data is the computer fit to a double exponential equation with exponents of 513 and 34.1 s^{-1} for the decreasing and increasing phases respectively.

Results

Generation of hemiacetals

The hemiacetals were generated by the aqueous bromination of α-aryloxystyrenes. This method of studying the kinetics of breakdown of hemiacetals was discussed previously in the context of α-alkoxystyrenes (22). The basis of the approach is that the two reaction stages preceding the decomposition of the hemiacetal are very fast. For α-alkoxystyrenes there was ample precedent. The bromination stage had been established to occur with a bimolecular rate constant approaching the diffusion limit (23), and the hydration of the oxocarbocations was also known to be very rapid (24–26). Thus, on mixing aqueous solutions of vinyl ether and bromine, the first two



[3]

stages occur very quickly, resulting in the buildup of the hemiacetal. The rate-limiting stage in the formation of the product α-bromoacetophenone is the breakdown of the hemiacetal, and rate constants measured by following the appearance of this ketone are the rate constants specifically for this stage.

With the α-aryloxystyrenes the bromination stage is possibly slower, since there is not as much stabilization of the incipient oxocarbocation. We were therefore initially concerned that the rate-limiting stage with these vinyl ethers may have shifted towards the first stage. However, the kinetic evidence suggested that this was not the case. In particular, the rate constants for the formation of the α-bromoacetophenone were independent of the initial concentrations of bromine, but did show general acid–base catalysis. Both these observations are consistent with rate-limiting hemiacetal breakdown and are not expected for rate-limiting bromination. It was in fact possible to observe with α-aryloxystyrenes with electron-withdrawing substituents a very rapid *decrease* in absorbance, which we presume represents the disappearance of vinyl ether in the bromination stage. A kinetic trace illustrating this is shown in Fig. 1. The absorbance decreases were extremely rapid, occurring with rates corresponding to half-lives of ~1 ms that are just at the limit of the stopped-flow apparatus. In fact a considerable portion of this decrease must have occurred in the 2-ms dead time, where it would have not have been observed. As shown in Fig. 1 the decrease was followed by a slower exponential *increase* in absorbance with the kinetic characteristics mentioned above consistent with hemiacetal breakdown. Thus, although the bromination stage may have been slowed somewhat, even with these compounds it is faster than hemiacetal breakdown.

One further note concerns the relative ratio of bromine and vinyl ether in the kinetic experiments. While with the α-alkoxystyrenes we had employed excess bromine, similar conditions with the α-aryloxystyrenes resulted in kinetic traces with drifting infinity absorbances. This was traced to a reaction of the excess bromine with the substituted phenol that is one of the products of the bromination of these vinyl ethers. This problem was not encountered when the kinetic experiments were carried out with α-aryloxystyrene in excess, such that the bromine was completely consumed in the first reaction stage.

Kinetics of the breakdown of hemiacetals

Kinetic experiments were carried out at 25.0°C and ionic strength 0.1 in solutions containing HCl, and chloroacetate,

Can. J. Chem. Downloaded from www.nrcresearchpress.com by 123.30.183.119 on 09/08/12
For personal use only.

Can. J. Chem. Downloaded from www.nrcresearchpress.com by 123.30.183.119 on 09/08/12
For personal use only.

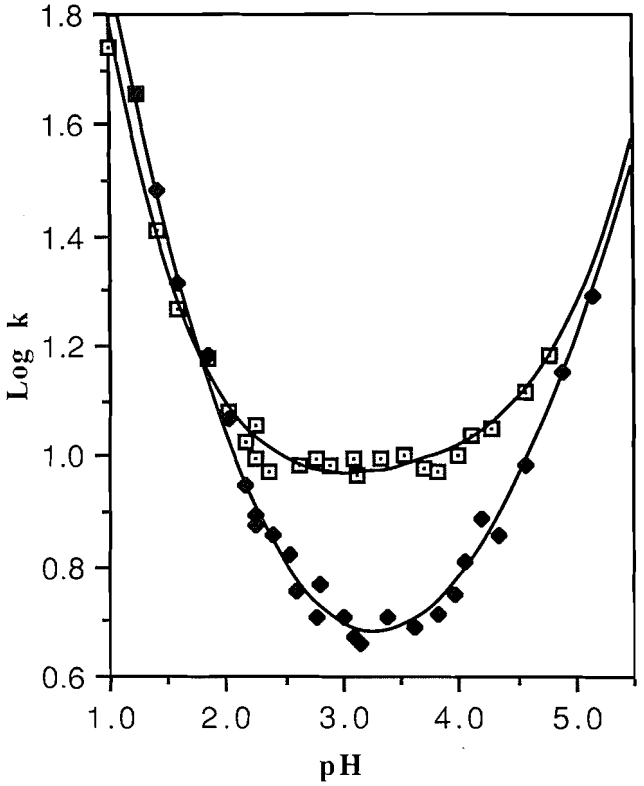


FIG. 2. Rate–pH profiles for the breakdown of α-bromoacetophenone hemiacetals: (⊡) phenyl; (◆) *p*-methoxyphenyl. Rate constants below pH 3 were measured in HCl solutions; above pH 3, they were determined by extrapolation to zero buffer concentration.

3-chloroproponiate, and acetate buffers. These buffers were chosen since they are unreactive towards bromine. More basic buffers could not be employed since rate constants associated with the catalysis by the base component became so large that, even at the minimal concentrations required to maintain buffering capacity, the observed rates were too fast for accurate measurement even by the stopped-flow technique. As noted in the previous section, an exponential increase in the absorbance of the α-bromoacetophenone was observed in each solution. First-order rate constants followed the rate law

$$[4] \quad k(\text{obs}) = k_{\text{H}}[\text{H}^+] + k_0 + k_{\text{OH}}[\text{OH}^-] + k_{\text{HA}}[\text{HA}] + k_{\text{A}}[\text{A}^-]$$

typical of hemiacetal breakdown. In all buffers the buffer dilution plots (k(obs) versus total buffer concentration) were excellently linear. This included chloroacetate and chloropropionate where quite high buffer concentrations could be employed. Rate–pH profiles based upon extrapolation to zero buffer concentration are shown for two of the systems in Fig. 2. Catalytic coefficients are listed in Table 1. There was pronounced catalysis by the base component of the buffer. This was particularly true for acetate buffers, a solution containing 0.001 M CH_3COO^-, for example, reacting with the phenyl hemiacetal with a contribution of 64 s^{-1} from the buffer alone. These accelerations made it difficult to obtain accurate intercepts in the buffer dilution plots in the more basic acetate buffers. These are the solutions where the term in hydroxide becomes important, and thus there were considerable errors in evaluating k_{OH}. In fact with the 3-MeO, 4-Cl, and 3-Cl systems this constant could not be evaluated with reliable precision.

TABLE 1. Rate constants for the breakdown of aryl hemiacetals of α-bromoacetophenone (PhC(OH)(OAr)CH_2Br). Conditions are 25°C, ionic strength = 0.1. Units are M^{-1} s^{-1}, except for water where units are s^{-1}

	Aryl group						
Catalyst	4-$MeOC_6H_4$	4-MeC_6H_4	3-MeC_6H_4	C_6H_5	3-$MeOC_6H_4$	4-ClC_6H_4	3-ClC_6H_4
H_3O^+	$(6.3 \pm 0.3) \times 10^2$	$(6.4 \pm 0.2) \times 10^2$	$(5.3 \pm 0.1) \times 10^2$	$(4.5 \pm 0.1) \times 10^2$	$(4.1 \pm 0.1) \times 10^2$	$(3.6 \pm 0.1) \times 10^2$	$(4.0 \pm 0.2) \times 10^2$
$ClCH_2COOH$	$(3.3 \pm 0.5) \times 10^1$	$(2.3 \pm 0.6) \times 10^1$	$(2.4 \pm 0.4) \times 10^1$	$(1.8 \pm 0.5) \times 10^1$	[a]	[a]	[a]
H_2O	$(4.1 \pm 0.2) \times 10^0$	$(4.2 \pm 0.2) \times 10^0$	$(6.5 \pm 0.1) \times 10^0$	$(9.0 \pm 0.9) \times 10^0$	$(1.9 \pm 0.1) \times 10^1$	$(3.2 \pm 0.1) \times 10^1$	$(6.8 \pm 0.2) \times 10^2$
$ClCH_2CO_2^-$	$(6.9 \pm 0.3) \times 10^1$	$(7.5 \pm 0.5) \times 10^1$	$(8.9 \pm 0.4) \times 10^1$	$(1.2 \pm 0.1) \times 10^2$	$(2.4 \pm 0.2) \times 10^2$	$(4.4 \pm 0.4) \times 10^2$	$(1.1 \pm 0.1) \times 10^3$
$Cl(CH_3)_2CO_2^-$	$(1.1 \pm 0.1) \times 10^3$	$(1.1 \pm 0.1) \times 10^3$	$(1.5 \pm 0.1) \times 10^3$	$(1.6 \pm 0.1) \times 10^3$	$(3.0 \pm 0.3) \times 10^3$	$(5.5 \pm 0.2) \times 10^3$	$(1.2 \pm 0.1) \times 10^4$
$CH_3CO_2^-$	$(4.6 \pm 0.3) \times 10^3$	$(4.3 \pm 0.1) \times 10^3$	$(5.1 \pm 0.2) \times 10^3$	$(6.4 \pm 0.3) \times 10^3$	$(1.2 \pm 0.1) \times 10^4$	[a]	[a]
OH^-	$(8 \pm 2) \times 10^9$	$(7 \pm 2) \times 10^9$	$(9 \pm 3) \times 10^9$	$(8 \pm 2) \times 10^9$	[a]	[a]	[a]

[a]Rate constant could not be accurately measured.

TABLE 2. Brønsted β values and β_{lg} values for the general base-catalyzed breakdown of aryl hemiacetals of α-bromoacetophenone

Aryl group	β(RCOOH + H_2O)[a]	β(RCOOH only)[b]	Catalyst	β_{lg}
4-$CH_3OC_6H_4$	0.86	1.02	H_2O	−1.03
4-$CH_3C_6H_4$	0.85	0.99	$CH_2ClCO_2^-$	−1.00
3-$CH_3C_6H_4$	0.83	0.99	$Cl(CH_2)_2CO_2^-$	−0.87
C_6H_5	0.82	0.97	$CH_3CO_2^-$	−0.77
3-$MeOC_6H_4$	0.81	0.95		
4-ClC_6H_4	0.80	0.91		
3-ClC_6H_4	0.80	0.86		

[a]Based upon the rate constants for the three carboxylic acids plus the pH-independent rate constant divided by 55.

[b]Based upon the three carboxylic acids only.

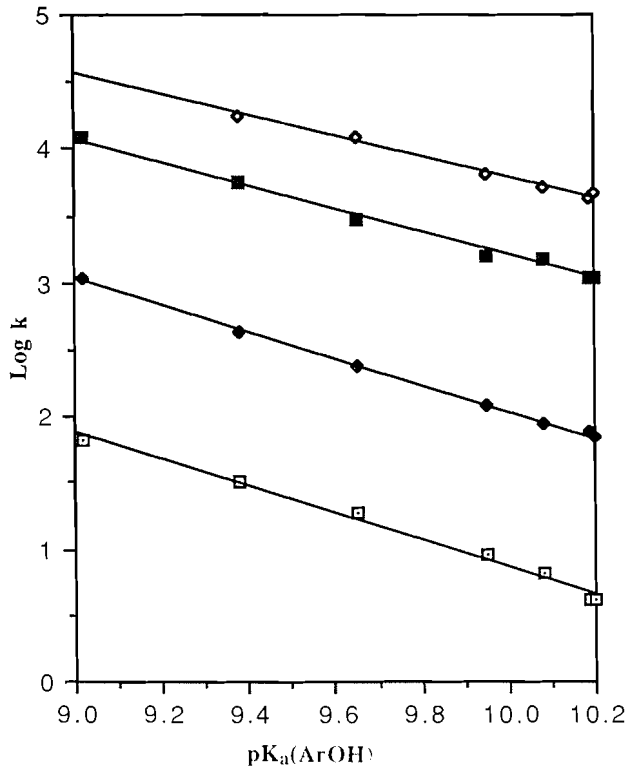


FIG. 3. Brønsted-type correlation of rate constants for base catalysis with the acidity constant of the leaving phenol for the breakdown of aryl hemiacetals of α-bromoacetophenone. Points, in increasing order of rate constant, refer to water (the pH-independent term in the rate law), $CH_2ClCO_2^-$, $ClCH_2CH_2CO_2^-$, and $CH_3CO_2^-$.

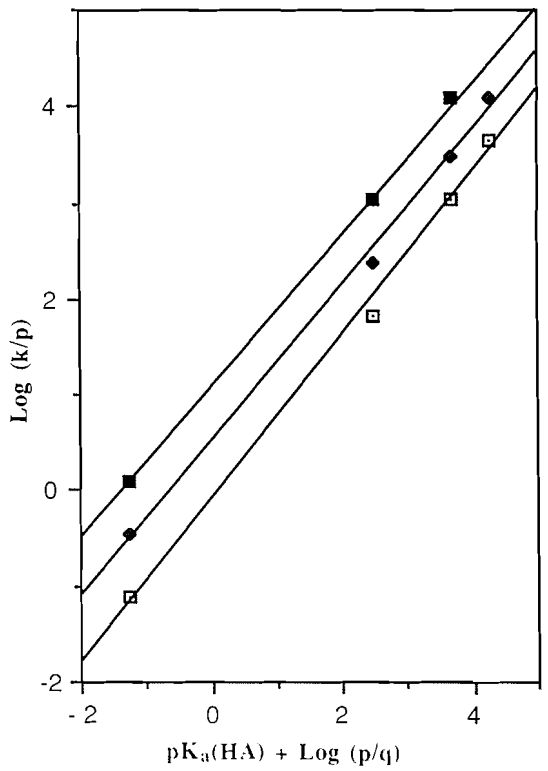


FIG. 4. Brønsted plots for general base catalysis of the breakdown of aryl hemiacetals of α-bromoacetophenone. Points, in increasing order of rate constant, refer to *p*-methoxyphenyl, *m*-methoxyphenyl, and *m*-chlorophenyl hemiacetals. The point for water has been calculated by dividing k_0 by 55. The lines are based upon linear regression including the water point.

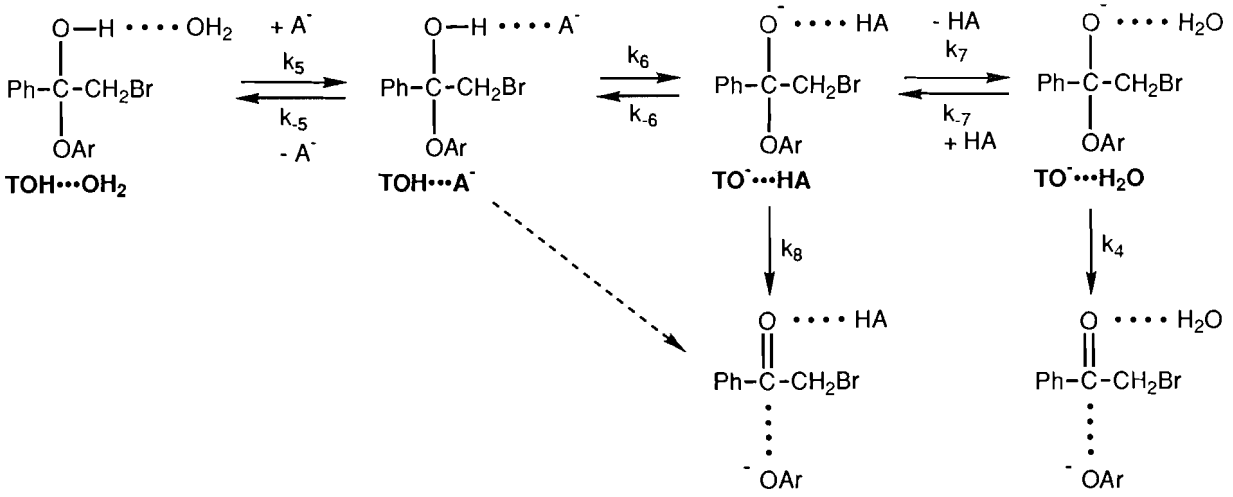
Discussion

Mechanism of general base catalysis

The rate constants for base catalysis are strongly affected by both the substituent in the aryl ring and the nature of the catalyzing base. These features are illustrated in Figs. 3 and 4, which show respectively Brønsted-like plots of log k versus pK_a(ArOH), and Brønsted plots of log k versus the pK_a of the conjugate acid of the catalyzing base. Values of β_{lg} and β obtained from these correlations are given in Table 2. Both are large, having absolute magnitudes in the range 0.8–1.0. These are indicative of transition states in which there is almost complete proton transfer to the catalyzing base and, at the same time, substantial rupture of the C—OAr bond forming the aryloxide anion.

In the base catalysis of the breakdown of the alkyl hemiacetals of α-bromoacetophenone, the ethyl and chloroethyl derivatives proceed by the normal class n mechanism, but there is a change with the trifluoroethyl compound to a mechanism where the deprotonation step has become rate-limiting (15). The latter behaviour arises from a situation where the rate constant k_4 of eq. [2*b*] becomes very large with the good trifluoroethoxide leaving group, so that the hemiacetal anion, once it is formed, proceeds on to products faster than it can protonate and revert to the neutral hemiacetal. The occurrence of a rate-limiting proton transfer was indicated experimentally by a Brønsted β value near unity, with more compelling evidence being supplied by the observation of breaks in both the rate–

Can. J. Chem. Downloaded from www.nrcresearchpress.com by 123.30.183.119 on 09/08/12
For personal use only.



SCHEME 1

TABLE 3. Acidity constants of hemiacetals of α-bromoacetophenone, and rate constants k_4 for the expulsion of alkoxide or aryloxide from their conjugate bases

Alcohol/phenol (ROH)	pK_a(ROH)[a]	pK_a(TOH)[b]	k_4, s^{-1}
CH_3CH_2OH[c]	16.00	12.39	8×10^5
$ClCH_2CH_2OH$[c]	14.31	12.05	1.4×10^7
CF_3CH_2OH[c]	12.37	11.66	8×10^8
4-$CH_3OC_6H_4OH$	10.20	11.23	4.5×10^{10}[d]
4-$CH_3C_6H_4OH$	10.19	11.23	4.6×10^{10}[d]
3-$CH_3C_6H_4OH$	10.08	11.21	5.7×10^{10}[d]
C_6H_5OH	9.95	11.18	7.3×10^{10}[d]
3-$MeOC_6H_4OH$	9.65	11.12	1.3×10^{11}[d]
4-ClC_6H_4OH	9.38	11.07	2.2×10^{11}[d]
3-ClC_6H_4OH	9.02	10.99	4.3×10^{11}[d]

[a]pK_a values for phenols taken from W.P. Jencks and J. Regenstein. Handbook of Biochemistry. 1968, p. J-158.
[b]Acidity constant of hemiacetal. See text for method of calculation.
[c]See ref. 15 for origin of values for these hemiacetals.
[d]Determined by extrapolation of the plot of log k_4 versus pK_a(ROH) for the alkyl derivatives.

pH profile and buffer dilution plots. The latter are associated with a change in rate-limiting step at the higher concentrations of hydronium ion or the buffer acid, where protonation of the hemiacetal anion by the acid begins to compete with its breakdown. At very high acid concentrations deprotonation becomes reversible, and the rate-limiting step is the breakdown.

With the aryl hemiacetals the Brønsted β values are also large. However, there are no signs of breaks or curvature even with 0.5 M buffer acid. Moreover, the β_{lg} values imply that there is substantial aryloxide ion character in the transition state. A much smaller dependence on the nature of OAr is expected for a rate-limiting proton transfer, since the substituents are remote from the charged center in the hemiacetal anion. The implication is that yet another mechanistic behavior is being followed.

One clue comes in considering what the magnitude of the rate constant k_4, for breakdown of the hemiacetal anion, is likely to be with the aryloxide leaving groups. Values of this rate constant were obtained with the alkyl derivatives, and it was found that a plot of log k_4 versus the pK_a value of the leaving alcohol was linear, with a β_{lg} of −0.87 (15). The rate constants are provided in Table 3, where it can be seen that for the trifluoroethyl derivative k_4 is large, approaching 10^9 s^{-1}. With the assumption that the log k_4 – pK_a correlation extends to aryloxide leaving groups, values of k_4 can be estimated for the latter. These are also given in Table 3, where it can be seen that there is a further increase over the trifluoroethoxide k_4 by about two orders of magnitude to numbers in the 10^{11} s^{-1} range. With breakdown this fast, a further change in reaction mechanism is expected, to a preassociation mechanism (2).

In terms of acid–base catalysis a "preassociation mechanism" arises when the substrate molecule in a complex with the catalyst undergoes some reaction at a rate that is faster than the catalyst separates away by diffusion. The consequence is that the catalyst is associated with the substrate in the rate-limiting step of the overall reaction, although there is no proton transfer component to that step. Such a mechanism for hemiacetal breakdown is provided in Scheme 1. The species $TOH\cdots OH_2$ and $TO^-\cdots H_2O$ are the starting hemiacetal and conjugate base associated only with solvent water molecules, and the rate constant k_4 of eq. [2*b*] and Table 3 refers to the breakdown of the latter anion. Conversion of $TOH\cdots OH_2$ to $TO^-\cdots H_2O$ by reaction with a base such as carboxylate ion proceeds in three steps: step 5, diffusional encounter of the base and the hemiacetal to form the hydrogen-bonded complex $TOH\cdots A^-$; step 6, proton transfer within this complex to form a new hydrogen-bonded complex $TO^-\cdots HA$; and step 7, diffusional separation of TO^- and HA. When the proton transfer is in the thermodynamically unfavorable direction, as it is for a hemiacetal and $RCOO^-$, the rate-limiting step in this three-step sequence is the diffusional separation, step 7. This situation arises since the thermodynamically favorable proton transfer converting the complex $TO^-\cdots HA$ back to $TOH\cdots A^-$ is very fast, having virtually no barrier. Thus the rate constant k_{-6} is around 10^{13} s^{-1} and is greater than k_7, the rate constant for the diffusional separation. The consequence is that the species $TO^-\cdots HA$ forms reversibly from $TOH\cdots OH_2$ and A^-, most of the time reverting to $TOH\cdots A^-$. Net proton transfer only occurs on those occasions when the acid diffuses away. In a preassociation mechanism, breakdown of the complex $TO^-\cdots HA$ by expulsion of ArO^- (step 8 of Scheme 1) becomes faster than diffusional separation ($k_8 > k_7$). This provides a route to products that involves deprotonation by A^-, but does not require separation of the catalyst prior to the

Can. J. Chem. Downloaded from www.nrcresearchpress.com by 123.30.183.119 on 09/08/12
For personal use only.

TABLE 4. Estimated equilibrium constants and rate constants for the base-catalyzed breakdown of aryl hemiacetals of α-bromoacetophenone by the mechanism of Scheme 1

Aryl group	K_5,[a] M^{-1}	$(1/K_7)$,[b] M^{-1}	K_6[c]	k_7[d], s^{-1}	k_8(ClPr)[e,f]	k_8(ClAc)[e,g]	k_8(Ac)[e,h]
$4\text{-}CH_3OC_6H_4OH$	0.012	0.76	3.5×10^{-6}	6.6×10^9	1.9×10^{10}	1.2×10^{10}	2.7×10^{10}
$4\text{-}CH_3C_6H_4OH$	0.012	0.76	3.5×10^{-6}	6.6×10^9	1.9×10^{10}	1.3×10^{10}	2.5×10^{10}
$3\text{-}CH_3C_6H_4OH$	0.012	0.75	3.7×10^{-6}	6.7×10^9	2.7×10^{10}	1.6×10^{10}	2.9×10^{10}
C_6H_5OH	0.012	0.75	3.9×10^{-6}	6.7×10^9	2.7×10^{10}	2.1×10^{10}	3.6×10^{10}
$3\text{-}CH_3OC_6H_4OH$	0.012	0.73	4.3×10^{-6}	6.9×10^9	5.0×10^{10}	4.1×10^{10}	6.6×10^{10}
$4\text{-}ClC_6H_4OH$	0.012	0.71	4.8×10^{-6}	7.0×10^9	8.7×10^{10}	7.1×10^{10}	9.2×10^{10}
$3\text{-}ClC_6H_4OH$	0.012	0.69	5.5×10^{-6}	7.2×10^9	1.7×10^{11}	1.6×10^{11}	

[a] $[TOH\cdots A^-]/[TOH][A^-] = 0.013(pK_a(TOH) - 15.7)(-1.7 - pK_a(HA)) - 2.04$, for A^- = 3-chloropropionate.
[b] $[TO^-\cdots HA]/[TO^-][HA] = 0.013(pK_a(HA) - 15.7)(-1.7 - pK_a(TOH)) - 2.04$, for HA = 3-chloropropionic acid.
[c] $[TO^-\cdots HA]/[TOH\cdots A^-] = K_a(TOH)/(K_a(HA) \times K_5 \times K_7)$ for HA = 3-chloropropionic acid.
[d] Rate constant for diffusional separation of TO^- and 3-chloropropionic acid from the hydrogen-bonded complex $TO^-\cdots HA$; calculated as $k_{-7} \times K_7$, taking $k_{-7} = 5 \times 10^9\ M^{-1}\ s^{-1}$.
[e] Calculated from the relationship: $k_A(obs) = (k_8 + k_7)K_5K_6$, where $k_A(obs)$ = experimentally determined catalytic coefficient for base catalysis.
[f] 3-Chloropropionic acid.
[g] Chloroacetic acid.
[h] Acetic acid.

C—O cleavage. There is still a barrier to the expulsion of ArO^-, so that $k_8 < k_{-6}$. Thus the rate-limiting step is the breakdown of the hydrogen-bonded complex $TO^-\cdots HA$, step 8, with the catalyst still associated with the substrate. If k_8 were to become greater than k_{-6}, the intermediate $TO^-\cdots HA$ would not exist and loss of ArO^- would be concerted with the proton transfer in $TOH\cdots A^-$ (see dashed arrow in Scheme 1).

Jencks has defined several criteria that point to a preassociation mechanism (2), and these are met with the aryl hemiacetals. Such mechanisms require that the Brønsted β values approach unity, since the proton is completely transferred in the transition state (although values exactly unity are not expected since the conjugate acid of the catalyzing base is present in the rate-limiting step and this can have a small effect (see below)). The rate-limiting step involves cleavage of the C—OAr bond, and thus there should be a substantial leaving-group effect, as is also observed. Finally, a preassociation mechanism is expected to have a larger rate constant than one calculated for an overall proton transfer to the catalyzing base. As argued above, the rate-limiting step for this proton transfer is the diffusional separation of $TO^-\cdots HA$. The preassociation mechanism short-circuits this and thus has a faster rate. This is also the case for the aryl hemiacetals. For example, for 3-chloropropionate removing a proton from the 4-chlorophenyl hemiacetal, a rate constant of $4 \times 10^2\ M^{-1}\ s^{-1}$ is calculated considering the relative acidities of the hemiacetal (see below for calculation) and 3-chloropropionic acid, and using $5 \times 10^9\ M^{-1}\ s^{-1}$ for the proton transfer in the reverse, thermodynamically favorable, direction $\{k(TOH\cdots OH_2 + A^- \rightarrow TO^-\cdots H_2O + HA) = 5 \times 10^9 \times K_a(TOH)/K_a(HA)\}$. The observed catalytic coefficient for the breakdown of this hemiacetal catalyzed by 3-chloropropionate is $5.5 \times 10^3\ M^{-1}\ s^{-1}$, over 10 times larger.

Preassociation mechanisms for base-catalyzed breakdown of a hemiacetal are expected in a rather narrow window of lifetimes of the hemiacetal anion. For such a mechanism to occur, the breakdown of this species must be faster than diffusional separation of $TO^-\cdots HA$, but slower than the reverse proton transfer. This requires that $k_8 > k_7$ and $k_8 < k_{-6}$. The value of k_7 should be around $10^{10}\ s^{-1}$ while k_{-6} should be around $10^{13}\ s^{-1}$. The estimates of $\sim 10^{11}\ s^{-1}$ arrived at by extrapolation of the data for the alkyl hemiacetal anions (Table 3) are obviously consistent with this idea. The following analysis provides additional support, and in fact shows that reasonable numbers for k_8 emerge by considering equilibrium constants expected for this system.

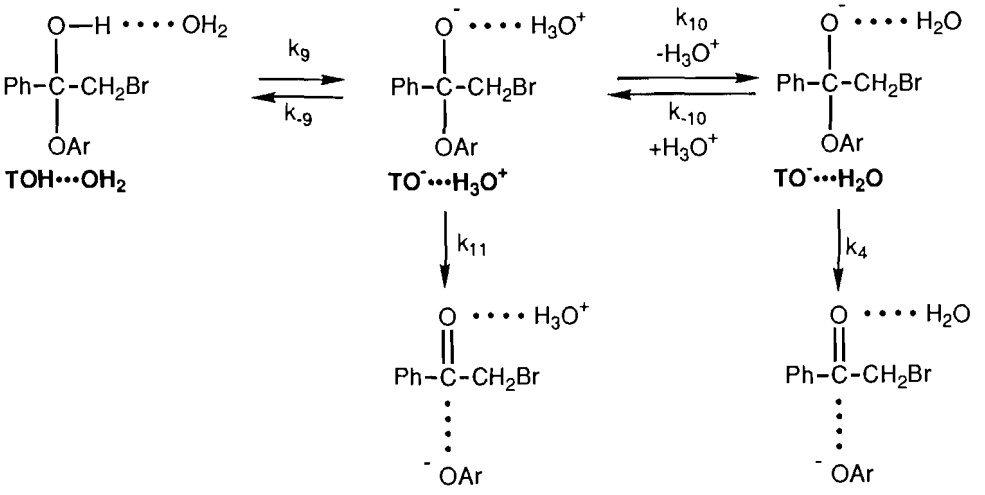
We first estimate the acidity constants of the hemiacetal ($K_a(TOH) = [TO^-][H^+]/[TOH]$, Table 3, using a previously described method. This involves the application of an equation of Hine and Koser (27) for carbonyl hydrates to provide the pK_a for the hydrate of α-bromoacetophenone, statistically correcting this number to obtain a value of the ethyl hemiacetal, and then assuming that a correlation of $pK_a(TOH)$ with $pK_a(ROH)$ has a slope of 0.2 (3, 4, 15). The constant $pK_a(ROH)$ refers to the acidity constant of the alcohol or phenol leaving group. The acid and base that are referred to in the acidity constant $K_a(TOH)$ are the species $TOH\cdots OH_2$ and $TO^-\cdots H_2O$ of Scheme 1, the hemiacetal and conjugate base solvated by water, and the following relationship with the equilibrium constants of the individual steps then applies

$$[5] \quad K_5K_6K_7 = K_a(TOH)/K_a(HA)$$

where $K_a(HA)$ is the acidity constant of the buffer acid HA. The constants K_5 and K_7 refer to equilibria involving the formation or breakdown of hydrogen-bonded complexes in water. To estimate these we have made use of a general equation suggested by Stahl and Jencks (28), as modified from an original proposal of Hine (29). This equation is based upon observations that the strengths of hydrogen-bonded complexes in water follow Brønsted relationships in the acidities and basicities of the two pairs of reagents. The third equilibrium constant K_6 refers to proton transfer within the hydrogen-bonded complexes. This can be calculated from K_5 and K_7 using eq. [5].

For the processes in Scheme 1 the inequality $k_{-6} > k_7 + k_8$ applies, as discussed previously. Moreover, with k_4 of the order of magnitude suggested by the extrapolation from the alkyl series, the intermediate $TO^-\cdots H_2O$, if it forms, must proceed on to products. This corresponds to a situation $k_4 > k_{-7}[HA]$, and it can be seen that even if [HA] were to approach 1 M, the inequality would hold. Thus, in terms of Scheme 1, proton transfer to a buffer base A^- can result in products in two ways, through breakdown of $TO^-\cdots HA$ by the pathway of step 8, or through diffusional separation to form $TO^-\cdots H_2O$

Can. J. Chem. Downloaded from www.nrcresearchpress.com by 123.30.183.119 on 09/08/12
For personal use only.



SCHEME 2

and HA···OH_2, followed by the rapid breakdown of the former by step 4. Since $TO^- \cdots HA$ forms reversibly,

[6] Rate = k_A(obs)[TOH][A^-] = $\{(k_7+k_8)K_5K_6\}$[TOH][A^-]

and the catalytic coefficient for general base catalysis is equal to $(k_7+k_8)K_5K_6$. As discussed in the previous paragraph, values of the two equilibrium constants can be calculated. The rate constant k_7 can also be estimated from the relationship $K_7 = k_7/k_{-7}$ using a value for k_{-7}, the rate constant for diffusional encounter of TO^- and HA, of 5×10^9 M^{-1} s^{-1} (30, 31). Thus only k_8 remains, and this can be calculated from the experimentally determined catalytic coefficients.

Results of these calculations are illustrated in Table 4, where it can be seen that the numbers so produced are consistent with the requirements of the preassociation mechanism. The values of k_8 are greater than k_7, and, moreover, lie in the range expected on the basis of the extrapolation from the alkyl hemiacetals (compare to k_4 values in Table 3). The values of k_8 also show a small effect due to the presence of HA, and this is expected. The hydrogen bond involving the oxygen and HA effectively disappears in the breakdown of $TO^- \cdots HA$, since the interaction of a carboxylic acid and a weakly basic C=O is very weak. Thus there should be a negative Brønsted α for the actual breakdown step. In fact the α values calculated using the rate constants k_8 given in Table 4 lie in the range from −0.10 to −0.15, typical of hydrogen-bonded complexes (28, 32).

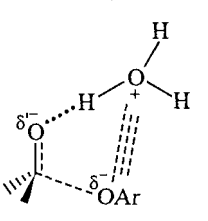
Water catalysis

The β_{lg} values for the pH-independent reaction is −1.03, similar to values for the carboxylates (Fig. 3). Moreover, the rate constant fits reasonably well along with the carboxylates on the Brønsted plot for base catalysis (Fig. 4). The conclusion therefore is that the pH-independent reaction is similar to that of the carboxylates, a preassociation with water acting as a general base. Such a mechanism is shown in Scheme 2. Proton transfer within the hydrated hemiacetal TOH···OH_2 produces the hydrogen-bonded ion pair $TO^- \cdots H_3O^+$, and breakdown of this species before diffusional separation of TO^- and H_3O^+ would correspond to a preassociation reaction exhibiting pH-independent kinetics. Using arguments similar to those discussed in the previous section, the rate law for this scheme is

[7] Rate = k_0[TOH] = $(k_{10} + k_{11})K_9$[TOH]

where the reversibly formed intermediate $TO^- \cdots H_3O^+$ proceeds on to products either by direct breakdown via step 11, or through diffusional separation of the two ions. As argued previously, if $TO^- \cdots H_2O$ forms, it will proceed to products faster than it will protonate. The back proton transfer in $TO^- \cdots H_3O^+$ is also extremely fast so that the formation of this species from TOH···OH_2 is reversible ($k_{-9} > k_{10} + k_{11}$).

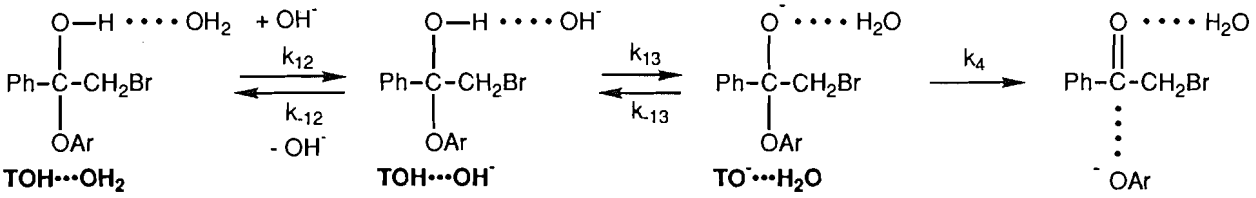
Using procedures similar to above, values of the individual rate constants can be estimated. This is illustrated here for the phenyl hemiacetal. The equilibrium constant $1/K_{10}$ for formation of the hydrogen-bonded complex $TO^- \cdots H_3O^+$ is calculated as 6.7 M^{-1} using the equation of Stahl and Jencks. This in turn provides $K_9 = 4.4 \times 10^{-11}$ through the relationship K_a(TOH) = K_9K_{10}, and $k_{10} = 3.0 \times 10^9$ s^{-1} through the relationship $K_{10} = k_{10}/k_{-10}$ using $k_{-10} = 2 \times 10^{10}$ M^{-1} s^{-1} (30). The experimental $k_0 = 9$ $s^{-1} = (k_{10}+k_{11})K_9$ from eq. [7], from which k_{11} is calculated as 2.0×10^{11} s^{-1}. As with the carboxylates, this rate constant is indeed found to be significantly larger than the rate constant k_{10} for diffusional separation, consistent with a preassociation mechanism. Moreover, the value is within the range expected on the basis of the extrapolation from the alkyl compounds. Interestingly, k_{11} is calculated to be larger than k_8, the rate constant for breakdown within the complex $TO^- \cdots HA$. A number of assumptions have gone into these calculations, so that this difference may not be real. It can, however, be explained by a stabilizing electrostatic interaction (33) between the spectator H_3O^+ and the departing aryloxide in the transition state for breakdown of $TO^- \cdots H_3O^+$.



Hydroxide ion catalysis

The mechanism for this reaction, shown in Scheme 3, is analogous to those of the carboxylates and water, with hy-

Can. J. Chem. Downloaded from www.nrcresearchpress.com by 123.30.183.119 on 09/08/12
For personal use only.



SCHEME 3

droxide ion functioning as the base catalyst. There is, however, an important difference, in that step 12, the formation of the initial hydrogen-bonded complex TOH···OH^- is now the rate-limiting step in the overall reaction. This situation arises since the proton transfer, TOH···OH^- → TO^-···H_2O, has become thermodynamically favored with the much stronger base. Thus k_{13} is greater than k_{-12} that is, proton transfer within TOH···OH^- occurs faster than the diffusional separation of TOH and OH^-. Furthermore, k_{-13} can be estimated to be around 10^9 s^{-1}, smaller than k_4, so that TO^-···H_2O, once it is formed, goes on to products. (To calculate k_{-13}, K_{12} was calculated using the Stahl and Jencks equation, K_{13} from the relation $K_{12}K_{13} = K_a(TOH)/K_w$, and k_{-13} from K_{13} using $k_{13} = 10^{13}$ s^{-1}.) Thus once TOH···OH^- forms, it will proceed on to products faster than the hydroxide can diffuse away. The consequence is that the catalytic coefficient for hydroxide ion is simply equal to k_{12}, the rate constant for diffusional encounter of OH^- and TOH. The experimental values are 8×10^9 M^{-1} s^{-1}, independent of the aryl substituent, consistent with this interpretation.

Lifetimes of hemiacetal anions

Within the series of α-bromoacetophenone hemiacetals we have now seen a progression from a normal class n mechanism to a mechanism with rate-limiting proton transfer, essentially the reverse of a "trapping" mechanism (2, 15), to a preassociation mechanism, as the lifetime of the conjugate base of the hemiacetal decreases with better leaving groups. Further decreases in lifetime are still possible. For example, the anion of the 4-nitrophenyl hemiacetal is estimated to have a rate constant of k_4 of 2×10^{13} s^{-1}, while with acetate as leaving group k_4 is estimated to be 10^{15} s^{-1}. Both of these numbers are greater than the rate constant for a vibration, and thus the anion in each case cannot exist. With these systems, therefore, proton transfer and C—OR bond cleavage will be concerted and TOH···A^- will proceed directly to the product without the intermediacy of TO^-···HA, as illustrated by the dashed arrow of Scheme 1. There is precedence for this from a study of the breakdown of a cyclic hemiacylal, where it was concluded that proton transfer to a base and loss of carboxylate were concerted (11).

Acid catalysis

Because of the very efficient base catalysis and the limitations on the buffers that can be employed with bromine, data were obtained for acid catalysis with only one buffer acid, chloroacetic acid, as well as H_3O^+. A plot of log k_H for the latter catalysis versus pK_a(ArOH) is curved, with rate acceleration for the hemiacetals with electron-donating substituents but, then, little change with the electron-withdrawing ones (Fig. 5). There are insufficient data to make a conclusive statement about such a plot for chloroacetic acid, although there again appears to be acceleration by electron donors. Based upon the two catalysts, the Brønsted α is 0.20–0.25. The catalysts are of different charge type, so that this must be regarded as an approximation. A reasonable conclusion is that α is low.

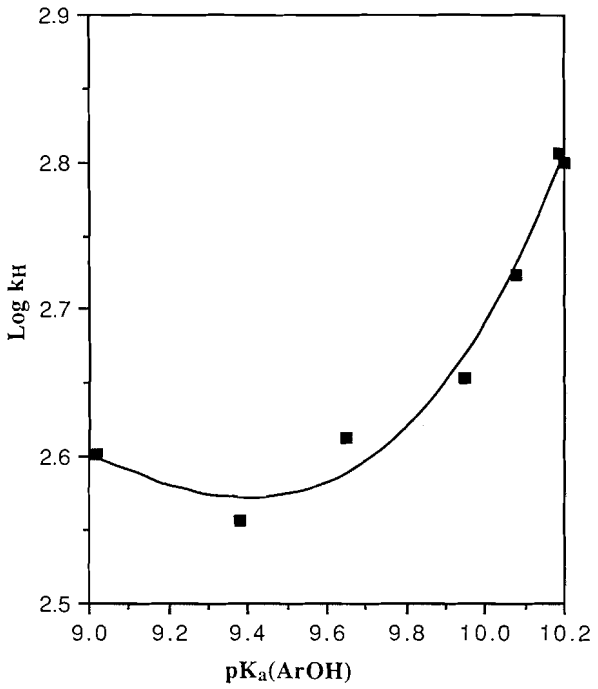
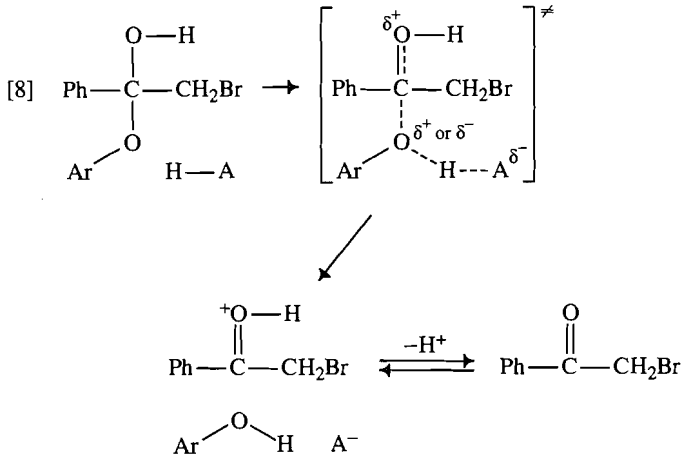


FIG. 5. Brønsted-type correlation of rate constants for H_3O^+ catalysis with the acidity constant of the leaving phenol for the breakdown of hemiacetals of α-bromoacetophenone.

One conclusion that can certainly be made is that these catalysts are *not* acting by the class e mechanisms of eq. [1]. This statement is made on considering the values expected for $K_a(SH^+)$, the acidity constant for the hemiacetal protonated on the phenolic oxygen. Acidity constants for protonated aromatic ethers are in fact not known, since anisole and its derivatives C-protonate in concentrated acids to form resonance-stabilized cyclohexadienyl cations (34, 35). If the simple assumption is made that the onium ions $CH_3CH_2OH_2^+$ and $PhOH_2^+$ have the same difference in pK_a as is observed for deprotonation of the neutral acids CH_3CH_2OH and C_6H_5OH, then pK_a for $PhOH_2^+$ is about −8, since the value for $CH_3CH_2OH_2^+$ is −2 (36). The protonated hemiacetal of this study has additional electron-withdrawing substituents; the OH group, for example, will have an effect of 2–2.5 pK_a units on its own (37). The consequence is that $pK_a(SH^+)$ for the phenyl hemiacetal can be estimated to be −11. To account for the experimental catalytic coefficients with such a number, the rate constant of k_1 of eq. [1] must be 2×10^{15} M^{-1} s^{-1} for chloroacetate, and k_2, 5×10^{13} s^{-1}. Both these rate constants are well above the diffusional limit, particularly k_1, which cannot be greater than $\sim 10^{10}$ M^{-1} s^{-1}. Thus, even if the acidity constant $K_a(SH^+)$ has been overstimated, the class e mechanism cannot apply.

This leaves the alternative class n mechanism (1, 3), in which the acid catalyzes the departure of the substituted phenol. This mechanism is directly analogous to that of a general acid-catalyzed hydrolysis of a full acetal, for which proton

Can. J. Chem. Downloaded from www.nrcresearchpress.com by 123.30.183.119 on 09/08/12
For personal use only.



transfer is concerted with C—OR bond cleavage forming an intermediate oxocarbocation (38). Interestingly, for acetals such as benzaldehyde aryl methyl acetals with aryl leaving groups (39), plots of log k versus pK_a(ArOH) are curved in the same manner as observed in this study.

This class n mechanism for the hemiacetal can be considered to be forced on the system by the very high energy of the fully protonated species, coupled with the ease of cleavage of the C—OAr bond. As shown in eq. [8], the oxygen of the leaving group can bear a partial positive charge or a partial negative charge in the transition state depending on whether proton transfer or bond cleavage has progressed to the greater extent. The curved pK_a(ArOH) correlation observed for H_3O^+ catalysis (Fig. 5) indicates that the actual situation depends on substituent, proton transfer being more important for the electron donors but then, with better leaving groups, bond breaking catching up. The low α value indicates that not a great deal of proton transfer is in fact required to reach the transition state.

Conclusion

Phenols or phenolates as leaving groups in the breakdown of α-bromoacetophenone hemiacetals result in dramatically different mechanistic behavior from that observed with simple alkyl derivatives. The changes are a direct consequence of the effect of the phenyl ring on the energies and lifetimes of important reaction intermediates. General base catalysis and water catalysis occur by preassociation mechanisms, in which a hydrogen-bonded intermediate loses aryloxide faster than diffusional separation of acid–base pair. This mechanism is enforced by the short lifetime of the hemiacetal anion when it has an aryloxide leaving group. Acid catalysis occur by a class n mechanism in which the acid assists departure of the phenol. Alkyl hemiacetals break down by class e mechanisms where the leaving group is fully protonated before bond cleavage. The different mechanism with the aryl hemiacetals avoids this intermediate, which, being of an O-protonated anisole structure, is of very high energy.

Acknowledgement

The continued financial support of the Natural Sciences and Engineering Research Council of Canada is gratefully acknowledged.

1. R. P. Bell. Adv. Phys. Org. Chem. **4**, 1 (1966).
2. W. P. Jencks. Acc. Chem. Res. **9**, 425 (1976).
3. L. H. Funderburk, W. P. Aldwin, and W. P. Jencks. J. Am. Chem. Soc. **100**, 5444 (1978).
4. P. E. Sorensen and W. P. Jencks. J. Am. Chem. Soc. **109**, 4675 (1987).
5. R. A. McClelland and M. Coe. J. Am. Chem. Soc. **105**, 2718 (1983).
6. E. Grunwald. J. Am. Chem. Soc. **107**, 4710 (1985).
7. C. A. Coleman and C. J. Murray. J. Am. Chem. Soc. **113**, 1677 (1991).
8. C. J. Murray and T. Webb. J. Am. Chem. Soc. **113**, 1684 (1991).
9. E. Grunwald. J. Am. Chem. Soc. **107**, 4715 (1985).
10. R. A. McClelland, D. B. Devine, and P. E. Sorensen. J. Am. Chem. Soc. **107**, 5459 (1985).
11. R. A. McClelland and P. E. Sorensen. Can. J. Chem. **64**, 1196 (1986).
12. R. A. McClelland. J. Am. Chem. Soc. **106**, 7579 (1984).
13. R. A. McClelland, V. M. Kanagasabapathy, and S. Steenken. Can. J. Chem. **68**, 375 (1990).
14. W. P. Jencks. Acc. Chem. Res. **13**, 161 (1980).
15. P. E. Sorensen, K. J. Pedersen, P. R. Pedersen, V. M. Kanagasabapathy, and R. A. McClelland. J. Am. Chem. Soc. **110**, 5118 (1988).
16. F. M. Irvine and J. C. Smith. J. Chem. Soc. 74 (1972).
17. A. J. Vogel. A textbook of practical organic chemistry. Longman, London. 1978. p. 844.
18. F. N. Tebbe, G. W. Parshall, and G. S. Reddy. J. Am. Chem. Soc. **100**, 3611 (1978).
19. S. H. Pine, R. Zahler, D. A. Evans, and R. H. Grubbs. J. Am. Chem. Soc. **102**, 3270 (1980).
20. S. H. Pine, R. J. Pettit, G. D. Geib, S. G. Cruz, C. H. Gallego, T. Tijerina, and R. D. Pine. J. Org. Chem. **50**, 1212 (1985).
21. A. Oku, T. Yokoyama, and T. Harada. Tetrahedron. Lett. **24**, 4699 (1983).
22. V. M. Kanagasabapathy and R. A. McClelland. J. Chem. Soc. Chem. Commun. 691 (1985).
23. M. F. Ruasse, A. Argile, and J. E. Dubois. J. Am. Chem. Soc. **106**, 4846 (1984).
24. P. R. Young and W. P. Jencks. J. Am. Chem. Soc. **99**, 8238 (1977).
25. R. A. McClelland and M. Ahmad. J. Am. Chem. Soc. **100**, 7031 (1978).
26. T. L. Amyes and W. P. Jencks. J. Am. Chem. Soc. **111**, 7888 (1989).
27. J. Hine and G. F. Koser. J. Org. Chem. **36**, 1348 (1971).
28. N. Stahl and W. P. Jencks. J. Am. Chem. Soc. **108**, 4196 (1986).
29. J. Hine. J. Am. Chem. Soc. **94**, 5766 (1972).
30. M. Eigen. Angew. Chem. Int. Ed. Engl. **3**, 1 (1964).
31. J. P. Guthrie, J. Cossar, and A. Klym. J. Am. Chem. Soc. **106**, 1351 (1984).
32. C. J. Murray and W. P. Jencks. J. Am. Chem. Soc. **110**, 7561 (1988).
33. A. J. Kresge and Y. Chiang. J. Am. Chem. Soc. **95**, 803 (1973).
34. A. J. Kresge and L. E. Hakka. J. Am. Chem. Soc. **88**, 3868 (1966).
35. A. J. Kresge, Y. Chiang, and L. E. Hakka, J. Am. Chem. Soc. **93**, 6167 (1971).
36. D. G. Lee and R. Cameron. J. Am. Chem. Soc. **93**, 4724 (1971).
37. J. P. Guthrie. J. Am. Chem. Soc. **100**, 5892 (1978).
38. N. Gravitz and W. P. Jencks. J. Am. Chem. Soc. **96**, 507 (1974).
39. B. Capon and K. Nimmo. J. Chem. Soc. Perkin Trans 2, 1113 (1975).

Can. J. Chem. Downloaded from www.nrcresearchpress.com by 123.30.183.119 on 09/08/12
For personal use only.

Gas-phase heteroaromatic substitution. 14.[1] Attack of dimethylfluoronium ion on 2- and 3-methyl-pyrroles, -furans, and -thiophenes

PATRIZIO CECCHI,[2] ADRIANO PIZZABIOCCA, AND GABRIELE RENZI
Dipartimento di Chimica, Università di Camerino, Camerino (MC), Italy

CINZIA SPARAPANI
Istituto di Chimica Nucleare del CNR, Area della Ricerca di Roma, Rome, Italy

AND

MAURIZIO SPERANZA[3]
Dipartimento di Agrobiologia ed Agrochimica, Università della Tuscia, Viterbo, Italy

Received March 28, 1991

PATRIZIO CECCHI, ADRIANO PIZZABIOCCA, GABRIELE RENZI, CINZIA SPARAPANI, and MAURIZIO SPERANZA. Can. J. Chem. **69**, 2094 (1991).

The gas-phase methylation of 2- and 3-methyl-pyrroles (**2P** and **3P**), -furans (**2F** and **3F**), and -thiophenes (**2T** and **3T**) by $(CH_3)_2F^+$ ions, from γ radiolysis of CH_3F, has been investigated at pressures ranging from 50 to 760 Torr, in the presence of a thermal radical scavenger (O_2) and variable concentrations of an added base (NMe_3: 0–10 Torr). The mechanism of the methylation process is discussed and the intrinsic positional selectivity of the $(CH_3)_2F^+$ ions evaluated in the framework of the Charge and Frontier Orbital Control concept. Owing to the very large energy gap between the LUMO of $(CH_3)_2F^+$ and the HOMOs of the selected heteroaromatic substrates, their gas-phase methylation is characterized by a distinct affinity of the ionic electrophile toward those substrate positions with the highest net negative charge, i.e., the C3 in **2P** (100%), the C4 in **3P** (100%), the heteroatom of **2F** and **3F** (>80%), the C5 of **2T** (32%), and the C2 of **3T** (47%). Analysis of the methylated product distribution from **2F** and **3F** as a function of the experimental conditions reveals that the interaction of the $(CH_3)_2F^+$ with the heteroatom of furans gives rise to the reversible formation of two sets of electrostatic adducts, i.e., a "chelate" adduct (**III**) and a single proton-bonded adduct (**IV**), the first rapidly evolving to the α-substituted heteroarenium intermediate by proximity effects and the latter slowly rearranging to the chelate structure **III**. Formation of these categories of electrostatic adducts from furans, which is much less extensive in the case of thiophenes and absent in pyrroles, accounts for the apparent pronounced affinity of gaseous alkylating electrophiles, irrespective of their LUMO energy, for the α carbons of furans.

Key words: gas-phase ion chemistry, electrophilic aromatic substitutions, radiolysis, dimethylfluoronium ions, methylated heteroarenes.

PATRIZIO CECCHI, ADRIANO PIZZABIOCCA, GABRIELE RENZI, CINZIA SPARAPANI et MAURIZIO SPERANZA. Can. J. Chem. **69**, 2094 (1991).

Opérant à des pressions allant de 50 à 760 Torr, en présence d'un piège thermique à radicaux (O_2) et à des concentrations variables de base ajoutée (NMe_3 : 0–10 Torr), on a étudié la méthylation en phase gazeuse des 2- et 3-méthyl-pyrroles (**2P** et **3P**), -furanes (**2F** et **3F**) et -thiophènes (**2T** et **3T**) par les ions $(CH_3)_2F^+$ obtenus par radiolyse γ du CH_3F. On discute du mécanisme du processus de méthylation et on a évalué la sélectivité positionnelle intrinsèque des ions $(CH_3)_2F^+$ à l'aide du concept du contrôle de la charge et des orbitales frontières. À cause de la grande différence d'énergie entre l'OM BV du $(CH_3)_2F^+$ et les OM HO des substrats hétéroaromatiques choisis, leur méthylation en phase gazeuse est caractérisée par une affinité distincte de l'électrophile ionique pour les positions du substrat qui portent les charges négatives nettes les plus élevées, soit les positions C3 du **2P** (100%), C4 du **3P** (100%), C5 du **2T** (32%), C2 du **3T** (47%) et l'hétéroatome de **2F** et **3F** (>80%). L'analyse de la distribution des produits de méthylation des produits **2F** et **3F** en fonction des conditions expérimentales révèle que l'interaction entre le $(CH_3)_2F^+$ et l'hétéroatome des furanes donne lieu à la formation réversible des deux ensembles d'adduits électrostatiques, soit un adduit de nature «chélatée» (**III**) et un adduit liant un seul proton (**IV**); sous l'influence d'effets de proximité, le premier évolue rapidement vers une intermédiaire hétéroarénium α-substitué alors que le second se transpose lentement vers la structure chélatée **III**. La formation de ces catégories d'adduits électrostatiques avec les furanes, qui est beaucoup moins importante dans le cas des thiophènes et qui est absente avec les pyrroles, permet d'expliquer l'affinité apparemment très prononcée des électrophiles alkylants gazeux, quelle que soit l'énergie de leur OM BV, pour les carbones α des furanes.

Mots clés : chimie ionique en phase gazeuse, substitutions aromatiques électrophiles, radiolyse, ions diméthylfluoronium, hétéroarènes substitués.

[Traduit par la rédaction]

Introduction

In the preceding papers of this series, the intrinsic reactivity features of unsubstituted five-membered heteroaromatic rings toward a variety of alkylating cations have been evaluated in the dilute gas state, i.e., in a reaction environment entirely free from those complicating factors, such as solvation, ion pairing, etc., which normally prevent meaningful kinetic measurements of the same processes in solution (2). The emerging reactivity picture is consistent with quantitative predictions based upon a simplified version of the Shaik and Pross Curve Crossing model (3), whose quantitative applicability till now appears restricted exclusively to gas-phase alkyl-cation additions to five-membered heteroaromatic rings (1).

In the gas-phase alkylation of heteroarenes by onium ions,

[1]For Part 13, see ref. 1.

[2]Present address: University of Tuscia, 01100 Viterbo, Italy.

[3]Author to whom correspondence may be addressed.

Printed in Canada / Imprimé au Canada

Can. J. Chem. Downloaded from www.nrcresearchpress.com by 123.30.183.119 on 09/08/12
For personal use only.

Can. J. Chem. Downloaded from www.nrcresearchpress.com by 123.30.183.119 on 09/08/12
For personal use only.

such as the dimethylfluoronium ion $(CH_3)_2F^+$ (4), the mode of attack of the electrophile cannot be regarded as a genuine addition process, such as for carbenium ions, but rather as a nucleophilic displacement. As a consequence, the simplified version of the Curve Crossing model used in the preceding paper of this series for rationalizing gas-phase addition of carbenium ions to heteroarenes (1) hardly applies in this case since the model neglects the contribution of the leaving CH_3F moiety to the activation barrier of the $(CH_3)_2F^+$ methylation of the heteroaromatic substrate.

To enlarge the experimental kinetic evidence on which to base any verification of the applicability of the Curve Crossing model (3) to $(CH_3)_2F^+$ ion attack on heteroarenes, the investigation has been now extended to estimating the reactivity features of the onium electrophile toward 2- (**2P**) and 3-methylpyrrole (**3P**), 2- (**2F**) and 3-methylfuran (**3F**), and 2- (**2T**) and 3-methylthiophene (**3T**). It is expected that this study will allow a first experimental assessment of the reactivity and orienting properties of the selected heteroaromatic substrates toward a typical Friedel–Crafts methylating reactant, the $(CH_3)_2F^+$ ion (5). In fact, any attempt to kinetically investigate the same process in the condensed phase under Friedel–Crafts conditions has met with no success to date.

Furthermore, additional interest is attached to $(CH_3)_2F^+$ regarding the nature and the stability of the primary adducts generated from the interaction of the gaseous electrophile with the heteroatom of furans and thiophenes (2). It was, indeed, generally observed, at variance with the behavior of pyrroles and with model predictions (1), that these substrates undergo predominant α substitution from alkylating electrophiles, either alkyl carbenium and alkyl onium ions, irrespective of their LUMO energy. A comparative analysis of the positional selectivity of $(CH_3)_2F^+$ toward isomeric methyl-furans and -thiophenes may help in elucidating the origin of the surplus of α substitution observed for this class of heteroaromatics in the gas phase.

The kinetic approach adopted in this study has been already presented (4). It is based upon the preparation of stationary concentrations of $(CH_3)_2F^+$ ions from γ-radiolysis of CH_3F gaseous mixtures, containing an effective thermal radical scavenger, i.e., O_2. Their attack on selected methylheteroarenes is investigated under conditions, i.e., 50–760 Torr (1 Torr = 133.3 Pa) and presence of a powerful cation trap (NMe_3: 0–10 Torr), ensuring efficient collisional thermalization and rapid deprotonation of the onium reactant and its daughter heteroarenium intermediates, whose isomeric distribution can therefore be determined from the relative abundance of the corresponding alkylated neutral derivatives.

Experimental section

Materials

Methyl fluoride (>99%), oxygen (>99.99%), and trimethylamine (>99%) (Matheson Co.) were used without further purification. 2-, 3-Methylthiophene, 2,5-dimethylthiophene, 2-methylfuran, 2,5-dimethylfuran, and 2,5-dimethylpyrrole were research grade chemicals from Aldrich Chemical Co. 2,3-, 2,4-, and 3,4-Dimethylthiophene (6), 3-methylfuran (7), 2,3- (8), 2,4- (9), 3,4-dimethylfuran (10), 2- (11), 3-methylpyrrole (12), 2,3- (13), 2,4- (14), 3,4- (15), 1,2- (16), an 1,3-dimethylpyrrole (17) were prepared according to established procedures. All these compounds were purified by preparative GLC on the same columns employed in the analysis of the reaction mixture and their identity checked by conventional mass spectrometric and NMR analyses.

Procedure

The procedure for the preparation of the radiolytic samples has previously been reported (4). Typical experimental conditions were as follows: CH_3F, 50–760 Torr; heteroaromatic substrate, 0.5–2.0 Torr; O_2, 5 Torr; NMe_3, 0–10 Torr. The irradiations were carried out at 37.5°C in a 220 Gammacell from Nuclear Canada Ltd. to a dose of 1.5×10^4 Gy at a rate of 5×10^5 Gy h^{-1}, as determined by a Fricke dosimeter. Control experiments, carried out at doses ranging from 1×10^4 to 1×10^5 Gy, showed that the relative yields of products are largely independent of the dose. The analysis of the irradiated mixtures was performed with a Perkin–Elmer Sigma 1B or a Hewlett–Packard 5730 gas chromatograph equipped with a flame ionization detector. The following columns were employed: (*i*) a 6 m long, 2 mm i.d. glass column, packed with SP 1200:Bentone 34 5%:1.75% on 80–100 mesh Supelcoport, operated at temperatures ranging from 80 to 90°C, 1°C min^{-1}; (*ii*) a 50 m long, 0.2 mm i.d. fused silica WCOT-UCON LB 550X capillary column, operated at 60°C; (*iii*) a 3.5 m long, 2 mm i.d. glass column, packed with 5% Carbowax 20M on 80–100 Carbopack, operated at temperatures ranging from 120 to 130°C, 1°C min^{-1}; (*iv*) a 30 m long, 0.32 mm i.d. stainless steel Carbowax 20M column, operated at 100°C.

The products were identified by comparison of their retention volumes with those of authentic standard compounds and their identity confirmed by GLC–MS (Hewlett–Packard 5988A). Their yields were measured from the area of the gas chromatographic elution peaks, using individual calibration factors.

Results

Gas-phase attack of radiolytic $(CH_3)_2F^+$ ions on 2- (**2P**) and 3-methylpyrrole (**3P**) yields the corresponding β-methylated derivatives, namely 2,3- (**23P**) and 3,4-dimethylpyrrole (**34P**), respectively, as the only detectable methylation products. Their absolute yield, expressed as the number of molecules M produced per 100 eV of energy absorbed by the gaseous mixture ($G_{(M)}$ values), was measured under various experimental conditions, at the constant temperature of 37.5°C and for the total dose of 1.5×10^4 Gy (dose rate: 5×10^5 Gy h^{-1}). For both substrates, the $G_{(M)}$ value of the corresponding β-methylated derivative, measured in the absence of added bases (NMe_3), is found to decrease at low pressure, ranging from ca. 0.3 at 760 Torr to ca. 0.1 at 50 Torr. At 760 Torr and in the presence of NMe_3, the absolute yields of **23P** from **2P** and of **34P** from **3P** decrease significantly, dropping by a factor ranging from 10 to 20 at the highest base concentration (10 Torr). Under these conditions, however, the sharp decrease of the β-methylated derivatives of **2P** and **3P** is in part counterbalanced by the formation of appreciable amounts of the corresponding β-*N*,*N*-dimethylaminomethyl derivatives, whose $G_{(M)}$ value is found to increase from ca. 0.02, at $P(NMe_3) = 1$ Torr, to ca. 0.12, at $P(NMe_3) = 10$ Torr.

Dimethylfluoronium ion attack on 2-methylfuran (**2F**) produces all the expected methylated derivatives, namely 2,3- (**23F**), 2,4- (**24F**), and 2,5-dimethylfuran (**25F**), but no detectable formation of the 3,4-dimethylated isomer (**34F**) is observed. Their overall $G_{(M)}$ value, measured in the absence of added NMe_3, increases from 1.2 at 760 Torr to 2.1 at 50 Torr. In the presence of variable concentrations of NMe_3, the overall $G_{(M)}$ value of the methylated products sharply decreases, levelling off to ca. 0.002 at $P(NMe_3) = 10$ Torr. No concomitant formation of *N*,*N*-dimethylaminomethyl derivatives of **2F** is observed, at variance with the behavior of pyrroles **2P** and **3P**. A similar picture arises from the $(CH_3)_2F^+$ ion attack on 3-methylfuran (**3F**), which leads to the exclusive formation of **23F**, **24F**, and **34F**.

Similarly, dimethylfluoronium ion methylation of 2- (**2T**) and 3-methylthiophene (**3T**) yields the corresponding methylated derivatives, namely 2,3- (**23T**), 2,4- (**24T**), and 2,5-dimethylthiophene (**25T**) (from **2T**) and 2,3- (**23T**), 2,4- (**24T**),

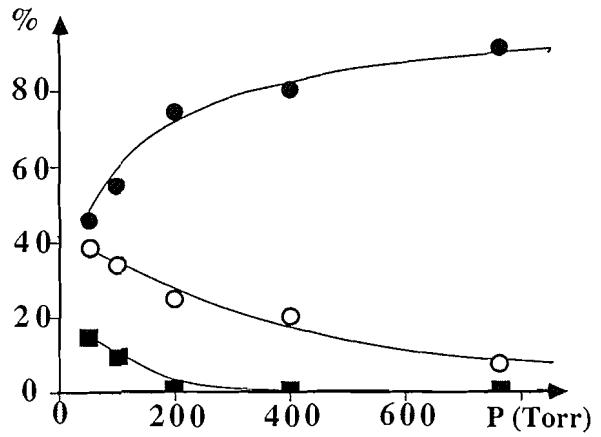


FIG. 1. Relative yields of isomeric dimethylfurans from $(CH_3)_2F^+$ attack on 2-methylfuran **2F** as a function of the total pressure (P) of the system in the absence of NMe_3: 2,5-dimethylfuran (**25F**, full circles); 2,3-dimethylfuran (**23F**, open circles); 2,4-dimethylfuran (**24F**, full squares).

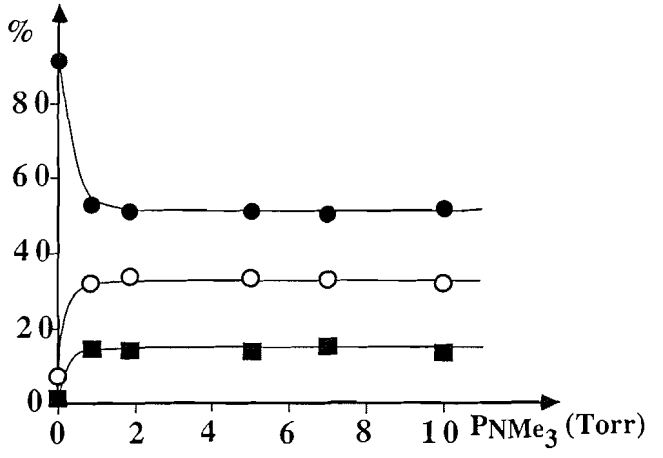


FIG. 2. Relative yields of isomeric dimethylfurans from $(CH_3)_2F^+$ attack on 2-methylfuran **2F** at 760 Torr as a function of the partial pressure of NMe_3 ($P(NMe_3)$): 2,5-dimethylfuran (**25F**, full circles); 2,3-dimethylfuran (**23F**, open circles); 2,4-dimethylfuran (**24F**, full squares).

and 3,4-dimethylthiophene (**34T**) (from **3T**). Their overall $G_{(M)}$ value, measured in the absence of NMe_3, increases from ca. 0.7 at 760 Torr to ca. 1.5 at 50 Torr. A dramatic lowering of the overall $G_{(M)}$ value of the methylated products is determined by addition of NMe_3 to the gaseous mixtures, a decrease by a factor of over 5 being observed at $P(NMe_3)$ = 10 Torr. In analogy with the results from isomeric methylfurans, no appreciable amounts of N,N-dimethylaminomethyl derivatives of **2T** and **3T** are formed in the irradiated mixtures with NMe_3.[4]

The isomeric distributions of the products from $(CH_3)_2F^+$ methylation of methylfurans and methylthiophenes were measured under largely different experimental conditions and are reported in Figs. 1–8. The relative yields of the methylated products from both isomeric methylfurans and methylthiophenes markedly depend upon the total pressure of the system (Figs. 1, 3, 5, and 7) and the presence of the added NMe_3 (Figs.

[4]The absolute and relative yields of products have an uncertainty level of ca. 10%.

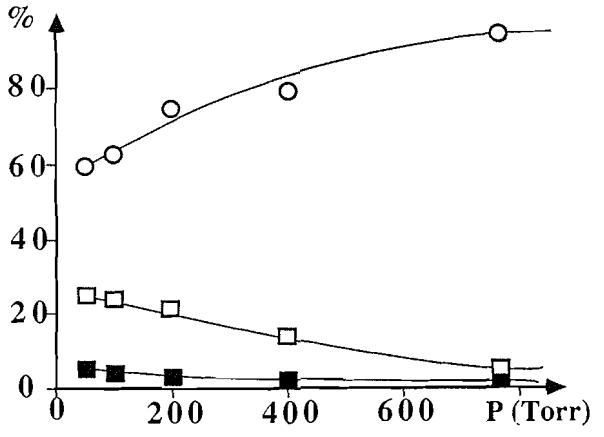


FIG. 3. Relative yields of isomeric dimethylfurans from $(CH_3)_2F^+$ attack on 3-methylfuran **3F** as a function of the total pressure (P) of the system in the absence of NMe_3: 2,3-dimethylfuran (**23F**, open circles); 3,4-dimethylfuran (**34F**, open squares); 2,4-dimethylfuran (**24F**, full squares).

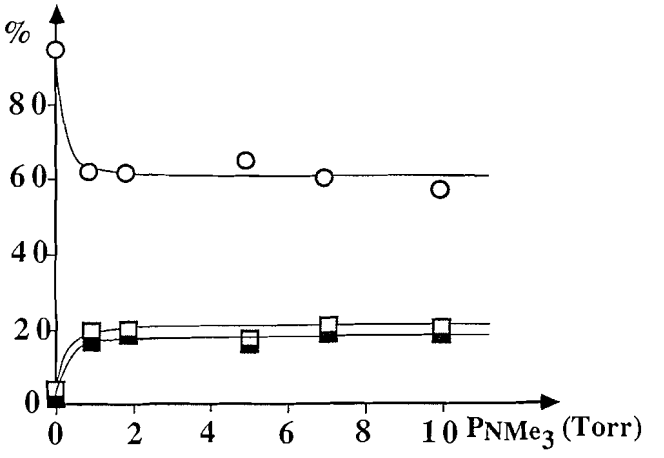


FIG. 4. Relative yields of isomeric dimethylfurans from $(CH_3)_2F^+$ attack on 3-methylfuran **3F** at 760 Torr as a function of the partial pressure of NMe_3 ($P(NMe_3)$): 2,3-dimethylfuran (**23F**, open circles); 3,4-dimethylfuran (**34F**, open squares); 2,4-dimethylfuran (**24F**, full squares).

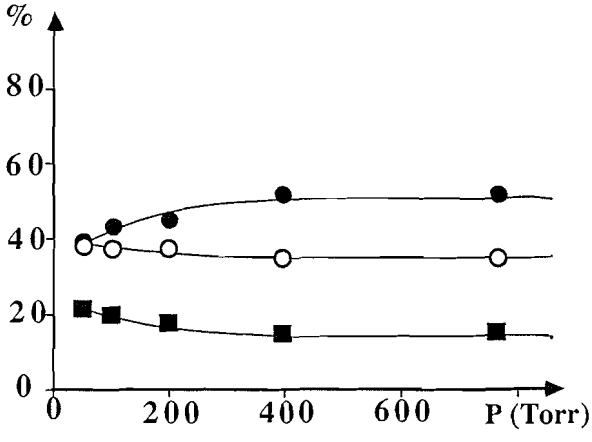


FIG. 5. Relative yields of isomeric dimethylthiophenes from $(CH_3)_2F^+$ attack on 2-methylthiophene **2T** as a function of the total pressure (P) of the system in the absence of NMe_3: 2,5-dimethylthiophene (**25T**, full circles); 2,3-dimethylthiophene (**23T**, open circles); 2,4-dimethylthiophene (**24T**, full squares).

Can. J. Chem. Downloaded from www.nrcresearchpress.com by 123.30.183.119 on 09/08/12
For personal use only.

Can. J. Chem. Downloaded from www.nrcresearchpress.com by 123.30.183.119 on 09/08/12
For personal use only.

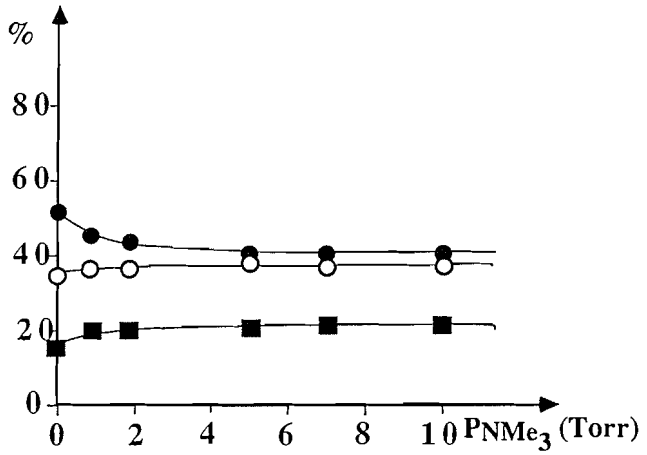


FIG. 6. Relative yields of isomeric dimethylthiophenes from $(CH_3)_2F^+$ attack on 2-methylthiophene **2T** at 760 Torr as a function of the partial pressure of NMe_3 ($P(NMe_3)$): 2,5-dimethylthiophene (**25T**, full circles); 2,3-dimethylthiophene (**23T**, open circles); 2,4-dimethylthiophene (**24T**, full squares).

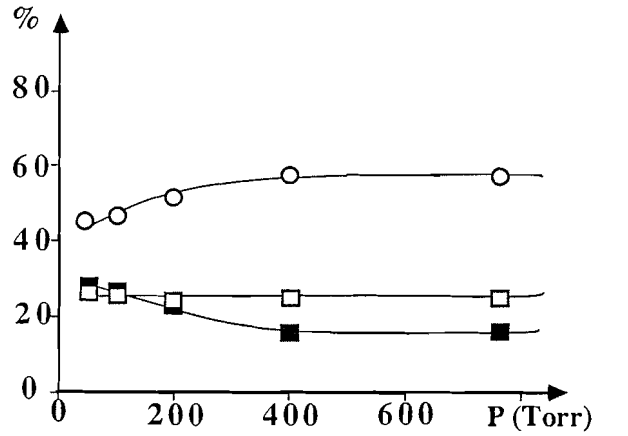


FIG. 7. Relative yields of isomeric dimethylthiophenes from $(CH_3)_2F^+$ attack on 3-methylthiophene **3T** as a function of the total pressure (P) of the system in the absence of NMe_3: 2,3-dimethylthiophene (**23T**, open circles); 3,4-dimethylthiophene (**34T**, open squares); 2,4-dimethylthiophene (**24T**, full squares).

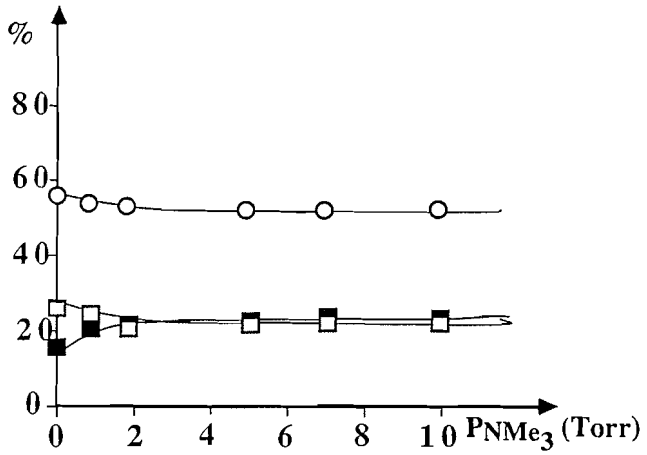


FIG. 8. Relative yields of isomeric dimethylthiophenes from $(CH_3)_2F^+$ attack on 3-methylthiophene **3T** at 760 Torr as a function of the partial pressure of NMe_3 ($P(NMe_3)$): 2,3-dimethylthiophene (**23T**, open circles); 3,4-dimethylthiophene (**34T**, open squares); 2,4-dimethylthiophene (**24T**, full squares).

2, 4, 6, 8). In fact, a **25F**:**23F**:**24F** = 53%:33%:14% distribution is observed in the **2F** systems irradiated at 760 Torr in the presence of NMe_3 (Fig. 2). At the same pressure, but in the absence of added bases, the product composition changes dramatically to **25F**:**23F**:**24F** = 92%:7%:1% (Fig. 2). A decrease of the total pressure of the gaseous mixture leads again to an increase of the relative yield of **23F** and **24F** at the expense of **25F** until, at total pressure of 50 Torr, approximately the same distribution, measured in the presence of NMe_3, is restored (Fig. 1). The same qualitative behavior is observed for the methylated products from **3F** (Figs. 3 and 4), whose isomeric distribution, measured at atmospheric pressure, changes from **25F**:**34F**:**24F** = 61%:20%:19%, in the presence of NMe_3, to 95%:5%:1%, in the absence of added bases (Fig. 4).

Relative to the methylfuran systems, the effect of NMe_3 upon the isomeric distribution of the methylated products from **2T** (Figs. 5 and 6) and **3T** (Figs. 7 and 8) is less pronounced. In fact, the isomeric composition of the methylated derivatives of **2T** changes from **25T**:**23T**:**24T** = 40%:38%:22%, in the presence of NMe_3, to 51%:35%:14%, in the absence of the base (Fig. 6). Similarly, the product distribution from **3T** changes from **23T**:**24T**:**34T** = 53%:24%:23%, in the systems with NMe_3, to 57%:17%:26%, in the systems without added bases (Fig. 8). In all methylthiophene systems, however, approximately the same original product composition, measured in the presence of NMe_3, is restored as the total pressure of the samples is lowered to 50 Torr (Figs. 5 and 7).

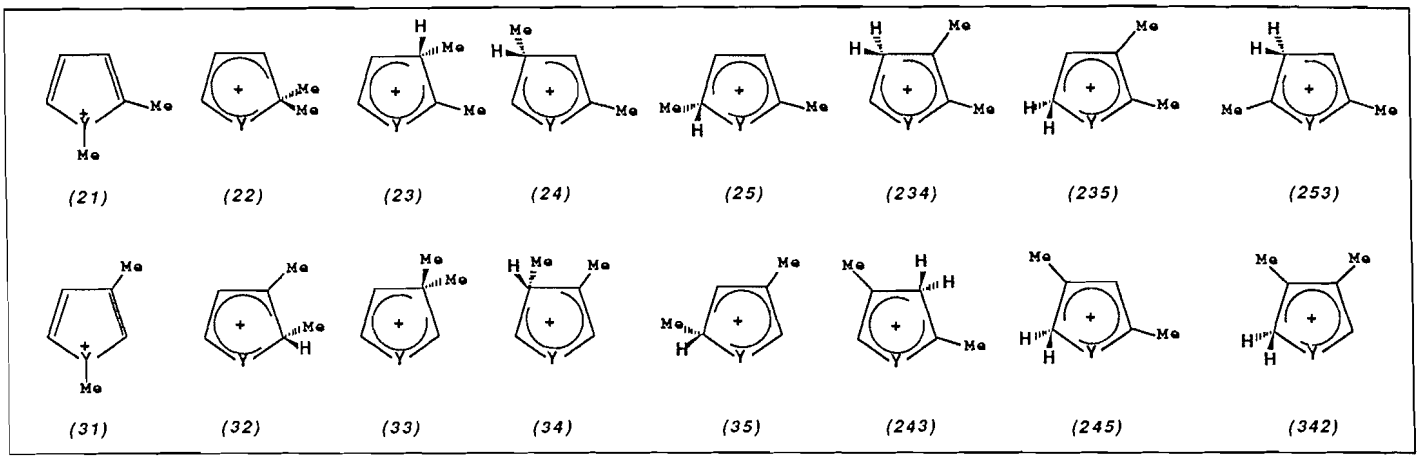
Discussion

Nature of the substitution process

As outlined in previous papers (4), the conditions typical of the present experiments, in particular the low concentrations of the heteroaromatic substrate (0.2–1.0 mol%) diluted with a large excess of CH_3F, exclude direct radiolysis of the starting compound as a significant route to its methylated products. The presence of an efficient thermal radical scavenger, such as oxygen, in the gaseous samples strongly inhibits possible free-radical pathways in favor of the competing ionic reaction pattern, whose role is testified to by the marked effect of the ion trap NMe_3 on the methylated product yields.

The pure Lewis-acid nature of the stable $(CH_3)_2F^+$ ions (ΔH_f^0 = 146 kcal mol^{-1}) (18) from the γ-radiolysis of CH_3F has been amply demonstrated by mass spectrometric (19) as well as radiolytic studies (4, 20). Accordingly, the radiolytic $(CH_3)_2F^+$ ions, thermalized by many unreactive collisions with the parent CH_3F molecules, are able to attack the heteroaromatic substrate, present in trace amounts in the gaseous mixture, yielding eventually the corresponding isomeric methylated heteroarenium intermediates **I** (eq. [1]). Their formation is energetically allowed, as shown in Figs. 9 and 10, and represents the only significant reaction channel available to the $(CH_3)_2F^+$ reactant.

Several reaction channels are open to the heteroarenium intermediates, excited by the exothermicity of their formation process. A direct route to the methylated products is represented by the collisional stabilization of the excited intermediate, followed by loss of a proton to a suitable base B (NMe_3 or other gaseous bases formed from γ-radiolysis of the batch gas), as illustrated in eq. [1] (a). In competition with collisional quenching, the excited intermediate may undergo several secondary reactions, including isomerization or fragmentation with loss of a H_2 molecule to the benzyl-type ion **II** (eq. [1] (b)). Extensive occurrence of this latter pro-



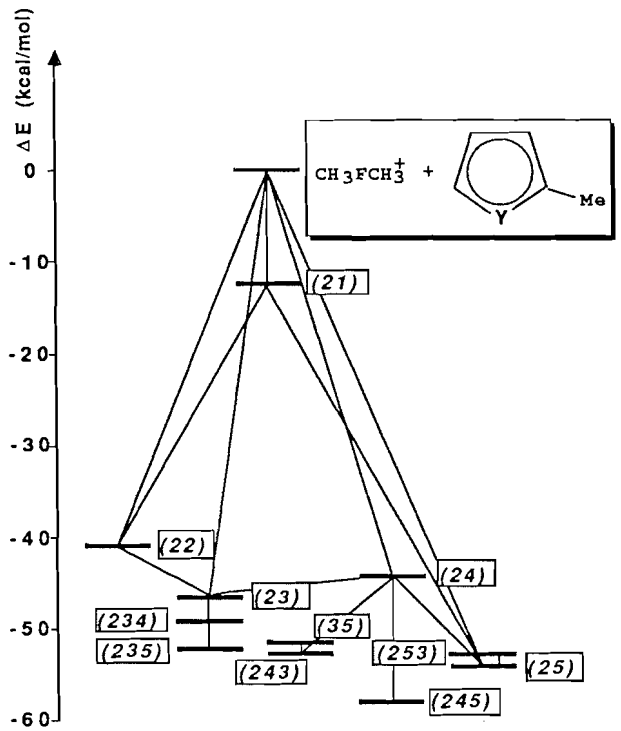


FIG. 9. Energetics of the gas-phase $(CH_3)_2F^+$ attack on 2-methylfuran **2F** to form its primary methylated intermediates (*21*, *22*, *23*, *24*, and *25*) and their isomerized forms (*234*, *235*, *243*, *35*, *253*, and *245*). The first and second figures of the italic numbers refer to the positions of the two methyl groups, whereas the last figure refers to the position of the sp^3-hybridized carbon. Thermochemical data taken from refs. 18 and 21. The formation enthalpies of the heteroarenium intermediates were obtained by lowering the overestimated MNDO calculated values (cf. refs. 18 and 21*b*) by 15 kcal mol^{-1}. Similar energetics are involved in the methylation of 2-methylthiophene, whereas the exothermicity of the methylation of 2-methylpyrrole is ca. 10 kcal mol^{-1} higher.

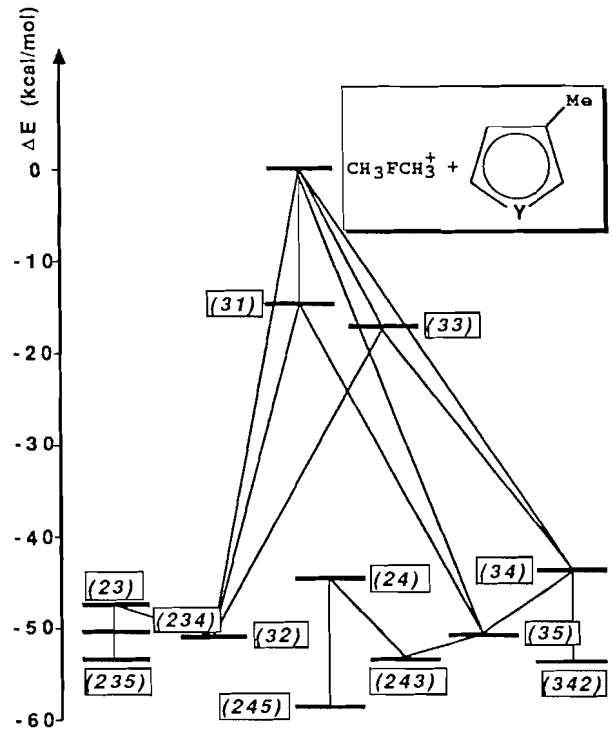


FIG. 10. Energetics of the gas-phase $(CH_3)_2F^+$ attack on 3-methylfuran **3F** to form its primary methylated intermediates (*31*, *32*, *33*, *34*, and *35*) and their isomerized forms (*23*, *234*, *235*, *243*, *24*, *245*, and *342*). The first and second figures of the italic numbers refer to the positions of the two methyl groups, whereas the last figure refers to the position of the sp^3-hybridized carbon. Thermochemical data taken from refs. 18 and 21. The formation enthalpies of the heteroarenium intermediates were obtained by lowering the overestimated MNDO calculated values (cf. refs. 18 and 21*b*) by 15 kcal mol^{-1}. Similar energetics are involved in the methylation of 2-methylthiophene, whereas the exothermicity of the methylation of 2-methylpyrrole is ca. 10 kcal mol^{-1} higher.

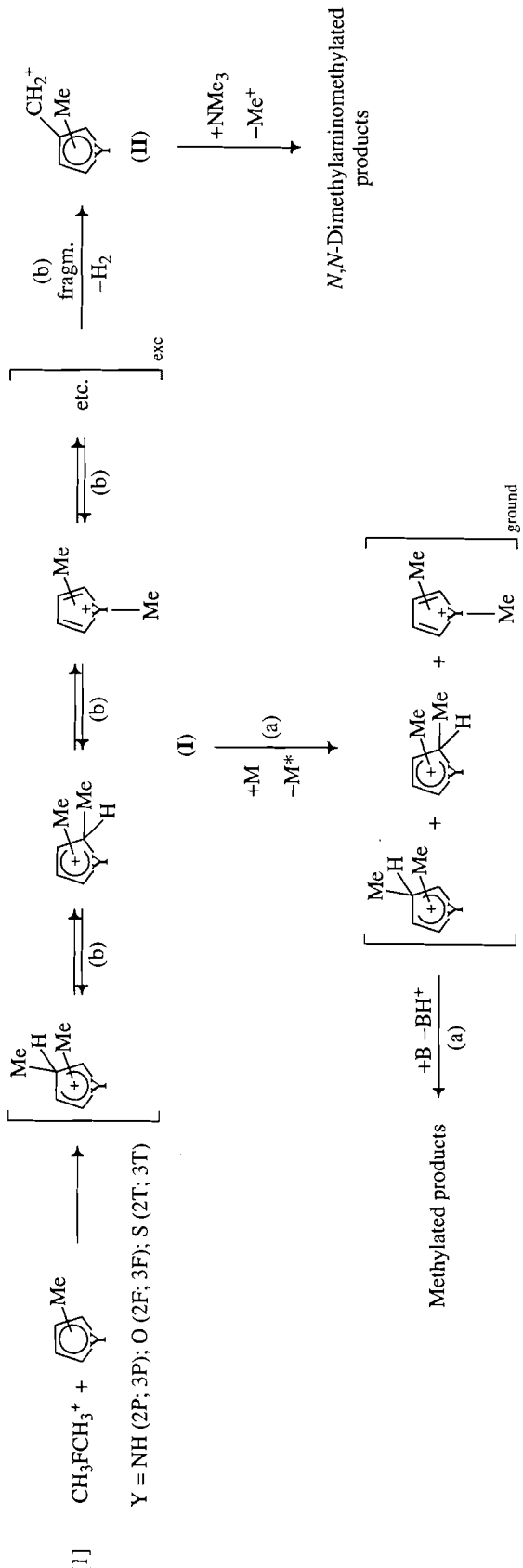
cess under chemical-ionization mass spectrometric conditions (0.1–1.0 Torr) was observed in previous related studies (4).

The relative extent of the competing processes, shown in eq. [1], appears regulated by changes in the reaction environment. Isomerization and fragmentation processes of intermediates **I** are expected to be depressed in systems at atmospheric pressure and with the highest concentrations of NMe_3, where their efficient quenching and rapid neutralization can take place.

The relatively constant methylated product distribution measured in the systems with NMe_3 (see, for instance, Figs. 2, 4, 6, and 8) corroborates the above expectation with regard to the isomerization of the ionic intermediates **I** under such con-

Can. J. Chem. Downloaded from www.nrcresearchpress.com by 123.30.183.119 on 09/08/12
For personal use only.

Can. J. Chem. Downloaded from www.nrcresearchpress.com by 123.30.183.119 on 09/08/12
For personal use only.



ditions. Concerning the fragmentation of the methylation intermediates **I** from methyl-furans and -thiophenes, the lack of any measurable amounts of their *N*,*N*-dimethylaminomethyl derivatives in the presence of NMe_3 and the relatively high yields of their methylated neutral products in the absence of added bases ($G_{(M)}$ = 1.2–2.1 (dimethylfurans); 0.7–1.5 (dimethylthiophenes)) indicate effective collisional quenching and neutralization of the corresponding primary methylation intermediates **I** prior to fragmentation to **II** and H_2. No similar conclusion can be reached regarding the extent of fragmentation of the methylated intermediates **I** from methylpyrroles under the same conditions. In fact, isolation of appreciable amounts of the β-*N*,*N*-dimethylaminomethyl derivatives of **2P** and **3P**, even at 760 Torr and in the presence of 10 Torr of NMe_3, points to extensive fragmentation of the corresponding methylated heteroarenium ions **I** to **II** and H_2 occurring in a time comparable with that of their effective collisional quenching and neutralization under such conditions (eq. [1]). As suggested by the comparatively low $G_{(M)}$ values of the methylated products from pyrroles (0.1–0.3), the extent of fragmentation of their β-methylated heteroarenium precursors **I** is likely increased in the absence of NMe_3 and at low pressures, yielding substantial amounts of their benzyl-type daughter species **II** whose occurrence cannot, however, be monitored by the formation of isolable products. Under such conditions, in fact, the benzyl-type fragments **II** cannot be trapped by NMe_3 to eventually yield their *N*,*N*-dimethylaminomethyl derivatives, but rather may further attack another molecule of pyrrole giving rise to an oligomerization process.

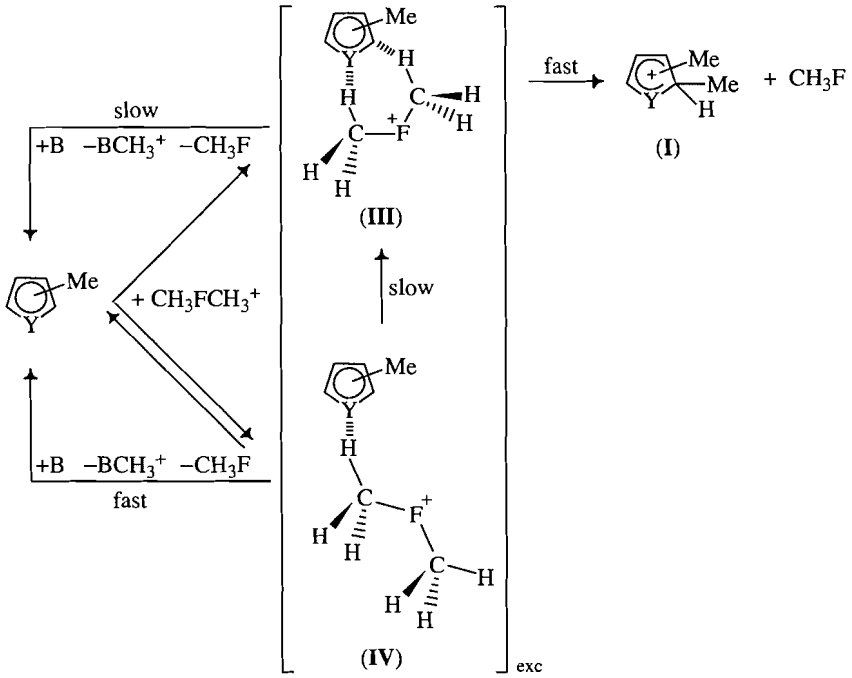
The residual fragmentation of the methylated heteroarenium intermediates from **2P** and **3P** at 760 Torr and in the presence of NMe_3, namely under conditions where the same process involving the corresponding intermediates from methyl-furans and -thiophenes is prevented, is probably due to the relatively high excess energy deposited in the methylation intermediates. In fact, thermochemical calculations show that $(CH_3)_2F^+$ ion methylation of methylpyrroles is over 10 kcal mol^{-1} more exothermic (ΔH^0 = −66 kcal mol^{-1}) relative to the same reactions with methyl-furans (ΔH^0 = −55 kcal mol^{-1}) and -thiophenes (21).

From the above considerations, it can be concluded that the isomeric composition of the methylated products (and the *N*,*N*-dimethylaminomethylated ones as well, in the case of methylpyrroles **2P** and **3P**) recovered from the systems at the highest total (760 Torr) and NMe_3 partial pressure (10 Torr) closely reflects the relative population of the primary *C*-methylated intermediates from attack of $(CH_3)_2F^+$ on the carbon centers of the selected substrates.

In the absence of NMe_3, namely under longer-lived ion conditions, while β-substituted products are still exclusively formed from methylpyrroles (100% **23P** from **2P**; 100% **34P** from **3P**), significant modifications in the relative distribution of the methylated products from methyl-furans and -thiophenes are observed (Figs. 2, 4, 6, and 8). Thus, the relative yield of **25F** from **2F** increases from 53 to 92% and that of **23F** from **3F** from 61 to 95% at the expense of the other relevant isomers. The variations in the relative yields of the corresponding methylated isomers from methylthiophenes are less pronounced, but still significant (from 40 to 51% for **25T** from **2T** and from 53 to 57% for **23T** from **3T**).

In analogy with the conclusions reached in previous related investigations (2, 4), such behavior is due to the presence of the

[2]



n-electrons of the heteroatom of furans and thiophenes, which can establish more or less effective electrostatic interactions with the proton centers of the ionic electrophile. Proximity factors may favor evolution of a properly oriented fraction of these electrostatic adducts, i.e., **III** of eq. [2], to the C_α-substituted σ-bonded heteroarenium intermediates **I** with a frequency that is high if compared to the collision frequency between the adduct and B = NMe_3. This accounts for the apparent discrepancy of a high-energy LUMO electrophile, such as $(CH_3)_2F^+$ (SCF STO-3G calculated $\varepsilon_{(LUMO)} = +1.77$ eV) (1), displaying a high affinity for the α positions of furans (53% at C5 of 2-methylfuran and 61% at C2 of 3-methylfuran). The remaining fraction of electrostatic adducts, i.e., **IV** of eq. [2], does not present an appropriate orientation for its rapid evolution to σ-bonded intermediates **I** before colliding with NMe_3 and, therefore, is readily destroyed by the base. In the absence of NMe_3, under longer-lived ion conditions, however, this latter fraction of electrostatic adducts, if stabilized by unreactive collision with the bath gas molecules, may also slowly acquire the appropriate configuration of structure **III** and thence evolve to the corresponding C_α-substituted σ-bonded heteroarenium intermediates **I**. This behavior accounts for the apparent increase of the relative yield of **25F** from **2F** and of **23F** from **3F**, in the gaseous samples containing no added bases irradiated at 760 Torr. In this perspective and in agreement with previous conclusions (2, 4), the much less pronounced increase of the relative yields of **25T** from **2T** and of **23T** from **3T**, observed under the same conditions, is consistent with the much lower tendency of the sulfur atom of thiophenes to establish electrostatic interactions with the proton centers of the ionic electrophile (22).

As the total pressure of the reaction mixtures decreases (Figs. 1, 3, 5, and 7), namely under long-lived *excited-ion* conditions, a methylated product distribution, which closely approaches that measured in the presence of NMe_3, is obtained from both methylfurans and methylthiophenes. Such a pressure effect is reminiscent of that observed in the $(CH_3)_2F^+$ methylation of unsubstituted furan and thiophene (4), which found a simple rationale in the extensive isomerization of the excited primary heteroarenium intermediates to the thermodynamically most stable structure via multiple intramolecular 1,2-methyl group shifts. However, such an isomerization route, although not excludable *a priori*, appears unlikely in the present case owing to the following considerations.

According to the thermochemical data reported in Figs. 9 and 10, isomer *245* is the thermodynamically most stable structure accessible in the isomerization via intramolecular 1,2-methyl group shifts of primary methylated heteroarenium intermediates of eq. [1], excited by the exothermicity of their formation process. By virtue of this isomerization pathway favoring formation of *245*, a distinct increase of its neutral 2,4-dimethylated product should be observed under long-lived excited-ion conditions, i.e., at low pressure in the absence of NMe_3, in contrast with experimental evidence. Contrariwise, the product distribution obtained under these conditions closely approaches that measured under kinetically controlled conditions, i.e., at 760 Torr and in the presence of 10 Torr of NMe_3 (cf. Figs. 1–8). Such a pressure effect on the product composition is better accounted for by the alternative hypothesis of a reversible formation of the electrostatic adducts **III** and **IV**, which, if not stabilized by collision with the bath gas molecules, may back-dissociate, although to a different extent, yielding again the heteroarene and the ionic electrophile (eq. [2]). Increase of the excitation level of the electrostatic adducts, i.e., by decreasing the system pressure, is reflected in their more extensive back-dissociation to reactants. The resulting onium ion has a high probability of attacking another molecule of substrate, by far the most abundant nucleophile present in the gaseous mixture. It may attack again the heteroatom of the substrate, yielding once more the readily dissociable electrostatic adducts **III** and **IV**. Alternatively, it may attack the ring carbons of the heteroarene, producing the methylated heteroarenium ions **I** with loss of a CH_3F moiety, an event which makes the attack irreversible.

The consequence of the reversible attack of the onium ion on the heteroatom of the substrate is that the ring carbons of

Can. J. Chem. Downloaded from www.nrcresearchpress.com by 123.30.183.119 on 09/08/12
For personal use only.

Can. J. Chem. Downloaded from www.nrcresearchpress.com by 123.30.183.119 on 09/08/12
For personal use only.

the heteroarene represent the reaction sink for the $(CH_3)_2F^+$ ions, which therefore are able to produce the primary distribution of *C*-methylated heteroarenium intermediates in high yields. The observation that approximately the same distribution of their primary methylated intermediates **I** is obtained at 50 Torr implies relatively high energy barriers for any conceivable methyl group shifts in the primary excited heteroarenium intermediates (23), in contrast with our previous hypothesis (4).

As mentioned above, the initial population of the electrostatic adducts **IV** emerges directly from a comparative analysis of the isomeric distribution of the neutral *C*-methylated products, as measured under kinetically controlled conditions, i.e., at 760 Torr and in the presence of NMe_3, where conversion of adducts **IV** to the α-methylated heteroarenium intermediates **I** is minimized, and at the same pressure, but in the absence of NMe_3, where back-dissociation of the adducts **IV** (and **III**) is prevented and their conversion to the heteroarenium ions **I** is allowed. The increase of the relative yield of **25F** from **2F** (from 53 to 92%), as the NMe_3 partial pressure decreases from 10 Torr to zero, is consistent with the relative extent of direct interaction of the $(CH_3)_2F^+$ on the oxygen of **2F** to give the electrostatic adducts **III** and **IV** exceeding 80%. By the same procedure, the corresponding increase of the relative yield of **23F** from **3F** (from 61 to 95%) can be accounted for by the relative extent of attack of the ionic electrophile on the oxygen of **3F** as exceeding 80%. Furthermore, the fact that such an increase is reflected in the accompanying decrease of not only **34F** (from 20 to 4%) *but also* **24F** (from 19 to 1%) suggests that the methyl substituent in the ensuing electrostatic adducts **III** and **IV** directs their conversion predominantly to the σ-bonded heteroarenium intermediate *32*, rather than to its isomer *35* (Figs. 9 and 10). The relatively minor increase in the abundance of **25T** from **2T** (from 40 to 51%), as the NMe_3 partial pressure decreases from 10 Torr to zero, indicates that establishment of electrostatic interactions between $(CH_3)_2F^+$ and the sulfur atom of **2T** is comparatively much less effective (>20%), in conformity with expectations (22). Similarly, in **3T**, direct attack of the ionic electrophile on the heteroatom of the substrate does not exceed 10%, as indicated by the increase of the relative yield of **23T** from 53 to 57%. The observation that such an increase takes place at the expense of the **24T** isomer (from 24 to 17%) suggests, in analogy with the conclusion reached for **3F**, that the methyl substituent in the adducts formed (**III** and **IV**) induces their total conversion to the σ-bonded heteroarenium intermediate *32*. Concerning the *N*-center of methylpyrroles **2P** and **3P**, the lack of any detectable amounts of both the α- and *N*-substituted derivatives under all experimental conditions reflects the lack of *n*-electrons on the heteroatom of pyrroles and, therefore, its low propensity to electrostatically interact with the incoming electrophile.

In conformity with the above considerations, the intrinsic positional selectivity of the $(CH_3)_2F^+$ ion toward the selected heteroaromatic substrates can be evaluated as reported in Fig. 11.

Positional selectivity

The intrinsic regiospecificity of gaseous $(CH_3)_2F^+$ toward pyrroles **2P** and **3P** demonstrates the tendency of the heteroaromatic molecule to drive the ionic electrophile toward the ring carbons with the highest value of the net negative charge (the C3 in **2P** and the C4 in **3P**) (24). This tendency conforms

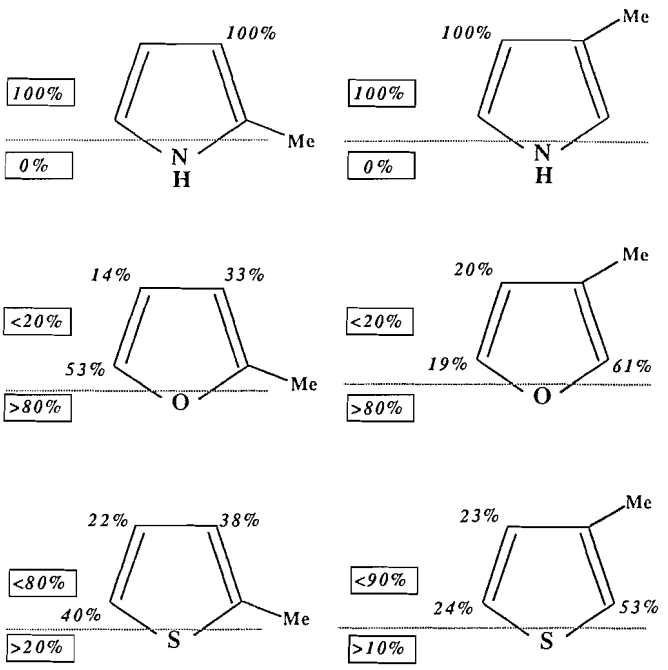


FIG. 11. Positional selectivity of gaseous $(CH_3)_2F^+$ ions toward isomeric methyl-pyrroles, -furans, and -thiophenes.

to that expected on the grounds of the Charge and Frontier Orbital Control Concept (25). Within this model, which is included in the more general Curve Crossing model (3), the reactivity properties of the ionic electrophile toward the selected methylpyrroles are essentially determined by the energy gap between the HOMO of the donor ($\varepsilon_H > -6.6$ eV)[5] and the LUMO of the ionic acceptor ($\varepsilon_L = +1.8$ eV) (1). Accordingly, the total perturbation energy in the orbital interaction between the methylpyrrole molecule and the $(CH_3)_2F^+$ electrophile is essentially determined by electrostatic interactions within the encounter pair, owing to the very large energy gap ($\varepsilon_H - (\varepsilon_L > -8.4$ eV) between the HOMO of the heteroarene and the LUMO of the electrophile, which is somewhat proportional to the difference between the vertical ionization potential of the donor and the vertical electron affinity of the acceptor (1). Hence, since $(CH_3)_2F^+$ methylation of isomeric methylpyrroles is a "charge-controlled" reaction, the $(CH_3)_2F^+$ electrophile is primarily oriented toward the reaction sites of pyrroles with the highest net negative charge (the C3 of **2P** and the C4 of **3P**).

The same model may also account for the apparent predominant formation of the α-methylated products **25F** from **2F** and **23F** from **3F**, once the preferential interaction between the ionic electrophile and the most negatively charged site of methylfurans, i.e., their oxygen atom, to yield the electrostatic adducts **III** and **IV** of eq. [2], is considered. In fact, rapid evolution of the "chelate" adducts **III** to the corresponding σ-bonded α-methylated intermediates **I** is favored by proximity of the CH_3 moiety of the electrophile to the C_α's of furans. The observation that, in spite of such an electrostatic coordination of the electrophile by the oxygen of **3F**, the **24F** derivative is formed with a yield (19%) slightly lower than that of **34F** (20%) points to some preference for a direct attack of the

[5]The HOMO energy of methylpyrroles is estimated as slightly higher than the STO-3G SCF calculated HOMO eigenvalue of pyrrole ($\varepsilon_H = -6.64$ eV) (1).

$(CH_3)_2F^+$ electrophile on the ring carbon of methylfurans with the highest net negative charge, e.g., the C4 of **3F** (26). The same factor determines as well the predominant pathway for evolution of the chelate adducts **III** from **3F** to the σ-bonded intermediate *32*, instead of to its isomer *35*.

Preliminary electrostatic interactions between the sulfur atom of methylthiophenes **2T** and **3T** and an ionic electrophile, such as $(CH_3)_2F^+$, are much less significant relative to furans (Fig. 11). This observation agrees well with others concerning unsubstituted thiophene and is attributable to the predominant localization of the net negative charge at the ring carbons of thiophenes, rather than at the heteroatom (27). As a result, the methylating electrophile is essentially directed to the ring carbons of methylthiophenes, wherein the combined effect of the electron-releasing methyl substituent and sulfur atom is maximized, i.e., at the C5 of **2T** and at the C2 of **3T** (28).

Conclusions

The intrinsic reactivity properties of gaseous $(CH_3)_2F^+$ ion toward methylated pyrroles, furans, and thiophenes qualitatively correspond to the expected behavior of a typical high-energy LUMO electrophile, which is electrostatically oriented toward the ring positions of the heteroaromatic substrate with the highest net negative charge. In methylpyrroles, the electron-releasing character of the methyl substituent adjacent to a β carbon significantly enhances the already distinct affinity of the $(CH_3)_2F^+$ ion for these positions of the pyrrolic ring. A similar activating effect of the methyl group is observed toward the most negatively charged unsubstituted α positions of methylthiophenes. Intense attractive interactions between the methylating electrophile and the heteroatom of methylfurans favor reversible formation of two different sets of electrostatic adducts with either a chelate structure **III** or a single proton-bonded form **IV** (eq. [2]). While rapid evolution of the first structure to the α-substituted heteroarenium intermediate is favored by proximity effects, relatively slow rearrangement of the open form **IV** to **III** takes place in competition with its back-dissociation or reaction with an external base. Reversible formation of electrostatic adducts **III** and **IV** in furans better accounts for the pronounced sensitivity of the relative composition of the substituted products to the experimental conditions adopted, ruling out a previously advanced alternative hypothesis of extensive intramolecular 1,2-methyl group shifts in their excited heteroarenium precursors.

It should be finally mentioned that the present gas-phase results represent the only meaningful kinetic measurement of the intramolecular selectivity of ionic alkylating reactants toward methyl-substituted five-membered heteroarenes, since the corresponding measurements under Friedel–Crafts conditions are complicated by the high sensitivity of the substrates to highly acidic media and to their tendency to undergo extensive polymerization (29).

Acknowledgments

The authors wish to express their gratitude to the Ministero dell'Università e della Ricerca Scientifica e Tecnologica (MURST) and the Consiglio Nazionale delle Ricerche (CNR; Progetto Finalizzato "Chimica Fine II") of Italy for financial support.

1. R. BUCCI, F. GRANDINETTI, A. FILIPPI, G. LAGUZZI, G. OCCHIUCCI, and M. SPERANZA. J. Am. Chem. Soc. **113**, 4550 (1991).
2. (*a*) M. SPERANZA. Adv. Heterocycl. Chem. **40**, 25 (1986); (*b*) J. Chem. Soc. Chem. Commun. 1177 (1981); (*c*) A. MARGONELLI and M. SPERANZA. J. Chem. Soc. Perkin Trans. 2, 1491 (1983); (*d*) G. LAGUZZI and M. SPERANZA. J. Chem. Soc. Perkin Trans. 2, 857 (1987); (*e*) G. ANGELINI, C. SPARAPANI, and M. SPERANZA. J. Am. Chem. Soc. **112**, 3060 (1990); (*f*) G. LAGUZZI, R. BUCCI, F. GRANDINETTI, and M. SPERANZA. J. Am. Chem. Soc. **112**, 3064 (1990); (*g*) M. E. CRESTONI, S. FORNARINI, and M. SPERANZA. J. Am. Chem. Soc. **112**, 6929 (1990); (*h*) A. FILIPPI, G. OCCHIUCCI, and M. SPERANZA. Can. J. Chem. **69**, 732 (1991).
3. (*a*) S. S. SHAIK. J. Am. Chem. Soc. **103**, 3692 (1981); (*b*) A. PROSS and S. S. SHAIK. Acc. Chem. Res. **16**, 361 (1983); (*c*) S. S. SHAIK. Prog. Phys. Org. Chem. **15**, 197 (1985); (*d*) A. PROSS. Adv. Phys. Org. Chem. **21**, 99 (1985).
4. (*a*) G. ANGELINI, C. SPARAPANI, and M. SPERANZA. J. Am. Chem. Soc. **104**, 7084 (1982); (*b*) G. ANGELINI, G. LILLA, and M. SPERANZA. J. Am. Chem. Soc. **104**, 7091 (1982).
5. (*a*) G. A. OLAH. Halonium ions. *Edited by* G. A. Olah. Wiley, New York. 1975; (*b*) G. A. OLAH and J. R. DEMEMBER. J. Am. Chem. Soc. **92**, 718 (1970); (*c*) G. A. OLAH and E. G. MELBY. J. Am. Chem. Soc. **94**, 6220 (1972); (*d*) G. A. OLAH, Y. YAMADA, and R. J. SPEAR. J. Am. Chem. Soc. **97**, 680 (1975); (*e*) P. E. PETERSON, R. BROCKINGTON, and D. W. VIDRINE. J. Am. Chem. Soc. **98**, 2060 (1976); (*f*) G. A. OLAH, D. J. DONOVAN, and H. C. LIN. J. Am. Chem. Soc. **98**, 2661 (1976).
6. M. JANDA, J. SROGL, I. STIBOR, M. NEMEC, and P. VOPATRNA. Synthesis, 545 (1972).
7. D. M. BURNESS, J. CASON, and R. B. HUTCHINSON. Org. Synth. **39**, 46 (1959).
8. (*a*) H. E. WINBERG, F. S. FAWCETT, W. E. MOCHEL, and C. W. THEOBOLD. J. Am. Chem. Soc. **82**, 1428 (1960); (*b*) K. C. RICE and J. R. DYER. Heterocycl. Chem. 1325 (1975).
9. T. H. MOREL and P. E. VERDAKE. Recl. Trav. Chim. Pays-Bas, **70**, 35 (1951).
10. D. I. RAWSON, B. K. CARPENTER, and H. M. R. HOFFMAN. J. Am. Chem. Soc. **101**, 1786 (1963).
11. A. J. CASTRO, J. F. DECK, M. T. HUGO, E. J. LOWE, J. P. MARSH, JR., and R. J. PFEIFFER. J. Org. Chem. **28**, 857 (1963).
12. R. E. LANCASTER, JR., and C. A. VAN DER WERF. J. Org. Chem. **23**, 1208 (1958).
13. G. P. BEAN. J. Org. Chem. **32**, 228 (1967).
14. J. P. NAGARKATTI and K. R. ASHLEY. Synthesis, 186 (1974).
15. R. L. HINMAN and S. THEODOROPULOS. J. Org. Chem. **28**, 3052 (1963).
16. R. M. ACHESON and J. M. VERNON. J. Chem. Soc. 1008 (1963).
17. B. E. MARYANOFF. J. Org. Chem. **44**, 4410 (1979).
18. J. K. HOVEY and T. B. MCMAHON. J. Am. Chem. Soc. **108**, 528 (1986).
19. (*a*) Z. LUCZYNSKY and J. A. HERMAN. J. Phys. Chem. **89**, 179 (1978); (*b*) S. A. BENEZRA, M. K. HOFFMAN, and M. M. BURSEY. J. Am. Chem. Soc. **92**, 7501 (1970); (*c*) M. J. K. PABST, H. S. TAN, and J. L. FRANKLIN. Int. J. Mass Spectrom. Ion Phys. **20**, 191 (1976); (*d*) R. J. BLINT, T. B. MCMAHON, and J. L. BEAUCHAMP. J. Am. Chem. Soc. **96**, 1269 (1974); (*e*) J. L. BEAUCHAMP, D. HOLTZ, S. D. WOODGATE, and S. L. PATT. J. Am. Chem. Soc. **94**, 2798 (1972); (*f*) D. HOLTZ, J. L. BEAUCHAMP, and S. D. WOODGATE. J. Am. Chem. Soc. **92**, 7484 (1970); (*g*) A. A. HEROD, A. G. HARRISON, and N. A. MCASKILL. Can. J. Chem. **49**, 2217 (1971).
20. (*a*) M. SPERANZA, N. PEPE, and R. CIPOLLINI. J. Chem. Soc. Perkin Trans. 2, 1179 (1979); (*b*) N. PEPE and M. SPERANZA. J. Chem. Soc. Perkin Trans. 2, 1430 (1981); (*c*) M. SPERANZA and G. ANGELINI. J. Am. Chem. Soc. **102**, 3115 (1980); (*d*) G. ANGELINI and M. SPERANZA. J. Am. Chem. Soc. **103**, 3792 (1981); (*e*) J. Am. Chem. Soc. **103**, 3800 (1981); (*f*) M. COLOSIMO and R. BUCCI. J. Phys. Chem. **83**, 1952 (1979).
21. (*a*) S. G. LIAS, J. E. BARTMESS, J. F. LIEBMAN, J. L. HOLMES, R. D. LEVIN, and W. G. MALLARD. J. Phys. Chem. Ref. Data, **17**, Suppl. 1 (1988); (*b*) R. HOURIET, E. ROLLI, G. BOUCHOUX, and Y. HOPPILLIARD. Helv. Chim. Acta, **68**, 2037 (1985).
22. (*a*) P. SCHUSTER, G. ZUNDEL, and C. SANDORFY. The hydrogen bond. North-Holland Publishing Co., Amsterdam. 1976; (*b*) P. J.

Can. J. Chem. Downloaded from www.nrcresearchpress.com by 123.30.183.119 on 09/08/12
For personal use only.

DESMUELES and L. C. ALLEN. J. Chem. Phys. **72**, 4731 (1980); (*c*) R. C. KERNS and L. C. ALLEN. J. Am. Chem. Soc. **100**, 6587 (1978); (*d*) K. F. PURCELL and R. S. DRAGO. J. Am. Chem. Soc. **89**, 2874 (1967); (*e*) T. B. VISHNYAKOVA, V. V. LOBANOV, and V. K. POGORELYI. Teor. Eksp. Khim. **16**, 534 (1980).

23. H. E. AUDIER, Y. HOPPILLIARD, and R. ROBIN. New. J. Chem. **12**, 217 (1988).
24. (*a*) M. V. SIGALOV, B. A. TROFIMOV, A. I. MIKHALEVA, and G. A. KALABIN. Tetrahedron, **37**, 3051 (1981); (*b*) R. J. ABRAHAM, R. D. LAPPER, K. M. SMITH, and J. F. UNSWORTH. J. Chem. Soc. Perkin Trans. 2, 1004 (1974).
25. (*a*) G. KLOPMAN. J. Am. Chem. Soc. **90**, 223 (1968); (*b*) R. G. PEARSON. Proc. Natl. Acad. Sci. USA, **83**, 8440 (1986).
26. (*a*) I. STIBOR, P. TRSKA, J. SROGL, and M. JANDA. Collect. Czech. Chem. Commun. **43**, 2170 (1978); (*b*) J. SROGL, M. JANDA, I. STIBOR, V. SKALA, P. TRASKA, and M. RYSKA. Collect. Czech. Chem. Commun. **39**, 3109 (1974).
27. (*a*) V. GELIUS, B. ROOS, and P. SIEGBAHN. Theor. Chim. Acta, **27**, 171 (1972); (*b*) F. BERNARDI, A. BOTTONI, and A. MANGINI. Gazz. Chim. Ital. **101**, 55 (1977).
28. (*a*) M. JANDA, J. SROGL, I. STIBOR, P. TRSKA, and P. VOPATRNA. Collect. Czech. Chem. Commun. **39**, 3522 (1974); (*b*) M. J. NANJAN, V. KANNAPPAN, and R. GANESAN. Z. Phys. Chem. (Munich), **127**, 13 (1981).
29. R. NICOLETTI and C. GERMANI. Ric. Sci. **36**, 1343 (1966).

Can. J. Chem. Downloaded from www.nrcresearchpress.com by 123.30.183.119 on 09/08/12
For personal use only.

Nucleic acid related compounds. 67. Synthesis of 5′-amino and 5′-methylthio chain-extended nucleosides from uridine[1]

STANISLAW F. WNUK, N. KENT DALLEY, AND MORRIS J. ROBINS[2]

Departments of Chemistry, Brigham Young University, Provo, UT 84602, U.S.A., Academy of Agriculture, 60625 Poznan, Wojska Polskiego 75, Poland, and University of Alberta, Edmonton, Alta., Canada T6G 2G2

Received April 23, 1991

STANISLAW F. WNUK, N. KENT DALLEY, and MORRIS J. ROBINS. Can. J. Chem. **69**, 2104 (1991).

Treatment of 2′,3′-*O*-isopropylideneuridine-5′-aldehyde with the stabilized Wittig reagent, (*p*-toluenesulfonylmethylene)triphenylphosphorane, gave high yields of 1-[5,6-dideoxy-2,3-*O*-isopropylidene-6-(*p*-toluenesulfonyl)-β-D-*ribo*-hex-5(*E*)-enofuranosyl]uracil (**2**). This vinylsulfone (**2**) underwent isomerization readily in base to give the allylic sulfone, 1-[5,6-dideoxy-2,3-*O*-isopropylidene-6-(*p*-toluenesulfonyl)-β-D-*erythro*-hex-4(*Z*)-enofuranosyl]uracil (**3**). Treatment of **2** or **3** with aqueous trifluoroacetic acid gave the corresponding deprotected vinyl (**5**) or allylic (**6**) sulfones, and **5** was converted to **6** readily in basic solutions. Treatment of **2** with sodium borohydride, sodium thiomethoxide, or ammonia resulted in conjugate addition (at C5′ of the vinyl sulfone) to give the 5′-hydro, 5′-methylthio, or 5′-amino-5′,6′-dideoxy-6′-(*p*-toluenesulfonyl) nucleosides. The 5′-substituted diastereomers were deprotected, separated, and the configuration of a 5′-amino derivative was established by X-ray crystallography.

Key words: allylic sulfones, amino-nucleosides, 5′,6′-dideoxynucleosides, nucleosides, uridine, vinyl sulfones.

STANISLAW F. WNUK, N. KENT DALLEY et MORRIS J. ROBINS. Can. J. Chem. **69**, 2104 (1991).

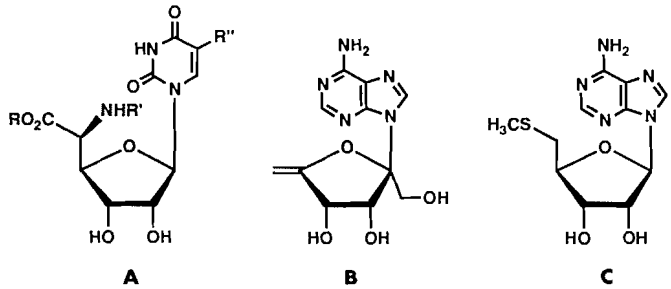
Le traitement du 2′,3′-*O*-isopropylidène-uridine-5′-aldéhyde avec le réactif de Wittig stabilisé, (*p*-toluènesulfonylméthylène)triphénylphosphorane, fournit des rendements élevés du 1-[5,6-didésoxy-2,3-*O*-isopropylidène-6-(*p*-toluènesulfonyl)-β-D-*ribo*-hex-5(*E*)-énofuranosyl]uracil (**2**). En présence de base, cette vinylcétone (**2**) subit une isomérisation conduisant à la sulfone allylique, 1-[5,6-didésoxy-2,3-*O*-isopropylidène-6-(*p*-toluènesulfonyl)-β-D-*érythro*-hex-4(*Z*)-énofuranosyl]uracil (**3**). Le traitement des composés **2** ou **3** avec de l'acide trifluoroacétique aqueux fournit les sulfones correspondantes déprotégées vinylique **5** et allylique **6**; le composé **5** est facilement transformé en produit **6** en solutions basiques. Le traitement du composés **2** par le borohydrure de sodium, du thiométhylate de sodium ou de l'ammoniac conduit à une addition conjuguée (en C5′ de la vinylcétone) et à la formation des 5′-hydro-, 5′-méthylthio- ou 5′-amino-5′,6′-didésoxy-6′-(*p*-toluènesulfonyl)-nucléosides. Les diastéréoisomères substitués en 5′ ont été déprotégés, séparés et la configuration d'un dérivé 5′-amino a été déterminé par diffraction des rayons-X.

Mots clés : sulfones allyliques, amino-nucléosides, 5′,6′-didésoxynucléosides, nucléosides, uridine, vinylsulfones.

[Traduit par la rédaction]

Introduction

Among the varied structural features present in nucleoside antibiotics (1*a*, 2*a*), the polyoxin and nikkomycin complexes (**A**) have a substituted 5′-amino-5′-deoxyhexofuranosyl uronic acid sugar backbone with a uracil or 5-substituted-uracil base (1*b*, 2*b*). Other nucleoside antibiotics (e.g., decoyinine (**B**)) have unsaturated sugar moieties and (or) further modifications at C5′ (1*c*, 2*c*). Methylthioadenosine phosphorylase catalyzes the glycosyl cleavage of 5′-*S*-methyl-5′-thioadenosine (**C**), and



A **B** **C**

the resulting 5-*S*-methyl-5-thioribose 1-phosphate is converted to methionine by salvage pathway enzymes (3). Pyrimidine nucleoside phosphorylases effect analogous cleavage of uridine nucleosides (4). Thus, the synthesis and biological evaluation of uridine nucleoside analogues modified at C5′ with amino or methylthio substituents is of current interest.

Chain extensions and other carbon–carbon bond forming reactions at C5′ of nucleosides have generally involved oxidation to 5′-aldehyde derivatives and treatment with Wittig-type reagents, or nucleophilic conversions with 5′-deoxy-5′-halonucleosides (5, 6). Wittig reactions of nucleoside 5′-aldehydes with stabilized ylides have provided 6′-substituted-5′,6′-unsaturated hexofuranosyl nucleosides (7–12). However, direct introduction of the methylene group at C5′ has met with limited success, and only recently has the direct synthesis of 5′-deoxy-5′-methyleneadenosine been reported (13). Seebach's silyl nitronate (nitro-aldol) methodology was used for chain extension of aldehyde sugars including a uridine 5′-aldehyde derivative (14). Barton *et al.* developed radical-mediated chemistry for the stereocontrolled synthesis of chain-lengthened nucleoside phosphonates (15*a*), vinyl sulfones (15*b*), and a phosphonate analogue of 3′-azido-3′-deoxythymidine 5′-monophosphate (AZTMP) (15*c*). A multistep synthesis of 5′-homo-AZT from 1,2;5,6-di-*O*-isopropylidene-3-*O*-mesyl-α-D-allofuranose (4% overall yield) was reported recently (16).

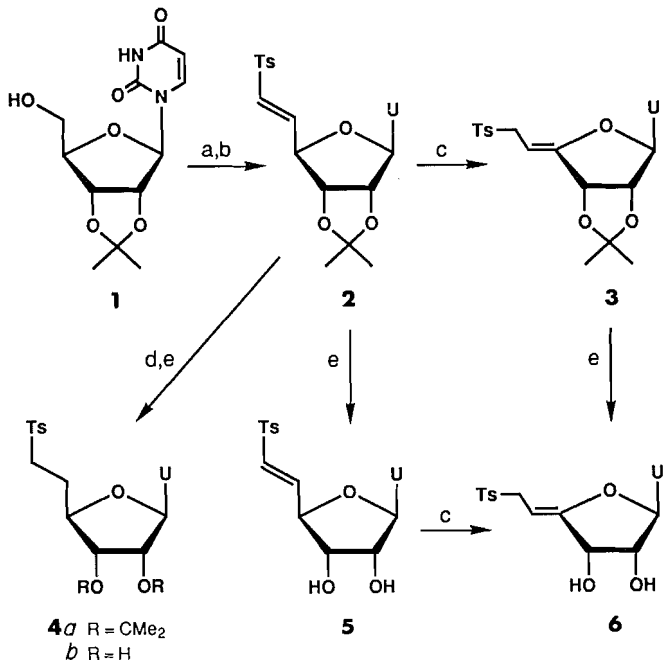
Chattopadhyaya and co-workers prepared 1-(2,3-dideoxy-3-*p*-toluenesulfonyl-β-D-*glycero*-pent-2-enofuranosyl)uracil and its adenine analogue (17) and the uracil 3′-phenylselenone analogue (18). These powerful Michael acceptors (vinyl 3′-sulfone or selenone) were utilized to functionalize the carbohydrate moiety of nucleosides. The chemistry of vinyl sulfones was reviewed recently (19). We now describe the efficient synthesis of a uridine vinylsulfone derivative (**2**), its use as a synthetic intermediate for Michael addition products, and its base-catalyzed rearrangement to the 4′,5′-unsaturated allylic sulfone (**3**).

[1]For the previous paper in this series see ref. 37.

[2]Author to whom correspondence may be addressed at Brigham Young University.

Printed in Canada / Imprimé au Canada

Can. J. Chem. Downloaded from www.nrcresearchpress.com by 123.30.183.119 on 09/08/12
For personal use only.



(a) DCC/DMSO/PTFA or DCC/DMSO/Cl_2CHCO_2H. (b) Ph_3P=CHTs. (c) NaOH/H_2O/CH_3CN or DBU/THF. (d) $NaBH_4$/MeOH/H_2O. (e) CF_3CO_2H/H_2O.

SCHEME 1

Results and discussion

Moffatt oxidation of 2′,3′-*O*-isopropylideneuridine (**1**, Scheme 1) (7, 20), followed by treatment of the resulting 5′-aldehyde with the stabilized ylid, (*p*-toluenesulfonylmethylene)triphenylphosphorane (21, 22), gave the vinyl sulfone, 1-[5,6-dideoxy-2,3-*O*-isopropylidene-6-(*p*-toluenesulfonyl)-β-D-*ribo*-hex-5(*E*)-enofuranosyl]uracil (**2**, 85%). The ^1H NMR spectrum of **2** in Me_2SO-d_6 had a "collapsed" broad singlet for H5′ and H6′ whereas its spectrum in $CDCl_3$ had two doublets of doublets. The large vinyl coupling constant ($^3J_{5'-6'}$ = 15.0 Hz) was in harmony with the *E* configuration. Deprotection of **2** with aqueous trifluoroacetic acid gave 1-[5,6-dideoxy-6-(*p*-toluenesulfonyl)-β-D-*ribo*-hex-5(*E*)-enofuranosyl]uracil (**5**, 89%).

Attempted application of methods for the reductive cleavage of carbon–sulfur bonds in saturated (23–25) and α,β-unsaturated (26–29) sulfones to **2** failed to give 5′-deoxy-2′,3′-*O*-isopropylidene-5′-methyleneuridine. The Corey sulfone cleavage conditions (23) with sodium (24) or aluminum (26) amalgam resulted in rearrangement of the vinyl to allylic sulfones (**2** → **3**) and (or) recovery of starting material. Formation of more complex mixtures was observed under more vigorous conditions. Attempted desulfonylation of **2** via conjugate addition of tributylstannyllithium (29) also failed, possibly resulting from interactions between the reagent and the uracil ring, in contrast to results with the adenosine analogue (13). The sodium dithionite procedure of Julia and co-workers (27, 28) caused loss of UV absorption, presumably resulting from nucleophilic addition of the reagent to C6 of uracil as anticipated from sodium bisulfite addition studies of Shapiro *et al.* (30).

Base-catalyzed isomerization of the vinyl sulfone **2** to a single allylic sulfone (**3**, 91%, exocyclic double bond tentatively assigned the less hindered *Z* configuration) occurred by stirring **2** in aqueous sodium hydroxide in acetonitrile or in the presence of 1,8-diazabicyclo[5.4.0]undec-7-ene (DBU) in THF. The bathochromic shift (λ_{max} 237 to 258 nm) and hypochromic effect (ε 22 200 to 10 300) accompanying conversion of the conjugated vinyl sulfone (**2**) into the allylic sulfone (**3**) was monitored by UV spectroscopy.

Attempted deprotection of 1-[5,6-dideoxy-2,3-*O*-isopropylidene-6-(*p*-toluenesulfonyl)-β-D-*erythro*-hex-4(*Z*)-enofuranosyl]uracil (**3**) at ambient temperature resulted in the expected acid-catalyzed decomposition of the exocyclic vinyl ether (31, 32). However, treatment of **3** with aqueous trifluoroacetic acid at 0°C for 25 min afforded **3**, uracil, and 1-[5,6-dideoxy-6-(*p*-toluenesulfonyl)-β-D-*erythro*-hex-4(*Z*)-enofuranosyl]uracil (**6**, 22%) after silica column purification. Longer reaction times resulted in formation of greater quantities of uracil. The deprotected vinyl sulfone (**5**) underwent clean isomerization to **6** (81%) in aqueous sodium hydroxide. This provides an efficient route to **6** (61% from **1**), which differs from the usual methodologies for preparation of 4′,5′-unsaturated nucleosides that involve elimination of hydrogen and an activated O5′ function or halide from C4′ and C5′ (5, 6, 31, 32).

Conjugate reduction of **2** occurred with sodium borohydride in aqueous methanol to give **4***a* (83%). Deprotection with aqueous trifluoroacetic acid gave 1-[5,6-dideoxy-6-(*p*-toluenesulfonyl)-β-D-*ribo*-hexofuranosyl]uracil (**4***b*, 71%). Treatment of **2** with sodium thiomethoxide in THF gave the 5′-methylthio-5′,6′-dideoxy diastereomers **7** (~1:1, >70%, Scheme 2). One diastereomer crystallized preferentially (19:1) during "diffusion crystallization" (33) from hexane/ethyl acetate. The mother liquor was purified by silica column chromatography and the second diastereomer then crystallized predominantly (1:4). Deprotection of the two mixtures with aqueous trifluoroacetic acid and crystallization afforded **8** (5′*R*, mp 219–220°C) and **9** (5′*S*, mp 125–128°C), respectively. The 5′-stereochemistry is tentatively assigned by parallel ^{13}C NMR shifts of C5′ relative to spectra of the 5′-amino analogues whose configurations were defined by X-ray crystallography of **12***b*(5′*R*). The ^{13}C NMR peak for C5′ of **8**(5′*R*) was at 1.2 ppm higher field than that of **9**(5′*S*). Shifts for C5′ of **10***b* (0.8 ppm) and **12***b* (0.6 ppm) (5′*R*) also were at higher fields than those of their *S* isomers.

Treatment of **2** with methanolic ammonia or aqueous ammonia in ethanol gave the 5′-amino-5′,6′-dideoxy diastereomers **10***a*(5′*R*) and **11***a*(5′*S*) (~1:1, 77%) plus the isomerization product **3** (19%). Purification by silica column chromatography resulted in partial separation of **10***a* and **11***a*. Treatment of a mixture of these diastereomers with 4-dimethylaminopyridine/acetic anhydride (34) gave the 5′-*N*-acetylamino derivatives **12***a*(5′*R*) and **13***a*(5′*S*), which were separated readily by chromatography. Deprotection of separated **10***a* and **11***a*, and **12***a* and **13***a* with aqueous trifluoroacetic acid gave **10***b* and **11***b*, and **12***b* and **13***b*, respectively. X-ray crystallography established the *R* configuration at C5′ of **12***b*. Removal of the *N*-acetyl group from **13***b*(5′*S*) was effected by heating with 1 M hydrochloric acid at ~90°C for 30 h to give **11***b*(5′*S*).

Attempted removal of the *p*-toluenesulfonyl group from a mixture of **10***a*/**11***a* by heating at reflux with magnesium turnings in MeOH as described recently (25) gave low yields (~14%) of slightly less polar (TLC) products. Although this mixture could be shown (^1H NMR and MS) (13) to contain 5′-deoxy-2′,3′-*O*-isopropylidene-5′-methyleneuridine, it was contaminated (10–15%) with by-products and was not investigated further.

In summary, Moffatt oxidation of 2′,3′-*O*-isopropylideneuridine and Wittig treatment of the resulting 5′-aldehyde with (*p*-toluenesulfonylmethylene)triphenylphosphorane gave efficient conversion to the chain-extended (*E*)vinyl sulfone. This in-

Can. J. Chem. Downloaded from www.nrcresearchpress.com by 123.30.183.119 on 09/08/12
For personal use only.

TABLE 1. ^{1}H NMR spectral data[a,b]

Compound	H1′[c] ($J_{1'-2'}$)	H2′[d] ($J_{2'-3'}$)	H3′[d] ($J_{3'-4'}$)	H4′[e] ($J_{4'-5'}$)	H5′[e] or H5′,5″ ($J_{5'-6'}$)	H6′ or H6′,6″	H5[c] (J_{5-6})	H6[c]	NH[f]	Aromatic[c] (J_{A-B})	Others[g]
2	5.80 (1.8)	5.12[e] (6.0)	4.88[e] (4.0)	4.66 (4.0)	6.93[f,h,i]		5.56 (8.0)	7.69	11.44	7.72, 7.44 (8.5)	1.26, 1.46 (CH_3's) 2.39 ($PhCH_3$)
3	5.84[g]	5.25[c] (6.3)	5.05[c]		4.45[j] (8.2)[k]	3.95[c]	5.59 (8.0)	7.68	11.42	7.71, 7.40 (8.5)	1.27, 1.29 (CH_3's) 2.37 ($PhCH_3$)
4*a*[l]	5.68 (2.2)	4.98[e] (6.2)	4.62[e] (5.0)	3.93[d] (6.5)[n]	1.91[m]	3.30[m]	5.60 (8.0)	7.66	11.40	7.74, 7.45 (8.5)	1.24, 1.42 (CH_3's) 2.41 ($PhCH_3$)
4*b*	5.62 (4.4)	4.03 (5.6)	3.77[m]	3.77[m]	1.93[m]	3.32[m]	5.59 (8.1)	7.56	11.40	7.78, 7.42 (8.5)	2.40 ($PhCH_3$) 5.13[c] (5.4,[o] OH3′) 5.35[c] (5.5,[o] OH2′)
5	5.72 (4.4)	4.16 (5.5)	3.99 (6.0)	4.39 (4.6)	6.98 (15.0)	6.87[c]	5.60 (8.0)	7.63	11.40	7.78, 7.44 (8.5)	2.40 ($PhCH_3$) 5.48[c] (6.2,[o] OH3′) 5.53[c] (5.3,[o] OH2′)
6	5.83 (4.8)	4.04 (5.1)	4.40[e]		4.53[j] (8.2)[k]	3.92[c]	5.58 (8.1)	7.10	11.42	7.72, 7.41 (8.5)	2.38 ($PhCH_3$) 5.56 (5.9,[o] OH3′) 5.63[c] (5.5,[o] OH2′)
7 (5′*R*)[p]	5.70[f]	5.05[c] (6.3)	4.89[e] (3.9)	3.96 (9.3)	3.18[d] (8.1)	[q]	5.61 (8.0)	7.67	11.40	7.73, 7.40 (8.5)	1.28, 1.45 (CH_3's) 1.92 (CH_3S) 2.38 ($PhCH_3$)
7 (5′*S*)[p]	5.68 (3.1)	4.98[e] (6.5)	4.79[e] (4.8)	4.13 (4.4)	3.22[d] (5.9)[k]	3.63[j]	5.67 (8.0)	7.61	11.41	7.80, 7.41 (8.5)	1.28, 1.46 (CH_3's) 2.03 (CH_3S) 2.38 ($PhCH_3$)
8 (5′*R*)[r]	5.78 (6.0)	4.22 (5.6)	4.16 (3.8)	3.98 (6.1)	3.21[d] (5.9)[k]	3.68[c]	5.75 (7.9)	7.74	11.42	7.89, 7.52 (8.5)	1.99 (CH_3S) 2.43 ($PhCH_3$) 5.34[c] (5.1,[o] OH3′) 5.50[c] (5.6,[o] OH2′)
9 (5′*S*)[r]	5.78 (5.8)	4.22[g]	4.17[g]	4.17[g] (6.0)	3.25[d] (6.0)[k]	3.74[c]	5.79 (8.0)	7.62	11.43	7.92, 7.54 (8.5)	2.07 (CH_3S) 2.44 ($PhCH_3$) 5.38[c] (4.8,[o] OH3′) 5.52[c] (5.1,[o] OH2′)
10*a* (5′*R*)	5.70 (3.0)	4.85[e] (6.5)	4.78[e] (5.0)	3.88 (3.0)	3.30[m]	3.30[m]	5.61 (8.0)	7.82	11.40	7.76, 7.43 (8.5)	1.24, 1.44 (CH_3's) 1.75[f] (NH_2) 2.38 ($PhCH_3$)
10*b* (5′*R*)	5.66 (6.3)	4.00[m]	4.00[m]	3.74[m]	3.50[m]	3.24[m]	5.62 (8.0)	7.93	11.40	7.79, 7.45 (8.5)	1.9[f] (NH_2) 2.40 ($PhCH_3$) 5.10[c] (5.0,[o] OH3′) 5.33[c] (5.4,[o] OH2′)
11*a* (5′*S*)	5.68 (2.0)	4.91[m]	4.91[m] (6.0)	3.74 (3.0)	3.25[m]	3.25[m]	5.54 (8.0)	7.66	11.32	7.72, 7.40 (8.5)	1.24, 1.43 (CH_3's) 1.8[f] (NH_2) 2.38 ($PhCH_3$)
11*b* (5′*S*)	5.68 (5.9)	4.04[m]	4.04[m]	3.61[m]	3.38[m]	3.19[m]	5.56 (8.0)	7.68	11.48	7.80, 7.43 (8.5)	1.9[f] (NH_2) 2.41 ($PhCH_3$)

termediate underwent Michael addition of hydrogen (sodium borohydride), thiomethanol, and ammonia to give the corresponding 5′-substituted-5′,6′-dideoxy derivatives. Removal of the isopropylidene group was effected with aqueous trifluoroacetic acid. Base-catalyzed isomerization of the vinyl sulfone to give a single geometric isomer of the 4′,5′-unsaturated allylic sulfone occurred readily. Attempted desulfonylation by various methods failed. New 5′-substituted-6′-*p*-toluenesulfonyl-5′,6′-dideoxy nucleoside analogues have been prepared and characterized, including determination of C5′ stereochemistry by X-ray crystallography. Biological testing results will be reported separately.

Single crystal X-ray structure determination

The single crystal structural study was performed with a Siemens R3m/V automated diffractometer that utilized graphite monochromated Mo Kα radiation (λ = 0.71073 Å). The compound (**12***b*) crystallized in the orthorhombic space group $P2_12_12_1$ with $a = 7.302(2)$, $b = 11.352(4)$, and $c = 25.813(9)$ Å with $Z = 4$. A total of 2359 unique data points were taken of which 1443 were considered observed, $F > 3\sigma(F)$.

The structure was solved using direct methods and refined using a full-matrix least-squares procedure. All non-hydrogen atoms were refined anisotropically. Positional parameters for hydrogen atoms of the nucleoside were calculated using known stereochemical geometry or obtained from difference maps, and these parameters were not refined. The isotropic thermal parameter of each hydrogen atom was set equal to 1.2 times the equivalent isotropic thermal parameter of the atom to which it was bonded, and these parameters were not refined. The phenyl ring was refined as a rigid body with C—C bond lengths fixed at 1.395 Å and C—C—C angles fixed at 120°. A partial water of hydration was located in the difference map. Its oxygen atom was refined anisotropically with an occupancy factor of

Can. J. Chem. Downloaded from www.nrcresearchpress.com by 123.30.183.119 on 09/08/12
For personal use only.

TABLE 1 (*concluded*)

Compound	H1′[c] ($J_{1'-2'}$)	H2′[d] ($J_{2'-3'}$)	H3′[d] ($J_{3'-4'}$)	H4′[e] ($J_{4'-5'}$)	H5′[e] or H5′,5″ ($J_{5'-6'}$)	H6′ or H6′,6″	H5[c] (J_{5-6})	H6[c]	NH[f]	Aromatic[c] (J_{A-B})	Others[g]
											5.10[c] (4.1,[o] OH3′) 5.32[c] (5.7,[o] OH2′)
12*a* (5′*R*)	5.72 (2.5)	5.01[e] (6.5)	4.61[e] (5.6)	3.98 (3.3)	4.47[m,s] (3.0)	[t]	5.70 (8.0)	7.70	11.45	7.75, 7.50 (8.5)	1.28, 1.52 (CH_3's) 1.64 (Ac) 2.38 ($PhCH_3$) 7.81[c] (8.5,[u] NH)
12*b* (5′*R*)	5.58 (5.5)	3.79[m]	3.79[m]	3.79[m] (3.0)	4.39[m,s] (2.6)	[v]	5.62 (8.0)	7.65	11.38	7.72, 7.43 (8.5)	1.63 (Ac) 2.40 ($PhCH_3$) 5.15[c] (5.2,[o] OH3′) 5.37[c] (5.7,[o] OH2′) 7.81[c] (8.2,[u] NH)
13*a* (5′*S*)	5.75 (2.0)	5.10[e] (6.5)	4.78[e] (4.7)	3.83 (7.2)	4.44[m,s] (9.0)	[w]	5.68 (8.0)	7.65	11.43	7.74, 7.48 (8.5)	1.30, 1.50 (CH_3's) 1.60 (Ac) 2.40 ($PhCH_3$) 7.92[c] (8.5,[u] NH)
13*b* (5′*S*)	5.66 (6.2)	4.03 (5.9)	3.86 (3.8)	3.56 (7.6)	4.31[m]	3.40[m]	5.61 (8.0)	7.38	11.40	7.66, 7.41 (8.5)	1.52 (Ac) 2.37 ($PhCH_3$) 5.16[c] (5.4,[o] OH3′) 5.41[c] (5.9,[o] OH2′) 7.84[c] (8.1,[u] NH)

[a]Chemical shifts at 200 MHz (Me_2SO-d_6 unless otherwise noted).
[b]"Apparent" first-order coupling constants (in parentheses).
[c]Doublet (unless otherwise noted).
[d]Doublet of doublets of doublets (unless otherwise noted).
[e]Doublet of doublets (unless otherwise noted).
[f]Broad singlet.
[g]Singlet (unless otherwise noted).
[h]"Collapsed" signals for H5′ and H6′.
[i]Spectrum in $CDCl_3$ revealed dd's at δ 6.48 ($J_{6'-5'}$ = 15 Hz, $J_{6'-4'}$ = 1.9 Hz, H6′), 7.05 ($J_{5'-4'}$ = 4.5 Hz, H5′).
[j]Triplet.
[k]($^3J_{5'-6',6''}$).
[l]Irradiation of the signal at δ 3.93 (H4′) simplified the multiplet at δ 1.91 (H5′,5″) into a triplet ($J_{5'-6'}$ = 8.0 Hz).
[m]Multiplet.
[n]($^3J_{4'-5',5''}$).
[o]($^3J_{HO-CH}$).
[p]Signals assigned from spectrum of diastereomeric mixture (correlated with integrated intensities).
[q]δ 3.66 (dd, $J_{6'-6''}$ = 15.2 Hz, H6′), 3.49 (dd, $J_{6''-5'}$ = 3.0 Hz, H6″).
[r]Spectrum at 500 MHz.
[s]ddd after D_2O exchange.
[t]δ 3.64 (dd, $J_{6'-6''}$ = 15.0 Hz, H6′), 3.51 (dd, $J_{6''-5'}$ = 9.0 Hz, H6″).
[u]($^3J_{5'-NH}$).
[v]δ 3.58 (dd, $J_{6'-6''}$ = 14.7 Hz, H6′), 3.36 (dd, $J_{6''-5'}$ = 9.6 Hz, H6″).
[w]δ 3.51 (dd, $J_{6'-6''}$ = 15.0 Hz, H6′), 3.43 (dd, $J_{6''-5'}$ = 2.0 Hz, H6″).

0.5. The water hydrogen atoms could not be located in difference maps and were not included in the refinement. The final R values were R = 0.0641 and R_w = 0.0574. All computer programs used in the structure solution, refinement, and display are included in the "SHELXTL PLUS" (35) program package. Standard atomic scattering factors (36) were used.

The drawing of the structure of **12***b* in Fig. 1 clearly established the *R* configuration at C5′. The pseudorotation angle of the furanose ring is 47.2°, indicating a $_4T^3$ conformation very close to $_4E$. The C6—N1–C1′—O4′ glycosyl torsion angle is 67.0(8)° and the C3′—C4′–C5′—N5′ torsion angle is 60.0(8)°. There are no intramolecular hydrogen bonds in the structure, but HO2′ and HN3 are involved in intermolecular hydrogen bonds. Also, HO3′ is hydrogen-bonded to the water of hydration. Details of the experimental procedure, structure solution, and refinement along with atomic positional and thermal parameters, bond lengths and angles, important torsion angles, and hydrogen bond data are included in the supplementary material.[3]

Experimental section

Uncorrected melting points were determined on a microstage block. UV spectra were recorded on a Hewlett Packard 8951A spectrophotometer. ^1H (200 MHz) and ^{13}C (50 MHz) NMR spectra were recorded on a Varian Gemini-200 spectrometer. ^1H spectra at 500 MHz were determined on a Varian VXR-500S spectrometer.

[3]Supplementary X-ray crystallography material may be purchased from: The Depository of Unpublished Data, Document Delivery, CISTI, National Research Council Canada, Ottawa, Canada K1A 0S2.

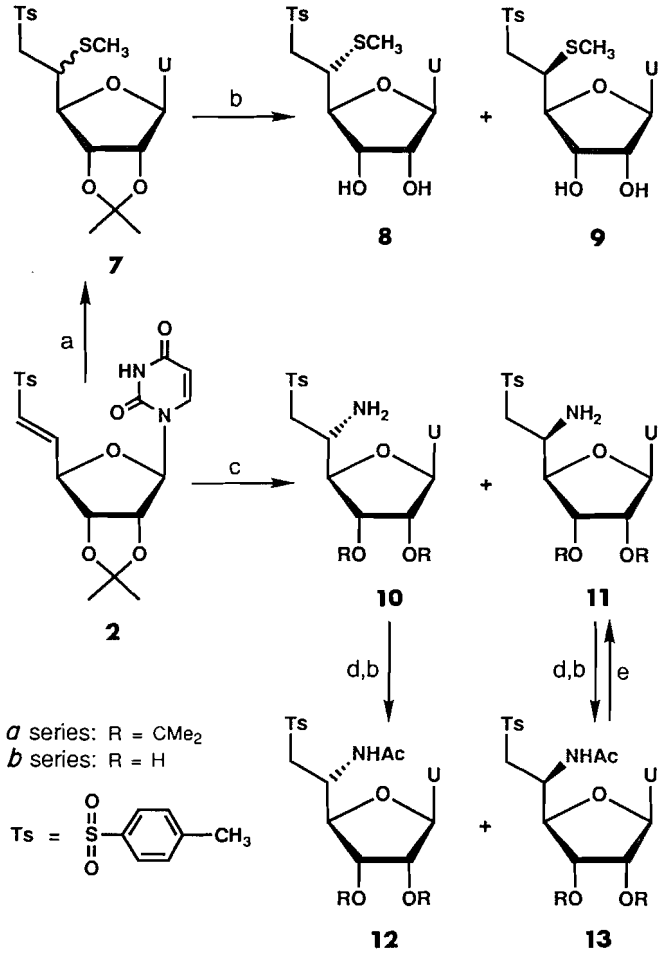
Tables of atomic coordinates, bond lengths and angles, and details of the structure determination have also been deposited with the Cambridge Crystallographic Data Centre, and can be obtained on request from The Director, Cambridge Crystallographic Data Centre, University Chemical Laboratory, Lensfield Road, Cambridge, CB2 1EW, U.K.

Can. J. Chem. Downloaded from www.nrcresearchpress.com by 123.30.183.119 on 09/08/12
For personal use only.

TABLE 2. ^{13}C NMR spectral data[a,b]

Compound	C2	C4	C5	C6	C1′	C2′,[c]	C3′,[c]	C4′	C5′	C6′	Aromatic C1″	Aromatic C2″	Aromatic C3″	Aromatic C4″	CH_3
4*b*	150.79	163.55	102.28	141.90	89.58	72.38[d]	72.38[d]	80.95	26.09	51.60	136.01	128.01	130.30	144.98	21.04
5	150.90	163.42	102.32	142.03[e]	90.32	73.13	72.39	81.08	142.50[e]	132.35	137.42	127.67	130.41	144.79	21.07
6	150.58	163.48	102.53	140.42	89.68	71.78	69.04	161.04	87.60	52.58	136.02	128.30	129.96	144.77	21.06
8 (5′*R*)[f]	150.98	163.58	102.42	141.91	88.91	71.74	70.26	84.83	41.94	55.91	136.88	128.12	130.19	145.03	21.10
9 (5′*S*)[f]	150.72	163.94	102.47	141.54	88.62	72.54	70.52	83.96	43.16	57.46	136.16	128.05	130.20	145.43	21.31
10*b* (5′*R*)	150.97	163.59	102.17	142.07	88.37	72.59	69.63	86.02	47.50	59.22	136.82	127.90	130.28	144.92	21.05
11*b* (5′*S*)	150.98	163.70	102.22	141.73	88.09	72.36	68.97	86.14	48.30	58.73	136.53	127.89	130.32	145.10	21.02
12*b* (5′*R*)[g]	150.94	163.75	102.04	142.21	88.76	72.30	69.44	84.71	45.32	55.94	136.17	128.15	130.10	145.03	21.01
13*b* (5′*S*)[h]	150.90	163.72	102.40	141.24	88.48	71.57	69.59	84.47	45.90	55.14	136.05	128.08	130.13	145.13	20.99

[a]Chemical shifts at 50 MHz.
[b]Proton-decoupled singlets.
[c]Assignments might be reversed.
[d]Peaks not resolved.
[e]Peak at δ 13.51 (CH_3S).
[f]Peak at δ 14.50 (CH_3S).
[g]Peaks at δ 22.23, 170.37 (Ac).
[h]Peaks at δ 22.14, 170.32 (Ac).



(a) $NaSCH_3$/THF. (b) CF_3CO_2H/H_2O. (c) NH_3/MeOH or NH_3/H_2O/EtOH. (d) DMAP/Ac_2O. (e) HCl/H_2O/Δ.

SCHEME 2

Mass spectra (MS) were obtained with an AEI MS-12 instrument. Elemental analyses were determined by the microanalytical laboratories of the University of Alberta, Adam Mickiewicz University, Poznan, or M-H-W Laboratories. Reagents and solvents were of reagent quality, and solvents were purified and dried before use. Diffusion crystallization was performed with the solvent combinations noted as described previously (33) except the diffusion solvent is listed first, and the dissolving solvent or mixture second, in the present paper. (*p*-Toluenesulfonylmethylene)triphenylphosphorane (73%, crystallized from CH_2Cl_2/hexane, mp 182–183°C (lit. (21) mp 186–187°C, (22) 182–184°C)) was prepared (21) from triphenylphosphine and bromomethyl *p*-toluylsulfone (22). Thin-layer chromatography (TLC) was performed on Merck Kieselgel 60 F_{254} sheets with the following systems: S1 (MeOH/$CHCl_3$, 1:16), S2 ($Me_2CO/CHCl_3$, 1:3), S3 (EtOAc/*i*-PrOH/H_2O, 4:1:2, upper layer), S4 (MeOH/$CHCl_3$, 1:8), with sample observation under 254-nm light. Column chromatography was performed with Merck Kieselgel 60 (230–400 mesh).

*1-[5,6-Dideoxy-2,3-*O*-isopropylidene-6-(*p*-toluenesulfonyl)-*β*-D-ribo-hex-5*(E)*-enofuranosyl]uracil* **2**

Method A

A solution of **1** (2.84 g, 10 mmol), dicyclohexylcarbodiimide (DCC, 8.25 g, 40 mmol), and pyridinium trifluoroacetate (PTFA, 0.96 g, 5 mmol) in anhydrous Me_2SO (40 mL) was stirred at ambient temperature overnight. (*p*-Toluenesulfonylmethylene)triphenylphosphorane (21, 22) (5.17 g, 12 mmol) was added and stirring continued at ~35°C for 5 h. Me_2SO was evaporated *in vacuo* and the residue partitioned (EtOAc/H_2O). The organic phase was

Can. J. Chem. Downloaded from www.nrcresearchpress.com by 123.30.183.119 on 09/08/12
For personal use only.

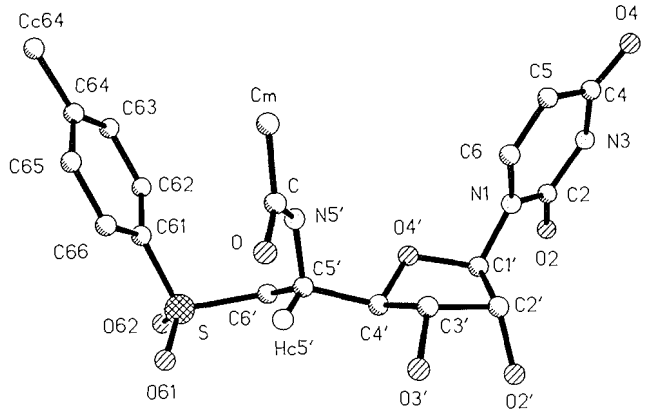


FIG. 1. Computer drawing of compound **12***b*. All hydrogen atoms except Hc5′ have been deleted for clarity and to emphasize the configuration at C5′.

washed (NaCl/H_2O), filtered (*N*,*N*′-dicyclohexylurea, DCU), dried ($MgSO_4$), evaporated, and the residue chromatographed (MeOH/$CHCl_3$, 1.5:98.5). Evaporation of appropriate fractions gave a white solid that was dissolved in $CH_2Cl_2/CHCl_3$ (20 mL, 1:1), filtered (traces of DCU), and the product precipitated with hexane. Recrystallization (MeOH) gave **2** (3.69 g, 85%) as white needles; mp 195–196°C; UV (MeOH) max: 237 nm (ε 22 200), min: 219 nm (ε 12 500); MS *m/z*: 434.1155 (1.6, M^+ = 434.1148). Anal. calcd. for $C_{20}H_{22}N_2O_7S$ (434.5): C 55.29, H 5.10, N 6.45, S 7.38; found: C 55.05, H 4.94, N 6.58, S 7.31.

Method B

A solution of **1** (4.26 g, 15 mmol) and DCC (12.36 g, 60 mmol) in anhydrous Me_2SO (60 mL) was stirred with cooling (ice-bath) while Cl_2CHCO_2H (0.62 mL, 0.97 g, 7.5 mmol) was added, and stirring was continued at ambient temperature for 2 h. (*p*-Toluenesulfonylmethylene)triphenylphosphorane (21, 22) (6.88 g, 16 mmol) was added and, after stirring overnight, TLC (S1) indicated complete conversion to a more rapidly migrating product. Oxalic acid dihydrate (5.67 g, 45 mmol) in MeOH (50 mL) was added and, after 30 min, DCU was filtered and the filtrate evaporated *in vacuo*. The residue was partitioned (EtOAc/H_2O) and the organic layer washed with H_2O (2 × 50 mL), $NaHCO_3/H_2O$, and NaCl/H_2O, dried ($MgSO_4$), and evaporated to give a yellow solid foam. Column chromatography (MeOH/$CHCl_3$, 1.5:98.5) and crystallization (MeOH) gave **2** (5.47 g, 84%) with identical data.

*1-[5,6-Dideoxy-6-(*p*-toluenesulfonyl)-β-D-*ribo*-hex-5(*E*)-enofuranosyl]uracil* **5**

A solution of **2** (217 mg, 0.5 mmol) in CF_3CO_2H/H_2O (9:1, 5 mL) was stirred at ~0°C for 25 min, evaporated, and coevaporated with EtOH. Crystallization of the residue (MeOH) gave **5** (175 mg, 89%) as white needles; mp 212–213°C; UV (MeOH) max: 238 nm (ε 21 000), shoulder: 260 nm (ε 9900), min: 221 nm (ε 12 600); MS *m/z*: 394 (1, M^+), 239 (25), 221 (100), 155 (43), 112 (56). Anal. calcd. for $C_{17}H_{18}N_2O_7S$ (394.4): C 51.77, H 4.60, N 7.10; found: C 51.79, H 4.65, N 7.03.

*1-[5,6-Dideoxy-2,3-*O*-isopropylidene-6-(*p*-toluenesulfonyl)-β-D-*erythro*-hex-4(Z)-enofuranosyl]uracil* **3**

To a stirred solution of **2** (217 mg, 0.5 mmol) in CH_3CN/H_2O (1:1, 15 mL) was added 1 M NaOH/H_2O (1 mL) (alternatively, DBU (0.075 mL, 76 mg, 0.5 mmol) in THF (10 mL) was used) and stirring was continued at ambient temperature for 4 h. TLC (S2) indicated complete conversion to one slightly slower migrating product. The solution was concentrated to half volume and EtOAc (30 mL) and 0.1 M HCl/H_2O (10 mL) were added. The organic layer was separated and the aqueous layer washed with EtOAc (2 × 10 mL). The combined organic phase was washed with $NaHCO_3/H_2O$, NaCl/H_2O, dried ($MgSO_4$), and evaporated to a white foam that was diffusion crystallized (hexane/EtOH) to give **3** (198 mg, 91%) as a white solid; mp 119–121°C; UV (MeOH) max: 258 nm (ε 10 300), min: 241 nm (ε 8000); MS *m/z*: 419.0897 (3, M − CH_3 [$C_{19}H_{19}N_2O_7S$] = 419.0913), 279.0979 (100, M − Ts [$C_{13}H_{15}N_2O_5$] = 279.0981). Anal. calcd. for $C_{20}H_{22}N_2O_7S$ (434.5): C 55.29, H 5.10, N 6.45, S 7.38; found: C 55.41, H 5.12, N 6.51, S 7.49.

*1-[5,6-Dideoxy-6-(*p*-toluenesulfonyl)-β-D-*erythro*-hex-4(Z)-enofuranosyl]uracil* **6**

Method A

A solution of **5** (100 mg, 0.25 mmol) in MeOH/H_2O (1:1, 30 mL) was treated with 1 M NaOH/H_2O (1 mL) and stirred at ambient temperature for 8 h (TLC (S3) showed a single slightly more polar product). Dried Dowex 50W-X8 (H^+) resin (0.3 g, 200–400 mesh) was added, stirred for 1 h, filtered, and washed with MeOH (2 × 10 mL). The combined filtrates were evaporated and the residue crystallized (MeOH) to give **6** (71 mg, 71%). Evaporation of the mother liquor and diffusion crystallization (hexane/MeOH) of the residue gave a second crop of **6** (10 mg, 10%); mp 196–197°C (dec.); UV (MeOH) max: 260 nm (ε 10 200), min: 243 nm (ε 8100); MS *m/z* 239 (38, M − Ts), 221 (100), 156 (60), 112 (84), 92 (82). Anal. calcd. for $C_{17}H_{18}N_2O_7S$ (394.4): C 51.77, H 4.60, N 7.10; found: C 51.95, H 4.66, N 7.18.

Method B

A solution of **3** (100 mg, 0.23 mmol) in CF_3CO_2H/H_2O (22:3, 5 mL) was stirred at ~0°C for 25 min, evaporated (<10°C), and coevaporated with EtOH. TLC (S4) of the residue showed three components with R_f 0.8 (**3**, ~40%), 0.48 (**6**, ~35%), and 0.39 (uracil, ~25%), which were separated by column chromatography (MeOH/$CHCl_3$, 1:24). Evaporation of appropriately pooled fractions gave **6** (20 mg, 22%) with identical data.

Extension of the deprotection time to 45 min resulted in formation of additional uracil without complete consumption of **3**.

*1-[5,6-Dideoxy-2,3-*O*-isopropylidene-6-(*p*-toluenesulfonyl)-β-D-ribo-hexofuranosyl]uracil* **4**a

To a magnetically stirred solution of **2** (260 mg, 0.6 mmol) in MeOH/H_2O (1:1, 60 mL) was added sodium borohydride (45 mg, 1.2 mmol). TLC (S2, two developments) after 18 h at ambient temperature indicated ~95% conversion to a slightly more polar product. The solution was concentrated to half volume and the residue was partitioned ($CHCl_3/H_2O$). The organic layer was washed with NaCl/H_2O, H_2O, dried ($MgSO_4$), and evaporated to give a foam that was purified by column chromatography ($Me_2CO/CHCl_3$, 1:9). Evaporation of appropriately pooled fractions and diffusion crystallization (hexane/EtOH) gave **4***a* (218 mg, 83%) as an amorphous powder; mp 108–110°C; UV (MeOH) max: 258, 223 nm (ε 10 200, 14 700), min: 238, 212 nm (ε 5900, 12 900); MS *m/z*: 436.1309 (1.2, M^+ = 436.1304), 421.1063 (19, M − CH_3), 325.1106 (89, M − B). Anal. calcd. for $C_{20}H_{24}N_2O_7S$ (436.5): C 55.04, H 5.54, N 6.42, S 7.35; found: C 54.79, H 5.68, N 6.55, S 7.58.

*1-[5,6-Dideoxy-6-(*p*-toluenesulfonyl)-β-D-ribo-hexofuranosyl]uracil* **4**b

A solution of **4***a* (174 mg, 0.4 mmol) in CF_3CO_2H/H_2O (9:1, 8 mL) was stirred at ~0°C for 40 min, evaporated, and coevaporated with EtOH to give an amorphous glass. Column chromatography (MeOH/$CHCl_3$, 1:24) and diffusion crystallization (hexane//EtOAc/MeOH) gave **4***b* (112 mg, 71%); mp 177–179°C; UV (MeOH) max: 260, 224 nm (ε 9300, 14 600), min: 239 nm (ε 6100); MS *m/z*: 284 (5, M − BH), 246 (20), 156 (24), 112 (100). Anal. calcd. for $C_{17}H_{20}N_2O_7S$ (396.4): C 51.51, H 5.09, N 7.07; found: C 51.40, H 5.29, N 7.05.

*1-[5,6-Dideoxy-2,3-*O*-isopropylidene-6,5-methylthio-(*p*-toluenesulfonyl)-β-D-ribo-hexofuranosyl]uracil 7(5′R/S)*

A solution of **2** (660 mg, 1.52 mmol) in anhydrous THF (20 mL) was added to a solution of sodium thiomethoxide (128 mg, 1.83 mmol) in anhydrous THF (10 mL) under N_2 and stirring was continued at ambient temperature for 7 h. Acetic acid (0.105 mL, 110 mg,

Can. J. Chem. Downloaded from www.nrcresearchpress.com by 123.30.183.119 on 09/08/12
For personal use only.

Can. J. Chem. Downloaded from www.nrcresearchpress.com by 123.30.183.119 on 09/08/12
For personal use only.

1.83 mmol) was added, the solution evaporated, and the residue partitioned ($CHCl_3$//$NaHCO_3$/H_2O). The organic layer was washed with NaCl/H_2O, dried ($MgSO_4$), evaporated, and the residue diffusion crystallized (hexane/EtOAc) to give **7** (210 mg, 29%, 5′(*R*/*S*) ~19:1) with mp 201–203°C; MS *m/z*: 467 (12, M − CH_3), 327 (100), 279 (82), 157 (91). Purification of the mother liquor by column chromatography (Me_2CO/$CHCl_3$, 1:9) and diffusion crystallization of the residue (hexane/EtOAc), gave **7** (325 mg, 44% 5′(*R*/*S*) ~1:4).

*1-[5,6-Dideoxy-5(*R*)-methylthio-6-(*p*-toluenesulfonyl)-β-D-ribo-hexofuranosyl]uracil {1-[6-deoxy-5-*S*-methyl-5-thio-6-(*p*-toluenesulfonyl)-α-L-talofuranosyl]uracil} **8**(5′R)*

A solution of **7** (150 mg, 0.31 mmol, 5′(*R*/*S*) ~19:1) in CF_3CO_2H/H_2O (9:1, 5 mL) was stirred at ~0°C for 30 min, evaporated, coevaporated with EtOH, and crystallized (EtOH, two crops) to give **8**(5′*R*) (116 mg, 85%) as fine white needles; mp 219–220°C; UV (MeOH) max: 260, 222 nm (ε 10 200, 15 400), min: 240 nm (ε 6100); MS *m/z*: 442 (1, M^+), 358 (24), 287 (93), 239 (72), 271 (58), 221 (100), 155 (52), 113 (66). Anal. calcd. for $C_{18}H_{22}N_2O_7S_2$ (442.5): C 48.86, H 5.01, N 6.33; found: C 48.84, H 5.07, N 6.36.

*1-[5,6-Dideoxy-5(*S*)-methylthio-6-(*p*-toluenesulfonyl)-β-D-ribo-hexofuranosyl]uracil {1-[6-deoxy-5-*S*-methyl-5-thio-6-(*p*-toluenesulfonyl)-β-D-allofuranosyl]uracil} **9**(5′S)*

A solution of **7** (200 mg, 0.41 mmol, 5′(*R*/*S*) ~1:4) in CF_3CO_2H/H_2O (9:1, 5 mL) was stirred at ~0°C for 30 min, evaporated, coevaporated with EtOH, and the resulting brown glass purified on a short silica column (MeOH/$CHCl_3$, 1:24). The residue was crystallized (hexane/EtOH) and recrystallized (MeOH, two crops) to give **9**(5′*S*) (114 mg, 63%) as cream-colored crystals; mp 125–128°C; UV (MeOH) max: 260, 224 nm (ε 9800, 14 500), min: 240 nm (ε 5900); MS *m/z*: 287 (28, M − Ts), 221 (45), 155 (100), 91 (82), 113 (52). Anal. calcd. for $C_{18}H_{22}N_2O_7S_2$ (442.5): C 48.86, H 5.01, N 6.33; found: C 48.71, H 5.19, N 6.42.

*1-[5-Amino-5,6-dideoxy-2,3-*O*-isopropylidene-6-(*p*-toluenesulfonyl)-β-D-ribo-hexofuranosyl]uracil **10**a(5′R)/**11**a(5′S)*

A solution of **2** (326 mg, 0.75 mmol) in anhydrous MeOH (30 mL) was treated with saturated NH_3/MeOH (30 mL) (or concentrated NH_3/H_2O (2 mL) in EtOH (20 mL)) and stirring was continued at ambient temperature for 4 h. TLC (S2) indicated complete consumption of **2** (R_f 0.53) with formation of more polar components (R_f 0.48 (**3**, minor), R_f 0.16/0.14 (**11***a*/**10***a*, ~1:1)). The reaction mixture was evaporated and subjected to column (80 g, 3.5 × 30 cm) chromatography. Slow elution (Me_2CO/$CHCl_3$, 3:22, 700 mL; followed by MeOH/$CHCl_3$, 1.5:98.5, 1200 mL) and evaporation of appropriately pooled fractions gave **3** (62 mg, 19%), **11***a* (115 mg, 34%), overlapping fractions of **11***a*/**10***a* (37 mg, 11%), and **10***a* (108 mg, 32%). The more rapidly eluted diastereomer was crystallized (MeOH) to give 1-[5-amino-5,6-dideoxy-2,3-*O*-isopropylidene-6-(*p*-toluenesulfonyl)-β-D-allofuranosyl]uracil (**11***a*(5′*S*)) (96 mg, 28%); mp 230–231°C; UV (MeOH) max: 224, 258 nm (ε 16 600, 10 800), min: 239, 212 nm (ε 6100, 13 600); MS *m/z*: 436.1175 (2, M − CH_3 [$C_{19}H_{22}N_3O_7S$] = 436.1178), 296.1244 (15, M − Ts), 198.0590 (100, $TsCH_2CHNH_2$); MS (ci, NH_3) *m/z*: 452 (100, M + 1). Anal. calcd. for $C_{20}H_{25}N_3O_7S$ (451.5): C 53.21, H 5.58, N 9.31, S 7.10; found: C 53.26, H 5.58, N 9.26, S 7.14. The more slowly eluted 1-[5-amino-5,6-dideoxy-2,3-*O*-isopropylidene-6-(*p*-toluenesulfonyl)-α-L-talofuranosyl]uracil (**10***a*(5′*R*)) failed to crystallize; UV (MeOH) max: 224, 258 nm (ε 16 000, 10 400), min: 239, 213 nm (ε 6100, 14 000); MS *m/z*: 436.1181 (1.8, M − CH_3 [$C_{19}H_{22}N_3O_7S$] = 436.1178), 296.1247 (13, M − Ts), 198.0592 (100, $TsCH_2CHNH_2$); MS (ci, NH_3) *m/z*: 452 (100, M + 1).

*1-[5(*R*)-Acetamido-5,6-dideoxy-2,3-*O*-isopropylidene-6-(*p*-toluenesulfonyl)-β-D-ribo-hexofuranosyl]uracil **12**a(5′R) and 1-[5(*S*)-acetamido-5,6-dideoxy-2,3-*O*-isopropylidene-6-(*p*-toluenesulfonyl)-β-D-ribo-hexofuranosyl]uracil **13**a(5′S)*

A mixture of **10***a*/**11***a* (~1:1, 157 mg, 0.35 mmol) in Ac_2O (1.5 mL) was treated with 4-dimethylaminopyridine (DMAP, 4 mg, 0.032 mmol) and stirred at ambient temperature for 5 h. TLC (S4) indicated complete consumption of **10***a*/**11***a* (R_f ~0.53) with formation of two well-resolved products (R_f 0.57 and 0.49). MeOH (3 mL) was added, the solution stirred for 1 h, evaporated *in vacuo*, and the residue partitioned ($CHCl_3$/(AcOH/H_2O, 1:99)). The organic phase was washed with $NaHCO_3$/H_2O, NaCl/H_2O, dried (Na_2SO_4), evaporated, and the residue subjected to column chromatography (MeOH/$CHCl_3$, 1.5:98.5). Evaporation of sequentially pooled fractions and diffusion crystallization (hexane/EtOAc) gave 1-[5-*N*-acetyl-5-amino-5,6-dideoxy-2,3-*O*-isopropylidene-6-(*p*-toluenesulfonyl)-α-L-talofuranosyl]uracil **12***a*(5′*R*) (81 mg, 47%); mp 110–115 (transition), 164–167°C; UV (MeOH) max: 258, 226 nm (ε 9800, 14 200), min: 240 nm (ε 5800); MS *m/z*: 478.1281 (7.7, M − CH_3 [$C_{21}H_{24}N_3O_8S$] = 478.1284), 338.1353 (11, M − Ts), 198.0589 (100, $TsCH_2CHNH_2$); MS (ci, NH_3) *m/z*: 494 (100, M + 1). Anal. calcd. for $C_{22}H_{27}N_3O_8S$ (493.5): C 53.54, H 5.51, N 8.51; found: C 53.61, H 5.58, N 8.49.

Further elution gave 1-[5-*N*-acetyl-5-amino-5,6-dideoxy-2,3-*O*-isopropylidene-6-(*p*-toluenesulfonyl)-β-D-allofuranosyl]uracil **13***a*-(5′*S*) (79 mg, 46%); MS *m/z*: 493.1505 (0.3, M^+ [$C_{22}H_{27}N_3O_8S$] = 493.1518), 478.1279 (8, M − CH_3), 338.1351 (7, M − Ts), 198.0586 (100, $TsCH_2CHNH_2$). It was confirmed that acetylation of a purified sample of **11***a*(5′*S*) gave **13***a*(5′*S*).

*1-[5(*R*)-Amino-5,6-dideoxy-6-(*p*-toluenesulfonyl)-β-D-ribo-hexofuranosyl]uracil **10**b(5′R) and 1-[5(*S*)-amino-5,6-dideoxy-6-(*p*-toluenesulfonyl)-β-D-ribo-hexofuranosyl]uracil **11**b(5′S)*

Solutions of **10***a*(5′*R*) (55 mg, 0.12 mmol) and **11***a*(5′*S*) (60 mg, 0.13 mmol) in CF_3CO_2H/H_2O (9:1, 5 mL) were stirred at ~0°C for 7 h and 8 h, respectively. Evaporation and coevaporation (EtOH) gave amorphous products that were purified on dry-packed silica columns (S3) to give 1-[5-amino-5,6-dideoxy-6-(*p*-toluenesulfonyl)-α-L-talofuranosyl]uracil **10***b*(5′*R*) (41 mg, 83%) (MeOH/EtOAc); mp 196–198°C; UV (MeOH) max: 260, 224 nm (ε 10 200, 15 200), min: 240 nm (ε 5000); MS *m/z*: 394 (1, M − NH_3), 264 (2), 170 (36), 156 (18), 155 (20), 112 (52), 92 (100). Anal. calcd. for $C_{17}H_{21}N_3O_7S$ (411.4): C 49.63, H 5.14, N 10.21; found: C 49.53, H 5.14, N 10.11. The diffusion crystallized (hexane/MeOH/EtOAc) 1-[5-amino-5,6-dideoxy-6-(*p*-toluenesulfonyl)-β-D-allofuranosyl]uracil **11***b*(5′*S*) (39 mg, 73%) had mp 203–206°C (dec.); UV (MeOH) max: 260, 224 nm (ε 9900, 15 100) min: 240 nm (ε 4900); MS *m/z*: 394 (1, M − NH_3), 264 (5), 239 (6), 198 (56), 156 (55), 112 (82), 92 (100). Anal. calcd. for $C_{17}H_{21}N_3O_7S$ (411.4): C 49.63, H 5.14, N 10.21; found: C 49.86, H 5.29, N 10.04.

*1-[5(*R*)-Acetamido-5,6-dideoxy-6-(*p*-toluenesulfonyl)-β-D-ribo-hexofuranosyl]uracil **12**b(5′R) and 1-[5(*S*)-acetamido-5,6-dideoxy-6-(*p*-toluenesulfonyl)-β-D-ribo-hexofuranosyl]uracil **13**b(5′S)*

Solutions of **12***a*(5′*R*) (65 mg, 0.13 mmol) and **13***a*(5′*S*) (60 mg, 0.12 mmol) in CF_3CO_2H/H_2O (9:1, 5 mL) were stirred at ~0°C for 3 h and 2 h, respectively. Evaporation and coevaporation (EtOH) gave amorphous products that were diffusion crystallized to give 1-[5-*N*-acetyl-5-amino-5,6-dideoxy-6-(*p*-toluenesulfonyl)-α-L-talofuranosyl]uracil **12***b*(5′*R*) (48 mg, 88%, hexane/MeOH/EtOAc); mp 259–260°C (dec.); UV (MeOH) max: 260, 226 nm (ε 9700, 14 100), min: 241 nm (ε 5100); MS *m/z*: 453 (2, M^+), 342 (11), 240 (31), 198 (94), 156 (38), 112 (100). Anal. calcd. for $C_{19}H_{23}N_3O_8S$ (453.5): C 50.33, H 5.11, N 9.27; found: C 50.13, H 5.05, N 9.05. For the X-ray study, this product was recrystallized (MeOH) to give near cubic crystals with mp 261–262°C. The 1-[5-*N*-acetyl-5-amino-5,6-dideoxy-6-(*p*-toluenesulfonyl)-β-D-allofuranosyl]uracil (**13***b*(5′*S*)) (37 mg, 68%, MeOH two crops) had mp 166–169°C; UV (MeOH) max: 260, 224 nm (ε 9800, 14 500), min: 240 nm (ε 5100); MS *m/z*: 342 (15, M − B), 240 (22), 198 (42), 155 (32), 112 (100), 92 (78). Anal. calcd. for $C_{19}H_{23}N_3O_8S{\cdot}0.5H_2O$ (462.5): C 49.34, H 5.23, N 9.09; found: C 49.25, H 5.49, N 8.96.

*Deacetylation of **13**b(5′S) to **11**b(5′S)*

A solution of **13***b*(5′*S*) (45 mg, 0.1 mmol) in MeOH (0.5 mL) was treated with 1 M HCl/H_2O (4 mL) and heated at ~90°C for 30 h. The reaction mixture was cooled, neutralized to pH ~7 with solid

$NaHCO_3$, and evaporated. The residue was extracted (hot MeOH) and purified by column chromatography (S3) to give **11***b*(5′*S*) (25 mg, 61%) with data identical to those of the product of the reaction of **11***a*(5′*S*) → **11***b*(5′*S*) described above.

Acknowledgements

We thank the American Cancer Society (Grant No. CH-405), the Natural Sciences and Engineering Research Council of Canada, Brigham Young University development funds, and the Academy of Agriculture for generous support. We thank Mrs. Kathryn M. Rollins for assistance with the manuscript.

1. (*a*) R. J. SUHADOLNIK. Nucleoside antibiotics. Wiley–Interscience, New York. 1970; (*b*) pp. 218–234; (*c*) pp. 115–119.
2. (*a*) R. J. SUHADOLNIK. Nucleosides as biological probes. Wiley–Interscience, New York. 1979; (*b*) pp. 30–37, 43–45; (*c*) pp. 279–281.
3. (*a*) F. SCHLENK. Adv. Enzymol. Relat. Areas Mol. Biol. **54**, 195 (1983); (*b*) R. W. MYERS and R. H. ABELES. J. Biol. Chem. **265**, 16913 (1990).
4. J. G. NIEDZWICKI, M. H. EL KOUNI, S. H. CHU, and S. CHA. Biochem. Pharmacol. **32**, 399 (1983).
5. J. G. MOFFATT. *In* Nucleoside analogues: chemistry, biology, and medical applications. *Edited by* R. T. Walter, E. De Clercq, and F. Eckstein. Plenum Press, New York. 1979. pp. 71–164.
6. T. UEDA. *In* Chemistry of nucleosides and nucleotides. Vol. 1. *Edited by* L. B. Townsend. Plenum Press, New York. 1988. pp. 1–112.
7. G. H. JONES and J. G. MOFFATT. J. Am. Chem. Soc. **90**, 5337 (1968).
8. P. HOWGATE, A. S. JONES, and J. R. TITTENSOR. Carbohydr. Res. **12**, 403 (1970).
9. J. A. MONTGOMERY, A. G. LASETER, and K. HEWSON. J. Heterocycl. Chem. **11**, 211 (1974).
10. R. A. SHARMA and M. BOBEK. J. Org. Chem. **43**, 367 (1978).
11. J. M. J. TRONCHET and M. J. VALERO. Helv. Chim. Acta, **62**, 2788 (1979).
12. J.-D. ZHANG and L.-H. ZHANG. Synthesis, 909 (1990).
13. S. F. WNUK and M. J. ROBINS. Can. J. Chem. **69**, 334 (1991).
14. O. R. MARTIN, F. E. KHAMIS, H. A. EL-SHENAWY, and S. P. RAO. Tetrahedron Lett. **30**, 6139 (1989).
15. (*a*) D. H. R. BARTON, S. D. GÉRO, B. QUICLET-SIRE, and M. SAMADI. J. Chem. Soc. Chem. Commun. 1000 (1989); (*b*) D. H. R. BARTON, S. D. GÉRO, B. QUICLET-SIRE, and M. SAMADI. J. Chem. Soc. Chem. Commun. 1372 (1988); (*c*) D. H. R. BARTON, S. D. GÉRO, B. QUICLET-SIRE, and M. SAMADI. Tetrahedron Lett. **30**, 4969 (1989).
16. J. HIEBL and E. ZBIRAL. Tetrahedron Lett. **31**, 4007 (1990).
17. J.-C. WU, T. PATHAK, W. TONG, J.-M. VIAL, G. REMAUD, and J. CHATTOPADHYAYA. Tetrahedron, **44**, 6705 (1988).
18. J.-C. WU and J. CHATTOPADHYAYA. Tetrahedron, **45**, 4507 (1989).
19. N. S. SIMPKINS. Tetrahedron, **46**, 6951 (1990).
20. K. E. PFITZNER and J. G. MOFFATT. J. Am. Chem. Soc. **87**, 5661 (1965).
21. A. J. SPEZIALE and K. W. RATTS. J. Am. Chem. Soc. **87**, 5603 (1965).
22. A. M. VAN LEUSEN, B. A. REITH, A. J. W. IEDEMA, and J. STRATING. Recl. Trav. Chim. Pays Bas, **91**, 37 (1972).
23. E. J. COREY and M. CHAYKOVSKY. J. Am. Chem. Soc. **87**, 1345 (1965).
24. B. M. TROST, H. C. ARNDT, P. E. STREGE, and T. R. VERHOEVEN. Tetrahedron Lett. **17**, 3477 (1976).
25. A. C. BROWN and L. A. CARPINO. J. Org. Chem. **50**, 1749 (1985).
26. V. PASCALI and A. UMANI-RONCHI. J. Chem. Soc. Chem. Commun. 351 (1973).
27. J. BREMNER, M. JULIA, M. LAUNAY, and J.-P. STACINO. Tetrahedron Lett. **23**, 3265 (1982).
28. M. JULIA, H. LAURON, J.-P. STACINO, J.-N. VERPEAUX, Y. JEANNIN, and Y. DROMZEE. Tetrahedron, **42**, 2475 (1986).
29. M. OCHIAI, T. UKITA, and E. FUJITA. J. Chem. Soc. Chem. Commun. 619 (1983).
30. R. SHAPIRO, R. E. SERVIS, and M. WELCHER. J. Am. Chem. Soc. **92**, 422 (1970).
31. J. P. H. VERHEYDEN and J. G. MOFFATT. J. Am. Chem. Soc. **88**, 5684 (1966).
32. J. R. MCCARTHY, JR., R. K. ROBINS, and M. J. ROBINS. J. Am. Chem. Soc. **90**, 4993 (1968).
33. M. J. ROBINS, R. MENGEL, R. A. JONES, and Y. FOURON. J. Am. Chem. Soc. **98**, 8204 (1976).
34. M. J. ROBINS, M. MACCOSS, S. R. NAIK, and G. RAMANI. *In* Nucleic acid chemistry. Improved and new synthetic procedures, methods and techniques. Vol. 3. *Edited by* L. B. Townsend and R. S. Tipson. Wiley–Interscience, New York. 1986. pp. 58–60.
35. G. M. SHELDRICK. SHELXTL PLUS™ Siemens Analytical X-ray Instruments, Inc., Madison, WI. 1990.
36. J. A. IBERS and W. C. HAMILTON (*Editors*). International tables for X-ray crystallography. Vol. 4. Kynoch Press, Birmingham, England. 1974. p. 99.
37. M. J. ROBINS, F. HANSSKE, S. F. WNUK, and T. KANAI. Can. J. Chem. **69**, 1468 (1991).

Can. J. Chem. Downloaded from www.nrcresearchpress.com by 123.30.183.119 on 09/08/12
For personal use only.

A voltammetric study of the kinetics of the hexacyanomanganate(III) disproportionation in acidic medium

GUILLERMO LÓPEZ-CUETO[1] AND CARLOS UBIDE[2]

División de Química Analítica, Facultad de Ciencias, Universidad de Alicante, Apdo. 99, 03080-Alicante, Spain

Received March 11, 1991

GUILLERMO LÓPEZ-CUETO and CARLOS UBIDE. Can. J. Chem. **69**, 2112 (1991).

The fast disproportionation of hexacyanomanganate(III) in acidic medium yields $Mn(CN)_6^{2-}$ and $Mn(H_2O)_6^{2+}$. The reaction has been studied by amperometry, with a rotating platinum-disk electrode, at a 1.0 V (vs. SCE) constant potential, in the acidity range 0.01–2.0 M and at temperatures between −5 and 15°C. A reversible one-electron process takes place with a 0.85 V (vs. SCE) half-wave potential that is not dependent on acidity. The reaction kinetics is pseudo-first order in $[Mn(CN)_6^{3-}]$ and the rate constant depends on acidity according to the equation: $k_{obs} = k_a + k_b[H_3O^+] + k_c[H_3O^+]^2$. At 5°C and ionic strength 2.0, the determined values of k_a, k_b, and k_c were $(2.20 \pm 0.08) \times 10^{-3}$ s^{-1}, $(4.9 \pm 0.2) \times 10^{-3}$ s^{-1} M^{-1}, and $(1.40 \pm 0.10) \times 10^{-3}$ s^{-1} M^{-2}, respectively. A mechanism is proposed where the three terms of k_{obs} are assigned to pathways involving hexacyanomanganate(III) in three different states of protonation. From the effect of temperature the activation parameters, $\Delta H^{\neq}$ and $\Delta S^{\neq}$, for each pathway are also reported.

Key words: hexacyanomanganate(IV), disproportionation, kinetics, amperometry, rotating platinum-disk electrode.

GUILLERMO LÓPEZ-CUETO et CARLOS UBIDE. Can. J. Chem. **69**, 2112 (1991).

La dismutation rapide de l'ion hexacyanomanganate(III), en milieu acide, fournit du $Mn(CN)_6^{2-}$ et du $Mn(H_2O)_6^{2+}$. On a étudié la réaction par ampérométrie, à l'aide d'une électrode de platine à disque tournant, à un potentiel constant de 1,0 V (vs. SCE), à des acidités allant de 0,01 à 2,0 M et à des températures allant de −5 à 15°C. Il se produit un processus réversible à un électron avec un potentiel de demi-vague de 0,85 V (vs. SCE) qui ne dépend pas de l'acidité. La cinétique de la réaction est du pseudo-premier ordre en $[Mn(CN)_6^{3-}]$ et la constante de vitesse est liée à l'acidité par l'équation : $k_{obs} = k_a + k_b[H_3O^+] + k_c[H_3O^+]^2$. À 5°C et à une force ionique de 2,0, les valeurs déterminées pour k_a, k_b et k_c sont respectivement $(2{,}20 \pm 0{,}08) \times 10^{-3}$ s^{-1}, $(4{,}9 \pm 0{,}2) \times 10^{-3}$ s^{-1} M^{-1} et $(1{,}40 \pm 0{,}10) \times 10^{-3}$ s^{-1} M^{-2}. On propose un mécanisme dans lequel les trois termes de k_{obs} sont attribués à des voies réactionnelles impliquant de l'hexacyanomanganate(III) dans trois états différents de protonation. En se basant sur l'effet de la température, on a aussi déterminé les paramètres d'activation, $\Delta H^{\neq}$ et $\Delta S^{\neq}$, pour chacune des voies réactionnelles.

Mots clés : hexacyanomanganate(IV), dismutation, cinétique, ampérométrie, électrode de platine à disque tournant.

[Traduit par la rédaction]

Introduction

The oxidation state 3+ of manganese is known to be very unstable because it is a strong oxidant, and thus it has been widely used as a one-electron oxidizing agent (1, 2). Mn(III) can often be made less oxidizing by complex formation (3), but in some cases these complexes show a thermodynamic tendency to disproportionate to Mn(IV) and Mn(II) (4–6), and therefore the disproportionation processes of Mn(III) compounds have special relevance. Nevertheless, the number of kinetic studies on Mn(III) disproportionation reactions is rather scarce in the literature (5, 6).

Cyanide ion strongly stabilizes Mn(III) as $Mn(CN)_6^{3-}$ in alkaline-cyanide medium (7–9). However, when $K_3Mn(CN)_6$ is dissolved in acidic solution it rapidly disproportionates to yield $Mn(H_2O)_6^{2+}$ and $Mn(CN)_6^{2-}$ (10, 11) and this explains why a change in the uv–visible spectra of the fresh acidic solutions of $Mn(CN)_6^{3-}$ is observed. The manganese(IV) cyano complex formed decomposes to $Mn(H_2O)_6^{2+}$ and $(CN)_2$, but the reaction is quite slow at room temperature (11) and thus the $Mn(CN)_6^{2-}$ solution can be used for oxidizing purposes for a period of time (12). The kinetics of the decomposition reaction of $Mn(CN)_6^{2-}$ has already been studied and a mechanism has been proposed (11). Trageser and Eysel (10) proposed a reaction scheme for the $Mn(CN)_6^{3-}$ disproportionation in which some part of $Mn(CN)_6^{3-}$ undergoes acid hydrolysis to yield $Mn(H_2O)_6^{3+}$ and this species oxidizes $Mn(CN)_6^{3-}$ to $Mn(CN)_6^{2-}$. This scheme is chiefly based on some thermodynamic considerations, but no kinetic evidence was reported on this reaction. In a previous paper (11) we reported that the kinetics of this reaction appeared to be close to a pseudo-first-order dependence, which seems to agree with the Trageser and Eysel scheme rather than with a bimolecular direct disproportionation. In the present paper the kinetics of the $Mn(CN)_6^{3-}$ disproportionation reaction in acidic medium is studied and a reaction mechanism is proposed. The reaction is quite fast at room temperature (at 25°C, half-life ~ 13 s) and thus the measurements have been taken well under room temperature using amperometric monitoring (spectrophotometric monitoring needs some extra care to avoid condensation of water on the outside of the cell). The amperometric measurements allowed some extra information about the redox properties of the involved species. Moreover, the voltammetric behavior of both the $Mn(CN)_6^{3-}$ and the $Mn(CN)_6^{2-}$ complexes at a rotating platinum-disk electrode in the same medium is described.

Experimental section

Apparatus

A 506 E Metrohm polarograph with a Metrohm 628-10 rotating platinum-disk electrode as working electrode, a platinum wire as auxiliary electrode, and a homemade saturated calomel electrode as reference electrode were used. The electrode rotation speed was 500 r.p.s. A 50 mL EA 880 Metrohm vessel was used as the reaction cell. The temperature in the vessel was continuously monitored by means of a Pt 100 temperature probe and kept constant (±0.1°C) by circulating an ethanol–water mixture from a thermostatic bath controlled by the probe.

[1]To whom correspondence should be addressed.

[2]Permanent address: Departamento de Química Aplicada, Universidad del País Vasco, 20080-San Sebastián, Spain.

Printed in Canada / Imprimé au Canada

Can. J. Chem. Downloaded from www.nrcresearchpress.com by 123.30.183.119 on 09/08/12
For personal use only.

Can. J. Chem. Downloaded from www.nrcresearchpress.com by 123.30.183.119 on 09/08/12
For personal use only.

Reagents

Potassium hexacyanomanganate(III) was prepared according to the method of Lower and Fernelius (13) and characterized as described previously (14). Nitric acid, sodium nitrate, and manganese(II) sulfate of analytical reagent grade and distilled, deionized water were used throughout.

Procedure

The reaction mixtures were prepared by adding the proper amount of solid $K_3Mn(CN)_6$ to 50 mL of a stirred solution having the required concentrations of Mn(II), nitric acid, and sodium nitrate (to adjust the ionic strength), and thermostated to the desired temperature (whenever $K_3Mn(CN)_6$ is taken into acidic solution HCN is produced, so *care* should be taken). After the solid was completely dissolved (between 5 and 60 s depending on the temperature) the magnetic stirrer was stopped. Then alternatively either current–voltage curves at different times or the current–time curve (the kinetic curve) were taken. The current–time curve was recorded, at least for three half-lives, at a 1.0 V (vs. SCE) constant potential. The pseudo-first-order rate constant, k_{obs}, was determined by plotting ln i_l vs. time (where i_l is the value of the limiting current) and linear regression analysis was applied (the value of i_∞ can be considered negligible). The temperature was varied between −5 and 15°C, the ionic strength between 0.1 and 2.0, the acidity between 0.01 and 2.0 M, the initial Mn(II) concentration between 0 and 0.01 M, and the initial $K_3Mn(CN)_6$ concentration between 3×10^{-4} and 3×10^{-3} M. Each kinetic run was usually repeated once, with the replicate measurement agreeing to within ±4% for 95% of the cases, and the value of k_{obs} was taken as the mean of the two runs.

Results and discussion[3]

Current–potential curves

The voltammogram obtained at a rotating platinum-disk electrode from a fresh acidic solution of $K_3Mn(CN)_6$ shows a one-electron anodic wave with a half-wave potential of about 0.85 V (vs. SCE) (Fig. 1, where anodic currents are considered positive and cathodic currents negative). Then a rapid change is spontaneously produced in the described voltammogram; the anodic current decreases while, at the same time, a cathodic current is produced, so that a composite anodic–cathodic current–potential curve is formed (Fig. 1). When the described transformation goes to completion only a cathodic current–voltage curve remains with a half-wave potential of about 0.85 V (vs. SCE). These electrochemical reactions involve the reversible couple $Mn(IV) + e^- \rightleftharpoons Mn(III)$, where Mn(IV) and Mn(III) represent the corresponding cyano complexes.

The variation of the limiting currents (i_l), of both the anodic and the cathodic processes, with time is shown in Fig. 2. As can be seen, the cathodic current tends towards a final value of about half the initial anodic current value. That is consistent with the following stoichiometry

$$[1] \qquad 2Mn(III) = Mn(IV) + Mn(II)$$

The manganese(IV) produced will remain in the form of cyano complex (Fig. 1), while manganese(II) will form the aquo complex (10, 11). Though the remaining acidic solution of the Mn(IV) cyano complex decomposes, this reaction proceeds very slowly at low temperature (11) and therefore only quite slow changes are observed in the voltammogram after the disproportionation reaction has gone to completion.

[3]Values of k_{obs}, k_{calc}, k_{calc}/k_{obs} for the disproportionation reaction may be purchased from the Depository of Unpublished Data, Document Delivery, CISTI, National Research Council of Canada, Ottawa, Ont., K1A 0S2.

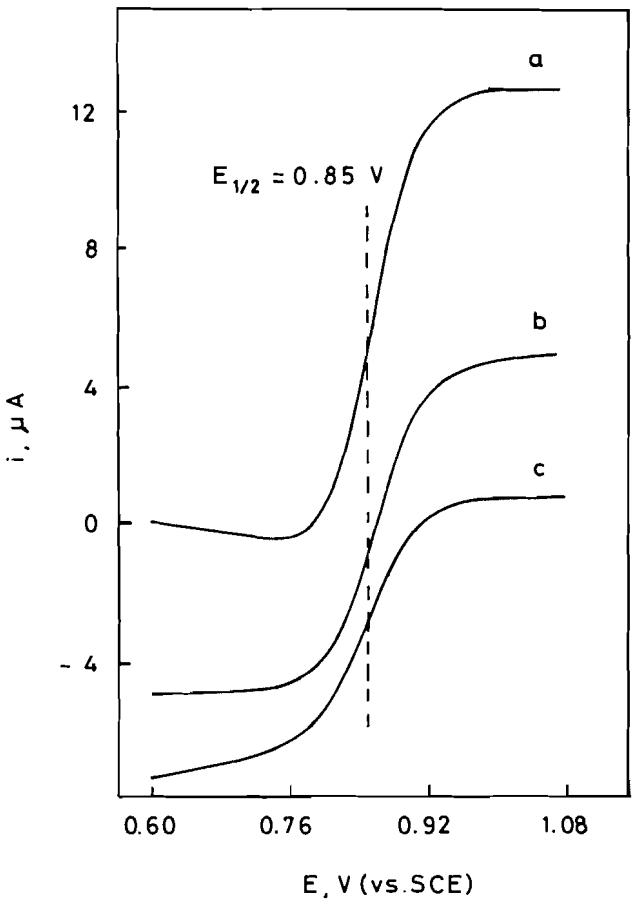


FIG. 1. Evolution of the current–potential curves of a fresh acidic solution of the Mn(III) cyano complex. Scan starting time: (*a*), 0; (*b*) 4; (*c*) 15 min. HNO_3, 0.1 M; *T*, 5°C. (Along the recording of the curve (*a*) the effect of the disproportionation reaction on the cathodic currents can clearly be observed. This effect is compensated for in curves (*b*) and (*c*) by the background current).

The half-wave potential remains essentially constant (0.85 ± 0.01 V, $n = 4$) when the H_3O^+ concentration varies in the range from 0.1 to 2.0 M (theoretically a one-proton reversible dependence in the mentioned acidity range would produce a change of about 0.077 V on the half-wave potential). This seems to indicate that protons are not involved in the electrode reaction.

Kinetics of disproportionation

Plots of ln i_l vs. time were linear for at least three half-lives. A first-order dependence on [Mn(III)] can therefore be inferred

$$[2] \qquad -\frac{d[Mn(III)]}{dt} = k_{obs}[Mn(III)]$$

The value of k_{obs} decreased about 30% when ionic strength increased from 0.1 to 1.0 and tended to level off for higher values (up to 2.0). On the other hand, k_{obs} was found to be independent of the $Mn(CN)_6^{3-}$ and Mn(II) initial concentrations (at least within the range studied) and thus the reaction does not seem to follow kinetics similar to that of the Mn(III) disproportionation in weakly complexing acidic medium, in which an equilibrium is involved (3):

$$[3] \qquad Mn(III) + Mn(III) \rightleftharpoons Mn(IV) + Mn(II)$$

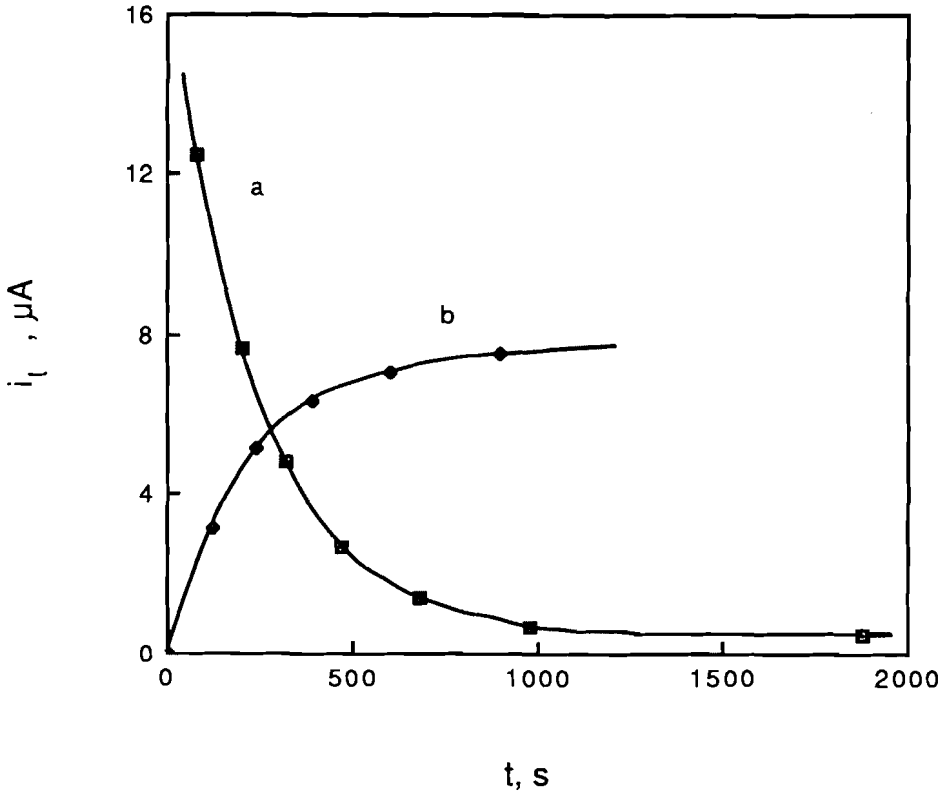


FIG. 2. Variation of the (*a*) anodic and (*b*) cathodic limiting current (i_l) with time during the disproportionation of the Mn(III) cyano complex. HNO_3 = 0.1 M; T = 5°C.

On the contrary, the $Mn(CN)_6^{3-}$ disproportionation seems to follow a scheme such as

$$[4] \qquad Mn(III) \underset{k_{-1}}{\overset{k_1}{\rightleftharpoons}} Mn(III)^* \quad \text{(intermediate)}$$

$$[5] \qquad Mn(III)^* + Mn(III) \xrightarrow{k_2} Mn(IV) + Mn(II)$$

and then, according to reactions [4] and [5]

$$[6] \qquad v = -\frac{d[Mn(III)]}{dt} = \frac{2k_1k_2[Mn(III)]^2}{k_{-1} + k_2[Mn(III)]}$$

But if reaction [5] is fast enough, $k_2[Mn(III)] \gg k_{-1}$. Therefore

$$[7] \qquad v = k_{obs}[Mn(III)]$$

k_{obs} being $2k_1$.

The value of k_{obs} depends on acidity. This dependence was found to lie between first and second order. Thus the following tentative equation was tested:

$$[8] \qquad k_{obs} = k_a + k_b[H_3O^+] + k_c[H_3O^+]^2$$

Following this equation a plot of $(k_{obs} - k_a)/[H_3O^+]$ vs. $[H_3O^+]$ should be straight. Figure 3 shows such a plot for temperatures ranging between −5 and 15°C. The values of k_a, k_b, and k_c at each temperature were obtained by non-linear regression analysis applied to the experimental points according to eq. [8]. Values of $k_a = (2.20 \pm 0.08)\ 10^{-3}\ s^{-1}$, $k_b = (4.9 \pm 0.2)\ 10^{-3}\ s^{-1}\ M^{-1}$, and $k_c = (1.40 \pm 0.10)\ 10^{-3}\ s^{-1}\ M^{-2}$ were obtained at 5°C and ionic strength 2.0. On the other hand, plots of $\ln (k/T)$ vs. $1/T$ for each rate constant allowed us to calculate the activation parameters $\Delta H^{\neq}$ and $\Delta S^{\neq}$ of the three reaction paths (Table 1).

If eq. [8] applies and the activation parameters are known, the value of the overall rate constant can be calculated theoretically (k_{calc}):

$$[9] \qquad k_{calc} = \frac{RT}{Nh}\left\{\exp\left(\frac{\Delta S_a^{\neq}}{R} - \frac{\Delta H_a^{\neq}}{RT}\right) + \exp\left(\frac{\Delta S_b^{\neq}}{R} - \frac{\Delta H_b^{\neq}}{RT}\right)[H_3O^+] + \exp\left(\frac{\Delta S_c^{\neq}}{R} - \frac{\Delta H_c^{\neq}}{RT}\right)[H_3O^+]^2\right\}$$

where R is the gas constant, T the absolute temperature, N is Avogadro's number, h is Planck's constant, and a, b, and c refer to the three paths given by eq. [8].

The values of k_{calc} obtained from eq. [9] were compared with the experimental ones (k_{obs}) by obtaining the k_{calc}/k_{obs} relation for different reaction conditions (the k_{obs} values ranged between 4.37×10^{-4} and 9.23×10^{-2}). The average value obtained for the k_{calc}/k_{obs} ratio was 0.995 with a standard deviation of 0.005 (assuming a gaussian distribution of the quotients). These results prove that both eq. [8] and the obtained values for the activation parameters hold throughout the ranges studied.

Reaction mechanism

According to eqs. [2] and [8] a mechanism with three par-

Can. J. Chem. Downloaded from www.nrcresearchpress.com by 123.30.183.119 on 09/08/12
For personal use only.

Can. J. Chem. Downloaded from www.nrcresearchpress.com by 123.30.183.119 on 09/08/12
For personal use only.

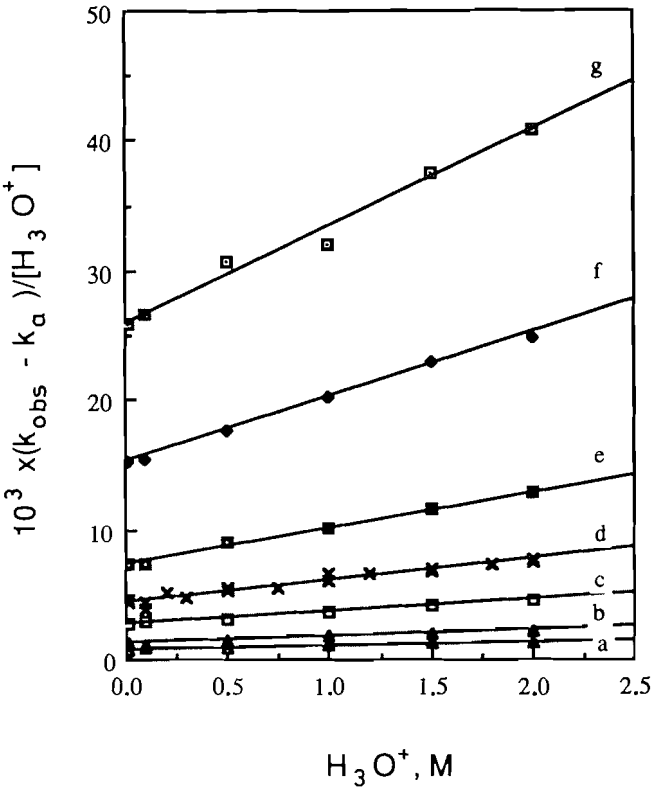


FIG. 3. Plots of $(k_{obs} - k_a)/[H_3O^+]$ vs. $[H_3O^+]$ for the disproportionation reaction of hexacyanomanganate(III) in acidic solution at ionic strength 2.0. Temperatures, °C: (*a*), −5; (*b*), −2; (*c*), 2; (*d*), 5; (*e*), 8; (*f*), 12; (*g*), 15.

allel pathways involving zero, one, and two protons, respectively, may be considered. The predominant species of the Mn(III) and Mn(IV) cyano complexes should have the same number of protons because it has already been shown above that the reversible electrode reaction $Mn(III) \rightleftarrows Mn(IV) + e^-$ involves zero protons. According to previous work (15), the predominant species of the Mn(IV) cyano complex in acidic solution should be at least monoprotonated, and so the Mn(III) and Mn(IV) predominant species will be $Mn(CN)_5(CNH)^{2-}$ and $Mn(CN)_5(CNH)^-$, respectively, both of them being species partially protonated on the nitrogen of some of the coordinated cyano groups as previously reported (11) and stated for some other cyano complexes (16).

The following equilibria should be considered before the rate-determining step

[10] $Mn(CN)_5(CNH)^{2-} + H_3O^+ \overset{\beta_1}{\rightleftharpoons} Mn(CN)_4(CNH)_2 + H_2O$

[11] $Mn(CN)_5(CNH)^{2-} + 2H_3O^+ \overset{\beta_2}{\rightleftharpoons} Mn(CN)_3(CNH)_3 + H_2O$

Each one of the three manganese(III) species will participate in a mechanism like the one schematized by reactions [4] and [5]. According to the scheme three parallel pathways will have to be considered, and the determining steps will be:

[12] $Mn(CN)_5(CNH)^{2-} \underset{k_{-a}'}{\overset{k_a'}{\rightleftharpoons}}$ intermediate (a)

[13] $Mn(CN)_4(CNH)_2^- \underset{k_{-b}'}{\overset{k_b'}{\rightleftharpoons}}$ intermediate (b)

TABLE 1. Activation parameters for the disproportionation reaction of hexacyanomanganate(III) in acidic solution at ionic strength 2.0 (each value is accompanied by its standard error)

Rate constant	$\Delta H^{\ddagger}$/kJ mol^{-1}	$\Delta S^{\ddagger}$/J mol^{-1} K^{-1}
k_a/s^{-1}	99.6 ± 1.0	63 ± 4
k_b/s^{-1} M^{-1}	109.4 ± 1.2*	105 ± 4*
k_c/s^{-1} M^{-2}	104 ± 2*	74 ± 7*

*These values are apparent since the rate constant includes a protonation equilibrium constant.

[14] $Mn(CN)_3(CNH)_3 \underset{k_{-c}'}{\overset{k_c'}{\rightleftharpoons}}$ intermediate (c)

Finally, each of the intermediate species will react quickly with the predominant Mn(III) cyano complex:

[15] $Mn(CN)_5(CNH)^{2-}$ + intermediate (a), (b), (c) $\overset{\text{fast}}{\rightleftharpoons}$ Mn(II) + Mn(IV)

The resulting Mn(II) species should be labile cyano-aquo complexes that rapidly lose the coordinated cyanides to give $Mn(H_2O)_6^{2+}$. As far as the Mn(IV) species is concerned, all of them will be transformed into $Mn(CN)_5(CNH)^-$, as this appears to be the predominant species in an acidic medium (15).

We have been looking for some experimental proof of the existence of the postulated intermediates (steps [12]–[14]), but neither spectral (uv–visible) nor electrochemical (cyclic voltammetry) evidence has been found, probably because the steady-state concentrations lie under their detection limits. Nonetheless, the existence of the intermediates has been postulated to explain the pseudo-first-order kinetics found. Unidentified steady-state intermediates of rearranged structure have sometimes been proposed to justify the experimental results (15, 17). The intermediates proposed here should have an oxidizing power high enough to oxidize the manganese(III) cyano complex to manganese(IV). These intermediates would probably be Mn(III) species at least partially dissociated (cyano-aquo complexes) in such a way that their oxidation potentials would approach that of the $Mn(H_2O)_6^{3+}/Mn(H_2O)_6^{2+}$ couple so that reaction [15] would be thermodynamically favorable. On the other hand, and according to thermodynamic considerations, Trageser and Eysel (10) proposed that the $Mn(CN)_6^{3-}$ disproportionation may take place through its oxidation to $Mn(CN)_6^{2-}$ via the $Mn(H_2O)_6^{3+}$ species formed in the previous hydrolytic decomposition of some part of the manganese(III) cyano complex. Our results seem to agree with these proposals.

From the proposed mechanism a pseudo-first-order rate law can be deduced, where the observed rate constant will have the form

$$[16] \quad k_{obs} = 2\,\frac{k_a' + k_b'\beta_1[H_3O^+] + k_c'\beta_2[H_3O^+]^2}{1 + \beta[H_3O^+] + \beta_2[H_3O^+]^2}$$

The monoprotonated species of the Mn(III) cyano complex, $Mn(CN)_5(CNH)^{2-}$, has been proposed above as predominant,

and from here: $1 \gg \beta_1[H_3O^+] \gg \beta_2[H_3O^+]^2$, and eq. [16] reduces to

$$[17] \quad k_{obs} = 2k_a' + 2k_b' + 2k_b'\beta_1[H_3O^+] + 2k_c'\beta_2[H_3O^+]^2$$

which may be written as

$$[8] \quad k_{obs} = k_a + k_b[H_3O^+] + k_c[H_3O^+]^2$$

where $k_a = 2k_a'$, $k_b = 2k_b'\beta_1$, and $k_c = 2k_c'\beta_2$.

The constants k_b and k_c include protonation equilibrium constants. Therefore the activation enthalpies and entropies for paths *b* and *c* are actually apparent and not much can be said on their numerical values (Table 1). On the other hand, k_a is a true rate constant and at low acidities it is the main part of k_{obs}. The activation enthalpy value of k_a appears to be rather high for a reaction in solution; from this a low rate constant could be expected. Nevertheless, relatively high values for k_a at not too high temperatures have been found ($k_a = 1.07 \pm 0.07) \times 10^{-2}$ s^{-1} at 15°C). This must be attributed to the high positive value of $\Delta S_a^{\neq}$, which suggests a strong dissociation in the activated complex formation. This result supports the hypothesis of a partially aquated cyano complex.

A number of disproportionation reactions have been reported to follow second-order kinetics (including uranium(V) (18), plutonium(V) (19), and americium(V) (20)) and it has been interpreted in terms of a bimolecular determining step, but some other disproportionation reactions have been reported to follow pseudo-first-order dependences. This appears to happen especially when the metal ion is in a complexed form, as Mo(V) complexes with EDTA, cysteine, histidine, and citric acid (21), neptunium(V) bonded in an inert cation–cation complex (22), and americium(V) in phosphoric acid (23) and in phosphotungstate solutions (24). On the other hand, the complexes of manganese(III) with $H_2P_2O_7^{2-}$ (6) and CyDTA in methanolic base (5) media also disproportionate following pseudo-first-order kinetics. In our case and according to reaction [4] only one Mn(III) is involved in the rate-determining step. It can be argued that [4] does not really correspond to a disproportionation. Nevertheless, considering the whole process (reactions [4] and [5]), two Mn(III) are involved and so it can be considered a disproportionation, in the same way as some precedences (5, 6, 10, 21–24).

Acknowledgement

One of us, C.U., is grateful to the Consejería de Educación del Gobierno Vasco for the award of a grant which enabled his stay in the University of Alicante where the experimental work was done.

1. J. Barek and A. Berka. CRC Crit. Rev. Anal. Chem. **9**, 55 (1980).
2. J. Barek and A. Berka. CRC Crit. Rev. Anal. Chem. **15**, 163 (1984).
3. G. Davies. Coordin. Chem. Rev. **4**, 199 (1969).
4. R. E. Hamm and M. A. Suwyn. Inorg. Chem. **6**, 139 (1967).
5. B. L. Poh and R. Stewart. Can. J. Chem. **50**, 3432 (1972).
6. N. Calu, A. Popa-Rang, and M. Calenciuc. Rev. Roum. Chem. **19**, 1889 (1974) (Chem. Abstr. **83**, 52598*j* (1975)).
7. W. P. Griffith. Q. Rev. (London), **16**, 188 (1962).
8. A. G. Sharpe. The chemistry of the cyano complexes of the transition metals. Academic Press, New York, NY. 1976. p. 86.
9. G. López-Cueto, and J. E. Gil-Pérez. Analyst, **109**, 637 (1984).
10. G. Trageser and H. H. Eysel. Inorg. Chim. Acta, **26**, L56 (1978).
11. G. López-Cueto and C. Ubide. Can. J. Chem. **64**, 2301 (1986).
12. G. López-Cueto and C. Ubide. Talanta, **37**, 849 (1990).
13. J. A. Lower and W. C. Fernelius. Inorg. Synth. **2**, 213 (1946).
14. G. López-Cueto, A. Alonso-Mateos, C. Ubide, and G. del Campo-Martínez. Talanta, **35**, 795 (1988).
15. G. López-Cueto and C. Ubide. Can. J. Chem. **66**, 2855 (1988).
16. R. J. Gillespie and R. Hulme. J. Chem. Soc. Dalton Trans. 1261 (1973). *In* Advanced inorganic chemistry. 4th ed. *Edited by* F. A. Cotton and G. Wilkinson. Wiley, New York, NY. 1980. p. 755.
17. P. L. Stanghellini, R. Rossetti, O. Gambino, and G. Cetini. Inorg. Chem. **10**, 2672 (1971).
18. A. Ekstrom. Inorg. Chem. **13**, 2237 (1974).
19. S. W. Rabideau. J. Am. Chem. Soc. **79**, 6350 (1957).
20. J. S. Coleman. Inorg. Chem. **2**, 53 (1963).
21. P. R. Robinson and C. R. Landis. Inorg. Chim. Acta, **33**, 63 (1979).
22. A. A. Frolov and A. G. Rykov. Radiokhimiya, **21**, 598 (1979) (Chem. Abstr. **91**, 163644*f* (1979)).
23. V. Ya. Frenkel, I. A. Levedev, M. F. Tikhonov, Yu. M. Kulyato, and T. I. Trofinov. Radiokhimiya, **23**, 844 (1981) (Chem. Abstr. **96**, 92441*c* (1982)).
24. E. A. Erin, V. V. Kopytov, V. Ya. Vasil'ev, and A. G. Rykov. Radiokhimiya, **25**, 51 (1983) (Chem. Abstr. **98**, 114485*r* (1983)).

Can. J. Chem. Downloaded from www.nrcresearchpress.com by 123.30.183.119 on 09/08/12
For personal use only.

Excess Gibbs energy for binary mixtures of acetonitrile with acetic acid, propionic acid, isobutyric acid, and trimethylacetic acid

T. S. BANIPAL,[1,2] B. S. LARK, AND S. SINGH
Department of Chemistry, Guru Nanak Dev University, Amritsar — 143005, Punjab, India
Received December 21, 1989[3]

T. S. BANIPAL, B. S. LARK, and S. SINGH. Can. J. Chem. **69**, 2117 (1991).

Total vapour pressures for binary mixtures containing acetic acid, propionic acid, isobutyric acid, and trimethylacetic acid with acetonitrile have been measured for the entire composition range at 298.15 and 318.15 K using a static manometric method. All systems show positive deviations from Raoult's law, enhanced by both an increase in temperature and an increase in the methylation of acetic acid. Activity coefficients have been calculated by taking into consideration the dimerization of these carboxylic acids in the vapour phase. TS^E values obtained from G^E and earlier reported H^E values are found to be negative for acetic acid, about zero for propionic and isobutyric acids, and positive for trimethylacetic acid for the whole composition range. The results have been interpreted in terms of various contributions such as depolymerization, heteromolecular dipole–dipole interactions, and the increasing dimerization constant and steric hindrance with increase of complexity of the acid.

Key words: excess Gibbs energy, carboxylic acids, acetonitrile, activity coefficients.

T. S. BANIPAL, B. S. LARK et S. SINGH. Can. J. Chem. **69**, 2117 (1991).

Utilisant une méthode manométrique statique et opérant à 298,15 et 318,15 K, on a mesuré les pressions de vapeur totales de mélanges binaires d'acétonitrile avec les acides acétique, propanoïque, isobutyrique et triméthylacétique sur l'ensemble des compositions. Tous les systèmes présentent des déviations positives par rapport à la loi de Raoult et elles sont majorées tant par une augmentation de la température que par le degré de méthylation de l'acide acétique. On a calculé les coefficients d'activité en tenant compte de la dimérisation de ces acides en phase vapeur. On a trouvé que, pour l'ensemble des compositions, les valeurs de TS^E obtenues à partir des valeurs de G^E et des valeurs de H^E rapportées antérieurement sont négative pour l'acide acétique, approximativement égales à zéro pour les acides propanoïque et isobutyrique et positive pour l'acide triméthylacétique. On a interprété les résultats en fonction de diverses contributions comme : la dépolymérisation, les interactions hétéromoléculaires dipôle–dipôle et l'augmentation de la constante de dimérisation ainsi que de l'empêchement stérique avec une augmentation de la complexité de l'acide.

Mots clés : énergie de Gibbs dans l'excès, acides carboxyliques, acétonitrile, coefficients d'activité.

[Traduit par la rédaction]

Introduction

Carboxylic acids are strongly associated liquids showing peculiar mixing properties with various solvents (1–15). The mixing behaviour of these acids with non-polar solvents is characterised by double or even higher magnitude of positive G^E values as compared to corresponding H^E values, resulting in negative TS^E values. This behaviour has been explained by the breaking up of acid trimers to dimers and monomers, and the formation of dimers from the monomers thus set free on the addition of an increasing proportion of non-polar solvents (1–3, 9). In the case of protic solvents like CH_3OH, in spite of the evidence that AB and AB_2 (A = acid monomer, B = CH_3OH) types of species are formed (16, 17), entropy changes are large and positive (10, 11). Predominant depolymerization of both acid and CH_3OH molecules explains this trend. As a continuation of our work in which we have reported V^E and H^E values of acetic acid, propionic acid, isobutyric acid, and trimethylacetic acid with acetonitrile (4), in this paper we report total vapour pressures and free energy results for such mixtures. Acetonitrile is an aprotic and purely polar solvent with high dielectric constant ($\epsilon = 36.01$) and dipole moment ($\mu = 3.37$ D) at 298.15 K and, unlike CH_3OH, is non-hydrogen bonding in nature (18). Thus the results may help us to sort out the various contributions and explain the magnitude of excess thermodynamic functions of carboxylic acid mixtures.

Experimental

Acetic acid (AR, BDH), propionic acid (AR, BDH), isobutyric acid (LR, SRL), trimethylacetic acid (GR, Tokyo Kasei Kogyo Co., Ltd., Japan), and acetonitrile (LR, E. Merck) were further purified by the methods reported earlier (1–5).

Details of the static manometric method used for the measurement of total vapour pressures appear elsewhere (1, 2, 19). The temperature of the water thermostat, in which the mixing cell was kept, was controlled to ±0.005 K with the help of a 0.001 K Beckmann thermometer. The Beckmann thermometer was calibrated by determining the transition temperature of Glauber's salt (32.384°C). The manometer was housed in the air thermostat kept at 50 ± 0.1°C and the necessary correction was applied to convert the pressures to 0°C. The pressures were read with a 0.001 cm cathetometer.

Results and discussion

Measured total vapour pressures for all the systems as a function of mole fraction of acid at 298.15 and 318.15 K are presented in Table 1 and illustrated in Figs. 1–4 along with the partial pressures (at 298.15 K). All the systems show positive deviations from Raoult's law with maximum lying in the acid-rich region, and shifting to higher mole fraction with increasing complexity of the acid and magnitude have the following order:

acetic acid < propionic acid < isobutyric acid < trimethylacetic acid

This order is just opposite to that for non-polar solvents (cyclohexane and *n*-heptane) as reported earlier (1–3). Furthermore, these deviations increase with the rise in temperature. It may also be seen that the positive deviations in the acetonitrile-rich

[1]To whom all correspondence should be addressed.
[2]Present address: Department of Chemistry, Indian Institute of Technology, Hauz Khas, New Delhi – 110016, India.
[3]Revision received June 29, 1991.

Printed in Canada / Imprimé au Canada

Can. J. Chem. Downloaded from www.nrcresearchpress.com by 123.30.183.119 on 09/08/12
For personal use only.

Can. J. Chem. Downloaded from www.nrcresearchpress.com by 123.30.183.119 on 09/08/12
For personal use only.

TABLE 1. Vapour pressures, activity coefficients, mole fractions of acid in the vapour phase (y), and residual pressures (P^R) for various systems

	298.15 K					318.15 K				
x	P/Torr	$\ln \gamma_A$	$\ln \gamma_B$	y	P^R	P/Torr	$\ln \gamma_A$	$\ln \gamma_B$	y	P^R
					$x CH_3COOH + (1 - x)CH_3CN$					
0.0000	88.99	1.4362	0.0000	0.0000	0.00	211.83	1.2086	0.0000	0.0000	0.00
0.0896	83.74	0.8606	0.0230	0.0203	−0.29	199.33	0.7847	0.0172	0.0223	−0.02
0.1486	80.75	0.6949	0.0488	0.0374	−0.40	192.58	0.6495	0.0351	0.0420	0.35
0.1902	79.71	0.6229	0.0594	0.0519	0.69	186.80	0.5839	0.0484	0.0581	−0.41
0.2367	76.66	0.5610	0.0761	0.0704	0.05	181.47	0.5227	0.0850	0.0779	−0.25
0.3131	72.64	0.4679	0.1115	0.1024	−0.24	173.88	0.4284	0.1008	0.1115	0.56
0.3728	70.62	0.3906	0.1520	0.1255	0.27	167.47	0.3534	0.1401	0.1363	0.06
0.4539	66.79	0.2827	0.2283	0.1526	−0.54	159.43	0.2540	0.2102	0.1676	−0.45
0.5205	64.80	0.2031	0.3039	0.1747	0.04	153.12	0.1834	0.2772	0.1948	−0.06
0.5812	62.45	0.1459	0.3737	0.1997	0.67	145.99	0.1335	0.3382	0.2253	0.34
0.6381	57.66	0.1084	0.4319	0.2323	−0.36	136.77	0.1005	0.3894	0.2632	0.06
0.7015	51.54	0.0904	0.4893	0.2932	−0.18	122.24	0.0747	0.4423	0.3298	−0.31
0.7901	43.74	0.0625	0.5433	0.3904	0.20	104.88	0.0566	0.4972	0.4306	0.18
0.8833	33.89	0.0360	0.6883	0.5394	−0.06	83.37	0.0312	0.6350	0.5818	0.04
1.0000	15.60	0.0000	1.4324	1.0000	0.00	43.35	0.0000	1.2704	1.0000	0.00
					$\sigma = 0.48$					$\sigma = 0.38$
					$x CH_3CH_2COOH + (1 - x)CH_3CN$					
0.0000	88.99	1.2826	0.0000	0.0000	0.00	211.83	1.1230	0.0000	0.0000	0.00
0.0973	82.32	0.9633	0.0160	0.0078	0.23	195.54	0.8633	0.0131	0.0099	0.30
0.1536	78.78	0.8129	0.0375	0.0133	−0.13	187.29	0.7364	0.0313	0.0167	−0.01
0.2236	75.46	0.6612	0.0725	0.0201	0.17	178.26	0.6051	0.0616	0.0257	0.09
0.2844	71.94	0.5569	0.1079	0.0264	−0.23	170.05	0.5128	0.0929	0.0340	−0.32
0.3295	69.84	0.4928	0.1362	0.0315	0.05	164.61	0.4551	0.1185	0.0407	0.13
0.3928	66.22	0.4166	0.1792	0.0393	−0.07	155.83	0.3858	0.1576	0.0510	−0.12
0.4820	61.22	0.3263	0.2495	0.0578	0.08	143.39	0.3028	0.2252	0.0676	−0.10
0.5417	57.74	0.2712	0.3073	0.0611	0.09	135.40	0.2523	0.2752	0.0801	0.40
0.6186	53.22	0.2029	0.4020	0.0739	0.04	123.99	0.1899	0.3618	0.0977	−0.01
0.7175	46.89	0.1202	0.5696	0.0930	−0.27	108.78	0.1142	0.5151	0.1246	−0.39
0.8440	36.69	0.0370	0.8684	0.1372	0.49	83.85	0.0367	0.7942	0.1844	0.46
0.8928	28.85	0.0168	1.0021	0.1776	−0.44	67.82	0.0171	0.9235	0.2357	−0.26
0.9442	19.32	0.0041	1.1435	0.2806	0.18	46.08	0.0044	1.0659	0.3568	0.07
1.0000	3.90	0.0000	1.2824	1.0000	0.00	12.75	0.0000	1.2166	1.0000	0.00
					$\sigma = 0.30$					$\sigma = 0.32$
					$x(CH_3)_2CHCOOH + (1 - x)CH_3CN$					
0.0000	88.99	1.6816	0.0000	0.0000	0.00	211.83	1.5959	0.0000	0.0000	0.00
0.0807	83.53	1.3473	0.0136	0.0056	0.30	198.69	1.2295	0.0145	0.0069	0.13
0.1373	79.28	1.1602	0.0364	0.0104	−0.85	190.60	1.0473	0.0366	0.0127	−0.58
0.2134	76.45	0.9512	0.0806	0.0164	−0.19	181.55	0.8593	0.0763	0.0203	−0.67
0.2664	75.25	0.8267	0.1198	0.0201	0.76	175.94	0.7516	0.1102	0.0255	0.58
0.3263	72.00	0.7016	0.1725	0.0238	−0.26	170.60	0.6435	0.1557	0.0312	0.52
0.4203	69.35	0.5312	0.2739	0.0290	0.33	161.08	0.4923	0.2458	0.0393	0.13
0.4905	66.59	0.4208	0.3663	0.0325	−0.08	154.34	0.3908	0.3308	0.0449	−0.19
0.5908	62.55	0.2850	0.5263	0.0376	−0.48	144.40	0.2629	0.4816	0.0529	−0.62
0.7166	57.07	0.1490	0.7840	0.0462	0.30	129.62	0.1353	0.7230	0.0665	0.65
0.7740	52.76	0.0997	0.9234	0.0525	0.26	118.34	0.0922	0.8553	0.0765	0.19
0.8413	44.87	0.0528	1.1261	0.0648	−0.39	99.97	0.0478	1.0337	0.0961	−0.49
0.9154	32.32	0.0165	1.3904	0.0984	0.22	70.72	0.0151	1.2717	0.1474	0.31
1.0000	2.12	0.0000	1.7756	1.0000	0.00	7.36	0.0000	1.6285	1.0000	0.00
					$\sigma = 0.56$					$\sigma = 0.61$
					$x(CH_3)_3CCOOH + (1 - x)CH_3CN$					
0.0000	88.99	2.3156	0.0000	0.0000	0.00	211.83	2.1222	0.0000	0.0000	0.00
0.0764	84.67	1.7470	0.0212	0.0025	0.60	200.44	1.5871	0.0193	0.0039	0.41
0.1310	81.75	1.4613	0.0539	0.0043	−0.05	194.81	1.3272	0.0496	0.0068	0.62
0.1892	79.76	1.2270	0.0983	0.0057	−0.08	188.79	1.1179	0.0892	0.0093	0.02
0.2361	78.57	1.0733	0.1397	0.0066	0.13	184.22	0.9813	0.1260	0.0112	−0.43
0.3128	76.26	0.8643	0.2185	0.0078	−0.14	178.18	0.7942	0.1966	0.0138	−0.39
0.3722	74.94	0.7261	0.2905	0.0085	−0.09	174.58	0.6678	0.2624	0.0154	0.20

TABLE 1 (*concluded*)

	298.15 K				318.15 K				
x	P/Torr	ln γ_A	ln γ_B	y	P^R	P/Torr	ln γ_A	ln γ_B	y	P^R
0.4639	73.14	0.5400	0.4242	0.0093	−0.12	169.14	0.4943	0.3871	0.0174	0.27
0.5790	71.34	0.3464	0.6352	0.0101	0.26	161.89	0.3120	0.5858	0.0195	−0.06
0.5952	70.92	0.3227	0.6690	0.0103	0.22	161.00	0.2898	0.6174	0.0199	0.26
0.6529	68.93	0.2452	0.7976	0.0108	−0.03	154.94	0.2181	0.7365	0.0214	−0.45
0.7198	65.44	0.1688	0.9650	0.0118	−0.41	146.31	0.1487	0.8882	0.0239	0.10
0.7993	59.89	0.0954	1.1976	1.0139	0.30	129.09	0.0838	1.0938	0.0292	0.09
0.8918	45.58	0.0327	1.5448	0.0199	−0.02	94.78	0.0291	1.3969	0.0438	−0.17
1.0000	0.55	0.0000	2.1584	1.0000	0.00	2.69	0.0000	1.9488	1.0000	0.00
					$\sigma = 0.32$					$\sigma = 0.41$

TABLE 2. Values of constants in eqs. [1] and [2]

T/K	A	B	C	D	E
		xCH$_3$COOH + $(1-x)$CH$_3$CN			
298.15	1.0120	−0.1080	−0.1460	0.1061	0.5683
318.15	0.9195	−0.1051	−0.1013	0.1360	0.4213
		xCH$_3$CH$_2$COOH + $(1-x)$CH$_3$CN			
298.15	1.1503	0.0872	0.2201	−0.0873	−0.0879
318.15	1.0488	0.1004	0.1949	−0.0536	−0.0739
		x(CH$_3$)$_2$CHCOOH + $(1-x)$CH$_3$CN			
298.15	1.5736	0.0538	0.1183	−0.0068	0.0367
318.15	1.4427	0.0683	0.0821	−0.0520	0.0874
		x(CH$_3$)$_3$CCOOH + $(1-x)$CH$_3$CN			
298.15	1.9192	−0.0209	0.1666	−0.0577	0.1512
318.15	1.7542	−0.0237	0.1014	−0.0630	0.1799

$l_1 = x_2^2$
$m_1 = -x_2^2(1 - 4x_1)$
$n_1 = x_2^2(1 - 8x_1 + 12x_1^2)$
$o_1 = -x_2^2(1 - 12x_1 + 36x_1^2 - 32x_1^3)$
$p_1 = x_2^2(1 - 16x_1 + 72x_1^2 - 128x_1^3 + 80x_1^4)$

$l_2 = x_1^2$
$m_2 = x_1^2(1 - 4x_2)$
$n_2 = x_1^2(1 - 8x_2 + 12x_2^2)$
$o_2 = x_1^2(1 - 12x_2 + 36x_2^2 - 32x_2^3)$
$p_2 = x_1^2(1 - 16x_2 + 72x_2^2 - 128x_2^3 + 80x_2^4)$

region are much smaller than those in the acid-rich region and the mixtures approach ideality as $x \rightarrow 0$.

The activity coefficients of the components in the mixtures were calculated from the total vapour pressures and the composition in the liquid phase, taking into consideration the dimerization constants (3, 11, 12) of the carboxylic acids in the vapour phase, by the method reported earlier (1–3). Estimated activity coefficients fitted to the following equations

$$[1] \quad \ln \gamma_A = Al_1 + Bm_1 + Cn_1 + Do_1 + Ep_1$$

$$[2] \quad \ln \gamma_B = Al_2 + Bm_2 + Cn_2 + Do_2 + Ep_2$$

by the method of least squares are included in Table 1. Equations [1] and [2] satisfy the Gibbs–Duhem equation and the values of constants A, B, C, etc., are given in Table 2. l_1, m_1, n_1, $\cdots$ and l_2, m_2, n_2, $\cdots$ are functions of mole fractions

TABLE 3. G^E, H^E, and TS^E values[a]

	G^E/(J mol^{-1})		H^E/(J mol^{-1})	TS^E/(J mol^{-1})
x	298.15 K	318.15 K	308.15 K	308.15 K
		xCH$_3$COOH + $(1-x)$CH$_3$CN		
0.1	246.0	248.0	119.6 (503.0)	−136.4
0.2	426.4	411.1	191.4 (655.2)	−227.4
0.3	541.2	526.3	247.3 (764.1)	−286.5
0.4	611.5	594.3	295.8 (868.8)	−307.1
0.5	627.2	608.1	330.3 (912.9)	−287.4
0.6	586.8	569.0	337.0 (853.1)	−240.9
0.7	503.3	489.2	302.6 (714.2)	−193.7
0.8	393.1	382.6	222.8 (550.2)	−165.0
0.9	249.7	241.1	109.7 (378.3)	−135.7
		xCH$_3$CH$_2$COOH + $(1-x)$CH$_3$CN		
0.1	274.4	259.5	237.7 (497.0)	−47.3
0.2	469.9	448.9	461.3 (783.8)	1.9
0.3	600.7	578.5	629.1 (932.6)	39.5
0.4	679.6	658.2	721.7 (999.7)	52.8
0.5	712.9	693.6	736.8 (1001.7)	33.6
0.6	699.5	683.2	682.6 (943.5)	−8.8
0.7	631.2	619.3	572.6 (809.4)	−52.7
0.8	496.4	490.1	419.9 (590.9)	−73.4
0.9	285.6	284.8	230.9 (297.8)	−54.3
		x(CH$_3$)$_2$CHCOOH + $(1-x)$CH$_3$CN		
0.1	362.5	357.8	274.7 (433.0)	−85.5
0.2	630.7	615.3	575.5 (861.2)	−47.5
0.3	818.5	796.6	816.4 (1146.2)	8.8
0.4	932.7	909.7	958.4 (1276.9)	37.2
0.5	975.2	954.1	995.9 (1291.1)	31.2
0.6	945.4	926.5	942.0 (1228.4)	6.1
0.7	840.5	823.3	816.1 (1098.1)	−15.8
0.8	655.1	640.4	629.7 (875.2)	−18.1
0.9	380.1	371.2	372.7 (513.3)	−3.0
		x(CH$_3$)$_3$CCOOH + $(1-x)$CH$_3$CN[b]		
0.1	476.1	462.0	517.0[c] (687.0)	55.0
0.2	802.7	799.5	938.8 (1149.8)	159.3
0.3	1021.2	993.5	1211.7 (1435.6)	218.2
0.4	1148.7	1119.7	1330.0 (1582.7)	210.3
0.5	1189.4	1160.1	1318.2 (1627.9)	158.1
0.6	1143.2	1113.1	1212.9 (1593.6)	99.8
0.7	1008.7	978.5	1044.6 (1460.4)	66.1
0.8	782.9	756.0	819.9 (1185.4)	63.9
0.9	455.5	438.4	503.5 (711.2)	65.1

[a] Calculated H^E values in parentheses.
[b] G^E values at 318.15 K have been used for TS^E values.
[c] H^E at 313.15 K.

Can. J. Chem. Downloaded from www.nrcresearchpress.com by 123.30.183.119 on 09/08/12
For personal use only.

Can. J. Chem. Downloaded from www.nrcresearchpress.com by 123.30.183.119 on 09/08/12
For personal use only.

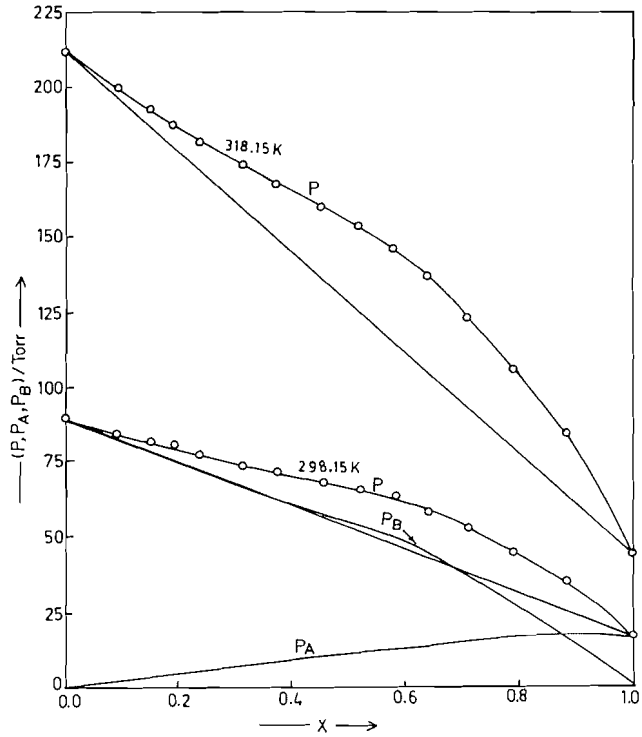


FIG. 1. Plot of total pressure (P) and partial pressures (P_A, P_B) vs. x for acetic acid + acetonitrile.

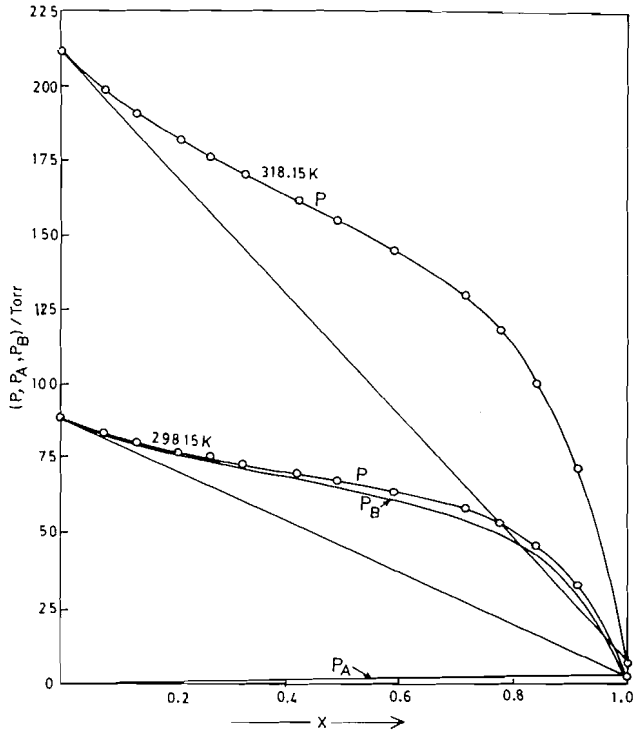


FIG. 3. Plot of total pressure (P) and partial pressures (P_A, P_B) vs. x for isobutyric acid + acetonitrile.

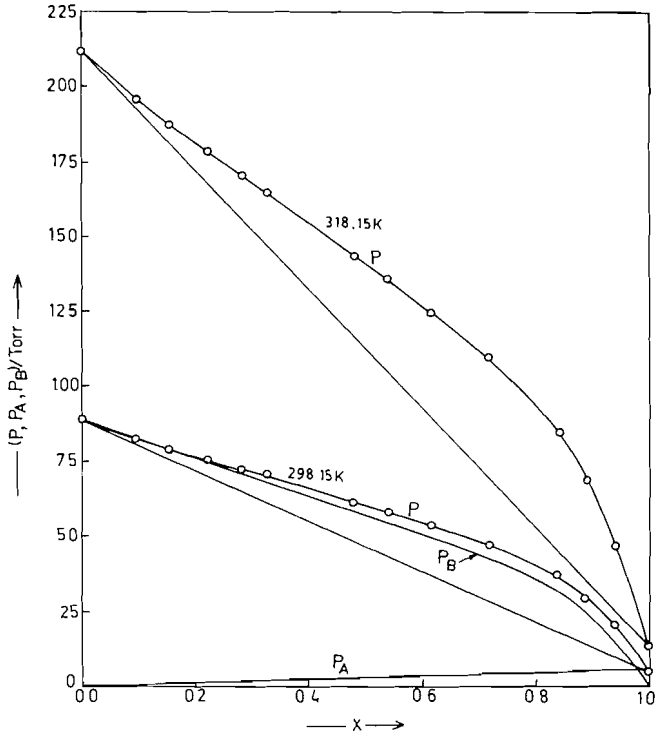


FIG. 2. Plot of total pressure (P) and partial pressures (P_A, P_B) vs. x for propionic acid + acetonitrile.

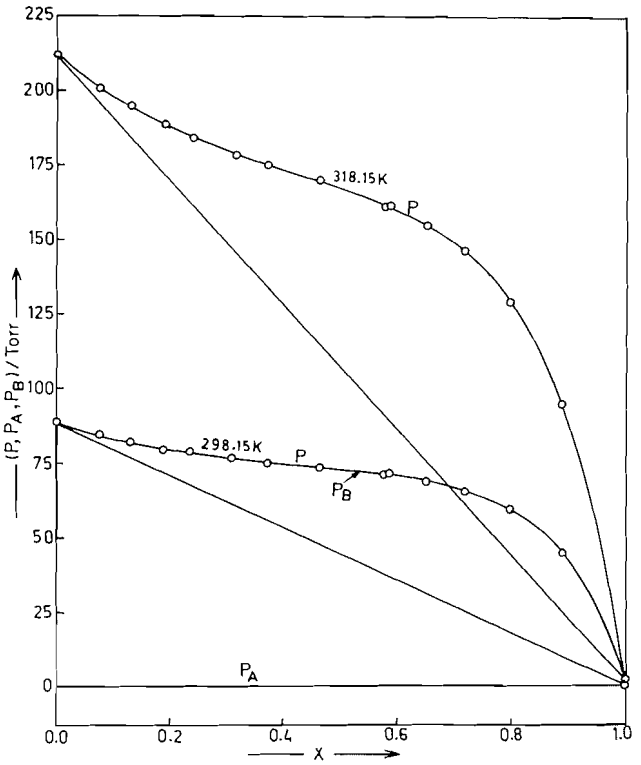


FIG. 4. Plot of total pressure (P) and partial pressures (P_A, P_B) vs. x for trimethylacetic acid + acetonitrile.

only and are given at the bottom of Table 2. Mole fractions of the acid in the vapour phase, residual pressures (the difference between the observed and calculated pressures), and standard deviations are also included in Table 1. Consistency of the activity data was checked from the plots of ln (γ_A/γ_B) vs. x, where negligible area was found under the curves for each system.

The excess Gibbs free energies derived from activity coef-

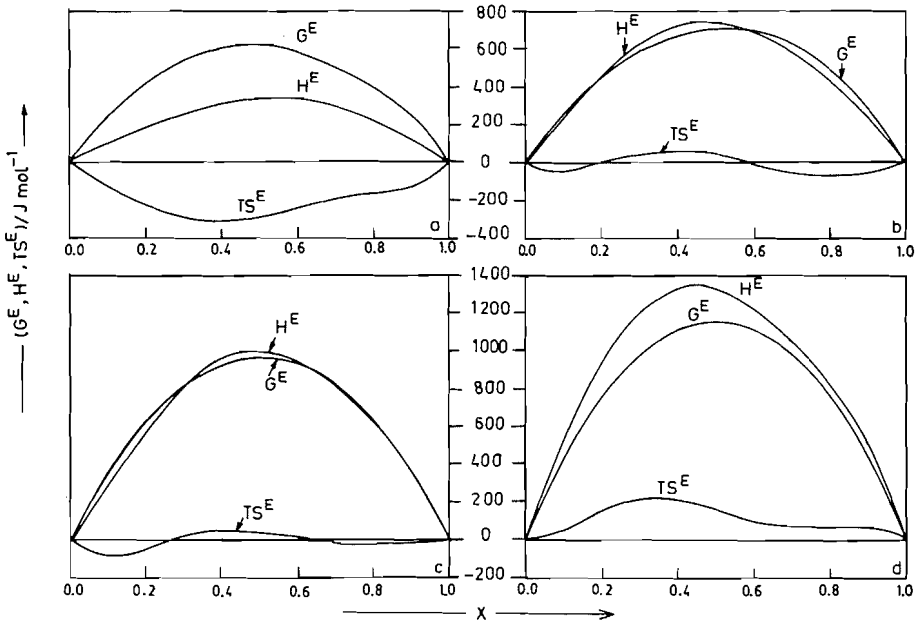


FIG. 5. Plot of G^E, H^E, and TS^E vs. x: (*a*) acetic acid + acetonitrile; (*b*) propionic acid + acetonitrile; (*c*) isobutyric acid + acetonitrile; (*d*) trimethylacetic acid + acetonitrile.

ficients at rounded mole fractions at 298.15 and 318.15 K and experimental excess enthalpies taken from our earlier report (4) at 308.15 K for all the systems are summarized in Table 3. A slight decrease in G^E values with the increase of temperature for all the systems, which may be due to the increased dipole–dipole interactions, is in line with the previously reported excess volume results (4) where the negative magnitude of V^E becomes more negative with the rise in temperature. H^E values calculated from the temperature dependence of G^E are included in Table 3 and the agreement with experimental values is good, considering the inherent large uncertainties associated with this method. TS^E values, estimated by utilizing the mean G^E, at 308.15 K (obtained as average of the corresponding values at 298.15 and 318.15 K), are summarized in Table 3 and illustrated along with the plots of G^E and H^E values in Fig. 5.

It may be seen that for acetic acid + acetonitrile: $G^E > H^E$ and $TS^E < 0$; for propionic acid + acetonitrile and isobutyric acid + acetonitrile: $G^E \approx H^E$ and $TS^E \approx 0$; and for trimethylacetic acid + acetonitrile: $G^E < H^E$ and $TS^E > 0$.

Further observation is that G^E and H^E increase with the complexity of the acid and H^E is increasing at a much faster rate to reverse the negative sign of TS^E for acetic acid to positive for trimethylacetic acid. This trend is quite in line with the increasing dimerization constants of the acids with their complexity (dimerization constants for acetic acid, propionic acid, isobutyric acid, and trimethylacetic acid are 1.982, 2.301, 7.755, and 842.9 Torr^{-1}, respectively, at 298.15 K). Negative TS^E in the case of acetic acid may be because of strong hetero dipole–dipole interactions. However, being impeded through increasing steric hindrance by the successive methylation of acetic acid results in almost zero TS^E values for propionic acid and isobutyric acid, and positive for trimethylacetic acid.

1. B. S. LARK, T. S. BANIPAL, S. SINGH, and R. C. PALTA. J. Chem. Eng. Data, **29**, 277 (1984).
2. B. S. LARK, T. S. BANIPAL, and S. SINGH. J. Chem. Eng. Data, **30**, 286 (1985).
3. B. S. LARK, T. S. BANIPAL, and S. SINGH. J. Chem. Eng. Data, **32**, 402 (1987).
4. B. S. LARK and T. S. BANIPAL. Can. J. Chem. **63**, 3269 (1985).
5. B. S. LARK and T. S. BANIPAL. Thermochim. Acta, **91**, 141 (1985).
6. B. S. LARK and R. C. PALTA. J. Chem. Thermodyn. **12**, 101 (1980).
7. B. S. LARK and R. C. PALTA. J. Chem. Thermodyn. **12**, 287 (1980).
8. B. S. LARK and R. C. PALTA. Malay. J. Sci. **6**(B), 159 (1980).
9. G. MIKSCH, F. RATKOVICS, and F. KOHLER. J. Chem. Thermodyn. **1**, 257 (1969).
10. M. WAGNER, A. APELBLAT, and A. TAMIR. J. Chem. Thermodyn. **12**, 181 (1980).
11. A. APELBLAT and F. KOHLER. J. Chem. Thermodyn. **8**, 749 (1976).
12. H. E. AFFSPRUNG, G. H. FINDENEGG, and F. KOHLER. J. Chem. Soc. A, 1364 (1968).
13. A. N. CAMPBELL and J. M. T. M. GIESKES. Can. J. Chem. **43**, 1004 (1965).
14. J. M. T. M. GIESKES. Can. J. Chem. **43**, 2448 (1965).
15. F. KOHLER, R. GOPAL, G. GOTZE, H. ATROPS, M. A. DEMIRIZ, E. LIEBERMANN, E. WILHELM, F. RATKOVICS, and B. PALAGYL. J. Phys. Chem. **85**, 2524 (1981).
16. N. A. IZMAILOV. Electrochemistry of solutions. 2nd ed. Izd. Khimya, Moscow. 1966. pp. 275–284, 563–564.
17. A. J. APELBLAT. J. Phys. Chem. **74**, 2214 (1970).
18. S. N. VINOGRADOV and R. H. LINNELL. Hydrogen bonding. Van Nostrand Reinhold Co., New York. 1971. p. 15.
19. B. S. LARK. Ph.D. Dissertation. Punjab University, Chadigarh-14, India. 1970.

Can. J. Chem. Downloaded from www.nrcresearchpress.com by 123.30.183.119 on 09/08/12
For personal use only.

The ^{119}Sn Mössbauer and solid-state NMR and the crystal and molecular structure of tin(II) bisfluorosulfate, $Sn(OSO_2F)_2$

DAVID C. ADAMS, THOMAS BIRCHALL,[1] ROMOLO FAGGIANI, RONALD J. GILLESPIE,[2] AND JOHN E. VEKRIS
Department of Chemistry, McMaster University, 1280 Main Street West, Hamilton, Ont., Canada L8S 4M1

Received November 26, 1990[3]

DAVID C. ADAMS, THOMAS BIRCHALL, ROMOLO FAGGIANI, RONALD J. GILLESPIE, and JOHN E. VEKRIS. Can. J. Chem. **69**, 2122 (1991).

The reaction of tin(II) fluoride with fluorosulfuric acid has been shown to produce tin(II) bisfluorosulfate. Crystals of $Sn(OSO_2F)_2$ are monoclinic, space group $P2_1/c$ with a = 5.195(1), b = 9.709(1), c = 13.861(1) Å, β = 110.12(1)°, Z = 4, R = 0.029, and R_w = 0.030 for 1461 unique reflections. The structure consists of a three-dimensional framework of fluorosulfate groups linked by O—Sn—O bridges with the two crystallographically independent fluorosulfates acting as tridentate bridging ligands between tin atoms. There are four short bonds (Sn—O = 2.338(3), 2.350(3), 2.398(4), and 2.427(3) Å) and two longer ones (Sn—O = 2.695(3) and 2.702(3) Å) around tin. The four short bonds have a disphenoidal, AX_4E, primary geometry with the lone pair occupying an equatorial site. If the two longer interactions are also considered the geometry is distorted octahedral, AX_4Y_2E. Two more non-bonding contacts of 3.420(4) and 3.319(4) Å complete an approximately dodecahedral arrangement of oxygen atoms around the tin. The fluorosulfate groups deviate significantly from C_{3v} symmetry and have the mean dimensions, S(1)—O = 1.419(4), S(1)—F = 1.541(4), S(2)—O = 1.435(3), S(2)—F = 1.539(3) Å, O—S(1)—O = 114.3(2)°, F—S(1)—O = 104.1(3)°, O—S(2)—O = 114.2(2)°, and F—S(2)—O = 104.1(2)°, respectively. The solid-state ^{119}Sn nmr spectrum shows only one single resonance with a shift of −1534 ppm which is substantially different from that of a solution in HSO_3F. The ^{119}Sn Mössbauer spectrum shows an unresolved quadrupole splitting as a result of a distorted environment around tin, produced by the stereochemically active non-bonding electron pair.

Key words: tin(II) bisfluorosulfate, ^{119}Sn Mössbauer, solid-state nmr, X-ray crystallography.

DAVID C. ADAMS, THOMAS BIRCHALL, ROMOLO FAGGIANI, RONALD J. GILLESPIE et JOHN E. VEKRIS. Can. J. Chem. **69**, 2122 (1991).

On démontre que la réaction du fluorure d'étain(II) avec l'acide fluorosulfurique conduit au bisfluorosulfate d'étain(II). Les cristaux du $Sn(OSO_2F)_2$ sont monocliniques, groupe d'espace P_1/c, avec a = 5,195(1), b = 9,709(1) et c = 13,861(1) Å, β = 110,12(1)°, Z = 4, R = 0,029 et R_w = 0,030 pour 1461 réflexions uniques. La structure comporte un squelette à trois dimensions de groupes fluorosulfates liés par des ponts O—Sn—O avec deux fluorosulfates cristallographiquement indépendants qui agissent comme ponts coordinants tricoordinés entre les atomes d'étain. Autour de l'étain, il existe quatre liaisons courtes (Sn—O = 2,338(3), 2,350(3), 2,398(4) et 2,427(3) Å) et deux liaisons plus longues (Sn—O = 2,695(3) et 2,702(3) Å). Les quatre liaisons plus courtes possèdent une géométrie primaire disphénoïdale, AX_4E, dans laquelle la paire d'électron libre occupe un site équatorial. Si les deux interactions plus longues sont aussi considérées, la géométrie est alors celle d'un octaèdre déformé, AX_4Y_2E. Deux autres contacts non-liants de 3,420(4) et 3,319(4) Å complètent un arrangement approximativement dodécaédrique des atomes d'oxygène autour de l'étain. La symétrie des groupes fluorosulfates s'éloigne beaucoup de C_{3v}; les dimensions moyennes sont les suivantes : (S(1)—O = 1,419(4) Å, S(1)—F = 1,541(4) Å, S(2)—O = 1,435(3) Å, S(2)—F = 1,539(3) Å, O—S(1)—O = 114,3(2)°, F—S(1)—O = 104,1(3)°, O—S(2)—O = 114,2(2)° et F—S(2)—O = 104,1(2)°. Le spectre rmn du ^{119}Sn à l'état solide ne présente qu'une résonance, avec un déplacement de −1534 ppm, qui est assez différente de celle d'une solution de HSO_3F. Le spectre de Mössbauer du ^{119}Sn présente un couplage quadripolaire non-résolu d'un environnement déformé autour de l'étain et qui est produit par la paire d'électron non-liée qui est stéréochimiquement active.

Mots clés : bisfluorosulfate d'étain(II), Mössbauer du ^{119}Sn, rmn de l'état solide; diffraction des rayons-X.

[Traduit par la rédaction]

Introduction

In an earlier paper we reported some spectroscopic studies of compounds prepared by the reaction of tin(II) fluoride with strong Lewis acids (1). $Sn(OSO_2F)_2$ was among the compounds studied at that time. Its vibrational and ^{119}Sn Mössbauer spectra indicated an appreciable covalent cation–anion interaction and, in addition, a detectable distortion of the environment about the central tin(II) nucleus was observed from the latter spectrum. However, no information regarding the structure of $Sn(OSO_2F)_2$ was obtained. In view of the improvements in spectrometers since the early seventies and of the superior counting statistics and better fitting procedures that are now available we have remeasured the Mössbauer spectrum of $Sn(OSO_2F)_2$ and we report this together with its X-ray crystal structure and the ^{119}Sn nmr spectra of the solid and its solution in HSO_3F.

Experimental

Materials and general procedures

Tin(II) fluoride (Ultrapure, Ventron, Alfa Products) was dried by heating to 60°C under vacuum overnight. Fluorosulfuric acid (Technical grade, J. T. Baker Chemical Co. N.J.) was purified by double distillation in an all-glass apparatus (2). A saturated solution of tin(II) bisfluorosulfate (1) in fluorosulfuric acid was allowed to stand overnight at room temperature. Well-formed colourless crystals obtained from this solution were filtered and dried by pumping on a vacuum line. A portion of this sample was pulverised to a fine powder in a nitrogen dry box and appropriate quantities of this portion were used for Mössbauer, solid-state, and solution nmr studies.

Crystallography

Colourless crystals of $Sn(OSO_2F)_2$ were sealed in Lindemann capillaries in a dry box equipped with a microscope. Precession photographs gave preliminary cell and symmetry information and accu-

[1]Deceased.
[2]Author to whom correspondence may be addressed.
[3]Revision received July 25, 1991.

Can. J. Chem. Downloaded from www.nrcresearchpress.com by 123.30.183.119 on 09/08/12
For personal use only.

Can. J. Chem. Downloaded from www.nrcresearchpress.com by 123.30.183.119 on 09/08/12
For personal use only.

TABLE 1. Fractional atomic co-ordinates ($\times 10^4$) and temperature factors ($Å^2 \times 10^3$) for $Sn(OSO_2F)_2$

Atom	x	y	z	U_{eq}[a]
Sn	148.4(5)	1927.1(3)	1795.7(2)	23
S(1)	1759(3)	1847(1)	−597(1)	28
S(2)	4616(2)	4791(1)	1906(1)	19
O(11)	1607(9)	2338(4)	357(2)	45
O(12)	1241(8)	2886(3)	−1360(2)	34
O(13)	401(10)	593(4)	−934(3)	51
O(21)	6808(7)	4077(3)	1755(3)	38
O(22)	2650(6)	3979(3)	2180(2)	30
O(23)	5400(6)	6009(3)	2555(2)	28
F(11)	4819(8)	1514(5)	−351(3)	79
F(21)	2949(6)	5380(3)	845(2)	38

[a] $U_{eq} = (1/3)(U_{11} + U_{22} + U_{33} + 2U_{13} \cos \beta)$.

rate cell parameters were obtained on a Nicolet P3 diffractometer from a least-squares refinement of x, ϕ, and 2θ for 15 well-centered high angle, $19° \leq 2\theta \leq 38°$, reflections.

Crystal data are as follows:

$Sn(OSO_2F)_2$, $M = 316.8$

Monoclinic, space group $P2_1/c$, $a = 5.195(1)$, $b = 9.709(1)$, $c = 13.861(1)$ Å, $\beta = 110.12°(1)$, $U = 656.4(2)$ $Å^3$, $Z = 4$, $D_c = 3.206$ g cm^{-3}, $F(000) = 592$, graphite-monochromated MoKα($\lambda = 0.71069$ Å), $\mu = 45.5$ cm^{-1}, $T = 296$ K.

Collection of the X-ray data and solution of the structure

An almost spherical crystal of 0.2 mm diameter was used for analysis. Intensities were measured on the Nicolet diffractometer using a θ(crystal)–2θ counter scan method, for the total of 1785 reflections with $3° \leq 2\theta \leq 55°$, (*hkl* range: $0 \leq h \leq 6$, $0 \leq k \leq 12$, $-18 \leq l \leq 16$). Two standard reflections were measured every 49 reflections and showed no variation with time (−2,0,6 (esd 1%) and 2,−3,−3 (1.2%)). The methods of selection of scan rates and initial data treatment have been described before (3). Lorentz, polarization (4), and ψ-scan absorption correction, PSI (5), were applied to all reflections. A total of 167 reflections of the 1785 collected were systematically absent and were removed from the data set. Equivalent reflections were averaged for a total of 1461 independent unique reflections ($R_{Int} = 0.017$). A three-dimensional Patterson map located the position of the tin atom and the remaining atoms were identified from a series of difference Fourier syntheses and least-squares refinements, using the program SHELX (6). Anisotropic thermal parameters were then assigned to all atoms and further refinement with full-matrix least-squares routines minimizing $\Sigma w(|F_o| - |F_c|)^2$, with the weight $w = 1/[\sigma^2(F) + 0.0005F_o^2]$, was terminated when the maximum shift/error fell to 0.005. Final R and R_w values were 0.029 and 0.030, respectively, for all measured unique reflections and 101 variables ($R = \Sigma||F_o| - |F_c||/\Sigma|F_o|$ and $R_w = [\Sigma w(|F_o| - |F_c|)^2/\Sigma_w|F_o|^2]^{1/2}$). Residual electron density in the final difference map was <1 e $Å^{-3}$. Corrections were made for secondary extinction by the SHELX method (6), and scattering factors were those stored in this program. Density was not determined because of the instability of the compound in air. Fractional atomic coordinates are given in Table 1 and selected bond distances and angles in Table 2 (7).[4,5]

[4]A complete list of observed and calculated structure factors, anisotropic thermal parameters, and details of least-squares planes may be purchased from the Depository of Unpublished Data, CISTI, Document Delivery, National Research Council of Canada, Ottawa, Ont., Canada K1A 0S2.

[5]All computations were carried out on a Cyber 170/815 and VAX 8600 computer. Programs used for initial data treatment are XRAY 76 (7*a*) and XTAL system of crystallographic programs (7*b*), University of Maryland, College Park, MD. 1983. Planes were calculated with the program LSQPL (7*c*). Diagrams were prepared from the program ORTEP-II (7*d*).

TABLE 2. Selected bond lengths and intra- and intermolecular distances (Å)[a] and angles (deg) for $Sn(OSO_2F)_2$[b]

Bond	Length	Bond	Length
Sn—O(11)	2.398(4)	S(1)—O(11)	1.432(4)
Sn—O(12′)	2.427(3)	S(1)—O(12)	1.420(3)
Sn—O(13′)	2.695(3)	S(1)—O(13)	1.404(4)
Sn—O(21′)	2.702(3)	S(1)—F(11)	1.541(4)
Sn—O(22)	2.338(3)	S(2)—O(21)	1.408(4)
Sn—O(23′)	2.350(3)	S(2)—O(22)	1.440(4)
Sn.....O(23″)	3.420(3)	S(2)—O(23)	1.457(3)
Sn.....F(11′)	3.319(4)	S(2)—F(21)	1.539(3)

Bonds	Angle	Bonds	Angle
O(22)—Sn—O(23′)	80.7(1)	O(11)—Sn—O(23′)	80.2(1)
O(22)—Sn—O(21′)	69.5(1)	O(12′)—Sn—O(22)	77.7(1)
O(21′)—Sn—O(13′)	136.3(1)	O(12′)—Sn—O(21′)	83.1(1)
O(13′)—Sn—O(23′)	76.4(1)	O(12′)—Sn—O(13′)	119.1(1)
O(11)—Sn—O(22)	74.8(1)	O(12′)—Sn—O(23′)	77.4(1)
O(11)—Sn—O(21′)	103.8(1)	O(23′)—Sn—O(21′)	147.3(1)
O(11)—Sn—O(13′)	78.3(1)	O(22)—Sn—O(13′)	147.2(1)
O(23″)—Sn—O(13′)	84.8(1)	O(11)—Sn—O(12′)	146.9(1)
O(23″)—Sn—O(11)	142.9(1)	F(11′)—Sn—O(22)	122.3(1)
O(23″)—Sn—O(12′)	69.8(1)	F(11′)—Sn—O(21′)	75.1(1)
O(23″)—Sn—O(23′)	127.5(1)	F(11′)—Sn—O(13′)	64.2(1)
		F(11′)—Sn—O(23′)	134.8(1)
O(23″)—Sn—F(11′)	71.7(1)	F(11′)—Sn—O(11)	71.3(1)
O(23″)—Sn—O(21′)	67.3(1)	F(11′)—Sn—O(12′)	140.7(1)
O(23″)—Sn—O(22)	128.0(1)		
O(11)—S(1)—O(12)	113.3(2)	O(21)—S(2)—O(23)	115.0(2)
O(11)—S(1)—O(13)	114.5(3)	O(21)—S(2)—F(21)	105.0(2)
O(11)—S(1)—F(11)	104.3(3)	F(21)—S(2)—O(22)	103.8(2)
F(11)—S(1)—O(12)	103.3(3)	O(22)—S(2)—O(23)	110.7(2)
O(12)—S(1)—O(13)	115.0(2)	O(23)—S(2)—F(21)	103.5(2)
O(13)—S(1)—F(11)	104.7(3)	S(1)—O(11)—Sn	147.8(2)
O(21)—S(2)—O(22)	117.0(2)	S(2)—O(22)—Sn	142.7(2)

[a]Length of Sn.....O,F ≤ 3.424 Å.

[b]Symmetry operations: O(13′), $-x, -y, -z$; O(23′) $1 - x, -1/2 + y, 1/2 - z$; O(12′) $x, 1/2 - y, 1/2 + z$; O(23″) $-x, -1/2 + y, 1/2 - z$; O(21′) $-1 + x, y, z$; F(11′) $-1 + x, y, z$.

Mössbauer spectroscopy

A powdered absorber sample of $Sn(OSO_2F)_2$ containing approximately 10 mg cm^{-2} of ^{119}Sn was pressed into a 20 mm i.d. threaded Kel-F Mössbauer cell under an atmosphere of dried nitrogen. The ^{119}Sn spectrum was recorded with the absorber sample at 77 K in a Technology Systems cryostat. Cooling of the sample was maintained by 30 mbar of He exchange gas between the sample and the liquid N_2 reservoir. The source, $Ca^{119m}SnO_3$ (10 mCi, Amersham), was maintained at ambient temperature. An Elscint MFG-N-5 Mössbauer function generator, an Elscint MDF-N-5 driver/generator, and an Elscint MVT-4 velocity transducer operating in the constant-acceleration triangular-waveform mode were used. The transmitted radiation was detected by a NaI(Tl) (6.35 mm), scintillation counter (Harshaw), and the pulses fed through a Tennelec TC 211A linear amplifier to a CMTE Multichannel Data Processor (operating in the multiscaling mode), controlled by an IBM PC/AT microcomputer. The velocity scale was calibrated using a standard iron foil and a $^{57}Co/Rh$ source mounted on the reverse end of the transducer, calibration spectra are thus recorded without interruption of the drive sequence. The calibration spectra were computer fitted to give a linear velocity scale and folding point. Folded ^{119}Sn spectra were fitted using the program GMFP (8), using a Lorentzian line-shape approximation. All isomer shifts were referenced to $Ca^{119}SnO_3$ at ambient temperature.

Can. J. Chem. Downloaded from www.nrcresearchpress.com by 123.30.183.119 on 09/08/12
For personal use only.

^{119}Sn solid state and solution nmr measurements

The solid state ^{119}Sn nmr spectrum was obtained on a Varian VXR-300 spectrometer equipped with a Doty Scientific 7 mm standard probe. The spectrometer operated at a field of 7 T and at ^{119}Sn frequency of 111.702 MHz. The sample was packed in a sapphire rotor equipped with Kel-F endcaps. The magic angle spinning technique was used along with the following acquisition parameters: 90° ^{119}Sn pulse, 4 μs; recycle delay, 2 s; spinning speed, 3545 Hz. The reference was external $Sn(CH_3)_4$. A solution of $Sn(OSO_2F)_2$ in fluorosulfuric acid was prepared in a 10 mm precision nmr tube, and the ^{119}Sn nmr spectrum was run on a Bruker WM 250 spectrometer operating at a field of 5.872 T and at ^{119}Sn frequency of 93.276 MHz. The reference was external $Sn(CH_3)_4$.

Results and discussion

Description of the structure

The coordination around the Sn(II) atom is shown in Fig. 1 and a stereoscopic view of the unit cell is illustrated in Fig. 2. There are one tin atom and two crystallographically independent fluorosulfate groups in the asymmetric unit. It has previously been suggested that the ir spectrum of $Sn(OSO_2F)_2$ may be interpreted in terms of two non-equivalent SO_3F^- groups (1, 9). The structure consists of a three-dimensional network wherein each fluorosulfate group is bonded through its oxygens to three different tin(II) atoms. The Sn atom forms two short bonds to the oxygens O(22) and O(23)′ of lengths 2.338(3) and 2.350(3) Å and two longer ones to O(11) and O(12)′ of lengths 2.398(4) and 2.427(3) Å, respectively. The primary geometry about Sn can be described as AX_4E, disphenoidal, with the longer bonds in the axial positions and the lone pair presumably occupying one of the equatorial sites of a trigonal bipyramidal arrangement of five electron pairs in accordance with the VSEPR model (10). Because the lone pair occupies more space in the valence shell of the tin atom than the bond pairs, the O(11)—Sn—O(12)′ angle (146.9°) is less than 180° and the O(22)—Sn—O(23)′ angle (80.7°) is less than 120°. In $Sn(OSO_2F)$, the tin atom also forms two long bonds to the oxygens O(21)′ and O(13)′ of lengths 2.702(3) and 2.695(3) Å, respectively. Atom O(21)′ lies below and atom O(13)′ lies above the plane which is defined by atoms O(23)′, O(22), and Sn and at distances of 0.603(5) and 1.055(6) Å, respectively. These long Sn...O bonds complete a distorted octahedral, AX_4Y_2E (11), arrangement of oxygen atoms around tin. Two more long contacts, Sn...O(23)″ = 3.420(4) and Sn...F(11)′ = 3.319(4) Å, complete the environment of the Sn(II) ion. A least-squares plane defined by atoms O(11), Sn, O(12)′, O(23)″, and F(11)′ shows that the maximum displacement of any of these atoms from the mean plane is 0.182 Å. This is also shown by the sum of the angles O(11)—Sn—F(11)′ = 71.3°(1), F(11)′—Sn—O(23)″ = 71.7(1)°, O(23)″—Sn—O(12)′ = 69.8(1)° and O(11)—Sn—O(12)′ = 146.9(1)° which is 359.7(1)°. This geometry suggests that the Sn...O(23)″ and Sn...F(11)′ contacts bisect two of the XE edges of the disphenoid so that there is an approximately dodecahedral arrangement of oxygen atoms around the tin.

The AX_4E primary geometry found in $Sn(OSO_2F)_2$ has also been observed for a number of other compounds of Sn(II) coordinated by oxygen (Table 3). This well-defined geometry is consistent with the Sn—O bonds having substantial covalent character as was previously concluded from the vibrational spectrum (1). However, the Sn—O primary bonds in the present compound are longer than in the other compounds in Table 3 presumably because these bonds are more ionic. The two secondary bonds (average 2.70 Å) are considerably shorter than the sum of the van der Waals radii, which is 3.62 Å (16).

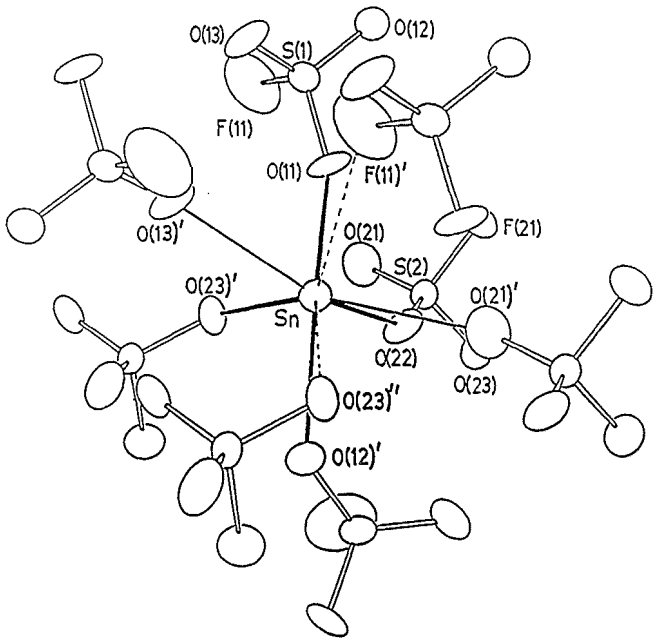


FIG. 1. The environment of the tin atom in $Sn(OSO_2F)_2$.

The fluorine atoms in the fluorosulfate groups were distinguished initially in the refinement on the basis of their significantly greater distances from the sulphur atoms and the final results indicate that these groups are ordered in the crystal. Potassium and ammonium fluorosulfates have ionic structures in which the SO_3F^- ions are disordered (17, 18) but in the more covalent structures of $Me_2Sn(OSO_2F)_2$ (19) and $I(OSO_2F)_2I$ (20) the fluorosulfate groups are ordered. The three S—O bond lengths are not equal and have the mean dimensions S(1)—O = 1.419(4) and S(2)—O = 1.435(3) Å. The S(1)—F(11) and S(2)—F(21) distances are 1.541(4) and 1.539(3) Å, respectively. The fluorosulfate groups deviate significantly from C_{3v} symmetry and this reduction in symmetry has been predicted earlier from spectroscopic results (1, 9). The angles O—S(1)—O, F—S(1)—O, O—S(2)—O, and F—S(2)—O have the mean values of 114.3(2)°, 104.1(3)°, 114.2(2)°, and 104.1(2)°, respectively, with the larger angles between the partially doubly bonded oxygens.

Mössbauer spectroscopy

The ^{119}Sn Mössbauer spectrum of $Sn(OSO_2F)_2$ was measured at 77 K. It consists of a single resonance in the tin(II) region, which has been successfully fitted to a small unresolved quadrupole splitting: $\delta = 4.19(1)$, $\Delta = 0.65(1)$, and $\Gamma = 0.97(2)$ mm s^{-1}. The present spectrum has a much narrower line width and is of considerably higher quality than our previously reported spectrum. This is a reflection of the improvements in instrumentation since 1971 and of the use of better counting statistics and fitting procedures. The unresolved quadrupole splitting may be attributed to a distortion of the environment of the tin nucleus from ideal cubic symmetry. The magnitude of the isomer shift ($\delta = 4.19$ mm s^{-1}) is high, showing that tin has considerable cationic character. However, the shift is smaller than that predicted for a "bare" tin(II) ion (21–23) or that observed for $Sn(SbF_6)_2$ ($\delta = 4.63$ mm s^{-1}) (24), $Sn(SbF_6)_2.2AsF_3$ ($\delta = 4.66$ mm s^{-1}) (25), or $Sn(II)[Sn(SO_3CF_3)_6]$ ($\delta = 4.69$ mm s^{-1}) (26), which appear

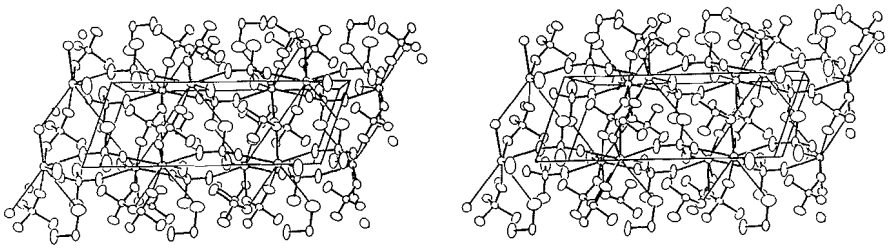


FIG. 2. A stereoscopic view of the unit cell of $Sn(OSO_2F)_2$.

TABLE 3. Comparison of Sn—O distances and angles in $Sn(OSO_2F)_2$ with other compounds having a similar primary geometry

	O_{eq}—Sn—O_{eq}		O_{ax}—Sn—O_{ax}		
Compound	Bond (Å)	Angle (deg)	Bond (Å)	Angle (deg)	Reference
$Sn(O_2CH)_2$	2.17(av.)	79.7(av.)	2.36(av.)	158.2(av.)	12
Sn_2OSO_4	2.19(av.)	78.6(av.)	2.44(av.)	150.6(av.)	13
$[Sn(PhCOCHCOMe)_2]$	2.13	94.7	2.29	150.4	14
$SnO_5C_4H_4$	2.19(av.)	80.7	2.38(av.)	152.9	15
$Sn(OSO_2F)_2$	2.34(av.)	80.7	2.41(av.)	146.9	This work

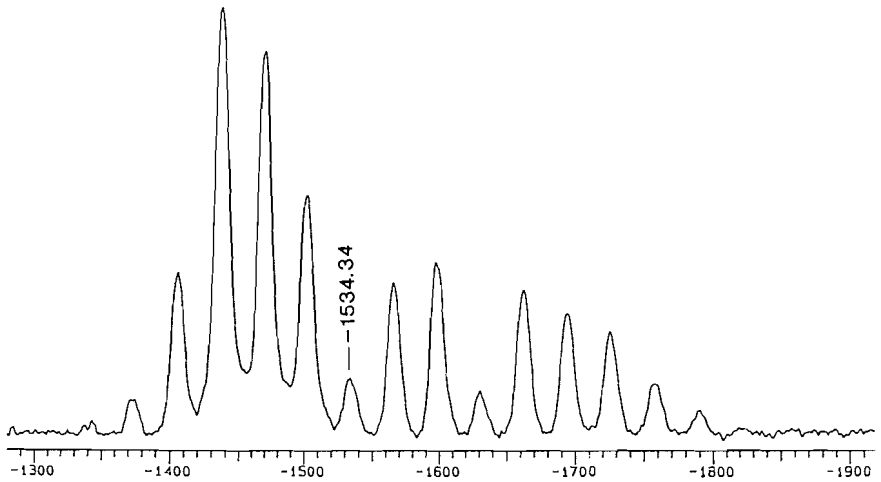


FIG. 3. ^{119}Sn SP-MAS spectrum of $Sn(OSO_2F)_2$; 90° ^{119}Sn pulse, 4 μs; recycle delay, 2 s; number of transients, 7620; spinning speed, 3545 Hz. The centre band is indicated.

to be highly ionic. Thus we conclude that the SnO bonds in $Sn(OSO_2F)_2$, while predominately ionic, have somewhat more covalent character than the SnF bonds in $SN(SbF_6)_2$.

Solid and solution-state nuclear magnetic resonance

The solid-state ^{119}Sn nmr spectrum of $Sn(OSO_2F)_2$ is shown in Fig. 3 with the centre band indicated. A comparison of the chemical shifts in the solid and in solution in HSO_3F is given in Table 4. No splitting of the ^{119}Sn resonance due to coupling with fluorine is observed in either the solid state or solution. It has been concluded from conductivity measurements that $Sn(OSO_2F)_2$ is partially ionized in solution in HSO_3F (27):

$$Sn(SO_3F)_2 \rightleftharpoons Sn(SO_3F)^+ + SO_3F^-$$

$$Sn(SO_3F)^+ \rightleftharpoons Sn^{2+} + SO_3F^-$$

The difference in the chemical shift between the solid state and the solution and its concentration dependence are consistent with this proposed ionization. The lack of any Sn—F coupling in solution as well as the observation of a single resonance in the ^{19}F nmr spectrum of a solution of $Sn(OSO_2F)_2$ in fluorosulfuric acid are also consistent with this ionization.

TABLE 4. ^{119}Sn nmr data for $Sn(OSO_2F)_2$

	Conc. M L^{-1}	δ, ppm[a]	$\Delta W_{1/2}$, Hz
Solid	—	−1534	ca. 1000
Solution in HSO_3F	0.34	−1628	125
	Saturated	−1636	85

[a]Relative to $Sn(CH_3)_4$.

The observation that there is only one tin signal in the ^{119}Sn solid-state nmr spectrum indicates that there is only one unique tin atom in the unit cell, and this is in accordance with the present X-ray structural analysis. The lack of an observable three-bond Sn—F coupling in the solid state is not surprising

Can. J. Chem. Downloaded from www.nrcresearchpress.com by 123.30.183.119 on 09/08/12
For personal use only.

in view of the ca. 1000 Hz line width of the Sn signal. Although not many examples are known, Harris *et al.* (28) list several Sn—F couplings in solution as being less than 30 Hz. A coupling of this magnitude would be unresolvable with the line width found for $Sn(OSO_2F)_2$ in the solid state.

Acknowledgments

We thank the Natural Sciences and Engineering Research Council of Canada for providing operating grants. Professor R. K. Harris and the Chemistry Department of Durham University are thanked for providing solid-state nmr facilities.

1. T. BIRCHALL, P. A. W. DEAN, and R. J. GILLESPIE. J. Chem. Soc. (A), 1777 (1971).
2. J. BARR, R. J. GILLESPIE, and R. C. THOMPSON. Inorg. Chem. **3**, 1149 (1964).
3. R. P. HUGHES, N. KRISHNAMACHARI, C. J. L. LOCK, J. POWELL, and J. TURNER. Inorg. Chem. **16**, 314 (1977); B. LIPPERT, C. J. L. LOCK, B. ROSENBERG, and M. ZVAGULIS. Inorg. Chem. **16**, 1525 (1977).
4. International tables for X-ray crystallography. Vol. II. Kynoch Press, Birmingham. 1974.
5. PSI. A local adaptation of the Nicolet R3 ψ-scan program.
6. G. M. SHELDRICK. SHELX: A program for crystal structure determination. University of Cambridge. 1976.
7. (*a*) J. M. STEWART. XRAY 76. Technical Report Tr-446, University of Maryland, College Park, MD. 1976; (*b*) J. M. STEWART and S. R. HALL. XTAL system of crystallographic programs, University of Maryland, College Park, MD. 1983; (*c*) G. DAVENPORT. LSQPL. 1989. XTAL 2.6. User's manual. *Edited by* S. R. Hall and J. M. Stewart. Universities of Western Australia and Maryland; (*d*) C. K. JOHNSON. ORTEP-II. Report ORNL-5138, Oak Ridge National Laboratory, Oak Ridge, TN. 1976.
8. K. RUEBENBAUER and T. BIRCHALL. Hyperfine Interact. **7**, 125 (1979).
9. C. S. ALLEYNE, K. O'SULLIVAN, and R. C. THOMPSON. Can. J. Chem. **52**, 336 (1974).
10. R. J. GILLESPIE. Molecular geometry. Van Nostrand Reinhold, London. 1972; R. J. GILLESPIE and I. HARGITTAI. The VSEPR model of molecular geometry. Allyn and Bacon, Boston. 1991.
11. J. F. SAWYER and R. J. GILLESPIE. Prog. Inorg. Chem. **34**, 65 (1986).
12. P. G. HARRISON and E. W. THORNTON. J. Chem. Soc. Dalton. 1274 (1978).
13. G. LUNDGREN, G. WERNFORS, and T. YAMAGUCHI. Acta Crystallogr. B**38**, 2357 (1982).
14. P. F. R. EWINGS, P. G. HARRISON, and T. J. KING. J. Chem. Soc. Dalton, 1455 (1975).
15. J. C. DEWAN, J. SILVER, R. H. ANDREWS, J. D. DONALDSON, and D. R. LAUGHLIN. J. Chem. Soc. Dalton, 368 (1977).
16. A. BONDI. J. Phys. Chem. **68**, 441 (1964).
17. K. O'SULLIVAN, R. C. THOMPSON, and J. TROTTER. J. Chem. Soc. (A), 2024 (1967).
18. K. O'SULLIVAN, R. C. THOMPSON, and J. TROTTER. J. Chem. Soc. (A), 1814 (1970).
19. F. H. ALLEN, J. A. LERBSCHER, and J. TROTTER. J. Chem. Soc. (A), 2507 (1971).
20. T. BIRCHALL, G. DENES, R. FAGGIANI, C. S. FRAMPTON, R. J. GILLESPIE, R. KAPOOR, and J. E. VEKRIS. Inorg. Chem. **29**, 1527 (1990).
21. O. C. KISTNER, V. JACCARINO, and L. R. WALKER. Proc. 2nd. Int. Conf. Mössbauer Effect. Saclay, France. 264 (1962).
22. J. LEES and P. A. FLINN. Phys. Lett. **19**, 186 (1965).
23. J. D. DONALDSON and B. J. SENIOR. J. Chem. Soc. (A), 1798 (1966).
24. T. BIRCHALL, B. FRLEC, D. GANTAR, D. HANZEL, and J. E. VEKRIS. J. Fluorine Chem. **27**, 61 (1985).
25. A. J. EDWARDS and K. I. KHALLOW. J. Chem. Soc. Chem. Commun. 51 (1984).
26. R. J. BATCHELOR, J. N. R. RUDDICK, J. R. SAMS, and F. AUBKE. Inorg. Chem. **16**, 1414 (1977).
27. S. P. MALLELA, S. T. TOMIC, K. LEE, J. R. SAMS, and F. AUBKE. Inorg. Chem. **25**, 2939 (1986).
28. R. K. HARRIS, J. P. KENNEDY, and W. MCFARLANE. NMR and the periodic table. *Edited by* R. K. Harris and B. E. Mann. Academic Press, New York/London. 1978. Chap. 10.

Can. J. Chem. Downloaded from www.nrcresearchpress.com by 123.30.183.119 on 09/08/12
For personal use only.

Sulfonyl esters 3. The formation of sulfone-sulfonates in the reactions of aryl methanesulfonates with sodium hydride

JAMES CLAYTON BAUM, KATHLEEN ANNE DURKIN, AND LAURA PRECEDO
Department of Chemistry, Florida Institute of Technology, Melbourne, FL 32901-6988, U.S.A.

AND

STACY BRIAN O'BLENES, JOHN EDWARD GOEHL, RICHARD FRANCIS LANGLER,[1]
GERALD KENDALL MACCORMACK, AND LANA LOUISE SMITH
Department of Chemistry, Mount Allison University, Sackville, N.B., Canada E0A 3C0

Received February 21, 1991

JAMES CLAYTON BAUM, KATHLEEN ANNE DURKIN, LAURA PRECEDO, STACY BRIAN O'BLENES, JOHN EDWARD GOEHL, RICHARD FRANCIS LANGLER, GERALD KENDALL MACCORMACK, and LANA LOUISE SMITH. Can. J. Chem. **69**, 2127 (1991).

Sodium hydride reductions of aryl methanesulfonates afford dimeric sulfone-sulfonate esters as well as products arising from SO bond rupture. SO bond rupture becomes more competitive as the LUMO energy of the sulfonate ester declines. Exploration of the chemistry of a sulfone-sulfonate ester revealed a complex novel reaction that resulted in the formation of, *inter alia*, a dichloromethanesulfonate ester and a trichloromethanesulfonate ester. The first successful approaches to the synthesis of the heretofore unknown trichloromethanesulfonates and dichloromethanesulfonates are reported.

Key words: sodium hydride reductions, sulfenes, sulfone-sulfonate esters.

JAMES CLAYTON BAUM, KATHLEEN ANNE DURKIN, LAURA PRECEDO, STACY BRIAN O'BLENES, JOHN EDWARD GOEHL, RICHARD FRANCIS LANGLER, GERALD KENDALL MACCORMACK et LANA LOUISE SMITH. Can. J. Chem. **69**, 2127 (1991).

Les réductions des méthanesulfonates d'aryles par l'hydrure de sodium fournissent les esters sulfone-sulfonates dimères ainsi que des produits provenant de la rupture de la liaison SO. La rupture de la liaison SO devient plus importante lorsque l'énergie des OM BV des sulfonates diminue. Une exploration de la chimie d'un ester sulfone-sulfonate a révélé l'existence d'une nouvelle réaction complexe qui conduit à la formation, entre autres choses, d'esters dichloro- et trichloro-méthanesulfonates. On rapporte les premières approches réussies à la synthèse de ces dichloro- et trichloro-méthanesulfonates qui étaient inconnus jusqu'à maintenant.

Mots clés : réductions par l'hydrure de sodium, sulfènes, esters sulfone-sulfonate.

[Traduit par la rédaction]

Introduction

Phenyl methanesulfonate induces the condensation of *p*-toluenethiol and primary alcohols to afford sulfides (1). In pursuit of a variation of that approach to sulfide synthesis, phenyl benzenethiosulfonate was allowed to react with alkoxide ions. The expected sequence involved transformation of the thiosulfonate into a sulfonate ester and a thiolate anion with sequential thiolate anion alkylation by the newly formed sulfonate ester. Equation [1] depicts the outcome of such an experiment.

$$[1] \quad CH_3OH + PhSO_2SPh \xrightarrow[HMPA]{NaH} PhSCH_3 + (PhS)_2$$

The formation of disulfide led us to explore the possibility that direct hydride reduction of the thiosulfonate was responsible for formation of some disulfide. Although sodium hydride is best known as a base, there is some precedent indicating that it may act as a reducing agent (2).

A brief investigation of phenyl benzenethiosulfonate reductions established that better reducing hydrides dramatically increase the yield of disulfide (see Table 1). In consonance with our previous experience (3), yields of benzenesulfinate anions (trapped with methyl iodide and isolated as methyl phenyl sulfone) tended to be low.

Reaction of phenyl benzenethiosulfonate with potassium metal afforded diphenyl disulfide in 23% yield, reminiscent of the sodium hydride result included in Table 1. This experiment suggests that sodium hydride may well react by the single electron transfer mechanism one would presume for potassium metal. Although it seemed reasonable to expect that sodium hydride should be able to reduce related sulfur functionalities, phenyl benzenesulfonate would not react with sodium hydride under our reaction conditions.

On the basis of this preliminary experience, we have undertaken a study of reactions between substituted aryl methanesulfonates and sodium hydride under the conditions of eq. [1].

TABLE 1. Yields of diphenyl disulfide and benzenesulfinate anions[a] isolated from reaction of phenyl benzenethiosulfonate with various hydrides in HMPA

Yield%)		
Diphenyl disulfide	Benzenesulfinate anions[a]	Hydride
32	36	NaH
58	21	$NaBH_4$
87	38	$LiAlH_4$

[a]Benzenesulfinate anions were isolated as phenyl methyl sulfone after trapping with methyl iodide.

Results and discussion

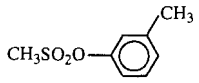
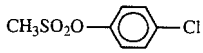
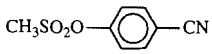
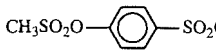
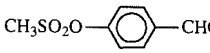
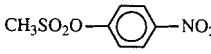
A series of aryl methanesulfonates **1***a*–**1***g* were prepared and allowed to react with sodium hydride in HMPA. Equation [2] depicts our results and Table 2 provides the product yields.

[1]Author to whom correspondence may be addressed.

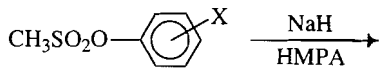
Printed in Canada / Imprimé au Canada

Can. J. Chem. Downloaded from www.nrcresearchpress.com by 123.30.183.119 on 09/08/12
For personal use only.

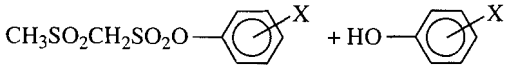
TABLE 2. Reaction of various methanesulfonates with sodium hydride in HMPA (eq. [2])

Methanesulfonate (**1**)		LUMO[a] eigenvalue (eV)	Yield[b] (%) Sulfone-sulfonate ester	Yield[b] (%) Corresponding phenol[c]
	(**1***a*)	+0.4030	**2***a* (54)	—
CH_3SO_2OPh	(**1***b*)	+0.3516	**2***b* (68)	43
	(**1***c*)	−0.0201	**2***c* (60)	47
	(**1***d*)	−0.5714	**2***d* (25)	76
	(**1***e*)	−0.6193	**2***e* (30)	64
	(**1***f*)	−1.0468	(0)	11
	(**1***g*)	−1.9839	(0)	55

[a]LUMO eigenvalues were calculated using the ZINDO program (*5b*).
[b]Starting methanesulfonates were completely consumed in these reactions.
[c]Yields calculated on the basis that 100% yield represents one mole of phenol obtained from 1 mole of starting methanesulfonate.

[2] 

1



2

Phenols cannot be formed exclusively by the processes that lead to the sulfone-sulfonate esters **2** because the phenolic yields are too high. An alternative pathway for phenol formation may involve single electron transfer (SET). SET from sodium hydride to the sulfonate esters **1** leading to products explicable through methylsulfonyl radicals and phenoxide anions would be consistent with our results on phenyl benzenethiosulfonate and previously reported results (3, 4, *5a*). In accord with this view, calculated sulfonate ester LUMO eigenvalues (Table 2) decline as observed yields of sulfone-sulfonate esters **2** decline. Thus, expected increases in facility for electron transfer correlate with increasing yields of sulfonate ester reduction products.

In contrast, the formation of a sulfone-sulfonate ester **2** seemed likely to begin with an acid–base step in which sodium hydride abstracts a proton from the methyl group of the starting methanesulfonate **1**. Skeletal assembly of the sulfone-sulfonate esters **2** may, thereafter, be imagined to proceed in three ways as shown in Scheme 1. Pathways *a* and *b* invoke sulfene intermediacy whereas pathway *c* envisions simple S_N2 attack of the carbanion at sulfonyl sulfur. Truce and Christensen (6) previously considered this dichotomy without adducing evidence for either possibility. When the reaction shown in eq. [2] was conducted on the methanesulfonate of phenol **1***b*, starting sulfonate ester was always completely consumed. Repetition of the reaction in the presence of an equivalent of sodium phenoxide gave the results shown in eq. [3].

[3] $CH_3SO_2OPh + NaOPh + NaH \xrightarrow{HMPA}$

1*b*

$CH_3SO_2CH_2SO_2OPh + CH_3SO_2OPh$

2*b* (3%) **1***b* (38%)

It seems unlikely that added phenoxide ion would impair the pathway *c* reaction (Scheme 1) whereas it would substantially reduce the amount of sulfene available for product formation by either pathway *a* or *b*. Furthermore, when the reaction shown in eq. [2] was repeated in the presence of an equivalent of phenyl benzenesulfonate, only **2***b* was isolated:

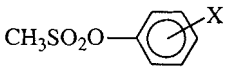
[4] $CH_3SO_2OPh + PhSO_2OPh + NaH \xrightarrow{HMPA}$

1*b*

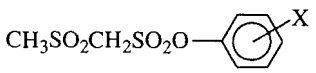
$PhSO_2CH_2SO_2OPh$

The failure of phenyl methanesulfonate carbanions to attack at sulfonyl sulfur in phenyl benzenesulfonate while the usual formation of **2***b* proceeded normally is inconsistent with the S_N2 process in pathway *c*. On this basis, we have dismissed pathway *c* from further consideration.

A brief computational study of sulfene[2] showed that both the



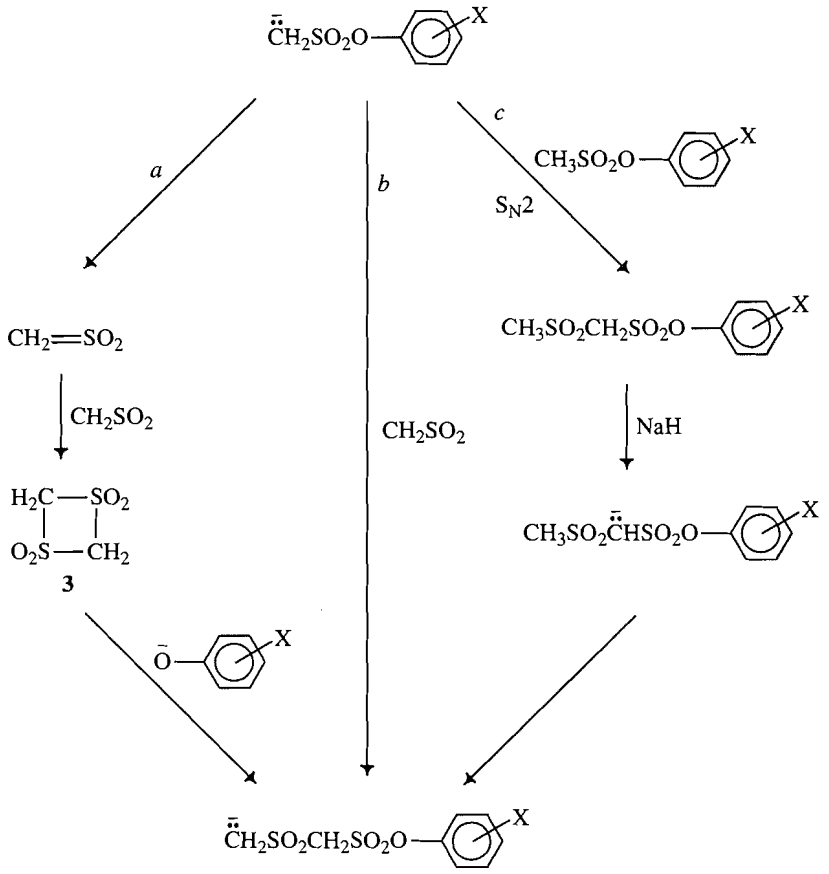
1*a* X = *m*CH_3
1*b* X = H
1*c* X = *p*Cl
1*d* X = *p*CN
1*e* X = *p*CH_3SO_2
1*f* X = *p*CHO
1*g* X = *p*NO_2



2*a* X = *m*CH_3
2*b* X = H
2*c* X = *p*Cl
2*d* X = *p*CN
2*e* X = *p*CH_3SO_2

[2]R. F. Langler and L. Precedo, unpublished results. Procedural details for MNDO computations were provided earlier, see ref. 7.

Can. J. Chem. Downloaded from www.nrcresearchpress.com by 123.30.183.119 on 09/08/12
For personal use only.



SCHEME 1

planar and the nonplanar energy-minimized structures assign the largest LUMO coefficient to carbon. This result suggests that carbon is the preferred soft base site in sulfene. It would seem unlikely that an α-sulfonate carbanion (soft base) would attack sulfene at sulfur (hard acid) as required by pathway *b*. Possible soft base attack at carbon in sulfenes has some precedent (8). The sulfene dimer might be $CH_3SO_2CHSO_2$ (9) or the dithiacyclobutane tetraoxide structure **3** (10*a*, *b*). Although Scheme 1 depicts the cyclic sulfene dimer structure, both **3** and $CH_3SO_2CHSO_2$ provide the necessary hard acid sites at sulfur to permit completion of the sulfone-sulfonate ester skeletal assembly by reaction with phenoxide ion (hard base). The importance of phenoxide ion exophilicity for efficient sulfene formation is demonstrated by results in eq. [5].

[5] $CH_3SO_2OCH_2CH(CH_3)_2 \xrightarrow[\text{HMPA}]{\text{NaH}}$ no reaction

This result[3] is consistent with the very large difference in pK_a's for a primary alcohol, CH_3OH (pK_a 29.0), and phenol (18.0) in DMSO, a solvent similar in nature to HMPA (10*c*). We conclude that (i) pathway *a* (Scheme 1) is the most reasonable rationale for sulfone-sulfonate ester **2** formation and (ii) sodium hydride can reduce selected sulfonate esters, probably by a SET mechanism.

[3]At the suggestion of a referee, isobutyl methanesulfonate was also treated with sodium hydride in the presence of sodium phenoxide. Again, no sulfone-sulfonate ester was formed. The product was a 5:3 mixture of isobutyl phenyl ether and unchanged methanesulfonate, respectively.

Subsequent efforts focused on the structure and reactivity of the sulfone-sulfonate esters **2**. Although sulfone-sulfonate esters have been known for some time (6, 9*d*, 11), this report includes details of the first mass spectrometric results for such compounds. The earlier studies (6, 9*d*, 11) dealt almost exclusively with the preparation of differently substituted systems: $ArCH_2SO_2CHXSO_3ArY$. Those systems which *do not* bear a π-acceptor on the ring show fragmentation, depicted in Scheme 2, strongly reminiscent of the Rämberg–Bäcklund process (12). Those systems which bear a π-acceptor appended to the ring do not undergo Rämberg–Bäcklund-like fragmentation but instead give $CH_3SO_2CH_2SO_2^+$ as the base peak of the spectrum. These divergent fragmentations are consistent with the requirement that the migrating phenoxy group be able to support substantial charge during the Rämberg–Bäcklund-like process.

The central methylene protons of sulfone-sulfonate esters **2** are so acidic that **2***b*, for example, can be quantitatively extracted into 2.5% aqueous sodium hydroxide solution (from chloroform solution) with a single extraction.[4] Consequently, before attempting nucleophilic substitution at sulfonyl sulfur, we have replaced the central protons with chlorine atoms:

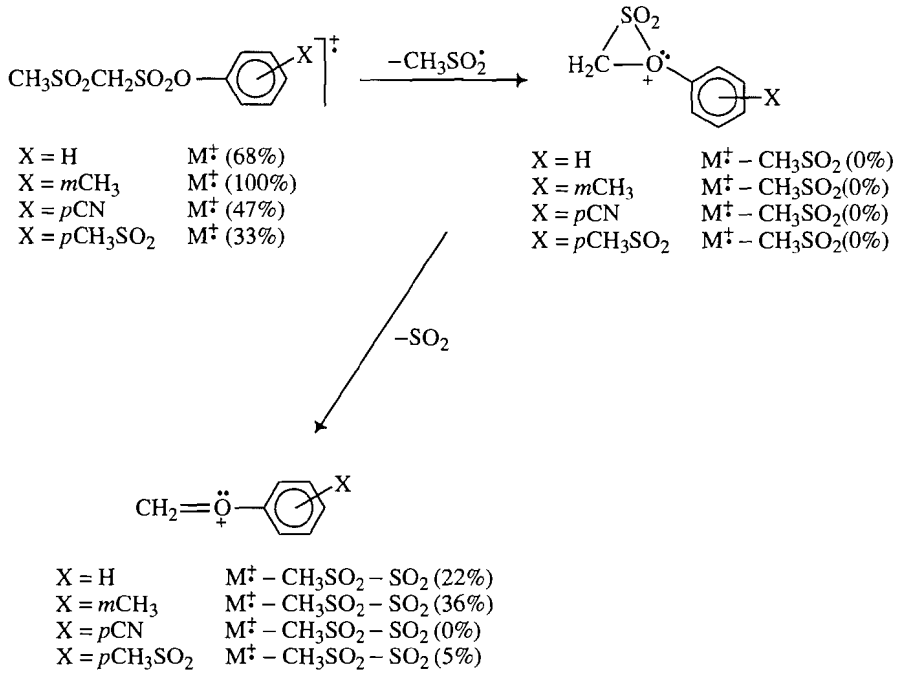
[6] $CH_3SO_2CH_2SO_2OPh \longrightarrow CH_3SO_2CCl_2SO_2OPh$

2*b* **3***b*

Reaction of **3***b* with two equivalents of sodium methoxide gave the following surprising results:

[4]Compare this result with the requirement that the analogous benzylic β-disulfone have four such extractions to remove the bulk of it from chloroform solution (13).

Can. J. Chem. Downloaded from www.nrcresearchpress.com by 123.30.183.119 on 09/08/12
For personal use only.



SCHEME 2

[7] $CH_3SO_2CCl_2SO_2OPh + 2CH_3ONa \longrightarrow$

3*b*

$CH_3SO_2CHClSO_2OPh + CH_3SO_2C(CH_3)ClSO_2OPh$

4 **5**

$+ CH_3SO_3Na + CHCl_2SO_2OPh + Cl_2CSO_2OPh$

6 **7**

The sodium salt of methanesulfonic acid was identified by comparison with authentic material obtained by reaction of ethyl methanesulfonate with sodium methoxide. The structures of the oily chlorosulfone-sulfonate esters **4** and **5** were assigned on the basis of spectroscopic data and independent synthesis. A brief exploration of structural dependence for this reaction involved subjecting the dichlorodisulfone **8** (14) to the same

[8] $CH_3SO_2CCl_2SO_2Ph + 2CH_3ONa \longrightarrow$

8

$CH_3SO_2C(CH_3)ClSO_2Ph$

9

reaction conditions. The crystalline chlorodisulfone **9** was fully characterized and independently synthesized. At this point, we were satisfied with the structural assignments for **4**, **5**, and **9**.

Apparently neither the dichloromethanesulfonate **6** nor the trichloromethanesulfonate **7** are previously known compounds. Attempts to prepare authentic samples by (i) reaction of phenol with the appropriate sulfonyl chloride in pyridine/triethylamine or (ii) reaction of sodium phenoxide with the appropriate sulfonyl chloride in acetone were unsuccessful. Both methods have been used to prepare other sulfonate esters (3).

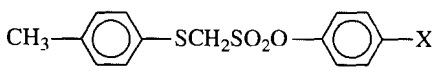
In an earlier study (14), we showed that sulfone-sulfides will furnish trichloromethyl sulfones upon exhaustive aqueous chlorinolysis (e.g., see eq. [9]).

[9] $pCH_3PhSCH_2SO_2Ph \xrightarrow[HOAc]{Cl_2/H_2O}$

$Cl_3CSO_2Ph + pCH_3PhSO_2Cl$

90%

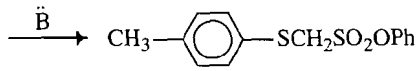
From this result, it seemed likely that a good yield of the trichloromethanesulfonate **7** might be obtained by chlorinolysis of an appropriate sulfide-sulfonate ester such as **10***a*. Since these



10*a* X = H
10*b* X = Cl

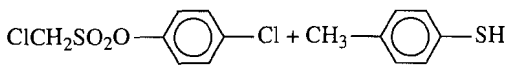
sulfide-sulfonate esters appear to be unknown compounds, we have selected **10***a* and **10***b* as targets.

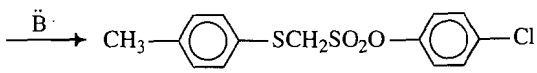
[10] $CH_3SO_2OPh + (CH_3C_6H_4S)_2$



10*a*

[11]

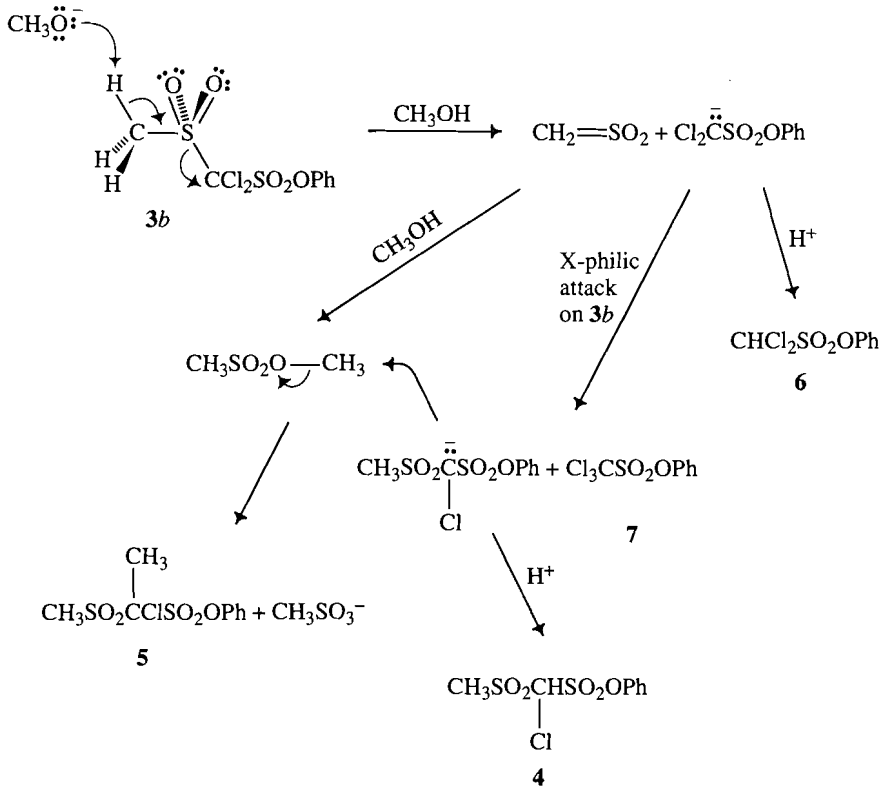




10*b*

Exhaustive chlorinolysis of **10***a* or **10***b* did indeed furnish the corresponding trichloromethanesulfonates in reasonable yields.

Can. J. Chem. Downloaded from www.nrcresearchpress.com by 123.30.183.119 on 09/08/12
For personal use only.



SCHEME 3

[12] $CH_3-C_6H_4-SCH_2SO_2O-C_6H_4-X \xrightarrow[HOAc]{Cl_2/H_2O}$

10*a* X = H
10*b* X = Cl

$Cl_3CSO_2O-C_6H_4-X + CH_3-C_6H_4-SO_2Cl$

The dichloromethanesulfonate **6** was obtained by thiolate anion induced dechlorination[5] of **7** as shown below:

[13] $Cl_3CSO_2OPh + 2PhSNa \longrightarrow CHCl_2SO_2OPh + (PhS)_2$

7 **6**

Since the dichloromethanesulfonate **6** is a new compound, we have converted it into the known phenyl chloromethanesulfonate by thiolate anion induced dechlorination.

Scheme 3 presents a proposed mechanism for the series of reactions leading to the product array in eq. [7]. Analogous processes would readily rationalize the formation of the chlorodisulfone **9** in eq. [8].

Conclusions

1. Aryl methanesulfonates react with sodium hydride to form sulfone-sulfonate esters and products arising from SO bond rupture.

2. SO bond rupture becomes more competitive as the sulfonate ester LUMO becomes lower in energy, thereby implicating SET as the most likely mechanism.

3. Reaction of a dichlorosulfone-sulfonate ester with methoxide ions has produced a dichloromethanesulfonate ester and a trichloromethanesulfonate ester. Neither functionality was previously known.

4. Rational synthesis of trichloromethanesulfonates through sulfide-sulfonate esters has been shown to be effective. Synthesis of the sulfide-sulfonate esters themselves requires further attention.

5. Thiolate anion induced dechlorination of trichloromethanesulfonates appears to be a satisfactory approach to the preparation of dichloromethanesulfonates.

Experimental

General

The ir spectra were recorded on a Perkin–Elmer 710B grating spectrophotometer. The ^1H nmr spectra were obtained on a Varian EM360L instrument using TMS as the internal standard. The ^{13}C nmr spectra were recorded on a Nicolet 360 N.B. highfield nmr spectrometer and are decoupled. Mass spectra were obtained on a Kratos MS 80 GC/MS. Melting points were determined on a Gallenkamp MFB-595 capillary melting point apparatus and are uncorrected.

Standard work-up

The crude reaction mixture was poured into water (100 mL) and concentrated hydrochloric acid (10 mL). The resultant mixture was washed with diethyl ether (three 100-mL aliquots). The combined wet ether layers were concentrated. The residue was poured into water (100 mL) and washed with diethyl ether (three 100-mL aliquots). The combined ether layers were dried ($MgSO_4$) and concentrated.

Hydride reductions of phenyl benzenethiosulfonate

The results presented in Table 1 were obtained in a similar manner. The reaction with sodium hydride will serve as the example.

A solution of phenyl benzenethiosulfonate (2.039 g, 8.15 mmol) in HMPA[6] (20 mL) was added dropwise to a suspension of sodium

[5]X-philic reactions have ample precedent in the chemistry of chlorosulfones (15*a*). For a review, see ref. 15*b*.

[6]HMPA (hexamethylphosphoramide) is toxic and carcinogenic (16).

Can. J. Chem. Downloaded from www.nrcresearchpress.com by 123.30.183.119 on 09/08/12
For personal use only.

Can. J. Chem. Downloaded from www.nrcresearchpress.com by 123.30.183.119 on 09/08/12
For personal use only.

hydride (0.388 g, 16.1 mmol) in HMPA (20 mL). Upon completion of the addition, the reaction mixture was stirred at ambient temperature for 1.5 h. A solution of methyl iodide (1.174 g, 8.27 mmol) in HMPA[6] (10 mL) was added dropwise to the reaction mixture. The reaction mixture was stirred at ambient temperature for 3 days.

Standard work-up afforded crude product, which was chromatographed on silica gel (200 g) employing a 3:2 mixture of carbon tetrachloride/methylene chloride (47 50-mL fractions). Thereafter the column was eluted with chloroform (50-mL fractions). Fractions 10–14 were combined and concentrated, yielding diphenyl disulfide (0.286 g, 1.31 mmol, 32%). Fractions 53–81 were combined and concentrated, furnishing phenyl methyl sulfone (0.459 g, 2.94 mmol, 36%).

Preparation of p-*methylsulfonylphenyl methanesulfonate* **1***e*

4-(Methylmercapto)phenol (5.005 g, 35.6 mmol) was converted to 4-(methylmercapto)phenyl methanesulfonate in standard fashion (3). Recrystallization from methanol afforded clean sulfide-sulfonate (6.115 g, 28.0 mmol, 79%, mp 75–77°C). The sulfide-sulfonate ester had ir ($CHCl_3$): 1380 and 1160 cm^{-1}; ^1H nmr ($CDCl_3$) δ: 7.26 (4H, s), 3.13 (3H, s), and 2.47 (3H, s).

A solution of 4-(methylmercapto)phenyl methanesulfonate (5.008 g, 22.9 mmol) in chloroform (100 mL) was cooled with an ice/water bath. *m*-Chloroperoxybenzoic acid (85%, 12.46 g) was added in small portions over 1 h. The reaction mixture was stirred at ambient temperature for 5 days. Chloroform (100 mL) was added and the resultant mixture washed with 2.5% NaOH (100-mL aliquots) until the aqueous pH remained basic. The organic layer was dried ($MgSO_4$) and concentrated. The residue was recrystallized from methanol yielding clean sulfone-sulfonate ester **1***e* (4.181 g, 16.7 mmol, 73%, mp 117.5–118.5°C). The sulfone-sulfonate ester **1***e* had ir ($CHCl_3$): 1380, 1360, 1150 cm^{-1}; ^1H nmr ($CDCl_3$) δ: 8.03 (2H, d, J = 9 Hz), 7.50 (2H, d, J = 9 Hz), 3.23 (3H, s), and 3.06 (3H, s). Anal. calcd. for $C_8H_{10}O_5S_2$: C 38.39, H 4.02; found: C 38.42, H 4.03.

The reaction of methanesulfonates **1**a–**1**g *with sodium hydride*

The appropriate methanesulfonate was reacted with sodium hydride in HMPA as outlined below for the cyanomesylate **1***d*. Final purification of products from reaction of **1***b* and **1***c* employed column chromatography. Results for these experiments are detailed in Table 2.

p-Cyanophenyl methanesulfonate **1***d* (1.005 g) in HMPA[6] (5 mL) was added dropwise to a suspension of sodium hydride (0.213 g) in HMPA (10 mL). Upon completion of the addition, the reaction mixture was stirred at ambient temperature for 1 h.

Standard work-up yielded a crude concentrate, which was dissolved in 2.5% sodium hydroxide solution (50 mL). The solution was acidified with concentrated hydrochloric acid (3 mL) and cooled with an ice/water bath. Crude *p*-cyanophenyl methylsulfonylmethanesulfonate **2***d* (0.173 g) was filtered off and the aqueous solution set aside. Recrystallization of crude sulfone-sulfonate ester from methanol afforded clean **2***d*.

The aqueous layer was concentrated to a final volume of 10 mL using hot benzene and a Dean–Stark trap. The aqueous concentrate was acidified with concentrated HCl (0.5 mL) and washed with diethyl ether (three 50-mL aliquots). The combined organic layers were dried ($MgSO_4$) and concentrated, yielding *p*-cyanophenol (0.458 g).

Recrystallized *m*-$CH_3PhOSO_2CH_2SO_2CH_3$ **2***a* (mp 63.9–64.3°C) had ir ($CHCl_3$): 1390, 1340, 1190, 1150, and 1120 cm^{-1}; ^1H nmr ($CDCl_3$) δ: 7.26 (4H, s), 4.70 (2H, s), 3.30 (3H, s), and 2.40 (3H, s); ^{13}C nmr ($CDCl_3$) δ: 149.01, 140.85, 129.93, 128.88, 122.50, 118.95, 67.11, 42.40, and 21.28; ms *m*/*e*: M^+ 264 (100%), 157 (12%), 121 (37%), and 108 (79%). Anal. calcd. for $C_9H_{12}O_5S_2$: C 40.89, H 4.57; found: C 40.95, H 4.58.

Recrystallized $PhOSO_2CH_2SO_2CH_3$ **2***b* (mp 73.9–74.8°C) had ir ($CHCl_3$): 1390, 1340, 1150 cm^{-1}; ^1H nmr ($CDCl_3$) δ: 7.43 (5H, s), 4.60 (2H, s), and 3.26 (3H, s); ^{13}C nmr ($CDCl_3$) δ: 148.98, 130.25, 128.11, 122.07, 66.84, and 42.31; ms *m*/*e*: M^+ 250 (68%), 157 (26%), 107 (22%), and 94 (100%). Anal. calcd. for $C_8H_{10}O_5S_2$: C 38.39, H 4.02; found: C 38.40, H 4.02.

Recrystallized *p*-$ClPhOSO_2CH_2SO_2CH_3$ **2***c* (mp 106.5–108°C) had ir ($CHCl_3$): 1395, 1345, 1150 cm^{-1}; ^1H nmr ($CDCl_3$) δ: 7.40 (4H, s), 4.70 (2H, s), and 3.33 (3H, s); ^{13}C nmr ($CDCl_3$) δ: 147.15, 133.94, 130.33, 123.49, 67.09, and 42.35; ms *m*/*e*: M^+ + 2 286 (59%), 284 (75%), 157 (37%), 143 (31%), 141 (48%), 130 (62%), and 128 (100%). Anal. calcd. for $C_8H_9ClO_5S_2$: C 33.74, H 3.18; found: C 33.84, H 3.10.

Recrystallized *p*-$NCPhOSO_2CH_2SO_2CH_3$ **2***d* (mp 158.4–159.2°C) had ir (KBr): 1390, 1330, 1160 cm^{-1}; ^1H nmr (CD_3COCD_3) δ: 7.96 (2H, d, J = 8 Hz), 7.60 (2H, d, J = 8 Hz), 5.46[7] (2H, s), and 3.26 (3H, s); ms *m*/*e*: M^+ 275 (48%), 157 (100%), 149 (90%), and 119 (53%). Anal. calcd. for $C_9H_9NO_5S_2$: C 39.26, H 3.29; found: C 39.30, H 3.34.

Recrystallized *p*-$CH_3SO_2PhOSO_2CH_2SO_2CH_3$ **2***e* (mp 160.7–161.8°C) had ir (KBr): 1390, 1315, 1150 cm^{-1}; ^1H nmr (CD_3COCD_3) δ: 8.23 (2H, d, J = 9 Hz), 7.83 (2H, d, J = 9 Hz), 5.63[7] (2H, s), 3.40 (3H, s), and 3.23 (3H, s); ms *m*/*e*: M^+ 328 (33%), 185 (5%), 172 (46%), and 157 (100%). Anal. calcd. for $C_9H_{12}O_7S_3$: C 32.91, H 3.68; found: C 32.93, H 3.58.

Preparation of $CH_3SO_2CCl_2SO_2OPh$ **3**b

The sulfone-sulfonate ester **2***b* (1.002 g, 4.01 mmol) was dissolved in glacial acetic acid (25 mL). Chlorine (ca. 200 mL/min) was bubbled into the solution for 30 min.

Chloroform (100 mL) was added and the resultant solution washed with 2.5% NaOH (three 100-mL portions). The organic layer was dried ($MgSO_4$) and concentrated. The product was recrystallized from methanol, giving clean dichlorosulfone-sulfonate ester **3***b* (0.899 g, 2.82 mmol, 71%, mp 67.1–69°C). **3***b* had ir ($CHCl_3$): 1420, 1370, 1220, 1180, 1150 cm^{-1}; ^1H nmr ($CDCl_3$) δ: 7.50 (5H, s) and 3.53 (3H, s); ms *m*/*e*: M^+ + 4 322 (9%), 320 (38%), 318 (51%), 179 (9%), 177 (36%), and 175 (52%). Anal. calcd. for $C_8H_8Cl_2O_5S_2$: C 30.10, H 2.52; found: C 30.14, H 2.57.

Reaction of $CH_3SO_2CCl_2SO_2OPh$ **3**b *with methoxide ions*

Sodium metal (0.080 g, 3.47 mmol) was dissolved in methanol (50 mL). The dichlorosulfone-sulfonate ester **3***b* (0.505 g, 1.58 mmol) was added and the reaction mixture stirred at ambient temperature for 24 h.

Water (50 mL) and 10% HCl (6 mL) were added and the resultant mixture washed with chloroform (three 100-mL aliquots). The combined chloroform layers were dried ($MgSO_4$) and concentrated, affording crude product (0.432 g).

The crude was chromatographed on silica gel (43 g), and 45-mL fractions were collected. Initially products were eluted with carbon tetrachloride (25 fractions).

Fractions 4–6 were concentrated and combined, yielding the trichloromethanesulfonate **7** (0.143 g, 0.52 mmol, 33%). The trichloromethanesulfonate **7** (bp 160°C/55 Torr; 1 Torr = 133.3 Pa) had ir ($CHCl_3$): 1400, 1120 cm^{-1}; ^1H nmr ($CDCl_3$) δ: 7.46 (s); ^{13}C nmr (CD_3COCD_3) δ: 151.81, 131.15, 129.02, 122.26, 100.92; ms *m*/*e*: M^+ + 4 278 (5%), 276 (12%), 274 (11%), 179 (7%),[8] 177 (37%),[8] 175 (56%),[8] 121 (32%), 119 (95%), and 117 (100%). Anal. calcd. for $C_7H_5Cl_3O_3S$: C 30.51, H 1.82; found: C 30.51, H 1.81.

Fractions 11–16 were concentrated and combined, yielding the dichloromethanesulfonate **6** (0.055 g, 0.23 mmol, 15%). The dichloromethanesulfonate **6** (bp 159°C/15 Torr) had ir ($CHCl_3$): 1400, 1150 cm^{-1}; ^1H nmr ($CDCl_3$) δ: 7.46 (5H, s) and 6.40 (1H, s); ^{13}C nmr (CD_3COCD_3) δ: 150.65, 131.14, 128.86, and 77.07; ms *m*/*e*: M^+ +6 244 (3%), 242 (16%), 240 (22%), 143 (31%),[8] and 141 (100%).[8] Anal. calcd. for $C_7H_6Cl_2O_3S$: C 34.87, H 2.50; found: C 34.89, H 2.60.

---

[7]The methylene signal for **2***b* (δ 4.60 in $CDCl_3$) shifts to δ 5.43 in CD_3COCD_3. The shift is accompanied by significant broadening of the signal.

[8]These ions may be rationalized by the Rämberg–Bäcklund-like process discussed in the text of this article (see Scheme 2).

Can. J. Chem. Downloaded from www.nrcresearchpress.com by 123.30.183.119 on 09/08/12
For personal use only.

Another 15 fractions (chloroform) were collected. Fractions 28–30 were combined and concentrated, affording the methylated chlorosulfone-sulfonate ester **5** (0.110 g, 0.36 mmol, 23%). The methylated sulfonate ester **5** had R_f 0.81 on analytical tlc plates developed with chloroform; ir ($CHCl_3$): 1380, 1345, 1160, and 1140 cm^{-1}; ^1H nmr ($CDCl_3$) δ: 7.53 (5H, s), 3.43 (3H, s), and 2.38 (3H, s). Fractions 32–37 were combined and concentrated, affording the chlorosulfone-sulfonate ester **4** (0.055 g, 0.19 mmol, 12%). The chlorosulfone-sulfonate ester had R_f 0,46 on analytical tlc plates developed with chloroform; ir ($CHCl_3$): 1400, 1350, 1140 cm^{-1}; ^1H nmr ($CDCl_3$) δ: 7.43 (5H, s), 5.63 (1H, s), and 3.33 (3H, s).

Preparation of authentic $CH_3SO_2CHClSO_2OPh$ 4

Sodium metal (0.036 g, 1.56 mmol) was dissolved in methanol (50 mL) and benzenethiol (0.176 g, 1.60 mmol) was added. The dichlorosulfone-sulfonate ester **3***b* (0.504 g, 1.58 mmol) was added and the mixture stirred at ambient temperature for 1 h.

Acidification with 10% HCl (3 mL) and routine extraction with chloroform gave a mixture of **3***b* and **4**. The crude product mixture was dissolved in chloroform solution (three 50-mL aliquots). The aqueous layer was acidified with concentrated hydrochloric acid (9 mL) and backwashed with chloroform (three 100-mL aliquots). The combined backwash layers were concentrated, affording the monochlorosulfone-sulfonate ester **4** (0.223 g, 0.78 mmol, 49%); **4** was chromatographed on silica gel, furnishing homogeneous product that was identical with **4** described under "Reaction of $CH_3SO_2CCl_2SO_2OPh$ **3***b* with methoxide ions" by double spotted tlc, ir, and nmr.

Preparation of $CH_3SO_2CH(CH_3)SO_2OPh$

Sodium metal (0.093 g, 4.04 mmol) was dissolved in methanol (50 mL) and the sulfone-sulfonate ester **2***b* (0.999 g, 3.99 mmol) added. Methyl iodide (1.716 g, 12.1 mmol) in methanol (10 mL) was added dropwise. The reaction mixture was stirred overnight at ambient temperature.

Water (60 mL) was added and the resultant mixture washed with chloroform (five 50-mL aliquots). The combined organic layers were dried ($MgSO_4$) and concentrated, affording a mixture of starting **2***b*, monomethylated sulfone-sulfonate ester, and dimethylated sulfone-sulfonate ester.

The crude was dissolved in chloroform (50 mL) and the resultant solution washed with 2.5% NaOH (one 50-mL aliquot), which completely removed **2***b* (0.194 g).

The organic layer was washed with an additional set of 2.5% NaOH extractions (15 50-mL aliquots). The combined aqueous layers were acidified with concentrated hdyrochloric acid (55 mL). The aqueous solution was concentrated with benzene and a Dean–Stark trap. The organic solution was dried ($MgSO_4$) and concentrated, affording monomethylated sulfone-sulfonate ester (0.356 g). The partially purified product was chromatographed on silica gel (40 g) employing chloroform elution. Homogeneous, chromatographed $CH_3SO_2CH(CH_3)SO_2OPh$ (0.267 g, 1.01 mmol, 25%) had ir ($CHCl_3$): 1380, 1335, 1145 cm^{-1}; ^1H nmr ($CDCl_3$) δ: 7.50 (5H, s), 4.73 (1H, q, J = 8 Hz), 3.26 (3H, s), and 1.96 (3H, d, J = 8 Hz); ms m/e: M^+ 264 (64%), 171 (23%), 121 (51%),[8] and 94 (100%).

Preparation of authentic $CH_3SO_2CCl(CH_3)SO_2OPh$ 5

$CH_3SO_2CH(CH_3)SO_2OPh$ (0.124 g, 0.47 mmol) was subjected to chlorinolysis and work-up as described under "Preparation of $CH_3SO_2CCl_2SO_2OPh$ **3***b*". Homogeneous **5** (0.128 g) had R_f 0.55 on analytical tlc developed with 3:1 chloroform/carbon tetrachloride. Spectra were identical with those described for **5** under "Reaction of $CH_3SO_2CCl_2SO_2OPh$ **3***b* with methoxide ions."

Reaction of $CH_3SO_2CCl_2SO_2Ph$ 8 with methoxide ions

The dichlorodisulfone **8** (0.500 g, 1.65 mmol) (14) was allowed to react as described for **3***b* under "Reaction of $CH_3SO_2CCl_2SO_2OPh$ **3***b* with methoxide ions".

Crude product was chromatographed on silica gel (50 g) employing carbon tetrachloride elution (50 mL fractions). Fractions 18–24 were concentrated and combined, affording trichloromethyl phenyl sulfone (0.016 g, 0.065 mmol, 4%). Fractions 35–38 were combined and concentrated, giving dichloromethyl methyl sulfone (0.009 g, 0.055 mmol, 3%). Fractions 39–44 provided a mixture of dichloromethyl methyl sulfone (0.022 g, 0.135 mmol, 8%) and the monochlorodisulfone **9** (0.079 g, 0.280 mmol, 17%). Fractions 45, 46 gave clean **9** (0.056 g, 0.198 mmol, 12%). A full description of **9** is provided under "Preparation of authentic $CH_3SO_2CCl(CH_3)SO_2Ph$ **9**".

Preparation of $CH_3SO_2CH_2SO_2Ph$

CrO_3 (13.500 g, 135 mmol) in glacial acetic acid (50 mL) was vigorously stirred at ambient temperature. $CH_3SO_2CH_2SPh$ (11.017 g, 54.5 mmol) (14) in glacial acetic acid (50 mL) was added dropwise. Upon completion of the addition, the reaction mixture was maintained at 90–100°C for 1 h.

Water (200 mL) was added and the resultant mixture washed with chloroform (three 100-mL portions). The combined organic layers were washed with 2.5% NaOH (100-mL aliquots) until the aqueous layer remained basic. The organic layer was dried ($MgSO_4$) and concentrated. Crude disulfone was recrystallized from methanol, furnishing clean product (7.477 g, 31.9 mmol, 59%, mp 150.1–152.1°C). The disulfone had ir ($CHCl_3$): 1340, 1140 cm^{-1}; ^1H nmr ($CDCl_3$) δ: 7.81 (2H), 7.55 (3H), 4.45 (2H, s), and 3.20 (3H, s). Anal. calcd. for $C_8H_{10}O_4S_2$: C 41.01, H 4.30; found: C 41.13, H 4.37.

Preparation of authentic $CH_3SO_2CCl(CH_3)SO_2Ph$ 9

$CH_3SO_2CH_2SO_2Ph$ (3.019 g, 12.9 mmol) was methylated as described for **2***b* under "Preparation of $CH_3SO_2CH(CH_3)$ SO_2OPh". Crude product, which contained a mixture of starting disulfone and monomethylated product, was dissolved in chloroform (200 mL) and washed with 2.5% NaOH (eight 200-mL aliquots). The organic layer was dried (Na_2SO_4) and concentrated. The monomethylated disulfone was recrystallized from methanol, affording $CH_3SO_2CH(CH_3)SO_2Ph$ (1.886 g, 7.6 mmol, 59%, mp 103.7–105°C). The monomethylated disulfone had ir ($CHCl_3$): 1340, 1140 cm^{-1}; ^1H nmr ($CDCl_3$) δ: 8.15 (2H), 7.85 (3H), 4.46 (1H, q), 3.36 (3H, s), and 1.73 (3H, d).

$CH_3SO_2CH(CH_3)SO_2Ph$ (1.087 g, 4.38 mmol) was chlorinated as described under "Preparation of $CH_3SO_2CCl_2SO_2OPh$ **3***b*". Crude **9** was recrystallized from methanol (2×), affording impure **9** (0.986 g). Impure **9** (0.3 g) was spotted on three preparative tlc plates. Each plate was developed (2×) with chloroform). The large band centered at R_f 0.61 was scraped from each plate. The combined bands were covered with 10% methanol in chloroform (100 mL). The mixture was stirred at ambient temperature for 1 h and filtered (0.240 g, 64%). Clean disulfone **9** was recrystallized from methanol (0.101 g, mp 105.8–106.1°C). **9** had ir ($CHCl_3$): 1330, 1150 cm^{-1}; ^1H nmr ($CDCl_3$) δ: 7.96 (2H), 7.60 (3H), 3.40 (3H, s), and 2.20 (3H, s). Anal. calcd. for $C_9H_{11}ClO_4S_2$: C 38.22, H 3.92; found: C 38.45, H 3.90. The chlorodisulfone **9** obtained in this way was identical to **9** obtained from eq. [8] by ir, nmr, mp, and double spotted tlc.

*Preparation of p-CH_3-$PhSCH_2SO_2OPh$ 10*a

p-Tolyl disulfide (2.804 g, 11.4 mmol) in HMPA[6] (10 mL) was added to a suspension of sodium hydride (0.688 g, 28.6 mmol) in HMPA[6] (80 mL). Phenyl methanesulfonate **1***b* (2.342 g, 13.6 mmol) was added and the reaction mixture stirred at ambient temperature for 1 h 10 min.[9].

Standard work-up was augmented with a single washing of the organic layer with 2.5% NaOH (100 mL). The crude, so obtained, was chromatographed on silica gel (300 g) employing carbon tetrachloride (100-mL fractions) for elution. Fractions 85–113 were combined and concentrated, furnishing clean sulfide-sulfonate ester **10***a* (0.133 g, 0.452 mmol, 4%, mp 69.0–70.7°C). The sulfide-sulfonate ester had ir ($CHCl_3$): 1380, 1365, 1145 cm^{-1}; ^1H nmr ($CDCl_3$) δ: 7.30 (9H, m), 4.40 (2H, s), and 2.33 (3H, s); ms m/e: M^+ 294 (11%) and 137 (100%). Anal. calcd. for $C_{14}H_{14}O_3S_2$: C 57.11, H 4.79; found: C57.32, H 4.80.

[9]Reaction times are critical for preparations of sulfide-sulfonate esters.

Can. J. Chem. Downloaded from www.nrcresearchpress.com by 123.30.183.119 on 09/08/12
For personal use only.

Preparation of p-*chlorophenyl chloromethanesulfonate*

A solution of *p*-chlorophenol (17.278 g, 135 mmol) and triethylamine (13.75 g, 136 mmol) in dry pyridine (150 mL) was cooled with an ice/water bath. Chloromethanesulfonyl chloride (19.936 g, 135 mmol) (17) was added dropwise. The reaction mixture was stirred at ambient temperature for 7 days.

Chloroform (300 mL) was added and the resultant mixture washed with 5% HCl (100-mL aliquots) until the aqueous pH remained acidic. The organic layer was washed with 2.5% NaOH solution (150 mL), dried ($MgSO_4$), and concentrated. The residue was rectified at reduced pressure, yielding a dark brown liquid (19.70 g).

A sample of the brown liquid (3 g) was chromatographed on silica gel (50 g) employing carbon tetrachloride elution (100-mL aliquots). Fractions 4–14 were combined and concentrated and the residue distilled, furnishing colorless *p*-chlorophenyl chloromethanesulfonate (1.809 g, bp 140°C/1.4 Torr). The chloromethanesulfonate had ir ($CHCl_3$): 1395, 1180, and 1160 cm^{-1}; ^1H nmr ($CDCl_3$) δ: 7.36 (4H), 4.70 (2H, s); ms *m/e*: $M^{\cdot+}$ + 4 244 (5%), 242 (26%), 240 (37%), 143[8] (17%), 141[8] (51%), 129 (33%), and 127 (100%). Anal. calcd. for $C_7H_6Cl_3O_3S$: C 34.87, H 2.50; found: C 34.94, H 2.49.

Preparation of p-$CH_3PhSCH_2SO_2OPh$-*Cl*-p ***10****b*

p-Toluenethiol (0.413 g, 3.33 mmol) in HMPA[6] (5 mL) was added dropwise to a suspension of sodium hydride (0.077 g, 3.20 mmol) in HMPA[6] (5 mL). *p*-Chlorophenyl chloromethanesulfonate (0.685 g, 2.85 mmol) in HMPA (15 mL) was added dropwise and the reaction mixture stirred overnight.

Standard work-up provided crude product, which was chromatographed on silica gel (100 g) employing 1:1 carbon tetrachloride/methylene chloride for elution (100-mL fractions). Fractions 4–6 were combined and concentrated, giving impure **10***b* (0.359 g).

Impure **10***b* was rechromatographed on silica gel (50 g) employing carbon tetrachloride elution (50-mL fractions). Fractions 25–28 were combined and concentrated, affording sulfide-sulfonate ester **10***b* (0.244 g, 0.743 mmol, 26%). Recrystallized sulfide-sulfonate ester **10***b* had mp 74.6–75.2°C; ir ($CHCl_3$): 1380, 1360, 1170, 1150 cm^{-1}; ^1H nmr ($CDCl_3$) δ: 7.33 (8H, m), 4.40 (2H, s), and 2.33 (3H, s); ms *m/e*: $M^{\cdot+}$ + 2 330 (0.4%), 328 (1.2%), and 137 (100%). Anal. calcd. for $C_{14}H_{13}ClO_3S_2$: C 51.13, H 3.98; found: C 51.03, H. 4.00.

Preparation of phenyl trichloromethanesulfonate and p-*chlorophenyl trichloromethanesulfonate*

The appropriate sulfide-sulfonate ester **10***a* or **10***b* provided the corresponding trichloromethanesulfonate (see eq. [12]). The procedure is exemplified by the details provided below for the chlorinolysis of **10***b*.

The sulfide *p*-chlorophenyl sulfonate ester **10***b* (1.020 g, 3.10 mmol) was suspended in glacial acetic acid (25 mL) and water (5 mL). Chlorine (ca. 200 mL/min) was bubbled into the solution for 8 h. Ice/water cooling was deployed as necessary to keep the reaction temperature between 20 and 30°C.

Water (50 mL) and chloroform (100 mL) were added to the reaction mixture and the layers separated. The organic layer was washed with 2.5% w/v sodium hydroxide solution (two 50-mL aliquots), dried ($MgSO_4$), and concentrated. The crude was chromatographed on silica gel (100 g) employing carbon tetrachloride elution (100-mL aliquots).

Fractions 4–10 were combined and concentrated, affording clean *p*-chlorophenyl trichloromethanesulfonate (0.536 g, 1.74 mmol, 56%, bp 166–170°C/35 Torr). The trichloromethanesulfonate had ir ($CHCl_3$): 1410, 1150 cm^{-1}; ^1H nmr ($CDCl_3$) δ: 7.40 (s); ms *m/e*: $M^{\cdot+}$ + 8 316 (1%), 314 (3%), 312 (16%), 310 (26%), 308 (23%), 213 (5%),[8] 211 (16%),[8] 209 (17%),[8] 123 (6%), 121 (36%), 119 (80%), and 117 (100%). Anal. calcd. for $C_7H_4Cl_4O_3S$: C 27.12, H 1.30; found: C 27.16, H 1.20.

Fractions 17–24 were combined and concentrated, yielding *p*-toluenesulfonyl chloride (0.133 g, 0.700 mmol, 23%).

Chlorinolysis of **10***a* (0.961 g, 3.27 mmol) provided phenyl trichloromethanesulfonate **7** (0.580 g, 2.11 mmol, 65%), which was identical to **7** as described under "Reaction of $CH_3SO_2CCl_2SO_2OPh$ **3***b* with methoxide ions."

Preparation of phenyl dichlormethanesulfonate ***6***

Sodium metal (0.175 g, 7.61 mmol) was dissolved in methanol (100 mL). Benzenethiol (0.800 g, 7.27 mmol) was added to the reaction mixture. Phenyl trichloromethanesulfonate **7** (0.954 g, 3.48 mmol) was added and the reaction mixture stirred at ambient temperature for 1 h.

Water (100 mL) and 10% HCl (1 mL) were added and the resultant mixture washed with chloroform (three 50-mL aliquots). The combined organic layers were dried ($MgSO_4$) and concentrated. The residue was chromatographed on silica gel (200 g) employing 2:1 carbon tetrachloride/cyclohexane for elution (100-mL fractions). Fractions 18–50 were combined and concentrated, yielding clean phenyl dichloromethanesulfonate **6** (0.709 g, 2.95 mmol, 85%). The dichloromethanesulfonate **6** had bp 158–160°C/15 Torr; ir ($CHCl_3$): 1403, 1150 cm^{-1}; ^1H nmr ($CDCl_3$) δ: 7.46 (5H, s) and 6.50 (1H, s); ^{13}C nmr (CD_3COCD_3) δ: 150.65, 131.14, 128.86, 122.61, and 77.07; ms *m/e*: $M^{\cdot+}$ +4 244 (3%), 242 (15%), 240 (22%), 143 (31%),[8] 141 (100%).[8] Anal. calcd. for $C_7H_6Cl_2O_3S$: C 34.87, H 2.50; found: C 34.89, H 2.60.

Conversion of ***6*** *into phenyl chloromethanesulfonate*

Sodium metal (0.186 g, 8.08 mmol) was dissolved in methanol (100 mL) and benzenethiol (0.929 g, 8.44 mmol) added. The dichloromethanesulfonate **6** (1.010 g, 4.20 mmol) was added and the reaction mixture stirred at ambient temperature for 7 days.

Water (100 mL) and 10% HCl (1 mL) were added and the reaction mixture washed with chloroform (three 50-mL aliquots). The combined organic layers were dried ($MgSO_4$) and concentrated. The residue was chromatographed on silica gel (100 g) employing carbon tetrachloride elution (100-mL fractions). Fractions 2–8 were concentrated and combined, affording diphenyl disulfide (0.611 g, 2.80 mmol, 66%). Fractions 13–22 were combined and concentrated, yielding unchanged dichloromethanesulfonate **6** (0.297 g, 1.23 mmol, 29%). Fractions 35–53 were combined and concentrated, providing phenyl chloromethanesulfonate, which was rectified at reduced pressure (0.116 g, 0.56 mmol, 13%, bp 122°C/1.7 Torr). This material was identical to that described under "Preparation of phenyl chloromethanesulfonate".

Preparation of phenyl chloromethanesulfonate

Phenyl chloromethanesulfonate was prepared following the procedure outlined for "Preparation of *p*-chlorophenyl chloromethanesulfonate". Phenyl chloromethanesulfonate had bp 122°C/1.7 Torr; ir ($CHCl_3$): 1390, 1190, 1170, 1140 cm^{-1}; ^1H nmr ($CDCl_3$) δ: 7.33 (5H, s) and 4.66 (2H, s).

Acknowledgements

The authors acknowledge some technical assistance from B. Webb and W. Bonafacia. Mass spectra were run by D. Drummond at the University of New Brunswick. The ^{13}C nmr spectra were obtained at the Atlantic Regional Magnetic Resonance Center, Dalhousie University, by M. Yeats. We are grateful to the Florida Institute of Technology and Mount Allison University for financial support.

1. R. F. Langler and N. A. Morrison. Can. J. Chem. **65**, 2385 (1987).
2. (*a*) M. Natsume, S. Kumadaki, Y. Kanda, and K. Kiuchi. Tetrahedron Lett. 2335 (1973); (*b*) J. Moreau and P. Caubere. Tetrahedron, **27**, 5741 (1971); (*c*) Y. L. Lee and W. D. Closson. Tetrahedron Lett. 381 (1974); (*d*) F. W. Swamer and C. R. Hauser. J. Am. Chem. Soc. **68**, 2647 (1946).
3. K. A. Durkin, R. F. Langler and N. A. Morrison. Can. J. Chem. **66**, 3070 (1988).
4. J. C. Baum, J. Bolhassan, R. F. Langler, P. J. Pujol and R. K. Raheja. Can. J. Chem. **68**, 1450 (1990).
5. (*a*) J. C. Carnahan, Jr., W. D. Closson, J. R. Ganson, D. A. Juckett, and K. S. Quaal. J. Am. Chem. Soc. **98**, 2526 (1976);

(*b*) J. RIDLEY and M. ZERNER. Theoret. Chim. Acta, **32**, 111 (1973).
6. W. E. TRUCE and C. W. CHRISTENSEN. J. Org. Chem. **35**, 3968 (1970).
7. J. L. GINSBURG and R. F. LANGLER. Can. J. Chem. **61**, 589 (1983).
8. (*a*) J. F. KING, E. G. LEWARS, and L. J. DANKS. Can. J. Chem. **50**, 866 (1972); (*b*) J. F. KING and T. DURST. Tetrahedron Lett. 585 (1963).
9. (*a*) J. CIABATTONI and M. CABELL. Tetrahedron Lett. 2693 (1968); (*b*) G. OPITZ, M. KLEEMAN, D. BÜCHER, G. WALZ, and K. RIETH. Angew. Chem. Int. Ed. Engl. **5**, 598 (1966); (*c*) S. THEA, G. GUANTI, A. R. HOPKINS, and A. WILLIAMS. J. Org. Chem. **50**, 5592 (1985); (*d*) A. SENNING. Synthesis, 211 (1973).
10. (*a*) G. OPITZ and H. R. MOHL. Angew. Chem. Int. Ed. Engl. **8**, 73 (1969); (*b*) E. BLOCK, E. R. COREY, R. E. PENN, T. L. RENKEN, P. F. SHERWIN, H. BOCK, T. HIRABAYASHI, S. MOHMAND, and B. SOLOUKI. J. Am. Chem. Soc. **104**, 3119 (1982); (*c*) F. G. BORDWELL. Acc. Chem. Res. **21**, 456 (1988).
11. Y. SHIROTA, T. NAGAI, and N. TOKURA. Tetrahedron, **25**, 3193 (1969).
12. (*a*) W. R. HARDSTAFF and R. F. LANGLER. Org. Mass. Spectrom. **10**, 215 (1975); (*b*) R. F. LANGLER, W. S. MANTLE, and M. J. NEWMAN. Org. Mass. Spectrom. **10**, 1135 (1975).
13. R. F. LANGLER, Z. A. MARINI, and J. A. PINCOCK. Can. J. Chem. **56**, 903 (1978).
14. D. G. KAY, R. F. LANGLER, and J. E. TRENHOLM. Can. J. Chem. **57**, 2185 (1979).
15. (*a*) R. F. LANGLER and J. A. PINCOCK. Can. J. Chem. **55**, 2316 (1977); (*b*) N. S. ZEFIROV and D. I. MAKHONKOV. Chem. Rev. **82**, 615 (1982).
16. N. I. SAX. Dangerous properties of industrial materials. Van Nostrand Rheinhold, New York. 1979. p. 721.
17. J. S. GROSSERT, W. R. HARDSTAFF, and R. F. LANGLER. Chem. Commun., 50 (1973).

Can. J. Chem. Downloaded from www.nrcresearchpress.com by 123.30.183.119 on 09/08/12
For personal use only.

Preparation of $Cr_2(CO)_8(NO)_2$ and X-ray crystal structures of $Cr_2(CO)_8(NO)_2$ and $Cr_2(CO)_9NO^-$. Stereochemical comparisons to $Cr_2(CO)_{10}^{2-}$

A. P. MASTERS, M. PARVEZ, AND T. S. SORENSEN[1]

The Department of Chemistry, University of Calgary, Calgary, Alta., Canada T2N 1N4

Received May 31, 1991

A. P. MASTERS, M. PARVEZ, and T. S. SORENSEN. Can. J. Chem. **69**, 2136 (1991).

$Cr_2(CO)_8(NO)_2$ (**1**) has been prepared and characterized, and the crystal structure determined, along with that of the related salt $Cr_2(CO)_9NO^-$ monoanion (**2**) as the CH_2Cl_2-solvated PPN^+ salt (where PPN^+ denotes the $(PPh_3)_2N^+$ monocation). Both **1** and **2** possess a metal–metal bonded structure analogous to that of $Mn_2(CO)_{10}$ and the electronically equivalent $Cr_2(CO)_{10}^{2-}$ dianion. Although $Cr_2(CO)_8(NO)_2$ (**1**) is slowly formed in poor yield from $Cr(CO)_4NO^-$ and $Cr(CO)_4NOBr$, it can be prepared in an almost quantitative yield by the one-electron oxidation of the monoanion with trityl hexafluorophosphate. The slowness of the former reaction makes $Cr(CO)_4NO^-$ useful as a two-electron reductant of organohalide bonds. Triclinic crystals of **1** incorporate two distinct molecules in the $P\bar{1}$ space group, although the geometries of each are almost identical. Triclinic crystals of monoanion (**2**) also belong to the $P\bar{1}$ space group. The Cr—Cr bond length is 3.00–3.02 Å in **1** and 2.995 Å in **2**, compared to 2.904 Å for the central Mn—Mn bond in $Mn_2(CO)_{10}$.

Key words: chromium nitrosyl, chromium carbonyl, X-ray crystal structure, metalate anion, metal–metal dimer.

A. P. MASTERS, M. PARVEZ et T. S. SORENSEN. Can. J. Chem. **69**, 2136 (1991).

On a préparé le $Cr_2(CO)_8(NO)_2$ (**1**), on l'a caractérisé et on a déterminé sa structure cristalline ainsi que celle du monoanion $Cr_2(CO)_9NO^-$ (**2**), sous la forme de sel du PPN^+ (où PPN^+ = monocation $(PPh_3)_2N^+$), solvaté par le CH_2Cl_2. Les composés **1** et **2** possèdent tous les deux une structure comportant une liaison métal–métal analogue à celle que l'on rencontre dans le $Mn_2(CO)_{10}$ et ils sont électroniquement équivalents au dianion $Cr_2(CO)_{10}^{2-}$. Même si le composé $Cr_2(CO)_8(NO)_2$ ne se forme que lentement et avec un faible rendement à partir du $Cr(CO)_4NO^-$ et du $Cr(CO)_4NOBr$, on peut le préparer avec un rendement pratiquement quantitatif par le biais d'une oxydation du monoanion par un électron avec l'hexafluorophosphate de trityle. La lenteur de la réaction précédente fait que le $Cr(CO)_4NO^-$ est utile comme réducteur à deux électrons des liaisons des halogénures organiques. Les cristaux tricliniques du composé **1** incorporent deux molécules distinctes dans le groupe d'espace $P\bar{1}$, même si les géométries de chacune de ces molécules sont pratiquement identiques. Les cristaux tricliniques du monoanion **2** appartiennent aussi au groupe d'espace $P\bar{1}$. La longueur de la liaison Cr—Cr est égale à 3,00–3,02 Å dans le composé **1** et à 2,995 Å dans le composé **2**; ces valeurs se comparent à la valeur de 2,904 Å que l'on observe pour la liaison centrale Mn—Mn du $Mn_2(CO)_{10}$.

Mots clés : nitrosyle de chrome, carbonyle de chrome, structure cristalline par rayons-X, anion métalate, dimère métal–métal.

[Traduit par la rédaction]

Introduction

In the reaction of $Mn(CO)_5^-$ with hindered α-bromo carbonyl compounds, one can get a facile two-electron reduction of the C—Br bond, resulting in $Mn(CO)_5Br$ and an enolate (1). However, a side product of this reaction is $Mn_2(CO)_{10}$, which appears to be formed from $Mn(CO)_5Br$ and $Mn(CO)_5^-$ in a reaction which can be competitive with the enolate-forming reaction.

In reactions of the isoelectronic anion $Cr(CO)_4NO^-$ (2) with α-bromo carbonyl compounds, similar complications have not been observed; however, we have occasionally seen traces of a very mobile light yellow TLC spot when analyzing crude reaction mixtures. Since $Mn_2(CO)_{10}$ behaves very similarly on TLC elution, there was a possibility that traces of the isoelectronic compound $Cr_2(CO)_8(NO)_2$ (**1**) were being observed in the former case. We were therefore interested in preparing and characterizing an authentic sample of $Cr_2(CO)_8(NO)_2$.

Several mixed monomeric chromium carbonyl nitrosyl complexes have been prepared under low-temperature photolysis conditions, including a possible $Cr(CO)_4NO$ species (3). Dimeric cyclopentadienylchromium carbonyl nitrosyl complexes are also known (4).

Results and discussion

Initial attempts to prepare **1** from $Cr(CO)_4NO^-$ and $Cr(CO)_4NOBr$ (reaction [1]) were beset by poor and variable yields along with slow reaction rates. Nevertheless, sufficient

[1] $PPN^+Cr(CO)_4NO^- + Cr(CO)_4NOBr \rightarrow Cr_2(CO)_8(NO)_2$ (generated *in situ*) $+ PPN^+Br^-$

information via mass spectral analysis was obtained to verify that **1** was indeed being formed and did in fact correspond to the unknown TLC spot referred to earlier. The fact that $Cr(CO)_4NOBr$ is unstable at room temperature and had to be generated *in situ* may partially account for the poor results. In the corresponding $W(CO)_4NOI$, the halide ligand has been successfully replaced (5) to generate W—M compounds, where M is a group IVA metal. However, $W(CO)_4NOI$ is a much more robust compound.

By analogy with manganese chemistry (6), the one-electron oxidation of $PPN^+Cr(CO)_4NO^-$ by carbocation salts was next projected as a route to $Cr_2(CO)_8(NO)_2$. Initial attempts to oxidize the monoanion with tropylium fluoroborate in THF solution did in fact produce $Cr_2(CO)_8(NO)_2$ (**1**) in some cases (together with bitropyl), but the reaction was unpredictable. Since tropylium fluoroborate is not very soluble in THF solution, reaction of the partly heterogeneous mixture was carried out at −80°C with slow warming to −20°C and then eventually to room temperature. Besides **1**, a second yellow metal-containing compound was also produced in quite variable yield; this compound was subsequently identified as $PPN^+Cr_2(CO)_9NO^-$ (denoted as PPN^+**2**) which was previously

[1]To whom correspondence should be addressed.

Can. J. Chem. Downloaded from www.nrcresearchpress.com by 123.30.183.119 on 09/07/12
For personal use only.

TABLE 1. Crystal data and structural parameters for $Cr_2(CO)_8(NO)_2$ (**1**)

Formula	$C_8N_2O_{10}Cr_2$	M_r	388.08
Space group	$P\bar{1}$	Crystal system	Triclinic
Cell dimensions:			
a, Å	7.898(1)	α, deg	78.07(2)
b, Å	13.516(4)	β, deg	73.00(2)
c, Å	13.966(4)	γ, deg	88.15(2)
V, Å^3	1394.29	Z	4
D_{cal}, Mg m^{-3}	1.849	$F(000)$	760
Radiation	Mo Kα	λ, Å	0.71069
μ, mm^{-1}	1.525	T, K	165
θ range, deg	2–25	Scan method	ω/2θ
ω-scan width, deg	(1.00 + 0.35 tan θ)	Crystal decay	8.2%
Variable scan speed, deg min^{-1}	(1.54–6.67)	Agreement on F's: R_f	0.10
Absorption correction:			
Minimum correction factor	0.683		
Maximum correction factor	1.383		
Total data measured	5403	Independent data	4888
Data used [$I > 3\sigma(I)$]	3118	No. of variables	397
Data:parameter ratio	7.9		
R, wR	0.061, 0.067		
$(\Delta/\sigma)_{max}$ in last cycle	<0.01		
Δρ, e Å^{-3} in final ΔF map	−1.2 to 1.0		

Can. J. Chem. Downloaded from www.nrcresearchpress.com by 123.30.183.119 on 09/07/12
For personal use only.

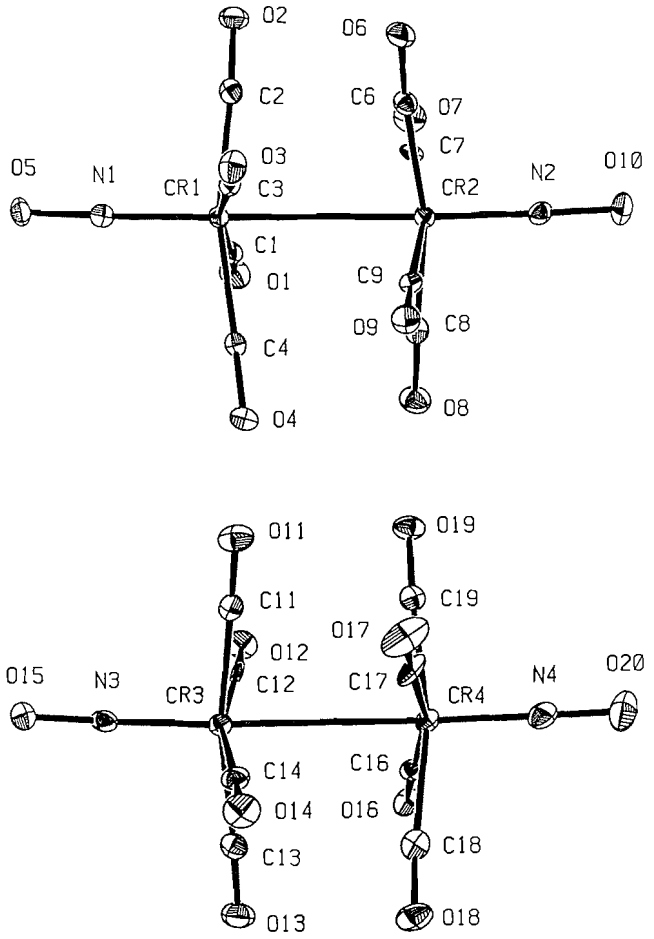


FIG. 1. ORTEP drawing (50% probability level) of $Cr_2(CO)_8(NO)_2$ (**1**). Two crystallographically independent molecules of **1** occupy the triclinic unit cell of $P\bar{1}$ symmetry.

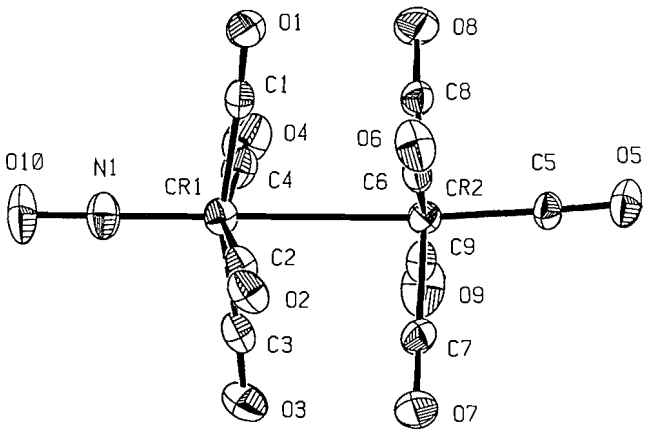


FIG. 2. ORTEP drawing (50% probability level) of the $Cr_2(CO)_9(NO)^-$ monoanion (**2**).

prepared in a rational route by Mantell and Gladfelter (2). Since this salt corresponds to a disproportionation-type process, which may in turn be associated with the heterogeneous nature of the reaction, we decided to use trityl hexafluorophosphate, which is more soluble in THF. In this case, the yield of $Cr_2(CO)_8(NO)_2$ (**1**) was good, the reaction was rapid, and none of the anionic dimer (**2**) was produced. Other reaction products are the well-known trityl radical dimer and (or) the peroxidation products of this, depending on how anaerobic the work-up is (7).

Relatively air-stable orange crystals of pure $Cr_2(CO)_8(NO)_2$ (**1**) were obtained from the crude reaction mixture by flash chromatography on silica gel. An infrared spectrum in *n*-hexane shows two main C—O stretches, at 1987 and 2023 cm^{-1}, along with a weak shoulder at 2032 cm^{-1}. The N—O stretch occurs at 1739 cm^{-1}. This simple infrared spectral pattern indicates a symmetrical structure, most probably with four equa-

TABLE 2. Crystal data and structural parameters for **2** as the CH_2Cl_2-solvated PPN^+ salt

Formula	$[C_9NO_{10}Cr_2][C_{36}H_{30}NP_2].0.25CH_2Cl_2$	M_r	945.91
Space group	$P\bar{1}$	Crystal system	Triclinic
Cell dimensions:			
a, Å	10.773(2)	α, deg	81.29(1)
b, Å	13.566(2)	β, deg	81.39(1)
c, Å	16.405(2)	γ, deg	88.24(1)
V, Å^3	2343.1	Z	2
D_{cal}, Mg m^{-3}	1.341		
Radiation	Mo Kα	λ, Å	0.71069
μ, mm^{-1}	0.590	T, K	295(1)
θ range, deg	2–24	Scan method	$\omega/2\theta$
ω-scan width, deg	(0.80 + 0.35 tan θ)	Crystal decay	None
Variable scan speed, deg min^{-1}	(1.25–4.00)	Agreement on F's: R_f	0.032
Absorption correction:	Ignored		
Total data measured	7991	Independent data	7337
Data used [$I > 3\sigma(I)$]	4992	No. of variables	491
Data:parameter ratio	10.2		
R, wR	0.0777, 0.0804		
$(\Delta/\sigma)_{max}$ in last cycle	<0.10		
$\Delta\rho$, e Å^{-3} in final ΔF map	0.80		

Can. J. Chem. Downloaded from www.nrcresearchpress.com by 123.30.183.119 on 09/07/12
For personal use only.

torial carbonyls on each chromium together with an apical nitrosyl on each chromium. Crystals of the dimer **1** suitable for X-ray diffraction were obtained by recrystallization from pentane.

Since the crystal structure of the PPN^+ salt of the isoelectronic $Cr_2(CO)_{10}^{2-}$ dianion has been reported (8), and since the isoelectronic $Cr_2(CO)_9(NO)^-$ monoanion (**2**) was also available, we obtained the X-ray structures of both **1** and **2** in order to compare the structural features of all three compounds.

An unsuccessful attempt was made to prepare $Fe_2(CO)_6(NO)_2$, isoelectronic with $Fe_2(CO)_8^{2-}$ and $Co_2(CO)_8$, from the reaction of $Fe(CO)_3NO^-$ and tropylium fluoroborate. Also, an attempted reaction between $Cr(CO)_4NO^-$ and $Mn(CO)_5Br$ did not yield the unknown mixed Cr—Mn dimer $ON(CO)_4Cr—Mn(CO)_5$.

$Cr_2(CO)_8(NO)_2$ (**1**) forms triclinic crystals with four molecules in a centrosymmetric unit cell. The two crystallographically independent molecules (Fig. 1) have a very similar D_{4d}-type $Mn_2(CO)_{10}$ geometry. A summary of the low temperature data collection is given in Table 1. The $Cr_2(CO)_9(NO)^-$ monoanion (**2**) as the PPN^+ salt also forms triclinic crystals with two formula species and two solvated methylene chloride molecules of one-quarter occupancy in the unit cell. An ORTEP drawing of the crystallographically independent $Cr_2(CO)_9(NO)^-$ monoanion (**2**), which is of approximate C_{4v} symmetry, is shown in Fig. 2. A summary of the data collection parameters is given in Table 2. Summaries of selected bond lengths and angles for **1** and **2** are given in Tables 3 and 4.

Both structures are similar to the prototype $Mn_2(CO)_{10}$ structure, containing an electron pair metal–metal bond and a staggered arrangement of the equatorial carbonyls. As expected, each nitrosyl ligand in **1** and **2** occupies an apical position. This same overall geometry is also found in the $Cr_2(CO)_{10}^{2-}$ dianion (8). As with $Mn_2(CO)_{10}$ and $Cr_2(CO)_{10}^{2-}$, each of the two sets of four equatorial carbonyls points slightly inward. In **1**, this inward bending from the perpendicular averages 5.85 and 6.2° for the two independent molecules in the unit cell, while for **2**, the values are 8.3 and 2.7° for the one independent monoanion, with the largest distortion on the nitrosyl side. In $Mn_2(CO)_{10}$, the corresponding angle is about 3.5° while in $Cr_2(CO)_{10}^{2-}$ it is about 3°. The larger distortion in the apical NO ligand relative to the apical CO ligand is expected because of the greater metal electron back-donation associated with the nitrosyl ligand.

In the case of the $M(CO)_5$ fragment in the monoanion (**2**), or in the $Cr_2(CO)_{10}^{2-}$ dianion, this equatorial-belt CO distortion is accompanied by a significantly shorter apical M—CO bond length: of 1.81 Å vs. an average of 1.88 Å for the four M—$C_{eq}O$ bond distances in **2**, as compared to 1.84 vs. 1.87 Å in the dianion (8). In the dinitrosyl complex (**1**), the equatorial M—C bond lengths average to 1.93 and 1.94 Å in the two independent molecules (it is noteworthy that these distances are for 165 K vs. 295 K for the former structures). The M—NO bond lengths are virtually identical in **1** and **2**, as are the N—O bond lengths. The C—O bond lengths (apical vs. equatorial) in **2** are also the same within experimental error.

Finally, the Cr—Cr bond length is similar in all three cases, viz., 2.97 Å in the dianion, 2.995 Å in **2**, and 3.001 and 3.020 in the two crystallographically independent molecules of **1**. A comparison of the isoelectronic neutral complexes $Cr_2(CO)_8(NO)_2$, **1**, and $Mn_2(CO)_{10}$ (Mn—Mn = 2.9038(6) Å) (9, 10) shows a much larger difference.

A tentative identification of $Cr(CO)_4NO$ was made in a low-temperature matrix photochemical study (3). Cyclic voltammetric studies of $Cr(CO)_4NO^-$ and $Cr_2(CO)_8(NO)_2$ (**1**) are planned to test the lifetime of this species at room temperature.

Experimental

Preparation of $Cr_2(CO)_8(NO)_2$ (1)

The salt, $PPN^+Cr(CO)_4NO^-$, was prepared essentially as described by Mantell and Gladfelter (2). Under a nitrogen atmosphere in a Schlenk tube was added 0.250 g (0.34 mmol) of this salt and 2 mL of THF (purified over sodium-benzophenone ketyl). The solution was cooled to 0°C, and 0.133 g (0.34 mmol) of solid trityl hexafluorophosphate (Aldrich) was added. Upon being stirred for 10 min, the solution–suspension gradually changed color from red to brown and also formed a precipitate. Hexane (10 mL) was added, and the solution allowed to warm to room temperature. The resulting suspension

Can. J. Chem. Downloaded from www.nrcresearchpress.com by 123.30.183.119 on 09/07/12
For personal use only.

TABLE 3. Selected bond lengths (Å) for **1** and **2**

1		**2**	
Bond	Length	Bond	Length
Cr(1)—N(1)	1.698(8)	C(1)—O(1)	1.141(8)
Cr(1)—C(3)	1.92(1)	C(2)—O(2)	1.143(7)
Cr(1)—C(1)	1.93(1)	C(3)—O(3)	1.140(8)
Cr(1)—C(4)	1.93(1)	C(4)—O(4)	1.116(8)
Cr(1)—C(2)	1.94(1)	C(5)—O(5)	1.152(7)
Cr(1)—Cr(2)	3.001(3)	C(6)—O(6)	1.149(8)
Cr(2)—N(2)	1.690(9)	C(7)—O(7)	1.149(8)
Cr(2)—C(6)	1.92(1)	C(8)—O(8)	1.139(8)
Cr(2)—C(8)	1.93(1)	C(9)—O(9)	1.142(8)
Cr(2)—C(7)	1.96(2)	N(1)—O(10)	1.189(7)
Cr(2)—C(9)	1.96(1)	Cr(2)—Cr(1)	2.995(1)
O(1)—C(1)	1.14(1)	N(1)—Cr(1)	1.704(6)
O(2)—C(2)	1.14(2)	C(1)—Cr(1)	1.902(8)
O(3)—C(3)	1.16(1)	C(2)—Cr(1)	1.882(7)
O(4)—C(4)	1.13(2)	C(3)—Cr(1)	1.913(9)
O(5)—N(1)	1.18(1)	C(4)—Cr(1)	1.916(8)
O(6)—C(6)	1.15(1)	C(5)—Cr(2)	1.806(6)
O(7)—C(7)	1.10(2)	C(6)—Cr(2)	1.874(8)
O(8)—C(8)	1.15(1)	C(7)—Cr(2)	1.884(7)
O(9)—C(9)	1.11(2)	C(8)—Cr(2)	1.873(7)
O(10)—N(2)	1.18(1)	C(9)—Cr(2)	1.890(8)
Cr(3)—N(3)	1.69(1)		
Cr(3)—C(11)	1.90(1)		
Cr(3)—C(12)	1.90(1)		
Cr(3)—C(14)	1.95(2)		
Cr(3)—C(13)	1.96(1)		
Cr(3)—Cr(4)	3.020(3)		
Cr(4)—N(4)	1.68(1)		
Cr(4)—C(17)	1.91(1)		
Cr(4)—C(16)	1.95(1)		
Cr(4)—C(19)	1.96(1)		
Cr(4)—C(18)	1.96(1)		
O(11)—C(11)	1.16(1)		
O(12)—C(12)	1.14(2)		
O(13)—C(13)	1.13(1)		
O(14)—C(14)	1.14(2)		
O(15)—N(3)	1.18(1)		
O(16)—C(16)	1.14(1)		
O(17)—C(17)	1.15(2)		
O(18)—C(18)	1.12(2)		
O(19)—C(19)	1.10(2)		
O(20)—N(4)	1.18(1)		

TABLE 4. Selected bond angles for **1** and **2**

1		**2**	
Bonds	Angle	Bonds	Angle
N(1)—Cr(1)—C(3)	94.6(4)	N(1)—Cr(1)—Cr(2)	176.2(2)
N(1)—Cr(1)—C(1)	95.9(4)	C(1)—Cr(1)—Cr(2)	81.3(2)
N(1)—Cr(1)—C(4)	97.5(4)	C(1)—Cr(1)—N(1)	97.4(3)
N(1)—Cr(1)—C(2)	95.0(4)	C(2)—Cr(1)—Cr(2)	79.4(2)
N(1)—Cr(1)—Cr(2)	179.0(3)	C(2)—Cr(1)—N(1)	97.1(3)
C(3)—Cr(1)—C(1)	169.5(4)	C(2)—Cr(1)—C(1)	88.7(3)
C(3)—Cr(1)—C(4)	89.6(5)	C(3)—Cr(1)—Cr(2)	82.9(2)
C(3)—Cr(1)—C(2)	91.3(5)	C(3)—Cr(1)—N(1)	98.6(3)
C(3)—Cr(1)—Cr(2)	84.9(3)	C(3)—Cr(1)—C(1)	163.9(3)
C(1)—Cr(1)—C(4)	88.2(5)	C(3)—Cr(1)—C(2)	91.3(3)
C(1)—Cr(1)—C(2)	88.6(5)	C(4)—Cr(1)—Cr(2)	83.2(2)
C(1)—Cr(1)—Cr(2)	84.6(3)	C(4)—Cr(1)—N(1)	100.3(3)
C(4)—Cr(1)—C(2)	167.3(4)	C(4)—Cr(1)—C(1)	89.2(3)
C(4)—Cr(1)—Cr(2)	83.3(3)	C(4)—Cr(1)—C(2)	162.6(3)
C(2)—Cr(1)—Cr(2)	84.1(3)	C(4)—Cr(1)—C(3)	86.1(3)
N(2)—Cr(2)—C(6)	96.3(4)	C(5)—Cr(2)—Cr(1)	176.6(2)
N(2)—Cr(2)—C(8)	95.5(4)	C(6)—Cr(2)—Cr(1)	87.9(2)
N(2)—Cr(2)—C(7)	95.3(5)	C(6)—Cr(2)—C(5)	91.4(3)
N(2)—Cr(2)—C(9)	96.3(5)	C(7)—Cr(2)—Cr(1)	87.9(2)
N(2)—Cr(2)—Cr(1)	178.4(3)	C(7)—Cr(2)—C(5)	95.4(3)
C(6)—Cr(2)—C(8)	168.1(4)	C(7)—Cr(2)—C(6)	89.5(3)
C(6)—Cr(2)—C(7)	88.9(5)	C(8)—Cr(2)—Cr(1)	86.1(2)
C(6)—Cr(2)—C(9)	90.1(5)	C(8)—Cr(2)—C(5)	90.6(3)
C(6)—Cr(2)—Cr(1)	82.1(3)	C(8)—Cr(2)—C(6)	89.4(3)
C(8)—Cr(2)—C(7)	88.6(5)	O(1)—C(1)—Cr(1)	176.1(6)
C(8)—Cr(2)—C(9)	89.9(5)	O(2)—C(2)—Cr(1)	175.1(6)
C(8)—Cr(2)—Cr(1)	86.0(3)	O(3)—C(3)—Cr(1)	176.5(6)
C(7)—Cr(2)—C(9)	168.4(4)	O(4)—C(4)—Cr(1)	177.6(7)
C(7)—Cr(2)—Cr(1)	84.6(3)	O(5)—C(5)—Cr(2)	177.6(6)
C(9)—Cr(2)—Cr(1)	83.8(3)	O(6)—C(6)—Cr(2)	177.9(6)
O(5)—N(1)—Cr(1)	178.0(9)	O(7)—C(7)—Cr(2)	178.8(7)
O(10)—N(2)—Cr(2)	177.7(8)	O(8)—C(8)—Cr(2)	177.1(6)
O(1)—C(1)—Cr(1)	176.7(9)	O(9)—C(9)—Cr(2)	177.3(6)
O(2)—C(2)—Cr(1)	175.5(9)	O(10)—N(1)—Cr(1)	176.7(6)
O(3)—C(3)—Cr(1)	176.8(9)	C(8)—Cr(2)—C(7)	173.9(3)
O(4)—C(4)—Cr(1)	178.7(8)	C(9)—Cr(2)—Cr(1)	87.3(2)
O(6)—C(6)—Cr(2)	175.0(9)	C(9)—Cr(2)—C(5)	93.4(3)
O(7)—C(7)—Cr(2)	175.8(9)	C(9)—Cr(2)—C(6)	175.2(3)
O(8)—C(8)—Cr(2)	177(1)	C(9)—Cr(2)—C(7)	90.4(3)
O(9)—C(9)—Cr(2)	177.7(9)		

was filtered, the solid washed with a further 5 mL of hexane, and the combined yellow filtrate evaporated to yield a pale yellow solid. This mixture was flash chromatographed (CH_2Cl_2/silica, 1 cm × 25 cm column) to give 0.0676 g (0.17 mmol, 100%) of the title compound as the first eluted material, followed by several compounds derived from the trityl portion of the reaction. Trial reactions were initially conducted at −78°C, but the reaction is quite slow at this temperature.

Crystals of **1** suitable for X-ray analysis were obtained by recrystallization from pentane at low temperatures. Crystals of **1** decomposed at about 88°C in a melting point tube. Mass spectral analysis showed a molecular ion (M^+) at m/z = 388, with prominent fragment ions at 360 ($M - CO^+$), 332 ($M - 2CO^+$), 304 ($M - 3CO^+$), 220 ($Cr_2(CO)_2(NO)_2^+$), 192 ($Cr_2(CO)(NO)_2^+$), 162 ($Cr_2(CO)(NO)^+$), 160 ($Cr_2(CO)_2^+$), 134 (Cr_2NO^+), 132 (Cr_2CO^+), 104 (Cr_2^+), 80 ($CrCO^+$), 57, 56 ($Cr(NO)_2^{2+}$), 55 ($Cr(NO)(CO)^{2+}$). Compound **1** was also produced in 18% isolated yield (reaction [1]) in a reaction of 2,4-dibromo-3-pentanone, trimethylsilyl chloride, and two molar equivalents of $PPN^+Cr(CO)_4NO^-$ in methylene chloride solvent (carried out on a 0.14 mmol scale in a Schlenk tube with 2 mL of solvent), starting at −78°C and stirring for 1 h, allowing to warm to −15°C over 1 h, and then stirring a further 1 h.

Preparation of $Cr_2(CO)_9(NO)^-$ (2) as the PPN^+ salt

A suspension of 0.52 g (0.71 mmol) of $PPN^+Cr(CO)_4NO^-$, 0.12 g (0.68 mmol) of tropylium fluoroborate (Aldrich), and 4 mL of purified THF was stirred overnight at room temperature under a N_2 atmosphere and then left in a refrigerator for 4 days. Hexane (2 mL) was added, and the heterogeneous mixture was filtered to yield, after evaporation, a yellow oil. Most of this oil, which was hexane insoluble, was taken up in methylene chloride and flash chromatographed on silica gel; elution with methylene chloride gave 0.0443 g (0.048 mmol, 21%, based on the most favorable disproportionation stoichiometry) of an orange crystalline product. Crystals suitable for X-ray diffraction were obtained by recrystallization from 3:2 hexane – methylene chloride. A mass spectrum and ^1H NMR spectrum indicated that PPN^+ was present. An IR spectrum in methylene chloride showed C—O stretches at 1980 (sh), 1961, 1891, and 1863 cm^{-1}, with a possibly very weak band at 2059 cm^{-1}; an N—O stretching frequency was observed at 1670 cm^{-1}. When the X-ray crystal structure was solved, it became apparent that the anion was

Can. J. Chem. Downloaded from www.nrcresearchpress.com by 123.30.183.119 on 09/07/12
For personal use only.

TABLE 5. Fractional coordinates ($\times 10^4$) and equivalent U_{iso} ($\times 10^3$) for $Cr_2(CO)_8(NO)_2$ (**1**)

Atom	x/a	y/b	z/c	U_{iso}
Cr(1)	0.6456(2)	0.7518(1)	0.7830(1)	0.023(1)
Cr(2)	0.6795(2)	0.9717(1)	0.6815(1)	0.026(2)
Cr(3)	0.9772(2)	0.6414(1)	1.1273(2)	0.028(2)
Cr(4)	0.7133(2)	0.6585(1)	1.3287(2)	0.028(2)
O(1)	0.4046(10)	0.8201(6)	0.9717(7)	0.046(8)
O(2)	0.9624(10)	0.7963(6)	0.8549(6)	0.039(8)
O(3)	0.8831(11)	0.7148(6)	0.5758(7)	0.046(8)
O(4)	0.3226(9)	0.7542(5)	0.7040(6)	0.036(7)
O(5)	0.6248(9)	0.5410(5)	0.8802(6)	0.036(7)
O(6)	1.0743(10)	0.9292(6)	0.6085(7)	0.044(8)
O(7)	0.7273(11)	1.0106(6)	0.8805(7)	0.047(9)
O(8)	0.2762(10)	0.9791(6)	0.7742(7)	0.046(8)
O(9)	0.6205(10)	0.8968(6)	0.5002(7)	0.042(8)
O(10)	0.7277(11)	1.1809(6)	0.5801(8)	0.054(9)
O(11)	0.9484(10)	0.4150(6)	1.2208(7)	0.049(9)
O(12)	0.6487(10)	0.6334(6)	1.0576(6)	0.040(8)
O(13)	0.9715(10)	0.8740(6)	1.0676(7)	0.052(9)
O(14)	1.2566(11)	0.6594(7)	1.2380(8)	0.06(1)
O(15)	1.2266(10)	0.6104(6)	0.9406(7)	0.047(8)
O(16)	0.5454(10)	0.8148(6)	1.1913(6)	0.036(7)
O(17)	0.9309(14)	0.4963(7)	1.4227(9)	0.08(1)
O(18)	0.9609(11)	0.8313(7)	1.3260(8)	0.055(9)
O(19)	0.5036(11)	0.4874(6)	1.2978(6)	0.042(8)
O(20)	0.4665(13)	0.6672(7)	1.5228(8)	0.07(1)
N(1)	0.6304(10)	0.6273(6)	0.8400(7)	0.025(8)
N(2)	0.7046(11)	1.0953(7)	0.6232(7)	0.031(8)
N(3)	1.1240(11)	0.6248(6)	1.0164(9)	0.036(9)
N(4)	0.5666(13)	0.6647(7)	1.4418(9)	0.04(1)
C(1)	0.4953(13)	0.7978(8)	0.9003(9)	0.03(1)
C(2)	0.8484(14)	0.7820(8)	0.8243(9)	0.03(1)
C(3)	0.7962(13)	0.7314(8)	0.6534(10)	0.03(1)
C(4)	0.4428(13)	0.7539(7)	0.7319(8)	0.023(9)
C(6)	0.9252(14)	0.9407(8)	0.6382(9)	0.03(1)
C(7)	0.7105(13)	0.9928(8)	0.8102(12)	0.04(1)
C(8)	0.4272(15)	0.9747(8)	0.7415(9)	0.03(1)
C(9)	0.6410(13)	0.9218(8)	0.5669(10)	0.03(1)
C(11)	0.9525(13)	0.5006(9)	1.1847(9)	0.03(1)
C(12)	0.7674(14)	0.6346(8)	1.0878(8)	0.025(9)
C(13)	0.9719(14)	0.7893(9)	1.0922(10)	0.04(1)
C(14)	1.1511(15)	0.6523(8)	1.1990(11)	0.04(1)
C(16)	0.6072(13)	0.7552(8)	1.2406(10)	0.03(1)
C(17)	0.8539(17)	0.5583(9)	1.3806(10)	0.04(1)
C(18)	0.8763(15)	0.7672(9)	1.3239(10)	0.04(1)
C(19)	0.5837(15)	0.5490(8)	1.3057(9)	0.03(1)

2, a compound previously prepared by Mantell and Gladfelter (2). Stirring **1** in purified THF solution, overnight at 20°C under N_2, with $PPN^+BF_4^-$ did not produce any reaction, suggesting that **2** is not formed directly from **1**.

Crystal structure determination of ***1***

Accurate cell dimensions and a crystal orientation matrix were determined on an Enraf-Nonius CAD-4 diffractometer by a least-squares refinement of the setting angles of 25 reflections with θ in the range 10–15°. Intensity data were collected by the $\omega/2\theta$ scan method using variable scan speed (1.54–6.67° min^{-1}), scan width (1.00 + 0.35 tan θ)°, and monochromatized Mo Kα radiation in the range $2° < \theta < 25°$ with h 0 to 9, k −16 to 16, and l −16 to 16. Three reflections monitored every 2 h of exposure time decreased by 8.2%; data were corrected for decay by appropriate scaling. The intensities of 5403 reflections were measured, of which 3118 had $I > 3\sigma(I)$, where $\sigma^2 I = S + 2B + [0.04(S - B)]^2$ with S = scan count and B = time-averaged background count extended 25% on each side. Data were corrected for Lorentz-polarization effects and absorption

TABLE 6. Fractional coordinates ($\times 10^4$) and equivalent U_{iso} ($\times 10^3$) for $PPN^+Cr_2(CO)_9NO^- \cdot 0.25CH_2Cl_2$

Atom	x/a	y/b	z/c	s.o.f.	U_{iso}
Cr(1)	380(1)	1124(1)	1532(1)		64(1)
Cr(2)	874(1)	−596(1)	2822(1)		60(1)
P(1)	4143(1)	5908(1)	7788(1)		40(1)
P(2)	6540(1)	5198(1)	6974(1)		43(1)
O(1)	2852(6)	441(4)	623(3)		82(4)
O(2)	1890(5)	2195(4)	2534(3)		88(4)
O(3)	−2062(6)	1328(4)	2707(4)		93(4)
O(4)	−1004(6)	−410(5)	851(4)		117(5)
O(5)	1473(5)	−2361(4)	3997(3)		92(4)
O(6)	3543(5)	121(4)	2652(4)		100(4)
O(7)	89(7)	737(5)	4140(4)		115(5)
O(8)	1670(7)	−1765(4)	1408(4)		119(5)
O(9)	−1820(6)	−1233(5)	2908(4)		117(5)
O(10)	101(6)	2864(5)	315(4)		115(5)
N(1)	181(6)	2140(5)	813(4)		84(4)
N(2)	5534(4)	5975(3)	7298(3)		48(3)
C(1)	1920(7)	664(5)	979(4)		63(4)
C(2)	1307(6)	1758(5)	2186(4)		63(4)
C(3)	−1131(8)	1242(5)	2290(5)		72(5)
C(4)	−489(7)	139(6)	1116(4)		76(5)
C(5)	1218(6)	−1669(5)	3551(4)		62(4)
C(6)	2521(7)	−133(5)	2713(4)		67(4)
C(7)	376(7)	236(6)	3637(4)		71(5)
C(8)	1363(7)	−1301(5)	1928(4)		70(4)
C(9)	−812(7)	−971(5)	2864(4)		69(3)
C(11)	3975(3)	6806(3)	8490(2)		47(3)
C(12)	4713(3)	7661(3)	8298(2)		60(4)
C(13)	4516(3)	8410(3)	8801(2)		77(5)
C(14)	3582(3)	8304(3)	9495(2)		86(5)
C(15)	2844(3)	7449(3)	9686(2)		82(5)
C(16)	3041(3)	6701(3)	9183(2)		67(4)
C(21)	3741(4)	4717(3)	8390(2)		47(3)
C(22)	4284(4)	4441(3)	9112(2)		73(4)
C(23)	4064(4)	3496(3)	9575(2)		91(6)
C(24)	3302(4)	2827(3)	9315(2)		91(6)
C(25)	2759(4)	3104(3)	8593(2)		84(5)
C(26)	2978(4)	4049(3)	8130(2)		61(4)
C(31)	3017(3)	6237(3)	7093(2)		43(3)
C(32)	1734(3)	6181(3)	7389(2)		51(3)
C(33)	865(3)	6498(3)	6851(2)		64(4)
C(34)	1279(3)	6870(3)	6018(2)		72(4)
C(35)	2562(3)	6925(3)	5722(2)		70(5)
C(36)	3431(3)	6609(3)	6259(2)		54(3)
C(41)	7676(4)	4931(3)	7660(2)		50(3)
C(42)	7607(4)	5424(3)	8352(2)		64(4)
C(43)	8492(4)	5221(3)	8896(2)		88(5)
C(44)	9446(4)	4523(3)	8748(2)		95(6)
C(45)	9515(4)	4029(3)	8056(2)		92(6)
C(46)	8630(4)	4233(3)	7512(2)		70(4)
C(51)	7360(4)	5746(2)	5982(2)		50(3)
C(52)	7461(4)	6782(2)	5805(2)		60(4)
C(53)	8115(4)	7225(2)	5046(2)		71(4)
C(54)	8668(4)	6634(2)	4464(2)		73(5)
C(55)	8567(4)	5598(2)	4640(2)		76(5)
C(56)	7913(4)	5154(2)	5399(2)		68(4)
C(61)	5902(4)	4038(4)	6844(2)		54(4)
C(62)	5214(4)	4034(4)	6189(2)		76(5)
C(63)	4615(4)	3166(4)	6104(2)		122(8)
C(64)	4704(4)	2302(4)	6675(2)		129(9)
C(65)	5391(4)	2307(4)	7330(2)		102(6)
C(66)	5990(4)	3175(4)	7415(2)		70(5)
Cl(I)	4783(23)	838(19)	4654(16)	0.25	236(9)
Cl(2)	6378(28)	142(22)	4868(18)	0.25	281(12)
C(S)	5437(44)	453(34)	4233(29)	0.25	120(13)

[a]Atoms of the solvent molecule had 0.25 site occupancy factors. $U_{iso}(A^2)$-$[(8/3)\pi^2(U_{11} + U_{22} + U_{33})]$.

effects (DIFABS (11)), with absorption coefficients ranging from 0.683 to 1.383.

The structure was solved by direct methods. Refinement of the structure was by full-matrix least-squares calculations, initially with isotropic and finally with anisotropic temperature factors. Refinement converged with $R = 0.061$ and $wR = 0.067$. In the refinement cycles, weights were derived from the counting statistics. Scattering factors were those of Cromer and Mann (12), and allowance was made for anomalous dispersion (Cromer and Liberman (13)). A difference map calculated at the conclusion of the refinement had no chemically significant features. All computer programs used in this study were part of XTAL2.6 (Hall and Stewart (14)), and Fig. 1 was plotted with ORTEP II (15). A list of the final fractional coordinates of **1** is given in Table 5.[2]

Crystal structure determination of **2**

Accurate cell dimensions and a crystal orientation matrix were determined on an Enraf-Nonius CAD-4 diffractometer by a least-squares refinement of the setting angles of 25 reflections with θ in the range 10–15°. Intensity data were collected by the $\omega/2\theta$ scan method using variable scan speed (1.25–4.00° min^{-1}), scan width (0.80 + 0.35 tan θ)°, and monochromatized Mo Kα radiation in the range $2° < \theta < 24°$ with h 0 to 12, k −15 to 15, and l −18 to 18. Three reflections monitored every 2 h of exposure time showed insignificant variations. The intensities of 7991 reflections were measured, of which 4992 had $I > 3\sigma(I)$, where $\sigma^2 I = S + 2B + [0.04(S - B)]^2$ with S = scan count and B = time-averaged background count extended 25% on each side. Data were corrected for Lorentz polarization; an absorption correction was deemed unnecessary.

The structure was solved by direct methods. Refinement of the structure was by full-matrix least-squares calculations, initially with isotropic and finally with anisotropic temperature factors for the non-hydrogen atoms except for the solvent atoms, which had only partial occupancy and which were refined with isotropic temperature factors. At an intermediate stage in the refinement, a difference map revealed most of the H atoms which were included in the subsequent cycles at geometrically idealized positions (C—H 0.95 Å) with a fixed overall isotropic temperature factor; H atoms of the solvent molecule were ignored. Refinement converged with $R = 0.0777$ and $wR = 0.0804$. In the refinement cycles, weights were derived from the counting statistics. Scattering factors were those of Cromer and Mann (12) and Stewart, Davidson, and Simpson (16) with corrections for anomalous dispersion (Cromer and Liberman (13)). A difference map calculated at the conclusion of the refinement had no chemically significant features. The computer programs used in this study were SHELX'76 (17), and ORTEP II (15). A list of the final fractional coordinates of **2** is given in Table 6.[2]

[2]A complete set of structure factor listings, anisotropic thermal parameters, and hydrogen atom parameters is available for **1** and **2** and may be purchased from the Depository of Unpublished Data, Document Delivery, CISTI, National Research Council Canada, Ottawa, Ont., Canada K1A 0S2.

Acknowledgement

We thank the Natural Sciences and Engineering Research Council of Canada for generous financial support.

1. A. P. MASTERS and T. S. SORENSEN. Can. J. Chem. **68**, 492 (1990).
2. D. R. MANTELL and W. L. GLADFELTER. J. Organomet. Chem. **347**, 333 (1988).
3. S. K. SATIJA, B. I. SWANSON, O. CRICHTON, and A. T. REST. Inorg. Chem. **17**, 1737 (1978).
4. G. B. RICHTER-ADDO and P. LEGZDINS. Chem. Rev. **88**, 991 (1988) and references therein.
5. E. E. ISAACS and W. A. G. GRAHAM. J. Organomet. Chem. **99**, 119 (1975).
6. E. W. ABEL, M. A. BENNETT, R. BURTON, and G. WILKINSON. J. Chem. Soc. 4559 (1958).
7. H. LANKAMP, W. TH. NAUTA, and C. MACLEAN. Tetrahedron Lett. 249 (1968).
8. L. B. HANDY, J. K. RUFF, and L. F. DAHL. J. Am. Chem. Soc. **92**, 7312 (1970).
9. L. F. DAHL and R. E. RUNDLE. Acta Crystallogr. **16**, 419 (1963).
10. M. R. CHURCHILL, K. N. AMOH, and H. J. WASSERMAN. Inorg. Chem. **20**, 1609 (1981).
11. N. WALKER and D. STUART. Acta Crystallogr. A**39**, 158 (1983).
12. D. T. CROMER and J. B. MANN. Acta Crystallogr. A**24**, 321 (1968).
13. D. T. CROMER and D. LIBERMAN. J. Chem. Phys. **53**, 1891 (1970).
14. S. R. HALL and J. M. STEWART (*Editors*). XTAL 2.6 User's manual. Universities of Western Australia and Maryland. 1989.
15. C. K. JOHNSON. ORTEP II. Report ORNL-5138. Oak Ridge National Laboratory, TN, U.S.A. 1976.
16. R. F. STEWART, E. R. DAVIDSON, and W. T. SIMPSON. J. Chem. Phys. **42**, 3175 (1965).
17. G. M. SHELDRICK. SHELX'76, A program system for crystal structure determination. University of Cambridge, Cambridge, England. 1976.

Can. J. Chem. Downloaded from www.nrcresearchpress.com by 123.30.183.119 on 09/07/12
For personal use only.

High-resolution amplified spontaneous emission (ASE) gain spectroscopy to study excited state complexation

R. W. YIP[1] AND Y-X. WEN

Département de chimie, Université du Québec à Montréal, C.P. 8888, Succ. A, Montréal (Québec), Canada H3C 3P8

Received June 3, 1991

This paper is dedicated to Dr. Richard Norman Jones

R. W. YIP and Y-X. WEN. Can. J. Chem. **69**, 2142 (1991).

Weakly bound excited state complexes involving 7-diethylamino-4-methylcoumarin have been studied by ASE gain spectroscopy to explore the applicability of the method for studying excited state complexation. Comparative steady state spectrofluorometric and ASE gain measurements showed that ASE gain measurements are capable of giving information on excited state complexation of the laser dye but with greater ease and frequency resolution.

Key words: excited state complex, amplified spontaneous emission, laser gain, ASE gain spectroscopy.

R. W. YIP et Y-X. WEN. Can. J. Chem. **69**, 2142 (1991).

Dans le but d'explorer la champ d'application de la méthode pour l'étude de la complexation d'états excités, on a examiné des complexes d'états excités faiblement liés, impliquant la 7-diéthylamino-4-méthylcoumarine par spectroscopie du gain d'émissions spontanées amplifiées. Une comparaison des états stationnaires tels que mesurés par spectrofluorométrie et par le gain d'émissions spontanées amplifiées montre que ces dernières mesures peuvent donner de l'information sur la complexation de l'état excité de lasers á colorant; la mesure est plus facile et la résolution des fréquences est meilleure.

Mots clés : complexe d'état excité, émission spontanée amplifiée, gain de laser, spectroscopie du gain d'émission spontanée amplifiée.

[Traduit par la rédaction]

Introduction

Since the 1960's, spectrofluorimetry has been widely applied to study excited state molecular complexation (1). The systems studied include the biologically important indoles in polar solvents (2, 3), coumarin dyes in solvent mixtures (4), and *trans-n*-styrylphenanthrene isomers in *n*-hexane/amines (5). Highly sensitive, conventional spectrofluorimetric measurements on solution molecular complexes often lack spectral resolution; thus, in order to resolve the overlapping fluorescence bands into their components, extremely precise measurements and assumptions regarding the shapes of the component bands are necessary.

By contrast, the bands from amplified spontaneous emission (ASE) gain spectroscopy introduced by Silfvast and coworkers (6*a*, *b*), are intrinsically narrower than those of the corresponding fluorescence emission. Although almost exclusively used since the 1970's to study the fundamental characteristics of lasers (6*b*, *c*–10), ASE spectroscopy may be a useful spectroscopic technique to resolve normally heavily overlapping bands due to "free" and complexed dyes or dyes in heterogeneous environments. In a recent study of the dual ASE bands of 7-aminocoumarin dyes in different solvents, distinctly resolved bands (9) due to uncomplexed species and hydrogen-bonded complexes (10) were observed.

The objective of the present work is to explore the applicability of ASE gain spectroscopy to the study of excited state complexation. Towards this objective we have (i) established a relationship between a constant derived from ASE gain measurements and the Stern–Volmer constant for fluorescence quenching or the ground state complexation constant from uv/vis absorption study, and (ii) carried out ASE gain measurements on weakly bound complexes comprising excited state 7-diethylamino-4-methylcoumarin (coumarin-1) in solvent systems containing either dichloromethane or *n*-butyl acetate as cosolvents. In these solvent systems, the steady state fluorescence spectra show no or extremely small frequency shifts with concentrations of dichloromethane. The clearly resolved bands observed in the ASE gain spectra in the same systems demonstrate the superior frequency resolution of the method.

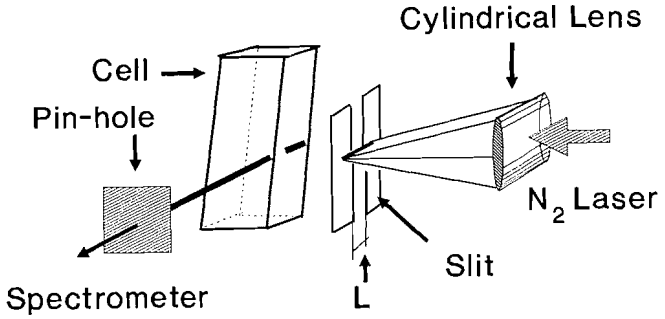


FIG. 1. ASE gain spectrometric system.

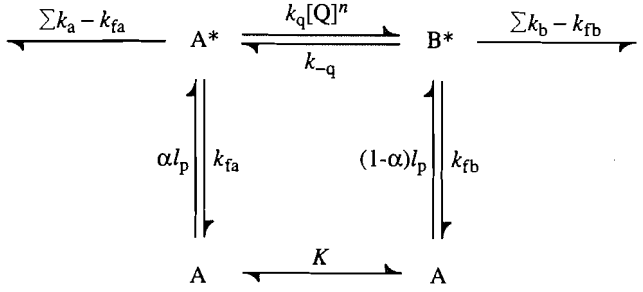
Experimental section

ASE gain studies used a PRA LN100 N_2 laser (60 μJ, pulse width ≈0.3 ns) for transverse excitation (2 in. focal length cylindrical quartz lens) of a dye solution contained in an upright 1-cm rectangular 4-window quartz fluorescence cell, and a JY HR 320 monochromator and a silicon diode array/OMA (EG&G 1412F/1461) system for detection of the emission. The transverse excitation geometry illustrated in Fig. 1 is as previously described (6, 10). For increased signal/noise ratio, at least 15 spectra measured under the same conditions were used to get the average spectrum. A pumping intensity of 100 kW was chosen for most of the studies by using a specific filter; this is slightly higher than the threshold pumping intensity for the laser dye. The ratio (R) of the average spectra with full cell width L and partial cell width (2/3)L ($R = I_L(\mathrm{WL})/I_{(2/3)L}(\mathrm{WL})$), has been used to transfer to its ASE gain spectrum by eq. [1] (8, 10):

$$[1] \qquad G(\mathrm{WL}) = (3/L)\ln\{1/2((R-1)+[(R-1)^2+4(R-1)]^{1/2})\}$$

[1]Author to whom correspondence may be addressed.

Can. J. Chem. Downloaded from www.nrcresearchpress.com by 123.30.183.119 on 09/08/12
For personal use only.



SCHEME 1

n-Butyl acetate (*n*BuOAc) (Fisher reagent) was refluxed over CaH_2 for 1 h and distilled. 1-Butanol (Fisher Certified A.C.S.), dichloromethane (CH_2Cl_2) (Anachemia spectro), and 2,2,4-trimethyl pentane (isooctane) (Matheson Coleman & Bell spectro) were used without further treatment. Preliminary studies of the ASE of coumarin-1 in untreated and CaH_2-treated dichloromethane gave, in contrast with *n*BuOAC, identical results. The 7-diethylamino-4-methylcoumarin (coumarin-1) (Exciton Corp.) was recrystallized from methanol–water and sublimed. Absorption and fluorescence spectra were measured with a Cary-2000 uv/vis spectrophotometer and a Perkin–Elmer-44 spectrofluorimeter, respectively.

Steady state fluorescence and ASE gain kinetics

A. Fluorescence quenching

For a normal two-component system, the ratio of fluorescence intensity at wavelength WL with and without quencher (I(WL) and I^0(WL) respectively), can be considered as the sum of two contributions by the free and complexed species (refer to Scheme 1) (10):

$$[2] \qquad I(\mathrm{WL})/I^0(\mathrm{WL}) = \Phi_a/\Phi_a^0 + \beta(\mathrm{WL})(\Phi_b/\Phi_b^0)$$

where Φ_i and Φ_i^0 (i = a or b) are the quantum yields with and without quencher (of free or complexed species respectively), and β(WL) is the ratio of the intensity in neat quencher and in neat solvent.

In the far blue region shown in Fig. 2, the contribution of the complex can be eliminated ($\beta(\mathrm{WL} \rightarrow 0)$. Thus, the intensity ratio in eq. [2] can be simply replaced by the quantum yield ratio of the free species, which should satisfy eq. [3] (10, 11):

$$[3] \qquad I(\mathrm{WL})/I^0(\mathrm{WL} = \Phi_a/\Phi_a^0 = (1-\alpha)/(1+K_{SV}[Q]^n)$$

where α is the fraction of light absorbed by ground state complex **B** and satisfies (10, 11)

$$[4] \qquad \alpha = K[Q]^m/(\sigma_{pa}/\sigma_{pb} + K[Q]^m)$$

where $\sigma_{pi}(WL_p)$ (i = a, b) are absorption cross sections of species **A** and **B**, WL_p is the pumping (excitation) wavelength, and K_{SV} is the Stern–Volmer constant defined by

$$[5] \qquad K_{SV} = k_q\tau_a/(1+k_{-q}\tau_b)$$

where τ_a, τ_b are the lifetimes of excited state free and complexed species defined as the reciprocal of $\sum k_a$ and $\sum k_b$, respectively, and K, k_q, and k_{-q} are the equilibrium and kinetic constants illustrated in Scheme 1; m and n are the stoichiometric constants of ground and excited state complexes, respectively.

B. Gain coefficient

The small-signal ASE gain is proportional to the population of the excited state as described in eq. [6] (6*c*, 8):

$$[6] \qquad g(\mathrm{WL}, t) = \sigma_e(\mathrm{WL})N(t) - g_{ai}(\mathrm{WL}, t)$$

where σ_e(WL) is the stimulated emission cross section, N is the population of the fluorescing state, and g_{ai} is the sum of possible losses due to the internal transitions between excited singlet–singlet and triplet–triplet states. In view of the location of the singlet–singlet absorption band (12) and the near-unity quantum yields of coumarin-1 in aprotic and moderately polar protic solvents (13), the gain of coumarin-1 in aprotic (isooctane, *n*BuOAc, and CH_2Cl_2) or moderately polar protic (*n*BuOH) solvents can be approximated by eq. [7]:

$$[7] \qquad g(\mathrm{WL}, t) = \sigma_e(\mathrm{WL})N(t)$$

The experimentally observable ASE gain in eq. [1] is the integral of eq. [7] with respect to the exposure time of the detector as expressed below:

$$[8] \qquad G(\mathrm{WL}) = \int_0^\infty g(\mathrm{WL}, t)\mathrm{d}t = \sigma_e(\mathrm{WL}) \int_0^\infty N(t)\mathrm{d}t$$

The ASE gain ratio of excited state species $\mathbf{B}^*$ and $\mathbf{A}^*$ can be represented by

$$[9] \qquad R_g = G_b(WL_b)/G_a(WL_a)$$
$$= (\sigma_{eb}/\sigma_{ea})\left(\int_0^\infty [\mathbf{B}^*(t)]\mathrm{d}t \Big/ \int_0^\infty [\mathbf{A}^*(t)]\mathrm{d}t\right)$$
$$= (\sigma_{eb}/\sigma_{ea}) \cdot R_p$$

where σ_{ei} (i = a, b) are stimulated emission cross sections of species $\mathbf{A}^*$ and $\mathbf{B}^*$, respectively, and R_p is the ratio of the integral populations of species $\mathbf{B}^*$ and $\mathbf{A}^*$.

C. Relationship between the gain ratio R_g *and* K_{SV} *or* K

The gain ratio (R_g) determined from ASE gain experiments is proportional to the ratio (R_p) of integral populations as described in eq. [9]. Based on the kinetics illustrated in Scheme 1, the differential populations of $\mathbf{A}^*$ and $\mathbf{B}^*$ with respect to time can be expressed by the following equations:

$$[10a] \qquad \mathrm{d}[\mathbf{A}^*]/\mathrm{d}t = (1-\alpha)I_p + k_{-q}[\mathbf{B}^*] - (\sum k_a + k_q[Q^n + \sigma_{ea}I_{ea})[\mathbf{A}^*]$$

$$[10b] \qquad \mathrm{d}[\mathbf{B}^*]/\mathrm{d}t = \alpha I_p + k_q[Q]^n[\mathbf{A}^*] - (\sum k_b + k_{-q} + \sigma_{eb}I_{eb})[\mathbf{B}^*]$$

where $[\mathbf{A}^*]$, $[\mathbf{B}^*]$ are the populations of excited states; σ_{ei} (i = a, b) are the stimulated cross sections of species $\mathbf{A}^*$ and $\mathbf{B}^*$; I_p is the pumping photon rate, and I_{ei} (I_p dependent) are the stimulated emission photon rates per area of species $\mathbf{A}^*$ and $\mathbf{B}^*$; and the remaining terms are defined in Scheme 1.

1. Pumping at threshold ($I_{ei} \rightarrow 0$, i = a, b)

Under transient conditions corresponding to excitation at t = 0 by a δ-function laser pumping of negligible duration (14), which is valid for the short duration N_2 laser pulse ($t_p \approx 300$ ps) in comparison to the lifetimes of fluorescent species ($t_i \approx 3$ ns), a zero pumping rate per area ($I_p = 0$) in the equation set [10] can be assigned for $t > 0$. Therefore, the equation set [10]

Can. J. Chem. Downloaded from www.nrcresearchpress.com by 123.30.183.119 on 09/08/12
For personal use only.

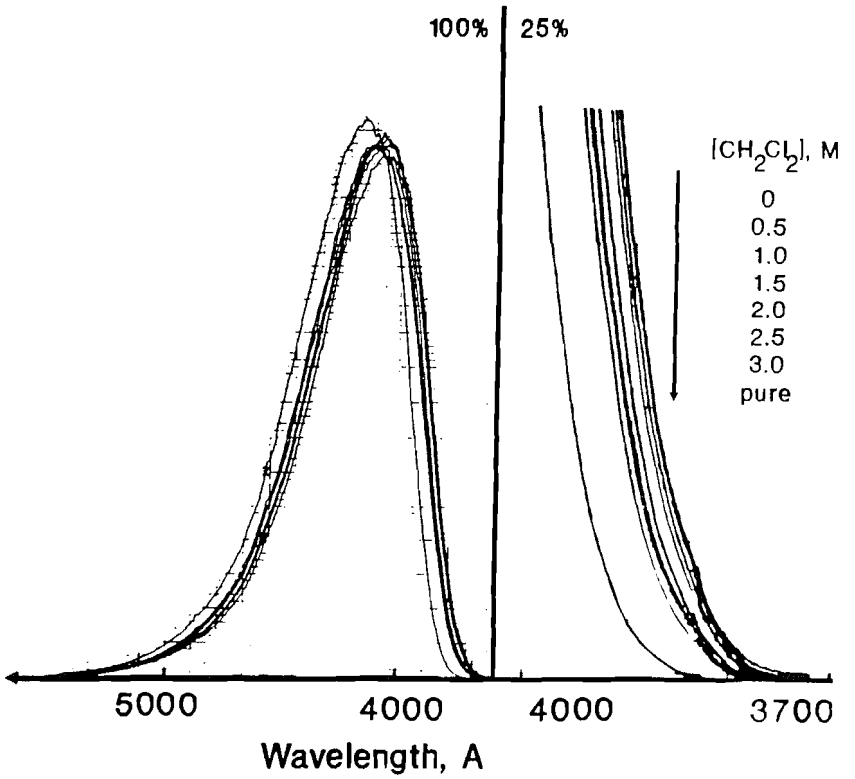


FIG. 2. Fluorescence spectra (excited at 361.2 nm) of coumarin-1 (0.035 mM) in *n*BuOAc containing different amounts of CH_2Cl_2 (0–3.0 M), and in pure CH_2Cl_2 at room temperature; right part is the amplified spectra from 3700 Å to 4000 Å.

can be simplified by eliminating the first terms and stimulated emissions (I_{ei}, i = a, b) as follows:

$$[11a] \quad d[\mathbf{A}^*]/dt = k_{-q}[\mathbf{B}^*] - k_1[\mathbf{A}^*]$$

$$[11b] \quad d[\mathbf{B}^*]/dt = k_q[Q]^n[\mathbf{A}^*] - k_2[\mathbf{B}^*]$$

where the coefficients are

$$[11c] \quad k_1 = \sum k_a + k_q[Q]^n$$

$$[11d] \quad k_2 = \sum k_b + k_{-q}$$

From eq. [11*a*], the population of species $\mathbf{B}^*$ can be represented by the population of species $\mathbf{A}^*$ as follows:

$$[12] \quad [\mathbf{B}^*] = (d\mathbf{A}^*]/dt + k_1[\mathbf{A}^*])/k_{-q}$$

Introducing the first-order derivative of eq. [12] with respect to time into eq. [11*b*], and replacing $[\mathbf{B}^*]$ in eq. [11] by [12], the simple second-order differential equation of $[\mathbf{A}^*]$ with respect to time is given by the following equation:

$$[13] \quad \frac{d^2[\mathbf{A}^*]}{dt^2} + B\frac{d[\mathbf{A}^*]}{dt} + C[\mathbf{A}^*] = 0$$

where $B = k_1 + k_2$, and $C = k_1k_2 - k_{-q}k_q[Q]^n$.

Since $B^2 - 4C = (k_1 - k_2)^2 + 4k_{-q}k_q[Q]^2 > 0$, the population of species $\mathbf{A}^*$ can be solved from eq. [13] (15):

$$[14a] \quad [\mathbf{A}^*] = C_1 \exp(S_1t) + C_2 \exp(S_2t)$$

where $C_{1,2}$ are the constants that can be found by considering the initial conditions, the parameters $S_{1,2}$ are

$$[14b] \quad S_1 = [-B^2 + (B^2 - 4C)^{1/2}]/2$$

$$[14c] \quad S_2 = [-B^2 - (B^2 - 4C)^{1/2}]/2$$

and B and C are as defined in eq. [13].

With eqs. [12] and [14], the population of species $\mathbf{B}^*$ can be expressed in the form of

$$[15] \quad [\mathbf{B}^*] = [(S_1 + k_1)C_1 \exp(S_1t) + (S_2 + k_1)C_2 \exp(S_2t)]/k_{-q}$$

Under the transient conditions, the initial populations of species $[\mathbf{A}^*(0)]$ and $[\mathbf{B}^*(0)]$ excited by a δ-function laser pulse at $t = 0$ can be presented by

$$[16a] \quad [\mathbf{A}^*(0)] = (1 - \alpha)I_0$$

$$[16b] \quad [\mathbf{B}^*(0)] = \alpha I_0$$

where I_0 is the total number of incident photons absorbed by both species.

By introducing the initial conditions (eqs. [16]) into eqs. [14] and [15], we get

$$[17a] \quad [\mathbf{A}^*(0)] = C_1 + C_2 = (1 - \alpha)I_0$$

$$[17b] \quad [\mathbf{B}^*(0)] = [(S_1 + k_1)C_1 + (S_2 = k_1)C_2]/k_{-q} = \alpha I_0$$

Replacing C_2 in eq. [17*b*] by eq. [17*a*], and dividing the

Can. J. Chem. Downloaded from www.nrcresearchpress.com by 123.30.183.119 on 09/08/12
For personal use only.

Can. J. Chem. Downloaded from www.nrcresearchpress.com by 123.30.183.119 on 09/08/12
For personal use only.

non-zero common factors of C_1 in both sides, the constant C_1 can be obtained:

$$[18a] \quad C_1 = [k_{-q}\alpha - (S_2 + k_1)(1 - \alpha)]I_0/(S_1 - S_2)$$

and the constant C_2 is given by

$$[18b] \quad C_2 = [(S_1 + k_1)(1 - \alpha) - k_{-q}\alpha]I_0/(S_1 - S_2)$$

Since the experimentally observable ASE gain ratio R_g is proportional to the ratio of the integral populations of species $\mathbf{B}^*$ and $\mathbf{A}^*$ as described in eq. [9], the integral populations of both species, which can be solved from eqs. [14], [15], and [18], are as follows:

$$[19a] \quad \int_0^\infty [\mathbf{A}^*]dt = \int_0^\infty \{C_1 \exp(S_1 t) + C_2 \exp(S_2 t)\}dt = (I_0/C)[\alpha k_{-q} + (1 - \alpha)k_2]$$

$$[19b] \quad \int_0^\infty [\mathbf{B}^*]dt = \int_0^\infty \{[(S_1 + k_1)C_1 \exp(S_1 t) + (S_2 + k_1)C_2 \exp(S_2 t)]/k_{-q}\}dt = (I_0/C)[(1 - \alpha)k_q[Q]^n + \alpha k_1]$$

Therefore, the gain ratio can be derived from eqs. [9] and [19] as

$$[20] \quad R_g = (\sigma_{eb}/\sigma_{ea})\frac{\alpha k_1 + (1 - \alpha)k_q[Q]^n}{(1 - \alpha)k_2 + \alpha k_{-q}}$$

where $k_{1,2}$ are defined in eq. [11*c*, *d*].

(i) Excited state complexation at $\alpha \rightarrow 0$ *(or* $K \rightarrow 0$*).* For the dynamic quenching process, the ASE gain ratio R_g in eq. [20] can be simply expressed by

$$[21a] \quad R_g = (\sigma_{eb}/\sigma_{ea})\frac{k_q[Q]^n}{\sum k_b + k_{-q}} = (\sigma_{eb}/\sigma_{ea})(\tau_b/\tau_a)K_{SV}[Q]^n = K_{ASE}[Q]^n$$

where $k_{1,2}$ have been replaced by the terms $\sum k_a + k_q[Q]^n$ and $\sum k_b + k_{-q}$, respectively. Hence the K_{ASE} obtained from ASE gain measurement is related to the Stern–Volmer constant K_{SV} (defined in eq. [5]) by

$$[21b] \quad K_{ASE} = (\sigma_{eb}/\sigma_{ea})(\tau_b/\tau_a)K_{SV}$$

where $\tau_i(\tau_i = 1/\sum k_i$, i = a, b) are lifetimes of species $\mathbf{A}^*$ and $\mathbf{B}^*$.

(ii) Ground state complexation only. By ignoring the excited state complexation ($k_q[Q]^n \ll \alpha \sum k_a$, $k_{-q} \ll (1 - \alpha)\sum k_b$), the ASE gain ratio can be obtained from eq. [20] by eliminating the terms with $k_q[Q]^n$ and k_{-q}, as expressed by the following equation:

$$[22a] \quad R_g = (\sigma_{eb}/\sigma_{ea}) \cdot \frac{\alpha \sum k_a}{(1 - \alpha)\sum k_b} = (\sigma_{eb}/\sigma_{ea})(\sigma_{pb}/\sigma_{pa})(\tau_b/\tau_a) \cdot K \cdot [Q]^m = K_{ASE}[Q]^m$$

where $\alpha/(1 - \alpha)$ has been replaced by the term of $(\sigma_{pb}/\sigma_{pa})K[Q]^m$ from eq. [4]. Therefore, the K_{ASE} constant obtained from ASE gain measurement can derive the information about the ground state complexation by

$$[22b] \quad K_{ASE} = (\sigma_{eb}/\sigma_{ea})(\sigma_{pb}/\sigma_{pa})(\tau_b/\tau_a) \cdot K$$

Hence K is the ground state complexation constant with stoichiometric constant m.

2. Effect of pumping intensity

In the above discussion, the pumping intensity effect (16–20) represented by the stimulated emission rates (I_{ea} and I_{eb}) in equation set [10] was not considered. Since the stimulated emission rate (I_{ea} or I_{eb}) is a function of the excited state population as well, the solution of the equation set [10], which could only be solved numerically, is very complicated. However, for moderate pumping intensities over the threshold, the stimulated emission rate (I_{ea} or I_{eb}) can be considered as a function of the pumping intensity with a small perturbation of the excited state population, which can be assumed constant for a specific pumping intensity. Therefore, the solution to the moderate pumping case can be found by derivations similar to those used for the threshold pumping case, except that the coefficients $k_{1,2}$ in eqs. [11]–[20] are now given by

$$[23a] \quad k_1 = \sum k_a + k_q[Q]^n + \sigma_{ea}I_{ea}$$

$$[23b] \quad k_2 = \sum k_b + k_{-q} + \sigma_{eb}I_{eb}$$

instead of eqs. [11*c*, *d*].

As the pumping intensity is increased above the threshold value (W_{th}), stimulated emission will compete with spontaneous emission and radiationless deactivation of species $\mathbf{A}^*$ and $\mathbf{B}^*$, which leads not only to a shortening of the decay time but also to strong non-exponential decay (18). For the purpose of extrapolation to K_{ASE} at the pumping intensity threshold value, $K_{ASE}(W_{th})$, eq. [20] can be simplified for the dynamic quenching process ($\alpha \rightarrow 0$):

$$[24a] \quad R_g = (\sigma_{eb}/\sigma_{ea})(k_q/k_2)[Q]^n = K_{ASE}[Q]^n$$

Here the K_{ASE} constant obtained from ASE gain measurement can be described by

$$[24b] \quad K_{ASE} = (\sigma_{eb}/\sigma_{ea})(k_q/k_2) = (\sigma_{eb}/\sigma_{ea})[k_q/(\sum k_b + k_{-q} + \sigma_{ea}I_{ea})] = (\sigma_{eb}/\sigma_{ea})(\tau_b/\tau_a)\frac{1 + k_{-q}\tau_b}{1 + k_{-q}\tau_b + \tau_b\sigma_{ea}I_{ea}}K_{SV}$$

Since the stimulated emission $\sigma_{eb}I_{eb}$ is pumping intensity dependent, eq. [24*b*] can be expressed in the simple form of

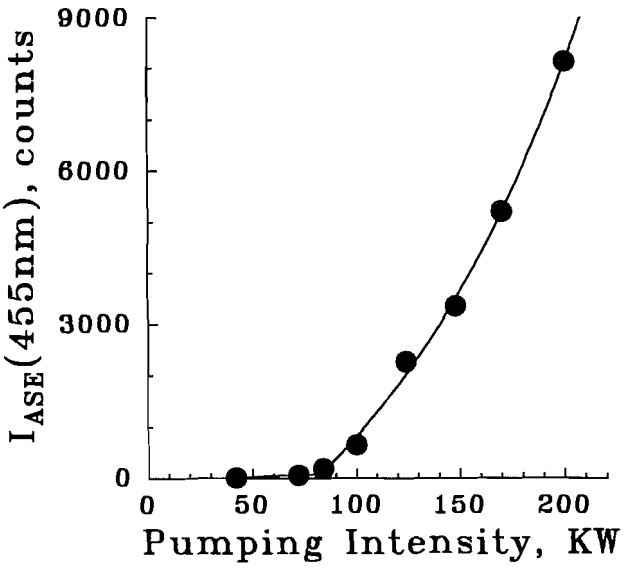


FIG. 3. ASE intensity (I_{ASE}) of coumarin-1 (8.0 mM) in pure *n*BuOH vs. pumping intensity (W) (dark circles) fitted by solid line as expressed by eq. [26].

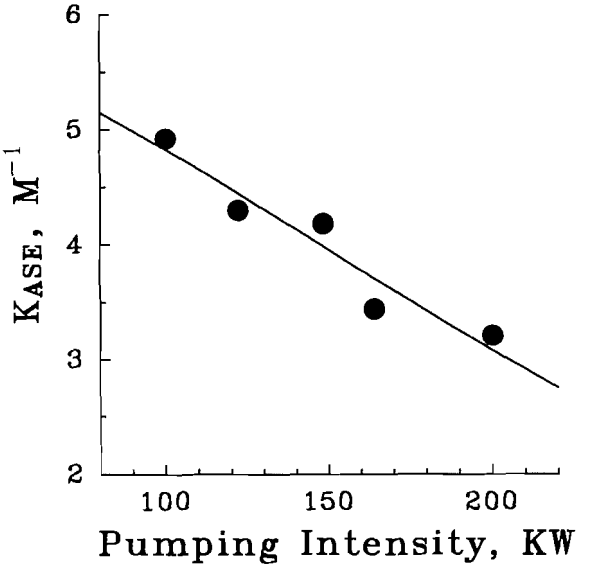


FIG. 4. Pumping intensity effects on K_{ASE} of coumarin-1 (8.0 mM) in *n*BuOAc containing different amounts of *n*BuOH (dark circles) fitted by solid line as described by eq. [25*b*].

$$[25a] \quad K_{ASE} = K_{ASE}(W_{th})/\{1 + \Gamma \cdot I_{eb}(W)\}$$

where Γ is a constant and $K_{ASE}(W_{th})$ is as defined in eq. [21*b*].

At intensities above the pumping threshold ($W \geq W_{th}$), we expect and observe an exponential function with respect to the pumping intensity for relatively small ASE signals (20). The dependence of the total ASE (I_{ASE}) of coumarin-1 in pure *n*BuOH at peak position (WL_b = 455 nm) on the pumping intensity (W) is shown in Fig. 3. The circles are the experimental points and the solid line is the best fit computed from the equation

$$[25b] \quad I_{ASE} = 4103 \cdot \{\exp(0.00909 \cdot (W - W_{th})) - 1\}$$

with $W_{th} = 80 \pm 5$ kW.

TABLE 1. Kinetic constants of coumarin-1 in different solvent mixtures

Solvent	Quencher	E_T^N of quencher[a]	Quenching constants (M^{-1}) K_{SV}[b]	K_{ASE}[c]	K[d]
*n*BuOAc	*n*BuOH	0.602	5.3	4.9	0.2[e]
*n*BuOAc	CH_2Cl_2	0.309	0.36	0.33	0.09
Isooctane	*n*BuOAc	0.241	0 (2.26)[f]	0.4	0.33

[a]Reference 21.
[b]From conventional spectrofluorimetric study (eq. [3]).
[c]Under 100-kW pumping intensity, if not specified.
[d]From uv/vis absorption study.
[e]In units of M^{-2}; ref. 10.
[f]No dynamic contribution; K = 0.26 M^{-1} was obtained from fluorescence spectra using eq. [27*b*].

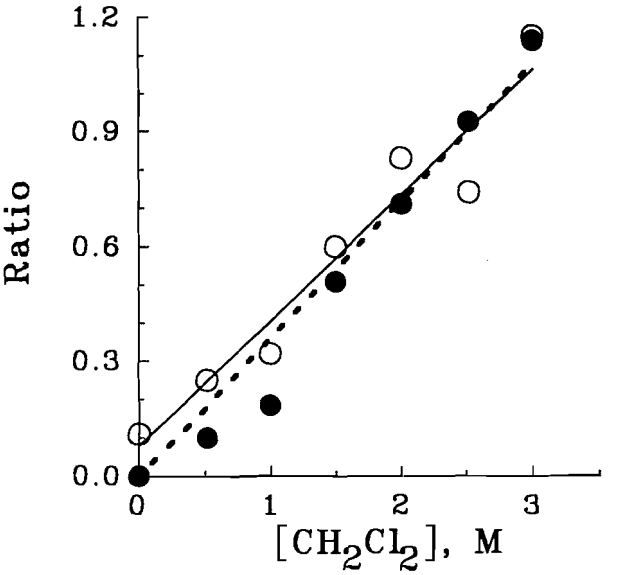


FIG. 5. Plot of Φ_a^0/Φ_a^{-1} and R_g versus $[CH_2Cl_2]$. Dark circles: Φ_a^0/Φ_a^{-1} ([coumarin-1]:0.035 mM) from conventional spectrofluorimetry fitted by dark dots line (K_{SV} = 0.36 M^{-1}); blank circles: R_g ([coumarin-1]:8.0 mM) from ASE gain spectroscopy fitted by solid line (K_{ASE} = 0.33 M^{-1}).

Since the spontaneous emission (I_{sb}) contribution is negligible ($I_{sb} \ll I_{eb}$) for pumping intensities $W > W_{th}$, the stimulated emission (I_{eb}) can be considered as the total ASE ($I_{eb} = I_{ASE}$). Applying eq. [25*a*] to simulate the experimental values of K_{ASE} by considering eq. [26] as the pumping intensity dependence of the stimulated emission (I_{eb}) in eq. [25*a*] for pumping intensities $W \geq W_{th}$, we obtained

$$[26] \quad K_{ASE} = K_{ASE}(W_{th})/\{1 + 0.341 \times [\exp(0.00909 \cdot (W - W_{th})) - 1]\}$$

where $K_{ASE}(W_{th}) = 5.2 \pm 0.3$ M^{-1}. The results are shown in Fig. 4 where the filled circles are the experimental values from the slopes of gain ratio (R_g) vs. concentration of *n*BuOH using eq. [21*a*], and the solid curve is calculated from eq. [25*b*].

Discussion

The fluorescence spectra of coumarin-1 in *n*BuOAc containing different amounts of CH_2Cl_2 (refer to Fig. 2) show

Can. J. Chem. Downloaded from www.nrcresearchpress.com by 123.30.183.119 on 09/08/12
For personal use only.

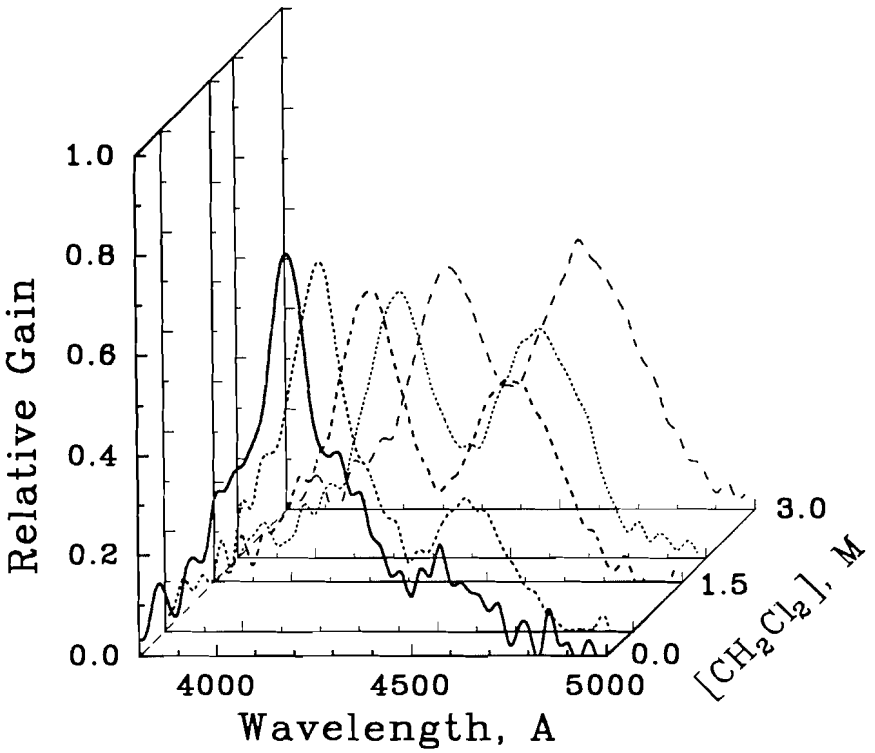


FIG. 6. Relative ASE gain spectra of coumarin-1 (8.0 mM) in *n*BuOAc containing different amounts of CH_2Cl_2 (0–3.0 M) at room temperature using eq. [1].

Can. J. Chem. Downloaded from www.nrcresearchpress.com by 123.30.183.119 on 09/08/12
For personal use only.

slight shifts in the peak position with changing concentration of CH_2Cl_2, which is mainly due to the excited state complexation between dye and quencher (CH_2Cl_2). The Stern–Volmer constant K_{SV} determined from eq. [3] is much larger than the ground state constant K from uv/vis absorption study (as listed in Table 1), which implies a higher capability of complexation in the excited state than in the ground state. In a system containing *n*BuOH, significant changes in the fluorescence spectra have been observed due to its strong H-bonding effect between alcohol and dye in the excited state (10).

In the isooctane/*n*BuOAc system, where there is no H-bonding effect in the excited state, there is only a slight shift in the fluorescence spectra of coumarin-1 with increasing concentration of *n*BuOAc. The value of the Stern–Volmer constant for dynamic quenching in the excited state determined from eq. [3] was found to be zero. With $K_{SV} = 0$, eq. [3] for the fluorescence quenching becomes:

$$[27a] \quad \Phi_a/\Phi_a^0 = 1 - \alpha$$

Since the sample is excited at the isosbestic wavelength ($WL_p = WL_{iso}$), the ratio of $\sigma_{pa}/\sigma_{pb} = 1$ in eq. [4] defining α, and eq. [27*a*] for the ground state equilibrium becomes:

$$[27b] \quad \Phi_a/\Phi_a^0 = 1/(1 + K[Q]^m)$$

The value of $K = 0.26\ M^{-1}$ obtained from the fluorescence quenching using eq. [27*b*] is similar to that obtained from the absorption measurement (Table 1).

Similarly, the weak binding effect of coumarin-1 in isooctane mixed with *n*BuOAc is also observed from their ASE gain spectra. To increase the signals, 200-kW pumping intensity was applied to get a gain ratio that satisfies eq. [22*a*] ($m = 1$). A value of K_{ASE} obtained by using eq. [22*a*] in Table 1 is comparable to the ground state complexation constant K from uv/vis absorption studies as presented by eq. [22*b*].

Table 1 also shows that the Stern–Volmer constants increase in the order:

$$[28] \quad K_{SV}\ (n\text{BuOAc}) < K_{SV}\ (CH_2Cl_2) < K_{SV}\ (n\text{BuOH})$$

which parallels quencher polarity (E_T^N (21)). The most significant factor, however, appears to be H-bonding between dye and quencher, consistent with our earlier conclusion (10).

As discussed in the previous section, the gain ratio of complexed and free species should satisfy eq. [21*a*]. A linear relation between R_g and concentration of CH_2Cl_2 is observed in Fig. 5 as expected. The ASE quenching constants K_{ASE} obtained experimentally in *n*BuOAc with CH_2Cl_2 and *n*BuOH (Table 1) are comparable to the K_{SV} from conventional spectrofluorimetry. Since the increase of the gain ratio R_g with CH_2Cl_2 or *n*BuOH is mainly due to excited state complexation between dye and CH_2Cl_2 or *n*BuOH (dynamic quenching), the K_{ASE} constant should satisfy eq. [21*b*] with unit stoichiometric constant ($n = 1$) as observed experimentally. Similarly, the K_{ASE} constant of coumarin-1 in the cosolvents isooctane and *n*BuOAc should be directly related to its ground state constant K (refer to eq. [22*b*]), because of the dominance of the static quenching over ground state complexation constant. When only the dynamic contribution is considered, the values of K_{ASE} for the different quenchers parallel those of the Stern–Volmer constant (eq. [28]).

When the dominant process is dynamic quenching, as in the case of coumarin-1 in *n*BuOAc mixed with *n*BuOH (10), the value of K_{ASE} at threshold, $5.2 \pm 0.3\ M^{-1}$, should be consistent with that determined from the Stern–Volmer quenching as discussed below.

TABLE 2. Comparison of K_{ASE} of coumarin-1 in *n*BuOAc[a] containing different amount of *n*BuOH[b] from ASE gain spectroscopy to that from conventional spectrofluorimetry

σ_{eb}/σ_{ea}[a]	τ_b/τ_a[b]	K_{SV}[c] (M^{-1})	K_{ASE}[d] (M^{-1})
1.4	0.85	5.3 ± 0.8	5.2 ± 0.3 (5.8 ± 1.7)[e]

[a]See footnote 2 of text.
[b]Equal to its quantum yield ratio in ref. 13*a*.
[c]Reference 10.
[d]Obtained from the best fit (eq. [25*b*]).
[e]Estimated from the Stern–Volmer constant using eq. [21*b*].

By estimating the ratios of $\sigma_{eb}(455\text{ nm})/\sigma_{ea}(420\text{ nm})$, τ_b/τ_a of coumarin-1 in pure *n*BuOH and *n*BuOAc as listed in Table 2, an ideal value of the K_{ASE} constant ($K_{ASE} = 5.8 \pm 1.7$ M^{-1}) can be estimated from the K_{SV} determined from conventional spectrofluorimetry by means of eq. [21*b*]. This value is similar to the K_{ASE} constant determined by extrapolation to the threshold intensity (W_{th}) using eq. [25*b*] ($K_{ASE}(W_{th}) = 5.2 \pm 0.3$ M^{-1}). The agreement between these two K_{ASE} constants also confirms the anticipated equivalence of these two techniques for the study of excited state complexation.

In Fig. 6, the separated two-component ASE gain spectra of coumarin-1 in *n*BuOAc with different amounts of CH_2Cl_2 were obtained directly from eq. [1]. By comparison with their fluorescence spectra in Fig. 2, a significantly higher resolution is observed for the gain spectra, which is very useful to identify multicomponent spectra with close peak positions.

During the sample preparation, the gain ratio (R_g) was found to be relatively insensitive to the variation of the coumarin-1 concentration ($\pm 10^{-4}$ M). By comparison, the quantum yield ratio measurements from conventional spectrofluorimetry were carried out with coumarin-1 concentrations of 0.035 mM and the difference between each sample and reference had to be less than 0.5% or $\approx \pm 10^{-7}$ M.

In conclusion, excited and ground state complexation of coumarin-1 in different solvents with or without quenchers has been investigated and a correlation between ASE gain spectroscopy and conventional spectrofluorimetry has been established, which has been confirmed in both experiment and theory. Although obviously limited to fluorophores capable of undergoing stimulated emission, the advantage of ASE gain spectroscopy over conventional spectrofluorimetry was found to be (a) higher frequency resolution to permit identification of multicomponents with close band positions; (b) easier sample preparation (no precise requirement about the dye concentration); (c) fast data treatment.

By comparing the excited state quenching constants with the empirical parameters for quencher polarity E_T^N (21), the reduction of the ASE gain of free species or enhancement of the ASE gain of complexes with respect to the quencher polarity E_T^N can be explained in terms of H-bonding formation between dye and quencher.

[2]The stimulated emission cross section $\sigma_{ei}(WL_i)$ (i = a, b) is given by the relationship (17):

$$\sigma_{ei}WL_i\ {}^4E_i(WL_i)/(8\pi\tau_i c n_i^2)$$

where $E_i(WL_i)$ is the fluorescence line shape function, n_i the refractive index of the solution at WL_i, τ_i is the lifetime of the fluorescing state without stimulated emission, and c the velocity of light *in vacuo*. Therefore, the ratio of the stimulated emission cross section of coumarin-1 in *n*BuOH to that in *n*BuOAc can be estimated by

$$\sigma_{eb}/\sigma_{ea} = (WL_b/WL_a)^4(\tau_a/\tau_b)(n_a/n_b)^2(E_b(WL_b)/E_a(WL_a))$$
$$\approx (WL_b/WL_a)^4(\Phi_a/\Phi_b)(n_a/n_b)^2(\Phi_b/\Phi_a)$$
$$= (WL_b/WL_a)^4(n_a/n_b)^2$$
$$= (455/420)^4 \cdot 1 = 1.4$$

Here the fluorescence line shape ratio of peaks $WL_b = 455$ nm and $WL_a = 420$ nm is approximated by its quantum yield ratio under assumption of equal band width, and the index ratio can be assumed to be unity.

Acknowledgements

R.W.Y. wishes to thank R. Norman Jones for his friendship, encouragement, and advice during their long association, which began in his section at NRC. The authors are indebted to the Natural Sciences and Engineering Research Council of Canada for financial support.

1. (*a*) I. WEINRYB and R. F. STEINER. The luminescence of the aromatic amino acids. *In* Excited states of proteins and nucleic acids. *Edited by* R. F. Steiner and I. Weinryb. Plenum Press, New York. 1971. Chap. 5; (*b*) S. GEORGHIOU. Fluorometric studies of biologically important molecular complexes. *In* Modern Fluorescence spectroscopy. Vol. 3. *Edited by* E. L. Wehry. Plenum Press, New York. 1981. Chap. 5; (*c*) R. F. CHEN. Proteins and peptides. *In* Practical fluorescence. 2nd. ed. *Edited by* G. G. Guilbault. Marcel Dekker, New York. 1990. p. 595.
2. R. LUMRY and M. HERSHBERG. Photochem. Photobiol. **27**, 819 (1978).
3. B. SKALSKI, D. M. RAYNER, and A. G. SZABO. Chem. Phys. Lett. **70**, 587 (1980).
4. M. S. A. ABDEL MOTTALEB, M. S. ANTONIOUS, M. M. ABO-ALY, L. F. M. ISMAIEL, B. A. EL-SAYED, and A. M. K. SHERIEF. J. Photochem. Phototobiol. A: **50**, 259 (1989).
5. G. G. ALOISI and F. ELISER. J. Phys. Chem. **94**, 5813 (1990).
6. (*a*) W. T. SILFVAST and J. S. DEECH. Appl. Phys. Lett. **11**, 97 (1967); (*b*) C. V. SHANK, A. DIENES, and W. T. SILFVAST. Appl. Phys. Lett. **17**, 307 (1970); (*c*) C. V. SHANK. Rev. Mod. Phys. **47**, 649 (1975).
7. (*a*) G. MAROWSKY, F. K. TITTEL, W. L. WILSON, and E. FRENKEL. Appl. Opt. **19**, 138 (1980); (*b*) P. CHOU, D. MCMORROW, T. J. AARTSMA, and M. KASHA. J. Phys. Chem. **88**, 4596 (1984); (*c*) P. FABENI, R. LINARI, G. P. PAZZI, and A. RANFAGNI. Appl. Opt. **26**, 5317 (1987).
8. J. HELDT, J. R. HELDT, J. SZCZEPANSKI, and H. A. DIEHL. Appl. Phys. B: **B46**, 339 (1988).
9. (*a*) V. MASILAMANI and B. M. SIVARAM. J. Lumin. **27**, 137 (1982); (*b*) V. MASILAMANI, V. CHANDRASEKAR, B. M. SIVARAM, B. SIVASANKAR, and S. NATARAJAN. Opt. Commun. **59**, 203 (1986); (*c*) Opt. Commun. **62**, 389 (1987); (*d*) A. RAMALINGAM. P. K. PALANISAMY, V. MASILAMANI, and B. M. SIVARAM. J. Photochem. Photobiol. A: **49**, 89 (1989).
10. R. W. YIP and Y-X. WEN. Can. J. Chem. **69**, 1414 (1991).
11. (*a*) G. PORTER and B. STEVENS. Progress in reaction kinetics. Vol. 1. Pergamon Press, Oxford. 1961. p. 189; (*b*) J. B. BIRKS. Photophysics of aromatic molecules. J. Wiley, London. 1970. p. 441; (*c*) J. N. DEMAS. Excited states lifetime measurements. Academic Press, New York. 1983. pp. 53–69.
12. R. W. YIP and Y-X. WEN. J. Photochem. Photobiol. A: **54**, 263 (1990).
13. (*a*) W. RETTIG and A. KLOCK. Can. J. Chem. **63**, 1649 (1985);

Can. J. Chem. Downloaded from www.nrcresearchpress.com by 123.30.183.119 on 09/08/12
For personal use only.

(*b*) G. J. JONES II, W. R. JACKSON, C-Y. CHOI, and W. R. BERGMARK. J. Phys. Chem. **89**, 294 (1985).
14. J. B. BIRKS, D. J. DYSON, and I. H. MUNRO. Proc. R. Soc. A, **275**, 575 (1963).
15. G. A. KORN and T. M. KORN. Mathematical handbook for scientists and engineers. McGraw–Hill, New York. 1968. p. 266.
16. A. PENZKOFER and W. FALKENSTEIN. *In* Picosecond phenomena. *Edited by* C. V. Shank, E. P. Ippen, and S. L. Shapiro. Springer-Verlag, Berlin, Heidelberg, New York. 1978. p. 71.
17. L. G. NAIR. Prog. Quantum Electron. **7**, 153 (1982).
18. H. E. LESSING, E. LIPPERT, and W. RAPP. Chem. Phys. Lett. **7**, 247 (1970).
19. E. SAHAR and D. TREVES. IEEE J. Quantum Electron. **13**, 962 (1977).
20. U. GANIEL, A. HARDY, G. NEUMANN, and D. TREVES. IEEE J. Quantum Electron. **11**, 881 (1975).
21. C. REICHARDT. Solvents and solvent effects in organic chemistry. VCH Verlagsgesellschaft mbH, Weinheim. 1988. p. 359.

Can. J. Chem. Downloaded from www.nrcresearchpress.com by 123.30.183.119 on 09/08/12
For personal use only.

Zongchao Jia, Guy Tourigny, Louis T. J. Delbaere, Allan L. Stuart, and Sagar V. Gupta. Structure and conformation of 5-methyoxymethyl-2′-deoxycytidine. Can. J. Chem. **68**, 836 (1990).

In Table 5 of this paper, the coordinates of one atom and the negative signs were inadvertently omitted. The corrected Table 5 is as follows:

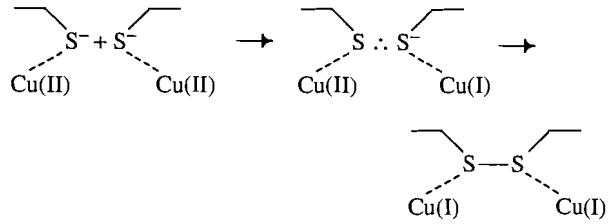
TABLE 5. Fractional coordinates and average thermal parameters for MMdCyd molecule A and molecule B (estimated standard deviation of the last digit is given in parentheses)

Atom	x/a	y/b	z/c	U
N(1A)	−0.0066(3)	0.8191(2)	0.4692(2)	0.0312
C(2A)	−0.1654(4)	0.8562(3)	0.4702(3)	0.0355
O(2A)	−0.1859(3)	0.8844(3)	0.5771(2)	0.0544
N(3A)	−0.2898(3)	0.8594(2)	0.3533(3)	0.0365
C(4A)	−0.2616(3)	0.8263(3)	0.2401(3)	0.0306
N(4A)	−0.3890(3)	0.8311(3)	0.1291(3)	0.0409
C(5A)	−0.0986(3)	0.7879(3)	0.2363(3)	0.0287
C(5, 1A)	−0.0601(4)	0.7606(3)	0.1063(3)	0.0345
O(5, 2A)	−0.1882(3)	0.7038(2)	0.0415(2)	0.0427
C(5, 3A)	−0.1819(5)	0.6897(3)	−0.0943(3)	0.0481
C(6A)	0.0225(4)	0.7861(3)	0.3539(3)	0.0302
C(1′A)	0.1343(4)	0.8241(3)	0.5955(3)	0.0331
C(2′A)	0.1461(4)	0.7506(3)	0.6887(3)	0.0401
C(3′A)	0.3399(4)	0.7415(3)	0.7483(3)	0.0371
O(3′A)	0.4015(3)	0.7911(3)	0.8662(2)	0.0508
C(4′A)	0.4169(4)	0.7707(3)	0.6335(3)	0.0388
O(4′A)	0.2936(3)	0.8296(2)	0.5572(2)	0.0388
C(5′A)	0.4573(5)	0.7035(3)	0.5426(4)	0.0542
O(5′A)	0.3115(3)	0.6517(3)	0.4971(3)	0.0584
N(1B)	0.0177(3)	0.9890(2)	0.0045(2)	0.0294
C(2B)	0.1758(3)	0.9529(2)	0.0007(3)	0.0316
O(2B)	0.2031(3)	0.9314(2)	−0.1092(2)	0.0490
N(3B)	0.2976(3)	0.9438(−)	0.1183(2)	0.0354
C(4B)	0.2648(3)	0.9668(2)	0.2358(3)	0.0304
N(4B)	0.3915(3)	0.9587(2)	0.3469(2)	0.0453
C(5B)	0.0981(3)	0.9991(2)	0.2437(3)	0.0294
C(5, 1B)	0.0574(4)	1.0199(2)	0.3757(3)	0.0353
O(5, 2B)	0.1652(3)	1.0859(2)	0.4381(2)	0.0446
C(5, 3B)	0.1552(5)	1.0969(3)	0.5741(4)	0.0615
C(6B)	−0.0188(3)	1.0090(2)	0.1250(3)	0.0293
C(1′B)	−0.1116(3)	1.0059(2)	−0.1233(2)	0.0283
C(2′B)	−0.2616(3)	0.9450(2)	−0.1516(3)	0.0287
C(3′B)	−0.4088(3)	0.9970(2)	−0.2344(3)	0.0300
O(3′B)	−0.4003(3)	1.0042(1)	−0.3729(2)	0.0373
C(4′B)	−0.3707(3)	1.0821(2)	−0.1679(3)	0.0338
O(4′B)	−0.1847(2)	1.0850(1)	−0.1134(2)	0.0335
C(5′B)	−0.4635(4)	1.1022(2)	−0.0580(3)	0.0484
O(5′B)	−0.4210(3)	1.0476(2)	0.0530(2)	0.0527

Stephen P. Mezyk and David A. Armstrong. Radical reductions of Cu(II)–penicillamine complexes: Evidence for a Cu(II)– disulphide anion intermediate. Can. J. Chem. **69**, 533 (1991).

Page 537, the line immediately after eq. [21] should read "The values of k_{17}, k_{18}, k_{19}, and k_{21} as reported in ref. 6 were...".

Page 539, reaction [24] should read

[24] 

Can. J. Chem. Downloaded from www.nrcresearchpress.com by 123.30.183.119 on 09/07/12
For personal use only.

Zongchao Jia, Guy Tourigny, Louis T. J. Delbaere, Allan L. Stuart, and Sagar V. Gupta. Structure and conformation of 5-methyoxymethyl-2′-deoxycytidine. Can. J. Chem. **68**, 836 (1990).

In Table 5 of this paper, the coordinates of one atom and the negative signs were inadvertently omitted. The corrected Table 5 is as follows:

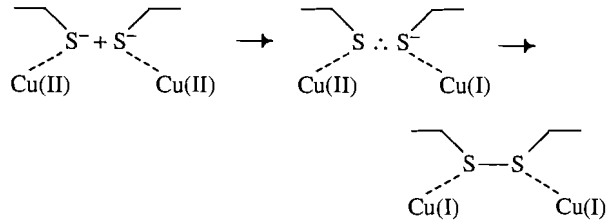
TABLE 5. Fractional coordinates and average thermal parameters for MMdCyd molecule A and molecule B (estimated standard deviation of the last digit is given in parentheses)

Atom	x/a	y/b	z/c	U
N(1A)	−0.0066(3)	0.8191(2)	0.4692(2)	0.0312
C(2A)	−0.1654(4)	0.8562(3)	0.4702(3)	0.0355
O(2A)	−0.1859(3)	0.8844(3)	0.5771(2)	0.0544
N(3A)	−0.2898(3)	0.8594(2)	0.3533(3)	0.0365
C(4A)	−0.2616(3)	0.8263(3)	0.2401(3)	0.0306
N(4A)	−0.3890(3)	0.8311(3)	0.1291(3)	0.0409
C(5A)	−0.0986(3)	0.7879(3)	0.2363(3)	0.0287
C(5, 1A)	−0.0601(4)	0.7606(3)	0.1063(3)	0.0345
O(5, 2A)	−0.1882(3)	0.7038(2)	0.0415(2)	0.0427
C(5, 3A)	−0.1819(5)	0.6897(3)	−0.0943(3)	0.0481
C(6A)	0.0225(4)	0.7861(3)	0.3539(3)	0.0302
C(1′A)	0.1343(4)	0.8241(3)	0.5955(3)	0.0331
C(2′A)	0.1461(4)	0.7506(3)	0.6887(3)	0.0401
C(3′A)	0.3399(4)	0.7415(3)	0.7483(3)	0.0371
O(3′A)	0.4015(3)	0.7911(3)	0.8662(2)	0.0508
C(4′A)	0.4169(4)	0.7707(3)	0.6335(3)	0.0388
O(4′A)	0.2936(3)	0.8296(2)	0.5572(2)	0.0388
C(5′A)	0.4573(5)	0.7035(3)	0.5426(4)	0.0542
O(5′A)	0.3115(3)	0.6517(3)	0.4971(3)	0.0584
N(1B)	0.0177(3)	0.9890(2)	0.0045(2)	0.0294
C(2B)	0.1758(3)	0.9529(2)	0.0007(3)	0.0316
O(2B)	0.2031(3)	0.9314(2)	−0.1092(2)	0.0490
N(3B)	0.2976(3)	0.9438(−)	0.1183(2)	0.0354
C(4B)	0.2648(3)	0.9668(2)	0.2358(3)	0.0304
N(4B)	0.3915(3)	0.9587(2)	0.3469(2)	0.0453
C(5B)	0.0981(3)	0.9991(2)	0.2437(3)	0.0294
C(5, 1B)	0.0574(4)	1.0199(2)	0.3757(3)	0.0353
O(5, 2B)	0.1652(3)	1.0859(2)	0.4381(2)	0.0446
C(5, 3B)	0.1552(5)	1.0969(3)	0.5741(4)	0.0615
C(6B)	−0.0188(3)	1.0090(2)	0.1250(3)	0.0293
C(1′B)	−0.1116(3)	1.0059(2)	−0.1233(2)	0.0283
C(2′B)	−0.2616(3)	0.9450(2)	−0.1516(3)	0.0287
C(3′B)	−0.4088(3)	0.9970(2)	−0.2344(3)	0.0300
O(3′B)	−0.4003(3)	1.0042(1)	−0.3729(2)	0.0373
C(4′B)	−0.3707(3)	1.0821(2)	−0.1679(3)	0.0338
O(4′B)	−0.1847(2)	1.0850(1)	−0.1134(2)	0.0335
C(5′B)	−0.4635(4)	1.1022(2)	−0.0580(3)	0.0484
O(5′B)	−0.4210(3)	1.0476(2)	0.0530(2)	0.0527

Stephen P. Mezyk and David A. Armstrong. Radical reductions of Cu(II)–penicillamine complexes: Evidence for a Cu(II)– disulphide anion intermediate. Can. J. Chem. **69**, 533 (1991).

Page 537, the line immediately after eq. [21] should read "The values of k_{17}, k_{18}, k_{19}, and k_{21} as reported in ref. 6 were...".

Page 539, reaction [24] should read

[24] 

Can. J. Chem. Downloaded from www.nrcresearchpress.com by 123.30.183.119 on 09/07/12
For personal use only.

Wolfgang Kliegel, Ulf Riebe, Steven J. Rettig, and James Trotter. Structural studies of organoboron compounds. XLVIII. 1,4-Diphenyl-3,3:6,6-bis(tetramethylene)-2,5,7-trioxa-3,6-diazonia-1,4-diboratabicyclo[2.2.1]heptane. Can. J. Chem. **69**, 1222 (1991).

In this paper, the correct Fig. 1 (p. 1226) should be the following:

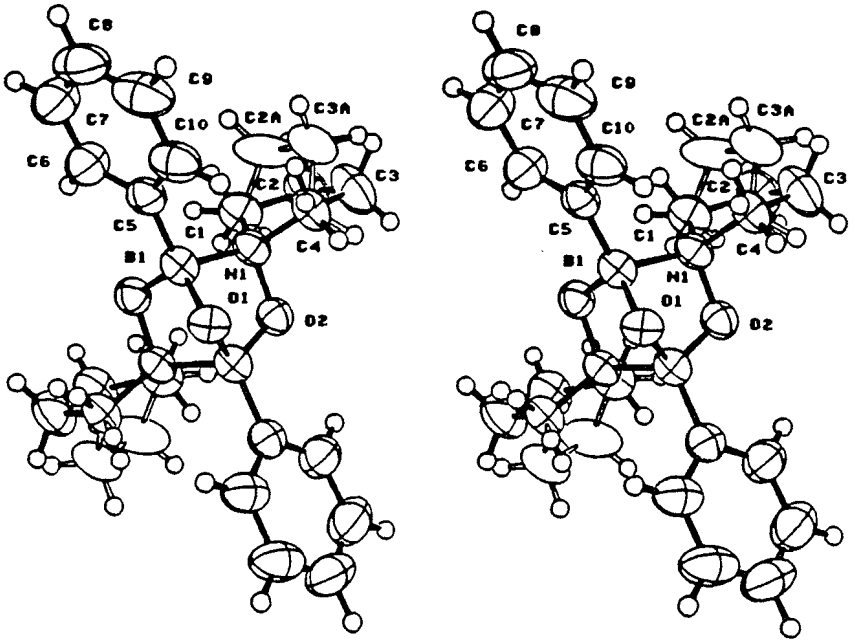


FIG. 1. Stereoview of **3***C*; 50% probability thermal ellipsoids are shown for the non-hydrogen atoms.

Can. J. Chem. Downloaded from www.nrcresearchpress.com by 123.30.183.119 on 09/08/12
For personal use only.